 © 1984 The Chemical Society of Japan Bull. Chem. Soc. Jpn., 57, 1—7 (1984)

Kinetic Isotope and Pressure Effects in the Reaction of Leucocrystal Violet with Tetracyanoethylene and Chloranil

Norio NISHIMURA* and Takushi MOTOYAMA
Department of Chemistry, School of Science, Okayama University, Tsushima, Okayama 700
(Received March 25, 1983)

The rates of reaction of Leucocrystal Violet (LCV) with chloranil (CA) and tetracyanoethylene (TCNE) were measured, and the kinetic isotope and pressure effects were examined. In the LCV-CA system, a very large isotope effect ($k_H/k_D \approx 11$) was observed, while in the LCV-TCNE system, it was not so large ($k_H/k_D = 5$—6) suggesting the tunnel effect is not substantial. For both systems, the formation of a CT complex in equilibrium with the reactants was observed at low temperatures (<−50 °C). From the rate law, the isotope effect, the electronic and ESR spectra observed during the reaction, and their time dependence, possible reaction processes are proposed.

When hydrogen(H·, H^+, or H^-) undergoes transfer in a rate-determining step, it is sometimes observed that the kinetic isotope effects are larger than those expected from differences in the zero-point energy of the isotopic bonds undergoing fission ($k_H/k_D > 7$). This has been regarded as evidence for the occurrence of quantum-mechanical tunneling, a highly mass-dependent property. Besides abnormally large kinetic isotope effects, isotopic dependence of the Arrhenius pre-exponential factor and curved Arrhenius plots are believed to be criteria of tunneling.

In 1977, Isaacs *et al.*[1] found abnormally large isotope effect ($k_H/k_D = 11.2$) in the reaction between Leucocrystal Violet (LCV) and chloranil (CA), but it levels off at a value near the maximum normal ratio of about 7.5 when the external pressure is raised to 2 kbar. According to them, the external pressure serves to lower the free energy barrier, thus the relative importance of tunneling diminishes with increasing pressure. They considered that the rate-determining step of the reaction involves a direct hydride ion transfer to produce a Crystal Violet cation and a tetrachlorohydroquinone anion(one-step process):

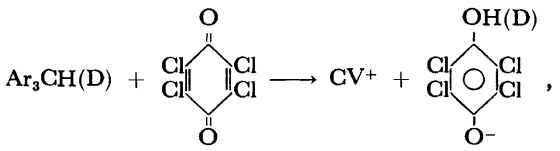

Ar = *p*-NMe_2-C_6H_4-

Indeed, reactions of *N*-benzyl-1,4-dihydronicotinamide and related compounds, recognized as models of dihydronicotinamide coenzymes for biological redox reactions, were believed to involve direct hydride transfer.[2,3] However, Steffens and Chipman[4] presumed, based on the kinetic isotope effects, that these reactions involve a two-step process and the intermediate may be a CT complex. Ohno and Kito,[5] and Fukuzumi and Tanaka[6] demonstrated that a CT complex is really formed as an intermediate product in these reactions.

This study has been undertaken to reexamine the direct hydride transfer mechanism in the LCV-CA system in the hope that similar pressure dependence of the kinetic isotope effect might be observed also in the reaction between LCV and tetracyanoethylene (TCNE).

Experimental

Reagents. LCV(H) was prepared as follows: dried Crystal Violet chloride was mortared in dry tetrahydrofuran and then lithium aluminium hydride powder was added slowly until the purple color of the solution diminished. The preparation was carried out under nitrogen in a dry-box. The product was poured into deoxygenated water and the precipitated Leucocrystal Violet was collected and dried. The LCV was recrystallized from benzene-ethanol mixture to give colorless needles. The same method was used with lithium aluminium deuteride to obtain LCV(D). Deuteration was ascertained by NMR. Commercial TCNE was purified by repeated sublimations. Chloroform of the reagent grade which contains *ca.* 1% ethanol for stabilization, was used as received, since no appreciable kinetic effect was observed compared with freshly distilled chloroform. Other solvents were purified as usual.

Procedures. A high-pressure reaction vessel, which is made of 17-4PH stainless steel and equipped with a water-circulating jacket and a stop-valve, was used. The vessel consists of two compartments, one for sample solutions and the other for reference solvents, with optical windows.

After a solution containing LCV and TCNE, and the solvent had been charged, same pressure was applied on them by a hand-pump through liquid separation pistons. After reading the pressure by a Heise Bourdon gauge, the stop-valve was closed and the vessel was separated from the pump system, and placed in a cell compartment of a Hitachi 105 double-beam spectrophotometer. The reaction was followed by monitoring the Crystal Violet cation (CV^+, $\lambda_{max} = 586$ nm), and the absorbance was recorded. Most of the runs were carried out under the conditions that the pseudo first-order plots could be realized. All runs were carried out in air. The kinetic data were checked by duplicate or triplicate runs.

In order to estimate the partial molar volumes of LCV and Crystal Violet chloride, and the molar volume of bulk Crystal Violet chloride, Ostwald-Sprengel and Weld types of pycnometers were used. By measuring the density of their chloroform solutions at various concentrations, the partial molar volumes at infinite dilution were estimated. Liquid paraffin was used for the determination of the molar volume of bulk Crystal Violet chloride.

Product Analysis. An equimolar mixture of LCV and TCNE in dichloromethane was allowed to stand at room temperature overnight, and the solution was chromato-

graphed on silica gel(Wakogel C-200). Two kinds of Crystal Violet salts (F_1 and F_2) were obtained. F_1: mp 225—227 °C, golden metallic flakes, λ_{max}/nm (ε) in $CHCl_3$, 305(30000), 398(22000), 416(21800), 586(140000); IR(Nujol) 2196 cm^{-1} (C≡N str). F_2: mp 164—166 °C, dark blue powder, λ_{max}/nm in $CHCl_3$: 305, 586; IR (Nujol) 2200 cm^{-1} (C≡N str).

Results

The reaction between LCV and CA in acetonitrile was carried out in a thermostated cell and the spectral change with time in the visible region is shown in Fig. 1. By means of the initial-rate method, the reaction order was confirmed to be first-order with respect to each reactant (Fig. 2). The reaction proceeds, in the initial stage, in accordance with the second-order rate law strictly. Figure 3 shows the Arrhenius plots based on the data of Isaacs *et al.*[1] and ours. The spectral change with time for the reaction between LCV and TCNE in chloroform is shown in Fig. 4. The absorption maxima at 305 and 586 nm are attributed to CV^+. These absorption bands increase with time at the expense of the bands due to TCNE (λ_{max}=266 and 276 nm), the isosbestic point being at 277 nm. Most of the reactions were carried out in excess of TCNE. Under such condition, the plot of $\ln(A_\infty - A_t)$ *versus* time t, where A_∞ and A_t are the absorbance at λ=586 nm at t=∞ and t, gave a straight line. The slope of the line was then plotted against the initial concentration of TCNE as shown in Fig. 5, giving a straight line passing the origin. We can therefore conclude that the overall order of reaction is second order. Similar pseudo-first-order plots were made for the reaction under various pressures (Fig. 6). As seen in Fig. 6, the external pressure accelerates the rate remarkably. In Table 1, the second-order rate constants for the reaction between LCV (H and D) and TCNE at various temperatures and under various pressures are listed. On the basis of the data in the table, the Arrhenius parameters were evaluated and they are given in Table 2. In Fig. 7, the rate constants in the logarithmic scale are plotted against

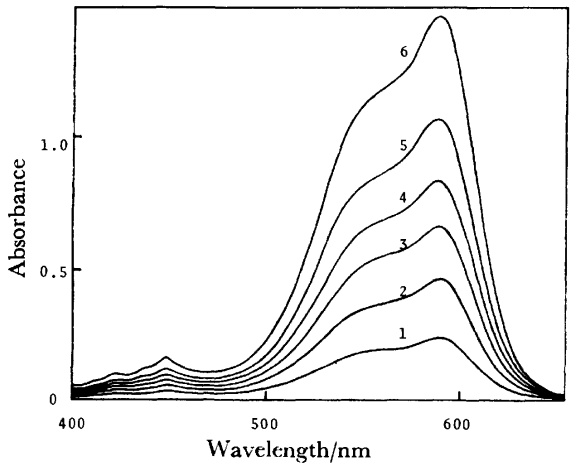

Fig. 1. Spectral change as a function of time for reaction between LCV and CA in acetonitrile at 20 °C. $[LCV(H)]_0 = 5.73 \times 10^{-4}$ mol dm^{-3}; $[CA]_0 = 4.80 \times 10^{-5}$ mol dm^{-3}. Time (min): 1, 5; 2, 10; 3, 15; 4, 20; 5, 30; 6, 60.

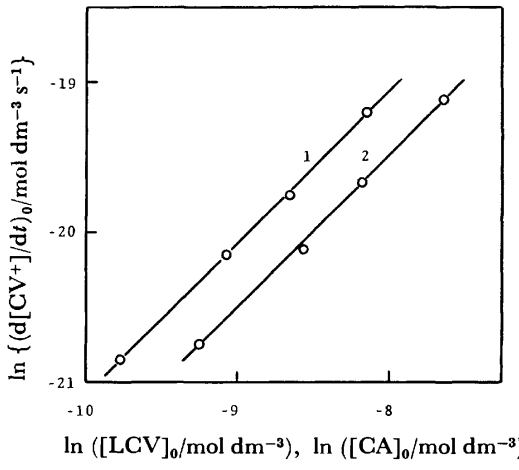

Fig. 2. Determination of the order of reaction by means of the initial-rate method. 1, $[CA]_0 = 1.82 \times 10^{-4}$ mol dm^{-3}; 2, $[LCV]_0 = 1.17 \times 10^{-4}$ mol dm^{-3}; 20 °C in acetonitrile.

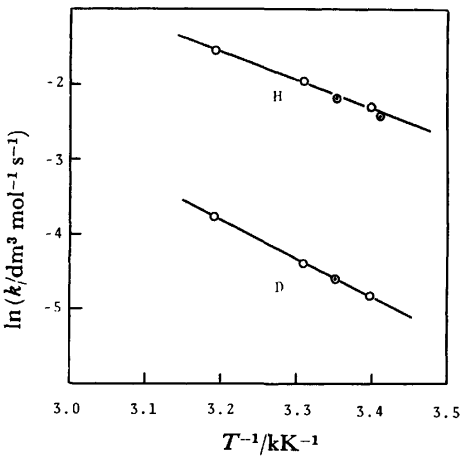

Fig. 3. The Arrhenius plots for the reaction of LCV (H or D) with CA. ⊙: Present results; ○: Isaacs *et al.*

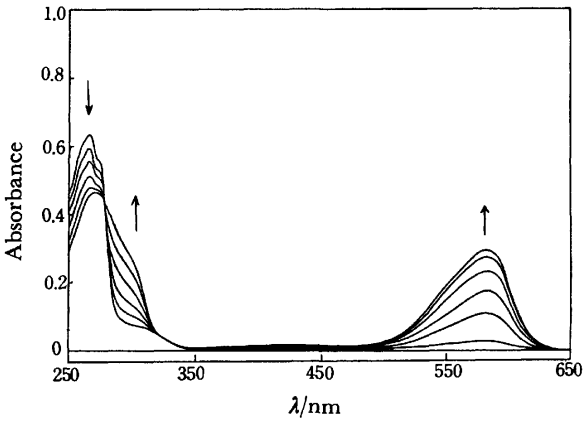

Fig. 4. Spectral change (every 30 min) during the reaction between LCV(H) and TCNE in chloroform at 30 °C. $[LCV]_0 = 6.76 \times 10^{-6}$ mol dm^{-3}; $[TCNE]_0 = 3.65 \times 10^{-5}$ mol dm^{-3}.

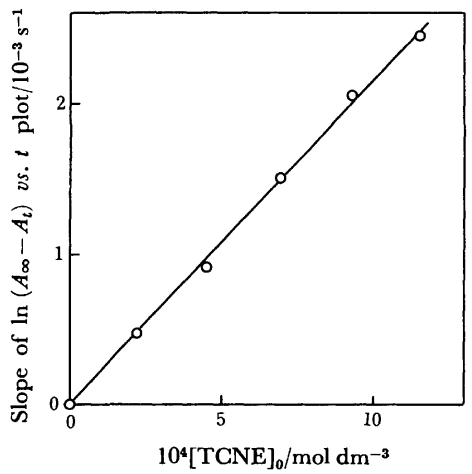

Fig. 5. Determination of the order of reaction with respect to [TCNE] by means of the isolation method. $[LCV]_0=6.90\times10^{-6}$ mol dm^{-3}; 30 °C.

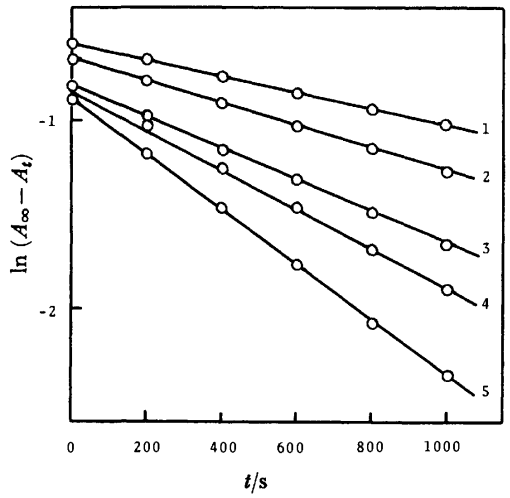

Fig. 6. Pressure dependence of the pseudo-first-order plot for the reaction between LCV(H) and TCNE in chloroform at 25 °C. $[LCV]_0=6.76\times10^{-6}$ mol dm^{-3}, $[TCNE]_0=2.43\times10^{-4}$ mol dm^{-3}; pressure (10^5 Pa): 1, 1; 2, 300; 3, 600; 4, 900; 5, 1200.

the external pressures. The solid lines represent the following quadratic regression equation:

$$\ln k_p = a + bp + cp^2. \quad (1)$$

The activation volumes at the atmospheric pressure were estimated according to the following equation:

$$\left(\frac{\partial \ln k_p}{\partial p}\right)_T = -\frac{\Delta V^*}{RT} + \Delta n\kappa_0 \approx b, \quad (2)$$

where Δn is the difference in the number of species between the activated complex and reactants, and κ_0 is the isothermal compressibility of the system ($\kappa_0=1.54\times10^{-9}$ Pa^{-1} for chloroform). In Table 3, the volumes of activation are given. Auxiliary kinetic data in benzene, benzene-toluene and benzene-*p*-xylene binary mixtures are given in Table 4.

Discussion

Reacion of LCV with CA. The maximum absorption at 586 nm (Fig. 1) is assigned to Crystal Violet cations, since the band and its shape agree with

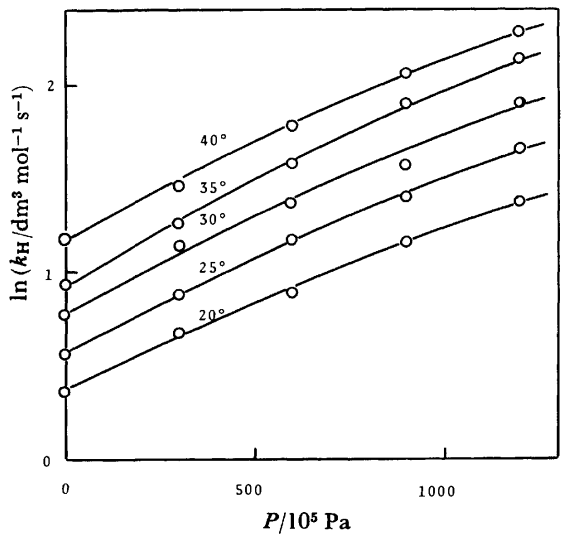

Fig. 7. Pressure dependence of k_H.

Table 1. Rate constants for the reaction between Leucocrystal Violet and tetracyanoethylene in chloroform

	P/10^5 Pa	k/dm^3 mol^{-1} s^{-1}				
		20 °C	25 °C	30 °C	35 °C	40 °C
H	1	1.44±0.20	1.73±0.08	2.13±0.10	2.50±0.11	3.20±0.18
	300	1.95	2.36	3.09	3.43	4.19
	600	2.39	3.18	3.88	4.75	5.89
	900	3.13	4.01	4.74	6.67	7.79
	1200	3.95	5.27	6.64	8.44	9.78
D	1	0.237±0.019	0.295±0.012	0.383±0.025	0.460±0.031	0.580±0.022
	300	0.328	0.396	0.535	0.680	0.792
	600	0.437	0.571	0.672	0.912	1.16
	900	0.564	0.745	0.846	1.16	1.32
	1200	0.694	0.863	1.08	1.46	1.80

those of an authentic sample. As for the assignment of the band system in the region 400—500 nm with maxima at 448 and 20 nm in acetonitile, there has been a confusion. Braude *et al.*[7] reported that the reaction of 1,2-dihydro-1-methylquinoline with CA can occur only by removal of a hydride ion from the position next to the nitrogen atom, followed by quaternization,

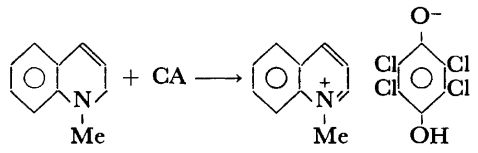

1 **2**

and the salt (**1**+**2**) in an acidic solution has one of its absorption maxima at 452 nm. Hajdu and Sigman[8] followed the rate of reaction between CA and a series of dihydronicotinamides by monitoring the absorption maximum at 448 nm in acetonitrile. They considered that tetrachlorohydroquinone anion **2** is responsible for the band. Very recently, Fukuzumi and Tanaka[6] also reported that in the same system a 1 : 1 CT complex is formed at first as an intermediate product, followed by a hydride transfer to afford **2** which is characterized by the absorption spectrum (λ_{max}=448 nm in acetonitrile).

On the other hand, Kainar and Überle[9] demonstrated that a mixture of *N,N,N',N'*-tetramethyl-*p*-phenylenediamine (TMPD) and CA acetonitrile solutions exhibits spectrum similar to that of CA-Na system in the range 400—500 nm. They considered that the complete transfer of an electron from TMPD to CA takes place to produce radical ions as ascertained by magnetic susceptibility measurements. Foster and Thomson[10] reported the visible absorption spectra for systems of TMPD-halobenzoquinones and considered that the band in question is due to CA semiquinone anion (**3**)

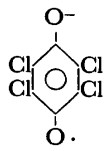

3

Iida[11] and Tsubomura *et al.*[12] also reported that the band can be assigned to **3**. The *g*-value of **3** is reported as 2.0058[13] and 2.0056±0.0002.[14]

When a mixture of LCV and CA acetonitrile solutions was subjected to ESR spectroscopy at room temperature, signals shown in Fig. 8 were recorded. The signal centered at 3337 G† has the *g*-value of 2.0058 in agreement with the reported one. From the above discussion and findings, the band system in the range 400—500 nm can unequivocally be assigned to **3**. The time dependence of the radical concentration is shown in Fig. 9. The radical concentration increases in parallel with the concentration of CV^+ at first, reaches a maximum and then decreases gradually. Therefore we regard **3** as the main product of the reaction.

Table 2. Activation parameters for the reaction between LCV and TCNE in chloroform

	P / 10^5 Pa	E_a / kJ mol^{-1}	$\Delta S^{\ddagger}$ / J K^{-1} mol^{-1}	r[a]
H	1	30.0±0.8	−148±3	0.997
	300	29.1±1.3	−148±4	0.994
	600	33.6±0.8	−131±3	0.998
	900	35.6±1.5	−123±5	0.994
	1200	34.5±1.2	−123±4	0.996
D	1	34.1±0.6	−149±4	0.999
	300	35.2±1.3	−143±5	0.996
	600	36.9±1.3	−134±5	0.996
	900	32.8±1.6	−146±4	0.992
	1200	37.1±1.1	−130±4	0.997

a) Correlation coefficient for the plot of ln k *versus* $1/T$.

Table 3. Volumes of activation($\Delta V^{\ddagger}$/cm^3 mol^{-1}) for the reaction between LCV and TCNE in chloroform

Temp / °C	20	25	30	35	40
H	−25.4	−29.6	−28.6	−33.7	−32.0
D	−31.4	−35.7	−29.2	−37.0	−34.1

Table 4. Rate constants for the reaction between Leucocryatal Violet and tetracyanoethylene in benzene and in binary mixtures

Solvent	Temp / °C	k_H / 10^{-2} dm^3 mol^{-1} s^{-1}	k_D / 10^{-2} dm^3 mol^{-1} s^{-1}	k_H/k_D
Benzene	25	5.63±0.05	1.01±0.05	5.57
Benzene	30	7.46±0.14	1.40±0.03	5.43
Benzene	35	9.77±0.03	1.86±0.04	5.25
Benzene	40	12.60±0.05	2.56±0.02	4.92
Benzene-Toluene (6:4 v/v)	30	4.98±0.01	0.95±0.03	5.25
Benzene-Toluene (2:8 v/v)	30	3.35±0.05	—	—
Benzene-*p*-Xylene (6:4 v/v)	30	1.11±0.02	0.24±0.01	4.70

† 1 G=10^{-4} T.

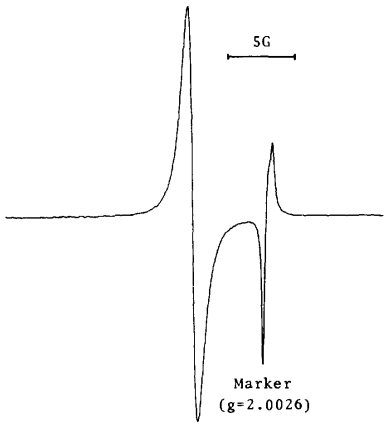

Fig. 8. ESR spectrum of CA anion radical in acetonitrile.

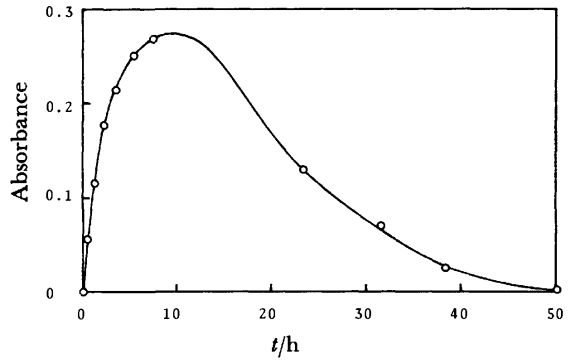

Fig. 9. Time dependence of CA anion radical concentration. $[LCV]_0=5.73\times10^{-4}$ mol dm^{-3}, $[CA]_0=4.80\times10^{-5}$ mol dm^{-3}, 20 °C in acetonitrile.

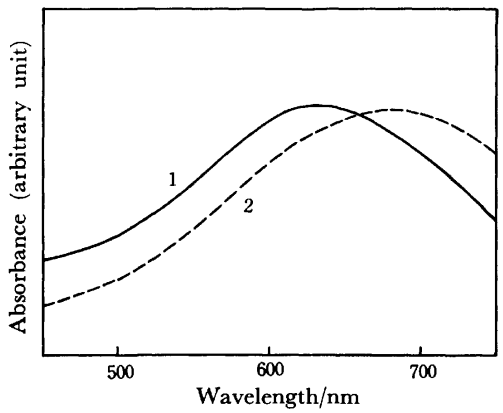

Fig. 10. Absorption spectra appeared when the mixture of LCV and TCNE (1) and LCV and CA (2) in EPA are cooled to ≈77 K.

There is a number of reports on the formation of CT complexes between CA and TCNE as electron acceptors, and bases. Since LCV may be regarded as a base, we expected the formation of CT complexes in our reaction systems. At room temperatures, there was no indication of the formation. However, when the reaction mixtures were cooled to below −50 °C, the solution turned deep blue. The color faded when warmed, and appeared again when cooled. The absorption spectra at ≈77 K are shown in Fig. 10. Judging from the position and the shape these absorption bands could be assigned to outer CT complexes in equilibrium with their components.

Nagakura *et al.*[15] found that an outer complex which is characterized by the absorption band at λ_{max}=560 nm (ε=1250) exists as a stable species in equilibrium with component CA and aniline below 200 K. On the basis of the time delay between the decay of the outer complex and the formation of a product, they further postulated the existence of an inner complex which is a precursor of the product.

Taking these situations into account, together with the substantial isotope effect and the kinetic law, the following alternative reaction schemes may be proposed.

$$LCV + CA \rightleftharpoons X_1 \rightleftharpoons X_2$$
$$X_1 \text{ or } X_2 \xrightarrow{\text{slow}} CV^+ + \mathbf{2}$$

Scheme 1.

$$LCV + CA \rightleftharpoons X_1 \rightleftharpoons X_2$$
$$\searrow^{\text{slow}}$$
$$CV^+ + \mathbf{2}$$

Scheme 2.

where X_1 and X_2 represent outer and inner complexes, respectively and their structures may be as follows:

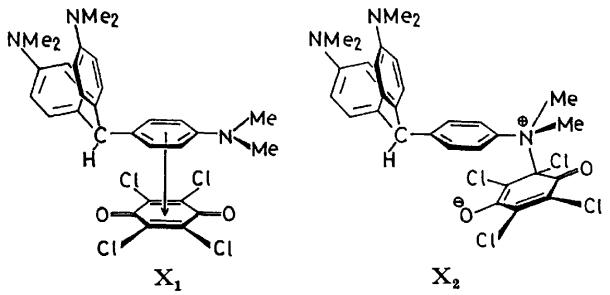

We have not ascertained the existence of X_2 yet.

If X_1 or X_2 is a precursor of CV^+, the transfer of an electron from the LCV-moiety to the CA-moiety, followed by the hydrogen atom transfer, is more likely than the direct hydride transfer. In Scheme 2, a highly polarized partial bond formation of the type $\equiv C^{\delta+}\cdots H\cdots^{\delta-}O=$ in the transition state may be involved. The remarkable kinetic pressure effect[1] could better be accounted for by this scheme rather than Scheme 1. In any way, the preference and detailed discussion for the reaction mechanism are open to future investigations. Steady-state assumption for **2** could explain the simultaneous formation of CV^+ and **3**.

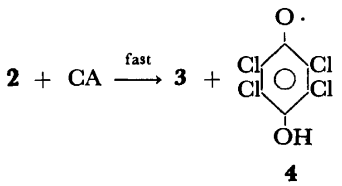

4

4 ⟶ dimerization, disproportionation

Reaction of LCV with TCNE. As seen in Fig. 4, a very weak band appears in the region λ=350—500 nm.

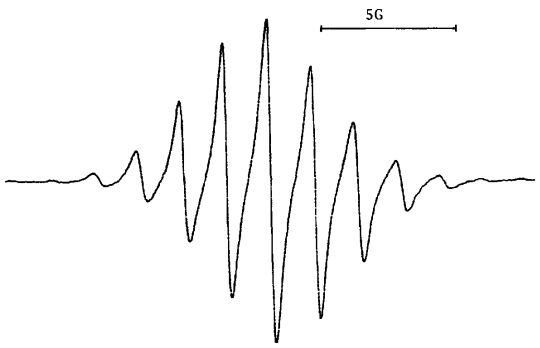

Fig. 11. ESR spectrum of TCNE anion radical.

The band spectrum becomes well-characterized in acetonitrile, and is assigned to TCNE anion radical, since the spectrum coincides with the reported one.[16] This is supported by the appearance of ESR signals when a mixture of LCV and TCNE solutions was subjected to ESR spectroscopy at room temperature (Fig. 11). The spectrum consists of nine lines (and two ^{13}C satellites) with a spacing of 1.6 G, and is assigned to TCNE anion radical, since the spectrum and the splitting constant agree with those reported.[17,18]

As seen in Table 3, the pressure effect on the rate of reaction is remarkable, suggesting also a large polarity change on going from the initial to the transition state in this system.

However, the ratios k_H/k_D in the LCV-TCNE system under various pressures are considerably smaller than those in the LCV-CA system,[1] and no systematic change in the ratio with increasing pressure was observed. The Arrhenius plots are not curved and the isotopic dependences of $\Delta S^{\ddagger}$ and $\Delta V^{\ddagger}$ (Tables 2 and 3) are not substantial. Therefore, we can conclude that the isotopic tunnel effect is, if any, immaterial in this system. As far as we inspected our data and those of Isaacs *et al.*, the reason why the tunnel effect is observed in the LCV-CA system alone has not been clarified.

When the reaction was carried out in benzene, the rate decreased a great deal (Table 4), while the isotope effect is similar to that in $CHCl_3$. The formation of CT complexes involving TCNE and various aromatic compounds are well known. Therefore, the very small rate constants in benzene compared with those in $CHCl_3$ may be attributed to the complex formation rather than the kinetic solvent effects. This is supported by the fact that the rate further decreased in the binary benzene-toluene and benzene-xylene systems in which more stable complexes are formed.[19]

The final electronic spectrum in the visible region for both the LCV-CA and LCV-TCNE systems agreed with the spectrum of authentic Crystal Violet in the case of kinetic runs. Under much more concentrated conditions, two kinds of salts (F_1 and F_2) were obtained (see Experimental section). The spectrum of F_1 involves extra maxima at 398 and 416 nm. Middleton *et al.*[20] reported that 1,1,2,3,3-pentacyano-2-propenide anion (PCP) in aqueous solutions is characterized by the absorption maxima at 393 nm (ε=22600) and 412 nm (ε=22100). Since our data for F_1 coincide with these values, the counter anion of the Crystal Violet cation may be PCP. The structure of F_2 has not been clarified yet.

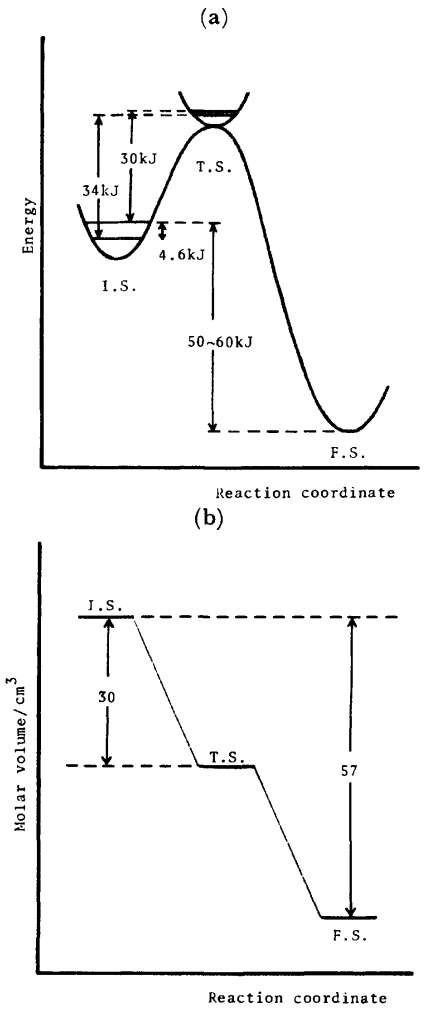

Fig. 12. (a) Energy profile. (b) Volume profile.

Potential and Volume Profiles. We finally wish to draw approximate potential and volume profiles. The zero point energy difference between C-H and C-D stretching vibrations of LCV was estimated to be *ca.* 4.6 kJ on the basis of the data for $CHCl_3$ (ν_{C-H}=3019 cm^{-1}, ν_{C-D}=2256 cm^{-1}). This might be responsible for the difference in the activation energy between the isotopic species (Table 2). Blanch *et al.*[22] studied the proton transfer reaction of 4-nitrophenylnitromethane with pentamethylguanidine to give an ion pair. According to them, the heat of reaction is -59.8 kJ mol^{-1} in acetonitrile and -54.0 kJ mol^{-1} in toluene. From the difference in the activation energy for the forward and backward reactions of *N*-ethyl-*N*-methylaniline with methyl iodide in nitrobenzene, Stewart and Weale[22] estimated the heat of forward reaction as -64.0 kJ mol^{-1}. If the overall heat of reaction in LCV-TCNE system is similar to those observed in perfect charge transfer reactions, it would be -50—-60 kJ mol^{-1}. In Fig. 12 (a), the potential profile for the reaction of LCV with TCNE is shown.

On the other hand, the partial molar volumes of LCV and CV^+ Cl^- in chloroform were estimated to be 349±6 and 320±10 cm^3 mol^{-1}, respectively. These values may be compared with the molar volume of bulk Crystal

Violet, 344.9 cm^3 mol^{-1}. The van der Waals volume of Cl_2 was estimated as 25.7 cm^3 mol^{-1}. The molar volume of Cl_2 may be twice as large as its van der Waals volume.[23] From the density data,[24] the partial molar volume of HCl in 40% aqueous solution was estimated as 23 cm^3 mol^{-1}. If we tentatively use these values, the volume change for the following reaction can be estimated as $\Delta V = -57$ cm^3.

$$\text{LCV} + \text{Cl}_2 \xrightarrow{\Delta\overline{V}} \text{CV}^+\text{Cl}^- + \text{HCl}$$

It is noted that the estimated volume change is similar to those observed in Menschutkin reactions (50—60 cm^3).[25] The volume of activation for the LCV-TCNE reaction are about -30 cm^3 mol^{-1} for both isotopic species (Table 3), indicating that the transition state is considerably polar. It was reported that in the LCV(H or D)-CA system, the volumes of activation in acetonitrile are -25(H) and -35(D) cm^3 mol^{-1}, respectively, the difference having been ascribed to the tunnel effect.[1] By using the above values, we can draw the volume profile for a reaction involving the nominal transfer of a hydride ion from LCV to a base, as shown in Fig. 12(b).

The authors wish to express their thanks to Mr. M. Kohno (JEOL) for the ESR measurements.

References

1) N. S. Isaacs, K. Javaid, and E. Rannala, *Nature*, **268**, 372 (1977); *J. Chem. Soc., Parkin Trans. 2*, **1978**, 709.

2) D. Mauzerall and F. H. Westheimer, *J. Am. Chem. Soc.*, **77**, 2261 (1955).

3) R. H. Abeles, R. F. Hutton, and F. H. Westheimer, *J. Am. Chem. Soc.*, **79**, 712 (1957).

4) J. J. Steffens and D. M. Chipman, *J. Am. Chem. Soc.*, **93**, 6694 (1971).

5) A. Ohno and N. Kito, *Chem. Lett.*, **1972**, 369.

6) S. Fukuzumi and T. Tanaka, *Chem. Lett.*, **1982**, 1513.

7) E. A. Braude, J. Hannah, and R. Linstead, *J. Chem. Soc.*, **1960**, 3249.

8) J. Hajdu, D. S. Sigman, *J. Am. Chem. Soc.*, **97**, 3524 (1975).

9) H. Kainer and A. Überle, *Ber.* **88**, 1147 (1955).

10) R. Foster and T. J. Thomson, *Trans. Faraday Soc.*, **58**, 860 (1962).

11) Y. Iida, *Bull. Chem. Soc. Jpn.*, **43**, 2772 (1970).

12) Y. Shirota, K. Kawai, N. Yamamoto, K. Tada, T. Shida, H. Mikawa, and H. Tsubomura, *Bull. Chem. Soc. Jan.*, **45**, 2683 (1972).

13) J. E. Wertz and J. L. Vivo, *J. Chem. Phys.*, **23**, 2441 (1955).

14) J. W. Eastman, G. Engelsma, and M. Calvin, *J. Am. Chem. Soc.*, **84**, 1339 (1962).

15) T. Nogami, K. Yoshihara, H. Hosoya, and S. Nagakura, *J. Phys. Chem.*, **73**, 2670 (1969).

16) M. R. Ronayne, J. P. Guarino, and W. H. Hamill, *J. Am. Chem. Soc.*, **84**, 4230 (1962).

17) W. D. Phillips and J. C. Rowell, *J. Chem. Phys.*, **33**, 626 (1960).

18) P. H. Rieger, I. Bernal, and G. K. Fraenkel, *J. Am. Chem. Soc.*, **83**, 3918 (1961).

19) R. E. Merrifield and W. D. Phillips, *J. Am. Chem. Soc.*, **80**, 2778 (1958).

20) W. J. Middleton, E. L. Little, D. D. Coffman, and V. A. Engelhardt, *J. Am. Chem. Soc.*, **80**, 2795 (1958).

21) J. H. Blanch, O. Rogne, and L. I. Rossemyr, *J. Chem. Soc., Faraday Trans. 1*, **76**, 1905 (1980).

22) M. S. Stewart and K. E. Weale, *J. Chem. Soc.*, **1965**, 2854.

23) T. Asano and W. J. leNoble, *Rev. Phys. Chem. Jpn.*, **43**, 85 (1973).

24) "International Critical Table," (1900), Vol. 3, p. 54.

25) K. E. Weale, "Chemical Reactions at High Pressures," E. and F. N. Spon Ltd., London (1967), Chap. 6.

Lithium Salt Effects on Extractions of 15-Crown-5, 18-Crown-6, or Their Silver(I) Complexes as Picrates

Yuko HASEGAWA,* Takahisa NAKANO, Yoshihiro ODORI, and Yūkō ISHIKAWA
Department of Chemistry, Science University of Tokyo, Kagurazaka, Shinjuku-ku, Tokyo 162
(Received May 18, 1983)

The extractions of 15-crown-5, 18-crown-6, or their silver(I) or lithium(I) complexes as picrates from lithium salt solutions into chloroform have been studied at 25 °C. The extractions of these crown ethers were impaired by an increase in the lithium perchlorate or nitrate concentration. A small salting-out effect was observed in the presence of lithium chloride. The extraction of silver(I) was also impaired by the addition of lithium perchlorate or nitrate. In the lower-concentration region of the lithium salts, the extraction of silver(I) was affected more markedly than that of crown ether itself.

The extraction of metal ions with crown ethers and anions has been measured under uncontrolled ionic media, although the extraction from constant ionic media should be useful in keeping the activity coefficients of all species constant. This fact is mainly caused by the facts that the extraction with crown ethers has been measured in rather dilute solutions, and that such suitable background salts as sodium perchlorate, which is employed in most extraction systems, can not be used because any cations may interact with the crown ethers.

However, information on the effects of salt on the extraction is necessary to treat the data quantitatively or to attempt the extraction and separation of trace elements such as the uranyl ion from seawater or concentrated salt solutions.

Recently, Kolthoff has made a preliminary report on the effect of salt on the extraction into dichloromethane of 18C6 (18-crown-6) and of the ion pair between the potassium ion complexed with the ether and the picrate anion.[1] According to his report, the extraction of 18C6 increased in the presence of lithium chloride, while the extraction of the complexed potassium ion decreased.

The present paper will describe the effect of lithium nitrate on the extraction of 15C5(15-crown-5), B15C5 (benzo-15-crown-5), 18C6, and DB18C6 (dibenzo-18-crown-6) and will extend to the effects of such anions as chloride and perchlorate ions on the extraction of 15C5 and 18C6. The effects of salt on the extraction of crown ether itself will be compared with the effect on the extraction of an ion pair consisting of silver(I) or lithium(I), a crown ether, and a picrate ion.

Experimental

Reagents. The lithium chloride and nitrate were recrystallized from water. The lithium perchlorate was prepared from lithium carbonate and perchloric acid and was then recrystallized from water. The concentration of the stock solutions, prepared by dissolving the salts in deionized water, was determined from the balance between the weight of an aliquot of each stock solution and that after it had dried up. The chloroform was washed with deionized water just before use. The benzo-15-crown-5 and DB18C6 were recrystallized from heptane and benzene respectively. The other reagents were used without further purification. The concentration of 15C5 or 18C6 was checked from the balance between the weight of the solution and that after it had dried up.

Procedures. Distribution constants of crown ethers: a portion of a salt stock solution at a certain concentration between 0 and 3 M (M=mol dm^{-3}) and a certain amount of a 15C5 or 18C6 aqueous solution were placed in a stoppered glass tube, together with chloroform, agitated mechanically for 1 h, and centrifuged. Then, a portion of each phase was transferred into another glass tube containing lithium dipicrylamide (7×10^{-4} M), a potassium chloride aqueous solution for 18C6 or a sodium chloride solution for 15C5, and a given volume of chloroform. After both phases had attained distribution equilibria, the absorbance of each chloroform phase was measured at 460 nm. Lambert-Beer's law holds to at least 2×10^{-5} M for 18C6 and 4×10^{-5} M for 15C5.

The distribution constant of a crown ether was calculated from the ratio of the total concentration between the two phases:

$$K_D = [E]_o/[E], \quad (1)$$

where E denotes crown ethers and where the subscript "o" and the lack of a subscript denote the organic phase and the aqueous phase respectively.

The distribution constant of B15C5 or DB18C6 was determined in a similar way except that we then employed the chloroform solution and the concentrations in the two phases were determined by measuring the absorption at 275 nm directly.

Distribution ratio of Ag^I or Li^I: Silver nitrate, lithium picrate, 15C5, or 18C6, and various amounts of lithium nitrate or perchlorate were placed in a stoppered glass tube together with an equal volume of chloroform. The two phases were then agitated vigorously. The concentration of silver(I) distributed between the two phases was determined by means of atomic absorption spectrometry. The extraction with DB18C6 was measured in a similar way except that we then used a chloroform solution containing DB18C6. The amount of lithium(I) extracted into the organic phases was measured by means of emission spectrometry. The distribution ratio of silver(I) or lithium(I), D, was defined as:

$$D = [M(I)]_o/[M(I)]. \quad (2)$$

Results and Discussion

Effect of Lithium Salts on the Distribution Constants of Crown Ethers. The distribution constants of crown ethers between water and chloroform, K_{D0}, are listed in Table 1. Figure 1 shows the change in the distribution constants (K_D) of 15C5, B15C5, 18C6, and DB18C6 as a function of the lithium nitrate concentration when the distribution constant (K_{D0}) between water and chloroform was employed as a reference (K_D/K_{D0}). The introduction of a benzene ring into crown

Table 1. Distribution constants of crown ethers and extraction constants of silver(I) with picrate anion and the ethers between water and chloroform

Crown ether	log K_{D0}	log K_{ex_0}
18C6	0.8	4.6
DB18C6	3.9[a)]	3.3[a)]
15C5	0.9	4.4
B15C5	2.4	3.5[b)]

a) Taken from Ref. 2. b) Taken from Ref. 3.

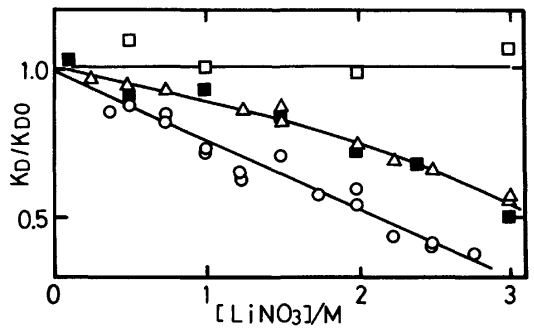

Fig. 1. The influence of $LiNO_3$ on the change in the distribution constant of 15C5 (○), 18C6 (△), DB18C6 (□), and B15C5 (■) when the distribution constant of each crown ether obtained from water was employed as a reference.
The total concentration of crown ether employed: 3.8×10^{-4} M (15C5), 1×10^{-4} M (18C6), 3×10^{-2} M (B15C5), and 1.8×10^{-2} M (DB18C6).

ether seems to lessen the salt effect. The different basicity of each crown ether would be one of the reasons why the effects of salt on the extraction of different crown ethers are not similar, as was suggested by Long and McDevit[4] with reference to the salt effect on simple molecules in aqueous solutions. Actually, the fact that the distribution constant of 15C5 changes more than that of B15C5 may be explained simply in terms of the higher basicity of 15C5. However, the extraction of 15C5 seems to be affected more markedly by the salt than that of 18C6, although 18C6 should be a little more basic than 15C5. If the difference in the effects of salt on different crown ethers is caused by the complexation of the ethers with the lithium ion in the background salt, the use of a more hydrophobic anion as a counter ion should improve the extraction. Figure 2-a shows the ratio of the distribution constants of 15C5 and 18C6 obtained from a salt solution to that of one obtained from water as a function of the lithium salt concentration. As may be seen from the figure, the anion effect does not seem to support the above expectation; *e.g.*, the value of the distribution ratio of 15C5 in the presence of 1 M lithium perchlorate is smaller than one-half the value of the distribution ratio in the absence of the salt, and in 2 M lithium perchlorate the value of the distribution ratio is only 20% of the value without the salt, while the presence of lithium chloride does not change the constant, although a rather large salting-out effect with lithium chloride was reported[1] (*e.g.*, the

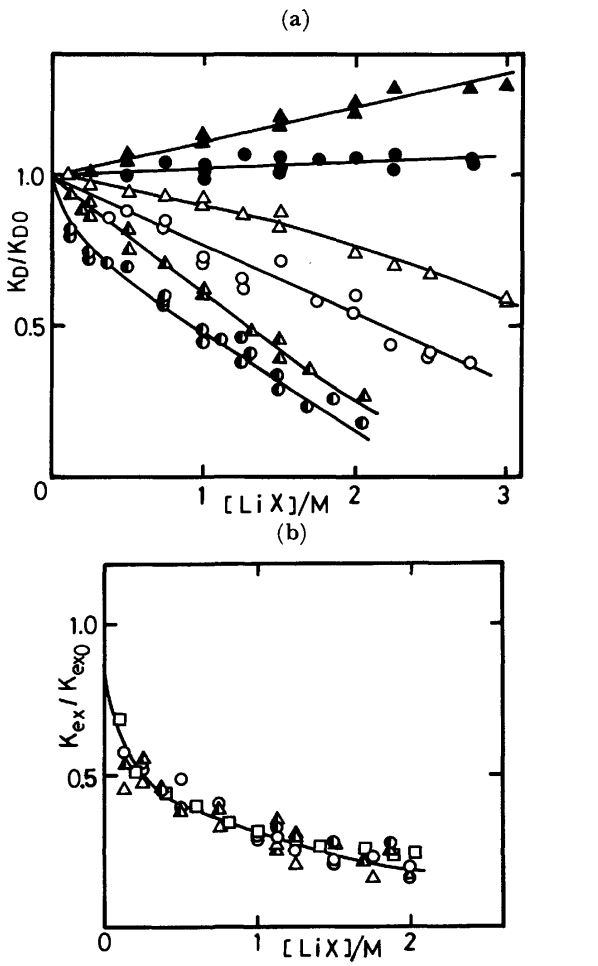

Fig. 2. Change in the distribution constant of crown ethers (denoted in Eq. 1) and the extraction constant of Ag^I with picrate ion and the crown ether (Eq. 5) by an addition of lithium chloride (closed symbols), nitrate (open symbols), or perchlorate (semiclosed symbols).
The K_{D0} and K_{ex_0} are listed in Table 1.
(a): The influence of lithium salts on the distribution constants of 15C5 (circles) and 18C6 (triangles).
(b): The influence of lithium salts on the extraction of Ag^I picrate with 15C5, 18C6 or DB18C6.
Aq phase: lithium salt solutions containing Ag^I of 5×10^{-5} M, 15C5 (circles) or 18C6 (triangles) of 1.1×10^{-3} M and 9.4×10^{-3} M lithium picrate. Org phase: $CHCl_3$ for 15C5 and 18C6 or $CHCl_3$ containing DB18C6 (squares) of 2.5×10^{-3} M.

distribution constant of 18C6 between water and dichloromethane, 4.5, increased to 7.4 even upon the addition of lithium chloride of only 0.4 M).

The tendency of the anion effect on the distribution constants of crown ethers is similar to that on the aqueous solutions of many nonelectrolytes, which was comprehensively reviewed by Long and McDevit.[4] The anion effect may not, however, be quantitatively explained by their theory, since they indicated that the theory is essentially valid only for nonpolar nonelectrolytes. They reported that the order of anions which exert greater salting-out effects on nonelectrolytes in aqueous solutions is in the sequence of $Cl^->NO_3^->ClO_4^-$.

The order of destroying the water structure by salt anions was also reported to be $ClO_4^->NO_3^->Cl^-$ on the basis of the IR measurements of various aqueous solutions.[5] Therefore, the order of anions whose presence leads to greater salting-in effects in the present extraction system, $ClO_4^->NO_3^->Cl^-$, seems reasonable.

Furthermore, it was confirmed by measuring the lithium(I) concentration in the organic phases that the increase in the extraction of the crown ethers is not caused by the extraction of the lithium ion complexed with crown ethers: when the concentrations of lithium(I) extracted with 15C5 or 18C6 into chloroform from lithium salt solutions were measured, it was observed that the concentrations increased with the increase in the salt concentration in the sequence of $ClO_4^->NO_3^->Cl^-$, as is generally observed in the extraction system of ion pairs. On the other hand, lithium(I) was not extracted without crown ether. Therefore, strictly speaking, the concentration ratio of crown ethers between organic and aqueous phases should be described as $D_E=([E]_o+[LiEX]_o)/[E]$ instead of Eq. 1. However, since even the concentration of lithium(I) in chloroform extracted from a 2 M lithium perchlorate solution containing 2.5×10^{-2} M 18C6 was less than 2×10^{-3} M, the proportion of $(LiE)^+ClO_4^-$ to the total crown ether in the organic phase would be 10% at a maximum under the present experimental conditions. Accordingly, the concentration ratio of the crown ether may be substantially represented as Eq. 1, and it may be concluded that the change in the distribution ratio of crown ether with the increase in the salt concentration is due to the change in the activity coefficients of crown ether, but not to the extraction of the lithium(I) complexed with crown ethers.

A simple method to determine activity coefficients using the solvent extraction method has previously been reported;[4,6] that is, the distribution constants of crown ethers, as represented by activity units, are always identical, as obtained either from water or from a salt solution:

$$\frac{\{E\}_o}{\{E\}}=\frac{\gamma_o[E]_o}{\gamma[E]}=\frac{\gamma_{0,o}[E]_{0,o}}{\gamma_0[E]_0}, \quad (3)$$

where γ or [E] denotes a value obtained from a lithium salt solution and where the subscript "0" denotes a value obtained from water. Since γ_o can be essentially regarded as $\gamma_{0,o}$ when the crown ether concentration in the organic phases is not high, $\gamma/\gamma_0=K_D/K_{D0}$. Therefore, the ratio of K_D to K_{D0} in Fig. 2-a should be nothing but the change in the activity coefficients of crown ether in lithium salt solutions at various concentrations.

Effect of the Salts on Extraction of the Ion Pair of Ag^I or Li^I with the Crown Ethers and the Picrate Ion. When silver(I) is distributed between aqueous solutions containing a crown ether and a picrate ion and chloroform, the extraction equilibrium and the extraction constant can be described as:

$$M^+ + E_{(o)} + A^- \rightleftarrows ME^+A^-_{(o)},$$

$$K_{ex}=\frac{[ME^+A^-]_o}{[M^+][E]_o[A^-]}, \quad (4)$$

$$=D[E]_o^{-1}[A^-]^{-1}, \quad (5)$$

where $[E]_o=[E]_{total}/(1+1/K_D)$ and the values of K_D at the different salt concentrations were obtained from Fig. 2-a.

Figure 2-b shows the change in the extraction constant of silver(I) as a function of the concentration of the background lithium salt when the extraction constant obtained from an aqueous solution containing no lithium salt was employed as the reference. The extraction of silver(I) also lessens upon the addition of lithium salts. It does not seem that there is a big difference with the sort of salt added or the sort of crown ether used as an extractant, although the extraction of the crown ether itself is affected by them, as may be seen in Fig. 2-a. Moreover, it is also observed that the addition of a small amount of the salt leads to a larger change in the extraction of silver(I) than in the extraction of the crown ethers. For example, the rate of the change in the extraction of the crown ethers to the extraction from a no-salt aqueous solution is only 5—20% upon the addition of the salts of 0.3 M, while that of silver(I) may be more than 50%.

The extraction constants of lithium(I) are plotted as a function of the salt concentration in Fig. 3. The extraction constants were calculated by using Eq. 5. The extraction constants of lithium(I) do not seem to change greatly with an increase in the salt concentration or with the sort of salt. The extraction with 18C6 would, though, be a little better than that with 15C5. The distribution ratio in the absence of a lithium salt such as nitrate or perchlorate could not be determined, because the amount of lithium(I) extracted into chloroform was too small to be determined.

As has been mentioned above, the salting-in effect with background salts on the extraction of the ion pairs can not be explained in terms of the decrease in the crown ether concentration which is effective in forming extractable complexes in aqueous phases. The different salt effect on the extraction of silver(I) from that of lithium(I) may suggest that cations may be affected by

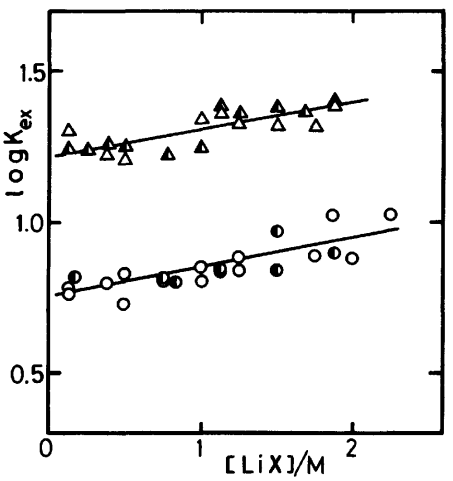

Fig. 3. The influence of lithium nitrate or perchlorate on the extraction constant of Li^I with 18C6 or 15C5 and picrate ion as a function of lithium salt concentration.
All symbols are the same in Fig. 2. The log D was around −4.

the background salt, because picrate ion is common to these systems. Besides, a metal ion trapped in a crown ether would not be as greatly affected as an untrapped metal ion. Salt effects on the extraction of an ion pair would thus be caused by a complex combination of many factors. Further information will be necessary before a detailed discussion of the salt effects on the ion pair extraction will become possible.

The authors wish to thank Professor Tatsuya Sekine of Science University of Tokyo for his valuable discussion. They would also like to thank Mr. Mitsuhiko Kase for his experimental aid.

References

1) I. M. Kolthoff, *Can. J. Chem.*, **59**, 1548 (1981).
2) Y. Hasegawa, N. Iizima, and T. Sekine, *J. Inorg. Nucl. Chem.*, **43**, 633 (1980).
3) Y. Hasegawa *et al.*, unpublished data.
4) F. A. Long and W. F. McDevit, *Chem. Rev.*, **51**, 119 (1952).
5) G. R. Choppin and K. Buijs, *J. Chem. Phys.*, **39**, 2042 (1963).
6) Y. Hasegawa and T. Sekine, *Bull. Chem. Soc. Jpn.*, **38**, 117 (1965).

Decrease in the Quantum Efficiency of a Cadmium Sulfide Photoanode Due to Sulfur Deposition. Determination of Quantum Efficiency by Temperature Measurement

Akira FUJISHIMA,* Tian-kai LI,† Yau-ning ZHU,† Guo-ding ZHOU,† and Xue-ping LI†
Department of Synthetic Chemistry, Faculty of Engineering, The University of Tokyo, Bunkyo-ku, Tokyo 113
†*Institute of Photographic Chemistry, Academia Sinica, Peking, People's Republic of China*
(Received June 23, 1983)

CdS photoelectrodes dissolve during photoanode reactions in a supporting electrolyte solution, and the quantum efficiency changes due to sulfur deposition. Temperature measurement technique has been used in this work to determine the quantum efficiency of the CdS photoelectrode. It has been found that decreases in the quantum efficiency can be monitored easily by this method.

A number of photoelectrochemical cells based on semiconductor electrodes for the purpose of converting solar energy either to chemical energy (*e.g.* the photodecomposition of water) or to electrical energy have been reported.[1-3] Most investigations to date have focused on the more familiar semiconductor compounds, *e.g.* Si, GaAs, GaP, ZnO, CdS, and TiO_2. Stable electrodes, such as TiO_2, have a large bandgap $Eg \geqslant 3$ eV, while materials with a smaller bandgap, such as CdS, tend to be unstable.

In the case of a CdS photocell, the electrode itself can be oxidized by photogenerated positive holes, so that the Cd^{2+} ions dissolve into the solution and atomic sulfur is deposited onto the electrode surface.[4] Hence, the photocurrent and the quantum efficiency of the electrochemical photocell dacay rapidly with time due to the filtering effect of the deposited sulfur.

The energy conversion efficiencies and quantum effiiencies of electrochemical photocells are very important factors in the effective utilization of solar energy. Recently Fujishima *et al.*[5] used a new method to measure the temperature change on a semiconductor electrode during photoelectrochemical reaction for determining the intrinsic quantum efficiency of the photoelectrochemical cell. When the semiconductor electrode is illuminated with a monochromatic light pulse having an energy E, with an average absorbed intensity I for a time t, consideration of the energy balance within the semiconductor photoelectrode in the limiting photocurrent region will result in the equation:

$$E\frac{\Delta T}{\Delta T^\circ} = \frac{Q_{sc}+T\Delta S}{It} + \eta e(V-V_{fb}), \qquad (1)$$

where ΔT is temperature change of the semiconductor surface; ΔT°, temperature change of the semiconductor surface in the open circuit; ΔS, entropy change for the semiconductor electrode reaction; Q_{sc}, heat evolved in the semiconductor *via* recombination and radiationless processes; η, quantum efficiency of photoelectrode reaction; V, applied potential *vs.* reference electrode; V_{fb}, flatband potential *vs.* reference electrode.

Therefore, under constant conditions of illumination (*i.e.* EIt held constant) a plot of $E\frac{\Delta T}{\Delta T^\circ}$ against $(V-V_{fb})$[5,6] yields the quantum efficiency η from the slope of the straight line and the loss term, $(Q_{sc}+T\Delta S)/It$, is obtained from the intercept of the $E\frac{\Delta T}{\Delta T^\circ}$ axis at $V=V_{fb}$.

To understand the quantum efficiency obtained from the relationship between temperature change and applied potential, two model cases are shown in Fig. 1. When $\eta=1.0$ the slope of $E\frac{\Delta T}{\Delta T^\circ}$ against V should be 1.0, since all the electrons excited into the conduction band by light irradiation move from the surface into the bulk of the semiconductor through the space charge layer generating heat. When $\eta=0.5$, the slope should be 0.5, since half of the excited electrons are recombined with the holes in the surface region.

In this study we used this method for measuring the change in the quantum efficiency of the photoelectrochemical reaction of the CdS photocell because of its great simplicity and the fact that there is no need to count the number of photons irradiated and/or absorbed.

Experimental

Electrode Preparation. The resistivity of the *n*-CdS single crystal used was 0.4 Ω cm, and the carrier concentration was 6×10^{16} cm^{-3}. The ohmic contact was made by rubbing In-Ga alloy on the back surface of the crystal and then attaching a copper wire to the contact with conducting Ag epoxy. The back and sides of the crystal were insulated and mounted on a flat piece of glass attached to a glass rod with epoxy resin.

Thermistors (Shibaura Electronics, Model BSB4-41A; nominal resistance 4 kΩ, sensitivity 0.052 °C/Ω), having a time constant 0.4 s when immersed in still water were used in matched pairs, in a differential arrangement with one held against the front surface of the semiconductor electrode and the other placed behind the electrode but not touching it.[5] The cell was carefully positioned so that the monochromatic light beam struck the electrode but none of the thermistors.

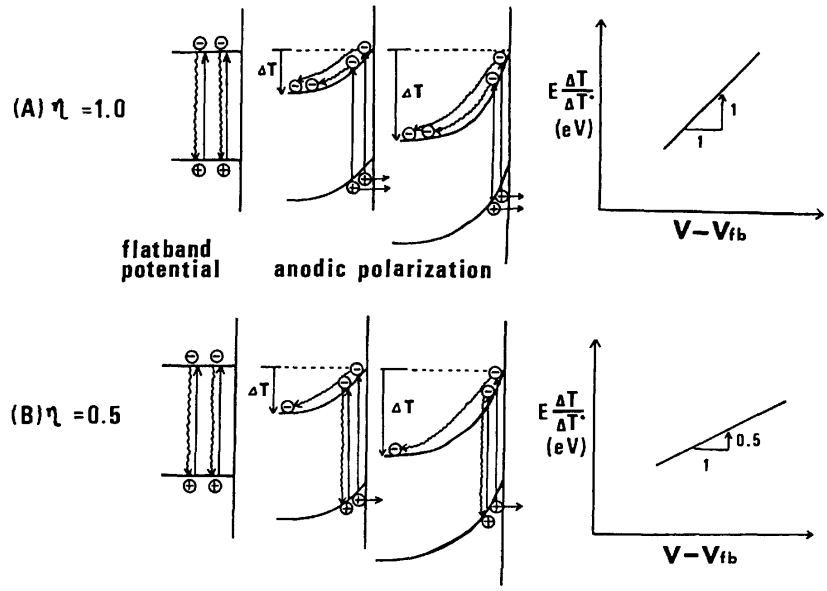

Fig. 1. Theoretical behavior of temperature change *vs.* potential.

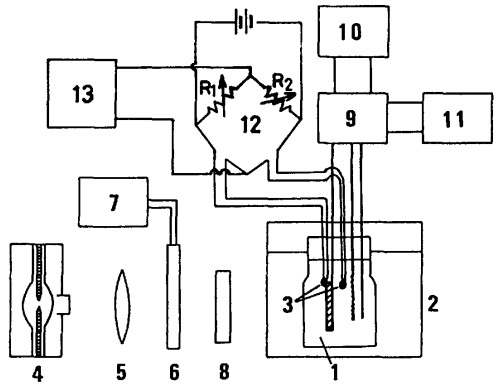

Fig. 2. Experimental apparatus.
1: cell, 2: water bath, 3: thermistor, 4: 500 W Hg lamp, 5: lens, 6: shutter, 7: timer, 8: filter, 9: potentiostat, 10: potential sweeper, 11: X-Y recorder, 12: D.C. bridge, 13: polyrecorder.

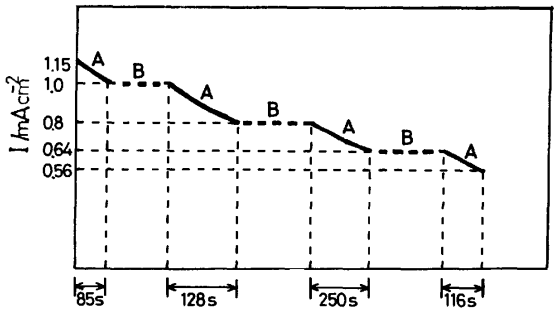

Fig. 3. Illustration of the experiment procedure.
A: Decrease of photocurrent in 0.2 M Na_2SO_4. B: Measurement of photothermal response in 0.1 M Na_2SO_3–0.2 M Na_2SO_4.

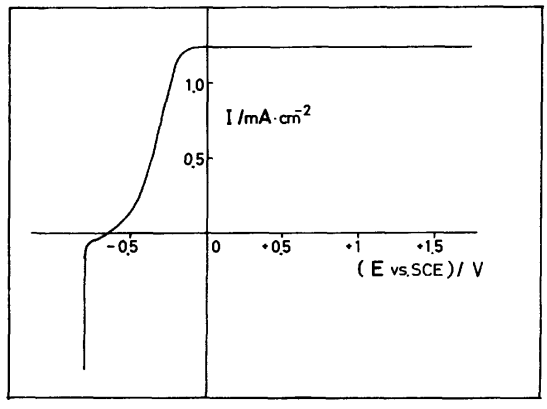

Fig. 4. Photocurrent *vs.* potential of CdS single crystal electrode in 0.1 M Na_2SO_3–0.2 M Na_2SO_4.

The CdS electrode was polished with sandpaper and etched for 10 s in concentrated HCl prior to use.

Apparatus. Figure 2 shows a block diagram of the experimental apparatus. The light source used was a 500 W Xenon lamp (Type SQ500) in an Ushio Model UI-501C lamp housing. Other apparatus included a lens to focus the light beam, a shutter to fix the irradiation period, and an interference filter (Koshin Kogaku) to select the wavelength of the exciting light.

Current-potential and current-time curves were measured under potentiostatic conditions with a Type HDV-7 potentiostat and Type KS-1 single scanner. These curves were displayed on an X-Y recorder (Type L23-24).

The electrochemical cell was a conventional three-electrode cell with a saturated calomel electrode (SCE) as the reference electrode and a Pt plate counter electrode.

All chemicals were of reagent grade and used without further purification.

Procedure. Figure 3 shows the experimental procedure. A photothermal experiment on surface-fresh *n*-CdS photoelectrode in 0.1 M Na_2SO_3–0.2 M Na_2SO_4 (1 M=

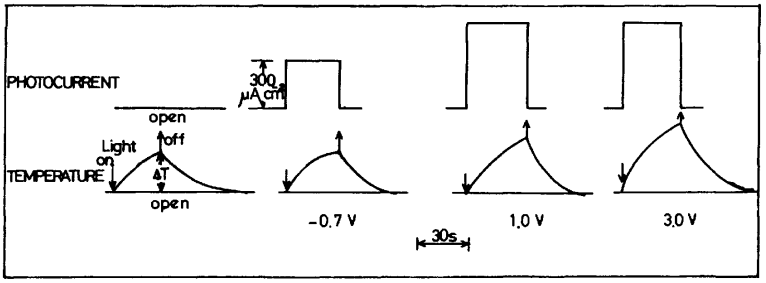

Fig. 5. Change in temperature *vs.* time (bottom) and anodic photocurrent *vs.* time (top) of the CdS anode in 0.1 M Na_2SO_3–0.2 M Na_2SO_4.

1 mol dm^{-3}) was first carried out according to the method reported.[5] The photothermal response and the saturated photocurrent, 1.15 mA/cm^2, were obtained. Then the electrode was put in 0.2 M Na_2SO_4 and the current-time was measured. The photocurrent gradually decreased because of sulfur deposition on the surface of the photoelectrode, and when it had decreased to a certain value (*e.g.* 1.0 mA/cm^2), the experiment was stopped. The electrode was immediately replaced in the 0.1 M Na_2SO_3–0.2 M Na_2SO_4 and the corresponding photothermal response was obtained. After that, the experiment was carried out alternately in the two solutions until the saturated photocurrent decreased to the lowest value in the experiment (*e.g.* 0.55 mA/cm^2).

Results are given for monochromatic irradiation at wavelengths shorter than that corresponding to the bandgap energy (*e.g.* 480 nm for CdS). Photothermal responses were obtained for the photoelectrode during anodic polarization, and under open circuit conditions in the electrolyte solutions. A change in temperature of the electrode caused a resistive change in the thermistor and produced a voltage imbalance in the DC bridge. The corresponding current and temperature changes were then plotted as a function of applied potential.

Results and Discussion

Figure 4 shows the current-potential characteristics of the CdS single crystal photoanode by using the 480 nm interference filter in 0.1 M Na_2SO_3–0.2 M Na_2SO_4 solution. In the dark, anodic photocurrent does not appear, but under illumination it does. The onset potential of the anodic photocurrent corresponds to the flatband potential of the photoanode, −0.75 V. The saturated photocurrent is stabilized at about 1.2 mA/cm^2.

The quantum efficiency of the CdS electrode was determined by temperature measurement in 0.1 M Na_2SO_3–0.2 M Na_2SO_4. Figure 5 shows the time dependency of changes in photocurrent and temperature of the CdS photoanode at each applied potential. Temperature increased when the light was turned on, and decreased when it was turned off. The relationship of temperature changes to applied potential is given in Fig. 6. The slope for CdS without deposited sulfur in the saturated photocurrent regions was approximately 1, nearly the same as reported by Maeda *et al.*,[6] but the slope decreased as sulfur was deposited on the electrode surface. In the absence of the reducing agent (Na_2SO_3) in the electrolyte solution (0.2 M Na_2SO_4), the photocurrent at the CdS photo-

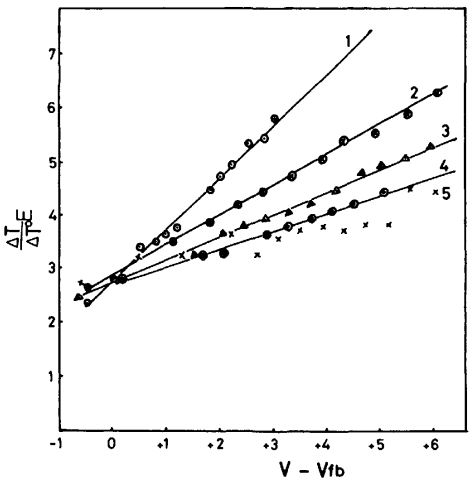

Fig. 6. Temperature change *vs.* potential of CdS single crystal electrode.
1: On fresh surface, 2—5: On surfaces with varying amounts of sulfur deposition. The photocurrents were observed in Na_2SO_3 solution. Therefore their values were almost constant as shown in dotted lines in Fig. 3; 1: 1.29(mA/cm^2), 2: 0.77, 3: 0.49, 4: 0.46, 5: 0.2—0.3

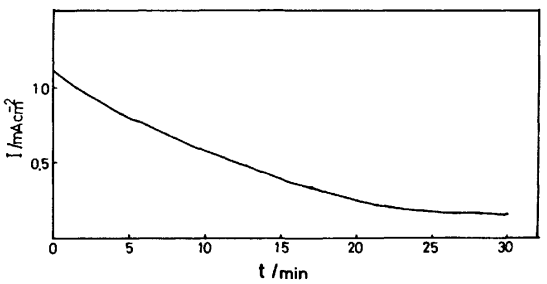

Fig. 7. Photocurrent *vs.* time of exposure of CdS single crystal electrode in 0.2 M Na_2SO_4.

anode resulted in the decomposition of the CdS according to the equation,[7]

$$CdS + 2p^+ \longrightarrow Cd^{2+} + S$$

and sulfur was deposited on the surface of the photoanode. Because the sulfur layer absorbed light, the intensity of the light penetrating it to impinge on the CdS single crystal decreased, so that the saturated photocurrent was reduced. The photocurrent decreased with the amount of sulfur, and with the time of

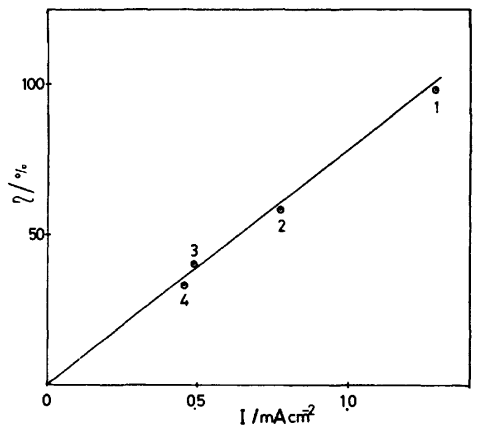

Fig. 8. Quantum efficiency *vs.* photocurrent of the CdS single crystal electrode. Number 1—4 was the same as Fig. 6.

exposure as shown in Fig. 7. Thus the saturated photocurrent corresponds to the amount of deposited sulfur. As the CdS photoanode decomposed in 0.2 M Na_2SO_4 to produce varying amounts of sulfur, a family of $E\frac{\Delta T}{\Delta T^\circ}$ *vs.* potential curves may be plotted (see Fig. 6). These lines corresponding to the amounts of sulfur deposited, remained linear in the saturated photocurrent regions, but their slopes varied with photocurrent. However, it was found at curve 5 in Fig. 6 that points at 0.35 mA did not form a straight line. Moreover, the saturated photocurrent increased during temperature measurement from 0.35 mA to 0.50 mA. It is suggested that in this case the deposited sulfur may not have adhered so strongly to the CdS surface, or may have broken off in part. A plot was made of slope, *i.e.*, quantum efficiency η, *vs.* photocurrent i, and it was found that η was also linear with i, as shown in Fig. 8. We assumed that it was the absorption of light by the deposited sulfur that resulted in the change of slope, since if the deposition layer was reflective, as for the reason of decrease of photocurrent, the slope would have been constant.

If the deposition layer adheres fully to the electrode surface, the amount of deposited sulfur, and presumably the average thickness of deposition layer will, in accordance with Faraday's law, be proportional to the number of coulombs. Therefore, the quantum efficiency of photocurrent will decreare with the number of coulombs flowed for surfur deposition. Actually we observed the decrease of quantum efficiency with the charge flowed for sulfur deposition.

This experiment indicates that the temperature measurement is also applicable to CdS photoanode on which sulfur is deposited.

The authors wish to express their thanks to Academia Sinica, People's Republic of China.

References

1) A. Fujishima and K. Honda, *Nature*, **238**, 37 (1972).
2) T. Watanabe, A. Fujishima, and K. Honda, *Bull. Chem. Soc. Jpn.*, **49**, 355 (1976).
3) H. Gerischer and J. Gobrecht, *Ber. Bunsenges. Phys. Chem.*, **80**, 327 (1976).
4) T. Inoue, T. Watanabe, A. Fujishima, and K. Honda, *J. Electrochem. Soc.*, **124**, 719 (1977).
5) A. Fujishima, Y. Maeda, and K. Honda, *J. Electrochem. Soc.*, **127**, 840 (1980).
6) Y. Maeda, A. Fujishima, and K. Honda, *Chem. Lett.*, **1980**, 271.
7) T. Inoue, T. Watanabe, A. Fujishima, and K. Honda, *Bull. Chem. Soc. Jpn.*, **52**, 1243 (1979).

Infrared Intensities in Methyl Chloride. II. Binary Overtone and Combination Bands

Shigeo KONDO,* Yoshinori KOGA, Taisuke NAKANAGA, and Shinnosuke SAËKI
National Chemical Laboratory for Industry, Tsukuba Research Center, Yatabe, Ibaraki 305
(Received June 25, 1983)

Infrared intensities of binary overtones and combinations of CH_3Cl and CD_3Cl molecules have been measured by the pressure broadening technique. Simplified formulas for the intensities of binary overtone and combination bands of symmetric top molecules were given. Contribution from the mechanical anharmonicity was calculated by use of these equations. Contribution from the electric anharmonicity was estimated by *ab initio* MO method (4-31 G*). The calculated intensities were compared with the observed values and discussed.

In Part I, we have analyzed the fundamental band intensities of CH_3Cl and CD_3Cl molecules to determine the values of the first derivatives of the dipole moment with respect to the normal coordinates ($\partial \boldsymbol{P}/\partial Q_i$).[1] The result of Part I is applied in the present study to analyze the intensities of binary overtone and combination bands of this molecule. The general expressions have been developed for the absorption intensities of two quantumn transitions in polyatomic molecules using the contact transformation method.[2-4] Up to the second order of approximation, the transition moments of the binary overtone and combination bands can be calculated if both the first and second partial derivatives of the molecular dipole moment with respect to the normal coordinates together with the cubic normal coordinate force constants are known. In Part I, we have determined the values of the first derivatives of the dipole moment including their signs. Furthermore the cubic force constants have also been obtained by the present authors[5] through the analysis of the vibration-rotation interaction constants. Therefore, it may be possible to gain some information on the values of the second derivatives of the dipole moment from the intensities of the two quantumn transitions.

The present paper reports the result of such analysis for methyl chloride molecule.

Theoretical

The dipole moment function of a molecule is expanded as a Taylor series in the dimensionless normal coordinates and is written as,

$$\boldsymbol{P} = \boldsymbol{P}_0 + \sum_r \boldsymbol{P}_r q_r + (1/2)\sum_{rs} \boldsymbol{P}_{rs} q_r q_s + \cdots, \quad (1)$$

where $\boldsymbol{P}_r$ stands for $(\partial \boldsymbol{P}/\partial q_r)$, $\boldsymbol{P}_{rs}$ for $(\partial^2 \boldsymbol{P}/\partial q_r \partial q_s)$, *etc.*[3] On the other hand, the potential function may also be expanded in dimensionless normal coordinates to give:

$$V/hc = (1/2)\sum_r \omega_r q_r^2 + (1/6)\sum_{rst} \varphi_{rst} q_r q_s q_t + \cdots, \quad (2)$$

where ω_r is rth normal frequency and φ_{rst} is a cubic force constant.[6]

In order to evaluate matrix elements of the dipole moment operator for anharmonic vibrational wave functions, we may use a contact transformation, T, to obtain,

$$\boldsymbol{P}' = T\boldsymbol{P}T^{-1}, \quad (3)$$

where

$$T = \exp(i\lambda S). \quad (4)$$

All details of the contact transformation calculations are given in Refs. 2, 3, and 4, and are not repeated here.

Then, according to Overend,[4] the integrated intensities of binary combination bands may be expressed by the following equation:

$$A_{ss'} = (8\pi^3 N/3hc)(\omega_s + \omega_{s'}) d_f (Q_{ss'})^2 \times Z_s Z_{s'} [1 - \exp\{-\beta(\omega_s + \omega_{s'})\}], \quad (5a)$$

where

$$Q_{ss'} = |\langle v_s = v_{s'} = 0 | \boldsymbol{P}' | v_s = v_{s'} = 1 \rangle|. \quad (5b)$$

Similarly, for binary overtone bands,

$$A_{ss} = (8\pi^3 N/3hc)(2\omega_s) d_f (Q_{ss})^2 Z_s^2 \{1 - \exp(-2\beta\omega_s)\}, \quad (6a)$$

where

$$Q_{ss} = |\langle v_s = 0 | \boldsymbol{P}' | v_s = 2 \rangle|. \quad (6b)$$

Here, N is Avogadro's number, c is the velocity of light, h is Plank's constant, ω_s is the sth normal frequency, d_f is the degeneracy of the upper vibrational state, β is $1/kT$, Z_s is the partition function for the sth normal vibration, $Z_s = 1/\{1 - \exp(-\beta\omega_s)\}$, and $\boldsymbol{P}'$ is the transformed molecular dipole moment.

By substituting appropriate expressions for the transition moments, Q_{ss} and $Q_{ss'}$, we can also use these equations for the absorption intensities of different kind of two quantumn transitions of symmetric top molecules. The method of evaluating the transition moments was shown by Overend.[7] The result is as follows:

$$Q_{ss}^z = (1/2\sqrt{2})[P_{ss}^z + \sum_{s'} P_{s'}^z \varphi_{sss'} \omega_{s'}/(4\omega_s^2 - \omega_{s'}^2)], \quad (7)$$

$$Q_{ss'}^z = (1/2)[P_{ss'}^z + \sum_{s''} P_{s''}^z \varphi_{ss's''} \omega_{s''}/\{(\omega_s + \omega_{s'})^2 - \omega_{s''}^2\}], \quad (8)$$

$$Q_{st}^x = (1/2)[P_{st}^x + \sum_{t'} P_{t'}^x \varphi_{stt'} \omega_{t'}/\{(\omega_s + \omega_t)^2 - \omega_{t'}^2\}], \quad (9)$$

$$Q_{tt}^z = (1/2)[P_{tt}^z + \sum_s P_s^z \varphi_{tts} \omega_s/(4\omega_t^2 - \omega_s^2)], \quad (10)$$

$$Q_{tt}^x = (1/2)[P_{tt}^x + \sum_{t'} P_{t'}^x \varphi_{ttt'} \omega_{t'}/(4\omega_t^2 - \omega_{t'}^2)], \quad (11)$$

$$Q_{tt'}^z = (1/\sqrt{2})[P_{tt'}^z + \sum_s P_s^z \varphi_{tt's} \omega_s/\{(\omega_t + \omega_{t'})^2 - \omega_s^2\}], \quad (12)$$

$$Q^{x}_{tt'} = (1/\sqrt{2})[P^{x}_{tt'} + \sum_{t''} P^{x}_{t''}\varphi_{tt't''}\omega_{t''}/ \{(\omega_t+\omega_{t'})^2-\omega_{t''}^2\}]. \quad (13)$$

In these equations, all of the summations are unrestricted, so that $\Sigma_{s'}$ includes the term with $s'=s$ and $\Sigma_{t'}$ includes the term with $t'=t$, *etc.* However, the index s runs only over nondegenerate modes and the index t runs only over degenerate modes. The numerical subscripts on t for the other dipole moment expansion coefficients are as follows; $P^{x}_{t}=P^{x}_{ta}=P^{y}_{tb}$, $P^{x}_{tt'}=P^{z}_{tat'a}=P^{z}_{tbt'b}$, and $P^{x}_{tt'}=P^{x}_{tat'a}=-P^{x}_{tbt'b}=-P^{y}_{tat'b}=-P^{y}_{tbt'a}$.[7] Similarly, the numerical subscripts on t for the other cubic anharmonic force constants are as follows; $\varphi_{stt'}=\varphi_{stat'a}=\varphi_{stbt'b}$; $\varphi_{tt't''}=\varphi_{tat'at''a}=-\varphi_{tat'bt''b}=-\varphi_{tbt'at''b}=-\varphi_{tbt'bt''a}$.[8]

These equations are by no means new but have a definite advantage over the previous ones[7] in that the expressions are given for the individual cases in much simpler forms.

Experimental Results

The sample gases of CH_3Cl and CD_3Cl are the same as those used in Part I which were purchased from Takachiho Chemical Co. and Merck Sharp & Dohme Co. Canada, respectively. The purity of CH_3Cl was stated as 99.5% and that of CD_3Cl was 99 atom%. As will be described later inspection of full region of the infrared spectra of these gases well guaranteed the stated sample purities.

Spectra were all observed with a Nicolet model 7199 FT-IR spectrophotometer accomodated with a mercury-cadmium telluride detector. Optical resolution of 0.25 cm^{-1} was used (maximum path difference of 4 cm, with Happ-Genzel apodization). For intensity measurements, a 6 cm high pressure cell with KBr windows was used under a total pressure of 1.11×10^6 Pa. In order to investigate rotational fine structure of the bands, a conventional 10 cm glass body cell was used. The sample pressure was measured with an MKS baratron type 220, which covers a pressure range of 1.333×10^5 to 1.333×10^2 Pa with a stated accuracy of 0.25% of reading.

Integration of the "isolated" band area were carried out in a manner similar to the one described in Ref. 9 according to the following equation:

$$B_l = (1/nl)\int_{\text{band } l} \ln (T_0/T)d\nu, \quad (14)$$

where n is the sample concentration (mol m^{-3}), l is the optical path length (m), T and T_0 are the transmittance values of the cell with and without the sample gas, respectively. The band intensity is given by units of km $mol.^{-1}$

In many places in the spectra of both CH_3Cl and CD_3Cl, overtone and combination bands were observed to be overlapping with each other. Therefore, whenever possible use was made of a simulation technique to obtain individual band intensities. As usual, the simulation calculation was carried out for the spectra taken under the pressurized sample condition.[1,9] In the calculations, the ground state values of the rotational constants A and B were assumed for the excited vibrational states unless otherwise described. On the other hand, the values of the band centers ν^0 and Coriolis zeta constants ζ^z were obtained from the analysis of the spectra when they were not available in the literature.

For CH_3Cl molecule, the spectral region from 6300 through 500 cm^{-1} has been investigated. There are several things to be noticed in the spectrum. One is a fact that strongly absorbing bands are all due to the fundamentals. Only exception is a parallel component of the $2\nu_5$ band. The fact that the intensity of this particular band is by far the largest among the (binary) overtones and combinations strongly suggests that it is due to the Fermi resonance with the neighboring ν_1 band. This is in accord with the conclusion obtained by Bensari-Zizi and Alamichel.[10] Secondly, as regards the remaining bands, the large majority of them can be assigned to binary overtones and combinations. Also we can find a few of the ternary combinations such as $(\nu_2+2\nu_5^0)$, $(2\nu_2+\nu_5)$, $(\nu_6+2\nu_5^0)$, and $(\nu_3+2\nu_5^0)$.[11] It is most probable that their intensities are borrowed from the neighboring binary combinations through the Fermi resonances. Almost nothing is left to be assigned to impurity bands.

In the 6200—5800 cm^{-1} region, $2\nu_4$, $(\nu_1+\nu_4)$, and $2\nu_1$ bands are expected. The parallel component of the $2\nu_4$ band is clearly observed at 6015.1 cm^{-1}. The band center of the perpendicular component, $2\nu_4(\perp)$, was tentatively located at 6062 cm^{-1}. Since the $2\nu_4(\perp)$ band is strongly perturbed by the Fermi resonance with $(\nu_4+3\nu_6)$ band, the intensity of the $2\nu_4(//)$ was first determined by a simulation calculation for the spectral region of 6050—5980 cm^{-1}. And then the $2\nu_4(\perp)$ intensity was determined by subtracting the parallel component from the total area for these two bands. On the other hand, $(\nu_1+\nu_4)$ band is distributed over obscured $2\nu_1$ band, and the intensities for these two bands were not determined separately.

In a large bush observed between 4600 and 4300 cm^{-1}, $(\nu_4+\nu_5)$, $(\nu_1+\nu_5)$, $(\nu_2+\nu_4)$, and $(\nu_1+\nu_2)$ bands are expected. Since the spectrum of this region is so complicated that their individual intensities were not obtained separately. Towards the lower frequency skirts of this complicated structure, $(\nu_2+2\nu_5^0)$ band is observed.[11]

$(\nu_4+\nu_6)(\perp)$ and $(\nu_4+\nu_6)(//)$ bands are distributed over a region of 4120—4000 cm^{-1}. For these bands, since peaks of the $(\nu_4+\nu_6)(\perp)$ band are not apparent, only the total absorption area was determined from the spectrum. On the other hand, $(\nu_1+\nu_6)$ band appears with a neat band contour at 3979.66 cm^{-1}.[12] The $(\nu_1+\nu_6)$ intensity was obtained through simulating the spectrum from 3990 to 3910 cm^{-1}, by use of the molecular parameters reported in Ref. 12. Also the intensity of $(\nu_3+\nu_4)$ band was obtained through simulation calculation for the spectrum from 3830 to 3730 cm^{-1}. $(\nu_1+\nu_3)$ band is located at 3700.67 cm^{-1}.[12] The intensity of this band was obtained through calculation of the spectrum between 3730 and 3650 cm^{-1}.

The strong $2\nu_5^0$ band is located at 2879.25 cm^{-1},[10] and $(\nu_2+\nu_5)$ band is found at 2803.39 cm^{-1}.[13] Separation of the $(\nu_2+\nu_5)$ intensity from the $2\nu_5^0$ absorption was car-

ried out through comparison of the observed and calculated areas for both 2920—2820 and 2820—2720 cm^{-1} regions.

For the $(\nu_5+\nu_6)$ and $(\nu_2+\nu_6)$ region, a rotational analysis has been carried out by DiLauro and Alamichel.[14] Therefore, the molecular constants determined by them have been utilized to make simulation analysis of the spectrum. $(\nu_2+\nu_3)$ band was observed independently from other bands,[15] and its intensity was obtained in a straightforward manner. Due to the weakness of the absorptions, none of the intensities of the $(\nu_3+\nu_5)$,[15] $(\nu_3+\nu_6)$, and $2\nu_6$ bands were determined accurately. The observed intensities for CH_3Cl are summarized in Table 1.

For CD_3Cl molecule, the spectral region from 4800 through 500 cm^{-1} has been investigated. The general feature of the spectrum is very similar to that for CH_3Cl. However, in this case, we have observed three distinct bands at 3012,1300, and 1250 cm^{-1}, respectively. These bands seems to be due to CHD_2Cl species. From their intensities, the concentration of CHD_2Cl can be considered to be less than 1%.

The perpendicular component of $2\nu_4$ band is located at 4550.9 cm^{-1}, and the parallel one at 4515.5 cm^{-1}. The

TABLE 1. OBSERVED BAND INTENSITIES FOR CH_3Cl[a]

Band	ν_i / cm^{-1}	ζ_i	B_i[b] / km mol^{-1}	Band	ν_i / cm^{-1}	ζ_i	B_i[b] / km mol^{-1}
$2\nu_4(//)$	6015.1	—	0.290(15)	$2\nu_5(//)$	2879.25[e]	—	4.16(34)[a]
$2\nu_4(\perp)$	6062	−0.10	0.429(43)	$2\nu_5(\perp)$	2892.33	?	
$\nu_1+\nu_4$	5923.7	0.11	0.92(18)	$\nu_2+\nu_5$	2803.39[f]	−0.262[f]	0.316(32)
$2\nu_1$	?	—		$2\nu_2$	?	—	0.0[c]
$\nu_4+\nu_5(//,\perp)$	?	?		$\nu_5+\nu_6(//)$	2466.26[g]	0.518[g]	0.004(4)
$\nu_1+\nu_5$	?	?	3.02(30)	$\nu_5+\nu_6(\perp)$	2461.88[g]	−0.012[g]	0.433(43)
$\nu_2+\nu_4$	?	?		$\nu_2+\nu_6$	2367.72[g]	0.242[g]	0.255(13)
$\nu_1+\nu_2$	?	—		$\nu_3+\nu_5$	2182.38[h]	−0.247[h]	0.0[c]
$\nu_4+\nu_6(//)$	4042	?	0.369(37)	$\nu_2+\nu_3$	2080.54[h]	—	0.087(5)
$\nu_4+\nu_6(\perp)$	?	?		$2\nu_6(//,\perp)$	?	?	0.0[c]
$\nu_1+\nu_6$	3979.66[d]	0.252[d]	0.134(7)	$\nu_3+\nu_6$	?	?	0.0[c]
$\nu_3+\nu_4$	3773.6	0.08	0.164(8)	$2\nu_3$	?	—	?
$\nu_1+\nu_3$	3700.67[d]	—	0.205(10)	ν_5	1452.12	—	11.38(78)[a]
ν_4	3038.91	—	10.77(120)[a]	ν_2	1354.95	—	8.41(68)[a]
ν_1	2967.76	—	19.15(144)[a]	ν_6	1017.26	—	3.85(42)[a]
				ν_3	732.88	—	23.69(94)[a]

a): For the fundamental bands, see Ref. 1. b): Numbers in parentheses are estimated errors. c): These bands were not observed because of the noise level; althought the noise level was dependent on the spectral region, their intensities may not utmost exceed 0.1 km mol^{-1}. d): Ref. 12. e): Ref. 10. f): Ref. 13. g): Ref. 14. h): Ref. 15.

TABLE 2. OBSERVED BAND INTENSITIES FOR CD_3Cl[a]

Band	ν_i / cm^{-1}	ζ_i	B_i[b] / km mol^{-1}	Band	ν_i / cm^{-1}	ζ_i	B_i[b] / km mol^{-1}
$2\nu_4(//)$	4515.5	—	0.202(10)	$2\nu_5(//)$	2104.0	—	2.56(13)[a]
$2\nu_4(\perp)$	4550.9	−0.33	0.284(14)	$2\nu_5(\perp)$	?	?	
$\nu_1+\nu_4$	4405.3	0.17	0.224(45)	$\nu_2+\nu_5$	?	?	?
$2\nu_1$	?	—		$2\nu_2$	2034.4	—	1.29(10)[a]
$\nu_4+\nu_5(//)$	3322	?		$\nu_5+\nu_6(//)$	1813	?	
$\nu_4+\nu_5(\perp)$	3310?	0.10	0.91(9)	$\nu_5+\nu_6(\perp)$	1801	0.08	0.384(38)
$\nu_2+\nu_4$	?	?		$\nu_3+\nu_5$	?	?	
$\nu_1+\nu_5$	?	?		$\nu_2+\nu_6$	?	?	?
$\nu_1+\nu_2$	?	—	0.0[c]	$\nu_2+\nu_3$	1725.7	—	0.125(13)
$\nu_4+\nu_6(//)$	3046	?	?	$2\nu_6(//,\perp)$	?	?	0.0[c]
$\nu_4+\nu_6(\perp)$	?	?	?	$\nu_3+\nu_6$	?	?	0.0[c]
$\nu_3+\nu_4$	?	?	0.0[c]	$2\nu_3$	1394.9	—	0.124(12)
$\nu_1+\nu_6$	?	?	0.0[c]	ν_5	1059.97	—	5.76(46)[a]
$\nu_1+\nu_3$	2859.2	—	0.119(6)	ν_2	1028.67	—	12.37(37)[a]
ν_4	2283.29	—	5.42(12)[a]	ν_6	767.61	—	0.57(10)[a]
ν_1	2160.24	—	1.96(24)[a]	ν_3	701.36	—	17.70(35)[a]

a): For the fundamental bands, see Ref. 1 b): Numbers in parentheses are estimated errors. c): These bands were not observed because of the noise level; although the noise level was dependent on the spectral region, their intensities may not utmost exceed 0.1 km mol^{-1}

Table 3. Values of the cubic force constants φ_{rst} for methyl chloride [a] (Units are cm^{-1})

rst	CH_3Cl	CD_3Cl	rst	CH_3Cl	CD_3Cl
A group[b]			255	−60.7	−5.1
111	−1106.3	−669.9	256	−203.5	−150.5
112	−7.1	−11.8	266	−176.1	−152.5
113	17.6	−2.4	344	19.5	2.8
122	−102.6	−68.6	345	−6.6	14.9
123	−14.2	15.5	346	−70.5	−25.2
133	48.5	52.7	355	−49.4	6.7
222	204.2	104.5	356	−242.6	−144.5
223	−20.9	−55.6	366	−84.3	−64.2
233	−21.9	−61.6	C group[b]		
333	−260.5	−221.3	444	−820.4	−532.1
B group[b]			445	−58.9	−43.8
144	−1035.5	−648.6	446	9.6	−5.7
145	−11.9	18.5	455	−183.5	−128.4
146	−18.8	−34.5	456	156.3	63.7
155	95.5	62.8	466	166.3	99.0
156	−2.2	−19.8	555	−460.6	−204.6
166	623.8	372.5	556	−295.8	−208.0
244	50.6	28.2	566	−19.4	−47.9
245	−79.6	−26.4	666	86.3	55.4
246	−281.6	−180.9			

a): Calculated from the cubic symmetry force constants in Ref. 5. b): See Ref. 5 for the classification of the force constants.

individual intensities of these two bands were easily obtained by the simulation method. The feature of the $(\nu_1+\nu_4)$ and $2\nu_1$ band region is quite similar to that in CH_3Cl, and the intensities of these bands were not separately determined. Also the spectral region for $(\nu_4+\nu_5)$, $(\nu_2+\nu_4)$, and $(\nu_1+\nu_5)$ shows a very complicated appearance, and the individual intensities were not determined either.

Althogh $(\nu_4+\nu_6)(//)$ band appears with an appreciable intensity,peaks due to the perpendicular component were not identified, as in the case of CH_3Cl. Instead, there was an extra parallel type band at 3011.6 cm^{-1}, presumably due to CHD_2Cl molecule. In fact, we have also observed a structure which seemed to be due to the "perpendicular" component of the same band. Due to the weakness, neither of $(\nu_3+\nu_4)$ and $(\nu_1+\nu_6)$ bands were clearly identified.

The parallel band of $(\nu_1+\nu_3)$ is clearly observed at 2861.6 cm^{-1}, which is accompanied by $(2\nu_2+\nu_3)$ and $(\nu_3+2\nu_5^0)$ bands. Intensities for $2\nu_5(//)$ and $2\nu_2$ have already been determined in Part I.[1] In this case however the intensity value for the $2\nu_5$ band should be considered as to include contributions both from $2\nu_5^0$ and $2\nu_5^2$.

Peaks due to the perpendicular component of $(\nu_5+\nu_6)$ band are apparent in the region between 1900 and 1750 cm^{-1}. However, the individual band intensities contributing to this region can not separately be obtained because of the spectral complexity. The $(\nu_2+\nu_3)$ band is clearly seen at 1725.7 cm^{-1}. Also $2\nu_3$ band is apparent at 1394.9 cm^{-1}, although we did not find clearly the $2\nu_6$ band anywhere. As mentioned above, a pair of parallel and perpendicular type bands appear at 1300 and 1250 cm^{-1}, respectively, which may

Table 4. Calculated values of the second derivatives of the transformed dipole moment for CH_3Cl (in 1 D≈3.3356×10^{-30} C m)

rs(α)	Calcd I[a]	Calcd II[b]	Calcd III[c]
11(z)	0.0094	−0.0099	−0.0005
12(z)	−0.0005	−0.0017	−0.0022
13(z)	−0.0005	0.0074	0.0069
22(z)	−0.0105	−0.0329	−0.0434
23(z)	−0.0021	0.0185	0.0164
33(z)	−0.0247	0.0193	−0.0054
14(x)	0.0042	−0.0191	−0.0149
15(x)	0.0006	−0.0143	−0.0137
16(x)	−0.0013	0.0078	0.0065
24(x)	−0.0003	0.0172	0.0169
25(x)	−0.0048	−0.0077	−0.0125
26(x)	−0.0110	0.0179	0.0069
34(x)	−0.0003	0.0093	0.0090
35(x)	0.0009	−0.0001	0.0008
36(x)	−0.0202	0.0005	−0.0197
44(z)	0.0083	−0.0223	−0.0140
44(x)	0.0030	−0.0182	−0.0152
45(z)	−0.0002	−0.0030	−0.0032
45(x)	−0.0005	−0.0130	−0.0135
46(z)	−0.0017	0.0106	0.0089
46(x)	0.0003	0.0028	0.0031
55(z)	0.0326	0.0055	0.0381
55(x)	−0.0214	0.0069	−0.0145
56(z)	−0.0095	−0.0065	−0.0160
56(x)	−0.0007	−0.0121	−0.0128
66(z)	0.0193	−0.0240	−0.0047
66(x)	0.0016	0.0002	0.0018

a): Contribution from the mechanical anharmonicity. b): The electrical anharmonicity. c): Calcd I+II.

be due to CHD_2Cl.

The observed band intensities for the CD_3Cl molecule are summarized in Table 2.

Numerical Calculations and Discussion

As is apparent in the equations shown in a previous section, the intensities of binary overtone and combination bands contain contributions both from electrical and mechanical anharmonicities. If the second derivatives of the dipole moment are neglected, we can calculate the intensities of these bands by using the values of $(\partial P/\partial Q_r)$ and cubic force constants. The former has been determined in Part I, and the latter can be calculated from the cubic symmetry force field determined in Ref. 5. The cubic force constants obtained from the symmetry force constants are shown in Table 3. Calcd I in Tables 4 and 5 shows thus derived mechanical anharmonicity correction to the second derivatives of the dipole moment. Calcd I in Tables 6 and 7 shows the calculated intensities from these values. However, comparison of these values with the observed ones reveals that the agreement is not so good. Indeed, this is not surprising because we did not consider the second derivatives themselves to obtain the calculated intensities.

In order to obtain some estimates of the dipole moment derivatives, *ab initio* calculations may be useful. In fact, Scanlon *et al.* have calculated the second derivatives of the dipole moment for CH_4[16] and SF_6[17] with some success. In the following, a similar calculation will be carried out to obtain the values of the second derivatives of the dipole moment for methyl chloride.

The calculations were carried out by using the HONDO program[18] (IMS version) with the 4-31 G* basis set, where d-functions with $\alpha=0.80$ were used for both C and Cl atoms. The dipole moment derivatives were calculated with the experimental normal coordinates[19,21] for the optimized molecular geometry: CH=1.0775 Å, CCl=1.7775 Å, and ∠HCH=110.29°. The displacements for the second derivatives were obtained by addition of the simple harmonic motion of the two normal coordinates involved. Distorsions of 0.02 $u^{1/2}$ Å were employed in each case.

Calcd II in Tables 4 and 5 shows the resulting *ab initio* values of the second derivatives of the dipole moment. The numbers for Calcd III in the same tables are the sums of the numbers for Calcd I and II. On the other hand, Calcd II in Tables 6 and 7 shows the calculated intensities for the overtones and combinations using

Table 5. Calculated values of the second derivatives of the transformed dipole moment for CD_3Cl (in 1 D≈3.3356×10^{-30} C m)

$rs(\alpha)$	Calcd I[a]	Calcd II[b]	Calcd III[c]
11(z)	0.0076	−0.0075	0.0001
12(z)	−0.0002	−0.0002	−0.0004
13(z)	0.0010	0.0045	0.0055
22(z)	−0.0199	−0.0142	−0.0341
23(z)	−0.0038	0.0225	0.0187
33(z)	−0.0185	0.0124	−0.0061
14(x)	0.0031	−0.0154	−0.0123
15(x)	0.0001	−0.0051	−0.0050
16(x)	0.0000	0.0033	0.0033
24(x)	−0.0002	0.0125	0.0123
25(x)	−0.0014	−0.0011	−0.0025
26(x)	−0.0085	0.0136	0.0051
34(x)	0.0001	0.0052	0.0053
35(x)	0.0014	0.0087	0.0101
36(x)	−0.0068	−0.0008	−0.0076
44(z)	0.0064	−0.0177	−0.0113
44(x)	0.0022	−0.0148	−0.0126
45(z)	−0.0006	−0.0017	−0.0023
45(x)	−0.0002	−0.0038	−0.0040
46(z)	−0.0012	0.0077	0.0065
46(x)	0.0003	0.0002	0.0005
55(z)	0.0396	0.0056	0.0452
55(x)	−0.0123	0.0208	0.0085
56(z)	−0.0137	−0.0039	−0.0176
56(x)	−0.0021	−0.0006	−0.0027
66(z)	0.0104	−0.0160	−0.0056
66(x)	0.0000	−0.0008	−0.0008

a): Contribution from the mechanical anharimonicity. b): The electrical anharmonicity. c): Calcd I+II.

Table 6. Comparison of the observed band intensities with the calculated values for CH_3Cl (Units are km mol^{-1})

Band	Obsd	Calcd I[a]	Calcd II[b]
$2\nu_4(//)$	0.290(15)	0.260	0.750
$2\nu_4(\perp)$	0.429(43)	0.070	1.751
$\nu_1+\nu_4$	0.92(18)	0.131	1.679
$2\nu_1$		0.163	0.001
$\nu_4+\nu_5(//,\perp)$	3.02(30)	0.003	2.106
$\nu_1+\nu_5$		0.002	1.047
$\nu_2+\nu_4$		0.001	1.568
$\nu_1+\nu_2$		0.001	0.013
$\nu_4+\nu_6(//)$	0.369(37)	0.014	0.409
$\nu_4+\nu_6(\perp)$		0.001	0.097
$\nu_1+\nu_6$	0.134(7)	0.008	0.215
$\nu_3+\nu_4$	0.164(8)	0.000	0.396
$\nu_1+\nu_3$	0.205(10)	0.001	0.113
$2\nu_5(//)$	4.16(34)	1.934	2.642
$2\nu_5(\perp)$		1.677	0.771
$\nu_2+\nu_5$	0.316(32)	0.081	0.550
$2\nu_2$	0.0[c]	0.094	1.605
$\nu_5+\nu_6(//)$	0.004(4)	0.283	0.801
$\nu_5+\nu_6(\perp)$	0.433(43)	0.003	1.029
$\nu_2+\nu_6$	0.255(13)	0.361	0.144
$\nu_3+\nu_5$	0.0[c]	0.002	0.002
$\nu_2+\nu_3$	0.087(5)	0.006	0.361
$2\nu_6(//,\perp)$	0.0[c]	0.487	0.037
$\nu_3+\nu_6$	0.0[c]	0.926	0.881
$2\nu_3$	?	0.296	0.014

a): Contribution from mechanical anharmonicity only was taken into account. b): The second derivatives of the dipole moment estimated through *ab initio* method (4-31 G*) were also taken into consideration. c): See footnote c) to Table 1.

Table 7. Comparison of the observed band intensities with the calculated values for CD_3Cl (Units are km mol^{-1})

Band	Obsd	Calcd I[a]	Calcd II[b]
$2\nu_4(//)$	0.202(10)	0.118	0.364
$2\nu_4(\perp)$	0.284(14)	0.027	0.911
$\nu_1+\nu_4$	0.224(45)	0.053	0.844
$2\nu_1$		0.077	0.000
$\nu_4+\nu_5(//)$	0.91(9)	0.001	0.022
$\nu_4+\nu_5(\perp)$		0.000	0.133
$\nu_2+\nu_4$		0.000	0.628
$\nu_1+\nu_5$		0.000	0.102
$\nu_1+\nu_2$	0.0[c]	0.000	0.000
$\nu_4+\nu_6(//)$	?	0.006	0.165
$\nu_4+\nu_6(\perp)$	?	0.001	0.002
$\nu_3+\nu_4$	0.0[c]	0.000	0.108
$\nu_1+\nu_6$	0.0[c]	0.000	0.041
$\nu_1+\nu_3$	0.119(6)	0.002	0.056
$2\nu_5(//)$	2.56(13)	2.103	2.740
$2\nu_5(\perp)$		0.404	0.196
$\nu_2+\nu_5$	?	0.005	0.016
$2\nu_2$	1.29(10)	0.258	0.759
$\nu_5+\nu_6(//)$	0.384(38)	0.442	0.730
$\nu_5+\nu_6(\perp)$		0.022	0.035
$\nu_3+\nu_5$		0.004	0.232
$\nu_2+\nu_6$	?	0.168	0.060
$\nu_2+\nu_3$	0.125(13)	0.016	0.393
$2\nu_6(//,\perp)$	0.0[c]	0.109	0.033
$\nu_3+\nu_6$	0.0[c]	0.090	0.113
$2\nu_3$	0.124(12)	0.160	0.017

a): Contribution from mechanical anharmonicity only was taken into account. b): The second derivatives of the dipole moment estimated by 4-31 G* were also taken into consideration. c): See footnote c) Table 2.

these estimated values of the dipole derivatives. On the whole, agreement of the calculated intensities with the observed ones improved much by the inclusion of the *ab initio* values of the second derivatives. The agreement is almost semi-quantitative for all bands expect $2\nu_2$, $(\nu_5+\nu_6)(//)$, and $(\nu_3+\nu_6)$ of CH_3Cl molecule. Therefore, the *ab initio* values of the second derivatives should at least be of correct orders of magnitude.

However, the discrepancies are still much larger than we expected. In this concern, it should be noted that the effect of Fermi resonance has not been taken into account exactly in the expressions given in this paper. The intensity values calculated from these equations may contain large errors when there are close resonances. For example, in the case of $2\nu_5(//)$ band of CH_3Cl and CD_3Cl, a part of discrepancy between the observed and calculated intensities must be due to Fermi resonance with the respective ν_1 band. Discrepancies are, however, also noted for some of those which are free from such resonances. It is possible that a considerable part of the discrepancy is due to the errors in the normal coordinate force constants used here. In fact, in order to determine the force constants through the least-squares calculation, we were forced to constrain some of the 38 independent force constants.[5] Moreover, the resulting errors for many of the force constants were more or less of the same magnitudes as or even larger than the derived values of the constants themselves.[5]

At any rate, it is clear that a further effort to refine the cubic force field is required before definite values are obtained for the second derivatives of the dipole moment of this molecule.

The *ab initio* calculations of the dipole moment derivatives were carried out by the HONDO program from Institute for Molecular Science through the courtesy of Professor Keiji Morokuma and Dr. Shigeki Kato.

References

1) S. Kondo, Y. Koga, T. Nakanaga, and S. Saëki, *Bu. Chem. Soc. Jpn.*, **56**, 416 (1983).
2) C. Secroun, A. Barbe, and P. Jouve, *J. Mol. Spectrosc.* **45**, 1 (1973).
3) S. J. Yao and J. Overend, *Spectrochim. Acta, Part A*, **32**, 1059 (1976).
4) J. Overend, *J. Chem. Phys.*, **64**, 2878 (1976).
5) S. Kondo, Y. Koga, T. Nakanaga, and S. Saëki, *J. Mol. Spectrosc.*, **100**, 332 (1983).
6) A. R. Hoy, I. M. Mills, and G. Strey, *Mol. Phys.*, **24**, 1265 (1972).
7) J. Overend, "Vibrational Intensities in Infrared and Raman Spectroscopy," ed by W. B. Person and G. Zerbi, Elsevier, Amsterdam (1982), p. 203.
8) I. M. Mills, "Molecular Spectroscopy: Modern Research," ed by K. N. Rao and C. W. Mathews, Academic Press, New York (1972), p. 115.
9) For example, see S. Kondo and S. Saëki, *J. Chem. Phys.*, **74**, 6603 (1981).
10) N. Bensari-Zizi and C. Alamichel, *Mol. Phys.*, **43**, 1255 (1981).
11) N. Bensari-Zizi, C. Alamichel, and G. Guelachvili, *Spectrochim. Acta, Part A*, **37**, 773 (1981).
12) N. Bensari-Zizi, C. Alamichel, and G. Guelachvili, *Can. J. Phy.*, **59**, 994 (1981).
13) M. Morillon-Chapey, G. Graner, C. Alamichel, C. Betrencourt-Stirnemann, M. Betrencourt, and J. Pinard, *J. Phys. (Paris)*, **31**, 519 (1970).
14) C. DiLauro and C. Alamichel, *J. Mol. Spectrosc.*, **81**, 390 (1980).
15) N. Bensari-Zizi, C. Alamichel, and G. Guelachvili, *Mol. Phys.*, **46**, 171 (1982); **34**, 1131 (1977).
16) K. Scanlon, R. A. Eades, D. A. Dixon, and J. Overend, *J. Phys. Chem.*, **85**, 2878 (1981).
17) K. Scanlon, R. A. Eades, and D. A. Dixon, *Spectrochim. Acta, Part A*, **38**, 849 (1982).
18) M. Dupuis and H. F. King, *J. Chem. Phys.*, **68**, 3998 (1978).
19) In part I, the harmonic force field of Duncan, Allan, and McKean[20] was used. In the present work, a slightly modified one by Duncan, McKean, and Speirs[21] is utilized. See Ref. 5.
20) J. L. Duncan, A. Allan, and D. C. Mckean, *Mol. Phys.*, **18**, 289 (1970).
21) J. L. Duncan, D. C. McKean, and G. K. Speirs, *Mol. Phys.*, **24**, 553 (1972).

Electrical Conductivities of the Complexes of Naphthaceno[5,6-*cd*:11,12-*c'd'*]-bis[1,2]dithiole and Its Analogs Obtained by Electrochemical Crystallization and Diffusion Method

Takashi NOGAMI,* Hidekazu TANAKA, Shigeo OHNISHI, Yoshihiko TASAKA, and Hiroshi MIKAWA
Department of Applied Chemistry, Faculty of Engineering, Osaka University, Yamada-oka, Suita, Osaka 565
(Received July 8, 1983)

Electrochemical crystallizations of the complexes of naphthaceno[5,6-*cd*:11,12-*c'd'*]bis[1,2]dithiole (TTT), anthra[1,9-*cd*:4,10-*c'd'*]bis[1,2]dithiole (TTA), anthra[1,9-*cd*:4,10-*c'd'*]bis[1,2]diselenole (TSA), and naphtho[1,8-*cd*:4,5-*c'd'*]bis[1,2]dithiole (TTN) were made in 1,1,2-trichloroethane or tetrahydrofuran as a solvent. Most of the crystals were obtained with non-stoichiometric compositions, and they included the solvent. Some charge-transfer complexes including the above donors were also made by a diffusion method. The electrical conductivities of the crystals were measured by a two-probe or four-probe method. TTT-$(PF_6)_{0.61}$ was found to be the most conductive materials in the complexes studied. Its electrical conductivity was 762 $(\Omega\,cm)^{-1}$ at room temperature, and it showed metallic behavior above 220 K. The conductivities of the other complexes varied widely in the range 10^2—10^{-7} $(\Omega\,cm)^{-1}$

The studies on the highly conductive organic materials have progressed greatly in the past few years.[1] The first organic superconductors were discovered for complexes of tetramethyltetraselenafulvalene (TMTSF).[2] Another organic superconductor has recently been reported for the complex of bis(ethylenedithio)tetrathiafulvalene (BEDT-TTF), (BEDT-TTF)$_4$(ReO_4)$_2$.[3] The crystals of these organic superconductors were grown by an electrochemical method.[4] However, most of the electrochemical crystallizations have been conducted on the complexes of tetrathiafulvalene (TTF) and its analogs. Naphthaceno[5,6-*cd*:11,12-*c'd'*]bis[1,2]dithiole (TTT) is known to give highly conductive organic complexes.[5] The TTT analogs are planar molecules with four chalcogen atoms stretched out from the aromatic ring. Interchain coupling through chalcogen atoms is expected for the complexes of TTT analogs; this might suppress Peierls transitions. Thus, these complexes are expected to be highly conductive down to low temperatures. We have made electrochemical crystallizations of TTT, anthra[1,9-*cd*:4,10-*c'd'*]bis[1,2]diselenole (TSA), anthra[1,9-*cd*:4,10-*c'd'*]bis[1,2]dithiole (TTA), and naphtho[1,8-*cd*:4,5-*c'd'*]bis[1,2]dithiole (TTN). We have also made some charge-transfer complexes by use of these donor molecules by diffusion method. Their electrical conductivities were measured by a two-probe or four-probe method. We have also measured the half-wave oxidation potentials and electronic absorption spectra of the above donor molecules to get their basic data.

Experimental

Materials. TTT,[6] TSA,[7] TTA,[8] and TTN[9] were synthesized by the procedures reported. Tetrabutylammonium perchlorate was recrystallized from ethanol. Tetrabutylammonium hexafluorophosphate was synthesized according to the reported procedures.[10] Tetrabutylammonium hexafluoroarsenate was synthesized by mixing equimolar amounts of aqueous solutions of tetrabutylammonium bromide with potassium hexafluoroarsenate. The white powder was filtered, dried in vacuum, and recrystallized twice from the mixed solution of ethyl acetate and hexane (7:3). Tetrabutylammonium hexafluoroantimonate was synthesized by the reported procedures.[11] Tetrabutylammonium tetrafluoroborate was obtained by mixing equimolar amounts of aqueous tetrabutylammonium bromide with tetrafluoroboric acid (40%) at 0 °C in a polyethylene vessel. The crude product was recrystallized from ethyl acetate in the polyethylene vessel. Tetrabutylammonium triiodide was synthesized by the procedures reported.[12] 1,1,2-Trichloroethane was purified by refluxing it over phosphorus pentaoxide, followed by distillation. Tetrahydrofuran was purified by refluxing it over calcium hydride, followed by distillation. Benzonitrile was steam distilled, the organic layer was shaken with aqueous sodium carbonate, and the solution was mixed with diethyl ether. The organic solution was shaken with water, and the resulting mixture was dried over calcium chloride overnight. Diethyl ether was then distilled out, and the remaining liquid was distilled in vacuum.

Electrochemical Crystallization. Electrochemical crystallization was conducted under galvanostatic conditions (1—5 μA). The detailed procedures were described before.[13]

Crystal Growth by Diffusion Method. The single crystals of TCNQ complexes and iodine complexes of TTT and its analogs were grown by diffusion method in organic solvents. For the crystal growths of iodine complexes, tetrabutylammonium triiodide was used instead of iodine. The detailed procedures are similar to those of the literature.[14]

Cyclic Voltammetry. Cyclic voltammetry was made by a Potentiostat/Galvanostat (Hokuto Denko, HA-501), and by

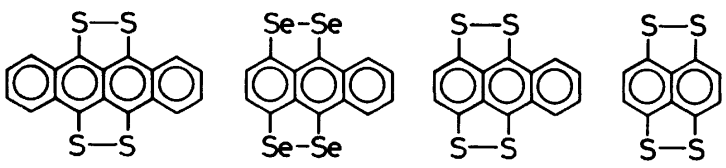

a Function Generator (Hokuto Denko, HB-104).

Measurement of Electrical Conductivity. Electrical conductivities of the crystals were measured by a two-probe or four-probe method. Temperature dependence of the electrical conductivity was measured by a Type D Cryo Mini (Osaka Sanso Co. Ltd).

Results and Discussion

Cyclic Voltammetries of Donor Molecules. The electrochemical half-wave potentials were measured *vs.* SCE at a platinum electrode in benzonitrile-Bu_4NAsF_6 (0.1 mol dm^{-3}). Table 1 summarizes the first and second half-wave oxidation potentials and their differences ($E_{1/2}(2)-E_{1/2}(1)$) of TTT, TTA, and TSA, together with the reported values of TTN, TSN, TTF, TMTTF, TMTSF, and HMTTeF for comparison.[15] Here, TSN, TMTTF, and HMTTeF denote naphtho-[1,8-*cd*:4,5-*c'd'*]bis[1,2]diselenole,[16] tetramethyltetrathiafulvalene, and bis(trimethylene)tetratellurafulvalene, respectively. The first oxidation potentials increase in the order: TTT≃TMTTF<TTF<TSA≃TTA≃TMTSF≃HMTTeF<TSN<TTN.

Electronic Absorption Spectra of Donor Molecules. The electronic absorption spectra of a series of TTT analogs were measured in several solvents at room temperature. Figure 1 shows the electronic absorption spectra of TTT, TSA, TTA, TTN, and TSN.[16] Table 2 summarizes the absorption peak positions and logarithms of extinction coefficients. The absorption peak positions of the lowest energy transition of selenium derivatives showed bathochromic shifts relative to the corresponding sulfur derivatives.

Electrochemical Crystallization. Electrochemical crystallization was conducted for the donor molecules TTT, TSA, TTA, and TTN. The counter anions were Cl^-, Br^-, I^-, ClO_4^-, BF_4^-, PF_6^-, AsF_6^-, and SbF_6^-. Table 3 summarizes the complexes obtained, their decomposition temperatures, elemental analyses, solvents, appearances, and electrical conductivities at room temperature. Since the elemental analyses of chalcogen atoms and halogen atoms could not be made when they coexist in the same sample, elemental analyses were made only for carbon and hydrogen. The content of the solvent was estimated from the analyses by the least-squares method. Most of the complexes contained the solvent in non-stoichiometric ratios. The solvent could not be removed merely by drying the complex *in vacuo* at room temperature. The ratio of the donor molecule and the counter anion was also non-stoichiometric. The reason why $TTT(ClO_4)_{0.56}$, $TTT(PF_6)_{0.61}$, and $TTT(SbF_6)_{0.64}$ do not contain the solvent, 1,1,2-trichloethane, is not clear.

Electrical Conductivities of the Complexes. Electrical conductivities of the complexes were measured by a two-probe or four-probe method. Table 3 summarizes

Table 1. Electrochemical half-wave oxidation potentials of donor molecules in benzonitrile

Molecules	(Oxidation potentials *vs.* SCE)/V $E_{1/2}(1)$	$E_{1/2}(2)$	ΔE
TTT	0.24	0.67	0.43
TTA	0.41	0.85	0.44
TSA	0.42	0.84	0.42
TTN[a]	0.55	0.93	0.38
TSN[b]	0.40	—	—
TTF[a]	0.34	0.71	0.37
TMTTF[a]	0.24	0.73	0.49
TMTSF[a]	0.42	0.81	0.39
HMTTeF[a]	0.40	0.69	0.29

a) Ref 15; b) Ref 16. We could not measure $E_{1/2}(2)$ of TSN because of the irreversible chemical reaction.

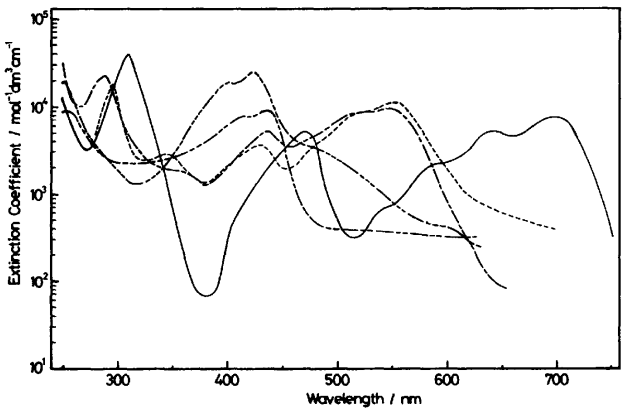

Fig. 1. Electronic absorption spectra of donor molecules.
—— TTT, ---- TSA, — — — TTA, — — — — TSN, — — — — — TTN

Table 2. Electronic absorption peak positions and extinction coefficients of donor molecules

Molecules	λ_{max}/nm (log ε)
TTT[a]	316 (4.62), 462 (4.0), 596 (2.67), 649 (3.45)
TST[b]	321 (4.13), 465 (3.29), 598 (1.73), 656 (2.75)
TTA[a]	288 (4.36), 437 (3.71), 520 (3.93), 548 (3.98)
TSA[a]	297 (4.20), 430 (3.57), 520 (3.93), 552 (4.05)
TTN[c]	251 (4.16), 420 (4.26)
TSN[d]	256 (3.94), 415 (3.88), 436 (3.96)

a) Solvent: chloroform; b) TST denotes naphthaceno-[5,6-*cd*:11,12-*c'd'*]bis[1,2]diselenole. Solvent: 1,2,4-trichlorobenzene (Ref. 6). c) Solvent: acetonitrile; d) Solvent: 1,2-dichloroethane.

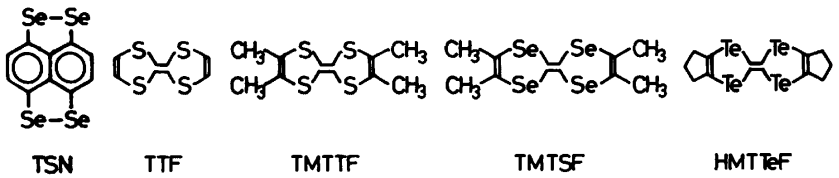

Table 3. The complexes obtained, and their elemental analyses, decomposition temperatures, solvents, appearances, and electrical condutivities at room temperature

Complex	Found(Calcd) (%)		Dp/°C[a]	Solvent	Appearance	Conductivity $(\Omega\ cm)^{-1}$
TTT $Cl_{0.75}(TCE)_{0.52}$	50.78 (51.00)	2.56 (2.17)	220	TCE	Dark brown needles	1.47
TTT $Br_{0.70}(TCE)_{0.16}$	51.27 (51.24)	2.25 (2.00)	259	TCE	Dark brown needles	45
TTT $I_{0.90}(TCE)_{0.20}$	44.78 (44.79)	1.74 (1.76)	274	TCE	Black needles	158
TTT$(ClO_4)_{0.56}$	52.86 (52.98)	2.20 (1.98)	259	TCE	Dark brown needles	6×10^{-3}
TTT$(BF_4)_{0.25}(TCE)_{0.20}$	55.49 (55.20)	2.25 (2.17)	283	TCE	Black needles	2.5×10^{-2}
TTT$(PF_6)_{0.61}$	49.33 (49.13)	2.28 (2.53)	>300	TCE	Black needles	762
TTT$(SbF_6)_{0.64}$	42.85 (42.60)	2.16 (2.42)	264	TCE	Black needles	40
TTT$(PF_6)_{0.58}(THF)_{0.66}$	51.22 (51.20)	2.74 (2.76)	>300	THF	Black needles	5
TTT$(AsF_6)_{0.68}(THF)_{1.1}$	48.03 (48.02)	3.00 (3.02)	210	THF	Black needles	8.4
TTT$(SbF_6)_{0.47}(THF)_{0.64}$	48.48 (48.47)	2.63 (2.59)	263	THF	Black needles	4.9
TTT$(ClO_4)_{0.61}(THF)_{0.48}$	53.45 (53.43)	2.69 (2.67)	273	THF	Black needles	0.31
TTT$(BF_4)_{0.55}(THF)_{0.16}$	54.40 (54.37)	2.25 (2.27)	300	THF	Black needles	0.12
TTA$(PF_6)_{0.33}(TCE)_{0.96}$	39.99 (39.99)	1.88 (1.87)	—	TCE	Dark green needles	2.3×10^{-4}
TSA$(PF_6)_{0.41}(TCE)_{1.97}$	26.23 (26.53)	1.45 (1.48)	260	TCE	Violet plate	2.5×10^{-5}
TSA$(ClO_4)_{0.61}(TCE)_{1.12}$	27.86 (27.86)	1.35 (1.35)	143	TCE	Dark brown powder	1.7×10^{-5}
TTN$(PF_6)_{0.39}(TCE)_{1.07}$	32.28 (32.28)	1.61 (1.61)	205	TCE	Dark green powder	1.25×10^{-7}
TTN$(ClO_4)_{0.86}(TCE)_{0.27}$	33.85 (33.85)	1.31 (1.30)	269	TCE	Dark green powder	2.56×10^{-7}
TTN$(SbF_6)_{0.88}(TCE)_{0.84}$	24.53 (24.53)	1.15 (1.15)	262	TCE	Dark green powder	7.69×10^{-7}
TTN$(AsF_6)_{0.55}(TCE)_{0.94}$	29.62 (29.62)	1.43 (1.43)	280	TCE	Dark green powder	1.92×10^{-7}
TTN$(PF_6)_{0.81}(THF)_{0.41}$	35.02 (35.01)	1.84 (1.84)	232	THF	Dark green needles	1.40×10^{-7}
TTN$(ClO_4)_{0.99}(THF)_{0.14}$	35.13 (35.14)	1.43 (1.43)	272	THF	Dark green needles	1.58×10^{-7}
TTN$(AsF_6)_{0.69}(THF)_{0.68}$	35.39 (35.38)	2.21 (2.21)	261	THF	Dark green needles	3.22×10^{-6}
TTA·$I_{1.2}$	36.62 (36.98)	1.30 (1.33)	225	CH_3CN[b] $C_6H_5NO_2$[b]	Dark green needles	4.2
TSA·TCNQ	45.38 (44.98)	1.61 (1.45)	250	C_6H_5CN[c]	Black needles	15
TTN·$I_{2.4}$	21.51 (21.57)	0.73 (0.71)	187	CH_3CN[b] $C_6H_5NO_2$[b]	Dark green needles	1.45×10^{-2}

a) Decomposition temperature. b) Diffusion method: the solvents of Bu_4NI_3 and donor molecule are acetonitrile and nitrobenzene, respectively. c) Diffusion method: the solvent is benzonitrile.

the observed results. Roughly speaking, the order of the electrical conductivities obtained by electrochemical method is as follows: TTT complexes (10^{-3}—$10^{3}(\Omega\ cm)^{-1}$)>TTA complexes ($10^{-4}(\Omega\ cm)^{-1}$)>TSA complexes ($10^{-5}(\Omega\ cm)^{-1}$)>TTN complexes (10^{-6}—$10^{-7}(\Omega\ cm)^{-1}$). That is to say, the larger the aromatic ring is, the higher is the conductivity. The charge carrier in these complexes is considered to be a hole. The above orders of the conductivities arise partly from the weaker on-site Coulomb repulsion energy between holes for large aromatic systems than that for small aromatic systems, because the average distance between the holes becomes larger in going from TTN to TTT.[17] The electrical conductivities of the complexes which do not

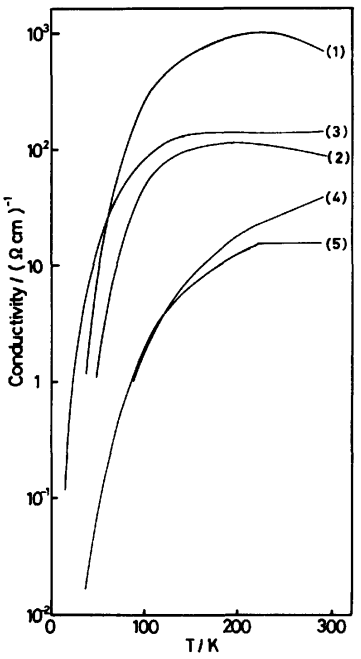

Fig. 2. Temperature dependences of the electrical conductivities of the complexes.
(1) $TTT(PF_6)_{0.61}$ (crystal 1), (2) $TTT(PF_6)_{0.61}$ (crystal 2), (3) $TTT\ I_{0.90}(TCE)_{0.20}$, (4) $TTT(SbF_6)_{0.64}$, (5) TSA·TCNQ

contain the solvents were high in general. The steric effect of the solvent prevents the overlap of the π-electron clouds between adjacent donor molecules; this leads to the low conductivity. Thus, we must select a proper solvent or a special condition of electrocrystallization in order to prevent the coordination of the solvent to the complex. Electrochemical crystallizations of TTT complexes were conducted both in 1,1,2-trichloroethane (TCE) and in tetrahydrofuran (THF). Most of the TTT complexes obtained in the former solvent were more conductive than those obtained in the latter solvent. Temperature dependences of the electrical conductivities of $TTT(PF_6)_{0.61}$, $TTT{\cdot}I_{0.90}(TCE)_{0.20}$, and $TTT(SbF_6)_{0.64}$ are shown in Fig. 2. $TTT(PF_6)_{0.61}$ gave two kinds of crystals, which could be distinguished from the appearances. The thin crystal (crystal 1 in Fig. 2) was more conductive than the thick one (crystal 2 in Fig. 2). $TTT(PF_6)_{0.61}$ (crystal 1) was the most conductive material, and its electrical conductivity was $762(\Omega\ cm)^{-1}$ at room temperature. The conductivity increased gradually with lowering the temperature which is a characteristic behavior of metallic conductivity, and showed the maximum value of $1050(\Omega\ cm)^{-1}$ at 220 K. $TTT(PF_6)_{0.61}$ (crystal 2) also showed metallic behavior above 190 K. $TTT{\cdot}I_{0.90}(TCE)_{0.20}$ showed almost no activation energy of the conductivity above 160 K. The conductivities of $TTT(PF_6)_{0.61}$ and $TTT{\cdot}I_{0.90}(TCE)_{0.20}$ decreased gradually at the lower temperature range due to a phase transition, like many low-dimensional conductors.

The complexes obtained by the diffusion method showed higher conductivities than those obtained by the electrochemical method, especially in TTA-, TSA-, and TTN-complexes; *e.g.*, $TTA{\cdot}I_{1.2}$, $4.2(\Omega\ cm)^{-1}$; TSA·TCNQ, $15(\Omega\ cm)^{-1}$; $TTN{\cdot}I_{2.4}$, $1.45\times10^{-2}(\Omega\ cm)^{-1}$. Temperature dependence of the electrical conductivity of TSA·TCNQ is shown in Fig. 2. The conductivity was almost constant above 220 K, at which temperature the phase transition gave rise to a low conductive phase. In view of the high electrical conductivities of the following complexes,[18] we can get highly conductive complexes more easily by the diffusion method than by the electrochemical method if we use TTT and its analogs as donor molecules: TTT_2I_3, $10^3(\Omega\ cm)^{-1}$; $TTT(TCNQ)_2$, $10^2(\Omega\ cm)^{-1}$; TTN·TCNQ, $40(\Omega\ cm)^{-1}$.

We are grateful to Prof. F. Wudl, University of California at Santa Barbara, for teaching us the detailed synthetic procedures of TTN.

References

1) "Extended Linear Chain Compounds," ed by J. S. Miller, Plenum Press, New York (1982).
2) D. Jerome, M. Mazaud, M. Ribault, and K. Bechgaard, *J. Phys.*, **41**, L95 (1980).
3) S. S. Parkin, E. M. Engler, R. R. Schumaker, R. Lagier, V. Y. Lee, J. C. Scott, and R. L. Greene, *Phys. Rev. Lett.*, **50**, 270 (1983).
4) E. M. Engler, R. L. Greene, P. Haen, Y. Tomkiewicz, K. Mortensen, and J. Berenzen, *Mol. Cryst. Liq. Cryst.*, **79**, 371 (1982).
5) R. B. Somoano, S. P. S. Yen, V. Hadek, S. K. Khanna, M. Novotony, T. Datta, A. M. Hertman, and J. A. Woollman, *Phys. Rev. B*, **17**, 2853 (1978).
6) E. P. Gooding, D. A. Mitchard, and G. Owen, *J. Chem. Soc., Perkin Trans. 1*, **1972**, 1310; B. Hilti and C. W. Mayer, *Helv. Chim. Acta*, **61**, 501 (1978); B. Hilti, C. W. Mayer, and M. G. Rihs, *ibid.*, **61**, 1462 (1978).
7) S. Ohnishi, T. Nogami, and H. Mikawa, *Chem. Lett.*, **1982**, 1841.
8) S. Ohnishi, T. Nogami, and H. Mikawa, *Tetrahedron Lett.*, **24**, 2401 (1983).
9) F. Wudl, D. E. Schafer,and B. Miller, *J. Am. Chem. Soc.*, **98**, 252 (1976).
10) J. E. Lind, Jr., and H. A. Abdel-Rehim, *J. Phys. Chem.*, **70**, 3610 (1966).
11) V. W. Lange and K. Askitopoulos, *Z. Anorg. Allg. Chem.*, **223**, 369 (1935).
12) R. E. Buckles and J. P. Yuk, *J. Am. Chem. Soc.*, **75**, 5048 (1953).
13) H. Tanaka, T. Nogami, and H. Mikawa, *Chem. Lett.*, **1982**, 727.
14) H. Endres, H. J. Keller, J. Queckborner, J. Veigel, and D. Schweitzer, *Mol. Cryst. Liq. Cryst.*, **86**, 111 (1982).
15) TTN: Ref. 9; TTF: D. C. Green, *J. Org. Chem.*, **44**, 1476 (1979); TMTTF, TMTSF, and HMTTeF: F. Wudl and E. A. Shalom, *J. Am. Chem. Soc.*, **104**, 1154 (1982).
16) A. Yamahira, T. Nogami, and H. Mikawa, *J. Chem. Soc., Chem. Commun.*, **1983**, 904.
17) J. B. Torrance, *Acc. Chem. Res.*, **12**, 79 (1979).
18) J. Riga, J. J. Verbist, F. Wudl, and A. Kruger, *J. Chem. Phys.*, **69**, 3221 (1978).

Temperature Dependence of Magnetic Susceptibilities of (TTT)(TCNQ) and (TTT)(TCNQ)$_2$

Masashi TAKAHASHI, Tadashi SUGANO, and Minoru KINOSHITA*
The Institute for Solid State Physics, The University of Tokyo, Roppongi, Minato-ku, Tokyo 106
(Received July 19, 1983)

Static magnetic susceptibility and ESR studies of 1:1 and 1:2 charge-transfer complexes of naphthaceno-[5,6-*cd*:11,12-*c'd'*]bis[1,2]dithiole and 2,2'-(2,5-cyclohexadiene-1,4-diylidene)bis(propanedinitrile) [(TTT)-(TCNQ) and (TTT)(TCNQ)$_2$] in the temperature region of 2—310 K are described. (TTT)(TCNQ)$_2$ exhibits a temperature dependent spin susceptibility, while the spin susceptibility of (TTT)(TCNQ) is almost independent of temperature. Spin susceptibilities of the TTT and TCNQ chains, which are evaluated with a *g*-value decomposition technique, are interpreted in terms of a one-dimensional Hubbard model. In both complexes, the on-site Coulomb repulsion is comparable with or larger than the band width on the TCNQ chains and is smaller on the TTT chains. Two magnetic phase transitions are observed in (TTT)(TCNQ)$_2$. The transition is driven in each chain independently by the Peierls instability. The amount of charge transfer in (TTT)-(TCNQ) is determined to be 0.73±0.05 from an X-ray photoelectron spectroscopic study.

Naphthaceno[5,6-*cd*: 11,12-*c'd'*]bis[1,2]dithiole [tetrathiotetracene; abbreviated as TTT hereafter] is known to be a powerful donor and forms many highly conductive low dimensional organic solids with some organic acceptors and inorganic anions.[1-7] TTT forms two distinct charge-transfer complexes with 2,2'-(2,5-cyclohexadiene-1,4-diylidene)bis(propanedinitrile) [tetracyanoquinodimethan; abbreviated as TCNQ]. One is (TTT)(TCNQ)[3,4] and the other is (TTT)(TCNQ)$_2$.[2,4] Electrical conductivity of a single crystal of (TTT)-(TCNQ)$_2$ has been found to be about 100 Ω^{-1} cm^{-1} at room temperature and shows metallic temperature dependence down to about 90 K, but becomes semiconductive below 90 K.[2] Room temperature conductivity of a powdered sample of (TTT)(TCNQ) has been found to be 0.1—1 Ω^{-1} cm^{-1},[2,4] and is comparable with that of (TTT)(TCNQ)$_2$. Therefore (TTT)(TCNQ) is also regarded as a highly conductive compound, though its single crystal conductivity has not yet been reported.

The temperature dependence of magnetic susceptibility is an important physical property for an organic conductor because it provides information on the band width and the on-site Coulomb correlation effects. The temperature dependences of magnetic susceptibilities of (TTT)(TCNQ) and (TTT)(TCNQ)$_2$ have been reported previously by two groups.[2,3] In these reports, a large contribution ((2—8)×10^{-2} spins per molecule) of paramagnetism described by Curie law inhibits an accurate evaluation of intrinsic paramagnetism. Furthermore, it is necessary to decompose total spin susceptibilities into individual contributions from the two chains in order to discuss quantitatively the band width and the Coulomb correlation effects. For this purpose, a decomposition technique has been developed which uses the *g*-value observed in electron spin resonance.[8] Therefore, we have reexamined the temperature dependence of the magnetic susceptibilities and, for the first time, measured ESR of (TTT)(TCNQ) and (TTT)-(TCNQ)$_2$ in the temperature range of 2—310 K.

In this report we describe the relation between the band width and the on-site Coulomb correlation in detail using the results of magnetic susceptibility and ESR measurements. Insight into magnetic phase transition is also provided. Moreover to evaluate the band width, the amount of charge transfer in (TTT)-(TCNQ) is estimated from the results of X-ray photoelectron spectroscopy.

Experimental

Materials. TTT was synthesized by using the procedures described in the literature[5,9] with a slight modification and purified by repeated vacuum sublimation.

TCNQ (Aldrich) was purified twice by recrystallization from an acetonitrile solution and for several times by sublimation under reduced pressure.

(TTT)(TCNQ) was obtained by the following procedures. A 50 cm^3 of hot toluene solution containing 20 mg (0.1 mmol) of TCNQ was added to a boiling solution of 35 mg (0.1 mmol) of TTT in 350 cm^3 of toluene and refluxed for 30 min. The solution stood for overnight and the precipitated crystals were collected, washed with ethanol, and dried in atmosphere. Yield; 48 mg. Found: C, 65.70; H, 2.09; N, 10.16; S, 20.92%. Calcd for $C_{30}H_{12}N_4S_4$: C, 64.72; H, 2.18; N, 10.67; S, 23.04%. Room temperature resistivity on a compressed powder sample was 1.8 Ω cm.

(TTT)(TCNQ)$_2$ was obtained in the same manner as (TTT)(TCNQ) except for using twice amount of TCNQ. Yield; 71 mg. Found: C, 65.98; H, 2.11; N, 13.54; S, 16.14%. Calcd for $C_{42}H_{16}N_8S_4$: C, 66.29; H, 2.12; N, 14.73; S, 16.85%. Resistivity at room temperature on a compressed powder sample was 4.5 Ω cm.

M(TCNQ) (M=Na, K, Rb) and (tetraethylammonium)-(TCNQ)$_2$ were prepared by the method in the literature.[10] The complex of 2,2'-bi(1,3-dithiolylidene), [tetrathiafulvalene; abbreviated as TTF], and TCNQ was prepared by direct reaction of equimolar amounts of TTF and TCNQ in purified hot acetonitrile solutions.

Magnetic Susceptibility. Static magnetic susceptibility of powder samples was measured with a Faraday susceptometer described below. The construction of the susceptometer system is schematically illustrated in Fig. 1. The susceptometer is composed of three main parts; a cryostat in combination with superconducting magnets (Oxford Instruments Limited), an electric microbalance (Cahn model 2000), and a temperature control unit.

The superconducting magnets consist of a main solenoid coil which produces homogeneous field up to 50 kOe[11] and a couple of quadrupole-type gradient coils which produces

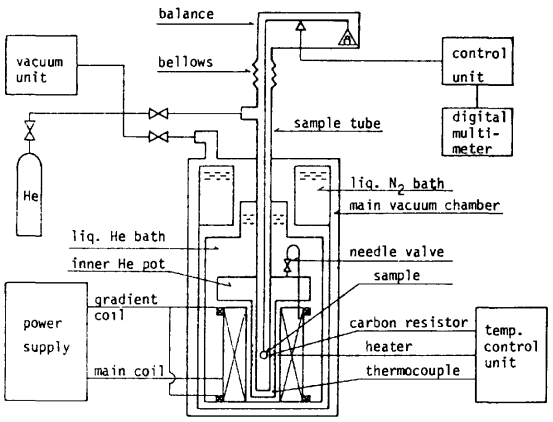

Fig. 1. Construction of the Faraday magnetosusceptometer system.

field gradient up to 1 kOe cm^{-1}. The solenoid and gradient coils are wound from NbTi filamentary wire. The magnets allow the field and field gradient to be set at desired values independently. The two magnets are used in superconducting state; in paticular, the main coil is used in a persistent current state for susceptibility measurements, and consequently fluctuation of the field strength is almost completely suppressed. The relation between a loading current and generated field was calibrated by measuring the susceptibility of sodium chloride.

The maximum loading capacity of the balance is 1 g and the magnetic force is reproducible within 1 μg, giving a maximum precision of the present system of 1×10^{-8} erg Oe^{-1} g^{-1} [11] for magnetization and 2×10^{-11} emu g^{-1} [11] for magnetic susceptibility.

A compressed powder sample of about 50 mg was contained in a quartz bucket and suspended from the balance beam with tungsten wire 30 μm in diameter. The output from the balance was read with a digital multimeter (Takeda Riken TR 6840). The sample and balance were pumped to less than 2×10^{-3} Pa to remove adsorbed oxygen and water. Typically evacuation for 90 h was necessary for (TTT)(TCNQ) to be free from paramagnetism of adsorbed oxygen. During the measurement, the sample tube was filled with purified helium gas at about 3 Pa to keep thermal contact between the sample and a copper heat sink.

Temperature below 20 K was measured with a carbon resistor and from 20 to 300 K with a 0.03% Fe-Au/chromel thermocouple. Temperature was controlled with an Oxford DTC2 temperature controller and calibrated by measuring the magnetic susceptibility of *N,N,N',N'*-tetramethyl-1,2-ethanediammonium tetrachlorocuprate(II).[12] The accuracy of temperature was to ±0.2 and ±0.5 K at 10 and 100 K, respectively.

Electron Spin Resonance. Temperature dependence of X-band electron spin resonance (ESR) spectra from 120 to 310 K were recorded on a JES-FX-1 equipped with a cryostat of cold gas nitrogen flow type. Spectra in the temperature region of 7—260 K were measured using a JES-FX-3AX with an Oxford ESR 900 continuous flow cryostat. In every measurement the modulation width was kept to be within 0.05 Oe in order to prevent a distortion of lineshape due to overmodulation.

X-Ray Photoelectron Spectroscopy (XPS). X-Ray photoelectron spectra of (TTT)(TCNQ) were measured by means of a McPherson ESCA 36 electron spectrometer on powder samples pressed onto aluminum plates employing Mg *Kα* (1253.6 eV) as the stimulating radiation. The binding energy was calibrated against the Au4f$_{7/2}$ peak (83.8 eV) of a thin film deposited on the sample surface in the spectrometer. Data for neutral TTT and (TTT)ClO$_4$ measured under the same conditions were kindly supplied by Professor Ikemoto.

Infrared Spectra. Infrared (IR) spectra were recorded using KBr disks of powdered samples with a Perkin-Elmer PE684 spectrometer.

Evaluation of the Amount of Charge Transfer

The amount of charge transfer, ρ, is one of the important quantities to consider physical properties of organic conductors, because it is related to the filling of electrons in an electron energy band. Several methods are proposed for estimation of ρ; X-ray[13,14] and neutron[15] scattering techniques, Raman[16] and IR[17] spectroscopies and XPS[18-21] method. Ikemoto *et al.*[20] have already evaluated ρ of (TTT)(TCNQ)$_2$ to be 0.93±0.05 with XPS. However, since ρ of (TTT)(TCNQ) has been left unknown, we have estimated it by means of XPS method.

The Nls core level peak of (TTT)(TCNQ) observed in this measurement has a broadened and asymmetric shape which is evidence for the presence of two kinds of TCNQ (*i.e.*, TCNQ^0 and TCNQ$^-$) in this solid as observed in (TTF)(TCNQ) and related compounds.[18-21] Since (TTT)(TCNQ) has the stoichiometry of 1 : 1, this observaton suggests that an incomplete charge transfer from TTT to TCNQ occurs in this complex.

Ikemoto *et al.* have suggested that the S2p peak is suitable for estimation of ρ for sulfur containing charge transfer complexes, because this peak is not accompanied with any strong satellite and is free from radiation damage in contrast to the Nls peak.[19,20] Our analysis is carried out by following the method proposed by them. We use the S2p peak profiles of TTT and (TTT)ClO$_4$ as standards for TTT^0 and TTT$^+$, respectively. ρ is estimated by trying to reproduce the observed (TTT)(TCNQ) peak as a sum of the TTT$^+$ and TTT^0 peaks by varying the relative intensities and separation of the two component peaks. The best fit profile is shown in Fig. 2. From the ratio of the cation peak area to the total one, ρ is estimated to be 0.73±0.05.

Chappell *et al.* have proposed an alternative method for estimation of ρ from IR spectra.[17] According to their result, wavenumber, ω, of the highest frequency vibration among those of the nitrile stretching bands has a linear relation to ρ.

We have measured the IR spectra of neutral TCNQ, alkali metal(Na, K, and Rb)-TCNQ, (TTF)(TCNQ) and tetraethylammonium(TCNQ)$_2$. The observed spectra for Na-, K-, and Rb(TCNQ) are in good agreement with the reported ones.[22-24] However, agreement with those of Chappell *et al.* is not satisfactory: For example, our results for the nitrile stretching mode are 2202 cm^{-1} for Na(TCNQ) and 2196 cm^{-1} for K-(TCNQ), while the values reported by Chappell *et al.* are 2185 and 2183 cm^{-1}, respectively. Our plot of ρ *versus* ω in several TCNQ salts shows a poor linearlity so that the evaluation of ρ from this plot would include larger error.

The value of ω=2183 cm^{-1} for K(TCNQ), which has been used as the standard for TCNQ$^-$ by them, seems to

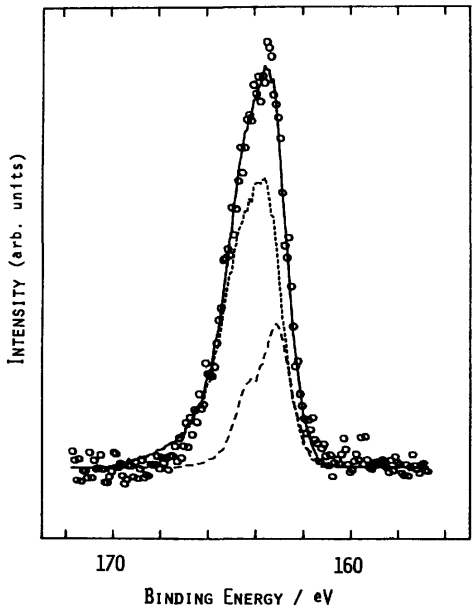

Fig. 2. Observed and calculated S2p peak profiles of X-ray photoelectron spectrum of (TTT)(TCNQ). ○: Observed data; ----: TTT^+ component; — — —: TTT^0 component; ——: superimposed peak.

correspond to the middle band among the three observed bands in the nitrile stretching band region. This band becomes allowed by vibronic coupling on the TCNQ chain[25,26] and the frequency is influenced by the strength of the coupling. Thus this band seems to be unsuitable for a reference.

For the reasons mentioned above, we employ the values of 0.73±0.05 derived from the XPS measurement as the amount of charge transfer. It has been shown that careful applicaton of the XPS method provides the ρ values in good agreement with those derived from other methods.[19-21]

Magnetic Susceptibilities

Temperature dependences of the total paramagnetic susceptibilities (χ_P) of (TTT)(TCNQ) and (TTT)-$(TCNQ)_2$ obtained by subtracting the diamagnetic contribution are shown in Fig. 3. The contribution of core diamagnetism to the observed susceptibility is estimated from the reported values of 2.15×10^{-4} emu mol^{-1} [11] for TTT[7] and 1.21×10^{-4} emu mol^{-1} for TCNQ.[27]

The temperature dependences of the susceptibilities of both complexes are different above 20 K and similar below there. To clarify the behavior in the low temperature region, $\log(\chi_P/\text{emu mol}^{-1})$ is plotted against $\log(T/\text{K})$ in Fig. 4. Below 20 K, the susceptibilities increase steadily with decreasing temperature according to the equation,

$$\chi_P = AT^{-\alpha}, \quad (1)$$

where A and α are constants. The values of $\alpha = 0.64$ and $A=1.37\times10^{-2}$ emu K mol^{-1} for (TTT)(TCNQ) and $\alpha=0.82$ and $A=4.35\times10^{-3}$ emu K mol^{-1} for $(TTT)(TCNQ)_2$ are obtained from the plots of Fig. 4. Either value of

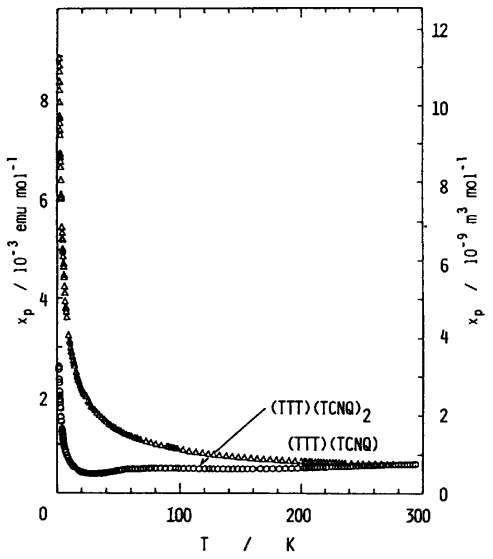

Fig. 3. Temperature dependence of total paramagnetic susceptibility. △: (TTT)(TCNQ); ○: (TTT)-$(TCNQ)_2$.

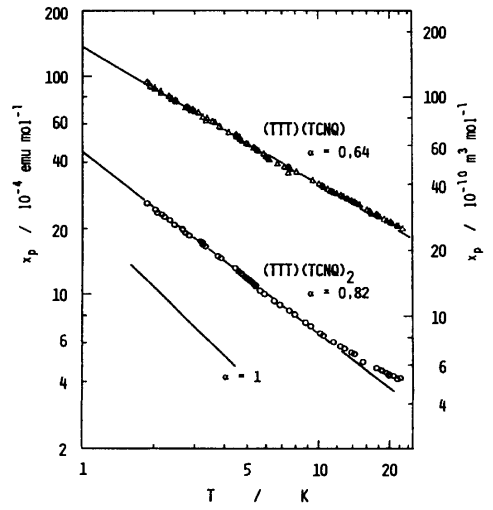

Fig. 4. Total paramagnetic susceptibility at low temperature. △: (TTT)(TCNQ); ○: $(TTT)(TCNQ)_2$; solid lines represent the least squares fit susceptibilities with T-power law.

α is unexpectedly less than unity, indicating that neither of the complexes obeys the Curie law in the low temperature region.

Some groups of organic conductors have been shown recently to exhibit the susceptibility obeying the power law expressed by Eq. 1 at low temperatures. This behavior has been interpreted in terms of a random exchange Heisenberg antiferromagnetic chain with $S=1/2$ spins.[28-32] One of the groups is represented by TCNQ complexes with asymmetric donors such as N-methylphenazinium(TCNQ),[29,33] acridinium $(TCNQ)_2$,[29] and quinolinium$(TCNQ)_2$.[29,33-36] The other group is comprised of complexes involving disorders additionally introduced by chemical doping or X-ray or neutron irradiation. Typical examples are $(HMTTF)_x$-

(HMTSF)$_{1-x}$(TCNQ), $x<1$,[35] and irradiated (TTF)-(TCNQ),[34,35] where HMTTF and HMTSF stand for 2,2′-bi(5,6-dihydro-4*H*-cyclopenta[1,3]dithiolylidene) and its selenium derivative.

Our samples seem to belong to the latter group because of the symmetric shape of TTT and TCNQ molecules. Disorder may be introduced by solvent molecules randomly included or by deviation from ideal stoichiometry. Our mass spectroscopic measurements have shown that (TTT)(TCNQ) and (TTT)(TCNQ)$_2$ include toluene, used as the solvent, in the crystals. The molar ratios of TCNQ to TTT are 1.1 for (TTT)-(TCNQ) and 1.9 for (TTT)(TCNQ)$_2$ with slight deviations among batches. This nonstoichiometry makes up kinks and missfits of the array of molecules in the molecular stacks to violate the periodic potential of the lattice and thus spins are trapped near the kinks or defects. In a similar way randomly included solvent molecules would also create the randomly trapped spins.

The reproducibility of α is good and the values of 0.63±0.05 for (TTT)(TCNQ) and 0.82±0.05 for (TTT)(TCNQ)$_2$ are obtained from the several measurements for each complex, while the magnitude of A, which corresponds to the Curie constant when $\alpha=1$, varies from sample to sample.

Regarding A as the Curie constant, though $\alpha\neq1$, we may estimate the spin concentration contributing to the susceptibility at low temperature. In spite of careful preparations of the samples, the spin concentrations estimated range from 1×10^{-2} to 4×10^{-2} spins per molecule for several batches of the both complexes. These values are comparable with or slightly less than those reported previously (about (2—8)$\times10^{-2}$ spins per molecule[4,5]). Therefore, we believe that the low temperature paramagnetism is inherent nature to the two complexes and is ascribed to the disorder mentioned above.

The spin susceptibilities (χ_s) of the two complexes in the higher temperature region are obtained by subtracting the low-temperature disorder paramagnetism discribed by Eq. 1 from the total paramagnetism. They are shown in Fig. 5. It will be shown later from the results of ESR study on powdered samples that this separation of susceptibility is appropriate for these complexes.

The χ_s values of the two complexes are quite different in temperature dependence and magnitude from each other. In (TTT)(TCNQ), χ_s is almost independent of temperature above 30 K, suggesting that no magnetic phase transition occurs in this temperature range. The value of about 2×10^{-4} emu mol^{-1} is rather smaller than that of various TCNQ complexes.

On the other hand, χ_s of (TTT)(TCNQ)$_2$ is similar to that of (TTF)(TCNQ) in temperature dependence and magnitude. The feature of temperature dependence of the observed spin susceptibility is in good agreement with the reported one in the whole temperature range, though the magnitude of our result is larger by about 30% than that.[2] The spin susceptibility increases rapidly with increase of temperature in the semiconducting region ($T\leq55$ K). Two sudden changes in χ_s are observed at about 55 and 85 K, implying occurrence

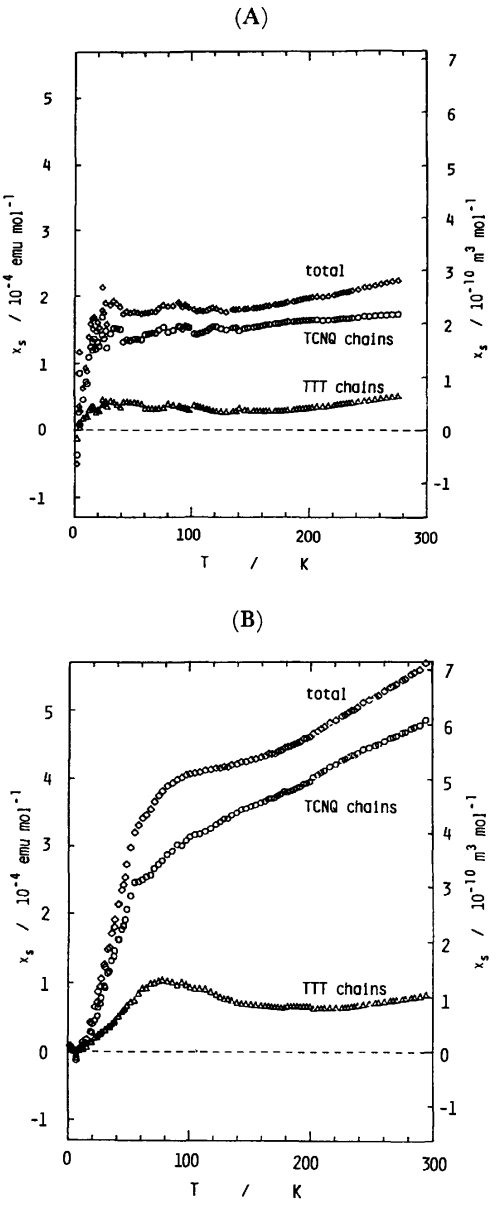

Fig. 5. Temperature dependence of total and individual spin susceptibilities. (A): (TTT)(TCNQ); (B): (TTT)(TCNQ)$_2$. ◇: Total susceptibilities; △: TTT chains; ○: TCNQ chains.

of magnetic phase transitions like those found in (TTF)-(TCNQ).[27,37] In the metallic region above 90 K, χ_s increases rather slowly with increasing temperature as observed with other organic conductors in their metallic region. We would be able to regard (TTT)(TCNQ)$_2$ as a characteristic organic conductor which is subject to a phase transition into semiconducting state at low temperature.

Decomposition of Total Spin Susceptibility into Contributions from Individual Chains

The observed spin susceptibilities of (TTT)(TCNQ) and (TTT)(TCNQ)$_2$ are total ones, namely the sums of spin susceptibilities of the TTT and TCNQ chains.

Both of the TTT and TCNQ chains are expected to exhibit finite magnetic susceptibilities almost independently. Thus separation of total susceptibilities into the individual components becomes important for further discussion. Two techniques for such separation have been proposed. One is the technique to use the g-values of ESR spectra.[8] The other is the method to make use of Knight-shift in ^{13}C-NMR spectra[38] The former technique is readily available to us and is employed here.

The observed ESR spectra at various temperatures are shown in Fig. 6. The structure appearing in the spectrum at high temperature is attributed to a g-value anisotropy for both complexes, because the lineshape cannot be reproduced by a superposition of absorption lines of TTT^+ and $TCNQ^-$ radicals. Indeed, a preliminary ESR measurement on a single crystal of (TTT)-(TCNQ)$_2$ shows a single narrow absorption.

Lineshapes of the spectra of the two complexes are clearly different and their temperature dependence reflects the presence or absence of magnetic phase transition. In (TTT)(TCNQ), the lineshape varies continuously from 300 K down to 7.8 K. There is no indication of magnetic phase transition in this temperature range. This behavior is consistent with the result of magnetic susceptibility in the preceding section. The low field line additionally appears below 200 K with $g'=2.0073$ and seems to be arising from the spins mainly localized on TTT, because the observed value of g' is close to the g-value of the TTT cation radical.[39] Since the intensity of this line increases rapidly on cooling, this line is likely caused by the localized paramagnetic centers introduced by disordered nature of the solid observed in the static susceptibility.

In (TTT)(TCNQ)$_2$, the lineshape varies suddenly at some temperatures. On cooling, the depth of the dip near g_1 increases and the width narrows gradually. Sud-

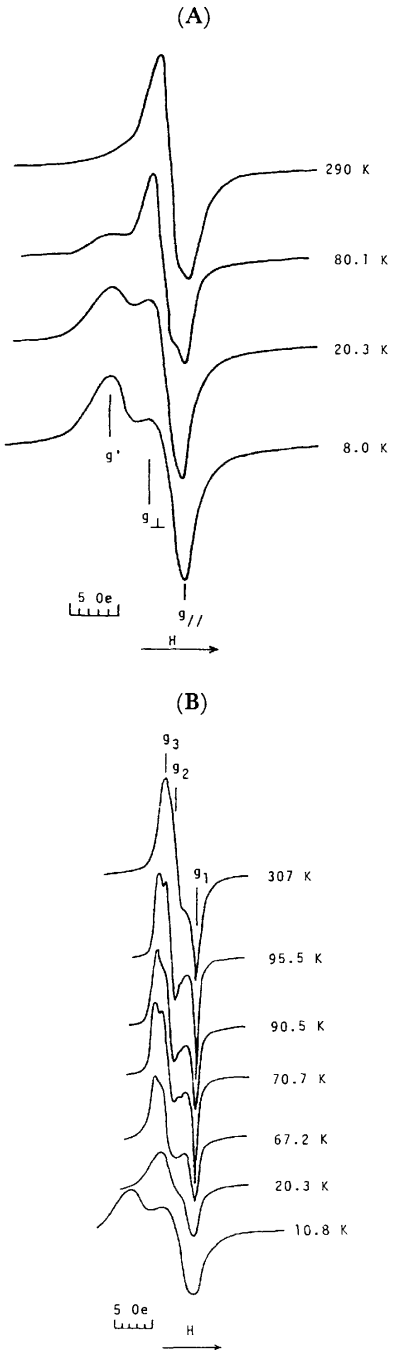

Fig. 6. ESR signals on powdered samples at various temperatures. (A): (TTT)(TCNQ); (B): (TTT)-(TCNQ)$_2$. Assignment of anisotorpic g-values is tentative.

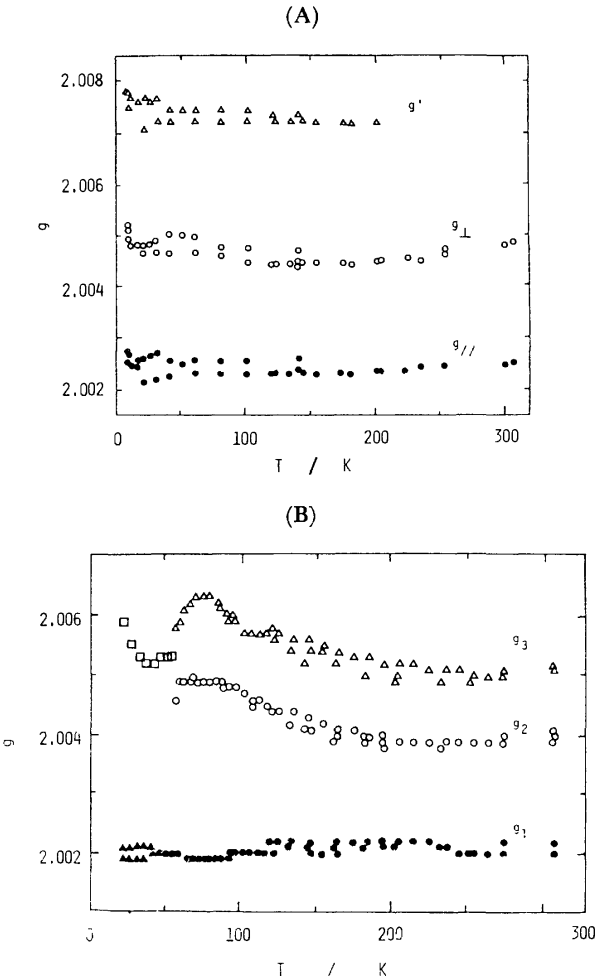

Fig. 7. Temperature dependence of g-values. (A): (TTT)(TCNQ); (B): (TTT)(TCNQ)$_2$.

den decrease in depth and increase in width are observed near 90 and 67 K, indicating the presence of phase transitions. The variation below 55 K is rather continuous, though the linewidth becomes broadened with decreasing temperature. A new line appearing below 15 K at the lower magnetic field would also be attributed to the signal due to the spin on disordered TTT site as discussed for (TTT)(TCNQ).

The temperature dependences of g-values shown in Fig. 7 support the results of the measurements of the temperature dependences of lineshape and magnetic susceptibility. Variation is continuous in (TTT)(TCNQ), while two irreguralities are found at 65 and 90 K in the temperature dependence of g_2 and g_3 in (TTT)(TCNQ)$_2$.

Since the main structures of the ESR spectra of (TTT)(TCNQ) and (TTT)(TCNQ)$_2$ are only due to the g-value anisotropy, the magnetic exchange interaction between TTT and TCNQ chains is expected to exceed the difference in the Larmor frequency, and averages out the g-values of the component radicals. Tomkiewicz *et al.* have shown that the observed g-value of such a complex is determined by a weighted average of the g-values of the component radicals,[8] where weight is proportional to χ_s of the donor and acceptor chains. Thus we may expect the following relationship to our complexes.

$$\bar{g} = \frac{\chi_{s,T}\bar{g}_T + \chi_{s,Q}\bar{g}_Q}{(\chi_{s,T} + \chi_{s,Q})}, \tag{2}$$

where $\bar{g}$, $\bar{g}_T$, and $\bar{g}_Q$ are the averaged g-values of the complex, the TTT^+ radical, and the $TCNQ^-$ radical, respectively, and $\chi_{s,T}$ and $\chi_{s,Q}$ are the spin susceptibility of the TTT and TCNQ chains. The value of 2.0029 is known as the average g-value of tetraethylammonium $(TCNQ)_2$.[40] The value of $\bar{g}_T$ is presently determined to be 2.0083 for $(TTT^+)(CH_3CO_2^-)$.[39] Using the relation of Eq. 2, we may estimate $\chi_{s,T}$ and $\chi_{s,Q}$ from these g-values. In this estimation, we have assumed that the $\bar{g}_T$ and $\bar{g}_Q$ are independent of temperature. The results are shown in Fig. 5 together with total χ_s.

In both complexes, $\chi_{s,Q}$ is larger than $\chi_{s,T}$. In particular the temperature dependence of χ_s of (TTT)(TCNQ)$_2$ is primarily dominated by the susceptibility of the TCNQ chains. It is clearly seen from Fig. 5 that the phase transition near 90 K is related to the TTT chains and that near 60 K is to the TCNQ chains, and moreover each phase transition does not seem to influence the other.

Estimation of Band Width and On-site Coulomb Repulsive Energy

Spin susceptibilities of organic conductors have often been explained in terms of a one-dimensional Hubbard model,[41] which takes into account of transfer of electron between neighboring sites and on-site Coulomb repulsion between two electrons on the same site. The magnetic properties on this model are known for the following three limiting cases which are characterized by the relation between the band width ($4t$) and the on-site Coulomb repulsive energy (U), where t is the transfer integral between neighboring sites; (a) non-interacting case ($U=0$), (b) small U limit ($U \ll 4t$), and (c) large U limit ($U \gg 4t$).

In the non-interacting case, the system is in metallic state and the magnetic susceptibility would be given by the Pauli paramagnetism. Assuming a tight-binding approximation, the Pauli susceptibility at $T=0$ K is given by[42]

$$\chi_{Pauli}(0) = \frac{N_A\mu_B^2}{t\pi \sin(\pi\rho/2)}, \tag{3}$$

where N_A is the Avogadro constant, μ_B is the Bohr magneton and ρ is the electron-to-site ratio. The temperature dependence of Pauli paramagnetism, $\chi_{Pauli}(T)$, has been calculatd only for $\rho=1$ by Shiba.[43] Therefore we have to assume that the temperature dependence of Pauli susceptibility for arbitrary ρ is given by dividing $\chi_{Pauli}(T)$ by filling factor, $\sin(\pi\rho/2)$.

In the small U limit ($U \ll 4t$), the spin susceptibility due to the Pauli paramagnetism would be enhanced by the on-site Coulomb repulsion and is given by[44]

$$\chi_s = \frac{\chi_{Pauli}(T)}{(1-U/4\pi t)\sin(\pi\rho/2)}. \tag{4}$$

As the on-site Coulomb repulsion increases, electrons tend to be scattered with each other and localized character of them gradually increases. In the large U limit ($U \gg 4t$), electrons are strongly localized on each site and this situation just coincides with the one-dimensional Heisenberg antiferromagnetic chain. In this case, the exchange coupling constant, J, is related to U, $4t$, and ρ by the equation,[45]

$$J = \frac{2t^2}{U + (4t/\pi)\sin\pi\rho}\left(1 - \frac{\sin 2\pi\rho}{2\pi\rho}\right). \tag{5}$$

The band width and the Coulomb repulsion energy may be estimated from these equations by examining the susceptibilities at various temperatures. Representative results of such fittings are shown in Fig. 8 for the spin susceptibilities of TTT and TCNQ chains in (TTT)(TCNQ) and (TTT)(TCNQ)$_2$, performed by using the values of ρ derived from the XPS study. Unfortunately, however, the agreement between the calculated and observed susceptibilities are not satisfactory in the whole temperature region in either case. In (TTF)(TCNQ), Torrance *et al.*[44] have also found lack of agreement in the temperature dependence of calculated susceptibilities with those observed. We concentrate then our attention on getting agreement in the magnitude of χ_s only at room temperature in order to see what is the most reasonable case as discussed by Torrance *et al.*

We examine the TCNQ chains at first. For the non-interacting case, agreements are obtained when we choose $4t$ to be 0.3 eV for (TTT)(TCNQ) and 0.15 eV for (TTT)(TCNQ)$_2$. Since most of the band widths of organic conductors have been estimated to be 0.4—1.5 eV from different experiments and calculations,[46,47] these obtained values seem to be too small. If we intend to apply the reasonable band width, we have to take into account of enhancement of χ_s by introducing a finite on-site Coulomb repulsive interaction.

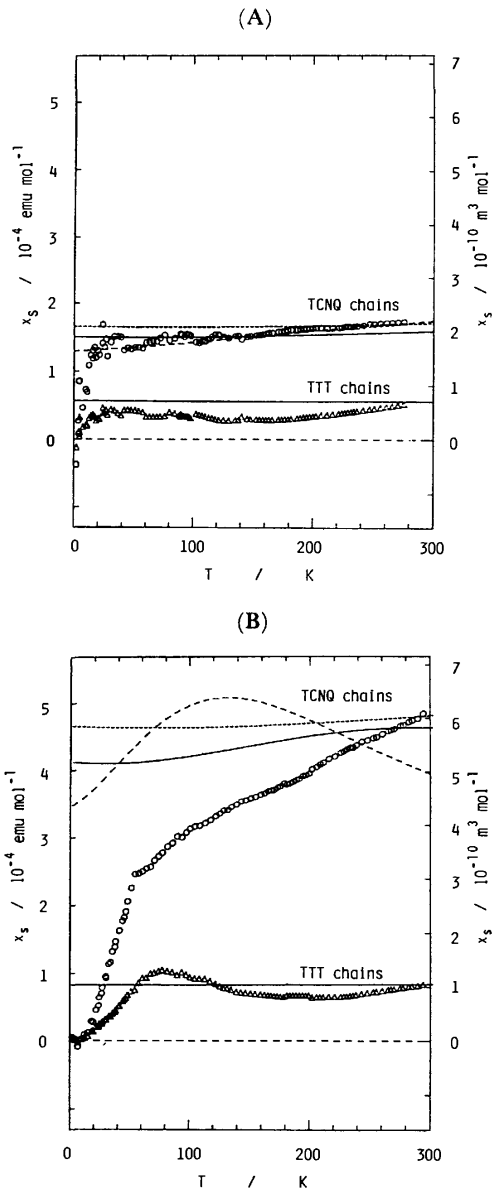

Fig. 8. Estimated spin susceptibilities with the one-dimensional Hubbard model for three limits. (A): (TTT)(TCNQ): △; $\chi_{s,T}$ observed, ——; non-interacting case (U=0, $4t$=0.8 eV), ○; $\chi_{s,Q}$ observed, ——; non-interacting case (U=0, $4t$=0.3 eV), ----; small U limit ($4t$=0.4 eV, $U/4t$=1.0), — — —; large U limit (J=420 K, $U/4t$=1.2), (B) (TTT)(TCNQ)$_2$: △; $\chi_{s,T}$ observed, ——; non-interacting case (U=0, $4t$=0.5 eV), ○; $\chi_{s,Q}$ observed, ——; non-interacting case (U=0, $4t$=0.15 eV), ----; small U limit ($4t$=0.4 eV, $U/4t$=2.1), — — —; large U limit (J=100 K, $U/4t$=2.1).

Berlinsky *et al.*[47] have estimated $4t$ of TCNQ chains in (TTF)(TCNQ) to be 0.44 eV based on extended Hückel MO calculation. The X-ray analysis of (TTT)(TCNQ)$_2$[2,48] shows that the manner of overlap of the TCNQ molecules is similar to that of (TTF)(TCNQ),[49] *i.e.*, so called ring-external bond type. The interplanar spacing between TCNQ molecules (318 pm) is nearly the same as that of (TTF)(TCNQ)(317 pm). By expecting that a value of $4t$ is not much influenced by the change in the manner of stacking, the band width of the TCNQ chains of the two complexes may be assumed to be 0.4 eV. On this assumption, the best fit is obtained when $U/4t$ is 1.0 for (TTT)(TCNQ) and 2.1 for (TTT)(TCNQ)$_2$ in the small U limit.

For the large U limit, fitting with Bonner-Fisher susceptibility[50] gives the J value of 420 K for (TTT)(TCNQ) and 100 K for (TTT)(TCNQ)$_2$. From these J, the values of $U/4t$ is estimated to be 1.2 for (TTT)(TCNQ) and 2.5 for (TTT)(TCNQ)$_2$.

In each limit, the estimated $U/4t$ falls into the range of 1—2.5 and contradicts the initially assumed condition, that is, small or large U. This fact suggests that the magnitude of U is comparable with that of $4t$; *i.e.*, the relation between U and $4t$ is in an intermediate case, since the behavior of susceptibility for intermediate U is simply intermediate between the behavior calculated for small U and that for large U. Torrance *et al.* have suggested that the intermediate U can be expected for (TTF)(TCNQ) and the role of the on-site Coulomb repulsion is important in magnetic properties of one-dimensional organic conductors.[44] Similar findings on χ_s have also been reported for organic conductors such as (TSF)(TCNQ) and (HMTTF)(TCNQ).[51]

For the TTT chains, the situation seems to be different. In the non-interacting limit, $4t$ of the TTT chains are evaluated to be 0.8 eV for (TTT)(TCNQ) and 0.5 eV for (TTT)(TCNQ)$_2$. These values seem to be in agreement with the reported values of 0.6—1.5 eV for (TTT)$_2$I$_3$.[5,6,52] Therefore, the on-site Coulomb repulsion seems to be very small on the TTT chains in both complexes.

It is of interest to compare the evaluated spin susceptibilities with those of other two-chains organic conductors. The spin susceptibilities of donor ($\chi_{s,d}$) and acceptor chains ($\chi_{s,a}$) of some two-chains conductors at 300 K are listed in Table 1 together with those of (TTT)(TCNQ) and (TTT)(TCNQ)$_2$. Table 1 indicates that the variation of $\chi_{s,d}$ among these complexes is larger than that of $\chi_{s,a}$. Since the TCNQ molecules in these complexes make stacking in the similar manner,[49,57-60] it is reasonably expected that $\chi_{s,Q}$ does not differ too much, though the interplanar spacings are varied from 317 to 331 pm. For the donor stacks, on

Table 1. Total ($\chi_{s,t}$), donor ($\chi_{s,d}$), and acceptor ($\chi_{s,a}$) spin susceptibilities of two-chains organic conductors at 300 K. Susceptibilities are given in 10^{-4} emu mol^{-1}

	$\chi_{s,t}$	$\chi_{s,d}$	$\chi_{s,a}$	Reference
(TTF)(TCNQ)	6.0	3.2	2.8	27), 51)
(TSF)(TCNQ)	3.3	0.7	2.6	51), 56)
(TMTTF)(TCNQ)[a]	4.8	2.6	2.2	27), 53)
(HMTTF)(TCNQ)	2.4	0.7	1.7	51), 54)
(TMTSF)(DMTCNQ)[b,c]	5.5	1.65	3.85	55)
(TTT)(TCNQ)$_2$	5.8	0.9	4.9	This work
(TTT)(TCNQ)	2.3	0.5	4.9	This work

a) TMTTF=2,2′-Bi(4,5-dimethyl-1,3-dithiolylidene). b) TMTSF=2,2′-Bi(4,5-dimethyl-1,3-diselenolylidene). c) DMTCNQ=2,2′-(2,5-Dimethyl-2,5-cyclohexadiene-1,4-diylidene)bis(propanedinitrile).

the other hand, the large variation of $\chi_{s,d}$ may be ascribed to the large difference in molecular structure and chemical properties of the donors.

Among these compounds, the susceptibility of donor chains in (HMTTF)(TCNQ) exhibits behavior similar to that in (TTT)(TCNQ) and (TTT)(TCNQ)$_2$ in temperature dependence and magnitude. The spin susceptibility of HMTTF chains in (HMTTF)(TCNQ) is almost independent of temperature above the transition temperature of 50 K and its magnitude is 0.75×10^{-4} emu mol^{-1}, which corresponds to the Pauli paramagnetism with $4t$=0.57 eV. Tomkiewicz *et al.* have explained this finding in terms of reduction of U arising from the following two possible ways;[51] (1) reduction of bare U, caused by chemical modification of donor molecule and (2) effective reduction of U, arising from a screening effect of counter ions which has been first proposed by LeBlanc.[61]

Since the interplanar distance of the donor in (TTT)(TCNQ)$_2$ (352 pm) is larger to a small extent than that in (TTF)(TCNQ) (347 pm), the band width of TTT is expected to be comparable with or slightly narrower than that of TTF. Therefore the flat temperature dependence of the small magnitude of susceptibility would have to be attributed to the reduction of the on-site Coulomb repulsion as discussed in the case of (HMTTF)(TCNQ). It is plausible to assume that the reduction of U arises from the chemical modification of donor molecule, because it is rather difficult to see that the screening effect of TCNQ as a counter ion contributes markedly to reduction of U from its molecular and crystal structure.

Spin density distribution calculations[62] on sulfur containing organic cation radicals would support this idea. The calculation on the TTT$^+$ radical has revealed that more than 70% of unpaired electron spins are distributed on the 5-, 6-, 11-, and 12-carbon atoms and the four sulfur atoms of the TTT molecule. In the TTF$^+$ radical, most of the spins are located on the 2- and 2′-carbon atoms and the four sulfur atoms. A comparison of the spin distributions allows us to regard TTT as a molecule similar to TTF, but the four sulfur atoms in TTF are pulled apart from 1,1′,3,3′-positions to 4,4′,5,5′-positions. Since the sulfur-sulfur distance between different five-membered rings is prolonged in TTT in comparison with that of TTF, U is expected to be reduced. At the same time, the four benzene rings in TTT also contribute to reduction of U as a result of the delocalization of electrons

Phase Transitions and Low-temperature Spin Susceptibility

As discussed in previous sections, the presence of the magnetic phase transition becomes apparent in (TTT)(TCNQ)$_2$ by the measurements of magnetic susceptibility and ESR. In (TTT)(TCNQ), however, no evidence for a phase transition has been found at least above 20 K. Thus our discussion about the phase transition is limited only to (TTT)(TCNQ)$_2$.

The temperature-dependent $\chi_{s,T}$ and $\chi_{s,Q}$ are shown in Fig. 9. On lowering the temperature below

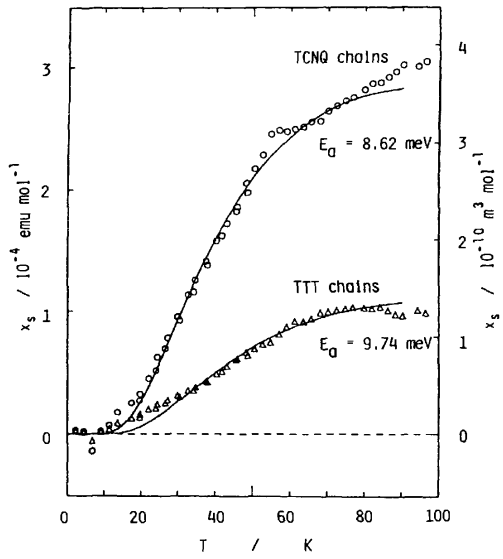

Fig. 9. Spin susceptibilities of TTT and TCNQ chains in (TTT)(TCNQ)$_2$ below the transition temperature. Solid lines are calculated susceptibilities with $\chi_s = (C/T)\exp(-E_a/k_BT)$, E_a=9.74 meV for TTT chains and 8.62 meV for TCNQ chains.

the transition temperature, the spin susceptibilities of both chains decrease monotonously with the activation-type equation,

$$\chi_s = (C/T)\exp(-E_a/k_BT), \quad (6)$$

where C is a constant and E_a is an activation energy. The values of C and E_a are found to be 0.034 emu K mol^{-1} and 9.74 meV for the TTT chains and 0.077 emu K mol^{-1} and 8.62 meV for the TCNQ chains. The temperature dependence of the susceptibilities arises from the spins which are thermally excited across a gap that is formed by a phase transition. This type of temperature dependence of susceptibility has often been found in the low temperature region of organic conductors which become semiconductive by the Peierls transition.[53,63] Indeed, the conductivity measurement carried out by Buravov *et al.* has shown that (TTT)(TCNQ)$_2$ is semiconductive below the transition temperature of about 90 K.[2] Thus the phase transition may be attributed to a metal-semiconductor transition driven by the Peierls instability.

The activation energies of paramagnetism of the TCNQ chains for (TTF)(TCNQ)[63] and (HMTTF)(TCNQ)[53] are known to be 36 and 21.5 meV, respectively, in the semiconductive region. The observed E_a of 8.62 meV for the TCNQ chains of (TTT)(TCNQ)$_2$ is smaller than these values. Since a magnetic activation energy is related to the strength of electron-phonon coupling,[64] the small value for (TTT)(TCNQ)$_2$ suggests a weaker electron-phonon coupling on the TCNQ chains in (TTT)(TCNQ)$_2$. The activation energies of the donor chains for (TTF)(TCNQ) and (TMTTF)(TCNQ) have been estimated to be 10.8 and 13.8 meV, respectively, and are slightly larger than those for the TTT chains of (TTT)(TCNQ)$_2$ (9.74 meV). Thus the magnitude of electron-phonon coupling on the TTT

chains in(TTT)(TCNQ)$_2$ seems to be close to that on TTF in (TTF)(TCNQ), whose donor chains are distorted at 49 K.[38,63]

The transition temperature of the TTT chains in (TTT)(TCNQ)$_2$ is rather high compared with that of the donor chains in other two-chains complexes, while that of the TCNQ chains is not so different from that of (TTF)(TCNQ). A transition temperature driven by the Peierls instability is associated with the strength of the electron-phonon coupling and the dimensionality, namely the strength of interchain interactions. The stronger the electron-phonon coupling and the weaker the interchain interaction, the higher phase transition temperature is expected. The crystal structure analysis suggests that the interchain interaction is weak in (TTT)(TCNQ)$_2$. The shortest interchain distances are 344 and 348 pm, and are considerably longer than those of (TTF)(TCNQ) (320 and 325 pm)[49] and (HMTTF)(TCNQ) (325 pm).[55] The weak interchain interaction is also suggested by our preliminary ESR measurements on a single crystal of this complex. The peak-to-peak linewidth of ESR signal at room temperature is quite narrow (1.1 Oe) among the sulfur containing organic conductors.[53,55] This finding indicates that the spin relaxation is suppressed, because if interchain interaction is too weak to transfer effectively the magnetic energy three-dimensionally, the correlation among spins is generally kept for rather long time.

Therefore high transition temperature of TTT chains reflects the low-dimensional character of this complex. For the TCNQ chains, the observed weak electron-phonon coupling would lower the transition temperature, whereas weak interchain interaction would raise the transition temperature. The two effects on the TCNQ chains counteract each other and consequently, the transition temperature of the TCNQ chains would not change much from that of (TTF)-(TCNQ).

Summary

The susceptibilities of both of the donor and acceptor chains extracted by the manipulation of the data indicate that, in the metallic region, the susceptibility of the TCNQ chains is considerably enhanced by the on-site Coulomb repulsion and dominates the magnitude of the total susceptibility, while the susceptibility of the TTT chains is explained by the Pauli paramagnetism.

The discontinuities in the temperature dependence of the spin susceptibility in (TTT)(TCNQ)$_2$ are driven by the Peierls instability, resulting in the thermally activated paramagnetism below the transition temperature. The susceptibility of (TTT)(TCNQ) is almost temperature independent above 20 K. Although some insight into electronic state is given in the latter complex, further experiments such as conductivity measurement on a single crystal and structure analysis are indispensable for detailed discussion.

The authors are thankful to Professor Kazuo Morigaki and Dr. Izumi Hirabayashi of the Institute for Solid State Physics and Drs. Mikio Hoshino and Hisaharu Hayashi of the Institute of Physical and Chemical Research for the kindness in putting the ESR spectrometers at their disposal. Thanks are also due to Professors Haruo Kuroda and Isao Ikemoto of the Department of Chemistry for their support in XPS measurements. The authors are grateful to Dr. Gunji Saito of the Institute for Molecular Science for measurements of mass spectra and Mr. Kenji Suzuki for his help in synthesis of TTT. A part of this work was supported by a Grant-in-Aid for Scientific Research from the Ministry of Education, Science and Culture (No. 57740230).

References

1) For reviews see a) L. C. Isett and E. A. Perez-Albuerne, *Ann. N. Y. Acad. Sci.*, **313**, 395 (1978); b) I. F. Shchegolev and E. B. Yagubskii, "Extended Linear Chain Conductors," ed by J. S. Miller, Plenum Press, New York (1982), Vol. 2, p. 385.

2) L. I. Buravov, O. N. Eremenko, R. B. Lyubovskii, L. P. Rozenberg, M. L. Khidekel', R. P. Shibaeva, I. F. Shchegolev, and E. B. Yagubskii, *Pis'ma Zh. Eksp. Teor. Fiz.*, **20**, 457 (1974). (*JETP Lett.*, **20**, 208 (1974).)

3) P. Delhaès, S. Flandrois, G. Keryer, and P. Dupuis, *Mater. Res. Bull.*, **10**, 825 (1975).

4) R. C. Wheland and J. L. Gillson, *J. Am. Chem. Soc.*, **98**, 3916 (1976).

5) L. C. Isett and E. A. Perez-Albuerne, *Solid State Commun.*, **21**, 433 (1977).

6) G Mihály, A. Jánossy, and G. Grüner, *Solid State Commun.*, **22**, 771 (1977).

7) L. C. Isett, *Phys. Rev. B*, **18**, 439 (1978).

8) a) Y. Tomkiewicz, A. R. Taranko, and J. B. Torrance, *Phys. Rev. Lett.*, **36**, 751 (1976); b) *Phys. Rev. B*, **22**, 3113 (1980).

9) C. Marschalk and C. Stumm, *Bull. Soc. Chim. Fr.*, **1948**, 418; E. P. Goodings, D. A. Mitchard, and G. Owen, *J. Chem. Soc., Perkin Trans. 1*, **1972**, 1310.

10) L. R. Melby, R. J. Harder, W. R. Hertler, W. Mahler, R. E. Benson, and W. E. Mochel, *J. Am. Chem. Soc.*, **84**, 3374 (1962).

11) We employed in this report the c.g.s. electromagnetic units, in the interest of comparison with values in references. To convert into the SI unit, the following relations should be used; 1 A m^{-1}=4π×10^{-3} Oe, 1 A m^2 kg^{-1}=1 erg Oe^{-1} g^{-1}, 1 m^3 kg^{-1}=10^3/4π emu g^{-1}, and 1 m^3 mol^{-1}=10^6/4π emu mol^{-1}.

12) D. B. Brown, V. H. Crawford, J. W. Hall, and W. E. Hatfield, *J. Phys. Chem.*, **81**, 1303 (1977).

13) F. Denoyer, R. Comès, A. F. Garito, and A. J. Heeger, *Phys. Rev. Lett.*, **35**, 445 (1975).

14) S. Kagoshima, H. Anzai, K. Kajimura, and T. Ishiguro, *J. Phys. Soc. Jpn.*, **39**, 1143 (1975).

15) G. Shirane, S. M. Shapiro, R. Comès, A. F. Garito, and A. J. Heeger, *Phys. Rev. B*, **14**, 2325 (1976).

16) S. Matsuzaki, R. Kuwata, and K. Toyoda, *Solid State Commun.*, **33**, 403 (1980); S. Matsuzaki, T. Moriyama, and K. Toyoda, *ibid.*, **34**, 857 (1980).

17) J. S. Chappell, A. N. Bloch, W. A. Bryden, M. Maxfield, T. O. Poehler, and D. O. Cowan, *J. Am. Chem. Soc.*, **103**, 2442 (1981).

18) W. D. Grobman and B. D. Silverman, *Solid State Commun.*, **19**, 319 (1976).

19) I. Ikemoto, T. Sugano, and H. Kuroda, *Chem. Phys. Lett.*, **49**, 45 (1977).

20) I. Ikemoto, M. Yamada, T. Sugano, and H. Kuroda, *Bull.Chem. Soc. Jpn.*, **53**, 1871 (1980).

21) M. Tokumoto, N. Koshizuka, H. Anzai, and T.

Ishiguro, *J. Phys. Soc. Jpn.*, **51**, 332 (1982).
22) M. S. Khantkale and J. P. Devlin, *J. Chem. Phys.*, **70**, 1851 (1979).
23) Z. Iqbal, C. W. Christoe, and D. K. Dawson, *J. Chem. Phys.*, **63**, 4485 (1975).
24) R. Bozio, A. Girlando, and C. Pecile, *J. Chem. Soc., Faraday Trans. 2*, **71**, 1237 (1972).
25) R. Bozio, I. Zanon, A. Girlando, and C. Pecile, *J. Chem. Soc., Faraday Trans. 2*, **74**, 235 (1978).
26) G. R. Anderson and J. P. Devlin, *J. Phys. Chem.*, **79**, 1100 (1978).
27) J. C. Scott, A. F. Garito, and A. J. Heeger, *Phys. Rev. B*, **10**, 3131 (1974).
28) For review articles; W. G. Clark, J. Jamann, J. Sanny, and L. C. Tippie, "Lecture Notes in Physics," ed by S. Barišić, A. Bjeliš, J. R. Cooper, and B. Leontić, Springer-Verlag, Berlin (1979), Vol. 96, p. 255; W. G. Clark, "Physics in One Dimension," ed by Bernasconi and T. Schneider, Springer-Verlag, Berlin (1981), p. 289.
29) L. N. Bulaevskii, A. V. Zvarykina, Yu. S. Karimov, R. B. Lybovskii, and I. F. Shchegolev, *Zh. Eksp. Tero. Fiz.*, **62**, 725 (1972). (*Sov. Phys. JETP*, **35**, 384 (1972).)
30) W. G. Clark and L. C. Tippie, *Phys. Rev. B*, **20**, 2914 (1979).
31) G. Theodorou, *Phys. Rev. B*, **16**, 2254, 2264 (1977).
32) L. P. Gor'kov, O. N. Dorokhov, and F. V. Prigara, *Solid State Commun.*, **37**, 869 (1981); C. Dasgupta and S. Ma, *Phys. Rev. B*, **22**, 1305 (1980); Z. G. Soos and S. R. Bondeson, *Mol. Cryst. Liq. Cryst.*, **85**, 1409 (1982); J. E. Hirsch and J. V. José, *J. Phys. C*, **13**, L53 (1980).
33) G. Theodorou, *Phys. Rev. B*, **16**, 2273 (1977).
34) M. Miljak, B. Korin, J. R. Cooper, K. Holczer, G. Grüner and A. Jánossy, *J. Mag. Mag. Mater.*, **15-18**, 219 (1980).
35) M. Miljak, B. Korin, J. R. Cooper, K. Holczer, and A. Jánossy, *J. Phys. (Paris)*, **41**, 639 (1980).
36) L. C. Tippie and W. G. Clark, *Phys. Rev. B*, **23**, 5846 (1981).
37) Y. Tomkiewicz, B. A. Scott, L. J. Tao, and R. S. Title, *Phys. Rev. Lett.*, **32**, 1363 (1974).
38) E. F. Rybaczewski, L. S. Smith, A. F. Garito, A. J. Heeger, and B. G. Silbernagel, *Phys. Rev. B*, **14**, 2746 (1976); E. F. Rybaczewski, A. F. Garito, A. J. Heeger, and E. Ehrenfreund, *Phys. Rev. Lett.*, **34**, 524 (1975).
39) Measured values on $(TTT^+)(CH_3CO_2^-)$; $g_{//}$=2.0034(1), $g_\perp$=2.0107(1), and $\bar{g}$=2.0083(1).
40) J. Kurti and G. Menczel, *Phys. Status Solidi B*, **102**, 639 (1980); g_1=2.00236 g_2=2.00276, g_3=2.00355, and $\bar{g}$=2.00289.
41) J. Hubbard, *Proc. R. Soc. London, Ser. A*, **276**, 238 (1963); *ibid.*, **281**, 401 (1964).
42) H. Shiba, *Phys. Rev. B*, **6**, 930 (1972).
43) H. Shiba, *Prog. Theor. Phys.*, **48**, 2171 (1972).
44) J. B. Torrance, Y. Tomkiewicz, and B. D. Silverman, *Phys. Rev. B*, **15**, 4738 (1977).
45) D. J. Klein and W. A. Seitz, *Phys. Rev. B*, **10**, 3217 (1974).
46) For example, proposed 4t for (TTF)(TCNQ) is in the range of 0.2—0.7 eV; A. A. Bright, A. F. Garito, and A. J. Heeger, *Phys. Rev. B*, **10**, 1328 (1974); P. M. Grant, R. L. Greene, G. C. Wrighton, and G. Castro, *Phys. Rev. Lett.*, **31**, 1311 (1973); D. R. Salahub, P. R. Messmer, and F. Herman, *Phys. Rev. B*, **13**, 4252 (1976); A. Karpfen, J. Ladik, G. Stollhoff, and P. Fulde, *Chem. Phys.*, **8**, 215 (1975).
47) A. J. Berlinsky, J. F. Carolan, and L. Weiler, *Solid State Commun.*, **15**, 795 (1974).
48) R. P. Shibaeva and L. P. Rozenberg, *Kristallografiya*, **20**, 943 (1975). (*Sov. Phys. Cryst.*, **20**, 581 (1976).)
49) T. J. Kistenmacher, T. E. Phillips, and D. O. Cowan, *Acta Crystallogr., Sect. B*, **30**, 763 (1974).
50) J. C. Bonner and M. E. Fisher, *Phys. Rev.*, **135**, A640 (1964).
51) Y. Tomkiewicz, B. Welber, P. E. Seiden, and R. Schumaker, *Solid State Commun.*, **23**, 471 (1977).
52) R. B. Somoano, S. P. S. Yen, V. Hadek, S. K. Khanna, M. Novotny, T. Datta, A. M. Hermann, and J. A. Woollam, *Phys. Rev. B*, **17**, 2853 (1978).
53) Y. Tomkiewicz, A. R. Taranko, and D. C. Green, *Solid State Commun.*, **20**, 767 (1976).
54) Y. Tomkiewicz, A. R. Taranko, and R. Schumaker, *Phys. Rev. B*, **16**, 1380 (1977).
55) Y. Tomkiewicz, J. R. Andersen, and A. R. Taranko, *Phys. Rev. B*, **17**, 1579 (1978).
56) R. L. Greene, J. J. Mayerle, R. Schmaker, G. Castro, P. M. Chaikin, S. Etemad, and S. J. LaPlaca, *Solid State Commun.*, **20**, 943 (1977).
57) L. I. Buravov, R. N. Lybovskaya, R. B. Lybovskii, and M. L. Khidekel', *Zh. Eksp. Teor. Fiz.*, **70**, 1982 (1976). (*Sov. Phys. JETP*, **43**, 1033 (1977).)
58) K. Bechgaard, T. J. Kistenmacher, A. N. Bloch, and D. O. Cowan, *Acta Crystallogr., Sect. B*, **33**, 417 (1977).
59) T. E. Phillips, T. J. Kistenmacher, A. N. Bloch, J. P. Ferraris, and D. O. Cowan, *Acta Crystallogr., Sect. B*, **33**, 422 (1977).
60) J. R. Andersen, K. Bechgaard, C. S. Jacobsen, G. Rindorf, H. Soling, and N. Thorup, *Acta Crystallogr., Sect. B*, **34**, 1901 (1978).
61) O. H. LeBlanc, Jr., *J. Chem. Phys.*, **42**, 4307 (1965).
62) F. B. Bramwell, R. C. Haddon, F. Wudl, M. L. Kaplan, and J. H. Marshall, *J. Am. Chem. Soc.*, **100**, 4612 (1978); W. E. Geiger, Jr., *J. Phys. Chem.*, **77**. 1862 (1973).
63) Y. Tomkiewicz, A. R. Taranko, and J. B. Torrance, *Phys. Rev. Lett.*, **36**, 751 (1976).
64) Ref. 55 and the references cited therein.

Dinuclear Cobalt(II) Complexes with Various Dinucleating Ligands and Their Dioxygen Complexes

Masatatsu SUZUKI,*,† Hajime KANATOMI, and Ichiro MURASE
Laboratory of Chemistry, College of General Education, Kyushu University, Ropponmatsu, Chuo-ku, Fukuoka 810
(Received July 21, 1983)

Various types of dinuclear cobalt(II) complexes, $[Co_2L(CH_3COO)_2]ClO_4$, $[Co_2L(CH_3COO)](ClO_4)_2$, $[Co_2L(OH)](ClO_4)_2$, $[Co_2L(C_3H_3N_2)](ClO_4)_2$($C_3H_3N_2^-$=pyrazolate), and $[Co_2LX_2](ClO_4)_n$, were prepared, where HL represents 2,6-bis[bis(2-pyridylmethyl)aminomethyl]-4-methylphenol(Hbpmp), 2,6-bis[*N*-(2-pyridylmethyl)-2-(2-pyridyl)ethylaminomethyl]-4-methylphenol(Hbpmep), 2,6-bis[bis[2-(2-pyridyl)ethyl]aminomethyl]-4-methylphenol(Hbpep), and 2,6-bis[bis(2-benzimidazolylmethyl)aminomethyl]-4-methylphenol(Hbbimp), and X is N_3^-, NCS^-, Cl^-, Br^-, H_2O, or py(pyridine). The electronic spectra and magnetic moments of the complexes revealed that $[Co_2L(CH_3COO)_2]ClO_4$ (L=bpmp, bpmep, or bpep) are high-spin octahedral, whereas the other complexes have five-coordinate structure of high-spin configuration. Some of the bpmp and the bpmep complexes reacted reversibly with molecular oxygen more or less. The $P_{1/2}$ of some complexes were determined spectrometrically. The oxygen affinities of the complexes are highly dependent on the natures of the dinucleating ligands and additional bridging or unidentate ligands.

It has been demonstrated that a number of metal complexes with sterically and electronically controlled ligand environment reversibly bind molecular oxygen. Dinuclear metal complexes in which two metal ions are in suitable positions can bind molecular oxygen to form 2:1 (metal:O_2) dioxygen adducts.[1,2]

In biological system, hemocyanine and hemerythrin contain two metal ions (copper for hemocyanine and iron for hemerythrin) at each oxygen binding site and form 2:1 dioxygen adducts. For those complexes, it has been postulated that two metal ions are linked by such bridging ligands as phenolate, carboxylate, hydroxide, or oxide.[3,4]

In the previous studies,[5,6] we demonstrated that dinuclear cobalt(II) complexes having phenolate and carboxylate bridges, $[Co_2(bpmp)(CH_3COO)_2]ClO_4$ and $[Co_2(bpmp)(CH_3COO)](ClO_4)_2$, react with molecular oxygen to form 2:1 dioxygen adduct, $[Co_2(bpmp)(CH_3COO)(O_2)](ClO_4)_2\cdot 2H_2O$. The X-ray analysis of $[Co_2(bpmp)(benzoato)(O_2)](BF_4)_2\cdot 2H_2O$ showed that two cobalt ions are linked by three bridging ligands, *viz.* dioxygen, phenolate, and benzoate, and the O-O bond distance is 1.43 Å which is in the range of those of the μ-peroxo complexes.[6]

As an extension of the above studies, we have synthesized various types of dinuclear cobalt(II) complexes with the dinucleating ligands shown in Fig. 1, and their reactivities toward molecular oxygen have been investigated spectrometrically.

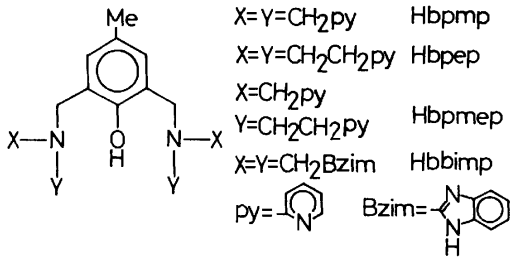

Fig. 1. Dinucleating ligands.

Experimental

Preparation of Ligands. Bis[2-(2-pyridyl)ethyl]amine was prepared according to the literature.[7] Bis(2-benzimidazolylmethyl)amine was synthesized by heating a mixture of iminodiacetic acid and *o*-phenylenediamine at 200 °C. *N*-(2-pyridylmethyl)-2-(2-pyridyl)ethylamine was prepared as follows. An ethanol solution of 2-(2-pyridyl)ethylamine (0.1 mol) and 2-pyridinecarbaldehyde (0.1 mmol) was refluxed for 30 min. The resulting Schiff base was hydrogenated under 4 atm pressure (1 atm=1.013×10^5 Pa) at room temperature using 1 g of 5% Pd-C catalyst. Approximately one molar equivalent of hydrogen was absorbed during 2 h. The filtered solution was distilled and fraction, bp 155—160 °C (133 pa), was collected. This was used for the preparation of Hbpmep without further purifications.

Hbpmep and Hbpep were prepared in the same way as that of Hbpmp.[5] Those ligands were used without further purifications. Hbbimp was prepared as follows. To a dimethylformamide solution (200 cm^3) of bis(2-benzimidazolylmethyl)amine (0.1 mol) and triethylamine (0.1 mol) was added 2,6-bis(chloromethyl)-4-methylphenol (0.05 mol) with stirring in small portions during 1 h at −30 °C. The solution was stirred for 1 h at 0 °C and then dimethylformamide was removed under reduced pressure. The residue was dissolved in 200 cm^3 of hot methanol and after cooling, white powder was obtained.

Preparation of Complexes. For the preparation of the bpmp and the bpmep cobalt(II) complexes, all the manipulations were carried out under argon atmosphere.

$[Co_2L(CH_3COO)_2]ClO_4$ (L=bpmp, bpmep, bpep, or bbimp). The complexes were prepared by the same method as that of $[Co_2(bpmp)(CH_3COO)_2]ClO_4$.[5]

$[Co_2L(CH_3COO)](ClO_4)_2$ (L=bpmp or bpep). Sodium acetate (0.5 mmol) was mixed with a methanol solution (30 cm^3) containing HL (0.5 mmol) and $Co(ClO_4)_2\cdot 6H_2O$ (1 mmol). Pink crystals deposited were collected by filtration, washed with methanol, and dried *in vacuo*. The bpmp complex was air-sensitive and exposure to air caused a color change from pink to brown. The elemental analysis was carried out for the brown compound.

$[Co_2L(OH)](ClO_4)_2$ (L=bpmp or bbimp). The prepar-

† Present address: Department of Chemistry, Faculty of Science, Kanazawa University, Kanazawa 920.

ation of the bpmp complex is exemplified. To a methanol solution (30 cm^3) containing Hbpmp (0.5 mmol) and $Co(ClO_4)_2 \cdot 6H_2O$ (1 mmol) was added a methanol solution (20 cm^3) of CH_3ONa (1 mmol) with stirring. The complex was obtained as green powder, which was filtered, washed with methanol, and dried *in vacuo*.

$[Co_2(bpmp)X_2]ClO_4$ ($X=N_3^-$, NCS^-, Cl^-, or Br^-). The complexes were prepared in a similar way. The typical procedure of the preparation is as follows. To a methanol solution (30 cm^3) of Hbpmp (0.5 mmol) and NaBr (1 mmol) was added a methanol solution (20 cm^3) of $Co(ClO_4)_2 \cdot 6H_2O$ (1 mmol). Violet crystals deposited were collected by filtration, washed with methanol, and dried *in vacuo*.

$[Co_2L(C_3H_3N_2)]ClO_4)_2$ (L=bpmp or bpmep). To a mixture of HL (0.5 mmol), $Co(ClO_4)_2 \cdot 6H_2O$ (1 mmol), and pyrazole (0.5 mmol) in hot ethanol was added dropwise a methanol solution (20 cm^3) of CH_3ONa (1 mmol) with stirring and then the solution was concentrated to 20 cm^3 under reduced pressure. Reddish brown powder deposited was collected by filtration, washed with cold ethanol, and dried *in vacuo*. The complexes were air-sensitive and exposure to air caused a color change from reddish brown to brown. The elemental analysis of the bpmp complex was carried out for the brown compound. For the bpmp complex, the elemetal analysis was carried out for the dioxygen complex (*vide infra*).

$[Co_2(bbimp)(OH_2)_2](ClO_4)_3$. Addition of Hbbimp (0.5 mmol) to 30 cm^3 of ethanol solution of $Co(ClO_4)_2 \cdot 6H_2O$ (1 mmol) gave violet crystals, which were filtered, washed with ethanol, and dried *in vacuo*.

$[Co_2(bbimp)(py)_2](ClO_4)_3 \cdot 2H_2O$. Addition of ethanol (50 cm^3) to a methanol solution (20 cm^3) containing Hbbimp (0.5 mmol), $Co(ClO_4)_2 \cdot 6H_2O$ (1 mmol), and 500 mg of pyridine afforded violet crystals, which were filtered, washd with ethanol, and dried *in vacuo*.

$[Co_2L(CH_3COO)(O_2)](ClO_4)_2$ (L=bpmp or bpmep). A brown methanol solution (100 cm^3) containing HL (0.5 mmol), $Co(ClO_4)_2 \cdot 6H_2O$ (1 mmol), and CH_3COONa (0.5 mmol) was left to stand overnight in air atmosphere. Brown crystals deposited were filtered, washed with ethanol, and dried.

$[Co_2(bpmp)(C_3H_3N_2)(O_2)](ClO_4)_2 \cdot 2H_2O$. To a methanol solution (50 cm^3) containing Hbpmp (0.5 mmol), $Co(ClO_4)_2 \cdot 6H_2O$ (1 mmol), and pyrazole (0.5 mmol) was added dropwise a methanol solution of CH_3ONa (1 mmol) with stirring. The resulting solution was exposed to air and allowed to stand overnight. The brown powder deposited was filtered, washed with ethanol, and dried.

$[Co_2(bpmp)(OH)(O_2)](Bph_4)_2 \cdot CH_3CN \cdot H_2O$. Sodium tetraphenylborate ($NaBph_4$)(1.5 mmol) was added to an acetonitrile solution of $[Co_2(bpmp)(OH)](ClO_4)_2 \cdot 0.5H_2O$ (0.5 mmol) in air atmosphere. The resulting brown solution was allowed to stand overnight to give brown crystals, which were filtered, washed with methanol, and dired.

Measurements. The electronic spectra of solutions and of solids were obtained with a Hitachi EPS-3T recording spectrophotometer and infrared spectra were recorded with a Hitachi 295 infrared spectrophotometer by means of KBr disks. Electrolytic conductivities at 25 °C on approximately 10^{-3} M (1 M=1 mol dm^{-3}) acetonitrile and methanol solutions were obtained using Yokogawa-Hawlett-Packard 4261 LCR meter. Magnetic susceptibilities were measured by Faraday method in a temperature range from liquid nitrogen temperature to room temperature. Magnetic moments were calculated by the expression, $\mu_{eff}=2.828\sqrt{\chi_a \times T}$, where χ_a is the magnetic susceptibility per one cobalt ion corrected for diamagnetism using Pascal's constants.

Oxygen Uptake Measurement. The equilibrium constants (K) for the reaction

$$[Co_2] + O_2 \rightleftharpoons [Co_2 \cdot O_2] \quad (1)$$

were determined at 25 °C(±0.5) in acetonitrile or methanol using visible spectroscopy. In a typical measurement, 7×10^{-6} mol of $[Co_2(bpmp)(N_3)_2]^+$ was dissolved in 50 cm^3 of acetonitrile in a specially designed reaction cell equipped with a quartz cell (1 cm path length). The reaction cell was evacuated and filled with argon gas, and heated at 70 °C until almost colorless solution was obtained. Then the reaction cell was evacuated for a while. Subsequently, after temperature equilibration, various pressures of oxygen were added to the reaction cell, and the contents were stirred until the constant absorbance was obtained. In the case of $[Co_2(bpmp)(CH_3COO)]^{2+}$, $[Co_2(bpmp)(C_3H_3N_2)]^{2+}$, $[Co_2(bpmp)(OH)]^{2+}$, and $[Co_2(bpmp)(CH_3COO)_2]^+$, various pressures of argon gas containing known oxygen partial pressure were added. Equilibrium constants were calculated by the method of Collman *et al.*[8] using the following equation,

$$P_{O_2} = [Co_2]_T \cdot l \cdot \Delta\varepsilon \cdot P_{O_2}/(A-A_0) - K^{-1},$$

where P_{O_2} is the partial pressure of O_2, $[Co_2]_T$ is the total complex concentraton, l is the path length of the cell, A is the absorbance of the solution at the oxygen pressure P_{O_2} and A_0 is the absorbance of the solution in the absence of oxygen, $\Delta\varepsilon$ is the difference between molar extinction coefficients of the oxy and the deoxy complexes. A plot of P_{O_2} *vs.* $P_{O_2}/(A-A_0)$ should be a straight line with slope of $[Co_2]_T \cdot l \cdot \Delta\varepsilon$ (constant) and intercept of $-K^{-1}$. Straight lines were then computor fit and the equilibrium constants (K) were determined from the intercepts.

The slopes of the plots of $\log((A-A_0)/(A_\infty-A))$ *vs.* $\log(P_{O_2})$ were 1.0—1.2, indicating a 1:1 stoichiometry for the oxygenation reaction (1). In the cases where complete oxygenation was not obtained at O_2 pressure of *ca.* 700 Torr (1 Torr=133.322 Pa), the values of A_∞ were determined by extrapolating a plot of A *vs.* P_{O_2} to infinite pressure.[9]

In the case of $[Co_2(bpmp)(CH_3COO)]^{2+}$, $[Co_2(bpmp)(C_3H_3N_2)]^{2+}$, and $[Co_2(bpmp)(OH)]^{2+}$ the values for K could not be obtained because of very small amount of O_2 involved for those measurements and $P_{1/2}$ values are only roughly estimated numbers, where $P_{1/2}$ represents a partial oxygen pressure at which 50% of the complex is oxygenated.

Results and Discussion

Dinuclear Cobalt(II) Complexes. The magnetic moments of the dinuclear cobalt(II) complexes are given in Table 1 (4.1—4.8 BM, 1 BM=9.274×10^{-24} J T^{-1}). Those values indicate that all the complexes have the high-spin configuration.

The electronic spectral data of the dinuclear cobalt(II) complexes are summarized in Table 2 and the representative electronic spectra are shown in Fig. 2. The electronic spectra of the complexes indicate that $[Co_2L(CH_3COO)_2]^+$ (L=bpmp, bpmep, or bpep) are six-coordinate, whereas all the other complexes are five-coordinate.

The complexes, $[Co_2L(CH_3COO)_2]^+$, show two d-d bands at *ca.* 9000 and 21000 cm^{-1}, except for $[Co_2(bbimp)(CH_3COO)_2]^+$ (Table 2 and Fig. 2). The spectra are closely similar to that of octahedral hexaaquacobalt(II).[10] In these six-coordinate complexes, two acetate ions can coordinate to cobalt ions in two way, *viz.* as chelating ligands or as bridging ligands in syn-syn configuration.[11] An examination of a Dreiding model suggested that the two acetate ions function as

Table 1. Elemental analyses and magnetic moments of complexes at room temperature

Complex	Found(Calcd)(%)			μ_{eff}/BM
	C	H	N	
$[Co_2(bpmp)(CH_3COO)_2]ClO_4$	51.10(51.37)	4.65(4.54)	9.42(9.71)	4.6
$[Co_2(bpmp)(CH_3COO)](ClO_4)_2$	45.15(45.52)	4.08(3.93)	8.85(9.10)	
$[Co_2(bpmp)(OH)](ClO_4)_2\cdot 0.5H_2O$	45.54(45.43)	4.14(4.04)	9.44(9.63)	4.1
$[Co_2(bpmp)(N_3)_2]ClO_4\cdot H_2O$	46.57(46.68)	4.00(4.15)	19.38(19.79)	4.2
$[Co_2(bpmp)(NCS)_2]ClO_4\cdot H_2O$	47.67(47.71)	3.84(4.00)	12.48(12.71)	4.4
$[Co_2(bpmp)Br_2]ClO_4$	43.51(43.71)	3.65(3.67)	9.18(9.28)	4.3
$[Co_2(bpmp)Cl_2]ClO_4\cdot 3H_2O$	45.51(45.46)	4.69(4.51)	9.29(9.64)	4.6
$[Co_2(bpmp)(CH_3COO)(O_2)](ClO_4)_2\cdot 2H_2O$	43.04(43.18)	3.96(4.14)	8.55(8.63)	0.5
$[Co_2(bpmp)(C_3H_3N_2)(O_2)](ClO_4)_2\cdot 2H_2O$	44.06(44.05)	3.89(4.11)	11.28(11.42)	0.7
$[Co_2(bpmp)(OH)(O_2)](Bph_4)_2\cdot CH_3CN\cdot H_2O$	71.87(71.72)	5.60(5.73)	6.84(6.96)	0.2
$[Co_2(bpmep)(CH_3COO)_2]ClO_4\cdot H_2O$	51.75(51.41)	5.22(4.98)	9.00(9.22)	4.7
$[Co_2(bpmep)(CH_3COO)(O_2)](ClO_4)_2\cdot 2.5H_2O$	43.95(43.98)	4.41(4.49)	8.44(8.32)	
$[Co_2(bpmep)(C_3H_3N_2)](ClO_4)_2\cdot 2H_2O$	46.61(46.69)	4.33(4.54)	11.19(11.46)	
$[Co_2(bpep)(CH_3COO)_2]ClO_4\cdot H_2O$	52.20(52.43)	5.04(5.26)	8.92(8.95)	4.8
$[Co_2(bpep)(CH_3COO)](ClO_4)_2\cdot 1.5H_2O$	47.35(47.38)	5.04(4.79)	8.27(8.50)	4.5
$[Co_2(bbimp)(CH_3COO)_2]BF_4\cdot 3H_2O$	50.63(50.86)	4.47(4.65)	12.99(13.18)	4.2
$[Co_2(bbimp)(OH)](ClO_4)_2\cdot 3H_2O$	45.90(45.87)	3.80(4.13)	13.14(13.05)	4.4
$[Co_2(bbimp)(OH_2)_2](ClO_4)_3$	43.09(43.27)	3.68(3.63)	12.27(12.31)	4.3
$[Co_2(bbimp)(py)_2](ClO_4)_3\cdot 2H_2O$	47.08(47.26)	4.03(3.97)	12.84(12.97)	4.3

Table 2. Absorption spectral data

Complex	Absorption[a] $\tilde{\nu}/10^3$ cm^{-1}					
$[Co_2(bpmp)(CH_3COO)_2]ClO_4$	21.00[b]	19.60[s]	18.60[s]		9.40	
$[Co_2(bpmp)(CH_3COO)](ClO_4)_2$	22.20	19.92	17.50		10.58	≈6.5
$[Co_2(bpmp)(OH)](ClO_4)_2\cdot 0.5H_2O$	22.00	21.10	16.60	15.90[s]	14.20[s]	≈6.5
$[Co_2(bpmp)(N_3)_2]ClO_4\cdot H_2O$	21.60	19.60	18.80[s]	17.90	9.20	≈6.7
$[Co_2(bpmp)(NCS)_2]ClO_4\cdot H_2O$	22.50	19.20	17.90		11.00	6.58
$[Co_2(bpmp)Br_2]ClO_4$	21.40	19.80	17.50	14.80[s]	8.70	≈6.7
$[Co_2(bpmp)Cl_2]ClO_4\cdot 3H_2O$	21.50	20.00[s]	18.30[s]	17.80	14.30	≈8.0—6.3[b]
$[Co_2(bpmp)(C_3H_3N_2)]^{2+}$	CT			17.50[s]	10.50	≈6.0
$[Co_2(bpmep)(CH_3COO)_2]ClO_4\cdot H_2O$	21.50[s]	20.50	19.80[s]	18.70[s]	8.80	
$[Co_2(bpmep)(CH_3COO)]^{2+}$	CT	22.00[s]			10.40	≈6.0
$[Co_2(bpmep)(C_3H_3N_2)](ClO_4)_2\cdot 2H_2O$	21.70[s]	19.80	18.90[s]	11.40[s]		≈7.4—5.9[b]
$[Co_2(bpep)(CH_3COO)_2]ClO_4\cdot H_2O$	21.10[s]	20.20	19.50[s]	18.50[s]	8.70	
$[Co_2(bpep)(CH_3COO)](ClO_4)_2\cdot 1.5H_2O$	22.00[s]	19.00	18.10	14.30[s]	9.0	≈5.3
$[Co_2(bbimp)(CH_3COO)_2]BF_4\cdot 3H_2O$	20.40[s]	17.90		12.90		≈6.0
$[Co_2(bbimp)(OH)](ClO_4)_2\cdot 3H_2O$	20.40	19.60	16.90	12.90		6.06
$[Co_2(bbimp)(OH_2)_2](ClO_4)_3$	20.40[s]	18.50		13.70		6.20
$[Co_2(bbimp)(py)_2](ClO_4)_3\cdot 2H_2O$	20.60[s]	18.70		13.90		6.30

a): In acetonitrile. b): Broad band. s: Shoulder.

bridging ligands. Therefore, we assumed that the six-coordinate complexes possess the structure given in Fig. 3a, where two cobalt ions are linked by three bridging ligands, *viz.* two acetates and one phenolate.

In contrast to the above complexes, $[Co_2(bbimp)(CH_3COO)_2]^+$ shows several d-d bands in the visible and the near infrared regions (Fig. 2). In general, five-coordinate cobalt(II) complexes exhibit several d-d bands in 5000—25000 cm^{-1}.[12] Thus the electronic spectrum of the complex indicates the presence of a five-coordinate cobalt(II) chromophere. The two acetate ions in this complex, therefore, coordinate to cobalt ions as unidentate ligands. A possible structure of the complex is given in Fig. 3e. Of particular interest is that bbimp forms five-coordinate bis(acetato) complex, whereas the other dinucleating ligands form six-coordinate bis(acetato) complexes. Such structural change in the bbimp complex seems to be attributed to a steric requirement in the bbimp complex; a steric interaction between bulky benzimidazolyl groups and methyl groups of the acetate ions may enforce five-coordinate structure.

The electronic spectra of $[Co_2(bpmp)X_2]$ ($X=N_3^-$, NCS^-, Cl^-, or Br^-) show that the complexes have five-

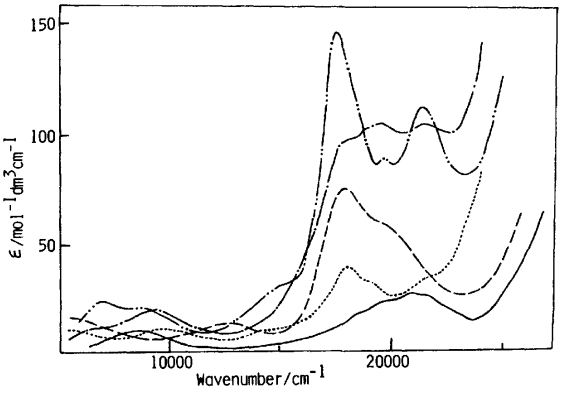

Fig. 2. Absorption spectra of $[Co_2(bpep)(CH_3COO)_2]^+$ (——), $[Co_2(bbimp)(CH_3COO)_2]^+$ (----), $[Co_2(bpep)(CH_3COO)]^{2+}$ (·····), $[Co_2(bpmp)(N_3)_2]^+$ (—·—), and $[Co_2(bpmp)Br_2]^+$ (—··—) in acetonitrile.

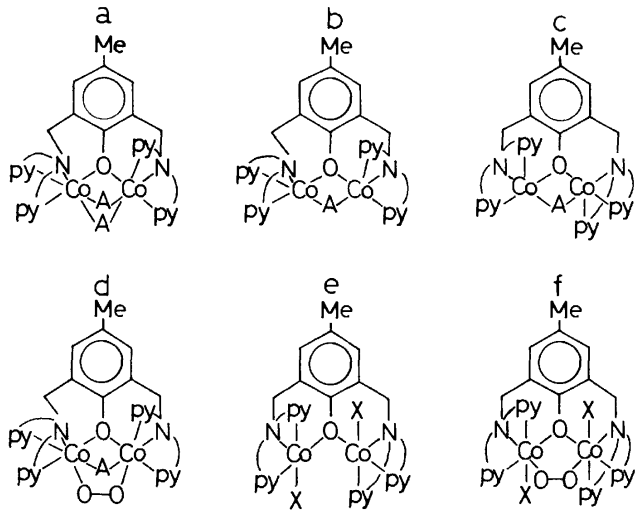

Fig. 3. Proposed structures of dinuclear complexes. A is CH_3COO^-, $C_3H_3N_2^-$, or OH^-, and X is N_3^-, NCS^-, Cl^-, or Br^-.

coordinate structure. The molar conductivities of the complexes in acetonitrile are 134—139 Ω^{-1} cm^2 mol^{-1}, which are typical for 1 : 1 electrolytes in acetonitrile,[13] supporting the above formula, $[Co_2(bpmp)X_2]^+$. The structure of the complexes seem to be essentially identical to that of $[Co_2(bbimp)(CH_3COO)_2]^+$ (Fig. 3e), where the two cobalt(II) ions are bridged by only phenolate.

The electronic spectra of the mono(acetato), mono(pyrazolato), mono(hydroxo) complexes also revealed that all the complexes are five-coordinate. In these complexes, the acetate, pyrazolate, and hydroxide ions seem to function as bridging ligands as found in the dinuclear copper(II) complexes containing such ions.[14]

For those complexes, there are two possible structures shown in Fig. 3b and c. Judging from the reactivities of the mono(acetato) and mono(pyrazolato) complexes with molecular oxygen in the solid state (*vide infra*), the structure b seems to be preferable. On the other hand, the structure (c) seems to be preferable for the hydroxo complex (*vide infra*).

In general, the magnetic moments of six-coordinate complexes are larger than those of five-coordinate complexes because of an extensive contribution from an orbital angular momentum in $^4T_{1g}$ ground state in octahedral symmetry. Such tendency can be observed for the present complexes (Table 1).

Table 3. Magnetic data

Complex	μ_{eff} BM		θ K
	82 K	291 K	
$[Co_2(bpmp)(CH_3COO)_2]ClO_4$	4.37	4.61	−15
$[Co_2(bpmp)(OH)](ClO_4)_2\cdot 0.5H_2O$	3.75	4.12	−27
$[Co_2(bpmp)(NCS)_2]ClO_4\cdot H_2O$	3.73	4.37	−51
$[Co_2(bbimp)(OH_2)_2](ClO_4)_3$	3.73	4.28	−36
$[Co_2(bbimp)(OH)](ClO_4)_2\cdot 3H_2O$	4.16	4.40	−12

The magnetic susceptibilities of the complexes listed in Table 3 were measured in the temperature range 80—300 K. The magnetic moment of the six-coordinate complex, $[Co_2(bpmp)(CH_3COO)_2]ClO_4$, decreases with temperature. However, this does not necessarily imply antiferromagnetic interaction between the cobalt(II) ions, since monomeric six-coordinate cobalt(II) complexes show such a decrease of magnetic moments because of an extensive contribution from an angular orbital momentum in $^4T_{1g}$ ground state in octahedral symmetry.[15] The magnetism of the complex obeys the Curie-Weiss law in the temperature range 80—300 K and the Weiss constant is −15 K. The Weiss constants of the monomeric cobalt(II) complexes have been shown to be in the range −10—−40 K.[15] Thus the magnetic interaction between the cobalt(II) ions must be negligibly small. The magnetisms of the five-coordinate complexes also obey the Curie-Weiss law. The Weiss constants are −10—−50 K. These values suggest that the antiferromagnetic interactions in the complexes are weak.

Oxygenation Reactions. Since all the oxygenated complexes showed intense brown color, the oxygenation can be easily followed spectrometrically. Brown color of the oxygenated complexes may be attributable to the charge transfer transitions from dioxygen and/or phenolic oxygen to the cobalt centers. The representative spectral change upon oxygenation is given in Fig. 4. The dioxygen complexes isolated are essentially diamagnetic (Table 1). The X-ray structure determination of $[Co_2(bpmp)(benzoato)(O_2)](BF_4)_2\cdot 2H_2O$ has shown that the O-O bond distance is 1.43 Å and the two cobalt ions are bridged by three ligands, dioxygen, phenolate, and benzoate (see Fig. 3d). These observations suggest that the dioxygen complexes are of μ-peroxo type.

The six-coordinate complex, $[Co_2(bpmp)(CH_3COO)_2]ClO_4$, was stable on exposure to air in the solid state, whereas the complex underwent oxygenation in methanol. The molar conductivity of the complex in methanol gradually increased by bubbling O_2 (90 → 150 Ω^{-1} cm^2 mol^{-1}), indicating the formation of a 2 : 1 electrolyte upon oxygenation.[13] The addition of sodium perchlorate in methanol solution in air atmosphere afforded brown crystals, $[Co_2(bpmp)(CH_3COO)(O_2)]$-

Table 4. Equilibrium constants for the reaction $[Co_2]+O_2 \rightleftarrows [Co_2 \cdot O_2]$[a] at 20 °C

Complex 7×10^{-6} mol	Solvent	$\log(K/\mathrm{Torr}^{-1})$	$P_{1/2}$/Torr
$[Co_2(bpmp)(CH_3COO)_2]^+$	CH_3OH	-0.8 ± 0.1[b]	6
$[Co_2(bpmp)(CH_3COO)]^{2+}$	CH_3CN		≈ 0.1[c]
$[Co_2(bpmp)(C_3H_3N_2)]^{2+}$	CH_3CN		≈ 0.1[c]
$[Co_2(bpmp)(N_3)_2]^+$	CH_3CN	-1.70 ± 0.02	50
$[Co_2(bpmep)(CH_3COO)]^{2+}$	CH_3CN	-1.39 ± 0.03	24

a): Standard state of 1 Torr. b): For the reaction, $[Co_2(bpmp)(CH_3COO)_2]^+ + O_2 \rightleftarrows [Co_2(bpmp)(CH_3COO)(O_2)]^{2+} + CH_3COO^-$, K is calculated by the following equation, $K=[Co_2 \cdot O_2]/[Co_2] \cdot P_{O_2}$, where the concentration of the acetate ion dissociated is omitted. c): Only roughly estimated number.

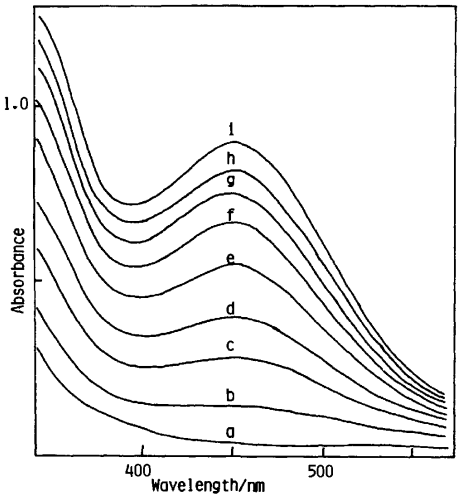

Fig. 4. Spectral change as a function of oxygen pressure for the reversible oxygenation of $[Co_2(bpmp)(N_3)_2]^+$ in acetonitrile at 20 °C. Spectra of a—i are at partial pressure of oxygen: 0, 6, 19, 32, 60, 104, 172, 284, and 692 Torr, respectively.

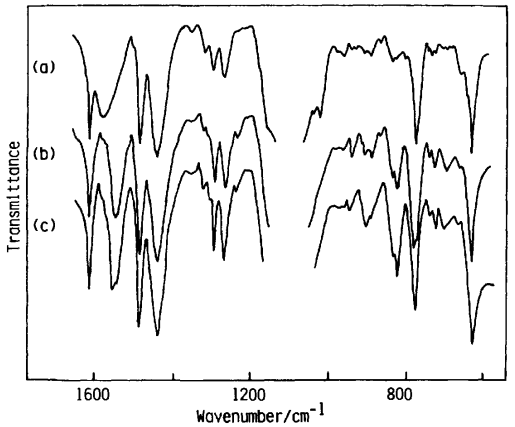

Fig. 5. Infrared spectra of $[Co_2(bpmp)(CH_3COO)](ClO_4)_2$ (a and b), and $[Co_2(bpmp)(CH_3COO)(O_2)](ClO_4)_2 \cdot 2H_2O$(c). a, freshly prepared; b, after 24 h.

$(ClO_4)_2 \cdot 2H_2O$, the structure of which is given in Fig. 3d. It is noteworthy that no oxygenation was observed in acetonitrile and dichloromethane. In addition, the oxygenation in a methanol solution was suppressed by the addition of sodium acetate. Those observations suggest that the oxygenation proceeds *via* the five-coordinate complex, $[Co_2(bpmp)(CH_3COO)]^{2+}$, and the dissociation of the acetate ion from $[Co_2(bpmp)(CH_3COO)_2]^+$ is suppressed in acetonitrile and dichloromethane. Therefore, it is likely that the oxygenation of the complex proceeds as follows,

$$[Co_2(bpmp)(CH_3COO)_2]^+ \rightleftharpoons [Co_2(bpmp)(CH_3COO)]^{2+} + CH_3COO^-$$

$$[Co_2(bpmp)(CH_3COO)]^{2+} + O_2 \rightleftharpoons [Co_2(bpmp)(CH_3COO)(O_2)]^{2+}.$$

$P_{1/2}$ for the complex is 6 Torr in methanol at 20 °C and may be controlled by the addition of sodium acetate. $[Co_2(bpmep)(CH_3COO)_2]^+$ also reacted reversibly with molecular oxygen in methanol. However, the oxygen affinity is too low to determine $P_{1/2}$ at 20 °C. For $[Co_2(bpep)(CH_3COO)_2]^+$, no oxygenation was observed in methanol even at −40 °C.

In contrast to the above six-coordinate complex with bpmp, the five-coordinate complex, $[Co_2(bpmp)(CH_3COO)]^{2+}(ClO_4)_2$, is air-sensitive in the solid state. Finely powdered compound gradually changed its color from pink to brown in the presence of O_2. The magnetic moment of the pink compound gradually decreased from 4.3 to 1.4 BM with color change at room temperature in air atmosphere. The pink compound also showed an infrared spectral change (Fig. 5). The brown compound resulted on exposure to air for 24 h shows a spectrum almost identical to that of $[Co_2(bpmp)(CH_3COO)(O_2)](ClO_4)_2 \cdot 2H_2O$. Heating the brown compound at *ca.* 140 °C *in vacuo* regenerated pink compound. Thus $[Co_2(bpmp)(CH_3COO)](ClO_4)_2$ reacts reversibly with molecular oxygen in the solid state. Such reversible O_2 binding in the solid state suggests that the coordination sites of the two cobalt ions should be close enough to bind O_2 in μ-peroxo fashion without extensive rearrangement of the structure. A possible structure of the five-coordinate complex is sketched in Fig. 3b.

The complex also underwent reversible oxygenation in acetonitrile. The deoxygenation by bubbling of argon gas was extremely slow at room temperature, whereas it was much accelerated by heating a solution at about 70 °C. No decomposition was observed after ten oxygenation-deoxygenation cycles. The $P_{1/2}$ of the complex is ≈0.1 Torr at 20 °C in acetonitrile. The dioxygen complex with bpmep, $[Co_2(bpmep)(CH_3COO)(O_2)](ClO_4)_2 \cdot 2H_2O$, also underwent reversible

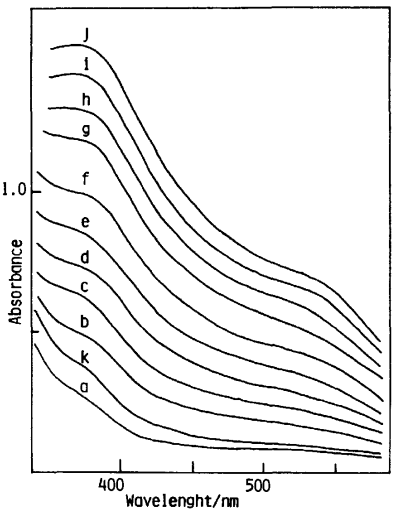

Fig. 6. Spectral change as a function of oxygen pressure for the oxygenation of $[Co_2(bpmep)(C_3H_3N_2)]^{2+}$ in acetonitrile at 20 °C. The spectra of a—j are at partial pressure of oxygen: 0, 10, 22, 42, 74, 119, 201, 301, 483, and 655 Torr, respectively. The spectrum k is at 0 Torr O_2 after oxygenation-deoxygenation cycle.

deoxygenation-oxygenations in acetonitrile. The $P_{1/2}$ is 25 Torr at 20 °C, which is considerably larger than that of the corresponding bpmp complex. In contrast to the above complexes, $[Co_2(bpep)(CH_3COO)]^{2+}$ did not react with molecular oxygen even at −40 °C in acetonitrile.

The pyrazolato-bridged complexes with bpmp and bpmep were also air-sensitive in the solid state. Reddish brown compounds turned brown upon exposure to air. For the bpmep complex, heating the brown compound at 140 °C regenerated the reddish brown compound, whereas the bpmp complex decomposed without the color change to reddish brown by heating. However, the reversible O_2 binding was observed for the bpmp complex in acetonitrile. The $P_{1/2}$ is ≈0.1 Torr at 20 °C, which is comparable to that of the mono(acetato) complex, with bpmp. On the other hand, for the bpmep complex, the oxygenation was not completely reversible in acetonitrile at 20 °C (Fig. 6) and a plot of P_{O_2} *vs.* $P_{O_2}/(A-A_0)$ did not give a straight line. Under such conditions, the $P_{1/2}$ was roughly estimated as ≈80 Torr.

In contrast to the above five-coordinate acetato- and pyrazolato-bridged complexes, $[Co_2(bpmp)(OH)](ClO_4)_2 \cdot 0.5H_2O$ was stable on exposure to air in the solid state. The complex reacted with molecular oxygen in acetonitrile to give brown solution and heating the brown solution at about 70 °C under argon atmosphere regenerated green solution. The addition of sodium tetraphenylborate to an acetonitrile solution in air atmosphere afforded brown crystals, $[Co_2(bpmp)(OH)(O_2)](Bph_4)_2 \cdot CH_3CN \cdot H_2O$. A possible structure of the oxygenated complex is given in Fig. 3d, which is essentially identical to those of the corresponding acetato and pyrazolato complexes.

An attempt to determine the $P_{1/2}$ was made in acetonitrile at 20 °C. The oxygenation was very slow as compared with those of the acetato and pyrazolato complexes at low oxygen pressure (0.2 Torr) and some decomposition was observed during the measurement. Under such conditions, the $P_{1/2}$ was roughly estimated as smaller than 0.2 Torr which is comparable to those of the acetato and pyrazolato complexes with bpmp.

There are two possible structures for $[Co_2(bpmp)(OH)]^{2+}$ as shown in Fig. 3b and c. The structure (b) is essentially identical to those of the acetato and pyrazolato complexes and the oxygen binding sites are close to each other. Therefore, the complex having the structure (b) would be expected to react with molecular oxygen in the solid state. On the other hand, for the structure (c), an extensive rearrangement of the structure is necessary for O_2 binding. Since the complex did not react with molecular oxygen in the solid state and the oxygenation was extremely slow as compared with those of the acetato and pyrazolato complexes in acetonitrile, the structure (c) seems to be plausible.

The complexes, $[Co_2(bpmp)X_2]^+$ ($X=N_3^-$ or NCS^-), reversibly reacted with molecular oxygen in acetonitrile. However, the oxygenated complexes could not be isolated. Conductivity measurement of the azido complex showed that the oxygenated complex is a 1:1 electrolyte in acetonitrile (135 Ω^{-1} cm^2 mol^{-1}) and can be formulated as $[Co_2(bpmp)(N_3)_2(O_2)]^+$. A possible structure is given in Fig. 3f. The $P_{1/2}$ of the complex is 50 Torr at 20 °C, whereas that of the isothiocyanato complex could not be determined because of its low oxygen affinity. The chloro and bromo complexes did not react with molecular oxygen even at −40 °C. Thus, in a series of $[Co_2(bpmp)X_2]^+$, the order of the oxygen affinity is $N_3^- > NCS^- > Cl^-$, Br^-. This order reflects the differences in the electron donor abilities of the unidentate ligands to the cobalt centers; the stronger the electron donor ability of the ligand, the greater the amount of the electron density on the cobalt centers, and the greater the oxygen affinity.

The oxygen affinities of the complexes studied are highly dependent on the nature of the dinucleating ligand. The order of the oxygen affinities for changes in the dinucleating ligands is bpmp>bpmep>bpep. The order can be explained by considering the effect of the chelate ring size of the dinucleating ligand. Martell *et al.*[16] demonstrated that, in a series of the cobalt(II) complexes with various quinquedentate ligands, the nitrogen donor atoms in the six-membered chelate rings are weaker electron donors than those in the corresponding five-membered chelate rings. This is also the case for the present complexes. In addition, it is likely that the observed differences in the oxygen affinities of the present complexes are also attributed to the steric requirement of the dinucleating ligand. The oxygen binding sites of the two cobalt ions must be held in suitable positions for the O_2 binding in μ-peroxo fashion and such a steric requirement which is governed by the nature of the dinucleating ligand would be also responsible to the stability of the dioxygen complex.

Martell *et al.*[17] also suggested that the total basicities of the ligands are important in determining whether a cobalt(II) complex will form a dioxygen adduct, and the presence of three aliphatic nitrogen donors is suffi-

cient but not necessary for dioxygen adduct formation. It should be noted that all the bbimp complexes (even $[Co_2(bbimp)(py)_2]^{3+}$ which has N_4O donor set for each cobalt ion) did not react with molecular oxygen even at −40 °C. Although the total basicities of Hbbimp and Hbpmp are not known, it is reasonable to assume that the total basicity of Hbbimp is larger than that of Hbpmp, because benzimidazole (pK_a=5.4) is stronger base than pyridine (pK_a=5.2). Stynes *et al.*[18] demonstrated that in 1 : 1 dioxygen adduct formation of LCoP (P=protoporphyrin IX dimethyl ester and L=various bases), pyridine is a better base than benzimidazole. In the above system, therefore, the lower oxygen affinity of the benzimidazole complex is ascribed not to the electronic effect but to the steric effect between benzimidazole and the porphyrine ring, which prevents close approach of benzimidazole to the cobalt center. It is likely that no reactivity of the bbimp complexes with molecular oxygen is also due to such a steric effect of benzimidazolyl groups.

It is interesting that the oxygen affinities of $[Co_2L(C_3H_3N_2)]^{2+}$ are comparable to or smaller than those of $[Co_2L(CH_3COO)]^{2+}$ (L=bpmp or bpmep). It is well known that the nitrogen donors tend to promote oxygenation, whereas the oxygen donors such as carboxylates tend to retard the dioxygen adduct formation.[17] Pyrazolate is a moderately strong base (pK_a's of the following equilibria, pyrazolium $\rightleftharpoons$ pyrazole+H^+ and pyrazole $\rightleftharpoons$ pyrazolate+H^+, are 2.5 and 14.2, respectively)[19] and therefore pyrazolate must be a more effective σ donor than acetate. However,the observed oxygen affinities of the pyrazolato complexes seem to be much weaker than those expected from the above general concept and the basicity argument. It is possible that pyrazolate plays a role as a strong π acceptor and/or pyrazolate-bridge prevents optimum binding of O_2 in μ-peroxo fashion.

Our thanks are due to Prof. S. Kida, Prof. H. Okawa, and Dr. Y. Nishida for their helpful discussions, and to Prof. A. Matsubara and Dr. K. Nomura for conductivity measurement.

References

1) a) C. K. Chang, *J. Chem. Soc., Chem. Commun.*, **1977**, 800; b) J. P. Collman, P. Denisevich, Y. Konai, M. Marrocco, C. Koval, and F. C. Anson, *J. Am. Chem. Soc.*, **102**, 6027 (1980).
2) Y. Nishida, T. Takahashi, H. Kuramoto, and S. Kida, *Inorg. Chim. Acta*, **54**, L103 (1981).
3) R. S. Himmelwright, N. C. Eickman, and E. I. Solomon, *J. Am. Chem. Soc.*, **101**, 1576 (1979).
4) J. W. Dawson, H. B. Gray, H. E. Hoeing, G. R. Rossman, J. M. Schredder, and R. H. Wang, *Biochemistry*, **11**, 461 (1972).
5) M. Suzuki, H. Kanatomi, and I. Murase, *Chem. Lett.*, **1981**, 1745.
6) M. Suzuki, I. Ueda, H. Kanatomi, and I. Murase, *Chem. Lett.*, **1983**, 185.
7) E. Uhlig, B. Bovek, and H. Glaenzer, *Z. Anorg. Allg. Chem.*, **348**, 189 (1966).
8) J. P. Collman, J. I. Brauman, K. M. Doxsee, T. R. Halbert, S. E. Hayes, and K. S. Suslick, *J. Am. Chem. Soc.*, **100**, 2761 (1978).
9) L. S. Chen, M. E. Koehler, B. C. Pestel, and S. C. Commings, *J. Am. Chem. Soc.*, **100**, 7243 (1978).
10) O. G. Holmes and D. S. McClure, *J. Chem. Phys.*, **26**, 1686 (1957).
11) G. B. Deacon and R. J. Phillips, *Coord. Chem. Rev.*, **33**, 227 (1980).
12) M. Ciampolini and I. Bertini, *J. Chem. Soc., A*, **1968**, 2241.
13) W. J. Geary, *Coord. Chem. Rev.*, **7**, 81 (1971).
14) a) H. Okawa, *Bull. Chem. Soc. Jpn.*, **43**, 3019 (1970); b) R. Robson, *Aust. J. Chem.*, **23**, 2217 (1970); c) K. D. Karlin, P. L. Dalstrom, S. N. Cozzette, P. M. Scensng, and J. J. Zubieta, *J. Chem. Soc., Chem. Commun.*, **1981**, 881; d) V. Mckee, J. V. Dagdigian, R. Bau, and C. A. Reed, *J. Am. Chem. Soc.*, **103**, 7000 (1981); e) W. Marzurek, K. J. Berry, K. S. Murray, M. J. O'connor, M. R. Snow, and A. G. Wedd, *Inorg. Chem.*, **21**, 3071 (1982).
15) P. W. Ball and A. B. Blake, *J. Chem. Soc., Dalton Trans.*, **1974**, 852.
16) a) W. R. Harris, I. Murase, J. H. Timmons, and A. E. Martell, *Inorg. Chem.*, **17**, 889 (1978); b) J. H. Timmons, R. H. Niswander, A. Clearfield, and A. E. Martell, *ibid.*, **18**, 2977 (1979).
17) G. Mclendon and A. E. Martell, *Coord. Chem. Rev.*, **19**, 1 (1976).
18) D. V. Stynes, H. C. Stynes, J. A. Ibers, and B. R. James, *J. Am. Chem. Soc.*, **95**, 1142 (1973).
19) G. Yagil, *Tetrahedron*, **23**, 2855 (1967).

 © 1984 The Chemical Society of Japan Bull. Chem. Soc. Jpn., 57, 43—46 (1984)

Ylide-Metal Complexes. VIII.[1] The Preparation and Properties of Metal (Cu, Ag, Au, Zn, Cd, Hg, Ge, Sn, Pb, Pd, and Pt) Complexes with Methylenetris(dimethylamino)phosphorane

Yoshihisa YAMAMOTO
Faculty of Pharmaceutical Sciences, Higashi Nippon Gakuen University, Ishikari-Tobetsu, Hokkaido 061-02
(Received March 15, 1983)

Bis[methylenetris(dimethylamino)phosphorane]metal chlorides, $[(Me_2N)_3PCH_2\text{-}M\text{-}CH_2P(NMe_2)_3]Cl_n$ (M: Cu, Ag, Au, Zn, Cd, Hg; n: 1 or 2), have been isolated from a reaction mixture of methylenetris(dimethylamino)phosphorane $(Me_2N)_3P{=}CH_2$ (**L**) and CuCl, AgCl, $(C_6H_5)_3PAuCl$, $ZnCl_2$, $CdCl_2$, or $HgCl_2$ in the mole ratio of 2:1 or 3:1. The reactions of **L** with R_3MCl (M: Sn, Pb; R: Me, C_6H_5) in the mole ratio 1:1 yield new monomeric compounds of [methylenetris(dimethylamino)phosphorane]trimethyl(or triphenyl)-metal chloride, $[(Me_2N)_3PCH_2\text{-}MR_3]Cl$. The reactions of **L** with $PdCl_2$ or PtI_4 in the mole ratio of 2:1 or 4:1 yield $[(Me_2N)_3PCH_2]_2PdCl_2$ and $[(Me_2N)_3PCH_2]_4PtI_4$, respectively. The Ag, Au, Sn, and Pb complexes are stable. Their properties are compared with those of the metal complexes with methylenetriphenylphosphorane, $(C_6H_5)_3P{=}CH_2$.

Many investigations of the metal complexes[2-4] with phosphonium ylides, *e.g.*, with methylenetrimethyl- or methylenetriphenylphosphorane, have been reported. Their complexes have the $\begin{matrix}C\\ \diagdown\\ C\text{-}\overset{+}{P}\text{-}C\text{-}M\text{-}\\ \diagup\\ C\end{matrix}$ structure. However, few investigations of the ylide-metal complexes which have the $\begin{matrix}N\\ \diagdown\\ N\text{-}\overset{+}{P}\text{-}C\text{-}M\text{-}\\ \diagup\\ N\end{matrix}$ structure have been described: only the nitridobis(methylenedimethylphosphorane)metal complexes[5] and bis[methylenetris(dimethylamino)phosphorane]gold chloride.[6]

The present paper deals with the preparation and properties of group IB, IIB, IVA, and VIII metal complexes with methylenetris(dimethylamino)phosphorane, $(Me_2N)_3P{=}CH_2$ (**L**). Their properties are compared with those of the metal complexes,[4,7-9] with methylenetriphenylphosphorane, $(C_6H_5)_3P{=}CH_2$. In the previous paper[2] of this series, we have reported the preparation and properties of group IIA (Be, Mg) and IIIA (Al, Ga, In) complexes with methylenetriphenylphosphorane.

Results and Discussion

Bis[methylenetris(dimethylamino)phosphorane]group IB and IIB metal complexes (**1—6**) have been isolated from a reaction mixture of methylenetris(dimethylamino)phosphorane (**L**) and CuCl, AgCl, $(C_6H_5)_3PAuCl$, $ZnCl_2$, $CdCl_2$, or $HgCl_2$ in the mole ratio of 2:1 or 3:1. Complex **2** is stable in dichloromethane, though unstable in chloroform, and is sensitive to light.

$$\underset{\textbf{L}}{m(Me_2N)_3P{=}CH_2} + MCl_n \longrightarrow [(Me_2N)_3PCH_2\text{-}M\text{-}CH_2P(NMe_2)_3]Cl_n$$

m: 2 or 3 ; n: 1 or 2

1—6

No.	1	2	3	4	5	6
M	Cu	Ag	Au	Zn	Cd	Hg

Complex **3**[6] is highly hygroscopic. It is soluble in water and organic solvents, and is stable in air and solution.

The ^1H NMR spectra of **2** and **3** showed a doublet signal for the methylene group at 1.3 ppm for **2** (0.99 ppm for **3**) and a doublet signal for the methyl group at 2.6 ppm in a ratio of 4:36 at room temperature (r.t.) in dichloromethane-d_2. The chemical shifts of the methylene group are at a lower field than that[10] (0.1 ppm) of **L**. In the ^{13}C NMR spectra of **2** and **3**, the chemical shifts (+9 ppm) of the methylene carbon are at a lower field than that (−9 ppm) of **L**. Their coupling constants ($^1J_{CP}$: 97 for **2** and 89 Hz for **3**) are much smaller than that (176 Hz) of **L**. These spectral properties are similar to those[4,7,8] of bis(methylenetriphenylphosphorane)metal chloride, $[(C_6H_5)_3P\overset{R}{\overset{|}{C}}H\text{-}M\text{-}\overset{R}{\overset{|}{C}}HP(C_6H_5)_3]Cl_n$ (**7**) (M: group IB and IIB; R: H; n: 1, 2). Thus, the ylide is bonded to the metal atom through the carbanionic donor atom.

The following differences between **3** and **7** (M: Au; R: H) are significant: i) the chemical shift (δCH_2P) of **3** is at a higher field than that[7] of **7** as shown in Fig. 1; ii) the coupling constant ($^2J_{HCP}$) of **3** is similar to that of **L**, but that[7] (14 Hz) of **7** is larger than that[11] (7.5 Hz) of methylenetriphenylphosphorane, $(C_6H_5)_3P{=}CH_2$ (**L'**); iii) the coupling constant (J_{CP}) of **3** is much larger than that[7] (39 Hz) of **7**. The coupling constants ($^3J_{HCNP}$, $^2J_{CNP}$) and chemical shifts ($\delta PNCH_3$) of the methyl groups in **2** and **3** are similar to those of **L**, as shown in Table 1. Complexes **1** and **4—6** are unstable in dichloromethane and chloroform at r.t.; they give a methyltris(dimethylamino)phosphonium chloride, $[(Me_2N)_3PCH_3]Cl$ (**8**).

[Methylenetris(dimethylamino)phosphorane]silver chloride (**9**) and the corresponding zinc dichloride (**10**) have been prepared from the reaction mixture of **L** with AgCl or $ZnCl_2$ in the mole ratio of 1:1. Complexes **9** and **10** are also unstable in dichloromethane and chloroform at r.t.; they give the corresponding phosphonium chloride (**8**). Though their structures are un-

TABLE 1. ^1H AND ^{13}C NMR DATA OF COMPLEXES, YLIDE AND RELATED COMPOUNDS

^1H Complex No.	$CH_{2(3)}P$ δ	$^2J_{HCP}$/Hz	NCH_3 δ	$^3J_{HCNP}$/Hz	C_6H_5 δ	CH_3 δ	Solvent and Standard	
2	1.32 d(4H)	14.5	2.63 d(36H)	9.8			CD_2Cl_2	1)
3	0.99 d(4H)	13.5	2.68 d(36H)	9.8			D_2O	2)
11	1.94 d(2H)	13.7	2.70 d(18H)	9.3		0.69 s(9H)	CD_2Cl_2	1)
12	1.68 d(2H)	14.0	2.50 d(18H)	9.8	7.2—8.2 m(15H)		CD_2Cl_2	1)
13	1.64 d(2H)	14.0	2.52 d(18H)	9.8	7.2—8.2 m(15H)		CD_2Cl_2	1)
8	1.9 d(3H)	14.0	2.68 d(18H)	9.8			D_2O	2)
	2.25 d(3H)	14.0	2.77 d(18H)	10.0			CD_2Cl_2	1)
L	0.1 d(2H)	13.0	2.45 d(18H)	10.0			C_6D_6	1)
L'	0.76 d(2H)	7.5			6.9—8.0 m(15H)		C_6D_6	1)
L'*	0.13 d(2H)	7.5			6.1—7.2 m(15H)		C_6D_6	3)

^{13}C	$CH_{2(3)}P$ δ	$^1J_{CP}$/Hz	NCH_3 δ	$^2J_{CNP}$/Hz		
2	9.13 d	96.6	36.7 d	3.9	CD_2Cl_2	4)
3	9.48 d	88.9	37.4 d	2.0	D_2O	5)
	7.9 d	87.9	37.2 d	2.93	$CDCl_3$	6)
8	11.2 d	113.3	36.6 d	3.9	D_2O	5)
	9.04 d	112.3	36.6 d	3.9	$CDCl_3$	6)
L	−9.15 d	175.8	37.0 d	2.93	C_6D_6	7)

Standard: 1) internal TMS, 2) internal DSS, 3) external TMS, 4) CD_2Cl_2 (δ=53.6), 5) dioxane (δ=67.4), 6) $CDCl_3$(δ=77.1), 7) C_6D_6 (δ=128). *: Ref. 11.

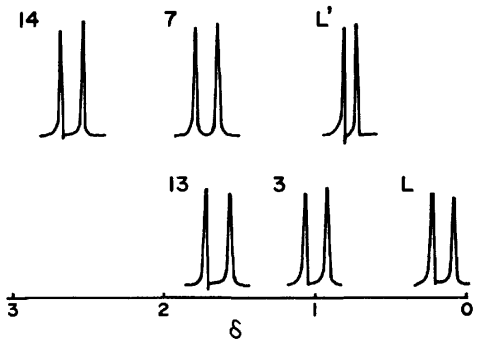

Fig. 1. ^1H NMR spectra of ylides **L**, **L'** and complexes **3**, **7**, **13**, **14**.
L: $(Me_2N)_3P{=}CH_2$ in C_6D_6, **L'**: $(C_6H_5)_3P{=}CH_2$ in C_6D_6, **3**: $[(Me_2N)_3PCH_2{-}Au{-}CH_2P(NMe_2)_3]Cl$ in CD_2Cl_2, **7**: $[(C_6H_5)_3PCH_2{-}Au{-}CH_2P(C_6H_5)_3]Cl$ in CD_2Cl_2, **13**: $[(Me_2N)_3PCH_2{-}Pb(C_6H_5)_3]Cl$ in CD_2Cl_2, **14**: $[(C_6H_5)_3PCH_2{-}Pb(C_6H_5)_3]Cl$ in CD_2Cl_2.

$$m(Me_2N)_3P{=}CH_2 + mMCl_n \longrightarrow [(Me_2N)_3PCH_2{-}MCl_n]_m$$
n: 1 or 2 **9**, **10**

No.	**9**	**10**
M	Ag	Zn

certain, they should not be polymers because they are soluble in dichloromethane. The elemental analyses of **9** and **10** agree with that of $[(Me_2N)_3PCH_2{-}MCl_n]_m$ (n: 1 or 2). Thus they can be a oligomer.[4a)]

[Methylenetris(dimethylamino)phosphorane]triphenyltin chloride (**11**) and [methylenetris(dimethylamino)phosphorane]triphenyltin (**12**) or -lead (**13**) chloride have been isolated from the reaction mixture of **L** and trimethyltin chloride or triphenyltin (or lead) chloride. They are stable in dichloromethane and air at r.t. The ^1H NMR spectra of **11**—**13** showed the dou-

$$(Me_2N)_3P{=}CH_2 + R_3MCl \longrightarrow [(Me_2N)_3PCH_2{-}MR_3]Cl$$
11—**13**

No.	**11**	**12**	**13**
M	Sn	Sn	Pb
R	Me	Ph	Ph

blet signals for the methylene group at 1.6—1.9 ppm and the doublet signals for the methyl group ($PNCH_3$) at 2.5—2.7 ppm in a ratio of 2:18 at r.t. in dichloromethane-d_2. The methyl protons (MCH_3) of **11** and the phenyl protons of **12** and **13** are assigned to a singlet signal at 0.69 ppm (9H) and the multiplet signals at 7.2—8.2 ppm (15H), respectively. The chemical shifts of the methylene group of **11**—**13** are at a lower field than that of **L**. This is similar to that[9)] of (methylenetriphenylphosphorane)triphenyllead chloride, $[(C_6H_5)_3PCH_2{-}MPh_3]Cl$ (**14**) M: Pb. The chemical shift of the methylene group of **12** is at a higher field than that of **11**. This difference is ascribed to the methyl (MCH_3) and phenyl groups. The chemical shift (δCH_2-P) of **13** is at a higher field than that[9)] of **14** (M: Pb), as shown in Fig. 1.

Tetrakis[methylenetris(dimethylamino)phosphorane]-germanium tetrachloride (**15**), tris[methylenetris-(dimethylamino)phosphorane]tin dichloride (**16**), bis-[methylenetris(dimethylamino)phosphorane]lead dichloride (**17**), bis[methylenetris(dimethylamino)phosphorane]paradium dichloride (**18**) and tetrakis[methylene-

tris(dimethylamino)phosphorane]platinum tetraiodide (**19**) have been isolated from the reaction mixture of **L** and $GeCl_4$, $SnCl_2$, $PbCl_2$, $PdCl_2$, or PtI_4. They are unstable in dichloromethane or chloroform at r.t., and give the corresponding phosphonium salt (**8**). Complexes **17** and **19** are stable in air. The melting points or decomposition temperatures of both the complexes differ from those of the ylide and **8**. They are thermally stable in the solid state. These properties resemble those[4,7,8] of **7** (M: group IB, IIB metal; R: Me, *i*-Pr) and **14**[9] (M: Ge, Sn). Thus, the ylide seems to be

$$m(Me_2N)_3P{=}CH_2 + MCl_n \longrightarrow [(Me_2N)_3PCH_2]_mMCl_n \quad (n: 2, 4;\ \mathbf{15}\text{—}\mathbf{18})$$

$$\downarrow PtI_4$$

$$[(Me_2N)_3PCH_2]_4PtI_4 \quad \mathbf{19}$$

No.	15	16	17	18
M	Ge	Sn	Pb	Pd
m	4	3	2	2
n	4	2	2	2

bonded to the metal atom in the solid state,[9] though the structures are uncertain. Complexes **16** and **17** are not so stable as complexes **11**—**13** in dichloromethane. This property is similar to those[9] of other lead complexes such as $[Ph_3PCH_2PbPh_3]Cl$ and $[Ph_3PCH_2]_2PbCl_2$.

In the complexes of the methylenetris(dimethylamino)phosphorane and methylenetriphenylphosphorane, the most remarkable difference between them is solubility in water: *i.e.*, the gold complex (**3**) is soluble but complex (**7**) is insoluble.

The feature of the stable metal complexes with methylenetris(dimethylamino)phosphorane and alkylidenetriphenylphosphorane is ascribed to three factors of metals, ylides, and structures as follows. i) Metals: the metals of stable complexes are Cu(I), Ag(I), Au(I), Zn(II), Cd(II), Be(II), Mg(II), Al(III), Ga(III), In(III), Sn(IV), and Pb(IV). ii) Ylides: *e.g.*, the zinc complex with methylenetriphenylphosphorane is stable, though the complex with methylenetris(dimethylamino)phosphorane is unstable. iii) Structures: the silver complex (**2**) with the composition ratio 2:1 is stable, though the complex (**7**) with the composition ratio 1:1 is unstable; the tin and lead complexes (**11** and **13**) with the coexisting methyl and phenyl ligands are stable, though those complexes (**16** and **17**) with the coexisting chloride ion are unstable.

Experimental

Measurements. The NMR spectra were recorded with an R-40 spectrometer (Hitachi) for ^1H NMR and an FX-60 (JEOL) for ^{13}C NMR.

Starting Materials. Methylenetris(dimethylamino)-phosphorane (**L**) was prepared from methyltris(dimethylamino)phosphonium bromide and sodium in liquid ammonia by Issleib's method.[12] Methyltris(dimethylamino)-phosphonium bromide was prepared from the reaction mixture of tris(dimethylamino)phosphine[13] and methyl bromide.

Ylide-Metal Complexes. Bis[methylenetris(dimethylamino)phosphorane]copper Chloride (1): The ylide of 0.22 g (1.24 mmol) was added to dry THF (10 cm^3) under nitrogen. To the solution was added CuCl of 0.045 g (0.455 mmol). The mixture was stirred for 1 d at room temperature. The white complex which formed was filtered and dried under vacuum. Yield: 0.15 g (72.8%). Found: C, 36.73; H, 9.07%. Calcd for $C_{14}H_{40}N_6P_2CuCl$ (MW 453.46) C, 37.08; H, 8.89%.

Bis[methylenetris(dimethylamino)phosphorane]silver Chloride (2): The ylide of 0.56 g (3.16 mmol) was added to dry THF (5 cm^3) under nitrogen. To the solution was added AgCl (0.15 g, 1.05 mmol). The mixture was stirred for 1 d at r.t. The white complex which formed was filtered and dried under vacuum. Yield: 0.40 g (76.8%). Found: C, 34.02; H, 8.08%. Calcd for $C_{14}H_{40}N_6P_2AgCl$ (MW 497.78) C, 33.78; H, 8.10%.

Bis[methylenetris(dimethylamino)phosphorane]gold Chloride (3): Triphenylphosphinegold chloride of 0.36 g (0.727 mmol) and ylide of 0.39 g (2.2 mmol) were added to dry benzene of 20 cm^3 under nitrogen. The mixture was stirred for approximately 1 d at room temperature. The white complex which precipitated was filtered, washed with dry benzene and dried under vacuum. Yield: 0.33 g (77.3%). Found: C, 29.00; H, 6.86%. Calcd for $C_{14}H_{40}N_6P_2AuCl$ (MW 586.88) C, 28.65; H, 6.87%.

Bis[methylenetris(dimethylamino)phosphorane]zinc Dichloride (4): Zinc chloride of 0.15 g (1.10 mmol) was added to the dry THF (20 cm^3) solution of ylide (0.40 g, 2.26 mmol). The mixture was stirred at r.t. under nitrogen. After 1 d, the solution was filtered and ether was added to the filtrate at −60 °C. The white complex which formed was filtered and dried. Yield: 0.11 g (20.4%). Found: C, 33.62; H, 8.38%. Calcd for $C_{14}H_{40}N_6P_2ZnCl_2$ (MW 490.74) C, 34.26; H, 8.22%.

Bis[methylenetris(dimethylamino)phosphorane]cadmium Dichloride (5): Cadmium chloride of 0.17 g (0.93 mmol) was added to the dry THF (20 cm^3) solution of ylide (0.51 g, 2.88 mmol). The mixture was stirred for 3 d. Pentane was added to the solution and the resulting white precipitated complex was filtered and dried. Yield: 0.1 g (20.1%). Found: C, 31.48; H, 7.29%. Calcd for $C_{14}H_{40}N_6P_2CdCl_2$ (MW 537.76) C, 31.27; H, 7.50%.

Bis[methylenetris(dimethylamino)phosphorane]mercury Dichloride (6): Mercury(II) chloride of 0.2 g (0.74 mmol) was added to the dry THF (9 cm^3) solution of ylide of 0.34 g (1.92 mmol) and the mixture was stirred for 3 d. The white precipitated complex was filtered, washed with dry pentane and dried under vacuum. Yield: 0.43 g (93.3%). Found: C, 27.10; H, 6.21%. Calcd for $C_{14}H_{40}N_6P_2HgCl_2$ (MW 625.95) C, 26.86; H, 6.44%. This complex is hygroscopic. Decomp 188 °C under nitrogen.

[Methylenetris(dimethylamino)phosphorane]silver Chloride (9): Silver chloride of 0.17 g (1.19 mmol) was added to the dry THF solution (5 cm^3) of ylide 0.23 g (1.30 mmol) and the mixture was stirred for 16 h under nitrogen at r.t. The white complex which formed was filtered and dried under vacuum. Yield: 0.31 g (81.5%). Found: C, 26.40; H, 6.75%. Calcd for $C_7H_{20}N_3PAgCl$ (MW 320.55) C, 26.23; H, 6.29%. Complex **9** was sensitive to light.

[Methylenetris(dimethylamino)phosphorane]zinc Dichloride (10): Zinc chloride of 0.15 g (1.10 mmol) was added to the dry THF (8 cm^3) solution of ylide (0.20 g, 1.13 mmol) and the mixture was stirred 1 d under nitrogen. Ether was added to the solution and the white complex which precipitated was filtered and dried under vacuum. Yield: 0.15 g (43.5%). Found: C, 26.73; H, 6.43%. Calcd for $C_7H_{20}N_3PZnCl_2$ (MW 313.51) C, 26.82; H, 6.43%.

[Methylenetris(dimethylamino)phosphorane]trimethyltin Chloride (11): Trimethyltin chloride of 0.53 g (2.66 mmol) was added to the dry THF (7 cm^3) solution of ylide of 0.48 g (2.71 mmol) at 0 °C. The mixture was stirred for 1 d at r.t. The white complex which precipitated was filtered, washed with pentane and dried. Yield: 0.5 g (50.0%). Found: C, 30.93; H, 7.57%. Calcd for $C_{10}H_{29}N_3PSnCl$ (MW 376.48) C, 31.90; H,

7.76%. Mp 215—218 °C.

[Methylenetris(dimethylamino)phosphorane]triphenyltin Chloride (12): The ylide (0.10 g, 0.56 mmol) and triphenyltin chloride (0.21 g, 0.54 mmol) were added to dry THF (10 cm^3) and the resulting mixture was stirred 1 d at 0 °C. The white complex which precipitated was filtered and washed with pentane of 10 cm^3. Yield: 0.16 g (52.2%). Found: C, 52.94; H, 6.70%. Calcd for $C_{25}H_{35}N_3PSnCl$ (MW 562.69) C, 53.36; H, 6.27%. Mp 267—270 °C.

[Methylenetris(dimethylamino)phosphorane]triphenyllead Chloride (13): The mixture of the ylide (0.34 g, 1.92 mmol) and triphenyllead chloride (0.89 g, 1.88 mmol) in dry THF (8 cm^3) were stirred for 1 d at r.t. The white precipitate was filtered, washed with pentane and dried. Yield: 0.55 g (45.0%). Found: C, 46.40; H, 5.87%. Calcd for $C_{25}H_{35}N_3PPbCl$ (MW 651.12) C, 46.12; H, 5.42%. Mp 258—261 °C.

Tetrakis[methylenetris(dimethylamino)phosphorane]germanium Tetrachloride (15): Germanium tetrachloride (0.051 g, 0.24 mmol) was added to the dry THF (8 cm^3) solution of ylide of 0.17 g (0.96 mmol) at 0 °C, and the mixture was stirred 1 d at r.t. The white complex which precipitated was filtered and dried under vacuum. Yield: 0.14 g (63.7%). Found: C, 35.79; H, 8.89%. Calcd for $C_{28}H_{80}N_{12}P_4GeCl$ (MW 923.32) C, 36.42; H. 8.73%.

Tris[methylenetris(dimethylamino)phosphorane]tin Dichloride (16): Tin(II) chloride of 0.14 g (0.73 mmol) was added to the dry THF (8 cm^3) solution of ylide (0.4 g, 2.26 mmol). The mixture was stirred for 3 d at r.t. The white precipitate was filtered, washed with dry pentane and dried. Yield: 0.23 g (60.5%). Found: C, 34.80; H, 8.15%. Calcd for $C_{21}H_{60}N_9P_3SnCl_2$ (MW 721.28) C, 34.97; H, 8.38%.

Bis[methylenetris(dimethylamino)phosphorane]lead Dichloride (17): To the dry THF (18 cm^3) solution of ylide of 0.27 g (1.52 mmol) was added $PbCl_2$ (0.21 g, 0.76 mmol) at 0 °C and the mixture was stirred 1 d at r.t. The white complex which formed was filtered and dried. Yield: 0.36 g (75.0%). Found: C, 25.86; H, 6.18%. Calcd for $C_{14}H_{40}N_6P_2PbCl_2$ (MW 632.48) C, 26.59; H, 6.37%. Decomp 248 °C.

Bis[methylenetris(dimethylamino)phosphorane]paradium Dichloride (18): To the dry THF (12 cm^3) solution of ylide of 0.46 g (2.60 mmol) was added $PdCl_2$ (0.18 g, 1.02 mmol) at r.t. and the mixture was stirred 1 d. The precipitated complex was filtered, washed with pentane and dried. Yield: 0.42 g (77.8%). Found: C, 32.00; H, 8.06%. Calcd for $C_{14}H_{40}N_6P_2PdCl_2$ (MW 531.76) C, 31.62; H, 7.58%.

Tetrakis[methylenetris(dimethylamino)phosphorane]platinum Tetraiodide (19): Platinum(IV) iodide of 0.30 g (0.43 mmol) was added to the dry THF (10 cm^3) solution of ylide (0.35 g, 1.97 mmol) and the mixture was stirred 1 d at r.t. The yellow precipitate which formed was filtered, washed with dry ether and dried. Yield: 0.46 g (75.8%). Found: C, 24.23; H, 6.15%. Calcd for $C_{28}H_{80}N_{12}P_4PtI_4$ (MW 1411.62) C, 23.82; H, 5.71%. Mp 189—191 °C.

All complexes are soluble in dichloromethane and chloroform. Complexes **2**, **3**, **6**, **11**, and **16** are soluble in water and organic solvents such as acetone, alcohols, DMF, and DMSO. Complexes **12** and **13** are soluble in the organic solvents and insoluble in water. Complex **17** is slightly soluble in dichloromethane-chloroform (1 : 1) and insoluble in water and the organic solvents. Complex **19** is soluble in DMSO and MeOH, but insoluble in water, acetone, and DMF.

The authors thank Professor Hubert Schmidbaur of the Technical University of Munich, West Germany for his encouragement. The present work was partially supported by Grant-in-Aid for Scientific Research No. 554190 from the Ministry of Education, Science and Culture.

References

1) Part VII. Ref. 2.
2) Y. Yamamoto, *Bull. Chem. Soc. Jpn.*, **56**, 1772 (1983).
3) a) H. Schmidbaur, *Acc. Chem. Res.*, **8**, 62 (1975); b) H. Schmidbaur and J. Eberlein, *Z. Anorg. Allg. Chem.*, **434**, 145 (1977); c) H. Schmidbaur and R. Franke, *Inorg. Chim. Acta*, **13**, 79 (1975); d) H. Schmidbaur and R. Franke, *ibid.*, **13**, 85 (1975); e) H. Schmidbaur and K. H. Räthlein, *Chem, Ber.*, **107**, 102 (1974); f) W. Malisch, *J. Organomet. Chem.*, **77**, C15 (1974); g) W. Malisch, *ibid.*, **61**, C15 (1973); h) D. Seyferth and S. O. Grim, *J. Am. Chem. Soc.*, **83**, 1610 (1961).
4) a) Y. Yamamoto and H. Schmidbaur, *J. Organomet. Chem.*, **97**, 479 (1975); b) Y. Yamamoto and H. Schmidbaur, *ibid.*, **96**, 133 (1975).
5) H. Schmidbaur, H. J. Füller, V. Bejenke, A. Franck and G. Huttner, *Chem. Ber.*, **110**, 3536 (1977).
6) Y. Yamamoto, *Chem. Lett.*, **1980**, 311.
7) Y. Yamamoto and Z. Kanda, *Bull. Chem. Soc. Jpn.*, **52**, 2560 (1979).
8) Y. Yamamoto and H. Sugimoto, *Bull. Chem. Soc. Jpn.*, **53**, 3176 (1980).
9) Y. Yamamoto, *Bull. Chem. Soc. Jpn.*, **55**, 3025 (1982).
10) K. Issleib, M. Lischewski, and A. Zschunke, *Org. Magn. Reson.*, **5**, 401 (1973).
11) H. Schmidbaur, H. Stühler, and W. Vornberger, *Chem. Ber.*, **105**, 1084 (1972).
12) K. Issleib and M. Lischewski, *J. Prakt. Chem.*, **312**, 135 (1970).
13) V. Mark, *Org. Synth.*, Coll. Vol. V, 602 (1973).

The Preparation and Properties of Ethylenediamine(2-methyl-8-quinolinolato)cobalt(III) Complexes†

Yoshihisa YAMAMOTO* and Eiko TOYOTA
Faculty of Pharmaceutical Sciences, Higashi Nippon Gakuen University, Ishikari-Tobetsu, Hokkaido 061-02
(Received May 14, 1983)

Ethylenediaminebis(2-methyl-8-quinolinolato)cobalt(III) complexes and bis(ethylenediamine)(2-methyl-8-quinolinolato)cobalt(III) complexes have been isolated and characterized by analytical and spectroscopic methods. In the former complexes, the NMR spectra indicate that the two nitrogen atoms of the coordinated 2-methyl-8-quinolinolato ligands are in the *trans* positions, whereas the two oxygen atoms are in the *cis* positions.

A few investigations of the stereochemistry of bis(8-quinolinolato)metal complexes, $[M(oxine)_2X_2]$, in an octahedral configuration have been reported by some authors.[1-6] The configuration of the coordinated 8-quinolinolato ligands in their complexes is in the *trans* positions for two oxygen atoms and in the *cis* positions for two nitrogen atoms except for the dicarbonyl complex[6] which is in the *cis* positions for both the two oxygen atoms and the two nitrogen atoms. However, a complex of the configurations in the *cis* positions for two oxygen atoms and in the *trans* positions for two nitrogen atoms of the coordinated 8-quinolinolato ligands has not yet been reported.

Previously, we have been concerned with ethylenediaminebis(8-quinolinolato)cobalt(III) complexes,[7] which are in the *cis* positions for the two oxygen atoms of the coordinated 8-quinolinolato ligands. However, it has not been resolved whether the two nitrogen atoms of the coordinated 8-quinolinolato ligands are in the *trans* or the *cis* positions. An X-ray study of the complexes has not yet been made, because the crystals could not be obtained. We have found that the two methyl groups of the coordinated 2-methyl-8-quinolinolato ligands in the complexes have a steric hindrance against the amine protons of the coordinated ethylenediamine ligand. Thus, the present paper describes the preparation and properties of the ethylenediaminebis(2-methyl-8-quinolinolato)cobalt(III) complexes and bis(ethylenediamine)(2-methyl-8-quinolinolato)cobalt(III) complexes, and deals with the identification of the configuration of the former complexes.

Results and Discussion

Ethylenediaminebis(2-methyl-8-quinolinolato)cobalt(III) chloride hydrate, $[Co(\text{ 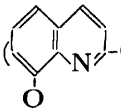 }-CH_3)(en)_2]Cl\cdot H_2O$ (**1**) has three isomers A, B, and C as is shown in Fig. 1. The isomers of A and C have C_2 symmetry, while that of B has C_1 symmetry. In isomer A, the two methyl groups of the coordinated 2-methyl-8-quinolinolato ligands are far from both the *N*-Ha and *N*-Hb amine protons of the coordinated ethylenediamine ligand. Thus, in the ^1H NMR spectrum of isomer A, the amine proton signals of the coordinated ethylenediamine ligand can differ little from those of the corresponding 8-quinolinolato chloride dihydrate $[Co(oxine)_2en]Cl\cdot 2H_2O$ (**2**), previous reported.[7] While, in the isomer C, the two methyl groups of the coordinated 2-methyl-8-quinolinolato ligands are very near both the *N*-Ha and *N*-Hb amine protons of the coordinated ethylenediamine ligand, *i.e.*, the amine proton signals of the ^1H NMR spectrum should be different from those of **2**. The two methyl groups in the isomer B are at different positions from those of A and C. Accordingly, the distinction between isomers A, B, or C should be evident in the NMR spectrum.

Complex **1** has been isolated by chromatographic separation from a reaction mixture of *trans*-$[CoCl_2en_2]Cl$,[8] Ag_2O, and 2-methyl-8-quinolinol. The corresponding nitrate (**3**) or picrate (**4**) has been prepared from the reaction mixture of **1** and silver nitrate or picric acid, respectively. The color of **1** in the solid state is brown, **3** is dark brown and **4** is yellowish green. Complexes **1** and **3** are soluble in alcohols, DMSO, CF_3COOH and water, though complex **4** is soluble in DMSO, and somewhat soluble in acetone and methanol.

^1H NMR and ^{13}C NMR spectra of **1** are suggestive of the present of C_2 symmetry[5,9] from Figs. 2 and 3, *i.e.*, the isomer of **1** can be suggested to be either A or C. In the ^1H NMR spectrum of **1**, the signals at 6.9—8.2 ppm (10H) are assigned to the protons of the coordinated 2-methyl-8-quinolinolato ligand. The signals (10H) at 2.55 ppm and 2.54—2.70 ppm are assigned to the methyl and methylene protons of the coordinated ligands. The amine protons of the coordinated ethylenediamine ligand showed two singlet signals at 4.88 ppm (2H) and 5.87 ppm (2H). A clear distinction of **1** and **2** was found in the amine proton signals of their ^1H NMR spectra as is shown in Fig. 2. The amine proton signals at 4.88 and 5.87 ppm of **1** shift to 5.27 and 5.79 ppm of **2**, respectively in the same conditions ($6.2\pm0.05\times10^{-2}$ mol dm^{-3} DMSO-d_6 solution). Also, this behavior occurs in 50% ($CF_3COOH+D_2O$) solution as is shown in Table 1. The shift of signal at 4.88 ppm is larger than that of 5.87 ppm. This behavior can be based on the steric effect of the methyl groups upon the amine protons. Then, the signal at 4.88 ppm is assigned to the *N*-Ha amine protons, because they are near both methyl groups. The signal at 5.87 ppm is assigned to *N*-Hb amine protons. Thus, complex **1** has been assigned to isomer C, which has been in the *trans* position for the two nitrogen atoms and in the *cis* position for the two oxygen atoms

† Part III: Cobalt(III) Complexes with $[N_{6-n}X_n]$ Type Ligand. Part I: Ref. 5; Part II: Ref. 7.

TABLE 1. SOME PHYSICAL PROPERTIES OF COMPLEXES **1**—**8**

^1H / No.	$NH_2CH_2CH_2NH_2$ δ			2-Methyl-8-quinolinolato δ		Picrate δ	Absorption bands in methanol λ/nm (ε)			Electro conductivity of aqueous solutions S cm² equiv.⁻¹
	$[CH_2]$ CH_2+CH_3	$[NH_2]$ Ha	Hb	8-Quinolinolato	CH_3					
1	2.54—2.70 (10H)	4.88 (2H)	5.87 (2H)	6.9—8.2 (10H)	2.55[1]		326 (1980)	342 (2240)	398 (5220)	125
	[3.06(4H)]	3.99 (2H)	5.22 (2H)	7.1—8.2 (10H)	2.47 (6H)[2]					
2	[2.75(4H)]	5.27 (2H)	5.79 (2H)	6.9—8.4 (12H)[1]	—		325 (2400)	339 (2960)	404 (5730)	130
	[3.27(4H)]	4.62 (2H)	5.21 (2H)	7.1—8.3 (12H)[2]	—					
3	2.50—2.75 (10H)	4.87 (2H)	5.83 (2H)	6.8—8.2 (10H)	2.55[1]		326 (2080)	341 (2360)	398 (5420)	
4	2.54—2.84 (10H)	4.91 (2H)	5.87 (2H)	6.8—8.2 (10H)	2.57	8.51 (2H)[1]		362 (19530)	393 (18370)	
5	2.59—3.18 (11H)	[4.19—5.92 (8H)]		7.1—8.4 (5H)	2.94[3]		320 (985)	341 (975)	398 (2690)	230
6	2.55—3.12 (11H)	[4.03—5.80 (8H)]		7.0—8.3 (5H)	2.91[3]		320 (1090)	341 (1070)	398 (2900)	
7	2.55—2.90 (11H)	[4.00—6.06 (8H)]		6.8—8.2 (5H)	2.78	8.49 (4H)[1]		357 (22300)	390 (17620)	
8*	2.92(8H)	[4.12—5.34 (8H)]		7.0—8.7 (6H)[3]	—		324 (1150)	338 (1250)	407 (2900)	270

^{13}C	$NH_2CH_2CH_2NH_2$ δ				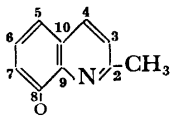 δ						
					C-2	C-3	C-4	C-5	C-6	C-7	C-8	C-9	C-10	CH_3
1	45.5				164.8	114.6	139.6	127.3	117.3	129.7	145.9	165.6	129.0	22.2[4]
5	43.9	44.6	45.7	46.7	164.4	115.1	140.9	127.3	116.4	129.8	145.7	164.8	129.8	24.0[4]

Solvents and Standard: 1) DMSO-d_6, internal TMS; 2) 50% ($CF_3COOH+D_2O$), internal DSS; 3) 1.8 mol dm^{-3} D_2SO_4, internal DSS; 4) D_2O, internal dioxane (δ=67.4). *: Ref. 7.

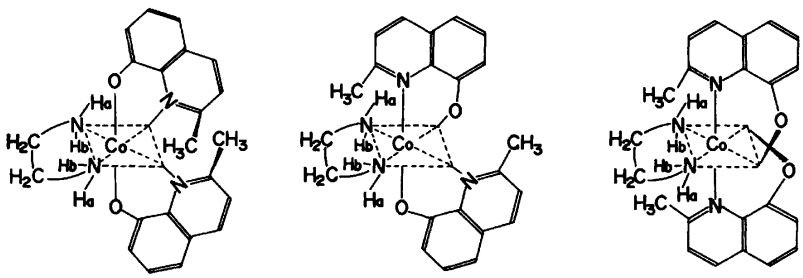

A B C

Fig. 1. The isomers of $[Co(2\text{-Me-oxine})_2cn]Cl\cdot H_2O$.

of the coordinated 2-methyl-8-quinolinolato ligands. In the ^{13}C NMR spectrum of **1** as is shown in Fig. 3, the chemical shifts of the coordinated 2-methyl-8-quinolinolato ligands were assigned on the basis of the results of the complex **2**;[7] they are collected in Table 1.

Bis(ethylenediamine)(2-methyl-8-quinolinolato)cobalt(III) chloride dihydrate, $[Co(\text{ 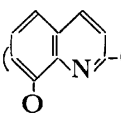 })(en)_2]Cl\cdot 2H_2O$ (**5**) has been isolated from a reaction mixture of *trans*-$[CoCl_2en_2]Cl$, Ag_2O, and 2-methyl-8-quinolinol. The corresponding nitrate (**6**) or picrate (**7**) has been prepared from the reaction mixture of **5** and silver nitrate or picric acid, respectively. The color of **5** in the solid state is russet brown, **6** is brown, and **7** is yellowish brown. Complexes **5** and **6** are soluble in DMSO, methanol and water, and they are somewhat soluble in ethanol, though complex **7** is soluble in acetone and DMSO and somewhat soluble in methanol. The signals of the methyl, metyhlene, and 8-quinolinolato

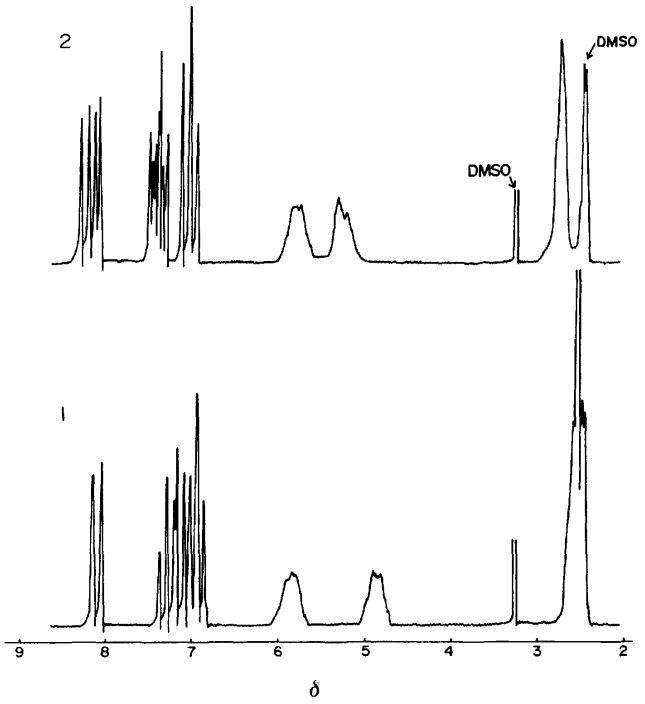

Fig. 2. The ^{1}H NMR spectra of [Co(2-Me-oxine)$_2$en]Cl·H_2O (**1**) and [Co(oxine)$_2$en]Cl·$2H_2O$ (**2**) in DMSO-d_6.

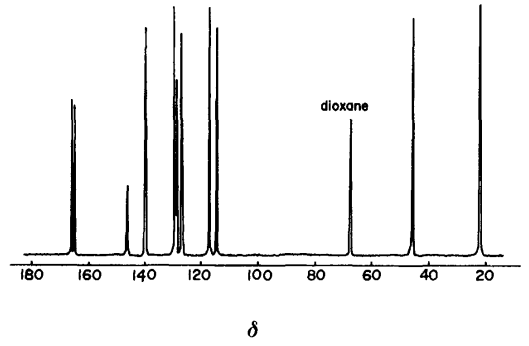

Fig. 3. The ^{13}C NMR spectrum of [Co(2-Me-oxine)$_2$-en]Cl·H_2O in D_2O.

protons and carbons and of amine protons of the coordinated ligands in **5**—**7** were assigned on the basis of the results of the bis(ethylenediamine)(8-quinolinolato)-cobalt(III) chloride dihydrate, [Co(oxine)en$_2$]Cl·$2H_2O$ (**8**), in the previous paper,[7] and collected in Table 1.

Absorption spectra of **1**—**3**, **5**, **6**, and **8** show three absorption bands at around 325, 340, and 400 nm in methanol as is shown in Table 1. The absorption bands at 340 nm of **1**—**3** complexes are stronger than those at 325 nm, though those at 325 nm of **5** and **6** are stronger than those at 340 nm. The ε's of three bands of **1** or **3** and **5** or **6** are smaller than those of **2** and **8**, respectively because it can be based on the inductive effect of the methly group of the chelate ligand. The absorption bands at around 400 nm are charge transfer band.[5] All complexes are diamagnetic. Their electric conductivities in an aqueous solution were collected in Table 1.

Experimental

Measurements. The NMR spectra were recorded with an FX-60 spectrometer (JEOL) for ^{13}C NMR and R-40 (Hitachi) for ^{1}H NMR. The visible absorption spectra were recorded with a Shimadzu MPS-5000 recording spectrophotometer. The electric conductivities of an aqueous solution were determined by the use of a conductometric meter CM-30 (Shimadzu) at room temperature. The magnetic susceptibilities were measured by Faraday's method using a magnetic balance (Shimadzu) at room temperature.

Preparation of Complexes. Ethylenediaminebis(2-methyl-8-quinolinolato)cobalt(III) Chloride Hydrate (1) and Bis(ethylenediamine)(2-methyl-8-quinolinolato)cobalt(III) Chloride Dihydrate (5): To 100 cm^3 of an aqueous solution of [CoCl(OH)en$_2$]$^+$ which was prepared from *trans*-[CoCl$_2$en$_2$]-Cl (10.0 g, 35.0 mmol) and Ag_2O (4.05 g, 17.5 mmol), a methanol solution (120 cm^3) of 2-methyl-8-quinolinol (5.5 g, 34.5 mmol) was added dropwise. The liquid was stirred for 45 h at 60 °C. The reaction mixtures were concentrated on a rotary evaporator and dried over silica gel. Complexes **1** and **5** were extracted with methanol from the dried mixture. The methanol extract was concentrated, and the solution was chromatography on a column of alumina. On elution with ethanol, the first band (complex **1**) was collected and the solution concentrated. The precipitated complex was recrystallized from ethanol-ether twice. The second band (complex **5**) was eluted with methanol and the solution was concentrated. This complex was recrystllized from methanol-ethanol (1:2) twice. Yields: 7.72 g (45.1%) for **1**, 0.62 g (4.0%) for **5**. Found **1**: C, 54.59; H, 5.27; N, 11.05; Cl, 7.76%. **5**: C, 37.80; H, 6.39; N, 16.06; Cl, 16.40%. Calcd for **1**: $CoC_{22}H_{26}N_4O_3Cl$ (MW 488.86) C, 54.05; H, 5.36; N, 11.46; Cl, 7.25%. **5**: $CoC_{14}H_{28}N_5O_3Cl_2$ (MW 444.25) C, 37.85; H, 6.35; N, 15.76; Cl, 15.96%.

Ethylenediaminebis(2-methyl-8-quinolinolato)cobalt(III) Nitrate (3): To an aqueous solution of **1** (0.5 g, 1.0 mmol) was added an aqueous solution silver nitrate (0.17 g, 1.0 mmol). The mixture was stirred, and the silver chloride precipitated was filtered. The filtrate was concentrated on a rotary evaporator. A small amount of silver complex in the filtrate was removed by column chromatography on alumina. The elution band of methanol was collected and the solution was concentrated. Complex **3**, thus precipitated, was recrystallized from ethanol-ether twice. Yield: 0.35 g (70.4%). Found: C, 52.69; H, 5.15; N, 14.12%. Calcd for $CoC_{22}H_{24}N_5O_5$ (MW 497.40) C, 53.12; H, 4.86; N, 14.08%.

Ethylenediaminebis(2-methyl-8-quinolinolato)cobalt(III) Picrate (4): An aqueous solution of **1** (0.5 g, 1.0 mmol) was added to a solution of picric acid (0.23 g, 1.0 mmol); the mixture was stirred, and the separated yellowish green complex was filtered and recrystallized from methanol. Yield: 0.60 g (90.4%). Found: C, 50.01; H, 3.99; N, 15.25%. Calcd for $CoC_{28}H_{26}N_7O_9$ (MW 663.50) C, 50.69; H, 3.95; N, 14.78%.

Bis(ethylenediamine)(2-methyl-8-quinolinolato)cobalt(III) Nitrate Hydrate (6): This complex was prepared from the reaction mixture of **5** (0.5 g, 1.1 mmol) and silver nitrate (0.38 g, 2.2 mmol) by the method of complex **3**, and recrystallized from water-ethanol twice. Yield: 0.31 g (58.8%). Found: C, 34.90; H, 5.58; N, 20.64%. Calcd for $CoC_{14}H_{26}N_7O_8$ (MW 479.35) C, 35.08; H, 5.47; N, 20.45%.

Bis(ethylenediamine)(2-methyl-8-quinolinolato)cobalt(III) Picrate (7): An aqueous solution of **5** (0.5 g, 1.1 mmol) was added to a solution of picric acid (0.51 g, 2.2 mmol), the mixture was stirred, and the separated russet brown complex was filtered and recrystallized from methanol. Yield: 0.59 g (67.6%). Found: C, 39.54; H, 4.17; N, 19.14%. Calcd for $CoC_{26}H_{28}N_{11}O_{15}$ (MW 793.52) C, 39.35; H, 3.56; N, 19.42%.

References

1) E. O. Schlemper, *Inorg. Chem.*, **6**, 2012 (1967).
2) B. F. Studd and A. G. Swallow, *J. Chem. Soc., A*, **1968**, 1961.
3) L. O. Atovmyan and Y. A. Sokolova, *J. Chem. Soc., Chem. Commun.*, **1969**, 649.
4) J. D. Matthews, N. Singer, and A. G. Swallow, *J. Chem. Soc., A*, **1970**, 2545.
5) Y. Yamamoto, *Chem. Lett.*, **1980**, 1555.
6) J. A. Van Doorn and P. W. N. M. Van Leeuwen, *J. Organomet. Chem.*, **222**, 299 (1981).
7) Y. Yamamoto, R. Kataoka, S. Imahara, and T. Amano, *Bull. Chem. Soc. Jpn.*, **54**, 2972 (1981).
8) J. C. Bailar. Jr., *Inorg. Synth.*, Coll. Vol. II, 222 (1946).
9) a) S. Utsuno, A. Hayashi, S. Kondo, and M. Utsumi, *Chem. Lett.*, **1979**, 351; b) S. Utsuno and M. Sekizaki, *Inorg. Nucl. Chem. Lett.*, **15**, 259 (1979).

Mössbauer Effect of ^{119}Sn in Tin Sulfides Produced through Thermal Decomposition of SnS_2

Sumio ICHIBA* and Kazushi KUNITA
Department of Chemistry, Faculty of Science, Hiroshima University, Higashisenda-machi, Naka-ku, Hiroshima 730
(Received May 9, 1983)

The intermediate tin sulfides produced through thermal decomposition of SnS_2 were studied by quenching and Mössbauer spectroscopy. The thermal decomposition of SnS_2 in a nitrogen gas flow proceeded to SnS *via* Sn_2S_3. The existing phases of the decomposition products in the range of the S/Sn ratio less than 1.50 were Sn_2S_3 and $Sn_{1-x}S$. A new peak observed in the Mössbauer spectrum of tin sulfides with the S/Sn ratio less than 1.04 was assigned to Sn^{4+} in the nonstoichiometric compound $Sn_{1-x}S$.

The tin-sulfur system was studied by many workers.[1-8] Albers *et al.* gave a phase diagram (Fig. 1).[1] In the diagram, the existence of the compounds SnS_2 and SnS is clearly indicated. The intermediates Sn_2S_3, Sn_3S_4, Sn_4S_5, and $Sn_{1-x}S$ have been reported so far, but there are inconsistencies. G. H. Moh identified Sn_2S_3 and $Sn_{1-x}S$ as the intermediate compounds on the basis of his detailed studies by quenching, high-temperature X-ray powder diffraction, and differential thermal analysis; however he refuted the existence of Sn_3S_4 and Sn_4S_5.[7] Bartenov *et al.* studied the Sn–S system by Mössbauer spectroscopy and reported that the intermediate compound such as Sn_2S_3 and Sn_3S_4 did not exist.[8] On the other hand, P. I. Seregin *et al.* asserted the existence of Sn_2S_3 and Sn_3S_4 with intrinsic crystal lattice structures by Mössbauer spectroscopy.[9]

Previously the authors have examined the tin sulfides produced through thermal decomposition of SnS_2 and identified Sn_2S_3 as an intermediate by quenching, Mössbauer spectroscopy, thermogravimetry, differential thermal analysis, and X-ray powder diffraction.[10,11] In this study, the existing phases of tin sulfides in the range S/Sn=1.5 to 1.0 produced through thermal decomposition of SnS_2 in a nitrogen gas flow are examined by Mössbauer spectroscopy.

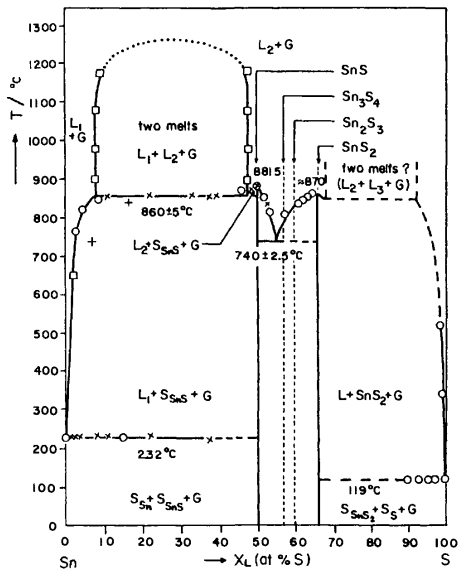

Fig. 1. The phase diagram of Sn–S system. (From Ref. 1)

Experimental

Preparation of the Tin Sulfide Sample. The tin sulfide samples were prepared by thermal decomposition of tin(IV) sulfide. The tin(IV) sulfide to be decomposed was prepared by the addition of 2 mol dm^{-3} -HCl to an aqueous solution of $Na_4SnS_4 \cdot 14H_2O$. To remove the reaction products NaCl and S throughly the crystals were washed with distilled water several times, then with methanol and carbon disulfide alternately. The thermal decomposition of SnS_2 was carried out by heating SnS_2 to 878 K at a rate of 3 K/min in a nitrogen gas flow and maintaining it at this temperature from 2 min to 60 min. After heating the decomposition products were quenched to room temperature without breaking the inert atmosphere. The S/Sn ratio of the sulfides was determined by analysing the tin in the sample gravimetrically in which the sample was calcined at 1173 K for 5 h in air.

Measurements. The Mössbauer spectra were measured using a constant acceleration type spectrometer with an accuracy within 0.05 mm s^{-1}. The γ-ray source of calcium stannate was used at room temperature and the absorber was cooled at 93 K in a liquid nitrogen cryostat. The velocity scale was calibrated against the spectra of $BaSnO_3$ and β-tin at room temperature. All isomer shifts are reported relative to $BaSnO_3$. Mössbauer parameters were deduced from Lorentzian curves computer-fitted to the spectra by a least-squares method.

Results and Discussion

The Mössbauer spectra of tin sulfides in the ranges S/Sn=1.50 to 1.07 and less than 1.04 are shown in Figs. 2 and 3, respectively. The spectra are apparently superposition of two spectra, *i.e.* the spectrum characteristic of SnS and the spectrum characteristic of SnS_2. Mössbauer parameters deduced from the spectra are shown in Table 1 along with the area ratio of Sn^{IV} to total. In Table 1, Sn_2S_3 with intrinsic lattice are distinguished from the other for the reason that the isomer shift and quadrupole splitting for Sn^{II} at S/Sn=1.50 are larger than those of SnS as reported previously.[10] Sn_2S_3 was decomposed further by heating the sulfide at 878 K for various times. The heating durations and the S/Sn ratios of the sulfides obtained are also shown in Table 1. The absorption peak for Sn^{IV} at about 1.1 mm s^{-1} decreased with the decreasing S/Sn ratio and disappeared at S/Sn=1.04. On the other hand, the peak for Sn^{II} increased with the decreasing S/Sn ratio. The value of the isomer shift for Sn^{IV} was almost the same in the range

Table 1. Mössbauer parameters for tin sulfides produced through thermal decomposition or SnS_2

Duration of heating at 878 K (min)	Atomic ratio (S/Sn)	Sn^{IV}		Sn^{II}			$\frac{Sn^{IV}}{Sn(total)}$
		δ / mm s^{-1}	Γ / mm s^{-1}	δ / mm s^{-1}	Δ / mm s^{-1}	Γ / mm s^{-1}	
0	1.50±0.02	1.12	1.20	3.55	1.01	1.12	0.50
2	1.38±0.02	1.17	1.23	3.45	0.95	1.15	0.37
4	1.33±0.03	1.18	1.21	3.47	0.96	1.15	0.32
7	1.24±0.02	1.10	1.23	3.41	0.92	1.14	0.28
12	1.23±0.02	1.16	1.54	3.38	0.96	1.13	0.27
17	1.20±0.01	1.01	1.43	3.42	0.91	1.14	0.20
22	1.07±0.03	1.12	1.56	3.38	0.88	1.11	0.15
23	1.04±0.02	−0.01	3.65	3.38	0.92	1.15	0.13
25	1.03±0.03	−0.51	2.88	3.39	0.93	1.18	0.09
27	1.02±0.03	−0.24	2.05	3.38	0.96	1.16	0.06
32	1.01±0.02	−0.44	1.54	3.36	0.90	1.15	0.05
57	1.01±0.02	—	—	3.38	0.93	1.17	—

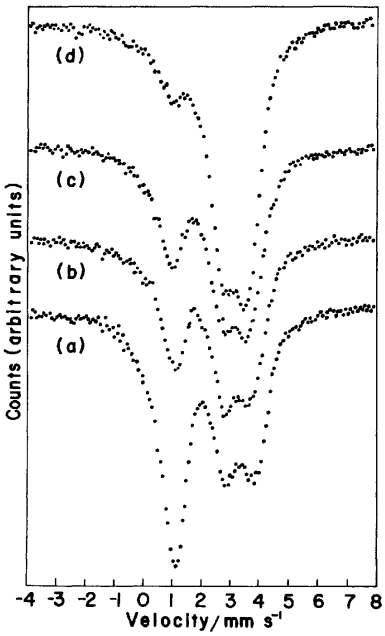

Fig. 2. Mössbauer spectra for tin sulfides produced through thermal decomposition of SnS_2. S/Sn ratio, (a) 1.50; (b) 1.33; (c) 1.24; (d) 1.07.

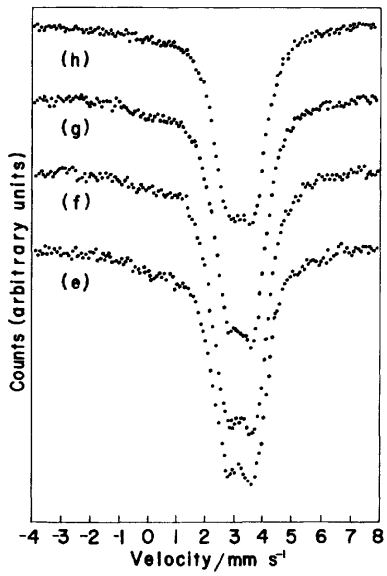

Fig. 3. Mössbauer spectra for tin sulfides produced through thermal decomposition of SnS_2. S/Sn ratio, (e) 1.04; (f) 1.03; (g) 1.02; (h) 1.0.

S/Sn=1.50 to 1.07, but the values of the shift and quadrupole splitting for Sn^{II} decreased with decreasing S/Sn ratio and approached the values for SnS. The area ratio coincided with the corresponding S/Sn ratio in the range S/Sn=1.50 to 1.33, however, in the range less than 1.24 the area ratio exceeded the corresponding S/Sn ratio.

Gerasimov *et al.* reported the existence of Sn_2S_3 and Sn_4S_5 as the intermediate products through thermal decomposition of higher sulfides, *viz.* $SnS_2 \rightarrow Sn_2S_3 \rightarrow Sn_4S_5 \rightarrow SnS$.[2] G. H. Moh synthesized the sulfides in evacuated, sealed silica tubes in which weighed amounts of tin and sulfur were heated at a predetermined temperature and the reaction products examined by X-ray powder diffraction and optical reflectivity. All the reaction products in the range of S/Sn ratio smaller than 1.50 were Sn_2S_3 and $Sn_{1-x}S$; but Sn_3S_4 and Sn_4S_5 did not exist.[7] P. I. Seregin *et al.* synthesized tin sulfides by melting initial components of tin and sulfur in evacuated quartz capsules and investigated the reaction products by Mössbauer spectroscopy. They assert the existence of Sn_3S_4 and Sn_2S_3, because the spectra of Sn_3S_4 and Sn_2S_3, obtained by different methods, have the same isomer shifts and quadrupole splittings, but the ratio of the area below the spectra of Sn^{II} and Sn^{IV} depends on the method of synthesis.[9]

In the present work, it seems likely that the existing phases of the decomposition products in the range of S/Sn less than 1.50 are Sn_2S_3 and $Sn_{1-x}S$, because the parameters were not anomalous at S/Sn=1.33 and 1.24, and the peak for nonstoichiometric $Sn_{1-x}S$ manifested itself in the range of S/Sn less than 1.04. The peak for Sn^{IV} characteristic of $Sn_{1-x}S$ becomes distinct at about 0

mm s^{-1} as the peak for Sn^{IV} characteristic of Sn_2S_3 disappeared and it diminished as the S/Sn ratio approached to the stoichiometric value, as shown in Fig. 3. The excess value of the area ratio to the corresponding S/Sn ratio in the range of S/Sn less than 1.24 may be caused by superposition of the peak in the spectrum characteristic of $Sn_{1-x}S$ to the spectrum of Sn_2S_3 if the recoilless fraction of Sn^{II} is equal in both $Sn_{1-x}S$ and Sn_2S_3.

Albers *et al.* showed that the existence region of solid SnS probably lies entirely on the excess sulfur side on the basis of their Hall effect measurements.[1] Rau also reported the sulfur rich boundary of the homogeneity region of SnS as the result of their measurement of the variation of sulfur pressure by a chemical method and that the doubly negatively charged tin vacancy is probably the prevailing imperfection at equilibrium.[12]

The lower thermal decomposition product of Sn_2S_3 can justifiably be refered to the formula $Sn_{1-x}S$. In $Sn_{1-x}S$ metal vacancies exist. The single metal vacancies act as acceptors with a level near the valence band and leave positive holes in the valence band. Trapping holes give rise to Sn^{4+} in $Sn_{1-x}S$. Besides this, association of the neutral vacancies will take place.

The pertinent quasi-chemical equations by the use of the Kröger's notation[13] are

$$V_{Sn}^{x} \rightleftarrows V_{Sn}'' + 2h\cdot, \quad (1)$$

$$2V_{Sn}^{x} \rightleftarrows (V_{Sn})_i^{x}, \quad (2)$$

with neutrality condition $[h\cdot]=2[V_{Sn}'']$.

The deviation from stoichiometry, x, is

$$x = [V_{Sn}^{x}] + [V_{Sn}''] + 2[(V_{Sn})_i^{x}]. \quad (3)$$

At high temperature, 878 K, where $Sn_{1-x}S$ was formed the association will be relatively unimportant and Eq. 3 may be approximated by $x \approx [V_{Sn}''] = [Sn^{4+}]$. Thus, the concentration of Sn^{4+} will be defined by the deviation from stoichiometry. In Table 1, the excess area ratio to the corresponding S/Sn ratio in the lower range may also be caused by still existing Sn_2S_3 as shown in the large line width of the peak.

References

1) W. Albers, C. Haas, H. J. Vink, and J. D. Wasscher, *J. Appl. Phys. Suppl.* **32**, 2220 (1961).

2) J. I. Gerasimov, E. V. Kruglova, and N. D. Rosenblum, *Moskau, Zurnal Obscej Chimii*, **7**, 1520 (1937).

3) L. D. C. Bok and J. C. A. Boeyens, *J. South African Chem. Inst.*, **10**, 49 (1957).

4) M. I. Karakhanova, A. S. Pashinkin, and A. V. Novoselova, *Izv. Akad. Nauk SSSR, Neorg. Matr.*, **2**, 991 (1966).

5) D. Mootz and R. Kunzmann, *Acta Crystallogr.*, **15**, 913 (1962).

6) J. Oftedal, *Z. Phys. Chem.*, **134**, 301 (1928).

7) G. H. Moh, *Neues Jahrb. Mineral., Abh.*, **111**, 277 (1969).

8) G. M. Bartenev, A. D. Tsyganov, S. A. Dembovskii, and V. I. Mikhailov, *Izv. Akad. Nauk SSSR, Neorg. Matr.*, **7**, 1442 (1971).

9) P. I. Seregin, M. Sagatov, B. T. Melekh, Yu. P. Kostikov, and L. N. Vasil'ev, *Inorg. Mater. (U.S.S.R.)*, **9**, 119 (1973).

10) S. Ichiba, M. Katada, and H. Negita, *Chem. Lett.*, **1974**, 979.

11) M. Katada, *J. Sci. Hiroshima Univ., Ser. A*, **39**, 45 (1975).

12) H. Rau, *J. Phys. Chem. Solids*, **27**, 761 (1966).

13) F. A. Kröger, "The Chemistry of Imperfect Crystals," North-Holland, Amsterdam (1974), Vol. 2, Chap. 7, p. 14.

 © 1984 The Chemical Society of Japan Bull. Chem. Soc. Jpn., 57, 54—57 (1984) [Vol. 57, No. 1

Studies of the Selective Adsorption of Anions by Metal Ion Loaded Ion-exchange Resin. VI.[1] The Adsorption Behavior of the Phosphate Ion on the Iron(III) Loaded Ion-exchange Resin

Isao YOSHIDA,* Ryoichi TAKESHITA, and Keihei UENO
Department of Industrial Chemistry, Kumamoto Institute of Technology, Ikeda 4-22-1, Kumamoto 860
(Received June 6, 1983)

Adsorption isotherms for the phosphate ion by various iron(III)-loaded ion-exchange resins(IRC-Fe(III)), which are different in iron(III)-ion concentrations, were prepared at 5—35 °C in aqueous systems with pH values of 3 and 4.6 by means of the batch method. These isotherms could be represented by the $C_p = Q_\infty(C_p/Q) - 1/K$ equation in the phosphate-ion-concentration range from 3.23×10^{-4} to 3.23×10^{-2} mol dm^{-3} (10 ppm to 1000 ppm as P), where C_p and Q are the phosphate-ion concentrations of the aqueous phase and the adsorbent respectively; Q_∞ is the saturated phosphate concentration of the adsorbent, and K is the equilibrium constant. From the analysis of adsorption isotherms, the values for Q_∞ and K were determined on each adsorbent, and the nature of the adsorbent IRC-Fe(III) was discussed, with consideration paid to these two parameters and the pH-dependency of the distribution ratio of the phosphate ion between the aqueous phase and the adsorbent.

In a previous paper,[2] we reported on the adsorption behavior of the phosphate ion on the iron(III)-loaded chelating resin(UR 10-Fe(III)) and on the evidence that the resin-bound iron(III) was the site for phosphate adsorption. While iron(III) is tightly held on UR 10 resin through the chelate formation with the *N*-(*o*-hydroxybenzyl)iminodiacetate moiety, our investigation was extended to find a better phosphate adsorbent using other types of chelating resins or cation-exchange resins. We finally found that the iron(III)-loaded weakly acidic carboxylate-type cation-exchange resins, such as Amberlite IRC-50 or diaion WK, were the most advantageous adsorbents for phosphate with regards to their adsorption capacity, thermal stability, iron-binding property, and recycling perfomances.[3] This paper describes the results of our detailed investigation of the adsorption behavior of the phosphate ion on the iron(III)-loaded Amberlite IRC-50.

Experimental

Materials. The weakly acidic carboxylate-type cation-exchange resin, Amberlite IRC-50(30 to 50 mesh; proton-exchange capacity, 10.62 mequiv g^{-1}), was washed with 2 mol dm^{-3} of sodium hydroxide and hydrochloric acid alternatively three times, and finally converted to the sodium form. Fifteen grams of the sodium-form resin was suspended for 24 h in 200 cm^3 of a 0.03 mol dm^{-3} sodium acetate–acetic acid buffer solution of pH 3.0 containing from 0.7 to 5 g of iron(III) chloride hexahydrate. The resulting iron(III)-loaded Amberlite IRC-50(hereafter abbreviated as IRC-Fe(III)) was washed with deionized water until the washing became free from iron(III); it was then sucked and centrifuged. The IRC-Fe(III) adsorbent was sealed in a bottle and stored in a refrigerator.

The iron(III) content in the resin was determined spectrophotometrically on the acid eluate as has been described in a previous paper;[3] it was expressed in terms of C_{Fe}(mmol g^{-1} of the dry adsorbent). The iron(III) contents ranged from 0.323 to 1.97 mmol g^{-1}, as is shown in Table 1. The water content of IRC-Fe(III) was determined on each batch by measuring the weight loss after drying to a constant weight at 110 °C immediately before the adsorption study.

A stock solution of phosphate was prepared from potassium dihydrogenphosphate. All the other reagents were of an analytical grade.

Procedure for Adsorption Study. An exactly weighed amount of IRC-Fe(III)(*ca.* 0.5 g) was shaken with 50 cm^3 of a buffered solution containing phosphate at a constant temperature for 48 h. This shaking time was found to be sufficient to attain an approximate equilibrium. For the observation of the adsorption isotherms, the pH of the aqueous phase was adjusted to 3.0 or 4.6 with 0.09 mol dm^{-3} sodium sulfate or with 0.1 mol dm^{-3} acetic acid–sodium acetate respectively. However, in the experiment at pH 3.0, the pH of the solution after equilibration deviated over the range from 2.5 to 3.3 because of the poor buffering capacity of the reagent. For the measurements of the distribution ratio, D, at various pHs, the pHs of the aqueous phases were adjusted with the use of 2 mol dm^{-3} sodium hydroxide and 1 mol dm^{-3} hydrochloric acid. The ionic strength of the aqueous phase was maintained at 0.3 and 0.15 with sodium chloride for the study of the adsorption isotherm and the distribution ratio respectively. After equilibration, the phoshate concentrations were determined spectrophotometrically by the molybdenum blue method on both aqueous and resin phases, the latter being analyzed on the eluate with 2 mol dm^{-3} sodium hydroxide.[3] The percentages of the recovery of phosphate found in the adsorbent and in the aqueous phase against the initial phosphate concentration were 97.0 to 103%, with an average of 99.72±1.27% for 170 measurements.

The distribution ratio, D, of phosphate between the aqueous phase and the adsorbent is expressed as $D=Q/C_p$, where C_p and Q represent the phosphate-ion concentrations in the aqueous phase(mol dm^{-3}) and in the adsorbent(mmol g^{-1} of dry adsorbent) respectively. While the wet adsorbent was used throughout the experiment, the corrections were made for the dry-adsorbent base by taking into account the water content of each wet adsorbent.

Instruments. A TOA HM-5A pH meter was used for the pH measurements, while a Shimadzu MPS-50L spectrophotometer was used for the absorbance measurements.

Results and Discussion

Adsorption Isotherms. The effect of the iron(III) concentration of the resin, C_{Fe}, on the adsorption isotherms of phosphate at 35 °C is shown in Figs. 1(at pH

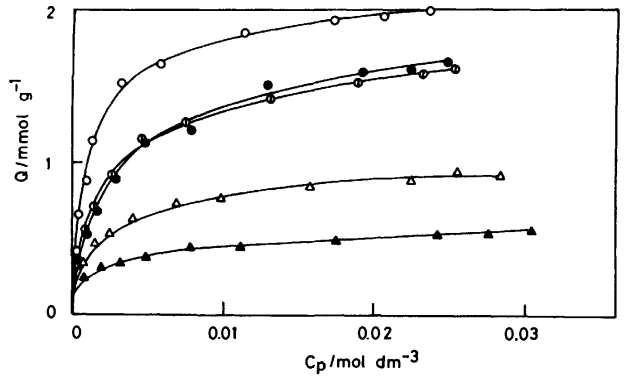

Fig. 1. Adsorption isotherms of phosphate ion by IRC-Fe(III) at 35 °C. pH 3, I=0.3.
—○—: C_{Fe}=1.97 mmol g^{-1}, —●—: 1.81, —◑—: 1.64, —△—: 0.950, —▲—: 0.726.

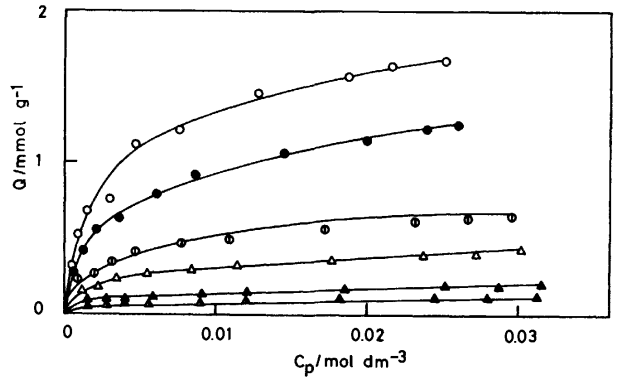

Fig. 2. Adsorption isotherms of phosphate ion by IRC-Fe(III) at 35 °C. pH 4.6, I=0.3.
—○—: C_{Fe}=1.97 mmol g^{-1}, —●—: 1.75, —◑—: 1.34, —△—: 0.993, —▲—: 0.469, —◭—: 0.323.

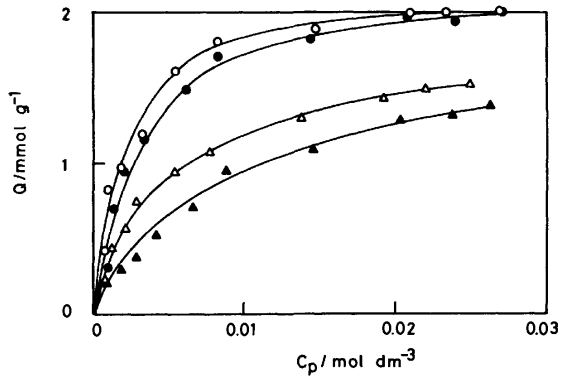

Fig. 3. Adsorption isotherms of phosphate ion by IRC-Fe(III) (C_{Fe}=1.97 mmol g^{-1}). I=0.3.
—○—: 20 °C, pH 3, —●—: 5 °C, pH 3, —△—: 20 °C, pH 4.6, —▲—: 5 °C, pH 4.6.

3) and 2(at pH 4.6). The adsorbed phosphate concentration, Q, increased with an increase in the concentration of iron in the resin, C_{Fe}, and of the phosphate ion in the aqueous phase, C_P, approaching the saturation point at higher phosphate concentrations. The value of Q also increased with a rize in the temperature in the range from 5 to 35 °C as is shown in Figs. 1 to 3.

Thus, the adsorption of phosphate is attributable to

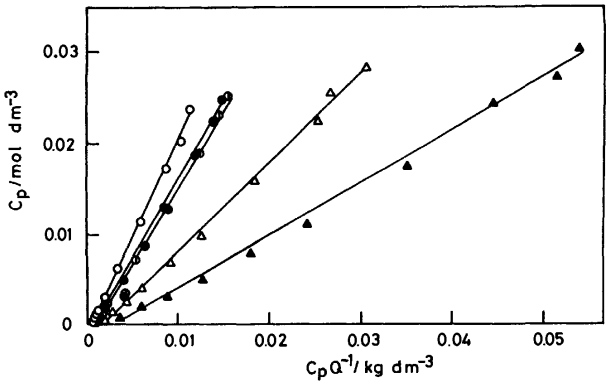

Fig. 4. C_p *vs.* C_p/Q plots on the adsorbent of different iron(III) concentration at 35 °C. pH 3, I=0.3.
—○—: C_{Fe}=1.97 mmol g^{-1}, —●—: 1.81, —◑—: 1.64, —△—: 0.950, —▲—: 0.726.

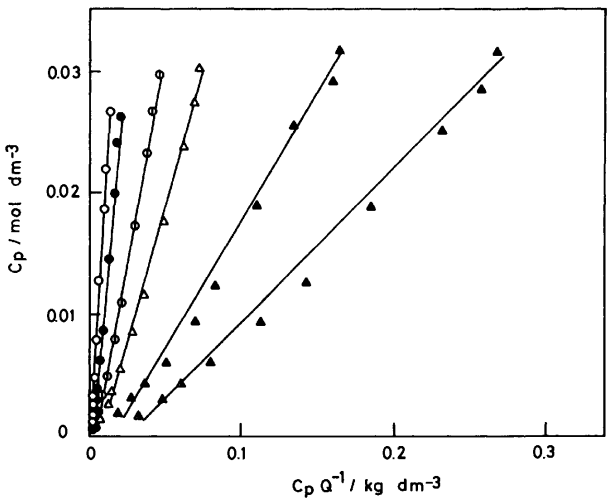

Fig. 5. C_p *vs.* C_p/Q plots on the adsorbent of different iron(III) concentration at 35 °C. pH 4.6, I=0.3.
—○—: C_{Fe}=1.97 mmol g^{-1}, —●—: 1.75, —◑—: 1.34, —△—: 0.993, —▲—: 0.469, —◭—: 0.323.

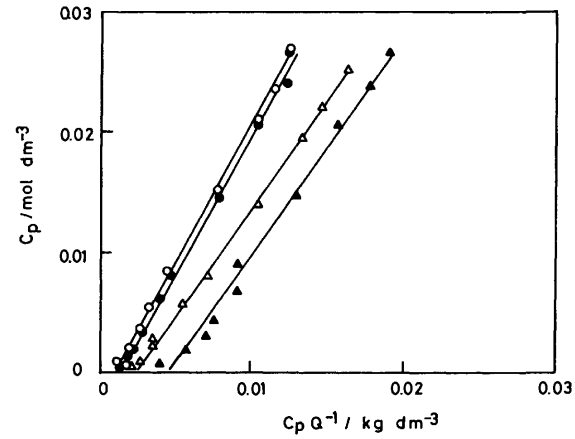

Fig. 6. C_p *vs.* C_p/Q plots on the adsorbent of C_{Fe}= 1.97 mmol g^{-1}. I=0.3.
—○—: 20 °C, pH 3, —●—: 5 °C, pH 3, —△—: 20 °C, pH 4.6, —▲—: 5 °C, pH 4.6.

the ligand-exchange reaction of phosphate with the coordinated water on the resin-bound iron(III), as has been reported previously.[2] Accordingly, the adsorp-

Table 1. Adsorption parameters for phosphate by various IRC-Fe(III)

Temp °C	pH	C_{Fe} mmol g^{-1}	Q_∞ mmol g^{-1}	K dm^3 mol^{-1}	$Q_\infty C_{Fe}^{-1}$
35	3	1.97	1.97±0.04	618±41	1.00±0.02
20	3	1.97	1.99±0.04	478±19	1.01±0.02
5	3	1.97	2.19±0.09	240±11	1.11±0.05
35	3	1.81	1.78±0.05	400±12	0.983±0.03
35	3	1.64	1.69±0.02	548±14	1.03±0.01
35	3	0.950	0.979±0.016	518±18	1.03±0.02
35	3	0.726	0.578±0.010	481±18	0.796±0.014
35	4.6	1.97	1.87±0.03	294±25	0.949±0.015
20	4.6	1.97	1.76±0.03	239±15	0.893±0.015
5	4.6	1.97	1.81±0.06	111±10	0.918±0.03
35	4.6	1.75	1.39±0.03	265±24	0.793±0.015
35	4.6	1.34	0.692±0.012	309±30	0.516±0.009
35	4.6	0.993	0.440±0.010	293±38	0.443±0.010
35	4.6	0.469	0.204±0.000	292±35	0.435±0.000
35	4.6	0.323	0.123±0.003	285±34	0.381±0.009

tion isotherms can be treated by the linearized adsorption equation 1(in this equation, Q_∞ and K are the concentration of the saturated adsorbed phosphate and the equilibrium constant for the adsorption reaction respectively):

$$C_p = Q_\infty(C_p/Q) - 1/K. \quad (1)$$

Thus, the plots of C_P against C_P/Q should give a straight line with an intercept of $-1/K$ and a slop of Q_∞. Such plots, corresponding to Figs. 1 to 3, are shown in Figs. 4 to 6 respectively. The values of K and Q_∞ were evaluated from these plots by the least-squares method; the results are summarized in Table 1.

In the experiment at pH 3, the concentration, Q_∞, increased with the increase in the iron(III) concentration, C_{Fe}, while the molar ratio Q_∞/C_{Fe} was nearly equal to unity over the range from C_{Fe}=0.726 to 1.97, indicating that the resin-bound iron(III) is the adsorption site for phosphate. The adsorption equilibrium constant, K, was found to be from 400 to 618 at 35 °C, irrespective of the value of C_{Fe}.

In the experiment at pH 4.6, the value of Q_∞ also increased with the increase in C_{Fe}, but the molar ratio of Q_∞/C_{Fe} was smaller than unity at lower iron concentrations and approached unity with the increase in the iron concentration. The value of K was, in this case, evaluated as from 265 to 309 at 35 °C, irrespective of the value of C_{Fe}.

If one considers the molecular structure of Amberlite IRC-50, which is a cross-linked poly(acrylic acid), the different behavior of the adsorbent at pH 3 and 4.6 may be explained by the presence of free carboxyl groups in the adsorbent of a lower iron concentration. In the pH 3 region, these carboxyl groups remained undissociated, having little interaction with the resin-bound iron. At pH 4.6, however, the carboxyl groups, after deprotonation, became available for coordination to the resin-bound iron, giving the negatively charged tetracoordinated iron sites, which are not capable of ligand exchange with phosphate. The lower the iron concentration in the resin, the larger the fraction of inactivated adsorption sites in this pH region.

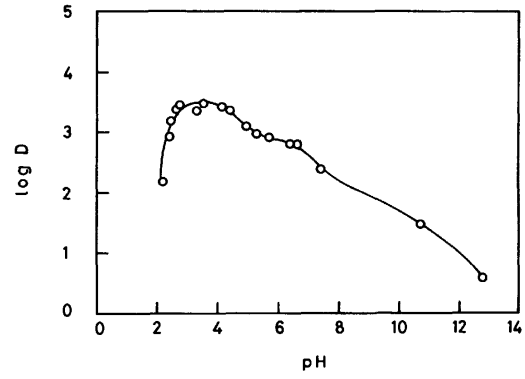

Fig. 7. pH profile of distribution ratio, D, of phosphate ion by IRC-Fe(III)(C_{Fe}=1.97 mmol g^{-1}) at 35 °C. I=0.15.

Effect of Temperature. It may be seen from Figs. 1 to 3 that the Q value increases with the rize in the temperature, while the Q_∞ value remains almost constant over the temperature range from 5 to 35 °C, as shown in Table 1. Thus, the increase in the Q value may be said to be due to the increase in the K value in this temperature range.

Effect of pH on the Distribution Ratio. The distribution ratio of phosphate, D, at 35 °C on IRC-Fe(III)(C_{Fe}=1.97 mmol g^{-1}) was markedly dependent upon the pH of the aqueous phase, as is illustrated in Fig. 7. In this experiment, the pH of the aqueous phase was adjusted with hydrochloric acid and sodium hydroxide, while the concentration of the phosphate ion in the aqueous phase, C_p, was kept in the range from 9.04×10^{-5} to 1.90×10^{-3} mol dm^{-3} (2.8 to 59 ppm) after equilibration to make Q considerably less than Q_∞.

It may be seen from Fig. 7 that the adsorption of the phosphate ion is most appreciable in the pH range from 2.5 to 4.0. The D value rapidly decreases beyond this optimum pH range. The pH profile of the distri-

bution ratio is similar to that of UR10-Fe(III) reported previously,[2] whereas the D values of IRC-Fe(III) are about twenty times larger than those of UR10-Fe(III).

The decrease in the D value in the pH region below 2.5 may be ascribed to the increasing concentration of phosphoric acid(H_3PO_4, pK_{a1}=2.1), which is not adsorbed on the resin, while that in the pH range above 4.0 may be due to the protolysis of hydrated water on the resin-bound iron.

Comparison of Adsorption Behavior of IRC-Fe(III) with That of UR10-Fe(III). In both adsorbents, the Q_∞ value increased with an increase in the C_{Fe} value, indicating that the resin-bound iron is the adsorption site of the phosphate ion. However, in the case of UR10-Fe(III), Q_∞/C_{Fe} decreased from 1.08 to 0.61 when C_{Fe} increased from 0.12 to 1.34 mmol g^{-1} at pH 6; this behavior was explained by the electrostatic and spatial interaction of the phosphate ion in the adsorbent with high C_{Fe} value. On the other hand, Q_∞/C_{Fe} remained unity regardless of the C_{Fe} value(0.726 to 1.97 mmol g^{-1}) at pH 3, while it increased from 0.381 to 0.949 with an increase in the C_{Fe} value from 0.323 to 1.97 mmol g^{-1} at pH 4.6. This behavior is opposite to that of UR10-Fe(III) at pH 6. The different behavior of IRC-Fe(III) in comparison with that of UR10-Fe(III) is presumably caused by the different nature of the resin matrices; that of the former and that of the latter being MR-type and gel-type respectively.

References

1) Part V: I. Yoshida, M. Nishimura, K. Matsuo, and K. Ueno, *Sep. Sci. Tech.*, **18**, 73 (1983).
2) R. Takeshita, I. Yoshida, and K. Ueno, *Bull. Chem. Soc. Jpn.*, **52**, 2577 (1979).
3) I. Yoshida, R. Takeshita, and K. Ueno, *Nippon Kagaku Kaishi*, **1980**, 220.

Proton Chemical Shift Study of the Hydrophobic Interaction between Tris(1,10-phenanthroline)ruthenium(II) Ions in Aqueous Solutions

Yuichi MASUDA and Hideo YAMATERA*,†
Department of Chemistry, Faculty of Science, Nagoya University, Chikusa-ku, Nagoya 464
(Received June 18, 1983)

The proton NMR chemical shifts were measured in the D_2O solutions of $[Ru(phen)_3]SO_4$. The proton resonances of the phenanthroline ligand showed up-field shifts with increasing concentration of $[Ru(phen)_3]SO_4$, but they were not significantly affected by the addition of Na_2SO_4. The profile of the up-field shifts for the *Λ*-$[Ru(phen)_3]SO_4$ solution was different from that for the *rac*-$[Ru(phen)_3]SO_4$ solution. These results prove that the up-field shifts were caused by the interaction between $[Ru(phen)_3]^{2+}$ ions. Assuming the formation of the triple and quadrupole aggregates containing two $[Ru(phen)_3]^{2+}$ ions, the association constants of these aggregates and the up-field shifts of the proton signals in the aggregates were determined. A probable structure of the aggregates was deduced from the measured chemical shifts by attributing the up-field shift in the aggregates to the ring-current effect of the phenanthroline ligand. The importance of the hydrophobic interaction between $[Ru(phen)_3]^{2+}$ ions in aqueous solution was thus indicated.

Tris(1,10-phenanthroline) complex ions of bivalent metals, $[M(phen)_3]^{2+}$, are known to be hydrophobic with respect to their hydration[1,2] and also with respect to their interaction with hydrophobic anions in aqueous solutions.[3,4] The ion-pair between the complex cation and the alkanesulfonate anion shows an anomalously large ion-association constant[3] and has a structure which demonstrates the importance of the hydrophobic interaction between these ions.[4] Moreover, the $[Fe(phen)_3]^{2+}$ ions interact with alkyltrimethylammonium ions of a large alkyl group to form cation-cation pairs in aqueous solutions.[5] These findings suggest that the hydrophobic nature of the phenanthroline ligands might cause some mutual interaction between the ions of the $[M(phen)_3]^{2+}$type.

The object of the present study is to investigate how the $[M(phen)_3]^{2+}$ ions interact with each other. We observed the proton NMR of the 1,10-phenanthroline ligand of $[Ru(phen)_3]^{2+}$in aqueous solutions; evidence was obtained for a noticeable cation-cation interaction and information was gained about the structure of the aggregate containing two $[Ru(phen)_3]^{2+}$ ions.

Experimental

Materials. The preparation of tris(phenanthroline)-ruthenium(II)[6] and -cobalt(III)[7] chlorides and optical resolution for obtaining *Λ*-$[Ru(phen)_3]^{2+}$[8] were performed by the literature methods. The sulfate of each metal complex was obtained by double decomposition of Ag_2SO_4 and the chloride of the complex.

NMR Measurements. The ^1H NMR spectra were obtained on a JEOL FX-100 Fourier-transform spectrometer operating at 100 MHz with the D_2O and CD_3OD solutions of $[M(phen)_3](SO_4)_n$ (M=Ru(II) and Co(III)) at 28.0±0.5 °C. The chemical shifts, δ, were measured in ppm down-field from the central peak of the triplet resonance of the tetramethylammonium ion, which was added in the form of the nitrate as the internal reference. The concentration of the tetramethylammonium ion was 1/20 of that of the metal complex ion. The sample solutions for measuring NMR were prepared as follows. The sulfate of the metal complex was dissolved in D_2O and dried up by a rotary evaporator at room temperature. This procedure was repeated. The resulting complex salt was dissolved in D_2O. The methanol solutions were prepared in a similar manner, with CD_3OD in place of D_2O.

† Adjunct Professor of the Institute of Molecular Science, Okazaki (April 1981—March 1983).

Results and Discussion

Effect of the Ion-Ion Interaction on the Proton Chemical Shifts of the Ligands in $[Ru(phen)_3]^{2+}$. Figure 1 shows the representative examples of the proton NMR spectrum for the phenanthroline ligand of $[Ru(phen)_3]SO_4$ in D_2O. Different profiles of the spectra are found for different concentrations of the complex salt. The concentration dependence of the chemical shift was greatest for protons in the 5 and 6 positions. The dependences of the proton shifts on the concentration of $[Ru(phen)_3]SO_4$ in D_2O and CD_3OD are quantitatively shown in Fig. 2, where $\Delta\delta$ indicates the down-field shift with reference to each δ value at infinite dilution, $\delta(0)$. Each proton signal of the phenanthroline ligand of $[Ru(phen)_3]^{2+}$ in D_2O showed monotonous up-field shifts with increasing concentration of $[Ru(phen)_3]SO_4$. The magnitude of the up-field shifts increased in the order of the 2,9<3,8<4,7<5,6 positions of the protons.

If these up-field shifts were caused by the interaction with the sulfate ion, a similar change of the proton shifts of the phenanthroline ligands should be observed when Na_2SO_4 are added to the solution of $[Ru(phen)_3]SO_4$. However, only slight changes were observed in the proton shifts on the addition of Na_2SO_4 (up to about 0.25 mol dm^{-3}) to 0.0025 mol dm^{-3} $[Ru(phen)_3]SO_4$ solution in D_2O (Fig. 2, ◑). This indicates that the up-field shifts with the increase in the concentration of $[Ru(phen)]_3]SO_4$ (Fig. 2, ●) are not due to the interaction with the sulfate ion.

Then the change in the proton shifts may have arisen from interaction of $[Ru(phen)_3]^{2+}$ ions with each other.

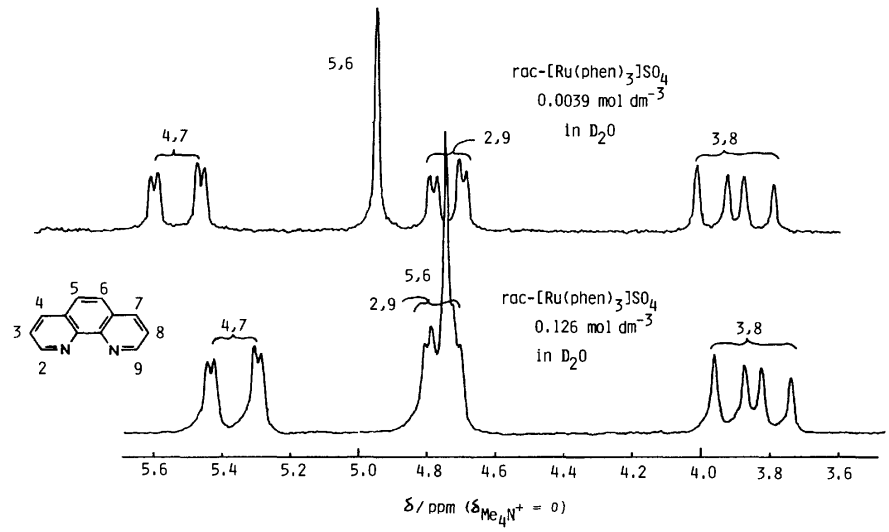

Fig. 1. ^1H NMR spectra of *rac*-$[Ru(phen)_3]SO_4$ in D_2O. (A) 0.0039 mol dm^{-3}. (B) 0.126 mol dm^{-3}. The chemical shift, δ, represents the down-field shift from the proton resonance of Me_4N^+.

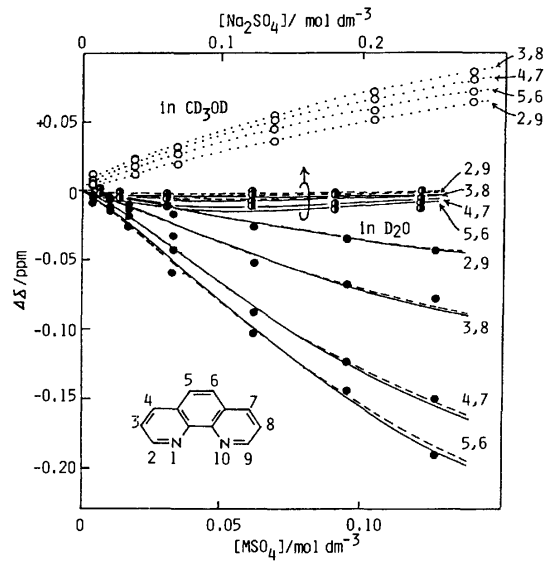

Fig. 2. Plots of the $\Delta\delta$ values *vs.* the concentration of *rac*-$[Ru(phen)_3]SO_4$ in D_2O (●) and in CD_3OD (○), and *vs.* the concentration of Na_2SO_4 added to 0.0025 mol dm^{-3} *rac*-$[Ru(phen)_3]SO_4$ in D_2O (◑). Broken and solid lines indicate the $\Delta\delta$ values calculated with the $\Delta\delta_{t,a}$ values for ion-size parameters, $a=10$ and 12 Å, respectively (Table 1).

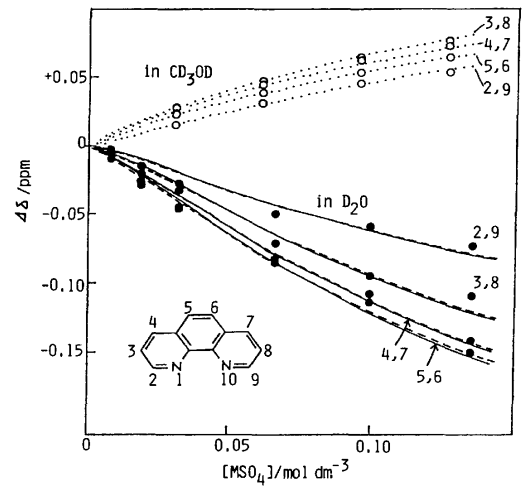

Fig. 3. Plots of the $\Delta\delta$ values *vs.* the concentration of *Λ*-$[Ru(phen)_3]SO_4$ in D_2O (●) and in CD_3OD (○). Broken and solid lines indicate the $\Delta\delta$ values calculated with the $\Delta\delta_{t,a}$ values for ion-size parameters, $a=10$ and 12 Å, respectively (Table 1).

Hydrophobic interaction between the ions may outweigh the coulombic repulsion between them. In order to confirm this, the proton shifts of the phenanthroline ligand were measured with optically active *Λ*-$[Ru(phen)_3]SO_4$ at various concentrations in D_2O (Fig. 3, ●). While the trend of the changes in the proton shifts of *Λ*-$[Ru(phen)_3]SO_4$ is similar to that for *rac*-$[Ru(phen)_3]SO_4$, the magnitudes of the changes are distinctly different. This difference between the racemate and the optical isomer indicates that these up-field shifts are caused by the interaction between two $[Ru(phen)_3]^{2+}$ ions. Either the manner of their interaction or the equilibrium constant for the aggregate formation may differ between the aggregate of a *Δ* and a *Λ*-$[Ru(phen)_3]^{2+}$ ion and that of two *Λ* ions. A further discussion of this problem will be given below.

In the CD_3OD solution of $[Ru(phen)_3]SO_4$, on the other hand, the proton resonances of the phenanthroline ligands (Fig. 2, ○) showed small down-field shifts with increasing concentration of the complex salt, and no meaningful differences were detected between the *Λ* isomer and the racemate. The D_2O solutions of $[Co(phen)_3](SO_4)_{3/2}$ showed only slight down-field shifts (within 0.02 ppm) when the concentration of the complex salt increased up to 0.1 mol dm^{-3} and when Na_2SO_4 was added up to 0.25 mol dm^{-3}. These results indicate that no significant short-range interaction exists

between the metal complex ions in these solutions. The stronger electrostatic repulsion between the complex cations in methanol solutions and that between the tripositive cations of the cobalt complex most probably prevented the complex ions from approaching each other.

Quantitative Treatment of the Proton Chemical Shifts. For the quantitative treatment of the proton shifts of $[Ru(phen)_3]SO_4$ in D_2O, the equilibria between chemical species existing in the solution are considered. The $[Ru(phen)_3]^{2+}$ ion forms the 1:1 ion-pair with the sulfate ion:

$$M + X \rightleftharpoons MX, \tag{1a}$$

where M, X, and MX indicate the $[Ru(phen)_3]^{2+}$ ion, the sulfate ion, and their ion-pair, respectively. The ion association constant at infinite dilution, K, is expressed by:

$$K = \frac{[MX]}{y_M y_X [M][X]}, \tag{1b}$$

where y_M and y_X represent the activity coefficient of each species. Among the species containing two $[Ru(phen)_3]^{2+}$ ions, the aggregate only of two $[Ru(phen)_3]^{2+}$ ions, M_2, is less probable than the triple ions, M_2X, and the quadrupole ions, M_2X_2, because of the large coulombic repulsion between the ions. Thus, the formation of the M_2 ion-pair is disregarded here. Equilibria and equilibrium constants for M_2X and M_2X_2 are:

$$MX + M \rightleftharpoons M_2X, \tag{2a}$$

$$K_t = \frac{y_{M_2X}[M_2X]}{y_M[MX][M]}, \tag{2b}$$

$$M_2X + X \rightleftharpoons M_2X_2, \tag{3a}$$

$$K' = \frac{[M_2X_2]}{y_X y_{M_2X}[M_2X][X]}, \tag{3b}$$

$$2MX \rightleftharpoons M_2X_2, \tag{4a}$$

$$K_q = \frac{[M_2X_2]}{[MX]^2}. \tag{4b}$$

The following relation exists between the four association constants:

$$\frac{K_q}{K_t} = \frac{K'}{K}. \tag{5}$$

For the sake of simplicity, we assume that the value of K' is equal to K. This assumption is justified as an approximation if the ion association in Eqs. 1a and 3a is caused by electrostatic interaction. Since both K and K' are association constants between dipositive and dinegative ions, it can be expected that their values are nearly equal. Substituting $K'=K$ in Eq. 5, we obtain $K_t=K_q$. This result is also reasonable even if hydrophobic interaction between two $[Ru(phen)_3]^{2+}$ ions is involved in the aggregation shown by Eqs. 2a and 4a. Similar results were obtained by Yokoyama and Yamatera by measuring the vapor pressure of aqueous $[Ru(phen)_3]SO_4$ solutions.[9]

Next, we consider the $\Delta\delta$ value for each aggregate. As shown in Fig. 2, the addition of sodium sulfate had only trivial effects on the proton shifts of $[Ru(phen)_3]^{2+}$. Therefore, we assume that the change in each proton chemical shift of the $[Ru(phen)_3]_2^{+}$ ion in D_2O is solely caused by the interaction between the $[Ru(phen)_3]^{2+}$ ions. We further assume for simplicity's sake that the $\Delta\delta$ values are the same for M_2X and M_2X_2 and denote them by $\Delta\delta_{t,q}$. This assumption is justified if the formation of these aggregates is essentially caused by the hydrophobic interaction between the $[Ru(phen)_3]^{2+}$ ions. Then, the observed $\Delta\delta$ value is represented by:

$$\Delta\delta = (x_t + x_q)\Delta\delta_{t,q}. \tag{6}$$

Here x_t and x_q denotes the mole fractions of $[Ru(phen)_3]^{2+}$ existing in the forms of the M_2X and M_2X_2 aggregates, respectively, defined by:

$$x_t = 2[M_2X]/c_M \text{ and } x_q = 2[M_2X_2]/c_M,$$

where c_M is the total concentration of $[Ru(phen)_3]^{2+}$.

If the K value (Eq. 1b) is known,[9] we have here two unknown parameters, $\Delta\delta_{t,q}$ and K_t ($=K_q$). (The activity coefficient, y, was calculated with the Debye-Hückel equation). The unknown parameters for the racemic solution, $K_t(rac)$ ($=K_q(rac)$) and $\Delta\delta_{t,q}(rac)$ and those for the Λ-isomer solution, $K_t(\Lambda)$ ($=K_q(\Lambda)$) and $\Delta\delta_{t,q}(\Lambda)$ were determined so as to give the best fit to the measured proton shifts for the racemic and the Λ-isomer solutions, respectively. The association constant obtained for the racemic solution, $K_t(rac)$ ($=K_q(rac)$), was practically identical with that for the Λ-isomer solution, $K_t(\Lambda)$ ($=K_q(\Lambda)$). The *rac*-$[Ru(phen)_3]SO_4$ solution contains two chemically different species of paired $[Ru(phen)_3]^{2+}$ ions, Λ-Λ and Λ-Λ (or Δ-Δ). The approximate equality of $K_t(rac)$ and $K_t(\Lambda)$ indicates that no significant difference exists between the values of the association constants for the Δ-Λ pair ($K_t(\Delta$-$\Lambda)$) and for the Λ-Λ pair ($K_t(\Lambda$-$\Lambda)$). This gives the relation:

$$\Delta\delta_{t,q}(rac) = (1/2)[\Delta\delta_{t,q}(\Delta\text{-}\Lambda) + \Delta\delta_{t,q}(\Lambda\text{-}\Lambda)]. \tag{7}$$

With Eq. 7, we obtained the $\Delta\delta_{t,q}(\Delta$-$\Lambda)$ value from the experimental values of $\Delta\delta_{t,q}(rac)$ and $\Delta\delta_{t,q}(\Lambda)$($=\Delta\delta_{t,q}$-$(\Lambda$-$\Lambda)$). Table 1 summarizes the association constants and the chemical-shift changes for M_2X and M_2X_2 in each case, where the ion-size parameter (a) in Debye-Hückel equation is assumed to be 10 or 12 Å[10] (1 Å= 10^{-10} m). The values in Table 1 were used to calculate the gross $\Delta\delta$ values for each solution (broken and solid lines in Figs. 2 and 3).

In the case of the Δ-Λ aggregate, the proton up-field shifts strongly depend on the position of the proton in the phenanthroline ligand; the magnitude of the up-field shifts increases in the order of 2,9<3,8<4,7<5,6. For the Λ-Λ aggregate, the up-field shifts were less strongly dependent on the position of the proton, although the order was the same as the Δ-Λ case. These results can be taken as the evidence for the operation of short-range interaction between the cations.

The Structure of the Aggregate Containing Two [Ru(phen)$_3$]$^{2+}$ Ions. The up-field shifts in the M_2X and M_2X_2 aggregates probably result from the ring-current effect[11] of the phenanthroline ligand. Such up-field shifts were previously observed for the ^{13}C chemical shifts of the hexanesulfonate ion in the ion-pair with the $[Fe(phen)_3]^{2+}$ ion,[4] and on the methyl proton shift of the amino acid with a large alkyl group in a mixed-ligand Zn(II) complex containing phenanthroline.[12] If

TABLE 1. THE UP-FIELD SHIFTS OF THE PROTONS IN THE M_2X AND M_2X_2 AGGREGATES AND THE ASSOCIATION CONSTANTS FOR THESE AGGREGATES (28 °C)

	$K(=K')$/mol^{-1} dm^3	$K_t(=K_q)$/mol^{-1} dm^3			$-\Delta\delta_{t,q}$/ppm			
a/Å[a]	Lit[b]	This work	Lit[b]	M^{2+}-M^{2+}	2.9	3.8	4.7	5.6
10	25	5	5	Δ-Δ	0.18	0.49	0.96	1.11
				Λ-Λ	0.21	0.30	0.38	0.40
12	40	4	3	Δ-Δ	0.13	0.40	0.83	1.06
				Λ-Λ	0.17	0.25	0.32	0.34

a) Ion size parameter. b) Ref. 10.

the ring-current effect is responsible for the up-field shifts, the proton of a $[Ru(phen)_3]^{2+}$ ion placed just above the aromatic rings of a phenanthroline ligand of another $[Ru(phen)_3]^{2+}$ ion will show the largest up-field shift, and increasing distance from this position will decrease the magnitude of the shift. Thus, the difference in the up-field shifts between the Δ-Δ and the Λ-Λ aggregate reflects the difference in the configuration between them. This result is similar to Yamagishi's recent report that the arrangement of the Λ-$[Fe(phen)_3]^{2+}$ ions adsorbed on soil from a solution of the Λ isomer is largely different from the alternate arrangement of the Δ and Λ ions adsorbed from a solution of the racemate.[13]

We first consider the aggregate containing the Λ and Δ complex ions. In the M_2X or M_2X_2 aggregate, the 5 and 6 protons with the largest up-field shifts are considered to be placed closest to the position just above the aromatic rings of a phenanthroline ligand of the other $[Ru(phen)_3]^{2+}$ ion and the other protons are farther from that position in the order of 5,6<4,7<3,8 <2,9. Figure 4 shows a probable configuration of two $[Ru(phen)_3]^{2+}$ ions in the aggregate, where the edge of a phenanthroline ligand (**A**) of one $[Ru(phen)_3]^{2+}$ ion is placed in an opening between two phenanthroline ligands of the other $[Ru(phen)_3]^{2+}$ ion. Then the 5 and 6 protons of the **A** phenanthroline ligand are considerably influenced by the ring-current of those two phenanthroline ligands. Either the 4 or the 7 proton of the **A** phenanthroline ligands is placed above one of those phenanthroline ligand and none of the 2, 3, 8, and 9 protons are placed above them. The same applies to the protons of the **B** phenanthroline ligand.

For estimating the up-field shifts of the 5 and 6 protons, we assumed that the ring-current effect of phenanthroline is approximated by that of phenanthrene. Then, Hazato's theory[14] predicts an up-field shift of 4.1—4.3 ppm for the 5 and 6 protons of the **A** and **B** ligands.[15] Since only a single signal was observed for the 5 and 6 protons (Fig. 1), the observed chemical shift corresponds to the average over six equivalent protons of $[Ru(phen)_3]^{2+}$. Then, assuming that the proton chemical shifts of the ligands other than the **A** or **B** ligand are not affected by the aggregate formation, the average up-field shift of the 5 and 6 protons was estimated to be about 1.4 ppm. The experimental value of about 1.1 ppm (Table 1) shows a reasonable agreement with this value; the small difference may be explained if the aggregate does not always take the optimum configuration. Such flexibility of the configuration will also explain the small but appreciable up-field shifts for the 2, 3, 8, and 9 protons in the aggregate.

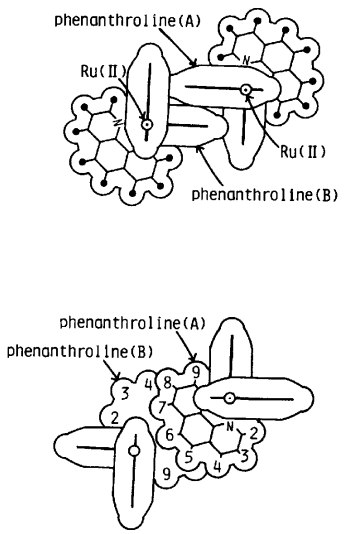

Fig. 4. Probable configuration of a pair of Λ- and Δ-$[Ru(phen)_3]^{2+}$ ions in the M_2X and M_2X_2 aggregates: the elevation (top) and the plan (bottom).

The up-field shifts of the protons of the Λ-Λ aggregate span an obviously narrower range than spanned by those of the Δ-Λ aggregate. This may indicate that the configuration of the Λ-Λ aggregate is more labile and/or more manifold than that of the Δ-Λ one. Actually, examinations with the CPK model demonstrated that a well-fitted structure like that shown in Fig. 4 is not possible for the Λ-Λ aggregate because of the steric hindrance between the phenanthroline ligands.

This work was carried out as a Cooperative Research (1982) of the Institute for Molecular Science. The authors thank the Ministry of Education, Science and Culture for the support of this work (Grant-in-Aid for Scientific Research No. 56470039).

References

1) G. Wada, E. Nagao, N. Kawamura, and K. Kinumoto, *Bull. Chem. Soc. Jpn.*, **51**, 1937 (1978).
2) Y. Yamamoto, T. Tominaga, and S. Tagashira, *Inorg. Nucl. Chem. Lett.*, **11**, 825 (1975).
3) S. Tachiyashiki and H. Yamatera, *Chem. Lett.*, **1981**,

1681.

4) Y. Masuda, S. Tachiyashiki, and H. Yamatera, *Chem. Lett.*, **1982**, 1065.

5) S. Tachiyashiki and H. Yamatera, *Bull. Chem. Soc. Jpn.*, **55**, 759 (1982).

6) P. Pfeiffer and B. Werdelmann, *Z. Anorg. Chem.*, **263**, 31 (1950).

7) F. H. Burstall, *J. Chem. Soc.*, **1936**, 173.

8) K. Sasaki and H. Yamatera, *Radiochim. Acta*, **31**, 121 (1982).

9) H. Yokoyama and H. Yamatera, *Bull. Chem. Soc. Jpn.*, **48**, 2708 (1975).

10) The sum of the ionic radii of the $[Ru(phen)_3]^{2+}$ ion and the sulfate ion is about 10.1 Å.

11) L. Jackman, "Application of Nuclear Magnetic Resonance Spectroscopy in Organic Chemistry," Pergamon Press, London (1959), Chap. 7.

12) B. E. Fischer and H. Sigel, *J. Am. Chem. Soc.*, **102**, 2998 (1980); H. Sigel, *Angew. Chem., Int. Ed. Engl.*, **21**, 389 (1982).

13) A. Yamagishi, *J. Phys. Chem.* **86**, 2472 (1982).

14) G. Hazato, *J. Chem. Phys.*, **27**, 605 (1957).

15) The distance of a proton from the plane of the phenanthroline is taken as 2.8 Å, which is the sum of half the thickness of the phenanthroline molecule and the Van der Waals radius of the hydrogen atom.

 © 1984 The Chemical Society of Japan Bull. Chem. Soc. Jpn., 57, 63—67 (1984)

Synthesis and Physicochemical Properties of Dioxathia[*n*]ferrocenophanes

Sadatoshi Akabori,* Sumio Shibahara, Yoichi Habata, and Masaru Sato†
Department of Chemistry, Fuculty of Science, Toho University, Funabashi, Chiba 274
†*Chemical Analysis Center, Saitama University, Urawa, Saitama 338*
(Received April 23, 1983)

The reaction of 1,1′-bis(2-chloroethoxy)ferrocene with 1,2-ethanedithiolate in absolute ethanol gave mononuclear 1,10-dioxa-4,7-dithia[10]ferrocenophane and binuclear 1,10,21,30-tetraoxa-4,7,24,27-tetrathia-[10,10]ferrocenophane, along with a small amount of unexpected 1,13-dioxa-4,7,10-trithia[13]ferrocenophane and 1,16-dioxa-4,7,10,13-tetrathia[16]ferrocenophane. Extraction of aqueous metal picrates (M; alkali, alkaline earth, Ag^+, Tl^+, Cd^{2+}, Co^{2+}, Cu^{2+}, Ni^{2+}, and Hg^{2+}) with dioxathia[*n*]ferrocenophanes was examined and also with the corresponding ring membered polyoxa[*n*]ferrocenophanes. Dioxathiaferrocenophanes showed a highly selective extraction ability towards bivalent mercury and copper ions.

While investigations of crown ethers and their cation complexes have been steadily gaining interest during the past decade, most attention has been focused so far on the synthesis of a new type of ligand.[1] The preparation and physicochemical properties of several kinds of polyoxa- and polythia[*n*]ferrocenophanes (**1**—**4**) have been previously reported.[2-7] It was shown that some of these compounds, particularly those containing five and six heteroatoms in the macrocyclic ring, form complexes with alkali-metal, thallium, and silver cations. Many methods for the synthesis of polythiacrown ethers have been reported.[8-11] However, with the exception of thioformaldehyde polymerization,[12] all other methods of thioether ring closure were based on α-mercaptide displacement of ω-halide function. We wish here to report a novel finding concerning the synthesis and extraction ability of dioxathia[*n*]ferrocenophanes.

Synthesis and Structure. The following reactions were carried out in order to obtain 1,1′-bis(2-mercaptoethoxy)ferrocene (**6**) as a starting material. 1,1′-Bis(2-chloroethoxy)ferrocene (**5**) was readily synthesized by reaction of the disodium salt of 1,1′-ferrocenediol, which was prepared by the hydrolysis of 1,1′-diacetoxyferrocene, with large excess of 1-bromo-2-chloroethane. An attempt to convert **5** into the corresponding dithiol (**6**) by a reaction with sodium hydrogensulfide failed. Instead 1,7-dioxa-4-thia[7]ferrocenophane (**4b**) was obtained in 49% yield, doutless by incursion of the cyclization mechanism accompanying an intramolecular attack of the thiolate anion to the halogenated carbon atom.[11] Compound **4b** was found to be identical with an authentic sample[7] prepared by the reaction of **5** with sodium sulfide. Therefore, dioxathia[*n*]ferrocenophanes were prepared according to the following method.

A solution of 5 (1.0 molar equiv) in absolute ethanol was added at once to a solution of disodium 1,2-ethanedithiolate (3.0 molar equiv) in absolute ethanol and the resulting solution was stirred at refluxing temperature for 14 h. After the usual work-up, the reaction mixture was separated by silica-gel thinlayer chromatography. From the reaction mixture, mononuclear 1,10-dioxa-4,7-dithia[10]ferrocenophane (**9**) and

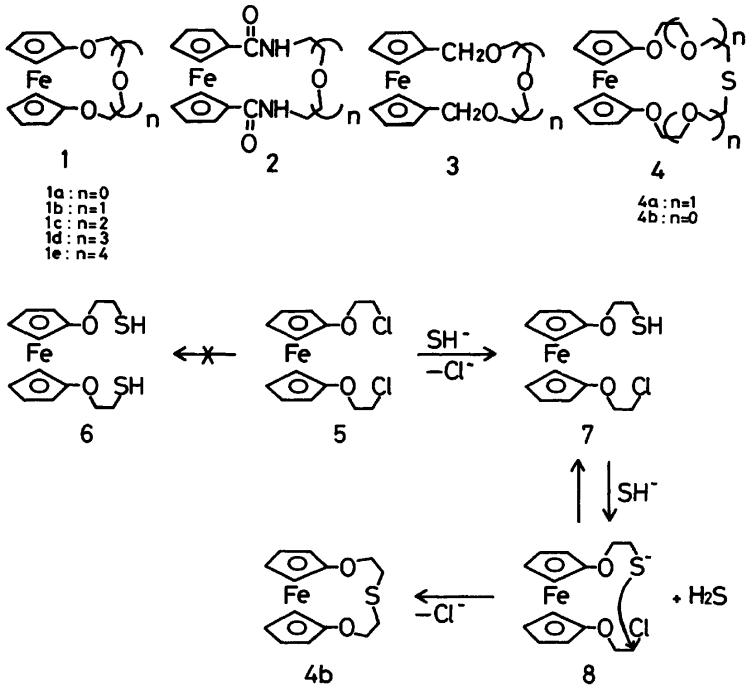

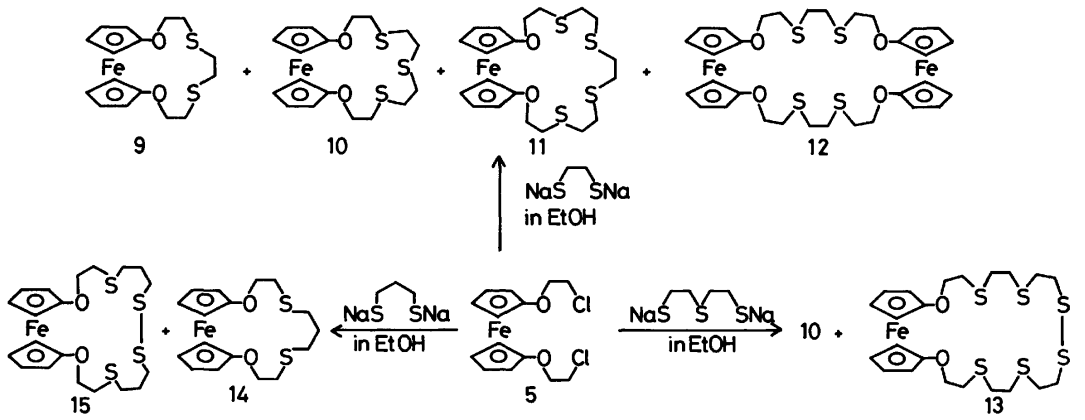

binuclear 1,10,22,31-tetraoxa-4,7,25,28-tetrathia[10.10]ferrocenophane (**12**) were obtained in 38 and 3.2% yields, respectively. Moreover, a small amount of unexpected 1,13-dioxa-4,7,10-trithia[13]ferrocenophane (**10**, 6.1%) and 1,16-dioxa-4,7,10,13-tetrathia-[16]ferrocenophane (**11**, 1.9%) were isolated.[13] When **5** was treated with equimolar of 1,2-ethanedithiol under similar conditions, compounds **9**, **10**, and **12** were obtained, although the yields of those were somewhat low and **11** could not be isolated. Interestingly, the reactions of **5** with bis(2-mercaptoethyl) sulfide did not yield the unexpected ring enlarged dioxathia[*n*]ferrocenophanes, but gave normal mononuclear ferrocenophane (**10**) and disulfide (**13**) in 51 and 2.9% yields, respectively. Such an abnormal reaction was not observed in the reaction of **5** with 1,3-propanedithiol. Isolation of the disulfide (**13** and **15**) suggest that the dithiolate, which was formed by a nucleophilic attack of two molar of 1,2-ethanedithiolate at the halogenated carbons of **5**, was easily oxidized by the trace amount of oxygen in an atmosphere of nitrogen to give the corresponding disulfide in low yield. The results obtained by the reactions of **5** with dithiols are listed in Table 1, along with the physical data of the products.

The possible mechanism of the unexpected formation of compounds **10** and **11** is shown in Scheme. The initial reaction may be a nucleophilic attack of two molar of 1,2-ethanedithiolate on the halogenated carbons of **5** to give the dithiolate **16**. The second step of the reaction is considered to be single proton elimination from the methylene next to the sulfur atom followed by elimination of S^{2-} to give the vinyl sulfide intermediate **17**. Thus, the formation of **10** can be interpreted by an intramolecular attack of $-S^-$ at the double bond followed by addition of a proton to the resulting sulfur-stabilized anion. Moreover, the addition of another disodium 1,2-ethanedithiolate to **17** would form the ferrocenophane **11** by the same mechanism. Support for this mechanism is provided by the following results. The reaction of **5** with disodium 1,3-propanedithiolate gave 1,11-dioxa-4,8-dithia[11]ferrocenophane (**14**) in 64% yield, but no abnormal product corresponding to **10** and **11**, because the dithiolate intermediate corresponding **17** in this reaction have no leaving group (S or SH) for forming a vinyl sulfide group. On the other hand, **5** reacted with the disodium salt of bis(2-mercaptoethyl) sulfide to afford

Table 1. Yield, Mp, mass spectral data of dioxapolythia[*n*]ferrocenophanes

Compd	Yield %	Mp θ_m/°C	Mass (M^+, *m/e*)
4a	49	104—106 (104—106)[7]	
9	38	115—116.6	364
10	6.1 (51)[a]	114—116	424
11	1.9	69—70	484
12	3.2	129—131	728
13	2.9	79—81	576
14	64	149—150	378
15	8.6	84—86	484

a) The value in parenthesis showed the yield obtained by the reaction of **5** with bis(2-mercaptoethyl) sulfide.

10 and **13**. This is probably due to the large ring size of the possible cyclization intermediate which would make the template effect impossible, and this can help the intramolecular nucleophilic attack to the cyclization to ferrocenophane. However, many attempts to isolate intermediates such as **17** and **18** from the reaction mixture failed. Thus, the resulting intermediates (**17** and **18**) must be unstable or too reactive and might react easily with an intermediate mercapto group.

Structural assignment of these ferrocenophanes **9**—**15** and **6** was achieved by their elemental analyses, spectral inspection, and partly on the basis of the unequivocal synthesis. In particular all of their elemental analyses were in good accord with the proposed compositions, and the IR spectra showed a cyclopentadienyl C-H absorption band at near 1485 cm^{-1}, an ether linkage band near 1015 cm^{-1} and a C-S stretching vibration band near 610 cm^{-1}. In addition to the above bands, the IR spectra of compounds **13** and **15** also showed an S-S stretching band near 490 cm^{-1}. In the ^{1}H-NMR spectra of **9**—**11**, the signal for methylene protons next to the oxygen atom appeared as a triplet (4H, J=*ca.* 6 Hz) near δ 4.10 and the signal for the methylene protons α to the sulfur atom appeared as a triplet (4H, J=*ca.* 6 Hz) near δ 2.9. The signals for the other methylene protons appeared at δ 3.03—2.62, respectively. Furthermore, ferrocene ring protons resonanced as a pair of triplets (each 4H, J=*ca.* 1.8 Hz)

Table 2. Extraction of metal picrates from the aqueous to the organic phase (%)[a)]

Compd	Li^+	Na^+	K^+	Rb^+	Cs^+	Mg^{2+}	Ca^{2+}	Sr^{2+}
4a	1.2	1.2	1.4	0.8	1.5	0.6	0.8	0.7
9	0.5	0.9	0.8	0.3	2.1	0.5	0.1	0.8
10	0.5	1.3	1.3	1.7	2.6	1.4	1.2	0.7
1d	0.5	1.5	4.5	4.6	5.6	1.2	0.5	0.4
B15C5	1.2	23.9	50.1	27.5	12.8	0.3	0.5	0.4

Compd	Ba^{2+}	Cd^{2+}	Hg^{2+}	Tl^+	Pb^{2+}	Ag^+	Cu^{2+}	Co^{2+}	Ni^{2+}
4a	0.4	0.9	,30.4	8.3	2.0	Decomp	1.9	1.1	1.1
9	1.3	0.8	38.1	1.4	1.5	Decomp	27.8	0.6	0.5
10	1.6	1.0	76.1	2.1	1.5	Decomp	50.9	2.0	0.7
1d	0.6	0.8	11.7	25.2	3.3	Decomp	17.9	1.3	0.9
B15C5	1.2	1.0	0.5	56.0	2.2	Decomp	0.6	1.2	0.5

a) Solvent: Water and dichloromethane(1 : 1). Concentration of polyether: 7×10^{-4} M. Concentration of picric acid: 7×10^{-5} M. Concentration of metal nitrates: 0.1 M.

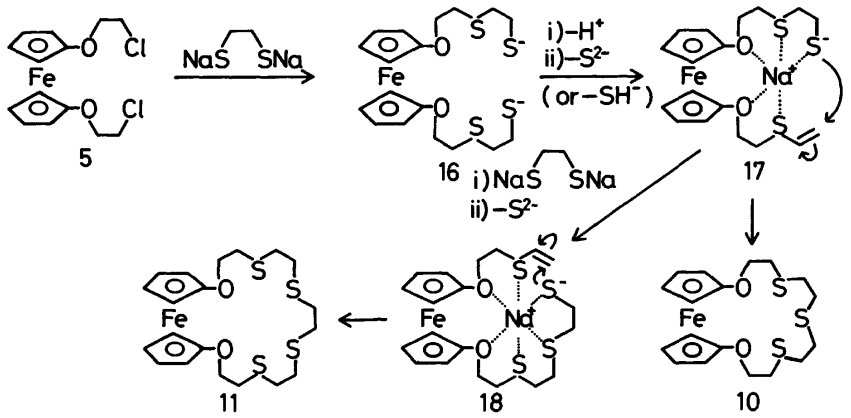

at near δ 4.10 (Fc-H$_\alpha$) and 3.88 (Fc-H$_\beta$). The ^{1}H-NMR spectrum of binuclear ferrocenophane (**12**) and disulfide (**13** and **15**) are similar to those of mononuclear ferrocenophanes.

Extraction Ability. The extraction ability of ferrocenophanes (**4a**, **9**, and **10**) for alkali, alkaline-earth metals, and several other metal cations was measured by Pedersen's method.[15)] The data are summarized in Table 2, along with those of polyoxaferrocenophane (**1d**) and benzo-15-crown-5. The dioxathia[*n*]ferrocenophanes (**4a**, **9**, and **10**) showed little extraction ability toward alkali metal ions (hard cation), although benzo-15-crown-5 showed relatively high extraction ability. The extraction ability of the dioxathiaferrocenophanes toward alkaline-earth metal ions is also low and these result are similar to those of polyoxaferrocenophane (**1d**) and benzo-15-crown-5.

The extraction ability of dioxathiaferrocenophanes (**4a**, **9**, and **10**) toward transition metal cations was more complex. A soft mercury(II) ion was extracted by **9** and **10** very well. The extraction ability of the ferrocenophanes (**1d**, **4a**, and **10**) having the same ring member toward mercury(II) ion in the following order: **10**(76.1)>**4a**(30.4)>**1d**(11.7). The phenomenon may be explained by the HSAB rule.[16)] That is, the successive displacement of an oxygen atom in the macrocyclic ring of the ferrocenophanes by a sulfur atom, which is softer compared with an oxygen atom, increases the affinity to a soft mercury(II) ion. However, the extraction ability of a thallium(I) ion, which is classified in a soft ion, by the ferrocenophanes (**1d**, **4a**, and **10**) rather showed the reverse order: **1d**(25.2)>**4a**(8.3)> **10**(2.1). So, the extraction ability of metal ions by the ferrocenophanes must be influenced by other factors, such as the conformation of the macrocycles, the size of the hole in the macrocycles, and so on, as well as a soft-hard characterization of the metal ions. Interestingly, benzo-15-crown-5 extracted a thallium(I) ion more efficiently than **1d**, while it scarcely extracted a mercury(II) ion. These obsevations indicated that **10** has a specifically high extraction ability toward a mercury(II) ion. A similar trend was observed in the extraction ability of 18-crown-6 and its sulphur analog toward silver(I) ion.[10)] The extraction ability of **4a**, **9**, and **10** toward a silver(I) ion was then examined. However, their extraction ability could not be measured, because of a rapid decomposition, in which the iron atom of ferrocene might be oxidized by the incorporated silver(I) ion. A similar result was also observed in polyoxa[*n*]ferrocenophanes.[3)]

The extraction ability of these ferrocenophanes toward the borderline ions, nickel(II) and cobalt(II) ions,

was very low, while that of a copper(II) ion was relatively high. The remarkable extraction ability of **9** and **10** toward a copper(II) ion is noteworthy, since the extraction ability of a copper(II) ion by a crown-type compound has rarely been reported. In connection with this observation, it is interesting that cyclic polythiaethers formed the complex having a high stability constant with copper(II) ion.[18]

Experimental

The melting points are uncorrected. The mass spectra were taken on a Hitachi M-80 mass spectrometer. The ^{1}H-NMR spectra were obtained on a Hitachi R-90 spectrometer, with TMS as the internal standard. The optical spectra were obtained on a Hitachi Model 200-10 spectrometer. The IR spectra were measured on a JASCO IRA-2 Diffraction Grating Infrared Spectrometer.

Materials and Reagents. 1,1'-Bis(2-chloroethoxy)ferrocene (**5**) is prepared according to the previously reported method. The other reagents employed were commercial materials or were prepared by the usual methods.

Reaction of 5 with Sodium Hydrogensulfide. To a solution of **5** (0.243 g, 0.71 mmol) in *n*-butanol (150 ml) was added sodium hydrogensulfide hydrate (0.7 g, 7.1 mmol) and the mixture was stirred for 13 h at 120 °C under nitrogen. After the solution had been cooled to room temperature, the solvent was evaporated *in vacuo*. The residue was extracted with ether. The extracts were combined and filtered. The filtrate was concentrated and the residue chromatographed on silica gel TLC (hexane:acetone=3:1). The main fraction was extracted with acetone, followed by filtration and evaporation of the solvent, to give yellow crystals. Recrystallization of the crude material from hexane gave **4a** as yellow crystals, mp 104—106 °C (lit, 104—106 °C) in 49% yield. Compound **4b** was identified by direct comparison with the spectral data of an authentic sample.

Reaction of 5 with 1,2-Ethanedithiol. 1,2-Ethanedithiol (1.5 ml, 17 mmol) was added to 500 ml of absolute ethanol containing 0.53 g (13.3 mmol) of sodium hydroxide under nitrogen, and the mixture was stirred at room temperature. After 10 min, a solution of **5** (1.43 g, 4.17 mmol) in 100 ml of absolute ethanol was added all at once, and then the mixture was stirred for 13 h at refluxing temperature. After the solution had cooled to room temperature, the solvent was evaporated *in vacuo*. The residue was extracted with ether and chloroform. The extracts were combined, followed by filtration and evaporation of the solvent to give a yellow oil. The residue was chromatographed on silica gel TLC (hexane: acetone: chloroform=6:1:trace). The first fraction was extracted with acetone, followed by filtration and evaporation of the solvent, to give yellow crystals. Recrystallization of the crude material from hexane gave **9** as yellow crystals, mp 115—116 °C, in 38% yields. ^{1}H-NMR (in $CDCl_3$): δ 4.11 (t, J=1.8 Hz, H$_\alpha$, 4H), 3.89 (t, J=1.8 Hz, H$_\beta$, 4H), 4.12 (t, J=6.3 Hz, -OCH_2, 4H), 3.03 (s, -SCH_2CH_2S-, 4H), 2.91 (t, J=6.3 Hz, -SCH_2, 4H), MS (70 eV): m/e 364 (M^+). IR (KBr): 3100, 2930, 1485, 1275, 1080, and 610 cm^{-1}. Found: C, 52.72; H, 5.58%. Calcd for $C_{16}H_{20}O_2S_2Fe$: C, 52.75; H, 5.53%. The second fraction was extracted with acetone. Evaporation of the solvent gave yellow crystals. Recrystallization of the crude material from hexane gave pure **10**, mp 114—116 °C, in 6.1% yield. ^{1}H-NMR (in $CDCl_3$): δ 4.08 (t, J=2.0 Hz, H$_\alpha$, 4H), 3.88 (t, J=2.0 Hz, H$_\beta$, 4H), 4.05 (t, J=6.1 Hz, -OCH_2, 4H), 2.62—3.02 (t+m, -SCH_2, 12H). MS (70 eV): m/e 424 (M^+). IR (KBr): 3100, 2940, 1480, 1250, 1085, and 610 cm^{-1}. Found: C, 50.89; H, 5.75%. Calcd for $C_{18}H_{24}O_2S_3Fe$: C, 50,94; H, 5.70%. The third fraction was extracted with acetone. Evaporation of the solvent gave yellow crystals. Recrystallization of the crude material from ethanol gave pure **11**, mp 69—70 °C, in 1.9% yield. ^{1}H-NMR (in $CDCl_3$): δ 4.12 (t, J=1.8 Hz, H$_\alpha$, 4H), 3.88 (t, J=1.8 Hz, H$_\beta$, 4H), 4.05 (t, J=6.4 Hz, -OCH_2, 4H), 2.80—3.02 (s+m, -SCH_2, 16H). MS (70 eV): m/e 484 (M^+). IR (KBr): 3100, 2930, 1485, 1245, 1050, and 620 cm^{-1}. Found: C, 49.41; H, 5.99%. Calcd for $C_{20}H_{28}O_2S_4Fe$: C, 49.58; H, 5.82%. The fourth fraction was extracted with acetone. Evaporation of the solvent gave a yellow oil which was rechromatographed on silica gel TLC (hexane: acetone: chloroform=3:1:trace). The main band was extracted with acetone. Evaporation of the solvent gave a yellow oil. Recrystallization of the crude material from ethanol gave pure **12**, mp 129—131 °C, in 3.2% yield. ^{1}H-NMR (in $CDCl_3$): δ 4.07 (t, J=1.8 Hz, H$_\alpha$, 8H), 3.84 (t, J=1.8 Hz, H$_\beta$, 4H), 4.00 (t, J=6.5 Hz, -OCH_2, 8H), 2.77—2.97 (s+t, -SCH_2, 16H). MS (70 eV): m/e 728 (M^+). IR (KBr): 3100, 2920, 1480, 1245, 1085, and 610 cm^{-1}. Found: C, 52.91; H, 5.76%. Calcd for $C_{32}H_{40}O_4S_4Fe$: C, 52.75; H, 5.53%.

Reaction of 5 with Bis(2-mercaptoethyl) Sulfide. Bis(2-mercaptoethyl) sulfide (1.8 ml, 12.4 mmol) was added all at once to 240 ml of absolute ethanol containing sodium hydroxide (0.33 g, 8.2 mmol) under nitrogen and the mixture was stirred at room temperature. After 10 min, a solution of **5** (0.814 g, 2.4 mmol) in 60 ml of absolute ethanol was added all at once, then the mixture was stirred for 15 h at reflux temperature. After the solution had been cooled to room temperature, the solvent was evaporated *in vacuo*. The residue was extracted with chloroform. The extract was filtered off and the filtrate was concentrated *in vacuo*. The residue was chromatographed on silica gel (hexane: acetone: chloroform=6:1:trace). The first fraction was extracted with acetone. Evaporation of the solvent gave a yellow oil. Recrystallization of the crude material from hexane gave pure **10** as yellow crystals, mp 114—116 °C in 51% yield. The pure **10** was identified by direct comparison with the spectral data of an authentic sample obtained by reaction of 1,2-ethanedithiol with **5**. The second fraction was extracted with acetone. Evaporation of the solvent gave a yellow oil. The crude material was recrystallized from hexane to give **13** as yellow crystals, mp 79—81 °C, in 2.9% yield. ^{1}H-NMR (in $CDCl_3$): δ 4.10 (t, J=1.9 Hz, H$_\alpha$, 4H), 4.03 (t, J=6.5 Hz, 4H, -OCH_2), 3.87 (t, J=1.9 Hz, H$_\beta$, 4H), 2.78—3.00 (m, 20H). MS (70 eV): m/e 576 (M^+). IR (KBr): 3100, 2930, 1485, 1250, 1015, and 490 cm^{-1}. Found: C, 46.12; H, 5.70%. Calcd for $C_{22}H_{32}O_2S_6Fe$: C, 45.83; H, 5.56%.

Reaction of 5 with 1,3-Propanedithiol. 1,3-Propanedithiol (1.0 ml, 9.6 mmol) was added to 250 ml of absolute ethanol containing sodium hydroxide (0.277 g, 6.9 mmol) under nitrogen, and the mixture was stirred at room temperature. After 10 min, a solution of **5** (0.711 g, 2.07 mmol) in 100 ml of absolute ethanol was added all at once, and the mixture then stirred for 14 h at reflux temperature. The usual work-up gave a yellow oil, which was chromatographed on alumina using dichloromethane as eluent. The fraction gave yellow crystals. Recrystallization of the crude product from hexane gave pure **14**, mp 149—150 °C, in 64% yield. ^{1}H-NMR (in $CDCl_3$): δ 4.19 (t, J=2.0 Hz, H$_\alpha$, 4H), 3.91 (t, J=2.0 Hz, H$_\beta$, 4H), 4.10 (t, J=6.5 Hz, -OCH_2, 4H), 2.70—3.03 (m, -SCH_2, 8H), 2.08 (q, J=6.3 Hz, CH_2, 2H). MS (70 eV): m/e 378 (M^+). IR (KBr): 3080, 2910, 1485, 1245, 1075, and 610 cm^{-1}. Found: C, 53.69; H, 5.70%. Calcd for $C_{17}H_{22}O_2S_2Fe$: C, 53.97; H, 5.82%. The second fraction gave crude **15** as a yellow oil. Recrystallization of the crude material from hexane gave pure **15**, mp 84—86 °C, in 8.6% yield. ^{1}H-NMR (in $CDCl_3$): δ 4.07 (t, J=1.9 Hz, H$_\alpha$, 4H), 4.00 (t, J=6.4 Hz, -OCH_2 4H), 3.83 (t, J=1.9 Hz, H$_\beta$, 4H), 2.66—2.98 (m, 12H), 2.05 (q, J=6.2 Hz, CH_2, 4H). MS (70 eV): m/e 484 (M^+). IR (KBr): 3100, 2910, 1485, 1245, 1075, and 490 cm^{-1}.

Found: C, 49.77; H, 5.73%. Calcd for $C_{20}H_{28}O_2S_4Fe$: C, 49.58; H, 5.82%.

Extraction Ability. Extraction ability of the ferrocenophanes and benzo-15-crown-5 with metal picrate was examined by the method described in a previous paper.[3]

References

1) R. E. Izatt and J. J. Christensen, "Synthetic Multidentate Macrocyclic Componds," Academic Press, New York (1978).

2) J. F. Biernat and T. Wilczewski, *Tetrahedron*, **36**, 2521 (1980); G. Oepen and F. Vogtle, *Liebigs Ann. Chem.*, **1979**, 1094; A. P. Bell and C. D. Hall, *J. Chem. Soc., Chem. Commun.*, **1980**, 163; P. J. Hammond, A. P. Bell, and C. D. Hall, *J. Chem. Soc., Perkin Trans. 1*, **1983**, 707.

3) S. Akabori, Y. Habata, Y. Sakamoto, M. Sato, and S. Ebine, *Bull. Chem. Soc. Jpn.*, **56**, 537 (1983).

4) M. Sato, M. Kubo, S. Ebine, and S. Akabori, *Tetrahedron Lett.*, **23**, 185 (1982).

5) M. Sato, H. Watanabe, S. Ebine, and S. Akabori, *Chem. Lett.*, **1982**, 1753.

6) S. Akabori, H. Fukuda, Y. Habata, M. Sato, and S. Ebine, *Chem. Lett.*, **1982**, 1393.

7) S. Akabori, Y. Habata, M. Sato, and S. Ebine, *Bull. Chem. Soc. Jpn.*, **56**, 1459 (1983).

8) D. St. C. Black and I. A. McLean, *Tetrahedron Lett.*, **1969**, 3961.

9) W. Rosen and D. H. Busch, *J. Am. Chem. Soc.*, **91**, 4694 (1970).

10) C. J. Pedersen, *J. Org. Chem.*, **36**, 254 (1971).

11) L. A. Ochrymowycz, C. -P. Mak, and J. D. Michna, *J. Org. Chem.*, **39**, 2079 (1974).

12) M. Russo, L. Mortillaro, L. Credari, and C. de Checchi, *Polym. Lett.*, **3**, 455 (1965).

13) The purity of 1,2-ethanedithiol was carefully checked by gas chromatography and mass spectrometry (99.5%). It does not contain any bis(2-mercaptoethyl) sulfide.

14) In the reaction of 1,1′-bis(hydroxymethyl)ferrocene with α-(2-haloethyl)-ω-halopoly(oxyethylene), the vinyl derivatives corresponding to **17** and **18** were isolated. Ref. 6.

15) C. J. Pedersen, *Fed. Proc.*, **27**, 1305 (1968).

16) T. -L. Ho, "Hard and Soft Acids and Bases Principles in Organic Chemistry," Academic Press, New York and London (1977), p. 163.

17) H. F. Frendorff, *J. Am. Chem. Soc.*, **93**, 600 (1971).

18) T. E. Jones, D. B. Rorabacher, and L. A. Ochrymowycz, *J. Am. Chem. Soc.*, **97**, 7486 (1975).

Crystal Structure and NMR Spectral Studies of Alkali Thiocyanate Complexes with Polyoxa[*n*]ferrocenophanes

Sadatoshi AKABORI,* Yoichi HABATA, and Masaru SATO†
Department of Chemistry, Faculty of Science, Toho University, Funabashi, Chiba 274
†*Chemical Analysis Center, Saitama University, Urawa, Saitama 338*
(Received June 17, 1983)

^{1}H- and ^{13}C-NMR spectra of free ligands and their alkali metal complexes with a new type of crown ethers containing a ferrocene unit have been recorded. The change of chemical shifts in ^{1}H- and ^{13}C-NMR spectra was attributed to an electronic field effect and a conformational change on the metal complexation, respectively. The crystal structure of the complex of 1,4,7,10,13-pentaoxa[13]ferrocenophane with sodium thiocyanate was determined by the X-ray method. The crystals are orthorhombic, space group Cccn, with a=20.579(4), b=25.622(8) c=7.606(1) Å, U=4010(2) Å^3, Z=8, D_c=1.48 g cm^{-3}. The distances between the iron atom of a ferrocene nucleus and the incorporated sodium cation and between the sodium cation and the nitrogen atom of a counter anion are 4.129 and 2.541 Å, respectively. The results suggest that the iron atom of the ferrocene does not take part directly in complex formation and that the sodium cation forms a contact ion pair with the nitrogen atom of a counter anion.

Polyoxa- and polythia[*n*]ferrocenophanes are a kind of crown ether-like compounds including a ferrocene subunit as a ring member; in it, the iron atom may act as a coordinatable heteroatom. Recently, several research groups have treated the interaction between the iron atom of ferrocene nucleus and the complexed cation,[1-3] and have synthesized polyoxa- and polythia[*n*]ferrocenophanes. Biernat *et al.* concluded that there is no interaction between the iron atom of **1a** and the complexed rubidium cation in methanol by only the UV spectral studies.[1] However, we ourselves previously observed a certain interaction between the iron atom of oxathia[*n*]ferrocenophane and the complexed silver cation.[4] In a previous paper,[5] we have reported the preparation and some spectroscopic and physicochemical properties of the polyoxa[*n*]ferrocenophanes and its alkali thiocyanate complexes. Polyoxa[*n*]ferrocenophanes (**1**) show a weak complexing ability to alkali, alkaline-earth cations (hard ions), and a higher complexing ability to silver and thallium cations (soft ions). It is of interest to know what kind of interaction can be expected between the iron atom of a ferrocene nucleus and the complexed cation. In continuation of our investigations about the complexes of polyoxaferrocenophanes with metal cations, we now report the ^{1}H-NMR, ^{13}C-NMR, and the crystal structure of the complexes of polyoxa[*n*]ferrocenophanes with alkali-metal thiocyanates.

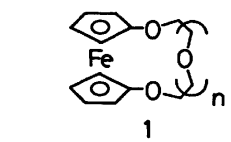

1

1a : n=4
1b : n=3

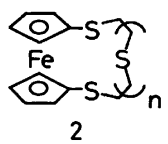

2

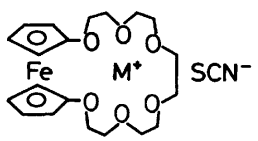

3

3a : M=Li
3b : M=Na
3c : M=K

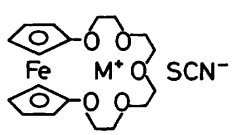

4

4a : M=Li
4b : M=Na

Results and Discussion

Ligands (**1a** and **1b**) form complexes with various alkali metal thiocyanates.[5] Suitable crystals for the X-ray analysis of **4b** were obtained by slow addition of hexane to the chloroform solution containing the ligand and sodium thiocyanate.

^{1}H-NMR Spectra of the Complexes 3 and 4. In the ^{1}H-NMR spectrum of **1a**, the signals at δ 4.14 and 3.86 which appear as triplets (J=2.0 Hz) are attributable to α- and β-protons of cyclopentadienyl rings, respectively, while the two singlets at δ 3.70 and 3.78 and the two triplets at δ 3.86 and 4.05 (J=4.6 Hz) are attributable to the methylene protons of the macrocycle. The ^{1}H-NMR spectra of compounds **1** were compared with those of alkali metal thiocyanate complexes **3** and **4**. The chemical shift of the complexes are shown in Table 1, together with those of uncomplexed ligands (**1a** and **1b**). The differences in the chemical shifts between the free ligands and the complexes are also shown in parentheses in Table 1. The change of chemical shifts of the ferrocenophanes on complexation with alkali metals seems to be attributable to a) an electronic field effect caused by the metal cation and the counter anion, b) perturbation of the electron density on the carbon atom through M$^+$-Fe-cyclopentadienyl rings, and c) factors due to the conformational change on complexation. The downfield shift was observed not only on the methylene protons but also on all protons of the cyclopentadienyl rings of ferrocene nucleus. In **4a** and **4b**, the change of chemical shifts of the cyclopentadienyl ring protons seems to depend on the distance of each proton from the complexation site, that is, the downfield shift of α-protons is more enhanced than those of β-protons. By contrast, the chemical shift differences between α- and β-protons in **3a**—**c** were approximately the same. The cavity of the macrocyclic polyether ring of **1a** seems to be too large for Li$^+$ and Na$^+$, and the complexes may take a folded geometry as pictured by Poonia.[6] The above results are in good

Table 1. ^{1}H-NMR spectral data of compounds **1a** and **1b** and their alkali metal thiocyanate complexes[a, b]

Compd	Cp-ring protons		Methylene protons		
	H_α	H_β			
1a	4.09(t)	3.82(t)	3.66(s)	3.68(s)	3.93—4.04 (m)
3a(LiSCN)	4.17(t) (+0.08)	3.92(t) (+0.10)	3.75(s) (+0.09)	3.72(s) (+0.04)	4.04—3.78 (m)
3b(NaSCN)	4.13(t) (+0.04)	3.85(t) (+0.03)	3.66(s) (±0.0)	3.71(s) (+0.03)	4.06—3.77 (m)
3c(KSCN)	4.14(t) (+0.05)	3.90(t) (+0.08)	3.74(s)	(*ca.* +0.10)	4.04—3.78 (m)
1b	4.11(t)	3.81(t)	3.68(s)	4.06—3.92 (m)	
4a(LiSCN)	4.31(t) (+0.20)	3.86(t) (+0.05)	3.76(s) (+0.08)	4.11—3.79 (m)	
4b(NaSCN)	4.41(t) (+0.30)	3.89(t) (+0.08)	3.71(s) (+0.03)	3.98—3.76 (m)	

a) Chemical shifts as δ values. A downfield shift is denoted as a positive value. b) Deuteriochloroform was used as solvent.

Table 2. ^{13}C-NMR spectral data of compounds **1a** and **1b** and their alkali metal thiocyanate complexes[a, b]

Compd	C_b	C_α	C_β	Methylene carbons			
1a	127.1	56.2	61.9	71.2	70.6	70.1	
3a(LiSCN)	126.6 (−0.5)	56.8 (+0.6)	62.3 (+0.4)	70.6	70.5 (−0.1—−0.6)	70.4	70.0
3b(NaSCN)	126.2 (−0.9)	56.9 (+0.7)	62.5 (+0.6)	69.5	69.4 (*ca.* −0.7)		
3c(KSCN)	126.2 (−0.9)	57.3 (+1.1)	62.4 (+0.5)	71.1	70.2 (−0.1—−0.6)	69.5	
1b	126.9	56.4	61.9	71.3	70.7	70.3	70.0
4a(LiSCN)	125.0 (−21.9)	58.4 (+2.0)	63.0 (+1.1)	71.1	69.1 (−0.2—−1.6)	68.4	
4b(NaSCN)	124.9 (−2.0)	59.9 (+3.5)	63.6 (+1.7)	73.4	69.1 (+2.1—−3.0)	68.7	

a) Chemical shifts as δ values. A downfield shift is denoted as a positive value. b) Deuteriochloroform was used as solvent. c) Shift changes are presented in parentheses.

agreement with the hole size estimated from Corey-Pauling-Koltum stereomolecular model (**1a**: 2.8—3.4 Å and **1b**: 2.2 Å) with the ionic diameters[7] of Li^+ (1.20 Å), Na^+ (1.90 Å), and K^+ (2.66 Å). It has already been reported[8] that in an 18-membered crown ether, such as dibenzo-18-crown-6, the addition of more than one equivalent of KSCN caused no further chemical shift change, although the resonances of all protons were successively shifted until done equivalent of the metal salt was added. The above results suggest that the electronic field effect of the counter anion, SCN^-, on all the protons of the host crown ether is small and negligible. Therefore, the chemical shifts of the complexes seems to be best interpreted in terms of an electronic field effect due to the incorporated metal cation and a perturbation of the electron density on the carbon atom through the C-O bond due to the coordination of an oxygen atom to the metal cation.

^{13}C-NMR Spectra. It is well known[9] that ^{13}C-NMR chemical shifts are sensitive to conformational changes, and relatively less sensitive to perturbation such as solvent effect than proton chemical shifts are. Therefore, the ^{13}C-NMR spectra of compounds **1a**, **1b**, and their alkali thiocyanate complexes (**3a—c** and **4a—b**) were recorded using deuteriochloroform as solvent. These results are listed in Table 2. The changes of the chemical shifts of the complexes are also shown in Table 2 in parentheses. The carbon resonances of cyclopentadienyl ring were assigned according to the literature.[10] Methylene carbon resonances were not rigorously assigned. In the ^{13}C-NMR spectra of **1b** the bridgehead carbon, α- and β-carbons of the cyclo-

pentadienyl rings showed their resonances at 126.9, 56.4, and 61.9 ppm, respectively, together with methylene carbons at 71.3, 70.7, 70.3, and 70.0 ppm. However, the ^{13}C-NMR spectrum of lithium thiocyanate complex (**4a**) showed resonances at 125.0, 58.4 (C_α), and 63.0 (C_β) ppm, together with the resonances of methylene carbons at 71.1. 69.1, and 68.4 ppm. Contrary to the upfield shifts of the bridgehead carbon of cyclopentadienyl rings, the α- and β-carbon resonances were shifted downfield on the metal complexation. The methylene carbon resonances were also shifted upfield on complexation except for the one methylene carbon of **4a**. In particular, the bridgehead carbon, C_b and methylene carbons at 2- and 12-positions showed a remarkable shift.

However, the spectral changes were slight for the alkali metal complexes containing six oxygen atoms, **3**, compared with the shift changes of **4**. The large shifts of bridgehead, C_α and methylene carbons at 2- and 12-position may be attributed to a special conformational change in which two oxygen lobes point inward. The upfield shifts of the bridgehead and methylene carbons and the downfield shifts of C_α- and C_β- resonances are in fair agreement with the results of alkali metal thiocyanate complexes of benzo-crown ethers.[8]

Crystal Structure of 4b. The molecular conformation and the coordinative aspects of the complex **4b** and the numbering are shown in Fig 1. Bond lengths and bond angles are summarized in Table 4. The complex can be divided into two parts: the roughly planar complexing unit containing O(1) through O(5) and the ferrocene unit. In the complexing unit, the bonding from the sodium ion to the ligand is directed to the five oxygen atoms and nitrogen atom of counter anion. The Na^+-O(1), -O(2), -O(3), -O(4), and -O(5) bond lengths are 2,439(10), 2.449(9), 2.474(10), 2.396(9), and 2.631(9) Å, respectively. These distances are in fair agreement with the sum of the ionic radius of Na^+ (0.95 Å) and the van der Waals radius of an oxygen atom (1.4 Å). Similar distances have found in the sodium complexes of dibenzo-18-crown-6[11] and 18-crown-6.[12] The distance between Na^+ and a nitrogen atom of a thiocyanate anion is 2.541(12) Å, which is slightly longer than the sum of the ionic radius of Na^+ (0.95 Å) and the van der Waals radius of a nitrogen atom (1.5 Å). Such results suggest that the sodium cation is coordinated by five coplanar oxygen atoms and a nitrogen atom of a thiocyanate anion, to give a contact ion pair. The interatomic O-O distances between adjacent oxygen atoms (mean, 2.73 Å) are appropriately equal to the sum (2.80 Å) of the van der Waals radius of an oxygen atom. Thus, the neighboring oxygen atoms are in contact with each other. The distance between the iron atom of a ferrocene nucleus and the incorporated sodium cation is 4.129(5) Å: this value is too long compared with the sum of the van der Waals radius of the iron atom and ionic radius of a sodium cation (0.95 Å). The result suggests that the iron atom of the ferrocene unit does not take part directly in complex formation, although we can not rule out some very weak interactions between the iron atom and the incorporated sodium cation.

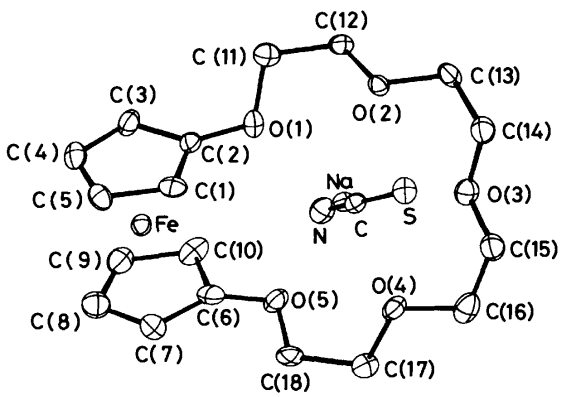

Fig. 1. Molecular structure of **4b** with atom numbering scheme.

Table 3. Fractional atomic coordinates ($\times 10^{-5}$), with estimated standard deviations in parentheses

Atom	x	y	z	B_{eq}/Å^2 a)
Na	55879(1)	11879(0)	18749(0)	3.0
N	53806(56)	12528(45)	-14110(151)	3.7
C	57022(56)	11971(43)	-26109(156)	2.4
S	61791(17)	11055(15)	-43583(49)	3.5
Fe	36373(8)	13426(6)	30355(23)	2.3
C(1)	39398(71)	10516(49)	6754(179)	3.3
C(2)	41081(57)	7038(45)	20679(196)	2.9
C(3)	35204(60)	5437(50)	29567(199)	3.4
C(4)	29971(60)	7968(52)	20409(195)	3.3
C(5)	32432(67)	11197(60)	6938(198)	3.8
C(6)	42977(69)	19024(50)	38353(188)	3.3
C(7)	37352(63)	21446(51)	31281(215)	3.7
C(8)	31886(79)	19702(62)	41905(245)	4.2
C(9)	34295(74)	16226(60)	54709(213)	4.3
C(10)	41332(70)	15595(56)	52664(174)	3.7
C(11)	48533(64)	271(49)	23712(173)	2.9
C(12)	55737(63)	-384(46)	26774(170)	2.9
C(13)	66238(62)	2048(50)	17051(195)	3.3
C(14)	69414(68)	6324(62)	5999(215)	4.0
C(15)	70194(70)	15541(61)	4615(228)	4.2
C(16)	67671(71)	20356(61)	14325(208)	4.2
C(17)	57772(63)	24754(55)	21654(172)	3.2
C(18)	50533(61)	23882(41)	21788(177)	2.9
O(1)	47254(40)	5666(35)	25541(141)	3.8
O(2)	59301(38)	2780(30)	15309(110)	2.6
O(3)	67750(42)	11187(37)	14141(119)	3.4
O(4)	60682(39)	20276(31)	13900(117)	2.9
O(5)	49233(40)	19551(32)	33088(119)	3.1

a) Equivalent isotropic temperature factor as defined by W. C. Hamilton (*Acta Crystallogr.*, **12**, 609(1959)).

The C-C bond lengths of the cyclopentadienyl rings in the ferrocene unit were in the range of 1.410—1.444 Å in the A[C(1)-C(5)] ring and 1.409—1.465 Å in theB-[C(6)-C(10)] ring, with the average values of 1.432(48) Å and 1.437(47) Å, respectively. The valency angle in the A and B rings ranged over 107.0—110.3° and 104.2—111.2°, with the average values of 108.0(2)° and 108.0(2)°, respectively. The average length of the C-C bonds in the cyclopentadienyl rings is slightly longer than that found in ferrocene (1.40 Å)[13] but in good agreement with that of bridgehead ferrocenophanes.[14] The distance between the iron atom and the ring carbons ranged from 2.038 to 2.065 Å for the A ring and from 2.031 to 2.067 Å for the B ring; the average distance was 2.049 (30) Å for the A ring and 2.054(33) Å for the B ring. The perpendicular distances from the iron atom to the least square planes of the A and B rings, 1.647 and 1.651Å, respectively, are both slightly longer than that found in ferrocene itself but agree well with those of some bridged ferrocenophanes.[14]

TABLE 4. BOND LENGTHS AND ANGLES WITH ESTIMATED STANDARD DEVIATIONS IN PARENTHESES

Bond length	l/Å	Bond length	l/Å	Bond length	l/Å
Fe-C(1)	2.041(13)	C(4)-C(5)	1.410(21)	C(16)-O(4)	1.438(17)
Fe-C(2)	2.039(12)	C(6)-C(7)	1.419(20)	O(4)-C(17)	1.422(16)
Fe-C(3)	2.062(13)	C(7)-C(8)	1.455(22)	C(17)-C(18)	1.506(18)
Fe-C(4)	2.065(13)	C(8)-C(9)	1.409(23)	C(18)-O(5)	1.428(15)
Fe-C(5)	2.038(15)	C(9)-C(10)	1.465(21)	O(5)-C(6)	1.355(16)
Fe-C(6)	2.067(14)	C(10)-C(6)	1.439(19)	Na-O(1)	2.439(10)
Fe-C(7)	2.066(13)	C(2)-O(1)	1.369(15)	Na-O(2)	2.449(9)
Fe-C(8)	2.051(17)	O(1)-C(11)	1.413(16)	Na-O(3)	2.474(10)
Fe-C(9)	2.031(16)	C(11)-C(12)	1.510(19)	Na-O(4)	2.396(9)
Fe-C(10)	2.056(14)	C(12)-O(2)	1.398(15)	Na-O(5)	2.631(9)
Fe-Na	4.129(5)	O(2)-C(13)	1.445(15)	Na-N	2.541(12)
C(1)-C(2)	1.426(19)	C(13)-C(14)	1.527(21)	C-N	1.136(16)
C(1)-C(5)	1.444(30)	C(14)-O(3)	1.432(18)	C-S	1.668(12)
C(2)-C(3)	1.444(18)	O(3)-C(15)	1.422(19)		
C(3)-C(4)	1.437(19)	C(15)-C(16)	1.528(22)		

Bond angle	ϕ/°	Bond angle	ϕ/°	Bond angle	ϕ/°
C(1)-Fe-C(2)	40.9(1)	C(3)-Fe-C(9)	110.6(1)	C(1)-C(2)-C(3)	108.8(1)
C(1)-Fe-C(5)	41.5(1)	C(3)-Fe-C(10)	110.5(1)	C(2)-C(3)-C(4)	105.8(1)
C(1)-Fe-C(3)	69.3(1)	C(4)-Fe-C(5)	40.2(1)	C(3)-C(4)-C(5)	110.3(1)
C(1)-Fe-C(4)	68.0(1)	C(4)-Fe-C(6)	175.6(1)	C(4)-C(5)-C(1)	107.0(1)
C(1)-Fe-C(5)	41.5(1)	C(4)-Fe-C(7)	138.4(1)	C(7)-C(6)-C(10)	111.2(1)
C(1)-Fe-C(6)	108.2(1)	C(4)-Fe-C(8)	113.6(1)	C(6)-C(7)-C(8)	106.6(1)
C(1)-Fe-C(7)	111.3(1)	C(4)-Fe-C(9)	116.0(1)	C(7)-C(8)-C(9)	107.8(1)
C(1)-Fe-C(8)	143.1(1)	C(4)-Fe-C(10)	143.3(1)	C(8)-C(9)-C(10)	110.1(1)
C(1)-Fe-C(9)	174.2(1)	C(5)-Fe-C(6)	135.5(1)	C(9)-C(10)-C(6)	104.2(1)
C(1)-Fe-C(10)	132.3(1)	C(5)-Fe-C(7)	110.3(1)	C(1)-C(2)-O(1)	125.9(1)
C(2)-Fe-C(3)	41.2(1)	C(5)-Fe-C(8)	114.5(1)	C(3)-C(2)-O(1)	125.3(1)
C(2)-Fe-C(4)	68.1(1)	C(5)-Fe-C(9)	144.3(1)	C(2)-O(1)-C(11)	113.4(1)
C(2)-Fe-C(5)	69.4(1)	C(5)-Fe-C(10)	173.7(1)	O(1)-C(11)-C(12)	106.0(1)
C(2)-Fe-C(6)	110.5(1)	C(6)-Fe-C(7)	40.2(1)	C(11)-C(12)-O(2)	110.7(1)
C(2)-Fe-C(7)	139.8(1)	C(6)-Fe-C(8)	68.0(1)	C(12)-O(2)-C(13)	112.7(1)
C(2)-Fe-C(8)	175.7(1)	C(6)-Fe-C(9)	68.0(1)	C(13)-C(14)-O(3)	106.5(1)
C(2)-Fe-C(9)	135.4(1)	C(6)-Fe-C(10)	40.8(1)	C(14)-O(3)-C(15)	112.2(1)
C(2)-Fe-C(10)	106.2(1)	C(7)-Fe-C(8)	41.4(1)	O(3)-C(15)-C(16)	105.5(1)
C(3)-Fe-C(4)	40.8(1)	C(7)-Fe-C(9)	68.8(1)	C(16)-O(4)-C(17)	113.6(1)
C(3)-Fe-C(5)	69.5(1)	C(7)-Fe-C(10)	69.8(1)	C(17)-C(18)-O(5)	107.7(1)
C(3)-Fe-C(6)	140.7(1)	C(8)-Fe-C(9)	40.4(1)	C(18)-O(5)-C(6)	115.7(1)
C(3)-Fe-C(7)	178.9(1)	C(8)-Fe-C(10)	70.0(1)	C(10)-C(6)-O95)	120.5(1)
C(3)-Fe-C(8)	137.6(1)	C(2)-C(1)-C(5)	108.0(1)	C(7)-C(6)-O(5)	128.3(1)

It is well known[15] that the tilt angle between two cyclopentadienyl rings varies greatly with the number of bridging methylenes of the bridged ferrocenophanes. A deformation strain resulting from an interannular bridge shorter than four carbons in length can not be accomodated in the ferrocene nucleus without distortion of the prefered coplanar molecular geometry by the ring tilting. It is noteworthy that the cyclopentadienyl rings in the present complex (**4b**), containing thirteen atoms in an interannular bridge, deviates from planality, and its tilting angles are 3.30°. This may be because the crown ether part wrings the sodium cation. Finally it is also noteworthy that, although the nearest neighbor atoms between the intermolecules is C(11) and carbon atom of SCN^- and the distance (3.34(17) Å) is roughly equal to the sum of the appropriate van der Waals radii, the smallest distance in the host molecule is C(18) and O(5) and this distance (3.41(18) Å) is longer than the sum of the van der Waals radii. These results suggest that there is no strong interaction between the intermolecules.

Experimental

Polyoxa[n]ferrocenophanes (**1a** and **1b**) and their alkali metal complexes (**3a—c** and **4a, b**) were prepared by the procedures described previously.[5] ^{1}H-NMR spectra (90 MHz) and the ^{13}C-NMR spectra (22.5 MHz) were recorded in deuteriochloroform with tetramethylsilane as an internal standard on a JEOL-FX-90Q spectrometer.

X-Ray Crystallography. A crystal of dimensions 0.4×0.4×0.1 mm, obtained from hexane-chloroform, was used for the intensity measurements. Intensity data were obtained on a Rigaku four-circle automatic difractometer, equipped with graphite-monochromated Mo $K\alpha$ radiation, and using the θ-2θ scan technique ($2\theta \leq 60°$). 2539 independent reflections ($F_o \geq 3.0\sigma F_o$) were corrected for Lorentz and polarization factors but not for absorption. The crystal data are as follows: $C_{19}H_{14}O_5FeNSNa$, mol wt 457.3, orthorhombic, space group Cccn, a=20.579(4), b=25.622(8), c=7.606(1) Å, U=4010(2) Å^3, Z=8, D_c=1.48 g cm^{-3}. The structure was solved by the direct methods. The positional and thermal

parameters were refined by the block-diagonal least-squares methods. The final discrepancy index R is 0.10. The positional parameters for nonhydrogen atoms are listed in Table 3. Thermal parameters and observed and calculated structure factors are kept at the Chemical Society of Japan (Document No. 8352).

The authors wish to thank Professor Hayao Kobayashi, Department of Chemistry, Toho University, for the X-ray analyses.

References

1) J. F. Biernat and T. Wilczewski, *Tetrahedron*, **36**, 2521 (1980).

2) G. Oepen and F. Vogtle, *Justus Liebigs Ann. Chem.*, **1974**, 1094; A. P. Bell and C. D. Hall, *J. Chem. Soc., Chem. Commun.*, **1980**, 193.

3) S. Akabori, H. Fukuda, Y. Habata, M. Sato, and S. Ebine, *Chem. Lett.*, **1982**, 1393.

4) M. Sato, M. Kubo, S. Ebine, and S. Akabori, *Tetrahedron Lett.*, **23**, 2717 (1982); M. Sato, H. Watanabe, S. Ebine, and S. Akabori, *Chem. Lett.*, **1982**, 1753.

5) S. Akabori, Y. Havbata, Y. Sakamoto, M. Sato, and S. Ebine, *Bull. Chem. Soc. Jpn.*, **56**, 537 (1983).

6) N. S. Poonia, *J. Am. Chem. Soc.*, **96**, 1012 (1974).

7) L. Pauling, "The Nature of the Chemical Bond," Third ed, Cornell University Press, Ithaca, New York (1960), Chap. 13.

8) D. Live and S. I. Chan, *J. Am. Chem. Soc.*, **98**, 3769 (1976).

9) D. Bright and M. R. Truter, *J. Chem. Soc., B*, **1970**, 1544. N. K. Dalley, D. E. Smith, R. M. Izatt, and J. J. Christensen, *J. Chem. Soc., Chem. Commun.*, **1972**, 90; P. R. Mallinson and M. R. Truter, *J. Chem. Soc., Perkin Trans. 2*, **1972**, 1818.

10) A. A. Koridze, P. V. Petrovskii, A. I. Mokhov, and A. I. Lutsenko, *J. Organomet. Chem.*, **136**, 57 (1977).

11) D. Bright and M. R. Truter, *Nature*, **225**, 176 (1970).

12) "Structure and Bonding," ed by J. D. Dunitz, Springer-Verlag, Berlin (1973), Vol. 16, p. 98.

13) P. Seiler and J. D. Dunitz, *Acta Crystallogr., Sect. B*, **35**, 1068 and 2020 (1979).

14) M. Hillman and E. Fujita, *J. Organomet. Chem.*, **155**, 87, 99 (1978); L. D. Spaulding, M. Hillman, and G. J. B. Williams, *ibid.*, **155**, 109 (1978).

15) G. B. Sul'pin and M. I. Rybinskaya, *Russian Chem. Revs.*, **43**, 716 (1974).

Indole Syntheses Utilizing *o*-Methylphenyl Isocyanides

Yoshihiko Ito, Kazuhiro Kobayashi, Norihiko Seko, and Takeo Saegusa
Department of Synthetic Chemistry, Faculty of Engineering, Kyoto University, Sakyo-ku, Kyoto 606
(Received April 28, 1983)

New indole synthesis starting with *o*-methylphenyl isocyanides such as *o*-tolyl, 2,4-xylyl, and 2,6-xylyl isocyanide is described in full detail. Treatment of *o*-tolyl isocyanide with LDA in diglyme at −78 °C generated selectively *o*-(lithiomethyl)phenyl isocyanide in an almost quantitative yield, which on warming up to room temperature was cyclized to indole after aqueous workup. Similary, 2,4-xylyl and 2,6-xylyl isocyanides were cyclized to 5-methylindole and 7-methylindole quantitatively. The *o*-(lithiomethyl)phenyl isocyanides reacted with electrophiles such as alkyl halides and alkylene oxides to give *o*-alkylphenyl isocyanides, which were cyclized *via* the lithiation at the orthobenzylic carbon to afford 3-substituted indoles. On the other hand, the *o*-(lithiomethyl)phenyl isocyanides generated *in situ* at −78 °C was first warmed up to room temperature and then treated with electrophiles to furnish 1-substituted indoles. The *o*-(lithiomethyl)phenyl isocyanides were acylated in a fairly good yield with *N*-acylaziridines to give *o*-(acylmethyl)phenyl isocyanides, which were readily alkylated in the presence of sodium hydride to produce *o*-(1-acylalkyl)phenyl isocyanides. On acid hydrolysis followed by neutralization, *o*-(1-acylalkyl)phenyl isocyanides were converted to 2,3-disubstituted indoles.

Since Schöllkopf[1] discovered the lithiation of isocyanides at the α-carbon, isocyanides have been useful and versatile reagents in organic syntheses.[2] The carbon-carbon bond formation with the α-metalated isocyanides provides a new methodology for nucleophilic introduction of masked α-aminoalkyl groups because the resulting isocyanides are readily converted to primary amine derivatives by acid hydrolysis.

On the other hand, isocyanide functional group itself, which may be regarded formally as carbene, has reacted with various polar reagents in an α-addition manner.[3] Isocyanides, which have no α-hydrogen, react with organolithium to afford lithiated aldimines, which are able to be used as acyl anion equivalents.[4]

The reactions of electrophiles with α-metalated isocyanides coupled with intramolecular α-addition to isocyanide carbon lead to the formation of heterocycles. The heterocycle syntheses have permitted rapid and efficient preparation of a variety of heterocyclic ring systems, which are otherwise accessible with difficulty.

On the background of isocyanide chemistry mentioned above, we have attempted a selective lithiation at the ortho-methyl group of *o*-tolyl isocyanide with the expectation that the resulting *o*-(lithiomethyl)-phenyl isocyanide might be cyclized by the intramolecular α-addition. In the preliminary paper,[5] we reported a successful selective lithiation at the ortho-methyl group of *o*-tolyl isocyanide and its intramolecular cyclization leading to indole. This paper describes the full scope of syntheses of indole derivatives by elaboration of *o*-(lithiomethyl)phenyl isocyanides. The selective lithiation and nucleophilic elaboration of *o*-methylphenyl isocyanides such as *o*-tolyl isocyanide 2,4- and 2,6-xylyl isocyanides, which are readily prepared from commercially available toluidine derivatives, make the present indole syntheses more flexible. The indole syntheses have many advantages of simplicity, versatility and high yields over the reported synthetic methods.[6]

Selective Lithiation at the Benzylic Carbon of o-Alkylphenyl Isocyanides. Lithiation at the methyl group of *o*-tolyl isocyanide (**1a**) was achieved in an almost quantitative yield by treatment of **1a** with 2 equiv of lithium diisopropylamide (LDA) in diglyme at −78 °C. The deep-red *o*-(lithiomethyl)phenyl isocyanide (**2a**) thus generated was quenched at −78 °C with D_2O to yield *o*-tolyl isocyanide (>95% yield) with deuterium incorporation of >93%. The use of 2 equiv of LDA was required for the quantitative lithiation of **1a**. The silimar treatment of **1a** with 1 equiv of LDA followed by deuterolysis regenerated *o*-tolyl isocyanide (>95% yield) with deuterium incorporation of *ca.* 50%. The

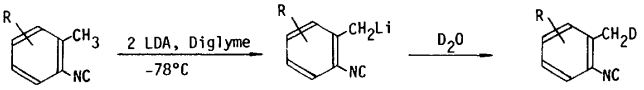

1 2 1-d_1

a : R = H
b : R = 4-Me
c : R = 5-Me
d : R = 6-Me
e : R = 4-MeO
f : R = 4-Cl

o-(lithiomethyl)phenyl isocyanide (**2a**) generated was stable at −78 °C under nitrogen in diglyme for several days. The selective lithiation of **1a** was solvent dependent. Use of monoglyme and heptane instead of diglyme gave **2a** but in somewhat decreased yields. In these solvents **2a** was slightly unstable and cyclized even at −78 °C within several hours, resulting in the formation of indole as mentioned later. The lithiation of **1a** in ether and THF solvents generated **2a** in a low yield, being substantially accompanied by an adduct (**3**) of LDA to the isocyano carbon of **1a**, of which hydrolysis furnished N^1,N^1-diisopropyl-N^2-(*o*-tolyl)formamidine (**4**). Similarly, the selective lithiation at the ortho-

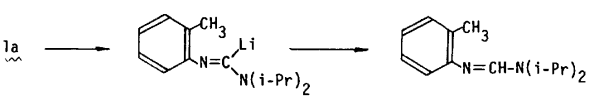

3 4

methyl group of 2,4- (**1b**), 2,5- (**1c**), and 2,6-dimethylphenyl isocyanide (**1d**), 2-methyl-4-methoxyphenyl

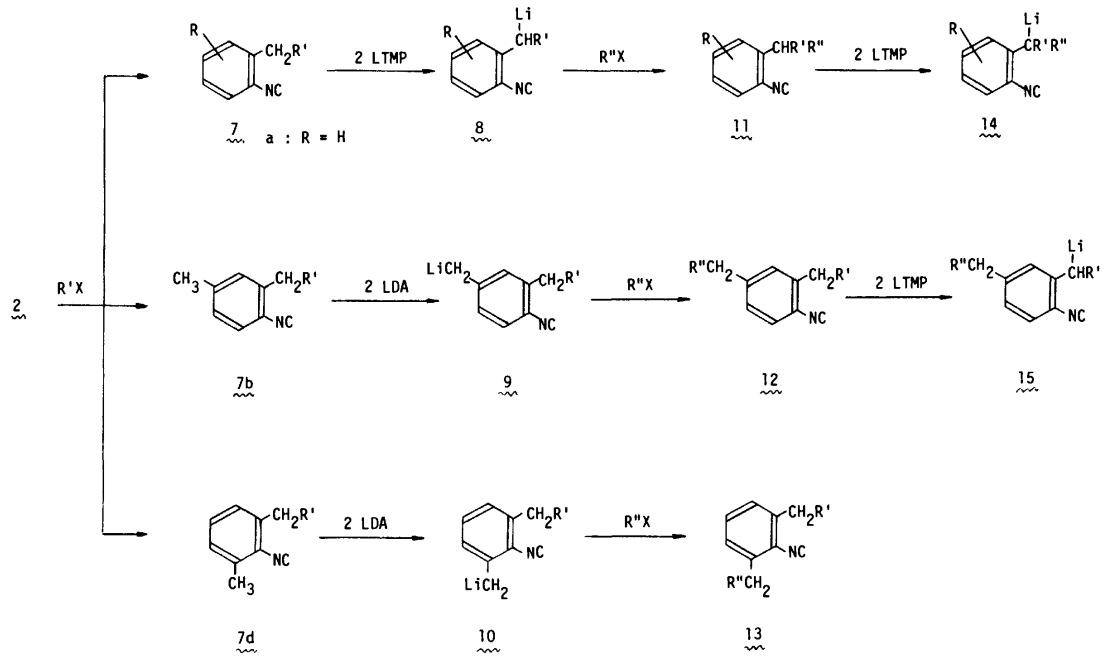

Scheme 1.

isocyanide (**1e**), and 2-methyl-4-chlorophenyl isocyanide (**1f**) was performed with 2 equiv of LDA in diglyme at −78 °C. The selective lithiation at the ortho-methyl group of **1b** may suggest that the lithiation at the ortho-methyl group of *o*-methylphenyl isocyanide (**1**) is assisted to some extent by the neighboring isocyano function. But, the treatment of **1b** and **1d** with 4 equiv of LDA in diglyme at −78 °C generated the respective dianions (**5**) and (**6**). Lithiation at the

ortho-benzylic carbon of *o*-alkylphenyl isocyanides (**7**), which are readily prepared by alkylations of **2**, can be selectively achieved by means of 2 equiv of lithium 2,2,6,6-tetramethylpiperidide (LTMP). The benzylic lithiation of *o*-alkylphenyl isocyanides (**7**) with LDA was accompanied by an adduct of LDA onto the isocyano carbon of **7**. For instance, the treatment of *o*-pentylphenyl isocyanide (**7a-iii**) with LDA at −78 °C followed by warming up to room temperature produced, after aqueous workup, N^1, N^1-diisopropyl-N^2-(*o*-pentylphenyl)formamidine (60%) and 3-butylindole (30%), which is formed by the intramolecular cyclization of *o*-(α-lithiopentyl)phenyl isocyanide (**8a-iii**).

Noteworthy is that the lithiation of 2-alkyl-4-methylphenyl isocyanide (**7b**) and 2-alkyl-6-methylphenyl isocyanide (**7d**) with 2 equiv of LDA took place selectively at the 4-methyl and the 6-methyl groups, respectively, leading to 2,4-dialkylphenyl isocyanide (**12**) and 2,6-dialkylphenyl isocyanide (**13**) by alkylations (Scheme 1).

As expectedly, further lithiation of 2,4-dialkylphenyl isocyanides (**12**) with 2 equiv of LTMP occurred at the ortho-benzylic carbon with high selectivities.

Alkylations and Cyclizations of o-Alkylphenyl Isocyanides via the Selective Lithiation at the ortho-Benzylic Carbon. i) Syntheses of 3-Alkylindoles: *o*-(Lithiomethyl)phenyl isocyanide (**2a**), which is stable at −78 °C in diglyme, was cyclized on warming to give indole, after aqueous workup. Deep red characteristic of **2a** in diglyme at −78 °C gradually turned light brown as the temperature was raised up above −25 °C to room temperature. The light brown solution was quenched with H_2O at room temperature to produce indole in an almost quantitative yield. Similarly, the cyclizations of substituted *o*-methylphenyl isocyanides (**1b**—**f**) *via* the lithiation at the ortho-methyl group afforded indoles with substituents on the benzene ring in high yields.

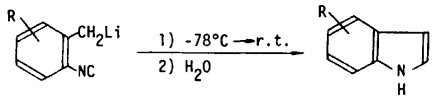

2	**16**
a : R = H	a : 100%
b : R = 4-Me	b : 100%
c : R = 5-Me	c : 82%
d : R = 6-Me	d : 100%
e : R = 4-MeO	e : 91%
f : R = 4-Cl	f : 100%

The *o*-(lithiomethyl)phenyl isocyanides can be elaborated at −78 °C with electrophiles such as alkyl halides, aldehydes,[7] ketones,[7] epoxides, α, β-unsaturated carboxylic esters,[8] allyl carboxylates,[9] *N*-acylaziridines *etc.*, leading to a variety of *o*-substituted phenyl isocyanides. Some alkylations of *o*-(lithiomethyl)phenyl isocyanide (**2a**) including silylation and sulfenylation are summarized in Table 1.

The reactions of **2a** with alkyl halides are immedi-

Table 1. Alkylations and cyclizations of *o*-tolyl isocyanide (**1a**)

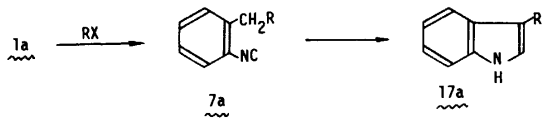

Entry	RX[a]	**7a** (%)	**17a**[b] (%)
1	CH_3I	95 (**7a-i**)	95 (**17a-i**)
2	CH_2=$CHCH_2Br$	82 (**7a-ii**)	95 (**17a-ii**)
3	*n*-C_4H_9Br	83 (**7a-iii**)	85 (**17a-iii**)
4	*i*-C_4H_9Br	78 (**7a-iv**)	78 (**17a-iv**)
5	*i*-C_3H_7I	89 (**7a-v**)	65 (**17a-v**)
6	$(EtO)_2CHCH_2Br$	68 (**7a-vi**)	62 (**17a-vi**)
7	Me_3SiCl	95 (**7a-vii**)	90 (**17a-vii**)
8	MeSSMe[c]	67 (**7a-viii**)	84 (**17a-viii**)

a) Two equivalents of electrophile was used unless otherwise stated. b) Isolated yields from **7a**. c) One equivalent of electrophile was used.

ately complete at −78 °C except for that **2a** reacted slowly with α-bromoacetaldehyde diethy acetal at −78 °C over 8—10 h. The reactions of **2a** with trimethylsilyl chloride and dimethyl disulfide permitted introductions of trimethylsilyl and methanesulfenyl groups on the methyl group of *o*-tolyl isocyanide (**1a**), both of which in turn are capable of stabilizing benzylic carbanion.

o-Alkylphenyl isocyanides (**7a-i**—**7a-iv** and **7a-vi**) thus prepared were cyclized to 3-substituted indoles in good yields by the selective lithiation at the ortho-benzylic carbon with 2 equiv of LTMP at −78 °C followed by raising the reaction temperature. Some syntheses of 3-alkylindoles (**17a**) are summarized in Table 1.

The cyclization of **7a-vi** presents a convenient synthesis of diethyl acetal (**17a-vi**) of indole-3-acetaldehyde, which is a metabolite from Helianthus Annuus. No cyclization of **7a-v** occurred on the similar treatment, because of the failure in the lithiation at the benzylic carbon with LTMP. Its cyclization was realized by successful lithiation at the ortho-benzylic carbon of **7a-v** with LTMP in the presence of HMPA. Cyclizations of **7a-vii** and **7a-viii**, of which the benzylic carbanions are stabilized by silicon and sulfur atoms, are readily accomplished *via* the lithiation with LDA.

All attempts to synthesize 3-alkylindoles (**17a**) in one-flask *via* alkylation and cyclization starting with *o*-methylphenyl isocyanide (**1a**) were, however, unsuccessful.

The present methodology also provides a convenient synthetic route to 1,3,4,5-tetrahydrobenz[*cd*]indole (**17g**), which constitutes the skeleton of ergot alkaloid, from 5,6,7,8-tetrahydro-1-naphthylamine *via* the lithiation of the corresponding isonitrile (**1g**) with LTMP as shown below.

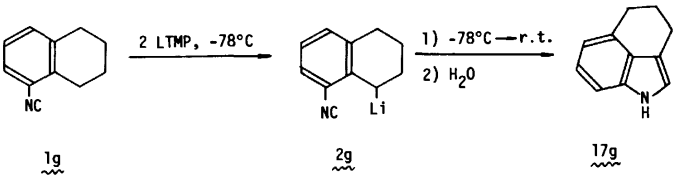

The alkylation and cyclization using 2,4- and 2,6-dimethylphenyl isocyanides (**1b**) and (**1d**) make the present indole syntheses more applicable. 2,4-Dialkylphenyl isocyanides (**12**) were prepared *via* the stepwise selective lithiation (**2b** and **9**) or the direct lithiation (**5**) of **1b**, followed by alkylations. The 2,4-dialkylphenyl isocyanides (**12**) were cyclized *via* the selective lithiation at the ortho-benzylic carbon with 2 equiv of LTMP to 3,5-dialkylindoles (**18**) but in somewhat low yields.

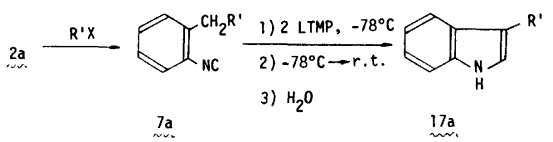

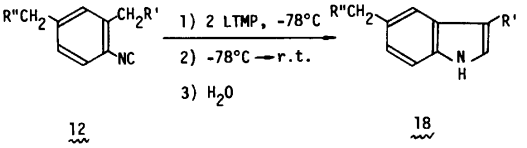

Table 2. Alkylations and cyclizations of 2,4-dimethylphenyl isocyanides (**1b**)

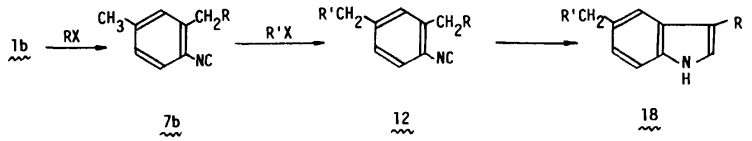

Entry	RX	R'X	**7b** (%)[a]	**12** (%)[a]	**18** (%)[d]
1	CH_3I	—	93 (**7b-i**)		
2	*n*-C_4H_9Br	—	99 (**7b-ii**)		
3	CH_2=$CHCH_2Br$	—	98 (**7b-iii**)		
4	CH_3I	CH_3I		78[b] (64)[c] (**12-i**)	39 (**18-i**)
5	*n*-C_4H_9Br	*n*-C_4H_9Br		79[b] (75)[c] (**12-ii**)	30 (**18-ii**)
6	*n*-C_4H_9Br	CH_2=$CHCH_2Br$		86[b] (**12-iii**)	40 (**18-iii**)
7	CH_2=$CHCH_2Br$	*i*-C_3H_7I		69[b] (**12-iv**)	47 (**18-iv**)

a) Yields based on **1b**. b) Yields are of stepwise alkylation *via* **7b**. c) Yields in parenthesis are of dialkylation *via* the direct dilithiation (**5**). d) Yields based on **12**.

Table 3. Alkylations and cyclizations of 2,6-dimethylphenyl isocyanides (**1d**)

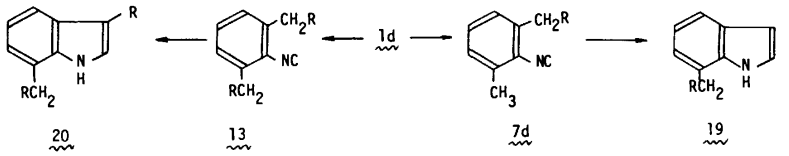

Entry	RX	**7d** (%)[a]	**13** (%)[a]	**19** (%)[d]	**20** (%)[e]
1	n-C_4H_9Br	87 (**7d-i**)		66 (**19-i**)	
2	i-C_3H_7I	75 (**7d-ii**)		74 (**19-ii**)	
3	n-C_4H_9Br		60[b] (70)[c] (**13-i**)		43 (**20-i**)
4	CH_3I		75[b] (**13-ii**)		63 (**20-ii**)

a) Yields based on **1d**. b) Yields are of the direct alkylation *via* **6**. c) Yields in parenthesis is of the stepwise alkylation *via* **10**. d) Yields based on **7d**. e) Yields based on **13**.

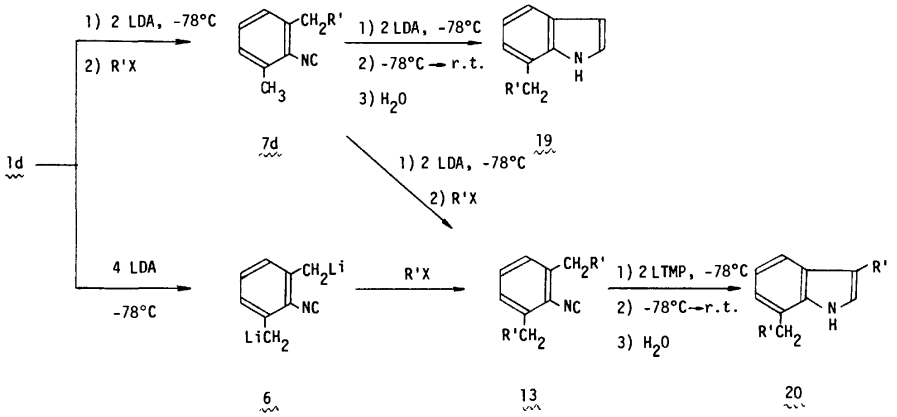

Scheme 2.

Similarly, mono- and dialkylations of 2,6-dimethylphenyl isocyanide (**1d**) were carried out *via* the stepwise selective lithiation (**2d** and **10**) or the direct lithiation (**6**). The monoalkylations of **1d** and subsequent cyclizations *via* the selective lithiation at the remaining methyl group provided a convenient synthesis of 7-alkylindoles (**19**) (Table 3).

2,6-Dialkylphenyl isocyanides (**13**) were also cyclized to 3,7-dialkylindoles (**20**) *via* the benzylic lithiation with LTMP (Table 3). But the cyclization of unsymmetrical 2,6-dialkylphenyl isocyanide was less significant from synthetic viewpoint, because of difficulty in the selective lithiation at either of two ortho-benzylic carbons. Another interesting elaboration of **1d** *via* **21** is illustrated in preparation of **19-iii**.

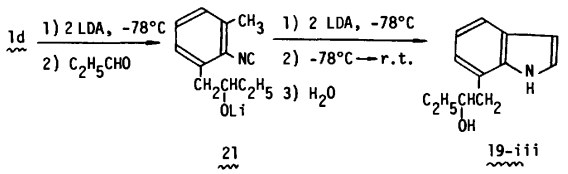

o-Alkylphenyl isocyanides **7a** were further alkylated by treatment with 2 equiv of lithium amide followed by addition of alkyl halides to afford *o*-(*s*-alkyl)phenyl isocyanides (**22**) in moderate to good yields (Table 4). Various attempts to cyclize *o*-(*s*-alkyl)phenyl isocyanides (**22**) to indolenine derivatives (**23**), however, failed, in spite of success of the benzylic lithiation.[10]

Table 4. Alkylations of **7a**[a]

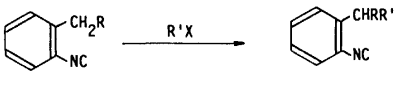

Entry	R	R′X	**22** (%)
1	CH_3	n-C_4H_9Br	72 (**22-i**)
2	n-C_4H_9	CH_3I	66 (**22-i**)
3	CH_3	CH_3I	68 (**22-ii**)
4	CH_3	CH_3SSCH_3	75 (**22-iii**)
5	SCH_3[b]	CH_3I	78 (**22-iii**)
6	SCH_3[b]	CH_3SSCH_3	65 (**22-iv**)
7	$Si(CH_3)_3$[b]	CH_3I	88 (**22-v**)

a) LTMP was used for the ortho-benzylic lithiation of **7a** unless otherwise noted. b) LDA was used for the ortho-benzylic lithiation.

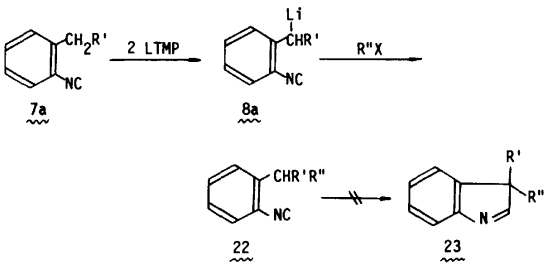

ii) One-flask Synthesis of Tryptophol Derivatives: The carbon-carbon bond formation of *o*-(lithiomethyl)-phenyl isocyanides (**2**) with alkylene oxide and subsequent cyclization of the resultant *o*-(3-hydroxyalkyl)-phenyl isocyanide (**24**) *via* the ortho-benzylic lithiation provided a rapid synthetic route to tryptophol derivatives.

Unlike the synthesis of 3-alkylindoles by the alkylation and cyclization of **1** as mentioned above, the synthesis of tryptophol derivatives starting with *o*-methylphenyl isocyanides (**1**) was accomplished in one-flask without isolation of any intermediates. In the reaction of **2a** generated *in situ* from **la** and 2 equiv of LDA at −78 °C in diglyme with 2 equiv molar of alkylene oxide for 2 h, *o*-(3-hydroxyalkyl)phenyl isocyanide (**24**) was produced together with tryptophol derivatives (**25**) as a minor product, after aqueous workup at room temperature. The formation of **25** suggested

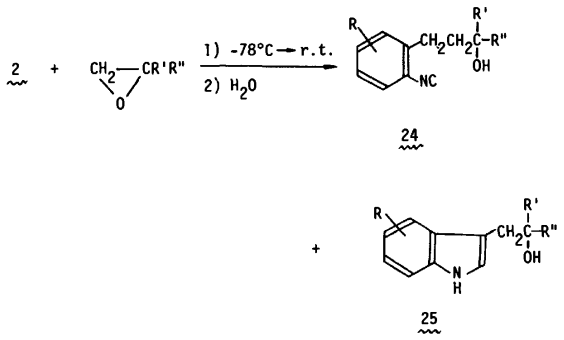

that lithium alkoxide of **24** initially formed from **2** and alkylene oxide underwent the ortho-benzylic lithiation with LDA during the reaction. Expectedly, *o*-(3-hydroxyalkyl)phenyl isocyanide (**24**) once isolated was converted to tryptophol derivative *via* the ortho-benzylic lithiation by 3 equiv of LDA. In this case, use of LTMP was not necessary. On the basis of these observations, one-flask synthesis of tryptophol derivatives was realized as follows. To the mixture of **1** and 2 equiv of LDA, which had been stirred at −78°C for 3 h, another 2 equiv of LDA was added at the same temperature and stirred for 2 h. The reaction mixture was warmed up to room temperature and quenched with water to furnish tryptophol derivative (**25**) in moderate yields. With unsymmetrical alkylene oxides, isomeric tryptophol derivatives, which may be derived by nucleophilic attack of **2** at the more substituted site of alkylene oxides, was produced in negligible yields as a by-product as judged by NMR analysis. Some syntheses of tryptophol derivatives starting with **1** are summarized in Table 5.

The tryptophol syntheses with 2,4- and 2,6-dimethylphenyl isocyanide (**1b**) and(**1d**) were accompanied by side reactions, which were caused from the lithiation at 4-methyl and 6-methyl of 2-(3-hydroxyalkyl)-4-methylphenyl isocyanide and 2-(3-hydroxyalkyl)-6-methylphenyl isocyanide. Accordingly, 2,4-bis(3-hydroxyalkyl)phenyl isocyanide (**26b**) and 7-(3-hydroxyalkyl)-indole (**27d**) were isolated with the desired tryptophol derivatives (**25b**) and (**25d**), respectively.

Table 5. One-flask synthesis of tryptophol derivatives (**25**)

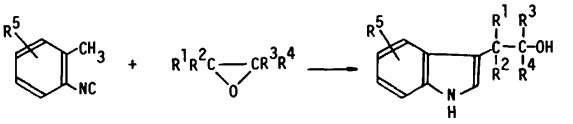

Entry	R^1	R^2	R^3	R^4	R^5		Yield/%
1	H	H	CH_3	CH_3	H	(**25a-i**)	68
2	H	H	H	C_2H_5	H	(**25a-ii**)	61
3	H	H	H	CH_3	H	(**25a-iii**)	65
4	H	$-(CH_2)_4-$			H	(**25a-iv**)	42
5	H	H	CH_3	CH_3	5-CH_3	(**25b-v**)	48
6	H	H	H	CH_3	5-CH_3	(**25b-vi**)	48
7	H	H	CH_3	CH_3	7-CH_3	(**25d-vii**)	23
8	H	H	CH_3	CH_3	5-Cl	(**25e-viii**)	78

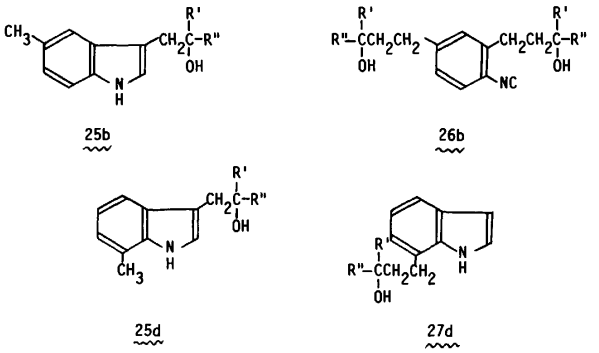

iii) Syntheses of 1-Alkylinodoles: The present indole synthesis presents an interesting example of a "5-*endo*-digonal" ring closure as classified by Baldwin,[11] in which the benzylic carbanion **8**, adds intramolecularly to the adjacent isocyano carbon, resulting in the formation of lithiated aldimine derivative (**28**). Attempts to

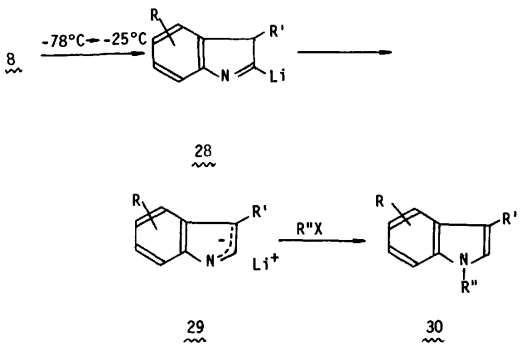

trap the lithiated aldimine **28** with electrophiles which could provide an entry to 2-substituted indoles, were, however, unsuccessful. When **8** generated *in situ* in diglyme at −78 °C was allowed to warm up to −25 °C, the characteristic color of **8** (R=H: deep red; R=alkyl: purple) gradually changed to light brown. The solution at −25 °C was treated with electrophiles such as alkyl halides, alkylene oxides, *etc.*, to afford the corresponding 1-substituted indoles (**30**) in good yields

Table 6. Synthesis of 1-substituted indoles

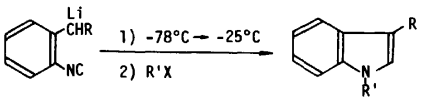

8a 30a

Entry	R	R'X	**30a** (%)[a]
1	H	CH_3I	82 (**30a-i**)
2	H	n-C_4H_9Br	82 (**30a-ii**)
3	H	CH_3OCOCH_2Br	52 (**30a-iii**)
4	H	$(CH_3)_3SiCl$	87 (**30a-iv**)
5	H	C_2H_5COCl	79 (**30a-v**)
6	H	CH_3OCOCl	76 (**30a-vi**)
7	H	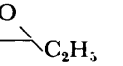	84 (**30a-vii**)[b]
8	H	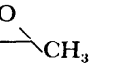	72 (**30a-viii**)[b]
9	H	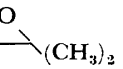	65 (**30a-ix**)[b]
10	H	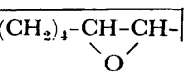	18 (**30a-x**)
11	CH_3	n-C_4H_9Br	65 (**30a-xi**)

a) Yields based on **7a**. b) Isomeric 1-(2-hydroxyalkyl)-indoles, which may be formed by nucleophilic attack of **29** at the more substituted carbon of alkylene oxide, were produced in negligible yields.

Table 7. Acylations of **2**

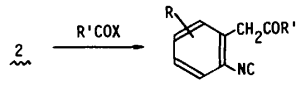

31

Entry	R	R'	**31** (%)[a]
1	H	CH_3	92 (**31-i**)[b]
2	H	t-C_4H_9	86 (**31-ii**)[b]
3	H	$Cl(CH_2)_3$	52 (**31-iii**)[c]
4	H	$HO(CH_2)_3$	47 (**31-iv**)[d]
5	4-CH_3	t-C_4H_9	85 (**31-v**)[b]
6	6-CH_3	t-C_4H_9	80 (**31-vi**)[b]

a) Ref. 9. b) The corresponding N-acylaziridine was used. c) Ethyl 4-chlorobutyrate was used. d) γ-Butyrolactone was also used.

(Table 6). The observation indicates that the lithiated aldimine **28** was rapidly converted to **29** even at −25 °C. Consequently, this procedure provided a convenient synthetic method of 1-substituted indoles starting with o-methylphenyl isocyanides (**1**).

Acylations and Cyclizations of o-Methylphenyl Isocyanides. Syntheses of 2,3-Disubstituted Indoles: Unlike the alkoxycarbonylation[4] of **2** with chloroformate, acylation of **2** was not successful with acyl halides. Carboxylic esters were conveniently employed for the acylations of **2** to afford o-(acylmethyl)-phenyl isocyanides (**31**). Allyl carboxylates gave better yields, but alkyl carboxylates including γ-butyrolactone were also usable. High-yielding acylations of **2** were accomplished with N-acylaziridines, as listed in Table 7.

As already reported,[9] 2-(acylmethyl)phenyl isocyanides (**31**) thus prepared were useful synthetic intermediates, which were cyclized to 3-acylindoles (**32**) by a Cu_2O catalyst and to 2-alkylindoles (**33**) on acid hydrolysis followed by neutralization. Usefulness of

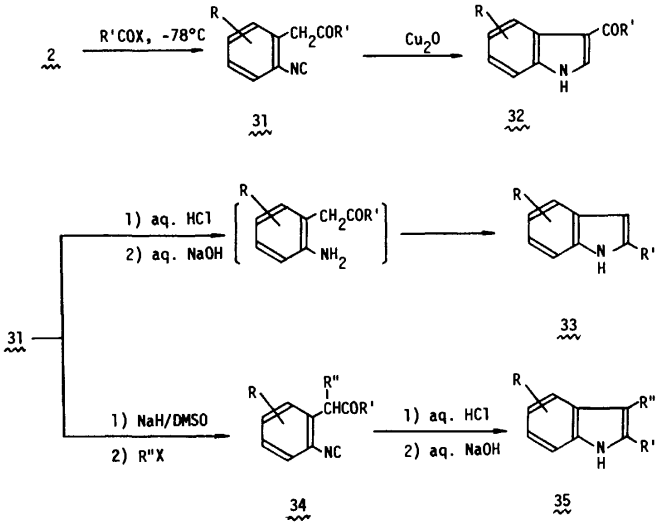

31 was further demonstrated by cyclization coupled with alkylation of **31**, producing 2,3-disubstituted indoles (**35**). Alkylations of **31** having an active methylene group were conducted more easily by means of NaH, producing 2-(1-acylalkyl)phenyl isocyanides (**34**). (Table 8) The isocyanides **34** prepared were unexpectedly not cyclized by Cu_2O catalyst.[9] Moreover, **34-i** was treated with NaH at −78 °C followed by warming up to room temperature to give 3-methylindole and 1-acetyl-3-methylindole in good yield. But, **34** was cleanly converted to 2,3-disubstituted indole (Table 8) in good yield on treatment with aqueous HCl. This reaction presents an expedient and versatile preparative method of 2,3-disubstituted indoles.

Experimental

Measurements. The ^1H NMR spectra were recorded in $CDCl_3$ with tetramethylsilane as an internal standard, unless otherwise stated. The IR spectra were measured of neat samples, unless otherwise stated. Thin layer chromatography was performed using Merck Silica Gel 60 GF_{254}.

Materials. All solvents were dried over drying agents and distilled under nitrogen. Butyllithium (1.6 M† solution in hexane) was purchased from aldrich Inc. Alkyl halides and alkylene oxides were all purified by distillation under nitrogen. Starting o-methylphenyl isocyanides (**1a—f**) were prepared according to the Ugi's procedure[12] or the modified procedure (*vide infra*) from the corresponding formamides, which were prepared by formylation of commercially available o-toluidines with formic acid or acetic formic anhydrid.[13]

5-Isocyano-1,2,3,4-tetrahydronaphthalene (1g). To a solution of 6.0 g (34 mmol) of 5-formamido-1,2,3,4-tetra-

† 1 M=1 mol dm^{-3}.

TABLE 8. ALKYLATIONS AND CYCLIZATIONS OF **31**

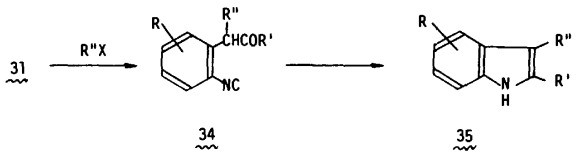

Entry	R	R'	R"X	**34** (%)[a]	**35** (%)[b]
1	H	CH_3	CH_3I	84 (**34-i**)	62 (**35-i**)
2	H	*i*-C_4H_9	CH_3I	90 (**34-ii**)	77 (**35-ii**)
3	H	*t*-C_4H_9	CH_3I	85 (**34-iii**)	86 (**35-iii**)
4	H	*t*-C_4H_9	*i*-C_3H_7I	63 (**34-iv**)	90 (**35-iv**)
5	H	*t*-C_4H_9	CH_3COCH_2Br	56 (**34-v**)	59 (**35-v**)
6	H	*t*-C_4H_9	$NCCH_2I$	89 (**34-vi**)	75 (**35-vi**)
7	H	Ph	CH_2=$CHCHBr$	70 (**34-vii**)	66 (**35-vii**)
8	4-CH_3	*t*-C_4H_9	$C_2H_5OCOCH_2Br$	77 (**34-viii**)	46 (**35-viii**)
9	6-CH_3	*t*-C_4H_9	CH_2=$CHCH_2Br$	78 (**34-ix**)	67 (**35-ix**)
10	H	$Cl(CH_2)_3$	R"=H	—	55 (**33-i**)
11	H	$HO(CH_2)_3$	R"=H	—	53 (**33-ii**)

a) Isolated yield based on **31**. b) Isolated yield based on **34**.

hydronaphthalene, which was prepared from 5,6,7,8-tetrahydro-1-naphthylamine[14] and formic acid, and 14 mL of triethylamine in 40 mL of THF, was added dropwise 5.2 g (34 mmol) of phosphoryl chloride at 0 °C. After stirring at the same temperature for 30 min, the mixture was stirred for additional 30 min at room temperature, and poured into diluted aq $NaHCO_3$, extracted with ether and washed with water. The extract was dried over KOH pellet, filtered and evaporated. The residue was distilled to afford 4.7 g (88%) of 5-isocyano-1,2,3,4-tetrahydronaphthalene (**1g**), bp 86—87 °C (0.4 mmHg[††]). **1g**: IR 2110 cm^{-1}; NMR δ=1.55—2.10 (m, 4H), 2.46—3.10 (m, 4H), 6.75—7.30 (m, 3H). Found: C, 83.90; H, 7.21; N, 9.11%. Calcd for $C_{11}H_{11}N$: C, 84.04; H, 7.05; N, 8.91%.

*5-Methylindole (**16b**).* *General Procedure*: To a solution of 304 mg (3 mmol) of diisopropylamine in 4 mL of diglyme was added dropwise 3 mmol of butyllithium (1.6 M solution in hexane) at −78 °C, and stirred for 15 min at the same temperature. To the mixture, 197 mg (1.5 mmol) of 2,4-xylyl isocyanide (**1b**) was added and stirred for 30 min at −78 °C. The resultant red solution was allowed to warm up to room temperature, and quenched with aq NH_4Cl. The mixture was extracted with ether, washed with water three times and dried over anhydrous Na_2SO_4. After the ether extract was evaporated, the residual solid was recrystallized from hexane to furnish 5-methylindole in an almost quantitative yield, mp 57 °C (lit,[6d] 55.0—56.5 °C). IR (KBr disk) 3400 cm^{-1}; NMR(CCl_4 with Me_4Si) δ=2.36 (s, 3H), 6.22 (m, 1H), 6.61 (m, 1H), 6.83 (br s, 2H), 7.0 (br s, 1H), 7.22 (br s, 1H).

Indole (**16a**),[15a] 6-methylindole (**16c**),[16] 7-methylindole (**16d**),[15b] 5-methoxyindole (**16e**),[15c] and 5-chloroindole (**16f**)[15d] were synthesized according to the above procedure, and purified by recrystallization from hexane except for **16c** which was distilled, bp 60 °C (0.2 mmHg) [lit,[16] 148—155 °C (20 mmHg)]. Identities of **16a—f** were established by comparison of their spectral data with those reported. **16c**: IR 3400 cm^{-1}; NMR(CCl_4 with Me_4Si) δ=2.42 (s, 3H), 6.31 (m, 1H), 6.7—7.5 (m, 5H).

*o-Ethylphenyl Isocyanide (**7a-i**).* *General Procedure for Alkylations of o-Tolyl Isocyanide (**1a**)*: To a stirring solution of 3 mmol of LDA in 4 mL of diglyme at −78 °C was added dropwise 176 mg (1.5 mmol) of *o*-tolyl isocyanide (**1a**). After 30 min, 426 mg (3 mmol) of methyl iodide was added dropwise. The characteristic red color of *o*-(lithiomethyl)-phenyl isocyanide (**2a**) disappeared immediately. The reaction mixture was quenched with aq NH_4Cl at −78 °C, extracted with ether, washed with water three times and dried over anhydrous Na_2SO_4. The ether extract was evaporated and distilled using Kugelrohr apparatus to afford *o*-ethylphenyl isocyanide (**7a-i**) [bp 85 °C (10 mmHg)] in 95% yield. **7a-i**: IR 2115 cm^{-1}; NMR δ=1.28 (t, 3H), 2.77 (q, 2H), 7.20 (s, 4H). Found: C, 82.62; H, 7.09; N, 10.85%. Calcd for C_9H_9N: C, 82.40; H, 6.92; N, 10.68%. *o*-Alkylphenyl isocyanides (**7a-ii**)—(**7a-viii**) were prepared according to the above procedure.

*o-(3-Butenyl)phenyl Isocyanide (**7a-ii**)*: [Bp 70 °C (1 mmHg)]: IR 2120, 1641 cm^{-1}; NMR (CCl_4 with Me_4Si) δ=2.40 (t, 2H), 2.6—3.0 (m, 2H), 4.8—5.2 (m, 2H), 5.5—6.0 (m, 1H), 7.0—7.5 (m, 4H). Found: C, 84.19; H, 7.20; N, 9.01%. Calcd for $C_{11}H_{11}N$: C, 84.04; H, 7.05; N, 8.91%.

*o-Pentylphenyl Isocyanide (**7a-iii**)*: [Bp 85 °C (4 mmHg)]: 2120 cm^{-1}; NMR(CCl_4 with Me_4Si) δ=0.95 (t, 3H), 1.1—1.8 (m, 6H), 2.72 (t, 2H), 7.16 (s, 4H). Found: C, 83.45; H, 8.90; N, 8.04%. Calcd for $C_{12}H_{15}N$: C, 83.19; H, 8.73; N, 8.09%.

*o-Isopentylphenyl Isocyanide (**7a-iv**)*: [Bp 86 °C (5 mmHg)]: IR 2110 cm^{-1}; NMR δ=0.95 (d, 6H), 1.3—1.7 (m, 3H), 2.72 (t, 2H), 7.23 (s, 4H). Found: C, 83.01; N, 8.89; N, 8.32%. Calcd for $C_{12}H_{15}N$: C, 83.19; H, 8.73; N, 8.09%.

*o-Isobutylphenyl Isocyanide (**7a-v**)*: [Bp 80 °C (4 mmHg)]: IR 2115 cm^{-1}; NMR(CCl_4 with Me_4Si) δ=0.94 (d, 6H), 1.95 (m, 1H), 2.58 (d, 2H), 7.19 (s, 4H). Found: C, 83.01; H, 8.50; N, 8.66%. Calcd for $C_{11}H_{13}N$: C, 82.97; H, 8.23; N, 8.80%.

*o-(3,3-Diethoxypropyl)phenyl Isocyanide (**7a-vi**)*: [Bp 120 °C (0.8 mmHg)]: The reaction of *o*-(lithiomethyl)phenyl isocyanide (**2a**) with bromoacetaldehyde diethyl acetal was slow at −78 °C and took about 10 h before the red color of **2a** diasppeared. IR 2115 cm^{-1}; NMR(CCl_4 with Me_4Si) δ= 1.19 (t, 6H), 1.7—2.1 (m, 2H), 2.6—2.9 (m, 2H), 3.2—3.7 (m, 4H), 4.3—4.6 (m, 1H), 7.20 (s, 4H). Found: C, 71.98; H, 8.34; N, 5.79%. Calcd for $C_{14}H_{19}NO_2$: C, 72.07; H, 8.21; N, 6.00%.

†† 1 mmHg≈133.322 Pa.

*o-(Trimethylsilylmethyl)phenyl Isocyanide (**7a-vii**)*: [Bp 105 °C (4 mmHg)]: IR 2130, 1252, 852 cm^{-1}; NMR (CCl_4 with Me_4Si) δ=−0.06 (s, 9H), 2.15 (s, 2H), 6.7—7.2 (m, 4H). Found: C, 69.54; H, 7.74; N, 7.40%. Calcd for $C_{11}H_{15}NSi$: C, 69.78; H, 7.99; N, 7.40%.

*o-(Methylthiomethyl)phenyl Isocyanide (**7a-viii**)*: [Bp °C (1 mmHg)]: IR 2115 cm^{-1}; NMR(CCl_4 with Me_4Si) δ= 1.97 (s, 3H), 3.69 (s, 2H), 7.1—7.4 (m, 4H). Found: C, 66.41; H, 5.31; N, 8.60%. Calcd for C_9H_9NS: C, 66.22; H, 5.56; N, 8.58%.

*3-Methylindole (**17a-i**). General Procedure for Preparation of 3-Alkylindoles*: To a solution of 424 mg (3 mmol) of 2,2,6,6-tetramethylpiperidine in 4 mL of diglyme was added dropwise 3 mmol of butyllithium (1.6 M solution in hexane) at −78 °C, and stirred for 15 min at the same temperature. To the mixture, 197 mg (1.5 mmol) of *o*-ethylphenyl isocyanide (**7a-i**) was added and stirred for 30 min at −78 °C. The purple solution was then allowed to warm up to room temperature and quenched with aq NH_4Cl. The mixture was worked up in the same way mentioned for the preparation of **16b**. 3-Methylindole (**17a-i**) was recrystallized from hexane (95% yield) and identified by comparison of spectral data[15e] with those of the authentic sample.

3-Alkylindoles (**17a-ii**)—(**17a-vi**) and (**17g**) were prepared from the corresponding **7** according to the above procedure.

*3-Allylindole (**17a-ii**)*:[17] TLC(Silica gel, $CHCl_3$) R_f=0.79.

*3-Butylindole (**17a-viii**)*:[18] [Bp 130 °C (1 mmHg)]: IR 3400 cm^{-1}; NMR δ=0.93 (t, 3H), 1.1—1.8 (m, 4H), 2.72 (t, 2H), 6.9—7.6 (m, 5H), 7.9 (br 1H).

*3-Isobutylindole (**17a-iv**)*: [Mp 32 °C recrystallization from hexane (lit,[19] 31—32 °C)]: IR 3400 cm^{-1}; NMR(CCl_4 with Me_4Si) δ=0.96 (d, 6H), 1.96 (m, 1H), 2.61 (d, 2H), 6.86 (m, 1H), 7.0—7.3 (m, 3H), 7.5—7.7 (m, 1H), 7.9 (br 1H).

*Indole-3-acetaldehyde Diethyl Acetal (**17a-vi**)*: [Bp 140 °C (0.4 mmHg)]: IR 3400 cm^{-1}; NMR(CCl_4 with Me_4Si) δ= 1.09 (t, 6H), 2.90 (d, 2H), 3.39 (m, 4H), 4.63 (t, 1H), 6.7—6.9 (m, 4H), 7.2—7.5 (m, 1H), 8.0—8.2 (br 1H). Found: C, 72.33; H, 8.11; N, 6.23%. Calcd for $C_{14}H_{19}NO_2$: C, 72.07; H, 8.21; N, 6.00%.

*1,3,4,5-Tetrahydrobenz[cd]indole (**17g**)*: [Mp 53—54 °C, recrystallization from hexane (lit,[20] 50—52 °C)]: IR 3410 cm^{-1}; NMR δ=1.75 (m, 2H), 2.63—3.10 (m, 4H), 6.55—7.15 (m, 4H), 7.38—8.05 (br 1H).

*3-Isopropylindole (**17a-v**)*: To a solution of 3 mmol of LTMP in 4 mL of diglyme at −78 °C, 3 mL of hexamethylphosphoric triamide (HMPA) was added, and then 239 mg (1.5 mmol) of **17a-v** was dropwise added. After the mixture was stirred at −78 °C for 30 min, it was allowed to warm up to room temperature and quenched with aq NH_4Cl. 3-Isopropylindole (**17a-v**)[17] was isolated by preparative TLC [TLC(Silica gel, C_6H_6) R_f=0.85].

*3-Trimethylsilylindole (**17a-vii**)*: [Bp 104 °C (0.2 mmHg)] was prepared from **7a-vii** according to the procedure for the preparation of 3-methylindole (**17a-i**) except for that LDA was used in place of LTMP. IR 3410, 1252, 847 cm^{-1}; NMR (CCl_4 with Me_4Si) δ=−0.04 (s, 9H), 6.37 (m, 1H), 6.8—7.2 (m, 3H), 7.3—7.7 (m, 2H). Found: C, 69.54; H, 7.76; N, 7.18%. Calcd for $C_{11}H_{15}NSi$: C, 69.78; H, 7.99; N, 7.40%.

*3-(Methylthio)indole (**17a-viii**)*: [Bp 120 °C (0.1 mmHg)] [lit,[6d] bp 112—113 °C (0.15 mmHg)] was prepared from **7a-viii** according to the procedure for the preparation of **17a-vii**.

*2-Ethyl-4-methylphenyl Isocyanide (**7b-i**). General Procedure for Selective Alkylations at the ortho-Methyl Group of 2,4-Dimethylphenyl Isocyanide (**1b**)*: To a solution of 3 mmol of LDA in 4 mL of diglyme at −78 °C was added 197 mg of 2,4-dimethylphenyl isocyanide (**1b**). After 30 min, 426 mg (3 mmol) of methyl iodide was added to the mixture at −78 °C. The reaction mixture was worked up in the usual way and distilled to afford 2-ethyl-4-methylphenyl isocyanide (**7b-i**) [bp 70 °C (1 mmHg)] in 93% yield. IR 2125 cm^{-1}; NMR(CCl_4 with Me_4Si) δ=1.26 (t, 3H), 2.32 (s, 3H), 2.69 (q, 2H), 6.8—7.2 (m, 3H). Found: C, 82.66; H, 7.85; N, 9.88%. Calcd for $C_{10}H_{11}N$: C, 82.72; H, 7.64; N, 9.65%.

2-Alkyl-4-methylphenyl Isocyanide (**7b-ii**) and (**7b-iii**) were prepared according to the above procedure.

*2-Pentyl-4-methylphenyl Isocyanide (**7b-ii**)*: [Bp 80 °C (1 mmHg)]: IR 2120 cm^{-1}; NMR (CCl_4 with Me_4Si) δ=1.88 (t, 3H), 1.2—1.6 (m, 6H), 2.30 (s, 3H), 2.63 (t, 2H), 6.8—7.2 (m, 3H). Found: C, 83.51; H, 9.29; N, 7.62%. Calcd for $C_{13}H_{17}N$: C, 83.37; H, 9.15; N, 7.48%.

*2-(3-Butenyl)-4-methylphenyl Isocyanide (**7b-iii**)*: [Bp 54 °C (0.6 mmHg)]: IR 2115, 1638 cm^{-1}; NMR (CCl_4 with Me_4Si) δ=2.37 (s, 3H), 2.44 (m, 2H), 2.88 (m, 2H), 4.8—5.2 (m, 2H), 5.5—6.1 (m, 1H), 6.8—7.2 (m, 3H). Found: C, 84.36; H, 7.89; N, 8.00%. Calcd for $C_{12}H_{13}N$: C, 84.17; H, 7.65; N, 8.18%.

*2,4-Diethylphenyl Isocyanide (**12-i**). General Procedure for Selective Alkylations at the 4-Methyl Group of 2-Alkyl-4-methylphenyl Isocyanide (**7b**)*: To a solution of 3 mmol of LDA in 4 mL diglyme at −78 °C was added 218 m (1.5 mmol) of 2-ethyl-4-methylphenyl isocyanide (**7b-i**) and stirred for 30 min at the same temperature. To the red colored mixture, 426 mg (3 mmol) of methyl iodide was added. The usual work-up of the reaction mixture afforded 2,4-diethylphenyl isocyanide (**12-i**) [bp 57 °C (0.5 mmHg)] in 84% yield. IR 2120 cm^{-1}; NMR (CCl_4 with Me_4Si) δ= 1.20 (t, 3H), 1.28 (t, 3H), 2.56 (q, 2H), 2.68 (q, 2H), 6.8—7.2 (m, 3H). Found: C, 82.78; H, 8.43; N, 9.03%. Calcd for $C_{11}H_{13}N$: C, 82.97; H, 8.23; N, 8.80%.

Similarly, 2,4-dialkylphenyl isocyanides (**12-ii**), (**12-iii**), and (**12-iv**) were prepared by alkylations of **7b**

*2,4-Dipentylphenyl Isocyanide (**12-ii**)*: [Bp 120 °C (0.4 mmHg)]: IR 2120 cm^{-1}; NMR (CCl_4 with Me_4Si) δ=0.88 (t, 6H), 1.1—1.8 (m, 12H), 2.3—2.8 (m, 4H), 6.8—7.2 (m, 3H). Found: C, 83.69; H, 10.49; N, 5.95%. Calcd for $C_{17}H_{25}N$: C, 83.89; H, 10.35; N, 5.76%.

*2-Pentyl-4-(3-butenyl)phenyl Isocyanide (**12-iii**)*: [Bp 116 °C (0.4 mmHg)]: IR 2120, 1640 cm^{-1}; NMR (CCl_4 with Me_4Si) δ=0.92 (t, 3H), 1.2—1.6 (m, 6H), 2.1—2.8 (m, 6H), 4.7—5.0 (m, 2H), 5.3—5.8 (m, 1H), 6.7—7.2 (m, 3H). Found: C, 84.30; H, 9.08; N, 6.09%. Calcd for $C_{16}H_{21}N$: C, 84.53; H, 9.31; N, 6.16%.

*2-(3-Butenyl)-4-isobutylphenyl Isocyanide (**12-iv**)*: [Bp 115 °C (0.6 mmHg)]: IR 2120, 1638 cm^{-1}; NMR(CCl_4 with M_4eSi) δ=0.93 (d 6H), 1.85 (m, 1H), 2.2—2.8 (m, 6H), 4.8—5.1 (m, 2H), 5.4—5.9 (m, 1H), 6.8—7.2 (m, 3H). Found: C, 84.75; H, 8.70; N, 6.34%. Calcd for $C_{15}H_{19}N$: C, 84.45; H, 8.98; N, 6.57%.

*2,4-Diethylphenyl Isocyanide (**12-i**). General Procedure for Direct Dialkylations of 2,4-Dimethylphenyl Isocyanide (**1b**)*: To a solution of 6 mmol of LDA in 8 mL of diglyme at −78 °C was added 197 mg (1.5 mmol) of 2,4-dimethylphenyl isocyanide (**1b**) and stirred for 30 min at the same temperature. To the red solution was added 852 mg (6 mmol) of methyl iodide and worked up in the usual way. 2,4-Diethylphenyl isocyanide (**12-i**) was obtained in 64% yield.

*3-Methyl-5-ethylindole (**18-i**). General Procedure for Preparations of 3,5-Dialkylindoles (**18**)*: To a solution of 3 mmol of LTMP in 4 mL of diglyme at −78 °C was added dropwise 239 mg (1.5 mmol) of 2,4-diethylphenyl isocyanide (**12-i**), and stirred for 30 min at the same temperature. The reaction mixture was allowed to warm up to room temperature and quenched with aq NH_4Cl. After the usual work-up, 3-methyl-5-ethylindole (**18-i**) was isolated in 39% yield by preparative TLC [TLC (Silica gel, $CHCl_3$) R_f=0.63]. IR 3400 cm^{-1}; NMR (CCl_4 with Me_4Si) δ=1.27 (t, 3H), 2.25 (d,

3H), 2.69 (q, 2H), 6.62 (m, 1H), 6.85 (m, 2H), 7.16 (m, 1H), 7.8 (br 1H). Found: C, 83.01; H, 8.11; N, 8.99%. Calcd for $C_{11}H_{13}N$: C, 82.97; H, 8.23; N, 8.80%.

2,4-Dialkylindoles (**18-ii**)—(**18-iv**) were prepared according to the above procedure.

*3-Butyl-5-pentylindole (**18-ii**)*: [TLC (Silica gel, $CHCl_3$) R_f=0.84]: IR 3400 cm^{-1}; NMR δ=0.88 (t, 3H), 0.90 (t, 3H), 1.2—1.8 (m, 10H), 2.67 (t, 4H), 6.80 (m, 1H), 7.00 (m, 1H), 7.08 (m, 1H), 7.28 (m, 1H), 7.6 (br, 1H). Found: C, 83.78 H, 10.08; N, 5.49%. Calcd for $C_{17}H_{25}N$: C, 83.89; H, 10.35; N, 5.76%.

*3-Butyl-5-(3-butenyl)indole (**18-iii**)*: [TLC (Silica gel, C_6H_6-hexane (1:1)) R_f=0.65] IR 3400, 1638cm^{-1}; NMR δ=0.96 (t, 3H), 1.2—1.6 (m, 4H), 2.19 (m, 2H), 2.67 (m, 4H), 4.8—5.1 (m, 2H), 5.4—6.0 (m, 1H), 6.84 (m, 1H), 6.96 (m, 1H), 7.09 (m, 1H), 7.30 (m, 1H), 7.7 (br, 1H). Found: C, 84.82; H, 9.17; N, 6.00%. Calcd for $C_{16}H_{21}N$: C, 84.53; H, 9.31; N, 6.16%.

*3-Allyl-5-isobutylindole (**18-iv**)*: [TLC (Silica gel, $CHCl_3$) R_f= 0.82]: IR 3400, 1636 cm^{-1}; NMR (CCl_4 with Me_4Si) δ=0.85 (d, 6H), 1.85 (m, 1H), 2.45 (d, 2H), 3.34 (d, 2H), 4.8—5.1 (m, 2H), 5.6—6.1 (m, 1H), 6.54 (m, 1H), 6.79 (m, 2H), 7.09 (m, 1H), 7.3 (br, 1H). Found: C, 84.30; H, 8.72; N, 6.44%. Calcd for $C_{15}H_{19}N$: C, 84.45; H, 8.98; N, 6.57%.

*2-Methyl-6-pentylphenyl Isocyanide (**7d-i**). General Procedure for Monoalkylations of 2,6-Dimethylphenyl Isocyannide (**1d**)*: To a solution of 2.5 mmol[21] of LDA in 4 mL of diglyme at −78 °C was added dropwise 197 mg (1.5 mmol) of 2,6-dimethylphenyl isocyamide (**1d**) in 1 mL of diglyme and stirred for 30 min at the same temperature. 343 mg (2.5 mmol) of butyl bromide was added to the mixture, and then worked up in the usual way and distilled to give 2-methyl-6-pentylphenyl isocyanide (**7d-i**) [bp 95 °C (0.6 mmHg)] in 87% yield. IR 2110 cm^{-1}; NMR (CCl_4 with Me_4Si) δ=0.93 (t, 3H), 1.2—1.6 (m, 6H), 2.38 (s, 3H), 2.64 (m, 2H), 6.94 (m, 3H). Found: C, 83.11; H, 8.95; N, 7.32%. Calcd for $C_{13}H_{17}$-N: C, 83.37; H, 9.15; N, 7.48%.

2-Methyl-6-isobutylphenyl isocyanide (**7d-ii**) was prepared according to the above procedure. **7d-ii** [bp 62 °C (0.4 mmHg)] : IR 2110 cm^{-1}; NMR (CCl_4 with Me_4Si) δ=0.92 (d, 6H), 1.92 (m, 1H), 2.35 (s, 3H), 2.53 (d, 2H), 6.94 (m, 3H). Found: C, 83.09; H, 8.51; N, 7.85%. Calcd for $C_{12}H_{15}N$: C, 83.19; H, 8.73; N, 8.09%.

*2,6-Dipentylphenyl Isocyanide (**13-i**). General Procedure for Selective Alkylation at the 2-Methyl Group of 2-Methyl-6-alkylphenyl Isocyanide (**7d**)*: To a solution of 3 mmol of LDA in 4 mL of diglyme at −78 °C, 281 mg (1.5 mmol) of 2-methyl-6-pentylphenyl isocyanide (**7d-i**) was added dropwise, and stirred for 30 min at the same temperature. To the mixture, 411 mg (3 mmol) of butyl bromide was added then worked up in the usual way. 2,6-Dipentylphenyl isocyanide (**13-i**) [bp 112 °C (0.6 mmHg)] was distilled in 80% yield. IR 2110 cm^{-1}; NMR (CCl_4 with Me_4Si) δ=0.92 (t, 6H), 1.2—1.7 (m, 12H), 2.63 (m, 4H), 6.94 (m, 3H). Found: C, 83.74; H, 10.01; N, 5.48%. Calcd for $C_{17}H_{25}N$: C, 83.89; H, 10.35; N, 5.76%.

*2,6-Diethylphenyl Isocyanide (**13-ii**). General Procedure for Direct Dialkylations of 2,6-Dimethylphenyl Isocyanide (**1d**)*: To a solution of 6 mmol of LDA in 8 mL of diglyme at −78 °C was added 197 mg (1.5 mmol) of **1d** and stirred for 30 min at the same temperature. To the red colored solution of the dianion **6**, 852 mg (6 mmol) of methyl iodide was added, and worked up in the usual way. 2,6-Diethylphenyl isocyanide (**13-ii**) [bp 55 °C (0.4 mmHg)] was distilled in 75% yield. IR 2115 cm^{-1}; NMR (CCl_4 with Me_4Si) δ=1.27 (t, 6H), 2.70 (q, 4H), 6.99 (m, 3H). Found: C, 82.81; H, 8.01; N, 8.57%. Calcd for $C_{11}H_{13}N$: C, 82.97; H, 8.23; N, 8.80%.

2,6-Dipentylphenyl isocyanide (**13-i**) was prepared in 60% yield by the procedure for direct dialkylations.

*7-Pentylindole (**19-i**). General Procedure for Preparations of 7-Alkylindoles (**19**)*: To a solution of 3 mmol of LDA in 4 mL of diglyme at −78 °C was added 281 mg (1.5 mmol) of 2-methyl-6-pentylphenyl isocyanide (**7d-i**) and stirred for 30 min at the same temperature. The mixture was allowed to warm up to room temperature, quenched with aq NH_4Cl, and worked up in the usual way. 7-Pentylindole [TLC (Silica gel, $CHCl_3$) R_f=0.59] was isolated in 66% yield by preparative TLC. IR 3410 cm^{-1}; NMR (CCl_4 with Me_4Si) δ=0.85 (t, 3H), 1.1—1.7 (m, 6H), 2.52 (t, 2H), 6.25 (dd, 1H), 6.6—7.3 (m, 4H), 7.4 (br, 1H). Found: C, 83.55; H, 9.31; N, 7.35%. Calcd for $C_{13}H_{17}N$: C, 83.37; H, 9.15; N, 7.48%.

7-Isobutylindole (**19-ii**)[22] was similarly prepared and isolated by preparative TLC [TLC (Silica gel, $CHCl_3$) R_f= 0.68]. IR 3410 cm; NMR δ=0.98 (d, 6H), 2.03 (m, 1H), 2.64 (d, 2H), 6.42 (dd, 1H), 6.7—7.1 (m, 3H), 7.40 (m, 1H), 7.9 (br, 1H).

*3-Methyl-7-ethylindole (**20-ii**). General Procedure for Preparations of 3,7-Dialkylindoles (**20**)*: To a solution of 3 mmol of LTMP in 4 mL of digylme at −78 °C was added 239 mg (1.5 mmol) of 2,6-diethylphenyl isocyanide (**13-ii**) and stirred for 30 min at the same temperature. The purple solution was allowed to warm up to room temperature, and stirred for 30 min at room temperature. After the mixture was quenched with aq NH_4Cl, it was worked up in the usual way. 3-Methyl-7-ethylindole [bp 90 °C (0.6 mmHg)] was distilled in 63% yield. IR 3400 cm^{-1}; NMR δ=1.31 (t, 3H), 2.32 (d, 3H), 2.68 (q, 2H), 6.39 (q, 1H), 6.7—7.4 (m, 3H), 7.5 (br, 1H). Found: C, 82.77; H, 8.05; N, 8.95%. Calcd for $C_{11}H_{13}N$: C, 82.97; H, 8.23; N, 8.80%.

3-Butyl-7-pentylindole (**20-i**) was similarly prepared and isolated by preparative TLC [TLC (Silica gel, C_6H_6) R_f= 0.79]: IR 3400 cm^{-1}; NMR δ=0.91 (t, 3H), 0.96 (t, 3H), 1.2—1.7 (m, 10H), 2.76 (m, 4H), 6.50 (m, 1H), 6.8—7.5 (m, 3H), 7.6 (br, 1H). Found: C, 83.59; H, 10.30; N, 5.49%. Calcd for $C_{17}H_{25}N$: C, 83.89 ; H, 10.35; N, 5.76%.

*α-Ethylindole-7-ethanol (**19-iii**)*: To a solution of 3 mmol of LDA in 4 mL of diglyme at −78 °C, 197 mg (1.5 mmol) of 2,6-dimethylphenyl isocyanide (**1d**) was added and stirred at the same temperature for 30 min. To the red solution, 174 mg (3 mmol) of propionaldehyde was added at −78 °C. The red color of **2d** turned light yellow soon. Next, a solution of 3 mmol of LDA in 4 mL at −78 °C was added to the light yellow solution, and stirred for 30 min at −78 °C. The reaction mixture, which became red again, was allowed to warm up to room temperature and quenched with aq NH_4Cl. The usual work-up afforded α-ethylindole-7-ethanol in 57% yield [TLC (Silica gel, $CHCl_3$-AcOEt (1:4)) R_f= 0.36]: IR 3400, 3300 cm^{-1}; NMR (CCl_4 with Me_4Si) δ= 0.94 (t, 3H), 1.39 (m, 2H), 2.5 (br, 1H), 2.77 (d, 2H), 3.54 (m, 1H), 6.25 (m, 1H), 6.6—6.9 (m, 3H), 7.20 (m, 1H), 9.1 (br, 1H). Found: C, 76.41; H, 8.18; N, 7.26%. Calcd for C_{12}-$H_{15}NO$: C, 76.15; H, 7.99; N, 7.40%.

*o-(1-Methylpentyl)phenyl Isocyanide (**22-i**). General Procedure for Alkylations of o-Alkylphenyl Isocyanide(**7a**)*: To a solution of 3 mmol of LTMP in 4 mL of diglyme at −78 °C, was added 197 mg (1.5 mmol) of *o*-ethylphenyl iso cyanide (**7a-i**), and stirred for 30 min at the same temperature. To the purple solution, 322 mg (3 mmol) of butyl bromide was added at −78 °C and worked up in the usual way. *o*-(1-Methylpentyl)phenyl isocyanide (**22-i**) [bp 68 °C (2 mmHg)] was isolated in 72% yield by distillation. IR 2115 cm^{-1}; NMR (CCl_4 with Me_4Si) δ=0.88 (t, 3H), 1.1—1.8 (m, 9H), 2.5—3.3 (m, 1H), 6.9—7.4 (m, 4H). Found: C, 83.51; H, 9.00; N, 7.63%. Calcd for $C_{13}H_{17}N$: C, 83.37; H, 9.15; N, 7.48%.

o-(1-Methylpentyl)phenyl isocyanide (**22-i**) was also pre-

pared by methylation of *o*-pentylphenyl isocyanide (**7a-iii**). *o*-Alkylphenyl isocyanides (**22-ii**) and (**22-iii**) were prepared according to the above procedure.

o-Isopropylphenyl Isocyanide (22-ii): [Bp 50 °C (0.1 mmHg)]: IR 2120 cm^{-1}; NMR (CCl_4 with Me_4Si) δ=1.32 (d, 6H), 3.1—3.5 (m, 1H), 7.19 (m, 4H). Found: C, 82.60; H, 7.44; N, 9.37%. Calcd for $C_{10}H_{11}N$: C, 82.72; H, 7.64; N, 9.65%.

o-(1-Methylthioethyl)phenyl Isocyanide (22-iii): [Bp 86 °C (1 mmHg)]: IR 2110 cm^{-1}; NMR (CCl_4 with Me_4Si) δ=1.53 (d, 3H), 1.93 (s, 3H), 4.26 (q, 1H), 7.2—7.7 (m, 4H). Found: C, 67.93; H, 6.05; N, 7.71%. Calcd for $C_{10}H_{11}NS$: C, 67.76; H, 6.25; N, 7.90%.

o-(1-Methylthioethyl)phenyl Isocyanide (22-iii): To a solution of 3 mmol of LDA in 4 mL of diglyme at −78 °C was added 245 mg (1.5 mmol) of *o*-(methylthiomethyl)phenyl isocyanide (**7a-iii**), and stirred for 30 min at the same temperature. To the mixture, 426 mg (3 mmol) of methyl iodide was added at −78 °C and worked up in the usual way.

o-[Bis(methylthio)methyl]phenyl isocyanide (**22-iv**) and *o*-(1-trimethylsilylethyl)phenyl isocyanide (**22-v**) were prepared in the similar way.

o-[Bis(methylthio)methyl]phenyl Isocyanide (22-iv): [Bp 90 °C (0.4 mmHg)]: IR 2115 cm^{-1}; NMR (CCl_4 with Me_4Si) δ= 2.08 (s, 6H), 5.00 (s, 1H), 7.1—7.5 (m, 4H). Found: C, 57.19; H, 5.12; N, 7.01%. Calcd for $C_{10}H_{11}NS_2$: C, 57.38; H, 5.30; N, 6.69%.

o-(1-Trimethylsilylethyl)phenyl Isocyanide (22-v): [Bp 52 °C (0.6 mmHg)]: IR 2130, 1250, 835 cm^{-1}; NMR (CCl_4 with Me_4Si) δ=−0.06 (s, 9H), 1.30 (d, 3H), 2.71 (q, 1H), 6.7—7.2 (m, 4H). Found: C, 70.77; H, 8.40; N, 6.85%. Calcd for $C_{12}H_{17}NSi$: C, 70.87; H, 8.42; N, 6.89%.

α-α-Dimethylindole-3-ethanol (25a-i). General Procedure for One Pot Syntheses of Tryptophol Derivatrives (25): To a solution of 3 mmol of LDA in 4 mL of diglyme at −78 °C was added 176 mg (1.5 mmol) of *o*-tolyl isocyanide (**1a**) and stirred for 30 min at the same temperature. 216 mg (3 mmol) of 2,2-dimethyloxirane was added to the mixture at −78 °C and stirred. After 3 h, 3 mmol of LDA in 2 mL of diglyme was added to the mixture at −78 °C and stirred for additional 2 h. The resulting mixture was allowed to warm up to room temperature and worked up in the usual way. α,α-Dimethylindole-3-ethanol (**25a-i**) [bp 150 °C (0.5 mmHg); mp 92—93 °C (lit,[23] 93—94 °C)] was produced in 68% yield. IR 3400, 3300 cm^{-1}; NMR δ=1.24 (s, 6H), 1.51 (s, 1H), 2.80 (s, 2H), 6.8—7.6 (m, 5H), 8.20 (br, 1H). Tryptophol derivatives (**25a-ii**)[24]—(**25e-viii**) were prepared according to the above procedure.

α-Methylindole-3-ethanol (25a-iii): [Bp 155 °C (0.5 mmHg) (lit,[23] 140—145 °C (0.05 mmHg)); mp 129—133 °C]: IR 3400, 3300 cm^{-1}; NMR δ=1.26 (d, 3H), 2.2 (br, 1H), 2.85 (m, 2H), 4.03 (m, 1H), 7.0—7.7 (m, 5H), 8.0 (br, 1H).

2-(3-Indolyl)cyclohexanol (25a-iv):[25] [Bp 170 °C (0.1 mmHg); mp 168 °C]: IR 3450, 3220 cm^{-1}; NMR δ=1.0—2.0 (m, 9H), 2.5 (m, 1H), 3.8 (m, 1H), 6.9—7.7 (m, 5H), 8.1 (br, 1H). The reaction of *o*-(lithiomethyl)phenyl isocyanide (**2a**) and cyclohexene oxide was slow and took 5 h at −78 °C before the second addition of LDA.

α,α,5-Trimethylindole-3-ethanol (25b-v) (48% yield) was produced together with 2,4-bis(3-hydroxy-3-methylbutyl)-phenyl isocyanide (**26b-v**) (15% yield), which were separated and isolated by preparative TLC. **25b-v** [TLC (Silica gel, $CHCl_3$-AcOEt (5:2)) R_f=0.46]: IR 3400, 3300cm^{-1}; NMR δ=1.09 (s, 6H), 1.79 (br s, 1H), 2.32 (s, 3H), 2.65 (s, 2H), 6.57 (m, 1H), 6.80 (m, 2H), 7.17 (m, 1H), 8.2 (br, 1H). Found: C, 76.56; H, 8.20; N, 6.65%. Calcd for $C_{13}H_{17}NO$: C, 76.81; H, 8.43; N, 6.89%. **26b-v** [TLC (Silica gel, $CHCl_3$-AcOEt (5:2)) R_f=0.12]: IR 3350, 2121 cm^{-1}; NMR δ=1.17 (br s, 12H), 1.70 (m, 4H), 2.32 (br, 2H), 2.72 (m, 4H), 6.8—7.2 (m, 3H). Found: C, 73.96; H, 9.22; N, 5.28%. Calcd for $C_{17}H_{25}NO_2$: C, 74.14; H, 9.15; N, 5.09%.

α,5-Dimethylindole-3-ethanol (**25b-vi**) (48% yield) was produced with 2,4-bis(3-hydroxybutyl)phenyl isocyanide (**26b-vi**) (17% yield). **25b-vi** [Bp 160 °C (0.5 mmHg)]: IR 3400, 3300 cm^{-1}; NMR δ=1.25 (d, 3H), 1.85 (br s, 1H), 2.39 (s, 3H), 2.78 (m, 2H), 4.03 (m, 1H), 6.93 (d, 1H), 7.0—7.4 (m, 3H), 8.1 (br, 1H). Found: C, 75.94; H, 8.08; N, 7.57%. Calcd for $C_{12}H_{15}NO$: C, 76.15; H, 7.99; N, 7.40%. **26b-vi** [TLC (Silica gel, $CHCl_3$-AcOEt (5:2)) R_f=0.14]: IR 3350, 2120 cm^{-1}; NMR δ=1.18 (d, 3H), 1.21 (d, 3H), 1.77 (m, 4H), 2.4—2.9 (m, 6H), 3.6—4.0 (m, 2H), 6.8—7.2 (m, 3H). Found: C, 72.63; H, 8.34; N, 5.88%. Calcd for $C_{15}H_{21}NO_2$: C, 72.84; H, 8.56; N, 5.66%.

α,α,7-Trimethylindole-3-ethanol (**25d-vii**) (23% yield) was produced with 7-(3-hydroxy-3-methylbutyl)indole (**27d-vii**) (33% yield). **25d-ii** [TLC (Silica gel, $CHCl_3$-AcOEt (4:1)) R_f=0.49]: IR 3400, 3350 cm^{-1}; NMR δ=1.23 (s, 6H), 1.82 (s, 1H), 2.38 (s, 3H), 2.80 (s, 2H), 6.90 (m, 3H), 7.35 (m, 1H), 8.1 (br, 1H). Found: C, 76.55; H, 8.22; N, 6.51%. Calcd for $C_{13}H_{17}NO$: C, 76.81; H, 8.43; N, 6.89%. **27d-vii** [TLC (Silica gel, $CHCl_3$-AcOEt (4:1)) R_f=0.18]: IR 3400, 3300 cm^{-1}; NMR δ=1.27 (s, 6H), 1.94 (m, 2H), 2.42 (br s, 1H), 2.80 (m, 2H), 6.7—7.4 (m, 5H), 9.4 (br, 1H). Found: C, 76.64; H, 8.18; N, 6.66%. Calcd for $C_{13}H_{17}NO$: C, 76.81; H, 8.43; N, 6.89%.

1-Methylindole (30a-i). General Procedure for Preparations of 1-Substitued Indoles (30): To a solution of 3 mmol of LDA in 4 mL of diglyme at −78 °C was added 176 mg (1.5 mmol) of **1a**, and stirred for 30 min at the same temperature. After the reaction mixture was allowed to warm up to room temperature, 426 mg (3 mmol) of methyl iodide was added dropwise to the resulting light yellow solution, and stirred for 1 h at room temperature. The progress of the alkylation can be monitored by TLC or GLC. The mixture was worked up in the usual way to give 1-methylindole (**30a-i**) [bp 85 °C (1 mmHg) (lit,[26] 103—105 °C (2 mmHg))] in 82% yield. NMR δ=3.69 (s, 3H), 6.42 (d, 1H) 6.9—7.3 (m, 4H), 7.5—7.7 (m, 1H).

1-Substituted indoles (**30a-ii**)—(**30a-x**) were prepared according to the above procedure.

1-Butylindole (30-ii):[27] [Bp 114 °C (2 mmHg)]: NMR δ=0.93 (t, 3H), 1.0—2.0 (m, 4H), 4.02 (t, 2H), 6.31 (d, 1H), 6.8—7.2 (m, 4H), 7.4—7.6 (m, 1H).

1-(Methoxycarbonylmethyl)indole (30a-iii):[28] [Bp 119 °C (2 mmHg)]: IR 1733 cm^{-1}; NMR (CCl_4 with Me_4Si) δ= 3.56 (s, 3H), 4.66 (s, 2H), 6.32 (d, 1H), 6.82 (d, 1H), 6.9—7.1 (m, 2H), 7.3—7.5 (m, 1H).

1-(Trimethylsilyl)indole (30a-iv): [Bp 74 °C (0.4 mmHg) (lit,[29] 82—84 °C (0.4 mmHg))].

1-Propionylindole (30a-v): [Bp 93 °C (1 mmHg); mp 59—60 °C (lit,[30] 60.5—61 °C)]: IR 1697 cm^{-1}; NMR (CCl_4 with Me_4Si) δ=1.21 (t, 3H), 2.74 (q, 2H), 6.40 (d, 1H), 6.9—7.4 (m, 4H), 8.2—8.4 (m, 1H).

1-(Methoxycarbonyl)indole (30a-vi):[31] [Bp 100 °C (2 mmHg)]: IR 1736 cm^{-1}; NMR δ=3.96 (s, 3H), 6.55 (d, 1H), 7.1—7.6 (m, 4H), 8.0—8.2 (m, 1H).

α-Ethylindole-1-ethanol (30a-vii): [Bp 125 °C (1 mmHg)]: IR 3350 cm^{-1}; NMR δ=1.02 (t, 3H), 1.2—1.7 (m, 2H), 2.0 (br, 1H), 3.8—4.2 (m, 3H), 6.56 (d, 1H), 7.1—7.8 (m, 5H). Found: C, 75.95; H, 7.84; N, 7.15%. Calcd for $C_{12}H_{15}NO$: C, 76.15; H, 7.99; N, 7.40%.

α-Methylindole-1-ethanol (30a-viii): [Bp 117 °C (1 mmHg)]: IR 3350cm^{-1}; NMR δ=1.08 (d, 3H), 1.98 (s, 1H), 3.7—4.1 (m, 3H), 6.42 (d, 1H), 6.9—7.7 (m, 5H). Found: C, 75.19; H, 7.62; N, 7.77%. Calcd for $C_{11}H_{13}NO$: C, 75.40; H, 7.48; N, 7.99%.

α,α-Dimethylindole-1-ethanol (30a-ix): [TLC (Silica gel,

$CHCl_3$-AcOEt (4:1)) R_f=0.76]: IR 3400 cm^{-1}; NMR δ= 1.24 (s, 6H), 1.42 (s, 1H), 4.00 (s, 2H), 6.43 (d, 1H), 6.9—7.6 (m, 5H). Found: C, 76.01; H, 7.72; N, 7.58%. Calcd for $C_{12}H_{15}NO$: C, 76.15; H, 7.99; N, 7.40%.

*1-(2-Hydroxycyclohexyl)indole (**30a-x**)*: [TLC (Silica gel, $CHCl_3$) R_f=0.49]: IR 3400 cm^{-1}; NMR δ=1.0—2.1 (m 9H), 3.2—4.1 (m, 2H), 6.32 (d, 1H), 6.9—7.6 (m, 5H). Found: C, 78.27; H, 8.12; N, 6.37%. Calcd for $C_{14}H_{17}NO$: C, 78.10; H, 7.96; N, 6.51%.

*1-Butyl-3-methylindole (**30a-xi**)*: To a solution of 3 mmol of LTMP in 4 mL of diglyme at −78 °C was added 197 mg (1.5 mmol) of *o*-ethylphenyl isocyanide (**7a-i**) and stirred for 30 min at the same temperature. After the mixture was allowed to warm up to room temperature, 322 mg (3 mmol) of butyl bromide was added dropwise and stirred for 1 h. The usual work-up of the reaction mixture afforded 1-butyl-3-methylindole (**30a-xi**)[31] [bp 170 °C (1 mmHg)] in 65% yield.

*o-(Acetylmethyl)phenyl Isocyanide (**31**). General Procedure for Acylations of **2** with N-Acylaziridines*: To a stirring solution of **2a** (7.5 mmol) in 20 mL of diglyme at −78 °C was added dropwise 1.28 g (15 mmol) of *N*-acetylaziridine. After the reaction mixture was stirred at the same temperature for 10 min, it was worked up in the usual way. *o*-(Acetylmethyl)phenyl isocyanide (**31-i**) (92%) was distilled at bp 105 °C (1 mmHg).[9]

o-[(4-Chlorobutyryl)methyl]phenyl isocyanide (**31-iii**) and *o*-[(4-hydroxybutyryl)methyl]phenyl isocyanide (**31-iv**) were prepared by the reaction of **2a** with ethyl 4-chlorobutyrate and γ-butyrolactone according to the procedure reported.[9]

31-iii [TLC (Silica gel, $CHCl_3$-AcOEt (100:1)) R_f=0.44]: IR 2110, 1718 cm^{-1}; NMR (CCl_4 with Me_4Si) δ=2.15 (m, 2H), 2.80 (t, 2H), 3.61 (t, 2H), 3.91 (s, 2H), 7.0—7.8 (m, 4H). Found: C, 64.84; H, 5.59; N, 6.48%. Calcd for $C_{12}H_{12}NOCl$: C, 65.02; H, 5.46; N, 6.32%.

31-iv [TLC (Silica gel, $CHCl_3$-AcOEt (1:1)) R_f=0.43]: IR 3400, 2120, 1713 cm^{-1};NMR δ=1.83 (quintet, 2H), 2.2 (br, 1H), 2.67 (t, 2H), 3.59 (t, 2H), 3.87 (s, 2H), 7.27 (m, 4H). Found: C, 71.19; H, 6.70; N, 6.75%. Calcd for $C_{12}H_{13}NO_2$: C, 70.91; H, 6.45; N, 6.89%.

*o-(1-Acetylethyl)phenyl Isocyanide (**34-i**). General Procedure for Alkylations of o-(Acylmethyl)phenyl Isocyanide (**31**)*: To a stirring suspension of 48 mg (1 mmol, 50% in Oil) of NaH in 3 mL of DMSO-THF (1:1) at −20 °C was added 159 mg (1 mmol) of *o*-(acetylmethyl)phenyl isocyanide (**31-i**) in 1 mL of THF. After stirring for 15 min, the mixture was treated with 142 mg (1 mmol) of methyl iodide for 30 min. An extractive work-up gave 146 mg (84%) of *o*-(1-acetylethyl)phenyl isocyanide (**34-i**), bp 95 °C (0.4 mmHg). **34-i**: IR 2105, 1718 cm^{-1}; NMR δ=1.42 (d, 3H), 2.13 (s, 3H), 4.15 (q, 1H), 7.1—7.5 (m, 4H). Found: C, 76.44; H, 6.70; N, 8.22%. Calcd for $C_{11}H_{11}NO$: C, 76.27; H, 6.40; N, 8.09%.

*o-(1-Isovalerylethyl)phenyl Isocyanide (**34-ii**)*: [Bp 109 °C 0.2 mmHg)]: IR 2105, 1722 cm^{-1}; NMR δ=0.85 (d, 6H), 1.35 (d, 3H), 2.00—2.45 (m, 3H), 4.05 (q, 1H), 7.0—7.4 (m, 4H). Found: C, 78.03; H, 8.12; N, 6.68%. Calcd for $C_{14}H_{17}NO$: C, 78.10; H, 7.96; N, 6.51%.

*o-(1-Pivaloylethyl)phenyl Isocyanide (**34-iii**)*: [Bp 120 °C (0.6 mmHg)]: IR 2105, 1710 cm^{-1}; NMR δ=1.05 (s, 9H), 1.44 (d, 3H), 4.57 (q, 1H), 7.1—7.5 (m, 4H). Found: C, 77.91; H, 8.15; N, 6.68%. Calcd for $C_{14}H_{17}NO$: C, 78.10; H, 7.96; N, 6.51%.

*o-(1-Pivaloyl-2-methylpropyl)phenyl Isocyanide (**34-iv**)*: [Bp 105 °C (0.3 mmHg)]: IR 2105, 1703 cm^{-1}; NMR (CCl_4 with Me_4Si) δ=0.91 (d, 6H), 1.00 (s, 9H), 2.0—2.5 (m, 1H), 4.11 (d, 1H), 7.0—7.5 (m, 4H). Found: C, 79.03; H, 8.98; N, 5.54%. Calcd for $C_{16}H_{21}NO$: C, 78.97; H, 8.70; N, 5.76%.

*o-(1-Pivaloyl-3-oxobutyl)phenyl Isocyanide (**34-v**)*: [TLC (Silica gel, $CHCl_3$) R_f=0.62]: IR 2105, 1720, 1705 cm^{-1}; NMR δ= 1.13 (s, 9H), 2.15 (s, 3H), 2.56 (dd, 1H), 3.36 (dd, 1H), 5.03 (dd, 1H), 7.1—7.5 (m, 4H). Found: C, 74.44; H, 7.30; N, 5.66%. Calcd for $C_{16}H_{19}NO_2$: C, 74.68; H, 7.44; N, 5.44%.

*2-(1-Pivaloyl-2-cyanoethyl)phenyl Isocyanide (**34-vi**)*: [TLC (Silica gel, $CHCl_3$-AcOEt (40:1)) R_f=0.47]: IR 2238, 2115, 1700 cm^{-1}; NMR δ=1.09 (s, 9H), 2.56 (dd, 2H), 4.94 (t, 1H), 7.2—7.7 (m, 4H). Found: C, 74.81; H, 6.52; N, 11.85%. Calcd for $C_{15}H_{16}N_2O$: C, 74.97; H, 6.71; N, 11.66%.

*o-(1-Benzoyl-3-butenyl)phenyl Isocyanide (**34-vii**)*: [TLC (Silica gel, hexane-C_6H_6 (1:1)) R_f=0.80]: IR 2110, 1725, 1645 cm^{-1};NMR δ=2.4—2.9 (m, 2H), 4.6—5.5 (m, 3H), 5.5—6.4 (m, 1H), 7.1—7.6 (m, 6H), 7.8—8.1 (m, 3H). Found: C, 82.89; H, 5.55; N, 5.58%. Calcd for $C_{18}H_{15}NO$: C, 82.73; H, 5.79; N, 5.36%.

*2-[1-Pivaloyl-2-(ethoxycarbonyl)ethyl]-4-methylphenyl Isocyanide (**34-viii**)*: [TLC (Silica gel, $CHCl_3$-AcOEt (10:1)) R_f=0.54]: IR 2110, 1730, 1715 cm^{-1}; NMR δ=1.10 (s, 9H), 1.28 (t, 3H), 2.26 (s, 3H), 2.43 (dd, 1H), 3.02 (dd, 1H), 4.03 (q, 2H), 4.90 (dd, 1H), 6.8—7.9 (m, 3H). Found: C, 71.63; H, 7.88; N, 4.50%. Calcd for $C_{18}H_{23}NO_3$: C, 71.73; H, 7.69; N, 4.65%.

*2-(1-Pivaloyl-3-butenyl)-6-methylphenyl Isocyanide (**34-ix**)*: [Bp 130 °C (0.4 mmHg)]: IR 2105, 1709, 1640 cm^{-1}; NMR δ=1.06 (s, 9H), 2.45 (s, 3H), 2.4—3.0 (m, 2H), 4.5—5.2 (m, 3H), 5.4—6.0 (m, 1H), 7.1—7.6 (m, 3H). Found: C, 80.09; H, 8.38; N, 5.72%. Calcd for $C_{17}H_{21}NO$: C, 79.96; H, 8.29; N, 5.49%.

*2,3-Dimethylindole (**35-i**). General Procedure for Preparations of 2,3-Disubstituted Indole (**35**)*: A mixture of 173 mg (1 mmol) of *o*-(1-acetylethyl)phenyl isocyanide (**34-i**) and 6 mL of *ca.* 6% HCl in 5:1 methanol-water was stirred for 30 min at room temperature. Then, the mixture was made alkaline by adding 10% aqueous NaOH and stirred for 30 min. An extractive work-up, followed by recrystallization from hexane afforded 90 mg (62%) of 2,3-dimethylindole (**35-i**), mp 106—107 °C (lit,[15b] 105—107 °C).

*2-Isobutyl-3-methylindole (**35-ii**)*: [TLC (Silica gel, $CHCl_3$) R_f=0.85]: IR 3400 cm^{-1}; NMR δ=0.99 (d, 6H), 2.20 (s, 3H), 2.54 (d, 2H), 1.95—2.62 (m, 1H), 7.1—8.1 (m, 5H). Found: C, 83.38; H, 9.30; N, 7.61%. Calcd for $C_{13}H_{17}N$: C, 83.37; H, 9.15; N, 7.48%.

*2-t-Butyl-3-methylindole (**35-iii**)*:[32] [TLC (Silica gel, hexane-C_6H_6 (1:1)) R_f=0.60]: IR 3420 cm^{-1}: NMR δ= 1.40 (s, 9H), 2.31 (s, 3H), 6.8—7.5 (m, 4H), 7.5—7.9 (br, 1H). Found: C, 83.52; H, 9.01; N, 7.30%. Calcd for $C_{13}H_{17}N$: C, 83.37; H, 9.15; N, 7.48%.

*2-t-Butyl-3-isopropylindole (**35-iv**)*: [TLC (Silica gel, hexane-C_6H_6 (1 : 1)) R_f=0.74] (mp 100—102.5 °C): IR (KBr disk) 3430 cm^{-1}; NMR δ=1.42 (s, 9H), 1.45 (d, 6H), 3.44 (m, 1H), 6.8—7.3 (m, 3H), 7.5—7.8 (m, 2H). Found: C, 83.83; H, 10.02; N, 6.73%. Calcd for $C_{15}H_{21}N$: C, 83.66; H, 9.83; N, 6.51%.

*2-t-Butyl-3-(2-oxopropyl)indole (**35-v**)*: [TLC (Silica gel, $CHCl_3$-AcOEt (10:1)) R_f=0.57]: IR 3380, 1697 cm^{-1}; NMR δ=1.40 (s, 9H), 2.05 (s, 3H), 3.84 (s, 2H), 6.9—7.5 (m, 4H), 8.1—8.5 (br, 1H). Found: C, 78.72; H, 8.18; N, 5.96%. Calcd for $C_{15}H_{19}NO$: C, 78.56; H, 8.35; N, 6.11%.

*2-t-Butyl-3-(cyanomethyl)indole (**35-vi**)*: [TLC (Silica gel, $CHCl_3$-AcOEt (40:1)) R_f=0.53]: IR 3375, 2235 cm^{-1}: NMR δ=1.41 (s, 9H), 3.90 (s, 2H), 7.0—7.6 (m, 4H), 7.8—8.5 (br, 1H). Found: C, 79.50; H, 7.81; N, 13.32%. Calcd for $C_{14}H_{16}N_2$: C, 79.21; H, 7.60; N, 13.20%.

*2-Phenyl-3-allylindole (**35-vii**)*: [TLC (Silica gel, hexane-C_6H_6 (1:1)) R_f=0.53]: IR 3390, 1635 cm^{-1}; NMR δ=3.5—3.8 (m, 2H), 4.8—5.3 (m, 2H), 5.8—6.5 (m, 1H), 6.9—8.8

(m, 10H). Found: C, 87.35; H, 6.71; N, 5.98%. Calcd for $C_{17}H_{15}N$: C, 87.51; H, 6.48; N, 6.00%.

*2-t-Butyl-3-(ethoxycarbonylmethyl)-5-methylindole (**35-viii**)*: [TLC (Silica gel, $CHCl_3$) R_f=0.22]: IR 3390, 1725 cm^{-1}; NMR δ=1.29 (t, 3H),1.41 (s, 9H), 2.42 (s, 3H), 3.90 (s, 2H), 4.15 (q, 2H), 6.9—7.5 (m, 3H), 8.0 (br, 1H). Found: C, 74.85; H, 8.58; N, 5.01%. Calcd for $C_{17}H_{23}NO_2$: C, 74.69; H, 8.48; N, 5.12%.

*2-t-Butyl-3-allyl-7-methylindole (**35-ix**)*: [TLC (Silica gel, hexane-C_6H_6 (1:1)) R_f=0.63]: IR 3470, 1638 cm^{-1}; NMR δ= 1.43 (s, 9H), 2.47 (s, 3H), 3.61 (m, 2H), 4.7—5.2 (m, 2H), 5.6— 6.4 (m, 1H), 6.8—7.5 (m, 3H), 7.7 (br 1H). Found: C, 84.28; H, 9.11; N, 6.01%. Calcd for $C_{16}H_{21}N$: C, 84.53; H, 9.31; N, 6.16%.

*2-(3-Chloropropyl)indole (**33-i**)*: [TLC (Silica gel, $CHCl_3$) R_f=0.64]: IR 3375 cm^{-1}; NMR δ=2.11 (quintet, 2H), 2.88 (t, 2H), 3.58 (t, 2H), 6.30 (m, 1H), 7.1—7.7 (m, 4H), 7.8 (br, 1H). Found: C, 68.44; H, 6.40; N, 7.29%. Calcd for $C_{11}H_{12}NCl$: C, 68.22; H, 6.25; N, 7.23%.

*2-(3-Hydroxypropyl)indole (**33-ii**)*: [TLC (Silica gel. $CHCl_3$-AcOEt (10:1)] R_f=0.24] (mp 53—55 °C): IR (KBr disk) 3390, 3300 cm^{-1}; NMR δ=1.6—2.1 (m, 3H), 2.65 (t, 2H), 3.54 (t, 2H), 6.14 (m, 1H), 6.9—7.6 (m, 4H), 8.2 (br, 1H). Found: C, 75.59; H, 7.31; N, 8.10%. Calcd for $C_{11}H_{13}NO$: C, 75.40; H, 7.48; N, 7.99%.

References

1) U. Schöllkopf and F. Gerhart, *Angew. Chem.*, **80**, 842 (1968).

2) D. Hoppe, *Angew. Chem., Int. Ed. Engl.*, **13**, 789 (1974); U. Schöllkopf, *ibid.*, **16**, 339 (1977).

3) T. Saegusa and Y. Ito, "Isonitrile Chemistry," Academic Press, New York, N. Y. (1971), pp. 65—92, and references cited therein.

4) H. M. Walborsky and G. E. Niznik, *J. Am. Chem. Soc.*, **91**, 7778 (1969).

5) Y. Ito, K. Kobayashi, and T. Saegusa, *J. Am. Chem. Soc.*, **99**, 3532 (1977).

6) a) E. Fischer and F. Jourden, *Chem. Ber.*, **16**, 2241 (1883); b) E. Fischer, *Justis Liebigs Ann. Chem.*, **236**, 126 (1886); c) R. J. Sundberg, "The Chemistry of Indoles," Academic Press, New York, N. Y. (1970); d) P. G. Gassmann, T. J. van Bergen, D. P. Gilbert, and B. W. Cue, Jr., *J. Am. Chem. Soc.*, **96**, 5495 (1974); e) J. Bakke, H. Heikman, and E. B. Hellgran, *Acta Chem. Scand., Ser. B*, **28**, 134 (1974); f) L. S. Hegedus, G. S. Allen, and E. L. Watermann, *J. Am. Chem. Soc.*, **98**, 2673 (1976); g) M. Mori and Y. Ban, *Tetrahedron Lett.*, **1976**, 1803; h) R. R. Bard and J. F. Bunnett, *J. Org. Chem.*, **45**, 1546 (1980).

7) *o*-(Lithiomethyl)phenyl isocyanides (**2**) reacted at −78 °C with ketones and aldehydes to give *o*-(2-hydroxyalkyl)phenyl isocyanides in excellent yields. Attempts to cyclize *o*-(2-hydroxyalkyl)phenyl isocyanides *via* the ortho-benzylic lithiation afforded indole-3-methaol derivatives in low yields. Y. Ito, K. Kobayashi, and T. Saegusa, *Tetrahedron Lett.*, **1978**, 2087.

8) *o*-(Lithiomethyl)phenyl isocyanides (**2**) reacted with α,β-unsaturated esters in a conjugate addition to furnish 4-(*o*-isocyanophenyl)butyrates in good yields, which were converted on the ortho-benzylic lithiation to indole-3-propionates in low yields. Y. Ito, K. Kobayashi, M. Maeno, and T. Saegusa, *Chem. Lett.*, **1980**, 487.

9) Y. Ito, K. Kobayashi, and T. Saegusa, *J. Org. Chem.*, **44**, 2030 (1979).

10) The addition of *o*-(s-alkyl)phenyl isocyanides (**22**) to 2 equiv of LTMP in diglyme at −78 °C gave rise to a purple solution, suggesting the formtion of the expected benzylic carbanions. No cyclization product was obtained on warming up the purple solution. Unexpectedly, *o*-(1-methylthioethyl)phenyl isocyanide (**22-iii**) was treated with LTMP at −78 °C followed by warming up to room temperature to give 3-methylindole in good yield.

11) J. E. Baldwin, *J. Chem. Soc., Chem. Commun.*, **1976**, 734.

12) I. Ugi and R. Meyer, *Org. Synth.*, Coll. Vol. V, 1060 (1973).

13) M. Fieser and L. F. Fieser, "Reagents for Organic Synthesis," Wiley, New York, N. Y. (1969), Vol. 2, p. 10.

14) O. M. H. El Dusouqui, M. Hassan, A. R. H. El Nad, and G. Yousif, *J. Chem. Soc., Perkin Trans. 2*, **1976**, 359.

15) C. J. Pouchert, "The Aldrich Library of Infrared Spectra," 2nd ed, Aldrich Chemical Co., Milwaukee, Wis. (1975), and C. J. Pouchert and J. R. Campbell, "The Aldrich Library of NMR Spectra," Aldrich Chemical Co., Milwaukee, Wis. (1974). a) Vol. 2, 1079A and Vol. 8, 51A. b) Vol. 2, 1079E and Vol. 8, 51D. c) Vol. 2, 1082A and Vol. 8, 55A. d) Vol. 2, 1081C and Vol. 8, 54B. e) Vol. 2, 1079B and Vol. 8, 51B.

16) R. R. Lorenz, B. F. Tullar, C. F. Kaelsch, and S. Arether, *J. Org. Chem.*, **30** 2531 (1965).

17) B. Cardillo, G, Casnati, A. Pochini, and A. Ricca, *Tetrahedron*, **23**, 3771 (1967).

18) G. P. Buldrini, M. P. Panunzio, and A. Umani-Rocnch, *J. Chem. Soc., Chem. Commun.*, **1975**, 359.

19) J. Szmuszkovicz, *J. Org. Chem.*, **27**, 515 (1962).

20) A. B. A. Jansen, J. M. Johnson, and J. R. Sortees, *J. Chem. Soc.*, **1964**, 5573.

21) The use of 2 equiv of LDA resulted in the formation of a small amount of 2,6-dialkylphenyl isocyanides (**13**).

22) C. A. Demerson, L. G. Humber, and A. H. Philipp, *J. Med. Chem.*, **19**, 391 (1976).

23) M. Julia, H. Igolen, and J. Lenzi, *Bull. Soc. Chim. Fr.*, **1966**, 2291.

24) M. N. Preobrazhenskaya, K. K. Zhirnova, and N. P. Kostyuchenko, *Zh. Org. Khim.*, **8**, 994 (1972).

25) B. Heath-Brown and P. G. Philpott, *J. Chem Soc.*, **1965**, 7165.

26) N. Nakazaki and K. Yamamoto, *J. Org. Chem.*, **41**, 1877 (1976).

27) H. Plieninger, H. P. Kraemer, and C. Roth, *Chem. Ber.*, **108**, 1776 (1975).

28) S. Naruto, *Mem. Int. Sci. Ind. Res., Osaka Univ.*, **7**, 143 (1950).

29) R. J. Sundberg and H. F. Russell, *J. Org. Chem.*, **38**, 3324 (1973).

30) A. G. Anastassiou, R. L. Eliott, and A. Lichtenfeld, *Tetrahedron Lett.*, **1972**, 4569.

31) N. E. Schore and N. J. Turro, *J. Am. Chem. Soc.*, **97**, 2488 (1975).

32) B. Robinson, *Chem. Ind.*, **1962**, 1291.

N,N'-Carbonyldi[2(3*H*)-benzoxazolethione]: New, Reactive Condensing Agent for the Synthesis of Amides, Esters, Peptides, and Polyamides

Mitsuru UEDA,* Naomi KAWAHARASAKI, and Yoshio IMAI†
Department of Polymer Chemistry, Faculty of Engineering, Yamagata Universtiy, Yonezawa, Yamagata 992
†*Department of Textile and Polymeric Materials, Tokyo Institute of Technology, Meguro-ku, Tokyo 152*
(Received June 7, 1983)

A new condensing agent, *N,N'*-carbonyldi[2(3*H*)-benzoxazolethione] (**3**), was readily prepared by the reaction of 2-benzoxazolethiol and trichloromethyl chloroformate in benzene. The condensing agent **3** is shown to be useful for the preparation of amides, esters, and dipeptides under mild conditions. A successful polyamide synthesis by the polycondensation of isophthalic acid with diamines using **3** is also described.

Dicyclohexylcarbodiimide (DCC) (**1**) and *N,N'*-carbonyldiimidazole (**2**) are useful and popular condensing agents. However, they have some disadvantages in acylation reactions; **1** is accompanied by the formation of *N*-acylurea which causes a purification problem as well as reducing the yield, and **2** is very sensitive to moisture, and must be handled with care. To overcome these problems, many condensing agents have been reported.[1]

As a part of our continuing research program on the preparation of amides, esters, and polyamides under mild conditions,[2] our group has recently initiated the synthesis of new active condensing agents. One requirement for an improved condensing agent is that the conversion of carboxylic acids to the active intermediates should occur readily under mild conditions. In the preceding paper, we showed that 3-substituted 1,2-benzisothiazole 1,1-dioxides and *N,N'*-carbonyldi[1,2-benzisoxazol-3(2*H*)-one] are new reactive condensing agents for the synthesis of amides and esters.[3,4]

We now report that amides, esters, dipeptides, and polyamides can be easily obtained from carboxylic acids and nucleophiles by a one-pot procedure using the new condensing agent, *N,N'*-carbonyldi[2(3*H*)-benzoxazolethione] (**3**).

Results and Discussion

Synthesis of N,N'-*Carbonyldi[2(3H)-benzoxazolethione] (3).* *N*-Acyl derivatives of imidazoles, pyrazoles, and triazoles are highly reactive acylating agent which are involved in numerous condensing methods.[5] For example, carbonyldiimidazole (**2**) has been used for direct condensing method as in Scheme 1. The actual acylating agent is an *N*-acyl imidazole.

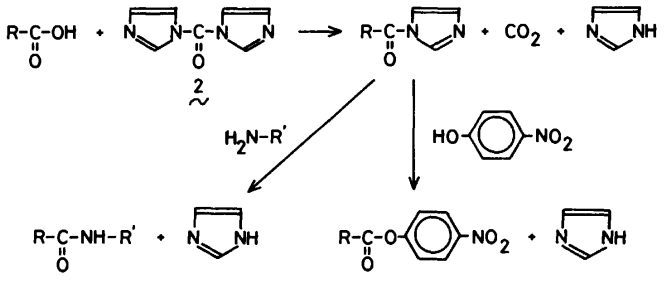

Scheme 1.

Recently we reported that *N*- or *S*-acyl derivatives of 2-benzoxazolethiol (**4**) is a new highly reactive acylating agent for amines and alcohols.[6] This finding prompted us to develop further new condensing agent, *N,N'*-carbonyldi[2(3*H*)-benzoxazolethione] (**3**) for the synthesis of amides and esters *via* *N*- or *S*-acyl derivatives of **4** as an active intermediate.

The condensing agent **3** was conveniently prepared from trichloromethyl chloroformate (**5**) and **4** in a 1:1 molar ratio in benzene (Scheme 2). Recrystallization from cyclohexane gave white needles melting point at 160—161 °C. It is stable even if exposed to atmospheric moisture for a long time. Acylation of **4** might be expected to yield the *S*- or *N*-acyl product, because of the tautomerism of **4**. The more thermodynamically stable isomers (*N*-acyl products) were obtained under a variety of reaction conditions,[7] but *S*-acyl products were obtained with a careful control of the reaction conditions.[6] The reaction of **4** and **5** in benzene under reflux conditions gave preferentially the more thermodynamically stable *N*-acyl product **3**. The structure of **3** was assigned on the basis of IR spectroscopy and elemental analysis. The IR spectrum exhibited a strong carbonyl absorptin at 1680 cm^{-1} and a C=S stretching absorption at 1350 cm^{-1}.

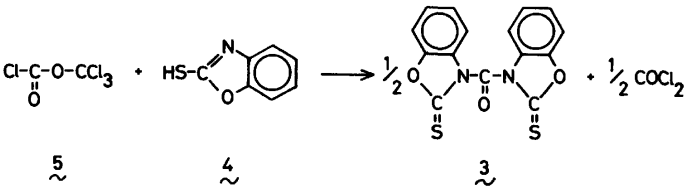

Scheme 2.

Reaction of 3 with Benzoic Acid (6a). In order to clarify the reaction pathway, the reaction of **3** with benzoic acid (**6a**) was carried out in *N*-methyl-2-pyrrolidone (NMP) at room temperature for 2 h in the presence of pyridine as a tertiary base. **3** reacted rapidly with **6a** with liberation of CO_2, and gave 3-benzoyl-2(3*H*)-benzoxazolethione (**7**) together with a

Table 1. Preparation of amides **10** and esters **11** using condensing agent **3**[a]

Carboxylic acid R-COOH, **6** R-	Amine or Alcohol	Reaction time (Step 2)	Product	Yield[b] %
C_6H_5	Aniline	1 h	Benzanilide	83[c]
C_6H_5	Aniline	1 h	Benzanilide	95
C_6H_5	Benzylamine	1 h	*N*-Benzylbenzamide	91
C_5H_{11}	Aniline	1 h	*N*-Phenylhexanamide	85
C_5H_{11}	Benzylamine	1 h	*N*-Benzylhexanamide	84
C_6H_5	Phenol	1 d	Phenyl benzoate	90
C_6H_5	Benzyl alcohol	4 d	Benzyl benzoate	80
C_6H_5	*p*-Nitrophenol	1 d	*p*-Nitrophenyl benzoate	98
C_6H_5	*p*-Aminophenol	1 h	4′-Hydroxybenzanilide	88
C_6H_5	1/2 *p*-Aminophenol	1 h/1 d	4′-Benzoyloxybenzanilide	88

a) Reaction was carried out with 2 mmol of the reactants in 4 ml of NMP at room temperature. Pyridine was used as a tertiary base at step 1. Reaction time: Step 1, 2 h. b) Isolated yields. c) Triethylamine as a tertiary base was used at the step 1.

small amount of benzoic anhydride (**8**). The intermediate **7** has been characterized by high reactivity toward aminolysis. The above observations point to the following pathway (Scheme 3). **3** reacts first with

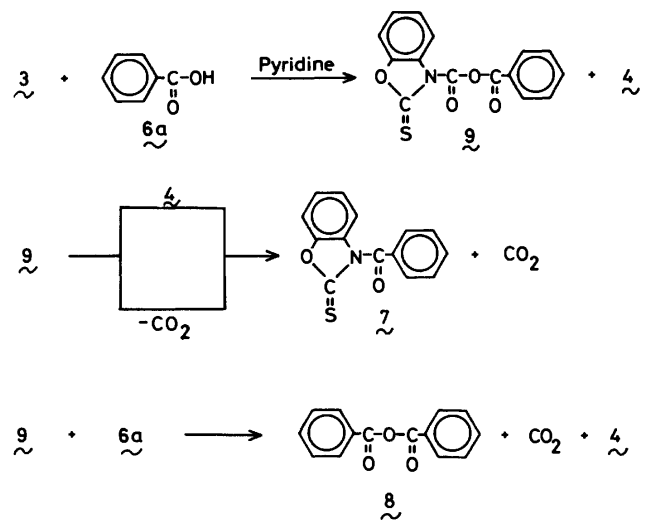

Scheme 3.

6a to form the mixed anhydride **9**, a highly activated acylating agent. The product **9** was less stable and it's enhanced reactivity causes it to react more rapidly with available nucleophiles, **4** and **6a**. These reactions yield the active intermediates **7** and **8**.

Synthesis of Amides (10) and Esters (11). The conversions of carboxylic acids into amides **10** or esters **11** using new condensing agent **3** were carried out by a one-pot procedure at room temperature in the presence of a tertiary base. Equimolar amounts of carboxylic acids, nucleophiles, and the condensing agent **3** are used. This efficient procedure involves two separate steps; (1) "activation" of the carbonyl component, *i.e.* generation of active intermediate **7** and **8** described above; and (2) "condensing" with the nucleophilic reagent (Scheme 4). The rections proceeded smoothly to give the corresponding amides **10**

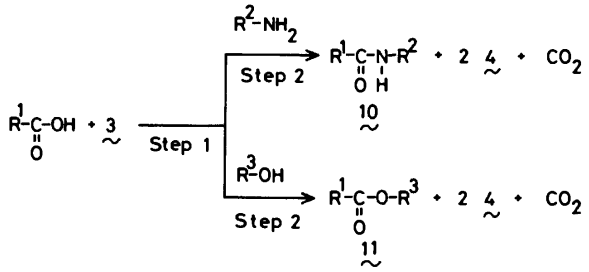

Scheme 4.

and esters **11** in good yields. Pyridine as a base was more favorable than triethylamine (TEA) in step 1. The alcoholysis required an equimolar amount of TEA at step 2.

The amines, as expected from their generally greater reactivity in nucleophilic reactions, react more rapidly than the alcohols with the active intermediates **7** and **8**. With this different reactivity cited above between the reactions of the active intermediates with amines and alcohols, next, the selective *N*-acylation and *N,O*-diacylation of *p*-aminophenol (**12**) were performed either in the absence or in the presence of TEA, respectively. The corresponding amide **13** or amide ester **14** were obtained in good yields (Scheme 5). These results are summarized in Table 1.

Synthesis of Dipeptides (15). Futher it was found that the present reaction was applicable to the preparation of dipeptides **15**. Thus, the reaction of an *N*-protected α-amino acid (**16**) with an α-amino acid ester hydrochloride (**17**) was carried out with **3** in the presence of TEA. The *N*-protected α-amino acid **16** reacted with an equimolar amount of **3** in dichloromethane in the presence of TEA at room temperature. After several hours, the α-amino acid ester hydrochloride **17** and TEA, an acid acceptor, were added. The dipeptide product **15** was isolated in the ordinary manner. The optical purity of the dipeptides was estimated by comparison with the specific rotation of the reported values. *N*-Protected dipeptide esters **15** were prepared in good yields with the suppressed racemization (Table 2), (Scheme 6).

Table 2. Preparation of dipeptide esters **15** using condensing agent **3**[a)]

N-Protected α-amino acid	α-Amino acid ester	Product	Yield[b)] %	Mp θ_m/°C Found	Mp θ_m/°C Reported	$[\alpha]_D$/°(Temp/°C, *c*, Solv.) (Reported)
Z-Ala	Gly-OEt	Z-Ala-Gly-OEt	81	99—100	99—100	−21.0(22, 3.33, EtOH) −22.3(3.65, EtOH)[8)]
Z-Val	Gly-OEt	Z-Val-Gly-OEt	91	169—170	170—171	−30.0(22, 3.33, Dioxane) −32.4(20, 1.85, Dioxane)[3)]
Boc-Leu	Leu-OMe	Boc-Leu-Leu-OMe	77	129—131	131—132	−49.4(22, 2.33, MeOH) −50.0(22, 0.39, MeOH)[9)]
Boc-Phe	Val-OMe	Boc-Phe-Val-OMe	82	115—117	117—118	−10.7(20, 3.00, DMF) −11.0(1.89, DMF)[8)]
Z-Val	Val-OMe	Z-Val-Val-OMe	81	114—116	116	−23.0(22, 1.52, MeOH) −24.3(25, 0.3, MeOH)[10)]

a) Reaction was carried out with 1 mmol of the reactants in 5 ml of dichloromethane. Reaction time: Step 1, 3 h, Step 2, 12 h. b) Isolated yields.

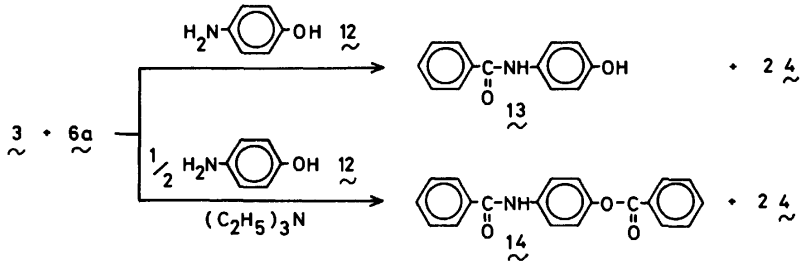

Scheme 5.

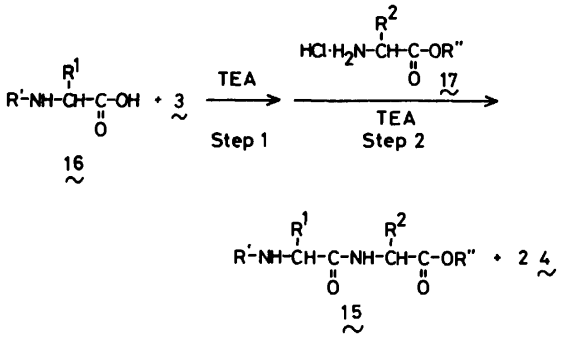

Scheme 6.

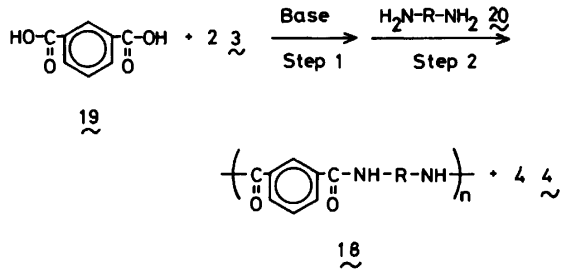

Scheme 7.

Synthesis of Polyamides (18). The direct polycondensation of diamines with dicarboxylic acids to form polyamides under mild conditions has received considerable attention. Most of them are based on phosphorylation reactions. Facile one-pot amide synthesis using the condensing agent **3** provides a promising route to polyamides. The polycondensation of isophthalic acid (**19**) with aromatic diamines (**20**) using **3** was investigated by the two methods, the one-pot polycondensation and the direct polycondensation. The one-pot polycondensation was carried out in solution at low temperature using 4,4′-oxydianiline and 4,4′-methylenedianiline as diamines **20**. The polar aprotic solvents, NMP and hexamethylphosphoric triamide (HMPA), were used as polymerization media (Scheme 7). The activation of isophthalic acid **19** (step 1) was carried out by the addition of the condensing agent **3** to a cold solution of **19** in a polar solvent in the presence of tertiary base. After several hours, the diamine was added. The solution was stirred at room temperature for a specified time. Although the polymers were isolated in excellent yields the molecular weights remained low. In order to determine the influence of base strength in these polymerizations, tertiary amines with a wide range of pK_a values were tested. But, there is no correlation between base strength and the resulting viscosity of the polymer. These results are summarized in Table 3.

To prevent the formation of a small amount of anhydride, the direct polycondensation of **19** with **20** was carried out at temperatures of 0—25 °C in the presence of the condensing agent **3** (Scheme 8). As

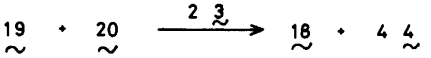

Scheme 8.

Table 3. Synthesis of polyamides **18** by the one-pot polycondensation of isophthalic acid with diamines **20** using the condensing agents **3**[a)]

Diamine H_2N-R-NH_2	Reaction conditions				Polymer		
	Base	Solvent	Time/h		Type	Yield %	η_{inh}[b)] dl g^{-1}
			Step 1	Step 2			
20a -C_6H_4-O-C_6H_4-	TEA	NMP	3	24	**18a**	99	0.10
20a -C_6H_4-O-C_6H_4-	TEA	NMP	24	48	**18a**	99	0.15
20a -C_6H_4-O-C_6H_4-	Pyridine	NMP	3	1	**18a**	99	0.20
20a -C_6H_4-O-C_6H_4-	2-Ethyl pyridine	NMP	15	3	**18a**	99	0.13
20a -C_6H_4-O-C_6H_4-	2-Ethyl pyridine	NMP	48	6	**18a**	99	0.12
20a -C_6H_4-O-C_6H_4-	2,4,6-Trimethyl pyridine	NMP	0.5	24	**18a**	90	0.14
20a -C_6H_4-O-C_6H_4-	Imidazole	NMP	3	16	**18a**	99	0.16
20a -C_6H_4-O-C_6H_4-	Quinoline	NMP	1	12	**18a**	99	0.15
20a -C_6H_4-O-C_6H_4-	Tributyl amine	HMPA	24	24	**18a**	99	0.18
20a -C_6H_4-O-C_6H_4-	*N*-Ethyl piperidine	HMPA	1	24	**18a**	99	0.15
20b -C_6H_4-CH_2-C_6H_4-	Pyridine	HMPA	3	24	**18b**	92	0.10
20b -C_6H_4-CH_2-C_6H_4-	TEA	HMPA	3	24	**18b**	90	0.10

a) Polymerization was carried out with 1 mmol of the monomers using the condensing agent **3** (2 mmol) in the solvent at room temperature. b) Measured at a concentration of 0.5 g dl^{-1} in concentrated sulfuric acid at 30 °C.

Table 4. Synthesis of polyamides **18** by the direct polycondensation of isophthalic acid with diamines **20** using the condensing agent **3**[a)]

Diamine H_2N-R-NH_2	Reaction conditions		Polymer		
	Time h	Temperature °C	Type	Yield %	η_{inh}[b)] dl g^{-1}
20a -C_6H_4-O-C_6H_4-	24	r. t	**18a**	99	0.37
20a -C_6H_4-O-C_6H_4-	48	r. t	**18a**	98	0.35
20a -C_6H_4-O-C_6H_4-	24	0—r. t	**18a**	99	0.50
20a -C_6H_4-O-C_6H_4-	24	40	**18a**	92	0.27
20b -C_6H_4-CH_2-C_6H_4-	15	r. t	**18b**	98	0.23

a) Polymerization was carried out with 1 mmol of the monomers using the condensing agent **3** (2 mmol) in HMPA (2 ml). b) Measured at a concentration of 0.5 g dl^{-1} in concentrated sulfuric acid at 30 °C.

can be seen from the inherent viscosities in Table 4, the polymers were produced in quantitative yields with inherent viscosities up to 0.5 dl g^{-1}. The polymers were identified as polyamides by comparison of their IR spectra with those of the authentic polyamides.

In summary, our studies indicate that the condensing agent **3** is very useful reagent for the formation of amides, esters, peptides, and polyamides. The new condensing agent **3** is a crystalline solid having excellent hydrolytic stability and therefore it is handled more easily than conventional agents. Futhermore 2-benzoxazolethiol **4**, a leaving group, is readily removed from the reaction products by washing the reaction mixture with cold 1% aqueous sodium hydrogencarbonate.

Experimental

Melting points were uncorrected. Infrared spectra were obtained using potassium bromide pellets with a JASCO IRA-1 spectrophotometer. 4,4'-Oxydianiline, and 4,4'-methylenedianiline were recrystallized from tetrahydrofuran and benzene respectively. *N*-Methyl-2-pyrrolidone (supplied by Mitsubishi Chemical Industries Ltd.), hexamethylphosphoric triamides were purified by vacuum distillation and stored 4-Å Molecular Sieves. *N*-Protected α-amino acids and α-amino acid ester hydrochlorides were prepared by usual procedures. Trichloromethyl chloroformate was purchased from Hodogaya Chemical Industries Ltd. The other reagents were used without futher purification.

N,N'-Carbonyldi[2(3H)-benzoxazolethione] (3). A mixture of **4** (15 g, 0.1 mol) and trichloromethyl chloroformate (**5**) (12 ml, 0.1 mol) in benzene (100 ml) was refluxed with stirring for 3 h. Then the solvent was removed *in vacuo*, and the residue was allowed to stand overnight. Purification by recrystallization from cyclohexane gave white needles. Yield: 7.4 g (45%). Mp 160—161 °C; IR (KBr), 1680 and 1350 cm^{-1}.

Found: C, 55.0; H, 2.7; N, 8.6%. Calcd for $C_{15}H_8O_3N_2S_2$: C, 54.87; H, 2.46; N, 8.53.

Reaction of 3 with Benzoic Acid (6a). To a stirred solution of **6a** (0.244 g, 2.0 mmol), pyridine (0.18 ml, 2.0 mmol) in NMP (4 ml) was added **3** (0.657 g, 2.0 mmol), followed by stirring at room temperature for 2 h. The reaction mixture was poured into water (100 ml). The precipitate formed was collected by filtration, washed with water,

and dried *in vacuo*. 3-Benzoyl-2(3*H*)-benzoxazolethione (**7**) was the major product, and a small amount of benzoic anhydride (less than 5%) was formed. The crude product was recrystallized from ethanol to give yellow needles (**7**). Yield: 0.45 g (88%), mp 117—118 °C (lit,[6] 117 °C); IR (KBr), 1695 and 1340 cm^{-1}.

Amide (10). *General Procedure*: The condensing agent **3** (2 mmol) was added to a stirred solution of the carboxylic acid (2 mmol) and pyridine (2 mmol) in NMP (4 ml) at room temperature. After 2 or 3 h, the amine (2 mmol) was added. Stirring was continued for 1 h. The mixture was poured into 1% aqueous sodium hydrogencarbonate. The precipitate was filtered and washed with water and dried.

Ester (11). *General Procedure*: A mixture of **3** (2 mmol), benzoic acid (2 mmol), and pyridine (2 mmol) in NMP (4 ml) was stirred at room temperature for 2 h. To this mixture, the alcohol (2 mmol) and TEA (2 mmol) were added. Stirring was continued for several hours. The reaction mixture was worked up as described above.

Amide Ester (14). The condensing agent **3** (2 mmol) was added with stirring to a solution of benzoic acid (2 mmol) and pyridine (2 mmol) in NMP (4 ml) at room temperature. After 2 h, *p*-aminophenol (**12**) (1 mmol) was added to this mixture. After stirring 2 h, TEA (1 mmol) was added, the mixture was stirred for 4 d, and worked up as described. The compound (**13**) was obtained when TEA was omitted.

N-*Protected Dipepide Ester (15).* *General Procedure*: To a solution of the *N*-protected α-amino acid (1 mmol) and TEA (1 mmol) in dichloromethane (5 ml), **3** (1 mmol) was added under nitrogen. The solution was stirred for 3 h at 0 °C, then the α-amino acid ester hydrochloride (1 mmol) and TEA (1 mmol) were added. The solution was stirred for 12 h at room temperature. After removal of the solvent *in vacuo*, the residue was dissolved in ethyl acetate, and the organic solution was successively with 5% aqueous sodium hydrogencarbonate, 1 M hydrochloric acid and saturated brine, and then dried ($MgSO_4$). After evaporation of ethyl acetate, the dipeptide ester was purified by recrystallization.

Polyamide (18). *One-pot Polycondensation*: The condensing agent **3** was added to a stirred solution of isophthalic acid (**19**) (1 mmol) and pyridine (2 mmol) in NMP (2 ml). The mixture was stirred for a defined time at room temperature, then diamine (1 mmol) was added at room temperature. Stirring was continued for several hours. The resulting solution was poured into 1% aqueous sodium hydrogencarbonate (200 ml) and the precipitated polymer was collected and dried *in vacuo* at 60 °C for 2 d. The inherent viscosity was measured at a concentration of 0.5 g dl^{-1} in concentrated sulfuric acid at 30 °C.

Direct Polycondensation. To a solution of **19** (1 mmol) and diamine (1 mmol) in HMPA (2 ml), the condensing agent **3** (2 mmol) was added at 0 °C. The mixture was stirred for 10 h at 0 °C, and then for 14 h at room temperature. The polymer solution was worked up as described above.

We are indebted to Mr. Sadao Kato for the performance of the elemental analyses.

References

1) "The Peptides," ed by E. Gross and J. Meienhofer, Academic Press, New York (1979), Vol. 1.

2) Y. Imai and M. Ueda, *Yuki Gosei Kagaku Kyokai Shi*, **39**, 312 (1981).

3) M. Ueda, N. Kawaharasaki, and Y. Imai, *Synthesis*, **1982**, 933.

4) M. Ueda, H. Oikawa, N. Kawaharasaki, and Y. Imai, *Bull. Chem. Soc. Jpn.*, **56**, 2485 (1983).

5) H. A. Staab and W. Rohr, "Newer Methods of Preparative Organic Chemistry," ed by W. Forest, Verlag Weinheim (1967), Vol. V, p. 61.

6) M. Ueda, K. Seki, and Y. Imai, *Synthesis*, **1981**, 991.

7) F. Pagani and G. Romussi, *Bull. Chim. Farm.*, **111**, 409 (1972); G. Wagner and S. Leistner, *Pharmazie*, **28**, 25 (1973); G. Wagner and S. Leistner, *ibid.*, **27**, 547 (1972).

8) H. Kinoshita, K. Inomata, O. Miyano, and H. Kotake, *Bull. Chem. Soc. Jpn.*, **52**, 2619 (1979).

9) D. E. Nitecki, B. Halpern, and J. W. Westley, *J. Org. Chem.*, **33**, 864 (1968).

10) J. E. Shields, S. T. McDowell, J. Pavlos, and G. R. Gray, *J. Am. Chem. Soc.*, **90**, 3549 (1968).

Studies of Bitter Peptides from Casein Hydrolyzate. IV.[1] Relationship between Bitterness and Hydrophobic Amino Acids Moiety in the C-Terminal of BPIa (Arg-Gly-Pro-Pro-Phe-Ile-Val)[2]

Ken OTAGIRI, Toshiaki SHIGENAGA, Hidenori KANEHISA, and Hideo OKAI*
Department of Fermentation Technology, Faculty of Engineering, Hiroshima University, Shitami, Saijo-cho, Higashihiroshima 724
(Received June 15, 1983)

In the synthetic studies of bitter peptide BPIa (Arg-Gly-Pro-Pro-Phe-Ile-Val), we synthesized several BPIa analogs to elucidate the participation of the hydrophobic amino acids moiety in the C-terminal in the bitter taste exhibited by BPIa. The syntheses of the peptides were performed by the usual MA (mixed anhydride) and DCC (dicyclohexylcarbodiimide)-HOBt (1-hydroxybenzotriazole) method,[3] and the bitterness of the peptides was organoleptically determined. The BPIa analogs in which more than two hydrophobic amino acids were located in the C-terminal exhibited a bitter taste as strong as that of BPIa.

In 1972, Minamiura *et al.*[4] isolated a bitter heptapeptide named BPIa from casein hydrolyzate by alkaline proteinase of *Bacillus subtilis*. They decided its amino acid sequence as follows: Arg-Gly-Pro-Pro-Phe-Ile-Val. In our laboratory, the authors have investigated the relationship between the bitterness and the chemical structure of BPIa. In a previous paper,[5] we explained that at least two hydrophobic amino acid residues in the C-terminal group are necessary for the intense bitter taste exhibited by BPIa. However, we did not deal with the relationship between the bitterness and the position of the hydrophobic amino acids in the C-terminal group of BPIa in that paper. In order to elucidate this, we synthesized several C-terminal analogs of BPIa, as shown in the Table.

Figure 1 indicates the route for the synthesis of the compound **1** (Arg-Gly-Pro-Pro-Gly-Gly-Val). *N*-(*t*-Butoxycarbonyl)glycylglycylvaline benzyl ester (**12**) was prepared by the reaction of *N*-(*t*-butoxycarbonyl)glycylglycine with valine benzyl ester by means of a mixed anhydride method. The subsequent treatment of **12** with hydrogen chloride in dioxane gave the tripeptide benzyl ester hydrochloride (**13**). *N*-(*t*-Butoxycarbonyl)prolylproline and **13** were coupled by the mixed anhydride method to yield *N*-(*t*-butoxycarbonyl)prolylprolylglycylglycylvaline benzyl ester (**14**). After treatment of **14** with hydrogen chloride, the pentapeptide benzyl ester hydrochloride (**15**) and N^{α}-benzyloxycarbonyl-N^{G}-nitroarginylglycine were coupled by the mixed anhydride method to yield N^{α}-benzyloxycarbonyl-N^{G}-nitroarginylglycylprolylprolylglycylglycylvaline benzyl ester (**16**). The protected heptapeptide was hydrogenated in the presence of palladium black to give the desired heptapeptide (H-Arg-Gly-Pro-Pro-Gly-Gly-Val-OH) (**1**).

Figure 2 indicates the route for the synthesis of the compound **2** (Arg-Gly-Pro-Pro-Gly-Ile-Gly). *N*-(*t*-Butoxycarbonyl)isoleucine and glycine benzyl ester were coupled by the mixed anhydride method to

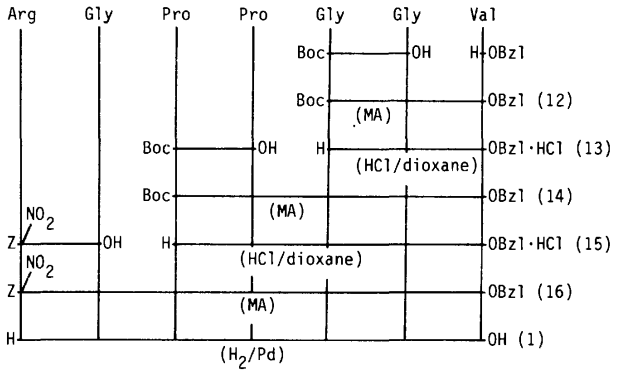

Fig. 1. Synthesis of compound **1**.

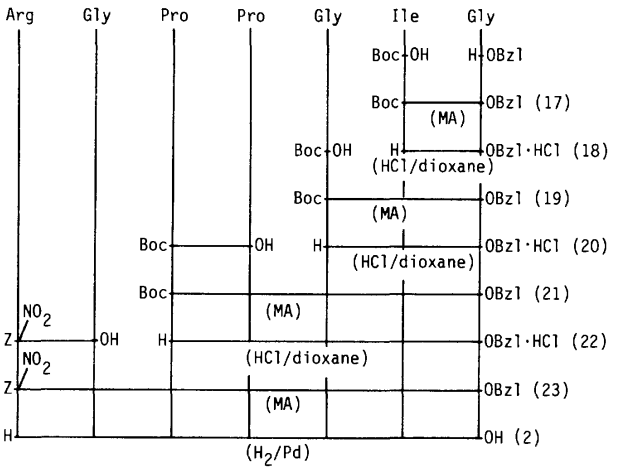

Fig. 2. Synthesis of compound **2**.

TABLE. THE THRESHOLD VALUE FOR BITTER TASTE OF THE SYNTHETIC PEPTIDES

Compound	T.V./mM	$R_{caf.}$[b]
1. Arg-Gly-Pro-Pro-Gly-Gly-Val	3.30	0.3
2. Arg-Gly-Pro-Pro-Gly-Ile-Gly	1.70	0.6
3. Arg-Gly-Pro-Pro-Phe-Gly-Gly	0.60	1.7
4. Arg-Gly-Pro-Pro-Gly-Phe-Gly	0.21	4.8
5. Arg-Gly-Pro-Pro-Gly-Gly-Phe	0.82	1.2
6. Arg-Gly-Pro-Pro-Phe-Phe	0.06	17.0
7. Arg-Gly-Pro-Pro-Gly-Phe-Phe	0.04	25.0
8. Arg-Gly-Pro-Pro-Gly-Gly-Phe-Phe	0.08	13.0
9. Arg-Gly-Pro-Pro-Gly-Gly-Gly-Phe-Phe	0.11	9.0
10. Arg-Gly-Pro-Pro-Phe-Phe-Phe	0.01	100.0
11. Arg-Gly-Pro-Pro-Phe-Ile-Val[a]	0.05	20.0

a) BPIa, isolated by Minamiura *et al.* b) Ratio of caffeine.

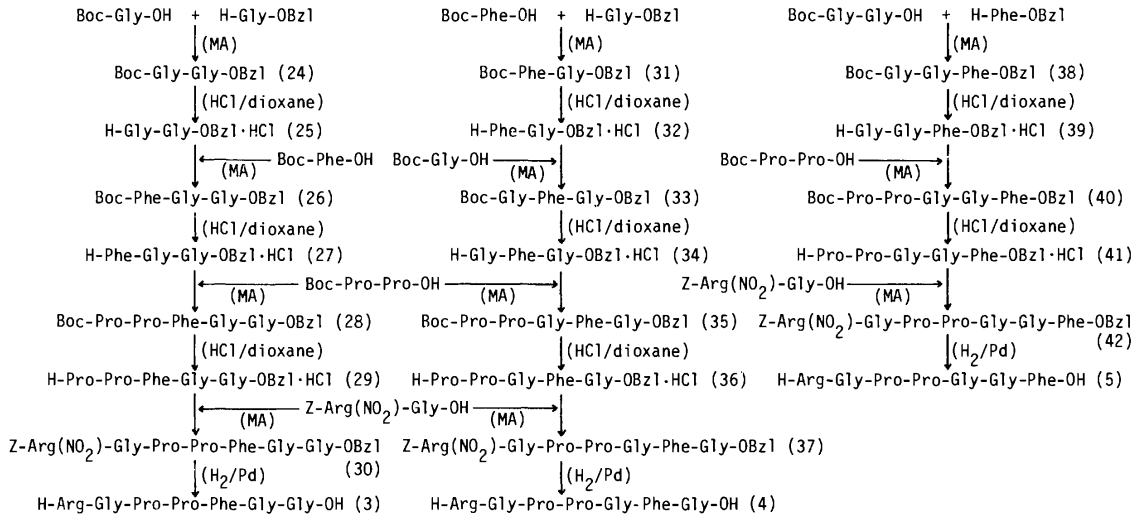

Fig. 3. Syntheses of compounds **3**, **4**, and **5**.

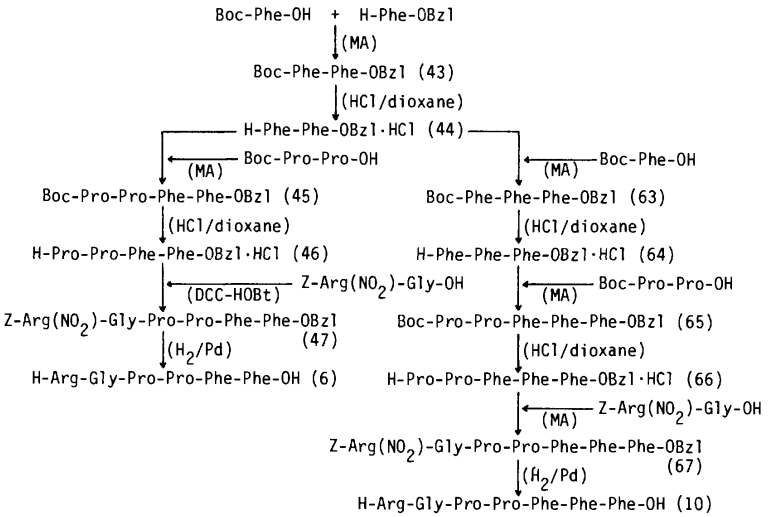

Fig. 4. Syntheses of compounds **6** and **10**.

yield *N*-(*t*-butoxycabonyl)isoleucylglycine benzyl ester (**17**). The subsequent treatment of **17** with hydrogen chloride in dioxane gave the dipeptide ester hydrochloride (**18**). The reaction of *N*-(*t*-butoxycarbonyl)glycine and **18** gave the tripeptide derivative (**19**). After treatment of **19** with hydrogen chloride in dioxane, the tripeptide benzyl ester hydrochloride (**20**) and *N*-(*t*-butoxycarbonyl)prolylproline were coupled by the mixed anhydride method to yield *N*-(*t*-butoxycarbonyl)prolylprolylglycylisoleucylglycine benzyl ester (**21**). The removal of the *t*-butoxycarbonyl group from **21** with hydrogen chloride in dioxane afforded the corresponding pentapeptide benzyl ester hydrochloride (**22**). N^{α}-Benzyloxycarbonyl-N^{G}-nitroarginylglycine and **22** were coupled by the mixed anhydride method to yield N^{α}-benzyloxycarbonyl-N^{G}-nitroarginylglycylprolylprolylglycylisoleucylglycine benzyl ester (**23**). The protected heptapeptide was hydrogenated in the presence of palladium black to give the desired compound (H–Arg–Gly–Pro–Pro–Gly–Ile–Gly–OH) (**2**).

The details of the synthetic routes to other peptides (compounds **3**—**10**) are shown in Figs. 3—5, and are described in the Experimental part. The purity of the synthetic peptides and their intermediates was confirmed by thin-layer examinations in two solvent systems, elemental analyses, and amino acid analyses.

The bitterness of the synthetic peptides was organoleptically determined by a panel evaluation of five people (see Table). Compounds **1**—**3** were synthesized to confirm the participation of the hydrophobic moiety in the bitter taste exhibition; bitterness of these compounds was weaker than that of BPIa. Compounds **3**, **4**, and **5** in which an L-phenylalanine residue is located at 5, 6, and 7 position[6] respectively, also exhibited a weak bitter taste. On the other hand, the bitterness of compounds **6**—**9**, in which two L-phenylalanine residues are located in the C-terminal, was on the same level as that of BPIa.

We treated the relationship between bitterness and the position of the hydrophobic amino acid residue. The bitterness of compound **4**, in which an L-phenylalanine residue locates at 6 position, was stronger than that of compounds **3** and **5**, which contain the hydrophobic amino acid residue at 5 and 7 posi-

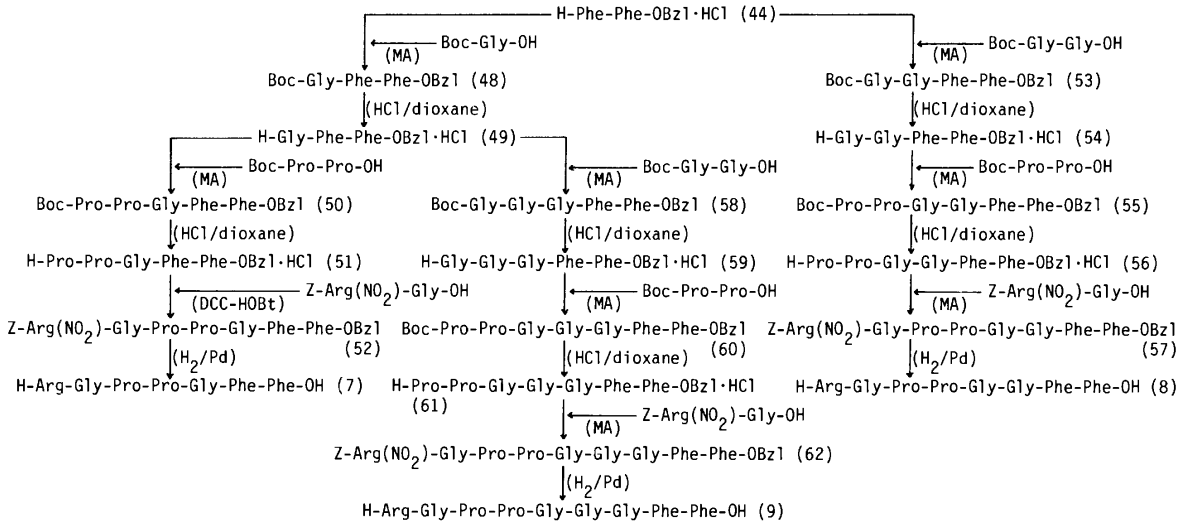

Fig. 5. Syntheses of compounds **7**, **8**, and **9**.

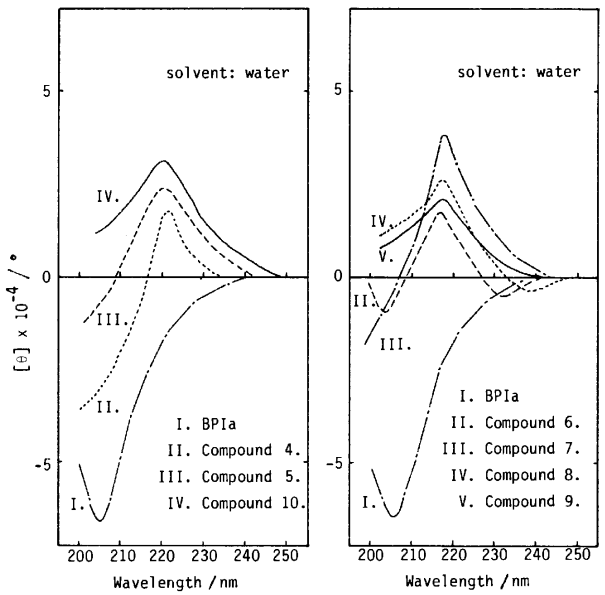

Fig. 6. CD curves of BPIa and its C-terminal analogs.

tion respectively. For compounds **6**—**9**, similar results obtained. In the previous paper,[5] we reported that the des-Gly[2]-BPIa, des-Pro[4]-BPIa, and des-Val[7]-BPIa, in which an L-hydrophobic amino acid residue is located at 6-position, exhibited a bitter taste as strong as that of BPIa.

The bitterness of compound **10**, in which three L-phenylalanine residues are located in the C-terminal, was five times stronger than that of BPIa. The result indicated that the strength of the bitterness increased with an increase of the hydrophobicity in the C-terminal. In conclusion, the presented data suggest that the hydrophobicity of the C-terminal moiety and the L-hydrophobic amino acid at 6-position were necessary for an intense bitter taste to be exhibited by BPIa.

The authors measured the circular dichroism (CD) of the synthetic peptides in this study, as shown in Fig. 6. In the previous papers,[1,5] the BPIa analogs that exhibited as strong and bitter a taste as BPIa have similarly shaped CD curves, with a negative trough at about 205 nm just as BPIa possesses. However, both the BPIa analogs in this study, the one which exhibited a strong bitter taste and the one with a weak bitter taste, have CD curves shaped oppositely to those of the BPIa analogs in the previous papers.[1,5] Further studies of this question are now in progress.

Experimental

All the melting points are uncorrected. Thin-layer chromatography (TLC) was carried out on Merck silica gel G with the following solvent systems: R_f^1, 1-butanol–acetic acid–pyridine–water (4:1:1:2, v/v); R_f^2, chloroform–methanol (5:1, v/v). Materials possessing a free amino group on a thin-layer plate were detected by spraying with ninhydrin. Compounds with blocked amino groups were detected by spraying with 25% hydrogen bromide in acetic acid and then with ninhydrin. The optical rotations were measured on a Union PM-101 polarimeter. Amino acid analyses were performed on a Hitachi amino acid analyzer KLA-5 type, after hydrolysis in a mixture of 6 M HCl (1 M=1 mol dm^{-3}) and propionic acid (1:1) at 110 °C for 72 h.

Boc-Gly-Gly-Val-OBzl (12). To a solution of Boc-Gly-Gly-OH[1] (2.32 g, 10 mmol) in DMF (20 ml) and NMM (1.1 ml, 10 mmol), ECF (1.0 ml, 10 mmol) was added at −5 °C. After 10 min, a solution of H-Val-OBzl·TsOH[7,8] (3.80 g, 10 mmol) and NMM (1.1 ml, 10 mmol) in chloroform (20 ml) was added. The reaction mixture was stirred in an ice bath for 1 h, then at room temperature overnight. The mixture was evaporated *in vacuo*, and the oily residue was dissolved in ethyl acetate. The solution was washed with water, 4% citric acid, 4% sodium hydrogencarbonate, and water successively, then dried over anhydrous sodium sulfate. Sodium sulfate was removed by filtration, and the filtrate was evaporated *in vacuo*. The oily residue was crystallized with ether–petroleum ether: yield 2.82 g (84%); mp 127—130 °C; $[\alpha]_D^{20}$ −21.0° (*c* 1, methanol); R_f^1 0.93 and R_f^2 0.67.

Found: C, 59.50; H, 7.43; N, 9.95%. Calcd for $C_{21}H_{31}O_6N_3$: C, 59.84; H, 7.41; N, 9.97%.

H-Gly-Gly-Val-OBzl·HCl (13). To a solution of compound **12** (2.40 g, 5.7 mmol) in dioxane (10 ml), 4 M HCl/dioxane (20 ml) was added. The reaction mixture was allowed to stand at room temperature. After 1.5 h, the solution was evaporated *in vacuo*. The residual oil was crystallized with ether: yield 1.82 g (89%); mp 205—206 °C; $[\alpha]_D^{20}$ −32.0° (*c* 1, methanol); R_f^1 0.80 and R_f^2 0.25.

Found: C, 53.16; H, 6.74; N, 11.63%. Calcd for $C_{16}H_{23}O_4N_3 \cdot HCl \cdot 1/4\ H_2O$: C, 53.03; H, 6.82; N, 11.60%.

Boc-Pro-Pro-Gly-Gly-Val-OBzl (14). Boc-Pro-Pro-OH[7,9] (1.25 g, 4 mmol) and compound **13** (1.43 g, 4 mmol) were coupled by the same method as described for the preparation of **12**: yield 2.12 g (86%); mp 73—76 °C; $[\alpha]_D^{20}$ −67.5° (*c* 1, methanol): R_f^1 0.82 and R_f^2 0.52.

Found: C, 59.16; H, 7.21; N, 10.72%. Calcd for $C_{31}H_{45}O_8N_5 \cdot H_2O$: C, 58.75; H, 7.47; N, 11.05%.

H-Pro-Pro-Gly-Gly-Val-OBzl·HCl (15). Compound **14** (2.11 g, 3.4 mmol) was treated as described in the case of **13**: yield 1.93 g (99%); mp 97—101 °C; $[\alpha]_D^{20}$ −50.0° (*c* 1, methanol); R_f^1 0.71 and R_f^2 0.55.

Found: C, 54.96; H, 6.87; N, 12.29%. Calcd for $C_{26}H_{37}O_6N_5 \cdot HCl \cdot H_2O$: C, 54.77; H, 7.07; N, 11.73%.

Z-Arg(NO$_2$)-Gly-Pro-Pro-Gly-Gly-Val-OBzl (16). Z-Arg(NO$_2$)-Gly-OH[7,10] (0.82 g 2 mmol) and compound **15** (1.10 g 2 mmol) were coupled by the same method as described for the preparation of **12**: yield 1.52 g (84%); mp 114—117 °C; $[\alpha]_D^{20}$ −69.0° (*c* 1, methanol); R_f^1 0.71 and R_f^2 0.55.

Found: C, 54.40; H, 6.30; N, 16.46%. Calcd for $C_{42}H_{57}O_{12}N_{11} \cdot H_2O$: C, 54.47; H, 6.42; N, 16.64%.

H-Arg-Gly-Pro-Pro-Gly-Gly-Val-OH (1). A solution of **16** (0.79 g, 1 mmol) in methanol (2 ml) and acetic acid (2 ml) was hydrogenated in the presence of palladium black at room temperature for 24 h. The catalyst was removed by filtration, then the filtrate was evaporated *in vacuo*. The residue was crystallized with acetone: yield 0.39 g (94%); mp 176—178 °C $[\alpha]_D^{20}$ −83.5° (*c* 1, H_2O); R_f^1 0.26 and R_f^2 0.00.

Found: C, 48.70; H, 7.20; N, 19.36%. Calcd for $C_{27}H_{46}O_8N_{10} \cdot H_2O \cdot CH_3COOH$: C, 48.59; H, 7.33; N, 19.55%.

Amino acid ratios in acid hydrolyzate: Arg 0.95, Gly 2.89, Pro 2.08, Val 1.00.

Boc-Ile-Gly-OBzl (17). Boc-Ile-OH·DCHA,[7,11] (13.62 g, 33 mmol) and H-Gly-OBzl·TsOH[12] (10.12 g, 30 mmol) were coupled by the same method as described for the preparation of **12**: yield 9.28 g (82%); mp 99—100 °C; $[\alpha]_D^{20}$ −22.5° (*c* 1, methanol); R_f^1 0.98 and R_f^2 0.71.

Found: C, 63.63; H, 8.09; N, 7.40%. Calcd for $C_{20}H_{30}O_5N_2$: C, 63.47; H, 7.99; N, 7.40%.

H-Ile-Gly-OBzl·HCl (18). Compound **17** (3.78 g, 10 mmol) was treated as described in the case of **13**: yield 2.96 g (94%); mp 52—56 °C; $[\alpha]_D^{20}$ +4.0° (*c* 1, methanol); R_f^1 0.78 and R_f^2 0.62.

Found: C, 56.48; H, 7.48; N, 8.79%. Calcd for $C_{15}H_{22}O_3N_2 \cdot HCl \cdot 1/4\ H_2O$: C, 56.42; H, 7.42; N, 8.77%.

Boc-Gly-Ile-Gly-OBzl (19). Boc-Gly-OH[13] (1.75 g, 10 mmol) and compound **18** (3.20 g, 10 mmol) were coupled by the same method as described for the preparation of **12**: yield 3.47 g (87%); mp 97—99 °C; $[\alpha]_D^{20}$ −28.5° (*c* 1, methanol); R_f^1 0.98 and R_f^2 0.43.

Found: C, 60.61; H, 7.69; N, 9.61%. Calcd for $C_{22}H_{33}O_6N_3$: C, 60.67; H, 7.64; N, 9.65%.

H-Gly-Ile-Gly-OBzl·HCl (20). Compound **19** (2.62 g, 6 mmol) was treated as described in the case of **13**: yield 2.21 g (99%); mp 185—187 °C; $[\alpha]_D^{20}$ −33.0° (*c* 1, methanol); R_f^1 0.77 and R_f^2 0.43.

Found: C, 53.25; H, 6.99; N, 11.19%. Calcd for $C_{17}H_{25}O_4N_3 \cdot HCl \cdot 2/3\ H_2O$: C, 53.18; H, 7.17; N, 10.95%.

Boc-Pro-Pro-Gly-Ile-Gly-OBzl (21). Boc-Pro-Pro-OH[7,9] (1.56 g, 5 mmol) and compound **20** (1.86 g, 5 mmol) were coupled by the same method as described for the preparation of **12**: yield 2.90 g (92%); 80—82 °C; $[\alpha]_D^{20}$ −63.0° (*c* 1, methanol); R_f^1 0.85 and R_f^2 0.50.

Found: C, 60.00; H, 7.52; 10.56%. Calcd for $C_{32}H_{47}O_8N_5 \cdot 3/4\ H_2O$: C, 59.75; H, 7.60; N, 10.89%.

H-Pro-Pro-Gly-Ile-Gly-OBzl·HCl (22). Compound **21** (2.79 g, 4.4 mmol) was treated as described in the case of **13**: yield 2.48 g (98%); mp 96—100 °C; $[\alpha]_D^{20}$ −62.0° (*c* 1, methanol); R_f^1 0.75 and R_f^2 0.40.

Found: C, 55.23; H, 6.97; N, 11.72%. Calcd for $C_{27}H_{39}O_6N_5 \cdot HCl \cdot H_2O$: C, 55.52; H, 7.08; N, 11.99%.

Z-Arg(NO$_2$)-Gly-Pro-Pro-Gly-Ile-Gly-OBzl (23). Z-Arg(NO$_2$)-Gly-OH[7,10] (0.82 g, 2 mmol) and compound **22** (1.14 g, 2 mmol) were coupled by the same method as described for the preparation of **12**: yield 0.78 g (85%); mp 114—117 °C; $[\alpha]_D^{20}$ −70.0° (*c* 1, methanol); R_f^1 0.85 and R_f^1 0.53.

Found: C, 55.20; H, 6.41; N, 16.34%. Calcd for $C_{43}H_{59}O_{12}N_{11} \cdot H_2O$: C, 54.94; H, 6.51 N, 16.39%.

H-Arg-Gly-Pro-Pro-Gly-Ile-Gly-OH (2). Compound **23** (0.92 g, 1 mmol) was treated as described in the case of **1**: yield 0.62 g (87%); mp 183—185 °C; $[\alpha]_D^{20}$ −116.0° (*c* 1, H_2O); R_f^1 0.20 and R_f^2 0.00.

Found: C, 50.47; H, 7.41; N, 19.80%. Calcd for $C_{28}H_{48}O_8N_{10} \cdot CH_3COOH$: C, 50.54; H, 7.35; N, 19.65%.

Amino acid ratios in acid hydrolyzate: Arg 0.93, Gly 3.01, Pro 1.97, Ile 1.00.

Boc-Gly-Gly-OBzl (24). Boc-Gly-OH[13] (5.26 g, 30 mmol) and H-Gly-OBzl·TsOH (10.12 g, 30 mmol) were coupled by the same method as described for the preparation of **12** : yield 8.89 g (92%); mp 84—85 °C; R_f^1 0.98 and R_f^2 0.76.

Found: C, 59.61; H, 6.91; N, 8.68%. Calcd for $C_{16}H_{22}O_5N_2$: C, 59.61; H, 6.88; N, 8.69%.

H-Gly-Gly-OBzl·HCl (25). Compound **24** (6.45 g, 20 mmol) was treated as described in the case of **13**: yield 4.93 g (95%); mp 158—160 °C (lit,[14] 160 °C) R_f^1 0.76 and R_f^2 0.26.

Found: C, 51.00; H, 5.87; N, 10.86%. Calcd for $C_{11}H_{14}O_3N_2 \cdot HCl$: C, 51.07; H, 5.84; N, 10.83.

Boc-Phe-Gly-Gly-OBzl (26). Boc-Phe-OH·DCHA[15] (4.91 g, 11 mmol) and compound **25** (2.59 g, 10 mmol) were coupled by the same method as described for the preparation of **13**: yield 4.01 g (85%); mp 100—102 °C; $[\alpha]_D^{20}$ +8.5° (*c* methanol); R_f^1 0.97 and R_f^2 0.75.

Found: C, 64.06; H, 6.71; N, 9.03%. Calcd for $C_{25}H_{31}O_6N_3$: C, 63.94; H, 6.66; N, 8.95%.

H-Phe-Gly-Gly-OBzl·HCl (27). Compound **26** (3.29 g, 7 mmol) was treated as described in the case of **13**: yield 2.69 g (92%); mp 60—63 °C; $[\alpha]_D^{20}$ −35.5° (*c* 1, methanol); R_f^1 0.80 and R_f^2 0.49.

Found: C, 55.42; H, 6.25; N, 9.98%. Calcd for $C_{20}H_{23}O_4N_3 \cdot HCl \cdot 3/2\ H_2O$: C, 55.48; H, 6.29; N, 9.71%.

Boc-Pro-Pro-Phe-Gly-Gly-OBzl (28). Boc-Pro-Pro-OH[7,9] (1.25 g, 4 mmol) and compound **27** (1.63 g, 4 mmol) were coupled by the same method as described for the preparation of **12**: yield 2.32 g (89%); mp 78—81 °C; $[\alpha]_D^{20}$ −73.0° (*c* 1, methanol); R_f^1 0.91 and R_f^2 0.50.

Found: C, 61.65; H, 6.86; N, 10.00%. Calcd for $C_{35}H_{45}O_8N_5 \cdot H_2O$: C, 61.66; H, 6.95; N, 10.27%.

H-Pro-Pro-Phe-Gly-Gly-OBzl·HCl (29). Compound **28** (2.77 g, 4.2 mmol) was treated as described in the case of **13**: yield 2.37 g (93%); mp 102—107 °C; $[\alpha]_D^{20}$ −68.5° (*c* 1, methanol); R_f^1 0.78 and R_f^2 0.42.

Found: C, 57.62; H, 6.33; N, 10.88%. Calcd for $C_{30}H_{37}O_6N_5 \cdot HCl \cdot 3/2\ H_2O$: C, 57.45; H, 6.59; N, 11.17%.

Z-Arg(NO$_2$)-Gly-Pro-Pro-Phe-Gly-Gly-OBzl (30). Z-Arg(NO$_2$)-Gly-OH[7,10] (0.82 g, 1 mmol) and compound

29 (1.20 g, 1 mmol) were coupled by the same method as described for the preparation of **12**: yield 0.70 g (72%); mp 114—117 °C; $[\alpha]_D^{20}$ −72.5° (*c* 1, methanol); R_f^1 0.86 and R_f^2 0.56.

Found: C, 56.88; H, 6.00; N, 15.79%. Calcd for $C_{46}H_{57}O_{12}N_{11}\cdot H_2O$: C, 56.71; H, 6.11; N, 15.81%.

H-Arg-Gly-Pro-Pro-Phe-Gly-Gly-OH (3). Compound **30** (0.96 g, 1 mmol) was treated as described in the case of **1**: yield 0.61 g (81%) mp 180 °C (decomp); $[\alpha]_D^{20}$ −106.0° (*c* 1, H_2O); R_f^1 0.21 and R_f 0.00.

Found: C, 51.98; H, 6.81; N, 17.95%. Calcd for $C_{31}H_{46}O_8N_{10}\cdot H_2O\cdot CH_3COOH$: C, 51.82; H, 6.87; N, 18.32%.

Amino acid ratios in acid hydrolyzate: Arg 0.92, Gly 3.00, Pro 1.99, Phe 1.00.

Boc-Phe-Gly-OBzl (31). Boc-Phe-OH·DCHA[15] (9.83 g, 22 mmol) and H-Gly-OBzl·TsOH[12] (6.75 g, 20 mmol) were coupled by the same method as described for the preparation of **12**: yield 7.76 g (94%); mp 134—135 °C; $[\alpha]_D^{20}$ −7.0° (*c* 1, methanol); R_f^1 0.94 and R_f^2 0.91.

Found: C, 66.99; H, 6.81; N, 6.84%. Calcd for $C_{23}H_{28}O_5N_2$: C, 66.96: H, 6.86; N, 6.79%.

H-Phe-Gly-OBzl·HCl (32). Compound **31** (6.18 g, 15 mmol) was treated as described in the case of **13**. This product was obtained in a hygroscopic form: yield 5.37 g (98%); R_f^1 0.72 and R_f^2 0.61.

Boc-Gly-Phe-Gly-OBzl (33). Boc-Gly-OH[13] (1.75 g, 10 mmol) and compound **32** (3.65 g, 10 mmol) were coupled by the same method as described for the preparation of **12**. This product was obtained in an oily form: yield 4.51 g (96%); R_f^1 0.96 and R_f^2 0.77.

H-Gly-Phe-Gly-OBzl·HCl (34). Compound **33** (4.51 g, 9.6 mmol) was treated as described in the case of **13**. This product was obtained in an oily form: yield 3.76 g (97%); R_f^1 0.70 and R_f^2 0.41.

Boc-Pro-Pro-Gly-Phe-Gly-OBzl (35). Boc-Pro-Pro-OH[7,9] (2.91 g, 9.33 mmol) and compound **34** (3.76 g, 9.33 mmol) were coupled by the same method as described for the preparation of **12**. This product was obtained in an oily form: yield 4.70 g (76%); R_f^1 0.85 and R_f^2 0.69.

H-Pro-Pro-Gly-Phe-Gly-OBzl·HCl (36). Compound **35** (4.71 g, 7.09 mmol) was treated as described in the case of **13**: yield 4.00 g (94%); mp 76—78 °C; $[\alpha]_D^{20}$ −36.5° (*c* 1, methanol); R_f^1 0.72 and R_f^2 0.33.

Found: C, 58.27; H, 6.60; N, 11.29%. Calcd for $C_{30}H_{37}O_6N_5\cdot HCl\cdot H_2O$: C, 58.28; H, 6.53; N, 11.33%.

Z-Arg(NO₂)-Gly-Pro-Pro-Gly-Phe-Gly-OBzl (37). Z-Arg(NO₂)-Gly-OH[7,10] (0.82 g, 2 mmol) and compound **36** (1.19 g, 2 mmol) were coupled by the same method as described for the preparation of **12**: yield 1.39 g (73%); mp 125—128 °C; $[\alpha]_D^{20}$ −77.0° (*c* 1, acetic acid); R_f^1 0.75 and R_f^2 0.53.

Found: C, 57.21; H, 6.11; N, 16.02%. Calcd for $C_{46}H_{57}O_{12}N_{11}\cdot 1/2\ H_2O$: C, 57.25; H, 6.07; N, 15.97%.

H-Arg-Gly-Pro-Pro-Gly-Phe-Gly-OH (4). Compound **37** (0.96 g, 1 mmol) was treated as described in the case of **1**: yield 0.59 g (79%); mp 87—89 °C; $[\alpha]_D^{20}$ −83.0° (*c* 1, H_2O); R_f^1 0.20 and R_f^2 0.00.

Found: C, 52.01; H, 6.89; N, 18.24%. Calcd for $C_{31}H_{46}O_8N_{10}\cdot H_2O\cdot CH_3COOH$: C, 51.82; H, 6.87; N, 18.32%.

Amino acid ratios in acid hydrolyzate: Arg 0.93, Gly 2.99, Pro 1.98, Phe 1.00.

Boc-Gly-Gly-Phe-OBzl (38). Boc-Gly-Gly-OH[1] (2.58 g, 8 mmol) and H-Phe-OBzl·TsOH[16,17] (3.42 g, 8 mmol) were coupled by the same method as described for the preparation of **12**. This product was obtained in an oily form: yield 2.59 g (69%); R_f^1 0.93 and R_f^2 0.69.

H-Gly-Gly-Phe-OBzl·HCl (39). Compound **38** (2.59 g, 5.49 mmol) was treated as described in the case of **13**: yield 2.15 g (97%); mp 122—123 °C; $[\alpha]_D^{20}$ −2.0° (*c* 1, methanol); R_f^1 0.67 and R_f^2 0.27.

Found: C, 56.61; H, 6.02; N, 9.87%. Calcd for $C_{20}H_{23}O_4N_3\cdot HCl\cdot H_2O$: C, 56.65; H, 5.96; N, 9.91%.

Boc-Pro-Pro-Gly-Gly-Phe-OBzl (40). Boc-Pro-Pro-OH[7,9] (1.56 g, 5 mmol) and compound **39** (2.02 g, 5 mmol) were coupled by the same method as described for the preparation of **12**. This product was obtained in a hygroscopic form: yield 2.13 g (64%); R_f^1 0.76 and R_f^2 0.65.

H-Pro-Pro-Gly-Gly-Phe-OBzl·HCl (41). Compound **40** (2.13 g, 3.2 mmol) was treated as described in the case of **13**: yield 1.80 g (94%); mp 94—97 °C; $[\alpha]_D^{20}$ −35.0° (*c* 1, methanol); R_f^1 0.68 and R_f^2 0.32.

Found: C, 59.08; H, 6.44; N, 11.59%. Calcd for $C_{30}H_{37}O_6N_5\cdot HCl\cdot 1/2\ H_2O$: C, 59.14; H, 6.47; N, 11.50%.

Z-Arg(NO₂)-Gly-Pro-Pro-Gly-Gly-Phe-OBzl (42). Z-Arg(NO₂)-Gly-OH[7,10] (0.82 g 2 mmol) and compound **41** (1.19 g, 2 mmol) were coupled by the same method as described for the preparation of **12**: yield 1.43 g (79%); mp 121—123 °C; $[\alpha]_D^{20}$ −63.0° (*c* 1, acetic acid); R_f^1 0.75 and R_f^2 0.53.

Found: C, 56.11; H, 6.13; N, 15.72%. Calcd for $C_{46}H_{57}O_{12}N_{11}\cdot 3/2\ H_2O$: C, 56.19; H, 6.16; N, 15.67%.

H-Arg-Gly-Pro-Pro-Gly-Gly-Phe-OH (5). Compound **42** (0.96 g, 1 mmol) was treated as described in the case of **1**: yield 0.63 g (84%); mp 124 °C; $[\alpha]_D^{20}$ −72.0° (*c* 1, H_2O); R_f^1 0.19 and R_f^2 0.00.

Found: C, 52.35; H, 6.85; N, 18.47%. Calcd for $C_{31}H_{46}O_8N_{10}\cdot 1/2\ H_2O\cdot CH_3COOH$: C, 52.43; H, 6.81; N, 18.53%.

Amino acid ratios in acid hydrolyzate: Arg 0.92, Gly 3.01, Pro 1.98, Phe 1.00.

Boc-Phe-Phe-OBzl (43). Boc-Phe-OH·DCHA[15] (14.74 g, 33 mmol) and H-Phe-OBzl·TsOH[16] (12.82 g, 30 mmol) were coupled by the same method as described for the preparation of **12**: yield 13.01 g (86%); mp 144—146 °C (lit,[17] 148—149 °C); $[\alpha]_D^{20}$ −6.0° (*c* 1, DMF); R_f^1 0.99 and R_f^2 0.95.

Found: C, 71.61; H, 6.87; N, 5.55%. Calcd for $C_{30}H_{34}O_5N_2$: C, 71.68; H, 6.83; N, 5.58%.

H-Phe-Phe-Bzl·HCl (44). Compound **43** (10.05 g, 20 mmol) was treated as described in the case of **13**: yield 7.89 g (83%); mp 155—157 °C; $[\alpha]_D^{20}$ +10° (*c* 1, DMF); R_f^1 0.87 and R_f^2 0.71.

Found: C, 63.15; H, 5.79; N, 6.01%. Calcd for $C_{25}H_{26}O_3N_2\cdot HCl$: C, 63.21; H, 5.74; N, 5.90%.

Boc-Pro-Pro-Phe-Phe-OBzl (45). Boc-Pro-Pro-OH[7,9] (1.56 g, 5 mmol) and compound **46** (2.37 g, 5 mmol) were coupled by the same method as described for the preparation of **12**: yield 3.03 g (87%); mp 130—131 °C; $[\alpha]_D^{20}$ −80.0° (*c* 1, methanol); R_f^1 0.98 and R_f^2 0.68.

Found: C, 69.20; H, 6.81; N, 7.99%. Calcd for $C_{40}H_{48}O_7N_4$: C, 68.93; H, 6.96; N, 8.04%.

H-Pro-Pro-Phe-Phe-OBzl·HCl (46). Compound **45** (2.09 g, 3 mmol) was treated as described in the case of **13**: yield 1.89 g (98%); mp 78—79 °C; $[\alpha]_D^{20}$ −79.0° (*c* 1, methanol); R_f^1 0.69 and R_f^2 0.35.

Found: C, 65.57; H, 6.71; N, 8.68%. Calcd for $C_{35}H_{40}O_5N_4\cdot HCl\cdot 1/2\ H_2O$: C, 65.46; H, 6.61; N, 8.73%.

Z-Arg(NO₂)-Gly-Pro-Pro-Phe-Phe-OBzl (47). To a solution of Z-Arg(NO₂)-Gly-OH[7,10] (0.82 g, 2 mmol) in DMF (10 ml), DCC (0.41 g, 2 mmol), and HOBt (0.27 g, 2 mmol) were added at 0 °C. After 20 min, a solution of compound **46** (1.27 g, 2 mmol) and NMM (0.22 ml, 2 mmol) in DMF (10 ml) was added to the mixture. The mixture was cooled at 0 °C for 1 h and allowed to stand overnight at room temperature. The DCUrea was removed by filtration, and the filtrate was evaporated *in vacuo*. The oily residue was dissolved in ethyl acetate and the solution was

washed with water, 2% hydrochloric acid, 4% sodium hydrogencarbonate, and water successively. The solution was dried over anhydrous sodium sulfate. Sodium sulfate was removed by filtration, and the filtrate was evaporated *in vacuo*. The residue was crystallized with ether–petroleum ether: yield 1.07 g (54%); mp 115—117 °C; $[\alpha]_D^{20}$ −64.0° (*c* 1, acetic acid); R_f^1 0.69 and R_f^2 0.42.

Found: C, 60.35; H, 6.21; N, 13.68%. Calcd for $C_{51}H_{60}O_{11}N_{10}\cdot 3/2\ H_2O$: C, 60.27; H, 6.26; N, 13.79%.

H-Arg-Gly-Pro-Pro-Phe-Phe-OH (6). Compound **47** (0.79 g, 0.8 mmol) was treated as described in the case of **1**: yield 0.50 g (80%); mp 108—111 °C; $[\alpha]_D^{20}$ −73.0° (*c* 1, H_2O); R_f^1 0.25 and R_f^2 0.00.

Found: C, 54.91; H, 6.98; N, 14.21%. Calcd for $C_{36}H_{49}O_7N_9\cdot 2CH_3COOH\cdot 2H_2O$: C, 54.83; H, 7.03; N, 14.39%.

Amino acid ratios in acid hydrolyzate: Arg 0.93, Gly 1.01, Pro 1.98, Phe 2.00.

Boc-Gly-Phe-Phe-OBzl (48). Boc-Gly-OH[13] (1.75 g, 10 mmol) and compound **44** (4.75 g, 10 mmol) were coupled by the same method as described for the preparation of **12**: yield 5.26 g (94%); mp 129—130 °C; $[\alpha]_D^{20}$ −11.0° (*c* 1, methanol); R_f^1 0.89 and R_f^2 0.63.

Found: C, 68.74; H, 6.62; N, 7.55%. Calcd for $C_{32}H_{37}O_6N_3$: C, 68.67; H, 6.68; N, 7.51%.

H-Gly-Phe-Phe-OBzl·HCl (49). Compound **48** (4.48 g, 8 mmol) was treated as described in the case of **13**: yield 3.56 g (90%); mp 143—145 °C; $[\alpha]_D^{20}$ −2.0° (*c* 1, methanol); R_f^1 0.70 and R_f^2 0.63.

Found: C, 63.37; H, 6.25; N, 8.24%. Calcd for $C_{27}H_{29}O_4N_3\cdot HCl\cdot H_2O$: C, 63.44; H, 6.32; N, 8.22%.

Boc-Pro-Pro-Gly-Phe-Phe-OBzl (50). Boc-Pro-Pro-OH[7,9] (1.56 g, 5 mmol) and compound **49** (2.47 g, 5 mmol) were coupled by the same method as described for the preparation of **12**: yield 3.17 g (84%); mp 75—76 °C; $[\alpha]_D^{20}$ −54.0° (*c* 1, methanol); R_f^1 0.77 and R_f^2 0.46.

Found: C, 66.97; H, 6.75; N, 9.33%. Calcd for $C_{42}H_{51}O_8N_5$: C, 66.91; H, 6.83; N, 9.29%.

H-Pro-Pro-Gly-Phe-Phe-OBzl·HCl (51). Compound **50** (2.26 g, 3 mmol) was treated as described in the case of **13**: yield 1.90 g (92%); mp 95—97 °C; $[\alpha]_D^{20}$ −44.0° (*c* 1, methanol); R_f^1 0.46 and R_f^2 0.30.

Found: C, 62.83; H, 6.42; N, 9.77%. Calcd for $C_{37}H_{43}O_6N_5\cdot HCl\cdot H_2O$: C, 62.74; H, 6.49; N, 9.81%.

Z-Arg(NO$_2$)-Gly-Pro-Pro-Gly-Phe-Phe-OBzl (52). Z-Arg(NO_2)-Gly-OH[7,10] (0.82 g, 2 mmol) and compound **51** (1.38 g, 2 mmol) were coupled by the same method as described for the preparation of **47**: yield 1.68 g (80%); mp 93—96 °C; $[\alpha]_D^{20}$ −54.0° (*c* 1, acetic acid); R_f^1 0.94 and R_f^2 0.50.

Found: C, 60.35; H, 6.13; N, 14.54%. Calcd for $C_{53}H_{63}O_{12}N_{11}\cdot 1/2\ H_2O$: C, 60.32; H, 6.13; N, 14.60%.

H-Arg-Gly-Pro-Pro-Gly-Phe-Phe-OH (7). Compound **52** (1.05 g, 1 mmol) was treated as described in the case of **1**: yield 0.74 g (88%); mp 110 °C; $[\alpha]_D^{20}$ −71.0° (*c* 1, H_2O); R_f^1 0.22 and R_f^2 0.00.

Found: C, 57.36; H, 6.80; N, 16.77%. Calcd for $C_{38}H_{52}O_8N_{10}\cdot CH_3COOH$: C, 57.40; H, 6.76; N, 16.74%.

Amino acid ratios in acid hydrolyzate: Arg 0.92, Gly 2.00, Pro 1.98, Phe 2.00.

Boc-Gly-Gly-Phe-Phe-OBzl (53). Boc-Gly-Gly-OH[1] (2.32 g, 10 mmol) and compound **44** (4.74 g, 10 mmol) were coupled by the same method as descried for the preparation of **12**: yield 5.24 g (85%); mp 81—82 °C; $[\alpha]_D^{20}$ −6.0° (*c* 1, methanol); R_f^1 0.93 and R_f^2 0.55.

Found: C, 63.39; H, 6.71; N, 8.74%. Calcd for $C_{34}H_{40}O_7N_4\cdot 3/2\ H_2O$: C, 63.43; H, 6.75; N, 8.71%.

H-Gly-Gly-Phe-Phe-OBzl·HCl (54). Compound **53** (4.32 g, 7 mmol) was treated as described in the case of **13**: yield 3.76 g (97%); mp 159—161 °C; $[\alpha]_D^{20}$ −13.0° (*c* 1, methanol); R_f^1 0.75 and R_f 0.43.

Found: C, 61.05; H, 6.14; N, 9.80%. Calcd for $C_{29}H_{32}O_5N_4\cdot HCl\cdot H_2O$: C, 60.98; H, 6.19; N, 9.81%.

Boc-Pro-Pro-Gly-Gly-Phe-Phe-OBzl (55). Boc-Pro-Pro-OH[7,9] (1.56 g, 5 mmol) and compound **54** (2.77 g, 5 mmol) were coupled by the same method as described for the preparation of **12**: yield 3.51 g (87%); mp 88—90 °C; $[\alpha]_D^{20}$ −53.0° (*c* 1, methanol); R_f^1 0.74 and R_f^2 0.41.

Found: C, 63.70; H, 6.79; N, 10.17%. Calcd for $C_{44}H_{54}O_9N_6\cdot H_2O$: C, 63.75; H, 6.82; N, 10.14%.

H-Pro-Pro-Gly-Gly-Phe-Phe-OBzl·HCl (56). Compound **55** (2.43 g, 3 mmol) was treated as described in the case of **13**: yield 2.09 g (93%); mp 101—103 °C; $[\alpha]_D^{20}$ −38.0° (*c* 1, methanol); R_f^1 0.58 and R_f^2 0.39.

Found: C, 61.17; H, 6.52; N, 10.95%. Calcd for $C_{39}H_{46}O_7N_6\cdot HCl\cdot H_2O$: C, 61.21; H, 6.47; N, 10.98%.

Z-Arg(NO$_2$)-Gly-Pro-Pro-Gly-Gly-Phe-Phe-OBzl (57). Z-Arg(NO_2)-Gly-OH[7,10] (0.82 g, 2 mmol) and compound **56** (1.49 g, 2 mmol) were coupled by the same method as described for the preparation of **12**: yield 1.79 g (81%); mp 116—119 °C; $[\alpha]_D^{20}$ −48.0° (*c* 0.5, acetic acid); R_f^1 0.90 and R_f^2 0.32.

Found: C, 59.30; H, 6.02; N, 15.17%. Calcd for $C_{55}H_{66}O_{13}N_{12}\cdot 1/2\ H_2O$: C, 59.39; H, 6.08; N, 15.12%.

H-Arg-Gly-Pro-Pro-Gly-Gly-Phe-Phe-OH (8). Compound **57** (1.10 g, 1 mmol) was treated as described in the case of **1**: yield 0.72 g (81%); mp 128—130 °C; $[\alpha]_D^{20}$ −61.0° (*c* 1, H_2O); R_f^1 0.19 and R_f^2 0.00.

Found: C, 54.81; H, 6.85; N, 16.70%. Calcd for $C_{40}H_{55}O_9N_{11}\cdot 3/2\ H_2O\cdot CH_3COOH$: C, 54.76; H, 6.80; N, 16.73%.

Amino acid ratios in acid hydrolyzate: Arg 0.93, Gly 2.99, Pro 2.02, Phe 2.00.

Boc-Gly-Gly-Gly-Phe-Phe-OBzl (58). Boc-Gly-Gly-OH[1] (2.32 g, 10 mmol) and compound **49** (4.93 g, 10 mmol) were coupled by the same method as described for the preparation of **12**: yield 5.46 g (81%); mp 175—176 °C; $[\alpha]_D^{20}$ −11.0° (*c* 1, methanol); R_f^1 0.93 and R_f^2 0.58.

Found: C, 64.15; H, 6.49; N, 10.39%. Calcd for $C_{36}H_{43}O_8N_5$: C, 64.17; H, 6.45; N, 10.40%.

H-Gly-Gly-Gly-Phe-Phe-OBzl·HCl (59). Compound **58** (4.72 g, 7 mmol) was treated as described in the case of **13**: yield 4.03 g (94%); mp 170—173 °C; $[\alpha]_D^{20}$ −12.0° (*c* 1, methanol); R_f^1 0.63 and R_f^2 0.34.

Found: C, 60.97; H, 5.99; N, 11.53%. Calcd for $C_{31}H_{35}O_6N_5\cdot HCl$: C, 61.02; H, 5.96; N, 11.50%.

Boc-Pro-Pro-Gly-Gly-Gly-Phe-Phe-OBzl (60). Boc-Pro-Pro-OH[7,9] (1.56 g, 5 mmol) and compound **59** (3.05 g, 5 mmol) were coupled by the same method as described for the preparation of **12**: yield 3.63 g (84%); mp 130—131 °C; $[\alpha]_D^{20}$ −52.0° (*c* 1, methanol) R_f^1 0.73 and R_f^2 0.54.

Found: C, 63.60; H, 6.81; N, 11.33%. Calcd for $C_{46}H_{57}O_{10}N_7\cdot H_2O$: C, 63.64; H, 6.86; N, 11.30%.

H-Pro-Pro-Gly-Gly-Gly-Phe-Phe-OBzl·HCl (61). Compound **60** (2.60 g, 3 mmol) was treated as described in the case of **13**: yield 2.34 g (97%); mp 137—140 °C; $[\alpha]_D^{20}$ −29.0° (*c* 1, methanol); R_f^1 0.58 and R_f^2 0.30.

Found: C, 59.93; H, 6.31; N, 11.90%. Calcd for $C_{41}H_{49}O_8N_7\cdot HCl\cdot H_2O$: C, 59.88; H, 6.37; N, 11.93%.

Z-Arg(NO$_2$)-Gly-Pro-Pro-Gly-Gly-Gly-Phe-Phe-OBzl (62). Z-Arg(NO_2)-Gly-OH[7,10] (0.82 g, 2 mmol) and compound **61** (1.61 g, 2 mmol) were coupled by the same method as described for the preparation of **12**. This product was obtained in a hygroscopic form: yield 1.72 g (74%); R_f^1 0.85 and R_f^2 0.52.

H-Arg-Gly-Pro-Pro-Gly-Gly-Gly-Phe-Phe-OH (9). Compound **62** (1.15 g, 1 mmol) was treated as described in the case of **1**: yield 0.67 g (70%); mp 137—140 °C; $[\alpha]_D^{20}$

$-50.0°$ (c 1, H_2O); R_f^1 0.21 and R_f^2 0.00.

Found: C, 54.55; H, 6.61; N, 17.33%. Calcd for $C_{42}H_{58}O_{10}N_{12}\cdot H_2O\cdot CH_3COOH$: C, 54.52; H, 6.67; N, 17.35%.

Amino acid ratios in acid hydrolyzate: Arg 0.93, Gly 3.98, Pro 1.99, Phe 2.00.

Boc-Phe-Phe-Phe-OBzl (63). Boc-Phe-OH·DCHA[15] (5.36 g, 12 mmol) and compound **49** (4.74 g, 10 mmol) were coupled by the same method as described for the preparation of **12**: yield 5.78 g (89%); mp 170—172 °C; $[\alpha]_D^{20}$ $-27.5°$ (c 1, methanol); R_f^1 0.99 and R_f^2 0.89.

Found: C, 72.13; H, 6.76; N, 6.49%. Calcd for $C_{39}H_{43}O_6N_3$: C, 72.09; H, 6.77; N, 6.46%.

H-Phe-Phe-Phe-OBzl·HCl (64). Compound **63** (5.30 g, 8.15 mmol) was treated as described in the case of **13**: yield 4.55 g (95%); mp 186 °C (decomp); $[\alpha]_D^{20}$ $-9.0°$ (c 1, methanol); R_f^1 0.91 and R_f^2 0.81.

Found: C, 69.70; H, 6.19; N, 7.15%. Calcd for $C_{34}H_{35}O_4N_3\cdot HCl$: C, 69.67; H, 6.19; N, 7.13%.

Boc-Pro-Pro-Phe-Phe-Phe-OBzl (65). Boc-Pro-Pro-OH[7,9] (1.56 g, 5 mmol) and compound **64** (2.93 g, 5 mmol) were coupled by the same method as described for the preparaton of **12**: yield 3.46 g (82%); mp 109—112 °C; $[\alpha]_D^{20}$ $-66.5°$ (c 1, methanol); R_f^1 0.99 and R_f^2 0.84.

Found: C, 69.80; H, 6.83; N, 8.26%. Calcd for $C_{49}H_{57}O_8N_5$: C, 69.76; H, 6.81; N, 8.30%.

H-Pro-Pro-Phe-Phe-Phe-OBzl·HCl (66). Compound **65** (2.53 g, 3 mmol) was treated as described in the case of **13**: yield 2.22 g (95%); mp 100—103 °C; $[\alpha]_D^{20}$ $-76.5°$ (c 1, methanol); R_f^1 0.82 and R_f^2 0.40.

Found: C, 66.92; H, 6.48; N, 8.88%. Calcd for $C_{44}H_{49}O_6N_5\cdot HCl\cdot 1/2\ H_2O$: C, 66.95; H, 6.51; N, 8.87%.

Z-Arg(NO$_2$)-Gly-Pro-Pro-Phe-Phe-Phe-OBzl (67). Z-Arg(NO_2)-Gly-OH[7,10] (0.82 g, 2 mmol) and compound **66** (1.56 g, 2 mmol) were coupled by the same method as described for the preparation of **12**: yield 1.75 g (77%); mp 114—117 °C; $[\alpha]_D^{20}$ $-69.5°$ (c 1, methanol); R_f^1 0.84 and R_f 0.55.

Found: C, 62.47; H, 6.27; N, 13.32%. Calcd for $C_{60}H_{70}O_{12}N_{11}\cdot H_2O$: C, 62.43; H, 6.30; N, 13.35%.

H-Arg-Gly-Pro-Pro-Phe-Phe-Phe-OH (10). Compound **67** (1.14 g, 1 mmol) was treated as described in the case of **1**: yield 0.74 g (76%); mp 127—130 °C; $[\alpha]_D^{20}$ $-64.0°$ (c 1, acetic acid); R_f^1 0.29 and R_f^2 0.00.

Found: C, 60.25; H, 6.79; N, 15.03%. Calcd for $C_{45}H_{58}O_8N_{10}\cdot 1/2\ H_2O\cdot CH_3COOH$: C, 60.29; H, 6.80; N, 14.96%.

Amino acid ratios in acid hydrolyzate: Arg 0.95, Gly 1.00, Pro 2.08, Phe 2.99.

CD Measurement. The measurements were performed with a JASCO J-20 Automatic Recording Spectropolarimeter over a wavelength range of 200 to 250 nm. A cell of path length 0.2 mm was used and the runs were made at ambient temperature. Patterns in a solvent of distilled water are shown in Fig. 6.

Sensory Test. The bitterness of the synthetic BPIa analogs was organoleptically determined *via* panel evaluation by five people. A series of solution of decreasing concentration was prepared in which each solution was half as strong as its proceeding one. Before testing the sample, the tester's month was thoroughly rinsed with distilled water. The sample size was usually 2—3 ml. The sample solution was held in the mouth for *ca.* 10 s and then spit out. The threshold values of synthetic BPIa analogs are shown in the Table.

The authors wish to express their thanks to Professor Sakuzo Fukui of Hiroshima University for his helpful discussion in the course of this study. Thanks are also due to Associate Professor Michio Kondo of Saga University for his help in the CD measurements, and to Dr. Shinji Okumura of Ajinomoto Co. Inc., for supplying some amino acids.

References

1) Part III. I. Miyake, K. Kouge, H, Kanehisa, and H. Okai, *Bull. Chem. Soc. Jpn.*, **56**, 1678 (1983).

2) The abbreviations recommended by the IUPAC-IUB commission of Biochemical Nomenclature (*J. Biol. Chem.*, **247**, 977 (1972)) have been used. Amino acid symbols except glycine denote the L-configuration. Additional abbreviations: DCC, dicyclohexylcarbodiimide; DCHA, dicyclohexylamine; DCUrea, *N,N'*-dicyclohexylurea; DMF, *N,N*-dimethylformamide; ECF, ethyl chloroformate; HOBt, 1-hydroxybenzotriazole; MA, mixed anhydride; NMM, *N*-methylmorpholine; TsOH, *p*-toluenesulfonic acid; THF, tetrahydrofurane.

3) W. König, R. Geiger, "Peptides," ed by E. Scoffone, North-Holland Publ. Co., Amsterdam (1969), p. 17.

4) N. Minamiura, Y. Matsumura, J. Fukumoto, and T. Yamamoto, *Agric. Biol. Chem.*, **36**, 588 (1972).

5) K. Otagiri, I. Miyake, N. Ishibashi, H. Fukui, H. Kanehisa, and H. Okai, *Bull. Chem. Soc. Jpn.*, **56**, 1116 (1983).

6) The numbers indicate the position of the individual amino acid residues. For example: BPIa, Arg(1)-Gly(2)-Pro(3)-Pro(4)-Phe(5)-Ile(6)-Val(7).

7) H. Fukui, H. Kanehisa, N. Ishibashi, I. Miyake, and H. Okai, *Bull. Chem. Soc. Jpn.*, **56**, 766 (1983).

8) H. Gibian and E. Schröder, *Justus Liebigs Ann. Chem.*, **642**, 145 (1961).

9) G. R. Pettit and S. K. Das Gupta, *Can. J. Chem.*, **45**, 1600 (1967).

10) M. E. Cox, H. G. Garg, J. Hollowood, J. M. Hugo, P. M. Scopes, and G. T. Young, *J. Chem. Soc.*, **1965**, 6806.

11) H. C. Beyerman, C. A. M. Boers-Boonekamp, and H. Maassen van den Brink-Zimmermannova, *Recl. Trav. Chim. Pays-Bas*, **87**, 257 (1968).

12) B. F. Erlanger and E. Brand, *J. Am. Chem. Soc.*, **73**, 3508 (1951).

13) E. Schnabel, *Justus Liebigs Ann. Chem.*, **702**, 188 (1967).

14) L. Zervas and D. M. Theodoropoulos, *J. Am. Chem. Soc.*, **78**, 1359 (1956).

15) M. Fujino and C. Hatanaka, *Chem. Pharm. Bull. (Tokyo)*, **15**, 2015 (1967).

16) L. Zervas, M. Winitz, and J. P. Greenstein, *J. Org. Chem.*, **22**, 1515 (1957).

17) F. Weygand and E. Frauendorfer, *Chem. Ber.*, **103**, 2437 (1970).

 © 1984 The Chemical Society of Japan Bull. Chem. Soc. Jpn., 57, 97—102 (1984)

Studies of Bitter Peptides from Casein Hydrolyzate. VI.[1] Syntheses and Bitter Taste of BPIc (Val-Tyr-Pro-Phe-Pro-Pro-Gly-Ile-Asn-His) and Its Analogs and Fragments[2]

Hidenori KANEHISA
Research and Development Division, Sunstar Inc., Asahi-cho, Takatsuki, Osaka 569
(Received June 15, 1983)

In order to investigate the relationship between chemical structure and bitter taste, the bitter peptide BPIc (Val-Tyr-Pro-Phe-Pro-Pro-Gly-Ile-Asn-His) isolated from casein hydrolyzate by Minamiura *et al.* and its analogs and fragments were synthesized. BPIc, whose threshold value of bitter taste was 0.05 mM, was found to be one of the most bitter compounds, like quinine and phenylthiourea. However, [Gly^{5,6}]- and [Gly^{9,10}]-BPIc, and N-terminal octa- and heptapeptide fragments of BPIc possessed much weaker bitterness than BPIc. The results suggested that 5,6-proline and the basic nature of C-terminal are necessary for the strong bitterness exhibited by BPIc.

In a series of studies of bitter peptides, the first paper[3] described the synthesis of bitter peptide BPIa (H-Arg-Gly-Pro-Pro-Phe-Ile-Val-OH) isolated from enzymatic hydrolyzate of cow milk casein by Minamiura *et al.*[4] The peptide possessed an extremely bitter taste of the same level as well known bitter substances such as quinine and phenylthiourea. The threshold value of bitter taste of BPIa was found to be 0.05 mM (1 M=1 mol dm^{-3}). To elucidate the structure-taste relationship of BPIa, its numerous fragments and analogs were prepared and their tastes were measured.[1,5-7] All the fragments except N-terminal hexapeptide fragment exhibited a weaker bitterness than BPIa itself.[5] Des-Gly^2-BPIa was the same as BPIa,[5] whereas the analogs in which prolylproline residue was substituted for glycylglycine or D-prolyl-D-proline residues exhibited a weaker bitterness than BPIa.[6] The results of their CD examinations in water also suggested that at least six amino acid residues are necessary for the exhibition of strong bitterness and that the spatial structure of BPIa molecule attributed to L-proline residue at 3-position contributes to its bitter taste.[5,6] In order to clarify the nature of the N-terminal arginine residue, the strength of bitterness for Arg^1-substituted analogs were compared with that of des-Gly^2-BPIa.[1] When the position of arginine was filled by another basic amino acid, the analogs possessed a bitter taste. However, the strength of bitterness decreased with reducing of the side-chain length of the basic amino acid residues. On the other hand, the analogs in which the position of arginine was replaced by hydrophobic or bulky side chain amino acid still possessed a bitter taste. However its strength was slightly weaker than that of basic amino acid-substituted analogs. The C-terminal moiety in the sequence of BPIa was studied; the analog in which C-terminal tripeptide moiety of BPIa was substituted for triphenylalanine residue possessed the strongest bitterness in the series of BPIa analogs.[7] The results suggested that both basic amino acid residue in N-terminal position and hydrophobic amino acid residues in C-terminal moiety are necessary for an intense bitterness in BPIa. This finding is also supported from taste behavior results: that des-Arg^1-BPIa and the N-terminal pentapeptide fragment of BPIa exhibited a much weaker bitterness than BPIa.[5]

Minamiura *et al.* isolated a bitter decapeptide named BPIc from casein hydrolyzate in addition to BPIa and decided that its amino acid sequence was H-Val-Tyr-Pro-Phe-Pro-Pro-Gly-Ile-Asn-His-OH.[4] It is interesting to compare the structure of BPIc with that of BPIa. They have several characteristic features in common. These peptides include prolylproline residue in the center of the molecules. Also, they include a basic amino acid residue (histidine or arginine) and some hydrophobic amino acid residues (valine, phenylalanine, isoleucine, and/or tyrosine) on both terminal positions in these molecules. Although BPIc is extremely bitter according to Minamiura *et al.*,[4] no study has made on the synthesis of BPIc.

In order to elucidate the relationship between chemical structure and bitterness of peptides, the author prepared BPIc. The author also prepared [Gly^{5,6}]-BPIc, in which prolylproline residue at 5,6-position was replaced by glycylglycine, and [Gly^{9,10}]-BPIc and N-terminal octa- and heptapeptide fragments, based on the findings in the synthetic studies of BPIa. The present paper describes the syntheses and bitter taste of BPIc and its analogs and fragments.

The sequence of reactions employed for the synthesis of BPIc is shown in Fig. 1. Acyldipeptide acid (**2**), derived from the corresponding methyl ester (**1**), was condensed with H-Pro-Phe-OEt·HCl (**4**) to yield the protected N-terminal tetrapeptide derivative (**5**) by means of the dicyclohexylcarbodiimide-1-hydroxybenzotriazole (DCC-HOBt) method. It was converted to the corresponding acid (**6**) by saponification with sodium hydroxide. Acyltripeptide ester (**8**) was prepared from Boc-Pro-Pro-OH (**7**) and H-Gly-OBzl·TsOH by the mixed anhydride (MA) method, and then the N-terminal protected group of **8** was removed by the action of hydrogen chloride in dioxane to yield the tripeptide ester hydrochloride (**9**).

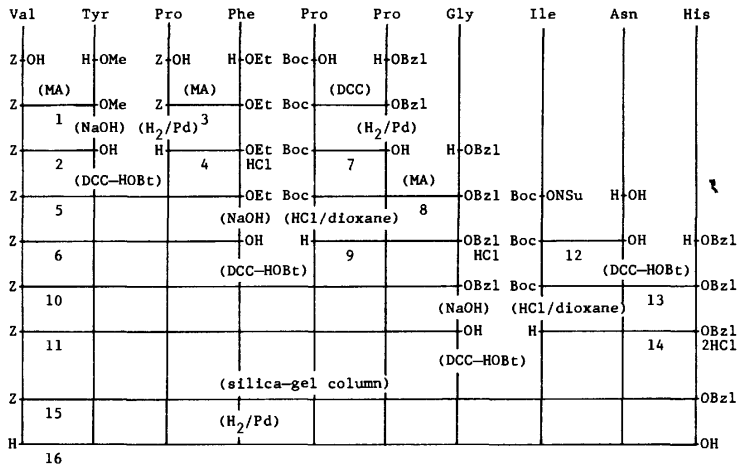

Fig. 1. Synthesis of BPIc.

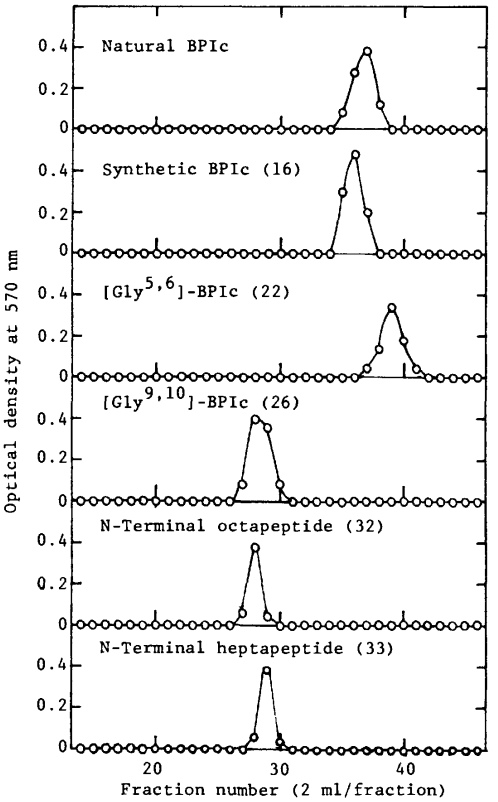

Fig. 2. Carboxymethylcellulose column chromatography of synthetic and natural BPIc. Solvent: 0.2 M pyridinium acetate, pH 5.0.

9 was coupled with **6** by the DCC-HOBt method and the resulting acylheptapeptide ester (**10**) was easily converted to the corresponding acid (**11**) by saponification. Asparagine was acylated to Boc-Ile-Asn-OH (**12**) with Boc-Ile-ONSu, then **12** and H-His-OBzl·2TsOH were coupled to yield acyltripeptide ester (**13**) by the DCC-HOBt method. The amino protection of **13** was removed by the action of hydrogen chloride in 98% formic acid. The compound **14** thus obtained and **11** were condensed by the DCC-HOBt method in DMF. The resulting acyldecapeptide ester (**15**) was purified with extraction of 1-butanol, and then the extract was placed on a silica-gel column and eluted with chloroform-methanol (5:1, v/v). The catalytic hydrogenation of pure **15** in methanol containing hydrogen chloride gave decapeptide BPIc (**16**).

The preparation of [Gly^{5,6}]-BPIc was described as follows. **6** was condensed with triglycine ethyl ester (**18**) by the DCC-HOBt method and the obtained heptapeptide (Z-Val-Tyr-Pro-Phe-Gly-Gly-Gly-OEt, **19**) was easily saponified to yield the corresponding acid (**20**), which was made to condense with **14** by the DCC-HOBt method. The Z-Val-Tyr-Pro-Phe-Gly-Gly-Gly-Ile-Asn-His-OBzl (**21**) thus obtained was hydrogenated in the presence of palladium black to give [Gly^{5,6}]-BPIc (**22**).

[Gly^{9,10}]-BPIc was prepared as described below. Boc-Ile-OH was coupled with H-Gly-Gly-OBzl·HCl by the MA method to give Boc-Ile-Gly-Gly-OBzl (**23**). It was converted to the corresponding tripeptide ester hydrochloride (**24**) by the treatment of hydrogen chloride in dioxane. Then **24** and **11** were condensed by the DCC-HOBt method to yield Z-Val-Tyr-Pro-Phe-Pro-Pro-Gly-Ile-Gly-Gly-OBzl (**25**). It was hydrogenated to give [Gly^{9,10}]-BPIc (**26**).

N-Terminal octapeptide fragment of BPIc was synthesized by the following procedures. Boc-Gly-OH and H-Ile-OBzl·TsOH were coupled by the MA method to give Boc-Gly-Ile-OBzl (**27**). This was converted to the corresponding dipeptide ester hydrochloride (**28**) by the action of hydrogen chloride in dioxane. **28** and **7** were condensed by the MA method to yield Boc-Pro-Pro-Gly-Ile-OBzl (**29**). This was converted to the corresponding tetrapeptide ester hydrochloride (**30**) by the action of hydrogen chloride in dioxane. **30** and **6** were then condensed by the DCC-HOBt method to give Z-Val-Tyr-Pro-Phe-Pro-Pro-Gly-Ile-OBzl (**31**). Catalytic hydrogenation of **31** gave N-terminal octapeptide fragment of BPIc (**32**). The N-terminal heptapeptide fragment of BPIc, H-Val-Tyr-Pro-Phe-Pro-Pro-Gly-OH (**33**), was obtained from **9** by hydrogenation.

The purity of synthetic BPIc, its analogs and fragments, and their intermediates was confirmed by thin-layer examinations on two solvent systems, and by elemental analyses. The homogeneity of the final products was also confirmed by paper electrophoresis, carboxymethylcellulose column chromatography, and amino acid analysis.

The taste of final products was organoleptically determined by panel evaluation employing several persons. The results are listed in the Table. All the synthetic peptides possessed a bitter taste. BPIc, whose threshold value of bitterness was 0.05 mM, was the same as BPIa. However, the strength of bitterness of BPIc analog **22** was *ca.* 1/5 of that of BPIc. This means that 5,6-proline residues are necessary

Table. The threshold values for bitter taste of BPIc and its analogs and fragments

Compound		Threshold values for bitter taste/mM
Val-Tyr-Pro-Phe-Pro-Pro-Gly-Ile-Asn-His	(BPIc, **16**)	0.05
Val-Tyr-Pro-Phe-Gly-Gly-Gly-Ile-Asn-His	(**22**)	0.23
Val-Tyr-Pro-Phe-Pro-Pro-Gly-Ile-Gly-Gly	(**26**)	0.30
Val-Tyr-Pro-Phe-Pro-Pro-Gly-Ile	(**32**)	0.15
Val-Tyr-Pro-Phe-Pro-Pro-Gly	(**33**)	0.30
Ile-Asn-His[8]		25.00
Asn-His[8]		100.00

for the strong bitterness of BPIc. The analog **26** was one-sixth as bitter as BPIc. Also, bitterness of BPIc fragments (**32** and **33**) was weaker than that of BPIc. Further, H-Ile-Asn-His-OH and H-Asn-His-OH were nearly tasteless. These results indicate that the basic nature of C-terminal position in BPIc, in addition to the hydrophobic nature of its N-terminal contributes to its bitter taste. The findings obtained from BPIc are equivalent to those from BPIa. Therefore, BPIc can be regarded as a retro form of BPIa possessing a reverse sequence of BPIa; in bitter peptides contain prolylproline residue in the center of the molecule and both basic and hydrophobic amino acid residues in N- and C-terminal positions respectively, it is possible for N- and C-terminal amino acid residues to change places with each other. Further studies of this problem are in progress.

Experimental

All melting points are uncorrected. Thin layer chromatography was carried out on Merck silica-gel G. Developing solvents commonly used were (1) 1-butanol-acetic acid-pyridine-water (4:1:1:2, v/v), and (2) chloroform-methanol (5:1, v/v). Materials possessing free amino groups on a thin layer plate were detected by spraying with ninhydrin. Compounds with blocked amino groups were detected by spraying with 25% hydrogen bromide in acetic acid and then with ninhydrin. Optical rotations were measured on a JASCO automatic polarimeter, DIR-SL type. Amino acid analyses were performed with a Hitachi amino acid analyzer, KLA-5 type. Prior to analysis, compounds were dried over phosphorus pentaoxide at 66 °C and 2 mmHg (1 mmHg≈133.332 Pa) for 2 h.

Synthesis of BPIc. *Z-Val-Tyr-OMe (1)*: A solution of Z-Val-OH[9] (10.05 g, 40 mmol) and NMM (4.4 ml, 40 mmol) in THF (100 ml) was chilled to −5 °C, then ECF (4 ml, 40 mmol) was added to it. After 10 min, a precooled solution of H-Tyr-OMe·HCl[10] (14.64 g, 40 mmol) and NMM (4.4 ml, 40 mmol) in DMF (100 ml) was added to it. The reaction mixture was refrigerated for 1 h and then allowed to stand overnight at room temperature. The mixture was evaporated *in vacuo*, and the oily residue was dissolved in ethyl acetate (400 ml). The solution was washed successively with 4% sodium hydrogencarbonate, 0.5 M hydrochloric acid and water, and then dried over anhydrous sodium sulfate. The solution was concentrated to an oily residue which was crystallized by addition of ether; yield 15.13 g (88%); mp 152—153 °C (lit,[11] 150 °C); $[\alpha]_D^{20}$ +14.0° (*c* 1, pyridine) (lit,[11] +12.1° (*c* 1, pyridine)); R_f^1 0.98 and R_f^2 0.69.

Found: C, 64.30; H, 6.74; N, 6.53%. Calcd for $C_{23}H_{28}O_6N_2$: C, 64.47; H, 6.59; N, 6.54%.

Z-Val-Tyr-OH (2): To a solution of **1** (12.9 g, 30 mmol) in methanol (40 ml), 2 M sodium hydroxide (31 ml) was added. The reaction mixture was allowed to stand for 1 h at room temperature and then diluted with water (40 ml). The mixture was then extracted with ether. The aqueous layer was acidified to pH 2 with 2 M hydrochloric acid. The oily product was extracted with ethyl acetate (400 ml). The organic layer was washed with water and dried with anhydrous sodium sulfate. The filtrate was evaporated *in vacuo*, the oily residue was crystallized by ether and petroleum ether; yield 8.60 g (69%); mp 163—164 °C (lit,[12] 161—163 °C); $[\alpha]_D^{20}$ +26.5° (*c* 1, pyridine) (lit,[12] +26.0° (*c* 1, pyridine)); R_f^1 0.85 and R_f^2 0.24.

Found: C, 63.91; H, 6.52; N, 6.73%. Calcd for $C_{22}H_{26}O_6N_2$: C, 63.75; H, 6.32; N, 6.76%.

Z-Pro-Phe-OEt (3): This compound was obtained from Z-Pro-OH[13] (9.95 g, 40 mmol) and H-Phe-OEt·TsOH[14] (16.45 g, 45 mmol), as described for the preparation of **1**; yield 12.68 g (75%) mp 67—68 °C (lit,[15] 65—68 °C); $[\alpha]_D^{20}$ −39.8° (*c* 1, methanol) (lit,[15] −33° (alcohol)); R_f^1 0.96 and R_f^2 0.92.

Found: C, 67.79; H, 6.65; N, 6.62%. Calcd for $C_{24}H_{28}O_5N_2$: C, 67.90; H, 6.65; N, 6.60%.

H-Pro-Phe-OEt·HCl (4): Compound **3** (11.46 g, 27 mmol) was hydrogenated in the presence of palladium black and 0.3 M methanolic hydrogen chloride (100 ml). The filtrate from catalyst was evaporated *in vacuo*, and the residue was crystallized from ether. It was recrystallized from ethanol-ether; yield 8.35 g (94%); 149—150 °C; $[\alpha]_D^{20}$ −41.5° (*c* 1, water) (lit,[16] −40.9° (*c* 2, water)); R_f^1 0.79 and R_f^2 0.66.

Found: C, 58.69; H, 7.16; N, 8.56%. Calcd for $C_{16}H_{23}O_3N_2Cl$: C, 58.77; H, 7.09; N, 8.56%.

Z-Val-Tyr-Pro-Phe-OEt (5): To a chilled solution of **2** (9.95 g, 24 mmol), **4** (8.17 g, 25 mmol), NMM (2.75 ml, 25 mmol) and HOBt (3.38 g, 25 mmol) in THF (100 ml), DCC (4.95 g, 24 mmol) was added. The reaction mixture was held overnight at 0 °C and the DCUrea which formed was filtered off. The filtrate was evaporated *in vacuo*, and the residual oil was dissolved in ethyl acetate. The solution was washed with 4% sodium hydrogencarbonate, 0.5 M hydrochloric acid and water, and dried over sodium sulfate. The filtrate was evaporated *in vacuo*, and the residue was crystallized by addition of ether and petroleum ether; yield 14.42 g (88%); mp 122—124 °C; $[\alpha]_D^{20}$ −67.0° (*c* 1, methanol); R_f^1 0.97 and R_f^2 0.64.

Found: C, 66.20; H, 6.73; N, 8.25%. Calcd for $C_{38}H_{46}O_8N_4$: C, 66.45; H, 6.75; N, 8.16%.

Z-Val-Tyr-Pro-Phe-OH (6): Compound **5** (13.73 g, 20 mmol) was saponified by 2 M sodium hydroxide (21 ml) and methanol (50 ml) for 1 h. Purification of the product

was done by the procedure used for the preparation of **2**; yield 9.17 g (70%); mp 121—124 °C; $[\alpha]_D^{20}$ −52.8° (*c* 1, methanol); R_f^1 0.88 and R_f^2 0.46.

Found: C, 65.81; H, 6.45; N, 8.47%. Calcd for $C_{36}H_{42}O_8N_4$: C, 65.64; H, 6.43; N, 8.51%.

Boc-Pro-Pro-OH (7): To a chilled solution of Boc-Pro-OH[17] (4.26 g, 20 mmol), H-Pro-OBzl·HCl[18] (5.06 g, 22 mmol) and NMM (2.4 ml, 22 mmol) in acetonitrile (50 ml), DCC (4.12 g, 20 mmol) was added. The reaction mixture was held overnight at 0 °C, then DCUrea was separated by filtration. The filtrate was evaporated *in vacuo*, the residue was dissolved in ethyl acetate and washed successively with 4% sodium hydrogencarbonate, 4% citric acid and water, and then dried over anhydrous sodium sulfate. The filtrate was evaporated *in vacuo*, and the residue was dissolved in methanol (100 ml). It was subjected to hydrogenolysis in the presence of palladium black. The filtrate from the catalyst was evaporated *in vacuo*, and the residue was crystallized with ether. It was recrystallized from hot ethyl acetate; yield 3.74 g (60%); mp 181—182 °C (lit,[19] 187—187.5 °C); $[\alpha]_D^{20}$ −118.0° (*c* 1, methanol); R_f^1 0.77 and R_f^2 0.40.

Found: C, 57.58; H, 7.90; N, 8.92%. Calcd for $C_{15}H_{24}O_5N_2$: C, 57.67; H, 7.74; N, 8.97%.

Boc-Pro-Pro-Gly-OBzl (8): This was prepared from **7** (4.69 g, 15 mmol) and H-Gly-OBzl·TsOH[20] (5.07 g, 15 mmol) as described for the preparation of **1**; yield 4.76 g (70%); mp 107—109 °C; $[\alpha]_D^{20}$ −127.8° (*c* 1, methanol); R_f^1 0.90 and R_f^2 0.74.

Found: C, 62.57; H, 7.28; N, 9.18%. Calcd for $C_{24}H_{33}O_6N_3$: C, 62.72; H, 7.24; N, 9.14%.

H-Pro-Pro-Gly-OBzl·HCl (9): Compound **8** (4.60 g, 10 mmol) was dissolved in 4 M hydrogen chloride in dioxane (25 ml) and held for 1 h at room temperature. The solution was evaporated *in vacuo*, dissolved in dioxane (20 ml), and evaporated again. A precipitate was obtained by the addition of ether. This precipitate was filtered off and dried over pellets of potassium hydroxide *in vacuo*; yield of hygroscopic powder was 3.96 g (98%); mp 65—67 °C; $[\alpha]_D^{20}$ −113.5° (*c* 1, methanol); R_f^1 0.65 and R_f^2 0.38.

Found: C, 57.38; H, 6.64; N, 10.43%. Calcd for $C_{19}H_{26}O_4N_3Cl$: C, 57.64; H, 6.62; N, 10.62%.

Z-Val-Tyr-Pro-Phe-Pro-Pro-Gly-OBzl (10): A solution of of DCC (2.06 g, 10 mmol) in THF was added to a chilled solution of **6** (6.59 g, 10 mmol), **9** (3.90 g, 10 mmol), NMM (1.1 ml, 10 mmol), and HOBt (1.48 g, 11 mmol) in THF (100 ml). The reaction mixture was held overnight at 0 °C. DCUrea was filtered off and the filtrate was evaporated *in vacuo*. The residue was dissolved in ethyl acetate. The solution was washed with 4% sodium hydrogencarbonate, 0.5 M hydrochloric acid and water, and dried over anhydrous sodium sulfate. The filtrate was evaporated *in vacuo*, and the product was obtained by addition of ether; yield 8.68 g (76%); mp 115—117 °C; $[\alpha]_D^{20}$ −118.5° (*c* 1, methanol); R_f^1 0.91 and R_f^2 0.63.

Found: C, 65.74; H, 6.62; N, 9.72%. Calcd for $C_{55}H_{65}O_{11}N_7$: C, 66.05; H, 6.55; N, 9.80%.

Z-Val-Tyr-Pro-Phe-Pro-Pro-Gly-OH (11): To a solution of **10** (8.00 g, 8 mmol) in methanol (70 ml), 2 M sodium hydroxide (9 ml) was added. The reaction mixture was held for 2 h at room temperature, then diluted with 150 ml water and extracted with ethyl acetate. The aqueous layer was acidified with 2 M hydrochloric acid and extraced with ethyl acetate. The organic layer was washed with water and then dried over anhydrous sodium sulfate. The filtrate was evaporated *in vacuo* and then was crystallized from ether; yield 5.79 g, (80%); mp 148—150 °C (decomp); $[\alpha]_D^{20}$ −128.0° (*c* 1, methanol); R_f^1 0.81 and R_f^2 0.36.

Found: C, 63.14; H, 6.46; N, 10.56%. Calcd for $C_{48}H_{59}O_{11}N_7$: C, 63.35; H, 6.54; N, 10.78%.

Boc-Ile-Asn-OH (12): Asparagine monohydrate (3.3 g, 22 mmol) and Et_3N (2.8 ml, 20 mmol) were dissolved in water (50 ml). Boc-Ile-ONSu[21] (6.65 g, 20 mmol) dissolved in dioxane (50 ml) was added at room temperature while the solution was being stirred. The mixture was stirred overnight, and then diluted with 5% sodium hydrogencarbonate (100 ml) and extracted with ether. The aqueous layer was acidified with citric acid and extracted with 1-butanol (300 ml). The butanol layer was washed with water and concentrated to 50 ml. The product was crystallized with ether and petroleum ether, then recrystallized from ethanol-ether; yield 4.69 g (68%); mp 159—161 °C; $[\alpha]_D^{20}$ −10.5° (*c* 1, methanol); R_f^1 0.86 and R_f^2 0.10.

Found: C, 52.34; H, 8.05; N, 11.88%. Calcd for $C_{15}H_{27}O_6N_3$: C, 52.16; H, 7.88; N, 12.17%.

Boc-Ile-Asn-His-OBzl (13): To a chilled solution of **12** (5.18 g, 15 mmol) and HOBt (2.44 g, 18 mmol) in THF (40 ml), DCC (3.09 g, 15 mmol) was added, then a solution of H-His-OBzl·2TsOH[22] (9.0 g, 15 mmol) and NMM (3.3 ml, 30 mmol) in DMF (20 ml) was added. The reaction mixture was held for 2 h at −5 °C and then refrigerated overnight at 0 °C. DCUrea was filtered off and washed with a small amount of DMF. The filtrate and the washing were combined and evaporated *in vacuo*, then dissolved in 1-butanol. The solution was washed successively with 4% sodium hydrogencarbonate and water, then dried over anhydrous sodium sulfate. The filtrate was evaporated *in vacuo*, the product was crystallized by the addition of ether and recrystallized from methanol-ether; yield 5.38 g (63%); mp 181—182 °C (decomp); $[\alpha]_D^{20}$ −9.5° (*c* 1, DMF); R_f^1 0.77 and R_f^2 0.57.

Found: C, 58.50; H, 7.12; N, 14.69%. Calcd for $C_{29}H_{40}O_7N_6$: C, 58.72; H, 7.04; N, 14.68%.

H-Ile-Asn-His-OBzl·2HCl (14): Compound **13** (5.15 g, 9 mmol) was dissolved in 98% formic acid (50 ml) and the solution was cooled in an ice bath. A solution of 4 M hydrogen chloride in dioxane (50 ml) was added to it, and the mixture was held for 1 h at 10 °C. The solution was then evaporated *in vacuo* below 25 °C. A residue was obtained by the aid of ether as a hygroscopic solid and was recrystallized from methanol-ether; yield 4.79 g (94%); mp 156—157 °C; $[\alpha]_D^{20}$ +8.5° (*c* 1, pyridine); R_f^1 0.67 and R_f^2 0.11.

Found: C, 50.55; H, 6.56; N, 15.67%. Calcd for $C_{23}H_{34}O_5N_6Cl_2$: C, 50.64; H, 6.28; N, 15.41%.

Z-Val-Tyr-Pro-Phe-Pro-Pro-Gly-Ile-Asn-His-OBzl (15): To a solution of **11** (3.64 g, 4 mmol), **14** (2.53 g, 4.5 mmol), HOBt (0.54 g, 4 mmol) and NMM (1.0 ml, 9 mmol) in DMF (40 ml), DCC (0.83 g, 4 mmol) was added. The reaction mixture was held overnight at 0 °C, then DCUrea was filtered off. The filtrate was dissolved in 1-butanol and washed with 4% sodium hydrogencarbonate and water. The solution was evaporated *in vacuo* and the crude product was precipitated with ether to give 4.43 g (81%, mp 135—140 °C). Two g of the crude product were dissolved in methanol (2 ml) and applied to a silica-gel column (Merck silica-gel G) (2×35 cm), then developed with a mixture of chloroform and methanol (5:1, v/v). The fractions (175—300 ml) which gave a single spot on thin-layer chromatography were collected and evaporated *in vacuo*. The residue was crystallized with ether; yield 1.15 g (57%); mp 144—145 °C; $[\alpha]_D^{20}$ −91.0° (*c* 1, methanol) R_f^1 0.79 and R_f^2 0.68.

Found: C, 62.77; H, 6.51; N, 13.06%. Calcd for $C_{71}H_{89}O_{15}N_{13}$: C, 62.49; H, 6.57; N, 13.35%.

H-Val-Tyr-Pro-Phe-Pro-Pro-Gly-Ile-Asn-His-OH·2HCl (16): Compound **15** (0.45 g, 0.33 mmol) in 0.035 M methanolic hydrogen chloride (20 ml) was hydrogenated in the presence of palladium black. The filtrate was evaporated

in vacuo and the residue was crystallized from acetone. It was reacrystallized from methanol-acetone; yield of the air-dried product was 0.39 g (95%); $[\alpha]_D^{20}$ −96.4° (*c* 1.3, water); R_f^1 0.51. Amino acid ratios in acid hydrolyzate:[23] Val 1.0; Tyr 1.0; Pro 3.1; Phe 1.0; Gly 1.0; Ile 1.1; Asp 1.1; His 1.1.

Found: C, 50.13; H, 7.26; N, 13.31%. Calcd $C_{56}H_{79}O_{13}N_{13}Cl_2 \cdot 7H_2O$: C, 50.29; H, 7.01; N, 13.47%. The air-dried product lost 8.7% of its weight after drying for 2 h at 110 °C and 2 mmHg. Calcd for $7H_2O$: 8.8%.

Syntheses of BPIc Analogs and Fragments. Z-Gly-Gly-Gly-OEt (17): A solution of Z-Gly-OH[24] (1.88 g, 9 mmol) and NMM (0.99 ml, 9 mmol) in THF (20 ml) was chilled to −5 °C, and ECF (0.9 ml, 9 mmol) was added under stirring. After 10 min, the precooled solution of H-Gly-Gly-OEt·HCl[25] (1.77 g, 9 mmol) and NMM (0.99 ml, 9 mmol) in DMF (20 ml) was added to it. The reaction mixture was kept for 1 h in a refrigerator and then kept overnight at room temperature. The mixture was added to 4% sodium hydrogencarbonate (100 ml) and the precipitate was collected by filtration, then washed with 4% sodium hydrogencarbonate, 0.5 M hydrochloric acid and water. It was recrystallized ethanol-ether; yield 2.11 g (67%); mp 166 °C (lit,[26] 167 °C); R_f^1 0.91 and R_f^2 0.64.

Found: C, 54.76; H, 6.04; N, 11.92%. Calcd for $C_{16}H_{21}O_6N_3$: C, 54.69; H, 6.02; N, 11.96%.

H-Gly-Gly-Gly-OEt·HCl (18): A solution of **17** (2.0 g, 5.7 mmol) dissolved in 0.3 M methanolic hydrogen chloride (30 ml) was hydrogenated in the presence of palladium black. The filtrate from the catalyst was evaporated *in vacuo* and the residue was crystallized by addition of ether; yield 1.25 g (87%); mp 219—220 °C (decomp) (lit, [27] 214—217 °C (decomp)); R_f^1 0.64 and R_f^2 0.08.

Found: C, 37.98; H, 6.43; N, 16.79%. Calcd for $C_8H_{16}O_4N_3Cl$: C, 37.87; H, 6.36; N, 16.56%.

Z-Val-Tyr-Pro-Phe-Gly-Gly-Gly-OEt (19): To a chilled solution of **6** (2.64 g, 4 mmol) and HOBt (0.57 g, 4.2 mmol) in THF (20 ml), DCC (0.83 g, 4 mmol) was added. After 20 min, the precooled solution of **18** (1.01 g, 4 mmol) and NMM (0.44 ml, 4 mmol) in DMF (20 ml) was added and the mixture was kept for 5 h at 0 °C, then stood overnight at room temperature. DCUrea was filtered off and the filtrate was evaporated *in vacuo* and then dissolved in ethyl acetate. The solution was washed successively with 4% sodium hydrogencarbonate, 0.5 M hydrochloric acid and water, then dried over anhydrous sodium sulfate. The filtrate was evaporated *in vacuo* and the residue was solidified by addition of petroleum ether. It was recrystallized from ethanol and petroleum ether; yield 2.78 g (81%); mp 96 °C; $[\alpha]_D^{20}$ −59.0° (*c* 1, methanol); R_f^1 0.92 and R_f^2 0.63.

Found: C, 61.07; H, 6.73; N, 11.11%. Calcd for $C_{34}H_{55}O_{11}N_7 \cdot 1/2\,H_2O$: C, 60.95; H, 6.51; N, 11.31%.

Z-Val-Tyr-Pro-Phe-Gly-Gly-Gly-OH (20): Compound **19** (2.53 g, 3 mmol) was subjected to the saponification in the mixture of methanol (10 ml) and 2 M sodium hydroxide (3.3 ml) for 1 h. The following procedure was employed for the preparation of **11**; yield 2.07 g (83%); mp 114—116 °C; $[\alpha]_D^{20}$ −65.0° (*c* 1, methanol); R_f^1 0.73 and R_f^1 0.29.

Found: C, 59.76; H, 6.22; N, 11.43%. Calcd for $C_{32}H_{51}O_{11}N_7 \cdot H_2O$: C, 59.45; H, 6.30; N, 11.55%.

Z-Val-Tyr-Pro-Phe-Gly-Gly-Gly-Ile-Asn-His-OBzl (21): This compound was prepared from **20** (1.25 g, 1.5 mmol) and **14** (0.98 g, 1.8 mmol) as described for the preparation of **15**; yield 1.36 g (71%); mp 153—155 °C; $[\alpha]_D^{20}$ −58.5° (*c* 1, methanol); R_f^1 0.84 and R_f^2 0.48.

Found: C, 60.92; H, 6.29; N, 14.13%. Calcd for $C_{65}H_{81}O_{15}N_{13}$: C, 60.78; H, 6.36; N, 14.18%.

H-Val-Tyr-Pro-Phe-Gly-Gly-Gly-Ile-Asn-His-OH·HCl (22): A solution of **20** (1.0 g, 0.78 mmol) in 0.3 M methanolic hydrogen chloride (4 ml) was subjected to the hydrogenation as described for **16**; yield 0.75 g (79%); mp 184—187 °C; $[\alpha]_D^{20}$ −39.5° (*c* 1, methanol); R_f^1 0.60. Amino acid ratios in acid hydrolyzate:[23] Val 1.1; Tyr 1.0; Pro 1.1; Phe 1.0; Gly 3.1; Ile 1.0; Asp 1.0; His 1.0.

Found: C, 51.43; H, 6.53; N, 15.45%. Calcd for $C_{50}H_{70}O_{13}N_{13}Cl \cdot 4H_2O$: C, 51.38; H, 6.73; N, 15.58%.

Boc-Ile-Gly-Gly-OBzl (23): This compound was prepared from Boc-Ile-OH·DCHA[28] (4.14 g, 10 mmol) and H-Gly-Gly-OBzl·HCl[29] (2.60 g, 10 mmol) as described for the preparation of **1**; yield 3.70 g (85%); mp 93—94 °C; $[\alpha]_D^{20}$ +3.0° (*c* 1, methanol); R_f^1 0.95 and R_f^2 0.67.

Found: C, 60.68; H, 7.73; N, 9.67%. Calcd for $C_{22}H_{33}O_6N_3$: C, 60.67; H, 7.64; N, 9.65%.

H-Ile-Gly-Gly-OBzl·HCl (24): This was prepared from **23** (1.74 g, 4 mmol) as described for the preparation of **9**; yield 1.40 g (94%); mp 186—187 °C; $[\alpha]_D^{20}$ +29.0° (*c* 1, methanol); R_f^1 0.80 and R_f^2 0.50.

Found: C, 54.58; H, 7.23; N, 11.49%. Calcd for $C_{17}H_{26}O_4N_3Cl$: C, 54.90; H, 7.31; N, 11.30%.

Z-Val-Tyr-Pro-Phe-Pro-Pro-Gly-Ile-Gly-Gly-OBzl (25): This was prepared from **11** (1.86 g, 2 mmol) and **24** (0.78 g, 2.2 mmol) as described for the preparation of **15**. Purification of the product was done by the recrystallization from ethanol-ether; yield 2.06 g (84%); mp 115—118 °C; $[\alpha]_D^{20}$ −91.0° (*c* 1, methanol); R_f^1 0.92 and R_f^2 0.57.

Found: C, 62.43; H, 6.90; N, 11.15%. Calcd for $C_{65}H_{82}O_{14}N_{10} \cdot H_2O$: C, 62.53; H, 7.02; N, 11.22%.

H-Val-Tyr-Pro-Phe-Pro-Pro-Gly-Ile-Gly-Gly-OH (26): Compound **25** (1.23 g, 1 mmol) was hydrogenated as described for the preparation of **16**; yield 0.95 g (85%); mp 168—171 °C; $[\alpha]_D^{20}$ −89.0° (*c* 1, methanol); R_f^1 0.71 and R_f^2 0.31. Amino acid ratios in acid hydrolyzate:[23] Val 1.0; Tyr 1.0; Pro 2.9; Phe 1.0; Gly 3.2; Ile 1.0.

Found: C, 56.77; H, 6.95; N, 13.05%. Calcd for $C_{50}H_{70}O_{12}N_{10} \cdot 3H_2O$: C, 56.80; H, 7.25; N, 13.25%.

Boc-Gly-Ile-OBzl (27): This was prepared from Boc-Gly-OH[30] (3.50 g, 20 mmol) and H-Ile-OBzl·TsOH[31] (9.00 g, 22 mmol) as described for the preparation of **1**. The product was obtained as an oily form; yield 7.50 g (100%); R_f^1 0.97 and R_f^2 0.81.

H-Gly-Ile-OBzl·HCl (28): Compound **27** (7.50 g, 20 mmol (oily form)) was treated with hydrogen chloride as described for the preparation of **9**; yield 5.10 g (81%); mp 108—110 °C; $[\alpha]_D^{20}$ −19.5° (*c* 1, methanol); R_f^1 0.81 and R_f^2 0.47.

Found: C, 55.52; H, 7.66; N, 8.95%. Calcd for $C_{15}H_{23}O_3N_2Cl \cdot 1/2\,H_2O$: C, 55.64; H, 7.47; N, 8.65%.

Boc-Pro-Pro-Gly-Ile-OBzl (29): This was prepared from **7** (1.87 g, 6 mmol) and **28** (1.88 g, 6 mmol) as described for the preparation of **1**. The product was obtained as an oily form; yield 3.43 g (100%) R_f^1 0.91 and R_f^2 0.63.

H-Pro-Pro-Gly-Ile-OBzl·HCl (30): Compound **29** (3.43 g, 6 mmol (oily form)) was treated with hydrogen chloride as described for the preparation of **9**; yield 2.54 g (83%); mp 68—70 °C; $[\alpha]_D^{20}$ −99.0° (*c* 1, methanol); R_f^1 0.77 and R_f^2 0.35.

Found: C, 58.08; H, 7.42; N, 10.59%. Calcd for $C_{25}H_{37}O_5N_4Cl \cdot 1/2\,H_2O$: C, 57.96; H, 7.39; N, 10.82%.

Z-Val-Tyr-Pro-Phe-Pro-Pro-Gly-Ile-OBzl (31): This compound was prepared from **6** (3.29 g, 5 mmol) and **30** (2.40 g, 5 mmol) as described for the preparation of **10**; yield 4.21 g (76%); mp 114—116 °C; $[\alpha]_D^{20}$ −104.0° (*c* 1, methanol); R_f^1 0.86 and R_f^2 0.71.

Found: C, 65.29; H, 7.01; N, 9.98%. Calcd for $C_{61}H_{76}O_{12}N_8 \cdot 1/2\,H_2O$: C, 65.28; H, 6.92; N, 9.98%.

H-Val-Tyr-Pro-Phe-Pro-Pro-Gly-Ile-OH (32): A solution of **31** (3.34 g, 3 mmol) in methanol (8 ml) and acetic acid (8 ml) was hydrogenated in the presence of palladium black. The filtrate from the catalyst was evaporated *in vacuo* and

the residue was crystallized from ether; yield 2.54 g (92%); mp 164—168 °C (decomp); $[\alpha]_D^{20}$ −124.5° (*c* 0.92, water); R_f^1 0.76 and R_f^2 0.40. Amino acid ratios in acid hydrolyzate:[23] Val 0.9; Tyr 1.0; Pro 3.1; Phe 1.0; Gly 1.0; Ile 1.0.

Found: C, 60.06; H, 7.10; N, 12.21%. Calcd for $C_{46}H_{64}O_{10}N_8 \cdot 3/2\ H_2O$: C,60.31; H, 7.37; N, 12.23%.

H-Val-Tyr-Pro-Phe-Pro-Pro-Gly-OH (33): Compound **11** (1.36 g, 1.5 mmol) was hydrogenated as described for the preparation of **32**; yield 1.15 g (91%); mp 172—174 °C (decomp); $[\alpha]_D^{20}$ −125.9° (*c* 0.84, water); R_f^1 0.67 and R_f^2 0.28. Amino acid ratios in acid hydrolyzate:[23] Val 1.0; Tyr 1.0; Pro 2.9; Phe 1.0; Gly 0.9.

Found: C, 58.63; H, 6.65; N, 11.93%. Calcd for $C_{40}H_{53}O_9N_7 \cdot 1/2\ CH_3COOH \cdot 2H_2O$: C, 58.49; H, 7.06; N, 11.65%.

A Comparison of Synthetic and Natural BPIc.[32] *Thin Layer Chromatography*: Both compounds gave a single spot and identical R_f values. R_f^1 values of both are 0.51.

Paper Electrophoresis: This was carried out under the following conditions. Paper, Toyo Roshi No. 51A chromatography paper; solvent, pyridine–acetic acid–water (10:0.4:90, v/v) (pH 6.4); voltage gradient, 15 V/cm; charge period, 2 h. Electrophoretic mobilities were recorded as R_{His}, the ratio of the distance the compounds moved to that which a standard histidine spot moved on the same electrophoreogram. BPIc migrated toward the cathode and gave a single spot. The R_{His} value of both natural and synthetic BPIc was 0.82. The R_{His} values of **22**, **26**, **32**, and **33** were 0.83, 0.70, 0.70, and 0.69 respectively.

Carboxymethylcellulose Column Chromatography: A portion (*ca.* 1 mg) of synthetic or natural BPIc was dissolved in 0.3 ml of 0.2 M pyridinium acetate (pH 5.0). The solution was applied to a column (1.0×60 cm) of carboxymethylcellulose. Elution was carried out with the same solvent and 2 ml fractions were collected at a flow rate of 8 ml h^{-1}. The peptide content was determined by the method described by Yemm and Cocking.[33] The results shown in Fig. 2 indicate that the pattern of the chromatogram of synthetic BPIc is indistinguishable from that of the natural material. The cochromatography of synthetic and natural BPIc was carried out under the same conditions and a single peak was obtained. The chromatographic patterns of other synthetic peptides are also presented in Fig. 2.

Sensory Test. Bitterness of the synthetic peptides was organoleptically determined by panel evaluation employing four people. A series of solutions of decreasing concentration, each half as strong as the proceeding one, were prepared. Before tasting the sample, the mouth was thoroughly rinsed with deionized water. The sample solution was held in the mouth for *ca.* 10 s and then spit out and the threshold value was determined. The results are listed in the Table.

The author wishes to express his thanks to Professor Nobuo Izumiya of Kyushu University and Associate Professor Hideo Okai of Hiroshima University for their helpful discussions. The author would like to thank Dr. Noshi Minamiura of Osaka City University for his kind offer of the natural sample of BPIc. Thanks are also due to Dr. Shinji Okumura of Ajinomoto Co. Inc., for supplying some amino acids.

References

1) Part V. H. Kanehisa and H. Okai, *Bull. Chem. Soc. Jpn.*, **57**, 301 (1984).

2) The abbreviations recommended by IUPAC-IUB commission of Biochemical Nomenclature (*J. Biol. Chem.*, **247**, 977(1972)) have been used. Amino acid symbols except glycine denoted L-configuration unless otherwise noted. Additional abbreviations: DCC, dicyclohexylcarbodiimide; DCHA, dicyclohexylamine; DCUrea, *N,N'*-dicyclohexylurea; DMF, *N,N*-dimethylformamide; ECF, ethyl chloroformate; Et_3N, triethylamine; HOBt, 1-hydroxybenzotriazole; HONSu, *N*-hydroxysuccinimide; NMM, *N*-methylmorpholine; THF, tetrahydrofuran; TsOH, *p*-toluenesulfonic acid.

3) Part I. H. Fukui, H. Kanehisa, N. Ishibashi, I. Miyake, and H. Okai, *Bull. Chem. Soc. Jpn.*, **56**, 766 (1983).

4) N. Minamiura, Y. Matsumura, J. Fukumoto, and T. Yamamoto, *Agric. Biol. Chem.*, **36**, 588 (1972).

5) Part II. K. Otagiri, I. Miyake, N. Ishibashi, H. Fukui, H. Kanehisa, and H. Okai, *Bull. Chem. Soc. Jpn.*, **56**, 1116 (1983).

6) Part. III. I. Miyake, K. Kouge, H. Kanehisa, and H. Okai, *Bull. Chem. Soc. Jpn.*, **56**, 1678 (1983).

7) Part IV. K. Otagiri, T. Shigenaga, H. Kanehisa, and H. Okai, *Bull. Chem. Soc. Jpn.*, **57**, 90 (1984).

8) These peptides were synthesized in the usual manners. Details of di-, tri-, and tetrapeptide fragments of BPIc will be described in another investigation.

9) E.Shröder, *Ann. Chem.*, **692**, 241 (1966).

10) E. Wünsch, G. Friss, and A. Zwick, *Chem. Ber.*, **91**, 543 (1958).

11) H. Ramachandran and C. H. Li, *J. Org. Chem.*, **28**, 173 (1963).

12) R. Schwyzer, B. Iselin, H. Kappeler, B. Riniker, W. Rittel, and H. Zuber, *Helv. Chim. Acta*, **41**, 1273 (1958).

13) W. Grassmann and E. Wünsch, *Chem. Ber.*, **91**, 462 (1958).

14) T. Kato, S. Makisumi, M. Ohno, and N. Izumiya, *Nippon Kagaku Zasshi*, **83**, 1151 (1962).

15) H. Aoyagi, K. Arakawa, and N. Izumiya, *Bull. Chem. Soc. Jpn.*, **41**, 433 (1968).

16) N. Izumiya and J. S. Fruton, *J. Biol. Chem.*, **218**, 59 (1956).

17) E. Boyer, G. Jung, and H. Hagenmaier, *Tetrahedron*, **24**, 4853 (1968).

18) R. E. Newman and E. L. Smith, *J. Biol. Chem.*, **193**, 97 (1951).

19) G. R. Pettit and S. K. Das Gupta, *Can. J. Chem.*, **45**, 1600 (1967).

20) C. R. Harington and T. H. Mead, *Biochem. J.*, **30**, 1598 (1936).

21) G. W. Anderson, J. E. Zimmerman, and F. M. Callahan, *J. Am. Chem. Soc.*, **86**, 1839 (1964).

22) S. Akabori, S. Sakakibara, and S. Shiina, *Bull. Chem. Soc. Jpn.*, **31**, 784 (1958).

23) The synthetic peptides were hydrolyzed with 6 M hydrochloric acid in a sealed tube at 110 °C for 65 h. Molar ratios of amino acids are based on isoleucine or valine value.

24) M. Bergmann and L. Zervas, *Chem. Ber.*, **65**, 1192 (1932).

25) A. H. Cook and A. L. Levy, *J. Chem. Soc.*, **1950**, 646.

26) P. M. Hardy, B. Ridge, H. N. Rydon, and F. O. Dos. S. P. Seräo, *J. Chem. Soc.*, **1971**, 1722.

27) J. C. Sheehan and W. L. Richardson, *J. Am. Chem. Soc.*, **76**, 6329 (1954).

28) H. C. Beyerman, C. A. M. Boers-Boonekamp, and H. Maassen van den Brink-Zimmermannova, *Recl. Trav. Chim. Bays-Bas*, **87**, 257 (1968).

29) L. Zervas and D. M. Theodoropoulos, *J. Am. Chem. Soc.*, **78**, 1359 (1959).

30) G. W. Anderson and A. C. McGregor, *J. Am. Chem. Soc.*, **79**, 6180 (1957).

31) L. Zervas, M. Winitz, and J. P. Greenstein, *J. Org. Chem.*, **22**, 1515 (1957).

32) Natural BPIc was received from Dr. N. Minamiura.

33) E. W. Yemm and E. C. Cocking, *Analyst*, **80**, 209 (1955).

Studies of Bitter Peptides from Casein Hydrolyzate. VII.[1] Bitterness of the retro-BPIa (Val-Ile-Phe-Pro-Pro-Gly-Arg) and Its Fragments[2]

Toshiaki SHIGENAGA, Ken OTAGIRI, Hidenori KANEHISA, and Hideo OKAI*
Department of Fermentation Technology, Faculty of Engineering, Hiroshima University, Shitami, Saijo-cho, Higashihiroshima 724
(Received August 1, 1983)

To explain the bitter taste exhibited by BPIa (Arg-Gly-Pro-Pro-Phe-Ile-Val) which was isolated from casein hydrolyzate, we have proposed the following requirement: its characteristic spatial structure: the basic moiety in the N-terminal and the hydrophobic moiety in the C-terminal were affected to each other by prolylprolyl residue, is necessary for the bitterness to be exhibited. As for BPIc (Val-Tyr-Pro-Phe-Pro-Pro-Gly-Ile-Asn-His), which is the other fraction, although it exhibited as strong and bitter a taste as BPIa, the basic moiety of BPIc is located in the C-terminal and its hydrophobic moiety is located in the N-terminal. The authors synthesized retro-BPIa with the reverse peptide sequence and its fragments. The retro-BPIa exhibited as strong and bitter a taste as BPIa. However, the bitterness of the fragments of retro-BPIa was far weaker than that of retro-BPIa.

In studies of the relationship between bitterness and chemical structure of BPIa (Arg-Gly-Pro-Pro-Phe-Ile-Val) which was isolated by Minamiura *et al.*,[3] the authors reported that the basic amino acid residue in the N-terminal, the hydrophobic amino acid residues in the C-terminal, and its characteristic spatial structure, which may derive from prolylprolyl residues at 3 and 4 positions of BPIa, are necessary for an intense bitter taste to be exhibited by BPIa.[4-7] In the previous paper,[1] we reported that a decapeptide BPIc (Val-Tyr-Pro-Phe-Pro-Pro-Gly-Ile-Asn-His) in which basic moiety is located in the C-terminal and hydrophoic moiety is located in the N-terminal exhibited an extremely bitter taste on the same level as that of BPIa. From those results, it was expected that the retro-BPIa (Val-Ile-Phe-Pro-Pro-Gly-Arg) possessing the reverse amino acid sequence of BPIa would exhibit as bitter a taste as BPIa. Thus the authors synthesized retro-BPIa and its fragments, as shown in the Table, and investigated their bitterness.

The synthetic route to compound **1** (retro-BPIa) is shown in Fig. 1. *N*-(Benzyloxycarbonyl)isoleucine and phenylalanine benzyl ester were coupled by the mixed anhydride method to yield *N*-(benzyloxycarbonyl)-isoleucylphenylalanine benzyl ester (**12**). The free dipeptide (**5**) was given by the catalytic hydrogenation of **12**. *N*-(Benzyloxycarbonyl)valine *N*-hydroxysuccinimide ester and **5** were coupled to yield *N*-(benzyloxycarbonyl)valylisoleucylphenylalanine (**13**). *N*-(*t*-Butoxycarbonyl)prolylproline and glycine benzyl ester were coupled by the mixed anhydride method to yield *N*-(*t*-butoxycarbonyl)prolylprolylglycine benzyl ester (**14**). After treatment of **14** with hydrogen chloride in dioxane, the tripeptide benzyl ester hydrochloride (**15**) and **13** were coupled by the DCC-HONSu method to yield *N*-(benzyloxycarbonyl)valylisoleucylphenylalanylprolylprolylglycine benzyl ester (**16**). *N*-(Benzyloxycarbonyl)valylisoleucylphenylalanylprolylprolylglycine (**17**) was obtained by the saponification of **16**. **17** and N^G-nitroarginine benzyl ester were coupled by the DCC-HOBt method to yield *N*-(benzyloxycarbonyl)valylisoleucylphenylalanylprolylprolylglycyl-N^G-nitroarginine benzyl ester (**18**). The protected heptapeptide was hydrogenated in the presence of palladium black to give the retro-BPIa (**1**).

The synthetic route to compounds **2** and **3** is shown in Fig. 2. These compounds were obtained by the catalytic hydrogenation of **16** and **13**, which are the intermediates in the synthesis of retro-BPIa. The details

TABLE. THE THRESHOLD VALUE FOR BITTER TASTE OF THE SYNTHETIC PEPTIDES

	Compound	Taste	T.V./mM	$R_{caf.}$[a]
1.	Val-Ile-Phe-Pro-Pro-Gly-Arg	Bitter	0.08	12.50
2.	Val-Ile-Phe-Pro-Pro-Gly	Bitter	2.10	0.48
3.	Val-Ile-Phe	Bitter	1.30	0.77
4.	Val-Ile	Bitter	6.00	0.17
5.	Ile-Phe	Bitter	1.50	0.67
6.	Pro-Pro	Bitter	4.50	0.22
7.	Pro-Pro-Gly	Bitter	9.50	0.11
8.	Pro-Gly	Sweet	—	—
9.	Pro-Gly-Arg	Bitter	25.00	0.04
10.	Gly-Arg	Bitter	75.00	0.01
11.	Arg-Gly-Pro-Pro-Phe-Ile-Val	Bitter	0.05	20.00

a) Ratio of caffeine.

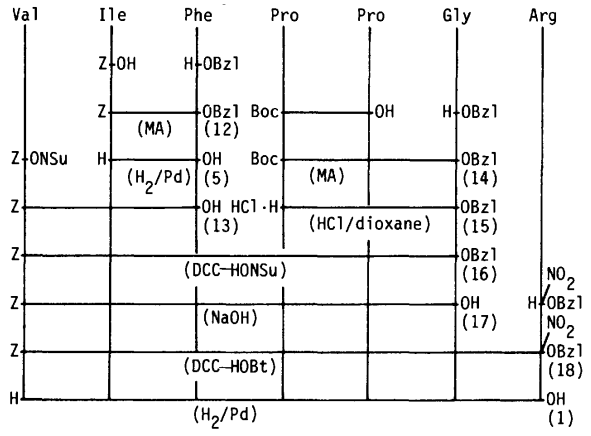

Fig. 1. Syntheses of compound **1** (retro-BPIa) and **5**.

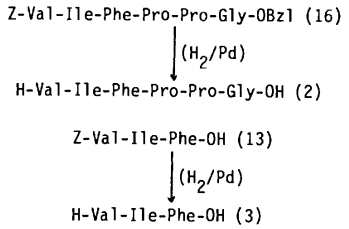

Fig. 2. Syntheses of compounds **2** and **3**.

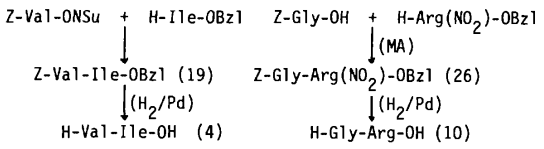

Fig. 3. Syntheses of compounds **4** and **10**.

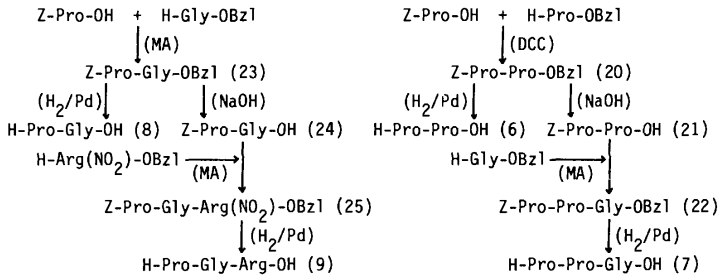

Fig. 4. Syntheses of compounds **6**, **7**, **8**, and **9**.

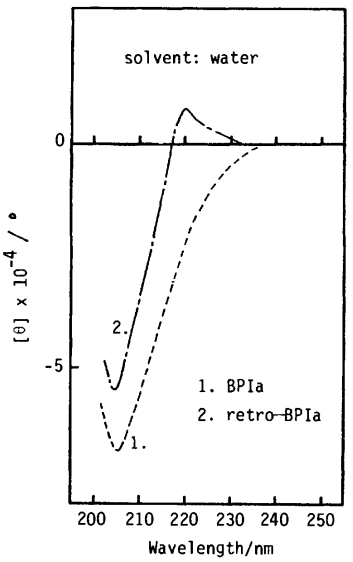

Fig. 5. CD curves of BPIa and retro-BPIa.

of the synthetic route to other peptides (compounds **4**—**10**) are shown in Figs. 3 and 4, and are described in the Experimental part. The purity of the synthetic peptides and their intermediates was confirmed by thin-layer chromatography in two solvent systems, elemental analyses, and amino acid analyses.

The bitterness of the synthetic peptides were organoleptically determined by panel evaluation of five people (see Table). The threshold value of retro-BPIa (compound **1**) was 0.08 mM (1 M=1 mol dm^{-3}). The value is about the same as that of BPIa. On the other hand, the bitterness of des-Arg^7-retro-BPIa (**2**) was far weaker than that of retro-BPIa. In the previous paper,[4] we reported that des-Arg^1-BPIa also exhibited a weakly bitter taste. The result indicated that the arginine residue plays an important role for the bitter taste exhibited by BPIa and retro-BPIa, as has been described in the previous papers.[4,7] As for the other fragments (**4**—**10**), they did not exhibit as strong and bitter a taste as BPIa.

We have reported that the strong bitter taste exhibited by BPIa may derive from its characteristic spatial structure.[4,5] In order to investigate that requirement, we measured the circular dichroism (CD) of the retro-BPIa, and compared its CD curves with that of BPIa, as shown in Fig. 5. The CD curves of BPIa and retro-BPIa were similar in shape.

The results described above suggest that the spatial structure of retro-BPIa possessing the reverse amino acid sequence may be similar to that of BPIa. Thus, in order for the bitter taste to be exhibited by BPIa, the spatial structure of the molecule is more important than the position of the basic and hydrophobic moieties.

Experimental

All the melting points are uncorrected. Thin-layer chromatography (TLC) was carried out on Merck silica gel G with the following solvent systems: R_f^1, 1-butanol-acetic acid-pyridine-water (4:1:1:2, v/v); R_f^2, chloroform-methanol (5:1, v/v). Materials possessing a free amino group on a thin-layer plate were detected by spraying with ninhydrin. Compounds with blocked amino groups were detected by spraying with 25% hydrogen bromide in acetic acid and then with ninhydrin. The optical rotations were measured on a Union PM-101 polarimeter. Amino acid analyses were performed on a Hitachi amino acid analyzer KLA-5 type, after hydrolysis in a mixture of 6 M hydrochloric acid and propionic acid (1:1) at 110 °C for 72 h.

Z-Ile-Phe-OBzl (12). Z-Ile-OH·DCHA (14.74 g, 33 mmol) was dissolved in ethyl acetate (100 ml), and 0.5 M sulfic acid (50 ml) was added to the mixture during stirring. The organic layer was washed with water and dried over anhydrous sodium sulfate. The solution was con-

centrated to dryness *in vacuo*, and the oily residue was dissolved in THF (50 ml) and NMM (3.3 ml, 30 mmol). ECF (3.0 ml, 30 mmol) was added to the mixture at −5 °C. After 10 min, a solution of H-Phe-OBzl·TsOH[8] (12.80 g, 30 mmol) in chloroform (50 ml) was added to the mixture. The reaction mixture was stirred in an ice bath for 1 h, then at room temperature overnight. The reaction mixture was evaporated *in vacuo*, and the oily residue was dissolved in ethyl acetate. The solution was washed with water, 0.5 M hydrochloric acid, 4% sodium hydrogencarbonate, and water successively, then dried over anhydrous sodium sulfate. Sodium sulfate was removed by filtration, and the filtrate was evaporated *in vacuo*. The oily residue was crystallized with ether-petroleum ether: yield 11.88 g (71%); mp 158 °C; $[\alpha]_D^{15}$ −15.5° (*c* 1, *N,N*-dimethylformamide); R_f^1 0.99 and R_f^2 0.97.

Found: C, 71.63; H, 7.01; N, 5.50%. Calcd for $C_{30}H_{34}O_5N_2$: C, 71.69; H, 6.82; N, 5.57%.

H-Ile-Phe-OH (5). A solution of compound **12** (10.05 g, 20 mmol) in methanol (20 ml) and acetic acid (5 ml) was hydrogenated in the presence of palladium black at room temperature overnight. The catalyst was removed by filtration, and the filtrate was evaporated *in vacuo*. The residue was crystallized by the aid of acetone: yield 4.96 g (90%); mp 250 °C (decomp); $[\alpha]_D^{15}$ +68.0° (*c* 1, acetic acid); R_f^1 0.83 and R_f^2 0.06.

Found: C, 65.16; H, 7.87; N, 10.11%. Calcd for $C_{15}H_{22}O_3N_2$: C, 64.72; H, 7.97; N, 10.07%.

Z-Val-Ile-Phe-OH (13). To a solution of Z-Val-ONSu[9] (4.20 g, 12 mmol) in THF (20 ml), a solution of compound **5** (2.78 g, 10 mmol) and Et_3N (1.4 ml, 10 mmol) in water (20 ml) was added. The reaction mixture was allowed to stand at room temperature for 24 h, and then suspended by the aid of water (200 ml). The insoluble product was collected by filtration and recrystallized from hot ethanol and ether: yield 3.58 g (70%); mp 208—210 °C; $[\alpha]_D^{15}$ +7.5° (*c* 1, *N,N*-dimethylformamide); R_f^1 0.89 and R_f^2 0.74.

Found: C, 65.10; H, 7.63; N, 8.40%. Calcd for $C_{28}H_{37}O_6N_3 \cdot 1/3\ H_2O$: C, 64.97; H, 7.34; N, 8.12%.

Boc-Pro-Pro-Gly-OBzl (14). Boc-Pro-Pro-OH[10] (6.24 g, 20 mmol) and H-Gly-OBzl·TsOH[11,12] (6.74 g, 20 mmol) were coupled by the same method as described for the preparation of **12**: yield 6.95 g (76%); mp 108—109 °C; $[\alpha]_D^{15}$ −122.5° (*c* 1, methanol); R_f^1 0.85 and R_f^2 0.67.

Found: C, 62.71; H, 7.36; N, 9.04%. Calcd for $C_{24}H_{33}O_6N_3$: C, 62.72; H, 7.24; N, 9.14%.

H-Pro-Pro-Gly-OBzl·HCl (15). To a solution of compound **14** (4.60 g, 10 mmol) in dioxane (20 ml), 4 M HCl/dioxane (50 ml) was added. The solution was allowed to stand at room temperature. After 2 h, the solution was evaporated *in vacuo*. The residual oil was solidified with ether: yield 3.92 g (99%); mp 65—67 °C; $[\alpha]_D^{15}$ −115.0° (*c* 1, methanol); R_f^1 0.62 and R_f^2 0.13.

Found: C, 56.74; H, 6.83; N, 10.38%. Calcd for $C_{19}H_{25}O_4N_3 \cdot HCl \cdot 1/3\ H_2O$: C, 56.78; H, 6.68; N, 10.45%.

Z-Val-Ile-Phe-Pro-Pro-Gly-OBzl (16). To a solution of compound **13** (2.56 g, 5 mmol) and compound **15** (1.98 g, 5 mmol) and NMM (0.55 ml, 5 mmol) and DMF (20 ml), DCC (1.55 g, 7.5 mmol) and HONSu (0.86 g, 7.5 mmol) were added to the mixture. The reaction mixture was cooled at −10 °C for 1 h and allowed to stand at room temperature for 48 h. The DCUrea was removed by filtration, and the filtrate was evaporated *in vacuo*. The oily residue was dissolved in ethyl acetate and the solution was washed with water, 0.5 M hydrochloric acid, 4% sodium hydrogencarbonate, and water successively. The solution was dried over anhydrous sodium sulfate. Sodium sulfate was removed by filtration and the filtrate was evaporated *in vacuo*. The residue was crystallized with ether-petroleum ether: yield 4.12 g (97%); mp 108—109 °C; $[\alpha]_D^{15}$ −54.5° (*c* 1, *N,N*-dimethylformamide); R_f^1 0.94 and R_f^2 0.60.

Found: C, 66.00; H, 7.33; N, 10.02%. Calcd for $C_{47}H_{60}O_9N_6$: C, 66.17; H, 7.09; N, 9.85%.

Z-Val-Ile-Phe-Pro-Pro-Gly-OH (17). To a solution of compound **16** (2.56 g, 3 mmol) in methanol (15 ml), 2 M sodium hydroxide (1.8 ml, 3.6 mmol) was added under stirring. The solution was allowed to stand at room temperature. After 2 h, the solution was evaporated *in vacuo*, and then diluted with water. The solution was washed with ethyl acetate. The aqueous layer was acidified to pH 4 with 2 M hydrochloric acid. The precipitate thus obtained was collected and washed with water. It was recrystallized from hot ethanol-ether: yield 2.16 g (92%); mp 130—134 °C; $[\alpha]_D^{15}$ −56.0° (*c* 1, *N,N*-dimethylformamide); R_f^1 0.78 and R_f^2 0.35.

Found: C, 62.01; H, 7.19; N, 10.84%. Calcd for $C_{40}H_{54}O_9N_6 \cdot 1/3\ H_2O$: C, 62.08; H, 7.12; N, 10.86%.

Z-Val-Ile-Phe-Pro-Pro-Gly-Arg(NO$_2$)-OBzl (18). To a solution of compound **17** (0.77 g, 1 mmol) and H-Arg(NO$_2$)-OBzl·2TsOH[13] (0.65 g, 1 mmol) in NMM (0.22 ml, 2 mmol) and DMF (10 ml), DCC (0.31 g, 1.5 mmol) and HOBt (0.20 g, 1.5 mmol) were added. The reaction mixture was cooled in an ice bath for an hour and allowed to stand at room temperature overnight. The DCUrea was removed by filtration, and the filtrate was evaporatd *in vacuo*. The oily residue was dissolved in ethyl acetate and the solution was washed with water, 0.5 M hydrochloric acid, 4% sodium hydrogencarbonate, and water successively. The solution was dried over anhydrous sodium sulfate. Sodium sulfate was removed by filtration, and the filtrate was evaporated *in vacuo*. The oily residue was crystallized with ether-petroleum ether: yield 0.75 g (71%); mp 130—133 °C; $[\alpha]_D^{15}$ −39.5° (*c* 1, *N,N*-dimethylformamide); R_f^1 0.98 and R_f^2 0.57.

Found: C, 59.93; H, 7.00; N, 14.17%. Calcd for $C_{53}H_{71}O_{12}N_{11} \cdot 1/2\ H_2O$: C, 59.87; H, 6.82; N, 14.49%.

H-Val-Ile-Phe-Pro-Pro-Gly-Arg-OH (1). Compound **18** (0.53 g, 0.5 mmol) was treated as described for the preparation of **5**: yield 0.37 g (87%); mp 180 °C (decomp); $[\alpha]_D^{15}$ −124.5° (*c* 1, H_2O); R_f^1 0.47 and R_f^2 0.00.

Found: C, 56.32; H, 7.82; N, 16.15%. Calcd for $C_{38}H_{60}O_8N_{10} \cdot CH_3COOH \cdot 1/2\ H_2O$: C, 56.25; H, 7.75; N, 16.40%.

Amino acid ratios in acid hydrolyzate: Val 1.03, Ile 1.00, Phe 1.01, Pro 2.02, Gly 1.00, Arg 0.96.

H-Val-Ile-Phe-Pro-Pro-Gly-OH (2). Compound **16** (0.85 g, 1 mmol) was treated as described in the case of **5**: yield 0.48 g (77%); mp 162—164 °C; $[\alpha]_D^{15}$ −86.5° (*c* 1, acetic acid); R_f^1 0.62 and R_f^2 0.03.

Found: C, 57.30; H, 7.75; N, 12.39%. Calcd for $C_{32}H_{48}O_7N_6 \cdot 7/3\ H_2O$: C, 57.29; H, 7.91; N, 12.53%.

Amino acid ratios in acid hydrolyzate: Val 1.02, Ile 1.00, Phe 0.99, Pro 2.01, Gly 1.01.

H-Val-Ile-Phe-OH (3). Compound **13** (0.51 g, 1 mmol) was treated as described in the case of **5**: yield 0.30 g (80%); mp 233 °C (decomp); $[\alpha]_D^{15}$ +9.0° (*c* 1, acetic acid); R_f^1 0.80 and R_f^2 0.13.

Found: C, 62.53; H, 8.23; N, 10.88%. Calcd for $C_{20}H_{31}O_4N_3 \cdot 1/3\ H_2O$: C, 62.63; H, 8.32; N, 10.95%.

Amino acid ratios in acid hydrolyzate: Val 1.01, Ile 1.00, Phe 0.99.

Z-Val-Ile-OBzl (19). Z-Val-ONSu[9] (2.10 g, 6 mmol) and H-Ile-OBzl·TsOH[8] (1.97 g, 5 mmol) were coupled by the same method as described for the preparation of **13**: yield 1.38 g (61%); mp 108—109 °; $[\alpha]_D^{15}$ −14.0° (*c* 1, methanol); R_f^1 0.98 and R_f^2 0.95.

Found: C, 68.74; H, 7.59; N, 6.20%. Calcd for $C_{26}H_{34}$-

O_5N_2: C, 68.70; H, 7.63; N, 6.14%.

H-Val-Ile-OH (4). Compound **19** (0.91 g, 2 mmol) was treated as described in the case of **5**: yield 0.44 g (96%); melting point above 250 °C; $[\alpha]_D^{15}$ +17.0° (*c* 1, H_2O); R_f^1 0.71 and R_f^2 0.21.

Found: C, 57.28; H, 9.68; N, 12.14%. Calcd for $C_{11}H_{22}O_3N_2$: C, 57.36; H, 9.65; N, 12.21%.

Amino acid ratios in acid hydrolyzate: Val 1.02, Ile 1.00.

Z-Pro-Pro-OBzl (20). To a solution of Z-Pro-OH[14-16] (2.49 g, 10 mmol) in CH_3CN (10 ml), DCC (2.48 g, 12 mmol) was added to the mixture at 0 °C. After 20 min, a solution of H-Pro-OBzl·HCl[17,18] (2.42 g, 10 mmol) and NMM (1.1ml, 10 mmol) in CH_3CN (10 ml) was added to the mixture. The resulting mixture was cooled at 0 °C for 1 h and allowed to stand overnight at room temperature. The DCUrea was removed by filtration, and the filtrate was evaporated *in vacuo*. The oily residue was dissolved in ethyl acetate and the solution was washed with water, 0.5 M hydrochloric acid, 4% sodium hydrogencarbonate, and water successively. The solution was dried over anhydrous sodium sulfate. Sodium sulfate as removed by filtration, and the filtrate was evaporated *in vacuo*. This compound was obtained in an oily form, while Appel *et al.*[19] reported that they obtained this compound as a crystalline form: yield 3.93 g (90%); R_f^1 0.89 and R_f^2 0.94.

H-Pro-Pro-OH (6). Compound **20** (3.93 g, 9 mmol) was treated as described in the case of **5**: yield 1.70 g (89%); mp 130—132 °C (lit, 125—127 °C,[19] 144—145 °C,[20] and 220—222 °C[21]); $[\alpha]_D^{15}$ −167.5° (*c* 1, H_2O) (lit, −166° (H_2O),[19] −169° (H_2O),[20] and −87° (H_2O)[21]); R_f^1 0.33 and R_f^2 0.10.

Found: C, 56.63; H, 7.58; N, 13.15%. Calcd for $C_{10}H_{16}O_3N_2$: C, 56.59; H, 7.63; 13.23%.

Z-Pro-Pro-OH (21). Compound **20** (5.13 g, 11.75 mmol) was treated as described for the preparation of **17**: yield 3.30 g (81%); mp 186 °C (lit, 187—190 °C[22] and 191.5—193.5 °C[23]); $[\alpha]_D^{15}$ −84.5° (*c* 1, *N,N*-dimethylformamide) (lit, −83° (*N,N*-dimethylformamide[23])); R_f^1 0.69 and R_f^2 0.17.

Found: C, 59.47; H, 6.58; N, 7.77%. Calcd for $C_{18}H_{22}O_5N_2 \cdot H_2O$: C, 59.32; H, 6.65; N, 7.69%.

Z-Pro-Pro-Gly-OBzl (22). Compound **21** (1.73 g, 5 mmol) and H-Gly-OBzl·TsOH[11,12] (1.69 g, 5 mmol) were coupled by the same method as described for the preparation of **12**: yield 2.42 g (98%); mp 121—124 °C (lit, 120—122 °C[24]); $[\alpha]_D^{15}$ −113.0° (*c* 1, methanol) (lit, −115° (methanol)[24]); R_f^1 0.87 and R_f^2 0.71.

Found: C, 65.82; H, 6.31; N, 8.61%. Calcd for $C_{27}H_{31}O_6N_3$: C, 65.70; H, 6.34; N, 8.52%.

H-Pro-Pro-Gly-OH (7). Compound **22** (0.99 g, 2 mmol) was treated as described for the preparation of **5**: yield 0.50 g (93%); mp 108—111 °C (lit, 112—114 °C[24]); $[\alpha]_D^{15}$ −97.0° (*c* 1, H_2O); R_f^1 0.27 and R_f^2 0.07.

Found: C, 51.89; H, 7.13; N, 14.98%. Calcd for $C_{12}H_{19}O_4N_3 \cdot 1/2\ H_2O$: C, 51.79; H, 7.26; N, 15.10%.

Amino acid ratios in acid hydrolyzate: Pro 2.10, Gly 1.00.

Z-Pro-Gly-OBzl (23). Z-Pro-OH[14-16] (4.99 g, 20 mmol) H-Gly-OBzl·TsOH[11,12] (6.75 g, 20 mmol) were coupled by the same method as described for the preparation of **12**: yield 6.99 g (88%); mp 81—83 °C (lit, 88—89 °C[19]); $[\alpha]_D^{15}$ −65.0° (*c* 1, methanol); R_f^1 0.90 and R_f^2 0.74.

Found: C, 66.58; H, 6.02; N, 7.18%. Calcd for $C_{22}H_{24}O_5N_2$: C, 66.65; H, 6.11; N, 7.07%.

H-Pro-Gly-OH (8). Compound **23** (0.79 g, 2 mmol) was treated as described in the case of **5**: yield 0.30 g (87%); mp 225—228 °C (lit, 230—232 °C[25]); $[\alpha]_D^{15}$ −23.5° (*c* 1, H_2O) (lit, −23° (H_2O[26])); R_f^1 0.23 and R_f^2 0.07.

Found: C, 46.27; H, 7.21; N, 15.38%. Calcd for $C_7H_{12}O_3N_2 \cdot 1/2\ H_2O$: C, 46.39; H, 7.25; N, 15.46%.

Amino acid ratios in acid hydrolyzate: Pro 1.07, Gly 1.00.

Z-Pro-Gly-OH (24). Compound **23** (5.95 g, 15 mmol) was treated as described in the case of **17**. This compound was obtained in an oily form:[27] yield 2.48 g (54%); R_f^1 0.77 and R_f^2 0.34.

Z-Pro-Gly-Arg(NO$_2$)-OBzl (25). Compound **24** (2.48 g, 8.1 mmol) and H-Arg(NO_2)-OBzl·TsOH[13] (5.29 g, 8.1 mmol) were coupled by the same method as described for the preparation of **12**: yield 4.02 g (83%); mp 75—79 °C; $[\alpha]_D^{15}$ −30.5° (*c* 2, methanol); R_f^1 0.90 and R_f^2 0.50.

Found: C, 53.70; H, 6.08; N, 15.83%. Calcd for $C_{28}H_{35}O_8N_7 \cdot 3/2\ H_2O$: C, 53.84; H, 6.14; N, 15.70%.

H-Pro-Gly-Arg-OH (9). Compound **25** (1.20 g, 2 mmol) was treated as described for the preparation of **5**. This compound was obtained in a hygroscopic form: yield 0.58 g (89%); R_f^1 0.23 and R_f^2 0.00.

Z-Gly-Arg(NO$_2$)-OBzl (26). Z-Gly-OH[28-30] (1.15 g, 5.5 mmol) and H-Arg(NO_2)-OBzl·2TsOH[13] (3.60 g, 5.5 mmol) were coupled by the same method as described for the preparation of **12**: yield 1.84 g (67%); mp 117—119 °C; $[\alpha]_D^{15}$ −14.0° (*c* 1, methanol); R_f^1 0.95 and R_f^2 0.53.

Found: C, 55.11; H, 5.68; N, 16.74%. Calcd for $C_{23}H_{28}O_7N_6$: C, 55.19; H, 5.65; N, 16.80%.

H-Gly-Arg-OH (10). Compound **26** (1.00 g, 2 mmol) was treated as described in the case of **5**: yeld 0.47 g (80%); mp 68—72 °C; $[\alpha]_D^{15}$ +4.0° (*c* 1, H_2O); R_f^1 0.19 and R_f^2 0.00.

Found: C, 38.71; H, 8.07; N, 22.74%. Calcd for $C_8H_{19}O_3N_5 \cdot CH_3COOH \cdot H_2O$: C, 38.83; H, 8.16; N, 22.65%.

Amino acid ratios in acid hydrolyzate: Pro 1.05, Gly 1.00, Arg 0.97.

CD Measurement. The measurements were performed with JASCO J-20 Automatic Recording Spectropolarimeter over a wavelength range of 200 to 250 nm. A cell of path length 0.2 mm was used and the runs were made at ambient temperature. Patterns in solvent of distilled water are shown in Fig. 5.

Sensory Test. The bitterness of the synthetic peptide was organoleptically determined *via* panel evaluation by five people. A series of solutions of decreasing concentration was prepared in which each solution was half as strong as its proceeding one. Before testing the sample, the panelist's mouth was thoroughly rinsed with distilled water. The sample size was usually 2—3 ml. The sample solution was held in the mouth for *ca.* 10 seconds and then spit out. The threshold value and the $R_{caf.}$ (ratio of caffeine) value, which expresses the extent of the strength of bitterness of the synthetic peptides, are shown in the Table.

The authors wish to express their thanks to Professor Sakuzo Fukui of Hiroshima University for his helpful discussion in the course of this study. Thanks are also due to Associate Professor Michio Kondo of Saga University for his help in the CD measurements, and to Dr. Shinji Okumura of Ajinomoto Co. Inc., for supplying some amino acids.

References

1) Part VI. H. Kanehisa, *Bull. Chem. Soc. Jpn.*, **57**, 97 (1984).

2) The abbreviations recommended by the IUPAC-IUB commission of Biochemical Nomenclature (*J. Biol. Chem.*, **247**, 977 (1972)) have been used. Amino acid symbols except glycine denote the L-configuration. Additional abbreviations: DCC, dicyclohexylcarbodiimide; DCHA, dicyclohexylamine; DCUrea, *N,N'*-dicyclohexylurea; DMF, *N,N*-dimethylformamide; ECF, ethyl chloroformate; Et_3N, triethylamine; HOBt, 1-hydroxybenzotriazole; HONSu, *N*-hydroxysuccinimide; MA, mixed anhydride; NMM, *N*-meth-

ylmorpholine; TsOH, *p*-toluenesulfonic acid; THF, tetrahydrofuran.

3) N. Minamiura, Y. Matsumura, J. Fukumoto, and T. Yamamoto, *Agric. Biol. Chem.*, **36**, 588 (1972).

4) K. Otagiri, I. Miyake, N. Ishibashi, H. Fukui, H. Kanehisa, and H. Okai, *Bull. Chem. Soc. Jpn.*, **56**, 1116 (1983).

5) I. Miyake, K. Kouge, H. Kanehisa, and H. Okai, *Bull. Chem. Soc. Jpn.*, **56**, 1678 (1983).

6) K. Otagiri, T. Shigenaga, H. Kanehisa, and H. Okai, *Bull. Chem. Soc. Jpn.*, **57**, 90 (1984).

7) H. Kanehisa and H. Okai, *Bull. Chem. Soc. Jpn.*, **57**, 301 (1984).

8) L. Zervas, M. Winitz, and J. P. Greenstein, *J. Org. Chem.*, **22**, 1515 (1957).

9) G. W. Anderson, J. E. Zimmerman, and F. M. Callahan, *J. Am. Chem. Soc.*, **86**, 1839 (1964).

10) H. Fukui, H. Kanehisa, N. Ishibashi, I. Miyake, and H. Okai, *Bull. Chem. Soc. Jpn.*, **56**, 766 (1983).

11) C. R. Harington and T. H. Mead, *Biochem. J.*, **30**, 1598 (1936).

12) B. F. Erlanger and E. Brand, *J. Am. Chem. Soc.*, **73**, 3508 (1951).

13) H. Otsuka, K. Inouye, M. Nakayama, and F. Shinozaki, *Bull. Chem. Soc. Jpn.*, **39**, 882 (1966).

14) A. Berger, J. Kutz, and E. Katchalski, *J. Am. Chem. Soc.*, **76**, 5552 (1954).

15) W. Grassmann and E. Wünsch, *Chem. Ber.*, **91**, 462 (1958).

16) E. Schröder, *Ann. Chem.*, **692**, 241 (1966).

17) R. E. Newman and E. L. Smith, *J. Biol. Chem.*, **193**, 97 (1951).

18) J. Ramachandran and C. H. Li, *J. Org. Chem.*, **28**, 173 (1963).

19) R. Appel, G. Bäumer, and W. Strüver, *Chem. Ber.*, **108**, 2680 (1975).

20) M. Rothe, R. Theysohn, and K. D. Steffen, *Tetrahedron Lett.*, **1970**, 4603.

21) M. Rothe and J. Mażanek, *Tetrahedron Lett.*, **1972**, 3795.

22) S. Lande, *J. Org. Chem.*, **27**, 4558 (1962).

23) P. Bruckner, B. Rutschmann, J. Engel, and M. Rothe, *Helv. Chim. Acta*, **58**, 1276 (1975).

24) E. Wünsch, H-G. Heidrich, and W. Grassmann, *Chem. Ber.*, **97**, 1818 (1964).

25) T. R. Govindachari, K. Nagarajan, S. Rajappa, A. S. Akerkar, and V. S. Lyer, *Tetrahedron*, **22**, 3367 (1966).

26) F. Weyand, A. Prox, M. A. Tilak, D. Hoffter, and H. Fritz, *Chem. Ber.*, **97**, 1024 (1964).

27) K. Suzuki, T. Abiko, and M. Asaka, *Chem. Pharm. Bull. (Tokyo)*, **14**, 217 (1966).

28) M. Bergmann and L. Zervas, *Chem. Ber.*, **65**, 1192 (1932).

29) F. H. C. Stewart, *Aust. J. Chem.*, **18**, 1699 (1965).

30) D. F. DeTar, R. Silverstein, and F. F. Rogers, Jr., *J. Am. Chem. Soc.*, **88**, 1024 (1966).

Cross-coupling Reaction between Enol Phosphates and Organoaluminium Compounds in the Presence of Palladium(0) Catalyst

Kazuhiko TAKAI, Mitsuyoshi SATO, Koichiro OSHIMA,* and Hitosi NOZAKI
Department of Industrial Chemistry, Faculty of Engineering, Kyoto University, Yoshida, Sakyo-ku, Kyoto 606
(Received June 25, 1983)

The title reaction in the presence of a catalytic amount of tetrakis(triphenylphosphine)palladium(0) affords alkylative coupling products in good to excellent yields in 1,2-dichloroethane at room temperature. This coupling reaction under C(sp^2)-O cleavage proceeds stereospecifically. The reaction does not affect a coexisting vinyl sulfide group. This feature enables 1,2- and 1,3-carbonyl transposition with or without alkylation *via* phenylthio-substituted enol phosphates.

The regioselective transformation of ketones into alkyl-substituted olefins is an important process in organic synthesis. The classical Grignard addition to ketones or organolithium version, followed by dehydration of the resultant alcohols, generally gives isomeric olefins and/or skeletal rearrangement products.[1] We report here (1) regioselective olefin formation[2] and (2) keto carbonyl 1,2- and 1,3-transposition[3] by palladium(0)-promoted cross-coupling of enol diphenyl phosphates and organoaluminium compounds.

(1) Regioselective Olefin Formation from Ketones. During the past decade, cross-coupling of alkenyl halides with organolithium and organomagnesium compounds has been achieved in the presence of Pd(0) or Ni(0) catalyst.[4,5] However there are few examples of the replacement of an enolate oxygen by an alkyl substituent.[6] We have found that organoaluminium compounds cause alkylation of enol phosphates under the C(sp^2)-O bond fission in the presence of a catalytic amount of $Pd(PPh_3)_4$ (Scheme 1). The results are summarized in Table 1.

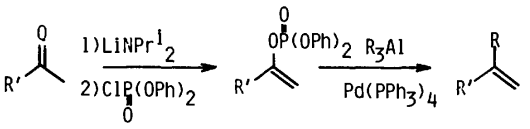

Scheme 1.

Alkynyl (Runs, 3, 4, 8, and 10) and alkenyl group (Run 5) were introduced selectively in preference to the ubiquitous alkyl substituents on aluminium. The reaction of (*E*)-1-heptenyldiisobutylaluminium (Run 5) prepared *in situ* from 1-heptyne and Bu^i_2AlH in hexane,[7] gave a diene having and (*E*) olefinic linkage as the sole product.

Organolithium and magnesium compounds were not suitable for this reaction, as these organometallics caused nucleophilic attack on phosphorus atom of 1-phenylethenyl diphenyl phosphate (**1**), produc-

TABLE 1. COUPLING REACTION BETWEEN ENOL DIPHENYL PHOSPHATES AND ORGANOALUMINIUM REAGENTS CATALYZED BY $Pd(PPh_3)_4$[a]

Run	Enol phosphate	Aluminium reagent	Reaction time / h	Yield[b] of coupling product / %
1	$CH_3(CH_2)_9C(OP(O)(OPh)_2)=CH_2$	Me_3Al	2	91
2		Et_3Al	3	71
3		$PhC{\equiv}C\text{-}AlEt_2$	3	82[c]
4		$CH_3(CH_2)_3C(H){\equiv}C\text{-}AlEt_2$	3	59[c]
5		$CH_3(CH_2)_4C(H)=C(H)\text{-}AlBu^i_2$	4	66
6	$PhC(OP(O)(OPh)_2)=CH_2$	Me_3Al	2	94[d]
7		Et_3Al	2	80
8		$PhC{\equiv}C\text{-}AlEt_2$	3	67[c]
9	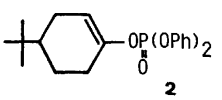	Me_3Al	5	72
10		$PhC{\equiv}C\text{-}AlEt_2$	6	70[c]

1

2

a) Reactions were performed on 2.0 mmol scale at 25 °C. Four mmol of aluminium reagent and 0.2 mmol of $Pd(PPh_3)_4$ were employed. b) Yields are based on isolated, purified products. c) Ethylated products were not detected. The sole product was the respective 2-substituted ethynylation product. d) GLPC yield.

ing acetophenone upon workup. In contrast, the less nucleophilic organoaluminium compounds effectively induce the desired replacement of diphenyl phosphate group under new C-C bond formation.[8]

The reaction did not occur in the absence of the Pd(0) catalyst. Yields in the reaction between enol phosphate **2** and trimethylaluminium in the presence of various kinds of catalysts are given below: [Ni(acac)$_2$] (80 °C, 6 h, 12%), [Ni(acac)$_2$]-PPh$_3$-Bu$^i_2$AlH (80 °C, 6 h, 18%), [NiBr$_2$(PPh$_3$)$_2$] (80 °C, 6 h, <5%), [PdCl$_2$(PhCN)$_2$] (80 °C, 8 h, <5%), [Pd(acac)$_2$] (80 °C, 8 h, <5%).

The cross-coupling reactions proceed stereospecifically, analogously as those of alkenyl halides and organolithium compounds (or Grignard reagents).[5a] For example, methylation of (*Z*)- and (*E*)-1-phenyl-1-propenyl diethyl phosphates[9] afforded (*E*)- and (*Z*)-2-phenyl-2-butene in 88 and 84% yield; their isomeric purities are over 96 and 92% respectively (Scheme 2). The diethyl phosphate group is less effective than diphenyl phosphate as a leaving group. The reaction between diethyl phosphates and Me$_3$Al did not proceed at 25 °C but required heating at reflux in 1,2-dichloroethane.

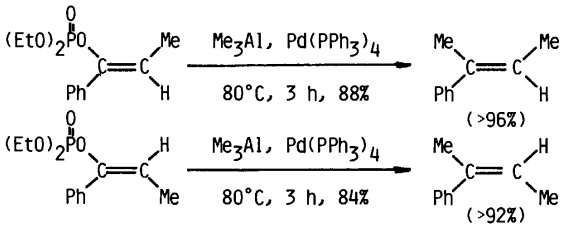

Scheme 2.

An enol phosphate was prepared alternatively by 1,4-addition of lithium dialkylcuprate(I) to an α,β-unsaturated carbonyl compound, followed by trapping of the resulting enolate with diphenyl phosphorochloridate.[10] Treatment of the enol phosphate furnished selective 1,3-dialkylation of the original conjugated enone (Scheme 3).

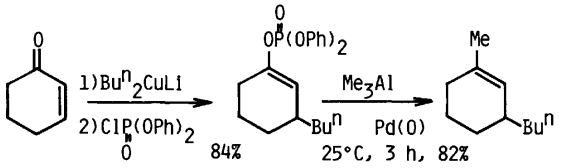

Scheme 3.

(2) 1,2- and 1,3- Transposition of a Keto Group. Scheme 4 shows that the present procedure does not affect the coexisting vinyl sulfide group, in sharp contrast to the Takei's analogous sp^2 carbon alkylation with Ni(0) catalyst.[11] Since alkenyl sulfides are valuable synthetic precursors of carbonyl compounds,[12,13] further extension of this reaction has been explored.

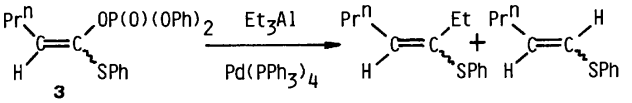

Scheme 4.

Treatment of phenylthio-substituted enol phosphate with organoaluminium compounds bearing a β-hydrogen, such as triethylaluminium, has afforded a mixture of the alkylated product and the hydrogenated one (Scheme 4). The ratios of these two products heavily depended on the solvents used. The reaction of the enol phosphate **3** and Et$_3$Al gave the following ratios of ethylated and hydrogenated products in solvents given in parentheses: 29:71 (hexane), 48:52 (1,2-dichloroethane), 62:38 (benzene), 71:29 (ether), 60:40 (THF), 71:29 (THF-HMPA, 9:1). The ethylated product was favored by using more

Table 2. Coupling reaction between enol phosphates derived from thiocarboxylic *S*-esters and organoaluminium reagents catalyzed by Pd(PPh$_3$)$_4$[a]

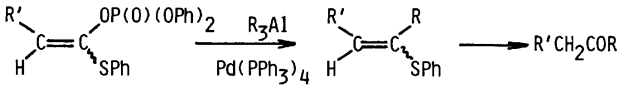

Enol phosphate R′	Aluminium reagent	Reaction time h	Yield of sulfide %	Yield of ketone %
$CH_3CH_2CH_2$	Me_3Al	1	83	70[b]
	Et_3Al	2	82[c]	—
	$PhC{\equiv}C\text{-}AlEt_2$	2	83[d]	—
	$CH_3(CH_2)_4\overset{H}{\underset{|}{C}}{=}C\text{-}AlBu^i_2$	3	62[d]	65[e]
Ph	Me_3Al	1	64	89[b]
	Et_3Al	2	55[c]	—

a) Reactions were performed on 2.0 mmol scale at 25 °C in benzene. Four mmol of aluminium reagent and 0.2 mmol of Pd(PPh$_3$)$_4$ were employed. b) Hydrolysis with TiCl$_4$. See Ref. 13. c) Mixture of ethylated and hydrogenated products in 3:2 ratio. d) Ethynylation or ethenylation product was obtained exclusively. e) Hydrolysis with HgCl$_2$. See Ref. 14.

polar solvents.

Coupling reactions between enol phosphates derived from thiocarboxylic *S*-esters and organoaluminium reagents are shown in Table 2. Hydrolysis of the resulting vinyl sulfides with $TiCl_4$[13] or $HgCl_2$[14] proceeded easily to give the corresponding ketones.

Scheme 5 provides 1,2-transposition[15] of a carbonyl group, accompanied by alkylation. Treatment of the enol phosphate **4** derived from α-phenylthio ketone with Me_3Al and a catalytic amount of $Pd(PPh_3)_4$ afforded the methylated alkenyl sulfide **5** in 80% yield. Hydrolysis with $TiCl_4$ gave the ketone **6**, which completed its 1,2-carbonyl transposition under methylation. The enol phosphate **10** was converted into benzyl methyl ketone in nearly 60% overall yield upon treatment with Et_3Al-$Pd(PPh_3)_4$ reagent and hydrolysis of the simple reduction product **11** isolated in 64% yield (Scheme 6). The ethylated sulfide, PhC(Et)=C(SMe)Me, was isolated in less than 4% yield.

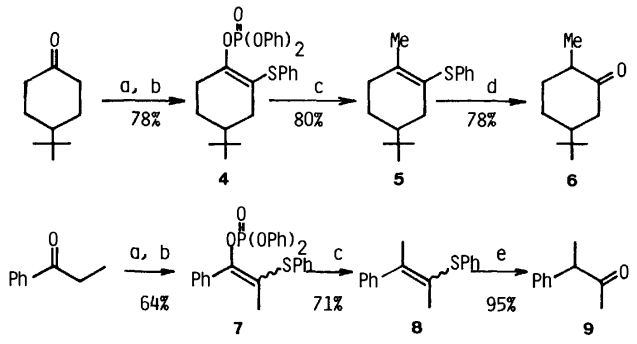

(a) $LiNPr^i_2$, PhSSPh (b) NaH, $ClP(O)(OPh)_2$ (c) Me_3Al, $Pd(PPh_3)_4$, CH_2ClCH_2Cl, 80 °C (d) $TiCl_4$-H_2O, CH_2Cl_2 (e) $TiCl_4$-H_2O, CH_3COOH

Scheme 5.

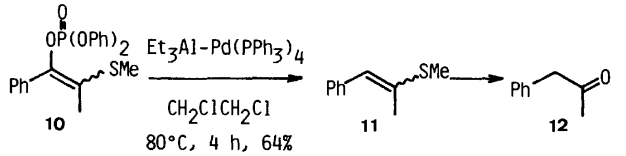

Scheme 6.

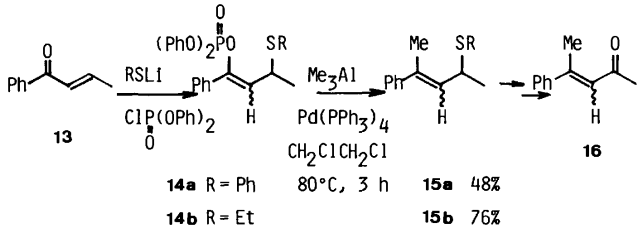

Scheme 7.

Alkylative 1,3-transposition[16] of a carbonyl group could be also achieved (Scheme 7). Enol phosphates **14a, b** prepared by 1,4-addition of RSLi (R=Ph, Et) to an enone **13** and successive phosphorylation were submitted to alkylation with the Me_3Al-$Pd(PPh_3)_4$ system. The alkylated product **15a** was transformed into an enone **16** by the procedures previously reported.[16a]

Experimental

The IR spectra were determined on Shimadzu IR-27-G spectrometer, the mass spectra, on a Hitachi M-80 machine, and the NMR spectra, on a Varian EM-360 spectrometer. The chemical shifts are given in δ, with TMS as the internal standard. The analyses were carried out by the staff at the Elemental Analyses Center of Kyoto University. 1,2-dichloroethane was dried on P_2O_5 and distilled. All the experiments were carried out under an argon atmosphere. Purification of product were performed by preparative thin layer chromatography (TLC) or column chromatography on silica gel (Merck Kieselgel 60). Analytical GLPC was performed with a Yanagimoto GCG-550-F or Shimadzu GC-4CPT. Preparative GLPC was performed with a JEOL-JGC-20K apparatus.

Preparation of Enol Diphenyl Phosphates. A solution of a ketone (5.0 mmol) in THF (30 ml) was treated with lithium diisopropylamide (5.5 mmol) at −78 °C for 30 min. To this was added at −78 °C a THF solution of diphenyl phosphorochloridate (1.3 g, 5.5 mmol) and the solution was allowed to warm to 0 °C. After being stirred for 20 min, the mixture was diluted with ether (20 ml), poured into ice-cold water (50 ml), and extracted with ether. The separated organic layer was washed with brine (2×20 ml), dried (Na_2SO_4), and concentrated. The crude product was purified by silica-gel column chromatography(hexane-ethyl acetate).

1-Decylethenyl Diphenyl Phosphate: Bp 168 °C (bath temp, 0.15 Torr, 1 Torr=133.322 Pa); IR (neat): 2950, 2870, 1665, 1600, 1498, 1300, 1190, 1025, 960, 755, 690 cm^{-1}; NMR (CCl_4): δ 0.75—1.00 (bt, *J*=6 Hz, 3H), 1.15—1.50 (m, 16H), 2.17 (t, *J*=7 Hz, 2H), 4.50—4.60 (bm, 1H), 4.88 (t, *J*=5 Hz, 1H), 7.10—7.40 (m, 10H); MS *m/e* (%): 416 (M^+, 4), 252 (20), 251 (100), 250 (16), 166 (17), 116 (16), 94 (30), 77 (24); Found: C, 69.38; H, 8.13%. Calcd for $C_{24}H_{33}O_4P$: C, 69.21; H, 7.99%.

1-Phenylethenyl Diphenyl Phosphate (1): Bp 174 °C (bath temp, 0.1 Torr); IR (neat): 3080, 1642, 1595, 1495, 1465, 1300, 1188, 1010, 960, 770, 690 cm^{-1}; NMR (CCl_4): δ 5.25—5.38 (m, 2H), 7.05—7.65 (m, 15H); MS *m/e* (%): 353 (M^++1, 5), 352 (M^+, 23), 261 (18), 249 (17), 178 (57), 105 (100), 103 (76), 94 (77), 77 (88); Found: C, 67.89; H, 4.86%. Calcd for $C_{20}H_{17}O_4P$: C, 68,18; H, 4.86%.

4-t-Butyl-1-cyclohexenyl Diphenyl Phosphate (2): Bp 168 °C (bath temp, 0.15 Torr); IR (neat): 2980, 1695, 1595, 1495, 1295, 1190, 1115, 950, 770, 752, 688 cm^{-1}; NMR (CCl_4): δ 0.90 (s, 9H), 1.10—2.35 (m, 7H), 5.35—5.54 (bs, 1H), 7.10—7.45 (m, 10H); MS *m/e* (%): 387 (M^++1, 11), 386 (M^+, 47), 329 (12), 251 (100), 94 (24), 77 (44); Found: C, 68.37; H, 7.10%. Calcd for $C_{22}H_{27}O_4P$: C, 68.38; H, 7.04%.

General Procedure for the Reaction between Enol Diphenyl Phosphates and Organoaluminium Compounds in the Presence of $Pd(PPh_3)_4$. Palladium tetrakis(triphenylphosphine) was prepared according to the literature.[17] To a solution of an enol diphenyl phosphate (2.0 mmol) and a catalytic amount of $Pd(PPh_3)_4$ (0.23 g, 0.2 mmol) in 1,2-dichloroethane (10 ml) was added at 25 °C a hexane solution of an organoaluminium compound (4.0 mmol) under an argon atmosphere. The yellow color of the solution turned red immediately in the case of trialkylaluminium. After being stirred for an appropriate time as listed in Table 1, the resulting mixture was diluted with ether (20 ml), poured into 1 M† hydrochloric acid (20 ml), and extracted with

† 1 M=1 mol dm^{-3}

ether. The separated organic layer was washed with brine (2×20 ml), dried over anhydrous sodium sulfate, and concentrated under reduced pressure. The crude product was purified by column chromatography or preparative TLC on silica gel using hexane as an eluent.

2-Methyl-1-dodecene: Bp 82 °C (bath temp, 5 Torr); IR (neat): 2930, 2850, 1654, 1470, 1460, 1374, 882 cm^{-1}; NMR (CCl_4): δ 0.89 (bt, J=7 Hz, 3H), 1.10—1.45 (m, 16H), 1.69 (s, 3H), 1.96 (t, J=7 Hz, 2H), 4.61 (s, 2H); MS m/e (%): 183 (M^++1, 2), 182 (M^+, 10), 126 (5), 97 (11), 83 (14), 69 (41), 56 (100), 41 (61); Found: C, 85.39; H, 14.37%. Calcd for $C_{13}H_{26}$: C, 85.63; H, 14.37%.

2-Ethyl-1-dodecene: Bp 86 °C (bath temp, 4 Torr); IR (neat): 2925, 2860, 1648, 1468, 1375, 960, 884 cm^{-1}; NMR (CCl_4): δ 0.87 (m, 3H), 1.00 (t, J=7 Hz, 3H), 1.15—1.45 (m, 16H), 1.70—2.15 (m, 4H), 4.62 (s, 2H); MS m/e (%): 196 (M^+, 4), 168 (5), 167 (5), 111 (9), 97 (15), 83 (25), 70 (100), 55 (70); Found: C, 85.55; H, 14.55%. Calcd for $C_{14}H_{28}$: C, 85.63; H, 14.37%.

2-Decyl-4-phenyl-1-buten-3-yne: Bp 176 °C (bath temp, 2 Torr); IR (neat): 2920, 2850, 1610, 1490, 1468, 1442, 890, 750, 686 cm^{-1}; NMR (CCl_4): δ 0.88 (bt, J=6 Hz, 3H), 1.15 1.80 (m, 16H), 2.22 (bt, J=6 Hz, 2H), 5.23 (s, 1H), 5.35 (s, 1H), 7.20—7.53 (m, 5H); MS m/e (%): 268 (M^+, 4), 210 (4), 168 (9), 154 (14), 142 (15), 141 (100), 140 (29); Found: C, 89.61; H, 10.74%. Calcd for $C_{20}H_{28}$: C, 89.49; H, 10.51%.

2-Decyl-1-octen-3-yne: Bp 128 °C (bath temp, 2 Torr); IR (neat): 2940, 2860, 1614, 1468, 1375, 885 cm^{-1}; NMR (CCl_4): δ 0.75—1.05 (m, 6H), 1.15—1.75 (m, 20H), 2.05 (t, J=7 Hz, 2H), 2.24 (t, J=6 Hz, 2H), 5.04 (s, 1H), 5.08 (s, 1H); MS m/e (%): 248 (M^+, 2), 191 (11), 149 (11), 135 (11), 122 (63), 108 (33), 107 (100), 93 (88), 79 (52); Found: C, 87.17; H, 13.20%. Calcd for $C_{18}H_{32}$: C, 87.02; H, 12.98%.

(E)-*2-Decyl-1,3-nonadiene*: Bp 175 °C (bath temp, 2 Torr); IR (neat): 2970, 2925, 2855, 1608, 1468, 1460, 962, 880 cm^{-1}; NMR (CCl_4): δ 0.73—1.07 (m, 6H), 1.07—1.73 (m, 22H), 1.73—2.27 (m, 4H), 4.77 (s, 2H), 5.57 (dt, J=15, 6 Hz, 1H), 5.97 (d, J=15 Hz, 1H); MS m/e (%): 264 (M^+, 8), 193 (14), 138 (82), 95 (91), 82 (72), 81 (100), 55 (58); Found: C, 86.57; H, 13.74%. Calcd for $C_{19}H_{36}$: C, 86.28; H, 13.72%.

2-Phenyl-1-butene: Bp 104 °C (bath temp, 15 Torr); IR (neat): 3090, 2960, 2930, 1630, 1498, 1465, 1445, 890, 770, 698 cm^{-1}; NMR (CCl_4): δ 1.01 (t, J=7.5 Hz, 3H), 2.47 (q, J= 7.5 Hz, 2H), 4.98 (s 1H), 5.18 (s, 1H), 7.00—7.40 (m, 5H); MS m/e (%): 132 (M^+, 66), 117 (100), 115 (28), 103 (53), 91 (33), 78 (36), 77 (46), 51 (62). The compound was identical with the authentic sample.[18]

2,4-Diphenyl-1-buten-3-yne: This compound (clear liquid) polymerized easily at 0 °C to give a pale yellow viscous liquid. IR (neat): 3070, 1604, 1576, 1494, 1448, 1335, 892, 753, 688 cm^{-1}; NMR (CCl_4): δ 5.64 (s, 1H), 5.86 (s, 1H), 7.15—7.75 (m, 10H); MS m/e (%): 205 (M^++1, 31), 204 (M^+, 100), 203 (54), 202 (54), 126 (23), 77 (39); Found: m/e 204.0895. Calcd for $C_{16}H_{12}$: M, 204.0940.

4-t-Butyl-1-methyl-1-cyclohexene: Bp 60 °C (bath temp, 9 Torr); IR (neat): 2975, 1675, 1390, 1360, 1242, 1175, 800 cm^{-1}; NMR (CCl_4): δ 0.86 (s, 9H), 1.00—1.43 (m, 3H), 1.60 (s, 3H), 1.67—1.98 (m, 4H), 5.29 (bs, 1H); MS m/e (%): 152 (M^+, 14), 137 (7), 123 (5), 109 (17), 95 (59), 81 (40), 57 (100); Found: C, 86.95; H, 13.00%. Calcd for $C_{11}H_{20}$: C, 86.76; H, 13.24%.

4-t-Butyl-1-(phenylethynyl)-1-cyclohexene: Bp 152 °C (bath temp, 2 Torr); IR (neat): 2950, 1598, 1492, 1364, 750, 688 cm^{-1}; NMR (CCl_4): δ 0.89 (s, 9H), 1.04—1.50 (m, 3H), 1.65—2.37 (m, 4H), 6.06 (bs, 1H), 7.12—7.50 (m, 5H); MS m/e (%): 238 (M^+, 23), 181 (18), 167 (27), 166 (21), 154 (66), 153 (26), 57 (100); Found: C, 90.89; H, 9.51%. Calcd for $C_{18}H_{22}$: C, 90.70; H, 9.30%.

(E)- *and (Z)-1-Phenyl-1-prophenyl Diethyl Phosphate*.[9] A mixture of α-bromopropiophenone (4.26 g, 20 mmol) and triethyl phosphite (4.15 g, 25 mmol) was heated at 100 °C for 24 h and washed with water (2×50 ml) to give a crude mixture containing two isomeric enol phosphates and *O,O'*-diethyl 1-benzoylethyl phosphonate in a ratio of *ca.* 3:1:1. The product was carefully separated by column chromatography (benzene–diethyl ether, 20:1) on silica gel (500 g). (*E*)-Isomer: Minor product (8% isolated yield); bp 96 °C (bath temp, 0.1 Torr); IR (neat): 3000, 1670, 1450, 1368, 1270, 1200, 1020, 884, 765, 698 cm^{-1}; NMR (CCl_4): δ 1.27 (t, J= 6 Hz, 6H), 1.75 (dd, J_{H-H}=7 Hz, J_{P-H}=3 Hz, 3H), 4.00 (dt, J_{H-H}=6 Hz, J_{P-H}=6 Hz, 4H), 5.68 (dq, J_{P-H}=2 Hz, J_{H-H}=7 Hz, 1H), 7.15—7.53 (m, 5H); MS m/e (%): 270 (M^+, 34), 155 (100), 127 (45), 116 (50), 115 (34), 99 (46). (*Z*)-Isomer: Major product (48% isolated yield); bp 94 °C (bath temp, 0.1 Torr); IR (neat): 2980, 1668, 1495, 1446, 1390, 1268, 1160, 1020, 882, 760, 690 cm^{-1}; NMR (CCl_4): δ 1.23 (t, J=6 Hz, 6H), 1.85 (dd, J_{H-H}=7 Hz, J_{P-H}=3 Hz, 3H), 4.00 (dt, J_{P-H}=6 Hz, J_{H-H}=6 Hz, 4H), 5.57 (dq, J_{P-H}=1.5 Hz, J_{H-H}=7 Hz, 1H), 7.05—7.55 (m, 5H); MS m/e(%): 270 (M^+, 32), 155 (100), 127 (45), 116 (55), 115 (34), 99 (50).

(E)-*2-Phenyl-2-butene*:[19] A hexane solution of trimethylaluminium (1.0 M, 40 ml, 4.0 mmol) was added at 25 °C to a stirred solution of (Z)-1-phenyl-1-propenyl diethyl phosphate (0.54 g, 2.0 mmol) and a catalytic amount of $Pd(PPh_3)_4$ (0.23 g, 0.2 mmol) in 1,2-dichloroethane (15 ml). The resulting mixture was heated at 80 °C for 3 h. After a usual workup, the crude product was purified by silica-gel column chromatography using hexane as an eluent to give (*E*)-2-phenyl-2-butene in 88% yield (0.23 g) as a colorless liquid: Bp 98 °C (bath temp, 20 Torr); IR (neat): 3040, 2930, 1650, 1600, 1500, 1448, 1382, 1022, 826, 750, 694 cm^{-1}; NMR (CCl_4): δ 1.79 (d, J=7 Hz, 3H), 2.02 (s, 3H), 5.76 (q, J=7 Hz, 1H), 7.03—7.37 (m, 5H); MS m/e (%): 132 (M^+, 86), 117 (100), 115 (20), 91 (18).

The isomeric purity of the crude product was determined by GLPC analysis (10% PEG 20 M, 2 m, 100 °C). (*E*)-Isomer: T_r=8.5 min. (*Z*)-Isomer: T_r=4.1 min.

(Z)-*2-Phenyl-2-butene*:[19] Treatment of (*E*)-1-phenyl-1-propenyl diethyl phosphate (0.54 g, 2.0 mmol) dissolved in 1,2-dichloroethane (15 ml) with trimethylaluminium (1.0 M of a hexane solution, 4.0 ml, 4.0 mmol) and a catalytic amount of $Pd(PPh_3)_4$ (0.23 g, 0.2 mmol) at 80 °C for 3 h gave the title (*Z*)-olefin in 84% yield (0.22 g). Bp 100 °C (bath temp, 20 Torr); IR (neat): 3040, 2930, 1650, 1602, 1500, 1450, 1380, 1260, 1024, 785, 750 cm^{-1}; NMR (CCl_4): δ 1.53 (d, J=7 Hz, 3H), 2.00 (s, 3H), 5.49 (q, J=7 Hz, 1H), 6.95—7.40 (m, 5H); MS m/e (%): 132 (M^+, 100), 117 (77), 91 (22).

3-Butyl-1-cyclohexenyl Diphenyl Phosphate. Butyllithium (2.5 ml of a 1.6 M hexane solution, 4.0 mmol) was added to a suspension of copper(I) iodide (0.19 g, 2.0 mmol) in ether (20 ml) at −23 °C under an argon atmosphere. After stirring at −23 °C for 20 min, the reaction mixture was cooled to −78 °C. A solution of 2-cyclohexen-1-one (0.19 g, 2.0 mmol) in ether (3.0 ml) was added and the resulting mixture was kept there for 1 h. A solution of diphenyl phosphorochloridate (0.59 g, 2.2 mmol) in ether (3.0 ml) was added and the mixture was stirred at −78 °C for 1 h, then warmed to 25 °C. Water (5.0 ml) was added and the mixture was filtered through a pad of Celite 545. The filtrate was washed with water (2×10 ml), dried over anhydrous sodium sulfate, and concentrated to give a pale yellow oil. Purification by column chromatography on silica gel (50 g) with hexane–ethyl acetate (10:1) as an eluent afforded a milky oil (0.61 g, 78%): Bp 162 °C (bath temp, 0.15 Torr); IR (neat): 2950, 1682, 1595, 1495, 1296, 1190, 950, 770, 750, 688 cm^{-1}; NMR (CCl_4): δ 0.87 (bt, J=6

Hz, 3H), 1.03—1.42 (m, 6H), 1.50—1.90 (m, 4H), 1.97—2.30 (m, 3H), 5.37 (bs, 1H), 7.04—7.42 (m, 10H); MS *m/e* (%): 386 (M^+, 27), 330 (20), 329 (100), 251 (71), 136 (23), 94 (17), 79 (32), 77 (61); Found: C, 68.50; H, 7.12%. Calcd for $C_{22}H_{27}O_4P$: C, 68.38; H, 7.04%.

3-Butyl-1-methyl-1-cyclohexene: Bp 127 °C (bath temp, 1 atm); IR (neat): 2950, 2860, 1460, 1380, 810 cm^{-1}; NMR (CCl_4): δ 0.91 (t, J=5 Hz, 3H), 1.05—1.46 (bm, 6H), 1.50—2.04 (m, 10H), 5.21 (bs 1H); MS *m/e* (%): 152 (M^+, 54), 96, (53), 95 (100), 81 (43), 79 (33), 67 (77), 55 (47); Found: C, 86.81; H, 13.30%. Calcd for $C_{11}H_{20}$: C, 86.76; H, 13.24%.

1-Phenylthio-1-pentenyl Diphenyl Phosphate (3). *S*-Phenyl pentanethioate was prepared by the reaction of the acid chloride with an excess of benezenethiol in pyridine. *S*-Phenyl pentanethioate (0.97 g, 5.0 mmol) dissolved in THF (25 ml) was treated with lithium diisopropylamide (5.5 mmol) at −78 °C. The resulting lithium enolate was trapped by diphenyl phosphorochloridate (1.48 g, 5.5 mmol) at 0 °C. The mixture was diluted with ether (20 ml) and poured into ice-cold water. The separated organic layer was washed with brine (2×20 ml), dried (Na_2SO_4), and concentrated. Purification of the crude product by silica-gel column chromatography (hexane-ethyl acetate, 10:1) gave the desired phosphate **3** in 89% yield (1.89 g). This compound decomposes at 140 °C (0.05 Torr). IR (neat): 3080, 2975, 1640, 1596, 1499, 1302, 1192, 960 cm^{-1}; NMR (CCl_4): δ 0.92 (t, J=7 Hz, 3H), 1.10—1.67 (m, 2H), 1.90—2.44 (m, 2H), 5.89 (dt, J=3, 7 Hz, 1H), 6.90—7.35 (m, 15H); MS *m/e* (%): 426 (M^+, 12), 251 (89), 177 (96), 176 (100), 147 (90), 143 (74), 110 (90), 99 (79), 77 (87); Found: C, 64.74; H, 5.46%. Calcd for $C_{23}H_{23}O_4PS$: C, 64.78; H, 5.44%.

2-Phenyl-1-(phenylthio)ethenyl Diphenyl Phosphate: This compound was prepared by treating *S*-phenyl 2-phenylethanethioate first with lithium diisopropylamide and then with diphenyl phosphorochloridate in THF. This phosphate decomposes at 150 °C (0.05 Torr). IR (neat): 3080, 1620, 1595, 1498, 1280, 1188, 945 cm^{-1}; NMR (CCl_4): δ 6.80—7.60 (m, 20H), 6.86 (d, J=2 Hz, 1H); MS *m/e* (%): 460 (M^+, 0.2), 342 (73), 306 (51), 250 (71), 109 (80), 94 (77), 86 (100), 77 (88), 65 (92); Found: *m/e* 460.0861. Calcd for $C_{26}H_{21}O_4PS$: M, 460.0899.

Cross-coupling Reactions between Organoaluminium Reagents and Enol Phosphates Derived from Thiocarboxylic S-Esters. A hexane solution of trimethylaluminium (1.0 M, 4.0 ml, 4.0 mmol) was added at 25 °C to a benzene (15 ml) solution of enol phosphate (2.0 mmol) derived from thiocarboxylic *S*-ester containing a catalytic amount of $Pd(PPh_3)_4$ (0.23 g, 0.2 mmol) under an argon atmosphere. After being stirred at 25 °C for an appropriate time, as listed in Table 2, the mixture was diluted with ether (20 ml) and poured into 1 M hydrochloric acid (20 ml). The separated organic layer was washed with brine (2×20 ml), dried over sodium sulfate, and concentrated. The crude product was purified by silica-gel column chromatography (hexane-ethyl acetate).

(E)- *and* (Z)-*1-Methyl-1-pentenyl Phenyl Sulfide.* TLC (hexane) showed two UV active bands, R_f=0.50 (23%, isolated yield) and R_f=0.40 (60%, isolated yield). Faster moving band: Bp 75 °C (bath temp, 0.08 Torr); IR (neat): 2970, 1634, 1588, 1484, 1442, 1380, 1056, 1025, 736, 686 cm^{-1}; NMR (CCl_4): δ 0.95 (t, J=7 Hz, 3H), 1.42 (tq, J=7, 7 Hz 2H), 1.87 (s, 3H), 2.27 (dt, J=7, 7 Hz, 2H), 5.71 (bt, J=7 Hz, 1H); MS *m/e* (%): 192 (M^+, 96), 163 (100), 136 (52), 130 (42), 110 (24); Found: C, 75.19; H, 8.43%. Calcd for $C_{12}H_{16}S$: C, 74.94; H, 8.39%. Slower moving band: Bp 72 °C (bath temp, 0.08 Torr); IR (neat): 2970, 1636, 1588, 1482, 1442, 1380, 1150, 1070, 1026, 896, 736, 686 cm^{-1}; NMR (CCl_4): δ 0.94 (t, J=7 Hz, 3H), 1.43 (tq, J=7, 7 Hz, 2H). 1.84 (s, 3H), 2.24 (dt, J=7, 7 Hz, 1H), 5.74 (bt, J=7 Hz, 1H), 6.94—7.30 (m, 5H); MS *m/e* (%): 192 (M^+, 99), 163 (100), 136 (57), 130 (41), 110 (26); Found: C, 74.89; H, 8.44%. Calcd for $C_{12}H_{16}S$: C, 74,94; H, 8.39%.

1-Pentenyl Phenyl Sulfide. GLPC analysis Silicone OV-17, 2 m, 140 °C) of the product generated by the reaction of enol phosphate **3** and triethylaluminium indicated two peaks, T_r=5.5 min (1-pentenyl phenyl sulfide) and T_r=7.3 min (1-ethyl-1-pentenyl phenyl sulfide). The analytically pure samples of both compounds were prepared by preparative GLPC (3% Silicone OV-17, 2 m). Bp 100 °C (bath temp, 1 Torr); IR (neat): 2970, 1612, 1590, 1488, 1444, 1092, 1026, 952, 734, 684 cm^{-1}; NMR (CCl_4): δ 0.94 (bt, 3H), 1.18—1.72 (m, 2H), 1.93—2.35 (m, 2H), 5.55—6.22 (m, 2H), 6.98—7.33 (m, 5H); MS *m/e* (%): 178 (M^+, 87), 149 (100), 110 (27); Found: C, 74.16; H, 8.01%. Calcd for $C_{11}H_{14}S$: C, 74.10; H, 7.91%.

1-Ethyl-1-pentenyl Phenyl Sulfide: Bp 75 °C (bath temp, 0.08 Torr); IR (neat): 2970, 1634, 1588, 1484, 1442, 1380, 1068, 1025, 895, 736, 686 cm^{-1}; NMR (CCl_4): δ 0.93 (t, J=7 Hz, 3H), 1.03 (t, J=7 Hz, 3H), 1.17—1.64 (m, 2H), 1.97—2.44 (m, 2H), 5.79 (bt, J=7 Hz, 1H), 6.85—7.27 (m, 5H); MS *m/e* (%): 206 (M^+, 100), 177 (68), 135 (85), 110 (33), 67 (43), 55 (84); Found: C, 75.83; H, 8.94%. Calcd for $C_{13}H_{18}S$: C, 75.67; H, 8.79%.

1-(Phenylethynyl)-1-pentenyl Phenyl Sulfide: Bp 106 °C (bath temp, 0.04 Torr); IR (neat): 3070, 2970, 2210, 1588, 1495, 1485, 1445, 1280, 1070, 1024 cm^{-1}; NMR (CCl_4): δ 1.03 (t, J=7.5 Hz, 3H), 1.28—1.76 (m, 2H), 2.39 (dt, J=7, 7 Hz, 2H), 6.23 (t, J=7 Hz, 1H), 6.85—7.50 (m, 10H); MS *m/e* (%): 278 (M^+, 100), 249 (77), 235 (15), 216 (18), 154 (35), 141 (33), 115 (34), 91 (35); Found: *m/e* 278.1139. Calcd for $C_{19}H_{18}S$: M, 278,1128.

(E)-*1-Butylidene-2-heptenyl Phenyl Sulfide*: Bp 104 °C (bath temp, 0.07 Torr); IR (neat): 2920, 2850, 1645, 1586, 1480, 1440, 1026, 960, 899 cm^{-1}; NMR (CCl_4): δ 0.73—1.68 (m, 14H), 1.87—2.15 (m, 2H), 2.36 (dt, J=7, 7 Hz, 2H), 5.93—6.27 (m, 3H), 7.05—7.35 (m, 5H); MS *m/e* (%): 274 (M^+, 79), 259 (32), 245 (50), 231 (21), 203 (54), 197 (23), 109 (59). 79 (100); Found: *m/e* 274.1775. Calcd for $C_{18}H_{28}S$: M, 274.1709.

1-Phenyl-2-phenylthio-1-propene: Bp 115 °C (bath temp, 0.09 Torr); IR (neat): 3070, 1600, 1584, 1478, 1442, 1023, 904, 845, 745, 690 cm^{-1}; NMR (CCl_4): δ 2.00, 2.07 (s, 3H, (*E*) and (*E*)-isomeric mixture), 6.58 (bs, 1H), 7.03—7.53 (m, 10H); MS *m/e* (%): 226 (M^+, 84), 211 (25), 115 (100), 91 (53); Found: C, 79.75; H, 6.29%. Calcd for $C_{15}H_{14}S$: 79.60; H, 6.23%.

1-Phenyl-2-(phenylthio)ethene and 1-Phenyl-2-phenylthio-1-butene. These compounds could not be separated well by GLPC (PEG 20M, PEG 6000, Silicone OV-17, or SE-30). The ratio of ethylated and hydrogenated products was determined by NMR analysis. Spectral data of the mixture are as follows. NMR (CCl_4): δ 1.13 (t, J=7 Hz, $C{=}C(SPh)CH_2C\underline{H}_3$), 2.27 (q, J=7 Hz, $C{=}C(SPh)C\underline{H}_2CH_3$), 6.3, 6.45 (d, J=11 Hz, $C{=}C\begin{matrix}\diagup\underline{H}\\ \underline{H}\diagdown\end{matrix}$), 6.68 (s, $PhC\underline{H}{=}C(SPh)$-Et), 6.61, 6.74 (d, J=15 Hz, $C{=}C\begin{matrix}\underline{H}\diagup & \diagdown\underline{H}\end{matrix}$), 7.03—7.54 (m, 10H); MS *m/e* (%): 240 (M^+ of ethylated compound, 64), 212 (M^+ of hydrogenated product 100). Hydrogenated product, 1-phenyl-2-(phenylthio)ethene ((*E*)- and (*Z*)-isomeric mixture), was prepared independently according to the literature.[20] NMR (CCl_4): δ 6.35 and 6.45 (d, J=11 Hz, 2H of (*Z*)-isomr), 6.61 and 6.74 (d, J=15 Hz, 2H of (*E*)-isomer), 6.99—7.53 (m, 10H); MS *m/e* (%): 212 (M^+, 100, 178 (29), 167 (29), 121 (39), 77 (50).

Hydrolysis of Vinyl Sulfide Derivatives with $TiCl_4$-H_2O System.[13] To a stirred dichloromethane (5 ml) solution of vinyl sulfide substrate (1.0 mmol) was added at 25 °C a

dichloromethane solution of titanium tetrachloride (1.0 M, 2.0 ml, 2.0 mmol) and water (72 mg, 4.0 mmol) successively. The mixture was stirred at 25 °C for several hours. Then ether (10 ml) was added to the reaction mixture and the whole was poured into water (10 ml). The separated organic layer was washed with brine (2×10 ml), dried (Na_2SO_4), and concentrated. Purification was carried out by preparative TLC (hexane-ether).

2-Hexanone and benzyl methyl ketone were identical with the authentic samples.

(E)-6-Dodecen-5-one: Mercury(II) chloride (0.54 g, 2.0 mmol) was added to a solution of (*E*)-1-butylidene-2-heptenyl phenyl sulfide (0.14 g, 0.5 mmol) in CH_3CN-H_2O (3:1, 8 ml) at 25 °C. The resulting mixture was heated at 100 °C for 8 h with rapid stirring. The cold mixture was filtered and the residue was washed with ethyl acetate (2×10 ml). The separated organic layer was washed with water (10 ml) and brine (2×10 ml), dried over magnesium sulfate, and concentrated. Purification by preparative TLC (hexane-ethyl acetate, 10:1) afforded the enone in 65% yield (59 mg). Bp 89 °C (bath temp, 1.5 Torr); IR (neat): 2975, 2950, 1700, 1680, 1635, 1472, 982, 726 cm^{-1}; NMR (CCl_4): δ 0.93 (bt, J=7 Hz, 6H), 1.07—1.80 (m, 10H), 2.00—2.51 (m, 4H) 5.92 (d, J=16 Hz, 1H), 6.65 (dt, J=16, 7 Hz, 1H); MS *m/e* (%): 182 (M^+, 1), 153 (1), 140 (15), 125 (40), 111 (17), 55 (100); Found: C, 78.95; H, 12.39%. Calcd for $C_{12}H_{22}O$: C, 79.06; 12.16%.

4-t-Butyl-2-phenylthio-1-cyclohexenyl Diphenyl Phosphate (4). Treatment of 4-*t*-butyl-2-phenylthiocyclohexanone (0.79 g, 3.0 mmol) with sodium hydride (60%, 0.13 g, 3.3 mmol) and diphenyl phosphorochloridate (0.89 g, 3.3 mmol) in THF (15 ml) at 0 °C afforded the title phosphate **4** (78% yield from 4-*t*-butylcyclohexanone) as a pale yellow liquid: Bp 175 °C (bath temp, 0.05 Torr); IR (neat): 3080, 2980, 1666, 1595, 1492, 1365, 1290, 1185, 950, 770, 750 cm^{-1}; NMR (CCl_4): δ 0.84 (s, 9H), 1.20—2.00 (m, 2H), 2.00—2.50 (m, 3H), 2.68—3.00 (m, 2H), 7.00—7.50 (m, 15H); MS *m/e* (%): 494 (M^+, 100), 329 (52), 251 (42), 187 (58), 160 (71), 57 (59); Found: C, 68.07; H, 6.31%. Calcd for $C_{28}H_{31}O_4PS$: C, 68.00; H, 6.32%.

1-Phenyl-2-phenylthio-1-propenyl Diphenyl Phosphate (7). Treatment of 2-phenylthiopropiophenone (0.73 g, 3.0 mmol) dissolved in THF with lithium diisopropylamide (3.3 mmol) and diphenyl phosphorochloridate (0.89 g, 3.3 mmol) at °C gave title phosphate **7** (64% yield from propiophenone) as a pale yellow liquid: Bp 176 °C (bath temp, 0.05 Torr); IR (neat): 3070, 1592, 1492, 1442, 1298, 1186, 1060, 955, 686 cm^{-1}; NMR (CCl_4): δ 1.78 and 2.00 (d, J=3 and 2 Hz respectively, 3H, (*E*)- and (*Z*)-isomeric mixture), 6.95—7.60 (m, 20H); MS *m/e* (%): 474 (M^+, 4), 326 (100), 325 (67), 251 (18), 233 (18), 170 (28), 94 (29); Found: C, 68.47; H, 5.15%. Calcd for $C_{27}H_{23}O_4PS$: C, 68.34; H, 4.89%.

5-t-Butyl-2-methyl-1-cyclohexenyl Phenyl Sulfide (5). To a solution of enol diphenyl phosphate **4** (0.99 g, 2.0 mmol) and $Pd(PPh_3)_4$ (0.23 g, 0.2 mmol) in 1,2-dichloroethane (10 ml) was added at 25 °C a hexane solution of trimethylaluminium (1.0 M, 5.0 ml, 5.0 mmol). The resulting mixture was heated at 80 °C for 4 h. After the usual workup, as described above, the crude product was purified by silica-gel column chromatography (hexane-ethyl acetate, 10:1) to give the sulfide **5** (0.42 g, 80%) as a colorless liquid: Bp 132 °C (bath temp, 2 Torr); IR (neat): 2960, 1752, 1588, 1482, 1442, 1364, 1220, 1020, 735, 688 cm^{-1}; NMR (CCl_4): δ 0.83(s, 9H), 1.13—1.46 (m, 3H), 1.92 (s, 3H), 1.46—2.35 (m, 4H), 7.00—7.40 (m, 5H); MS *m/e* (%): 260 (M^+, 100), 203 (8), 95 (44), 93 (42), 57 (78); Found: *m/e* 260.1582. Calcd for $C_{17}H_{24}S$: M, 260.1600.

2-Phenyl-3-phenylthio-2-butene (8): Bp 138 °C (bath temp, 2 Torr); IR (neat): 3080, 2940, 1590, 1484, 1445, 1024, 738, 700, 690 cm^{-1} NMR (CCl_4): δ 1.80, 2.03, 2.16, 2.30 (s, total 6H, (*E*)- and (*Z*)-isomeric mixture), 7.00—7.50 (m, 10H); MS *m/e* (%): 240 (M^+, 60), 132 (23), 131 (100), 91 (76); Found: C, 79.90; H, 6.75%. Calcd for $C_{16}H_{16}S$: C, 79.95; H, 6.71%.

2-Methyl-5-t-butylcyclohexanone (6).[21] Alkenyl sulfide **5** was subjected to hydrolysis with titanium tetrachloride according to the literature.[13] Bp 108 ° (bath temp, 3 Torr); IR (neat): 2970, 1708, 1448, 1364, 1220, 1052 cm^{-1}; NMR (CCl_4): δ 0.95 (s, 9H), 0.82—2.55 (m, 11H); MS *m/e* (%): 168 (M^+, 17), 112 (55), 111 (40), 57 (100), 55 (72).

3-Phenyl-2-butanone (9):[22] Bp 98 °C (bath temp, 5 Torr); IR neat): 3030, 2975, 2935, 1715, 1492. 1358, 1195, 950, 765, 702 cm^{-1}; NMR (CCl_4): δ 1.34 (d, J=7 Hz, 3H), 1.96 (s, 3H), 3.64 (q, J=7 Hz, 1H), 7.00—7.45 (m, 5H); MS *m/e* (%): 148 (M^+, 11), 133 (5), 105 (100), 79 (10), 77 (10), 43 (16).

2-Methylthio-1-phenyl-1-propenyl Diphenyl Phosphate (10). The enol phosphate **10** was prepared by treating α-(methylthio)propiophenone with lithium diisopropylamide and diphenyl phosphorochloridate in THF. TLC analysis (hexane-ethyl acetatea, 2:1) of the crude product showed two UV active bands, R_f=0.61 (49%, isolated yield) and R_f=0.51 (36%, isolated yield). The two isomers were separated by silica-gel column chromatography (hexane-ethyl acetate, 10:1). Faster moving band (**10a**): Bp 160 °C (bath temp, 0.15 Torr); IR (neat): 1590, 1488, 1294, 1184, 1055, 945, 684 cm^{-1}; NMR (CCl_4): δ 2.02 (d, J=2 Hz, 3H), 2.06 (s, 3H), 6.80—7.42 (m, 15H); MS *m/e* (%): 412 (M^+, 12), 306 (56), 251 (83), 250 (89), 170 (37), 147 (25), 94 (100); Found: *m/e* 412.0871. Calcd for $C_{22}H_{21}O_4PS$: M, 412.0899. Slower moving band (**10b**): Bp 160 °C (bath temp, 0.15 Torr); IR (neat): 1600, 1500, 1304, 1200, 1092, 955, 688 cm^{-1}; NMR (CCl_4): δ 1.92 (d, J=3 Hz, 3H), 2.22 (s, 3H), 6.80—7.40 (m, 15H); MS *m/e* (%): 412 (M^+, 50), 251 (19), 162 (46), 147 (100), 115 (26); Found: *m/e* 412.0882. Calcd for $C_{22}H_{21}O_4PS$: M, 412.0899.

(E)- and (Z)-1-Methyl-2-phenylethenyl Methyl Sulfide (11).[23] Treatment of enol phosphate **10a** dissolved in 1,2-dichloroethane with triethylaluminium (2.0 equiv) and a catalytic amount of $Pd(PPh_3)_4$ (0.1 equiv) at 80 °C for 4 h gave the hydrogenated sulfide **11** in 59% yield (*E*/*Z*=68/32). Meanwhile enol phosphate **10b** afforded (*E*)-isomer in 72% yield as the sole product under the same conditions. (*E*)-Isomer: Bp 94 °C (bath temp, 4 Torr); R_f=0.21 (hexane): IR (neat): 2920, 1618, 1500, 1440, 1376, 1002, 764, 692 cm^{-1}; NMR (CCl_4): δ 2.06 (s, 3H), 2.30 (s, 3H), 6.10 (s, 1H), 7.10—7.45 (m, 5H); MS *m/e* (%): 164 (M^+, 100), 149 (69), 134 (42), 115 (29), 91 (21). (*Z*)-Isomer: Bp 96 °C (bath temp, 4 Torr); R_f=0.17 (hexane); IR (neat): 2940, 1600, 1500, 1448, 1118, 746, 688 cm^{-1}; NMR (CCl_4): δ 2.17 (s, 3H), 2.24 (s, 3H), 6.33 (s, 1H), 6.95—7.42 (m, 5H); MS; *m/e* (%): 164 (M^+, 100), 149 (68), 134 (59), 115 (69), 91 (27).

1-Phenyl-3-phenylthio-1-butenyl Diphenyl Phosphate (14a). A solution of 1-phenyl-2-buten-1-one (**13**, 0.73 g, 5.0 mmol) in THF (20 ml) was added at −78 °C to a THF solution of lithium benzenethiolate (5.0 mmol) and the whole was stirred at 0 °C for 15 min. To this mixture was added a THF solution of diphenyl phosphorochloridate (5.0 mmol). After being stirred at 0 °C for 20 min, the mixture was diluted with ether (20 ml) and poured into ice-cold water (30 ml). The separated organic layer was washed with brine (2×20 ml), dried (Na_2SO_4), and concentrated. Purification of the crude product gave the desired phosphate **14a** in 74% yield (1.80 g). Bp 166 °C (bath temp, 0.05 Torr); IR (neat): 3075, 1662, 1595, 1498, 1302, 1188, 950 cm^{-1}; NMR (CCl_4): δ 1.36 (d. J=7 Hz, 3H), 4.30 (dq, J=10, 7 Hz, 1H), 5.44 (dd, J=2, 10 Hz, 1H), 6.84—7.50 (m, 20H); MS *m/e* (%): 488 (M^+, 1), 380 (33), 379 (100), 342 (35), 252 (49), 251 (98), 129 (99), 128 (97), 109 (95), 77 (93), 65 (95); Found: C, 68.60; H, 5.33%. Calcd for $C_{28}H_{25}O_4PS$: C, 68.84; H, 5.16%.

1-Phenyl-3-ethylthio-1-butenyl Diphenyl Phosphate (14b). This compound was prepared by using lithium ethanethiolate instead of lithium benzenethiolate in a manner similar to that described above. Bp 160 °C (bath temp, 0.05 Torr); IR (neat): 3070, 2975, 1660, 1592, 1495, 1186, 950 cm^{-1}; NMR (CCl_4): δ 1.16 (t, J=7 Hz, 3H), 1.27 (d, J=7 Hz,3H), 2.38 (q, J=7 Hz, 2H), 3.95 (dq, J=10, 7 Hz, 1H), 5.46 (dd, J=2, 10 Hz, 1H), 6.83—7.57 (m, 15H); MS m/e (%): 440 (M^+, 6), 379 (15), 251 (100), 190 (47), 175 (37), 129 (66), 77 (58); Found: C, 65.17; H, 5.68%. Calcd for $C_{24}H_{25}O_4PS$: C, 65.44; H, 5.72%.

2-Phenyl-4-phenylthio-2-pentene (15a). Enol diphenyl phosphate **14a** (0.97 g, 2.0 mmol) dissolved in benzene (15 ml) was treated with trimethylaluminium (1.0 M of a hexane solution, 5.0 ml, 5.0 mmol) and a catalytic amount of $Pd(PPh_3)_4$ (0.23 g, 0.2 mmol) at 80 °C for 3 h. After a usual workup,the crude product was purified by preparative TLC (hexane-ethyl acetate, 5:1) to afford the title coupling product **15a** in 48% yield (0.24 g). Bp 117 °C (bath temp, 0.09 Torr); IR (neat): 3080, 2985, 1606, 1592, 1502, 1445, 1200, 1024, 872 cm^{-1}; NMR (CCl_4): δ 1.27, 1.38 (d, J=7 Hz each, 3H, (*E*)- and (*Z*)-isomeric mixture), 1.68, 1.93 (s, 3H), 3.70, 4.00 (dq, J=11, 7 Hz each, 1H), 5.29, 5.53 (bd, J=10 Hz each, 1H), 7.01—7.46 (m, 10H); MS m/e (%): 254 (M^+, 1), 145 (100), 129 (9), 117 (12), 91 (8); Found: m/e 254.1128. Calcd for $C_{17}H_{18}S$: M, 254.1130.

2-Phenyl-4-ethylthio-2-pentene (15b): Bp 95 °C (bath temp, 0.1 Torr); IR (neat): 2980, 2940, 1605, 1503, 1452, 1385, 1272, 1213, 874, 758, 693 cm^{-1}; NMR (CCl_4): δ 1.22 (t, J=7 Hz, 3H), 1.31 (d, J=7 Hz, 3H), 2.05 (s, 3H), 2.41 (q, J=7 Hz, 2H), 3.75 (dq, J=10, 7 Hz, 1H), 5.54 (bd, J=10 Hz, 1H), 7.05—7.43 (m, 5H); MS m/e (%): 206 (M^+, 3), 145 (100), 128 (28), 117 (24), 91 (11); Found: C, 75.69; H, 8.92%. Calcd for $C_{13}H_{18}S$: C, 75.67; H, 8.79%.

(E)-*4-Phenyl-3-penten-2-one (16).* Treatment of allyl sulfide **15a** dissolved in methanol-water with sodium periodate (1.05 equiv) at 0 °C for 4 h afforded the corresponding sulfoxide (**17**, UV active, R_f=0.32 (hexane-ethyl acetate, 1:1)) in 74% yield. The sulfoxide **17** was treated with lithium diisopropylamide (1.5 equiv) and diphenyl disulfide (1.5 equiv) in THF at −78—0 °C for 1 h to give 2-phenyl-4-phenylthio-3-penten-2-ol (**18**, UV active, R_f=0.30 (hexane-ethyl acetate, 5:1). Hydrolysis of the crude sulfide **18** with mercury(II) chloride (1.05 equiv) in acetonitrile-water at 50 °C for 6 h gave the title enone **16** (E/Z=95/5) in 68% yield from **17**. Bp 85 °C (bath temp, 1 Torr); IR (neat): 1730, 1675, 1597, 1490, 1370, 1352, 1240, 1035, 955 cm^{-1}; NMR (CCl_4): δ 2.17 (s, 3H), 2.47 (s, 3H), 6.34 (s, 1H), 7.10—7.52 (m, 5H); MS m/e (%): 160 (M^+, 66), 159 (100), 145 (87), 117 (45), 115 (36), 91 (24). The compound was identical with the authentic sample.[24]

Financial support by the Ministry of Education, Science and Culture (Grant-in-Aid Nos. 403022, 530706) is gratefully acknowledged.

References

1) R. Askani in Houben-Weyl, "Methoden der Organischen Chemie," Georg Thieme Verlag, Stuttgart (1972), Vol. V/1b, pp. 44—104.

2) K. Takai, K. Oshima, and H. Nozaki, *Tetrahedron Lett.*, **21**, 2531 (1980).

3) M. Sato, K. Takai, K. Oshima, and H. Nozaki, *Tetrahedron Lett.*, **22**, 1609 (1981).

4) For reviews, see: J. Tsuji, "Organic Synthesis by Means of Transition Metal Complexes," Springer-Verlag, Brlin (1975); R. Noyori, "Transition Metal Organometallics in Organic Synthesis," Academic Press, New York (1976), Vol. 1, pp. 83—187; B. M. Trost, *Tetrahedron*, **33**, 2615 (1977); E. Negishi, "Current Trends in Organic Synthesis," ed by H. Nozaki, Pergamon Press, Oxford (1983), pp. 269—280.

5) A variety of organometallics are reported to couple aryl halides and alkenyl halides in the presence of Pd(0) catalyst. a) Mg and Li: S. Murahashi, M. Yamamura, K. Yanagisawa, N. Mita, and K. Kondo, *J. Org. Chem.*, **44**, 2408 (1979). b) Cu: H. P. Dang and G. Linstrumelle, *Tetrahedrn, Lett.*, **1978**, 191. c) B: N. Miyaura and A. Suzuki, *J. Chem. Soc., Chem, Commun.*, **1979**, 866; H. Yatagai, Y. Yamamoto, and K. Maruyama, *ibid.*, **1977**, 852. d) Zn: E. Negishi, A. O. King, and N. Okukado, *J. Org. Chem.*, **42**, 1821 (1977); A. O. King, E. Negishi, F. J. Villani, Jr., and A. Silveira, Jr., *ibid.*, **43**, 358 (1978).

6) Ni(0) catalyzed coupling reaction of organomagnesium reagents under C-O bond fission have been reported. Enol ether: E. Wenkert, E. L. Michelotti, and C. S. Swindelli, *J. Am. Chem. Soc.*, **101**, 2246 (1979); Enol silyl ether: T. Hayashi, Y. Katsuro, and M. Kumada, *Tetrahedron Lett.*, **21**, 3915 (1980).

7) G. Zweifel and C. C. Whitney, *J. Am. Chem. Soc.*, **89**, 2753 (1967).

8) A. Itoh, S. Ozawa, K. Oshima, S. Sakaki, H. Yamamoto, T. Hiyama, and H. Nozaki, *Bull. Chem. Soc. Jpn.*, **53**, 2357 (1980). See also, H. Yamamoto and H. Nozaki, *Angew. Chem., Int. Ed. Engl.*, **17**, 169 (1978); K. Oshima and H. Nozaki, *Yuki Gosei Kagaku Kyokai Shi*, **38**, 450 (1980).

9) Prepared from α-bromopropiophenone and triethyl phosphite according to the reported procedure: F. W. Lichtenthaler, *Chem. Rev.*, **61**, 607 (1961); I. J. Borowitz, K. C. Yee, and R. K. Crouch, *J. Org. Chem.*, **38**, 1713 (1973).

10) R. E. Ireland and G. Pfister, *Tetrahedron Lett.*, **1969**, 2145.

11) H. Okamura, M. Miura, and H. Takei, *Tetrahedron Lett.*, **1979**, 43.

12) K. Oshima, K. Shimoji, H. Takahashi, H. Yamamoto, and H. Nozaki, *J. Am. Chem. Soc.*, **95**, 2694 (1973); R. C. Cookson and P. J. Parsons, *J. Chem. Soc. Chem. Commun.*, **1976**, 990; **1978**, 821; R. Muthukrishnam and M. Schlosser, *Helv. Chim. Acta*, **59**, 13 (1976). See also Ref. 15a.

13) T. Mukaiyama, K. Kamio, S. Kobayashi, and H. Takei, *Bull Chem. Soc. Jpn.*, **45**, 3723 (1972).

14) D. Seebach, N. R. Jones, and E. J. Corey, *J. Org. Chem*, **33**, 300 (1968).

15) 1,2-Carbonyl transposition has been reported. a) T. Nakai and T. Miura, *Tetrahedron Lett.*, **1979**, 531; *Chem. Lett.*, **1980**, 931; b) W. E. Fristad, T. R. Bailey, and L. A. Paquette, *J. Org. Chem.*, **45**, 3028 (1980); c) T. Shono, I. Nishiguchi, and M. Nitta, *Chem. Lett.*, **1976**, 1319; d) B. M. Trost, K. Hiroi, and S. Kurozumi, *J. Am. Chem. Soc.*, **97**, 438 (1975); e) Alkylative 1,2-carbonyl transposition: S. Kato, T. Yokomatsu, T. Ono, S. Hibino, and S. Shibuya, *J. Chem. Soc., Chem. Commun.*, **1978**, 414.

16) For 1,3-carbonyl transposition, see: a) B. M. Trost and J. L. Stanton, *J. Am. Chem. Soc.*, **97**, 4018 (1975); b) D. Liotta, G. Zima, *J. Org. Chem.*, **45**, 2551 (1980); c) W. C. Still, *J. Am. Chem. Soc.*, **99**, 4836 (1977).

17) "Shin Jikken Kagaku Koza," ed by the Chem. Soc. Jpn., Maruzen, Tokyo (1976), No. 12, pp. 236—237.

18) S. Danno, I. Moritani, and Y. Fujiwara, *Tetrahedron*, **25**,4809 (1969).

19) S. A. Theine and J. G. Traynham, *J. Org. Chem.*, **39**, 153 (1974).

20) E. P. Kohler and H. Potter, *J. Am. Chem. Soc.*, **57**, 1316

(1935).
21) H. O. House and M. J. Umen, *J. Org. Chem.*, **38**, 1000 (1973).
22) E. J. Corey and D. Enders, *Chem. Ber.*, **111**, 1337 (1978).
23) E. J. Corey and J. I. Shulman, *J. Org. Chem.*, **35**, 777 (1970).
24) J. Klein and R. Levene, *J. Chem. Soc., Perkin Trans. 2*, **1973**, 1971.

Synthesis of Sydnone Compounds Having Alternating Carbon-Nitrogen Chain and Heterocyclic Groups at the 4-Position[1)]

Toshio FUCHIGAMI,* Mou-Yung YEH,† Takushi GOTO,
Tsutomu NONAKA,* and Hsien-Ju TIEN†
Department of Electronic Chemistry, Graduate School at Nagatsuta, Tokyo Institute of Technology, Nagatsuta, Midori-ku, Yokohama 227
†*Department of Chemistry, National Cheng Kung University, Tainan, Taiwan, Republic of China*
(Received July 11, 1983)

Entirely new type sydnones having alternating carbon-nitrogen chain groups such as 3-aryl-4-(arylcarbonimidoylcarbamoyl)sydnones, 3-aryl-4-(dimethylaminomethylenecarbamoyl)sydnones, and 4-(dimethylaminomethylenethiocarbamoyl)-3-phenylsydnone were prepared in high yields from 3-aryl-4-chloroformylsydnone, 3-aryl-4-carbamoylsydnone, and 3-phenyl-4-thiocarbamoylsydnone, respectively. The cyclization of the alternating carbon-nitrogen chain groups provided new sydnone derivatives having heterocyclic substituents such as 1,2,4-oxadiazol-5-yl, 1,2,4-triazol-3-yl, and 1,2,4-thiadiazol-5-yl groups in good yields.

Sydnone is a typical mesoionic compound and its chemical and physical properties are very unique.[2,3)] Recently, many sydnone derivatives have been found to have biological and pharmacological activities.[2,4)] In addition, alternating carbon-nitrogen chain and nitrogen-containing heterocyclic compounds are also well known to show similar activities.

It therefore should be significant to establish some methods for synthesizing sydnone compounds having alternating carbon-nitrogen chain and heterocyclic groups as their substituents. However, a sydnone ring is so sensitive to acids, alkalies, and heat that reaction conditions for the preparation of sydnone compounds seem to be limited in cases. One of excellent methods for preparing alternating carbon-nitrogen chain compounds is to start from amino compounds but 4-aminosydnone compounds have been unknown, though some attempts had been done.[5)] Both amidines and imidates are also useful as precusors for the alternating carbon-nitrogen chain compounds, but their preparations have been unsuccesfully tried in the case of sydnone compounds.[6)]

In this work, the synthesis of sydnones attached to a carbon atom of the alternating carbon-nitrogen groups was aimed.

Results and Discussion

Synthesis of Sydnone Compounds Having Alternating Carbon-Nitrogen Chain Groups. 3-Aryl-4-(arylcarbonimidoylcarbamoyl)sydnones (1): Using a method similar to the preparation of *N*-acylamidines,[7,8)] the reaction of amidine hydrochloride with 3-aryl-4-chloroformylsydnone was carried out in aqueous solution in the presence of sodium hydroxide at room temperature. However, the yield was very low because of low solubility of the chloride and its instability in an alkaline solution. It was found that **1** could be prepared in good yields by changing the solvent and base into DMF and two equiv of triethylamine, respectively. Table 1 summarizes synthetic results of **1**.

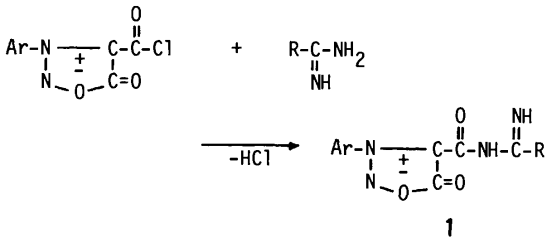

Scheme 1.

*3-Aryl-4-(dimethylaminomethylenecarbamoyl)sydnones (**2a**, **2b**) and 3-Aryl-4-(dimethylaminomethylenethiocarbamoyl)sydnone (**2c**)*: Recently Lin *et al.*[8)] found that amides reacted readily with *N*,*N*-dimethylalkanamide dimethyl acetal to give N^2-acyl-N^1,N^1-dimethylamidines in good yields. Using this new amination method, **2a** and **2b** were prepared quantitatively by heating 3-aryl-4-carbamoylsydnone in large excess amount of *N*,*N*-dimethylformamide dimethyl acetal. In a similar manner, **2c** was also obtained quantitatively from 3-phenyl-4-thiocarbamolsydnone at room temperature. Physical properties and spectral data of **2** are summarized in Table 2.

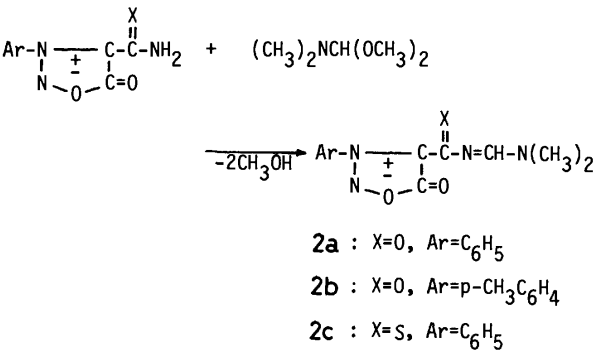

Scheme 2.

Cyclization of Sydnone Compounds Having Alternating Carbon-Nitrogen Chain Groups. The alternating carbon-nitrogen chains of the sydnone compounds synthesized above could be converted into the corresponding heterocyclic groups without any decomposition of their sydnone rings.

*Synthesis of Sydnone Derivatives Having 1,2,4-Oxadiazol-5-yl Groups (**3**) from 1*: We previously developed a novel synthesis of 1,2,4-oxadiazoles from *N*-haloamidino compounds.[7,8)] In this work, this synthetic reaction could be successfully extended to the

TABLE 1. SYNTHESIS OF 3-ARYL-4-(ARYLCARBONIMIDOYLCARBAMOYL) SYDNONES (1)

	Compd 1		Yield	Mp	MS	IR (KBr)		
	Ar	R	%	θ_m/°C	(*m/e*)	ν_{NH}/cm^{-1}	$\nu_{C=O}$/cm^{-1}	$\nu_{C=N}$/cm^{-1}
1a	C_6H_5	C_6H_5	74	198—199	—[a]	3380 3280	1780, 1765 1630	1600
1b	C_6H_5	*p*-$NO_2C_6H_4$	60	193—193.5	353 (M^+)	3370 3200	1765 1625	1580
1c	*p*-$CH_3C_6H_4$	C_6H_5	74	185.5—186	322 (M^+)	3390 3295	1765 1630	1600
1d	*p*-$CH_3C_6H_4$	*p*-$NO_2C_6H_4$	71	193—194.5	366 (M^+)	3400 3225	1755 1625	1625 1590
1e	C_6H_5		48	228.5—229	—[a]	3400 3270	1780, 1765 1610	1570

a) No molecular ion was observed.

TABLE 2. PHYSICAL PROPERTIES AND SPECTRAL DATA OF 2

Sydnone compd	Yield	Mp	MS	^{1}H NMR (DMSO-d_6) δ			
	%	θ_m/°C	(*m/e*)	$(CH_3)_2N$	Ar-H	$CH_3C_6H_4$	-N=CH-
2a	100	192—193.5	260 (M^+)	2.60 (s, 3H) 3.10 (s, 3H)	7.72 (s, 5H)	—	8.43 (s, 1H)
2b	97	175—176	274 (M^+)	2.64 (s, 3H) 3.13 (s, 3H)	7.41 (d, 2H) 7.63 (d, 2H)	2.47 (s, 3H)	8.40 (s, 1H)
2c	100	146.5—147	—[a]	2.67 (s, 3H) 3.03 (s, 3H)	7.53 (s, 5H)	—	8.32 (s, 1H)

a) No molecular ion was observed.

TABLE 3. SYNTHETIC RESULTS OF SYDNONE COMPOUNDS (3) FROM 1

	Sydnone compd		Yield	Mp	IR (KBr)	
	Ar	R	%	θ_m/°C	ν_{ring}/cm^{-1}	$\nu_{C=O}$/cm^{-1}
3a	C_6H_5	C_6H_5	75	168.5—170	1600	1790
3b	C_6H_5	*p*-$NO_2C_6H_4$	92	204.5—205.5	1620 1600	1795
3c	*p*-$CH_3C_6H_4$	C_6H_5	89	169—171	1600	1790
3d	*p*-$CH_3C_6H_4$	*p*-$NO_2C_6H_4$	89	192—192.5	1610	1800
3e	C_6H_5		0	—	—	—

conversion of **1** into **3**, as shown in Scheme 3. The cyclization was found to proceed in DMF only when accurately equivalent amounts of both *t*-butyl hypochlorite and sodium hydroxide were used. When either reagent was used in excess, no sydnone derivatives having 1,2,4-oxadiazol-5-yl group (**3**) were obtained because the sydnone ring is very unstable to oxidation and alkali. In this reaction, attempts to isolate *N*-chloro intermediate (**4**) failed because of its instability. As shown in Table 3, **3** was thus prepared from **1** in excellent yields except for **3e**.

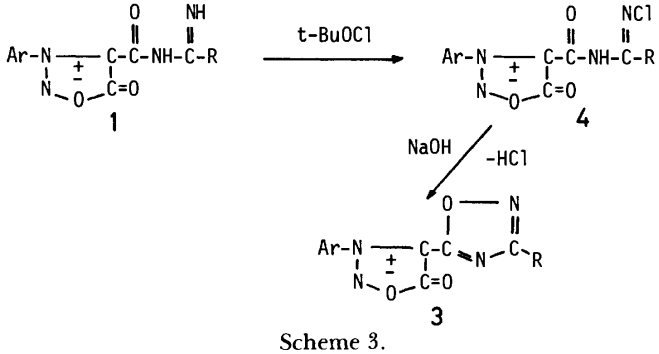

Scheme 3.

The cyclization seems to proceed *via* a nitrene intermediate as proposed previously by us.[7,8,10]

Attempts to Synthesize Sydnone Derivatives (3) Having 1,2,4-Oxadiazol-5-yl Group from 2: Recently Lin *et al.*[9] have reported a facile synthesis of 1,2,4-oxadiazoles and 1,2,4-triazoles by the reaction of N^2-acyl-N^1,N^1-dimethylamidines with hydroxylamine and hydrazine. Using their procedure, the cyclization of **2** to the corresponding (1,2,4-oxadiazol-5-yl)sydnone was attempted. However, when heated **2a** with hydroxylamine in an aq acetic acid solution, 4-carbamoylsydnone was formed instead of desired **3f**.

On the other hand this reaction was carried out at room temperature to give an open-chain intermediate (**5a**) in 90% yield. The cyclization was attempted by heating **5a** at 100 °C for 1 h in acetic acid, at 90 °C for 1 h in a mixed solution of acetic acid and dioxane (1 : 1), and for 2 h in boiling toluene, respectively. However all our

attempts failed and the starting material was recovered. The reaction seemed quite different from that of ordinary *N*-acylamidines with hydroxylamine. In a manner similar to the preparation of **5a**, **5b** was obtained in a high yield. When **5b** was heated in acetic acid at 90 °C, evolution of hydrogen sulfide was observed. However, **3b** expected could not be isolated.

Synthesis of Sydnone Derivatives (6) Having 1,2,4-Triazol-5-yl Groups from 2: Sydnone compounds (**6**) could be obtained in good yields by heating **2** and hydrazine hydrate in acetic acid at 90—100 °C for 1 h, as shown in Table 4.

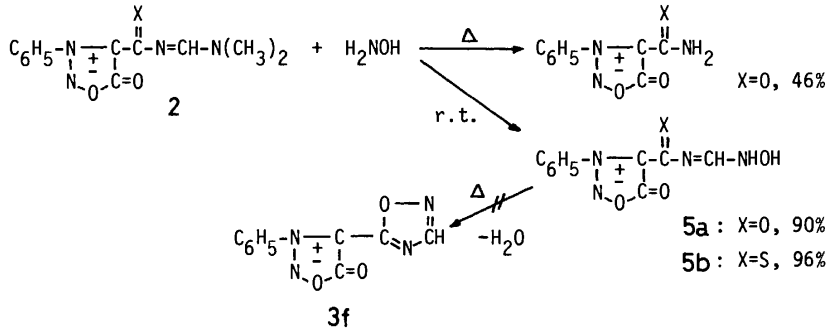

Scheme 4.

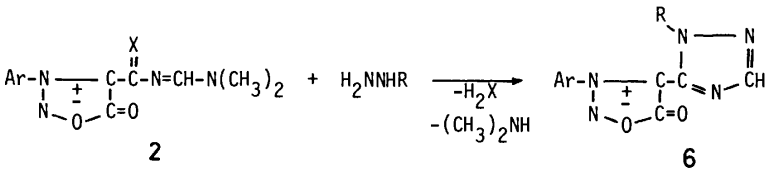

Scheme 5.

Table 4. Synthesis of sydnone compounds (**6**) from **2**

	Sydnone		Hydrazine	Product	Yield	Mp	IR (KBr)
	Ar	X	R		%	θ_m/°C	$\nu_{C=N}$/cm^{-1}
2a	C_6H_5	O	H	**6a**	85	268—269	1565
2c	C_6H_5	S	H	**6a**	88	268—269	1565
2a	C_6H_5	O	C_6H_5	**6b**	87	161—162.5	1560
2b	*p*-$CH_3C_6H_4$	O	H	**6c**	88	278—279	1570
2b	*p*-$CH_3C_6H_4$	O	C_6H_5	**6d**	82	193—194	1570

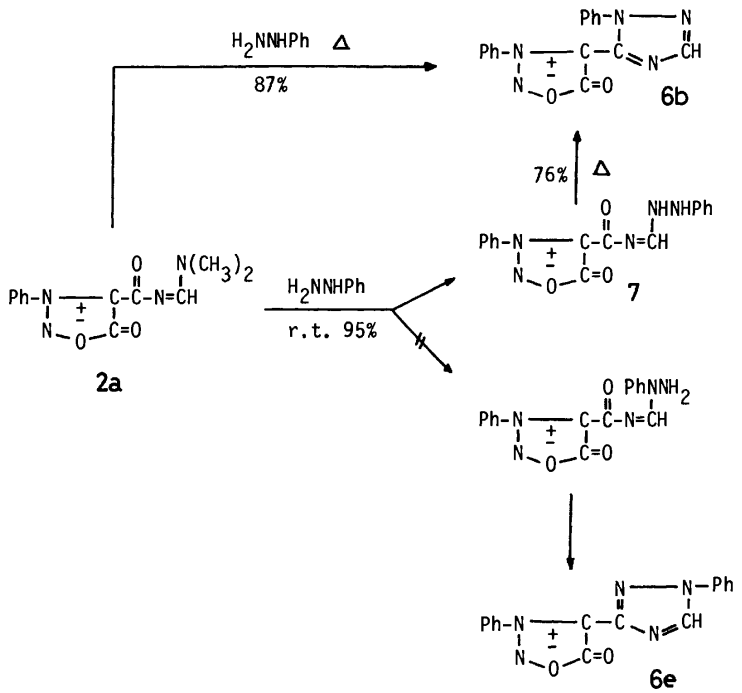

Scheme 6.

Since **2c** provided **6a** in an approximately same yield as **2a**, no remarkable difference in the reactivity was observed between the carbonyl and thiocarbonyl groups of **2**.

A sole product, **6b** was obtained in a good yield by heating **2** and phenylhydrazine although two possible products (**6b** and **6e**) were expected to be formed as shown in Scheme 6. The structure of **6b** was established by the NMR spectral study of an open-chain intermediate (**7**) which was obtained by the same reaction at room temperature. The proton NMR spectrum (DMSO-d_6) of the intermediate shows two doublets (C<u>H</u> and N<u>H</u>) at 8.25 and 9.55 ppm and one singlet (N<u>H</u>C_6H_5) at 9.81 ppm. The latter two signals disappeared while the former did not and changed to singlet by addition of deuterium oxide. On this bases, the structure of the open-chain intermediate was identified as **7**. When heated, **7** cyclized to give **6b**.

Synthesis of a Sydnone Derivative (8) Having 1,2,4-Thiadiazol-5-yl Group from 4-(Dimethylaminomethylenethiocarbonyl)-3-phenylsydnone (2c). Most recently, N^2-arylthiocarbonyl-N^1,N^1-dimethylamidines have been found to be transformed to 1,2,4-thiadiazoles by treatment with hydroxylamine-*O*-sulfonic acid in the presence of pyridine.[11] Using this new cyclization method, the transformation of **2c** to **8** was attempted. According to recommendation of the literature,[11] the reaction of **2c** was first run in a dichloromethane-ethanol mixture at room temperature, but the desired **8** was not formed and the starting **2c** was almost completely recovered. The reaction then was run under refluxing conditions to afford the formation **8** in a low yield as 35%. In this case, the starting **2c** still remained unreacted and 3-phenyl-4-thiocarbamoylsydnone was found to be formed. These results indicate that the thiocarbonyl group of **2c** is fairly less reactive than that of ordinary aromatic compounds.

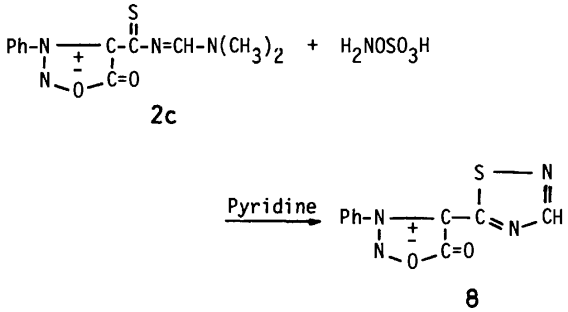

Scheme 7.

The new types of sydnone compounds thus prepared are expected to be pharmacologically active and screening tests of several biological activities of these sydnones are currently under investigation.

Experimental

^{1}H NMR spectra were recorded at 60 MHz on a Hitachi R24B spectrometer using DMSO-d_6 and Me_4Si as solvent and an internal standard, respectively. IR spectra were obtained on a Hitachi 295 infrared spectrometer. Electron impact mass spectra were determined at 30 eV on a JEOL JMS-D100 mass spectrometer by direct introduction *via* solid probe.

3-Phenyl-4-*thio*carbamoylsydnone was prepared as follows: Hydrogen sulfide was passed into the solution of 4-cyano-3-phenylsydnone (2.20 g, 11.8 mmol) and triethylamine (1.44 g, 14.3 mmol) in 50 ml of ethanol at 0 °C for 1 h. The precipitating yellow solid was collected by filtration and washed with ether. The yield was 1.23 g (47%); mp 161 °C. Recrystallization from ethanol provided 0.96 g (37%) of the pure thiocarbamoylsydnone as orange-yellow needles; mp 161 °C (decomp). (Ref,[12] 133 °C).

4-Benzimidoylcarbamoyl-3-phenylsydnone (1a). To a stirred solution of benzamidine hydrochloride (0.44 g, 2.3 mmol) and triethylamine (0.73 g, 7.2 mmol) in 10 ml of DMF, gradually added a solution of 4-chloroformyl-3-phenylsydnone[13] (0.50 g 2.2 mmol) in 2 ml of DMF at 0 °C. After addition, the reaction mixture was stirred for 1.5 h at room temperature and was poured into about 100 ml of ice-water. The precipitates were collected by filtration. The yield was 0.51 g; mp 192—194 °C (decomp). Recrystallization from methanol provided 0.40 g (58%) of pure **1a** as a white solid. ^{1}H NMR δ=7.12—7.97 (m, 10H, C_6<u>H</u>$_5$), 9.36 (br s, 1H, N<u>H</u>), and 9.89 (br s, 1H, N<u>H</u>). Found: C, 62.28; H, 3.65; N, 18.04%. Calcd for $C_{16}H_{12}N_4O_3$: C, 62.34; H, 3.92; N, 18.17%.

4-(p-Nitrobenzimidoyl)-3-phenylsydnone (1b). Using the same procedure, the crude product was obtained; mp 169.5 —171.5 °C (decomp). Recrystallization from methanol provided pure **1b** (38%) as white needles. ^{1}H NMR δ=7.78—8.65 (m, 9H, Ar-<u>H</u>) and 10.05 (br s, 2H, N<u>H</u>). Found: C, 54.24; H, 3.49; N, 19.68%. Calcd for $C_{16}H_{11}N_5O_5$: C, 54.40; H, 3.14: N, 19.82%.

4-Benzimidoylcarbamoyl-3-(p-tolyl)sydhone (1c). Using the same procedure, the crude product was obtained from benzamidine and 4-chloroformyl-3-(*p*-tolyl)sydnone:[3e] mp 184—185 °C (decomp). Recrystallization from methanol provided pure **1c** (45%) as white needles. ^{1}H NMR δ=2.48 (s, 3H, C<u>H</u>$_3$), 7.40—7.80 (m, 9H, Ar-<u>H</u>), 9.42 (br s, 1H, N<u>H</u>), and 9.85 (br s, 1H, N<u>H</u>). Found: C, 63.13; H, 4.44; N, 17.08%. Calcd for $C_{17}H_{14}N_4O_3$: C, 63.35; H, 4.38; N, 17.38%.

4-(p-Nitrobenzimidoylcarbamoyl)-3-(p-tolyl)sydnone (1d). By the similar procedure, pure **1d** was obtained as white needles after recrystallization from methanol. ^{1}H NMR δ=2.30 (s, 3H, C<u>H</u>$_3$), 7.36 (d, 2H, J=8.4 Hz, Ar-<u>H</u>), 7.72 (d, 2H, J=8.4 Hz, Ar-<u>H</u>), 7.95 (d, 2H, J=11.4 Hz, Ar-<u>H</u>), 8.28 (d, 2H, J=11.4 Hz, Ar-<u>H</u>), and 9.75 (br s, 2H, N<u>H</u>). Found: C, 55.90; H, 3.46; N, 19.08%. Calcd for $C_{17}H_{13}N_5O_5$: C, 55.59; H, 3.57; N, 19.07%.

3-Phenyl-4-(piperidinocarbonimidoylcarbamoyl)sydnone (1e). By the similar method, pure **1e** was obtained as white needles after recrystallization from aq methanol. ^{1}H NMR δ=1.38 (br s, 6H, C<u>H</u>$_2$), 3.13 (br s, 4H, C<u>H</u>$_2$), 7.62 (s, 5H, C_6<u>H</u>$_5$), and 8.27 (br s, 2H, N<u>H</u>). Found: C, 57.27; H, 5.37; N, 22.30%. Calcd for $C_{15}H_{17}N_5O_3$: C, 57.14; H, 5.43; N, 22.21%.

4-(Dimethylaminomethylenecarbamoyl)-3-phenylsydnone (2a). A suspension of 4-carbamoyl-3-phenylsydnone[13] (4.07 g, 19.9 mmol) in *N*,*N*-dimethylformamide dimethyl acetal (4.68 g, 37.3 mmol) was heated at 110—120 °C for 1 h. After evaporation under reduced pressure, 5.16 g of a white solid was obtained. Recrystallization from ethanol provided 4.08 g (79%) of pure **2a** as white prisms. Found: C, 55.43; H, 4.49; N, 21.76%. Calcd for $C_{12}H_{12}N_4O_3$: C, 55.38; H, 4.65; N, 21.53%.

4-(Dimethylaminomethylenecarbamoyl)-3-(p-tolyl)sydnone (2b). Using the same procedure, the crude product was obtained; mp 175—176 °C. Recrystallization from ethanol provided pure **2b** as white prisms. Found: C, 56.67; H, 4.78; N, 20.15%. Calcd for $C_{13}H_{14}N_4O_3$: C, 56.93; H, 5.15; N, 20.43%.

4-(Dimethylaminomethylenethiocarbamoyl)-3-phenylsydnone (2c). A suspension of 3-phenyl-4-thiocarbamoylsydnone (1.00 g, 4.52 mmol) in *N*,*N*-dimethylformamide dimethyl acetal (0.68 g, 5.4 mmol) was allowed to stand at room

temperature for 1 h. Evaporation under reduced pressure provided 1.25 g of a reddish solid, mp 147 °C (decomp). Recrystallization from methanol gave 0.94 g (75%) of pure **2c** as reddish prisms. Found: C, 52.49; H, 4.45; N, 20.36; S, 11.56%. Calcd for $C_{12}H_{12}N_4O_2S$: C, 52.16; H, 4.38; N, 20.28; S, 11.60%.

*3-Phenyl-4-(3-phenyl-1,2,4-oxadiazol-5-yl)sydnone (**3a**).* To a stirred solution of **1a** (0.50 g, 1.61 mmol) in 20 ml of DMF was gradually added a solution of *t*-butyl hypochlorite (0.17 g, 1.60 mmol) in 5 ml of DMF at 0 °C. The color of the solution gradually changed to yellow. After the mixture had been stirred at the same temperature for 1 h, 1.6 ml of 1 M sodium hydroxide was added and the solution was stirred for additional 1 h. After the mixture had been warmed at 70—80 °C for 30 min, it was poured into about 100 ml of ice-water. After cooling the precipitates were separated by filtration and washed with water. The yield was 0.37 g, mp 163—166 °C (decomp). Recrystallization from dichloromethane-hexane provided pure **3a** as white needles. ^{1}H NMR δ=7.78—8.33 (m, 10H, C_6H_5). *m/e* 306 (M^+) and 248 (M^+—NO—CO). Found: C, 62.73; H, 3.02; N, 18.12%. Calcd for $C_{16}H_{10}N_4O_3$: C, 62.75; H, 3.29; N, 18.29%.

*4-[3-(p-Nitrophenyl)-1,2,4-oxadiazol-5-yl]-3-phenylsydnone (**3b**).* By the same procedure, the crude product was obtained; mp 205—206 °C (decomp). Recrystallization from dichloromethane-ether provided pure **3b** as white needles. ^{1}H NMR δ=7.85—8.53 (m, 9H, Ar-H). *m/e* 351 (M^+) and 293 (M^+—NO—CO). Found: C, 54.61; H, 2.47; N, 19.89%. Calcd for $C_{16}H_9N_5O_5$: C, 54.71; H, 2.58; N, 19.94%.

*4-(3-Phenyl-1,2,4-oxadiazol-5-yl)-3-(p-tolyl)sydnone (**3c**).* By the same procedure, the crude product was obtained; mp 159—163 °C (decomp). Recrystallization from dichloromethane-hexane provided pure **3c** as white needles in 60% yield. ^{1}H NMR δ=2.53 (s, 3H, CH_3), 7.52—7.95 (m, 9H, Ar-H). *m/e* 320 (M^+) and 262 (M^+—NO—CO). Found: C, 63.49; H, 3.68; N, 17.23%. Calcd for $C_{17}H_{12}N_4O_3$: C, 63.75; H, 3.78; N, 17.49%.

*4-[3-(p-Nitrophenyl)-1,2,4-oxadiazol-5-yl]-3-(p-tolyl)sydnone (**3d**).* By the same procedure, the crude product was obtained; mp 186—186.5 °C (decomp). Recrystallization from dichloromethane-ether provided pure **3d** as white needles. ^{1}H NMR δ=2.30 (s, 3H, CH_3), 7.63 (d, 2H, J=9.0 Hz, Ar-H), 7.93 (d, 2H, J=9.0 Hz, Ar-H), 8.15 (d, 2H, J=9.0 Hz, Ar-H), and 8.48 (d, 2H, J=9.0 Hz, Ar-H). *m/e* 365 (M^+) and 307 (M^+—NO—CO). Found: C, 55.82; H, 2.79; N, 19.04%. Calcd for $C_{17}H_{11}N_5O_5$: C, 55.90; H, 3.04; N, 19.17%.

*4-Hydroxyaminomethylenecarbamoyl-3-phenylsydnone (**5a**).* To a stirred solution of 0.30 g (4.3 mmol) of hydroxylamine hydrochloride, 10 ml of acetic acid, and 4.4 ml of 1 M sodium hydroxide was added **2a** (1.10 g, 4.2 mmol) and the mixture was stirred at room temperature for 1 h. The yellow precipitates were separated by filtration and washed with water. The yield was 0.94 g (90%), mp 180.5—182 °C (decomp). Recrystallization from ethanol provided pure **5a**; mp 180.5—182 °C (decomp). IR (KBr) 1775, 1695 (C=O), and 1660 cm^{-1} (C=N). ^{1}H NMR δ=7.61 (d, 1H, J=10.2 Hz, Ar-CH), and 7.75 (s, 5H, C_6H_5), 10.14 (d, 1H, J=10.2 Hz, NH), and 11.11 (s, 1H, OH). *m/e* 248 (M^+) and 190 (M^+—NO—CO). Found: C, 48.65; H, 3.18; N, 22.32%. Calcd for $C_{10}H_8N_4O_4$: C, 48.39; H, 3.25; N, 22.57%.

*4-Hydroxyaminomethylenethiocarbamoyl-3-phenylsydnone (**5b**).* The mixture of hydroxylamine hydrochloride (0.27 g, 3.9 mmol) and **2c** (1.00 g, 3.6 mmol) in 10 ml of acetic acid and 3.6 ml of 1 M sodium hydroxide was stirred at room temperature for 1 h. The resulting solid was separated by filtration and washed with ethanol to provide 0.79 g (83%) of a crude product, mp 142—145 °C (decomp). After addition of about 100 ml of water to the filtrate, the resulting precipitates were collected by filtration and washed with ethanol to provide the additional product, 0.12 g (13%); mp 141—143 °C (decomp). Recrystallization from aq acetone provided pure **5b** as orange needles; mp 142—144 °C (decomp). IR (KBr) 1755 (C=O), and 1655 cm^{-1} (C=N). ^{1}H NMR δ=7.68 (s, 5H, C_6H_5), 8.14 (d, 1H, J=8.4 Hz, CH), 11.55 (s, 1H, OH), and 11.78 (d, 1H, J=8.4 Hz, NH). *m/e* 264 (M^+), 246 (M^+—H_2S—NO—CO). Found: C, 45.85; H, 3.20; N, 21.02%; S, 12.15%. Calcd for $C_{10}H_8N_4O_3S$: C, 45.45; H, 3.05; N, 21.20; S, 12.13%.

*3-Phenyl-4-(1,2,4-triazol-3-yl)sydnone (**6a**).* *Synthesis of **6a** from **2a**:* The mixture of **2a** (1.00 g, 3.8 mmol) and hydrazine hydrate (0.20 g, 3.9 mmol) in 10 ml of acetic acid was heated at 90—100 °C for 1 h. After cooling, water was added to the reaction mixture. The precipitates were separated by filtration and washed with water. The yield was 0.75 g; mp 269—269.5 °C (decomp). Recrystallization from ethanol provided pure **6a** as white needles. IR (KBr) 1760 cm^{-1} (C=O). ^{1}H NMR δ=7.71 (s, 5H, C_6H_5), 8.52 (s, 1H, triazole C-H), and 14.36 (br s, 1H, NH). *m/e* 229 (M^+) and 171 (M^+—NO—CO). Found: C, 52.62; H, 2.85; N, 30.42%. Calcd for $C_{10}H_7N_5O_2$: C, 52.40; H, 3.80; N, 30.56%.

*Synthesis of **6a** from **2c***: The mixture of hydrazine hydrate (0.60 g, 1.1 mmol) and **2c** (0.30 g, 1.1 mmol) in 2 ml of acetic acid was heated at 90—100 °C for 1 h. After cooling about 50 ml of water was added to the reaction mixture. The needle precipitates were separated by filtration and washed with ethanol. The yield of **6a** was 0.22 g

*3-Phenyl-4-(1-phenyl-1,2,4-triazol-5-yl)sydnone (**6b**).* To a stirred solution of phenylhydrazine (0.13 g, 1.2 mmol) in 3 ml of acetic acid was added **2a** (0.30 g, 1.2 mmol). The color of the mixture changed to red and precipitates began to appear. Then, the mixture was heated at 90—100 °C for 1 h. The color gradually changed to yellow. About 100 ml of water was added to the reaction mixture and the resulting precipitates were separated and washed with ethanol. The yield was 0.31 g; mp 160.5—162 °C. Recrystallization from ethanol provided pure **6b** as pale yellow needles. IR (KBr) 1790 and 1780 cm^{-1} (C=O). ^{1}H NMR δ=7.56 (s, 5H, C_6H_5), 7.66 (s, 5H, C_6H_5), and 8.39 (s, 1H, triazole C-H). *m/e* 305 (M^+) and 247 (M^+—NO—CO). Found:, 63.20; H, 3.50; N, 23.20%. Calcd for $C_{16}H_{11}N_5O_2$: C, 62.95; H, 3.63; N, 22.94%.

*3-(p-Tolyl)-4-(1,2,4-triazol-3-yl)sydnone (**6c**).* Using the same procedure, the crude product was obtained; mp 278—279.5 °C (decomp). Recrystallization from ethanol provided pure **6c** as white needles. IR (KBr) 1775 cm^{-1} (C=O). ^{1}H NMR δ=2.45 (s, 3H, CH_3), 7.51 (d, 2H, J=9.0 Hz, tolyl CH), 7.74 (d, 2H, J=9.0 Hz, tolyl C-H), 8.70 (s, 1H, CH), and 14.74 (br s, 1H, NH). Found: C, 54.37; H, 3.57; N, 28.77%. Calcd for $C_{11}H_9N_5O_2$: C, 54.32; H, 3.73; N, 28.79%.

*4-(1-Phenyl-1,2,4-triazol-5-yl)-3-(p-tolyl)sydnone (**6d**).* Using the same prcedure, the crude product was obtained; mp 185—187 °C. Recrystallization from ethanol provided pure **6d** as white needles. IR (KBr) 1785 cm^{-1} (C=O). ^{1}H NMR δ=2.43 (s, 3H, CH_3), 7.48, 7.58 (two s, 9H, Ar-H), and 8.41 (s, 1H, triazol C-H). *m/e* 319 (M^+) and 261 (M^+—NO—CO) Found: C, 64.16; H, 3.98; N, 21.76%. Calcd for $C_{17}H_{13}N_5O_2$: C, 63.94; H, 4.10; N, 21.93%.

*3-Phenyl-4-(phenylhydrazinomethylenecarbamoyl)sydnone (**7**).* The mixture of phenylhydrazine (0.13 g, 1.2 mmol) and **2a** (0.30 g, 1.2 mmol) in 3 ml of acetic acid was allowed to stand at room temperature for 5 min. The resulting precipitates were separated by filtration and washed with ethanol. The yield was 0.34 g (90%); mp 182.5—184.5 °C. Recrystallization from acetone-hexane provided pure **7** as orange needles; mp 183—184.5 °C. IR (KBr) 1760 and 1675 cm^{-1} (C=O). ^{1}H NMR δ=6.56—7.30 (m, 5H, C_6H_5), 7.75 (s, 5H, C_6H_5) 8.25 (d, 1H, J=8.4 Hz, CH), 9.55 (d, 1H, J=8.4 Hz, NH), and 9.81 (s, 1H, NHC_6H_5). *m/e* 323 (M^+), 305 (M^+—H_2O) and 247 (M^+—H_2O—NO—CO). Found: C, 59.43; H, 3.99; N, 21.81%.

Calcd for $C_{16}H_{13}N_5O_3$: C, 59.44; H, 4.05; N, 21.66%.

Cyclization of **7** *to* **6b**. A mixture of **7** (84 mg, 0.26 mmol) in 1 ml of acetic acid was heated at 90—100 °C for 20 min. After cooling, about 100 ml of water was added to the reaction mixture. The resulting pale yellow precipitatees (60 mg, 76%) were separated by filtration. The product was identified as **6b** by comparison with IR spectrum.

3-Penyl-4-(1,2,4-thiadiazol-5-yl)sydnone (8). To a solution of **2c** (0.76 g, 2.8 mmol) and pyridine (0.49 g, 6.1 mmol) in 15 ml of dry dichloromethane was added a solution of hydroxylamine-*O*-sulfonic acid (0.35 g, 3.1 mmol) in 5 ml of absolute methanol. The reaction mixture was refluxed for 5 h. After cooling, about 30 ml of dichloromethane was added and the dichloromethane solution was washed with 2 M hydrochloric acid (50 ml×2), and water (50 ml), and then dried over sodium sulfate. After removal of the dichloromethane, the residue was chromatographed on silica gel (70—230 mesh). Elution with dichloromethane provided 0.24 g (35%) of the crude product. Recrystallization from dichloromethane-hexane provided 0.13 g (19%) of pure **8** as white needles, mp 144—145 °C. IR (KBr) 1775 cm^{-1} (C=O). ^1H NMR δ=7.73 (s, 5H, $C_6\underline{H}_5$) and 8.17 (s, 1H, thiazole C-$\underline{H}$). *m/e* 246 (M^+) and 188 ($M^+ -NO-CO$). Found: C, 48.68; H, 2.25; N, 22.57; S, 13.02%. Calcd for $C_{10}H_6N_4O_2S$: C, 48.78; H, 2.46; N, 22.75; S, 13.02%.

References

1) A Part of this work is "Organic *N*-Halogeno Compounds. Part 15." Part 14: T. Fuchigami and T. Nonaka, *J. Org. Chem.*, **46**, 5215 (1981).

2) M. Ohta and H. Kato, "Non-benzenoid Aromatics," Academic Press, New York, N. Y. (1969), Vol. 1, Chap. 4.

3) F. H. C. Stewart, *Chem. Rev.*, **64** 129 (1964).

4) a) L. B. Kier and E. B. Roche., *J. Pharm. Sci.*, **56**, 149 (1967); b) L. B. Kier, D. Dhawan, and M. J. Flegry, *ibid.*, **53**, 677 (1964); c) S. G. Boots and C. C. Cheng, *J. Heterocycl. Chem.*, **4**, 272 (1967); d) T. Bruzzese, S. Casadio, E. Marazzi-Uberti, and C. Turba, *J. Pharm. Sci.*, **54**, 1041 (1965); e) L. B. Kier, A. Al-shama, D. Campbell, P. Patil, and A. Tye, *Nature*, **210**, 742 (1966); f) T. Naito, S. Nakagawa, T. Takahashi, and K. Masuko, *J. Antibiot. (Tokyo)*, **21**, 290 (1968); g) H. Wagner and J. B. Hill, *J. Med. Chem.*, **17**, 1337 (1974).

5) a) H. Kato and M. Ota, *Bull. Chem. Soc. Jpn.*, **32**, 282 (1959); b) M. Hashimoto, Dr. Dissertation, Tokyo Institute of Technology, 1969; c) H.-J. Tien *Cheng-kung Ta Hsueh Pao*, **14**, 19 (1979); *Chem. Abstr.*, **92**, 181090x (1980); d) M.-Y. Yen, H.-J. Tien, and T. Nonaka, *J. Org. Chem.*, **48**, 1382 (1983).

6) M.-Y. Yeh, T. Nonaka, T. Goto, M.-C. Hsu, T. Fuchigami, and H.-J. Tien, *Bull. Chem. Soc. Jpn.*, **56**, 3535 (1983).

7) T. Fuchigami and K. Odo, *Chem. Lett.*, **1974**, 1139.

8) T. Fuchigami and K. Odo, *Bull. Chem. Soc. Jpn.*, **49**, 3607 (1976).

9) Y. Lin, S. A. Lang, Jr., M. F. Lovell, and N. A. Perkinson, *J. Org. Chem.*, **44**, 4160 (1979)

10) T. Fuchigami and K. Odo, *Bull. Chem. Soc. Jpn.*, **50**, 1739 (1977).

11) Y. Lin, S. A. Lang, Jr., and S. R. Petty, *J. Org. Chem.*, **45**, 3750 (1980).

12) S. A. Zotova and V. G. Yashunskii, *Zh. Org. Khim.*, **1**, 2218 (1965).

13) K. Kishimoto and M. Ota, *Nippon Kagaku Zasshi*, **83**, 833 (1962).

Infrared Spectroscopic Studies on the Resilium of a Surf Clam, *Spisula (Pseudocardium) sachalinensis*

Yasuo KIKUCHI* and Nobuo TAMIYA
Department of Chemistry, Faculty of Science, Tohoku University, Aobayama, Sendai, Miyagi 980
(Received July 11, 1983)

Sulfinyl group was detected in the resilium (internal hinge-ligament) of surf clam by IR spectrometry. The results reconfirm the previous reports on the presence of methionine *S*-oxide in the intact resilium protein. Aragonite structure was deduced for $CaCO_3$ in the resilium because the IR spectrum of the resilium was reproduced from those of decalcified resilium and aragonite ($CaCO_3$). The IR spectrum of intact protein component in the resilium was simulated from those of the resilium and aragonite ($CaCO_3$).

The hinge-ligaments of molluscan bivalves are elastic and function to open the shells. The resilium (internal hinge-ligament) of surf clam species (Mactridae family) consists of protein (40% of the dry weight) and calcium carbonate ($CaCO_3$). The resilium protein contains 50 mol% of glycine and 20 mol% of methionine of total amino acids.[1,2] Methionine in the resilium protein was suggested to be in an oxidized form, methionine *S*-oxide, by amino acid analysis of the alkaline hydrolysate of the resilium[1] and by solid-state ^{13}C-NMR spectroscopy on powdered resilium preparation without any chemical treatment.[2] It was the first solid evidence for the presence of methionine *S*-oxide in the intact natural proteins.

In the present study, an additional evidence for the presense of methionine *S*-oxide was obtained by infrared (IR) spectrometry and the aragonite structure of $CaCO_3$ was deduced by simulation method applied on IR spectra.

Experimental

Materials *Resilium*: Sakhalin surf clams, *Spisula (Pseudocardium) sachalinensis*, were collected at the north east coast of the main island of Japan. The resiliums were removed from the shells, dried *in vacuo* and stored at −20 °C.

Reduced Resilium: The powdered resilium (8.9 g) was stirred in 50% (v/v) aqueous *N*-methylmercaptoacetamide[3] (100 ml) at room temperature for 7 d, washed successively with water (50 ml×5), 50% (v/v) methanol (50 ml×5), methanol (50 ml×5) and acetone (50 ml×5) and dried *in vacuo* (7.1 g). The amino acid compositions of the resilium before and after the reduction are shown in Table 1.

TABLE 1. AMINO ACID COMPOSITION OF THE RESILIUM[a] BEFORE AND AFTER THE REDUCTION WITH *N*-METHYLMERCAPTOACETAMIDE

Amino acid[12]	Composition/mol%	
	Resilium	Reduced resilium
Met (O)	16	1
Met	0	19
Gly	53	52
Others	31	28

a) The resilium (about 2 mg) was hydrolyzed with 2.5 mol dm^{-3} NaOH at 105 °C for 15h. Amino acids were analyzed on JLC 10-D amino acid analyzer (JEOL Co. Ltd., Tokyo). No correction was made for hydrolytic losses.

Decalcified Resilium: The powdered resilium (2g) was stirred in 10% acetic acid (20 ml) for 15 h, washed with water (20 ml×5) and dried *in vacuo* (0.8 g).

Calcite and Aragonite: The authentic specimens of $CaCO_3$, calcite and aragonite, were provided by Dr. M. Akizuki of the Geology Department of this faculty.

Infrared Spectra. Infrared spectra were measured on a Hitachi 260-10 IR spectrophotometer (Hitachi Co. Ltd., Tokyo, Japan) by KBr disk method.

Combination of IR Spectra. The spectral data were digitized into absorbance values at every 50 cm^{-1} between 4000 cm^{-1} and 2000 cm^{-1} and at every 10 cm^{-1} between 2000 cm^{-1} and 650 cm^{-1}. The combination of the spectra was accomplished according to the additivity of absorbance values. The combination ratio was determined to give the smallest squared deviation of the differences between the resilium spectrum and the artificially prepared spectrum.

Results and Discussion

Methionine S-Oxide. While only 20 amino acids are involved as monomer building blocks in the protein synthesis, more than 140 amino acids have been identified in natural proteins because some amino acids are modified after they are incorporated into the peptide chain of proteins.[4] Methionine *S*-oxide had been detected in some proteins,[5-7] but it was not included in the list of post-translational modification products[4] because its contents were low and methionine can be oxidized *in vitro* during the isolation procedures of proteins.[8] Therefore, the presence of methionine *S*-oxide in an intact protein should be demonstrated excluding the possibility of formation as an artifact or, preferably, without any chemical treatment. In the previous studies, about 90% of methionine in the resilium protein was detected in sulfoxide form after alkaline hydrolysis of the resilium.[1] To exclude the posibility that methionine was oxidized during the alkaline hydrolysis, the presence of methyl group attached to sulfinyl group was demonstrated by solid-state ^{13}C-NMR using cross-polarization and magic angle spinnig techniques.[2]

In the IR spectrum (Fig. 1-a) of the resilium of a surf clam, *S.* (*Ps.*) *sachalinensis*, the absorption band at 1020 cm^{-1} was assigned to S-O stretching vibration of sulfinyl group. The corresponding band was not observed in the spectrum (Fig.1-b) of the reduced resilium, in which methionine *S*-oxide had been converted into methionine with reducing reagent (Table 1). The S-O stretching vibration band of authentic methionine *S*-oxide appeared at 1030 cm^{-1} and 1020 cm^{-1} as splitted

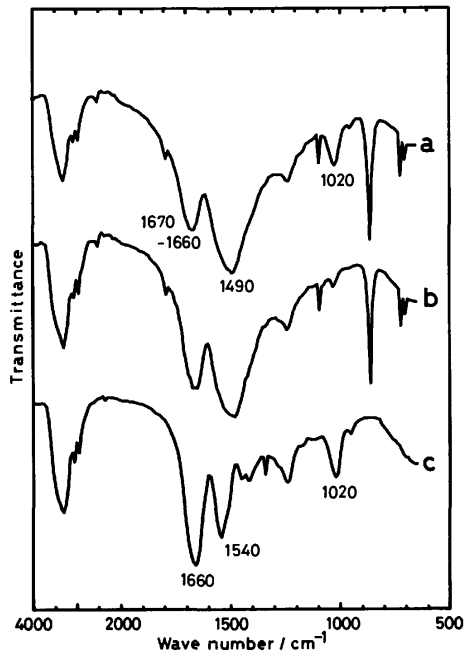

Fig. 1. IR spectra of (a) resilium, (b) reduced resilium, and (c) decalcified resilium.

peaks (not shown). These results indicate the presence of sulfinyl group in the resilium and recomfirm the presence of methionine *S*-oxide in the intact resilium protein.

Aragonite Structure of $CaCO_3$. In Fig.1-a, the absorption band at 1670—1660 cm^{-1} is assigned to amide I band of the resilium protein, but that at 1490 cm^{-1} is unusual as a typical amide II band because it is more intense than amide I band and it is at lower wave number than 1500 cm^{-1}. When the resilium was decalcified with 10% acetic acid, most of the protein remained insoluble. The decalcified resilium showed a typical amide II band at 1540 cm^{-1} (Fig.1-c). Therefore, the unusual band at 1490 cm^{-1} in Fig. 1-a was concluded to contain amide II band of protein and C-O stretching band of $CaCO_3$. Calcite and aragonite are the major crystal types of polymorphic $CaCO_3$ and they are distinguishable by IR spectrometry (Fig. 2-a and b) as reported by Adler and Kerr.[9] If a mixture containing the decalcified resilium and one of the $CaCO_3$ polymorphs could afford the IR spectrum of the resilium (Fig. 1-a), that type of $CaCO_3$ would be the one present in the resilium. In the present study, the spectra of decalcified resilium (Fig. 1-c) and $CaCO_3$ (Fig. 2-a or b) were combined to simulate the spectrum of the mixture. The combination ratio was determined to give the closest spectrum to that of the resilium (Fig. 1-a). Figure 3-a shows the spectrum prepared artificially from those of the decalcified resilium (Fig. 1-c) and calcite ($CaCO_3$) (Fig. 2-a). The amide II band of protein (1540 cm^{-1}) and C-O stretching band of $CaCO_3$ (1430 cm^{-1}) were observed separately. On the other hand, the combination of the spectra of the decalcified resilium (Fig. 1-c) and aragonite ($CaCO_3$) (Fig. 2-b) gave a single absorption band (1490 cm^{-1}) which contained amide II band and C-O band (Fig. 3-b). The IR spectrum of the resilium (Fig. 1-a) was reproduced with the spectra of the decalcified resilium and aragonite ($CaCO_3$). Calcite is the most stable form of $CaCO_3$ at normal temperature, but aragonite is more popular than calcite in the biologically derived structures such

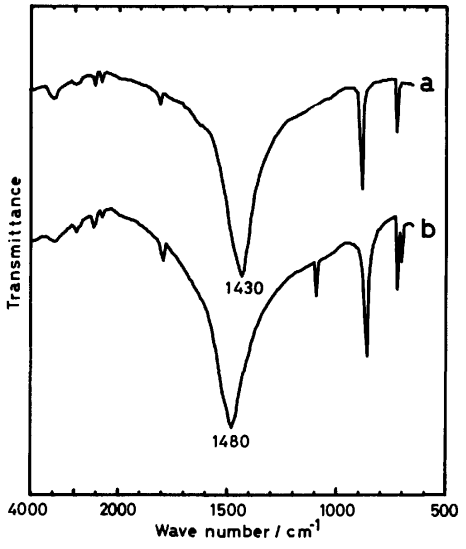

Fig. 2. IR spectra of (a) calcite and (b) aragonite.

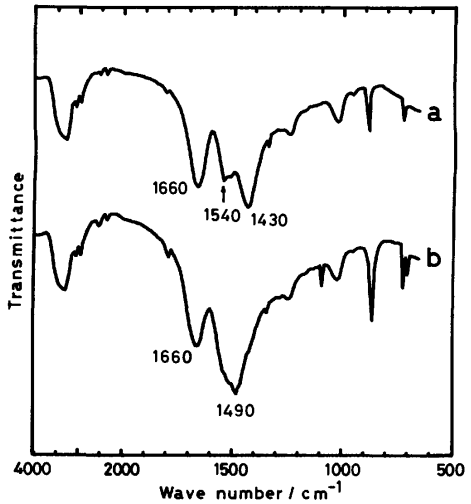

Fig. 3. IR spectra of resilium simulated with (a) decalcified resilium (Fig. 1-c) and calcite (Fig. 2-a) and (b) decalcified resilium (Fig. 1-c) and aragonite (Fig. 2-b).

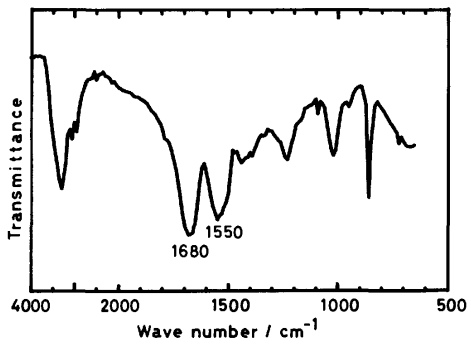

Fig. 4. Simulated spectrum of the protein component in the resilium. The spectrum of aragonite (Fig. 2-b) was subtracted from that of the resilium (Fig. 1-a).

as coral reefs and shells of molluscus.[10] Calcium carbonate in the resilium of surf clams appeared to be in the aragonite form as shown above.

The spectrum of aragonite ($CaCO_3$) (Fig. 2-b) was subtracted from that of the resilium (Fig. 1-a) to simulate the spectrum of the protein component in the resilium (Fig. 4). In Fig. 4, amide I and II bands are observed at 1680 cm^{-1} and 1550 cm^{-1}, while the corresponding bands of the decalcified resilium are at 1660 cm^{-1} and 1540 cm^{-1}, respectively (Fig 1-c). As the amide I and II vibrations are affected by the protein conformation,[11] the small shifts observed above might result from the conformational change of protein caused by decalcification. The amide I and II bands of the decalcified resilium (Fig. 1-c) are close to those assigned to the random-structured protein. The bands in the simulated spectrum of protein component of the resilim (Fig. 4) do not coincide with those proposed for α-helical or β-sheet structure. The protein conformation in the resilium is supposed to be stabilized with calcium ions and contribute to the elasticity of the resilium.

We thank Dr. Mizuhiko Akizuki of Geology Department for providing the specimens of calcite and aragonite. We also thank Professor Satoshi Kanisawa of College of General Education, Dr. Kei Mori of Geology Department and Dr. Yoshiyuki Morioka of this department for helpful discussions.

References

1) Y. Kikuchi and N. Tamiya, *J. Biochem.*, **89**, 1975 (1981)
2) Y. Kikuchi, N. Tamiya, T. Nozawa, and M. Hatano, *Eur. J. Biochem.* **125**, 575 (1982)
3) R. A. Houghten and C. H. Li, *Anal. Biochem.*, **98**, 36 (1979)
4) R. Uy and F. Wold, *Science*, **198**, 890 (1977)
5) B. G. Hudson and R. G. Spiro, *J. Biol. Chem.*, **247**, 4299 (1972)
6) B. H. Brewer, Jr., H. T. Keutmann, J. T. Potts, Jr., R. A. Reisfeld, R. Schleuter, and P. L. Munson, *J. Biol. Chem.*, **243**, 5739 (1968)
7) R. S. Adelstein and W. M. Kuehl, *Biochemistry*, **9**, 1355 (1970)
8) M. S. Doscher and H. W. Hirs, *Biochemistry*, **6**, 304 (1967)
9) H. H. Adler and P. F. Kerr, *Am. Mineral.*, **47**, 700 (1962)
10) I. Kobayashi, "The Mechanism of Biomineralization in Animals and Plants," ed by M. Omori and N. Watabe, Tokai University Press, Tokyo (1980) p. 145; Y. Kitano, N. Kanamori, and S. Yoshioka, *ibid.*, p. 269.
11) T. Miyazawa and E. R. Blout, *J. Am. Chem Soc.*, **83**, 712 (1961)
12) Abbreviations for amino acids are according to the IUPAC-IUB Commission on Biochemical Nomenclature, *J. Biol. Chem.*, **247**, 977 (1972). Met(O) represents methionine *S*-oxide.

 © 1984 The Chemical Society of Japan Bull. Chem. Soc. Jpn., 57, 125—133 (1984)

Chemical Synthesis of a Heat-stable Enterotoxin Produced by Enterotoxigenic *Escherichia coli* Strain 18D

Shoko YOSHIMURA, Makoto MIKI, Haruo IKEMURA, Saburo AIMOTO, Yasutsugu SHIMONISHI,*
Tae TAKEDA,† Yoshifumi TAKEDA,† and Toshio MIWATANI†
Institute for Protein Research, Osaka University, Suita, Osaka 565
†*Research Institute for Microbial Diseases, Osaka University, Suita, Osaka 565*
(Received July 26, 1983)

Two peptides with the two primary structures of 18 amino acid residues proposed for a heat-stable enterotoxin from enterotoxigenic *Escherichia coli* strain 18D were synthesized by solution methods and their physicochemical and biological properties were compared with those of native toxin. One of these peptides (Asn-Thr-Phe-Tyr-Cys-Cys-Glu-Leu-Cys-Cys-Asn-Pro-Ala-Cys-Ala-Gly-Cys-Tyr) showed the same heat-stability and ^{1}H-NMR spectrum as those of the native toxin and evoked fluid secretion in suckling mice at a dose of 1.5—2.0 ng, which is similar to the effective dose of native toxin. Moreover, its toxicity was neutralized by antisera against the native toxin. The other peptide (Asn-Thr-Phe-Tyr-Cys-Cys-Glu-Leu-Cys-Cys-Tyr-Pro-Ala-Cys-Ala-Gly-Cys-Asn) showed different physicochemical and biological behaviors from those of the native toxin and exhibited toxic activity at a dose of 50—80 ng, which is about thirty times the effective dose of the native toxin. Moreover, its toxicity was not neutralized by antisera against the native toxin. These observations indicate that the former peptide is identical to native toxin but that the latter peptide differs in properties from the native toxin.

Enterotoxigenic *Escherichia coli* (ETEC) produces two types of enterotoxin, singly or together, which cause acute diarrhea in man and various domestic animals: a high-molecular-weight, heat-labile enterotoxin (LT) and a low-molecular-weight, heat-stable enterotoxin (ST).[1] There are several reports[2,3] that LT shows similar immunological properties to those of cholera toxin and exerts its effect by stimulating adenylate cyclase in the epithelial cells of the small intestine. However, little is known about ST, except that it may affect the guanylate cyclase-cyclic GMP system.[4-7] This absence of information is mainly because the large quantities of pure ST necessary for biological studies cannot be obtained from a natural source.

In 1981, Chan and Giannella[8] reported that the amino acid sequence of an ST isolated from the culture supernatant of ETEC strain 18D was as illustrated in Fig. 1. Slightly before their report, So and McCarthy[9] determined the nucleotide sequence of DNA encoding an ST produced by a bovine strain of ETEC and hence deduced the amino acid sequence of the ST. The amino acid sequence reported by Chan and Giannella[8] was very similar to that of the C-terminal 18 residues in the amino acid sequence deduced from the nucleotide sequence by So and McCarthy,[9] but differed in two residues at positions 11 and 18 from the N-terminus. To examine this difference in the two sequences, we[10] reinvestigated the amino acid sequence of an ST (named ST_p in this paper) produced by the strain of ETEC used by Chan and Giannella.[8] We found that the sequence of ST_p was different from that proposed by Chan and Giannella,[8] but identical to that deduced from the nucleotide sequence of DNA by So and McCarthy,[9] as illustrated in Fig. 1. Recently, Lazure *et al.*[11] purified an ST produced by a porcine strain F11 (P155) of ETEC and reported the amino acid sequence (Fig. 1). Their sequence was identical to that for ST_p determined by us. Thus, the amino acid sequence of ST_p produced by ETEC strain 18D was established. However, it seemed interesting to confirm the structure of ST_p by chemical synthesis and also to study the effect of amino acid substitution in the sequence of ST_p on its biological properties. Since it is difficult to obtain much toxin by cultivation of bacteria, chemical synthesis of ST_p also seemed useful in providing a way to obtain the large amounts of toxin necessary for biological studies.

In this paper, we describe the chemical syntheses of two peptides with the amino acid sequences proposed by Chan and Giannella[8] (designated as ST_p[Tyr,[11] Asn[18]]) and by us[10] (designated as ST_p) for an ST isolated from strain 18D of ETEC. We also report some physicochemical and biological properties of the synthetic peptides.

Experimental

All chemicals used for preparative experiments were of reagent grade. Chemicals used for analysis were of special grade and solvents were redistilled before use. All amino acids used were of the L-configuration except glycine. DEAE-Sephadex ion-exchanger was purchased from Pharmacia Japan. LiChrosorb RP-8 was obtained from Merck Japan. Melting points were measured by the capillary method and are given as uncorrected values. Optical rotations were determined with a Perkin-Elmer Model 241 polarimeter. Peptide samples were hydrolyzed in 6 M HCl†† in evacuated sealed tubes at 105 °C for 24 or 48 h, and amino acids in the hydrolysates were analyzed in a Hitachi KLA-5 analyzer. Proton NMR spectra were recorded with a JEOL GX-500 spectrometer. Samples were dissolved in 0.3 ml of dimethyl-d_6 sulfoxide containing 15% acetonitrile-d_3 at a concentration of 1—3 mM and measurements were made at 10 °C after addition of 33 μl of D_2O. Chemical shifts were measured from tetramethylsilane added as an internal standard. A large peak caused by remaining H_2O was saturated by the ^{1}H-homo gated decoupling method. Fast atom bombardment (FAB) mass spectra were recorded with a JEOL double-focusing mass spectrometer JMS-HX100 equipped with an FAB ion source, as described previously.[10] Native ST_p was isolated from the culture supernatant of ETEC strain 18D and purified by high-performance liquid chromatography, as described previously.[10] The abbreviations used in this paper are those recommended by the IUPAC-IUB: *J. Biol. Chem.*, **247**, 977 (1972). Additional abbrevitions: MBzl, *p*-methylbenzyl; TFA, trifluoroacetic acid; TEA, triethylamine; DMF, *N,N*-dimethylformamide; DMSO, dimethyl

†† 1 M = 1 mol dm^{-3}.

sulfoxide.

*Boc-Cys(MBzl)-Asn-OBzl (**Ia-1**).* Boc-Asn-OBzl[12] (32.2 g, 0.1 mol) was dissolved in TFA (150 ml) and stirred at room temperature for 30 min. The solution was concentrated under reduced pressure to a syrup, which was mixed with dioxane containing 1 equiv of HCl. The mixture was treated with ether and the resulting precipitate was redissolved with TEA (14.0 ml, 0.1 mol) in DMF (200 ml) and mixed with Boc-Cys(MBzl)-ONSu (46.5 g, 0.11 mol) in DMF (100 ml). The solution was stirred at room temperature for 1 d and then concentrated to a syrup under reduced pressure. The syrup was dissolved in AcOEt and washed successively with 0.1 M HCl, 5% aq $NaHCO_3$ and water. The washed solution was dried over anhydrous Na_2SO_4 and concentrated under reduced pressure to a solid, which was crystallized from a mixture of AcOEt, ether and hexane; wt 50.8 g (96.0 %), mp 124—125 °C, $[\alpha]_D^{23}$ −28.0° (*c* 1.0, DMF).

Found: C, 60.99; H, 6.74; N, 7.82; S, 5.98%. Calcd for $C_{27}H_{35}O_6N_3S$: C, 61.23; H, 6.66; N, 7.93; S, 6.04%.

*Boc-Gly-Cys(MBzl)-Asn-OBzl (**Ia-2**).* Compound **Ia-1** (42.4 g, 80 mmol) was treated with TFA (150 ml) at room temperature for 30 min. The solution was concentrated to dryness under reduced pressure and the residue was mixed with dioxane containing 1 equiv of HCl. The mixture was concentrated under reduced pressure to a syrup, which was solidified in ether. The solid was dissolved in DMF (200 ml) and mixed with TEA (11.2 ml) and Boc-Gly-ONSu (24.0 g, 88 mmol). After 1 d at room temperature, the solution was concentrated to a syrup under reduced pressure. The syrup was dissolved in AcOEt, washed successively with 0.1 M HCl, 5% aq $NaHCO_3$ and water, and dried over anhydrous Na_2SO_4. The dried solution was concentrated under reduced pressure to a solid, which was recrystallized from a mixture of AcOEt, ether and hexane; wt 40.5 g (86.4%), mp 119.5—120.5 °C, $[\alpha]_D^{23}$ −26.8° (*c* 1.0, DMF). Found: C, 59.17; H, 6.48; N, 9.38; S, 5.38%. Calcd for $C_{29}H_{38}O_7N_4S$: C, 59.37; H, 6.53; N, 9.55; S, 5.45%.

*Boc-Ala-Gly-Cys(MBzl)-Asn-OBzl (**Ia-3**).* Compound **Ia-2** (38.1 g, 65 mmol) was treated with TFA (150 ml) at room temperature for 25 min and then concentrated to dryness under reduced pressure. The residue was dissolved with dioxane containing 1 equiv of HCl and precipitated by adding ether. The precipitate was redissolved in DMF (150 ml), mixed with TEA (9.1 ml) and Boc-Ala-ONSu (20.0 g, 70 mmol) and stirred at room temperature for 1 d. The solution was concentrated to dryness under reduced pressure, redissoved in AcOEt, and then washed with 0.1 M HCl, 5% aq $NaHCO_3$ and water. The washed solution was dried over anhydrous Na_2SO_4 and then concentrated under reduced pressure to a solid, which was recrystallized from AcOEt, ether and hexane; wt 41.5 g (97.0%), mp 148—149 °C, $[\alpha]_D^{23}$ −33.8° (*c* 1.0, DMF).

Found: C, 57.84; H, 6.59; N, 10.65; S, 4.75%. Calcd for $C_{32}H_{43}O_8N_5S \cdot 0.5H_2O$: C, 57.65; H, 6.65; N, 10.51; S, 4.80%.

*Boc-Ala-Gly-Cys(MBzl)-Tyr-OBzl (**Ib-3**).* Boc-Gly-Cys(MBzl)-Tyr-OBzl[13] (41.3 g, 65 mmol) was dissolved in TFA (160 ml) and stirred at room temperature for 35 min. The solution was concentrated under reduced pressure to a syrup, which was treated with 1 equiv of HCl in dioxane and then with ether. The precipitate formed was dissolved in DMF (100 ml) and mixed with TEA (9.1 ml) and Boc-Ala-ONSu (21.0 g, 72 mmol). The solution was stirred at room temperature for 2 h and then concentrated to a syrup under reduced pressure. The syrup was redissolved in AcOEt and washed successively with 0.2 M HCl, 5% aq $NaHCO_3$ and water. The washed solution was dried over anhydrous Na_2SO_4 and then concentrated under reduced pressure to a semisolid material, which was recrystallized from AcOEt and ether; wt 34.5 g (75.2%), mp 126—128 °C, $[\alpha]_D^{18}$ −31.3° (*c* 1.0, DMF).

Found: C, 62.04; H, 6.53; N, 7.91; S, 4.39%. Calcd for $C_{37}H_{46}O_8N_4S \cdot 0.5H_2O$: C, 62.08; H, 6.62; N, 7.83; S, 4.47%.

*Boc-Cys(MBzl)-Ala-Gly-Cys(MBzl)-Asn-OBzl (**Ia**).* Compound **Ia-3** (30.0 g, 45 mmol) was dissolved in TFA (150 ml), stirred at room temperature for 20 min, and concentrated to a syrup under reduced pressure. The syrup was treated with dioxane containing 1 equiv of HCl and material was precipitated with ether. The precipitate was dissolved in DMF (150 ml) and mixed with TEA (6.3 ml) and Boc-Cys(MBzl)-ONSu (21.2 g, 50 mmol). The solution was stirred at room temperature for 1 d and then concentrated to dryness under reduced pressure. The residue was dissolved in AcOEt, washed with 0.1 M HCl, 5% aq $NaHCO_3$ and water, and then dried over anhydrous Na_2SO_4. The dried solution was concentrated under reduced pressure to a gelatinous solid, which was recrystallized from a mixture of MeOH and ether; wt 32.5 g (83.6 %), mp 187—188 °C, $[\alpha]_D^{23}$ −24.6° (*c* 1.0, DMF).

Found: C, 59.32; H, 6.56; N, 9.42; S, 7.29%. Calcd for $C_{43}H_{56}O_9N_6S_2 \cdot 0.5H_2O$: C, 59.09; H, 6.57; N, 9.62; S, 7.32%.

*Boc-Cys(MBzl)-Ala-Gly-Cys(MBzl)-Tyr-OBzl (**Ib**).* Compound **Ib-3** (31.8 g, 45 mmol) was dissolved in TFA (100 ml) and stirred at room temperature for 40 min. The solution was concentrated under reduced pressure to a syrup, which was solidified in ether. The solid was dissolved with TEA (6.3 ml) and Boc-Cys(MBzl)-ONSu (21.1 g, 50 mmol) in DMF (200 ml) and stirred at room temperature for 1 d. The solution was concentrated under reduced pressure to a syrup, which was redissolved in AcOEt and washed with 0.3 M HCl, 5% aq $NaHCO_3$ and water. The washed solution was dried over anhydrous Na_2SO_4 and concentrated to a syrup under reduced pressure. The material was crystallized from $CHCl_3$ and ether; wt 39.0 g (94.9 %), mp 89—91 °C (decomp), $[\alpha]_D^{14}$ −19.6° (*c* 1.0, DMF).

Found: C, 61.72; H, 6.71; N, 7.60; S, 6.67%. Calcd for $C_{48}H_{59}O_9N_5S_2 \cdot H_2O$: C, 61.85; H, 6.60; N, 7.52; S, 6.87%.

*Boc-Tyr-Pro-Ala-OMe (**IIa-1**).* Z-Pro-Ala-OMe[14] (16.7 g, 50 mmol) was dissolved in MeOH (300 ml) containing 1 equiv of HCl and hydrogenated over 5% palladium-charcoal catalyst under atmospheric pressure. The catalyst was filtered off and the filtrate was concentrated to dryness under reduced pressure. The residue was dissolved in DMF (20 ml). Meanwhile, Boc-Tyr-N_2H_3 (16.2 g, 55 mmol) was dissolved in DMF (100 ml), cooled below −20 °C and mixed with 4.39 M HCl in dioxane (29.5 ml). The solution was stirred with isopentyl nitrite (7.8 ml, 60 mmol) at the same temperature for 20 min and mixed with the above DMF solution and TEA (25.2 ml). The solution was stirred at 0 °C for 4 d in a refrigerator. The precipitate formed was removed by filtration and the filtrate was concentrated under reduced pressure to an oil, which was redissolved in AcOEt. The solution was washed successively with 0.5 M HCl, 5% aq $NaHCO_3$ and water. Then it was dried over anhydrous Na_2SO_4 and concentrated under reduced pressure to a syrup, which was crystallized from ether and hexane; wt 21.2 g (91.4%), mp 74—76 °C, $[\alpha]_D^{23}$ −33.5° (*c* 1.0, DMF).

Found: C, 59.89; H, 7.66; N, 8.76%. Calcd for $C_{23}H_{33}O_7N_3$: C, 59.60; H, 7.18; N, 9.07%.

*Boc-Cys(MBzl)-Cys(MBzl)-Tyr-Pro-Ala-OMe (**IIa-2**).* Compound **IIa-1** (18.5 g, 40 mmol) was treated with TFA (80 ml) at room temperature for 25 min and concentrated to dryness under reduced pressure. The residue was dissolved in DMF (80 ml). Meanwhile, Boc-Cys(MBzl)-Cys(MBzl)-N_2H_3[13] (24.1 g, 44 mmol) was dissolved in DMF (80 ml) and cooled below −20 °C. The solution was mixed with 4.39 M HCl in dioxane (23.6 ml) and isopentyl nitrite (6.5 ml, 50 mmol) and stirred at −20 °C for 35 min. The solution was mixed with the above solution and TEA (20.1 ml) and then stirred at 0 °C for 3 d in a refrigerator. The precipitate formed

was removed by filtration and the filtrate was concentrated to an oil under reduced pressure. The oil was dissolved in AcOEt and washed successively with 0.1 M HCl, 5% aq $NaHCO_3$ and water. The washed solution was dried over anhydrous Na_2SO_4 and then concentrated to an oil under reduced pressure. The oil was purified by chromatography on a column of silica gel using a mixture of AcOEt: benzene (v/v, 1/1) as eluent. The purified material was crystallized from AcOEt and hexane; wt 28.1 g (80.0%) mp 102—103 °C, $[\alpha]_D^{23}$ −52.4° (*c* 0.5, DMF).

Found: C, 61.38; H, 6.95; N, 7.73; S, 7.15%. Calcd for $C_{45}H_{59}O_9N_5S_2$: C, 61.56; H, 6.77; N, 7.98; S, 7.29%.

*Boc-Cys(MBzl)-Cys(MBzl)-Tyr-Pro-Ala-N_2H_3 (**IIa**).* Compound **IIa-2** (26.3 g, 30 mmol) was dissolved in MeOH (300 ml), mixed with 100% hydrazine hydrate (60 ml), and then stirred at room temperature for 1 d. The solution was concentrated to dryness under reduced pressure and mixed with water. The precipitate formed was collected and crystallized from MeOH and ether; wt 21.3 g (81.0%), mp 122—123 °C, $[\alpha]_D^{23}$ −42.8° (*c* 0.5, DMF).

Found: C, 59.06; H, 6.46; N, 10.80; S, 7.05%. Calcd for $C_{44}H_{59}O_8N_7S_2 \cdot H_2O$: C, 58.98; H, 6.86; N, 10.94; S, 7.14%.

*Boc-Cys(MBzl)-Cys(MBzl)-Tyr-Pro-Ala-Cys(MBzl)-Ala-Gly-Cys(MBzl)-Asn-OBzl (**IIIa**).* Compound **Ia** (8.65 g, 10.0 mmol) was dissolved in TFA (100 ml) in an ice-bath. The solution was stirred at room temperature for 20 min and concentrated under reduced pressure to a syrup, which was solidified in ether. The solid was dissolved in DMF (30 ml). Meanwhile, compound **IIa-3** (10.52 g, 12.0 mmol) was dissolved in DMF (50 ml), cooled below −20 °C and mixed with 4.39 M HCl in dioxane (14.7 ml) and isopentyl nitrite (1.82 ml, 14.0 mmol). The solution was stirred below −20 °C for 30 min, and then mixed with TEA (10.4 ml) and the solution described above. The mixture was stirred at 0 °C for 2 d in a refrigerator. The precipitate formed was removed by filtration and the filtrate was concentrated to a syrup under reduced pressure. The syrup was dissolved in hot AcOEt and kept at room temperature. The precipitate formed was collected and recrystallized from MeOH, DMF and ether; wt 15.1 g (93.8%), mp 173—175 °C, $[\alpha]_D^{19}$ −57.6° (*c* 0.5, DMSO).

Found: C, 60.00; H, 6.06; N, 9.24; S, 7.86%. Calcd for $C_{82}H_{103}O_{15}N_{11}S_4 \cdot 2H_2O$: C, 59.79; H, 6.55; N, 9.36; S, 7.79%.

*Boc-Cys(MBzl)-Cys(MBzl)-Asn-Pro-Ala-Cys(MBzl)-Ala-Gly-Cys(MBzl)-Tyr-OBzl (**IIIb**).* Boc-Cys(MBzl)-Cys(MBzl)-Asn-Pro-Ala-N_2H_3[13] (14.1 g, 17 mmol) was dissolved in DMF (50 ml), cooled below −20 °C and mixed with 4.39 M HCl in dioxane (14.7 ml) and then with isopentyl nitrite (2.5 ml, 19 mmol). The solution was stirred at −20 °C for 30 min. Meanwhile, compound **Ib** (13.7 g, 15 mmol) was dissolved in TFA (100 ml), stirred at room temperature for 40 min and then concentrated under reduced pressure to a syrup, which was solidified in ether. The solid and TEA (11.2 ml) were added to the azide solution described above and stirred at 0 °C for 1 d in a refrigerator. The precipitate was removed by filtration and the filtrate was concentrated to an oil under reduced pressure. The oil was solidified in a mixture of AcOEt and ether and recrystallized repeatedly from EtOH; wt 19.0 g (78.5%), mp 213—214 °C, $[\alpha]_D^{14}$ −41.6° (*c* 0.5, DMSO)

Found: C, 61.18; H, 6.66; N, 9.78; S, 8.09%. Calcd for $C_{82}H_{103}O_{15}N_{11}S_4$: C, 61.14; H, 6.45; N, 9.57; S, 7.95%.

*Boc-Cys(MBzl)-Cys(MBzl)-Glu(OBu^t)-Leu-Cys(MBzl)-Cys(MBzl)-Tyr-Pro-Ala-Cys(MBzl)-Ala-Gly-Cys(MBzl)-Asn-OBzl (**IVa**).* Compound **IIIa** (6.44 g, 4.00 mmol) was dissolved with anisole (2.5 ml) in TFA (75 ml) and stirred at room temperature for 60 min. The solution was concentrated under reduced pressure to a syrup, which was solidified in ether. The solid was dissolved in DMF (50 ml). Meanwhile, Boc-Cys(MBzl)-Cys(MBzl)-Glu(OBu^t)-Leu-N_2H_3[13] (4.06 g, 4.80 mmol) was dissolved in DMF (50 ml), cooled below −20 °C, and mixed with 4.39 M HCl in dioxane (5.5 ml) and isopentyl nitrite (0.62 g, 5.28 mmol). The solution was stirred at −20—−30 °C for 30 min and mixed with TEA (4.0 ml) and the solution described above. The mixture was stirred at 2—3 °C for 3 d in a refrigerator. The precipitate formed was collected with MeOH, boiled repeatedly in hot EtOH and collected; wt 7.60 g (81.7%), mp 225—227 °C, $[\alpha]_D^{19}$ −39.2° (*c* 0.5, DMF).

Found: C, 60.69; H, 6.82; N, 8.69; S, 8.26%. Calcd for $C_{119}H_{155}O_{21}N_{15}S_6 \cdot 3H_2O$: C, 60.61; H, 6.88; N, 8.91; S, 8.16%.

*Boc-Cys(MBzl)-Cys(MBzl)-Glu(OBu^t)-Leu-Cys(MBzl)-Cys(MBzl)-Asn-Pro-Ala-Cys(MBzl)-Ala-Gly-Cys(MBzl)-Tyr-OBzl (**IVb**).* Compound **IIIb** (8.05 g, 5.0 mmol) was dissolved in TFA (100 ml). The solution was stirred at room temperature for 30 min and concentrated under reduced pressure to a syrup, which was solidified in ether. The solid was dissolved in DMSO (40 ml). Meanwhile, Boc-Cys(MBzl)-Cys(MBzl)-Glu(OBu^t)-Leu-N_2H_3[13] (5.07 g, 6 mmol) was dissolved in DMF (30 ml), cooled below −20 °C, and mixed with 4.39 M HCl in dioxane (8.85 ml) and isopentyl nitrite (0.91 ml, 7 mmol). The solution was stirred at −20—−30 °C for 35 min and mixed with the solution described above and TEA (6.2 ml). The mixture was stirred at 0 °C for 2 d in a refrigerator. The precipitate formed was removed by filtration and the filtrate was concentrated to a syrup. The syrup was mixed with 0.2 M HCl and the precipitate formed was collected and recrystallized from EtOH; wt 11.0 g (94.8%), mp 236 °C (decomp), $[\alpha]_D^{18}$ −51.3° (*c* 0.32, DMSO).

Found: C, 61.01; H, 6.89; N, 8.90; S, 8.28%. Calcd for $C_{119}H_{155}O_{21}N_{15}S_6 \cdot H_2O$: C, 61.04; H, 6.76; N, 8.97; S, 8.20%.

*Z(OMe)-Phe-Tyr-OEt (**V-1**).* H-Tyr-OEt·HCl (8.1 g, 33 mmol) was dissolved with TEA (4.6 ml) in DMF (70 ml) and mixed with Z(OMe)-Phe-ONp (13.5 g, 30 mmol) in DMF (30 ml). The solution was stirred at room temperature for 6 d and concentrated to dryness under reduced pressure. The residue was dissolved in AcOEt and washed successively with 5% aq $NaHCO_3$, 0.5 M HCl and water. The washed solution was dried over anhydrous Na_2SO_4 and then concentrated under reduced pressure to a syrup, which was crystallized from AcOEt, EtOH and hexane; wt 15.5 g (99.4%), mp 139.5—140.5 °C, $[\alpha]_D^{19}$ −9.0° (*c* 1.0, DMF).

Found: C, 66.36; H, 6.24; N, 5.32%. Calcd for $C_{29}H_{32}O_7N_2$: C, 66.91; H, 6.20; N, 5.38%.

*Boc-Asn-Thr-OEt (**V-2**).* H-Thr-OEt·HCl (7.34 g, 40 mmol) was dissolved with TEA (5.6 ml) and Boc-Asn-ONp (12.4 g, 35 mmol) in DMF (30 ml). The solution was stirred at room temperature for 1 d and concentrated to dryness under reduced pressure. The residue was dissolved in 1-butanol and washed with 5% aq $NaHCO_3$, 0.1 M HCl and water. The washed solution was dried over anhydrous Na_2SO_4 and concentrated to a syrup under reduced pressure. The syrup was crystallized from AcOEt, hexane and ether: wt 8.70 g (69.0%), mp 150—151 °C, $[\alpha]_D^{23}$ −15.6° (*c* 1.0, DMF).

Found: C, 49.85; H, 7.68; N, 11.57%. Calcd for $C_{15}H_{27}O_7N_3$: C, 49.85; H, 7.53; N, 11.63%.

*Boc-Asn-Thr-N_2H_3 (**V-3**).* Compound **V-2** (8.67 g, 24.0 mmol) was dissolved in MeOH (100 ml) and mixed with 100% hydrazine hydrate (30 ml). The solution was stirred at room temperature for 1 d and then concentrated to an oil under reduced pressure. The oil was crystallized from MeOH and ether; wt 7.90 g (94.8%), mp 186—188 °C (decomp), $[\alpha]_D^{23}$ −25.2° (*c* 1.0, DMF).

Found: C, 44.10; H, 7.22; N, 20.33%. Calcd for $C_{13}H_{25}O_6N_5 \cdot 0.5H_2O$: C, 44.18; H, 7.30; N, 19.82%.

*Boc-Asn-Thr-Phe-Tyr-OEt (**V-4**).* Compound **V-1** (10.4 g, 20.0 mmol) was dissolved with anisole (5 ml) in TFA (30 ml), stirred at room temperature for 30 min and then

concentrated to a syrup under reduced pressure. The syrup was dissolved in DMF (60 ml). Meanwhile, compound **V-3** (7.63 g, 22.0 mmol) was dissolved in DMF (50 ml) and cooled below −20 °C. The solution was mixed with 4.39 M HCl in dioxane (14.8 ml) and isopentyl nitrite (3.25 ml, 25 mmol). The solution was stirred below −20 °C for 30 min and mixed with the solution described above and TEA (11.9 ml). The mixture was stirred at 0 °C for 6 d in a refrigerator. The precipitate formed was removed by filtration and the filtrate was concentrated to a syrup under reduced pressure. The syrup was dissolved in AcOEt and washed successively with 0.5 M HCl, 5% aq $NaHCO_3$ and water. The washed solution was dried over anhydrous Na_2SO_4 and concentrated to a gelatinous solid under reduced pressure. The solid was crystallized from EtOH and ether; wt 11.3 g (84.3%), mp 139.5—140.5 °C, $[\alpha]_D^{23}$ −27.5° (*c* 1.0, DMF).

Found: C, 58.03; H, 6.94; N, 10.19%. Calcd for $C_{33}H_{45}O_{10}N_5 \cdot 0.5H_2O$: C, 58.22; H, 6.81; N, 10.29%.

Boc-Asn-Thr-Phe-Tyr-N_2H_3 (V). Compound **V-4** (10.1 g, 15.0 mmol) was dissolved in MeOH (150 ml) and mixed with 100% hydrazine hydrate (20 ml). The solution was stirred at room temperature for 1 d and then concentrated to a crystalline solid under reduced pressure. The solid was collected with water and recrystallized from DMF and ether; wt 9.0 g (91.8%), mp 204—205 °C, $[\alpha]_D^{23}$ −42.3° (*c* 1.0, DMF).

Found: C, 54.80; H, 6.74; N, 14.25%. Calcd for $C_{31}H_{43}O_9N_7 \cdot H_2O$: C, 55.10; H, 6.71; N, 14.51%.

*Boc-Asn-Thr-Phe-Tyr-Cys(MBzl)-Cys(MBzl)-Glu-Leu-Cys(MBzl)-Cys(MBzl)-Tyr-Pro-Ala-Cys(MBzl)-Ala-Gly-Cys-(MBzl)-Asn-OBzl (**VIa**).* Compound **IVa** (2.3 g, 1.0 mmol) was dissolved in TFA (20 ml) and stirred at room temperature for 60 min. The solution was concentrated to dryness under reduced pressure and the residue was dissolved in DMF (10 ml). Meanwhile, compound **V** (0.79 g, 1.2 mmol) was dissolved in DMF (5 ml) and cooled below −20 °C. The solution was mixed with 4.39 M HCl in dioxane (1.5 ml) and isopentyl nitrite (0.18 ml, 1.4 mmol) and stirred below −20 °C for 30 min. The solution was mixed with the solution described above and TEA (1.1 ml) and stirred at 0 °C for 5 d in a refrigerator. The precipitate formed was removed by filtration and the filtrate was concentrated to an oil under reduced pressure. The oil was mixed with 0.1 M HCl and the resulting precipitate was collected with water. The precipitate was crystallized from DMF and ether; wt 2.50 g (89.6%), mp 225 °C (decomp), $[\alpha]_D^{23}$ −34.7° (*c* 0.34, DMSO). Amino acid ratio in the acid hydrolysate: Asp, 1.96 (2); Thr, 0.84 (1); Glu, 0.91 (1); Pro, 1.03 (1); Gly, 1.00 (1); Ala, 2.03 (2); Leu, 0.92 (1); Tyr, 1.75 (2); Phe, 0.93 (1).

Found: C, 60.09; H, 6.62; N, 9.77; S, 6.60%. Calcd for $C_{141}H_{178}O_{28}N_{20}S_6 \cdot H_2O$: C, 60.24; H, 6.45; N, 9.97; S, 6.83%.

*Boc-Asn-Thr-Phe-Tyr-Cys(MBzl)-Cys(MBzl)-Glu-Leu-Cys(MBzl)-Cys(MBzl)-Asn-Pro-Ala-Cys(MBzl)-Ala-Gly-Cys(MBzl)-Tyr-OBzl (**VIb**).* Compound **IVb** (4.65 g, 2 mmol) was dissolved in TFA (100 ml) and stirred at room temperature for 45 min. The solution was concentrated under reduced pressure to a syrup, which was solidified in ether. Meanwhile, compound **V** (1.58 g, 2.4 mmol) was dissolved in DMF (20 ml) and cooled below −20 °C. The solution was mixed with 6.72 M HCl in dioxane (1.75 ml) and isopentyl nitrite (0.37 ml) and stirred below −20 °C for 35 min. Then, the mixture was stirred at 0 °C for 4 d in a refrigerator with TEA (2.0 ml) and the solid prepared as described above and dissolved in DMSO (5 ml). The precipitate was removed by filtration and the filtrate was concentrated to a syrup under reduced pressure. The syrup was precipitated from EtOH and ether; wt 5.0 g (89.6%), mp 243 °C (decomp), $[\alpha]_D^{18}$ −39.4° (*c* 0.35, DMF). Amino acid ratio in the acid hydrolysate: Asp, 1.95 (2); Thr, 0.89 (1); Glu, 0.99 (1); Pro, 1.02 (1); Gly, 1.00 (1); Ala, 1.95 (2); Leu, 0.95 (1); Tyr, 1.85 (2); Phe, 0.97 (1).

Found: C, 60.14; H, 6.74; N, 9.77; S, 6.99%. Calcd for $C_{141}H_{178}O_{28}N_{20}S_6 \cdot H_2O$: C, 60.24; H, 6.45; N, 9.97; S, 6.83%.

HF-treatment and Air-oxidation: Compound **VIa** or **VIb** (69.8 mg, 25 μmol) was treated in the presence of anisole (0.1 ml) with anhydrous liquid hydrogen fluoride (3 ml) at 0 °C for 60 min. The HF-reagent was evaporated under reduced pressure. The residue was dissolved in 99% formic acid (1 ml) and washed three times with hexane. The solution was diluted to 5×10^{-5} M with distilled water and rapidly adjusted to pH 8.0 with aqueous ammonia. The solution was kept at room temperature for 4 d with occasional stirring. Free thiol became undetectable during this period. The solution was freeze-dried to a powder. The powder was dissolved in a small amount of water, applied to a column (2×90 cm) of Sephadex G-25, and eluted with 0.01 M NH_4HCO_3. The toxic fractions were collected and lyophilized. The lyophilized material was dissolved in water, applied to a column (2×33 cm or 1.6×25 cm) of DEAE-Sephadex A-25 (acetate form), and washed sufficiently with water. The adsorbed material was eluted with a linear-gradient of 0 to 0.5 M acetic acid. The toxic fractions were collected, lyophilized and purified on a reversed-phase column of HPLC, as described below.

High-performance Liquid Chromatography (HPLC): HPLC was performed on LiChrosorb RP-8 (Merck, 5 μm). Two columns (8×300 mm and 4×250 mm) were packed in our laboratory for semipreparative separation and for analysis, respectively. Both columns were equilibrated with 0.01 M ammonium acetate (pH 5.7) containing 10% acetonitrile and the sample solution was injected onto one of these columns. The column was developed at a flow rate of 1 ml/min with a linear-gradient of 10—30% acetonitrile in 0.01 M ammonium acetate (pH 5.7) with increase in the acetonitrile concentration at a rate of 1%/min.

Biological Assay: ST activity was assayed in suckling mice of 2—4 d old, as described previously.[16] The fluid accumulation ratio of each animal was calculated as the ratio of the weight of the entire intestine to that of the rest of the body. The minimal amount of ST giving a fluid accumulation ratio of over 0.09 was designated as 1 mouse unit, as described previously.[16]

Results and Discussion

Isolation of Biologically Active Synthetic Peptides. We recently determined the amino acid sequence of an ST (named ST_h in this paper) isolated from a human strain SK-1 of ETEC.[16,17] The sequence was identical with that of ST_p except for the N-terminal three residues and the fourth residue from the C-terminus, as shown in Fig. 1. Interestingly, six half-cystine residues were found at common positions and joined intramolecularly. The disruption of the disulfide bonds in ST_p by reduction destroyed the biological activity of ST.[8] Furthermore, we found that native ST_p and ST_h have the same potency in a fluid accumulation test using suckling mice[10,17] and their toxicity is neutralized by homologous and heterologous *anti*-ST_p and *anti*-ST_h antisera.[22] These findings suggested that ST_p and ST_h have the similar secondary structures including disulfide linkages, which play an important part for expression of the toxicity of ST, although the mode of disulfide bond formation has not yet been determined. Moreover, we recently prepared the protected peptide with the amino acid sequence of ST_h and deprotected all the protecting groups from the peptide followed by air-oxidation. We found that the crude air-oxidized product is highly toxic and that the purified

```
                1               5                  10                  15
(a)     Asn-Thr-Phe-Tyr-Cys-Cys-Glu-Leu-Cys-Cys-Tyr-Pro-Ala-Cys-Ala-Gly-Cys-Asn        Chan and Giannella[8]

(b)  ---ACC-ACA-TTT-TAC-TGC-TGT-GAA-CTT-TGT-TGT-AAT-CCT-GCC-TGT-GCT-GAA-TGT-TAT       So and McCarthy[9]
       -Asn-Thr-Phe-Tyr-Cys-Cys-Glu-Leu-Cys-Cys-Asn-Pro-Ala-Cys-Ala-Gly-Cys-Tyr

(c)     Asn-Thr-Phe-Tyr-Cys-Cys-Glu-Leu-Cys-Cys-Asn-Pro-Ala-Cys-Ala-Gly-Cys-Tyr        Takao et al.[10]

(d)     Asn-Thr-Phe-Tyr-Cys-Cys-Glu-Leu-Cys-Cys-Asn-Pro-Ala-Cys-Ala-Gly-Cys-Tyr        Lazure et al.[11]

(e)  Asn-Ser-Ser-Asn-Tyr-Cys-Cys-Glu-Leu-Cys-Cys-Asn-Pro-Ala-Cys-Thr-Gly-Cys-Tyr     Aimoto et al.[17]
```

Fig. 1. Comparison of amino acid sequences proposed for ST: (a) Data reported for an ST isolated from ETEC strain 18D in Ref. 8; (b) deduced from the nucleotide sequence encoding an ST of bovine origin;[9] (c) data proposed for an ST (=ST_p) isolated from ETEC strain 18D by us;[10] (d) data proposed for an ST isolated from a porcine strain F11(P155) of ETEC in Ref. 11; (e) data proposed for an ST (=ST_h) isolated from a human strain SK-1 of ETEC by us.[17]

peptide shows the same biological and physicochemical properties as native ST_h.[18] Hence, we considered that two peptides with the amino acid sequences proposed for ST_p, which have similar amino acid sequences to that of ST_h, can be synthesized by a similar method to that used for synthesis of ST_h. The sequences were first divided into four segments and the protected derivatives of these fragments were prepared separately by conventional solution methods. Then, the segments were coupled sequentially from the C-terminus to the N-terminus by an azide method[19] to reduce undesirable racemization, as illustrated in Fig. 2. The protected fragments Boc-Cys(MBzl)-Cys(MBzl)-Glu(OBu^t)-Leu-N_2H_3[13] and **V** were used for the syntheses of both the two protected peptides **VIa** and **VIb**.

Then, all the protecting groups were removed by the HF-method[15] and free peptides were air-oxidized under similar conditions to those described previously.[18] The air-oxidized solutions of peptides were directly applied to a reversed-phase column of HPLC, as illustrated in

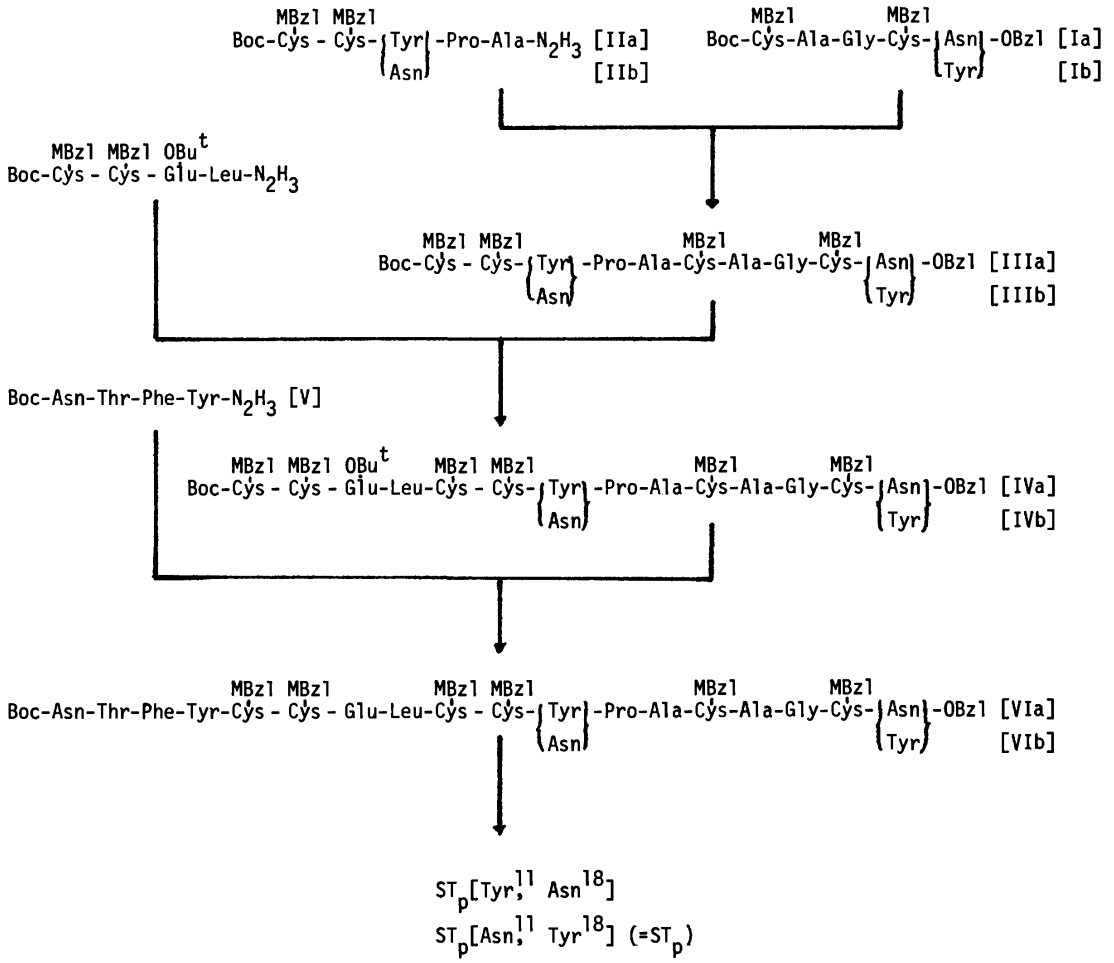

Fig. 2. Scheme for syntheses of $ST_p[Tyr^{11}, Asn^{18}]$ and ST_p.

Figs. 3A and 4A. Materials in the peaks obtained by HPLC were fractionated and subjected to biological assay. Toxic materials were mainly recovered in the peaks shown by bars in Figs. 3A and 4A, respectively, and the materials in these peaks were compared with native ST_p,[10] isolated from ETEC strain 18D,[8] as illustrated in Figs. 3B and 3C, and 4B and 4C, respec-

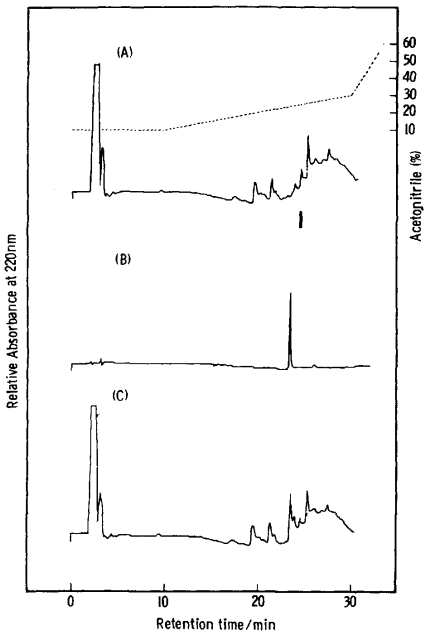

Fig. 3. HPLC profiles on a LiChrosorb RP-8 column (5 μm, 4×250 mm) of: (A) HF-treated and air-oxidized solution of **VIa**; (B) purified native ST_p;[10] (C) a mixture of (A) and (B). The toxic activity was found in the peak marked by a bar in (A).

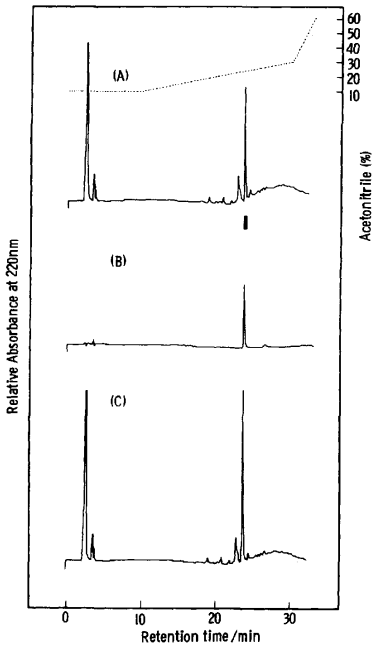

Fig. 4. HPLC profiles on a LiChrosorb RP-8 column (5 μm, 4×250 mm) of: (A) HF-treated and air-oxidized solution of **VIb**; (B) purified native ST_p;[10] (C) a mixture of (A) and (B). The main toxic activity was observed in the peak marked by a bar in (A).

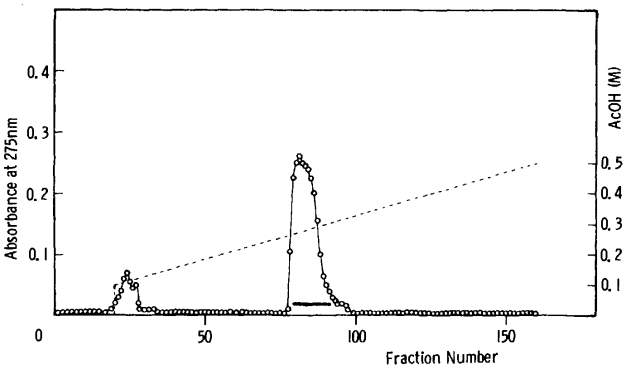

Fig. 5. Chromatography on DEAE-Sephadex A-25 of HF-treated and air-oxidized solution of compound **VIa**. The toxic fraction is shown by a horizontal bar. Column size: 2×33 cm; fractionation size: 10 ml/tube; flow rate: 100 ml/h.

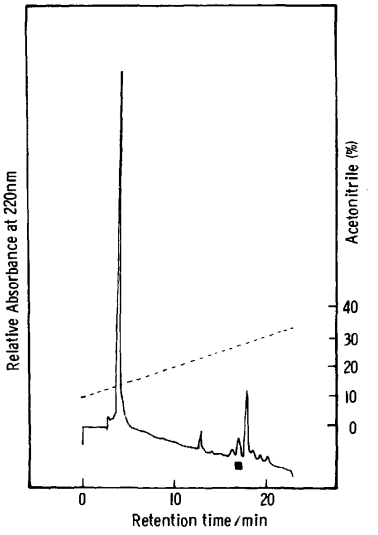

Fig. 6. Semipreparative HPLC of the toxic fraction shown by a horizontal bar in Fig. 5 on a LiChrosorb RP-8 column (5 μm, 8×300 mm). The toxicity was observed in the peak fraction shown by a horizontal bar.

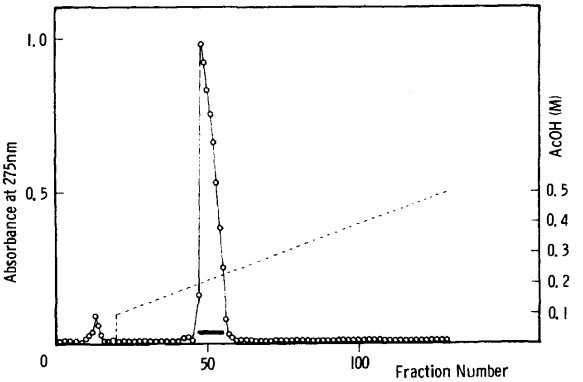

Fig. 7. Chromatography on DEAE-Sephadex A-25 of HF-treated and air-oxidized solution of compound **VIa**. The toxic fraction shown by a horizontal bar was collected. Column size: 1.6×25 cm; fractionation size: 5 ml/tube; flow rate: 35 ml/h.

tively. In Fig. 3A, the toxic fraction was eluted later than native ST_p; the peak fraction eluted at the same retention time as that of native ST_p showed no toxic activity. On the contrary, the toxic peak was eluted with the same retention time as that of native ST_p, in Fig. 4A. Furthermore, the total toxic activity of the air-oxidized solution of compound **VIa** was only one-hundredth of that of compound **VIb**.

The HF-treated and air-oxidized solution of **VIa** was purified on DEAE-Sephadex A-25 and toxic fractions were collected, as shown in Fig. 5. The toxic fractions shown by a horizontal bar were collected and purified further on a semipreparative HPLC column by the reversed-phase mode, as illustrated in Fig. 6. The purity of the separated fraction shown by a bar was also confirmed by analytial HPLC, as shown in Fig. 9A. The toxic peptide $ST_p[Tyr^{11}, Asn^{18}]$ was obtained in about 1—2% yield from compound **VIa**.

The HF-treated and air-oxidized solution of compound **VIb** was also purified on DEAE-Sephadex A-25, as illustrated in Fig. 7. The toxic fractions shown by a horizontal bar were combined, lyophilized and purified further on a semipreparative column of reversed-phase HPLC, as shown in Fig. 8. The purity of the toxic fraction was examined by analytical HPLC, as illustrated in Fig. 9B. The yield of purified synthetic peptide ST_p was about 13%, based on the amount of compound **VIb**. As illustrated in Fig. 9C, definite differences were observed between the retention times of the two synthetic peptides $ST_p[Tyr^{11}, Asn^{18}]$ and ST_p on a reversed-phase column of HPLC. The amino acid compositions of purified synthetic $ST_p[Tyr^{11}, Asn^{18}]$ and ST_p are summarized in Table 1.

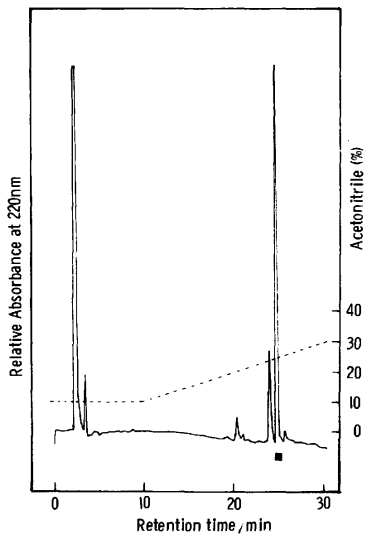

Fig. 8. HPLC profile on a LiChrosorb RP-8 (5 μm, 8×300 mm) of the fraction shown by a horizontal bar. The toxicity was observed in the peak fraction shown by a horizontal bar.

Table 1. Amino acid compositions of synthetic $ST_p[Tyr^{11}, Asn^{18}]$ and $ST_p[Asn^{11}, Tyr^{18}]$[a)]

	Synthetic		Native
	$ST_p[Tyr^{11}, Asn^{18}]$	$ST_p[Asn^{11}, Tyr^{18}]$	ST_p[b)]
Asp	2.00	2.04	2.01 (2)
Thr	1.00	0.90	0.99 (1)
Glu	1.11	0.98	1.16 (1)
Pro	1.07	1.01	1.27 (1)
Gly	0.99	1.01	1.16 (1)
Ala	2.00	2.00	2.00 (2)
1/2·Cys	5.25	3.08	4.92 (6)
Leu	0.96	0.96	1.13 (1)
Tyr	1.86	1.87	1.92 (2)
Phe	0.98	0.90	0.99 (1)

a) Values are expressed as molar ratios to alanine.
b) Data cited from Ref. 10.

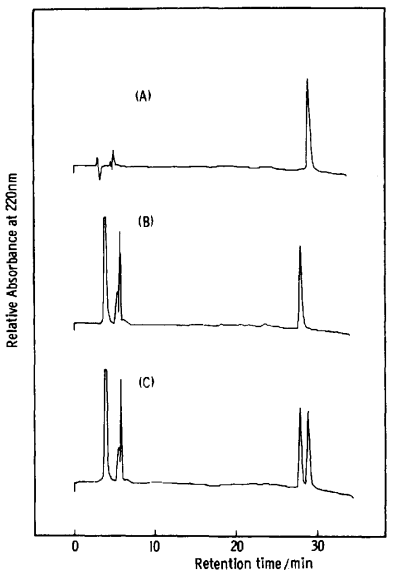

Fig. 9. HPLC profiles of two synthetic preparations on LiChrosorb RP-8 (5 μm, 8×300 mm); (A) Purified synthetic $ST_p[Tyr^{11}, Asn^{18}]$; (B) purified synthetic ST_p; (C) a mixture of (A) and (B).

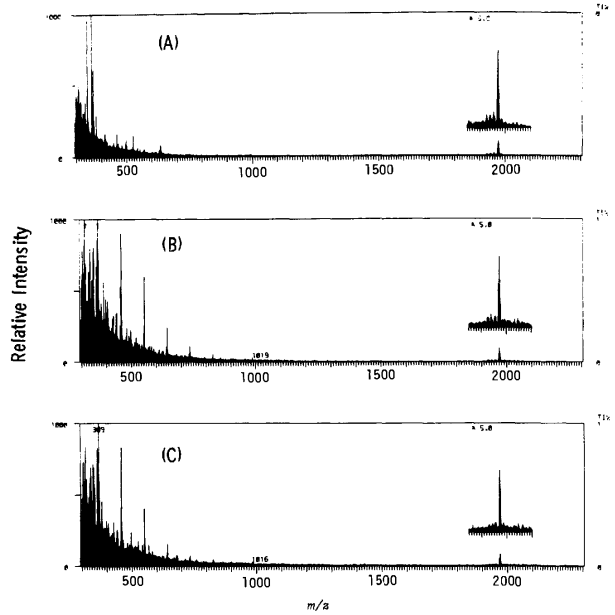

Fig. 10. Positive FAB mass spectra of A) synthetic $ST_p[Tyr^{11}, Asn^{18}]$; B) synthetic ST_p; and C) purified native ST_p.

Physicochemical Properties of Synthetic Peptides $STp[Tyr^{11}, Asn^{18}]$ and STp. *i) Mass Spectra*: Purified synthetic peptides $STp[Tyr^{11}, Asn^{18}]$ and STp were subjected to mass measurement by FAB mass spectrometry[20] and the mass spectra were compared with that of native toxin as shown in Fig. 10. Like native STp, both $STp[Tyr^{11}, Asn^{18}]$ and STp gave strong signals at $m/z=1971$ (m/z means the ratio of the mass number of an ion m to the number of charges of ion z). The results indicate that the two synthetic $STp[Tyr^{11}, Asn^{18}]$ and STp both have the same molecular weight (M_r: 1970) as native STp and are intramolecularly linked by three disulfide bonds, although the positions of the disulfide linkages were not determined.

ii) Proton NMR Spectra: To determine whether either of the synthetic peptides had the same steric features as the native toxin, we compared the ^{1}H-NMR spectra of the two synthetic preparations ($STp[Tyr^{11}, Asn^{18}]$ and STp) with that of the native toxin. As illustrated in Fig. 11, proton chemical shifts of synthetic STp were superimposable on those of the native toxin, but the spectrum of synthetic $STp[Tyr^{11}, Asn^{18}]$ was different from that of the native toxin. The results strongly indicate that synthetic STp has the same three dimensional structure, including three disulfide linkages, as native toxin.

Comparison of Heat-stabilities by High-performance Liquid Chromatography (HPLC). Recently we reported a method for testing the heat-stability of ST by HPLC.[18] We found that synthetic STh had the same heat-stability as native STh and the peak heights on HPLC of synthetic and native STh were greatly decreased, although not abolished completely, by heating the compounds at 100°C for 30 min. Using this procedure, we compared the heat-stabilities of synthetic $STp[Tyr^{11}, Asn^{18}]$ and STp with that of native STp. Figure 12 shows HPLC profiles of synthetic and native peptides heated at 100°C for various periods. Both synthetic peptides showed similar heat-stability to that of native toxin, although synthetic $STp[Tyr^{11}, Asn^{18}]$ had lower toxic activity than native STp and its toxicity could not be neutralized by antiserum raised against native STp, as described below.

Biological Activities of Synthetic Peptides. Synthetic peptides $STp[Tyr^{11}, Asn^{18}]$ and STp were examined by the fluid accumulation test in suckling mice.[16] The minimum effective dose of synthetic peptide $STp[Tyr^{11}, Asn^{18}]$ was 50—80 ng, which was about 30 times that of native STp. On the other hand, the minimum effective dose of synthetic peptide STp was 1.5—2 ng, which was almost the same as that of native STp.

The immunological properties of synthetic peptides $STp[Tyr^{11}, Asn^{18}]$ and STp were tested by measuring neutralization of their ST activities with antisera against purified native STh[21] and STp.[22] The toxic activity of synthetic $STp[Tyr^{11}, Asn^{18}]$ was not neutralized by either of these antisera, but those of native STp and synthetic STp were both neutralized by these antisera.

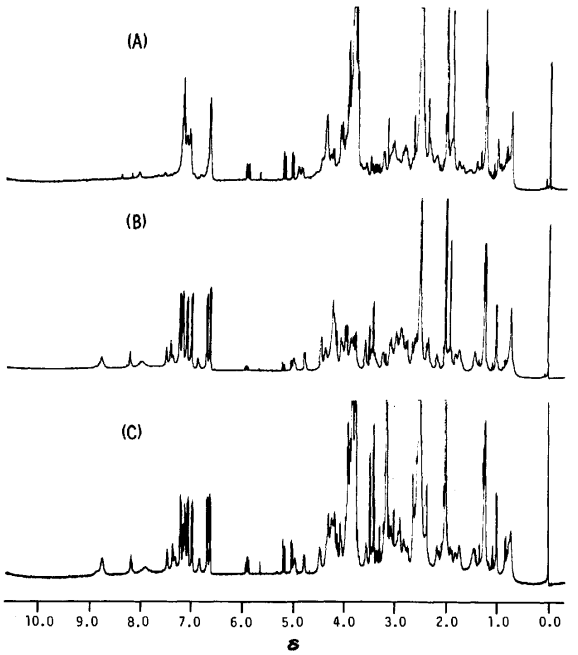

Fig. 11. 500 MHz ^{1}H-NMR spectra of (A) synthetic $STp[Tyr^{11}, Asn^{18}]$, (B) synthetic STp, (C) native STp, measured under the conditions described in the text.

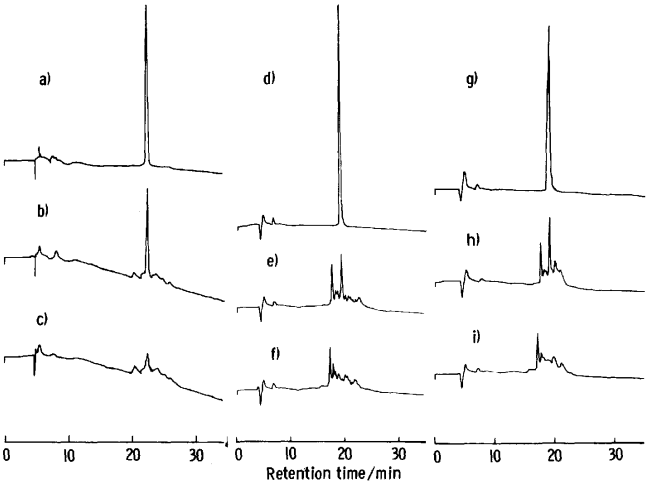

Fig. 12. Comparison of heat-stabilities of synthetic and native ST: (first column) synthetic $STp[Tyr^{11}, Asn^{18}]$ a) untreated, b) after 10 min at 100°C, c) after 30 min at 100°C; (second column) synthetic STp d) untreated, e) after 10 min at 100°C, f) after 30 min at 100°C; (third column) native STp g) untreated, h) after 10 min at 100°C, i) after 30 min at 100°C.

TABLE 2. SUMMARY OF BIOLOGICAL PROPERTIES OF SYNTHETIC PEPTIDES $STp[Tyr^{11}, Asn^{18}]$ AND STp

	MED[a]	Neutralization of ST Activity	
	ng	*anti*-STh Antiserum[b]	*anti*-STp Antiserum[c]
Native STp	2.5	+	+
Synthetic $STp[Tyr^{11}, Asn^{18}]$	50—80	−	−
Synthetic STp	1.5—2.0	+	+

a) Minimum effective dose. b) Antiserum against native STh raised in rabbits [21] was used. c) Antiserum against native STp raised in rabbits [22] was used.

The results, summarized in Table 2, strongly suggest that ST_p[Tyr^{11}, Asn^{18}] with the amino acid sequence proposed by Chan and Giannella[8] did not have the same biological and immunological activities as those of native ST_p, whereas ST_p with the sequence proposed by us[10] had similar biological and immunological properties indistinguishable from those of native toxin. The biologial and immunological properties of these synthetic peptides will be reported in detail elsewhere.

In this work, two peptides (ST_p[Tyr^{11}, Asn^{18}] and ST_p) with the amino acid sequences proposed in Ref. 8 and 10 for an ST produced by ETEC strain 18D were synthesized. Analyses of these synthetic peptides gave the following interesting results: 1) Synthetic ST_p was indistinguishable from native ST_p in all physicochemical and biological properties examined, 2) Synthetic ST_p[Tyr^{11}, Asn^{18}] differed in properties from native ST_p, although Klipstein *et al.*[24] recently reported that synthetic ST_p[Tyr^{11}, Asn^{18}] had similar properties to those of native ST_p, 3) In spite of its difference from native ST_p, synthetic ST_p[Tyr^{11}, Asn^{18}] had ST activity, although its toxicity was lower than that of native ST_p and could not be neutralized by antiserum against native ST_p. Using the synthetic preparation, it will be possible to examine the structure-activity relationship and the biological and immunological properties of the toxin.

This work was partly supported by a Grant-in-Aid for Scientific Research No. 58122002 from the Ministry of Education, Science and Culture.

References

1) H. W. Smith and C. L Gyles, *J. Med. Microbiol.*, **3**, 387 (1970).
2) C. L. Gyles, *J. Infect. Dis.*, **129**, 277 (1974).
3) R. L. Guerrant, L. L. Brunton, T. C. Schnaitman, L. I. Rebhun, and A. G. Gilman, *Infect. Immun.*, **10**, 320 (1974).
4) M. Field, L. H. Graf, Jr., W. J. Laird, and P. L. Smith, *Proc. Natl. Acad. Sci. U.S.A.*, **75**, 2800 (1978).
5) J. M. Hughes, F. Murad, B. Chang, and R. L. Guerrant, *Nature*, **271**, 755 (1978).
6) P. M. Newsome, M. N. Burgess, and N. A. Mullan, *Infect. Immun.*, **22**, 290 (1978).
7) M. C. Rao, S. A. Orellan, M. Field, D. C. Robertson, and R. A. Giannella, *Infect. Immun.*, **33**, 165 (1981).
8) S.-K. Chan and R. A. Giannella, *J. Biol. Chem.*, **256**, 7744 (1981).
9) M. So and B. J. McCarthy, *Proc. Natl. Acad. Sci. U.S.A.*, **77**, 4011 (1980).
10) T. Takao, T. Hitouji, S. Aimoto, Y. Shimonishi, S. Hara, T. Takeda, Y. Takeda, and T Miwatani, *FEBS Lett.*, **152**, 1 (1983).
11) C. Lazure, N. G. Seidah, M. Chretien, R. Lallier, and S. St-Pierre, *Can. J. Biochem. Cell Biol.*, **61**, 287 (1983).
12) S.-S. Wang, B. F. Gisin, D. P. Winter, R. Makofske, I. D. Kulesha, C. Tzougraki, and J. Meienhofer, *J. Org. Chem.*, **42**, 1286 (1977).
13) H. Ikemura, unpublished.
14) E. Schroeder, *Ann. Chem.*, **679**, 207 (1964).
15) S. Sakakibara, Y. Shimonishi, Y. Kishida, M. Okada, and H. Sugihara, *Bull. Chem. Soc. Jpn.*, **40**, 2164 (1967).
16) Y. Takeda, T. Takeda, T. Yano, K. Yamamoto, and T. Miwatani, *Infect. Immun.*, **25**, 978 (1979).
17) S. Aimoto, T. Takao, Y. Shimonishi, S. Hara, T. Takeda, Y. Takeda, and T. Miwatani, *Eur. J. Biochem.*, **129**, 257 (1982).
18) H. Ikemura, S. Yoshimura, S. Aimoto, Y. Shimonishi, T. Takeda, Y. Takeda, and T. Miwatani, *Chem. Lett.*, **1983**, 101.
19) J. Honzl and J. Rudinger, *Collect. Czech. Chem. Commun.*, **26**, 2333 (1961).
20) M. Barber, R. S. Bordori, R. D. Sedgwick, and A. N. Tyler, *J. Chem. Soc., Chem. Commun.*, **1981**, 325.
21) K. Okamoto, A. Miyama, T. Takeda, Y. Takeda, and T. Miwatani, *FEMS Microbiol. Lett.*, **16**, 85 (1983).
22) T. Takeda, Y. Takeda, S. Aimoto, T. Takao, H. Ikemura, Y. Shimonishi, and T. Miwatani, submitted to *FEMS Microbiol. Lett.*, (1983).
23) S. Aimoto, H. Watanabe, H. Ikemura, Y. Shimonishi, T. Takeda, Y. Takeda, and T. Miwatani, *Biochem. Biophys. Res. Commun.*, **112**, 320 (1983).
24) F. A. Klipstein, R. F. Engert, and R. A. Houghten, *Infect. Immun.*, **39**, 117 (1983).

Intra- and Intermolecular [3⁺+2] Cycloadditions of Aldehyde or Ketohydrazones[1)]

Tomio SHIMIZU,* Yoshiyuki HAYASHI, Mineo NAKANO, and Kazuhiro TERAMURA
Department of Color Chemistry and Technology, Faculty of Industrial Arts, Kyoto Technical University, Matsugasaki, Sakyo-ku, Kyoto 606
(Received August 1, 1983)

The reaction of several 2-(alkenyloxy)benzaldehydes (or 1-naphthaldehydes) (**1**) with arylhydrazine hydrochlorides leads to intramolecular [3⁺+2] cycloadducts, 3-substituted 2-aryl-1,2,3,3a,4,9b(or 1,2,3,3a,4,11c)hexahydro[1]benzopyrano (or naphtho[1′,2′:5,6]pyrano)[4,3-*c*]pyrazole hydrochlorides (**4**), in good yields. Free bases (**5**) were obtained in high yields after the treatment of **4** with triethylamine. The thermal treatment of **5** at 150 °C gave 3-substituted 2-aryl-2,3,3a,4-tetrahydro[1]benzopyrano (or naphtho[1′,2′:5,6]pyrano)[4,3-*c*]pyrazoles. The reaction of **1** with methylhydrazine sulfate gave the corresponding 2-methyl derivatives. Analogous intramolecular [3⁺+2] cycloadducts were obtained from the reaction of 2′-(alkenyloxy)acetophenones with arylhydrazine hydrochlorides. Intermolecular [3⁺+2] cycloadducts were also obtained from a reaction mixture of 1-naphthaldehyde, arylhydrazine hydrochlorides, and styrene.

Many heterocyclic compounds containing nitrogen atoms show a broad range of phermacological activities and industrially useful chemical properties. Several studies aimed at the synthesis of biologically important [1]benzopyrano[4,3-*c*]pyrazoles have been done by a number of investigators.[2-4)] In a series of investigations of the intramolecular 1,3-dipolar cycloaddition reactions of 2-(alkenyloxy)benzaldehyde arylhydrazones,[5)] we ourselves have prepared several [1]benzopyranopyrazoles in relatively good yields, but some desirable cycloadducts could not be brought about because of the weak reactivity of some substrates. (see Routes a and b in Scheme 1)

The acid-catalyzed [3⁺+2] 1,3-dipolar cycloaddition of hydrazones with olefins reported recently by Hamelin *et al.*[6)] is a fruitful alternative for the prepatation of the cycloadducts *via* an interesting type of dipole bearing a cationic center. However, their method, using an excess amount of sulfuric acid as a catalyst, is unsuitable for substrates bearing substituents which are labile in a strong acid. In the course of the application of their method to the synthesis of benzopyranopyrazoles, we have found that hydrochloride or sulfate of aryl(or alkyl)hydrazines itself acts as an acid-catalyst and that cycloadducts were obtained very easily from the reaction in good yields. (Route c in Scheme 1)

Results and Discussion

The reaction of 2-(alkenyloxy)benzaldehydes(or 1-naphthaldehydes) (**1**) with an equimolar amount of arylhydrazine hydrochlorides was carried out in ethanol for several hours at room temperature. 3-Substituted 2-aryl-1,2,3,3a,4,9b (or 1,2,3,3a,4,11c)hexahydro[1]benzopyrano(or naphtho[1′,2′:5,6]pyrano)[4,3-*c*]pyrazole hydrochlorides (**4**) were obtained from the reaction mixture in the yields shown in Table 1. The structure of **4** was established on the basis of elemental analyses and spectral data; the IR spectra show an NH-streching vibration of quarternary ammonium salts around 2500 cm^{-1} and no carbonyl-streching vibration of the formyl group observed at **1**. The NMR spectra show saturated methine and methylene protons at δ 3.0—5.0 and no alkenyl protons. The assignment of the structure was further supported by the transformation to known compounds, 3-substituted 2-aryl-2,3,3a,4-tetrahydro[1]benzopyrano(or 1-naphtho[1′,2′:5,6]-pyrano)[4,3-*c*]pyrazoles (**6**).[5c,d)] The treatment of **4** with triethylamine in chloroform at room temperature afforded the free bases (**5**) and/or further dehydrogenated compounds (**6**). Refluxing a xylene solution of pyrazolidines (**5**) at 150 °C for several hours resulted in pyrazolines (**6**) and/or further dehy-

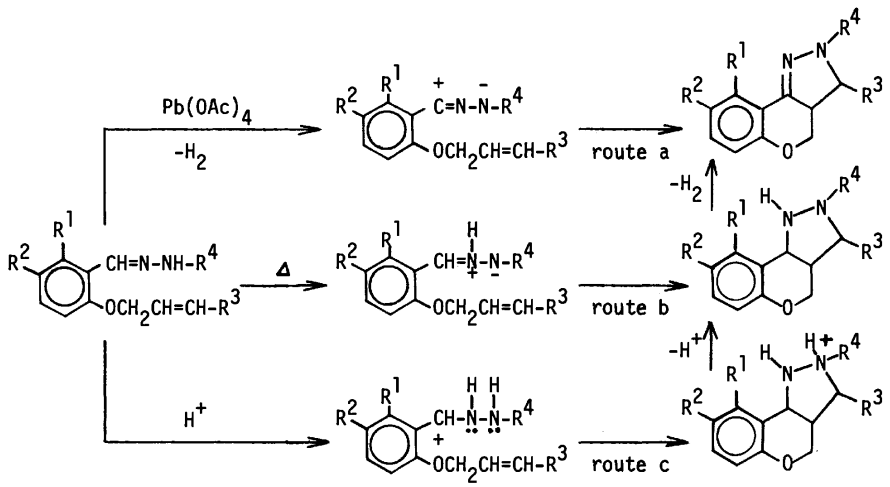

Scheme 1.

TABLE 1. YIELDS, MELTING POINTS, AND SPECTRAL DATA OF 4

	R^1 R^2	R^3	R^4	Yield %	Mp θ_m/°C	IR($\tilde{\nu}$/cm^{-1})	NMR (δ) in DMSO-d_6
4a	-(CH)$_4$-	CO_2Et	CH_3	82	168—188	2450 (N^+H) 1750 (COO)	1.2(t, 3H, J=7 Hz), 2.2(s, 3H), 3.12—3.7 (m, 1H), 4.0—4.73(m, 5H), 5.33(d, 1H, J=7 Hz), 6.6—8.1(m, 9H), 8.53(d, 1H, J=8 Hz)
4c	-(CH)$_4$-	CO_2Et	Cl	55	103—109	2450 (N^+H) 1730 (COO)	1.2(t, 3H, J=7 Hz), 3.2—3.57(m, 1H), 4.0—4.53(m, 5H), 5.12(d, 1H, J=7 Hz), 6.6—7.9(m, 9H), 8.43(d, 1H, J=8 Hz)
4e	-(CH)$_4$-	CN	H	95	120—125	2700 (N^+H) 2230 (CN)	3.0—3.8(m, 1H), 4.0—4.6(m, 2H), 4.85—5.3(m, 2H), 6.8—8.4(m, 10H), 9.2(d, 1H, J=8 Hz)
4f	-(CH)$_4$-	CN	Cl	96	a)	2430 (N^+H) 2230 (CN)	3.0—3.6(m, 1H), 4.15—4.53(m, 2H), 4.9—5.3(m, 2H), 6.85—8.75(m, 9H), 9.27(d, 1H, J=8 Hz)
4g	-(CH)$_4$-	Ph	CH_3	80	a)	2430 (N^+H)	2.2(s, 3H), 2.85—3.3(m, 1H), 4.0—4.5 (m, 2H), 4.8(d, 1H, J=6 Hz), 5.65(d, 1H, J=8 Hz), 6.9—8.0(m, 14H), 8.3(d, 1H, J=8 Hz)
4h	-(CH)$_4$-	Ph	H	81	112—116	2480 (N^+H)	2.7—3.4(m, 1H), 4.0—5.0(m, 3H), 5.6 (d, 1H, J=7 Hz), 6.8—8.1(m, 15H), 8.75 (d, 1H, J=8 Hz)
4i	-(CH)$_4$-	Ph	Cl	64	148—150	2460 (N^+H)	2.7—3.35(m, 1H), 4.0—4.6(m, 2H), 4.8 (d, 1H, J=6 Hz), 5.4(d, 1H, J=8 Hz), 6.7—8.0(m, 14H), 8.23(d, 1H, J=8 Hz)
4j	-(CH)$_4$-	H	CH_3	74	147—150	2550 (N^+H)	2.3(s, 3H), 3.7—5.0(m, 5H), 5.46(d, 1H, J=6 Hz), 7.0—8.0(m, 9H), 8.25(d, 1H, J=8 Hz)
4k	-(CH)$_4$-	H	H	82	133—137	2500 (N^+H)	3.0—3.5(m, 1H), 4.15—4.53(m, 2H), 4.9—5.3(m, 2H), 6.85—8.75(m, 10H), 9.27(d, 1H, J=8 Hz)
4l	-(CH)$_4$-	H	Cl	74	150—155	2550 (N^+H)	2.9—3.5(m, 1H), 3.6—4.6(m, 4H), 5.1 (d, 1H, J=6 Hz), 6.9—8.0(m, 9H), 8.2(d, 1H, J=8 Hz)
4m	-(CH)$_4$-	CH_3	CH_3	85	155—167	2470 (N^+H)	1.55(d, 3H, J=6 Hz), 2.2(s, 3H), 3.46—5.0(m, 5H), 7.0—8.03(m, 9H), 9.2(d, 1H, J=8 Hz)
4n	-(CH)$_4$-	CH_3	H	80	135—139	2460 (N^+H)	1.41(d, 3H, J=6 Hz), 2.7—3.2(m, 1H), 3.46—4.8(m, 3H), 5.56(d, 1H, J=7 Hz), 7.0—8.0(m, 9H), 9.2(d, 1H, J=8 Hz)
4o	-(CH)$_4$-	CH_3	Cl	83	135—140	2460 (N^+H)	1.43(d, 3H, J=6 Hz), 2.7—3.3(m, 1H), 3.85—4.7(m, 3H), 5.53(d, 1H, J=7 Hz), 6.85—8.1(m, 9H), 8.7(d, 1H, J=8 Hz)
4p	H H	CO_2Et	CH_3	77	a)	2460 (N^+H) 1750 (COO)	1.3(t, 3H, J=7 Hz), 2.17(s, 3H), 2.6—3.0(m, 1H), 3.95—4.75(m, 6H), 6.7—7.55(m, 8H)
4q	H H	CO_2Et	H	64	a)	2660 (N^+H) 1720 (COO)	
4s	H H	Ph	CH_3	69	193—195	2550 (N^+H)	2.2(s, 3H), 4.2—5.9(m, 5H), 6.77—7.8 (m, 13H)
4t	H H	Ph	H	56	133—135	2540 (N^+H)	4.1—6.4(m, 5H), 6.7—7.8(m, 14H)
4u	H H	Ph	Cl	91	161—163	2490 (N^+H)	4.1—6.2(m, 5H), 6.7—7.6(m, 13H)
4v	H H	H	CH_3	39	127—130	2550 (N^+H)	2.23(s, 3H), 3.1—5.2(m, 6H), 6.9—8.1 (m, 8H)
4x	H H	H	Cl	37	117—124	2530 (N^+H)	2.9—5.7(m, 5H), 6.7—8.4(m, 8H)

a) The melting-point range was very broad because of the contamination of a small amount of **5** and/or **6**.

drogenated pyrazoles (**7**). (Table 3) The structure of **5** was established on the basis of elemental analyses and spectral data. (Table 2) Some of the **4** and **5** are so hygroscopic or easily oxidized to **5** or **6** that they are difficult to isolate in a pure state; thus, the range of the melting points of those compounds is relatively broad. **4** could also be obtained after the treatment of hydrazones (**2**) with ethanolic hydrogen chloride. The formation of **4** can not be accounted for in terms of the [3+2] 1,3-dipolar cycloaddition reaction after the thermal isomerization of hydrazones (**2**) to azomethine imine tautomers, for such isomerization can not be observed under the thermal conditions up to 100 °C.[5c] In fact, **2** are infinitely stable in refluxing ethanol. From these results, it is most plausible to explain the formation of **4** in terms of a [3⁺+2] 1,3-dipolar

TABLE 2. YIELD, MELTING POINTS, AND SPECTRAL DATA OF 5[a)]

	R^1	R^2	R^3	R^4	Yield[b)] %	Mp[c)] θ_m/°C	IR($\tilde{\nu}$/cm^{-1})	NMR (δ)[d)]
5a	-(CH)$_4$-		CO_2Et	CH_3	80	104—105	3130 (NH)	1.33(t, 3H, J=7 Hz), 2.17(s, 3H), 2.88—3.33(m, 1H), 3.67—4.56(m, 5H),4.66—5.2(m, 1H), 6.54—7.9(m, 9H), 8.43(d, 1H, J=8 Hz)
5d	-(CH)$_4$-		CN	CH_3	72	222—225	3270 (NH) 2250 (CN)	2.48(s, 3H), 2.8—3.5(m, 1H), 3.9—4.95 (m, 4H), 7.15—8.1(m, 9H), 8.38(d, 1H, J=8 Hz)
5e	-(CH)$_4$-		CN	H	31	208—210	3270 (NH) 2250 (CN)	2.9—3.56(m, 1H), 4.1—4.6(m, 2H), 5.12 (d, 1H, J=7 Hz), 5.8(d, 1H, J=13 Hz), 6.7—8.0(m, 10H), 8.33(d, 1H, J=8 Hz)
5f	*-(CH)$_4$-*		*CN*	*Cl*	*85*	*203—205*	*3270 (NH)* 2230 (CN)	*3.0—3.2(m, 1H), 3.8—6.0(m, 4H), 6.95—* 7.95(m, 9H), 8.25(d, 1H, J=8 Hz)
5i	-(CH)$_4$-		Ph	Cl	84	180—182	3170 (NH)	2.5—3.0(m, 1H), 3.6—4.5(m, 3H), 4.85 (dd, 1H, J=6 and 10 Hz), 6.45—7.8(m, 9H), 8.49(d, 1H, J=8 Hz)
5p	H	H	CO_2Et	CH_3	62	130—131	3230 (NH) 1740 (COO)	1.46(t, 3H, J=7 Hz), 2.23(s, 3H), 2.68 (hex, 1H, J=5 Hz), 3.7—4.5(m, 6H), 4.65(dd, 1H, J=5 and 10 Hz), 6.7—7.5 (m, 8H)
5s	H	H	Ph	CH_3	71	188—190	3280 (NH)	2.2(s, 3H), 2.77—4.66(m, 5H), 6.67—7.42(m, 13H)
5t	H	H	Ph	H	70	184—194	3250 (NH)	2.7—3.2(m, 1H), 3.6—5.0(m, 4H), 6.6—7.8(m, 13H), 8.2(d, 1H, J=8 Hz)
5u	H	H	Ph	Cl	60	101—103	3270 (NH)	3.6—4.8(m, 5H), 6.4—8.2(m, 13H)
5v	H	H	H	CH_3	40	116—123	3260 (NH)	2.2(s, 3H), 2.4—4.8(m, 6H), 6.8—7.6 (m, 8H)

a) Satisfactory anlytical data were obtained for these compounds. b) **5d** was obtained in the yield from **1b** without isolation of **4d**; the yields of the other substances were based on **4**. c) Recrystallized from ethanol. d) **5e** was dissolved in DMSO-d_6; the other substances were dissolved in $CDCl_3$.

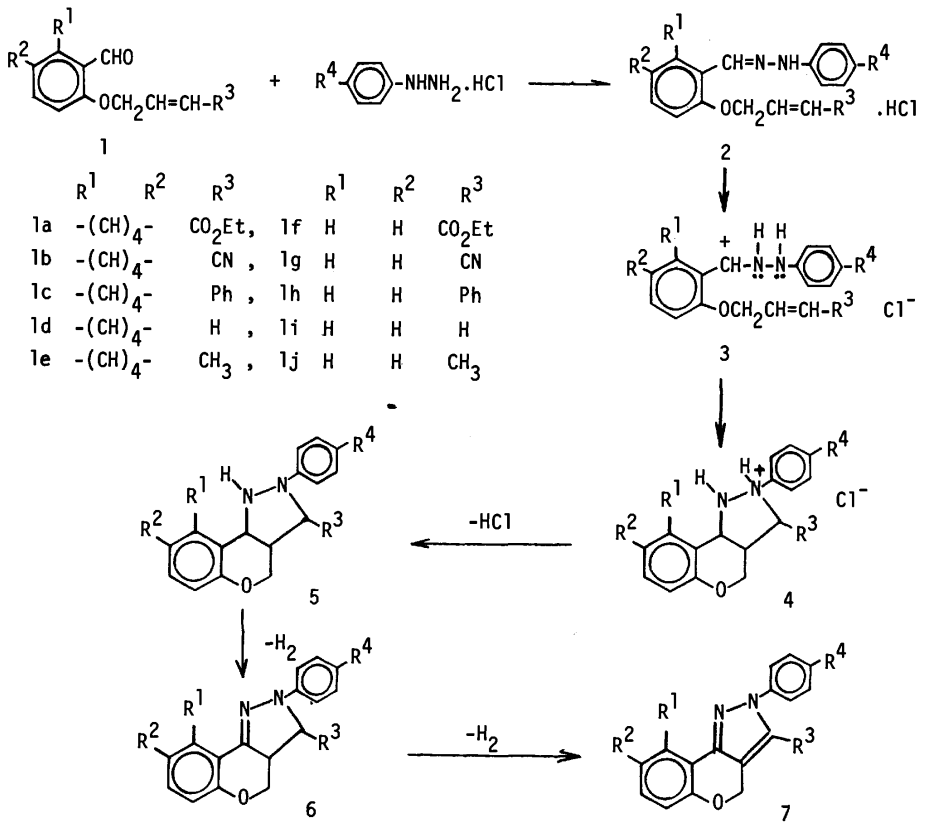

Scheme 2.

Table 3. Yield, melting points, and spectral data of **6** and **7**[a]

	R^1 R^2	R^3	R^4	Yield[b] %	Mp θ_m/°C[c] (lit)	NMR (δ) in $CDCl_3$
6a	-$(CH)_4$-	CO_2Et	CH_3	81	145—147 (148—151)[d]	
6b	-$(CH)_4$-	CO_2Et	H	28	133—136 (134—136)[d]	
6c	-$(CH)_4$-	CO_2Et	Cl	58	166—168 (162—165)[d]	
6g	-$(CH)_4$-	Ph	CH_3	67	206—208 (208—210)[d]	
6h	-$(CH)_4$-	Ph	H	51	199—201 (194—195)[d]	
6i	-$(CH)_4$-	Ph	Cl	74	206—208 (206—208)[d]	
6j	-$(CH)_4$-	H	CH_3	71	103—105	2.43(s, 3H), 3.0—3.3(m, 1H), 3.4—4.9(m, 4H), 6.95—7.9(m, 9H), 9.2(d, 1H, J=8 Hz)
6k	-$(CH)_4$-	H	H	57	72—76	2.84—4.82(m, 5H), 6.66—7.9(m, 10H), 9.35 (d, 1H, J=8 Hz)
6l	-$(CH)_4$-	H	Cl	75	117—119	3.1—4.85(m, 5H), 6.8—7.8(m, 9H), 9.2(d, 1H J=8 Hz)
6m	-$(CH)_4$-	CH_3	CH_3	73	128—129	1.6(d, 3H, J=7 Hz), 2.3(s, 3H), 3.1—4.8(m, 4H), 6.9—7.8(m, 9H), 9.33(d, 1H, J=8 Hz)
6n	-$(CH)_4$-	CH_3	H	50	102—103	1.63(d, 3H, J=7 Hz), 3.2—4.9(m, 4H), 6.8—7.9 (m, 10H), 9.25(d, 1H, J=8 Hz)
6o	-$(CH)_4$-	CH_3	Cl	83	129—131	1.63(d, 3H, J=7 Hz), 3.15—4.8(m, 4H), 6.63—7.9(m, 9H), 9.1(d, 1H, J=8 Hz)
6r	H H	CO_2Et	Cl	8	128—129 (121—122)[e]	
6s	H H	Ph	CH_3	50	143—145 (148—150)[d]	
6t	H H	Ph	H	70	143—146 (146—147)[d]	
6u	H H	Ph	Cl	34	180—183 (180—183)[d]	
6v	H H	H	CH_3	71	127—128	2.25(s, 3H), 2.9—4.4(m, 3H), 4.76(q, 1H, J=7 Hz), 6.73—7.95(m, 8H)
6x	H H	H	Cl	44	105—107	2.93—4.84(m, 5H), 6.74—7.93(m, 8H)
7q	H H	CO_2Et	H	5	129—131 (129—130)[e]	

a) Satisfactory analytical data were obtained for the new compounds. b) **6b, r,** and **7q** were obtained in these yields from **1** without the isolation of any precursors; **6c, j, k, l, m, n, o, t,** and **6x** were obtained in these yields from **4**; the yields of the other substances were based on **5**. c) Recrystallized from ethanol. d) Lit, 5c. e) Lit, 5d.

cycloaddition reaction of the cationic intermediate (**3**) (see Scheme 2). No remarkable substituent effects in these cycloaddition were observed except for the few examples described below. In the cases of $R^1=R^2=H$ and $R^3=CN$, hydrazones (**2**) were the only isolable products, and no cycloadducts were detected. However, the cycloadducts (**4**) could be obtained in good yields after the treatment of the hydrazones (**2**) in ethanol containing 8% hydrogen chloride. While the quantitative formation of hydrazones was also observed in the case of $R^4=NO_2$, these hydrazones were stable even in refluxing ethanol containing 8% hydrogen chloride. This result may be explained in terms of the electronic effect of the nitro group; the same effect was observed in the relatively poor 1,3-dipolar reactivity of *N*-(*p*-nitrophenyl)nitrilimines.[7]

A 1,3-dipolar cycloaddition reaction can generally be explained in terms of the frontier molecular orbital (FMO) theory,[8] but so far the FMO of the cationic dipole **3** has not been calculated accurately. The observed good reactivity toward both the electron-rich and electron-poor alkenes is consistent with the interactions of a relatively low LUMO and a high HOMO in the 1,3-dipole and alkenes, and Sustmann, Type-II behavior.[9] An alternative explanation for the reactivity of **3** may be proposed on the basis of the entropically favoured intramolecular reaction, while previous studies of an intramolecular 1,3-dipolar cycloaddition[5c,d] with analogous compounds showed a substantial rate dependence on substituents.

The method described here can readily be effected with olefins and hydrazones bearing many types of functional groups, thus greatly extending the usefulness of the cycloaddition. Much better yields of **6** were obtained after consecutive treatment with the base and the thermal treatment of the reaction mixture without the isolation of **4** and **5**.

It is now shown that the [3+2] cycloaddition is not restricted to some aldohydrazones but also to a variety of hydrazones, derived from ketones and alkylhydrazines. Some of the results are shown below.

The reaction of a suspension of methylhydrazine sulfate

in ethanol with **1** proceed to completion within a few hours at room temperature. A subsequent work-up of the reaction mixtures gave the expected salts (**10**) and/or free bases (**11**) (Scheme 3). The same procedure in the case of **4** also gave **11**,**12**, and/or **13** (Table 4).

The reaction of 2′-(alkenyloxy)acetophenones(**14**) with arylhydrazine hydrochlorides in ethanol proceeded sluggishly at room temperature, but occurred smoothly at 80°C to give cycloadducts (**17**) in the yields shown in Table 5. The structure of **17** was

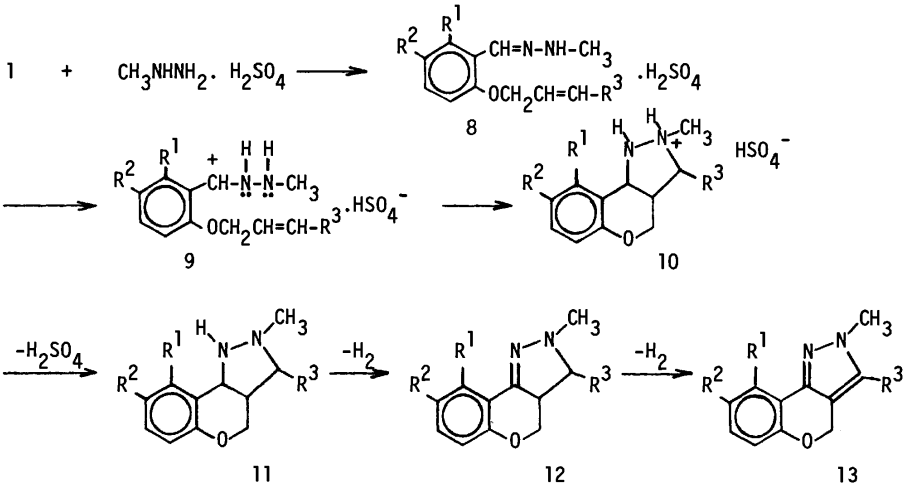

Scheme 3.

TABLE 4. YIELDS, MELTING POINTS, AND SPECTRAL DATA OF **10**—**13**[a]

	R^1 R^2	R^3	Yield[b] %	Mp[c] θ_m/°C	NMR (δ)[d]
10c	-$(CH)_4$-	Ph	66	275—277	2.67(s, 3H), 3.0—5.2(m, 5H), 6.2—8.3(m, 11H)
11g	H H	CN	48	*ca.* 160	2.9(s, 3H), 3.0—5.0(m, 4H), 6.8—8.0(m, 4H)
11b	-$(CH)_4$-	CN	35	167—169	2.8(s, 3H), 3.0—3.2(m, 1H), 3.8—4.8(m, 5H), 7.0—7.8 (m, 5H), 8.3(d, 1H, J=8 Hz)
12c	-$(CH)_4$-	Ph	70	177—178	2.9(s, 3H), 3.65—4.75(m, 4H), 6.85—7.8(m, 10H), 9.4 (d, 1H, J=8 Hz)
12g	H H	CN	22	127—128	3.0(s, 3H), 3.36—4.15(m, 3H), 4.66—4.85(m, 1H), 6.7—8.0(m, 4H)
13a	-$(CH)_4$-	CO_2Et	24	179—180	1.33(t, 3H, J=7 Hz), 4.2(q, 2H, J=7 Hz), 5.26(s, 2H), 7.0—7.8(m, 5H), 10.27(d, 1H, J=8 Hz)

a) Satisfactory analytical data were obtained for these compounds. b) **12c** was obtained in this yield from **10c**; **12g** was obtained in this yield from **11g**; the yields of the other substances were based on **1**. c) Rectystallized from ethanol. d) **10c** was dissolved in DMSO-d_6; the other substances were dissolved in $CDCl_3$.

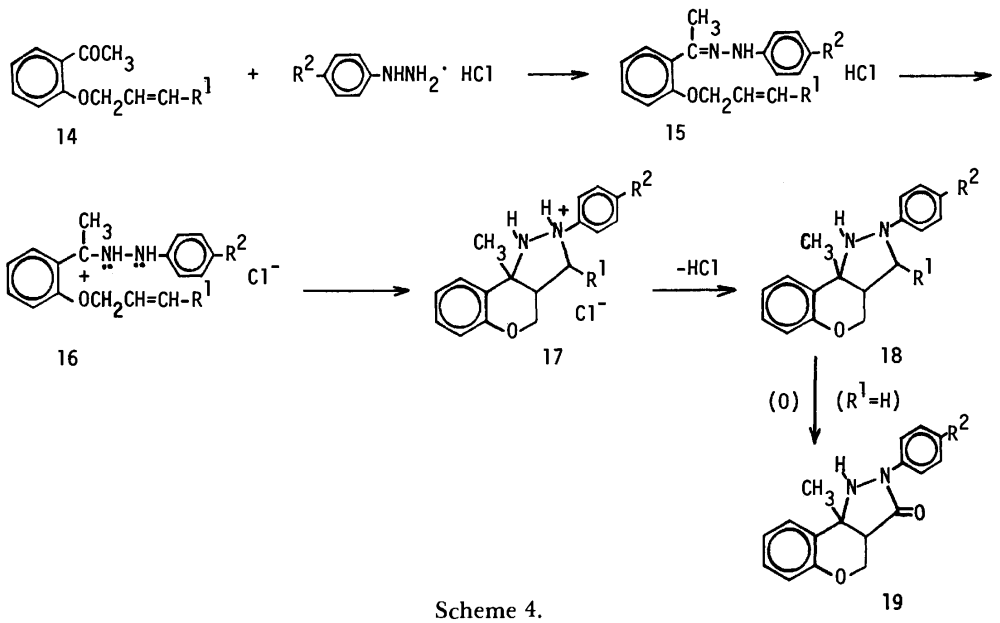

Scheme 4.

Table 5. Yields, melting points, and spectral data of **17**, **18**, and **19**[a]

	R^1	R^2	Yield %	Mp[b] θ_m/°C	IR($\tilde{\nu}$/cm^{-1})	NMR (δ)[c]
17a	H	CH_3	61	120—130 (decomp)	2400 (N^+H)	1.87(s, 3H), 2.17(s, 3H), 2.7—4.3(m, 5H), 7.1—7.6 (m, 7H), 8.13(dd, 1H, J=2 and 8 Hz)
17b	H	H	62	130—150 (decomp)	2450 (N^+H)	1.9(s, 3H), 2.8—3.8(m, 2H), 3.85—4.5(m, 3H), 6.85—7.6(m, 8H), 8.23(dd, 1H, J=2 and 8 Hz)
17c	H	Cl	42	107—108 (decomp)	2450 (N^+H)	1.83(s, 3H), 2.7—3.5(m, 1H), 3.7—4.4(m, 2H), 4.56 (d, 1H, J=5 Hz), 6.8—7.7(m, 7H), 8.06(dd, 1H, J=2 and 7 Hz)
17d	CH_3	CH_3	31	167—169 (decomp)	2430 (N^+H)	1.43(d, 3H, J=6 Hz), 1.85(s, 3H), 2.17(s, 3H), 3.45—3.93(m, 1H), 4.05—4.63(m, 3H), 6.8—7.6(m, 7H), 8.1 (dd, 1H, J=2 and 7 Hz)
18b	H	H	77	131—132	3170 (NH)	1.33(s, 3H), 2.52(heptet, 1H, J=4 Hz), 3.22(dd, J=4 and 10 Hz), 3.45—4.05(m, 2H), 4.15(dd, 1H, J=12 and 5 Hz), 6.63—7.63(m, 8H), 7.5(dd, 1H, J=7 and 2 Hz)
19a	H	CH_3	25	239—240	3230 (NH) 1680 (CON)	1.66(s, 3H), 2.23(s, 3H), 2.94(t, 1H, J=4 Hz), 4.33—4.85(m, 2H), 6.65—7.85(m, 8H)
19c	H	Cl	37	202—203	3230 (NH) 1690 (CON)	1.66(s, 3H), 2.9(t, 1H, J=3 Hz), 4.23(dd, 1H, J=4 and 12 Hz), 4.53(dd, 1H, J=4 and 12 Hz), 6.7—7.8(m, 8H)

a) Satisfactory analytical data were obtained for these compounds. b) **17a—d** were recystallized from benzene; the other substances were recrystallized from ethanol. c) **17a—d** were dissolved in DMSO-d_6; the other substances were dissolved in $CDCl_3$.

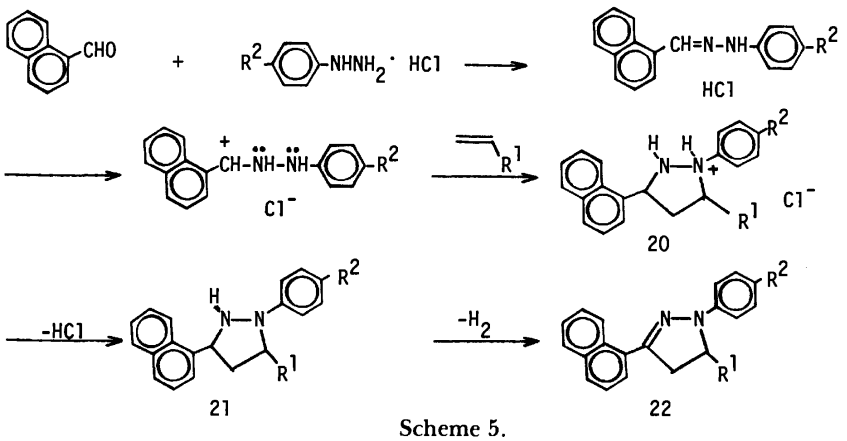

Scheme 5.

Table 6. Yields, melting points, and spectral data of **20** and **22**[a]

	R^1	R^2	Yield %	Mp[b] θ_m/°C	NMR (δ)[c]
20a	Ph	CH_3	53	177—178	2.23(s, 3H), 2.4—2.9(m, 1H), 3.0—3.7(m, 1H), 4.9—5.4(m, 1H), 5.7—6.2(m, 1H), 6.9—8.2(m, 15H), 8.3—8.6(m, 1H)
20c	Ph	Cl	64	134—138	2.8—3.4(m, 2H), 3.7—4.3(m, 1H), 4.8—5.6(m, 2H), 6.4—8.4 (m, 15H), 8.1—8.4(m, 1H)
20d	CO_2Et	Cl	64	d)	1.15(t, 3H, J=7 Hz), 3.2—4.3(m, 7H), 5.75(d, 1H, J=6 Hz), 7.3—8.2(m, 10H), 9.5—9.8(m, 1H)
22a	Ph	CH_3	87	172—173	2.36(s, 3H), 2.7—4.2(m, 2H), 4.75(dd, 1H, J=7 and 10 Hz), 6.9—7.9(m, 15H), 8.3—8.6(m, 1H)
22b	Ph	H	80	167—168	2.9—4.2(m, 2H), 5.05(dd, 1H, J=7 and 12 Hz), 6.7—8.0(m, 16H), 9.4—9.7(m, 1H)
22c	Ph	Cl	100	155—157	2.1—4.3(m, 2H), 4.56(dd, 1H, J=7 and 10 Hz), 6.8—7.9(m, 15H), 8.2—8.3(m, 1H)
22d	CO_2Et	Cl	50	d)	1.2(t, 3H, J=7 Hz), 3.5—5.8(m, 5H), 6.9—8.0(m, 10H), 8.9—9.3 (m, 1H)

a) Satisfactory analytical data were obtained for **20a, c, 22a, b,** and **22c**. b) The compounds **20** were recystallized from benzene; the compounds **22** were recrystallized from ethanol. c) **20a, c,** and **20d** were dissolved in DMSO-d_6; the other compounds were dissolved in $CDCl_3$. d) The melting points of **20d** and **22d** were very broad because a contamination of alcohol, which could not be removed completely by recrystallization from other solvents or by drying under reduced pressure at 80 °C.

assigned on the basis of the results of elemental analyses and the spectral data. Although some of the **17** gave crystalline free bases (**18**) upon treatment of triethylamine, some of the oily free bases (**18**) gave air-oxidation products (**19**) after the reaction mixture had been allowed to stand at room temperature for several days. The structure of **19** was assigned on the basis of the results of elemental analyses and the spectral data (see Table 5). The methylene at the 3-position of **18** is labile to air-oxidation. Thus, **18a**—**c** gave the 3-oxo products, while **18d** (with methyl substituted for one hydrogen) was stable for the oxidation under the same conditions.

While an intermolecular [3^++2] cycloaddition proceeds well in the presence of an excess of sulfuric acid,[6] our procedure under much milder conditions also gave the intermolecular cycloadducts (**20**) in higher yields (see Scheme 5 and Table 6). 1-Aryl-3-(1-naphthyl)-5-phenyl-2-pyrazolines (**22**) were obtained after the treatment of **20** with triethylamine. The intermediate, 1-aryl-3-(1-naphthyl)-5-phenylpyrazolidines (**21**), would be unstable and oxidized to **22** under the reaction conditions. The assignment of the structure was supported by a comparison of the physical properties of **22** with those of authentic specimens prepared according to the previously published procedures.[10] The cycloaddition with such dipolarophiles as acrylonitrile, methyl methacrylate, dimethyl maleate, dimethyl fumarate, *N*-phenylmaleimide, norbornene, dimethyl acethylenedicarboxylate, and phenylacetylene afforded cycloadducts in poor yields. The cycloadducts (**20**) were also obtained in good yields after the treatment of 1-naphthaldehyde arylhydrazones with olefins in ethanol containing 8% hydrogen chloride at room temperature.

Experimental

All the melting points are uncorrected. The IR spectra were recorded on a Hitachi 215 Infrared Spectrophotometer. The NMR spectra were measured on a Varian T-60A instrument, using suitable solvents and TMS as an internal standard.

Materials. The 2-(alkenyloxy)benzaldehydes(or 1-naphthaldehydes) (**1**) and their arylhydrazones were prepared according to the method previously reported.[5] The arylhydrazine hydrochlorides and methylhydrazine sulfate were commercially available (Nakarai Chem. Co.) and were used without further purification. The 2′-(alkenyloxy)-acetophenones (**14**) were prepared by the reaction of 2′-hydroxyacetophenone and ω-bromoalkenes in acetone in the presence of an equimolar amount of anhydrous potassium carbonate at 60°C for 20h. The 2′-allyloxyacetophenone (**14a**) was obtained in an 83% yield; bp 125—126°C (7mmHg), IR (neat): 1670cm^{-1} (C=O) and NMR ($CDCl_3$): δ 2.6 (s, 3H), 4.6 (d, 2H, J=5Hz), 5.1—5.6 (m, 2H), 5.75—6.4 (m, 1H), and 6.75—7.85 (m, 4H). The 2′-(2-butenyloxy)acetophenone(**14b**) was obtained in an 81% yield; bp 136—138°C (7mmHg), IR (neat): 1670cm^{-1} and NMR ($CDCl_3$) δ 1.7 (d, 3H, J=5Hz), 2.6 (s, 3H), 4.5 (d, 2H, J=4Hz), 5.6—5.95 (m, 2H), and 6.75—7.85 (m, 4H).

Reaction of 1 with Arylhydrazine Hydrochlorides. General Procedure: An equimolar mixture (5 mmol) of **1** and arylhydrazine hydrochlorides was stirred in ethanol (50ml) for several hours at room temperature. The crystals of arylhydrazine hydrochlorides are only slightly soluble in the solvent at this temperature, but the mixture became homogenous after 1 h, and then a crystalline precipitate of 3-substituted 2-aryl-1,2,3,3a,4,9b(or 1,2,3,3a,4,11c)hexahydro[1]-benzopyrano(or naphtho[1′,2′:5,6]pyrano)[4,3-*c*]pyrazole hydrochlorides (**4**) appeared within additional few hours. The evaporation of the solvent gave another corp of **4** or an oily residue. Scratching a benzene solution of the oily residue gave **4**. The yields, melting points, and spectral data are shown in Table 1. Almost all the **4** which could be recrystallized from ethanol gave correct elemental analyses. A solution of **1** and arylhydrazine hydrochlorides in warm ethanol (50—60°C) gave results similar to those described above.

The Treatment of 2-(Alkenyloxy)benzaldehyde(or 1-naphthaldehyde) Arylhydrazones in Ethanol Containing 8% HCl. 2-(Alkenyloxy)benzaldehyde (or 1-naphthaldehyde) arylhydrazones (**2**)[5c,d] was added to an ethanol containing 8% HCl at room temperature and the mixture was stirred for an additional hour after the complete dissolution of **2**. The subsequent evaporation of the solvent and the hydrogen chloride at 70°C in a rotary evaporator gave an oily residue. The residue was recrystallized from benzene to afford **4** in 90—100% yields.

The Treatment of 4 with Triethylamine. Into a suspension of **4** in chloroform we added an excess mol of triethylamine, after which the mixture was stirred for 30min. The reaction mixture was then washed with water several times, and the organic layer was dried over anhydrous sodium sulfate. The subsequent evaporation of the solvent yielded 3-substituted 2-aryl-1,2,3,3a,4,9b(or 1,2,3,3a,4,11c) hexahydro[1]benzopyrano(or naphtho[1′,2′,:5,6]pyrano)[4,3-*c*]pyrazoles (**5**) in the yields shown in Table 2.

Preparation of 3-Substituted 2-Aryl-2,3,3a,4-tetrahydro(or -2,4-dihydro)[1]benzopyrano(or naphtho[1′,2′:5,6]pyrano)[4,3-c] pyrazoles (6 and/or 7). A xylene solution (50ml) of **5** (1mmol) was refluxed for 4h. After the evaporation of the solvent, the residue was mixed with a small amount of ehtanol (10ml) and allowed to stand for several hours, and the precipitate (**6**) that thus formed was filtered off. The filtrate was chromatographed (silica gel) with chloroform to give another crop of **6** and/or **7**.

The Reaction of 1 with Methylhydrazine Sulfate. Into a suspension of methylhydrazine sulfate (10mmol) in ethanol (50ml) we added **1** (10mmol), after which the mixture was stirred at room temperature. After the complete dissolution of the methylhydrazine sulfate, the mixture was stirred for an additional 4 h. The subsequent work-up of the reaction mixture gave 3-substituted 2-methyl-1,2,3,3a,4,9b (or 1,2,3,3a,4,11c)hexahydro[1]benzopyrano(or naphtho[1′2′:5,6]-pyrano)[4,3-*c*]pyrazole sulfates (**10**) in a rather impure crystalline or oily state because of the contamination of a small amount of **11** and/or **12**. Free bases (**11**) and dehydrogenated products (**12** and **13**) were prepared following procedures similar to those described in the cases of **4**→**7**.

The Reaction of 14 with Arylhydrazine Hydrochlorides. A mixture of **14** (10mmol) and arylhydrazine hydrochloride (10mmol) in ethanol (70ml) was refluxed for 20h. After the evaporation of the solvent, benzene was added (30ml) to the residue; crystalline **17** was then precipitated immediately from the benzene solution. Recrystallization from benzene gave pure **17**. 2′-(3-Phenyl-2-propenyloxy)acetophenone arylhydrazones were the only isolable products from the reaction of 2′-(3-phenyl-2-propenyloxy)acetophenone (**14c**) with arylhydrazine hydrochlorides; no cycloadducts were detected.

The Treatment of 17 with Triethylamine. To a solution of **17b** (1.8g) in chloroform (70ml) we added triethylamine (1ml), after which the mixture was stirred for 30 min at room temperature. The reaction mixture was then washed with water several times, and the organic layer was dried over

anhydrous sodium sulfate. The subsequent evaporation of the solvent yielded crystals of 9b-methyl-2-phenyl-1,2,3,3a,4,9b-hexahydro[1]benzopyrano[4,3-*c*]pyrazole (**18b**) in a 77% yield (1.22 g). Recrystallization from ethanol gave pure **18b**. On the other hand, an oily mass was obtained after the similar treatment of **17a** (or **17c**) with triethylamine. The exposure of the ethanol solution of the oily mass to the atmosphere for several days yielded white crystals of 2-aryl-9b-methyl-1,2,3,3a,4,9b-hexahydro[1]benzopyrano[4,3-*c*]pyrazol-3-ones (**19a** or **19c**) in the yields shown in Table 5.

The Reaction of 1-Naphthaldehyde with Arylhydrazine Hydrochlorides in the Presence of Dipolarophiles. An ethanol solution (80 ml) of an equimolar (10 mmol) mixture of 1-naphthaldehyde and arylhydrazine hydrochlorides was stirred for 20 h at room temperature in the presence of dipolarophile (4 ml of dipolarophiles which exhibit boiling points less than 150 °C, and an equimolar amount (10 mmol) of other high-boiling dipolarophiles). After the evaporation of the solvent, the residue was mixed with hot benzene (20 ml) and the mixture was cooled to room temperature. The 5-substituted 1-aryl-3-(1-naphtyl)pyrazolidine hydrochlorides (**20**) thus precipitated filtered and were recrystallized from benzene. The yields and melting points are shown in Table 6.

The Reaction of 1-Naphthaldehyde p-*Chlorophenylhydrazone and Styrene in Ethanol Containing 8% HCl.* The reaction of 0.3 g (2 mmol) of 1-naphthaldehyde *p*-chlorophenylhydrazone and 1.0 g (10 mmol) of styrene was carried out in ethanol (30 ml) containing 8% HCl at toom temperature for 20 h. After the evaporation of the solvent and the excess amount of HCl and styrene, the residue was mixed with benzene (10 ml) to give white crystals (0.34 g, 82% yield) which shows the same physical properties as those of **20c**.

References

1) Presented in part at the 46th National Meeting of the Chemical Society of Japan, Niigata, October 1982, Abstr. 725.

2) a) W. Oppolzer, Ger. Offen., 1926023 (1969); *Chem. Abstr.*, **72**, 43671 (1970); b) R. E. Brown and J. Shavel, Jr., U. S. Patent 3624102 (1971); *Chem. Abstr.*, **76**, 59618 (1972); c) M. T. Di Parsia, C. Suarez, M. J. Vitolo, V. E. Marguez, C. Urbina, and I. Hurtado, *J. Med. Chem.*, **24** 117 (1981); d) F. Eiden and I. Breugst, Ger. Offen., 2917575 (1980); *Chem. Abstr.*, **94**, 139801 (1981); e) N. K. Sangwan and S. N. Rastogi, *Indian J. Chem., Sec. B*, **20**, 135 (1981).

3) a) Imperial Industries, Ltd., Neth. Appl., 6511492 (1966); *Chem. Abstr.*, **65**, 2271 (1966); b) T. Kamino and H. Kato, Jpn. Kokai Tokkyo Koho, 79126114 (1979); *Chem. Abstr.*, **92**, 119745 (1980).

4) a) H. Meier, W. Heinzelman, and H. Heimgartner, *Chimica*, **34**, 506 (1980); b) A. Padwa, S. Nahn, and E. Kato, *J. Org. Chem.*, **43**, 1664 (1978); c) G. Schmitt and B. Laude, *Tetrahedron Lett.*, **1978**, 3727; d) F. M. Dean, K. B. Hindley, S. Murray, and W. Taylor, *J. Chem. Soc., Perkin Trans. 1*, **1976**, 2444; e) H. Meier and H. Heimgartner, *Helv. Chim. Acta*, **60**, 3035 (1977); f) W. Oppolzer, *Tetrahedron Lett.*, **1971**, 3091; g) W. Kirmse and H. Dietrich, *Chem. Ber.*, **100**, 2710 (1967).

5) a) T. Shimizu, Y. Hayashi, Y. Nagano, and K. Teramura, *Bull. Chem. Soc. Jpn.*, **53**, 429 (1980); b) T. Shimizu, Y. Hayashi, K. Yamada, T. Nishio, and K. Teramura, *ibid.*, **54**, 217 (1981); c) T. Shimizu, Y. Hayashi, Y. Kitora, and K. Teramura, *ibid.*, **55**, 2450 (1982); d) T. Shimizu, Y. Hayashi, S. Ishikawa, and K. Teramura, *ibid.*, **55**, 2456 (1982).

6) a) G. Le Fevre, S. Sinbandhit, and J. Hamelin, *Tetrahedron*, **35**, 1821 (1979); b) G. Le Fevre and J. Hamelin, *Tetrahedron Lett.*, **1979**, 1757.

7) R. S. Tewari and P. Parihar, *Tetrahedron*, **39**, 129 (1983).

8) a) I. Fleming, "Frontier Orbitals and Organic Chemical Reactons," John Wiley and Sons, New York (1976); b) K. N. Houk, J. Sims, R. E. Duke, Jr., R. W. Stronzier, and J. K. George, *J. Am. Chem. Soc.*, **95**, 7287 (1973); c) K. N. Houk in "Pericyclic Reactions, II," ed by R. E. Lehr and A. P. Marchand, Academic Press, New York (1977).

9) R. Sustmann, *Tetrahedron Lett.*, **1971**, 2717.

10) R. Huisgen, M. Siedel, G. Wallbillich, and H. Knupfer, *Tetrahedron*, **17**, 3(1962).

Structural and Stereochemical Study of Galantinic Acid, a New Amino Acid from Peptide Antibiotic Galantin I

Tateaki WAKAMIYA, Toshihiko ANDO, Tadashi TESHIMA, and Tetsuo SHIBA*
Department of Chemistry, Faculty of Science, Osaka University, Toyonaka, Osaka 560
(Received August 3, 1983)

A new amino acid, galantinic acid, was found as one of the constituent amino acids in a peptide antibiotic galantin I. The structure of galantinic acid was determined to be (2*S*,4*S*,5*S*)-5-amino-2-carboxymethyl-4-hydroxytetrahydropyran on the basis of NMR and CD studies.

A peptide antibiotic galantin I effective against both Gram positive and Gram negative bacteria was isolated from the culture broth of *Bacillus pulvifaciensis* by Shoji and his co-workers.[1] Recently, we succeeded to determine the chemical structure of galantin I as shown in Fig. 1.[2]

From the hydrolyzate of galantin I, two new amino acids named galantinic acid (**1**) and galantinamic acid (**2**), were isolated and their primary structures had been preliminarily reported.[2] In the present paper, we describe the details about the structural determination as well as the assignment of steric configuration of galantinic acid.

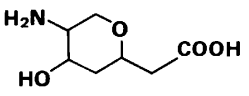

1 galantinic acid

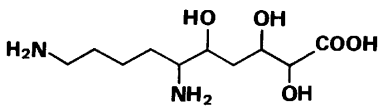

2 galantinamic acid

The isolation of galantinic acid from galantin I hydrolyzate was carried out by the use of ion-exchange chromatography and preparative paper electrophoresis. Galantinic acid was assumed to be a neutral amino acid taking into account the mobility on paper electropherogram and the retention time in amino acid analysis. However, its faster mobility or longer retention time compared with those of Gly or Ala indicated that galantinic acid would not be α-amino acid.

Characterization of galantinic acid was first achieved by NMR analyses. (Table 1) ^{13}C-NMR of this amino acid showed seven carbon signals which are of one carbonyl and six alkane carbons. Four of six alkane carbons were expected to carry heteroatoms such as *N* or *O* being classified into one carbon at higher field (51.8ppm) and three ones at lower field (64.7—73.6ppm). In general, the substitution of oxygen atom causes larger deshielding effect to the chemical shift of carbon atom than that of nitrogen atom. Therefore, we could deduce that amino group is attached on carbon atom at 51.8ppm and other three carbons are presumably bound to oxygen atoms.

^{1}H-NMR of galantinic acid revealed the presence of at least nine protons which are unexchangeable with deuterium. No protons were observed in olefinic or aromatic region. Of these protons, simple doublet centering at 2.39ppm (J=5Hz) was assumed to be methylene protons such as -X-C<u>H$_2$</u>-CH- (X=CO, NR$_2$, SR, *etc*). On the other hand, another seven protons appeared in complex multiplets which were expected from a ring structure. The correlations between carbon and proton signals were determined by the measurement of ^{13}C-NMR using selective decoupling method as summarized in Table 1.

Table 1. Correlations between ^{13}C and ^{1}H signals

δ		Supposed partial structure
^{13}C	Related ^{1}H	
37.6	1.43, 2.14	-C-<u>CH$_2$</u>-C-
41.6	2.39 (2H)	-C-<u>CH$_2$</u>-CO-
51.8	3.10	-C-<u>CH</u>-N-
64.7	3.44	-C-<u>CH$_2$</u>-O-, -C-<u>CH</u>-O- (×2)
67.2	3.82 (2H)	
73.6	4.11	
177.1	—	-C-<u>C</u>OOH

FD-MS spectrum of galantinic acid gave two peaks at m/z 175 and 176 which correspond to M^+ and $(M+H)^+$, respectively. When galantinic acid was *N*-benzoylated, the product gave two peaks at m/z 279 (M^+) and 280 ($(M+H)^+$) in FD-MS spectrum. This result clearly showed the introduction of one residue of benzoyl group indicating that galantinic acid is an aliphatic monoamino monocarboxylic acid.

From considerations of the molecular weight, carbon and proton numbers as well as the number of amino group, we could deduce unequivocally the molecular formula of galantinic acid to be $C_7H_{13}NO_4$. Therefore,

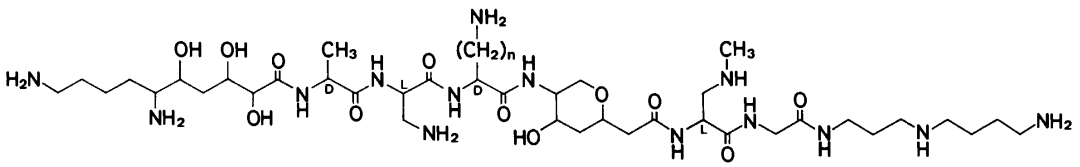

Fig. 1. The structure of galantin I. Galantin I is a mixture of two congeners differing at the fourth amino acid residue from N-terminal. Lysine (n=4) and ornithine (n=3) are found in a ratio of 9:1.

TABLE 2. ASSIGNMENTS OF PROTON SIGNALS AND THEIR SPIN COUPLING CONSTANTS (J/Hz)

δ	Multiplicity	Assignment	Coupled with							
			H_{2a}	H_{3a}	H_{3e}	H_{4a}	H_{5a}	H_{6a}	H_{6e}	H_7, H_7
			3.82	1.43	2.14	3.82	3.10	3.44	4.11	2.39
1.43	dt	H_{3a}	11	—	12	11	—	—	—	—
2.14	ddd	H_{3e}	2 or 5	12	—	5 or 2	—	—	—	—
2.39	d	H_7, H_7	7	—	—	—	—	—	—	—
3.10	dt	H_{5a}	—	—	—	11	—	11	4	—
3.44	t	H_{6a}	—	—	—	—	11	—	11	—
3.82	m	H_{2a} [a]	—	(11)	(2 or 5)	—	—	—	—	(7)
3.82	m	H_{4a} [a]	—	(11)	(5 or 2)	—	(11)	—	—	—
4.11	dd	H_{6e}	—	—	—	—	4	11	—	—

a) The analyses of multiplicity of H_{2a} and H_{4a} were impossible because of their complete overlapping. Therefore, the coupling constants only deducible from those of the related protons are shown in parentheses.

the degree of unsaturation of galantinic acid is two. Namely, one is of carboxylic acid and another one is of cyclic structure. The molecular formula also suggested that galantinic acid would be a hydroxyamino acid. When galantinic acid was oxidized with periodate and permanganate, no positive product to ninhydrin reaction was observed in amino acid analysis and on paper electropherogram. This result proposed the presence of vicinal amino alcohol moiety in galantinic acid.

Based on the facts mentioned above, a structure having tetrahydropyran skeletone was proposed for galantinic acid. The presence of three carbon atoms carrying oxygen atom, the multiplicity of proton signals, and their large coupling constants could be explained from the structure **1**. The assignments of proton signals in ^{1}H-NMR (Fig. 2) were achieved by use of the decoupling method as summarized in Table 2. The position of each proton was exactly determined and the relative configuration of galantinic acid was then estimated by

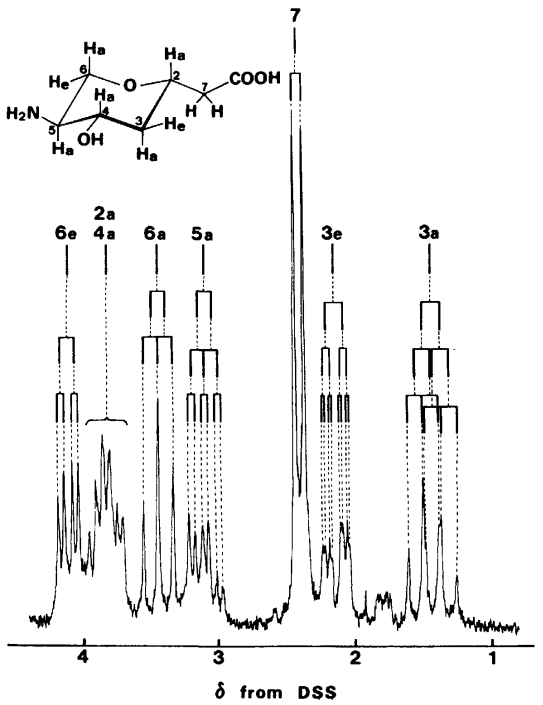

Fig. 2. ^{1}H-NMR of galantinic acid in D_2O (100 MHz).

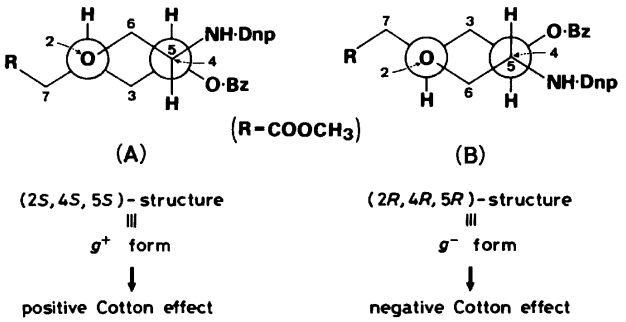

Fig. 3. Plausible stereo structures of galantinic acid and expected sign of Cotton effect of *N*-Dnp-*O*-Bz derivative. Dnp=2,4-dinitrophenyl; Bz=benzoyl.

precise analysis of the coupling constant of each proton. The fact that all the methine protons on C_2, C_4, and C_5 showed at least one large coupling constant over 10 Hz due to 1,2-diaxial protons might be elucidated from the steric structure mentioned in Fig. 2. For the purpose of determination of the absolute configuration of galantinic acid, Dnp-aromatic rule developed by Kawai and his co-workers was effectively applied.[3] The absolute configuration of vicinal amino alcohol part is thus deducible from the sign of CD spectrum of *N*-Dnp and *O*-Bz derivative. According to this rule, the structure **A** (g^+ form) of the two plausible stereo structures (Fig. 3), would show a positive Cotton effect, while the

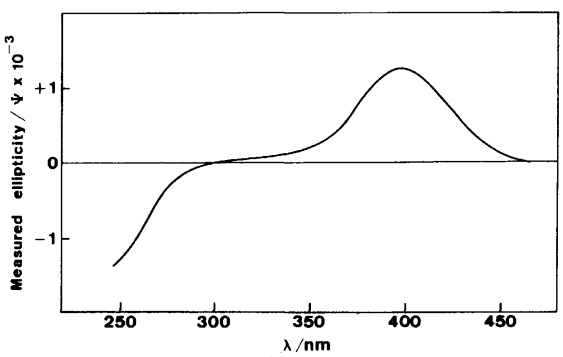

Fig. 4. CD spectrum of *N*-Dnp-*O*-Bz-galantinic acid methyl ester obtained in $CHCl_3$. The Cotton effect around 240 nm was not observed because of the disturbance due to solvent absorption.

structure **B** (g^- form) which corresponds to an enantiomeric form of the structure **A** would be expected to show a negative Cotton effect around 400 nm in CD spectrum.[4] *N*-Dnp-*O*-Bz-galantinic acid methyl ester prepared from the natural sample gave clearly a positive Cotton effect suggesting the g^+ form. (Fig. 4) As a result, the absolute structure of galantinic acid was defined to be (2*S*,4*S*,5*S*)-5-amino-2-carboxymethyl-4-hydroxytetrahydropyran.[5]

Experimental

The NMR spectra were obtained with Varian XL-100-15 and JEOL JNM-FX-90Q spectrometers for ^1H and ^{13}C in D_2O, respectively. Sodium 2,2-dimethyl-2-silapentane-5-sulfonate (DSS) was used as the external standard and the chemical shift were given in δ value (ppm) from the standard. FD and EI mass spectra were measured with a JEOL JMS-O1SG-2 mass spectrometer. CD spectra were recorded with a JASCO ORD/UV-5 spectrometer in $CHCl_3$.

Isolation of Galantinic Acid. Crude galantin I (0.44 g) was hydrolyzed for 5 h at 110 °C with 10 ml of constant boiling 6 M† hydrochloric acid in a sealed tube after deaeration. The hydrolyzate obtained from 1.76 g of galantin I was concentrated *in vacuo* and the residue was applied to Amberlite IRCG-50 column (type I, NH_4^+ form, 1.5×140 cm). The elution was carried out with a gradient method from 0.1% to 1.5% aqueous ammonia. Thus, a mixture of neutral amino acids was obtained in a yield of 0.21 g.

The mixture of neutral amino acids (1.4 g) obtained by the above procedure was dissolved in a small amount of 1 M HCl and 95% ethanol was added to the solution. The precipitate was deposited by centrifugation and the supernatant was concentrated *in vacuo*. A powdery residue obtained was applied to Amberlite IRCG-120 column (type I, pyridine form, 1.8×50 cm) which was eluted with a linear gradient method from 0.125 M to 0.50 M pyridine-acetate buffer (pH 3.5). The fractions containing galantinic acid were pooled and concentrated *in vacuo*. The residue was dissolved in a small amount of 1 M HCl and ethanol was added. The supernatant after centrifugation was concentrated *in vacuo* and the residue was purified by preparative paper electrophoresis (pyridine-acetic acid-water=1:10:89, pH 3.5, 13 V/cm, 2 h, Toyo Roshi No. 50 filter paper). Galantinic acid was extracted from the paper with 0.1 M acetic acid. The extract was lyophilized and the lyophilization was repeated twice after dissolving the residue in a small amount of water. Pure galantinic acid (26 mg) was obtained as hygroscopic powder which showed a single spot on paper electropherogram and TLC (cellulose plate, developing solvent: *n*-BuOH-pyridine-AcOH-H_2O=15:5:8:12, R_f 0.68).

N-Benzoylgalantinic Acid for FD-MS Measurement. To a solution of galantinic acid (1.0 mg, 5.7 μmol) in 0.1 ml of water were added benzoyl chrolide (2.1 mg, 15 μmol) and 4.8% Na_2CO_3 solution (0.05 ml, 22.5 μmol). The reaction mixture was stirred overnight at room temperature and then once extracted with ether to remove exess benzoyl chloride. The aqueous layer was acidified with hydrochloric acid and extracted with ethyl acetate. The extract was washed with water, dried over $MgSO_4$ and then concentrated *in vacuo*. A solution of the residue in 0.1 ml of DMSO was subjected to FD-MS measurement: *m/z* 279 (M^+) and 280 ($(M+H)^+$).

N-(2,4-Dinitrophenyl)-O-benzoylgalantinic Acid Methyl Ester. To a solution of galantinic acid (1.0 mg, 5.7 μmol) in 50 μl of H_2O were added $NaHCO_3$ (1.4 mg, 17 μmol) and 0.5 mM 2,4-dinitrofluorobenzene (DNFB) in acetone (34 μl, 17 μmol). The mixture was stirred for 4 h at room temperature in the dark. The reaction was followed by TLC (silica gel plate, developing solvent: $CHCl_3$-MeOH-AcOH=6:2:1). Extra reagents (0.4 mg of $NaHCO_3$; 10 μl of DNFB in acetone) were added every a few hours until the starting material disappeared.

After the completion of the reaction, the mixture was extracted with ether several times and the aqueous layer acidified with 2 M HCl was concentrated *in vacuo*. The residue in ethyl acetate was washed with saturated NaCl solution several times and organic layer was dried over $MgSO_4$. To the solution was added an excess of CH_2N_2 in ether. The mixture was allowed to stand for 1 h and then concentrated *in vacuo*.

To the residue in CH_2Cl_2 (0.2 ml) were added benzoic anhydride (10 mg, 44 μmol), triethylamine (6.1 μl, 44 μmol), and 4-dimethylaminopyridine (0.3 mg, 2.5 μmol). The mixture was stirred overnight at room temperature in the dark and then subjected to preparative TLC. The reaction mixture was applied to silica gel plate (Merck, 0.25 mm thickness, 20×20 cm) which was developed with benzene-ethyl acetate (4:1). Yellow band corresponding to the desired product was extracted with $CHCl_3$ and the extract was concentrated *in vacuo*. The crystalline residue thus obtained gave a peak at *m/z* 459 (M^+) in both FD and EI mass spectra. This sample was used for the measurement of CD spectrum.

Periodate-permanganate Oxidation of Galantinic Acid. Galantinic acid (0.43 mg) was dissolved in 0.05 M sodium acetate buffer (pH 7.7, 200 μl). To the solution was added 0.1 M sodium periodate solution (100 μl). The mixture was allowed to stand for 2 d at 4 °C in the dark and then 0.2% potassium permanganate solution was slowly added until a pale purple color remained. MnO_2 formed was removed off by centrifugation. The supernatant was subjected to an amino acid analysis and a paper electrophoresis.

The authors wish to express their thanks to Dr. Junichi Shoji, Shionogi Research Laboratory, Shionogi & Co. Ltd., for his kind supply of galantin I. We are grateful to Dr. Masao Kawai, Nagoya Institute of Technology, for the valuable suggestions and discussions about Dnp-aromatic rule. We also appreciate to Dr. Yasufumi Ohfune, Suntory Institute for Bioorganic Research, for his information of the results obtained from his synthetic work of galantinic acid.

References

1) J. Shoji, R. Sakazaki, Y. Wakisaka, K. Koizumi, M. Mayama, and S. Matsuura, *J. Antibiot.*, **28**, 122 (1975).

2) T. Ando, S. Terashima, M. Kawata, T. Teshima, T. Wakamiya, and T. Shiba, "Peptide Chemistry 1980," ed by K. Okawa, Protein Research Foundation, Osaka (1981), p. 113.

3) a) M. Kawai, U. Nagai, M. Katsumi, and A. Tanaka, *Tetrahedron*, **34**, 3435 (1978); b) M. Kawai, U. Nagai, and A. Tanaka, *Bull. Chem. Soc. Jpn.*, **55**, 1213 (1982).

4) (1*R*,2*R*)-2-Aminocyclohexanol, an example of g^- form, showed a negative Cotton effect. (Private communication from Dr. M. Kawai.) Abbreviations: Dnp=2,4-dinitrophenyl; Bz=benzoyl; g^+ and g^-=*gauche* forms possessing positive and negative bond chirality, respectively.

5) Synthetic (2*S*,4*S*,5*S*)-compound was completely identical with natural product in all respects. (Private communication from Dr. Y. Ohfune)

† 1 M=1 mol dm^{-3}.

 © 1984 The Chemical Society of Japan Bull. Chem. Soc. Jpn., 57, 145—150 (1984)

The Photoionization Mechanism of *N,N,N′,N′*-Tetramethyl-*p*-phenylenediamine in Acetonitrile

Shigemasa NAKAMURA, Nobuaki KANAMARU, Sawako NOHARA, Hiroki NAKAMURA, Yasuyoshi SAITO, Jiro TANAKA,* Minoru SUMITANI,† Nobuaki NAKASHIMA,† and Keitaro YOSHIHARA†

Department of Chemistry, Faculty of Science, Nagoya University, Chikusa-ku, Nagoya, 464

†*Institute for Molecular Science, Myodaiji, Okazaki 444*

(Received April 13, 1983)

The photoionization mechanism of *N,N,N′,N′*-tetramethyl-*p*-phenylenediamine (TMPD) in an acetonitrile solution was investigated by means of the fluorescence lifetime measurement, picosecond and nanosecond laser photolyses, and photocurrent measurement. The temperature dependence of the fluorescence lifetime was interpreted in terms of the thermally activated monophotonic ionization or the ion-pair-formation mechanism from the $S_{1,0}$ excited level. Picosecond laser photolysis clearly showed that a direct ionization from higher S_1 levels took place before relaxation into the $S_{1,0}$ level. The relative yields of triplet, ion-pair, and cation formation were estimated from analyses of the transient spectra and the photocurrent.

Considerable efforts have been devoted to the study of the photoionization mechanism of *N,N,N′,N′*-tetramethyl-*p*-phenylenediamine (TMPD) in nonpolar and polar solvents. Tsubomura and his co-workers[1,2] have found a biphotonic ionization process in a nonpolar solvent by means of microsecond flash photolysis, and have suggested a monophotonic process in an acetonitrile solution on the basis of photocurrent measurements.[3] Ottolenghi[4-6] and his group performed an extended spectral study indicating the importance of the singlet-intermediate state. Richards and Thomas[7] have used microsecond and nanosecond flash photolysis techniques for studying the photoionization in cyclohexane, ethanol, and water; they established the characters of the triplet and ion-pair states and discussed a possible mechanism of photoionization in water. Ottolenghi[8] suggested a charge transfer to the solvent (CTTS) state as an intermediate in the photoionization of several organic molecules. The importance of the CTTS state has been shown in the decay and photoionization of sodium 8-anilino-1-naphthalenesulfonate.[9,10] In spite of many investigations so far performed, however, no fast method of analyzing the monophotonic ionization process in a polar solvent has yet appeared.

In this paper we present a combined investigation of the photoionization mechanism of TMPD in an acetonitrile solution by using the results of picosecond and nanosecond laser photolyses and photocurrent and fluorescence-lifetime measurements.

Experimental

Materials. The TMPD was obtained from the Aldrich Chem. Co., and was purified by vacuum sublimation in a furnace with a temperature gradient. The acetonitrile was refluxed over P_2O_5 and distilled. The hexane was a spectrograde product of Merck. The 1,3-pentadiene, a mixture of cis and trans isomers from Wako Pure Chem., was purified, while a zone-refined naphthalene from Tokyo Kasei was used without further purification.

Fluorescence-lifetime Measurements. The fluorescence-lifetime measurements were performed by two methods. One was a photon-counting technique employing a discriminator and a TAC (Canberra 1443A) combined with a MCA system. The light source was a free-running lamp in air at 1 atm; the 337-nm light was selected after passing it through a Nikon G250 monochromator. The half-band width of the pulse duration was 2.5 ns. Picosecond laser (a mode-locked Nd-YAG laser) excitation, followed by recording the fluorescence decay with a streak camera (HTV C-1000), was also used for the lifetime measurements in the range of a few nanoseconds. The temperature dependence of the fluorescence lifetimes was measured by circulating cooled nitrogen gas around the sample cell, while the temperature was kept constant with an accuracy of ±0.5 °C. The results obtained with the photon-countig method are tabulated in Table 1.

Nanosecond Laser-flash Photolysis. The transient absorption in the nanosecond and microsecond time domain was measured by means of nanosecond laser-flash-photolysis apparatus. The nitrogen laser was a home-made TEA type with a peak power of 500 kW and a time duration of 2 ns. All the solutions used for the fluorescence-lifetime and laser-photolysis experiments were degassed at least five times by means of a freeze-pump-and-thaw method. The temporal changes in the absorbance were recorded with an oscilloscope (Tektronix 485) at twenty points of significant absorbance; these data were then used to obtain the time-resolved transient absorption spectra.

Picosecond Laser-flash Photolysis. The transient absorption in the picosecond time region was measured by

TABLE 1. FLUORESCENCE LIFETIMES IN VARIOUS SOLVENTS AT DIFFERENT TEMPERATURES, AND ACTIVATION ENERGY FOR THE DECAY RATE OF THE TMPD $S_{1,0}$ STATE

Temperature	Lifetime/ns										Activation energy
K / Solvent	313	298	274	260	246	232	217	202	186	168	kJ mol^{-1}
Acetonitrile	0.8	1.3	3.5	6.9	9.5	12.4					33.9
Methanol	3.0	4.0	7.2	10.1	11.6	12.1	13.1	13.2	13.0		30.1
Ethanol	6.9	7.8	9.0	9.6	9.8	10.2	11.0	11.5	12.1	12.3	5.0
Hexane	4.9	4.9	4.9								—

means of a laser excitation of a third harmonics of a mode-locked Nd:YAG laser (355 nm) with a 20-ps pulse width. The laser light from the YAG oscillator was amplified and used for excitation and for recording transient absorption by means of multichannel photo-diode system with a pulsed-continuum light source (D_2O+2-propanol) or a fast-photomultiplier tube system (HTV R1294U), with a Xe arc lamp as a monitoring light. The Xe lamp was fired by a strong laser pulse focussed onto the arc electrode.[11]

Photocurrent Measurements. The photocurrents induced in irradiated solutions were measured in order to determine the decay of the transient carrier. The induced current in the solution was measured with Pt-electrodes separated by 0.3 mm after excitation from a YAG laser. The transient current was amplified through a preampifier (model 115, PAR) and recorded by means of an oscilloscope (Hewlett-Packard, 1744A). Between the electrodes, a constant voltage of 20 V was applied during the photocurrent measurements. All solutions were bubbled with nitrogen gas at least for 30 min or longer, because otherwise the dissolved oxygen would quench the photocurrent.

Results and Discussions

Fluorescence Lifetime. As is shown in Table 1, a temperature dependence of fluorescence lifetimes was found in ethanol, methanol, and acetonitrile; however, it was not observed in hexane. This observation might be correlated with the temperature independence of the intersystem crossing and the absence of monophotonic ionization in hexane. Richards and Thomas[7] reported that the triplet yield of TMPD in cyclohexane was 0.96± 0.10 and that the fluorescence yield was 0.09. Since hexane is as inert as cyclohexane, all excited species may decay either into the triplet state through intersystem crossing at the rate k_{ISC} or to the ground state at the fluorescence rate k_f in hexane. Then the fluorescence lifetime in hexane, τ_h, is given as:

$$\tau_h = 1/(k_{ISC} + k_f) = 4.9 \text{ ns},$$

where $k_{ISC}=\phi_T/\tau_h=1.96\times10^8$ s^{-1}, $k_f=\phi_f/\tau_h=0.18\times10^8$ s^{-1}, and other radiationless processes are ignored. In a polar solvent such as acetonitrile, the monophotonic ionization process with the rate k_{ion} is involved, as will be discussed later, and the fluorescence lifetime, τ_f, will be shrunk as is described by:

$$\tau_f = 1/(k_{ion} + k_{ISC} + k_f) = 1.0 \text{ ns}.$$

k_{ion} is estimated as 8×10^8 s^{-1} at 300 K if k_{ISC} and k_f are assumed to be independent of the solvent and the temperature (Here the value of τ_f is obtained with a streak camera after picosecond excitation.). If we assume that the temperature dependence of the fluorescence lifetime is to be ascribed to the activation of the ionization process, then k_{ion} will be represented as $k_{ion}=k_0\exp(-\Delta E/RT)$, where other processes are considered to be temperature-independent. These assumptions are supported by the variation in the activation energies for acetonitrile, methanol, and ethanol (Table 1).

From the slope of $\ln(1/\tau_f-1/\tau_0)$ shown in Fig. 1, the activation energies for the temperature-dependent

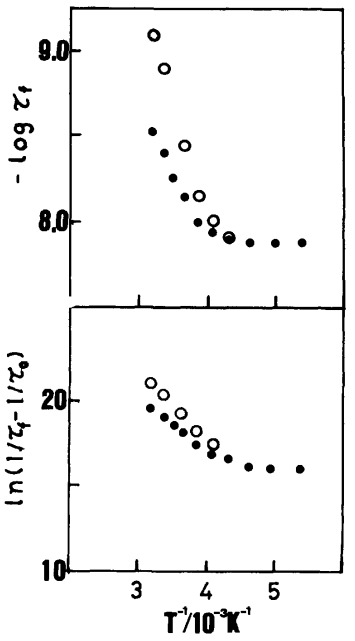

Fig. 1. Temperature dependence of fluorescence lifetime (τ_f) and $\ln(\tau_f^{-1}-\tau_0^{-1})$. ○: Acetonotrile and ●: methanol solutions.

ionization process are determined to be as is shown in Table 1. Here, τ_0 is the fluorescence lifetime obtained at a lower temperature, where the thermal process can be neglected. In an acetonitrile solution, the thermally activated decay process is most evident; below it will be connected with thermally activated monophotonic ionization process found by means of picosecond laser photolysis.

Picosecond Laser-flash Photolysis. Hexane Solution: The transient absorption spectra after picosecond-laser excitation are illustrated in Fig. 2. In a

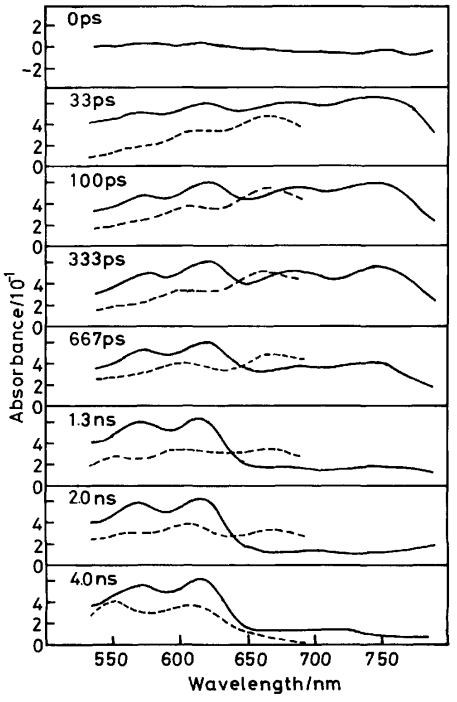

Fig. 2. Transient spectra of photolyzed TMPD measured with MCPD system in acetonitrile (——) and hexane (------) solutions.

hexane solution, the $S_n \leftarrow S_1$ absorption bands were observed immediately after excitation to have peaks at 670, 610, and 560 nm (the 700-nm region was not recorded); all these bands decayed with a time constant of 5 ns. The fluorescence lifetime (Table 1) in hexane was 4.9 ns; therefore, these bands were assigned to the $S_n \leftarrow S_1$ absorption. In the transient spectra in the 610—520 nm region, new bands grew with a time constant of $\simeq$5 ns, and the spectral shape was coincident with the previously reported $T_n \leftarrow T_1$ absorption.[1)]

In a hexane solution, the biphotonic ionization may occur via the siglet- or triplet-excited states under a high-intensity light, but the present laser has not enough power and has the very short duration of 20 ps; therefore, the biphotonic process can be neglected.

When the temporal changes in the transient spectra are superposed, an isosbestic point of the $S_n \leftarrow S_1$ and $T_n \leftarrow T_1$ absorptions is found at 620 nm. The molar-extinction coefficient of the $T_n \leftarrow T_1$ at 570 nm was determined by Richards and Thomas[7)] to be 11900. The molar absorption coefficient of the $S_n \leftarrow S_1$ absorption at 670 nm could be determined as 18000 by using the data at a time delay of 100 ps and the above-mentioned value for the $T_n \leftarrow T_1$ absorption. Thus, the picosecond laser photolysis in hexane showed the band shapes of the $S_n \leftarrow S_1$ and $T_n \leftarrow T_1$ absorptions and their molar-absorption coefficients.

Acetonitile Solution: In an acetonitrile solution, the spectra immediately after the excitation show peaks at 750, 680, 620, and 570 nm. The longer-wavelength peaks at 750 and 680 nm decayed with a lifetime of 1 ns, which indicated that these bands were due to the $S_n \leftarrow S_1$ absorption since the lifetime of the fluorescence was determined as 1 ns. The peaks at 620 and 570 nm should be assigned to the absorption bands of the photoionized product, either the cation or the ion-pair or the CTTS state, because these band positions coincide with those reported for cations.[1)] No distinction between the spectra of the ion-pair and the CTTS states with a cation is discernible, but we consider that the ion-pair state is the only singlet intermediate before the ionization because the CTTS state may have a similar electronic structure. Moreover, we can not say simply at this moment that the product is a cation, because there are several decay processes for this transient absorption. In the spectrum at 33 ps after the excitation, these peaks were already found, implying that a direct ionization or ion-pair formation took place before relaxation to the $S_{1,0}$ state. In the spectrum of the 4-ns time lag, some contribution of the triplet state might overlap. As is well known,[1)] the cation spectra and the $T_n \leftarrow T_1$ absorption bands are very close to each other, and so the separation of the transient spectra into these components is rather difficult without the aid of other means. The results of nanosecond flash photolysis and the photocurrent measurements were used for this analysis. In the picosecond photolysis spectra, the cation-like species were found immediately after the excitation; in addition to this, another process to produce this species was indicated because the cation-like band increased in intensity with a time constant of 1.2 ns. This temporal change in the spectra was also confirmed by the measurement of the transient absorbance with a fast photomultiplier tube, as is shown in Fig. 3. The analysis of the growth of the absorbance at 610 and 540 nm showed the rise time of 1.1 ns, which is in perfect agreement with the fluorescence lifetime in acetonitrile. After subtracting the contributions of the $S_n \leftarrow S_1$ and $T_n \leftarrow T_1$ transitions and the direct ionization from the transient spectra, the second process was found to have a yield twice that of the first direct ionization process. Thus, the cation-like band grows accompanied by the decay of the $S_{1,0}$ state. As has been discussed in the fluorescence-lifetime section, this decay process is thermally activated. Thus, the monophotonic ionization occurred by means of the 355-nm excitation, either from the higher S_1 level or from the bottom of the S_1 state ($S_{1,0}$), with the aid of thermal activation.

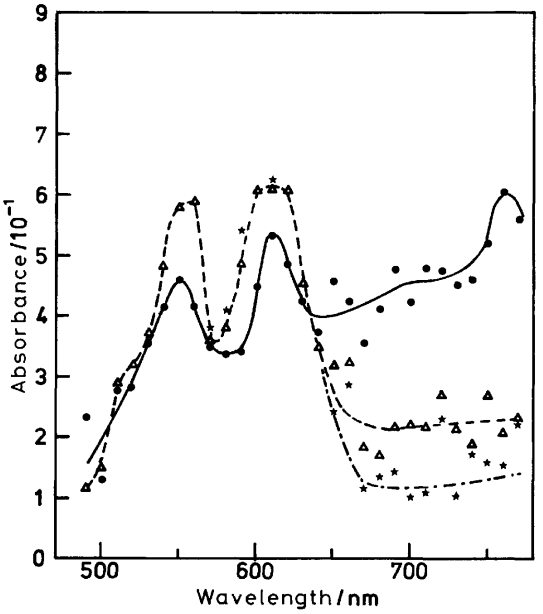

Fig. 3. Transient spectra measured by a fast photomultipler system at zero (●), 3 ns (△), and 10 ns (*) time delay.

Another important experiment to find the overall reaction scheme is that of the power dependence of the transient absorption. The intensity of the transient absorption at 620 nm was measured by varying the laser power in the range of 0.3—2 mJ; the absorbance was shown to be linear with the excitation energy as is shown in Fig. 4. This measurement was made with a photomultiplier tube with a rise time of 2 ns (RU928); therefore, the results showed that the overall ionization process is monotonic rather than the biphotonic process which was considered to occur in ethanol.[1)]

In the photolysis spectra above the 700-nm region, there remained a broad, residual transient absorption with a lifetime longer than the $S_n \leftarrow S_1$ transition; its lifetime was estimated as about 50 ns. In the literature, the spectra of CH_3CN^- is reported to have a maximum at 1.45 μm;[12)] therefore, we may observe the tail of the absorption band of CH_3CN^- in the 700-nm range. The short lifetime as compared with the literature value ($\simeq$900 ns) might be due to the presence of an efficient scavenger or a fast reaction with the cation produced.

Nanosecond Laser-flash Photolysis. The transient

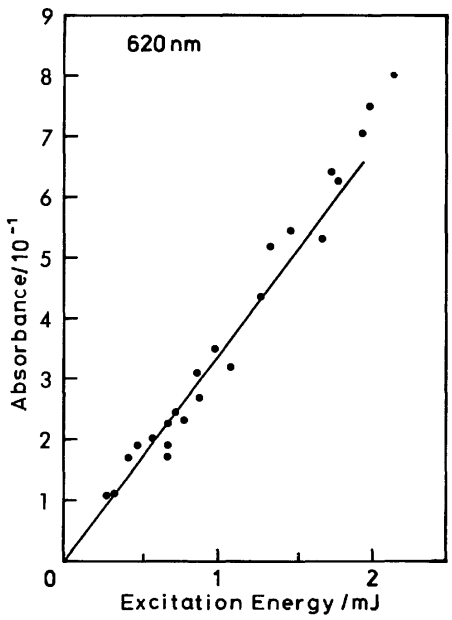

Fig. 4. Laser power dependence of transient absorption measured at 620 nm.

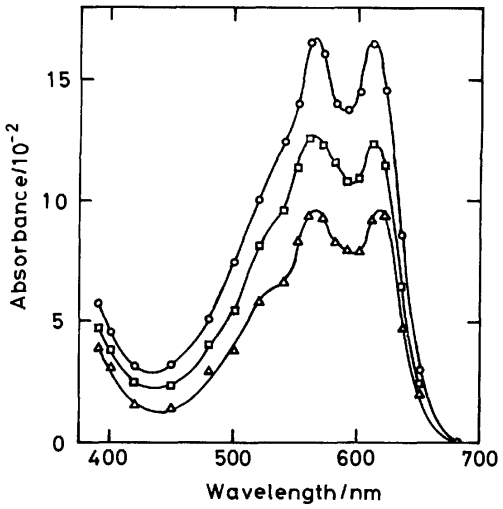

Fig. 5. Transient spectra obtained by nanosecond laser photolysis at 0.1 μs (—O—O—), 1.0 μs (—□—□—) and 4.0 μs (—△—△—) time delay.

absorption spectra as determined by nanosecond laser-flash photolysis, are shown in Fig. 5. The time-resolved absorption spectra after time delays of 100 ns, 1 μs, and 4 μs are illustrated. The decay of the absorbance at each wavelength was analyzed by a linear combination of several first-order decay curves, and at least three or four components were confirmed. The extrapolation to $t=0$ after the excitation gave three different absorption curves, as is shown in Fig. 6, where the height of the absorption represents the relative quantities of the photoproducts. The spectrum of the longest-lifetime component ($\tau>1$ s) is exactly the same as that of the cation; the medium-lifetime ones ($\tau\simeq2$ μs and $\simeq50$ μs) also resemble the cation spectrum.

The shortest-lifetime component ($\tau\simeq500$ ns) has a slightly different spectral shape; it is very close to the $T_n\leftarrow T_1$ absorption reported in the literature.[1]

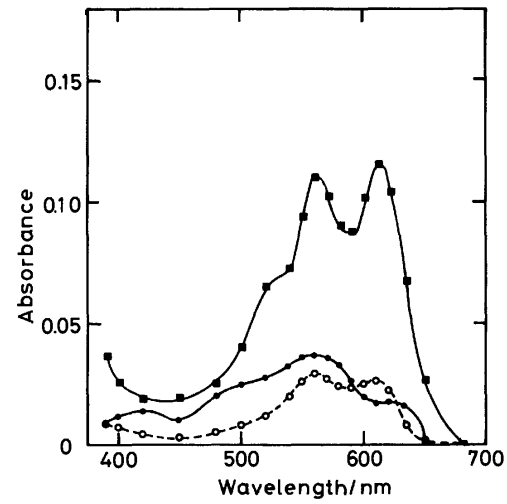

Fig. 6. Absorption spectra of the stable cation (—O—O—), the long lived component ($\tau=2$ and 50 μs (—■—■—), and the short lived component ($\tau=0.5$ μs) (—●—●—).

Therefore, this shortest component in the nanosecond flash photolysis is ascribed to the triplet state. Quite recently, Tokumura *et al.*[13] reported the decay of the T_1 state in acetonitrile to have a lifetime of 660 ns, thereby confirming our finding that the shortest-lifetime component of $\tau\simeq$ 500 ns is ^{3}TMPD. The relative yields of these three components have been estimated by an extrapolation to $t=0$; the yields and lifetimes are summarized in Table 2.

TABLE 2. LIFETIMES AND YIELDS OF LASER-PHOTOLYSIS PRODUCTS IN MICROSECOND TIME RANGE

Species	Lifetime	τ	Yield/%
^{3}TMPD	Shortest	0.5 μs	0.22±0.07
Cation and ion-pair or CTTS state	Medium	14 μs (2 and 50)	0.60±0.06
Stable cation	Longest	> 1 s	0.18±0.07

In this table the medium-lifetime components are represented as having a common decay time of 14 μs, but the detailed analysis showed that these are at least two components with 2 and 50 μs. It is apparent, therefore, that there are several decay processes of the cation and ion-pair state. However, the lifetimes of these intermediates are independent of the laser power; accordingly, these decays might be first-order processes. It is conceivable that a geminate recombination of the ion pair is a major decay process.

Photocurrent. In order to determine the mechanism of transient phenomena in detail, the photocurrent produced after the YAG laser excitation was measured with a time resolution of $\simeq$ 10 ns. The current was found to be linear with the intensity of the exciting light, which is in good agreement with the results of an earlier study.[3] The transient current was analyzed with a linear combination of several components with different lifetimes; it may be described as:

$$I_p(t) = \sum_j A_j e^{-t/\tau_j},$$

where A_j is a preexponential factor for the j-th decay component of the lifetime τ_j and where numerical values are as follow:

τ_j	0.08	0.7	1.6	40	240	(μs)	$>$1 ms
A_j	0.24	0.26	0.18	0.08	0.07		0.18

These lifetimes are independent of the power of the laser light. The shortest lifetime coincides with those of CH_3CN^- in transient spectra. The origin of the second component is not clear, but it may be due to the free cation produced immediately after the excitation. The third and fourth components have decay times similar to that found by nanosecond laser photolysis; therefore, they may be related to the ion-pair state. Although no report has yet been presented on the current originating from the ion-pair without a rise time, the present coincidence of the decay of the transient-cation spectra with that of the current might indicate that the ion-pair gives a current under an electric field near the electrode surface. The independence of the decay times of the power intensity may indicate that most of the ejected electrons are still bound close to the cation, forming an ion-pair or a CTTS state, and that they exhibit a photocurrent under the applied field by dissociation. The presence of several decay times may mean the existence of inhomogeneous electron-trapped states, in which electrons are loosely bound to the cation but give a transient current under the applied electric field. Although all these measurements were carried out with nitrogen-bubbled samples, the effect of oxygen on the photocurrent was also examined. The shortest- and the medium-lifetime transient currents were significantly quenched, the former being reduced to one-tenth, and the latter, to about one-fifth. Therefore, both the CH_3CN^- and the ion-pair were shown to be quenched by oxygen.

Conclusion

The photoionization mechanism of TMPD in an acetonitrile solution was investigated by means of picosecond and nanosecond laser photolyses and photocurrent and fluorescence-lifetime measurements. Although the monophotonic ionization from the higher S_2 state has been studied by several groups,[14,15] little attention has been given to that from the higher S_1 level except for the work by Siomos *et al.*[16] They showed the photocurrent in a heptane solution excited by a two-photon process, but the photoionization from the $S_{1,0}$ level was not indicated. In this study, however, both the monophotonic direct ionization from the higher S_1 level and the thermally activated process from the $S_{1,0}$ is confirmed by picosecond laser photolysis. However, not all the cation-like species in the transient spectra may be due to the free cation, since the final yield after the photolysis is $\simeq$0.18. In the initial stage of photolysis, the yield of the cation-like species is $\simeq$0.77 as a whole; the direct ionization is estimated as $\simeq$0.25, and the second thermal process is $\simeq$0.52, as is shown in Fig. 7. The yield of the triplet state was estimated by nanosecond laser photolysis to be $\simeq$0.21. The fluorescence yield was evaluated as 0.02 by comparing the fluorescence lifetimes in acetonitrile and cyclohexane and the quantum yield in cyclohexane.

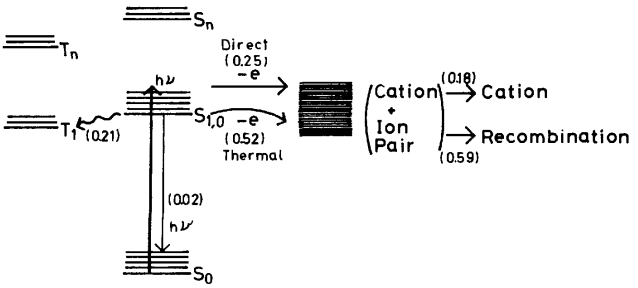

Fig. 7. Monophotonic ionization scheme of TMPD in acetonitrile solution.

In order to estimate the relative yields of the decay processes, quenching experiments with 1,3-pentadiene (1.0×10^{-3} M), naphthalene (1.2×10^{-3} M), and an air-saturated solution were performed. About one-third of the transient absorptions were quenched, indicating that most of the triplet absorption and some of the cation-like absorptions disappeared upon the use of the quenchers. The triplet yield of TMPD was found to be $\simeq$0.20 by means of the $T_n\leftarrow T_1$ absorption of naphthalene. This value was consistent with the value estimated by the nanosecond laser photolysis. Summarizing the whole photoionization scheme, the overall processes are illustrated in Fig. 7. The relative yields for each process might have uncertainties of $\pm$0.05.

In the initial statge of photolysis, two independent pathways leading to the ionization or the ion-pair formation were indicated, but 80% of the cation-like absorption decayed through the recombination process. The photo-ejected electrons in an acetonitrile solution may exist in several different environmental conditions, which means that some of them are bound to acetonitrile molecules; some are closely connected with $TMPD^+$, forming an ion-pair; some are free, and some decay rapidly by reacting with scavengers. The monophotonic ionization process from the S_1 state of TMPD in a polar solvent is thus found to be the main process, and the present analysis may throw light on the unsolved problems regarding the photoionization mechanism of TMPD in polar media.

The authors are grateful to Mr. Toshiaki Noda for making the photocurrent cell and to Mr. Atsuo Kawai for his contribution in the initial statge of this work. They also wish to thank Professor Michiya Itoh of Kanazawa University for his kind comments on this manuscript.

References

1) N. Yamamoto, Y. Nakato, and H. Tsubomura, *Bull. Chem. Soc. Jpn.*, **39**, 2603 (1966).
2) Y. Nakato, N. Yamamoto, and H. Tsubomura, *Bull. Chem. Soc. Jpn.*, **40**, 2480 (1967).
3) T. Imura, N. Yamamoto, H. Tsubomura, and K. Kawabe, *Bull. Chem. Soc. Jpn.*, **44**, 3185 (1971).
4) R. Potashnik, M. Ottolenghi, and R. Bensasson, *J. Phys. Chem.*, **73**, 1912 (1969).
5) A. Alchalal, M. Tamir, and M. Ottolenghi, *J. Phys. Chem.*, **76**, 2229 (1972).
6) A. Alchalal and M. Ottolenghi, *Chem. Phys. Lett.*, **17**,

117 (1972).
7) J. T. Richards and J. K. Thomas, *Trans. Faraday Soc.*, **66**, 621 (1970).
8) M. Ottolenghi, *Chem. Phys. Lett.*, **12**, 339 (1971).
9) H. Nakamura, J. Tanaka, N. Nakashima, and K. Yoshihara, *Chem. Phys. Lett.*, **77**, 419 (1981).
10) H. Nakamura and J. Tanaka, *Chem. Phys. Lett.*, **78**, 57 (1981).
11) M. Sumitani and K. Yoshihara, *Bull. Chem. Soc. Jpn.*, **55**, 85 (1982).
12) I. P. Bell, M. A. Rodgers, and H.D. Burrows, *J. Chem. Soc., Faraday Trans. 1*, **73**, 315 (1977).
13) K. Tokumura, K. Endo, and M. Itoh, Presented at the National Meeting of Chem. Soc. Jpn., Spring, 1983.
14) J. Bullot, P. Cordier, and M. Gauthier, *J. Phys. Chem.*, **84**, 3516 (1980).
15) H. T. Choi, D.S. Sethi, and C.L. Braun, *J. Chem. Phys.*, **77**, 6027 (1982).
16) K. Siomos, G. Kourouklis, and L.G. Christophorou, *Chem. Phys. Lett.*, **80**, 504 (1981).

 © 1984 The Chemical Society of Japan Bull. Chem. Soc. Jpn., 57, 151—155 (1984)

The Electronic Structure of the Fulvalene Trication Radical. A Localization of the Unpaired Electron

Azumao TOYOTA*,† and Takeshi NAKAJIMA

†*Department of Chemistry, Faculty of General Education, Yamagata University, Yamagata 990*
Department of Chemistry, Faculty of Science, Tohoku University, Sendai 980
(Received April 15, 1983)

The restricted Hartree-Fock (RHF) solution for the trication radical of fulvalene, obtained by using the open-shell SCF formalism of the Pariser-Parr-Pople-type MO method, is found to be doublet unstable at the conventional D_{2h} nuclear arrangement. We calculate the broken-symmetry charge-density wave solution lower in energy than the usual symmetry-adapted RHF solution and examine its properties. It is predicted that the unpaired electron should be localized on the single five-membered ring having a smaller positive charge. Finally, on the basis of the second-order Jahn-Teller effect, we examine the molecular-symmetry reduction of the trication radical from the fully-symmetrical D_{2h} to the C_{2v} nuclear arrangement.

On the basis of the doublet instability of the restricted Hartree-Fock (RHF) solution,[1,2] we have examined the origin of the anomalous phenomena that in the monoanion and trianion radicals of heptafulvalene the unpaired electron is localized on a single seven-membered ring.[3,4] It has been shown that the RHF solutions for the anion radicals, obtained by using the open-shell SCF formalism of the Pariser-Parr-Pople (PPP) type MO method, are doublet unstable at the conventional D_{2h} nuclear arrangement and the spin-density distributions obtained from the resulting broken-symmetry charge-density wave (CDW) solutions are in good agreement with the experimental ones.[5,6]

The monoanion radical of fulvalene has recently been prepared by Davies *et al.*[7,8] The spin-density distribution of this radical is of interest in connection with that of the heptafulvalene monoanion radical. In order to obtain information about the behavior of unpaired electron, they have made the ESR studies of the radical and it is revealed that the unpaired electron is delocalized over the entire molecule, showing a sharp contrast to the situation observed with the heptafulvalene monoanon radical.[3]

Although neither the monocation nor the trication radical of fulvalene has so far been prepared, both of the radicals are of great interest from theoretical and experimental points of view, because our previous research suggests that the localization of unpaired electron similar to those in the heptafulvalene monoanion and trianion radicals should occur: As to the monocation radical, we have partly studied the problem in view of the doublet instability of the RHF solution at the conventional D_{2h} nuclear arrangement.[5]

In this paper, we investigate the behavior of unpaired electron and the distribution of charge density in the trication radical of fulvalene by examining the instability of the RHF solution and by using the second-order Jahn-Teller theory. On the basis of the results obtained, we point out a distinct difference with regard to the distributions of the unpaired spin density and the ring charge density between the monocation and trication radicals.

Theoretical

The Stability Conditions of the RHF Solution. The stability conditions of the RHF solution for the open-shell case were formulated by Paldus and Cizek.[1,2] Since the conditions are well discussed in several literatures, we give here only the outline of the theory.

Using the usual real molecular orbitals, the question of whether the RHF solution is doublet stable or not resolves itself into the solution of the lowest-lying eigenvalue of the following two eigenvalue problems:

$$(A+B)D_+ = \lambda_+ D_+,$$
$$(A-B)D_- = \lambda_- D_-. \quad (1)$$

That is, if $\lambda_+ < 0$ or $\lambda_- < 0$, a doublet instability occurs in the usual symmetry-adapted RHF solution and a new RHF solution becomes a real CDW solution or a complex CDW solution, respectively.

In Eq. 1, elements of the square matrices, A and B, represent the configuration interactions between spin unflip singly excited configurations and those between the RHF ground state and spin unflip bi-excited states, respectively. The elements of the column matrix D_+ or D_- are the mixing coefficients which give the weights with which the virtual RHF molecular orbitals are admixed to the occupied ones. If the occupied and virtual orbitals belong to different irreducible representations, the symmetry properties of the new orbitals are broken (see Eq. 2): The molecular orbitals do not transform according to the irreducible representations of the molecular point group and, as a result, the new HF solution becomes the so-called broken-symmetry CDW solution.

Results and Discussion

The Broken-symmetry CDW Solution and Its Properties. The optimum nuclear arrangement of the trication radical with the D_{2h} symmetry was

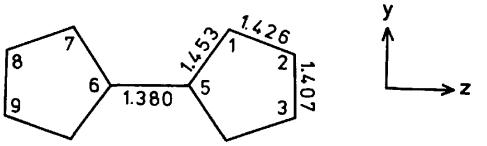

Fig. 1. The optimized bond lengths (in Å) of the fulvalene trication radical at the D_{2h} nuclear arrangement, the numberings of atomic positions, and the choice of molecular axes.

calculated by using Longuet-Higgins and Pople's MO method[9] in conjunction with the variable bond-length technique.[10] The RHF solution to which the stability conditions will be applied is the one corresponding to the molecular geometry thus optimized with respect to carbon nuclear arrangement (Fig. 1).

It turns out that the lowest-lying eigenvalue λ_{min}, obtained from the λ_+ subproblem of Eq. 1, is -1.227 eV and the electronic configurations that play an important role in the RHF instability are those including the orbital jumps from the highest doubly occupied orbital ϕ_3 (b_{3u}) to the next lowest vacant orbital ϕ_6 (b_{2g}) and from the singly occupied orbital ϕ_4 (a_u) to the lowest vacant orbital ϕ_5 (b_{1g}). As noted above, since the eigenvector d_{min} is of b_{1u} symmetry, a new HF solution becomes a real CDW solution having the C_{2v} spatial symmetry.

Let us now treat the CDW solution according to the same procedure as used in a previous paper.[5] For obtaining the CDW solution we take into account only the two orbital jumps above. This approximate procedure is justified, for the eigenvalue λ'_{min} (-1.130 eV) thus obtained reproduces well the eigenvalue λ_{min}(-1.227 eV) obtained by including all the singly excited configurations. By using the mixing coefficients of the eigenvector d'_{min} corresponding to the eigenvalue λ'_{min} the new occupied orbitals are formed as:

$$\begin{aligned}\phi_i &= \phi_i \ (i=1,2),\\ \phi_3 &= \mu_1\phi_3 + \mu_2\phi_6,\\ \phi_4 &= \nu_1\phi_4 + \nu_2\phi_5,\end{aligned} \tag{2}$$

and

$$\begin{aligned}\mu_1 &= \{1-(0.3135k)^2\}^{1/2},\ \mu_2 = -0.3135\,k\\ \nu_1 &= \{1-(0.9496k)^2\}^{1/2},\ \nu_2 = 0.9496\,k\end{aligned} \tag{3}$$

where k is the dimensionless mixing parameter, which indicates the degree of deformation of the CDW solution from the symmetry-adapted RHF solution. Using the molecular orbitals above, we can write the CDW solution as:

$$\begin{aligned}{}^2\Psi_{CDW}(k) &= \mu_1^2\nu_1^2\Psi_{RHF}(A_u) + \mu_1^2\nu_2^2\Psi_1(B_{1g}: 4\rightarrow5)\\ &+\sqrt{2}\,\mu_1\mu_2\nu_1^2\Psi_1(B_{1g}: 3\rightarrow6) + \mu_2^2\nu_1^2\Psi_2(A_u: 3,3\rightarrow6,6)\\ &+\sqrt{2}\,\mu_1\mu_2\nu_2^2\Psi_2(A_u: 3,4\rightarrow6,5)\\ &+ \mu_2^2\nu_2^2\Psi_3(B_{1g}: 3,3,4\rightarrow6,6,5),\end{aligned} \tag{4}$$

where notations used are the same as those in a previous paper.[5] It is seen that the CDW solution comprises the configurations of A_u and B_{1g} symmetries. Evidently, the symmetry-breaking components are the configurations of B_{1g} symmetry, for the RHF ground state is of A_u symmetry.

We now examine the dependence of the energy expectation value of the broken-symmetry CDW solution on the mixing parameter k. The result shows that the energy minimum point, *i.e.*, the stable CDW solution, is found at $k=0.66$, the energy lowering from the symmetry-adapted RHF solution being calculated to be 0.249 eV.

In Fig. 2 are shown the dependence of the electron densities and bond orders of the CDW solution on k. It is seen that the electron densities at 1 and 7, 2 and 8, and 5 and 6 and the bond orders between 1—5 and 6—7, 1—2 and 7—8, and 2—3 and 8—9 become separated as k increases. Included in Table 1 are the detailed values of electron density and bond order of the symmetry-adapted RHF and stable CDW solutions. It is found that there is a notable difference in the distribution of the density matrix elements between the two solutions: If we take the electron densities of the RHF solution as the reference values, a charge-density alternation can be seen along the longer molecular axis(z) in the electron-density distribution of the CDW solution. As to the

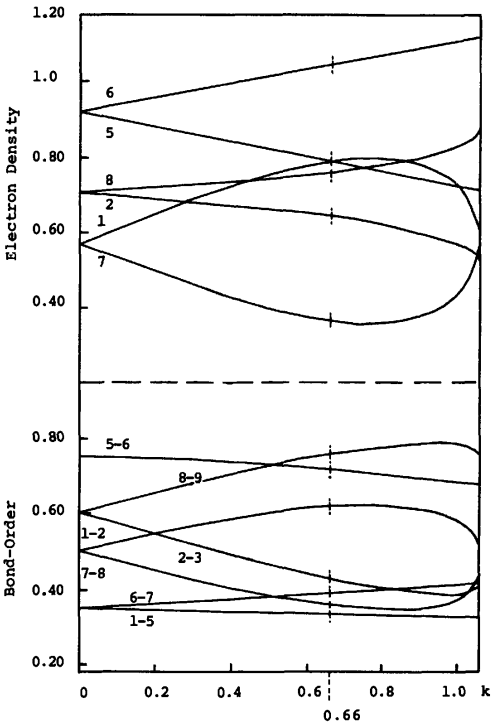

Fig. 2. The dependence of the electron densities and bond orders of the broken-symmetry CDW solution on the mixing parameter k.

Table 1. Electron densities bond orders of the fulvalene trication radical

RHF solution (C_{2v} molecular geometry)		CDW solution (D_{2h} molecular geometry)	RHF solution
Atom	Electron density		
1	0.750	0.791	0.579
7	0.410	0.374	
2	0.671	0.649	0.710
8	0.758	0.765	
5	0.779	0.796	0.921
6	1.043	1.048	
Bond	Bond order		
1-2	0.628	0.624	0.504
7-8	0.360	0.366	
2-3	0.424	0.438	0.607
8-9	0.752	0.763	
1-5	0.351	0.347	0.361
6-7	0.434	0.396	
5-6	0.693	0.726	0.753

distribution of bond orders, a similar behavior can be seen.[11] It is noted that the positive ring charges of the broken-symmetry CDW solution are unequal: The charge of the left-hand ring is 1.676(e) and that of the other ring is 1.324.

In Fig. 3 is depicted the dependence of the unpaired spin densities of the broken-symmetry CDW solution on k. This shows that the unpaired spin densities of the stable CDW solution ($k=0.66$) are localized essentially on a single five-membered ring. It is remarked that such a localization of the unpaired electron has also been found out theoretically in the monocation radical of fulvalene.[5] However there is a distinct difference with regard to the distributions of the unpaired spin density and the ring charge density between the trication and monocation radicals. In the latter, the unpaired spin density is localized in the five-membered ring having a larger positive charge, while in the former it is localized in the ring having a smaller positive charge. This difference will be explained by using Eq. 2 as follows. In the trication radical, the occupied orbital that is affected greatly by the appearance of the doublet instability is the singly occupied orbital ψ_4, whereas in the monocation radical such orbitals are the doubly occupied orbital ψ_4 and the singly occupied orbital $\psi_5(=\nu_1\phi_5-\nu_2\phi_4)$. As shown in Fig. 4, the atomic-orbital coefficients for the symmetry-adapted RHF orbitals, ϕ_4 and ϕ_5, are almost equal in absolute value and opposite on the respective carbon atoms. Thus, as k increases, orbitals ψ_4 and ψ_5 will be localized in the different five-membered rings. Consequently, in the trication radical the unpaired electron is localized in the ring having a smaller positive charge, while in the monocation radical it is localized in the ring having a larger positive charge.

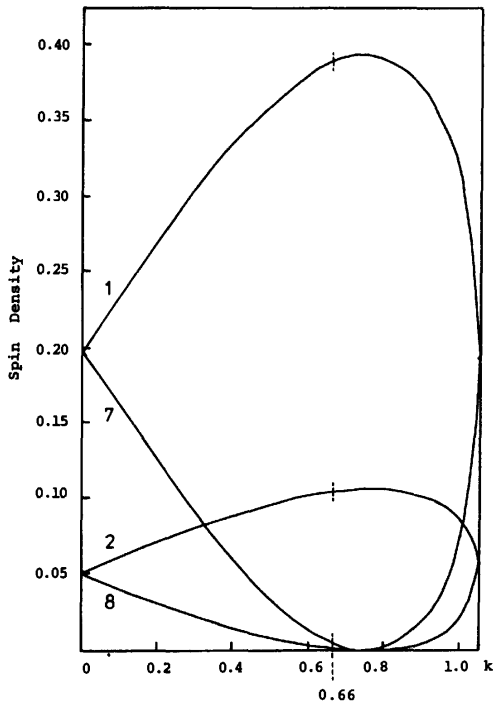

Fig. 3. The dependence of the unpaired spin densities of the broken-symmetry CDW solution on the mixing parameter k. The spin densities on the carbon atoms 5 and 6 are zero by symmetry.

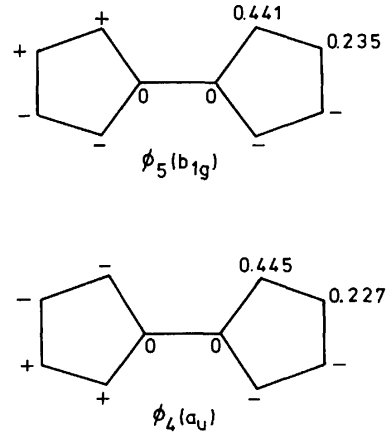

Fig. 4. The atomic-orbital coefficients of the usual symmetry-adapted RHF orbitals, ϕ_4 and ϕ_5, for the fulvalene trication radical.

TABLE 2. SPIN DENSITIES AND PROTON HYPERFINE SPLITTINGS OF THE FULVALENE TRICATION RADICAL

Atom	Broken-symmetry CDW solution (D_{2h} molecular geometry)		Symmetry-adapted RHF solution (C_{2v} molecular geometry)	
	Spin density	Hyperfine splitting/G[a]	Spin density	Hyperfine splitting/G
1	0.3887	8.16	0.3559	7.47
2	0.1054	2.21	0.1235	2.59
5	0	0	0	0
6	0	0	0	0
7	0.0050	0.11	0.0174	0.36
8	0.0009	0.02	0.0032	0.07

a) 1 G=10^{-4} T.

The detailed spin densities of the stable CDW solution are listed in Table 2, together with the proton hyperfine splittings calculated by using McConnell's relationship[12] with $|Q|=21$ G (1G=10^{-4}T). It is predicted that the proton hfs constant on the carbon atom 1 is greater than that on the carbon atom 2.

It has thus been shown that the distribution of the density matrix elements inherent in the stable CDW solution is lower in symmetry than that of the nuclear arrangement used. Such an effect has been recognized in the theory of chemical reaction as the electron-cloud preceding.[13] Since it is known that such a preceding behavior of electron cloud brings about the change in nuclear configuration from unstable to stable one, we may expect that the broken-symmetry CDW solution is further stabilized by relaxation of the nuclear framework such that it may match up with the symmetry of the CDW solution.[14] This implies that a lattice instability similar to the second-order Jahn-Teller effect[15] may occur, as is very often the case.

The Second-order Jahn-Teller Effect. From the above argument, it is suggested that the trication radical may undergo the second-order Jahn-Teller distortion.[15] In order to elucidate this problem, we examine the lower electronic states of the trication

radical by assuming the optimized D_{2h} molecular geometry (Fig. 1). It turns out that the ground state is of A_u symmetry and the lowest excited doublet state corresponding to a single MO transition $\phi_4(a_u)\rightarrow\phi_5(b_{1g})$ is of B_{1g} symmetry, the energy separation between the two states being only 0.03 eV. Since both the states are nearly degenerate, the nuclear deformation of $B_{1u}(A_u\times B_{1g})$ symmetry should cause a strong vibronic interaction between them. Accordingly, we can expect that the ground state of the trication radical would undergo the second-order Jahn-Teller distortion from the D_{2h} to the C_{2v} nuclear arrangement. Of the three types of C-C bond distortion belonging to the B_{1u} symmetry, the one actually effective for the molecular-symmetry reduction can be given by examining the distribution of the transition density ρ between the ground and the lowest excited doublet state.[16-18] The nearest two-center components of the transition density, $\phi_4\phi_5$, are shown in Fig. 5.

We now calculate the geometrical structure with respect to C-C bond lengths of the trication radical as follows: As a starting geometry for iterative PPP-type SCF MO calculation, we adopt a nuclear configuration in which C-C bond lengths are distorted so that the set of displacement vectors may match up with the distribution of the transition density shown in Fig. 5. Then, self-consistency has been achieved at a set of C-C bond lengths corresponding to a lower symmetrical nuclear arrangement (C_{2v}). The obtained bond lengths and ring charges for the C_{2v} nuclear arrangement are shown in Fig. 5. Here, the stabilization energy, defined as the difference in total energy between the fully-symmetrical D_{2h} and the reduced C_{2v} molecular geometry,[16,17,19] is calculated to be 0.403 eV. In Table 1 are summarized the electron densities and bond orders for comparision with those of the broken-symmetry CDW solution. Moreover, the unpaired spin densities and the associated proton hfs constants calculated by assuming the C_{2v} nuclear arrangement are listed in Table 2. It is clear from Tables 1 and 2 that the density matrix elements of the symmetry-adapted RHF solution corresponding to the C_{2v} nuclear arrangement show a striking resemblance to those of the stable

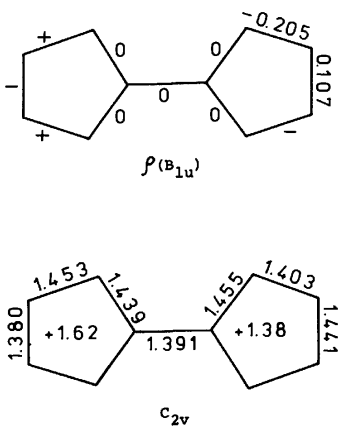

Fig. 5. The distribution of the nearest two-center components of transition density ρ and the optimized bond lengths (in Å) and ring charges at the C_{2v} nuclear arrangement.

broken-symmetry CDW solution and the unpaired electron is confined to the single five-membered ring having a ring charge of 1.38 (see Fig. 5). It is further proved that the present symmetry-adapted RHF solution (C_{2v}) is lower in energy than the stable CDW solution by 0.154 eV. From these aspects, it can be said that the broken-symmetry CDW solution is realized in the C_{2v} nuclear arrangement, becoming to be symmetry adapted.

The Ion Radicals of Fulvalene and Heptafulvalene. In connection with the fulvalene trication radical, it is noted that the RHF solution for the trianion radical, as well as that for the monoanion radical, is doublet stable ($\lambda_{min}=0.619$ eV) at the optimum nuclear arrangement with the D_{2h} symmetry. This shows a sharp contrast to the cases of the trication and monocation radicals. The explanation for this distinct difference between the anion radicals and the cation radicals of fulvalene can be given qualitatively as follows. From the stability conditions of the RHF solution, it is seen that the occurrence of the RHF instability depends on the magnitudes of energy separation between the RHF ground state and the singly excited doublet configurations. In fulvalene with the D_{2h} symmetry, the highest two occupied orbitals are nearly degenerate (in the HMO approximation those orbitals are accidentally degenerate). For the monocation and trication radicals, which are formed respectively by taking off one and three electrons from those orbitals, the RHF ground states are nearly degenerate with the respective lowest singly excited configurations. For this reason, the RHF solutions turn out to be doublet unstable. While, for the monoanion and trianion radicals the lowest singly excited configurations are well separated from the respective RHF ground states, so that the RHF solutions turn out to be doublet stable. In this connection, we also refer to the characteristic features of the RHF instabilities found in the ion radicals of heptafulvalene.[5,6] In heptafulvalene, the situation of the orbital pattern is quite different from that in fulvalene: The molecular orbitals that are accidentally degenerate in the HMO approximation are the lowest two unoccupied orbitals. Hence, for the monoanion and trianion radicals, which are formed respectively by adding the extra one and three electrons to those orbitals, the RHF ground states turn out to be nearly degenerate with the respective lowest singly excited configurations, resulting in the occurrence of the doublet instabilities in the RHF solutions. In cases of the monocation and trication radicals, the RHF solutions turn out to be double stable since the lowest singly excited configurations in question are well separated from the respective RHF ground states. Therefore, the origin of the instabilities of the RHF solutions and related phenomena, especially the anomalies in the spin-density distributions in the ion radicals of fulvalene systems, can be ascribed to the near degeneracy of the highest two occupied or the lowest two unoccupied orbitals inherent in the respective fulvalene systems.

Concluding Remarks. In the framework of the HF approximation, we have been concerned with the problem of the localization of unpaired electron in the

fulvalene trication radical. The results of the present calculations based on the RHF instability and the second-order Jahn-Teller theory show that the ground-state geometrical structure of the trication should be of C_{2v} symmetry and in the stable nuclear arrangement the unpaired electron is localized essentially on the single five-membered ring having a smaller positive charge. It has also been demonstrated that the occurrence of the RHF instability provides useful information about the type of wave function and the symmetry of nuclear framework. Especially, the resulting broken-symmetry CDW solution is shown to give a good account of the mechanism how the localization of unpaired electron occurs.

It is noted that the trication radical of 2,5-bis(2,4-cyclopentadien-1-ylidene)-1,4-cyclohexadiene, [5.6.5]quinarene, is expected to undergo a molecular symmetry reduction ($D_{2h} \rightarrow C_{2v}$) and exhibit an anomalous spin-density distribution similar to that of the fulvalene trication radical.

References

1) J. Cizek and Paldus, *J. Chem. Phys.*, **47**, 3976 (1967).
2) J. Paldus and J. Cizek, *Chem. Phys. Lett.*, **3**, 1 (1969).
3) M. D. Sevilla, J. H. Flajer, G. Vincov, and H. J. Dauben, *J. Am. Chem. Soc.*, **91**, 4139 (1969).
4) N. L. Bauld, C. S. Chang, and J. H. Eilert, *Tetrahedron Lett.*, **1973**, 153.
5) A. Toyota, M. Saito, and T. Nakajima, *Theoret. Chim. Acta*, **56**, 231 (1980).
6) A. Toyota and T. Nakajima, *Theor. Chim. Acta*, **61**, 505 (1982)
7) W. von E. Doering, "Theoretical Organic Chemistry. The Kekulé Symposium," Butterworths, London (1959).
8) A. G. Davies, J. R. M. Giles, and J. Lusztyk, *J. Chem. Soc., Perkin Trans. 2*, **1981**, 747.
9) H. C. Longuet-Higgins and J. A. Pople, *Proc. Phys. Soc. London, Sect. A*, **68**, 591 (1955).
10) H. Yamaguchi, T. Nakajima, and T. L. Kunii, *Theor. Chim. Acta*, **12**, 349 (1968).
11) J. Paldus and J. Cizek, *J. Polym. Sci.*, **29**, 199 (1970).
12) H. M. McConnell, *J. Chem. Phys.*, **24**, 632, 764 (1956).
13) H. Nakatsuji, *J. Am. Chem. Soc.*, **96**, 24, 30 (1974).
14) A. Toyota, T. Tanaka, and T. Nakajima, *Int. J. Quantum Chem.*, **10**, 917 (1976).
15) H. A. Jahn and E. Teller, *Proc. R. Soc. London, Ser. A*, **161**, 220 (1937).
16) T. Nakajima, A. Toyota, and S. Fujii, *Bull. Chem. Soc. Jpn.*, **45**, 1022 (1972).
17) T. Nakajima, *Top. Curr. Chem.*, **32**, 1 (1972).
18) L. Salem, *Chem. Phys. Lett.*, **3**, 99 (1969).
19) L. C. Snyder, *J. Phys. Chem.*, **66**, 2299 (1962).

Water Photolysis by Means of Visible Light with a System Composed of Prussian Blue and the Tris(2,2′-bipyridine)ruthenium(II) Complex

Masao KANEKO,* Naoki TAKABAYASHI, Yukio YAMAUCHI, and Akira YAMADA*
The Institute of Physical and Chemical Research,
Hirosawa, Wako, Saitama 351
(Received May 2, 1983)

A water-photolysis system composed of Prussian Blue (PB) and the tris(2 2′-bipyridine)ruthenium(II) complex([Ru(bpy)$_3$]$^{2+}$)which evolves hydrogen and oxygen simultaneously was studied. Both the components worked catalytically in the photolysis. PB provides active sites for both H_2 and O_2 evolution. The dependence on the pH showed optimum conditions at pH 2. The photolysis required the presence of a cation, and only such cations as K^+ and Rb^+ whose hydrated ions are smaller than the pore size of the PB lattice were active for the reaction. The dependene on the KCl concentraition showed an optimum point at 0.5 mol dm^{-3}. The oxidative quenching of [Ru(bpy)$_3$]$^{2+*}$ by PB was suggested, but its ratio in the total quenching process was estimated to be only 8.5%. The static quenching of [Ru(bpy)$_3$]$^{2+*}$ by PB was demonstrated, and an interaction between the two components was shown by NMR spectroscopy. The effect of oxygen on the photolysis suggested that the reduction sites are located inside the PB lattice. A mechanism for the photolysis was proposed.

Water photolysis by visible light is attracting much attention in the chemical conversion of solar energy. Many studies of solar-energy conversion have been related to this subject.[1,2] The tris(2,2′-bipyridine)-ruthenium(II) complex ([Ru(bpy)$_3$]$^{2+}$) is the most promising photocatalyst for decomposing water photochemically.[1,3,4] Water photolysis with this complex requires, though, both electron mediator and catalysts. Methylviologen (MV^{2+}; 1,1′-dimethyl-4,4′-bipyridinium dichloride) has been studied as a promising electron mediator; however, the cation radical formed in its reaction system is too sensitive to oxygen oxidation for it to be used in a system evolving oxygen simultaneously. Moreover, the rather complicated system composed of [Ru(bpy)$_3$]$^{2+}$, MV^{2+}, and two kinds of catalysts for hydrogen and oxygen evolution (*e.g.*, Ref. 5) involves the problem of getting reproducible results.

It was found by the present authors[6] that Prussian Blue (PB) induces water photolysis to give hydrogen and oxygen simultaneously with the combination of [Ru(bpy)$_3$]$^{2+}$. PB is a polynuclear mixed-valent iron complex whose composition has been proposed to be $Fe^{III}_4[Fe(CN)_6]_3$;[7] it forms a colloidal aqueous solution. The studies of this simple photolysis system have shown that the PB works as a kind of electron mediator as well as a catalyst for both hydrogen and oxygen evolution.[6] Such multifunctionalities of PB must be due to its polynuclear and mixed-valent sturcture. In this paper the factors affecting the photochemical reaction as well as the reaction mechanism are reported.

Experimental

Materials. The potassium hexacyanoferrate(III), $K_3[Fe(CN)_6]$, and iron(II) chloride, $FeCl_2 \cdot 3.8\ H_2O$, were the purest commercially available grade. The PB was prepared by mixing aqueous solutions of both the iron salts at an equimolar ratio. The molar concentration (M=mol dm^{-3}) of PB in the text represents the concentration of each of the iron salts contained in the solution. The colloidal solution of PB thus prepared was stirred continuously before use in order to prevent the aggregation of the colloids, and used within 1 d. The [Ru(bpy)$_3$]$^{2+}$Cl$_2$ was prepared by the reaction of ruthenium(III) chloride and 2, 2′-bipyridine in methyl alcohol, and recrystallized twice from methyl alcohol.

Photochemical Reaction. A 10-ml aqueous solution of 5 mM PB and 10 μM [Ru(bpy)$_3$]$^{2+}$ containing 0.5 M KCl at pH 2 (HCl-KCl buffer) was stirred and irradiated with visible light under argon atmosphere in a sealed vessel with a volume of about 20 ml equipped with a silicone stopper for the gas sampling. The irradiation was made with a 500-W Xenon lamp through UV and IR cutoff filters (Toshiba VY-42 and IRQ-80). The light intensity at the illuminated surface was 78 mW cm^{-2}.

Measurements. The gases formed were analyzed mainly by gas chromatography with a column consisting of a Molecular Sieve 5 A, using argon as the carrier gas. The O_2 evolved by the photochemical reaction was calculated by subtracting the content of O_2 coming from the air. For this calculation, the blank O_2/N_2 ratio was obtained by measuring the ratio (O_2/N_2) in the same vessel containing the same solution without irradiation. The errors in the determinations were ±0.01 μl for H_2 and ±0.02 μl for O_2. The lifetime was measured by a single-photon-counting method, with an exciting light pulse of about 1 ns from a 12-atm hydrogen lamp. The particle size of the PB colloids was studied by means of transmission electron microscope (Hitachi H-3000), using phosphotungstic acid as the negative staining agent.

Results and Discussion

The mass spectrum of the gases evolved by the reaction of water containing D_2O and $H_2{}^{18}O$ in the presence of PB, [Ru(bpy)$_3$]$^{2+}$, and KCl showed that hydrogen and oxygen came from water.[6] The ratio of H_2 to O_2 was almost 2 to 1, corresponding to the theoretical value of water decomposition.[6] The time dependencies of the water photolysis, as represented by the amount of H_2 evolved at various concentrations of PB and [Ru(bpy)$_3$]$^{2+}$, are shown in Fig. 1. The photolysis occurs almost linearly with the time. The turnover number of [Ru(bpy)$_3$]$^{2+}$ in the photolysis with 1 μM [Ru(bpy)$_3$]$^{2+}$ and 500 μM PB is calculated to be 11 after 90 h. The visible spectrum of the solution after that reaction showed no actual change in the absorptions of either PB or [Ru(bpy)$_3$]$^{2+}$ indicating that both the reactants work as catalysts.

As has been described in the previour paper[6] the excitations of both the complexes were required for the water photolysis to occur. The irradiation of an aque-

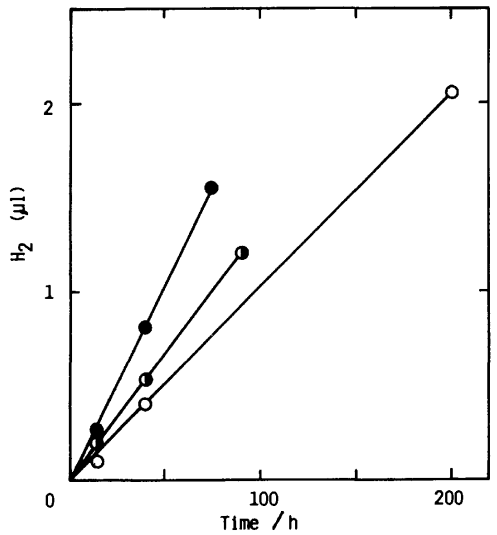

Fig. 1. Time dependencies of H_2 evolved by irradiation of the photolysis system composed of PB and $[Ru(bpy)_3]^{2+}$ in the presence of 0.5 M KCl at pH 2. Under argon at room temperature. Solution; 10 ml.

	PB (μM)	$[Ru(bpy)_3]^{2+}$ (μM)
◑	500	1
○	500	10
●	5000	100

ous solution containing EDTA, $[Ru(bpy)_3]^{2+}$, and PB gave H_2[6], suggesting that PB works as the H_2-evolving catalyst. The irradiation of an aqueous solution containing 10 μM ascorbic acid and 5 mM PB gave a small amount of H_2 (0.03 μl), while no H_2 was formed in the dark. An excess ascorbic acid brought about the formation of Prussian White, which is a Fe^{2+}-Fe^{2+}-type polynuclear cyanide complex, but H_2 was not formed even under irradiation. These results lead to the conclusion that H_2 is formed only by the irradiation of partially reduced PB. As will be shown later (Fig. 7), the ground state of Prussian White (entirely reduced PB) can not reduce protons because of its redox potential, but the excited state of a partially reduced PB must induce proton reduction to give H_2. The excitation of PB at the λ_{max} of 700 nm is known to be due to an intervalent charge transfer (ICT) between the adjacent Fe^{2+} and Fe^{3+} ions through the antibonding π orbitals of the bridging CN ligand.[8] Since the Fe^{2+} ion itself can not reduce protons, the reduction of the protons must occur through the antibonding π orbitals of CN groups under excited conditions. The partially reduced PB would bring about the excitation of the adjacent CN ligands under ICT conditions, and such activated states of the adjacent CN groups would reduce two near-by protons to give H_2.

It has been shown that the $[Ru(bpy)_3]^{3+}$ complex alone can not oxidize water in the absence of a catalyst.[9] The oxidation of water to give O_2 by $[Ru(bpy)_3]^{3+}$ in the presence of PB has led to the conclusion that PB works also as a catalyst for water oxidation.[6] Table 1 shows that a small amount of $[Ru(bpy)_3]^{3+}$ with respect to PB produces a high yield of O_2 when PB is used as the catalyst. The use of a higher concentration of

Table 1. Oxygen evolution by $[Ru(bpy)_3]^{3+}(ClO_4^-)_3$ with PB as the catalyst

$[Ru(bpy)_3]^{3+}$/M	(μl)	O_2 evolved Yield/%[a]
10^{-4}	4.5	74
10^{-3}	5.3	8.8
10^{-2}	11.5	1.9

PB: 5 mM, pH 2 (HCl-KCl buffer); solution: 10 ml; reaction for 1 h at 21 °C. a) Based on $[Ru(bpy)_3]^{3+}$.

$[Ru(bpy)_3]^{3+}$ increased the amount of O_2 evolved; however, its yield rather decreased. This is due to the oxidative degradation of PB, *i.e.*, the formation of a Fe^{3+}-Fe^{3+}-type complex (so-called Berlin Green), which was observed to form upon adding an excess of $[Ru(bpy)_3]^{3+}$ to PB. When a small amount of $[Ru(bpy)_3]^{3+}$ is used PB works as a good catalyst for O_2 formation by means of water oxidation. Considering the redox potential of $[Ru(bpy)_3]^{3+/2+}$ (1.27 V at pH 7), it can oxidize water to give O_2 only in the presence of a 4-electron oxidation catalyst.[10] Therefore, PB would work as a 4-electron oxidation catalyst to oxidize two molecules of water to form one molecule of O_2 through its polynuclear structure. The 4-electron catalytic reduction of O_2 by means of electrode reaction with PB-coated glassy carbon[11] supports the occurrence of a multi-electron process in the polynuclear PB lattice.

For the water photolysis, an excess of PB with respect to $[Ru(bpy)_3]^{2+}$ is required. Table 2 shows that at least a

Table 2. Dependencies of water photolysis on the PB and $[Ru(bpy)_3]^{2+}$ concentrations

$[Ru(bpy)_3]^{2+}$/M	[PB]/M	H_2(μl)
10^{-4}	5×10^{-3}	0.36
10^{-4}	5×10^{-4}	0
10^{-4}	5×10^{-5}	0
10^{-5}	5×10^{-3}	0.27
10^{-5}	5×10^{-4}	0.21
10^{-5}	5×10^{-5}	0

KCl: 0.5 M, pH 2 (HCl-KCl buffer); solution: 10 ml; reaction for 15 h at 21 °C.

50-fold excess of PB is needed. As will be shown later (Fig. 5), a low concentration of PB can efficiently quench the excited state of the Ru complex. It can, therefore, be concluded that a large excess of PB is necessary not for the quenching process, but for the catalytic redox reactions.

Colloidal particles of PB were studied by means of an electron micrograph. The average diameter of the particles was about 23 nm. Studies by means of optical and electron microscopes showed that the particles aggregate to *ca.* 1 μm in the presence of KCl, even when stirred. The standing of the colloidal solution in the presence of KCl induced the growth of the aggregates to tens of μm, and at last caused the sedimentation of almost 90% of the PB. The rates of aggregation and sedimentation depend on the KCl concentration. The aggregation and sedimentation of PB lower its activity markedly. The presence of KCl in the solution hinders the study by means of microscope; however, since PB

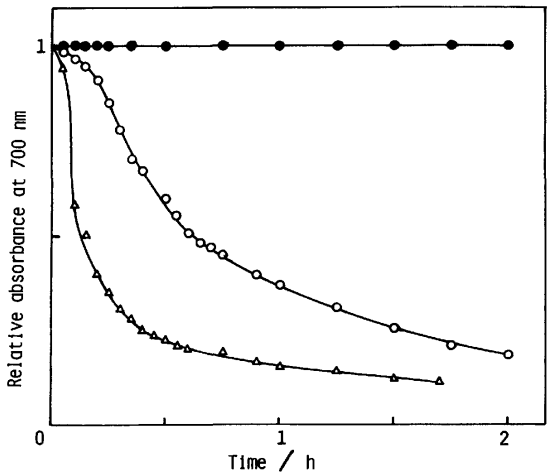

Fig. 2. Decrease of absorbance at 700 nm induced by aggregation and sedimentation of PB at pH 2. PB; 0.5 mM, $[Ru(bpy)_3]^{2+}$; 10 μM. KCl concentration (M): ●; 0, ○; 0.5, △; 0.9.

aggregation brings about a decrease of its absorbance at 700 nm, the aggregation can be followed by means of visible spectroscopy. The decrease in the absorbance at 700 nm on standing is shown in Fig. 2. No absorbance change was observed in the absence of KCl, while the addition of KCl remarkably enhanced the absorbance decrease; *i.e.*, the aggregation becomes very rapid on the addition of KCl when there is no stirring. During a photochemical reaction, no spectrum change is observed, since the reaction mixture is stirred vigorously. However, the results of Fig. 2 reflect at least the effect of KCl on the aggregation of PB, which is not observed as a spectrum change under stirring.

The pH dependency of the H_2 formation is shown in Fig. 3. No photochemical reaction was observed below pH 1.5 or above 3.5. Since H_2 is formed by the reduction of protons, a lower pH should give a higher H_2 yield. However, the O_2 evolution by the $[Ru(bpy)_3]^{3+}$ oxidation of water showed its optimum point at pH values from 2 to 3, and no O_2 was formed at pH 1.[9] If O_2 is not evolved efficiently, the back-electron transfer shown

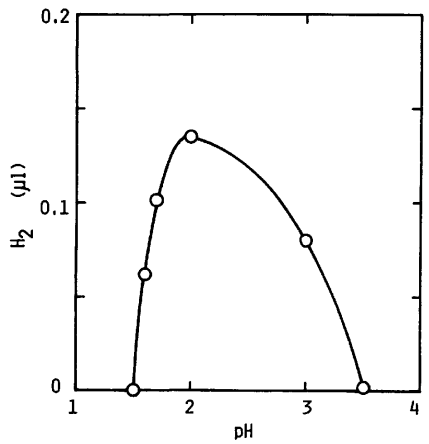

Fig. 3. pH dependency of H_2 formation. PB; 1 mM, $[Ru(bpy)_3]^{2+}$; 10 μM, KCl; 0.5 M, Buffer solution: pH 1.5—2 (HCl-KCl), pH 2.5—3 (CH_3COONa-HCl), pH 3.5 (CH_3COONa-CH_3COOH). Irradiated under argon for 15 h. Solution; 4 ml.

later as Eq. 4 lowers the efficiency of the photolysis. Thus, the low efficiency of O_2 evolution would be one of the reasons for the low activity below pH 2 in Fig. 3. Since the redox potential of PB^+/PB is only slightly more positive than that of H_2O/O_2 at pH 2 as shown later in Fig. 7, the shift of the latter potential to more positive value at lower pH than 2 (*e.g.*, 1.17 V for H_2O/O_2 at pH 1) might be the reason for the lower activity at the pH lower than 2.

In the present water-photolysis system, the addition of KCl enhances the reaction rate. The effect of a neutral salt on the photolysis is shown in Table 3. RbCl and KCl were effective, but NaCl, LiCl, and $BaCl_2$ did not induce photolysis. For the reduction of PB, a cation (Cat^+) must enter into the PB lattice in order to compensate the negative charge of the electron (Eq. 1):

Table 3. Effect of neutral salt on water photolysis with PB and $[Ru(bpy)_3]^{2+}$

Neutral salt	Diameter (nm) of hydrated cation	H_2(μl)
RbCl	0.24	0.2
KCl	0.25	0.2
NaCl	0.37	0
LiCl	0.47	0
$BaCl_2$	0.58	0

PB: 5 mM, $[Ru(bpy)_3]^{2+}$; 10 μM; salt: 0.4 M, pH 2; solution: 10 ml; reaction for 15 h at 21 °C.

$$(Cat^+)Fe^{III}[Fe^{II}(CN)_6]^{4-} + e^- + Cat^+ \longrightarrow (Cat^+)_2Fe^{II}[Fe^{II}(CN)_6]^{4-} \quad (1)$$

Itaya *et al.* recently studied the electrochemical reduction of PB coated on a platinum electrode in the presence of various neutral salts.[12] They found that neutral salts composed of cations whose hydrated ions are smaller than the pore size of the PB lattice (0.35 nm) can induce PB reduction, but neutral salts composed of larger cations are entirely ineffective. The results in Table 3 also shows that only the cations whose hydrated ions are smaller than the PB pore size are effective for the water photolysis.

The dependence of the photochemical reaction on the concentration of KCl is shown in Fig. 4. It has an optimum point at about 0.5 M. As has been described above, the present photolysis system demands the presence of a neutral salt such as KCl. On the other hand, neutral salt makes colloidal dispersions aggregate (see Fig. 2), because colloids are stabilized by an electrostatic repulsion of the charged particles. The decrease in photolysis at the higher concentration of KCl in Fig. 4 is thus explained by the easy aggregation of PB.

The excited state of the $[Ru(bpy)_3]^{2+}$ is efficiently quenched by PB. The formation of H_2 by the irradiation of the mixture of EDTA, $[Ru(bpy)_3]^{2+}$, and PB in water[6] indicated that the oxidative quenching of $[Ru(bpy)_3]^{2+*}$ by PB is involved. The Stern-Volmer plots of the $[Ru(bpy)_3]^{2+*}$ quenching by PB in the presence of 0.5 M KCl are shown in Fig. 5 (a). The quenching-rate constant is calculated to be 1.99×10^{10} ($M^{-1}\,s^{-1}$), using the lifetime (528 ns) of the $[Ru(bpy)_3]^{2+*}$ under these conditions. If the quenching is entirely due

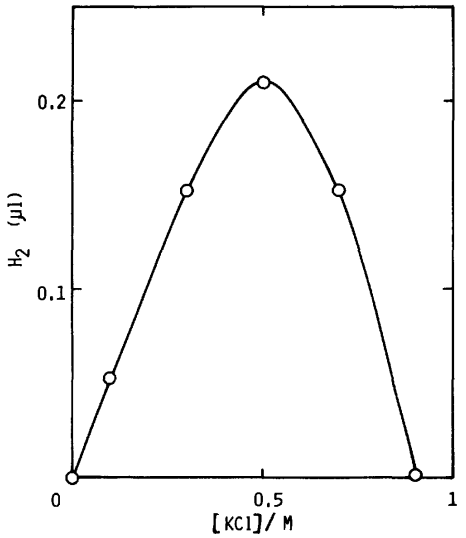

Fig. 4. Dependency of H_2 formation on KCl concentration. PB; 5 μM, $[Ru(bpy)_3]^{2+}$; 10 μM, pH 2. Irradiated under argon for 15 h. Solution; 10 ml.

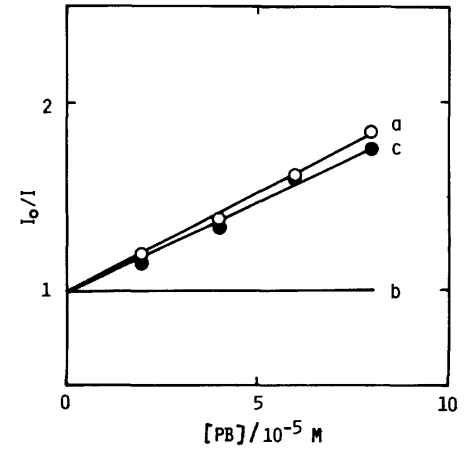

Fig. 5. Stern-Volmer plots for the quenching of $[Ru(bpy)_3]^{2+}$ by PB measured by emission intensity at 600 nm. $[Ru(bpy)_3]^{2+}$; 20 μM, pH 2, under argon, excited at 450 nm. (a) KCl; 0.5 M, (b) Theoretical line when no quenching occurs, (c) NaCl; 0.5 M.

to electron transfer from $[Ru(bpy)_3]^{2+*}$ to PB, it would not occur in the presence of NaCl instead of KCl, because PB can not be reduced in the presence of NaCl.[12] The plots must fall on the (b) line of Fig. 5 in this case. If the quenching is only partly due to the electron transfer, the Stern-Volmer plots measured in the presence of NaCl would fall between (a) and (b) lines. The quenching of $[Ru(bpy)_3]^{2+*}$ in the presence of NaCl without KCl was measured; it is shown in Fig. 5(c). The (c) line lies between (a) and (b), indicating that the quenching is partly due to electron transfer. The ratio of the electron-transfer quenching is estimated to be 8.5% from the ratio of the difference in the (a) and (c) slopes to the slope of (a), assuming that the other quenching process of the $[Ru(bpy)_3]^{2+*}$ by PB is not affected by the cation species of the neutral salt present.

The Stern-Volmer plots, as measured by means of emmision quenching and the lifetime, are shown in Fig. 6. The two plots fall on quite different lines,

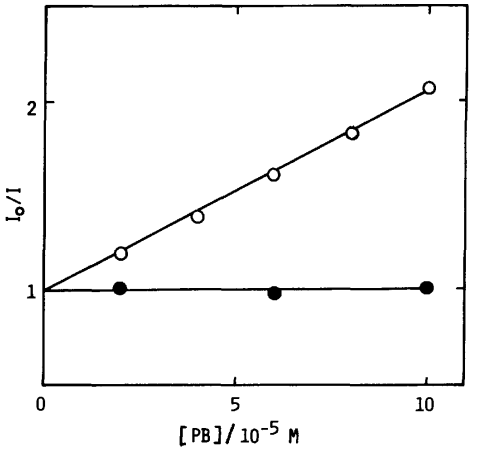

Fig. 6. Stern-Volmer plots measured by emission quenching (○) and lifetime (●) of $[Ru(bpy)_3]^{2+}$ with PB as a quencher. $[Ru(bpy)_3]^{2+}$; 20 μM, KCl; 0.5 M, pH 2, under argon, at 25 °C, excited at 450 nm.

indicating that static quenching occurs. It is suggested that there is an interaction between PB and $[Ru(bpy)_3]^{2+}$. No such interaction was observed in the visible spectrum, but the ^1H NMR spectrum showed an evidence of it. The proton signals of the bpy rings of the Ru complex shown in Table 4, that were observed at the δ values of 7—9, did not appear in the presence of PB at δ=0—15. It was observed that the proton signals of benzoic acid, which does not form any complex with PB, are not affected by the presence of PB. These results indicate some strong interaction, probably complex formation, between $[Ru(bpy)_3]^{2+}$ and PB. Such an interaction must cause the static quenching of $[Ru(bpy)_3]^{2+*}$ by PB.

Table 4. ^1H NMR of $[Ru(bpy)_3]^{2+}$ in the absence and presence of PB

Proton	δ in the absence of PB	δ in the presence of PB
H_a	9.04 (Doublet)	Not observed between δ=0—15
H_c	8.56 (Triplet)	
H_d	8.34 (Triplet)	
H_b	7.88 (Doublet)	

Measured in D_2O:

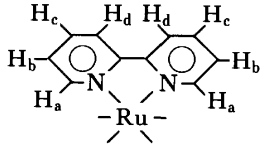

In a photochemical conversion system using MV^{2+} as an electron mediator, the presence of even a trace of oxygen inhibits the photochemical reaction, because O_2 very rapidly oxidizes the cation radical of MV^{2+} formed as an internediate. For the same reason, MV^{2+} is not suited as an electron mediator for a system that aims at simultaneous O_2 and H_2 evolution. The effect of O_2 on the water photolysis by PB and $[Ru(bpy)_3]^{2+}$ is shown in Table 5. It is interesting that H_2 was evolved even in the presence of O_2, although the efficiency decreased to one-third that of the system containing no O_2. The shape of the O_2 molecule can be approximated as a cylinder which has a diameter of about 0.28 nm and a length of 0.4 nm. The O_2 molecule can, therefore,

TABLE 5. EFFECT OF O_2 ON THE WATER PHOTOLYSIS WITH PB AND $[Ru(bpy)_3]^{2+}$

Atmosphere	H_2(μl)
Argon	0.27
Air	0.09

PB: 5 mM, $[Ru(bpy)_3]^{2+}$; 10 μM; KCl: 0.5 M, pH 2 (HCl-KCl buffer); reaction: 15 h.

enter into the PB lattice only from the direction of its axis, the inside of the lattice being fairly protected against O_2 attack. From a thermodynamic point of view, the active site of H_2 evolution must be sensitive to O_2 oxidation, leading to inactivation. The fact of H_2 evolution in spite of the presence of O_2 shown in Table 5 suggests, then, that the active reduction sites are located inside the PB lattice, allowing the water photolysis even under air.

The mechanism of the present water-photolysis system can be summarized as follows:

$$[Ru(bpy)_3]^{2+} \xrightarrow{450\ nm} [Ru(bpy)_3]^{2+*}, \quad (2)$$

$$[Ru(bpy)_3]^{2+*} + PB \longrightarrow [Ru(bpy)_3]^{3+} + PB^-, \quad (3)$$

$$[Ru(bpy)_3]^{3+} + PB^- \longrightarrow [Ru(bpy)_3]^{2+} + PB, \quad (4)$$

$$[Ru(bpy)_3]^{2+*} + PB^- \longrightarrow [Ru(bpy)_3]^{3+} + PB^{2-}, \quad (5)$$

$$PB^{2-} + 2H^+ \xrightarrow{700\ nm} PB + H_2, \quad (6)$$

$$2[Ru(pby)_3]^{3+} + H_2O \xrightarrow{PB} 2[Ru(bpy)_3]^{2+} + 1/2\ O_2 + 2\ H^+. \quad (7)$$

The excited state of $[Ru(bpy)_3]^{2+}$ is quenched by PB by means of a static process. A part of the quenching occurs by means of electron transfer from $[Ru(bpy)_3]^{2+*}$ to PB in the presence of cation such as K^+ or Rb^+, thus giving $[Ru(bpy)_3]^{3+}$ and PB^- (Eq. 3). Although back-electron transfer (Eq. 4) might prevail, the electron-transfer quenching of $[Ru(bpy)_3]^{3+*}$ by PB^- would also occur to form $[Ru(bpy)_3]^{3+}$ and PB^{2-} (Eq. 5). The PB^{2-} thus formed would reduce two protons under excited ICT-conditions to give H_2 (Eq. 6). The active site for this reduction process would be located inside the lattice, protected against O_2 attack. When four molecules of $[Ru(bpy)_3]^{3+}$ are accumulated, they oxidize water with the PB catalyst to give O_2 (Eq. 7).

As has been shown before (Fig. 6), strong static quenching occurs in the present photolysis system. In addition, the entire shift of the $[Ru(bpy)_3]^{2+}$ proton peaks of the NMR spectrum in the presence of PB (shown in Table 3), and the almost complete quenching of the excited state of $[Ru(bpy)_3]^{2+}$ by PB under usual reaction conditions, show that almost all the Ru complexes are interacting with PB. Assuming that PB has a spherical form, one particle 23 nm in diameter contains about 6×10^3 unit cells. One PB particle then interacts with 2.4×10^2 $[Ru(bpy)_3]^{2+}$ molecules under the usual conditions of a 10 μM Ru complex and 1 mM PB. Since $[Ru(bpy)_3]^{2+*}$ is entirely quenched by PB under these conditions, the occurrence of the multi-electron reduction of PB shown in Eq. 5 is possible. The mixing of $[Ru(bpy)_3]^{2+}$ with PB before or after the formation of the latter complex did not affect the catalysis. Considering this result and the fact that the Ru Complex is too large to be included in the PB lattice, the Ru complex must be present on the surface of the PB particle. The location of the oxidation sites has not been elucidated by the experiments so far; however, it might be located on or near the PB surface, considering that the oxidation and reduction sites must be located separately.

The presence of Pt colloids and/or RuO_2 (powders or sol) in the reaction mixture did not increase the rate of water photolysis. These results would support the above-mentioned mechanism, the idea that the inner or surface structure of PB colloids plays an important role in the H_2 and O_2 evolution.

The potential diagram of the present photolysis system (at pH 2) is shown in Fig. 7. The redox

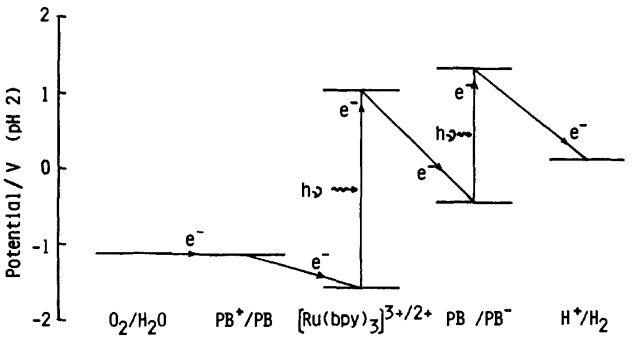

Fig. 7. Potential diagram of the water photolysis system with PB and $[Ru(bpy)_3]^{2+}$.

potentials of PB are the values at pH 4 reported by Itaya *et al.*[12] It could be assumed that the potentials of PB are almost pH-independent. Since the ground state of PB^- can not reduce protons potentially, the excitation of the partially reduced PB is necessary in order to reduce H^+ to give H_2. Such a diagram is regarded as a model for the photoinduced electron flow of the photosyntesis, where two steps of excitation brings about an endoergic electron transfer from water to CO_2.

PB thus works as a kind of electron mediator and also as a catalyst for both H_2 and O_2 evolution. These multifunctionalities of PB are due to its polynuclear and mixed-valent structure.

The authors are grateful to Prof. Y. Inoue and Dr. M. Ikeuchi for the measurements using the electron microscope.

References

1) M. Grätzel, *Ber. Bunsenges. Phys. Chem.*, **84**, 981 (1980).

2) Abstract of the 4th International Conference on Photochemical Conversion and Storage of Solar Energy (Israel, 1982).

3) C. Creutz and N. Sutin, *Proc. Natl. Acad. Sci. U.S.A.*, **72**, 2858 (1975).

4) J. -M. Lehn, "Photochemical Conversion and Storage of Solar Energy," ed by J. S. Connoly, Academic Press, New York (1981), p.161.

5) K. Kalyanasundaram and M. Grätzel, *Angew. Chem.*, **91**, 759 (1979).

6) M. Kaneko, N. Takabayashi, and A. Yamada, *Chem.*

Lett., **1982**, 1647.
7) H. J. Buser, D. Schwarzenbach, W. Petter, and A. Ludi, *Inorg. Chem.*, **16**, 2704 (1977).
8) M. B. Robin, *Inorg. Chem.*, **1**, 337 (1962).
9) M. Kaneko, N. Awaya, and A. Yamada, *Chem. Lett.*, **1982**, 619.
10) M. Kaneko and A. Yamada, *Adv. Polym. Sci.*, in press.
11) K. Itaya and I. Uchida, 46th National Meeting of the Chem. Soc. of Jpn., Oct. 1982, Abstr. p. 131.
12) K. Itaya, T. Ataka, and S. Toshima, *J. Am. Chem. Soc.*, **104**, 4767 (1982).

Polarized Absorption Spectra of Aromatic Radicals in Stretched Polymer Film. V. The Benzophenone Radicals

Tsuneyuki MINEGISHI, Hiroshi HIRATSUKA,* Yoshie TANIZAKI,† and Yuji MORI
Department of Chemistry, Faculty of Science, Tokyo Institute of Technology, Ohokayama, Meguro-ku, Tokyo 152
(Received May 25, 1983)

Benzophenone radical anions and ketyl radicals have been prepared in poly(vinyl alcohol) [PVA] films by means of γ-ray irradiation at 77 K. The polarized absorption spectra have been measured and used to determine the resolved spectra of these radicals. The spectrum of radical anions in the PVA film is very similar to that of ketyl radicals and can also be well explained by the calculated results for the hydrogen-bonding model of radical anions. The intense near-UV and visible absorption bands of radical anions in the PVA film are both correlated with those of ketyl radicals.

In previous papers we have reported the polarized absorption spectra of some aromatic radicals, determined by the stretched polymer film technique combined with γ-irradiation.[1-4] It was shown that the information on the direction of transition moments is useful for the assignment of the electronic transitions of these radicals.

A number of investigations have been reported on the preparation and the electronic structure of benzophenone radicals.[5-18] Porter and Wilkinson studied the visible absorption spectra of benzophenone ketyl radicals and radical anions prepared in an acidic or alkaline solution by means of flash photolysis.[5] They also studied the equilibrium between these radicals and determined the pK_a value of this equilibrium. The molar-extinction coefficients of these radicals in an acidic or alkaline solution have been determined by Hayon *et al.*, using the technique of pulse radiolysis-absorption spectroscopy.[11] McCelland investigated the electronic spectra of metal ion-paired ketyls by taking into account the effect of alkali metal ions as the perturbing electrostatic potential and semiquantitatively showed the spectroscopic blue shift of the visible absorption band.[7] Shida *et al.* measured the electronic absorption spectra of benzophenone radicals prepared by γ-irradiation in rigid glassy matrices and discussed the visible and near-UV bands in comparison with the results of MO calculations.[14] They suggested that the near-UV absorption bands of benzophenone radical anions and ketyl radicals have different polarization directions, though their spectra are quite similar in appearance. The polarization study of the electronic transition, however, has not been carried out for these radicals. It is desirable to determine experimentally the assignments of these absorption bands from the point of view of the direction of the transition moment.

In this study we investigate the polarized absorption spectra of benzophenone ketyl radicals and radical anions, prepared by the γ-irradiation of benzophenone in poly(vinyl alcohol) [PVA] films. The results are discussed in comparison with the results of MO calculations.

† Present address: The Department of Materials Science and Technology, Technological University of Nagaoka, Nagaoka, Niigata 949-54.

Experimental

Guaranteed reagent-grade benzophenone and methanol from Tokyo Kasei Co. Ltd., were used as received. PVA films were prepared by the method described previously.[2] Benzopheone was introduced into PVA films with the aid of methanol. The acidic sample film was prepared by immersing a PVA film into an acidic methanol solution of benzophenone containig 2 vol% of concd hydrochloric acid. The alkaline sample film was prepared by immersing a PVA film into an alkaline methanol solution of benzophenone containing 0.05 mol dm^{-3} of sodium hydroxide. These sample films were irradiated by ^{60}Co γ-ray for 2 h at a dose rate of 1.0×10^6 rad/h in liquid nitrogen. To control the concentrations of the ketyl radicals and radical anions of benzophenone, the irradiated films were taken out from liquid nitrogen and kept for tens of seconds. After this warming at room temperature, the films were again immersed in liquid nitrogen. The absorption spectrum of the radicals produced in the film was determined as the difference in the absorbances of the film before and after irradiation. In this experiment, the error introduced by the decrease of the parent molecule by the formation of radicals is less than 2% in absorbances below 360 nm because of the small molar-extinction coefficient ($\varepsilon\approx300$)[19] of the parent molecule. The absorption spectra from 300 to 850 nm were measured with a spectrophotometer (JASCO SS-50) equipped with a Rochon polarizer. For the polarization measurements, the sample films were stretched about 4 times before irradiation.[2]

Roothaan's restricted Hartree-Fock open-shell calculations were carried out in the pi-electron approximation for benzophenone ketyl radicals and radical anions. The configuration interaction calculations were limited to all the singly excited and ground configurations. In order to take into account the effects of the hydrogen bond, the point charge, Z_{eff} e, was located at the distance of 1.72 Å from the oxygen atom. The value of Z_{eff} was changed from 0 to 0.8. The valence-state ionization potentials (I_p), electron affinities (E_a), and resonance integrals (β) used were as follows; $I_p(C)=11.22$, $E_a(C)=0.62$, $I_p(=O)=11.76$, $E_a(=O)=3.87$, $I_p(-OH)=33.00$, $E_a(-OH)=11.47$, $\beta_{C-C}=-2.318$, $\beta_{C=O}=-2.70$, and $\beta_{C-OH}=-2.30$ in eV.

Results and Discussion

Curve a in Fig. 1 shows the absorption spectrum of the benzophenone radicals at 77 K produced by the γ-irradiation of the sample PVA films. By making reference to the spectra of benzophenone radical anions [$BP^{-\cdot}$] and ketyl radicals [$BPH^{\cdot}$] reported by Porter and

Wilkinson,[5] this is ascribed to the mixture of $BP^{-\cdot}$ and BPH$^{\cdot}$. The absorption maxima appearing at about 18×10^3 cm^{-1} and 16×10^3 cm^{-1} are assigned to BPH$^{\cdot}$ and $BP^{-\cdot}$ respectively. Assuming the values of the molar-extinction coefficients reported by Hayon *et al.* for these peaks,[11] the concentrations of $BP^{-\cdot}$ and BPH$^{\cdot}$ are estimated to be $(2.8\pm0.2)\times10^{-3}$ mol dm^{-3} and 1.1 ± 0.1 mol dm^{-3} respectively. Curve a′ in Fig. 1 is the spectrum measured at 77 K after a slight warming. The concentrations of $BP^{-\cdot}$ and BPH$^{\cdot}$ are estimated to be $(1.3\pm0.1)\times10^{-3}$ mol dm^{-3} and $(1.9\pm0.2)\times10^{-3}$ mol dm^{-3} respectively. It should be noted here that $BP^{-\cdot}$ was converted to BPH$^{\cdot}$ by warming, though some of the radicals disappeared. This change has been attributed to the acid-base equilibrium between benzophenone radicals.[5]

Curve b in Fig. 1 shows the spectrum of the γ-irradiated benzophenone in the PVA film containing methanol and hydrochloric acid. It is similar to curve a′ in appearance. The concentrations of $BP^{-\cdot}$ and BPH$^{\cdot}$ are estimated to be $(3.0\pm0.3)\times10^{-3}$ mol dm^{-3} and $(2.8\pm0.3)\times10^{-3}$ mol dm^{-3} respectively. After a slight warming, the spectrum of curve b′ was also observed. This is similar to that of BPH$^{\cdot}$ in an ethanol glass reported by Shida *et al.*[14] The peak of $BP^{-\cdot}$ disappeared. The concentration of BPH$^{\cdot}$ is $(6.0\pm0.5)\times10^{-3}$ mol dm^{-3}. Curve c in Fig. 1 shows the spectrum of the γ-irradiated benzophenone in the PVA film containing methanol and sodium hydroxide. After a slight warming, the spectrum of curve c′ was observed. Though there remains a shoulder at about 18×10^3 cm^{-1} which is assigned to BPH$^{\cdot}$, $BP^{-\cdot}$ is predominant after this warming. The concentrations of $BP^{-\cdot}$ and BPH$^{\cdot}$ are estimated to be $(2.2\pm0.2)\times10^{-3}$ mol dm^{-3} and $(0.2\pm0.1)\times10^{-3}$ mol dm^{-3} respectively. It should be noted that only 5% of the absorbance of the intense near-UV band at 29.5×10^3 cm^{-1} (curve c′) is due to BPH$^{\cdot}$.

Thus, under acidic or alkaline conditions benzophenone ketyl radicals or radical anions are predominantly prepared in the PVA films. The sample films for the polarization measurements of BPH$^{\cdot}$ and $BP^{-\cdot}$ were prepared in the same manner as those of b′ and c′ in Fig. 1.

Figure 2 shows the polarized absorption spectra of BPH$^{\cdot}$ (a) and $BP^{-\cdot}$ (b) in the stretched PVA films. The sample films (a) and (b) contain hydrochloric acid and sodium hydroxide respectively, as in curves 1b and 1c. In Fig. 2b there remains the absorption due to BPH$^{\cdot}$ and the molar ratio of BPH$^{\cdot}$ to $BP^{-\cdot}$ is about 0.13. The behavior of the dichroic ratio ($R_d=A_{/\!/}/A_{\perp}$) of these spectra is similar; the R_d values in the regions of the intense near-UV and visible bands are large. It is usually admitted that the molecular long axis is preferentially inclined to the stretching direction of the film. This has been confirmed by the analysis of the polarized absorption spectra for the radicals produced in the PVA films by γ-irradiation and for the parent molecule, benzophenone.[1-4,19] This means that the transition moments of these bands are polarized parallel to the molecular long axis. In order to show this situation more clearly, the resolved spectra were determined by making use of the polarized absorption spectra, according to a method described in a previous paper.[4] Figure 3 shows the resolved spectra of BPH$^{\cdot}$ (a) and $BP^{-\cdot}$ (b). The extreme values used to determine the resolved spectra were as follows; $R_d^1=1.86$ and

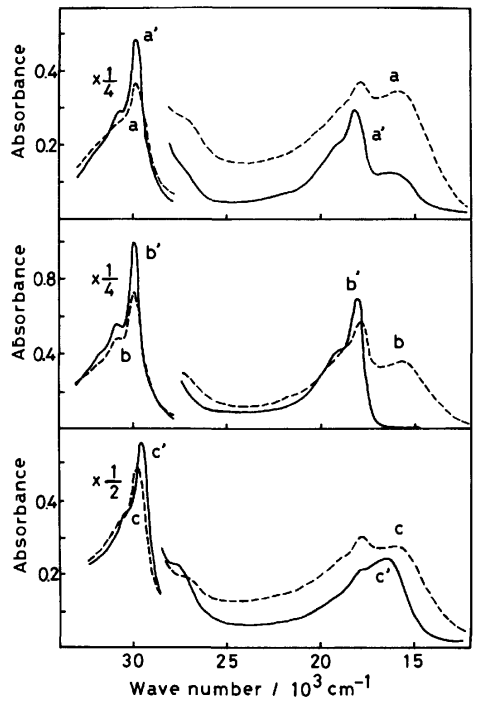

Fig. 1. Absorption spectra of the γ-irradiated benzophenone in the neutral (curve a), acidic (b) and alkaline (c) PVA films. Curves a′, b′, and c′ are the spectra observed after slight warming at room temperature.

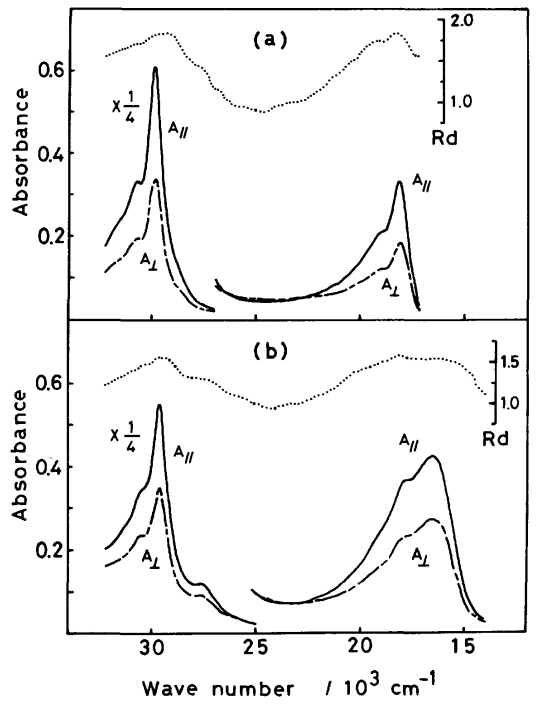

Fig. 2. Polarized absorption spectra of benzophenone ketyl radicals (a) and radical anions (b) in the stretched PVA films.

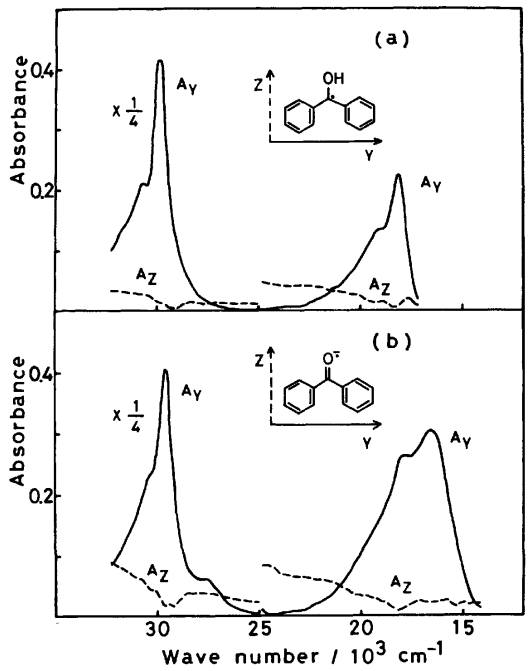

Fig. 3. Resolved spectra of benzophenone ketyl radicals (a) and radical anions (b). A_Y and A_Z curves are the molecular long- and short-axis polarized components, respectively.

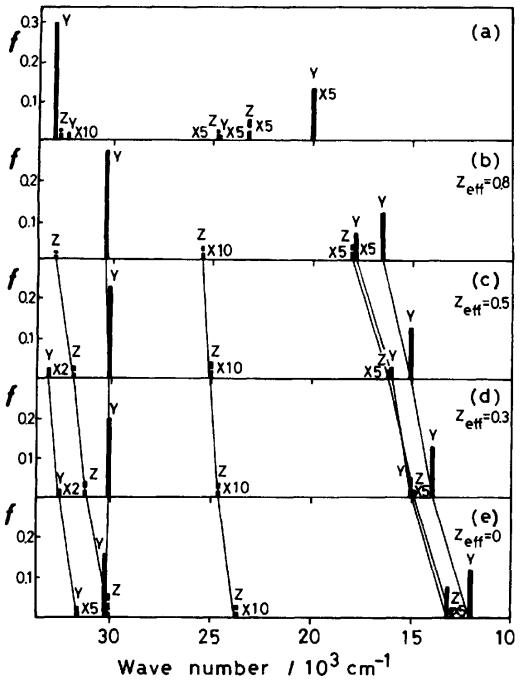

Fig. 4. Calculated results for benzophenone ketyl radicals (a) and radical anions (b)—(e). A point charge, Z_{eff} e, was set at the distance of 1.72 Å from the oxygen atom in order to take into accounts the effects of hydrogen bond.

R_d^s=0.87 for BPH·, and R_d^1=1.60 and R_d^s=0.94 for $BP^{-\cdot}$. As may be seen in Fig. 3, the main parts of the intense UV and visible bands of both radicals are long-axis (Y-) polarized components. No intense peak is found for the short-axis (Z-) polarized component.

The calculated results for BPH· are shown in Fig. 4a. The results are similar to those obtained by the Longuet-Higgins and Pople type MO calculation.[10,14] By comparison of Figs. 3a with 4a, it may be seen that the calculated transition energies are greater than the experimental values by $(2—3)\times10^3$ cm^{-1}, but the correspondence of the intense bands is fairly good. The Y-polarized bands at 18×10^3 cm^{-1} and 30×10^3 cm^{-1} are assigned to the first and seventh transitions respectively. The upper-state wave functions of these electronic transitions are represented by the following two main configurations; $\Psi_I=0.638\,\Phi_{8\to9}-0.383\,\Phi_{6\to8}+\cdots$ and $\Psi_{VII}=0.504\,\Phi_{8\to9}+0.424\,\Phi_{6\to8}+\cdots$, where the subscripts 6, 7, and 8 refer to the number of MO's and where MO ϕ_8 is the singly occupied orbital. Thus, these transitions originate mainly from two configurations, $\Phi_{8\to9}$ and $\Phi_{6\to8}$, and are similar to each other in characteristics. This assignment agrees well with those of other authors.[10,14]

The calculated results for $BP^{-\cdot}$ are shown in Fig. 4e. As $BP^{-\cdot}$ is considered to form a hydrogen bond in the PVA film, model calculations were carried out by locating a point charge, Z_{eff} e, at a distance of 1.72 Å from the oxygen atom of radical anions. These results are shown in Fig. 4b—d (Z_{eff}=0.8 to 0.3). On going from Z_{eff}=0 (Fig. 4e) to Z_{eff}=0.8, the first four transitions shift to blue, whereas the intense UV transition does not. The results for Z_{eff}=0.8 explain well the resolved spectra of Fig. 3b. The intense Y-polarized visible and near-UV bands at about 16.5×10^3 cm^{-1} and 29.5×10^3 cm^{-1} are, respectively, assigned to the first and the fifth transitons, the excited states of which are represented by the following two charge-resonance configurations; $\Psi_I=0.837\,\Phi_{8\to9}-0.278\,\Phi_{7\to8}+\cdots$ and $\Psi_V=0.402\,\Phi_{8\to9}+0.637\,\Phi_{7\to8}+\cdots$, where MO ϕ_8 is the singly occupied orbital.

The coefficients of the atomic orbitals of MO's, ϕ_6, ϕ_8, and ϕ_9 of BPH·, and ϕ_7, ϕ_8, and ϕ_9 of $BP^{-\cdot}$, are shown schematically in Fig. 5. As can be seen in Fig. 5, the

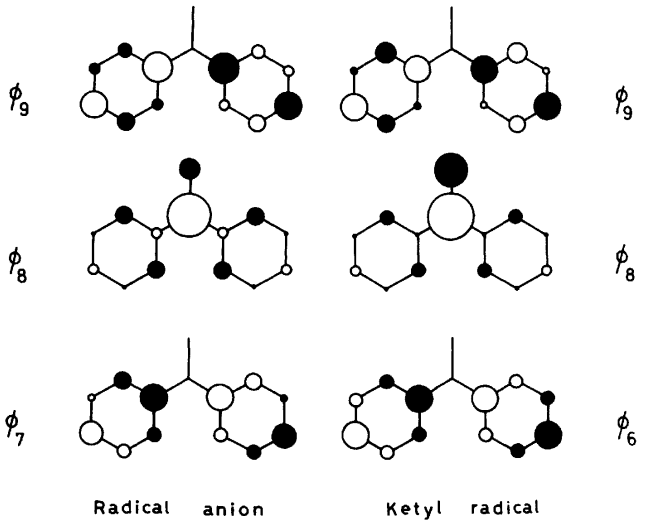

Fig. 5. Correlations of MO's ϕ_6, ϕ_8, and ϕ_9 of benzophenone ketyl radicals with the corresponding ones of radical anions (Z_{eff}=0.8). MO ϕ_8 is the singly occupied orbital. The size of the circle represents the relative value of the coefficient of the atomic orbitals. Open circles indicate positive sign and full circles negative sign.

MO's ϕ_6, ϕ_8, and ϕ_9, of $BPH^{\cdot}$ are similar to the ϕ_7, ϕ_8, and ϕ_9 of $BP^{-\cdot}$ respectively. Therefore, the $\Phi_{8\to9}$ and $\Phi_{7\to8}$ configurations of $BP^{-\cdot}$ are correlated with the $\Phi_{8\to9}$ and $\Phi_{6\to8}$ of $BPH^{\cdot}$ respectively. As a result,the Ψ_I and Ψ_V of $BPH^{\cdot}$ are correlated with the Ψ_I and Ψ_{VII} of $BPH^{\cdot}$. According to the results of the polarization measurement and the above discussion, the near-UV and visible bands of $BPH^{\cdot}$ in the PVA films can be said to be similar to those of $BP^{-\cdot}$ not only in spectral appearance, but also in the direction of the transition moments.

According to the Longuet-Higgins and Pople type MO calculation on $BP^{-\cdot}$, two transitions with large oscillator strengths are calculated to be located in the near-UV region.[14,20] The intense near-UV band observed in an MTHF glass was assigned to the Z-polarized transition by Shida *et al.*[14] However, in our caluclation (Fig. 4e, $Z_{eff}=0$) the Y-polarized transition is calculated to appear in this region with an oscillator strength larger than that of the Z-polarized one by a factor of 3. On going from $Z_{eff}=0$ to 0.8, this Z-polarized transition shifts to blue, while the Y-polarized one remains. Furthermore, the direction of the transition moment of the near-UV band of $BP^{-\cdot}$ in the PVA film is parallel to the molecular long axis (Y). Therefore, the main part of the intense near-UV band in an MTHF glass may be assigned to the Y-polarized transition.

References

1) H. Hiratsuka, K. Sekiguchi, Y. Hatano, and Y. Tanizaki, *Chem. Phys. Lett.*, **55**, 358 (1978).
2) H. Hiratsuka and Y. Tanizaki, *J. Phys. Chem.*, **83**, 2501 (1979).
3) K. Sekiguchi, H. Hiratsuka, Y. Hatano, and Y. Tanizaki, *J. Phys. Chem.*, **84**, 452 (1980).
4) H. Hiratsuka, H. Nakamura, Y. Tanizaki, and K. Nakajima, *Bull. Chem. Soc. Jpn.*, **55**, 3407 (1982).
5) G. Porter and F. Wilkinson, *Trans. Faraday Soc.*, **57**, 1686 (1961).
6) A. Beckett and G. Porter, *Trans. Faraday Soc.*, **59**, 2038 (1963).
7) B. J. McCelland, *Trans. Faraday Soc.*, **57**, 1458 (1961).
8) G. E. Adams, J. H. Baxedale, and J. W. Boag, *Proc. R. Soc. London, Ser. A*, **277**, 549 (1964).
9) K. Nakamura and N. Hirota, *Chem. Phys. Lett.*, **3**, 134, 137 (1969).
10) N. Kanamaru and S. Nagakura, *Bull. Chem. Soc. Jpn.*, **43**, 3443 (1970).
11) E. Hayon, T. Ibata, N. N. Lichtin, and M. Simic, *J. Phys. Chem.*, **76**, 2072 (1972).
12) S. Arimitsu and H. Tsubomura, *Bull. Chem. Soc. Jpn.*, **45**, 1357 (1972).
13) T. Shida and W. H. Hamill, *J. Am. Chem. Soc.*, **88**, 3683 (1966).
14) T. Shida, S. Iwata, and M. Imamura, *J. Phys. Chem.*, **78**, 741 (1974).
15) H. Murai and K. Obi, *J. Phys. Chem.*, **79**, 2446 (1975).
16) K. Obi and H. Yamaguchi, *Chem. Phys. Lett.*, **54**, 448 (1978).
17) M. Hoshino, S. Arai, M. Imamura, K. Ikehara, and Y. Hama, *J. Phys. Chem.*, **84**, 2576 (1980).
18) J. L. Marignier and B. Hickel, *Chem. Phys. Lett.*, **86**, 595 (1982).
19) J. Yoshino, T. Hoshi, H. Ogawa, T. Minegishi, and Y. Tanizaki, *Ber. Bunsenges. Phys. Chem.*, **81**, 748 (1977).
20) The MO diagram of ϕ_9 in Fig. 7 in Ref. 14 is erroneous (private communication).

Carbon Monoxide Absorption by Aqueous CuCl–$MgCl_2$ Absorbent

Masayuki KATSUMOTO,* Keiichi KANEHORI, and Taiji KAMIGUCHI†
Central Research Laboratory, Hitachi Ltd., Kokubunji, Tokyo 185
†*Kure Research Laboratory, Babcock-Hitachi K. K., Kure, Hiroshima 737*
(Received June 1, 1983)

Carbon monoxide absorption characteristics of an aqueous CuCl–$MgCl_2$ solution system are clarified. A CuCl 3.7 mol/l-$MgCl_2$ 4.7 mol/l solution is found to absorb 2.2 mol of CO per liter at 30 °C and $P_{CO}=2\times10^4$ Pa. This is 8 times greater than a CuCl 3.2 mol/l-HCl 8.2 mol/l solution and 16 times greater than a CuCl 4.8 mol/l-KCl 5.9 mol/l solution. The CO absorption of the concentrated aqueous solution of CuCl–$MgCl_2$ is accompanied with fine particle precipitation. This precipitate, which consists of CO, Cu^+, Mg^{2+}, Cl^-, and H_2O, is estimated to be $CO\cdot CuMgCl_3\cdot nH_2O$. The complex completely releases CO at 70 °C or above. Chloride ion influence on the formation of $CO\cdot CuMgCl_3\cdot nH_2O$ is discussed.

The carbon monoxide absorption properties of an aqueous copper(I) chloro-complex solution and aqueous CuCl–MCl_n (M=H^+, NH_4^+, metal ion and $n=1-3$) suspension systems have long been known.[1,2] Among these systems, the CuCl–$MgCl_2$ suspension was reported by Deringer[3] as absorbing a larger amount of CO at relativey low CO partial pressure region (above 20 kPa) than the aqueous solution of copper(I) chloro-complex. Decomposition pressure of the CO complex was said to be lowered only in the CuCl–$MgCl_2$ suspension absorbent, which contains solid $MgCl_2\cdot 6H_2O$.[3,4] The solid CO complex thus formed may contain $MgCl_2$, since the appearance of solid $MgCl_2\cdot 6H_2O$ changes after CO absorption.[3] However, neither the details of these phenomena nor the absorption behavior of CuCl–$MgCl_2$ solution has been clarified.

Aqueous absorbent that does not contain an acid or alkali, is quite promising for industrial use in recovering carbon monoxide from gas mixtures containing H_2O and CO_2. It includes no inflammable organic solvent and requires no pre-dehydration or pre-decarbonation of gas mixtures.[5,6]

The present work clarifies the CO absorption phenomena of the aqueous CuCl–$MgCl_2$ solution system.

Experimental

Materials. Copper(I) chloride and other chloride salts listed in Table 1 were purchased as reagent grade (Kanto Chemical Co., Inc.) and used as received. Carbon monoxide gas (99% pure) was used without further purification.

Copper(I) solutions were prepared by the following procedure. The desired amounts of chloride salts were weighed and transferred into a flask in a nitrogen box. Oxygen-free deionized water was added to the flask. Then, the flask was sealed and stirred. The flask was permitted to stand at 30 °C overnight to settle either the excess chloride or the impurities. The upper portion was used as a solution absorbent.

Metal ion concentration of the solution was determined by atomic absorption analysis. Chloride ion concentration was determined by spectrophotometry using mercury(II) thiocyanate and iron(III) ion,[7] after eliminating the metal ion as hydroxide precipitates.

The copper(II) ion content was checked by redox titration, using $TiCl_3$ standard solution as the reductant and monitoring the redox potential, for several solutions prepared as described above. Copper(II) ion content was always below 1% of the total copper ion concentration. Copper(II) ion does not form a compound with CO, and was ignored in the following discussion.

CO Absorption Measurement. Carbon monoxide absorption was measured using a constant pressure apparatus. The absorption vessel was connected to the apparatus *via* a tapered joint and immersed in temperature regulated water. The solution or suspension was rigorously stirred with a magnetic stirrer.

The amount of CO absorbed at $P_{CO}=1.01\times10^5$ Pa was determined as follows. Twenty ml of copper(I) solution or suspension was transferred to an absorption vessel. The apparatus was degassed quickly to the vapor pressure of the solution, and then CO gas was introduced to the apparatus. Pressure decrease due to absorption was detected by manometric pressure sensor and more CO gas was fed automatically to keep the pressure constant.

Dependence of the amount of CO absorbed on the CO pressure was determined as follows. After evacuation to a vapor pressure, measured quantities of CO were added. After each addition of CO, the equilibrium pressure and amount of CO absorbed were determined. The absorption equilibrium was attained within 1 h when the amount of CO absorbed was below 1.5 mol/l, after the precipitation occurred. It was considered that the maximum CO absorption under given conditions was obtained when the pressure change was less than 133 Pa within 30 min. No precipitation was observed before the CO absorption occurred.

To separate fine particles or a flake precipitate formed by

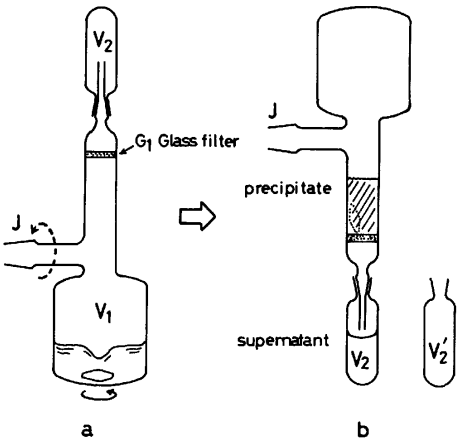

Fig. 1. Apparatus and procedure for precipitate separation from supernatant liquid.
V_1: Absorption vessel, V_2 and V_2': vessel for recuperation of liquid obtained after CO release, J: ground glass joint, a: CO absorption, b: separation of precipitate.

CO absorption in some cases, a vessel V_1, equipped with a glass filter (Fig. 1) was used. After CO absorption, V_1 was rotated around joint J. The supernatant portion dropped to vessel V_2, leaving the fine particles or flakes on the glass filter. Then, V_2 was replaced by V_2', previously filled with CO. The fine particles or the flakes remained on the glass filter were warmed and the quantity of CO released was measured with a gas buret. The liquid, obtained after CO release from the fine particles, dropped into vessel V_2'. During these procedures, the supernatant liquid and the precipitate were kept under an atmosphere of CO ($P_{CO}=1.01\times10^5$ Pa). This was done because the CO complex formed in the liquid phase as well as in the solid phase releases CO when the partial pressure of CO decreases. The white solid remained after CO release from the flake was dissolved in HCl solution. The total amount of CO released from the supernatant liquid and the precipitate corresponds to the amount of CO absorbed within the experimental errors.

Results and Discussion

Comparison of CO Absorption Behavior. The characteristics of CO absorption by aqueous CuCl-$MgCl_2$ solution (not including solid $MgCl_2\cdot6H_2O$) are compared with those of other CuCl-MCl_n solutions in terms of the maximum amount of CO absorbed, the molar ratio of CO absorbed to Cu^+, CO/Cu^+, and the appearance of precipitate. Results are summarized in Table 1.

Maximum Amount of CO Absorbed: The maximum amount of CO absorbed under given conditions increases with the dissolved CuCl concentration. It is noteworthy that the maximum amount of CO absorbed by the concentrated CuCl-$MgCl_2$ solution is larger than that by CuCl-MCl_n solution which contain nearly the same amount of dissolved CuCl as the CuCl-$MgCl_2$ solution.

CO/Cu^+ Ratio: The CO/Cu^+ ratio decreases as the dissolved CuCl concentration increases in the CuCl-HCl system.[1] All systems, except CuCl-$MgCl_2$, show the same tendency at 30 °C, regardless of whether flakes of CuCl-CO complex are formed.[1,8] The CO/Cu^+ ratio of the CuCl-$MgCl_2$ system decreases in the low concentration region. In high concentration region, the ratio increases with the dissolved CuCl concentration.

Appearance of Precipitate: When the concentration of CuCl and $MgCl_2$ was high, the precipitation of fine particles, which were considered as the CO complex, was observed. This kind of precipitate with a fine particle form has not been previously reported. This precipitate differs from the flake of CuCl-CO solid complex in both size and shape. The former is much smaller (about one-tenth that of the latter). It is also more spherical as opposed to flaky.

These observations clearly indicate that the CO absorption characteristics of the CuCl-$MgCl_2$ system are quite different from other CuCl-MCl_n systems.

Composition of the Precipitate with Fine Particle Form: The composition of supernatant solution, the content of precipitates, and the amount of CO released from the supernatant solution and the precipitate are summarized in Table 2.

Table 1. Maximum amount of CO absorbed by CuCl-MCl_n solutions (30 °C, $P_{CO}=1.01\times105$ Pa)

Concentration mol l^{-1}		Amount of CO absorbed	CO/Cu^+	Appearance of precipitate
CuCl	MCl_n	mol l^{-1}		
CuCl-$MgCl_2$				
0.79	1.95	0.32	0.40	—
2.20	3.27	0.62	0.28	—
2.57	3.46	1.03	0.40	Fine particle
2.61	3.64	1.24	0.47	Fine particle
2.30	3.93	1.43	0.62	Fine particle
2.80	3.92	1.86	0.66	Fine particle
3.00	4.80	1.83 (3×10^4 Pa)	0.61 (3×10^4 Pa)	Fine particle
3.70	4.70	2.23 (2×10^4 Pa)	0.60 (2×10^4 Pa)	Fine particle
CuCl-HCl				
0.26	2.00	0.15	0.57	—
0.98	4.62	0.40	0.48	—
2.24	6.77	0.91	0.41	—
3.15	8.15	1.30	0.41	Flake
CuCl-LiCl				
0.54	3.50	0.23	0.43	—
1.90	6.10	0.47	0.25	—
2.70	7.60	0.68	0.25	Flake
3.50	9.20	0.88	0.25	Flake
CuCl-NaCl				
0.76	3.24	0.28	0.37	—
2.20	5.40	0.44	0.20	—
3.20	6.40	0.95	0.29	Flake
CuCl-NH_4Cl				
0.77	2.33	0.30	0.39	—
2.04	4.16	0.62	0.28	—
4.31	6.97	0.65	0.15	—
5.30	7.71	0.64	0.12	—
CuCl-KCl				
0.23	1.34	0.12	0.52	—
1.53	3.32	0.38	0.24	—
2.61	4.44	0.56	0.22	—
3.93	5.52	0.88	0.22	Flake
4.84	5.88	1.07	0.22	Flake
CuCl-$CaCl_2$				
0.16	0.75	0.08	0.53	—
1.65	2.84	0.53	0.31	Flake
2.77	3.64	0.73	0.26	Flake
CuCl-$SrCl_2$				
0.26	0.93	0.16	0.63	—
1.02	1.97	0.35	0.34	—
2.69	3.30	0.78	0.29	Flake
CuCl-$CoCl_2$				
0.22	0.93	0.13	0.59	—
1.42	3.07	0.41	0.29	—
1.90	4.58	0.57	0.30	Flake
CuCl-$NiCl_2$				
0.26	1.04	0.14	0.53	—
1.65	3.05	0.43	0.26	Flake
2.17	3.80	0.53	0.25	Flake

For the CuCl-$MgCl_2$ and CuCl-$MgCl_2$-MCl_n solutions, the following results were obtained.

(1) About 80% of CO absorbed, was released from the fine particles.

(2) CO/Cu^+ ratio was about 0.8 for the precipitate and 0.2 for the supernatant solution.

TABLE 2. COMPOSITION OF SUPERNATANT LIQUID AND FINE PARTICLE PRECIPITATE
(30 °C, P_{CO}=1.01×10^5 Pa, volume of absorbent:20 ml)

Absorbent (mol/l)			Supernatant							Precipitate					
			Composition (mol/l)				volume (ml)	CO released (mmol)	CO / Cu^+	Content (mmol)				CO released (mmol)	CO / Cu^+
CuCl	$MgCl_2$	MCl_n	Cu^+	Mg^{2+}	M^{n+}	Cl^-				Cu^+	Mg^{2+}	M^{n+}	Cl^-		
2.9	4.0	—	2.2	3.6	—	9.4	10	4.4	0.2	37	44	—	131	28.3	0.76
2.4	3.1	0.6 $CrCl_3$	1.9	2.6	0.75	9.8	13.5	5.3	0.2	23	26	2.9	83	19.6	0.73
3.1	3.1	1.0 $CaCl_2$	2.5	2.6	1.3	10.3	13	5.9	0.2	28	28	5.3	95	23.2	0.83
2.8	3.3	1.1 $CoCl_2$	2.1	2.6	1.2	10.2	12	5.3	0.2	28	29	6.7	106	21.4	0.77
3.0	3.1	2.0 LiCl	2.4	2.4	2.3	10.1	12	5.9	0.2	31	32	11	104	24.8	0.80
4.8	—	5.1 KCl	4.4	—	5.0	10.0	18.5	7.9	0.1	15	—	8.9	a)	10.2	0.66

a) Amount of Cl^- could not be determined because the solid remaining after CO release was dissolved in HCl solution.

(3) The amount of chloride ion A_{Cl^-}, was expressed as $A_{Cl^-}=A_{Cu^+}+2A_{Mg^{2+}}+n\,A_{M^{n+}}$ where A_{Cu^+}, $A_{Mg^{2+}}$, and $A_{M^{n+}}$ are Cu^+, Mg^{2+}, and M^{n+} content in mol/l, respectively.

(4) As much Mg^{2+} as Cu^+ was contained in the precipitate.

(5) The Mg^{2+} concentration of the supernatant solution was always lower than that of the absorbent before CO absorption, while the M^{n+} concentration was always higher despite the rough separation process.

These results indicate that the precipitate with fine particle form consists of CO, Cu^+, Mg^{2+}, Cl^-, and H_2O. Since the M^{n+} distribution between a supernatant and a precipitate is opposite that of Mg^{2+}, M^{n+} is not considered as a precipitate compounent.

This precipitate might be expressed as the rational formula: $CO{\cdot}CuMgCl_3{\cdot}nH_2O$.

Flake formed when CO is absorbed by a concentrated CuCl–KCl solution, was analyzed in a simillar way. In this case, residue remained after release of CO from the flake was dissolved in HCl solution and the ratio of K^+ to Cu^+, K^+/Cu^+, was determined. As this ratio is much smaller than unity (0.58), the flake appears to be composed essentially of CuCl-CO as previously reported.[2,8]

Partial Pressure Dependence of CO Absorption. Pressure dependene of CO absorption by CuCl 3 mol/l-$MgCl_2$ 4.8 mol/l solution is shown in Fig. 2 (curve A). The amount of CO absorbed, A_{CO}, increases abruptly when CO partial pressure surpasses the threshold pressure, P^*_{CO}; and CO absorption above P^*_{CO} is accompanied with fine particle precipitation.

The pressure dependence of CO absorption by CuCl-$MgCl_2$ suspension and that by CuCl-KCl solution are also shown in Fig. 2. Curves C and D show the results obtained by Deringer.[3] This figure clearly shows that the dependence of the amount of CO absorbed on CO partial pressure is substantially the same for each CuCl-$MgCl_2$ system, regardless of whether it is a solution or a suspension. Furthermore, when CO was absorbed by CuCl 3 mol/l-$MgCl_2$ 5 mol/l suspension absorbent above P^*_{CO}, precipitate with fine particle form was also observed at the wall of the absorption vessel, in the vicinity of gas-liquid interface. Therefore, the CO complex pointed out by Deringer, which might contain $MgCl_2{\cdot}6H_2O$, is considered to be $CO{\cdot}CuMgCl_3{\cdot}nH_2O$.

The amount of CO absorbed by the concentrated CuCl-KCl system changes gradually with increasing CO partial pressure (curve E) in quite a different

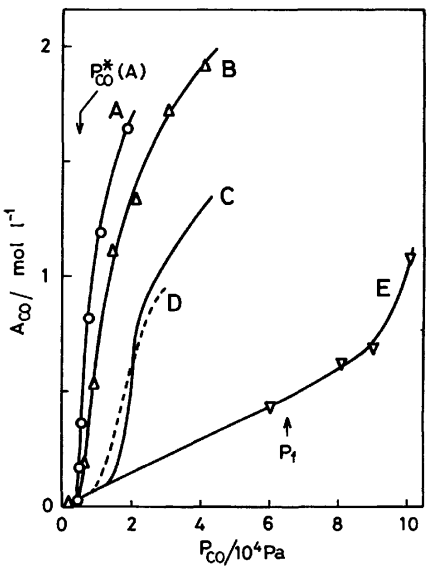

Fig. 2. Pressure dependence of CO amount absorbed, A_{CO}, by CuCl-$MgCl_2$ and CuCl-KCl (30 °C).
A: CuCl 3 mol/l-$MgCl_2$ 4.8 mol/l, B: CuCl 3 mol/l-$MgCl_2$ 5 mol/l (suspension), C: CuCl 1 g+3 ml of $MgCl_2$ suspension (Deringer[3]), D: CuCl 1 g+3 ml of Carnallite suspension (Deringer[3]), E: CuCl 4.8-KCl 5.9 mol/l.
P^*_{CO} (A): Threshold pressure for absorbent A above the amount of CO absorbed increases remarkably with increased CO partial pressure. CO absorption above P^*_{CO} is accompanied with fine particle precipitation. P^f_{CO}: Flake formation pressure for absorbent E. CO absorption above P^f_{CO} is accompanied with flake formation.

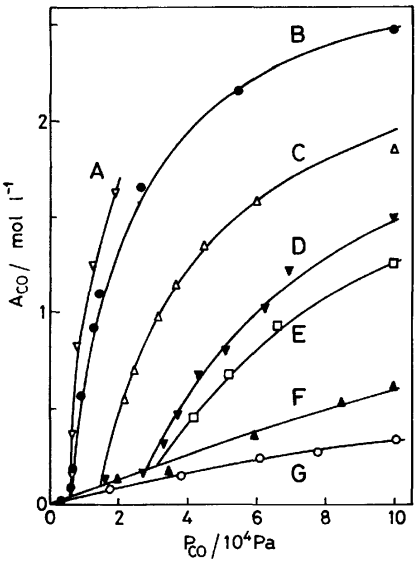

Fig. 3. Pressure dependence of CO amount absorbed, A_{CO}, for several CuCl-$MgCl_2$ solutions and suspensions (30°C).
A: CuCl 3 mol/l-$MgCl_2$ 4.8 mol/l, B: CuCl 3 mol/l-$MgCl_2$ 5 mol/l (suspension), C: CuCl 2.8 mol/l-$MgCl_2$ 3.9 mol/l, D: CuCl 3 mol/l-$MgCl_2$ 4 mol/l (suspension), E: CuCl 2.7 mol/l-$MgCl_2$ 3.7 mol/l, F:CuCl 2.2 mol/l-$MgCl_2$ 3.3 mol/l, G: CuCl 0.8 mol/l-$MgCl_2$ 2.0 mol/l.
Solid lines A to E were calculated using Eq. 4 with $K_2=8.86\times10^{-5}$ Pa^{-1} and $P^*_{CO}=5\times10^3$ Pa for A, $K_2=5.196\times10^{-5}$ Pa^{-1} and $P^*_{CO}=5\times10^3$ Pa for B, $K_2=2.625\times10^{-5}Pa^{-1}$ and $P^*_{CO}=1.16\times10^4$Pa for C, $K_2=1.26\times10^{-5}$ Pa^{-1} and $P^*_{CO}=2.33\times10^4$ Pa for D, and $K_2=1.191\times10^{-5}$ Pa^{-1} and $P^*_{CO}=2.43\times10^4$ Pa for E. Solid lines F and G were calculated using Eq. 2 with $K_1=3.725\times10^{-6}$ Pa^{-1} for F and $K_1=6.771\times10^{-6}$ Pa^{-1} for G.

manner than with CuCl-$MgCl_2$ system.

The partial pressure dependence of CO absorption by several CuCl-$MgCl_2$ solutions and suspensions are summarized in Fig. 3. There, P^*_{CO} increases as either CuCl or $MgCl_2$ content decrease, in either solution or suspension. Furthermore, the change in amount of CO absorbed with the CO pressure above P^*_{CO}, is smaller for more dilute absorbents.

These phenomena can be explained as follows. In solutions F and G, CO absorption proceeds *via* Reaction 1 as previously reported.[1,8]

$$\text{Cu(I)·chloro-complex(dissolved)} + \text{CO} \longrightarrow \text{CO·Cu(I)·chloro-complex(dissolved)} \quad (1)$$

The physical solubility of CO in this system is expected to be very low as in the case of the CuCl–HCl system.[8] Thus, the amount of CO absorbed, *i.e.* amount of CO·Cu(I)·chloro-complex dissolved, α in mol/l, is expressed by Eq. 2:

$$\alpha = \frac{K_1 P_{CO} A^\circ_{Cu^+}}{(1+K_1 P_{CO})}, \quad (2)$$

where K_1 denotes the absorption coefficient in Pa^{-1}, which depends on the absorbent composition and the temperature, and $A^\circ_{Cu^+}$, the total concentration of Cu^+ in mol/l.

The solid lines, F and G in Fig. 3, calculated using Eq. 2 and K_1, agree with the experimental results (K_1 was determined with the amount of CO absorbed at $P_{CO}=1.01\times10^5$ Pa).

For absorbents A to E, the amount of CO absorbed increases gradually with CO partial pressure below P^*_{CO}, in the same manner as for solutions F and G. Therefore, CO absorption in this region also proceeds *via* Reaction 1 .

Above P^*_{CO}, fine particle precipitation might occur *via* Reaction 3:

$$\text{CO·Cu(I)·chloro-complex(dissolved)} + Mg^{2+} + m\text{Cl}^- + n\text{H}_2\text{O} \longrightarrow \text{CO·CuMgCl}_3\cdot n\text{H}_2\text{O}\downarrow. \quad (3)$$

The pressure dependence of CO absorption in this region is expressed by Eq. 4:

$$A_{CO} = \frac{K_2(P_{CO}-P^*_{CO})A^\circ_{Cu^+}}{1+K_2(P_{CO}-P^*_{CO})}, \quad (4)$$

where K_2 is the absorption coefficient above P^*_{CO}, which depends on absorbent composition and temperature. Solid lines A to E of Fig. 3 calculated using Eq. 4, agree with the experimetal results. Values for K_2 and P^*_{CO}, used in the calculation are summarized in the figure caption.

To precipitate CO·$CuMgCl_3\cdot n\text{H}_2\text{O}$ a certain concentration of CO·Cu(I)·chloro-complex (dissolved) as well as Mg^{2+} and/or Cl^-, may be required. Once CO·$CuMgCl_3\cdot n\text{H}_2\text{O}$ precipitation occurs, the concentration of CO·Cu(I)·chloro-complex (dissolved), Mg^{2+} and Cl^- decrease. When CO partial pressure increases, the concentration of CO·Cu(I)·chloro-complex increases *via* Reaction 1. Then, precipitation occurs again *via* Reaction 3.

Temperatre Dependence of CO Absorption. The changes in the amount of CO absorbed, A_{CO}, by the CuCl 3 mol/l-$MgCl_2$ 5 mol/l suspension absorbent at $P_{CO}=4\times10^4$ Pa and at 1.01×10^5 Pa are shown in Fig. 4. The amount of CO absorbed decreases especially above

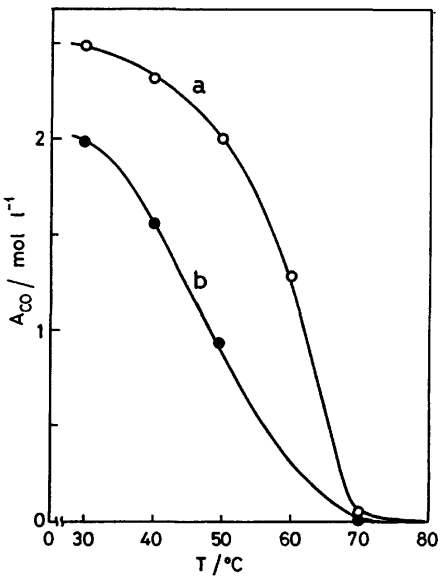

Fig. 4. Temperature dependence of amount of CO absorbed, A_{CO}, by CuCl 3 mol/l-$MgCl_2$ 5 mol/l (suspension).
a: $P_{CO}=1.01\times10^5$ Pa, b: $P_{CO}=4\times10^4$ Pa.

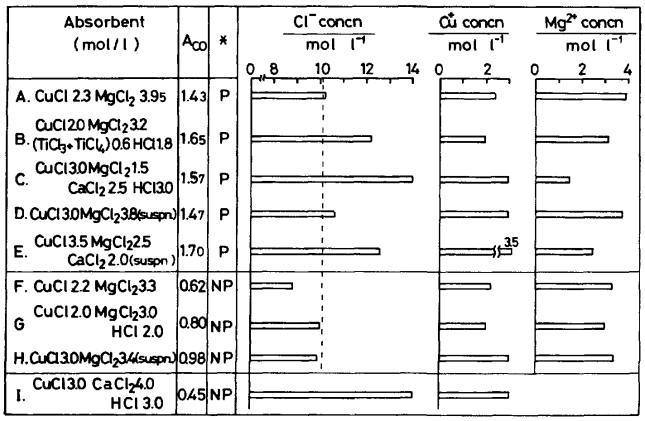

Fig. 5. Dependence of CO absorption behavior on ion concentration of solutions (30 °C: $P_{CO}=1.01\times10^5$ Pa).
* P: Precipitation was observed. NP: No precipitation was observed.

50 °C, becoming nearly zero at 70 °C. This means that the decomposition temperatre of the CO·$CuMgCl_3$·nH_2O complex at $P_{CO}=1.01\times10^5$ Pa is around 70 °C.

Influences of Chloride Ion Concentration on CO·CuMgCl₃·nH₂O Formation. Deringer claimed that only CuCl–$MgCl_2$ suspension absorbent containing solid $MgCl_2\cdot6H_2O$ absorbs a large amount of CO in the relatively low CO partial pressure range. As mentioned above, the amount of CO absorbed increases drastically above P^*_{CO} for both the CuCl–$MgCl_2$ solution and suspension absorbents. Therefore, the conditions proposed by Deringer are not always necessary for absorption of large amounts of CO by the CuCl–$MgCl_2$ system. Furthermore, this absorption of CO above P^*_{CO} closely relates to the formation of CO·$CuMgCl_3$·nH_2O.

The dependence of the absorption behavior of the CuCl-$MgCl_2$ system on the concentration of Cu^+, Mg^{2+}, and Cl^- is shown in Fig. 5. There is no threshold value for Cu^+ and Mg^{2+}, above that CO absorption accompanied with CO·$CuMgCl_3$·nH_2O precipitation.

On the contrary, absorbents containing more than 10 mol/l chloride ions manifest the CO absorption characteristic that is accompanied with the precipitation of CO·$CuMgCl_3$·nH_2O. Solution I, which contains 14 mol/l of chloride ion but no Mg^{2+}, absorbs only 0.45 mol/l of CO and no precipitation is observed.

Summary

The CO absorption by the concentrated aqueous CuCl-$MgCl_2$ solution system is characterized by (i) a large amount of CO absorbed per unit volume of absorbent, and (ii) precipitation of fine particles different from the flake complex of CuCl-CO. A chloride ion concentration of more than 10 mol/l in the CuCl-$MgCl_2$ system results in the formation of fine particles estimated to be CO·$CuMgCl_3$·nH_2O.

References

1) "Gmelins Handbuch der Anorganischen Chemie," Kupfer, Verlag Chemie, GmbH., Germany, (1958), Teil B, pp. 233—237.
2) M. I. Bruce, *J. Organomet. Chem.*, 44, 209 (1972).
3) H. Deringer, *Chimia*, 1, 125 (1947)
4) U. S. Patent, 2580527 (1952).
5) A. L. Kohl and F. C. Riesenfeld, "Gas Purification," McGraw-Hill, New York (1960), pp. 485—505.
6) D. J. Haase and D. G. Walker, *Chem. Eng. Prog.*, **70**(5), 74, (1974).
7) I. Iwasaki, S. Utsumi and T. Ozawa, *Bull. Chem. Soc. Jpn.*, **25**, 226 (1952)
8) W. Backen and R. Westin, *Acta Chem. Scand., Ser. A*, **33**, 85 (1979).

 © 1984 The Chemical Society of Japan Bull. Chem. Soc. Jpn., 57, 171—174 (1984)

Hydrates of Organic Compounds. VIII. The Effect of Carboxylate Anions on the Formation of Clathrate Hydrates of Tetrabutylammonium Carboxylates

Haruo NAKAYAMA* and Shigeru TORIGATA

Department of Chemistry, Faculty of Engineering, Yokohama National University, Tokiwadai, Hodogaya-ku, Yokohama 240

(Received June 28, 1983)

The solid-liquid phase diagrams of binary mixtures of tetrabutylammonium carboxylates, $(n\text{-}C_4H_9)_4$ NOOCR (R=H-n-$C_{10}H_{21}$ including various alkyl groups replaced by either methyl or ethyl group), with water were examined in order to confirm the formation of clathrate-like hydrates. The results can be summarized as follows: (1) for 14 carboxylates the formation of a clathrate-like hydrate is newly confirmed; (2) judging from melting points and hydration numbers, the hydrates can be classified into three groups: I, II, and III; (3) the group I hydrates, formed by the carboxylates with R=H, CH_3, C_2H_5, n-C_3H_7, i-C_3H_7, and t-C_4H_9, have hydration numbers around 30 and are the most stable hydrates among those examined in this experiment, with the exceptions of 2-methylpropionate and 2,2-dimethylpropionate hydrates; (4) the group II hydrates, with hydration numbers around 39, are formed by the salts with R=n-C_4H_9, s-C_4H_9, i-C_4H_9, and all the C_5H_{11}, and are relatively unstable (mp=5—11 °C); (5) the group III hydrates, with hydration numbers around 30 like the group I hydrates, are formed by the carboxylates with long alkyl chains from n-C_6H_{13} to n-$C_{10}H_{21}$ and are generally unstable; and (6) judging from the hydration number, the crystal structure of the group I and III hydrates seems to be isomorphous with a tetrabutylammonium fluoride hydrate, and that of the group II hydrates with a tetrabutylammonium benzoate hydrate.

As early as 1940, the formation of unusual hydrates of tetrabutylammonium carboxylates like formate and benzoate, which had a large number of water molecules per one salt molecule, was reported by Kraus *et al.*[1] In the subsequent crystallographic studies made by Jeffrey and his coworkers, it was concluded that hydrates of tetrabutylammonium acetate[2] and of tetrabutylammonium benzoate[3] had a clathrate-like structure similar in general character to the gas hydrates: the structure of the acetate hydrate is isomorphous with tetrabutylammonium fluoride hydrate,[4] in which each butyl group of the ammonium cation is located in a hydrogen-bonded framework of water molecules; and in the tetragonal benzoate hydrate, not only four butyl groups of the cation but also one benzyl group of the anion is surrounded by a hydrogen-bonded water framework.

Thus, there are at least two types of tetrabutylammonium carboxylate hydrates. However, we have no sufficient data to draw any conclusion as to the influence of an alkyl chain of a carboxylate anion on both the stability and the structure of the tetrabutylammonium carboxylate hydrates. In this paper, from the solid-liquid phase diagrams for 19 binary mixtures of tetrabutylammonium carboxylate-water, the effect of the shape and/or length of the alkyl group of a carboxylate anion on the stability (*i.e.*, melting point) and the crystal structure (*i.e.*, hydration number) of their clathrate hydrates has been systematically examined. These fundamental data would also offer a guiding principle, for example, for highly selective separation of a specific carboxylate anion from an aqueous solution containing several kinds of carboxylate anions by means of the formation of a mixed clathlate hydrate of tetrabutylammonium carboxylates.[5]

Experimental

Aqueous solutions of tetrabutylammonium carboxylates, except for formate, were prepared by a reaction between tetrabutylammonium iodide and the corresponding silver carboxyates in water, followed by filtration of AgI precipiate. Tetrabutylammonium iodide was synthesized by reacting tributylamine with butyl iodide in ethyl acetate and purifie by recrystallization from ethyl acetate-acetone mixture. Each silver carboxylate was obtained by mixing an aqueous solution of silver nitrate with an aqueous carboxylic acid solution after neutralization with NaOH, followed by repeated washing with water in order to remove the resultant sodium nitrate. An aqueous solution of tetrabutylammonium formate was prepared by neutralizing tetrabutylammonium hydroxide solution with formic acid solution. The hydroxide solution was obtained by treating tetrabutylammonium iodide with freshly prepared silver hydroxide in water. The silver hydroxide was obtained by reacting silver nitrate solution with sodium hydroxide solution, followed by filtration and by repeated washing with water. All the carboxylic acids were purchased from Tokyo Kasei Kogyo Co. Ltd. and were used without further purification. Some impurities contained in the carboxylic acid could be removed during the precipitation procedure of the silver salt of the carboxylic acid.

Solid-liquid phase diagrams for the binary systems of water-tetrabutylammonium carboxylate were determined in the same manner as described in the previous paper[6] (an ampoule method). The concentration of each mother solution was determined by a titration method using a standard sodium tetraphenylborate solution.[6]

Results and Discussion

The solid-liquid phase diagrams for tetrabutylammonium carboxylate-water binary systems are shown in Figs. 1, 2, and 3. The logarithm of the concentration expressed in mole fraction (X) is plotted against the reciprocal of the absolute temperature. The temperature expressed in ordinary Celsius units is shown on the upper side of each figure. For comparison, Fig. 1 includes the phase diagram of the tetrabutylammonium fluoride-water system reported earlier.[6,7] Because of the similarity of the data with each other, some of the results

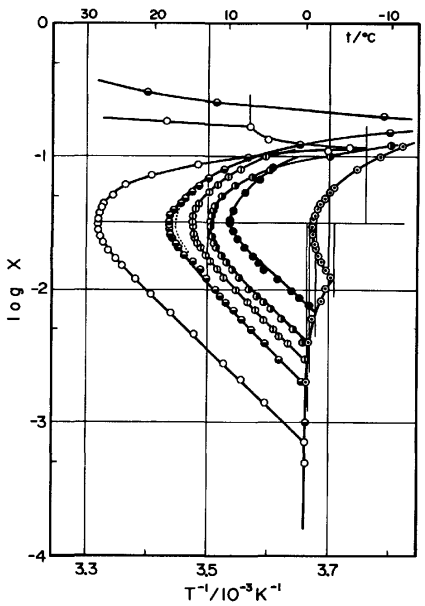

Fig. 1. Solid-liquid phase diagrams for the water-(n-$C_4H_9)_4NX$ systems.
○: X=F, ◑:X=HCOO, ⓓ: X=CH_3COO, ◒: X=C_2H_5COO, ·····: X=n-C_3H_7COO, ●: X=i-C_3H_7COO, ⊙: X=$(CH_3)_3CCOO$.

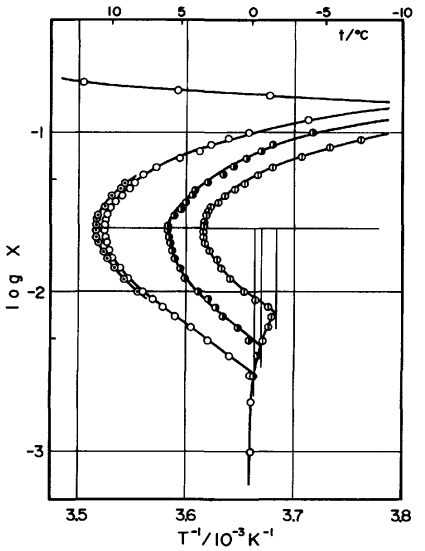

Fig. 2. Solid-liquid phase diagrams for the water-(n-$C_4H_9)_4NOOCR$ systems.
○: R=n-C_4H_9, ⊙: R=i-C_4H_9, ⓓ: R=n-C_5H_{11}, ◑: R=i-C_5H_{11}.

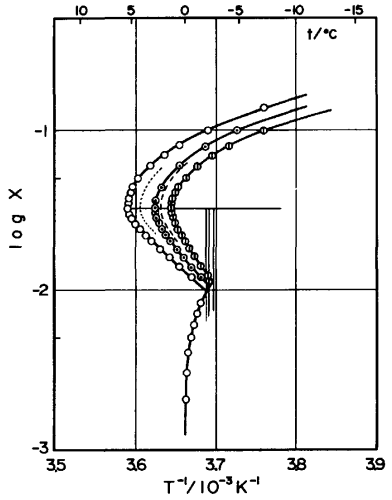

Fig. 3. Solid-liquid phase diagrams for the water-(n-$C_4H_9)_4NOOCR$ systems.
-----: R=n-C_6H_{13}, ⓓ: R=n-C_7H_{15}, ○: R=n-C_8H_{17}, ⊙: R=n-C_9H_{19}, ------: R=n-$C_{10}H_{21}$.

TABLE 1. MELTING POINTS AND HYDRATION NUMBERS OF THE CLATHRATE HYDRATES FORMED BY A SERIES OF TETRABUTYLAMMONIUM CARBOXYLATES (n-$C_4H_9)_4NOOCR$

R	Mp θ_m/°C	Hydration number
H	12.2(11.8[8])	30±1(32[8])
CH_3	14.8(14.9[8], 15.1[2])	30±1(32[8], 30.7[2])
C_2H_5	18.0(16.8[8], 18.1[8])	30±1(32[8])
n-C_3H_7	17.0(15.5[8])	31±1(32[8])
i-C_3H_7	9.8	30±1
n-C_4H_9	10.6(10.2[8])	40±1(40[8])
s-C_4H_9	7.7	40±1
i-C_4H_9	11.3	39±1
t-C_4H_9	−0.7	30±2
n-C_5H_{11}	3.4	40±1
$CH_3(CH_2)_2CH(CH_3)$	5.1	39±2
$CH_3CH_2CH(CH_3)CH_2$	5.1	39±2
$CH_3CH(CH_3)(CH_2)_2$	6.0	39±2
$CH_3CH_2CH(C_2H_5)$	10.6	39±1
n-C_6H_{13}	2.3	30±2
n-C_7H_{15}	1.3	29±2
n-C_8H_{17}	5.4	29±2
n-C_9H_{19}	2.8	31±2
n-$C_{10}H_{21}$	4.3	30±2

are either excluded from these figures or represented by a dotted or a broken line only in the vicinity of each congruent point. These figures clearly show that all the salts examined in this experiment can form clathrate-like hydrates similar to that of the fluoride, although their congruent melting points are considerably lower than that of the fluoride hydrate (Fig. 1). All the melting points and the hydration numbers, determined from each congruent melting point and congruent composition, are summarized in Table 1, together with those previously reported by other authors.[2,8] Among these hydrates, 14 hydrates which have not been reported earlier are confirmed in this experiment.

In Fig. 4, the melting point of the clathrate hydrate is plotted against the number of carbon atom in the main alkyl chain of each carboxylate anion. The points corresponding to the hydrates of a series of normal alkanoates are connected by a solid line. A filled circle indicates a hydrate with hydration number around 30 and an open circle indicates one with hydration number around 39. From this figure it is clear that the effect of an alkyl chain in the carboxylate anion on the formation of the clathrate hydrate of the tetrabutylammonium carboxylates is fairly complicated and also that all the

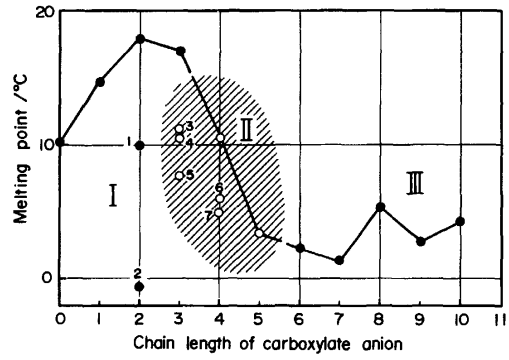

Fig. 4. Relatioship between the melting points of the tetrabutylammonium carboxylate, $(n\text{-}C_4H_9)_4NOOCR$, hydrates and the chain length of R in the carboxylate anion. Filled circle indicates the hydrate with hydration number of 30 and open circle indicates the one with hydration number of 39. All points not numbered indicate that R is normal alkyl group. Numbered point means as follows:
1: $R=CH_3CH(CH_3)$; 2: $R=(CH_3)_3C$; 3: $R=CH_3CH(CH_3)CH_2$; 4: $R=CH_3CH_2C(C_2H_5)$; 5: $R=CH_3CH_2CH(CH_3)$; 6: $R=CH_3CH(CH_3)CH_2CH_2$; 7: $R=CH_3(CH_2)_2CH(CH_3)$ and $R=CH_3CH_2CH(CH_3)CH_2$. Three groups shown by I, II, and III are explained in the text.

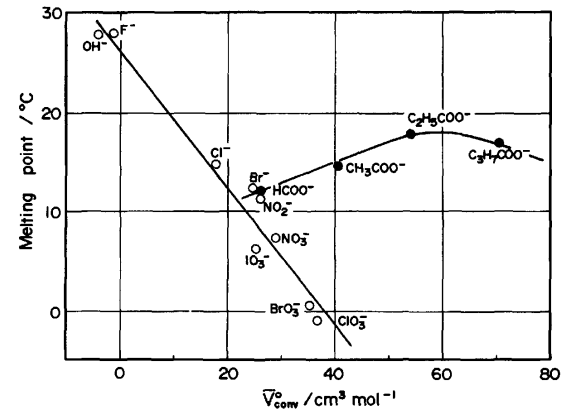

Fig. 5. Relationship between the melting points of the hydrates of tetrabutylammonium salt, $(n\text{-}C_4H_9)_4NX$, and the conventional partial molal ionic volumes of the anion X.

points corresponding to the hydrates of hydration number 39 (open circles) gather in a limited region (shown by the hatched area). Thus, we analyze these results by classifying, tentatively, these hydrates into three groups: I, II, and III, as also indicated in Fig. 4.

The group I hydrates include the hydrates formed by the carboxylates with R=H, CH_3, C_2H_5, $n\text{-}C_3H_7$, $i\text{-}C_3H_7$, and $t\text{-}C_4H_9$. These hydrates, except for the 2,2-dimethylpropionate hydrate, are fairly stable as compared with hydrates in the other groups. The fact that the hydration number of these hydrates is around 30, just as the fluoride hydrate, suggests that the crystal structue of the group I hydrate is isomorphous with that of the fluoride hydrate.[4] In fact McMullan and Jeffrey[2] have reported that the tetrabutylammonium acetate hydrate forms the same tetragonal crystal as those of such salts as fluoride, chloride, and bromide. Very recently, in the course of our investigation Dyadin *et al.*[8] have also reported that four tetrabutylammonium carboxylates having $HCOO^-$, CH_3COO^-, $C_2H_5COO^-$, and $n\text{-}C_3H_7OO^-$ anion can form a clathrate-like hydrate which is tetragonal and has 32 mol of water per one mole of the salt.

However, the effect of carboxylate anions on the stability of these group I hydrates cannot be explained by the same consideration as that applied to the hydrates of ordinary tetrabutylammonium inorganic salts.[6] In the previous paper,[6] we pointed out that the stability of the ordinary $(n\text{-}C_4H_9)_4NX$ (X=monovalent inorganic anion) hydrates approximately decreased with increasing the ionic volume of the X. This relationship is represented in Fig. 5, in which the melting point of each hydrate is plotted against the conventional partial molal anionic volume ($\bar{V}^\circ_{conv}$) at 25 °C as an indication of the effective volume of an anion within the hydrate solid. This nearly linear relationship between the melting point (*i.e.*, the stability) of the hydrate and $\bar{V}^\circ_{conv}$ of its anion[9] indicates that the stability of the hydrate is mainly governed by the distortion effect of the anion on the hydrogen-bonded water framework in the hydrate. In Fig. 5, similar plots are also given for the group I hydrates. The conventional partial molal volume of each carboxylate anion was obtained from the partial molal volumes of each sodium salt[10–12] at infinite dilution using the relation that $\bar{V}^\circ_{conv}$ for Na^+ is equal to -1.21 cm³/mol at 25 °C.[9] As is obvious from this figure, these plots, except for the formate hydrate, appreciably deviate from the simple, linear relationship found for the ordinary inorganic salt hydrate. This indicates that the stability of the group I hydrate, except for the formate hydrate, cannot be explained by a simple distortion effect caused by the presence of the carboxylate anion within the hydrate lattice.

A reasonable explanation for this behavior will be that such alkyl groups as CH_3, C_2H_5, and C_3H_7 are located in a pentagonal dodecahedron, which exists in a gap between the arrangement of larger polyhedra (tetrakaidecahedra and/or pentakaidecahedra filled by one of the butyl group of the tetrabutylammonium cation) and is believed to be either vacant or partially filled by a small molecule such as free water, oxygen, and nitrogen. Very recently, a similar consideration has been proposed by Dyadin *et al.*[8] on the basis of X-ray diffraction characteristics.

Our reasons derived from this investigation are summarized as follows: (1) the occupation of a pentagonal dodecahedron by an akyl group of a carboxylate anion will not cause any change in the crystal structure or the hydration number of the hydrate since the fundamental network of the hydrogen-bonded water molecules has nothing to do with the occupation of a pentagonal dodecahedron; (2) the best fitness of $CH_3CH_2COO^-$ anion to a pentagonal dodecahedron, as revealed by the highest melting point of the propionate hydrate, can be reasonably explained since the mean free diameter of a pentagonal dodecahedron is about 5.0 Å[13] and the van der Waals diameter of $CH_3CH_2COO^-$ anion is estimated to be 4.7Å if we take into account the fact that the oxygen atoms of the carboxylate anion are hydrogen-bonded to the water framework and form part of the polyhedral structure;[3] and (3) low stability of both 2-

methylpropionate and, especially, 2,2-dimethylpropionate hydrates can be interpreted by a distortion of pentagonal dodecahedron due to the presence of these bulky, methyl-substituted anions.

The group II hydrates include all the hydrates with the hydration number of 39. They are formed exclusively by all the carboxylates with R=C_4H_9 and C_5H_{11} except for *t*-C_4H_9, and are newly confirmed in this experiment except for the pentanoate hydrate.[8] The large hydration number, 39, as compared with that of the group I hydrate, 30, indicates that one more hydrogen-bonded water cage will be present in order to enclathrate such a fairly large carboxylate anion as $C_4H_9COO^-$ or $C_5H_{11}COO^-$, which is too large to be accommodated in a pentagonal dodecahedron just as considered for the group I hydrate. Although there is no more evidence about the crystal structure of the group II hydrate than the hydration number, the crystal structure seems to be essentially the same as that of the tetrabutylammonium benzoate hydrate, which is tetragonal and has an ideal composition of $(n\text{-}C_4H_9)_4NOOCC_6H_5 \cdot 39.5H_2O$.[3]

The effect of the length and/or shape of an alkyl chain of a carboxylate anion on the stability of the group II hydrates are summarized as follows:

(1) Among the hydrates with R=C_4H_9, except for *t*-C_4H_9, the melting points of the pentanoate and the 3-methylbutanoate hydrate are approximately equal and higher than that of the 2-methylbutanoate hydrate (7.7 °C). This suggests that the methyl group attached to the carbon atom of 2-position causes a considerable distortion in the hydrogen-bonded water framework.

(2) The hydrates of the salt with $C_5H_{11}COO^-$ anion are generally unstable, as compared with those of the salt with $C_4H_9COO^-$ anion, presumably because the alkyl chain is a little too long to be accommodated stably within a water framework structure and, in addition, because of a distortion effect caused by the substituted methyl group. However, the 2-ethylbutanoate hydrate is exceptionally stable (mp=10.6 °C). This would partly be due to the fact that the main alkyl chain is shorter by either one or two carbon atoms than in the rest of the salts. Another interesting reason is that the distortion effect caused by a ethyl group attached to the carbon atom of 2-position is expected to be smaller than that caused by a methyl group, since the carbon atom of 2-position is connected with the small and flexible methylene group and not with the bulky methyl group.

(3) As is seen from Table 1, the pentanoate hydrate (mp=10.6 °C) is more stable than the 4-methylpentanoate hydrate (mp=6.0 °C). This indicates that the *n*-$C_4H_9COO^-$ ion can be more suitably enclathrated by the hydrogen-bonded water framework than the *i*-$C_5H_{11}COO^-$ ion, in striking contrast to the fact that, in the hydrates of ordinary tetraalkylammonium salts with the same inorganic anion like F^- tetraisopentylammonium salt hydrate is more stable than tetrabutylammonium salt hydrate.[7]

The formation of a clathrate-like hydrate for the tetrabutylammonium carboxylates with such long alkyl chains as *n*-$C_6H_{13}COO$-*n*-$C_{10}H_{21}COO^-$ is clearly confirmed from the phase diagrams shown in Fig. 3. The existence of these hydrates has never been known before. They are classified as the group III hydrates. The characteristic features of the group III hydrates are summarized as follows: (1) the hydration number is around 30; (2) the melting points are low; and (3) there is no simple relationship between the melting point and the alkyl chain length of the carboxylate anion. From the fact that the hydration number is around 30, the possible crystal structure of these hydrates would be isomorphous with a distorted $(n\text{-}C_4H_9)_4NF$ hydrate just as the group I hydrate. The main difference between the structure of the group I hydrate and that of the group III hydrate would be the existence of the interpenetration of a long alkyl chain into two or three pentagonal dodecahedra, which are face-sharing with each other, in the group III hydrate crystal.

Referenes

1) D. L. Fowler, W. V. Loebenstein, D. B. Pall, and C. A. Kraus, *J. Am. Chem. Soc.*, **62**, 1140 (1940).
2) R. McMullan and G. A. Jeffrey, *J. Chem. Phys.*, **31**, 1231 (1959).
3) M. Bonamico, G. A. Jeffrey, and R. K. McMullan, *J. Chem. Phys.*, **37**, 2219 (1962).
4) R. K. McMullan, M. Bonamico, and G. A. Jeffrey, *J. Chem. Phys.*, **39**, 3295 (1963).
5) H. Nakayama, M. Asano, Y. Nakajima, and K. Hanno, *Nippon Kagaku Kaishi*, **1983**, 269.
6) H. Nakayama, *Bull. Chem. Soc. Jpn.*, **56**, 877 (1983).
7) H. Nakayama, *Bull. Chem. Soc. Jpn.*, **54**, 3717 (1981).
8) Yu. A. Dyadin, L. S. Aladko, L. A. Gaponenko, and T. M. Polyanskaya, *Izv. Sib. Otd. Akad. Nauk SSSR, Ser. Khim. Nauk*, **1981**, (9), 19.
9) F. J. Millero, "The Partial Molal Volumes of Electrolytes in Aqueous Solutions," in "Water and Aqueous Solutions," ed by R. A. Horne, Wiley-Interscience, London (1972), Chap. 13, pp.519—595.
10) E. J. King, *J. Phys. Chem.*, **73**, 1220 (1969).
11) O. Redlich and L. E. Nielson, *J. Am. Chem. Soc.*, **64**, 761 (1942).
12) G. M. Watson and W. A. Felsing, *J. Am. Chem. Soc.*, **63**, 410 (1941).
13) D. W. Davidson, "Clathrate Hydrates," in "Water," ed by F. Franks, Plenum Press, New York (1973), Vol. 2, Chap. 3, pp. 115—234.

 © 1984 The Chemical Society of Japan Bull. Chem. Soc. Jpn., 57, 175—178 (1984)

Pressure Effects on the Hydrolysis of Acetanilide Catalyzed by Cyclodextrins

Syoichi MAKIMOTO, Keizo SUZUKI, and Yoshihiro TANIGUCHI*

Department of Chemistry, Faculty of Science and Engineering, Ritsumeikan University, Kita-ku, Kyoto 603

(Received July 18, 1983)

The rates of the hydrolysis of *p*-nitrotrifluoroacetanilide (pNFA) catalyzed by α- and β-cyclodextrins (α-, β-CD) were measured at pressures up to 2 kbar at 25 °C and at pH 6.9 in a 0.05 M† Tris buffer solution. The substrate binding constants, K, and the rate constants of the acylation process, k_{acyl}, increased monotonically up to 2 kbar. From the pressure dependence of K, the volume changes (ΔV) accompanying the formation of the inclusion complexes at 1 bar were -3 ± 2 cm^3/mol for α-CD-pNFA and -2 ± 2 cm^3/mol for β-CD-pNFA. The activation volumes (ΔV) for the cleavage of the anilide molecule in the acylation process were -25 ± 2 cm^3/mol for α-CD-pNFA and -18 ± 2 cm^3/mol for β-CD-pNFA. The reaction mechanisms of the cleavage of the anilide substrte by CDs were discussed on the basis of the volume parameters (ΔV and ΔV^*).

Cyclodextrins have served as a good model of a serine protease, as has been reviewed by Bender *et al.*[1] The reactions of the CD-acceleated cleavage of the phenyl ester and anilide proceed *via* the three steps of the substrate binding, the acylation of CD, and the deacylation of acyl-CD as well as by means of the chymotrypsin reaction. The first reason for the great interest in these reactions is that the rate determining step of anilide hydrolysis is acylation, whereas that of ester hydrolysis is deacylation.[2—4] Secondly, the general acid catalysis in the acylation step has been observed only in the anilide substrate.[4] Therefore, the CD-catalyzed hydrolysis of anilide can be a means to discuss the reaction mechanism of the hydrolysis of amide compounds catalyzed by hydrolytic enzymes. In order to consider such a mechanism of the acylation of CD related to general acid catalysis, the volume changes and activation volumes (ΔV and ΔV^*) given by the pressure dependence of the rate process are useful, because a proton transfer in the general-acid catalysis is accompanied by a volume decrease of 5 cm^3/mol with one hydrogen-bonding formation[5,6] Thirdly, the difference in the reaction mechanism between meta and para substrates is reflected in the stereospecificity. It is well known that meta-substituted compounds are cleaved much faster than the corresponding para-substituted ones in the ester substrates.[2] In the anilide substrates, the reverse results have been reported.[4]

In the previous reports,[7,8] the most important difference in the stereospecific cleavage of the phenyl ester catalyzed by CDs between para- and meta-substrates has been regarded as the solvation effect; the para type is solvated, while the meta type is hardly solvated at all, in the activation state from the point of view of the ΔV^* values.

In this paper, the hydrolysis rates of pNFA catalyzed by α- and β-CDs were measured at pressures up to 2 kbar at 25 °C in order to obtain the ΔV value for the formation of the inclusion complex and the ΔV^* value for the acylation process. The difference in the reaction mechanism between an ester and an anilide is discussed in terms of the ΔV and ΔV^* values for the two kinds of substrates by comparing them with the findings of previous studies.[7,8]

† 1 M=1 mol dm^{-3}.

Experimental

Materials. The purification of the α- and β-CDs has been described previously.[7] The pNFA was synthesized from trifluoroacetic anhydride and *p*-nitroaniline and recrystallized 4 times from hexane-acetone; mp 149—150 °C (lit,[4] 150 °C). The ionized water was distilled. The acetonitrile was distilled over phosphorus pentaoxide before use.

Apparatus and Procedure. The method of measuring the rate of hydrolysis reactions under a high pressure has been described in a previous report.[9] The rate was measured at pH 6.9 in a 0.05 M Tris buffer solution up to 2 kbar at 25± 0.5 °C. The pressure dependence of the pH value is negligible, as the volume change of the dissociation process is −1 cm^3/mol.[10] By the use of a Hitachi 340-type spectrophotometer, the hydrolysis was monitored by means of the optical density at 390 nm attributable to the *p*-nitroaniline formed as a product. The initial concentrations of the cyclodextrins varied from 4.0×10^{-3} M to 2.0×10^{-2} M for α-CD and from 2.0×10^{-3} M to 1.0×10^{-2} M for β-CD respectively. The concentration of pNFA was 1.0×10^{-4} M.

Results and Discussion

At 1 bar, the apparent rate constant, k_{app} increased with an increase in the concentrations of the α- and β-CDs. The hydrolysis of pNFA catalyzed by CD has been shown by VanEtten *et al.*[2] to proceed *via* the scheme of Eq. 1, where S, P, K, and

$$\begin{array}{ccccccc} \mathrm{CD} + \mathrm{S} & \overset{K}{\rightleftharpoons} & \mathrm{CD{\cdot}S} & \xrightarrow{k_{acyl}} & \text{acyl-CD} & \xrightarrow{k_{deacyl}} & \mathrm{CD} + \mathrm{P_2} \\ \downarrow k_w & & & & + & & \\ \mathrm{P_1} + \mathrm{P_2} & & & & \mathrm{P_1} & & \end{array} \quad (1)$$

ks′ denote the anilide, the products, the binding constant, and the rate constants of each process respectively. K and k_{acyl} values at various pressures and at 25 °C, as determined by means of the Lineweaver-Burk plots[7] in Fig. 1 (pNFA, α-CD), are shown in Table 1. From the linear relations of log K and log k_{acyl} *vs.* the pressure established for each system in Figs. 2 and 3, the ΔV values for the formation of the CD complexes and ΔV^* values for the process of the product formation at 1 bar were determined to be as shown in Table 2, along with the previous data on the α-CD- and β-CD-*p*-

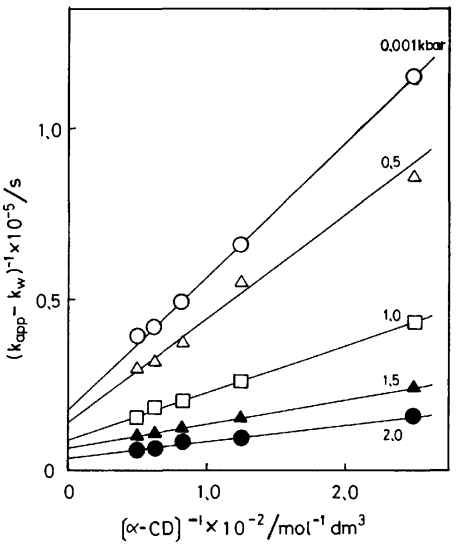

Fig. 1. Lineweaver-Burk plots for the hydrolysis of pNFA catalyzed by α-CD at each pressures, pH 6.9 (0.05 M Tris buffer) and 25 °C.

TABLE 1. RATE CONSTANTS, k_{acyl}, AND EQUILIBRIUM CONSTANTS, K, FOR THE INCLUSION-COMPLEX FORMATION OF pNFA CATALYZED BY CD AT VARIOUS PRESSURES AND AT 25 °C[a]

P/kbar	α-CD		β-CD	
	K/M^{-1}	$10^4\times k_{acyl}/s^{-1}$	K/M^{-1}	$10^4\times k_{acyl}/s^{-1}$
0.001	55.2	0.601 (0.119)[b]	95.9	0.235 (0.119)[b]
0.5	57.1	0.826	97.0	0.347
1.0	62.6	1.33	103	0.538
1.5	74.8	2.31	108	0.852
2.0	70.0	3.73	87.8	1.02

a) 1% acetonitrile solutions, pH 6.9 in a 0.05 M Tris buffer. b) k_W, spontaneous hydrolysis of pNFA.

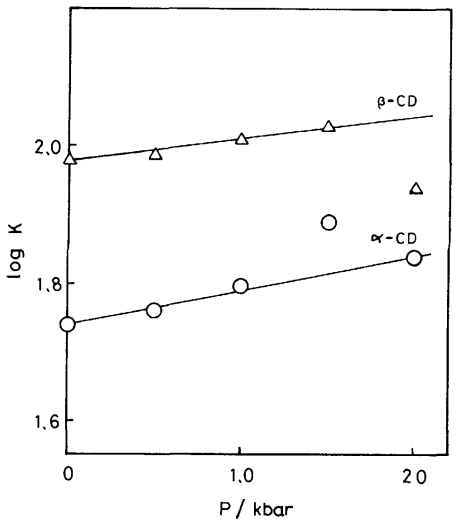

Fig. 2. Pressure dependence of log K at 25 °C.

nitrophenyl acetate (pNPA) systems.[7]

Substrate Binding. The ΔV values in the anilide substrate, as shown in Table 2, are −3 cm³/mol for α-CD and −2 cm³/mol for β-CD; those values are slightly more negative than those of the ester substrate (0 cm³/mol for α- and β-CDs).[7] This volume difference is

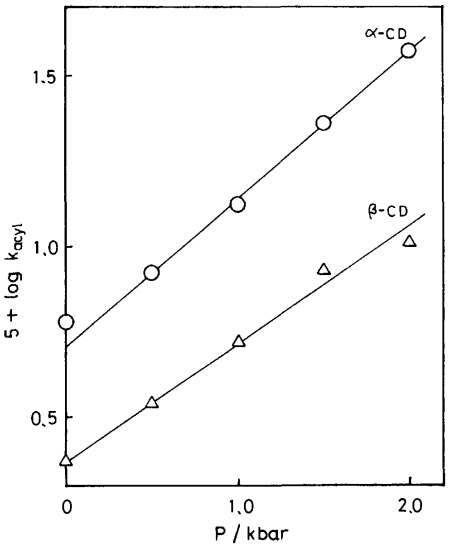

Fig. 3. Pressure dependence of log k_{acyl} at 25 °C.

TABLE 2. VOLUME CHANGES FOR INCLUSION-COMPLEX FORMATION AND ACTIVATION VOLUMES IN THE ACYLATION STEP AT 25 °C AND AT 1 bar

	pNFA		pNPA[a]	
	α-CD	β-CD	α-CD	β-CD
ΔV[b]/cm³ mol⁻¹	−3	−2	0	0
ΔV^*[b]/cm³ mol⁻¹	−25	−18	−16	−13

a) From Ref. 7. b) ±2 cm³/mol.

probably attributable to the differences in the inclusion mechanism between the NH group of anilide and the ether oxygen atom of the ester.

The X-ray analysis[11] of the β-CD-inclusion complex of *p*-nitroaniline (pNA) as a model for the β-CD·pNFA complex has shown that the pNA molecule is wholly included in the cavity of β-CD. If the *p*-nitrophenol (pNP) part of pNPA is wholly included in the cavity of CD, the ΔV value of pNFA for the inclusion process decreases to be 2.5 cm³/mol larger than that of pNPA, because the value of 2.5 cm³/mol is the difference in the molar volumes between the NH_2 group (10.54 cm³/mol) and the OH group (8.04 cm³/mol).[12] The estimated value is in good agreement with the experimental value of the volume difference of 2 cm³/mol.

From the X-ray analysis of the α-CD-inclusion complexes of *p*-iodoaniline (pIA)[13] and pNP[14] as models for the pNFA- and pNPA-α-CD complexes, both the NH_2 group of pIA and the OH group of pNP molecules are seen to stick out from the cavity of α-CD. Since both groups exist in the aqueous media before and after the complexation, the volume differences between the NH_2 and OH groups must be cancel each other out. The difference in the electron-donating power in the NH_2 and OH groups related to the hydrogen-bonding formation may be estimated from the bond-dissociation energy of the charge-transfer (CT) complex between I_2 and an electron-donor molecule. The energy of I_2-diethyl ether as the model for the ether oxygen of pNPA is 2.1 kcal/mol,[††] and that

†† 1 cal=4.184 J.

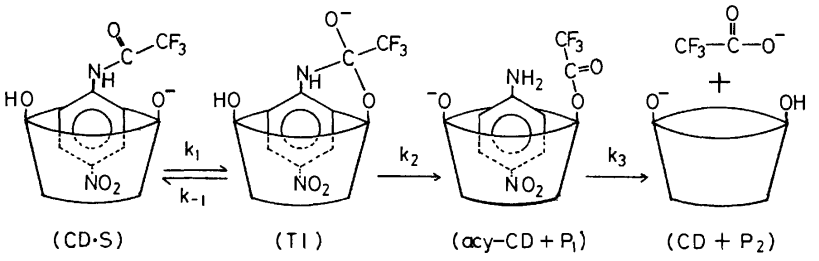

Fig. 4. Schematic drawing of the proposed reaction scheme of α-CD-catalyzed hydrolysis of pNFA after the complexation.

of I_2-*N*,*N*-dimethylaniline for the NH group of pNFA is 8.2 kcal/mol.[16] The amino nitrogen atom of the NH_2 group is more than 0.4 nm apart from any atom in α-CD.[13] After the complexation with pNFA, a hydrogen-bonding bridge among the NH group of pNFA, a water molecule, and the OH group of α-CD may be formed by the strong electron-donating power of the NH group. As the O···O distance between the water molecule and its second neighboring water molecue in an aqueous solution is approximately 0.4—0.5 nm,[15] the hydrogen-bonding system can form between the NH group of pNFA and the OH group of the α-CD through the bridge of a water molecule. Such a hydrogen-bonding system is supported by the X-ray analysis of the α-CD·pIA complex.[13] On the other hand, the ether oxygen atom of pNPA probably can not form such a hydrogn bond because of the lower power of its hydrogen-bonding formation than that of the NH group of pNFA. The volume change for a hydrogen-bonding formation is −5 cm^3/mol.[5,6] This value is in agreement with the value of −3 cm^3/mol for the volume difference between the ester and anilide substrates.

Acylation Process. The mechanism of the α-CD-catalyzed hydrolysis of pNFA after the complexation, as proposed by Komiyama and Bender,[4] is shown in Fig. 4 (Scheme 1). Here, TI is the tetrahedral intermediate produced as a result of the nucleophillic attack by the oxide ion from the secondary hydroxyl group of CD on the carbonyl carbon atom of pNFA. Then, the rate constant of the acylation step is given by Eq. 2, where $K_1=k_1/k_{-1}$:

$$k_{acyl} = K_1 \cdot k_2. \quad (2)$$

The activation volume in the acylation step is given by Eq. 3:

$$\Delta V^* = \Delta V_1 + \Delta V_2^*. \quad (3)$$

Since there is no difference in the volume change on the K_1 process between the ester and the anilide, the ΔV_1 values were estimated to be −16 cm^3/mol for α-CD and −13 cm^3/mol for β-CD in a previous report.[7] From these values and Eq. 3, we can determine that the ΔV_2^* values in the process of k_2 are −9 (=−25—(−16)) cm^3/mol for α-CD and −5(=−18—(−13)) cm^3/mol for β-CD.

From the isotope effects in the acylation step, Komiyama and Bender reported[4] that, in the breakdown of the TI (k_2 process), an un-ionized secondary hydroxyl (OH) group functions as an intracomplex general acid catalyst, either directly or *via* water molecules. From the discussion of the substrate

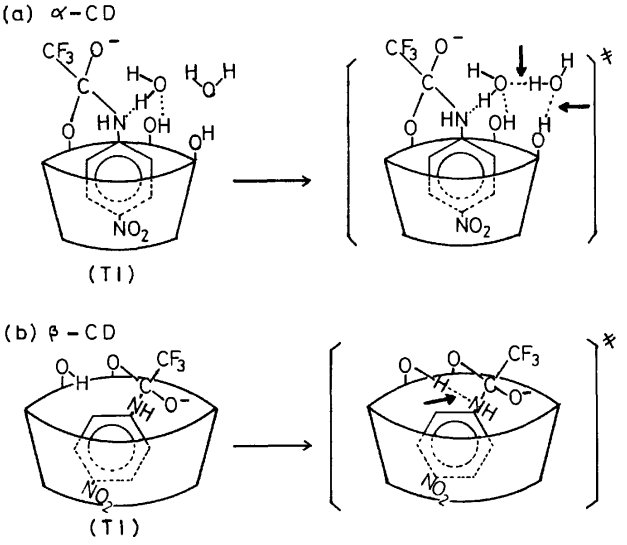

Fig. 5. Schematic drawing of the reaction mechanism of CD on the process of TI cleavage.

binding, the formation of the hydrogen-bonding bridge [(α-CD)-OH···O(H)-H···NH-(pNFA)] in the TI for α-CD has already been expected, but for β-CD, the NH group of pNFA located in the hydrophobic cavity of β-CD has already been dehydrated. If the proposed general acid catalyst functions *via* water molecules except for the hydrated water molecules, the formation of a hydrogen bond between the hydrated water molecule and the secondary water molecule can be expected to be related to the general acid catalysis on the basis of the value of −5 cm^3/mol.[5,6] The value of ΔV_2^*=−9 cm^3/mol for α-CD suggests the formation of two hydrogen bonds, while the value of −5 cm^3/mol for β-CD suggests one hydrogen bond. Following the discussion of the substrate-binding and acylation process, we can propose the reaction mechanism shown in Fig. 5 (Scheme 2). That is, an OH group of α-CD in the activation state is expected to function *via* a free (not hydrated) water molecule through the oxygen atom of a water molecule in the hydrogen-bonding system in TI. Accordingly, it is considered that two water molecules may exist between the OH group of α-CD and the NH group of pNFA. On the other hand, the OH group of β-CD functions directly as a intracomplex general acid catalyst.

We are grateful to Mr. Yoshio Yamaguchi of Ritsumeikan University for the synthesis of the anilide

and for his experimental assistance.

References

1) M. L. Bender and M. Komiyama, "Cyclodextrin Chemistry," Springer Verlag, New York (1977).
2) R. L. VanEtten, J. F. Sebastin, G. A. Clowes, and M. L. Bender, *J. Am. Chem. Soc.*, **89**, 3242 (1967).
3) R. L. VanEtten, G. A. Clowes, J. F. Sebastin, and M. L. Bender, *J. Am. Chem. Soc.*, **89**, 3253 (1967).
4) M. Komiyama and M. L. Bender, *J. Am. Chem. Soc.*, **99**, 8021 (1977).
5) E. Fishman and H. G. Drickamer, *J. Chem. Phys.*, **24**, 568 (1956).
6) Y. Taniguchi and K. Suzuki, *J. Phys. Chem.*, **78**, 759 (1974).
7) Y. Taniguchi, S. Makimoto, and K. Suzuki, *J. Phys. Chem.*, **85**, 3469 (1981).
8) S. Makimoto, K. Suzuki, and Y. Taniguchi, *J. Phys. Chem.*, **86**, 4544 (1982).
9) Y. Taniguchi, S. Makimoto, and K. Suzuki, *J. Phys. Chem.*, **85**, 2218 (1981).
10) R. C. Neuman, Jr., W. Kauzmann, and A. Zipp, *J. Phys. Chem.*, **77**, 2689 (1973).
11) M. M. Harding, J. M. McLennan, and R. M. Paton, *Nature*, **274**, 621 (1978).
12) A. Bondi, *J. Phys. Chem.*, **68**, 441 (1964).
13) K. Harata, *Bull. Chem. Soc. Jpn.*, **48**, 2409 (1975).
14) K. Harata, *Bull. Chem. Soc. Jpn.*, **50**, 1416 (1977).
15) a) A. H. Narten, M. D. Danford, and H. A. Levy, *Discuss. Faraday Soc.*, 43, 97 (1967); b) A. H. Narten and H. A. Levy, *J. Chem. Phys.*, **55**, 2263 (1971); c) A. H. Narten, *ibid.*, **56**, 5681 (1972).
16) T. Kagiya, Y. Sumida, and T. Inoue, *Bull. Chem. Soc. Jpn.*, **41**, 767 (1968).

Molecular Motion and Phase Transitions in 2-Methyl-2-nitropropane as Studied by Proton Magnetic Resonance and Relaxation

Tooru HASEBE, Nobuo NAKAMURA,† and Hideaki CHIHARA*,†

Department of Chemistry, Faculty of Education, Fukushima University, Matsukawa-machi, Fukushima 960-12

†*Department of Chemistry, Faculty of Science, Osaka University, Toyonaka, Osaka 560*

(Received August 31, 1983)

Proton spin-lattice relaxation times (T_1 and $T_{1\rho}$) were measured in solid and liquid phases of 2-methyl-2-nitropropane. In the lowest temperature solid phase (Phase III) a broad, asymmetric minimum in T_1 as well as a large reduction in the second moment was observed due to the coupled reorientations of methyl and *t*-butyl groups. The analyses of the T_1 and $T_{1\rho}$ in Phase III gave the activation parameters E_a=14.6±0.2 kJ mol^{-1} and τ_0=(6.45±0.10)×10^{-14} s for the methyl reorientation and E_a=15.1±0.3 kJ mol^{-1} and τ_0=(1.35±0.10)×10^{-13} s for *t*-butyl reorientation. In Phase II, the T_1 is governed by the *t*-butyl reorientation with the activation parameters E_a=15.3±0.1 kJ mol^{-1} and τ_0=(5.85±0.10)×10^{-14} s. In the low temperature region of the highest temperature plastic phase (Phase I) the molecular overall reorientation governs the T_1 and the molecular translational self-diffusion becomes the dominant relaxation mechanism near melting point. The $T_{1\rho}$ results were analyzed with the isotropic translational diffusion model and the activation parameters were determined to be E_a=46.5±0.9 kJ mol^{-1} and τ_0=(4.6±1.8)×10^{-15} s. The mean jump time of the molecule at the melting point, 6×10^{-7} s, is slightly longer than those in other plastic crystals. The activation energy for the translational diffusion is 9.7±1.5 kJ mol^{-1} in the liquid phase.

t-Butyl compounds ($(CH_3)_3CX$ (where X=Cl, Br, NO_2, and CN) are globular molecules with relatively large electric dipole moments[1,2] and they commonly exist in three solid phases which are named Phase I, Phase II, and Phase III in the decreasing order of temperature. The highest temperature phase, Phase I, of these compounds except $(CH_3)_3CCN$ is a plastic crystal. Although the unit cell of the most plastic crystals has a high symmetry like fcc, hcp, and bcc, Phase I of 2-methyl-2-nitropropane ($(CH_3)_3CNO_2$) belongs to an orthorhombic system with two molecules in the unit cell. This phase exists between the melting point (299.2 K) and 260.1 K. The intermediate phase, Phase II, that appears between 260.1 and 215.3 K and the lowest temperature phase (Phase III) below 215.3 K are both triclinic.[3] Structure and properties of solid $(CH_3)_3CNO_2$ have been studied by many experimental methods.[2-13] The molecular motions in solid $(CH_3)_3CNO_2$ were examined by dielectric measurement,[9-11] pulsed NMR method[12] and quasi-elastic neutron scattering method.[13] Mazur and Nosel[12] measured the proton T_1 at 25.5 MHz from about 150 K to the melting point and derived the activaion energy for methyl reorientation about its C_3 axis, 15.5±0.3 kJ mol^{-1}.

We measured proton magnetic resonance and relaxation (T_1 and $T_{1\rho}$) on the liquid and crystalline phases of $(CH_3)_3CNO_2$. The present paper reports its results and their interpretation in relation to the molecular motion and the phase transitions.

Experimental

2-Methyl-2-nitropropane obtained from Aldrich Chemical Co., Inc. was purified by a preparative gas chromatograph, followed by dehydration using Molecular Sieve 4A, vacuum distillation, and degassing by usual freeze-pump-thaw technique. The specimen was sealed under vacuum in a glass ampule of the outside diameter of 10 mm. The purity of the specimen was estimated to be higher than 99.87 mol per cent by a gas chromatographic analysis.

The melting point and the two transition points of this specimen were determined to be 298.7±0.3, 260.1±0.3, and 216.1±0.3 K, respectively by differential thermal analysis (DTA).

The line-shape of ^{1}H-NMR was measured as a function of temperature between 77 and 260.1 K at 12.1 MHz using a Robinson-type spectrometer. The proton relaxation times in the laboratory frame, T_1, and in the rotating frame, $T_{1\rho}$, were measured by the use of Bruker CXP 4—60 MHz pulsed NMR spectrometer. T_1 was measured at 10.0 MHz and 15.0 MHz by the saturation recovery method {$(\pi/2)_{comb}-\tau-\pi/2$ pulse sequences} for the liquid and the plastic phase (Phase I), and by the inversion recovery method ($\pi-\tau-\pi/2$ pulse sequences) for Phase II and Phase III.

The magnetization recovered exponentially in the whole temperature range of the measurements. $T_{1\rho}$ was measured at 15.0 MHz with a rotating rf magnetic field (H_1) of 7.0 and 3.0 G†† (also with H_1=2.0 and H_1=10.0 G for Phase I) by the spin-locking method. Generally, T_1 and $T_{1\rho}$ measurements were carried out between 100 K and the melting point but T_1 at 10 MHz was measured up to 320 K.

The temperature was measured with a Chromel-P/Constantan thermocouple** and was controlled to within 0.1 K.

Experimental Results and Their Analysis

Line-shape. The derivative of the proton resonance line together with its integrated line-shape in the solid phases at a few selected temperatures are shown in Fig. 1. The line-shape at 84 K corresponds to a typical three proton system in the rigid lattice indicating that rotational motion of the methyl and the *t*-butyl groups are frozen at this temperature, whereas those at 173.2 and 225.5 K show that some large amplitude motions of molecules are excited at these temperatures.

The second moment of the absorption line at each temperature was calculated, corrected for the modulation width, and given in Fig. 2. One sees in this figure that the second moment decreases sharply

†† 1 G=10^{-4} T.

** This thermocouple with its temperature scale was kindly donated by Chemical Thermodynamics Laboratory, Faculty of Science, Osaka University.

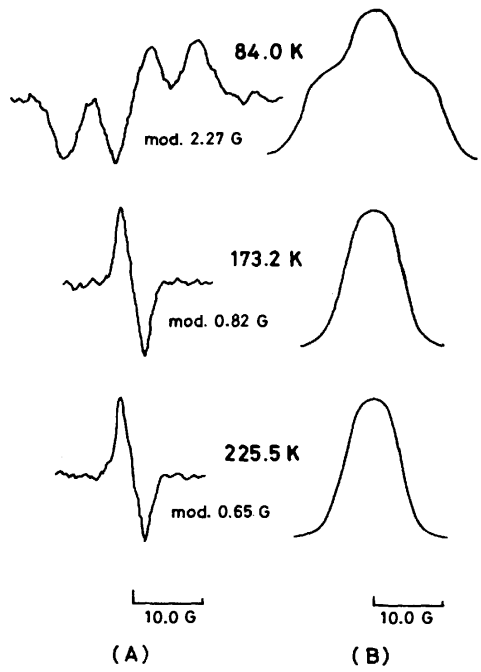

Fig. 1. Observed line shapes (A) and its integrated line shapes (B) at selected temperatures. The 'mod.' denotes modulation width of magnetic field.

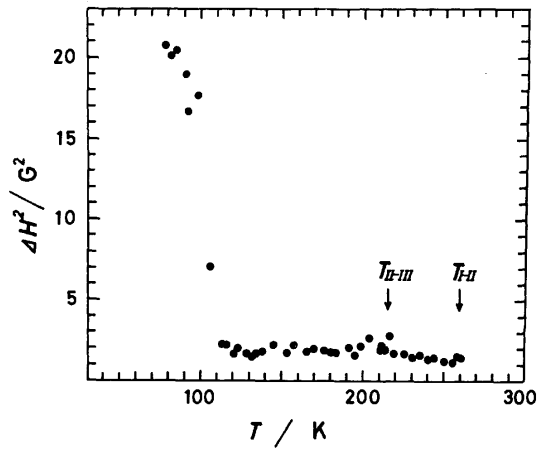

Fig. 2. Temperature dependence of the second moment.

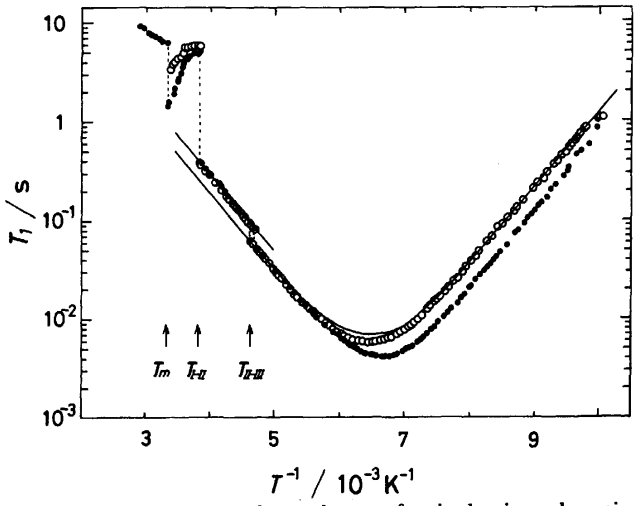

Fig. 3. Temperature dependence of spin-lattice relaxation times at 10 MHz (●) and 15 MHz (○).

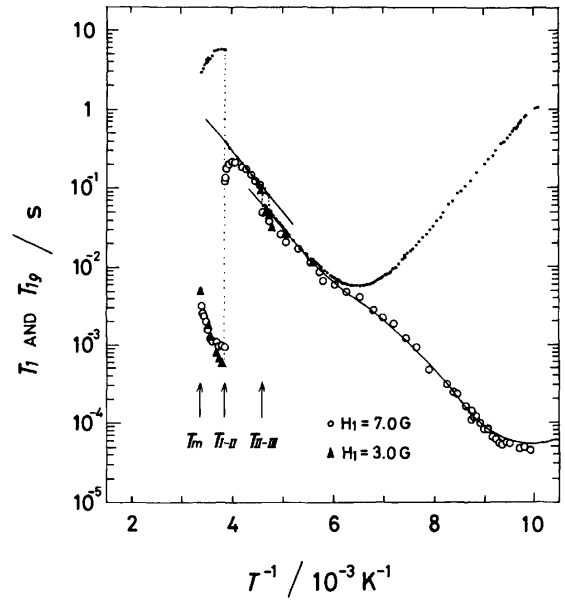

Fig. 4. Temperature dependences of the T_1(●) and the $T_{1\rho}$ at 15 MHz for rotating magnetic rf field of 7.0 G (○) and 3.0 G (▲).

between 80 and 110 K from 21 G^2 to 1.9 G^2. The intramethyl second moment calculated for a rigid lattice in a polycrystalline sample is 22.4 G^2, if the usual interproton distance, 0.178 nm, is used. The dipolar interaction between the methyl groups within one molecule contributes to the second moment by 1.8 G^2 which is based upon the tetrahedral and the staggered conformation of methyl groups in the molecule. Therefore, we obtain a value of 24.2 G^2 for the limiting low-temperature second moment without including the intermolecuar contribution.

If the methyl and the *t*-butyl groups rotate simultaneously, the intramethyl group second moment is reduced to 0.6 G^2 corresponding to the reduction factor 0.026.[14] The intermethyl second moment in one molecule becomes a quarter of 1.8 G^2. Therefore the concurrent reorientation of methyl groups about its C_3 axis and about the C_3' axis (C(Me)-C bond) causes the motional narrowing below 100 K in Phase III. Second moments of similar magnitude have been reported for a number of other compounds[15–19] containing *t*-butyl groups. Above 216 K, which is the phase transition point from Phase III to Phase II, the second moment further decreases gradually until the transition into Phase I occurs at 260.1 K, beyond which temperature the resonance line becomes narrower than the modulation width.

Spin-lattice Relaxation Times (T_2 and $T_{1\rho}$). Figure 3 shows the temperature dependence of the T_1 at 10 and 15 MHz in different phases of $(CH_3)_3CNO_2$. Discontinuities in the T_1 were observed at 298, 260, and 216 K due to the first order phase transitions. Among these discontinuities only the T_1 at the phase transition between Phase III and Phase II (216 K) showed a significant thermal hysteresis. The dielectric permitivity[9] in solid $(CH_3)_3CNO$ also showed a similar hysteresis at this phase transition.

The rotating frame relaxation times, $T_{1\rho}$, at the spin-locking field intensity (H_1) of 7.0 and 3.0 G

together with the T_1 at 15 MHz are shown in Fig. 4. Discontinuity is also seen in the $T_{1\rho}$ at each transition point.

Relaxation in Phase III: In Phase III, a broad, slightly asymmetric minimum in the T_1 was observed. The minimum value was 4.2±0.2 ms at 149.3 K and 10 MHz, and 5.6±0.2 ms at 153.8 K and 15 MHz. These values are consistent with the results by Mazur and Nosel[12] at 25.5 MHz, *i.e.* 11.5 ms at 170.9 K. As was discussed in the preceding section, we infer that the motion responsible for the relaxation in Phase III is the simultaneous excitation of the C_3- and the C_3'-rotations. In this case we obtain the expression for T_1 as follows,

$$1/T_1 = (1/T_1)_{\text{intra}} + (1/T_1)_{\text{inter}} + (1/T_1)_{\text{intermol}}, \quad (1)$$

where 'intra' and 'inter' denote intramethyl and intermethyl (intramolecular) contributions to the T_1, respectively, and 'intermol' denotes intermolecular contribution to the T_1. However, since the intermolecular contribution to the T_1 is very difficult to estimate accurately when the molecular motion involves different types of reorientations and since this contribution is expected to be small compared with other contributions, we ignore it in the following analysis. The relaxation rate for dipolar interaction within the molecule undergoing C_3- and C_3'-rotations is given by

$$(1/T_1)_{\text{intra}} = (\gamma^4\hbar^2/60r^6)\{8B(\tau_m) + 8B(\tau_M) + 19B(\tau_c)\}, \quad (2)$$

where r is the interproton distance in a methyl group, γ is the gyromagnetic ratio, τ_m and τ_M are the correlation times for C_3- and C_3'-rotations, respectively, and τ_c is defined by

$$1/\tau_c = 1/\tau_m + 1/\tau_M. \quad (3)$$

Here we used an approximation that C_3- and C_3'-rotations are mutually independent and ignored any correlation between these motions.[20,21]. The spectral density function $B(\tau)$ has the form

$$B(\tau) = \tau/(1+\omega^2\tau^2) + 4\tau/(1+4\omega^2\tau^2), \quad (4)$$

where ω is the Larmor frequency. The intermethyl contribution to the T_1 in the presence of the t-butyl reorientation is significantly large. In order to calculate this contribution, we assumed that the three protons in each methyl group reside at the center of the three proton system set. We can then calculate the relaxation rate due to the dipolar interaction between these hypothetical methyl groups as

$$(1/T_1)_{\text{inter}} = (27\,\gamma^4\hbar^2/20\,l^6)B(\tau_M), \quad (5)$$

where l is the distance between the centers of the methyl groups in a t-butyl group. The relaxation rate; $1/T_1$, is the sum of Eqs. 2 and 5;

$$1/T_1 = (2\,\gamma^4\hbar^2/15\,r^6)\{B(\tau_m) + B(\tau_M)\} + (19\,\gamma^4\hbar^2/60\,r^6)B(\tau_c) + (27\,\gamma^4\hbar^2/20\,l^6)B(\tau_M). \quad (6)$$

Under the same assumption for the molecular motion as in the calculation of T_1 we calculated the $T_{1\rho}$ in the weak collision limit[22] as

$$1/T_{1\rho} = (\gamma^4\hbar^2/15\,r^6)\{G(\tau_m) + G(\tau_M)\} + (19\,\gamma_4\hbar^2/120\,r^6)G(\tau_c) + (27\,\gamma^4\hbar^2/40\,l^6)G(\tau_M), \quad (7)$$

where $G(\tau)$ is the spectral density function,

$$G(\tau) = 5\,\tau/(1+\omega^2\tau^2) + 2\,\tau/(1+4\omega^2\tau^2) + 3\,\tau/(1+4\omega_1^2\tau^2), \quad (8)$$

and $\omega_1=\gamma H_1$.

Activation parameters for these two types of motions were obtaind by fitting the data of Fig. 3 to Eq. 7 using r=0.178 nm and l=0.310 nm, and by assuming the Arrhenius equation for the temperature dependence of the correlation time for each of C_3-rotation and C_3'-rotation,

$$\tau = \tau_0 \exp(E_a/RT),$$

where τ_0 is the pre-exponential factor and E_a the activation energy. Here we used a following assumption: The straight line portion of the T_1 curve in the temperature region below the temperature of T_1(min) is mainly governed by the methyl reorientation and T_1 on the high temperature side of the T_1(min) by the t-butyl reorientation. The activation parameters thus obtained for the methyl reorientation and the t-butyl reorientation are tabulated in Table 1 and the T_1 reproduced with these parameters is shown in Fig. 3 by the solid line. The minimum value (6.7 ms at 154 K at 15 MHz) of the theoretical T_1 is somewhat larger than that of the observed T_1. The descrepancy is due to the simple nature of our theoretical model in which cross correlation effect of methyl and t-butyl group reorientation as well as intermolecular dipolar contribution to the T_1 were ignored. The solid line in Fig. 4 is the calculated $T_{1\rho}$ using Eq. 7 and the activation parameters obtained from the analysis of the T_1, data. The theoretical $T_{1\rho}$ in Fig. 4 is in reasonable agreement with the experimental $T_{1\rho}$. The minimum value of the calculated $T_{1\rho}$ is 54 μs which occurs at 100 K.

Similarity in the activation parameters for the two motions gives the broad minimum instead of a reported double minimum of the T_1 responsible for each of these motions.

Relaxation in Phase II: The T_1 jumps from 65 ms to 95 ms at the transition point, T_{II-III}, and then increases

Table 1. Activation parameters (E_a and τ_0) obtained in this study for the various motions in $(CH_3)_3CNO_2$

	Motion	E_a/kJ mol^{-1}	τ_0/s
Phase III	Methyl reorientation	14.6±0.2	$(6.45\pm0.10)\times10^{-14}$
	t-Butyl reorientation	15.1±0.3	$(1.35\pm0.10)\times10^{-13}$
Phase II	t-Butyl reorientation	15.3±0.1	$(5.85\pm0.10)\times10^{-14}$
Phase I	Translational diffusion	46.5±0.9	$(4.6\pm1.8)\times10^{-15}$
Liquid	Translational diffusion	9.7±1.5	

monotonously in Phase II with increasing temperature as is seen in Fig. 3. The $T_{1\rho}$ shows a similar jump in T_1 at T_{II-III} but assumes a maximum value of 200 ± 20 ms at 250 K, and then decreases with increasing temperature in Phase II. The decrease in the $T_{1\rho}$ above 250 K is due to the onset of an additional mode of molecular motion, probably the overall molecular tumbling. The activation energy obtained from the slope of log T_1 against reciprocal temperature below 250 K in Phase II is 15.3 ± 0.1 kJ mol^{-1}. It agrees well with the E_a for the *t*-butyl reorientation in Phase III and gives support to the interpretation that the molecular motion governing the T_1 below 250 K is C_3'-rotation. As the change in the unit cell volume on going from Phase III to Phase II must be very small, considering the change of the second moment value (0.5 G^2), we can infer that the magnitude of intermolecular dipolar interaction does not change significantly. Hence we fitted the T_1 data in Phase II to Eq. 6 using the same E_a and the same molecular constants as in Phase III to estimate τ_0 for C_3'-rotation in Phase II. We obtained the τ_0 value of $(5.85\pm0.10)\times10^{-14}$ s which is shown in Table 1. At the transition point, T_{II-III} (216.1 K), the correlation time for the *t*-butyl reorientation is changed discontinuously from 6.1×10^{-10} s to 3.0×10^{-10} s. It is interesting to see that the rate of C_3'-rotation increases by a factor of two at the transition from Phase III to Phase II, whereas the activation energy controlling this mode does not undergo any significant change. For Phase II, a study[13] of quasi-elastic broadening in neutron scattering (QENS) led to the correlation time of about 1.6×10^{-12} s at 237 K for the 120° jump model for *t*-butyl group, which is larger than $\tau_c=1.4\times10^{-10}$ s at the same temperature deduced by using E_a and τ_0 in Table 1 by a factor of 100. It is hardly conceivable that the τ_c from NMR has such a large error since our value is consistent also with the narrowing condition. Thus, in Phase III, the *t*-butyl rotation has $\tau_c=1.0\times10^{-5}$ s at 100 K where the motional narrowing occurs. A difference by a factor of 100 means that the narrowing would occur when τ_c is as small as 10^{-7} s, which does not seem plausible. A similar discrepancy has been recognized in the solid phase of $(CH_3)_3CCl$: NMR measurements[23] reported the correlation time of the order of 10^{-8} s for *t*-butyl reorientation, whereas QENS measurements[24] reported the correlation time of the order of 10^{-12} s.

At the transition point, T_{I-II} (260.1 K), a jump in $T_{1\rho}$ by a factor of 100 and the corresponding jump in T_1 by a factor of 10 were observed as seen in Figs. 3 and 4. The correlation time of C_3'-rotation in Phase II is 6.9×10^{-11} s at T_{I-II}. This value is much smaller than that (4.3×10^{-9} s)[23] at the corresponding transition point of $(CH_3)_3CCl$. It was pointed out by Boden[25] that the correlation time of reorientational jumps between equivalent sites (*e.g.* for *t*-butyl compounds it is the C_3'-rotation.) in the ordered phase of some plastic crystals tends to converge into the value of 5×10^{-9} s at the brittle-plastic phase transition. The deviation in the case of $(CH_3)_3CNO_2$ is probably related to the non-cubic structure in its Phase I.

Relaxation in Phase I: In the plastic crystal phase, Phase I, the T_1 has a maximum which is frequency-dependent as can be seen in Fig. 3. On the low temperature side of this

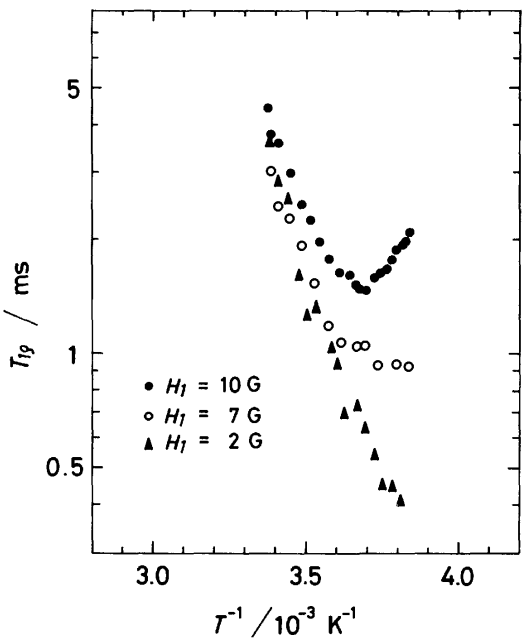

Fig. 5. Temperature dependence of the $T_{1\rho}$ (at 15 MHz) for three different rotating magnetic rf fields (H_1) in Phase I.

maximum the dominant relaxation mechanism is the overall molecular reorientation while the translational diffusion (self-diffusion) is responsible for the relaxation on the high temperature side as revealed by a study[26] of the pressure dependence of the T_1. This assignment of motion was also put forward by Mazur and Nosel.[12] When such two different relaxation mechanisms work, the experimental relaxation rate $1/T_{1\,obsd}$ can be written as

$$1/T_{1\,obsd} = 1/T_{1\,trans} + 1/T_{1\,rot}, \tag{9}$$

where $1/T_{1\,trans}$ and $1/T_{1\,rot}$ are the relaxation rate due to the translational diffusion and the overall molecular reorientation, respectively. According to Torrey's isotropic diffusion model,[27]

$$1/T_{1\,trans} = 2.67\,\gamma^2\delta\langle\Delta H^2\rangle/\omega^2\tau, \tag{10}$$

when $\omega\tau\gg1$, where τ is the mean time between successive diffusional jumps and $\delta\langle\Delta H^2\rangle$ is the change in second moment due to the translational diffusion. The activation energy for the translational diffusion was determined to be 47 ± 8 kJ mol^{-1} from the slope of the semilog plot of the $T_{1\,trans}$ against the inverse temperature. The temperature dependence of the $T_{1\rho}$ data at three different rotating rf fields is shown in Fig. 5. $T_{1\rho}$ measured at $H_1=10$ G assumes a minimum value of 1.50 ± 0.05 ms at 271 K and $T_{1\rho}$ measured at 7 G shows a less obvious minimum 0.94 ± 0.03 ms at 263 K. Isotropic diffusion model predicts that the minimum value of $T_{1\rho}$ is given by

$$1/T_{1\rho\,minimum} = 0.25\,\gamma^2\delta\langle\Delta H^2\rangle/\omega_1, \tag{11}$$

and on the high temperature side of the minimum, it is approximated by

$$1/T_{1\rho} = 0.5\,\gamma^2\delta\langle\Delta H^2\rangle\tau. \tag{12}$$

By substituting the experimental $T_{1\rho}$ minimum cited above and the appropriate value of $\omega_1=\gamma H_1$, $\delta<\Delta H^2>$ is estimated to be 1.0 ± 0.1 G^2 which agrees fairly well with the reduction of second moment 1.4 G^2 mentioned earlier. Activation parameters for the translational diffusion were determined by assuming the Arrhenius-type activation process (Eq. 8) for the correlation time τ and using $\delta<\Delta H^2>=1.0$ G^2 and are listed in Table 1. For this motion the result obtained from the $T_{1\rho}$ data is consistent with the result obtained from the T_1 data within the experimental error. The mean jump time at the melting point is about 6×10^{-7} s .

Relaxation in Liquid Phase: The T_1 in the liquid phase shows a monotonous increase on heating as shown in Fig. 3. The activation energy obtained from the slope of the T_1 was 9.7 ± 1.5 kJ mol^{-1} due to the translational motion (self-diffusion). Our result agreed with the result[7] of NMR spin echo method for the self-diffusion ($E_a=10.8$ kJ mol^{-1}) in the liquid phase of $(CH_3)_3CNO_2$.

Discussion

The result of analysis of the nuclear magnetic relaxation is summarized in Table 1. In Phase II, the relaxation due probably to the overall molecular tumbling is also seen although it was not possible to derive a value of its activation energy. Whether or not the *t*-butyl reorientation is accompanied by the reorientation of the NO_2 group was difficult to determine by experiment.

The large electric dipole moment (12.35 C m) is responsible for the unique properties of 2-methyl-2-nitropropane among *t*-butyl compounds which form a plastic phase. The fact that the Phase I is not of cubic symmetry indicates that the molecular reorientation in this phase is not rapid enough to eliminate the effect of anisotropy of intermolecular forces.

Such an anisotropy in molecular interaction is even more prominent in Phase II, where the structure is reported to be triclinic.[3] If the NO_2 group is also reorienting or even the molecule undergoes reorientation about its C_3 axis very vigorously, the molecule would assume on the average a cylindrical symmetry which would in turn lead to a crystal structure of higher symmetry.

These properties are probably related to the small value of the correlation time for *t*-butyl reorientation at T_{I-II} as compared with many other plastic crystals. In other words, the molecular motion in 2-methyl-2-nitropropane is not as rapid as one would expect for a typical plastic crystal and as a result the lattice is a little harder.

The change in NMR properties at the III—II transition is much smaller than that at the II—I transition although the corresponding entropy changes are comparable (2.36*R* and 2.16*R*, respectively). The packing factor change is greater at T_{III-II} than at T_{II-I}.[11] To rationalize all these behaviors and even the existence of Phase II requires more elaborate studies including detailed crystal structures of all the solid phases.

References

1) A. H. McLellan, "Tables of Experimental Dipole Moments," Freeman, San Francisco (1963).
2) P. R. R. Langridge-Smith, R. Stevens, and A. P. Cox, *J. Chem. Soc., Faraday Trans. 2*, **76**, 330 (1980)
3) S. Urban, Z. Tomkowicz, J. Mayer, and T. Waluge, *Acta Phys. Pol.*, **A48**, 61 (1975).
4) R. W. Crowe and C. P. Smyth, *J. Am. Chem. Soc.*, **72**, 4009 (1950).
5) E. E. Toops, Jr., *J. Phys. Chem.*, **60**, 304 (1956).
6) C. Clemett and M. Davies, *Trans. Faraday Soc.*, **58**, 1705 (1962).
7) D. Kessler, A. Weiss, and H. Witte, *Ber. Bunsenges. Phys. Chem.*, **71**, 3 (1967).
8) R. Haffmans and I. W. Larkin, *J. Chem. Soc., Faraday Trans. 2*, **68**, 1729 (1972).
9) P. Freundlich, J. Kalenid, E. Narewski, and L. Soczyk, *Acta Phys. Pol.*, **A48**, 701 (1975).
10) S. Urban, *Acta Phys. Pol.*, **A49**, 741 (1976).
11) P. Freundlich and L. Sobczyk, *Mol. Cryst. Liq. Cryst.*, **65**, 197 (1981).
12) J. Mazur and W. Nosel, *Acta Phys. Pol.*, **A52**, 477 (1977).
13) J. Mayer, I. Natkaniec, and J. Sciesinski, *Acta Phys. Pol.*, **A52**, 665 (1977).
14) J. G. Powles and H. S. Gutowsky, *J. Chem. Phys.*, **21**, 1695 (1953).
15) H. Chihara, M. Otsuru, and S. Seki, *Bull. Chem. Soc. Jpn.*, **39**, 2145 (1966).
16) G. W. Smith, *J. Chem. Phys.*, **51**, 3569 (1969).
17) Y. Yukitoshi, H. Suga, S. Seki, and J. Itoh, *J. Phys. Soc. Jpn.*, **12**, 515 (1957).
18) G. W. Smith, *J. Chem. Phys.*, **54**, 174 (1971)
19) Z. M. El Saffer, J. Kalenik, and E. F. Meyer, *J. Chem. Phys.*, **56**, 1477 (1972).
20) D. E. Woessner, *J. Chem. Phys.*, **36**, 1 (1962).
21) S. Albert, H. S. Gutowsky, and J. A. Ripmeester, *J. Chem. Phys.*, **56**, 1332 (1972).
22) D. C. Look and I. J. Lowe, *J. Chem. Phys.*, **44**, 2995 (1966).
23) D. E. O'Reilly, E. M. Peterson, C. E. Scheie, and E. Seyfarth, *J. Chem. Phys.*, **59**, 3576 (1973).
24) P. S. Goyal, W. Nawrocik, S. Urban, J. Domoslawski, and I. Natkaniec, *Acta Phys. Pol.*, **A46**, 399 (1974).
25) N. Boden, *Chem. Phys. Lett.*, **46**, 141 (1977).
26) T. Hasebe and H. Chihara, unpublished.
27) H. C. Torrey, *Phys. Rev.*, **92**, 962 (1953); **96**, 690 (1954).

Equilibrium and Rate Data on Some Arsenite Transesterification Reactions

John O. Edwards,* Akiko Okumura,*,† Philip H. Rieger, Catherine M. Taylor, and Yuiko Toyomi
Department of Chemistry, Brown University, Providence, Rhode Island 02912, U.S.A.
†*Department of Chemistry, Nara Women's University, Nara 630*
(Received Februaty 21, 1983)

The arsenite transesterification reaction $As(OCH_3)_3 + HOR \rightleftharpoons As(OCH_3)_2OR + HOCH_3$ (with R equaling benzyl and *t*-butyl) has been studied in acetonitrile solvent. With benzyl alcohol, K, $\Delta H°$, and $\Delta S°$ are 3.6 (25 °C), 5.0 kJ mol^{-1} and 27 J mol^{-1} K^{-1} respectively; with *t*-butyl alcohol, the values are 0.36 (25 °C), 4.0 kJ mol^{-1}, and 5 J mol^{-1} K^{-1} respectively. The rate law for the approach to equilibrium in the case of benzyl alcohol is:

$$\frac{-d[As(OCH_3)_3]}{dt} = k_f'[As(OCH_3)_3][HOCH_2Ph]^2 - k_r'[As(OCH_3)_2(OCH_2Ph)][HOCH_3][HOCH_2Ph].$$

A mechanism which explains the unusual law has been postulated. The slower *t*-butyl alcohol reaction proceeds by a different mechanism which apparently involves catalysis by small amounts of water in the solvent. The steric effects are very significant.

Arsenious acid $As(OH)_3$ and related arsenic(III) compounds are potent inhibitors of enzymes which have a mercaptan function near the active site. Thus, understanding the rates and equilibria of these arsenic compounds is important.

A few studies of replacement rates in arsenic(III) compounds have been carried out. These include an ^{17}ONMR line-broadening investigation of the exchange between arsenite ions and water[1] and a quantitative study of the hydrolysis of arsenite triesters.[2] In both instances, the rates were too fast for classical rate techniques. Some less definitive studies of the glycol complexing of arsenite ions,[3] of the arsenite catalysis of arsenate-oxygen exchange with water,[4] and 2-mercaptoethanol complexing of arsenite ions[5] gave results also indicating rapid replacement in the arsenic coordination sphere.

In the present work, data on the arsenite transesterification reaction:

$$As(OCH_3)_3 + HOR \rightleftharpoons As(OCH_3)_2(OR) + HOCH_3, \quad (1)$$

with R equaling benzyl and *t*-butyl, have been obtained. With benzyl alcohol, the rates have been found to be rapid; on the other hand, with *t*-butyl alcohol, the reactions are much slower. The mechanisms are strikingly different.

Experimental

Chemicals. Trimethyl arsenite, also known as trimethoxyarsine, $As(OCH_3)_3$, was prepared by two methods,[6,7] both of which were found satisfactory. $AsCl_3$ (Aldrich, ultrapure) was used as obtained. All the other materials for the preparations (ether, hexane, triethylamine, and methanol) were dried according to standard procedures.[8] The product was characterized by NMR and chloride-ion analysis to see if any side products such as $As(OCH_3)_2Cl$ were present. The $As(OCH_3)_3$ was found to be at least 99.993% pure.

Benzyl alcohol and *t*-butyl alcohol were dried by the usual methods.[8] Acetonitrile, which was employed as the reaction solvent, was normally distilled twice from P_2O_5; drying is important because any significant amount of water in acetonitrile will cause cloudiness or turbidity when the arsenite ester is dissolved. In some experiments, we used acetonitrile vigorously dried by the following procedure: 1) The acetonitrile was distilled. 2) It was then stirred with P_2O_5 (about 0.04 g per 10 g of CH_3CN). 3) It was redistilled, collected over 4 Å Molecular Sieves (which had been previously dried by heating in a vacuum oven), and shaken occasionally for 2 h. 4) It was again distilled, and then stored over Molecular Sieves. The dried solvent was taken up just before use by means of a Pasteur pipet with a glass-wool filter.

Equipment. For the benzyl alcohol kinetic runs, a Bruker WP60 FT NMR apparatus was coupled to a specially constructed stopped-flow apparatus based on the design of Couch *et al.*[9] The glass tips of the syringes were constructed so that the two solutions were fed directly into the NMR tube. The equilibrium data and kinetic results for the slower *t*-butyl alcohol runs were obtained with the Bruker instrument or with a Varian EM-360 NMR apparatus.

Reaction Analyses. The concentration of the reactant and product species were determined by measuring their NMR peak heights and by comparing them with the known initial concentration of trimethyl arsenite. These peak heights correlated well with the integrated areas, and mass balance was also tested.

Results

Proton NMR. For both equilibrium and rate experiments, the analysis were based on the proton-NMR-line intensities. The chemical-shift assignments in acetonitrile are as follows: $C\underline{H}_3OH$, 3.31 ppm; $(C\underline{H}_3O)_3As$ and $(C\underline{H}_3O)_2AsOCH_2Ph$, both 3.53±0.03 as one line; $PhC\underline{H}_2OH$, 4.59 ppm; $PhC\underline{H}_2OAs(OCH_3)_2$, 4.87 ppm; $C_6\underline{H}_5CH_2OH$, 7.35 ppm; $(C\underline{H}_3)_3COH$, 1.19 ppm; and $(C\underline{H}_3)_3COAs(OCH_3)_2$, 1.37 ppm.

Table 1. Equilibrium constants with benzyl alcohol

t/°C	$[As(OCH_3)_3]_0$/M	$[HOCH_2Ph]_0$/M	*K*
25	2.75	0.93	3.66
	2.71	1.21	3.58
	2.21	1.70	3.69
	2.06	1.87	3.51
	2.02	1.87	3.51
−25	2.06	1.87	2.34
−20	2.06	1.87	2.38
−15	2.06	1.87	2.65
−11	2.06	1.87	2.93
20	2.06	1.87	3.43
28	2.06	1.87	3.51

Equilibria. The transesterification reaction, Eq. 1, proceeds rapidly to a convenient degree when trimethyl arsenite and the alcohol are in the concentration range from 1 to 3 M.†

Some results for the benzyl-alcohol reaction are given in Table 1. At 25 °C, the average value or K from these data is 3.59±0.08 (standard deviation), while from the results in Table 3 it is 3.49±0.04. The temperature dependence of K gives $\Delta H°=5.0\pm0.3$ kJ mol^{-1} and $\Delta S°=27\pm1$ J mol^{-1} K^{-1}. It is important to mention that the evidence for the formation of some $(PhCH_2O)_2As(OCH_3)$ was indicated by a significant increase in the apparent binding constant when there was an excess of benzyl alcohol, therefore, all of the present results are given for the condition, $[PhCH_2OH]_0<[As(OCH_3)_3]_0$ so as to minimize this complication.

Some results with t-butyl alcohol are presented in Table 2. The average of the first three values of K therein is 0.364±0.010. Under the kinetics conditions (see below), the observed value was 0.29±0.03. The thermodynamic quantities based on the Table 2 data are $\Delta H°=4.0\pm0.4$ kJ mol^{-1} and $\Delta S°=5.2\pm1.1$ J mol^{-1} K^{-1}. From the equilibrium constant based on the kinetic data in Table 5, the values of $\Delta H°$ and $\Delta S°$ were found to be 4.2±0.5 kJ mol^{-1} and 6±2 J mol^{-1} K^{-1} respectively; these values are considered somewhat less accurate than those based on the Table 2 data.

Kinetics with Benzyl Alcohol. The stoichiometry of the reaction may be represented as:

$$A + B \underset{k_r}{\overset{k_f}{\rightleftharpoons}} 2C \qquad (2)$$

with C standing for each product (since they are present in equal concentrations). For purposes of calculation and plotting, it is initially assumed that the orders match the stoichiometry; this assumption can be checked in order to obtain the correct rate law. Thus, the tentative law;

$$\frac{-d[A]}{dt} = k_f[A][B] - k_r[C]^2 \qquad (3)$$

is employed. This is converted to the integrated form:

$$\frac{1}{Q}\ln\left\{\frac{([A]_0-[A]_e)([A]-[A]_e+Q)}{([A]-[A]_e)([A]_0-[A]_e+Q)}\right\} = (k_f-k_r)t, \qquad (4)$$

where $Q=[1/(K-1)]\{K^2([B]_0-[A]_0)^2+4[A]_0[B]_0K\}^{1/2}$, where the subscripts 0 and e designate the initial and equilibrium states, and where K is obtained for each run separately. If the left-hand side is plotted *versus* the time t, (k_f-k_r) is obtained from the slope; with $K=k_f/k_r$ on the basis of microscopic reversibility, k_f and k_r can be evaluated.

Table 2. Equilibrium constants with t-butyl alcohol

t/°C	$[As(OCH_3)_3]_0$/M	$[HOC(CH_3)_3]_0$/M	K
25	3.10	1.65	0.362
	2.82	2.74	0.374
	2.43	3.01	0.355
28	2.82	2.74	0.374
36	2.82	2.74	0.382
45	2.82	2.74	0.404
56	2.82	2.74	0.419
66	2.82	2.74	0.448

† 1 M=1 mol dm^{-3}.

As may be seen in Fig. 1a, the plots are linear, with the results from experiments at variable concentrations given in Table 3. The values of k_f and k_r at variable $[As(OCH_3)_3]$ and constant $[PhCH_2OH]$ are essentially constant. On the other hand, when the benzyl alcohol concentration is varied, k_f and k_r both increase in proportion to the concentration; this indicates that the true order is larger by one than the assumed order. Furthermore, the fact the rate plots shown in Fig. 1a are linear over the measured course of reaction suggests that both forward and reverse reactions involve the initial concentration of benzyl alcohol, $[PhCH_2OH]_0$, which may be equated the total alcohol concentration at any time t, $\{[PhCH_2OH]_t+[CH_3OH]_t\}$.

Employing the corrected rate law consistent with the observed results:

$$\frac{-d[As(OCH_3)_3]}{dt} = k_1[As(OCH_3)_3][HOCH_2Ph][HOCH_2Ph]_0 - k_2[As(OCH_3)_2(OCH_2Ph)][HOCH_3][HOCH_2Ph]_0, \qquad (5)$$

and the preliminary data in Table 3, the average values of k_1 and k_2 obtained are 0.349±0.008 M^{-2} s^{-1} and 0.100±0.002 M^{-2} s^{-1}. The values of k_1 and k_2 are calculated by using the relations, $k_1=k_f/[HOCH_2Ph]_0$

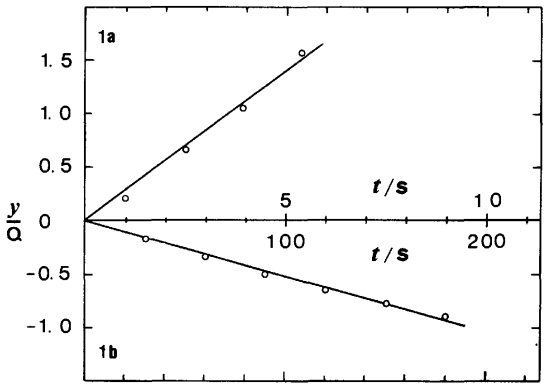

Fig. 1. Rate plots for arsenite transesterification reactions with (a) $[As(OCH_3)_3]=2.02$ M, $[HOCH_2Ph]=1.16$ M, and (b) $[As(OCH_3)_3]=1.69$ M, $[HOC(CH_3)_3]=1.07$ M. The ordinate is the left side of Eq. 4.

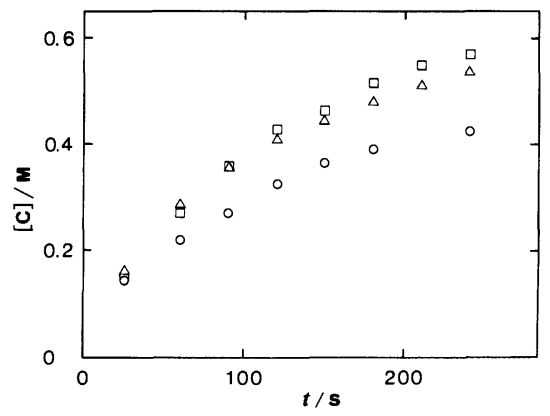

Fig. 2. Plot of $[As(OCH_3)_2OC(OCH_3)_3]$ as a function of time for $[As(OCH_3)_3]_0=2.02$ M, and ○: $[HOC(CH_3)_3]=1.07$, △: 1.67, and □; 2.07 M.

Table 3. Rate results for benzyl alcohol[a)]

$[As(OCH_3)_3]_0$/M	$[PhCH_2OH]_0$/M	k_f/M^{-1} s^{-1}	k_r/M^{-1} s^{-1}	K[b)]	k_1/M^{-2} s^{-1}[c)]	k_2/M^{-2} s^{-1}[d)]
2.02	1.16	0.397	0.115	3.45	0.342	0.099
2.02	1.40	0.497	0.145	3.48	0.355	0.102
2.02	1.87	0.651	0.186	3.50	0.348	0.099
1.17	1.16	0.394	0.113	3.49	0.340	0.097
1.51	1.16	0.415	0.117	3.55	0.358	0.101

a) At 25 °C in the acetonitrile solvent. b) $K=k_f/k_r$. c) $k_1=k_f/[HOCH_2Ph]_0$. d) $k_2=k_r/[HOCH_2Ph]_0$.

Table 4. Rate results for *t*-butyl alcohol[a)]

$[As(OCH_3)_3]_0$/M	$[HOC(CH_3)_3]_0$/M	10^3k_f/M^{-1} s^{-1}	10^3k_f/M^{-1} s^{-1}	K[b)]	10^3k_3/s^{-1}[c)]	10^3k_4/s^{-1}[d)]
2.03	2.07	1.12	3.60	0.31	2.32	7.45
2.03	1.67	1.51	4.63	0.33	2.52	7.73
2.03	1.07	1.87	7.11	0.26	2.00	7.61
1.69	1.07	1.92	7.04	0.27	2.05	7.53
1.25	1.07	1.95	7.11	0.28	2.09	7.61

a) At 25 °C in acetonitrile. b) $K=k_f/k_r$. c) $k_3=k_f[HOC(CH_3)_3]_0$. d) $k_4=k_r[HOC(CH_3)_3]_0$.

and $k_2=k_r/[HOCH_2Ph]_0$ respectively.

It was not possible to obtain the activation parameters because the stopped-flow injector did not have a temperature-control attachment.

The catalysis of the transesterification reaction is important. 1-Pentanethiol, *p*-toluenesulfonic acid, and 2,4-dimethylpyridine, all at concentrations near 10^{-2} M, accelerated the reaction to such an extent that equilibrium was reached in times comparable to or less than the time necessary for getting the first data point.

Kinetics with t-*Butyl Alcohol.* It is possible to treat the initial rate data for this alcohol in a manner (*i.e.*, Eq. 4) identical with that used for benzyl alcohol. However, the slope is now negative (as would be expected for $K<1$), and the alcohol concentration effect on the slope was in the opposite direction.

A typical plot is shown in Fig. 1b, and the data are presented in Table 4. As the *t*-butyl alcohol concentration increased, the preliminary rate constants decreased. This change in the rate constant indicates that the order assumed in the derivation is too large; these constants vary in such a manner as to indicate that the correct order in *t*-butyl alcohol is zero. This surprising conclusion can be visualized in the plots of the concentration of the product against the time shown in Fig. 2. The initial slopes must be essentially identical because the 30-second points for all three alcohol concentrations are the same, within the limits of experimental error.

The recalculation of the k_f and k_r data in Table 4 on the basis of the corrected rate law:

$$\frac{-d[As(OCH_3)_3]}{dt} = k_3\frac{[As(OCH_3)_3][HOC(CH_3)_3]}{[HOC(CH_3)_3]_0} - k_4\frac{[As(OCH_3)_2(OC(CH_3)_3][HOCH_3]}{[HOC(CH_3)_3]_0} \quad (6)$$

was then carried out. The two constants, k_3 and k_4, from Table 4 have values of $(2.20\pm0.22)\times10^{-3}$ s^{-1} and $(7.59\pm0.10)\times10^{-3}$ s^{-1} respectively.

The rates for the *t*-butyl alcohol reaction were measured at five temperatures from 30 to 60 °C; these are given in Table 5. The values of ΔH^* and ΔS^* for k_3 are 15 ± 1 kJ mol^{-1} and -253 ± 4 J mol^{-1} K^{-1}; for k_4, the corresponding numbers are 10 ± 1 kJ mol^{-1} and -258 ± 5 J mol^{-1} K^{-1} respectively.

Table 5. Dependence of *t*-butyl alcohol rate constant on temperature[a)]

t/°C	10^3k_3/s^{-1}	10^3k_4/s^{-1}	K[b)]
30.0	1.20	3.24	0.369
36.5	1.41	3.59	0.392
45.0	1.77	4.45	0.397
53.0	1.98	4.78	0.414
61.0	2.25	5.15	0.438

a) In acetonitrile, $[As(OCH_3)_3]=2.025$ M, and $[HOC(CH_3)_3]=1.073$ M. b) $K=k_3/k_4$.

The *t*-butyl alcohol reaction with $As(OCH_3)_3$ was found not to be catalyzed by 2,4-dimethylpyridine, *p*-toluenesulfonic acid, or 1-pentanethiol.

The rate law (Eq. 6) in the forward direction shows a dependence on only a single species: this might suggest a unimolecular reaction. However, the activation parameters give evidence that such a suggestion can not be correct. A low ΔH^* value and a very negative ΔS^* value can only be explained if considerable bond formation between several species is taking place in the transition state and in equilibria prior to the transition state. A further piece of evidence that other species are present in the transition state is the slight difference in rate constants in Tables 4 and 5, the data for which were obtained using different batches of a solvent. It seems possible that the rate-limiting step in the transesterification reaction was the reaction of $As(OCH_3)_3$ with a trace amount of water in the acetonitrile. This hypothesis was tested by treating the solvent so as to dry it beyond the normal purification procedure. The rate decreased greatly, by about three powers of ten; the resulting halftime was about one week at room temperature. Because of other complications, however, the further study of this very slow transesterification was not possible.

Discussion

General. From prior arsenite-rate studies,[1-5] it

was expected that the transesterification reaction would be rapid, with a cleavage of the arsenic-oxygen bond. The observed rates with benzyl alcohol are indeed rapid, although slightly slower than the oxygen-exchange process[1] and the ester hydrolysis.[2] Low values of $\Delta H^{\ddagger}$ and negative values of $\Delta S^{\ddagger}$ are found for all three reactions; presumably this is a characteristic of replacements in the arsenite-coordination sphere.

Equilibria. The K value found for benzyl alcohol is 3.6. This can be converted (using the appropriate statistical factor of 3) to the corrected value of 1.2. The reaction is slightly endothermic (5.0 kJ mol^{-1}). The entropy is (after correction for the statistical factor) $+18$ J mol^{-1} K^{-1}.

For t-butyl alcohol, the value of K is near 0.3; after statistical correction, it is 0.1. An enthalpy (4.0 kJ mol^{-1}) comparable to the case of benzyl alcohol was found. The decrease of a power of ten in the equilibrium constant shows up as a lower entropy ($\Delta S°=+5$ J mol^{-1} K^{-1}; after correction, -4).

The difference in the equilibrium constants can be traced completely to the entropy contribution. It seems probable that As–O free rotations, which are probably active in $As(OCH_3)_3$, may be shut down in $As(OCH_3)_2OC(CH_3)_3$ because of the large t-butyl group. For one carbon-carbon free rotation, the entropy contribution is about 16 J mol^{-1} K^{-1};[10] even if the rotation about the arsenic-oxygen bond is less important, three such rotations could easily be sufficiently active to explain a loss of 22 J mol^{-1} K^{-1}.

Kinetics with Benzyl Alcohol. The rate of this transesterification was rapid as expected; on the other hand, the rate law was somewhat of a surprise. Nevertheless, it is readily explicable in terms of a mechanism. The second benzyl alcohol molecule is presumably present in order to accomplish the necessary proton transfer (without an energy-costly charge-separation process) in a transition state of this type:

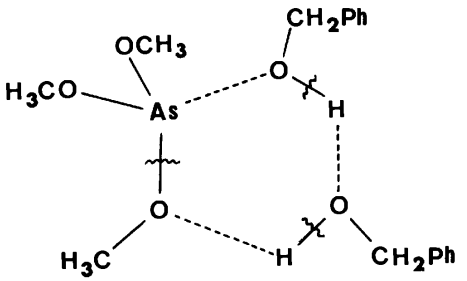

The dashed lines indicate bonds being formed; bonds being cleaved are denoted by a bond line crossed by a wavy line. A recent study of the arsenate ester/alcohol transesterification reaction indicated hydrogen-bonding, and a transition state similar to the above had to be considered.[11]

The energetic basis for additional (over stoichiometry) molecules has been discussed in some detail in relation to the peroxide oxidation of neutral nucleophiles.[12] Two examples of reactions which are catalyzed by extra protic molecules and involve proton transfer in the transition state are the oxidation of dialkyl sulfides by hydrogen peroxide[13] and the hydration of carbonyl compounds in mixed solvents.[14]

In the present case, at least two proton transfers are involved; these could take place synchronously or in a stepwise fashion. One arsenic-oxygen bond is being broken, while another is being formed, at essentially the same time. Since the rate plots as shown in Fig. 1a are linear over the measured course of the reaction, it appears that benzyl alcohol and methanol have similar proton-transrer capabilities.

Kinetics with t-Butyl Alcohol. For this alcohol, the half-time for the reaction is about one power of ten longer (in a normally purified solvent) than for benzyl alcohol; this slower rate makes it possible to follow the process using normal NMR line-intensity techniques. Now, however, the initial rate is independent of the entering alcohol concentration, and the experimental rate law given in Eq. 6 which was found to give a quantitative fit of the data most certainly cannot be complete. The activation parameters show that other particles must be present in the transition state, and evidence has been presented that the trace of water in the acetonitrile solvent acts as a catalyst. This leads to the following mechanism:

$$As(OCH_3)_3 + H_2O \underset{k_2'}{\overset{k_1'}{\rightleftharpoons}} As(OCH_3)_2OH + HOCH_3,$$

$$As(OCH_3)_2OH + HOC(CH_3)_3 \underset{k_4'}{\overset{k_3'}{\rightleftharpoons}} As(OCH_3)_2OC(CH_3)_3 + H_2O. \quad (7)$$

The steady-state rate law derived from Eq. 7 is:

$$-\frac{d[As(OCH_3)_3]}{dt} = k_1'[H_2O][As(OCH_3)_3]R/(1+R) - k_4'[H_2O][As(OCH_3)_2OC(CH_3)_3]/(1+R), \quad (8)$$

where $R=k_3'[HOC(CH_3)_3]/k_2'[HOCH_3]$. Equation 8 reduces to Eq. 6 if $R \gg 1$ to give $k_3=k_1'[H_2O]$ and $k_4=k_2'k_4'[H_2O]/k_3'$.

The fit to Eq. 6 was, in fact, not perfect (notice the slight curvature of the points in Fig. 1b). A three-parameter fit to Eq. 8 is considerably better. The results of a nonlinear least-squares fit are:[15] $k_1'[H_2O]=3.5\times10^{-3}$ s^{-1}, $k_4'[H_2O]=1.5\times10^{-3}$ s^{-1} and $k_3'/k_2'=0.15$. Since k_1' is just the rate constant for hydrolysis, we can use the known value, 4.4 M^{-1} s^{-1},[2] to obtain an estimate of the water concentration in the acetonitrile solvent, 8×10^{-4} M, which is not an unreasonable value.

For this transesterification study, t-butyl alcohol was chosen because the bulk of the large alkyl group was expected to bring about interesting effects; such turned out to be the case. Compared to the benzyl-alcohol results, the K value is very low and this is reflected in the fact that k_4 is larger than k_3. The binding difference of a factor of ten is due wholly to the lower value of ΔS, and this may be related to the loss of internal rotations in the product, the mixed ester.

The direct reaction of t-butyl alcohol with trimethyl arsenite is exceedingly slow, if it occurs at all, and this allows the entry of a mechanism which seems to be based on catalysis by very small concentrations of water in the solvent. Finally, the discrimination constant, k_3'/k_2', reflects the fact that t-butyl alcohol (in spite of

its probably larger nucleophilicity) is larger than the competing methanol.

Acknowledgement is made to the Brown University Biomedical Research Support Grant Committee for its partial support of this work. One of us (A. O.) is indebted to Nara Women's University for a twelve-month leave. The machinists and glass blower at Brown University aided us with their technical skill. We have enjoyed helpful conversations with Professor Carl Baer.

References

1) W. C. Copenhafer and P. H. Rieger, *J. Am. Chem. Soc.*, **100**, 3776 (1978).
2) C. D. Baer, J. O. Edwards, P. H. Rieger, and C. M. Silva, *Inorg. Chem.*, accepted for publication.
3) G. L. Roy, A. L. Laferriere, and J. O. Edwards, *J. Inorg. Nucl. Chem.*, **4**, 106 (1957).
4) A. Okumura, N. Yamamoto, and N. Okazaki, *Bull. Chem. Soc. Jpn.*, **46**, 3633 (1973).
5) J. O. Edwards, T. Mallouk, and P. H. Rieger, unpublished results.
6) M. Moedritzer, *Inorg. Syn.*, **14**, 181 (1968).
7) T. B. Brill and N. C. Campbell, *Inorg. Chem.*, **12**, 1884 (1973).
8) J. A. Riddick and W. S. Bunger, "Organic Solvents," in "Techniques of Chemistry, " 3rd ed, ed by A. Weissberger, Wiley, New York (1971), Vol. 2, Chap. V, pp. 572—877.
9) D. A. Couch, O. W. Howarth, and P. Moore, *J. Phys. E. Sci. Inst.*, **8**, 831 (1975).
10) J. O. Edwards, unpublished calculations.
11) a) C. D. Baer, J. O. Edwards, M. J. Kaus, T. G. Richmond, and P. H. Rieger, *J. Am. Chem. Soc.*, **102**, 5793 (1980); b) C. D. Baer, Ph. D. Thesis, Brown university, 1980.
12) R. Curci, R. DiPrete, J. O. Edwards, and G. Modena, "Hydrogen-Bonded Solvent Systems," ed by A. K. Covington and P. Jones, Taylor and Francis, London (1968), pp. 303—321.
13) M. A. P. Dankleff, R. Curci, J. O. Edwards, and H. Y. Pyun, *J. Am. Chem. Soc.*, **90**, 3209 (1968).
14) R. P. Bell, J. P. Millington, and J. M. Pink, *Proc. R. Soc. London, Ser. A*, **303**, 1 (1968).
15) Although the overall fit of Eq. 8 to the experimental data is good, the parameters are strongly correlated; the values given are, therefore, rough estimates at best.

 © 1984 The Chemical Society of Japan Bull. Chem. Soc. Jpn., 57, 189—193 (1984)

The Selective Extraction and Spectrophotometric Determination of Copper and Silver by the Use of a Thiocrown Compound 1,4,8,11-Tetrathiacyclotetradecane

Keiitsu SAITO, Yoshitaka MASUDA,† and Eiichi SEKIDO*,†

The Graduate School of Science and Technology, Kobe University, Nada-ku, Kobe 657
†Department of Chemistry, Faculty of Science, Kobe University, Nada-ku, Kobe 657
(Received May 23, 1983)

A highly selective solvent extraction and spectrophotometric determination of copper and/or silver is proposed; it is based on the extraction of the ion-pair formed by the copper(I)- or silver(I)-thiocrown ether complex cation and the appropriate dye anion. A comparative study of Bromocresol Green (BCG), Thymol Blue (TB), and picrate ions as the pairing ions for the extraction of copper using a 1,4,8,11-tetrathiacyclotetradecane (TTCT) solution of 1,2-dichloroethane is described. The use of BCG gave the highest sensitivity among these three kinds of anions and made it possible to determine copper in the range of 0.6—3.2 $\mu g\,ml^{-1}$. The interferences of six kinds of cations and four kinds of anions were examined; only Ni^{2+} and ClO_4^- interfered, and they slightly. The separation by the extraction of silver and/or copper with TTCT solution of 1,2-dichloroethane from an aqueous solution containing seven kinds of metal ions (Mn^{2+}, Co^{2+}, Ni^{2+}, Cu^{2+}, Zn^{2+}, Cd^{2+}, and Ag^+) in the presence of picrate ion (Pic^-) was also examined. Silver was first extracted quantitatively as the ion-pair compound, $[Ag(ttct)_2]^+Pic^-$, and then copper as $[Cu(ttct)]^+Pic^-$ after having been reduced to copper(I). The absorption maximum of both extracted species lies at 378 nm (ε: 1.8×10^4), and the spectrophotometric determination of these metals is possible. This method was successfully applied to the determination of copper and silver in standard samples of steel.

Although the solvent extraction of alkali metals using crown-ether compounds has been widely studied,[1-7] there have been few studies of metals using thiocrown ether compounds.[8-10] We tried to examine the solvent extraction of various metal ions with TTCT, which is a typical thiocrown ether.[11] Consequently, it was found that the Class *b* metals classified by Ahrland,[12] in particular copper(I) and silver(I), are extracted; on the other hand, the Class *a* metals are not extracted at all, and the Class *ab* metals are practically not extracted at all.

In the present study, the extraction-spectrophotometric determination of copper and silver using TTCT as the ligand, the dye anion(BCG or picrate) as the pairing anion, and 1,2-dichoroethane as the extracting solvent, was examined. Therefore, it was confirmed that TTCT is a useful selective reagent to separate the Class *b* metals, especially copper and silver, from other metals. It was also found that the use of the dye anion makes the spectrophotometric determination of copper and/or silver possible. Hitherto,such reagents as neocuproine, diethyldithiocarbamic acid (DDTC), and dithizone for copper and those such as *p*-dimethylaminobenzidinerhodanine and dithizone for silver have usually been employed as the spectrophotometric reagents in the routine analysis of these metals. By comparing the proposed method with conventional methods, it was found that the proposed method is more sensitive than the neocuproine method and more selective than the DDTC and dithizone methods for copper, and is more reproducible than the *p*-dimethylaminobenzidinerhodanine method and more selective than the dithizone method for silver.

Experimental

Reagents. The TTCT was synthesized by the method described by Rosen and Bush[13] and recrystallized three times from ethanol. A 5×10^{-5} M (1 M=1 mol dm^{-3}) TTCT 1,2-dichloroethane solution was prepared; it was stable for a week at least. After we had prepared the 1×10^{-2} M copper(II) and silver(I) sulfate solutions, we determined their concentrations by EDTA titration and by potentiometric titration with sodium chloride respectively. The 1,2-dichloroethane was shaken three times with 2 M potassium hydroxide and then with distilled water. After drying with calcium chloride anhydride, it was distilled. The other reagents used were of analytical-reagent grade.

Apparatus. A Taiyo M incubator was used for shaking a 50-ml glass cylindrical tube equipped with a glass stopper. An Iwaki KM-shaker was used for shaking a 100-ml separatory funnel. A Seiko SAS-725 atomic absorption spectrophotometer was used for the determination of the copper and silver concentrations. The absorption spectra were measured with a Hitachi 124 double-beam spectrophotometer and a Shimadzu UV-240 self-recording spectrophotometer. The pH of the aqueous phase was measured with a Hitachi-Horiba H-5 PH meter.

Solvent Extraction of Copper(I). An aqueous solution containing 5×10^{-5} M copper(II) sulfate, the 5×10^{-5} M dye anion(BCG, TB or picrate), a 1×10^{-2} M buffer, and 0.1 M hydroxylammonium sulfate was prepared; its ionic strength was kept at 0.1 with sodium sulfate. The buffer solutions were prepared with acetic acid–sodium acetate in the weak acidic region and sodium tetraborate and sodium hydroxide in the weak basic region. Ten ml of this aqueous solution was placed in a 50-ml glass cylindrical tube equipped with a glass stopper. After the addition of 10 ml of the 5×10^{-3} M TTCT solution of 1,2-dichloroethane, the mixture was shaken for 30 min at 200 strokes/min at 25±0.1 °C and then centrifuged for 5 min at 2000 min^{-1}. The absorption spectra of the 1,2-dichloroethane phase were measured against a reagent blank in the range from 250 to 550 nm. The pH of the aqueous phase was measured, and the copper concentration of the aqueous phase was measured by means of atomic-absorption spectrophotometry. The copper concentration of the 1,2-dichloroethane phase was determined as follows: a five ml portion of the organic phase was placed in a beaker and allowed to evaporate. The residue was dissolved in concentrated nitric acid and diluted to 25 ml or 10 ml with water. The copper concentration was determined by means of atomic-absorption spectrophotometry.

Separation of Silver and Copper from a Mixed Solution Containing Various Metal Ions. An aqueous solution

containing various metal ions(Mn^{2+}, Co^{2+}, Ni^{2+}, Cu^{2+}, Zn^{2+}, Cd^{2+}, and Ag^{+}), a picrate (1×10^{-3} M), and an acetic acid-sodium acetate buffer (1×10^{-2}M, pH 5.4) was prepared. Ten ml of this aqueous solution was introduced into a 50-ml glass cylindrical tube equipped with a glass stopper, and then 10 ml of the 5×10^{-3} M TTCT solution of 1,2-dichloroethane was added. The mixture was shaken for 30 min at 200 strokes/min at 25±0.1 °C and then centrifuged for 5 min at 2000 min^{-1}. A 5 ml portion of the aqueous phase was introduced into a 50-ml glass cylindrical tube equipped with a glass stopper, and then 5-ml of an aqueous solution containing 0.2 M hydroxylammonium sulfate,the 1×10^{-3} M picrate, and the 1×10^{-2} M acetic acid-sodium acetate buffer were added. After the addition of 10 ml of the 5×10^{-3} M TTCT solution of 1,2-dichloroethane, the mixture was shaken for 30 min at 200 strokes/min at 25±0.1 °C and then centrifuged for 5 min at 2000 min^{-1}. All the metals were determined by means of atomic-absorption spectrophotometry. The concentration of the metal ion in the organic phase was determined as has been described above.

Preparation of a Standard Sample Solution of Steel. A standard sample of steel (0.1 g) was dissolved in 20 ml of (1+4) nitric acid by heating. After the addition of 10 ml of (1+9) sulfuric acid, the solution was heated gently until fumes of sulfuric acid had been evolved. The residue was cooled to room temperature, and then the walls of the beaker were washed with a small portion of water. After the addition of several drops of a hydrogen-peroxide solution (30%), the solution was heated gently until fumes of sulfuric acid had been evolved. The residue was cooled and then dissolved in water. Finally the solution was diluted to 100 ml with water.

Recommended Procedure for the Determination of Copper and Silver. (I) Determination of Copper in a Standard Sample of Steel in the Absence of Silver: Pipette an aliquot of a sample solution containing up to 32 μg of copper(II) into a 100-ml separatory funnel. Add 5 ml of 1 M hydroxylammonium sulfate and 5 ml of a 1×10^{-2} M picric acid or 2.5×10^{-3} M BCG solution. Adjust the pH in the range of pH 4—5 with a 1.5 M sodium acetate solution, and then dilute with water to 50 ml. After the addition of 10 ml of the TTCT solution of 1,2-dichloroethane, shake for 10 min. Allow it to stand and the layers to separate, and then place the yellow extract in a 1-cm cell. Measure the absorbance at 378 nm for picrate or at 408 nm for BCG against the reagent blank as the reference solution.

(II) Determination of Silver and Copper in a Standard Sample of Steel in the Presence of Silver and Copper: Pipette an aliquot of a sample solution containing up to 54 μg of silver(I) into a 100-ml separatory funnel. Add 5 ml of 1×10^{-2} M picric acid, and then adjust the pH in the range of pH 4—6 with 1.5 M sodium acetate. Dilute it with water to 50 ml, and then shake with 10 ml of the TTCT solution of 1,2-dichloroethane for 10 min. Allow it to stand and the layers to separate, and then place the yellow extract in a 1-cm cell. Measure the absorbance at 378 nm against the reagent blank. Pipette an aliquot of the aqueous phase containing up to 32 μg of copper(II) into a 100-ml separatory funnel. Finally, add 5 ml of 1 M hydroxylammonium sulfate and the 1×10^{-2} M picric acid solution to make a 1×10^{-3} M. The subsequent procedure was the same as that used for the determination of copper in a standard sample of steel in the absence of silver.

Results and Discussion

Extraction Behavior of Copper(I) with TTCT in the Presence of BCG, TB, or Picrate. The extraction of copper(I) with TTCT from the aqueous solution in the presence of BCG, TB, or picrate ions into 1,2-dichloroethane was examined in the pH range from 3—8. Plots of the logarithm of the distribution ratio of copper(I) (log D) *vs.* the pH of the aqueous solution are shown in Fig. 1. For the extraction of copper(I) in the presence of BCG, TB, or picrate ions, almost the same pH dependence was observed. Each extractability is kept constant at a value of more than 99% (log D>2) in the pH range from 4 to 6, but it decreases with the decrease in pH value below 4 and with the increase above 6. It is considered that the decrease in the extraction on the acidic side is due to the decrease in the amount of copper(I), accompanied by the decrease in the reducing power of hydroxylammonium sulfate; on the other hand, the decrease in the extraction on the basic side is considered to be due to the hydrolysis of copper(I).

It was found in the previous study[11] that copper(I) was extracted with TTCT into organic solvents by forming an ion-pair compound, $[Cu(ttct)]^{+}Pic^{-}$, in the presence of picrate. In the present study, the composition of the extracted species in the presence of BCG or TB was checked. The logarithmic plot of the distribution ratio of copper(I) *vs.* the concentration of TB in the aqueous phase, which was determined by means of the absorbance at 431 nm, is shown in Fig. 2.

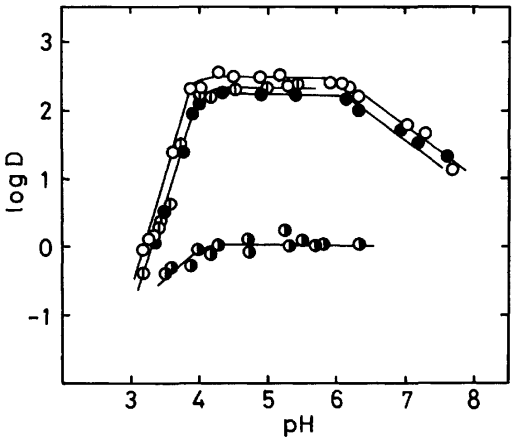

Fig. 1. Plots of log D *vs.* pH. Initial concentration; TTCT: 5×10^{-3}M.
-○-; $[Cu^{+}]_i=5\times10^{-5}$M, $[BCG]_i=5\times10^{-4}$M. -●-; $[Cu^{+}]_i=5\times10^{-5}$M, $[TB]_i=5\times10^{-4}$M. -Φ-; $[Cu^{+}]_i=5\times10^{-5}$M, $[Pic]_i=5\times10^{-4}$M. -◑-; $[Cu^{2+}]_i=5\times10^{-5}$M, $[BCG]_i=5\times10^{-4}$M.

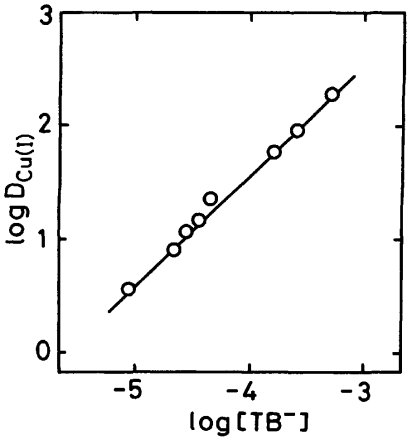

Fig. 2. Plot of log $D_{Cu(I)}$ *vs.* log $[TB^{-}]$. pH 4.5. Initial concentration; copper(I): 5×10^{-5}M, TTCT: 5×10^{-3}M.

The straight line with the slope of +1 thus obtained, indicates the 1 : 1 ratio of copper to TB. The molar ratio of copper to BCG was examined by the continuous-variation method; the results are shown in Fig. 3. As may be seen in Fig. 3, the maximum absorbance is found at the 1 : 1 molar ratio of copper to BCG. These results suggest that the species extracted into 1,2-dichloroethane are $[Cu(ttct)]^+A^-$, where A^- is the TB or BCG anion.

Absorption Spectra. The absorption spectra of the organic extracts, as measured against a reagent blank, are shown in Fig. 4. It was found that the absorption maxima lie at 408, 391,and 378 nm for BCG, TB, and picrate ions respectively. BCG exhibited the maximum absorbance among these three kinds of pairing ions. Although the extracted complexes are stable, the absorbance of the organic phase was measured within 4 h after the extraction.

Effect of pH. The effect of the pH of the aqueous phase was also examined. Plots of the absorbance at the maximum wavelength of the organic phase *vs.* the pH of the aqueous phase are shown in Fig. 5. As is shown in Fig. 5, the absorbance is constant over the pH range from 4.0 to 5.0 for BCG, from 3.8 to 7.0 for TB, and from 4.0 to 5.5 for picrate in the examined pH. It seems that the decreases in absorbance in the range of pH 5—6 for BCG is related to the pH range of color change interval of BCG from pH 3.7 to 5.4. Figure 5 also shows that among the three kinds of pairing ions, BCG is most favorable for the spectrophotometric determintion of copper.

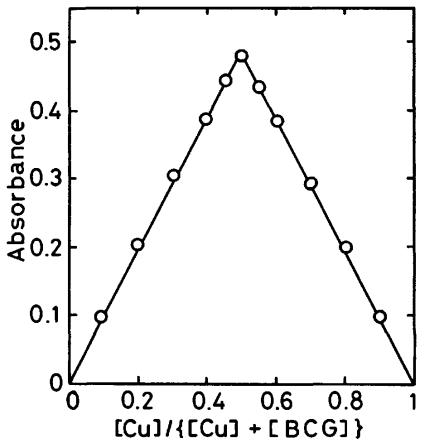

Fig. 3. Continuous variation method.
$[Cu]+[BCG]=2.5\times10^{-5}$M, $[TTCT]_o=5\times10^{-3}$M.
Wavelength; 408 nm. Reference; reagent blank.

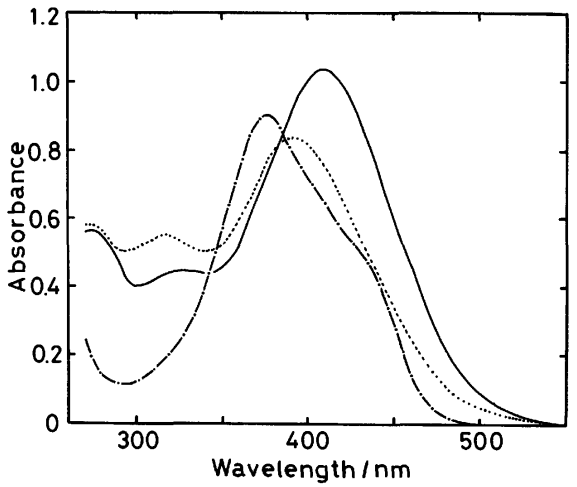

Fig. 4. Absorption spectra of 1,2-dichloroethane extracts from aqueous solution containing 5×10^{-4}M BCG^- (—), TB^-(····), or Pic^-(– –). Initial concentration; copper(I): 5×10^{-5} M, TTCT: 5×10^{-3} M.

Calibration, Sensitivity, and Precision. When the procedure described for the solvent extraction of copper(I) (Experimental section) was used, Beer's law was followed in the range of 0.6—3.2 μg Cu ml^{-1}. When BCG or picrate ions were used, the molar absorptivity was 2.01×10^4 or 1.80×10^4 l $mol^{-1}cm^{-1}$ respectively. These values are higher than the molar absorptivity for the neocuproine method; 7.95×10^3 at 454 nm in isoamyl alcohol, bathocuproine method; 1.42×10^4 at 479 nm in *n*-hexyl alcohol and diethyldithiocarbamic acid method; 1.42×10^4 at 432 nm in chloroform. The sensitivity for the 0.001 absorbance was 3.16 or 3.53 ng cm^{-2} respectively. When 10 solutions containing 15.9 μg of copper were deter-

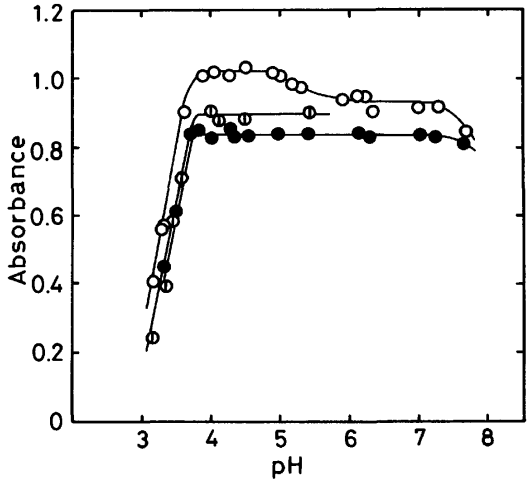

Fig. 5. Absorbance of the 1,2-dichloroethane extracts at the wavelength of absorption maximum as a function of pH. Reference; reagent blank. Initial concentration; copper(I) 5×10^{-5}M, TTCT: 5×10^{-3}M, dye: 5×10^{-4}M.
-○-; BCG, wavelength 408 nm. -●-; TB, wavelength 391 nm. -Φ-; Pic, wavelength 378 nm.

Table 1. Effects of diverse ions

Ion	Concentration/M	Absorbance at 408 nm
None	—	0.505
Mn^{2+}	2.5×10^{-2}	0.050
Fe^{2+}	2.5×10^{-2}	0.504
Co^{2+}	2.5×10^{-2}	0.510
Ni^{2+}	2.5×10^{-2}	0.535
	2.5×10^{-3}	0.507
Zn^{2+}	2.5×10^{-2}	0.504
Cd^{2+}	2.5×10^{-2}	0.510
ClO_4^-	5.0×10^{-2}	0.482
	2.5×10^{-2}	0.491
	5.0×10^{-3}	0.495
NO_3^-	0.1	0.493
Cl^-	0.1	0.502
SO_4^{2-}	0.1	0.508

Concentration of copper(I) in each case: 2.5×10^{-5} M.
Reference: reagent blank.

mined using the BCG or the picrate as the pairing ion, the relative standard deviation was 1.5% or 0.6% respectively.

Effect of Foreign Ions. The interference from the following metal ions and anions were examined by using BCG; Mn^{2+}, Fe^{2+}, Co^{2+}, Ni^{2+}, Zn^{2+}, and Cd^{2+}, ClO_4^-, NO_3^-, Cl^-, and SO_4^{2-}. All the metal ions were added as sulfates, while all the anions were added as their sodium salts. The results are shown in Table 1. Mn^{2+}, Fe^{2+}, Co^{2+}, Zn^{2+}, and Cd^{2+} in a 1000-fold excess over the copper concentration did not interfere, whereas Ni^{2+} in a 1000-fold excess serves to increase the absorbance by 5.9%. However, Ni^{2+} in a 100-fold excess did not interfere with the determination of copper. The presence of 0.1 M sulfate, chloride, and nitrate ions did not affect the determination of copper significantly, whereas the perchlorate ion when present in a quantity of more than 2.5×10^{-3} M gave a negative error.

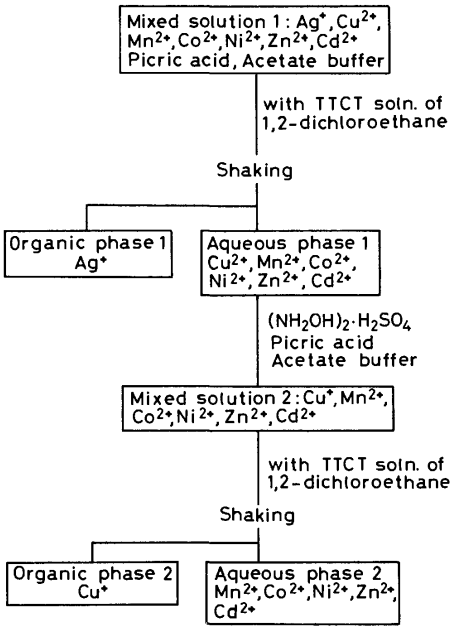

Fig. 6. Procedure of separation for silver and copper.

Separation of Silver and Copper from Aqueous Solution Containing Various Metal Ions. As has been mentioned above, it seems that among the dye anions examined, the BCG is most advantageous for both the ion-pair extraction and the spectrophotometric determination. However, from the fact that about 50% of the copper(II) was extracted when the BCG was used as the pairing ion (Fig. 1), it seems that the selectivity for silver(I) toward copper(II) decrease. Little copper(II) is extracted with TTCT in the presence of the picrate, whereas silver(I) is completely extracted.[11] Consequently a procedure was devised for separating silver and copper from an aqueous solution containing various metal ions using the picrate as the pairing ion. This separation scheme is shown in Fig. 6. Silver was first extracted as the ion-pair compound, $[Ag(ttct)_2]^+Pic^-$, the composition of which will be clarified in another paper, and then copper was extracted as $[Cu(ttct)]^+Pic^-$ after reducing the copper(II) to copper(I) with hydroxylammonium sulfate. The results are shown in Table 2. Silver(I) in a mixed solution containig Mn^{2+}, Co^{2+}, Ni^{2+}, Cu^{2+}, Zn^{2+}, Cd^{2+}, and Ag^+ (each metal ion concentration: 5×10^{-5} M) was more than 99% extracted by a single extraction. The other metal ions remained in the aqueous phase. In the case of the extraction from an aqueous solution containing 5×10^{-5} M Ag^+ and 1×10^{-2} M of other metal ions, almost the same results were obtained except that only a little copper(II) was extracted (3.8×10^{-6} M). The ion-pair compound, $[Ag(ttct)_2]^+Pic^-$, was completely back-extracted with 3 M HCl into the aqueous phase. In order to reduce copper(II) to copper(I), a hydroxylammonium sulfate solution was added to an aqueous phase into which silver(I) was extracted into the 1,2-dichloroethane phase, and then the extraction of copper(I) with TTCT was carried out. Ninety-nine percent of the copper(I) in the mixed solution was extracted by the single extraction in this procedure. All the other metal ions remained in the aqueous phase.

Table 2. Results of the separation of Ag^+ and Cu^+

Mixed solution 1		Organic phase 1		Recovery of Ag
Mn^{2+}, Co^{2+}, Ni^{2+}, Cu^{2+}, Zn^{2+}, Cd^{2+}	Ag^+	Cu^{2+}	Ag^+	%
5×10^{-5} M	5×10^{-5} M		4.98×10^{-5} M	99.6
1×10^{-2} M	5×10^{-5} M	3.8×10^{-6}	4.99×10^{-5} M	99.8
Mixed solution 2		**Organic phase 2**		**Recovery of Cu**
Mn^{2+}, Co^{2+}, Ni^{2+}, Zn^{2+}, Cd^{2+}	Cu^+	Cu^+		%
2.5×10^{-5} M	2.5×10^{-5} M	2.48×10^{-5} M		99.2
5×10^{-3} M	2.5×10^{-5} M	2.46×10^{-5} M		98.4

Table 3. Analytical values of standard steel samples

Sample	Chemical composition (wt%)[a]										
	C	Si	Mn	Ni	Cr	S	Cu	P	V	Mo	Ag
No. 1	0.35	0.61	0.10	0.064	3.00	0.033	0.30	0.016	0.43	0.42	—
No. 2	0.521	0.258	0.807	0.137	1.00	0.027	0.181	0.036	0.054	0.414	0.090

a) Cited from standard values of JSS 155-1 for Sample No. 1, and from standard values of NBS 159 for Sample No. 2.

TABLE 4. ANALYSIS OF STANDARD STEEL SAMPLES FOR COPPER AND SILVER

Sample	Cu(wt%)			Ag(wt%)	
	Standard value	Present work		Standard value	Present work
		BCG	Pic		Pic
No. 1	0.30	0.30	0.31	—	—
No. 2	0.181	—	0.181	0.090	0.093

The absorption spectrum of the extracted species of silver(I) was almost the same as that of copper(I) in Fig. 4, and the absorption maximum lay at 378 nm.

These results show that the selective extraction-spectrophotometric determination of silver and copper from an aqueous solution containing first-transition metal ions (Mn^{2+}, Fe^{2+}, Ni^{2+}, Co^{2+}) and post-transition metal ions (Zn^{2+}, Cd^{2+}) is possible.

Practical Application. Two kinds of standard samples (No. 1 and 2) of steel were used in this study. Sample No. 1 contains copper, but no silver, while sample No. 2 contains both copper and silver. The chemical compositions of these samples are shown in Table 3. Sample No. 1 was analysed for copper using the BCG or picrate as the pairing anion (Table 4). The values in Table 4 are the averages of five measurements. The results show a reasonable agreement with the standard values. This sample contains a relatively large percentage of copper, so that 5 ml of the sample solution is sufficient for the determination of the copper. Therefore, the determination of copper is possible according to the procedure described in the solvent extraction of copper(I) (Experimental section), in which the volume of the aqueous phase is 10 ml. However, in the case of a sample containing a small percentage of copper, we adopted the recommended procedure for the determination of copper and silver, in which the volume of the aqueous phase was 50 ml. The absorbance of the organic phase did not change, although the volume of the aqueous phase increased from 10 to 50 ml.

Sample No. 2 was analyzed for copper and silver according to the procedure described for the separation of silver and copper from a mixed solution containing various metal ions (Table 4). The values in Table 4 are the averages for five measurements. The copper and silver contents (0.181% and 0.093% respectively) obtained by proposed method compare reasonably well with the standard values of 0.181 and 0.090% for copper and silver respectively.

The proposed method is so selective that the determinations of copper(I) and silver(I) are not interfered with the first-transition metal ions even when no masking reagent is present.

The authors are grateful to the Central Research Laboratory, Sumitomo Metal Industries, Ltd., for the supply of the standard samples of steel.

References

1) C. J. Pedersen, *J. Am. Chem. Soc.*, **89**, 7017 (1967).
2) H. K. Frensdorff, *J. Am. Chem. Soc.*, **93**, 4684 (1971).
3) J. J. Christensen, D. J. Eatough, and R. M. Izatt, *Chem. Rev.*, **74**, 351 (1974).
4) A. Sadakane, T. Iwachido, and K. Toei, *Bull. Chem. Soc. Jpn.*, **48**, 60 (1975).
5) J. W. Mitchell and D. L. Sanks, *Anal. Chem.*, **47**, 642 (1975).
6) Y. Takeda and H. Kato, *Bull. Chem. Soc. Jpn.*, **52**, 1027 (1979).
7) H. Sumiyoshi, K. Nakahara, and K. Ueno, *Talanta*, **24**, 763 (1977).
8) D. Sevdic and H. Mieder, *J. Inorg. Nucl. Chem.*, **39**, 1403 (1977).
9) D. Sevdic and H. Mieder, *J. Inorg. Nucl. Chem.*, **39**, 1409 (1977).
10) D. Sevdic L. Fekete, and H. Mieder, *J. Inorg. Nucl. Chem.*, **42**, 885 (1980).
11) K. Saito, Y. Masuda, and E. Sekido, *Anal. Chim. Acta*, **151**, 447 (1983).
12) S. Ahrland, J. Chatt, and N. R. Davies, *Quart. Rev. London*, **12**, 265 (1958).
13) W. Rosen and D. H. Bush, *J. Am. Chem. Soc.*, **91**, 4694 (1969).

Mechanism of the Reactions of Oxomolybdenum(V) Tetraphenylporphyrin Complex with Alcohols in the Presence of Superoxide

Taira IMAMURA,* Koichi HASEGAWA, Tetsuya TANAKA, Wataru NAKAJIMA, and Masatoshi FUJIMOTO*
Department of Chemistry, Faculty of Science, Hokkaido University, Sapporo 060
(Received June 6, 1983)

The successive addition of ROH (R=CH_3 and C_2H_5) to the dichloromethane solution of Mo^VO(tpp)Br (tpp=*meso*-tetraphenylporphinato) causes two-step reactions at 25 °C. The products of the first and the second step of the reactions are alcohol complex, [Mo^VO(tpp)(ROH)]Br, and alkoxo complex, Mo^VO(tpp)OR, respectively. In the presence of superoxide ion, O_2^-, in the dichloromethane solution of Mo^VO(tpp)X (X=Br and NCS) containing alcohol, Mo^VO(tpp)OR is formed through competitive two reaction paths where O_2^- acts as a proton acceptor and a reducing agent. The reaction steps of the two paths were confirmed by optical and ESR studies.

Much attention has been given to the studies of the reactions of metal complexes with superoxide to elucidate the mechanisms of the formation reaction and the electronic structure of dioxygen complex and of disproportionation reactions of superoxide by superoxide dismutases.[1,2] Superoxide possesses versatile reactivities as a ligand, a reductant, an oxidant, and a base depending on the reaction conditions such as solvents and temperature.[2,3]

Recently, the authors reported that Mo^VO(tpp)Br was reduced to $Mo^{IV}O$(tpp) by superoxide ion in aprotic solvents *via* an intermediate which was suggested to be a dioxygen complex.[4] When the reaction system contained a small amount of alcohol, alkoxo complex, Mo^VO(tpp)OR, was finally formed.[5,6] The present paper reports the mechanism of the reaction of Mo^VO(tpp)X with alcohols (CH_3OH and C_2H_5OH) in the presence of superoxide ion. In this reaction system, superoxide ion acts as a base to remove a proton from alcohol and a reducing agent for Mo^VO(tpp)X.

Experimental

The syntheses of the complexes, Mo^VO(tpp)X,[5] Mo^VO(tpp)OC_2H_5,[5] Mo^VO(tpp)OCH_3,[7] and $Mo^{IV}O$(tpp),[4] were reported previously. Dichloromethane was distilled, passed through a column of basic alumina to remove stabilizer,[8] and again distilled immediately before use. Methanol and ethanol were purified by the usual methods.[9] Dimethyl sulfoxide was kept with calcium hydride for several days, distilled at 37 °C under reduced pressure, and stored under Ar atmosphere. Potassium superoxide (ICN Pharmaceuticals) and 18-crown-6 (Nippon Soda) were used without further purification. The solution of superoxide was prepared from potassium superoxide solubilized by 18-crown-6 in dimethyl sulfoxide under Ar atmosphere.[10] The concentration of superoxide in dimethyl sulfoxide was determined by photometric titration with iodine.[6]

Visible absorption spectra were measured at 25.0±0.1 °C with a Hitachi 808 spectrophotometer. ESR spectra were recorded with a JEOL JES-FE1X spectrometer at 25 °C.

Results and Discussion

Reactions of Mo^VO(tpp)X with Alcohols. The successive addition of methanol to the dichloromethane solution of Mo^VO(tpp)Br at 25 °C causes two-step reactions. In the first step, the absorbance of the Soret band of Mo^VO(tpp)Br at 508 nm is decreased with increasing absorbance of a new Soret band at 478 nm (spectra 1—4 in Fig. 1). This spectral change has isosbestic points. Asmus plot[11] for this spectral change indicates that the reaction is the type of A+B⇄C, where A and B denote the reactants (Fig. 2). By the further addition of a large excess of methanol, the Soret band at 478 nm diminishes with appearance of a new absorption band at 454 nm (spectrum 5 in Fig. 1). The absorption spectrum of the final product agrees with that of the complex, Mo^VO(tpp)OCH_3, synthesized and isolated independently.[7] The product of the first step of the reaction is assigned to the alcohol complex, [Mo^VO(tpp)(CH_3OH)]Br, which is namely formed by the substitution of Br^- in Mo^VO(tpp)Br with methanol.[12] The spectral change shown in Fig. 1 suggests that the second step reaction is the deprotonation

Table 1. Absorption peaks in UV and visible regions

Complex	λ_{max}/nm ($\varepsilon/10^4$ mol^{-1} dm^3 cm^{-1}) in CH_2Cl_2 at 25 °C					
Mo^VO(tpp)Br[a]	350 (6.40)	375, 390 (sh)	421 (2.63)	508 (3.45)	638 (0.71)	686 (0.86)
Mo^VO(tpp)NCS[a]	333 (5.42)	370 (sh)	410 (sh)	493 (4.55)	622 (0.91)	667 (0.93)
[Mo^VO(tpp) (dmso)]Br[b]	330 (4.6)	375 (sh)	405 (sh)	477 (6.0)	604 (1.0)	648 (0.9)
[Mo^VO(tpp) (CH_3OH)]Br	340 (5.1)	375 (sh)	407 (sh)	478 (5.4)	600 (1.0)	645 (0.8)
$Mo^{IV}O$(tpp)[c]	320 (0.9)			428 (29.0)	554 (1.59)	589 (0.31)
Mo^VO(tpp)OC_2H_5[a]	320 (3.42)	385 (sh)		454 (15.8)	582 (1.51)	622 (1.04)
Mo^VO(tpp)OCH_3[d]				454 (17.0)	581 (1.57)	621 (1.08)

a) Ref. 5 b) Ref. 12 c) Ref. 4 d) Ref. 19

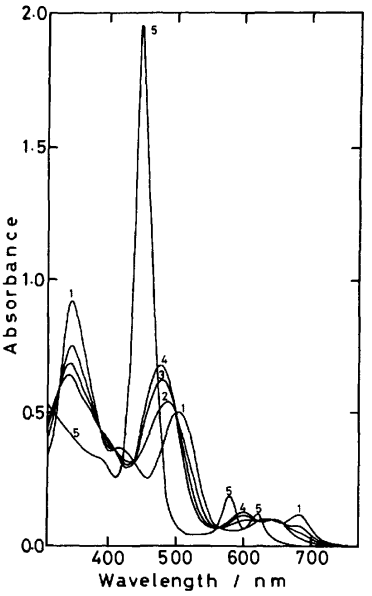

Fig. 1. The spectral change in the reaction of $Mo^{V}(tpp)Br$ with methanol in dichloromethane at 25 °C. The initial concentrations are $[Mo^{V}O(tpp)Br]_0=1.44\times10^{-5}$ mol dm^{-3} and $[CH_3OH]_0$=0 (0) (1); 0.2 (0.049) (2); 0.5 (0.12) (3); 0.9 (0.22) (4); 5.0%(v/v) (1.24 mol dm^{-3}) (5).

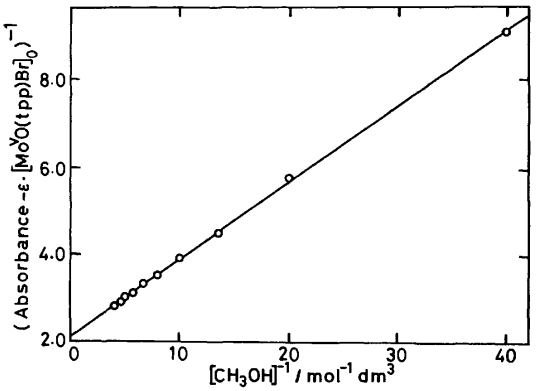

Fig. 2. Asmus plot at 478nm for the reaction of $Mo^{V}O(tpp)Br$ with methanol at 25 °C.

reaction of $[Mo^{V}O(tpp)(CH_3OH)]Br$ enhanced by the presence of a large amount of alcohol in the reaction system. This deprotonation reaction could be resulted from the change in the dielectric constant of the solution or the role of alcohol as a base.

The formation constant, K_s, of the first step of the reaction,

$$Mo^{V}O(tpp)Br + CH_3OH \overset{K_s}{\rightleftharpoons} [Mo^{V}O(tpp)(CH_3OH)]Br$$
$$\lambda_{Soret} = 508\ nm \qquad \lambda_{Soret} = 478\ nm$$
$$\overset{+CH_3OH}{\rightleftharpoons} Mo^{V}O(tpp)OCH_3 + HBr \qquad (1)$$
$$\lambda_{Soret} = 454\ nm$$

and the molar absorption coefficient at 478 nm of $[Mo^{V}O(tpp)(CH_3OH)]Br$ were determined to be K_s= 12.5 mol^{-1} dm^3 and $\varepsilon_{478\,nm}=5.4\times10^4$ mol^{-1} dm^3 cm^{-1} from Asmus plot at 25 °C.

By the reaction of $Mo^{V}O(tpp)Br$ with ethanol, $Mo^{V}O(tpp)OC_2H_5$ is also formed *via* the formation of $[Mo^{V}O(tpp)(C_2H_5OH)]Br$. The formation constant of the $[Mo^{V}O(tpp)(C_2H_5OH)]Br$ is $K_s=2.8\pm0.2$ mol^{-1} dm^3 at 25 °C. The spectral change of the reaction does not show any isosbestic points since the first step of the reaction is not discriminated from the second step owing to the small value of the formation constant, K_s.

The solution of the complex, $[MoO(tpp)(CH_3OH)]Br$, resulted from the reaction of $Mo^{V}O(tpp)Br$ with methanol shows ESR signals due to molybdenum which indicates that the oxidation state of the central molybdenum atom of the complex is 5+ as that of the complexes, MoO(tpp)Br and MoO(tpp)OR.[13]

The successive addition of methanol to the dichloromethane solution of $Mo^{V}O(tpp)NCS$ causes the shift of absorption peak from 493 to 480 nm followed by the appearance of a new band at 454 nm. The bands at 480 and 454 nm are ascribed to $[Mo^{V}O(tpp)(CH_3OH)]NCS$ and $Mo^{V}O(tpp)OCH_3$, respectively. The amount of the alcohol complex, $[Mo^{V}O(tpp)(CH_3OH)]NCS$, formed in the course of the reaction is relatively small compared to that of the reaction system of $Mo^{V}O(tpp)Br$, which is due to the small value of the formation constant, $K_s<1.0$ at 25 °C. The order of the magnitude of the formation constant of the dimethyl sulfoxide complexes, $[Mo^{V}O(tpp)(dmso)]X$, was also found to be $K^{DMSO}_{X=NCS} \ll K^{DMSO}_{X=Br}$.[12]

Mechanisms of the Reactions between $Mo^{V}O(tpp)X$, Alcohols, and Superoxide. The complex, $Mo^{V}O(tpp)X$, is present as the reaction species, $Mo^{V}O(tpp)X$, $[Mo^{V}O(tpp)(ROH)]X$, and $Mo^{V}O(tpp)OR$, in dichloromethane solutions containing 10^{-3}—2% (v/v) alcohol at 25 °C. By the addition of dimethyl sulfoxide solution of superoxide to the solution, the absorption peak of the alkoxo complex, $Mo^{V}O(tpp)OR$, is rapidly increased (Fig. 3).[5,6] The formation reaction of $Mo^{V}O(tpp)OR$ proceeds through competitive two

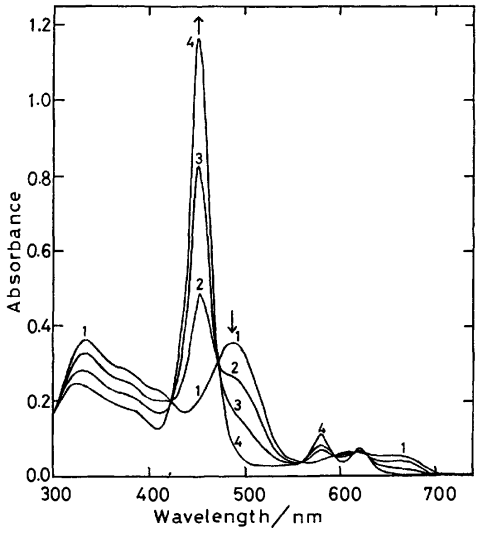

Fig. 3. The spectral change in the reaction between $Mo^{V}O(tpp)NCS$, methanol, and superoxide in dichloromethane at 25 °C. The initial concentrations are $[Mo^{V}O(tpp)NCS]_0=7.54\times10^{-6}$ mol dm^{-3}, $[CH_3OH]_0$=2%(v/v) (0.49 mol dm^{-3}), $[DMSO]_0$=1% (v/v) (0.14 mol dm^{-3}), and $[O_2^-]_0$=0 (1); 3.05×10^{-6} (2); 5.59×10^{-6} (3); 1.12×10^{-5} mol dm^{-3} (4).

reaction paths, A and B.

Reaction path A

$$ROH + O_2^- \rightleftarrows RO^- + HO_2 \quad (2)$$

$$Mo^VO(tpp)X + DMSO \rightleftarrows [Mo^VO(tpp)(dmso)]X \quad (3)$$

$$Mo^VO(tpp)X + ROH \rightleftarrows [Mo^VO(tpp)(ROH)]X \quad (4)$$

$$[Mo^VO(tpp)(ROH)]X \rightleftarrows Mo^VO(tpp)OR + HX \quad (5)$$

$$Mo^VO(tpp)X + RO^- \rightleftarrows Mo^VO(tpp)OR + X^- \quad (6)$$

$$[Mo^VO(tpp)(dmso)]X + RO^- \rightleftarrows Mo^VO(tpp)OR + X^- + DMSO \quad (7)$$

$$[Mo^VO(tpp)(ROH)]X + RO^- \rightleftarrows Mo^VO(tpp)OR + X^- + ROH \quad (8)$$

$$[Mo^VO(tpp)(ROH)]X + O_2^- \rightleftarrows Mo^VO(tpp)OR + X^- + HO_2 \quad (9)$$

Reaction path B

$$Mo^VO(tpp)X + O_2^- \rightleftarrows Mo^{IV}O(tpp) + O_2 + X^- \quad (10)$$

$$[Mo^VO(tpp)(dmso)]X + O_2^- \rightleftarrows Mo^{IV}O(tpp) + O_2 + X^- + DMSO \quad (11)$$

$$Mo^{IV}O(tpp) + O_2 + ROH \rightleftarrows Mo^VO(tpp)OR + HO_2 \quad (12)$$

The reaction path A starts with the formation of alkoxide ion, RO^-. The RO^- is first formed by the reaction of alcohol with superoxide (Eq. 2).[14,15] The formation of the dimethyl sulfoxide complex, $[Mo^VO(tpp)(dmso)]X$, is confirmed by adding dimethyl sulfoxide to the dichloromethane solution of $Mo^VO(tpp)X$ (Eq. 3).[12] The spectral change of the reaction of the complex, $Mo^VO(tpp)X$ or $[Mo^VO(tpp)(dmso)]X$, with $C_2H_5O^-$ derived from C_2H_5ONa solubilized by 18-crown-6 to dichloromethane reveals the occurrence of the reactions 6 and 7.[13] Reaction 8 was also confirmed by the spectral change in the reaction of $[Mo^VO(tpp)(CH_3OH)]Br$ with $C_2H_5O^-$ ion. The reaction of alcohol with superoxide (Eq. 2) suggests the presence of the reaction 9 in which superoxide directly reacts with the coordinated alcohol in $[Mo^VO(tpp)(ROH)]X$ to form $Mo^VO(tpp)OR$.

The reaction path B is started by the direct reduction of the complex, $Mo^VO(tpp)X$ and $[Mo^VO(tpp)(dmso)]X$, by an excess of superoxide to $Mo^{IV}O(tpp)$ (Eqs. 10 and 11); the reaction was confirmed by spectral and ESR measurements.[4] The ESR spectrum of the dichloromethane solution of $Mo^VO(tpp)X$ consists of a strong central line ($\bar{g}$=1.967) due to $^{94,96,98,100}Mo$ nuclei (I=0)(natural abundance *ca.* 75%) which is split to nine lines by coordinated four nitrogens of the ligand.[13] By the addition of an excess of superoxide to the solution of $Mo^VO(tpp)X$, ESR signal due to $Mo^V(d^1)$ diminished, owing to the formation of $Mo^{IV}O(tpp)$ which is ESR silent. Equation 12[16] was also confirmed by adding alcohol to the dichloromethane solution of $Mo^{IV}O(tpp)$ synthesized and isolated independently.[4]

The reaction ratio of the paths A to B to form $Mo^VO(tpp)OR$ largely depends on the concentrations of alcohol and superoxide ion. The reaction path through A is of greater advantage than that through B and completes within 1 min under the conditions of high alcohol concentration, *e.g.* 2%(v/v) methanol (0.49 mol dm^{-3}).

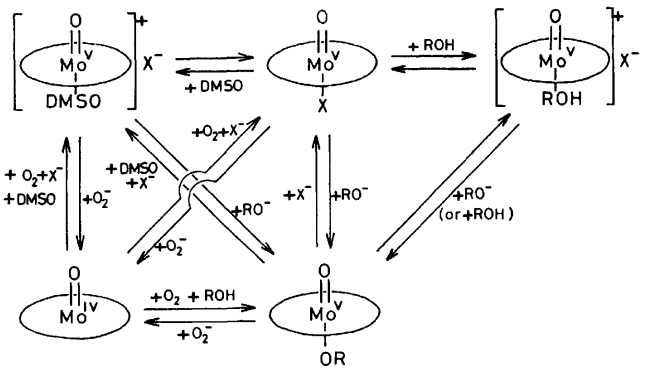

Scheme 1.

The stoichiometry of the $Mo^VO(tpp)OCH_3$ formation reaction in 2%(v/v) methanol–dichloromethane was determined to be $Mo^VO(tpp)NCS: O_2^- = 1:1$ by the molar ratio method.[6] Equations 10 and 11 which reveal respectively the reduction reactions of $Mo^VO(tpp)X$ and $[Mo^VO(tpp)(dmso)]X$ with superoxide lie on the left. More than tenfold excess of superoxide over the complex is required to complete the reduction. It takes more than 20 min at 25 °C to complete the reactions 10 and 11 with the initial concentrations of $[O_2^-]_0 = 2.2\times10^{-4}$ and $[Mo^VO(tpp)Br]_0 = 7.9\times10^{-6}$ mol dm^{-3}.[4] Thus, under the conditions of 2%(v/v) methanol and $[CH_3OH]_0 \gg [O_2^-]_0$, the formation reaction of $Mo^VO(tpp)OCH_3$ proceeds almost (>90%) through the reaction path A. The lower the concentration of methanol becomes, the more the reaction through the path B increases. The complex, $Mo^VO(tpp)OR$, formed finally is relatively stable in the solution but is reduced by a very large excess, *e.g.* 10^{-1}—10^{-2} mol dm^{-3}, of superoxide over the initial concentrations of $[Mo^VO(tpp)X]_0$ and $[ROH]_0$ (Eq. 13).

$$Mo^VO(tpp)OR + O_2^- \rightleftarrows Mo^{IV}O(tpp) + RO^- + O_2 \quad (13)$$

Under the experimental conditions such as in Fig. 3, this equilibrium lies far on the left, which is supported by the large differences of the oxidation-reduction potentials between the O_2/O_2^- couple (−0.5—−0.65 V *vs.* NHE in aprotic solvents)[17] and $Mo^VO(tpp)OCH_3/Mo^{IV}O(tpp)$ couple (−0.74—−0.89 V *vs.* SCE in dichloromethane).[18] All reactions among $Mo^VO(tpp)X$, ROH, and superoxide and the absorption spectral data are shown in Scheme 1 and Table 1, respectively.

Addition of an excess of superoxide to the dichloromethane solution of $Mo^VO(tpp)X$ containing a trace amount of water gives the hydroxo complex, $Mo^VO(tpp)OH$, which has the Soret peak at 464 nm.[19] The equilibrium of the reaction 15 also depends on the concentration of superoxide.

$$Mo^VO(tpp)X + H_2O + O_2^- \rightleftarrows Mo^VO(tpp)OH + X^- + HO_2 \quad (14)$$

$$Mo^VO(tpp)OH + O_2^- \rightleftarrows Mo^{IV}O(tpp) + OH^- + O_2 \quad (15)$$

The hydroxo complex, $Mo^VO(tpp)OH$, should be formed through the same competitive two reaction paths of A and B as in the formation reaction of the alkoxo complex, $Mo^VO(tpp)OR$. The slow reaction of superoxide ion with dichloromethane[20] does not affect the mechanism of the reaction between $Mo^VO(tpp)X$, alcohol, and superoxide.

References

1) "Superoxide and Superoxide Dismutases," ed by A. M. Michelson, J. M. McCord, and I. Fridovich, Academic Press, New York, N. Y. (1977).

2) D. T. Sawyer and J. S. Valentine, *Acc. Chem. Res.*, **14**, 393 (1981).

3) J. S. Valentine, "Biochemical and Clinical Aspects of Oxygen," ed by W. S. Caughey, Academic Press, New York, N. Y. (1979), pp. 659—677.

4) T. Imamura, K. Hasegawa, and M. Fujimoto, *Chem. Lett.*, **1983**, 705.

5) T. Imamura, T. Numatatsu, M. Terui, and M. Fujimoto, *Bull. Chem. Soc. Jpn.*, **54**, 170 (1981).

6) K. Kitamura, K. Hasegawa, K. Mochizuki, T. Imamura, and M. Fujimoto, *Bull. Chem. Soc. Jpn.*, **54**, 1400 (1981).

7) $Mo^{V}O(tpp)OCH_3$ was synthesized according to the modified method of the synthesis of $Mo^{V}O(tpp)OC_2H_5$.[5]

8) G. Wohlleben, *Angew. Chem.*, **68**, 752 (1956).

9) J. A. Riddick and W. B. Bunger, "Organic Solvents," 3rd ed, Wiley-Interscience, New York, N. Y. (1970).

10) J. S. Valentine and A. B. Curtis, *J. Am. Chem. Soc.*, **97**, 224 (1975).

11) E. Asmus, *Fresenius' Z. Anal. Chem.*, **178**, 104 (1960).

12) The dimethyl sulfoxide complex, $[Mo^{V}O(tpp)(dmso)]X$, is also formed by the reaction of $Mo^{V}O(tpp)X$ with dimethyl sulfoxide in dichloromethane. The order of the magnitude of the formation constant of $[Mo^{V}O(tpp)(dmso)]X$ is

$$K_{X=F}^{DMSO} \ll K_{X=NCS}^{DMSO} \approx K_{X=Cl}^{DMSO} \ll K_{X=Br}^{DMSO}.$$

T. Imamura, T. Tanaka, and M. Fujimoto, unpublished data.

13) T. Imamura, M. Terui, Y. Takahashi, T. Numatatsu, and M. Fujimoto, *Chem. Lett.*, **1980**, 89.

14) A. Le Berre and Y. Berguer, *C. R. Acad. Sci., Paris*, **260**, 1995 (1965).

15) A. Le Berre and Y. Berguer, *Bull. Soc. Chim. Fr.*, **1966**, 2363.

16) H. J. Ledon, M. Bonnet, and D. Galland, *J. Am. Chem. Soc.*, **103**, 6209 (1981).

17) D. T. Sawyer and J. L. Roberts, Jr., *J. Electroanal. Chem.*, **12**, 90 (1966); M. E. Peover and B. S. White, *Electrochim. Acta*, **11**, 1061 (1966); D. L. Maricle and W. G. Hodgson, *Anal. Chem.*, **37**, 1562 (1965); E. L. Johnson, K. H. Pool, and R. E. Hamm, *ibid.*, **38**, 183 (1966).

18) These values are half-wave potentials obtained by cyclic voltammetry. K. M. Kadish, T. Malinski, and H. Ledon, *Inorg. Chem.*, **21**, 2982 (1982).

19) H. J. Ledon, M. C. Bonnet, Y. Brigandat, and F. Varescon, *Inorg. Chem.*, **19**, 3488 (1980).

20) J. L. Roberts, Jr., and D. T. Sawyer, *J. Am. Chem. Soc.*, **103**, 712 (1981).

A Study of the Mechanism for the Extraction of Uranium, Water, and Nitric Acid with Trioctylphosphine Oxide Using a Binary Molten Mixture of Biphenyl and Naphthalene as the Solvent

Takehiro KOJIMA

Department of Chemistry, Okayama College of Science, 1-1, Ridai-chō, Okayama 700

(Received June 23, 1983)

Liquid-liquid distribution with trioctylphosphine oxide (TOPO) and a binary molten mixture of biphenyl and naphthalene (weight ratio=3:1) has been examined for the extraction of uranium from a 0.1 mol kg^{-1} nitric acid solution. The stoichiometry of the TOPO complex of uranyl nitrate in the molten biphenyl-naphthalene phase was established to be $UO_2(NO_3)_2(TOPO)_2$. The extracted species of water and nitric acid are $H_2O \cdot TOPO$ and $H_3O^+ \cdot TOPO \cdot NO_3^-$ at concentrations of TOPO of less than 0.1 mol kg^{-1}. The thermodynamic quantities ($\Delta H°$, $\Delta G°$, and $\Delta S°$) were obtained for the extraction of uranyl nitrate, nitric acid, and water into TOPO-biphenyl-naphthalene and TOPO-cyclohexane solutions from the temperature dependence of the extraction constants. More exothermic enthalpy and smaller entropy changes were observed for the binary molten mixture; these differences were attributed to the aromatic and viscous properties of the solvent.

Solvent extraction systems with organophosphorus compounds, such as trioctylphosphine oxide (TOPO) and tributylphosphate (TBP), have been reported in many papers[1–5] and have been documented in books.[6–7] Furthermore, to clarify the mechanism of the selective extraction many fundamental investigations have been done: the competitive extraction of uranium complexes and acid,[8–9] the extraction of water and acids,[10–16] and the thermodynamic quantities of the free energy, enthalpy, and entropy changes in the extraction process.[17–21]

A method involving solid-liquid separation after liquid-liquid extraction has been developed by Fujinaga *et al.*[22] The method has been applied to the spectrophotometric determination of micro amounts of metals by using a molten organic compound, such as biphenyl (mp 70 °C)[22] or naphthalene (mp 80 °C),[23–25] combined with appropriate chelating agents such as 8-quinolinol. The extraction method with molten solvents has some advantages: metal ions can be efficiently concentrated, since only an organic/aqueous volume ratio of 1/1000 is available, the phase separation is easily facilitated by cooling without a separatory funnel, and high distribution ratios are obtained.

Recently we have studied the process of capturing uranium from sea water by adsorption on adsorbents made of polyacrylamide and hydrous titanium oxide.[26–27] Although the solvent extraction with TOPO and ordinary liquid solvents such as toluene has been carried out by others,[4–5] we ourselves have efficiently applied solvent extraction with a molten solvent to the concentration of uranium in the eluent in order to determine uranium or zirconium spectrophotometrically.[28–32]

However, the molten-solvent method suffers from two disadvantages: the volatilization of naphthalene and the adhesion of the extractants to the walls of vessels. It is desirable to do extraction at as low a temperature as possible to minimize volatilization. Therefore, the mixed molten solvent of molten biphenyl and naphthalene was chosen because the melting point of the extraction phase become lower, reaching a minimum temperature of 52 °C at a biphenyl-naphthalene weight ratio of 3/1. There have, however, been few reports on the mechanism of the extraction with molten solvents, especially with the binary molten solvent.

The present paper investigates the separation of uranium as the TOPO complex by solvent extraction with a binary molten mixture of biphenyl and naphthalene and elucidates the mechanism of the extraction more thermodynamically than the extraction by cyclohexane. There is an appreciable difference in the enthalpy and entropy changes of extraction between the binary molten-mixture solvent and cyclohexane. The enthalpy and entropy changes for the extraction process indicate that the extracted species, $UO_2(NO_3)_2(TOPO)_2$, is more stable in the binary molten solvent than in cyclohexane.

Experimental

Reagents. TOPO (Doindo Co., Ltd.) of a reagents grade was used without further purification. A standard uranium solution (10^{-2} mol kg^{-1}) was prepared by dissolving 0.502 g of uranyl nitrate hexahydrate ($UO_2(NO_3)_2 \cdot 6H_2O$, Yokozawa Chemical Co., Ltd.) in deionized water and then diluting it to 100 cm^3. The binary molten mixture solvent with a melting point of 52 °C was prepared by mixing 100 g of naphthalene (mp 80 °C) and 300 g of biphenyl (mp 70 °C). The other reagents used were of an analytical grade.

Procedure

Extraction of Uranium(VI). Twenty cm^3 of 10^{-3} mol kg^{-1} uranium in a 0.1 mol kg^{-1} nitric acid solution was transferred to a 50-cm^3 glass-stoppered flask. Then 5 g of the mixture of biphenyl-naphthalene containing TOPO(0.01—0.3 mol kg^{-1}) was added to it, and the flask was heated on a water bath at 60 °C until the TOPO-biphenyl-naphthalene had melted completely. The mixture was stirred for 3 h with a magnetic stirrer (Toyo Kagaku Sangyo Co., Ltd., Model SS-5) and then allowed to stand for 3 h for the phase-separation.

Determinaton of Distribution Ratio of Uranium. The determination of the uranium(VI) remaining in the aqueous phase was carried out spectrophotometrically with 1-(2-pyridylazo)-2-naphthol (PAN).[33] After the phase-separation, an aliquot

of the aqueous phase was transferred into a 100-cm^3 separatory funnel by means of a pipet. A 100 mg part in sulphamic acid was then added, followed by appropriate amounts of concentrated nitric acid and water to give 2 mol kg^{-1} nitric acid in a final volume of 20 cm^3. Five cm^3 of the 0.05 mol dm^{-3} TOPO cyclohexane solution was then added, and the funnels were vigorously shaken for 1 min. After phase-separation, the aqueous phase was removed and the organic phase was transferred to a 10-cm^3 volumetric flask containing 1 cm^3 of the 0.1% PAN solution and 2 cm^3 of a 10% triethanolamine ehtanol solution. The solution was adjusted to 10 cm^3 with ethanol. After mixing well, the absorbance of the solution at 555 nm was measured against a reagent blank. The distribution ratio was calculated according to this relation: $D=$ (concentration of uranium(VI) in the organic phase)/(concentration of uranium(VI) in the aqueous phase) × (weight of aqueous phase)/(weight of organic phase).

Determination of Water Content in the Organic Phases. After phase-separation, an aliquot of the molten organic phase (TOPO–biphenyl–naphthalene) was transferred into a 10-cm^3 Erlenmyer flask with a heated pipet, because the molten organic phase is solidified at room temperature. The amount of the organic phase was weighed. Then the solidified organic phase was dissolved in a constant amount of cyclohexane. The water content in the organic phase was measured coulometrically by using a Hiranum AQ-3C aquacounter. In the case of the binary molten solvent, the water content was corrected for the amount of water contained in cyclohexane alone.

Determination of Acid Content in the Organic Phase. The content of acid in the organic phase was determined by back-titration with the standard nitric acid solution (0.1 mol dm^{-3}) after the addition of a constant excess of 0.1 mol dm^{-3} potassium hydroxide solution. Phenolphthalein was used as the indicator.

Results and Discussion

Extraction of Acid and Water. The uranium nitrate and acid are extracted competitively from an aqueous solution.[8-9] It is well known that a trace amount of water is also extracted with an organophosphorus compound.[10-16] Therefore, it is necessary to examine the extraction behavior of acid and water into the binary molten solvent prior to the extraction of uranium(VI). The total concentration of water in the organic phase is written as:

$$[H_2O]_{org} = [H_2O]_{org,blank} + [H_2O]_{org,ext}, \quad (1)$$

where $[H_2O]_{org,blank}$ and $[H_2O]_{org,ext}$ are the concentrations of the water in the binary molten solvent and of the water extracted with TOPO. The relation of the concentration of extracted water to that of TOPO in the organic phase is shown in Fig. 1. The extraction equilibrium is:

$$m\text{TOPO}_{org} + nH_2O_{aq} \rightleftharpoons m\text{TOPO}\cdot nH_2O_{org}, \quad (2)$$

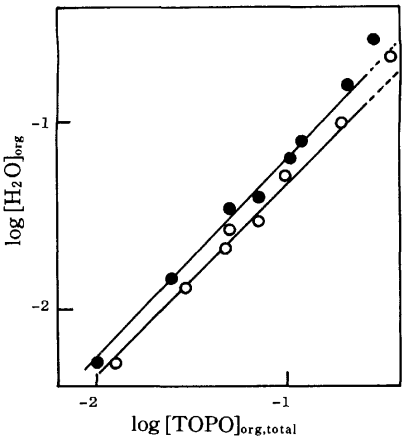

Fig. 1. Variation of water content of the organic phase with total TOPO concentration in cyclohexane or biphenyl-naphthalene, after correction for the dissolved water by the diluent.
Aqueous phase: 10 g, organic phase: 5 g, -●- cyclohexane, at 50 °C, -O- biphenyl-naphthalene, at 55 °C.

with the corresponding extraction constant K_{H_2O}:

$$K_{H_2O} = [m\text{TOPO}\cdot nH_2O]_{org}/[\text{TOPO}]^m_{org}[H_2O]^n_{aq}. \quad (3)$$

In view of the low solubility of the studied TOPO in water and its relatively low initial concentration in the organic phase, the water activity of the aqueous phase may be assumed to be unity; the plot of $\log[H_2O]_{org,ext}$ *vs.* $\log[\text{TOPO}]_{org}$ thus reflects the number of water molecules per TOPO molecule. In Fig. 1 the free TOPO concentration is calculated on the basis of its initial concentration in the organic phase and the amount of the water extracted. It can be seen that the log-log plot is linear from 0.01 to 0.1 mol kg^{-1} TOPO, with a slope of 1.0 corresponding to $m=n$. From the dependence of the amount of coextracted water on that of TOPO and from the IR studies,[15] we can say that the 1-1 species TOPO · H_2O is the predominant species in various solvents, such as cyclohexane and carbon tetrachloride.[14] From Eqs. 1 and 3 with $m=n=1$, we get the following relation:

$$[H_2O]_{org,ext} = [K_{H_2O}/(1+K_{H_2O})][\text{TOPO}]_{org}. \quad (4)$$

The K_{H_2O} values at various temperatures were evaluated by using the log-log plot of Eq 4, the results obtained are given in Table 1. The K_{H_2O} value of 3.13 for cyclohexane is comparable with the value reported

Table 1. Extraction constants of water and nitric acid with TOPO at various temperatures

t/°C	Cyclohexane			
	25	30	40	50
K_{H_2O}	2.12	1.80	1.89	1.64
K_{HNO_3}	42.0	38.7	35.0	31.8
t/°C	Biphenyl-naphthalene			
	55	60	65	
K_{H_2O}	0.73	0.70	0.61	
K_{HNO_3}	24.9	12.3	—	

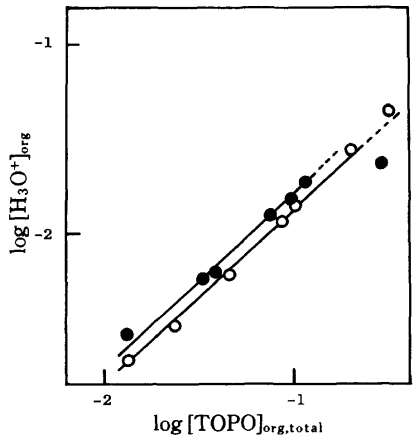

Fig. 2. Variation of organic phase acid with TOPO ncentration in cyclohexane or biphenyl-naphthale.
-●- Cyclohexane, at 50°C, -O- biphenyl-naphthalene, at 55°C.

(3.57) at 25°C[14]: the slightly smaller K_{H2O} values for TOPO in the binary solvent system have also been reported for carbon tetrachloride (0.85,[10] 0.56,[10] 0.68,[11] at 25°C). Binary molten biphenyl-naphthalene or cyclohexane containing quantities of TOPO ranging from 0.01 to 0.3 mol kg^{-1} was equilibrated with the 0.1 mol kg^{-1} nitric acid solution. The results are shown in Fig. 2. The amount of nitric acid extracted into the binary molten solvent and cyclohexane without TOPO was confirmed to be negligibly small. The 1:1 stoichiometry for nitric acid-TOPO extraction has been well established,[15] and the above results in the binary solvent are compatible with the 1:1 stoichiometry. Therefore, the extraction equilibrium for nitric acid is written by Eq 5:

$$H^+_{aq} + NO_3^-{}_{aq} + TOPO_{org} \rightleftharpoons HNO_3 \cdot TOPO_{org}, \quad (5)$$

and the extraction constant is:

$$K_{HNO_3} = [HNO_3 \cdot TOPO]_{org} / [H^+]_{aq}[NO_3^-]_{aq}[TOPO]_{org} f_{H^+} f_{NO_3^-}. \quad (6)$$

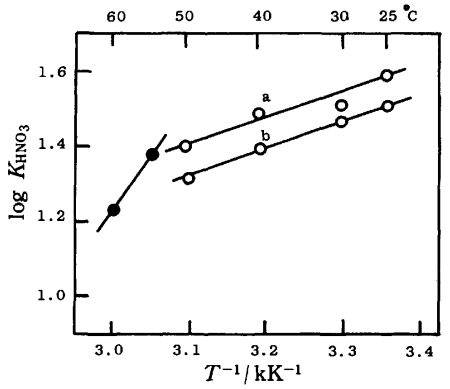

Fig. 3. Effect of varying temperature on extraction of nitric acid by TOPO in cyclohexane or biphenyl-naphthalene.
-●- Biphenyl-naphthalene, TOPO concentration in mol kg^{-1}: 0.013 to 0.3, -O- cyclohexane, TOPO concentration in mol kg^{-1}: a, 0.12; b, 0.09.

In a way similar to that for water extraction, the K_{HNO_3} values were estimated; they are given in Table 1. The mean activity coefficients of nitric acid were estimated by the extrapolation of values at concentrations of more than 0.1 mol kg^{-1} at 25°C;[34] their temperature dependences were neglected.

Figure 3 shows the temperature dependence of nitric-acid extraction; the thermodynamic quantities ($\Delta H°$, $\Delta G°$, and $\Delta S°$) for extracton were calculated by means of the following equations:

$$\Delta G° = -2.303\,RT \log K_{ex}, \quad (7)$$

$$\Delta H° = -2.303\,R(\mathrm{d} \log K_{ex}/\mathrm{d}(1/T)), \quad (8)$$

$$\Delta S° = (\Delta H° - \Delta G°)/T, \quad (9)$$

where R is the gas constant and T is the absolute temperature. The results obtained are given, together with those for the water extraction, in Table 4. It should be noted that the enthalpy and entropy changes for the binary system are much larger han those for cyclohexane. The extraordinarily large enthalpy changes accompanying the large entropy loss for nitric acid should be attributed to the solvation of the TOPO nitrate complex by the molten solvent of an aromatic character. Similar aspects were observed for the uranium extraction, as will be described later.

Extraction of Uranium(VI). The distribution ratios of the uranium-TOPO complex at a uranium concentration of 1×10^{-3} mol kg^{-1} from a 0.1 mol kg^{-1} nitric acid solution were determined as a function of the TOPO concentrations, ranging from 0.01 to 0.3 mol kg^{-1}. The results are shown in Fig. 4. The slope of the line in Fig. 4 is 2.1, indicating the composition of the extracted species to be $UO_2(TOPO)_2(NO_3)_2$, just as in cyclohexane.[35]

The distribution ratio for the extraction of uranium(Vl) from a 0.1 mol kg^{-1} nitric acid solution was obtained as a function of the TOPO concentration at different temperatures. The results are given in Tables 2 and 3. The D value decreases with an increase in the temperature under all sets of conditions examined. The equilibrium expression for the extrac-

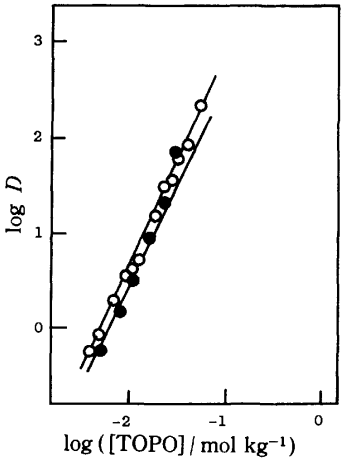

Fig. 4. Effect of TOPO concentration on the extraction of uranium(VI).
U(VI): 10^{-3} mol kg^{-1}, HNO^3: 10^{-1} mol kg^{-1}, Organic phase: 5 g, aqueous phase: 20 g, -●- cyclohexane, at 50 °C, -O-biphenyl-naphthalene, at 55 °C.

Table 2. Variation in the distribution ratio of U(VI) for cyclohexane with the TOPO concentration at different temperatures

TOPO(mol kg^{-1})	0.005	0.007	0.008	0.010	0.013	0.015	0.033	0.067
D, at 20 °C	1.4	—	3.7	7.2	—	18	—	—
25	—	2.9	—	—	11	—	1.2×10^2	8.6×10^2
30	1.2	2.5	2.6	4.7	9.0	11	1.0×10^2	4.9×10^2
40	0.9	—	1.6	3.4	—	8.7	—	—
50	0.6	1.7	1.4	2.9	4.7	8.3	23	1.9×10^2
60	—	—	—	—	2.2	—	14	1.0×10^2

U(VI): 10^{-3} mol kg^{-1}, HNO_3: 10^{-1} mol kg^{-1}, organic phase/aqueous phase: 5/20, solvent: cyclohexane.

Table 3. Variation in the distribution ratio of U(VI) for molten biphenyl–naphthalene with the TOPO concentration at different temperatures

TOPO(mol kg^{-1})	0.010	0.018	0.032	0.054
D, at 55 °C	3.2	12	53	1.8×10^2
60	2.3	7.4	44	1.7×10^2
65	2.0	6.7	32	1.3×10^2

U(VI): 10^{-3} mol kg^{-1}, HNO_3: 10^{-1} mol kg^{-1}, organic phase/aqueous phase: 5/20, solvent: molten biphenyl-napthalene (weight ratio=3:1).

tion of uranium is given by Eq. 10:

$$UO_2^{2+}{}_{aq} + 2NO_3^-{}_{aq} + 2TOPO_{org} \rightleftharpoons UO_2(NO_3)_2(TOPO)_{2\,org}. \quad (10)$$

Thus, the corresponding extraction constant can be expressed by Eq.11:

$$K_{ex} = [UO_2(NO_3)_2(TOPO)_2]_{org}/[UO_2]_{aq}[NO_3^-]^2_{aq}\,[TOPO]^2_{org}\,f_{UO_2^{2+}}f^2_{NO_3^-} \quad (11)$$

where the square brackets refer to the concentrations and where f is the activity coefficient of the respective species. The extraction constant was estimated from the distribution ratio D by Eq.12:

$$K_{ex} = D(1+\sum_1^n \beta_n[NO_3^-]^n_{aq})/[NO_3^-]^n_{aq}[TOPO]^2_{org}\,f_{UO_2^{2+}}f^2_{NO_3^-}, \quad (12)$$

where the $(1+\sum_1^n\beta_n[NO_3^-]^n_{aq})$ term takes into account the formation of uranyl nitrate complexes with the formation constant for $UO_2(NO_3)_n^{(2-n)+}$ in the aqueous phase. Thus, $D(1+\sum_1^n\beta_n[NO_3^-]^n_{aq})$ is equal to the ratio of the concentration of $UO_2(NO_3)_2(TOPO)_2$ in the organic phase (assuming that this is the only species extracted) to that of free UO_2^{2+} in the aqueous phase.

From the temperature dependence of the extractability of 0.1 mol kg^{-1} nitric acid, it was found that, at a TOPO concentation of 0.05 mol kg^{-1} the aqueous nitric acid concentration in mol kg^{-1} varies from 0.0982 at 25 °C to 0.0984 at 50 °C for cyclohexane and from 0.0981 at 55 °C to 0.0982 at 60 °C for the molten mixed solvent.

Therefore, it is reasonable to assume that the equilibrium concentrations of the nitrate ion in the aqueous phase and of free TOPO in the organic phase would remain practically constant over the temperature range studied. A value of 0.02 for $(1+\sum_1^n\beta_n[NO_3^-]^n_{aq})$ in a 0.1 mol kg^{-1} nitric acid solution was reported at 25 °C by Patil *et al.*[19] The values of $(1+\sum_1^n\beta_n[NO_3^-]^n_{aq})$ for uranium(VI) were estimated by using the method of cation exchange: 1.02 (25 °C) in a 0.1 mol dm^{-3} nitric acid solution,[19] and 2.1 (25 °C) and 2.3 (40 °C) in a 3 mol dm^{-3} nitric acid solution.[36] If the correction term $(1+\sum_1^n\beta_n[NO_3^-]^n_{aq})$ and activity coefficients do not change significantly over the temperature range investigated, the enthalpy change, $\Delta H°$, associated with the extraction of uranium can be calculated from Eq. 8.

The logarithms of the distribution ratio at different concentrations of TOPO were plotted against the reciprocal temperature. Some typical plots for the extraction of nitric acid and uranium with cyclohexane and the molten mixture solvent are shown in Figs. 3 and 5 respectively. All the plots were linear. The $\Delta H°$ values obtained from these plots by using a least-square procedure are given in Table 4. It was found that the $\Delta H°$ values are independent of the concentration of TOPO, supporting the above assumptions. The $\Delta H°$ values for uranium in the binary molten solvent are two times higher than that in cyclohexane.

The Gibbs-free-energy and entropy changes for uranium extraction obtained by using Eq. 7 are given in Table 4. A mean activity coefficient of 0.60 for the UO_2^{2+} ions in *ca.* 0.1 mol kg^{-1} nitric acid, which was

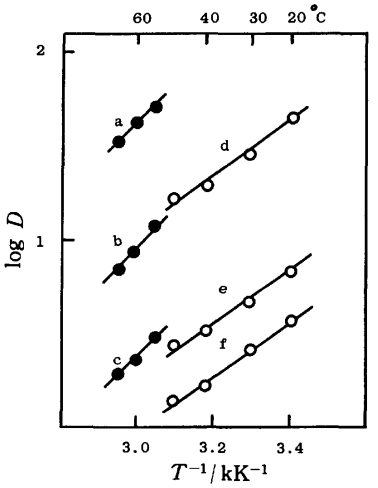

Fig. 5. Effect of varying temperature on extraction of uranium(VI) by TOPO in cyclohexane and biphenyl-naphthalene.
-●- Biphenyl-naphthalene, TOPO concentration in mol kg^{-1}: a, 0.032; b, 0.018; c, 0.009, -○- cyclohexane, TOPO concentration in mol kg^{-1}: d, 0.015; e, 0.010; f, 0.008.

TABLE 4. THERMODYNAMIC QUANTITIES ($\Delta H°$, $\Delta G°$, AND $\Delta S°$) ASSOCIATED WITH THE EXTRACTION OF WATER, NITRIC ACID, AND URANIUM(VI) INTO THE TOPO-ORGANIC PHASE

		$\Delta H°$/kJ mol^{-1}	$\Delta G°$/kJ mol^{-1}	$\Delta S°$/J K mol^{-1}
H_2O-TOPO in cyclohexane,	at 25 °C	−8.5	−1.9	−22
	at 50 °C	−8.5	−1.3	−22
H_2O-TOPO in the binary molten biphenyl-naphthalene,	at 55 °C	−17	0.9	−53
HNO_3-TOPO in cyclohexane,	at 25 °C	−14	−8.9	−16
		(−16.3)	(−5.4)	(−36.5)
	at 50 °C	−14	−9.2	−14
HNO_3-TOPO in the binary molten biphenyl-naphthalene,	at 55 °C	−63	−8.8	-1.6×10^2
$UO_2(NO_3)_2(TOPO)_2$ in cyclohexane,	at 25 °C	−23	−42	63
		(−24.3)	(−48.1)	(79.8)
	at 50 °C	−23	−42	58
$UO_2(NO_3)_2(TOPO)_2$ in the binary molten biphenyl-naphthalene,	at 55 °C	−44	−45	1.2

The values in paremtheses are quoted from Ref. 35.

calculated by means of the modified Debye-Hückel equation,[34] was used over the temperature range studied.

From Table 3 it may be seen that uranium is a little more extractable in the binary molten solvent, with a more negative enthalpy and smaller entropy changes, than in cyclohexane. As has been stated earlier, a more exothermic enthalpy change is also observed for the nitric acid–molten solvent system; it may be due to the stronger solvation of the extracted TOPO complex by aromatic solvents, with additional interactions of π-electrons, compared with the case for alicylic cyclohexane.

In addition to the strong solvation effect, the viscous characteristics of the binary molten solvent can also be responsible for the smaller entropy changes. However, in the cyclohexane phase the extracted species disperse easily, resulting in larger entropy changes.

In conclusion, the extraction behavior of uranium(VI), water, and nitric acid for the molten biphenyl–naphthalene solvent is similar to that for cyclohexane. However, the metal UO_2^{2+} ion is extracted in the molten solvent with more exothermic enthalpy and smaller entropy changes than those for the cyclohexane system.

The author is deeply indebted to professor Y. Yamamoto and Dr. E. Iwamoto, Hiroshima University, for their helpful discussions and suggestions, and to professor Y. Shigetomi, Okayama College of Science, for his helpful suggestions and warm encouragement.

References

1) T. Ishimori, K. Watanabe, and E. Nakamura, *Bull. Chem. Soc. Jpn.*, **33**, 639 (1960).
2) T. Ishimori, K. Watanabe, and L. Kimura, *Nippon Genshiryoku Gakkai Shi*, **2**, 750 (1960).
3) H. Umezawa and R. Hara, *Anal. Chim. Acta*, **25**, 360 (1961).
4) J. C. White and W. J. Ross, NAS-NA 3102 (1961).
5) C. A. Blake, K. B. Brown, and C. F. Coleman, ORNL, 26 (1965).
6) Y. Marcus and A. S. Kerts, "Ion Exchange and Solvent Extraction of Metal Complexes," Wiley, New York (1969).
7) M. Tanaka, "Youbai Chyushutsu No Kagaku," Kyoritsu, Tokyo (1979).
8) K. Watanabe, *J. Nucl. Sci. Technol.*, **1**, 155 (1964).
9) T. Sato and T. Nishida, *J. Inorg. Nucl. Chem.*, **36**, 2087 (1974).
10) T. J. Conocchioli, M. I. Tocher, and R. M. Diamond, *J. Phy. Chem.*, **69**, 1106 (1965).
11) J. W. O'Laughlin, J. J. Richard, J. W. Ferguson, and C. V. Banks, *Anal. Chem.*, **40**, 146 (1968).
12) M. Niitsu, N. Iritani, and T. Sekine, *Bull. Chem. Soc. Jpn.*, **52**, 1799 (1979).
13) M. Niitsu and T. Sekine, *Bull. Chem. Soc. Jpn.*, **50**, 1015 (1977).
14) C. Klofyter, S. Palik, M. Sfnegacnik, and B. Jerkovic, *J. Inorg. Nucl. Chem.*, **34**, 3873 (1972).
15) M. Senegacnik, C. Klofuter, S. Paljk, and L. Smrekar, *J. Inorg. Nucl. Chem.*, **32**, 1659 (1970).
16) J. R. Johnson, S. D. Christian, and H. E. Affsprung, *J. Chem. Soc., A*, **1966**, 77.
17) A. Ramanujam, V. V. Ramakrishna, and S. K. Patil, *J. Inorg. Nucl. Chem.*, **40**, 1167 (1978).
18) T. H. Siddall, *J. Am. Chem. Soc.*, **81**, 4176 (1959).
19) S. V. Bagawde, P. R. Vasudava Rao, V. V. Ramakrishna, and S. A. Patil, *J. Inorg. Nucl. Chem.*, **40**, 1913 (1978).
20) S. A. Pai, J. P. Shukla, and M. S. Subramanian, *J. Inorg. Nucl. Chem.*, **43**, 1045 (1981).
21) D. G. Kalina, G. W. Mason, and E. P. Horeitz, *J. Inorg. Nucl. Chem.*, **43**, 159 (1981).
22) T. Fujinaga, T. Kuwamoto, E. Nakayama, and M. Satake, *Bunseki Kagaku*, **18**, 398 (1969).
23) M. Satake, Y. Matsumura, and T. Fujinaga, *Talanta*, **25**, 71, (1978).
24) T. Fujinaga, M. Satake, and T. Yonekubo, *Bull. Chem. Soc. Jpn.*, **46**, 2090 (1976).
25) T. Fujinaga, M. Satake, and M. Shimizu, *Bunseki Kagaku*, **26**, 313 (1976).
26) Y. Shigetomi, T. Kojima, and M. Shinagawa, *J. Nucl. Sci. Technol.*, **14**, 811 (1977).
27) Y. Shigetomi, T. Kojima, and M. Shinagawa, *Bunseki Kagaku*, **26**, 167 (1977).
28) Y. Shigetomi, T. Kojima, H. Kamba, and Y. Yamamoto, *Anal. Chim. Acta*, **116**, 199 (1980).
29) Y. Shigetomi, T. Kojima, and H. Kamba, *J. Nucl. Sci. Technol*, **20**, 120 (1983).
30) T. Kojima, Y. Shigetomi, H. Kamba, H. Iwashiro, T. Sakamoto, and A. Doi, *Analyst*, **107**, 519 (1982).
31) Y. Shigetomi, T. Kojima, and H. Kamba, *Talanta*, **27**,

1079 (1980).
32) Y. Shigetomi and T. Kojima, *Bull. Chem. Soc. Jpn.*, **54**, 1887 (1981).
33) R. J. Baltisberger, *Anal. Chem.*, **36**, 2369 (1964).
34) R. A. Robinson and R. H. Stokes, "Electrolyte Solutions," Butterworth, London (1965).
35) A. H. A. Heyn and Y. D. Soman, *J. Inorg. Nucl. Chem.*, **26**, 287 (1964).
36) S. K. Patil, V. V. Ramakrishna, G. V. N. Avadhny, and M. V. Ramaniah, *J. Inorg. Nucl. Chem.*, **35**, 2537 (1973).

 © 1984 The Chemical Society of Japan Bull. Chem. Soc. Jpn., 57, 204—208 (1984) [Vol. 57, No. 1

Kinetics and Mechanism of Copper(II), Zinc(II), and Cadmium(II) Incorporation into 5,10,15,20-Tetraphenylporphine and *N*-Methyl-5,10,15,20-tetraphenylporphine in *N,N*-Dimethylformamide

Shigenobu FUNAHASHI, Yūshi YAMAGUCHI, and Motoharu TANAKA*
Laboratory of Analytical Chemistry, Faculty of Science, Nagoya University, Chikusa-ku, Nagoya 464
(Received August 4, 1983)

The kinetics of reactions of 5,10,15,20-tetraphenylporphine (H_2(tpp)) and *N*-methyl-5,10,15,20-tetraphenylporphine (H(metpp)) with Cu^{II}, Zn^{II}, and Cd^{II} ions was studied spectrophotometrically in *N,N*-dimethylformamide. The rate of incorporation of metal ions (M^{2+}: Cu^{2+}, Zn^{2+}, Cd^{2+}) into H(metpp) is first order with respect to both H(metpp) and metal ion: $d[M(metpp)^+]/dt=k[H(metpp)][M^{2+}]$ with k(25 °C)=11.5±0.5 mol^{-1} dm^3 s^{-1} for Zn^{2+} and (5.8±0.8)×10^2 mol^{-1} dm^3 s^{-1} for Cd^{2+}. The rate of incorporation of copper and zinc into H_2(tpp) is first order in H_2(tpp) and the conditional first-order rate constants are expressed as follows: $k_{0(M)}=K[M^{2+}](1+K[M^{2+}])^{-1}(k_1+k_2[M^{2+}])$ where for Cu^{2+} and Zn^{2+} K/mol^{-1} dm^3, k_1/s^{-1}, and k_2/$mol^{-1}dm^3$ s^{-1} at 25 °C are (1.6±0.2)×10^4 and (7.2±1.5)×10^2, (1.2±0.1)×10^{-4} and (3.5±0.7)×10^{-5}, and (5.2±0.2)×10^{-2} and (8.6±0.2)×10^{-4}, respectively. Metal ion incorporation into H_2(tpp) proceeds through the formation of intermediates prior the rate-limiting step. For the H(metpp) system, the methyl group on the pyrrole in H(metpp) prevents the formation of such an intermediate. On the other hand, the rate of cadmium incorporation into H_2(tpp) is first order with respect to Cd^{2+} and H_2(tpp) and its second order rate constant k is (6.5±1.0)×10^{-3} mol^{-1} dm^3 s^{-1}. The large cadmium(II) ion can not fit into the porphyrin nucleus and its reaction proceeds through a pathway involving a mononuclear activated complex.

The mechanisms of complexation of labile metal ions have attracted a good deal of attention. Now one can make a reasonable accurate assessment of the rate constant for the reaction of a particular metal ion–ligand system.[1,2] More recently attention has been directed to the more unusual ligands such as macrocycles,[3,4] cryptands,[5–7] and porphyrins.[8–12] Their steric restrictions are likely to slow down the "normal" rates and introduce mechanistic novelties.

A number of kinetic studies of metalloporphyrin formation have been published and the work has been reviewed by Schneider,[13] Hambright,[14] and Longo.[15] A classification of kinetics of metalloporphyrin formation has been presented recently.[16] Since the solvents, metal salts, porphyrins, and other conditions are different in these kinetic studies, a quantitative comparison of the available data is difficult. A number of studies have been addressed to the question of how metal ions are incorporated into porphyrin molecules to form metalloporphyrins. A particularly attractive idea was that of "sitting-atop" (SAT) complexes, produced by reaction of metal ions with free base porphyrins prior to metal ion incorporation.[17] Evidence for SAT complexes has been presented in various types of systems.[18–20] On the other hand, there are some papers to show evidence for the nonexistence of SAT complexes.[21,22]

Previously we have investigated the rate of reaction of 5,10,15,20-tetra(4-pyridyl)porphine with cobalt(II) in acetic acid and demonstrated the variation of the reaction order in metal ion with varying metal ion concentration.[8] We have emphasized that it is indispensable to conduct experiments over as wide a concentration range as possible. In order to elucidate the origin of previously reported differences in mechanisms of metalation, reactions of copper(II), zinc(II), and cadmium(II) ions with 5,10,15,20-tetraphenylporphine (H_2(tpp)) and *N*-methyl-5,10,15,20-tetraphenylporphine (H(metpp)) have been studied over a wide range of metal ion concentrations in *N,N*-dimethylformamide (DMF).

X = H, H_2(tpp)
X = CH_3, H (metpp)

Two of the most significant studies which we will refer to are those of Bain-Ackerman and Lavallee,[9] who have provided data for complexation of H(metpp) by Cu^{II}, Zn^{II}, Co^{II}, Mn^{II}, and Ni^{II} and Longo *et al.*,[23] who have provided activation parameters for reactions of H_2(tpp) and its derivatives with metal chloride in DMF.

Experimental

Reagents. In order to prepare sample solutions as dry as possible, extreme care was taken in purification and preparation of all reagents and solutions.

DMF: Reagent grade DMF was dried over calcium hydride and distilled twice under reduced pressure. The water content in DMF was determined to be less than 3×10^{-3} mol dm^{-3} by the Karl-Fisher titration.

Porphyrins: H_2(tpp) (Strem Chemicals) was chromatographed on an alumina column by elution with chloroform. H(metpp) was prepared from methylation of H_2(tpp) by methylfluorosulfonate (Aldrich Chemical Co., "Magic methyl") according to literature procedures.[24] H(metpp) was isolated and purified by a thin-layer chromatograph twice. H(metpp) is characterized by ^{1}H NMR spectrum and electronic spectra. The distinctive NMR spectrum shows a sharp singlet due to *N*-methyl group at 4.1 ppm upfield from

$SiMe_4$ in $CDCl_3$.

Copper(II) Perchlorate DMF Solution: Crystals of hydrated copper(II) perchlorate were obtained by treating copper metal (99.999%) and perchloric acid of special purity (Wakojunyaku) The crystals were dissolved in DMF in the presence of 3A Molecular Sieves and allowed to stand for 1 d under reduced pressure. Then the Molecular Sieves were removed by filtration.

Calcium(II) Perchlorate DMF Solution: Crystals of hydrated calcium(II) perchlorate were obtained from reagent grade calcium(II) carbonate and perchloric acid, and recrystallized twice from distilled water. The crystals were placed in an oven at 110 °C for 1 h and then at 240 °C at least for 24 h. The anhydrous calcium(II) perchlorate was dissolved in DMF.

DMF Solutions of Zinc(II), Cadmium(II), and Calcium(II) Nitrates: Reagent grade zinc(II) nitrate was recrystallized twice from distilled water. Crystals of hydrated zinc(II) nitrate were dissolved in DMF. The water involved was removed by 3A Molecular Sieves under vacuum line. The DMF solutions of cadmium(II) nitrate and calcium(II) nitrate were prepared by the same procedure as above.

The amounts of water involved in the DMF solutions were determined to be less than 5×10^{-3} mol dm^{-3}. The concentrations of copper(II), zinc(II), cadmium(II), and calcium(II) solutions were determined complexometrically by EDTA.

The purification of DMF and the preparation of DMF solutions were carried out just before kinetic measurements.

Measurements. The slow reactions were monitored spectrophotometrically by a Union Giken (Type SM401) spectrophotometer or a Hitachi (Type 124) spectrophotometer with a thermostated cell compartment maintained within $\pm$0.1 °C. The formation of metalloporphyrins was carried out in 1 cm cells by mixing a porphyrin solution and a metal ion solution preequilibrated at the reaction temperature. The absorption spectra change as a function of time with distinct isosbestic points until completion of the reaction. The faster reactions in the H(metpp) system were followed by a Union Giken (Type RA1100) stopped-flow spectrophotometer. Addition of calcium(II) nitrate or perchlorate as an electrolyte did not affect visible spectra and rates.

The kinetics were run under pseudo-first-order conditions at 25 °C with the metal ion concentration at a large excess over the free base porphyrin concentration (10^{-6}—10^{-5} mol dm^{-3}). Pseudo-first-order plots showed good linearity untill three half-lives. Conditional first-order rate constants were obtained from the slope of such plots. The half-life times for the fastest and slowest reaction in the present reaction systems were 1 s and 120 h, respectively.

Results

Kinetics of Metal Ion Incorporation into H_2(tpp). The kinetics of reactions of H_2(tpp) with copper(II) perchlorate and zinc(II) nitrate in DMF at 25 °C was studied. The rate for the formation of metalloporphyrin is first order in porphyrin:

$$\frac{d[M(tpp)]}{dt} = -\frac{d[H_2(tpp)']}{dt} = k_{o(M)}[H_2(tpp)'], \qquad (1)$$

where $k_{o(M)}$ is the conditional first-order rate constant involving the metal concentration and $[H_2(tpp)']$ is the total concentration of porphyrin (C_P) minus the concentration of metalloporphyrin. The values of $k_{o(Cu)}$ are plotted against total concentration of copper C_{Cu} and its square root $C_{Cu}^{1/2}$(Fig. 1). As apparent from Fig. 1 the rate is proportional to neither the concentration of metal ion nor its half power.

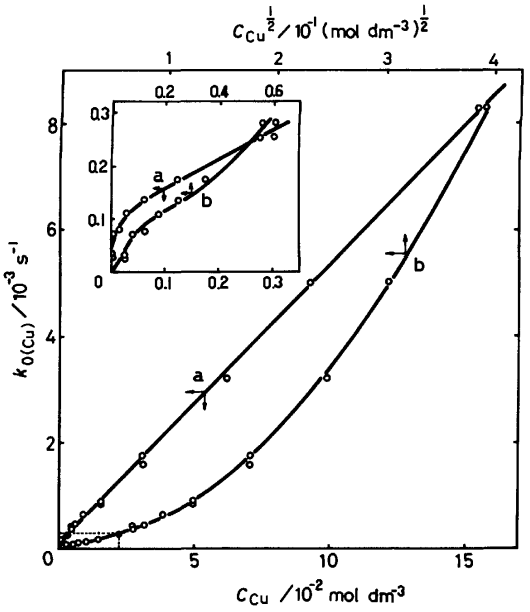

Fig. 1. Relationship between $k_{o(Cu)}$ and copper(II) ion concentration. (a): Plot of $k_{o(Cu)}$ *vs.* C_{Cu}; (b) Plot of $k_{o(Cu)}$ *vs.* $C_{Cu}^{1/2}$. The solid curves are calculated with the rate constants and formation constants obtained. The inset shows the plots in the range of lower concentration.

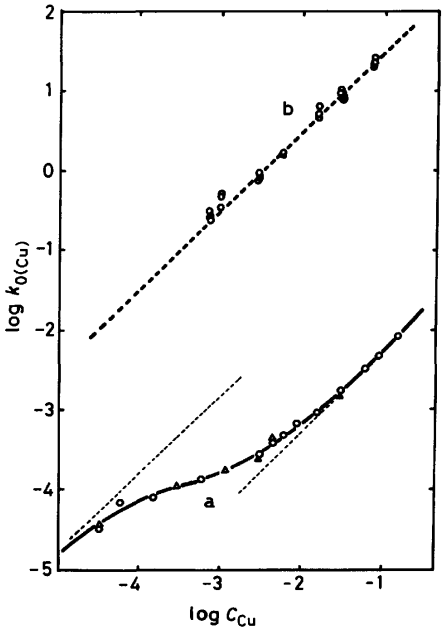

Fig. 2. Plots of log $k_{o(Cu)}$ *vs.* log C_{Cu} for the H_2(tpp) system (a) and the H(metpp) system (b). (a): The data at 25.0 °C in the absence (○) and in the presence (△) of 0.0924 mol dm^{-3} calcium(II) perchlorate; (b): the data given in ref 9.

The logarithmic relationship between rate constants and copper concentrations is shown in Fig. 2a. At lower and higher copper concentration, the reaction tends to be first order in C_{Cu}, while at the intermediate copper concentration $k_{o(Cu)}$ changes with C_{Cu} to a lesser extent. This concentration dependence of the rate constants indicates a mechanism involving a rapid preequilibrium between copper(II) ion and H_2(tpp) prior to metal insertion and proton release:[8]

$$H_2(tpp) + Cu^{2+} \overset{K}{\rightleftharpoons} Cu^{2+}\cdots H_2(tpp), \quad (2)$$

$$Cu^{2+}\cdots H_2(tpp) \xrightarrow{k_1} Cu(tpp) + 2H^+, \quad (3)$$

$$Cu^{2+}\cdots H_2(tpp) + Cu^{2+} \xrightarrow{k_2} Cu(tpp) + Cu^{2+} + 2H^+, \quad (4)$$

where $Cu^{2+}\cdots H_2(tpp)$ is an intermediate. DMF is sufficiently basic to absorb the low concentration of protons released from the free-base porphyrins as the complexation reaction proceeds. In addition, DMF should strongly solvate metal ions and compete well against trace levels of water for coordination sites on the metal ions. Assuming a rapid preequilibrium step of Eq. 2 and two parallel rate-determining steps of Eqs. 3 and 4, Eq. 5 can be readily derived.

$$k_{0(Cu)} = \frac{K[Cu^{2+}]}{1+K[Cu^{2+}]}(k_1 + k_2[Cu^{2+}]) \quad (5)$$

This equation reproduces very nicely the experimental rate data as illustrated in Fig. 2.

The important role of water in the formation of metalloporphyrins has been demonstrated in some systems.[11] We checked the effect of water on the rate in the present systems. An introduction of small amounts of water ($[H_2O]$/mol dm^{-3}=0.0608, 0.151, 0.209, 0.453, 0.867) into the copper(II)-H_2(tpp) system did not appreciably affect the rate constants. Since the water concentration of our systems is at most *ca.* 5×10^{-3} mol dm^{-3}, we believe with confidence that the presence of water, if any, did not affect our results.

Since there are some reports about effects of ionic strength on the rate of metalloporphyrin formation, we studied the effect of added salt on the rate in the present systems. The addition of 0.0924 mol dm^{-3} calcium(II) perchlorate has no effect on the reaction rate (see Fig. 2a). The absence of salt effect on the rate is consistent with the porphyrin reacting as the free-base porphyrin H_2(tpp).

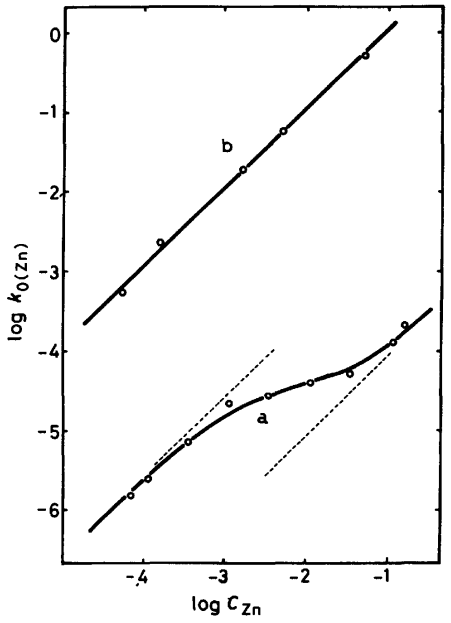

Fig. 3. Plots of log $k_{0(Zn)}$ *vs.* log C_{Zn} for the H_2(tpp) system (a) and the H(metpp) system (b). (a): At 25.0 °C in the presence of 0.30 mol dm^{-3} calcium(II) nitrate; (b): at 25.0 °C in the presence of 0.34 mol dm^{-3} calcium(II) nitrate.

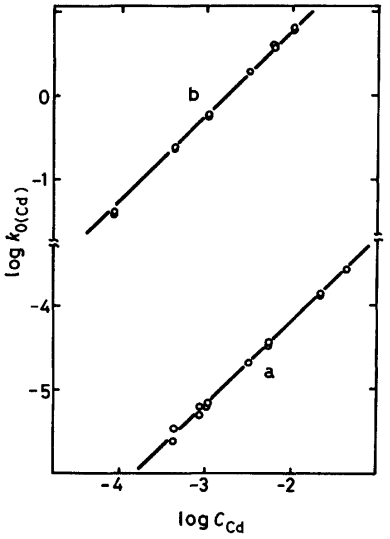

Fig. 4. Plots of log $k_{0(Cd)}$ *vs.* log C_{Cd} for the H_2(tpp) system (a) and the H(metpp) system (b). (a): At 25.0 °C in the presence of 0.42 mol dm^{-3} calcium(II) nitrate; (b): at 25.0 °C in the presence of 0.11 mol dm^{-3} calcium(II) nitrate.

TABLE 1. RATE CONSTANTS (25 °C) FOR METAL(II) ION INCORPORATION INTO H_2(tpp) AND H(metpp) IN DMF

Reaction system	K/mol^{-1} dm^3	k_1/s^{-1}	k_2/mol^{-1} dm^3 s^{-1}	k/mol^{-1} dm^3 s^{-1}	Ref
H_2(tpp) sytem					
Copper(II) perchlorate	$(1.6\pm0.2)\times10^4$	$(1.2\pm0.1)\times10^{-4}$	$(5.2\pm0.2)\times10^{-2}$		This work
Copper(II) perchlorate				1.03×10^{-1} a)	25
Copper(II) chloride				8.47×10^{-2}	23
Zinc(II) nitrate	$(7.2\pm1.5)\times10^2$	$(3.5\pm0.7)\times10^{-5}$	$(8.6\pm0.2)\times10^{-4}$		This work
Zinc(II) perchlorate				9×10^{-4} b)	11
Zinc(II) perchlorate				1.25×10^{-3} a)	26
Zinc(II) chloride				5.62×10^{-3}	23
Cadmium(II) nitrate				$(6.5\pm1.0)\times10^{-3}$	This work
H(metpp) system					
Copper(II) perchlorate				289	9
Zinc(II) nitrate				11.5±0.5	This work
Zinc(II) perchlorate				10.4	9
Cadmium(II) nitrate				$(5.8\pm0.8)\times10^2$	This work

a) At 30 °C. b) For D_2(tpp) the same rate constant was obtained (no kinetic effect).

As shown in Fig. 3a, the dependence of $k_{0(Zn)}$ on zinc(II) concentration is the same as for the Cu(II)-H_2(tpp) system. On the other hand, the cadmium(II)-concentration dependene of $k_{0(Cd)}$ is clearly linear over a wide range of cadmium concentrations, as illustrated in Fig. 4a.

Rate constants were determined by a nonlinear least-squares fitting with weight. The constants obtained are summarized in Table 1.

Kinetics of Metal(II) Ion Incorporation into H(metpp). The kinetics of reaction of H(metpp) with an excess of zinc(II) nitrate was studied in DMF solution containing 0.34 mol dm^{-3} calcium(II) nitrate. The rate for formation of metalloporphyrin is first order in porphyrin:

$$\frac{d[Zn(metpp)^+]}{dt} = -\frac{d[H(metpp)]}{dt} = k_{0(Zn)}[H(metpp)]. \quad (6)$$

The values of $k_{0(Zn)}$ determined in the wide range from 10^{-1} mol dm^{-3} to 10^{-5} mol dm^{-3} of zinc nitrate are proportional to the total concentration of zinc nitrate C_{Zn} (Fig. 3b).

For the Cd^{II}-H(metpp) system the dependence of $k_{0(Cd)}$ on cadmium nitrate concentration is clearly linear (see Fig. 4b) as in the case of the Cd^{II}-H_2(tpp) system. In Fig. 2b, the values of $k_{0(Cu)}$ obtained by Bain-Ackerman and Lavallee[9] are plotted against C_{Cu}. All the reactions for the H(metpp) system obey a second-order rate law: first order in porphyrin and first order in metal ion. The rate constants obtained are listed in Table 1.

Discussion

Results obtained in the present system are summarized in Table 1 together with data reported previously.[9,11,23,25,26] In the Zn^{II}-H(metpp) system the rate constant in the perchlorate medium[9] is in good agreement with ours in the nitrate medium. It has been reported that the reaction order of metal ion in the metalation of porphyrins is not always unity.[8] The earlier workers, working over a narrow range of metal ion concentration, may have deduced the first order or half order in metal ion as obvious from Fig. 1. The second-order rate constant k obtained previously in the Cu^{II}- and Zn^{II}-H_2(tpp) systems should be regarded as k_2 in the present work. In fact, as apparent from figures in Table 1, the reported k values are in good agreement with the corresponding k_2 values.

In the Cu^{II}- and Zn^{II}-H_2(tpp) systems, the formation constants (K) of intermediates given by Eq. 2 are considerably large and the K for copper(II) is greater than that for zinc(II). The intermediate may be regarded as a kinetically detected SAT complex. In the k_2 path (Eq. 4), a second metal should be inserted from the opposite side of the metal in the SAT complex with a homodinuclear activated complex. On the other hand, in the k_1 path, the metal ion in the SAT complex just drops into the porphyrin ring. Such a mechanism has been proposed previously for the cobalt incorporation into 5,10,15,20-tetra(4-pyridyl)porphine in acetic acid.[8]

In the H(metpp) systems the rate is first order with respect to metal ion over a wide range of metal ion concentrations. Recent study[27] on the crystal structures of mono-chloro-*N*-methyl metalloporphyrins of Mn, Fe, Co, and Zn shows the out-of-plane displacement of metal ion and deviation of *N*-methylated pyrrole ring from the plane of reminder of the porphyrin core. Judging from these structures, in the metalation of H(metpp) a second metal can not attack from the opposite side due to steric hindrance of the methyl group. Therefore the reaction does not involve a homodinuclear activated complex as observed in the Cu^{II}- and Zn^{II}-H_2(tpp) system: the rate of metal ion incorporation into H(metpp) is invariably first order in metal ion.

The rate of cadmium incorporation into H_2(tpp) is first order in Cd^{2+} and H_2(tpp). A large metal ion such as Cd^{2+} ion (its crystal ionic radius is 97 pm[28]) can not fit into the porphyrin nucleus because the N-N distance in H_2(tpp) is 408 pm[29] and its reaction proceeds through a pathway involving a mononuclear activated complex.

In the H(metpp) systems the rate of cadmium incorporation is faster than in the H_2(tpp) systems, whereas the rate is much slower than that for the solvent exchange at this cation.[30] In common to all mechanisms, the porphyrins form an outer-sphere complex with the metal ions (K_{os}) and then the porphyrin nucleus deforms to provide a suitable configuration to complex the metal ion (K_D). The rapid K_{os} and K_D preequilibria should be followed by the rate-determining step involving a mono-nuclear activated complex.

K_{os} for porphyrins should be smaller than those for small ligands as estimated by the Fuoss theory,[31] because the outer-sphere interaction of solvated metal ions with porphyrins occurs effectively only in the vicinity of the central part of porphyrins.

The *N*-methylated porphyrin is largely deformed in comparison with the non-methylated porphyrin. This deformation enhances both the coordinating ability of the lone pairs by directing them away from the central porphyrin cavity and the acidity of the central protons by destroying the N-H tautomerism.[32] The predeformed *N*-methylated porphyrin incorporates metal ions up to five orders of magnitude faster than the corresponding non-*N*-methylated analogue, pointing to the importance of porphyrin deformation in the metal ion incorporation into porphyrins.

References

1) R. G. Wilkins, "The Study of Kinetics and Mechanism of Reactions of Transition Metal Complexes," Allyn and Bacon, Boston (1974).

2) D. W. Margerum, G. R. Cayley, D. C. Weatherburn, and G. K. Pagenkopf, "Kinetics and Mechanism of Complex Formation and Ligand Exchange," in "Coordination Chemistry," ed by A. E. Martell, American Chemical Society, Washington, D. C. (1978), ACS Monogr. No. 174, Chap. 1, pp. 1—220.

3) M. Kodama and E. Kimura, *J. Chem. Soc., Dalton Trans.*, **1977**, 1473 and 2269.

4) L. Hertli and T. A. Kaden, *Helv. Chim. Acta*, **64**, 33 (1981).

5) J.-M. Lehn, *Acc. Chem. Res.*, **11**, 49 (1978).

6) C. C. Chen and S. Petrucci, *J. Phys. Chem.*, **86**, 2601 (1982).
7) E. Schmidt and A. I. Popov, *J. Am. Chem. Soc.*, **105**, 1873 (1983).
8) S. Funahashi, K. Saito, and M. Tanaka, *Bull. Chem. Soc. Jpn.*, **54**, 2695 (1981).
9) M. J. Bain-Ackerman and D. K. Lavallee, *Inorg. Chem.*, **18**, 3358 (1979).
10) J. Turay and P. Hambright, *Inorg. Chem.*, **19**, 562 (1980).
11) D. K. Lavallee and G. M. Onady, *Inorg. Chem.*, **20**, 907 (1981).
12) R. F. Pasternack, G. C. Vogel, C. A. Skowronek, R. K. Harris, and J. G. Miller, *Inorg. Chem.*, **20**, 3763 (1981).
13) W. Schneider, *Struct. Bonding (Berlin)*, **23**, 123 (1975).
14) P. Hambright, "Dynamic Coordination Chemistry of Metalloporphyrins," in "Porphyrins and Metalloporphyrins," ed by K. M. Smith, Elsevier, New York (1975), Chap. 6, pp. 233—278.
15) F. R. Longo, E. M. Brown, W. G. Rau, and A. D. Adler, "Kinetic and Mechanistic Studies of Metalloporphyrin Formation," in "The Porphyrins," ed by D. Dolphin, Academic Press, New York (1979), Vol. V, Chap. 10, pp. 459—481.
16) M. Tanaka, *Pure Appl. Chem.*, **55**, 151 (1983).
17) E. B. Fleischer and J. H. Wang, *J. Am. Chem. Soc.*, **82**, 3498 (1960).
18) K. Letts and R. A. Mackay, *Inorg. Chem.*, **14**, 2993 (1975).
19) E. B. Fleischer and F. Dixon, *Bioinorg. Chem.*, **7**, 129 (1977).
20) H. J. Callot, B. Chevrier, and R. Weiss, *J. Am. Chem. Soc.*, **101**, 7729 (1979).
21) H. Baker, P. Hambright, and L. Wagner, *J. Am. Chem. Soc.*, **95**, 5942 (1973).
22) D. K. Lavallee and M. J. Bain-Ackerman, *Bioinorg. Chem.*, **9**, 311 (1978).
23) F. R. Longo, E. M. Brown, D. J. Quimby, A. D. Adler, and M. Meot-Ner, *Ann. N. Y. Acad. Sci.*, **206**, 420 (1973).
24) D. K. Lavallee and A. E. Gebala, *Inorg. Chem.*, **13**, 2004 (1974).
25) S. Sugata and Y. Matsushima, *J. Inorg. Nucl. Chem.*, **39**, 729 (1977); **40**, 1269 (1978).
26) S. Sugata and Y. Matsushima, *Chem. Pharm. Bull.*, **26**, 1071 (1978).
27) O. P. Anderson, A. B. Kopelove, and D. K. Lavallee, *Inorg. Chem.*, **19**, 2101 (1980) and references cited therein.
28) R. C. Weast, Ed, "Handbook of Chemistry and Physics," 60th ed, CRC Press, Boca Raton, FL (1979).
29) E. B. Fleischer, *Acc. Chem. Res.*, **3**, 105 (1970).
30) S. Yamada and R. E. Verrall, *J. Phys. Chem.*, **85**, 3145 (1981).
31) S. Funahashi and M. Tanaka, *Inorg. Chem.*, **8**, 2159 (1969).
32) C. B. Storm, Y. Teklu, and E. A. Sokoloski, *Ann. N. Y. Acad. Sci.*, **206**, 631 (1973).

 © 1984 The Chemical Society of Japan Bull. Chem. Soc. Jpn., 57, 209—213 (1984)

A Novel Synthesis of Internal Alkenyldialkylborane by the Reaction of 1-Halo-1-alkenyldialkylborane with Grignard Reagent

Akira ARASE,* Masayuki HOSHI, and Yuzuru MASUDA
Department of Applied Chemistry, Kitami Institute of Technology, Kitami 090
(Received December 11, 1982)

To synthesize internal alkenyldialkylboranes, coupling reactions were carried out by using 1-halo-1-alkenyldialkylboranes and Grignard reagents. Hydrogen peroxide oxidation and protonolysis with acetic acid of the reaction product revealed that internal (*E*)-alkenyldialkylborane was formed in 60—90% yield.

Organoborane is readily prepared by hydroboration, in which borane adds to a carbon-carbon double or triple bond in a regio- and stereoselective manner.[1] The skeleton of the alkyl or alkenyl group of organoborane formed by hydroboration is specified by the starting unsaturated compound. If the structure of the alkyl or alkenyl group of organoborane could be transformed to a desired one, the synthetic utility of organoborane would be greatly enhanced, although it is presently unavailable *via* hydroboration.

By the coupling reaction of 1-bromoalkyldialkoxyborane with alkylmagnesiumhalides, substitution of bromine with alkyl group has been reported,[2,3] and the application of this reaction to 1-halo-1-alkenylborane seems to be a successful route to regio- and stereoselective synthesis of internal alkenylboranes.[4] In this paper, we wish to report a synthesis of internal alkenyldialkylboranes by the coupling reaction of 1-halo-1-alkenylborane with a Grignard reagent (Scheme 1).

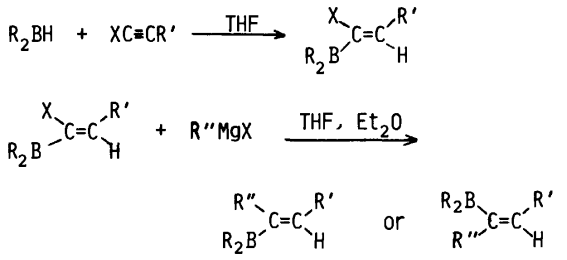

Scheme 1.

Results and Discussion

We have no suitable means to estimate directly the formation of internal alkenyldialkylborane at present. Fortunately, however, the internal alkenyl group of organoborane can be almost quntitatively transformed to the corresponding ketone by alkaline hydrogen peroxide oxidation.[5,6] Thus the yield of the internal alkenyldialkylborane was estimated indirectly from the amount of ketone formed by the above oxidation of the reaction product.

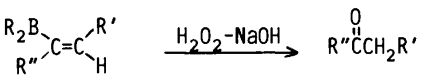

The reaction was carried out in the following way. To a THF solution of 2 mmol of 1-halo-1-alkenyldialkylborane, prepared from dialkylborane and 1-halo-1-alkyne,[7] diethyl ether solution of 2 mmol of alkylmagnesium halide was added at −50 °C and the solution was stirred at this temperature for 1 h. Then the reaction mixture was treated with alkaline hydrogen peroxide, and the product was analyzed by GLC.

In the reaction of 1-bromo-1-hexenyldicyclohexylborane with methylmagnesium iodide, 2-heptanone was obtained in 74% yield based on dicyclohexylborane employed. This result indicated that the expected 1-methyl-1-hexenyldicyclohexylborane was formed at least in this yield by the coupling reaction depicted in Scheme 2. In addition to 2-heptanone, cyclohexyl-

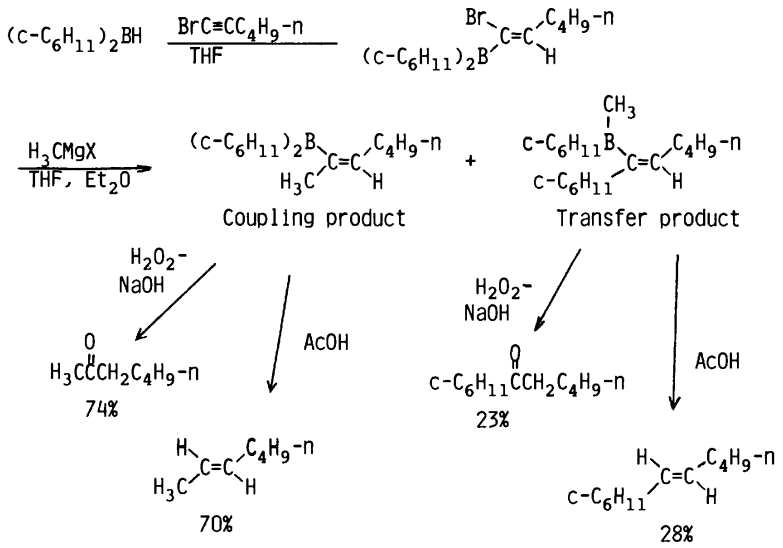

Scheme 2.

pentylketone was formed in 23% yield. This fact suggests that the transfer of the cyclohexyl group from the boron atom to the hexenyl carbon atom competed with the coupling reaction, to give 1-cyclohexyl-1-hexenylmethylcyclohexylborane (Transfer product in Scheme 2).

Brown *et al.* reported that the protonolysis of internal alkenylborane with carboxylic acid provided corresponding alkenes in retention of the configuration.[8] Thus to obtain further evidence for the formation of 1-methyl-1-hexenyldicyclohexylborane and to reveal the configuration of the alkenyl moiety of this com-

Table 1. 1-Alkyl-1-alkenyldialkylboranes obtained by the reactions of 1-bromo-1-alkenyldialkylboranes with Grignard reagents[a] and their yields[b]

R and R′ of 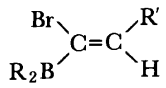	R″X for the Grignard reagent	Product and yield/% 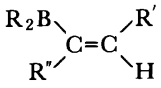 (Coupling)	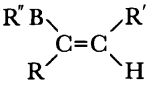 (Transfer)
R=cyclohexyl R′=n-C_4H_9	CH_3I[d]	74	23
	$CH_3CH_2CH_2Br$	60	36
	$(CH_3)_2CHBr$	12	40
	$CH_3(CH_2)_3CH_2Br$	52	35
	$CH_3(CH_2)_6CH_2Br$	54	37
	$H_2C{=}CHCH_2Br$	70	27
	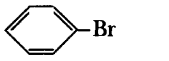	0	88
	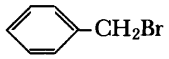	21	58
R=C_5H_{11}[c] R′=n-C_4H_9	$CH_3CH_2CH_2Br$	64	18
	$CH_3(CH_2)_3CH_2Br$	68	20
	$CH_3(CH_2)_6CH_2Br$	64	35
	$H_2C{=}CHCH_2Br$[d]	60	28
	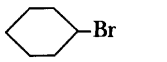	9	34
R=cyclohexyl R′=n-C_6H_{13}	CH_3I[d]	72	24

a) Carried out by using 5 mmol of 1-bromo-1-alkenyldialkylborane and 5 mmol of the Grignard reagent in THF at −50 °C. b) Estimated from the amount of ketone in the oxidized solution and based on dialkylborane used. c) 1,2-Dimethylpropyl. d) Diethyl ether was used as the solvent for the Grignard reagent.

Table 2. 1-Alkyl-1-alkenyldialkylboranes obtained by the reactions of 1-iodo-1-alkenyldialkylboranes with Grignard reagents[a] and their yields[b]

R and R′ of 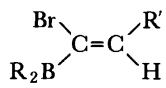	R″X for the Grignard reagent	Product and yield/% 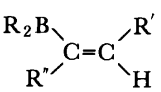 (Coupling)	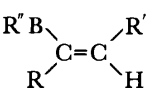 (Transfer)
R=cyclohexyl R′=n-C_4H_9	$CH_3CH_2CH_2Br$	70	30
	$CH_3(CH_2)_3CH_2Br$	66	31
	$CH_3(CH_2)_6CH_2Br$	66	30
	$H_2C{=}CHCH_2Br$[d]	90	9
R=C_5H_{11}[c] R′=n-C_4H_9	$CH_3CH_2CH_2Br$	75	8
	$CH_3(CH_2)_3CH_2Br$	70	8
	$CH_3(CH_2)_6CH_2Br$	70	12
	$H_2C{=}CHCH_2Br$[d]	62	10
R=cyclohexyl R′=n-C_6H_{13}	CH_3I[d]	85	13
R=C_5H_{11}[c] R′=n-C_6H_{13}	CH_3I[d]	82	14

a) Carried out by using 5 mmol of 1-iodo-1-alkenyldialkylborane and 5 mmol of the Grignard reagent in THF at −50 °C. b) Estimated from the amount of ketone in the oxidized solution and based on dialkylborane used. c) 1,2-Dimethylpropyl. d) Diethyl ether was used as the solvent for the Grignard reagent.

pound, the reaction mixture was treated with acetic acid at room temperature for 3 h, and the products were analyzed by GLC.

In this case (*E*)-2-heptene was formed in 70% yield based on dicyclohexylborane employed. The above fact supported the formation of (*E*)-1-methyl-1-hexenyldialkylborane. Thus, inversion of the configuration must be involved in the coupling reaction because 1-bromo-1-hexenyldicyclohexylborane has the *Z*-configuration as depicted in Scheme 2.[7]

Several coupling reactions of 1-bromo-1-alkenyldialkylboranes with some Grignard reagents were examined. The results are shown in Table 1.

In most cases, two (*E*)-1-alkyl-1-alkenyldialkylboranes were formed. One was the expected coupling product and the other was the transfer product. The size of the alkyl group of the Grignard reagent had an appreciable influence on the distribution of these products. Thus in the case of small groups, such as methyl, propyl and allyl, the coupling reaction proceeded predominantly, while in the case of bulky groups, such as cyclohexyl, phenyl and benzyl, the transfer reaction proceeded predominantly.

Much better results were obtained when 1-iodo-1-alkenyldialkylboranes were employed instead of 1-bromo-1-alkenyldialkylboranes. 1-Alkyl-1-alkenyldialkylborane formed in these reactions and their yields estimated in a similar manner as described above are presented in Table 2.

To clarify the configuration of the alkenyl moiety of these internal alkenylboranes, the reaction mixtures were protonolyzed with acetic acid and the resulting alkenes are presented in Table 3. In all cases examined, (*E*)-alkenes were formed, indicating that these internal alkenyldialkylboranes have the *E*-configuration.

Campbell *et al.* reported that in the reaction of (*Z*)-1-halo-1-alkenyldialkylborane with *t*-butyllithium, an inversion of the configuration occured *via* an ate-complex with hydride.[9] On the other hand, Zweifel *et al.* revealed that an internal (*E*)-alkenylborinate, having one alkyl group and one methoxl group on the boron atom, was formed in the reaction of 1-halo-1-alkenyldialkylborane with sodium methoxide.[10] In this reaction one of the two alkyl groups on the boron atom is transfered to the α-carbon atom of the alkenyl group *via* an ate-complex.

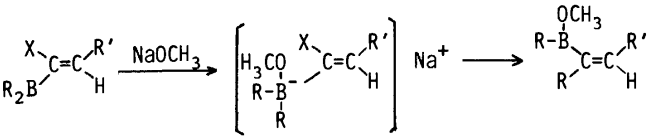

In the present reaction, it seems probable that a similar ate-complex of 1-halo-1-alkenyldialkylborane with the carbanion from the Grignard reagent would be formed at the first stage of the reaction, and then R'and R" may be transfered to the alkenyl carbon atom in a competitive manner, path 1 in Scheme 3. Initially, we attempted to couple directly 1-halo-1-alkenyldialkylborane and the Grignard reagent, path 2 in Scheme 3. However, we have no clear evidence for such a coupling reaction at the moment. In any event, it was revealed that (*E*)-1-alkyl-1-alkenyldialkylborane was formed in the present reaction.

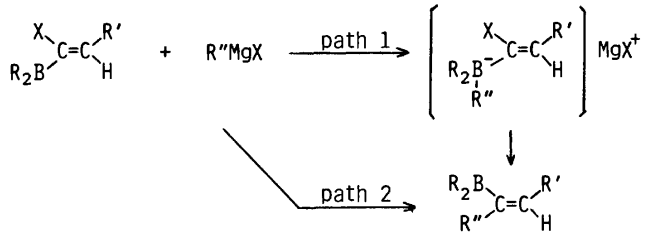

Scheme 3.

Internal alkenyldialkylborane can be synthesized by hydroboration of internal alkyne with sterically hindered dialkylborane.[7] However, in this reaction the regioselective addition of the boron atom to the triple bond is impossible for an internal alkyne whose two alkyl groups are of a similar structure. Thus the reac-

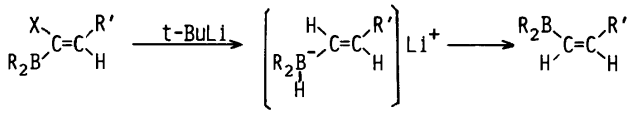

Table 3. (*E*)-Alkenes formed by the protonolysis of 1-alkyl-1-alkenyldialkylborane with acetic acid[a]

R and R' of 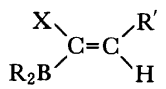	R"X for the Grignard reagent	Product and yield/%[b] 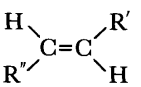	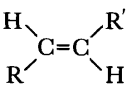
R=cyclohexyl R'=*n*-C_4H_9	CH_3I[d,e]	70	28
	$CH_3(CH_2)_3CH_2Br$[e]	54	37
	$CH_3(CH_2)_6CH_2Br$[e]	56	38
	$CH_3(CH_2)_3CH_2Br$[e]	69	22
	$CH_3(CH_2)_6CH_2Br$[e]	69	22
	$CH_3(CH_2)_6CH_2Br$[f]	70	16
	$CH_3(CH_2)_6CH_2Br$[f]	73	18
R=cyclohexyl R'=*n*-C_6H_{13}	H_2=$CHCH_2Br$[d,f]	67	20

a) Protonolyzed at room temperature for 3 h. b) Based on dialkylborane used. c) 1,2-Dimethylpropyl. d) Diethyl ether was used as the solvent for the Grignard reagent. e) 1-Bromo-alkenyldialkylborane was used. f) 1-Iodo-alkenyldialkylborane was used.

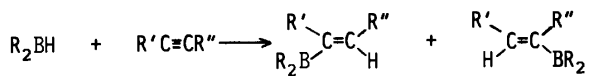

tion can be successfully applied only for alkynes in which the steric hindrance and/or electronic character of the two alkyl groups differ largely from each other, or for completely symmetrical alkynes. Further, internal alkenyldialkylborane, thus obtained has the *Z*-configuration. The present reaction has the feature that two alkyl groups on the alkenyl double bond can be chosen arbitrarily. One is from relatively unhindered Grignard reagent and the other is from 1-halo-1-alkyne. In addition, the resulting internal alkenyldialkylborane has the *E*-configuration.

Several attempts were made to increase the yield of the internal alkenyldialkylborane. For, example, metal-triphenylphosphine compounds $NiCl_2(PPh_3)$[11] and $Pd(PPh_3)_4$,[12] known to have a remarkable promoting effect on the coupling reaction of alkenyl halide with the Grignard reagent, were added to the reaction mixture. Also 9-BBN was used as the hydroborating agent instead of dicyclohexylborane and bis(1,2-dimethylpropyl)borane. However, these failed to give satisfactory results.

Although the purpose of the present work is to synthesize internal alkenyldialkylborane, the regioselective formation of ketones and the regio- and stereoselective formation of internal alkenes observed in the examination of 1-alkyl-1-alkenyldialkylborane is also of interest to organic synthesis. Brown *et al.* obtained ketones or internal (*E*)-alkenes by the successive treatment of (1,1,2-trimethylpropyl)chloroborane with alkene, potassium triisopropoxyborohydride, 1-halo-1-alkyne and alkaline hydrogen peroxide or a carboxylic acid.[7,13] In this reaction the alkyl group introduced into the alkenyl double bond is derived from alkene *via* hydroboration.

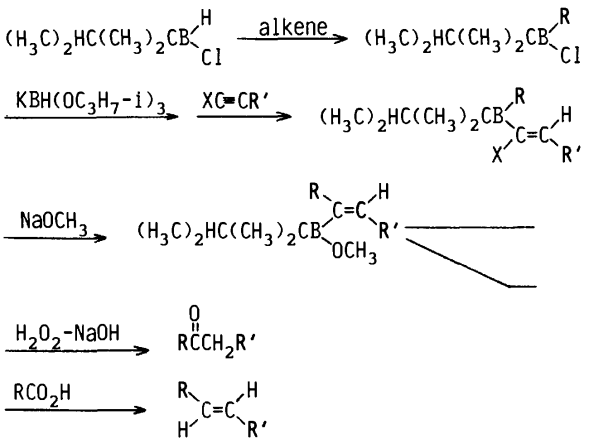

However, in the present reaction such an alkyl group is derived from the Grignard reagent. Accordingly the reaction is applicable to the introduction of such alkyl groups as methyl and allyl, which cannot be introduced *via* hydroboration. For example, in the preparative scale experiment using 1-bromo-1-hexenyldicyclohexylborane and methyl magnesium iodide 2-heptanone was obtained in 68% yield by distillation of the oxidized products. Similarly (*E*)-2-heptene was also obtained in 65% yield by distillation of the protonolyzed products.

Experimental

Instruments. IR spectra (film) were recorded by using a Hitachi 285 spectrometer. ^1H NMR (CCl_4, TMS) spectra were run on a Hitachi R-20A spectrometer. Mass spectra were recorded by using a Hitachi M-52 mass spectrometer.

Reagents. Cyclohexene and 2-methyl-2-butene were distilled under argon stream after drying over lithium aluminium hydride. 1-Bromo-1-hexyne,[14] 1-bromo-1-octyne,[14] 1-iodo-1-hexyne,[15] and 1-iodo-1-octyne[16] were prepared by the methods described in the literatures. Dicyclohexylborane and bis(1,2-dimethylpropyl)borane[17] in THF were prepared as described in the literature. Alkyl halides were dried over Molecular Sieve 5A and distilled before use.

Representative Procedure. A 100-ml round bottomed flask, equipped with a gas inlet for argon, a septum inlet with a serum cap and a magnetic stirring bar, was flushed with argon. 1-Bromo-1-hexenyldicyclohexylborane was prepared by the addition of cyclohexene (0.82 g, 10 mmol) to BH_3 (5 mmol) in THF. 1-Bromo-1-hexyne (0.81 g, 5 mmol) was added slowly to the solution at −10 °C and the solution was stirred for 3 h at 0 °C. To this stirred solution, a diethyl ether solution of methylmagnesium iodide (5 mmol), prepared separately, was transfered with the aid of a syringe at −50 °C and the stirring was continued at this temperature for 1 h. Then the solution was allowed to warm to room temperature and oxidized with alkaline hydrogen peroxide, neutralized with hydrochloric acid, washed three times with NaCl-saturated water and dried over anhydrous magnesium sulfate. The solution was analyzed by GLC (10% PEG-20M, Diasolid M) using the internal standard method.

In the preparative reaction, the amounts of reagents and solvents used were four times those in the analytical reaction. After work-up diethyl ether and THF were evaporated, and the residue was put on a silica-gel column (Wako Q-50). From a mixture of two ketones, eluted by a mixture of benzene and diethyl ether (95:5), 1.55 g of 2-heptanone was distilled at 147 °C/753 Torr (68% yield) nearly free from cyclohexylpentyl ketone. ^1H NMR δ=0.88 (3H, t), 1.08—1.90 (6H, m), 2.05 (3H, s) and 2.31 (2H, t); IR 1712 cm^{-1}; MS *m/e* 142 (M^+).

The protonolysis was performed in the following way. To the reaction mixture, obtained as described above, 5 ml of acetic acid was added and the solution was stirred at room temperature for 3 h. Then the solution was washed three times with NaCl-saturated water and dried over anhydrous calcium chloride. The solution was analyzed by GLC (10% PEG-20M, Diasolid M) using the internal standard method. The preparative reaction was carried out by using four times the amounts of reagents and solvents used in the analytical reaction. After work-up 1.27 g of (*E*)-2-heptene was distilled at 97 °C/754 Torr (65% yield) uncontaminated by (*E*)-1-cyclohexyl-1-hexene. ^1H NMR δ=0.88 (3H, t), 1.00—1.50 (4H, m), 1.59 (3H, d), 1.70—2.25 (2H, m) and 5.00—5.72 (2H, m); IR 964 cm^{-1} (HC=CH); MS *m/e* 98 (M^+).

Analytical data of ketones and alkenes obtained in the examination of internal alkenyldialkylboranes are as follows.

2-Nonanone: ^1H NMR δ=0.88 (3H, t), 1.08—1.90 (10H, m), 2.05 (3H, s) and 2.30 (2H, t); IR 1713 cm^{-1}; MS *m/e* 142 (M^+).

4-Nonanone: ^1H NMR δ=0.83 (6H, t), 1.05—2.00 (8H, m) and 2.28 (4H, t); IR 1718 cm^{-1}; MS *m/e* 142 (M^+). Found: C, 76.01; H, 12.74%. Calcd for $C_9H_{18}O$: C, 75.99; H, 12.76%.

6-Undeuanone: ^1H NMR δ=0.83 (6H, t), 1.05—2.00 (12H,

m) and 2.28 (4H, t); IR 1718 cm^{-1}; MS *m/e* 170 (M^+). Found: C, 77.55; H, 13.00%. Calcd for $C_{11}H_{22}O$: C, 77.58; H, 13.02%

1-Nonen-4-one: ^1H NMR δ=0.83 (3H, t), 1.00—2.00 (6H, m), 2.30 (2H, m), 3.00 (2H, d) and 4.65—6.20 (3H, m); IR 1720 and 915 cm^{-1} (-CH=CH_2); MS *m/e* 140 (M^+). Found: C, 77.12; H, 11.50%. Calcd for $C_9H_{16}O$: C, 77.09; H, 11.50%.

1-Undecen-4-one: ^1H NMR δ=0.87 (3H, t), 1.00—2.00 (10H, m), 2.30 (2H, m), 3.00 (2H, d) and 4.65—6.20 (3H, m); IR 1719 and 916 cm^{-1} (-CH=CH_2); MS *m/e* 168 (M^+). Found: C, 78.48; H, 11.97%. Calcd for $C_{11}H_{20}O$: C, 78.51; H, 11.98%.

(E)-*5-Undecene*: ^1H NMR δ=0.81 (6H, t), 1.00—1.70 (10H, m), 1.70—2.20 (4H, m) and 5.18—5.40 (2H, m); IR 965 cm^{-1} (CH=CH): MS *m/e* 154 (M^+). Found: C, 85.66; H, 14.33%. Calcd for $C_{11}H_{22}$: C, 85.63; H, 14.33%.

(E)-*5-Tetradecene*: ^1H NMR δ=0.85 (6H, t), 1.00—1.70 (16H, m), 1.70—2.30 (4H, m) and 5.20—5.40 (2H, m); IR 964 cm^{-1} (HC=CH); MS *m/e* 196 (M^+). Found: C, 85.60; H, 14.34%. Calcd for $C_{14}H_{28}$: C, 85.63; H, 14.34%.

(E)-*1,4-Undecadiene*: ^1H NMR δ=0.84 (3H, t), 1.10—1.70 (8H, m), 1.70—2.20 (2H, m), 2.50—2.75 (2H, m) and 4.60—6.10 (5H, m); IR 914 (-CH=CH_2) and 965 cm^{-1} (CH=CH); MS *m/e* 152 (M^+). Found: C, 86.80; H, 13.21%. Calcd for $C_{11}H_{20}$: C, 86.76; H, 13.24%.

References

1) For reviews see: a) H. C. Brown, "Hydroboration," W. A. Benjamin, Inc., New York (1962); b) G. M. L. Cragg, "Organoborane in Organic Synthesis," Marcel Dekker, New York (1973); c) H. C. Brown, G. W. Kramer, A. B. Levy, and M. M. Midland, "Organic Synthesis via boranes," John Wiley and Sons, New York (1975); T. Onak, "Organoborane Chemistry," Academic Press, New York (1975).

2) D. S. Matteson and R. W. Mah, *J. Am. Chem. Soc.*, **85**, 2599 (1963).

3) H. C. Brown and N. R. Delue, *J. Org. Chem.*, **42**, 4088 (1977).

4) For Reviews see: H. C. Brown, "Organic Synthesis Today and Tomorrow," ed by B. M. Trost and G. R. Hutchinson, Pergamon Press, London (1980), p. 121.

5) H. C. Brown and S. K. Gupta, *J. Am. Chem. Soc.*, **44**, 4370 (1972).

6) S. U. Kulkarni, H. D. Lee, and H. C. Brown, *Synthesis*, **1982**, 193.

7) a) G. Zweifel, R. P. Fisher, J. T. Snow, and C. C. Whitney, *J. Am. Chem. Soc.*, **93**, 6309 (1971); b) E. Negishi, J. J. Katz, and H. C. Brown, *Synthesis*, **1972**, 555.

8) H. C. Brown and G. Zweifel, *J. Am. Chem. Soc.*, **83**, 3834 (1961).

9) J. B. Campbell Jr., and G. A. Molander, *J. Organomet. Chem.*, **156**, 71 (1978).

10) G. Zweifel and Arzoumanian, *J. Am. Chem. Soc.*, **89**, 5086 (1967).

11) a) K. Tamao, A. Minato, N. Miyake, Y. Kiso, and M. Kumada, *Chem. Lett.*, **1975**, 133; b) K. Tamao, K. Sumitani, Y. Kiso, M. Zenbayashi, A. Fujioka, S. Komada, I. Nakajima, A. Minato, and M. Kumada, *Bull. Chem. Soc. Jpn.*, **49**, 1958 (1976).

12) M. Yamamura, I. Moritani, and S. Murahashi, *J. Organomet. Chem.*, **91**, C39 (1975).

13) H. C. Brown, H. D. Lee, and S. U. Kulkarni, *Synthesis*, **1982**, 195.

14) K. E. Schulte and M. Goes, *Arch. Pharm.*, **290**, 118, (1959).

15) P. L. Southwick and J. R. Kirchiner, *J. Org. Chem.*, **27**, 3305 (1962).

16) G. Zwefel, H. Arzoumanian, and C. C. Whitney, *J. Am. Chem. Soc.*, **89**, 3652 (1967).

17) H. C. Brown and A. W. Moerikofer, *J. Am. Chem. Soc.*, **83**, 3471 (1961).

Enantioselectivity Enhancement in the Deacylation of *N*-Acyl Amino Acid Esters by Vesicular Systems of Long Chain Dipeptide Nucleophiles and a Cationic Double Chain Surfactant

Katsutoshi OHKUBO,* Noriko MATSUMOTO, Masaru NAGASAKI, Kazuhiro YAMAKI, and Harumi OGATA
Department of Synthetic Chemistry, Faculty of Engineering, Kumamoto University, Kurokami, Kumamoto 860
(Received April 25, 1983)

The enantioselective deacylation of short chain and long chain *N*-acyl amino acid *p*-nitrophenyl esters, $CH_3(CH_2)_nCONH\overset{*}{C}H(R)\text{-}CO_2C_6H_4NO_2\text{-}p$ (R=$C_6H_5CH_2$, $(CH_3)_2CHCH_2$, CH_3; n=0, 8, 12), was carried out at 4—25 °C (pH 7.68) with the vesicular systems composed of *N,N*-didodecyl-*N,N*-dimethylammonium bromide and long chain nucleophiles, N^{α}-dodecanoyl-L-histidine, N^{α}-(*N*-dodecanoyl-L-leucyl)-L-histidine (**3a**), N^{α}-(*N*-dodecanoyl-L-phenylalanyl)-L-histidine (**3b**), and *N*-(N^{α}-dodecanoyl-L-histidyl)-L-leucine (**3c**). Both the deacylation rate and the enantioselectivity were the largest in the deacylation of the substrates possessing a long *N*-acyl chain (n=8) with the efficient dipeptide nucleophiles (**3a** and **3b**) including the L-histidine moiety in their terminal position, and the neighboring amino acid binding to the L-histidine in **3a**, **3b**, and/or **3c** was found to play an important role in the enhancement of enantioselectivity. The lowering of the reaction temperature decreased the deacylation rate and increased the enantioselectivity. The maximum enantiomer rate ratio of 24.5 was obtained in the deacylation of *p*-nitrophenyl *N*-dodecanoylphenylalaninates with the dipeptide nucleophile **3b**. The characteristic features of the present reaction are discussed on the basis of kinetic parameters (binding constants and activation parameters) and isokinetic relationships.

The enantioselective hydrolysis of ester substrates by chiral bilayer membranes has recently received considerable attention in the biomimetic chemistry. There are four reports dealing with the following reactions: (a) the deacylation of *p*-nitrophenyl *N*-benzyloxycarbonylphenylalaninates by a synthetic functionalized membrane including L-histidine moiety with a maximum enantiomer rate ratio (k_L/k_D) of 4.4 (4 °C),[1] (b) the deacylation of *p*-nitrophenyl *N*-acylphenylalaninates by the vesicles including N^{α}-palmitoyl-L-histidine with a maximum rate ratio of 5.6 (25 °C),[2] (c) the deacylation of di- or tripeptide type amino acid *p*-nitrophenyl esters by the mixed vesicles of *N,N*-dihexadecyl-*N,N*-dimethylammonium bromide and 1-hexadecanethiol surfactant with a maximum ratio of 4.53 (25 °C),[3] and (d) the deacylation of *p*-nitrophenyl *N*-acylphenylalaninates by the vesicular systems of N^{α}-(*N*-benzyloxycarbonyl-L-leucyl)-L-histidine and a cationic double chain surfactant with maximum rate ratios of 29.6 (25 °C) and 83.6 (10 °C).[4] In this paper, we wish to report the enantioselective deacylation of *N*-acyl amino acid esters by vesicular systems composed of long chain dipeptide nucleophiles and *N,N*-didodecyl-*N,N*-dimethylammonium bromide.

$$CH_3(CH_2)_nCONH\overset{*}{C}HCO_2C_6H_4NO_2\text{-}p$$
$$\quad\quad\quad

Table 1. Deacylation rate and enantioselectivity[a)]

Nucleophile		k/1 mol^{-1}s^{-1}																
		1a (n=0)				**1a** (n=8)				**1a** (n=12)				**1b** (n=8)				**1c** (n=8)
		25 °C	15 °C	10 °C	4 °C	25 °C	15 °C	10 °C	4 °C	25 °C	15 °C	10 °C	4 °C	25 °C	15 °C	10 °C	4 °C	25 °C
2	L	392	262	200	49	1768	1398	1100	315	1550	738	598	188	1874	1332	1088	110	392
	D	240	146	114	12	380	256	200	26	398	176	144	16	426	254	190	9.0	230
	L/D	1.6	1.8	1.8	4.1	4.7	5.5	5.5	12.1	3.9	4.2	4.2	11.8	4.4	5.2	5.7	12.2	1.7
3a	L	1084	644	542	224	4318	3030	2148	1439	1654	1044	764	264	4118	2704	2126	620	
	D	156	74	56	13	654	386	270	128	538	254	190	52	620	330	260	53	
	L/D	6.9	8.7	9.8	17.2	6.6	7.8	8.0	11.2	3.0	4.1	4.0	5.1	6.6	8.1	8.2	11.7	
3b	L	764	556	436	128	3156	2254	2030	1520	1664	802	546	228	2040	1556	1172	471	
	D	118	54	38	5.4	340	226	172	62	352	154	106	21	360	226	158	37	
	L/D	6.5	10.3	11.5	23.7	9.3	10.0	11.8	24.5	4.7	5.2	5.2	10.9	5.7	6.9	7.4	12.7	
3c	L	122	68	58	17	844	536	456	229	576	326	210	56	722	526	420	37	
	D	120	66	56	6.0	136	68	56	20	90	52	32	2.4	112	72	60	2.8	
	L/D	1.0	1.0	1.0	2.8	6.4	7.9	8.1	11.5	6.4	6.3	6.6	23.3	6.4	6.9	7.0	13.2	

a) Tris buffer (0.083 mol dm^{-3}) containing 0.083 mol dm^{-3} KCl at 4—25 °C (pH 7.68) in 3% (v/v) CH_3CN-H_2O: [1]=1×10^{-5} mol dm^{-3}, [2 or 3]=5×10^{-5} mol dm^{-3}, and [4]=1×10^{-3} mol dm^{-3}.

chain. The suitably long hydrophobic chain of **1a** (n=8), **1b** (n=8), or **1c** (n=8) contributes to the incorporation of **1a** (n=8), **1b** (n=8), or **1c** (n=8) *per se* into the vesicles and intensifies the approximation between the nucleophile and the substrate. However, the substrate **1a** (n=12) has an excessively long *N*-acyl chain which might refuse the close approach of the susceptible carbonyl group in **1a** (n=12) to the imidazolyl moiety in the nucleophile; thus **1a** showed a decreased rate and lower enantioselectivity. It is unlikely that all parts of the substrate and the nucleophile are incorporated into the vesicle layer out of the aqueous phase. Thus such an interaction between the hydrophobic benzyl group (substrate) and imidazolyl moiety (nucleophile) seems important for making the reacting positions of the nucleophile and the substrate come closer together. In this sense, the order of the deacylation rate and of the enantioselectivity in the deacylation of **1a** (n=8), **1b** (n=8), and **1c** (n=8) with **2**, **1a** (n=8)>**1b** (n=8)>**1c** (n=8), might reflect the extent of the magnitude of the interaction between the hydrophobic imidazolyl part (nucleophile) and the apolar R (R=$C_6H_5CH_2$, $(CH_3)_2CHCH_2$, or CH_3) substituent (substrate).

We studied the structural effects of the nucleophiles. The dipeptide nucleophiles (**3a** and **3b**) including the L-histidine moiety in their terminal position resulted in the large deacylation rate and the high enantioselectivity as compared with those of the nucleophile (**2**). The L-leucine or L-phenylalanine moiety, which is adjacent to the L-histidine part, might intensify the hydrophobic interaction between **3a** or **3b** and the substrate so as to enhance the deacylation rate and the enantioselectivity, even in the deacylation of the short chain substrate **1a** (n=0) which is condensed or partly incorporated by the vesicles. The chirality of the neighboring group of L-leucine or L-phenylalanine in **3a** or **3b** is also important, because the use of the D-isomer instead of the above neighboring group decreases both the deacylation rate and the enantioselectivity considerably.

The dipeptide nucleophile **3c**, which includes a L-leucine unit in its terminal position, showed low hydrolyzing activity in the deacylation of the present substrates and resulted in little or no enantioselectivity for the short chain substrate **1a** (n=0). Presumably the

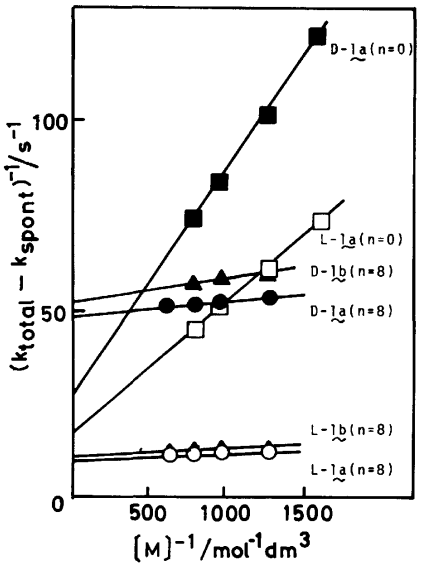

Fig. 1. Typical examples of the linear relationships between the reciprocal values of (k_{total}—k_{spont}) and [M] ([M]=[surfactant]+[nucleophile]—[surfactant]$_{cmc}$). The deacylation of 1 (1×10^{-3} mol dm^{-3}) with **2** ((3.0—7.5×10^{-5} mol dm^{-3}) and **4** ((0.6—1.5)×10^{-3} mol dm^{-3}; [**4**]/[**2**]=20) at 25 °C (pH 7.68).

steric hindrance of the terminal L-leucine part in **3c** against the reaction of **3c** itself with the substrates decreased the deacylation rate (and/or enantioselectivity), especially in the case of the deacylation of the weakly hydrophobic short-chain substrate **1a** (n=0). However, the relatively high enantioselection of the hydrophobic, long-chain substrates (**1a** (n=8, 12) and **1b** (n=8)) by **3c** suggested the contribution of the L-leucine part to the enhancement of enantioselectivity for the long chain substrates which bind strongly to the vesicles. The deacylation rate and enantioselectivity were also influenced by the reaction temperature, which affects the mobility of the substrate and the nucleophile and the liquid crystal-gel equilibrium of the vesicles. As can be seen from Table 1, the lowering of the reaction temperature decreased the deacylation rate and increased the enantioselectivity. These reaction circumstances were well reflected in the binding

Table 2. Kinetic parameters[a]

Nucleophile	parameters[b]	1a (n=0) L	1a (n=0) D	1a (n=8) L	1a (n=8) D	1b (n=8) L	1b (n=8) D
2	K_b/N	634	538	10245	9448	8031	7878
	$10^2\,k_v$	6.1	4.4	11.6	4.0	10.7	2.8
	k_v^L/k_v^D	1.4		2.9		3.8	
3a	K_b/N	1109	766				
	$10^2\,k_v$	10.5	2.2				
	k_v^L/k_v^D	4.8					
3c	K_b/N	399	389	4721	2024	4352	3300
	$10^2\,k_v$	3.1	3.1	7.0	2.9	5.4	1.6
	k_v^L/k_v^D	1.0		2.4		3.4	

a) The reaction conditions are the same as in Table 1 except [2 or 3]=(3—7.5)×10^{-5} mol dm^{-3}, [4]=(0.6—1.5)×10^{-3} mol dm^{-3}, and [4]/[2 or 3]=20. b) The binding parameters (K_b/N and k_v) are given for the reactions at 25 °C, and the units of parameters are K_b/N (dm^3 mol^{-1}), and k_v (s^{-1}).

constant K_b/N (N is the aggregation number) and the rate constant k_v; these kinetic parameters were obtained in the usual way,[5] as indicated in Fig. 1, by taking the deacylation of **1a** (n=0, 8) and **1b** (n=8) with **2** as an example. They are listed in Table 2. The fast deacylation rate and high selectivity of the long-chain substrates are well reflected in the large values of K_b/N and k_v^L/k_v^D obtained in the deacylation of **1a** (n=8) and **1b** (n=8) with **2** or **3c**. The dipeptide nucleophile **3a** which possesses a higher enantioselective activity than that of **2** or **3c**, showed large values of K_b/N and k_v^L/k_v^D in the deacylation of short chain substrate **1a** (n=0). Furthermore, the relatively small K_b/N values of the dipeptide nucleophile **3c**, as compared with those of **2**, are in harmony with the low deacylation ability of **3c**, and the negligibly small enantioselection of the short chain substrate **1a** (n=0) by **3c** is also reflected in the markedly small K_b/N and k_v values.

The change of deacylation rate due to the temperature decrease from 25 to 4 °C was expressed by closely linear Arrhenius plots in which all the plots obtained at 4 °C deviated from linear Arrhenius plots (Fig. 2). Such a deviation of the plots at 4 °C from the Arrhenius relation might be related to the liquid crystal-gel phase transition.[6] The temperature decrease from 10 to 4 °C remarkably increased the enantioselectivity with the maximum enantiomer rate ratio 24.5 in the hydrolysis of **1a** (n=8) by the efficient dipeptide nucleophile **3b**. The characteristic features of the present reaction were also reflected in the activation parameters (ΔH^* and ΔS^*) for the reaction at 10—25 °C (Table 3); that is, the smaller (or negatively larger) ΔH^* (or ΔS^*) values of the L-substrates, as compared with those of the D-substrates, indicate the preferential attack of the nucleophile on the L-substrate, and the small ΔH^* (or ΔS^*) values for the deacylation of **1a** (n=8) or **1b** (n=8) supported the intensified interaction between the efficient dipeptide nucleophile and the substrates possessing the N-acyl chain of appropriate length (n=8). In this respect, the relatively low deacylation rate of **1a** (n=12) was reflected in the relatively large ΔH^* or ΔS^* values of **1a** (n=12). These aspects of the present reaction were also deduced from the isokinetic relation between the ΔH^* and ΔS^* values (Fig. 3). The extent of enantioselectivity can be seen in the difference of the

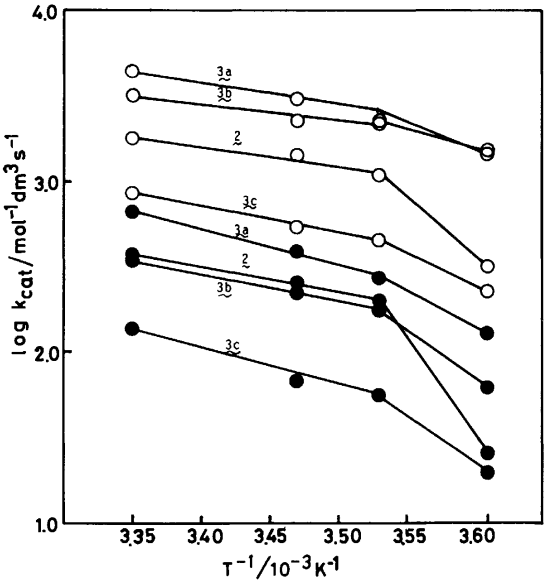

Fig. 2. Typical examples of Arrhenius plots (the deacylation of **1a** (n=8) with **2** or **3**).
○: L ●: D

Table 3. Activation parameters[a]

No.	Nucleophile	Activation parameter	1a (n=0) L	1a (n=0) D	1a (n=8) L	1a (n=8) D	1a (n=12) L	1a (n=12) D	1b (n=8) L	1b (n=8) D
1	2	ΔH^*	6.9	7.8	4.6	6.5	10.3	11.1	4.7	5.9
		ΔS^*	−43.3	−41.3	−48.0	−44.4	−28.9	−29.2	−47.7	−46.7
2	3a	ΔH^*	7.3	11.0	7.0	9.2	7.9	11.2	6.8	9.3
		ΔS^*	−39.8	−31.2	−38.1	−34.4	−36.2	−28.2	−39.0	−34.4
3	3b	ΔH^*	5.6	12.2	4.4	6.9	11.9	12.9	5.4	8.5
		ΔS^*	−46.2	−27.9	−47.3	−43.3	−23.7	−23.2	−44.9	−38.1
4	3c	ΔH^*	8.0	8.1	6.9	9.6	10.9	19.4	5.8	7.5
		ΔS^*	−41.7	−41.4	−41.6	−36.2	−28.9	−2.9	−45.6	−43.5

a) Obtained for the reaction performed under the conditions in Table 1 at 10—25 °C. The units are kcal/mol for ΔH^* and e.u. for ΔS^* (1 cal=4.184 J).

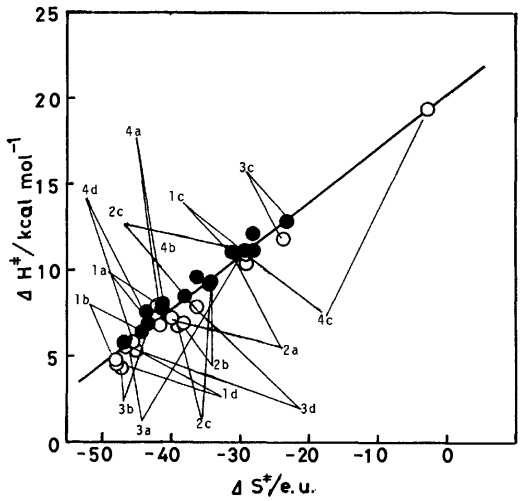

Fig. 3. A isokinetic relation obtained for the deacylation of **1a** (n=0—12) and **1b** (n=8) with **2** and **3**.
○: L, ●: D; a. **1a** (n=0), b. **1a** (n=8), c. **1a** (n=12), d. **1b** (n=8); 1. **2**, 2. **3a**, 3. **3b**, 4. **3c**.

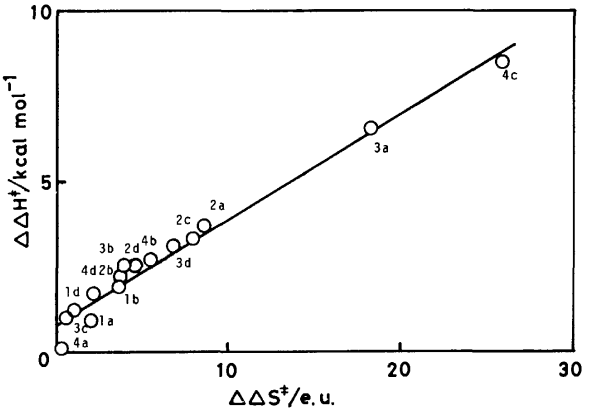

Fig. 4. A linear correlation between $\Delta\Delta H^{\ddagger}$ and $\Delta\Delta S^{\ddagger}$ values.
(Notations are the same in Fig. 3).

activation parameters between the enantiomers ($\Delta\Delta H^{\ddagger}=\Delta H^{\ddagger}_{D}-\Delta H^{\ddagger}_{L}$ or $\Delta\Delta S^{\ddagger}=\Delta S^{\ddagger}_{D}-\Delta S^{\ddagger}_{L}$). The high enantioselectivity was well reflected in the large $\Delta\Delta H^{\ddagger}$ (or $\Delta\Delta S^{\ddagger}$) values, and there is an approximately linear correlation between the $\Delta\Delta H^{\ddagger}$ and $\Delta\Delta S^{\ddagger}$ values (Fig. 4).

The present vesicular system including the dipeptide nucleophile exhibited a relatively high enantioselectivity through the efficient interaction between the L-phenylalanyl(or L-leucyl)-L-histidine moiety in the nucleophile and the hydrophobic substrates incorporated (or condensed) by the vesicles.

Experimental

Materials. N^{α}-dodecanoyl-L-histidine (**2**) and *N*-(N^{α}-dodecanoyl-L-histidyl)-L-leucine (**3c**) were obtained by the acylation of commercially available L-histidine and L-histidyl-L-leucine with dodecanoyl chloride.[7,8] N^{α}-(*N*-dodecanoyl-L-leucyl)-L-histidine (**3a**) and N^{α}-(*N*-dodecanoyl-L-phenylalanyl)-L-histidine (**3b**) were prepared from *N*-hydroxysuccinimide ester of *N*-benzyloxycarbonyl-L-leucine and *N*-benzyloxycarbonyl-L-phenylalanine by the coupling with L-histidine, the hydrobromination of the *N*-benzyloxycarbonyl group, and then the acylation of the NH_2HBr group with dodecanoic anhydride. Satisfactory elemental analyses were obtained for the nucleophiles, and those for new compounds are shown below. **3a**: Found: C, 63.18; H, 9.39; N, 12.30%. Calcd for $C_{24}H_{42}N_4O_4$: C, 63.97; H, 9.39; N, 12.43%. **3b**: Found: C, 66.32; H, 8.74; N, 10.50%. Calcd for $C_{27}H_{40}N_4O_4$: C, 66.91; H, 8.32; N, 11.56%. **3c**: Found: C, 63.81; H, 9.17; N, 12.33%. Calcd for $C_{24}H_{42}N_4O_4$: C, 63.97; H, 9.39; N, 12.43%.

The ester substrates (**1**) were prepared by the method described previously,[9] and the double chain surfactant **4** was obtained by the reaction of *N*,*N*-dimethyldodecylamine and dodecyl bromide.[9] Satisfactory elemental analyses were also obtained for **1** and **4** (C, H, N).

Hydrolysis and Kinetic Measurements. The hydrolysis of 1×10^{-5} mol dm^{-3} substrates (**1**) by the vesicles of 5×10^{-5} mol dm^{-3} nucleophile (**2** or **3**) and 1×10^{-3} mol dm^{-3} surfactant (**4**) were carried out at 4—25°C, pH 7.68 in 0.083 mol dm^{-3} tris(hydroxymethyl)aminomethane buffer involving 0.083 mol dm^{-3} KCl (μ=0.083) in H_2O including 3 vol% CH_3CN, where the stock solutions were prepared by dissolving **2** (or **3**) and **4** in the buffer by sonication at 45°C for 1 h.

The hydrolysis rate, which obeyed a good pseudo-first-order rate law (up to *ca.* 80% conversion), was followed by the spectrophotometric determination of *p*-nitrophenolate (400 nm). The second-order catalytic rate constant k was evaluated from the pseudo-first-order rate constants k_{total} (obtained with the nucleophile) and k_{spont} (obtained without the nucleophile) in the usual way ($k=(k_{total}-k_{spont})/[\text{nucleophile}]$). The binding constant K_b/N and the rate constant k_v were obtained (correlation coefficient>0.990) in the deacylation of 1×10^{-5} mol dm^{-3} substrate (**1**) by the vesicles of $(3-7.5)\times10^{-5}$ mol dm^{-3} nucleophile (**2** or **3**) and $(0.6-1.5)\times10^{-3}$ mol dm^{-3} surfactant (**4**) ([**4**]/[**2** or **3**]=20) at 25°C (pH 7.68) in the usual way with the following simplified reactions.[5]

$$S + V \underset{}{\overset{K_b}{\rightleftharpoons}} SV \xrightarrow{k_v} V + P$$

$$S \xrightarrow{k'} P,$$

where S=substrate, V=vesicles, SV=substrate-vesicle complex, and P=*p*-nitrophenolate.

References

1) Y. Murakami, A. Nakano, A. Yoshimatsu, and K. Fukuya, *J. Am. Chem. Soc.*, **103**, 728 (1981).
2) R. Ueoka, Y. Matsumoto, Y. Ninomiya, K. Inoue, and K. Ohkubo, *Chem. Lett.*, **1981**, 785.
3) R. A. Moss, T. Taguchi, and G. O. Bizzigotti, *Tetrahedron Lett.*, **23**, 1985 (1982).
4) K. Ohkubo, N. Matsumoto, and H. Ohta, *J. Chem. Soc., Chem. Commun.*, **1982**, 738.
5) T. Inoue, K. Nomura, and H. Kimizuka, *Bull. Chem. Soc. Jpn.*, **49**, 719 (1976).
6) The phase transition temperature (T_c) of **4** has already been reported as follows: T_c=5—10°C (estimated by means of a DSC method. T. Kunitake, Y. Okahata, R. Ando, S. Shinkai, and S. Hirakawa, *J. Am. Chem. Soc.*, **102**, 7877 (1980)), 10°C (a fusion experiment. M. Shimomura and T. Kunitake, *Chem. Lett.*, **1981**, 1001), 16°C (a DSC method. Y. Okahata, R. Ando, and T. Kunitake, *Ber. Bunsenges. Phys. Chem.*, **85**, 789 (1981)), and 18°C (a DSC method. S. Honda,

N. Kusumoto, T. Hirayama, T. Kunitake, and Y. Motozato, *Nippon Kagaku Kaishi*, **1983**, 428). The kinetic analysis for the estimation of T_c is also available, and the present kinetic results might be in harmony with the first two reported T_c values (T_c=5—10°C and 10°C) of **4**.

7) C. Gitler, and A. Ochoa-Solano, *J. Am. Chem. Soc.*, **90**, 5004 (1968).

8) K. Ohkubo, K. Sugahara, H. Ohta, K. Tokuda, and R. Ueoka, *Bull. Chem. Soc. Jpn.*, **54**, 576 (1981).

9) R. A. Moss, and W. L. Sunshine, *J. Org. Chem.*, **39**, 1083 (1974).

 © 1984 The Chemical Society of Japan Bull. Chem. Soc. Jpn., 57, 219—221 (1984)

The Addition Reaction of Substituted Benzenesulfinic Acids to *N*-Phenylmaleimide

Itsuo MATSUDA,* Keiichi AKIYAMA, Hiroyuki FURUTA,† and Masateru MIZUTA†

Developing and Engineering Group, Toshiba Chemical Products Co., Ltd., Chidori-cho, Kawasaki, Kanagawa 210

†*Department of Industrial Chemistry, Faculty of Engineering, Gifu University, Yanagido, Gifu 500*

(Received May 10, 1983)

The reaction of substituted benzenesulfinic acids with *N*-phenymaleimide has been carried out, and the products obtained have been identified as sulfones from analyses of their IR, UV, and NMR spectra. From the kinetic investigation, a linear Hammett relationship between the σ-value and log K_2/K_0 has been confirmed. It is concluded that the nucleophilic attack of the sulfinic acid sulfur atom on the carbon of the C=C bond of *N*-phenylmaleimide is the rate-determining step.

The addition reaction of benzenesulfinic acid to seven *N*-substituted phenylmaleimides was studied in the preceding paper.[1] A U-shaped Hammett plot was reported, but the reaction mechanism was not clearly confirmed. It was assumed that the substituent effect was not directly transferred toward the carbon atom of the C=C bond of *N*-(substituted phenyl)maleimide.

In order to pursue this point by using substituted benzenesulfinic acids, in which the substituent effect is directly conveyed toward the sulfur atom, the reaction of five substituted benzenesulfinic acids with *N*-phenylmaleimide has been studied.

The present paper will deal with the kinetic investigation of the addition reaction of *p*-substituted benzenesulfinic acids with *N*-phenylmaleimide. By measuring the unreacted sulfinic acid by means of neutralization titration, the rate constants of the reaction have been determined in the same manner as in the preceding paper.[1]

The Hammett plot, the ρ-value, and the correlation coefficient (r) have also been studied, and the activation parameters for the reaction have been calculated.

Experimental

Materials. The *N*-phenylmaleimide has been prepared by the literature method[2] and recrystallized from ethanol; mp 89.5—90.3 °C (88.0—88.5 °C[2]). The five substituted benzenesulfinic acids have been prepared in the same manner as in the literature. The following materials have been used; benzenesulfinic acid, mp 74.0—76.0 °C (74.0—76.0 °C[1]); *p*-methylbenzenesulfinic acid, mp 82.3—83.5 °C (84—85 °C[3]); *p*-methoxybenzenesulfinic acid, mp 95.5—99.0 °C (97—98 °C[4]); *p*-chlorobenzenesulfinic acid, mp 92.0—94.0 °C (93—94 °C[4]); *p*-bromobenzenesulfinic acid, mp 94.0—97.0 °C (94.0—97.0 °C[5]).

The Confirmation and Analysis of Adducts of Five Substituted Benzenesulfinic Acids with N*-Phenylmaleimide.* The adducts have been prepared in the same manner as in the preceding paper[1] and recrystallized from dichloromethane/hexane. The structural formulas have been confirmed by means of IR, UV, NMR, and elemental analyses. The yields, mps, results of elemental analyses, and NMR are summarized in Table 1.

Measurement of the Rate Constant for the Reaction The rate constants have been determined in the same way as in the preceding paper[1] by the measurement of the remaining

TABLE 1. ANALYTICAL DATE AND PHYSICAL PROPERTIES OF 3 ADDUCTS

Compd No.	X	Mp θ_m/°C	Yield %	Found (Calcd) (%) C	H	N	S	Cl Br	IR (KBr water, ν/cm^{-1}) νC=O	νC=N	νC=C	νSO$_2$
3a	*p*-CH_3O	192.0—193.0	97	59.01	4.36	4.07	9.13		1719	1400	1598	1327
				(59.12)	(4.38)	(4.06)	(9.28)				1503	1144
3b	*p*-CH_3	180.0—183.0	96	61.68	4.51	4.21	9.60		1718	1396	1600	1327
				(61.99)	(4.59)	(4.25)	(9.74)				1498	1159
3c	H	195.0—196.0	96	60.89	4.10	4.47	10.05		1716	1396	1588	1326
				(60.94)	(4.15)	(4.44)	(10.17)				1505	1148
3d	*p*-Cl	227.0—228.0	94	54.87	3.45	4.03	9.17	10.19	1719	1394	1586	1329
				(54.94)	(3.46)	(4.00)	(9.17)	(10.13)			1505	1156
3e	*p*-Br	231.0—232.0	94	48.67	3.06	3.51	8.06	20.31	1719	1395	1578	1329
				(48.74)	(3.07)	(3.55)	(8.13)	(20.27)			1505	1157

Compd No.	UV (CH_2Cl_2) λ_{max}/nm	(ε_{max})		NMR ($CDCl_3$+DMSO-d_6) δ Aromatic		CH	CH_2	CH_3
3a	278 Shoulder			8.06—7.86 (2H)	7.60—7.06 (7H)	4.88	3.39—3.14	3.90
3b	275 (915)	262 Shoulder		7.98—7.58 (2H)	7.58—7.02 (7H)	4.79	3.40—3.16	2.46
3c	273 (1232)	266 (1813)	260 (1891)	8.07—7.52 (5H)	7.42—7.02 (5H)	4.50	3.40	
3d	278 (831)	269 Shoulder	265 Shoulder	8.12—7.58 (4H)	7.58—7.06 (5H)	5.08	3.42—3.18	
3e	278 (926)	270 Shoulder	267 Shoulder	8.08—7.68 (4H)	7.58—7.04 (5H)	5.08	3.46—3.20	

TABLE 2. THE SECOND-ORDER RATE CONSTANTS, THE ρ-VALUES, AND THE CORRELATION COEFFICIENTS (r) OF ADDITION REACTIONS OF N-PHENYLMALEIMIDE WITH SUBSTITUTED BENZENESULFINIC ACIDS IN ETHANOL-WATER (1/1)

X	$k_2 \times 10^2$/mol^{-1} l s^{-1}				
	1 °C	5 °C	10 °C	15 °C	20 °C
p-CH_3O	2.10±0.10	2.84±0.17	3.75±0.25	4.57±0.26	—
	(2.00)	(3.00)	(4.00)	(5.00)	
p-CH_3	—	2.27±0.05	3.34±0.34	4.17±0.17	4.88±0.30
		(2.50)	(3.00)	(4.00)	(5.00)
H	—	1.42±0.09	1.68±0.15	2.35±0.08	2.92±0.09
		(1.50)	(2.00)	(2.50)	(3.00)
p-Cl	—	0.77±0.02	0.98±0.02	1.30±0.10	1.72±0.05
		(0.50)	(1.00)	(1.50)	(1.50)
p-Br	—	0.70±0.03	1.12±0.05	1.50±0.10	1.71±0.04
		(1.00)	(1.00)	(1.50)	(1.50)
ρ	—	−1.20	−1.15	−1.09	−1.03
r	—	−0.99	−0.99	−0.98	−0.98

The values in parentheses have been calculated by the least-squares method.
ρ: The reaction constant. r: The correlation coefficient.

unreacted substituted benzenesulfinic acid *via* neutralization titration with a 0.025 M alcholic KOH solution (1 M= 1 mol dm^{-3}), using phenolphthalein as the indicator. All the kinetic runs have been conducted in the same way as in the preceding paper.[1] All the rate constants have been calculated from the second-rate equation as follows:

$$k_2 t = \frac{1}{A_0}\left(\frac{a}{a_0 - a}\right) = \frac{1}{A_0}\left(\frac{a_0}{a_0 - a} - 1\right).$$

$a_0 - a$: The titre of the 0.025 M alcoholic KOH solution at time (t).
a_0 : The initial titre of the 0.025 M alcoholic KOH solution.
A_0 : The initial concentration (mol/l) of N-substituted maleimide.

The second-order plots of the reaction of substituted benzenesulfinic acids with N-phenylmaleimide are obtained. All the rate constants, ρ-values, and r-values are noted in Table 2.

Results and Discussion

The Structural Identification of Adducts. The structural formulas of the adducts have been identified from the IR, UV, NMR, and elemental analyses, as noted in Table 1. The absorption peak at 1719—1716 cm^{-1}, assigned to C=O vibrations, and the absorption peaks at 1159—1144 cm^{-1} and at 1329—1326 cm^{-1}, assigned to S=O vibrations of the sulfones,[6], have been confirmed in the infrared spectra of all the adducts. As far as the ultraviolet spectra are concerned, λ_{max} (log ε 3.4—4.09) was observed at 218—245 nm in the UV spectra of sulfinic acids and sulfinates,[7,8] whereas λ_{max} (log ε 2.8—2.9) was observed at 266—273 nm in those of sulfones.[7,8] The values of the molar-extinction coefficients are nearly 1000 (log ε=3.00), and λ_{max} has been observed at 260—278 nm in the UV spectra of all the adducts. These data prove that the adducts are sulfones.

In the NMR spectra, the observed values agree well with the theoretical values as to the number of protons of all the adducts. The results obtained indicate that the adducts are sulfones.

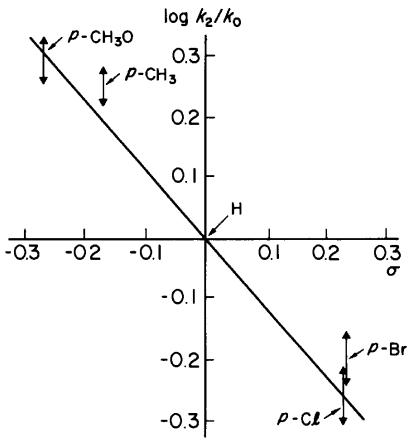

Fig. 1. Hammett plots with σ at 15 °C.

The Investigation of the Hammett Plot. The Hammett plot (log k_2/k_0 *vs.* σ-value) has been examined from the rate constants of the reactions of the five substituted benzenesulfinic acids with N-phenylmaleimide.

As be shown in Fig. 1, a plot of log k_2/k_0 against the σ-value gives a straight line. The linear Hammett relationship has been confirmed from the calculation of the ρ-value and the correlation coefficient (r). As a result, it is evident that the reaction rate is accelerated by an electron-donating group on the benzene nucleus of benzenesulfinic acid, whereas it is retarded by an electron-withdrawing group.

The Calculation of the Activation Entropy. The Arrehenius equation is as follows:

$$k = A \exp(-E_A/\mathbf{R}T),$$
$$\log k = -E_A/4.576\,T + \log A.$$

The activation energy, E_A(kcal/mol, 1 cal=4.184 J), and the logarithm of the fequency factor, log A(s^{-1}), have been obtained by plotting log$k$ against $1/T$. The activation entropy, ΔS^*(e.u.) has been calculated from the following equation:

Table 3. Activation parameters

X	E_A/kcal mol^{-1}	log(A/s^{-1})	ΔS^{*}/e.u.^{288K}
p-CH_3O	9.15±0.57	5.7±0.4	−33±2
	[8.63]	(5.2)	(−35)
p-CH_3	8.90±0.51	5.4±0.3	−34±2
	[8.17]	(4.8)	(−37)
H	8.48±0.47	4.8±0.3	−37±2
	[8.12]	(4.5)	(−38)
p-Cl	8.94±0.22	4.9±0.2	−36±1
	[8.70]	(4.7)	(−37)
p-BR	9.42±0.27	5.3±0.2	−34±1
	[8.86]	(4.9)	(−36)

The values in brackets have been calculated by the least-squares method.

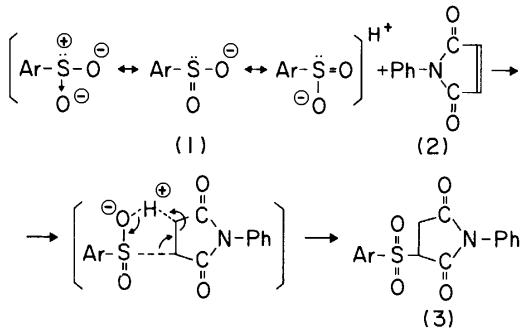

Scheme 1.

$$\Delta S^{*} = 2.303\,\mathbf{R}\,(\log A - \log \mathbf{K}T/\mathbf{h}).$$

The results obtained are shown in Table 3.

The Reaction Mechanism. In the preceding paper[1] it was presumed that the nucleophilic addition of benzenesulfinic acid takes place only at the carbon-carbon double bond of *N*-substituted maleimide. However the reaction mechanism was not clearly confirmed from the substituent effect of *N*-(substituted phenyl)maleimide.

From the investigation of the Hammett plot in the present paper, it is evident that the nucleophilic attack of the sulfur atom of the sulfinic acid on the carbon atom of the ethylene linkage of *N*-substituted maleimide is the rate-determining step. As be noted in Table 3, all the activation entropies have large negative values.[9,10] It can be presumed that the degree of freedom of the transition state is smaller than that of the initial state and that the intermediate is cyclic.[5] It may be concluded that, as be shown in Scheme 1, the reaction of the substituted benzenesulfinic acid with *N*-(substituted phenyl)maleimide proceeds *via* the ionic process, and that the nucleophilic attack of the sulfur atom of sulfinic acid on the carbon atom of the ethylene linkage of *N*-substituted maleimide forms sulfone *via* a cyclic transition state.

References

1) I. Matsuda, K. Akiyama, Y. Toyoshima, S. Kato, and M. Mizuta, *Bull. Chem. Soc. Jpn.*, **48**, 3675 (1975).
2) D. Bryce-Smith and M. A. Hems, *J. Chem. Soc., B*, **1968**, 812.
3) R. K. Burkland, D. E. Sellers, F. DeCou, and J. L. Lambert, *J. Org. Chem.*, **24**, 767 (1959).
4) M. Kobayashi and N. Koga, *Bull. Chem. Soc. Jpn.*, **39**, 1788 (1966).
5) I. Matsuda, K. Akiyama, S. Kobayashi, T. Katada, and M. Mizuta, *Nippon Kagaku Kaishi*, **1981**, 405.
6) L. J. Bellamy, "The Infrared Spectra of Complex Molecules," John Wiley & Sons, New York (1966), pp. 360, 316.
7) S. Oae, "Yuki Iou Kagoobutsu No Kagaku," "Ge," Kagaku Doojin, Kyoto (1969), p. 360.
8) S. Detoni and D. Hodzi, *J. Chem. Soc.*, **1955**, 3163.
9) K. Okamoto, "Kyukaku Chikan Hanno," Tokyo Kagaku Doojin, Tokyo (1972), p. 36.
10) T. Hueno, "Kagaku Hanno Ron," Asakura Syoten, Tokyo (1975), pp. 203, 204.

Kinetic Studies of the Oxidation of 2,3-Dihydroxy-2-propenal (Triose Reductone) by the Peroxodisulfate Ion

Yasuo Abe,* Hideo Horii, and Setsuo Taniguchi
Radation Center of Osaka Prefecture, Shinke-cho, Sakai 593
(Received May 13, 1983)

Kinetic studies of the oxidation of 2,3-dihydroxy-2-propenal (triose reductone) by the peroxodisulfate ion ($S_2O_8^{2-}$) were carried out between pH 4.1 and 5.9 at various temperatures (10—30 °C) and for ionic strengths (I) (0.07 to 1.07 M (1 M=1 mol dm^{-3})) which were adjusted using $NaClO_4$. The pH dependence of the reaction rates revealed that the singly-charged anion (RH^-) was chiefly responsible for the reaction, while undissociated reductone was inactive to peroxodisulfate ion. The rate constant (k_2) of RH^- with $S_2O_8^{2-}$ was 0.79 $M^{-1}s^{-1}$ at 25 °C and I=1.07 M (ΔH^*=37 kJ mol^{-1}, ΔS^*=−123 J deg^{-1} mol^{-1}). A relationship of $\log k_2 = -0.95 + 1.88I^{1/2}/(1+I^{1/2})$ was found at 30 °C.

The 2,3-dihydroxy-2-propenal produced from dextrose by alkaline hydrolysis is called triose reductone because of its strong reducing ability. The reductone is the simplest in structure of the compounds having an enediol group; the physiologically important L-ascorbic acid is a typical compound of this structure. Thus kinetic studies on the reaction of triose reductone would help to clarify the mechanisms of the physiological activities of enediol compounds. Previously, we studied the kinetics of the autoxidation of triose reductone in an aqueous solution and compared the rate constants with those of L-ascorbic acid.[1] The peroxodisulfate ion is known as a powerful two-electron oxidizing agent which employes an electron-transfer mechanism. The reaction with alcohol gives alcohol radicals and sulfate anion radicals.[2] In an effort to resolve whether the sulfate anion radicals work as an oxidizing species in the present experiment, we have studied the kinetics of the oxidation of triose reductone by aqueous peroxodisulfate ion in the pH range 4.1—5.9 and have compared the kinetic parameters with those for the reaction of L-ascorbic acid.[3]

Experimental

Materials. Triose reductone was prepared and purified by the method described in the literature.[4] Potassium peroxodisulfate and sodium perchlorate of analytical grade of E. Merck were used without further purification. All the other chemicals used were guaranteed reagents of the Wako Pure Chemicals Co. Ltd.

Reaction Solution. The triose reductone solution was prepared by dissolving 2 mg of the compound in 0.5 dm^3 of the aqueous solution saturated with argon (a high-purity argon gas was bubbled through the solution to remove the dissolved oxygen) and containing 50 mM of acetate buffer, 5 mM of disodium dihydrogen ethylenediaminetetraacetate (EDTA), and a given weight of sodium perchlorate; the bubbling of an argon gas was continued to avoid oxygen contamination. The potassium peroxodisulfate solution was prepared by dissolving 0.9 g of the solid in 0.25 dm^3 of water and then the dissolved oxygen was removed by the bubbling of argon through the solution.

Kinetic Method. Since the triose reductone is sensitive to oxygen, the reductone solution was transferred into a quartz cell under replacement with argon gas. The reaction was started by mixing the peroxodisulfate solution with the reductone solution. The pH value, ionic strength, and temperature of the reaction solution were kept constant during the reaction. Kinetic data were obtained spectrophotometrically by using a Hitachi 323 Recording Spectrophotometer. The temperature was controlled by circulating thermostated water around the cell housing. The reaction were followed by measuring the decreasing absorption of triose reductone at a wavelength between 268 and 293 nm. The pH values of the reaction solutions were measured with a Toa Dempa HM-20E digital pH meter immediately after the measurement of the absorption. The activity coefficients f_i for protons at varying ionic strengths (I) were obtained by using $\log f_i = -0.358 z_i^2 I^{1/2}/(1+10^8 a_i \times 0.2325 I^{1/2})$ with a_i=900 pm and z_i=1.[5] The activity coefficients used in this paper were 0.83 (0.17), 0.79 (0.57), and 0.76 (1.07): the ionic strength is given in parentheses.

Results and Discussion

Dissociation Constant of Triose Reductone. The first dissociation constants (pK_1) of triose reductone (RH_2) for the equilibrium, $RH_2 \rightleftharpoons RH^- + H^+$, were determined by the spectrophotometric method reported previously[1] at an ionic strength of 1.07 M (with the temperature (°C) in parentheses): 4.83 (10), 4.83 (15), 4.78 (20), 4.74 (25), and 4.70 (30), and at 30 °C (with the I in parentheses): 4.78 (0.57) and 4.88 (0.17).

Kinetics of the Reactions. The kinetic runs were carried out over the pH range from 4.1 to 5.9. In this pH range, the thermal decomposition of either peroxodisulfate or triose reductone was so slow under 30 °C that the decomposition could be neglected.[2] When pseudo-first-order conditions ($[TR]_0 \ll [S_2O_8^{2-}]_0$) were adopted, plots of $\ln A_t$ *vs.* t were linear for at least 60% of the whole reaction; here $[TR]_0$ indicates the initial concentrations of all the forms of triose reductone ($[TR]_0$ can be put as $[RH_2]_0 + [RH^-]_0$ in the present pH range), $[S_2O_8^{2-}]_0$ indicates the initial concentration of peroxodisulfate ion, and A_t indicates the absorbance of triose reductone at time t. The observed first-order rate constants were proportional to the concentration of peroxodisulfate ion. When second-order conditions ($[TR]_0 = [S_2O_8^{2-}]_0$) were employed, the second-order plots were also linear; *i.e.* the plots of $[TR]^{-1}$ *vs.* t were rectilinear. Thus, the empirical rate equation may be written as follows:

$$-\frac{d[TR]}{dt} = k_0[TR][S_2O_8^{2-}], \quad (1)$$

where k_0 is the observed second-order rate constant. The conventional treatment of the reaction involving the acid dissociation equilibrium gives k_0 as in Eq. 2.

$$k_0 = k_1 + (k_2 - k_1)\frac{K_1}{[H^+] + K_1}, \quad (2)$$

$$RH_2 \overset{K_1}{\rightleftharpoons} RH^- + H^+, \quad (3)$$

where K_1 is the first dissociation constant of triose reductone, and k_1 and k_2 are rate constants of the reaction of RH_2 and RH^- with $S_2O_8^{2-}$, respectively. The plots of k_0 *vs.* $K_1/(K_1+[H^+])$ showed a proportional relationship; the plots are given in Figs. 1 and 2. The k_1 values calculated from the experimental data are considered to be zero within the experimental errors. Hence, the rate equation becomes:

$$-\frac{d[TR]}{dt} = \frac{k_2K_1[TR][S_2O_8^{2-}]}{[H^+] + K_1}. \quad (4)$$

The k_2 values are listed in Table 1. The rate equation 4 can be simplified to Eq. 5:

$$-\frac{d[TR]}{dt} = k_2[RH^-][S_2O_8^{2-}]. \quad (5)$$

Equation 5 shows that the reactive species of triose reductone against peroxodisulfate is the monoanion of the reductone in the present pH range.

Mechanism of the Reaction. The presence of $RH^{\cdot}$ radical in the autoxidation of triose reductone catalyzed by peroxidase has been confirmed by ESR measurements.[6] For the purpose of examining whether the present reaction occurs *via* successive one-electron transfers involving the $RH^{\cdot}$ radical, the acrylonitrile (2×10^{-4} dm^3) was added as a radical scavenger to the reaction solution (3×10^{-3} dm^3) at the start of the reaction. The observed second-order rate constant decreased to only 90% of the value in the absence of acrylonitrile. No observable white sediment of polyacrylonitriles was found in the reaction solution in the course of reaction. Although there are some possibilities that the sulfate anion radicals produced in Eq. 6 oxidize triose reductone by chain reactions, the effect of the radical scavenger is not so strong as to indicate the importance of $RH^{\cdot}$ radical. This fact suggests that the reaction occurs *via* a two-electron oxidation instead of successive one-electron oxidations. But it is reasonable to suppose that triose reductone radical and sulfate anion radical are produced by a one-electron oxidation once in a cage, then they react rapidly to consume the radicals. The following scheme can be written to account for the experimental results:

$$RH^- + S_2O_8^{2-} \xrightarrow{k_2} (RH^{\cdot} + SO_4^{-\cdot} + SO_4^{2-}), \quad (6)$$

$$\xrightarrow[\text{very fast}]{} 2SO_4^{2-} + DR + H^+, \quad (7)$$

where DR represents dehydroreductone hydrate, 2,2-dihydroxypropane-1,3-dial. Dehydroreductone is known as an unstable product in the oxidation of triose reductone by many oxidizing agents to give formic acid,

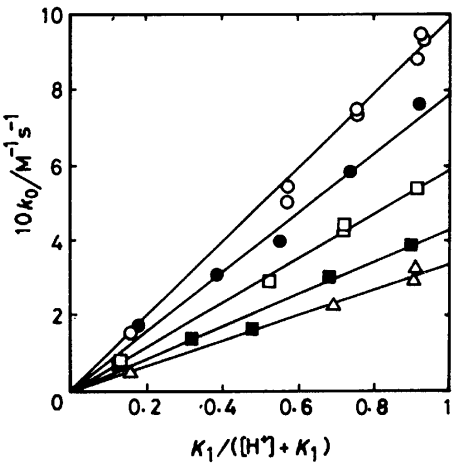

Fig. 1. Relation between k_0 and $K_1/([H^+]+K_1)$ for the oxidation of triose reductone with peroxodisulfate at ionic strength 1.07 M and various temperatures. ○: 30°C, ●: 25°C, □: 20°C, ■: 15°C, △: 10°C.

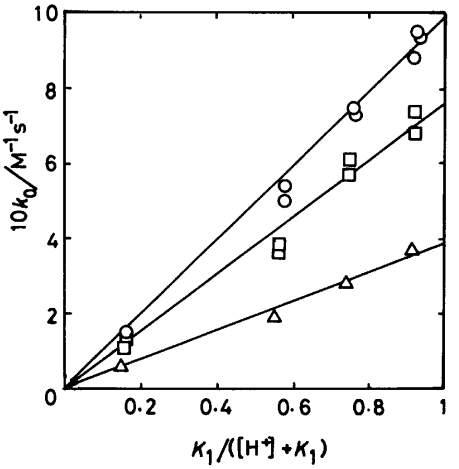

Fig. 2. Relation between k_0 and $K_1/([H^+]+K_1)$ for the oxidation of triose reductone with peroxodisulfate at 30°C and various ionic strengths. ○: 1.07 M, □: 0.57 M, △: 0.17 M.

Table 1. The second-order rate constant, k_2 in Eq. 2, and the kinetic parameters[a]

Temp	Ionic strength	$10k_2$
°C	M	$M^{-1}\,s^{-1}$
10	1.07	3.4±0.1
15	1.07	4.3±0.2
20	1.07	5.9±0.1
25	1.07	7.9±0.3
30	1.07	9.9±0.2
30	0.57	7.6±0.2
30	0.17	3.9±0.2
$\Delta H_2^{\ddagger}$	37±1 kJ mol^{-1}	
$\Delta S_2^{\ddagger}$	−123±5 J deg^{-1} mol^{-1}	

a) The initial concentrations are 6.0×10^{-5} M for triose reductone and 4.5×10^{-4} M for potassium peroxodisulfate, 5×10^{-3} M in EDTA, 0.05 M in sodium acetate, and the given concentrations of acetic acid and sodium perchlorate.

glyoxylic acid, and carbon dioxide.[7-9] Therefore, DR produced in this reaction may also be decomposed by the following equations.

$$DR + 2H_2O + S_2O_8^{2-} \xrightarrow{\text{very slow}} HCOCOOH + 2SO_4^{2-} + HCOOH + 2H^+, \quad (8)$$

$$HCOCOOH + H_2O + S_2O_8^{2-} \xrightarrow{\text{very slow}} HCOOH + 2SO_4^{2-} + CO_2 + 2H^+. \quad (9)$$

Although the reaction of triose reductone with peroxodisulfate is complicated by competitive and successive reactions with the peroxodisulfate, it is reasonably supposed that the decomposition reactions of DR, Eqs. 8 and 9, occur very slowly compared with Eq. 6, since the experimental rate law for the reaction scheme (Eqs. 6—9) is in agreement with Eq. 5.

Temperature Dependence. The activation parameters correspnding to the specific rate constants are shown in Table 1. Both ΔH_2^* and ΔS_2^* values in the reaction of triose reductone (37 ± 1 kJ mol^{-1} and -123 ± 5 J deg^{-1} mol^{-1}) are smaller than those (45 ± 1 kJ mol^{-1} and -102 ± 4 J deg^{-1} mol^{-1}, respectively) obtained in the reaction of L-ascorbic acid with peroxodisulfate ion.[3] The k_2 values in the reaction of triose reductone are larger than those obtained in the reaction of L-ascorbic acid over the temperature range of 10—30 °C. Although it has no practical significance, it is worth mentioning that the k_2 for triose reductone should become smaller than the k_2 for L-ascorbic acid at temperatures higher than 108 °C.

Ionic-strength Dependence. Although the ionic-strength values employed in this work lie outside the Debye-Hückel region, the plots of $\log k_2$ *vs.* $I^{1/2}/(1+I^{1/2})$ showed a straight line, with a relationship of $\log k_2 = -(0.95 \pm 0.07) + (1.88 \pm 0.17) I^{1/2}/(1+I^{1/2})$. This dependence is of a kind which is expected for the reaction between two ions of the same sign; the positive value of 1.88 is in good agreement with that of 2.04 which is obtained from the theoretical term of $1.02 z_a z_b \times I^{1/2}/(1+I^{1/2})$ with $z_a = -1$ for RH^- and $z_b = -2$ for $S_2O_8^{2-}$. The ionic-strength dependence suggests that the reaction between RH^- and $S_2O_8^{2-}$ (Eq. 6) is the rate-determining step.

The authors wish to express their thanks to Professor Masaru Kimura of Nara Women's University and to Dr. Takaaki Dohmaru for their helpful discussions and to Dr. Shin-ichi Fujita for kindly offering his data processing system.

References

1) Y. Abe, H. Horii, S. Taniguchi, K. Kamai, and M. Takagi, *Bull. Chem. Soc. Jpn.*, **56**, 467 (1983).
2) D. A. House, *Chem. Rev.*, **62**, 185 (1962).
3) M. Kimura, A. Kobayashi, and K. Boku, *Bull. Chem. Soc. Jpn.*, **55**, 2068 (1982).
4) H. v. Euler and C. Martius, *Justus Liebigs Ann. Chem.*, **505**, 73 (1933).
5) J. Kielland, *J. Am. Chem. Soc.*, **59**, 1675 (1937).
6) I. Yamazaki and L. H. Piette, *Biochim. Biophys. Acta*, **77**, 47 (1963).
7) J. R. Holker, *J. Chem. Soc.*, **1955**, 579.
8) P. Szabo and L. Szabo, *C. R. Acad. Sci., Ser. C*, **262**, 513 (1966).
9) K. Kretzscmar and W. Jaenicke, *Tetrahedron Lett.*, **1969**, 3811.

 © 1984 The Chemical Society of Japan Bull. Chem. Soc. Jpn., 57, 225—231 (1984)

ortho-Disubstituted *F*-Benzenes. V. Intramolecular Heteroatom-facilitated ortho-Substitution of *F*-Benzene Derivatives with Oxazolinyl and Oxazinyl Groups

Yoshinari INUKAI,† Keisuke TAKUMA, Koji TORITANI,††
Takaaki SONODA, and Hiroshi KOBAYASHI*
Research Institute of Industrial Science, Kyushu University 86, Kasuga, Fukuoka 816
††*Department of Molecular Science and Technology, Interdisciplinary Graduate School of Engineering Sciences, Kyushu University 39, Kasuga, Fukuoka 816*
(Received June 6, 1983)

The oxazinyl and oxazolinyl substituents on an *F*-benzene ring facilitated the substitution of fluorine ortho to the heterocyclic functional groups by carbon and nitrogen nucleophiles. Alkylmagnesium halides and alkyllithium compounds were employed as the carbon nucleophile, and lithium *N*-methylanilide and *N*-methylanilinomagnesium halide as the nitrogen nucleophile. The selective ortho-substitution was accomplished by the complexing interaction between the ring-membered nitrogen on the functional substituents and the anionic nucleophile through the interposing metal cation. Effects of the substituents in the orientations and rates of the reactions depended upon the polarity of the reaction solvent and the kinds of anionic nucleophile and counter metal cation.

The reaction of monosubstituted *F*-benzene[1] with nucleophiles affords predominantly para-disubstituted derivatives, except for a few cases of the formation of meta-disubstituted products.[2] Some attempts at the specific formation of ortho-disubstituted *F*-benzenes are available in the literature. Most of them can be classified as intramolecular cyclization followed by cleavage of the resulting (*F*-benzo)-heterocyclic ring, as shown in Scheme 1.[3-16] Such heterocyclic rings, however, sometimes have been difficult to cleave.

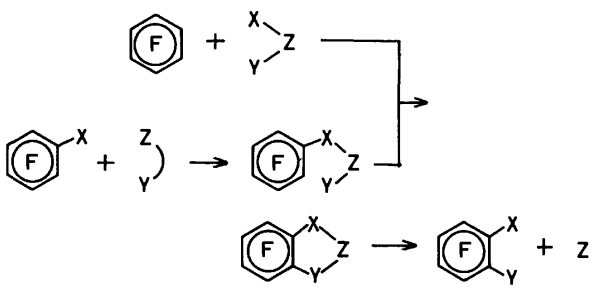

Scheme 1.

There are also some exceptional cases where the ortho-substitution dominates. Actually nitro, carbonyl, sulfone, and amine oxide substituents direct the ortho-substitution in nonpolar solvents.[2c,17] This anomalous behavior was interpreted in terms of a particular affinity of such substituents for the counter cation paired with an anionic nucleophile at the transition stage; namely, the cation is pulled towards the close neighborhood of such a substituent, so that the anionic nucleophile is oriented to attack preferentially the sterically favorable ortho-position.

Meyers and Gschwend showed that an oxazolinyl substituent on an aromatic ring was highly efficient in directing the lithiodeprotonation at the ortho-position,[18,19] and accelerated the nucleopuhilic displacement of a methoxyl group or fluorine ortho to the oxazolinyl substituent.[18,20] The ortho-activation by the oxazolinyl group in deprotonation and nucleophilic displacement was attributable to the strong ion-dipole interaction between the oxazolinyl group and lithium cation.

In the present study, 2-oxazolin-2-yl (OX5) and 1,3-oxazin-2-yl (OX6) groups on an *F*-benzene ring were examined as to how well they promoted nucleophilic attack of carbon and nitrogen nucleophiles on the ortho-position prior to the para-one (Scheme 2).

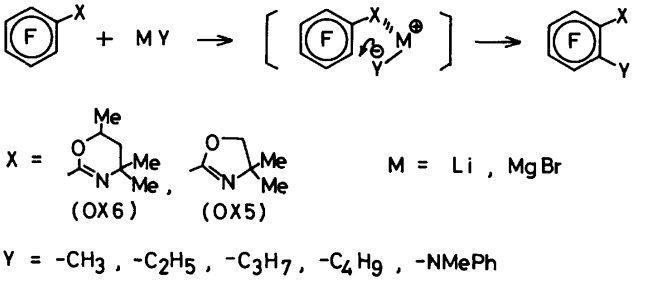

Scheme 2.

Results

The starting 2-(*F*-phenyl)-4,4,6-trimethyl-5,6-dihydro-4*H*-oxazine (**1**) and 2-(*F*-phenyl)-4,4-dimethyl-2-oxazoline (**2**) were obtained according to the methods for the preparation of the corresponding hydrocarbon analogues.[21]

Reaction with C-Nucleophile. Lithium and magnesium ions were favorable for the complex formation with the oxazoline and oxazine groups.[18] Organolithium and Grignard reagents were therefore employed as carbon nucleophiles.

Both Grignard and lithio reagents attacked exclusively the aromatic carbon ortho to the oxazolinyl and oxazinyl groups. The efficacies in the ortho-orientation caused by these functional substituents are evident in the formation of 2′-alkyl-*F*-phenyl derivatives (locations on the *F*-phenyl ring are primed) and 2′,6′-dialkyl-*F*-phenyl ones, while no 4′-monoalkylated products nor 2′,4′-dialkylated ones form at all.

† Present address: Government Industrial Research Institute in Kyushu, Shukumachi, Tosu, Saga 841.

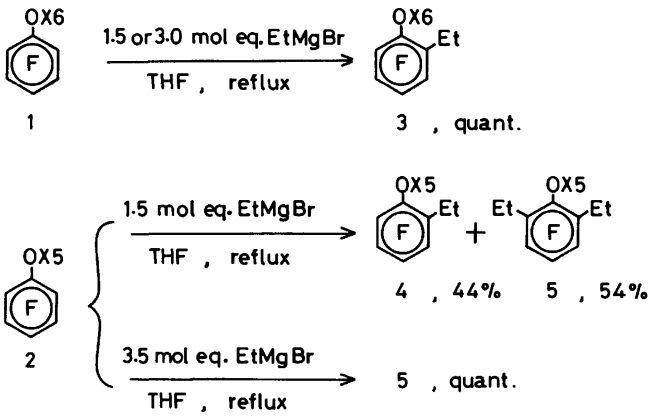

Scheme 3.

In the reaction of the oxazine **1** and the oxazoline **2** with 1.5 times molar amounts of ethylmagnesium bromide in THF, the corresponding ortho-substituted *F*-phenyl derivatives, **3**, **4**, and **5**, were exclusively afforded, as shown in Scheme 3. The ethyl derivatives **3** and **4** each show four ^{19}F-NMR signals of equal intensity. Even if an excess of ethylmagnesium bromide was added, the oxazine **1** in THF gave only the 2′-monoalkylated product **3** quantitatively, while the oxazoline **2** gave the 2′,6′-dialkylated product **5** also in quantitative yield by use of an excess of ethylmagnesium bromide. The latter product exhibits two ^{19}F-NMR signals with relative intensities of one to two. These results indicate that the oxazine **1** and the oxazoline **2** are both highly ortho-directing, no para-substituted products being formed at all.

When an excess amount of ethylmagnesium bromide was used in benzene, which is less polar and has a higher boiling point than THF, the oxazine **1** and oxazoline **2** both afforded only the 2′,6′-disubstituted products, **5** and **6**, quantitatively (Scheme 4).

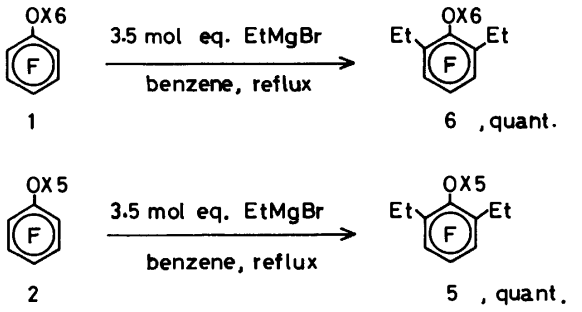

Scheme 4.

These substrates **1** and **2** reacted with butyllithium to give the corresponding ortho-substituted products, as shown in Scheme 5. The reactions with butyllithium, however, could be controlled only with some difficulty, so that the selectivity and yield of the products were less reproducible than those with the Grignard reagent.

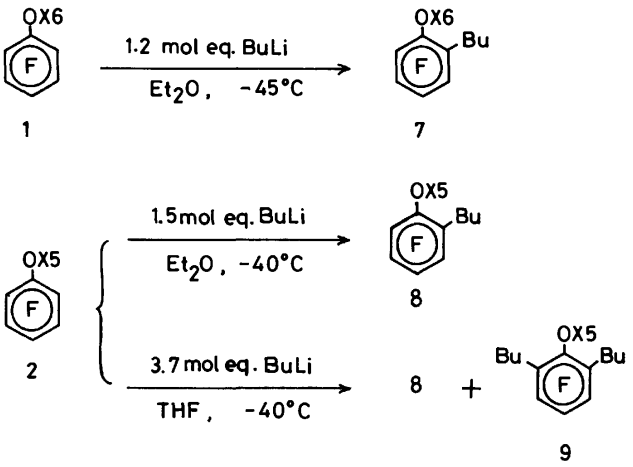

Scheme 5.

TABLE 1. ^{19}F-NMR SPECTRAL DATA OF THE (ortho-ALKYL-*F*-PHENYL) OXAZINES AND OXAZOLINES IN CCl_4 SOLUTIONS

	Compound	Chemical shifts/ppm against an internal C_6F_6			
		$F^{3'}$	$F^{4'}$	$F^{5'}$	$F^{6'}$
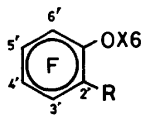	**10**; R=Me	19.6 (m)	5.4 (ddd)	2.0 (ddd)	19.8 (m)
	3; Et	17.0 (ddd)	5.5 (ddd)	2.1 (ddd)	19.6 (ddd)
	7; *n*-Bu	17.7 (ddd)	5.3 (ddd)	2.1 (ddd)	19.5 (ddd)
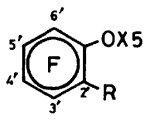	**11**; R=Me	20.4 (dddq)	8.1 (ddd)	2.9 (ddd)	23.1 (ddd)
	4; Et	17.9 (ddd)	8.3 (ddd)	3.0 (ddd)	23.2 (ddd)
	12; *n*-Pr	19.0 (ddd)	8.2 (ddd)	3.1 (ddd)	23.0 (ddd)
	8; *n*-Bu	18.8 (ddd)	8.2 (ddd)	2.9 (ddd)	23.2 (ddd)

	F-F Coupling constants/ Hz				
3′-4′	3′-5′	3′-6′	4′-5′	4′-6′	5′-6′
17.9	0.9	12.0	21.3	2.3	21.3
20.7	1.9	12.5	20.7	2.9	21.6
21.1	1.9	12.5	21.6	3.4	22.1
20.9	2.4	7.3	20.9	4.4	20.9
21.0	2.9	12.2	21.0	4.4	21.0
21.5	2.0	12.2	21.5	4.4	21.5
20.7	2.2	11.9	21.2	4.4	21.2

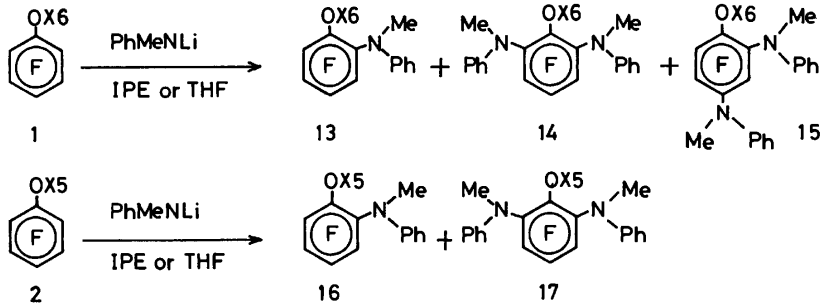

Scheme 6.

Table 2. Reactions of the oxazine (**1**) and the oxazoline (**2**) with lithium *N*-methylanilide

Run No.	Substrate	Molar ratio[a)]	Solvent	Temp °C	Reaction time/h	Products (Yield/%)		
						o-mono-	*o,o'*-di-	*o,p*-di-
1	**1**	2.0	IPE[b)]	50	19.5	**13** (73)	—	—
2	**1**	3.0	IPE[b)]	50	68	**13** (3)	**14** (86)	—
3	**1**	1.6	THF	Reflux	2	**13** (12)	—	**15** (36)
4	**2**	2.0	IPE[b)]	Reflux	13.3	**16** (87)	**17** (10)	—
5	**2**	3.0	IPE[b)]	Reflux	19.5	**16** (49)	**17** (46)	—
6	**2**	1.5	THF	Reflux	4.5	**16** (17)	**17** (40)	—

a) Molar ratio of lithium *N*-methylanilide to the subtrate. b) IPE, for diisoproryl ether.

These difficulties would be due to the reactivity of alkyllithium being higher than that of the alkylmagnesium halide.

Methyl and propyl groups could be also introduced to the ortho-position on the *F*-phenyl group of the oxazine **1** and the oxazoline **2** by use of their lithio and Grignard reagent to give 2'-alkyl derivatives **10**, **11**, and **12**.[22)]

Comparisons of ^{19}F-NMR spectra of the present (2'-alkyl-*F*-phenyl)oxazines, **3**, **7**, and **10**, and -oxazolines **4**, **8**, **11**, and **12**, indicated that the chemical shifts of one fluorine varied with the alteration of the alkyl substituents, while those of the other fluorines remained within a range of 0.2 ppm, as shown in Table 1. Thus, the former signals could be assigned tentatively to the 3'-fluorine adjacent to such alkyl substituents. The assignment of fluorine chemical shifts was compatible with the relatively large downfield shifts at the adjacent 3'-fluorine caused by the monoalkylation and at the 3'- and 5'-fluorines by the dialkylation, and also the presence of the long-range coupling between 3'-fluorine and 2'-methyl hydrogens of **11** in its ^{19}F-NMR spectrum.

Reaction with N-*Nucleophile.* In the reactions with lithium *N*-methylanilide as a nitrogen nucleophile, the oxazine **1** and the oxazoline **2** gave the corresponding ortho-substituted *F*-phenyl derivatives in diisopropyl ether and THF solutions, as shown in Scheme 6.

The monoanilino derivatives, **13** and **16**, each show four ^{19}F-NMR signals of equal intensity. Their structures were interpreted on the basis of the ^{19}F-NMR chemical shifts which were assigned in an analogous manner with those of the ortho-alkylated *F*-phenyloxazines and -oxazolines. The mass spectra of **14**, **15**, and **17** indicate that the dianilino substitutions also occurred in the above reactions. ^{19}F-NMR spectra of **14** and **17**, which showed two signals of one to two in intensity ratio indicated that the disubstituted *F*-phenyloxazine and -oxazoline were of the vicinal 1',2',6'-trisubstituted *F*-benzene structure. On the other hand, three ^{19}F-signals of equal intensity of **15** indicated

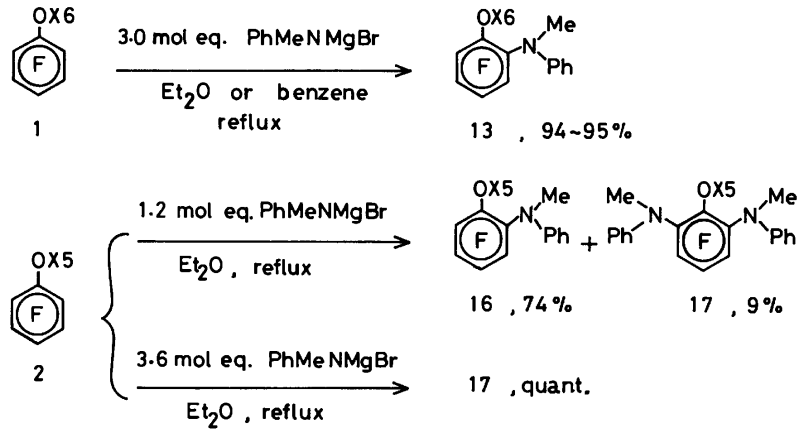

Scheme 7.

that the disubstituted *F*-phenyloxazine structure was the unsymmetrical 1′,2′,4′-trisubstituted *F*-benzene structure. Lithium *N*-methylanilide in a THF solution attacked the oxazine **1** on the 2′- and 4′-positions (Run 3 in Table 2), while in diisopropyl ether, which is less polar than THF, it attacked the 2′- and 6′-positions (Run 2 in Table 2). The oxazoline **2** did not afford any 4′-substituted product, even in a THF solution (Compare Run 6 with Run 3 in Table 2), and was superior in the regioselectivity than was the oxazine **1**.

With *N*-methylanilinomagnesium bromide, on the other hand, both the reaction of the oxazine **1** and that of the oxazoline **2** proceeded, in analogy with those with alkylmagnesium bromide, to give 2′-mono- and 2′,6′-disubstituted products, **13**, **16**, and **17**, predominantly, in both diethyl ether and benzene solutions (Scheme 7).

Discussion

The oxazinyl and oxazolinyl groups on an *F*-benzene ring are effective to facilitate the carbon-carbon and carbon-nitrogen bond formation exclusively at the ortho-position on the *F*-benzene ring relative to those heterocyclic functional groups. Such ortho-directing effects, however, seemed to be remarkable among the carbon and nitrogen nucleophiles studied so far, since the reaction with other nucleophilic reagents such as lithium aluminum hydride and lithium phenoxide took a longer reaction period and afforded an appreciable yield of the para-substituted product, though the ortho-substituted one was major.[23]

The ring-membered nitrogens of the oxazinyl and the oxazolinyl groups seem to play the indispensable role in the interacion with the metal cation, since the oxolanyl group in 2-methyl-2-(*F*-phenyl)-1,3-dioxolane (**18**) is less effective not only in the regioselectivity but also in the acceleration of reactions, as shown in Scheme 8, where the dioxolane **18** were not alkylated with ethylmagnesium bromide under reflux in benzene.

Complexation of the metal cation at the ring-membered nitrogen would lead the nucleophilic agent, which was tightly paired with the metal cation, to attack the ortho-position nearest to the heterocyclic substituent. The coordination of the nitrogen to metal cation would also induce the mesomeric polarization of the C–N double bond of the heterocyclic substituents. The effect would promote not only the nucleophilicity of the anionic agent at the beginning stage of the attack, but also the mesomeric stabilization of an intermediary anionic σ-complex at the subsequent stage, and facilitate the bond formation between the ortho-carbon and nucleophiles as illustrated in Scheme 9.

The oxazolinyl group of a smaller ring size seemed more effective in promoting the reaction than the larger oxazinyl group; once the substitution occurred on an ortho-position, the former allowed the successive substitution on the opposite ortho-position even under milder conditions, in contrast to the latter in which no additional ortho-substitution occurred.

Such differences in the reactivity and selectivity might be due to the restricted rotation about the bond between the heterocyclic ring and the ortho-monosubstituted *F*-phenyl ring; *i.e.*, a coplanar conformation which would be required for mesomeric stabilization upon the subsequent substitution might be hindered by the ortho-substituent on the *F*-phenyl ring, and such a steric hindrance would be more pronounced with a larger ring size than a smaller one.

Polarity of the reaction solvent also affected the reaction path. In a less polar solvent such as benzene, the substitution proceeded to a higher extent. Such increased reactivity was understandable as follows: The less polar was the reaction solvent, the more tightly the metal cation would be coordinated with the substrate molecule at the donating nitrogen atom, so that the anionic nucleophile attacked preferably the nearest ortho-position.

The participation of the oxazinyl and oxazolinyl substituents depended also upon the kind of anionic nucleophiles; lithium amide, hydroxide, and bromide in benzene solutions caused no reactions; the starting compounds remaining intact, presumably due to very low solubility of these lithium salts in the reaction solvent.

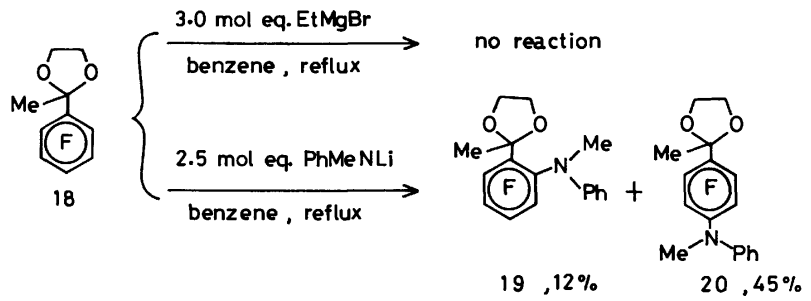

Scheme 8.

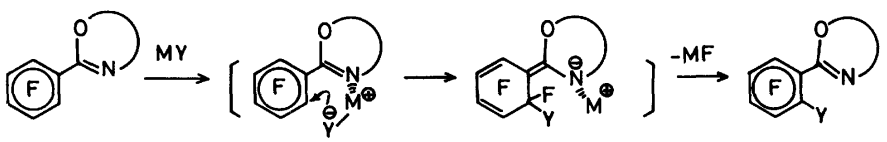

Scheme 9.

Experimental

Melting points were uncorrected. IR spectra were measured with a JASCO DS-403G spectrometer. ^{1}H- and ^{19}F-NMR chemical shifts were recorded on a HITACHI 24-B against the internal TMS reference, and on JEOL FX-100 and HITACHI 24-F as the positive values downfield from the internal *F*-benzene reference, respectively. Mass spectra were obtained with JEOL JMS-07 and 01SG spectrometers. Electronic spectra were measured with a HITACHI 200-20 instrument. *F*-Benzonitrile[24] and *F*-benzoyl chloride[25] were prepared according to the literature methods.

2-(F-Phenyl)-4,4,6-trimethyl-5,6-dihydro-4H-oxazine (1). *F*-Benzonitrile (5.79 g, 30 mmol) was added dropwise to concentrated sulfuric acid (15 g, 220 mmol) over a 5-min period at 0 °C. To the mixture was added 2-methyl-2,4-pentanediol (3.54 g, 30 mmol) over a 15-min period at 0 °C. The resulting mixture was stirred at 0 °C for an additional 30 min, then at room temperature for another additional 30 min, and poured into ice-water. The aqueous mixture was basified by sodium hydroxide and extracted with diethyl ether. The ethereal extract was washed with water and dried over sodium sulfate. The dried extract was distilled, and the fraction boiling at 113 °C/1200 Pa gave 2-(*F*-phenyl)-4,4,6-trimethyl-5,6-dihydro-4*H*-oxazine (**1**) (4.48 g, 51%) in colorless oil. ^{1}H-NMR (neat): δ=1.05—2.10 (m, 11H, CH_3, CH_2) and 4.00—4.60 (m, 1H, CH)). ^{19}F-NMR (CCl_4): —0.7 (m, 2F, F$^{3'}$ and F$^{5'}$), 7.6 (tt, 1F, F$^{4'}$), and 20.4 ppm (m, 2F, F$^{2'}$, and F$^{6'}$), ($J_{2'4'}$=3.4 and $J_{3'4'}$=21.2 Hz). UV (EtOH): λ_{max} (log ε); 207 (2.94) and 263 nm (2.16). Found: C, 53.12; H, 4.20; N, 4.50%; M$^+$, 293. Calcd for $C_{13}H_{12}NF_5O$: C, 53.25; H, 4.13; N, 4.78%; M, 293.

2-(F-Benzoylamino)-2-methyl-1-propanol (21). A solution of *F*-benzoyl chloride (1.74 g, 7.6 mmol) in anhydrous dichloromethane (5 cm^3) was added dropwise to a stirred solution of 2-amino-2-methyl-1-propanol (1.35 g, 15 mmol) in anhydrous dichloromethane (10 cm^3) over a 30-min period at 0 °C. The mixture was kept stirred at room temperature for an additional 12 h, and then evaporated to dryness *in vacuo*. The residue was washed with water, and recrystallization from benzene gave 2-(*F*-benzoylamino)-2-methyl-1-propanol (**21**) (1.86 g, 87%) in colorless plates, mp 126 °C. IR (KBr): 3350 and 3200 (OH, NH), and 1660 cm^{-1} (C=O). ^{1}H-NMR ($CDCl_3$–DMSO-d_6): δ=1.34 (s, 6H, CH_3), 3.54 (d, J=5.3 Hz, 2H, CH_2), 4.28 (br. t, J=5.3 Hz, 1H, OH), and 7.25 (br. s, 1H, NH). Found: M$^+$, 283. Cacld for $C_{11}H_{10}NF_5O_2$: M, 283.

2-(F-Phenyl)-4,4-dimethyl-2-oxazoline Hydrochloride (22). A mixture of the propanol **21** (9.52 g, 33.7 mmol) and thionyl chloride (7.1 cm^3, 100 mmol) was stirred at room temperature for 1 d. The mixture was poured into diethyl ether, and evaporated to dryness *in vacuo*. The residue was 2-(*F*-phenyl)-4,4-dimethyl-2-oxazoline hydrochloride (**22**) (7.47 g, 72%) in a colorless solid, mp 119—120 °C. ^{1}H-NMR ($CDCl_3$): δ=1.45 (s, 6H, CH_3), 3.85 (s, 2H, CH_2), and 6.15 (br. s, 1H, HCl). Found: M$^+$, 303 and 301. Calcd for $C_{11}H_9NClF_5O$: M, 303 and 301.

2-(F-Phenyl)-4,4-dimethyl-2-oxazoline (2). A solution of the hydrochloride **22** (3.35 g, 11.1 mmol) in anhydrous THF (10 cm^3) was added dropwise to a stirred mixture of sodium hydride (17.7 mmol) and anhydrous THF (10 cm^3) over a 5-min period at room temperature under a dry nitrogen atmosphere. The mixture was stirred at room temperature for an additional 10 min and poured into diethyl ether. The ethereal solution was washed with water, dried over sodium sulfate, and evaporated *in vacuo*. The residue was distilled, and the fraction boiling at 96—97 °C/1600 Pa gave 2-(*F*-phenyl)-4,4-dimethyl-2-oxazoline (**2**) (2.68 g, 91%) in colorless oil. ^{1}H-NMR (CCl_4): δ=1.32 (s, 6H, CH_3), and 4.03 (s, 2H, CH_2). ^{19}F-NMR (CCl_4): 0.3 (m, 2F, F$^{3'}$ and F$^{5'}$), 10.5 (tt, 1F, F$^{4'}$), and 24.6 ppm (m, 2F, F$^{2'}$ and F$^{6'}$), ($J_{2'4'}$=2.1 and $J_{3'4'}$=21.1 Hz). UV (EtOH): λ_{max} (log ε); 211 nm (2.92). Found: C, 49.66; H, 3.06; N, 5.26%; M$^+$, 265. Calcd for $C_{11}H_8NF_5O$: C, 49.82; H, 3.04; N, 5.28%; M, 265. Isolation of the free oxazoline **2** from the hydrochloride **22** failed with aqueous and methanolic alkalis.

Reaction of the Oxazine 1 with Ethylmagnesium Bromide. The Reaction in THF: A solution of the oxazine **1** (1.17 g, 4.0 mmol) in anhydrous THF (10 cm^3) was added dropwise to a stirred mixture of ethylmagnesium bromide (6.0 mmol) and anhydrous THF (20 cm^3) over a 5-min period at room temperature under a dry nitrogen atomosphere. The mixture was refluxed for 10 h with stirring, poured into water after being cooled, and extracted with dichloromethane. The extract was washed with water, dried over sodium sulfate, and evaporated *in vacuo*. The residue was developed on a silica-gel TLC plate with dichloromethane. The fraction of R_f=0.15—0.20 afforded 2-(2-ethyl-*F*-phenyl)-4,4,6-trimethyl-5,6-dihydro-4*H*-oxazine (**3**) (1.16 g, 93%) in colorless oil. Found: M$^+$, 303. Calcd for $C_{15}H_{17}NF_4O$: M, 303. Elemental analysis was carried out in the form of its hydrochloride monohydrate. Found: C, 50.34; H, 5.63; N, 3.91%. Calcd for $C_{15}H_{18}NClF_4O \cdot H_2O$: C, 50.36; H, 5.63; N, 3.92%.

The Reaction in Benzene: A solution of the oxazine **1** (1.17 g, 4.0 mmol) in dry benzene (20 cm^3) was added dropwise to a stirred mixture of ethylmagnesium bromide (14 mmol) and anhydrous diethyl ether (30 cm^3) over a 10-min period at room temperature under a dry nitrogen atmosphere. Diethyl ether was distilled out of the mixture by adding portions of dry benzene. The resulting benzene solution was refluxed for an additional 10 h and worked up in a similar manner. 2-(2,6-Diethyl-*F*-phenyl)-4,4,6-trimethyl-5,6-dihydro-4*H*-oxazine (**6**) was obtained quantitatively, in colorless oil. ^{19}F-NMR (CCl_4): 1.1 (t, 1F, F$^{4'}$) and 18.9 ppm (d, 2F, F$^{3'}$ and F$^{5'}$), ($J_{3'4'}$=21.2 Hz). Found: M$^+$, 313. Calcd for $C_{17}H_{22}NF_3O$: M, 313. Found: (Hydrochloride monohydrate): C, 55.41; H, 6.83; N, 3.77%. Calcd for $C_{17}H_{23}NClF_3O \cdot H_2O$: C, 55.51; H, 6.85; N, 3.81%.

Reaction of the Oxazoline 2 with Ethylmagnesium Bromide. The Reaction in THF: The oxazoline **2** (1.06 g, 4 mmol) reacted with ethylmagnesium bromide (6 mmol) in anhydrous THF (30 cm^3) like the oxazine **1** did. The reaction mixture was distilled, and the fraction boiling at 95—96 °C/1200 Pa gave colorless oily 2-(2-ethyl-*F*-phenyl)-4,4-dimethyl-2-oxazoline (**4**) in 44% yield. Found: C, 56.85; H, 4.91; N, 4.94%; M$^+$, 275. Calcd for $C_{13}H_{13}NF_4O$: C, 56.73; H, 4.76; N, 5.09%; M, 275. The residue was developed on a silica-gel TLC plate with dichloromethane. The fraction of R_f=0.2—0.3 afforded 2-(2,6-diethyl-*F*-phenyl)-4,4-dimethyl-2-oxazoline (**5**) in 54% yield, colorless oil. ^{19}F-NMR (CCl_4): 3.5 (t, 1F, F$^{4'}$) and 19.7 ppm (d, 2F, F$^{3'}$ and F$^{5'}$), ($J_{3'4'}$=21.6 Hz). Found: M$^+$, 285. Calcd for $C_{15}H_{18}NF_3O$: M, 285. Found (Hydrochloride): C, 56.06; H, 6.02; N, 4.26%. Calcd for $C_{15}H_{19}NClF_3O$: C, 55.99; H, 5.95; N, 4.35%.

The Reaction in Benzene: The reaction in dry benzene was carried out in a similar manner to that in diethyl ether. The residue was purified by TLC on a silica-gel plate. The fraction of R_f=0.2—0.3 gave the diethyl derivative **5** quantitatively.

Reaction of the Oxazine 1 with Butyllithium. A mixture of butyllithium (1.17 mmol, *ca.* 15% hexane solution) and anhydrous diethyl ether (3 cm^3) was added dropwise to a stirred solution of the oxazine **1** (298 mg, 1 mmol) in anhydrous diethyl ether (5 cm^3) over a 5-min period at —45 °C under a dry nitrogen atmosphere. The mixture was kept stirred at —45 °C for 21 h and at room temperature for an additional 3 h, and poured into diethyl ether. The ethereal solution was washed with water, dried over sodium sulfate, and evaporated *in vacuo*. The residue was purified by TLC to give 2-(2-butyl-*F*-phenyl)-4,4,6-trimethyl-5,6-dihydro-4*H*-oxazine (**7**) in 65%

yield, a colorless oil. Found: M+ 331. Calcd for $C_{17}H_{21}NF_4O$: M, 331. Found (Hydrochloride): C, 55.41; H, 6.05; N, 3.76%. Calcd for $C_{17}H_{22}NClF_4O$: C, 55.51; H, 6.03; N, 3.81%.

Reaction of the Oxazoline **2** *with Butyllithium.* A mixture of butyllithium (2.3 mmol, *ca.* 15% hexane solution) and anhydrous diethyl ether (5 cm³) was added dropwise to a stirred mixture of the oxazoline **2** (396 mg, 1.5 mmol) and anhydrous diethyl ether (5 cm³) over a 25-min period at −40 °C under a dry nitrogen atmosphere. The mixture was stirred at −40 °C for 6.5 h and then at room temperature for an additional 3 h, and then was worked up as above. The residue was chromatographed on a silica-gel column. The earlier fraction eluted with dichloromethane gave 2-(2-butyl-*F*-phenyl)-4,4-dimethyl-2-oxazoline (**8**) (49 mg, 11%) in colorless oil. Found: C, 59.33; H, 5.69; N, 4.50%; M+, 303. Calcd for $C_{15}H_{17}NF_4O$: C, 59.40; H, 5.65; N, 4.62%; M, 303. The later fraction eluted with dichloromethane was the starting compound **2** (266 mg, 67%).

When treated with 3.7 times molar amounts of butyllithium, the compound **8** (40%) and 2-(2,6-dibutyl-*F*-phenyl)-4,4-dimethyl-2-oxazoline (**9**) (15%) was obtained. ^{19}F-NMR (CCl_4): 3.1 (t, 1F, F$^{4'}$) and 19.4 ppm (d, 2F, F$^{3'}$ and F$^{5'}$), ($J_{3'4'}$ = 21.5 Hz). Found: C, 66.86; H, 7.63; N, 4.11%; M+, 341. Calcd for $C_{19}H_{26}NF_3O$: C, 66.84; H, 7.68; N, 4.10 %; M, 341.

Reaction of the Oxazine **1** *with Lithium* N-*Methylanilide.* A solution of the oxazine **1** (0.1 g, 0.36 mmol) in anhydrous diisopropyl ether (6 cm³) was added dropwise over a 10-min period at room temperature under a dry nitrogen atmosphre to a stirred mixture of lithium *N*-methylanilide (0.72 mmol), which was prepared from *N*-methylaniline and lithium amide in anhydrous diisopropyl ether (7 cm³). The mixture was stirred at 50 °C for an additional 19.5 h, and poured into diethyl ether after being cooled. The ethereal solution was washed with water. The aqueous washings were acidified and again extracted with diethyl ether. The ethereal extract and the original ethereal solution were combined, washed with water, dried over sodium sulfate, and evaporated *in vacuo*. The residue was chromatographed on a silica-gel column. The fraction eluted with dichloromethane gave 2-[2-(*N*-methylanlino)-*F*-phenyl]-4,4,6-trimethyl-5,6-dihydro-4*H*-oxazine (**13**) (73%) in pale yellow oil. ^{19}F-NMR ($CDCl_3$): 3.89 (ddd, 1F, F$^{5'}$), 7.59 (ddd, 1F, F$^{4'}$), 15.79 (ddd, 1F, F$^{3'}$), and 20.44 ppm (ddd, 1F, F$^{6'}$) ($J_{3'4'} = J_{4'5'} =$ 22.59, $J_{3'6'} = 10.99$, and $J_{4'6'} = J_{3'5'} = 2.44$ Hz). Found: C, 63.30; H, 5.45; N, 7.29%; M+, 380. Calcd for $C_{20}H_{20}N_2F_4O$: C, 63.14; H, 5.31; N, 7.37%; M, 380.

When 3.0 times molar amounts of the reagent were used in the same solvent, a mixture of the monoanilino derivative **13** and 2-[2,6-bis(*N*-methylanilino)-*F*-phenyl]-4,4,6-trimethyl-5,6-dihydro-4*H*-oxazine (**14**) was obtained in the yields of 13 and 86%, respectively. The latter was a yellow oil. ^{19}F-NMR ($CDCl_3$): 6.79 (t, 1F, F$^{4'}$) and 20.28 ppm (d, 2F, F$^{3'}$ and F$^{5'}$), ($J_{3'4'}$=21.97 Hz). Found M+, 467. Calcd for $C_{27}H_{28}N_3F_3O$; M, 467. Found (Hydrochloride): C, 64.41; H, 5.84; N, 8.42%. Calcd for $C_{27}H_{29}N_3ClF_3O$: C, 64.35; H, 5.80; N, 8,34%.

When the reaction was carried out in anhydrous THF with 1.5 times molar amounts of the reagent, the mixture of the monoanilino derivative **13** and 2-[2,4-bis(*N*-methylanilino)-*F*-phenyl]-4,4,6-trimethyl-5,6-dihydro-4*H*-oxazine (**15**) was afforded in the yields of 12 and 36%, respectively. ^{19}F-NMR (CCl_4) of the latter **15**: 20.6 (dd, 1F, F$^{6'}$), 21.0 (d, 1F, F$^{5'}$), and 33.9 ppm (d, 1F, F$^{3'}$), ($J_{3'6'} = 13.0$, $J_{5'6'} = 24.0$ Hz). Found: M+ 467. Calcd for $C_{27}H_{28}N_3F_3O$: M, 467.

Reaction of the Oxazoline **2** *with Lithium* N-*Methylanilide.* The reaction was carried out in anhydrous diisopropyl ether with 2.0 times molar amounts of the reagent as described above. The reaction mixture was chromatographed on a silica-gel column, then eluted with dichloromethane. The earlier fraction gave 2-(2-*N*-methylanilino-*F*-phenyl)-4,4-dimethyl-2-oxazoline (**16**) (87%), which was isolated in the form of the yellow picrate, mp 149—150 °C (decomp). ^{19}F-NMR ($CDCl_3$): 4.17 (ddd, 1F, F$^{5'}$), 12.15 (ddd, 1F, F$^{4'}$), 17.27 (ddd, 1F, F$^{3'}$) and 24.43 ppm (ddd, 1F, F$^{6'}$), ($J_{3'4'} = J_{4'5'} = J_{5'6'} = 21.97$, $J_{3'6'} = 10.98$, $J_{3'5'} = 4.88$, and $J_{4'6'} = 2.44$ Hz). Found (Picrate): C, 49.71; H, 3.31; N, 12.02%. Calcd for $C_{24}H_{19}N_5F_4O_8$: C, 49.58; H, 3.29; N, 12.05%. The later fraction afforded 2-[2,6-bis(*N*-methylanilino)-*F*-phenyl]-4,4-dimethyl-2-oxazoline (**17**) (10%) in pale yellow powder, mp 102—103.5 °C. ^{19}F-NMR ($CDCl_3$): 9.41 (t, 1F, F$^{4'}$) and 21.16 ppm (d, 2F, F$^{3'}$ and F$^{5'}$, ($J_{3'4'}$ = 21.97 Hz). Found: C, 68.26; H, 5.66; N, 9.32%; M+, 439. Calcd for $C_{25}H_{24}N_3F_3O$: C, 68.31; H, 5.52; N, 9.56%; M, 439.

When 3.0 times molar amounts of the reagent were used in the same reaction solvent, a mixture of the same products, **16** and **17**, was obtained, while the yields varied to 49 and 46%, respectively; these values were determined by GLC peak areas and ^{19}F-NMR signal intensities. The reaction which was carried out in anhydrous THF with 1.5 times molar amounts of the reagent, also afforded the same products, **16** and **17**, in the yields of 17 and 40%, respectively.

Reaction of the Oxazine **1** *with* N-*Methylanilinomagnesium Bromide.* A solution of the oxazine **1** (0.3 g, 1.19 mmol) in anhydrous diethyl ether (8 cm³) was added dropwise to the solution of *N*-methylanilinomagnesium bromide (3.57 mmol), which was prepared by adding ethereal *N*-methylaniline into ethylmagnesium bromide in diethyl ether over a 10-min period under a dry nitrogen atmosphere. The mixture was refluxed for 14.5 h, and the formation of the product **13** was determined by GLC to be in 96% yield. When the reaction solvent was altered into dry benzene, the same product **13** was formed in 95% yield.

Reaction of the Oxazoline **2** *with* N-*Methylanilinomagnesium Bromide.* The reaction was carried out in anhydrous diethyl ether with 1.2 times molar amounts of the reagent, and the resulting mixture was worked up as above. The yields of ortho-substituted products, **16** and **17**, were 74 and 9%, respectively, and the starting oxazoline **2** was recovered in 17% yield; the yields were determined by the ^{19}F-NMR signal ratio of the reaction mixture.

When 3.0 times molar amounts of the reagent was used, 2′,6′-disubstituted product **17** was obtained quantitatively.

2-Methyl-2-(F-phenyl)-1,3-dioxolane (18). A solution of 2,3,4,5,6-pentafluoroacetophenone (4.62 g, 22 mmol), ethylene glycol (1.24 g, 20 mmol), and *p*-toluenesulfonic acid (0.1 g, 1 mmol) in anhydrous methanol (50 cm³) was refluxed for 22 h under a nitrogen atmosphere. Cyclohexane (230 cm³) was added to the resulting mixture, which was distilled to remove water as an azeotropic mixture. The residue was then distilled and the fraction boiling at 113 °C/6300 Pa gave 2-methyl-2-(*F*-phenyl)-1,3-dioxolane (**18**) (1.85 g, 36%). IR (neat): 1208 and 1168 cm^{-1} (C-O-C). ^{1}H-NMR (neat): δ = 1.7 (s, 3H, CH_3) and 3.8—4.4 (m, 4H, CH_2). ^{19}F-NMR (neat): —0.3 (m, 2F, F$^{3'}$ and F$^{5'}$), 6.7 (tt, 1F, F$^{4'}$), and 21.4 ppm (m, 2F, F$^{2'}$ and F$^{4'}$), ($J_{2'4'} = 3.7$, $J_{3'4'} = 20.8$ Hz). Found: C, 47.25; H, 2.79%; M+, 254. Calcd for $C_{10}H_7F_5O_2$: C, 47.26; H, 2.77%; M, 254.

Reaction of the Dioxolane **18** *with Ethylmagnesium Bromide.* The dioxolane **18** (0.4 g, 1.6 mmol) reacted with ethylmanesium bromide (4.8 mmol) in anhydrous benzene like the oxazine **1** did. The starting dioxolane **18** was confirmed by GLC to remain intact under such conditions.

Reaction of the Dioxolane **18** *with Lithium* N-*Methylanilide.* A solution of the dioxolane **18** (0.3 g, 1.2 mmol) in dry benzene (5 cm³) was added dropwise to a stirred mixture of lithium *N*-methylanilide (3.0 mmol) and anhydrous benzene (5 cm³) over a 10-min period at room temperaure under a nitrogen atmosphere. The mixture was refluxed for 29 h, and poured into diethyl ether (50 cm³) after being cooled. The ethereal solution was washed with water, dried over

magnesium sulfate, and evaporated *in vacuo*. An addition of a small amount of heptane into the residue afforded the precipitates of 2-methyl-2-(4-*N*-methylanilino-*F*-phenyl)-1,3-dioxolane (**20**), mp 113—115 °C. ^{19}F-NMR ($CDCl_3$): 16.89 dd, 2F, $F^{2'}$ and $F^{6'}$) and 18.72 ppm (dd, 2F, $F^{3'}$ and $F^{5'}$), ($J_{2'3'}$ = 21.97 and $J_{2'5'}$ = 10.99 Hz). Found: C, 59.94; H, 4.51; N, 4.18%. Calcd for $C_{17}H_{15}NF_4O_2$: C, 59.82; H, 4.44; N, 4.10%. The residue after separating the dioxolane **20** contained 2-methyl-2-(2-*N*-methylanilino-*F*-phenyl)-1,3-dioxolane (**19**), which could not be isolated in its pure form; the structure was assigned by its ^{19}F-NMR spectrum. ^{19}F-NMR ($CDCl_3$): 3.99 (dd, 1F, $F^{5'}$), 10.43 (ddd, 1F, $F^{4'}$), 16.80 (dd, 1F, $F^{3'}$), and 23.89 ppm (ddd, 1F, $F^{6'}$), ($J_{3'4'} = J_{4'5'} = J_{5'6'} = 21.97$, $J_{3'6'} = 10.79$, and $J_{3'5'} = 4.89$ Hz). Overall yields of **19** and **20** were 12 and 45%, respectively.

This study was supported by the Grant-in-Aid for Developmental Scientific Research (Project No. 00585221) from the Ministry of Education, Science and Culture, to whom the authors are grateful.

References

1) According to the revised nomenclature of highly fluorinated organic compounds by J. A. Young, *J. Chem. Document.*, **14**, 98 (1974); *J. Fluorine Chem.*, **6**, 571 (1975).

2) a) R. D. Chambers, "Fluorine in Organic Chemistry," Wiley-Interscience, New York (1973), p. 261; b) J. Miller, "Aromatic Nucleophilic Substitution," Elsevier, Amsterdam (1968), p. 124; c) L. S. Kobrina, "Fluorine Chemistry Reviews," Marcel Dekker, New York (1974), Vol. 7, Chap. 1.

3) J. Burdon, V. A. Damedaran, and J. C. Tatlow, *J. Chem. Soc.*, **1964**, 763.

4) N. N. Vorozhtsov, V. A. Barkhash, A. T. Prudchenko, and T. I. Khonenko, *J. Gen. Chem. USSR.*, **35**, 1504 (1965).

5) A. T. Prudchenko, L. P. Vordenko, V. A. Barkhash, and N. N. Vorozhtsov, *Khim. Geterotsikl. Soedin.*, **1968**, 967; *Chem. Abstr.*, **70**, 106308s (1968).

6) S. A. Osadchii and V. A. Barkhash, *J. Org. Chem. USSR.*, **6**, 1639 (1970).

7) V. A. Vlasov and G. G. Yakobson, *Bull. Acad. Sci. USSR, Div. Chem. Sci.*, **18**, 812 (1969).

8) G. S. Shchegoleva, A. K. Petrov, V. A. Barkhash, and N. N. Vorozhtsov, *Khim. Geterotsikl. Soedin.*, **1970**, 278; *Chem. Abstr.*, **76**, 140675t (1972).

9) G. S. Shchegoleva, J. S. Isaev, T. F. Ardyukova, and V. A. Barkhash, *Izv. Sibirsk. Otd. Akad. Nauk SSSR*, **1**, 90 (1971); *Chem. Abstr.*, **76**, 13587r (1972).

10) G. S. Shchegoleva, E. D. Krivosova, and V. A. Barkhash, *Izv. Sibirsk. Otd. Akad. Nauk SSSR*, **1**, 95 (1971); *Chem. Abstr.*, **76**, 24470j (1972).

11) V. P. Molosnova, V. A. Barkhash, and N. N. Vorozhtsov, *J. Gen. Chem. USSR.*, **39**, 1737 (1969).

12) T. D. Petrova, V. P. Mamaev, G. G. Yakobson, and N. N. Vorozhtsov, *Khim. Geterotsikl. Soedin.*, **1968**, 771; *Chem. Abstr.*, **71**, 13104c (1969).

13) T. D. Petrova, V. P. Mamaev, G. G. Yakobson, and N. N. Vorozhtsov, *Khim. Geterotsikl. Soedin.*, **1968**, 777; *Chem. Abstr.*, **71**, 12929v (1969).

14) Y. Inukai, Y. Oono, T. Sonoda, and H. Kobayashi, *Bull. Chem. Soc. Jpn.*, **52**, 516 (1979).

15) Y. Inukai, T. Sonoda, and H. Kobayashi, *Bull. Chem. Soc. Jpn.*, **52**, 2657 (1979).

16) Y. Inukai, T. Sonoda, and H. Kobayashi, *Bull. Chem. Soc. Jpn.*, **55**, 337 (1982).

17) T. N. Gerasimova, I. I. Baturina, T. V. Fomenko, V. S. Chertek, V. F. Kollegov, and E. P. Fokin, *J. Org. Chem. USSR*, **10**, 2181 (1974); T. N. Gerasimova, N. A. Orlova, T. V. Fomenko, and E. P. Fokin, *Izv. Sibirsk. Otd. Akad. Nauk SSSR.*, **1975**, 54; *Chem. Abstr.*, **84**, 121337h (1976); T. N. Gerasimova, T. V. Fomenko, and E. P. Fokin, *ibid.*, **1975**, 100; *Chem. Abstr.*, **84**, 16902r (1976); *Bull. Acad. Sci. USSR, Div. Chem. Sci.*, **26**, 1742 (1977); *J. Org. Chem. USSR*, **13**, 1439 (1977); T. N. Gerasimova, N. V. Semikolenva, and E. P. Fokin, *ibid.*, **14**, 91 (1978).

18) A. I. Meyers and E. D. Mihelich, *Angew. Chem., Int. Ed. Engl.*, **15**, 270 (1976).

19) H. W. Gschwend and A. Hamdam, *J. Org. Chem.*, **40**, 2008 (1975).

20) A. I. Meyers and D. E. Williams, *Tetrahedron Lett.*, **1978**, 223.

21) J. J. Pitter and E. J. Tillmans, *J. Org. Chem.*, **22**, 839 (1957); P. Allen and J. Ainos, *ibid.*, **28**, 2759 (1963).

22) Reactions of the oxazine (**1**) with methyllithium and the oxazoline (**2**) with methylmagnesium iodide and propylmagnesium bromide were performed like those with butyllithium and ethylmagnesium bromide, respectively, and afforded 2-(2-methyl-*F*-phenyl)-4,4,6-trimethyl-5,6-dihydro-4*H*-oxazine (**10**), and 2-(2-methyl-*F*-phenyl)- and 2-(2-propyl-*F*-phenyl)-4,4-dimethyl-2-oxazoline, (**11**) and (**12**), in 95, 15, and 25% yields, respectively. Enough of these alkyl derivatives could not be isolated in their pure forms for elemental analyses, so their structures were assigned by ^{19}F-NMR and mass spectra.

23) Unpublished data, details of which will be published elsewhere.

24) L. V. Belf, M. W. Buxton, and G. Fuller, *J. Chem. Soc.*, **1965**, 3372.

25) A. K. Barbour, M. W. Buxton, P. L. Coe, R. Stephens, and J. C. Tatlow, *J. Chem. Soc.*, **1961**, 808.

Reduction of Sulfonic Acids with Triphenylphosphine–Diaryl Disulfide System

Shigeru OAE*,† and Hideo TOGO
Department of Chemistry, The University of Tsukuba, Sakura, Niihari, Ibaraki 305
(Received, July 18, 1983)

Diaryl disulfides are effective catalysts to reduce arenesulfonic acids with triphenylphosphine to the corresponding arenethiols in good yields, while alkanesulfonic acids are transferred into the corresponding alkyl aryl sulfides. Arenesulfonic acids bearing electron-donating substituents can be reduced more readily than those having electron-withdrawing substituents, while diaryl disulfides bearing electron-withdrawing substituents are more effective catalysts than diaryl disulfides with electron-donating ring substituents.

The first example of one-pot reduction of sulfonic acids to thiols was recently reported from this laboratory, by using $(CF_3CO)_2O/(n\text{-}Bu)_4N^+I^-$. This method is the first break through in the direct deoxygenative reduction of sulfonic acids to thiols and thiol derivatives. However, it not only requires a large excess of expensive reagents but also affords a mixture of reduction products, *i.e.* thiols and thiol trifluoroacetates.[1] G. A. Olah *et al.* reported recently a second successful one-pot reduction of sulfonic acids to the corresponding disulfides with BX_3 (X=Cl, Br, I)/KI.[2] In the previous paper, we reported another facile and quantitative deoxygenative reduction of sulfonic acids and its derivatives by a new reducing system, *i.e.* triphenylphosphine-iodine system.[3] This paper deals with another facile and attractive reduction of sulfonic acids with triphenylphosphine–diaryl disulfide system. Although triphenyphosphine is known to be a relatively strong reducing agent, it does not react directly with sulfonic acids. Meanwhile, the mixture of triphenylphosphine with halogen[4] and that of triphenylphosphine with disulfide[5] respectively are known to give phosphonium salts. Several reactions are known to utilize such phosphonium salts *e.g.* the conversion of alcohol and phenol derivatives to the corresponding halides by treatment with the phosphine and halogen,[6] the desulfurization of disulfides to the corresponding sulfides with the phosphine,[7] the condensation of carboxylic acids and alcohols or amines to the corresponding esters or amides by treatment of the phosphine and diaryl disulfide[8] or diselenide,[9] and the conversion of alcohols to the corresponding sulfides by treatment with a mixture of the phosphine and the disulfide.[10] Thus a mixture of triphenylphosphine and a catalytic amount of diaryl disulfide or diaryl diselenide was our choice system for the reduction of sulfonic acids.

Results and Discussion

Reduction of Arenesulfonic Acids and Alkanesulfonic Acids to the Corresponding Arenethiols and Alkyl Aryl Sulfides with Triphenylphosphine and Diaryl Disulfide. Arenesulfeyltriphenylphosphonium arenethiolate is known to be formed upon treatment of diaryl disulfide with triphenylphosphine and has been utilized for the synthetic organic chemistry, *e.g.* syntheses of alkyl aryl sulfides,[10] peptide synthesis, *etc.*[8] This reagent system was found to reduce also arenesulfonic acids. The reducing ability of the system appears to depend on the choice of the disulfide used for the reduction. Some disulfides showed nearly the same activity as iodine, while others were found to be much weaker reducing catalysts than iodine.[3] In this reducing system, the amount of the disulfide did not affect the yield (Table 2) of the thiol, the reduction product, but changed the time to complete the reaction, suggesting that the disulfide acts as a catalyst. GLC analysis after the completion of reaction showed two kinds of thiols and three kinds of disulfides. These disulfides were then heated with an enough amount of triphenylphosphine and water, to be reduced to the thiols of which the yields were determined by GLC or isolation (Eq. 1).

$$ArSO_3H + \left(3+\frac{1}{2}\right)Ph_3P + \frac{1}{2}(Ar'S)_2 \xrightarrow[2)\ H_2O]{1)\ \text{reflux in benzene}} ArSH + Ar'SH + \left(3+\frac{1}{2}\right)Ph_3PO \quad (1)$$

The reaction is considered to be resulted by the following consecutive reactions (Eqs. 2—7) as postulated in the reaction of triphenylphosphine/iodine system.[3]

$$Ar'SSAr' + Ph_3P \rightleftharpoons Ar'S\text{–}\overset{+}{P}Ph_3\ Ar'S^- \quad (2)$$

$$ArSO_3H + Ar'S\text{–}\overset{+}{P}Ph_3\ Ar'S^- \overset{K_3}{\rightleftharpoons} ArSO_3^-\ Ar'S\text{–}\overset{+}{P}Ph_3 + Ar'SH \quad (3)$$

$$ArSO_3^-\ Ar'S\text{–}\overset{+}{P}Ph_3 \overset{K_4}{\rightleftharpoons} ArSO_2\text{–}O\text{–}\overset{+}{P}Ph_3\ Ar'S^- \quad (4)$$

$$ArSO_2\text{–}O\text{–}\overset{+}{P}Ph_3\ Ar'S^- \longrightarrow ArSO_2SAr' + Ph_3PO \quad (5)$$

$$ArSO_2SAr' + 2\,Ph_3P \longrightarrow \frac{1}{3}[ArSSAr + ArSSAr' + Ar'SSAr'] + 2\,Ph_3PO \quad (6)$$

$$ArSSAr + ArSSAr' + Ar'SSAr' + 3\,Ph_3P + 3\,H_2O \longrightarrow 3\,ArSH + 3\,Ar'SH + 3\,Ph_3PO \quad (7)$$

The reaction of alkanesulfonic acid such as 1-phentanesulfonic acid with triphenylphosphine/di-2-pyridyl disulfide gave the alkyl pyridyl sulfide.

$$CH_3(CH_2)_4SO_3H + (PyS)_2 + 4\,Ph_3P \longrightarrow CH_3(CH_2)_4\text{–}S\text{–}Py + 3\,Ph_3PO + Ph_3PS + PySH \quad (8)$$

† Present address: Okayama University of Science, Ridai-cho 1-1, Okayama 700.

Table 1. Reaction of sulfonic acid with triphenylphosphine/diaryl disulfide in benzene under nitrogen atmosphere[a)]

$ArSO_3H$	$ArSO_3H/Ph_3P/(Ar'S)_2$	$(Ar'S)_2$	Time/h (Reflux)	Yields of products/%		
				$ArSH$[b)]	$Ar'SH$[b)]	Ph_3PO
2,4-$(CH_3)_2C_6H_3SO_3H$	2/8/1	$(p\text{-}ClC_6H_4S)_2$	21	(60)[c)]	(76)[c)]	—
p-$CH_3C_6H_4SO_3H$	2/10/1	$(p\text{-}ClC_6H_4S)_2$	24	75(60)[c)]	100(90)[c)]	—
$C_6H_5SO_3H$	2/10/1	$(p\text{-}ClC_6H_4S)_2$	24.5	90	94	—
p-$ClC_6H_4SO_3H$	2/8/1	$(p\text{-}ClC_6H_4S)_2$	24	26	100	—
2,4-$(CH_3)_2C_6H_3SO_3H$	2/8/1	$(p\text{-}CH_3C_6H_4S)_2$	28	46(42)[c)]	(78)[c)]	—
p-$CH_3C_6H_4SO_3H$	2/8/1	$(p\text{-}CH_3C_6H_4S)_2$	23.5	90(90)[c)]	100	90
$C_6H_5SO_3H$	2/8/1	$(p\text{-}CH_3C_6H_4S)_2$	36	14	85	—
p-$ClC_6H_4SO_3H$	2/8/1	$(p\text{-}CH_3C_6H_4S)_2$	22	Trace	100	—
p-$CH_3C_6H_4SO_3H$	2/8/1	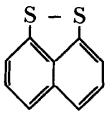	24	63	—	—
p-$CH_3C_6H_4SO_3H$	1/4/0.5	$(C_6H_5Se)_2$	24	29	—	—
p-$ClC_6H_4SO_3H$	2/14(Bu_3P)/1.5	$(p\text{-}CH_3C_6H_4S)_2$	18	No reaction		
p-$CH_3C_6H_4SO_3H$	2/8/1/0.2(Bu_4NI)	$(p\text{-}ClC_6H_4S)_2$	2	91	100	—
$CH_3CH_2SO_3H$	2/11/3	$(p\text{-}ClC_6H_4S)_2$	29	No reaction		

a) After this reaction, the mixture of 300 mg of water and 2 ml of dioxane was added and refluxed for 0.5—1.0 h. b) GLC yield (20% OV-1, 10 m glass column). c) Isolated yield.

Table 2. Reaction of sulfonic acid with triphenylphosphine/diaryl disulfide in benzene under nitrogen atmosphere[a)]

$ArSO_3H$	$ArSO_3H/Ph_3P/(Ar'S)_2$	$(Ar'S)_2$	Time/h (Reflux)	Yields of products/%		
				$ArSH$[b)]	$Ar'SH$[b)]	Ph_3PO
2,4-$(CH_3)_2C_6H_3SO_3H$	2/8/1	$(PyS)_2$[e)]	2	(92)[c)]	—	(88)[c)]
p-$CH_3C_6H_4SO_3H$	2/8/1	$(PyS)_2$[e)]	2	87(73)[c)]	—	—
2-$C_{10}H_7SO_3H$	2/8/1	$(PyS)_2$[e)]	4	(76)[c)]	—	—
p-$ClC_6H_4SO_3H$	2/8/1	$(PyS)_2$[e)]	4	60(53)[c)]	—	(65)[c)]
$C_6H_5SO_3H$	2/8/1	$(PyS)_2$[e)]	2	85	—	(76)[c)]
p-$CH_3C_6H_4SO_3H$	2/8/0.2	$(PyS)_2$[e)]	5	(73)[c)]	—	—
p-$CH_3C_6H_4SO_3H$	2/8(Bu_3P)/1	$(PyS)_2$[e)]	4	(26)[c)]	—	—
$CH_3(CH_2)_4SO_3H$	2/10/2	$(PyS)_2$[e)]	3.5 (room temperature)		60 [$CH_3(CH_2)_4S$][d)]	
$C_6H_5SO_3H$	2/9/1/2(Bu_3N)	$(PyS)_2$[e)]	2	18	—	—
2-$C_{10}H_7SO_3H$	2/8/1	$(Cl_3C_6H_2S)_2$[f)]	32	Trace	—	—
p-$CH_3C_6H_4SO_3H$	2/8/1	$(Cl_3C_6H_2S)_2$[f)]	3	75(60)[c)]	(100)[c)]	(75)[c)]
$C_6H_5SO_3H$	2/8/1	$(Cl_3C_6H_2S)_2$[f)]	5	68	—	—
2,4-$(CH_3)_2C_6H_3SO_3H$	2/8/1	$(Cl_3C_6H_2S)_2$[f)]	5	(66)[c)]	(97)[c)]	(61)[c)]
p-$ClC_6H_4SO_3H$	2/8/1	$(Cl_3C_6H_2S)_2$[f)]	25	Trace	—	—

a) After this reaction, the mixture of 300 mg of water and 2 ml of dioxane was added and refluxed for 0.5—1.0 h. GLC yield (20% OV-1, 10 m glass column). c) Isolated yield. d) Pentyl 2-pyridyl sulfide was obtained, and Ph_3PS was also obtained in 83% isolated yield. e) Di-2-pyridyl disulfide. f) Bis(2,4,5-trichlorophenyl) disulfide.

When dialkyl disulfide, such as lipoic acid or dibutyl disulfide was used, the following known desulfurization reaction took place rather than the reduction to the thiol.[11]

$$RSSR + Ph_3P \longrightarrow RSR + Ph_3PS \quad (9)$$

Thus, diaryl disulfides had to be used for this purpose. Inspection of the data in Tables 1, 2, and Fig. 1 reveals that the diaryl disulfide which bears a stronger electron-withdrawing aryl group is a better catalyst in the reduction of sulfonic acids with triphenylphosphine; *e.g.* unsubstituted diphenyl disulfide exhibits only a trivial catalytic activity, however, the catalytic ability of bis(2,4,5-trichlorophenyl) disulfide is nearly as strong as that of iodine.[3] Di-2-pyridyl disulfide was found to be the best among several disulfides tested (Tables 1 and 2), while 1,2-dithiaacenaphthene was not a good catalyst, probably due to the unfavorable equilibrium (Eq. 2) because of its unusually high stability of the stereoelectronic arrangement, or due to the formation of a very stable phosphorane intermediate by the reaction between triphenylphosphine and 1,2-dithiaacenaphthene. Diphenyl diselenide displayed only a weak catalytic

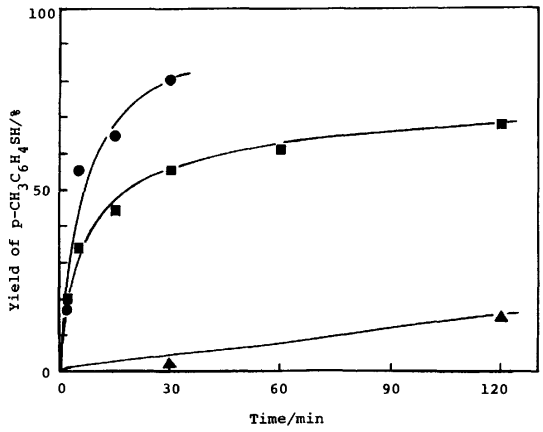

Fig. 1. Reaction of p-$CH_3C_6H_4SO_3H$ with Ph_3P/$(ArS)_2$ in benzene under reflux conditions.
p-$CH_3C_6H_4SO_3H/Ph_3P/(ArS)_2$=2/8/1 (mmol).
●: Di-2-pyridyl disulfide, ■: Bis(2,4,5-trichlorophenyl) disulfide, ▲: Bis(p-chlorophenyl) disulfide.

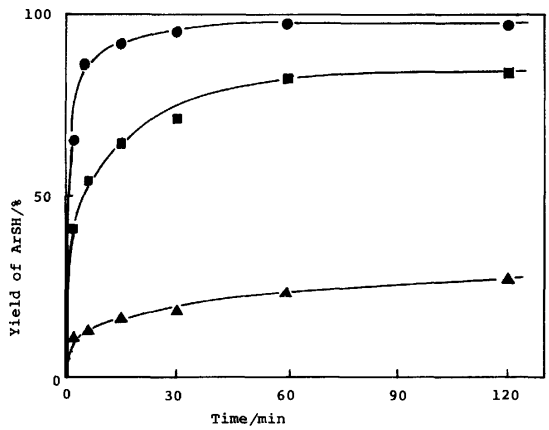

Fig. 2. Reaction of $ArSO_3H$ with $Ph_3/(PyS)_2$ in benzene at 15 °C.
p-$CH_3C_6H_4SO_3H/C_6H_5SO_3H/p$-$ClC_6H_4SO_3H/Ph_3P/(PyS)_2$=1/1/1/13/1.5 (mmol).
●: p-$CH_3C_6H_4SO_3H$, ■: $C_6H_5SO_3H$, ▲: p-$ClC_6H_4SO_3H$.
$(PyS)_2$: Di-2-pyridyl disulfide.

activity. The use of tributylphosphine instead of triphenylphosphine led to a sluggish reaction even when it was used in combination with di-2-pyridyl disulfide.

Inspection of the data in Tables 1, 2, and Fig. 2, reveals that the introduction of an electron-releasing substituent on the aromatic ring of arenesulfonic acid accelerates the reduction with $Ph_3P/(Ar'S)_2$ system. Typical examples are shown in Fig. 2. In contrast to the reaction with triphenylphosphine/iodine system, addition of tertiaryl amine in the reaction of the arenesulfonic acid with triphenylphosphine/diaryl disulfide system did not accelerate the reaction but slightly retarded the reaction (Table 2). The rate of the reaction of sodium arenesulfonate in the presence of crown ether was found to be much lower than that of the corresponding acid. This opposite behavior with bases in the reaction of $Ph_3P/(Ar'S)_2$ system to that with Ph_3P/I_2 system suggests that since arenethiolate anion is a much stronger base than sulfonate anion in the reduction with $Ph_3P/(Ar'S)_2$ system, K_3 is quite large and hence a higher concentration of the sulfonate anion can be maintained, however K_4 is very small. Whereas in the case of Ph_3P/I_2 system, since hydrogen iodide would be a strong acid comparable to the sulfonic acid in an aprotic solvent, K_{10} would not be sufficiently large

$$ArSO_3H + Ph_3\overset{+}{P}\text{–}I\ I^- \overset{K_{10}}{\rightleftharpoons} ArSO_3^-\ Ph_3\overset{+}{P}\text{–}I + HI \quad (10)$$

$$ArSO_3^-\ Ph_3\overset{+}{P}\text{–}I \overset{K_{11}}{\rightleftharpoons} ArSO_2\text{–}O\text{–}\overset{+}{P}Ph_3\ I^- \quad (11)$$

enough to maintain a high concentration of the sulfonate anion in the absence of any base catalyst, however, K_{11} is larger than K_4.[3] These considerations along with the actual observations would suggest that the rate-determining step involves the nucleophilic substitution on the phosphorus atom of the arenesulfenyltriphenylphosphonium ion by the sulfonate anion. This hypothesis is also in accordance with the observation that a diaryl disulfide bearing an electron-withdrawing group is a better catalyst than that which bears an electron-donating substituent in the reduction of arenesulfonic acids with triphenylphosphine as shown in Figs. 1 and 2; *i.e.* the better leaving ability of $Ar'S^-$ and the stronger nucleophilicity of $ArSO_3^-$ facilitate the reactions Eqs. 2 and 4. If the following elemental reaction, Eq. 5, is the rate-determining step of this reaction, the observed electronic demand should be the opposite, since the nucleophilicity of $Ar'S^-$ increases with the decrease of electronegativity of Ar' group and any electron-withdrawing substituent on Ar group should accelerate the nucleophilic displacement on the sulfonyl sulfur. The retardation of the rate of the reaction, Eq. 3, by addition of any base can be rationalized in terms of our postulate that the rate-determining step is the reaction shown by Eq. 4. If the reaction shown by Eq. 5 would be the rate-determining step, the addition of a base would have to accelerate the reaction, since the base ionizes the thiol, generating the thiolate anion which is a much stronger nucleophile than the thiol, toward the sulfonyl sulfur. Once the thiosulfonic S-ester is formed, this can be very readily reduced by either triphenylphosphine[3] or thiol.

Alkyl arenesulfonate, sodium arenesulfonate, and tetraethylammonium benzenesulfonate, however, could not be reduced to the corresponding thiols even with triphenylphosphine/dipyridyl disulfide which was the best catalyst.

Experimental

Preparation of Disulfide. Disulfides, which are not commercially available, were synthesized by a known method.[12] To a benzene solution (150 ml) of a thiol (0.05 mol) and pyridine (0.055 mol), was added dropwise iodine (0.025 mol) dissolved in benzene (50 ml). When the color of the solution changed to brown by excess iodine, the addition was stopped. The reaction mixture was washed with water, 5% HCl solution, $Na_2S_2O_3$ solution, and then water again, and the organic layer was dried over $MgSO_4$. After evaporation of benzene, the residual disulfide was purified by

recrystallization usually from hexane. Yields were nearly quantitative. Di-*p*-tolyl disulfide mp 44—45 °C (lit,[13] 46 °C). Bis(*p*-chorophenyl) disulfide mp 70—71 °C (lit,[14] 73 °C). 1,2-Dithiaacenaphthene was prepared according to the method of Zweig and Hoffmann, starting with commercial 8-amino-1-naphthalenesulfonic acid *via* initial formation of yellow crystals of 1,8-naphthalenedithiol[7.1%, NMR ($CDCl_3$) δ= 4.11 (2H, s), 7.0—7.8 (6H, m)] and subsequent autoxidation of the dithiol (84%). The product was recrystallized from ethanol. Mp 116—117 °C (lit,[15] 116 °C).

Competitive Reduction of p-*Substituted Benzenesulfonic Acids with $Ph_3P/(PyS)_2$ System.* A mixture of 190.2 mg (1 mmol) of *p*-toluenesulfonic acid, 176 mg (1 mmol) of benzenesulfonic acid, and 192.5 mg (1 mmol) of *p*-chlorobenzenesulfonic acid was dissolved in 5 ml of benzene, and the mixture was refluxed in a reactor which was equipped with a condenser and a calcium chloride tube. These sulfonic acids were dehydrated to nearly completely dry prior to the reaction by way of azeotropic distillation with benzene. After 3406 mg (13 mmol) of triphenylphosphine and 154 mg (1 mmol) of biphenyl (standard) were added to the mixture of these sulfonic acids, this reactor was equipped with another condenser and a nitrogen balloon and then substituted with this inert gas with a vacuum pump. Then, 330 mg (1.5 mmol) of di-2-pyridyl disulfide which was dissolved in 5 ml of dry benzene was added into the mixture which was stirred at 75 °C. A small portion, 0.1 ml, of the reaction mixture was picked up by a microsyringe and quenched with a mixture of water–dioxane–benzene (v=1/1/2) at every fixed time (2, 6, 15, 30, 60, and 120 min from initial reaction time respectively). The yields of three thiols obtained by this method were determined by comparison of the GLC curve with the predetermined calibration curve by gas chromatography (SE-30, using biphenyl as the standard).

Relative Catalytic Effects of Various $(Ar'S)_2$ Catalysts in the Reduction of p-*Toluenesulfonic Acid with $Ph_3P/(Ar'S)_2$ System.* *p*-Toluenesulfonic acid monohydrate 381 mg (2 mmol) was dissolved in 5 ml of benzene, refluxed, and dehydrated to nearly completely dry by the same procedure. After 2100 mg (8 mmol) of triphenylphosphine and 300 mg (2 mmol) of biphenyl were added to this dried sulfonic acid, this reactor was equipped with another condenser and a nitrogen balloon, and was substituted with this inert gas with a vacuum pump. Then, 3 ml of dry benzene was added to this mixture and 1 mmol of a chosen diaryl disulfide (di-2-pyridyl disulfide, bis(2,4,5-trichlorophenyl) disulfide, or bis(*p*-chlorophenyl) disulfide) which was dissolved in 5 ml of dry benzene was added to this mixture (total benzene 8 ml) and the whole mixture was stirred, and refluxed (bath temperature 112 °C). A small portion, 0.1 ml, of reaction mixture was picked up by a microsyringe and quenched with a mixture of water–dioxane–benzene (v=1/1/2) at fixed time intervals. The yields of thiols obtained by this procedure were determined by comparison of the GLC curve with the predetermined calibration curve by gas chromatography (SE-30, using biphenyl as the standard).

Reductive Conversion of Alkanesulfonic Acid with $Ph_3P/(PyS)_2$ System. 1-Pentanesulfonic acid, 304 mg (2 mmol) of which was dried completely by a vacuum pump and 2620 mg (10 mmol) of triphenylphosphine were added into a reactor which was equipped with a condenser and a nitrogen balloon. Then, 440 mg (2 mmol) of di-2-pyridyl disulfide which was dissolved in 5 ml of dry benzene was added to this mixture which was then stirred for 3.5 h at room temperature; the reaction was monitored by GLC. After the reaction, the yields of triphenylphosphine sulfide, pentyl 2-pyridyl sulfide were determined by GLC (SE-30). Pentyl 2-pyridyl sulfide 60% IR (NaCl) 750, 1120, 1400, 1440, 1570 cm^{-3}. GC-MS: m/e 181, TLC (benzene) R_f=0.4, bp 104—106 °C/5.5 mmHg (1 mmHg=133.322 Pa). Found: C, 66.33; H, 8.35; N, 7.77. Calcd for $C_{10}H_{15}NS$: C, 66.25; H, 8.33; N, 7.72. NMR (CCl_4) δ=8.3 (m, 1H), 6.7—7.5 (m, 3H), 0.9 (t, 3H, J=6 Hz), 1.1—2.9 (m, 6H), 3.15 (t, 2H, J=6 Hz).

Triphenyphosphine sulfide 83%. The yield of triphenylphosphine oxide was determined through a silica-gel column chromatography with benzene as eluent (85%).

Preparation of Diphenyl Diselenide. Diphenyl diselenide was prepared according to a known procedure[16,17] by autoxidation of benzeneselenol which was prepared by treating phenyl Grignard reagent with black selenium in an excellent yield. Mp 57—58 °C (lit,[17] 61—63 °C).

Reduction of Arenesulfonic Acid with $Ph_3P/(PyS)_2$/Amine System. To a carefully dehydrated mixture of 352 mg (2 mmol) of benzenesulfonic acid and 371 mg (2 mmol) of tributylamine, 2360 mg (9 mmol) of triphenylphosphine was added into a reactor which was equipped with a condenser and a nitrogen balloon and substitued thoroughly with this inert gas with a vacuum pump. Then, 220 mg (2 mmol) of di-2-pyridyl disulfide which was dissolved in 5 ml of dry benzene was added to this mixture. The reaction mixture was stirred and refluxed for 2 h, following the reaction by GLC. Then a mixture of 3 ml of water and 3 ml of dioxane was added to this reaction mixture which was refluxed for 0.5 h. Benzenethiol was obtained in 18% yield by GLC.

References

1) T. Numata, H. Awano, and S. Oae, *Tetrahedron Lett.*, **21**, 1235 (1980).

2) G. A. Olah, S. C. Narang, L. D. Field, and R. Karpeles, *J. Org. Chem.*, **46**, 2408 (1981).

3) S. Oae and H. Togo, *Bull. Chem. Soc. Jpn.*, **56**, 3802 (1983).

4) A. D. Beveridge, G. S. Harris, and F. Inglis, *J. Chem. Soc., Perkin Trans. 1* , **1966**, 520; L. Horner and H. Nickel, *Ann. Chim. (Paris)*, **597**, 20 (1955).

5) D. N. Harpp, J. G. Gleason, *J. Am. Chem. Soc.*, **93**, 2437 (1971).

6) G. A. Wiley, R. L. Hershkowitz, B. M. Rein, and B. C. Chung, *J. Am. Chem. Soc.*, **86**, 964 (1964); G. A. Wiley, B. M. Rein, and R. L. Hershkowitz, *Tetrahedron Lett.*, **1964**, 2509; R. Michinek and W. Liittke, *Synthesis*, **1975**, 255.

7) D. N. Harpp and J. G. Gleason, *J. Org. Chem.*, **35**, 3259 (1970); D. N. Harpp, J. G. Gleason, and J. P. Snyder, *J. Am. Chem. Soc.*, **90**, 4181 (1968); I. L. Knunyants, *Dokl. Chem.*, **224**, 521 (1975); D. N. Harpp and J. G. Gleason, *J. Org. Chem.*, **36**, 73 (1971); D. N. Harpp and J. G. Gleason, *J. Am. Chem. Soc.*, **93**, 2437 (1971).

8) S. Kobayashi, T. Iimori, T. Izawa, and M. Ohno, *J. Am. Chem. Soc.*, **103**, 2406 (1981); R. Matsueda, H. Maruyama, M. Ueki, and T. Mukaiyama, *Bull. Chem. Soc. Jpn.*, **44**, 1373 (1971); T. Endo, S. Ikenaga, and T. Mukaiyama, *ibid.*, **43**, 2632 (1970); T. Mukaiyama, K. Goto, R. Matsueda, and T. Ueki, *Tetrahedron Lett.*, **1970**, 5293; E. J. Corey and D. J. Brunelle, *ibid.*, **1976**, 3409; T. Mukaiyama, M. Ueki, H. Maruyama, and R. Matsueda, *J. Am. Chem. Soc.*, **90**, 4490 (1968); T. Takaku and Y. Shimada, *Chem. Lett.*, **1975**, 873; T. Mukaiyama and M. Hashimoto, *J. Am. Chem. Soc.*, **94**, 8528 (1972).

9) H. Takaku, T. Konishi, and H. Hata., *Chem. Lett.*, **1977**, 655.

10) I. Nakagawa and T. Hata., *Tetrahedron Lett.*, **1975**, 1409.

11) D. N. Harpp, J. G. Gleason, and J. P. Snyder, *J. Am. Chem. Soc.*, **90**, 4181 (1968); D. N. Harpp and J. G. Gleason, *J. Org. Chem.*, **36**, 73 (1971).

12) D. T. McAllen, T. V. Cullum, R. A. Dean, and F. A. Fidler, *J. Am. Chem. Soc.*, **73**, 3629 (1951).

13) L. Field, *J. Am. Chem. Soc.*, **74**, 394 (1954).
14) M. B. Sparke, J. L. Cameron, and N. Kharasch, *J. Am. Chem. Soc.*, **75**, 4907 (1953).
15) A. Zweig and A. K. Hoffmann, *J. Org. Chem.*, **30**, 3997 (1965).
16) E. C. Horning, *Org. Synth.*, Coll. Vol. III, 771 (1965).
17) Aldrich Chemical Co.

Optical Resolution of Pyridoxal-like Pyridinophanes

Yoji TACHIBANA,† Toshihiko KOMATSU,†† Makoto ANDO, and Hiroyoshi KUZUHARA*
The Institute of Physical and Chemical Research, Wako, Saitama 351
(Received July 22, 1983)

Racemic modifications of the pyridoxal-like ansa compounds such as 15-formyl-14-hydroxy-2,8-dithia-[9](2,5)pyridinophanes prepared as a pontential catalyst for stereospecific nonenzymatic reactions were optically resolved through formation of Schiff bases by treatment with amino sugar derivatives or amino acids. Resolutions with the amino sugar derivatives were ascribable to the difference of the solubilities of the diastereomeric Schiff bases, whereas those with the amino acids resulted from the difference of the reaction rates for the formation of the diastereomeric Schiff bases. As the amino sugar resolving agents, 3-amino-3-deoxy-1,2:5,6-di-*O*-isopropylidene-β-D-idofuranose and the corresponding α-D-glucofuranose isomer were employed and gave (*R*)- and (*S*)-pyridoxal-like pyridinophanes, respectively. On the other hand, chiral valine was the most efficient resolving agent among the amino acid tested and the presence of half equimolar Fe^{3+} markedly increased the optical purities of the products. Employment of (*S*)-valine gave (*R*)-pyridinophanes in excess and *vice versa*.

In a series of studies pursuing systems mimicking vitamin B_6-dependent enzymes capable of enantio-face differentiation, we have reported the synthesis of pyridoxal-like pyridinophanes with planar chirality due to restricted rotation; *i.e.*, (*S*)-15-formyl-14-hydroxy-2,8-dithia[9](2,5)pyridinophane ((*S*)-**1**)[1] and (*S*)-15-formyl-14-hydroxy-5,5-dimethyl-2,8-dithia-[9](2,5)-pyridinophane ((*S*)-**2**).[2] Compound (*S*)-**1** was an active catalyst for the stereospecific racemization of a chiral amino acid[1] and both (*S*)-**1** and (*S*)-**2** were important precursors of the corresponding chiral pyridoxamine-like pyridinophanes,[2,3] which played a main role in the stereoselective transamination reactions.[4]

We now wish to describe some interesting additional findings concerning the optical resolutions of the racemate of these pyridoxal-like pyridinophanes. Amino sugar derivatives or amino acids could be employed as the resolving agents but their resolution mechanisms were completely different.

Results and Discussion

Resolution with Amino Sugar Derivatives. As described in the previous paper,[1] the attempt to resolve racemic **1** *via* formation of a Schiff base by treatment with commercial chiral α-methylbenzylamine failed because the Schiff base resisted crystallization; whereas 3-amino-3-deoxy-1,2:5,6-di-*O*-isopropylidene-α-D-glucofuranose (**3**) served as an efficient resolving agent for racemic **1**[1] or **2**[2] because it gave a crystalline Schiff base mixture (**4**), from which one diastereomer could be readily isolated in a pure state by recrystallization. Acidic hydrolysis of the less soluble diastereomer gave levorotatory **1** or **2** that was later assigned as the *S*-enantiomer on the basis of X-ray analyses[5] and other data on ORD and CD spectra.[2]

One of the disadvantages of using the amino sugar derivatives such as **3** as the resolving agent was the inaccessibility to its antipode, L-glucofuranose derivative (**5**). This meant that the *R*-enantiomer of the pyridinophanes could not be readily obtainable in a pure state. This situtation prompted us to develop more readily accessible resolving agent in the place of **5**. As a result, 3-amino-3-deoxy-1,2:5,6-di-*O*-isopropylidene-D-idofuranose (**6**) proved to be a good candidate. The only difference between **5** and **6** is the configuration of the substituent at C-5 and, therefore, their approximate molecular shapes are quite similar. The preparation of **6** was performed *via* the corresponding 3-azido-3-deoxy derivative (**7**) from the known 1,2:5,6-di-*O*-isopropylidene-β-D-talofuranose (**8**).[6] Thus, **8** was methylsulfonylated at 0 °C to the syrupy 3-*O*-mesylate (**9**), which was treated with sodium azide in hexamethylphosphoric triamide to give the crystalline 3-azido-3-deoxy-D-idofuranose derivative (**7**). The azido sugar derivative was catalytically hydrogenated with Raney Ni, giving **6**. Optical resolution of racemic **1** using **6** was conducted in a similar way to the resolution using **3** reported previously. A mixture of racemic **1** and **6** was refluxed in benzene with azeotropic removal of the water produced, giving a Schiff base mixture (**10**) as crystals. Recrystallization of **10** from a benzene–cyclohexane mixture was conducted twice, giving the less soluble diastereomer (**10a**) of sharp melting

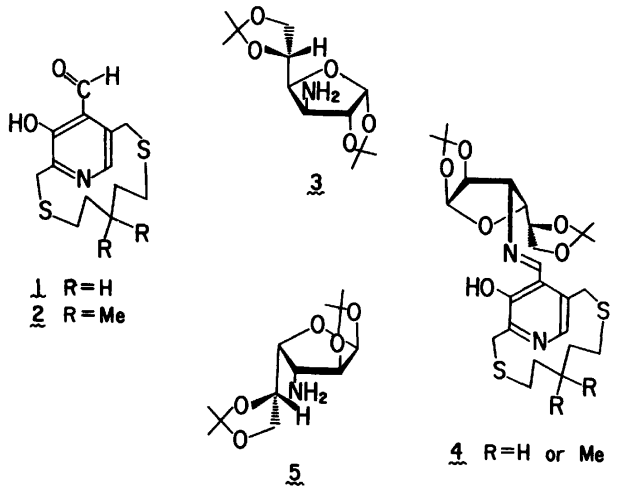

† Present address: Central Research Laboratory, Nisshin Flour Milling, Co., Ltd., Ohimachi, Iruma-gun, Saitama 354.

†† Present address: Zenyaku Kogyo, Co., Ltd., 2-33-7 Ohizumi, Nerima-ku, Tokyo 177.

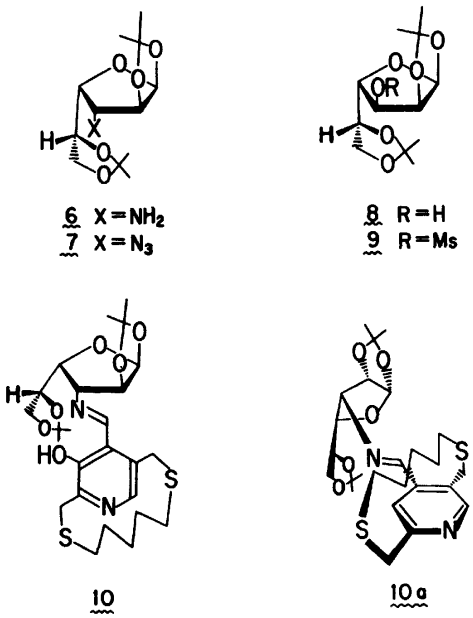

point (150 °C). There was a couple of doublets around δ 6.17 assignable to the anomeric proton of the sugar moiety in the ^{1}H NMR spectrum of **10** as shown in Fig. 1, whereas one doublet at δ 6.18 completely disappeared in the spectrum of **10a**, suggesting that separation between the two diastereomers had been attained. In contrast to the Schiff base isolatable in a homogeneous state from the diastereomeric mixture (**4**, R=H)[1] prepared from **1** and **3**, the crystals of **10a** incorporated 2/3 equimolar benzene and 1/2 equimolar cyclohexane; this was suggested by the results of elemental analyses and the ^{1}H NMR spectra. After acidic hydrolysis of **10a**, the regenerated pyridinophane was extracted with an organic solvent and purified by chromatography, giving the dextrorotary species ((*R*)-**1**) as expected. The absolute value of the specific rotation of this specimen was a little lower than that of the alternative enantiomer previously obtained by using **3** as the resolving agent. This was probably because the *gluco* configuration was superior to the *ido* configuration for the resolution of racemic **1** and since the solubility of **10** was too low to provide smooth fractional crystallization. However, it was interesting that the D-idose derivative (**6**) could substitute the antipode of **3** having the L-*gluco* configuration (**5**). This suggests that optical resolution of atropisomers might depend on the approximate molecular shape of the resolving agent.

Althouth both enantiomers of pyridoxal-like pyridinophanes could be obtained by employing the **3** and **6** pair as the resolving agents, there was still a problem; *i.e.*, acidic hydrolysis of the Schiff base including the moieties of **3** or **6** for reproduction of the pyridoxal-like pyridinophanes accompanied hydrolysis of the isopropylidene groups in **3** or **6**, making their recovery difficult. These facts further prompted us to develop other type of resolution method.

Resolution with Amino Acids. Generally, pyridoxal and its analogs can condense with free amino acids owing to their great tendency to form Schiff bases.[7,8] As amino acids belong to the most readily obtainable chiral compounds, it would be convenient if they could be utilized for the optical resolu-

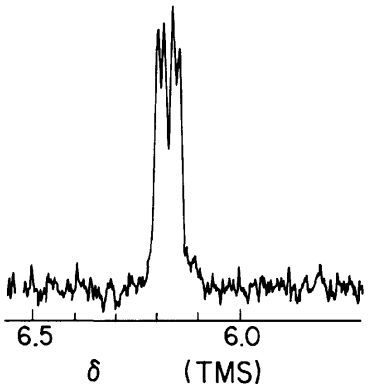

Fig. 1. ^{1}H 100-MHz NMR spectrum of **10**. Signals are anomeric protons of sugar moiety of **10**.

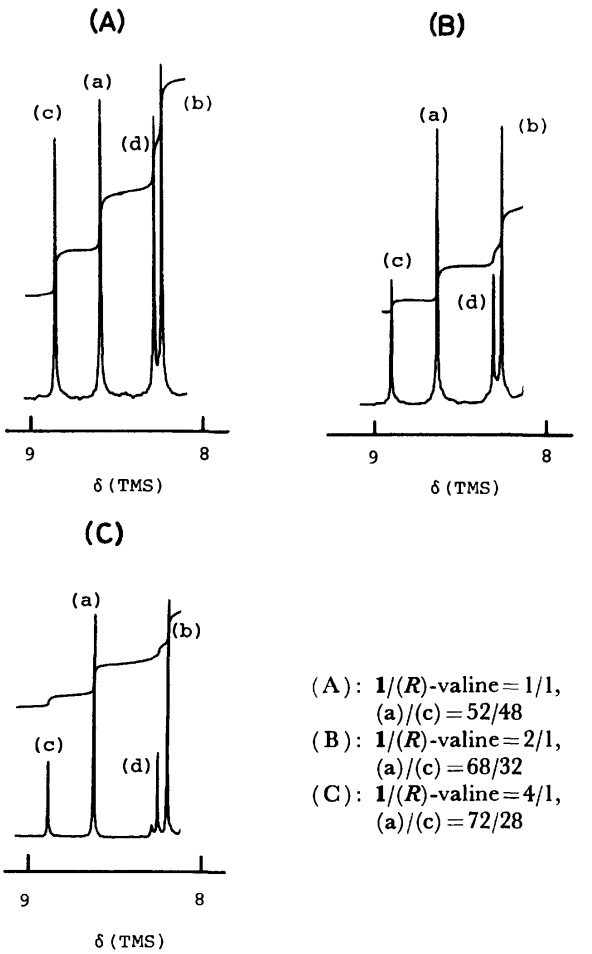

(A): **1**/(*R*)-valine=1/1, (a)/(c)=52/48
(B): **1**/(*R*)-valine=2/1, (a)/(c)=68/32
(C): **1**/(*R*)-valine=4/1, (a)/(c)=72/28

Fig. 2. ^{1}H 400-MHz NMR spectra of C_6D_6 solution of the Schiff bases derived from **1** and (*R*)-valine in various molar ratios in methanol. (A): **1**/(*R*)-valine=1/1, (B): **1**/(*R*)-valine=2/1, (C): **1**/(*R*)-valine=4/1. The signals (a—d) are; (a), (c): azomethine protons of **11** and **12**, (b), (d): 6-H protons of pyridine ring of **11** and **12**, respectively.

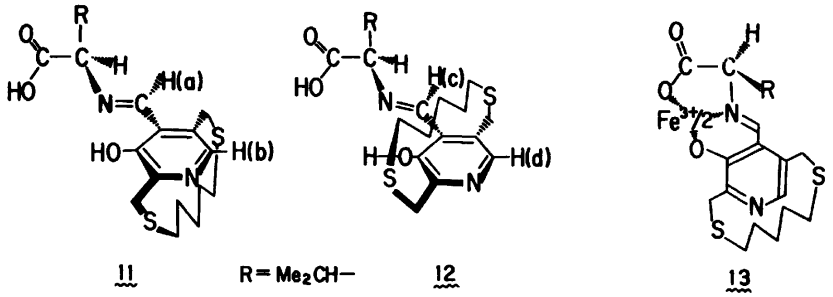

11 R=Me$_2$CH- 12 13

tion of racemic **1** or **2**. The problem is that racemization of the amino acid moieties may proceed within such Schiff bases, especially when some heavy metal ions are coexisting and the media is basic.[9,10] Therefore, we first examined the capability of the resolution of racemic **1** and **2** with chiral amino acids in the absence of metal ions in neutral media. Racemic **1** was condensed with (*R*)-valine[11] in methanol, changing the molar ratio of both reactants. Figure 2 shows 400 MHz ^{1}H NMR spectra of the C_6D_6 solution of the resulted mixture. Two pairs of signals, (a), (b) and (c), (d), were assigned to the azomethine and pyridine ring protons of the Schiff bases (**11** and **12**) derived from (*S*)-**1** and (*R*)-**1** respectively by referring them to those in the spectra of the Schiff bases derived from the authentic chiral pyridoxal-like pyr-

Table 1. Optical resolution of **1** and **2** with chiral amino acids in the absence of Fe^{3+}

Pyridoxal analog	Amino acid (confign.)	**1** or **2** / Amino acid	Product		
			Confign.[a]	o.p./%[b]	c.y./%[c]
1	Valine (*S*)	1/1	*R*	4	73
1	Valine (*S*)	2/1	*R*	21	71
1	Valine (*S*)	4/1	*R*	31	76
1	Valine (*R*)	4/1	*S*	35	78
1	Isoleucine (*S*)	2/1	*R*	26	67
1	Isoleucine (*R*)	2/1	*S*	24	68
1	Leucine (*S*)	2/1	*R*	11	64
1	Phenylalanine (*S*)	1/1		0	80
1	Phenylalanine (*S*)	2/1	*R*	6	70
2	Valine (*S*)	2/1	*R*	26	65
2	Alanine (*S*)	2/1	*R*	5	70
2	Phenylalanine (*S*)	2/1	*R*	7	68

a) Major enantiomer. b) The optical purities were determined on the basis of the specific rotations observed by reference to the values of the authentic samples.[1,2] c) The chemical yields were calculated on the basis of the amount of the amino acids used.

Table 2. Optical resolution of **1** and **2** with chiral amino acids in the presence of Fe^{3+}

Pyridoxal analog	Amino acid (confign.)	Fe^{3+} / Amino acid	**1** or **2** / Amino acid	Product		
				Confign.[a]	o.p./%[b]	c.y./%[c]
1	Valine (*S*)	1/1	2/1	*R*	20	87
1	Valine (*S*)	0.5/1	2/1	*R*	51	70
1	Valine (*S*)	0.5/1	4/1	*R*	70	76
1	Valine (*S*)	0.5/1	8/1	*R*	76	80
1	Valine (*R*)	0.5/1	2/1	*S*	54	68
1	Valine (*R*)	0.5/1	4/1	*S*	69	70
1	Leucine (*S*)	0.5/1	2/1	*R*	29	71
1	Leucine (*S*)	0.5/1	4/1	*R*	34	70
1	Leucine (*R*)	0.5/1	4/1	*S*	38	67
1	Isoleucine (*S*)	0.5/1	2/1	*R*	42	63
1	Isoleucine (*S*)	0.5/1	4/1	*R*	55	67
2	Valine (*S*)	0.5/1	2/1	*R*	50	72

a) Major enantiomer. b) The optical purities were determined on the basis of the specific rotations observed by reference to the values of the authentic samples.[1,2] c) The chemical yields were calculated on the basis of the amount of the amino acids used.

idinophanes. As the molar ratio of **1**/(*R*)-valine was increased, the apparent predominance of the intensity of the signals (a), (b) over (c), (d) was observed. These data sugested that (*R*)-valine coupled with (*S*)-**1** more preferentially than with (*R*)-**1**. In fact, the acidic hydrolysis of the Schiff base obtained through the reaction between (*R*)-valine and excess of racemic **1** and the subsequent removal of the unreacted **1** gave partially resolved **1** containing the (*S*)-enantiomer in excess. In the same way, employment of (*S*)-valine gave (*R*)-**1** in excess and employment of other chiral amino acids also resulted in the partial resolution of racemic **1**. The racemate of **2** was similarly resolved. The optical purities of the pyridinophanes isolated were determined by measuring their optical rotations. These results are shown in Table 1. The highest optical purities achieved by using valine indicated that the bulkiness of the α-substituents of the amino acids was important factor[12,13] dominating the optical purity of the products resolved. Throughout all runs, the efficiency of the resolution with amino acids seemed not so high.

In expectation of the enhancement of the optical purities of the resolution products, our attention was next directed towards addition of heavy metal ions to the reaction mixture for the Schiff base formation. It is known that some metal ions accelerate the formation of such Schiff bases, finally producing the chelate compounds of the Schiff bases.[14-17] Following preliminary experiments changing the metal ions employed, addition of iron(III) salt half equimolar to the amino acids served most effectively for the resolution of **1**. Furthermore, we found no racemization of the amino acid moiety in the Schiff base chelate complex (**13**) in the experiment using the system composed of **1**, chiral amino acid, and Fe^{3+} (4:1:0.5 in the molar ratio) under neutral conditions. On the basis of these preliminary results, the resolutions of racemic **1** and **2** were attempted in the presence of Fe^{3+} under neutral conditions, varying the kind and amount of the amino acid employed. The results are tabulated in Table 2. Again, the optical purity of the resolved pyridinophane (**1**) increased as the ratio of **1**/chiral amino acid increased, suggesting that this resolution is also ascribable to a kinetic asymmetric transformation.[18] The optical purities of **1** so obtained were almost twice obtained under similar conditions in the absence of Fe^{3+} (Table 1). In both cases, use of (*S*)-amino acids gave (*R*)-**1** in excess and *vice versa*. Use of a ratio larger than 4/1 for **1**/chiral amino acid resulted in no appreciable improvement in the optical purity of the product. Therefore, a combination of racemic pyridinophane–chiral valine–Fe^{3+} (4:1:0.5 in molar ratio) was regarded as the practical resolution system. Two treatments by this system were enough to give pure enantiomers of **1** and **2**.

The foregoing two types of resolution procedures using amino sugars and amino acids as the resolving agents differ from each other in several aspects. Concerning the resolution mechanisms, the former is based on the difference of the solubilities between the diastereomeric Schiff bases; whereas the later owes its specificity to the preferencial formation of one diastereomer; *i.e.*, to a difference in the reaction rate. In contrast to the readily available chiral amino acids, amino sugar derivatives are difficult to prepare. However, the efficiency of the optical resolution was much higher with the amino sugars than with amino acids.

Experimental

Solutions were evaporated under reduced pressure. Melting points are uncorrected. ^1H NMR spectra were recorded with a JEOL HA-100 spectrometer for amino sugar derivatives and with a JEOL JNM-FX 400 spectrometer for amino acid derivatives, using tetramethylsilane as the internal standard. Optical rotations were determined with a Perkin-Elmer Model 241 MC polarimeter. The racemic specimens of the pyridoxal-like pyridinophanes (**1** and **2**) were prepared according to our previous papers.[1,2]

3-Azido-3-deoxy-1,2:5,6-di-O-isopropylidene-β-D-idofuranose (7). Methanesulfonyl chloride (3.5 g) was added in portions at 0 °C to a solution of **8** (5.8 g) in dry pyridine (20 ml). The mixture was kept at the ambient temperature overnight, poured into ice-water, and extracted with chloroform. The extract was washed with 3% H_2SO_4, water, dried (Na_2SO_4) and evaporated to give **9** (6.4 g) as a yellow syrup: IR (film) 1185 cm^{-1}. To the solution of **9** in HMPA (35 ml) was added sodium azide (4.0 g). The mixture was heated at 100 °C with stirring for 11 h, cooled, diluted with ice-water (500 ml), and extracted with diethyl ether. The extract was washed with water, dried (Na_2SO_4) and evaporated to give a syrup (4.0 g). The syrup was chromatographed on silica gel with 5:1 (v/v) benzene–diethyl ether as the eluent to give **7** (3.3 g, 52% on the basis of **8**) as colorless crystals: mp 66—66.5 °C; $[\alpha]_D^{23}$ +74° (*c* 0.9, $CHCl_3$); IR(KBr) 2100 cm^{-1}. Found: C, 50.49; H, 6.76; N, 14.70%. Calcd for $C_{12}H_{19}O_5N_3$: C, 50.52; H, 6.71; N, 14.73%.

3-Amino-3-deoxy-1,2:5,6-di-O-isopropylidene-β-D-idofuranose (6). A solution of **7** (400 mg) in ethanol (20 ml) was stirred with Raney Ni (W-IV) in hydrogen atmosphere for 2 h. After filtration, the filtrate was evaporated to give crystalline **6** which was recrystallized from cyclohexane: yield 360 mg (99%); mp 98—98.5 °C; $[\alpha]_D^{22}$ +40° (*c* 0.26, $CHCl_3$); IR (KBr) 3380, 3330, and 1630 cm^{-1}; ^1H NMR ($CDCl_3$) δ= 1.24 (2H, s, NH_2), 3.35 (1H, d, $J_{3,4}$=4.0 Hz, H-3), and 5.93 (1H, d, $J_{1,2}$=3.5 Hz, H-1). Found: C, 55.68; H, 8.18; N, 5.24%. Calcd for $C_{12}H_{21}NO_5$: C, 55.58; H, 8.16; N, 5.40%.

Preparation of Schiff Base Mixture (10) and Isolation of Less Soluble Diastereomer (10a). A solution of racemic **1** (100 mg) and **6** (100 mg) in benzene (10 ml) was placed in an open flask and heated for 1 h under gentle boiling. Evaporation of the residual solvent gave **10** as yellow powder: ^1H NMR ($CDCl_3$) δ=6.16 (0.5H, d, $J_{1',2'}$=4.0 Hz, H-1'), and 6.18 (0.5H, d, $J_{1',2'}$=4.0 Hz, H-1'). This powder was dissolved in a hot mixture of benzene (10 ml) and cyclohexane (6 ml) and then cooled, giving yellow crystals (78 mg): mp 139—140 °C. The crystals were recrystallized from a mixture of benzene (3.5 ml) and cyclohexane (3.5 ml) to give **10a**: yield 60 mg (65% on the basis of half of **1** used); mp 149—150 °C; $[\alpha]_D^{26}$ +236° (*c* 0.064, $CHCl_3$); IR (KBr) 3470 and 1620 cm^{-1}; ^1H NMR ($CDCl_3$) δ=6.16 (1H, d, $J_{1',2'}$= 4.0 Hz, H-1'), the doublet at 6.18 completely disappeared, 8.01 (1H, s, H-6 of the pyridine ring), 8.79 (1H, s, -CH= N-), and signals due to the solvent: 1.42 (6H, s, cyclohexane), and 7.32 (4H, s, benzene). Found: C, 62.31; H, 7.50; N, 4.17; S, 10.23%. Calcd for $C_{25}H_{36}O_6N_2S_2 \cdot 2/3\ C_6H_6 \cdot 1/2\ C_6H_{12}$: C, 62.11; H, 7.49; N, 4.53; S, 10.36%.

Acidic Hydrolysis of 10a to (R)-*1.* The Schiff base **10a** (400 mg) was dissolved in hot 1,4-dioxane (40 ml) and cool-

ed. After addition of 1 M (1 M=1 mol dm^{-3}) HCl (10 ml), the mixture was kept at room temperature for 40 min, diluted with water (250 ml), and extracted with ethyl acetate (300 ml). The extract was washed with aq $NaHCO_3$ and water successively, dried (Na_2SO_4), and evaporated to give (*R*)-**1** as a syrup, which was chromatographed on silica gel with 6:1 (v/v) benzene–diethyl ether as the eluent: yield 169 mg (92%); $[\alpha]_D^{17}$ +347° (*c* 1.05, $CHCl_3$) (lit[1]) for the antipode $[\alpha]_D^{24}$ −366°); IR (film) 3100 and 1660 cm^{-1}. Found: C, 55.64; H, 5.92; N, 4.86; S, 22.30%. Calcd for $C_{13}H_{17}O_2NS_2$: C, 55.09; H, 6.05; N, 4.94, S, 22.63%.

^1H NMR Measurement of the Schiff Bases Derived from **1** *and* (R)-*Valine.* A methanol solution (5 ml) of **1** (20.4 mg) and (*R*)-valine (4.1 mg) was stirred at room temperature overnight and evaporated. The resulting residue was dissolved in C_6D_6 (1 ml) and the NMR spectrum of the solution was recorded at 400 MHz.

Attempt for the Resolution of **1** *and* **2** *with Amino Acids in the Absence of Fe^{3+}.* A typical procedure for the resolution of **1** is exemplified in the following. A methanol solution (100 ml) containing (*S*)-valine (59 mg) and **1** (283 mg) was stirred at room temperature overnight. The methanol was evaporated and the residue was washed with 1:1 (v/v) benzene–hexane to remove the unreacted **1**, which was recycled. After addition of ethyl acetate (200 ml), the mixture was adjusted to pH 1 with 1 M HCl. The ethyl acetate solution was washed with water, dried ($MgSO_4$), and evaporated to give a yellow syrup, which was chromatographed on silica gel with 5:1 (v/v) benzene–diethyl ether as the eluent to give (*R*)-rich **1**: yield 100 mg (71% on the basis of valine); $[\alpha]_D^{23}$ +76° (*c* 0.16, $CHCl_3$); optical purity 21%.

Resolution of **1** *and* **2** *with Amino Acids in the Presence of Fe^{3+}.* A typical procedure is exemplified in the following. To a stirred solution of (*S*)-valine (47 mg), 0.1 M methanolic sodium methoxide (4 ml), and **1** (453 mg) in methanol (200 ml) was added dropwise a solution of $Fe(ClO_4)_3 \cdot 8H_2O$ (100 mg) in methanol (50 ml). The mixture was stirred at room temperature overnight. The pH value of the media was around 7 during the reaction. Methanol was evaporated and the resulting residue was washed with chloroform. Ethyl acetate was added to the residue and the mixture was adjusted to pH 1 with 1 M HCl. The ethyl acetate solution was washed with water, dried ($MgSO_4$), and evaporated to dryness. The resulting residue was chromatographed on silica gel with 5:1 (v/v) benzene–diethyl ether as the eluent to give (*R*)-rich **1**: yield 86 mg (76% on the basis of valine), $[\alpha]_D^{24}$ +256° (*c* 0.12, $CHCl_3$); optical purity 70%. The aqueous layer underwent ion-exchange chromatography as described in the previous paper[3] to give 38 mg of valine; $[\alpha]_D^{23}$ +27.6° (*c* 0.90, 6 M HCl) (authentic (*S*)-valine $[\alpha]_D^{23}$ +28.8° (*c* 1.10, 6 M HCl)). The 70% optically pure (*R*)-**1** (80 mg), (*S*)-valine (28 mg), 0.1 M methanolic sodium methoxide (2.4 ml), and $Fe(ClO_4)_3 \cdot 8H_2O$ (60 mg) were treated again in methanol (200 ml). After a similar work up to the first resolution, almost pure (*R*)-**1** was obtained: yield 46 mg (68% on the basis of valine); $[\alpha]_D^{23}$ +360° (*c* 0.13, $CHCl_3$).

The authors express their gratitude to Dr. Jun Uzawa and Mrs. Tamiko Chijimatsu for recording and measuring the ^1H NMR spectra. Also, they are indebted to Dr. Haruo Homma and his collaborators for elemental analyses.

References

1) H. Kuzuhara, M. Iwata, and S. Emoto, *J. Am. Chem. Soc.*, **99**, 4173 (1977).
2) M. Ando, Y. Tachibana, and H. Kuzuhara, *Bull. Chem. Soc. Jpn.*, **55**, 829 (1982).
3) H. Kuzuhara, T. Komatsu, and S. Emoto, *Tetrahedron Lett.*, **1978**, 3563.
4) Y. Tachibana, M. Ando, and H. Kuzuhara, *Chem. Lett.*, **1982**, 1765.
5) T. Sakurai, H. Kuzuhara, and S. Emoto, *Acta Crystallogr., Sect. B*, **35**, 2984 (1979).
6) K. N. Slessor and A. S. Tracy, *Can. J. Chem.*, **47**, 3989 (1969).
7) O. A. Gansow and R. H. Holm, *J. Am. Chem. Soc.*, **91**, 573 (1969).
8) E. H. Abott and A. E. Martell, *J. Am. Chem. Soc.*, **92**, 5845 (1970).
9) Y. Numata, H. Okawa, and S. Kida, *Chem. Lett.*, **1979**, 293.
10) Yu. N. Belokon, I. E. Zel'tzer, N. N. Loim, V. A. Tsiryapkin, Z. N. Parnes, D. N. Kursanov, and V. M. Belikov, *J. Chem. Soc., Chem. Commun.*, **1979**, 789.
11) As far as the amino acids in this paper are concerned, *R*-enantiomers correspond to D-amino acids and *vice versa*.
12) M.-D. Tsai, S. R. Byrn, C.-j. Chang, H. G. Floss, and H. J. R. Weintraub, *Biochemistry*, **17**, 3177 (1978).
13) M.-D. Tsai, H. J. R. Weintraub, S. R. Byrn, C.-j. Chang, and H. G. Floss, *Biochemistry*, **17**, 3183 (1978).
14) E. Cesarotti, A. Pasini, and R. Ugo, *J. Chem. Soc., Dalton Trans.*, **1981**, 2147.
15) Y. Fujii, M. Matsufuru, A. Sato, and S. Tsuchiya, *Bull. Chem. Soc. Jpn.*, **54**, 2029 (1981).
16) L. Casella and M. Gullotti, *J. Am. Chem. Soc.*, **103**, 6338 (1981).
17) Y. Fujii, Y. Kuwana, S. Takahashi, K. Shimizu, and K. Hiroi, *Bull. Chem. Soc. Jpn.*, **55**, 2598 (1982).
18) E. L. Eliel, "Stereochemistry of Carbon Compounds," McGraw-Hill, New York (1962), p. 65.

Arylation and 1-Alkenylation on α-Position of Ketones *via* Tributyltin Enolates Catalyzed by Palladium Complex

Masanori KOSUGI, Isao HAGIWARA, Takao SUMIYA, and Toshihiko MIGITA*
Department of Chemistry, Faculty of Technology, Gunma University, Kiryu, Gunma 376
(Received August 8, 1983)

The reaction of tributyltin enolates, prepared from tributyltin methoxide and enol acetates *in situ*, with aryl and 1-alkenyl bromides in the presence of dichlorobis(tri-*o*-tolylphosphine)palladium was found to give α-aryl and α-(1-alkenyl) ketones, respectively, in good yields with essentially complete retention of the enol acetate regiochemistry.

Aryl and 1-alkenyl halides, except those bearing electron-withdrawing groups at the ortho and/or para positions, are usually unreactive toward nucleophilic displacement reactions, and thus fail to react with metal enolates under usual conditions.[1] Various methods of α-phenylation[2] and α-vinylation[3] of metal enolates are now developed. However, these require the strong basic conditions or multistep operations.

While organotin enolates have been shown to react both with carbonyl compounds to give addition products[4] and with alkyl halides to give coupling products,[4,5] there is no example of the reaction with aryl and 1-alkenyl halides. In our previous communications, we briefly reported that tributyltin enolates, irrespective of their tautomeric structures, α-stannyl ketones or enol stannyl ethers, reacted with aryl and 1-alkenyl halides in the presence of a catalytic amount of dichlorobis(tri-*o*-tolylphosphine)palladium to give α-aryl and α-(1-alkenyl) ketones in good yields.[6] Trial for similar coupling reaction with enol silyl ether *via* tin enolates was also reported by Kuwajima *et al.*[7] This paper describes the details of our results. The reaction is thought to proceed through the oxidative-adduct of the halides to palladium, followed by metathesis with tin compounds, and then reductive elimination.

Results and Discussion

Acetonylation of Aryl Bromides. Initial studies were focused on the palladium-catalyzed acetonylation of aryl bromides with the isolated acetonyltributyltin. The yield of phenylacetone, however, is rather low and substantial amounts of acetone are produced. These imply that the desired coupling competes with thermal decomposition of acetonyltributyltin under the prolonged heating conditions. Then, it may be desirable that relative concentration of acetonyltributyltin to organic halides is kept as small as possible. Indeed the best procedure was found to be the method in which acetonyltributyltin was prepared *in situ*.

$$Bu_3SnOMe + AcOCMe{=}CH_2 \longrightarrow [Bu_3SnCH_2COMe] + AcOMe$$

$$[Bu_3SnCH_2COMe] + ArBr \xrightarrow{[Pd]} ArCH_2COMe + Bu_3SnBr$$

Table 1. Pd-Catalyzed acetonylation of aryl bromides *via* acetonyltributyltin

R-C_6H_4-Br	Catalyst	Yield of $ArCH_2COMe$/%[a]		
H-	$Pd(Ph_3P)_4$		(22)	
H-	$PdCl_2(Ph_3P)_2$		(15)	
H-	$PdCl_2[(o\text{-}MeC_6H_4)_3P]_2$	78	(83)	(30)[b] (0)[c]
H-	$PdCl_2[(p\text{-}MeC_6H_4)_3P]_2$		(16)	
H-	$PdCl_2[(o\text{-}ClC_6H_4)_3P]_2$		(68)	
H-	$PdCl_2[(Me_2C_6H_3)_3P]_2$		(0)	
o-Me-	$PdCl_2[(o\text{-}MeC_6H_4)_3P]_2$	91		
m-Me-		88		
p-Me-		80		(27)[b]
o-Me-		90		(61)[b]
p-MeO-		51		
o-Cl-		80		
p-Cl-		73		
p-Me_2N-		71		
2,4,6-Me_3-		94		
o-Ac-		0		
p-Ac-		64		
p-CN-		0		
p-NO_2-		0		

a) Isolated yield based on bromide, GLC yield in parenthesis. b) Reaction with PhI. c) Reaction with PhCl.

The procedure is quite simple. Thus, just heating of a stirred solution of tributyltin methoxide (15 mmol), isopropenyl acetate (15 mmol), aryl bromide (10 mmol), and palladium complex (0.1 mmol) in toluene (5 ml) under argon at 100 °C for 5 h, followed by usual work up gave arylacetone. The results are shown in Table 1.

The reaction was fairly sensitive to the nature of the ligand on the dichloropalladium catalyst. The best ligand was tri-*o*-tolylphosphine. The reaction using dichlorobis(tri-*p*-tolylphosphine)palladium as a catalyst, gave only poor yield, although tri-*p*-tolylphosphine may have an electronic effect resembling to that of tri-*o*-tolylphosphine. Tris(*o*-chlorophenyl)phosphine ligand providing almost the same steric situation around palladium with that of tri-*o*-tolylphosphine was the next better ligand, but more bulkier trimesitylphosphine was not proper as ligands. Tri-*o*-tolylphosphine was previously demonstrated by Heck *et al.* to be more suitable ligand than triphenylphosphine for the palladium-catalyzed vinylation of aryl halides.[8] They explained this in terms of difference in easiness of phosphonium salt formation between the two ligands. However, even with triphen-

ylphosphine, it was found that aryl bromide did not form phosphonium salt effectively although aryl iodide did.[9] Then, phosphonium salt formation seems not to be an essential factor influencing the efficiency of the catalyst. Although the reason why tri-*o*-tolylphosphine was effective for the present reaction is not made clear comprehensively, we feel that steric situation around palladium provided by ligand is responsible.

As shown in Table 1, among halobenzenes, bromobenzene was the best substrate. Chlorobenzene did not react with this reagent, and iodobenzene which was considered to be more reactive, gave the product in poor yields. The isolated yields were reasonably high irrespective of the substituent (Me_2N–, MeO–, Me–, Cl–, or Ac–) in aryl bromide, indicating that the reaction can be used for the preparation of arylacetone. However, there were some limitations, that is, the reaction cannot be applied to the bromide having *p*-NO_2, *p*-CN, and *o*-Ac. The presence of nitrobenzene in the reaction mixture for the acetonylation of bromobenzene did not affect the yield of phenylacetone. This means that the presence of nitro group in reacting systems does not disturb the catalytic cycle. Since the aryl bromide bearing electron-withdrawing substituent easily reacts with palladium to form the oxidative-adduct,[10] these substituent groups seem to retard subsequent steps, metathesis or reductive-elimination.

The reaction can be carried out with the substrates bearing Me–, MeO–, and Cl– at an ortho position, and even with mesityl bromide. Thus, the reaction is not sensitive to the steric effect of ortho substituents, except *o*-Ac– group, in aryl bromides.

Stepwise acetonylation of *p*- and *m*-dibromobenzene could be attained by changing the molar ratio of the reactants. Usage of three molar excess of the tin enolates gave the diacetonylbenzene in 81 and 84% yield based on the corresponding dibromobenzene, respectively, while usage of three molar excess of dibromobenzenes gave *p*- and *m*-acetonylbromobenzenes in 65 and 57% yields based on the reagent, respectively. The reaction of *o*-dibromobenzene was rather complicated. Under the conditions of monoacetonylation, *o*-acetonylbromobenzene was obtained in 56% yield, but under the conditions of double acetonylation the sole isolated product was phenylacetone (13%), indicating that *o*-acetonylbromobenzene once formed was reduced under the conditions.

α-Phenylation of Ketones. Even though the α-arylation of ketones has received much attention,[2] there is still a need for a simple and regio-controlled procedure for this conversion. Since arylated acetone was effectively produced by palladium-catalyzed reaction between α-stannylacetone and aryl bromide, we tried to extend the reaction to various stannyl ketones, and to utilize the reaction for α-phenylation of ketones by the following two steps.

$$R^1COCHR^2R^3 \longrightarrow R^1\overset{OAc}{\overset{|}{C}}{=}CR^2R^3 \xrightarrow[[Pd],\ PhBr]{Bu_3SnOMe} R^1COCPhR^2R^3 + Bu_3SnBr + AcOMe$$

Table 2. Preparation of enol acetate

Ketone	Method[a]	Enol acetate	Yield/%[b]
$MeCOBu^t$	A	$CH_2{=}C(OAc)Bu^t$	44
MeCOPh	A	$CH_2{=}C(OAc)Ph$	69
$MeCOCH{=}CMe_2$	A	$CH_2{=}C(OAc)CH{=}CMe_2$	78
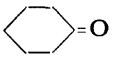	A	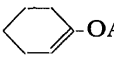	88
MeCOEt	C	$CH_2{=}C(OAc)Et$	—
	A	$Me(AcO)C{=}CHMe$	47
$MeCOPr^i$	A	$CH_2{=}C(OAc)Pr^i$	34
	B	$Me(AcO)C{=}CMe_2$	76

a) A: Reaction with ketene. B: Reaction with acetic anhydride and perchloric acid. C: See Experimental part. b) Isolated yield.

Table 3. Pd-Catalyzed α-phenylation of ketones *via* tributyltin enolates

Enol acetate	Product	Yield/%[a]
$CH_2{=}C(OAc)Bu^t$	$PhCH_2COBu^t$	86
$CH_2{=}C(OAc)Ph$	$PhCH_2COPh$	90
$CH_2{=}C(OAc)CH{=}CMe_2$	$PhCH_2COCH{=}CMe_2$	64
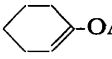	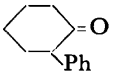	54
$CH_2{=}C(OAc)Et$	$PhCH_2COEt$	(67)
$Me(AcO)C{=}CHMe$	MeCOCHPhMe	60
$CH_2{=}C(OAc)Pr^i$	$PhCH_2COPr^i$	87
$Me(AcO)C{=}CMe_2$	$MeCOCPhMe_2$	33(38)

a) Isolated yield, GLC yield in parenthesis.

The first step has been investigated thoroughly, including its regiochemistry.[11] The following method was particularly useful to prepare enol acetates used here: (A) treatment of ketone with ketene and (B) treatment of ketone with acetic anhydride and perchloric acid. Enol acetates thus prepared are shown in Table 2.

The second step is a one-pot reaction involving tributyltin enolates prepared *in situ* from the enol acetates and tributyltin methoxide as cited above. The tin enolate which would be formed *in situ* have been known to exist in either or both of tautomeric structures, α-stannyl ketones or enol stannyl ethers.[12] α-Phenyl ketones, irrespective of the tautomeric structure of the tin reagents, were obtained in reasonably high yields with complete retention of the acetate regiochemistry.

Thus, as shown in Table 3, the reaction with 2-acetoxy-1-butene and -2-butene gave exclusively 1-phenyl and 2-phenyl-butanone, respectively. Low yields from enol acetates bearing methyl substituents on the reaction site (particularly 3-methyl-2-acetoxy-2-butene) may be due to the steric hindrance. The enol ester of aldehyde cannot be used, because the produced α-phenyl aldehyde adds tributyltin methoxide.

Thus, α-arylation of ketones with complete retention of the acetate regiochemistry could be attained by two steps starting from ketones.

1-Alkenylation on α-Position of Ketones. The

Table 4. Pd-Catalyzed 1-alkenylation on α-position of ketones *via* tributyltin enolates

Enol acetate	Bromide	Product	Yield/%[a]
CH_2=C(OAc)Me	Me_2C=CHBr	Me_2C=$CHCH_2COMe$	62
CH_2=C(OAc)Bu^t	CH_2=CMeBr	CH_2=$CMeCH_2COBu^t$	53
	Me_2C=CHBr	Me_2C=$CHCH_2COBu^t$	81
	Me_2C=CMeBr	Me_2C=$CMeCH_2COBu^t$	86
	(*E*) MeCH=CMeBr	(*E*) MeCH=$CMeCH_2COBu^t$	76
	(*Z*) MeCH=CMeBr	(*Z*) MeCH=$CMeCH_2COBu^t$	90
CH_2=C(OAc)Ph	Me_2C=CHBr	Me_2C=$CHCH_2COPh$[b]	74
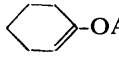		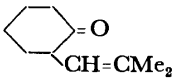	32
CH_2=C(OAc)Et		Me_2C=$CHCH_2COEt$	(53)
Me(AcO)C=CHMe		MeCOCHMeCH=CMe_2	35
CH_2=C(OAc)Pr^i		Me_2C=$CHCH_2COPr^i$	74
Me(AcO)C=CMe_2		MeCOCMe_2CH=CMe_2	(8)

a) Isolated yield based on bromide, GLC yield in parenthesis. b) α,β-Unsaturated ketone was detected by NMR. (*ca.* 5%).

success of α-arylation of ketones *via* tin enolates catalyzed by palladium complex suggests that similar reaction can be applied to the reaction between tin enolates and 1-alkenyl bromides, which may give allylic ketones. We found that various allylic ketones were obtained in good yields under the conditions similar to those for the reaction of aryl bromide. Results are shown in Table 4.

The reaction seems sensitive to steric hindrance caused by substituent on enol acetate. The reaction of enol acetates bearing terminal methylene gave the 1-alkenylated ketones generally in high yields, while lower yields were obtained for the substrates having substituents on the reaction site. Number and position of substituents on 1-alkenyl bromide seem not to give the serious effect on the product yield. The configuration of 1-alkenyl bromide was completely retained. Thus from (*E*)- and (*Z*)-2-bromo-2-butene, (*E*)- and (*Z*)-2,2,5-trimethyl-5-hepten-3-one were obtained exclusively, respectively.

Experimental

Materials. Tributyltin methoxide was prepared by the reaction of tributyltin chloride with sodium methoxide.[13] *o*-Bromotoluene,[14] *o*-chlorobromobenzene,[15] *o*-bromoanisole,[15] mesityl bromide,[16] 2-bromopropene,[17] 3-methyl-2-bromo-2-butene,[18] 2-methyl-1-bromo-2-propene,[18] (*E*)-2-bromo-2-butene,[18] (*Z*)-2-bromo-2-butene,[17] triarylphosphines,[19] tetrakis(triphenylphosphine)palladium,[20] and dichlorobis(triarylphosphine)palladium[21] were prepared from the method described in literatures. 3,3-Dimethyl-2-acetoxy-1-butene, α-acetoxystyrene, 1-cyclohexenyl acetate, 4-methyl-2-acetoxy-1,3-pentadiene, 2-acetoxy-2-butene, and 3-methyl-2-acetoxy-1-butene were prepared by treatment of the corresponding ketones with ketene in the presence of small amounts of sulfuric acid.[11a] 3-Methyl-2-acetoxy-2-butene was prepared by treatment of the ketone with acetic anhydride and perchloric acid.[11b] 2-Acetoxy-1-butene which could be prepared by treatment of the ketone with triphenylmethyllithium followed by acetic anhydride was not obtained by the method.[11c,d] Then it was prepared by the addition of acetic acid to 1-butyne in the presence of mercury(II) acetate.[11e] Other substrates were available commercially and used after distillation or recrystallization.

Reaction Procedures. A stirred solution of tributyltin methoxide (15 mmol), a particular enol acetate (15 mmol), bromobenzene or 1-alkenyl bromide (10 mmol), and $PdCl_2$-[(*o*-$MeC_6H_4)_3P]_2$ (0.1 mmol) in toluene (5 ml) was heated under argon at 100 °C for 5 h. After evaporation of the solvent and methyl acetate, column chromatograph of the residue (silica gel; cyclohexane followed by diethyl ether as eluants) provided the α-phenyl or α-(1-alkenyl) ketone in the ethereal elute, from which the products were isolated by distillation under reduced pressure. Some α-(1-alkenyl) ketones were obtained by distilling the reaction mixture directly under reduced pressure.

Products. The structure of the products were deduced based on the analytical and spectroscopic data recorded here. Boiling points were uncorrected.

Phenylacetone: Bp 88—92 °C/15 mmHg (1 mmHg= 133.322 Pa). IR Aldrich 742A.[22] ^{1}H NMR (CCl_4) δ=2.00 (s, 3H), 3.50 (s, 2H), and 7.30 (s, 5H).

o-Tolylacetone: Bp 97—99 °C/16 mmHg. IR (neat) 1718 (C=O), 1605 (C=C), and 1498 cm^{-1} (C=C). ^{1}H NMR (CCl_4) δ=2.01 (s, 3H), 2.25 (s, 3H), 3.62 (s, 2H), and 7.14 (s, 4H). MS (20 eV) *m/e* (rel intensity) 148 (M^+, 73), 106 (82), 105 (100), and 43 (100). Found: C, 81.16; H, 8.08%. Calcd for $C_{10}H_{12}O$: C, 81.08; H, 8.16%.

m-Tolylacetone: Bp 95—97 °C/14 mmHg. IR (neat) 1715 (C=O), 1605 (C=C), and 1490 cm^{-1} (C=C). ^{1}H NMR (CCl_4) δ=2.04 (s, 3H), 2.31 (s, 3H), 3.51 (s, 2H), and 6.80—7.35 (m, 4H). MS (20 eV) *m/e* (rel intensity) 148 (M^+, 98), 106 (100), 105 (100), and 43 (100). Found: C, 80.67; H, 8.05%. Calcd for $C_{10}H_{12}O$: C, 81.04; H, 8.16%.

p-Tolylacetone: Bp 122—125 °C/35 mmHg. IR (neat) 1710 (C=O), 1605 (C=C), and 1512 cm^{-1} (C=C). ^{1}H NMR (CCl_4) δ=2.00 (s, 3H), 2.30 (s, 3H), 3.49 (s, 2H), and 7.00 (s, 4H). MS (30 eV) *m/e* (rel intensity) 148 (M^+, 15), 106 (32), 105 (100), and 43 (100). Found: C, 81.38; H, 8.46%. Calcd for $C_{10}H_{12}O$: C, 81.04; H, 8.16%.

p-Methoxyphenylacetone: Bp 88—90 °C/3 mmHg. IR (neat) 1710 (C=O), 1610 (C=C), 1512 (C=C), and 1248 cm^{-1} (C-O-C). ^{1}H NMR (CCl_4) δ=2.02 (s, 3H), 3.49 (s, 2H), 3.80 (s, 3H), and 6.61, 6.94 (ABq, *J*=9 Hz, 4H). MS

(20 eV) *m/e* (rel intensity) 164 (M^+, 7) 149 (10), 121 (33), and 43 (100). Found: C, 72,77; H, 7.43%. Calcd for $C_{10}H_{12}O_2$: C, 73.15; H, 7.37%.

o-*Methoxyphenylacetone*: Bp 118 °C/15 mmHg. IR (neat) 1718 (C=O), 1603 (C=C), 1498 (C=C), and 1250 cm^{-1} (C-O-C). ^1H NMR (CCl_4) δ=2.00 (s, 3H), 3.55 (s, 2H), 3.80 (s, 3H), and 6.67—7.35 (m, 4H). MS (20 eV) *m/e* (rel intensity) 164 (M^+, 100), 122 (100), 121 (100), and 43 (100).

p-*Chlorophenylacetone*: Bp 115—117 °C/15 mmHg. IR (neat) 1717 (C=O), 1598 (C=C), and 1491 cm^{-1} (C=C). ^1H NMR (CCl_4) δ=2.05 (s, 3H), 3.51 (s, 2H), and 6.97, 7.20 (ABq, *J*=8 Hz, 4H). MS (20 eV) *m/e* (rel intensity) 170 (M^+, 3), 168 (10), 127 (9), 125 (30), and 43 (100). Found: C, 64.15; H, 5.56%. Calcd for C_9H_9OCl: C, 64.11; H, 5.38%.

o-*Chlorophenylacetone*: Bp 119 °C/18 mmHg. IR (neat) 1726 (C=O), 1573 (C=C), and 1473 cm^{-1} (C=C). ^1H NMR (CCl_4) δ=2.09 (s, 3H), 3.71 (s, 2H), and 7.05—7.60 (m, 4H). MS (20 eV) *m/e* (rel intensity) 168 (1), 127 (9), 125 (27), and 43 (100).

p-*(Dimethylamino)phenylacetone*: Bp 103—104 °C/2.5 mmHg. IR (neat) 1710 (C=O), 1610 (C=C), 1520 (C=C), and 1350 cm^{-1} (C-N). ^1H NMR (CCl_4) δ=1.95 (s, 3H), 2.95 (s, 6H), 3.44 (s, 2H), and 6.61, 7.01 (ABq, *J*=9 Hz, 4H). MS (20 eV) *m/e* (rel intensity) 177 (M^+, 13), 134 (100), and 43 (7).

p-*Acetylphenylacetone*: Bp 128—130 °C/2.5 mmHg, mp 43—44 °C. IR (neat) 1718 (C=O), 1680 (C=O), 1603 (C=C), and 1508 cm^{-1} (C=C). ^1H NMR (CCl_4) δ=2.01 (s, 3H), 3.45 (s, 3H),3.59 (s, 2H), and 7.16, 7.79 (ABq, *J*=8 Hz, 4H). MS (30 eV) *m/e* (rel intensity) 176 (M^+, 2), 161 (9), 134 (100), 133 (10), 119 (20), 91 (49), and 43 (100). Found: C, 75.17; H, 6.85%. Calcd for $C_{11}H_{12}O_2$: C, 74.98; H 6.86%.

Mesitylacetone: Bp 130 °C/10 mmHg, mp 60 °C. IR (neat) 1720 (C=O), 1611 (C=C), and 1487 cm^{-1} (C=C). ^1H NMR (CCl_4) δ=1.98 (s, 3H), 2.20 (s, 9H), 3.53 (s, 2H), and 6.75 (s, 2H). MS (20 eV) *m/e* (rel intensity) 176 (M^+, 24), 134 (16), 133 (100), and 43 (18). Found: C, 81.81; H, 9.54%. Calcd for $C_{12}H_{16}O$: C, 81.77; H, 9.15%.

p-*Diacetonylbenzene*: Bp 118 °C/0.5 mmHg, mp 46—47 °C. IR (neat) 1715 (C=O), 1610 (C=C), and 1511 cm^{-1} (C=C). ^1H NMR (CCl_4) δ=2.07 (s, 6H), 3.58 (s, 4H), and 7.10 (s, 4H). MS (20 eV) *m/e* (rel intensity) 190 (M^+, 13), 148 (78), 147 (13), 105 (40), and 43 (100). Found: C, 75.75; H, 7.65%. Calcd for $C_{12}H_{14}O_2$: C, 75.76; H, 7.42%.

m-*Diacetonylbenzene*: Bp 127 °C/2 mmHg. IR (neat) 1712 (C=O), 1602 (C=C), and 1487 cm^{-1} (C=C). ^1H NMR (CCl_4) δ=2.08 (s, 6H), 3.59 (s, 4H), and 6.93—7.28 (m, 4H). MS (20 eV) *m/e* (rel intensity) 190 (M^+, 9), 148 (18), 147 (21), 105 (21), and 43 (100). Found: C, 75.57; H, 7.24%. Calcd for $C_{12}H_{14}O_2$: C, 75.76; H, 7.42%.

p-*Bromophenylacetone*: Bp 91—92 °C/1 mmHg. IR (neat) 1718 (C=O), 1592 (C=C), and 1488 cm^{-1} (C=C). ^1H NMR (CCl_4) δ=2.10 (s, 3H), 3.58 (s, 2H), and 7.05, 7.47 (ABq, *J*=9 Hz, 4H). MS (20 eV) *m/e* (rel intensity) 214 (M^+, 27), 212 (28), 171 (32), 169 (30), and 43 (100). Found: C, 50.62; H, 4.71%. Calcd for C_9H_9OBr: C, 50.73; H, 4.26%.

m-*Bromophenylacetone*: Bp 83 °C/0.3 mmHg. IR (neat) 1718 (C=O), 1591 (C=C), and 1471 cm^{-1} (C=C). ^1H NMR (CCl_4) δ=2.10 (s, 3H), 3.59 (s, 2H), and 7.05—7.50 (m, 4H). MS (20 eV) *m/e* (rel intensity) 214 (M^+, 63), 212 (64), 171 (14), 169 (14), and 43 (100).

o-*Bromophenylacetone*: Bp 88—92 °C/0.6 mmHg. IR (neat) 1722 (C=O), 1597 (C=C), and 1472 cm^{-1} (C=C). ^1H NMR (CCl_4) δ=2.11 (s, 3H), 3.73 (s, 2H), and 6.90—7.70 (m, 4H). MS (20 eV) *m/e* (rel intensity) 171 (100), 169 (100), and 43 (100).

1-Phenyl-2-butanone: Bp 102—103 °C/15 mmHg. IR Aldrich 742C.[22] ^1H NMR (CCl_4) δ=0.96 (t, *J*=7 Hz, 3H), 2.35 (q, *J*=7 Hz, 2H), 3.55 (s, 2H), and 7.19 (s, 5H).

3-Phenyl-2-butanome: Bp 94—95 °C/14 mmHg. (107 °C/22 mmHg)[23] IR (neat) 1718 (C=O), 1600 (C=C), and 1496 cm^{-1}(C=C). ^1H NMR (CCl_4) δ=1.35 (d, *J*=7 Hz, 3H), 1.97 (s, 3H), 3.68 (q, *J*=7 Hz, 1H), and 7.25 (s, 5H). MS (20 eV) *m/e* (rel intensity) 148 (M^+, 29), 133 (9), 106 (25), 105 (100), and 43 (100). Found: C, 80.62; H, 8.25%. Calcd for $C_{10}H_{12}O$: C, 81.04; H, 8.16%.

1-Phenyl-3-methyl-2-butanone: Bp 114—115 °C/25 mmHg. IR (neat) 1712 (C=O), 1602 (C=C), and 1496 cm^{-1} (C=C). ^1H NMR (CCl_4) δ=1.05 (d, *J*=7 Hz, 6H), 2.61 (h, *J*=7 Hz, 1H), 3.61 (s, 2H), and 7.18 (s, 5H). MS (20 eV) *m/e* (rel intensity) 162 (M^+, 27), 119 (5), 92 (22), 91 (100), 71 (100), 44 (19), and 43 (100). Found: C, 81.79; H, 8.45%. Calcd for $C_{11}H_{14}O$: C, 81.44; H, 8.70%.

3-Phenyl-3-methyl-2-butanone: Mp 99—101 °C/16.5 mmHg, Ir, (neat) 1710 (C=O), 1599 (C=C), and 1495 cm^{-1} (C=C). ^1H NMR (CCl_4) δ=1.43 (s, 6H), 1.81 (s, 3H), and 7.19 (s, 5H). MS (20 eV) *m/e* (rel intensity) 162 (M^+, 6), 120 (36), 119 (100), 43 (25), and 15 (9). Found C, 80.86; H, 8.78%. Calcd for $C_{11}H_{14}O$: C, 81.44; H, 8.70%.

1-Phenyl-3,3-dimethyl-2-butanone: Bp 110—111 °C/18 mmHg. IR (neat) 1710 (C=O), 1600 (C=C), and 1493 cm^{-1} (C=C). ^1H NMR (CCl_4) δ=1.15 (s, 9H), 3.70 (s, 2H), and 7.20 (s, 5H). MS (20 eV) *m/e* (rel intensity) 176 (M^+, 2), 119 (1), 92 (26), 91 (28), 85 (100), 58 (25), and 57 (100). Found: C, 82.14; H, 9.00%. Calcd for $C_{12}H_{16}O$: C, 81.77; H, 9.15%.

2-Phenylcyclohexanone: Bp 143—145 °C/14 mmHg, mp 58—59 °C (155 °C/13 mmHg, 60 °C)[24] IR Aldrich 742E.[22]

1-Phenyl-4-methyl-3-penten-2-one: Bp 80—81 °C/1.5 mmHg. IR (neat) 1685 (C=O), 1618 (C=C), and 1496 cm^{-1} (C=C). ^1H NMR (CCl_4) δ=1.79 (s, 3H), 2.07 (s, 3H), 3.52 (s, 2H), 5.88 (s, 1H), and 7.19 (s, 5H). MS (20 eV) *m/e* (rel intensity) 174 (M^+, 14), 119 (3), 92 (3), 91 (34), 83 (100), 56 (5), and 55 (69). Found: C, 82.37; H, 8.26%. Calcd for $C_{12}H_{14}O$: C, 82.77; H, 8.10%.

Phenylacetophenone: Bp 115—117 °C/1 mmHg, mp 54—55 °C (160 °C/5 mmHg, 56 °C)[25] IR Aldrich 748E.[22]

5-Methyl-4-hexen-2-one: Bp 43—45 °C/17 mmHg. IR (neat) 1720 cm^{-1} (C=O). ^1H NMR (CCl_4) δ=1.65 (s, 3H), 1.73 (s, 3H), 2.06 (s, 3H), 2.98 (d, *J*=7 Hz, 2H), and 5.23 (t, *J*=7 Hz, 1H). MS (20 eV) *m/e* (rel intensity) 112 (M^+, 100), 97 (100), 70 (100), 69 (100), 43 (100), and 15 (13). Found: C, 75.31; H, 11.12%. Calcd for $C_7H_{12}O$: C, 74.95; H, 10.78%.

4,5-Dimethyl-4-hexen-2-one: Bp 53 °C/21 mmHg. IR (neat) 1712 cm^{-1} (C=O). ^1H NMR (CCl_4) δ=1.69 (s, 9H), 2.01 (s, 3H), and 3.01 (s, 2H). MS (20 eV) *m/e* (rel intensity) 126 (M^+, 93), 111 (100), 84 (100), 83 (100), 43 (100), and 15 (8). Found: C, 75.83; H, 11.18%. Calcd for $C_8H_{14}O$: C, 76.14; H, 11.18%.

6-Methyl-5-hepten-3-one: IR (neat) 1718 cm^{-1}(C=O). ^1H NMR (CCl_4) δ=1.03 (t, *J*=7 Hz, 3H), 1.67 (s, 3H), 1.79 (s, 3H), 2.38 (q, *J*=7 Hz, 2H), 3.01 (d, *J*=7 Hz, 2H), and 5.30 (t, *J*=7 Hz, 1H). MS (20 eV) *m/e* (rel intensity) 126 (M^+, 10), 97 (7), 70 (2), 69 (23), 57 (100), and 29 (74). Found: C, 75.63; H, 11.20%. Calcd for $C_8H_{14}O$: C, 76.14; H, 11.18%.

3,5-Dimethyl-4-hexen-2-one: Bp 56—58 °C/20 mmHg. IR (neat) 1715 cm^{-1} (C=O). ^1H NMR (CCl_4) δ=1.05 (d, *J*=7 Hz, 3H), 1.73 (s, 6H), 3.29 (d of q, *J*=10 and 7 Hz, 1H), and 4.98 (d, *J*=10 Hz, 1H). Found: C, 76.34; H, 11.51%. Calcd for $C_8H_{14}O$: C, 76.14; H, 11.18%.

2,6-Dimethyl-5-hepten-3-one: Bp 69—70 °C/20 mmHg. IR (neat) 1712 cm^{-1} (C=O). ^1H NMR (CCl_4) δ=1.09 (d, *J*=7 Hz, 6H), 1.62 (s, 3H), 1.74 (s, 3H), 2.55 (h, *J*=7 Hz, 1H), 3.05 (d, *J*=7 Hz, 2H), and 5.27 (t, *J*=7 Hz, 1H). MS (20 eV) *m/e* (rel intensity) 140 (M^+, 69), 97 (59), 71 (100), 70 (63), 69 (100), 44 (93), and 43 (100). Found: C, 76.85; H, 11.44%. Calcd

for $C_9H_{16}O$: C, 77.09; H, 11.50%.

3,3,5-Trimethyl-4-hexen-2-one: IR (neat) 1709 cm^{-1} (C=O). ^1H NMR (CCl_4) δ=1.17 (s, 6H), 1.49 (s, 3H), 1.71 (s, 3H), 2.02 (s, 3H), and 5.27 (s, 1H). MS (20 eV) *m/e* (rel intensity) 140 (M^+, 37), 95 (100), and 43 (62). Found: C, 76.65; H, 11.70%. Calcd for $C_9H_{16}O$: C, 77.09; H, 11.50%.

2,2,5-Trimethyl-5-hexen-3-one: Bp 62—63 °C/34 mmHg. IR (neat) 1713 cm^{-1} (C=O). ^1H NMR (CCl_4) δ=1.15 (s, 9H), 1.71 (s, 3H), 3.11 (s, 2H), 4.67 (s, 1H), and 4.81 (s, 1H). MS (20 eV) *m/e* (rel intensity) 140 (M^+, 53), 85 (100), 83 (100), 58 (38), 57 (100), 56 (38), and 55 (68). Found: C, 76.81; H, 11.63%. Calcd for $C_9H_{16}O$: C, 77.09; H, 11.50%.

2,2,6-Trimethyl-5-hepten-3-one: Bp 72—73 °C/19 mmHg. IR (neat) 1710 cm^{-1} (C=O). ^1H NMR (CCl_4) δ=1.10 (s, 9H), 1.60 (s, 3H), 1.73 (s, 3H), 3.11 (d, J=7 Hz, 2H), and 5.24 (t, J=7 Hz, 1H). MS (20 eV) *m/e* (rel intensity) 154 (M^+, 4), 97 (19), 85 (77), 70 (18), 69 (46), 58 (18), and 57 (100). Found: C, 77.93; H, 11.95%. Calcd for $C_{10}H_{18}O$: C, 77.87; H, 11.76%.

2,2,5,6-Tetramethyl-5-hepten-3-one: Bp 79—80 °C/16 mmHg. IR (neat) 1715 cm^{-1} (C=C). ^1H NMR (CCl_4) δ=1.17 (s, 9H), 1.58 (s, 6H), and 1.70 (s, 3H). MS (20 eV) *m/e* (rel intensity) 168 (M^+, 19), 111 (29), 85 (99), 84 (28), 83 (64), 58 (28), and 57 (100). Found: C,78.42; H, 11.97%. Calcd for $C_{11}H_{20}O$: C, 78.51; H, 11.98%.

(E)-*2,2,5-Trimethyl-5-hepten-3-one*: Bp 70—71 °C/15 mmHg. IR (neat) 1710 cm^{-1} (C=O). ^1H NMR (CCl_4) δ= 1.15 (s, 9H), 1.58 (s, 3H), 1.60 (d, J=7 Hz, 3H), 3.08 (s, 2H), and 5.15 (t, J=7 Hz, 1H). ^{13}C NMR 26.4 (q), 214 (s), 47 (t), 130 (s), 123 (d), 13.5 (q), 16.1 (q), and 44.4 (s), MS (20 eV) *m/e* (rel intensity) 154 (M^+, 20), 97 (64), 85 (100), 70 (82), 69 (100), 58 (79), and 57 (100). Found: C, 77.72; H, 11.79%. Calcd for $C_{10}H_{18}O$: C, 77.87; H, 11.76%.

(Z)-*2,2,5-Trimethyl-5-hepten-3-one*: Bp 67—69 °C/14 mmHg. IR (neat) 1711 cm^{-1} (C=O). ^1H NMR (CCl_4) δ= 1.16 (s, 9H), 1.50 (d, J=7 Hz, 3H), 1.60 (s, 3H), 3.12 (s, 2H), and 5.30 (q, J=7 Hz, 1H). ^{13}C NMR 26.4 (q), 44.5 (s), 213 (s), 39.3 (t), 129.9 (s), 123.0 (d), 13.5 (q), and 24.1 (q). MS (20 eV) *m/e* (rel intensity) 154 (M^+, 15), 97 (61), 85 (100), 70 (75), 69 (97), 58 (71), and 57 (100). Found: C, 77.62; H, 11.78%. Calcd for $C_{10}H_{18}O$: C, 77.87; H, 11.76%.

2-(2-methyl-1-propenyl)cyclohexanone: Bp 95—97 °C/15 mmHg. IR (neat) 1710 cm^{-1} (C=O). ^1H NMR (CCl_4) δ=1.60 (s, 3H), 1.75 (s, 3H), 1.50—2.15 (m, 6H), 2.15—2.50 (m, 2H), and 2.70—3.55 (m, 1H). MS (20 eV) *m/e* (rel intensity) 152 (M^+, 15), 137 (26), 109 (36), 95 (37), 93 (30), 81 (57), 67 (100), and 43 (36).

The present work was partially supported by a Grant-in-Aid for Scientific Research No. 56540291 from the Ministry of Education, Science and Culture.

References

1) D. Caine, "Carbon-Carbon Bond Formation," ed by R. L. Augustine, Marcel Dekker, New York (1979), Vol. 1. pp. 152—153.

2) R. A. Rossi and J. F. Bunnett, *J. Org. Chem.*, **38**, 1407 (1973); L. S. Hegedus and R. K. Stiverson, *J. Am. Chem. Soc.*, **96**, 3250 (1974); M. F. Semmelhack, B. P. Chong, R. D. Stauffer, T. D. Rogerson, A. Chong, and R. D. Jones, *ibid.*, **97**, 2507 (1975); M. W. Rathke and A. A. Millard, *ibid.*, **99**, 4833 (1977); J. F. Bunnett and J. E. Sunberg, *J. Org. Chem.*, **41**, 1702 (1976); J. T. Pinhey and B. A. Rowe, *Aust. J. Chem.*, **33**, 113 (1980); C. E. Sacks and P. L. Fuchs *J. Am. Chem. Soc.*, **97**, 7372 (1975); A. A. Milard and M. W. Rathke, *ibid.*, **97**, 4833 (1975).

3) P. F. Hudrlik and A. K. Kulkarni, *J. Am. Chem. Soc.*,**103**, 6251 (1981) and references cited therein; D. L. J. Clieve and C. G. Russell, *J. Chem. Soc., Chem. Commun.*, **1981**, 434; C. J. Kowalski snd J. S. Dunk, *J. Am. Chem. Soc.*, **102**, 7950 (1980); T. C. T. Chang, M. Rosenblum, and S. B. Samuels, *ibid.*, **102**, 5931 (1980).

4) M. Pereyre and J-C. Pommier, "New Application of Organometallic Reagents in Organic Synthesis," ed by Seyferth, Elsevier (1976) and references cited therein.

5) E. M. Jung and R. B. Blum, *Tetrahedron Lett.*, **1977**, 3791; B. M. Trost and E. Keinan, *ibid.*, **21**, 2591 (1980).

6) M. Kosugi, M. Suzuki, I. Hagiwara, K. Goto, K. Saitoh, and T. Migita, *Chem. Lett.*, **1982**, 939; M. Kosugi, I. Hagiwara, T. Sumiya, and T. Migita, *J. Chem. Soc., Chem. Commun.*, **1983**, 344; M. Kosugi, I. Hagiwara, and T. Migita, *Chem. Lett.*, **1983**, 839.

7) I. Kuwajima and H. Urabe, *J. Am. Chem. Soc.*, **104**, 6831 (1982).

8) J. E. Plevyak and R. Heck, *J. Org. Chem.*, **43**, 2454 (1978); C. B. Ziegler, Jr., and R. Heck, *ibid.*, **43**, 2941 (1978).

9) T. Migita, T. Nagai, K. Kiuchi, and M. Kosugi. *Bull. Chem. Soc. Jpn.*, **56**, 2869 (1983).

10) P. Fitton and E. A. Rick, *J. Organomet. Chem.*, **28**, 287 (1971).

11) a) B. H. Gwynn and E. F. Degering, *J. Am.Chem. Soc.*, **64**, 2216 (1942); b) H. O. House, M. Gall, and H. D. Olmstead, *J. Org. Chem.*, **36**, 2361 (1971); c) H. O. House and V. Kramer, *ibid.*, **28**, 3362 (1963); d) H. O. House and B. M. Trost, *ibid.*, **30**, 1341 (1965); e) P. F. Hudrlik and A. M. Hudrlik, *ibid.*, **38**, 4254 (1973); f) J. K. Rasmussen, *Syntheses*, **1977**, 98.

12) M. Pereyre, B. Bellegarde, J. Mendelsohn, and J. Valade, *J. Organomet. Chem.*, **11**, 97 (1968).

13) R. K. Ingham, S. D. Rosenberg, and H. Gilman. *Chem. Rev.*, **60**, 459 (1960); R. Ueeda, Y. Kawasaki, T. Tanaka, and R. Okawara, *J. Organomet. Chem.*, **5**, 194 (1966).

14) L. A. Bigelow, J. R. Johnson, and L. T. Sandborn, *Org. Synth.*, Coll. Vol. I, 133 (1956).

15) J. L. Hartwell, *Org. Synth.*, Coll. Vol. III, 185 (1955).

16) L. I. Smith, *Org. Synth.*, Coll. Vol. II, 95 (1950).

17) J. K. Farrell and G. B. Bachman, *J. Am. Chem. Soc.*, **57**, 1281(1935); G. B. Bachman, *ibid.*, **55**, 4279 (1933).

18) B. A. Patel, J. I. Kim, D. D. Bender, L-C. Kao, and R. F. Heck, *J. Org. Chem.*, **46**, 1061 (1981).

19) F. G. Mann and E. J. Ehapline, *J. Chem. Soc.*, **1937**, 527.

20) D. R. Coulson, *Inorg. Synth.*, **13**, 121 (1972).

21) J. Chatt and F. G. Mann, *J. Chem. Soc.*, **1939**, 1631.

22) "The Aldrich Library of Infrared Spectra," second ed, (1975).

23) A. Haller, *Ann. Chim. (Paris)*, **29**, 313 (1913).

24) M. S. Newman and M. D. Farbman, *J. Am. Chem. Soc.*, **66**, 1550 (1944).

25) C. F. H. Allen and W. E. Barker, *Org. Synth.*, Coll. Vol. II, 156 (1950).

Effect of the Base Stacking Association on the Phosphate Ionization of 2′-Deoxyguanosine 5′-Monophosphate

Kazumi HIROTA, Yoshio INOUE, and Riichirô CHÛJÔ*
Department of Polymer Chemistry, Tokyo Institute of Technology, O-okayama 2, Meguro-ku, Tokyo 152
(Received August 16, 1983)

The concentration dependence of ^{31}P chemical shifts at neutral pH has been measured for 2′-deoxyguanosine 5′-monophosphate and deoxyribose 5-monophosphate. The chemical shifts are sensitive to the variation of concentration, and are affected by the presence or absence of the base. The variations of ^{31}P chemical shifts correspond to those of $pK_{a'}$ values. The concentration dependence of ^{31}P chemical shift of deoxyribose 5-monophosphate can be explained by the ionic strength change accompanied by the concentration change, whereas that of the nucleotide can not be interpreted with the aid of it alone. The phosphate group of the nucleotide ionizes more readily at higher concentration. There is an additional effect other than ionic strength on the $pK_{a'}$ eand it is caused by the presence of the base. The appearance of the concentration effect owing to the base is attributable to the base stacking association. The measurements at different temperatures support this conclusion.

The association of naturally occurring nucleotides in aqueous solution has been studied by various experimental techniques such as microcalorimetry[1] and UV[2-4] and NMR[5-12] spectroscopy. It is now generally accepted that base stacking is a possible mode of self-association of nucleotides and it proceeds beyond dimer stages.[6,7,9] It is also well established that the stacking affinity of the nucleobases contributes greatly to the free energy sustaining the nucleic acid secondary structure.[13,14] The majority of studies have based on the concentration dependence of ^1H NMR chemical shift. A change of concentration should, however, affect the phosphate ionization of nucleotides through a change of ionic strength of solutions. The base stacking is also expected to affect the phosphate ionization through the formation of new molecular assemblies, since assembly of electrolytes in solution affects the pK_a value.[15] It seems that an understanding of the effect of the base stacking association on the phosphate ionization and on the conformation of nucleotides would promote the understanding of the secondary structure of DNA. In this work, we will focus on the phosphate ionization.

^{31}P NMR is a useful technique for studying an ionization state of phosphate group, since the chemical shift is a very sensitive function of pH.[16,17] The effect of pH on ^{31}P chemical shifts of mononucleotides has been studied by Cozzone and Jardetzky,[17] where the nucleotides were 0.5×10^{-2} M or less to avoid possible effects of self-associations.

In order to clarify the effect of the base stacking on the phosphate ionization of nucleotides, it is necessary to differentiate the effect of ionic strength from that of self-association both of which are included in the concentration dependence of ^{31}P chemical shifts. For the purpose of this subject, we will study, based on ^{31}P and ^1H NMR, the effect of concentration, ionic strength, and temperature on the phosphate ionization of 2′-deoxyguanosine 5′-monophosphate (5′-dGMP) and deoxyribose 5-monophosphate (5-dRP).

Experimental

Sample Preparation. Sodium salts of 5′-dGMP and 5-dRP were purchased from Sigma Chemical Co. Deuterium oxide (isotope purity >99.7%) was from Merck Sharp& Dohme, Canada Ltd.. Paramagnetic contaminants were removed from NMR samples by chromatography on Chelex-100 (Bio-Rad Laboratory), followed by lyophilization. All NMR sample tubes were soaked in 40% nitric acid prior to use. NMR samples were prepared in D_2O, containing 0.5×10^{-2} M† ethylenediaminetetraacetic acid (EDTA). The addition of EDTA did not affect the ^{31}P and ^1H chemical shifts. The pH of solution was adjusted to a desired value by an addition of very small amount of concentrated DCl and/or NaOD solutions in D_2O. The pH was measured with an accuracy of ±0.01 pH unit, both before and after the NMR experiments, using a Toko TP-101 pH meter with a combination electrode of Type CE-103 which can be directly used for NMR sample tube. No correction was made for the deuterium isotope effect on pH value. Concentrations were determined by dry weight and then adjusted to desired values, typically from 0.5×10^{-2} M to 0.2 M, by dilution using a volumetrically variable pipette 4710 (Eppendolf).

NMR Measurements. ^{31}P NMR spectra were obtained in the Fourier transform mode on a JEOL PS-100 NMR spectrometer operating at 40.5 MHz, equipped with a PFT-100 Fourier transform system and a JEOL EC-100 computer. Heteronuclear proton noise decoupling was achieved with a JEOL JNM HD-SC. The spectrometer was field-frequency locked on the deuterium resonance of deuterium oxide used as a solvent. ^{31}P chemical shifts were measured in Hz from 85% H_3PO_4 as an external reference, without any correction of bulk susceptibility. Digital resolution was 0.2 Hz.

Fourier transformed ^1H NMR spectra were taken at 100 MHz on the same spectrometer. All ^1H chemical shifts were measured from 2-methyl-2-propanol as an internal reference. Although this reference is known to be shifted upfield in the presence of high concentration of aromatic solute,[18] the shift is negligibly small in the concentration range of our experiments (up to 0.2 M).

All spectra were recorded at 27 °C, unless specified other-

† 1 M=1 mol dm^{-3}.

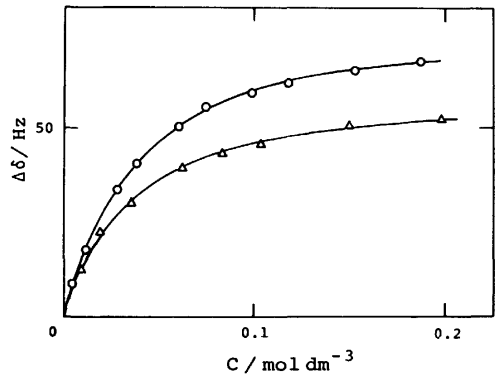

Fig. 1. Variation of the ^{31}P chemical shift differences ($\Delta\delta$) for 5'-dGMP(○) and 5-dRP(△) as a function of concentration(C) at pH 6.60, where $\Delta\delta$ is the difference between the ^{31}P chemical shift at each concentration and that at an infinite dilution.

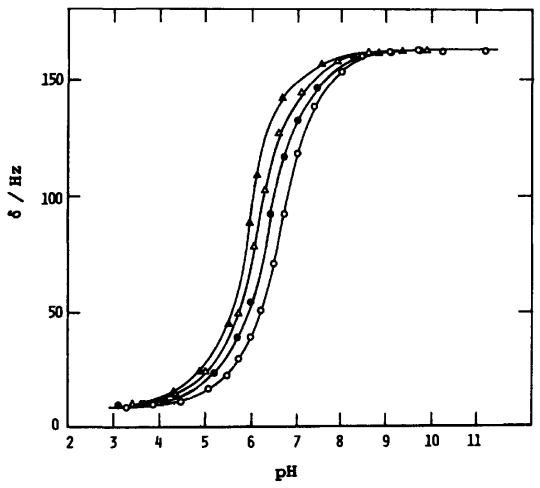

Fig. 2. ^{31}P chemical shift(δ) of 5'-dGMP as a function of pH at various 5'-dGMP concentrations, 0.5×10^{-2} M(○), 4×10^{-2} M(●), 0.1 M(△), and 0.2 M (▲).

wise. A JES VT-3 temperature controller was used for the stabilization, with an accuracy of ±2 °C.

Results and Discussion

Concentration dependence of ^{31}P chemical shifts of 5'-dGMP and 5-dRP was measured at a constant pH (6.60) near the pK_a for secondary ionization of phosphate groups (Fig.1). The ^{31}P resonances of these compounds show remarkable downfield shifts with increasing concentration. ^{31}P chemical shifts of these compounds are identical with each other at lower concentration (<0.02 M), but they are differentiated at higher concentration and the difference increases with increasing concentration. The magnitude of shift is larger for 5'-dGMP than for 5-dRP.

In order to clarify whether the concentration dependence of the chemical shift of each compound is owing to a change of pK_a value or not, titration curves were measured for 5'-dGMP at various concentrations (Fig. 2). The pK_a value decreased with increasing concentration. The ^{31}P resonance at pH 6.60 undergoes a remarkable downfield shift with a small decrease of the pK_a value. At an alkaline pH (>9), the ^{31}P chemical shift is independent of the concentration. It was found that 5'-dGMP and 5-dRP have the same thermodynamic pK_a (6.87±0.01) and chemical shift at an infinite dilution (65±0.5 Hz). The variation of chemical shifts of these compounds with concentration corresponds to the change of pK_a value. The concentration dependence of ^{31}P chemical shifts in Fig. 1, therefore, shows that the phosphate group of 5'-dGMP ionizes more readily than that of 5-dRP. The presence of base moiety may influence on the ^{31}P chemical shift.

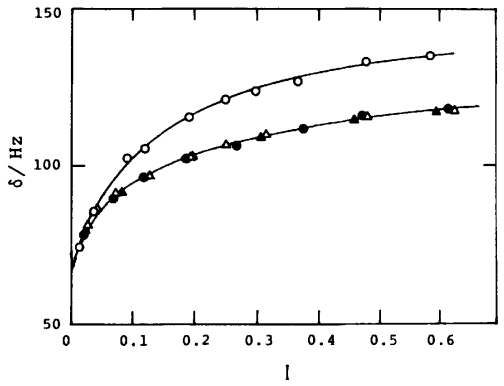

Fig. 3. Dependence of ^{31}P chemical shifts(δ) of 5'-dGMP (circle) and 5-dRP(triangle) on ionic strength (I) at pH 6.60. Open symbols, the ionic strengths calculated from the concentration of each compound in Fig. 1; filled symbols, those adjusted by adding NaCl to 0.5×10^{-2} M solution of each compound.

The conditional pK_a($pK_{a'}$) changes with concentration by the change in the activity coefficient induced by that of the ionic strength.[15,19] To estimate the extent of this effect, the dependence of ^{31}P chemical shift on the ionic strength is observed at pH 6.60 by adding neutral salt (NaCl) to the 0.5×10^{-2} M solution of each compound (Fig. 3, all of filled symbols). At this concentration, the degree of self-association of nucleotides is negligibly small. The ionic strength dependence of ^{31}P chemical shift in this case is little affected by the presence of the base. In Fig. 3 is also shown the dependence of ^{31}P chemical shifts of both compounds on the ionic strength in which the ionic strength is changed with its own concentration (open symbols). As can be seen in Fig. 3, ^{31}P chemical shift change of 5-dRP lacking the base moiety depend only on the ionic strength, while those of 5'-dGMP can not be interpreted by the ionic strength alone. This also indicates that the concentration dependence of ^{31}P chemical shift of 5-dRP represents an concentration effect on the phosphate ionization of the nucleotide in the case where any self-association does not occur. There is an additional effect other than ionic strength in the concentration effect on the phosphate ionization of the nucleotide, which should be owing to the existence of base moiety of the nucleotide.

Above results suggest that the additional effect is

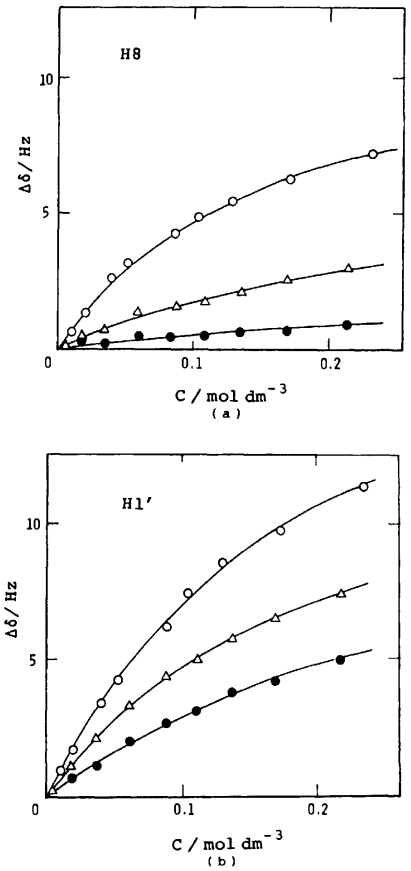

Fig. 4. Effect of temperature on the concentration(C) dependence of H-8(a) and H-1′(b) ^{1}H chemical shift differences($\Delta\delta$) of 5′-dGMP at pH 6.60. 27 °C(○); 45 °C(△); 60 °C(●). $\Delta\delta$ is the difference between the chemical shift of a particular proton at each concentration and that at an infinite dilution.

owing to the formation of the base stacking aggregates. Effects of temperature on the phosphate ionization of the nucleotide were studied to confirm this view. It is known that base stacking aggregates break down with increasing temperature.[11] First the concentration dependence was measured for H-8 and H-1′ chemical shifts of 5′-dGMP at three temperature, 27, 45, and 60 °C (Fig. 4). These resonances shift upfield with increasing concentration. The chemical shift changes are consistent with the isodesmic model of indefinite non-cooperative stacking.[20] The magnitude of shift decreases with increasing temperature. From the concentration dependence of ^{1}H chemical shifts at each temperature, the association constants (K) for the base stacking were estimated with the aid of the isodesmic model (Table 1). The K values derived from both ^{1}H chemical shifts decrease with increasing temperature, indicating the decrease of the stacking affinity.

If the additional reduction of p$K_{a'}$ value for the phosphate group of 5′-dGMP with increasing concentration is owing to the base stacking association, the magnitude of ^{31}P shift at pH 6.60 should decrease with increasing temperature. To verify this idea, the concentration dependence of ^{31}P chemical shift of 5′-dGMP was observed at different temperatures, 27, 45, 60 °C (Fig. 5). With increasing temperature, a reduction of induced shift is observed and the variation of shift with concentration at 60 °C agrees well with that of 5-dRP at 27 °C, indicating a validity of the interpretation based on the base stacking association. An essential effect of temperature on the p$K_{a'}$ value of 5′dGMP must be considered, but it was very small (d pK_a/ d T=0.5×10^{-3}).[21] Previous ^{1}H NMR studies have demonstrated that temperature variation has little effect on the nucleotide conformation.[22-24] There is, therefore, little contribution of conformational changes to the temperature variation of ^{31}P chemical shift.

Table 1. Effect of temperature on the association constant K[a] for the base stacking of 5′-dGMP at pH 6.60

T/°C	K/M^{-1}		K_{av}/M^{-1} [b]
	H-8	H-1′	
27	2.6	2.8	2.7
45	2.0	2.2	2.1
60	1.2	1.4	1.3

a) Estimated errors for these association constants are 10—15%. b) K_{av} is the mean of the individual results. (1 M = 1 mol dm^{-3})

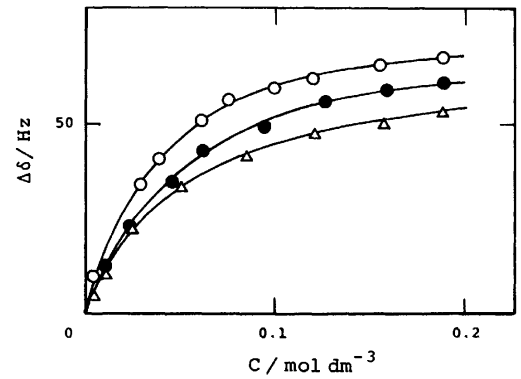

Fig. 5. Effect of temperature on the concentration(C) dependence of the ^{31}P chemical shift differences($\Delta\delta$) of 5′-dGMP at pH 6.60. 27 °C(○); 45 °C(●); 60 °C(△). $\Delta\delta$ is defined as in Fig. 2.

Base stacking should cause a change of nucleotide conformation: the ribose-phosphate backbone,[24-26] the ribose ring[25,26] and the ribose-base torsion.[26-29] One can postulate that ^{31}P chemical shift could be affected by these changes. However, the influence of these conformational changes is not large enough to affect significantly ionization of the phosphate groups, since the same pK_a value can be obtained from the titration curves for various nucleoside 5′-monophosphates with different conformation.[17,24] Identical percentages of the preferred "gauche-gauche" rotamers around C$_{5'}$–O$_{5'}$ and C$_{4'}$–C$_{5'}$ bonds are found for various nucleoside-5′-monophosphates.[24] Although a change of the rotamer populations around the C$_{5'}$–O$_{5'}$ and C$_{4'}$–C$_{5'}$ bonds, determining

the statistically preferred orientation of the 5′-phosphate group, should affect the chemical shift of the corresponding ^{31}P signal, constancy of conformer populations was found from the measurements of coupling constants $^{3}J_{PH}$ (*ca.* 4.8 Hz) and $^{4}J_{PH}$ (*ca.* 1.5 Hz) for 5′-dGMP over the range of experimental concentration at pH 6.60.

The effects on the ^{31}P shift of the ring current fields, as well as the diamagnetic and paramagnetic components of the atomic magnetic anisotropy, seem also insignificant, since ^{31}P chemical shifts are independent of concentration at alkaline pH (>9) (Fig. 2). Even in this pH region, base stacking can also occur.[7]

The effect of concentration on the 5′-phosphate ionization of 5′-dGMP should be attributed to the molecular condensation effect owing to the base stacking association.

References

1) L. Soccorsi and M. Cignitti, *Bioelectro. Bioenerg.*, **9**, 219 (1982).
2) E. Gallego, A. R. de Bodas, and F. Peral, *An. Quim., Ser. A*, **77**, 98 (1981).
3) A. Bascones, F. Peral, and E. Gallego. *An. Quim., Ser. A*, **77**, 105 (1981).
4) E. Gallego, F. Peral, and J. Morcillo., *An. Quim., Ser. A*, **77**, 118 (1981).
5) A. D. Broom, M. P. Schweizer, and P. O. P. Ts'o, *J. Am. Chem. Soc.*, **89**, 3612 (1967).
6) G. P. Rosetti and K. E. Van Holde, *Biochem. Biophys. Res. Commun.*, **26**, 717 (1967).
7) M. P. Schweizer, A. D. Broom, P. O. P. Ts'o, and D. P. Hollis, *J. Am. Chem. Soc.*, **90**, *1042 (1968)*.
8) T. D. Son and C. Chachaty, *Biochim. Biophys. Acta*, **335**, 1 (1973).
9) F. E. Evans and R. H. Sarma, *Biopolymers*, **13**, 2117 (1974).
10) W. J. Egan, *J. Am. Chem. Soc.*, **98**, 4091 (1976).
11) K. J. Neurohr and H. H. Mantsh, *Can. J. Chem.*, **57**, 1986 (1979).
12) M. Borzo, C. Detellier, P. Laszlo, and A. Paris, *J. Am. Chem. Soc.*, **102**, 1124 (1980).
13) G. Felsenfeld and H. T. Miles, *Ann. Rev. Biochem.*, **36**, 407 (1967).
14) R. H. Sarma and S. S. Danyluk, *Int. J. Quantum Chem.*, **4**, 269 (1977).
15) R. G. Bates, "Determination of pH, Theory and Practice," John Wiley & Sons, New York (1964), pp. 95—130.
16) K. Moedritzer, *Inorg. Chem.*, **6**, 936 (1967).
17) P. J. Cozzone and O. Jardetzky, *Biochemistry*, **15**, 4853 (1976).
18) R. A. Y. Jones, A. R. Kartritzky, J. N. Murrell, and N. J. Sheppard, *J. Chem. Soc.*, **1962**, 2576.
19) R. Philips, S. J. Eisenberg, P. George, and R. J. Rutman, *J. Biol. Chem.*, **246**, 4393 (1965).
20) J. L. Dimicoli and C. Hélène, *J. Am. Chem. Soc.*, **95**, 1036 (1973).
21) The value of d pK_a/d T was determined from the temperature variation (27—60 °C) of pK_a of 5′-dGMP at 0.5×10^{-2} M.
22) P. O. P. Ts'o, N. S. Kondo, M. P. Schweizer, and D. P. Hollis, *Biochemistry*, **8**, 997 (1969).
23) T. Schleich, B. J. Blackburn, R. D. Lapper, and I. C. P. Smith, *Biochemistry*, **11**, 137 (1972).
24) P. J. Cozzone and O. Jardetzky, *Biochemistry*, **15**, 4860 (1976).
25) R. H. Sarma and R. J. Mynott, *Org. Magn. Reson.*, **4**, 577 (1972).
26) D. B. Davies, *Prog. Nucl. Magn. Reson. Spec.*, **12**, 135 (1978).
27) I. D. Bobruskin, M. P. Kirpichnikov, M. Yu. Pokrovskaya, and V. L. Florent'ev, *Mol. Biol.*, **14**, 830 (1980).
28) I. D. Bobruskin, M. P. Kirpichnikov, M. Yu. Pokrovskaya, and V. L. Florent'ev, *Biorg. Khim.*, **6**, 1163 (1980).
29) C. F. G. C. Geraldes, H. Santos, and A. V. Xavier, *Can. J. Chem.*, **60**, 2976 (1982).

 © 1984 The Chemical Society of Japan Bull. Chem. Soc. Jpn., 57, 251—253 (1984)

Oxidative Carbonylation of Piperidine in the Presence of Palladium(II)-Copper(II) Catalytic System

Yuri L. Sheludyakov and Valentin A. Golodov*
Institute of Organic Catalysis and Electrochemistry 480100, Alma-Ata, K. Marx str., 142, USSR
(Received January 14, 1982)

A kinetic study on oxidative carbonylation of piperidine to give 1,1'-carbonyldipiperidine in the presence of Pd(II) and Cu(II) complexes at 40 °C has been investigated.

Carbonylation of amines depending on the conditions of the reaction and the catalyst nature produces various oxygen-containing derivatives.[1-4] Thermodynamic characteristics of the reaction are most favorable in case of the oxidative carbonylation.[3] A new catalytic system of the oxidative carbonylation of amines, based on Pd(II) and Cu(II) complexes in mild conditions, was reported previously.[5] Its high activity is due to the development of the synergistic effect of the mixed catalyst.

This paper is aimed at the elucidation of the reaction mechanism and causes of the synergistic effect by studying in detail the kinetics of the oxidative carbonylation of piperidine to give 1,1'-carbonyldipiperidine in the same catalytic system.

A static system under volumetric and potentiometric control was adopted. During the kinetic study, the reactor was energetically shaked up to provide good mixing of gas and liquid. In the study of the mechanism of separate stages, the solution of the complexes from the reactor was periodically fed to the cell of UR-20 spectrometer.

Results and Discussion

The rate of the reaction (1)

$$2C_5H_{10}NH + CO + 2Cu\,(II) \xrightarrow{Pd(II)} 2Cu(I) + (C_5H_{10}N)_2CO + 2H^+ \quad (1)$$

increased linearly with both Pd(II) concentration and CO partial pressure (Fig. 1a, c) and nonlinearly with Cu(II) concentration (Fig. 1b). At the ratio of Cu(II) : Pd(II) = 2 the reaction order was 1, but it approached to zero at the ratio >40. It was found that the reaction rate was independent of the piperidine concentration in the 4.2×10^{-3}—1.4×10^{-1} mol l^{-1} range. The kinetic equation is thus represented in the following form:

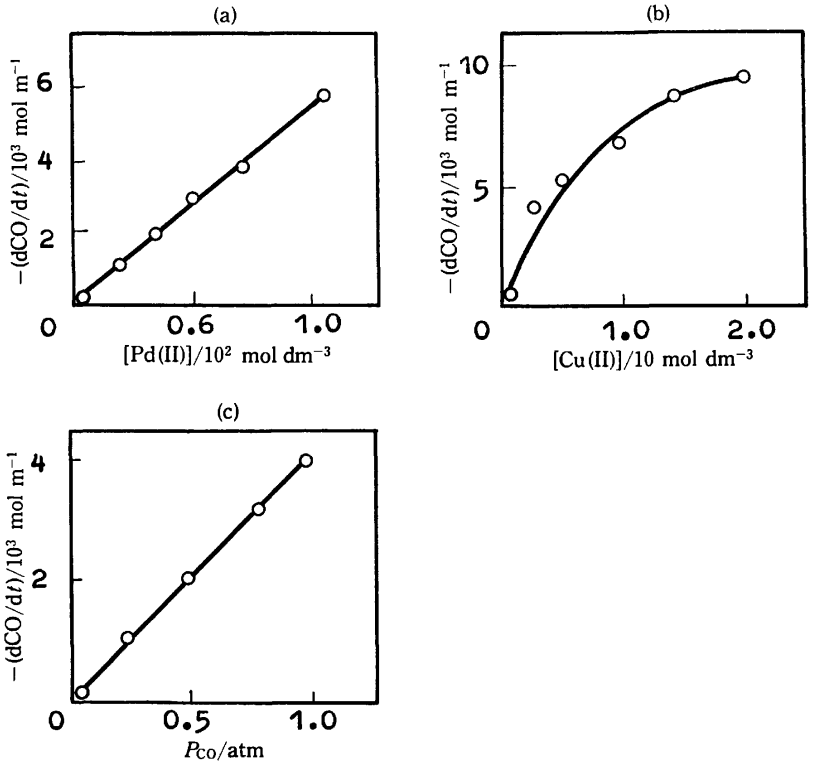

Fig. 1. Dependences of oxidative carbonylation rate of piperidine on Pd(II) (a), Cu(II) (b) concentrations and CO partial pressure (c). Pyridine, 40 °C, $[Pd(II)]=7.2\times10^{-3}$ mol dm^{-3}, $[Cu(II)]=7.2\times10^{-2}$ mol dm^{-3}, $P_{CO}=1$ atm.

$$-\frac{dCO}{dt} = k_{ef}\cdot[Cu(II)]^n\cdot[Pd(II)]\cdot[CO], \quad (2)$$

$n = 0—1$

Our data and those cited in the paper of Brakman[6] on piperidine carbonylation in the Cu(II)–Cu(I) catalyst system can be described by the kinetic Eq. 3:

$$-\frac{dCO}{dt} = k_{ef}\cdot[Cu(I)CO]\cdot[C_5H_{10}NH], \quad (3)$$

which shows that autocatalysis is carried out in the reaction till the complete consumption of Cu(II) with accumulation of 1,1′-carbonyldipiperidine and copper-(I) carbonyl in the solution (bands in the IR spectrum at 1650 and 1970 cm^{-1}).

In the absence of copper(II), $PdCl_2(C_5H_{10}NH)_2$ in the excess of piperidine with CO gives a product having a number of bands in the "carbonyl" region, *i.e.* 1595, 1895, 2010, and 2045 cm^{-1}.

If the excess of piperidine was replaced by two equivalents of triphenylphosphine, then the IR spectrum would show only one intensive band at 1590 cm^{-1} which, on the basis of literature data,[7] may be attributed to the carbamoyl complex. The band at 1595 cm^{-1} in the above-mentioned group is attributed to the same complex. The relation of other bands is not quite clear.

Literature[8] and our experimental data show that the key-complex of palladium in the catalytic reaction is represented by the carbamoyl complex which is stable to the action of the excess of amine and air oxygen at a room temperature but is easily decomposed by water forming metallic palladium and by piperidine complex of copper(II) forming 1,1′-carbonyldipiperidine (ν_{CO}= 1650 cm^{-1}).

$$Pd(II)(CONC_5H_{10}) + 2Cu(II) \xrightarrow{k_4} 2Cu(I) + Pd(II) + (C_5H_{10}N)_2CO \quad (4)$$

(Cl^- and amine ligands are omited for Simplicity) Presynthesized carbamoyl complex of palladium(II) can be titrated potentiometrically by copper(II) chloride in the excess of piperidine and in the absence of CO (Fig. 2).

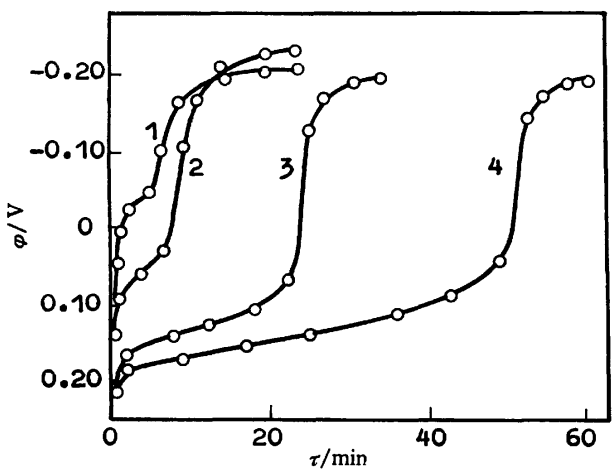

Fig. 2. Potentiometric curves of the interaction of carbamoyl complex of palladium with copper(II) amine complex. Pyridine, 25 °C, $[Pd(II)]=4.0\times10^{-2}$ mol dm^{-3}, $[Cu(II)]=0.8\times10^{-2}$ (1), 1.6×10^{-2} (2), 2.4×10^{-2} (3), 4.0×10^{-2} mol dm^{-3} (4).

According to the stoichiometric Eq. 4, 2 mol Cu(II) are necessary for the formation of 1,1′-carbonyldipiperidine. However, the first order for copper(II) obtained experimentally, indicates that the reaction (4) consists of minimum two stages where the interaction with the second complex of copper(II) proceeds, probably, fast and does not affect the rate of the process as a whole.

When the reaction is carried out directly in the IR spectrometer, palladium carbonyl preceding the carbamoyl complex is not observed. The formation of carbamoyl can be supposed to be carried out by CO incorporation into Pd–N bond despite the fact that in a similar Cu(I)–Cu(II) system the reaction proceeds through the stage of the formation of carbonyl; this reaction route is considered as a key reaction for the synthesis of carbamoyl complex.[9]

$$Pd(II)(C_5H_{10}NH) + CO \underset{k_5}{\overset{k_{-5}}{\rightleftharpoons}} Pd(II)(CONC_5H_{10}) + H^+ \quad (5)$$

The kinetic Eq. 6 corresponding to the stages (5) and (4) qualitatively agrees with the experimental one (2).

$$-\frac{dCO}{dt} = \frac{k_5\cdot k_4\cdot[Pd(II)]\cdot[CO]\cdot[Cu(II)]}{k_{-5}[H^+]+k_4\cdot[Cu(II)]} \quad (6)$$

By the graphic method the constants of the Eq. 6 have been determined as $k_5=117$ dm^3 mol^{-1} min^{-1} and $k_{-5}/k_4=1.82\times10^{-3}$. The k_4 can be determined independently by the initial rate of the reaction product of Pd(II) with carbon monoxide and copper(II). The constant k_4 thus obtained is 17 dm^3 mol^{-1} min^{-1}, which gives the value of $K_5=k_5/k_{-5}=3.8\times10^3$.

As the values of k_5 and k_4 are similar the change of the reaction order of Cu(II) from 0 to 1 in a relatively narrow range of copper(II) concentrations would be accounted for. In fact at low Cu(II) concentrations the reaction rate is limited by the reaction (4) and we find the first order for copper, while at high Cu(II) concentrations the products of Pd(II) and CO interaction are quickly transformed to urea derivatives and the process is limited by the reaction (5).

The synergistic effect in Pd(II)–Cu(II) system (Fig. 3) can be accounted for the fact that in the presence of Pd(II) the stage of the formation of the carbamoyl

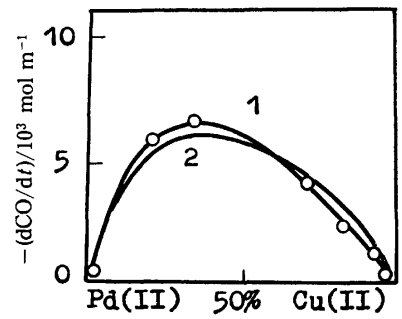

Fig. 3. Dependence of the initial rate of the oxidative carbonylation of piperidine on the ratio of palladium and copper complexes. $Pd(II)+Cu(II)=5.0\times10^{-4}$ mol CO, $C_5H_{10}NH$: $(Pd(II)+Cu(II))=20$. 1: Experimental points, 2: calculated curve.

complex is accelerated while Cu(II) additions accelerate its redox decomposition, *i.e.* an oxidizer is necessary for the stage of redox decomposition of the carbamoyl complex. In the classification offered,[10] this is a third type of synergism.

Hence, by the present study we managed to confirm the scheme of the process of piperidine carbonylation using a new mixed Pd(II)–Cu(II) catalyst for this reaction; to determine a key intermediate species *i.e.* the carbamoyl complex of palladium and to show that an oxidizer is necessary for the stage of redox decomposition of this complex which leads to the synergism in the system.

References

1) J. Tsuji and N. Iwamoto, *Chem. Commun.*, **1966**, 380.
2) E. W. Stern and M. L. Spector, *J. Org. Chem.*, **31**, 596 (1966).
3) V. A. Golodov, Yu. L. Sheludyakov, and D. V. Sokolsky "Fundamental Research in Homogeneous Catalysis," Plenum Press, New York (1979), Vol. 3, p. 239.
4) J. Falbe, "New Synthesis with Carbon Monoxide," Springer-Verlag, Berlin (1980).
5) Yu. L. Sheludyakov, V. A. Golodov, and D. V. Sokolsky *Dokl. Akad. Nauk SSSR*, **249**, 658 (1979).
6) W. Brakman, *Discuss. Faraday Soc.*, **46**, 122 (1968).
7) W. Beck and V. Purucker, *J. Organomet. Chem.*, **112**, 361 (1976).
8) R. J. Angelici, *Acc. Chem. Res.*, **5**, 335 (1972).
9) Ch. Green and R. J. Angelici, *Inorg. Chem.*, **11**, 2095 (1972).
10) V. A. Golodov, *J. Res. Inst. Catal., Hokkaido Univ.*, **29**, 49 (1981).

On the Physicomagnetic Properties of Some Nitro Compounds

Mohamed M. Abdel-Kader* and Safia M. Salem
Physics Department, Faculty of Science, University of Cairo Giza, Egypt
(Received January 12, 1983)

The mean molar susceptibilities of nine aromatic nitro compounds namely, *o*-, *m*-, *p*-dinitrobenzene; *o*-, *m*-, *p*-nitrobenzoic acid and *o*-, *m*-, *p*-nitrophenol have been measured. The semiexperimental anisotropies of these molecules have been calculated. The magnetic data are correlated with the positional isomerism of the nitro groups and the crystal structures of these molecules as well as their hydrogen bonding.

Introduction of a large group like that of the nitro group (NO_2) for hydrogen atom in a benzene ring generally resulted in a detectable change in various physical constants of the molecule. But the nature of the effect depends much on the position of the group in the ring. The mean molar susceptibilities of the nitro group and nitro compounds have been extensively considered theoretically or experimentally. Cabrena and Fahlenbrach[1] found that, in nitrotoluene, the *m*-compound had a higher value of the observed molar susceptibility (χ_M^{obsd}) than the other two isomers. French[2] after studying a large number of compounds, noticed an anomalous effect in the case of nitro-substituted compounds. This anomaly was explained by Badder and Mikhail[3] and later by Mikail,[4] as arising from the contribution of the quinonoid structures of the nitro group to the normal structure. From their measurements of the χ_M^{obsd} of seventeen aromatic nitro compounds, Sriraman *et al.*[5] found that the contribution of the nitro group to the mean susceptibilities depends on its position on the benzene ring.

We felt that, it is of interest to study the contribution of the nitro group to the magnetic anisotropies of some benzenoid molecules semiexperimentally. The large anisotropies of the diamagnetic susceptibilities of benzenoid molecules are usually interpreted in terms of ring currents[6–10] despite some criticism.[11,12] A recent paper on the use of the ring current concept has been given by Gomes.[13]

If K_1, K_2, and K_3 are the principal molecular susceptibilities, (K_1, K_2) are the in-plane susceptibility and K_3 is the out-of-plane susceptibility, then the magnetic anisotropy of a molecule is defined as:

$$\Delta K = K_3 - \frac{1}{2}(K_1+K_2) \qquad (1)$$

In general, the molecular susceptibilities (and hence the magnetic anisotropy) can be estimated by measuring the principal crystal susceptibilities (χ_1, χ_2, χ_3) combined with the information about the orientation of the molecules in it. The mathematical relations concerning the transition from crystalline to molecular susceptibilities were previously given by Lonsdale and Krishnan.[14]

In the present work, the magnetic anisotropies of these molecules have been calculated semiexperimentally. The details of this method have been discussed before by one of the present authors.[15] The equation used is

$$\Delta K_{semi} = 3[\chi_M^{obsd} - \frac{1}{2}(K_1+K_2)]. \qquad (2)$$

Experimental

The molecules studied in this paper can be classified into three groups:

1) Dinitro Benzenes: a) *o*-Dinitrobenzene.[16] b) *m*-Dinitrobenzene.[17] c) *p*-Dinitrobenzene.[18]

2) Nitrobenzoic Acids: a) *o*-Nitrobenzoic acid.[19] b) *m*-Nitrobenzoic acid.[20] c) *p*-Nitrobenzoic acid.[21]

3) Nitrophenols: a) *o*-Nitrophenol.[22] b) *m*-Nitrophenol. c) *p*-Nitrophenol.[23]

The crystal structure of these compounds are known except for *m*-nitrophenol. The purity of each compound was tested by measuring its melting point. Purification by recrystallization from solvents was carried out when the melting point of the compound is slightly different from that given in the literatures. The melting point (mp) of each compound has been given in Table 1.

The Gouy method was employed for the measurements of the susceptibility of each compound. Details of this method has been given elsewhere.[15]

Results and Discussion

In Table 1, the specific susceptibility χ_S, the observed

Table 1. Observed and calculated susceptibilities ($\times 10^{-6}$ emu mol^{-1})

Compound	Mp θ_m/°C	Mol wt	χ_S	χ_M^{obsd}	χ_M^{calcd}	$\Delta\chi_M$	Other values
o-Dinitrobenzene	118	168	−0.400±0.002	−67.20	−69.48	−2.28	−65.98[a], −66.91[b]
m-Dinitrobenzene	89—90	168	−0.424±0.001	−71.23	−69.48	+1.75	−70.53[a], −71.29[b]
p-Dinitrobenzene	173.5	168	−0.405±0.001	−68.04	−69.48	−1.44	−68.30[a], −67.08[b]
o-Nitrobenzoic acid	147	167	−0.462±0.001	−77.15	−77.54	−0.39	−76.11[a], −77.03[c]
m-Nitrobenzoic acid	140	167	−0.485±0.002	−80.99	−77.54	+7.45	−80.22[a], −77.19[c]
p-Nitrobenzoic acid	238	167	−0.468±0.002	−78.16	−77.54	+0.62	−78.81[a], −77.86[c]
o-Nitrophenol	45	139	−0.478±0.001	−66.44	67.04	−0.6	−67.39[b]
m-Nitrophenol	96	139	−0.494±0.002	−68.67	67.04	+1.63	−69.40[b]
p-Nitrophenol	113	139	−0.476±0.002	−66.16	67.04	−0.88	−67.00[b]

a): Ref. 2, b): Ref. 5, c): *Sci. Rep. Tohoku Imp. Univ.*, **24**, 701 (1936).

TABLE 2. SEMIEXPERIMENTAL MAGNETIC ANISOTROPIC ($\times 10^{-6}$ emu mol^{-1})

Compound	$\sum\chi_A$	$\frac{1}{2}(K_1+K_2)$ $=\chi_A+n\infty$	K_3	$\Delta K'^{a)}$ $=K_3-\sum\chi_A$	ΔK_{semi}
o-Dinitrobenzene	−70.68	−47.88	−105.84	−35.16	−57.96
m-Dinitrobenzene	−70.68	−47.88	−117.93	−47.25	−70.05
p-Dinitrobenzene	−70.68	−47.88	−108.36	−37.68	−60.48
o-Nitrobenzoic acid	−80.14	−53.54	−124.37	−44.23	−70.83
m-Nitrobenzoic acid	−80.14	−53.54	−135.89	−55.75	−82.35
p-Nitrobenzoic acid	−80.14	−53.54	−127.40	−47.26	−73.86
o-Nitrophenol	−68.14	−45.34	−108.64	−40.50	−63.30
m-Nitrophenol	−68.14	−45.34	−115.33	−47.19	−69.99
p-Nitrophenol	−68.14	−45.34	−107.86	−39.72	−62.46

a) The calculated values of $\Delta K'$ and/or ΔK_{semi} for the benzene ring and/or the acid molecule were given in Ref. 15.

molar susceptibility χ_M^{obsd} and the calculated molar susceptibility χ_M^{calcd} of each compound are presented.

The method used for the calculation of χ_M (in 10^{-6} emu mol^{-1}) is as follows:

a) The mean molar susceptibility of the benzene ring is −55.20.[10]

b) The drop in diamagnetism of the benzene ring due to the replacement of one hydrogen atom by another atom or group is 2.00.

c) The mean molar susceptibility of the $(NO_2)^{1+}$ group is −6.7,[5] using Yung method,[24] we get for the neutral NO_2 group the value $-(6.7+2.44)=-9.14$.

d) The mean molar susceptibility of the COOH group is −17.20[25] and of the OH group is 6.7.[25]

Thus the calculated molar susceptibility of any molecule of the compounds of the first series is $(-55.20+2.00\times2-9.14\times2)=-69.48$.

The most important fact emerging from the data shown in Table 1 is that, the *m*-compound has a markedly higher diamagnetic susceptibility than the other two isomers. Such a result is normally expected. According to French,[2] Sriraman *et al.*,[5,26] and Baliah *et al.*,[27] the nitro group is strong meta-directing. When such group is substituted in the benzene ring, it tends to withdraw electrons from the ring and the displacement of electrons is mainly from the *o*- and *p*-positions. As a result, the *m*-position is the point of relatively high electron density which will mean a higher χ_M^{obsd} value for the *m*-isomer. It can also be seen from Table 1 that, the order of χ_M^{obsd} for the members of the first and second series is:

meta>para>ortho,

as suggested by Baliah *et al.*[27] in a similar work. For the compounds of the third series, the OH group is *o*, *p*-directing and the NO_2 group is strong *m*-directing, so the order of χ_M^{obsd} is

meta>ortho>para.

Recently,[28] a different theoretical approach, where the susceptibility is represented as a sum of bond contributions and bond-bond interaction is capable of explaining difference between isomers.

The values of $\frac{1}{2}(K_1+K_2)$, K_3 or $K^{\perp}$, and ΔK_{semi} for each compound are listed in Table 2. The values of the atomic susceptibilities used in the calculations of $\sum\chi_{atomic}$ are:

$\chi_C = -7.4$,[29] $\chi_H = -2.0$,[29] $\chi_O = -4.6$.[30]

For the NO_2 group, its magnetic susceptibility depends on its position in the benzene ring,[5] its value is taken as −9.14.

Perhaps the most striking fact emerging from the magnetic data of the compounds of the first series given in Table 2 is that the semiexperimental magnetic anisotropy of the *m*-dinitrobenzene is numerically too high. Fortunately, the observed magnetic data of this compound have been determined by Lasheen.[31] Accordingly,

$$K_L \equiv (K_1) = -50 \pm 6.9,\ K_M \equiv (K_2) = -41.7 \pm 2.1,$$
$$K_N \equiv K_3 = -119.8 \pm 6.7 \text{ and } \Delta K_{obsd} = -74 \pm 7.6.$$

Unfortunately Lasheen did not give any explanation for his results because he was interested only in the molecular susceptibilities. The semiexperimental magnetic anisotropy of *m*-dinitrobenzene agrees closely with Lasheen value. Furthermore, our results for $K^{//}$ and $K^{\perp}$ are also in agreement with Lasheen values. This can be considered as a check on the accuracy of the semiexperimental method.

Since the *m*-dinitrobenzene crystals are orthrhombic, therefore the crystallographic axes agree with the axes of the triaxial ellipsoid representing the crystal susceptibilities (χ_a, χ_b, and χ_c). Assuming $K_1 \simeq K_2$, the values of χ_a, χ_b, and χ_c have been calculated by the present authors from the set of equations given in Ref. 15. Our values for χ_a, χ_b and χ_c are

$$\chi_a = -48.34,\ \chi_b = -59.40,\ \chi_c = -105.84.$$

In a good agreement with Lasheen experimental values namely,

$$\chi_a = -45.1 \pm 2.3,\ \chi_b = -58.9 \pm 2.4,$$
$$\chi_c = -107.05 \pm 4.6.$$

In the opinion of the present authors, there are two possibilities for the interpretation of the high value of ΔK for this compound:

a) The NO_2 group is not magnetically isotropic and may have a certain value of anisotropy like for example the carbonate or nitrate groups.[32]

b) The second possibility which seems to us more likely to exist is the dipole moment of the molecule. Since we have two NO_2 groups, therefore the dipole moment of the molecule will depend largely on the positions of the two NO_2 groups relative to each other. From

their measurements of the dipole moment of the nitro-substituted compounds, Jalkar and Phansalker[33] confirmed that the *m*-directing inductive effect of the nitro group had a considerable influence on the dipole moment.

At this point, it is necessary to calculate the delocalization anisotropy or the π-electron susceptibility. The results of calculations are given in Table 2. The empirical equation used for these calculations is that given by Davies,[34] namely

$$\Delta K' = K^{\perp} - \sum \chi_{\text{atomic}}.$$

From Table 2, it is clear that the delocalization anisotropy of the *m*-isomer is numerically much higher than that of the benzene ring and of the other two isomers. In other words the effect of the NO_2 groups in the *m*-position to the magnetic properties of the molecule is much more pronounced than that of the other two isomers.

For the members of the second and third series it is of interest to correlate the magnetic properties of these molecules with their structures and their hydrogen bonding systems. Refinements of the crystal structures of the nitrobenzoic acid molecules have been carried out by the Indian group, Pant *et al.*[19-21] The general feature of the crystal structures of these molecules is that, the acid groups are dimerized across intermolecular hydrogen bonds. The O–H···O are 2.645 and 2.653 Å for *o*- and *p*-nitrobenzoic acids respectively. For the *m*-nitrobenzoic acid, each dimeric unit consisting of crystallographically independent molecules A and B. The O–H···O hydrogen bonds linking molecules A and B are 2.630 and 2.666 Å.[29]

The contribution of the hydrogen bonding to both the magnetic susceptibilities and anisotropies of some aromatic compounds containing a benzene ring has been discussed by the present authors,[15,35] We have showed that the effect of the hydrogen bonding is to increase the values of $\Delta K'$ and/or ΔK of the acid molecule by about 5×10^{-6} emu mol^{-1}. from the calculated one. Thus for the *o*- and/or *p*-nitrobenzoic acid the numerical increase in $\Delta K'$ and/or ΔK of the molecule can be ascribed to the additional magnetic anisotropy of the electron delocalization resulting from the hydrogen bonding as suggested by Mason.[29]

The case of *m*-nitrobenzoic acid is very intersting. For this compound, the values of $\Delta K'$ and/or ΔK are numerically much greater than that of the other two isomers. Since the hydrogen bonding scheme of the three nitrobenzoic acid molecules are similar,[19-21] therefore one cannot attribute this large anisotropy to the effect of the hydrogen bonding alone. In other words, the contribution of the NO_2 group in this case (*i.e.* in the *m*-position) to the anisotropy of the molecule is very clear.

For the compounds of the third series, the hydrogen bonds are due to the OH and/or NO_2 group. This type of hydrogen bonding is much weaker than that of the COOH group. Thus the slight increase in the anisotropies of the *o*- and/or *p*-nitrophenol can be explained as resulting from the contribution of the weak hydrogen bonding of these molecule. On the other hand, the anisotropy of the *m*-nitrophenol is numerically much greater than that of the *o*- and/or *p*-isomers and cannot be ascribed to the effect of hydrogen bonding alone.

In conclusion, the observed molar susceptibilities and the magnetic anisotropies of the *m*-nitro compounds are numerically much greater than that of the *o*- and/or *p*-isomers. These peculiar magnetic properties of the *m*-nitro compounds may be attributable to the large dipole moments of the *m*-isomers or probably to the anisotropy of the nitro group in the *m*-position. Certain anomalous effects which agree and support this conclusion were found by other workers. Abe[36] found that *m*-dinitrobenzene showed the maximum absorption band at shorter wavelengths than nitrobenzene, such a result was also confirmed by Semba.[37] He also measured the equilibrium constants of isomeric nitroanilines and nitrophenol, and found that the meta compound had a very high value compared with other two isomers.

References

1) B. Cabrena and H. Fahlenbrach, *Z. Phys.*, **89**, 682 (1934).
2) C. M. French, *Trans. Faraday Soc.*, **41**, 676 (1945).
3) F. G. Baddar and H. Mikail, *J. Chem. Soc.*, **1949**, 2927.
4) H. Mikail, *J. Chem. Phys.*, **21**, 1004 (1953).
5) S. Sriraman, R. Sabesan, and S. Srinivasan, *Bull. Chem. Soc. Jpn.*, **36**, 1080 (1963).
6) L. Pauling, *J. Chem. Phys.*, **4**, 673 (1936).
7) F. London, *J. Phys. Rad.*, **8**, 397 (1937).
8) H. Akamatu and Y. Matsunaga, *Bull. Chem. Soc. Jpn.*, **26**, 364 (1953).
9) J. A. Pople, *Mol. Phys.*, **1**, 175 (1958).
10) A. T. Amos and Ff. Roberts, *J. Chem. Phys.*, **50**, 2375 (1969).
11) J. I. Musher, *J. Chem. Phys.* **43**, 4081 (1965); **46**, 1219 (1967).
12) J. M. Gaidis and R. West, *J. Chem. Phys.* **46**, 1219 (1967).
13) J. N. F. Gomes, *Mol. Phys.*, **40**, 765 (1980).
14) K. Lonsdale and K. S. Krishnan, *Proc. R. Soc. London, Ser. A*, **156**, 597 (1936).
15) M. M. Abdel-Kader, *Bull. Chem. Soc. Jpn.*, **56**, 3134 (1983).
16) A. M. Chandhury and S. K. Talapatra, *Pakistan J. Sci. Res.* **5**, 1246 (1953).
17) J. Trotter, *Acta Crystallogr.*, **14**, 244 (1961).
18) F. Di Rienzo and A. Domenicano, *Acta Crystallogr., Sect. B*, **36**, 586 (1980).
19) T. D. Sakore, S. S. Tavale, and L. M. Pant, *Acta Crystallogr.*, **22**, 720 (1967).
20) N. N. Dhaveshuar, S. S. Tavale, and L. M. Pant, *Acta Crystallogr., Sect. B*, **30**, 583 (1974).
21) T. D. Sakore and L. M. Pant, *Acta Crystallogr.*, **21**, 715 (1966).
22) F. Iwasaki and Y. Kawano, *Acta Crystallogr., Sect. B*, **34**, 1286 (1978).
23) Ph. Coppens, *Acta Crystallogr.*, **18**, 654 (1965).
24) Tai-Yuna Yang, *J. Chem. Phys.*, **16**, 865 (1949).
25) C. M. French, *Trans. Faraday Soc.*, **51**, 1320 (1954).
26) S. Sriraman and R. Sabesan, *Trans. Faraday Soc.* **58**, 1080 (1961).
27) V. Baliah, Abubucker, and M. Mohamed, *Indian J. Chem.*, **9**, 963 (1971).
28) S. O'Sullivan and H. F. Hameka, *J. Am. Chem. Soc.*, **92**,

25 (1970).
29) R. Mason, *Mol. Phys.*, **1961**, 191.
30) C. K. Ingold, "Structure and Mechanism in Organic Chemistry," Cornell University Press, New York (1953).
31) M. A. Lasheen, *Acta Crystallogr.*, **24**, 289 (1968).
32) J. A. Pople, *J. Chem. Phys.*, **38**, 1276 (1963).
33) S. K. K. Jalkar and V. K. Phansalker, *J. Univ. Poona*, **22**, Part II, 57 (1962).
34) D. W. Davies, *Nature*, **190**, 1102 (1961).
35) S. M. Salem, S. A. Abdel-Hadi, and M. M. Abdel-Kader, *Z. Phys. Chem. (Leipzig)*, **257**, **641**, 4, 5 (1976).
36) T. Abe, *Bull. Chem. Soc. Jpn.*, **33**, 220 (1960).
37) K. Semba, *Bull. Chem. Soc. Jpn.*, **33**, 1640 (1960).

Kinetics and Mechanism of the Oxidation of Alcohols by Pyridinium Fluorochromate

Manabendra N. BHATTACHARJEE, Mihir K. CHAUDHURI,* and Himadri S. DASGUPTA
Department of Chemistry, North-Eastern Hill University, Shillong 793003, India
(Received February 1, 1983)

Pyridinium fluorochromate, $C_5H_5NHCrO_3F$, oxidizes benzyl alcohol, ethanol, and cyclohexanol to benzaldehyde, acetaldehyde, and cyclohexanone, respectively. While each of the oxidation, studied in acetonitrile–nitrobenzene (1 : 1, v/v) medium, is first order with respect to the oxidant, the rate is almost independent of the substrate concentration. The reactions are catalyzed by acid, the acid-catalyzed reactions being very fast, precluded determination of their order in acid medium. The effects of temperatures and solvent compositions were studied and activation parameters evaluated. Probable mechanisms are discussed.

There has been a continued interest in the development of new chromium(VI) reagents[1–6] for the effective oxidation of organic substrates, particularly alcohols, under mild conditions, and significant improvements were achieved, in recent years, by the use of new oxidizing agents.[2–6] We have very recently developed[7] a new reagent pyridinium fluorochromate, $C_5H_5NHCrO_3F$ (PFC) and found several advantages of our reagent over similar oxidizing agents in respects of amounts of oxidant and solvent required, short reaction times, and high yields. The mechanism of oxidations involving this important reagent has not yet been reported. The present paper describes the kinetics of oxidation of three typical alcohols *viz.*, benzyl alcohol, ethanol, and cyclohexanol, studied in medium acetonitrile–nitrobenzene (1 : 1, v/v), evaluates the reaction constants and discusses the probable mechanism.

Experimental

All chemical used were reagent grade products. The solvents were purified and dried by the literature methods.[8] *p*-Toluenesulfonic acid (TsOH) and benzoic acid were used in the attempts to study the acid-catalyzed reactions. Pyridinium fluorochromate, PFC, was synthesized by the method originally described in our previous paper.[7]

The reaction products benzaldehyde, acetaldehyde and cyclohexanone were characterized by spectral analyses and estimated as their 2,4-dinitrophenylhydrazones.

For kinetic measurements, the reactions were performed under pseudo-first-order conditions by maintaining a large excess (×5 or greater) of alcohol over PFC. The reactions were carried out at constant temperature (±0.1 K) and progress of the reactions were followed by iodometric estimation of unreacted chromium(VI), after quenching the reaction. The medium of reactions was always 1 : 1 (v/v) acetonitrile: nitrobenzene, unless otherwise stated. Acetonitrile–nitrobenzene system was chosen as the solvent because it was observed in our previous studies[7] that acetonitrile did not react with PFC. The reaction mixtures were homogeneous for the total period of kinetic investigation.

Computations of the rate constants were made from the plot of log[oxidant] against time. The values reported are the mean of at least duplicate runs and are reproducible to within ±4%.

Dielectric constants for the varying proportions of acetonitrile–nitrobenzene mixtures were estmiated from the dielectric constants of the pure solvents[9] and are set out in Table 3. A constant ionic strength could not be maintained owing to the nonaqueous nature of the reaction medium. It may, however, be mentioned that the variation in ionic strength did not bring about any change[10] in the oxidation of benzyl alcohol by chromium(VI) oxide in aqueous acetic acid medium.

The uncatalyzed reactions were studied with varying temperatures of 303, 308, 313, and 318 K (error limit ±0.1 K) respectively for all the three alcohols (Table 4). The frequency factors were determined on the basis of the results obtained thereof. The activation parameters were evaluated by the standard procedure,[11] within allowable average error limit (at 303 K) (Table 5).

Results and Discussion

The oxidation of benzyl alcohol, ethanol and cyclohexanol by PFC in 1 : 1 (v/v) acetonitrile–nitrobenzene leads to the formation of benzaldehyde, acetaldehyde and cyclohexanone respectively in very high yields (>90%), showing no indication of further oxidation of the carbonyls conforming to our earlier synthetic studies involving PFC.[7]

The stoichiometry of various oxidations studied herein were estimated by the reaction of the respective alcohol with an excess of oxidant (PFC) followed by estimating the unreacted Cr^{VI}. In some runs, however, an excess of alcohols were used followed by the estimation of the carbonyl product. The stoichiometry of the reactions can be represented as follows:

$$3RCH_2OH + 2Cr^{VI} \longrightarrow 3RCHO + 6H^+ + 2Cr^{III}. \quad (1)$$

The stoichiometry of the reactions with cyclohexanol was determined in an analogous manner,

$$3C_6H_{11}OH + 2Cr^{VI} \longrightarrow 3C_5H_{10}CO + 6H^+ + 2Cr^{III}. \quad (2)$$

Like the analogous PCC[12–14] reactions, all the three alcohols studied herein were found to be first order with respect to time, because the first order rates were constant at different times. The reactions were also observed to be clearly first order with respect to the oxidant (PFC) as the rate constants were found to be practically unaltered for most of the reaction times (Table 1) with varying concentration of oxidant. The most prominent difference in the oxidations involving PCC[12–14] and those involving PFC is that the order of the reactions of the three alcohols with respect to the substrate concentrations was found to be practically constant enabling us to infer that the rates are almost independent of substrate concentrations. However, a small but steady increase in the rate constant values for all the three alcohols with increasing concentrations of the substrate

Table 1. Oxidant dependence of the reaction rate
T=303 K

[Oxidant] / 10^{-3} mol dm^{-3}	$k_1/10^{-4}$ s^{-1}		
	[Ethanol] / 0.1 mol dm^{-3}	[Benzyl alcohol] / 0.01 mol dm^{-3}	[Cyclohexanol] / 0.01 mol dm^{-3}
1	6.765	8.413 (0.075)[12]	9.233
2	6.77 (0.10)[13]	7.95 (0.075)[12]	9.5
3	6.62	8.41 (0.072)[12]	9.34
4	6.56 (0.973)[13]	8.27 (0.077)[12]	9.59
5	6.64	8.21 (0.076)[12]	9.60

PCC oxidation data in parentheses.

Table 2. Substrate dependence of the reaction rate
[PFC]=0.001 mol dm^{-3}; T=303 K

Ethanol		Benzyl alcohol		Cyclohexanol	
Concn / mol dm^{-3}	$k_1/10^{-4}$ s^{-1}	Concn / mol dm^{-3}	$k_1/10^{-4}$ s^{-1}	Concn / mol dm^{-3}	$k_1/10^{-4}$ s^{-1}
0.1	6.765 (0.10)[13]	0.01	8.413 (0.075[a])[12]	0.01	9.233
0.2	7.87 (0.207)[13]	0.02	9.66 (0.152[a])[12]	0.02	13.89
0.3	8.55	0.03	10.1	0.03	15.79
0.4	9.16 (0.41)[13]	0.04	10.52 (0.306[a])[12]	0.04	17.78
0.5	10.6	0.05	11.54	—	—

PCC oxidation data in parentheses: a) Values at 298 K.

Table 3. Dependence of reaction rate on solvent composition
[Oxidant]=0.002 mol dm^{-3}; T=303 K

Nitrobenzene (%)	Acetonitrile (%)	Dielectric constant	[Ethanol] / 0.2 mol dm^{-3} $k_1/10^{-5}$ s^{-1}	[Benzyl alcohol] / 0.02 mol dm^{-3} $k_1/10^{-4}$ s^{-1}	[Cyclohexanol] / 0.02 mol dm^{-3} $k_1/10^{-4}$ s^{-1}
30	70	36.7	1.01	1.05	3.08
40	60	36.4	1.997	1.77	5.31
50	50	36.16	4.05	3.15	7.2
60	40	35.9	7.97	4.3	10.27
70	30	35.6	15.82	5.51	12.95

Table 4. Rate constants for the uncatalyzed oxidation of alcohols by pyridinium fluorochromate
[PFC]=0.001 mol dm^{-3}

Substrate	Concentration of substrate/mol dm^{-3}	$k/10^{-4}$ l mol^{-1} s^{-1} [a]			
		303 K	308 K	313 K	318 K
Ethanol	0.1	6.765 (1.0)[13]	7.112 (1.4)[13]	7.447 (1.93)[13]	7.798 (2.63)[13]
Benzyl alcohol	0.01	8.413 (7.5)[12]	8.593 (11.2)[12]	8.811 (15.5)[12]	9.057 (21.6)[13]
Cyclohexanol	0.01	9.233 —	9.619 (88.3)[14]	10.0 (133.3)[14]	10.447 (208.3)[14]

a) PCC oxidation data in parentheses.

Table 5. Activation parameters for the oxidation of alcohols by pyridinium fluorochromate

Substrate	ΔH^*/kJ mol^{-1} [a]	$-\Delta S^*$/J mol^{-1} K^{-1} [a]	ΔF^*/kJ mol^{-1} [a]
Ethanol	7.657(51.8)[13]	280.51(153)[13]	92.65(98.2)[13]
Benzyl alcohol	3.89 (54.7)[12]	291.33(125)[12]	92.06(92.0)[12]
Cyclohexanol	6.127(93.0)[14]	282.98(−18)[14]	91.82(87.4)[14]

a) PCC oxidation data in parentheses.

has been observed (Table 2) and a plot of log k_{obsd} against log [substrate] shows that the rates increase in very small fractions with the sequential increase in substrate concentration. This most probably implies that complex formation between the substrate and oxidant is taking place in present cases.

Our attempts to study the acid-catalyzed oxidations of the three alcohols were unsuccessful. Attempted acid-catalyzed reactions involving *p*-Toluenesulfonic acid or benzoic acid, and varying proportions of solvent compositions were observed to be too fast to measure the rate.

The results of uncatalyzed reactions with varying composition of the solvent components (Table 3) shows that the reaction rate decreases with increase in dielectric constant (though small) of the medium suggesting that the more polar solvents may require larger reaction times for the oxidation reactions. A plot of log k_1 against the inverse of dielectric constants of the media is a straight line with positive slope and implies the occurrence of an interaction between a dipole and a positive ion,[15] and also indicates the probable involvement of a protonated Cr^{VI} species, in the presence of an acid, in the rate determining step. However, since the range of dielectric constants varies between 35.6 and 36.7 showing a large increase in the rate, the observed change could as well be solvent specific rather than owing to the effect of change in dielectric constant.

The near constancy of the values of the free energies of activation of the three reactions (Table 5) suggest that a similar mechanism is operative in each of the three oxidations. Free energies of the acid-catalyzed reactions appear to be lower, as there has been a pronounced increase in the rate of catalyzed reactions suggesting thereby that a protonated Cr^{VI} species may be involved in the rate determining step in the presence of an acid. This is in accord with the involvement of such species well established in chromium(VI) oxide oxidations.[16]

The large negative entropy values obtained in the present studies, suggest that the solvent molecules are strongly oriented or 'frozen' around the ions thereby resulting in the loss of entropy,[17] the effect being larger in nonpolar solvents. This conforms to the contention that the decrease of polarity of the medium results in increase of the entropy value and the number of unbound molecules in the solution increases.[18] This also accounts for the lowering of rate coefficient values with increasing polarity of the medium. Comparatively greater reactivity of pyridinium fluorochromate (PFC) over that of the corresponding chlorochromate (PCC), as shown in our previous paper,[7] can now be understood from the relatively higher negative entropy values of the reactions. We believe that the bonding of F with chromium in PFC facilitates larger charge distribution in the transition state in the cases of PFC oxidation and correlates well with the observed entropy values.

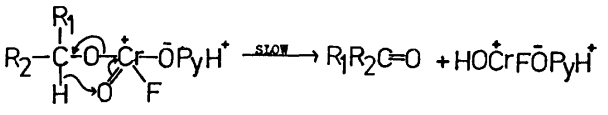

Scheme 1.

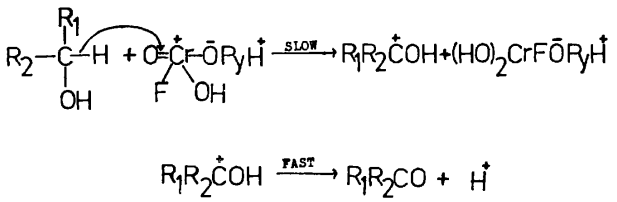

Scheme 2.

In view of the above results it appears that a hydride transfer mechanism is involved in the rate determining step of the PFC oxidations. It is possible that the hydride transfer may take place either through the prior formation of chromate (Scheme 1), or directly (Scheme 2). The present data also suggest, like the similar oxidations involving chromic acid,[16] a chromate formation in the rate-determining step (Scheme 1) although the chances of Scheme 2 can not be totally ruled out. It is also expected that the chromate intermediate will be better stabilised in the less polar medium and will enhance the oxidation rate, thus conforming to the observations made by us.

The authors wish to thank the University for the award of a fellowship (U. G. C.) to one of them (M. N. B.) and also to Dr. A. K. Sil, for his interest in the work.

References

1) J. C. Collins and W. W. Hess, *Org. Synth.*, **52**, 5, (1972).
2) E. J. Corey and J. W. Suggs, *Tetrahedron Lett.*, **1975**, 2647.
3) E. J. Corey and D. L. Boger, *Tetrahedron Lett.*, **1978**, 2461.
4) G. Piancatalli, A. Scettri, and M. D'Auria, *Synthesis*, **1982**, 245.
5) E. J. Corey and G. Schmidt, *Tetrahedron Lett.*, **1979**, 399.
6) F. S. Guziec and F. A. Luzzio, *Synthesis*, **1980**, 691.
7) M. N. Bhattacharjee, M. K. Chaudhuri, H. S. Dasgupta N. Roy, and D. T. Khathing, *Synthesis*, **1982**, 588.
8) D. D. Perrin, W. L. Armarego, and D. R. Perrin, "Purification of Organic Compounds," Pergamon Press, Oxford (1966).
9) C. N. R. Rao, "A Handbook of Chemistry and Physics," Affiliated East-West Press, New Delhi (1967), p. 169.
10) G. V. Bakore, K. K. Banerjee, and R. Shanker, *Z. Phys. Chem. (Frankfurt)*, **45**, 129 (1965).
11) A. A. Frost and R. G. Pearson, "Kinetics and Mechanism," Wiley-Eastern, New Delhi (1970), p. 99.
12) K. K. Banerjee, *J. Chem. Soc., Perkin Trans. 2*, **1978**, 639.
13) K. K. Banerjee, *Bull. Chem. Soc. Jpn.*, **51**, 2732, (1978).
14) G. P. Panigrahi and D. D. Mahapatra, *Indian J. Chem.*, **19A**, 579, (1980).
15) E. S. Amiss, "Solvent Effects on Reaction Rates and Mechanism," Academic Press, New York (1967), p. 42.
16) K. B. Wiberg, "Oxidation in Organic Chemistry," Academic Press, New York (1965), Part A, p. 99.
17) F. Basolo and R. G. Pearson, "Mechanism of Inorganic Reaction: A Study of Metal Complexes in Solution," 2nd ed, Wiley-Eastern, New Delhi (1973), p. 129.
18) F. A. Cotton and G. Wilkinson, "Advanced Inorganic Chemistry," 3rd ed, Wiley-Eastern, New Delhi (1976), p. 169.

Vibrational Spectra and Thermodynamic Functions of 2-Methoxypyridine and 2-Methoxy-d_3-pyridine

Kanak C. Medhi

Department of Physics, Gauhati University, Gauhati-781014, India

(Received February 4, 1983)

The infrared spectra in the liquid state (4000—50 cm^{-1}) and in the vapor phase (4000—400 cm^{-1}) and the polarized laser Raman spectra in the liquid state have been measured for 2-methoxypyridine and 2-methoxy-d_3-pyridine. Essentially complete assignments of the observed frequencies are presented. Ideal gas state thermodynamic functions of the molecules are also calculated in the temperature range 200—1500 K.

In continuation of the earlier work on the vibrational analysis of a few substituted pyridine molecules,[1-4] the investigation has now been extended to 2-methoxypyridine and 2-methoxy-d_3-pyridine. The infrared spectrum of 2-methoxypyridine in solution or in the pure liquid state was reported by Katritzky and Hands,[5] Katritzky and Coats,[6] and Spinner and White[7] in a limited range, and a partial assignment of only a few bands was given. The earlier work on the simple Raman spectrum of 2-methoxypyridine relate to that of Spinner and White.[7] There is however no previous study on the vibrational spectra of the deuterated species, 2-methoxy-d_3-pyridine.

The present investigation was undertaken with a view to making a detailed study of the infrared spectra of 2-methoxypyridine and 2-methoxy-d_3-pyridine in the liquid and vapor phases and the polarized Raman spectra of the two molecules in the liquid state. Assignments of the observed frequencies based on the infrared band contours, state of polarization of the Raman lines and comparison with the assignments for related molecules[8-12] are given. The ideal gas state thermodynamic functions of the molecules are also calculated on the basis of these assignments.

Experimental

Chemically pure sample of 2-methoxypyridine, used in this experiment, was obtained from Aldrich Chemical Company, U. S. A. and purified by fractional distillation. A sample of 2-methoxy-d_3-pyridine of 98 at.% isotopic purity was supplied by Merck Sharp and Dohme, Canada Ltd., and used as received.

The infrared spectra of the samples in the liquid and vapor states in the range 4000—400 cm^{-1} were recorded on a Carl-Zeiss Specord IR 75 spectrophotometer. The calibration of the instrument was checked by a polystyrene film run immediately after each record. The gas-phase spectra were taken at different temperatures using a 9 cm heated gas cell equipped with KBr windows. A Perkin-Elmer model 180 spectrophotometer and a DIGILAB FTS-15B Fourier Transform interferometer were employed to scan the far infrared spectra of the pure liquid samples in the region 500—50 cm^{-1}. The Raman spectra were measured on a Cary 82 laser Raman spectrophotometer using 488.0 nm (200 mW) line of an argon ion laser as the excitation source. Polarization measurements were made by the method described elsewhere.[4]

Results and Discussion

The frequencies observed in the infrared and Raman spectra of the two molecules, their approximate intensities and probable assignments are given in Table 3. The calculated values of the thermodynamic functions are listed in Tables 4 and 5. Assuming C_s symmetry for both the molecules, the thirty-nine normal vibrations, which are active both in the infrared and Raman spectra, are divided over the irreducible representation as follows:

$$\Gamma = 26a' + 13a''$$

The a′ modes should give rise to polarized Raman lines, whilst the depolarized lines are associated with the a″ modes.

Taking the ring as a planar regular hexagon, the principal moments of inertia of 2-methoxypyridine and 2-methoxy-d_3-pyridine molecules and the asymmetry parameters $\kappa=(2B-A-C)/(A-C)$ and $\rho^*=(A-C)/B$, where A, B, and C are the rotational constants, have been calculated (Table 1) with the following geometry on the assumption that the 2-methoxypyridine molecules exist in the cis (synperiplanar) conformation (Fig. 1).

$$r(\text{C–C}) = r(\text{C–N}) = 1.397\ \text{Å},\ r(\text{C–H}) = 1.084\ \text{Å},$$
$$\angle\text{CCC} = \angle\text{CCN} = \angle\text{CCO} = 120°,$$

and for OCH_3 group : $r(\text{C–H})=1.0936$ Å, $r(\text{C–O})=1.426$ Å, $\angle\text{COC}=109.47°$, and all other angles are tetrahedral (109.47°). The values of relative atomic masses recommended by IUPAC[13] were used in the calculation.

Making use of the results given in Table 1, the PR separations of the vapor-phase band envelopes in the infrared spectra have been calculated at $T=323$ K by the method of Seth-Paul and Dijkstra[14] and compared with the observed values (Table 2). While the normal

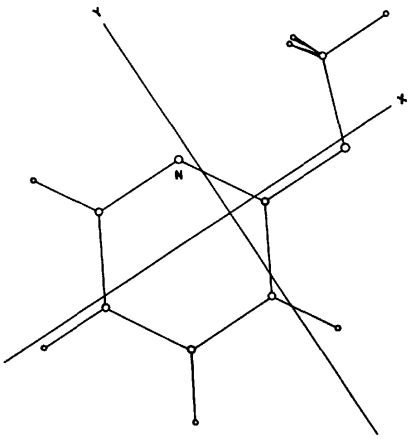

Fig. 1. Cis conformation of 2-methoxypyridine.

Table 1. Principal moments of inertia and asymmetry parameters for 2-methoxypyridine and 2-methoxy-d_3-pyridine

Molecule	I_x / 10^{-47} kg m^2	I_y / 10^{-47} kg m^2	I_z / 10^{-47} kg m^2	κ	ρ^*
2-Methoxypyridine	169.272	519.530	683.467	−0.7922	2.3091
2-Methoxy-d_3-pyridine	175.661	564.214	729.175	−0.8144	2.4382

The z axis is perpendicular to the plane of the ring.

Table 2. PR separations in the Infrared vapor-phase band envelopes

Band type	2-Methoxypyridine PR separation ν/cm^{-1}		2-Methoxy-d_3-pyridine PR separation ν/cm^{-1}	
	Calcd	Obsd	Calcd	Obsd
A (∥)	11.1	11.0, 11.5, 11.0, 11.0, 11.5, 11.5, 13.0, 12.0	10.7	11.0, 11.0, 11.0, 11.0, 11.5, 10.0, 10.0, 11.5, 11.0, 11.0
B (⊥)	9.1	10.5, 10.0	8.8	—
C (⊥)	16.7	18.0, 17.5, 18.0	16.1	≈18.0, 17.0, ≈17.0

modes of species a″ will have a contour of type-C with strong Q branch, the a′ modes will give rise to A- or B-contours or contours of the hybrid type-AB depending on the directions of the oscillating dipoles.

Species a′. The polarized Raman lines observed at 3013, 3062, 3072, and 3094 cm^{-1} in the case of 2-methoxypyridine and 3021, 3066, and 3078 cm^{-1} and the infrared band at 3088 cm^{-1} in 2-methoxy-d_3-pyridine are readily assigned to the C–H stretching vibrations. The Raman spectra of the two molecules show polarized lines at 1602 and 1572 cm^{-1}, and 1599 and 1571 cm^{-1} respectively; these are assigned to the C–C stretching modes of the highest energy. The infrared bands observed at 1481, 1419, and 1312 cm^{-1} and 1472, 1433, and 1316 cm^{-1} in 2-methoxypyridine and its deuterio analog respectively show type-A vapor-phase contours, and are attributed to the next ring stretching modes. The highly intense and polarized Raman shifts at 988 and 984 cm^{-1} observed in the spectra of the two molecules may be confidently assigned to the ring breathing mode.

The two components of the planar ring deformation mode are little affected by substitution in the present cases, and identified with the polarized Raman lines at 622 and 602 cm^{-1}, and 620 and 577 cm^{-1} in the case of the two molecules respectively. The three substituent-sensitive modes belonging to the a′ class may be represented by the polarized Raman lines at 1289, 811, and 254 cm^{-1} in 2-methoxypyridine and 1292, 786, and 232 cm^{-1} in 2-methoxy-d_3-pyridine. The remaining a′ modes that can be derived from pyridine may be assigned to the polarized Raman lines observed at 1256, 1143, 1098, and 1044 cm^{-1}, and 1257, 1144, 1075, and 1042 cm^{-1} in the case of the normal and deuterated molecules respectively.

Species a″. The infrared bands at 781, 738, and 526 cm^{-1} in 2-methoxypyridine and 779, 737, and 524 cm^{-1} in the deuterio analog show conclusively type-C vapor-phase contours, and are assigned as a″ fundamentals. Similarly, the infrared spectra of the two molecules show absorptions of medium strength at 862 and 861 cm^{-1} respectively which appear to have type-C structures with prominent central maxima in the gas-phase spectra. These are assigned to the a″ mode involving principally out-of-plane bending motions of the ring H atoms. The remaining fundamentals belonging to the a″ species may be identified with the weak or moderately intense infrared bands at 957, 827, 412, and 116 cm^{-1} in 2-methoxypyridine and 957, 837, 415, and 130 cm^{-1} in 2-methoxy-d_3-pyridine in agreement with the assignments proposed for other monosubstituted pyridines.[4,9,10]

The Internal Vibrations of the Methoxyl Group. There would appear twelve additional modes of vibration arising from the internal motions of the methoxyl group. The moderately intense infrared band at 2980 cm^{-1} appears to have type-C band contour in the gas-phase spectrum, while the Raman line at 2944 cm^{-1} is very strong and highly polarized. These are assigned to the a″ and a′ CH_3 asymmetric stretching modes respectively. Both of these frequencies are shifted to 2241 and 2263 cm^{-1} on OCH_3 deuteration. Again the infrared vapor-phase band contour of the 2241 cm^{-1} band shows a sharp central maximum characteristic of a type-C band, and its Raman counterpart is depolarized. It is, therefore, assigned to the a″ component of the CD_3 asymmetric stretching mode, while the a′ component may be identified with the polarized Raman line at 2263 cm^{-1}. The frequency at 2209 cm^{-1} appearing with comparable intensity both in the infrared and the Raman spectra may be explained as the overtone $2\times 1101=2202$ cm^{-1} (A′) enhanced by Fermi-resonance interaction with the fundamental at 2263 cm^{-1}. But the situation is complicated by the appearance of three polarized Raman lines of almost equal intensity at 2870, 2850, and 2828 cm^{-1} each having a counterpart in the infrared spectrum of 2-methoxypyridine. Since there occurs an infrared band at 2823 cm^{-1} in the deuterated species corresponding to the 2828 cm^{-1} frequency of the normal molecule, it must be assigned as a combination

TABLE 3. OBSERVED FUNDAMENTAL FREQUENCIES AND ASSIGNMENTS FOR 2-METHOXYPYRIDINE AND 2-METHOXY-d_3-PYRIDINE

2-Methoxypyridine			2-Methoxy-d_3-pyridine			
Infrared ν/cm^{-1}		Raman ν/cm^{-1}	Infrared ν/cm^{-1}		Raman ν/cm^{-1}	Assignment
Liquid	Vapor	Liquid	Liquid	Vapor	Liquid	
3095 (sh)	3107	3094 (sh)	3088 (sh)	3107		ν_1 (a′), 20b
3077 (mw)	3086	3072 (9) p	3077 (mw)	3084	3078 (sh) p	ν_2 (a′), 2
3058 (mw)	3060	3062 (sh) p	3057 (mw)	3061	3066 (10) p	ν_3 (a′), 20a
3014 (ms)	3023 3021 3012	3013 (2) p	3018 (mw)	3032	3021 (1) p	ν_4 (a′), 7b
2980 (ms)	2985		2241 (ms)	2248	2241 (0)dp	ν_{27} (a″), $-CH_3$ or $-CD_3$ asymmetric stretching
2945 (ms)	2960	2944 (8) p	2263 (ms)	2276 2271 A 2265	2263 (1) p	ν_5 (a′), $-CH_3$ or CD_3 asymmetric stretching
2849 (w)	2847	2850 (2) p	2075 (ms)	2090 2085 A 2079	2075 (4) p	ν_6 (a′), $-CH_3$ or $-CD_3$ symmetric stretching
1605 (s)	1613.5 1608.0 1602.0	1602 (1) p	1599 (vs)	1600	1599 (1) p	ν_7 (a′), 8a
1573 (s)	1573	1572 (3) p	1571 (s)	1572	1571 (2) p	ν_8 (a′), 8b
1481 (vs)	1491 1486 A 1480	1480 (0)	1472 (vs)	1481 1475 A 1470	1473 (0) p	ν_9 (a′), 19a
1464(mw)†	1466	1464 (0) dp	1049 (mw)	1048	1051 (sh) p	ν_{10} (a′) and ν_{28} (a″), $-CH_3$ or $-CD_3$ asymmetric deformation
1444 (s)	1452.0 1446.0 A 1440.5	1444 (2) p	1101 (vs)	1118 1113 A 1107	1100 (1) p	ν_{11} (a′), $-CH_3$ or $-CD_3$ symmetric deformation
1419 (vs)	1428 1422 A 1417	1419 (0)	1433 (vs)	1443.5 1438.0 A 1432.0	1434 (1) p	ν_{12} (a′), 19b
1312 (s)	1319 1314 A 1308	1310 (5) p	1316 (vs)	1325 1321 A 1315	1316 (5) p	ν_{13} (a′), 14
1289 (vs)	1296.0 1290.0 A 1284.5	1289 (4) p	1291 (vs)	1300 1295 A 1290	1292 (2) p	ν_{14} (a′), $-C-OCH_3$ or $-C-OCD_3$ stretching, 13
1252 (ms)	1260	1256 (2) p	1251 (mw)		1257 (2) p	ν_{15} (a′), 3
1143 (ms)	1147.5 1142.0 A 1136.0	1143 (1) p	1144 (ms)	1146.5 1141.0 A 1135.0	1144 (1) p	ν_{16} (a′), 9a
1098 (w)		1098 (2) p	1075 (w)		1075 (0) p	ν_{17} (a′), 15
			1040 (ms)	1044 1038 A 1033	1042 (3) p	ν_{18} (a′), 18a
1044 (s)	1049 1044 A 1036	1044 (5) p	894 (mw)		897 (0) dp	ν_{29} (a″), $-CH_3$ or $-CD_3$ out-of-plane rocking
1022 (s)	1024	1022 (1) p	996 (s)	997	997 (sh)	ν_{19} (a′), $-O-CH_3$ or $-O-CD_3$ stretching
988 (ms)	995.0 984.5 B	988 (10) p	983 (s)	981	984 (8) p	ν_{20} (a′), 1
957 (w)	955		957 (ms)	955		ν_{30} (a″), 17a
862 (mw)	≈869 861 ≈851		861 (mw)	862		ν_{31} (a″), 5
827 (mw)	832	828 (0)	837 (mw)	835		ν_{32} (a″), 10a
			802 (sh)		786 (5) p	ν_{21} (a′), 12
811 (ms)	818 813 807	811 (8) p	642 (mw)	642		ν_{22} (a′), $-CH_3$ or CD_3 in-plane-rocking

Table 3. (Continued)

2-Methoxypyridine			2-Methoxy-d_3-pyridine			
Infrared ν/cm^{-1}		Raman ν/cm^{-1}	Infrared ν/cm^{-1}		Raman ν/cm^{-1}	Assignment
Liquid	Vapor	Liquid	Liquid	Vapor	Liquid	
781 (s)	790, 782, 772 C	783 (0) dp	779 (s)	≈789, 780, ≈771 C		ν_{33} (a″), 10b
738 (ms)	744.5, 737.0, 727.0 C	729 (0)	737 (ms)	744, 736, 727 C		ν_{34} (a″), 4
621 (mw)	619	622 (1) p	618 (mw)	612	620 (1) p	ν_{23} (a′), 6b
601 (ms)	604, 600, 592 A	602 (1) p	575 (ms)	580, 577, 569 A	577 (1) p	ν_{24} (a′), 6a
526 (ms)	530, 522, 512 C	528 (0)dp	525 (mw)	≈527, 520, ≈510 C	527 (0) dp	ν_{35} (a″), 11
455 (mw)	458, 448 B	457 (3) p	438 (mw)		440 (2) p	ν_{25} (a′), ∠COC deformation
412 (mw)			415 (mw)*		414 (0) dp ?	ν_{36} (a″), 16a
256 (mw)		254 (0) p	240 (mw)*		232 (1) p	ν_{26} (a′), 18b
237 (sh)		234 (1) dp	234 (sh)*			ν_{37} (a″), ∠COC deformation
116 (mw)			130 (mw)*			ν_{39} (a″), 16b

(s)=strong, (m)=medium, (w)=weak, (v)=very, (sh)=shoulder, p=polarized, dp=depolarized.
*: Frequency observed in polycrystalline thin film at liquid nitrogen temperature.
†: Frequency observed in CCl_4 solution.

band. Of the remaining two frequencies, the 2850 cm^{-1} band is taken as the CH_3 symmetric stretching fundamental on the basis of the observed fact that a sharp band is usually occurs at about 2835 cm^{-1} when a methoxyl group is attached to the aromatic ring,[8,15-17] while the 2870 cm^{-1} band may be explained as the overtone $2\times 1444=2888$ cm^{-1} (A′) in Fermi-resonance[18] with the fundamental at 2850 cm^{-1}. These are shifted to 2124, 2105, and 2075 cm^{-1} on OCH_3 deuteration. Of these, the 2105 cm^{-1} band being weak must be explained as a combination tone. The polarized Raman line at 2075 cm^{-1} and its infrared counterpart at the same frequency showing type-A contour in the gas-phase spectrum are more intense, and may be reasonably assigned to the CD_3 symmetric stretching mode, while the 2124 cm^{-1} frequency appearing with smaller intensity both in the infrared and Raman spectra may be interpreted as the overtone $2\times 1049=2098$ cm^{-1} (A′) or the combination band $1101+996=2097$ cm^{-1} (A′) in Fermi-resonance with the 2075 cm^{-1} fundamental.

A moderately intense polarized Raman line at 1444 cm^{-1} with a strong infrared counterpart at the same frequency is observed in 2-methoxypyridine, but it is absent in the Raman spectrum of the deuterio analog, though an infrared band with much reduced intensity appears at 1451 cm^{-1}. It is also known that the CH_3 symmetric deformation frequency being somewhat sensitive to the electronegativity of the attached oxygen atom in OCH_3 group, shifts to higher frequency[15] as a result of changes in the HCO bending force constant.[19] These observations lead the 1444 cm^{-1} band to be assigned to the CH_3 symmetric deformation mode, while the 1451 cm^{-1} band in 2-methoxy-d_3-pyridine may be attributed to the combination $802+642=1444$ cm^{-1} (A′). The Raman line at 1464 cm^{-1} with its infrared counterpart of medium intensity is assigned to both the components of the CH_3 asymmetric deformation mode.

There appear two polarized Raman lines of almost equal strength at 1100 and 1051 cm^{-1} on OCH_3 deuteration. The infrared band at 1101 cm^{-1} showing type-A contour is very strong, while the band at 1049 cm^{-1} is comparatively weak. The former is therefore assigned to the CD_3 symmetric bending vibration and the latter to the CD_3 asymmetric bending mode in agreement with the assignments proposed for similar molecules.[20-23]

It is found that the 1044 and 811 cm^{-1} bands observed in the infrared and Raman spectra of 2-methoxypyridine, which are already assigned to the a′ fundamentals, decrease appreciably in intensity showing a small shift to lower frequency on OCH_3 deuteration. This may be taken as an evidence that two different fundamentals are overlapping at each of these positions. This frequency range being appropriate for CH_3 rocking modes, the bands at 1044 and 811 cm^{-1} are again assigned to the out-of-plane and in-plane CH_3 rocking modes respectively in agreement with the assignments for other molecules.[9,20,23,24] There appear two additional bands at 894 and 642 cm^{-1} in the infrared spectrum of 2-methoxy-d_3-pyridine. The corresponding Raman shift at 897 cm^{-1} being completely depolarized, is assigned to the CD_3 out-of-plane rocking mode, while the frequency at 642 cm^{-1} may be identified with the CD_3 in-plane rocking mode. The fundamental associated with the torsional mode remains unidentified in the present cases.

The strong infrared band at 1022 cm^{-1} and the polarized Raman line at 457 cm^{-1} in 2-methoxypyridine shift to 996 and 440 cm^{-1} respectively on OCH_3 deuteration. The former is assigned to the O–CH_3 stretching mode in agreement with the previous assignments,[7,25,26] while the latter may arise from the O–CH_3 in-plane bending vibration.[11] The O–CH_3 out-of-plane bend-

Table 4. Thermodynamic functions of 2-methoxypyridine[a)]

Temperature K	C_p° $cal_{th}\ K^{-1}\ mol^{-1}$	$(H^\circ-E_0^\circ)/T$ $cal_{th}\ K^{-1}\ mol^{-1}$	S° $cal_{th}\ K^{-1}\ mol^{-1}$	$-(F^\circ-E_0^\circ)/T$ $cal_{th}\ K^{-1}\ mol^{-1}$
200	19.20	12.92	74.03	61.11
250	23.40	14.59	78.76	64.17
273.15	25.44	15.42	80.92	65.50
298.15	27.65	16.35	83.24	66.89
300	27.82	16.43	83.41	66.99
400	36.31	20.35	92.60	72.25
500	43.54	24.29	101.50	77.21
600	49.44	28.01	109.98	81.98
700	54.23	31.42	117.97	86.55
800	58.17	34.53	125.48	90.95
900	61.46	37.34	132.53	95.19
1000	64.23	39.90	139.15	99.25
1100	66.58	42.22	145.38	103.17
1200	68.58	44.34	151.26	106.93
1300	70.30	46.27	156.82	110.56
1400	71.77	48.04	162.09	114.05
1500	73.04	49.66	167.08	117.42

a) Ideal gas state at standard pressure of 1 atm. 1 cal_{th}=4.184 J.

Table 5. Thermodynamic functions of 2-methoxy-d_3-pyridine[a)]

Temperature K	C_p° $Cal_{th}\ K^{-1}\ mol^{-1}$	$(H^\circ-E_0^\circ)/T$ $cal_{th}\ K^{-1}\ mol^{-1}$	S° $Cal_{th}\ K^{-1}\ mol^{-1}$	$-(F^\circ-E_0^\circ)/T$ $Cal_{th}\ K^{-1}\ mol^{-1}$
200	19.82	13.04	75.03	61.99
250	24.42	14.85	79.94	65.09
273.15	26.64	15.75	82.20	66.45
298.15	29.03	16.77	84.63	67.87
300	29.21	16.84	84.81	67.97
400	38.20	21.09	94.48	73.40
500	45.70	25.28	103.84	78.56
600	51.71	29.21	112.72	83.52
700	56.54	32.78	121.07	88.29
800	60.45	36.00	128.88	92.88
900	63.67	38.90	136.19	97.29
1000	66.33	41.52	143.04	101.53
1100	68.55	43.88	149.47	105.60
1200	70.42	46.01	155.51	109.51
1300	72.00	47.95	161.22	113.27
1400	73.35	49.72	166.60	116.89
1500	74.50	51.33	171.70	120.37

a) Ideal gas state at standard pressure of 1 atm. 1 cal_{th}=4.184 J.

ing mode may be represented by the depolarized Raman shift at 234 cm^{-1} in 2-methoxypyridine.

The Application of the Product Rule. When the Teller-Redlich product rule is applied to the assignments for the a′ species, it is found that the observed ratio is

$$\frac{\pi\nu^{\mathrm{I}}}{\pi\nu} = 0.192$$

and the calculated value of this ratio is 0.189.

Since the torsional frequencies are not identified, the product rule cannot be applied to the assignments for the a″ species.

Thermodynamic Functions

The thermodynamic functions of 2-methoxypyridine and 2-methoxy-d_3-pyridine were calculated at several temperatures assuming a rigid rotator, harmonic oscillator approximation and free internal rotation of the methyl group by utilising the fundamental frequencies given in Table 3. The reduced moments of inertia of the CH_3 and CD_3 groups were calculated to be 5.2627×10^{-47} kg m^2 and 10.4120×10^{-47} kg m^2 respectively.

The author wishes to thank Professor I. Haque and Professor J. R. Durig for their kind permission to use the infrared spectrophotometers. The author is also thankful to S. K. Barooah and K. K. Chatterjee for their assistance in recording some of the infrared spectra.

References

1) K. C. Medhi and D. K. Mukherjee, *Spectrochim. Acta*, **21**, 895 (1965).
2) K. C. Medhi, *Optika i Spektroskopiya*, **19**, 49 (1965).
3) K. C. Medhi, *Indian J. Phys.*, **46**, 300 (1972).
4) K. C. Medhi, *Indian J. Phys. A*, **51**, 399 (1977).
5) A. R. Katritzky and A. R. Hands, *J. Chem. Soc.*, **1958**, 2202.
6) A. R. Katritzky and N. A. Coats, *J. Chem. Soc.*, **1959**, 2062.
7) E. Spinner and J. C. B. White, *J. Chem. Soc.*, **1962**, 3115.
8) J. H. S. Green, *Spectrochim. Acta*, **18**, 39 (1962).
9) J. H. S. Green, W. Kynaston, and H. M. Paisley, *Spectrochim. Acta*, **19**, 549 (1963).
10) D. A. Long and W. O. George, *Spectrochim. Acta*, **19**, 1777 (1963).
11) A. Allan, D. C. Mckean, J. P. Perchard, and M. L. Josien, *Spectrochim. Acta, Part A*, **27**, 1409 (1971).
12) V. I. Berezin and M. D. Elkin, *Opt. Spectrosc.*, **34**, 395 (1973).
13) Atomic Weights of the Elements, *Pure Appl. Chem.* **30**, 637 (1972).
14) W. A. Seth-Paul and G. Dijkstra, *Spectrochim. Acta, Part A*, **23**, 2861 (1967).
15) N. B. Colthup, L. H. Daly, and S. E. Wiberley, "Introduction to Infrared and Raman Spectroscopy," Academic Press, New York (1975), pp. 225, 226.
16) H. B. Henbest, G. D. Meakins, B. Nicholls, and A. A. Wagland, *J. Chem. Soc.*, **1957**, 1462.
17) W. A. Seth-Paul, J. P. Tollenaere, H. Meeusen, and F. Höfler, *Spectrochim. Acta, Part A*, **30**, 193 (1974).
18) A. B. Dempster, D. B. Powell, and N. Sheppard, *Spectrochim. Acta, Part A*, **28**, 373 (1972).
19) N. Sheppard, *Trans. Faraday Soc.*, **51**, 1465 (1955).
20) A. B. Dempster, D. B. Powell, and N. Sheppard, *Spectrochim. Acta, Part A*, **31**, 245 (1975).
21) Jouko Korppi-Tommola, *Spectrochim. Acta, Part A*, **34**, 1077 (1978).
22) J. Overend, R. A. Nyquist, J. C. Evans, and W. J. Potter, *Spectrochim. Acta*, **17**, 1205 (1961).
23) A. Poletti, G. Paliani, M. G. Giorgin, and R. Cataliotti, *Spectrochim. Acta, Part A*, **31**, 1869 (1975).
24) W. C. Harris and I. W. Levin, *J. Mol. Spectrosc.*, **43**, 117 (1972).
25) L. H. Briggs, L. D. Colebrook, H. M. Fales, and W. C. Wildman, *Anal. Chem.*, **29**, 904 (1957).
26) K. J. Sax, W. S. Saart, C. L. Mahoney, and J. M. Gordon, *J. Org. Chem.*, **25**, 1590 (1960).

Extractive Separation of Osmium and Ruthenium from Thiocyanate Media

Sambamoorthy JAYA* and Tiruvesaloor V. RAMAKRISHNA
Department of Chemistry, Indian Institute of Technology, Madras-600 036, India
(Received January 25, 1983)

The sequential separation of osmium and ruthenium as thiocyanate complexes by extraction into mesityl oxide and cyclohexanone is described. The conditions for their re-extraction prior to determination from the respective organic layers have been established. Alternatively, the amounts of osmium and ruthenium were established spectrophotometrically from the coloured mesityl oxide and cyclohexanone layers respectively. The developed procedure has been applied to the separation of these metals present in synthetic samples of various minerals.

The reaction of thiocyanate with osmium and ruthenium has been extensively investigated for the spectrophotometric determination of these elements after extraction into diethyl ether, 2-octanone or isobutyl methyl ketone.[1-3] Though the extraction of osmium into diethyl ether or 2-octanone has been reported to be selective, the extraction behaviour of ruthenium has not been described.[1] In the extraction of ruthenium as tetraoxide into carbon tetrachloride,[2] osmium interferes demanding a separation prior to determination. Recently a method[3] has been described for the sequential separation of osmium and ruthenium when present together. This procedure is based on the extraction of the thiocyanate complex of osmium into peroxide containing ether and subsequently ruthenium into isobutyl methyl ketone. The extraction efficiency of osmium and ruthenium however are critically dependent on various experimental parameters such as acidity and duration of heating for complex formation in addition to peroxide content of ether. In the course of our study on the extraction behaviour of the thiocyanate complexes of osmium and ruthenium, it was found that osmium forms such complex at very low concentrations of thiocyanate and low acidities at room temperature itself while the formation of such extractable complex of ruthenium requires heating besides higher acidity and thiocyanate concentration. This formed the basis of the sequential solvent extractive separation procedure described here.

Experimental

Reagents. *Osmium(VIII) Solution*: Prepare by dissolving 1 g of osmium tetraoxide in 250 cm^3 of water as described elsewhere.[4] A working solution containing 100 $\mu g\ cm^{-3}$ of osmium is prepared by suitably diluting the stock solution with water.

Ruthenium(III) Solution: Dissolve 0.513 g of ruthenium trichloride (LOBA-CHEMIE-PURISS) in 25 cm^3 of concentrated hydrochloric acid and dilute with water to 250 cm^3 to get a solution 1000 ppm in ruthenium.

Potassium Thiocyanate Solutions (0.05 mol dm^{-3} and 4 mol dm^{-3}) Sulfuric Acid (3 and 10 mol dm^{-3}).

Solvents: Mesityl oxide, cyclohexanone and cyclohexane.

Apparatus: A carl Zeiss PMQ-II spectrophotometer with 10 mm quartz cells.

Recommended Procedure. *Separation*: Transfer a suitable aliquot of sample solution (upto 8 cm^3) into a 60 cm^3 separatory funnel, add 1 cm^3 each of 0.05 mol dm^{-3} potassium thiocyanate and 3.0 mol dm^{-3} sulfuric acid and dilute to 10 cm^3. Equilibrate the solution with 5 cm^3 of mesityl oxide for 5 min. Separate the organic layer and equilibrate the aqueous layer with 10 cm^3 of cyclohexanone to remov the traces of dissolved mesityl oxide. Drain the aqueous layer into a 25 cm^3 beaker. Add 1.5 cm^3 of 10 mol dm^{-3} sulfuric acid and 3 cm^3 of 4 mol dm^{-3} potassium thiocyanate and dilute to 15 cm^3. Heat the solution at 75 °C for 20 min. Transfer the cooled solution after diluting to 15 cm^3 with water into a 60 cm^3 separatory funnel and equilibrate with 5 cm^3 of cyclohexanone for 1 min.

Equilibrate the mesityl oxide layer with 10 cm^3 of 0.1 mol dm^{-3} sodium hydroxide for 5 min to re-extract osmium. Add 15 cm^3 of cyclohexane to cyclohexanone layer and equilibrate with 10 cm^3 of water for 5 min. Use suitable aliquots of the stripped layers, if necessary, after diluting to a known volume and proceed with the determination as follows:

Determination: Add with mixing 5% potassium thiocyanate solution (2.5 cm^3 for osmium[5] and 1 cm^3 for ruthenium[6]) and 2.5 cm^3 of 1 mol dm^{-3} sodium acetate. Adjust the pH to 3, dilute to about 15 cm^3 with water and heat on a boiling water bath for 20 min. Cool and transfer into 25 cm^3 volumetric flasks. Add 5 cm^3 of 0.005% Rhodamine 6G solution and 1 cm^3 of 1% gelatin. Make up the solutions to mark and measure the absorbance at 565 nm in 10 mm cells against the respective reagent blanks. Establish the concentration by reference to corresponding calibration graphs prepared by using 0 to 40 μg of osmium and 0 to 8 μg of ruthenium.

Results and Discussion

Extraction of Osmium: Preliminary studies were carried out by extracting 100 μg each of osmium or ruthenium into 5 cm^3 of mesityloxide from 10 cm^3 of weakly acidic and acidic solutions containing 0.05 mol dm^{-3} potassium thiocyanate. The per cent extraction was established by estimating the amounts of osmium and ruthenium left out in the aqueous phase using the procedures described under 'Determination.'

The effect of varying the potassium thiocyanate concentration on the extraction of osmium (curve A) and ruthenium (curve B) are shown in Fig. 1. It is evident that though a concentration of as low as 5×10^{-4} mol dm^{-3} potassium thiocyanate is sufficient for the quantitative extraction of osmium, higher concentrations upto 0.9 mol dm^{-3} do not affect the extraction. There is no extraction of ruthenium until the potassium thiocyanate concentration is raised to 0.4 mol dm^{-3}.

Curve A in Fig. 2 shows the effect of acidity on the extraction of osmium from which it is clear that the extraction of osmium is quantitative from 0.1 to 0.6 mol dm^{-3} sulfuric acid. Over the whole range of acidity studied, ruthenium is found to be not at all extracted

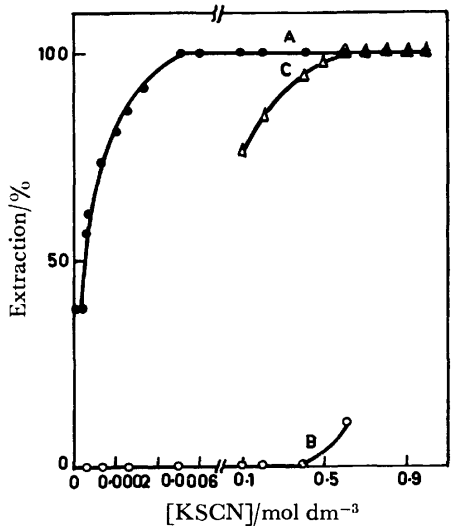

Fig. 1. Effect of potassium thiocyanate (0.30 mol dm^{-3} in H_2SO_4; 5 cm^3 mesityl oxide).
A: Osmium, B: ruthenium, C: ruthenium (1 mol dm^{-3} in H_2SO_4; 5 cm^3 cyclohexanone).

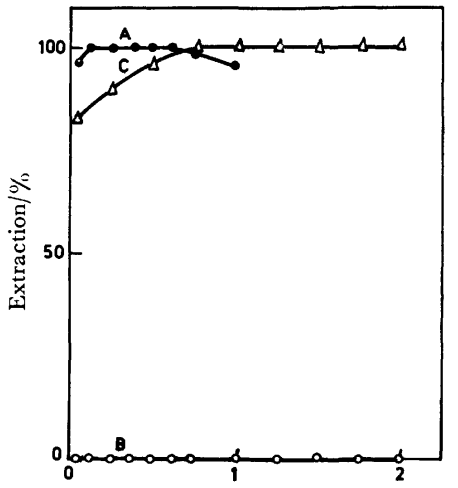

Fig. 2. Effect of acidity -H_2SO_4 (0.005 mol dm^{-3} in KSCN; 5 cm^3 mesityl oxide).
A: Osmium, B: ruthenium, C: ruthenium (0.8 mol dm^{-3} in KSCN; 5 cm^3 cyclohexanone).

TABLE 1. CHOICE OF SOLVENT–OSMIUM STAGE

Solvent	Distribution ratio	
	D_{Os}	D_{Ru}
Carbon tetrachloride	6.9	<0.01
Chloroform	7.5	<0.01
Benzene	<0.01	<0.01
Cyclohexane	6.4	<0.01
Isobutyl methyl ketone	18.0	<0.01
Cyclohexanone	98.0	<0.01
1-Butanol	10.3	<0.01
Cyclohexanol	14.0	<0.01
Pentyl acetate	7.2	<0.01
Diethyl ether	5.3	<0.01
Mesityl oxide	≫100	<0.01

(*cf.* curve B Fig. 2).

The extractability of osmium and ruthenium into a variety of solvents has been studied from a medium 0.005 mol dm^{-3} in potassium thiocyanate and 0.3 mol dm^{-3} in sulfuric acid. The results are summarised in Table 1 from which it is clear that only mesityl oxide extracted osmium quantitatively while none of the solvents extracted ruthenium under similar conditions. It is also established that a minimum of 3 min of equilibration is essential for the quantitative extraction of osmium into mesityl oxide and a ten-fold increase of the aqueous phase volume to that of the organic phase did not affect the extraction.

Extraction of Ruthenium. As ruthenium forms the extractable thiocyanate complex only on heating, extraction studies on ruthenium are carried out by heating 100 μg of ruthenium in a media which is 0.8 mol dm^{-3} in thiocyanate and 1 mol dm^{-3} in sulfuric acid to 70 °C in a water bath and equilibrating with 5 ml each of various solvents. As clear from Table 2, cyclohexanone alone extracts ruthenium quantitatively while mesityl oxide and cyclohexanol extract only partially. Other solvents like diethyl ether, benzene, cyclohexane, and pentyl acetate do not at all extract ruthenium. Cyclohexanone is preferred in further studies.

The effect of temperature on the formation of thiocyanate complex is established by heating the solution 0.8 mol dm^{-3} in potassium thiocyanate and 1 mol dm^{-3} in sulfuric acid for 20 min in a thermostat maintained at various temperatures and extracting into 5 cm^3 of cyclohexanone after cooling. The results indicate that for quantitative extraction the complex should be formed over the temperature range 70 to 85 °C. Higher temperatures are found to cause lower recoveries of ruthenium possibly due to the decomposition of the extractable species. It is also found that a minimum of 15 min of heating at 75 °C is essential for the complete formation of the complex while heating upto even one hour did not affect the extraction.

The effect of varying the concentration of thiocyanate (curve C, Fig. 1) indicates that a minimum of 0.6 mol dm^{-3} potassium thiocyanate is essential for the quantitative extraction of ruthenium. The effect of acidity on the extraction of ruthenium is studied using varying amounts of sulfuric acid in a medium 0.8 mol dm^{-3} in potassium thiocyanate. The results are indicated in

TABLE 2. CHOICE OF SOLVENT–RUTHENIUM STAGE

Solvent	Distribution ratio D_{Ru}
Carbon tetrachlride	0.286
Chloroform	0.174
Benzene	<0.01
Cyclohexane	<0.01
Isobutyl methyl ketone	0.667
Cyclohexanone	≫100
1-Butanol	1.704
Cyclohexanol	26.220
Pentyl acetate	<0.01
Diethyl ether	<0.01
Mesityl oxide	18.000

curve C, Fig. 2, from which it is clear that over the range of 0.75 to 2 mol dm^{-3} sulfuric acid, the extraction is quantitative. The extraction is found to be quantitative with equilibration times as low as 10 seconds and an aqueous to organic phase volume ratio of 3.5 : 1 does not affect the extraction.

Sequential Separation of Osmium and Ruthenium. From the studies on the individual extraction of osmium and ruthenium it is found that osmium forms a quantitatively extractable complex at concentrations of thiocyanate as low as 5×10^{-4} mol dm^{-3} from weakly acidic media at room temperature itself. Further, it is found that, under these conditions, increasing the thiocyanate concentration or acidity does not increase the extraction of ruthenium considerably. It has also been observed that ruthenium can form such extractable complex only on heating and the various parameters have been optimized for the quantitative extraction of ruthenium.

Table 3. Recovery studies

Sample No.	Composition of the mixture (μg)		Amount recovered (μg)		Recovery (%)	
	Os	Ru	Os	Ru	Os	Ru
1	10	10	10	9.8	100	98
2	50	50	49.5	50	99	100
3	100	100	100	100	100	100
4	1000	1000	1000	1000	100	100
5	1000	10	1000	9.8	100	98
6	500	20	495	19.8	99	99
7	50	1000	49	1000	98	100
8	50	200	50	200	100	100
9	10	100	9.9	100	99	100
10	20	1000	20	1000	100	100

Table 4. Analysis of synthetic mixtures after oxidative fusion

Sample No.	Sample composition (wt%)	Composition of the synthetic sample (μg)	Amount found (μg)	
			Os	Ru
	Osmiridium or Syserkite			
1	Columbia			
	Ir (57.8), Pd(0.63)	Ir(660), Pd(8)	396.5	70.1
	Ru (6.37), Os(35.1)	Ru(70), Os(400)	393.0	68.8
			400.0	70.7
2	California			
	Ir(53.5), Pd(2.6)	Ir(1000), Pd(50)	812.0	9.7
	Ru(0.5), Os(43.4)	Ru(10), Os(800)	784.8	10.0
			800.0	10.2
3	Urals			
	Pt(0.62), Ir(43.28)	Pt(8), Ir(540)	505.0	100.0
	Pd(5.73), Ru(8.49)	Pd(75), Ru(100)	490.4	98.7
	Os(40.11)	Os(500)	501.2	100.6
4	Australia			
	Ir(58.13), Pd(3.04)	Ir(700), Pd(40)	400.0	65.3
	Ru(5.22), Os(33.46)	Ru(65), Os(400)	405.2	64.8
			398.3	65.0
5	South Africa			
	Pt(0.2), Ir(17)	Pt(1.5), Ir(125)	496.4	65.7
	Ru(0.9), Os(69.9)	Ru(65), Os(500)	500.2	65.3
			505.2	64.8
	Iridioosmium or Nevjanskite			
6	Urals			
	Pt(1.1), Ir(77.2)	Pt(50), Ir(3700)	1012.3	9.8
	Pd(0.5), Ru(0.2),	Pd(25), Ru(10),	990.5	10.0
	Os(21)	Os(1000)	1003.1	10.1
7	South Africa			
	Pt(0.1—3.1),	Pt(120), Ir(4500),	2530	20.0
	Ir(46.8—77.2),	Ru(20), Os(2500)	2500	19.7
	Ru(0—0.5), Os(21—49.3),	Rh(30)	2482	20.3
	Rh(0.5—7.7)			

Hence the two individual extraction steps are combined and applied to the sequential separation of osmium and ruthenium from their mixtures in the following manner.

After the extraction of osmium, the thiocyanate concentration of the aqueous phase is increased to 0.8 mol dm^{-3} and acidity to 1 mol dm^{-3} in sulfuric acid, dilute to 15 cm^3 and heated in a boiling water bath at 75 °C for 20 min. The solution was then cooled, diluted to about 15 cm^3 and when equilibrated with 5 cm^3 of cyclohexanone gave lower recoveries of ruthenium. This can be attributed to the presence of dissolved mesityl oxide in the aqueous phase. Equilibration of the aqueous phase, after extracting off osmium, with 10 cm^3 of cyclohexanone renders it free of any dissolved mesityl oxide and in this instance the recoveries of ruthenium are found to be quantitative. The results of the extraction and re-extraction studies of binary mixtures of osmium and ruthenium over varying ratios are indicated in Table 3. From the table it is clear that the developed procedure works quite satisfactorily for the separation of osmium and ruthenium over a widely varying ratios and concentrations.

Estimation. Of the various stripping agents studied only sodium hydroxide (0.1 mol dm^{-3}) is found to re-extract osmium quantitatively while none of the reagents examined are effective for the quantitative stripping of ruthenium. Since hydrocarbons are found not to extract ruthenium (*cf.* Table 2), addition of such hydrocarbons to the organic phase is attempted to facilitate the quantitative re-extraction of ruthenium. Both benzene and cyclohexane are found to be effective. However, the latter is chosen, as in this instance, the phase separation is clean and rapid. A minimum ratio of 3 : 1 by volume of cyclohexane to cyclohexanone is found to be essential for the quantitative stripping of ruthenium into 10 cm^3 of water. The osmium and ruthenium contents are established by subjecting the respective strippings to 'Determination' as described earlier.

Further, it is observed that the organic extracts are coloured blue in the case of osmium and bluish violet in the case of ruthenium. Hence the amounts of osmium or ruthenium extracted are also determined by measuring the absorbance of these layers at 590 nm and 560 nm respectively after centrifuging. The Beer's law ranges are 0.4 to 24 ppm for osmium and 1 to 12 ppm for ruthenium. The molar absorptivities for the determination of osmium and ruthenium are 9.5×10^3 and 1.4×10^4 dm^{-3} mol^{-1} cm^{-1} respectively.

Analysis of Synthetic Samples. As no standard sample is available, the method developed is applied to synthetic samples of syserkite (osmiridium) and Nevjanskite (iridioosmium) containing both osmium and ruthenium, after oxidative fusion with potassium hydroxide and potassium nitrate.[7] The samples were prepared by mixing the respective metal solutions in proportions reported elsewhere.[8] To each sample 1 cm^3 of 5% hydrazine sulfate was added and heated gently almost to dryness to which about 1 g of 8 : 1 mixture of potassium hydroxide and potassium nitrate were added and heated at 800 °C for 30 min. The fused melt was leached with 5 cm^3 of 1 mol dm^{-3} hydrochloric acid and diluted to 50 cm^3. Aliquots of the made up solution are subjected to the separation and determination and the results are summarized in Table 4. The results show that the procedure developed can be directly applied to the analysis of osmium and ruthenium in these minerals.

One of us (S. J.) is thankful to CSIR, New Delhi for the financial assistance.

References

1) J. H. Wiersma and P. F. Lott, *Anal. Chem.*, **39**, 674 (1967).
2) W. L. Belew, G. R. Wilson, and L. T. Corben, *Anal. Chem.*, **33**, 886 (1961).
3) Z. Marczenko and M. Balcerzak, *Anal. Chim. Acta*, **109**, 123 (1979).
4) S. Jaya and T. V. Ramakrishna, *Talanta*, **29**, 619 (1982).
5) S. Jaya and T. V. Ramakrishna, *Bull. Chem. Soc. Jpn.*, **55**, 2633 (1982).
6) S. Jaya and T. V. Ramakrishna, *Analyst*, **107**, 828 (1982).
7) R. Bock, "A Handbook of Decomposition Methods in Analytical Chemistry," International Text Book Co., (1979), p. 416.
8) J. W. Mellor, "A Comprehensive Treatise on Inorganic and Theoretical Chemistry," Pt and General Index Longmans Green and Co., (1900), Vol. XVI, p. 6.

The Two-phase Oxidation of Some Aromatic Compounds with Cerium Ammonium Nitrate in the Presence of Surfactants

Jacek SKRŻEWSKI* and Ewa CICHACZ
Institute of Organic and Physical Chemistry, Technical University of Wroclaw, 50-370 Wroclaw, Poland
(Received December 24, 1982)

The two-phase oxidations of 3,6-dimethoxydurene and xylenes in cyclohexane solutions with the aqueous solution of cerium ammonium nitrate were carried out in the presence of cationic, nonionic, and anionic surfactants. Both cationic (ammonium salt) and nonionic (Dipodand) surfactants inhibited the reaction. The anionic surfactant (sodium dodecyl sulfate, SDS) catalyzed these oxidations. From the product distribution it was concluded that the catalytic action of SDS is due to the binding of aromatic compounds and the Ce(IV) ions to the surface of the SDS micelles. The micellar oxidant has the high oxidation potential which should allow to oxidize the comparatively nonreactive substrates.

Although there have been many investigations of micellar effects on electron transfer reactions,[1] only very few studies have since appeared which consider a micellar catalysis in the oxidation of organic substrates by metal ions.[2] However, it seems obvious that the aggregates of amphiphilic molecules should help to bring together hydrophobic substrates and hydrophilic, highly charged metal ion oxidants. This is particularly important when the reaction is run under the two-phase conditions, so there is a gap of hydrophobic repulsions between the reagents.

Our interest in the oxidation of aromatic compounds by cerium ions[3] prompted us to examine the influence of the complexing surfactants on the two-phase oxidation reactions. In a previous paper we reported the catalytic effect of a lipophilic complexone **6** bringing the Ce(IV) species into an organic phase.[4] This report describes our study of the title reactions carried out in the presence of typical cationic, anionic, and nonionic surfactants.

Results and Discussion

In the case of the two-phase system with the micelle-forming catalyst the reaction can take place at the interface, or in the bulk aqueous, bulk organic or micellar phases. With the catalyst located in an aqueous layer, one can expect that the lipophilic substrate will be solubilized partially in the micellar phase and in this way will be brought to the oxidant. In an organic phase the reversed micelles can be formed thus takeing the oxidant to the substrate. The micelles can also affect the reactivity of both organic substrate and metal ion, changing their redox potentials by the electrostatic interactions. The high ionic strength of the oxidant solution should favour an increase of density of surface charge of the aqueous micelles as well as the higher solubility of organic substrate in this micellar phase.

With these general considerations in mind we examined the catalytic activity of surfactants by determining the

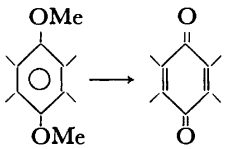

(1)

1 **2**

extent of reactions 1 and 2 with and without catalyst.

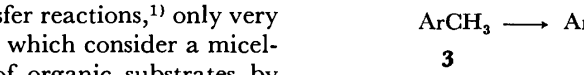

(2)

3 **4** **5**

Both reactions were carried out in cyclohexane–water system under mild, standard stirring at 20 °C and gave the same products as previously reported.[3-5] The following surfactants were tested: Dipodand **7**,[6] sodium dodecyl sulfate (SDS), and dodecyltriethylammonium nitrate (**8**). These compounds were compared with 4,4′ bis (octadecyloxy)-2,2′-bipyridine 1,1′-dioxide (**6**) which was used earlier.[4] The results are given in Table 1.

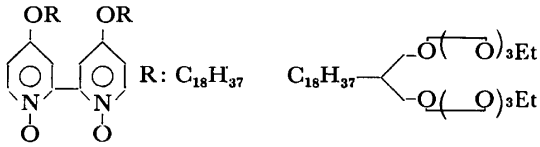

6 **7**

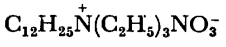

8

From Table 1 it can be seen that nonionic Podand **7** and cationic dodecyltriethylammonium nitrate (**8**) hinder the oxidation while lipophilic complexone **6** and SDS accelerate the reaction. The inhibitory effects are analogous to lowering of the rates of oxidation of phenothiazine by Fe^{3+} ions in the presence of both cationic (CTAB) and nonionic (Triton-X-100) surfactants reported by Pelizzetti and Pramauro.[2] They ascribed these effects to the difficulty of approach of the metal ion to the organic substrate in the micelle as well as to an increase of the apparent reduction potential of the substrate. The same effects can be responsible for the decrease of the reaction rate in our case. Additionally, the hampering effect of salt **8** on the oxidation in the presence of **6** (acting in the organic phase only[4]) suggests that some modification of the interface can take place as well. Such modification would prevent the reagents from reaching each other. In the presence of SDS, a remarkable increase of the oxidation rate was observed and this result was also in agreement with that of Pelizzetti and Pramauro.[2] In their case it was due to a concentration effect as well as to decrease of the reduction potential of substrate in the micelles.

Since only SDS showed the accelerating effect, this surfactant was used in all subsequent experiments. Thus,

TABLE 1. EFFECTS OF SURFACTANTS ON THE TWO-PHASE CAN OXIDATION OF 3,6-DIMETHOXYDURENE IN CYCLOHEXANE[a)]

Catalyst (10×No. of mol)	Consumption of CAN(%)	
	After 6 min	After 40 min
None	19.1	57
6(1.30)	41.3	—
7(5.84)	8.0	—
8(10.0)	10.2	42
6 and **8**(1.30, 10.0)	22.2	74
SDS(6.00)	57.0	—

a) A solution of **1** in cyclohexane (0.10 M, 2 ml) was oxidized with aqueous CAN (1.0 M, 1 ml) in the presence of catalyst at 20 °C. The consumptions of CAN based on organic substrate were determined by oxidimetry.

consumption of cerium ammonium nitrate (CAN) in the two-phase oxidation of **1** *vs.* SDS concentration was determined and shown in Fig. 1. This plot demonstrates that the rate enhancement was strongly affected by the concentration of surfactant in its CMC-range. Figure 2 presents the time dependent effects of SDS and SDS with **6** on the oxidation of *p*-xylene. The catalytic effects of SDS were higher than those of **6** and the competitive inhibition was observed when both catalysts were used together. The second effect can be due to the association of weaker oxidant [**6**. Ce(IV)][4] with the micelles.[8]

In order to learn about the new oxidant, we studied the oxidation of *p*-xylene (1 M† solution in cyclohexane) with aqueous CAN solution in the presence of SDS in various concentrations and under standard stirring conditions (magnetic stirrer, ellipsoid-like mixing bar, >300 min^{-1}). As in all experiments, so far described, if the stirring rate dropped below *ca.* 100 min^{-1}, the yields were much lower and hardly reproducible. The resulting mixture was analyzed (Ce^{4+}-by oxidimetry, organic products-by GLPC) and the reaction advancements were determined from the consumption of CAN and from the yields of **4** and **5**, respectively (Fig. 3). The yields of organic products *vs.* concentration of SDS are presented in Fig. 4. The experiments run under nitrogen gave the same results as those under air atmosphere.

From the results given in Fig. 3 it is apparent that the catalytic effect occurs at the concentration of surfactant which is much less (10^{-5} M) than the CMC value for diluted solution of SDS (8.1×10^{-3} M).[1] It seems to be caused by the extremelly high ionic strength of 1 M CAN solution (μ 12 M), thus "salting out" all the hydrophobic species and forming the micelles at very low concentration of surfactant. The discrepancy between CAN consumption and the yield of organic products observed for $c_{SDS}\approx10^{-4}$ M led us to check the possibility of the consecutive oxidation of *p*-tolualdehyde (**5**). This was the case and as can be seen from Table 2, the rate of this reaction increases sharply at higher concentration of SDS. Analysis of the product distribution (Fig. 4) shows that the micellar oxidant increases a contribution of aldehyde in the reaction mixture. The true increase

† 1 M=1 mol dm^{-3}.

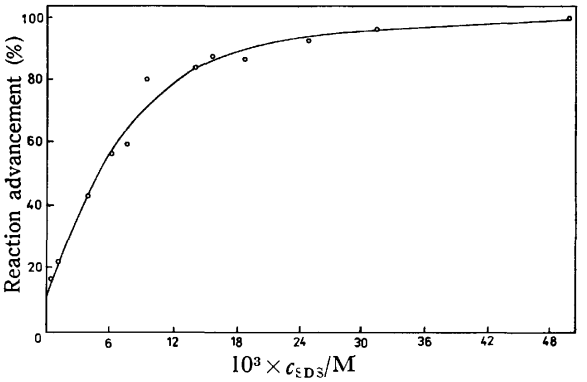

Fig. 1. Dependence of the yield of the two-phase oxidation on the concentration of SDS in water solution. Conditions: **1** (0.10 M in cyclohexane, 2 ml), CAN (1.00 M in an appropriate solution of SDS in water, 1 ml), 20 °C, 6 min.

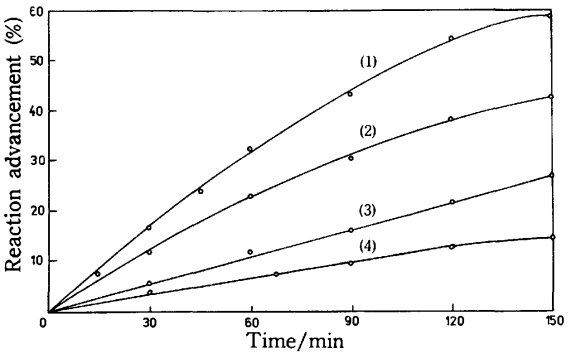

Fig. 2. Effects of SDS (6.0×10^{-5} M), **6** (6.0×10^{-5} M), and both catalysts on the oxidation of *p*-xylene (1.0 M) in cyclohexane with aqueous CAN (1.0 M) at 20 °C. (1): SDS, (2): SDS+**6**, (3): **6**, (4): none.

TABLE 2. OXIDATION OF *p*-TOLUALDEHYDE WITH AQUEOUS CAN[a)]

c_{SDS}/M	Comsumption of CAN (%)
0.0	3.6
5.0×10^{-5}	5.0
5.0×10^{-4}	9.6
5.0×10^{-3}	39

a) A solution of *p*-tolualdehyde (freshly distilled) (0.10 M, 5 ml) in cyclohexane was stirred under N_2 with aqueous CAN (1.0 M, 10 ml) for 1 h at 25 °C.

is even higher than this observed from the plot because of the consecutive oxidation of **5**. This result suggests that the catalyzed oxidation takes place in a hydrophilic medium (3).

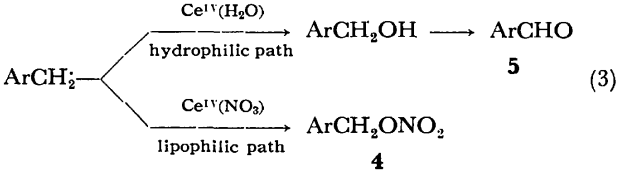

(3)

It is well known that aromatic compounds are located at the surface of micelles.[9] On the other hand, the recently investigated association of metal ions to SDS

Table 3. Oxidation of xylenes with aqueous CAN[a)]

Substrate(IP/eV)[b)]	SDS (M)	Yield			
		Nitrate (mmol)	Aldehyde (mmol)	Total/%	Unchanged substrate/%
p-Xylene (8.44)	—	2.7	3.6	78	20
	5×10^{-4}	1.7	3.0	58	0
o-Xylene (8.56)	—	1.9	1.9	46	41
	5×10^{-4}	3.5	4.1	93	7
m-Xylene (8.59)	—	1.4	1.4	35	33
	5×10^{-4}	2.7	3.3	74	19

a) Xylene (1.00 ml) was oxidized with CAN (20 g, *ca.* 10% oxcess) in water or SDS solution (16 ml) when the two-phase system was stirred for 6 h at 25 °C. The resulting mixture was treated as described earlier.[4)] b) R. P. Blaunstein and L. G. Christophorou, *Radiat. Res. Rev.*, **3**, 69 (1971).

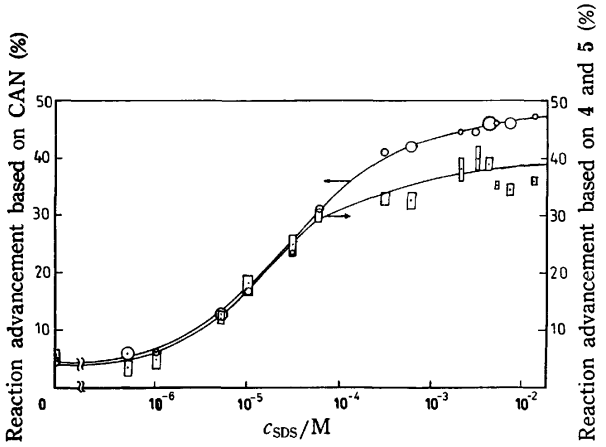

Fig. 3. The advancements of the oxidation (2) based on the consumption of CAN (⊙) and on the yields of **4** and **5** (⊡) *vs.* the concentrations of SDS.
Conditions: *p*-xylene (1.0 M in cyclohexane, 5 ml), CAN (1.00 M in the SDS solution), 25 °C, 1 h.

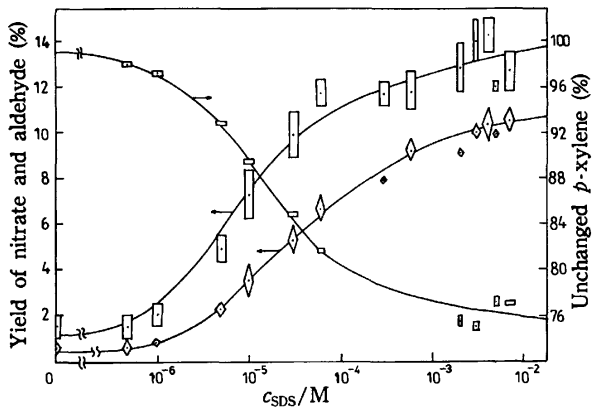

Fig. 4. The yields of nitrate and aldehyde formed in the oxidation (2) *vs.* the concentration of SDS.
⊡: Aldehyde, ◇: nitrate, ⊡: unchanged *p*-xylene.
Conditions: as for Fig. 3.

micelles has revealed that the metal ions were bound to the micellar surface. The association constant has been rationalized by considering the chemistry of the specific ion.[10)] The Ce(IV) ions associate more strongly to the sulface than to nitrate ions and the reduced metal ions form the weaker complexes.[11)] The above arguments suggest that the catalytic reaction site is located at the hydrophilic surface of micelles.

In order to gain insight into the properties of the new oxidizing system, we studied, as previously for **6**,[4)] the yields of benzylic nitrates (**4**) and aldehydes (**5**) obtained in the two-phase oxidation of xylenes without diluent in the presence and absence of SDS. The ionization potentials of these substrates differ slightly so the effectiveness of catalyst in each case can test the oxidation potential of the oxidant. The corresponding benzoic acids were formed as by-products and this fact was responsible for the lack of material balance (Table 3). The results in Table 3 indicate that catalyst has almost the same effectiveness for *o*- and *m*-xylene. For *p*-xylene there was the relatively high oxidation yield without SDS, so the addition of catalyst led to the consecutive oxidation of aldehyde. The observed lack of selectivity of the oxidant action implies its high oxidation potential, perhaps related to the potential of Ce(IV) in an equilibrium with the sulfate ions (1.44 V[12)]). All these facts support the evidence that the reaction takes place at the micellar surface.

Summarizing, we conclude that the two-phase oxidation of aromatic compounds with the aqueous CAN solution is inhibited by cationic and nonionic surfactants and catalyzed by the anionic one.

The catalytic action of SDS is due to the binding of aromatic compounds and the Ce(IV) ions to the surface of micelles. The micellar oxidant has the high oxidation potential which should allow to oxidize the comparatively nonreactive substrates. The catalyst is effective at the very low concentration level, so it does not disturb the phase separation process during the work up.

Experimental

Reagents. The following surfactants were prepared and purified as described in the literature: 4,4′-bis(octadecyloxy)-2,2′-bipyridine 1,1′-dioxide,[7)] Dipodand **7**,[6)] and dodecyltriethylammonium nitrate.[13)] Sodium dodecyl sulfate (Merck) was recrystallized twice from ethanol and dried in vacuum desiccator over P_2O_5. Cyclohexane was shaken with aqueous $KMnO_4$, concd. H_2SO_4, water, and $NaHCO_3$ soln, dried over $CaCl_2$ and distilled. 3,6-Dimethoxydurene was prepared and purified according to the literature.[14)] Xylenes (GLPC standard grades) were used as purchased. Cerium ammonium nitrate and other inorganic reagents were of highest available purity. Doubly distilled water was used.

Procedure. All the reactions were carried out in Erlen-

meyer flasks (Quickfit, ₹ 14/23) in sizes 5 and 10-ml with a Teflon-coated ellypsoidal stirring bar (5 mm × 15 mm) or in sizes 25 and 50-ml with the (7 mm × 21 mm) bar.

In a typical experiment, 5 ml of a solution of *p*-xylene (1.00 M) in cyclohexane, an appropriate quantity of SDS, and 10.0 ml of CAN solution (1.00 M) in water were introduced *via* pipette into a 25-ml flask. The flask was sealed with a ground joint stopper, placed in a water bath maintained at the desired temperature (20 or 25 °C), and stirring was started. After appropriate time the phases were separated in a small separatory funnel. Samples of CAN solution were quenched with an excess of a standardized iron(II) sulfate solution and then titrated with 0.1 M CAN. The organic phase was washed with the $FeSO_4$ solution, water, $NaHCO_3$ soln., water, dried over $MgSO_4$ and subjected to the GLPC analysis (GCHF-18.3.6, Gide apparatus, 20% Carbowax on Chromosorb W, 1 m -long column at 120 °C, FID-detector). The identified products were the same as observed earlier.[4]

In the reaction under nitrogen, the water solution was bubbled with a stream of N_2 and then organic substrate solution was injected, the flask was sealed and the reaction started. The work up was the same as described above. Cyclohexane itself was found not to undergo any changes under the conditions used.

The reproducibility of the results obtained was within a few per cent when the same flask and stirring bar were applied.

This work was supported by Grant R. 1.9 from the Polish Ministry of Science, Education and Technology.

References

1) J. H. Fendler and E. J. Fendler, "Catalysis in Micellar and Macromolecular Systems," Academic Press, New York (1975).

2) E. Pelizzetti and E. Pramauro, *Ber. Bunsenges. Phys. Chem.*, **83**, 996 (1979); C. A. Bunton and G. Cerichelli, *Int. J. Chem. Kinet.*, **12**, 519 (1980).

3) L. Syper, K. Kloc, and J. Mlochowski, *Tetrahedron*, **34**, 123 (1980) and references cited therein.

4) J. Skarzewski, *J. Chem. Res.*, (*S*), **1980**, 410.

5) L. A. Dust and E. W. Gill, *J. Chem. Soc., C*, **1970**, 1630; E. Baciocchi, S. Mei, and C. Rol, *J. Org. Chem.*, **43**, 2919 (1978) and references therein.

6) J. Skarzewski and J. Mlochowski, *Tetrahedron*, **39**, 309 (1983).

7) J. Skarzewski and J. Mlochowski, *Heterocycles*, **12**, 1403 (1979).

8) A Referee has pointed out that the reversed micelles in the organic phase can be responsible for the catalysis. In order to check this possibility we extracted a 1 M CAN solution (5×10^{-3} M in SDS) with an equal volume of cyclohexane. After the saturation a sample of cyclohexane was treated with the same volume of ferroin (1×10^{-5} M) solution in water which, in turn, did not lose its extinction at 510 nm. This experiment demonstrated that under the conditions used no appreciable amount of Ce(IV) was transferred to the organic phase so we belive that the reaction was catalyzed by the aqueous micelles, even if some aggregates of the surfactant were present in cyclohexane. The results of product distribution study support this conclusion (see the text).

9) P. Mukerjee and J. R. Cardinal, *J. Phys. Chem.*, **82**, 1620 (1978).

10) H. Ziemiecki and W. R. Cherry, *J. Am. Chem. Soc.*, **103**, 4479 (1981).

11) J. Inczedy, "Analytical Applications of Complex Equilibria," Akad. Kiado, Budapest (1976).

12) W. M. Latimer, "Oxidation Potentials," Prentice-Hall, New Jersey (1952).

13) The authors are indebted to Mr K. Kloc of this Laboratory for the preparation of this salt according to the general method.[1]

14) H. Schmid, A. Ebnöther, and Th. M. Meijer, *Helv. Chim. Acta*, **33**, 1751 (1950); L. I. Smith, *Org. Synth.*, Coll. Vol. II, 254 (1943).

© 1984 The Chemical Society of Japan

NOTES

Bull. Chem. Soc. Jpn., 57, 275—276 (1984)

The Crystal Structure of 4-Cyanoimino-3-methoxymethyl-perhydro-1,3,5-oxadiazine

Toichi EBISUNO,* Michiaki TAKIMOTO, and Ryuichi SHIBA†

Department of Chemistry, Faculty of Science, Toho University, Miyama 2-2-1, Funabashi, Chiba 274

†*Department of Applied Science, Faculty of Technology, Tokyo Denki University, Kanda, Chiyoda-ku, Tokyo 101*

(Received May 4, 1983)

Synopsis. The structure of 4-cyanoimino-3-methoxymethylperhydro-1,3,5-oxadiazine in the crystalline state was determined by X-ray crystal analysis. The crystal is triclinic, space group $P\bar{1}$, a=10.307(3), b=8.166(2), c=5.082(1) Å, α=97.34(2), β=91.98(2), γ=107.13(2)°, Z=2. The final R value was 0.061 for 1651 reflections.

In the reaction of cyanoguanidine (CG) with formaldehyde, only two hydroxymethylated CG have been isolated;[1] mono- and 1,3-bis(hydroxymethyl)-2-cyanoguanidine (CG-1F and CG-2F). No adducts of 3 mol or more of formaldehyde per mole of CG have been isolated. As reported in the previous paper,[2] the exhaustive hydroxymethylation of 1,3-bis(methoxymethyl)-2-cyanoguanidine (CG-2M), prepared by the methoxylation of CG-2F, was examined and two new products were isolated. They had the structure of a cyclic ether of perhydro-1,3,5-oxadiazine. One was assigned as 4-cyanoimino-3-methoxymethylperhydro-1,3,5-oxadiazine (CG-1Mcyc2F), an adduct of 3 mol of formaldehyde per mole of CG, and the other as 3,5-bis(methoxymethyl)-4-methoxymethyl (carbamoylimino)perhydro-1,3,5-oxadiazine (AU-3Mcyc2F) by the elemental analysis, FD-MS and ^{1}H- and ^{13}C-NMR spectrometry. The latter product was derived from the hydration of the cyano group in the former and further addition of 2 mol of formaldehyde, one by one, to the imino group and to the newly formed amino group. The former product was derived by the dehydration from two newly introduced hydroxymethyl groups in methoxylated CG-1F or by the MeOH elimination between a newly introduced hydroxymethyl group in one imino group and the methoxymethyl group in the other imino group in CG-2M.

In order to confirm the cyclic nature of CG-1Mcyc2F and to elucidate its structural characteristic, the crystal structure of CG-1Mcyc2F has been determined by the X-ray method. Intensity data were collected on a Rigaku automated four-circule diffractometer using Mo $K\alpha$ radiation (λ=0.7107 Å).

Results and Discussion

Crystal Data. $C_6H_{10}N_4O_2$, M.W.=170.17, triclinic, space group $P\bar{1}$, a=10.307(3), b=8.166(2), c=5.082(1) Å, α=97.34(2), β=91.98(2), γ=107.13(2)° U=404.3 Å^3, Z=2, D_C=1.40 g cm^{-3}, μ(Mo $K\alpha$)=1.0 cm^{-1}. The structure of CG-1Mcyc2F was solved by direct methods and refined to a final R value of 0.061 for 1651 unique reflections. All the scattering factors were taken from the International Tables for X-Ray Crystallography.[3] The final atomic parameters are listed in Table 1. The complete table of observed and calculated structure factors is kept as Document No. 8403 at the Office of the Editor of the Bulletin of the Chemical Society of Japan. A perspective drawing of the molecular structure of CG-1Mcyc2F is shown in Fig. 1, which is a view perpendicular to the plane of the guanidine moiety. The structure agrees with that deduced from the spectroscopic data.[2] The underscored numbers in Fig. 1 give the heights of the atoms above or below the plane in Å. The interatomic distances and bond angles are listed in Table 2. Figure 1 shows a plane char-

TABLE 1. FINAL ATOMIC PARAMETERS (POSITIONAL $\times 10^4$, FOR H $\times 10^3$) AND THERMAL PARAMETERS (B_{eq} FOR NON-H $\times 10$, B_{iso} FOR H $\times 10$), WITH THEIR ESTIMATED STANDARD DEVIATIONS IN PARENTHESES

Atom	x	y	z	$B_{eq}(B_{iso})$/Å^2
C_1	3342(3)	1736(3)	6160(5)	32(1)
C_2	2311(3)	-1156(4)	3771(7)	51(1)
C_3	1553(3)	1027(4)	2513(6)	43(1)
C_4	4894(3)	2402(3)	9690(6)	37(1)
C_5	2801(3)	4101(3)	4248(6)	38(1)
C_6	1286(3)	4629(4)	7441(7)	49(1)
N_1	3198(2)	42(3)	5908(5)	39(1)
N_2	2577(2)	2262(3)	4445(4)	35(1)
N_3	4164(2)	2912(3)	7997(5)	40(1)
N_4	5560(3)	2089(3)	11281(5)	48(1)
O_1	1171(2)	- 598(3)	3318(5)	56(1)
O_2	1602(2)	4547(2)	4719(4)	43(1)
H_1	199(4)	- 232(5)	424(7)	43(9)
H_2	273(4)	- 89(5)	189(8)	61(10)
H_3	72(3)	146(4)	249(7)	33(8)
H_4	199(4)	86(5)	75(7)	48(9)
H_5	363(3)	484(4)	559(6)	29(7)
H_6	301(3)	431(4)	233(6)	27(7)
H_7	108(3)	343(4)	797(7)	35(8)
H_8	210(4)	551(4)	861(7)	40(9)
H_9	48(4)	502(5)	780(8)	52(10)
H_{10}	364(3)	38(4)	705(6)	26(7)

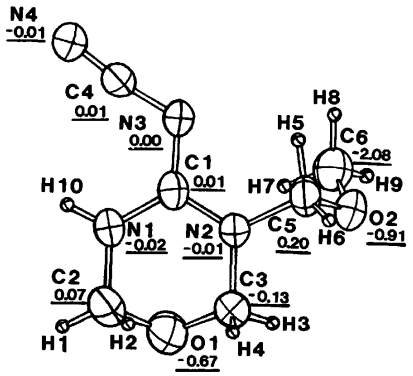

Fig. 1. The structure of CG-1Mcyc2F projected on the plane of the guanidine moiety composed of C_1, N_1, N_2, and N_3. Underscored numbers are heights in Å of the atoms above or below the plane.

acteristic of the structure which is composed of four nitrogen atoms (N_1, N_2, N_3, and N_4) and two carbon atoms (C_1 and C_4). Furthermore, two carbon atoms (C_2 and C_3) and one hydrogen atom (H_{10}) are placed near the plane. This planar structure is due to the triple bond character of the cyano group and to the resonated structure of the guanidine moiety and is similar to the molecular structure of CG.[4] The observed atomic distances for the cyanoimino group (1.308 Å (C_4–N_3) and 1.144 Å (C_4–N_4)) are in fair agreement with the previously predicted values,[5] 1.32 and 1.20 Å, but differ from those for the cyanoimino group in CG,[4] 1.28 and 1.22 Å. This difference in the atomic distances for the cyanoimino group between CG and CG-1Mcyc2F is probably due to the presence and absence of hydrogen bonds in CG and CG-1Mcyc2F, respectively. In CG, the terminal nitrogen of the cyanoimino group was reported to have three hydrogen bonds directed towards three amino groups in two adjacent molecules, while in CG-1Mcyc2F, most of the hydrogen atoms in the amino groups have already been substituted and the residual one hydrogen atom of H_{10} in the imino group is placed near the plane. The intra- and intermolecular distances and the bond angle of N_1–H_{10}– –X in CG-1Mcyc2F clearly indicate that there are no hydrogen bonds.

Table 2. Interatomic distances and angles for CG-1Mcyc2F

Bond distance	l/Å	Bond angle	ϕ/°	Bond angle	ϕ/°
C_1 N_1	1.336(5)	N_1-C_1-N_2	117.3(10)	O_2-C_6-H_7	109.1(21)
C_1-N_2	1.346(13)	N_1-C_1-N_3	124.4(8)	O_2-C_6-H_8	109.1(22)
C_1-N_3	1.323(20)	N_2-C_1-N_3	118.4(6)	O_2-C_6-H_9	113.9(25)
C_2-N_1	1.451(22)	N_1-C_2-O_1	108.5(8)	H_7-C_6-H_8	111.6(30)
C_2-O_1	1.402(9)	N_1-C_2-H_1	111.4(22)	H_7-C_6-H_9	106.6(32)
C_2-H_1	0.971(37)	N_1-C_2-H_2	108.9(19)	H_8-C_6-H_9	106.5(30)
C_2-H_2	1.085(41)	O_1-C_2-H_1	107.8(24)	C_1-N_1-C_2	120.9(8)
C_3-N_2	1.465(22)	O_1-C_2-H_2	95.3(26)	C_1-N_1-H_{10}	120.8(20)
C_3-O_1	1.388(10)	H_1-C_2-H_2	123.1(31)	C_2-N_1-H_{10}	118.3(19)
C_3-H_3	1.017(39)	N_2-C_3-O_1	110.4(8)	C_1-N_2-C_3	121.7(6)
C_3-H_4	1.026(39)	N_2-C_3-H_3	106.6(18)	C_1-N_2-C_5	122.0(10)
C_4-N_3	1.308(12)	N_2-C_3-H_4	108.8(19)	C_3-N_2-C_5	116.1(9)
C_4-N_4	1.144(11)	O_1-C_3-H_3	108.1(20)	C_1-N_3-C_4	118.5(6)
C_5-N_2	1.467(5)	O_1-C_3-H_4	104.6(23)	C_2-O_1-C_3	110.9(9)
C_5-O_2	1.407(8)	H_3-C_3-H_4	118.2(31)	C_5-O_2-C_6	113.8(10)
C_5-H_5	1.051(32)	N_3-C_4-N_4	174.5(3)		
C_5-H_6	1.029(33)	N_2-C_5-O_2	110.2(10)		
C_6-O_2	1.430(8)	N_2-C_5-H_5	108.7(22)		
C_6-H_7	1.010(36)	N_2-C_5-H_6	108.9(20)		
C_6-H_8	1.034(34)	O_2-C_5-H_5	112.4(21)		
C_6-H_9	0.987(44)	O_2-C_5-H_6	106.2(22)		
N_1-H_{10}	0.883(36)	H_5-C_5-H_6	110.4(25)		

The authors wish to express their hearty thanks to Professor Hayao Kobayashi of Toho University, for his kind support in the data collection on the Rigaku automated four-circle diffractometer at Toho University and computation.

References

1) M. Hamada, *Reports in Lab. of Toyo Reiyon*, **1**, 28 (1954); **2**, 25 (1955).
2) M. Takimoto, T. Ebisuno, and R. Shiba, *Bull. Chem. Soc. Jpn.*, **56**, 3319 (1983).
3) "International Tables for X-Ray Crystallography," Kynoch Press, Birmingham (1974), Vol. IV.
4) E. W. Hughes, *J. Am. Chem. Soc.*, **62**, 1258 (1940).
5) L. Pauling and J. Sturdivant, *Proc. Natl. Acad. Sci. U.S.A.*, **23**, 615 (1937).

Determination of the Rate Constant for the Reaction $NH_3+O\rightarrow NH_2+OH$

Nobuyuki FUJII,* Hisaaki SATO, Shiro FUJIMOTO,† and Hajime MIYAMA
Department of Materials Science and Technology, The Technological University of Nagaoka, Kamitomioka, Nagaoka, Niigata 949-54
(Received May 13, 1983)

Synopsis. The rate constant for the reaction $NH_3+O\rightarrow NH_2+OH$ was determined by the comparison of the calculated ammonia consumption rates with those observed in shock tube experiments in the range of 1690—2310 K, for NH_3-N_2O-Ar mixtures. The rate constant can be represented by the expression $k=3.1\times10^{12}\exp(-25.5\ \mathrm{kJ}/RT)\ \mathrm{cm^3\ mol^{-1}\ s^{-1}}$.

The rate constants for the reaction $NH_3+O\rightarrow NH_2+OH$ were measured at low temperatures below 1000 K by several researchers,[1,2] but those at high temperatures have not been measured accurately. The rate constants at higher temperatures in the range of 1690—2310 K were determined using the shock tube technique in this experiment.

Experimental

The shock tube consisted of a 2 m driver section and a 3.6 m experimental section. These were made of 46 mm inside diameter precision-bore stainless steel tubing. The shock velocity was measured by two piezogauges with a time counter. An observation section was placed at a position of 3 m apart from the diaphragm. Here, the change of absorption of NH_3 at 220 nm behind the incident shock wave was monitored by using an optical system consisting of a D_2 lamp, a monochromator, and a photomultiplier. Simultaneously at the same location, the infra-red emission of N_2O at 4.52 μm was measured with an InSb detector through an infra-red filter (half width: 0.18 μm). These signals were displayed on an oscilloscope and photographed. The composition of the gas mixtures, the temperature and the pressure range of incident shock waves are shown in Table 1. The shock parameters were calculated from the incident shock velocities.

Results and Discussion

Typical profiles of NH_3 and N_2O concentration change with reaction time behind the incident shock wave are shown in Fig. 1. In order to compare the profiles with those obtained by computer simulation, elementary reactions shown in Table 2 were selected as the important ones in this reaction system. Among the rate constants of these reactions shown in Table 2. Those of Reactions 1, 3, 7, and 8 were well established. From the preliminary calculation, the dissociation reaction of NH_3 was eliminated from the scheme, because the rate constant of this reaction[3] was smaller than that of Reaction 1 by about 200 times at 2000 K, and the rate of NH_3 consumption was hardly affected by the former reaction.

In order to examine the contribution of other elementary reaction to the rate of NH_3 consumption, the sensitivity checks described previously[4] were applied as follows. The calculated reaction time required for 10% consumption of NH_3, τ in Fig. 1, was found to be very sensitive to the change in the rate constants of Reactions 1—4, but not sensitive to those of other elementary reactions. However, when the N_2O concentration was not smaller than that of NH_3 and the temperature was higher than 2000 K, the calculated reaction time τ was not sensitive to the rate constant of Reaction 4. The conditions were satisfied only by mixture II.

Therefore, only Reactions 1—3 were used in the simulation for mixture II and the rate constant of Reaction 2 was determined accurately by choosing the value to fit best the calculate τ value of NH_3 consumption to the experimental one. In this calculation, the heat of reaction and the correction for the nonideality of shocked flow caused by the boundary layer behind the incident shock front[5] were taken into account. The rate constants of Reaction 2 obtained are shown in Fig.

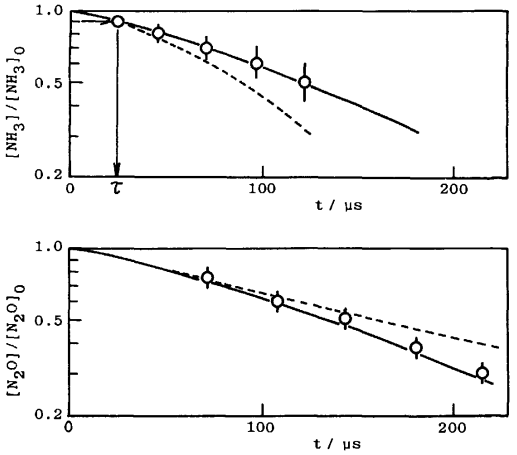

Fig. 1. Profiles of NH_3 and N_2O consumption for the mixture NH_3 : N_2O : Ar = 1 : 1 : 98 at T = 2000 K and p = 2.04 atm.
○: Experimentals, dotted lines: calculations by using Reactions 1—3, solid lines: calculations by using Reactions 1—8 and their reverse reactions.

TABLE 1. EXPERIMENTAL CONDITIONS

Mixture	NH_3	N_2O	Ar	T/K	p/atm[a]
I	1.0	0.3	98.7	1690—2310	1.78—2.04
II	1.0	1.0	98.0	2000—2260	2.04—2.14
III	2.0	0.4	97.6	1860—2290	0.91—1.05

a) 1 atm = 101 325 Pa.

† Present address: Department of Chemistry, National Defense Academy, Hashirimizu, Yokosuka 239.

Table 2. Reaction scheme and rate parameters
$k = AT^B \exp(-E/RT)$ cm^3 mol^{-1} s^{-1}

Elementary reactions	log A	B	E/kJ	Ref.
1) $N_2O + M \longrightarrow N_2 + O + M$	15.21	0	257.7	8
2) $NH_3 + O \longrightarrow NH_2 + OH$	12.49	0	25.5	
3) $NH_3 + OH \longrightarrow NH_2 + H_2O$	12.50	0	8.4	9
4) $NH_3 + NH_2 \longrightarrow N_2H_3 + H_2$	11.90	0.5	90.4	7
5) $O + NH_2 \longrightarrow NH + OH$	11.96	0.5	0	10
6) $N_2H_3 + M \longrightarrow NH_2 + NH + M$	12.80	0	41.8	7
7) $N_2O + O \longrightarrow NO + NO$	14.00	0	117.2	1
8) $N_2O + O \longrightarrow N_2 + O_2$	14.00	0	117.2	1

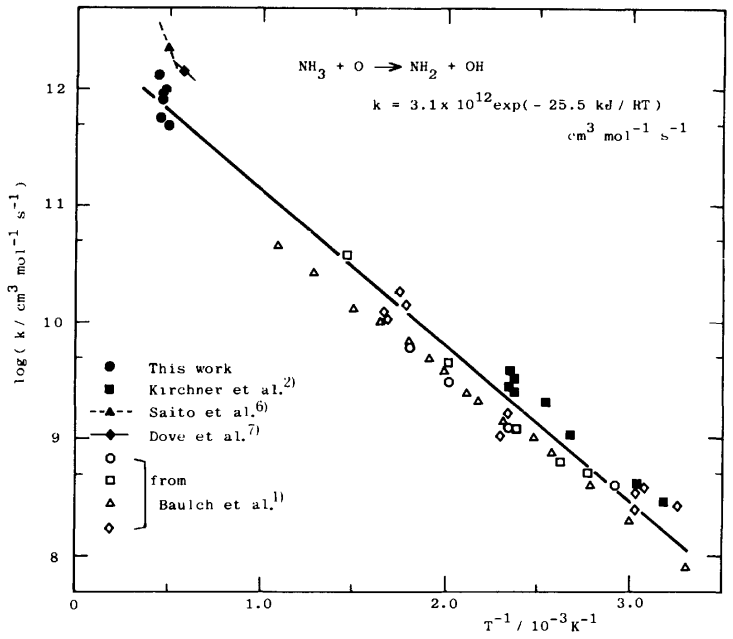

Fig. 2. Arrhenius plots of the rate constants for Reaction 2.

2. The values obtained recently by Satio and Bradley[6] and those obtained as the upper limit by Dove and Nip[7] are shown together in Fig. 2. Comparing the values obtained in the present work, both reported values are larger than the extrapolated value from those obtained in the lower temperature region.

A combination of our values with the mean values at low temperatures reported by Kirchner *et al.*[2] and by other researchers[1] yields the following Arrhenius expression for Reaction 2.

$$k_2 = 3.1 \times 10^{12} \exp(-25.5\ \text{kJ}/RT)\ \text{cm}^3\ \text{mol}^{-1}\ \text{s}^{-1}.$$

The NH_3 and N_2O consumption profiles calculated by using Reactions 1—3 are shown by the dotted lines in Fig. 1. The agreement between the calculated and experimental values at the initial stage of the reaction is good. In the figure, the deviations of the calculated curves from the experimental values after the reaction time τ were improved by adding subsequent Reactions 4—8 to the reaction scheme, as shown by the solid lines. The rate constants obtained for mixtures I and III, which did not satisfy the conditions, were also within the scattering of the above-obtained values.[8]

References

1) D. L. Baulch, D. D. Drysdale, D. G. Horne, and A. C. Lloyd, "Evaluated Kinetic Data for High Temperature Reactions," Butterworths, London (1973), Vol. 2.

2) K. Kirchner, N. Merget, and C. Schmidt, *Chem. Ing. Tech.*, **46**, 661 (1974).

3) M. Yumura and T. Asaba, "18th Int. Symp. Combust.," The Combustion Institute, Pittsburgh (1981), p. 863.

4) N. Fujii, H. Miyama, M. Koshi, and T. Asaba, "18th Int. Symp. Combust.," The Combustion Institute, Pittsburgh (1981), p. 873.

5) N. Fujii, M. Koshi, H. Ando, and T. Asaba, *Int. J. Chem. Kinet.*, **11**, 285 (1979).

6) K. Saito and J. N. Bradley, unpublished data.

7) J. E. Dove and W. S. Nip, *Can. J. Chem.*, **52**, 1171 (1974); **57**, 689 (1979).

8) N. Fujii, H. Sato, S. Fujimoto, and H. Miyama, *Int. J. Chem. Kinet.*, (to be published).

9) N. Fujii, H. Miyama, and T. Asaba, *Chem. Phys. Lett.*, **80**, 355 (1981).

10) J. Duxbury and N. H. Pratt, "15th Int. Symp. Combust.," The Combustion Institute, Pittsburgh (1975), p. 843.

Adsorption of Oligomer Type Surfactants on Iron Oxide

Kunio ESUMI,* Kimihiko OGIHARA, and Kenjiro MEGURO
Department of Applied Chemistry and Institute of Colloid and Interface Science, Science University of Tokyo, Kagurazaka, Shinjuku-ku, Tokyo 162
(Received June 14, 1983)

Synopsis. Adsorption of oligomer type surfactants synthesized from acrylic acid, acrylonitrile, and 1-dodecanethiol on α-Fe_2O_3 was examined by measuring adsorption isotherms and zeta potentials. It was found that the adsorption behavior of oligomer type surfactants on α-Fe_2O_3 was influenced by the pH of suspensions and further by the differences of composition of oligomer type surfactants.

Recently, from the standpoints of environment pollution and of conservation of resources, water-base paints[1] have been preferred instead of organic-base ones. The preparation of stable pigment dispersions requires the addition of dispersants. Many kind of surfactants[2-5] have been utilized for this purpose. Of these surfactants, oligomer type surfactants[6-10] have been developed and employed for dispersion of pigments due to suitable properties, such as improvement of film formation and resistance for water vapor.

In this work, to understand the interactions of oligomer type surfactant and pigment surface in aqueous solution, the adsorption of oligomer type surfactants synthesized from acrylic acid, acrylonitrile, and 1-dodecanethiol on α-Fe_2O_3 is examined by measuring adsorption isotherms and zeta potentials.

Experimental

Materials. The oligomer type surfactant used in this study was synthesized[10] by co-oligomerization of acrylic acid, acrylonitrile, and 1-dodecanethiol, followed by neutralization with potassium hydroxide. The chemical structure and analytical properties of the oligomers are given in Table 1. All the chemicals were of reagent grade. The water used was purified by passing through Milli-Q Reagent Grade Water Systems until its specific conductivity fell below 10^{-7} Ω^{-1} cm^{-1}.

As a pigment, α-Fe_2O_3 was supplied by Titan Chemicals; it was washed with water sufficiently to remove impurities and then dried. The specific surface area of this pigment was determined to be 6.35 m^2/g by nitrogen adsorption at its liquid temperature.

Measurements. A 20 ml portion of oligomer aqueous solution was placed in an L-shaped test tube and α-Fe_2O_3 (0.3 g) was added in; then the test tube was shaken at 25 °C. After at least 2 h, having reached adsorption equilibrium, the sample was separated by using a Milli-pore filter. The concentration of supernatant solution was determined with UV spectrophotometer by measuring the absorbancy at 215 nm.

The zeta potential of α-Fe_2O_3 after the adsorption was measured using a Pen Kem Laser 500.

The surface tensions of oligomer type surfactant aqueous solutions were determined by a modified Wilhelmy type surface tension meter (Shimadzu ST-1) at 25 °C.

Table 1. Chemical structure and analytical properties of oligomer type surfactants

$C_{12}H_{25}S$—$(CH_2CH)_x$—$(CH_2CH)_y$—$(CH_2CH)_z$—H
CN COOK COOH

	$\overline{M}_w$[a]	x	y	z	$\frac{y+z}{x+y+z}$
Oligomer(I)	1320	3.6	7.0	2.2	0.72
Oligomer(II)	1530	0.0	9.5	3.8	1.00

a) Mean molecular weight calculated from elemental analysis.

Results and Discussion

Before a study of adsorption of oligomer type surfactant on pigments, it is important to characterize the surface properties of the oligomer type surfactant aqueous solution. The surface tension of oligomer type surfactant(I) as a function of the concentration in the absence and in the presence of HCl was measured.[10] In the absence of HCl, the surface tension curve of oligomer type surfactant(I) was similar to that of an ordinary surfactant like sodium dodecyl sulfate, while the surface tension value over a relative low concentration became lower in the presence of HCl, indicating that some $-COO^-K^+$ groups in oligomer(I) molecule are converted to -COOH groups by addition of HCl, resulting in enhancement of surface activity due to decrease of repulsion forces between $-COO^-K^+$ groups and of the hydrophilicity of oligomer(I) molecule. Thus, oligomer type surfactant exhibits an appreciable surface activity.

Figure 1 gives the adsorption isotherms of oligomer(I) on α-Fe_2O_3 in the absence and in the presence of HCl. All three isotherms were Langmuir type; furthermore, the amount adsorbed of oligomer(I) on α-Fe_2O_3 increased with an increase of the concentration of HCl added. Also, to elucidate the interaction of oligomer(I) and the surface of α-Fe_2O_3, the zeta potential of α-Fe_2O_3 corresponding the adsorp-

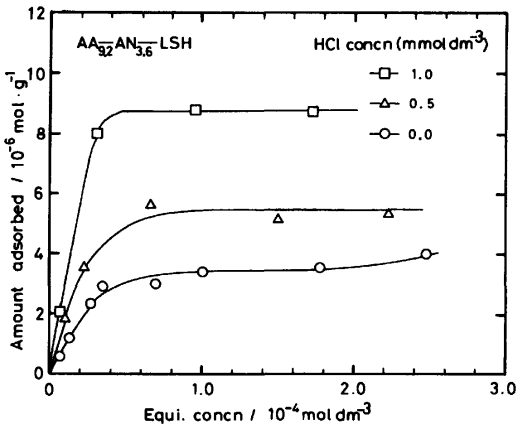

Fig. 1. Adsorption isotherms of oligomer type surfactant(I) on α-Fe_2O_3 in the absence and in the presence of HCl at 25 °C.

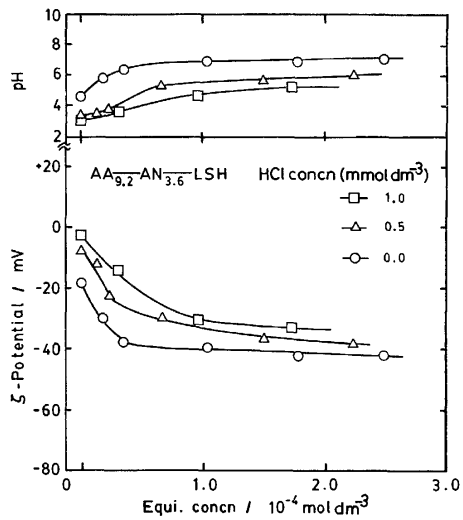

Fig. 2. Zeta potentials of α-Fe_2O_3 and pH values of suspension shown in Fig. 1.

tion isotherm was measured; the result is shown in Fig. 2. It can be seen that the zeta potential value decreases as a function of the equilibrium concentration of oligomer(I) in the absence and in the presence of HCl. The magnitude of zeta potential in the presence of higher concentrations of HCl was less negative than that in lower concentration of HCl. The above results can be interpreted as follows: since the pH of oligomer(I) aqueous solution without adding HCl is about 6, some $-COO^-K^+$ groups in oligomer(I) molecule are likely to dissociate easily. When such an oligomer is adsorbed on the surface of α-Fe_2O_3, an appreciable negative charge at the surface is provided in spite of the fact that less oligomer(I) is adsorbed; this may be due to repulsion of dissociable $-COO^-K^+$ groups in the molecule. On the other hand, with an increase of the concentration of HCl added, some $-COO^-K^+$ groups in oligomer(I) molecule are changed to undissociated -COOH groups, resulting in a decrease of negative charge density of the oligomer molecule. Accordingly, though the amount adsorbed with adding HCl is relatively large, the magnitude of zeta potential of α-Fe_2O_3 in the presence of HCl is less negative than that without HCl. Thus, the change in charge density of oligomer(I) molecule in the presence of various concentrations of HCl exhibits a different adsorption behavior. So, it seems interesting to study the adsorption behavior by different chemical structures of the oligomer.

Figure 3 demonstrates the adsorption isotherms of oligomer(II) containing no acrylonitrile groups on α-Fe_2O_3. This oligomer(II) has less surface active than oligomer(I). These isotherms are different from those of oligomer(I); the amount adsorbed of oligomer(II) in the presence of HCl increases with an increase of the concentration of oligomer(II), reaches a maximum, and then decreases. The isotherm is changed much remarkably in the presence of higher concentrations of HCl than in lower concentrations of HCl. This phenomenon might be explained by changes in the solubility of oligomer(II) with adding HCl and in the interaction between oligomer(II)

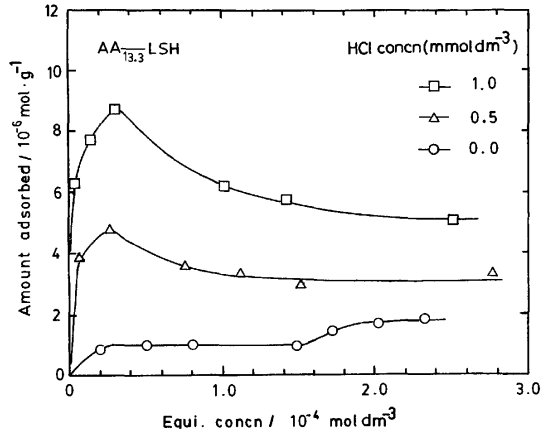

Fig. 3. Adsorption isotherms of oligomer type surfactant(II) on α-Fe_2O_3 in the absence and in the presence of HCl at 25 °C.

molecules and surface of α-Fe_2O_3. That is, some $-COO^-K^+$ groups in oligomer(II) molecule at lower concentration are converted by addition of HCl to -COOH groups, which reaction decreases the solubility of oligomer(II), resulting in an increase of amount adsorbed. Further, with an increase of the concentration of oligomer(II) in the presence of HCl, the conversion ratio from $-COO^-K^+$ to -COOH declines. As a result, the increment of solubility of oligomer(II) reduces the amount adsorbed. Also, as it is expected that repulsion forces between oligomer(II) molecule and surface of α-Fe_2O_3 charged negatively increase with an increase of the suspension's pH, so the amount adsorbed would decrease. Further, the zeta potential of α-Fe_2O_3 by the adsorption of oligomer(II) in the absence and in the presence of HCl was measured. These changes in zeta potential corresponded to those of the adsorption isotherms as shown in Fig. 3. The adsorption of oligomer(II) provided more negative charge on the surface of α-Fe_2O_3 than that of oligomer(I).

The occupied area per molecule at 2×10^{-4} mol dm^{-3} of the equilibrium concentration for two oligomers was calculated as a function of pH of the suspension. For both oligomers, the calculated area increases with an increase of pH of the suspension. The calculated area for oligomer(II) is larger than that for oligomer(I) in the region of above pH=6.

References

1) R. Kita and I. Kogure, *J. Jpn. Colour Mater.*, **53**, 299 (1980).
2) R. J. Akers and P. W. Piley, *J. Colloid Interface Sci.*, **48**, 162 (1974).
3) N. Moriyama, *J. Colloid Interface Sci.*, **50**, 80 (1975).
4) W. Carr, *J. Oil Col. Chem. Assoc.*, **54**, 155 (1971).
5) S. Kumagai and S. Fukushima, *J. Colloid Interface Sci.*, **56**, 227 (1976).
6) Y. Ishigami, S. Suzuki, S. Yamazaki, and H. Suzuki, *J. Jpn. Colour Mater.*, **54**, 671 (1981).
7) F. Tokiwa and T. Iwamura, *J. Am. Oil Chem. Soc.*, **46**, 571 (1969).
8) N. Moriyama, *Colloid Polym. Sci.*, **254**, 726 (1976).
9) K. Ogihara, S. Tomioka, K. Esumi, and K. Meguro, *J. Jpn. Colour Mater.*, **55**, 546 (1982).
10) K. Ogihara, H. Watanabe, K. Esumi, and K. Meguro, *Yukagaku*, **32**, 25 (1983).

The Tricritical Point in the n-$C_8H_{17}SO_3Na$/n-C_4H_9OH/H_2O/n-$C_{14}H_{30}$ System

Hironobu KUNIEDA* and Tsutomu ARAI†

Department of Applied Chemistry, Faculty of Engineering, Yokohama National University, Tokiwadai 156, Hodogaya-ku, Yokohama 240

(Received June 18, 1983)

Synopsis. The phase behavior of three coexisting liquid phases has been studied in the four-component system of n-$C_8H_{17}SO_3Na$/n-C_4H_9OH/H_2O/n-$C_{14}H_{30}$. With a rise in the temperature, the three-phase region shrinks to a tricritical point at which the three liquid phases become identical.

Since ultralow interfacial tensions are attained and a solubilizing power of a surfactant reaches its maximum around a three-phase region (water(W), surfactant(D), and oil(O) phases)[1,2] due to critical phenomena, it is very important to investigate the solution behavior of a surfactant around this region. In a three-liquid-phase system, two liquid phases (O-D or D-W phases) become identical in the presence of a third phase (W or O phase) at a critical end point which is located on the boundary between the two- and three-phase regions.[2] If the two critical end points of the O-D and D-W phases coincide with each other, the three coexisting phases become identical at a high-order critical point, the tricritical point.[3,4] This kind of critical phenomenon has been observed in some systems,[5] but not in a surfactant system.

We previously found a tricritical phenomenon in a bile-salt system.[4] In this paper, in order to find a tricritical point in an ordinary surfactant system, the phase behavior of the n-$C_8H_{17}SO_3Na$/n-C_4H_9OH/H_2O/n-$C_{14}H_{30}$ system has been investigated.

Experimental

Materials. Extra-pure-grade n-$C_8H_{17}SO_3Na$ and n-$C_{14}H_{30}$ were obtained from the Tokyo Kasei Kogyo Co., while extra-pure-grade n-C_4H_9OH was obtained from the Wako Chemicals Co. The procedures for the determination of the phase beoundaries have been described elsewhere.[4]

Results and Discussion

In the n-C_4H_9OH/H_2O/n-$C_{14}H_{30}$ system,[6] a three-phase region appears at a lower temperature in the absence of a surfactant, as is shown in Fig. 1 (●). In this case, a critical end point is an invariant point at a constant pressure (an atmospheric pressure).[2,7] By adding n-$C_8H_{17}SO_3Na$ to this three-component system, the maximum temperature of the three-phase region moves up to a higher temperature, as is also shown in Fig. 1 (○). This maximum temperature of a three-phase region is determined for a variety of over-all compositions; the maximum over all compositions of these maxima may be identified as the tricriti-

† Present address: Fuji Film Co., Nakanuma 210, Minamiashigara, Kanagawa 250-01.

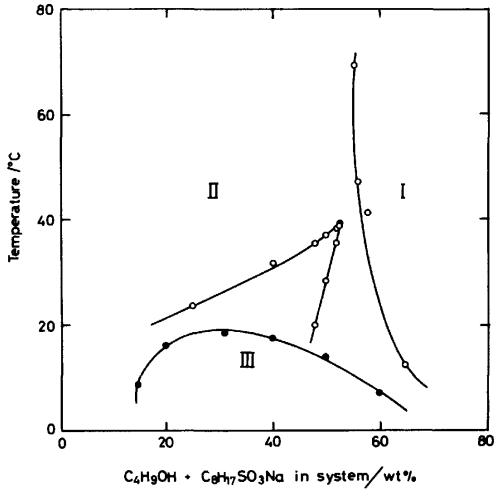

Fig. 1. Phase diagrams of equi-weight mixtures of H_2O–$C_{14}H_{30}$ containing C_4H_9OH (●) and 95 wt% C_4H_9OH+5 wt% $C_8H_{17}SO_3Na$ (○) as a function of temperature. I, II, and III denote one-, two-, and three-phase regions respectively.

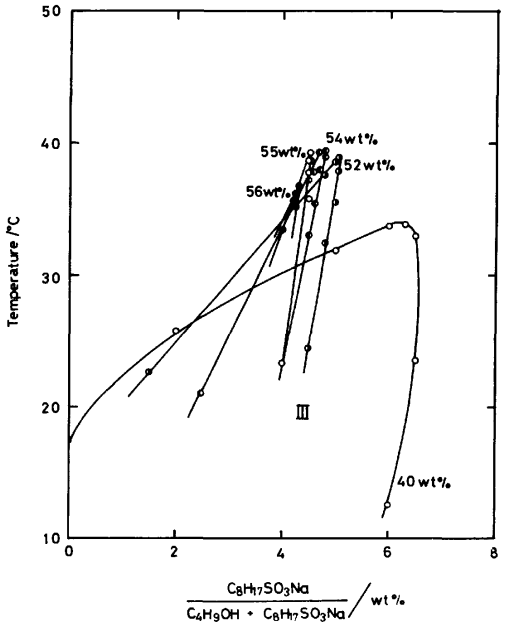

Fig. 2. The effect of concentration of $C_8H_{17}SO_3Na$ in $C_8H_{17}SO_3Na$+C_4H_9OH on the three-phase region of equi-weight mixture of H_2O–$C_{14}H_{30}$ containing $C_8H_{17}SO_3Na$+C_4H_9OH. Numerical number in the Figure indicates the concentration of $C_8H_{17}SO_3Na$+C_4H_9OH in system.

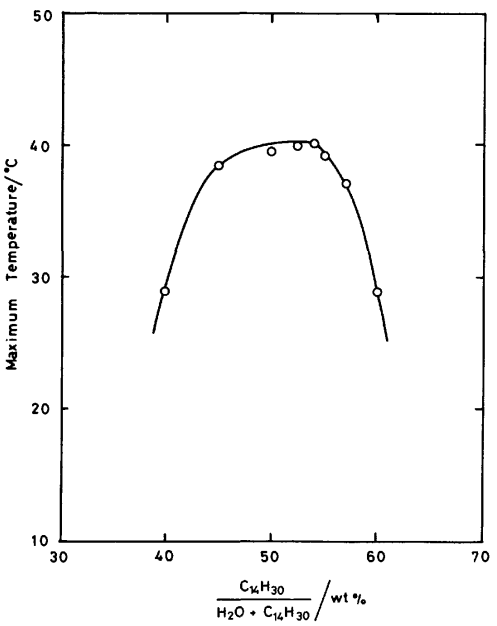

Fig. 3. The effect of $H_2O/C_{14}H_{30}$ ratio on the maximum temperature of the three-phase region.

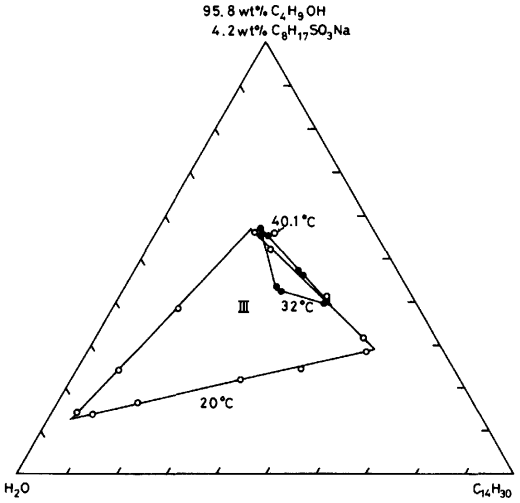

Fig. 4. The three-phase region of pseudo ternary system of (95.8 wt% $C_4H_9OH+C_8H_{17}SO_3Na)/H_2O/C_{14}H_{30}$. The three-phase region shrink to a tricritical point with the rise in temperature.

cal point.[3] This is because, in a four-component system, a line of critical end points exists in a certain space of temperature and compositions at a constant pressure, and the two critical end points of O-D and D-W exist at the respective temperatures as long as a three-phase region appears.[4] Since a three-phase region is a point in a composition tetrahedron at the maximum temperature, the two critical end points may coincide at this point, *i.e.*, the tricritical point. In Fig. 2, the three-phase region is determined as a function of n-$C_8H_{17}SO_3Na/(n$-$C_8H_{17}SO_3Na+n$-$C_4H_9OH)$ and the weight fraction of oil/water is unity. In this case, the maximum temperature of the three-phase region appears at the 54 wt%/system of (n-$C_8H_{17}SO_3Na+n$-C_4H_9OH). Similar maximum temperatures are determined for a variety of water/oil ratios and are plotted in Fig. 3. The maximum temperature of these maxima is 40.1 °C (n-$C_8H_{17}SO_3Na+n$-C_4H_9OH, 56 wt%/system. n-$C_{14}H_{30}/H_2O$, 0.54/0.46 (W/W). n-$C_8H_{17}SO_3Na/n$-C_4H_9OH, 0.042/0.958 (W/W)).

Therefore, at this temperature, the three-phase region is a point in this four-component system and is identified as the tricritical point. In fact, the critical opalescence is observed in all phases in the vicinity of this point. The three-phase region in the pseudo-three-component system of 95.8 wt% n-C_4H_9OH+4.2 wt% n-$C_8H_{17}SO_3Na)/H_2O/n$-$C_{14}H_{30}$ is shown at 20, 32, and 40.1 °C in Fig. 4. The three-phase region shrinks to a point on approaching 40.1 °C.

The authors wish to thank Prof. Kōzō Shinoda for his helpful discussion.

References

1) K. Shinoda and H. Kunieda, "Microemulsions," ed by L. M. Prince, Academic Press, New York and London (1977), Chap. 4.

2) H. Kunieda and K. Shinoda, *Bull. Chem. Soc. Jpn.*, **55**, 1777 (1982).

3) R. B. Griffiths, *J. Chem. Phys.*, **60**, 195 (1974).

4) H. Kunieda and K. Shinoda, *Bull. Chem. Soc. Jpn.*, **56**, 980 (1983).

5) G. D. Efremova and A. V. Shvarts, *Russ. J. Phys. Chem.*, **40**, 486 (1966).

6) B. M. Knickerbocker, C. V. Pesheck, H. T. Davis, and L. E. Scriven, *J. Phys. Chem.*, **86**, 393 (1982).

7) H. Kunieda, *Bull. Chem. Soc. Jpn.*, **56**, 625 (1983).

The Thermal Properties of (4-Substituted Cyclohexyl) 4-Substituted Cinnamates

Shigetsugu HAYASHI, Shunsuke TAKENAKA,* and Shigekazu KUSABAYASHI
Department of Applied Chemistry, Faculty of Engineering, Osaka University, Suita, Osaka 565
(Received July 13, 1983)

Synopsis. The thermal properties for a homologous series of 4-alkylcyclohexyl 4-alkoxy- and 4-cyanocinnamates are examined. They exhibit nematic phases with low melting points. The effect of the cyclohexyl group on the mesophase stability is discussed.

(4-Substituted phenyl) 4-substituted benzoates have been known to be good nematogens for devices employing a twisted nematic mode, as one of the substituents is a polar group, such as cyano, and the guest-host and dynamic scattering modes, as both substituents are the nonpolar groups, such as an alkyl and/or alkoxyl.[1] For practical purposes, (4-substituted cyclohexyl) 4-substituted benzoates are also good nematogens, because the cyclohexyl group tends to lower the melting point and increases the clearing point. In this paper, we will demonstrate the preparation and thermal properties of (4-substituted cyclohexyl) 4-substituted cinnamates; the effect of the cyclohexyl group on the thermal properties is also discussed.

Preparation

The 4-alkylcyclohexanols were obtained by the hydrogenation of the corresponding 4-alkylphenols in the presence of Ranney nickel under 150×10^5 Pa at 150 °C. The cis and trans mixtures of the cyclohexanols were reacted with benzoyl chloride, giving 4-alkylcyclohexyl benzoates. The esters were purified by column chromatography over silica gel, using a mixed solvent of hexane–ether (98:2—95:5). After repeating the chromatographic purification, the esters were hydrolyzed with methanol– 2 mol dm^{-3} potassium hydroxide (1:1), thus giving *trans*-4-alkylcyclohexanols. The purity was checked by means of the NMR spectrum. The NMR spectrum for *trans*-4-heptylcyclohexyl benzoate shows a multiplet at 4.7—5.1 ppm arising from the methine proton at the 1 position, and the cis form a broad singlet at 5.3 ppm (Δ) in $CDCl_3$. The yields of the materials with a purity of more than 99% were less than 20%. 4-Alkyl-, 4-alkoxy-, and 4-cyanocinnamoyl chlorides were reacted with *trans*-4-alkylcyclohexanols according to the usual method. The esters prepared here were purified by column chromatography over silicagel, using a mixed solvent of hexane–ether (98:2), followed by recrystallization from absolute ethanol. The data of elemental analysis are shown in Table 1.

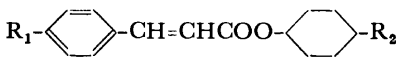

Results and Discussion

The melting points and mesomorphic transition temperatures for the cinnamate esters are given in Table 2. Compounds **1**—**11** have melting points that lie between 53 and 99 °C, while compounds **12** and **13** have somewhat lower melting points. The nematic-isotropic transition temperatures for the homologous series of 4-heptylcyclohexyl cinnamates show a typical even-odd effect. Compounds **12** and **13** have low melting points and enthalpies, being good nematogens.

TABLE 1. ELEMENTARY ANALYSIS DATA

Compound	R_1	R_2	Calcd (%)			Found (%)		
			C	H	N	C	H	N
1	CH_3O	C_7H_{15}	77.05	9.56		76.99	9.56	
2	C_2H_5O		77.37	9.74		77.28	9.71	
3	C_3H_7O		77.67	9.91		77.44	9.95	
4	C_4H_9O		77.95	10.07		78.12	9.87	
5	$C_5H_{11}O$		78.21	10.21		78.10	10.25	
6	$C_6H_{13}O$		78.45	10.35		78.28	10.33	
7	$C_7H_{15}O$		78.68	10.48		78.38	10.55	
8	CH_3O	C_3H_7	75.46	8.67		75.17	8.69	
9		C_4H_9	75.91	8.92		75.81	8.92	
10		C_5H_{11}	76.32	9.15		76.22	9.16	
11	$C_5H_{11}O$	C_5H_{11}	77.67	9.91		77.39	9.95	
12	C_5H_{11}	C_3H_7	80.65	10.01		80.60	10.03	
13		C_5H_{11}	81.03	10.34		81.25	10.40	
14	CN	C_4H_9	77.13	8.09	4.50	77.11	8.12	4.56
15		C_5H_{11}	77.50	8.36	4.30	77.35	8.42	4.19
16		C_7H_{15}	78.14	8.84	3.96	77.83	8.95	4.02

Table 2. Thermal properties

Compound	C	N	I	ΔH_{mp} / kJ mol^{-1}	ΔH_{NI} / kJ mol^{-1}
1	. 52.7 .	95.3 .		36.0	1.3
2	. 98.8 .	104.3 .		30.6	1.4
3	. 85.0 .	92.8 .		34.0	1.1
4	. 75.8 .	97.5 .		24.6	1.5
5	. 61.0 .	92.5 .		47.2	1.4
6	. 69.7 .	94.5 .		48.1	1.7
7	. 77.2 .	92.5 .		40.8	1.6
8	. 67.0 .	91.0 .		19.5	0.9
9	. 57.4 .	87.2 .		26.7	0.7
10	. 56.5 .	97.2 .		24.0	0.9
11	. 66.1 .	95.3 .		20.1	1.2
12	. 45.3 .	65.4 .		18.2	1.0
13	. 36.5 .	69.0 .		22.5	0.9
14	. 121.0 .	(104.0)[a] .		25.5	—
15	. 122.0 .	(109.0)[a] .		27.5	—
16	. 112.5 .	(110.0)[a] .		28.6	0.9

a) Parentheses indicate monotropic transition temperatures.

The transition temperatures were measured using a Nikon polarized microscope POH equipped with a Mettler FP 52 heating stage and a control unit. The transition enthalpies were measured by means of a Daini Seikosha SSC 560 differential scanning calorimeter, using indium (99.9%) as the calibration standard at a heating rate of 5 °C/min.

As the alkoxyl group is replaced by a cyano group, both melting and clearing points increase, showing monotropic nematic properties. These results may be compared with those of the corresponding phenyl cinnamates. It has been known that a cyclohexyl group is less favorable for the thermal stability of the mesophase than a phenyl, because the former is more flexible than the latter. For example, 4-alkylbenzoic acids have higher melting and clearing points than 4-alkylcyclohexanecarboxylic acids.

For compounds **1**—**13** having nonpolar substituents, the melting points are lower by 10—30 °C than those for the corresponding phenyl cinnamate esters.[3,4] On the other hand, the clearing points for the present series are also lower by 5—40 °C than those for the corresponding phenyl cinnamate esters. The difference tends to become larger with increase in the carbon number in the alkyl and alkoxyl chains. These trends are probably connected with the flexibility of the cyclohexyl group.

As the terminal group is replaced by a cyano group, the circumstances differ significantly. Usually, as the phenyl group with the alkyl chain in 4-cyano-4′-alkylbiphenyls and 4-cyanophenyl 4-alkylbenzoates is replaced by a cyclohexyl group, the clearing points increase by *ca.* 20 °C, whereas the melting points are almost unchanged. These trends have been interpreted in terms of the structural difference in the antiparallel dimer of the molecules in the mesophase.[5] Indeed, X-ray measurements indicate that the "overlapping core" formed by the 4-cyanobiphenyls and 4-cyanophenyl benzoates differs significantly from the "partially overlapping" one formed by the corresponding cyclohexyl compounds.[6] For the present series (**14**—**16**), by contrast, the melting points are higher by 30—40 °C, and the clearing points are lower by 10—20 °C than those for the corresponding 4-alkylphenyl 4-cyanocinnamates.[7,8] These facts indicate that the enhancement of the nematic stability upon the replacement of the phenyl group with the cyclohexyl one does not occur in this system. A possible explanation is that the "overlapping core" for the phenyl 4-cyanocinnamates differs from those for the 4-cyanobiphenyls and 4-cyanophenyl benzoates and is rather similar to those for the cyclohexyl compounds, while the flexibility of the cyclohexyl group decrease the stability of the nematic phase, as has been mentioned above.

In conclusion, the replacement of the phenyl ring by the cyclohexyl in the phenyl cinnamate core leads to a decrease in the thermal stability of the nematic phase, presumably because of an increase in the flexibility of the core, even though both terminal substituents are nonpolar alkyl and/or alkoxyl groups or a polar cyano.

References

1) G. J. Sprokel, "The Physics and Chemistry of Liquid Crystal Devices," Plenum Press, New York (1980).
2) D. Demus, H. Demus, and H. Zasche, "Flüssig Kristalle in Tabellen," VEB Deutscher Verlag für Grundstoff Industries, Leipzig (1974).
3) F. B. Jones, Jr., and J. J. Ratto, U. S. Patent 3926834 (1973).
4) F. J. Jun and J. Ratto, *J. Chem. Soc., Chem. Commun.*, **1973**, 841.
5) G. W. Gray, *Mol. Cryst. Liq. Cryst.*, **63**, 3 (1981).
6) A. J. Leadbetter and A. I. Mehta, *Mol. Cryst. Liq. Cryst.*, **72**, 51 (1981).
7) F. B. Jones, Jr., and J. J. Ratto, *J. Phys. C*, **36**, Cl-413 (1975).
8) V. V. Titov, E. I. Kovshev, A. I. Pavluchenko, V. T. Lazareva, and M. F. Grebenkin, *J. Phys. C*, **36**, Cl-387 (1975).

The Volume Profile for the Aquation Reactions of *trans*-[CoBr(NO$_2$)(en)$_2$]$^+$ and *trans*-[CoCl(N$_3$)(en)$_2$]$^+$ †

Yoichi KITAMURA,* Shinji NARIYUKI, and Toshiaki KONDO††
Department of Chemistry, Faculty of Science, Ehime University, Matsuyama, Ehime 790
(Received January 27, 1983)

Synopsis. For the aquation of *trans*-[CoBr(NO$_2$)(en)$_2$]$^+$, the activation volume at atmospheric pressure ($\Delta V^{\neq}$) is 0.3±0.2 cm^3 mol^{-1} at 10 °C, and the reaction volume (ΔV) is −10.4±0.1 cm^3 mol^{-1} at 7.4 °C, both in pure water. For *trans*-[CoCl(N$_3$)(en)$_2$]$^+$, $\Delta V^{\neq}$ is 0.7±0.6 cm^3 mol^{-1} at 30 °C in 0.011 M HClO$_4$ (1 M=1 mol dm^{-3}) and ΔV is −11.0±0.6 and −11.4±0.3 cm^3 mol^{-1} at 25 °C in 0.008 M HClO$_4$, thus yielding the trans and the cis aqua products respectively.

In a recent report, one (Y. K.) of the present authors has examined the magnitudes of $\Delta V^{\neq}$ and ΔV of 14 aquation reactions of the Co^{III} complex ion, where the leaving ligand is a monovalent anion.[1] It has been indicated that the ΔV's for 10 such reactions lie in the relatively limited range from −7 to −13 cm^3 mol^{-1} and are typically −10 cm^3 mol^{-1}. A general feature that has also been pointed out is that the $\Delta V^{\neq}$ is large (*ca.* 14 cm^3 mol^{-1}) when the initial complex contains the strongly electron-donating NH_2^- nonlabile ligand; moderate when the initial complex contains a moderately electron-donating Cl^- or N_3^-, or moderately electron-withdrawing NO_2^-, nonlabile ligand, and small (*ca.* −9 cm^3 mol^{-1}) and close to the corresponding ΔV when the initial complex does not contain any nonlabile ligand with electron-donating or -withdrawing power.

In the present work, $\Delta V^{\neq}$ and ΔV are obtained for two additional reactions, where the initial complex contains a nonlabile NO_2^- or N_3^- ligand:

trans-[CoBr(NO$_2$)(en)$_2$]$^+$ + H$_2$O ⟶
trans-[Co(NO$_2$)(en)$_2$H$_2$O]$^{2+}$ + Br$^-$, (1)[2]

trans-[CoCl(N$_3$)(en)$_2$]$^+$ + H$_2$O ⟶
80% *trans*-, 20% *cis*-[Co(N$_3$)(en)$_2$H$_2$O]$^{2+}$ + Cl$^-$. (2)[3]

It is tested whether or not the volume profiles of Reactions 1 and 2 are pertinent to the general tendency and whether or not the previous interpretation of the $\Delta V^{\neq}$ is also applicable in these cases. In Reaction 2 the trans configuration of the reactant is not retained. On the basis of this, the geometry of the transition state in Reaction 2 should differ from those in analogous reactions, where the geometries are retained.[4] We are further interested in whether or not this feature of Reaction 2 is remarkable in its $\Delta V^{\neq}$. The isomerization velocity of *trans*-[Co(NO$_2$)(en)$_2$H$_2$O]$^{2+}$ to the cis-isomer is sufficiently slow, and the kinetic course of Reaction 1 is not interrupted by this isomerization.[5] The *trans*- and *cis*- [Co(N$_3$)(en)$_2$H$_2$O]$^{2+}$ have an isosbestic point at 533 nm, where the velocity of Reaction 2 can be followed spectrophotometrically.[3]

Experimental

Materials. The *trans*-[CoBr(NO$_2$)(en)$_2$]ClO$_4$ (**1**)[2] and *trans*-[CoCl(N$_3$)(en)$_2$]ClO$_4$ (**2**)[6] were obtained by the published methods and identified by means of elemental analysis (C, H, N).

Kinetic Measurements and Dilatometry. The procedures were the same as in the previous report except that a Heise high-pressure gauge was used.[1]

Results and Discussion

Kinetic Results. The rate constants at each pressure are shown in Table 1. The k-values at each pressure are fitted to $\ln(k/k_o)/P=a+bP$ by the least-squares method, where k_o is the average rate constant at atmospheric pressure. $\Delta V^{\neq}$ is obtained by the use of $\Delta V^{\neq}=-RT(\mathrm{d}\ln k/\mathrm{d}P)=-RTa$. The rate constants are rather independent of the pressure, and the resultant $\Delta V^{\neq}$'s are close to zero (Table 2). Reaction 1 was followed in pure water and in an 0.01 M HClO$_4$ aqueous solution. The rate constants at each pressure are essentially the same in both.

Table 1. Rate constants (k/10^{-5} s^{-1}) of the aquation reaction at each pressure (P/bar)

1,[a] *trans*-[CoBr(NO$_2$)(en)$_2$]$^+$, 1 mM in H$_2$O,[b] 10 °C,[c] 376 nm,[d] $\ln(k/k_o)/P=-(0.12\pm0.07)\times10^{-4}-(1.6\pm0.5)\times10^{-8}P$[e]

P	1	1	400	800	1200	1600	2000
k	58.2	56.3	56.2	55.2	55.2	53.0	53.5
	55.8	57.8	56.7	56.2	54.8	54.5	51.2

1,[a] *trans*-[CoBr(NO$_2$)(en)$_2$]$^+$, 1 mM in 0.01 M HClO$_4$,[b] 10 °C,[c] 376 nm,[d] $\ln(k/k_o)/P=-(0.08\pm0.08)\times10^{-4}-(2.2\pm0.7)\times10^{-8}P$[e]

P	1	1	400	800	1200	1600	2000
k	58.5	57.5	58.2	57.0	55.2	53.8	53.7
	59.2	56.8	57.2	55.8	55.5	53.7	52.3

2,[a] *trans*-[CoCl(N$_3$)(en)$_2$]$^+$, 2.6 mM in 0.011 M HClO$_4$,[b] 30 °C,[c] 533 nm,[d] $\ln(k/k_o)/P=-(0.27\pm0.25)\times10^{-4}-(2.6\pm2.0)\times10^{-8}P$[e]

P	1	1	400	800	1200	1600	2000
k	37.7	35.5	35.3	34.8	33.3	32.8	32.3
	36.5	36.3	37.2	33.5	33.2	33.0	32.7

a) Reaction number. b) Concentration of the complex. c) Reaction temperature. d) Reaction was followed at this wavelength. e) Standard deviations are indicated.

† Presented at the 6th International Symposium on Solute-Solute-Solvent Interactions, July, 1982, at Minoo, Japan.

†† Present address: Kawanoe High School, Kawanoe, Ehime 799-01.

TABLE 2. VOLUME PROFILE (V/cm^3 mol^{-1}) FOR THE AQUATION OF $[CoXY(en)_2]^+$

Reaction No.	Reactant	Configuration[a]	ΔV^* (T/°C, solvent)	ΔV (T/°C, solvent)
1[b]	*trans*-$[CoBr(NO_2)(en)_2]^+$	100% trans	0.3±0.2 (10, H_2O) 0.2±0.2 (10, 10 mM $HClO_4$)	−10.4±0.1 (7.4, H_2O)
2[b]	*trans*-$[CoCl(N_3)(en)_2]^+$	80% trans, 20% cis	0.7±0.6 (30, 11 mM $HClO_4$)	−11.0±0.6 (25, 8 mM $HClO_4$)[c] −11.4±0.3 (25, 8 mM $HClO_4$)[d]
3[e]	*trans*-$[CoCl(NO_2)_2(en)_2]^+$	100% trans	0.1 (15, H_2O)	−10.4 (15, H_2O)
4[e]	*cis*-$[CoCl(NO_2)_2(en)_2]^+$	100% cis	0.9 (30, H_2O)	−9.3 (25, H_2O)
5[f]	*cis*-$[CoCl_2(en)_2]^+$	100% cis	−0.3±0.4 (30, 10 mM HNO_3)[g]	−14.2 (25, H_2O)
6[f]	*trans*$[CoCl_2(en)_2]^+$	65% trans, 35% cis	−1.7±1.1 (25, H_2O)	−13.9 (25, H_2O)

a) Configuration of the aqua product. b) This work. c) For the trans aqua product. d) For the cis aqua product. e) Ref. 1. f) Ref. 7. g) Ionic strength = 0.1 M ($NaClO_4$).

Dilatometric Results. Reaction 1 was followed at 7.4 °C in a 4.0 mM aqueous solution of **1** from a 52 to a 99% completion. ΔV was obtained from the intercept at t=0 of the $\ln(h_t-h_\infty)$ *vs.* t plot, where h_t is the meniscus height at the reaction time (t). The h_∞ value is calculated from h_t's, and k=40.7×10^{-5} s^{-1} is obtained from this plot. The volume change in a 4.0 mM solution of **2** in 0.008 M $HClO_4$ was followed at 25 °C from a 40 to a 90% completion. The total volume (V) of the solution is related to the partial molal volume ($\overline{V}_i$) and the mole number (n_i) of each component (i) in the solution as: $V=\sum n_i\overline{V}_i$. At several stages of Reaction 2, n_i's were calculated according to the following scheme, where the initial product of the aquation consists of 80% trans and 20% cis aqua complex:[3]

$$\begin{array}{l} \textit{trans}\text{-}[CoCl(N_3)(en)_2]^+ + H_2O \xrightarrow{k} \\ \qquad\qquad \textit{trans}\text{-}[Co(N_3)(en)_2H_2O]^{2+} + Cl^- \\ \qquad\qquad\qquad k_1 \downarrow \uparrow k_{-1} \\ \qquad\qquad \textit{cis}\text{-}[Co(N_3)(en)_2H_2O]^{2+} + Cl^-. \end{array}$$

We used the literature rate constants at 25 °C in an 0.01 M $HClO_4$ aqueous solution (k=22.0×10^{-5} s^{-1}, k_1=7.2×10^{-5} s^{-1}, k_{-1}=2.6×10^{-5} s^{-1}).[3] The ΔV's of Reaction 2 were obtained for the trans aqua and the cis aqua products respectively by solving a set of simultaneous equations for several reaction stages. Two independent runs were performed. ΔV is −10.7± 0.5 and −11.3±0.6 cm^3 mol^{-1} for the trans product, and −11.4±0.3 and −11.3±0.3 cm^3 mol^{-1} for the cis product. These results indicate that the difference between the $\overline{V}_i$'s of *trans*-$[Co(N_3)(en)_2H_2O]^{2+}$ and of *cis*-$[Co(N_3)(en)_2H_2O]^{2+}$ is small enough. Assuming this difference as zero, k=21.2×10^{-5} and 21.9×10^{-5} s^{-1} are obtained from the Guggenheim plots of the dilatometric data, which agree well with that in the literature.[3] The results are summarized in Table 2, along with four volume profiles of analogous reactions.

Discussion. It can be noticed that, in Reactions 1 and 2, the ΔV^*'s are close to zero and the ΔV's are close to −10 cm^3 mol^{-1}. Thus, the volume profiles of Reactions 1 and 2 are quite pertinent to the general tendency indicated in the previous report.[1] Therefore, these volume profiles can be interpreted along the previous line of arguments. The transition state is composed of an ion pair between the leaving ligand and the five-coordinate intermediate, $[Co(NO_2)(en)_2\cdots OH_2]^{2+}$ or $[Co(N_3)(en)_2\cdots OH_2]^{2+}$, where the entering water molecule is halfway between the vacant coordination site and the first solvation sphere. The volume profiles of Reactions 1—6 are quite similar to each other. The magnitudes of ΔV^* are not affected by the geometrical difference in the transition state between those for Reactions 2 and 6 and those for Reactions 1, 3, 4, and 5. This is further in accordance with the fact that the ΔV's of Reaction 2 are quite similar in both cases where cis and trans aqua products are formed. It seems that neither ΔV^* nor ΔV is sensitive to the stereochemical course of the reaction.

References

1) Y. Kitamura, *Bull. Chem. Soc. Jpn.*, **55**, 3625 (1982).
2) C. H. Langford and M. L. Tobe, *J. Chem. Soc.*, **1963**, 506.
3) P. J. Staples and M. L. Tobe, *J. Chem. Soc.*, **1960**, 4803.
4) M. L. Tobe, *Inorg. Chem.*, **7**, 1260 (1968).
5) M. N. Hughes, *J. Chem. Soc.*, **1967**, 1284.
6) P. J. Staples and M. L. Tobe, *J. Chem. Soc.*, **1960**, 4812.
7) G. Daffner, D. A. Palmer, and H. Kelm, *Inorg. Chim. Acta*, **61**, 57 (1982).

Cobalt(III) Complexes with Quadridentate Ligands. V.[1] The Preparation and Properties of Paramagnetic and Diamagnetic *cis*-β_2-Isomer of the 5-Nitrosalicylato(quadridentate amine)cobalt(III) Complexes

Yoshihisa YAMAMOTO* and Hiroko KUDO
Faculty of Pharmaceutical Sciences, Higashi Nippon Gakuen University, Ishikari-Tobetsu, Hokkaido 061-02
(Received April 15, 1983)

Synopsis. Several green paramagnetic 5-nitrosalicylato(quadridentate amine)cobalt(III) chloride nitrate hydrates, $[Co(5\text{-}NO_2sal)L]Cl\cdot NO_3\cdot nH_2O$ (L: 2,3,2-tet, 3,2,3-tet, and 3,3,3-tet) and the corresponding orange diamagnetic nitrate hydrates, $[Co(5\text{-}NO_2sal)L]NO_3\cdot nH_2O$, have been isolated and characterized by analytical, spectroscopic, and magnetic methods.

The preparation and properties of paramagnetic metal complexes with the quadridentate amine ligands such as 2,3,2-tet, 3,2,3-tet, and 3,3,3-tet, as is shown in Fig. 1, have not previously been described, except for iron(III) complexes[2] with sexadentate ligands derived from salicylaldehyde and 3,2,3-tet or 3,3,3-tet. The present paper deals with the preparation and properties of the green paramagnetic 5-nitrosalicylato(quadridentate amine)cobalt(III) complexes, $[Co(5\text{-}NO_2sal)L]^{n+}$ (L: 2,3,2-tet, 3,2,3-tet, and 3,3,3-tet; n=2) and of the corresponding orange diamagnetic cobalt(III) complexes (n=1).

Results and Discussion

The green paramagnetic *cis*-β_2-5-nitrosalicylato-(quadridentate amine)cobalt(III) chloride nitrate hydrates, $[Co(5\text{-}NO_2sal)L]Cl\cdot NO_3\cdot nH_2O$ (L: 2,3,2-tet (**1a**), 3,2,3-tet (**1b**), 3,3,3-tet (**1c**)), have been isolated from a reaction mixture of the diamagnetic *cis*-β_2-salicylato(quadridentate amine)cobalt(III) chloride hydrates,[3] $[Co(sal)L]Cl\cdot nH_2O$ (L: 2,3,2-tet (**2a**), 3,2,3-tet (**2b**), 3,3,3-tet (**2c**)), 60% HNO_3 and acetone. From the orange acetone filtrate, the orange diamagnetic *cis*-β_2-5-nitrosalicylato(quadridentate amine)-cobalt(III) nitrate hydrates, $[Co(5\text{-}NO_2sal)L]NO_3\cdot nH_2O$ (L: 2,3,2-tet (**3a**), 3,2,3-tet (**3b**), 3,3,3-tet (**3c**)) have been isolated. Their colors in the solid state are green (**1a—c**), organge (**3a** and **3b**), and pink-russet (**3c**). The effective magnetic moments of **1a—c** are 1.7—1.8 BM,† suggesting one unpaired electron. Complexes **3a—c** are diamagnetic. In the ^1H NMR spectra, the signals of the methylene protons, amine protons, and salicylato protons of **1a—c** and **3a—c** have been assigned by the comparison with those[3] of **2a—c**. Their form is *cis*-β_2-form from their ^1H NMR spectra, because both signals of the NH_2-side methylene protons (*cf.* Table 1) and the NH-side methylene protons (*cf.* Table 1) of the coordinated quadridentate ligands of **1a—c** and **3a—c** are distinguishable.[3,7]

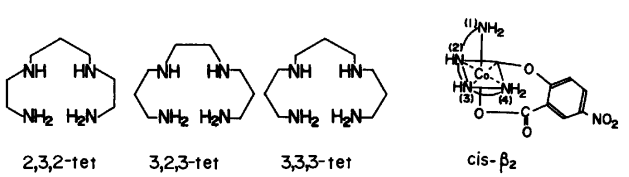

Fig. 1. The quadridentate amine ligands of 2,3,2-tet, 3,2,3-tet, and 3,3,3-tet, and the *cis*-β_2-form of complexes.

The properties of IR, ^1H-, ^{13}C NMR spectra, and magnetic moments of **1a—c** are similar to those of the green paramagnetic 5-nitrosalicylato(amine)cobalt(III) complexes, $[Co(5\text{-}NO_2sal)L]X_2\cdot nH_2O$ (L: trien (**4a**), en_2 (**4b**), $(bpy)_2$ (**4c**), and $(NH_3)_4$ (**4d**)), *i.e.*, an unpaired electron of **4a—d** is delocalized over the chelate ring containing the cobalt atom and the 5-nitrosalicylato ligand from the results of the IR spectra,[4] ^1H-, ^{13}C NMR spectra,[4] magnetic susceptibility,[5] the electric resistivity,[5] ESR,[5] and XPS.[6] Thus, an unpaired electron of **1a—c** is also delocalized over the chelate ring containing the cobalt atom and the 5-nitrosalicylato ligand.

A clear distinction between **1a—c** and **4a**[7] was found in the absorption spectra in 60% HNO_3. The ε's of the absorption bands at around 350 nm of **1a—c** are larger than those at 460 nm. The absorption bands at around 350 nm of **1a—c** show a hypsochromic shift from that (360 nm) of **4a** as is shown in Table 1. These properties have been ascribed to the coordinated quadridentate ligands.

The properties of **3a—c** are similar to those of the orange diamagnetic 5-nitrosalicylato(trien)cobalt-(III) complex,[7] $[Co(5\text{-}NO_2sal)trien]NO_3\cdot 3H_2O$ (**5**), in the IR, NMR spectra, and magnetic susceptibility. Both signals of the center methylene protons (*cf.* Table 1) and NH_2-side methylene protons of the coordinated quadridentate ligand in **3a—b** are distinguishable, but those of **1a—b** are indistinguishable, because of the paramagnetism. The first absorption bands of **3a—c** shift to 503 nm (**3a**) from 535 nm (**3c**). This shift is similar to that[3] of **2a—c**. Some physical properties of **1a—c**, **3a—c**, **4a**, and **5** are collected in Table 1.

Experimental

Measurements. The NMR spectra were recorded with an R-40 apparatus (Hitachi) for ^1H NMR. The IR spectra were recorded in potassium bromide disks with an IR-27G spectrophotometer (Shimadzu). The visible absorption spectra were recorded with a Shimadzu MPS-5000 recording spectrophotometer. The magnetic susceptibilities were measured by the Faraday method using a mag-

† 1 BM=9.274×10^{-24} A m^{-2}.

TABLE 1. SOME PHYSICAL PROPERTIES OF COMPLEXES **1a—c** AND **3a—c**

	Center methylene protons $NHCH_2CH_2CH_2NH_2$ $NHCH_2CH_2CH_2NH$ δ	NH_2-side methylene protons $NHCH_2CH_2NH_2$ $NHCH_2CH_2CH_2NH_2$ δ	NH-side methylene protons $-CH_2NHCH_2CH_2NH_2$ $-CH_2NHCH_2CH_2CH_2NH_2$ δ
4a[b]		2.33—2.82(3H)	2.82—3.84(9H)
1a	1.63—2.70(5H)		2.70—3.78(9H)
1b	1.31—2.38(7H)		2.38—3.21(9H)
1c	1.32—2.37(9H)		2.37—3.37(9H)
5[b]		2.56(3H)	3.14(9H)
3a	1.99(2H)	2.04—2.54(3H)	2.89(9H)
3b	2.02(4H)	2.24—2.46(3H)	2.46—3.28(9H)
3c	1.60—2.40(9H)		2.40—3.26(9H)

	$N(1)H_2$ δ	$N(4)H_2$ δ	N(3)H δ	N(2)H δ	Salicylato δ	Absorption bands λ/nm (ε)			Magnetic moments μ_{eff}/BM
4a[b]	4.48(2H)	5.14(1H) 5.38(1H)	6.35(1H)	a)	—[1]	360 (3240)	455 (3300)	663 (11800)	1.7
1a	4.46(3H)	5.34(2H)		6.07(1H)	—[2]	355 (5500)	460 (3100)	670 (8600)	1.7
1b	3.55(1H) 4.25(1H)	4.48—5.65(3H)		a)	—[1]	352 (5300)	460 (3100)	670 (8100)	1.7
1c	3.37—4.39 (2H)	4.67(3H)		5.47(1H)	—[1]	346 (5500)	453 (3200)	657 (10500)	1.8
5[b]	4.53(2H)	4.97(1H) 5.35(1H)	6.34(1H)	6.87(1H)	7.1—8.9 (3H)[3]	378 (13600)	498 (316)		dia
3a	4.42(2H)	4.96(2H)	5.24(1H)	6.34(1H)	7.1—8.6 (3H)[1]	375 (13200)	503 (337)		dia
3b	3.28—3.70 (1H) 3.83(1H)	4.52(2H)	5.16(1H)	5.91(1H)	7.2—a)[3]	370 (13000)	510 (254)		dia
3c	3.48—4.11 (2H)	4.63(3H)		5.38(1H)	7.2—8.8 (3H)[1]	375 (14100)	535 (246)		dia

Solvents and Standard: 1) 3.6 mol dm^{-3} D_2SO_4, internal DSS; 2) 65% DNO_3, internal DSS; 3) 1.8 mol dm^{-3} D_2SO_4, internal DSS. a) This signal is overlapped with the solvent. b) Ref. 7.

netic balance (Shimadzu) from liquid nitrogen to room temperature.

Materials. The quadridentate amine ligands of 2,3,2-tet, 3,2,3-tet, and 3,3,3-tet were purchased from Strem Chemicals Inc.

Preparation of Complexes. Diamagnetic *cis*-β_2-salicylato(quadridentate amine)cobalt(III) chloride hydrates, $[Co(sal)L]Cl \cdot nH_2O$ (L: 2,3,2-tet, n=2 (**2a**), L: 3,2,3-tet, n=3 (**2b**), and L: 3,3,3-tet, n=1 (**2c**)) were prepared from the reaction mixture of salicylic acid or sodium salicylate and $[CoCl_2L]Cl \cdot nH_2O$ (L: 2,3,2-tet, 3,2,3-tet, and 3,3,3-tet) according to the previous paper.[3]

*Paramagnetic β_2-5-Nitrosalicylato(3,7-diazanonane-1,9-diamine)cobalt(III) Chloride Nitrate Dihydrate (**1a**), Paramagnetic β_2-5-Nitrosalicylato(4,7-diazadecane-1,10-diamine)cobalt(III) Chloride Nitrate Dihydrate (**1b**), and Paramagnetic β_2-5-Nitrosalicylato(4,8-diazaundecane-1,11-diamine)cobalt(III) Chloride Nitrate Dihydrate (**1c**)*: One cubic centimeter of 60% nitric acid was added to **2a** (1.0 g, 2.34 mmol), **2b** (1.0 g, 2.18 mmol), and **2c** (1.0 g, 2.29 mmol), respectively. After the reaction, 60% nitric acid (1 cm^3) was added to the reaction mixture and stirred. Then the green solution was filtered using a glass filter (G-4), and the filtrate was added to acetone. The green complex thus precipitated was filtered off, washed with acetone, and dried. It was then precipitated twice more by dissolution in 60% nitric acid and by the addition of acetone. Complexes **1a—c** are soluble in water, DMSO, DMF, and acid solvents and slightly soluble in MeOH, though insoluble in common organic solvents. Yields: 0.28 g (22.4%) for **1a**, 0.15 g (12.6%) for **1b**, 0.29 g (22.5%) for **1c**. Found **1a**: C, 31.67; H, 5.42; N, 15.51; Cl, 6.61%. **1b**: C, 32.83; H, 5.23; N, 15.91; Cl, 6.79%. **1c**: C, 34.55; H, 5.95; N, 15.12; Cl, 6.69%. Calcd for **1a**: C, 31.50; H, 5.10; N, 15.74; Cl, 6.64%. **1b**: C, 32.89; H, 5.34; N, 15.34; Cl, 6.47%. **1c**: C, 34.20; H, 5.56; N, 14.96; Cl, 6.31%. Decomp 184 °C for **1a**, 183 °C for **1b** and 160 °C for **1c**. IR spectra, **1a**: 3050, 3080, and 3180 cm^{-1}; 1030(s), 1050(sh), 1055(s), and 1080(m) cm^{-1}. **1b**: 3050, 3100, and 3200 cm^{-1}; 1015(m), 1040(s), 1045(s), and 1080(m) cm^{-1}. **1c**: 3080, 3120, and 3200 cm^{-1}; 1025(sh), 1035(s), 1050(s), and 1080(s) cm^{-1}.

*β_2-5-Nitrosalicylato(3,7-diazanonane-1,9-diamine)cobalt(III) Nitrate (**3a**), β_2-5-Nitrosalicylato(4,7-diazadecane-1,10-diamine)cobalt(III) Nitrate Hydrate (**3b**), and β_2-5-Nitrosalicylato(4,8-diazaundecane-1,11-diamine)cobalt(III) Nitrate Hydrate (**3c**)*: The **1a**, **1b**, or **1c** complex was precipitated by the addition of acetone to a 60% nitric acid solution of the **2a**, **2b**, or **2c** (above section). From the orange acetone solution of the filtrate, complexes **3a**, **3b**, or **3c** crystallized directly on standing. Then, the orange complex thus separated was filtered off, washed with water and dried. Complexes **3a—c** isolated were recrystallized from water, twice and dried. Complexes **3a**, **3b** are soluble in DMSO and somewhat soluble in water, though complex **3c** is soluble in water, DMSO, DMF, and MeOH. Yields: 0.36 g (33.3%) for **3a**, 0.43 g (39.9%) for **3b**, 0.30 g (25.8%) for **3c**. Found **3a**: C, 36.27; H, 4.72; N, 18.65%. **3b**: C, 36.57; H, 5.54; N, 17.40%. **3c**: C, 38.16; H, 5.39; N, 17.05%. Calcd for **3a**: C, 36.37; H, 5.01; N, 18.18%. **3b**: C, 36.45; H, 5.50; N, 17.00%. **3c**: C, 37.80; H, 5.75; N, 16.53%. Decomp 233 °C for **3a**, 195 °C for **3b**, 208 °C for **3c**. IR spectra, **3a**: 3080, 3160, and 3220 cm^{-1}; 1005(sh), 1012(m), 1025(s), 1040(s), 1060(vs), and 1070(vs) cm^{-1}. **3b**: 3120, 3190, and 3230 cm^{-1}; 1015(m), 1040(sh), 1050(vs), 1070(vs), and 1080(sh) cm^{-1}. **3c**: 3080, 3120, and 3200 cm^{-1}; 1025(sh), 1035(s), 1050(s), 1070(sh), and 1080(s) cm^{-1}.

References

1) Part IV: Y. Yamamoto, E. Toyota, and Y. Yamamoto, *Bull. Chem. Soc. Jpn.*, **56**, 2721 (1983).

2) T. Ito, M. Sugimoto, H. Ito, K. Toriumi, H. Nakayama, W. Mori, and M. Sekizaki, *Chem. Lett.*, **1983**, 121.

3) Y. Yamamoto, H. Kudo, and E. Toyota, *Bull. Chem. Soc. Jpn.*, **56**, 1051 (1983).

4) Y. Yamamoto, *Bull. Chem. Soc. Jpn.*, **51**, 2894 (1978).

5) Y. Yamamoto, *Bull. Chem. Soc. Jpn.*, **42**, 999 (1969).

6) Y. Yamamoto, M. Mori, and H. Kudo, *Bull. Chem. Soc. Jpn.*, **54**, 1995 (1981).

7) Y. Yamamoto, E. Toyota, and N. Mitsudera, *Bull. Chem. Soc. Jpn.*, **53**, 3517 (1980).

Determination of a Small Amount of a Biological Constituent by the Use of Chemiluminescence. II. Determination of Albumin as a Model Protein by Means of the Flow-injection Analysis Using a Cobalt(III) Complex Compound as a Catalyst

Tadashi HARA,* Motohiro TORIYAMA, and Kazuhiko TSUKAGOSHI
Department of Chemical Engineering, Faculty of Engineering, Doshisha University, Karasuma Imadegawa, Kamigyo-ku, Kyoto 602
(Received April 15, 1983)

Synopsis. A new procedure for the determination of 8×10^{-9}—3×10^{-7} mol dm^{-3} bovine serum albumin as a model protein has been established on the basis of the fact that the catalytic activity of *cis*-tetraamminediaquacobalt(III) sulfate for the chemiluminescent reaction between luminol and hydrogen peroxide decreases in the presence of bovine serum albumin.

In the previous paper,[1] several proteins were determined by use of the fact that the catalytic activity of copper(II) for the chemiluminescent reaction between 5-amino-2,3-dihydro-1,4-phthalazinedione (luminol) and hydrogen peroxide (H_2O_2) decreased in the presence of those proteins. In the present work, *cis*-tetraamminediaquacobalt(III) sulfate which is known to give a longer luminescence time and more stable luminescence intensity than those in copper(II)[2,3] was used in place of copper(II) in the previous method. It was experimentally observed that the catalytic activity of the cobalt(III) complex compound for the chemiluminescent reaction between luminol and H_2O_2 decreased in the presence of bovine serum albumin (BSA), human serum albumin, bovine serum α-globulin, and bovine serum γ-globulin. BSA was chosen as a model protein. Though the present method is similar to the previous method in its detection limit and concentration range suitable for the determination, the standard curve of BSA in the present method is linear, and different from the non-linear one in the previous method. This means that the present method is superior to the previous method.

Experimental

All reagents were of commercially available special grade. Ion exchange water was distilled for use. A luminol solution, a H_2O_2 solution, and a buffer solution were prepared as in the previous paper. A 1.0×10^{-3} mol dm^{-3} cobalt(III) catalyst solution was prepared as a stock solution by dissolving *cis*-tetraamminediaquacobalt(III) sulfate[4] in water and it was diluted to 1.0×10^{-5} mol dm^{-3} with water, followed by the dilution with a buffer solution for use. BSA (Sigma Chemical Co., mol wt 66000) was used as a model protein.

The experiment was carried out as in the previous paper using the same apparatus. A sample solution containing BSA was dissolved and diluted with a buffer solution, and to it a cobalt(III) catalyst solution was added to give a definite concentration of cobalt(III) solution. After the solution was held at 30 °C for 50 min, an aliquot of the solution was subjected to the flow-injection analysis and the chemiluminescence (CL) intensity in the luminol-H_2O_2-cobalt(III) catalyst system was measured.

Results and Discussion

A calibration curve was obtained for the solution which contained only cobalt(III) catalyst (Fig. 1), and it is quite different from the non-linear calibration curve obtained for the copper(II) catalyst solution.

The relationship between reaction time and the CL intensity at 3.0×10^{-8}, 7.6×10^{-8}, and 3.0×10^{-7} mol dm^{-3} BSA was obtained (Fig. 2). Figure 2 shows that the reaction between cobalt(III) catalyst and BSA goes to completion in 50 min at 30 °C.

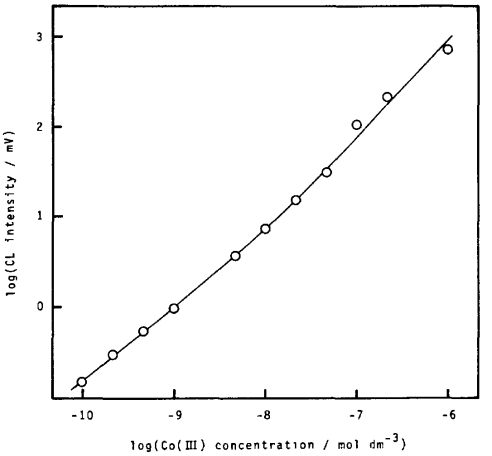

Fig. 1. Relationship between cobalt(III)[a] concentration and CL intensity. Conditions: 1.0×10^{-3} mol dm^{-3} luminol and 2.5×10^{-3} mol dm^{-3} H_2O_2. a) $[Co(NH_3)_4(H_2O)_2]_2(SO_4)_3$

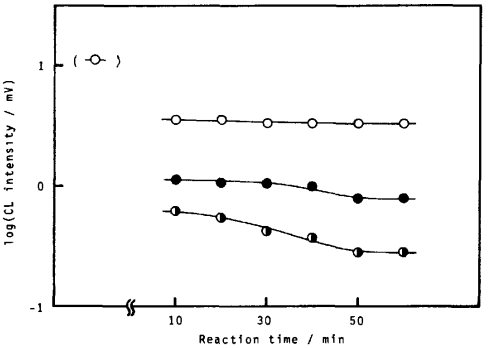

Fig. 2. Relationship between reaction time and CL intensity.
○: 3.0×10^{-8} mol dm^{-3}-, ●: 7.6×10^{-8} mol dm^{-3}-, ◑: 3.0×10^{-7} mol dm^{-3}-BSA, and (○): BSA free.
Conditions: 1.5×10^{-8} mol dm^{-3} Co(III), 1.0×10^{-3} mol dm^{-3} luminol, and 2.5×10^{-3} mol dm^{-3} H_2O_2.

Table 1. The concentration of species at equilibrium

Initial Co(III) concn/mol dm^{-3}	CL intensity / mV	[Co] / mol dm^{-3} a)	[Co·BSA] / mol dm^{-3}
1.00×10^{-8}	7.0	2.1×10^{-9}	7.9×10^{-9}
1.25×10^{-8}	9.8	2.8×10^{-9}	9.7×10^{-9}
1.50×10^{-8}	14	3.7×10^{-9}	1.13×10^{-8}
1.75×10^{-8}	15	4.4×10^{-9}	1.31×10^{-8}

Initial BSA concn = 3.0×10^{-8} mol dm^{-3}. a) Estimated from Fig. 1.

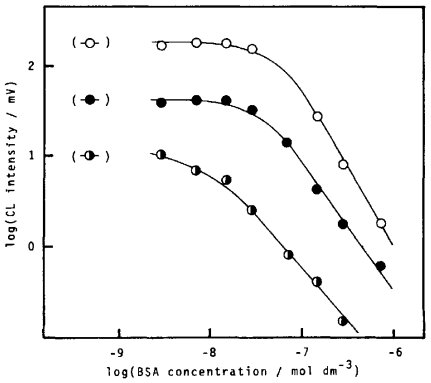

Fig. 3. Standard curves. ◑: 1.5×10^{-8} mol dm^{-3}-, ●: 5.0×10^{-8} mol dm^{-3}-, ○: 2.0×10^{-7} mol dm^{-3}-Co(III), and (○), (◑), (●): BSA free. Conditions: 1.0×10^{-3} mol dm^{-3} luminol and 2.5×10^{-3} mol dm^{-3} H_2O_2.

Standard curves were obtained by the reaction of BSA with 1.5×10^{-8}, 5.0×10^{-8}, and 2.0×10^{-7} mol dm^{-3} cobalt(III) catalyst solutions (Fig. 3). Lowering of the chemiluminescent activity of cobalt(III) catalyst solution in the presence of BSA seems to be due to the formation of cobalt(III)-polypeptide linkage similarly as in the copper(II) catalyst solution. As can be seen from Fig. 3, BSA in the concentration range of 8×10^{-9}—3×10^{-7} mol dm^{-3} could be determined, with a detection limit of 0.2 μg, by use of 1.5×10^{-8} mol dm^{-3} cobalt(III) catalyst solution. The present method is superior to the previous method since the standard curve in the present method is almost linear.

Lowry *et al.*[5] estimated an apparent dissociation constant between copper(II) and protein as 3×10^{-6} mol dm^{-3} on the assumption that they associated at the mole ratio 1:1 in the copper(II) concentration range of 8×10^{-6}—4×10^{-5} mol dm^{-3}. The authors also estimated an apparent association constant between cobalt(III) and BSA similarly as in the case of Lowry *et al.* The slope of the standard curve at 1.5×10^{-8} mol dm^{-3} cobalt(III) catalyst solution in Fig. 3 is approximately −1 and then the association between cobalt(III) and BSA is given by Eq. 1 as an equimolar reaction.

$$[\mathrm{Co}] + [\mathrm{BSA}] \rightleftharpoons [\mathrm{Co\cdot BSA}], \quad (1)$$

where [Co], [BSA], and [Co·BSA] are the concentrations of free cobalt(III), free BSA, and associated complex, respectively. An apparent association constant, K is defined by Eq. 2.

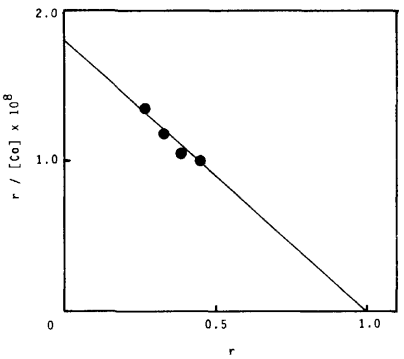

Fig. 4. Relationship between r and r/[Co]. Conditions: 1.0×10^{-3} mol dm^{-3} luminol and 2.5×10^{-3} mol dm^{-3} H_2O_2.

$$\frac{[\mathrm{Co\cdot BSA}]}{[\mathrm{Co}][\mathrm{BSA}]} = K. \quad (2)$$

From Eq. 2, Eq. 3 is derived.

$$r/[\mathrm{Co}] = K - rK, \quad (3)$$

where r means the mole ratio of bound cobalt(III) to total BSA. Figure 4 shows the plot of r/[Co] to r which was obtained by use of the data in Table 1. The straight line obtained by plotting r/[Co] against r on section paper passed through the point at r=1 in Fig. 4. This means that the derivation of Eqs. 1, 2, and 3 was reasonable. The value of K, 1.8×10^8 mol^{-1} dm^3 at 1.5×10^{-8} mol dm^{-3} cobalt(III) catalyst solution was found from the slope of the straight line in Fig. 4. The value of K thus obtained may be reasonable by considering the principle of the present method in which the concentration of a liberated cobalt(III) in the reaction between cobalt(III) and BSA is measured.

According to the present flow-injection analysis method, 8×10^{-9}—3×10^{-7} mol dm^{-3} BSA as a model protein can be determined at the rate of about 30 samples per hour after the reaction between cobalt(III) and BSA, with the detection limit of 0.2 μg BSA and with the standard curve which is almost linear in the range of 1×10^{-8}—3×10^{-7} mol dm^{-3} BSA.

The authors wish to thank Messrs. Masakatsu Imaki and Hirohumi Hashimoto for their help with the experiments.

References

1) T. Hara, M. Toriyama, and K. Tsukagoshi, *Bull. Chem. Soc. Jpn.*, **56**, 1382 (1983).
2) H. Ojima and R. Iwaki, *Nippon Kagaku Zasshi*, **78**, 1632 (1957).
3) S. Aida, Y. Yamashita, Y. Nishikawa, and T. Shigematsu, *Jpn. Anal.*, **22**, 1180 (1973).
4) S. M. Jorgensen, *Z. Anorg. Chem.*, **2**, 297 (1892).
5) O. H. Lowry, N. J. Rosebrough, A. L. Farr, and R. J. Randall, *J. Biol. Chem.*, **193**, 265 (1951).

The Magnetic Properties of $Cu(CH_3COO)_2 \cdot 2NH_4Cl$ and $NH_4Cu(HCOO)Cl_2$

Shuji EMORI* and Yoneichiro MUTO
Department of Chemistry, Faculty of Science and Engineering, Saga University, Honjo-machi, Saga 840
(Received May 19, 1983)

Synopsis. The temperature dependence of the magnetic susceptibility of $Cu(CH_3COO)_2 \cdot 2NH_4Cl$ obeys the Bleaney-Bowers equation, indicating the existence of the anionic copper(II) acetate dinuclear unit. The exchange integral, J/k, is equal to -205 K. For $NH_4Cu(HCOO)Cl_2$, the structure containing copper(II) formate layers connected by tetrachlorocuprate(II) bridges is presumed on the basis of the value of the Weiss constant.

It has been suggested that, in dinuclear copper(II) carboxylate adducts, the axial ligand (apical ligand of the square pyramidal coordination polyhedron) plays a role in determining the extent of spin-exchange interaction or the singlet-triplet separation ($-2J$).[1] Goodgame *et al.* have reported the magnetic properties of several dinuclear anionic copper(II) acetate complexes, $(R_4N)_2[Cu(CH_3COO)_2X]_2$ (X=NCS, NO_2, or Br).[2,3] However, insufficient data have been available to draw any precise conclusions regarding the role of the axial ligand in anionic copper(II) acetate complexes. In this work, we prepared three copper(II) acetate complexes, $Cu(CH_3COO)_2 \cdot 2KCl$, $Cu(CH_3COO)_2 \cdot 2NH_4Cl$, and $Cu(CH_3COO)_2 \cdot 3/2C_4H_9NH_3Cl$, and two copper(II) formate complexes, $KCu(HCOO)Cl_2$ and $NH_4Cu(HCOO)Cl_2$, and measured their magnetic susceptibilities in order to study the effect of the chloride ions upon the magnetic properties.

The compound with the stoichiometry of $Cu(CH_3COO)_2 \cdot nACl$, where $n=2$ for A=NH_4 or K and $n=3/2$ for A=*n*-$C_4H_9NH_3$, was precipitated in large green crystals when an excess of ACl was added to a hot aqueous solution of copper(II) acetate monohydrate with a few drops of acetic acid and the mixture was allowed to stand overnight at *ca.* 5 °C in a refrigerator. The magnetic moments of these compounds were evaluated from their susceptibilities observed at room temperature and the relevant Pascal constants.[4] They are low and practically the same as that of copper(II) acetate monohydrate (Table 1).

The temperature dependence of the magnetic susceptibility of the $Cu(CH_3COO)_2 \cdot 2NH_4Cl$ complex over the range of 77—300 K (Fig. 1) was also found to correspond well with the known behavior of copper(II) acetate monohydrate. A reasonably good agreement was found between the experimental results and the theoretical curve calculated from the usual expression[5] for the susceptibility of the copper(II) ions in the copper(II) acetate dimer (Bleaney-Bowers equation), using the following parameters: $g=2.14$, $J/k=-205$ K, and $N\alpha=60\times10^{-6}$ emu/mol (1 emu/mol$=4\pi\times10^{-6}$ m^3/mol). The variation in the value of $-2J$ on the replacement of H_2O by Cl is too small to confirm the suggestion that the exent of spin-exchange interaction increases as the axial ligand becomes stronger as an electron donor.[6] However, the obtained result is consistent with the assumption that the anionic copper(II) acetate is constructed by replacing the water molecules in $[Cu(CH_3COO)_2 \cdot H_2O]_2$ with chloride ions.

We attempted to prepare the analogous formate complexes by the method described above. However, the compounds with the stoichiometry of $ACu(HCOO)Cl_2$, where A=NH_4 or K, were obtained as fine yellowish

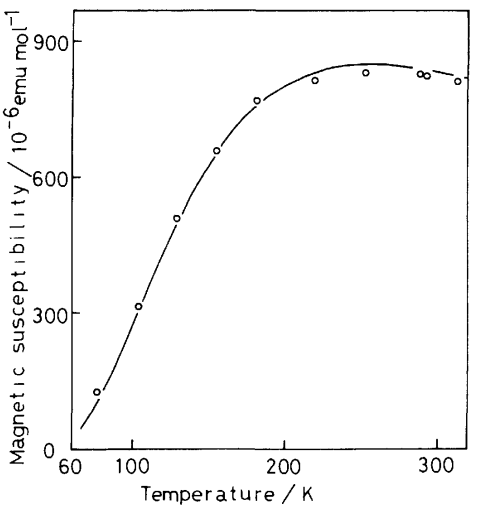

Fig. 1. Observed and calculated magnetic susceptibilities of $Cu(CH_3COO)_2 \cdot 2NH_4Cl$: experimental points and solid curve calculated by the Bleaney-Bowers equation.

TABLE 1. ANALYTICAL DATA AND EFFECTIVE MAGNETIC MOMENTS AT 17 °C

Compound	Cu (%)		Cl (%)		μ_{eff}/BM
	Calcd	Found	Calcd	Found	
$Cu(CH_3COO)_2 \cdot 2KCl$	19.21	19.16	21.44	21.29	1.38
$Cu(CH_3COO)_2 \cdot 2NH_4Cl$	22.02	22.05	24.57	24.76	1.39
$Cu(CH_3COO)_2 \cdot 3/2C_4H_9NH_3Cl$	18.34	18.45	15.35	15.17	1.41
$KCu(HCOO)Cl_2$	29.07	29.12	32.44	32.27	1.78
$NH_4Cu(HCOO)Cl_2$	32.46	32.17	35.90	35.81	1.77

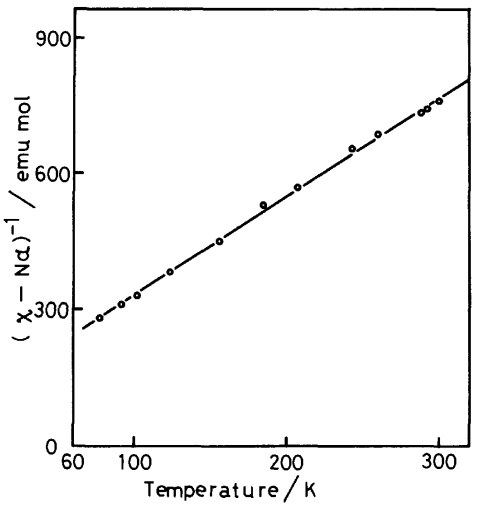

Fig. 2. A plot of inverse susceptibility data *vs.* temperature for the complex $NH_4Cu(HCOO)Cl_2$. The solid line shows the Curie-Weiss behavior.

green crystals. The room-temperature magnetic moments determined for these formates are slightly lower than those found for paramagnetic copper(II) compounds, indicating the existence of antiferromagnetic interactions among the copper(II) ions. Their values, however, are obviously different from those of dimeric copper(II) formate adducts with pyridine,[7,8] urea,[9] or thiocyanate ions.[2] The composition suggests that these compounds are 1 : 1 complexes between copper(II) formate and tetrachlorocuprates(II), $Cu(HCOO)_2 \cdot A_2CuCl_4$. This formulation is supported by the fact that these crystals can be obtained more efficiently by concentrating an aqueous solution of $Cu(HCOO)_2 \cdot 2H_2O$ and $A_2CuCl_4 \cdot 2H_2O$ on a water bath.

The temperature dependence of the magnetic susceptibility of the $NH_4Cu(HCOO)Cl_2$ complex over the range of 77—300 K (Fig. 2) obeys the Curie-Weiss law when the following parameters are used: g=2.21 and Θ=−52.8 K. The value of the weiss constant for this compound is almost half of the value for $Cu(HCOO)_2 \cdot 4H_2O$,[10] the X-ray crystal analysis of which has indicated that the metal ions are bridged in anti-anti-bonding arrangements of Cu-O-C-O-Cu links to form a two-dimensional lattice.[11] It is known that half of the water molecules interposed between the copper(II) formate layers can be replaced by urea[12] or pyridine,[8] and that the resultant compound has essentially the same configuration as does tetrahydrate. These facts suggest that the present formates are also formed by interposing A_2CuCl_4 between the copper(II) formate layers, because the paramagnetic ions between layers seem to diminish the value of the Weiss constant. Martin and Waterman[10] have suggested that the adduct ligands which most effectively reduce the residual charge on the copper(II) ion may favour a syn-syn-bonding arrangement of the Cu-O-C-O-Cu links, but the importance of the packing effects was also pointed out.[13] The above-mentioned structure can be explained by this packing effect.

References

1) M. Melnik, *Coord. Chem. Rev.*, **42**, 259 (1982).
2) D. M. L. Goodgame, N. J. Hill, D. F. Marsham, A. C. Skapski, M. L. Smart, and P. G. H. Thoughton, *Chem. Commun.*, **1969**, 629.
3) D. M. L. Goodgeme and D. F. Marsham, *J. Chem. Soc., A*, **1966**, 1167.
4) G. Foex, "Constants Sélectionées, Diamagnétisme et Paramagnétisme," Masson, Paris (1957).
5) J. Lewis, Y. C. Lin, L. K. Royston, and R. C. Thompson, *J. Chem. Soc.*, **1965**, 6464.
6) R. W. Jotham, S. F. A. Kettle, and J. A. Marks, *J. Chem. Soc., Dalton Trans.*, **1972**, 428.
7) R. L. Martin and H. Waterman, *J. Chem. Soc.*, **1959**, 2960.
8) M. A. Bernard, M. M. Borel, F. Busnot, and A. Leclaire, *Rev. Chem. Miner.*, **16**, 124 (1979).
9) D. B. Yawney and R. J. Doedens, *Inorg. Chem.*, **9**, 1626 (1970).
10) R. L. Martin and H. Waterman, *J. Chem. Soc.*, **1959**, 1359.
11) R. Kiriyama, H. Ibamoto, and K. Matsuo, *Acta Crystallogr.*, **7**, 482 (1954).
12) H. Kiriyama and K. Kitahara, *Acta Crystallogr., Sect. B*, **32**, 330 (1976).
13) E. Sletten and L. H. Jensen, *Acta Crystallogr., Sect. B*, **29**, 1752 (1973).

Vacuum Sublimation Behavior of Metal Complexes of Thio-β-diketones. Purification of Manganese(II), Iron(III), Cobalt(III), Nickel(II), Copper(II), Zinc(II), Palladium(II), Silver(I), and Cadmium(II) with 1,1,1-Trifluoro-4-(2-thienyl)-4-mercapto-3-buten-2-one

Takaharu HONJO* and Shigeki SHIMA
Department of Chemistry, Faculty of Science, Kanazawa Universty, Marunouchi, Kanazawa 920
(Received June 13, 1983)

Synopsis. A vacuum sublimation apparatus with a continuous temperature gradient (25—260 °C) along the tube (0—50 cm) at 2×10^{-2} Torr (1 Torr≈133.322 Pa) was used. STTA (1,1,1-trifluoro-4-(2-thienyl)-4-mercapto-3-buten-2-one) and its metal chelates of Mn^{II}, Fe^{III}, Co^{III}, Ni^{II}, Cu^{II}, Zn^{II}, and Pd^{II} sublimed quantitatively without thermal decomposition, while the chelates of Ag^{I} and Cd^{II} were accompanied by thermal decomposition.

The vacuum sublimation method is useful for the purification and separation of metal chelates.[1,2] Of the 14 chelating reagents other than β-thioxo ketones, diethyldithiocarbamates and oxine were found to offer the greatest promise for this purpose.[1] The present research aims to find suitable β-thioxo ketones for the purification of metals as their chelates by vacuum sublimator with continuous temperature gradient under low pressure. Some aspects of vacuum sublimation behavior of the chelate compounds will also be discussed.

Experimental

Materials. Various monothio analogs of β-diketones were synthesized by the reaction of hydrogen sulfide with β-diketones in an anhydrous ethanol in the presence of hydrogen chloride for 30—60 min, as described previously.[3,6] Nickel(II) chelate compounds with disulfur analogs of β-diketones were also prepared by the modification of the reaction of a corresponding β-diketone dissolved in an anhydrous ethanol with hydrogen sulfide in the presence of nickel(II) chloride and hydrogen chloride as a catalyst for 1—5 h.[7] Nickel(II) dithioacetylacetone was also prepared by the two electron reduction of 3,5-dimethyl-1,2-dithiolium cation with sodium tetrahydroborate in the presence of nickel(II) ion.[8] The chelating reagents and their nickel(II) chelates tested were as follows: SAA (4-mercapto-3-penten-2-one), SSAA (4-mercapto-3-penten-2-thione), SDBM (3-mercapto-1,3-diphenyl-2-propen-1-one), SBFA (1,1,1-trifluoro-4-mercapto-4-phenyl-3-buten-2-one), SSBFA (1,1,1-trifluoro-4-mercapto-4-phenyl-3-butene-2-thione), STTA (1,1,1-trifluoro-4-(2-thienyl)-4-mercapto-3-buten-2-one), SSTTA (1,1,1-trifluoro-4-(2-thienyl)-4-mercapto-3-butene-2-thione), and their parent β-diketones of AA (2,4-pentanedione), BA (1-phenyl-1,3-butanedione), DBM (1,3-diphenyl-1,3-propanedione), BFA (benzoyltrifluoroacetone), TTA (2-thenoyltrifluoroacetone). All other metal chelates were prepared by solvent extraction mentioned previously.[2] These materials were purified by recrystallization from carbon tetrachloride or by sublimation *in vacuo* before usage. The content of sulfur in the products was ascertained by using the Sn^{II}-strong phosphoric acid method;[9] the results were in good agreement with the theoretical values.

Sublimation Procedure. A vacuum sublimation apparatus providing a continuous temperature gradient (25—260 °C) along the tube (0—50 cm) at 2×10^{-2} Torr was used, as previously described.[1] The patterns of the rise in temperature along the sublimation tube are shown in Fig. 1. These patterns were obtained by supplying the following electric power through the mantle heaters; 50, 20, 10, and 4.2 V at 1.38 A. Metal chelates were placed inside the apparatus for 2 h after establishment of the thermal equilibrium. The temperature gradient along the sublimator is shown in Fig. 2; this was obtained after the thermal equilibrium. The temperature gradient in the region of 25 (room temperature) to 260 °C is about 4 °C/cm with the deviation of ±4 °C. The sublimate zone along the sublimation tube was decided from the color of the chelate and its position of deposition.

Results and Discussion

Effect of ligands on the sublimation-recrystallization temperatures for various nickel(II) chelates of β-thioxo ketones and their parent β-diketones are shown in Fig. 3. The temperature range of the deposited zones, the recovery, and the colors of the various nickel(II) chelates after sublimation are summarized in Table 1. The

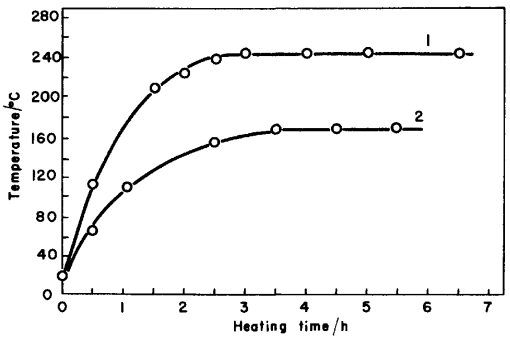

Fig. 1. Rate of rise in temperature along vacuum sublimator. Distance of the places from the high temperature end of the sublimator: (1) 15 cm, (2) 30 cm.

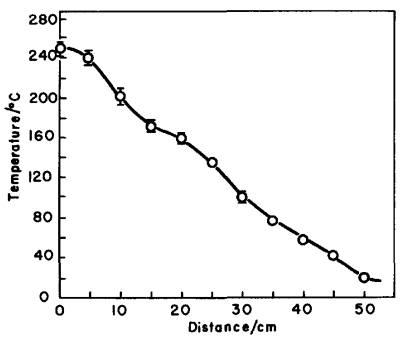

Fig. 2. Continuous temperature gradient along vacuum sublimator.

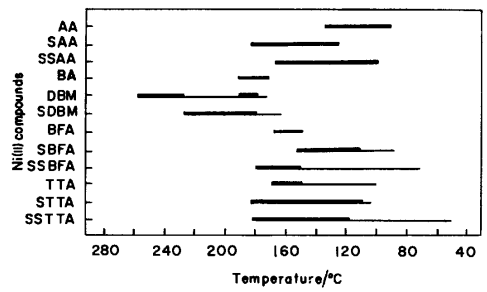

Fig. 3. Effect of ligands on the sublimation-recrystallization temperatures for nickel(II) chelates with various β-thioxo ketones and their parent β-diketones.

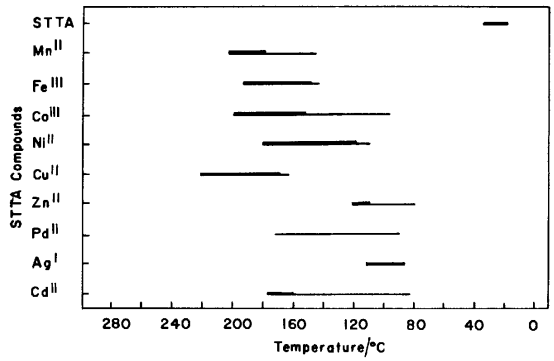

Fig. 4. Sublimation-recrystallization temperature for various metal STTA chelates.

sublimation-recrystallization temperature of nickel(II) chelates generally increased in the following order: AA<BFA, TTA<BA<DBM; SSAA, SBFA, SSBFA, STTA, SSTTA, SAA<SDBM. All of the chelates sublimed within 30 min to 2 h, and deposited inside the wall of the glass tube in the temperature range of 50 to 260 °C. The preliminary examination on the sublimation behavior of nickel(II) chelates of various β-thioxo ketones revealed that the STTA chelates were more volatile and stable on heating, so that a series of metal chelates of STTA was examined in detail. The results are schematically shown in Fig. 4, in which a thicker line indicates the deposited zone of uniformity with a large amount of metal chelate. The data are listed in Table 2. The STTA and its metal chelates of Mn^{II}, Fe^{III}, Co^{III}, Ni^{II}, Cu^{II}, Pd^{II}, and Zn^{II} sublimed quantitatively without thermal decomposition, while the chelates of Ag^{I} and Cd^{II} were accompanied by thermal decomposition. Berg and Reed reported that the STTA chelates of Cd^{II}, Co^{II}, Cu^{II}, Ni^{II}, Pb^{II}, Pd^{II}, and Zn^{II} partially sublimed with remarkable thermal decomposition at 1.3 Torr in a stream of air.[11] The thermal decomposition may be due to an air oxidation of STTA chelates under higher pressure. In the present investigation, it was found that the STTA chelates (1.6—53.5 mg) sublimed quantitatively without thermal decomposition at 2×10^{-2} Torr. The sublimation-recrystallization temperature of individual chelates increased in the following order: $Ag^{I}<Zn^{II}<Pd^{II}<Cd^{II}<Ni^{II}<Fe^{III}<Co^{III}<Mn^{II}<Cu^{II}$. In general, when a large amount of metal chelate (20—200 mg) sublimed, the deposited zone appeared at a temperature higher by about 50 °C than the ordinary position. Therefore the sublimation is useful for purification of each metal chelate, since highly pure crystals, especially large-sized pure crystals, can be obtained.

Table 1. Sublimation-recrystallization zone temperatures, amounts remaining, and colors of various nickel(II) chelates after sublimation at 2×10^{-2} Torr

Nickel chelates	Recrystallization zone temperature/°C	Color	Chelate taken (mg)	Metal chelate remaining[a]
AA	134— 91	yellow green	14.1	none
SAA	124—183	light gray	3.2	much
SSAA	168— 98	dark gray	12.2	much
BA	191—172	yellow green	5.6	none
DBM	258—171	yellow green	11.1	none
SDBM	228—164	dark brown	3.9	none
BFA	168—148	yellow green	6.4	none
SBFA	153— 88	brown	2.5	a little
SSBFA	178— 70	brown	4.8	much
TTA	170—100	yellow green	26.9	none
STTA	181—108	deep red	18.5	none
SSTTA	181— 50	brown	4.5	a little

a) None, 0—10%; a little, 10—30%; much, >30%.

Table 2. Sublimation-recrystallization zone temperatures, amounts remaining, and colors of various metal STTA chelates after sublimation at 2×10^{-2} Torr

STTA chelates	Recrystallization zone temperature/°C	Color	Chelate taken (mg)	Metal compound remaining[a]
STTA	< 45	red	11.3	none
Mn^{II}	204—145	brown	1.8	a little
Fe^{III}	194—144	deep orange	18.7	none
Co^{III} [b]	200— 96	dark orange	53.5	none
Ni^{II}	181—108	deep red	18.5	none
Cu^{II}	221—163	olive brown	1.6	none
Zn^{II}	121— 79	yellow orange	6.5	none
Pd^{II}	173— 90	deep orange	1.7	a little
Ag^{I}	112— 86	orange	4.5	much
Cd^{II}	178— 82	orange	4.4	much

a) None, 0—10%; a little, 10—30%; much, >30%. b) Ascertain the tervalent cobalt by spectrophotometry and solvent extraction method.[8,13,14]

The authors wish to thank Professor Emeritus Toshiyasu Kiba of Kanazawa University for his helpful advice.

References

1) T. Honjo, H. Imura, S. Shima, and T. Kiba, *Anal. Chem.*, **50**, 1545 (1978).
2) T. Honjo and S. Shima, *DOJIN News*, **1980**, 1.
3) T. Honjo and T. Kiba, *Bull. Chem. Soc. Jpn.*, **45**, 185 (1972).
4) T. Honjo and T. Kiba, *Bull. Chem. Soc. Jpn.*, **46**, 3768 (1973).
5) T. Honjo, H. Honnami, and T. Kiba, *Bull. Chem. Soc. Jpn.*, **51**, 1559 (1978).
6) T. Honjo and H. Freiser, *Anal. Chem.*, **53**, 1258 (1981).
7) R. L. Martin and I. M. Stewart, *Nature*, **210**, 522 (1966).
8) T. Honjo and T. Otaki, *Fresenius' Z. Anal. Chem.*, **300**, 413 (1980).
9) T. Honjo, Y. Fujioka, H. Itoh, and T. Kiba, *Anal. Chem.*, **49**, 2241 (1977).
10) E. W. Berg and K. P. Reed, *Anal. Chim. Acta*, **42**, 207 (1968).
11) E. W. Berg and K. P. Reed, *Anal. Chim. Acta*, **36**, 372 (1966).
12) L. Westgaad, *J. Inorg. Nucl. Chem.*, **31**, 3747 (1969).
13) T. Honjo, S. Yashima, and T. Kiba, *Bull. Chem. Soc. Jpn.*, **46**, 3772 (1973).
14) T. Honjo, R. Honda, and T. Kiba, *Anal. Chem.*, **49**, 2246 (1977).

The X-Ray Fluorescence Spectroscopy of Inorganic Solids. VI. The P $K\alpha$ Energy of Phosphate Glasses and Crystals

Takashi MAEKAWA,* Masakazu FURUKAWA, and Toshio YOKOKAWA
Department of Chemistry, Faculty of Science, Hokkaido University, Sapporo 060
(Received June 29, 1983)

Synopsis. The P $K\alpha$ emission spectra of several phosphorus compounds and phosphate glasses were examined. The P $K\alpha$ energies decrease with an increase in the basicities of the matrices. The results also suggest that in order to interprete the chemical shift one must take into account the effects due to changes in the short range structure around the phosphorus atom in the PO_4 tetrahedron.

The present note reports an extension of our earlier studies concerning the X-ray fluorescence spectroscopy of inorganic glasses. Phosphorus is one of the most important constituents of oxide glasses and slags. However, in contrast with silicates, there have been few spectroscopic studies of the chemical state of phosphorus in phosphates. As to the X-ray spectroscopy, Fichter reported the $K\alpha$ energies of phosphorus in various compound.[1] Although he found a relation between the effective charges on phosphorus and the P $K\alpha$ energies, no chemical shifts of the P $K\alpha$ energy among phosphates were observed. In this work, the P $K\alpha$ energy shifts are obtained for several phosphate glasses and crystals. The results are discussed in connection with the effective positive charges on phosphorus and the basicity of the glasses.

Experimental

Apparatus. The P $K\alpha$ from crystals and glasses were measured by means of a high resolution 2-crystal spectrometer (Toshiba AFV 701). The analyzing crystals were ADP. A Cr X-ray tube was used for the primary excitation. Pulses from a gas-flow proportional counter were stored in a multichannel analyzer. The other details including the procedure for determining the chemical shifts were described in previous papers.[2-4]

Samples. The glassy samples were prepared by melting desired quantities of commercial $NaH_2PO_4 \cdot 2H_2O$, P_2O_5, H_3BO_3, and Na_2CO_3 in a platinum crucible and then pouring them onto a stainless steel plate. The sodium ion concentration in glasses with a high P_2O_5 content was determined by the ion-selective electrode method. SiP_2O_7 and BPO_4 were synthesized by direct reactions of phosphoric acid with silica or boric acid. The other anhydrous phosphates were obtained by the dehydration of commercial reagents in an electric furnace. All the crystalline samples were examined by means of an X-ray diffraction method.

Results and Discussion

In Table 1 are compiled the results of the P $K\alpha$ energy shifts of phosphates (crystals and glasses) referred to that of $NaPO_3$ glass. In contrast to the results of the previous author,[1] it could be detected that the P $K\alpha$ energy depends on the kind and the content of the metal ion, even among phosphates. This behavior may become clearer when looking at the relation between the energy shifts of the glassy samples and their composition. In Fig. 1 the composition dependence of the P $K\alpha$ energy of Na_2O–P_2O_5 and Na_2O–P_2O_5–B_2O_3 glasses is shown. In the binary glasses, the P $K\alpha$ energy decreases with an increase in the Na_2O contents, which is consistent with the previous results for Si $K\alpha$.[3] The addition of B_2O_3 to $NaPO_3$ glass results in smaller shifts than in binary glasses.

It has been shown that the $K\alpha$ energies of the third period elements increase with an increase in the partial positive charges on the corresponding elements.[5] Therefore, the P $K\alpha$ energy reflects the degree of polarity of the phosphorus–oxygen bond in the PO_4 tetrahedron. Around an one-to-one mole ratio of Na_2O to P_2O_5, *i.e.*, $NaPO_3$, phosphate changes its form with an increase in the Na_2O contant as follows:

$$PO_{2.5} \longrightarrow PO_3^- \longrightarrow PO_{3.5}^{1-} .$$

Because of the rather strong acidic character of P_2O_5,

TABLE 1. PHOSPHORUS $K\alpha$ CHEMICAL SHIFTS OF PHOSPHATES
$\Delta E = E(\text{Sample}) - E(NaPO_3)$

Sample			ΔE/eV	
Crystals				
1	SiP_2O_7		0.079±0.007[a]	[10][b]
2	$AlPO_4$		0.079±0.005	[10]
3	$Mg_2P_2O_7$		0.054±0.007	[10]
4	BPO_4		0.048±0.007	[10]
5	$FePO_4$		0.040±0.007	[10]
6	$Zn_3(PO_4)_2$		0.016±0.004	[7]
7	$Mg_3(PO_4)_2$		0.010±0.005	[9]
8	Li_3PO_4		0.007±0.005	[10]
9	KH_2PO_4		−0.007±0.009	[11]
10	$Ca_3(PO_4)_2$		−0.008±0.009	[10]
11	Na_3PO_4		−0.009±0.005	[9]
12	K_3PO_4		−0.010±0.004	[13]
13	K_2HPO_4		−0.022±0.004	[7]
14	$Na_4P_2O_7$		−0.027±0.005	[7]
Glasses				
Na_2O(mol%)	P_2O_5	B_2O_3		
20.0	80.0	—	0.027±0.004	[7]
40.0	60.0	—	0.016±0.007	[10]
50.0	50.0	—	0.0 (reference)	
55.0	45.0	—	−0.005±0.004	[9]
60.0	40.0	—	−0.002±0.004	[9]
8.3	8.3	83.3	0.034±0.006	[11]
20.0	20.0	60.0	0.022±0.005	[8]
25.0	25.0	50.0	0.011±0.004	[12]
33.3	33.3	33.3	0.009±0.004	[10]
45.5	45.5	9.1	0.004±0.006	[10]

a) Error limit; t-distribution 95% certainty. b) Number of measurements.

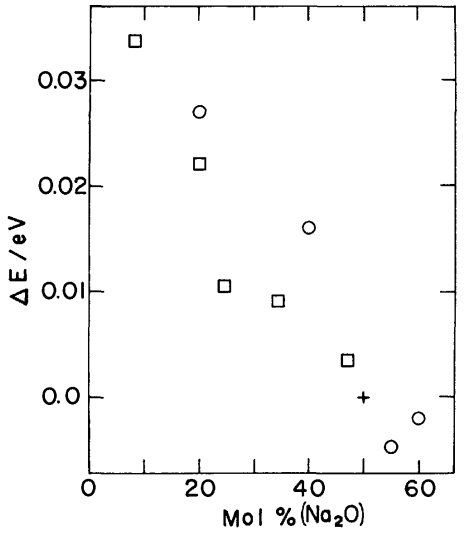

Fig. 1. Composition dependence of P $K\alpha$ energy shifts of Na_2O–P_2O_5 (○) and Na_2O–P_2O_5–B_2O_3 (□) glasses. The reference material is $NaPO_3$ (+).

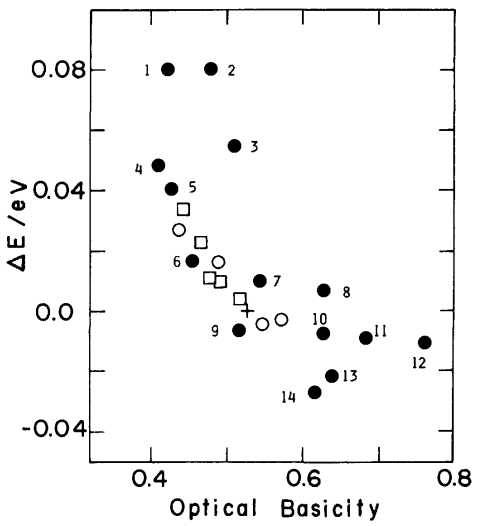

Fig. 2. The relation between P $K\alpha$ energy shifts and theoretical optical basicities of Na_2O–P_2O_5 (○), Na_2O–P_2O_5–B_2O_3 (□) and phosphates (●). The reference material is $NaPO_3$ (+). Numbers indicated in the figure correspond to the compounds in Table 1.

this sequential transformation is sensitive to the composition, especially at the equivalent points. This transformation naturally leads to the changes in the effective charge on the phosphorus atom. The effect of the B_2O_3 addition, therefore, is understandable, though B_2O_3 is a weak acid compared with P_2O_5.[6] Figure 2 shows the dependence of the P $K\alpha$ energy shifts on the theoretical optical basicity, as defined by Duffy and Ingram.[7] The P $K\alpha$ energy increases with a decrease in the optical basicities. However, the P $K\alpha$ energy shifts are larger in the Si and Al phosphates than in alkali phosphates, even with the same optical basicity.

The addition of alkali or alkaline earth metal oxides to a pure P_2O_5 causes the breakage of a P–O–P bond, giving rise to a non-bridging oxygen ion, accompanied by adjacent metal ions as charge compensators. In this case, the isostructural picture with the corresponding silicate can be expected. If more electronegative elements, such as silicon or aluminium, are located, they will form a linkage such as –P–O–Si–O– at the expence of the P=O double bond. The electrons which have been localized on a PO_4 tetrahedron as a double bond with oxygen then diffuse to adjacent polyhedra (SiO_6 in the above case). In other words, the effective positive charge on phosphorus should increase much more than would be expected from the average electronegativity or theoretical optical basicity. The $K\alpha$ energy increases in proportion to the increased positive charges on the phosphorus atom. A further quantitative discussion will be made after measuring the P $K\alpha$ spectra, which give direct information about the chemical bond in phosphates.

The present work was partially supported by a Grant-in-Aid for Foundamental Scientific Research from the Japan Society of Promotion Science. (T. Maekawa).

References

1) M. Fichter, *Spectrochim. Acta, Part B*, **30**, 417 (1975).

2) T. Maekawa, N. Kikuchi, N. Fukuda, and T. Yokokawa, *Bull. Chem. Soc. Jpn.*, **51**, 777 (1978).

3) T. Maekawa, N. Kikuchi, S. Sumita, and T. Yokokawa, *Bull. Chem. Soc. Jpn.*, **51**, 780 (1978).

4) N. Kikuchi, T. Maekawa, and T. Yokokawa, *Bull. Chem. Soc.Jpn.*, **52**, 1260 (1979).

5) G. Leonhardt and A. Meisel, *J. Chem. Phys.*, **52**, 6189 (1970).

6) T. Yokokawa and S. Kohsaka, *J. Chem. Eng. Data*, **24**, 167 (1979).

7) J. A. Duffy and M. D. Ingram, *J. Non-Cryst. Solids*, **21**, 373 (1976).

Studies of the Interaction of Isocyanides with Transition-metal Complexes.[1] XXVI. The Preparation of Octakis(aryl isocyanide)dirhodium

Yasuhiro YAMAMOTO* and Hiroshi YAMAZAKI
The Institute of Physical and Chemical Research, Wako, Saitama 351
(Received July 15, 1983)

Synopsis. The treatment of a mixture of $[Rh(cod)Cl]_2$ and aryl isocyanide with sodium amalgam afforded octakis(aryl isocyanide)dirhodium. A structure with two bridging and six terminal isocyanide ligands was deduced from the IR spectrum in comparison with that of the known cobalt analog. The temperature-dependent ^1H NMR spectrum of this complex suggested harder intramolecular and easier intermolecular ligand exchanges than those of the corresponding cobalt analog.

Previously Green *et al.*[2] and also the present authors[3] reported the synthesis of dinuclear zerovalent $Co_2(RNC)_8$ either by the reduction of alkyl and aryl isocanide complexes of cobalt(I) and cobalt(II) by the alkali metal amalgam, or by the substitution reaction of $Co_2(CO)_8$ or $Co_4(CO)_{12}$ with aryl isocyanide. Spectroscopic and X-ray crystallographic analyses showed that the molecule consists of two bridging and six terminal isocyanide ligands and that the molecule is fluxional in a solution. For comparison we attempted to prepare related rhodium complexes and to examine their structural features.

Results and Discussion

The treatment of dichloro-bis(η^4-1,5-cyclooctadiene)dirhodium(I) and 2,6-xylyl isocyanide with a sodium amalgam in THF at room temperature led to formation of zerovalent octakis(2,6-xylyl isocyanide)dirhodium (**1a**) in a moderate yield:

$$[Rh(cod)Cl]_2 + 8\,RNC \xrightarrow{Na/Hg} Rh_2(RNC)_8.$$
1a—c

Yellow crystals of **1a** which contain benzene as a solvate are fairly stable in the solid state and can be kept in a refrigerator under an inert-gas atmosphere. In contrast, $Rh_2(CO)_8$ has only been characterized spectroscopically under a high pressure of carbon monoxide[4] and also in a low-temperature matrix (*ca.* 35 K).[5] No isocyanide cluster complexes, such as $Rh_4(RNC)_{12}$ and $Rh_6(RNC)_{16}$ corresponding to the known binary carbonyl clusters were formed, probably for steric reasons. The use of mesityl or 2,6-dimethyl-4-bromophenyl isocyanide also afforded similar complexes (**1b**: 2,4,6-$Me_3C_6H_2NC$; **1c**: 2,6-Me_2-4-BrC_6H_2NC).

The IR spectrum of **1a** in nujol shows characteristic absorptions assignable to the terminal isocyanide groups [2125(sh), 2090(sh), 2070(s), and 1995(sh) cm^{-1}] and to the bridge-bonded isocyanide groups [1672(m) and 1653(s) cm^{-1}]. The IR spectrum in a solution also shows a similar absorption pattern. These spectra were similar to those of the known cobalt analog, $Co_2(2,6\text{-}Me_2C_6H_3NC)_8$, and suggest that **1a** has a dimeric structure consisting of two bridging and six terminal isocyanide ligands.

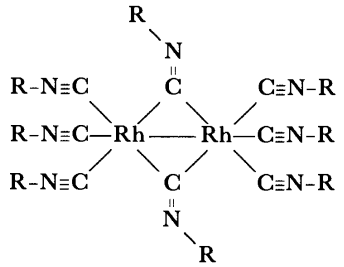

It has been known that binary rhodium carbonyl exists in the bridge-bonded form, and there is no evidene for the non-bridged form.[4,5]

The ^1H NMR spectrum of **1a** in PhCl at the ambient temperature shows only one sharp singlet, at δ 2.30, which is assigned to methyl protons. This simple spectrum implies a rapid intramolecular ligand exchange between bridging and terminal isocyanide ligands. Similar behavior has also been observed in the case of the cobalt analog. However, the sharp singlet at δ 2.30 broadened on cooling and at *ca.* −33 °C splitted into two signals in an intensity ratio of 3:1, showing slow intramolecular ligand exchange; this was in contrast to the case of the cobalt analog, which showed rapid ligand exchange even at −90 °C. The intermolecular ligand exchange with added 2,6-xylyl isocyanide was also observed. The spectrum at 14 °C showed two sharp, separated signals, at δ 2.30 and 2.17, due to coordinated and uncoordinated isocyanides respectively. No intermolecular ligand exchange occurs below this temperature, as is indicated by the sharpness of the two separated singlets. The two signals become broad on warming and coalesce to a broad singlet at 40 °C. The spectrum at 60 °C shows a sharp singlet, suggeting rapid intermolecular exchange. This temperature-dependent NMR behavior is reversible. The coalescence temperature of intermolecular exchange in the cobalt analog is 127 °C. Thus, the intramolecular ligand exchange is harder, and the intermolecular exchange is easier in **1a** than in the cobalt analog. The thermodynamic data for the ligand-exchange processes of **1a**, **1b**, and **1c** are listed in Table 1.

The electronic spectra of **1a** in cyclohexane, together with that of $Co_2(2,6\text{-}Me_2C_6H_3NC)_8$, are shown in Fig. 1. The band at 29670 cm^{-1} (337 nm) is assigned to the σ-σ^* transition by analogy with the electronic spectrum of $Co_2(2,6\text{-}Me_2C_6H_3NC)_8$. The energy of the σ-σ^* transition in **1a** is lower by 8790 cm^{-1} than that of $Rh_2(CO)_8$.[5] This difference can be associated with the weaker π-acid character of isocyanide than that of carbon monoxide. The

Table 1. Approximate coalescence temperatures, rate constants, and free energies for $Rh_2(2,6\text{-}Me_2\text{-}4\text{-}XC_6H_2NC)_8$[a]

X	Intermolecular			Intramolecular		
	T_c/°C	k/s^{-1}	ΔG^*/kcal m^{-1} [b]	T_c/°C	k/s^{-1}	ΔG^*/kcal m^{-1} [b]
Br	50	34.2	16.6	−25	20.4	12.8
H	40	31.1	16.1	−28	13.0	12.9
Me	40	39.1	16.0			

a) Measured in PhCl. b) 1 cal=4.184 J.

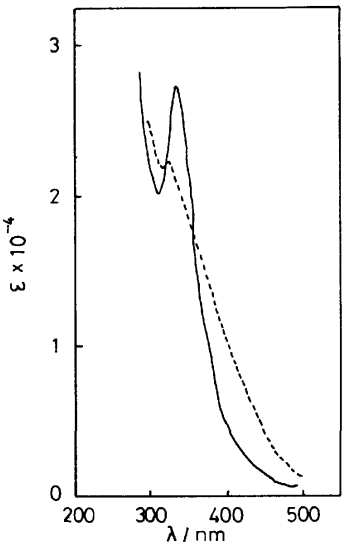

Fig. 1. Electronic spectra of $Rh_2(2,6\text{-}Me_2C_6H_3NC)_8$ (——) and $Co_2(2,6\text{-}Me_2C_6H_3NC)_8$ (----) in cyclohexane

isocyanide ligand promotes the accumulation of d-electron density on the rhodium atoms and so increases the d-d repulsive energies. The σ-σ^* transition band in the isocyanide complex red-shifts on passing from $Co_2(2,6\text{-}Me_2C_6H_3NC)_8$ to $Rh_2(2,6\text{-}Me_2C_6H_3NC)_8$; this is the reverse of the trend observed in binary carbonyls of cobalt and rhodium.[5]

Experimental

The reactions were carried out under an atmosphere of nitrogen. The IR and electronic spectra were obtained on Shimadzu IR-27G and Shimadzu UV-180 spectrophotometers respectively. The ^1H NMR spectra were recorded on a Varian HA-100B spectrometer, using tetramethylsilane as a reference. The isocyanides[6] and $[Rh(cod)Cl]_2$[7] were prepared by procedures described in the literature. The tetrahydrofuran was distilled from sodium ketyl just before use.

*Octakis(2,6-xylyl isocyanide)dirhodium (**1a**).* A mixture of $[Rh(cod)Cl]_2$ (0.20 g) and 2,6-xylyl isocyanide (0.50 g) (mole ratio: *ca.* 1:9.4) in dry tetrahydrofuran (50 ml) was stirred at room temperature with an excess of the sodium amalgam (1%) for 0.5 h. The solution was then decanted, and the solvent was evaporated to dryness under reduced pressure. The residue was chromatographed on alumina (deactivated by H_2O (10%), 2 cm×5 cm), using benzene as the eluent. The concentration of the orange eluate and the addition of hexane gave yellow crystals of the title cmpound containing a benzene molecule (0.36 g, 68%); mp *ca.* 120 °C (decomposing in a nitrogen filled capillary tube). Found: C, 70.29; H, 5.29; N, 8.42%. Calcd for $Rh_2C_{78}H_{78}N_8$: C, 70.26; H, 5.95; N 8.40%.

Similarly, octakis(2,6-dimethyl-4-bromophenyl isocyanide)-dirhodium (**1c**) was obtained in a 24% yield; mp *ca.* 150 °C (decomposing in a nitrogen filled capillary tube). Found: C, 48.38; H, 3.75; N, 5.69%. Calcd for $Rh_2C_{78}H_{70}N_8Br_8$ (containing a benzene molecule): C, 47.69; H, 3.59; N, 5.70%.

For the preparation of the mesityl isocyanide analog (**1b**), the reaction mixture was chromatographed on alumina, using tetrahydrofuran as the eluent.

The subsequent concentration of the eluate gave yellow crystals of **1b** in a 60% yield; mp *ca.* 130 °C (decomposing in a nitrogen filled capillary tube). Found : C, 69.91; H 6.81; N 7.57%. Calcd for $Rh_2C_{84}H_{96}N_8O$ (containing a tetrahydrofuran molecule): C, 70.09; H,6.72;N,7.78%.

Variable-temperature NMR. A mixture of **1a** (388 mg) and 2,6-xylyl isocyanide (12 mg) was dissolved in chlorobenzene and sealed under a nitrogen atmosphere in a 5-mm NMR tube. The temperatures were calibrated using the chemical-shift separation obtained from an ethylene glycol solution at high temperatures and using that obtained from a methanol solution at low temperatures. Similar variable-temperature NMR spectra of **1b** and **1c** were also measured; the results are summarized in Table 1.

References

1) A part of this paper was presented at the 28th Symposium on Organometallic Chemistry, November 5 (1981), Osaka. Part XXV: Y. Yamamoto and H. Yamazaki, *Inorg. Chim. Acta.*, in Press.

2) G. K. Barker, A. M. R. Galas, M. Green, F. G. A. Stone, T. W. Turney, A. J. Welch, and P. Woodward, *J. Chem. Soc., Chem. Commun.*, **1977**, 256; W. E. Carroll, M. Green, A. M. R. Galas, M. Murray, T. W. Turney, A. J. Welch, and P. Woodward, *J. Chem. Soc., Dalton Trans.*, **1980**, 80.

3) Y. Yamamoto and H. Yamazaki. *J. Organomet. Chem.*, **137**, C31(1977); *Inorg. Chem.*, **17**, 3111(1978).

4) R. Whyman, *J. Chem. Soc., Dalton Trans.*,**1972**, 1375.

5) A. J. L. Hanlan,G. A. Ozin, and H. B. Gray, *Inorg. Chem.*, **18**, 1790(1979).

6) H. M. Walborsky and G. E. Niznik, *J. Org. Chem.*, **37**, 187(1972).

7) R. B. King, "Organometallic Syntheses," Academic Press, New York (1965), Vol. 1, p. 132.

Theoretical Interpretation of the Mössbauer Parameter in [1]Ferrocenophanes

Shigeru IKUTA,* Izumi MOTOYAMA, and Hirotoshi SANO*
Department of Chemistry, Faculty of Science, Tokyo Metropolitan University, Fukasawa, Setagaya-ku, Tokyo 158
(Received August 20, 1983)

Synopsis. The smaller quadrupole splitting values in [1]ferrocenophanes than that in ferrocene were accounted for by assuming a lesser quantity of the nuclear part in the electric-field gradient at the iron nucleus; smaller quadrupole splitting could not be explained by the electron distribution among Fe 3d orbitals.

Mössbauer spectroscopy has been used as a very useful tool for probing the changes in the electronic environment around the iron nucleus.

Quadrupole splitting values (qs=2.0 mm s^{-1}) about 15% smaller than that in ferrocene were observed in (1,1′-ferrocenediyl)diphenylgermane, (1,1′-ferrocenediyl)phenylphosphine, and (1,1′-ferrocenediyl)diphenylsilane.[1] Stoeckli-Evans *et al.*[2] performed a three-dimensional X-ray analysis of these compounds, and determined the distances between the Fe and Ge atoms and between the Fe and P atoms to be 2.744 Å and 2.774 Å, respectively. They pointed out that there is clearly no bonding between these atoms, since these interatomic distances are appreciably longer than the bond lengths calculated from the metallic covalent radii ($l_{Fe\text{-}Ge}$=2.47 Å and $l_{Fe\text{-}P}$=2.37 Å).

On the other hand, Clemance *et al.*[3] stated that the Fe–P length of 2.77 Å does not preclude the possibility of bonding interaction between the Fe and P atoms, and that the contribution of the phosphorus' d orbitals can be present in (1,1′-ferrocenediyl)phenylphosphine.

These discussions indicate a lack of clear understanding of the reason why smaller qs values are to be expected in these [1]ferrocenophanes.

In the present note, the electronic structures and the electric-field gradients around the iron nucleus in (1,1′-ferrocenediyl)diphenylgermane and (1,1′-ferrocenediyl)phenylphosphine were estimated based on calculations by means of an *ab initio* (coreless) MO method. The smaller qs values than that in ferrocene are explained in terms of the lesser quantity of the nuclear part in the electric-field gradient at the iron nucleus.

Calculation

The pseudo-potential method of Barthelat and Durand[4] was used for the *ab initio* (coreless) MO calculations in order to account for the electronic structures and electric-field gradients around the iron nucleus. A one-electron-property-package of the MONSTERGAUSS program[5] was installed in the PSHONDO program[6] which has been revised by Daudey in order to apply the pseudo-potential method to an original HONDO program.[7] The basis sets used for the Fe, C, and H atoms were the same as those in the previous communications;[8] only the basis set for the Fe 3d orbital was of a double-zeta quality. The contracted [2s2pld] basis sets[9] optimized by Daudey were used for the valence of the Ge and P atoms.

The geometrical structures determined by Stoeckli-Evans *et al.*[2] were used for the calculations, but the phenyl groups were replaced by hydrogen atoms because of their large systems. These simplifications can not be expected to affect the electron distributions, especially in the 3d orbitals of the iron atom, which lies far from the phenyl groups. The original structures determined by Stoeckli-Evans *et al.*[2] were used without any modifications in calculating the nuclear part of the electric-field gradient at the iron nucleus in (1,1′-ferrocenediyl)diphenylgermane.

The usefulness of the coreless MO calculations with the pseudo-potential method has already been reported by several authors,[8,10–15] and we ourselves have discussed the ferrocene derivatives.[8]

All the calculations were performed by the use of a FACOM M380 computer at the Institute of Physical and Chemical Research.

Results and Discussion

The quadrupole splitting (qs) can be theoretically calculated by means of the principal component of the electric-field gradient (q_{zz}) around the iron nucleus: $qs=1/2\cdot eQV_{zz}(1+1/3\cdot\eta^2)^{1/2}$, where V_{zz} equals $-q_{zz}$, where Q is the nuclear electric quadrupole moment, and where η is the asymmetry parameter.[8] The qs value is, then, directly proportional to the q_{zz} values. The principal electric-field gradient (q_{zz}) is composed of the nuclear (q_{zz}^{NUC}) and electronic (q_{zz}^{ELF}) ones.

The q_{zz}^{ELF} values are proportional to the following amount, which corresponds to the electron distribution among iron's 3d orbitals: $q_{zz}^{ELF}\propto[p(d_{x^2-y^2}+d_{xy})-\{p(d_{z^2}+1/2\cdot p(d_{xz}+d_{yz})\}]$. Therefore, the qs values are also related to the electron distribution among the iron's 3d orbitals.

In Table 1, the total energies, the electron populations among iron's 3d orbitals, the net atomic charges, the electric-field gradients around the iron nucleus, and the asymmetry parameters are summarized. In the present *ab initio* (coreless) MO calculations, the phenyl moiety was replaced by a hydrogen atom because of its large system. The values in ferrocene, as calculated by means of the *ab initio* coreless MO method, have already been found to be in agreement with them obtained by using the all-electron MO method.[8]

The q_{zz}^{ELF} values in (1,1′-ferrocenediyl)diphenylgermane and (1,1′-ferrocenediyl)phenylphosphine are quite similar to that in ferrocene. These results come from the fact that the electron distribution among iron's 3d orbitals (in these molecules) agrees well with that in ferrocene, as is shown in the table. The η values in these compounds are quite small.

Table 1. Total energies, electron populations, net atomic charges, electric-field gradients, and asymmetry parameters in [1]ferrocenophanes

	Ferrocene	(1,1′-Ferrocenediyl)-diphenylgermane	(1,1′-Ferrocenediyl)-phenylphosphine (A)[a]	(1,1′-Ferrocenediyl)-phenylphosphine (B)[b]
E_t[c]	−81.1477	−84.6464	−86.4948	−86.6835
$p(d_{x^2-y^2})$[d]	1.891	1.888	1.898	1.892
$p(d_{xy})$	1.891	1.896	1.901	1.899
$p(d_{xz})$	0.433	0.433	0.429	0.427
$p(d_{yz})$	0.433	0.460	0.426	0.429
$p(d_{z^2})$	1.947	1.954	1.963	1.960
n(Fe)[e]	6.734	6.825	6.758	6.742
n(C)	4.359	4.38—4.39	4.35—4.50	4.35—4.39
n(H)	0.767	0.77—0.78	0.77—0.78	0.77—0.78
n(Ge)	—	3.272	—	—
n(P)	—	—	4.128	4.431
q_{zz}^{NUC}[f]	−0.97	−0.73(−0.69)[g]	−0.81	−0.81
q_{zz}^{ELE}[h]	−3.18	−3.12	−3.21	−3.20
q_{zz}	−4.15	−3.85(−3.81)	−4.01	−4.01
η[i]	0.00	0.12	0.01	0.00

a) 3d Function was not added on the P atom. b) 3d Function was added on the P atom. c) Total energies in a.u. d) Electron populations among Fe 3d orbitals. e) Net atomic charges. f) Nuclear part of the electricfield gradient in a.u. g) We used the geometrical structures determined by Stoeckli-Evans *et al.*,[2] in which diphenyl was not replaced by hydrogen atoms. h) Electronic part of the electric-field gradient in a.u. The correction due to core electrons (shielding effect) was not performed. See Ref. 8. i) Asymmetry parameters.

The nuclear part of the electric-field gradient (q_{zz}^{NUC}) does not show a negligible value. It is worthwhile to note that the q_{zz}^{NUC} value in (1,1′-ferrocenediyl)diphenylgermane, in which the experimetal geometry determined by Stoeckli-Evans *et al.*[2] is used without any modifications, is lower by about 0.3 a.u. than that in ferrocene. This quite important result indicates that the total electric-field gradient in (1,1′-ferrocenediyl)diphenylgermane is also lower by 0.30 a.u. than that in ferrocene. (The overlap populations between the Fe and Ge atoms are −0.030, showing that there is no bonding between these two atoms.) Therefore, the smaller *qs* value in (1,1′-ferrocenediyl)diphenylgermane than that in ferrocene cannot be ascribed to the change in the electron distribution among iron's 3d orbitals caused by a direct bonding between the Fe and Ge atoms, but it can clearly be accounted for by the contribution of a smaller quantity of the nuclear part of the electric-field gradient around the iron nucleus in (1,1′-ferrocenediyl)diphenylgermane.

For the (1,1′-ferrocenediyl)phenylphosphine, two types of the calculations were performed; one (A) does not include the 3d polarization function for the phosphorus atom, while the other (B) does include it. As is shown in the table, the two sets of data are almost identical, indicating that the contribution of the phosphorus' 3d polarization function to the electron distribution among the iron's 3d orbitals does not exist in this system; the same q_{zz}^{ELF} values are obtained in these two types of calculations. The nuclear part of the electric-field gradient (q_{zz}^{NUC}) is smaller by 0.2 a.u. than that in ferrocene. (The q_{zz}^{NUC} value is estimated to become even smaller if the experimental geometry determined by Stoeckli-Evans *et al.*[2] is used, for in it the phenyl group is not replaced by a hydrogen atom.)

In (1,1′-ferrocenediyl)phenylphosphine, also the smaller experimental *qs* value can be accounted for by assuming a lesser contribution of the nuclear part to the electric-field gradient.

In conclusion, the smaller experimental *qs* values can be ascribed by the lesser q_{zz}^{NUC} values, without using any unreasonable supposition such as that reported by Clemance *et al.*[3]

The authors gratefully acknowledge the help of Dr. P. Daudey, who provided his PSHONDO program to one of them (S.I.). They also wish to thank Professor M. Imamura, the Institute of Physical and Chemical Research, who gave them the chance to use the FACOM M380 computer.

References

1) A. G. Osborne, R. H. Whiteley, and R. E. Meads, *J. Organomet. Chem.*, **193**, 345 (1980).
2) H. Stoeckli-Evans, A. G. Osborne, and R. H. Whiteley, *J. Organomet. Chem.*, **194**, 91 (1980).
3) M. Clemance, R. M. G. Roberts, and J. Silver, *J. Organomet. Chem.*, **243**, 461 (1983).
4) J. C. Barthelat, PH. Durand, and A. Serafini, *Mol. Phys.*, **33**, 159 (1977).
5) M. Peterson and R. Poirier, Univ. of Toronto, Canada.
6) J. P. Daudey, Univ. of Paul Sabatier, France.
7) M. Dupuis, J. Rys, and H. F. King, *J. Chem. Phys.*, **65**, 111 (1976).
8) S. Ikuta, I. Motoyama, and H. Sano, *Radiochem. Radioanal. Lett.*, **58**, 329 (1983).
9) J. P. Daudey, private communication, 1983.
10) M. E. Ruiz, J. P. Daudey, and O. Novaro, *Mol. Phys.*, **46**, 853 (1982).
11) G. H. Jeung, J. P. Malrieu, and J. P. Daudey, *J. Chem. Phys.*, **77**, 3571 (1982).
12) G. H. Jeung, J. P. Daudey, and J. P. Malrieu, *Chem. Phys. Lett.*, **94**, 300 (1983).
13) G. Trinquier, J. P. Malrieu, and P. Riviere, *J. Am. Chem. Soc.*, **104**, 4529 (1982).
14) J. C. Barthelat, G. Trinquier, and G. Bertrand, *J. Am. Chem. Soc.*, **101**, 3786 (1979).
15) J. C. Barthelat, B. S. Roch, G. Trinquier, and J. Stage, *J. Am. Chem. Soc.*, **102**, 4080 (1980).

Studies of Bitter Peptides from Casein Hydrolyzate. V.[1] Bitterness of the Synthetic N-Terminal Analogs of des-Gly²-BPIa (Arg-Pro-Pro-Phe-Ile-Val)[2]

Hidenori KANEHISA† and Hideo OKAI*

Department of Fermentation Technology, Faculty of Engineering, Hiroshima University, Shitami, Saijo-cho, Higashihiroshima 724

(Received June 15, 1983)

Synopsis. In order to investigate how the basic amino acid residue in the N-terminal contributes to the bitter taste exhibited by BPIa (Arg-Gly-Pro-Pro-Phe-Ile-Val), we synthesized several kinds of N-terminal analogs of des-Gly²-BPIa (Arg-Pro-Pro-Phe-Ile-Val). The basic amino acid residue of BPIa was found to play an important role in its bitter taste.

In studies of the relationship between bitterness and chemical structure of BPIa (Arg-Gly-Pro-Pro-Phe-Ile-Val) which was isolated from casein hydrolyzate by Minamiura *et al.*,[3] BPIa and its various analogs and fragments have been synthesized in our laboratory.[1,4-6] In Previous papers,[1,5] we explained that the hydrophobic amino acids moiety in the C-terminal and the L-arginine residue in the N-terminal of BPIa are necessary for an intense bitter taste. However, the participation in the bitter taste of several basic amino acids other than L-arginine in the N-terminal of BPIa was not dealt with in those papers.[1,5] During the synthetic studies of BPIa, we found that des-Gly²-BPIa (Arg-Pro-Pro-Phe-Ile-Val) exhibited a strong bitter taste of the same level as BPIa.[5] We synthesized six kinds of des-Gly²-BPIa analogs, as shown in Table 1, and compared their bitterness with that of des-Gly²-BPIa.

The synthesis of compound **1** was as follows: Z-Lys(ε-Z)-OH·DCHA and H-Pro-Pro-Phe-Ile-Val-OBzl·HCl[4] that is an intermediate in the synthesis of BPIa were coupled by the mixed anhydride method to yield Z-Lys(ε-Z)-Pro-Pro-Phe-Ile-Val-OBzl. The protected hexapeptide was hydrogenated in the presence of palladium black to give H-Lys-Pro-Pro-Phe-Ile-Val-OH (**1**). Other peptides (compounds **2—6**) were prepared by the same procedures mentioned above, employing the corresponding acylamino acids instead of Z-Lys(ε-Z)-OH·DCHA. The purity of synthetic peptides and their intermediates was confirmed by thin-layer examinations on two solvent systems, elemental analyses, and amino acid analyses. The threshold value for bitter taste and the ratio of caffeine ($R_{caf.}$) value of the synthesized peptides were organoleptically determined by panel evaluation with five people, as shown in Table 1.

All the synthesized peptides possessed a bitter taste. However, their bitterness was weaker than that of des-Gly²-BPIa (**7**). By comparing the bitteness of compounds **1—3** and **7** with that of **4—6**, it is obvious that the basic nature in the N-terminal is important for showing the strong bitter taste in compound **7**. The strength of bitterness of compounds **1—3** decreased proportionally to the decreasing of the side chain length of the amino acid residue in the N-terminal. On the other hand, we found an interesting result for the bitter taste of compounds **5** and **6**. The bitter taste of compound **1** where L-lysine residue was located in the N-terminal was stronger than that of compound **2** in

TABLE 1. THE THRESHOLD VALUE FOR BITTER TASTE OF THE SYNTHETIC PEPTIDES

	Compound	T.V./mM	$R_{caf.}$[a]
1	Lys-Pro-Pro-Phe-Ile-Val	0.15	6.67
2	Orn-Pro-Pro-Phe-Ile-Val	0.31	3.33
3	Dab-Pro-Pro-Phe-Ile-Val	0.60	1.67
4	Phe-Pro-Pro-Phe-Ile-Val	0.30	3.33
5	Lys(ε-Ac)-Pro-Pro-Phe-Ile-Val	1.30	0.77
6	Orn(δ-Ac)-Pro-Pro-Phe-Ile-Val	0.60	1.67
7	Arg-Pro-Pro-Phe-Ile-Val[b]	0.08	12.50

a) Ratio of caffeine. b) des-Gly²-BPIa.

TABLE 2. YIELD AND ANALYTICAL DATA OF PROTECTED HEXAPEPITDES (Z-X-Pro-Pro-Phe-Ile-Val-OBzl)

X	Yield %	Mp θ_m/°C	$[\alpha]_D^{20}$/° (*c* 1, methanol)	Formula	Found(Calcd)(%) C	H	N	R_f^1	R_f^2
Lys(ε-Z)	82	74—76	−86.0	$C_{59}H_{75}O_{11}N_7 \cdot 1/2\,H_2O$	66.17 (66.39)	7.34 (7.18)	9.22 (9.19)	0.96	0.66
Orn(δ-Z)	74	78—80	−88.5	$C_{58}H_{73}O_{11}N_7 \cdot 1/2\,H_2O$	65.96 (66.14)	7.31 (7.08)	9.32 (9.31)	0.96	0.73
Dab(γ-Z)	78	84—86	−97.0	$C_{57}H_{71}O_{11}N_7 \cdot 1/2\,H_2O$	66.05 (65.85)	7.06 (6.98)	9.52 (9.44)	0.97	0.73
Phe	69	88—90	−99.5	$C_{54}H_{66}O_9N_7 \cdot 2H_2O$	68.16 (68.32)	7.13 (7.43)	8.85 (8.86)	0.97	0.85
Lys(ε-Ac)	91	78—80	−100.5	$C_{53}H_{71}O_{10}N_7 \cdot H_2O$	64.43 (64.48)	7.35 (7.48)	9.81 (9.96)	0.95	0.60
Orn(δ-Ac)	91	90—92	−101.0	$C_{52}H_{69}O_{10}N_7 \cdot H_2O$	64.65 (64.37)	7.19 (7.38)	9.99 (10.11)	0.93	0.65

† Present address: Research and Development Division, Sunstar Inc., Asahi-cho, Takatsuki, Osaka 569.

Table 3. Yield and analytical data of final products
(H-X-Pro-Pro-Phe-Ile-Val-OH)

Compd	X	Yield %	Mp θ_m/°C	$[\alpha]_D^{20}$/° (c 1, methanol)	Formula / Amino acid ratios in acid hydrolyzate	Found (Calcd) (%) C	H	N	R_f[1]
1	Lys	71	156—157	−89.0	$C_{36}H_{57}O_7N_7 \cdot CH_3COOH \cdot 3/2\,H_2O$ Lys 0.99, Pro 2.04, Phe 1.00, Ile 1.00, Val 1.04.	57.81 (57.99)	7.91 (8.20)	12.46 (12.46)	0.57
2	Orn	79	155—157	−93.0	$C_{35}H_{55}O_7N_7 \cdot CH_3COOH \cdot 3/2\,H_2O$ Orn 1.03, Pro 1.96, Phe 1.03, Ile 1.00, Val 1.05.	57.26 (57.49)	7.75 (8.08)	12.56 (12.67)	0.56
3	Dab	88	156—157	−86.5	$C_{34}H_{53}O_7N_7 \cdot CH_3COOH \cdot H_2O$ Dab 0.97, Pro 1.95, Phe 1.03, Ile 1.00, Val 1.02.	57.46 (57.66)	7.78 (7.93)	12.90 (13.08)	0.68
4	Phe	97	144—145	−88.0	$C_{39}H_{54}O_7N_6 \cdot H_2O$ Phe 2.10, Pro 2.13, Ile 1.00, Val 0.99.	63.64 (63.56)	7.65 (7.66)	11.35 (11.41)	0.75
5	Lys(ε-Ac)	73	140—142	−84.5	$C_{38}H_{59}O_8N_7 \cdot 1/2\,H_2O$ Lys 1.02, Pro 1.95, Phe 1.03, Ile 1.00, Val 1.00.	60.51 (60.78)	8.10 (8.05)	12.81 (13.06)	0.69
6	Orn(δ-Ac)	79	144—145	−86.0	$C_{37}H_{57}O_8N_7 \cdot 3/2\,H_2O$ Orn 1.01, Pro 1.97, Phe 1.05, Ile 1.00, Val 1.02.	59.10 (59.10)	7.96 (7.64)	12.76 (13.04)	0.68

which L-ornithine replaced L-lysine. However, N^{δ}-acetyl-L-orinithine N-terminal substituted analog (compound **6**) gave a stronger bitterness than N^{ε}-acetyl-L-lysine substituted one (compound **5**), which is due to the acetyl group introduction. From the results described above, the strong bitterness exhibited by BPIa depends on both basicity and side chain length of the amino acid in the N-terminal.

Experimental

All the melting points are uncorrected. Thin-layer chromatographies were performed on Merck silica gel G. Developing solvents commonly used were (1) 1-butanol-acetic acid-pyridine-water (4:1:1:2, v/v) and (2) chloroform-methanol (5:1, v/v). Materials possessing a free amino group on a thin-layer plate were detected by spraying with ninhydrin. Compounds with blocked amino groups were detected by spraying with 25% hydrogen bromide in acetic acid and then with ninhydrin. The optical rotations were measured on a Union PM-101 polarimeter. Amino acid analyses of peptides were carried out on samples that had been hydrolyzated with constant boiling hydrochloric acid for 65 h in evacuated, sealed tubes at 110 °C, and were recorded on a Hitachi amino acid analyzer KLA-5 type.

Syntheses of Protected Hexapeptides. Z-Lys(ε-Z)-Pro-Pro-Phe-Ile-Val-OBzl: A solution of Z-Lys(ε-Z)-OH·DCHA (0.89 g, 1.5 mmol) and *N*-methylmorpholine (0.16 ml, 1.5 mmol) in tetrahydrofuran (1.5 ml) was chilled to −5 °C. Ethyl chloroformate (0.15 ml, 1.5 mmol) was added, and then the mixture was kept for 15 min at −5 °C. A solution of H-Pro-Pro-Phe-Ile-Val-OBzl·HCl[4] (1.05 g, 1.5 mmol) and *N*-methylmorpholine (0.16 ml, 1.5 mmol) in *N*,*N*-dimethylformamide (10 ml) was added to the mixture and stirred for 1 h, then at room temperature overnight. The mixture was evaporated *in vacuo*, and the oily residue was dissolved in ethy acetate. The solution was washed with water, 0.5 M (1 M=1 mol dm^{-3}) hydrochloric acid, 4% sodium hydrogencarbonate, and water successively, then dried over anhydrous sodium sulfate. Sodium sulfate was removed by filtration, and the filtrate was evaporated *in vacuo*. The oily residue was crystallized with ether-petroleum ether; yield, physical constants, and elemetal analysis of this compound is given in Table 2. Other protected hexapeptides were prepared from the corresponding acylamino acids and H-Pro-Pro-Phe-Ile-Val-OBzl·HCl by the same method. Their yields and analytical data are also presented in Table 2.

Syntheses of Final Products. H-Lys-Pro-Pro-Phe-Ile-Val-OH (1): Z-Lys(ε-Z)-Pro-Pro-Phe-Ile-Val-OBzl (1.05 g, 1 mmol) was hydrogenated in methanol (2 ml) and acetic acid (2 ml) for 20 h by the aid of palladium black. The catalyst was filtered off, and the filtrate was evaporated *in vacuo*. The oily residue was crystallized from acetone-ether. It was recrystallized from methanol-acetone-ether; Compounds **2—6** were prepared from the corresponding hexapeptides by hydrogenation. Yields and analytical data of final products are given in Table 3.

Sensory Test. Taste of the peptides was organoleptically determined by the same manner as described in the previous papers.[1,4-6]

The authors wish to express thank to Dr. Shinji Okumura of Ajinomoto Co. Inc., for supplying some amino acids.

References

1) Part IV. K. Otagiri, T. Shigenaga, H. Kanehisa, and H. Okai, *Bull. Chem. Soc. Jpn.*, **57**, 90 (1984).

2) The abbreviations recommended by the IUPAC-IUB commission of Biochemical Nomenclature (*J. Biol. Chem.*, **247**, 977 (1972)) have been used. Amino acid symbols except glycine denote the L-configuration. Additional abbreviations: Ac, acetyl; Dab, 2,4-diaminobutyric acid; DCHA, dicyclohexylamine.

3) N. Minamiura, Y. Matsumura, J. Fukumoto, and T. Yamamoto, *Agric. Biol. Chem.*, **36**, 588 (1972).

4) H. Fukui, H. Kanehisa, N. Ishibashi, I. Miyake, and H. Okai, *Bull. Chem. Soc. Jpn.*, **56**, 766 (1983).

5) K. Otagiri, I. Miyake, N. Ishibashi, H. Fukui, H. Kanehisa, and H. Okai, *Bull. Chem. Soc. Jpn.*, **56**, 1116 (1983).

6) I. Miyake, K. Kouge, H. Kanehisa, and H. Okai, *Bull. Chem. Soc. Jpn.*, **56**, 1678 (1983).

Monodebromination of *gem*-Dibromocyclopropanes by Sodium Hydrogentelluride

Atsuhiro OSUKA,* Keita TAKECHI, and Hitomi SUZUKI*
Department of Chemistry, Faculty of Science, Ehime University, Bunkyo-cho 2-5, Matsuyama 790
(Received June 30, 1983)

Synopsis. *gem*-Dibromocyclopropanes were effectively reduced to monobromocyclopropanes by sodium hydrogentelluride.

Much attention has been focused in recent years on the application of tellurium in organic syntheses.[1] Among these, sodium hydrogentelluride (NaHTe),[2] which was prepared *in situ* from tellurium and sodium borohydride ($NaBH_4$), has been reported to possess considerable versatility as selective reagent for the reduction of a wide variety of organic molecules.[2-5] While NaHTe effects the hydrogenation of α,β-unsaturated carbonyl compounds, it does not reduce simple ketones or aldehydes.[3b,4] Several observations that anionic tellurium species have strong affinity toward activated halogen have led to the development of their uses for dehalogenation reactions.[3a,5,6,7] In this note, we wish to report an effective monodebromination of *gem*-dibromocyclopropanes by NaHTe.

Monobromocyclopropanes were obtained by treatment of *gem*-dibromocyclopropanes with 2.5 equiv. of NaHTe in refluxing ethanol. A further reduction of the resultant monobromides was not observed under the reaction conditions employed. For comparison, the reduction of *gem*-dibromocyclopropanes with $NaBH_4$ was also investigated. The yields and trans/cis ratios of the present reactions are given in the Table 1. Apparently, the reduction with NaHTe is faster and more selective than that with $NaBH_4$ in ethanol. A similar debromination may be expected in the reaction with NaHSe,[8] but neither 1,1-dibromo-2-phenylcyclopropane, nor 1,1-dibromo-2-methyl-2-phenylcyclopropane, nor 7,7-dibromobicyclo[4.1.0]heptane underwent reduction upon treatment with 2.5 equiv. of NaHSe in refluxing ethanol. It should be noted here that NaHTe has strong affinity for activated halogens, which property is not shared by NaHSe. 1,1-Dichloro-2-phenylcyclopropane and 7,7-dichlorobicyclo[4.1.0]heptane were quantitatively recovered after prolonged treatment with NaHTe, while dichlorodiphenylmethane was readily reduced by NaHTe to give tetraphenylethylene and diphenylmethane in 37 and 33% yields, respectively.

$$Ph_2CCl_2 \xrightarrow[EtOH]{NaHTe} Ph_2C{=}CPh_2 + Ph_2CH_2.$$

It was indeed true that numerous methods are availabe to bring about the monodebromination of *gem*-

Table 1. Reduction of *gem*-dibromocyclopropanes to monobromocyclopropanes by sodium hydrogentelluride[a]

Reactant	Reducing reagent	Reaction time/h	Conversion/%	Yield/%[b]	Trans/Cis[c]
	NaHTe	3.5	100	64	72:28
	$NaBH_4$	3.5	17	(14)[d]	65:35
	NaHTe	3	100	61	63:37
	$NaBH_4$	3	20	(16)[d]	54:46
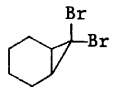	NaHTe	9	98	55	24:76
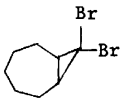	NaHTe	8	100	56	33:67
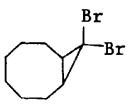	NaHTe	9	98	59	33:67
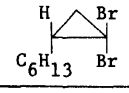	NaHTe	9	98	63	30:70

a) All reactions were performed as described in detail in the text. b) Values reported are isolated yields for mixtures of *trans*- and *cis*-bromocyclopropanes. c) The trans/cis ratios were determined by GLPC. d) GLPC yields.

dibromocyclopropanes[9] but the present method would be a simple and convenient addition to them.

Experimental

gem-Dibromocyclopropanes and *gem*-dichlorocyclopropanes were prepared according to the reported procedures.[10]

General Procedure for the Reduction of gem-*Dibromocyclopropanes with Sodium Hydrogentelluride.* To a hot solution of sodium hydrogentelluride, prepared in situ by reacting tellurium (1.30 g, 10 mmol) and sodium borohydride (0.90 g, 24 mmol) for 1 h in refluxing ethanol (40 ml) under argon atmosphere, *gem*-dibromocyclopropane (4 mmol) in 4 ml of ethanol was added. The resulting mixture was refluxed for a suitable time as indicated in the Table 1. The progress of the reaction was followed by GLPC (a Hitachi Model 163, using a 3 mm×2 m strainless steel column packed with 10% SE-30 on Celite 545 AW.) After completion of the reaction, the reaction mixture was cooled to room temperature, 50 ml of water was added, and the resulting mixture was left open to air with stirring. The solution became clear after about 3 h with the deposition of tellurium species as tellurium powder. It was then filtered through Celite 545 and the filtrate was extracted with three portions of hexane (30 ml). The extracts were washed with water, dried over Na_2SO_4, and evaporated to give the crude product, which was purified by Kugel-rohr distillation. The products were identified by comparison with authentic samples.

NaHSe was preprared by the method of Klayman[8] and used directly.

The present work was partially supported by a Grant-in-Aid for Scientific Research No. 58740233 from the Ministry of Education, Science and Culture.

References

1) S. Uemura, *Kagaku*, **36**, 381 (1981); K. J. Ingolic, *J. Organomet. Chem.*, **189**, 65 (1980).

2) D. H. R. Barton, and S. W. McCombie, *J. Chem. Soc., Perkin Trans. 1*, **1975**, 1574.

3) a) K. Ramasamy, S. K. Kalyanasundaram, and P. Shanmugam, *Synthesis*, **1978**, 311; b) K. Ramasamy, S. K. Kalyanasundaram, and P. Shanmugam, *ibid.*, **1978**, 545.

4) M. Yamashita, Y. Kato, and R. Suemitsu, *Chem. Lett.*, **1980**, 847

5) A. Osuka and H. Suzuki, *Chem. Lett.*, **1983**, 119.

6) G. Bergson, *Acta Chem. Scand.*, **11**, 571 (1957).

7) L. Engman, *Tetrahedron Lett.*, **23**, 3601 (1982); L. Engman and M. P. Cava, *J. Org. Chem.*, **47**, 3946 (1982).

8) D. L. Klayman and T. S. Griffin, *J. Am. Chem. Soc.*, **95**, 197 (1973).

9) D. Seyferth, H. Yamazaki, and D. L. Alleston, *J. Org. Chem.*, **28**, 703 (1963); C. L. Osborn, T. C. Shields, B. A. Shoulders, J. F. Krause, H. V. Cortez, and P. D. Gardner, *J. Am. Chem. Soc.*, **87**, 3158 (1965); C. L. Osborn, T. C. Shields, B. A. Shoulders, C. G. Gardenas, and P. D. Gardner, *Chem. Ind. (London)*, **1965**, 766; H. Nozaki, T. Aratani, and R. Noyori, *Tetrahedron*, **23**, *3645 (1967)*; *J. Monreau and P. Caubere, ibid.*, **27**, 5741 (1971); C. W. Jefford, D. Kirkpatrick, and F. Delay, *J. Am. Chem. Soc.*, **94**, 8905 (1972); H. Yamanaka, R. Oshima, K. Teramura, and T. Ando, *J. Org. Chem.*, **37**, 1734 (1972); J. T. Groves and K. W. Ma, *J. Am. Chem. Soc.*, **96**, 6527 (1974); R. M. Blankenship, K. A. Burdett, and J. S. Swenton, *J. Org. Chem.*, **39**, 2300 (1974); R. J. Kinney, W. D. Jones, and R. G. Bergman, *J. Am. Chem. Soc.*, **100**, 635 (1978) R. Barlet, *J. Org. Chem.*, **43**, 3500 (1978); T. Hirao, T. Masunaga, Y. Ohshiro, and T. Agawa, *ibid.*, **46**, 3745 (1981).

10) W. von E. Doering and A. K. Hoffmann, *J. Am. Chem. Soc.*, **76**, 6162 (1954); P. S. Skell and A. Y. Garner, *ibid.*, **78**, 5430 (1956).

The Alkylation of 1-Hydroxyanthraquinone with Visible-light Irradiation

Masahiro TAJIMA,* Haruo INOUE,† and Mitsuhiko HIDA†
General Education Course, Faculty of Engineering, Toyo University, Nakanodai Kujirai, Kawagoe 350
†*Department of Industrial Chemistry, Faculty of Technology, Tokyo Metropolitan University, Fukazawa, Setagaya-ku, Tokyo 158*
(Received July 2, 1983)

Synopsis. The 2-position of 1-hydroxyanthraquinone was alkylated by the use of tertiary amine or methanol with visible-light irradiation (λ>400 nm).

Recently various new reactions of anthraquinones with visible-light irradiation have been reported and have attracte much attention.[1] We ourselves have now found a photochemical alkylation of 1-hydroxy-9, 10-anthraquinone (**1**) by the use of tertiary amine or methanol with visible-light irradiation.

When **1** in aerated methanol was irradiated with the light of λ>400 nm in the presence of triethylamine, 1-hydroxy-2-methyl-9,10-anthraquinone (**2**) was obtained in a 54% yield (Table 1). The photoproduct, **2**, was identified by means of elemental analysis, IR, ^{1}H NMR, UV, and visible-absorption spectra in comparison with those of an authentic sample.[2] In acetonitrile or 2-propanol, however, a 2-ethyl-substituted product (**3**) and its dimer (**4**) were obtained in the photoreaction with triethylamine. All the spectral data suggested that the structure of the dimer was **4**. A similar alkylation was also observed when trioctylamine was used as the tertiary amine (Table 1). Without a tertiary amine, the photoalkylation was not observed at all in any solvent. The alkyl group of the tertiary amine was transferred into the quinone nucleus except for the reaction in methanol, which gave the methylated product regardless of the amine used.

No alkylation occurred in the cases of 1-methoxyanthraquinone (**6**) and 1-acetylaminoanthraquinone (**7**) each of which has an absorption maximum (**6**: λ_{max}=380 nm; **7**: λ_{max}=398 nm in ethanol) similar to that of **1** (λ_{max}=403 nm in ethanol). 1-Hydroxyanthraquinones have been revealed to have tautomerism and acid-base equilibria in their excited states,[3] and their photochemical behavior has been expected to be different from that of the other derivatives, which are unable to be converted to the 1,10-quinonoid form. The alkylation may be connected with the tautomer of **1**, 9-hydroxy-1,10-anthraquinone. Although we have no substantial evidence for the reaction mechanism, the alkylation seems to be closely related to the reactions between the tertiary amine and the benzene derivertives[4] which are induced by an electron transfer from the amine to the excited aromatics, followed by proton transfer. In methanol, the methoxide ion presumably behaves as an electron donor, for no reaction occurs in the absence of the tertiary amine, which can cause a dissociation of the methanol.

Experimental

Light irradiation was carried out by means of a 500 W high-pressure mercury lamp (Eikosha) through a solution filter (saturated aqueous solution of $NaNO_2$ (5 mm path length)), until the **1** in aerated methanol, acetonitrile, or 2-propanol disappeared completely. The initial concentration were 5.0×10^{-4} (in methanol), 3.0×10^{-3} (in acetonitrile), and 1.0×10^{-3} mol dm^{-3} (in 2-propanol). After the solvent and amine had been evaporated from the irradiated solutions, the products were separated by silica-gel column chromatography, using benzene as the eluent, and then recrystallized from benzene.

1-Hydroxy-2-methylanthraquinone (2): Mp 183.2—183.7 °C. Found: C, 75.46; H, 3.97%; M$^+$, 238. Calcd for $C_{15}H_{10}O_3$: C, 75.62; H, 3.97%; M$^+$, 238. IR(KBr) 2931, 2857, 1670, and 1637 cm^{-1}. ^{1}H NMR($CDCl_3$) δ=2.41 (3H, s, CH_3), 7.40 (1H, d, J=8 Hz), 7.5—7.9 (3H, m), 8.0—8.4 (2H, m), 12.93

Table 1. Photochemical alkylation of **1**[a]

$[R_3N]$/mol dm^{-3}		Solvent	Yield/%			
			2	**3**	**4**	**5**
R=C_2H_5	0.14	CH_3OH	54	—	—	—
R=C_2H_5	0	CH_3OH	0	—	—	—
R=C_2H_5	0.30	CH_3CN	—	43	19	—
R=C_2H_5	0.20	*i*-PrOH	—	43	4	—
R=$CH_2(CH_2)_6CH_3$	0.076	*i*-PrOH	—	—	—	67

a) Conversion was 100% in each run.

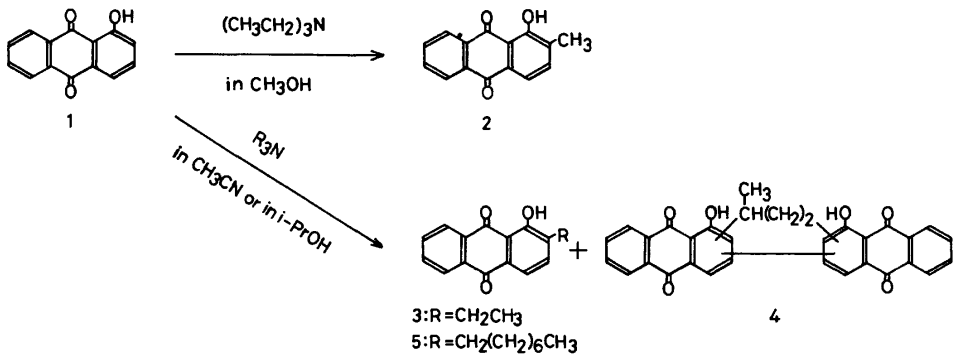

(1H, s, OH).

1-Hydroxy-2-ethylanthraquinone (3): Mp 167.9—168.8 °C. Found: C, 76.25; H, 4.60%. Calcd for $C_{16}H_{12}O_3$: C, 76.18; H, 4.79%. IR(KBr) 2960, 2920, 2878, 1672, and 1634 cm^{-1}. ^1H NMR ($CDCl_3$) δ=1.26 (3H, t, J=8 Hz, CH_3), 2.77 (2H, q, J=8 Hz, CH_2), 7.49 (1H, d, J=8 Hz), 7.6—7.9 (3H, m), 8.0—8.5 (2H, m), 12.83 (1H, s, OH).

Dimer(4): Mp 221.9—223.2 °C. Found: C, 76.50; H, 4.07%; M^+, 500. Calcd for $C_{32}H_{20}O_6$: C, 76.79; H, 4.03%: M^+,500. IR(KBr) 2964, 2926, 1667, and 1629 cm^{-1}. ^1H NMR ($CDCl_3$) δ=1.41 (3H, d, J=7 Hz, CH_3), 1.8—2.5 (2H, m, $CHC\underline{H}_2CH_2$), 2.85 (2H, t, J=7 Hz, $CHCH_2C\underline{H}_2$), 3.1—3.9 (1H, m, CH), 7.5—8.0 (6H, m), 8.1—8.4 (4H, m), 13.03 (1H, s, OH), 13.18 (1H, s, OH).

1-Hydroxy-2-octylanthraquinone (5): Mp 113.8—114.9 °C. Found: C, 78.34; H, 7.03%. Calcd for $C_{22}H_{24}O_3$: C, 78.54; H, 7.19%. IR(KBr) 2933, 2852, 1668, and 1629 cm^{-1}. ^1H NMR ($CDCl_3$) δ=0.87 (3H, t, J=4 Hz, CH_3), 1.0—2.0 (12H, m, $CH_2(C\underline{H}_2)_6CH_3$), 2.69 (2H, t, J=8 Hz, $C\underline{H}_2(CH_2)_6CH_3$), 7.40 (1H, d, J=8 Hz), 7.5—7.9 (3H, m), 8.0—8.4 (2H, m), 13.06 (1H, s, OH).

References

1) H. Inoue, T. D. Tuong, M. Hida, and T. Murata, *J. Chem Soc., D*, **1971**, 1347; J. Griffiths and C. Hawkins, *J. Chem. Soc., Chem. Commun.*, **1973**, 11; H. Inoue, A. Ezaki, H. Tomono, and M. Hida, *ibid.*, **1979**, 860.

2) An authentic sample of 1-hydroxy-2-methylanthraquinone was synthesized by the hydrolysis of diazotized 1-amino-2-methylanthraquinone, which had been obtained from 2-methylanthraquinone by nitration and subsequent reduction.

3) H. H. Richtol and B. R. Fitch, *Anal. Chem.*, **46**, 1749, 1860 (1974); H. Inoue, M. Tajima, M. Hida, N. Nakashima, and K. Yoshihara, *Chem. Phys. Lett.*, to be submitted.

4) D. Bryce-Smith, M. T. Clarke, A. Gilbert G. Klunklin, and C. Manning, *J. Chem. Soc., D*, **1971**, 916; M. Ohashi, K. Miyabe, and K. Tsujimoto, *Bull. Chem. Soc. Jpn.*, **53**, 1683 (1980).

The Dehydration of Ketohexoses into 5-Chloromethyl-2-furaldehyde. The Isolation of Diketohexose Dianhydrides

Kazuhiko HAMADA,* Hiroshi YOSHIHARA, Gohfu SUZUKAMO, and Osamu HIROAKI
Takatsuki Research Laboratory, Sumitomo Chemical Co., Ltd., Takatsuki, Osaka 569
(Received July 16, 1983)

Synopsis. The isolation of diketohexose dianhydrides, produced during the dehydration of D(−)-fructose and L(−)-sorbose with concentrated hydrochloric acid, in a mixture containing water, an organic solvent and a catalytic amount of a surface-active agent is described.

The chemistry of 2,5-disubstituted furan derivatives has attracted attention recently in connection with the transformation of carbohydrates into useful organic intermediates. We ourselves have previously reported an improved method for synthesizing 5-chloromethyl-2-furaldehyde (CFAL), a potent intermediate of synthetic pyrethroid, in a high yield from saccharides with mineral acids.[1] The present work will describe the isolation and structural determination of diketohexose dianhydrides produced during the early stage of the reaction.

Experimental

In a typical run, D(−)-fructose, 4 equiv. of concd hydrochloric acid, and a catalytic amount of a cationic surface-active agent ($C_{12}H_{25}N^+(CH_3)_3Cl^-$) were mixed and stirred at 15—20 °C for 2 h ("pre-reaction solution"). This "pre-reaction solution" was then added, drop by drop, to an inert organic solvent (benzene, toluene, or chlorobenzene), and maintained at 80 °C for about 30 min with stirring. After the temperature of the solution had been allowed to drop to room temperature under continuous stirring (1—2 h), a small amount of water and some active charcoal were added and the mixture was stirred further. The organic layer separated after filtration was washed with a saturated aqueous NaCl solution twice, dried over anhydrous sodium sulfate, and concentrated to obtain CFAL in a yield of 70%.[2]

Results and Discussion

The polarimetric analysis of the "pre-reaction solution" revealed that the addition of a catalytic amount of a surface-active agent accelerated the pyranose-furanose mutarotation rate of D(−)-fructose twice as much as in a solution containing D(−)-fructose and concd hydrochloric acid. The HPLC analysis of the "pre-reaction solution"[3] revealed that the two compounds, **1** and **2** (total 45%;[4] **1**/**2**=2.5/1) were equibrated with the remaining D(−)-fructose **3** (55%) at the end of the "pre-reaction." The isolation of these products using HPLC or cellulose-column chromatography[5] was carried out, and then they were studied spectroscopically. **1** and **2** were attributed to be difructose dianhydrides.[6] The D-fructose rings in **2** were found by periodate oxidation to be pyranoid moieties only; **1** possessed one pyranoid and one furanoid resudue. The proton signals of ^{1}H NMR[7] of the peracetylated difructose dianhydrides in benzene-d_6 were resolved to permit first-order analysis; each of these sugars was thus found to possess three rings, one substituted 1,4-dioxane and two D-fructose.[8] The conformations of the ring systems and the anomeric configurations were determined by means of ^{13}C NMR[7] (Table 1). The structures of **1** and **2** were found to be 1′,2-anhydro-1-*O*-α-fructopyranosyl-(1C)-β-D-fructofuranose-(E3) ($[\alpha]_D^{20}$ =−36°; *c* 3.5, H_2O) and 1′,2-anhydro-1-*O*-α-D-fructopyranosyl-(1C)-α-D-fructopyranose-(C1) ($[\alpha]_D^{20}$=−49°; *c* 3.1, H_2O) respectively, which coincided with the known difructose dianhydrides.[9] A ^{13}C NMR study[10] of the remaining D(−)-fructose fraction, **3** ($[\alpha]_D^{20}$=−41—−44°; *c* 2.6, H_2O, 2 h), by means of the measurement

Table 1. ^{13}C NMR chemical shifts[a] of **1** and **2**

Assignment	Chemical shifts of ^{13}C resonances of	
	1[b]	**2**[c]
C-2		
β-D-Fructofuranose	103.1	
β-D-Fructopyranose		
α-D-Fructopyranose	96.5	95.6, 94.2
C-3, C-4, C-5		
β-D-Fructofuranose	84.4, 82.7, 78.6	
D-Fructopyranose	69.8, 69.8, 69.4	71.6, 71.2, 69.3, 69.3
C-1, C-6		
Pyranose	64.3, 62.4	64.0, 63.6
Furanose	62.1, 62.1	61.6, 61.2, 60.0

a) Chemical shifts are expressed in δ downfield from the ^{13}C resonance of Me_4Si. b) Measured in D_2O. c) Measured in DMSO-d_6.

Table 2. Chemical shifts and coupling constants of the methine and methylene protons of hexaacetates[a] of **4** and **5**

Proton	Chemical shifts, δ (Coupling constants/Hz in benzene-d_6)	
	4	**5**
H-1	4.02	3.71
H-1	3.71	3.71
H-1′	3.65	3.84
H-1′	3.50	4.09
H-3 (*J* 3,4)	5.53(10.4)	5.62(10.5)
H-4 (*J* 4,5)	5.75(3.7)	5.82(3.6)
H-5 (*J* 5e,6a)	5.46(1.6)	5.48
H-6 (*J* 5e,6e)	3.42(1.7)	3.41
H-6 (*J* 6e,6a)	3.52(−12)	3.53(−11)
H-3′(*J* 3′,4′)[b]		5.44(1.7)
H-4′(*J* 4′,5′)[b]		5.23(5.6)
H-5′(*J* 5′,6′)	5.39(8.7)	4.09(3.6)
H-6′(*J* 5′,6′)	3.57(4.5)	4.30(4.5)
H-6′(*J* 6′,6′)	3.90(−10)	4.54(−11)

a) Acylation conditions: A 0.9-g portion of **4** (or **5**) in pyridine (12 ml) was reacted with acetic anhydride (8 ml) at 15 °C for 3 d (yield=70%). b) As the signals for H-3′, H-4′, and H-5′ in the second pyranoid ring of **4** were not resolved, its conformation was determined by an analysis of the H-6′ resonance patterns.

Table 3. ^{13}C NMR chemical shifts[a] of 4 and 5

Assignment	Chemical shifts of ^{13}C resonances of	
	4[b]	5[b]
C-2		
α-L-Sorbofuranose		100.5
β-L-Sorbopyranose	97.9, 97.7	
α-L-Sorbopyranose		95.2
C-3, C-4, C-5		
α-L-Sorbofuranose		83.9, 81.9, 77.0
C-3, C-4, C-5		
L-Sorbopyranose	74.0, 72.3, 72.3	74.1, 72.5, 70.0
	71.9, 69.9, 69.0	
C-1, C-6		
Pyranose	62.9, 62.5, 62.2	62.6, 62.6
Furanose	59.6	62.0, 61.9

a) Chemical shifts are expressed in δ downfield from the ^{13}C resonance of Me_4Si. b) Measured in D_2O.

of the integration of the peak intensities, clarified the equilibrium composition at 20 °C: α-D-fructofuranose 25%, β-D-fructofuranose 17%, β-D-fructopyranose 57%. It should be noted that the isolated **1** was converted into CFAL in a yield of only about 40%[2] under the present reaction conditions.

In the same way, the treatment of L(−)-sorbose with 4 equiv. of concd hydrochloric acid in the presence of a catalytic amount of a surface-active agent (*e.g.*, $C_{16}H_{33}N^+(CH_3)_3Cl^-$ or $C_{12}H_{25}N^+(CH_3)_3Cl^-$) under stirring at 20 °C for 4 h afforded two compounds, **4** and **5** (total 20%), equibrated with the remaining L(−)-sorbose (80%). The isolation of **4** and **5** using HPLC[3] was then carried, and the spectroscopic data were obtained. **4** and **5** were thus identified as disorbose dianhydrides.[11] The L-sorbose rings in **4** were found by periodate oxidation to be pyranoid moieties only; **5** possessed one furanoid and one pyranoid residue. A ^1H NMR[7] of the peracetylated disorbose dianhydrides (Table 2) showed the conformational structures of **4** and **5** to be 1′,2-anhydro-1-*O*-L-sorbopyranosyl-L-sorbopyranose and 1′,2-anhydro-1-*O*-L-sorbopyranosyl-L-sorbofuranose respectively. ^{13}C NMR was used to determine the anomeric configurations of the two compounds (Table 3). The structures of **4** and **5** were thus identified as new disorbose dianhydrides, 1′,2-anhydro-1-*O*-β-L-sorbopyranosyl-(1C)-β-L-sorbopyranose-(Cl) ($[\alpha]_D^{20}=-107°$; *c* 0.17, H_2O) and 1′,2-anhydro-1-*O*-α-L-sorbopyranosyl-(E3)-α-L-sorbopyranose-(1C) ($[\alpha]_D^{20}=-121°$; *c* 0.40, H_2O) respectively (Fig. 1).

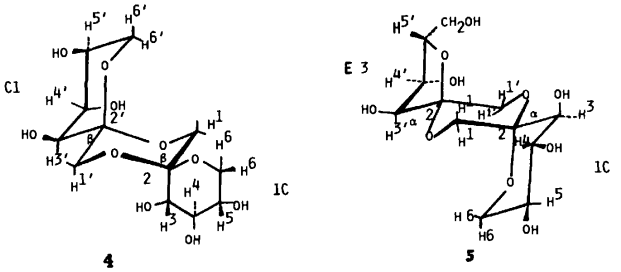

Fig. 1. Disorbose dianhydrides.

References

1) K. Hamada, H. Yoshihara, and G. Suzukamo, *Chem. Lett.*, **1982**, 617.

2) GC analysis: LAC-2R 446/H_3PO_4, 2 m, 130 °C.

3) HPLC study: μ-BONDAPAK, Carbohydrates, CH_3CN/H_2O=85/15, 2 ml/min, RI. The "pre-reaction solution" was neutralized with Et_3N. Maltose was used as the Internal Standard.

4) **1** and **2**: total 25%, **1**/**2**=1.5/1.0 ("pre-reaction solution" without the addition of a catalytic amount of a surface-active agent).

5) Cellulose: 4 cm$^\phi$×70 cm; $CH_3COOC_2H_5$/C_2H_5OH/H_2O=6/3/1–3/3/4.

6) **1**=**2**: CI-MS, *m*/*z* 163 ($C_6H_{12}O_6$ (fructose)−H_2O)+1; FD-MS, *m*/*z* 347 2 ($C_6H_{12}O_6$(fructose)−H_2O)+Na; elemental analysis; **1** Found: C, 46.4; H, 7.1%. **2** Found: C, 45.1; H, 6.3%.

7) ^1H NMR: 200 MHz, Varian XL-200, FT-NMR. ^{13}C NMR: 50.3 MHz, Varian XL-200, FT-NMR.

8) R. W. Binkley, W. W. Binkley, and A. A. Grey, *Carbohydr. Res.*, **28**, 365 (1973).

9) R. W. Binkley, W. W. Binkley, and B. Wickberg, *Carbohydr. Res.*, **36**, 196 (1974); K. Tanaka, T. Uchiyama, and A. Itoh, Japan Patent 117688 (1974).

10) D. Doddrell and A. Allerhand, *J. Am. Chem. Soc.*, **93**, 2779 (1971).

11) FD-MS: **4**, *m*/*z* 347; **5**, *m*/*z* 347. Elemental analysis: **4** Found: C, 45.3; H, 6.0%. **5** Found: C, 46.2; H, 6.1%. Calcd for $C_{12}H_{20}O_{10}$: C, 44.5; H, 6.2%.

The Formation and Solubility of Various Lead(II) Compounds Prepared by the Hydrolysis of Lead(II) Nitrate

Eiichi NARITA,* Hiroshi OKAYASU, and Hiroyuki NAITO†

Department of Applied Chemistry, Faculty of Engineering, Tohoku University, Aramaki, Sendai 980

†Mizusawa Factory, Mizusawa Industrial Chemicals, Ltd., Nishime, Tsuruoka 999-75

(Received January 10, 1983)

Synopsis. Lead(II) nitrate was hydrolyzed by mixing with sodium hydroxide solutions at 25 and 50 °C. Four kinds of lead(II) hydroxide nitrates and two kinds of lead(II) oxides (massicot and litharge) were formed, depending on the pH, temperature, lead(II) nitrate concentration, and aging time of the suspension. The solubility of the products was also measured.

It is generally known that the kind of product obtained by the hydrolysis of lead(II) salts strongly affected by coexisting anions in the resulting suspension,[1,2] and that various basic lead(II) compounds are formed according to the formation conditions.[3-11] Among these studies, the hydrolysis of lead(II) chloride[3] and lead(II) acetate[4] have been investigated in detail. On the hydrolysis of lead(II) nitrate, the formation of various lead(II) hydroxide nitrates has been reported by earlier workers.[5-9] However, some of them have been thought to be ambiguous. Although recent results on the chemical composition of the products were reported by Kwestroo *et al.*[10] and Brusset *et al.*,[11] both results were partially different. Therefore, reliable information about the kind of the product from the hydrolysis of lead(II) ion in the presence of nitrate ion is needed, together with data about these particle characteristics and solubilities. This study will deal with the hydrolysis of lead(II) nitrate, especially with the effects of changes in pH, temperature, concentration of lead(II) nitrate and aging time on the kind, particle characteristic and solubility of the products.

Experimental

A 300 cm^3 acrylic resin cylindrical reactor was equipped with a reflux condenser, a dropping funnel, a nitrogen gas inlet tube, a glass electrode of a pH meter, a thermometer, and a magnetic stirrer. A 50 cm^3 portion of NaOH solutions was transferred to the reactor and maintained at 25±0.2 or 50±0.2 °C. Then, a 200 cm^3 portion of $Pb(NO_3)_2$ solution in the dropping funnel was added to the stirred NaOH solution. Total lead concentration in the suspension obtained after the mixing was set to be 0.05 and 0.5 M (1 M=1 mol dm^{-3}). Unless otherwise stated, the resulting suspension was stirred for a further 1 h. All procedures were carried out under nitrogen atmosphere. After measuring the pH of the suspension, the product was filtered off, washed with distilled water, and then dried at room temperature under reduced pressure. The identification of the product and the quantitative analysis of binary mixtures were made by X-ray diffractometry using a Rigaku Denki Geigerflex 2013 with Ni filtered Cu $K\alpha$ radiation, with 30 kV and 10 mA. The observation of the product was performed using a Hitachi-Akashi Scanning Electron Microscope MSM 4C-102. The solubility of the product was determined by analyzing the filtrate for lead ion with atomic absorption spectroscopy.

Results and Discussion

The kind and solubility of the products at various pH values of the suspension are shown in Fig. 1. On the hydrolysis of 0.5 M $Pb(NO_3)_2$ at 25 °C (A in Fig. 1), the basicity in the chemical composition of the precipitated lead(II) hydroxide nitrates increased with increasing pH of the suspension, namely $Pb(NO_3)_2 \cdot Pb(OH)_2$ (phase **a**, white), $2Pb(NO_3)_2 \cdot 5Pb(OH)_2$ (phase **b**, white), and $Pb(NO_3)_2 \cdot 5Pb(OH)_2$ (phase **d**, white), or a binary mixture of these three at pH range of 6—13. The pH range of the formation of binary mixtures was negligible. This tendency was the same as the results reported by earlier workers.[10,11] The X-ray diffraction patterns of these lead(II) hydroxide nitrates were identical with those reported by Kwestroo *et al.*[10] However, the formation of $Pb(NO_3)_2 \cdot 2Pb(OH)_2$ and $3Pb(NO_3)_2 \cdot 7Pb(OH)_2$ identified as an intermediate by Brusset *et al.*[11] from potentiometric and conductimetric measurements was not observed here after aging of 1 h, because of the unstability of these compounds. If the resulting suspension contains no anions, for example, in the case of the hydrolysis of lead(II) alkoxide,[12,13] massicot (orthorhombic), litharge (tetragonal), or hydrous lead(II) oxide ($3PbO \cdot H_2O$, tetragonal) should be formed over the same pH range. It was also found that the solubility of lead(II) hydroxide nitrates decreased with increasing basicity of products and was minimized at the pH range of 10—11. At the pH values higher than 11, the solubility gradually increased, and massicot (phase **M**, yellow) and litharge (phase **L**, red) were formed. Figure 2 shows the scanning electron micrographs of typical lead(II) hydroxide nitrates obtained here. The particle sizes were considerably smaller than those of massicot (10—20 μm) and litharge (5—10 μm).

On the hydrolysis of 0.05 M $Pb(NO_3)_2$ at 25 °C (B in Fig. 1), the pH range of the formation of these lead(II) hydroxide nitrates was shifted, on the whole, to the pH side lower than that of A in Fig. 1. It was also found that the pH range of the formation of massicot was broadened. This means that the stable phase is easily formed by decreasing the concentration of $Pb(NO_3)_2$. The particle sizes of these precipitates became progressively greater as the concentration of $Pb(NO_3)_2$ became lower, as shown in Fig. 2(e), whereas no changes in the particle shape were observed.

At a higher temperature (50 °C, C in Fig. 1), the pH range of the formation of these lead(II) hydroxide nitrates was further shifted to the lower pH side and the particle sizes of these precipitates further increased, as shown in Fig. 2(f).

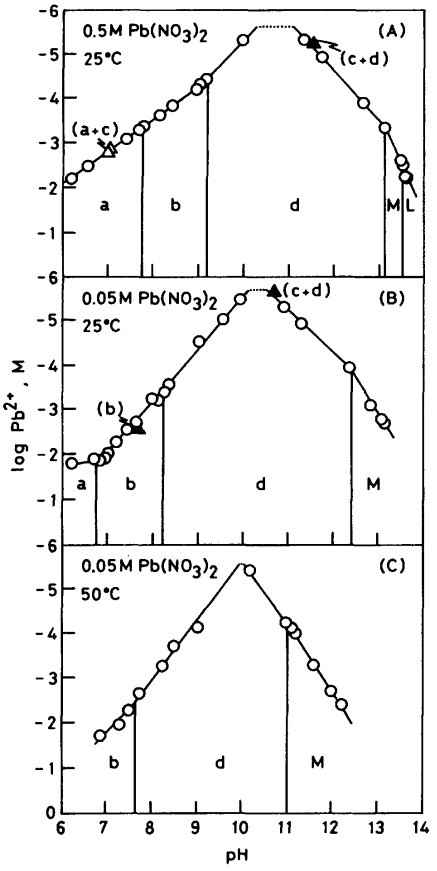

Fig. 1. Solubilities of lead(II) compounds at various pH values of the suspensions.
(a): $Pb(NO_3)_2 \cdot Pb(OH)_2$, (b): $2Pb(NO_3)_2 \cdot 5Pb(OH)_2$, (c): $Pb(NO_3)_2 \cdot 3Pb(OH)_2$, (d): $Pb(NO_3)_2 \cdot 5Pb(OH)_2$, (M): massicot, (L): litharge.
Aging time(h): ○ 1, △ 8, ▲ 24.

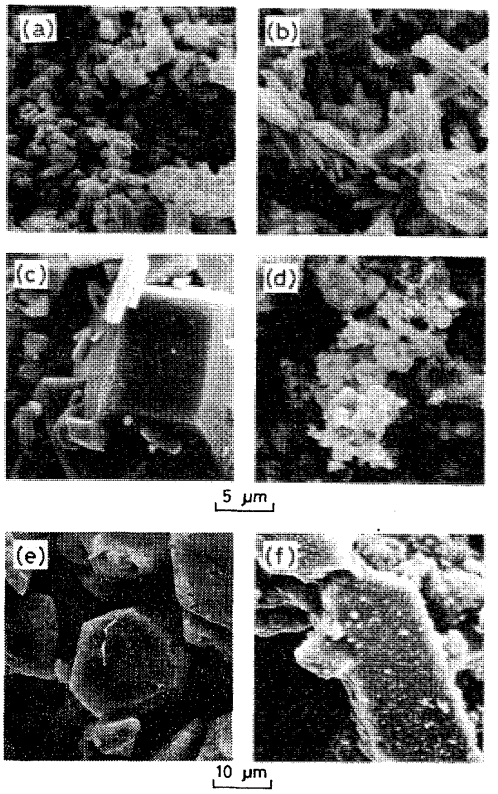

Fig. 2. Scanning electron micrographs of lead(II) hydroxide nitrates prepared by hydrolysis of lead(II) nitrate.
(a)—(d): samples in Fig. 1(A), (e): sample in Fig. 1(B), (f): sample in Fig. 1(C).
(a),(e): $Pb(NO_3)_2 \cdot Pb(OH)_2$, (b),(f): $2Pb(NO_3)_2 \cdot 5Pb(OH)_2$, (c): $Pb(NO_3)_2 \cdot 3Pb(OH)_2$, (d): $Pb(NO_3)_2 \cdot 5Pb(OH)_2$.

When the aging time was prolonged, the initial pH of the suspension of only 8—9 was occasionally changed; one of the reasons for this phenomenon is thought to be the occurrence of another phase during the aging. The kind and solubility of the products were changed with variation of pH. However, the solubility was found to change along with the solubility curves shown in Fig. 1 and there was no difference with the solubility values measured after 1 h. One other phase, $Pb(NO_3)_2 \cdot 3Pb(OH)_2$ (Phase c, white) was formed together with $Pb(NO_3)_2 \cdot 5Pb(OH)_2$, the formation ratio of c/d being as about 4 after 24 h. This phase was also formed together with $Pb(NO_3)_2 \cdot Pb(OH)_2$, the formation ratio of c/a being as about 6 after 8 h. Kwestroo *et al.*[10] identified it only in diluted reaction mixtures. In this experiment it was obtained by aging the resulting mixtures for a while. As can be seen in Fig. 2(c), the particle size of $Pb(NO_3)_2 \cdot 3Pb(OH)_2$ was larger than those of the coprecipitated $Pb(NO_3)_2 \cdot Pb(OH)_2$ and $Pb(NO_3)_2 \cdot 5Pb(OH)_2$.

The authors wish to thank Prof. Taijiro Okabe of the Department of Applied Chemistry, Tohoku University, for his helpful discussion.

References

1) "Gmelin's Handbuch der Anorganischen Chemie," No. 47, "Blei 1," Verlag Chemie, Weinheim-Bergstr. (1969), p. 58.
2) C. F. Baes, Jr., and R. E. Mesmer, "The Hydrolysis of Cation," John Wiley & Sons, Inc., New York (1976), p. 358.
3) M. Kiyama, K. Murakami, T. Takada, I. Sugano, and T. Tsuji, *Chem. Lett.*, **1976**, 23.
4) H. Torii, M. Kiyama, and T. Takada, *Bull. Inst. Chem. Res., Kyoto Univ.*, **56**, 247 (1978).
5) J. Bye, *Bull. Soc. Chim. Fr.*, **1947**, 205.
6) A. Berton, *Bull. Soc. Chim. Fr.*, **1947**, 289.
7) J. Heubel, *Ann. Chim.*, **4**, 699 (1949).
8) J. L. Pauley and M. K. Testerman, *J. Am. Chem. Soc.*, **76**, 4220 (1954).
9) E. Michell, *J. Appl. Chem. Biotechnol.*, **24**, 571 (1974).
10) W. Kwestroo, C. Langereis, and H. A. M. van Hal, *J. Inorg. Nucl. Chem.*, **29**, 33 (1967).
11) H. Brusset, J. J. P. Martin, C. Martin-Lefevre, Y. Repelin, E. Husson, and B. Despagne, *Can. J. Chem.*, **50**, 184 (1972).
12) O. Yamaguchi, M. Yamadera, and K. Shimizu, *Bull. Chem. Soc. Jpn.*, **50**, 2805 (1977).
13) E. Narita, M. Kobayashi, H. Shinjo, H. Tsuchida, and H. Naito, *Bull. Chem .Soc. Jpn.*, **56**, 3129 (1983).

Viscosity of the Quaternary Gaseous Mixture He-N_2-O_2-CO_2

Ali BOUSHEHRI* and Shahrbanoo RAHMANSETAYESH
Department of Chemistry, Shiraz University, Shiraz, Iran
(Received December 6, 1982)

Synopsis. The kinetic theory expressions for multicomponent gas mixtures are used in conjunction with the law of corresponding states formulated by Kestin, Ro and Wakeham to generate the viscosities of the quaternary gaseous mixture He-N_2-O_2-CO_2. The calculated viscosities are compared with direct measurements performed in a capillary flow apparatus.

The extended law of corresponding states of Kestin, Ro, and Wakeham[1-3] has provided the correlation of low-density equilibrium and transport properties of the monatomic gases and their mixtures with an uncertainty commensurate with the experimental accuracy. In an earlier paper[4] it has been established that the viscosity of the quaternary mixture N_2-O_2-CO_2-N_2O conforms to the extended law of corresponding states. In this work the kinetic-theory expressions for multicomponent gas mixture are used in conjunction with the law of corresponding states and the appropriate scaling parameters σ_{ij} and ε_{ij} to generate the viscosities of He-N_2-O_2-CO_2 mixture. The calculated viscosities are compared with direct measurements made by a capillary flow method at temperatures 0 and 40 °C. For the viscosity we can employ the known formula[5]

$$\mu(T) = (-1)\begin{vmatrix} H_{11} & H_{12}\cdots H_{1n} & X_1 \\ H_{21} & H_{22}\cdots H_{2n} & X_2 \\ H_{n1} & H_{n2}\cdots H_{nn} & X_n \\ X_1 & X_2\cdots X_n & 0 \end{vmatrix} \Bigg/ \begin{vmatrix} H_{11} & H_{12}\cdots H_{1n} \\ H_{21} & H_{22}\cdots H_{2n} \\ H_{n1} & H_{n2}\cdots H_{nn} \end{vmatrix}^{-1}, \quad (1)$$

where X_i is the fraction of component i, and the element H_{ij} are written as:

$$H_{ii} = \frac{X_i}{\mu_i} + \sum_{\substack{k=1 \\ k\neq i}}^{n} \frac{2X_iX_k}{\mu_{ik}} \frac{M_iM_k}{(M_i+M_k)^2}\left(\frac{5}{3A^*_{ik}} + \frac{M_k}{M_i}\right), \quad (1a)$$

$$H_{ij} = -\frac{2X_iX_j}{\mu_{ij}} \frac{M_iM_j}{(M_i+M_j)^2}\left(\frac{5}{3A^*_{ij}} - 1\right) i \neq j. \quad (1b)$$

Here M_i represents the molecular weight of species i in the mixture. The interaction viscosity μ_{ij} is determined from:

$$\mu_{ij} = 5/16(k\,M_{ij}\,T/\pi N)^{1/2}(1/\sigma_{ij}^2\Omega_{22}), \quad (2)$$

where $M_{ij}=2M_iM_j/(M_i+M_j)$ and σ_{ij} is a distance scaling parameter.

It should be mentioned that the recently determined scaling parameters for rare-gas pairs by Kestin and coworkers perform a discrepancy by a factor of 1.016 in the distance of zero potential.[6,7]

The best empirical expressions for the universal functions of the single parameter $T^*=k_BT/\varepsilon_{ij}$ determined by Kestin *et al.* are given as:

$$\Omega_{11} = \Omega^{(1,1)*} = \exp[0.347 - 0.444(\ln T^*) + 0.093(\ln T^*)^2 - 0.010(\ln T^*)^3], \quad 0.5<T^*<25, \quad (3)$$

$$\Omega_{22} = \Omega^{(2,2)*}/f_\mu = \exp[0.45667 - 0.53955(\ln T^*) + 0.18265(\ln T^*)^2 - 0.03629(\ln T^*)^3 + 0.00241(\ln T^*)^4], \quad 1<T^*<90, \quad (4)$$

where f_μ is higher-order correction to the viscosity and:

$$A^* = \Omega^{(2,2)*}/\Omega^{(1,1)*} \simeq \Omega_{22}/\Omega_{11}.$$

The quantities Ω_{22} and A^*_{ij} are functionals of the potential energy function describing the interaction of molecular pairs. Equations 1—4 together with a knowledge of the scaling parameters σ_{ij} and ε_{ij} characteristic of the i-j interaction permit the evaluation of the viscosity μ of He-N_2-O_2-CO_2 at any composition and any desired temperature.

With the aid of the scaling factors, the universal functions provide us with a sharp criterion which permits us to disqualify guessed analytic forms of the pair potential. The (11-6-8) potential proposed by Hanley and Klein[8] is acceptable as a correlator data (for $1\leq T^*\leq 20$), even this potential fails for helium at high reduced temperatures. For the temperature range considered here, we are able (within the precision of the experimental data) to neglect the quantum effects for the present gaseous mixtures.

Experimental

The measurements reported here were made with a constant-volume gas viscometer similar to that of McCoubrey and Singh.[9] The viscometer bulb and capillary were thermostated in a water bath except at 0 °C where an ice-slush was used. The bath was controlled to within ±0.1 °C. Pressures were measured with a travelling microscope reading to 0.05 mm and the times with a precision stopwatch (calibrated in tenths of a second). The apparatus constant at each temperature was determined from the wellknown Poiseuille equation modified for slip correction. The apparatus constant at each temperature was determined using nitrogen and checked with oxygen (whose viscosities are known). The pressure range in these measurements was 22—11 cm mercury.

Nitrogen was supplied by the Matheson Co. Oxygen and helium were obtained from Fluka Co. Carbon dioxide was

TABLE 1. VISCOSITY OF QUATERNARY MIXTURES

Compn (mole fraction)				Temp	Viscosity/μP		
He	N_2	O_2	CO_2	°C	Exptl	Calcd	Deviation(%)
0.10	0.50	0.25	0.15	0	178.5	176.3	1.25
				40	197.2	197.0	0.10
0.25	0.25	0.25	0.25	0	182.6	185.8	−1.72
				40	208.6	207.9	0.34

supplied by the Chemical Co., Shiraz, Iran. The minimum purities were 99%. For each mixture, viscosity results at each temperature were averaged from at least three runs.

Results and Discussion

The experimental results for He–N_2–O_2–CO_2 are given in Table 1. The viscosity of the two quaternary mixtures can be calculated with the aid of Eqs. 1—4 and scaling parameters, for the gases He, N_2, O_2, and CO_2, taken from Ref. 10. Evalution of the viscosity is made by using computer program developed by Kestin and co-workers. The scheme presented here may be used for the generation of viscosity for any mixtures of these same gases.

References

1) J. Kestin, S. T. Ro, and W. A. Wakeham, *Physica*, **58**, 165 (1972).

2) J. Kestin, S. T. Ro, and W. A. Wakeham, *J. Chem. Phys.*, **56**, 4119 (1972).

3) J. Kestin and E. A. Mason, "Transport Phenomena-1973," ed by J. Kestin, AIP Conf. Proc. (1973), Vol. 11, p. 137.

4) A. Boushehri and B. Najafi, *J. Chem. Eng. Data*, **24**, 24 (1979).

5) J. O. Hirschfelder, C. F. Curtiss, and R. B. Bird, "Molecular Theory of Gases and Liquids," 2nd ed, John Wiley and Sons, New York (1964).

6) A. Boushehri, L. A. Viehland, and E. A. Mason, *Physica*, **91A**, 424 (1978).

7) A. Boushehri, *Physica*, **97A**, 206 (1979).

8) H. J. M. Hanley and M. Klein, *J. Chem. Phys.*, **53**, 4722 (1970).

9) J. C. McCoubrey and N. M. Singh, *Trans. Faraday Soc.*, **53**, 877 (1957).

10) J. Kestin, H. E. Khalifa, S. T. Ro, and W. A. Wakeham, *Physica*, **88A**, 242 (1977).

Concentration Dependence of Transport Properties of Glass-forming Melts

Sheik MAHIUDDIN and Kochi ISMAIL*
Department of Chemistry, North-Eastern Hill University, Bijni Campus, Laitumkhrah, Shillong 793003, India
(Received March 10, 1983)

Synopsis. The Vogel-Tammann-Fulcher (VTF) equation has been derived from the Adam-Gibbs (AG) model after accounting for the empirical nature of the temperature dependence of configurational heat capacity. An expression for describing the concentration dependence of the preexponential parameter of the VTF equation and another two-parameter isothermal equation for describing such dependences of transport properties are obtained. The applicability of the newly derived equations has been verified using the data available for several hydrate melts. The present study emphasizes the view that the glass transition temperature controls the concentration dependence of transport properties of glass-forming melts.

A large amount of literature[1-8] on the transport properties of binary molten systems containing at least one component as the hydrated salt has been accumulated. The temperature dependence of the transport properties of all such molten salt systems has been described in terms of the VTF equation

$$Y = A_y T^{-1/2} \exp[-B_y/(T-T_{oy})], \quad (1)$$

where Y is the transport property, either fluidity (ϕ) or equivalent conductance (Λ). T is the absolute temperature. A_y, B_y, and T_{oy} are the three constant parameters. Empirically these three parameters have been found to have dissimilar types of concentration dependence. B_y remains almost independent of concentration in binary molten systems containing either anhydrous or hydrated salts (or both). The ideal glass transition temperature, T_{oy} has been found to vary linearly with concentration in almost all the binary melts studied.

On the other hand, the dependence of A_y parameter on concentration is comparatively less understood and the nature of this dependence is found to be inconsistent in the various systems studied. For instance, studies made by Islam and coworkers[4-7] have revealed a linear dependence of A_y on concentration. Instead, Moynihan *et al.*[3] observed a linear variation of $\ln A_y$ with concentration in the molten mixture of calcium nitrate tetrahydrate and cadmium nitrate tetrahydrate and this trend was found to be contrary to the be havior expected from the free volume model.[9]

The objective of this paper is therefore to obtain an analytical expression to describe the observed trend in the variation of A_y with concentration and then to derive an isothermal equation for representing the concentration dependence of fluidity and conductance of binary mixture containing hydrate melt or melts. The approach adopted to achieve this is to insert the temperature dependence of heat capacity in the AG equation.[10]

Derivation of the New Isothermal Equation. As adopted by others,[11-13] in the absence of a rigorous theoretical description for the variation of heat capacity, C_p of molten salt systems with temperature, an alternative approach to account for the temperature dependence of configurational heat capacity, ΔC_p would be to take into cognizance the general trend in the empirical behavior of C_p with T. It is interesting to note from the reported heat capacity data for hydrate melts[14] and molecular liquids[12,15] that their C_p exhibits a linear dependence on T in the glassy as well as liquid regions. Accordingly, ΔC_p may be written as

$$\Delta C_p = \Delta C_o + \Delta C_1(T-T_o), \quad (2)$$

where $\Delta C_o = C_{ol} - C_{og}$ and $\Delta C_1 = C_{1l} - C_{1g}$. C_{ol} is the extrapolated heat capacity of the melt at T_o, C_{1l} is the slope of the linear variation of melt heat capacity with T, C_{og} is the heat capacity of the corresponding glass at T_o, C_{1g} is the slope of the linear variation of glass heat capacity with temperature. It may be noted that ΔC_1 becomes a negative, zero, or positive term depending upon the relative rates of change (linear) of C_p of mels and glass with T. For example, in $Ca(NO_3)_2 \cdot 4H_2O$,[14] $Cd(NO_3)_2 \cdot 4H_2O$,[14] $Mg(OAc)_2 \cdot 4H_2O$,[14] *o*-terphenyl,[12,15] *o*-benzylphenol,[12] and phenyl salicylate[12] ΔC_1 is found to be a negative quantity and Eq. 2 resembles with the function used for ΔC_p by Laughlin and Uhlmann[12] as well as with one of the probable functiont suggested by Privalko.[13] Substituting Eq. 2 in the AG equation[10] and then by making a few approximations, we get for Y an expression of the form

$$Y = A_{1y} T^{-1/2} \exp(B_{1y}/T_{oy}) \times \exp[-B_{1y}(1-\Delta C_1 T_{oy}/\Delta C_2)/(T-T_{oy})], \quad (3)$$

where A_{1y} and B_{1y} are constant parameters and $\Delta C_2 = \Delta C_o - \Delta C_1 T_o$. It is interesting to find that Eq. 3 is similar to the VTF equation and comparison of Eqs. 1 and 3 gives

$$A_y = A_{1y} \exp(B_{1y}/T_{oy}), \quad (4)$$

$$\text{and } B_y = B_{1y}[1-(\Delta C_1/\Delta C_2)T_{oy}]. \quad (5)$$

The empirical fact that B_y remains almost independent of concentration appears to imply that in molten salt systems the term $\Delta C_1/\Delta C_2$ is proportional to $1/T_{oy}$. By taking into account in Eq. 3 the constancy of B_y and the linear variation of T_{oy} with mole fraction of the solute, x, we obtain an isothermal expression for describing the concentration dependence of Y which approximates after neglecting the higher powers of x to

$$Y = A_y^* \exp(\pm Q_y^* X), \quad (6)$$

A_y^* and Q_y^* are empirical constants. The negative sign of the exponent in Eq. 6 is valid when T_o increases with x and the positive sign corresponds to the case of T_o decreasing with x.

On the Application of Eqs. 5 and 7. To justify the suitability of Eq. 4 for describing the variation of A_y parameter with concentration, exemplary plots of $\ln A_y$ *versus* $1/T_{oy}$ using their reported values are drawn in Fig. 1 for some of the molten mixtures.[3,4b,5,6] The linearity of these plots justifies the validity of Eq. 4. Furthermore, on substituting the linear concentration dependence of T_o (decrease or increase) in Eq. 4 it approximates to (after

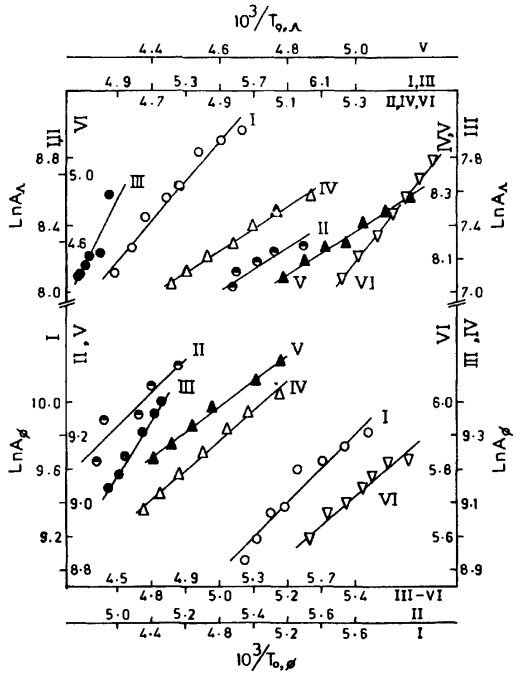

Fig. 1. Plots of $\ln A_y$ *versus* $1/T_{oy}$ for binary melts. The plots I to VI correspond to the six systems given in Table 1 and are in the same order.

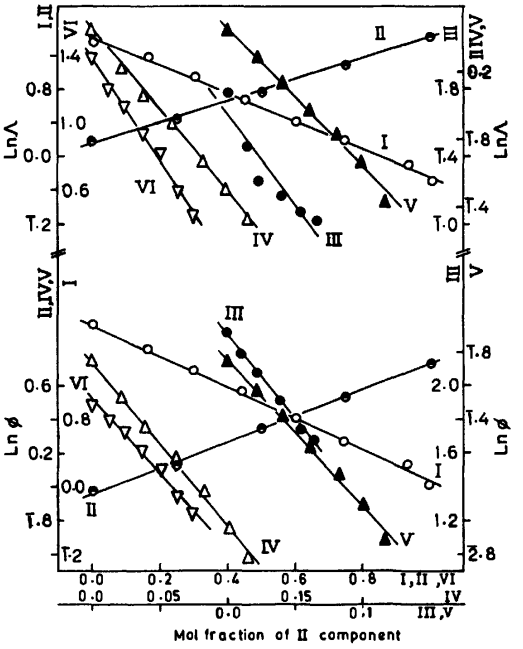

Fig. 2. Plots of $\ln Y$ *versus* mole fraction of the second component for binary melts. The plots I to VI correspond to the six systems given in Table 1 and are in the same order.

neglecting higher powers of x)

$$\ln A_y = A'_y \pm B'_y X, \qquad (7)$$

where A'_y and B'_y are another set of constant parameters. It is interesting to find that Eq. 7 explains the empirical behavior of A_y with concentration in molten $Ca(NO_3)_2 \cdot 4.09H_2O + Cd(NO_3)_2 \cdot 4.07H_2O$ mixture which could not be explained[3] on the basis of the free volume model[9] as mentioned above.

To verify the applicability of Eq. 6, the reported fluidity and equivalent conductance data at 313 K for the various molten mixtures cited above are least-squares fitted to Eq. 6. The values of A_y^* and Q_y^* so obtained are listed in Table 1. It is apparent from Table 1 and from the linearity of the plots of $\ln Y$ *versus* x (Fig. 2) that Eq. 6 describes satisfactorily the concentration dependences of transport properties of binary molten mixtures containing hydrate melts. It is worthwhile to note that the isothermal Eq. 6 has only two adjustable parameters unlike the cases with the expressions reported earlier.[4b,16,17] The applicability of Eqs. 4 and 6 also reinforces the view that the concentration dependence of transport properties of binary melts is completely governed by the behavior of the ideal glass transition temperature with concentration.

TABLE 1. BEST-FIT PARAMETERS FOR Eq. 6 FOR THE FLUIDITY AND EQUIVALENT CONDUCTANCE OF GLASS-FORMING MELTS

Melt	A_y^*	Q_y^*	Std. dev. in $\ln Y$
$Zn(NO_3)_2 \cdot 6.33H_2O + Ca(NO_3)_2 \cdot 4.1H_2O$	1.9401	−1.8714	0.029
	(1.4351)	(−1.6966)	(0.046)
$Ca(NO_3)_2 \cdot 4.09H_2O + Cd(NO_3)_2 \cdot 4.07H_2O$	−0.0498	0.7681	0.017
	(−0.2163)	(0.6215)	(0.012)
$Ca(NO_3)_2 \cdot 3.91H_2O + CoCl_2$	−0.1054	−9.8721	0.020
	(−0.3662)	(−10.6646)	(0.106)
$Cd(NO_3)_2 \cdot 4.1H_2O + NiCl_2$	0.7641	−10.0624	0.020
	(0.4589)	(−9.6243)	(0.016)
$Cd(NO_3)_2 \cdot 4.1H_2O + CoCl_2$	0.7797	−9.0010	0.036
	(0.4891)	(−8.4575)	(0.042)
$Zn(NO_3)_2 \cdot 6.27H_2O + CoCl_2$	1.9078	−2.1327	0.038
	(1.3715)	(−3.0096)	(0.033)

Parameters for equivalent conductance are within the parentheses.

References

1) C. A. Angell, *J. Electrochem. Soc.*, **112**, 1224 (1965).
2) J. Braunstein, *J. Chem. Educ.*, **44**, 223 (1967).
3) C. T. Moynihan, C. R. Smalley, C. A. Angell, and E. J. Sare, *J. Phys. Chem.*, **73**, 2287 (1969).
4) a) N. Islam and K. Ismail, *J. Phys. Chem.*, **78**, 2180 (1975); b) *ibid.*, **80**, 1929 (1976); c) *Indian J. Chem.*, **15A**, 857 (1977).
5) N. Islam, S. Kumar, and K. P. Singh, *Can. J. Chem.*, **56**, 1231 (1978).
6) a) N. Islam, K. P. Singh, and S. Kumar, *J. Chem. Soc., Faraday Trans. 1*, **75**, 1312 (1979); b) *Bull. Chem. Soc. Jpn.*, **52**, 579 (1979).
7) N. Islam and A. Ali, *Can. J. Chem.*, **57**, 2028 (1979).
8) S. K. Jain, *J. Phys. Chem.*, **82**, 1272 (1978).
9) M. H. Cohen and D. Turnbull, *J. Chem. Phys.*, **31**, 1164 (1959).
10) G. Adam and J. H. Gibbs, *J. Chem. Phys.*, **43**, 139 (1965).
11) C. A. Angell and R. D. Bressel, *J. Phys. Chem.*, **76**, 3244 (1972).
12) W. T. Laughlin and D. R. Uhlmann, *J. Phys. Chem.*, **76**, 2317 (1972).
13) V. P. Privalko, *J. Phys. Chem.*, **84**, 3307 (1980).
14) C. A. Angell and J. C. Tucker, *J. Phys. Chem.*, **78**, 278 (1974).
15) R. J. Greet and D. Turnbull, *J. Chem. Phys.*, **47**, 2185 (1967).
16) C. A. Angell, *J. Phys. Chem.*, **70**, 3988 (1966).
17) C. A. Angell, *J. Chem. Phys.*, **46**, 4673 (1967).

Desulfurization of *N,N'*-Diarylthioureas by Lead Tetraacetate Oxidation

Abhijit DEBROY, Sujit NANDY MAZUMDAR, Parag D. BARUA, and Mahinder P. MAHAJAN*
Department of Chemistry, North-Eastern Hill University, Shillong 793003, India
(Received January 5, 1983)

Synopsis. Lead tetraacetate oxidation of *N,N'*-diarylthioureas in refluxing dichloromethane and pyridine gave the corresponding *N,N'*-diarylureas. Sulfur was isolated during each oxidation reaction.

One of the interesting oxidation reactions in organic chemistry is the oxidation of thioureas. Depending on the substitution pattern of thioureas, the oxidizing agent, the polarity of the medium and reaction conditions, a variety of products have been isolated.[1-3]

Suitable synthetic methods are available for the chemical transformation of carbonyl into thiocarbonyl functions. In order to increase the synthetic versatility of this reaction investigation of the proper reagents for carrying out reverse conversion, *i.e.*, thiocarbonyl into carbonyl, is considered to be of great importance. Moreover, because of the discovery of 4-thiouridine in t-RNA of *E. Coli*,[4] it has recently inspired many groups to search for mild reagents for this transformation in order to elucidate the biochemical role of this minor component of t-RNA.[5] Apart from earlier reported reagents, a number of reagents have recently been discovered for conversion of thiocarbonyl compounds to carbonyl analogues. Almost all of them, having different limitations, have been used with varying degrees of success and include, DMSO–acids,[6,7] DMSO–iodine,[8] oxonium tetrafluoroborate,[9] manganese dioxide,[3] mesitylenecarbonitrile oxide,[10] diaryl selenooxides,[11,12] diaryl telluroxide,[13] benzeneseleninic anhydride,[14] thiophosgene,[15] potassium *t*-butoxide/Br_2 or I_2[16,17] and trimethyl phosphite or iron(O) pentacarbonyl.[18]

The oxidation of *N,N'*-diarylthioureas with lead tetraacetate/acetic acid has been reported to give disulfides.[19] Considering the significance of desulfurization reactions, *i.e.*, conversion of thiocarbonyl compounds into their carbonyl analogues, it was thought worthwhile to reinvestigate this reaction with the specific idea of carrying out this transformation. Also, keeping in mind the dependence of oxidation product on reaction conditions it was resolved to achieve this transformation by carrying out the oxidation in aprotic medium.

Thus in our laboratory we have carried out the oxidation of *N,N'*-diarylthioureas with lead tetraacetate in dichloromethane and pyridine at 80—90 °C. In every case, the corresponding urea and sulfur were isolated from the reaction mixture. The products were characterised with the help of IR spectra and melting points. The IR spectra of these compounds showed intense absorption in 1655—1700 cm^{-1} region due to carbonyl stretching. The desulfurization reaction and the formation of ureas is believed to proceed through carbodiimide intermediate(I) as shown in the Scheme 1.

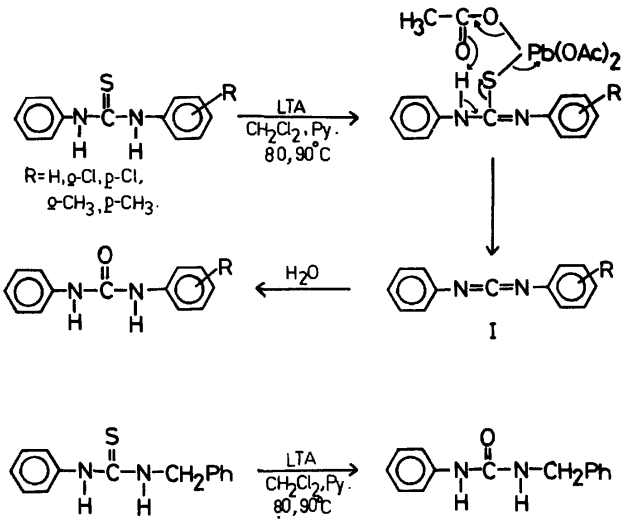

Scheme 1.

Experimental

Starting Materials. Lead tetraacetate was prepared according to literature method.[20] All the *N,N'*-diarylthioureas were prepared by mixing phenyl isothiocyanate and corresponding amines in molecular ratio in ethanol and stirring the mixture at room temperature.

Oxidation of N,N'-*Diphenylthiourea.* To a stirred solution of *N,N'*-diphenylthiourea (2.28 g; 0.01 mol) in dichloromethane (25 cm^3) and pyridine (5 cm^3) was added lead tetraacetate (4.88 g; 0.011 mol) in small portions over a period of 20 min. After complete addition of lead tetraacetate, the reaction mixture was refluxed in an oil bath (80—90 °C) for 1.5 h. The solvent was then removed under reduced pressure and the residue so obtained was chromatographed over a silica-gel column. Elution of the column with hexane gave 0.2 g of sulfur, identified by its undepressed mixed mp. After removal of the sulfur, further elution of the column with a mixture (4 : 1) benzene and ethyl acetate gave 1.8 g (86%) of a solid, identified as *N,N'*-diphenylurea, which was recrystallized from a mixture (1 : 1) of benzene and ethanol, mp 235—236 °C. (Lit,[21] mp 237 °C). IR (Nujol): ν_{max}: 3400 (ν_{N-H}); 3060, 3020, 2970 (ν_{C-H}); 1655 ($\nu_{C=O}$) and 1610, 1580 ($\nu_{C=C}$). These IR bands are common in all the *N*-phenyl-*N'*-arylureas reported here.

Other *N*-phenyl-*N'*-arylureas (Table 1, 2—6) were obtained similarly by lead tetraacetate oxidation of the corresponding *N*-phenyl-*N'*-arylthioureas.

Table 1. *N*-Phenyl-*N'*-arylureas

Sl. No.	Name of the compound	Mp θ_m/°C (Lit)	Yield %
1	*N,N'*-Diphenylurea	235—236 (237)[21]	86
2	*N*-Phenyl-*N'*-(*o*-chlorophenyl)urea	225	65
3	*N*-Phenyl-*N'*-(*p*-chlorophenyl)urea	236 (238)[21]	73
4	*N*-Phenyl-*N'*-benzylurea	166	73
5	*N*-Phenyl-*N'*-(*o*-tolyl)urea	193 (195)[21]	68
6	*N*-Phenyl-*N'*-(*p*-tolyl)urea	220 (219)[3]	73

References

1) C. P. Joshua and K. N. Rajasekharan, *Aust. J. Chem.*, **30**, 1819 (1977) and references therein.
2) C. Christopherson, T. Otterson, K. Seff, and S. Treppendahl, *J. Am. Chem. Soc.*, **97**, 5237 (1975) and references therein.
3) T. C. Sharma, N. S. Sahni, and Ambalal, *Bull. Chem. Soc. Jpn.*, **51**, 1245 (1978) and references therein.
4) M. N. Lipsett, *J. Biol. Chem.*, **240**, 3975 (1965).
5) R. H. Hall, "The Modified Nucleosides in Nucleic Acid," Columbia University Press, New York (1971), p. 347.
6) M. Mikolajezyk and J. Lucazak, *Synthesis*, **1974**, 491.
7) M. Mikolajezyk and J. Lucazak, *Chem. Ind. (London)*, **1974**, 701.
8) M. Mikolajezyk and J. Lucazak, *Synthesis*, **1975**, 114.
9) R. Mukherji, *Indian. J. Chem., B*, **15**, 502 (1977).
10) R. Grashey, G. Schroll, and M. Weidner, *Chem.-Ztg.*, **100**, 496 (1976).
11) M. Mikolajezyk and J. Lucazak, *J. Org. Chem.*, **43**, 2132 (1978).
12) S. Tamagahi, I. Hatanaka, and S. Kozuka, *Bull. Chem. Soc. Jpn.*, **50**, 3421 (1977).
13) D. H. R. Barton, S. V. Ley, and C. A. Meerholz, *J. Chem. Soc., Chem. Commun.*, **1979**, 755.
14) N. J. Cunam, S. V. Ley, and D. H. R. Barton, *J. Chem. Soc., Perkin Trans. 1*, **1980**, 1650.
15) R. Abugar, S. Sharma, and R. N. Iyer, *Indian J. Chem., B*, **19**, 211 (1980).
16) H. Singh, P. Singh, and N. Malhotra, *J. Chem. Soc., Perkin Trans. 1*, **1981**, 2647.
17) H. Singh and P. Singh, *Tetrahedron*, **1981**, 1215.
18) S. A. Kalonstian and W. C. Agorta, *Synth. Commun.*, **1981**, 1011.
19) L. Suchomelova and J. Zyka, *J. Electroanal. Chem.*, **5**, 57 (1963); *Chem. Abstr.*, **59**, 1482b (1963).
20) A. I. Vogel, "A Text Book of Practical Organic Chemistry," English Language Book Society and Longman, London (1978), p. 300.
21) H. H. Capps and W. M. Dehn, *J. Am. Chem. Soc.*, **54**, 4301 (1932).

 © 1984 The Chemical Society of Japan Bull. Chem. Soc. Jpn., 57, 317—321 (1984)

Studies on the Mechanism of Zeolite X Crystallization. II. Effect of Silica Sources of Starting Materials on the Gas-phase Adsorption at Solid Phases

Ryozi Hino,* Hiroyasu Aoi, and Kenzi Toki
Department of Chemistry, Faculty of Science, Shimane University, Nishikawatsu, Matsue 690
(Received January 31, 1983)

The mechanism of zeolite X crystallization was studied by using two kinds of silica sources, tetraethyl orthosilicate and silica sol. The adsorption of benzene and cyclohexane was subjected to a measurement to clarify the distribution of cation Na^+ and the change in the pore structure and surface of solid phases with reaction progress. The relation between specific surface area and reaction time has been revealed by means of adsorption of nitrogen gas, benzene, and cyclohexane as follows: 1) In the early stage of reaction or in the amorphous solid state, $N_2 \approx C_6H_6 \approx C_6H_{12}$ for tetraethyl orthosilicate and $N_2 \approx C_6H_6 > C_6H_{12}$ for silica sol; 2) for crystals in the early stage, $N_2 > C_6H_{12} > C_6H_6$ for tetraethyl orthosilicate and $N_2 > C_6H_{12} \approx C_6H_6$ for silica sol; 3) for crystals in a sufficiently developed stage, $N_2 \gg C_6H_{12} > C_6H_6$ for tetraethyl orthosilicate and $N_2 \approx C_6H_6 > C_6H_{12}$ for silica sol. In the case of silica sol, the crystallization mechanism is based on inhomogeneous nucleation; a number of critical nuclei may be generated but their dimension is small. In the case of tetraethyl orthosilicate critical nuclei are fewer in number and larger in size than in the case of silica sol; the mechanism of crystallization is based on homogeneous nucleation.

Zeolites are aluminosilicate crystals which are easily formed from gels composed of silica, alumina, soda, and water. However, because of the complexity of aluminosilicate gel in structure and reaction, the process of zeolite crystallization has not yet been made clear.

Many investigations concerning zeolite crystallization have been done in recent years.[1-10] Two representative hypotheses exist as follows: One is a zeolite crystallization which occurs in the solid phase in such a way that crystals are formed through interaction between the solid and liquid phases of a gel. This is supported by Breck and Flanigen,[5] McNicol *et al.*,[11] and Aiello *et al.*[12] The other is a crystallization which occurs in the liquid phase in such a way that an amorphous precursor is formed from a reaction mixture and then caused its constituents to be dissolved in the liquid phase prior to crystallization. This has been supported by Kerr,[1] Ciric,[7] Culfaz and Sand,[2] and Cournoyer *et al.*[13]

Some additional investigations in support of the latter hypothesis have recently been reported by Ueda and Koizumi[10] and Kageyama *et al.*[9] They pointed out that the presence of the solid-gel phase is not always needed in the crystallization process of zeolite Y, because crystals are grown in homogeneous solution. But, in general, the presence of solid phases as transient intermediates has been observed in many systems for zeolite synthesis.

The present authors[14,15] have reported that sources of silica remarkably influence the crystallization process. In this study, we made measurements on the adsorption of benzene or cyclohexane vapor to clarify the distribution of cation Na^+ and the change in pore and surface with reaction progress, and made an inference on the change in solid phases by considering both the interaction between the cation and the π-electrons of benzene and the physical adsorption of cyclohexane.

Experimental

The preparation of specimens, the chemical analysis of solid phases, and the adsorption of nitrogen gas were conducted as described in previous papers.[14,15] The absorption of benzene or cyclohexane vapor was subjected to volumetric measurements at 25 °C. The pretreatment of specimens was carried out in such a sequence that specimens were placed in a bath thermostated at 110 °C for 24 h, heated at 300 °C for 2 h, and finally degassed under a reduced pressure of 1×10^{-4} mmHg (1 mmHg≈133.322 Pa) at 300 °C. The adsorbates, benzene and cyclohexane, were obtained by purifying commercial guaranteed reagents by distillation.

Results and Discussion

The change in the chemical composition of solid phases with reaction time is shown in Fig. 1. Figure 1 indicates analytical values obtained for the solid phases during the process of aging with mechanical stirring at room temperature for 6—72 h followed by standing in the bath thermostated at 85 °C for 74—96 h. As can be seen from Fig. 1, the change in the analytical values for the solid phases derived from silica sol is abrupt as compared with those derived from tetraethyl orthosilicate.

The solid phases derived fom tetraethyl orthosilicate contain all constituents uniformly throughout the

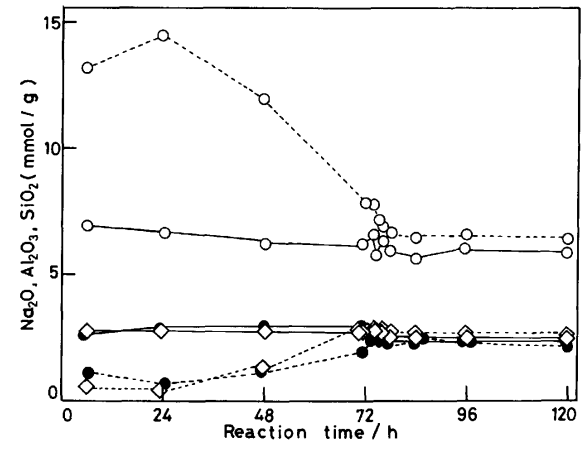

Fig. 1. Relation between reaction time and component concentrations in the solid phase.
——: Si $(OC_2H_5)_4$, ------: silica sol, ○: SiO_2, ◇: Al_2O_3, ●: Na_2O.

course of reaction. For example, the SiO_2/Al_2O_3 molar ratios of the solid phases obtained at 24, 72, and 96 h are 32.7, 2.89, and 2.60 in the case of silica sol in contrast to 2.34, 2.40, and 2.44 in the case of tetraethyl orthosilicate; thus the constituent concentration of the solid phases in the latter case changes little as compared with that in the former case.

Adsorption isotherms with benzene and cyclohexane vapors on the solid phases derived from tetraethyl orthosilicate are shown in Figs. 2 and 3, respectively. The adsorption isotherms in each figure are classified into three groups. The solid phases (24E-75E, where the figure denotes the reaction time and the symbol E indicates that the solid phase concerned has been obtained from tetraethyl orthosilicate) obtained in the early stage of reaction were amorphous and capable of adsorbing the vapors only in small quantities. The amount adsorbed increased greatly with the progress of crystallization.

The crystals obtained in the early stage (76E) and a sufficiently developed stage (84E-96E) gave the same adsorbed quantities at a relative pressure of 0.5 for benzene and at 0.25 for cyclohexane. Above these relative pressures, the former crystal caused no increased adsorption, whereas the latter ones resulted in adsorption in large quantities. This different behavior sug-

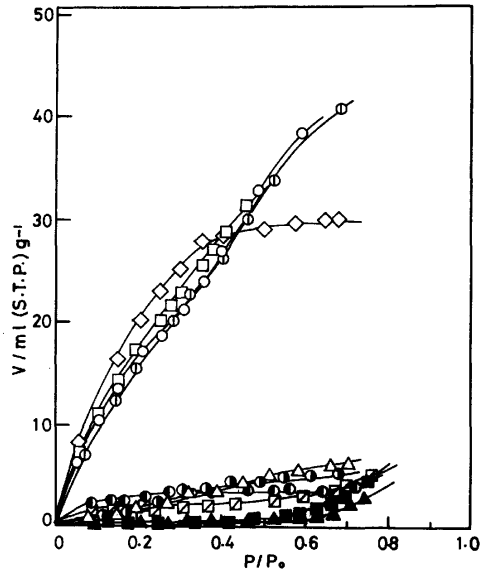

Fig. 2. Adsorption isotherms of benzene vapor on the solid phases derived from tetraethyl orthosilicate at 25°C.
○: 96E, ⊕: 84E, □: 78E, ◇: 76E, ⊠: 75E, △: 74E, ◐: 72E, ◑: 48E, ■: 24E, ▲: 6E.

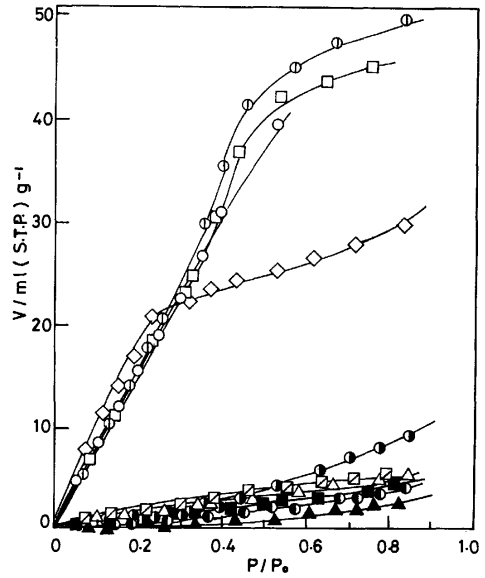

Fig. 3. Adsorption isotherms of cyclohexane vapor on the solid phases derived from tetraethyl orthosilicate at 25°C.
○: 96E, ⊕: 84E, □: 78E, ◇: 76E, ⊠: 75E, △: 74E, ◐: 72E, ◑: 48E, ■: 24E, ▲: 6E.

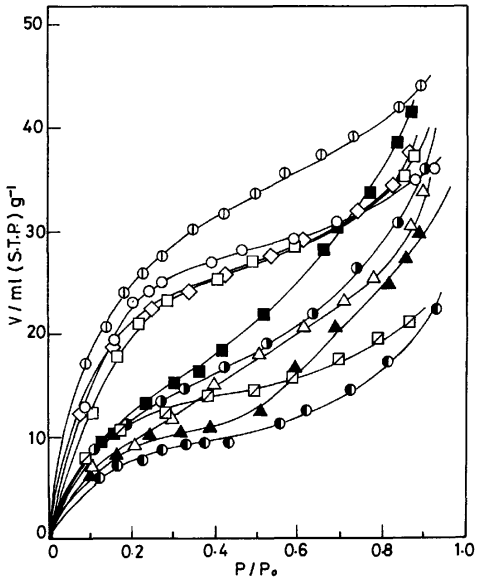

Fig. 4. Adsorption isotherms of benzene vapor on the solid phases derived from silica sol at 25°C.
○: 96C, ⊕: 84C, □: 78C, ◇: 76C, ⊠: 75C, △: 74C, ◐: 72C, ◑: 48C, ■: 24C, ▲: 6C.

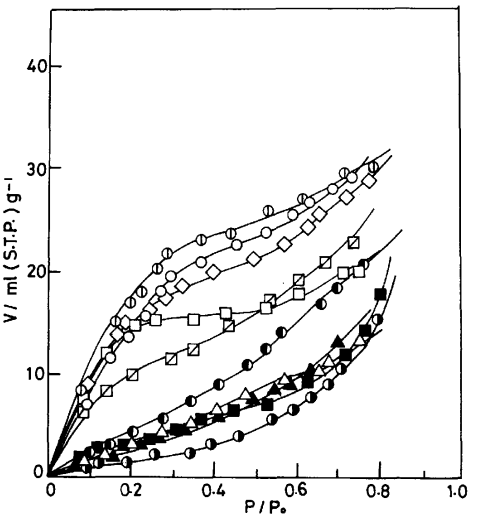

Fig. 5. Adsorption isotherms of cyclohexane vapor on the solid phases derived from silica sol at 25°C.
○: 96C, ⊕: 84C, □: 78C, ◇: 76C, ⊠: 75C, △: 74C, ◐: 72C, ◑: 48C, ■: 24C, ▲: 6C.

gests a difference in the developments of pore structure of the crystals.

The adsorption isotherms of benzene and cyclohexane on the solid phases derived from silica sol are shown in Figs. 4 and 5, respectively. The adsorption isotherms in each figure may be classified into three groups in the same way as in the case of tetraethyl orthosilicate. The solid phases in the early stage (6C-74C, where the figure denotes the reaction time and the symbol C indicates that the solid phase concerned has been derived from silica sol) adsorbed fairly large quantities of benzene and cyclohexane, as compared with the case of tetraethyl orthosilicate. In addition, the amount adsorbed increased steeply with increasing relative pressure. These features are consistent with the results obtained from a nitrogen-gas adsorption, that is, the measured quantities depend primarily on the particle size distribution of the amorphous solid phases.[15]

In Figs. 4 and 5, the crystal in the early stage (75C) and those in a sufficiently developed stage (78C-96C) exhibit somewhat similar patterns of isotherms, although the latter adsorb the adsorbates in larger quantities than the former. As mentioned in the case of tetraethyl orthosilicate, this difference is due primarily to the difference in pore-structure development.

By applying the BET method[16] to the adsorption isotherms, the monolayer capacity, V_m, for benzene or cyclohexane was calculated except the case of amorphous states (6E-48E). In this case (6E-48E), the BET method could not apply to the isotherms, because these solid phases adsorbed the vapors in too small a quantity. The monolayer capacity, specific surface area, and the constant C are listed in Table 1. The specific surface areas evaluated from the nitrogen-gas isotherms are tabulated in the same table.

For the calculation of the specific surface area for solid phases from the monolayer capacity, we used the molecular dimensions of 7.4 (l)×6.7 (b) for benzene and of 7.2 (l)×6.4 (b) for cyclohexane,[17,18] where the symbols (l) and (b) denote the length and breadth for the molecular dimensions in Å, respectively. We assumed that the molecules adsorbed are oriented nearly flat to the solid surface.[19-21]

In Table 1, the specific surface areas of the amorphous phases derived from tetraethyl orthosilicate are nearly equal for both the benzene and cyclohexane adsorptions. In addition, they are consistent with those as evaluated from the nitrogen adsorption. Therefore, the surface of the solid phases may be taken to be covered with these adsorbates in the same manner. In contrast, the crystal phases adsorb cyclohexane more than benzene. This different behavior suggests that the adsorption depends mainly on the molecular dimensions rather than the effect of the interaction between the cations and the π-electrons of benzene.

As seen from a comparison of data of the crystals formed in the early stage and those in a sufficiently developed stage, the specific surface area slightly decreases with reaction time. This seems due to the change in the particle size distribution with the development of crystal phase. The surface area as evaluated by the nitrogen-gas adsorption does not show any of the tendency mentioned above, because the degree of development of micro pores has a strong effect on the specific surface area, as compared with the change in the outer specific surface area. This agrees with the fact that the outer area of zeolite crystals is only about 1% of the total surface area.[22]

On the other hand, the solid phases derived from silica sol give larger specific surface areas by the benzene adsorption than by the cyclohexane adsorption. The degree of the difference in this case is somewhat smaller than that in the case of tetraethyl orthosilicate. But the amorphous phases (6C-74C) adsorb benzene in larger quantities than cyclohexane. Consequently, the interaction between adsorbates and cations has a somewhat

Table 1. Monolayeer capacity, specific surface area, and constant C of solid phases

Specimen	V_m	S_s	C[a]	S_s[b]
	mmol g^{-1}	m^2 g^{-1}		m^2 g^{-1}
Benzene				
96E	0.850	254	8.4	717
84E	0.844	252	8.3	746
78E	0.900	268	8.4	708
76E	0.976	291	11	457
75E	0.0546	16	13	19
74E	0.0609	18	13	4
72E	0.100	29	10	7
48E	—	—	—	3
24E	—	—	—	4
6E	—	—	—	4
Cyclohexane				
96E	1.17	325	3.4	
84E	1.34	371	2.9	
78E	1.50	416	2.4	
76E	1.31	363	3.4	
75E	0.107	30	5.9	
74E	0.0736	20	5.9	
72E	0.0378	1	12	
48E	—	—	—	
24E	—	—	—	
6E	—	—	—	
Benzene				
96C	1.13	337	7.7	324
84C	1.09	325	14	366
78C	0.940	281	7.7	257
76C	1.05	313	9.9	251
75C	0.399	119	39	141
74C	0.393	117	17	107
72C	0.296	88	54	112
48C	0.548	164	10	159
24C	0.621	185	5.6	174
6C	0.367	110	31	123
Cyclohexane				
96C	0.879	244	5.3	
84C	0.923	256	7.8	
78C	0.800	222	7.7	
76C	0.585	162	72	
75C	0.392	109	30	
74C	0.235	65	3.8	
72C	0.363	101	2.9	
48C	0.0708	19	34	
24C	0.154	43	19	
6C	0.215	60	4	

a) Evaluated by using the BET equation. b) Evaluated by means of nitrogen adsortion.

stronger effect than the molecular dimensions. This suggests that, as previously mentioned,[14,15] the crystal phase derived from silica sol includes an amorphous substance, and that the micro structure of crystals is not yet be developed sufficiently. Therefore, the large specific surface areas evaluated with benzene depend mainly on the amorphous substance included in crystals. This indicates that the surface of the solid phase can be covered with benzene, but that there is a portion on the surface that cannot be sufficiently covered with cyclohexane. On the whole, the amorphous phases prepared from silica sol give larger specific surface areas than those derived from tetraethyl orthosilicate. This depends on the interaction between adsorbates and cations in addition to the difference in the particle size distribution.

No regularity of constant C is found in the case of silica sol, in contrast to the case of tetraethyl orthosilicate. As previously pointed out,[14,15] the surface of the solid phase derived from tetraethyl orthosilicate is supposed to be made up of aluminosilicate with chemical and structural orderliness. On the contrary, the surface of the solid phase derived from silica sol is influenced by complex factors such as the heterogeneity of surface, the wide distribution of particle sizes, the presence of foreign substances, and the interaction between hydroxyl groups and adsorbate.

The relation between the monolayer capacity obtained with benzene, V_m, and the cation concentration is shown in Fig. 6. The monolayer capacity of the amorphous solid phases (72E–75E) derived from tetraethyl orthosilicate changes little with increase in cation concentration. But the monolayer capacity of the crystals in the early stage (76E) and those in a sufficiently developed stage (78E–96E) changes considerably in a steeply linear relationship with cation concentration.

In the case of the amorphous solid phases (6C–72C), the monolayer capacity somewhat decreases with change in cation concentration, and the crystal phases (75C–96C) exhibit an approximately linear relationship between the monolayer capacity and cation concentration. This result suggests that the interaction of π-electrons of benzene is stronger with cations existing in cavities of crystals than with those on the surface of solid phases.

The monolayer capacity obtained with cyclohexane shows none of such a relationship as that with benzene does. This result indicates the existence of a strong interaction between π-electrons of benzene and cations on the solid surface. It has been suggested that benzene is associated with a similarly strong interaction, whereas cyclohexane with some weak interaction.[23]

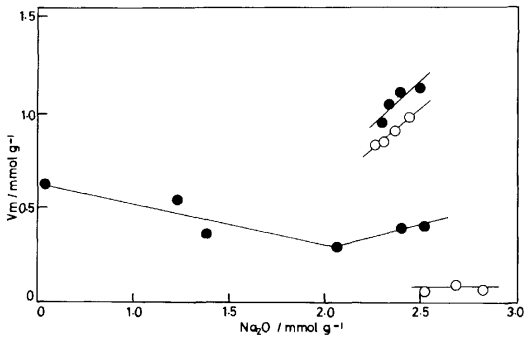

Fig. 6. Relation between monolayer capacity, V_m, and cation (Na_2O) concentration. —O—: $Si(OC_2H_5)_4$, —●—: silica sol.

On the basis of these results and discussions, the change in pores and channels of the solid phases and the mechanism of the crystallization of zeolite X are to be considered.

The schematic representation of the channel and pore formation is given in Fig. 7. The amorphous solid phases derived from tetraethyl orthosilicate are of the same chemical composition as the crystal phase, and therefore, Na^+ ions are contained in the solid phase in large quantities. These solids adsorb benzene and cyclohexane in rather small quantities.

The amorphous solid phases derived from silica sol contain Na^+ ions in small quantities but adsorb benzene more than the solid phases derived from tetraethyl orthosilicate; they adsorb benzene more than cyclohexane. In addition, taking into account the different particle size distribution and the relative specific surface areas $N_2 \approx C_6H_6 \approx C_6H_{12}$ for tetraethyl orthosiicate and $N_2 \approx C_6H_6 > C_6H_{12}$ for silica sol, we have given schematic representations of the surfaces of the amorphous solid states derived from silica sol and tetraethyl orthosilicate in A-1 and B-1, respectively. In the case of tetraethyl orthosilicate, the cations in the solid phase exist in a similar state as in the crystal phase or ordered aluminosilicate, whereas in the case of silica sol, a small quantity of cations are widely distributed on the

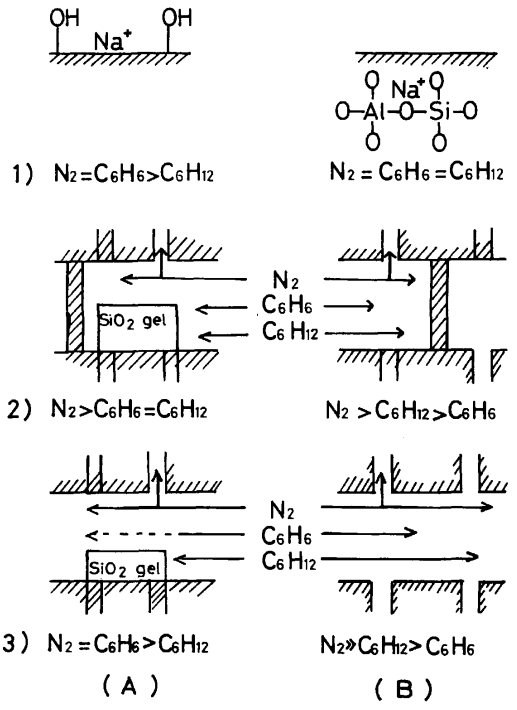

Fig. 7. Schematic diagram of channel and pore formations with reaction time. (A) and (B) are the solid phases derived from silica sol and tetraethyl orthosilicate respectively.
1) At early stage (amorphous), 2) crystals at early stage, 3) crystals at sufficiently developed stage.

outer surface of the solid phase. Furthermore, there seem to exist no less than the hydroxyl groups on the heterogeneous surface of the solid phase.[15]

The crystal phase derived from silica sol in the early stage give the order of specific surface areas: $N_2 > C_6H_{12} \approx C_6H_6$. This order suggests that the channels and pores characteristic of the zeolite structure have already been formed but not yet so much developed as to be able to adsorb benzene and cyclohexane in large quantities. This is due to a contamination of silicic polymers in the channel and pore structures, as previouly pointed out.[14,15]

The crystals derived from tetraethyl orthosilicate give the order of specific surface areas: $N_2 \gg C_6H_{12} > C_6H_6$. This differece in specific surface area is due to the molecular dimensions. The crystal phases derived from tetraethyl orthosilicate may be supposed not to be contaminated with amorphous substances such as a silicic polymer which will not be incorporated in the aluminosilicate framework; thus, these solid phases are capable of adsorbing nitrogen gas and cyclohexane in larger quantities than can be expected from the degree of crystallinity. This crystal phase adsorbs nitrogen gas and cyclohexane in fairly larger quantities than benzene. Therefore, the crystals in the early stage may be considered to have had their structure developed to a considerable extent with respect to channel and pore.

The crystals derived from tetraethyl orthosilicate in a sufficiently developed stage give the order of specific surface areas: $N_2 \gg C_6H_{12} > C_6H_6$. An increase in crystallinity is accompanied by development of the internal structure of crystals. On the whole, channels and pores, which can adsorb nitrogen gas but not appreciably benzene or cyclohexane, have been formed considerably in the crystal phase. This is in accord with the abrupt increase in the specific surface areas, evaluated by the nitrogen adsorption, from 460 for 76E to 720 m^2/g for 96E.

The crystals derived from silica sol in a developed stage give the order of specific surface areas: $N_2 \approx C_6H_6 > C_6H_{12}$. The channels and pores have fairly been developed. But the existene of amorphous substances in the crystal phase prevents cyclohexane to a higher degree from being adsorbed than nitrogen gas and benzene vapor. Because of the interaction between π-electrons of benzene and surface hydroxyl groups or cations distributed on the outer surface, benzene is adsorbed in larger quantities than cyclohexane. These considerations are in conformity with experimental results on IR spectra, chemical analyses, and crystallinity previously described.[14,15]

The authors wish to express their thanks to Professor Ryohei Matuura of Kyushu University for many helpful discussions during the course of this work and to Shimadzu Co., Ltd. for the measurement of the particle size distributions with a SediGraph type 5000-01.

References

1) G. T. Kerr, *J. Phys. Chem.*, **70**, 1047 (1966).
2) A. Culfaz and L. B. Sand, *Adv. Chem. Ser.*, **121**, 140, (1973).
3) B. D. McNicol, G. T. Pott, K. R. Loss, and N. Mulder, *Adv. Chem. Ser.*, **121**, 152, (1973).
4) W. Meise and F. E. Schwochow, *Adv. Chem. Ser.*, **121**,169, (1973).
5) D. W. Breck and E. M. Flanigen, "Molecular Sieves," Society of Chemical Industry, London (1968), p. 47.
6) S. P. Zhdanov and N. N. Samulevich, "Proceeding of the Fifth International Conference on Zeolites," Heyden and Son Ltd., London (1980), p. 75.
7) J. Ciric, *J. Colloid Interface Sci.*, **28**, 315 (1968).
8) A. Yoshida and K. Inoue, *Nippon Kagaku Kaishi*, **1982**, 1466.
9) N. Kageyama, S. Ueda, and M. Koizumi, *Nippon Kagaku Kaishi*, **1981**, 1510.
10) S. Ueda and M. Koizumi, *Am. Mineral.*, **64**, 172 (1979).
11) B. D. McNicol, G. T. Pott, and K. R. Loss, *J. Phys. Chem.*, **76**, 3388 (1972).
12) R. Aiello, R. M. Barrer, and I. S. Kerr, *Adv. Chem. Ser.*, **101**, 44 (1971).
13) R. A. Cournoyer, W. L. Kranich, and L. B. Sand, *J. Phys. Chem.*, **79**, 1578 (1975).
14) R. Hino and K. Toki, *Nippon Kagaku Kaishi*, **1977**, 593.
15) R. Hino, R. Matuura, and K. Toki, *Bull. Chem. Soc. Jpn.*, in press.
16) S. Brunauer, P. H. Emmett, and E. Teller, *J. Am. Chem. Soc.*, **60**, 309 (1938).
17) R. M. Barrer, "Zeolites and Clay Minerals as Sorbents and Molecular Sieves," Academic Press, London (1978), Chap. 8, p. 472.
18) R. M. Barrer and A. Sikand, *J. Chem. Soc., Faraday Trans. 1*, **75**, 2221 (1979).
19) T. Kagiya, Y. Sumida, and T. Tachi, *Bull. Chem. Soc. Jpn.*, **44**, 1219 (1971).
20) H. Matuo, Y. Moroi, and R. Matuura, *Mem. Fac. Sci., Kyushu Univ., C*, **9**, 45 (1974).
21) C. L. Angell and M. V. Howell, *J. Colloid Interface Sci.*, **28**, 279 (1968).
22) D. W. Breck, "Zeolite Molecular Sieves," John Wiley & Sons, New York (1974), Chap. 8, p. 595.
23) D. Barthomeuf and B. H. Ha, *J. Chem. Soc., Faraday Trans. 1*, **69**, 2147 (1973).

Theoretical Study of Relaxation Mechanism in Magnetic Field Effects on Chemical Reactions

Hisaharu HAYASHI* and Saburo NAGAKURA†
The Institute of Physical and Chemical Research, Wako, Saitama 351
†*The Institute for Molecular Science, Myodaiji, Okazaki, Aichi 444*
(Received May 30, 1983)

External magnetic field and magnetic isotope effects on the dynamic behavior of radical pairs in solutions have been studied theoretically, where the relaxation of their electron spins was taken into account. The decay observed with some radical pairs in micellar solutions under high magnetic fields is successfully interpreted in terms of the relaxation mechanism, and the magnetic field dependence of the relaxation rates is calculated for a model system.

Magnetic field effects on chemical reactions have been extensively studied during the last decade.[1-8] The effects observed for usual solvents are known to be classified and systematically explained in terms of the Δg, hyperfine coupling (HFC) and level-crossing (J) mechanisms[9] of the radical pair theory.[10,11]

Recently,we first succeeded in measuring the effect on photochemical reaction rates, taking the reactions of benzophenone (BP),[12-14] its derivatives,[15] and dibenzyl ketone (DBK)[14,16] in some micelles as examples. A similar effect was also observed in the reactions of 1,4-naphthoquinone (NQ) derivatives in a sodium dodecyl sulfate (SDS) micelle.[17] In these reactions, we have found some new external magnetic field and magnetic isotope effects on the decay of their intermediate radical pairs which cannot be explained in terms of only the Δg, HFC, and J mechanisms of the radical pair theory. The yields of their escaping radicals and reaction products were also found to show similar effects.

Among the new effects observed in the micellar solutions, the effects observed in the photodecomposition reaction of DBK[14] were explained in terms of the triplet (T) mechanism successfully applied to some chemically induced dynamic electron polarization (CIDEP).[18] On the other hand, the effects observed in the hydrogen abstraction reactions of BP's and NQ's could not be explained by this mechanism. In preceding papers,[14,15] we have suggested that the relaxation mechanism may explain these magnetic field effects. Brocklehurst studied theoretically the effect of the relaxation times (T_1 and T_2) of electron spins in a radical pair on the evolution of its singlet character.[19] However, it is not clear at present how the decay of the radical pair and the yields of escaping radicals and reaction products are influenced by a magnetic field when the relaxation mechanism is effective. Therefore, the purpose of the present study is to analyze theoretically the dynamic behavior of the radical pair through the relaxation mechanism and to explain the observed effects in micellar solutions with the developed theory.

Theoretical

Dynamic Behavior of Radical Pair. It has already been shown that a separated radical pair plays a very important role in the magnetic field effects on chemical reactions in solutions.[9,11,20] Thus, in the present paper, we also consider the dynamic behavior of the separated radical pair, in which the interaction between its component radicals (radicals a and b) is very small. In this paper, the separated radical pair is simply written as the radical pair.

The energy diagram of the radical pair is shown in Fig. 1. At the zero magnetic field, we assume that the energy (E_S) of its singlet state ($|S\rangle$) and that (E_{Ti}) of each sublevel (i=x, y, or z) of its triplet state are degenerate with each other. On this assumption, the singlet-triplet (S-T) separation ($2J$) of the radical pair and the energy splittings within the triplet sublevels are considered to be zero. This assumption is usually adopted for the theoretical studies of the above-mentioned mechanism except for the J one.

At a high field, where the high field approximation holds,[21,22] two of the triplet sublevels ($|T_{\pm1}\rangle$) are shifted from the central one ($|T_0\rangle$) through the Zeeman effect. In usual radical pairs, the magnetic flux density (B) of 0.04 T is enough for the high field approximation.[9,20]

In order to analyze exactly the dynamic behavior of the radical pair, a stochastic Liouville equation must be solved.[20] However, it cannot be solved analytically and a tedious calculation is necessary for its solution. On the other hand, many nuclear spin states of a radical pair can interfere with one another and the overall dynamics of its singlet and triplet states become very simple. Thus we can use the first order rate equations

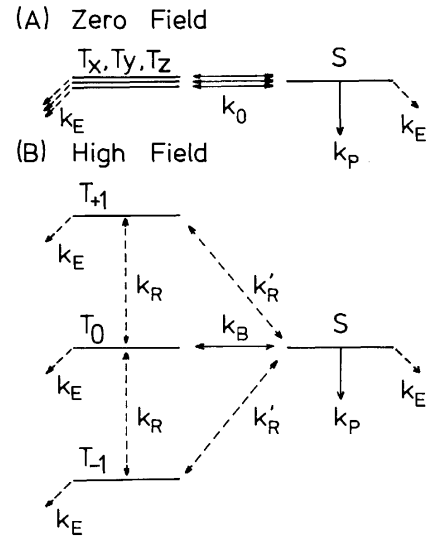

Fig. 1. Dynamic behavior of a radical pair at (A) the zero field and (B) a high field.

in order to understand the dynamics intuitively. In fact, all of the decay curves of radical pairs observed in micellar solutions with a laser-photolysis technique[13-17] have been expressed by combination of some exponential functions.

Therefore, we introduce rate equations for the populations of the singlet state and triplet sublevels ([S] and [T_i]) of a radical pair. At the zero field, they can be written as follows:

$$d[T]/dt = -(k_0+k_E)[T] + 3k_0[S], \quad (1)$$

$$d[S]/dt = k_0[T] - (k_P+3k_0+k_E)[S], \quad (2)$$

where $[T]=[T_x]+[T_y]+[T_z]$. Each rate constant (k_i) is shown in Fig. 1(A). The S-T conversion rate constant is written by k_0, which is determined by the HFC and has the order of 10^9—10^8 s^{-1}.[23] The reaction rate constant from the singlet state is written by k_P, which has the order of 10^{10}—10^7 s^{-1}.[23] The reaction from the triplet state is not considered in the present study for simplicity, although it is possible if necessary. The escaping rate constant of radicals from the radical pair, k_E, may have the order of 10^5 s^{-1} for the micellar solutions of BP's and NQ's. In usual solvents, it may be much larger.

At a high field, the following equations are introduced.

$$d[T_i]/dt = -(\sum_{i\neq i}' k_{ij}+k_{iS}+k_E)[T_i] + \sum_{j\neq i} k_{ji}[T_j] + k_{Si}[S], \quad (3)$$

$$d[S]/dt = \sum_i k_{iS}[T_i] - (k_P+\sum_i k_{Si}+k_E)[S], \quad (4)$$

where i, j=0 or ±1, k_{ij} is the conversion rate constant from the i-triplet sublevel to the j-one, and k_{Si} and k_{iS} are the S-T converson rate constants between the singlet state and the i-triplet sublevel. Since $k_{ij}=k_{ji}$,[21,22] and $k_{Si}=k_{iS}$,[9] Eqs. 3 and 4 are summarized as follows:

$$d[T']/dt = -(k_R+k_R'+k_E)[T'] + 2k_R[T_0] + 2k_R'[S], \quad (5)$$

$$d[T_0]/dt = k_R[T'] - (k_B+2k_R+k_E)[T_0] + k_B[S], \quad (6)$$

$$d[S]/dt = k_R'[T'] + k_B[T_0] - (k_P+k_B+2k_R'+k_E)[S], \quad (7)$$

where $[T']=[T_1]+[T_{-1}]$, $k_B=k_{S0}$, $k_R=k_{\pm10}$, and $k_R'=k_{\pm1S}$. As shown in Appendix, k_{10} is equal to k_{-10} and k_{1S} is equal to k_{-1S}. Each rate constant is shown in Fig. 1(B). It is noteworthy that the relaxation from the ±1-triplet sublevel to the singlet state must be taken into account besides that to the 0-one (see Appendix). In usual radicals, T_1^{-1} is 10^6—10^4 s^{-1}.[23] Thus k_R and k_R' may have similar values. According to the radical pair theory, k_B is based on the HFC and $\Delta g\beta B$ of the radical pair, where Δg is the difference between the isotropic g-values (g^a and g^b) of the component radicals and β is the electric Bohr magneton. Usually, k_B is larger than k_0.

Solution of Rate Equations. Equations 1 and 2 and Eqs. 5—7 are solved approximately for $k_P \gg k_0$, k_B (case a) and k_0, $k_B \gg k_P$ (case b), respectively. As already explained, in micellar solutions k_P, k_0, and k_B can be considered to be much larger than the other rate constants. This condition is considered in the present calculation. For the reaction from an S-precursor, the initial population ([ ]$_0$) can be taken as follows: $[S]_0=1$, $[T]_0=0$, or $[T_i]_0=0$ (i=0 or ±1). For the reaction from a T-precursor, the initial population can be taken as follows:[24] $[S]_0=0$, $[T]_0=1$, or $[T_i]=1/3$.

After calculation of [S], [T], [T'], and [T_0], the total population of the radical pair ([R]) is obtained, where $[R]=[S]+[T]$ at the zero field and $[R]=[S]+[T']+[T_0]$ at a high field. The results are as follows:

S-precursor:

At the zero magnetic field:

$$\text{Case a } (k_P \gg k_0)\text{: } [R] = \exp[-(k_P+3k_0+k_E)t], \quad (8)$$

$$\text{Case b } (k_0 \gg k_P)\text{: } [R] = \exp[-(k_P/4+k_E)t]. \quad (9)$$

At a high magnetic field:

$$\text{Case a } (k_P \gg k_B)\text{: } [R] = \exp(-r_1t), \quad (10)$$

$$\text{Case b } (k_B \gg k_P)\text{: } [R] = \exp(-r_2't). \quad (11)$$

T-precursor:

At the zero magnetic field:

$$\text{Case a } (k_P \gg k_0)\text{: } [R] = \exp[-(k_0+k_E)t], \quad (12)$$

$$\text{Case b } (k_0 \gg k_P)\text{: } [R] = \exp[-(k_P/4+k_E)t]. \quad (13)$$

At a high magnetic field:

$$\text{Case a } (k_P \gg k_B)\text{: } [R] = (1/3)\exp(-r_2t) + (2/3)\exp(-r_3t), \quad (14)$$

$$\text{Case b } (k_B \gg k_P)\text{: } [R] = (1/3)\exp(-r_2't) + (2/3)\exp(-r_3't), \quad (15)$$

where r_1, r_2, r_3 r_2', and r_3' are given as follows:

$$r_1 = k_P + k_B + 2k_R' + k_E, \quad (16)$$

$$r_2 = k_B + 2k_R + k_E, \quad (17)$$

$$r_2' = k_P/2 + k_R + k_R' + k_E, \quad (18)$$

$$r_3 = r_3' = k_R + k_R' + k_E. \quad (19)$$

From these solutions, the following predictions can be given for the reaction from the S-precursor: (1) The decay of the radical pair can be expressed by a single exponential function for all the cases under consideration. (2) The decay rate constant at the zero field shows no or very little isotope effect because k_P and k_E usually show no magnetic isotope effect.[7] (3) For case a, the magnetically induced change of its decay rate constant is $k_B-3k_0+2k_R'$. This value is negative at a relatively low field and increases with increasing B. The magnetic field effect on the rate constant, however, is very small because the main component of r_1 is k_P. (4) For case b, the change is $k_P/4+k_R+k_R'$. This value is positive and the decay rate constant rapidly increases with increasing B in the low field region ($B<0.04$ T). On the other hand, in the high field region ($B>0.04$ T) its magnetically induced change becomes very small because k_P is a main term for the decay rate constant.

For the reactions from the T-precursor, the following predictions are made: (1) The decay of the radical pair can be expressed by a single exponential function at the zero field and by a combination of two eponential functions at a high field. (2) At the zero field, the decay rate constant can be represented by k_0+k_E for case a and by $k_P/4+k_E$ for case b. Therefore, its magnetic isotope effect can be expected for the former case but not for the latter. (3) For case a, the change from the decay rate constant at the zero field to the larger one in the high field region (r_2) is $k_B-k_0+2k_R$. Its magnetic field effect

at a relatively low field is small but increases with increasing B. The smaller one (r_3) in the high field region is much smaller than the rate constant at the zero field. (4) For case b, the change from the decay rate constant at the zero field to r_2' is $k_P/4+k_R+k_R'$. This value is the same as that is given in the reaction from the S-precursor. On the other hand, the second component appears in the high field region for the reaction from the T-precursor. Its rate constant (r_3') is much smaller than that at the zero field.

The populations of one of the escaping radicals ([E]) and the product from the singlet radical pair ([P]) can also be obtained from the following equations:

$$d[E]/dt = k_E[R], \quad (20)$$

$$d[P]/dt = k_P[S]. \quad (21)$$

Results and Discussion

Summaries of Experimental Results. In the reactions of BP's and NQ's in micelles at room temperature,[12-15,17] the following characteristics were found for their magnetic field effects:

(a) The decay curves of their radical pairs observed at the zero field are expressed by single exponential functions. Some of the decay rate constants observed in an SDS micelle are listed in Table 1. They are about 3×10^6 s^{-1} for BP's and about 5×10^6 s^{-1} for NQ's. For BP, the magnetic isotope effect on the decay rate constant can scarcely be observed at the zero field.

(b) In the presence of a magnetic field above 0.04 T, the decay curves of the radical pairs are expressed by combinations of two eponential functions. The rate constants of the slow decay component observed with BP's and NQ's in the SDS micelle are listed in Table 1. They decrease with increasing B until 1.34 T at which the magnetic field effects become almost constant. They are about 2×10^6 s^{-1} at 0.04 or 0.05 T but are as small as about 3×10^5 s^{-1} at 1.34 T.

(c) As shown in Table 1, the magnetic isotope effects on the rate constants appeared clearly between 0.04 and 0.5 T, but the effects became small above 0.5 T again. Similar magnetic isotope effects were also obtained more accurately for the yields of the escaping radicals in the BP reaction.[15]

(d) The yields of the escaping radicals in the reactions of BP's and NQ's increase with increasing B until 1.34 T.[15,17]

The external magnetic field and magnetic isotope effects summarized above cannot be interpreted by the Δg, HFC, and J mechanisms for the following reasons: According to the Δg mechanism,[9] the decay rate constant of the radical pair in the reactions from the T-precursor should increase with increasing B. From the HFC mechanism,[9,20] the rate constant is expected to decrease with increasing B, which is saturated at a low magnetic field ($B\ll0.1$ T).[20] According to the J mechanism,[9] the rate constant should increase at a level-crossing field. These predictions clearly contradict the observed results (see summary b).

The observed results cannot be explained also by the T mechanism for the following reason: The initial population of each sublevel of the triplet radical pair ($[T_i]_0$) can be influenced by a magnetic field through the T mechanism. However, this mechanism cannot explain appearance of the two decay components of the radical pair in the presence of a magnetic field and the magnetically induced changes of the slow decay component. The magnetic field effects on this component are the main problem of the present paper.

Application of Relaxation Mechanism. Now let us consider the observed magnetic field effects on the reactions of BP's and NQ's, taking account of the relaxation mechanism developed in the present paper. The observed numbers of the decay components of [R] in the absence (one) and presence (two) of a magnetic field agree well with the prediction for the reaction from the T-precursor. For case a, the observed decay rate constan at the zero magnetic field should correspond to k_0+k_E. As explained above, k_0 should have the order of 10^9—10^8 s^{-1} and should show a magnetic isotope effect. This prediction contradict the observed results (see summary a).

For case b, the rate constant at the zero magnetic field should correspond to $k_P/4+k_E$ and may not show any appreciable isotope effect. The magnitudes of k_P and k_E are also reasonable for explaining the observed rate constants. Thus we can conclude that case b is

TABLE 1. THE DECAY RATE CONSTANTS OF THE RADICAL PAIRS (k) OBSERVED WITH THE SDS SOLUTIONS OF SOME BP AND NQ DERIVATIVES

Magnetic field B/T	$k/10^6$ s^{-1}					
	BP[a]	BP-d_{10}[b]	BP-^{13}C[c]	BP-F_2[d]	NQ[e]	MNQ[f]
0	2.8[g]	2.8[g]	2.8[g]	2.9	4.7	4.1
0.04	2.2	2.1	2.4	—	—	—
0.05	—	—	—	—	2.4	1.9
0.07	1.9	1.9	2.2	—	—	—
0.10	0.9_1	—	1.1	1.3	1.7	1.4
0.20	0.7_1	—	0.8_9	0.7_5	1.3	0.9_5
0.50	0.4_9	—	0.5_3	0.4_5	0.8_5	0.7_7
1.00	0.3_7	—	0.3_8	—	—	—
1.34	0.3_7	—	0.4_2	0.3_0	0.5_2	0.6_5

a) Benzophenone; Refs. 13 and 15. b) Benzophenone-d_{10}; Ref. 13. c) Benzophenone-carbonyl-^{13}C; Refs. 13 and 15. d) 4,4'-Difluorobenzophenone; Ref. 15. e) 1,4-Naphtoquinone; Ref. 17. f) 2-Methyl-1,4-Naphtoquinone; Ref. 17. g) The values measured under a residual magnetic field (0.12 mT) are listed.

applicable to the reactions of BP's and NQ's in the micellar solutions and the rate constants of the fast and slow decay components are assigned to r_2' and r_3', respectively. This means that the magnetic field and magnetic isotope effects observed with the slow decay component are due to $r_3'=k_R+k_R'+k_E$ (see Eq. 19). Since k_E can be considered to be insensitive to a magnetic field below 1.34 T, the observed magnetic field and magnetic isotope effects are considered to be due to k_R and k_R'.

It is noteworthy that these effects are not due to such direct S-T conversion rate constant as k_0 and k_B. This is a new situation in the study of the magnetic field effects on chemical reactions through radical pairs. The effects through the other mechanisms have been shown to be due to k_0 and k_B.[9,20]

Analytical Forms of Relaxation Rate Constants. The external magnetic field and magnetic isotope effects on k_R and k_R' of the radical pair have not yet been studied well. Therefore, we have undertaken to analyze them theoretically. The internal motions of a radical pair against the direction of an external magnetic field are shown in Fig. 2. Here Ω^i and Ω^{ab} represent the sets of the angular coordinates of the molecular axes of the i-th radical (X^i, Y^i, and Z^i) and the vector (r_{ab}) from an odd electron on radical b to that on radical a, respectively.

We have obtained the analytical forms of k_R and k_R' for the following simple model of a radical pair: (1) Each of the component radicals has its HFC with only one nucleus having spin 1/2. The principal values of the HFC tensor (A^i tensor) are given by A_X^i, A_Y^i, and A_Z^i. The nuclear spin quantum number is written by M^i. (2) The principal axes of the g tensor of the i-th radical (g^i tensor) are supposed to coincide with those of the A^i one. (3) The axial symmetry is assumed for g^i and A^i tensors. Their isotropic parameters are given by $g^i=g_\parallel^i/3+2g_\perp^i/3$ and $A^i=A_\parallel^i/3+2A_\perp^i/3$, respectively. Their anisotropic parameters are given by $\Delta g^i=g_\parallel^i-g_\perp^i$ and $\Delta A^i=A_\parallel^i-A_\perp^i$, respectively. Here $\parallel$ and $\perp$ represent the parallel and perpendicular components against the axis of symmetry, respectively. (4) The dipole-dipole interaction between the odd electrons is assumed to be due to that between the two points which are separated with each other by the averaged distance (R) of r_{ab}.

For the above model, k_R and k_R' are given as follows:

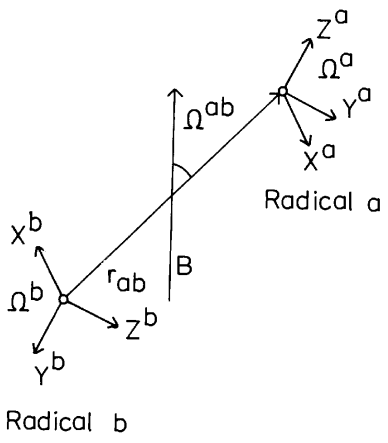

Fig. 2. Internal motions of a radical pair.

$$k_R=(1/4)\sum_{M^a}\sum_{M^{a'}}\sum_{M^b}\sum_{M^{b'}}P<T_{\pm1},M^a,M^b|T_0,M^{a'},M^{b'}>, \quad (22)$$

$$k_R'=(1/4)\sum_{M^a}\sum_{M^{a'}}\sum_{M^b}\sum_{M^{b'}}P<T_{\pm1},M^a,M^b|S,M^{a'},M^{b'}>, \quad (23)$$

where $P<m|l>$ is the transition probability from the m-th state to the l-th one. The derivations and analytical forms of the right sides of Eqs. 22 and 23 are given in Appendix.

Model Calculations of Relaxation Times. After hydrogen abstraction by the triplet state of BP or NQ from a micellar molecule, a radical pair of the ketyl or semiquinone radical with the alkyl one is produced. Thus the former and latter radicals can be written by radicals a and b, respectively.

Now let us calculate k_R+k_R' numerically with the aid of Eqs. 22 and 23. Since many parameters in these equations have not yet been measured, they are assumed adequately. The following parameters are fixed: $g^a=g^b=2.003$,[25] $\Delta g^b=0.002$,[25] $\tau_a=1\times10^{-10}$ s,[28] and $\tau_b=5\times10^{-9}$ s.[28] The others are changed. The calculated contributions of the motions of radicals a and b (V^a and V^b) and the relative motion of the two radicals (V^{ab}) to $\log(k_R+k_R')$ are plotted against B in Fig. 3.

From Fig. 3, the following characteristics are found: (1) Curves a—e show the contributions of V^a for some sets of parameters. From curve a which shows the contribution of Δg of 0.002, this contribution is proved to be neglibly small. The increases from curve a to curves b—d show the contributions of the increases in $\Delta A^a/g\beta$ from 0 to 0.002, 0.004, and 0.006 T, respectively, where g is $(g^a+g^b)/2$. This contribution is

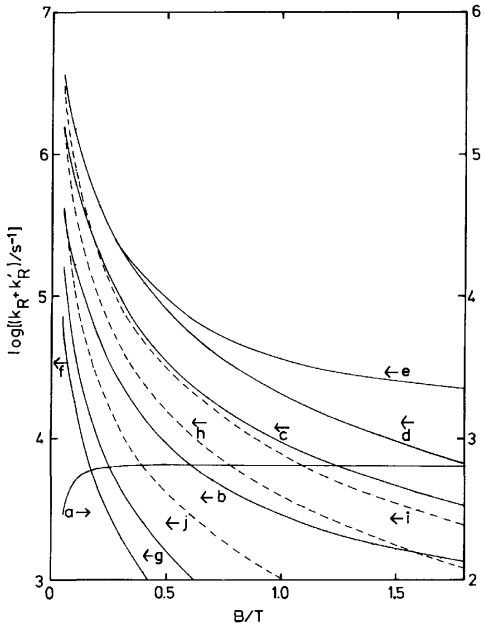

Fig. 3. Calculated contributions of V^a, V^b, and V^{ab} to k_R+k_R' with the following parameters: V^a: $g^a=2.003$ and $\tau_a=1\times10^{-10}$ s^{-1} (a) $\Delta g^a=0.002$ and $\Delta A^a/g\beta=0$ T; (b) $\Delta g^a=0.002$ and $\Delta A^a/g\beta=0.002$ T; (c) $\Delta g^a=0.002$ and $\Delta A^a/g\beta=0.004$ T; (d) $\Delta g^a=0.002$ and $\Delta A^a/g\beta=0.006$ T; (e) $\Delta g^a=0.01$ and $\Delta A^a/g\beta=0.006$ T. V^b: $g^b=2.003$, $\Delta g^b=0.002$, and $\tau_b=5\times10^{-9}$ (f) $\Delta A^b/g\beta=0.004$ T; (g) $\Delta A^b/B\beta=0.006$ T. V^{ab}: (h) $R=0.8$ nm and $\tau_{ab}=1\times10^{-9}$ s; (i) $R=0.8$ nm and $\tau_{ab}=5\times10^{-10}$ s; (j) $R=1.0$ nm and $\tau_{ab}=1\times10^{-9}$ s.

shown to be larger under low magnetic fields and to increase with increasing ΔA^a. This is the origin of the magnetic isotope effect on k_R+k_R' and the amount of the effect is also shown to decrease with increasing B because of the denominator $(1+\omega^2\tau_a^2)$ in Eqs. A7—A9. The differnce between curves e and d is the contribution of the increase of Δg from 0.002 to 0.01. This is also small.

(2) Curves f and g show the contribution of V^b. Thus the contribution of the alkyl radical is found to be negligibly small. This is due to the fact that its correlation time is assumed to be very long. Since this radical may take part in micellar formation, this assumption may be permitted.

(3) Curves h—j show the contribution of V^{ab}. This contribution is found to be comparable to that of V^a in magnitude. Thus this is also shown to play an important role in k_R. Figure 3 shows that this contribution decreases with inreasing B, R, and τ_{ab}. However, it is very difficult to determine the values of R and τ_{ab} from other experimental methods.

Comparison between the Observed and Calculated Rate Constants. In Fig. 4, the observed dependence of the decay rate constants on B is plotted for some typical reactions. In this figure, the rate constant values calculated for the adopted model are also shown. Here the contributions of V^a and V^{ab} are only taken into account because that of V^b has been shown to be much smaller than the former. The assumed parameters are as follows: $k_E=4\times10^5$ s^{-1}, $g^a=2.003$, $\Delta g^a=0.002$,[25] $\tau_a=1\times10^{-10}$ s, $R=0.8$ nm, and $\tau_{ab}=1\times10^{-9}$ s.[28] The value of ΔA^a is changed. The k_E, R, and τ_{ab} values are chosen in such a way as the calculated rate constant values agree with the observed ones. They seem to be reasonable for radical pairs considered in the present paper.

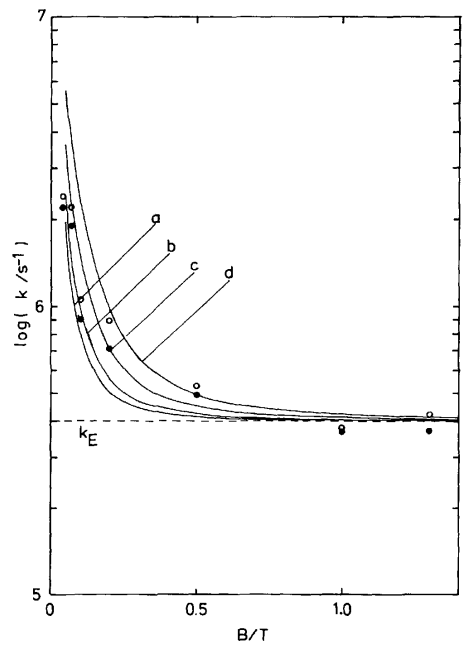

Fig. 4. The magnetic field dependences of the rate constants (k) of the slow decay components observed with the SDS solutions of (●) benzophenone and (○) benzophenone-carbonyl-^{13}C.[13,15] Calculated magnetic field dependences of the rate constants due to the combination of V^a and V^{ab} with the following parameters: (a) $\Delta A^a/g\beta=0$ T, (b) $\Delta A^a/g\beta=0.002$ T, (c) $\Delta A^a/g\beta=0.004$ T, and (d) $\Delta A^a/g\beta=0.006$ T. The other parameters are written in the text.

From the comparison among the results shown in Table 1 and Fig. 4, it is considered that this calculation can explain the observed characteristics of the decay rate constants in spite of the facts that the adopted model is very simple and that there are some ambiguities in assuming the parameters. The observed magnetic field dependence of the decay rate constant is well interpreted by the calculated k_R+k_R'. Its decrease with increasing B is due to the denominators in Eqs. A7—A9.

The observed magnitude of k_R+k_R' is also explained by this calculation. At magnetic fields below 0.1 T, the magnitude is calculated to be larger than 10^6 s^{-1}. At fields above 0.5 T, the magnitude is smaller than 10^5 s^{-1}. They agree well with the observed values if the observed decay rate constant at 1.34 T is nearly equal to k_E in each of the investigated reactions. The observed magnetic isotope effects on the decay rate constant in the BP reaction are also explained by the calculated curved in Fig. 4. They show that the decay rate constant increases with increasing ΔA^a and that the magnitude of the effects is appreciable at low magnetic fields and becomes small at high fields.

Thus the observed external magnetic field and magnetic isotope effects on the radical pair decay in each of the reactions of BP's and NQ's in micelles have been successfully interpreted in terms of the relaxation mechanism. At the zero magnetic field, the decay rate constant of the radical pair corresponds to $k_P/4+k_E$, which should not show any appreciable magnetic isotope effect. In the presence of a magnetic field where the high field approximation holds, the constant shows the external magnetic field and magnetic isotope effects which are due to the relaxations from the ±1-sublevel of the triplet radical pair to the 0-sublevel (k_R) and the singlet state (k_R'). The analytical forms for a model system are derived and numerical values of k_R and k_R' are calculated. The magnetic field effects on the yields of the escaping radicals and reaction products observed in these micellar solutions are also explained by the relaxation mechanism. Details of the effects on the yields will be published elsewhere.[15,17]

Appendix

The transition probability, $P<m|n>$, under a time dependent perturbation ($V(t)$) is given as follows:[21]

$$P<m|n> = \hbar^{-2}|V_{mn}|^2 2\tau_c/(1+\omega_{mn}^2\tau_c^2), \quad \text{(A1)}$$

where ω_{mn} is expressed by

$$\omega_{mn} = \hbar^{-1}(E_n-E_m), \quad \text{(A2)}$$

and $V(t)$ is supposed to take the form

$$V(t) = V\cdot f(t), \quad \text{(A3)}$$

where V is an operator which is independent of time and $f(t)$ is a fluctuating numerical factor. When the autocorrelation function ($G(\tau)$) of $f(t)$ decays exponentially with a correlation time of τ_c,

$$G(\tau) = \overline{f(t+\tau)f(t)} = \overline{f(t)^2} \exp(-|\tau|/\tau_c), \quad \text{(A4)}$$

Eq. A1 is obtained.

For a radical pair, various off-diagonal matrix elements among $|T_{\pm1}>$, $|T_0>$, and $|S>$ have been obtained previously (Eqs. 39 and 40 in Ref. 10b). They can be used for $V(t)$. In the presence of a magnetic field where the high field approximation holds, $P<T_{\pm1}|\Gamma>$ (Γ is T_0 or S) can be obtained as follows:

$$P<T_{\pm1}|\Gamma> = \sum_i \frac{|V^i|^2}{\hbar^2} \cdot \frac{2\tau_i}{1+\omega^2\tau_i^2} + \frac{|V^{ab}|^2}{\hbar^2} \cdot \frac{2\tau_{ab}\delta_{\Gamma T_0}}{1+\omega^2\tau_{ab}^2}, \quad \text{(A5)}$$

where $\delta_{T_0T_0}=1$ and $\delta_{ST_0}=0$. V^i (i=a or b) contains the contributions from the anisotropic terms of the g^i and A^i tensors and V^{ab} is due to the dipole-dipole interaction between radicals a and b. The correlation times of Ω^i and Ω^{ab} are given by τ_i and τ_{ab}, respectively. In this calculation, we consider the case where

$$\hbar\omega = |E_{T_{\pm1}} - E_{T_0}| = |E_{T_{\pm1}} - E_S| = (g^a+g^b)\beta B/2. \quad \text{(A6)}$$

From Eq. A5, the following equations can be derived: $k_{10}=k_{-10}$ and $k_{1S}=k_{-1S}$. It is shown that k_R' is comparable to k_R in magnitude. For the adopted model shown in the text, non-vanishing elements of P can be expressed as follows:

$$\hbar^2P<T_{\pm1},M^a,M^b|\Gamma,M^a,M^b> = \sum(\beta B\Delta g^i + M^i\Delta A^i)^2\tau_i/[30(1+\omega^2\tau_i^2)] + D^2\tau_{ab}\delta_{\Gamma T_0}/[7.5(1+\omega^2\tau_{ab}^2)], \quad \text{(A7)}$$

$$\hbar^2P<T_{\pm1},\pm 1/2,M^b|\Gamma,\mp 1/2,M^b> = (\Delta A^a)^2\tau_a/[30(1+\omega^2\tau_a^2)], \quad \text{(A8)}$$

$$\hbar^2P<T_{\pm1},\mp 1/2,M^b|\Gamma,\pm 1/2,M^b> = (\Delta A^a)^2\tau_a/[180(1+\omega^2\tau_a^2)]. \quad \text{(A9)}$$

$P<T_{\pm1}, M, M'|\Gamma, M, M''>$ has the same form as $P<T_{\pm1}, M', M|\Gamma, M'', M>$, where D is given as follow:[22]

$$D = -(3/2)(\mu_0/4\pi)(g^2\beta^2/R^3). \quad \text{(A10)}$$

Since k_R and k_R' are defined as the averaged transition probabilities about the nuclear spin states, they are given as shown in Eqs. 22 and 23.

We wish to thank Professor Koichi Itoh, Osaka City University, and Dr. Yoshio Sakaguchi, The Institute of Physical and Chemical Research, for their helpful discussions.

References

1) R. Z. Sagdeev, Yu. N. Molin, K. M. Salikhov, T. V. Leshina, M. A. Kamha, and S. M. Shein, *Org. Magn. Reson.*, **5**, 603 (1973).

2) B. Brocklehurst, R. S. Dixon, E. M. Gardy, V. J. Lopata, M. J. Quinn, A. Singh, and F. P. Sargent, *Chem. Phys. Lett.*, **28**, 361 (1974)

3) Y. Tanimoto, H. Hayashi, S. Nagakura, H. Sakuragi, and K. Tokumaru, *Chem. Phys. Lett.*, **41**, 267 (1976).

4) N. Hata, *Chem. Lett.*, **1976**, 547.

5) M. E. Michel-Beyerle, R. Haberkorn, W. Bybe, E. Steffens, H. Schröder, H. J. Neusser, E. W. Schlag, and H. Seidlitz, *Chem. Phys.*, **17**, 139 (1976).

6) K. Shulten, H. Staerck, A. Weller, H. J. Werner, and B. Nickel, *Z. Phys. Chem. (Frankfurt an Main)*, **101**, 371 (1976).

7) N. J. Turro and B. Kraeutler, *Acc. Chem. Res.*, **13**, 369 (1980).

8) H. Hayashi, *Chem. Phys. Lett.*, **87**, 113 (1982).

9) H. Hayashi and S. Nagakura, *Bull. Chem. Soc. Jpn.*, **51**, 2862 (1978); Y. Sakaguchi, H. Hayashi, and S. Nagakura, *ibid.*, **53**, 39 (1980).

10) a) H. Hayashi. K. Itoh, and S. Nagakura, *Bull. Chem. Soc. Jpn.*, **39**, 199 (1966); b) K. Itoh, H. Hayashi, and S. Nagakura, *Mol. Phys.*, **17**, 561 (1969). There are some misprints in Eq. 40 of this paper. In the denominators of $A_{01}(=A_{-10})$ and $A_{\pm1S}$, $2^{1/2}$ is dropped,

11) R. Kaptein, *J. Am. Chem. Soc.*, **94**, 6251 (1972).

12) Y. Sakaguchi, H. Hayashi, and S. Nagakura, *Chem. Phys. Lett.*, **72**, 420 (1980).

13) Y. Sakaguchi, S. Nagakura, A. Minoh, and H. Hayashi, *Chem. Phys. Lett.*, **82**, 213 (1981).

14) Y. Sakaguchi, H. Hayashi, and S. Nagakura, *J. Phys. Chem.*, **86**, 3177 (1982).

15) A preliminary report has appeared: Y. Sakaguchi and H. Hayashi, *Chem. Phys. Lett.*, **87**, 539 (1982). Details will be published elsewhere.

16) H. Hayashi, Y. Sakaguchi, and S. Nagakura, *Chem. Phys. Lett.*, **1980**, 1149.

17) A preliminary report has appeared: Y. Sakaguchi, H. Hayashi, and S. Nagakura, Symposium on Photochemistry 1982, Kanazawa, October 1982, Abstr. p. 209. Details will be published elsewhere: Y. Sakaguchi and H. Hayashi, *J. Phys. Chem.*, in press.

18) P. W. Akins and G. T. Evans, *Mol. Phys.*, **27**, 1633 (1974).

19) B. Brocklehurst, *J. Chem. Soc., Faraday Trans. 2*, **72**, 1869 (1976).

20) Z. Schluten and K. Shulten, *J. Chem. Phys.*, **66**, 4616 (1977).

21) A. Carrington and A. D. McLachlan, "Introduction to Magnetic Resonance," Harper & Row, New York (1967).

22) K. Kuwata and K. Itoh, "Denshi-supin-kyomei Nyumon," Nankodo, Tokyo (1980).

23) R. Kaptein, "Introduction to Chemically Induced Magnetic Polarization," in "Chemically Induced Magnetic Polarization," ed by L. T. Muus, P. W. Atkins, K. A. McLauchlan, and J. B. Pedersen, D. Reidel, Dordrecht, Holland (1977), Chap. 1.

24) The influence of the T mechanism on the initial population is not considered in the present study for simplicity, although it is possible if necessary.

25) For the BP ketyl and NQ semiquinone radicals, their isotropic g-values were measured to be 2.0030[26] and 2.00418,[27] respectively. The ESR parameters of the alkyl radicals from micellar molecules are not known. When an odd electron is localized on a carbon atom, its g and Δg values have been measured to be about 2.003 and 0.002, respectively.[21,22]

26) R. Wilson, *J. Chem. Soc., B*, **1968**, 1581.

27) S. Frydkjaer and L. T. Muus, *Chem. Phys.*, **51**, 365 (1980).

28) The correlation times of nitroxide radicals in an SDS micelle were estimated to be about 1×10^{-10} s at room temperature.[29] That of an SDS micelle was estimated to be 1.1×10^{-8} s,[30] the simple Stokes law relation being applied. Thus τ_a was assumed to be 1×10^{-10} s and τ_b was assumed to be

somewhat shorter than 1.1×10^{-8} s. Some values between τ_a and τ_b were taken for τ_{ab}.

29) N. M. Atherton and S. J. Strach, *J. Chem. Soc., Faraday Trans. 2*, **68**, 374 (1972).
30) A. S. Waggoner, O. H. Griffith, and C. R. Christensen, *Proc. Natl. Acad. Sci.*, **57**, 1198 (1969).

 © 1984 The Chemical Society of Japan Bull. Chem. Soc. Jpn., 57, 329—333 (1984)

The Structure of Liquid Water by Neutron Scattering. III. Calculations of the Partial Structure Factors

Norio Ohtomo,† Kazuo Tokiwano,† and Kiyoshi Arakawa*
Research Institute of Applied Electricity, Hokkaido University, Sapporo 060
†*Faculty of Engineering, Hokkaido University, Sapporo 060*
(Received June 8, 1983)

A formula for obtaining partial structure factors for fluid systems composed of molecular clusters with various sizes was derived according to the theoretical procedure proposed in the preceding papers (N. Ohtomo, K. Tokiwano, and K. Arakawa, *Bull. Chem. Soc. Jpn.*, **54**, 1802 (1981): **55**, 2788 (1982)). The formula was applied to calculate partial structure factors of liquid water, and from the good agreement between the calculated and observed values the pentamer-monomer mixture model for liquid water was confirmed as reasonable.

As the result of neutron diffraction studies of liquid water reported in the preceding papers,[1,2]†† the pentamer–monomer mixture model turned out to be the best structure model of water, where the total neutron structure factors obtained were interpreted successfully by that model.

Quite recently, two partial structure factor data of liquid water at 25°C were reported by Thiessen and Narten[3] and by Soper and Silver[4] using an isotope substitution technique of neutron diffraction. A comparison between calculated and observed partial structure factors will offer a very sensitive test for the structure model of liquid. However, no useful theoretical procedure has been proposed for the calculation of partial structure factors for associated liquids like water.

In the present study, thus, we attempt to derive a formula useful for obtaining partial structure factors for the fluid system composed of molecular clusters with various sizes based on the theoretical procedure proposed in paper I and II.[1,2] Then the partial structure factors of liquid water for the pentamer–monomer mixture model are calculated by the use of the formula derived, and the results are compared with the observed data.[3,4]

Procedure of Calculations of Partial Structure Factors

Partial Structure Factors for Fluids Composed of Molecular Clusters. For a r-component system, the partial structure factors $S_{ss'}(Q)$ are connected with the total structure factor $S_m(Q)$ by

$$S_m(Q) = \sum^{-2} \sum_{s,s'}^{r} c_s c_{s'} b_s b_{s'} S_{ss'}(Q), \quad (1)$$

where $\sum \equiv \sum_s^r c_s b_s$, b_s the coherent scattering length for the nucleus species s, c_s the number of the nuclei per molecular unit, and $Q \equiv |\vec{Q}|$ ($\vec{Q}$: the scattering vector).

We consider here the case of a fluid system consisting of molecular clusters with various sizes including monomers and, then, begin with Eq. 12 for $S_m(Q)$ in paper II,

$$S_m(Q) = \sum_\nu \frac{x_\nu}{\nu} f_1^\nu(Q) + \sum_{\nu \geqq 2} \frac{x_\nu}{\nu} f_c^\nu(Q) + \bar{f}_{2U}(Q)[S_c(Q) - 1], \quad (2)$$

where x_ν is the fraction of ν-mer clusters in molecular number, the $f_1^\nu(Q)$ the intramolecular contribution within the clusters (Eq. 13 in II), $f_\ell^\nu(Q)$ the factor originating from the orientational correlation of molecules within the clusters (Eq. 14 in II), $S_c(Q)$ the molecular-centers structure factor of the liquid (Eq. 10 in II), and $\bar{f}_{2U}(Q)$ an extended form of a factor resulting from the completely uncorrelated orientational configuration between molecules in the liquid (Eq. 11 in II). We rewrite $f_\ell^\nu(Q)$ as

$$f_c^\nu(Q) = \nu f_1^c(Q) - f_1^\nu(Q) - \nu f_3^\nu(Q) \cdot f_{2U}^\nu(Q), \quad (3)$$

where

$$f_1^c(Q) = \sum^{-2} \frac{1}{\nu} \left[\left\langle \sum_{l,l'} \sum_{n_l, n_{l'}} b_{n_l} b_{n_{l'}} \exp(i\vec{Q} \cdot \vec{r}_{n_l n_{l'}}) \right\rangle \right]_\nu, \quad (4)$$

$$f_3^\nu(Q) = \frac{1}{\nu} \left[\left\langle \sum_{l \neq l'} \exp(i\vec{Q} \cdot \vec{r}_{cll'}) \right\rangle \right]_\nu \quad (\nu \geqq 2), \quad (5)$$

and

$$f_{2U}^\nu(Q) = \sum^{-2} \frac{1}{\nu} \left[\sum_l^\nu \left[\sum_{n_l} b_{n_l} \left\langle \exp(i\vec{Q} \cdot \vec{r}_{cn_l}) \right\rangle \right]^2 \right]_\nu. \quad (6)$$

Suffix l denotes the l-th molecule within the ν-mer cluster and n_l the n-th nucleus in the molecule l. $\vec{r}_{n_l n_{l'}}$ is the vector distance from the n_l-th nucleus to the $n_{l'}$-th one, $\vec{r}_{cll'}$ the vector distance from the center of the l-th molecule to that of the l'-th one, and $\vec{r}_{cn_l}$ the vector distance from the center of the molecule l to its n_l-th nucleus, within the ν-mer cluster. $f_1^c(Q)$ is the contribution of atom-pairs within the ν-mer cluster (Eq. 8 in I), $f_3^\nu(Q)$ a factor resulting from the molecular-center pairs within the cluster (Eq. 11 in I), and $f_{2U}^\nu(Q)$ an extended form of a factor resulting from the completely-uncorrelated orientational configuration between molecules within the cluster.

Introducing Eq. 3 into Eq. 2, we obtain

$$S_m(Q) = \sum_\nu x_\nu \left[\frac{1}{\nu} f_1^\nu(Q) \delta_{\nu 1} + f_1^c(Q)(1 - \delta_{\nu 1}) - f_3^\nu(Q) \cdot f_{2U}^\nu(Q) \right] + \bar{f}_{2U}(Q)[S_c(Q) - 1], \quad (7)$$

where δ_{ik} is Kronecker's δ.

From Eqs. 1 and 7, we can obtain the partial structure factors $S_{ss'}(Q)$ for the liquid composed of molecular clusters of various sizes including monomers. The Eq. 1 has a quadratic form on b_s as well as the Eq. 7, though in Eq. 7 the b_s are contained in an implicit form. And then, we can obtain the formula of $S_{ss'}(Q)$ by comparing these two equations, when an explicit form of the total $S_m(Q)$ is given. Thus, the formula of $S_{ss'}(Q)$ is obtained for the practical model of the liquid under consid-

†† We cite Refs. 1 and 2 as paper I and II, respectively, in the following.

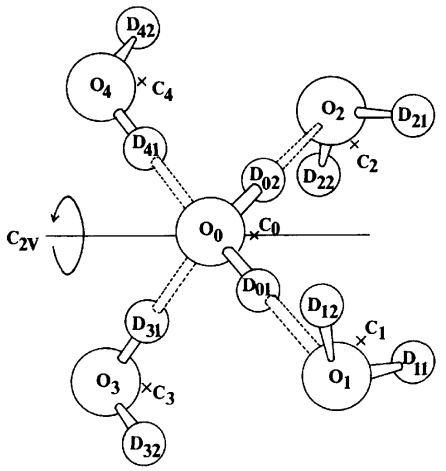

Fig. 1. The structure of the regular tetrahedral pentamer with the C_{2v} symmetrical coordination. The suffix O_i indicates oxygen in the i-th molecule within the pentamer, D_{ij} the j-th deuteron in the i-th molecule, and C_i the molecular center of the i-th molecule.

eration.

Partial Structure Factors for Pentamer-Monomer Mixture Model. For liquid water, using three partial structure factors $S_{OO}(Q)$, $S_{OD}(Q)$, and $S_{DD}(Q)$, Eq. 1 becomes

$$S_m(Q) = \sum^{-2}[b_O^2 S_{OO}(Q) + 4b_O b_D S_{OD}(Q) + 4b_D^2 S_{DD}(Q)], \quad (8)$$

where $\sum = b_O + 2b_D$.

In order to calculate the partial structure factors, we adopt the pentamer-monomer mixture model fully examined in paper II, which is composed of regular tetrahedral pentamers with the C_{2v} symmetrical coordination (Fig. 1) and monomers as its constituents. In this case, we put $x_1 \neq 0$ and $x_5 \neq 0$ (others=zero). Since $\bar{f}_{2U}(Q) = x_1 f_{2U}^1(Q) + x_5 f_{2U}^5(Q)$, Eq. 7 becomes

$$S_m(Q) = x_1\{f_1^1(Q) + f_{2U}^1(Q)[S_c(Q) - 1]\} + x_5\{S_m^p(Q) + f_{2U}^5(Q)[S_c(Q) - f_3^5(Q) - 1]\}. \quad (9)$$

The intra-pentamer contribution $S_m^p(Q)$ ($\equiv f_1^c(Q)$ for pentamer) is given from Eq. 13 in paper I as

$$S_m^p(Q) = \frac{1}{5} f_1^5(Q) + \sum^{-2}[b_O^2 S_{m,p}^{(OO)}(Q) + 4b_O b_D S_{m,p}^{(OD)}(Q) + 4b_D^2 S_{m,p}^{(DD)}(Q)]. \quad (10)$$

The factors $S_{m,p}^{(OO)}(Q)$, $S_{m,p}^{(OD)}(Q)$, and $S_{m,p}^{(DD)}(Q)$, are the intra-pentamer part of the contributions of the O-O, O-D, and D-D pairs, respectively, and the explicit expressions are written below when the orientational configuration of water molecules within the pentamer is specified. The intramolecular contribution $(1/\nu) f_1^\nu(Q)$ (ν=1 for monomer and ν=5 for pentamer) is

$$\frac{1}{\nu} f_1^\nu(Q) = \sum^{-2}[b_O^2 + 2b_D^2 + 4b_O b_D Y_{OD}^\nu(Q) + 2b_D^2 Y_{DD}^\nu(Q)], \quad (11)$$

and

$$Y_{nn'}^\nu(Q) = j_0(Q r_{nn'}^\nu) \exp(-\gamma_{nn'}^\nu Q^2), \quad (12)$$

where $j_0(x) = \sin x/x$, $r_{nn'}^\nu$ is the distance between two different nuclei n and n′ within a molecule and $2\gamma_{nn'}^\nu$ the mean-square variation to the distance $r_{nn'}^\nu$. The factor $f_{2U}^\nu(Q)$ is

$$f_{2U}^\nu(Q) = \sum^{-2}[b_O^2\{Y_{cO}^\nu(Q)\}^2 + 4b_O b_D Y_{cO}^\nu(Q) Y_{cD}^\nu(Q) + 4b_D^2\{Y_{cD}^\nu(Q)\}^2], \quad (13)$$

where the suffix c denotes the molecular center.

From Eqs. 8—13, the partial structure factors $S_{OO}(Q)$, $S_{OD}(Q)$, and $S_{DD}(Q)$ for liquid water are given explicitly as follows:

$$S_{OO}(Q) = x_1[1 + \{Y_{cO}^1(Q)\}^2[S_c(Q) - 1]] + x_5[1 + S_{m,p}^{(OO)}(Q) + \{Y_{cO}^5(Q)\}^2[S_c(Q) - f_3^5(Q) - 1]], \quad (14)$$

$$S_{OD}(Q) = x_1[Y_{OD}^1(Q) + Y_{cO}^1(Q) Y_{cD}^1(Q)[S_c(Q) - 1]] + x_5[Y_{OD}^5(Q) + S_{m,p}^{(OD)}(Q) + Y_{cO}^5(Q) Y_{cD}^5(Q)[S_c(Q) - f_3^5(Q) - 1]], \quad (15)$$

and

$$S_{DD}(Q) = x_1\left[\frac{1}{2}\{1 + Y_{DD}^1(Q)\} + \{Y_{cD}^1(Q)\}^2[S_c(Q) - 1]\right] + x_5\left[\frac{1}{2}\{1 + Y_{DD}^5(Q)\} + S_{m,p}^{(DD)}(Q) + \{Y_{cD}^5(Q)\}^2[S_c(Q) - f_3^5(Q) - 1]\right]. \quad (16)$$

For the C_{2v} symmetry pentamer (Fig. 1), $S_{m,p}^{(OO)}(Q)$, $S_{m,p}^{(OD)}(Q)$, and $S_{m,p}^{(DD)}(Q)$ are given as Eqs. 16, 17, and 18 in I, respectively, and the factor $f_3^5(Q)$ is

$$f_3^5(Q) = \frac{1}{5}[8Y_{c_0c_1}(Q) + 4\{Y_{c_1c_3}(Q) + Y_{c_1c_4}(Q)\} + 2\{Y_{c_1c_2}(Q) + Y_{c_3c_4}(Q)\}]. \quad (17)$$

For the $S_c(Q)$ required in the calculation of Eqs. 14—16, we can use the observed X-ray intensity data, considering from the fact that the first peak mainly expresses the averaged packing of water molecules in the liquid.

Parameters Used in the Present Calculation. According to the procedure described above, we can calculate the $S_{OO}(Q)$, $S_{OD}(Q)$, and $S_{DD}(Q)$ for the pentamer-monomer mixture model with an appropriate value of pentamer fraction x_5 and other several parameters (intramolecular distances, distances between molecular centers, mean-square variations, *etc*). The calculated curves are compared with the experimental data at 25 °C by Thiessen and Narten[3] and by Soper and Silver.[4]

According to the result in paper II the value of x_5 is 0.85 at 25 °C. Then, we use x_1=0.15 and x_5=0.85 in the present analysis.

The values of molecular parameters are identical with those in paper II: for pentamer, r_{OD}^5=0.98 Å, r_{DD}^5= 1.60 Å, and DOD angle=109.5° corresponding to the molecule in heavy ice-I, for monomer, r_{OD}^1=0.96 Å, r_{DD}^1 =1.52 Å, and DOD angle=104.5° corresponding to the molecule in the vapor, and for the hydrogen-bonding, $r_{O_1O_2}$ (=r_{OO} in paper II)=2.85 Å and the O-O-O angle=109.5°.

In performing calculations, the determination of molecular centers is required and there are three ways of defining the molecular center: the center of mass of the molecule $\vec{r}_G$, the definition as $\vec{r}_{c_1}=\Sigma b_n\vec{r}_n/\Sigma b_n$,[6] and

$$\vec{r}_{c_2}=\frac{\sum b_n^2\vec{r}_n}{\sum b_n^2}, \tag{18}$$

where n ranges over the nuclei in a molecule. Positions of the three types of molecular center in heavy water molecules ($b_O=0.58\times10^{-12}$ cm and $b_D=0.67\times10^{-12}$ cm)[7] are indicated in Fig. 2. As seen in the figure, $\vec{r}_{c_1}\simeq\vec{r}_{c_2}$ for heavy water molecule. Thus, we adopt here the two kinds of molecular centers, $\vec{r}_G$, and $\vec{r}_{c_2}$.

With respect to the magnitudes of Debye-Waller factors, assuming the mean-square variation $2\gamma_{nn'}^{\nu}\propto$ the inter-nucleus distance $r_{nn'}^{\nu}$,[8] we assign the following values to the rms variation $\{2\gamma_{nn}^{\nu}\}^{1/2}$ as: first, $D_1=0.06$ Å$^{1/2}$ per 1 Å for intramolecular distances (r_{OD}^1, r_{DD}^1, r_{OD}^5, r_{DD}^5, r_{cO}^1, r_{cD}^1, r_{cO}^5, and r_{cD}^5) and for hydrogen-bonded distances ($r_{O_0O_1}$, and $r_{O_1D_{01}}$); second, $D_2=0.07$ Å$^{1/2}$ per 1 Å for the seven intermolecular distances ($r_{O_1O_2}$, $r_{O_0D_{11}}$, $r_{O_1D_{31}}$, $r_{D_{01}D_{11}}$, $r_{D_{01}D_{21}}$, $r_{D_{01}D_{22}}$, and $r_{D_{31}D_{41}}$) and for five distances between molecular centers ($r_{c_0c_1}$, $r_{c_1c_2}$, $r_{c_1c_3}$, $r_{c_1c_4}$, and $r_{c_3c_4}$); third, $D_3=0.1$ Å$^{1/2}$ per 1 Å for four intermolecular (distances ($r_{O_1D_{21}}$, $r_{O_1D_{22}}$, $r_{D_{12}D_{41}}$, and $r_{D_{11}D_{31}}$); and, fourth, $D_4=0.2$ Å$^{1/2}$ per 1 Å for four intermolecular distances ($r_{D_{11}D_{21}}$, $r_{D_{11}D_{22}}$, $r_{D_{11}D_{42}}$, and $r_{D_{12}D_{22}}$).

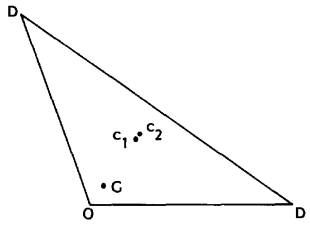

Fig. 2. Positions of molecular centers.
G: The center of mass, c_1: by Egelstaff,[6] c_2: by the authors (Eq. 18).

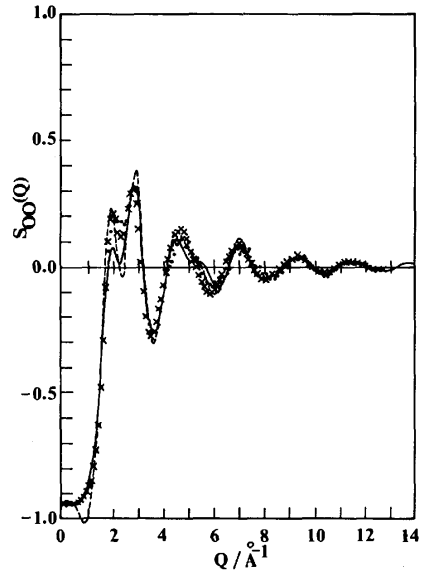

Fig. 3. Comparison between the calculated $S_{OO}(Q)$ for the C_{2v} symmetry model and observed data.
——: $S_{OO}^{c2}(Q)$ calculated, ------: $S_{OO}^{G}(Q)$ calculated, ●: neutron diffraction data by Thiessen and Narten,[3] ×: X-ray dffraction data by Narten.[9]

Results and Discussion

Comparison between Calculated Partial Structure Factors $S_{OO}(Q)$, $S_{OD}(Q)$, and $S_{DD}(Q)$ and Observed Data. Now, we can calculate the $S_{OO}(Q)$, $S_{OD}(Q)$, and $S_{DD}(Q)$, using Eqs. 14—18 together with the observed X-ray intensity data at 25 °C[9] for the $S_c(Q)$. The calculated O-O, O-D, and D-D structure factors are shown in Figs. 3, 4, and 5, respectively, and compared with the corresponding observed data. All calculated curves essentially reproduce the observed data successfully on the whole. Detailed features observed in these figures are described in the following.

Two calculated curves, $S_{OO}^{c2}(Q)$ and $S_{OO}^{G}(Q)$, are indicated in Fig. 3, where upper suffixes c2 and G shows the factor for the case when $\vec{r}_{c_2}$ and $\vec{r}_G$ is taken as the molecular center respectively. The $S_{OO}^{c2}(Q)$ is in agreement with the observed data on the whole, except for the deviation in the first peak at 2.1 Å^{-1} and that near $Q\simeq5$ Å^{-1}. On the other hand, an over oscillatory behavior appears in the calculated $S_{OO}^{G}(Q)$ curve, though a good agreement in the first peak. On the whole, the $S_{OO}^{c2}(Q)$ curve is somewhat better than $S_{OO}^{G}(Q)$ and the small difference between $S_{OO}^{c2}(Q)$ and $S_{OO}^{G}(Q)$ is attributed to the different magnitudes of the factors $Y_{cO}^{c2}(Q)$ and $Y_{cO}^{G}(Q)$ mainly.

With respect to the $S_{OD}(Q)$ shown in Fig. 4(a), the main features of the observed data are seen as: the

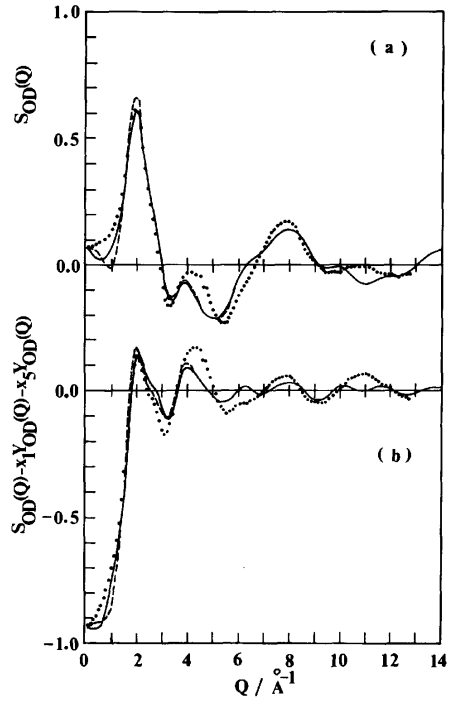

Fig. 4. Comparison between calculated O-D structure factors for the C_{2v} symmetry model and observed data.
(a) $S_{OD}(Q)$ (●: $S_{OD}(Q)$ observed by Thiessen and Narten[3]), (b) $S_{OD}(Q)-x_1Y_{OD}^1(Q)-x_5Y_{OD}^5(Q)$ (●: intermolecular part of $S_{OD}(Q)_{obsd}$ from which the intramolecular contribution of the pentamer-monomer mixture model is subtracted), ——: calculated curves ($\vec{r}_{c_2}$ as the molecular center), ------: calculated curves ($\vec{r}_G$ as the molecular center).

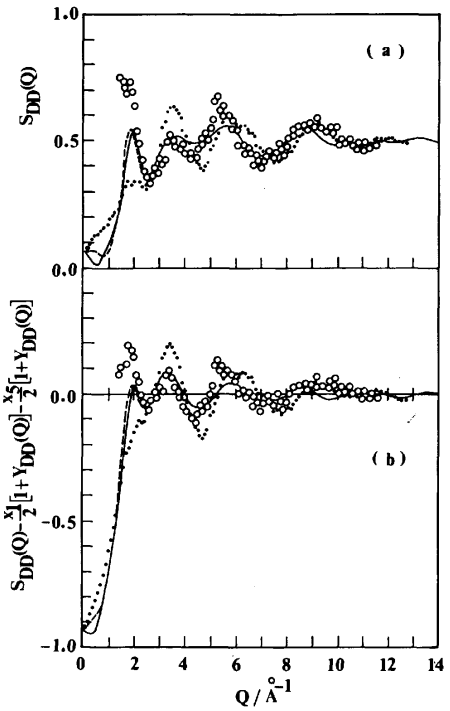

Fig. 5. Comparison between calculated D-D structure factors for the C_{2v} symmetry model and observed data.
(a) $S_{DD}(Q)$ (○: $S_{DD}(Q)$ observed by Soper and Silver,[4] ●: $S_{DD}(Q)$ observed by Thiessen and Narten[3]), (b) $S_{DD}(Q)-\frac{x_1}{2}[1+Y^1_{DD}(Q)]-\frac{x_5}{2}[1+Y^5_{DD}(Q)]$ (○: intermolecular part of $S_{DD}(Q)_{obsd}$ by Soper and Silver[4] from which the intramolecular contribution of the pentamer-monomer mixture model is subtracted, ●: intermolecular part of $S_{DD}(Q)_{obsd}$ by Thiessen and Narten[3] from which the intramolecular contribution of the pentamer-monomer mixture model is subtracted), ——: calculated curves ($\vec{r}_{c_2}$ as the molecular center), ------: calculated curves ($\vec{r}_G$ as the molecular center).

largest peak at 2 Å^{-1}, a bump at *ca.* 4 Å^{-1} a deep minimum at *ca.* 5 Å^{-1} and a broader peak ranging over 6—9 Å^{-1}. The calculated curve essentially reproduces these features of the $S_{OD}(Q)$ data. Especially, the agreement between the $S^{c_2}_{OD}(Q)$ and the observed data is excellent in the range of the first peak, 1—3 Å^{-1}. A large deviation of the calculated $S^{G}_{OD}(Q)$ curve from the data is seen in the lower Q range, like the case of O-O structure factor (Fig. 3). The same trend is found in the intermolecular part of the O-D structure factor, $S_{OD}(Q)-x_1Y^1_{OD}(Q)-x_5Y^5_{OD}(Q)$, shown in Fig. 4(b).

In Fig. 5, the calculated D-D structure factors are compared with the neutron diffraction data at reactor by Thiessen and Narten[3] and those at LINAC by Soper and Silver.[4] The two recent experimental data agree with each other on the whole. But, several noticeable deviations are observed. Taking account of the experimental difficulties in determining partial structure factors, we can see in Fig. 5(a) that the calculated $S^{c_2}_{DD}(Q)$ and $S^{G}_{DD}(Q)$ curves are in essential agreement with Soper and Silver's data on the whole. With respect to these features, the behavior of the intermolecular part of the $S_{DD}(Q)$ shown in Fig. 5(b) is quite similar to that of the $S_{DD}(Q)$ on the whole. Thus, we can state that the pentamer-monomer mixture model with the regular tetrahedral pentamer of the C_{2v} symmetrical structure reproduces the fundamental character of the D-D structure factors satisfactorily. In addition, the appearance of the first peak at 2 Å^{-1} in the calculated curves as well as in Soper and Silver's data is noticeable, though the magnitude of the calculated curves is only half that of their data.

Thus, the agreement between the calculated structure factor curves and observed data suggests the essential effectiveness of the pentamer-monomer mixture model with the regular tetrahedral pentamer as its dominant constituent.

We have taken so far the molecular center to be at the oxygen nucleus, similarly to the choice by Page and Powles,[5] and successfully interpreted the total structure factors of heavy water.[1,2] When the center is taken so, the $S_{OO}(Q)$ is reduced to $S_c(Q)$ resultantly as seen in Eq. 14, and then a reasonable estimation of the molecular center is required for the present calculation. As described in the preceding section, we have adopted two kinds of molecular centers for heavy water molecule, $\vec{r}_{c_2}$ and $\vec{r}_G$ (Fig. 2), and have calculated the partial structure factors (Figs. 3—5). The reasonable choice of the molecular center is practically important in obtaining successful results. Moreover, it is pointed out, as a noticeable feature, that the calculated curves are independent on the choice of molecular centers in this work, although only slight deviations of the $S^{G}_{ss}(Q)$ from $S^{c_2}_{ss}(Q)$ appear in lower Q region as seen in Figs. 3—5.

Freely Rotating Model. It is of much interesting whether the overall orientational configuration of water molecules in tetrahedral pentamer is the C_{2v} symmetry or the freely rotating, with respect to peripheral molecules. In paper I, we calculated the total structure factors for the freely rotating model in addition to the C_{2v} symmetry model. In the former model, the peripheral molecules are rotating freely around the axis on a straight line joining the central and peripheral oxygens. Here, we calculate the partial structure factors of the freely rotating model also. Then, for that model, we have assumed that the positions of outer six deuterons are reduced to those of peripheral oxygens on the average and also that the positions of all the molecular centers are reduced to those of oxygens within the molecule including its molecular center. Accordingly, the $S^{(OD)}_{m,p}(Q)$ and $S^{(DD)}_{m,p}(Q)$ are written as

$$S^{(OD)}_{m,p}(Q) = \frac{1}{5}[2Y_{O_1D_{01}}(Q) + 3Y_{O_1D_{31}}(Q) + 6Y_{O_0D_{11}}(Q) + 9Y_{O_1O_2}(Q)], \quad (19)$$

and

$$S^{(DD)}_{m,p}(Q) = \frac{1}{10}[Y_{D_{31}D_{41}}(Q) + 8Y_{O_0D_{11}}(Q) + 10Y_{O_1D_{31}}(Q) + 8Y_{O_1D_{01}}(Q) + 13Y_{O_1O_2}(Q)], \quad (20)$$

respectively, and $f^5_3(Q)$ (Eq. 20) is reduced to Eq. 17. Equations 19 and 20 are identical with Eqs. 19 and 20 in paper I, where a typographical error in Eq. 20 in paper I is corrected.[10] Then, for the freely rotating model, using Eqs. 14—20, we calculated the O-O, O-D, and

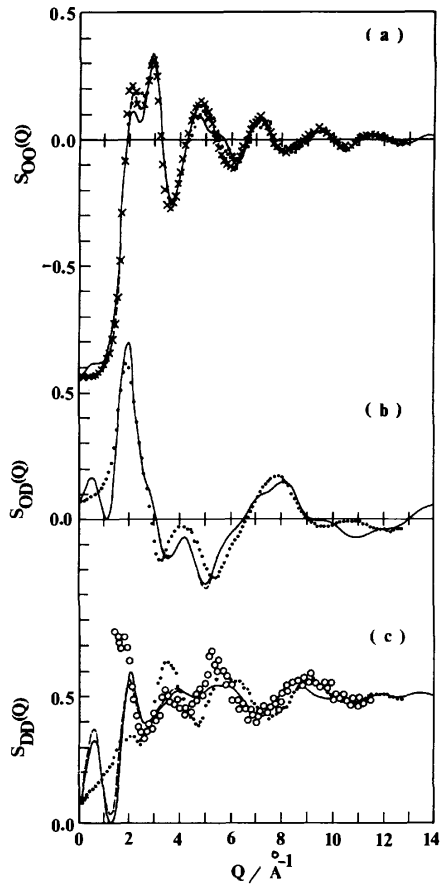

Fig. 6. Comparison between calculated partial structure factors for the freely rotating model and observed data.
○: Neutron diffraction data by Soper and Silver,[4] ●: neutron diffraction data by Thiessen and Narten,[3] ×: X-ray diffraction data by Narten,[9] ——: calculated curves ($\vec{r}_{c_2}$ as the molecular center), -------: calculated curves ($\vec{r}_G$ as the molecular center).

D–D structure factors. The calculated curves are shown in Fig. 6.

Compared Figs. 6(a)—(c) with Figs. 3—5, respectively, it is found that the difference between the results for the freely rotating model and those for the C_{2v} symmetry model is very slight, except the D–D structure factors in lower Q region. As seen in Figs. 5 and 6(c), the calculated $S_{DD}(Q)$ curves for both models are fairly different from each other in lower Q region ($\lesssim 1.5$ Å^{-1}). This means the fact that the D–D structure factors in low Q region dominantly reflect the orientational configuration of water molecules in the liquid. Thus, the marked deviation of the calculated $S_{DD}(Q)$ curve for the freely rotating model from the observed data is considered to indicate that the model behaves only as an approximate one.

References

1) N. Ohtomo, K. Tokiwano, and K. Arakawa, *Bull. Chem. Soc. Jpn.*, **54**, 1802 (1981).
2) N. Ohtomo, K. Tokiwano, and K.Arakawa, *Bull. Chem. Soc. Jpn.*, **55**, 2788 (1982).
3) W. E. Thiessen and A. H. Narten, *J. Chem. Phys.*, **77**, 2656 (1982).
4) A. K. Soper and R. N. Silver, *Phys. Rev. Lett.*, **49**, 471 (1982).
5) D. I. Page and Powles, *Mol. Phys.*, **21**, 901 (1971).
6) P. A. Egelstaff, "An Introduction to the Liquid State," Academic Press, New York and London (1967).
7) G. Kostorz and S. W. Lovessey, "Treatise on Materials Science and Technology," Academic Press, New York and London (1979), Vol. 15, pp. 5—8.
8) N. Ohtomo and K. Arakawa, *Bull. Chem. Soc. Jpn.*, **51**, 1649 (1978).
9) A. H. Narten, "X-Ray Diffraction Data on Liquid Water in Temperature Range 4—200 °C," ORNL-4578 (1970).
10) In paper I the calculations for the freely rotating model were performed by using the right expression Eq. 20 given in this text throughout, and then the curves shown in Figs. 6 and 7 in paper I are correct ones.

Studies of Polystyrene-based Ion Exchange Fiber. II. A Novel Fiber-form Catalyst for Sucrose Inversion and Methyl Acetate Hydrolysis†

Toshio YOSHIOKA* and Masaharu SHIMAMURA
Fibers Research Laboratories, Toray Industries, Inc., Sonoyama, Otsu 520
(Received June 9, 1983)

To obtain a novel acid-base catalyst of high activity and easy treatment, we have prepared polystyrene-based fibrous ion exchange catalysts which have large surface areas per unit of weight and which can be utilized in various forms. They are excellent in chemical stability and mechanical strength due to their composite structures, reinforced with polypropyrene. The reactions of sucrose inversion and methyl acetate hydrolysis were carried out by using these cation exchange fibers and ordinary cation exchange resins. The fiber has about sixteen times as high a catalytic activity per equivalent acid as the resin in the case of sucrose inversion. The intrinsic rate constant in the fiber phase is evaluated to be 2.4 times larger than that in the resin phase in terms of the solid-catalysis theory considering the catalytic effectiveness factor and the absorption coefficient. On the other hand, the catalytic activity per equivalent acid of the fiber is almost equal to that of the resin in the case of methyl acetate hydrolysis. It is suggested that this different behavior is attributable to the different molecular sizes of the reactants.

Polystyrene-based ion exchange resins have been intensively studied as solid acid-base catalysts in a number of organic reactions.[2] The use of ion exchange resins, however, has the disadvantage that their catalytic activities per equivalent acid or base are lower than those of free acids or bases in the case of a reaction controlled by intraparticle diffusion. Although catalytic activity is enhanced by using a fine or crushed resin, catalytic treatment becomes difficult.

In order to enhance the catalytic activity and to make catalytic treatment easier, we have undertaken an investigation of fibrous acid-base catalysts, which have large surface areas per unit of weight and which can be used in various forms. Polystyrene-based fibrous ion exchange catalysts have been prepared and used in the well-known reactions of sucrose inversion and methyl acetate hydrolysis.[3] These results will be discussed in terms of the solid-catalysis theory in this paper.

Experimental

Polystyrene (PSt; average molecular weight: 23×10^4) as the predominant *sea* ingredient and polypropylene (PP; average molecular weight: 20×10^4) as the *island* ingredient were spun into composite filaments having an *islands-in-a-sea* type sectional structure, as is shown in Fig. 1, in the conventional manner. Polystyrene-based ion exchange fibers, named IONEX, were prepared according to the process shown in Fig. 2 after spinning.[1] The crosslinking was performed by treating the fiber (10 g) with 100 ml of a solution consisting of 5 wt% paraformaldehyde, 25 wt% acetic acid, and 70 wt% concd. sulfuric acid at 80 °C for 2 h or at 90 °C for 4 h.[4] Fibrous acid or base catalysts were obtained by treating these fibers with an acid or a base in the usual manner.

These fibrous cation exchange catalysts were packed into a jacketed glass fixed-bed reactor with an inside diameter of 2 cm. The reactions of sucrose inversion and methyl acetate hydrolysis were carried out by pumping a 50 wt% sucrose aqueous solution at 60 °C and a 3.2 M (1 M=1 mol dm^{-3}) methyl acetate aqueous solution at 30 °C respectively through the reactor. For the purposes of comparison, the reactions were also carried out by using commercially available cation exchange resins (Amberlite IR-120B and IR-200) with radii of *ca.* 250 μm. The reaction ratio of sucrose was measured according to the usual polarimetric technique.[5] The acetic acid concentration was determined by the titration method.

† A preliminary report of this work was presented in *Shokubai*, **25**, 115 (1983).

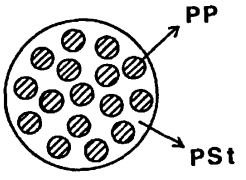

Fig. 1. Schematic cross section of composite fiber. PSt: polystyrene, *sea* ingredient; PP: polypropylene, *island* ingredient.

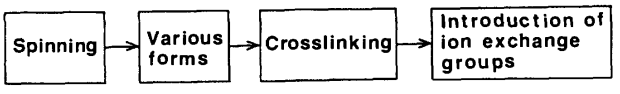

Fig. 2. Process of preparing the polystyrene-based ion exchange fiber (IONEX).[1]

Results and Discussion

Fibrous Acid-base Catalyst. The characteristic data of the filamentary IONEX are summarized in Table 1. Acid-base catalysts in various forms, such as cut fiber, knitted fabric, woven fabric, braid, felt, nonwoven fabric, and paper, can be obtained by processing the filaments before chemical reactions, as the filaments reinforced with polypropylene have high mechanical strengths. Figure 3 shows fibrous cation

Table 1. Characteristic data of filamentary IONEX

Ionic group[a]	Diameter μm	Strength g d^{-1}	Capacity[b] mequiv g^{-1}	Water content[c]
—	24	3.0	—	—
$-SO_3^-$	30	1.3	2.6	1.6
$-N^+(CH_3)_3$	32	1.4	2.4	1.9

a) Original filaments: *Sea* (PSt//PP)/*Islands* (PP)= (40//10)/50. b) Capacity of strong-acid (base) groups. c) $(W-W_0)/W_0$. W: wet weight, W_0: dry weight.

TABLE 2. RESULTS OF SUCROSE INVERSION BY VARIOUS ACID CATALYSTS

No.	Acid catalyst	Capacity	Water content	Bed volume[a]	Packed weight	Rate constant[b] $k\times10^3$
		mequiv g^{-1}		ml	g	ml s^{-1} mequiv^{-1}
1	Filamentary IONEX	2.5	2.0	37.5	4.0	12.4
2	Filamentary IONEX	2.5	1.6	25	2.9	12.7
3	Knitted IONEX	2.5	1.6	25	5.3	8.9
4	Amberlite IR-120B	5.0	0.9	25	10	0.80
5	Amberlite IR-200	4.8	1.0	25	10	0.88

a) Diameter: 2 cm. b) 60 °C, 50 wt% sucrose aqueous solution.

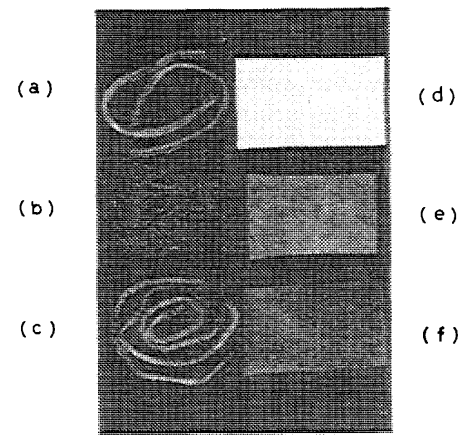

Fig. 3. Fibrous cation exchange catalyst in various forms of knitted cord (a), filament (b), braid (c), paper (d), knitted fabric (e), and needle punched felt (f).

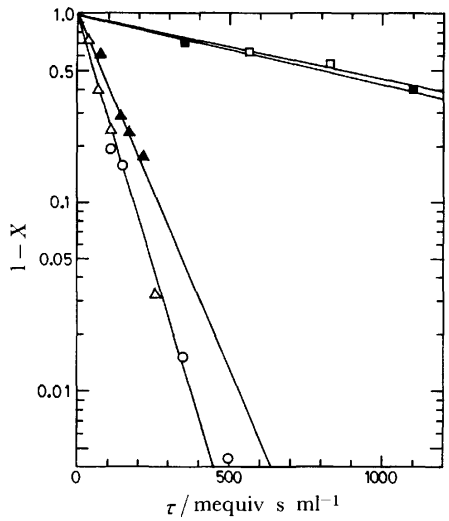

Fig. 4. Plots of $1-X$ *vs.* τ in sucrose inversion (Eq. 1). Reaction temperature, 60 °C; concentration of sucrose solution, 50 wt%.
○: Filamentary IONEX (water content 2.0), △: filamentary IONEX (water content 1.6), ▲: knitted IONEX (water content 1.6), □: Amberlite IR-120B, ■: Amberlite IR-200.

exchange catalysts in various forms. The ion exchange capacities per unit of weight of IONEX are lower than those of ordinary ion exchange resins by the amount of polypropyrene used for reinforcement.

Sucrose Inversion. The results of sucrose inversion by various acid catalysts are shown in Fig. 4 and Table 2. On the assumption of first-order kinetics, the apparent rate constant, k, was determined from the following equation:

$$\ln(1-X) = -k\tau, \tag{1}$$

where X is a reaction ratio of sucrose and where τ is a contact time.

The effect of the packing density of the fibers was also examined. In the density range above 0.1 g ml^{-1} the rate constant is close to the value of 13.4×10^{-3} ml s^{-1} mequiv^{-1} determined by a batch method. However, below 0.1 g ml^{-1} it decreases slightly as the density is lowered, probably because of the effect of an irregular flow. It was found that the height of the fixed-bed and the crosslinking degree of the fiber do not affect the rate constant. The catalytic activity of the knitted IONEX is 30% lower than that of the filamentary IONEX. This result may be interpreted by assuming that the effective surface area per unit of weight decreases or an irregular flow takes place because of the knitted structure.

The apparent rate constant of the filamentary IONEX is about sixteen times as large as that of the gel-type resin, IR-120B. According to the solid-catalysis theory, the apparent rate constant, k, can be described by the following equation:[6,7]

$$k = \lambda k_0 \eta, \tag{2}$$

where λ, k_0, and η are an absorption coefficient, an intrinsic rate constant, and a catalytic effectiveness factor respectively. Here, the catalytic effectiveness factors in the two cases of spherical and fibrous catalysts with a given radius, R, are given by:[8]

$$\eta(\text{sphere}) = \frac{3(mR\coth mR-1)}{(mR)^2} \tag{3}$$

and

$$\eta(\text{fiber}) = \frac{2I_1(mR)}{I_0(mR)} \tag{4}$$

respectively, where I_0 and I_1 are modified Bessel functions of zero and first-order and where $m=\sqrt{k_0/D}$, in which D is an effective diffusion coefficient of a reactant in a catalyst. The relation between m and η in the two cases of the spherical catalyst with a radius of 250 μm and the fibrous catalyst with a radius of 15 μm is shown in Fig. 5.

The value of η for IR-120B is larger than 0.25, judging from the results studied by Gilliland *et al.*,[7] so that the value of η for the fiber can be roughly evaluated

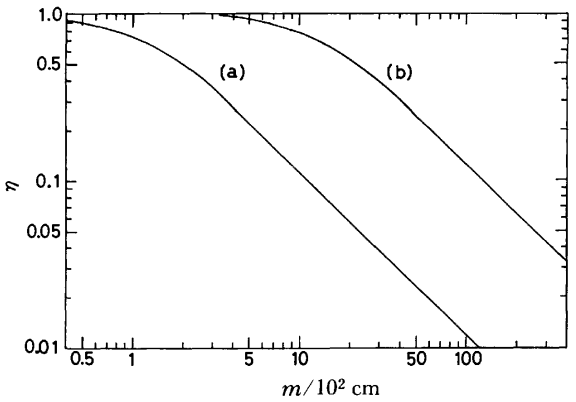

Fig. 5. Catalytic effectiveness factor η as a function of m (Eqs. 3 and 4).
(a) Spherical catalyst (R= 250 μm), and (b) fibrous catalyst (R=15 μm).

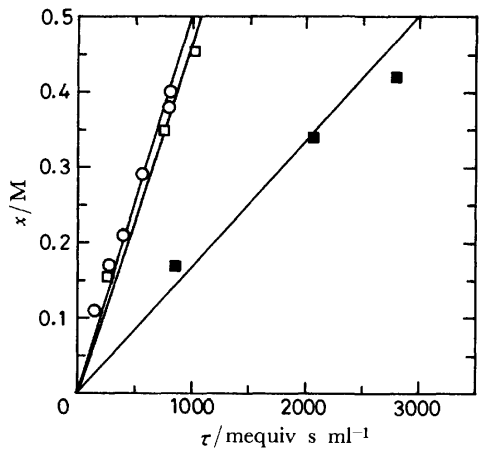

Fig. 6. Plots of x *vs.* τ in methyl acetate hydrolysis (Eq. 5).
Reaction temperature, 30°C; concentration of methyl acetate solution, 3.2 M.
○: Filamentary IONEX (water content 2.0), □: Amberlite IR-120B, ■: Amberlite IR-200.

to be almost equal to 1 at the corresponding m-value from Fig. 5. The sucrose-absorption coefficients for IR-120B and the fiber in a Na form were found to be 0.30±0.05 and 0.50±0.1 in a 50 wt% sucrose aqueous solution. The former value is much larger than that in a 20 wt/vol% sucrose aqueous solution determined by Gilliland *et al.*[7] It is, however, considered to be an adequate value, because the absorption coefficient generally increases as the concentration of sucrose in a solution increases. Probably the absorption coefficient of the fiber is larger than that of the resin because of the difference in water contents; that is, the fiber has a higher water content than the resin.[6]

In considering the results described above, the experimental data show that the intrinsic rate constant in the fiber phase is 2.4 times larger than that in the resin phase. It has been reported by Gilliland *et al.* that the intrinsic rate constants in the resin phase are only 60% as large as those determined in 3 M acid solutions.[7] The reason for the reduced effectiveness of the resin as a catalyst has been attributed to an irregular structure of the crosslinked resin and to steric hindrance due to a large reactant of the sucrose molecule. The fact that the fiber has a higher intrinsic rate constant than the resin may be explained by assuming that the fiber has such a crosslinked structure that the steric hindrance is relieved. That is, the fiber based on polystrene essentially has a less restricted one-dimensional structure although its chains are crosslinked by methylene bonds, while the resin based on a styrene–divinylbenzene polymer has a more restricted three-dimensional structure. The difference in the intrinsic rate constants may be enhanced by the high sucrose concentration of 50 wt%.

On the other hand, the catalytic effectiveness factor for IR-200 of the macroreticular type can be estimated to be 1 from its large surface area of 50 $m^2\ g^{-1}$. Its absorption coefficient for sucrose was measured as 0.40±0.05. Taking these facts into account, the intrinsic rate constant in the IR-200 phase is found to be only 20% as large as that in the IR-120B phase. This may be attributable to the large effect of the steric hindrance, which prevents a close approach of a sucrose molecule to an active site for inversion, because the macroreticular-type resin is three-dimensionally and tightly crosslinked.[7,9]

Methyl Acetate Hydrolysis. The reaction of methyl acetate hydrolysis was carried out by using the Nos. 1, 4, and 5 beds shown in Table 2. The acetic acid concentrations in effluent solutions as a function of the contact times are shown in Fig. 6. As this reaction is first-order, the apparent rate constant can be evaluated from the following equation:

$$\ln a/(a-x) = k\tau, \tag{5}$$

where x is an acetic acid concentration and a is its concentration in equilibrium. It is possible to evaluate the apparent rate constants directly from Fig. 6, since k is equal to $x/a\tau$ when x is sufficiently small.

No large difference in the apparent rate constants was observed between the fiber and IR-120B. This fact indicates that their catalytic effectiveness factors are both close to 1 because of the probable rapid diffusion of methyl acetate molecules in the catalysts, and that both the absorption coefficient and the intrinsic rate constant of the fiber are almost equal to those of the resin.[6,10] On the other hand, the apparent rate constant for IR-200 is only one third as large as that for IR-120B. This result can be interpreted by assuming that the former has a small absorption coefficient and also has a small intrinsic rate constant because of the steric hindrance in comparison with the latter, although their catalytic effectiveness factors are both close to 1.[11]

The fibrous catalyst is expected to be applicable to new reactors such as the reaction distiller of methyl acetate hydrolysis, since it can be used in various forms.[12,13]

Conclusion

1. Polystyrene-based fibrous ion exchange catalysts which are excellent in chemical stability and mechanical strength have been prepared. These fibrous acid-base catalysts have a large surface areas per unit of

weight and can be used in various forms.

2. These ion exchange fibers have not only much higher catalytic activities than ordinary ion exchange resins when the reactant is a large molecule such as sucrose, but also the advantage of easier catalytic treatment than a fine or crushed resin.

3. When the reactant is a small molecule such as methyl acetate, these ion exchange fiber show as high catalytic activities as ordinary ion exchange resins.

The authors would like to express their appreciation to Dr. Tatsuro Kawaguchi, Mr. Michihiko Tanaka, and Dr. Masaki Nishino for their continuous encouragement throughout this work. They are also much obliged to Mr. Kazuo Teramoto for his advice on the chemical treatments and to Mr. Seiichi Yoshikawa and other collaborators for the preparation of the composite fibers. The authors also wish to thank Toray Industries, Inc., for making this study possible.

References

1) For Part I., see T. Yoshioka and M. Shimamura, *Polym. Prepr. Jpn.*, **31**, 2025 (1982); *Bull. Chem. Soc. Jpn.*, **56**, 3726 (1983).

2) F. X. McGarvey and R. Kunin, "Ion Exchange Technology," ed by F. C. Nachod and J. Schubert, Academic Press, New York (1956), p. 272.

3) T. Yoshioka, K. Teramoto, and M. Shimamura, Japanese Laid-open Patent 123982 (1977); *Chem. Abstr.*, **88**, 106423x (1978).

4) K. Kashihara and M. Shimamura, Japanese Laid-open Patent 6587 (1975); *Chem. Abstr.*, **83**, 29388g (1975).

5) G. Bodamer and R. Kunin, *Ind. Eng. Chem.*, **43**, 1082 (1951).

6) H. Saito, F. Shimamoto, Y. Mishima, and O. Sataka, *Kogyo Kagaku Zasshi*, **64**, 1733 (1961).

7) E. R. Gilliland, H. J. Bixler, and J. E. O'Connell, *Ind. Eng. Chem. Fundam.*, **10**, 185 (1971).

8) O. Levenspiel, "Chemical Reaction Engineering," Wiley, New York (1962), Chap. 14.

9) Y. Murakami and O. Mori, *Kogyo Kagaku Zasshi*, **69**, 588 (1966).

10) H. Teshima, T. Sumi, and N. Morita, *Nippon Kagaku Kaishi*, **1972**, 711.

11) H. Teshima, T. Ido, and T. Kasahara, *Nippon Kagaku Kaishi*, **1977**, 769.

12) Y. Fuchigami, *Shokubai*, **24**, 178 (1982).

13) M. Chiwa, H. Shimizu, and M. Nozaki, Japanese Laid-open Patent 7259 (1982).

The Mercury Volatilization Rate from Water to the Atmosphere

Shoichi Okouchi,* Sokichi Sasaki, and Yoshio Harano†
Chemical Laboratory, College of Engineering, Hosei University, Koganei, Tokyo 184
†*Department of Applied Chemistry, Osaka City University, Sumiyoshi-ku, Osaka 558*
(Received June 20, 1983)

The volatilization rate of mercury was studied, together with the oxygen reaeration rate, in a laboratory scale under various mixing conditions. The rates of both mercury and oxygen were controlled by mass transfer in the aqueous phase. The obtained ratio of the mercury-volatilization rate constant to the oxygen-reaeration rate constant was 0.94 at temperatures ranging from 283 to 303. If the oxygen-reaeration rate constant is available in a real-water body or in a wastewater-treatment facility, multiplying its value by the ratio of 0.94 permits the determination of the volatilization rate constant of mercury without the direct measurement of the mercury.

It is well known that contaminants such as mercury, DDT, and PCB have been transported widely throughout global environments. The volatilization of contaminants from natural water bodies to the atmosphere has been considered to be a very important step in the environmental-pollution process.

A mass balance for the volatilization of a contaminant, i, from well-mixed water into the atmosphere is given by Eq. 1:

$$-dC^{(i)}/dt = K_V^{(i)}(C^{(i)} - p^{(i)}/H^{(i)}), \quad (1)$$

where C is the concentration of the contaminant in the water; t is the time; K_v is the volatilization rate constant; p is the partial pressure of the contaminant in the atmosphere, and H is Henry's law constant. The subscript (i) denotes the component i. According to the two-film model, $K_V^{(i)}$ is given by Eq. 2:

$$K_V^{(i)} = K_L^{(i)}a = [1/k_L^{(i)} + (RT/H^{(i)})(1/k_G^{(i)})]^{-1}a, \quad (2)$$

where K_L is the overall mass-transfer coefficient based on the liquid-phase concentration; k_L and k_G are the mass-transfer coefficients in liquid and gas films respectively; a is the interfacial contact area per liquid volume; R is the gas constant, and T is the absolute temperature.

The actual environmental-water body generally comes in contact with the atmosphere on its free surface; therefore, a is given by the reciprocal of the depth of the water, L. Thus, the overall volatilization rate constant of a component, i, from an environmental-water body, $K_{V(env)}^{(i)}$, is expressed by:

$$K_{V(env)}^{(i)} = (1/L)[1/k_{L(env)}^{(i)} + (RT/H^{(i)})(1/k_{G(env)}^{(i)})]^{-1}. \quad (3)$$

The subscript (env) means the environmental-water body. Since the coefficients, $k_{L(env)}$ and $k_{G(env)}$, depend greatly on the hydrodynamic situation of both water and atmosphere, it is necessary, for the direct evaluation of $K_{V(env)}^{(i)}$, according to Eq. 3, to grasp the mixing situation of the system quantitatively. This is, however, a very difficult matter, except the oxygen-reaeration rate constant, $K_{V(env)}^{(O_2)}$,[1-3] of $i = O_2$.

From these circumstances, the volatilization rates of some contaminants on the actual water body can be estimated indirectly, according to Eq. 4, by using the data on $K_{V(env)}^{(O_2)}$:

$$K_{V(env)}^{(i)} = K_{V(env)}^{(O_2)} \times (K_V^{(i)}/K_V^{(O_2)}), \quad (4)$$

where $K_V^{(O_2)}$ is the oxygen-reaeration rate constant defined by Eq. 5 and where both $K_V^{(i)}$ and $K_V^{(O_2)}$ can be measured experimentally under well-defined conditions:

$$dC^{(O_2)}/dt = K_V^{(O_2)}(C_S^{(O_2)} - C^{(O_2)}), \quad (5)$$

where $C_S^{(O_2)}$ is the solubility of oxygen in water for a partial of oxygen in the atmosphere.

The volatilization rate of mercury in the actual water body has not been estimated, although mercury is one of the most important environmental contaminants and can be anticipated to volatilize readily to the atmosphere.[4] In this work, the $K_V^{(i)}/K_V^{(O_2)}$ ratio, which is the determining factor for the volatility of the contaminants, was determined experimentally for mercury.

Experimental

All the chemicals used were of an analytical reagent grade. A schematic diagram of the experimental apparatus is shown in Fig. 1. The volatilization rate constant of mercury was measured as follows. An aqueous solution of mercury(II) chloride at the concentration of the ppb level (below the value of elemental mercury solubility[17] in water) was prepared in the vessel (V in Fig. 1) and was then stirred at a constant agitation speed by means of a magnetic stirrer. The vessel was maintained at a constant temperature, and air was made to flow through the space above the aqueous solution in the vessel, the absorption cell(C), and the absorber(S),

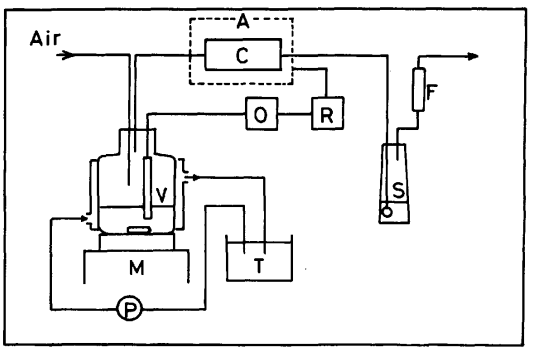

Fig. 1. Schematic diagram of apparatus.
A: Atomic absorption spectrophotometer, C: absorption cell, F: flow meter, M: magnetic stirrer, O: dissolved oxygen analyzer, P: pump, R: recorder, S: ($KMnO_4$+H_2SO_4) absorber, T: thermostat, V: volatilization vessel.

successively, at a constant flow rate throughout the measurements. By the addition of hydrazine hydrate to the aqueous solution as a reducing agent,[4] the mercury(II) species were reduced quickly and completely to elemental mercury. The elemental mercury thus formed began immidiately to volatilize into the flowing air. The concentration of mercury in air was continuously measured from the absorbance at 253.7 nm obtained by means of an absorption spectrophotometer(A). The volatilization rate constant of mercury was determined by fitting the concentration data to the integral form of Eq. 1.

As to the measurement of the oxygen-reaeration rate, the distilled water in the vessel(V) was purged with nitrogen to remove most of the dissolved oxygen. By agitating the water at a constant agitation speed, oxygen from the atmosphere was dissolved in the oxygen-deficient water. The oxygen-reaeration rate constant was determined by fitting the data of the oxygen concentration in the water, as measured by means of a dissolved oxygen analyzer, to the integral form of Eq. 5.

Results and Discussion

The volatilization rate constant of mercury, $K_v^{(Hg)}$, was unaffected by the mercury concentration over the range from 5×10^{-11} to 2.5×10^{-10} mol m^{-3}, as was to be expected from Eq. 2. The effect of turbulence in the gas phase on $K_v^{(Hg)}$ and on the oxygen-reaeration rate constant, $K_v^{(O_2)}$, was not observed over the air-flow rate range from 0.03 to 0.3 m^3 h^{-1} at 298 K, as shown in Fig.

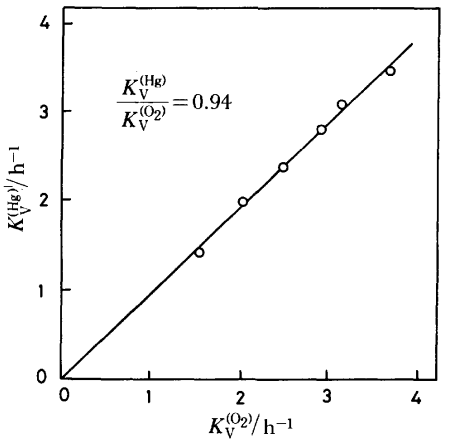

Fig. 4. Relation between $K_v^{(Hg)}$ and $K_v^{(O_2)}$ at 298 K.

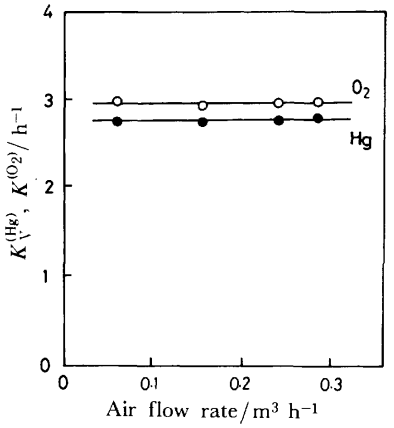

Fig. 2. Effect of air flow rate on $K_v^{(Hg)}$ and $K_v^{(O_2)}$ at 298 K.
Agitation speed: 320 min^{-1}, water depth: 3.7×10^{-2} m.

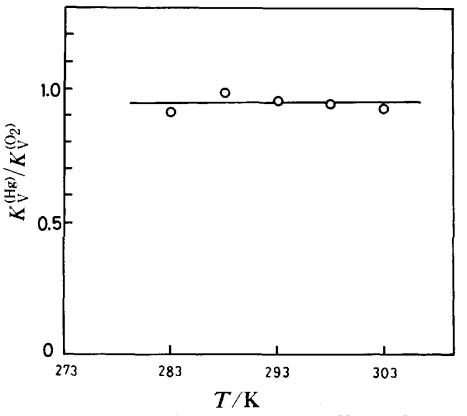

Fig. 5. Effect of temperature on $K_v^{(Hg)}/K_v^{(O_2)}$.
Air flow rate: 0.24 m^3 h^{-1}, water depth: 3.7×10^{-2} m, agitation speed: 320 min^{-1}.

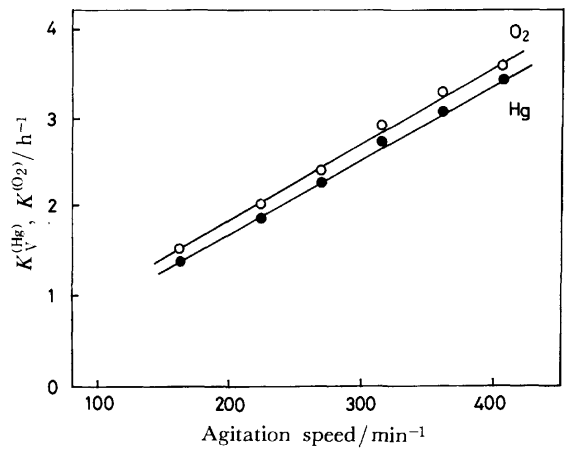

Fig. 3. Effect of agitation speed on $K_v^{(Hg)}$ and $K_v^{(O_2)}$ at 298 K.
Air flow rate: 0.24 m^3 h^{-1}, water depth: 3.7×10^{-2} m.

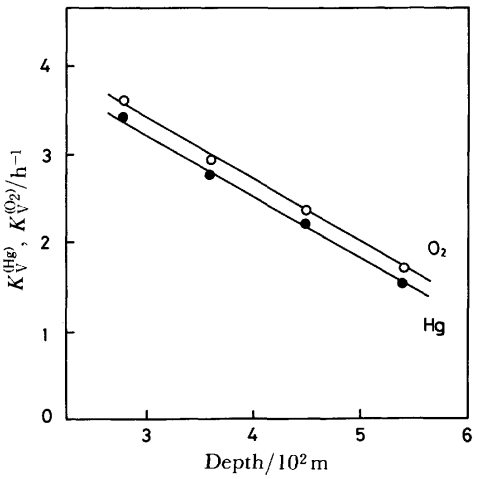

Fig. 6. Effect of water depth on $K_v^{(Hg)}$ and $K_v^{(O_2)}$ at 298 K.
Air flow rate: 0.24 m^3 h^{-1}, agitation speed: 320 min^{-1}.

Table 1. Volatilization rate constant and half-life of contaminants estimated as $K_{v(env)}^{(O_2)}=10^{-2}$ h^{-1}

Contaminant (i)	Molecular weight	$K_v^{(i)}/K_v^{(O_2)}$	$K_{v(env)}^{(i)}$/h^{-1}	$\tau^{(i)}$/d	Vapor pressure/Pa (at 298 K)
Mercury	200.59	0.94	9.4×10^{-3}	3.1	0.245
Benzene	78.11	0.56	5.6×10^{-3}	5.2	12700
Tetrachloroethylene	165.83	0.52	5.2×10^{-3}	5.6	2400

2. On the other hand, both the rate constants increased with an increase in the agitation rate in the aqueous phase, as shown in Fig. 3. From these data, the values of $K_v^{(Hg)}$ and $K_v^{(O_2)}$ at 298 K were related by a linear relationship with a slope of 0.94 ($=K_v^{(Hg)}/K_v^{(O_2)}$), as shown in Fig. 4. The $K_v^{(Hg)}/K_v^{(O_2)}$ ratio was observed to be independent of temperatures ranging from 283 to 303 K, as shown in Fig. 5, although both the rate constants increased with a rise in the temperatures. Figure 6 shows the effect of the depth of the solution on the rate constants, indicating that the greater the depth, the smaller the rate constants become at a constant agitation speed because of the smaller turbulence in the aqueous solution and the smaller interfacial area. However, the $K_v^{(Hg)}/K_v^{(O_2)}$ ratio did not change, regardless of the depth.

Mackay and Leinonen[5] have suggested that mass transfer in the liquid phase is rate-controlling when the value of Henry's law constant is greater than 500 m^3 Pa mol^{-1}. Henry's law constant of mercury and oxygen is 993[6] and 79240[7] m^3 Pa mol^{-1} respectively at 298 K. As has been mentioned above, the mercury-volatilization rate and the oxygen-reaeration rate were both much many affected by the turbulence in the liquid phase than by that in the gas phase; consequently, these results support the suggestion of Mackay and Leinonen. Therefore, most of the resistance to these mass-transfer rates is concluded to lie in the liquid-phase boundary layer; thus, the term of $(RT/H^{(i)})(1/k_G^{(i)})$ in Eq. 2 can be neglected.

Taking into account the fact that the mass-transfer coefficient is proportional to the n-th power of diffusivity,[8] together with the above consideration, Eq. 6 is obtained from Eq. 2:

$$K_V^{(Hg)}/K_V^{(O_2)} = K_L^{(Hg)}/K_L^{(O_2)} = (D_L^{(Hg)}/D_L^{(O_2)})^n, \quad (6)$$

where D_L is the diffusivity** in the liquid phase. The value of n is $0.5\leq n\leq 1$, where n becomes unity in the case based on the classical theory of the two-film mass-transfer model[9] and where n is equal to 0.5 according to the theories of the penetration model[10] or the surface-renewal model[11]. From Eq. 6, the value of $K_v^{(Hg)}/K_v^{(O_2)}$ is estimated to be 1.2 ($n=1$) or 1.1 ($n=0.5$) by using the Othmer-Thakar relation[12] of $D_L\propto V_b^{-0.6}$, where V_b is the molar volume at the boiling point, 0.83 ($n=1$) or 0.91 ($n=0.5$) by considering the inverse proportionality of D_L to the molecular diameter[13] and 1.3 ($m=-0.5$[14]) or 1.2 ($m=-0.31$[15]) by applying the relation of $K_v\propto V_c^m$, where V_c is the critical molar volume. Based on the Liss-Slater's relation[16] of $K_v\propto M^{-0.5}$, the value of 0.4 is obtained. Besides this, all the other estimated values are considered to support the value of 0.94 obtained experimentally in this work.

The values of the oxygen-reaeration rate constant in the representative environmental water bodies, $K_{v(env)}^{(O_2)}$ [h^{-1}], have been reported[1] to be 4.6×10^{-3}—9.6×10^{-3} for ponds, 4.2×10^{-3}—3.9×10^{-1} for rivers, and 4.2×10^{-3}—1.2×10^{-2} for lakes. Table 1 shows the $K_{v(env)}^{(i)}$ values calculated by Eq. 4 for some contaminants, taking the value of $K_{v(env)}^{(O_2)}$ to be 10^{-2} h^{-1} and the values of $K_v^{(i)}/K_v^{(O_2)}$ to be 0.94, 0.57,[7] and 0.52[7] for mercury (in this work), benzene, and tetrachloroethylene respectively. Table 1 also shows the half-life times of the contaminants, $\tau^{(i)}$, defined by Eq. 7:

$$\tau^{(i)} = \ln 2/K_{v(env)}^{(i)}. \quad (7)$$

As is apparent in Table 1, mercury volatilizes about 1.7—1.8 times more rapidly than benzene or tetrachloroethylene, although the latter has much higher vapor pressures and smaller molecular weights. In this work, it has been demonstrated that the volatiliation of mercury in a water body to the atmosphere occurs much faster than has generally been appreciated.

** The diffusivity of mercury has not been measured.

References

1) J. H. Smith, W. R. Mabey, N. Bohonos, B. R. Holt, S. S. Lee, T. W. Chou, D. C. Bomberger, and T. Mill, *U.S. Environ. Prot. Agency Rept., EPA*-600/7-77-113 (1977).
2) E. C. Tsivoglou and J. R. Wallance, *U.S. Environ. Prot. Agency Rept., EPA*-R3-72-012 (1972).
3) R. E. Rathbun and D. Y. Tai, *Water Res.*, **15**, 243 (1981).
4) S. Okouchi, Y. Itakura, and S. Sasaki, *Nippon Kagaku Kaishi*, **1979**, 1263.
5) D. Mackay and P. J. Leinonen, *Environ. Sci. Technol.*, **9**, 1178 (1975).
6) S. Okouchi and S. Sasaki, *Bull. Chem. Soc. Jpn.*, **54**, 2821 (1981).
7) R. F. Weiss, *Deep Sea Res.*, **17**, 721 (1970).
8) J. H. Smith, D. C. Bomberger, and D. L. Haynes, *Environ. Sci. Technol.*, **14**, 1332 (1980).
9) W. K. Lewis and W. G. Whiteman, *Ind. Eng. Chem.*, **16**, 1215 (1924).
10) R. Higbie, *Trans. Am. Inst. Chem. Eng.*, **31**, 365 (1935).
11) P. V. Danckwerts, *Ind. Eng. Chem.*, **43**, 1460 (1951).
12) D. F. Othmer and M. S. Thakar, *Ind. Eng. Chem.*, **45**, 589 (1953).
13) D. F. Paris, W. C. Steen, and G. L. Baughman, *Chemosphere*, **4**, 319 (1978).
14) C. M. Müller, W. Güjer, and W. Giger, *Water Res.*, **15**, 1271 (1981).
15) S. Kyosai, *Jpn. J. Water Pollut. Res.*, **4**, 205 (1981).
16) P. S. Liss and P. G. Slater, *Nature*, **247**, 181 (1974).
17) D. N. Glew and D. A. Hames, *Can. J. Chem.*, **49**, 3114 (1971).

 © 1984 The Chemical Society of Japan Bull. Chem. Soc. Jpn., 57, 341—348 (1984)

Magnetic Circular Dichroism Studies of Bipyridyls

Hiroyuki UCHIMURA, Akio TAJIRI, and Masahiro HATANO*
Chemical Research Institute of Non-aqueous Solutions, Tohoku University, Katahira, Sendai 980
(Received June 21, 1983)

The magnetic circular dichroism (MCD) and UV absorption spectra of 2,2′- and 4,4′-bipyridyl in cyclohexane and sulfuric acid were measured at room temperature. The MCD spectrum of 2,2′-bipyridyl is different from that of 4,4′-bipyridyl, reflecting the difference in molecular symmetry between them. The absorption and MCD spectral profiles of 2,2′-bipyridyl in cyclohexane are different from those of 2,2′-bipyridyl in mineral acids, in this system protonation taking place on the nitrogen atoms to give a mono- or di-cation with low symmetry. On the contrary, the MCD spectra of 4,4′-bipyridyl in cyclohexane and in acidic media at pH 0.98 exhibit a similar spectral profile to each other due to the D_2 symmetry being retained in 4,4′-bipyridyl. Theoretical calculations were carried out on the basis of the PPP-SCF-CI method to get a reasonable explanation for the observed MCD spectra. The assignments of the MCD bands of these compounds are given and their dihedral angles are estimated.

According to Fisher-Hjalmars' consideration,[1] the repulsion among ortho-protons in biphenyl plays an important role in determining its stable conformation. The twisted angle around the central bond (see Fig. 1) is given on a balance between two effects, the conjugation between the two benzene rings and the repulsion among the nonbonded atoms, especially among the ortho-protons. Accordingly, on substitution with bulky groups at the ortho-positions the dihedral angle of biphenyl will increase due to an appreciable increase in the steric repulsion, giving rise to a hypsochromic effect on the transition energy and a hypochromic effect on the intensity of the conjugation band.[2]

It has been known from an X-ray diffraction study that 2,2′-bipyridyl has a trans-planar structure.[3] The molecular structure in solvents where the protonation of the bipyridyl moiety is prevented is expected to be planar because of the absence of the repulsion among the protonated protons. On the other hand, in 4,4′-bipyridyl there exists a repulsion among the ortho-protons as in biphenyl. Accordingly, the two pyridine rings of 4,4′-bipyridyl in solution are expected to be twisted around the central bond.

For bipyridyls, abbreviated to B hereafter, the equilibria are expected to be established in acidic media,

$$BH_2^{2+} \overset{K_2}{\rightleftharpoons} BH^+ + H^+ \overset{K_1}{\rightleftharpoons} B + 2H^+,$$

where K_1 and K_2 are the acid dissociation constants. There exist three species, a neutral species B and protonated species BH^+ and BH_2^{2+}, in acidic solutions. Nakamoto[4] investigated the equilibrium between the neutral molecule B and the mono-cation BH^+ of 2,2′-bipyridyl by observing UV absorption spectra at various pH values. According to this investigation 2,2′-bipyridyl exists mainly in a mono-cationic form at pH≃1.80 and in a neutral form at pH>9.15. Krumholz[5] determined pK_1 of 2,2′-bipyridyl to be 4.44 based on the potentiometric titration method. This value is in good agreement with that obtained by Nakamoto.[4]

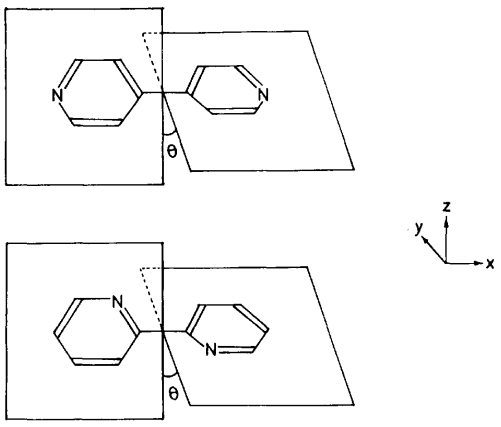

Fig. 1. Molecular skeletons and choice of axis for 4,4′-(top) and 2,2′-bipyridyl (bottom).

On the other hand, pK_1 and pK_2 for 4,4′-bipyridyl were evaluated to be 4.82 and 3.17, respectively.[5] Therefore, 4,4′-bipyridyl exists mainly as a di-cation at pH<2.0.

In 2,2′-bipyridyldium, two pyridinium rings seem to be twisted around the central bond due to the repulsion among the ortho-protons. However, Nakamoto[4] has suggested that the planar trans-configuration is preferable for 2,2′-bipyridyldium in view of the charge distribution. Borgen *et al.*[6] have drawn the same conclusion for the di-cation of 2,2′-bipyridyl on the basis of a CNDO calculation.

The 2,2′-bipyridylium cation was confirmed to have a cis-form by Nakamoto[4] based on a comparative absorption spectroscopic study between the mono-cation and the metal-chelate compound $[Ni(bypy)_3]Cl_2$ in which bipyridyl is forced to take a cis-form. In the mono-cation the two pyridine rings seem to be twisted to some extent around the central bond due to the repulsion among the ortho-protons.

In this work 2,2′- and 4,4′-bipyridyl in cyclohexane and acids were reexamined from the view point of MCD spectroscopy. A quantum mechanical calculation based on the PPP method was carried out to get a reasonable characterization and assignment of observed MCD bands. A comparison between experimental and theoretical results has led to an estimation of the dihedral angles of bipyridyls in solution.

Experimental

Commercially available 2,2′- and 4,4′-bipyridyl were purified by sublimation under reduced pressure. The cyclohexane and sulfuric acid were of spectro-grade and used

as solvents without further purification. The buffer solutions were $CH_3COOH+CH_3COOK$ with pH=3.0—6.0 and $NaOH+KH_2PO_4$ with pH=6.97.

MCD and UV spectra were measured with a JASCO-J500C recordig circular dichrometer equipped with a 1.14 T electromagnet and with a JASCO-UVIDEC-J510 recording spectrophotometer, respectively. All measurements were carried out at room temperature.

Theoretical

The electronic transition energies, oscillator strenghths, and Faraday B values of the bipyridyls and their cations were evaluatd by the use of the PPP method[7] together with configuration interaction among singly excited configurations with transition energies below 10 eV. One-center core and repulsion integrals were evaluated from valence state ionization potentials and electron affinities. Two-center core integrals, β_{pq}, were calculated by use of the Wolfsberg-Helmholz equation,[8] except β_{CN^+} for which the value of −2.74 eV was used.[9] Two-center repulsion integrals were evaluated by use of the Nishimoto-Mataga equation.[10] The repulsion integrals, γ_{pq}, within the pyridine ring, were evaluated according to the usual formula

$$\gamma_{pq} = \frac{14.397}{R_{pq} + a_{pq}}, \tag{1}$$

with

$$a_{pq} = \frac{28.794}{\gamma_{pp} + \gamma_{qq}}, \tag{2}$$

where R_{pq} is the distance between atoms p and q, and γ_{pp} stands for the one-center repulsion integral. The repulsion integral, γ_{pq}, in which atoms p and q belong to different pyridine rings was calculated using Eq. 1 with the following modification on a_{pq}:

$$a_{pq} = \frac{28.794}{(\gamma_{pp}+\gamma_{qq})\cos^2\theta + (\gamma'_{pp}+\gamma'_{qq})\sin^2\theta}, \tag{3}$$

$$\gamma'_{pp} = \gamma_{pp} - 6F_2, \tag{4}$$

where θ is the dihedral angle and F_2 is the Slater-Condon parameter. The bond distances and bond angles of 2,2′-bipyridyl were taken from X-ray diffraction data.[3] The molecular geometry for the pyridine ring in 4,4′-bipyridyl was taken from electron diffraction data for pyridine.[11] The molecular structure of the cation was assumed to be identical with that of the corresponding neutral molecule. The coordinate system is shown in Fig. 1. The x axis lies along the long molecular axis and the y axis bisects the dihedral angle, θ.

The theoretical Faraday B term associated with an electronic transition, $j \leftarrow a$, is expressed as[12]

$$\begin{aligned} B(j\leftarrow a) = \mathrm{Im}\Big[& \sum_{k\neq a} \{\langle k|\vec{\mu}|a\rangle/(E_k - E_a)\} \times \\ & \langle a|\vec{m}|j\rangle \times \langle j|\vec{m}|k\rangle \\ & + \sum_{k\neq j} \{\langle j|\vec{\mu}|k\rangle/(E_k - E_j)\} \times \\ & \langle a|\vec{m}|j\rangle \times \langle k|\vec{m}|a\rangle\Big], \end{aligned} \tag{5}$$

where $\vec{\mu}$ and $\vec{m}$ denote the magnetic and electric moment operators, respectively. The quantities in the denominator, *e.g.*, E_k, is the energy of the kth state. The transition dipole moments were estimated by the dipole length method using the Slater AO's. The atomic integrals of the electric and magnetic dipole moments were retained only for the nearest neighbor atoms, and were neglected for the distant atoms because they are too small to give any decisive effect on calculated results. The deorthogonalized set of atomic orbitals obtained by the inverse Löwdin procedure[13] was used for the calculation of these quantities. The calculation was carried out using an ACOS-700 computer at The Computer Center of Tohoku University.

Results and Discussion

2,2′-Bipyridyl and Its Cations. The UV absorption spectrum of 2,2′-bipyridyl in cyclohexane is illustrated in Fig. 2 (left), showing absorption maxima at 35400, 40800, and 42000 cm^{-1}. The MCD spectrum exhibits a negative peak at 36000 cm^{-1} and a positive extreme at 42300 cm^{-1}. Another MCD band appears in the wave number region higher than 47000 cm^{-1}. From a comparison of the 2nd MCD band with the corresponding absorption band, the fine structure of the latter is considered to be vibrational in origin. In fact, the UV absorption spectrum of 2,2′-bipyridyl in basic media shows a structureless single peak in the same region.

The calculated Faraday B values and oscillator strengths of 2,2′-bipyridyl are schematically represented in Fig. 2 (right). For convenience $-B$ is taken on the ordinate since the Faraday parameter B appears as $-B$ in the expression of the molar ellipticity, $[\theta]_M$. It is assumed in the present calculation that 2,2′-bipyridyl has the trans-planar structure (θ=0°). The 1st and 2nd MCD bands of 2,2′-bipyridyl are assigned to the 1st and 2nd $^1B_u \leftarrow {}^1A_g$ electronic transitions, respectively. The strong negative MCD band in the energy region higher than 47000 cm^{-1} is assigned to the predicted $^1B_u \leftarrow {}^1A_g$ (51100 cm^{-1}) transition.

The UV absorption spectra of 2,2′-bipyridyl in sulfuric acid of various concentrations between 0.102 and 3.87 M (1 M=1 mol dm^{-3}) are illustrated in Fig. 3, where three isosbestic points are observed, exhibiting the equilibrium $BH_2^{2+} \rightleftarrows BH^+ + H^+$. 2,2′-Bipyridyl in sulfuric acid of 0.102 M exists in a mono-cationic form, exhibiting the absorptions at 33300 and 41700 cm^{-1} (the dotted line in Fig. 3). Increasing the concentration of the acid causes the equilibrium to shift toward left so as to give the absorption at 35000 cm^{-1} characteristic of the di-cation (the solid line). No further change in spectral profile takes place at concentrations lower (higher) than 0.102 M (3.87 M). It is clear from these facts that 2,2′-bipyridyl in sulfuric acid with concentrations higher than 3.87 M exists as the di-cation, and that 2,2′-bipyridyl in sulfuric acid with pH's lower than 1.80 exists as the mono-cation.

The absorption spectrum of 2,2′-bipyridyl in sulfuric acid at pH 1.22 is included in Fig. 4, which reveals absorptions at 33300 and 41700 cm^{-1}, characteristic of the mono-cationic species. The intensity of the former

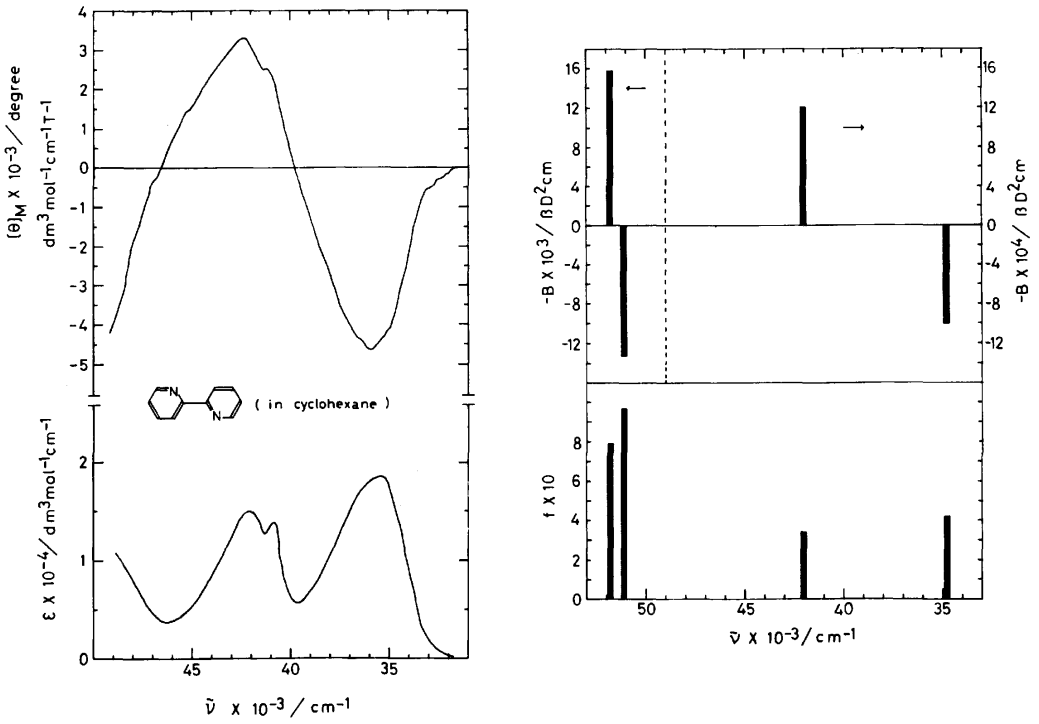

Fig. 2. The observed MCD (left top) and absorption (left bottom) spectra of 2,2′-bipyridyl in cyclohexane at room temperature. Theoretical B values (right top) and oscillator strengths (right bottom) calculated for a trans structure with $\theta=0°$.

TABLE 1. THEORETICAL TRANSITION ENERGIES ($\tilde{\nu}$), OSCILLATOR STRENGTHS (f), AND B VALUES (B) OF 2,2′-BIPYRIDYL

Compound	Symmetry	$\tilde{\nu}\times10^{-3}$ / cm^{-1}	f	$-B\times10^{5}$ / βD^{2}cm	$\tilde{\nu}\times10^{-3}$ / cm^{-1}	$[\theta]_M^{max}\times10^{-3}$
2,2′-Bipyridyl	$^1B_u \leftarrow {}^1A_g$	34.8	0.42	−100.9	35.97	−4.64
(θ=0°)	$^1A_g \leftarrow {}^1A_g$	37.5	forb.	0.0	—	—
	$^1B_u \leftarrow {}^1A_g$	42.1	0.34	120.4	42.28	−3.28
	$^1A_g \leftarrow {}^1A_g$	47.4	forb.	0.0	—	—
	$^1A_g \leftarrow {}^1A_g$	49.4	forb.	0.0	—	—
	$^1B_u \leftarrow {}^1A_g$	51.1	0.97	1335.3	—	—
2,2′-Bipyridyl		28.4	0.47	−6.1	33.70	−2.19
mono-cation		33.5	0.11	−96.0	—	—
(θ=30°)		39.0	0.08	−34.3	37.65	−1.81
		41.4	0.10	107.4	41.70	−1.77
		42.1	0.06	90.2	—	—
		46.0	0.06	−14.8	—	—
		48.3	0.06	−117.3	—	—
2,2′-Bipyridyl	$^1B \leftarrow {}^1A$	33.4	0.74	−62.9	34.80	−3.10
di-cation	$^1A \leftarrow {}^1A$	41.1	0.02	14.1	38.70	−0.60
(θ=40°)	$^1A \leftarrow {}^1A$	43.5	0.01	−23.3	41.80	−0.98
	$^1B \leftarrow {}^1A$	44.1	0.01	−33.6	—	—
	$^1A \leftarrow {}^1A$	46.3	0.03	−32.9	—	—

is twice as strong as that of the latter. The observed 1st and 2nd absorption bands are weak as compared with the corresponding bands of the neutral molecule on the whole.

The MCD spectrum of the mono-cation shows negative bands at 33700 and 37600 cm^{-1} and a positive band at 41700 cm^{-1}. The spectral profile of the mono-cation is much complicated as compared with that of the neutral molecule. This may be attributed to the increase in the dihedral angle and the reduction in the molecular symmetry on protonation.

In Table 2 the calculated transition energies, oscillator strengths, and Faraday B values for both the trans- and cis-form with a dihedral angle of 30° are listed and compared with experimental values. There appears an appreciable difference between the calculated Faraday B values of the cis- and trans-form. The evaluated MCD signs of the 3rd, 4th, and 6th transitions of the trans-form are opposite to those of the corresponding transitions of the cis-form. Since the

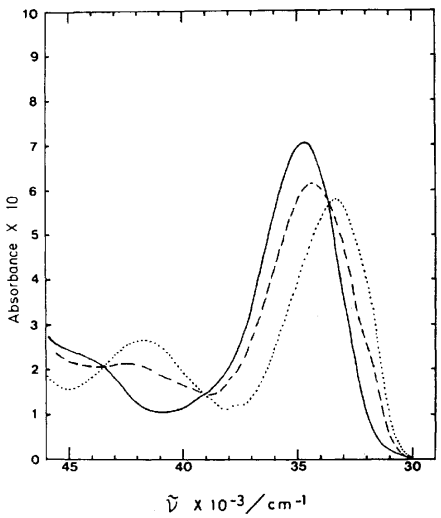

Fig. 3. The absorption spectra of 2,2′-bipyridyl (7.18×10^{-5} M) in sulfuric acid (3.87 M ——; 1.41 M -----; 0.102 M. ·····) at room temperature.

calculated result for the trans-structure is in better agreement with the observation than that for the cis-structure, the mono-cation of 2,2′-bipyridyl is considered to take the trans-configuration. The lowest transition energy of the mono-cation with the trans-structure is predicted to be 28400 cm^{-1}, which is considered to be assigned to the observed absorption band at 33300 cm^{-1} in view of the oscillator strengths.

The calculated Faraday B values and oscillator strengths of the mono-cation in the trans-form with the dihedral angle of 30° are included in Fig. 4 (right).

In Fig. 5 (left) the absorption and MCD spectra of 2,2′-bipyridyl in sulfuric acid of 7.04 M are represented. The absorption spectrum shows an intense band with its maximum at 34600 cm^{-1}. In the higher wave number region a discernible shoulder appears at *ca.* 43300 cm^{-1}. The MCD spectrum exhibits negative extrema at 34800 and 41800 cm^{-1} and a positive peak at 38700 cm^{-1}. The MCD spectral profile of the di-cation differs from that of the neutral molecule and also from that of the mono-cation. Especially, in the energy region of 41000—44000 cm^{-1} both the mono-cation and the neutral molecule exhibit positive MCD's, whereas the di-cation shows a negative band.

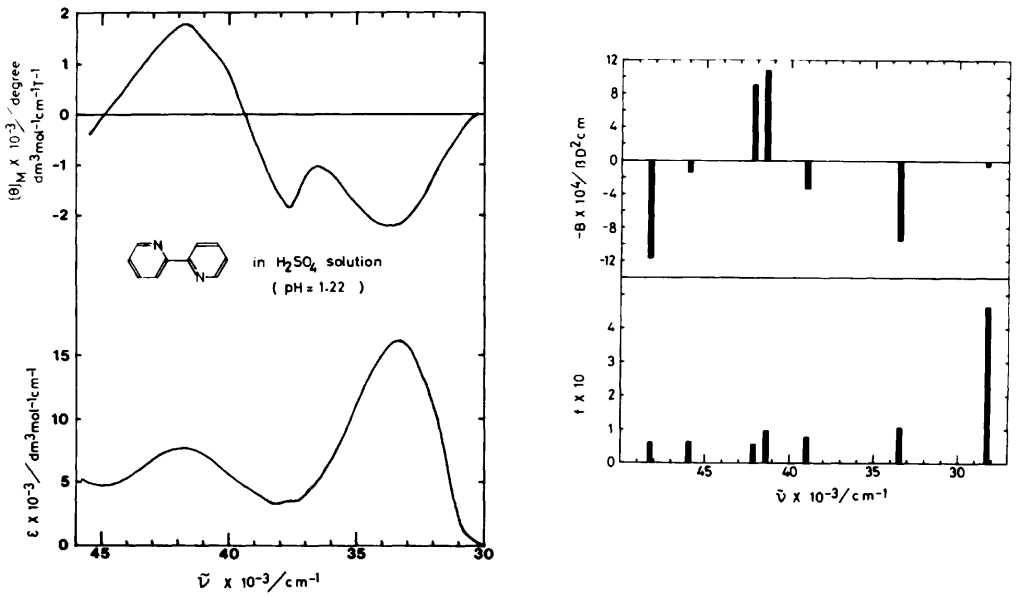

Fig. 4. The observed MCD (left top) and absorption (left bottom) spectra of 2,2′-bipyridyl in sulfuric acid at pH 1.22. Theoretical B values (right top) and oscillator strengths (right bottom) for a trans-structure with $\theta=30°$.

Table 2. Calculated transition energies and B values of the mono-cation of *trans*- and *cis*-2,2′-bipyridyl $\theta=30°$

Cis-form			Trans-form			Experimental	
$\tilde{\nu}\times10^{-3}$ / cm^{-1}	f	$-B\times10^5$ / βD^2cm	$\tilde{\nu}\times10^{-3}$ / cm^{-1}	f	$-B\times10^5$ / βD^2cm	$\tilde{\nu}\times10^{-3}$ / cm^{-1}	Sign of $[\theta]_M$
28.4	0.48	−14.1	28.4	0.47	−6.1	33.70	—
33.6	0.07	−88.9	33.5	0.11	−96.0	—	—
38.6	0.12	54.4	39.0	0.08	−34.3	37.65	—
41.4	0.06	−47.4	41.4	0.10	107.4	41.70	+
42.3	0.07	111.1	42.1	0.06	90.2		
46.0	0.07	46.7	46.0	0.06	−14.8	—	
48.5	0.04	−143.6	48.3	0.06	−117.3	—	

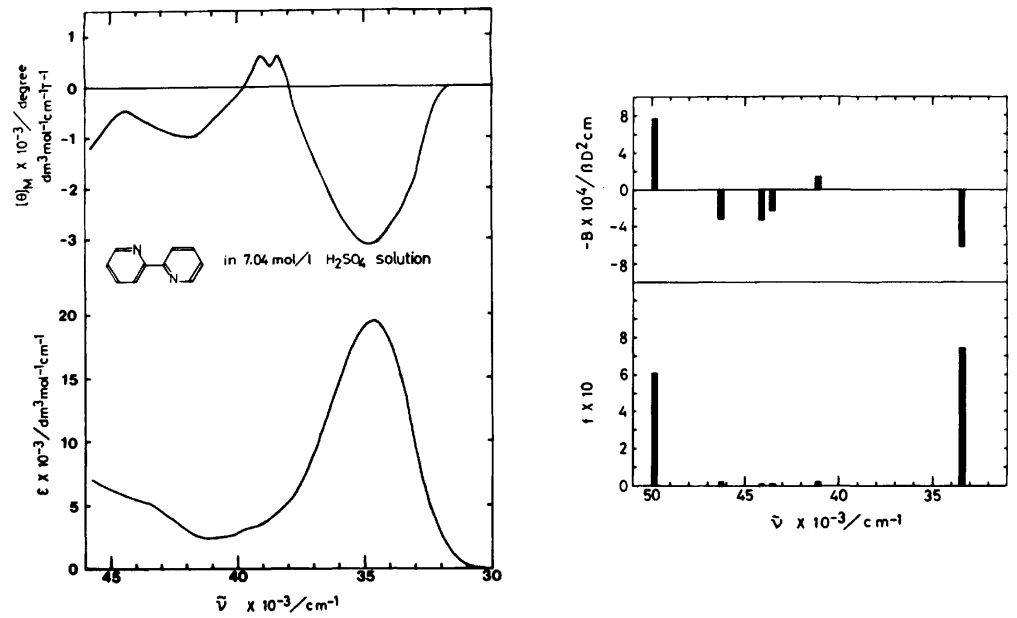

Fig. 5. The observed MCD (left top) and absorption (left bottom) spectra of 2,2′-bipyridyl in sulfuric acid of 7.04 M. Theoretical B values (right top) and oscillator strengths (right bottom) calculated for a trans-structure with θ=40°.

TABLE 3. ANGULAR DEPENDENCE OF CALCULATED TRANSITION ENERGIES AND B VALUES OF THE DI-CATION OF 2, 2′-BIPYRIDYL

	0°			10°			20°		
	$\tilde{\nu}\times10^{-3}$ / cm^{-1}	f	$-B\times10^{5}$ / βD^{2}cm	$\tilde{\nu}\times10^{-3}$ / cm^{-1}	f	$-B\times10^{5}$ / βD^{2}cm	$\tilde{\nu}\times10^{-3}$ / cm^{-1}	f	$-B\times10^{5}$ / βD^{2}cm
I	31.5	0.83	−69.1	31.6	0.83	−68.7	32.0	0.81	−67.6
II	40.8	0.00	0.0	40.8	0.00	0.9	41.0	0.01	3.7
III	43.0	0.15	−54.9	43.0	0.02	−61.1	43.3	0.01	−765.4
IV	43.2	0.00	0.0	43.2	0.00	6.0	43.3	0.01	709.8
V	46.2	0.00	0.0	46.2	0.00	−2.1	46.2	0.01	−8.5

	30°			40°			Experimental	
	$\tilde{\nu}\times10^{-3}$ / cm^{-1}	f	$-B\times10^{5}$ / βD^{2}cm	$\tilde{\nu}\times10^{-3}$ / cm^{-1}	f	$-B\times10^{5}$ / βD^{2}cm	$\tilde{\nu}\times10^{-3}$ / cm^{-1}	$-B\times10^{5}$ / βD^{2}cm
I	32.6	0.78	−65.7	33.4	0.74	−62.9	34.8	−78.8
II	41.1	0.01	8.4	41.1	0.02	14.1	38.7	8.1
III	43.4	0.01	−34.7	43.5	0.01	−23.3		
IV	43.6	0.01	−21.8	44.1	0.01	−33.6	41.8	—
V	46.3	0.02	−18.9	46.3	0.03	−32.9	—	—

In Table 3 the calculated Faraday B values and oscillator strengths of the di-cation in a trans-structure are listed along with experimental values. It is clear from Table 3 that the transition energies increase with an increase in the dihedral angle. The 1st, 2nd, and 3rd transitions show characteristic behavior depending on the variation of the dihedral angle. Both the Faraday B value and oscillator strength associated with the 1st transition decrease with an increase in the dihedral angle. On the other hand, those of the 2nd and 5th transitions increase with an increase in the dihedral angle, and are close to zero when θ=0°. The sign of the Faraday B values associated with the 2nd (38700 cm^{-1}) MCD band is calculated to be positive and assigned to the 2nd transition.

From comparison of the theoretical with experimental results, it is concluded that the di-cation of 2,2′-bipyridyl takes a structure twisted by 30—40° around the central bond. The calculated results for the di-cation with a dihedral angle of θ=40° are schematically represented in Fig. 5 (right) and summarized in Table 1. They are considered to be in good agreement with the experimental results.

It seems clear from the above discussion that the di-cation has a comparatively large dihedral angle, and accordigly that the conjugation between two pyridinium rings must be small. This is in contradiction with the inference by Nakamoto[4] and Borgen *et al.*[6] that the di-cation of 2,2′-bipyridyl has a planar structure.

4,4′-Bipyridyl and Its Cations. The UV absorption spectra of 4,4′-bipyridyl in acidic media at

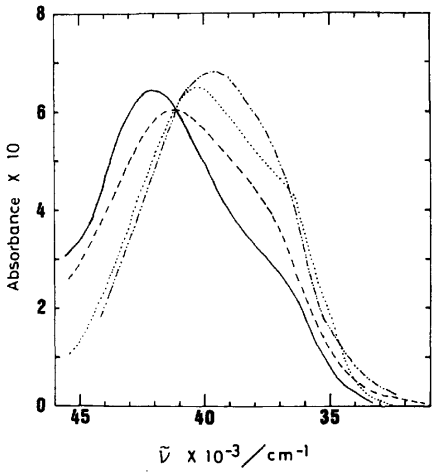

Fig. 6. The absorption spectra of 4,4′-bipyridyl (8.46×10^{-5} M) in sulfuric at pH 2.04 (·····), 3.20 (·····), 5.13 (-----), and 6.97 (——).

pH values between 2.06 and 6.97 are illustrated in Fig. 6. In basic conditions as well as in most organic solvents, 4,4′-bipyridyl exhibits an absorption at 42000 cm^{-1} characteristic of the neutral species.

On the other hand, in acidic solutions at pH<2.06, the UV absorption spectrum of 4,4′-bipyridyl exhibits the same spectral feature as the dotted line in Fig. 6 indicates. Accordingly, the UV absorption spectrum illustrated with the solid line in Fig. 6 is due to the neutral molecule and the one with the dotted line is ascribed to the di-cation.

The absorption and MCD spectra of 4,4′-bipyridyl in cyclohexane are represented in Fig. 7 (left). The negative MCD band at 42500 cm^{-1} corresponds to the absorption at 42500 cm^{-1}. The absorption shoulder at about 37500 cm^{-1} exhibits positive MCD. The MCD spectral profile of 4,4′-bipyridyl in cyclohexane is thus similar to that of substituted biphenyls with electron-attracting groups at the para-positions.

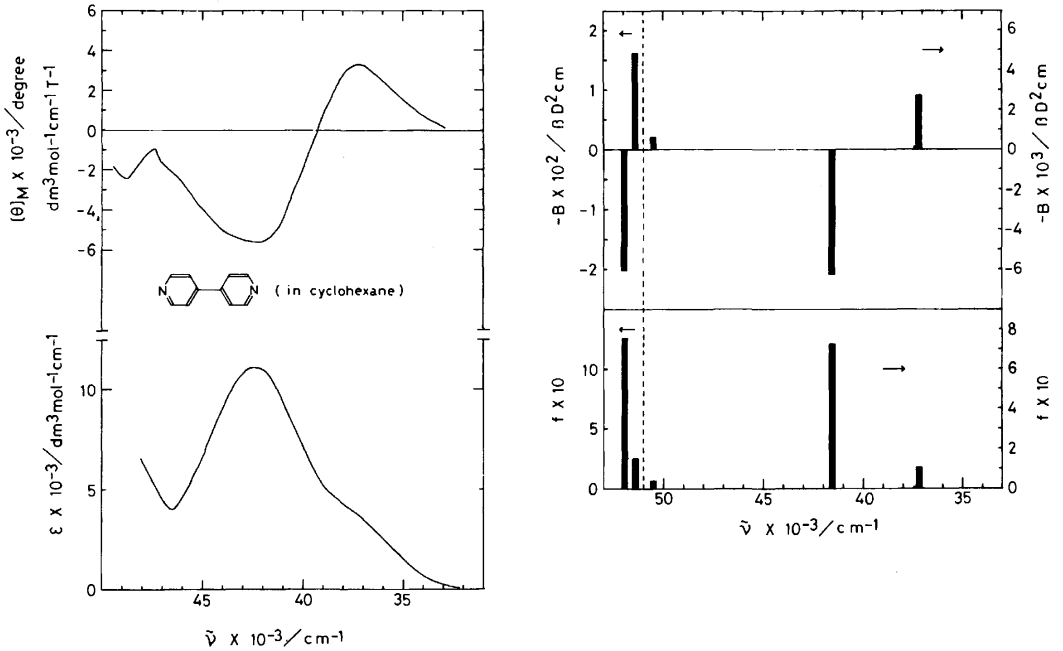

Fig. 7. The observed MCD (left top) and absorption (left bottom) spectra of 4,4′-bipyridyl in cyclohexane at room temperature. Theoretical B values (right top) and oscillator strengths (right bottom) calculated at $\theta=30°$.

Table 4. Theoretical transition energies ($\tilde{\nu}$), oscillator strengths (f), and B values (B) of 4,4′-bipyridyl

Compound	Symmetry	Theoretical $\tilde{\nu}\times10^{-3}$ / cm^{-1}	Theoretical f	Theoretical $-B\times10^5$ / D^{2}cm	Experimental $\tilde{\nu}\times10^{-3}$ / cm^{-1}	Experimental $[\theta]_M^{max}\times10^{-3}$
4,4′-Bipyridyl (θ=30°)	$^1B_2 \leftarrow {}^1A$	37.2	0.11	27.5	37.31	3.21
	$^1B_1 \leftarrow {}^1A$	37.2	0.01	2.0	—	—
	$^1B_3 \leftarrow {}^1A$	41.6	0.73	−62.5	42.46	−5.62
	$^1A \leftarrow {}^1A$	49.9	forb.	0.0	—	—
	$^1B_1 \leftarrow {}^1A$	50.5	0.04	6.6	—	—
4,4′-Bipyridyl di-cation (θ=30°)	$^1B_1 \leftarrow {}^1A$	36.5	0.04	3.1	—	—
	$^1B_2 \leftarrow {}^1A$	36.8	0.47	45.7	35.70	7.16
	$^1B_3 \leftarrow {}^1A$	40.4	0.59	−79.1	40.30	−11.00
	$^1B_1 \leftarrow {}^1A$	48.2	0.00	−1.1	—	—
	$^1B_2 \leftarrow {}^1A$	48.4	0.06	−14.6	—	—
	$^1A \leftarrow {}^1A$	48.8	forb.	0.0	—	—

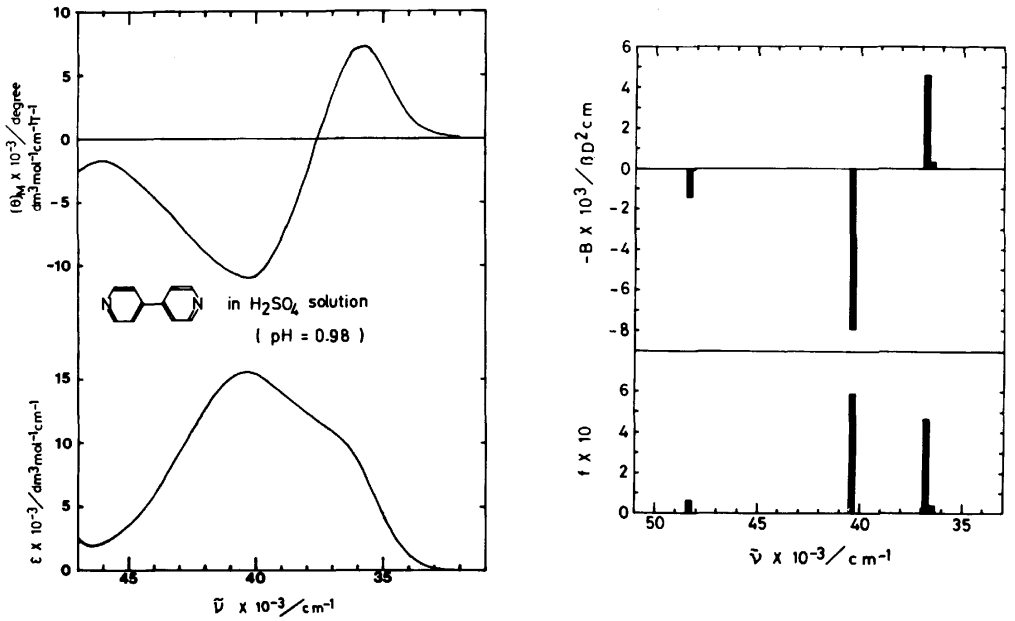

Fig. 8. The observed MCD (left top) and absorption (left bottom) spectra of 4,4′-bipyridyl in sulfuric acid at pH 0.98. Theoretical B values (right top) and oscillator strengths (right bottom) calculated at $\theta=30°$.

The Faraday B values and oscillator strengths of 4,4′-bipyridyl where the dihedral angle is assumed to be 30° are indicated in Fig. 7 (right). The agreement between experiment and theory is fairly good with respect to the sign, relative intensity, and transition energy. Accordingly, the dihedral angle of 4,4′-bipyridyl may be considered to be about 30°, larger than that of biphenyl in solution which has been found to be 20°.[15] The difference in dihedral angle between 4,4′-bipyridyl and biphenyl may be ascribed to the nitrogen atoms being incorporated in the biphenyl skeleton in the former so as to localize electrons on its para-positions. This leads to a less conjugation between the two rings. Then, 4,4′-bipyridyl exists in a more twisted form than biphenyl, although the repulsion among the ortho-protons seems to be nearly equal in both the cases.

The calculated result for 4,4′-bipyridyl is summarized in Table 4. The 1st and 2nd MCD bands of 4,4′-bipyridyl are assigned to the predicted $^1B_2\leftarrow{}^1A$ and $^1B_3\leftarrow{}^1A$ transitions, respectively. The assignment is identical with that for bipyridyl.[14] The absorption and MCD spectra of 4,4′-bipyridyl in sulfuric acid at pH 0.98 are represented in Fig. 8 (left). In the UV spectrum an absorption maximum is observed at 40300 cm^{-1} with a shoulder at about 36000 cm^{-1}. The MCD spectrum exhibits a positive band at 35700 cm^{-1} and a negative one at 40300 cm^{-1}. The intensity of the latter is greater than that of the former. Although the absorption and MCD extrema exhibit a red-shift in comparison with those of the neutral molecule, the di-cation of 4,4′-bipyridyl shows a similar spectral profile to the neutral molecule as a whole.

The calculated result for the di-cation of 4,4′-bipyridyl with $\theta=30°$ is included in Fig. 8 (right). It is found that the theoretical result is rather insensitive to the variation of the dihedral angle. The calculated result is summarized and listed in Table 4. The 1st, 2nd, and 3rd $\pi^*\leftarrow\pi$ transitions of the di-cation are calculated to be $^1B_1\leftarrow{}^1A$, $^1B_2\leftarrow{}^1A$, and $^1B_3\leftarrow{}^1A$, respectively, of which transitions $^1B_2\leftarrow A$ and $^1B_3\leftarrow{}^1A$ are assigned to the 1st and 2nd MCD bands.

Concluding Remarks

Bipyridyls exhibit characteristic spectra depending on the position of the nitrogen atoms and also on protonation. The observed absorption and MCD spectra are considered to have been reproduced fairly well by a theoretical calculation based on the PPP method, since the agreement between theory and experiment is acceptable in view of the approximation employed.

Calculated absorption and MCD spectra were compared with the observed spectra to get dihedral angles of 30—40° for di-cations of 2,2′- and 4,4′-bipyridyl. In the present work the dihedral angle of 2,2′- and 4,4′-bipyridyl have been estimated to be 0° and 30°, respectively.

This work was partially supported by Grant-in-Aid from the Ministry of Education, Science and Culture and by a grant from Nissan Science Foundation to M. H.

References

1) I. Fisher-Hjalmars, *Tetrahedron*, **19**, 1805 (1963).
2) G. H. Beaven and G. W. Gray, "Steric Effects in Conjugated Systems," Butterworths Scientific Publications, London (1958), Chap. 3, p. 22.
3) L. L. Merritt, Jr. and E. D. Schroeder, *Acta Crystallogr.*, **9**, 801 (1956).
4) K. Nakamoto, *J. Phys. Chem.*, **64**, 1420 (1960).
5) P. Kurmholz, *J. Am. Chem. Soc.*, **73**, 3487 (1951).
6) O. Borgen, B. Mestvedt, and I. Shaavik, *Acta Chem.*

Scand., Ser. A, **30**, 43 (1976).
7) R. Pariser and R. G. Parr, *J. Chem. Phys.*, **21**, 466, 767 (1953).
8) M. Wolfsberg and L. Helmholtz, *J. Chem. Phys.*, **20**, 837 (1952).
9) M. J. S. Dewar and L. Paolino, *Trans. Faraday Soc.*, **53**, 261 (1957).
10) K. Nishimoto and N. Mataga, *Z. Phys. Chem. (N.F.)*, **12**, 335 (1957).
11) B. Bak, L. Hansen-Nygaad, and J. Rastrup-Andersen, *J. Mol. Spectrosc.*, **2**, 361 (1958).
12) A. D. Buckingham and P. J. Stephens, *Ann. Rev. Phys. Chem.*, **17**, 399 (1966).
13) P. O. Löwdin, *J. Chem. Phys.*, **18**, 365 (1950).
14) H. Uchimura, A. Tajiri, and M. Hatano, *Bull. Chem. Soc. Jpn.*, **54**, 3279 (1981).
15) H. Suzuki, *Bull. Chem. Soc. Jpn.*, **32**, 1340 (1959).

Exponential Distribution of Aqueous 1-1 Electrolytes Due to Convective Thermal Diffusion in Vertical Columns

Naokata TAKEYAMA* and Kimie NAKASHIMA
Department of Industrial Chemistry, Faculty of Science and Engineering, Saga University, Saga 840
(Received July 11, 1983)

Using titanium columns of 10 cm length and glass columns of different lengths, the vertical exponential distribution of the concentration of aqueous 1-1 electrolytes in each column has been ascertained at the steady state of convective thermal diffusion. The value of $(a^4/L)\ln q$ is found to be characteristic of individual solutes, and possibly proportional to the thermal diffusion coefficients, where q is the quotient of the steady concentration of a solute at the bottom of column to that at the top, L is the effective column length, and a is the working column space. This fact has been also shown by jointed glass columns with and without top vessel, capable of multistep sampling from the top to the bottom through intermediate jointed parts along columns. The rate constants in processes to the steady state have been examined to be proportional to the square of temperature difference applied, and to decrease with increasing L. Although the enhancement of downward enrichment of solutes has been observed by attaching a large top vessel to the column top, the rate constants decrease inevitably and significantly thereby.

The thermal diffusion in liquid systems has been studied by measuring the Soret effect in a nonconvective cell,[1] and by using the Clusius-Dickel column settled vertically to utilize effectively natural convection induced by a temperature gradient applied horizontally.[2,3] The former is mainly directed to the determination of the Soret coefficient of solutes, while the latter is being examined to be applied to the separation of mixtures. Regarding aqueous ionic solutions, however, in spite of valuable efforts by several authors,[4-8] the basic principle of convective thermal diffusion in the column method is still unsolved in many respects. At present, various applications of the column method are being attempted by the present authors to seek a clue to effective utilization of thermal energy in a lower grade, concerning aqueous electrolytes.[9]

From a fundamental viewpoint, the thermal diffusion coefficient of aqueous electrolytes provides important information on the dissolved state of ions through the reduction rule in heats of transfer in connection with water structure-making and breaking properties of ions.[10] In the course of these applicative and basic studies, it grows as an important subject whether the thermal diffusion coefficient may be obtained by the column method in comparison with the Soret cell method established well.

Toward the subject, this paper describes basic experimental results by the column method to show the validity of exponential distribution of aqueous electrolytes along vertical columns, single and jointed, in a sedimentation-like way. From the exponential distribution of a solute at the steady state of convective thermal diffusion, a constant quantity having the dimension of volume, characteristic of the solute, may be obtained independently of column size to show a direct connection with the thermal diffusion coefficient from the Soret coefficient, in spite of large discrepancy in experimental conditions.

Experimental

Titanium Columns (Ti-I and Ti-II). Two columns made of titanium, Ti-I and Ti-II, were prepared by courtesy of the Nippon Kōgyo Co. and the Nikko Engineering Co., having a similar structure to that in Fig. 1 of a glass column. The outermost cylindrical wall was made by a poly (vinyl chloride) pipe equipped with two branches for circulation of cooling water, in which Ti made double annular part was fixed by sealing with poly(vinyl chloride) paste. The innermost Ti tube (1.00 mm thickness and 6.00 mm ϕ) and the outer Ti tube (1.00 mm thickness and 10.0 mm ϕ) were set to form the co-annular cylindrical space having 1.00 mm spacing for Ti-I and 0.97 mm for Ti-II,[11] in 10.0 cm length between the top and bottom reservoirs of 3.4 and 5.4 cm^3, respectively. Warm water at T_h°C was circulated into the innermost tube of column from a thermostatted bath. At the same time, colder water at T_c°C was circulated into the outermost space between the outer Ti tube and the outermost poly(vinyl chloride) pipe. Two by two branches were attached to the top and bottom reservoirs as an inlet of test solution and as an outlet of sample. As a reference column having 1.00mm spacing and 10.0cm length, Ti-I was selected. Both were individually used as single columns of total 10.5 ± 0.2 cm^3 volume.

Glass Columns. The structure of a Pyrex glass column, in Fig. 1, was composed of co-annular triple walls having 1 mm thickness in an outlook of Liebig condenser. Three main parts were the innermost tube, into which warm water was circulated, the co-annular cylindrical space between the top and bottom reservoirs of 6 cm^3, of which

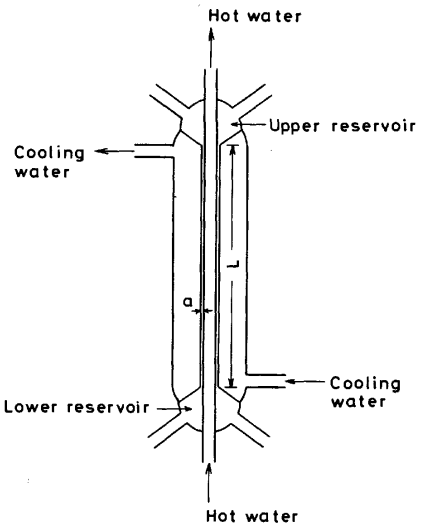

Fig. 1. Structure of a glass column. a; The spacing of working annular space, L: the effective length.

spacing a was kept at about 0.9 mm as constant as possible, and the outer space, in which cooling water was circulated. Two by two branches were attached to the top and bottom reservoirs for sampling outlets and for jointing branches. In some cases, a 500 cm^3 vessel was directly connected with one of two top branches to enhance downward enrichment of solutes. The working space was in the co-annular space of effective length L between the innermost (hotter) and outer (colder) walls. A unit column of L=10 cm was used to be jointed in series and in V-shape to lengthen total effective length as shown in Fig. 2, without and with top vessels. These jointed columns were very useful and effective for practical applications. In single column experiments, 4 glass columns

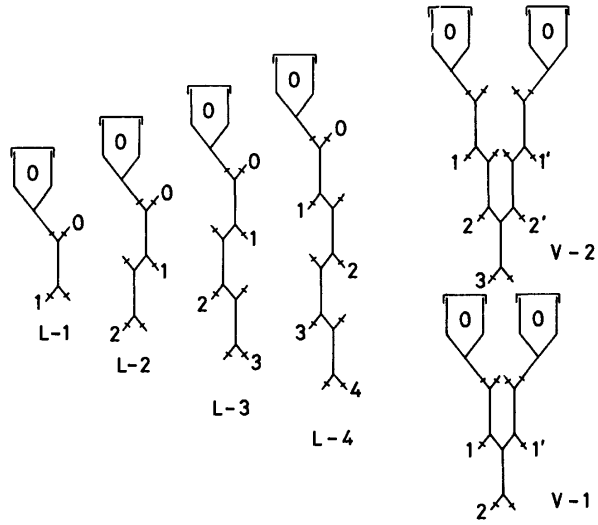

Fig. 2. Arrangement of jointed columns with and without top vessels.
The sampling outlets are denoted by 0, 1, ···, n for a column jointed linearly of n unit columns, and by 0, 1 and 1′, 2 and 2′, ···, n for a V-shape jointed column composed of $(2n-1)$ unit columns.

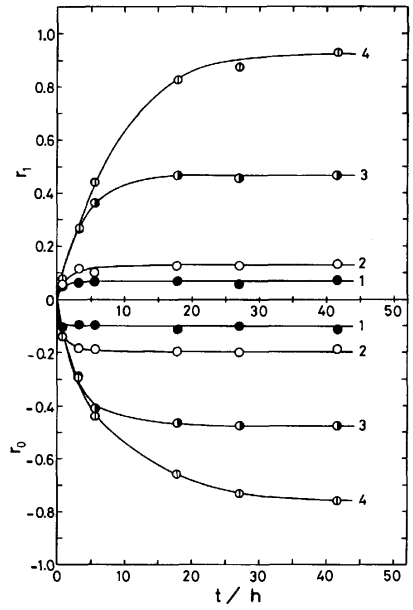

Fig. 3. Changes in the extents of dilution (r_0) at the top of column, and of enrichment (r_1) at the bottom with time, referring to 0.983 mol dm^{-3} HCl, at ΔT= 40.1, and T_m=54.0°C.
Column length L: 5.0 cm for (1), 10.0 cm for (2), 24.5 cm for (3), and 49.0 cm for (4).

of L=5.0, 10.0, 24.5, and 49.0 cm were used to examine the dependence of enrichment of solutes on the effective length. For the same purpose, jointed column experiments were successfully performed.

Sample Solutions. All of aqueous solutions were prepared from the purest available reagents using distilled and deionized water. Before and after a run of experiment, the concentration of a solute was volumetrically determined in each sample taken from the top and bottom outlets, including intermediate outlets in the case of jointed column experiments, shown in Fig. 2. Chemical analyses were performed according to the ordinary methods established well.

Procedure. A sample solution of the initial concentration C_i of an electrolyte was filled from the bottom inlet to the top of column using a leveler connected by a flexible tube with the inlet. After closing all stopcocks except one at the top, a run was started by circulating water at different temperatures from the bottom to the top. The top stopcock was closed after relaxation of thermal expansion of the solution filled. In a batch operation, test solutions were taken at a time t elapsed from the top outlet by a pipette, and then from the bottom outlet, after wasting a few drops to clean the part, by about 2 cm^3 in a dropping way. Such a sampling did not cause serious error. In a jointed column experiment, test solutions were taken from the top to the bottom through each intermediate outlet in order in a quite similar way.

When the concentration of the electrolyte under consideration was C_j at the j-th outlet, where j was numbered from the top j=0 to the bottom j=n as shown in Fig. 2, the result was expressed by the following relative deviation from the initial C_i at t:

$$r_j(t) = [C_j(t) - C_i]/C_i. \quad (1)$$

The duration of a run was changed in repetition of batch operations to be plotted $r_j(t)$ against t in a wide range. On a curve of $r_j(t)$ *versus* t, a time derivative $dr_j(t)/dt$ was evaluated by a graphical differentiation at t.[12] A linearity from plotting $dr_j(t)/dt$ against $r_j(t)$ showed

$$dr_j(t)/dt = A_j - k_j r_j(t), \quad (2.1)$$

which was characterized by constant A_j *and* k_j. The steady value $r_{j,st}$ was graphically determined as an intercept on the abscissa of $r_j(t)$, given by

$$r_{j,st} = A_j/k_j. \quad (2.2)$$

From Eqs. (2.1) and (2.2), the following equation was obtained:

$$dr_j(t)/dt = k_j[r_{j,st} - r_j(t)], \quad (2.3)$$

or

$$r_j(t) = r_{j,st}[1 - \exp(-k_j t)]. \quad (2.4)$$

Thus k_j was called the rate constant at the j-th outlet.

A set of experiments were specified by an average temperature difference $\Delta T = T_h - T_c$ applied and a mean temperature $T_m = (T_h + T_c)/2$ for the set of runs.

Results and Discussion

To clarify the nature of enrichment of solutes due to convective thermal diffusion in a vertical column, first of all, it is required to establish empirical relations from experimental results for the dependence of enrichment on column length and the working space. The subject is closely associated with the actual formulation of experimental results described below.

In the first place, the results from single column experiments are described, and then those by jointed columns without and with top vessels are reported.

Using 4 glass columns kept at $a \approx 0.9$ mm as constant as possible and having $L=5.0$, 10.0, 24.5, and 49.0 cm, the temporal changes of $r_j(t)$ for $j=0$ and 1 are studied to examine the dependence of $r_{j,st}$ on L, referring to aqueous 1-1 electrolytes, 4 alkalis, 3 acids, and 2 neutral salts, at *ca.* 1 mol dm^{-3}. In Fig. 3, the curves of $r_j(t)$ *versus* t for 0.983 mol dm^{-3} HCl are shown. In all columns used, the positive values of r_1 increase with time to individual steady values of $r_{1,st}$ to show the enrichment of HCl at the bottom of each column, while the negative values of r_0 decrease simultaneouly with time to individual steady values of $r_{0,st}$ to show the dilution of HCl at the top of individual columns. Such behavior is common to the cases of other species. Qualitatively, the extents of enrichment and dilution increase with increasing L. More quantitatively, firstly $r_{1,st}$ and $r_{0,st}$ are plotted in Fig. 4 against L for various electrolytes. Although $r_{1,st}$ increases with L almost linearly in all cases, $r_{0,st}$ decreases upward-concavely with L. Next, each pair of curves for an electrolyte in Fig. 4 may be transformed into one plait line, almost straight, by introducing

$$\ln q = \ln(C_{1,st}/C_{0,st}) = \ln[(r_{1,st}+1)/(r_{0,st}+1)], \quad (3)$$

as shown in Fig. 5, though the practical convenience of $r_{j,st}$ is inevitably lost. The values of ln q are individually proportional to L in all cases. The proportional constant for an electrolyte, given by $(\ln q)/L$, expresses an enriching power of column, still dependent on a, within experimental errors, partly due to slight difference in a. The values of $(\ln q)/L$ are tabulated in Table 1 as glass columns for 9 electrolytes at *ca.* 1 mol dm^{-3} and at $\Delta T=38.2\pm0.8$ °C and $T_m=55.1\pm0.8$ °C.

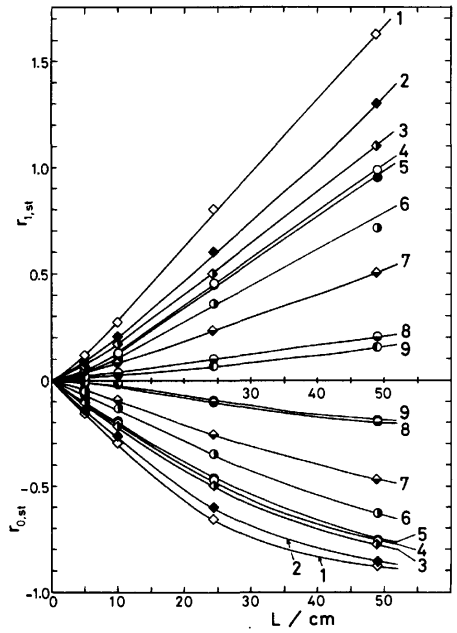

Fig. 4. Changes in the steady extents of dilution ($r_{0,st}$) at the column top, and of enrichment ($r_{1,st}$) at the bottom due to column length (L), at $\Delta T=38.2$, and $T_m=55.1$ °C.
1: 0.226 M CsOH, 2: 1.080 M KOH, 3: 1.044 M NaOH, 4: 1.530 M HBr, 5: 0.983 M HCl, 6: 0.999 M HNO_3, 7: 1.112 M LiOH, 8: 1.038 M KCl, and 9: 1.054 M NaCl (1M=1 mol dm^{-3}).

In Table 1, the data of $(\ln q)/L$ by Ti-I and Ti-II are shown for 12 electrolytes at *ca.* 1 mol dm^{-3} and at $\Delta T=49.7\pm0.5$ °C and $T_m=48.2\pm0.5$ °C. Moreover, for Ti-II and glass columns, the ratio of $(\ln q)/L$ to that of Ti-I is given in Table 1 to examine the constancy in the individual ratios by columns, because Ti-I is selected as a reference. The ratios are 1.14 ± 0.16 for Ti-II, and 1.91 ± 0.27 for glass columns as a whole, independently of the nature of electrolytes under consideration. According to the theoretical treatment of convective thermal diffusion in liquid mixtures,[2,3,13] the ratio may be mainly attributable to the difference in a in reference to a_0 of Ti-I as follows:

$$\frac{[(\ln q)/L]_{\text{for a column}}}{[(\ln q/L]_{\text{for Ti-I}}} = \left(\frac{a_0}{a}\right)^4 \quad (4)$$

This is valid in a crude approximation, at this stage, that other conceivable factors from differences in temperature, concentration, and column material do not seriously influence the ratio. The values of a, however, may be determined by Eq.(4) in reference to a_0; $a=0.97\pm0.03$ mm for Ti-II, and 0.85 ± 0.03 mm for glass columns on an average. These are reasonable values. Regarding the importance of this result, the dependence of ln q on ΔT and on the initial concentration of electrolytes is examined by using Ti-I. Figures 6 and 7 show that the values of ln q are independent of ΔT and initial concentrations, irrespectively of the nature of electrolytes investigated. Hence, the validity of Eq. (4) may be admitted.

Now, for a single column, the enriching power per unit length multiplied by a^4, $(a^4/L)\ln q$, represents an intrinsic quantity characteristic of an aqueous electrolyte solution, at least referring to single solutions, independently of experimental conditions and the column size a and L. Although the physicochemical content of characteristic volume $(a^4/L)\ln q$ at the steady state of convective thermal diffusion should be experimentally and theoretically clarified, it may be directly proportional to $(\eta/\beta\rho g)D'$ at the present status of theoretical treatment,[2,3,13] where

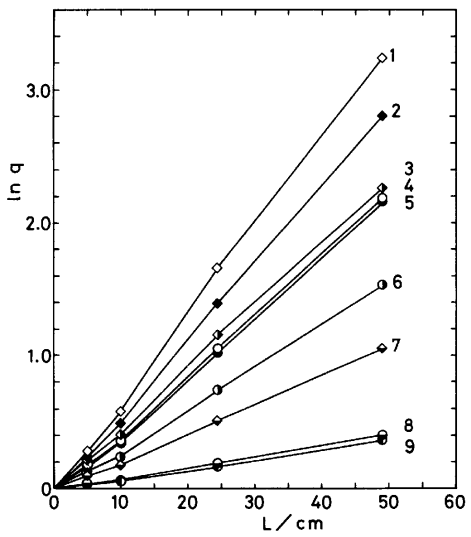

Fig. 5. Natural logarithms of the quotient of the steady concentration at the bottom to that at the top (ln q) *vs.* column length (L). The data are the same as Fig. 4.

TABLE 1. THE ENRICHING POWERS PER UNIT COLUMN LENGTH, $(\ln q)/L$, FOR TITANIUM AND GLASS COLUMNS

Aqueous electrolyte	Titanium columns Ti-I[a] $(\ln q)/L$ / cm^{-1}	Titanium columns Ti-II $(\ln q)/L$ / cm^{-1}	Ratio to Ti-I[c]	Glass columns having different lengths[b] $(\ln q)/L$ / cm^{-1}	Ratio to Ti-I[c]
CsOH				0.0618±0.0063	
KOH	0.0277	0.0315	1.14	0.0521±0.0057	1.88
NaOH	0.0220	0.0245	1.11	0.0430±0.0041	1.95
HBr	0.0194			0.0384±0.0041	1.98
HCl	0.0166			0.0379±0.0051	2.28
HNO_3				0.0273±0.0039	
LiOH	0.0117	0.0120	1.03	0.0195±0.0019	1.67
NaBr	0.0048	0.0050	1.04		
NaCl	0.0046	0.0050	1.09	0.0067±0.0006	1.46
KBr	0.0037	0.0055	1.49		
KCl	0.0034			0.0072±0.0015	2.12
NaI	0.0028	0.0030	1.07		
LiBr		0.0015			
LiCl	0.0004				
		Average	1.14		1.91
		Standard deviation	0.16		0.27

a) A reference column having 10.0 cm length and 1.00 mm spacing. b) L=5.0, 10.0, 24.5, and 49.0 cm, respectively. Refer to Fig. 5. c) The ratio of $(\ln q)/L$ in individual cases is taken to $(\ln q)/L$ for Ti-I column.

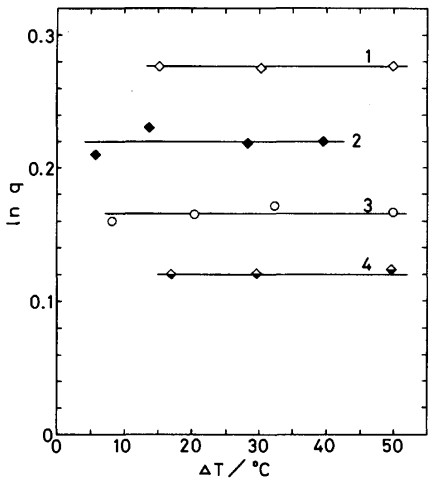

Fig. 6. $\ln q$ *vs.* temperature difference applied (ΔT), by a titanium column Ti-I. 1: 0.830 M KOH, 2: 1.013 M NaOH, 3: 1.054 M HCl, and 4: 1.114 M LiOH.

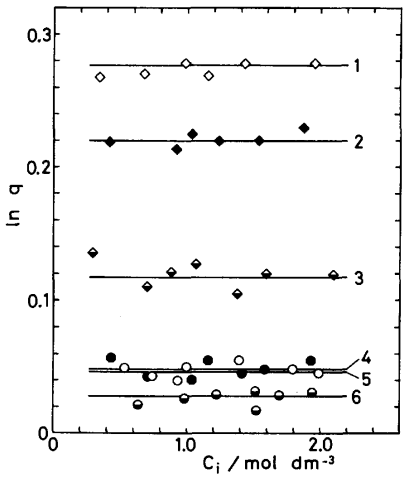

Fig. 7. $\ln q$ *vs.* initial concentration (C_i), by Ti-I column, at ΔT=49.7, and T_m=47.5 °C.
1: for KOH, 2: for NaOH, 3: for LiOH, 4: for NaCl, 5: for NaBr, and 6: for NaI.

η is the viscosity, β the thermal expansion coefficient, ρ the density of a sample solution, g the acceleration of gravity, and D' the thermal diffusion coefficient of an aqueous electrolyte. These physical properties should be estimated at the mean temperature and at the experimental conditions. It remains to be solved, however, whether the above expression for the characteristic volume, $(a^4/L)\ln q$, is compatible with the insensitibity to the experimental conditions mentioned above. At present, unfortunately, we cannot directly examine the validity because of no available data. In comparison with the thermal diffusion coefficients of 14 electrolytes at 0.01 mol kg^{-1} and at the mean temperature 25 °C, which are calculated from the Soret coefficients measured by Snowdon and Turner,[14] the values of $(a^4/L)\ln q$ in cm^3 are summarized in Table 2, obtained from the data in Table 1 by using the values of a estimated. The values for individual electrolytes are in good agreement with each other among columns used. Moreover, in spite of large discrepancies in experimental conditions, a parallelism between $(a^4/L)\ln q$ and D' may be seen, apart from a few inversions in order. This fact suggests $(f\eta/\beta\rho g)$ to be the order of magnitude of 10 cm s K by introducing a non-dimentional f. In this respect, it may be commented that for pure water at T_m=50 °C $(\eta/\beta\rho g)$ is 1.23×10^{-2} cm s K, thereby f is of the order of magnitude of 10^3.

Concerning the difference in column material between titanium and Pyrex glass, titanium is a good thermal conductor appropriate for the column material, especially best for aqueous alkaline and salt solu-

TABLE 2. THE VALUES OF $(a^4/L)\ln q$ MEASURED BY TITANIUM AND GLASS COLUMNS IN COMPARISON WITH THERMAL DIFFUSION COEFFICIENTS D' FROM SORET COEFFICIENTS AT 0.01 mol kg^{-1} AND 25 °C[a)]

Aqueous electrolyte	$(a^4/L)\ln q/10^{-7}$ cm^3 Columns			$D'/10^{-8}$ cm^2 s^{-1} K^{-1}
	Ti-I	Ti-II	Glass	
CsOH			32.3	40.7
KOH	27.7	27.9	27.2	36.5
NaOH	22.0	21.7	22.4	27.8
HBr	19.4		20.0	29.5
HCl	16.6		19.8	28.8
HNO_3			14.3	24.8
LiOH	11.7	10.6	10.2	19.5
NaBr	4.8	4.4		3.28
NaCl	4.6	4.4	3.5	3.15
KBr	3.7	4.9		2.78
KCl	3.4		3.8	2.69
NaI	2.8	2.7		0.878
LiBr		1.3		0.105
LiCl	0.4			0.027

a) From the date of Soret coefficients, observed by Snowdon and Turner[14], D' may be calculated using the limiting diffusion coefficient in the Nernst-Hartley approximation.

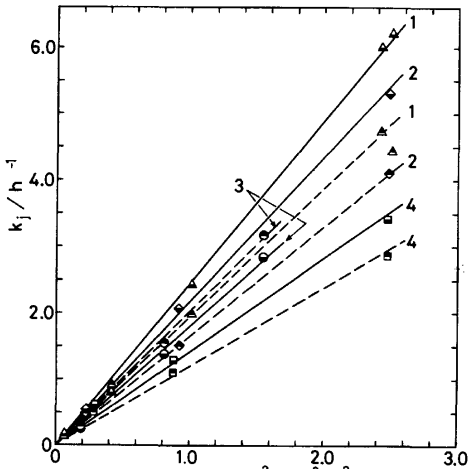

Fig. 8. Rate constants (k_j) *vs.* $(\Delta T)^2$, by Ti-I column. 1: 1.054 M HCl, 2: 0.830 M KOH, 3: 1.013 M NaOH, and 4: 1.114 M LiOH. k_0 at the top is denoted by broken lines, and k_1 at the bottom is by solid lines.

tions, capable of specifying $(\Delta T/a)$ for the gradient of temperature applied, while glass is a poorer one having the thermal conductivity comparable with that of aqueous solutions, and hence the effective temperature gradient may be $(1/3)(\Delta T/a)$, because in glass columns ΔT is applied to an aqueous layer in the working space of column between innermost and outer glass walls having the thickness comparable with a. Actually, the occurrence of convective thermal diffusion can be detected at $\Delta T \approx 1.5$ °C at the lowest in titanium columns, but at $\Delta T \approx 6$ °C at the lowest in glass columns.

The kinetic results by Ti-I are shown in Fig. 8. The rate constants k_0 at the top and k_1 at the bottom are proportional to $(\Delta T)^2$. This is true for glass columns, too, though the rate constants are smaller by 1/10 than

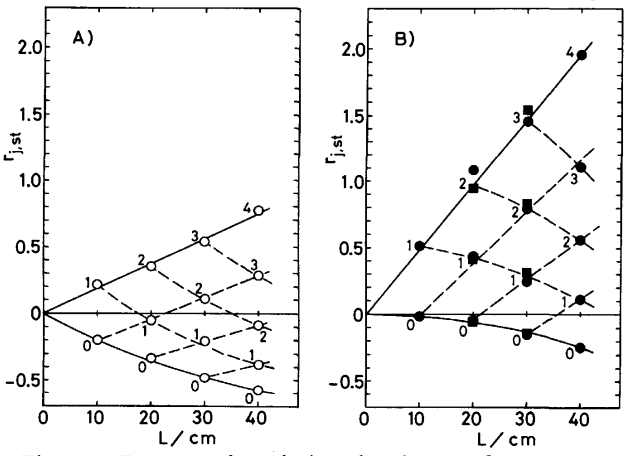

Fig. 9. Extents of variation in the steady concentration relative to the initial concentration ($r_{j,st}$) at the j-th outlet of jointed columns *vs.* total column length L, referring to 1.051 M HCl at $\Delta T=$ 49.8, and $T_m=49.0$ °C.
A): For the arrangements L-1, L-2, L-3, and L-4 without top vessel in Fig, 2, and B): for the same arrangements as in A) with top vessel (500 cm^3) denoted by solid circles and for V-shape arrangements V-1 and V-2 in Fig. 2 with two top vessels (each 500 cm^3) denoted by solid squares

those for Ti-I and Ti-II. Such a fact is consistent with the earlier theoretical prediction.[15]

In order to ascertain the relation of ln q proportional to L with jointed column experiments, the results for 1 mol dm^{-3} HCl are summarized in Fig. 9, in which $r_{j,st}$ in each jointed column of the number of jointed unit columns $n=1$ to 4 are plotted against total effective column length given by $L=10\times n$(cm) in A) referring to the cases without any top vessel, and B) for the cases with a top vessel (500 cm^3 volume) in the linear arrangements of L-1, L-2, L-3, and L-4 in Fig. 2, and also with two top vessels (each 500 cm^3) in the V-shape arrangements of V-1 and V-2 in Fig. 2.

In A) and B) in Fig. 9, curvilinear lattices are formed among the points of (L, $r_{j,st}$) in each jointed column. Connecting with the points of $r_{0,st}$ at the top in the cases of A), and in the top vessels for B), solid curves are drawn to show the changes in the extent of dilution. The extents of dilution in the top vessels in the cases of B) are lowered due to the presence of top vessels, while the extents of enrichment at the bottom are enhanced in each case in comparison with A). Such an enhancement of downward enrichment is clearly caused by the simple direct attachment of large vessels at the top of columns jointed. In the linear and V-shape arrangements of columns, L is taken as the effective height jointed column part except jointed parts and top vessels. Although the representation of $r_{j,st}$ is useful for the practical applicative purpose, the data in A) and B) are numerically examined in terms of ln q_j at the j-th outlet of jointed columns to compare with the results from single column experiments, where ln q_j has been defined by

$$\ln q_j = \ln[(r_{j,st}+1)/(r_{0,st}+1)] = \ln(C_{j,st}/C_{0,st}), \quad (5)$$

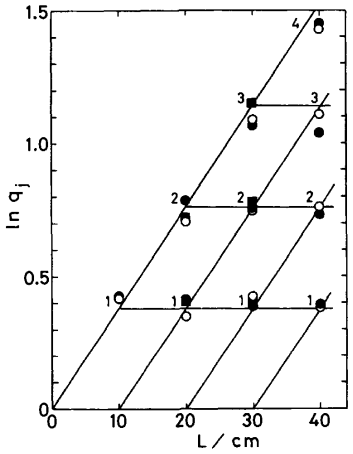

Fig. 10. Transformation of the data in Fig. 9, A) and B), into ln q_j for the j-th outlet of jointed columns against L.

in place of Eq. (3), for $j=1, 2, \cdots, n$, to investigate the vertical distribution of HCl from the top to the bottom through intermediate jointed parts. For jointed columns without any top vessel, the value of $(\ln q_j)/L_j$ is reduced to 0.0376 ± 0.0026 cm^{-1} averaged over 10 points, where L_j is the effective length from the top to the j-th outlet of an n-jointed column, $L_j=10\times j$(cm). For those with top vessels, it is 0.0380 ± 0.0024 cm^{-1} on average, in good agreement with the value mentioned above. As a whole, the average of $(\ln q_j)/L_j$ is 0.0379 ± 0.0025 cm^{-1} which is just equal to the value for HCl by single glass columns in Table 1. Using this average value, an inclined lattice is drawn in Fig. 10 by solid lines, in which the lattice points coincide satisfactorily with the observed points transformed from those in A) and B) in Fig. 9. Therefore, it may be mentioned that all of the points expressed by $r_{j,st}$ converge finally on one point averaged over those.

Regarding rate constants k_j at the j-th outlet of jointed columns, the dependence of k_j on L is numerically shown in Table 3. First, in the cases of jointed columns without and with top vessels, all k_j in each column are nearly constant independently of j, but k_0 in the top vessel is much smaller than other k_j at lower outlets presumably due to the large volume of top vessel, though such a trend vanishes gradually with increasing total L. Second, k_j for jointed columns with top vessel is smaller than that in the cases without top vessel by about 1/10 to 1/5. These facts show that, although the time required for one-half each $r_{j,st}$ to be attained are almost equal in a given total L except in top vessels, the rate constants decrease with increasing L, and the time required for each $r_{j,st}$ are prolonged with it.

TABLE 3. RATE CONSTANTS k_j OF CONVECTIVE THERMAL DIFFUSION FOR EACH OUTLET j NUMBERED FROM THE TOP TO THE BOTTOM OF JOINTED COLUMNS WITHOUT AND WITH A TOP VESSEL OF 500 cm^3 OPERATED AT $\Delta T=50.0\pm0.2$ °C AND $T_m=49\pm0.2$ °C, AND AT 1.0 mol dm^{-3} HCl

Total effective length L/cm	Number of outlet j	k/h^{-1} Without top vessel	k/h^{-1} With top vessel[a]
10.0	0	0.637	(0.01)
	1	0.605	0.130
20.0	0	0.537	(0.02)
	1	0.520	0.059
	2	0.540	0.053
30.0	0	0.260	(0.01)
	1	0.260	0.025
	2	0.265	0.022
	3	0.263	0.025
40.0	0	0.130	(0.02)
	1	0.102	0.015
	2	0.125	0.020
	3	0.102	0.022
	4	0.124	0.021

a) The values of k_0 at the top vessel in each case are shown in parentheses.

References

1) J. Chanu, *Electrochim. Acta*, **22**, 1025(1977) and the references cited therein.

2) R. C. Jones and W. H. Furry, *Rev. Mod. Phys.*, **18**, 151 (1946) and the references cited therein.

3) Regarding the recent theoretical studies, see, for example, J. L Navarro, J. A. Madariaga, and J. M. Saviron, *J. Phys. Soc. Jpn*, **52**, 478 (1983) and the references cited therein.

4) K. Hirota, *Bull. Chem. Soc. Jpn.*, **16**, 232, 475 (1941); *J. Chem. Phys.*, **18**, 396 (1950).

5) L. J Gillespie and S. Breck, *J. Chem. Phys.*, **9**, 370 (1941)

6) G. Guthrie, J. N. Wilson, and V. Schomaker, *J. Chem. Phys.*, **17**, 310 (1949).

7) K. F Alexander, *Z. Phys. Chem. (Leipzig)*, **203**, 213 (1954).

8) F. S. Gaeta, *Phys. Rev.*, **182**, 289 (1969); F. S. Gaeta, G. Perna, G. Scala, and F. Belluccl, *J. Phys. Chem.*, **86**, 2967 (1982); D. G. Mlta, F. Belluccl, M. G. Cutull, and F. S. Gaeta, *ibid.*, **86**, 2975 (1982). We cannot reproduce the unfamiliar concentration dependence of the Soret coefficient of aqueous electrolytes by the column method, reported by them.

9) N. Takeyama and K. Nakashima, *Kagaku To Kogyo (Osaka)*, **51**, 427(1977); N. Takeyama, Jpn. Patent 1013221 (1980); N. Takeyama and K. Nakashima, Jpn. Patent 1096034 (1982); 1107716 (1982); 1111846 (1982); 1149780 (1983).

10) N. Takeyama and K. Nakashima, *J. Phys. Soc. Jpn.*, **52**, 2692; 2699 (1983).

11) The accuracy may be within ±0.02 mm.

12) In the initial period of time changes of $r_j(t)$, the values of $dr_j(t)/dt$ are slightly larger than the values extrapolated from the later phase subject to Eq.(2.1), presumably due to unsteady temperature distribution applied to columns. On the contrary, an induction effect has been discussed by G. D. Rabinovich, *Chem. Eng. Sci.*, **32**, 791 (1977).

13) The theoretical expression may be written as $(a^4/L)\ln q=(504\,\eta\,/\,\beta\rho\,g)D'$ in the present notation, which has been previously used by K. Hirota, in the second paper of Ref. 4), on the basis of the result by P. Debye, *Ann. Phys.*, **36**, 284 (1939).

14) P. N. Snowdon and J. C. R. Turner, *Trans. Faraday Soc.*, **56**, 1409 (1960).

15) J. W. Hiby and K. Wirtz, *Phys. Z.*, **41**, 77 (1940).

 © 1984 The Chemical Society of Japan Bull. Chem. Soc. Jpn., 57, 355—360 (1984)

p-n Junction Silicon Electrode Coated with Noble Metal for Efficient Solar Photoelectrolysis of Hydrogen Iodide

Yoshihiro NAKATO,* Motomu YOSHIMURA,† Masahiro HIRAMOTO, Akira TSUMURA, Toshiaki MURAHASHI,† and Hiroshi TSUBOMURA*

Laboratory for Chemical Conversion of Solar Energy, Department of Chemistry, Faculty of Engineering Science, Osaka University, Toyonaka, Osaka 560

(Received July 16, 1983)

The photooxidation of iodide ions on n-type silicon electrodes highly doped with boron from the surface in hydrogen iodide or hydrogen iodide/iodine solutions was investigated. Two doping methods were employed: thermal diffusion and ion implantation. The electrode was remarkably stabilized by coating with a 2 to 3 nm-thick platinum layer, followed by heat-treatment at about 400 °C for *ca.* 10 min. The photocurrent was stable for more than 500 h at a density of the order of 10 mA cm^{-2}. The boron-doped and Pt-coated n-Si electrode also generated a photovoltage much higher than that for a Pt-coated n-Si electrode, showing an advantage of forming the p-n junction. Photoelectrochemical cells made of a boron-doped-Pt-coated n-Si electrode, a platinized Pt counter electrode, and a commercial cation exchange membrane were found to photoelectrolyze hydrogen iodide without externally applied voltage into hydrogen and iodine with a solar-to-chemical energy conversion efficiency (ϕ^{s}_{chem}) under simulated AM 1 solar radiation of 8.2%, probably the highest of the ϕ^{s}_{chem} values observed for the cells working without external voltage.

The semiconductor photoelectrochemical (PEC) cell is an interesting device for chemical conversion of solar energy. The basic idea of this device is to use the photovoltage generated in the semiconductor directly to drive electrochemical reactions at the semiconductor-solution interface. Extensive work has so far been made on such PEC cells,[1–7] but attention has been paid mostly to the photovoltaic effect at the Schottky junction formed at the semiconductor-solution (or semiconductor-overlayer) interface, and very little to the photovoltage arising from the p-n junction inside the semiconductor.

The use of semiconductors having the p-n junction in PEC cells is interesting because it has a merit in that the photovoltage is effectively generated irrespective of the presence of surface states often arising from surface defects, electrochemical reaction intermediates, *etc.* As is well known, the photovoltage at the p-n junction, together with that at the Schottky barrier, is widely used in the solid solar cells. The difference between the PEC cell and the solid cell lies in the fact that in the PEC cell the photogenerated holes (or electrons) arriving at the semiconductor surface directly react with the solution with little migration along the surface, while in the solid cell the holes (or electrons) have to travel along the surface for a macroscopic distance of a few mm until they reach the collecting grid on the cell surface. The PEC cell therefore has an advantage in that it has no restriction to have a conductive layer on the semiconductor surface so as to avoid the ohmic losses for the surface current. The photocurrent losses by electron-hole recombinations at crystal defects may also be minimized because the photogenerated holes (or electrons) coming to the surface mostly react with the solution before they drift along the surface and arrive at the defects. These advantages will be important when a polycrystalline or an amorphous material is used.

A problem, common to all semiconductor PEC cells, is that most of the available semiconductors having suitable band gaps are subject to photocorrosion in electrolyte solutions. Some trials have been made to stabilize the semiconductor electrodes. For example, an n-type silicon (n-Si) electrode was reported to be stabilized by coating with thin layers of noble metals,[8] metal oxides,[9,10] metal silicides,[11] or organic materials,[12–14] though the solar energy conversion efficiencies reported are in most cases unsatisfactory. Attempts to deposit metals on the surface for catalyzing desired electrode reactions have also been reported.[15–17]

In a recent letter[18] we reported that an n-Si electrode doped with boron from the surface and coated with a thin platinum (Pt) or palladium (Pd) layer was stable and a PEC cell with such an electrode efficiently decomposed hydrogen iodide into hydrogen and iodine under no external bias. A similar idea of photoelectrolyzing hydrogen iodide or bromide by use of electrodes composed of Si particles was proposed and high solar-to-chemical energy conversion efficiencies (6.3% in natural sunlight and *ca.* 10% by computer modelling) were reported at recent conferences by the Texas Instruments group.[19] In the present paper we will report on the electrochemical behavior of surface-boron-doped n-Si single crystal electrodes coated or not coated with a thin metal layer, together with their application to solar photoelectrolysis of hydrogen iodide.

Experimental

Two methods of boron-doping were employed: thermal diffusion and ion implantation. Thermally doped specimens were prepared from single crystal wafers of n-Si, cut perpendicular to the <111> axis and having the resistivity of 0.2 to 0.4 Ω cm and the donor (phosphorus) density of $(1-2)\times10^{16}$ *cm*$^{-3}$ *obtained from Shin-Etsu Handotai Co.* Chips of the n-Si wafer 0.5 to 1.0 cm^2 in area were cleaned ultrasonically in trichloroethylene, acetone, methanol, water, and 46% hydrofluoric acid, and doped with boron from the surface by coating with a saturated methanol solution of diboron trioxide (B_2O_3) and heating at 920 to 1000 °C for 0.5 to 2.0 h in the air. The chips thus doped were washed in water and etched in a 46% hydrogen fluoride (HF) solution for *ca.* 60 s.

† Central Research Laboratory, Mitsubishi Electric Corp., Amagasaki, Hyogo 661.

Specimens doped by ion implantation were obtained from Mitsubishi Electric Corp. Single crystal n-Si wafers cut perpendicular to the <100> axis and having the resistivity of 0.1 to 0.3 Ω cm were heated at 950°C in an atmosphere of water vapor in order to cover the surface with an oxide layer *ca.* 100 nm thick, then doped by irradiating a 50 keV $^{11}B^+$-ion beam at various doses from 10^{13} to 10^{16} cm^{-2}, annealed in vacuum at 1000°C for 20 min and etched in an HF solution.

The depth of the p-n junction formed was measured by employing the spherical drill method, namely, by slightly scraping the doped wafer with a rotating steel ball, staining by photoetching in a 46% HF solution, and inspecting the resultant concentric circles with a microscope. The p-n junction depth (x_j) was calculated from the radii of the concentric circles (R_1, R_2) and that of the steel ball (R) by using an equation $x_j=|R_1^2-R_2^2|/2R$. The sheet resistance (ρ_s) of the B-doped surface layer was measured with the four-point probe method. The surface density of boron was calculated from the above-obtained x_j and ρ_s values.[20]

A thin platinum or palladium layer was deposited by a method of thermal evaporation under $(1-2)\times10^{-5}$ Torr (1 Torr≈133.322 Pa). The Si wafer was etched in a 10% HF solution for *ca.* 60 s just before the metal evaporation. The average thickness of the metal layer was monitored with a quartz crystal oscillator. The Pt layers 2, 5, and 8 nm thick had the light transmittance at 700 nm of *ca.* 80, 50, and 30%, respectively.

ESCA spectra were obtained with a Shimadzu ESCA 750 spectrometer having a Mg *Kα* X-ray (1253.6 eV) source and a filter-type electron energy analyzer. The binding energies were corrected by taking the C1s peak as a standard, which always appeared due to sample contamination. The relative atomic concentrations were calculated from the integrated peak intensities, corrected for the relative ionization cross sections for the Si2p, O1s, B1s, N1s, $I3d_{5/2}$, Pd3d, and Pt4f peaks taken to be 0.86, 2.9, 0.49, 1.5, 19.3, 16.1, and 15.86, respectively. The depth profile was obtained by the ion etching technique using a 2.0 keV argon ion beam of a current density of 60 to 150 μA cm^{-2} under an argon pressure 5×10^{-6} Torr.

The p-n junction Si electrodes were prepared by making an ohmic contact on n-Si at the back face with indium-gallium alloy, attaching a copper wire with silver paste, and covering with epoxy resin. Current-potential curves were obtained with a commercial potentiostat and potential sweeper. The electrode not having a metal layer was in most cases etched in a 10% HF solution just before the experiment. A 120 V-300 W tungsten-halogen lamp was used as a light source, normally operated at 30 to 50 V and in some cases combined with glass filters transparent in wavelengths longer than 690 nm. Commercially available special grade chemicals were used without further purification.

Results

In the present paper, surface-boron-doped n-Si is abbreviated as p^+/n-Si. Similarly, surface-B-doped and Pt-deposited n-Si is abbreviated as Pt/p^+/n-Si, and Pt-deposited n-Si as Pt/n-Si. The depth of the p-n junction, x_j, for the thermally B-doped p^+/n-Si electrodes used in the present work was in a range from 0.3 to 1.5 μm. The surface boron concentration, c_s, determined from x_j and the sheet resistance of the doped layer took a nearly constant high value of *ca.* $(3-6)\times10^{20}$ cm^{-3}. The x_j for the B^+-ion implanted specimens ranged from 0.25 to 0.84 μm, and the c_s ranged from 10^{18} to 10^{21} cm^{-3}.

1. Photoelectrochemical Behavior of p^+/n-Si Electrodes in HI/I_2 Solutions. Figure 1A shows cyclic scanning of current density (j) *vs.* potential (U) curves for an n-Si electrode in a 7.6 M HI solution (M= mol/dm^3) under illumination. Although n-Si in this solution was more stable than in an HCl or H_2SO_4 solution, the j-U curve shifted with time toward the positive potential. The curve was restored to the initial state by dipping the electrode in an HF solution. These results suggest that the photocurrent in this case corresponds mostly to the oxidation of I^- ions and partly to the oxidation of the electrode surface.

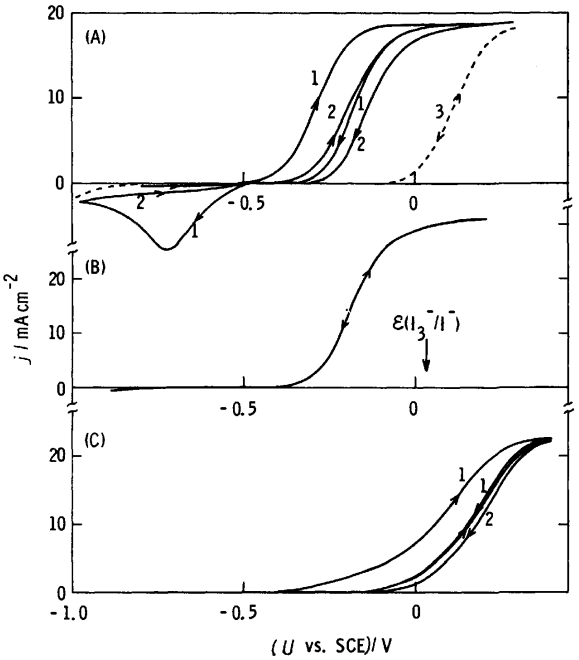

Fig. 1. Current density (j) *vs.* potential (U) curves: (A) for an n-Si electrode, 1; 1st scan, 2; 2nd scan, and 3; a curve after cyclic scanning for 60 min. (B) for a thermally B-doped p^+/n-Si electrode (x_j 0.9 μm and c_s 5×10^{20} cm^{-3}). (C) for a B^+-ion implanted p^+/n-Si electrode (x_j 0.8 μm and c_s 6×10^{20} cm^{-3}), 1 and 2 denote the 1st and 2nd scans, respectively. The electrolyte is a 7.6 M HI solution. The scan rate is 50 s/V. The illumination intensity is somewhat different in each case.

The j-U curve for a thermally B-doped p^+/n-Si electrode (Fig. 1B) was fairly stable during the repeated cyclic scans for more than 4h, the photoanodic current corresponding to the oxidation of the I^- ions,[18] while the j-U curve for an ion-implanted p^+/n-Si electrode changed at each scan (Fig. 1C). The surface of the thermally B-doped specimens showed the presence of a dark brown, lusterless, inhomogeneous thin layer, while the ion-implanted specimens gave no presence of such a layer. The layer could be removed by oxidizing the electrode surface either photoelectrochemically or by dipping in a concentrated HNO_3 solution or heating in the air at *ca.* 850°C followed by etching in a 46% HF solution and wiping. After such a treatment the electrode showed j-U curves similar to Fig. 1C. The x_j and c_s values were unchanged by removing the layer. The ESCA spectra of specimens having the brown layer showed that it was composed mainly of B, Si, and O atoms, the atomic ratio B/Si/O changing in a range

2/1/1 to 1/2/2 from specimen to specimen.

It is to be noted that the photocurrent for the p^+/n-Si electrode without the dark brown layer (Fig. 1C) shows very gradual increase with the potential even compared with that for the n-Si electrode (Fig. 1A). The ESCA studies of p^+/n-Si electrodes showed that they were easily oxidized only by immersing in an HI/I_2 solution in the dark for a few min, covered with a thin silicon oxide surface layer.

2. Photoelectrochemical Behavior of Pt (or Pd)/p^+/n-Si Electrodes in HI/I_2 Solutions. Figure 2 shows *j-U* curves for a Pt/p^+/n-Si electrode (ion-implanted specimen with a Pt layer *ca.* 3 nm thick) in a 7.5 M HI/0.01 M I_2 solution in the dark and under illumination, together with the curve for an illuminated Pt/n-Si electrode. The similar *j-U* curves were obtained for Pt/p^+/n-Si electrodes prepared from thermally B-doped specimens. The photocurrent for the Pt/p^+/n-Si electrode was quite stable, corresponding to the oxidation of the I^- ions.[18] The difference between the potential (U_0) at which the current under illumination is zero and the redox potential of an I_3^-/I^- couple, $\varepsilon(I_3^-/I^-)$, determined from a *j-U* curve at a Pt electrode was 0.55 to 0.59 V for the Pt/p^+/n-Si electrodes, much larger than that for the Pt/n-Si, as seen from Fig. 2. This means that the former electrode generates a photovoltage much higher than the latter, indicating an advantage of the p-n junction.

Nearly the same *j-U* curves were obtained when Pd was deposited on p^+/n-Si instead of Pt. The electrode in this case was stable during the cyclic scanning for several hours. Figure 3 shows the relative atomic concentrations (A) as well as the binding energy for a $Pd3d_{5/2}$ ESCA peak (B) as functions of the Ar^+-ion etching time for a Pd/p^+/n-Si electrode which was immersed in an HI/I_2 solution in the dark after the Pd deposition. Even though a thick Pd layer had been deposited, Fig. 3A shows that most of the Pd was dissolved. The binding energy for a $Pd3d_{5/2}$ peak lay *ca.* 1.5 to 1.9 eV higher than that for pure Pd metal (Fig. 3B). Based on the reported binding energies (336.8 to 337.0 eV) for silicide-forming Pd atoms,[21] these results indicate that most of the Pd atoms left without dissolving are penetrating into the Si crystal and form silicide bonds. It is interesting to note that such a small amount of Pd is effective to stabilize the electrode and catalyze the electron transfer reaction.

Figure 4 shows the photocurrent *vs.* time for three different Pt/p^+/n-Si electrodes which were prepared from the same ion-implanted p^+/n-Si wafer of x_j 0.6 μm and c_s 1×10^{20} cm^{-3}, obtained under continuous illumination in a 7.5 M HI/0.1 M I_2 stirred solution, with the Si electrode connected through a resistor of 80 to 100 Ω to a Pt counter electrode. Curve A stands for an electrode having a Pt layer *ca.* 7 nm thick. The photocurrent initially increased gradually, but in about 50 h decreased suddenly. The ESCA spectra of the degraded electrode showed almost complete disappearance of the deposited Pt metal and the growth of a considerable amount of silicon oxide.

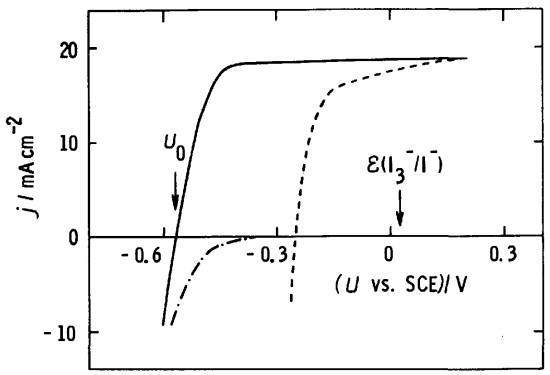

Fig. 2. Current density (*j*) *vs.* potential (*U*) curve for a Pt/p^+/n-Si electrode (B^+-ion implanted specimen, x_j 0.8 μm, c_s 6×10^{20} cm^{-3}, and the thickness of a Pt layer *ca.* 3 nm) in a 7.5 M HI/0.01 M I_2 solution in the dark (— · —) and under illumination (——), and the curve for an illuminated Pt/n-Si electrode (----).

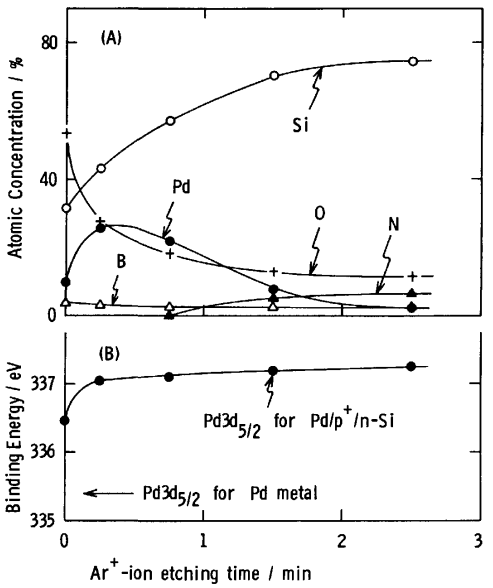

Fig. 3. Relative atomic concentrations (A) and the binding energy for a $Pd3d_{5/2}$ ESCA peak (B) as functions of the Ar^+-ion etching time for a Pd/p^+/n-Si electrode (thermally B-doped specimen) which was beforehand immersed in a 7.5 M HI/0.01 M I_2 solution in the dark for 40 s after the Pd deposition.

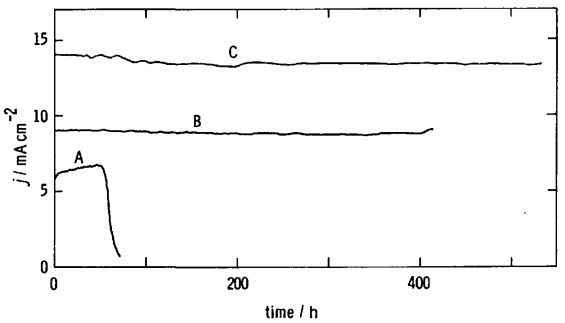

Fig. 4. Photocurrent *vs.* time curves for Pt/p^+/n-Si electrodes prepared from the same B^+-ion implanted p^+/n-Si wafer but coated with Pt in various ways: (A) A Pt layer *ca.* 7 nm thick as evaporated. (B) That *ca.* 7 nm thick heated at *ca.* 400 °C under $(2-5)\times10^{-5}$ Torr for 10 min. (C) Spotted Pt layers *ca.* 3 nm thick heated at *ca.* 400 °C under $(2-5)\times10^{-5}$ Torr for 6 min.

Curve B is for an electrode which was coated with a Pt layer *ca.* 7 nm thick and heated at about 400 °C under $(2-5)\times10^{-5}$ Torr for 10 min. The photocurrent in this case was steady for more than 400h. The *j-U* curves for this electrode (Fig. 5) observed before and after the stability test shows that the electrode is only slightly degraded by the prolonged illumination. The ESCA studies (Fig. 6) also show that a considerable amount of the deposited Pt still remains in this case after the prolonged illumination, though the oxygen concentration increases near the surfaces. These results indicate that the heat-treatment after the Pt deposition is effective for the electrode stabilization. It is also to be noted that the ESCA spectra of the heated and unheated specimens were almost the same, namely, the deposited Pt existed mostly in the form of pure metal, not silicide, even in the heated specimen, as seen from Fig. 6A.

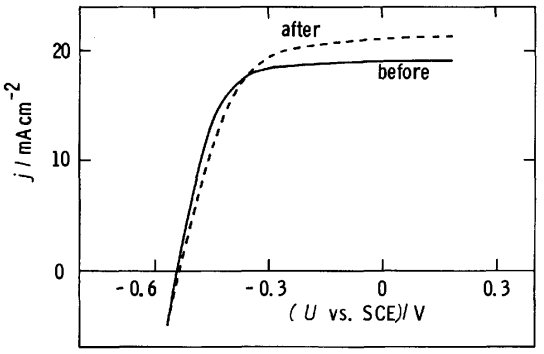

Fig. 5. Current density (j) *vs.* potential (U) curves for the Pt/p⁺/n-Si electrode observed before (——) and after (----) the stability test shown by curve B of Fig. 4.

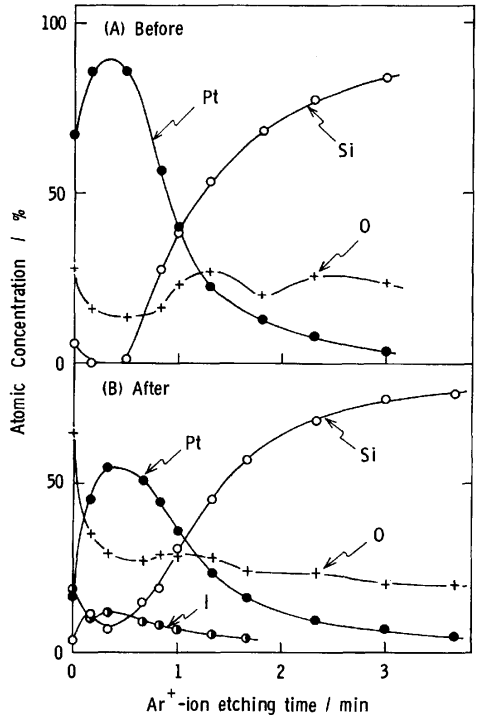

Fig. 6. Relative atomic concentrations as a function of the Ar⁺-ion etching time for the Pt/p⁺/n-Si electrode before (A) and after (B) the stability test shown by curve B of Fig. 4.

Curve C in Fig. 4 was obtained for a Pt/p⁺/n-Si electrode in which the Pt was deposited through a metal net so as to form metal layers in the form of small rectangles *ca.* 3 nm thick and *ca.* 0.3 mm² in area, spaced *ca.* 0.7 mm from each other, followed by heating at about 400 °C under $(2-5)\times10^{-5}$ Torr for 6 min. Although the Pt layer in this case did not cover the whole surface and was considerably thinner than the case of curve B, the photocurrent was stable for more than 500 h. It was also confirmed that the photocurrent was proportional to the averaged light transmittance of the Pt layer even in the case of spotted coating.

3. PEC Cells. A number of PEC cells of a photoelectric conversion type, consisting of a Pt/p⁺/n-Si electrode, a Pt counter electrode, and a 7.5 M HI/0.03 M I_2 stirred solution, were constructed by using various Pt/p⁺/n-Si electrodes. With the thermally B-doped electrodes, both the open-circuit voltage (V_{oc}) and the short-circuit current (I_{sc}) were almost independent of x_j in a range 0.3 to 0.9 μm. With the B⁺-ion implanted electrodes, nearly the same V_{oc} and I_{sc} were obtained, but the fill factor was in general somewhat better than that for the thermally doped electrodes. Under illumination of simulated AM 1 solar radiation at a power density of 100 mW cm⁻² by use of a Wacom Solar Simulator, the PEC cells having the B⁺-ion implanted electrodes generated the V_{oc} of 0.52 to 0.59 V, the I_{sc} of 21 to 29 mA

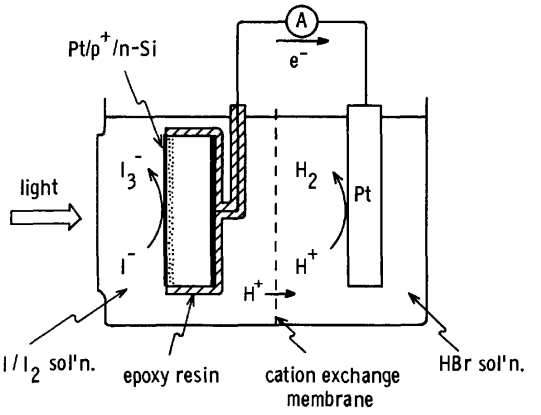

Fig. 7. A PEC cell for the HI photoelectrolysis.

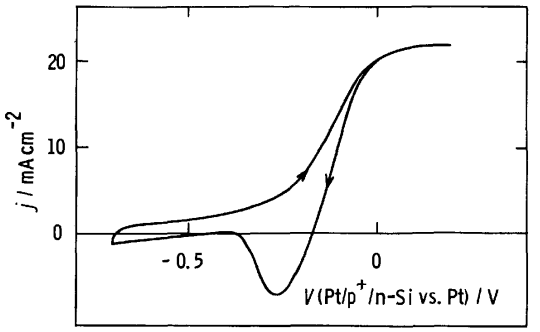

Fig. 8. Current density (j) for a Pt/p⁺/n-Si electrode in the PEC cell shown in Fig. 7 under illumination by a simulated 100 mW/cm² AM 1 solar radiation as a function of the voltage externally applied between the Si and the Pt counter electrode. The curve was obtained by cyclic scanning of the applied voltage at a rate 33 mV/s.

cm^{-2}, and the fill factor of 0.52 to 0.66. The solar-to-electric energy conversion efficiencies (ϕ^{s}_{elec}) calculated were 7.1 to 9.8%. These values are considerably high if we take account of the loss of incident light intensity due to the coloration of the HI/I_2 solution.

PEC cells for the photoelectrolysis of HI were also constructed using a $Pt/p^+/n$-Si electrode (ion-implanted specimen, x_j 0.6 μm, c_s 1×10^{20} cm^{-3}, and the thickness of a Pt layer *ca.* 2 nm) and a platinized Pt counter electrode (Fig. 7). 2 M HI/0.01 M I_2 and 2 M HBr solutions were used in the anode and the cathode compartment, respectively, by taking account of the overvoltage for the hydrogen evolution in the HBr solution smaller than that in the HI solution. The solutions were separated with a commercial cation exchange membrane (Asahi Glass Co., Selemion), both half cells stirred independently. Figure 8 shows the current density (j) for the $Pt/p^+/n$-Si electrode in the above cell under illumination by the Solar Simulator mentioned above as a function of the voltage (V) externally applied between the $Pt/p^+/n$-Si and the Pt electrode. The negative applied voltage implies that the PEC cell has an electrical output even in the photoelectrolysis of HI. The current at the zero applied voltage (*i.e.*, the short circuit current of the cell) was 20.0 mA cm^{-2}. During the current flow, the solution near the $Pt/p^+/n$-Si electrode became brown or red and gas evolved at the Pt counter electrode, showing that HI was photodecomposed into H_2 and I_2 (or I_3^-). The change in the Gibbs energy of this reaction was estimated both from current-potential curves for the two half-cell reactions at a platinized Pt electrode and from an open circuit voltage of a fuel cell operated with the same solutions as above and one atmosphere of hydrogen gas to be 0.41 eV/ion (or 79 kJ/mol). The chemical energy stored is then calculated to be 20 mA $cm^{-2}\times0.41$ V=8.2 mWcm^{-2}, and the solar-to-chemical energy conversion efficiency (ϕ^{s}_{chem}) to be 8.2%. When a 2 M HI/0.001 M I_2 solution was used in the anode compartment of the cell, the short circuit current increased to 21.7 mA cm^{-2} due to the better light transmittance of the solution.

Discussion

As mentioned before, the c_s values for the p^+/n-Si electrodes in the present work are so high, the order of 10^{20} cm^{-3} that the B-doped p^+-Si layer just beneath the surface should be degenerate at room temperature,[22] namely, the Fermi level of the layer (E^{p}_{F}) lies within the valence band. This implies that the surface p^+-Si layer behaves like a metal. Accordingly, when a p^+/n-Si electrode is in an HI/I_2 solution in the dark, the Fermi level (E^{p}_{F}) should coincide with the redox level of the I_3^-/I^- couple, $-e\varepsilon(I_3^-/I^-)$, with a negligibly thin Schottky barrier at an interface between the p^+-Si layer and the solution. It is therefore easily expected that the oxidation of the p^+-Si surface proceeds to some extent in an HI/I_2 solution even in the dark through the reaction of holes in the p^+-Si layer with water, followed by the hole injection by the I_3^- ions. This was really confirmed by the ESCA experiments, as described before. Very gradual increase of the photocurrent at the p^+/n-Si electrode with increasing the potential (Fig. 1C) can be understood on the basis of the presence of such an oxide layer at the surface.

The relatively stable j-U curve for the p^+/n-Si electrode prepared by the thermal diffusion method (Fig. 1B) was in a previous letter[18] explained by assuming the presence of a thin Schottky-type potential barrier at a p^+-Si-solution interface. It has been revealed in the present work that this stability is due to the presence of a dark brown overlayer consisting of the Si, B, and O atoms. It is interesting to note that such a brown layer plays a role in preventing further oxidation of the p^+-Si layer, contrary to the SiO_x layer which grows thicker and thicker with the passage of the photoanodic current (see Figs. 1A and C). This might suggest that the brown layer has a compact structure to be able to prevent the penetration of OH^- ions or H_2O molecules, though the holes may pass it by tunneling or thermal hopping. Unfortunately the brown layer-covered p^+/n-Si electrode is not sufficient both in the stability and the photocurrent efficiency in a potential

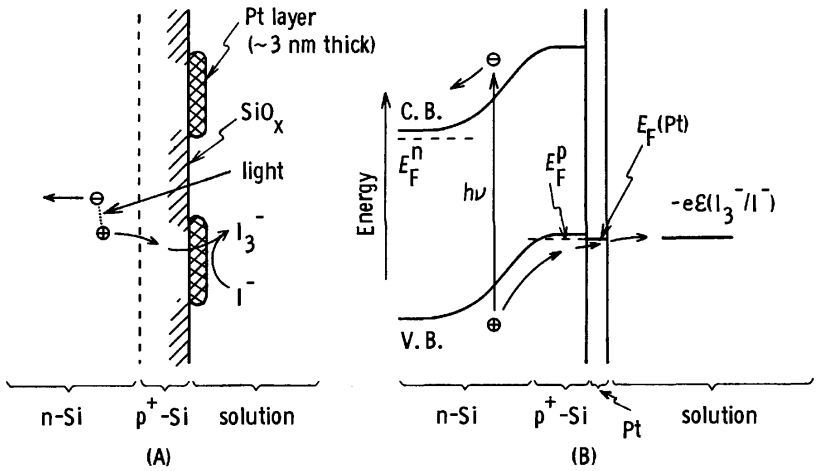

Fig. 9. Schematic cross section of a $Pt/p^+/n$-Si electrode (spotted Pt coating) in contact with an HI/I_2 solution (A) and energy band diagram under illumination (B). E^{n}_{F}: The Fermi level for the inside n-Si, E^{p}_{F}: that for the surface p^+-Si layer, and $E_F(Pt)$: that for the deposited Pt layer. ⊖ and ⊕: Photogenerated electron and hole, respectively.

range more negative than $\varepsilon(I_3^-/I^-)$.

The p^+/n-Si electrode coated with a Pt layer is very stable in an HI/I_2 solution (Fig. 4). This is true even for spotted coating with a relatively thin (2 to 3 nm thick) layer (curve C in Fig. 4). In such a case, the naked parts of the p^+-Si surface must be oxidized in the HI/I_2 solution, covered with insulating SiO_x layers, as mentioned above. Therefoe the photogenerated holes must be gathered into the Pt spots and react with the I^- ions, as shown in Fig. 9. Since the p^+-Si layer just beneath the surface is degenerate, as mentioned before, and is thought to be in ohmic contact with the Pt layer, the efficient photocurrent (Fig.2) can be explained by taking account of the effective photovoltage at the p-n junction and the low overvoltage for the I^- oxidation at the surface of the Pt layer.

As described before, the Pt layer as deposited by the vacuum evaporation is not sufficiently stable, disappearing during the prolonged flow of the photoanodic current in the HI/I_2, solution, and heat-treatment is necessary for stabilization. There was no difference between the heated and the unheated Pt layer in the ESCA spectra. Possibly, some change occurred in the structure of the Pt layer. This is contradictory to the results reporting the formation of Pt-silicide by heating.[11,23] In the present work a small amount of Pt-black on a boat-shaped tungsten heater was evaporated under 2×10^{-5} Torr quickly within several to 50 s. The Si wafer thus Pt-coated was then left in the air for, say, 1 d and heated at about 400 °C under $(2-5)\times10^{-5}$ Torr by use of an electric heater covered with mica plates. It was also confirmed that the silicide was really formed when Pt was deposited slowly by a method of electron-beam evaporation under 2×10^{-6} Torr, followed by heating of the Pt-deposited Si wafer at 350 to 450 °C without exposing to the air. Anyway, we can conclude from the results of Figs. 4 to 6 that the photocurrent of the Pt/p^+/n-Si electrode is stable as far as the deposited Pt is left at the electrode surface.

The solar-to-chemical energy conversion efficiency (ϕ^s_{chem}) obtained in the present work for the HI photoelectrolysis is encouragingly high, 8.2%. This value is, to our knowledge, the highest of the chemical conversion efficiencies ever obtained for the PEC cells working without external bias.[13,24-28] It will still be increased by optimizing various cell conditions. We can thus conclude that the use of the p-n junction semiconductors is an effective method for the solar energy conversion by use of PEC cells. Of course, there still lie many problems for the development of the presently proposed system to a practically feasible structure.

The authors express their thanks to Shin-Etsu Handotai Co. for offering n-Si single crystal wafers.

References

1) A. J. Nozik, *Ann. Rev. Phys. Chem.*, **29**, 189 (1978).
2) H. Gerischer, *Topics Appl. Phys.*, **31**, 115 (1979).
3) A. J. Bard, *J. Photochem.*, **10**, 59 (1979).
4) M. S. Wrighton, *Acc. Chem. Res.*, **12**, 303 (1979).
5) M. Tomkiewicz and H. Fay, *Appl. Phys.*, **18**, 1 (1979).
6) R. Memming, *Electrochim. Acta*, **25**, 77 (1980).
7) A. Heller, *Acc. Chem. Res.*, **14**, 154 (1981).
8) Y. Nakato, T. Ohnishi, and H. Tsubomura, *Chem. Lett.*, **1975**, 883.
9) a) P. A. Kohl, S. N. Franck, and A. J. Bard, *J. Electrochem. Soc.*, **124**, 225 (1977); b) M. Tomkiewicz and J. M. Woodall, *ibid.*, **124**, 1436 (1977); c) H. Morisaki, M. Ono, H. Dohkoshi, and K. Yazawa, *Jpn. J. Appl. Phys.*, **19**, L148 (1980).
10) a) F. Decker, J. Melsheimer, and H. Gerischer, *Israel J. Chem.*, **22**, 195 (1982); b) L. Thompson, J. DuBow, and K. Rajeshwar, *J. Electrochem. Soc.*, **129**, 1934 (1982).
11) F. -R. F. Fan, R. G. Keil, and A. J. Bard, *J. Am. Chem. Soc.*, **105**, 220 (1983).
12) a) J. M. Bolts, A. B. Bocarsly, M. C. Palazzotto, E. G. Walton, N. S. Lewis, and M. S. Wrighton, *J. Am. Chem. Soc.*, **101**, 1378 (1979); b) A. B. Bocarsly, E. G. Walton, and M. S. Wrighton, *ibid.*, **102**, 3390 (1980).
13) Y. Nakato, M. Shioji, and H. Tsubomura, *J. Phys. Chem.*, **85**, 1670 (1981).
14) a) R. Noufi, A. J. Frank, and A. J. Nozik, *J. Am. Chem. Soc.*, **103**, 1849 (1981); b) T. Skotheim, I. Lundström, and J. Prejza, *J. Electrochem. Soc.*, **128**, 1625 (1981); c) F. -R. F. Fan, B. L. Wheeler, and A. J. Bard, *ibid.*, **128**, 2042 (1981).
15) Y. Nakato, S. Tonomura, and H. Tsubomura, *Ber. Bunsenges. Phys. Chem.*, **80**, 1289 (1976).
16) H. D. Abruña and A. J. Bard, *J. Am. Chem. Soc.*, **103**, 6898 (1981).
17) R. N. Dominey, N. S. Lewis, J. A. Bruce, D. C. Bookbinder, and M. S. Wrighton, *J. Am. Chem. Soc.*, **104**, 467 (1982).
18) Y. Nakato, A. Tsumura, and H. Tsubomura, *Chem, Lett.*, **1982**, 1071.
19) W. R. McKee, K. R. Carson, and J. D. Levine, Conference Record of 16th IEEE Photovoltaic Specialists Conference, San Diego, California, September 1982, pp. 257—262. J. D. Luttmer and I. Trachtenberg, 161st Meeting of the Electrochemical Society (USA), Abstr., No. 448, p. 737 (1982). W. R. McKee, IEEE Transactions on Compounds, Hybrids, and Manufacturing Technology, Vol. CHMT-5, 336 (1982).
20) J. C. Irvin, *Bell System Tech. J.*, **41**, 387 (1962).
21) P. J. Grunthaner, F. J. Grunthaner, A. Madhukar, and J. W. Mayer, *J. Vac. Sci. Technol.*, **19**, 649 (1981).
22) F. J. Blatt, "Physics of Electronic Conduction of Solids," MaGraw-Hill, New York (1968).
23) K. N. Tu and J. W. Mayer, "Silicide Formation," in "Thin Films — Interdiffusion and Reactions," ed by J. M. Poate, K. N. Tu and J. W. Mayer, Wiley, New York (1978), Chap. 10, p. 359.
24) P. G. P. Ang and A. F. Sammells, *J. Electrochem. Soc.*, **129**, 233 (1982).
25) J. A. Baglio, G. S. Calabrese, E. Kamieniecki, R. Kershaw, C. P. Kubiak, A. J. Ricco, A. Wold, M. S. Wrighton, and G. D. Zoski, *J. Electrochem. Soc.*, **129**, 1461 (1982).
26) F. -R. F. Fan, H. S. White, B. L. Wheeler, and A. J. Bard, *J. Am. Chem. Soc.*, **102**, 5142 (1980).
27) C. Levy-Clement, A. Heller, W. A. Bonner, and B. A. Parkinson, *J. Electrochem. Soc.*, **129**, 1701 (1982).
28) A. Heller and R. G. Vadimsky, *Phys. Rev. Lett.*, **46**, 1153 (1981).

 © 1984 The Chemical Society of Japan Bull. Chem. Soc. Jpn., 57, 361—365 (1984)

Variational Determination of Molecular Orbital Energies in Independent Particle Models

Makoto ISIHARA

Department of General Education, Shotoku-Gakuen Women's Junior College, Nakauzura 1-38, Gifu 500

(Received August 3, 1983)

A simple construction formalism of molecular orbitals is presented in the context of partitioning of the electronic Hamiltonian. As a consequence of the formalism, a variational method of determining molecular orbital energies is proposed. The method is illustrated with the numerical example for the helium atom, whose result is reasonably meaningful.

Success of molecular orbital (MO) theory strongly suggests that the electronic Hamiltonian of a molecular system is often well represented by an independent particle model (IPM) Hamiltonian. Although MO's and MO energies are not inherently physical quantities, they are allowed to describe the physics of the system as conceptual tools of definite physical meanings under an IPM Hamiltonian. The IPM Hamiltonian is, however, almost always implicit in MO theory; MO's, their energies, wave functions, and state energies are determined usually through variational procedure. One may be tempted to think that the IPM Hamiltonian is merely a simple sum of the one-particle Hamiltonians determining MO's, but without any justification by the physical meaning of the one-particle Hamiltonian itself, the thought is generally incorrect. It seems natural to regard the IPM Hamiltonian as the best unperturbed Hamiltonian in the perturbation theory for electron correlation.

On the other hand, various perturbation methods aiming to go beyond the Hartree-Fock (HF) method have been developed using the so-called HF Hamiltonian as an unperturbed Hamiltonian.[1-5] However, irrelevance of that choice to molecular problems has been revealed in spite of the physically sound nature of the HF wave function as the zeroth order wave function.[6-9]

There are many unperturbed Hamiltonians having an identical wave function as an eigenfunction; what is the best unperturbed Hamiltonian? After Epstein's suggestive work on this problem,[10] taking the unphysical nature of the virtual HF orbitals into account, Silverstone and Yin have exploited the non-HF unperturbed Hamiltonian, the zeroth order wave function still remaining the HF one.[11] Davidson has also investigated some related aspects extensivly.[12] From a rather different viewpoint, partitioning the wave function space with projection operators,[13] an elaborate choice of the unperturbed Hamiltonian has been achieved for the correlation energy calculation by Kutzelnigg.[14,15]

This paper has two purposes: One is to present a simple construction formalism of MO's in the context of partitioning of the electronic Hamiltonian. Another is, as a consequence of the formalism, to propose that MO energies are to be adjusted through certain stability condition related to the perturbation left over. The former can be regarded as giving a prescription to extract some practical possibilities from the "unlimited variability"[10] concerning selection of the unperturbed Hamiltonian along Silverstone and Yin's way of thinking.[11]

Construction of MO's and Partitioning of the Electronic Hamiltonian

Let us start with the electronic Hamiltonian in the second quantized form as

$$H = \sum_{pq} h_{pq} a_p^\dagger a_q + \frac{1}{4} \sum_{pqrs} v_{qs}^{pr} a_p^\dagger a_r^\dagger a_s a_q, \tag{1}$$

where $a_p^\dagger$ and a_p stand for the creation and annihilation operators for the one-electron quantum state p, respectively. Whether the one-electron quantum states form a complete set or not, we regard that the space to be considered is defined by this Hamiltonian.[16] The hermiticity is brought in as requirements on the matrix elements:

$$h_{pq} = h_{qp}^* \tag{2}$$

and

$$v_{qs}^{pr} = v_{pr}^{qs}{}^*. \tag{3}$$

Further we assume that the electron repulsion matrix elements are antisymmetrized in the sense that

$$v_{qs}^{pr} = v_{sq}^{rp} = -v_{sq}^{pr} = -v_{qs}^{rp}. \tag{4}$$

When we have a starting set $\{p\}$ of one-electron quantum states other than MO's, say, site states, the first step is to generate MO's through an eigenvalue problem

$$\sum_q (h_{pq} + x_{pq}) c_{qj} = c_{pj} \varepsilon_j^{(0)}, \tag{5}$$

where $\{x_{pq}\}$ is selected so as to give a topologically appropriate nature to the MO's, namely, to $\{c_{pj}\}$; almost exclusively one imposes hermiticity upon $\{x_{pq}\}$ to obtain orthogonal MO's with real eigenvalues. The crucial point in this MO generation step is to separate the space under consideration into two parts, occupied and unoccupied spaces. Denoting sets of the whole, occupied, and unoccupied orbitals, respectively, by M, M_1, and M_2, we have

$$M = M_1 \oplus M_2. \tag{6}$$

Though this expression looks rather trivial, it is just an essence of MO theory. The most typical and plausible choice of $\{x_{pq}\}$ is

$$x_{pq} = \sum_{j \in M_1} v_{qj}^{pj}, \tag{7}$$

which leads us to the canonical HF orbitals. Such a choice makes Eq. 5 a pseud-eigenvalue problem; to work out the problem includes self-consistency procedure in general. Through the MO generation step we arrive at the Hamiltonian in the "MO representation"

$$H = \sum_j \varepsilon_j^{(0)} a_j^{(0)\dagger} a_j^{(0)} + \frac{1}{4}\sum_{jklm} v_{km}^{jl(0)} a_j^{(0)\dagger} a_l^{(0)\dagger} a_m^{(0)} a_k^{(0)} - \sum_{jk} x_{jk}^{(0)} a_j^{(0)\dagger} a_k^{(0)} \quad (8)$$

and the Fermi sea state

$$|F\rangle = \prod_{j\in M_1} a_j^{(0)\dagger} |\text{ vacuum }\rangle. \quad (9)$$

We label MO's with the indices $\{j,k,\cdots\}$.

Since any unitary transformation within the occupied or unoccupied orbital manifold keeps the Fermi sea state invariant, we can modify MO's (and MO energies) through the following eigenvalue problems.

$$\sum_{k\in M_{\xi\eta}} (\delta_{jk}\varepsilon_j^{(0)} + y_{jk}^{(0)}) u_{kl}^{(1)} = u_{jl}^{(1)} \varepsilon_l^{(1)} \quad (l\in M_{\xi\eta})(\xi = 1,2;\ \eta = 1,2,\cdots) \quad (10)$$

with

$$M_\xi = M_{\xi 1} \oplus M_{\xi 2} \oplus \cdots \quad (\xi = 1,2). \quad (11)$$

Note that MO indices $\{j,k,\cdots\}$ here are used for both modified(new) and unmodified(old) orbitals. It should be understood that they do not indicate any concrete one-electron function but label MO's flexibly in each orbital manifold. Representatives of MO modifications include the hole potential,[17,18] the electron-hole potential,[19,20] and the localized orbital [21] methods. By using the notation

$$a_j^{(n+1)} = \sum_k a_k^{(n)} u_{kj}^{(n+1)*}, \quad (12)$$

$$x_{jk}^{(n+1)} = \sum_{lm} u_{lj}^{(n+1)*} x_{lm}^{(n)} u_{mk}^{(n+1)}, \quad (13)$$

and so on, the Hamiltonian is rewritten as

$$H = \sum_j \varepsilon_j^{(1)} a_j^{(1)\dagger} a_j^{(1)} + \frac{1}{4}\sum_{jklm} v_{km}^{jl(1)} a_j^{(1)\dagger} a_l^{(1)\dagger} a_m^{(1)} a_k^{(1)} - \sum_{jk} x_{jk}^{(1)} a_j^{(1)\dagger} a_k^{(1)} - \sum_{\xi\eta}\sum_{jk\in M_{\xi\eta}} y_{jk}^{(1)} a_j^{(1)\dagger} a_k^{(1)}. \quad (14)$$

Of course, successive modifications are possible and to be utilized. For example, putting

$$M_{\xi\eta} = M_{\xi\eta 1} \oplus M_{\xi\eta 2} \oplus \cdots \quad (\xi = 1,2;\ \eta = 1,2,\cdots) \quad (15)$$

and solving

$$\sum_{k\in M_{\xi\eta\zeta}} (\delta_{jk}\varepsilon_j^{(1)} + z_{jk}^{(1)}) u_{kl}^{(2)} = u_{jl}^{(2)} \varepsilon_l^{(2)} \quad (l\in M_{\xi\eta\zeta})(\xi = 1,2;\ \eta,\zeta = 1,2,\cdots), \quad (16)$$

we have

$$H = \sum_j \varepsilon_j^{(2)} a_j^{(2)\dagger} a_j^{(2)} + \frac{1}{4}\sum_{jklm} v_{km}^{jl(2)} a_j^{(2)\dagger} a_l^{(2)\dagger} a_m^{(2)} a_k^{(2)} - \sum_{jk} x_{jk}^{(2)} a_j^{(2)\dagger} a_k^{(2)} - \sum_{\xi\eta}\sum_{jk\in M_{\xi\eta}} y_{jk}^{(2)} a_j^{(2)\dagger} a_k^{(2)} - \sum_{\xi\eta\zeta}\sum_{jk\in M_{\xi\eta\zeta}} z_{jk}^{(2)} a_j^{(2)\dagger} a_k^{(2)}. \quad (17)$$

Presumably it is suitable to call the process of modifications as a whole the MO modification step.

The "smallest" modification is the one-dimensional transformation; the MO does not change but the MO energy does. This is nothing other than level-shifting[22-26] and should be discussed separately from the above mentioned MO modification step. After any MO modification step consisting of g stages we are always still allowed to transform MO's as

$$\varepsilon_j = \varepsilon_j^{(g)} + \theta_j \quad (18)$$

with

$$u_{jk} = \delta_{jk}. \quad (19)$$

To rewrite $a_j^{(g)}$ as a_j, $x_{jk}^{(g)}$ as x_{jk}, and so on leads us to the resultant expression for the partitioned Hamiltonian

$$H = K + V \quad (20)$$

with

$$K = \sum_j \varepsilon_j a_j^\dagger a_j \quad (21)$$

and

$$V = \frac{1}{4}\sum_{jklm} v_{km}^{jl} a_j^\dagger a_l^\dagger a_m a_k - \sum_{jk} x_{jk} a_j^\dagger a_k - \sum_{\xi\eta}\sum_{jk\in M_{\xi\eta}} y_{jk} a_j^\dagger a_k - \sum_{\xi\eta\zeta}\sum_{jk\in M_{\xi\eta\zeta}} z_{jk} a_j^\dagger a_k - \cdots - \sum_j \theta_j a_j^\dagger a_j. \quad (22)$$

Apart from the MO modification step, which is to be based on physical reasoning, we can and should always adjust the MO energies by shifting in order to let the unperturbed Hamiltonian be the "best"; it must be emphasized that this MO energy shift step has nothing to do with the topological nature of the MO at all, as is obviously shown in Eq. 19. In the field of molecular quantum mechanics, the level shifting has been introduced and utilized in connection with the convergence problem in self-consistency procedure from a rather technical standpoint.[23] Another utilization worth referring to is seen in the degenerate perturbation approach.[22,24]

A Variational Determination of the MO Energy Shift

It is not very obvious how to determine the MO energy shift. In this section we describe one possible way of determining the MO energy shift for the canonical HF orbitals (without modification, for brevity), based on the quantum-mechanical variation principle. Hereafter the indices $\{j,k,l,m\}$ and $\{a,b,c,d\}$ are, respectively, used to label the occupied and unoccupied MO's: $j,k,l,m\in M_1$ and $a,b,c,d\in M_2$. The index i labels both: $i\in M$.

Let $|\psi\rangle$ be a trial correlated state corresponding to

the Fermi sea state. To take the first order perturbative state correction into account leads us to

$$|\Psi> = (1+C^\dagger)|F> \tag{23}$$

with

$$C^\dagger = -\frac{1}{4}\sum_{abjk} v_{jk}^{ab} w_{jk}^{ab} a_a^\dagger a_b^\dagger a_k a_j, \tag{24}$$

where the notation

$$w_{jk}^{ab} = 1/(\varepsilon_a+\varepsilon_b-\varepsilon_k-\varepsilon_j) \tag{25}$$

is used; of course, we have

$$w_{jk}^{ab} = w_{kj}^{ab} = w_{jk}^{ba} = w_{kj}^{ba} \tag{26}$$

and

$$w_{jk}^{ab} = -w_{ab}^{jk}. \tag{27}$$

The HF choice (Eq. 7) prevents any singly excited configuration from appearing in the first order state correction.[1] Denoting the exact ground state energy of H by E and abbreviating $<F|\cdots|F>$ to $<\cdots>$, we see the quantum-mechanical variation principle assert that[27-29]

$$E_0 + E_1 + (E_2+E_3)/(1+s) \geqq E \tag{28}$$

with

$$E_0 + E_1 = <K+V> = \sum_j \varepsilon_j^{(0)} - \frac{1}{2}\sum_{jk} v_{jk}^{jk}, \tag{29}$$

$$E_2 = <[C,V]> = -\frac{1}{4}\sum_{abjk} |v_{jk}^{ab}|^2 w_{jk}^{ab}, \tag{30}$$

$$\begin{aligned} E_3 &= <[[C,V],C^\dagger]> \\ &= \frac{1}{8}\sum_{abjk} v_{jk}^{ab} w_{jk}^{ab} (-2(\theta_a+\theta_b-\theta_k-\theta_j) v_{ab}^{jk} w_{jk}^{ab} \\ &\quad + \sum_{cd} v_{ab}^{cd} v_{cd}^{jk} w_{jk}^{cd} + \sum_{lm} v_{lm}^{jk} v_{ab}^{lm} w_{lm}^{ab} + 8\sum_{cl} v_{bl}^{kc} v_{ca}^{lj} w_{lj}^{ca}), \end{aligned} \tag{31}$$

and

$$s = <[C,C^\dagger]> = \frac{1}{4}\sum_{abjk} |v_{jk}^{ab}|^2 w_{jk}^{ab\,2}. \tag{32}$$

Now since E_0+E_1 is independent of $\{\theta_i\}$, that is,

$$\frac{\partial}{\partial\theta_i}(E_0+E_1) = 0 \quad (\text{any } i), \tag{33}$$

we require the "best" $\{\theta_i\}$ to fulfil the necessary condition

$$\frac{\partial}{\partial\theta_i}\left(\frac{E_2+E_3}{1+s}\right) = 0 \quad (\text{any } i), \tag{34}$$

which gives inhomogeneous simultaneous equations of variation parameters $\{\theta_i\}$. Generally speaking, they are to be solved only numerically, say, with the Newton-Raphson method. Here it should be noted that Eq. 34's for all i are not independent of each other, for the following equation identically holds.

$$\sum_i \frac{\partial}{\partial\theta_i}\left(\frac{E_2+E_3}{1+s}\right) = 0. \tag{35}$$

We can and should set, at least, one of $\{\theta_i\}$ arbitrarily.

The quantities needed in the numerical solution are the derivatives of E_2+E_3 and s with respect to $\{\theta_i\}$, which have expression as

$$\begin{aligned} \frac{\partial}{\partial\theta_m}(E_2+E_3) &= \frac{1}{2}\sum_{abj} w_{jm}^{ab\,2}\{-2|v_{jm}^{ab}|^2(\theta_a+\theta_b-\theta_m-\theta_j)w_{jm}^{ab} \\ &\quad + \sum_{cd} \mathrm{Re}(v_{jm}^{ab} v_{ab}^{cd} v_{cd}^{jm}) w_{jm}^{cd} + \sum_{kl} \mathrm{Re}(v_{jm}^{ab} v_{kl}^{jm} v_{ab}^{kl}) w_{kl}^{ab} \\ &\quad + 4\sum_{ck}(\mathrm{Re}(v_{jm}^{ab} v_{bk}^{jc} v_{ca}^{mk}) w_{mk}^{ca} + \mathrm{Re}(v_{jm}^{ab} v_{bk}^{mc} v_{ca}^{kj}) w_{kj}^{ca})\}, \end{aligned} \tag{36}$$

$$\begin{aligned} \frac{\partial}{\partial\theta_d}(E_2+E_3) &= -\frac{1}{2}\sum_{ajk} w_{jk}^{ad\,2}\{-2|v_{jk}^{ad}|^2(\theta_a+\theta_d-\theta_k-\theta_j)w_{jk}^{ad} \\ &\quad + \sum_{cd} \mathrm{Re}(v_{jk}^{ad} v_{lm}^{jk} v_{ad}^{lm}) w_{lm}^{ad} + \sum_{bc} \mathrm{Re}(v_{jk}^{ad} v_{ad}^{bc} v_{bc}^{jk}) w_{jk}^{bc} \\ &\quad + 4\sum_{bl}(\mathrm{Re}(v_{jk}^{ad} v_{al}^{kb} v_{db}^{lj}) w_{lj}^{db} + \mathrm{Re}(v_{jk}^{ad} v_{al}^{kb} v_{ba}^{lj}) w_{lj}^{ba})\}, \end{aligned} \tag{37}$$

$$\frac{\partial s}{\partial\theta_m} = \sum_{abj} |v_{jm}^{ab}|^2 w_{jm}^{ab\,3}, \tag{38}$$

and

$$\frac{\partial s}{\partial\theta_d} = -\sum_{ajk} |v_{jk}^{ad}|^2 w_{jk}^{ad\,3}. \tag{39}$$

Note that the quantities dependent on $\{\theta_i\}$ are only $\{w_{jk}^{ab}\}$ besides $\{\theta_i\}$ themselves in the above derivatives. The condition given by Eq. 34 is, of course, not sufficient as the minimum condition, but we have to be contented with describing such stationary one because of practical difficulty; numerical "checking" is possible.

Simplifications by reducing the number of the variation parameters may be worth being investigated. One is to set

$$\begin{cases} \theta_j = \theta & (\text{any } j) \\ \theta_a = \theta' & (\text{any } a), \end{cases} \tag{40}$$

which is actually one-parametric because of Eq. 35; the "distance" between the occupied and unoccupied spaces is arranged as a whole. Another is to use θ_i's only for specific orbitals, say, the highest occupied, the lowest unoccupied, and so on; the number of the variation parameters ranges from one to several. For example,

$$\theta_i = \begin{cases} \theta & (\text{the highest occupied}) \\ \theta' & (\text{the lowest unoccupied}) \\ 0 & \text{otherwise.} \end{cases} \tag{41}$$

Numerical Example

As an illustration we have applied the spin restricted version of the above mentioned methods to the ground state of the helium atom. The result of calculation is summarized in Tables 1, 2, and 3. The canonical HF orbitals are calculated by Roothaan's method[30] using the Slater-type s orbitals

$$\chi = ((2n)!)^{-1/2}(2\zeta)^{n+1/2} r^{n-1} e^{-\zeta r} Y_{00} \tag{42}$$

as a basis. The $1s$ ζ's are taken from best double-ζ calculation by Clementi and Roetti.[31] To the other ζ's we assign $1/n$ without any attempt of optimization.[17]

Table 1. Orbital energy shifts

		Orbital coefficients					Orbital energies and shifts		
		1s	1s	2s	3s	4s	ε^{o} [a]	θ	ε [b]/a.u.
	ζ	2.91093	1.45363	1/2	1/3	1/4			
A1	*1*	0.18069	0.84379				−0.91793		
	d	1.82122	−1.62404				2.82095	−0.67749	2.14346
A2	*1*	0.18086	0.84333	0.00110			−0.91810		
	c	0.03105	−0.30857	1.05129			0.06980	−0.18563	−0.11583
	d	1.91011	−1.78701	0.31414			3.06630	−0.72342	2.34288
A3	*1*	0.18090	0.84324	0.00138	−0.00040		−0.91813		
	b	−0.01332	−0.01401	−0.04517	1.02931		0.01178	−0.18337	−0.17156
	c	0.04443	−0.38961	1.43408	−0.89930		0.11414	−0.19084	−0.07670
	d	1.95601	−1.87274	0.51975	−0.27377		3.18699	−0.74597	2.44102
A4	*1*	0.18092	0.84321	0.00148	−0.00060	0.00019	−0.91814		
	a	0.00182	−0.02688	0.08660	−0.03389	1.00233	0.00406	−0.14505	−0.14099
	b	−0.01873	−0.01689	−0.07767	1.58261	−1.19772	0.02327	−0.18387	−0.16060
	c	0.05325	−0.43548	1.67783	−1.70916	0.81689	0.14095	−0.19761	−0.05666
	d	1.98484	−1.92706	0.66426	−0.56885	0.27001	3.26076	−0.75924	2.50152

a) ε° is the canonical HF orbital energy. b) $\varepsilon=\varepsilon^{\circ}+\theta$.

Table 2. Correlation corrections

	E_{HF} [a]	E_c° [b]	E_c [b]	ΔE_c [c]/a.u.
A1	−2.86167	−0.01329	−0.01374	−0.00045
A2	−2.86167	−0.01337	−0.01383	−0.00046
A3	−2.86168	−0.01343	−0.01389	−0.00046
A4	−2.86168	−0.01347	−0.01393	−0.00046

a) $E_{HF}=E_0+E_1$. b) E_c and E_c° are $(E_2+E_3)/(1+s)$ with and without shifting, respectively. c) $\Delta E_c=E_c-E_c^{\circ}$.

Table 3. One-parameter cases

	θ	E_c [a]	ΔE_c [a]/a.u.
A1	−0.67749	−0.01329	−0.00045
B2	−0.42354	−0.01369	−0.00032
B3	−0.38584	−0.01373	−0.00030
B4	−0.37144	−0.01376	−0.00029

a) See the footnote of Table 2.

The unoccupied orbitals are designated as *a*, *b*, *c*, and *d* in accordance with the characteristic of the orbital coefficients, the occupied orbital being named *1*. In the cases A1—A4 all of the unoccupied orbital energies are allowed to be variationally shifted, whereas the cases B2—B4 have only one variation parameter common to all the unoccupied orbitals (see Eq. 40); the shift of the occupied orbital energy is set to be zero in every case. Fulfillment of the minimum condition is checked numerically after variational solution for the stationary one.

The values of the orbital energy shifts obtained are neither extraordinary nor negligible. In A1—A4 we have the shifts similar to each other for the corresponding orbitals (the orbitals of the same name), which is the most impressive feature observed from the present example. It is more or less interesting that all the unoccupied orbital energies are shifted low and that the orbital energies of *a* and *b* in A4 are put in the reverse order by shifting. Although these are, of course, to be ascribed to the "nature" of the present example, the inclination reminds us of the hole potential treatment.[17]

The HF energies in A2—A4 scarcely differ from that of the double-ζ calculation (the HF energy in A1), the changes being 0.00001 a.u.; the correlation corrections with and without shifting, E_c and E_c°, vary clearly as the basis orbitals are added, though by the small amount of 0.00004—0.00009 a.u. On the other hand, the changes of the correlation corrections by shifting are about 0.00046 a.u. in A1—A4 and about 0.00030 a.u. in B2—B4, which are significantly large in comparison with the changes of the HF energies and the correlation corrections by the addition of the basis orbitals. The cases B2—B4 may be said to give passable result, if we take it into account that the method is merely one-parametric.

In spite of poorness of the additional basis, the result obtained here seems rather encouraging. We cannot, however, give any conclusive remark as to how the method proposed in the preceding section work in general. They are to be examined through further numerical calculations on leading systems, which is another enormous story.

Supplementary Remarks

First, we refer to a non-variational way of setting $\{\theta_i\}$. Putting

$$\theta_j = \frac{1}{2}\sum_k v_{jk}^{jk} - x_{jj} - y_{jj} - z_{jj} - \cdots, \tag{43}$$

we have

$$E_0 + E_1 = \sum_j \varepsilon_j. \tag{44}$$

Namely the state energy to first order can be written in terms of a sum of the occupied MO energies without regard to MO coefficients. Thus the Hückel model

Hamiltonian is obtained in a natural way. Especially, under the HF choice with no modification, the HF energy is expressed as

$$E_{\mathrm{HF}} = \sum_j \varepsilon_j \tag{45}$$

by setting

$$\theta_j = -\frac{1}{2}\sum_k v_{jk}^{jk}, \tag{46}$$

MO coefficients continuing to be the HF ones. The state energy shifting to give the HF energy as the zeroth order state energy has been early devised.[32]

Next, let us consider approximate evaluations of physical quantities with few terms in the Rayleigh-Schrödinger perturbation expansion.[27,28] The perturbation terms contain the MO energy differences in thier energy denominators to second and higher orders, so that the ambiguity due to the MO energy shift is not negligible but may be often significant. We should rather make use of it. Above all, the distance between the occupied and unoccupied spaces is to be treated carefully.

References

1) C. Møller and M. S. Plesset, *Phys. Rev.*, **46**, 618 (1934).
2) R. K. Nesbet, *Proc. R. Soc. London, Ser. A*, **230**, 312 (1955).
3) O. Sinanoğlu, *Proc. R. Soc. London, Ser. A*, **260**, 379 (1961).
4) H. J. Silverstone and O. Sinanoğlu, *J. Chem. Phys.*, **44**, 1899 (1966).
5) H. P. Kelly, *Phys. Rev.*, **144**, 39 (1966).
6) H. P. Kelly, *Phys. Rev.*, **131**, 684 (1963).
7) H. P. Kelly, *Phys. Rev.*, **136**, B896 (1964).
8) S. T. Epstein, *J. Chem. Phys*, **41**, 1045 (1964).
9) S. T. Epstein and J. H. Karl, *J. Chem. Phys.*, **44**, 4347 (1966).
10) S. T. Epstein, "Perturbation Theory and Its Applications in Quantum Mechanics," ed by C. H. Wilcox, Wiley, New York (1966), p. 49.
11) H. J. Silverstone and M.-L. Yin, *J. Chem. Phys.*, **49**, 2026 (1968).
12) E. R. Davidson, *J. Chem. Phys.*, **57**, 1999 (1972).
13) P.-O. Löwdin, *J. Math. Phys.*, **3**, 969 (1962).
14) W. Kutzelnigg, *Chem. Phys. Lett.*, **35**, 283 (1975).
15) W. H. Adams, *J. Chem. Phys.*, **45**, 3422 (1966).
16) K. McDowell, *J. Chem. Phys.*, **68**, 4151 (1978).
17) S. Huzinaga and C. Arnau, *Phys. Rev. A*, **1**, 1285 (1970).
18) S. Huzinaga and C. Arnau, *J. Chem. Phys.*, **54**, 1948 (1971).
19) K. Morokuma and S. Iwata, *Chem. Phys. Lett.*, **16**, 192 (1972).
20) S. Iwata and K. Morokuma, *Theor. Chim. Acta*, **33**, 285 (1974).
21) C. Edmiston and K. Ruedenberg, *Rev. Mod. Phys.*, **35**, 457 (1963).
22) B. H. Brandow, *Rev. Mod. Phys.*, **39**, 771 (1967).
23) V. R. Saunders and I. H. Hillier, *Int. J. Quatum Chem.*, **7**, 699 (1963).
24) I. Lindgren, *J. Phys. B*, **7**, 2441 (1974).
25) O. Matsuoka, *Mol. Phys.*, **30**, 1293 (1975).
26) R. Carbó, J. A. Hernández, and F. Sanz, *Chem. Phys. Lett.*, **47**, 581 (1977).
27) J. O. Hirschfelder, W. Byers Brown, and S. T. Epstein, *Adv. Quantum Chem.*, **1**, 255 (1964).
28) J. O. Hirschfelder, "Perturbation Theory and Its Applications in Quantum Mechanics," ed by C. H. Wilcox, Wiley, New York (1966), p. 3.
29) O. Sinanoğlu, *J. Chem. Phys.*, **34**, 1237 (1960).
30) C. C. Roothaan, *Rev. Mod. Phys.*, **23**, 69 (1951).
31) E. Clementi and C. Roetti, *At. Data Nucl. Data Tables*, **14**, 177 (1974).
32) D. F.-T. Tuan, S. T. Epstein, and J. O. Hirschfelder, *J. Chem. Phys.*, **44**, 431 (1966).

Kinetic Study of Proton Tunneling in the Reaction between 2,4,6-Trinitrotoluene and 1,8-Diazabicyclo[5.4.0]-undec-7-ene in Benzonitrile

Naoki SUGIMOTO, Muneo SASAKI,* and Jiro OSUGI

Department of Chemistry, Faculty of Science, Kyoto University, Oiwake-cho, Kitashirakawa, Sakyo-ku, Kyoto 606

(Received August 16, 1983)

The proton tunneling has been examined for the reaction between 2,4,6-trinitrotoluene and 1,8-diazabicyclo[5.4.0]undec-7-ene in benzonitrile in view of the solvent effect on the rate ratio k^H/k^D as well as on the various activation parameters. The reaction rate ratio k^H/k^D diminishes from 18.3 at 15 °C to 14.5 at 35 °C. The difference in the activation energies $E_a^D - E_a^H$ is 8.8 kJ mol^{-1} and the ratio of Arrhenius preexponential factors is 2.5. All these values are greater than the semiclassical limits of the primary kinetic isotope effects. According to Bell's equation the remarkable isotope effect is due to considerable contribution from tunneling in benzonitrile. The present results, being compared with those in other aprotic solvents, are discussed in relation with the effects of solvent polarity, specific acid-solvent interaction, and geometrical bulkiness in the vicinity of the reaction site.

Recently the primary kinetic isotope effect of the proton-transfer reaction in solution has been studied in detail from theoretical and phenomenological viewpoints.[1,2] The semiclassical theory of kinetic isotope effects, especially as applied to hydrogen and proton transfers, is well developed.[3-8] One of the recent topics is the quantum-mechanical tunneling phenomenon associated with a proton-transfer reaction.[9] The enormously large value of the kinetic isotope rate ratio has been almost explained on the basis of a tunneling contribution.[10-12]

In particular, the following proton/deuteron-transfers have attracted much interest because the experimental results of kinetic parameters and isotope effects are explained evidently by taking account of the appreciable tunneling effect; the reactions of (4-nitrophenyl)nitromethane (4NPNM) with tetramethylguanidine (TMG),[13-16] and pentamethylguanidine (PMG),[17] and the reactions of 2,4,6-trinitrotoluene (TNT) with TMG,[18-20] and 1,8-diazabicyclo[5.4.0]undec-7-ene (DBU).[21]

In the results of the reaction between 4NPNM and TMG[13] there appeared a sharp difference in the degree of kinetic isotope rate ratio k^H/k^D between the polar and nonpolar solvents: The larger was the dielectric constant, the smaller was the rate ratio. However, in the reaction of TNT with TMG,[18] a reverse tendency was found that k^H/k^D was 20.4 in acetonitrile (dielectric constant, $\varepsilon = 36$) and 13.7 in benzonitrile ($\varepsilon = 25.2$). It seems likely that a solvent character other than polarity also affects the degree of tunneling.

We reported previously proton tunneling of the reaction between TNT and DBU in acetonitrile (MeCN) and 1,2-dichloroethane (DCE).[21] In this paper we deal with the kinetics of the proton/deuteron-transfer reactions of the same system in benzonitrile (PhCN) for the purpose of investigating the steric effect of the medium. Benzonitrile is chosen as solvent because it is more bulky and less polar molecule than acetonitrile and so it might allow a greater contribution from tunneling.

Experimental

Materials. 2,4,6-Trinitrotoluene (TNT), 2,4,6-trinitrotoluene-α,α,α-d_3 (TNT-d_3), and 1,8-diazabicyclo[5.4.0]-undec-7-ene (DBU) were treated as described previously.[21] Benzonitrile (PhCN) was purified by the molecular sieves (type 5A), dried with phosphorus pentaoxide, then distilled several times. This treatment was repeated at frequent intervals.

Apparatus and Procedures. Absorption spectra were determined with a Shimadzu UV-200S spectrophotometer. Kinetic measurements were carried out with a Union Giken RA-401 stopped-flow apparatus. In all measurements the temperature was regulated within ±0.1 °C by circulating thermostated water. Solutions were freshly prepared before use and the following concentration of solutions were used: TNT, TNT-d_3, 0.02—0.08 mM; DBU, 1.3—14 mM. The apparent reaction rate was determined according to the same procedure as before.[21]

Results and Discussion

The reaction of TNT-d_3, as well as TNT, with DBU in PhCN gives a purple solution due to an ion pair. The absorption maxima of the product as a result of proton/deuteron-transfer from the methyl group of TNT to DBU are around 380, 535, and 645 nm in PhCN, and almost identical with those observed in other solvents.[21] The equilibrium constants K^H, K^D of the TNT, TNT-d_3+DBU reactions in PhCN were determined at 25 °C according to the Benesi-Hildebrand equation[22] (Fig. 1).

$$[AH]/a = 1/K\varepsilon[B] + 1/\varepsilon. \quad (1)$$

In this equation, [AH] is the initial concentration of TNT, [B] that of DBU, K the equilibrium constant, ε the molar absorption coefficient, and a the absorbance at 535 nm after equilibration. In kinetic measurement the stopped-flow trace fitted a first-order kinetic equation very well at each temperature when DBU existed in large excess over TNT or TNT-d_3. The plots of the observed first-order rate constant k_{obsd} against DBU concentration [B] are linear in agreement with Eqs. 2 and 3 (Figs. 2 and 3).

$$k_{obsd} = k_f^H[B] + k_b^H, \quad (2)$$

$$k_{obsd} = k_f^D[B] + k_b^D. \quad (3)$$

In these equations, k_f^H, k_f^D, k_b^H, and k_b^D denote the forward and backward rate constants of the proton- and deuteron-transfer reactions. The values of k_f^H, k_f^D, and k_f^H/k_f^D at each temperature are given in Table 1 together with those of K^H and K^D determined by equilibrium measurements at 25 °C. However, the values k_b^H and k_b^D are too small to be reliable and are not recorded. From the temperature dependence of the second-order rate constants (k_f^H and k_f^D), the activation parameters E_a, ΔH^*, ΔS^*, ΔG^*, and Arrhenius preexponential factors (A factors) were computed by a least-squares method (Table 2).

The result in Table 1 that K^H increases with solvent polarity suggests qualitatively that the ion pair is mainly stabilized by electrostatic interaction with the surrounding solvent molecules. On the other hand, increase of the activation energy E_a^H as well as the rate constant k_f^H is out of accord with increasing solvent polarity. E_a^H in PhCN is greater than those observed in MeCN and DCE by 8.0 and 18.4 kJ mol^{-1}, respectively, although solvent polarity increases in the order MeCN>PhCN>DCE. Contrary to ordinary cases, increasing solvent polarity tends to decrease k_f^H. These apparent differences in activation energy and rate constant between solvents originate from tunneling effect as described later.

The largely negative entropies of activation ΔS^*

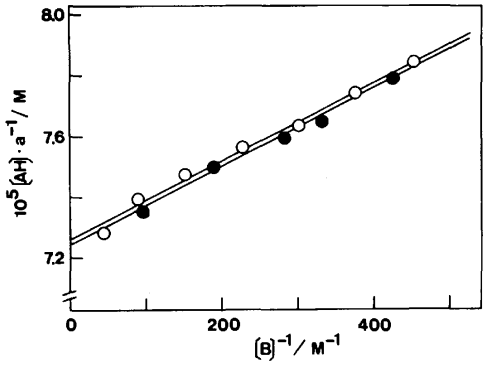

Fig. 1. Plots of [AH]/a against reciprocal of DBU concentrations in benzonitrile at 25 °C.
○: TNT+DBU, ●: TNT-d_3+DBU.

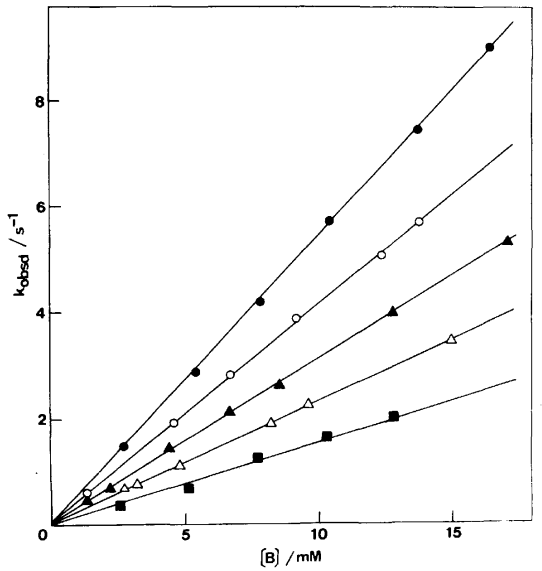

Fig. 2. Dependence of k_{obsd} on DBU concentration of the TNT+DBU reaction in benzonitrile.
●: 35 °C, ○: 30 °C, ▲: 25 °C, △: 20 °C, ■: 15 °C.

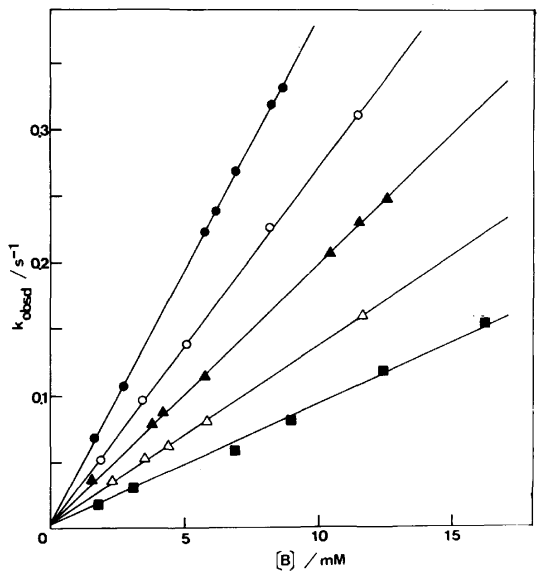

Fig. 3. Dependence of k_{obsd} on DBU concentration of the TNT-d_3+DBU reaction in benzonitrile.
●: 35 °C, ○: 30 °C, ▲: 25 °C, △: 20 °C, ■: 15 °C.

Table 1. Rate constants, equilibrium constants, and kinetic isotope rate ratios of the proton and deuteron transfer reactions in benzonitrile (ε=25.2)[a]

T / °C	k_f^H / M^{-1} s^{-1}	k_f^D / M^{-1} s^{-1}	k_f^H/k_f^D	K^H / M^{-1}	K^D / M^{-1}
35	554±10	38.3±0.8	14.5±0.5		
30	410±8	27.4±0.5	15.0±0.6		
25	310±6	19.5±0.4	15.9±0.6	5700±400	5500±350
	(204±4)[b]		(19.1±0.6)[b]	(6070±700)[b]	
	(565±10)[c]		(29.9±0.9)[c]	(1230±150)[c]	
20	233±5	13.5±0.3	17.3±0.8		
15	174±5	9.5±0.2	18.3±0.8		

a) Dielectric constant (ε) is 36.0 for acetonitrile and 10.4 for 1,2-dichloroethane. b) In acetonitrile (Ref. 21). c) In 1,2-dichloroethane (Ref. 21).

Table 2. Activation parameters of the proton and deuteron transfer reactions in benzonitrile at 25 °C

	H^+-Transfer	D^+-Transfer
E_a/kJ mol^{-1}	42.7±0.8 (34.7±0.8)[a] (24.3±0.7)[b]	51.5±0.8
ΔH^*/kJ mol^{-1}	40.2±0.8	49.0±0.8
ΔS^*/J K^{-1} mol^{-1}	−62.8±2.5 (−92.9±2.9)[a] (−119.7±3.8)[b]	−55.2±2.9
ΔG^*/kJ mol^{-1}	58.6±1.7	65.7±1.7
log A	9.9±0.1	10.3±0.1
$E_a^D-E_a^H$/kJ mol^{-1}	8.8±1.6	
A^D/A^H	2.5±1.5	

a) In acetonitrile (Ref. 21). b) In 1,2-dichloroethane (Ref. 21).

Table 3. Tunneling parameters for the TNF+DBU reaction in various solvents[a]

	CH_3CN[b]	C_6H_5CN	$C_2H_4Cl_2$[b]
E^H/kJ mol^{-1}	38.9±0.2	43.9±0.2	43.1±0.2
E^D/kJ mol^{-1}	44.8±0.2	49.8±0.2	49.0±0.2
$2b$/A	0.962±0.002	1.148±0.002	0.880±0.002
$2E^H/b^2$	20.1	15.9	26.6
E_a^H/E^H	0.89	0.97	0.56
ν^H/cm^{-1}	970	866	1116
Q^H (25 °C)	3.19±0.06	2.37±0.02	5.95±0.20
Q^D (25 °C)	1.79±0.03	1.56±0.02	2.23±0.10
$(k^H/k^D)_{calcd}$ (25 °C)	18.8±0.3	16.1±0.3	28.6±0.8
$(k^H/k^D)_{Arrh}$ (25 °C)	19.1±0.5	16.1±0.4	29.2±0.8

a) E_a: Activation energy; E: height of the barrier; $2b$: width of the barrier at base; ν: wave number along the reaction path; Q: tunneling factor. b) Ref. 21.

indicate that the transition state is solvated more strongly than the initial one. For the TNT+DBU reaction, $-\Delta S^*$ (H) in PhCN is smaller by about 30 J K^{-1} mol^{-1} in comparison with that in MeCN. Such a tendency, which is also found in the 4NPNM+TMG[13] and TNT+TMG reactions,[18] will suggest that the initial state in PhCN is more strongly solvated than that in MeCN. The stronger solvation in PhCN seems to be a result of the interaction of π electrons of PhCN with TNT rings.[18]

Tunneling in a proton/deuteron-transfer reaction is revealed by the following characteristic features;[1,2,9] a kinetic isotope rate ratio $k^H/k^D>11$ at 25 °C, an activation energy difference $E_a^D-E_a^H>5.8$ kJ mol^{-1}, and a ratio of the Arrhenius preexponential factors $A^D/A^H>1.4$. As found in Tables 1 and 2, the present results conform to the above mentioned features of tunneling. We have evaluated quantitatively the tunneling correction factor Q to manifest tunneling contribution according to the procedure described previously.[21] The tunneling factor Q is, in general, defined as the ratio of the actual rate constant k to the semiclassical rate constant k_s:

$$Q = k/k_s. \tag{4}$$

Assuming that the preexponential factor A is the same for H and D in the absence of tunneling, we obtain Eq 5:

$$Q^H/Q^D = (k^H/k^D)\exp[-(E^D-E^H)/RT]. \tag{5}$$

Further, Q is expressed by assuming a symmetrical parabolic potential barrier:

$$Q = 0.5u/\sin(0.5u) - \sum_{n=1}^{\infty}(-1)^n \exp[(u-2n\pi)\alpha/u]/[(u-2n\pi)/u], \tag{6}$$

where $\alpha=E/kT$, $u=h\nu/kT$, and $\nu=(E/2m)^{1/2}/\pi b$; k is Boltzmann's constant, h Planck's constant, E the height of barrier, b the half width of the barrier at the base, m the mass of the particle transferred, and ν the frequency of oscillation of a particle in parabolic potential. We calculated Q^H and Q^D under the same conditions described previously.[21] The values of E^H, E^D, and $2b$ were adjusted in Eqs. 5 and 6 by trial and error until the calculated rate ratios $(k^H/k^D)_{calcd}$ reproduced the experimental ones of $(k^H/k^D)_{Arrh}$ taken from the Arrhenius plots over the whole range of experimental temperature. These calculations fix the values of E^H and E^D within ±0.2 kJ mol^{-1} and those of $2b$ within ±0.002 A. The results in PhCN are given in Table 3 together with those in MeCN and DCE.[21] As seen in Table 3, Q^H at 25 °C in all these solvents is larger than unity, that is, the reaction is subjected to tunneling.

Tunneling factor Q is closely related with the curvature at the top of the potential barrier, $2E/b^2$, and so it also gives a criterion of tunneling. If we take $m^H=1$ and $m^D=2$ amu in continuum medium irrespective of solvent, E will decrease with increasing solvent polarity, and so Q^H will be smaller in more polar solvent. The comparison between DCE and MeCN will conform to this case. The barrier width $2b$ is a little longer in MeCN perhaps because of the partial specific interaction of CN group with TNT. But the difference of tunneling factors is mainly due to that of E. Besides electrostatic or specific interaction, the solvent environment in the vicinity of reaction site must affect the degree of tunneling. When geometrical bulkiness of a solvent molecule is significant, we have to consider two effects: One is the steric hindrance which will work so as to separate the acid-base distance, and the other is to form a solvent cage in which reaction takes place under much less electrostatic effect of solvent. The former case will depress the tunneling degree, while the latter will enhance. The present results in PhCN suggest that the solvent PhCN molecule works so as not to form a cage-like environment around the reactive site but to separate the barrier width $2b$. For the case of PhCN the interposition of solvent molecule enlarges the distance between proton donor and acceptor, and brings about the smaller degree of tunneling, because there may be the stronger solvation due to π electron interaction between PhCN and TNT ring.

In this study we could not unfortunately discriminate the purely steric effect of solvent molecule. For that purpose an experiment in a bulky and nonpolar solvent is required, but within the preliminary experiments in various solvents we could not find any solvent

in which the reaction took place effectively.

References

1) E. F. Caldin and V. Gold, "Proton-Transfer Reactions," Chapman and Hall, London (1975) and the references cited therein.
2) L. Melander and W. H. Saunder, Jr., "Reaction Rates of Isotopic Molecules," 2nd ed, Wiley, New York (1980).
3) L. Melander. "Isotope Effect on Reaction Rates," Ronald Press, New York (1960) and the literatures cited therein.
4) F. H. Westheimer, *Chem. Rev.*, **61**, 265 (1961).
5) J. Bigeleisen, *Pure Appl. Chem.*, **8**, 217 (1964).
6) W. J Albery, *Trans. Faraday Soc.*, **63**, 200 (1967).
7) R. A. M. O'Ferrall and J. Kouba, *J. Chem. Soc.*, **1967**, 985; R. A. M. O'Ferrall, *ibid.*, **1970**, 785.
8) A. J. Kresge, *J. Am. Chem. Soc.*, **102**, 7797 (1980).
9) R. P. Bell, *Trans. Faraday Soc.*, **55**, 1 (1959); "The Tunneling Effect in Chemistry," Chapman and Hall, London (1980).
10) S. B. Koldor and W. H. Saunders, Jr., *J. Chem. Phys.*, **68**, 2509 (1978); *J. Am. Chem. Soc.*, **101**, 7594 (1979).
11) R. J. Le Roy, H. Murai, and F. Williams, *J. Am. Chem. Soc.*, **102**, 2325 (1980).
12) V. Malatesta and K. U. Ingold, *J. Am. Chem. Soc.*, **103**, 3094 (1981).
13) E. F. Caldin and S. Mateo, *J. Chem. Soc., Faraday Trans. 1*, **71**, 1876 (1975).
14) A. J. Kresge and M. F. Powell, *J. Am. Chem. Soc.*, **103**, 201 (1981).
15) E. F. Caldin, S. Mateo, and P. Warrick, *J. Am. Chem. Soc.*, **103**, 202 (1981).
16) M. Sasaki, N. Sugimoto, and J. Osugi, *Chem. Lett.*, **1980**, 887; N. Sugimoto, M. Sasaki, and J. Osugi, *Bull. Inst. Chem. Res., Kyoto Univ.*, **59**, 63 (1981).
17) O. Rogne, *Acta Chem. Scand., Ser. A*, **32**, 559 (1978); J. H. Blanch and O. Rogne, *J. Chem. Soc., Faraday Trans. 1*, **74**, 1254 (1978); I. Heggen, J. Lindstron, and O. Rogne, *ibid.*, **74**, 1263 (1978); J. H. Blanch, O. Rogne, and L. I. Rossemyr, *ibid.*, **76**, 1905 (1980).
18) P. Pruszynski and A. Jarczewski, *Rocz. Chem.*, **51**, 2171 (1977).
19) A. Jarczewski, P. Pruszynski, and K. T. Leffek, *Can. J. Chem.*, **57**, 669 (1979).
20) N. Sugimoto, M. Sasaki, and J. Osugi, *Bull, Chem. Soc. Jpn.*, **54**, 2598 (1981).
21) N. Sugimoto, M. Sasaki, and J. Osugi, *J. Phys. Chem.*, **86**, 3419 (1982).
22) H. A. Benesi and J. H. Hildebrand, *J. Am. Chem. Soc.*, **71**, 2703 (1949).

A.c. Polarographic Study of Ion Transfer at the Water/Nitrobenzene Interface

Toshiyuki OSAKAI, Tadaaki KAKUTANI, and Mitsugi SENDA*
Department of Agricultural Chemistry, Faculty of Agriculture, Kyoto University, Sakyo-ku, Kyoto 606
(Received August 22, 1983)

The transfer of tetramethylammonium (TMA^+) ion across the interface between a 0.1 mol dm^{-3} LiCl aqueous solution and a 0.1 mol dm^{-3} tetrabutylammonium tetraphenylborate nitrobenzene solution was investigated by means of phase-selective a.c. polarography. In recording the a.c. polarographic current a two-electrode cell system was used and the ohmic drop due to solution resistance in the cell was compensated for by positive feedback. The ion-transfer admittance *vs.* potential curves were determined in the a.c. frequency range between 10 and 100 Hz and the kinetic parameters of the TMA^+-ion transfer across the water/nitrobenzene interface were determined.

Kinetics of the charge (ion or electron) transfer at the interface between two immiscible electrolyte solutions has been studied by several authors using electrochemical techniques. Gavach and his coworkers have employed chronopotentiometry[1-3] and impedance measurement methods[1] to determine the kinetic parameters of the transfer of alkylammonium ions at the water/nitrobenzene interface. Recently, Koczorowsky and Geblewicz[4] have also applied chronopotentiometry to the kinetic study of the transfer of tetrabutylammonium ion at the water/1,2-dichloroethane interface. On the other hand, Samec *et al.* have employed cyclic voltammetry, with or without convolution analysis, for the kinetic studies of the transfer of Cs^+ ion at the water/nitrobenzene interface[5,6] and the transfer of alkaline earth metal cations facilitated by synthetic neutral carriers at the water/nitrobenzene interface,[7] and also the electron transfer between ferrocene in nitrobenzene and hexacyanoferrate(II) in water.[6]

In this work we have applied a phase-selective a.c. polarographic technique to the study of the kinetics of ion (tetramethylammonium ion) transfer at the water/nitrobenzene interface; an a.c. voltage of small amplitude was superimposed on a linear sweep voltage applied to the interface, and the real and imaginary components of the resulting alternating current were recorded against the applied linear sweep voltage in the frequency range between 10 and 100 Hz and in the concentration range of transferring ion between 0.15×10^{-3} and 0.50×10^{-3} mol dm^{-3}. In recording phase-selective a.c. polarographic curves we used a two-electrode cell system and the ohmic drop due to the solution resistance in the cell was compensated for by a positive feedback circuit. The recorded phase-selective a.c. polarographic currents were transformed into the admittance of the test interface and the latter was corrected for the admittance of the base aqueous solution/base nitrobenzene solution interface to give the admittance due to the ion transfer at the interface. The resulting ion-transfer admittance *vs.* potential curves were analysed using the conventional theory of a.c. polarography, and the kinetic parameters of the ion transfer at the water/nitrobenzene interface were determined.

Experimental

Chemicals. The tetramethylammonium chloride (TMACl) was analytical grade (Wako Pure Chemical Industries, Ltd.), and used as received. The tetrabutylammonium chloride (TBACl) was analytical grade (Nakarai Chemicals Co.), and was purified as previously described.[8] The concentrations of TMACl and TBACl were determined by potentiometric titration with a standard silver nitrate solution. The analytical grade nitrobenzene (Nakarai) was distilled under reduced pressure; the middle 60% of the distillate was collected and shaken with active alumina overnight; after filtration of the suspension, the filtrate was washed with triply distilled water. The nitrobenzene solution of tetrabutylammonium tetraphenylborate (TBATPB) was prepared in the dark immediately before use. The other chemicals and the preparation of the aqueous solution have been described elsewhere.[9]

Electrolytic Cell. The electrolytic cell assembly is shown in Fig. 1. A glass tube A, which was filled with a 0.1 mol dm^{-3} LiCl aqueous solution containing $(0.15-0.50)\times10^{-3}$ mol dm^{-3} TMACl, was dipped into a 0.1 mol dm^{-3} TBATPB nitrobenzene solution. The test interface was formed at the end of the glass tube A with an area of 0.159 cm^2. A reproducible, flat water/nitrobenzene interface was formed by treating the edge and the outer surface of the glass tube with dimethyldichlorosilane.[9,10] The test interface was

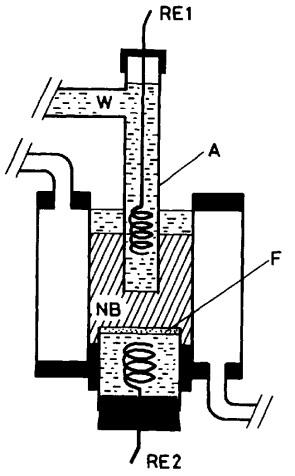

Fig. 1. Electrolytic cell. W, water phase; NB, nitrobenzene phase; A, glass tube; RE1 and RE2, reference electrodes; F, sintered glass.

renewed for each measurement of a single a.c. polarogram. The cell was water-jacketted at 25±0.1 °C.

The reference electrode for the nitrobenzene phase, RE2, was an Ag/AgCl/0.1 mol dm^{-3} TBACl (water) electrode with a large surface area (>6 cm^2), which was connected to the nitrobenzene phase through sintered glass. The other reference electrode for the aqueous phase, RE1, was an Ag/AgCl electrode with a large surface area (>4 cm^2), which was immersed in the aqueous phase. Accordingly, the cell to be studied can be expressed by:

$$\begin{array}{l} \qquad\qquad\qquad\qquad\quad \text{I} \qquad\qquad\quad \text{II} \\ \text{(RE2) Ag}\,|\,\text{AgCl}\,|\,0.1\ \text{mol dm}^{-3}\ \text{TBACl}\ \text{(W)}\,|\,0.1\ \text{mol dm}^{-3}\ \text{TBATPB}\ \text{(N)} \\ \qquad\qquad\qquad\quad \text{III} \\ |\,(0.15\text{—}0.50)\times 10^{-3}\ \text{mol dm}^{-3}\ \text{TMACl} + 0.1\ \text{mol dm}^{-3}\ \text{LiCl}\ \text{(W)} \\ |\,\text{AgCl}\,|\,\text{Ag (RE1)}, \qquad\qquad\qquad\qquad\qquad\qquad \text{(A)} \end{array}$$

where (W) and (N) represent the aqueous and the nitrobenzene phases. The interface between phases I and II is nonpolarizable and the potential difference across the interface is determined by the activities of TBA$^+$ ion in the two phases.[9,10]

Measurement of Solution Resistance. In a.c. polarographic measurements, we adopted a two-electrode cell system in which the ohmic drop due to the solution resistance between RE1 and RE2, R_u, was compensated for by means of positive feedback (see Fig. 3). For exact compensation of the ohmic drop, the value of R_u must be known accurately. We used a laboratory-made linear bridge[11] to determine R_u. Figure 2 shows the basic circuit of the bridge, which allowed accurate determination of resistance (a dummy cell resistance) using a 10 kHz a.c. generator with an error less than 10 Ω in the range between 0.5 and 5.0 kΩ. Determination of R_u was made every time the test interface was renewed. For a representative cell, as shown in Fig. 1, R_u was in the range between 1.41 and 1.54 kΩ.

A.c. Polarographic Measurement. The diagram of the basic electronic circuit for measurement of the interfacial impedance with a two-electrode cell system is shown in Fig. 3. The circuit bordered by broken lines is a conventional polarographic circuit (Yanako potentiostat PE21-TB2S). D.c. and a.c. voltages are generated by a sweep generator (Hokuto Denko HB-104) and an a.c. generator (YHP 3310B), respectively, and applied through R_1 to the summing point, e_s, of the inverting adder (OA1 and OA2), the output of which is applied to the terminal of RE1, while the terminal of RE2 is always held at virtual ground. The output voltage of OA3, E_o, is proportional to the current flowing through the cell, i, that is, $E_o=iR_i$. For the ohmic drop compensation, a part of this output voltage was fed back to the summing point. The feedback voltage was made equal to $\beta R_u i=\beta R_u E_o/R_i$ by adjusting a potentiometer, R_c, where β is the fraction of positive feedback and $\beta=1$ for 100% positive feedback. The real (in-phase) and imaginary (out-of-phase) components of the a.c. polarographic current flowing through the cell were determined by a lock-in amplifier (NF LI-574) and recorded against the linear sweep voltage applied to the test interface, usually at the voltage scan rate of $v=5$ mV s^{-1}, using an X-Y

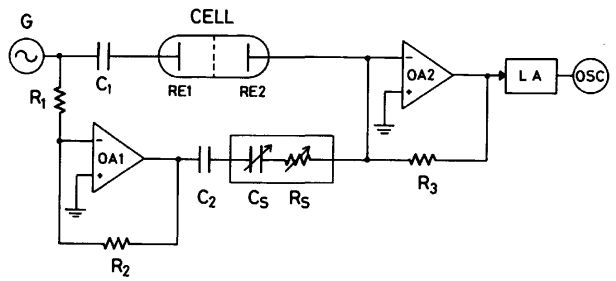

Fig. 2. Basic circuit of the linear bridge for measurement of the solution resistance. OA1 and OA2, operational amplifiers (Texas Instrument TLO82CP); G, a.c. generator (NF 572B); LA, lock-in amplifier (NF 572B); OSC, oscilloscope (Hitachi VC-801L); R_s and C_s, decade resistor and decade capacitor; $R_1=R_2=43$ kΩ; $R_3=100$ kΩ; $C_1=C_2=1$ μF.

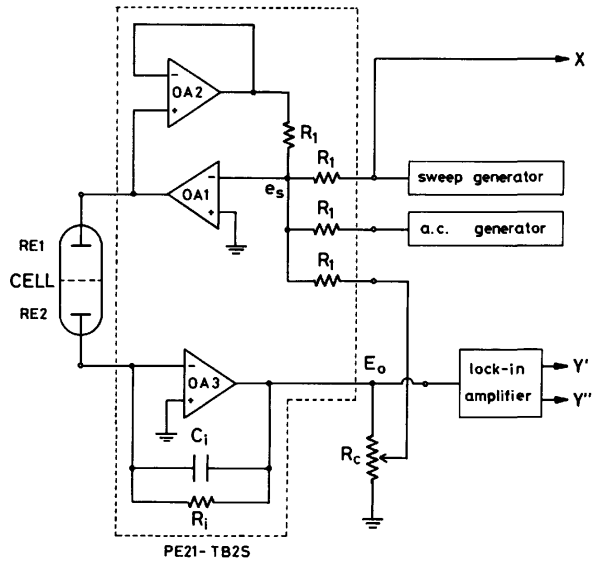

Fig. 3. Electronic circuit for d.c. and a.c. polarographic measurement with a two-electrode cell. X, Y', and Y'', inputs of recorder; RE1 and RE2, reference electrodes; OA1 to OA3, operational amplifiers (Burr Brown 3112/12C); R_i, current-measuring resistor (10 kΩ); C_i, damping capacitor (1000 pF); R_c, potentiometer (1 kΩ); R_1, resistor (10 kΩ).

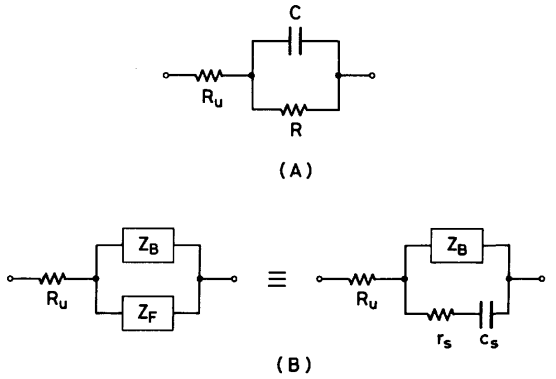

Fig. 4. (A) Dummy cell. R, C, and R_u correspond, respectively, to the resistance and capacitance of the test interface, and the solution resistance. (B) Equivalent circuit of the cell. R_u, solution resistance; Z_B, base impedance; $Z_F=r_s-j(1/\omega C_s)$, ion-transfer impedance.

recorder (Watanabe WX4302). The magnitude of the superimposed a.c. voltage (usually 5 mV peak to peak) was calibrated by replacing the cell with a known capacitor and measuring the a.c. current flowing through the capacitor by the lock-in amplifier.

The measuring circuit was calibrated by a dummy cell, which consists of R_u=1.5 kΩ, R=0.2 to 2 kΩ, and C=2 to 20 μF, as shown in Fig. 4(A), in the a.c. frequency range of 10 to 100 Hz. The error in measuring the dummy admittance ($1/R$ and ωC) with β being equal to 1 was not negligible, especially at high frequencies. Accordingly, the measured or apparent admittance was corrected for the non-ideal dynamic response of the measuring circuit, where the response was represented, in the first approximation, by the gain function of $G=K/(1+\tau_a s)$ of the control amplifier (OA1) with other amplifiers functioning ideally. The residual error in the corrected admittance was less than 1, 3, and 6% at 10, 50, and 100 Hz, respectively, in the calibrated range of R and C of the dummy cell.

Theoretical

In the following, the potential applied to cell A, E, is defined as the potential of RE1 against that of RE2, *i.e.*, $E=E_{RE1}-E_{RE2}$. The flow of the positive charge from the aqueous to the nitrobenzene phase is taken as the positive current.

Interfacial Admittance. The admittance of the test interface as determined by phase-selective a.c. polarography can be generally represented by:

$$Y_t = Y_t' + jY_t'', \tag{1}$$

where j is an operator $j=(-1)^{1/2}$. Let the base admittance, that is, the admittance of the base aqueous solution/base nitrobenzene solution interface, be $Y_B=Y_B'+jY_B''$. Then the admittance due to the ion transfer $Y_F=Y_F'+jY_F''$ can be estimated by:

$$Y_F' = Y_t' - Y_B', \tag{2}$$

$$Y_F'' = Y_t'' - Y_B''. \tag{3}$$

Finally, the ion-transfer admittance, Y_F, is related to a series combination of resistance and capacitance, r_s and c_s, due to the ion transfer (see Fig. 4(B)) by:

$$r_s = Y_F'/(Y_F'^2 + Y_F''^2), \tag{4}$$

$$1/\omega c_s = Y_F''/(Y_F'^2 + Y_F''^2), \tag{5}$$

where ω is the a.c. angular frequency ($\omega=2\pi f$, f being the a.c. frequency).

Ion-transfer Impedance. We suppose that the ion-transfer current I is a function of the surface concentrations of the ion in the aqueous and nitrobenzene phases, C^W and C^N, and of the interfacial potential difference, $\Delta_N^W\phi$, or the potential applied to the cell, $E=\Delta_N^W\phi+\Delta E_{ref}$, where ΔE_{ref} is determined by the reference electrode system:[9]

$$I = I(E,C^W,C^N). \tag{6}$$

In this and the following equations the terms containing activity coefficients of the ions are neglected for the sake of simplicity. When a small a.c. voltage is superimposed on the d.c. potential, E_{dc}, the ion-transfer impedance, $r_s-j(1/\omega c_s)$ (see Fig. 4(B)), can be generally expressed, by analogy with the faradaic impedance of an electrode reaction,[12-14] by:

$$r_s = r_{ct} + r^W + r^N, \tag{7}$$

$$1/\omega c_s = x^W + x^N, \tag{8}$$

with

$$r_{ct} = 1/\left(\frac{\partial I}{\partial E}\right)_{dc}, \tag{9}$$

$$r^\alpha = \pm\left[\left(\frac{\partial I}{\partial C^\alpha}\right)_{dc}\Big/\left(\frac{\partial I}{\partial E}\right)_{dc}\right](h_r)^\alpha(1/zFA), \tag{10}$$

$$x^\alpha = \pm\left[\left(\frac{\partial I}{\partial C^\alpha}\right)_{dc}\Big/\left(\frac{\partial I}{\partial E}\right)_{dc}\right](h_y)^\alpha(1/zFA), \tag{11}$$

where the superscript α (=W and N) stands for the aqueous (W) and nitrobenzene (N) phases, and the upper and lower signs in Eqs. 10 and 11 apply to W and N, respectively; z is the ionic valence, F the Faraday and A the surface area of the test interface. The expression $(\ )_{dc}$ means the partial differential coefficients with respect to the stated variable of Eq. 6 at $E=E_{dc}$, and $(h_r)^\alpha$ and $(h_y)^\alpha$ are the coefficients, which depend only on the mass transfer of the ion in the two phases and are given for semi-infinite linear diffusion by:

$$(h_r)^\alpha = (h_y)^\alpha = (2\omega D^\alpha)^{-1/2}, \tag{12}$$

where D^α is the diffusion coefficient of the ion in the α phase.

When the ion transfer is reversible or nernstian in d.c. cyclic voltammetry, the Nernst equation is valid for the d.c. components of surface concentration or the mean surface concentrations, $\bar{C}^W$ and $\bar{C}^N$:

$$E_{dc} = E^\circ + (RT/zF)\ln(\bar{C}^N/\bar{C}^W). \tag{13}$$

Here E° is the standard potential of the ion transfer at the test interface with respect to the reference electrode system in cell A and is defined by:

$$E^\circ = -\frac{\Delta G_{tr}^{\ominus,N\to W}}{zF} + \Delta E_{ref}, \tag{14}$$

where $\Delta G_{tr}^{\ominus,N\to W}$ is the standard Gibbs free energy of ion transfer from the nitrobenzene to the aqueous phase. Thus, we have $(\partial I/\partial C^W)_{dc}/(\partial I/\partial E)_{dc}=-(\partial E_{dc}/\partial \bar{C}^W)=(RT/zF)(1/\bar{C}^W)$ and $(\partial I/\partial C^N)_{dc}/(\partial I/\partial E)_{dc}=-(\partial E_{dc}/\partial \bar{C}^N)=-(RT/zF)(1/\bar{C}^N)$. For semi-infinite linear diffusion, we also have $(D^W)^{1/2}(C^{W,o}-\bar{C}^W)=(D^N)^{1/2}(\bar{C}^N-C^{N,o})$ where $C^{\alpha,o}$ is the bulk concentration of the ion in the α phase. Then we get from Eqs. 7 to 13, upon assuming that $C^{N,o}=0$:

$$r_s = (\sigma/\omega^{1/2})[1+(2\omega)^{1/2}\lambda^{-1}], \tag{15}$$

$$1/\omega c_s = \sigma/\omega^{1/2}, \tag{16}$$

where

$$\sigma = \frac{4RT\cosh^2(\xi/2)}{z^2F^2A(2D^W)^{1/2}C^{W,o}}, \tag{17}$$

$$\xi = zF(E_{dc} - E_{1/2}^r)/RT, \tag{18}$$

$$E_{1/2}^r = E^\circ + (RT/zF)\ln(D^W/D^N)^{1/2}, \tag{19}$$

and

$$\lambda = \frac{1}{zFA(D^W)^{1/2}}\left(\frac{\partial I}{\partial C^W}\right)_{dc} - \frac{1}{zFA(D^N)^{1/2}}\left(\frac{\partial I}{\partial C^N}\right)_{dc}. \tag{20}$$

Equations 15 and 16 can be rewritten as:

$$\lambda = (2\omega)^{1/2}/(r_s c_s \omega - 1). \quad (21)$$

For the sake of simplicity, we assume a simple linear kinetic equation:

$$I = zFA(\vec{k}C^W - \overleftarrow{k}C^N), \quad (22)$$

where $\vec{k}$ and $\overleftarrow{k}$ are the rate constants of the ion transfer from the aqueous to the nitrobenzene phase and from the nitrobenzene to the aqueous phase, respectively. We further assume Butler-Volmer type equations for $\vec{k}$ and $\overleftarrow{k}$:

$$\vec{k} = k_s \exp[\vec{\alpha}zF(E_{dc}-E^\circ)/RT], \quad (23)$$

$$\overleftarrow{k} = k_s \exp[-\overleftarrow{\alpha}zF(E_{dc}-E^\circ)/RT], \quad (24)$$

where k_s is the standard rate constant; $\vec{\alpha}$ and $\overleftarrow{\alpha}$ ($\vec{\alpha}+\overleftarrow{\alpha}=1$) are the transfer coefficients. Then Eq. 20 can be written as:

$$\lambda = \frac{\vec{k}}{(D^W)^{1/2}} + \frac{\overleftarrow{k}}{(D^N)^{1/2}}$$

$$= \Lambda[\exp(\vec{\alpha}\xi) + \exp(-\overleftarrow{\alpha}\xi)], \quad (25)$$

with

$$\Lambda = k_s\left(\frac{1}{(D^W)^{1/2}}\right)^{\overleftarrow{\alpha}}\left(\frac{1}{(D^N)^{1/2}}\right)^{\vec{\alpha}}, \quad (26)$$

Equation 25 can also be rewritten as:

$$\ln[\lambda/(1+\exp(-\xi))] = \ln\Lambda + \vec{\alpha}\xi. \quad (27)$$

Results and Discussion

Cyclic Voltammetry of TMA^+ Ion. Cyclic voltammograms for the transfer of TMA^+ ion across the interface between a 0.1 mol dm^{-3} LiCl aqueous solution and a 0.1 mol dm^{-3} TBATPB nitrobenzene solution were recorded, using the two-electrode cell system shown in Fig. 1, by means of the polarographic circuit shown in Fig. 3 with the ohmic drop compensation by positive feedback. Representative cyclic voltammograms are shown in Fig. 5. Reversible cyclic voltammograms were obtained when the solution resistance was compensated for by positive feedback of $\beta=1$; the positive and negative peak potentials were independent of the TMA^+-ion concentration between 0.15×10^{-3} and the 0.50×10^{-3} mol dm^{-3} and of the scan rate between 5 and 50 mV s^{-1}, and the peak separation was 60 ± 2 mV. The positive and negative peak currents, when corrected for the base current, were proportional to the TMA^+-ion concentration and to the square root of the voltage scan rate (data are not shown here). These results indicate that the two reference electrodes function as ideal non-polarized electrodes and that the ohmic drop compensation works correctly. The reversible half-wave potential, $E^r_{1/2,TMA}$ (or the midpoint potential between the positive and negative peak potentials) was determined to be 0.317 ± 0.001 V. This result agrees well with the previous result of $E^r_{1/2,TMA}=0.32$ V which was determined by potential-step chronoamperometry, cyclic voltammetry, and chronopotentiometry with a four-electrode electrochemical cell.[9]

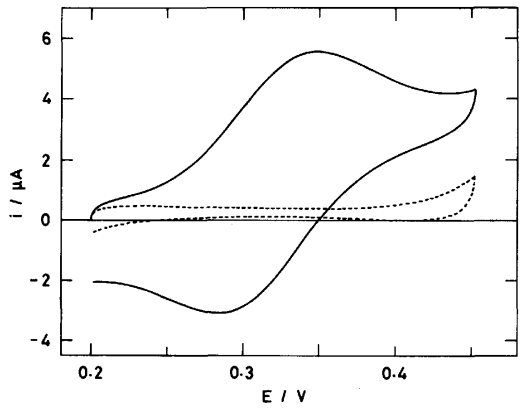

Fig. 5. Cyclic voltammogram obtained with the two-electrode cell system using the polarographic circuit as shown in Fig. 3 with positive feedback of $\beta=1$, for the transfer of 0.5×10^{-3} mol dm^{-3} TMA^+ ion from a 0.1 mol dm^{-3} LiCl aqueous solution to a 0.1 mol dm^{-3} TBATPB nitrobenzene solution at $v=5$ mV s^{-1}. Dashed line, cyclic voltammogram in the absence of TMA^+ ion.

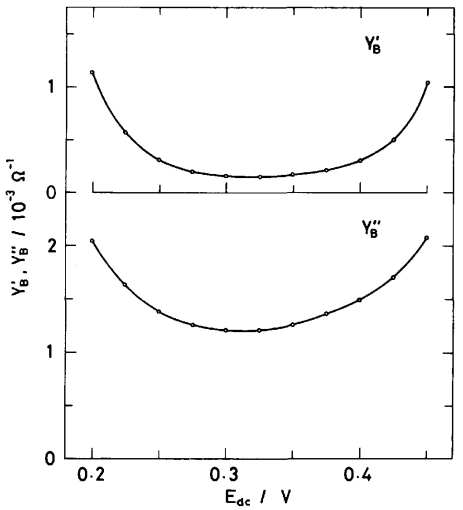

Fig. 6. Real (Y'_B) and imaginary (Y''_B) components of the base admittance at $f=50$ Hz for the interface between a 0.1 mol dm^{-3} LiCl aqueous solution and a 0.1 mol dm^{-3} TBATPB nitrobenzene solution.

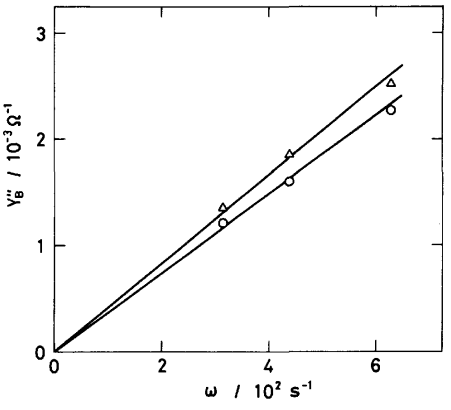

Fig. 7. Dependence of the imaginary components of the base admittance, Y''_B, on the angular frequency, ω, at $E_{dc}=0.300$ V (○) and 0.375 V (△).

Double-layer Capacity of Water/Nitrobenzene Interface. Figure 6 shows an example of Y'_B *vs.* E_{dc} and Y''_B *vs.* E_{dc} curves for the interface between a 0.1 mol dm^{-3} LiCl aqueous solution and a 0.1 mol dm^{-3} TBATPB nitrobenzene solution. Also, as seen in Fig. 7, Y''_B was proportional to ω in the frequency range between 50 and 100 Hz. From the slope of the plot of Y''_B *vs.* ω the double-layer capacity of the interface, C_{dl}, was determined by $Y''_B = A\omega C_{dl}$. The resultant C_{dl} *vs.* E curve is shown in Fig. 8. The potential of the capacity minimum, E_{min}, was about 0.30 V. This value is close to E_{min}=0.29 V reported by Samec *et al.*[15] The value of C_{dl} at E_{min}, $C_{dl,min}$, was 23.3 μF cm^{-2} , which is small compared with their 27 μF cm^{-2} (*cf.* Fig. 5 in Ref. 15).

Integration of the C_{dl} *vs.* E curve should yield the surface charge density on the water side of the interface,[8,16] q^W:

$$q^W = \int_{E_{pzc}}^{E} C_{dl}\, dE, \tag{28}$$

where E_{pzc} is the potential of zero charge. The value of E_{pzc} has been found to be 0.265 V in the present system by electrocapillary measurement.[8,16] The resultant q^W *vs.* E curve is shown in Fig. 9. Also plotted in Fig. 9 are the surface charge density data obtained from the electrocapillary measurement.[8,16] The two values of q^W obtained by the two different methods are in excellent agreement.

It has been shown that the residual current in the potential range between 0.20 and 0.45 V is mainly due to the transfer of TBA^+ and TPB^- ions across the interface.[8] However, the calculated values of Y'_B due to

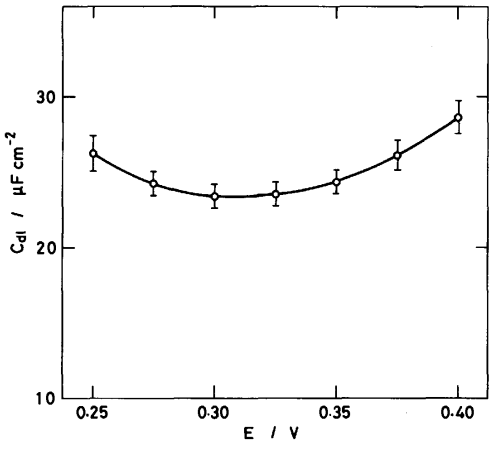

Fig. 8. Plot of the double-layer capacity, C_{dl}, against the potential, E, for the interface between a 0.1 mol dm^{-3} LiCl aqueous solution and a 0.1 mol dm^{-3} TBATPB nitrobenzene solution.

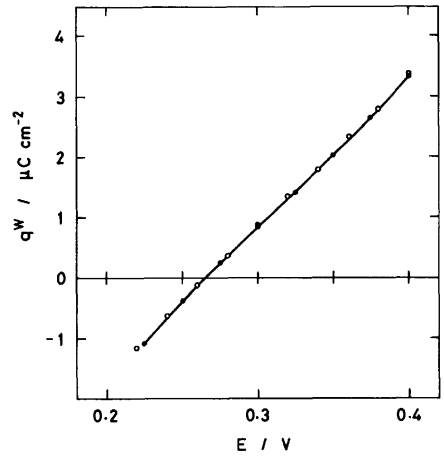

Fig. 9. Plot of the surface charge density on the water side of the interface, q^W, against the potential, E, for the interface between a 0.1 mol dm^{-3} LiCl aqueous solution and a 0.1 mol dm^{-3} TBATPB nitrobenzene solution, obtained by the integration of C_{dl} *vs.* E curve (●) and by the differentiation of the electrocapillary curve (○).[8]

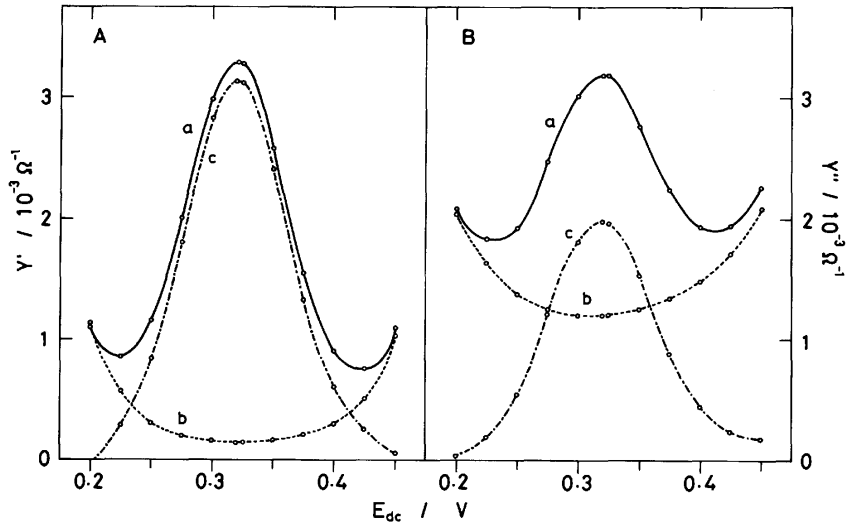

Fig. 10. Real (A) and imaginary (B) components of the admittance of the interface between a 0.1 mol dm^{-3} LiCl aqueous solution and a 0.1 mol dm^{-3} TBATPB nitrobenzene solution, at f=50 Hz, in the presence (a) and the absence (b) of 0.5×10^{-3} mol dm^{-3} TMA^+ ion in the aqueous phase. Curve c shows the ion-transfer admittance, Y'_F and Y''_F, for the TMA^+-ion transfer corrected for the base admittance.

the transfer of TBA^+ and TPB^- ion are too small to explain the observed values of Y'_B (Fig. 6); for example, the calculated value of Y'_B at 0.30 V and 50 Hz is 2.5×10^{-5} Ω^{-1}, while the observed value was 1.6×10^{-4} Ω^{-1} The reason for this discrepancy is left for further study.

Ion-transfer Impedance of TMA^+ Ion. In Fig. 10 the solid lines show representative plots of Y'_t and Y''_t *vs.* E_{dc} for the transfer of TMA^+ ion across the interface between a 0.1 mol dm^{-3} LiCl aqueous solution and a 0.1 mol dm^{-3} TBATPB nitrobenzene solution. Y'_F *vs.* E_{dc} and Y''_F *vs.* E_{dc} curves, obtained by Eqs. 2 and 3, are also shown in Fig. 10. The peak potentials of Y'_F and Y''_F coincided and were equal to 0.319 ± 0.002 V, irrespective of the frequency and the TMA^+-ion concentration, and agreed well with the reversible half-wave potential, $E^r_{1/2,TMA}=0.317\pm0.001$ V, obtained by cyclic voltammetry.

The real and imaginary components of the ion-transfer impedance, r_s and $1/\omega c_s$, at $E_{dc}=0.319$ V were calculated by Eqs. 4 and 5, and plotted against $\omega^{-1/2}$ in Fig. 11. Both plots are straight lines with a common slope, which gives $D^W_{TMA}=(1.46\pm0.05)\times10^{-5}$ cm^2 s^{-1} by Eqs. 17 and 18. This result agrees well with the previously reported value of 1.2×10^{-5} cm^2 s^{-1} determined by other electrochemical techniques.[9] Similar linear plots were also obtained for the ion-transfer impedances at several other d.c. potential in the range between 0.250 and 0.375 V.

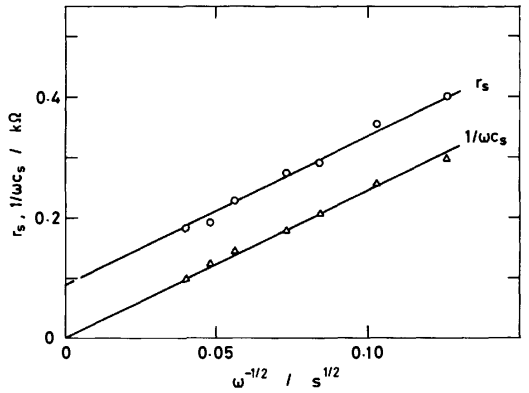

Fig. 11. Plot of the real (r_s) and imaginary ($1/\omega c_s$) components of the ion-transfer impedance against $\omega^{-1/2}$ for the transfer of 0.5×10^{-3} mol dm^{-3} TMA^+ ion at the interface between a 0.1 mol dm^{-3} LiCl aqueous solution and a 0.1 mol dm^{-3} TBATPB nitrobenzene solution at $E_{dc}=0.319$ V.

We calculated λ from r_s and $1/\omega c_s$ using Eq. 21. The results are shown in Table 1 for three different concentrations of TMA^+ ion. The figures are the average of the data obtained at seven different frequencies: 10, 15, 22.3, 30, 50, 70, and 100 Hz. As shown in this Table, λ is not very dependent on the TMA^+-ion concentration, indicating the approximate validity of the linear kinetic equation for the ion transfer (see Eq. 22).

In Fig. 12, $\ln[\lambda/(1+\exp(-\xi))]$ is plotted against ξ, giving an appreciably upward convex plot, instead of a linear or nearly linear one. Frumkin correction for the double-layer effect does not reform but rather intensifies the convex nature of the plot. Formally, this convex plot can be explained by the potential dependence of the transfer coefficients. Upon assuming that $\vec{\alpha}$ varies linearly with the potential: $\vec{\alpha}=\vec{\alpha}_0+\alpha'\xi$ so that $\overleftarrow{\alpha}=\overleftarrow{\alpha}_0-\alpha'\xi=(1-\vec{\alpha}_0)-\alpha'\xi$, where $\vec{\alpha}_0$ and $\overleftarrow{\alpha}_0$ are the transfer coefficients at $\xi=0$ and α' is the constant, the plot was fitted to Eq. 29, a modified form of Eq. 27, by adjusting three parameters, A', $\vec{\alpha}_0$ and α':

$$\ln[\lambda/(1+\exp(-\xi))] = \ln A' + \alpha'\xi \ln (D^W/D^N)^{1/2} + (\vec{\alpha}_0 + \alpha'\xi)\xi, \quad (29)$$

with

$$A' = k_s\left(\frac{1}{(D^W)^{1/2}}\right)^{\overleftarrow{\alpha}_0}\left(\frac{1}{(D^N)^{1/2}}\right)^{\vec{\alpha}_0}. \quad (30)$$

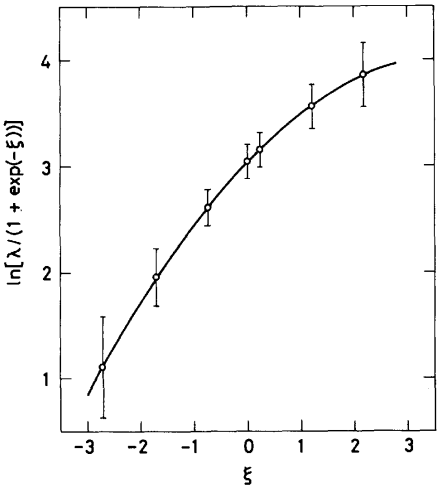

Fig. 12. Plot of $\ln[\lambda/(1+\exp(-\xi))]$ *vs.* ξ $(=zF(E_{dc}-E^r_{1/2})/RT)$. The solid line shows the regression line obtained by fitting the plot to Eq. 29. Vertical bars indicate the standard deviations.

Table 1. Dependence of λ ($s^{-1/2}$) values on the cell potential, E_{dc}, and the concentration of TMA^+ ion in the aqueous phase, $C^{W,o}_{TMA}$

E_{dc}	$C^{W,o}_{TMA}/10^{-3}$ mol dm^{-3}			
V	0.15	0.30	0.50	Mean
0.250	52.2(40.7)[a]	58.2(9.9)[a]	48.2(12.6)[a]	52.3(25.3)[a]
0.275	47.8(18.4)	50.7(5.4)	44.9(8.6)	47.8(12.2)
0.300	41.4(8.5)	45.8(3.6)	41.6(8.2)	42.9(7.1)
0.319[b]	41.2(8.6)	44.8(4.0)	40.6(7.3)	42.2(6.9)
0.325	40.4(9.1)	45.8(4.1)	40.4(7.8)	42.2(7.3)
0.350	46.9(16.0)	51.7(8.4)	43.5(6.1)	47.3(11.0)
0.375	50.6(18.5)	65.5(22.1)	50.6(7.8)	55.6(17.2)

a) The figures in parentheses are the standard deviations. b) The peak potentials: $E_p=0.319\pm0.002$ V.

Regression analysis was carried out using the SALS program[17] on the FACOM M-200 Computer in the Data Processing Center of Kyoto University. The result was $A'=20.8\pm2.1\ s^{-1/2}$, $\vec{\alpha}_0=0.55\pm0.08$, and $\alpha'=-0.067\pm0.047$ by taking $D^{W}_{TMA}=1.46\times10^{-5}\ cm^2\ s^{-1}$ and $D^{N}_{TMA}=D^{W}_{TMA}/2.07=7.05\times10^{-6}\ cm\ s^{-1}$.[18] Also k_s (the apparent standard rate constant) was tentatively determined to be 6.5×10^{-2} cm s^{-1} from A'. Further study is needed to find out whether the marked dependence of the transfer coefficents on the potential (as obtained here) is the common nature of the kinetic parameters of ion transfer at the interface of water and nitrobenzene (two immiscible electrolyte solutions), or a special case, indicating that the TMA^+-ion transfer at the 0.1 mol dm^{-3} LiCl(W)/0.1 mol dm^{-3} TBATPB(N) interface may involve complications which would require more complex equations of kinetics for the TMA^+-ion transfer in place of Eqs. 22 to 25.

In conclusion, phase-selective a.c. polarography is a promising technique for the kinetic study of the charge transfer at the interface between two immiscible electrolyte solutions.

This work was supported in part by a Grant-in-Aid from the Ministry of Education, Science and Culture.

References

1) C. Gavach, P. Seta, and F. Henry, *Bioelectrochem. Bioenerg.*, **1**, 329 (1974).
2) C. Gavach, B. d'Epenoux, and F. Henry, *J. Electroanal. Chem. Interfacial Electrochem.*, **64**, 107 (1975).
3) B. d'Epenoux, P. Seta, G. Amblard, and C. Gavach, *J. Electroanal. Chem. Interfacial Electrochem.*, **99**, 77 (1979).
4) Z. Koczorowski and G. Geblewicz, *J. Electroanal. Chem. Interfacial Electrochem.*, **139**, 177 (1982).
5) Z. Samec, V. Mareček, and J. Weber., *J. Electroanal. Chem. Interfacial Electrochem.*, **100**, 841 (1979).
6) Z. Samec, V. Mareček J. Weber, and D. Homolka, *J. Electroanal. Chem. Interfacial Electrochem.*, **126**, 105 (1981).
7) Z. Samec, D. Homolka, and V. Mareček *J. Electroanal. Chem. Interfacial Electrochem.*, **135**, 265 (1982).
8) T. Kakiuchi and M. Senda., *Bull. Chem. Soc. Jpn.*, **56**, 1322 (1983).
9) T. Kakutani, T. Osakai, and M. Senda, *Bull. Chem. Soc. Jpn.*, **56**, 991 (1983).
10) M. Senda, T. Kakutani, and T. Osakai., *Denki Kagaku*, **49**, 322 (1981).
11) R. Tamamushi, "Shin Jikken Kagaku Koza," ed by the Chemical Society of Japan, Maruzen, Tokyo (1977), Vol. 5, p. 370; K. Takahashi, S. Katayama, and R. Tamamushi, *Rikagaku Kenkyusho Hokoku*, **49**, 13 (1973).
12) D. C. Grahame, *J. Electrochem. Soc.*, **99**, 370C (1952).
13) M. Senda, *Kagaku No Ryoiki, Zokan*, **50**, 15 (1962).
14) M. Senda and P. Delahay, *J. Phys. Chem.*, **65**, 1580 (1961).
15) Z. Samec, V. Mareček, and D. Homolka, *J. Electroanal. Chem. Interfacial Electrochem.*, **126**, 121 (1981).
16) T. Kakiuchi and M. Senda, *Bull. Chem. Soc. Jpn.*, **56**, 1753 (1983).
17) T. Nakagawa and Y. Oyanagi, "SALS User's Manual," Computer Center of the University of Tokyo, 1979.
18) T. Osakai, T.Kakutani, Y. Nishiwaki, and M. Senda, *Bunseki Kagaku*, **32**, E81 (1983).

 © 1984 The Chemical Society of Japan Bull. Chem. Soc. Jpn., 57, 377—380 (1984)

Binding of 1-Decylpyridinium Bromide to Poly(vinyl sulfate)

Keishiro SHIRAHAMA* and Masatoshi TASHIRO
Department of Chemistry, Faculty of Science and Engineerig, Saga University, Saga 840
(Received September 12, 1983)

Binding of 1-decylpyridinium bromide onto poly(vinyl sulfate) in aqueous solution is measured by using a potentiometric titration method which employs propionyl-α-cyclodextrin as a neutral carrier in a 1-decylpyridinium selective electrode. Binding is highly cooperative and biphasic. The first step binding is reduced, while the second one increased on increasing added NaBr concentration. Temperaure dependence is very small giving an enthalpy of binding equal to −1.4 kJ mol^{-1}

Surfactants, a group of molecules possessing a large hydrophobic group as well as a strong hydrophilic group, show remarkable characters:[1,2] adsorption onto surfaces and aggregation into micelles. Furthermore surfactants are bound onto macromolecules, both natural and synthetic.[3,4] Recently relevant studies are being accumulated.[5–11] We also have reported binding isotherms for such systems as poly(ethylene oxide)-alkyl sulfates,[12,13] dodecyl sulfate-denatured proteins,[14] decyl sulfate-synthetic cationic polymer,[15] and DNA-1-dodecylpyridinium salt.[16] All the systems mentioned above are characterized by very marked cooperative binding: a sudden occurrence and completion of binding in a very narrow range of equilibrium concentration.

There are several methods in order to study surfactant–polymer interactions. We prefer a binding isotherm method which provides with a direct evidence of interaction and allows for thermodynamic interpretation by the aid of statistical mechanics. This kind of study can afford fundamental knowledges about interactions of various sorts of biomedical materials with biomacromolecules such as proteins and nucleic acids.

In the present study, binding of 1-decylpyridinium bromide (DePBr) to poly(vinyl sulfate) (PVS) was measured by a potentiometric titration method which employs a DeP-sensitive electrode to seek for a further understanding of the phenomena. A potentiometric method is superior to an equilibrium dialysis method in constructing a binding isotherm, because the former measures a thermodynamic activity directly and promptly, while the latter takes a very long time to reach an equilibrium followed by tedious analytical procedures, especially when a surfactant is used as a dialysate. A DeP-selective electrode prepared by using a hydrophobic cyclodextrin derivative dissolved in poly(vinyl chloride) (PVC) membrane was successfully used.[16]

Experimental

Materials. 1-Decylpyridinium bromide was synthesized by treating a fractionally distilled 1-bromodecane with dried pyridine and recrystallized from acetone three times followed by decolorization with active charcoal in a methanol solution. The critical micelle concentration as measured by an electric conductivity method is 51.6 mM† at 25 °C. Potassium poly(vinyl sulfate) (Wako Chemicals Co.) was converted into the sodium salt by dialysis in a concentrated sodium bromide solution (1 M) and then in pure water for days. The polymer solution was slightly acidic (pH 6). The sulfate content of the polymer solution was determined by a colloid titration method.[17]

Electrode. α-Cyclodextrin (Tokyo Kasei) was esterified with propionic anhydride in dried pyridine at room temperature for 1 d. Purification by precipitation with water followed by dissolution in acetone was repeated three times. The obtained white material is propionyl-α-cyclodextrin (prop-α-CD) working as a neutral carrier of the surfactant. Poly(vinyl chloride) (0.6 g), bis(2-ethylhexyl) phthalate (2.37 g), and the neutral carrier (0.03 g) are mixed well. Into the slurry mixture, 6 ml of tetrahydrofuran is added. The whole mixture is heated at 60 °C until it becomes a clear and viscous solution, which is then cast on a flat glass plate. After gradual evaporation of the solvent, the gel membrane (about 0.2 mm thick) is cut out and put on one end of a PVC tube (9 mm inner diameter and 11 cm long), where a 10% PVC tetrahydrofuran solution is a good adhesive. The electrode membrane is "annealed" at 40—50 °C under reduced pressure. A concentration cell is formed as follows:

$$\text{Calomel}\left|\begin{matrix}\text{1 M KCl}\\ \text{agar bridge}\end{matrix}\right|\begin{matrix}C_o\text{mM DePBr}\\ C_a\text{mM NaBr}\end{matrix}\Bigg|\mathbf{M}\Bigg|\begin{matrix}C_s\text{mM DePBr}\\ C_a\text{mM NaBr}\end{matrix}\left|\begin{matrix}\text{1 M KCl}\\ \text{agar bridge}\end{matrix}\right|\text{Calomel},$$

where **M** is the surfactant-selective membrane, C_S and C_O are the outer and inner surfactant concentrations respectively, and C_a is the added NaBr concentration. The polyelectrolyte concentation is usually about 1 mM residue. The potentiometric titration is carried out in a thermostated cocylindrical cell. The electromotive force (EMF) is measured with a digital voltmeter (Takeda Riken TR-6843). Asymmetric potential is usually less than ±2 mV and is not corrected for.

Results and Discussion

Figure 1 shows a relation between the EMF and logarithm of surfactant concentration. The electrode is excellently responsive from the cmc down to *ca.* 2×10^{-6} M with a slope of 58 mV per decade concentration difference at 20 °C. In the presence of 1 mM residue PVS, however, a deviation from the linearity is found suggesting that a part of surfactant is bound onto the polymer. Amount of binding, $\Delta C=C_s-C_f$ at an equilibrium concentration, C_f, is obtained by following the arrows shown. A degree of binding, X, is defined as ΔC/(total concentration of sulfate groups on polymer). A binding isotherm is constructed by plotting X against $\log C_f$.

† 1 M=1 mol dm^{-3}.

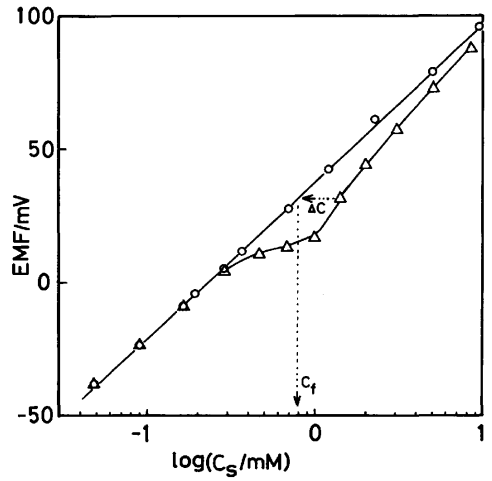

Fig. 1. Potentiogram of DePBr in 20 mM NaBr at 20°C.
○: Without polymer, △: with 1 mM PVS.

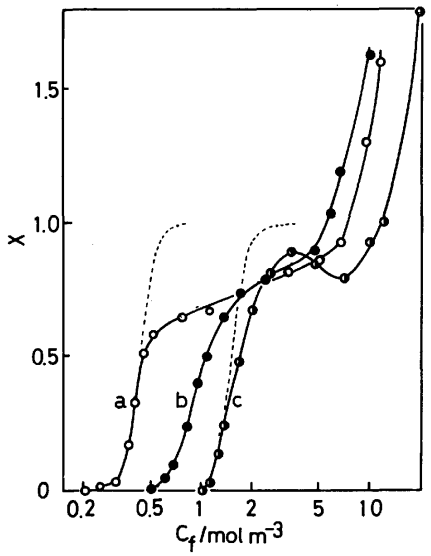

Fig. 2. Effect of added NaBr on binding isotherms at 20°C.
NaBr concentration in mM: a; 20, b; 50, and c; 100.

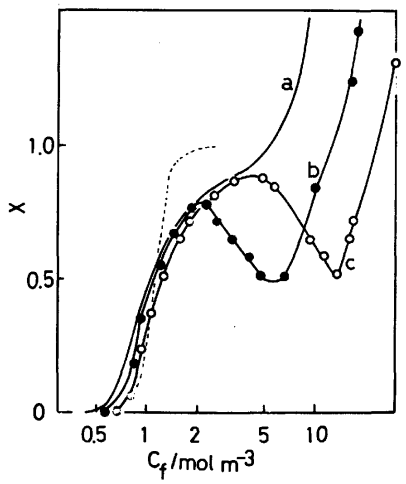

Fig. 3. Effect of temperature on binding isotherms in 50 mM NaBr.
Temperature in °C: a; 20, b; 40, and c; 50.

In Fig. 2, there are three binding isotherms in different NaBr concentrations at 20 °C. It is seen on an isotherm that there are two-step bindings: one occurring suddenly and sharply increasing until a shoulder around $X=1$, followed by another step binding. Titrated solution sometimes became turbid near $X=1$ due to neutralization of charges on the polymer and subsequent precipitation. The turbidity, however, soon disappears on further addition of surfactant. The hydrophobic precipitate is redispersed on further binding surfactants with their polar groups exposed to the bulk water phase, while their alkyl chains are in contact with the hydrophobic surfactant-polymer complex.

Now our analysis is mainly limited within the first step binding, since the second one is less reproducible probably because of the precipitation. The binding isotherm shifts right along the equilibrium concentration axis with increase in the added electrolyte concentration. This is the same tendency as we observed previously in the sodium decyl sulfate-cationic polymer system.[15] Added counterions suppress the electrostatic potential on a polyelectrolyte and reduce an affinity potential. It is a cooperative nature that the binding occurs suddenly and concludes within a very narrow range of equilibrium concentration: an already bound surfactant helps later coming surfactants bound through hydrophobic interaction between alkyl chains.

In Fig. 3, binding isotherms at three temperatures in the presence of 50 mM NaBr are shown. It is noted that isotherms slightly shift right on increasing temperature. Maxima and minima found at 40 and 50 °C: should be ascribed to precipitation mentioned above, which is apt to occur at higher temperature.

The following features are extracted from the binding isotherms semiquantitatively in accordance with the above discussion. According to the Ising's nearest neighbor interaction theory,[18] PVS may be viewed as one dimensional array of binding sites where surfactants are bound with mutual interaction. A partition function for such a system is explicitly expressed and yields a lot of important relations,[18] two of which are especially useful for the present purpose:

$$[dX/d\ln C_f]_{X=0.5} = \sqrt{u}/4, \tag{1}$$

$$K = [uC_f(0.5)]^{-1}, \tag{2}$$

where $C_f(0.5)$ is an equilibrium concentration corresponding to half binding ($X=0.5$), u the cooperative parameter, or an equilibrium constant for an aggregation process among bound surfactants, and K means a binding constant for a process that a surfactant ion is transferred from an aqueous solution phase onto an isolated binding site on a polyelectrolyte molecule. These thermodynamic parameters are obtained by fitting the lower half of the binding isotherms (actually $X<0.4$) to the theoretical formula (3), which is also derived from the original partition function.[15,18]

$$X = \frac{1}{2}\left[1 - \frac{1-s}{\sqrt{(1-s)^2+4s/u}}\right], \tag{3}$$

where $s=uKC_f$, or a kind of binding "pressure". Curve-fitting was carried out starting with an observed $C_f(0.5)$ and an assumed u, readjusting the two parameters until the best fit on a CRT display of a microprocessor was obtained. A small variation in the parameters (*ca.* 20% in u or 5% in K) results in appreciable deviation from the experimental points. Use of lower half of binding isotherm may be justified because the electrostatic potential of the polymer remains nearly constant there by the ion-condensaion effect as depicted by Manning.[19] So the Ising's theory may be applied. The calculated isotherms are plotted with dashed lines in Figs. 2 and 3. Deviation from the theoretical values at $X>0.5$ indicates a break down of the ion-condensation effect due to decreased ionization of the polyelectrolyte below a critical value predicted by the Manning's theory as a result of surfactant-binding. Electrostatic potential now is so much reduced on binding surfactants that a sort of negative cooperativity decreases actual binidng less than a theoretical one. The values of K and u are summarized in Table 1. It is a remarkable feature that u is insensitive to changes in added salt concentration as well as in temperature, albeit u contains substantial amount of uncertainty (some 30%). The insensitivity of u to added salt may be expected because a surfactant ion is discharged on binding and aggregation on polymer should be little influenced by changes in ionic atmosphere.[15] The aggregation is mainly promoted by hydrophobic interaction which usually accompanies very little thermal changes leading to a very small temperature-dependence of u values. If u is assumed to be constant then the observed variation in the binding isotherms is solely ascribed to the changes of K. The decrease in K with increasing C_a is evidently due to a diminished electrostatic potential at the polymer surface that is brought about by compression of electric double layer. Binding tendency is inversed, however, above $X=1$ where electric charges are accumulated on binding surfactant, while electric charges are reduced in the course of the first step binding. So the effect of added electrolyte on the second step binding is in the same direction as that for ordinary micelle formation in which electric charge is accumulated.

Table 1. Thermodynamic parameters

(1) Effect of added NaBr at 20 °C.

C_a/mM	20	50	100
u	200	150	150
K/M^{-1}	12	7.4	4.4

(2) Effect of temperature in 50 mM NaBr.

t/°C	20	40	50
u	150	150	150
K/M^{-1}	7.4	6.7	6.3

The values of K were calculated by using u and C_h instead of $C_f(0.5)$, where u and C_h are determined so that they give the best fit. C_h is usually about 10% smaller than $C_f(0.5)$.

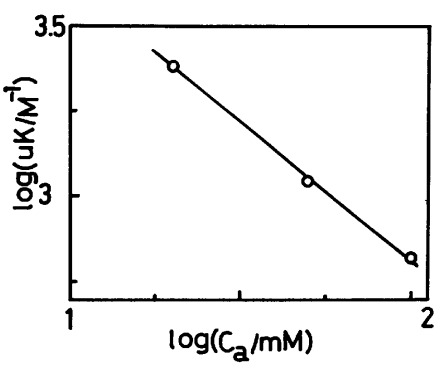

Fig. 4. Effect of added NaBr on binding affinity.

Temperature dependence of K is very small. van't Hoff plot gives an enthalpy change of the corresponding process -1.4 kJ mol^{-1} which may be a difference between exothermic discharging and endothermic rearrangement of hydration. The slightly negative enthalpy change suggests that some entropic effect also should contribute to promote the binding process.

Reciprocal of $K(K^{-1}=0.15$ M) is an equilibrium concentration that would be required to ensure a half-binding if the cooperativity were absent. In this context, it is easily understood why no binding is observed at such low C_f, *e.g.*, 0.1 mM. So it is stressed that the cooperativity is important for the binding process to appear in such a low equilibrium concentration.

A free energy of aggregation, or cooperativity, $\Delta G_u=-kT\ln(u)=-5kT$ is divided by a free energy of aggregation per methylene group, $\Delta\Delta G_u=-0.52$ kT/CH_2 which is half a difference of ΔG_u's between tetradecyltrimethylammonium and dodecyltrimethylammonium in their binding to DNA,[8] to result in 5/0.52=9.6. It is interpreted that almost all methylene groups are in action to gain cooperativity.

In Fig. 4, a $\ln(uK)$ *vs.* $\ln(C_a)$ plot shows a good linearity with a slope$=-0.81$, which is roughly interpreted as a fraction of released counterions (Na^+) having been condensed around charged sites on polyelectrolyte, when a surfactant cation is bound there. The condensed counterions are replaced with bound surfactant thus maintaining nearly constant electrostatic potential until the critical linear charge density is attained.[7,19]

References

1) K. Shinoda *et al.*, "Colloidal Surfactant," Academic Press, New York (1963).
2) E. Lucassen-Reynders, "Anionic Surfactants," Marcel Dekker, New York (1981), Surfactant Science Ser., Vol. 11.
3) J. Steinhardt and J. Reynolds, "Multiple Equilibria in Proteins," Academic Press, New York (1969), p. 234.
4) Ref. 2, p. 109.
5) G. Kresheck and W. Hargraves, *J. Colloid Interface Sci.*, **83**, 1 (1981).
6) D. Bloor and E. Wyn-Jones, *J. Chem. Soc., Faraday Trans. 2*, **78**, 657 (1982).
7) a) K. Hayakawa and J. Kwak, *J. Phys Chem.*, **86**, 3866 (1982); b) *ibid.*, **87**, 506 (1983).
8) K. Hayakawa, J. Santerre, and J. Kwak, *Biophys. Chem.*, **17**, 175 (1983).

9) I. Satake, T. Gondo, and H. Kimizuka, *Bull. Chem. Soc. Jpn.*, **52**, 361 (1979).
10) R. Chatterjee and D. Chattoraj, *Biopolymers*, **18**, 147 (1979).
11) K. Hiramatsu and J. T. Yang, *Biochim. Biophys. Acta*, **743**, 106 (1983).
12) K. Shirahama, *Colloid Polym. Sci.*, **252**, 978 (1974).
13) K. Shirahama and N. Ide, *J. Colloid Interface Sci.*,**54**, 451 (1976).
14) T. Takagi, K. Tsujii, and K. Shirahama, *J. Biochem. (Tokyo)*, **77**, 939 (1975).
15) K. Shirahama, H. Yuasa, and S. Sugimoto, *Bull. Chem. Soc. Jpn.*, **54**, 375 (1981).
16) K. Shirahama, "Microdomains in Polymer Solutions," ed by P. Dubin, Plenum Press, New York (1984), in press.
17) R. Senju, "Koroido Tekiteiho," Nankodo, Tokyo (1969).
18) G. Schwarz, *Eur. J. Biochem.*, **12**, 442 (1970).
19) G. Manning, *J. Chem. Phys.*, **51**, 924 (1969).

The Thermal Intramolecular Redox Reaction of *N,N'*-Ethylenebis(salicylideneaminato)(2,4-alkanedionato)cobalt(III) in the Solid State**

Setsuko KINOSHITA,* Kikuo MIYOKAWA, Hisanobu WAKITA, and Isao MASUDA
Department of Chemistry, Faculty of Science, Fukuoka University, Nanakuma, Jonan-ku, Fukuoka 814-01
(Received April 1, 1983)

The title complexes with the $[Co^{III}(salen)L^2]$ formula, where salen denotes *N,N'*-ethylenebis(salicylideneaminato) dianion and L^2, bidentate 2,4-alkanedionato anions, like the pent, hex, hept, or non anions,† underwent thermally induced, intramolecular one-electron transfer reaction from L^2 to Co(III) in the solid state to give $[Co^{II}(salen)]$ in a stoichiometric amount. The gaseous products evolved on the pyrolysis included 1/2 mol of free 2,4-alkanedione, corresponding to the L^2 of the complexes, per mole of the complexes. The pyrolysis reaction process was described by the contracting-disk equation for all the complexes. The rate constants increased in the following order of L^2: pent<hex<hept<non. The activation enthalpy values were found to increase in the same order. These solid-state reactions are found to be predominantly controlled by the activation entropy.

The thermally induced intramolecular electron-transfer reaction, which occurs in solid transition-metal complexes, is of interest in connection with the physical and chemical properties of such complexes. Many Co(III) complexes seem to have the potential to undergo an electron-transfer reaction from a ligand to Co(III) on heating; however, this reaction tends to be followed by complicated decomposition reactions. Hence, there are very few examples in which the redox reaction can be demonstrated to proceed stoichiometrically. For such complexes as $[Co(NH_3)_6]X_3$ ($X=Cl^-$, Br^-, I^-), $K_3[Co(C_2O_4)_3]$, and *trans*-$[Co(CH_3NH_2)_2(phbgH)_2]Cl_3$,† it has been revealed by the thermoanalytical technique that they undergo a thermally induced electron-transfer reaction from the NH_3, X, or phbgH ligands to the central Co(III) ion.[1] For the thermal dissociation of NO or O_2 from the nitrosyl or dioxygen complexes with a unitary formula, Co(III)-NO^-, Co(III)-O_2^-, or Co(III)-O_2^{2-}-Co(III), it was considered that the electron-transfer occurred from these ligands to Co(III).[2]

Podder and Biswas first prepared the series of complexes with the $[Co^{III}(salen)L^2]$ (L^2=2,4-alkanedionato) formula.[3] Subsequent investigations provided the extended series of analogous Co(III) complexes.[4] The crystal X-ray diffraction analysis of $[Co^{III}(salen)(pent)]\cdot 0.7H_2O$† has elucidated its octahedral structure, in which pent is coordinated as a bidentate ligand at the cis-position, and salen, as a tetradentate one at the remaining four positions.[5] In the present paper, the solid $[Co^{III}(salen)L^2]$ complexes are shown to undergo the thermally induced, intramolecular one-electron transfer reaction of $L^2 \rightarrow Co(III)$, affording oxygen-active crystals of $[Co^{II}(salen)]$ complex in a stoichiometric amount. Moreover, the kinetic analyses will disclose that the reaction rate is apparently dominated by the factor included in the activation entropy term.

This work was partly reported previously in *Polyhedron*, **2, 125(1983).

† The following abbreviations are used: pent, 2,4-pentanedionato; hex, 2,4-hexanedionato; hept, 2,4-heptanedionato; non, 2,4-nonanedionato anions; phbgH, phenylbiguanide; and salam, salicylideneaminato anion.

Experimental

Preparation of Complexes. The 2,4-pentanedione ligand was commercially available. The other 2,4-alkanediones were synthesized according to the literature.[6] The series of $[Co^{III}(salen)L^2]$ complexes, including newly prepared ones with L^2=hept and non, were prepared as follows: $[Co^{II}(salen)]$, obtained by following the literature method,[7] was heated with the appropriate 2,4-alkanedione in a water-acetone (2 : 3) solution on a steam bath for a few minutes. When the solution was cooled, it separated crystals; these were purified by recrystallization from chloroform. The crystals thus obtained were anhydrous; this was confirmed by thermal and elemental analyses. The crystals were hygroscopic in ordinary air and showed diamagnetism at room temperature.

Elemental analysis for $[Co(salen)L^2]$. Found, (Calcd for anhydride). For L^2=pent: C, 59.10 (59.43); H, 5.02 (4.95); N, 6.52 (6.60); Co, 13.80% (13.90%). For L^2=hex: C, 60.22 (60.28); H, 5.16 (5.29); N, 6.38 (6.40); Co, 13.38% (13.46%). For L^2=hept: C, 60.88 (61.06); H, 5.53 (5.57); N, 6.10 (6.19); Co, 12.81% (13.04%). For L^2=non: C, 62.29 (62.50); H, 6.08 (6.08); N, 5.89 (5.83); Co, 12.25% (12.28%).

The ^{1}H-NMR spectral investigation showed that the complex with L^2=pent had a "cis-β" coordination,[8] δ/ppm values of -CH=N- in the $CDCl_3$ solution: 7.80, 7.57. As for the complexes with L^2=hex, hept and non, three peaks were observed for -CH=N- in the $CDCL_3$ solution; δ/ppm: 7.82, 7.59, and 7.55 for each complex, and the δ values were not different among the three complexes. This observation suggested the two geometrical isomers, such as cis-β_1 and cis-β_2, were present.

Measurements. The TG and DTA curves were recorded in a flowing nitrogen atmosphere at a heating rate of 10 °C/min on a Rigaku Denki thermal analyzer, Model 8002. The kinetic analysis under dynamic conditions was carried out on the TG curves recorded by the use of a Sinku Riko TGD-3000-RH apparatus at a heating rate of 1 °C/min. The particle size of the samples provided for the measurements was under 200 mesh.

The powder X-ray diffractions were recorded on a Rigaku Denki Geigerflex diffractometer, using Co $K\alpha$ radiation and an iron filter.

Pyrolysis gas chromatographic (PGC) measurements[9] were made under the conditions cited in the footnote of Table 1. The calibration curves were drawn by means of the direct injection of known amounts of an appropriate, purified 2,4-alkanedione into the separation column of the

TABLE 1. THERMAL PROPERTIES OF [Co^{III}(salen)L^2]

L^2	Reaction temp/°C[a)]	Weight-loss/% Found	Weight-loss/% Calcd	Evolved HL^2 mol/mol[b)]
pent	216	23.4	23.3	0.47
hex	208	25.3	25.8	0.49
hept	204	27.8	28.1	0.50
non	203	31.7	32.3	0.50

a) Indicated the temperature at which the weight-loss amounted to one-half of the total weight-loss, *i.e.*, $\alpha=1/2$. b) PGC conditions: pyrolysis temperature, 220°C; column packing, DEGA(diethylene glycol adipate polyester); column temperature, 190°C.

instrument; the peak area was recorded on an integrator.

Results

Pyrolysis. The TG-DTA curves for the [Co^{III}(salen)L^2] complexes are shown in Fig. 1. The complexes undergo an endothermic change in the 170—230 °C range, the decrease in the weight corresponding to the elimination of one mol of L^2 per mole of the complexes. In the case of [Co^{III}(salen)(pent)], the elementary analytical results of the solid, pyrolysis product agreed with the results calculated for [Co(salen)]: Found, (Calcd): C, 58.62 (59.08); H, 4.21 (4.31); N, 8.30 (8.62); Co, 18.07% (18.12%). The effective magnetic moment μ_{eff}= 2.51 μ_B (300 K), of the product was consistent with the value, μ_{eff}=2.51 μ_B (296 K), previously reported for the authentic [Co^{II}(salen)];[10] it indicates that one unpaired electron was in the complex molecule. Moreover, the powder X-ray diffraction pattern for the resultant product agreed with that of authentic [Co^{II}(salen)], as is shown in Fig. 2. Similarly, the pyrolyses of the complexes with L^2=hex, hept, and non left behind a product that could be shown to be [Co^{II}(salen)] from the elementary analytical results and from the measurements of the magnetism and the X-ray diffraction.

The PGC analytical results clearly indicated that the gaseous products evolved by the pyrolysis included 1/2 mol of the corresponding free HL^2 per mole of the starting [Co(salen)L^2]. The data are given in Table 1. The production of free HL^2 was also indicated by the ^{1}H-NMR spectra in the DMSO-d_6 solution in which the gaseous products were trapped. In addition, when L^2=pent, the NMR spectral inspection indicated that the gaseous products included indefinite amounts of acetone, methanol and ethanol, besides the principal amount of Hpent.

From the above facts, the thermal reaction can be described as follows:

$$[Co^{III}(salen)L^2] \longrightarrow [Co^{II}(salen)] + 1/2\,HL^2 + X. \quad (1)$$

In Eq. 1, X represents a mixture of such volatile compounds as have been cited above; the further identification of X has not been undertaken here.

Kinetic Analysis. The kinetic analysis was carried out in order to ascertain the kinetic character of the reaction. As has been mentioned, the ^{1}H-NMR spectra suggested that the complexes with L^2=hex,

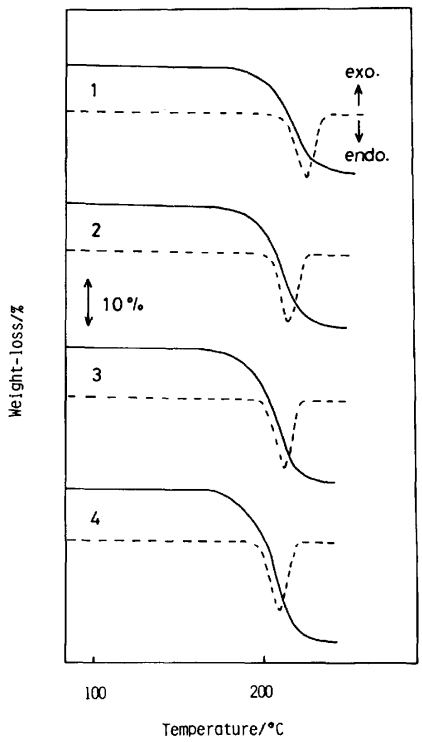

Fig. 1. TG (——) and DTA (----) curves of [Co^{III}(salen)L^2].
1: L^2=pent, 2: L^2=hex, 3: L^2=hept, 4: L^2=non.
No response appeared blow 100°C in the TG and DTA curves.

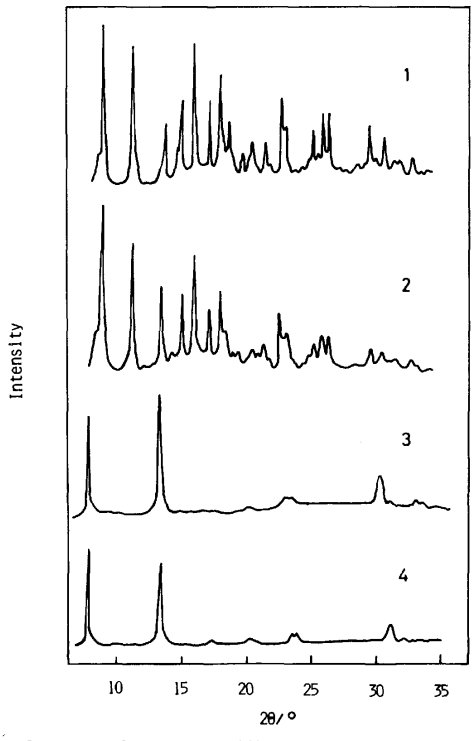

Fig. 2. Powder X-ray diffractograms.
1: [Co^{III}(salen)(pent)]·0.7H_2O, 2: [Co^{III}(salen)(pent)], 3: [Co^{II}(salen)] obtained by the pyrolysis of [Co^{III}-(salen)(pent)], 4: authentic [Co^{II}(salen)]; oxygen-active form crystal.

hept, and non in the solution existed in two isomeric forms. However, the TG and DTA curves showed only one-stage changes. Hence, it was assumed that these isomers were thermally indistinguishable in the solid state, if they were present there at all. Then, the rate plots under non-isothermal conditions were obtained by the use of Eq. 2, according to the method developed by Coats and Redfern:[11]

$$\log\{[1-(1-\alpha)^{1-n}]/T^2\} = \log\frac{AR(1-n)}{aE}\left[1-\frac{2RT}{E}\right]-\frac{E}{2.3RT}. \quad (2)$$

In Eq. 2, E is the activation energy; A, the pre-exponential factor; α, the molar fraction of [Co^{II}-(salen)]; T, the absolute temperature; R, the gas constant; a, the heating rate. Since, as is shown in Fig. 3, the rate plot of the reaction for [Co^{III}(salen)(pent)] under isothermal conditions was found to fit the contracting-disk equation, $1-(1-\alpha)^{1/2}=kt$ (k, the rate constant; t, the reaction time), n in Eq. 2 is replaced with a value of 1/2. Then, the rate plot, *i.e.*, the $\log\{[1-(1-\alpha)^{1/2}]/T^2\}$ *vs.* $1/T$ plot, gives a straight line, as is shown in Fig. 4. These facts indicate that the reaction fits the contracting-disk equation well for all the complexes investigated. The E and A values were calculated from, respectively, the slope and the intercept of these straight lines. For the sake of comparison, it is desirable to normalize the rate constants to those at a definite temperature. Therefore, the rate constants at 460 K were calculated from the Arrhenius equation, $k=A\exp(-E/RT)$, by using the above E and A values. The activation enthalpy ΔH^* value was calculated from the $\Delta H^*=E-RT$ relation; while the activation entropy ΔS^* value was obtained from Eq. 3, assuming the transmission coefficient κ to be 1;

$$\Delta S^* = R[\ln(Ah/\kappa kT) - 1]. \quad (3)$$

In Eq. 3, k is the Boltzman constant, and h, the Planck constant. The kinetic characteristics are tabulated in Table 2.

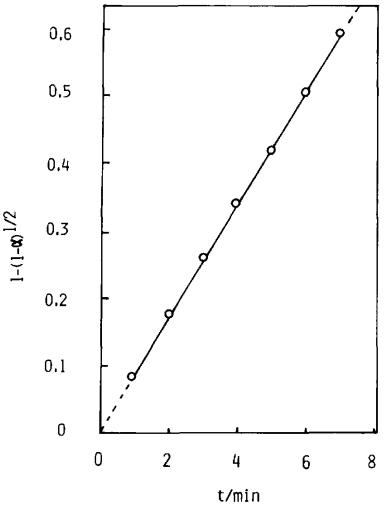

Fig. 3. Rate plots for thermal reaction of [Co^{III}-(salen)(pent)] under isothermal conditions. α; 0.17—0.84.

Discussion

It was shown by the mass spectrometric investigation that, upon pyrolysis, [$Co^{III}(pent)_3$] evolved gaseous products, including principally acetone and CO_2;[12] the redox process of the reaction was not elucidated, however. On the pyrolysis of the [Co^{III}(salen)L^2] complexes, the thermally induced one-electron transfer reaction, $L^2\rightarrow$Co(III), obviously occurred, producing [Co^{II}(salen)] and HL^2 in stoichiometric amounts, as is represented by Eq. 1. As may be seen in Fig. 2, the powder X-ray diffractogram of the anhydrous crystal of [Co^{III}(salen)(pent)], which was prepared here and subjected to pyrolysis, is almost entirely consistent with the diffractogram of the 0.7 hydrate crystal, for which crystal-structure analysis has been performed.[5] The other anhydrous crystals of the complexes investigated also showed well-defined diffractograms, although their crystal systems were not determined. For all the [Co^{III}(salen)L^2] complexes, the pyrolysis left behind [Co^{II}(salen)], which showed a diffraction pattern agreeing with that of authentic [Co^{II}(salen)]. Hence, it can be said that the thermal reaction described by Eq. 1 proceeds accompanied by a crystal-structure change in the pair of [Co^{II}(salen)] and respective [Co^{III}(salen)L^2].

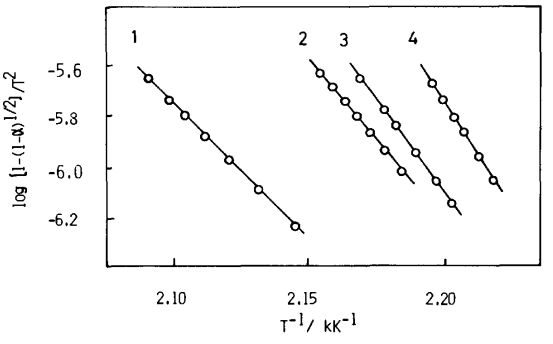

Fig. 4. Rate plots for thermal reactions of [Co^{III}-(salen)L^2] under non-isothermal conditions. 1: L^2=pent, 2: L^2=hex, 3: L^2=hept, 4: L^2=non.

Table 2. Kinetic data of thermal reactions of [Co^{III}(salen)L^2]

L^2	E/kJ mol^{-1}	log(A/s^{-1})	k(460 K)/s^{-1}	ΔH^*(460 K)/kJ mol^{-1}	ΔS^*(460 K)/J K^{-1} mol^{-1}
pent	197±3	18.7±0.5	(2.00±0.72)×10^{-4}	193±3	101±9
hex	231±6	23.4±0.6	(1.38±0.27)×10^{-3}	227±6	190±11
hept	256±9	26.6±0.9	(3.09±0.92)×10^{-3}	252±9	252±17
non	302±11	32.2±1.4	(7.75±2.45)×10^{-3}	298±11	359±26

E, Activation energy; A, pre-exponential factor; k, rate constant; ΔH^*, activation enthalpy; ΔS^*, activation entropy.

The volatile pyrolytic products consisting of HL^2 and other compounds are considered to diffuse through the system as rapidly as that the pyrolytic reaction can be described by only one equation, *i.e.*, the contraction-disk equation, over the range of α=0.17—0.84. In such cases as the thermal pyridine dissociation of Ni[*N*-(*p*-CH_3-C_6H_4)salam]$_2$(py)$_2$[†], the reaction proceeds, following the contracting-disk equation in the earlier stage of the reaction, α=0—0.35, and according to Jandar's equation in the later stage, α=0.35—0.75. This later stage of the reaction was interpreted as showing that the diffusion of the liberated pyridine was slow enough to be observed.[13]

The production of HL^2 can be explained as follows. The thermally induced, homolytic fission of the L^2-Co(III) bond causes a concomitant L^2→Co(III) one-electron transfer to form the $\cdot L^2$ radical; this derives a hydrogen atom from another $\cdot L^2$ radical to produce HL^2; the dehydrogenated $\cdot L^2$ radical decomposes into lower molecular compounds; these are represented by X in Eq. 1. It is noteworthy that HL^2 was produced quantitatively through such a reaction as occurs in the solid phase. The crystals of the [Co(salen)(pent)]$\cdot 0.7H_2O$ complex belong to the $P2_12_12_1$ space group, suggesting that, in these crystals, two complex molecules are packed as if they were a pair. In the anhydrous crystals, the molecular packing is considered not to be remarkably changed, as is indicated by the powder X-ray diffractograms shown in Fig. 2. Therefore, it may be speculated that this molecular arrangement, forming a pair as above, causes the reaction to proceed stoichiometrically, yielding one mole of Hpent from two moles of [Co(salen)(pent)]. Although the crystal structures for the other complexes have not yet been elucidated, a crystal structure analogous to that of [Co(salen)(pent)] might be suggested from their stoichiometric formation of HL^2.

As may be seen from the above discussion, the kinetic data apparently correspond to the change depicted by Eq. 4;

$$[Co^{III}(salen)L^2]\ (crystal) \rightarrow [Co^{II}(salen)]\ (crystal). \quad (4)$$

In Eq. 4 three processes are involved; i) the bond cleavage of L^2-Co(III), which occurs with a concomitant L^2→Co(III) electron-transfer, ii) the rearrangement in the coordination geometry from octahedron to square-plane, and iii) the change in the crystal packing from that of [Co^{III}(salen)L^2] to that of [Co^{II}-(salen)]. In the following argument, the effect on the kinetic data arising from the difference in the crystal packing of the starting complexes is assumed to be negligible among the complexes of the present series.

Generally speaking, the k value in most reactions decreases as the $\Delta H^{\ddagger}$ value increases. In the present complexes, the L^2-Co(III) bond can be expected to be more strengthened when the alkyl group substituted on L^2 has a longer chain; the electron-donating property (I-effect) of the alkyl group acts to increase the electron density on the O-atom in L^2 and hence, to strengthen the L^2- Co(III) coordination bond. Therefore, the complex with a longer chain alkyl group on L^2 can be expected to have larger $\Delta H^{\ddagger}$ values and smaller k values. Actually, however, the reaction

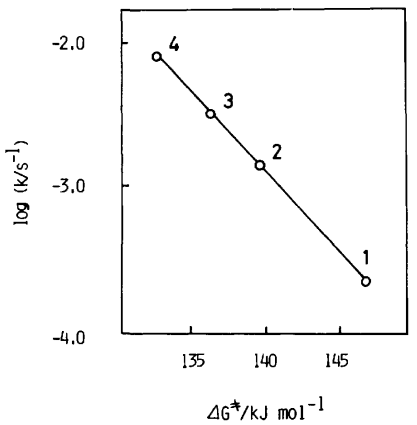

Fig. 5. Relation between log k and $\Delta G^{\ddagger}$ values at T= 460 K.
1: L^2=pent, 2: L^2=hex, 3: L^2=hept, 4: L^2=non.

examined here did not occur along these lines. That is, whereas the $\Delta H^{\ddagger}$ value increased in the order of L^2, pent<hex<hept<non, as predicted, the k value increased in the same order; this is numerically demonstrated in Table 2. This finding led us to consider that the activation entropy might involve a factor favoring the occurrence of these solid-state reactions. The $\Delta S^{\ddagger}$ value calculated in the case of a complex with L^2=non is *ca.* 3.5 times larger than that with L^2=pent. Therefore, for the complex with L^2=non, the $\Delta G^{\ddagger}$(=$\Delta H^{\ddagger}-T\Delta S^{\ddagger}$) value comes to be smallest and the k value, largest, among the complexes investigated; this relation between the $\Delta G^{\ddagger}$ value and the nature of L^2 is shown in Fig. 5.

As Table 2 shows, the $\Delta S^{\ddagger}$ value of the reaction is positive and rather large. This fact is not contrary to the assumption that the reaction rate is predominantly determined not by the electron-transfer, but by the L^2-Co(III) bond-cleavage reactions. In the transient structure, if the electrons participating in the L^2-Co(III) bonding were withdrawn toward the Co atom, this structure might have a lower entropy than usual. On the other hand, if the L^2-Co(III) bond were relaxed, this structure might have an increased entropy due to the increased freedom of L^2. By accepting the latter transient structure, it could be understood that the $\Delta S^{\ddagger}$ value of the reaction for the complex with L^2=non is larger than that for the complex with L^2=pent. In conclusion, L^2 ligands with longer alkyl chains cause the solid-state reaction of the complexes examined here to occur more easily through the entropic factor.

The crystalline [Co^{II}(salen)] complex obtained by the pyrolysis took up oxygen in a dry air or an oxygen atmosphere at room temperature. The O_2-adduct liberated oxygen endothermally at *ca.* 65 °C, thus decreasing the weight by 4.8%; this indicated that the composition of the adduct was [Co(salen)]$_2\cdot O_2$. There have appeared in the literatures two crystalline forms of the [Co^{II}(salen)] complex; one is active, and the other, inactive, toward oxygen-uptake;[7] the active form takes up oxygen reversibly in a molar ratio of Co(II) : O_2= 2 : 1. It has also been reported that the pyrolysis of the solid [Co^{II}(salen)(py)] or [Co^{II}-

(salen)($CHCl_3$)] leaves behind the oxygen-active complex of [Co^{II}(salen)].[14]

References

1) W. W. Wendlandt, *J. Inorg. Nucl. Chem.*, **25**, 1267 (1963); **25**, 545 (1963); G. W. Watt, *Inorg. Chem.*, **3**, 325 (1964); N. Tanaka and M. Nanjo, *Bull. Chem. Soc. Jpn.*, **37**, 1330 (1964); **40**, 330 (1967); **41**, 1143 (1968); Y. Ihara, A. Uehara, R. Tsuchiya, and E. Kyuno, *ibid.*, **51**, 2578 (1978); Y. Fujii and S. Takahashi, 37th National Meeting of the Chemical Society of Japan, Yokohama, April 1978, Abstr. No. 1 J26; Relf. 9a).

2) H. Masuda, K. Miyokawa, and I. Masuda, *Bull. Chem. Soc. Jpn.*, submitted for publication.

3) S. N. Poddar and D. K. Biswas, *J. Inorg. Nucl. Chem.*, **31**, 565 (1969).

4) R. J. Cozens and K. S. Murray, *Aust. J. Chem.*, **25**, 911 (1972); K. Dey and R. L. De, *Z. Anorg. Allg. Chem.*, **402**, 120 (1973); Y. Fujii, *Bull. Chem. Soc. Jpn.*, **43**, 1722 (1970).

5) M. Calligaris, G. Nordin, and L. Randaccio, *J. Chem. Soc., Chem. Commun.*, **1970**, 1079; M. Calligaris, G. Manzini, G. Nardin, and L. Randaccio, *J. Chem. Soc., Dalton Trans.*, **1972**, 543.

6) J. T. Adams and C. R. Hauser, *J. Am. Chem. Soc.*, **66**, 1220 (1944); R. Revine, J. A. Conroy, J. T. Adams, and C. R. Hauser, *J. Am. Chem. Soc.*, **67**, 1510 (1945).

7) T. Tsumaki, *Bull. Chem. Soc. Jpn.*, **13**, 252 (1938).

8) Diane Cummins, Brian M. Higson, and E. Donald Mckenzie, *J. Chem. Soc., Dalton Trans.*, **1973**, 1359.

9) a) K. Miyokawa, H. Masuda, and I. Masuda, *Bull. Chem. Soc. Jpn.*, **53**, 3573 (1980); b) K. Miyokawa, N. Abe, and I. Masuda, *J. Inorg. Nucl. Chem.*, **43**, 2791 (1981); *Bull. Chem. Soc. Jpn.*, **55**, 3647 (1982).

10) M. Calvin and C. H. Barkelew, *J. Am. Chem. Soc.*, **68**, 2267, (1946).

11) A. W. Coats and J. P. Redfern, *Nature(London)*, **201**, 68 (1964).

12) J. von Hoene, R. G. Charles, and W. M. Hickam, *J. Phys. Chem.*, **62**, 1098 (1958); **63**, 2084 (1959).

13) K. Miyokawa, H. Hirashima, and I. Masuda, *Bull. Chem. Soc. Jpn.*, **55**, 104 (1982).

14) R. H. Bailes and M. Calvin, *J. Am. Chem. Soc.*, **67**, 1886, (1947).

The Reactions of (Trichlorostannato)rhodates(III) with Trichlorostannate(II) in Hydrochloric Acid Solutions

Shigemi Iwasaki,* Takashi Nagai, Eiichi Miki, Kunihiko Mizumachi, and Tatsujiro Ishimori
Department of Chemistry, College of Science, Rikkyo University, Nishi Ikebukuro 3, Toshima-ku, Tokyo 171
(Received May 23, 1983)

(Trichlorostannato)rhodate(III) complexes, $[(CH_3)_4N]_3[RhCl_n(SnCl_3)_{6-n}]$ (n=2, 3, and 4), reacted with tin(II) in hydrochloric acid solutions to form a purple species. This purple species is assumed to be $[Rh^I(SnCl_3)_5]^{4-}$. The formation reaction of the purple species involved two independent paths, fast and slow paths. The main path was the fast one, in which the reactant mixture was in equilibria among $[RhCl_3(SnCl_3)_3]^{3-}$, $[RhCl_2(SnCl_3)_4]^{3-}$, $[RhCl(SnCl_3)_5]^{3-}$, and probably $[Rh(SnCl_3)_6]^{3-}$. The reaction orders in the formation of the purple species were 1, 2, and −2 with respect to the concentrations of the total rhodium(III) complexes, $SnCl_3^-$, and Cl^- respectively. The absorpton spectra of the reactant mixture showed an interaction absorption between $[RhCl_2(SnCl_3)_4]^{3-}$ and $SnCl_3^-$.

A series of six-coordinated (trichlorostannato)rhodate(III) complexes, $[(CH_3)_4N]_3[RhCl_n(SnCl_3)_{6-n}]$, where n=2, 3, and 4, have been prepared by Kimura.[1] The presence of $[RhCl(SnCl_3)_5]^{3-}$ (the pentakis complex) was confirmed in tin(II)–hydrochloric acid solutions by the use of Sn-119 NMR.[2] The complexes react with an excess of tin(II) in a hydrochloric acid solution to form a purple solution. In this paper, tentatively assuming the purple species in the solution to be $[Rh^I(SnCl_3)_5]^{4-}$, we will report an equilibrium mixture of the (trichlorostannato)rhodates(III) in tin(II)–hydrochloric acid solutions and the formation of the purple species from the equilibrium mixture.

Experimental

Materials. The rhodium(III)–trichlorostannato complexes (the rhodium(III) complexes), $[(CH_3)_4N]_3[RhCl_n(SnCl_3)_{6-n}]$, where n=2 and 3, were prepared by the methods of Kimura.[1] Reagents of a special grade were used.

Reaction Solution. The reaction solution was prepared by dissolving $[(CH_3)_4N]_3[RhCl_3(SnCl_3)_3]$ (the tris complex) or $[(CH_3)_4N]_3[RhCl_2(SnCl_3)_4]$ (the tetrakis complex) in a freshly prepared tin(II)–hydrochloric acid solution to give 2×10^{-4} mol dm^{-3}. The concentrations in the tin(II)–hydrochloric acid solution were adjusted to $[H^+]_{total}+[Li^+]_{total}$=3.0 mol dm^{-3}, $[Cl^-]_{total}+[ClO_4^-]_{total}$=3.4 mol dm^{-3}, and $[Sn^{II}]_{total}+[Zn^{II}]_{total}$=0.2 mol dm^{-3} by using zinc chloride, lithium chloride, and perchloric acid solutions respectively. In order to avoid the air oxidation of Sn^{II} in the reaction solution, a quartz cell was filled with the reaction solution and stoppered without any empty space, the stopper was then wrapped two-fold with polyethylene sheets. The concentration of Sn^{II} in the cell did not decrease more than a few per cent within 2 or 3 d. The total concentrations of Sn^{II} and Rh^{III} were determined in each run.

Measurements. The spectral change in the reaction solution was measured with a HITACHI 340 spectrophotometer equipped with a thermospacer cell compartment. The temperature of the reaction solution in the cell was thermostated at 25.0±0.3, 40.0±0.1, and 55.0±0.3 °C. A micro-computer was connected to the spectrophotometer to memorize the absorption curves at predetermined times and to calculate the rate constants by the method of least squares.

Kinetic Measurements. Figure 1 shows a typical example of the spectral change in the reaction solution. The absorptions at 402 and 560 nm were used independently for the kinetic analyses. Since Sn^{II}, Cl^-, and H^+ were in a large excess of the rhodium(III) complex, the pseudo-first-order method was used for the analyses. Because the absorption at 560 nm originated only from the product, the purple species, the change in the absorption at 560 nm(A_{560}) was used to determine the pseudo-first-order rate constant ($k_{obsd}(560)$) according to Eq. 1:

$$d(A_{560})/dt = k_{obsd}(560)\cdot(A_{560,\infty} - A_{560}). \quad (1)$$

When absorption curves during the reaction were corrected for the contribution of the purple species, the absorption curves showed a maximum around 402 nm. The corrected absorption at 402 nm(A_{402}) was assumed to be proportional to the total concentration of the rhodium(III) complexes, which were in rapid equilibria with each other; A_{402} was also used to determine the pseudo-first-order rate constant, $k_{obsd}(402)$, according to Eq. 2:

$$-d(A_{402})/dt = k_{obsd}(402)\cdot(A_{402}). \quad (2)$$

The spectral change at 402 nm was much greater than that at any other wavelength.

To determine the dependences of k_{obsd} on $[Sn^{II}]$ and $[H^+]$, $[Sn^{II}]_{total}$ was changed over the range of 0.02—0.06 mol dm^{-3} and $[H^+]_{total}$, over that of 0.25—3.0 mol dm^{-3}. The total concentration of Cl^- was changed over the range of 1.8—4.5 mol dm^{-3}. However, since the formation of the purple species was inhibited somewhat by the presence of perchloric acid, and since the reaction proceeded in a different way for $[HClO_4]$> 1.8 mol dm^{-3}, lithium chloride was added to the reaction solution, ignoring the increase in ionic strength in the cases of $[Cl^-]_{total}$>3.4 mol dm^{-3}.

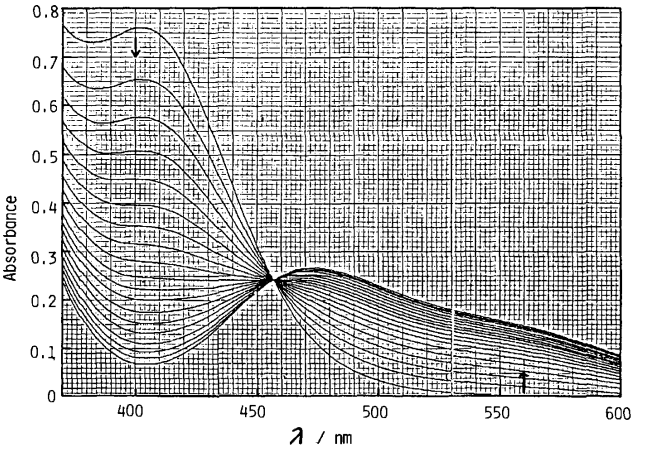

Fig. 1. An example of the spectral change of the reaction solution at 40.0 °C. $[Rh]_{total}=7.45\times10^{-5}$ mol dm^{-3}, $[Sn^{II}]_{total}$=0.0568 mol dm^{-3}

Results and Discussion

Reaction Product. The spectrum of the purple solution has been well established. The purple species can be assumed to be $[Rh(SnCl_3)_5]^{3-}$ (the rhodium(I) complex) on the basis of the complex salt obtained from the purple solution, $[Rh^{III}(NH_3)_6][Rh^{I}(SnCl_3)_4(SnCl_4)]\cdot[SnCl_6]\cdot 4H_2O$,[3] and on the basis of Sn-119 NMR studies of the Rh^{III}–Sn^{II} system in a hydrochloric acid solution.[2]

Reactants. Figure 2 shows an example of the conventional plots of the change in the absorptions at 402 and 560 nm. Two independent reaction paths, fast and slow ones, were generally observed under the conditions of $[Sn^{II}]_{total}>0.02$ mol dm^{-3}. The formation of the rhodium(I) complex through the slow path was only a few per cent, and its rate constant could not be determined accurately. Therefore, data on the slow path were used mainly for determining accurately the pseudo-first-order rate constant of the fast path.

Some of the kinetic results at 40.0 °C are listed in Table 1. In each run, $k_{obsd}(560)$ agrees with $k_{obsd}(402)$ within the limits of experimental error. This supports

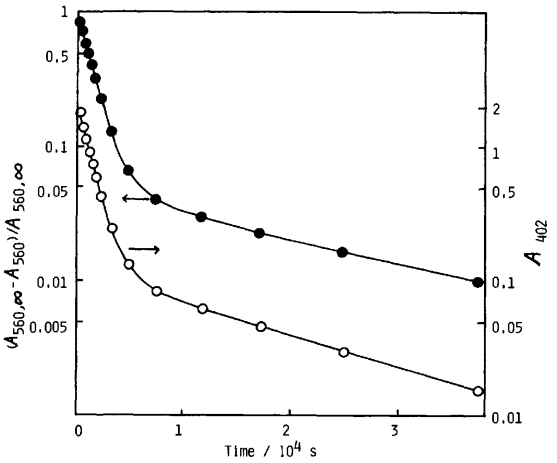

Fig. 2. The change in the absorptions at 402 and 560 nm.
log A_{402} *vs.* time(○), and log $(A_{560,\infty}-A_{560})/A_{560,\infty}$ *vs.* time(●). $[(CH_3)_4N]_3[RhCl_3(SnCl_3)_3]$ was dissolved at 55.0 °C. $[Rh]_{total}=1.96\times10^{-4}$ mol dm^{-3}, $[Sn^{II}]_{total}=0.0574$ mol dm^{-3}.

the assumption on the absorption at 402 nm in the Experimental section. When the absorption curves during the reaction were corrected for the contributions of the rhodium(I) complex and of the reaction mixture involved in the slow path and were expressed as the molar absorption curves with respect to the total rhodium(III) complexes involved in the fast path, all the absorption curves gave almost the same curve in a kinetic run except during the last period of the reaction. However, the curve did not agree with the absorption curves of the tris complex nor with that of the tetrakis complex, and it varied with such reaction conditions as $[Sn^{II}]_{total}$.

It is reasonable to consider that equilibria among the rhodium(III) complexes are present in relation to $[Sn^{II}]_{total}$, that one of the rhodium(III) complexes is the true reactant, and also that the equilibria are established rapidly enough for the rate of the reaction. The total rhodium(III) complexes in equilibria will hereafter be called "the yellow species" (Y); especially, the yellow species involved in the fast reaction path will be abbreviated as Y_I. The mean molar-absorption coefficients of Y_I, $\varepsilon(Y_I)$ were much greater than the molar-absorption coefficients of $[(CH_3)_4N]_3[RhCl_3(SnCl_3)_3]$ (the tris complex) or $[(CH_3)_4N]_3[RhCl_2(SnCl_3)_4]$ (the tetrakis complex), as is shown in Fig. 3. Furthermore, the absorptions of the pentakis and the hexakis complex are not expected to be large enough to explain the absorptions of Y_I. The molar-absorption coefficients of Y_I can be explained on the basis of the interaction absorption between $SnCl_3^-$ and the tetrakis complex, Y_4. The interaction absorption, IA, per mole of Y_4 can be defined as Eq. 3:

$$IA = \varepsilon(Y_I) - \varepsilon(Y_4), \quad (3)$$

where $\varepsilon(Y_I)$ is the mean molar-absorption coefficient of Y_I, and $\varepsilon(Y_4)$ is the molar-absorption coefficient of the tetrakis complex. Plots of IA at 402 nm *vs.* $[SnCl_3^-]$ are shown in Fig. 4. The values of $[SnCl_3^-]$ were calculated as will be described below. In Fig. 4, there is a linear relationship by which the straight line passes through the point of origin, the molar-absorption coefficient of Y_4. The relationship held at the other wavelengths as well. It is certain that these relationships are caused by the interaction absorption. It is also indicated that the tetrakis complex is the predominant species among the

TABLE 1. THE PSEUDO-FIRST-ORDER RATE CONSTANTS at 40.0±0.1 °C

Complex[a] (M=$[(CH_3)_4N]$)	$[Sn^{II}]_{total}$ / mol dm^{-3}	$k_{obsd}(560)$ / 10^{-4} s^{-1}	$k_{obsd}(402)$ / 10^{-4} s^{-1}
$M_3[RhCl_3(SnCl_3)_3]$	0.0197	0.442±0.001	0.401±0.006
	0.0280	1.42±0.00	1.41±0.00
	0.0288	1.38±0.16	1.27±0.01
	0.0449	3.08±0.01	3.03±0.01
	0.0568	5.23±0.09	5.19±0.04
$M_3[RhCl_2(SnCl_3)_4]$	0.0173	0.424±0.003	0.425±0.002
	0.0256	0.968±0.004	0.974±0.005
	0.0378	2.37±0.01	2.50±0.03
	0.0587	6.13±0.61	5.82±0.35

a) The complex used to prepare the reaction solution. Reaction solution: [HCl]=3.0 mol dm^{-3}. $[Sn^{II}]+[Zn^{II}]=0.2$ mol dm^{-3}.

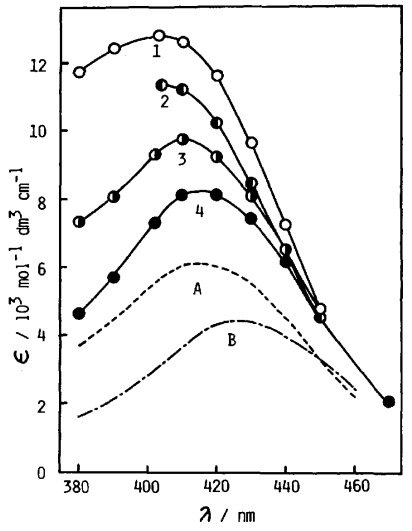

Fig. 3. The mean molar absorption coefficient of Y$_I$. $[(CH_3)_4N]_3[RhCl_3(SnCl_3)_3]$ was dissolved at 40.0°C in Sn^{II} solutions of various concentration of Sn^{II}: $[Sn]_{total}$/mol dm^{-3}; (1) 0.0568, (2) 0.0449, (3) 0.0280, (4) 0.0197. Spectrum of $[RhCl_2(SnCl_3)_4]^{3-}$ (A), and that of $[RhCl_3(SnCl_3)_3]^{3-}$ (B) were taken from Ref. 1.

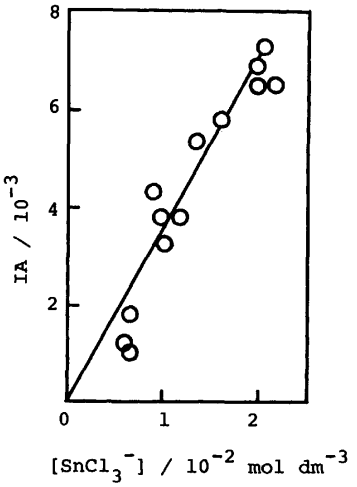

Fig. 4. The interaction absorption between the tetrakis complex and $SnCl_3^-$. $K_a(HSnCl_3)$=2. The absorptions at 402 nm were used.

rhodium(III) complexes in these reaction solutions.

The interaction absorption in Sn^{II}-Sn^{IV} in a hydrochloric acid solution[4] has been assumed to occur through a Cl^- bridge between Sn^{II} and Sn^{IV}.[5] The Mössbauer spectra of the rhodium(III) complexes suggested that the cooridnating Sn atoms were rather more similar to Sn^{IV} than to Sn^{II}.[1] Accordingly, the interaction absorption between $[RhCl_2(SnCl_3)_4]^{3-}$ and $SnCl_3^-$ in the reaction solution can be considered to occur with an associated species such as $[(SnCl_3)_3Cl_3RhSnCl_3{-}{-}SnCl_3]^{4-}$.

Rate Law. In Fig. 5, the logarithm of the means of k_{obsd}(560) and k_{obsd}(402), namely, k_{obsd}, are plotted against the total concentration of Sn^{II}. In the figure, the k_{obsd}'s for the reaction solutions prepared by dissolving the tris complex or the tetrakis complex are distributed on the same line. This also confirms the idea regarding the yellow species in the equilibria. The slopes of the

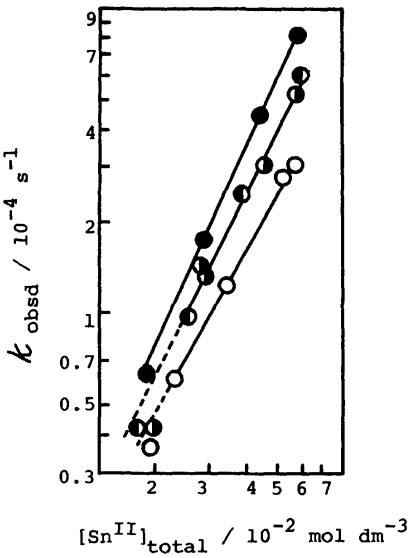

Fig. 5. The effect of $[Sn^{II}]_{total}$ on k_{obsd}.
○: 25.0°C, the starting materials (s.m.)=the tris complex, ◑: 40.0°C, s.m.=the tris complex, ◐: 40.0°C, s.m.=the tetrakis complex, ●: 55.0°C, s.m.=the tris complex.

lines were 1.82±0.02 at 25.0°C, 2.03±0.06 at 40.0 °C, and 2.31±0.02 at 55.0°C. The slopes increased with an increase in the temperature.

The slope for the plot of log k_{obsd} *vs.* log $[Cl^-]_{total}$ at 40.0°C was −2.0. Since the total concentration of Sn^{II} could not be kept absolutely constant in the series of experiments, the rate constants, k_{obsd}'s, obtained were corrected according to the dependence on the concentration of Sn^{II} described above. As perchlorate ions inhibited the progress of the formation of the rhodium(I) complex, the concentration of Cl^- was not changed over a wide range; the ionic strengths of the reaction solutions used ranges from 3.60 to 4.68 mol dm^{-3}. In order to examine the effect of the ionic strength, the solutions with the following compositions were compared: Soln A; [LiCl]=2.75 mol dm^{-3}, [HCl]=0.25 mol dm^{-3}, $[Cl^-]_{total}$=3.4 mol dm^{-3}, $[Sn^{II}]_{total}$= 0.038 mol dm^{-3}, $[Zn^{II}]_{total}$=0.16 mol dm^{-3}, I(ionic strength)=3.6 mol dm^{-3}. Soln B; $[CaCl_2]$= 1.375 mol dm^{-3}, [HCl]=0.25 mol dm^{-3}, $[Cl^-]_{total}$= 3.4 mol dm^{-3}, $[Sn^{II}]_{total}$=0.038 mol dm^{-3}, $[Zn^{II}]_{total}$= 0.16 mol dm^{-3}, I=4.98 mol dm^{-3}. The A and B solutions had the same concentrations of Cl^- and Sn^{II}, but different ionic strengths. The k_{obsd} was 6.7×10^{-4} s^{-1} for the A solution and 7.0×10^{-4} s^{-1} for the B. Consequently, the variation in the ionic strength to such an extent had little effect on k_{obsd}. The dependence was −1.95±0.04 for $[Cl^-]_{total}$ in the range from 2.55 to 4.47 mol dm^{-3}.

The slope for the plot of log k_{obsd} *vs.* log $[H^+]_{total}$ at 40.0 °C was −0.40±0.03. The corrections for slight variations in $[Sn^{II}]_{total}$ were made similarly to the case of the $[Cl^-]$ dependency.

A kinetic run was carried out in the presence of 1600 times as much $[Sn^{IV}]$ as [Rh^{III} complex]$_{total}$. The observed rate constant for the fast reaction path, k_{obsd}, was not influenced by the presence of $[Sn^{IV}]$; this suggested that the redox equilibrium, Rh^{III}+

$Sn^{II} \rightleftarrows Rh^{I} + Sn^{IV}$, was not involved in the processes before the rate-determining step.

These results for the fast reaction path at 40.0 °C can be summarized as in Eq. 4:

$$k_{obsd} \propto [Sn^{II}]^{2.0}_{total}[Cl^-]^{-2.0}_{total}[H^+]^{-0.4}_{total}[Sn^{IV}]^{0}_{total}. \quad (4)$$

We attemped to express the rate law in terms of the concentrations of definite species instead of the total concentrations. Since $SnCl_3^-$ behaved as a ligand, the concentraion of $SnCl_3^-$ was used in place of the total concentraion of Sn^{II}. In the calculation, the formation constants of $ZnCl^+$, $ZnCl_2$, and $ZnCl_3^-$,[6] and of $SnCl^+$, $SnCl_2$ and $SnCl_3^-$,[7] and the acid-dissociation constants of $HZnCl_3$ and $HSnCl_3$ were taken into account. The present experiments were carried out at temperatures different from those in the literature; the differences were corrected by using the thermodynamic data in the literature to estimate the formation constants of the zinc-chloro and tin-chloro complexes. Although hydrogen trichlorostannate(II), $HSnCl_3$, has been reported to be a weak acid, [8] the dissociation constant, $K_a(HSnCl_3)$, has not been measured. Therefore, $K_a(HSnCl_3)$ was assumed to be 0.1, 1, 2, 5, 10, and ∞. On the other hand, since the value of $K_a(HZnCl_3)$ previously reported[9] was considered to be too small, $K_a(HZnCl_3)$ was measured at $[Cl^-]_{total}=3$ mol dm^{-3} and found to be 4.9 ± 1.5 at 40.0 °C ($I=3.0$ mol dm^{-3}) by the potentiometric-titration method. By the use of these values, the dependencies were expressed at 40.0 °C as follows:

$$\begin{aligned}
K_a(HSnCl_3) = 0.1 \quad & k_{obsd} \propto [SnCl_3^-]^{2.0}[Cl^-]^{-1.8}[H^+]^{1.2} \\
1 \quad & [SnCl_3^-]^{2.0}[Cl^-]^{-1.9}[H^+]^{0.3} \\
2 \quad & [SnCl_3^-]^{2.0}[Cl^-]^{-2.0}[H^+]^{0.1} \\
5 \quad & [SnCl_3^-]^{2.0}[Cl^-]^{-2.1}[H^+]^{-0.1} \\
10 \quad & [SnCl_3^-]^{2.0}[Cl^-]^{-2.1}[H^+]^{-0.2} \\
\infty \quad & [SnCl_3^-]^{2.0}[Cl^-]^{-2.2}[H^+]^{-0.3}.
\end{aligned} \quad (5)$$

In the range of $K_a(HSnCl_3)$ values described above, the rate of the fast reaction path was always second-order with respect to the concentration of $SnCl_3^-$. When $K_a(HSnCl_3)$ was set at 2, the rate constant, k_{obsd} was almost independent of the hydrogen concentration. It was possible that H^+ participated only in the acid-dissociation equilibrium of $HSnCl_3$. The kinetic order of the concentration of Cl^- was in the range from -1.8 to -2.2. In the experiments concerning the effect of the Cl^- concentration on the fast reaction path, the concentration of Cl^- was somewhat changed. In the case of $K_a(HSnCl_3)=2$, the reaction order of $[Cl^-]$ was an integer, -2.0. It is probable that $K_a(HSnCl_3)=2$.

Reaction Routes. Several reaction routes were possible and so were considered. However, none of them could be chosen as the most probable one, because the reactant involved in the rate-determining step was not identified. As examples, two possible reaction routes are shown in Scheme 1.

In Route (1), the yellow species involved in the fast reaction path, Y_I, are considered to be an equilibrium mixture of the tris (Y_3), the tetrakis (Y_4), the pentakis (Y_5), and the hexakis(Y_6) complex. The rate-determining step is assumed to be the reaction of Y_6; it is assumed not to involve $SnCl_3^-$. The construction of a model of the hexakis complex shows that six trichlorostannato(II) ligands can coordinate to the rhodium(III) atom when the Cl–Sn–Cl angles are small enough.

Yellow Species: $Y = Y_I + Y_{II}$

Fast path

Route (1) K_4 K_5 K_6

$$Y_I: Y_3 \underset{Cl^-}{\overset{L^-}{\rightleftharpoons}} Y_4 \underset{Cl^-}{\overset{L^-}{\rightleftharpoons}} Y_5 \underset{Cl^-}{\overset{L^-}{\rightleftharpoons}} Y_6; Y_6 \xrightarrow{\text{r.d.s.}} [Rh^{I}L_5]^{4-} + Sn^{IV}Cl_3^+$$

Route (2)

$$Y_I: Y_3 \underset{Cl^-}{\overset{L^-}{\rightleftharpoons}} Y_4 \underset{Cl^-}{\overset{L^-}{\rightleftharpoons}} Y_5 \underset{Cl^-}{\overset{L^-}{\rightleftharpoons}} [Rh^{III}L_5]^{2-} \overset{L^-}{\rightleftharpoons} [L_4RhSnCl_3- -SnCl_3]^{3-}; Y_5'\text{–}SnCl_3$$

$$Y_5'\text{–}SnCl_3 \xrightarrow{\text{r.d.s.}} [Rh^{I}L_5]^{4-} + Sn^{IV}Cl_3^+$$

Slow path $Y_{II} \longrightarrow [Rh^{I}L_5]^{4-}$

Scheme 1. Possible reaction routes. $L = SnCl_3$, $Y_3 = [RhCl_3L_3]^{3-}$, $Y_4 = [RhCl_2L_4]^{3-}$, $Y_5 = [RhClL_5]^{3-}$, $Y_6 = [RhL_6]^{3-}$. r.d.s. represents rate-determining step. $K_4 = [Y_4][Cl^-]/[Y_3][L^-]$, $K_5 = [Y_5][Cl^-]/[Y_4][L^-]$, $K_6 = [Y_6][Cl^-]/[Y_5][L^-]$.

On the basis of the reaction Route (1) (in Scheme 1), k_{obsd} is expressed as follows:

$$k_{obsd} = \frac{k_1K_4K_5K_6[SnCl_3^-]^3}{[Cl^-]^3 + K_4[SnCl_3^-][Cl^-]^2 + K_4K_5[SnCl_3^-]^2[Cl^-] + K_4K_5K_6[SnCl_3^-]^3}. \quad (6)$$

In Eq. 6, the first term of the denominator is attributed to the tris complex(Y_3); the second term, to the tetrakis complex(Y_4); the third term, to the pentakis complex (Y_5), and the fourth term, to the hexakis complex(Y_6). When the tetrakis complex is the predominant species in the equilibrium mixture(Y_I), the following relationship is derived:

$$k_{obsd} = k_1K_5K_6[SnCl_3^-]^2[Cl^-]^{-2}. \quad (7)$$

This is in agreement with the derived rate law when $K_a(HSnCl_3)$ is assumed to be 2 in Eq. 5. In Fig. 5, the k_{obsd}'s obtained at low $[SnCl_3^-]$ values are found somewhat below the line with a slope of 2, which suggests that, in the reaction solution with a low $[SnCl_3^-]$, small amounts of the tris complex are present together with the major species, the tetrakis complex.

Route (2) (in Scheme 1) also satisfies the observed rate law when the tetrakis complex is predominant in the reactant mixture. The intermediate, $Y_5'\text{–}SnCl_3$, can be assumed because it is similar to the intermediate[5] in the exchange reaction of Sn^{II} and Sn^{IV} in hydrochloric acid solutions.

As to the temperature effect on the reaction, the slope of log k_{obsd} *vs.* log $[Sn^{II}]_{total}$ increased with the increase in the temperature, as may be seen from Fig. 5. This is explained by the shift of the equilibria among the rhodium(III) complexes due to the temperature; that is, at a higher temperature the tetrakis complex dissociates to the tris complex, whereas at a lower temperature the pentakis complex comes to be formed.[10]

It was found that the formation of the purple species

was generally accelerated by light irradiation. When $[(CH_3)_4N]_3[RhCl_4(SnCl_3)_2]$ was used as the starting material, the reaction was complicated and was greatly accelerated by light irradiation.

From this study, it was found clearly that the equilibria concerning the rhodium(III)-trichlorostannato complexes were rapidly established in the process of the formation reaction of the rhodium(I) complex. The reduction of the rhodium(III) complexes was not involved in the equilibria. It has been stated that anionic complexes of Rh^{III} are kinetically labile.[11] Our results were consistent with this view.

The present work was partially supported by a Grant-in-Aid for Scientific Research, No. 56470042, from the Ministry of Education, Science and Culture.

References

1) T. Kimura, *Sci. Papers I. P. C. R.*, **73**, 31(1979).
2) H. Moriyama, T. Aoki, S. Shinoda, and Y. Saito, *J. Chem. Soc., Dalton Trans.*, **1981**, 639.
3) T. Kimura, *J. Solid State Chem.*, **34**, 369(1980).
4) C. I. Browne, R. P. Craig, and N. Davidson, *J. Am. Chem. Soc.*, **73**, 1946(1951).
5) M. B. Robin and P. Day, "Mixed Valence Chemistry. A Survey and Classification," in "Advances in Inorganic Chemistry and Radiochemistry," ed by H. J. Emeléus and A. G. Sharpe, Academic Press, New York (1967), Vol. 10, pp. 374—375; R. P. Craig and N. Davidson, *J. Am. Chem. Soc.*, **73**, 1951(1951).
6) The formation constants of $ZnCl^+$, $ZnCl_2$ and $ZnCl_3^-$ at I=4.5 mol dm^{-3} used were the values reported by S. A. Chchukarev *et al.* (*Zh. Neorg. Khim.*, **1**, 225 (1956)) and presented in "Stability Constants of Metal Ion Complexes," The Chemical Society, London (1964), p. 289.
7) C. E. Vanderzee and D. E. Rhodes, *J. Am. Chem. Soc.*, **74**, 3552(1952).
8) S. J. Lachman and F. C. Tompkins, *Trans. Faraday Soc.*, **40**, 136(1944).
9) J. H. Hildebrand and W. G. Bowers, *J. Am. Chem. Soc.*, **38**, 785(1916).
10) When tetramethylammonium chloride was carefully added to the reaction solution at 0°C, a lemon-yellow precipitate was formed. The ratio of Rh to Sn in the precipitate was 1/4.0—1/4.7 in the range of tin(II) concentrations from 0.02 to 0.1 mol dm^{-3} in a 1—5 mol dm^{-3} hydrochloric acid solution.
11) F. A. Cotton and G. Wilkinson, "Advanced Inorganic Chemistry. A Comprehensive Text," 4th ed, John Wiley & Sons, New York (1980), p. 943.

 © 1984 The Chemical Society of Japan Bull. Chem. Soc. Jpn., 57, 391—394 (1984)

Potentiometric and Calorimetric Studies on the Formation of Ethylenediamine Complexes of Copper(II) Ion in Water and Aqueous Dioxane Solutions

Shin-ichi Ishiguro, Yoshihiro Oka, and Hitoshi Ohtaki*
Department of Electronic Chemistry, Tokyo Institute of Technology at Nagatsuta, 4259 Nagatsuta-cho, Midori-ku, Yokohama 227
(Received June 29, 1983)

Gibbs energies (or formation constants), enthalpies and entropies of formation of ethylenediamine complexes of copper(II) ions have been determined by means of potentiometric and calorimetric titrations at 25 °C in an aqueous solution and dioxane-water mixtures (dioxane contents are 0.1 and 0.2 mole fractions, which correspond to 35.2 and 55.0% w/w, respectively), all containing 3 mol dm^{-3} $LiClO_4$ as a constant ionic medium. The thermodynamic quantities of the reactions $CuL_{n-1}^{2+}+L=CuL_n^{2+}$ (L=ethylenediamine and n=1 and 2) determined in the solutions were as follows: ΔG_1°=−65.0 kJ mol^{-1} (dioxane content: 0.0 mole fraction), −66.8 kJ mol^{-1} (0.1 mole fraction), and −68.8 kJ mol^{-1} (0.2 mole fraction); ΔG_2°=−56.9 kJ mol^{-1} (0.0), −58.8 kJ mol^{-1} (0.1), and −61.1 kJ mol^{-1} (0.2); ΔH_1°=−67.7 kJ mol^{-1} (0.0), −68.6 kJ mol^{-1} (0.1), and −66.7 kJ mol^{-1} (0.2); ΔH_2°=−71.0 kJ mol^{-1} (0.0), −70.2 kJ mol^{-1} (0.1), and −68.8 kJ mol^{-1} (0.2); $T\Delta S_1^\circ$=−2.7 kJ mol^{-1} (0.0), −1.8 kJ mol^{-1} (0.1), and 2.1 kJ mol^{-1} (0.2); $T\Delta S_2^\circ$=−14.1 kJ mol^{-1} (0.0), −11.4 kJ mol^{-1} (0.1), and −7.7 kJ mol^{-1} (0.2). In any solvent examined the enthalpies contribute predominantly to the Gibbs energies. On the other hand, for a given complex with varying solvent compositions, the entropies mainly contribute to the change in the Gibbs energies of the complex formation reactions. With an increase in the dioxane content of the solvent, the Gibbs energies of the complex formation reactions become more negative, while the enthalpies of the reactions remain practically unchanged or even become less negative. Consequently, the entropies of the reactions increase with increasing dioxane content of the solvent, which is explained in terms of weakening of the hydrogen-bonded structure of water in the bulk solvent by the addition of dioxane.

In a previous paper,[1] we reported the solvent effect on the formation of ethylenediamine complexes of nickel(II) ions in an aqueous solution and in aqueous dioxane mixtures. The formation constants of the NiL^{2+}, NiL_2^{2+}, and NiL_3^{2+} complexes (L denotes ethylenediamine) increased with increasing dioxane content of the solvent, and the increment of the formation constants with varying solvent compositions was almost independent of the species. The solvent effect on the formation constants of the complexes was attributed mainly to the increase in the entropies of formation of the complexes. Enthalpies of the complex formation reactions became less negative at each stepwise reaction with the increase in the dioxane concentration in the solvents. The results have been explained in terms of the change in the hydrogen-bonded structure of water in the bulk solvent by the addition of dioxane.[1-3]

In the present study, we employed copper(II) ions in order to further examine solvent effects on the complex formation reaction of metal ions with neutral ligands in which the charges of the complexes remain unchanged in the course of the complex formation reaction. Ethylenediamine was used as the neutral ligand, as was demonstrated in the previous work.[1]

Experimental

Reagents. Copper(II) perchlorate was prepared from copper(II) oxide and perchloric acid of reagent grade. The copper(II) perchlorate thus prepared was recrystallized three times from water. A small amount of perchloric acid was added to the copper(II) perchlorate stock solution and pH of the stock solution was kept about 3. The concentration of free acid was determined coulometrically. The total concentration of copper(II) ions in the stock solution was determined electrogravimetrically.

Other chemicals used were prepared by the same methods as described previously.[1,4]

Method of Measurements and Analysis of Data. All potentiometric and calorimetric titrations were performed at 25 °C in a constant ionic medium of 3 mol dm^{-3} $LiClO_4$. The experimental method and the procedure of data analysis were described previously.[1]

Results and Discussion

Over the range of $-\log([H^+]/\text{mol dm}^{-3})$ from 3 to 10 in all the solvents examined, potentiometric titration curves of the copper(II)-ethylenediamine system could be well explained by assuming the formation of two mononuclear CuL^{2+} and CuL_2^{2+} complexes. The tris(ethylenediamine)copper(II) complex was not appreciably formed under the present experimental conditions. Typical titration curves obtained in the aqueous solution are shown in Fig. 1, where $-\log([H^+]/\text{mol dm}^{-3})$ values measured are plotted against X, the degree of neutralization of ethylenediammonium ions in the solution. The experimental points fitted well curves calculated (X_{calcd}) by using Eq. 1 over the whole range of the $-\log([H^+]/\text{mol dm}^{-3})$ values examined.

$$X_{calcd} = (2C_L - [H^+] + K_w[H^+]^{-1} - K_2^{-1}[H^+][L] - 2K_1^{-1}K_2^{-1}[H^+]^2[L])/C_L, \quad (1)$$

where K_1 and K_2 denote the dissociation constants of H_2L^{2+} and HL^+ ions, respectively. K_w represents the autoprotolysis constant of the solvent. Concentrations of free hydrogen ions and ethylenediamine molecules were calculated by using Eqs. 2 to 4.

$$C_M = [Cu^{2+}] + \beta_1[Cu^{2+}][L] + \beta_2[Cu^{2+}][L]^2, \quad (2)$$

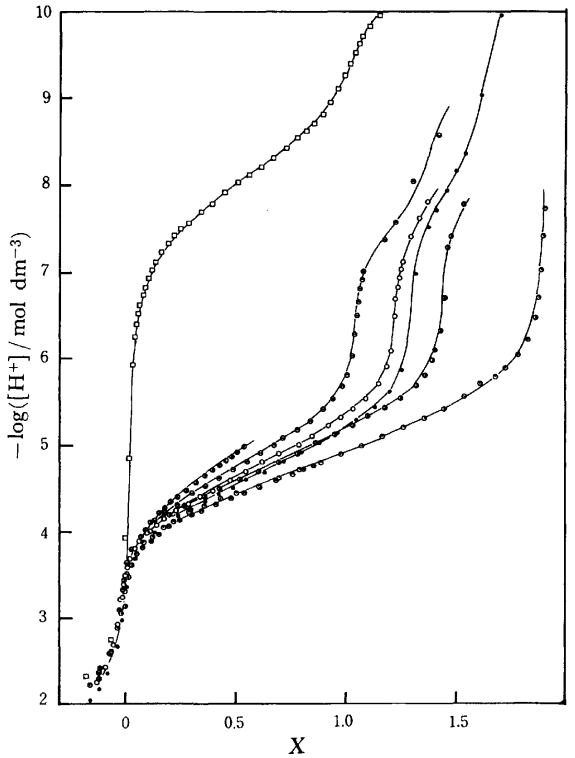

Fig. 1. Potentiometric titration curve of ethylenediamine and copper(II)-ethylenediamine aqueous solutions.
Curve □: C_M(mmol dm^{-3})=0.0, C_L(mmol dm^{-3})= 58.47; ○: 14.10, 45.75; ⊙: 16.53, 35.11; ⊖: 9.853, 37.46; ⊕: 22.96, 49.57; ●: 19.69, 61.06; ◑: 14.09, 38.57: ⓓ: 12.49, 59.60.
The concentrations of the metal ion and the ligand were changed by dilution during the titrations. The solid lines show calculated curves by using the constants in Table 1.

$$C_L = [L] + K_2^{-1}[H^+][L] + K_1^{-1}K_2^{-1}[H^+]^2[L] + \beta_1[Cu^{2+}][L] + 2\beta_2[Cu^{2+}][L]^2, \quad (3)$$

$$C_H = [H^+] - K_w[H^+]^{-1} + K_2^{-1}[H^+][L] + 2K_1^{-1}K_2^{-1}[H^+]^2[L]. \quad (4)$$

Here C_i denotes the total concentration of species i. β_1 and β_2 represent the overall formation constants of CuL^{2+} and CuL_2^{2+}, respectively. The values were optimized by using the least-squares method for searching the minimum error-square sum $U=\sum\{(C_M-C_{M,calcd})^2+(C_L-C_{L,calcd})^2+(C_H-C_{H,calcd})^2\}$, the program MINIQUAD[5] being employed for the calculation. The final values for the overall formation constants of the complexes are listed in Table 1.

In Fig. 2 typical results for the calorimetric titrations of aqueous copper(II)-ethylenediamine solutions are depicted, where heats evolved q_i at the addition of the i-th portion of a titrant are plotted against the average number $\bar{n}$ of ethylenediamine molecules bound per copper(II) ion in the solution. The solid lines are drawn by using the enthalpy values finally obtained with the aid of the least-squares program KALORI.[6] The results obtained are tabulated in Table 2.

Table 1. The formation constants, β_n, for the reactions, $Cu^{2+}+nL=CuL_n^{2+}$; $\beta_n=[CuL^{2+}]/[Cu^{2+}][L]^n$ (L=en) in aqueous dioxane containing 3 mol dm^{-3} $LiClO_4$ at 25 °C

	Complex	Concentration of dioxane/mole fraction 0.0 (0.0%w/w)	0.1 (35.2%w/w)	0.2 (55.0%w/w)
log β_1	CuL^{2+}	11.38(0.04)	11.70(0.04)	12.05(0.04)
log β_2	CuL_2^{2+}	21.35(0.09)	22.00(0.09)	22.76(0.09)

Values in parentheses refer to 3σ where σ denotes the standard deviation.

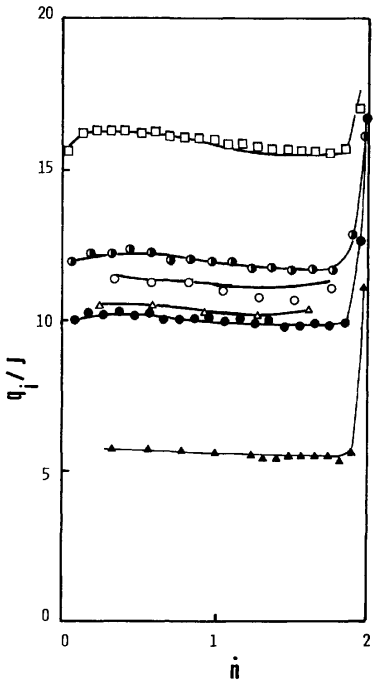

Fig. 2. Calorimetric titration curves of copper(II)-ethylenediamine aqueous solution.
Curve ▲: C_M(mmol dm^{-3})=8.0, C_L(mmol dm^{-3})=24.2; △: 3.6, 15.4; ○: 5.8, 18.6; ●: 9.6, 29.8; ◑: 10.9, 31.2; □: 19.6, 48.6.
The solid lines show calculated curve by using the constants in Table 2.

Table 2. The enthalpies, $\Delta H^\circ_{\beta n}$/kJ mol^{-1}, for the reactions, $Cu^{2+}+nL=CuL_n^{2+}$ (L=en) in aqueous dioxane containing 3 mol dm^{-3} $LiClO_4$ at 25 °C

	Complex	Concentration of dioxane/mole fraction 0.0 (0.0%w/w)	0.1 (35.2%w/w)	0.2 (55.0%w/w)
ΔH_{β_1}	CuL^{2+}	−67.7(0.4)	−68.6(0.4)	−66.7(0.5)
ΔH_{β_2}	CuL_2^{2+}	−138.7(0.4)	−138.8(0.5)	−135.5(0.6)

Values in parentheses refer to 3σ where σ denotes the standard deviation.

The thermodynamic quantities, ΔG_n°, ΔH_n°, and ΔS_n° for each successive complex formation reaction, $CuL_{n-1}^{2+}+L=CuL_n^{2+}$ (n=1 and 2) are summarized in Table 3.

TABLE 3. THE THERMODYNAMIC PARAMETERS, ΔG_n°, ΔH_n°/kJ mol^{-1} AND ΔS_n°/J K^{-1} mol^{-1}, FOR THE SUCCESSIVE REACTIONS, $CuL_{n-1}^{2+}+L=CuL_n^{2+}$, IN AQUEOUS DIOXANE CONTAINING 3 mol dm^{-3} $LiClO_4$ AT 25 °C

	Concentration of dioxane/mole fraction		
	0.0 (0.0%w/w)	0.1 (35.2%w/w)	0.2 (55.0%w/w)
$-\Delta G_1^\circ$	65.0	66.8	68.8
$-\Delta G_2^\circ$	56.9	58.8	61.1
$-\Delta H_1^\circ$	67.7	68.6	66.7
$-\Delta H_2^\circ$	71.0	70.2	68.8
ΔS_1°	−9.1	−6.0	7.1
ΔS_2°	−47.3	−38.3	−25.8

Aqueous Solution. Since the stepwise formation constants of the mono- and bis(ethylenediamine)-copper(II) complexes decrease with the ligand number within the complexes, the Gibbs energies of the first complex is more negative than the second one. However, the stepwise enthalpy of formation of the mono(ethylenediamine)copper(II) complex is less negative than that of the bis-complex. Therefore, the stepwise entropy of formation of the former complex is larger than that of the latter, although the values are both negative (see Table 3). Thus, $\Delta G_1^\circ<\Delta G_2^\circ$, $\Delta H_1^\circ>\Delta H_2^\circ$ and $\Delta S_1^\circ>\Delta S_2^\circ$. Similar trends in the variations of ΔG_n°, ΔH_n° and ΔS_n° have been observed in the formation of nickel(II)-ethylenediamine complexes.[1]

It may be generally accepted that metal-water bonds within an aquametal ion weaken when a part of water molecules within the aquametal ion are replaced with a ligand which has an atom or atoms with a stronger donor property than water.[7] Thus, we can expect that the Cu-OH_2 bonds within the mono(ethylenediamine)-copper(II) complex is weaker than those within the aquacopper(II) ion. Therefore, when we introduce the second ethylenediamine molecule to the mono-(ethylenediamine)copper(II) complex, an energy (enthalpy) to expell two water molecules from the coordination sphere of the mono-complex may be less than that of the aquacopper(II) ion. Consequently, the stepwise enthalpy of formation of the CuL_2^{2+} complex becomes more negative than that of the CuL^{2+} complex. On the contrary, when water molecules within the mono(ethylenediamine)copper(II) complex in which the water molecules combine relatively weakly with the metal ion are removed from the coordination sphere, a less entropy gain may be resulted compared with that for releasing water molecules from the aquacopper(II) ion. The negative values of the entropies of formation of the CuL^{2+} and CuL_2^{2+} complexes indicate that the complex formation is accompanied by the loss of entropy due to the combination of ethylenediamine molecules with the copper(II) ion and also to the recombination of dehydrating water molecules from the metal ion with those in the bulk solvent by the formation of hydrogen bonds.

The Solvent Effect on the Complex Formation. The Gibbs energies of formation of each complex became more negative with increasing dioxane content of the solvent. The decrease in the Gibbs energy of a given complex with varying solvent compositions is attributable to the increase in the entropy of formation of the complex, the enthalpy contributing to the Gibbs energy less favorably with the solvent effect.

As has been pointed out in the previous paper,[1] the secondary solvation of the both aquametal ion and metal-ethylenediamine complexes is enhanced in dioxane-water mixture and the degree of enhancement of the solvation is larger in the aquametal ion than in the metal-ethylenediamine complexes. Moreover, the enhancement become less significant within a complex with a larger number of the ethylenediamine molecules coordinated to the metal ion.

Although we have no experimental data for the enthalpy of transfer of copper(II) ions from water to a dioxane-water mixture and, therefore, we cannot calculate the enthalpies of transfer of each complex between the two solvents, we can expect that the secondary solvation of the aquacopper(II) ion is enhanced more strongly than that of a copper(II)-ethylenediamine complex in a given solvent mixture. Consequently, the formation of the copper(II)-ethylenediamine complexes becomes less favorable in the enthalpic point of view in a solvent with a larger dioxane content.

On the other hand, water molecules liberated from the coordination sphere of a complex can behave more freely in a dioxane-water mixture in which the hydrogen-bonded structure of water is partially destroyed. Therefore, the increase in the entropy of any copper(II)-ethylenediamine complex in a dioxane-water mixture is attributable mainly to an entropy gain of water liberated.

Such trends in the changes of the Gibbs energies, enthalpies and entropies of formation of complexes have also been observed in the nickel(II)-ethylenediamine system.[1]

The decrements of the Gibbs energies of formation of the copper(II)-ethylenediamine complexes with varying dioxane contents in the solvent are practically the same as those of the nickel(II)-ethylenediamine ones. Moreover, the changes are essentially independent of the number of ethylenediamine molecules coordinated. Such results are predictable from a simple Born equation by assuming the same ionic radii of the CuL_n^{2+} and NiL_n^{2+} ions. However, it should be noted that the increments of the both enthalpy and entropy of formation of each copper(II)-ethylenediamine complex are smaller than those of the corresponding nickel(II)-ethylenediamine ones (2.5 kJ mol^{-1} and 4.0 kJ mol^{-1} for the enthalpies of NiL^{2+} and NiL_2^{2+} complexes, respectively, at the transfer from water to the aqueous dioxane of 0.2 mole fraction dioxane content and 21.1 J K^{-1} mol^{-1} and 26.6 J K^{-1} mol^{-1} for the corresponding entropies of the respective species). The reason why the solvent effects on the enthalpies and entropies of formation of the CuL_n^{2+} complexes are smaller than those of the NiL_n^{2+} ones is not clear at the present stage.

The work has partially been supported by the Grant-in-Aid for Scientific Research No. 5740054 from the Ministry of Education, Science and Culture and by the Asahi Glass Foundation for Industrial Technology.

References

1) S. Ishiguro, Y. Oka, and H. Ohtaki, *Bull. Chem. Soc. Jpn.*, **56**, 2426 (1983).
2) D. N. Glew, H. D. Mak, and N. H. Rath, "Hydrogen-bonded Solvent Systems," Taylor and Francis Ltd., London (1968), p. 195.
3) D. Feakins and C. T. Allan, *J. Chem. Soc., Faraday Trans. 1*, **1976**, 314.
4) H. Ohtaki, *Inorg. Chem.*, **6**, 808 (1967).
5) S. Sabatini, A. Bacca, and P. Gran, *Talanta*, **21**, 53 (1974).
6) R. Karlsson and L. Kullberg, *Chem. Scr.*, **9**, 54 (1976).
7) V. Gutmann, "The Donor-Acceptor Approach to Molecular Interactions," Plenum, New York and London (1978).

Five-coordinate Bis(1,1,1,5,5,5-hexafluoro-2,4-pentanedionato)(tertiary phosphine)palladium(II) and -platinum(II) Complexes. X-Ray Crystal and Molecular Structures and Fluxional Motions in Solution

Seichi Okeya,*,† Toshiko Miyamoto, Shun'ichiro Ooi,* Yukio Nakamura, and Shinichi Kawaguchi*
Faculty of Science, Osaka City University, Sumiyoshi-ku, Osaka 558
†*Faculty of Education, Wakayama University, Fukiage, Wakayama 640*
(Received July, 29, 1983)

Five-coordinate complexes [M(hfac)$_2$L] (M=Pd, Pt; hfac=1,1,1,5,5,5-hexafluoro-2,4-pentanedionate anion) were produced by the reactions of [M(hfac)$_2$] with equimolar amounts of tertiary phosphines, phosphites, and triphenylarsine. They were characterized by ^{1}H, ^{13}C, ^{19}F, and ^{31}P NMR spectra in solution and several complexes containing bulky phosphines as L were isolated, and structures of [Pd(hfac)$_2${P(*o*-tolyl)$_3$}] and [Pt(hfac)$_2${P(cyclohexyl)$_3$}] were determined by X-ray analysis. Both complexes have very distorted square-pyramidal structures, one of the two hfac anions in either of them spanning the apical and basal coordination sites. NMR spectra at various temperatures disclosed the fluxional behaviors of these complexes which retain the solid-state structures at such low temperatures as −60 °C. Two kinds of twist mechanisms were proposed.

By our extensive studies, the ligand substitution reactions of bis(β-diketonato)palladium(II) and -platinum(II) with various nitrogen bases[1] and tertiary phosphines[2] were found to afford many types of complexes depending on the natures of the central metals, β-diketonate ligands, attacking Lewis bases, and solvents employed. In either case, a molecule of Lewis base L was considered to transform one of the chelating β-diketonate ligands (β-dik) into the *O*-unidentate state (β-dik-*O*) in the first stage of the overall reaction (Eq. 1). In fact several palladium(II) and

$$[M(\beta\text{-dik})_2] + L \longrightarrow [M(\beta\text{-dik})(\beta\text{-dik-}O)L] \quad (1)$$

platinum(II) complexes containing an *O*-unidentate 1,1,1-trifluoro-2,4-pentanedionate (tfac) ligand were isolated.[2]

The ligand substitution reactions of square-planar complexes usually proceed according to the associative mechanism[3] but the five-coordinate intermediate can hardly be detected experimentally,[4] although rather many stable five-coordinate palladium(II) and platinum(II) complexes have been prepared (*vide infra*). When the reaction between [Pd(tfac)$_2$] and tri-*o*-tolylphosphine was studied spectrophotometrically, a distinct isosbestic point was recorded, indicating that no intermediate was accumulated to an appreciable concentration.[5]

On the contrary, the reactions of bis(1,1,1,5,5,5-hexafluoro-2,4-pentanedionato)palladium(II) and -platinum(II) with bulky tertiary phosphines were found to give stable adducts [M(hfac)$_2$(PR$_3$)]. This paper reports the characterization of these five-coordinate complexes and their fluxional behaviors in solution as well as the molecular structures of two of them which were determined by the X-ray diffraction method.[6]

Experimental

Preparation of Compounds. The starting chelates [Pd(hfac)$_2$] and [Pt(hfac)$_2$] were prepared according to the previously reported method.[7] Commercially supplied tertiary phosphines were used without further purification except P(*o*-tolyl)$_3$ which was recrystallized from ethanol.

*Bis(1,1,1,5,5,5-hexafluoro-2,4-pentanedionato)(tri-o-tolylphosphine)palladium(II), [Pd(hfac)$_2${P(o-tolyl)$_3$}] (**1a**)*: After [Pd(hfac)$_2$] (494 mg, 0.949 mmol) and P(*o*-tolyl)$_3$ (293 mg, 0.963 mmol) were dissolved in hot hexane (10 cm^3), the mixture was kept at −5 °C in a refrigerator to precipitate dark red crystals, which were filtered, washed with a small amount of hexane, and dried *in vacuo* (530 mg). The filtrate was allowed to stand at room temperature to make the solvent evaporate spontaneously. Another crop of crystals was left on the wall of vessel. The combined yield was 669 mg (85%). Red plates obtained by recrystallization from hexane were subjected to X-ray analysis.

*Bis(1,1,1,5,5,5-hexafluoro-2,4-pentanedionato)(tri-o-tolylphosphine)platinum(II), [Pt(hfac)$_2${P(o-tolyl)$_3$}] (**2a**)*: A solution of [Pt(hfac)$_2$] (254 mg, 0.417 mmol) and P(*o*-tolyl)$_3$ (127 mg, 0.417 mmol) in diethyl ether (15 cm^3) was kept standing at ambient temperature to allow the solvent to vaporize spontaneously. Orange plates left on the wall of vessel were gathered, washed with a small amount of hexane, and dried *in vacuo*. The yield was 339 mg (89%).

*Bis(1,1,1,5,5,5-hexafluoro-2,4-pentanedionato)(phenyldi-o-tolylphosphine)palladium(II), [Pd(hfac)$_2${PPh(o-tolyl)$_2$}] (**1b**) and -platinum(II), [Pt(hfac)$_2${PPh(o-tolyl)$_2$}] (**2b**)*: Both compounds were prepared in a similar way and the yield was 70% in either case. Recrystallization from hexane gave red plates (**1b**) and yellow needles (**2b**), respectively.

*Bis(1,1,1,5,5,5-hexafluoro-2,4-pentanedionato)(tricyclohexylphosphine)platinum(II), [Pt(hfac)$_2$(PCy$_3$)] (**2g**)*: The complex was also prepared by the method similar to that for **2a** in a 93% yield. Orange columns obtained by recrystallization from hexane were used for X-ray analysis.

*(1,1,1,5,5,5-Hexafluoro-2,4-pentanedionato){2-(di-o-tolylphosphino)benzyl-C,P}palladium(II), [(hfac)PdCH$_2$(o-C$_6$H$_4$)P(o-tolyl)$_2$] (**3**)*: A solution of **1a** (350 mg, 0.424 mmol) in dichloromethane (5 cm^3) was left to stand at ambient temperature for 10 d and the solvent was then allowed to evaporate spontaneously to leave yellow oil. The crude product was dissolved in dichloromethane (0.5 cm^3). Petroleum ether (bp <60 °C) was added to the solution and the mixture was cooled to precipitate yellow plates, which were filtered and dried *in vacuo*. The yield was 124 mg (47%). When kept at ambient temperature for a long time, even the solid specimen of **1a** changed gradually to **3**. Anal. Found: C, 50.60; H, 3.40% M$^+$, 616 (^{106}Pd, 27%), 618 (^{108}Pd, 27%), 615 (^{105}Pd, 22%), and 614 (^{104}Pd, 11%). Calcd for $C_{26}H_{21}O_2PF_6Pd$: C, 50.63; H, 3.43%; M, 616.79. ^{1}H NMR in $CDCl_3$, δ(ppm from internal Me_4Si): 2.45 and 2.75 (6H, s, br, 2CH$_3$); 3.79 (2H, d,

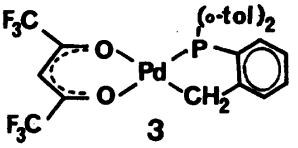

3

J(P-H)=4 Hz, CH_2); 6.8—7.3 (≈12H, ring protons). ^{13}C NMR in $CDCl_3$, δ(ppm from internal Me_4Si): 22.4 (d, br, ^3J(C-P)=10 Hz, ^1J(C-H)=*ca.* 130 Hz, CH_3); 32.1 (s, ^1J(C-H)=136 Hz, CH_2); 89.2 (s, br, ^1J(C-H)=164 Hz, CH of hfac). Other carbon signals are not analyzed. The ^{31}P NMR signal is observed in $CDCl_3$ as a singlet at 35.6 ppm downfield from external H_3PO_4. The above-mentioned splitting and broadening of methyl proton signals and broadening of methyl carbon signal seem to be caused by the restricted free rotation of the two tolyl groups around the P-C bonds. These signals became a broad singlet and a doublet, respectively at 50 °C.

X-Ray Analysis. The crystal data for [Pd(hfac)$_2${P(*o*-tolyl)$_3$}] (**1a**) and [Pt(hfac)$_2$(PCy$_3$)] (**2g**) are given in Table 1. The Laue symmetries and the space groups were determined from Weisenberg and precession photographs. The unit cell dimensions were obtained from the least-squares treatment of 20 θ values of higher angle reflections (θ=7—15°) measured on an automated diffractometer by use of Mo$K\alpha$ radiation.

The intensities were measured on the diffractometer by using graphite-monochromated Mo$K\alpha$ radiation. The background was counted at each side of the scan range. The intensities of three standard reflections monitored every 4 h for each compound showed no appreciable variation during the data collection. The intensity data from compound **2g** were corrected for absorption.[8]

The crystal structures were solved by the heavy atom technique. The positional and thermal parameters were refined by block-diagonal-matrix least-squares. The minimized function was $\sum\omega(F_O-|F_C|)^2$, where $\omega=1/\sigma^2(F_O)$. All H atoms in **1a** could be found on the difference Fourier map but the refinement of their parameters was unsuccessful. They were included in the least-squares calculation but the parameters were fixed, the isotropic temperature factor $B_H=B+1.0$ being assigned for individual H atom, where B is the isotropic temperature factor of the C atom (obtained at the final cycle of isotropic refinement) to which the H atom is bound. No attempt was made to locate H atoms in **2g**. All parameter shifts in the final cycle of the refinement were less than 0.5σ in either case.

Table 1. Crystal data and experimental details

Compound	**1a**	**2g**
Crystal system	Monoclinic	Orthorhombic
Space group	$P2_1$	Pcab
a/Å	13.998(3)	25.652(3)
b/Å	11.430(2)	20.397(3)
c/Å	10.897(3)	12.781(2)
β/°	108.48(2)	
D_m/g cm^{-3}	1.66	1.75
D_c/g cm^{-3}	1.675	1.768
Z	2	8
μ(Mo $K\alpha$)/cm^{-1}	7.12	45.7
Crystal size/mm^3	0.18×0.20×0.27	0.15×0.22×0.30
Scan type	ω-2θ	ω
Scan speed (ω/s^{-1})	0.025	0.025
Scan range (ω/°)	1.0+0.3tanθ	0.8+0.4tanθ
Background count/s^{-1}	20	16
$2\theta_{max}$/°	55.0	50.0
No. of unique data ($F_o^2>3\sigma(F_o^2)$)	3148	3270
R	0.039	0.045
R'(=[$\sum\omega\Delta^2/\sum\omega F_o^2$]$^{1/2}$)	0.052	0.052

The atomic scattering factors, with correction for real part of anomalous dispersion of Pd^0 and Pt^0, were taken from Ref. 9. Compound **1a** crystallizes in a chiral space group, being resolved spontaneously on the way of crystallization. However, no attempt was made to determine the absolute crystal structure. The atomic coordinates are given in Table 2. The F_O–F_C tables, the anisotropic thermal parameters, and the H atom coordinates in **1a** are preserved at the Chemical Society of Japan (Document No. 8409). The computation was performed by a FACOM 230-60 computer at Osaka City University and ACOS-700 computer at Crystallographic Reserch Center of Osaka University by use of the program in the UNICS[10] and ORTEP.[11]

Other Measurements. Infrared spectra were obtained in Nujol mull with a Hitachi 295 spectrophotometer. Electronic spectra were measured in dichloromethane or hexane with a Hitachi 200-20 spectrophotometer. NMR spectra were recorded on JEOL-C60HL (in the case of ^1H), FX60Q (for ^1H, ^{13}C, and ^{31}P), FX90Q (for ^{13}C, ^{19}F, and ^{31}P), and FX100 (for ^{13}C and ^{195}Pt) instruments. A vapor-pressure osmometer manufactured by Knauer in West Berlin, West Germany, was used for molecular weight determination.

Results and Discussion

The reactions of [M(hfac)$_2$] (M=Pd^{II} and Pt^{II}) with equimolar amounts of bulky tertiary phosphines such as P(*o*-tolyl)$_3$ and PCy$_3$ in hexane or diethyl ether gave crystalline adducts [M(hfac)$_2$(PR$_3$)] (M=Pd (**1**) and Pt (**2**)) in high yields, of which decomposition temperatures and analytical data are listed in Table 3. Of these products, crystals of [Pd(hfac)$_2${P(*o*-tolyl)$_3$}] (**1a**) and [Pt(hfac)$_2$(PCy$_3$)] (**2g**) were suitable for X-ray analysis.

Molecular Structures in Crystals. Both crystals are composed of discrete complex molecules. Figures 1 and 2 show their perspective views and projections along the normal of the coordination plane for each molecule, respectively. Figure 3 gives the views of the phosphine ligands along the respective M-P vectors. As both complexes have similar ligands, common atom numbering is used as is seen in these Figures. Bond lengths and bond angles are summarized in Tables 4 and 5, respectively. Average values are given for the parameters of CF_3 groups, since these groups have large thermal parameters indicative of a disorder (Table 2) and hence individual structural parameter is of less importance.

The metal atom in either complex is five-coordinate and has a very distorted square-pyramidal coordination. The apical atom [O(11)] largely deviates from the ideal site for tetragonal symmetry as is seen in Fig. 2. The M-O(11) bond intersects the basal coordination plane defined by the O(12), O(21), O(22), and P atoms at 65.3(2)° and 66.9(3)° in **1a** and **2g**, respectively. The apical M-O bond is much longer than the basal one, indicating the weaker interaction between M and the apical O in either case. The basal donor atoms show slight but significant deviations from the mean plane, being displaced toward tetrahedral disposition. The magnitude is more than three times larger in **2g** than in **1a**. Although the O(12)-Pt-O(22) angle is 178.6(3)°, the P-Pt-O(21) angle is 173.1(2)° and the P and O(21) atoms are distant from the idealized apical site.

Such a very flattened tetrahedral arrangement of the

basal atoms has also been found in the pseudo tetragonal five-coordinate Pd^{II} and Pt^{II} complexes such as [MBr$_2$L$_3$] (M=Pd and Pt, L=5-ethyl(or methyl)-5*H*-dibenzophosphole;[12] M=Pd, L=2-phenylisophosphindoline[13]), [PdCl$_2$(PMe$_2$Ph)$_3$],[14] [PtCN(phen)$_2$]NO$_3$,[15] [Pd(hfac)(triphos)](hfac) (triphos =Ph$_2$PCH$_2$CH$_2$P(Ph)CH$_2$CH$_2$PPh$_2$),[16] and [Pd(hfac)$_2$(PPh$_3$)].[17] Furthermore, the metal atom is displaced from the basal plane toward the apical site, the deviation of Pd in **1a** being about twice as much as that of Pt in **2g**. Such deviation is characteristic of a square-pyramidal coordination of transition metals.

The Pt-P bond in **2g** is slightly but significantly shorter than Pd-P in **1a**. The M-O(21) bond, in which O(21) lies trans to the phosphine ligand, is somewhat longer than the other basal M-O bonds probably owing to the trans influence of the phosphine.

Table 2a. Fractional coordinates and temperature factors for [Pd(hfac)$_2${P(*o*-tolyl)$_3$}] (**1a**). Standard deviations of the least significant figures are given in parentheses

Atom	*x*	*y*	*z*	B_{eq}/Å^2
Pd	0.21720(3)	0.0 (1)	0.19120(4)	3.59(1)
O(11)	0.2992(5)	-0.1622(6)	0.3885(5)	6.4(2)
O(12)	0.2184(4)	-0.1499(5)	0.0941(5)	4.3(1)
C(11)	0.240(1)	-0.321(1)	0.4796(9)	7.8(4)
C(12)	0.2524(6)	-0.2525(7)	0.3628(7)	4.8(2)
C(13)	0.2025(6)	-0.3036(7)	0.2380(8)	5.1(3)
C(14)	0.1924(5)	-0.2501(6)	0.1214(7)	3.7(2)
C(15)	0.1420(7)	-0.3173(9)	0.0018(9)	6.0(3)
F(11)	0.268(1)	-0.2709(8)	0.5794(7)	17.5(6)
F(12)	0.2883(7)	-0.4190(7)	0.4949(8)	11.9(3)
F(13)	0.1441(7)	-0.360(1)	0.4537(9)	16.2(5)
F(14)	0.1912(5)	-0.3243(8)	-0.0784(6)	9.5(3)
F(15)	0.1149(7)	-0.4248(6)	0.0200(7)	11.4(3)
F(16)	0.0510(4)	-0.2632(8)	-0.0623(6)	9.9(3)
O(21)	0.0942(4)	-0.0631(5)	0.2401(5)	4.7(2)
O(22)	0.2015(4)	0.1566(5)	0.2645(5)	5.1(2)
C(21)	-0.0442(6)	-0.0662(9)	0.3146(9)	5.8(3)
C(22)	0.0447(4)	-0.001(1)	0.2923(6)	4.1(2)
C(23)	0.0589(6)	0.1159(7)	0.3282(7)	4.4(2)
C(24)	0.1336(5)	0.1836(7)	0.3099(6)	3.9(2)
C(25)	0.1376(7)	0.3121(8)	0.3465(8)	5.3(3)
F(21)	-0.0177(5)	-0.1673(6)	0.3690(7)	9.4(3)
F(22)	-0.1114(5)	-0.0944(7)	0.2058(7)	10.4(3)
F(23)	-0.0920(5)	-0.0077(9)	0.3772(8)	10.8(3)
F(24)	0.2083(7)	0.3298(7)	0.4532(7)	13.9(4)
F(25)	0.0550(6)	0.3523(6)	0.3611(8)	10.9(3)
F(26)	0.1564(6)	0.3791(5)	0.2607(7)	8.9(3)
P	0.3399(1)	0.0692(2)	0.1182(2)	3.30(5)
C(31)	0.3670(5)	0.2188(7)	0.1726(7)	3.8(2)
C(32)	0.4091(6)	0.2433(8)	0.3038(7)	4.8(2)
C(33)	0.4295(9)	0.360(1)	0.341(1)	7.4(4)
C(34)	0.4016(8)	0.4486(8)	0.248(1)	7.6(4)
C(35)	0.3611(7)	0.4253(8)	0.126(1)	6.4(3)
C(36)	0.3439(7)	0.3100(8)	0.0850(8)	5.1(3)
C(37)	0.4423(8)	0.149(1)	0.4091(8)	6.9(3)
C(41)	0.2936(5)	0.0604(7)	-0.0589(7)	3.9(2)
C(42)	0.1994(6)	0.0952(8)	-0.1299(7)	4.7(2)
C(43)	0.1725(7)	0.079(1)	-0.2650(8)	6.3(3)
C(44)	0.2361(7)	0.030(1)	-0.3230(7)	6.3(3)
C(45)	0.3242(6)	-0.008(1)	-0.2532(6)	5.6(2)
C(46)	0.3592(5)	0.009(1)	-0.1191(6)	4.5(2)
C(47)	0.1216(7)	0.144(1)	-0.0728(9)	7.0(3)
C(51)	0.4595(5)	-0.010(1)	0.1698(5)	4.0(2)
C(52)	0.5512(5)	0.0382(7)	0.1625(7)	4.5(2)
C(53)	0.6337(6)	-0.0304(9)	0.2035(8)	5.9(3)
C(54)	0.6300(7)	-0.145(1)	0.2493(8)	7.2(3)
C(55)	0.5446(6)	-0.1908(9)	0.2563(8)	5.5(3)
C(56)	0.4586(7)	-0.1233(8)	0.2168(8)	5.7(3)
C(57)	0.5616(6)	0.1563(9)	0.1097(9)	5.9(3)
H13	0.17500(0)	-0.37900(0)	0.23700(0)	6.00(0)
H23	0.01500(0)	0.15100(0)	0.36900(0)	5.00(0)
H33	0.46200(0)	0.37900(0)	0.43000(0)	7.50(0)
H34	0.41200(0)	0.52800(0)	0.27600(0)	7.70(0)
H35	0.34400(0)	0.48700(0)	0.06400(0)	7.10(0)
H36	0.31600(0)	0.29400(0)	-0.00500(0)	6.00(0)
H371	0.39300(0)	0.08900(0)	0.39400(0)	7.40(0)
H372	0.45000(0)	0.18300(0)	0.49200(0)	7.40(0)
H373	0.50400(0)	0.11800(0)	0.40700(0)	7.40(0)
H43	0.10700(0)	0.10200(0)	-0.31800(0)	7.20(0)
H44	0.21500(0)	0.02100(0)	-0.41400(0)	6.80(0)
H45	0.36600(0)	-0.04900(0)	-0.29300(0)	6.40(0)
H46	0.42600(0)	-0.01400(0)	-0.06900(0)	5.40(0)

Table 2b. Fractional coordinates and temperature factors for [Pt(hfac)$_2$(PCy$_3$)] (**2g**). Standard deviations of the least significant figures are given in parentheses

Atom	*x*	*y*	*z*	B_{eq}/Å^2
Pt	0.13785(2)	0.15649(2)	0.08025(3)	2.88(1)
O(11)	0.0337(3)	0.1391(4)	0.1309(9)	6.6(3)
O(12)	0.1408(3)	0.0592(3)	0.0861(6)	3.5(2)
C(11)	-0.0353(9)	0.077(1)	0.162(2)	16.(1)
C(12)	0.0215(5)	0.0826(7)	0.143(1)	4.9(4)
C(13)	0.0510(5)	0.0224(6)	0.128(1)	4.8(4)
C(14)	0.1044(5)	0.0184(6)	0.1062(9)	4.2(4)
C(15)	0.1284(5)	-0.0517(6)	0.108(1)	5.5(4)
F(11)	-0.0296(5)	0.0441(7)	0.275(1)	17.2(7)
F(12)	-0.0572(3)	0.0238(6)	0.1351(9)	11.4(4)
F(13)	-0.0574(4)	0.1184(6)	0.207(1)	16.2(6)
F(14)	0.1571(4)	-0.0623(4)	0.0275(8)	9.0(3)
F(15)	0.0939(4)	-0.0986(4)	0.1093(9)	11.3(4)
F(16)	0.1580(4)	-0.0585(4)	0.1931(7)	9.4(4)
O(21)	0.0944(3)	0.1473(3)	-0.0581(5)	4.0(2)
O(22)	0.1333(3)	0.2538(3)	0.0761(6)	4.0(2)
C(21)	0.0444(8)	0.1800(7)	-0.204(1)	9.0(7)
C(22)	0.0756(5)	0.1955(6)	-0.1036(9)	4.0(4)
C(23)	0.0789(5)	0.2634(5)	-0.0749(9)	4.1(3)
C(24)	0.1063(4)	0.2844(5)	0.0091(9)	3.5(3)
C(25)	0.1038(6)	0.3578(6)	0.035(1)	5.3(4)
F(21)	0.0209(6)	0.1270(6)	-0.1998(9)	16.6(6)
F(22)	0.0788(5)	0.1660(8)	-0.2763(8)	16.4(6)
F(23)	0.0191(5)	0.2239(5)	-0.2453(9)	13.7(5)
F(24)	0.0859(6)	0.3935(4)	-0.0382(8)	12.5(5)
F(25)	0.1498(3)	0.3813(4)	0.0593(9)	9.7(4)
F(26)	0.0743(5)	0.3682(4)	0.1141(8)	10.6(4)
P	0.1925(1)	0.1637(1)	0.2155(2)	3.0(1)
C(31)	0.2364(4)	0.0916(5)	0.2194(8)	3.7(3)
C(32)	0.2621(5)	0.0779(6)	0.1125(9)	4.5(4)
C(33)	0.2927(5)	0.0116(6)	0.119(1)	4.5(4)
C(34)	0.3315(5)	0.0102(6)	0.204(1)	5.1(4)
C(35)	0.3068(6)	0.0254(7)	0.312(1)	6.2(5)
C(36)	0.2784(5)	0.0947(7)	0.3093(9)	5.6(4)
C(41)	0.1589(4)	0.1654(6)	0.3422(8)	3.9(3)
C(42)	0.1290(5)	0.0994(6)	0.3606(9)	4.4(4)
C(43)	0.0960(5)	0.1035(8)	0.462(1)	6.1(5)
C(44)	0.0578(5)	0.1606(8)	0.461(1)	5.9(4)
C(45)	0.0880(6)	0.2251(7)	0.4483(9)	5.8(5)
C(46)	0.1205(5)	0.2256(7)	0.343(1)	4.9(4)
C(51)	0.2267(5)	0.2438(5)	0.2081(8)	3.5(3)
C(52)	0.2596(6)	0.2600(6)	0.307(1)	5.3(4)
C(53)	0.2843(6)	0.3317(6)	0.290(1)	6.1(5)
C(54)	0.3167(5)	0.3363(6)	0.193(1)	6.3(5)
C(55)	0.2853(6)	0.3169(6)	0.097(1)	6.2(5)
C(56)	0.2631(5)	0.2457(6)	0.1089(9)	4.8(4)

Table 3. Isolated five-coordinate complexes [M(hfac)$_2$(PR$_3$)]

Compd			Decomposition temp	Found (Calcd)		
No.	M	PR$_3$	°C	C(%)	H(%)	Mol wt[a]
1a	Pd	P(*o*-tolyl)$_3$	113—114	45.54(45.14)	2.86(2.81)	818(825)
2a	Pt	P(*o*-tolyl)$_3$	136—137	40.90(40.75)	2.52(2.54)	901(914)
1b	Pd	PPh(*o*-tolyl)$_2$	*ca.* 100	44.56(44.44)	2.68(2.61)	
2b	Pt	PPh(*o*-tolyl)$_2$	130—135	40.10(40.06)	2.39(2.35)	
2g	Pt	PCy$_3$[b]	128—133	37.86(37.80)	3.94(3.97)	814(890)

a) Determined in dichloromethane at 25 °C. b) PCy$_3$ abbreviates P(cyclohexyl)$_3$.

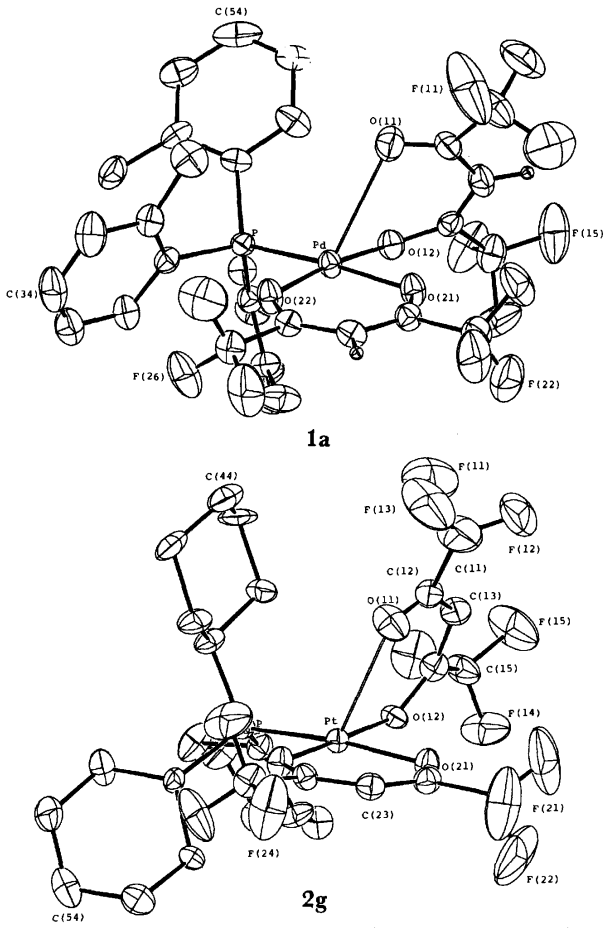

Fig. 1. ORTEP drawing of $[Pd(hfac)_2\{P(o\text{-tolyl})_3\}]$ (**1a**) and $[Pt(hfac)_2(PCy_3)]$ (**2g**). Thermal ellipsoids are drawn at 30% probability level. The H atom linked to the C(13) and C(23) atoms in **1a** are represented by spheres with arbitrary radius.

Table 4. Bond lengths

Bond length	l/Å	
	1a	**2g**
M-P	2.253(2)	2.232(3)
O(11)	2.796(6)	2.773(9)
O(12)	2.016(5)	1.988(6)
O(21)	2.086(6)	2.099(7)
O(22)	2.000(6)	1.990(7)
C(11)-C(12)	1.550(14)	1.48(3)
C(12)-O(11)	1.206(11)	1.203(16)
C(12)-C(13)	1.442(11)	1.455(18)
C(13)-C(14)	1.376(12)	1.399(17)
C(14)-O(12)	1.266(9)	1.275(14)
C(14)-C(15)	1.484(11)	1.557(16)
C(11), C(15)-F	1.302[a)]	1.34[a)]
C(21)-C(22)	1.537(13)	1.545(19)
C(22)-O(21)	1.251(11)	1.239(14)
C(22)-C(23)	1.384(14)	1.436(16)
C(23)-C(24)	1.366(11)	1.353(16)
C(24)-O(22)	1.242(10)	1.265(13)
C(24)-C(25)	1.519(12)	1.536(16)
C(21), C(25)-F	1.294[a)]	1.30[a)]
P-C(31)	1.810(8)	1.853(11)
C(41)	1.833(7)	1.835(11)
C(51)	1.830(8)	1.855(11)

a) Mean value of six C-F bond lengths.

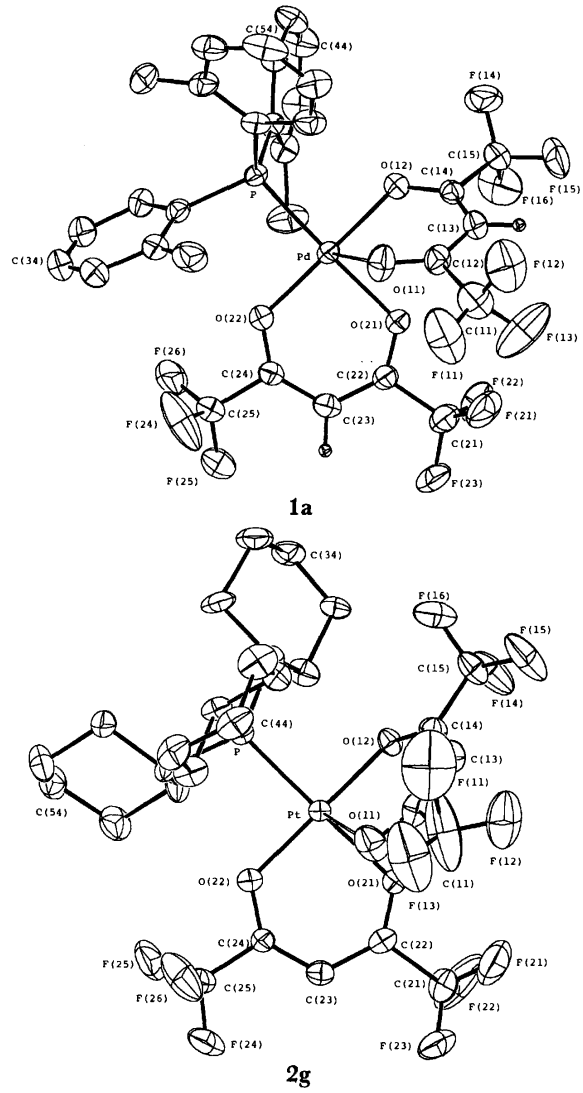

Fig. 2. Projection of each complex along the normal of coordination plane. Thermal ellipsoids are drawn at 30% probability level. The H atoms linked to the C(13) and C(23) atoms in **1a** are shown by spheres with arbitrary radius.

The hfac ligand lying on the basal plane in either complex forms a symmetrical planar chelate ring with the metal atom, and bond lengths indicate complete delocalization of π electrons within hfac. On the other hand, the hfac ligands which span the basal and apical sites in both complexes have structural parameters similar to each other. However, while the chelate ring in **2g** is totally planar, that in **1a** is folded along the line O(11)···O(12), the interplanar angle between the ligand plane (Plane 2 in Table 6) and the [Pd, O(11), O(12)] plane being 141.1(3)° as is seen in Fig. 2 and Table 6. Bond lengths clearly show the localization of π electrons in the latter ligand, indicating a greater contribution from the resonance structure $^{-}O\text{-}C(CF_3)=CH\text{-}C(CF_3)=O$. A detailed structural examination revealed that the two planar CF_3COC moieties are rotated with respect to each other through a dihedral angle of 9.2(4)°.

As stated already, the reactions of $[M(tfac)_2]$ with bulky tertiary phosphines afford four-coordinate

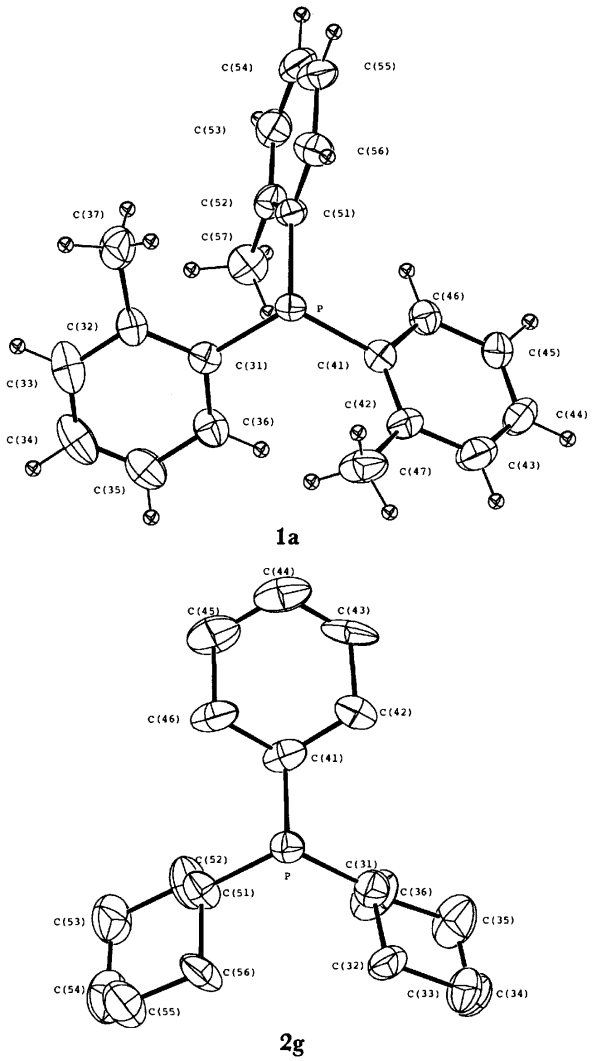

Fig. 3. The structures (30% ellipsoids) of the P(*o*-tolyl)$_3$ in **1a** and PCy$_3$ in **2g** viewed along the M-P vectors. Hydrogen atoms in **1a** are represented by spheres with arbitrary radius.

Table 5. Bond angles

Bond angle	ϕ/°	
	1a	**2g**
O(11)-M-O(12)	76.7(2)	84.2(3)
O(21)-M-O(22)	90.2(2)	92.0(3)
P-M-O(12)	88.8(2)	90.8(2)
P-M-O(22)	91.1(2)	89.5(2)
O(11)-M-O(21)	75.2(2)	70.9(3)
M-O(11)-C(12)	109.2(5)	113.7(8)
M-O(12)-C(14)	126.5(5)	129.1(7)
M-O(21)-C(22)	122.6(6)	122.2(7)
M-O(22)-C(24)	125.2(5)	122.8(7)
M-P-C(31)	108.7(3)	110.5(4)
M-P-C(41)	107.3(3)	112.9(4)
M-P-C(51)	116.3(3)	108.4(4)
C(11)-C(12)-C(13)	115.0(8)	118(1)
C(11)-C(12)-O(11)	115.9(7)	111(1)
C(13)-C(12)-O(11)	129.1(8)	131(1)
C(12)-C(13)-C(14)	124.7(8)	126(1)
C(13)-C(14)-O(12)	131.7(7)	136(1)
C(15)-C(14)-O(12)	110.7(7)	108(1)
C(15)-C(14)-C(13)	117.5(7)	116(1)
C(12)-C(11)-F C(14)-C(15)-F	112.6[a]	111[a]
F-C(11)-F F-C(15)-F	106[b]	102[b]
C(21)-C(22)-C(23)	118.4(8)	116(1)
C(21)-C(22)-O(21)	112.7(9)	116(1)
C(23)-C(22)-O(21)	128.9(8)	128(1)
C(22)-C(23)-C(24)	123.4(8)	123(1)
C(23)-C(24)-O(22)	129.5(7)	132(1)
C(25)-C(24)-O(22)	112.1(7)	111(1)
C(25)-C(24)-C(23)	118.4(8)	117(1)
C(22)-C(21)-F C(24)-C(25)-F	112.5[a]	113[a]
F-C(21)-F F-C(25)-F	106[b]	106[b]
C(31)-P-C(41)	111.4(3)	106.0(5)
C(31)-P-C(51)	107.0(4)	114.4(5)
C(41)-P-C(51)	106.3(3)	104.5(5)

a) Mean value of six C-C-F angles. b) Mean value of six F-C-F angles.

square-planar complexes [M(tfac)(tfac-*O*)(PR$_3$)] containing an *O*-unidentate tfac ligand, which is bound to the metal atom through the acetyl oxygen and the oxygen atom of the dangling trifluoroacetyl group is far from the metal atom, showing no sign of interaction.[18] On the other hand, an oxygen atom of hfac in [M(hfac)$_2$(PR$_3$)], which is obtained by a similar reaction, lies near the apical position of a square-pyramidal structure. The structural difference between these two types of complexes of similar composition may stem from (i) a greater net positive charge on the metal atom in the hypothetical complex [M(hfac)-(hfac-*O*)(PR$_3$)] caused by the lower basicity of the hfac anion than that of tfac, and (ii) preference of the *Z,Z*-form by hfac over either *E,E*-, or *E,Z*-form because of repulsions between bulky CF$_3$ groups or between CF$_3$ and the carbonyl oxygen. Thus it seems reasonable that when an hfac anion is allowed to occupy a single basal site to link to a metal atom through one of the two oxygens, the other oxygen atom of the dangling CF$_3$CO group is positioned around the apical site. The lone-pair electrons of the apical donor atom can interact with a net positive charge on the metal which is effected by incomplete neutralization of the metal charge due to low basicities of σ donors and/or by back donation through the M-L π bonding, thus completing a five-coordination. It is worth noting that the reactions between [M(hfac)$_2$] and various nitrogen bases have never given rise to five-coordinate complexes.[1]

Structures and Dynamic Behaviors of the Five-coordinate Complexes in Solution. Electronic and Infrared Spectra: The electronic spectrum of complex **1a** exhibits absorption maxima at 302 nm (ε=18200) and 410 nm (ε=2500) in dichloromethane at room temperature, and shows no appreciable change in hexane at −90 °C, suggesting that the structure of **1a** in solution does not vary in this temperature range. The absorption maxima of **2a** in dichloromethane at room temperature were observed at 275 nm (ε=11600), 280 nm (ε=11500), and 308 nm (ε=9600).

On addition of increasing amounts of P(*o*-tolyl)$_3$ to a solution of [Pd(hfac)$_2$] in hexane, the absorption

Table 6. Atom deviation from mean plane and interplanar angle

	1a	
Atom deviation (d/Å)		
Plane 1	[O(12), O(21), O(22), P]	
	Pd, 0.122(2); O(12), −0.020(5); O(21), 0.021(5); O(22), −0.020(5); P, 0.019(3)	
Plane 2	[O(11), O(12), C(11), C(12), C(13), C(14), C(15)]	
	O(11), 0.094(9); O(12), −0.114(8); C(11), −0.104(15); C(12), 0.042(12); C(13), 0.043(12); C(14), −0.012(10); C(15), 0.050(11)	
Plane 3	[O(11), C(11), C(12), C(13)]	
	O(11), −0.005(7); C(11), −0.003(14); C(12), 0.013(11); C(13), −0.004(9)	
Plane 4	[O(12), C(13), C(14), C(15)]	
	O(12), −0.000(6); C(13), −0.000(9); C(14), 0.001(9); C(15), −0.000(10)	
Plane 5	[O(21), O(22), C(21), C(22), C(23), C(24), C(25)]	
	O(21), −0.027(6); O(22), 0.015(6); C(21), −0.008(9); C(22), 0.009(8); C(23), 0.033(9); C(24), 0.015(8); C(25), −0.035(9)	
Interplanar angle (φ/°)		
	[Pd, O(11), O(12)]-Plane 2	141.1(3)
	[Pd, O(21), O(22)]-Plane 5	177.2(5)
	Plane 3–Plane 4	9.2(4)
Tortion angle (τ/°)		
	O(11)-C(12)···C(14)-O(12)	6.8(8)

Table 6. (Continued)

	2g	
Atom deviation (d/Å)		
Plane 1	[O(12), O(21), O(22), P]	
	Pt, 0.052(3); O(12), 0.077(8); O(21), −0.078(8); O(22), 0.075(8); P, −0.073(4)	
Plane 2	[O(11), O(12), C(11), C(12), C(13), C(14), C(15)]	
	O(11), 0.029(13); O(12), −0.031(11); C(11), −0.025(26); C(12), 0.045(18); C(13), −0.044(18); C(14), −0.025(15); C(15), 0.050(16)	
Plane 3	[O(21), O(22), C(21), C(22), C(23), C(24), C(25)]	
	O(21), −0.049(10); O(22), 0.042(10); C(21), 0.026(20); C(22), −0.009(16); C(23), 0.008(17); C(24), 0.026(15); C(25), −0.045(16)	
Interplanar angle (φ/°)		
	[Pt, O(11), O(12)]-Plane 2	178.9(3)
	[Pt, O(21), O(22)]-Plane 3	175.2(4)

spectrum changed stepwisely, exhibiting distinct isosbestic points at 341 and 369 nm (Fig. 4). Addition of the phosphine beyond the equimolar amount caused no further change in spectrum and the final spectrum closely resembles that of the authentic sample of **1a**. These results clearly indicate that the reaction between [Pd(hfac)$_2$] and P(o-tolyl)$_3$ affords no product other than **1a** and that the equilibrium constant of this addition reaction is very large. As is shown in Table 3, the molecular weight data for complexes **1a**, **2a**, and **2g** in dichloromethane at room temperature nearly coincide with the calculated values, indicating that these complexes are stable in solution and do not dissociate the phosphine to any appreciable extent.

Infrared spectrum of **1a** includes characteristic bands at 1690(s), 1633(vs), 1550(vs), and 1530(s) cm^{-1} and **2a** also absorbs at 1705(m), 1616(s), 1564(vs), and 1523(m) cm^{-1}. In either case, the highest-frequency band may be assigned to the ν(C=O) vibration of the CF_3CO group occupying the apical position. The other bands lie in the frequency region which is related with the ν(C=O)+ν(C=C) vibrations of the usually O,O'-chelated hfac ligand.

^{1}H NMR Spectra: The ^{1}H NMR data for the isolated complexes listed in Table 3 are given in Table 7. The ^{1}H NMR signals observed for reaction mixtures of [Pd(hfac)$_2$] with equimolar amounts of various tertiary phosphines, arsines, and phosphites are also included in Table 7. The spectra are quite similar to those of **1a** and **2g**, suggesting that the reaction products probably have the five-coordinate structures

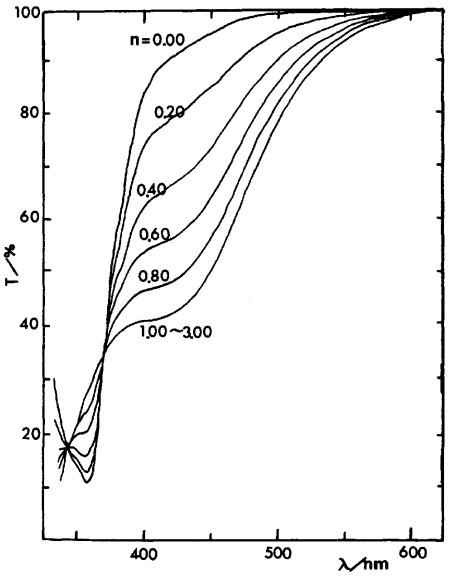

Fig. 4. Transmittance spectra of hexane solutions containing [Pd(hfac)$_2$] and n times molar amounts of P(o-tolyl)$_3$.
[complex]=1.50×10^{-4} mol dm^{-3}.

similar to those of **1a** and **2g**, although they were not isolated. Thus, in either case a single methine signal from the hfac ligands is observed at room temperature in the 5.8—6.1 ppm region except for **2i**, showing upfield shift by 0.3—0.6 ppm as compared with that from [M(hfac)$_2$]. Furthermore, the ^4J(Pt-H) values for the Pt^{II} complexes (**2**) are 5—7 Hz, about one half of 10.5 Hz for the parent bis-chelate, probably reflecting decrease in s-character of the platinum bonding with the change in structure from square to square-pyramid.

If the square-pyramidal structure in crystals is retained in solution, the two hfac ligands are not equivalent and should exhibit two methine proton

Table 7. ^{1}H NMR data for [M(hfac)$_2$L][a)]

Compd No.	M	L	Solvent	Temp °C	hfac-CH	L Me	L Ph
1a	Pd	P(*o*-tolyl)$_3$	CD_2Cl_2	27	5.85	2.31	7.2—8.1c
			CD_2Cl_2	−50	6.15, 5.47	2.94, 2.10, 1.72	7.25br, 7.57br 9.27d, br((16))
2a	Pt	P(*o*-tolyl)$_3$	CD_2Cl_2	27	5.89{5}	2.27	7.2—7.7c
			CD_2Cl_2	−60	6.34, 5.31	2.74, 2.13, 1.69	7.2br, 7.5br, 9.15d, br((18))
1b	Pd	PPh(*o*-tolyl)$_2$	$CDCl_3$	27	5.88	2.47	7.2—8.1c
2b	Pt	PPh(*o*-tolyl)$_2$	CD_2Cl_2	27	5.92{5}	2.37	7.2—8.1c
1c	Pd	PPh_3	CD_2Cl_2	27	5.87		7.3—7.9br
2c	Pt	PPh_3	CD_2Cl_2	27	5.96{5}		7.3—7.9c
2d	Pt	$PMePh_2$	$CDCl_3$	27	5.97{6}	1.90d((12)){31}	7.3—7.9c
2e	Pt	PMe_2Ph	$CDCl_3$	27	6.06{7}	1.76d((13)){33}	7.4—7.9c
2f	Pt	PEt_3	$CDCl_3$	27	6.08{5}	Et: 1.0—2.0c	
1g	Pd	PCy_3	$CDCl_3$	27	5.97	Cy: 1.9br, 1.3br	
2g	Pt	PCy_3	$CDCl_3$	27	6.04{5}	Cy: 1.9br, 1.3br	
2h	Pt	P(OPh)$_3$	$CDCl_3$	27	5.97{6}		7.1—7.5c
2i	Pt	P(OEt)$_3$	$CDCl_3$	27	6.28{6}	Et: 4.29dq(7)((7)),1.35dt(7)((2))	
1j	Pd	$AsPh_3$	$CDCl_3$	27	5.90		7.54br
2j	Pt	$AsPh_3$	$CDCl_3$	27	5.96[b)]		7.54br

a) Chemical shifts in ppm from internal Me_4Si. Figures in parentheses, double parentheses, and braces are $^3J(CH_2$-$CH_3)$, J(P-H), and J(Pt-H) in Hz, respectively. d: Doublet, t: triplet, q: quartet, br: broad, c: complex. b) The ^{195}Pt satellites are indiscernible.

signals. In fact, at lower temperatures (−50 and −60 °C) either of complexes **1a** and **2a** shows two methine and three methyl signals, indicating that the stereochemically rigid five-coordinate structure is retained in solution at low temperatures. If free rotation of the phosphine ligand around the M-P bond is prohibited, the three methyl groups attached to the phenyl rings may have different environments from each other since there exists no plane of symmetry involving the M-P bond. Signals from the phenyl-ring protons also show splitting and a 1H doublet is observed for either of **1a** and **2a** at such a low field as 9.27 and 9.15 ppm, respectively. The α-proton of a phenyl ring attached to phosphorus might exist near the sixth coordination site around the metal and suffer its paramagnetic anisotropic effect. Although such a conformation is not reallized in the crystal of **1a**, the M···H-C interaction is rather frequently noticed in metal complexes[19] especially as a prerequisite for orthometallation.[20]

At room temperature, besides the free rotation of the phosphine ligand, the five-coordinate complex may undergo some fluxional motion to average environments of the two hfac ligands. In the case of complexes **1c** and **2c** containing triphenylphosphine probably as a basal ligand, the hfac-CH signal does not show splitting even at −50 °C. The smaller steric hindrance of PPh_3 than that of P(*o*-tolyl)$_3$ may enhance the stereochemical nonrigidity of the five-coordinate complex.

^{19}F NMR Spectra: Figure 5 shows the ^{19}F{^{1}H}NMR spectra of complexes **1a** and **2a** in CD_2Cl_2 at various temperatures. At −60 °C both complexes exhibit four signals at 73.8_3, 74.6_3, 75.7_1, and 76.5_4 ppm upfield from internal $CFCl_3$ in the case of **1a** and at 73.5_4, 74.3_9, 79.5_0, and 76.9_9 ppm upfield for **2a**. These spectra are consistent with the molecular structure of **1a** in the solid, indicating nonequivalence of the four CF_3 groups. The signals from **1a** become broad with increasing temperature, coalesce at around −40 °C and give rise to a sharp singlet at -75.8_5 ppm at 22 °C. On the other hand, complex **2a** exhibits a little different behavior. Two signals in the lower field merge at 22 °C to a sharp singlet at -74.4_2 ppm (half-height width=1.6 Hz) flanked by the ^{195}Pt satellites (J(Pt-F)= 15 Hz), whereas the remaining two signals in the

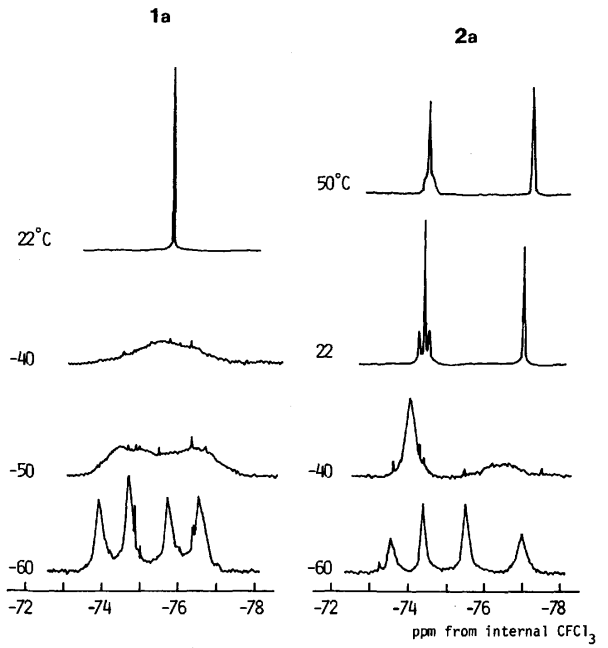

Fig. 5. ^{19}F{^{1}H} NMR spectra at 84.31 MHz of [Pd(hfac)$_2$-{P(*o*-tolyl)$_3$}] (**1a**) and [Pt(hfac)$_2${P(*o*-tolyl)$_3$}] (**2a**) in CD_2Cl_2 at several temperatures.

higher field are converted into a broader singlet at -77.0_1 ppm (half-height width=2.9 Hz). However, the two signals broaden at 50 °C, indicating that complex **2a** may behave in the same way as **1a** does but need much larger energy than **1a**.

Exchange between the basal and apical hfac ligands may be achieved by a twist motion via a trigonal-bipyramidal transition state as depicted in Eq. 1.

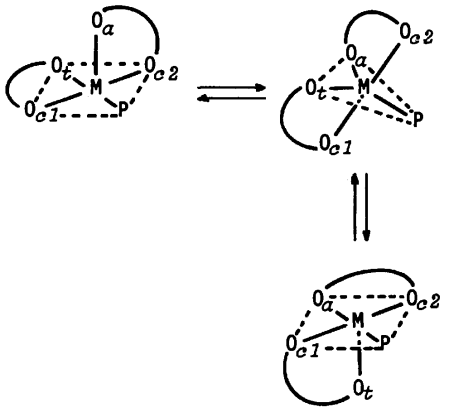

(1)

However, two halves of each hfac anion are not yet equivalent under this rapid motion. One half of each hfac is always near the site cis to phosphorus, while the other lies trans to P or at the apical site, being averaged. The ^1H and ^{19}F NMR spectra of complex **2a** at 22 °C are satisfactorily interpreted by this rapid intramolecular transformation (Eq. 1). Of the two ^{19}F signals, the lower-field one flanked by the ^{195}Pt satellites may be assigned to the CF_3 groups positioned cis to the phosphine, and the other broader high-field one to the average of CF_3 groups at the apical and trans sites, since the ^{19}F atoms around the positions cis to phosphine will couple to platinum more strongly than those around the apical and trans positions.

The ^{19}F NMR spectrum of **1a** at 22 °C can not be explained solely by Eq. 1, but needs another fluxional mode to average the cis and trans or apical positions. A simple oscillatory motion of the apical chelate ring as depicted in Eq. 2 may be sufficent to supplement mechanism (1) in averaging all four CF_3 groups.

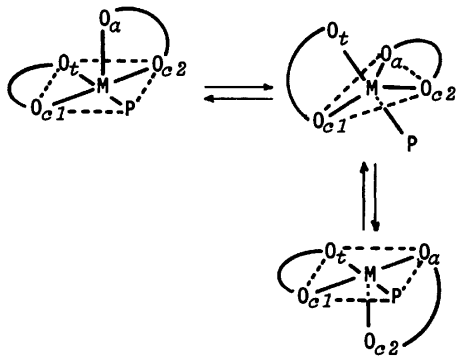

(2)

The ^1H NMR spectrum of a quasi square-pyramidal complex *cis*-$[PtCl(PEt_3)_2(phen)]BF_4$[21] showed that the two halves of phen are environmentally averaged in solution even at −80 °C.[22] The mechanism of the fluxional motion can not be dissociative, since couplings between Pt and both P and α-H of phen are retained in the fast-exchange limit NMR spectra. The ^{31}P NMR spectra also certified retention of the mutually cis arrangement of the PEt_3 ligands. All these findings are consistent with mechanism (2).[22] The fluxional process by which the metal changes its point of attachment to the α-diimine ligand in some *trans*-$[MCl_2L(dim)]$ complexes (M=Pd, Pt; L=unidentate tertiary phosphine or arsine) was also interpreted based on the same mechanism, that is oscillatory motion of the chelated α-diimine in a five-coordinate square-pyramidal intermediate.[23]

The observed ^{19}F NMR spectra of **1a** in Fig. 5 are rationalized if the Pd^{II} complex undergoes both modes of intramolecular rearrangement (Eqs. 1 and 2) concurrently. Alternatively, either one of the twist motions analogous to those proposed by Ray and Dutt, Bailar, and Springer and Sievers as the intramolecular mechanism for racemization of octahedral complexes[24] will also be effective for averaging environments of some fluorine atoms in **1a**. For example Eq. 3 shows the Ray-Dutt twist, in which the (O_{c1}, O_t) chelate ring rotates by 90 ° on the basal plane and the (O_a, O_{c2}) chelate ring moves synchronously on the plane perpendicular to the P-M axis.

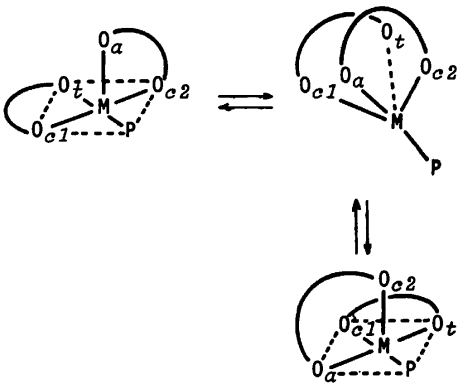

(3)

It should be noted that mechanism (3) does not exchange the basal and apical hfac ligands although both halves of each hfac are averaged. Therefore it is only supplementary to mechanism(1) in averaging all four CF_3 groups.

After we had completed this investigation,[6] Siedle and his collaborators[17] reported the X-ray structure of $[Pd(hfac)_2(PPh_3)]$ which is quite similar to that of **1a** and analyzed the dynamic ^{19}F NMR spectra of **1a** in CD_2Cl_2 to obtain the activation parameters, $\Delta H^{\ddagger}=7.7\pm1$ kcal mol^{-1} and $\Delta S^{\ddagger}=-20\pm5$ cal deg^{-1} mol^{-1} (1 cal=4.184 J). They preferred a transition state of the square-pyramidal structure with the phosphine ligand at the apical position which makes all CF_3 groups equivalent. However, this symmetrical transition state may need a much higher activation energy, since the five-coordinate $Pd^{II}$and Pt^{II} complexes cited above have the strongly-bonding ligands such as tertiary phosphines and the cyanide ion exclusively at the basal positions. Figure 5 clearly indicates that four CF_3 groups are averaged not simultaneously by a single process, but by two consecutive processes at least in the case of Pt^{II} complex **2a**. Wernberg and Hazell[15] found that $[PtCN(phen)_2]^+$ has a square-

pyramidal structure in the solid state with one of the phenanthroline nitrogens at the apical position, but its ^{13}C NMR spectrum showed no difference between the two phen ligands and furthermore both halves of each chelating molecule gave identical signals. They proposed the intramolecular transformation processes *via* trigonal bipyramids, denying a square-pyramidal transition state with the cyanide at the apical position because of the steric hindrance between the two phen molecules on the basal plane.[15]

^{13}C NMR Spectra: Table 8 lists the ^{13}C NMR data. Complex **1a** shows one set of signals. On the other hand, **2a**, **2b**, and **2g** exhibit two sets of signals from the CF_3 and CO carbons, although the CH signal is single in each case. These spectral features are quite similar to those observed for ^{1}H and ^{19}F NMR spectra and rationalized by mechanism (1) for the Pt^{II} complexes and combined (1) and (2) for the Pd^{II} complexes. The carbonyl-carbon signals from **2g** in $CDCl_3$ are composed of two quartets, of which only the higher-field set couples to platinum (^2J(Pt-C)=16 Hz) and is assigned to the two CO carbons positioned cis to the phosphine. The CF_3 carbons also exhibit two sets of signals. One is a quartet flanked by the ^{195}Pt satellites (J(Pt-C)=89 Hz) and assigned to the CF_3 groups positioned cis to the phosphine. The other is a doublet of quartets coupling to ^{31}P and is considered to be an averaged signal from the CF_3 groups at the trans and apical sites, of which the ^{195}Pt satellites are indiscernible.

The ^{13}C NMR spectrum of **2g** in C_6D_6 at room temperature is quite similar to that in $CDCl_3$, but the CF_3 carbon signal at 80 °C appears as a single doublet of quartets, indicating that environments of all four CF_3 groups are averaged at this temperature. The ^1J(F-C) (286 Hz) and ^4J(P-C) (2 Hz) values are also averaged. The fluxional motion is rapid at room temperature for all Pd^{II} complexes and [Pt(hfac)$_2$(PPh$_3$)] (**2c**), the averaged ^1J(C-F) value being 286 Hz in either case. The rate of fluxional motion decreases with increasing bulkiness of tertiary phosphines in the sequence $PPh_3 > PCy_3 > P(o\text{-tolyl})_3$. The ^{195}Pt NMR signal from **2a** in $CDCl_3$ was recorded as a doublet at 295.7 ppm upfield from external $K_2[PtCl_4]$, ^1J(Pt-P) being 448_5 Hz.

^{31}P NMR Spectra: The ^{31}P{^{1}H} NMR data are collected in Table 9. The ^1J(Pt-P) values are rather large lying in the range of 4130—4540 Hz. The δ_P and

Table 8. ^{13}C NMR Data for [M(hfac)$_2$L] at 30 °C[a]

Compd	Solvent	hfac			L	
		CF_3	CH	CO	Me	Ph
1a	$CDCl_3$	116.6q [286]	89.5 (165)	174.0q [34]	23.0 (127)((7))	C^1 121.9d((60)), C^2 143.0d((9)), C^3 132.2d(161)((9)), C^4 132.3d(164)((3)), C^5 126.2d(164)((13)), C^6 135.4d(162)((13))
2a	$CDCl_3$	116.3q [283]{90} 116.8dq [288]((5))	91.7 (164){44}	174.3q [34]{b} 169.4q [34]	22.7d (127)((6))	C^1 121.6d((66)){19}, C^2 142.9d((9)){19} C^3 132.2d(164)((12)), C^4 132.0d(164)((2)) C^5 125.9d(164)((12)), C^6 135.5d(168)((13)){21}
2b	CD_2Cl_2	b)	92.4 {45}	174.7 [34]{b} 170.1 [36]		
1c	$CDCl_3$	116.7dq [286]((3))	89.5 (164)	174.3q [34]		C^1 124.4d((58)), C^2,C^6 134.2d(164)((11)) C^3,C^5 128.9d(161)((12)), C^4 132.2d(163)((3))
2c	CD_2Cl_2	117.1dq [286]((2))	92.2 {45}	172br		C^1 125.2d((68)){27}, C^2,C^6 134.4d((11)){21} C^3,C^5 129.0d((12)), C^4 132.3d((3))
2e	$CDCl_3$	b)	92.3 {51}	b)	9.8d ((45)){29}	b)
2f	$CDCl_3$	117.0q [286]	92.2 {63}	174.7q {33}	Et: CH_3 6.8d((3)){21}, CH_2 13.2d((39)){31}	
1g	$CDCl_3$	117.0dq [286]((3))	89.5 (164)	174.1q [34]		Cy: C^1 31.7d((24)), C^2,C^6 27.3d((12)) C^3,C^5 28.4d((3)), C^4 26.1d((2))
2g	$CDCl_3$	117.1q [284]{89} 117.1dq [288]((4))	91.5 {44}	169.4q [34]{16} 174.5q [35]		Cy: C^1 30.5d((32)){24}, C^2,C^6 27.3d((12)) C^3,C^5 28.3d((2)){17}, C^4 26.3d((2))
	C_6D_6	117.6q [284]{b} 117.6dq [288]((4))	92.0 (163){44}	169.6q [34]{18} 176.3q [35]		Cy: C^1 30.6d(b)((33)){24}, C^2, C^6 27.5d(b)((11)) C^3,C^5 28.5d(b)((3)){20}, C^4 26.4d(b)((2))
	C_6D_6[c]	117.8dq [286]((2))	92.4 {43}	173br		Cy: C^1 31.2d((32)){25}, C^2,C^6 27.6d((12)) C^3,C^5 28.8d((3)){18}, C^4 26.5d((2))
1j	$CDCl_3$	116.4q [286]	89.8	174.3q [33]		C^1 126.8, C^2,C^6 133.3, C^3,C^5 129.5, C^4 131.7

a) Chemical shifts in ppm from internal Me_4Si. Figures in parentheses, double parentheses, braces, and brankets are ^1J(C-H), J(P-C), J(Pt-C), and J(F-C) in Hz, respectively. d=Doublet, q=quartet. b) Indiscernible. c) At 80 °C.

Table 9. $^{31}P\{^1H\}$ NMR data for $[M(hfac)_2(PR_3)]$[a]

Compd	Solvent	Temp °C	δ_P ppm	^1J(Pt-P) Hz
1a	CD_2Cl_2	30	18.7	
		−50	18.0	
2a	CD_2Cl_2	30	−7.4	447_4
		−50	−8.2	442_2
1c	CD_2Cl_2	30	20.9	
		−50	21.4	
2c	CD_2CL_2	30	−4.6	454_1
		−50	−4.1	448_0
2e	$CDCl_3$	30	−22.9	437_2
2f	$CDCl_3$	30	2.7	425_3
1g	$CDCl_3$	30	45.5	
		−30	46.3	
2g	$CDCl_3$	30	12.6	418_4
		−30	13.2	413_4

a) Chemical shifts (δ_P) in ppm from external H_3PO_4 at 30 °C (downfield positive).

^1J(Pt-P) values show no appreciable change with temperature in the −50 to +30 °C region, indicating retention of the five-coordinate structure. When an equimolar amount of PMe_2Ph or PEt_3 was added to $[Pt(hfac)_2]$ in $CDCl_3$, signals assignable to $[Pt(hfac)(PR_3)_2](hfac)$ appeared besides those from **2e** and **2f**, respectively, and increased with time in the expense of the latters. The disproportionation reactions of **2e** and **2f** to produce $[Pt(hfac)(PR_3)_2](hfac)$ and $[Pt(hfac)_2]$ were completed in about 2 d. The tertiary phosphines in the square-planar complexes $[Pt(hfac)(PR_3)_2](hfac)$ give the ^{31}P NMR signals in the 5—10 ppm lower field than those in the corresponding five-coordinate complexes and their ^1J(Pt-P) values are appreciably lower lying in the region of 3670—4020 Hz. On the other hand, $[Pd(hfac)_2]$ reacts with equimolar amounts of PMe_2Ph and PEt_3 rapidly with heat evolution to afford $[Pd(hfac)(PR_3)_2](hfac)$ exclusively. NMR signals assignable to the five-coordinate complexes were not detected.

When an equimolar amount of PPh_3 is added to $[M(hfac)_2]$ (M=Pd and Pt) and PCy_3 to $[Pd(hfac)_2]$ in CD_2Cl_2, complexes **1c**, **2c**, and **1g** are formed in equilibrium with small amounts of the $[M(hfac)(PR_3)_2](hfac)$-type complexes, respectively. (In the case of **1c**, signals attributable to $[Pd(hfac)(hfac\text{-}C^3)(PPh_3)]$ are also observed.) When another equivalent of phosphines is added to the solution, only the signals from $[M(hfac)(PR_3)_2](hfac)$ are observed. On the other hand, complexes **1a**, **2a**, and **2g** are quite stable in $CDCl_3$ and do not react with excess amounts of phosphines. These observations indicate that the thermodynamic stability of the five-coordinate complex becomes higher with increase in the bulkiness (cone angle[25]) of tertiary phosphine in the sequence $PPhMe_2 \approx PEt_3 < PPh_3 < PCy_3 < P(o\text{-tolyl})_3$. Difference in behaviors of **1g** and **2g** suggests that the stability of the five-coordinate complex is higher for platinum(II) than for palladium(II).

We wish to thank Mr. Junichi Gohda and Dr. Isamu Kinoshita for elemental analysis and measurements of electronic spectra at low temperatures, respectively. We also are grateful to Mr. Tetsu Hinomoto of JEOL, Ltd. for measurements of the ^{19}F and ^{195}Pt NMR spectra.

References

1) a) S. Okeya, H. Sazaki, M. Ogita, T. Takemoto, Y. Onuki, Y. Nakamura, B. K. Mohapatra, and S. Kawaguchi, *Bull. Chem. Soc. Jpn.*, **54**, 1978 (1981); b) S. Okeya, H. Yoshimatsu, Y. Nakamura, and S. Kawaguchi, *ibid.*, **55**, 483 (1982); c) S. Okeya, Y. Nakamura, and S. Kawaguchi, *ibid.*, **55**, 1460 (1982).
2) S. Okeya, Y. Nakamura, and S. Kawaguchi, *Bull. Chem. Soc. Jpn.*, **54**, 3396 (1981).
3) F. Basolo and R. G. Pearson, "Mechanisms of Inorganic Reactions," 2nd ed, Wiley, New York (1967), p. 351; L. Cattalini, *Progr. Inorg. Chem.*, **13**, 263 (1970).
4) In the reaction of $RhCl\{Sb(p\text{-tolyl})_3\}$(1,5-cyclooctadiene) with nitrogen bases, the five-coordinate intermediate is exceptionally stable and detected spectroscopically: L. Cattalini, R. Ugo, and A. Orio, *J. Am. Chem. Soc.*, **90**, 4800 (1968).
5) S. Matsumoto and S. Kawaguchi, *Bull. Chem. Soc. Jpn.*, **54**, 1704 (1981).
6) S. Okeya, T. Miyamoto, S. Ooi, Y. Nakamura, and S. Kawaguchi, *Inorg. Chim. Acta*, **45**, L135 (1980).
7) S. Okeya, S. Ooi, K. Matsumoto, Y. Nakamura, and S. Kawaguchi, *Bull. Chem. Soc. Jpn.*, **54**, 1085 (1981); S. Okeya and S. Kawaguchi, *Inorg. Synth.*, **20**, 65 (1980).
8) L. K. Templeton and D. H. Templeton, Abstracts, American Crystallographic Association Proceedings (1973), Series 2, Vol. 1.
9) "International Tables for X-Ray Crystallography," Kynoch Press, Birmingham, (1974), Vol. IV.
10) "UNICS," The Crystallographic Society of Japan (1969).
11) C. K. Johnson, ORTEP II, Report ORNL-5138, Oak Ridge National Laboratory, Oak Ridge, TN (1976).
12) K. M. Chui and H. M. Powell, *J. Chem. Soc., Dalton Trans.*, **1974**, 1879.
13) K. M. Chui and H. M. Powell, *J. Chem. Soc., Dalton Trans.*, **1974**, 2117.
14) W. J. Louw, D. J. A. de Waal, and G. J. Kruger, *J. Chem. Soc., Dalton Trans.*, **1976**, 2364.
15) O. Wernberg and A. Hazell, *J. Chem. Soc., Dalton Trans.*, **1980**, 973.
16) A. R. Siedle, R. A. Newmark, and L. H. Pignolet, *J. Am. Chem. Soc.*, **103**, 4947 (1981).
17) A. R. Siedle, R. A. Newmark, and L. H. Pignolet, *J. Am. Chem. Soc.*, **104**, 6584 (1982).
18) S. Ooi, T. Matsushita, K. Nishimoto, S. Okeya, Y. Nakamura, and S. Kawaguchi, *Bull. Chem. Soc. Jpn.*, **56**, 3297 (1983).
19) For example, A. Musco, W. Kuran, A. Silvani, and M. W. Anker, *J. Chem. Soc., Chem. Commun.*, **1973**, 938; W. Kuran and A. Musco, *Inorg. Chim. Acta*, **12**, 187 (1975); S. Otsuka, T. Yoshida, M. Matsumoto, and K. Nakatsu, *J. Am. Chem. Soc.*, **98**, 5850 (1976); Z. Dawoodi, M. L. H. Green, V. S. B. Mtetwa, and K. Prout, *J. Chem. Soc., Chem. Commun.*, **1982**, 802, 1410.
20) For example, G. L. Geoffroy and R. Pierantozzi, *J. Am. Chem. Soc.*, **98**, 8054 (1976); E. L. Muetterties, *Chem. Soc. Rev.*, **11**, 283 (1982).
21) G. W. Bushnell, K. R. Dixon, and M. A. Khan, *Can. J. Chem.*, **52**, 1367 (1974).
22) K. R. Dixon, *Inorg. Chem.*, **16**, 2618 (1977).
23) H. van der Poel, G. van Koten, and K. Vrieze, *Inorg. Chem.*, **19**, 1145 (1980).
24) C. S. Springer, Jr. and R. E. Sievers, *Inorg. Chem.*, **6**, 852 (1967).
25) C. A. Tolman, *Chem. Rev.*, **77**, 313 (1977).

Hydrophobic Vitamin B_{12}. II. Coordination Geometry and Redox Behavior of Heptamethyl Cobyrinate in Nonaqueous Media†

Yukito MURAKAMI,* Yoshio HISAEDA, Akiro KAJIHARA, and Teruhisa OHNO
Department of Organic Synthesis, Faculty of Engineering, Kyushu University, Hakozaki, Higashi-ku, Fukuoka 812
(Received August 12, 1983)

The nuclear cobalt(II) ion in heptamethyl cobyrinate iodide, Cob(II)ester·I, was found to assume a distorted square-planar geometry of $Co-N_4$ type with iodide as a counterion in a polar solvent (methanol) and a square-pyramidal one of $Co-N_4I$ type with the iodide ion coordinated at one of the axial positions in apolar solvents such as dichloromethane, benzene, and toluene. The redox chemistry of Cob(II)ester·I and heptamethyl cobyrinate perchlorate, [Cob(II)ester]ClO_4, was investigated in various organic solvents by means of cyclic voltammetry and controlled-potential electrolysis. The Co(II)/Co(I) and Co(III)/Co(II) redox potentials for [Cob(II)ester]ClO_4 exhibited cathodic shifts as either solvent basicity or polarity was raised, and were found to be in the anodic side relative to the corresponding potentials for Co^{II}(tpp) under identical conditions. The medium effect on the redox behavior of hydrophobic vitamin B_{12} was discussed in connection with the microenvironmental effect on vitamin B_{12} placed in the enzyme active sites.

We have been dealing with hydrophobic vitamin B_{12} derivatives in order to simulate various functions of vitamin B_{12} as exerted in the hydrophobic active sites of enzymes concerned. One of hydrophobic vitamin B_{12} derivatives involving a largely polarizable ion (iodide) shows different colors in solution as the solvent nature changes. Cob(II)ester·I has been prepared originally by Werthemann *et al.*,[1] and the X-ray diffraction analysis of its single crystal has shown that the complex is in a dimeric form which contains one bridging iodide per dimer complex and the second iodide ion is not coordinated.[2] However, any comprehensive structural clarification of the complex in solution has not been carried out yet. Thus, we studied firstly in this work the structures of Cob(II)ester·I in various organic solvents to clarify the origin of color change.

The redox behavior of vitamin B_{12} has recently been examined rather extensively,[3-9] and the studies on its catalytic reactions have been carried out by electrochemical means.[10-13] However, the redox chemistry of vitamin B_{12} in organic solvents has not been investigated because of its insolubility in most of such solvents. Thus, the redox behavior of hydrophobic vitamin B_{12} derivatives in various organic media was examined in this work by means of cyclic voltammetry in order to obtain useful information for the redox property of vitamin B_{12} under various microenvironmental conditions comparable to the enzyme active sites. In addition, the redox potentials of heptamethyl cobyrinate perchlorate, [Cob(II)ester]-ClO_4, were compared with those of (5,10,15,20-tetraphenylporphinato)cobalt(II), Co^{II}(tpp), evaluated under identical conditions, so that the intrinsic ligand effect on the redox behavior of vitamin B_{12} is to be characterized.

Experimental

Materials. Cob(II)ester·I was prepared by the

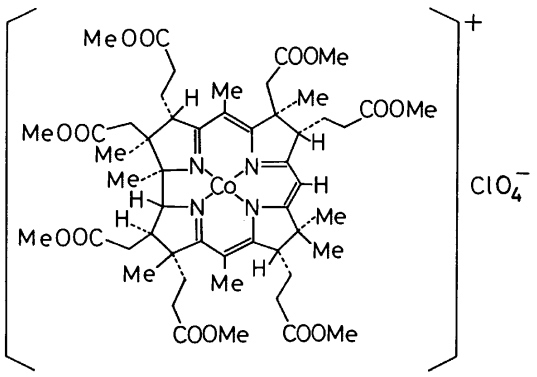

[Cob(II)ester] ClO_4

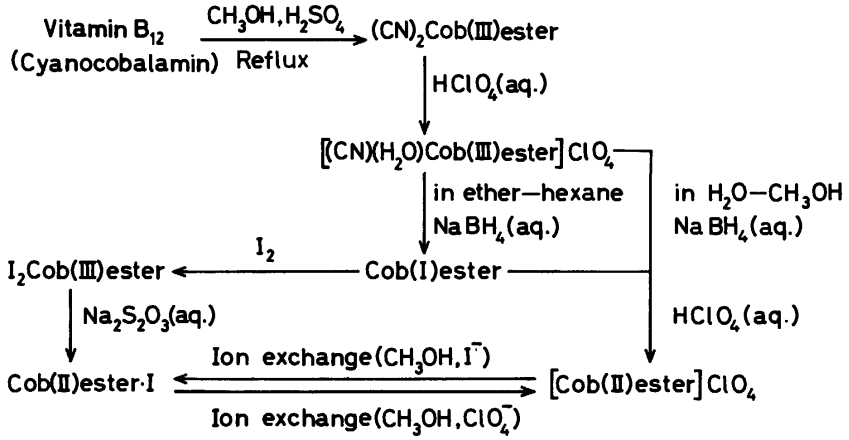

Scheme 1.

† Contribution No. 707 from this Department.

procedures outlined in Scheme 1 after the method of Werthemann *et al.*[1] [Cob(II)ester]ClO_4[14] and Co^{II}(tpp)[15] were synthesized according to the reported procedures. Tetrabutylammonium perchlorate (TBAP), tetrabutylammonium iodide (TBAI) of polarographic grade and ferrocene of guaranteed reagent grade were commercially obtained from Nakarai Chemicals. Organic solvents used for electrochemical measurements were purified and dried according to the standard procedures[16] and kept over 4-Å Molecular Sieves.

General Measurements. Electronic absorption spectra and diffuse reflectance spectra were recorded on a Hitachi 340 recording spectrophotometer. ESR spectra were obtained on a JEOL JES-ME 3 X-band spectrometer equipped with a 100-kHz field modulation unit; a standard MgO/Mn^{II} sample calibrated with a NMR magnetometer was employed for calibration of the magnetic field. Molecular weight measurements were carried out with a Hitachi Perkin-Elmer 115 vapor pressure osmometer by using benzene as a solvent.

Electrochemical Measurements. Cyclic voltammograms were obtained on a YANACO P-8 polarograph. An electrochemical cell similar to that reported in literature[17] was used and equipped with platinum wire of 0.5-mm diameter as working and auxiliary electrodes. A saturated calomel electrode (SCE) or an Ag/AgCl electrode was served as a reference which was separated from a bulk electrolyte solution by a salt bridge prepared with benzylidene-D-sorbitol[18] and a nonaqueous solution of TBAP (5.0×10^{-2} mol dm^{-3}). Nonaqueous solutions containing the cobalt complex (*ca.* 5×10^{-4} mol dm^{-3}) and TBAP (*ca.* 5×10^{-2} mol dm^{-3}) were deaerated prior to each measurement, and the inside of the cell was maintained under argon atmosphere throughout each measurement. All the measurements were carried out at 20 ± 2 °C. The scan rate was varied in a range from 10 through 200 mV s^{-1}. Half-wave potentials ($E_{1/2}$) and anodic and cathodic currents were evaluated according to the method described previously.[19]

Controlled-potential electrolysis was carried out in a three-electrode cell modified for electronic spectral measurements, as described previously.[19] An applied potential between the working and reference electrodes was maintained constant with a conventional potentiostat and monitored with a Takeda Riken TR-6656 digital multimeter.

Results and Discussion

Coordination Geometry of Cob(II)ester · I in Solution. Cob(II)ester · I shows two different kinds of electronic spectra in solution depending upon the nature of solvents (Figs. 1 and 2). The complex in methanol shows a spectral feature which is characteristic of the base-off vitamin B_{12r} in aqueous media and comparable to those of [Cob(II)ester]ClO_4 observed in methanol and dichloromethane. The diffuse reflectance spectrum of [Cob(II)ester]ClO_4 shown in Fig. 1 is apparently comparable to the spectrum of Cob(II)ester · I in methanol. Cob(II)ester · I has been known to be in a dimeric form with a single μ-iodo bridging between two cobalt atoms in the solid state as confirmed by the X-ray diffraction study.[2] The solution spectrum of Cob(II)ester · I in dichloromethane is apparently comparable to its diffuse reflectance spectrum as shown in Fig. 2. In order to identify the coordination geometry

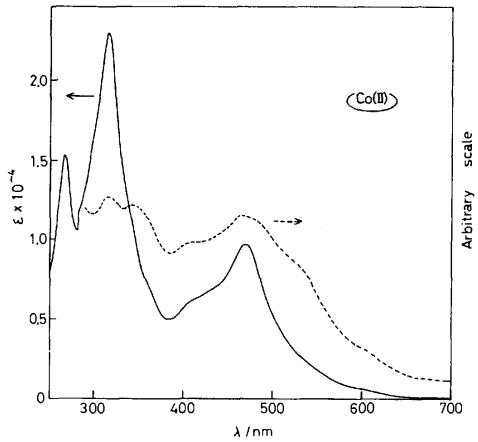

Fig. 1. Electronic absorption spectrum of Cob(II)ester · I (4.47×10^{-5} mol dm^{-3}) in methanol (solid line) and diffuse reflectance spectrum of [Cob(II)ester]ClO_4 (broken line) at room temperature.

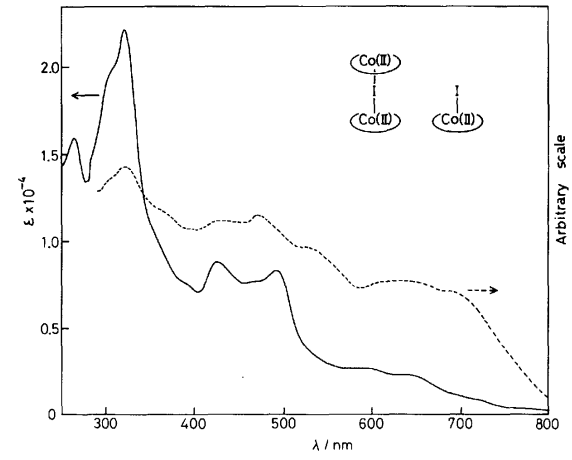

Fig. 2. Electronic absorption spectrum in dichloromethane (solid line; concentration of the complex, 4.90×10^{-5} mol dm^{-3}) and diffuse reflectance spectrum (broken line) of Cob(II)ester · I at room temperatue.

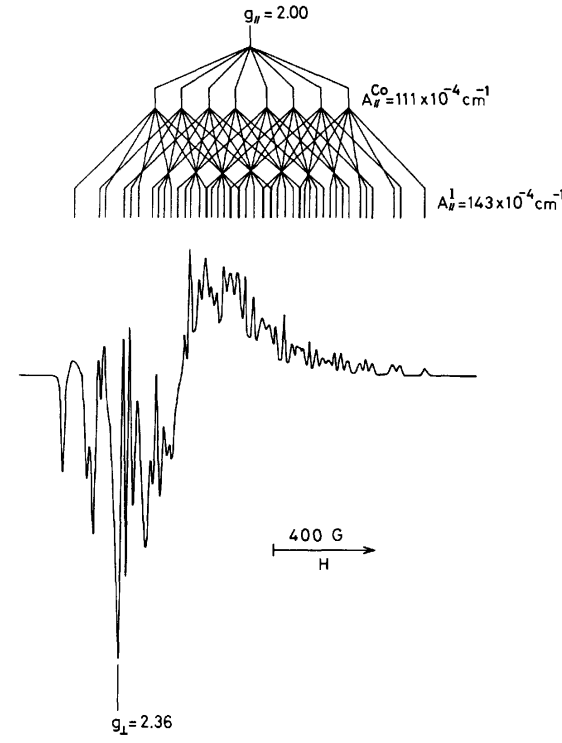

Fig. 3. ESR spectrum of Cob(II)ester · I (5.87×10^{-3} mol dm^{-3}) in toluene at 77 K.

of this complex in dichloromethane, another spectroscopic method was adopted in view of the advantageous property of Cob(II)ester · I in dichloromethane as being paramagnetic.

The ESR spectrum of Cob(II)ester · I in toluene at 77 K is shown in Fig. 3. Spin Hamiltonian parameters for the complex are as follows; $g_{\parallel}=2.00$, $g_{\perp}=2.36$, $A_{\parallel}^{Co}=11.1\times10^{-3}\,cm^{-1}$, and $A_{\parallel}^{I}=14.3\times10^{-3}\,cm^{-1}$. The superhyperfine structure observed in the $g_{\parallel}$ region is apparently due to the interaction between the iodine nucleus ($I=5/2$) and the cobalt nucleus ($I=7/2$). This indicates that one iodide ion is coordinated to the central cobalt at one of the axial positions of the latter. The spin Hamiltonian parameters thus evaluated are comparable to those for the same complex as measured by the Q-band ESR spectroscopy at 120 K in toluene; $g_{\parallel}=2.003$, $g_{\perp}=2.263$, $A_{\parallel}^{Co}=11.2\times10^{-3}\,cm^{-1}$, $A_{\parallel}^{I}=14.0\times10^{-3}\,cm^{-1}$, $A_{\perp}^{Co}\approx0$, and $A_{\perp}^{I}\approx0$.[20] An ESR signal due to forbidden transition, being characteristic of a dinuclear cobalt complex, was not observed for a wide scanning range of magnetic field. Consequently, the present complex is not associated with the interaction between cobalt-iodide-cobalt in dichloromethane. The ESR spectrum of Cob(II)ester · I measured in methanol at 77 K did not show such superhyperfine structure as caused by the interaction between the iodine and cobalt nuclei, but showed a spectral feature identical with that observed for [Cob(II)ester]ClO_4.[14] This again serves to confirm that the iodide ion is not coordinated to the cobalt atom at its axial position.

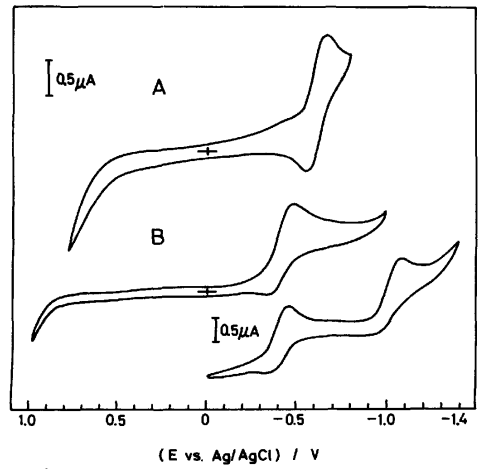

Fig. 4. Cyclic voltammograms of [Cob(II)ester]ClO_4 (5.0×10^{-4} mol dm^{-3}) containing 5.0×10^{-2} mol dm^{-3} TBAP in methanol (A) and dichloromethane (B) at 20±2 °C: scan rate, 100 mV s^{-1}.

Cob(II)ester · I in methanol was readily converted into [Cob(II)ester]ClO_4 by ion-exchange chromatography on a column of Amberlite IRA-401. This result also indicates that the iodide ion is acting only as a counteranion in methanol.

The molecular weight of Cob(II)ester · I was determined in benzene by vapor pressure osmometry: 1120±70; calcd for Cob(II)ester · I as monomer, 1164. This result further serves to confirm that Cob(II)ester · I is not dimeric but monomeric in apolar solvents.

In summarizing the above results, the coordination geometry around the nuclear cobalt of Cob(II)ester · I is subjected to change by the nature of solvents employed. In polar solvents such as methanol, the complex assumes a distorted square-planar geometry around the cobalt atom and the anion of weak coordination ability, iodide, simply acts as a counterion species even though solvent molecules would possibly occupy the axial positions of cobalt. In apolar solvents such as dichloromethane, benzene, and toluene, however, the complex assumes a square-pyramidal geometry around the nuclear cobalt having coordination number 5, the iodide ion being coordinated to the cobalt atom at its axial position, and exists as a mononuclear species in solution. Such coordination structures are closely correlated with the redox behavior of the complex as described below.

Electrochemical Behavior of Cob(II)ester Species. Cyclic voltammograms of [Cob(II)ester]ClO_4 and Cob(II)ester · I in methanol and dichloromethane are shown in Figs. 4 and 5. The Co(II)/Co(I) redox couple for [Cob(II)ester]ClO_4 is observed at −0.61 V *vs.* Ag/AgCl (−0.65 V *vs.* SCE) in methanol and at −0.41 V *vs.* Ag/AgCl (−0.45 V *vs.* SCE) in dichloromethane. The redox reversibility observed with [Cob(II)ester]ClO_4 and

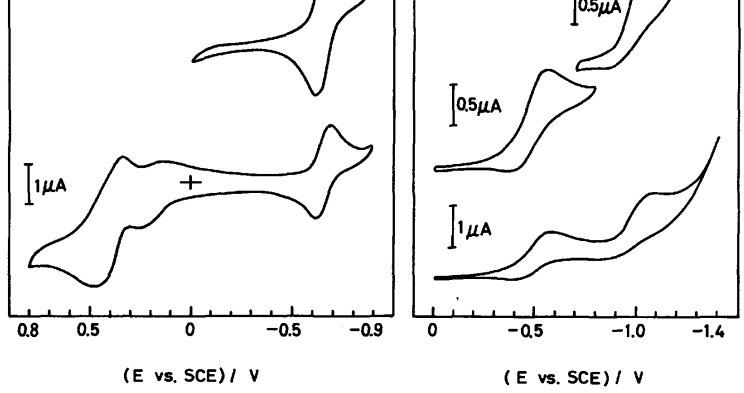

Fig. 5. Cyclic voltammograms of Cob(II)ester · I (7.0×10^{-4} mol dm^{-3}) containing 5.0×10^{-2} mol dm^{-3} TBAI in methanol (A) and dichloromethane (B) at 20±2 °C: scan rate, 100 mV s^{-1}.

Cob(II)ester·I in dichloromethane is less satisfactory as compared with that in methanol on the basis of relative potential peak intensities between the cathodic and anodic peaks; the redox process was irreversible in dichloromethane even at the scan rate as fast as 500 mV s^{-1} and the anodic peak disappeared at the slowest extreme. This is attributed to the fact that Cob(I)ester formed by electrochemical reduction undergoes reaction with dichloromethane to yield the corresponding alkylated complex [ClH_2C-Cob(III)ester] as confirmed independently by a preparative experiment. Scanning further to the cathodic side showed a one-electron reduction peak at −1.07 V *vs.* Ag/AgCl (−1.11 V *vs.* SCE). This reduction peak seems to be attributed to the alkyl complex derived from the reaction of Cob(I)ester with dichloromethane, ClH_2C-Cob(III)ester, in the light of the first reduction potential for [CH_3-Cob(III)ester]ClO_4 in dichloromethane (−1.23 V *vs.* SCE). The Co(III)/Co(II) redox peak was not observed under the above experimental conditions.

The cyclic voltammograms of Cob(II)ester·I in the presence of TBAI as a supporting electrolyte show redox peaks due to the iodide ion in the positive potential range (Fig. 5). The Co(II)/Co(I) redox peak for Cob(II)ester·I is observed at −0.65 V *vs.* SCE in methanol; comparable to that for [Cob(II)ester]ClO_4 in methanol. However, the same redox peak is observed at −0.52 V *vs.* SCE in dichloromethane; shifted by 70 mV to the cathodic side relative to the potential peak for [Cob(II)ester]ClO_4. Since the iodide ion acts as an axial ligand in dichloromethane, the reduction of Cob(II)ester·I requires greater cathodic potential relative to that of [Cob(II)ester]ClO_4. The Co(II)/Co(I) redox peak exhibits some anodic shift in dichloromethane relative to that in methanol even though the liquid junction potential difference between the two solvent systems is taken into consideration as described below. It is reasonable to expect that Cob(II)ester is more readily reduced in dichloromethane since this solvent is of noncoordinating nature and Cob(I)ester without charge on it is stabilized in highly apolar solvents.

Redox Potentials of [Cob(II)ester]ClO_4 in Various Solvents. The Co(II)/Co(I) and Co(III)/Co(II) redox potentials for [Cob(II)ester]ClO_4 in various organic solvents are summarized in Table 1. Cyclic voltammograms of the complex in dimethyl sulfoxide (DMSO) are shown in Fig. 6 as a typical example. The ratios between anodic and cathodic peak currents, i_{pa}/i_{pc}, were unity and independent of scan rate (from 10 to 200 mV s^{-1}) for the two redox couples in various organic solvents except dichloromethane. Plots of i_p ($=i_{pa}+i_{pc}$) *vs.* $v^{1/2}$(v for scan rate, mV s^{-1}) were linear, and potential separation between the anodic and cathodic peaks varied from 160 to 80 mV for the two redox couples, while $E_{1/2}$ values remained constant within an accuracy of ±3% regardless of scan rate variation. Thus, the present electrochemical redox reactions in various organic media except dichloromethane are consistent with reversible or quasi-reversible one-electron transfer processes.[21] In order to identify the complex species formed during each redox process, the controlled-potential electrolysis was performed at −1.20 and 0.80 V *vs.* SCE. The electrochemical reduction at −1.20 V *vs.* SCE was followed by electronic spectroscopy as shown in Fig. 7, where clear isosbestic points are observed at 308, 355, 417, and 547 nm. Since the developing absorption maximum at 394 nm during the reduction process is characteristic of Cob(I)ester, the redox potential at −0.64 V *vs.* SCE in DMSO is

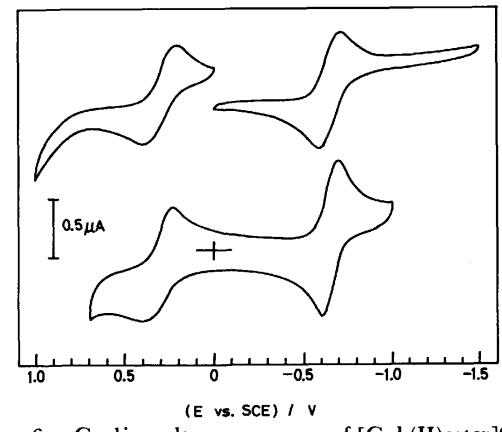

Fig. 6. Cyclic voltammograms of [Cob(II)ester]ClO_4 (5.2×10^{-4} mol dm^{-3}) in dimethyl sulfoxide containing 5.1×10^{-2} mol dm^{-3} TBAP at 20±2 °C: scan rate, 100 mV s^{-1}.

Table 1. Redox potentials for Cob(II)ester and Co^{II}(tpp) in nonaqueous media[a]

Complex	Medium[b]	Solvent parameters		*vs.* SCE/V		*vs.* (Fc^+/Fc)[c]/V	
		DN	*Z*	Co(III)/Co(II)	Co(II)/Co(I)	Co(III)/Co(II)	Co(II)/Co(I)
[Cob(II)ester]ClO_4[d]	CH_2Cl_2	0	64.2	—	−0.45	—	−1.00
	CH_3COCH_3	17.0	65.7	+0.77	−0.53	+0.30	−1.00
	DMF	26.6	68.5	*ca.* +0.40	−0.61	*ca.* −0.04	−1.05
	DMSO	29.8	71.1	+0.30	−0.64	−0.11	−1.05
	CH_3CN	14.1	71.3	*ca.* +0.45	−0.64	*ca.* +0.05	−1.04
	CH_3OH	19	83.6	—	−0.65	—	−1.05
Cob(II)ester·I[e]	CH_2Cl_2	0	64.2	—	−0.52	—	−1.07
	CH_3OH	19	83.6	—	−0.65	—	−1.05
Co^{II}(tpp)[d]	CH_2Cl_2	0	64.2	—	−0.88	—	−1.43
	DMF	26.6	68.5	+0.24	−0.83	−0.20	−1.27
	DMSO	29.8	71.1	+0.08	−0.87	−0.33	−1.28

a) Measured at 20±2 °C; scan rate, 100 mV s^{-1}. b) Abbreviations: DMF, *N*,*N*-dimethylformamide; DMSO, dimethyl sulfoxide. c) Abbreviations: Fc, ferrocene; Fc^+, ferricinium ion. d) TBAP, 5×10^{-2} mol dm^{-3}. e) TBAI, 5×10^{-2} mol dm^{-3}.

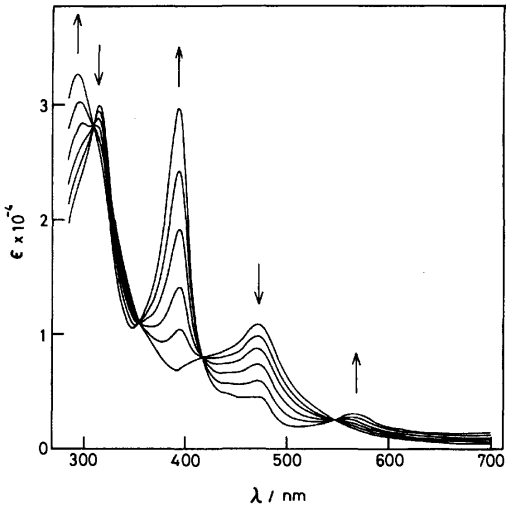

Fig. 7. Electrochemical reduction of [Cob(II)ester]ClO_4 (2.0×10^{-5} mol dm^{-3}) at −1.20 V *vs.* SCE in dimethyl sulfoxide containing 5.0×10^{-2} mol dm^{-3} TBAP at 20±2 °C: trends of spectral change with time are shown by arrows. About 80% of [Cob(II)ester]ClO_4 was reduced to Cob(I)ester after electrochemical reaction for 9 h.

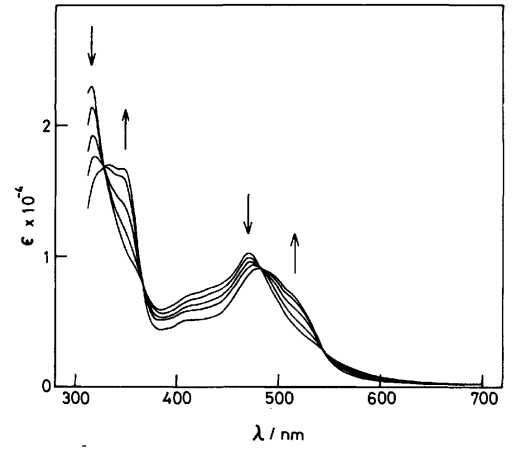

Fig. 8. Electrochemical oxidation of [Cob(II)ester]ClO_4 (2.0×10^{-5} mol dm^{-3}) at +0.80 V *vs.* SCE in dimethyl sulfoxide containing 5.0×10^{-2} mol dm^{-3} TBAP at 20±2 °C: trends of spectral change with time are shown by arrows. About 40% of [Cob(II)ester]$^+$ was oxidized to [Cob(III)ester]$^{2+}$ after electrochemical reaction for 3 h.

assigned to the Co(II)/Co(I) redox couple for the complex. Cob(I)ester thus produced was quantitatively reconverted into the original complex by oxidation at 0 V *vs.* SCE. The electronic spectral change during the electrochemical oxidation at 0.80 V *vs.* SCE in the same medium is shown in Fig. 8, and is accompanied with the increase in absorbance at 350, 490, and 520 nm. Since such absorption maxima are characteristic of Cob(III)ester, the redox potential at +0.30 V *vs.* SCE is assigned to the Co(III)/Co(II) redox couple.

Since the liquid junction potential is subjected to change by the nature of solvent system, the redox potentials observed in various solvents cannot be directly compared with each other among them. Though liquid junction potentials between electrolytic solutions in various solvents have been extensively investigated,[22] the most conventional and reliable means of eliminating the difference in liquid junction potential between various media is to adopt the observed redox potentials for the couple of ferrocene/ferricinium ion in various media as references. Because the true redox potential for the couple of ferrocene/ferricinium ion is considered to remain constant regardless of the nature of organic media,[23] the redox potentials corrected for the difference in liquid junction potential in the light of observed redox potentials for ferrocene/ferricinium ion are shown in Table 1. Gutmann investigated correlations between the half-wave potential of metal ion and the donor number of solvent (*DN*) for combination of various metal ions and solvents, and the half-wave potential for transition-metal ions was found to exhibit significant cathodic shift with the increase in solvent basicity (*DN*).[24] We claim here both polarity and basicity of solvents are primarily concerned with the redox potential after corrected for liquid junction potential. The solvent polarity is associated with the electrostatic stabilization of a metal complex; a polar solvent tends to favor the formation of a charged complex and such a solvent effect becomes more pronounced as the charge on a complex increases. On the other hand, the solvent basicity is concerned with the axial ligation behavior of solvent molecules; a sufficiently basic solvent tends to coordinate to the nuclear metal of a complex. Therefore, we discuss the Co(III)/Co(II) and Co(II)/Co(I) redox potentials for [Cob(II)ester]ClO_4 in correlation with both solvent polarity and basicity. Kosower's *Z*-value[25] and Gutmann's donor number (*DN*) are adopted here as polarity and basicity parameters, respectively. The correlations between the redox potential (Co(III)/Co(II) or Co(II)/Co(I)) and *DN* or *Z*-value are shown in Figs. 9 and 10. The Co(III)/Co(II) redox potential shows cathodic shift as the *DN* and *Z* parameters increase (Fig. 9); the higher the solvent basicity or polarity is, the more readily Cob(II)ester is oxidized. Such correlations are also observed for the Co(II)/Co(I) redox potential and level off beyond certain ranges of *DN* and *Z* parameters as shown in Fig. 10, but the extent of variation of the redox potential in various solvents is rather small as compared with that for the Co(III)/Co(II) couple. Since the overall charges on Cob(III)ester, Cob(II)ester, and Cob(I)ester are +2, +1, and 0, respectively, the tervalent cobalt complex is most stabilized in solvents of greater polarity. In addition, the tervalent cobalt in Cob(III)ester readily takes up the 5th and 6th ligand molecules at its axial sites while the univalent cobalt in Cob(I)ester has no tendency to interact with extra ligand molecules at its axial sites. Thus, the Co(III)/Co(II) redox potential is subjected to change by the variation of *DN* more effectively than the Co(II)/Co(I) couple. The correlations given in Figs. 9 and 10 apparently reflect such solvent effects. Similar solvent effects were observed on the Co(III)/Co(II) and Co(II)/Co(I) redox potentials for Co^{II}(tpp) (Table 1 and literature[26]). The Co(III)/Co(II) and Co(II)/Co(I) redox potentials for [Cob(II)ester]ClO_4 in various media appeared in the anodic side relative to the corresponding values for Co^{II}(tpp) as shown in Table 1. This must arise from the difference in ligand nature; the corrin and porphyrin

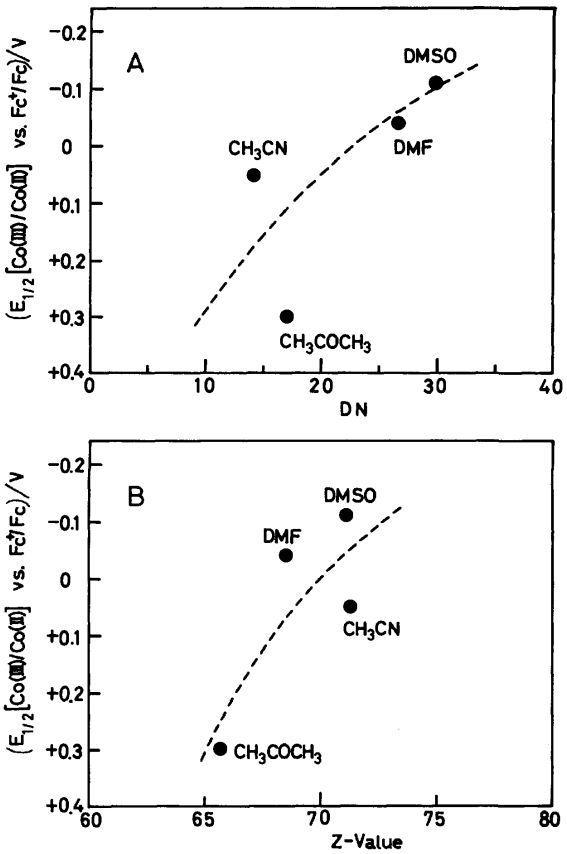

Fig. 9. Correlations of redox potential of [Cob(II)-ester]ClO_4 with solvent basicity and polarity: A, $E_{1/2}$[Co(III)/Co(II)] *vs. DN*; B, $E_{1/2}$[Co(III)/Co(II)] *vs. Z*-value.

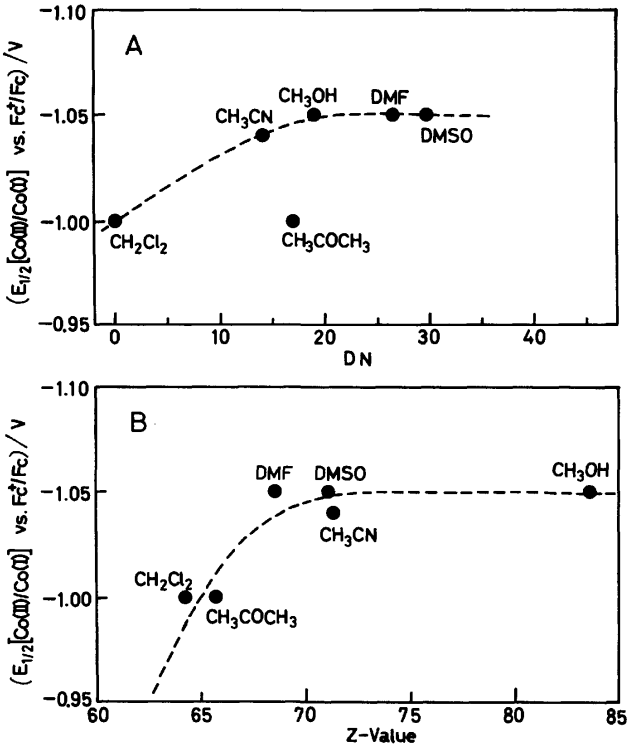

Fig. 10. Correlations of redox potential of [Cob(II)-ester]ClO_4 with solvent basicity and polarity: A, $E_{1/2}$[Co(II)/Co(I)] *vs. DN*; B, $E_{1/2}$[Co(II)/Co(I)] *vs. Z*-value.

ligands are mono- and dianionic, respectively, when coordinated to the cobalt ion. Thus, Co^{II}(tpp) is more readily oxidized and less readily reduced than Cob(II)ester. As reported in our previous paper,[14] the axial ligation behavior is subjected to change significantly by the nature of equatorial ligands, and the thermodynamic properties for the axial ligation of Cob(II)ester are much different from those observed for cobalt(II)-porphyrin. Such an equatorial ligand effect must be reflected on the redox behavior of cobalt.

The microenvironmental property effective on vitamin B_{12} in enzyme systems is considered to vary rather extensively by the nature of apoenzymes concerned. In the light of the present results, the redox behavior of the nuclear cobalt of vitamin B_{12} seems to be subjected to change from one enzyme to another depending upon the medium effects provided by the enzyme active sites. In particular, the Co(III)/Co(II) redox potential is sensitive to the nature of medium and the divalent cobalt state is more effectively stabilized in greater hydrophobic environments in the absence of coordinating ligands.

References

1) L. Werthemann, R. Keese, and A. Eschenmoser, unpublished results; see L. Werthemann, Dissertation, ETH Zürich (Nr. 4097), Juris Druck&Verlag, Zürich (1968).

2) J. M. Pratt, "Inorganic Chemistry of Vitamin B_{12}," Academic Press, London (1972), p. 105.

3) D. Lexa and J. M. Savéant, *J. Am. Chem. Soc.*, **98**, 2652 (1976).

4) D. Lexa, J. M. Savéant, and J. Zickler, *J. Am. Chem. Soc.*, **99**, 2786 (1977).

5) D. Lexa and J. M. Savéant, *J. Am. Chem. Soc.*, **100**, 3220 (1978).

6) N. R. de Tacconi, D. Lexa, and J. M. Savéant, *J. Am. Chem. Soc.*, **101**, 467 (1979).

7) D. Lexa, J. M. Savéant, and J. Zickler, *J. Am. Chem. Soc.*, **102**, 2654 (1980).

8) D. Lexa, J. M. Savéant, and J. Zickler, *J. Am. Chem. Soc.*, **102**, 4851 (1980).

9) K. A. Rubinson, E. Itabashi, and H. B. Mark, Jr., *Inorg. Chem.*, **21**, 3571 (1982).

10) L. Walder, G. Rytz, K. Meier, and R. Scheffold, *Helv. Chim. Acta*, **61**, 3013 (1978).

11) D. Lexa, J. M. Savéant, and J. P. Soufflet, *J. Electroanal. Chem. Interfacial Electrochem.*, **100**, 159 (1979).

12) R. Scheffold and E. Amble, *Angew. Chem.*, **92**, 643 (1980).

13) R. Scheffold, M. Dike, S. Dike, T. Herold, and L. Walder, *J. Am. Chem. Soc.*, **102**, 3642 (1980).

14) Y. Murakami, Y. Hisaeda, and A. Kajihara, *Bull. Chem. Soc. Jpn.*, **56**, 3642 (1983).

15) A. D. Adler, F. R. Longo, F. Kampas, and J. Kim, *J. Inorg. Nucl. Chem.*, **32**, 2443 (1970).

16) J. A. Riddick and W. B. Bunger, "Organic Solvents," Wiley-Interscience, New York (1970).

17) R. P. V. Duyne and C. N. Reilley, *Anal. Chem.*, **44**, 142 (1972).

18) F. Endo, *Yakugaku Zasshi*, **79**, 595 (1959).

19) Y. Matsuda, S. Yamada, and Y. Murakami, *Inorg. Chem.*, **20**, 2239 (1981).

20) A. V. Zelewsky, *Helv. Chim. Acta*, **55**, 2941 (1972).

21) R. Adams, "Electrochemistry at Solid Electrodes," Marcel Dekker, New York (1969), pp. 143—162.

22) See for example: a) B. G. Cox, A. J. Parker, and W. E. Waghorne, *J. Am. Chem. Soc.*, **95**,1010 (1973); b)K. Izutsu, T. Nakamura, T. Kitano, and C. Hirasawa, *Bull. Chem. Soc. Jpn.*, **51**, 783 (1978).
23) H. Strehlow, "The Chemistry of Non-aqueous Solvents," ed by J. J. Lagowski, Academic Press, London (1966), Vol. 1, p. 129.
24) V. Gutmann, *Monatsh. Chem.*, **100**, 2113 (1969).
25) E. M. Kosower, "An Introduction to Physical Organic Chemistry," John Wiley & Sons, New York (1968), Part 2.
26) F. A. Walker, D. Beroiz, and K. M. Kadish, *J. Am. Chem. Soc.*, **98**, 3484 (1976).

Synthesis of Azobenzo-crown Ethers and Their Complexation Behavior with Metal Ions

Masanobu SHIGA, Hiroshi NAKAMURA, Makoto TAKAGI,* and Keihei UENO†

Department of Organic Synthesis, Faculty of Engineering, Kyushu University, Hakozaki, Higashi-ku, Fukuoka 812

†*Department of Industrial Chemistry, Kumamoto Institute of Technology, 4-22-1 Ikeda, Kumamoto 860*

(Received September 1, 1983)

New crown ethers which have a benzeneazo group as a building block of a macrocyclic polyether ring. The complexation properties of these new azobenzo-crown ethers with alkali and alkaline earth metal iodide salts were investigated in acetonitrile solution spectrophotometrically. The complex formation constants were evaluated for alkali metal salts. The azo group is not particularly a favorable component of a crown ether macrocycle for stabilizing the metal complexes.

During the course of our investigation to develop the chromogenic crown ether reagents for the photometric determination of alkali and alkaline earth metal ions, a series of new crown ethers have been synthesized, in which 2,2′-positions of azobenzene were bridged by oligoethylene glycol to form a skeletal structure of crown ether. The crown ethers synthesized in this study are shown in structure **2**. They are conveniently named as azobenzo-crown ether or azobenzo-13-crown-4 for **2a** as an example, because the structure and hole size of **2a** is comparable with that of 13-crown-4 when azobenzene moiety takes trans-conformation.

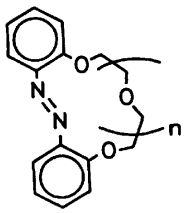

2a n = 1
b n = 2
c n = 3
d n = 4

In our previous communication,[1] we reported the photoisomerization of azobenzo-crown ethers. The trans-isomer was more favorable for metal ion complexation. The complexation behavior of azobenzo-crown ethers was also evaluated semiquantitatively by the ion-pair extraction of metal complex with tetrabromophenolphthalein ethyl ester. Lithium was not extracted by any of these crown ethers, but sodium was extracted by **2a** preferentially over potassium. **2b** preferred the extraction of potassium. Recently, Shinkai, Manabe and co-workers described the 4,4′-(oligoethylene glycol-linked) azobenzene, which showed a marked photo-responsive metal extraction properties in relation to their trans-cis isomerization of azo linkage.[2]

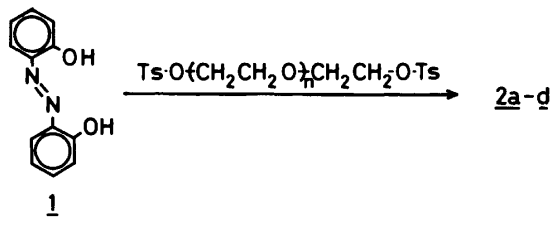

1

Scheme 1.

As we have found that considerable spectral change was observed for these azobenzo-crown ethers upon complexation with metal ion in aprotic solvents such as acetonitrile, a detailed photometric investigation has been done to evaluate the interaction quantitatively.

Experimental

Synthesis of Azobenzo-crown Ethers. The synthetic reaction is shown below, and the procedure for azobenzo-13-crown-4 is described below as an example.

*Azobenzo-13-crown-4 (**2a**).* To a 200 ml round bottomed flask containing 1.0 g (4.7 mmol) of 2,2′-dihydroxyazobenzene (**1**)[3] was added 1.1 g (9.8 mmol) of potassium *t*-butoxide in 50 ml THF under a nitrogen atmosphere at room temperature, and the mixture was stirred for 30 min. To this mixture, 2.0 g (4.8 mmol) of diethylene glycol ditosylate was added dropwise in 1 h, and refluxed for 16 h. After cooling, the precipitate in the reaction mixture was filtered off, and the filtrate was evaporated under a reduced pressure. The residue was taken into chloroform, and washed with water. After evaporation, the residual mass was applied on a silica-gel column (WAKO-gel C-200, 20×100 mm), and eluted with benzene, followed by chloroform. The red colored fraction was collected, and evaporated to obtain crystalline mass, which was recrystallized from heptane. Yield 0.36 g (27%). Mp 69.5—71 °C. IR (KBr disk) 2920 (CH), 1590 cm^{-1} (N=N). ^1H NMR (δ ppm from TMS; $CDCl_3$); δ=3.8—4.0 (4H, m, $-CH_2OCH_2-$), 4.12—4.35 (4H, m, $ArOCH_2-$), 6.63—7.50 (8H, m, Ar-H). Ms (*m/z*); 284 (M^+). Found: C, 67.36; H, 5.82; N, 9.56%. Calcd for $C_{16}H_{16}N_2O_3$: C, 67.59; H, 5.67; N, 9.85%.

*Azobenzo-16-crown-5 (**2b**), -19-crown-6 (**2c**), and -22-crown-7 (**2d**).* The procedures were almost the same as that of **2a**, except for the use of tri-, tetra- and pentaethylene glycol ditosylates for **2b**, **2c**, and **2d**, respectively, in place of diethylene glycol ditopsylate.

2b. Yield 11% (red crystal). Mp 67.5—68.0 °C. IR (KBr disk) 2900 (CH), 1590 cm^{-1}(N=N). ^1H NMR ($CDCl_3$); δ=3.62—4.00 (8H, m, $-CH_2OCH_2-$), 4.10—4.32 (4H, m, $ArOCH_2-$), 6.71—7.75 (8H, m, Ar-H). MS (*m/z*); 328 (M^+). Found: C, 65.84; H, 6.18; N, 8.49%. Calcd for $C_{18}H_{20}N_2O_4$: C, 65.84; H, 6.04; N, 8.53%

2c. Yield 23% (red plates). Mp 111.0—113.5 °C. IR (KBr disk) 2960 (CH), 1580 cm^{-1} (N=N). ^1H NMR ($CDCl_3$); δ=3.32—3.95 (12H, m, $-CH_2OCH_2-$), 4.10—4.42 (4H, m, $ArOCH_2-$), 6.71—7.45 (8H, m, Ar-H). MS (*m/z*); 372 (M^+). Found: C, 64.52; H, 6.45; N, 7.53%. Calcd for $C_{20}H_{24}N_2O_5$: C, 64.50; H, 6.50; N, 7.52%.

2d. Yield 31% (red syrup). IR (neat) 2900 (CH), 1590 cm^{-1} (N=N). ^1H NMR ($CDCl_3$); δ=3.51—4.00 (16H, m,

-CH_2OCH_2-), 4.15—4.48 (4H, m, $ArOCH_2$-), 6.75—7.60 (8H, m, Ar-H). MS (*m/z*); 416 (M^+). Found: C, 63.45; H, 6.78; N, 6.73%. Calcd for $C_{22}H_{18}N_2O_6$: C, 64.21; H, 6.63; N, 7.35%.

Reagents. Other reagents were of analytical grade.

Apparatus. Absorption spectra were recorded using a Hitachi-556 double wavelength spectrophotometer. ^1H NMR and IR spectra were obtained by Hitachi R-24B ^1H NMR spectrometer and JASCO DS 403GR infrared spectrophotometer, respectively.

Measurement of Complex Formation Constants. To a 1.0×10^{-4} M (1 M=1 moldm^{-3}) acetonitrile solution of azobenzo-crown ether, various amount of alkali iodide, was added to give a final concentration of $(0—1.0)\times10^{-2}$ M, and the resulting spectral change was measured using a standard 1 cm quartz cell. The optical absorbances were treated in a standard manner, and the complexation constants were calculated according to the Marquardt's nonlinear least square method.[4]

Results and Discussion

Synthesis. The syntheses of azobezo-crown ethers proceeded in a usual manner[5] and proposed structures of azobenzo-crown ethers were fully supported by the elemental analyses and the spectral informations.

Spectral Change and Complexation Behavior. Absorption spectra of azobenzo-13-crown-4, -16-crown-5, -19-crown-6, and -22-crown-7 in acetonitrile in the absence and in the presence of metal iodide are shown in Figs. 1, 2, 3, and 4, respectively. Acetonitrile was chosen as a common solvent for azobenzo-crown ethers and metal iodides. Since no spectral change was observed in a system of 2,2′-dimethoxyazobenzene and metal iodide in acetonitrile under comparable reaction conditions, such spectral change was understood to be due to the complexation of metal ions with the crown ether rings.

It is seen from Figs. 1 and 2 that the spectral changes occurred mainly in the increase of absorption intensity, but not much in the shift of absorption maxi-

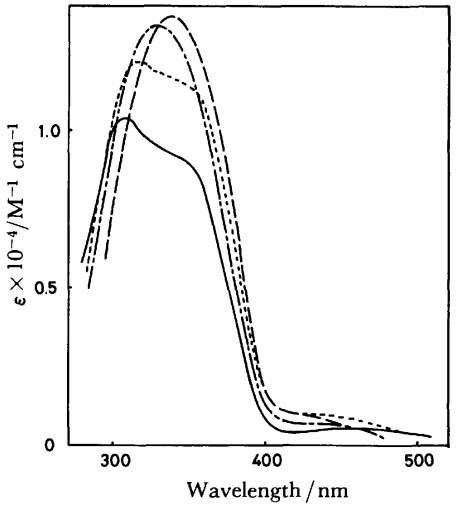

Fig. 1. Spectral change of azobenzo-13-crown-4 on the addition of metal salts. [L]=1×10^{-4} M, [MI]=1×10^{-3} M, [MI_2]=1×10^{-3} M, acetonitrile: ——, without salt; ----, LiI; ——, CaI_2; ——-, BaI_2.

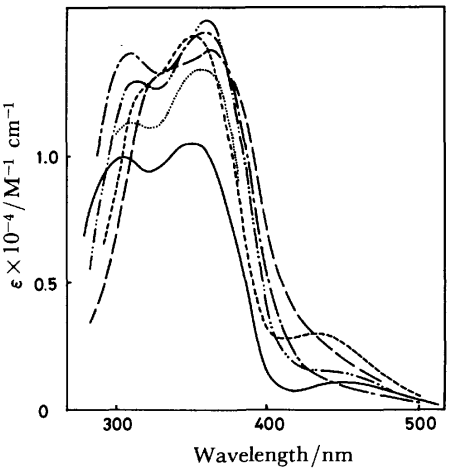

Fig. 2. Spectral change of azobenzo-16-crown-5 on the addition of metal salts. [L]=1×10^{-4} M, [MI]=1×10^{-3} M, [MI_2]=1×10^{-3} M, acetonitrile: ——, without salt; -----, LiI; —··—··—, NaI; ·····, KI; ——, CaI_2; —·—·—, BaI_2.

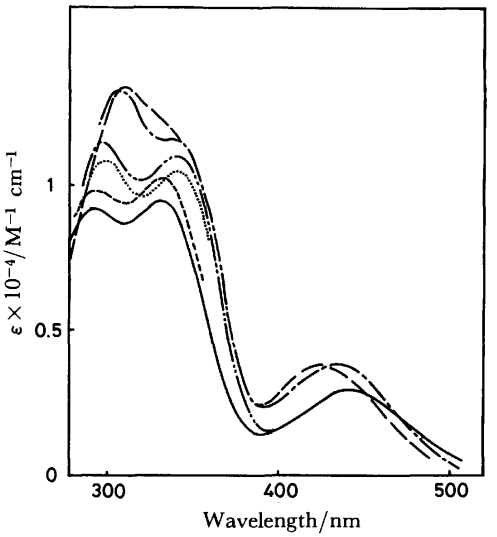

Fig. 3. Spectral change of azobenzo-19-crown-6 on the addition of metal salts. [L]=1×10^{-4} M, [MI]=1×10^{-3} M, [MI_2]=1×10^{-3} M, acetonitrile: ——, without salt; -----, LiI; —··—··—, NaI; ·····, KI; ——, CaI_2; ——, BaI_2.

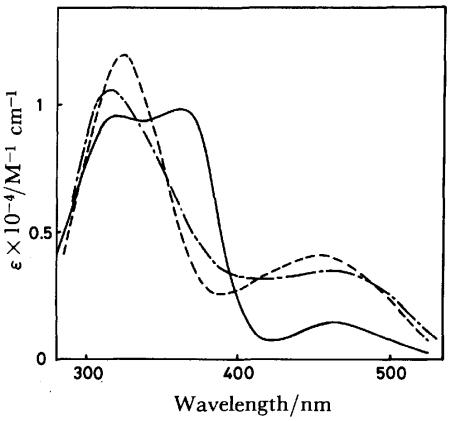

Fig. 4. Spectral change of azobenzo-22-crown-7 on the addition of metal salts. [L]=1×10^{-4} M, [MI]=1×10^{-3} M, acetonitrile: ——, without salt; ——, CaI_2; —·—·—, BaI_2.

mum. The change is more pronounced with divalent metal ions than with monovalent ions, indicating the importance of ion-dipole interaction between the metal and the chromophore group. Similar spectral changes have been also reported by Dix and Vögtle on monoaza-crown ethers with a pendent *p*-arylazophenyl group on the crown ether nitrogen.[6]

The extent of spectral changes depends on the nature of azobenzo-crown ethers and metal salts. It also depends on their concentrations. The association equilibrium constants of azobenzo-crown ethers with metal salts can be evaluated from these changes in absorption spectra. It should be recalled in the passing that the spectral shift widths on the rate of absorption enhancement can not be a measure of the energy of association between the crown ether and the metal salts. These may reflect the extent of interaction between the azo group and the metal, but not represent that between the crown ether entity and metal.

Spectrophotometrically, we have no way to differentiate metal ion (M^+) from metal iodide (MI), nor metal ion-crown ether complex (ML^+) from its iodide complex (MLI) in acetonitrile solution. Therefore the conditional association constant (K_{ML}) as defined by Eq. 1 was used to evaluate the extent of interaction between azobenzo-crown ether and metal iodide.

$$K_{ML}=\frac{[(MLI)_t]}{[L][(MI)_t]}, \quad (1)$$

where

$$[(MLI)_t]=[ML^+]+[MLI], \quad (2)$$

and

$$[(MI)_t]=[M^+]+[MI]. \quad (3)$$

The optical absorbance of the solution of this system can be expressed by Eq. 4,

$$A=\varepsilon_{MLI}[(MLI)_t]+\varepsilon_L[L], \quad (4)$$

where, ε_{MLI} and ε_L are molar absorption coefficients of metal complex and crown ether, respectively. The total concentrations of metal salt and crown ether are defined as follows:

$$C_M=[(MI)_t]+[(MLI)_t], \quad (5)$$

$$C_L=[L]+[(MLI)_t]. \quad (6)$$

By combining Eqs. 1—6, the mean molar absorption coefficient ε is derived as in Eq. 7.

$$\varepsilon = A/C_L = \{(\varepsilon_{MLI}-\varepsilon_L)((K_{ML}(C_M+C_L)+1) - \sqrt{(K_{ML}(C_M+C_L)+1)^2-4K_{ML}^2C_MC_L}\}/(2K_{ML}\cdot C_L) + \varepsilon_L. \quad (7)$$

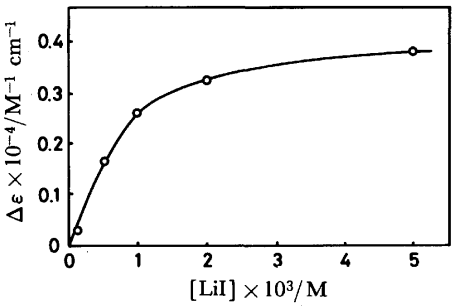

Fig. 5. Change of absorbance on the addition of lithium iodide to azobenzo-13-crown-4. 350 nm, [L]=1×10⁻³ M.

Experimentally, the value of $\varepsilon-\varepsilon_L$ ($\simeq\Delta\varepsilon$) is measured as a function of metal salt concentration as illustrated in Fig. 5. The values of K_{ML} and ε_{MLI} are then simultaneously determined from Eq. 7 by using Marquardt's non-linear least-squares method.

The constants obtained are summarized in Table 1. The spectral changes of **2a** on interaction with sodium iodide and potassium iodide and those of **2d** with alkali metal iodides were so small that the meaningful values of K_{ML} could not be obtained. As to the complexation with alkaline earth metal salts, the calculated values scattered and dependented on the wave lengths adopted for calculation. This indicates that the reactions can not be formulated in a simple manner as in Eqs. 1—6.

It is seen from the table that the association constant for lithium is highest with **2a** and decreases with increasing hole size of crown ether, indicating that (the trans form of) azobenzo-13-crown-4 (**2a**), whose hole size is approximately comparable with that of 12-crown-4, fits most well lithium ion. It is interesting to note that, among the alkali metal iodides investigated in this study, lithium ion forms about the most stable complexes with azobenzo-crown ethers, regardless of the hole size of crown ethers. Sodium then follows. This result does not agree with the generally accepted ion-cavity size fitness concept, suggesting that the energy of metal salt-crown ether interaction is primarily governed by a simple ion-dipole interaction (enthalpy contribution) rather than a macrocyclic encapsulating interaction (entropy contribution). The smallest lithium ion thus exercises the highest effective interaction with the crown ethers.

The complexation constants of **2b** and **2c** with sodium iodide or potassium iodide are unanimously lower than those of dibenzo-18-crown-6 (**3**) and "dicyclohexyl-18-crown-6" (**4**).[7] Even though **2c** has

Table 1. Complex formation constants in acetonitrile

Crown ether	LiI			NaI			KI				
	log K_{MLI}	$\varepsilon_{MLI}\times10^{-4}$ / M^{-1} cm^{-1}	λ_{max} / nm	log K_{MLI}	$\varepsilon_{MLI}\times10^{-4}$ / M^{-1} cm^{-1}	λ_{max} / nm	log K_{MLI}	$\varepsilon_{MLI}\times10^{-4}$ / M^{-1} cm^{-1}	λ_{max} / nm	$\varepsilon_L\times10^{-4}$ / M^{-1} cm^{-1}	λ_{max} / nm
2a	4.10	1.58	(327)	—	—		—	—		1.08	(310)
2b	4.00	1.28	(355)	3.69	1.40	(365)	3.15	1.37	(355)	0.99	(350)
2c	3.41	1.08	(320)	3.43	1.06	(295)	3.37	1.00	(300)	0.84	(331)
3	—			5.04[a]			4.83[a]				
4	—			5.20[a]			5.63[a]				

a) K_{ML} refers to the equilibrium, $M^+ + L \rightleftharpoons ML^+$. Ref. 7.

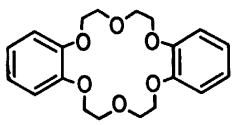

3

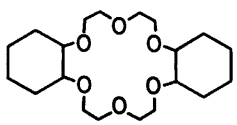

4

almost the same hole size as **3**, the K_{ML} value of **2c** is 40 times lower than that of **3**. A relatively low complexation ability of azobenzo-crown ethers as compared with normal crown ethers has been previously noticed.[1] The conformational structure of azobenzo-crown ether is suggested from CPK model considerations to be slightly distorted and disordered from that of standard crown ethers, and it is likely that the azo group does not contribute much to the stabilization of complexes. In the case of the azobenzo-crown ether having larger ether ring such as **2c** and **2d**, metal ion should be readily accomodated in the crown ether ring, but the spectral change upon metal complexation is less than that of **2a** and **2b**.

Dix and Vögtle synthesized a variety of crown ether dyes and described the spectral change upon interaction with metal salts in acetonitrile.[6] Some of the crown ethers showed a drastic spectral shift as large as 100 nm. Unfortunately, they did not treat the data in terms of the association equilibrium constants; however, the spectral pictures they showed suggest that the association constants are in the similar order of magnitude to the present study.

References

1) M. Shiga, M. Takagi, and K. Ueno, *Chem. Lett.*, **1980**, 1021.
2) S. Shinkai, T. Minami, Y. Kusano, and O. Manabe, *J. Am. Chem. Soc.*, **105**, 1851 (1983).
3) D. C. Freeman and C. E. White, *J. Am. Chem. Soc.*, **78**, 2678 (1956).
4) D. W. Marquardt, *J. Soc. Ind. Appl. Math.*, **11**, 431 (1963).
5) F. de Jong, M. G. Siegel, and D. J. Cram, *J. Chem. Soc., Chem. Commun.*, **1975**, 552.
6) J. P. Dix and F. Vögtle, *Angew. Chem., Int. Ed. Engl.*, **17**, 857 (1978); *Chem. Ber.*, **113**, 459 (1980); **114**, 638 (1981).
7) D. F. Evans, S. L. Wellington, J. A. Nadis, and E. L. Cussler, *J. Solution Chem.*, **1**, 499 (1972).

Cyclodienones. X. Reaction of Halo-cyclohexadien-1-ones with Phenols in the Presence of α-Picoline and Preparation of 4-Hydroxy- and 2-Hydroxyphenyl Aryl Ethers[1]

Masashi TASHIRO,* Takashi ITOH, and Gouki FUKATA†

Research Institute of Industrial Science, and Department of Molecular Science and Technology, Graduate School of Engineering Sciences, Kyushu University 86, Sakamoto, Kasuga, Kasuga, Fukuoka 816

†*Department of Food Science and Technology, Faculty of Engineering, Toa University, Kusuno, Shimonoseki, Yamaguchi 751*

(Received March 3, 1983)

Reaction of 4-halocyclohexadienones such as 4-bromo-(**1a**), 4-chloro-2,4,6-tri-*t*-butyl-(**1b**), 2,4-dichloro-4,6-di-*t*-butyl-2,5-cyclohexadien-1-one, and 2,4-dichloro-2,6-di-*t*-butyl-3,5-cyclohexadien-1-one with phenols in the presence of α-picoline was carried out under various conditions. The reaction of **1a** and **1b** with phenols afforded the corresponding 2-aryloxy-4,6-di-*t*-butyl phenols together with various by-products. The $AlCl_3$-catalyzed *trans*-*t*-butylation of 2-aroxy-4,6-di-*t*-butyl-phenols, which were obtained by the above reaction, afforded the corresponding 2-hydroxyphenyl aryl ethers. The similar reaction of 4-aroxy-2,4,6-tri-*t*-butyl-2,5-cyclohexadien-1-ones also afforded the corresponding 4-hydroxyphenyl aryl ethers.

It has been previously reported that[2] 4-bromo-2,4,6-tri-*t*-butyl-2,5-cyclohexadien-1-one (**1a**) reacted with sodium phenoxides to give 4-phenoxy dienones (**2**), which were easily converted to the corresponding 4-hydroxyphenyl aryl ethers (**3a**) by treatment with $AlCl_3$-CH_3NO_2 catalyst in toluene.

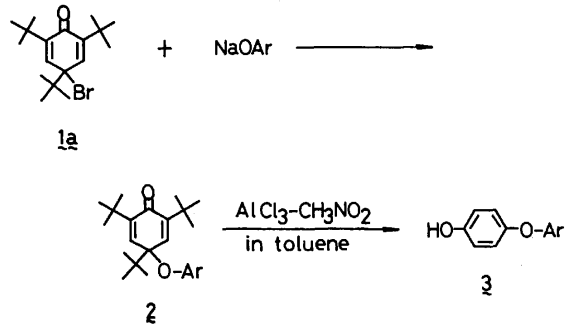

Reaction of **1a** with pyridine at 110 °C afforded *N*-(2-hydroxyphenyl)pyridinium bromide (**4**), but α-picoline did not react with **1a**.[3]

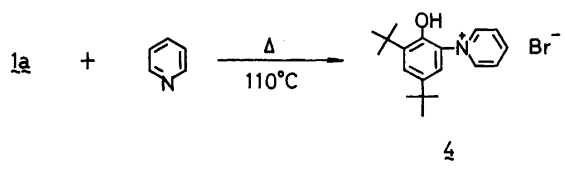

These results suggest that the reaction of **1a** with phenols at 110 °C might afford the corresponding 2,4-di-*t*-butyl-6-aryloxyphenols which would be suitable for the preparation of 2-hydroxyphenyl aryl ethers.

Results and Discussion

Reaction of Halocyclohexadienones with Phenols. Reaction of 4-bromo-(**1a**) and 4-chloro-2,4,6-tri-*t*-butyl-2,5-cyclohexadien-1-one (**1b**) with phenol (**5a**) was carried out at 110 °C under various conditions. The results are summarized in Table 1 and Scheme 1.

TABLE 1. REACTION OF 4-HALOCYCLOHEXADIENONES (**1a—b**) WITH PHENOL (**5a**) IN THE PRESENCE OF BASE[a)]

Run	Dienone	Base	Time/h	**6a** (%)
1	**1a**	α-Picoline	2	15
2	**1b**	α-Picoline	2	24
3	**1b**	α-Picoline	8	18
4	**1b**	2,6-Lutidine	2	23

a) A stirred mixture of **1** and **5a**, and base (molar ratio= 1:2:2) was heated at 110 °C (bath temperature). b) Isolated yields are shown.

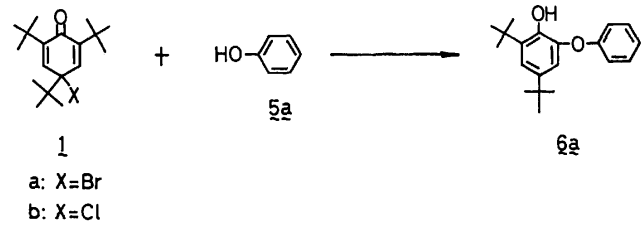

Scheme 1.

The data of the Table 1 show that reaction of **1a** with **5a** in the presence of α-picoline afforded the expected 2,4-di-*t*-butyl-6-phenoxyphenol (**6a**) in 15% yield together with by-products shown in following Scheme 2.

Compound **1b** gave the same product **6a** in higher yield than that of **1a**. Even under prolonged reaction time, **6a** was obtained in only 18% yield. It was also found that 2,6-lutidine afforded the same yield of **6a** as that of α-picoline though the former has a higher basicity than the latter.

The results of the reaction of **1b** with several phenols in the presence of α-picoline are summarized in Table 2 and Scheme 2.

The data of Table 2 show that **5b—o** as well as **5a** gave the expected **6b—o** together with by-products such as **8—12** respectively. It was also found that the phenols having ortho substituents afforded poor yields of **6**. It should be noted that the reactions with phenols **5k—o** having nitro, cyano, formyl, and acetyl

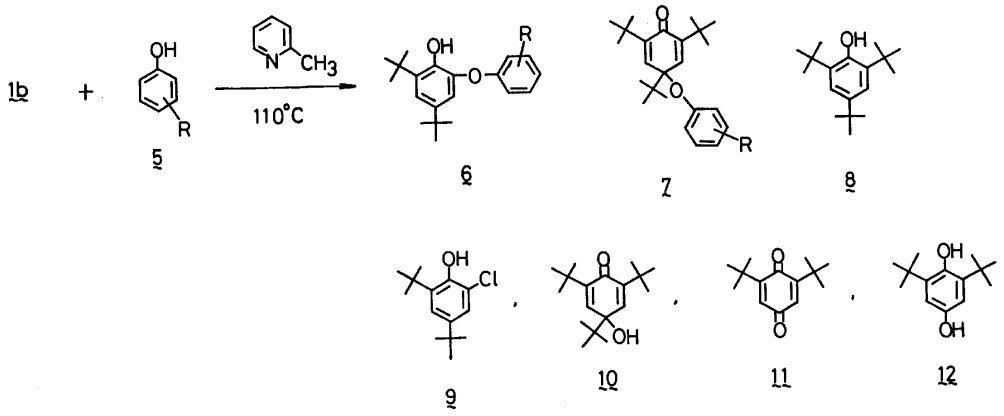

Scheme 2.

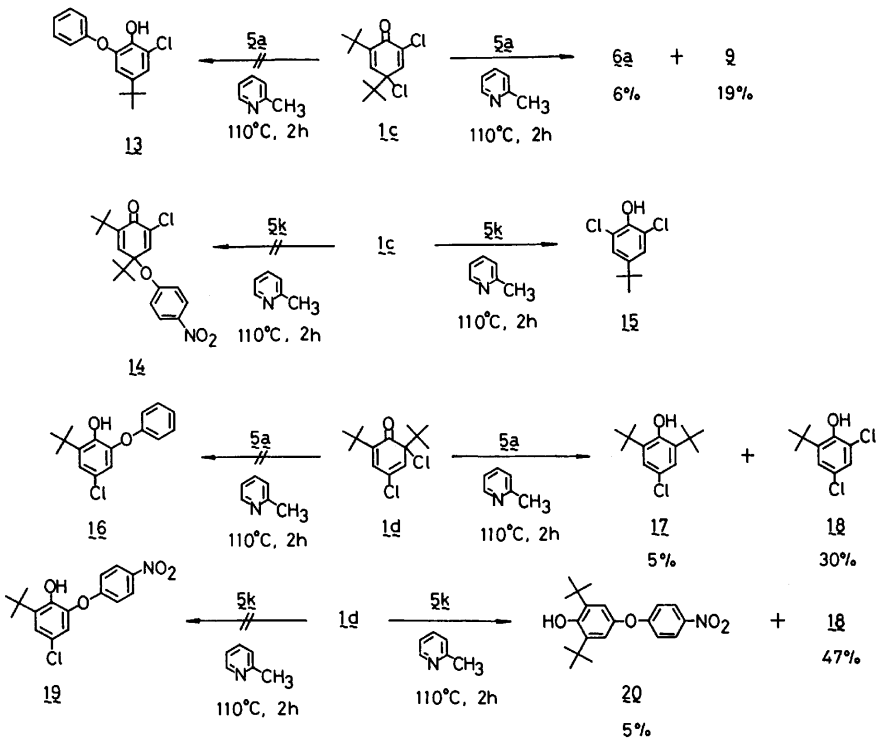

Scheme 3.

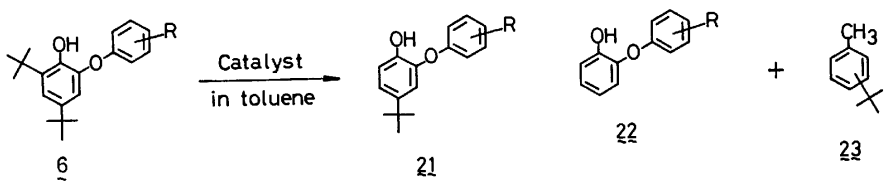

a: R=H
b: R=p-CH_3
c: R=p-F
d: R=o-Cl
e: R=p-Cl
f: R=p-Br
g: R=p-$CO_2C_2H_5$
h: R=p-NO_2
i: R=p-CN
j: R=p-CHO
k: R=p-$COCH_3$

Scheme 4.

Table 2. Reaction of **1b** with several phenols in the presence of α-picoline at 110 °C[a]

Run	Phenol	R	Product (%)[b]
1	**5a**	H	**6a** (24), **8** (25), **9** (13), **10** (2), **11** (2)
2	**5b**	*o*-CH_3	**6b** (6), **8** (50), **9** (7), **10** (1)
3	**5c**	*p*-CH_3	**6c** (32), **8** (32), **9** (13), **10** (13)
4	**5d**	*o*-F	**6d** (8), **8** (28), **9** (10), **10** (25)
5	**5e**	*p*-F	**6e** (51), **8** (18), **9** (+), **10** (3)
6	**5f**	*o*-Cl	**6f** (14), **8** (26), **9** (11)
7	**5g**	*p*-Cl	**6g** (36), **8** (28), **9** (28)
8	**5h**	*p*-Br	**6h** (51), **8** (29), **9** (13), **10** (8)
9	**5i**	*p*-C_6H_5	**6i** (7), **8** (52), **9** (+), **10** (+)
10	**5j**	*p*-$CO_2C_2H_5$	**6j** (36), **8** (7), **9** (33), **10** (+)
11	**5k**	*p*-NO_2	**6k** (21), **7a** (16), **8** (6), **9** (21), **10** (5)
12	**5l**	*m*-NO_2	**6l** (28), **7b** (15), **8** (8), **9** (19), **10** (9)
13	**5m**	*p*-CN	**6m** (28), **7c** (12), **8** (7), **9** (31), **10** (9)
14	**5n**	*p*-CHO	**6n** (18), **7d** (6), **8** (16), **9** (11), **10** (2)
15	**5o**	*p*-$COCH_3$	**6o** (12), **7e** (9), **8** (10), **9** (20), **10** (5)

a) Reaction time: 2 h, molar ratio of **1b**, **5**, and α-picoline is 1:2:2. b) Isolated yields are shown.

group afforded besides the corresponding **6**, cyclohexadienone derivatives **7a—e**, which could not be obtained by the reported method[2] described above.

The yields of by-products such as **8** and **9** increased with decrease in the yield of **6**. However, the reason for the above phenomena is still not clear.

Reactions of **1c** and **1d** with **5a** and **5k** were carried out under similar conditions (Scheme 3). However, the expected compounds such as **13, 14, 16,** and **19** were not formed in any case. Formation of **6a** from **1c** and **20** from **1d** might suggest that the chloro substituents of **1c** and **1d** migrated and then reacted with the phenols. However, the detailed reaction pathways of the formation of these compounds are still obscure.

trans-t-*Butylation.* The $AlCl_3$-catalyzed *trans-t*-butylation of **6** was carried out in order to obtain the corresponding 2-hydroxyphenyl aryl ethers. The results are summarized in Table 3 and Scheme 4.

When **6a** was treated with $AlCl_3$-CH_3NO_2 catalyst in toluene at 80 °C for 30 min, a mixture of **21a** and **22a** was obtained together with **23**. However, similar reaction of **6h** or **6k** afforded selectively **21f** or **21h** in good yield. These results suggest that the *t*-butyl group ortho to the hydroxyl group of **6** might be more easily removed than that in the para position. The same phenomenon was previously observed in *trans-t*-butylation of 3,3′,5,5′-tetra-*t*-butylbiphenyl-2,2′-diol.[4]

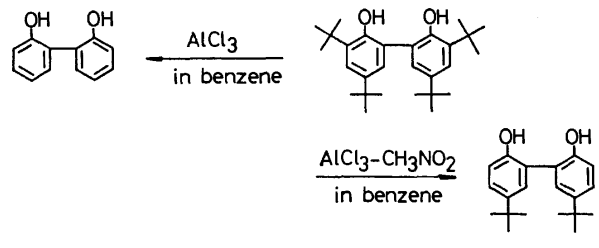

Table 3. *trans-t*-Butylation of **6** in toluene at 80 °C for 30 min[a]

Run	6	Catalyst	Product (%)[b]
1	**6a**	$AlCl_3$-CH_3NO_2	**21a** (80), **22a** (20)[c]
2	**6a**	$AlCl_3$	**22a** (85)
3	**6c**	$AlCl_3$	**22b** (80)
4	**6e**	$AlCl_3$	**22c** (89)
5	**6f**	$AlCl_3$	**22d** (96)
6	**6g**	$AlCl_3$	**22e** (99)
7	**6h**	$AlCl_3$-CH_3NO_2	**21f** (80)
8	**6h**	$AlCl_3$	**22f** (78)
9	**6j**	$AlCl_3$	**22g** (87)
10	**6k**	$AlCl_3$-CH_3NO_2	**21h** (69)
11	**6k**	$AlCl_3$	**22h** (52)
12	**6m**	$AlCl_3$	**22i** (91)
13	**6n**	$AlCl_3$	**22j** (61)
14	**6o**	$AlCl_3$	**22k** (97)

a) A mixture of 1 mmol of **6** and 2.2 mmol of $AlCl_3$ in 20 ml of toluene was heated. b) Isolated yields are shown. c) The yields shown were obtained by GC analysis.

The $AlCl_3$-catalyzed *trans-t*-butylation of **6** afforded only the expected **21** in good yields in all cases. Compound **23** was formed in all cases.

The $AlCl_3$-catalyzed *trans-t*-butylation of **7** was also carried out in order to obtain the corresponding 4-hydroxyphenyl aryl ethers (**24**). The results are summarized in the Scheme 5.

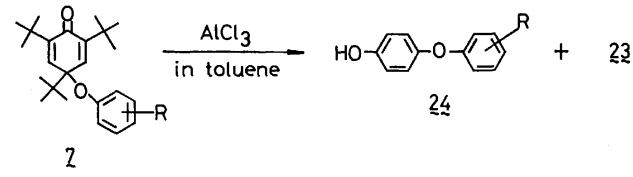

a: R=p-NO_2 86% d: R=p-CHO 68%
b: R=m-NO_2 68% e: R=p-$COCH_3$ 91%
c: R=p-CN 97%

Scheme 5.

The desired products **24a—e** were obtained together with **23** in good yields.

Experimental

All melting points are uncorrected. NMR spectra were determined at 100 MHz with a JEOL FT-100 NMR spectrometer with Me_4Si as an internal reference, and IR spectra were measured as KBr pellets or as liquid films on NaCl plates in a JASCO IR-A-102 spectrometer. Mass spectra were obtained on a JEOL JMS-OISA-2 spectrometer at 75 eV by using a direct inlet system.

Materials. Compounds **1a**,[5] **1b**,[5] **1c**, and **1d** were obtained according to Person's procedure.[5] **1c**: Mp 77—79 °C, **1d**: Mp 56—59 °C.

Reaction of Halocyclohexadienones (1) with Phenols (5). General Procedure: After a stirred mixture of **1** (2.5 mmol), **5** (50 mmol), and 0.5 ml of α-picoline was heated on an oil bath (110 °C) for specified reaction time under a stream of nitrogen gas, 50 ml of benzene was added. The benzene solution was washed with 10% hydrochloric acid (10

ml×2), 2.5% NaOH solution (20 ml×2) and water (20 ml), dried with Na_2SO_4 and evaporated *in vacuo* to leave a residue which was chromatographed on silica gel using hexane and a mixture of hexane and benzene as eluents to give the products shown in Tables 1 and 2, and Scheme 3. The melting points, elemental analyses, and spectral data of the products are summarized below.

6a: Colorless prisms (MeOH-H_2O), mp 38.5—40 °C; ^{1}H-NMR ($CDCl_3$); δ=1.22, 1.43 (each s, 9H), 5.67 (s, 1H, disappeared with D_2O), 6.78 (d, J=2.3 Hz, 1H), and 6.86—7.38 (m, 6H); Mass m/z 298 (M^+). Found: C, 80.41; H, 8.88%. Calcd for $C_{20}H_{26}O_2$: C, 80.50; H, 8.78%.

6b: Colorless crystals, mp 37—40 °C; ^{1}H-NMR ($CDCl_3$); δ=1.20, 1.44 (each s, 9H), 2.31 (s, 3H), 5.76 (s, 1H, disappeared with D_2O), 6.62 (d, J=2.2 Hz, 1H), and 6.71—7.28 (m, 5H); Mass m/z 312 (M^+). Found: C, 80.92; H, 9.29%. Calcd for $C_{21}H_{28}O_2$: C, 80.73; H, 9.03%.

6c: Colorless prisms (MeOH), mp 87—88 °C; ^{1}H-NMR ($CDCl_3$); δ=1.20 1.42 (each s, 9H), 2.32 (3H, s), 5.72 (s, 1H, disappeared with D_2O), and 6.86, 7.08 (each d, J=8.7 Hz, 2H); Mass m/z 312 (M^+). Found: C, 80.66; H, 8.97%. Calcd for $C_{21}H_{28}O_2$: C, 80.73; H, 9.03%.

6d: Colorless crystals, mp 50—53 °C; ^{1}H-NMR ($CDCl_3$); δ=1.22, 1.33 (each s, 9H), 5.76 (s, 1H, disappeared with D_2O), 6.70 (d, 1H, J=2.5 Hz), and 6.88—7.22 (m, 5H); Mass m/z 316 (M^+). Found: C, 75.55; H, 8.10%. Calcd for $C_{20}H_{25}FO_2$: C, 75.92; H, 7.96%.

6e: Colorless prisms (MeOH), mp 92—93 °C; ^{1}H-NMR ($CDCl_3$); δ=1.23, 1.44 (each s, 9H), 3.45 (s, 1H, disappeared with D_2O), 6.70 (d, J=2.5 Hz, 1H), 6.84—7.06 (m, 5H); Mass m/z 316 (M^+). Found: C, 76.04; H, 8.04%. Calcd for $C_{20}H_{25}FO_2$: C, 75.92; H, 7.96%.

6f: Pale yellow oil, ^{1}H-NMR ($CDCl_3$); δ=1.23, 1.44 (each s, 9H), 5.71 (s, 1H, disappeared with D_2O), 6.72 (d, J=2.3 Hz, 1H), and 6.80—7.48 (m, 5H); Mass m/z 334 (M^+), 332 (M^+). Found: C, 72.53; H, 7.75%. Calcd for $C_{20}H_{25}ClO_2$: C, 72.17; H, 7.57.

6g: Colorless prisms (MeOH), mp 110.5—111.5 °C; ^{1}H-NMR ($CDCl_3$); δ=1.23, 1.42 (each s, 9H), 5.60 (s, 1H, disappeared with D_2O), 6.74 (d, J=2.3 Hz, 1H), 7.05 (d, J=2.3 Hz, 1H), and 6.89, 7.24 (each d, J=9.2 Hz, 2H); Mass m/z 334 (M^+), 332 (M^+). Found: C, 72.31; H, 7.63%. Calcd for $C_{20}H_{25}ClO_2$: 72.17; H, 7.75%.

6h: Colorless needles (MeOH), mp 110.5—111 °C; ^{1}H-NMR ($CDCl_3$); δ=1.22, 1.42 (each s, 9H), 5.60 (1H, s, disappeared with D_2O), 6.74, 7.05 (each d, J=2.5 Hz, 1H), and 6.85, 7.38 (each d, J=9.0 Hz, 1H); Mass m/z 378 (M^+), 376 (M^+). Found: C, 63.63; H, 6.71%. Calcd for $C_{20}H_{25}BrO_2$: C, 63.66; H, 6.68%.

6i: Colorless needles (MeOH-H_2O), mp 93—94.5 °C; ^{1}H-NMR ($CDCl_3$); δ=1.22, 1.43 (each s, 9H), 5.72 (s, 1H, disappeared with D_2O), 6.75 (d, J=2.3 Hz, 1H), and 6.84—7.38 (m, 10H); Mass m/z 390 (M^+). Found: C, 79.84; H, 7.84%. Calcd for $C_{26}H_{30}O_3$: C, 79.97; H, 7.74%.

6j: Colorless prisms (MeOH-H_2O), mp 100—101 °C; ^{1}H-NMR ($CDCl_3$); δ=1.24, 1.43 (each s, 9H), 1.34 (t, J=7.0 Hz, 3H), 4.32 (q, J=7.0 Hz, 2H) 5.62 (s, 1H, disappeared with D_2O), 6.80, 7.10 (each d, J=2.0 Hz, 1H), and 6.97, 7.97 (each d, J=9.0 Hz, 2H); Mass m/z 370 (M^+). Found: C, 74.77; H, 8.23%. Calcd for $C_{23}H_{30}O_4$: C, 74.56; H, 8.16%.

6k: Pale yellow prisms (hexane), mp 126—127.5 °C; ^{1}H-NMR ($CDCl_3$); δ=1.25, 1.43 (each s, 9H), 5.41 (s, 1H, disappeared with D_2O), 6.82, 7.15 (each d, J=2.1 Hz, 1H), and 7.02, 8.17 (each d, J=9.0 Hz, 2H); Mass m/z 343 (M^+). Found: C, 70.22; H, 7.36; N, 4.26%. Calcd for $C_{20}H_{25}NO_4$: C, 69.95; H, 7.34; N, 4.08%.

6l: Colorless plates (MeOH-H_2O), mp 95.5—96.5 °C; ^{1}H-NMR ($CDCl_3$); δ=1.23, 1.41 (each s, 9H), 5.50 (s, 1H, disappeared with D_2O), 6.78 (d, J=2.2 Hz, 1H), 7.11 (d, J=2.2 Hz, 1H), 7.19—7.32 (m, 1H), 7.44 (t, J=8.0 Hz, 1H), and 7.76—7.97 (m, 1H); Mass m/z 343 (M^+). Found: C, 70.08; H, 7.32; N, 4.28%. Calcd for $C_{20}H_{25}NO_4$: C, 69.95; H, 7.34; N, 4.08%.

6m: Colorless prisms (hexane), mp 169—171 °C; IR (KBr) ν_{OH} 3450 and ν_{CN} 2210 cm^{-1}; ^{1}H-NMR ($CDCl_3$); δ=1.24, 1.42 (each s, 9H), 5.44 (s, 1H, disappeared with D_2O), 6.79, 7.13 (each d, J=2.5 Hz, 1H), and 7.00, 7.57 (each d, J=9.0 Hz, 2H); Mass m/z 323 (M^+). Found: C, 78.09; H, 7.82; N, 4.60%. Calcd for $C_{21}H_{25}NO_2$: C, 77.99; H, 7.79; N, 4.33%.

6n: Colorless prisms (hexane), mp 131—133 °C; IR (KBr) ν_{OH} 3410 and ν_{CO} 1658 cm^{-1}; ^{1}H-NMR ($CDCl_3$); δ=1.25, 1.44 (each s, 9H), 5.52 (s, 1H, disappeared with D_2O), 6.83, 7.12 (each d, J=2.2 Hz, 1H), 7.06, 7.83 (each d, J=8.8 Hz, 2H), and 9.87 (s, 1H); Mass m/z 326 (M^+). Found: C, 77.65; H, 8.02%. Calcd for $C_{21}H_{26}O_3$: C, 77.27; H, 8.06%.

6o: Colorless needles (hexane), mp 135—136 °C; IR (KBr) ν_{OH} 3400 and ν_{CO}1658 cm^{-1}; ^{1}H-NMR ($CDCl_3$); δ=1.23, 1.42 (each s, 9H), 2.54 (s, 3H), 5.54 (s, 1H, disappeared with D_2O), 6.80, 7.10 (each d, J=2.2 Hz, 1H), and 6.97, 7.89 (each d, J=8.8 Hz, 2H); Mass m/z 340 (M^+). Found: C, 77.83; H, 8.37%. Calcd for $C_{22}H_{30}O_3$: C, 77.61; H, 8.29%.

7a: Pale yellow prisms (MeOH), mp 140.5—142 °C; IR (KBr) $\nu_{C=O}$ 1660 and 1640 cm^{-1}; ^{1}H-NMR ($CDCl_3$); δ=1.06 (s, 9H), 1.21 (s, 18H), 6.40 (s, 2H), and 6.89, 8.03 (each d, J=9.0 Hz, 2H); Mass m/z 399 (M^+). Found: C, 72.17; H, 8.30; N, 3.38%. Calcd for $C_{24}H_{33}NO_4$: C, 72.15; H, 8.32; N, 3.32%.

7b: Pale yellow prisms (MeOH-H_2O), mp 102—103 °C; IR (KBr) $\nu_{C=O}$ 1660 and 1640 cm^{-1}; ^{1}H-NMR ($CDCl_3$); δ=1.05 (s, 9H), 1.19 (s, 18H), 6.60 (s, 2H), 7.08—7.37 (m, 2H), and 7.65—7.80 (m, 2H); Mass m/z 399 (M^+). Found: C, 72.34; H, 8.34; N, 3.36%. Calcd for $C_{24}H_{33}NO_4$: C, 72.15; H, 8.32; N, 3.15%.

7c: Colorless prisms (MeOH-H_2O), mp 152.5—154 °C; IR (KBr) $\nu_{C=O}$ 1658, 1638 and ν_{CN} 2220 cm^{-1}; ^{1}H-NMR ($CDCl_3$); δ=1.04 (s, 9H), 1.20 (s, 18H), 6.60 (s, 2H), and 6.87, 7.41 (each d, J=9.0 Hz, 2H); Mass m/z 380 (M^++1). Found: C, 79.02; H, 8.78; N, 4.30%. Calcd for $C_{25}H_{33}NO_2$: C, 79.12; H, 8.78; N, 3.69%.

7d: Pale yellow prisms (MeOH-H_2O), mp 109.5—111 °C; IR (KBr) $\nu_{C=O}$ 1690, 1658 and 1638 cm^{-1}; ^{1}H-NMR ($CDCl_3$); δ=1.07 (s, 9H), 1.22 (s, 18H), 6.64 (s, 2H), 6.94, 7.67 (each d, J=9.0 Hz, 2H), and 9.79 (s, 1H); Mass m/z 383 (M^++1). Found: C, 78.52; H, 8.90%. Calcd for $C_{25}H_{34}O_3$: C, 78.49; H, 8.96%.

7e: Colorless prisms (MeOH-H_2O), mp 113—113.5 °C; IR (KBr) $\nu_{C=O}$ 1680, 1660 and 1640 cm^{-1}; ^{1}H-NMR ($CDCl_3$); δ=1.05 (s, 9H), 1.21 (s, 18H), 2.11 (s, 3H), 6.64 (s, 2H), and 6.86, 7.74 (each d, J=9.0 Hz, 2H); Mass m/z 394 (M^+). Found: C, 78.52; H, 9.01%. Calcd for $C_{26}H_{36}O_3$: C, 78.74; H, 9.15%.

20: Pale yellow prisms (MeOH-H_2O), mp 126—127.5 °C; ^{1}H-NMR ($CDCl_3$); δ=1.42 (s, 18H), 5.13 (s, 1H, disappeared with D_2O), 6.91, 8.15 (each d, J=9.5 Hz, 2H), and 7.22 (s, 2H); Mass m/z 343 (M^+). Found: C, 70.10; H, 7.56; N, 4.18%. Calcd for $C_{20}H_{25}NO_4$: C, 69.95; H, 7.33; N, 4.08%.

As the other products such as **7**,[6] **8**,[7] **9**,[8] **10**,[9] **11**,[10] **12**,[11] **13**,[12] and **14**[13] which were obtained in the reaction described above are known compounds, their identification was carried out by comparison with authentic spectral data.

The $AlCl_3$-CH_3NO_2 Catalyzed trans-t-*Butylation. Typical Procedure*: To a stirred solution of 343 mg of **6k** in 20 ml of toluene was added a solution of 300 mg of $AlCl_3$ in 10 ml of nitromethane at room temperature. After the reaction mixture was heated at 80 °C for 1 h, it was poured into 50 ml of ice-water and extracted with benzene (20 ml×3). The benzene solution was dried with sodium sulfate and evaporated *in vacuo* to leave a residue which was chromatographed on silica gel using benzene as an eluent to give **23** and 200 mg (69%) of **21h**. Compound **21f** was also obtained in 80% yield

by this method. However, the case of **6a** afforded a mixture of **21a** and **22a** which could not be separated by the usual methods.

21f: Colorless needles (MeOH-H_2O), mp 85.5—87 °C ; ^{1}H-NMR ($CDCl_3$); δ=1.22 (s, 9H), 4.72 (s, 1H, disappeared with D_2O), 6.68—7.12 (m, 5H), and 7.38 (d, J=9.0 Hz, 2H), Mass m/z 322 (M^+), 320 (M^+). Found: C, 59.71; H, 5.18%. Calcd for $C_{14}H_{17}BrO_2$: C, 59.83; H, 5.33%.

21h: Colorless needles (hexane), mp 95.5—97 °C;^{1}H-NMR ($CDCl_3$); δ=1.25 (s, 9H), 5.14 (s, 1H, disappeared with D_2O), 6.80—7.15 (m, 5H) and 8.16 (d, J=9.2 Hz, 2H); Mass m/z 287 (M^+). Found: C, 66.62; H, 5.96; N, 4.88%. Calcd for $C_{16}H_{17}NO_3$: C, 66.89; H, 5.96; N, 5.08%.

The $AlCl_3$ Catalyzed trans-t-*Butylation. General Procedure*: After a mixture of 10 mmol of **6** or **7**, 30 mmol of $AlCl_3$ and 100 mmol of toluene was heated at 80 °C for 30 min, it was treated and worked up as described above to give the products shown in Table 3.

22a: Colorless granules (hexane), mp 100.5—103 °C; ^{1}H-NMR ($CDCl_3$); δ=5.54 (s, 1H, disappeared with D_2O), and 6.70—7.41 (m, 9H); Mass m/z 186 (M^+). Found: C, 76.93; H, 5.58%. Calcd for $C_{12}H_{10}O_2$: C, 77.40; H, 5.41%.

22b: Colorless needles (hexane), mp 61.5—62 °C; ^{1}H-NMR ($CDCl_3$); δ=2.51 (s, 3H), 5.58 (s, 1H, disappeared with D_2O), and 6.62—7.22 (m, 8H). Found: C, 77.12; H, 6.23%. Calcd for $C_{13}H_{12}O_2$: C, 77.10; H, 6.00%.

22c: Colorless prisms (hexane), mp 77—78 °C; ^{1}H-NMR ($CDCl_3$); δ=5.50 (s, 1H, disappeared with D_2O), and 6.68—7.06 (m, 8H); Mass m/z 204 (M^+). Found: C, 70.60; H, 4.54%. Calcd for $C_{12}H_9FO_2$: C, 70.58; H, 4.44%.

22d: Colorless crystals, mp 46.5—48 °C; ^{1}H-NMR ($CDCl_3$); δ=5.64 (s, 1H, disappeared with D_2O), and 6.64—7.52 (m, 8H); Mass m/z 222 (M^+) 220 (M^+). Found: C, 65.61; H, 4.18%. Calcd for $C_{12}H_9ClO_2$: C, 65.32; H, 4.11%.

22e: Colorless needles (hexane), mp 82—84 °C; ^{1}H-NMR ($CDCl_3$); δ=5.50 (s, 1H, disappeared with D_2O), 6.62—7.08 (m, 6H), and 7.28 (d, J=9.0 Hz, 2H); Mass m/z 222 (M^+), 220 (M^+). Found: C, 65.49; H, 4.19%. Calcd for $C_{12}H_9ClO_2$: C, 65.32; H, 4.11%.

22f: Colorless prisms (hexane), mp 58—59.5 °C; ^{1}H-NMR ($CDCl_3$); δ=5.68 (s, 1H, disappeared with D_2O), and 6.46—7.50 (m, 8H); Mass m/z 266 (M^+), 264 (M^+). Found: C, 54.40; H, 3.63%. Calcd for $C_{12}H_9BrO_2$: C, 54.37; H, 3.42%.

22g: Colorless needles (hexane), 95.5—97 °C; IR (KBr) $\nu_{C=O}$ 1695 cm^{-1}; ^{1}H-NMR ($CDCl_3$); δ=1.37 (t, J=7.0 Hz, 3H), 4.33 (d, J=7.0 Hz, 3H), 5.59 (s, 1H, disappeared with D_2O), 6.62—7.13 (m, 6H), and 7.96 (d, J=9.0 Hz, 2H), Mass m/z 258 (M^+). Found: C, 69.87; H, 5.27%. Calcd for $C_{15}H_{14}O_4$: C, 69.75; H, 5.46%.

22h: Colorless needles (benzene-hexane), mp 111—112 °C; ^{1}H-NMR ($CDCl_3$); δ=5.32 (s, 1H, disappeared with D_2O), 6.76—7.25 (m, 6H), and 8.19 (d, J=9.5 Hz, 2H); Mass m/z 231 (M^+). Found: C, 62.33; H, 3.98; N, 6.23%. Calcd for $C_{12}H_9NO_4$: C, 62.34; H, 3.92; N, 6.06%.

22i: Colorless needles (benzene-hexane), mp 104—105 °C; IR (KBr) ν_{CN} 2240 cm^{-1}; ^{1}H-NMR ($CDCl_3$); δ=5.50 (s, 1H, disappeared with D_2O), 6.72—7.22 (m, 6H), and 7.36 (d, J=9.0 Hz, 2H); Mass m/z 211 (M^+). Found: C, 73.81; H, 4.36; N, 6.54%. Calcd for $C_{13}H_9NO_2$: C, 73.92; H, 4.30; N, 6.63%.

22j: Colorless needles (benzene-hexane), mp 90.5—92 °C; IR (KBr) $\nu_{C=O}$ 1680 cm^{-1}; ^{1}H-NMR ($CDCl_3$); δ=5.56 (s, 1H, disappeared with D_2O), 6.76—7.20 (m, 6H), 7.80 (d, J=9.0 Hz, 2H), and 9.86 (s, 1H); Mass m/z 214 (M^+). Found: C, 73.17; H, 4.80%. Calcd for $C_{12}H_{10}O_3$: C, 72.89; H, 4.70%.

22k: Colorless needles (benzene), mp 84—85 °C; IR (KBr) $\nu_{C=O}$ 1660 cm^{-1}; ^{1}H-NMR ($CDCl_3$); δ=2.55 (s, 3H), 5.80 (s, 1H, disappeared with D_2O), 6.82—7.14 (m, 6H), and 7.89 (d, J=9.0 Hz, 2H); Mass m/z 228 (M^+). Found: C, 73.91; H, 5.29%. Calcd for $C_{14}H_{12}O_3$: C, 73.67; H, 5.30%.

24a: Yellow needles (benzene), mp 173.5—175 °C; ^{1}H-NMR ($CDCl_3$); δ=4.96 (s, 1H, disappeared with D_2O), 6.70—7.04 (m, 6H), and 8.14 (d, J=9.3 Hz, 2H); Mass m/z 281 (M^+). Found: C, 62.30; H, 3.95; N, 6.10%. Calcd for $C_{12}H_9NO_4$: C, 62.34; H, 3.92; N, 6.06%.

24b: Pale yellow oil; IR (NaCl) ν_{OH} 3440 cm^{-1}; ^{1}H-NMR ($CDCl_3$); δ=4.83 (br, s, 1H, disappeared with D_2O), and 6.72—7.93 (m, 8H); Mass m/z 231 (M^+).

Acetate of **24b** was prepared by treatment with acetic anhydride in order to obtain a crystalline compound.

The acetate: Colorless plates (ether-benzene), mp 62—63 °C; Mass m/z 273 (M^+). Found: C, 61.25; H, 3.98; N, 5.18%. Calcd for $C_{14}H_{11}NO_5$: C, 61.54; H, 4.06; N. 5.13%.

24c: Colorless prisms (benzene), mp 147—148.5 °C; IR (KBr) ν_{CN} 2340 cm^{-1}; ^{1}H-NMR ($CDCl_3$); δ=5.18 (s, 1H, disappeared with D_2O), 6.70—7.02 (m, 6H), and 7.54 (d, J=9.0 Hz, 2H); Mass m/z 211 (M^+). Found: C, 74.07; H, 4.34; N, 6.73%. Calcd for $C_{13}H_9NO_2$: C, 73.92; H, 4.29; N, 6.63%.

24d: Colorless plates (benzene-hexane), mp 129—130.5 °C; IR (KBr) $\nu_{C=O}$ 1675 cm^{-1}; ^{1}H-NMR ($CDCl_3$); δ=5.08 (s, 1H, disappeared with D_2O), 6.75—7.07 (m, 6H), 7.79 (d, J=9.0 Hz, 2H), and 9.85 (s, 1H); Mass m/z 214 (M^+). Found: C, 72.89; H, 4.74%. Calcd for $C_{12}H_{10}O_3$: C, 72.89; H, 4.70%.

24e: Colorless plates (benzene), mp 164—166.5 °C; IR (KBr) $\nu_{C=O}$ 1660 cm^{-1}; ^{1}H-NMR ($CDCl_3$); δ=2.55 (s, 3H), 5.38 (s, 1H, disappeared with D_2O), 6.72—7.03 (m, 6H), and 7.88 (d, J=9.0 Hz, 2H); Mass m/z 228 (M^+). Found: C, 73.56; H, 5.31%. Calcd for $C_{14}H_{12}O_3$: C, 73.67; H, 5.30%.

References

1) Part 10. M. Tashiro, G. Fukata, T. Itoh, and H. Yoshiya, to be published.

2) M. Tashiro, H. Yoshiya, and T. Yamato, *Synthesis*, **1978**, 399.

3) G. Fukata, T. Itoh, and M. Tashiro, *J. Org. Chem.*, **46**, 4454 (1981).

4) M. Tashiro, H. watanabe, and O. Tsuge, *Org. Prep. Proc. Int.*, **6**, 117 (1974).

5) D. E. Person, S. D. Venkaturamu, and W. E. Childers, Jr., *Syn. Commun.*, **9**, 5 (1979).

6) M. Tsubota, *Nippon Kagaku Zasshi*, **89**, 602 (1968).

7) M. Tashiro, H. Yoshiya, and G. Fukata, *J. Org. Chem.*, **46**, 3784 (1981).

8) N. Nishinaga, T. Itahara, and T. Matsuura, *Bull. Chem. Soc. Jpn.*, **48**, 1683 (1975).

9) A. McKillop, and B. P. Swann, *Tetrahedron*, **26**, 4031 (1970).

10) E. Müller and K. Ley, *Chem. Ber.*, **88**, 606 (1955).

11) D. R. Stevens, U. S. Patent, 2403748; *Chem. Abstr.*, **47**, 8093 (1953).

12) H. D. Kluge and E. C. Knowles, U. S. Patent, 2469469; *Chem. Abstr.*, **43**, 6406f (1949).

13 T. Zincke and N, Junney, *Justus Liebigs Ann. Chem.*, **398**, 354 (1913).

 © 1984 The Chemical Society of Japan Bull. Chem. Soc. Jpn., 57, 421—425 (1984)

Preparation and Spectral Behavior of Polyoxadithia[*n*]ferrocenophanes and Their Silver(I) Nitrate Complexes

Masaru SATO, Masao KUBO, Seiji EBINE,*,† and Sadatoshi AKABORI††

Chemical Analysis Center, Saitama University, Urawa, Saitama 338

†*Department of Chemistry, Faculty of Science, Saitama University, Urawa, Saitama 338*

††*Department of Chemistry, Faculty of Science, Toho University, Funabashi, Chiba 274*

(Received May 20, 1983)

Polyoxadithia[*n*]ferrocenophanes and polyoxatetrathia[*n.n*]ferrocenophanes were prepared by treatment of 1,1′-ferrocenedithiol with α,ω-dibromo polyethers. The ferrocenophanes formed efficiently a complex with a silver ion, but not with alkali and alkali-earth metal ions. The spectral data of the silver ion-complexed ferrocenophanes suggested the presence of a partial electron-transfer interaction between the iron atom and the complexed silver ion.

In order to develop a new functional ability, various attempts to prepare modified crown ethers have been made.[1] Incorporation of a certain heteroatom into a crown ether ring increases a complexing affinity with transition metals. For example, polythiamacrocycles are able to form a stable complex with silver(I),[2] nickel(II),[3] and copper(II) salts.[4] Polyoxathiaferrocenophane is a crown ether-like compound containing a ferrocene ring and a sulfur atom as ring members, in which the iron atom of the ferrocene may play a role of a coordinatable heteroatom to a complexed cation. A few were reported about this class of compounds. For example, 1,1′-ferrocenedicarbonyl dichloride reacted with a diazacrown ether and the product was reduced to give the ferrocene derivatives (**1**) of cryptand.[5] Polythia- (**2**)[6] and dithiaoxaferrocenophanes (**3**)[7] were prepared from 1,1′-ferrocenedimethanol and its derivatives. In these compounds, however, the distance between the iron atom of the ferrocene and the center of the macrocycle is too long to effect an interaction between the iron atom and the complexed metal ion. Polish workers[8] recently prepared polyoxaferrocenophanes (**4**) carrying oxygen atoms attached directly to a ferrocene nucleus, and suggested, from their electronic spectra, no interaction between the iron atom and the complexed rubidium cation. We also prepared polyoxaferrocenophanes and discussed their complexing ability and interaction between the iron atom and the complexed metal cations.[9] We now report the preparation and some complexing properties of polyoxadithiaferrocenophanes, carrying sulfur atoms attached to the ferrocene nucleus.[10]

Syntheses and Spectral Properties. Disodium 1,1′-ferrocenedithiolate, prepared from 1,1′-ferrocenedithiol[11] and aqueous sodium hydroxide in ethanol, reacted with α,ω-dibromo polyethers in ethanol at room temperature and the products were chromatographed by a silca-gel column to give two kinds of oxathiaferrocenophanes (**5**) and (**6**). The structures were determined by the elemental analyses and spectral data. For example, the molecular formula of **5c** was deduced to be $C_{18}H_{24}O_3S_2Fe$ by the elemental analysis and mass spectroscopy (M^+ 408). In the ^{1}H-NMR spectrum of **3d**, the α- and β-ring protons of the ferrocene nucleus appeared as a singlet (8H) at δ 4.24, while the methylene protons next to the oxygen atom appeared as a triplet (4H, J=6 Hz) at δ 3.74 and a singlet (8H) at 3.71, and those next to the sulfur atom resonated as a triplet (J=6.0 Hz) at δ 3.03. In the ^{13}C-NMR spectrum of **5c**, the bridgehead carbon (C_b), α- and β-carbons of the ferrocene nucleus resonated at δ 84.8, 72.7, and 68.8, respectively. In addition, the signal of the carbon next to the sulfur atom appeared at δ 35.8 and those next to the oxygen atoms appeared at δ 69.5, 70.5, and 70.7.

The yield of polyoxadithia[*n*]ferrocenophanes (**5**) amounted to maximum when n=3, but that of polyoxatetrathia[*n.n*]ferrocenophanes (**6**) decreased with the increase of the size of the macrocycle, which may indicate that a template effect of sodium cation plays a little role in the final cyclization step. As shown in the ^{1}H-NMR spectral data of Table 2, there is a remark-

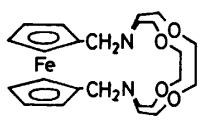

(1)

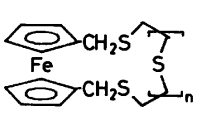

(2)

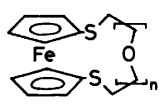

(5)

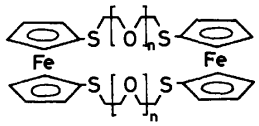

(6)

a : n=1, b : n=2, c : n=3, d : n=4

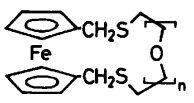

(3)

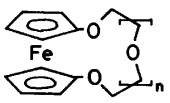

(4)

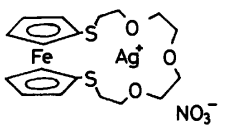

(7)

able difference in the pattern of ferrocene ring protones between mononuclear compounds **5** and dinuclear compounds **6**. In the former, the α- and β-ring protons of the ferrocene nucleus resonated as a singlet or a narrow multiplet, but in the latter the corresponding protons appeared as a pair of triplets. The methylene protons next to the sulfur atom in **5** resonated at lower field by 0.3 ppm than the corresponding ones in **6**. A similar trend was also observed in the methylene protons next to the oxygen atom. The low-field shift of the methylene protons in the mononuclear ferrocenophane **5** would be probably due to the fact that those protons exists in the deshielding zone of a ferrocene nucleus (an interannular area)[12] according to consideration of its stereomolecular model.

In the ^{1}H-NMR spectra of the ferrocene ring protons, **5a—d** have a similar chemical shift (δ *ca.* 4.2) to each other. In the ^{13}C-NMR spectra of the ferrocene ring carbons, however, **5a** showed a trend different from the other mononuclear ferrocenophanes **5b—d**, that is, the bridge-head carbon atom resonated at a lower field ($\Delta\delta$ *ca.* 6 ppm) and the α- and β-carbon atoms of **5a** resonated at a higher field ($\Delta\delta$ *ca.* 2 ppm) in **5a** than in the other **5b—d**. A similar specificity of **5a** was also observed in the electronic spectra of **5** (Table 1).

The absorption band near 440 nm of **5a**, assignable to a d-d transition of ferrocene nucleus,[13] shifted to a longer wavelength region ($\Delta\lambda$ *ca.* 10 nm) than that of **5b—d**, and its absorbance increased considerably (*ca.* 40%), the details of which will be discussed in another paper.[14]

Complexing Ability. The complexing ability of polyoxaferrocenophanes (**4**) with alkali metals was first reported to be conspicuous by the TLC method,[8] but was recently shown to be rather faint by the extraction method.[9] This trend is comparable with the fact that the complexing ability of benzocrown ether with alkali metal cations is smaller than that of crown ether itself, the reason of which has been rationalized by the HSAB principles.[15] On the basis of this principle, the displacement of some oxygen atoms of **4** by the sulfur atoms to **5** and **6** will results in a decrease in the affinity to hard cations and an increase in the affinity to soft heavy metal cations. The complexing ability of **5** and **6** with a variety of metals cation was examined by the extraction method described by Pedersen,[16] and the results were summarized in Table 3, alkali and alkali-earth metal cations being excluded because no extraction ability toward them was observed. This result is coincident with the expectation described above. The complexing ability of **5** and **6** was a little

Table 1. Electronic spectral data of **5** and **6**

Compd	5a	5b	5c	5d	6a	6b	6c
λ_{max}/nm	456	444	443	440	438	438	438
ε	242	198	198	192	351	363	379

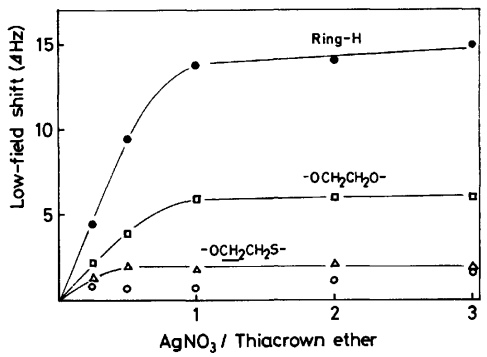

Fig. 1. ^{1}H-NMR spectral change of **5c** on addition of silver(I) nitrate in acetonitrile-d_3.

Table 2. ^{1}H-NMR and ^{13}C-NMR spectra of **5** and **6** ($CDCl_3$)

Compd	^{1}H-NMR (60 MHz)	^{13}C-NMR (22.5 MHz)
5a	4.20(m, 8H), 3.94(t, 4H, J=5.5), 3.07(t, 4H, J=5.5)	90.7(C_b), 66.9(C_α), 70.0(C_b), 34.7(SCH_2), 71.4(OCH_2)
5b	4.24(s, 8H), 3.86(t, 4H, J=6.2), 3.75(s, 8H), 3.06 t, 4H, J=6.2)	85.4(C_b), 68.3(C_α), 72.7(C_β), 35.6 (SCH_2), 69.6 and 71.0(OCH_2)
5c	4.25(s, 8H), 3.74(t, 4H, J=6.0), 3.71(s, 8H), 3.03(t, 4H, J=6.0)	84.8(C_b), 68.8(C_α), 72.7(C_β), 35.8 (SCH_2), 69.5, 70.5, 70.7(OCH_2)
5d	4.24(m, 8H), 3.69(t, 4H, J=6.0), 3.69(s, 12H), 2.75(t, 4H, J=6.0)	83.8(C_b), 69.3(C_α), 73.4(C_β), 36.5(SCH_2), 69.5, 70.5, 70.7(OCH_2)
6a	4.41(t, 8H, J=1.7), 4.25 (t, 8H, J=1.7), 3.64(t, 8H, J=5.8), 2.88(t, 8H, J=5.8)	
6b	4.35(t, 8H, J=1.7), 4.24 (t, 8H, J=1.7), 3.64(t, 8H, J=6.2), 3.59(s, 8H), 2.67(t, 8H, J=6.2)	
6c	4.34(t, 8H, J=1.7), 4.23 (t, 8H, J=1.7), 3.62(t, 8H, J=6.5), 3.61(s, 16H), 2.81 (t, 8H, J=6.5)	

Table 3. Extraction ability of **5** and **6**

Compd	Cd^{2+}	Pb^{2+}	Tl^+	Ag^+
5a	1.9	Nil	1.5	—
5b	2.9	Nil	1.5	49.1
5c	3.1	Nil	12.5	77.3
5d	3.3	19.2	43.9	78.9
6a	3.3	1.4	7.0	77.1
6b	2.9	1.0	20.0	84.7
6c	2.7	1.5	42.8	93.5

Table 4. Hypsochromic shift of electronic spectra in acetonitrile and low-field shift of ^{1}H-NMR spectra in acetonirile-d_3 of **5** in the presence of silver(I) nitrate (1 equiv)

Compd	Electronic spectra near 440 nm $\Delta\lambda_{max}$/nm	$\Delta\varepsilon$/%	^{1}H-NMR spectra (Δ, ppm) Ring-H		S-CH_2
5b	10	−10.1	0.32	0.20	0.15
5c	15	−18.3	0.17		0.01
5d	14	−13.1	0.21		0.08

or negligible with lithium, sodium, potassium, calcium, strontium, cadmium, and lead cations, while it was excellent with a silver cation and moderate with a thallium ion. The high complexing ability with a silver ion is comparable with that of benzooxathiacyclopolyethers.[2] It is also noteworthy that lead and thallium ions showed a remarkable dependence on the size of the macrocycle of **5** and **6**.

On addition of silver nitrate to **5** and **6** in acetonitrile, the absorption band near 440 nm showed a hypsochromic shift and a decrease in its absorbance, which are summarized in Table 4. There seems to be a parallel relationship between the hypsochromic shift and the decrease in absorbance in the mononuclear series **5b—d**, but not in the binuclear series **6a—c**. Both of the complexing ability and the electronic spectral change are large in **5c** and **5d**, but small in **5b**. This parallel relationship suggests an importance of the fitness of the macrocycles in **5** with a silver ion. The change of electronic spectra of a crown ether on addition of a metal cation is reported to be small.[17] So, a large electronic spectral change which depends on the complexing ability of those crown ether-type compounds presented here should be noticable.

In the ^{1}H-NMR spectrum of **5** in acetonitrile-d_3, the addition of silver nitrate causes a deshielding shift of the signals of methylene protons next to the sulfur atom and the ferrocene ring protons (Table 4). As shown in Fig. 2, the deshielding shift ($\Delta\delta$) increases almost linearly according to the increase of silver nitrate until the amount of the salt becomes equivalent to polyoxadithiaferrocenophanes **5**, but the addition of more silver ion results in little change of deshielding shift, which suggests the formation of a 1:1 complex of the ferrocenophanes 5 with silver nitrate in acetonitrile. The ferrocene ring protons of the complex of **5c** and **5d** with silver(I) nitrate appeared as a singlet just like those of free **5c** and **5d**, while the α- and β- protons of ferrocene ring protons of the complexed **5b** resonated as a separated pair of triplets. This is probably because the complex formation of **5b** with silver(I) nitrate demands the tilt-deformation of two cyclopentadienyl rings in order to put the silver(I) ion in the hole by spreading the macrocycle, because it is well known that the tilt-deformation of the cyclopentadienyl ring in ferrocenophanes causes the splitting of the α- and β-protons of ferrocene ring.[18] Since the tilting of two cyclopentadienyl rings results in some bathochromic shift,[18] the small change in the electronic spectrum of **5b** described above may reflect the difficulty on complexation of **5b** with a silver ion.

The deshielding of methylene protons on the complexation of **5** may be caused by the magnetic anisotropy of the silver ion. However, the large deshielding ($\Delta\delta$ *ca.* 0.2 ppm) of the ferrocene ring protons seems to be due to the electron density of the cyclopentadienyl rings decreased by a partial electron transfer from the iron atom to the complexed silver ion in **5**, since the α-and β-protons shifted to the same extent. If the deshielding shift is caused by the perturbation of the inductive and conjugative effect of the sulfur-substituent with coordination of a silver ion to a sulfur atom, the α-protons would be expected to resonate at a lower field than the β-protons. (The influence of an electron attracting substituent is well known to appear at the α-protons more remarkably.) Such a partial electron transfer has been observed in the complex of 1,1′-bis(diphenylphosphino)ferrocene with mercury(II) chloride.[19] An additional support was obtained from the ^{13}C-NMR spectra of **5b—d** and its benzene analog measured in the presence of silver(I) nitrate in acetonitrile-d_3 (Table 5).

Table 5. Low-field shift of ^{13}C-NMR spectra on additon of silver(I) nitrate to a solution of **5** in acetonitrile-d_3 (Δ, ppm)

Compd	C_b	C_α	C_β	SCH_2
5b	−3.2	1.1	2.0	1.3
5c	−8.2	4.2	2.8	3.9
5d	−6.4	3.5	2.2	3.2
8	−4.0	−1.5	1.5	2.7

a) C_b means the bridgehead carbon.

The signal of the α- and β-carbon of ferrocene ring in **5b—d** shifted down-field but those of the bridgehead carbon shifted up-field. The deshielding shift of methylene carbons next to a sulfur atom was similar to that of the ferrocene ring carbones, but the methylene carbons next to an oxygen atom showed only a little shift. In the benzene analog 4′-methyl-2,3-benzo-1,4-dithia-7,10,13-trioxa-2-cyclopentadecene (**8**),[2] on the other hand, the bridgehead carbon and methylene carbons next to sulfur atoms showed the same trend with in **5**, but the α-ring carbons showed some upfield shifts, suggesting a significant complexing of the silver ion with the sulfur atom. The fact that the ferrocene ring carbons (C_α and C_β) in **5** showed more deshielding shift than the corresponding benzene ring carbons in **8** suggest some electron transfer from the iron atom to the complexed silver ion on addition to the electron transfer *via* the sulfur atom from the cyclopentadienyl ring to the silver cation. Finally, the complexation of **5c**, among **5**, with silver(I) ion would be the strongest because the change of the carbon chemical shifts in the ^{13}C-NMR spectra was the largest in **5c**. The length of an oxyethylene chain in **5** would probably control the fitness of the macrocycle to a silver(I) ion.

Complex of 5c with Silver(I) Nitrate. A solution of **5c** and an equimolar silver(I) nitrate in acetonitrile was poured into anhydrous ether under nitrogen to give stable yellow crystalline precipitates of the 1:1 complex (7). However, **5b** and **5d** gave no crystalline complex. This result is coincident with suggestion described above that **5c** will form the most tight complex with silver(I) nitrate among **5**. The ^{1}H-NMR spectrum of **7** in $CDCl_3$ showed a pair of triplets corresponding to the H_α and H_β protons of a ferrocene nucleus at δ 4.50 and 4.33 (J=2.0 Hz), a pair of triplet assigned to the protons next to a sulfur atom and next to an oxygen atom at δ 3.04 and 3.74 (J=5.8 Hz) respectively, and a singlet at δ 3.77 (-OCH_2CH_2-). The difference in the chemical shift between free ligand **5c** and complex **7** is almost similar to that measured on

addition of silver(I) nitrate to a solution of **5c** in acetonitrile-d_6. The ferrocene ring protons appeared as a pair of triplet in the former but a broad singlet in the latter. This seems to be probably because in the latter, there is an equilibrium between the free ligand and the complex in acetonitrile and hence the signals of α- and β-protons are avaraged to an single signal. The fact that the splitting of the ferrocene ring protons was observed in the isolated silver-complex (**7**) indicates that the through-space electronic interaction between the iron atom of a ferrocene nucleus and the complexed silver ion in **7** described in the preceding section is too emphasized.

The ^{13}C-NMR spectrum of **7** in $CDCl_3$ showed the signals of bridge-head, α-, and β-carbons appeared at δ 77.7, 77.1, and 71.1 ppm, respectively. The carbons next to a sulfur atom appeared at δ 40.0 ppm, and those next to an oxygen atom appeared at δ 70.4, 69.7, and 67.2 ppm. The deshielding shifts of α- and β-carbons of ferrocene ring and the sulfur-attached carbons in **7** are almost similar to those measured on the addition of silver(I) nitrate to a solution of **5c** in acetonitrile-d_3. These NMR data of **7** indicate that **5c** and probably other polyoxadithiaferrocenophanes (**5b** and **5c**) also form a 1:1 complex in acetonitrile, and that the discussion about the nature of the complex of **5** with silver(I) nitrate described in the preceding and present section is reasonable enough.

Experimental

The melting points are uncorrected. The electronic spectra were measured on a Hitachi 340 Spectrometer. The IR spectra were measured on a JASCO IRA-2 Infrared Spectrometer. The ^{1}H-NMR and ^{13}C-NMR spectra were obtained on a JEOL FX-90Q Spectrometer, TMS being chosen as an internal standard. The mass spectra were taken by using a Hitachi M-80 Spectrometer.

Material. 1,1′-Ferrocenedithiol was prepared by reduction of 1,2,3-trithia[3]ferrocenophane with lithium aluminum hydride.[11] Bis(2-bromoethyl) ether,[20] 1,8-dibromo-3,6-dioxaoctane,[20] 1,11-dibromo-3,6,9-trioxaundecane,[21] and 1,14-dibromo-3,6,9,12-tetraoxatetradecane were prepared according to the literatures.

Polyoxadithia[n]*ferrocenophanes(5) and Polyoxatetrathia*-[n.n]*ferrocenophanes. General Procedure*: To a suspension of 1,1′-ferrocenedithiol (0.45 g, 1.8 mmol) in ethanol (90 ml) was added a solution of sodium hydroxide (0.18 ml of 20M** solution, 3.6 mmol) under stirring and bubbling of nitrogen. To the resulting red-orange solution was added a solution of the corresponding α,ω-dibromopolyether (1.8 mmol) in ethanol (3 ml). The solution was stirred for 4 h at room temperature under bubbling of nitrogen. After evaporating the solution, the residue was redissolved in benzene and filtered. The filtrate was condensed by an evaporator and charged on silica-gel column chromatography. Elution by toluene-ethyl acetate mixture gave **5** and **6**.

4-Oxa-1,7-dithia[7]ferrocenophane (5a). Red needles, 8%, mp 62—63 °C. Found: C, 52.70; H, 5.28%. Calcd for $C_{14}H_{16}OS_2Fe$: C, 52.51; H, 5.04%. MS (75 eV): *m/z* 320 (M^+, 100%). IR (KBr): 3100, 2940, 2850, 1420, 1120, 1035, and 807 cm^{-1}.

4,22-Dioxa-1,7,19,25-Tetrathia[7.7]ferrocenophane (6a). Orange needles, 30%, mp 112—113 °C. Found: C, 52.56; H, 5.09%. Calcd for $C_{28}H_{32}O_2S_4Fe_2$: C, 52.51; H, 5.04%. MS (75 eV): *m/z* 640 (M^+, 100%), 320 ($M^+/2$, 32%), and 304 (30%). IR (KBr): 3100, 2900, 2870, 1420, 1195, 1110, 1025, and 810 cm^{-1}.

4,7-Dioxa-1,10-dithia[10]ferrocenophane (5b). Orange oil, 26%. Found: C, 52.91; H, 5.44%. Calcd for $C_{16}H_{20}O_2S_2Fe$: C, 52.75; H, 5.53%. MS (75 eV): *m/z* 364 (M^+, 100%). IR (KBr): 3100, 2930, 2860, 1420, 1295, 1130, 1025, and 810 cm^{-1}.

4,7,25,28-Tetraoxa-1,10,22,31-tetrathia[10.10]ferrocenophane (6b). Orange oil, 12%. Found: C, 52.99; H, 5.60%. Calcd for $C_{32}H_{40}O_4S_4Fe_2$: C, 52.75; H, 5.53%. MS (75 eV): *m/z* 728 (M^+, 100%), 364 ($M^+/2$, 56%), and 304 (25%). IR (KBr): 3100, 2900, 2870, 1420, 1325, 1290, 1140, 1020, and 810 cm^{-1}.

4,7,10-Trioxa-1,13-dithia[13]ferrocenophane (5c). Orange oil, 63.8%. Found: C, 53.00; H, 6.42%. Calcd for $C_{18}H_{24}O_3S_2Fe$: C, 52.94; H, 5.92%. MS (75 eV): *m/z* 408 (M^+, 100%). IR (Neat): 3100, 2930, 2875, 1420, 1365, 1295, 1150—1100, 1030, 830, and 810 cm^{-1}.

4,7,10,28,31,34-Hexaoxa-1,13,25,37-tetrathia[13.13]ferrocenophane (6c). Orange cubes, mp 84—85 °C, 17.1%. Found: C, 53.10; H, 6.09%. Calcd for $C_{36}H_{48}O_6S_2Fe_2$: C, 52.94; H, 5.92%. MS (75 eV): *m/z* 816 (M^+, 100%) and 408 ($M^+/2$, 42%). IR (KBr): 3100, 2860, 1295, 1240, 1120, 835, and 820 cm^{-1}.

4,7,10,13-Tetraoxa-1,16-dithia[16]ferrocenophane (5d). Orange oil, 60.4%. Found: C, 52.81; H, 6.29%. Calcd for $C_{20}H_{28}O_4S_2Fe$: C, 53.10; H, 6.24%. MS (75 eV): *m/z* 452 (M^+, 100%). IR (Neat): 3100, 2925, 2870, 1420, 1360, 1295, 1150—1095, 1025, and 830 cm^{-1}.

The electronic, ^{1}H-NMR, and ^{13}C-NMR spectra of the compounds described above were summarized in Tables 1 and 2.

Method of Solvent Extraction. Extractability of polyoxathiaferrocenophanes **5** and **6** with metal cations was measured by the extraction method[9] which was the somewhat modified Pedersen method[16].

Measurement of the Electronic, ^{1}H- and ^{13}C-NMR Spectra in the Presence of Silver(I) Nitrate. The electronic spectra of **5b—d** (4.00×10^{-3}M) was recorded in the presence of silver(I) nitrate (2.00×10^{-3}M) in acetonitrile. The ^{1}H-NMR spectra of **5b—d** (0.08 mmol) was recorded in the presence of 0.25, 0.5, 1, 2, and 3 equivalents of silver(I) nitrate in acetonitrile-d_3 (*ca.* 0.3 ml). The results were summarized in Table 4 and Fig. 2. The ^{13}C-NMR spectra of **3b—d** and **8** (0.08 mmol) was recorded in the presence of silver(I) nitrate (0.1 mmol) in acetonitrile-d_3 (*ca.* 0.3 ml).

The Complex of 5c with Silver(I) Nitrate. **5c** (0.37 g, 0.9 mmol) and silver(I) nitrate (0.15 g, 0.9 mmol) were dissolved in acetonitrile (3 ml) under nitrogen. The resulting solution was heated for 3 min and then poured into anhydrous ether (40 ml). Yellow crystalline precipitates resulted.

Filtration and washing with anhydrous ether gave yellow crystals (0.43 g, 74%). The crystals were dissolved in chloroform and the resulting solution was filtered into anhydrous ether to give a pure complex. Mp 152 °C (decomp).

Found: C, 37.53; H, 4.32%. Calcd for $C_{18}H_{24}O_6NS_2FeAg$: C, 37.39; H, 4.18%. IR (KBr): 3090, 2870, 1390—1355, 1300, 1120, 1125, and 835 cm^{-1}.

**1 M=1 mol dm^{-3}.

References

1) R. M. Izatt and J. J. Christensen, "Synthetic Multidentate Macrocyclic Compounds," Academic Press, New York (1978).

2) C. J. Pedersen, *J. Org. Chem.*, **36**, 254 (1971).

3) W. Rosen and D. H. Busch, *Inorg, Chem.*, **9**, 262 (1970).

4) T. L. Jones, L. L. Zimmer, L. L. Diaddario, D. B. Rorabacher, and L. A. Ochrymowycz, *J. Am. Chem. Soc.*, **97**, 7163 (1975).

5) G. Oepen and F. Vögle, *Liebigs Ann. Chem.*, **1979**, 1094; A. P. Bell and C. D. Hall, *J. Chem. Soc., Chem. Commun.*, **1980**, 163.
6) A. Ratajczak and B. Czech, *Polish J. Chem.*, **54**, 57 (1980).
7) B. Czech and A. Ratajczak, *Polish J. Chem.*, **54**, 767 (1980).
8) J. F. Biernat and T. Wilczewski, *Tetrahedron*, **36**, 2521 (1980).
9) S. Akabori, Y. Habata, Y. Sakamoto, M. Sato, and S. Ebine, *Bull. Chem. Soc. Jpn.*, **56**, 537 (1982).
10) A preliminary report: M. Sato, M. Kubo, S. Ebine, and S. Akabori, *Tetrahedron Lett.*, **22**, 185 (1981).
11) J. J. Bishop, A. Davison, M. L. Katcher, D. W. Lichtenberg, R. E. Merrill, and J. C. Smart, *J. Organomet. Chem.*, **27**, 241 (1971).
12) L. N. Mulay and M. E. Fox, *J. Chem. Phys.*, **38**, 760 (1963)
13) D. R. Scott and R. S. Becker, *J. Chem. Phys.*, **35**, 516 (1961).
14) M. Sato, S. Tanaka, S. Ebine, K. Morinaga, and S. Akabori, to be submitted.
15) T. Ho, "Hard and Soft Acids and Bases Principle in Organic Chemistry," Academic Press, New York (1977).
16) C. J. Pedersen, *Fed. Proc.*, **27**, 1305 (1968).
17) C. J. Pedersen, *J. Am. Chem. Soc.*, **89**, 7017 (1967).
18) T. H. Barr and W. E. Watts, *Tetrahedron*, **34**, 6111 (1968).
19) K. R. Mann, W. H. Morrison, Jr., and D. N. Hendrickson, *Inorg. Chem.*, **13**, 1180 (1974).
20) A. Luttringhaus, F. Cramer, H. Prinzbach, and F. M. Henglein, *Justus Liebigs Ann. Chem.*, **613**, 185 (1958).
21) B. Dietrich, J. M. Lehn, J. P. Sauvage, and J. Blanzat, *Tetrahedron*, **29**, 1629 (1973).

Mechanism of Formation of α,β-Unsaturated Esters in the Reaction of Ethyl Mercaptoacetate Dianion with Carbonyl Compounds

Syuichi MATSUI
Department of Industrial Chemistry, Fukui Technical College, Geshi, Saboe, Fukui 916
(Received May 28, 1983)

Dianion derived from ethyl mercaptoacetate undergoes aldol type reaction with a carbonyl compound to give an adduct, which exhibited low diastereoselectivity. However, the adducts obtained by the reaction with a variety of aldehydes were subsequently treated with ethyl chloroformate in the presence of trivalent phosphorus compound to give (*E*)-isomers of α,β-unsaturated esters in high yields with greater than 85% stereoselectivity regardless of the stereochemistry of the diastereomers of the adducts. The stereochemical mechanism and application of this reaction were studied in detail.

Recently, it has been reported in the communication[1] that, when trivalent phosphorus compound was used as a desulfurization agent, the (*E*)-products of α,β-unsaturated esters can be synthesized in high yields with high stereoselectivity by treating aldehydes with dianion derived from ethyl mercaptoacetate (**1a**). This finding would account for the mechanism of this reaction which involves the intramolecular cyclization to thiirane as an intermediate, followed by extrusion of sulfur to **3**.

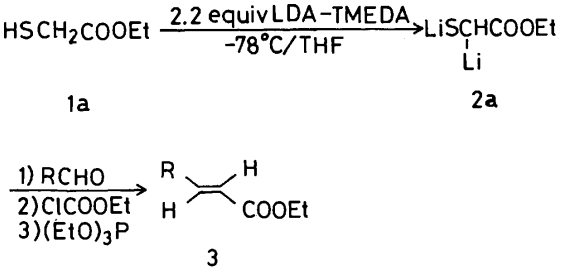

(1)

In the present study the author has observed that the aldol adducts were obtained in good yields by the reaction of **2a** with aldehydes, exhibiting consistently low diastereoselectivity. However, the reaction of the low diastereomeric mixture of the aldol products with 2.2 equiv of the base gave α,β-unsaturated esters of high stereoselectivity after treating with ethyl chloroformate and triethyl phosphite. In this paper the studies on the mechanism of the stereoselective formation of α,β-unsaturated esters and the application of this reaction to the synthesis of a component of royal jelly are described.

Results and Discussion

Aldol Condensation. Dianion (**2a**) undergoes aldol type reaction with a carbonyl compound to afford a mixture of diastereomers of an adduct (**4**). The conformations of aldol adduct, in which thiolate anion and alcoholate anion are gauche, are represented as **4T** and **4E** because of a chelation of lithium cation with both thiolate and alcoholate anion.[2] In order to determine the aldol diastereomer ratios (**4T** : **4E**), **2a** was treated with carbonyl compounds in THF at −78 °C for 2 h and quenched with saturated aqueous solution of ammonium chloride. The usual work-up and distillation afforded **5** in good yields.

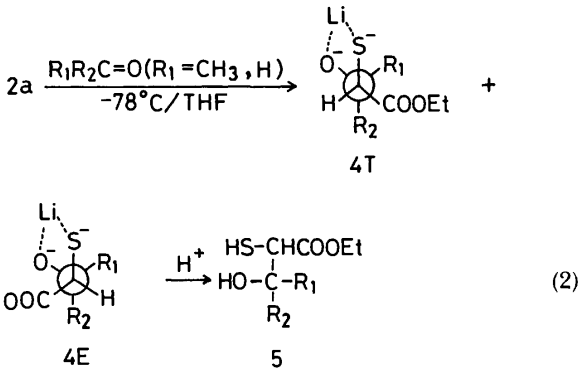

(2)

Diastereomer ratios were determined by the ^{1}H-NMR spectra of the purified aldol product, using the well-established results that $J_{threo} > J_{erythro}$ and a chemical shift of threo isomer is higher than that of erythro isomer.[2a,3] For example, the ^{1}H-NMR spectrum of **5** derived from benzaldehyde shows the hydroxymethine proton at δ 4.70 (J=8.0 Hz) for threo isomer and at δ 4.82 (J=6.0 Hz) for erythro isomer. Integration of these protons showed that the ratio of threo isomer and erythro isomer was 60 : 40, being identical with the ratio obtained by capirally column GLC analysis (ratio=61 : 39). The stereochemical compositions of **5** prepared from various carbonyl compounds are summarized in Table 1. Next, the effect of reaction time of aldol condensation on the diastereomer ratio (**5kT** : **5kE**) of aldol adduct derived from benzaldehyde was investigated (Table 2).

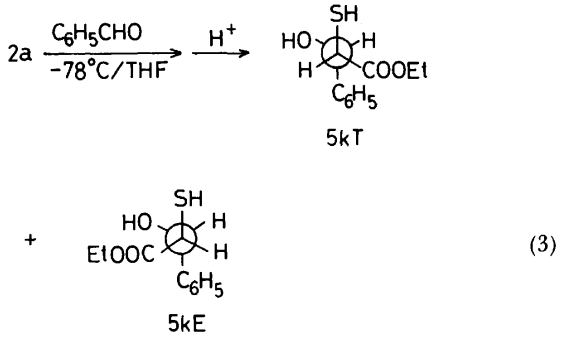

(3)

Tables 1 (Entry 12) and 2 show that there is no obvious effect of reaction time and temperature on the diastereomer ratios. Thus, this aldol reaction was pre-

TABLE 1. ALDOL CONDENSATIONS OF DIANION (**2a**) WITH CARBONYL COMPOUNDS

Entry No.	$R_1R_2C=O$		Aldol product HS-CHCOOEt / HO-C-R_1 (R_2)	Yield[a] %	erythro/threo[b] ratio
	R_1	R_2			
1	CH_3	n-C_4H_9	**5a**	73	38/62
2	CH_3	n-C_5H_{11}	**5b**	72	39/61
3	CH_3	n-C_6H_{13}	**5c**	85	43/57 (41/59)
4	CH_3	n-C_6H_{13}	**5d**	77[c]	54/46
5	CH_3	n-C_7H_{15}	**5e**	82	45/55
6	CH_3		**5f**	81	56/44
7	H	n-C_3H_7	**5g**	71	62/38 (62/38)
8	H	n-C_4H_9	**5h**	90	58/42 (54/46)
9	H	n-C_6H_{13}	**5i**	78	60/40
10	H	n-C_7H_{15}	**5j**	89	58/42 (59/41)
11	H		**5k**	73	40/60 (39/61)
12	H		**5k**	72[d]	31/69

a) Isolated yields. b) Determined by ^{1}H-NMR. Values in parentheses were determined by GLC with a 30 m glass capirally column. c) Ethyl 2-mercaptopropionate dianion was used in the place of **2a**. d) Yield obtained by quenching the reaction after stirring at −78 °C for 1 h and then at room temperature for 1 h.

TABLE 2. EFFECT OF REACTION TIME ON THE DIASTEREOMER RATIO OF **5k**

Entry No.	Reaction time h	Yield of **5k**[a] %	**5k**E/**5k**T[b]
1	0.02	64	41/59
2	2	73	40/60
3	5	78	41/59
4	24	75	35/65

a) Isolated yields. b) Determined by ^{1}H-NMR.

sumed to be kinetically controlled. Cross-over experiments which were attempted by adding another aldehydes to the reaction mixture produced no detectable cross-over product at −78 °C.

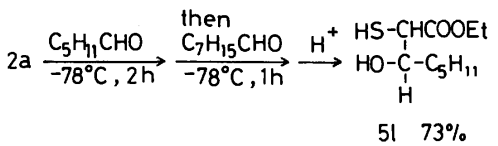

5l 73%

90%

(4)

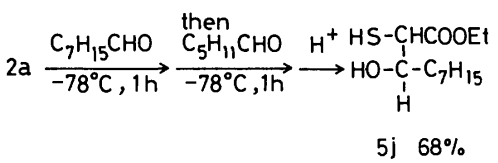

5j 68%

75%

(5)

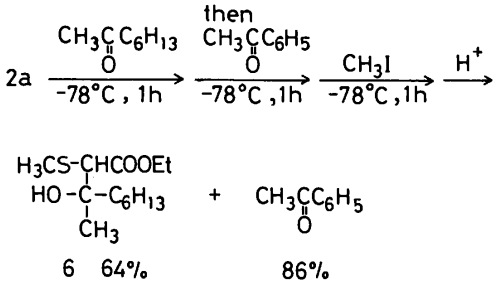

(6)

The carbonyl compound added first was always condensed with **2a** to afford **5l**, **5j**, and **6** in good yield, whereas the carbonyl compound added secondly was almost recovered. From these results, it is reasonable to consider that **4** is not in equilibrium with **2a** as follows (Eq. 7).

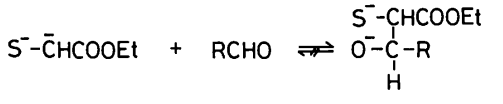

(7)

Generation of Thiirane Derivatives. It was found that a thioenol compound (**7**) could be isolated as a by-product in moderate yield in the reaction of **2a** with aldehydes, and that the formation of **7** was responsible for the low yield of **3** (Table 3). Yields of **7** were found to be strongly dependent on the reaction temperature after treating with ethyl chloroformate. For example, **7b** and **7d** were isolated in 41 and 68% yields respectively, by quenching the reaction at 10—15 °C after treating with ethyl chloroformate, whereas the yields of **7b** and **7d** were decreased to 22 and 53%, respectively, by quenching at 30—35 °C. On the other hand, **7** was not obtained by the reaction of **2a** with ketones. The structures of **7** were confirmed by their elemental analyses and spectral (IR, NMR) properties

(see Experimental). The *E*/*Z* ratio of **7** was determined by GLC and NMR analysis; *e.g.*, the ratio of (*E*)-isomer to (*Z*)-isomer of ethyl 2-mercapto-2-decenoate determined by integration of the olefinic proton at δ 6.59 and 5.83, respectively, is 93 : 7. Analysis of this material by GLC indicates a 94 : 6 mixture.

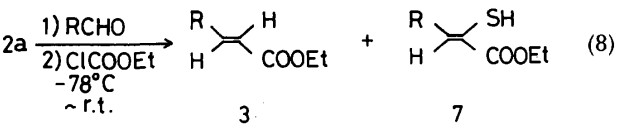

(8)

It is reasonable to assume that **7** is resulted from thiirane species (**8**) according to the following route (Eq. 9), since when trivalent phosphorus compound was added the formation of **7** was not observed and the yield of α, β-unsaturated ester (**3**) was increased.

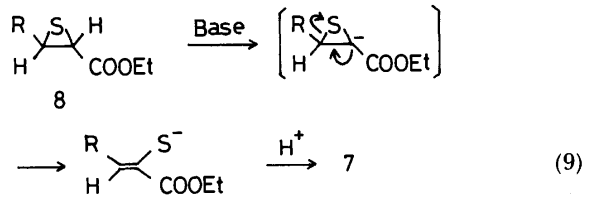

(9)

As anticipated, by the reaction of dianion derived from ethyl 2-mercaptopropionate (**9**) with aldehydes the thioenol compound was not obtained and α,β-unsaturated ester was isolated in high yield.

Attempts to isolate the thiirane species (**8**), however, were failed due to its unstability.

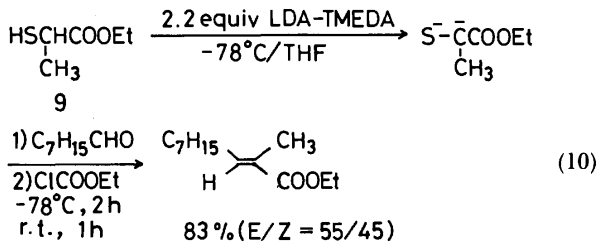

(10)

Retro-aldolization after Treating with ClCOOEt. When the adduct (**5j**) obtained by the reaction of **2a** with octanal was dilithiated with 2.2 equiv of LDA in the presence of TMEDA at −78 °C and followed by treating with hexanal and ethyl chloroformate in the presence of triethyl phosphite, ethyl 2-decenoate and ethyl 2-octenoate were obtained in 25 and 36% isolated yields, respectively. This scramble of carbonyl compound with **2a** demonstrates the retro-aldolization *after treating with ethyl chloroformate* (Eqs. 11, 12, 13, and 14).

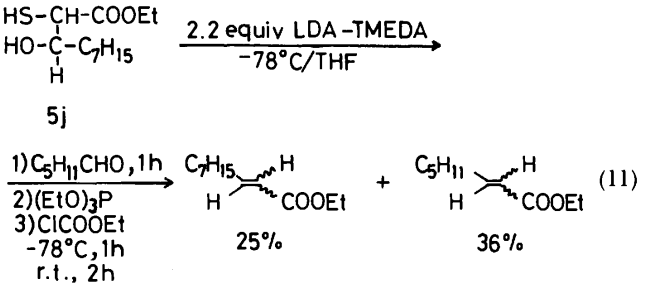

(11)

TABLE 3. PRODUCT YIELDS OBTAINED BY THE REACTION OF DIANION (**2a**) AND MONOANIONS (**2b** AND **2c**)[a] WITH CARBONYL COMPOUNDS

Entry No.	$XSCH_2COOEt$ X	$R_1R_2C=O$ R_1	R_2	Product (**3**)	Yield[b] %	*E*/*Z*[c] ratio	Product (**7**)	Yield[b] %	*E*/*Z*[c] ratio
1	H	H	n-C_5H_{11}	**3a**	51	92/8	**7a**	31	94/6
2	H	H	n-C_7H_{15}	**3b**	56 (54)[d]	91/9	**7b**	22 (41)[d]	94/6
3	H	H	n-C_9H_{19}	**3c**	50	90/10	**7c**	32	88/12
4	H	H	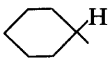	**3d**	35 (10)[d]	100/0	**7d**	53/(68)[d]	100/0
5	EtOC(=O)-	H	n-C_6H_{13}	**3e**	80	84/16	**7e**	18	82/18
6	EtOC(=O)-	H		**3f**	69	100/0	**7f**	11	100/0
7	EtOC(=O)-	H	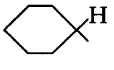	**3d**	59	100/0	**7d**	27	100/0
8	$(EtO)_2P(=O)$-	H	n-C_9H_{19}	**3c**	78	93/7	**7c**	8	94/6
9	H	CH_3	n-C_3H_7	**3g**	72[e]	39/61		0	
10	H	CH_3	n-C_6H_{13}	**3h**	66	43/57		0	
11	H	CH_3		**3i**	61	100/0		0	
12	H	CH_2CH_3		**3j**	48	95/5		0	

a) Monoanions **2d** and **2c** were prepared by adding *O*-ethyl *S*-ethoxycarbonylmethyl thiocarbonate and *S*-ethoxycarbonylmethyl diethyl phosphorothioate to 1.1 equiv LDA in THF at −78 °C, respectively.[1] b) Isolated yields by column chromatography. c) Determined by ^{1}H-NMR and GLC. d) All reactions were quenched at −30—35 °C after treating with ethyl chloroformate. Yields in parentheses were obtained by quenching the reaction at 10—15 °C. e) A mixture of THF and TMEDA (8.0 equiv) was used as a solvent.

Table 4. Prepartion of α, β-unsaturated esters (3) from aldol adducts (5)

Entry No.	Aldol adduct (5)	erythro/threo[a] ratio	Product (3)	Yield[b] %	E/Z[c] ratio
1	**5g**	62/38	**3k**	70	88/12
2	**5h**	58/42	**3l**	88	90/10
3	**5i**	60/40	**3e**	81	89/11
4	**5j**	58/42	**3b**	73	92/8
5	**5k**	40/60	**3f**	80	100/0

a) Determined by ^{1}H-NMR. b) Isolated yields. c) Determined by ^{1}H-NMR and GLC.

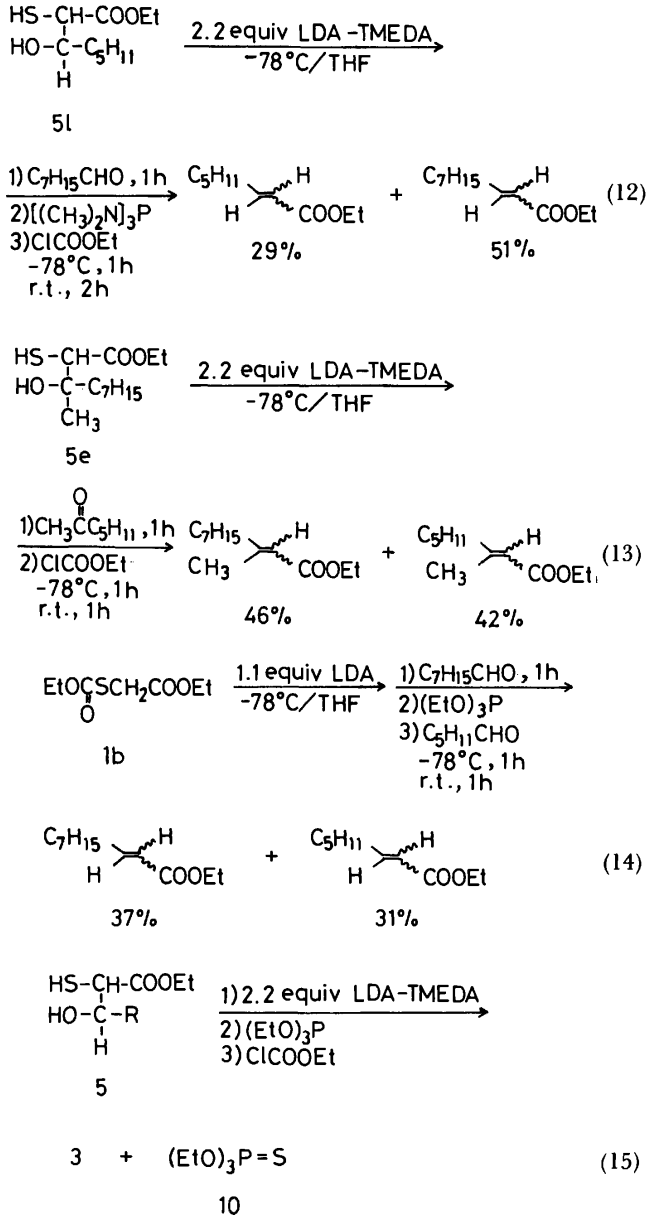

The aldol adducts (**5**) derived from carbonyl compounds afforded **3** in the following manner. These results were summarized in Table 4.

The substantial difference between the stereochemistry of **5** and the geometry of **3** was observed, that is, the predominant formation of (*E*)-α,β-unsaturated esters was observed.

Reaction Mechanism. It has been previously reported[4] that the mechanism of the reaction of **2a** with carbonyl compounds involves aldol type condensation, rearrangement of an adduct (**11**) to **12**, subsequent conversion of **12** to thiirane species (**8**), and elimination of sulfur to give α,β-unsaturated esters (**3**). The observations presented here would lead to the mechanism of the stereoselective formation of (*E*)-α,β-unsaturated esters.

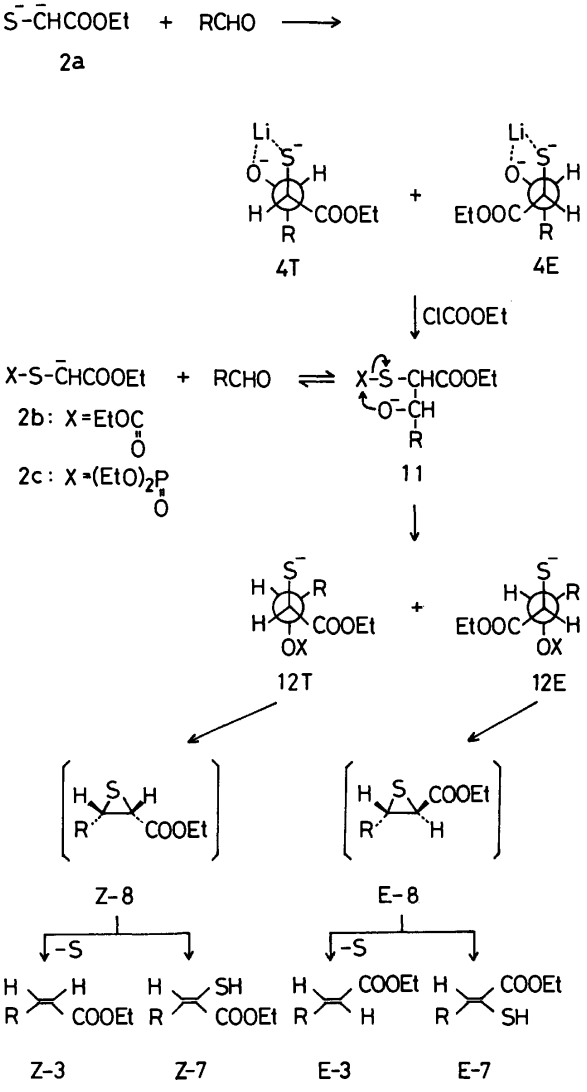

Scheme 1.

The aldol type condensation of **2a** with aldehydes exhibited low diastereoselectivity due to the kinetically controlled process, whereas the reaction after treating with ethyl chloroformate proceeded with high stereoselectivity to give (*E*)-isomer of **3**. This result can be rationalized by considering that a retroaldolization of **11** to **2b** is in competition with rearrangement of **11** to **12**, that is, the reaction after treating with ethyl chloroformate is the thermodynamically controlled process. In two possible stereoisomeric precursors (**12T** and **12E**) leading to **3** as shown in Scheme 1, if the conformer, in which the $O\overset{O}{\overset{\|}{C}}OEt$ and S^- groups are antiperiplaner, is favorable one for the subsequent intramolecular attack of S^- group and elimination of the $O\overset{O}{\overset{\|}{C}}OEt$ species, the orientation of R group is thus represented as **12T** and **12E**. The equiliblium between the stereoisomers **12T** and **12E** would surely favor **12E**, since the steric interaction between a bulky R group and an ethoxycarbonyl group is minimized in **12E**. On the other hand, the stereoisomer **12T**, in which the alkyl and ethoxycarbonyl group are gauche, would exhibit serve interactions. Thus, even if **12T** and **12E** should convert to (*Z*)-**3** and (*E*)-**3** stereospecifically, respectively,[5] the (*E*)-isomers of monosubstituted α,β-unsaturated esters would be predominantly obtained regardless of the stereochemistry of the aldol adduct (**4**) in the reaction of **2a** with aldehydes. On the other hand, in the reaction of **2a** with ketones, almost 1 : 1 mixture of geometrical isomers of disubstituted analogue was obtained.[4] Since in the conformers **13T** and **13E** (Scheme 2), the difference in steric interaction would be diminished by an introduction of methyl group in the place of hydrogen atom.

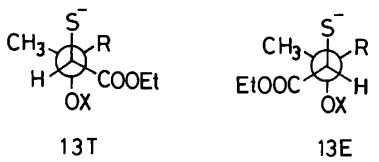

13T 13E

Scheme 2.

Reactivity of S-[1-(Ethoxycarbonyl)ethyl] Diethyl Phosphorothioate Carbanion. An already-published report described the efficient synthesis of trisubstituted α,β-unsaturated esters, starting from *S*-[1-(ethoxycarbonyl)ethyl] diethyl phosphorothioate (**14**).[6] To study the reactivity of **14**, the author treated *S*-[1-(ethoxycarbonyl)ethyl] diethyl phosphorothioate with 1.1 equiv of LDA in THF at −78 °C. The resulting

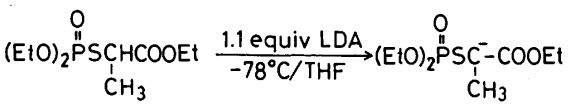

14 15

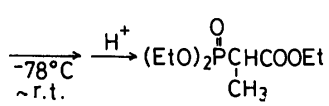

16 (16)

carbanion (**15**) afforded ethyl 2-(diethoxyphosphinyl)-propionate (**16**) in 88% yield upon quenching with saturated aqueous solution of ammonium chloride after warming to room temperature (Eq. 16).

The mechanism of the formation of **16** is proposed as follows (Scheme 3).

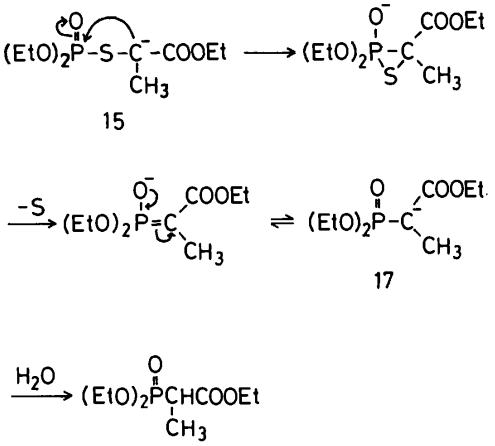

Scheme 3.

Therefore, two routes are taken into consideration for the reaction of **15** with carbonyl compounds to afford α,β-unsaturated esters (Scheme 4).

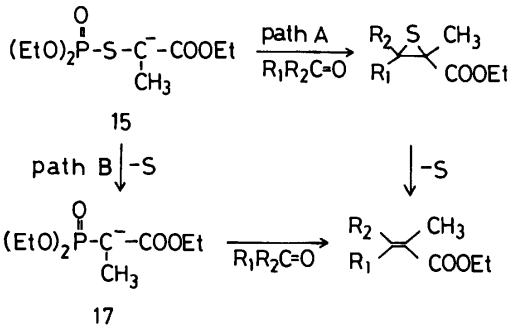

Scheme 4.

One is path A that proceeds *via* thiirane species as intermediate, another is path B where the product (**16**) acts as Emmons-Wadsworth reagent[7] and undergoes Wittig reaction.[8] In order to clarify the mechanism, the carbanion **18** was quenched with deuterium oxide and acetic acid-*d* at −78 °C, giving **19** in 89% yield (Eq. 17).

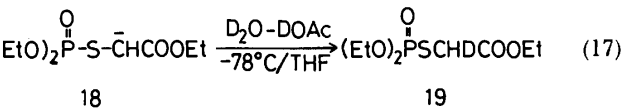

18 19 (17)

Furthermore, when **15** was treated with cyclohexanone at −78 °C for 1 h and at room temperature for 1 h, ethyl 2-cyclohexylidenepropionate (**20**) was isolated in 90% yield. Whereas **20** was obtained in only 33% yield from Emmons-Wadsworth reagent (**16**) under the same reaction conditions as those used for **14**.

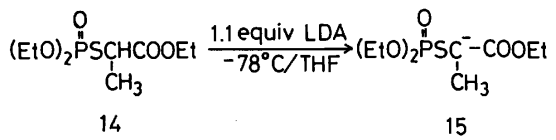

14 15

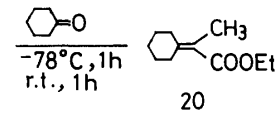

20 (18)

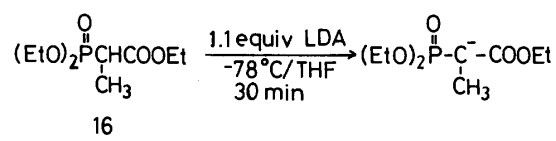

16

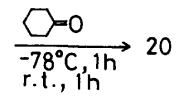

20 (19)

These results suggest that the reaction of *S*-[1-(ethoxycarbonyl)ethyl] diethyl phosphorothioate carbanion (**15**) with carbonyl compounds proceeds *via* path A.

Synthesis of (E)-*10-Hydroxy-2-decenoic Acid.* To demonstrate the utility of our novel methodology,[1] the author has carried out the synthesis of (*E*)-10-hydroxy-2-decenoic acid, a component of royal jelly from *Apis Melifica*.[9] Reaction of **2a** with **21** in the presence of triethyl phosphite gave pure **22** as a pale yellow oil in 63% isolated yield (*E*/*Z*=94/6). Acid hydrolysis of **22**[10] produced pure ethyl (*E*)-10-hydroxy-2-decenoate (**23**) as a viscous oil in 79% isolated yield after purification by silica-gel chromatography. Alkali hydrolysis of **23**[11] produced pure (*E*)-10-hydroxy-2-decenoic acid (**24**) in 73% isolated yield after recrystallization from ether.

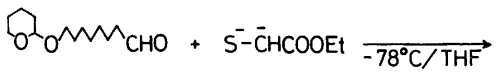

21 2a

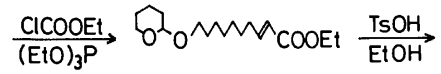

22

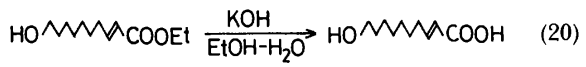

23 24 (20)

Experimental

General. Boiling points were determined during distillation and are uncorrected. Infrared spectra were determined on a Hitachi Model 260-30 spectrophotometer. Nuclear magnetic resonance spectra were determined on a JEOLCO MH-100 spectrometer. Gas chromatograms were obtained using a Varian Aerograph Model 920 instrument with a 0.15 cm×120 cm glass column (20% Silicone DC-550 on Celite 545). Tetrahydrofuran (THF) was dried by distillation from calcium hydride and by subsequent distillation from lithium aluminum hydride under a nitrogen atmosphere. Diisopropylamine and *N,N,N′,N′*-tetramethylethylenediamine (TMEDA) were distilled from calcium hydride and stored over molecular sieves. Triethyl phosphite and carbonyl compounds were purified by distillation under a nitrogen atmosphere. All reactions were performed under a nitrogen atmosphere. The glassware was dried by flaming in a nitrogen stream.

Preparation of Aldol Adduct (5). To a mixture of lithium diisopropylamide (LDA) (44 mmol) and TMEDA (44 mmol) in 40 ml of THF was added a solution of 2.4 g (20 mmol) of ethyl mercaptoacetate (**1a**) in 5 ml of THF at −78 °C. After being stirred for 1 h, a solution of 22 mmol of a carbonyl compound in 5 ml of THF was added and the reaction mixture was stirred at −78 °C for 2 h. The cooling bath was removed and the reaction mixture was quenched with 10 ml of saturated aqueous solution of ammonium chloride, poured into dilute hydrochloric acid, and extracted with ether (50×4 ml). The combined organic layer was washed twice with brine, dried on anhydrous sodium sulfate, and concentrated under reduced pressure. Distillation of the resulting oil gave **5**.

Ethyl 3-Hydroxy-2-mercapto-3-methylheptanoate (5a): Bp 93—96 °C/1 Torr (1 Torr≈133.322 Pa). ^{1}H-NMR (CCl_4); δ=4.16 (q, J=7 Hz, 2H, CH_2), 3.22 (s, 0.38H, erythro CH), 3.10 (s, 0.62H, threo CH), 2.93 (brs, 1H, OH), 2.23 and 2.14 (each d, J=6 and 5 Hz, total 1H, SH), 1.00—1.60 (m, 12H, $3CH_2$ and $2CH_3$), 0.70—1.00 (m, 3H, CH_3). IR (neat); 3500 (OH), 2560 (SH), 1710 cm^{-1} (COO). Found: C, 54.27; H, 9.16%. Calcd for $C_{10}H_{20}O_3S$: C, 54.51; H, 9.15%.

Ethyl 3-Hydroxy-2-mercapto-3-methyloctanoate (5b): Bp 96—100 °C/1 Torr. ^{1}H-NMR (CCl_4); δ=4.02 (q, J=7 Hz, 2H, CH_2), 3.10 (s, 0.39H, erythro CH), 2.99 (s, 0.61H, threo CH), 2.90 (brs, 1H, OH), 2.22 and 2.06 (each d, J=5 and 5 Hz, total 1H, SH), 1.12—1.58 (m, 14H, $4CH_2$ and $2CH_3$), 0.72—1.06 (m, 3H, CH_3). IR (neat); 3500 (OH), 2560 (SH), 1720 cm^{-1} (COO). Found: C, 56.17; H, 9.53%. Calcd for $C_{11}H_{22}O_3S$: C, 56.38; H, 9.46%.

Ethyl 3-Hydroxy-2-mercapto-3-methylnonanoate (5c): Bp 108—112.5 °C/1Torr. ^{1}H-NMR (CCl_4); δ=4.16 (q, J=7 Hz, 2H, CH_2), 3.20 (s, 0.43H, erythro CH), 3.09 (s, 0.57H, threo CH), 2.96 (brs, 1H, OH), 2.30 and 2.18 (each d, J=6 and 5 Hz, total 1H, SH), 1.18—1.60 (m, 16H, $5CH_2$ and $2CH_3$), 0.80—0.96 (m, 3H, CH_3). IR (neat); 3500 (OH), 2560 (SH), 1720 cm^{-1} (COO). Found: C, 57.87; H, 9.69%. Calcd for $C_{12}H_{24}O_3S$: C, 58.03; H, 9.74%.

Ethyl 3-Hydroxy-2-mercapto-2,3-dimethylnonanoate (5d): Bp 125—128 °C/2 Torr. ^{1}H-NMR (CCl_4); δ=4.10 (q, J=7 Hz, 2H, CH_2), 3.54 (brs, 1H, OH), 2.82 (brs, 0.54H, erythro SH), 2.66 (brs, 0.46H, threo SH), 1.10—1.60 (m, 19H, $5CH_2$ and $3CH_3$), 0.74—0.94 (m, 3H, CH_3). IR (neat); 3500 (OH), 2560 (SH), 1710 cm^{-1} (COO). Found: C, 59.47; H, 10.05%. Calcd for $C_{13}H_{26}O_3S$: C, 59.50; H, 9.99%.

Ethyl 3-Hydroxy-2-mercapto-3-methyldecanoate (5e): Bp 111.5—118 °C/1Torr. ^{1}H-NMR (CCl_4); δ=4.14 (q, J=7 Hz, 2H, CH_2), 3.18 (s, 0.45H, erythro CH), 3.02 (s, 0.55H, threo CH), 2.95 (brs, 1H, OH), 2.28 and 2.12 (each d, J=6 and 5 Hz, total 1H, SH), 1.14—1.60 (m, 18H, $6CH_2$ and $2CH_3$), 0.82—1.00 (m, 3H, CH_3). IR (neat); 3500 (OH), 2560 (SH), 1720 cm^{-1} (COO). Found: C, 59.38; H, 10.11%. Calcd for $C_{13}H_{26}O_3S$: C, 59.50; H, 9.99%.

Ethyl 3-Hydroxy-2-mercapto-3-phenylbutanoate (5f): Bp 123.0—126.5 °C/1 Torr. ^{1}H-NMR (CCl_4); δ=7.16—7.48 (m, 5H, aromatic), 4.18 (q, J=7 Hz, 2H, CH_2), 3.48—3.96 (m, 2H, CH and OH), 2.54 (d, J=2 Hz, 0.56H, erythro SH), 2.44 (d, J=3 Hz, 0.44H, threo SH), 1.40—1.70 (m, 3H, CH_3), 0.76—1.34 (m, 3H, CH_3). IR (neat); 3840 (OH), 2550 (SH), 1700 cm^{-1} (COO). Found: C, 59.92; H, 6.85%. Calcd for $C_{12}H_{16}O_3S$: C, 59.98; H, 6.71%.

Ethyl 3-Hydroxy-2-mercaptohexanoate (5g): Bp 83—86 °C/3 Torr. ^{1}H-NMR (CCl_4); δ=4.15 (q, J=7 Hz, 2H, CH_2), 3.50—3.88 (m, 1H, CH-OH), 3.00—3.30 (m, 2H, CH-SH and OH), 2.18 (d, J=4 Hz, 0.62H, erythro SH), 2.07 (d, 5 Hz, 0.38H, threo SH), 1.16—1.60 (m, 7H, $2CH_2$ and CH_3), 0.80—1.00 (m, 3H, CH_3). IR (neat): 3490 (OH), 2560 (SH), 1720 cm^{-1} (COO). Found: C, 49.72; H, 8.45%. Calcd for $C_9H_{18}O_3S$: C, 49.97; H, 8.39%.

Ethyl 3-Hydroxy-2-mercaptoheptanoate (5h): Bp 93.5—97 °C/2 Torr ^{1}H-NMR (CCl_4); δ=4.18 (q, J=7 Hz, 2H, CH_2), 3.52—3.84 (m, 1H, CH-OH), 3.04—3.30 (m, 2H, CH-SH and OH), 2.22 (d, J=4 Hz, 0.58H, erythro SH), 2.10 (d, J=5 Hz, 0.42H, threo SH), 1.20—1.60 (m, 9H, $3CH_2$ and CH_3), 0.80—1.00 (m, 3H, CH_3). IR (neat); 3500 (OH), 2560 (SH), 1710 cm^{-1} (COO). Found: C, 52.28; H,8.85%. Calcd for $C_9H_{18}O_3S$: C, 52.40; H, 8.79%.

Ethyl 3-Hydroxy-2-mercaptononanoate (5i): Bp 110—114.5 °C/2 Torr. ^{1}H-NMR (CCl_4); δ=4.14 (q, J=7 Hz, 2H, CH_2), 3.50—3.90 (m, 1H, CH-OH), 2.86—3.24 (m, 2H, CH-SH and OH), 2.18 (d, J=4 Hz, 0.60H, erythro SH), 2.08 (d, J=5 Hz, 0.40H, threo SH), 1.18—1.62 (m, 13H, $5CH_2$ and CH_3), 0.78—0.96 (m, 3H, CH_3). IR (neat); 3500 (OH), 2560 (SH), 1710 cm^{-1} (COO). Found: C, 56.31; H, 9.60%. Calcd for $C_{11}H_{22}O_3S$: C, 56.38; H, 9.46%.

Ethyl 3-Hydroxy-2-mercaptodecanoate (5j): Bp 114—118 °C/1 Torr. ^{1}H-NMR (CCl_4); δ=4.16 (q, J=7 Hz, 2H, CH_2), 3.54—3.90 (m, 2H, CH-OH and OH), 3.02—3.28 (m, 1H, CH-SH), 2.20 (d, J=4 Hz, 0.58H, erythro SH), 2.09 (d, J=5 Hz, 0.42H, threo SH), 1.18—1.70 (m, 15H, $6CH_2$ and CH_3), 0.76—1.00 (m, 3H, CH_3). IR (neat); 3500 (OH), 2560 (SH), 1700 cm^{-1} (COO). Found: C, 58.01; H, 9.79%. Calcd for $C_{12}H_{24}O_3S$: C, 58.03; H, 9.74%.

Ethyl 3-Hydroxy-2-mercapto-3-phenylpropionate (5k): Bp 128-131 °C/2 Torr. ^{1}H-NMR (CCl_4); δ=7.20 (s, 5H, aromatic), 4.82 (d, J=6 Hz, 0.40H, erythro CH-OH), 4.70 (d, J=8 Hz, 0.60H, threo CH-OH), 4.04 (q, J=7 Hz, 2H, CH_2), 3.72—3.84 (m, 1H, OH), 3.30—3.60 (m, 1H, CH-SH), 2.10 (d, J=9 Hz, 0.40H, erythro SH), 1.95 (d, J=10 Hz, 0.60H, threo SH), 1.00—1.30 (m, 3H, CH_3). IR (neat); 3490 (OH), 2560 (SH), 1730 cm^{-1} (COO). Found: C, 58.25; H, 6.39%. Calcd for $C_{11}H_{14}O_3S$: C, 58.39; H, 6.24%.

Ethyl 3-Hydroxy-2-mercaptooctanoate (5l): Bp 96.5—100 °C/2 Torr. ^{1}H-NMR (CCl_4); δ=4.16 (q, J=7 Hz, 2H, CH_2), 3.52—3.86 (m, 1H, CH-OH), 3.00—3.26 (m, 2H, CH-SH and OH), 2.20 (d, J=4 Hz, 0.60H, erythro SH), 2.08 (d, J=5 Hz, 0.40H, threo SH), 1.20—1.60 (m, 11H, $4CH_2$ and CH_3), 0.80—1.00 (m, 3H, CH_3). IR (neat): 3500 (OH), 2560 (SH), 1710 cm^{-1} (COO). Found: C, 54.35; H, 9.20%. Calcd for $C_{10}H_{20}O_3S$: C, 54.51; H, 9.15%.

Cross-over Experiment. Preparation of Ethyl 3-Hydroxy-3-methyl-2-(methylthio)nonanoate (6): Into a solution of 20 mmol of the dianion (**2a**) in 40 ml of THF, was added at −78°C a solution of 22 mmol of 2-octanone in 3 ml of THF. After being stirred for 1 h, a solution of 22 mmol of acetophenone in 3 ml of THF was added and the reaction mixture was stirred at −78 °C for 1 h. A solution of 22 mmol of methyl iodide in 3 ml of THF was then added with a syringe over a 3 min period. The resulting solution was stirred at −78 °C for 1 h before quenching with saturated aqueous solution of ammonium chloride (10 ml). The work-up similar to the preparation of **5** and silica-gel chromatography(benzene) gave 2.27 g of acetophenone and 3.36 g (64%) of **6**. ^{1}H-NMR (CCl_4); δ=4.28 (q, J=7 Hz, 2H, CH_2), 3.08 (s, 1H, CH), 3.07 (brs, 1H, OH), 2.20 (s, 3H, SCH_3), 1.20—1.72 (m, 16H, $5CH_2$ and $2CH_3$), 0.86—1.20 (m, 3H, CH_3). IR (neat); 3500 (OH), 1720 cm^{-1}(COO). Found: C, 59.39; H, 9.98%. Calcd for $C_{13}H_{26}O_3S$: C, 59.50; H, 9.99%.

General Procedure. Reaction of Dianion (2a) with Carbonyl Compounds: Into a solution of 20 mmol of the dianion (**2a**) in 40 ml of THF, was added at −78 °C a solution of 22 mmol of a carbonyl compound in 5 ml of THF. After being stirred for 2 h, ethyl chloroformate (20 mmol) in 3 ml of THF was added and the mixture was stirred at −78 °C for 30 min and at 30—35 °C or 15 °C for 1 h before it was quenched with saturated aqueous solution of ammonium chloride solution (10 ml). The reaction mixture was poured into dilute hydrochloric acid and extracted with ether (50× 4 ml). The combined organic layer was washed twice with brine, dried on anhydrous sodium sulfate, and concentrated under reduced pressure. Product isolation and purification by chromatography on silica-gel column (benzene) gave **3** and **7**. The dianion (**2a**) was treated with aldehydes in the presence of triethyl phosphite in a similar manner as described above to give **3** in high yields.

Reaction of Monoanions (2b, 2c) with Carbonyl Compounds: A solution of 20 mmol of *O*-ethyl *S*-ethoxycarbonylmethyl thiocarbonate (**1b**) or *S*-ethoxycarbonylmethyl diethyl phosphorothioate (**1c**) in 3 ml of THF was added to a stirred solution of 22 mmol of LDA in 40 ml of THF at −78 °C. The resulting solution was treating with 24 mmol of aldehydes in a similar manner as described above.

Ethyl (E)-2-Mercapto-2-octenoate (7a): ^{1}H-NMR (CCl_4); δ=6.72 (t, J=7 Hz, 1H, CH=C), 4.18 (q, J=7 Hz, 2H, CH_2), 3.94 (s, 1H, SH), 2.18 (q, J=7 Hz, 2H, CH_2), 1.10—1.60 (m, 9H, $3CH_2$ and CH_3), 0.86 (m, 3H, CH_3). IR (neat); 2560 (SH), 1710 (COO), 1610 cm^{-1} (C=C). Found: C, 59.31; H, 9.13%. Calcd for $C_{10}H_{18}O_2S$: C, 59.37; H, 8.97%.

Ethyl (E)-2-Mercapto-2-decenoate (7b): ^{1}H-NMR (CCl_4); δ=6.59 (t, J=7 Hz, 1H, CH=C), 4.06 (q, J=7 Hz, 2H, CH_2), 3.87 (s, 1H, SH), 2.14 (q, J=7 Hz, 2H, CH_2), 1.10—1.80 (m, 13H, $5CH_2$ and CH_3), 0.85 (m, 3H, CH_3). IR (neat); 2560 (SH), 1720 (COO), 1610 cm^{-1} (C=C). MS (20 eV); m/z 230 (M^+). Found: C, 62.60; H, 9.66%. Calcd for $C_{12}H_{22}O_2S$: C, 62.57; H, 9.63%.

Ethyl (E)-2-Mercapto-2-dodecenoate (7c): ^{1}H-NMR (CCl_4); δ=6.80 (t, J=7 Hz, 1H, CH=C), 4.24 (q, J=7 Hz, 2H, CH_2), 3.99 (s, 1H, SH), 2.20 (q, J=7 Hz, 2H, CH_2), 1.10—1.90 (m, 17H, $7CH_2$ and CH_3), 0.86 (m, 3H, CH_3). IR (neat); 2560 (SH), 1720 (COO), 1605 cm^{-1} (C=C). Found: C, 64.81; H, 10.22%. Calcd for $C_{14}H_{20}O_2S$: C, 65.07; H, 10.14%.

Ethyl (E)-3-Cyclohexyl-2-mercapto-2-propenoate (7d): ^{1}H-NMR (CCl_4); δ=6.40 (d, J=9 Hz, 1H, CH=C), 4.08 (q, J=7 Hz, 2H, CH_2), 3.87 (s, 1H, SH), 2.00—2.32 (m, 1H, CH), 0.80—1.80 (m, 13H, $5CH_2$ and CH_3). IR (neat); 2560 (SH), 1710 (COO), 1610 cm^{-1} (C=C). Found: C, 61.57; H, 8.35%. Calcd for $C_{11}H_{18}O_2S$: C, 61.65; H, 8.46%.

Ethyl (E)-2-Mercapto-2-nonenoate (7e): ^{1}H-NMR (CCl_4); δ=6.60 (t, J=7 Hz, 1H, CH=C), 4.08 (q, J=7 Hz, 2H, CH_2), 3.88 (s, 1H, SH), 2.14 (q, J=7 Hz, 2H, CH_2), 1.10—1.80 (m, 11H, $4CH_2$ and CH_3), 0.90 (m, 3H, CH_3). IR (neat); 2560 (SH), 1710 (COO), 1610 cm^{-1} (C=C). Found:C, 61.05; H, 9.41%. Calcd for $C_{10}H_{20}O_2S$: C, 61.07; H, 9.32%.

Ethyl (E)-2-Octenoate (3a): Bp 64—65 °C/2 Torr. ^{1}H-NMR (CCl_4); δ=6.82 (dt, J=7 Hz, 16 Hz, 1H, CH=C), 5.70 (d, J=16 Hz, 1H, CH=C), 4.08 (q, J=7 Hz, 2H, CH_2), 2.16 (m, 2H, CH_2), 1.47 (m, 9H, $3CH_2$ and CH_3), 0.90 (m, 3H, CH_3). IR (neat); 1640 cm^{-1} (C=C). Found: C, 70.38; H, 10.75%. Calcd for $C_{10}H_{18}O_2$:C, 70.55; H, 10.66%.

Ethyl 2-Decenoate (3b): Bp 87—88.5 °C/2 Torr. The *(E)*- and *(Z)*-isomers of **3b** were separated by silica-gel chromatography using benzene as eluent. *(E)*-isomer: ^{1}H-NMR (CCl_4); δ=6.76 (dt, J=7 Hz, 16 Hz, 1H, CH=C), 5.72 (d, J=16 Hz, 1H, CH=C), 4.12 (q, J=7 Hz, 2H, CH_2), 2.00—2.20 (m, 2H, CH_2), 1.10—1.80 (m, 13H, $5CH_2$ and CH_3), 0.90 (m, 3H, CH_3). IR (neat); 1645 cm^{-1} (C=C). Found: C, 72.51; H, 10.87%. Calcd for $C_{12}H_{22}O_2$: C, 72.67; H, 11.18%. *(Z)*-isomer: ^{1}H-NMR (CCl_4); δ=6.10 (dt, J=7 Hz, 16 Hz, 1H, CH=C), 5.72 (d, J=16 Hz, 1H, CH=C), 4.10 (q, J=7 Hz, 2H, CH_2), 1.98—2.00 (m, 2H, CH_2), 1.00—1.70 (m, 13H, $5CH_2$ and CH_3), 0.88 (m, 3H, CH_3).

Ethyl (E)-*2-Dodecenoate (3c)*: Bp 93—95 °C/2 Torr. ^{1}H-NMR (CCl_4); δ=6.88 (dt, J=7 Hz, 16 Hz, 1H, CH=C), 5.74 (d, J=16 Hz, 1H, CH=C), 4.12 (q, J=7 Hz, 2H, CH_2), 2.14 (m, 2H, CH_2), 1.45 (m, 17H, $7CH_2$ and CH_3), 0.90 (m, 3H, CH_3). IR (neat); 1650 cm^{-1} (C=C). Found: C, 74.03; H, 11.93%. Calcd for $C_{14}H_{26}O_2$: C, 74.29; H, 11.58%.

Ethyl (E)-*3-Cyclohexyl-2-propenoate (3d)*: Bp 57—58 °C/2 Torr. ^{1}H-NMR (CCl_4); δ=6.83 (dd, J=7 Hz, 16 Hz, 1H, CH=C), 5.70 (d, 16 Hz, 1H, CH=C), 4.13 (q, J=7 Hz, 2H, CH_2), 2.09 (m, 1H, CH), 1.75 (m, 4H, $2CH_2$), 0.90 (m, 9H, $3CH_2$ and CH_3). IR (neat); 1640 cm^{-1} (C=C). Found: C, 72.47; H, 9.95%. Calcd for $C_{11}H_{18}O_2$: C, 72.49; H, 9.95%.

Ethyl (E)-*2-Nonenoate (3e)*: Bp 71.5—73.5 °C/2 Torr. ^{1}H-NMR (CCl_4); δ=6.84 (dt, J=7 Hz, 16 Hz, 1H, CH=C), 5.70 (d, J=16 Hz, 1H, CH=C), 4.10 (q, J=7 Hz, 2H, CH_2), 2.17 (m, 2H, CH_2), 1.49 (m, 11H, $4CH_2$ and CH_3), 0.90 (m, 3H, CH_3). IR (neat); 1645 cm^{-1} (C=C). Found: C, 71.50; H, 11.02%. Calcd for $C_{11}H_{20}O_2$: C, 71.70; H, 10.94%.

Ethyl (E)-*3-Phenyl-2-propenoate (3f)*: Bp 99—100 °C/2 Torr. ^{1}H-NMR (CCl_4); δ=7.62 (d, J=16 Hz, 1H, CH=C), 7.40 (m, 5H, aromatic), 6.34 (d, J=16 Hz, 1H, CH=C), 4.18 (q, J=7 Hz, 2H, CH_2), 1.31 (t, J=7 Hz, 3H, CH_3). IR (neat); 1630 cm^{-1}(C=C). Found: C, 74.88; H, 6.87%. Calcd for $C_{11}H_{12}O_2$: C, 74.98; H, 6.86%.

Ethyl 3-Methyl-2-hexenoate (3g): Bp 51—55 °C/5 Torr. ^{1}H-NMR (CCl_4); δ=5.55 (brs, 1H, CH=C), 4.05 (q, J=7 Hz, 2H, CH_2), 2.56 (t, J=8 Hz, 1.22H, CH_2 for *(Z)*-isomer), 1.96—2.25 (m, 1.95H, CH_2 and CH_3 for *(E)*-isomer), 1.84 (m, 1.83H, CH_3 for *(Z)*-isomer), 1.30—1.72 (m, 2H, CH_2), 1.24 (t, J=7 Hz, 3H, CH_3), 0.94 (m, 3H, CH_3). IR (neat); 1640 cm^{-1} (C=C). Found: C, 69.07; H, 10.55%. Calcd for $C_9H_{16}O_2$: C, 69.19; H, 10.32%.

Ethyl 3-Methyl-2-nonenoate (3h): Bp 90—93.5 °C/6 Torr. ^{1}H-NMR (CCl_4); δ=5.60 (brs, 1H, CH=C), 4.06 (q, J=7 Hz, 2H, CH_2), 2.56 (m, 1.14H, CH_2 for *(Z)*-isomer), 1.92—2.32 (m, 2.15H, CH_2 and CH_3 for *(E)*-isomer), 1.86 (m, 1.71H, CH_3 for *(Z)*-isomer), 1.20—1.84 (m, 11H, $4CH_2$ and CH_3), 0.90 (m, 3H, CH_3). IR (neat); 1640 cm^{-1} (C=C). Found: C, 72.56; H, 11.25%. Calcd for $C_{12}H_{22}O_2$: C, 72.68; H, 11.18%.

Ethyl (E)-*3-Phenyl-2-butenoate (3i)*: Bp 115—116 °C/5 Torr. ^{1}H-NMR (CCl_4); δ=7.24 (m, 5H, aromatic), 6.05 (m, 1H CH=C), 4.10 (q, J=7 Hz, 2H, CH_2), 2.50 (s, 3H, CH_3), 1.24 (t, J=7 Hz, 3H, CH_3). IR (neat); 1625 cm^{-1} (C=C). Found: C, 75.65; H, 7.55%. Calcd for $C_{12}H_{14}O_2S$: C, 75.76; H, 7.42%. This product was judged as *(E)*-isomer by NMR spectra which is consistent with that of ethyl *(E)*-3-phenyl-2-butenoate reported previously.[4]

Ethyl (E)-*3-Phenyl-2-pentenoate (3j)*: Bp 91—94.5 °C/1 Torr. ^{1}H-NMR (CCl_4); δ=7.20—7.50 (m, 5H, aromatic), 5.96 (s, 1H, CH=C), 4.12 (q, J=7 Hz, 2H, CH_2), 3.08 (q, J=7 Hz, 2H, CH_2), 1.26 (t, J=7 Hz, 3H, CH_3), 1.04 (t, J=7 Hz, 3H, CH_3). IR (neat); 1620 cm^{-1} (C=C). Found: C, 76.38; H, 8.01%. Calcd for $C_{13}H_{16}O_2$: C, 76.44; H, 7.89%.

Ethyl (E)-*2-Hexenoate (3k)*: Bp 64—65 °C/10 Torr. ^{1}H-NMR (CCl_4); δ=6.80 (dt, J=7 Hz, 16 Hz, 1H, CH=C), 5.70 (d, J=16 Hz, 1H, CH=C), 4.08 (q, J=7 Hz, 2H, CH_2), 1.30—1.90 (m, 5H, CH_2 and CH_3), 0.97 (t, J=7 Hz, 3H, CH_3). IR (neat); 1650 cm^{-1} (C=C). Found: C, 67.51; H, 9.97%. Calcd for $C_8H_{14}O_2$: C, 67.57; H, 9.92%.

Ethyl (E)-*2-Heptenoate (3l)*: Bp 59—60 °C/5 Torr. ^{1}H-NMR (CCl_4); δ=6.82 (dt, J=7 Hz, 16 Hz, CH=C), 5.70 (d, J=16 Hz, 1H, CH=C), 4.08 (q, J=7 Hz, 2H, CH_2), 2.20 (m, 2H, CH_2), 1.50 (m, 7H, $2CH_2$ and CH_3), 0.90 (m, 3H, CH_3). IR (neat); 1640 cm^{-1} (C=C). Found: C, 69.03; H, 10.37%. Calcd for $C_9H_{16}O_2$: C, 69.19; H, 10.32%.

Preparation of S-[1-(Ethoxycarbonyl)ethyl] Diethyl Phosphorothioate (14):[12] To a stirred solution of 50.0g (0.36 mol) of diethyl phosphite in 250 ml of benzene was added 8.5 g (0.37 mol) of sodium metal under a nitrogen atmosphere. After the mixture has been stirred at room temperature for 2 h, 11.6 g (0.36 mol) of sulfur was added. Stirring was continued at room temperature for overnight and a solution of 65.2 g (0.36 mol) of ethyl 2-bromopropionate in 50 ml of benzene was added over a 20 min period. The reaction mixture was then refluxed for 3 h and the resulting precipitate was filtered. Evaporation and distillation under reduced pressure of the filtrate gave 35.3 g (36%) of **14**. Bp 126.5—127.5 °C/1.2—1.3 Torr. ^{1}H-NMR (CCl_4); δ=3.60—4.30 (m, 7H, $3CH_3\underline{CH_2}$ and CH), 1.00—1.70 (m, 12H, $4CH_3$). IR (neat); 1735 (C=O), 1015 cm^{-1} (P-O). MS (20 eV) m/z 270 (M^+).

Decomposition of S-[1-(Ethoxycarbonyl)ethyl] Diethyl Phosphorothioate Carbanion (15): The carbanion (**15**) was generated by treatment of 5.41g (20 mmol) of **14** with 22 mmol of LDA in 40 ml of THF at −78 °C. After being stirred for 30 min, the reaction mixture was allowed to warm from −78 °C to room temperature before it was quenched with saturated aqueous solution of ammonium chloride (10 ml). The usual work-up and distillation gave 4.1 g (88%) of ethyl 2-(diethoxyphosphinyl)propionate (**16**), bp 101—103 °C/1 Torr. The product was identified by comparison of ^{1}H-NMR and mass spectrum with the corresponding data for independently synthesized material.[7]

Generation of S-*(Ethoxycarbonylmethyl-1-*d*) Diethyl Phosphorothioate (19)*: To a solution of 9.5 mmol of LDA in 40 ml of THF was added a solution of 8.6 mmol of *S*-(ethoxycarbonylmethyl) diethyl phosphorothioate in 5 ml of THF at −78 °C. After stirring for 30 min, the cooling bath was removed, and a mixture of 30 mmol of acetic acid-*d* and 10 ml of deuterium oxide was added. The reaction mixture was then stirred for 15 min before it was quenched with saturated aqueous solution of ammonium chloride (20 ml), and extracted with ether (50×4 ml). The combined organic layer was washed with brine, dried on anhydrous sodium sulfate, and concentrated under reduced pressure. Distillation of the resulting oil gave 4.6 g (89%) of **19**, bp 129—131 °C/1.3 Torr. The degree of deuteration determined by means of ^{1}H-NMR was 87%.

Synthesis of Ethyl 2-Cyclohexilidenepropionate (20): To a solution of LDA (22 mmol) in 40 ml of THF was added dropwise a solution of 5.41 g (20 mmol) of **14** in 5 ml of THF at −78 °C. After being stirred for 30 min, a solution of 2.45 g (25 mmol) of cyclohexanone in 5 ml of THF was added dropwise over a 5 min period and stirred at −78 °C for 1 h and at room temperature for 1 h. The usual work-up and distillation gave 3.27 g (90%) of **20**. Bp 71—72 °C/1 Torr. ^{1}H-NMR (CCl_4); δ=4.06 (q, 2H, CH_2), 2.22—2.43 (m, 4H, $2CH_2$), 1.82 (s, 3H, $C{=}CCH_3$), 1.59 (m, 6H, $3CH_2$), 1.28 (t, J=7 Hz, 3H, $OCH_2\underline{CH_3}$). IR (neat); 1710 (C=O), 1635 cm^{-1} (C=C). MS (20 eV) m/z 182 (M^+). Found: C, 72.56; H, 10.00%. Calcd for $C_{11}H_{18}O_2$: C, 72.46; H, 9.95%.

Preparation of Ethyl 10-(2-Tetrahydropyranyloxy)-2-decenoate (22): 8-(2-Tetrahydropyranyloxy)octanal (**21**) was prepared from 8-(2-tetrahydropyranyloxy)-1-octanol by using chromium trioxide-pyridine complex by the reported procedure.[13] To a mixture of LDA (44 mmol) and TMEDA (44 mmol) in 40 ml of THF was added a solution of 2.4 g (20 mmol) of ethyl mercaptoacetate (**1a**) in 5 ml of THF at −78 °C. After being stirred for 1 h, a solution of 5.02 g (22 mmol) of **21** in 5 ml of THF was added and the reaction mixture was stirred in the presence of triethyl phosphite (30 mmol) at −78 °C for 2 h. Ethyl chloroformate (20 mmol) in 5 ml of THF was then added to the above solution with stirring and the mixture was kept at −78 °C for 30 min and at 30—35 °C for 1 h before it was quenched with saturated aqueous solution of ammonium chloride (10 ml). The usual work-up and silica-gel chromatography (benzene) gave **22** in 63% (3.75 g) isolated yield (*E*/*Z* =94/6). The (*E*)- and (*Z*)-isomers of **22** were separated by silica-gel chromatography using benzene as eluent.

Preparation of Ethyl (E)*-10-Hydroxy-2-decenoate (23)*: A solution of 3.50 g (16 mmol) of **22** and 0.35 g of *p*-toluensulfonic acid in 100 ml of ethanol was refluxed for 1 h, concentrated to half volume, diluted with water, and extracted with ether (50×4 ml). The combined organic layer was dried on anhydrous sodium sulfate and concentrated under reduced pressure. Silica-gel chromatography (ethyl acetate: chloroform=1 : 1) gave **23** as a viscous oil in 79% (2.70 g) isolated yield. ^{1}H-NMR (CCl_4); δ=6.65 (dt, J=7 Hz, 16 Hz, 1H, CH=C), 5.52 (d, 16 Hz, 1H, CH=C), 3.96 (q, J=7 Hz, 2H, CH_2), 3.40 (t, J=6 Hz, 2H, CH_2), 3.02 (brs, 1H, OH), 1.96—2.22 (m, 2H, CH_2), 1.08—1.62 (m, 13H, $5CH_2$ and CH_3).

Preparation of (E)*-10-Hydroxy-2-decenoic Acid (24)*: A solution of 2.57 g (12 mmol) of **23** and 1.40 g of potassium hydroxide in 16 ml of ethanol was refluxed for 1.5 h under a nitrogen atmosphere, concentrated to half volume, diluted with water, and acidified to pH 4.0 with 2.5 M sulfuric acid (1 M=1 mol dm^{-3}). The reaction solution was then extracted with ether (50×4 ml), dried on anhydrous sodium sulfate, and concentrated under reduced pressure. Silica-gel chromatography (ethyl acetate and chloroform) and recrystallization from ether gave pure **24** in 73% (1.63 g) isolated yield. Mp 62.5—63.5 °C. ^{1}H-NMR (CCl_4); δ=6.80 (dt, J=7 Hz, 16 Hz, 1H, CH=C), 6.07 (brs, 2H, OH and COOH), 5.58 (d, J=16 Hz, 1H, CH=C), 3.47 (t, J=6 Hz, 2H, CH_2), 2.05—2.24 (m, 2H, CH_2), 0.92—1.16 (m, 10H, $5CH_2$). IR (disk); 3420 (OH), 1685 (COOH), 1640 cm^{-1} (C=C). Found: C, 64.08; H, 9.51%. Calcd for $C_{10}H_{18}O_3$: C, 64.49; H, 9.74%.

The author would like to thank Drs. Aritsune Kaji and Kazuhiko Tanaka, Department of Chemistry, Faculty of Science, Kyoto University, for their helpful discussion during this work.

References

1) S. Matsui, K. Tanaka, and A. Kaji, *Synthesis*, **1983**, 127.

2) a) H. O. House, D. S. Crumrine, A. Y. Teranishi, and H. D. Olmstead, *J. Am. Chem. Soc.*, **95**, 3310 (1973); b) F. A. Carey and M. E. Kuehne, *J. Org. Chem.*, **47**, 3811 (1982); c) D. Seebach and V. Prelog, *Angew. Chem., Int. Ed. Eng.*, **21**, 654 (1982); d) C. H. Heathcock, C. T. Buse, W. A. Kleischick, M. C. Pirrung, J. E. Sohn, and J. Lampe, *J. Org. Chem.*, **45**, 1066 (1980).

3) a) T. Nakata and T. Oishi, *Tetrahedron Lett.*, **21**, 1640 (1980): b) M. Hirama and S. Masamune, *ibid.*, **1979**, 2225; c) S. Masamune, S. Mori, D. E. Vanhorn, and D. W. Brooks, *ibid.*, **1979**, 1665; d) D. E. Vanhorn and S. Masamune, *ibid.*, **1979**, 2229; e) M. Hirama, D. S. Garvey, L. D.-L. Lu, and S. Masamune, *ibid.*, **1979**, 3937.

4) K. Tanaka, N. Yamagishi, R. Tanikaga, and A. Kaji, *Chem. Lett.*, **1977**, 471; *Bull. Chem. Soc. Jpn.*, **52**, 3619 (1979).

5) a) M. Sander, *Chem. Rev.*, **66**, 297 (1966); b) N. P. Neureiter and F. G. Bordwell, *J. Am. Chem. Soc.*, **81**, 578 (1959); c) D. B. Denny and M. J. Boskin, *ibid.*, **82**, 4736 (1960).

6) K. Tanaka, H. Uneme, N. Ono, and A. Kaji, *Chem. Lett.*, **1979**, 1039.

7) W. S. Wadsworth, Jr., and W. D. Emmons, *J. Am. Chem. Soc.*, **83**, 1733 (1961).

8) G. Wittig and W. Haag, *Chem. Ber.*, **88**, 1654 (1955).

9) a) G. F. Tounsend and C. C. Lucas, *Biochem. J.*, **34**, 1155 (1940); b) G. I. Fray, R. H. Jaeger, R. Robinson, and A. D. B. Soan, *Tetrahedron*, **15**, 18 (1961); c) S. A. Barker, A. B. Foster, and D. C. Lamb, *Nature*, **184**, 634 (1959); S. A. Barker, A. B. Foster, D. C. Lamb, and L. M. Jackmann, *Tetrahedron*, **18**, 177 (1962); d) W. H. Brown and R. J. Freure, *Can. J. Chem.*, **37**, 2042 (1959).

10) W. G. Dauben, and H. L. Bradlow, *J. Am. Chem. Soc.*, **74**, 559 (1952).

11) C. F. Allen, and M. J. Kalm, *Org. Synth.*, IV, 608 (1963).

12) B. A. Arbuzov and D. Kh. Yarmkhametova, *Izv. Akad. Nauk SSSR, Otdel. Khim.*, **1960**, 1881.

13) a) R. Ratcliffe and R. Rodehorst, *J. Org. Chem.*, **35**, 4000 (1970); b) J. C. Collins, W. W. Hess, and F. J. Frank, *Tetrahedron Lett.*, **1968**, 3363; J. C. Collins and W. W. Hess, *Org. Synth.*, **52**, 5 (1972).

The Ruthenium Catalyzed Synthesis of Quinoline Derivatives from Nitroarenes and Aliphatic Alcohols

Yoshihisa WATANABE,* Yasushi TSUJI, and Jun SHIDA
Department of Hydrocarbon Chemistry, Faculty of Engineering, Kyoto University, Sakyo-ku, Kyoto 606
(Received June 3, 1983)

Nitroarenes are reductively converted into quinoline derivatives with aliphatic alcohols in the presence of a catalytic amount of ruthenium compound at 180 °C. Ruthenium(III) chloride is the most effective catalyst. The reaction of nitrobenzene with 1-propanol and 1-butanol gave 2-ethyl-3-methylquinoline and 3-ethyl-2-propylquinoline in 65 and 70% yields respectively. *p*-Methoxynitrobenzene gave 3-ethyl-6-methoxy-2-propylquinoline in 70% yield with 1-butanol. The reaction appears to include the redox reaction between the nitroarenes and the alcohols, that is, a catalytic hydrogen transfer reaction which generates the aminoarenes and aldehydes. Thus, the alcohol plays roles as both a reductant and an aldehyde precursor.

The Skraup synthesis is well known as the method for the preparation of quinoline derivatives.[1] This method, however, requires a large amount of strong acid and a high reaction temperature. Recently, transition metal-catalyzed synthesis of quinoline derivatives under non-acid conditions have been developed.[2,3] In the previous paper, we have reported. that several transiation metal catalysts are effective for the preparation of quinoline derivatives from aminoarenes. Aminoarenes react with aliphatic aldehydes to give quinoline derivatives in the presence of a rhodium complex such as di-μ-chlorobis(norbornadiene)-dirhodium ($[RhCl(NBD)]_2$),[4] or a rutheinum complex such as dichlorotris(triphenylphosphine)ruthenium ($[RuCl_2(PPh_3)_3]$).[5,6] Employing $[RuCl_2(PPh_3)_3]$ as the catalyst, the quinoline derivatives are also obtained from aminoarenes and allylic alcohols.[6]

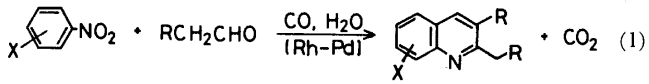

(1)

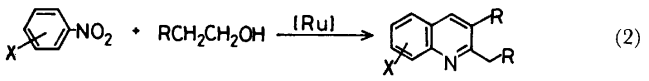

(2)

Although nitroarenes are also important as starting materials for preparations of *N*-heterocycles, few studies have been reported on the synthesis of quinoline derivatives from nitroarenes.[7] We have recently reported that nitroarenes were reductively converted into quinoline derivatives with aliphatic aldehydes in the presence of a rhodium–palladium binary catalyst system (Eq. 1).[8] In that reaction, conditions of water gas shift reaction (carbon monoxide pressure and presence of water) were effective. This reaction made a new entry in quinoline synthesis from nitroarenes.

For the preparation of the quinoline derivatives, we recently offered a new method. Aliphatic alcohols effectively reduced nitroarenes in the presence of a catalytic amount of ruthenium compound and the resulting aldehydes react with the corresponding aminoarenes to give quinoline derivatives (Eq. 2). The preliminary results have been reported with $[RuCl_2(PPh_3)_3]$ as catalyst.[9] Recently, Mares and Boyle published a similar quinoline synthesis from nitroarene and aliphatic alcohols using a binary catalyst, $[Rh(CO)_2Cl]_2$ and $MoCl_5$.[10] This method, however, required a much larger amount of each catalyst (10 mol% each).

In this work, we describe a new finding about a more effective catalyst and give full details of the results.

Results and Discussion

Nitrobenene reacted with aliphatic alcohols in the presence of ruthenium catalyst at 180 °C. Activities of various ruthenium catalysts for this reaction were

TABLE 1. EFFECT OF RUTHENIUM CATALYST PRECURSORS ON THE SYTHESIS OF QUINOLINE DERIVATIVES[a]

Run	Catalyst	Conversion	Yields of products[b]/%			
		%	**1a**	**2**	**3a**	**4a**
1	$RuCl_3 \cdot xH_2O$	92	42	9	8	0
2	$RuCl_3 \cdot xH_2O + P(n\text{-}Bu)_3$[c]	73	12	12	1	0
3	$RuCl_3 \cdot xH_2O + Ph_2P(CH_2)_2PPh_2$[d]	22	6	4	1	0
4	$RuCl_3 \cdot xH_2O + P(OPh)_3$[c]	16	2	0	0	tr
5	$[RuCl_2(PPh_3)_3]$	96	28	6	24	6
6	$[RuHCl(CO)(PPh_3)_3]$	91	11	14	7	tr
7	$[Ru(CO)_3(PPh_3)_2]$	97	10	14	13	0
8	$[Ru_3(CO)_{12}]$	95	9	8	25	tr
9	$[RuHCl(PPh_3)_3]$	52	4	5	8	0
10	$[RuH_2(PPh_3)_4]$	60	0	9	3	0

a) Nitrobenzene (40 mmol), 1-propanol (20 ml), ruthenium compound (0.40 mmol) at 180 °C for 4 h. b) Based on nitrobenzene used (GLC analysis): **1a**, 2-ethyl-3-methylquinoline; **2**, aniline; **3a**, *N*-propylaniline; **4a**, *N*,*N*-dipropylaniline. c) Phosphorus ligand, 2.40 mmol. d) Phosphorus ligand, 1.20 mmol.

TABLE 2. THE SYNTHESIS OF QUINOLINE DERIVATIVES UNDER VARIOUS REACTION CONDITIONS[a]

Run	Catalyst[b] (mol%)	Temp °C	Conversion[c] %	Yields of products[c]/% 1b	2	3b	4b
11[d]	1	180	91	(38)[e]	5	(6)[f]	(0)[g]
12	1	180	58	22	0	11	tr
13	3	180	90	56	2	15	2
14	5	180	96	70	0	14	5
15	10	180	94	39	7	3	0
16	5	150	30	5	tr	2	3
17	5	200	100	61	2	9	3
18[h]	5	180	100	(65)[i]	tr	(5)[j]	(8)[k]

a) Nitrobenzene (40 mmol), 1-butanol (20 ml) for 4 h. b) $RuCl_3 \cdot xH_2O$ based on nitrobenzene used. c) Based on nitrobenzene used (GLC analysis): **1b**, 3-ethyl-2-propylquinoline; 2, aniline; **3b**, *N*-butylaniline; **4b**, *N,N*-dibutylaniline. d) Ethanol was used as the alcohol. e) 2-Methylquinoline. f) *N*-Ethylaniline. g) *N,N*-Diethylaniline. h) 1-Propanol was used as the alcohol. i) 2-Ethyl-3-methylquinoline. j) *N*-Propylaniline. k) *N,N*-Dipropylaniline.

examined with 1-propanol as the alcohol. The results are summarized in Table 1. The yield of the product, 2-ethyl-3-methylquinoline (**1a**), strongly depends on the catalyst. Among the ruthenium catalysts examined, the highest catalytic activity is attained with ruthenium(III) chloride ($RuCl_3 \cdot xH_2O$). The addition of a phosphrous ligand on $RuCl_3 \cdot xH_2O$ suppressed the formation of the quinoline derivative (Runs 2—4). Dichlorotris(triphenylphosphine)ruthenium had some activity. With other ruthenium complexes, however, the yield of the quinoline was reduced considerably (Runs 6—10). Aniline (**2**), *N*-propylaniline (**3a**), and *N,N*-dipropylaniline (**4a**) were confirmed as the by-products.

Effects of reaction conditions were examined. The results are shown in Table 2. In Runs 12—17, 1-butanol was used as the alcohol. The yield of product, 3-ethyl-2-propylquinoline (**1b**), depends on the amounts of the catalyst. As the amount of catalyst increased from 1 mol% to 5 mol%, based on the amount of nitrobenzene used, the formation of the alkylquinoline was favored. Employing 5 mol% of $RuCl_3 \cdot xH_2O$ as the catalyst, the alkylquinoline was obtained in 70% yield (Run 14). The yield, however, decreased considerably with 10 mol% of the catalyst owing to side reactions. These results indicate that the optimum catalyst concentration is 5 mol%. 2-Ethyl-3-methylquinoline was obtained in 65% yield with 1-propanol with 5 mol% of catalyst concentration (Run 18).

As for the reaction temperature, the best result was realized at 180 °C. By lowering the reaction temperature to 150 °C, the conversion of nitrobenzene and the yield of the quinoline derivative were drastically reduced. The yield of the product was not improved by elevating the reaction temperature to 200 °C.

This procedure is applicable to a variety of nitroarenes. The results obtained with nitrobenzenes with methyl, methoxyl, and chloro substituents at para or ortho positions are listed in Table 3. *p*-Methoxynitrobenzene and *p*-methylnitrobenzene reacted with 1-butanol to give the corresponding 2,3,6-trisubstituted quinoline derivatives in 78 and 58% yield respectively. The chloro substituent reduced the reactivity of the substrate. On the other hand, *o*-substituted nitrobenzenes gave the quinoline derivatives in much lower yields, probably owing to the steric effect (Runs 22 and 23).

TABLE 3. THE RUTHENIUM-CATALYZED REACTION BETWEEN VARIOUS NITROARENES AND 1-BUTANOL

Run	Nitroarenes X[b]	Quinolines X (3-Et, 2-Pr)	Yield/%[c]
19	*p*-OCH_3	6-OCH_3	78
20	*p*-CH_3	6-CH_3	58
21	*p*-Cl	6-Cl	35
22	*o*-CH_3	8-CH_3	35
23	*o*-OCH_3	8-OCH_3	5

a) Nitrobenzene (40 mmol), 1-butanol (20 ml), $RuCl_3 \cdot xH_2O$ (2.0 mmol) at 180 °C for 4 h. b) See Eq. 2. c) Based on nitroarenes used (GLC analysis).

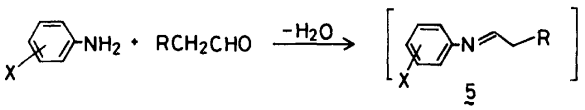

5

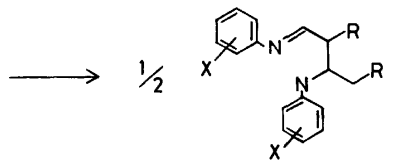

6 (3)

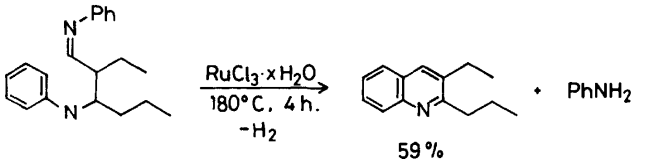

6a (4)

The group VIII metal complexes such as palladium,[11] rhodium,[12] and ruthenium[13] complexes catalyze the hydrogen transfer reaction from alcohols to various hydrogen acceptors. Several novel metal salts such as $RuCl_3 \cdot 3H_2O$, $RhCl_3 \cdot 3H_2O$, $PdBr_2$, and $PdCl_2$

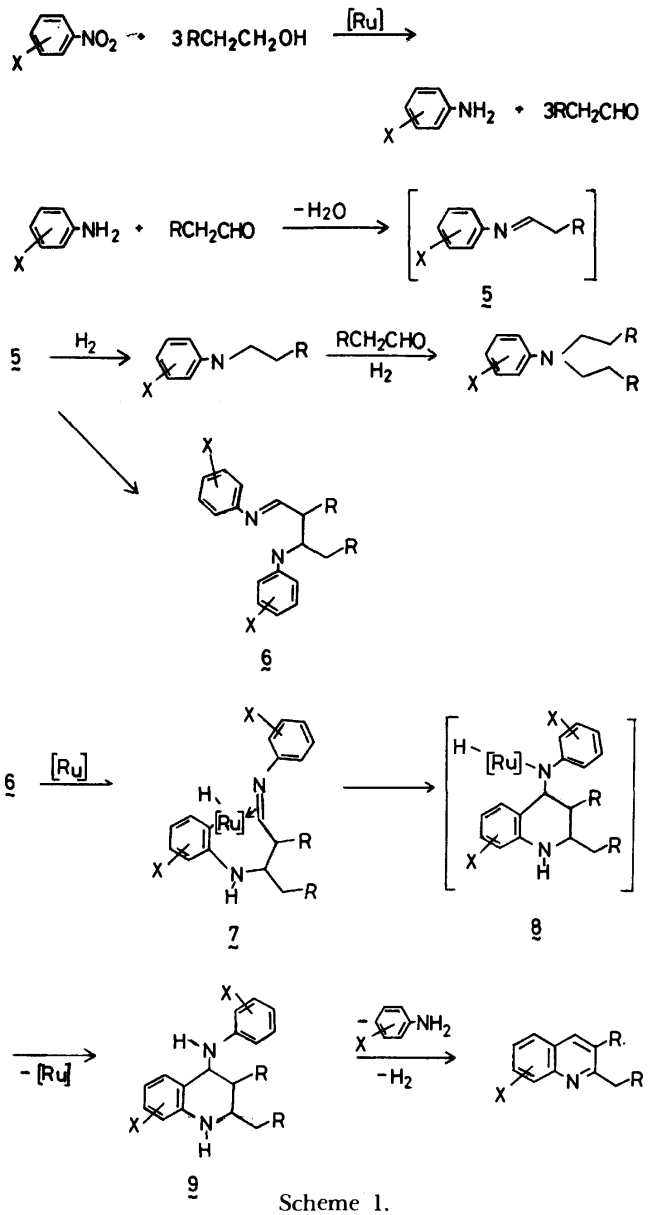

Scheme 1.

catalyze the hydrogen transfer from cyclic amines to nitrobenzenes to give corresponding aniline derivatives.[14]

In this study, the reaction appears to include reduction of nitroarenes with the alcohols by the catalytic hydrogen transfer from the alcohols, generating aminoarenes and aldehydes *in situ* (see the first equation in Scheme 1). Thus the alcohols play roles as both the reductants and aldehyde precursors in these reactions. The alkylquinolines would be formed by the ruthenium catalyzed reaction of the aminoarenes with the aldehydes. Actually, aminoarenes react with aliphatic aldehydes to the corresponding quinoline derivatives in the presence of ruthenium catalysts, as previously reported.[5,6]

It is well known that aminoarene reacts with aliphatic aldehyede to give a Schiff-base dimer on simply mixing at room temperature (Eq. 3).[15,16] In the previous paper,[6] we have suggested that the *N*-heterocyclization to the quinoline derivatives proceeds *via* these Schiff-base dimers (**6**). In a separate reaction, 3-ethyl-2-propylquinoline is obtained in 59% yield in the presence of $RuCl_3 \cdot xH_2O$ from the corresponding Schiff-base dimer (**6a** R=Et, X=H)(Eq. 4). Therefore, we consider that the present reaction also proceeds *via* a Schiff-base dimer (**6**). (Alkylamino)- and (dialkylamino)arenes were also obtained as by-products (Tables 1 and 2). These products could be formed *via* a Schiff-base monomer (**5**).[5] Such a Schiff-base monomer is liable to dimerize. The Schiff-base monomer could not be obtained and only the Schiff-base dimer (**6**) was isolated.[15,16] The Schiff-base dimer (**6**) may be activated at an elevated temperature by so called orthometallation (**7**)[17-23] as suggested in the previous paper,[6] and transformed into the corresponding quinoline derivative. The catalyst appears to be operative in the cyclization step (**7**→**8**), since (**6**) was obtained without catalyst and even at room temperature.

3-Ethyl-2-propylquinoline was also obtained in much lower yield from aniline and 2-ethyl-2-hexenal, an aldol condensate of butanal, in the presence of $RuCl_3 \cdot xH_2O$ (Eq. 5). Therefore the path *via* aldol condensation followed by Michael addition of aniline may be an alternative acceptable path in the present reaction (Scheme 2). Mares *et al.* suggested the path described in Scheme 2 as the most likely route, without positive evidence.[10]

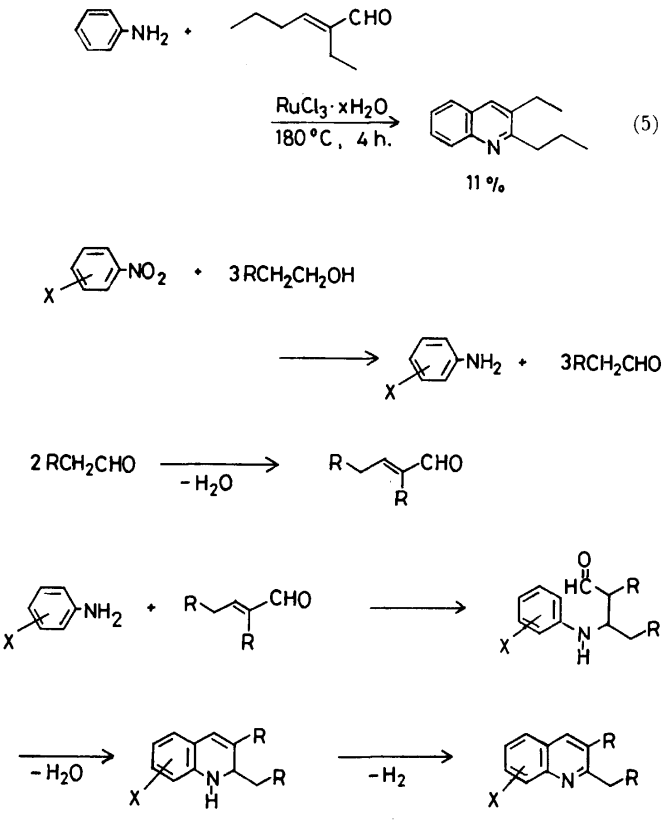

Scheme 2.

Thus, $RuCl_3 \cdot xH_2O$ is the effective catalyst for converting nitroarenes into quinoline derivatives with alcohols. In the reaction, the alcohol plays roles as both a reductant and an aldehyde precursor.

Experimental

Materials. The alcohols, the nitroarenes, and the phosphorus ligands were commercial materials and were purified by distillation or recrystallization before use. Ruthenium(III) chloride ($RuCl_3 \cdot xH_2O$, mainly $x=3$) was purchased from Wako Chemical and used without further purification. $[RuCl_2(PPh_3)_3]$,[24] $[RuHCl(PPh_3)_3]$,[25] $[RuHCl(CO)(PPh_3)_3]$,[26] $[RuH_2(PPh_3)_4]$,[27] $[Ru(CO)_3(PPh_3)_2]$,[26] and $[Ru_3(CO)_{12}]$[28] were prepared by published methods. 2-Ethyl-2-hexenal was prepared from butanal.[29] The Schiff-base dimer (**6a**) was synthesized with aniline and butanol by the method in the literature.[16]

Analytical Procedure. The ^{1}H-NMR spectra were obtained at 100 MHz with a JEOL JNM FX-100 or at 220 MHz with a Varian HR-220 spectrometer. The ^{13}C-NMR spectra were recorded at 25.05 MHz with a JEOL JNM FX-100 spectrometer, with tetramethylsilane as an internal standard. IR spectra were measured on a Hitachi model 215 grating spectrometer. Elemental analysis was performed at the Microanalytical Center of Kyoto University. The mass spectra were recorded on a JMS OISG mass spectrometer. The GLC analysis was performed on a Shimadzu-GC-3BT.

Reaction Procedure. An autoclave (100 ml; SUS 316) equipped with a magnetically driven stirrer was used in the reaction. A typical reaction with 1-butanol and nitrobenzene is described here to exemplify the general procedure adopted. A mixture of nitrobenzene (4.9 g, 40 mmol), 1-butanol (20 ml), and $RuCl_3 \cdot xH_2O$ (487 mg, 2.0 mmol, 5 mol% based on nitrobenzene used) was stirred under an argon atmosphere. The autoclave was heated in 20 min to 180 °C and held at this temperature for 4 h. After cooling, the autoclave was discharged and the reaction mixture was subjected to the GLC analysis with Apiezon Grease L supported on Neopak 1A 60—80 mesh (0.3 cmϕ×3 m). The products were isolated by vacuum fractional distillations. If the products were contaminated with other products, further purification was performed by means of medium pressure column chromatography (absorbent; Silica Gel 60, 0.040—0.063 mm, 230—400 mesh, Merck No. 9385: eluent; a mixture of hexane and ethyl acetate). The products were identified by means of ^{1}H-NMR, ^{13}C-NMR, IR, mass spectra, and elemental analysis. The identifications are confirmed by comparing the analytical date with those published elsewhere.[4-6] The conversion of the substrate and the yield of the product were determined by the internal standard method accordng to the calibration curve obtained for each sample. Biphenyl or triphenylmethane was employed as the internal standard.

Synthesis of 3-Ethyl-2-propylquinoline from Schiff-base Dimer (6a) A solution of **6a** (3.979 g, 13.5 mmol) in benzene (20 ml) was stirred under an argon atmosphere in the presence of nitrobenzene (1.546 g, 12.6 mmol) and $RuCl_3 \cdot xH_2O$ (299 mg, 1.23 mmol, 5 mol% based on nitrogen atom) at 180 °C for 4 h. The GLC analysis of the reaction mixture showed that 8.0 mmol (59% based on **6a**) of 3-ethyl-2-propylquinoline was formed.

Reaction of Aniline with 2-Ethyl-2-hexenal. A mixture of aniline (2.150 g, 23.1 mmol), 2-ethyl-2-hexenal (2.926 g, 23.2 mmol), benzene (10 ml), $RuCl_3 \cdot xH_2O$ (1.11 mmol, 4.8 mol% based on aniline), and nitrobenzene (2.625 g, 21.3 mmol) was stirred at 180 °C for 4 h. By the GLC analysis of the reaction products, 2.6 mmol (11% based on aniline) of 3-ethyl-2-propylquinoline was detected.

References

1) H. Skraup, *Chem. Ber.*, **13**, 2086 (1880).
2) S. E. Diamond, A. Szalkiewicz, and F. Mares, *J. Am. Chem. Soc.*, **101**, 493 (1979).
3) T. Joh and N. Hagihara, *Tetrahedron Lett.*, **1967**, 4199.
4) Y. Watanabe, S. C. Shim, and T. Mitsudo, *Bull. Chem. Soc. Jpn.*, **54**, 3460 (1981).
5) Y. Watanabe, Y. Tsuji, and Y. Ohsugi, *Tetrahedron Lett.*, **22**, 2667 (1981).
6) Y. Watanabe, Y. Tsuji, Y. Ohsugi, and J. Shida, *Bull. Chem. Soc. Jpn.*, **56**, 2452 (1983).
7) P. A. Claret, "Comprehensive Organic Chemistry," ed by P. G. Sammes, Pergamon Press, Oxford (1979), Vol. 4, p. 163.
8) Y. Watanabe, N. Suzuki, Y. Tsuji, S. C. Chim, and T. Mitsudo, *Bull. Chem. Soc. Jpn.*, **55**, 1116 (1982).
9) Y. Watanabe, Y. Tsuji, and N. Suzuki, *Chem. Lett.*, **1981**, 1067.
10) W. J. Boyle and F. Mares, *Organometallics*, **1**, 1003 (1982).
11) H. Imai, T. Nishiguchi, M. Tanaka, and K. Fukuzumi, *J. Org. Chem.*, **42**, 2309 (1977).
12) T. Nishiguchi, K. Tachi, and K. Fukuzumi, *J. Org. Chem.*, **40**, 237 (1975).
13) Y. Sasson and J. Blum, *J. Org. Chem.*, **40**, 1887 (1975).
14) H. Imai, T. Nishiguchi, and K. Fukuzumi, *Chem. Lett.*, **1976**, 655.
15) S. Dayagi and Y. Degani, "The Chemistry of the Carbon-Nitrogen Double Bond," ed by S. Patai, Interscience Publishers, London (1970), Chap. 2, pp. 61—67.
16) K. S. Kharash, I. Richlin, and R. Mayo, *J. Am. Chem. Soc.*, **62**, 494 (1940).
17) G. W. Parshall, *Acc. Chem. Res.*, **3**, 139 (1970) and the references cited therein.
18) H. D. Kaesz and R. B. Saillant, *Chem. Rev.*, **72**, 231 (1972).
19) I. Omae, *Chem. Rev.*, **79**, 237 (1979) and the references cited therein.
20) G. W. Parshall, W. H. Knoth, and R. A. Schunn, *J. Am. Chem. Soc.*, **91**, 4990 (1969).
21) T. Itoh, S. Kitazume, A. Yamamoto, and S. Ikeda, *J. Am. Chem. Soc.*, **92**, 3011 (970).
22) J. Chatt and J. M. Davidson, *J. Chem. Soc.*, **1965**, 843.
23) C. A. Tolman, S. D. Itell, A. D. English, and J. P. Jesson, *J. Am. Chem. Soc.*, **100**, 4080 (1978).
24) P. S. Hallman, T. A. Stephenson, and G. Wilkinson, *Inorg. Synth.*, **12**, 237 (1970).
25) P. S. Hallman, B. R. McGarvey, and G. Wilkinson, *J. Chem. Soc., A*, **1968** 3142.
26) N. Ahmad, J. J. Levison, S. D. Robinson, and M. F. Uttley, *Inorg. Synth.*, **15**, 48 (1974).
27) R. Young and G. Wilkinson, *Inorg. Synth.*, **17**, 75 (1977).
28) A. Mantorani and S. Cenini, *Inorg. Synth.*, **16**, 47 (1976).
29) H. Hausermann, *Helv. Chim. Acta*, **7**, 653 (1951).

 © 1984 The Chemical Society of Japan Bull. Chem. Soc. Jpn., 57, 439—441 (1984)

Synthesis of *N*-Tripeptidyl-D-glucosamine by the Stepwise Reaction of *N*-Carboxy α-Amino Acid Anhydride[1]

Masanao OYA* and Toshiyuki NEGISHI

Department of Industrial Chemistry, College of Technology, Gunma University, Tenjin-chō, Kiryu, Gunma 376

(Recieved June 14, 1983)

N-Peptidyl-D-glucosamines were synthesized by the stepwise reaction of *N*-carboxy α-amino acid anhydrides (4-alkyl-2,5-oxazolidinediones) with D-glucosamine hydrochloride in the presence of equimolar sodium methoxide in a mixture of acetonitrile and methanol, or in methanol, at a low temperature. Polymerization reaction of *N*-carboxy α-amino acid anhydrides (NCAs) did not occur at −50 °C. The mechanism of the reaction was then studied.

Proteins and peptides containing sugar residues, glycoproteins and glycopeptides, are widely distributed in nature, and have many bioactive properties.[2] Therefore, the syntnesis of models of glycoproteins and glycopeptides are important. In the carbohydrate-peptide linkage, the covalent linkage between the amino sugar-amino acid bonds, have been considered to be of two types. One is a peptide linkage which is formed between the amino residue of glucosamine and the carboxyl residue of amino acid. This bond is generally synthesized by the coupling reaction of an amino group of glucosamine with a carboxyl residue of an amino acid, the amino residue of which is protected, and following removal of protection.[3-8] However, many glycopeptides are unstable to acids or bases. They are decomposed with changing color by both acids or bases. It is therefore important to avoid the deprotecting reaction in strong acidic or basic media.

We attempted the synthesis of several *N*-peptidyl-D-glucosamines by the stepwise reaction of *N*-carboxy α-amino acid anhydrides (NCAs) with D-glucosamine having free hydroxyl groups in the mixed solvent of acetonitrile and methanol, or in methanol.

The mechanism of polymerization of NCAs have been studied extensively.[9] In comparison, there is little information on the stepwise reaction of an α-amino or hydroxyl residue with NCA. Bailey reports the synthesis of dipeptides by the stepwise reaction of NCAs with an amino acid ethyl ester in chloroform at −40 °C.[10] This reaction does not occur for any amino acid ester except glycine ethyl ester in chloroform because the polymerization reaction of NCAs occur.[11]

In a previous paper, we reported that the stepwise synthesis of oligopeptides with regular sequence by the method of controlled reaction of NCAs in an acetonitrile water heterogeneous system.[12,13] In another previous study, we reported the steric hindrance of the stepwise reaction of NCAs with the α-amino acid esters.[14] These stepwise syntheses of oligopeptides involves no, or limited removal of protecting groups. Further, these reactions did not lead to racemization.[15]

These studies suggest that NCAs can be utilized for the amino acylation of amino residues of many organic compounds.

When L-alanine was used in the reaction with D-glucosamine, polymerization of the NCA proceeded at −40 °C, but did not proceeded at −50 °C. However the stepwise reaction of L-alanine NCA (**2**; $R^1=CH_3$) with D-glucosamine (**1**) did proceed at −55 °C. It was considered that the steric hindrance of the side chains of both NCA and the compound having α-amino residue determine whether polymerization of NCA or the stepwise reaction proceeds at −20 °C.[11] As the polymerization of L-alanine NCA proceeded at −40 °C, the side chain of D-glucosamine must be more bulky than that of L-alanine NCA. The fact that the stepwise reaction of L-alanine NCA with D-glucosamine proceeded indicate that the steric hindrance of the side chains of both L-alanine NCA and the α-amino residue of the compound do not affect the reaction at −55 °C. The decarboxylation of the carbamic acid (**3**→**4**) must not occur below −54 °C., since carbamic acids are stable at a low temperature. NCAs are

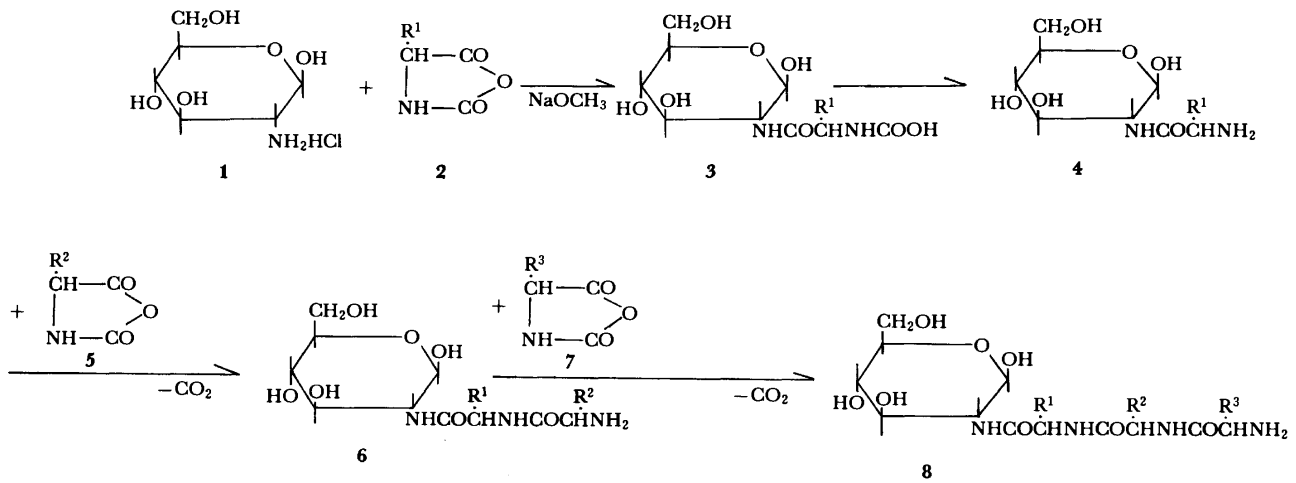

initiated with alcohols to produce dipeptides, polypeptides, and small amounts of amino acid esters.[9] However, the stepwise reaction of NCA with D-glucosamine does proceed in methanol at −55 °C. This indicates that the rate of reaction of NCA with the amino residue of D-glucosamine is faster than that of NCA with the hydroxyl group of methanol.

N-Dipeptidyl-D-glucosamine (**6**) was synthesized by addition of an acetonitrile solution of NCA (**5**) to the solution obtained by filtration of the reaction mixture of *N*-aminoacyl-D-glucosamine (**4**), followed by the same procedure as described above (**4**+**5**→**6**). *N*-Tripeptidyl-D-glucosamine (**8**) was synthesized by addition of the third NCA (**7**) with *N*-dipeptidyl-D-glucosamine (**6**) by the same synthetic procedure of *N*-dipeptidyl-D-glucosamine (**6**+**7**→**8**).

Experimental

D-Glucosamine hydrochloride and amino acids used were commercial products. NCAs were prepared as reported previously.[16]

NMR spectra were obtained on a Brucker WH-270 spectrometer, the chemical shifts are given in δ values (ppm) from sodium 2,2-dimethyl-2-silapentane-5-sulfonate.

N-L-*Alanyl*-D-*glucosamine* (*4*; $R^1=CH_3$). D-Glucosamine hydrochloride (1.5 g, 23.3 mmol) was dissolved in methanol solution (92 cm³) of sodium methoxide (1.3 g, 24 mmol). The solution of L-alanine NCA (2; $R^1=CH_3$, 2.7 g, 23 mmol) in acetonitrile (92 cm³) was then added, and stirred at −50 °C for 120 h. After the reaction, the mixture was raised to room temperature and filtered to remove a small amount of precipitate, and distilled *in vacuo* to remove the solvent. The residual product was dissolved in ethanol and water (90 : 10 v/v). The solution was filtered, and dried *in vacuo* to obtain pure *N*-L-alanyl-D-glucosamine: yield 6.2 g (80%); $[\alpha]_D^{22}$ −8.3° (*c* 0.012 CH_3OH); NMR[17] (0.04 g/ml D_2O) δ=1.36 (t Ala C<u>H</u>$_3$), 3.29 and 3.73 (m glucosamine OH), 4.4 (Ala CH), 7.23 (m CON<u>H</u> and N<u>H</u>$_2$). Found: C, 43.30; H, 6.88; N, 10.55%. Calcd for $C_9H_{18}O_6N_2$: C, 43.20; H, 6.88; N, 11.20%.

N-(L-*Alanyl*-L-*valyl*)-D-*glucosamine* (*6*; $R^1=(CH_3)_2CH$, $R^2=CH_3$). D-Glucosamine hydrochloride (**1**, 5 g, 23.3 mmol) was dissolved in a methanol solution (92 cm³) of sodium methoxide (1.3 g, 24 mmol). The solution of L-valine NCA (**2**; $R^1=(CH_3)_2CH$, 3.4 g, 24 mmol) in acetonitrile solution (92 cm³) was then added, and stirred for 120 h at −50 °C. After the reaction, the mixture was raised to room temperature and filtered to remove a small amount of precipitate. The filtrate was cooled to −50 °C, the solution of L-alanine NCA (2.6 g, 23 mmol) in acetonitrile (52 cm³) and methanol (52 cm³) was then added, and allowed to react as described above. The reaction mixture was raised to room temperature, filtered, and distilled *in vacuo* to obtain the crude product. The product was dissolved in the minimum amount of methanol, filtered, diluted with a half volume of diethyl ether, and filtered again. The solution part was distilled *in vacuo* to obtain crude *N*-(L-alanyl-L-valyl)-D-glucosamine. The crude product thus obtained was purified by columm chromatography, (Sephadex G-10, 2.5×45 cm). Elution with ethanol and water (1 : 1 v/v) separated contaminent, sodium chloride, and pure *N*-(L-alanyl-L-valyl)-D-glucosamine: yield 2.0 g (26%); $[\alpha]_D^{22}$ −22.7° (*c* 0.016 CH_3OH); NMR (2 mg/cm³ DMSO-d_6) δ=0.88 (q Val (C<u>H</u>$_3$)$_2$), 1.28 (t Ala C<u>H</u>$_3$), 1.59 (Val βC<u>H</u>), 3.38, 3.63, and 3.86 (glucosamine OH), 4.23 (Ala and Val αC<u>H</u>), 7.94, 8.02, 8.12, and 8.95 (N<u>H</u>CO and N<u>H</u>$_2$). Found: C, 48.89; H, 8.12; N, 12.12%. Calcd for $C_{14}H_{27}O_7H_3$: C, 48.14; H, 7.74; N, 12.02%.

N-(*γ-Methyl*-L-*α-glutamyl*-L-*phenylalanyl*-L-*alanyl*)-D-*glucosamine* (*8*; $R^1=CH_3$, $R^2=CH_2C_6H_5$, $R^3=CH_2CH_2COOCH_3$). D-Glucosamine hydrochloride (4.3 g, 20 mmol) was dissolved in a methanol solution (86 cm³) of sodium methoxide (1.1 g, 20 mmol). The solution was cooled to −50 °C. The solution of L-alanine NCA (2.5 g, 21 mmol) in acetonitrile (50 cm³) previously cooled to −50 °C was added to the solution of glucosamine, and allowed to react for 70 h at −50 °C, and subsequently for 70 h at −20 °C. After the reaction the resulting mixture was warmed to room temperature, and filtered to remove the precipitate. The filtrate was cooled to −20 °C. Crystals of L-phenylalanine NCA (3.1 g, 16.2 mmol) were added, and allowed to react for 70 h at −20 °C. After the reaction the system was warmed and filtered to separate the precipitate. The clear solution was cooled again to −20 °C, added to the solution of γ-methyl-L-glutamate NCA (3.3 g, 17.6 mmol) in acetonitrile (35 cm³), and allowed to react as above. After the reaction the resulting mixture was warmed, filtered, and distilled *in vacuo* to obtain the crude product (7.5 g, 71% yield). The crude product was purified as *N*-(L-valyl-L-alanyl)-D-glucosamine. Pure product: $[\alpha]_D^{22}$ −12.7° (*c* 0.0063 CH_3OH); NMR (2 mg/cm³ DMSO-d_6) δ=1.29 (Ala C<u>H</u>$_3$), 1.86 (Glu C<u>H</u>$_2$), 3.03 (Phe C<u>H</u>$_2$), 3.39 and 3.61 (glucosamine OH), 3.62 (Glu COOC<u>H</u>$_3$), 3.64 (glucosamine O<u>H</u>), 4.30 (Ala and Glu αCH), 7.25 (Phe C_6H_5), 7.75 and 8.59 (m CON<u>H</u> and N<u>H</u>$_2$). Found: C, 53.75; H, 5.96; N, 9.84%. Calcd for $C_{24}H_{36}O_{10}N_4$: C, 53.33; H, 6.67; N, 10.37%.

The other *N*-tripeptidyl-D-glucosamines were synthesized by the reactions of D-glucosamine (**1**) with the first NCA (**2**), following the second NCA (**5**), and the third NCA (**7**) under almost similar conditions to the tripeptidyl-D-glucosamine described above (Eq. 1).

N-(L-*Alanyl*-L-*leucyl*-L-*alanyl*)-D-*glucosamine* (*8*; $R^1=CH_3$, $R^2=(CH_3)_2CHCH_2$, $R^3=CH_3$). The pure product was obtained in a 40% yield: $[\alpha]_D^{22}$ −33.1° (*c* 0.0136 CH_3OH); NMR (DMSO-d_6 2 mg/cm³) δ=0.85, 0.87, and 0.90 (Leu (C<u>H</u>$_3$)$_2$), 1.22 (Ala C<u>H</u>$_3$), 1.47 and 1.59 (Leu βC<u>H</u>$_2$ and γC<u>H</u>), 3.38 and 3.63 (glucosamine O<u>H</u>), 4.29 (Ala αC<u>H</u>), 4.39 (Leu αC<u>H</u>), 7.93, 8.12, 8.22, and 8.29 (CON<u>H</u> and N<u>H</u>$_2$). Found: C, 48.78; H, 7.95; N, 12.21%. Calcd for $C_{18}H_{34}O_8N_4$: C, 49.76; H, 7.80; N, 12.12%.

N-(L-*Leucyl*-L-*leucyl*-L-*phenylalanyl*)-D-*glucosamine* (*8*; $R^1=CH_2C_6H_5$, $R^2=(CH_3)_2CHCH_2$, $R^3=(CH_3)_2CHCH_2$). This pure product was obtained in a 35% yield: $[\alpha]_D^{22}$ −22.5° (*c* 0.0142 CH_3OH): NMR (DMSO-d_6 2 mg/cm³) δ=0.92 (t Leu (C<u>H</u>$_3$)$_2$), 1.44 and 1.59 (Leu βCH$_2$ and γC<u>H</u>), 2.98 (Phe βCH$_2$), 3.24, 3.30, 3.36, and 3.39 (glucosamine O<u>H</u>), 4.39 (Leu αC<u>H</u>), 4.51 (Phe αC<u>H</u>), 7.24 (Phe C_6<u>H</u>$_5$), 7.81, 8.08, 8.22, and 8.33 (CON<u>H</u> and N<u>H</u>$_2$). Found: C, 59.83; H, 8.00; N, 10.11%. Calcd for $C_{27}H_{44}O_8N_4$: C, 58.70; H, 7.94; N, 10.37%.

N-(L-*Leucyl*-L-*phenylalanyl*-L-*leucyl*)-D-*glucosamine* (*8*; $R^1=(CH_3)_2CHCH_2$, $R^2=CH_2C_6H_5$, $R^3=(CH_3)_2CHCH_2$). The pure product was obtained in a 43% yield. NMR peaks were similar to those of *N*-(L-leucyl-L-leucyl-L-phenylalanyl)-D-glucosamine. $[\alpha]_D^{22}$ −21.6° (*c* 0.0176 CH_3OH). Found: C, 58.70; H, 7.72; N, 10.19%. Calcd for $C_{27}H_{44}O_8N_4$: C, 58.70; H, 7.94; N, 10.37%.

N-(*β-Benzyl*-L-*α-aspartyl*-*β-benzyl*-L-*α-aspartyl*-*β-benzyl*-L-*α-aspartyl*)-D-*glucosamine* (*8*; $R^1=R^2=R^3=CH_2COOCH_2C_6H_5$). Elution of the chromatograph (Sephadex G-10, 2.5×45 cm) was carried out with methanol and water (1 : 1 v/v). The pure product was obtained in a 36% yield. NMR (DMSO-d_6 2 mg/cm³) δ=2.66 and 2.77 (Asp βC<u>H</u>$_2$), 3.22 and 3.59 (glucosamine O<u>H</u>), 4.35 (Asp αC<u>H</u>), 5.13 (Asp Bz C<u>H</u>$_2$), 7.39 (Asp Bz C_6<u>H</u>$_5$), 8.19 (CON<u>H</u> and N<u>H</u>$_2$). Found: C, 57.99; H, 5.49; N, 7.05%. Calcd for $C_{39}H_{46}O_{10}N_4$: C, 58.94; H, 5.70; N, 7.05%. $[\alpha]_D^{22}$ −7.35° (*c* 0.0136 CH_3OH)

We wish to thank Dr. Tatsuo Miyazawa, Professor of The University of Tokyo, and Dr, Toshiya Endo of Gunma University, for helpful advice and measurement of the NMR spectra.

References

1) A part of this work was presented at 44th; Okayama Oct.1981, and 46th; Niigata Oct. 1982, National Meeting of the Chemical Society of Japan, Abstr. Nos. 1E24 and 3N23, respectively.

2) Robert G. Spiro, "Advance in Protein Chemistry" ed by C. B. Anfinsen, John T. Edsall, and M. Richard, Academic Press, New York (1973), Vol. 27, p. 349.

3) S. Okui and S. Suzuki, *Yakugaku Zasshi*, **79**, 471. (1959).

4) S. Suzuki, *Yakugaku Zasshi*, **81**, 222, 935, 938 (1961).

5) M. Bergman, *Ber.*, **1932**, 1199.

6) J. K. N. Jones, M. B. Perry, B. Shelton, and D. J. Watson, *Can. J. Chem.*, **40**, 2229 (1962).

7) N. K. Kochetkov, V. A. Dereviskaya, L. M. Kikhosherstov, N. V. Moldtsov, and S. G. Kara-Murza., *Tetrahedron*, **18**, 273 (1962).

8) David G. Doherty, Edwin A. Popenoe, and Karl Paul Link, *J. Am. Chem. Soc.*, **75**, 3469 (1953).

9) C. H. Bamford, A. Elliott, and W. E. Hamby, "Synthetic Polypeptides," Academic Press, New York (1965), p. 62.

10) J. L. Bailey, *J. Chem. Soc.*, **1950**, 3461.

11) K. Okawa, *Bull. Chem. Soc. Jpn.*, **29**, 486 (1956).

12) Y. Iwakura, K. Uno, M. Oya, and R. Katakai, *Biopolymers*, **9**, 1419 (1970).

13) R. Katakai, M. Oya, K. Uno, and Y. Iwakura, *Biopolymers*, **10**, 2199 (1971).

14) M. Oya and T Takahashi, *Bull. Chem. Soc. Jpn.*, **54**, 2705 (1981)

15) N. Izumiya, T. Katoh, M. Ohno, and H. Aoyagi, "Peptide Gosei," Maruzen, Tokyo (1975), p. 155.

16) M. Oya, K. Uno, and Y. Iwakura, *J. Polym. Sci., A-1*, **8**, 1851, (1970).

17) NMR spectra were obtained on a JEOL JNM-PMX-60 spectrometer.

Acylations of 2,2-Dimethyl-2*H*-chromenes

Seiji YAMAGUCHI, Satoru YAMAMOTO, Shoichi ABE, and Yoshiyuki KAWASE*
Department of Chemistry, Faculty of Science, Toyama University, Gofuku 3,190, Toyama 930
(Received June 22, 1983)

Orientation in acylation reactions of 2,2-dimethyl-2*H*-chromenes was studied. Five acetylchromenes were obtained with two methods and six formylchromenes were obtained with a third method. Demethylation of four acyl-methoxy-substituted chromenes gave the corresponding acylchromenols. 2,2-Dimethyl-2*H*-chromene-6-carboxylic acid (anofinic acid) was also obtained by oxidation of 6-formylchromene.

Many naturally occurring 2,2-dimethyl-2*H*-chromenes have an acetyl group in position 6 or 8.[1] But, the introduction of acetyl groups into 2,2-dimethyl-2*H*-chromenes has not been reported, because they were easily resinified with strong acids as acylating agents. We described a new preparative method of 2,2-dimethyl-2*H*-chromenes.[2] Now, we will report the acylation reactions of 2,2-dimethyl-2*H*-chromenes by using weak acids and their orientation. Acetylations were run in two methods; Method A: with acetic anhydride–zinc chloride in benzene at room temp for 3 h, at 80 °C for 20 min in a case of recovery, or at room temp for 1 h in a case that starting chromene was much resinified; Method B: with acetic acid–trifluoroacetic anhydride at room temp for 6 h. Formylations were run in a third method; Method C: with *N*-methylformanilide–phosphoryl chloride at 90 °C for 1 h. Their acylation yields are summarized in Table 1. In these reactions, both acetylations and formylations, similar orientations were observed (Chart 1). In all 2,2-dimethyl-2*H*-chromenes, except in 5-methoxy and 6-methoxy derivatives, the position 6 was the most reactive and the position 3, expected to be a styrene system, was not so reactive. 5-Methoxy derivative (**2**) afforded 8-formyl compound (para to methoxyl group) (**7b**), 6-methoxy derivative (**3**) afforded 7-acyl compounds (ortho to methoxyl group) (**8a, b**), and 8-methoxy derivative (**5**) gave a mixture of 5-acyl compounds (para to methoxyl group) (**10a, b**) and 6-acyl compounds (the most reactive position) (**11a, b**).

The structure of the acyl compounds were chiefly determined by the coupling constants of aromatic hydrogens in their ^{1}H-NMR spectra; other evidences are described below. 6-Acyl-2,2-dimethyl-2*H*-chro-

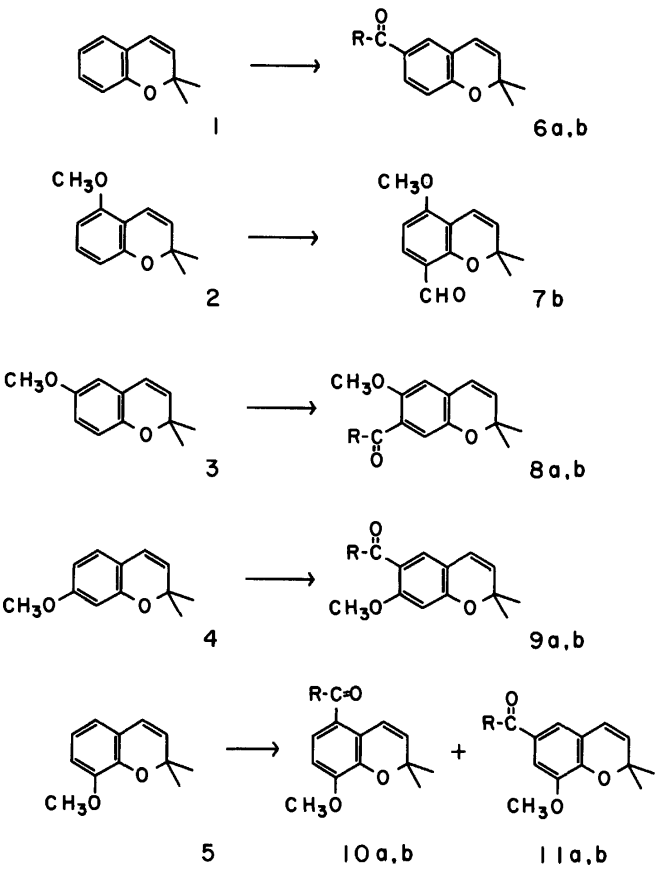

Chart 1.

Table 1. Acylations of 2,2-dimethyl-2*H*-chromenes

2,2-Dimethyl-2*H*-chromene	Acylated position	Yield/% Acetylation Method A	Acetylation Method B	Formylation Method C
1	6	64.3	64.4	39.6
2	8	0[a]	—	45.4
3	7	0[b] / 14.8[c]	35.5	51.9
4	6	8.5 / 25.4[d]	0[a]	55.3
5	5	9.7	8.2	38.2
	6	29.1	19.7	31.0

a) Only resin was obtained. b) Starting chromene was recovered. c) Acetylation was run at higher temp, 80 °C, for 20 min. d) Acetylation was run at room temp for a shorter period, 1 h.

menes (**6a ,b**) showed ortho and meta coupling in their ^{1}H-NMR spectra. There was no E.T. band due to a mesomery between C=O and C=C double bonds, such as 7-acylchromenes may show (Fig. 1). N. M. Venkama and R. G. S. Krishna reported the DDQ oxidation of 2,2,6-trimethyl-2*H*-chromene and 6-ethyl-2,2-dimethyl-2*H*-chromene to 6-formyl- and 6-acetyl-2,2-dimethyl-2*H*-chromene (**6a, b**).[3] Our compounds (**6a, b**) from 2,2-dimethyl-2*H*-chromene were identical with theirs which were obtained from the DDQ oxidation in their spectra. The structure of 8-formyl-5-methoxy-2,2-dimethyl-2*H*-chromene (**7b**) was assured by another synthetic method; dehydrogenetic cyclization of 2-hydroxy-4-methoxy-3-(3-methyl-2-butenyl)-benzaldehyde (**13**) to **7b**(Chart 2). The ^{1}H-NMR spectra of 5-acyl compounds(**10a, b**) showed two doublets with 9—10 Hz ortho coupling and deshielding by 5-acyl groups at 4-H proton.

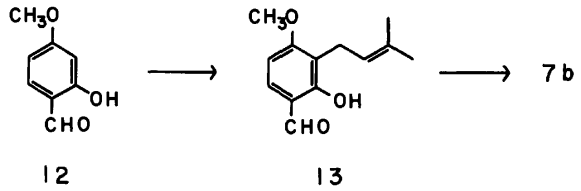

Chart 2.

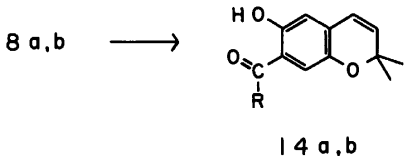

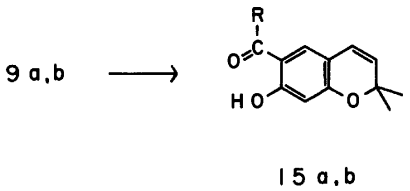

Chart 3.

Phosphoryl chloride is a weaker acid than zinc chloride or trifluoroacetic acid (derived from trifluoroacetic anhydride). Therefore, formylations could be run at higher temperatures than acetylations, and

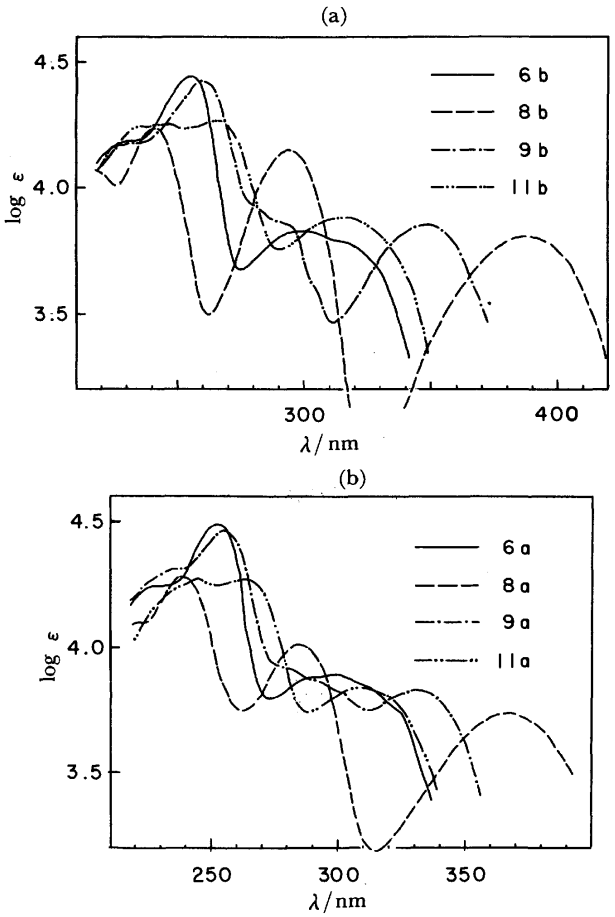

Fig. 1. (a) UV spectra of acetylchromenes, (b) UV spectra of formylchromenes.

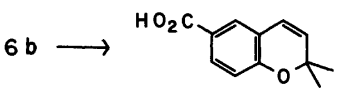

Chart 4.

Table 2. ^{1}H-NMR data of acylated chromenes

	2-H	3-H	4-H	5-H	6-H	7-H	8-H
6a	1.4 s	5.5 d(10)	6.2 d(10)	7.5 d(2)	2.4 s	7.6 dd(8+2)	6.6 d(8)
8a	1.3 s	5.6 d(10)	6.2 d(10)	6.4 s	3.8 s	2.4 s	7.0 s
9a	1.4 s	5.4 d(9)	6.2 d(9)	7.4 s	2.4 s	3.8 s	6.2 s
10a	1.4 s	5.6 d(10)	7.2 d(10)	2.4 s	7.2 d(9)	6.6 d(9)	3.8 s
11a	1.4 s	5.5 d(10)	6.2 d(10)	7.1 or 7.3 d(2)	2.4 s	7.1 or 7.3 d(2)	3.8 s
6b	1.5 s	5.8 d(10)	6.6 d(10)	7.7 d(2)	10.9 s	7.8 dd(8+2)	7.0 d(8)
7b	1.5 s	5.7 d(10)	6.7 d(10)	4.0 s	6.6 d(9)	7.6 d(9)	10.6 s
8b	1.4 s	5.9 d(10)	6.4 d(10)	6.6 s	4.0 s	10.5 s	7.3 s
9b	1.5 s	5.6 d(10)	6.5 d(10)	7.6 s	10.5 s	4.0 s	6.5 s
10b	1.6 s	7.3 d(10)	7.8 d(10)	10.3 s	8.1 d(11)	6.2 d(11)	4.2 s
11b	1.5 s	5.7 d(11)	6.4 d(11)	7.2 or 7.4 d(2)	10.0 s	7.2 or 7.4 d(2)	4.0 s

Chemical shifts: δ, in CCl_4 (Coupling constants: J/Hz).

formylations gave better yields than acetylations in all methoxy-substituted 2,2-dimethyl-2*H*-chromenes. Acetylations of 5-methoxy-2,2-dimethyl-2*H*-chromene (**2**) and 7-methoxy-2,2-dimethyl-2*H*-chromene (**4**) gave mainly resin. This result shows that the methoxyl group in 5- or 7-position enhanced the electron density in the C=C double bond and labilized 2*H*-chromenes against acids. The acetylations of 5,7-dimethoxy-2,2-dimethyl-2*H*-chromene to 6-acetyl-5,7-dimethoxy-2,2-dimethyl-2*H*-chromene (methylevodionol) or 8-acetyl-5,7-dimethoxy-2,2-dimethyl-2*H*-chromene (methylalloevodionol), as we would suppose, gave only resin.

The spectral data of **9a** and **11a** agreed with the reported data of natural methyleupariochromene[4] (encecalin[5]) and acetovanillochromene.[6] Demethylation reactions of **8a, b** and **9a, b** with anhydrous magnesium iodide gave the corresponding chromenols (**14a, b** and **15a, b**) (Chart 3); the spectral data of **15a** agreed with the reported data of natural eupariochromene.[4] Oxidation of **6b** with silver oxide gave 2,2-dimethyl-2*H*-chromene-6-carboxylic acid (**16**) (Chart 4), and its spectral data agreed with the reported data of natural anofinic acid.[7]

Experimental

The boiling points and melting points were uncorrected (in boiling points: 1 mmHg ≈133.322 Pa). The IR, UV, and ^{1}H-NMR spectra were measured on a Hitachi EPI-S2 spectrophotometer, a Hitachi 124 spectrophotometer, and a JEOL JNM-MH-60 spectrometer, respectively.

*Acetylations of 2,2-Dimethyl-2*H*-chromenes. Method A*: To a mixture of 2,2-dimethyl-2*H*-chromenes (10 mmol), zinc chloride (3.4 g, 25 mmol), and dry benzene (5 mL) was added acetic anhydride (1.0 g, 10 mmol) over a 20 min period. The mixture was stirred at room temp for 3 h, at 80 °C for 20 min, or at room temp for 1 h. After the reaction, the mixture was treated with 10% hydrochloric acid and then extracted with ether. The combined ether extracts was washed with 5% sodium hydroxide solution, and dried over anhydrous sodium sulfate. After the removal of the ether, the resulting oil was distilled to give acetylchromenes.

Method B: Under cooling in an ice-water bath, trifluoroacetic anhydride (4.2 g, 20 mmol) was added to a solution of 2,2-dimethyl-2*H*-chromenes (10 mmol) in acetic acid (1.2 g, 20 mmol). The mixture was then allowed to stand for 6 h at room temp. After the reaction, the mixture was treated with ice water, and alkalified with aqueous sodium hydrogencarbonate solution, and then extracted with ether. The ether extracts were dried over anhydrous sodium sulfate. After the removal of the ether, the resulting oil was distilled to give acetylchromenes.

*Formylations of 2,2-Dimethyl-2*H*-chromenes. Method C*: To a mixture of *N*-methylformanilide (30 g, 20 mmol) and phosphoryl chloride (4.4 g, 10 mmol), 2,2-dimethyl-2*H*-chromenes (10 mmol) were added. The mixture was then heated at 90 °C for 1 h with stirring. After cooling, the mixture was boiled with an aqueous sodium hydroxide solution (1.5 g, in 15 mL) for 1 min and then extracted with ether. The ethereal layer was washed with 10% hydrochloric acid and 5% sodium hydroxide solution, and then dried over anhydrous sodium sulfate. After the removal of the ether, the resulting oil was distilled to give formyl 2,2-dimethyl-2*H*-chromenes.

In case of the acylations of **5**, mixtures were obtained. These were separated into components, 5-acyl compounds (**10a, b**) and 6-acyl compounds (**11a, b**) by silica-gel chromatography. The yields and ^{1}H-NMR data of acyl chromenes are summarized in Tables 1 and 2, and some UV data are shown in Figs. 1a and 1b. Some other physical data are listed below.

6a, Bp 126—130 °C(4 mmHg); IR (neat): 1675 cm^{-1}.[3] **8a**, Bp *ca.* 126 °C (3 mmHg) (bath temp); mp 67—68.5 °C; IR (KBr disk): 1670 cm^{-1}; Found: C, 70.62; H, 6.67%. Calcd: C, 72.39; H, 6.94%. **9a**, Bp *ca.* 146 °C (2 mmHg) (bath temp); IR (neat): 1665 cm^{-1}; Found: C, 72.15; H, 6.93%. Calcd: C, 72.39; H, 6.94%. **10a**, Benzene-hexane eluted fractions; mp 85.5—87.5 °C (recrystallized from hexane); IR (KBr disk): 1665 cm^{-1}; UV (EtOH): 253 (log ε 4.36), 285 (4.06), 340 nm (3.60); Found: C, 72.29; H, 6.99%. Calcd: C, 72.39; H, 6.94%. **11a**, Benzene-hexane eluted fractions; mp 73—73.5 °C (recrystallized from hexane); IR (KBr disk): 1670 cm^{-1}; Found: C, 72.37; H, 6.94%. Calcd: C, 72.39; H, 6.94%. **6b**, Bp 95—103 °C (2 mmHg); IR (KBr disk): 1685 cm^{-1}.[3] **7b**, Benzene-hexane eluted fractions; bp 175—180 °C (23 mmHg); IR (neat): 1680 cm^{-1}; UV (EtOH): 264 (log ε 4.24), 277 (4.16), 291 nm (4.14); Found: C, 71.82; H, 6.46%. Calcd: C, 71.54; H, 6.47%. **8b**, Mp 87—88 °C (recrystallized from ether); IR (KBr disk): 1670 cm^{-1}; Found: C, 71.65; H, 6.52%. Calcd: C, 71.54; H, 6.47%. **9b**, Bp 130—133 °C (2 mmHg); mp 71.5—73 °C (recrystallized form cyclohexane); IR (KBr disk): 1675 cm^{-1}; Found; C, 71.29; H, 6.47%. Calcd:C, 71.54; H, 6.47%. **10b**, Benzene eluted fractions; bp 129—140 °C (5 mmHg) (bath temp); IR (neat): 1675 cm^{-1}; UV (EtOH); 252 (log ε 4.19), 293 (4.03), 347 nm (3.51); Found: C, 71.32; H, 6.57%. Calcd: C, 71.54; H, 6.47%. **11b**, Benzene eluted fractions; bp 135—150 °C (5 mmHg) (bath temp); IR (neat): 1680 cm^{-1}; Found: C, 71.29; H, 6.48%. Calcd: C, 71.54; H, 6.47%

Another Preparative Method of 7b. To a solution of 2-hydroxy-5-methoxybenzaldehyde (**12**) (2.5 g, 16.4 mmol) in dry benzene (20 mL) was added sodium hydride (53% dispersed in mineral oil; 1.5 g) and 4-bromo-2-methyl-2-butene (2.5 g, 16.8 mmol). The mixture was refluxed overnight. After the reaction, the mixture was poured into 10% hydrochloric acid, and the separated benzene layer was dried over anhydrous sodium sulfate. Removal of the benzene gave an oily residue, which was chromatographed on a silica-gel column. The benzene eluted fractions gave 2-hydroxy-4-methoxy-3-(3-methyl-2-butenyl)benzaldehyde (**13**) (217 mg, 5.8%); IR (neat): 1645 cm^{-1}; ^{1}H-NMR (CCl_4): δ=1.6 (3H, broad s), 1.7 (3H, broad s), 3.3 (2H, d, *J*=7 Hz), 3.9 (3H, S), 5.1 (1H, broad t, *J*=7 Hz), 6.5 (1H, d, *J*=9 Hz), 7.3 (1H, d, *J*=9 Hz), 9.7 (1H, s), 11.4 (1H, s). To a solution of **13** (150 mg, 0.681 mmol) in dry benzene (70 mL),DDQ (170 mg, 0.749 mmol) was added. This mixture was then refluxed for 1 h. After cooling, the mixture was filtered. The filtrate was washed with 5% sodium hydroxide solution and saturated sodium chloride aqueous solution and dried over anhydrous sodium sulfate. After removal of the benzene, the resulting oil was chromatographed on a silica-gel column. The benzene eluted fractions gave **7b** (26 mg, 17.5%). The IR and ^{1}H-NMR spectra were identical with those of **7b** from **2**.

Demethylations of 8a, b and 9a, b. In dry benzene (5 mL) and anhydrous ether (2 mL), magnesium metal (0.2 g, 8.2 mmol) was treated with iodine (1.1 g, 8.7 mmol). The mixture was slightly heated while stirring until the color disappeared. To this mixture was then added a solution of **8a, b** or **9a, b** (5 mmol) in dry benzene (10 mL). and the mixture was refluxed for 3 h with stirring. After cooling, the mixture was treated with 10% hydrochloric acid and then extracted with benzene. The benzene layer was washed with water and dried over anhydrous sodium sulfate. After removal of the benzene, the resulting oil was chromatographed on a silica-gel column . The benzene eluted fractions gave corresponding chromenols (**14a, b** or **15a, b**). **14a**, Yield:

22.1%; mp 66—68 °C (recrystallized from hexane); IR (KBr disk): 1645 cm^{-1}; UV (EtOH): 238 (log ε 4.26), 294 (4.14), 388 nm (3.68); ^{1}H-NMR (CCl_4): δ=1.4 (6H, s), 2.5(3H, s), 5.8(1H, d, J=10 Hz), 6.2 (1H, d, J=10 Hz), 6.6 (1H, s), 7.1 (1H, s), 11.8 (1H, s); Found: C, 71.63; H, 6.57%. Calcd: C, 71.54: H, 5.47%. **14b**, Yield: 20.4%; mp 97—99 °C (recrystallized from hexane); IR (KBr disk): 1645 cm^{-1}; UV (EtOH): 239 (log ε 4.23), 294 (4.16), 391 nm (3.76); ^{1}H-NMR (CCl_4): δ=1.5 (6H, s), 5.9 (1H, d, J=10 Hz), 6.4 (1H, d, J=10 Hz), 6.6 (1H, s), 7.0 (1H, s), 10.0 (1H, s), 10.8 (1H, s); Found: C, 70.68; H, 5.91%. Calcd: C, 70.57; H, 5.92%. **15a**, Yield: 43.9%; mp 72—73.5 °C (recrystallized from hexane); IR (KBr disk): 1655 cm^{-1}; UV (EtOH): 227 sh (log ε 4.16), 234 (4.27), 257 (4.54), 291 sh (3.81), 347 nm (3.79); ^{1}H-NMR (CCl_4); δ=1.5 (6H, s), 2.6 (3H, s), 5.7 (1H, d, J=10 Hz), 6.5 (1H, d, J=10 Hz), 6.5 (1H, s), 7.5 (1H, s), 13.2 (1H, s); Found: C, 71.32; H, 6.39%. Calcd: C, 71.54; H, 6.47%. **15b**, Yield: 54.2%; mp 97—99 °C (recrystallized from cyclohexane); IR (KBr disk): 1635 cm^{-1}; UV (EtOH): 228 sh (log ε 4.16), 235 (4.24), 259 (4.48), 282 sh (3.87), 293 sh (3.82), 349 nm (3.74); ^{1}H-NMR (CCl_4); δ=1.4 (6H, s), 5.5 (1H, d, J=10 Hz), 6.2 (1H, d, J=10 Hz), 6.2 (1H, s), 7.0 (1H, s), 9.6 (1H, s), 12.9 (1H, s); Found: C, 70.49; H, 5.87%. Calcd: C, 70.57; H, 5.92%.

*Oxidation of **6b** to Anofinic Acid.* To a solution of silver nitrate (2.3 g, 14.0 mmol) in water (20 mL), sodium hydroxide (1.0 g) was added. To this silver oxide suspension, a solution of **6b** (1.2 g, 6.38 mmol) in ethanol (20 mL) was added. The mixture was then refluxed for 2 h. After the reaction, the mixture was filtered. The filtrate was washed with ether and then acidified with 10% hydrochloric acid. The crystals thus obtained were collected and recrystallized from benzene-hexane (1 : 9) to give **16** (770 mg, 59.4%); mp 158.5—160 °C; IR (KBr disk): 1675 cm^{-1}; UV (EtOH): 239.5 (log ε 4.68), 280.5 (3.88), 306 (3.78), 318 nm (3.67); ^{1}H-NMR (CCl_4): δ=1.5 (6H, s), 5.8 (1H, d, J=10 Hz), 6.5 (1H, d, J=10 Hz), 7.0 (1H, d, J=9 Hz), 7.9 (1H, d, J=2 Hz), 8.1 (1H, dd, J=9+2 Hz), 10.3 (1H,s); Found: C, 70.75; H, 5.85%. Calcd: C, 70.57; H, 5.92%.

References

1) G. P. Ellis, "Chromenes, Chromanones, and Chromones," Wiley, New York, N. Y. (1976), p. 43.

2) Y. Kawase, S. Yamaguchi, H, Horita, J, Takeno, and H. Kameyama, *Bull. Chem. Soc. Jpn.*, **55**, 1153 (1982).

3) N. M. Venkama and R. G. S. Krishna, *Synthesis*, **1979**, 144; *Indian J. Chem.*, **17B**, 73 (1979).

4) T. Anthonsen, *Acta Chem. Scand.*, **23**, 3605 (1969).

5) L. F. Bjeldames and T. A. Geisman, *Phytochemistry*, **8**, 1293 (1969).

6) D. R. Taylor and J. A. Wright, *Phytochemistry*, **10**, 1665 (1971).

7) K. Shima, S. Hisada, and I. Inagaki, *Yakugaku Zasshi*, **91**, 1124 (1971).

Aliphatic Claisen Rearrangement Promoted by Organoaluminium Reagents

Kazuhiko TAKAI, Ichiro MORI, Koichiro OSHIMA,* and Hitosi NOZAKI
Department of Industrial Chemistry, Faculty of Engineering, Kyoto University, Yoshida, Sakyo-ku, Kyoto 606
(Received July 13, 1983)

Organoaluminium compounds, R_3Al, promote the Claisen rearrangement of allyl vinyl ether derivatives at room temperature under transfer of R or H as a nucleophile to the aldehydic carbon. Treatment of 1-butyl-2-propenyl vinyl ether with a hexane solution of Me_3Al (1.0 M†, 2.2 equiv) in CH_2ClCH_2Cl at 25 °C afforded 5-decen-2-ol (91% yield, E/Z=47/53), which was produced by the [3,3] sigmatropic rearrangement and successive methylation. The rearrangements with alkynylation, alkenylation, and hydrogenation are also achieved. The regular Claisen rearrangement products, or γ,δ-unsaturated aldehydes (ketones), are obtained at 25 °C in good to excellent yields with Et_2AlSPh (2.5 equiv) or the combination of Et_2AlCl (2.0 equiv) and PPh_3 (2.2 equiv).

Although aliphatic Claisen rearrangement[1] provides a means of introducing a carbon-carbon bond in a stereo- and regiospecific manner, higher temperature and longer reaction time limit the synthetic use of this reaction. Some modifications, such as amide-acetal,[2] orthoester,[3] and ester enolate method,[4] have been reported to overcome this difficulty. We report here that the treatment of simple allyl vinyl ether substrates with organoaluminium amphoteric reagents results in the [3,3] sigmatropic rearrangements under mild conditions.[5]

Addition of Lewis acid has been recently well documented as accelerating Diels-Alder reaction,[6] ene reaction,[7] and aromatic Claisen rearrangement.[8] The attempted aliphatic Claisen rearrangement in the presence of common Lewis acid, however, failed. For example, treatment of 1-butyl-2-propenyl vinyl ether (**1**) with $BF_3 \cdot OEt_2$, $TiCl_4$,[9] $SnCl_4$, or $ZnBr_2$ resulted in formation of complex mixtures containing 1-hepten-3-ol but none of the desired rearrangement products. In contrast, organoaluminium reagent, R_3Al or R_2AlSPh, proved to bring about the rearrangement at room temperature under transfer of R, H, or SPh[10] as a nucleophile to the aldehydic carbon.

Treatment of 1-butyl-2-propenyl vinyl ether (**1**) with 2.2 equiv of trimethylaluminium in 1,2-dichloroethane at 25 °C under an argon atmosphere gave 5-decen-2-ol (**2a**) in 91% yield (E/Z=47/53), this was apparently produced by the rearrangement and successive methylation. The use of triethylaluminium resulted in formation of a mixture of the corresponding ethylated alcohol **2b** (75% yield, E/Z=42/58) as well as a hydrogenated one **2c** (19% yield, E/Z=42/58). Meanwhile, the hydrogenated product was obtained exclusively with triisobutylaluminium or diisobutylaluminium hydride. The reactions between triisobutylaluminium and allyl vinyl ether substrates are shown in Table 1.

The E/Z ratios of newly developed double bonds were close to 1/1 and not affected by such solvents as hexane, benzene, dichloromethane, and 1,2-dichloroethane. In ethereal solvents like ether and THF, the reaction did not take place.

Neither methyllithium nor diethylzinc was effective for the transformation. Methylmagnesium iodide was marginal; for example, the reaction of **1** with 3 equiv of MeMgI took 2 h to be completed, affording **2a** in 78% yield (E/Z=52/48).

Because allyl vinyl ether substrates **3** and **4** gave the corresponding [3,3] sigmatropic products respectively

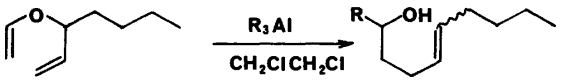

1

2a: R = CH_3
2b: R = CH_2CH_3
2c: R = H(*i*-Bu_3Al)

Scheme 1.

TABLE 1. REACTIONS BETWEEN Bu_3Al AND ALLYL VINYL ETHER SUBSTRATES[a]

Run	Ether[b] R^1	Ether[b] R^2	Conditions Temp/°C	Conditions Time/h	Yield[c] %	E/Z[d]
1	*n*-Bu	H	25	0.25	82	38/62
2	*n*-Bu	Me	25	0.25	89	45/55
3	Ph	H (**3**)	25	0.25	93	*E* only
4	H	Ph (**4**)	25	0.25	91	—
5	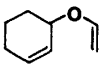		25	0.25	90	—
6	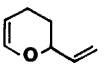		60	2	95	—
7	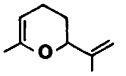		60	2	97	—
8	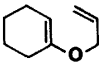		25	0.25	78	trans/cis 23/77

a) The substrates (2.0 mmol) dissolved in 1,2-dichloroethane (10 ml) were treated with a hexane solution of *i*-Bu_3Al (1.0 M, 4.4 mmol). b) Prepared by the mercury(II) acetate-catalyzed transetherification with ethyl vinyl ether (Runs 1—5). See Ref. 3b. c) Isolated yields. d) the crude prodcts were transformed into trimethylsilyl ethers whose isomeric ratios were determined by GLPC.

†1 M=1 mol dm^{-3}.

(Runs 3 and 4), the possibility of the following sequence of reactions was rejected: (1) A Lewis acid promoting C-O bond fission to give the ion pair of allylic cation and enolate ion, (2) recombination of the ion pair to afford the aldehyde, and (3) reduction of the aldehyde by i-Bu_3Al.[10]

Table 2 summarizes the reaction between trimethylaluminium and allyl vinyl ether derivatives.

Alkynyl and alkenyl groups were introduced in preference to an alkyl group, as shown in Scheme 2.

The reagent Et_2AlSPh[12] (method A) or a combination of Et_2AlCl and PPh_3 (method B) turned out to be effective for the rearrangement giving regular Claisen products, or γ,δ-unsaturated aldehydes (ketones), as shown in Table 3. The rearrangement did not occur in the presence of Et_2AlSEt, Et_2AlS^tBu, or $^iBu_2AlOPh$. Triphenylphosphine plays an important role in method B, since the reaction of **1** with diethylaluminium chloride alone afforded the same mixture of **2b** (56%, E/Z=46/54) and **2c** (12%, E/Z=48/52) as that with triethylaluminium. A similar combination of Et_2AlI and Et_3N was effective, but the yields were not so good as the yield of Et_2AlCl and PPh_3.

Almost the same yields and selectivities were obtained with Et_2AlSPh and Et_2AlCl-PPh_3 reagents.

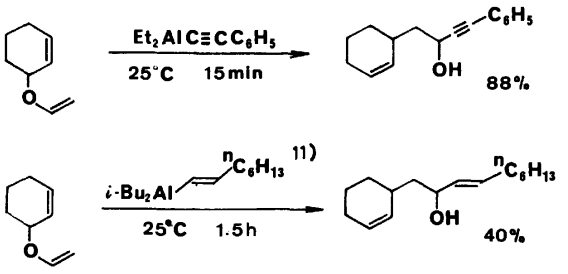

Scheme 2.

TABLE 2. REACTIONS BETWEEN Me_3Al AND ALLYL VINYL ETHER SUBSTRATES[a]

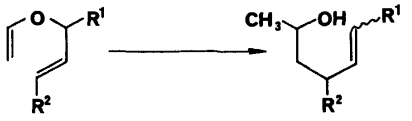

Run	Ether		Conditions		Yield[b]	E/Z[c]
	R^1	R^2	Temp/°C	Time/h	%	
1	n-Bu	H	25	0.25	91	47/53
2	Ph	H	25	0.25	78	E only
3	H	Ph	25	0.25	71	—
4	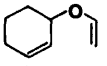		25	0.5	81	—
5	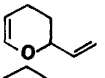		60	2	86	—
6	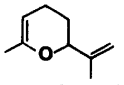		60	2	87	—

a) The substrates (2.0 mmol) dissolved in 1,2-dichloroethane (10 ml) were treated with a hexane solution of Me_3Al (1.0 M, 4.4 mmol). b) Isolated yields. c) The isomeric ratios of the corresponding trimethylsilyl ethers were determined by GLPC.

TABLE 3. CLAISEN REARRANGEMENT PROMOTED BY ORGANOALUMINIUM REAGENTS[a]

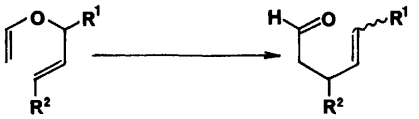

Run	Ether		Method	Time	Yield	E/Z
	R^1	R^2		h	%	
1	n-Bu	H	A[b]	0.25	84	39/61[c]
2			B[d]	0.25	81	43/57
3	n-Bu	Me	A	0.25	77	52/48[c]
4	Ph	H	A	0.5	67	E only
5	H	Ph	A	0.25	86	—
6			B	0.25	87	—
7	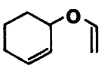		A	0.25	78	—
8	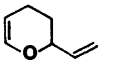		B[e]	1	61	—
9	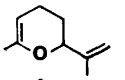		B[e]	0.5	69	—
10	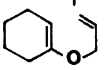		A[e]	0.5	76	—

a) Reactions were carried out in 1,2-dichloroethane at 25 °C. b) The substrates (2.0 mmol) were treated with Et_2AlSPh (5.0 mmol). c) The crude products were reduced with $LiAlH_4$ and transformed into trimethylsilyl ethers. The E/Z ratios of trimethylsilyl ethers were determined by GLPC. d) The substrates (2.0 mmol) were treated with a mixture of Et_2AlCl (4.0 mmol) and PPh_3 (4.4 mmol). e) Dichloromethane was used as a solvent.

It is worth noting that the rearrangement of 2-vinyl-3,4-dihydro-2*H*-pyran derivatives took place under extremely mild conditions (Runs 8 and 9) as compared with the pyrolysis (410—425 °C) without the catalyst described in the literature.[13]

Experimental

The IR spectra were determined on a Shimadzu IR-27-G spectrometer; the mass spectra, on a Hitachi M-80 machine; and the NMR spectra, on a Varian EM-360 spectrometer. The chemical shifts are given in δ, with TMS as the internal standard. The microanalyses were carried out at the Elemental Analyses Center of Kyoto University. 1,2-Dichloroethane and dichloromethane were dried over P_2O_5 and distilled. All the experiments were carried out under an argon atmosphere. Purification of products was performed by preparative thin-layer chromatography (TLC) or column chromatography on silica gel (Merck Kieselgel 60). Analytical GLPC was performed with a Yanagimoto GCG-550-F or Shimadzu GC-4CPT. Preparative GLPC was performed with a JEOL-JGC-20K apparatus.

Preparation of Allylic Vinyl Ethers by Transetherification.[3b] Mercury(II) acetate and ethyl vinyl ether were purified according to the literature.[14] Allylic alcohol (30 mmol), mercury(II) acetate (6.4 g, 20 mmol), and freshly distilled ethyl vinyl ether (150 ml) were boiled under reflux for 20—30 h under an argon atmosphere. The mixture was poured into 5% potassium hydroxide solution (30 ml) and extracted

with hexane. After being dried over anhydrous potassium carbonate, the solvent was evaporated. In order to remove the mercury compounds and the unreacted starting alcohol, the remaining liquid was purified by column chromatography on alumina (Merck Aluminiumoxid 90 aktiv neutral (Aktivitätsstufe III)) using hexane as an eluent.

1-Butyl-2-propenyl Vinyl Ether (1): Bp 52 °C (bath temp, 2 Torr, 1 Torr≈133.322 Pa); IR (neat): 2975, 2945, 1635, 1615, 1320, 1195, 1180, 1045, 990, 923, 825 cm^{-1}; NMR (CCl_4): δ=0.73—1.06 (m, 3H), 1.10—1.75 (m, 6H), 3.83 (d, J=6 Hz, 1H), 3.85—4.18 (m, 1H), 4.13 (d, J=15 Hz, 1H), 5.06 (d, J=11 Hz, 1H), 5.10 (d, J=15 Hz, 1H), 5.68 (ddd, J=15, 11, 6 Hz, 1H), 6.15 (dd, J=15, 6 Hz, 1H); MS m/z (%): 140 (M^+, 1), 97 (12), 96 (15), 81 (9), 55 (100), 54 (13); Found: C, 77.17; H, 11.72%. Calcd for $C_9H_{16}O$: C, 77.09; H, 11.50%.

(E)-*1-Butyl-2-butenyl Vinyl Ether*: Bp 53 °C (bath temp, 4 Torr); IR (neat): 2940, 2860, 1634, 1455, 1320, 1180, 1033, 960, 818 cm^{-1}; NMR (CCl_4): δ=0.92 (bt, J=6 Hz, 3H), 1.10—1.63 (m, 6H), 1.72 (d, J=5 Hz, 3H), 3.80 (d, J=6 Hz, 1H), 3.75—4.08 (m, 1H), 4.09 (d, J=15 Hz, 1H), 5.25 (dd, J=6, 15 Hz, 1H), 5.55 (dq, J=15, 5 Hz, 1H), 6.13 (dd, J=6, 15 Hz, 1H); MS m/z (%): 154 (M^+, trace), 111 (41), 69 (96), 55 (100); Found: C, 77.74; H, 11.94%. Calcd for $C_{10}H_{18}O$: C, 77.87; H, 11.76%.

1-Phenyl-2-propenyl Vinyl Ether (3): Bp 75 °C (bath temp, 2 Torr); IR (neat): 1645, 1620, 1500, 1462, 1320, 1188, 1172, 990, 930, 700 cm^{-1}; NMR (CCl_4): δ=3.90 (dd, J=2, 7 Hz, 1H), 4.17 (dd, J=2, 14 Hz, 1H), 5.00—5.30 (m, 3H), 5.87 (ddd, J=6, 10, 15 Hz, 1H), 6.23 (dd, J=6, 14 Hz, 1H), 7.15—7.30 (m, 5H); MS m/z (%): 160 (M^+, 7), 117 (100), 115 (24), 104 (17), 91 (40); Found: C, 82.60; H, 7.72%. Calcd for $C_{11}H_{12}O$: C, 82.46; H, 7.54%.

(E)-*3-Phenyl-2-propenyl Vinyl Ether (4)*: Bp 77 °C (bath temp, 1 Torr); IR (neat): 3040, 2870, 1640, 1620, 1500, 1457, 1320, 1194, 964, 820, 742, 692 cm^{-1}; NMR (CCl_4): δ=3.92 (dd, J=2, 6 Hz, 1H), 4.12 (dd, J=2, 15 Hz, 1H), 4.29 (d, J=5 Hz, 2H), 6.15 (dt, J=15, 5 Hz, 1H), 6.36 (dd, J=10, 15 Hz, 1H), 6.53 (d, J=15 Hz, 1H), 7.06—7.40 (m, 5H); MS m/z (%): 160 (M^+, 3), 117 (100), 115 (29), 91 (19); Found: C, 82.60; H, 7.67%. Calcd for $C_{11}H_{12}O$: C, 82.46; H, 7.55%.

2-Cyclohexenyl Vinyl Ether:[14] Bp 53 °C (bath temp, 18 Torr); IR (neat): 2940, 1635, 1612, 1190, 1065, 1012, 810 cm^{-1}; NMR (CCl_4): δ=1.00—2.23 (m, 6H), 3.97 (dd, J=1, 6 Hz, 1H), 4.22 (dd, J=1, 17 Hz, 1H), 4.20—4.47 (m, 1H), 5.70—5.98 (m, 2H), 6.36 (dd, J=6, 17 Hz, 1H); MS m/z (%): 124 (M^+, 6), 82 (13), 81 (100), 80 (37), 79 (43), 53 (23).

2-Vinyl-3,4-dihydro-2H-pyran:[13] Dry DMSO (50 ml) was added at 25 °C by a syringe to the washed sodium hydride (4.0 g of a 60% mineral oil dispersion, 0.10 mol). The mixture was heated at 75 °C and stirred until the hydrogen evolution ceased (*ca.* 1 h). Then, a solution of methyltriphenylphosphonium bromide (35.7 g, 0.10 mol) in warm DMSO (100 ml) was added to the methylsulfinylmethanide ion solution at 0 °C. The resulting greenish red solution was stirred at 25 °C for 15 min before freshly distilled acrylaldehyde dimer (11.2 g, 0.10 mol) was added at 25 °C. An immediate color change was observed. After stirring at 25 °C for 1 h, the reaction mixture was diluted with cold water (300 ml). The solids were removed by filtration and washed with pentane (3×100 ml). The concentrated crude product was distilled to afford the title compound (3.7 g, 34%) as a colorless liquid: Bp 57 °C (20 Torr); IR (neat): 3060, 2920, 2850, 1650, 1428, 1235, 1060, 985, 918, 900, 722 cm^{-1}; NMR (CCl_4): δ=1.47—2.13 (m, 4H), 4.09—4.32 (m, 1H), 4.45—4.63 (m, 1H), 5.03 (ddd, J=11, 10 Hz, 1H), 5.17 (ddd, J=1, 1, 15 Hz, 1H), 5.79 (ddd, J=4, 10, 15 Hz, 1H), 6.23 (d, J=6 Hz, 1H); MS m/z (%): 110 (M^+, 75), 95 (21), 92 (20), 81 (41), 79 (50), 54 (100).

2-Isopropenyl-6-methyl-3,4-dihydro-2H-pyran:[13] This material was prepared from methacrylaldehyde dimer as described for 2-vinyl-3,4-dihydro-2*H*-pyran in 63% yield as a colorless liquid: Bp 74 °C (28 Torr); IR (neat): 3080, 2960, 1722, 1684, 1655, 1462, 1440, 1380, 1238, 1045, 890, 800 cm^{-1}; NMR (CCl_4): δ=1.20—2.20 (m, 4H), 1.69 (s, 3H), 1.74 (s, 3H), 4.10 (dd, J=3, 8 Hz, 1H), 4.27—4.40 (bt, J=3 Hz, 1H), 4.78 (s, 1H), 4.89 (s, 1H); MS m/z (%): 138 (M^+, 12), 98 (20), 95 (90), 71 (49), 68 (100).

Allyl 1-Cyclohexenyl Ether:[15] To a stirred solution of Et_2AlI (1.2 M of a toluene solution, 4.2 ml, 5.0 mmol) and triethylamine (1.0 g, 10 mmol) in dichloromethane (20 ml) was added at 0 °C a dichloromethane solution of cyclohexanone diallyl acetal (0.98 g, 5.0 mmol). After stirring at 25 °C for 5 h, the resulting mixture was poured into 6 M sodium hydroxide solution (20 ml) and extracted with ether. The ethereal layer was washed with sat. sodium hydrogencarbonate (20 ml), dried over potassium carbonate, and concentrated. The crude product was purified by column chromatography on alumina (hexane-ether, 10 : 1) to give the ether (0.40 g, 58%) as a colorless liquid: Bp 72 °C (bath temp, 9 Torr); IR (neat): 2970, 1685, 1382, 1338, 1270, 1084, 910, 778 cm^{-1}; NMR (CCl_4): δ=1.33—1.80 (m, 4H), 1.80—2.14 (m, 4H), 4.05 (d, J=5 Hz, 2H), 4.44 (bt, J=4 Hz, 1H), 5.05 (d, J=10 Hz, 1H), 5.20 (d, J=15 Hz, 1H), 5.86 (ddt, J=10, 15, 5 Hz, 1H); MS m/z (%): 138 (M^+, 21), 109 (19), 105 (38), 95 (20), 94 (35), 79 (26), 55 (35), 41 (100).

Reactions between Triisobutylaluminium and Allyl Vinyl Ether Derivatives. A hexane solution of triisobutylaluminium (1.0 M, 5.0 ml, 5.0 mmol) was added to a solution of an allyl vinyl ether (2.0 mmol) in 1,2-dichloroethane (15 ml) at 25 °C under an argon atmosphere and the whole was stirred at 25 °C (60 °C) for 15 min (2 h). The mixture was diluted with ether (15 ml) and poured into 1 M hydrochloric acid (20 ml). The separated organic layer was washed with brine (2×20 ml), dried over anhydrous sodium sulfate, and concentrated. The crude product was purified by silica-gel column chromatography (hexane-ethyl acetate).

(E)- *and* (Z)-*4-Nonen-1-ol (2c)*: The crude product generated from 1-butyl-2-propenyl vinyl ether (**1**) and triisobutylaluminium was transformed into trimethylsilyl ether with *N*-(trimethylsilyl)imidazole (1.2 equiv) in dichloromethane. GLPC (5% PEG 20M, 2 m, 65 °C) indicated two peaks, T_r=16.0 min ((*Z*)-isomer, 62%) and T_r=17.5 min ((*E*)-isomer, 38%). The analytically pure samples of both isomers were prepared by preparative GLPC (20% PEG 20 M). These samples were identical to the authentic samples.[16] (*E*)-Alcohol: Bp 76 °C (bath temp, 5 Torr); IR (neat): 3350, 2940, 1470, 1380, 1055, 965 cm^{-1}; NMR (CCl_4); δ=0.90 (bt, J=6 Hz, 3H), 1.16—1.70 (m, 7H), 1.80—2.18 (m, 4H), 3.53 (t, J=7 Hz, 2H), 5.23—5.42 (m, 2H); MS m/z (%): 124 (M^+-H_2O, 17), 96 (27), 95 (42), 82 (51), 81 (100), 69 (32), 68 (97), 67 (65), 55 (69). (*Z*)-Alcohol: Bp 80 °C (bath temp, 5 Torr); IR (neat): 3350, 2950, 1475, 1380, 1060 cm^{-1}; NMR (CCl_4); δ=0.90 (bt, J=6 Hz, 3H), 1.04—1.78 (m, 7H), 1.80—2.23 (m, 4H), 3.52 (t, J=7 Hz, 2H), 5.05—5.48 (m, 2H); MS m/z (%): 124 (M^+-H_2O, 11), 96 (26), 95 (40), 82 (45), 81 (90), 68 (87), 67 (78), 55 (95), 41 (100).

(E)- *and* (Z)-*3-Methyl-4-nonen-1-ol*: GLPC analysis (10% PEG 20 M, 2 m, 100 °C) of the corresponding trimethylsilyl ethers indicated two peaks, T_r=20.0 min ((*E*)-isomer, 45%), T_r=17.9 min ((*Z*)-isomer, 55%). (*E*)-Alcohol: Bp 78 °C (bath temp, 1 Torr); IR (neat): 3350, 2990, 2950, 1460, 1376, 1050, 970 cm^{-1}; NMR (CCl_4): δ=0.88 (bt, 3H), 0.98 (d, J=6 Hz, 3H), 1.23—1.65 (m, 7H), 1.90—2.10 (m, 2H), 2.12—2.35 (m, 1H), 3.50 (t, J=7 Hz, 2H), 5.10—5.40 (m, 2H); MS m/z (%): 156 (M^+, 2), 138 (4), 109 (30), 95 (38), 81 (100), 69 (89); Found: C, 76.69; H, 13.20%. Calcd for $C_{10}H_{20}O$: C, 76.86; H, 12.90%. (*Z*)-Alcohol: Bp 75 °C (bath temp, 2 Torr); IR (neat): 3360, 2980, 2940, 1462, 1052, 1000, 968 cm^{-1}; NMR (CCl_4):

δ=0.78—1.05 (m, 6H), 1.10—1.55 (m, 7H), 1.80—2.18 (m, 2H), 2.35—2.85 (m, 1H), 3.46 (t, J=6 Hz, 2H), 4.85—5.40 (m, 2H); MS m/z (%): 156 (M^+, 3), 138 (5), 109 (32), 95 (33), 81 (100), 69 (84); Found: m/z 156.1572. Calcd for $C_{10}H_{20}O$: M, 156.1515.

(E)-*5-Phenyl-4-penten-1-ol*:[17] Bp 123 °C (bath temp, 1 Torr); IR (neat): 3325, 2940, 1600, 1498, 1450, 1050, 960, 735, 688 cm^{-1}: NMR (CCl_4); δ=1.70 (tt, J=7, 7 Hz, 2H), 1.83 (s, 1H), 2.25 (dt, J=6, 7 Hz, 2H), 3.57 (t, J=6 Hz, 2H), 6.06 (dt, J=15, 6 Hz, 1H), 6.33 (d, J=15 Hz, 1H), 7.00—7.33 (m, 5H); MS m/z (%): 162 (M^+, 43), 144 (22), 143 (23), 129 (100), 117 (59), 91 (46).

3-Phenyl-4-penten-1-ol: Bp 103 °C (bath temp, 2 Torr); IR (neat): 3350, 2950, 1642, 1608, 1500, 1460, 1048, 1026, 915, 702 cm^{-1}; NMR (CCl_4): δ=1.23 (s, 1H), 1.87 (dt, J=6, 6 Hz, 2H), 3.23—3.65 (m, 3H), 4.94 (ddd, J=1.5, 1.5, 10 Hz, 1H), 4.95 (ddd, J=1.5, 1.5, 17 Hz, 1H), 5.89 (ddd, J=7, 10, 17 Hz, 1H), 6.90—7.50 (m, 5H); MS m/z (%): 162 (M^+, 60), 144 (40), 143 (27), 129 (89), 117 (100), 115 (49), 91 (44); Found: C, 81.20; H, 8.74%. Calcd for $C_{11}H_{14}O$: C, 81.44; H, 8.70%.

3-(2-Hydroxyethyl)-1-cyclohexene:[18] Bp 80 °C (bath temp, 1 Torr); IR (neat): 3325, 2920, 1650, 1450, 1045, 784, 715 cm^{-1}; NMR (CCl_4); δ=1.03—2.33 (m, 10H), 3.74 (t, J=6 Hz, 2H), 5.33—5.70 (m, 2H); MS m/z (%): 126 (M^+, 1), 108 (48), 93 (78), 81 (45), 80 (33), 79 (100), 67 (30).

4-Hydroxymethyl-1-cyclohexene: Bp 75 °C (bath temp, 2 Torr); IR (neat): 3340, 3040, 2925, 1658, 1440, 1090, 1020, 965, 784 cm^{-1}; NMR (CCl_4); δ=1.10—2.53 (m, 8H), 3.40 (d, J=6 Hz, 2H), 5.56 (s, 2H); MS m/z (%): 112 (M^+, 1), 94 (28), 81 (24), 79 (100), 53 (23); Found: m/z 112.0904. Calcd for $C_7H_{12}O$: M, 112.0888.

4-(1-Hydroxyethyl)-2-methyl-1-cyclohexanol: Bp 75 °C (bath temp, 2 Torr); IR (neat): 3360, 2920, 1445, 1380, 1080, 930, 782 cm^{-1}; NMR (CCl_4); δ=1.14 (d, J=6 Hz, 3H), 1.00—2.15 (m, 8H), 1.62 (s, 3H), 3.54 (dq, J=6, 6 Hz, 1H), 5.30 (s, 1H); MS m/z (%): 140 (M^+, 2), 122 (10), 107 (35), 93 (100), 79 (36), 67 (31); Found: m/z 140.1209. Calcd for $C_9H_{16}O$: M, 140.1202.

cis-*and* trans-*2-Allyl-1-cyclohexene*: TLC analysis (hexane-ethyl acetate, 5 : 1) of the product derived from the reaction of allyl 1-cyclohexenyl ether and triisobutylaluminium showed two spots, R_f=0.42 (cis-isomer, 77%) and R_f=0.33 (trans-isomer, 23%). Analytically pure samples of both isomers were prepared by preparative TLC (hexane-ethyl acetate, 5 : 1). *cis*-Isomer:[19] Bp 90 °C (bath temp, 12 Torr); IR (neat): 3400, 3100, 2940, 1647, 1452, 1260, 975, 906, 785 cm^{-1}; NMR (CCl_4): δ=1.03—1.87 (m, 10H), 1.87—2.20 (m, 2H), 3.72—3.87 (bm, 1H), 4.90 (d, J=10 Hz, 1H), 4.93 (d, J=16 Hz, 1H), 5.71 (ddt, J=10, 16, 6 Hz, 1H); MS m/z (%): 140 (M^+, trace), 122 (54), 107 (35), 98 (79), 93 (45), 81 (100). *trans*-Isomer:[19] Bp 94 °C (bath temp, 12 Torr); IR (neat): 3350, 3075, 2940, 1640, 1450, 1055, 1030, 990, 902 cm^{-1}; NMR (CCl_4): δ=0.90—2.10 (m, 11H), 2.25—2.60 (m, 1H), 2.97—3.32 (m, 1H), 5.90 (d, J=10 Hz, 1H), 5.93 (d, J=16 Hz, 1H), 5.95 (ddt, J=10, 16, 6 Hz, 1H); MS m/z (%): 140 (M^+, trace), 122 (41), 107 (17), 98 (55), 93 (43), 81 (100), 67 (43).

Reactions between Trimethylaluminium and Allyl Vinyl Ether Derivatives. A solution of an allyl vinyl ether substrate (2.0 mmol) in 1,2-dichloroethane (15 ml) was treated with a hexane solution of trimethylaluminium (1.0 M, 4.4 ml, 4.4 mmol) at 25 °C (60 °C) for 15 min (2 h). The resulting mixture was diluted with ether (15 ml), and poured into 1 M hydrochloric acid (20 ml). The ethereal extracts were washed with brine (2×20 ml), dried over anhydrous sodium sulfate, and concentrated. The crude product was purified by silica-gel column chromatography (hexane-ethyl acetate).

(E)- *and* (Z)-*5-Decen-2-ol* (**2a**): The product was converted into trimethylsilyl ether, whose E/Z ratio was determined by GLPC (5% PEG 20 M, 2 m, 75 °C). GLPC showed a peak at 11.2 min, corresponding to (*Z*)-1-methyl-3-nonenyl trimethylsilyl ether (53%) and a peak at 12.3 min, corresponding to the (*E*)-isomer (47%). The authentic samples of both isomers were prepared by methylation of (*E*)- and (*Z*)-4-nonenal with MeMgI in THF. (*E*)-Alcohol: Bp 83 °C (bath temp, 5 Torr); IR (neat): 3350, 2940, 1470, 1460, 1375, 1120, 1080, 966 cm^{-1}; NMR (CCl_4); δ=0.89 (bt, J=5 Hz, 3H), 1.13 (d, J=6 Hz, 3H), 1.10—1.60 (m, 7H), 1.80—2.18 (m, 4H), 3.66 (tq, J=6, 6 Hz, 1H), 5.23—5.42 (m, 2H); MS m/z (%): 156 (M^+, 12), 138 (19), 109 (26), 95 (88), 82 (82), 81 (72), 71 (54), 68 (57), 67 (100); Found: C, 76.81; H, 13.09%. Calcd for $C_{10}H_{20}O$: C, 76.86; H, 12.90%. (*Z*)-Alcohol: Bp 59 °C (bath temp, 1 Torr); IR (neat): 3370, 2950, 1465, 1378, 1124, 1078, 955 cm^{-1}; NMR (CCl_4): δ=0.90 (bt, J=5 Hz, 3H), 1.13 (t, J=6 Hz, 3H), 1.10—1.53 (m, 7H), 1.80—2.20 (m, 4H), 3.68 (tq, J=6, 6 Hz, 1H), 5.07—5.47 (m, 2H); MS m/z (%): 156 (M^+, 9), 138 (11), 109 (17), 95 (58), 82 (58), 81 (56), 67 (90), 55 (79), 45 (100); Found: C, 76.74; H, 13.07%. Calcd for $C_{10}H_{20}O$: C, 76.86; H, 12.90%.

(E)-*6-Phenyl-5-hexen-2-ol*:[20] Bp 118 °C (bath temp, 1 Torr); IR (neat): 3375, 2950, 1602, 1498, 1452, 1125, 1068, 960, 740, 690 cm^{-1}; NMR (CCl_4): δ=1.13 (d, J=6 Hz, 3H), 1.40—1.70 (m, 2H), 1.80 (s, 1H), 2.15—2.43 (m, 2H), 3.74 (tq, J=6, 6 Hz, 1H), 6.05 (dt, J=15, 6 Hz, 1H), 6.30 (d, J=15 Hz, 1H), 7.00—7.30 (m, 5H); MS m/z (%): 176 (M^+, 30), 158 (13), 143 (32), 129 (100), 118 (31), 117 (45).

4-Phenyl-5-hexen-2-ol: Bp 86 °C (bath temp, 1 Torr); IR (neat): 3350, 3150, 3050, 1602, 1496, 1125, 910, 705 cm^{-1}; NMR (CCl_4): δ=1.08, 1.14 (d, J=6 Hz, total 3H diastereomeric mixture), 1.20 (bs, 1H), 1.73 (t, J=7 Hz, 2H), 3.16—3.90 (m, 2H), 4.80—5.20 (m, 2H), 5.60—6.25 (m, 1H), 6.88—7.30 (m, 5H); MS m/z (%): 176 (M^+, 1), 158 (13), 143 (50), 132 (53), 129 (23), 118 (26), 117 (100), 91 (16); Found: C, 81.88; H, 9.21%. Calcd for $C_{12}H_{16}O$: C, 81.77; H, 9.15%.

1-(2-Cyclohexenyl)-2-propanol: Bp 78 °C (bath temp, 1 Torr); IR (neat): 3350, 2940, 1650, 1450, 1372, 1126, 1014, 716, 672 cm^{-1}; NMR (CCl_4): δ=1.18 (d, J=6 Hz, 3H), 1.08-2.43 (m, 10H), 3.70—4.00 (m, 1H), 5.38—5.70 (m, 2H); MS m/z (%): 140 (M^+, 1), 122 (86), 107 (91), 93 (52), 81 (100), 79 (74); Found: C, 76.90; H, 11.79%. Calcd for $C_9H_{16}O$: C, 77.09; H, 11.50%.

4-(1-Hydroxyethyl)-1-cyclohexanol: Bp 70 °C (bath temp, 1 Torr); IR (neat): 3360, 3040, 2910, 1658, 1440, 1370, 1136, 1060, 942, 854, 650 cm^{-1}; NMR (CCl_4): δ=1.15 (d, J=6 Hz, 3H), 1.10—2.30 (m, 8H), 3.50 (q, J=6 Hz, 1H), 5.57 (s, 2H); MS m/z (%): 126 (M^+, trace), 108 (27), 93 (32), 79 (100), 78 (20), 67 (28); Found: C, 75.94; H, 11.44%. Calcd for $C_8H_{14}O$: C, 76.14; H, 11.18%.

4-(1-Hydroxy-1-methylethyl)-2-methyl-1-cyclohexanol: Bp 97 °C (bath temp, 2 Torr); IR (neat): 3390, 2980, 2925, 1440, 1378, 1150, 940, 910, 785 cm^{-1}; NMR (CCl_4): δ=1.13 (s, 6H), 1.10—2.27 (m, 8H), 1.60 (s, 3H), 5.30 (s, 1H); MS m/z (%): 154 (M^+, trace), 136 (16), 121 (21), 93 (86), 92 (36), 81 (32), 59 (100); Found: m/z 154.1352. Calcd for $C_{10}H_{18}O$: M, 154.1358.

(E)- *and* (Z)-*6-Undecen-3-ol* (**2b**): The reaction was carried out with triethylaluminium as described for trimethylaluminium to give the mixture of (*E*)- and (*Z*)-4-nonen-1-ol (**2c**) and the ethylated alcohols **2b**. The crude product was separated by preparative TLC (hexane-ether, 5 : 1). The isomeric alcohols **2b** were transformed into trimethylsilyl ethers. GLPC analysis (5% PEG 20 M, 2 m, 75 °C) of the trimethylsilyl ethers showed two peaks, T_r=19.8 min ((*E*)-isomer, 42%) and T_r=18.2 min ((*Z*)-isomer, 58%). The authentic samples of both isomers were prepared by ethylation of (*E*)- and (*Z*)-4-nonenal with EtMgBr in THF. (*E*)-Alcohol: Bp 79 °C (bath temp, 3 Torr); IR (neat): 3360, 2960, 1470, 970 cm^{-1}; NMR (CCl_4); δ=0.91 (t, J=7 Hz, 6H), 1.15—1.58 (m,

8H), 1.68 (s, 1H), 1.80—2.23 (m, 4H), 3.39 (tt, J=6, 6 Hz, 1H), 5.23—5.43 (m, 2H); MS m/z (%): 170 (M^+, 2), 152 (11), 123 (14), 109 (25), 96 (42), 81 (74), 67 (100); Found: C, 77.49; H, 13.24%. Calcd for $C_{11}H_{22}O$: C, 77.58; H, 13.02%. (*Z*)-Alcohol: Bp 68 °C (bath temp, 1 Torr); IR (neat): 3350, 2940, 1460, 1114, 964 cm^{-1}; NMR (CCl_4): δ=0.93 (t, J=7 Hz, 6H), 1.06—1.62 (m, 9H), 1.83—2.24 (m, 4H), 3.44 (tt, J=6, 6 Hz, 1H), 5.10—5.46 (m, 2H); MS m/z (%): 170 (M^+, 1), 123 (10), 109 (18), 96 (33), 81 (61), 67 (100); Found: C, 77.36; H, 13.30%. Calcd for $C_{11}H_{22}O$: C, 77.58; H, 13.02%.

1-(2-Cyclohexenyl)-4-phenyl-3-butyn-2-ol: To a stirred hexane solution of PhC≡CLi prepared from phenylacetylene (0.51 g, 5.0 mmol) and butyllithium (1.5 M of a hexane solution, 3.3 ml, 5.0 mmol) was added at 0 °C a hexane solution of diethylaluminium chloride (1.0 M, 5.0 ml, 5.0 mmol) and the whole was stirred at 25 °C for 20 min. After addition of 1,2-dichloroethane (15 ml), a solution of 2-cyclohexenyl vinyl ether (0.25 g, 2.0 mmol) in 1,2-dichloroethane (4 ml) was added to the aluminium reagent at 25 °C and the mixture was stirred for 15 min. After the usual workup, the crude product was purified by preparative TLC (hexane-ether, 5 : 1) to give the desired adduct in 88% yield (0.40 g) as a pale yellow liquid: Bp 130 °C (bath temp, 0.1 Torr); IR (neat): 3320, 2920, 2350, 1650, 1600, 1490, 1442, 1012, 750, 686 cm^{-1}; NMR (CCl_4): δ=1.05—2.62 (m, 10H), 4.16 (t, J=7 Hz, 1H), 5.46—5.74 (m, 2H), 7.13—7.50 (m, 5H); MS m/z (%): 226 (M^+, 1), 225 (12), 183 (19), 167 (19), 131 (100), 103 (25), 95 (35); Found: C, 84.87; H, 8.01%. Calcd for $C_{16}H_{18}O$: C, 84.91; H, 8.02%.

1-(2-Cyclohexenyl)-3-decen-1-ol: A solution of 2-cyclohexenyl vinyl ether (0.25 g, 2.0 mmol) in 1,2-dichloroethane (15 ml) was treated at 25 °C for 1.5 h with a hexane solution of (*E*)-1-octenyldiisobutylaluminium prepared from 1-octyne (0.60 g, 5.5 mmol) and diisobutylaluminim hydride (3.2 ml of a 1.7 M toluene solution, 5.5 mmol). After the usual workup and purification by silica-gel column chromatography gave the title alcohol in 40% yield (0.19 g) as a colorless liquid: Bp 95 °C (bath temp, 0.05 Torr); IR (neat): 3350, 2925, 1450, 960, 715 cm^{-1}; NMR (CCl_4); δ=0.89 (bt, J=6 Hz, 3H), 1.06—2.35 (m, 20H), 4.06 (dt, J=6, 6 Hz, 1H), 5.33—5.70 (m, 4H); MS m/z (%): 236 (M^+, 14), 218 (33), 151 (66), 134 (46), 109 (41), 95 (87), 94 (69), 81 (100); Found: C, 81.21; H, 12.05%. Calcd for $C_{16}H_{28}O$: C, 81.29; H, 11.94%.

Claisen Rearrangement of Allyl Vinyl Ether Derivatives Promoted by Et_2AlSPh (Method A). A solution of thiophenol (0.55 g, 5.0 mmol) in hexane (3 ml) was added at 25 °C to a hexane solution of triethylaluminium (1.0 M, 5.0 ml, 5.0 mmol) and the mixture was stirred at the same temperature for 20 min. After an addition of 1,2-dichloroethane (5 ml), a solution of allyl vinyl ether substrate (2.0 mmol) in 1,2-dichloroethane (3 ml) was added to the aluminium reagent at 25 °C and the whole was stirred for an appropriate time, as listed in Table 3. The reaction mixture was diluted with ether (20 ml) and poured into 1 M hydrochloric acid. The organic layer was separated, combined with three additional extracts of the aqueous layer, and washed with brine (2×20 ml). The ethereal layer was dried over anhydrous sodium sulfate and concentrated. The crude product was purified by column chromatography or preparative TLC (hexane-ethyl acetate).

Claisen Rearrangement of Allyl Vinyl Ether Derivatives Promoted by Et_2AlCl-PPh_3 System (Method B). A mixture of Et_2AlCl (1.0 M of hexane solution, 4.0 ml, 4.0 mmol) and triphenylphosphine (1.2 g, 4.4 mmol) was dissolved in 1,2-dichloroethane (5 ml) at 25 °C and stirred for 10 min. A solution of allyl vinyl ether substrate (2.0 mmol) in 1,2-dichloroethane (10 ml) was added to the reagent at 25 °C and the whole was stirred at the same temperature for an appropriate time, as listed in Table 3. The resulting mixture was diluted with ether (20 ml) and poured into 1 M hydrochloric acid (20 ml). The separated organic layer was washed with brine (2×20 ml), dried over anhydrous sodium sulfate, and concentrated. The crude product was purified by column chromatography or preparative TLC (hexane-ethyl acetate).

A small aliquot was treated with diisobutylaluminium hydride to yield the alcohols. The *E*/*Z* ratios of these aldehydes were calculated from GLPC peak area of the corresponding trimethylsilyl ethers of the alcohols.

(E)-*4-Nonenal*:[16] Bp 80 °C (bath temp, 2 Torr); IR (neat): 2940, 2725, 1730, 1470, 968 cm^{-1}; NMR (CCl_4); δ=0.91 (t, J=6 Hz, 3H), 1.06—1.50 (m, 4H), 1.76—2.13 (m, 2H), 2.13—2.53 (m, 4H), 5.20—5.43 (m, 2H), 9.66 (s, 1H); MS m/z (%): 140 (M^+, trace), 122 (8), 98 (20), 96 (35), 84 (100), 83 (49), 67 (43).

(Z)-*4-Nonenal*:[16] Bp 76 °C (bath temp, 2 Torr); IR (neat): 2970, 2940, 2720, 1730, 1470, 1415, 1055 cm^{-1}; NMR (CCl_4): δ=0.93 (t, J=6 Hz, 3H), 1.10—1.50 (m, 4H), 1.80—2.16 (m, 2H), 2.16—2.52 (m, 4H), 5.15—5.45 (m, 2H), 9.69 (s, 1H); MS m/z (%): 140 (M^+, trace), 122 (5), 98 (12), 96 (19), 84 (49), 67 (33), 55 (64), 41 (100).

(E)-*3-Methyl-4-nonenal*: Bp 72 °C (bath temp, 2 Torr); IR (neat): 3010, 2960, 2750, 1740, 1466, 1385, 976 cm^{-1}; NMR (CCl_4): δ=0.75—1.05 (m, 3H), 1.03 (d, J=6 Hz, 3H), 1.05—1.40 (m, 4H), 1.83—2.00 (m, 2H), 2.17—2.33 (m, 2H), 2.40—2.87 (m, 1H), 5.20—5.40 (m, 2H), 9.60 (t, J=2 Hz, 1H); MS m/z (%): 154 (M^+, 4), 111 (22), 110 (20), 98 (74), 97 (99), 69 (89), 55 (100); Found: C, 77.97; H, 11.86%. Calcd for $C_{10}H_{18}O$: C, 77.87, H, 11.76%.

(Z)-*3-Methyl-4-nonenal*: Bp 70 °C (bath temp, 2 Torr); IR (neat): 2960, 2700, 1728, 1455, 1255, 725 cm^{-1}; NMR (CCl_4): δ=0.76—1.08 (m, 3H), 1.04 (d, J=6 Hz, 3H), 1.13—1.60 (m, 4H), 1.90—2.07 (m, 2H), 2.30 (dd, J=2, 7 Hz, 2H), 2.75—3.18 (m, 1H), 5.08—5.45 (m, 2H), 9.57 (t, J=2 Hz, 1H); MS m/z (%): 154 (M^+, 2), 139 (10), 111 (20), 110 (20), 98 (67), 97 (83), 69 (85), 55 (100); Found: C, 77.94; H, 11.98%. Calcd or $C_{10}H_{18}O$: C, 77.87; H, 11.76%.

(E)-*5-Pheyl-4-pentenal*: Bp 118 °C (bath temp, 2 Torr); IR (neat): 3050, 2920, 2840, 2740, 1725, 1602, 1498, 1452, 962, 742, 690 cm^{-1}; NMR (CCl_4): δ=2.40—2.60 (m, 4H), 6.03 (m, 1H), 6.34 (d, J=15 Hz, 1H), 7.00—7.30 (m, 5H), 9.70 (s, 1H); MS m/z (%): 160 (M^+, 38), 132 (11), 129 (11), 117 (37), 104 (100), 91 (39). The compound was identical with the authentic sample.[21]

3-Phenyl-4-pentenal: Bp 86 °C (bath temp, 3 Torr); IR (neat): 3050, 2840, 2740, 1730, 1498, 1460, 915, 758, 700 cm^{-1}; NMR (CCl_4): δ=2.69 (dd, J=2, 6 Hz, 2H), 3.85 (dq, J=6, 6 Hz, 1H), 4.93 (d, J=16 Hz, 1H), 4.98 (d, J=10 Hz, 1H), 5.90 (ddd, J=6, 10, 16 Hz, 1H), 6.97—7.30 (m, 5H), 9.57 (s, 1H); MS m/z (%): 160 (M^+, 24), 142 (32), 132 (24), 131 (27), 117 (100), 115 (36), 91 (43); Found: C, 82.62; H, 7.59%. Calcd for $C_{11}H_{12}O$: C, 82.46; H, 7.55%.

3-Cyclohexene-1-carbaldehyde:[13] Bp 97 °C (bath temp, 20 Torr); IR (neat): 2940, 2710, 1732, 1662, 1442, 1372, 1240, 1044 cm^{-1}; NMR (CCl_4): δ=1.00—2.53 (m, 6H), 5.57 (s, 1H), 9.55 (s, 1H); MS m/z (%): 110 (M^+, 72), 95 (28), 92 (37), 81 (78), 79 (100), 67 (41), 54 (51), 53 (52).

4-Acetyl-2-methyl-1-cyclohexene:[13] Bp 88 °C (bath temp, 25 Torr); IR (neat): 2940, 1718, 1445, 1358, 1168, 775 cm^{-1}; NMR (CCl_4): δ=1.10—2.60 (m, 7H), 1.63 (s, 3H), 2.06 (s, 3H), 5.28 (s, 1H); MS m/z (%): 138 (M^+, 10), 95 (100), 79 (16), 67 (28), 43 (65).

2-Cyclohexene-1-acetaldehyde:[18] Bp 75 °C (bath temp, 20 Torr); IR (neat): 3040, 2950, 2740, 1730, 1445, 720 cm^{-1}; NMR (CCl_4): δ=1.03—2.10 (m, 6H), 2.30 (dt, J=1, 6 Hz, 1H), 2.38 (d, J=1 Hz, 1H), 2.43—2.83 (m, 1H), 5.25—5.80 (m, 2H), 9.70 (d, J=1 Hz, 1H); MS m/z (%): 124 (M^+, 21), 96 (19), 95 (40), 81 (56), 80 (100), 79 (51), 67 (71).

Financial support by the Ministry of Education, Science and Culture (Grant-in-Aid No. 56430027), is acknowledged.

References

1) For reviews, see: D. S. Tarbell, *Org. React.*, **2**, 1 (1966); S. J. Rhoads and N. R. Raulins, *ibid.*, **22**, 1 (1975); G. B. Bennett, *Synthesis*, **1977**, 589; F. E. Ziegler, *Acc. Chem. Res.*, **10**, 227 (1977); T. Hayashi, *Yuki Gosei Kagaku Kyokai Shi*, **34**, 396 (1976).

2) H. Meerwein, W. Florian, N. Schön, and G. Stopp, *Justus Liebigs Ann. Chem.*, **641**, 1 (1961); A. E. Wick, D. Felix, K. Steen, and A. Eschenmoser, *Helv. Chim. Acta*, **47**, 2425 (1964); D. Felix, K. Steen, A. E. Wick, and A. Eschenmoser, *ibid.*, **52**, 1030 (1969).

3) a) W. S. Johnson, L. Werthemann, W. R. Bartlett, T. J. Brocksom, T.-T. Li, D. J. Faulkner, and M. R. Petersen, *J. Am. Chem. Soc.*, **92**, 741 (1970); b) D. J. Faulkner and M. R. Petersen, *ibid.*, **95**, 553 (1973).

4) R. E. Ireland and R. H. Mueller, *J. Am. Chem. Soc.*, **94**, 5897 (1972); S. Danishefsky, R. L. Funk, and J. F. Kerwin, Jr., *ibid.*, **102**, 6889 (1980); M. M. Abelman, R. L. Funk, and J. D. Munger, Jr., *ibid.*, **104**, 4030 (1982).

5) K. Takai, I. Mori, K. Oshima, and H. Nozaki, *Tetrahedron Lett.*, **22**, 3985 (1981).

6) B. M. Trost, J. Ippen, and W. C. Vladuchick, *J. Am. Chem. Soc.*, **99**, 8116 (1977).

7) B. B. Snider, *Acc. Chem. Res.*, **13**, 426 (1980).

8) In Sharp contrast, there have been many reports published on aromatic Claisen rearrangement mediated by Lewis acids. a) BF_3-CH_3COOH: L. Y. Bryusova and M. L. Ioffe, *J. Gen. Chem. (U.S.S.R.)*, **11**, 722 (1941); *Chem. Abstr.*, **36**, 430 (1942). b) BCl_3: J. Borgulya, R. Madeja, P. Fahrni, H.-J. Hansen, H. Schmid, and R. Barner, *Helv. Chim. Acta*, **56**, 14 (1973). c) Et_2AlCl: F. M. Sonnenberg, *J. Org. Chem.*, **35**, 3166 (1970). d) $TiCl_4$-PhN=C(Me)OSiMe$_3$: K. Narasaka, E. Bald, and T. Mukaiyama, *Chem. Lett.*, **1975**, 1041.

9) It has been reported that $TiCl_4$ did not catalyze the rearrangement of crotyl vinyl ether; see: R. K. Hill and H. N. Khatri, *Tetrahedron Lett.*, **1978**, 4337.

10) We are tempted to assume the following mechanism (Scheme 3): (1) The oxygen atom of an allyl vinyl ether coordinates to an organoaluminium compound, and (2) [3,3] sigmatropic rearrangement occurs and a nucleophilic moiety R or H on the aluminium atom adds to the aldehydic carbon concomitantly.

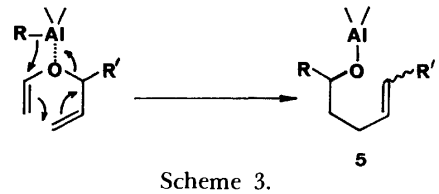

5

Scheme 3.

In the case of Et_2AlSPh, both diethylaluminium and SPh parts are eliminated from **5** (R=SPh) upon acidic workup to afford the regular Claisen rearrangement product, or γ,δ-unsaturated aldehyde.

11) G. Zweifel and C. C. Whitney, *J. Am. Chem. Soc.*, **89**, 2753 (1967).

12) A. Itoh, S. Ozawa, K. Oshima, and H. Nozaki, *Bull. Chem. Soc. Jpn.*, **54**, 274 (1981).

13) G. Büchi and J. E. Powell, Jr., *J. Am. Chem. Soc.*, **92**, 3126 (1970).

14) A. W. Burgstahler and I. C. Nordin, *J. Am. Chem. Soc.*, **83**, 198 (1961).

15) A. P. Davis, G. J. Hughes, P. R. Lowndes, C. M. Robbins, E. J. Thomas, and G. H. Whitham, *J. Chem. Soc., Perkin Trans. 1*, **1981**, 1934.

16) H. J. Bestmann, K. H. Koschatzky, W. Schätzke, J. Süß, and O. Vostrowsky, *Justus Liebigs Ann. Chem.*, **1981**, 1705.

17) C. G. Kruse, A. C. V. Janse, V. Dert, and A. van der Gen, *J. Org. Chem.*, **44**, 2916 (1979).

18) D. L. Garin, *J. Org. Chem.*, **34**, 2355 (1969).

19) V. Spéziale, M. M. Amat, and A. Lattes, *J. Heterocycl. Chem.*, **13**, 349 (1976).

20) B. Chantegrel and S. Gelin, *Bull. Soc. Chim. Fr.*, **1975**, 2639.

21) A. I. Meyers and J. L. Durandetta, *J. Org. Chem.*, **40**, 2021 (1975).

Mass-spectral Isotope Effects in the Metastable Transition of Benzene and Perdeuterio Benzene. Model Calculation

Ryuichi ARAKAWA and Yozaburo YOSHIKAWA*
Institute of Chemistry, College of General Education, Osaka University, Toyonaka, Osaka 560
(Received April 7 1983)

The abundances of $C_6H_5^+$, $C_6H_4^{+\cdot}$, $C_4X_4^{+\cdot}$, and $C_3X_3^+$ (X=H, D) fragments occurring in the metastable transition of benzene and perdeuterio benzene have been measured by means of electron-impact ionization. The isotope effects on the relative intensities were reproduced by the simple model calculation on the basis of the RRKM theory. The vibrational frequencies of the transition states for the deuteriated and the nondeuteriated were obtained by a vibrational analysis for the assumed geometries and force fields. The transition states for the $C_6H_5^+$ and $C_6H_4^{+\cdot}$ channels preferred a benzene structure while those for the $C_4H_4^{+\cdot}$ and $C_3H_3^+$ has a propargyl-cyclopropene structure. The calculated decay rates for the $C_6H_5^+$, $C_4H_4^{+\cdot}$, and $C_3H_3^+$ fragmentation were compared with those of the photoion photoelectron coincidence (PIPECO) results.

In the study of the metastable transitions of partly deuteriated ions, the isotope effect has been a tool in the structural assignment of both transition and reactant states. The application of the mass-spectral ion abundances of isotopically substituted molecules has been reviewed by Holmes.[1] The relative intensities of fragmentation from complex molecules have been readily explained by the statistical calculation without any serious discrepancy.[2,3] Systematic studies of the transition states have been done in the unimolecular reaction of the methyl radical and the hydrogen-atom loss from 1,3-butadiene and in that of its perdeuterio analog.[4] The model calculation of kinetic isotope effects showed the most plausible transition state for the methyl-elimination reaction to be a 2-methylcyclopropenium ion.

In the metastable transitions of benzene ions, the molecular ions lose $H^\cdot$, H_2, C_2H_2, and $C_3H_3^\cdot$ to yield fragments of $C_6H_5^+$, $C_6H_4^{+\cdot}$, $C_4H_4^{+\cdot}$, and $C_3H_3^+$ respectively. Mass spectral results on ^{13}C- and ^2H-labeled benzene have shown that there was a significant scrambling of carbon and hydrogen atoms prior to dissociation.[5] The first measurement concerning the dissociation rates for the benzene ion as a function of the internal energy was carried out by Andlauer and Ottinger using the charge-transfer reactions with ions of various ionization potentials.[6] Their results triggered arguments for the exsistence of two isolated $C_6H_6^{+\cdot}$ states, one producing $C_6H_5^+$ and $C_6H_4^{+\cdot}$, and the other giving $C_4H_4^{+\cdot}$ and $C_3H_3^+$.[7] Rosenstock *et al.*, by interpreting the photoionization mass spectrum,[8] suggested that the precursor ion for the $C_3H_3^+$ fragment was not the ground state of the benzene ion. Finally, Baer *et al.* measure the absolute fragmentation rates for internal-energy- selected $C_6H_6^{+\cdot}$ ions of several isomers, such as 2, 4- and 1, 5- hexadiyne, obtained by photoion photoelectron coincidence (PIPECO).[9] Their experimental and RRKM calculated rates indicate that benzene and these isomers rearrange to a common precursor and fragment to all product channels by competing pathways and that the existence of isolated states or noncommunicating isomeric structures is highly unlikely.

In the present communication, the mass-spectral isotope effects from metastable transitions were investigated in order to understand better the unimolecular process of benzene ions. The rates of unimolecular decomposition were calculated on the basis of the RRKM theory. The reaction paths were simulated by changing the structures of the transition state (TS) models, including a variety of reaction coordinates. The TS models were determined by changing the bond orders and the angles of the bonds involved in the reaction so as to reproduce the experimental isotope effects. The absolute rate constants of the $C_6H_5^+$, $C_4H_4^{+\cdot}$, and $C_3H_3^+$ fragments obtained from the PIPECO results[9] were helpful in constraining the assumed TS models.

Experimental

A home-built tandem mass spectrometer[10] was used to measure fragment ions. The temperature of the ion source was 150 °C. The electron-ionization energy was 30—50 eV, the electron current was 3 μA, and the ion-accelerating voltage was 1.2 kV. The pressure in the field-free region was always less than 1×10^{-6} Torr (1 Torr=133.32 N m^{-2}).

Fragment ions from metastable transitions occurring in the field-free region between two magnets were detected and their intensities integrated by mean of a multiscan system. For the measurement of the mass spectra, about one hundred scans over several hours were needed to accumulate 10^6 counts for molecular ions. The sample of benzene-d_6 (99% atom D; MERCK) was a commercially available one.

Results and Discussion

The peak-intensity ratios, P_X, of fragment ions for the metastable transitions of $C_6X_6^{+\cdot}$ (X=H,D) are summarized in Table 1. The error given shows the

Table 1. Relativa peak intensities of the fragment ions for the metastable transition of $C_6X_6^{+\cdot}$ (X=H,D)

X	E/eV	$C_6X_5^+$	$C_6X_4^{+\cdot}$	$C_4X_4^{+\cdot}$	$C_3X_3^+$
P_H	50	100	16±2	3.8±0.1	1.1±0.1
	40	100	18	4.2	1.2
	30	100	19	4.5	1.1
P_D	50	100	20±1	10±0.3	2.4±0.1
	40	100	20	11	2.5
	30	100	25	12	3.8

standard deviation after several runs. It is considered impossible to include the systematic error. There was no pressure effect on the measured peak ratios of the parent and metastable product ions. The main process is the hydrogen-atom elimination. The peak ratios did not change above the electron energy of 30 eV. The internal energy distribution, $P(E)$, of the molecular ions formed by electron impact is almost constant in this energy region of ionizing electrons.

The peak intensity of an i-th fragment ion in the mass spectra which does not undergo further decomposition is given by:

$$I_i = c\int_0^\infty P(E)k_i(E)T(E)/\sum k_j(E)\mathrm{d}E.$$

Here, c is a constant, E is the internal excitation energy of the molecular ion, $k_i(E)$ is the rate constant for decay into the i-th fragment, and $T(E)$ is the time factor, $T(E)=\exp(-t_1\sum k_j(E))-\exp(-t_2\sum k_j(E))$, where t_1 and t_2 are the entrance and exit times of the molecular ion in the field free region relative to the time of ion formation(t_1=3.6 and t_2=8.5 μs for $C_6H_6^{+\cdot}$).

The specific rate constant for unimolecular decomposition is given by

$$k(E)=L^*(I^*_{ABC}/I_{ABC})^{1/2}\sum P(E^*)/(hN(E_0+E^*)),$$

where h is Planck's constant, E_0 is the activation energy, $\sum P(E^*)$ is the total number of vibrational-rotational states of the activated complex at energy E^*, $N(E_0+E^*)$ is the level density of the reactant molecule at energy $E=E_0+E^*$, the I^* and I values are the products of the principal moments of inertia for the activated complex and reactant, and L^* is a statistical factor. An algorithm of Stein and Rabinovitch[11] was used for directly computing harmonic oscillator eigenstate sums and densities.

The internal energy of molecular ions consists of the internal thermal energy plus the energy transferred into the ion by the ionization process. Several methods of approximating the expression of $P(E)$ have been examined and these shortcomings analyzed.[12] In the present calculation, the energy-transfer probability was estimated by folding the photoionization cross-section[13] into the HeI photoelectron spectrum[14] under the optical approximation proposed by Miesels *et al.*[12]

The activation energies for the unimolecular decomposition of the benzene ion resulting in the loss of H$^\cdot$, C_2H_2, and $C_3H_3^\cdot$ are 3.60, 4.22, and 4.37 eV respectively, while the ionization energy of benzene is 9.24 eV.[9] That of the H_2 loss was estimated to be 3.86 eV.[15] The activation energies of the deuteriated species are estimated from applying the zero-point energy correction to the values for the nondeuteriated molecules. These corrections were all less than 0.05 eV.

The vibrational frequencies of the deuteriated and the non-deuteriated molecules for the reactant and the TS are obtained by a vibrational analysis for the assumed geometries and force fields.[16] The reactant and the TS models for the competing reactions are represented by the same internal coordinates. The relative rate constants yielding the relative intensities are thought to be independent of the influence of the approximate frequencies resulting from the approximate simple valence force field(diagonal force constant matrix), but one thought to be related to the TS structures. For the TS model, the reacting bond length r modified from the empirical length r_0 is described along the reaction coordinate and adjusted on the basis of Pauling's expression; $r=r_0-0.3\ln(n)$ where n is the bond order. The geometry of each model was most conveniently specified in terms of the bond orders and bond angles. The bond lengths of benzene are summarized in Table 2. The stretching force constants F_r° of the initial state for the reacting bond are modified for the TS model according to $F_r=nF_r^\circ$. The angle bending force constants are also given by $F_a=g(\theta)n_in_jF_a^\circ$, where n_i and n_j are the bond orders in the bending mode and F_a° is the initial bending force constant. The value of $g(\theta)$ refers to the hybridization factor, $g(\theta)=1.39+1.17\cos(\theta)$, where θ is the bond angle. Torsional and out-of-plane bending force constants are retained at the values of the reactant force constants for all the modes. The force constants employed in the frequency calculation are shown in Table 2. In the reaction coordinate, the decomposition frequency is imaginary when the curvature is negative at the barrier. For the reaction proceeding through a simple bond cleavage in the TS model, the force constant for the stretching mode of the reacting bond will be negative.

The reactant configuration of the $C_6X_6^{+\cdot}$ ion formed from benzene by ionization is taken to be identical with that of the neutral molecule. The TS models

Table 2. Bond lengths and force constants to be employed in the frequency calculation

Type of bond	r_0/Å	F_r/mdyn Å^{-1} [a]
sp^3C-sp^2C	1.5075	5.0
sp^2C-sp^2C	1.46	5.8
sp C-sp C	1.37	8.0
sp^3C-H	1.094	5.0
sp^2C-H	1.083	5.2
Type of angle		**F_a/mdyn Å rad^{-2} [b]**
HCH		0.55
HCC		0.65
CCC		1.0
Out-of plane		0.2
Torsion		0.072

a) Stretching force constants are given for bonds with an order of unity. b) Bending force constants correspond to angles of 109.47°, subtended by bonds with an order of unity.

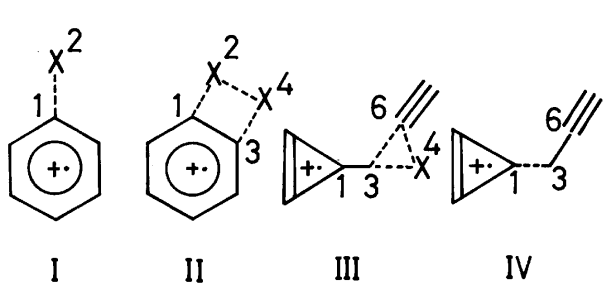

Fig. 1. Assumed geometries of the $C_6X_6^{+\cdot}$ ion for TS models of X$^\cdot$(I), X_2(II), C_2X_2(III), and $C_3X_3^\cdot$(IV) loss(X=H, D).

Table 3. Calculated isotope effect on peak intensities assuming various TS models

Models	Parameters	Fragment	Peak intensities	
			P_H	P_D
I	$n_{12}=0.1$[a] $F_S=-2.0$[b]	$C_6X_5^+$	100(100)[d]	100(100)
II	$n_{12}=0.1$ $n_{34}=0.5$ $F_S=-2.0$	$C_6X_4^{+\cdot}$	15(16)	20(20)
III	$n_{36}=0.2$ $n_{46}=1.0$ $F_S=-2.0$ $N_{rot}=3$[c]	$C_4X_4^{+\cdot}$	4.1(3.8)	7.1(10)
IV	$n_{13}=0.2$ $F_S=-2.0$ $N_{rot}=3$	$C_3X_3^+$	1.2(1.1)	2.6(2.4)

a) n_{ij} is the bond order of the i and j-th atoms: in Fig. 1. b) F_S means the force constant for the corresponding stretching mode of the reacting bond. c) Number of internal free rotations. d) Values in parentheses are experimental.

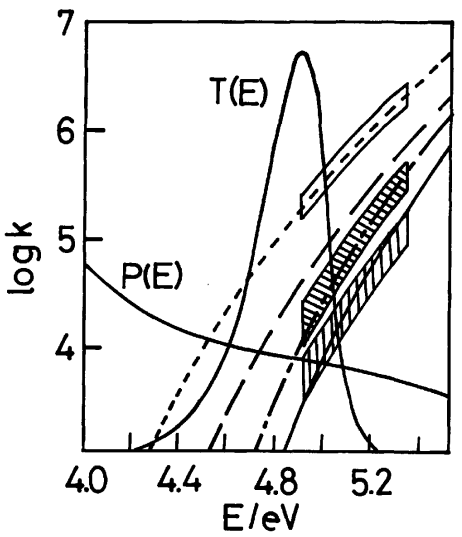

Fig. 2. Relationship among $P(E)$, $T(E)$ and decay rates for unimolecular decomposition of the $C_6H_6^{+\cdot}$ ion. Values of $P(E)$ and $T(E)$ are plotted on a linear scale versus the internal energy E. The decay curves show rate constants of $H^{\cdot}$(----), H_2(——), C_2H_2 (—·—), and $C_3H_3^{\cdot}$(——) loss. Wide lines are absolute rates obtained from PIPECO results of Baer *et al.* without the rate of H_2 loss.[9]

proceeding to the $C_6X_5^+$, $C_6X_4^{+\cdot}$, $C_4X_4^{+\cdot}$, and $C_3X_3^+$ products were assumed to be structures I—IV, they are shown in Fig. 1. The models of TS(I) and TS(II) are of a benzene molecule, and the others of a propargyl-1-cycloprop-2-ene structure similar to that chosen by Baer *et al.* The dissociations giving $C_6X_5^+$ and $C_3X_3^+$ are described as a simple-bond cleavage reactions of C_1–X_2 and C_1–C_3 as is shown in the TS(I) and TS(IV) models. In TS(II) and TS(III) models, a hydrogen-atom transition should occur. The relative motions of the migrating hydrogen atom and the loosing bond are defined by using an appropriate combination of interaction force constants(off-diagonal elements in F-matrix) for the coupling of the stretching modes of the reacting bonds. It requires a constant total bonding for the migrating atom, satisfying $n_{34}+n_{24}=1$ and $n_{34}+n_{46}=1$ for TS(II) and TS(III), respectively. For the sake of simplicity, however, the simple bond cleavage for the stretching modes of C_1–X_2, TS(II) and C_3–C_6, TS(III) are employed as the reaction coordinates. The interaction force constants were not considered. Structural parameters used here are shown in Table 3. The stretching force constants for the reacting bond are fixed at $F_S=-2.0$; the torsional modes of vibration are reduced to free internal rotations.

The calculated isotope effects on the peak intensities are shown in Table 3. The results agree well with the experimental isotope effects. The rate curves and P_X varied with the bond-order parameters, but the P_H/P_D ratio did not change greatly within the limit of the given TS model. The application of a linear structure such as a 1,5-hexadiyne ion to the $C_4H_4^{+\cdot}$ and $C_3H_3^+$ TS models gave insufficient results on isotope effects. The rate constants decaying to $C_6H_5^+$, $C_4H_4^{+\cdot}$, and $C_3H_3^+$ are compared with the results of Baer *et al.* in Fig. 2. Their rates were determined from the total decay rates and the branching ratios if the dissociation channels were in competition. The rate for the H_2 loss channel has not been presented. The vibrational frequencies for the TS(III) and TS(IV) models, obtained from the vibrational analysis, are not very different from those of Baer *et al.* used in the RRKM calculations for the $C_4H_4^{+\cdot}$ and $C_3H_3^+$ channels. The values of the peak intensities are derived from rate curves lying in a metastable window $T(E)$, 4.4—5.2 eV. There is always uncertainty on the $P(E)$ function followed by electron-impact ionization. The relative values of the $P(E)$ function, defined within narrow limits, are necessary to calculate the isotope effects. Therefore, it is improbable that the $P(E)$ curve estimated above causes a large error in the isotope effects. An increase of a few percent in the relative intensities, P_H and P_D can be calculated if the $P(E)$ function is constant. The intensity of $C_6X_5^+$ fragment is relatively reduced because of the smaller values of the $P(E)$ function in the lower-energy region of the window $T(E)$. Such a variation in $P(E)$ does not influence the isotope effects to any large extent. The decay rate for the $D^{\cdot}$ loss is slower by one order of magnitude than that for the $H^{\cdot}$ loss. The metastable window for the C_6D_6 dissociation shifts to a higher energy, 4.7—5.8 eV.

The mass spectral isotope effects support the conclusion that the dissociation of the benzene ion proceeds competitively to all products. The reactant model equivalent to the common precusor from the C_6H_6 isomers is of a benzene molecule, and the TS models are the product-like structures. The measured peak intensities can not directly reflect the absolute rate, but rather the relative TS density yielding the relative rate constant. This analysis requires the absolute decay rates in order to fix the TS model.

The authors wish to thank Mr. Masana Arimura for his helpful discussions.

References

1) J. L. Holmes, *MTP Int. Rev. Sci. Phys. Chem., Ser. II*, **5**, 207(1975).
2) H. M. Rosenstock, M. B. Wallenstein, A. L. Wahrhaftig, and H. Eyring, *Proc. Natl. Acad. Sci. U.S.A.*, **38**, 667(1962).
3) For recent general references, see C. Lifshitz, *Adv. Mass Spectro.*, **A**, 3(1978).
4) R. Arakawa, M. Arimura, and Y. Yoshikawa, *Int. J. Mass Spectrom. Ion Phys.*, **44**, 257(1982).
5) J. H. Beynon, R. M. Caprioli, W. O. Perry, and W. E. Baitinger, *J. Am. Chem. Soc.*, **94**, 6828(1972).
6) B. Andlauer and Ch. Ottinger, *J. Chem. Phys.*, **55**, 1471(1971).
7) J. H. D. Eland and H. Schulte, *J. Chem. Phys.*, **62**, 3835(1975).
8) H. M. Rosenstock, K. E. McCulloh, and F. P. Lossing, *Int. J. Mass Spectrom. Ion Phys.*, **25**, 327(1977).
9) T. Baer, G. D. Willett, D. Smith, and J. S. Phillips, *J. Chem. Phys.*, **70**, 4076(1979).
10) M. Arimura and Y. Yoshikawa, *Mass Spectro.(Japan)*, **30**, 183(1982).
11) S. E. Stein and B. S. Rabinovitch, *J. Chem. Phys.*, **58**, 2438(1973).
12) a) G. G. Meisels, C. T. Chan, B. G. Giessner, and R. H. Emmel, *J. Chem. Phys.*, **56**, 793(1972); b) H. Ehrhardt, F. Linder, and T. Tekaat, *Adv. Mass Spectro.*, **4**, 705(1969).
13) J. Momigny, C. Goffart, and L. D'or, *Int. J. Mass Spectrom. Ion Phys.*, **1**, 53(1968).
14) D. W. Turner, C. Baker, A.D. Baker, and C. R. Brundle, "Molecular Photoelectron Spectroscopy," Wiley, New York (1970).
15) H. M. Rosenstock, K. Draxl, B. W. Steiner, and J. T. Herron, *J. Phys. Chem. Ref. Data*, **6**, Suppl. 1 (1977).
16) For the frequency calculation, a frequency program in BEVOBIV-IV was used. a) L. B. Sims, G. W. Burton, and D. E. Lewis, BEVOBIV-IV, Quantum Chemistry Program Exchange No. 337 (1977); b) G. W. Burton, L. B. Sims, and D. J. McLennan, *J. Chem. Soc., Perkin Trans. 2*, **1963**, 1967; c) C. W. Burton, L. B. Sims, J. C. Wilson, and A. Fry, *J. Am. Chem. Soc.*, **99**, 3371 (1977); d) H. Yamataka and T. Ando, *J. Phys. Chem.*, **85**, 2281 (1981).

Palladium(II) Complexes Containing Both the Chelating β-Diketonato and σ-Pyridyl Ligands. Catalyzed Coordination-site Exchange Reactions

Hiroshi TANAKA, Kiyoshi ISOBE, Shinichi KAWAGUCHI,* and Seichi OKEYA†
Faculty of Science, Osaka City University, Sumiyoshi-ku, Osaka 558
†*Faculty of Education, Wakayama University, Fukiage, Wakayama 640*
(Received September 8, 1983)

A novel type of palladium(II) complexes, [Pd(β-dik)(pyridyl)(PPh_3)] and [Pd(β-dik)(pyridyl)]$_2$ containing a chelating acetylacetonate, trifluoroacetylacetonate, or hexafluoroacetylacetonate anion and 2-, 3-, or 4-pyridyl radical as the coexisting ligands were prepared and characterized by elemental analysis and molecular weight determination as well as ^1H and ^{13}C NMR spectroscopy. [Pd(acac)(C_5H_3(6-Cl)N-C^2)(PPh_3)] is stereochemically rigid in solution but undergoes the coordination-site exchange reaction catalyzed by nitrogen and phosphorus bases and donor solvents. Similar reaction of [Pd(acac)(C_5H_4N-C^2)(PPh_3)] is catalyzed by triphenylphosphine liberated by the dinuclear-complex formation reaction (autocatalysis). Intact molecules of [Pd(acac)(C_5H_4N-C^3 and -C^4) (PPh_3)] catalyze mutually their own coordination-site exchange (self-catalysis).

A stable dinuclear complex [PdBr(C_5H_4N-C^2)(PPh_3)]$_2$ (**3a**) was prepared by the reaction of [Pd(PPh_3)$_4$] (**1**) with 2-bromopyridine in toluene at 90°C[1,2] and was disclosed by X-ray analysis to have a novel structure in which two pyridyl ligands are bridging palladium atoms through the C^2 and N atoms.[2,3] A similar reaction of **1** with 2,6-dichloropyridine gave a mononuclear complex *trans*-[PdCl(C_5H_3(6-Cl)N-C^2)(PPh_3)$_2$] (**2d**), which coexists in equilibrium with a minute amount of the dinuclear complex [PdCl(C_5H_3(6-Cl)N-C^2)(PPh_3)]$_2$ in solution and is completely converted into the latter by oxidation of freed triphenylphosphine with hydrogen peroxide.[1,2] On the other hand, the reactions of **1** with 3- and 4-bromopyridines in toluene at 90°C afforded *trans*-[PdBr(C_5H_4N-C^3)(PPh_3)$_2$] (**2b**) and *trans*-[PdBr(C_5H_4N-C^4)(PPh_3)$_2$] (**2c**), respectively, and the corresponding dinuclear complexes have never been obtained.[4] Treatment of complexes **3a**, **2b**, and **2c** with triethylphosphine in diethyl ether at room temperature gave rise to a set of linkage isomers *trans*-[PdBr(C_5H_4N-C^2, -C^3, and -C^4)(PEt_3)$_2$], of which properties and molecular structures were compared with each other.[4]

In the present investigation, a new type of palladium(II) complexes [Pd(β-dik)(pyridyl)(PPh_3)] containing an *O,O'*-chelated β-diketonate anion and a carbon-bonded pyridyl ligand have been derived from complexes **3a**, **2b**, **2c**, and **2d**. This paper reports the properties of these mixed-ligand complexes, laying emphasis on their dynamic behaviors in solution catalyzed by Lewis bases including donor solvents.[5]

Experimental

Preparation of Complexes. [PdBr(C_5H_4N-C^2)(PPh_3)]$_2$ (**3a**), *trans*-[PdBr(C_5H_4N-C^3)(PPh_3)$_2$] (**2b**), *trans*-[PdBr(C_5H_4N-C^4)(PPh_3)$_2$] (**2c**), and *trans*-[PdCl(C_5H_3(6-Cl)N-C^2)(PPh_3)$_2$] (**2d**) were prepared by the methods reported previously.[2,4]

*[PdBr(C_5H_4N-C^3)(PPh_3)]$_n$ (**3b**)*: To a suspension of complex **2b** (6.35 g, 8.05 mmol) in acetone (50 cm^3) was added 12 cm^3 of 30% hydrogen peroxide solution (106 mmol) and the mixture was stirred at room temperature for 24 h. A white precipitate was filtered, washed with acetone and dietyl ether successively, and dried *in vacuo*. The yield was 4.15 g (97.9%).

*[PdBr(C_5H_4N-C^4)(PPh_3)]$_n$ (**3c**)*: White complex **3c** was obtained almost quantitatively (4.50 g, 98.8%) in a similar fashion by the reaction between **2c** (6.82 g, 8.64 mmol) and aqueous hydrogen peroxide (13 cm^3, 115 mmol).

*[PdCl(C_5H_3(6-Cl)N-C^2)(PPh_3)]$_2$ (**3d**)*: Yellow product **3d** from the reaction between **2d** (6.09 g, 7.82 mmol) and aqueous hydrogen peroxide (9 cm^3, 79.4 mmol) was purified by dissolution in dichloromethane and reprecipitation on addition of diethyl ether. The yield was 3.98 g (98.5%).

*[PdClO$_4$(C_5H_4N-C^2)(PPh_3)]$_2$ (**4a**)*: A solution of silver perchlorate (2.00 g, 9.65 mmol) in methanol (10 cm^3) was added to a dichloromethane (100 cm^3) solution of **3a** (3.00 g, 2.85 mmol) and the mixture was stirred at room temperature for 2 h. A precipitate of silver bromide was filtered off and the filtrate was treated three times with deionized water (50 cm^3 each) to extract residual silver perchlorate. The dichloromethane solution was passed through a column of anhydrous sodium sulfate and then concentrated to about 10 cm^3 under reduced pressure. On addition of diethyl ether to the concentrate, a yellow precipitate appeared, which was filtered, washed with the ether, dried *in vacuo*, and purified by reprecipitation from dichloromethane–diethyl ether. The yield was 2.56 g (82.0%).

*{[Pd(C_5H_4N-C^3)(PPh_3)(H_2O)]ClO$_4$}$_n$ (**4b**)*: *Method A*; A solution of silver perchlorate (1.02 g, 4.93 mmol) in methanol (10 cm^3) was added to a suspension of **3b** (2.03 g, 3.76 mmol when n=1) in dichloromethane (10 cm^3) and the mixture was stirred at room temperature for 50 min. After filtration of silver chloride, the filtrate was concentrated to about 2 cm^3. On scratching the wall of vessel with a glass rod after addition of methanol (20 cm^3) to the concentrate, a white precipitate appeared, which was filtered, washed with diethyl ether, and dried *in vacuo*. The yield was 1.84 g (86.7%).

Method B; After the reaction of **2b** (0.653 g, 0.838 mmol) with silver perchlorate (0.209 g, 1.01 mmol) in a mixture of dichloromethane (5 cm^3) and methanol (2 cm^3) at room temperature for 1 h, work up similar to method A gave a white precipitate. The yield was 0.215 g (45.5%) after reprecipitation from dichloromethane–ethanol.

*{[Pd(C_5H_4N-C^4)(PPh_3)(H_2O)]ClO$_4$}$_n$ (**4c**)*: Two preparative methods starting from **3c** and **2c** gave a light yellow powder of **4c** in 100 and 90.8% yields, respectively. The dichloromethane–benzene system was used for reprecipitation.

*[PdClO$_4$(C_5H_3(6-Cl)N-C^2)(PPh_3)]$_2$ (**4d**)*: Yellow complex **4d** was derived analogously from **3d** and **2d** in 89.0 and 81.6%

yields, respectively. Reprecipitation was performed from dichloromethane–diethyl ether.

Thus two methods were used for preparation of type-**4** complexes and method A was found better since products from method B were contaminated with a small amount of free triphenylphosphine. Analogously, the following type-**5** complexes were prepared by each of three methods: (method A) reactions of type-**2** complexes with thallium(I) β-diketonates, (method B) reactions of type-**3** complexes with thallium(I) β-diketonates, and (method C) reactions of type-**4** complexes with potassium β-diketonates. For brevity only the preferable methods are described here for each complex.

*[Pd(acac)(C$_5$H$_4$N-C^2)(PPh$_3$)] (**5a1**)*: *Method B*; Thallium(I) acetylacetonate, Tl(acac) (0.625 g, 2.06 mmol) was added to a solution of **3a** (0.986 g, 0.936 mmol) in dichloromethane (20 cm^3) and the mixture was stirred at room temperature for 30 min. After separation of thallium(I) bromide, the filtrate was concentrated to about 3 cm^3 under reduced pressure. A small amount of diethyl ether was added to the concentrate and crystallization was induced by scratching the flask. The product was filtered, washed with the ether, and recrystallized from dichloromethane–diethyl ether. The yield was 0.925 g (90.5%).

Method C; To a solution of **4a** (0.943 g, 0.863 mmol) in dichloromethane (30 cm^3) was added a methanol (10 cm^3) solution of potassium acetylacetonate (0.729 g, 5.28 mmol) and the mixture was stirred at room temperature for 20 min. After separation of potassium perchlorate by filtration, the solvent was evaporated to dryness under reduced pressure. Dichloromethane (30 cm^3) was added to the residue and insoluble material was filtered off. The filtrate was concentrated to about 2 cm^3 under reduced pressure. Crystallization was induced by scratching the flask after addition of diethyl ether (10 cm^3) to the concentrate. The product was filtered, washed with diethyl ether, and recrystallized from dichloromethane–diethyl ether. The yield was 0.802 g (85.2%).

*[Pd(tfac)(C$_5$H$_4$N-C^2)(PPh$_3$)] (**5a2**)*: The reaction of **3a** with thallium(I) trifluoroacetylacetonate, Tl(tfac) (method B) and that of **4a** with K(tfac) (method C) gave complex **5a2** in 68.7 and 46.9% yields, respectively. Petroleum ether (bp<60 °C) was used instead of diethyl ether for recrystallization.

*[Pd(hfac)(C$_5$H$_4$N-C^2)(PPh$_3$)] (**5a3**)*: Method B using **3a** and thallium(I) hexafluoroacetylacetonate, Tl(hfac), and method C using **4a** and K(hfac) afforded **5a3** in 51.9 and 44.3% yields, respectively.

*[Pd(acac)(C$_5$H$_4$N-C^3)(PPh$_3$)] (**5b1**), [Pd(tfac)(C$_5$H$_4$N-C^3)(PPh$_3$)] (**5b2**), and [Pd(hfac)(C$_5$H$_4$N-C^3)(PPh$_3$)] (**5b5**)*: These 3-pyridyl complexes were prepared by methods C,B, and B in 82.8, 78.6, and 53.2% yields, respectively.

*[Pd(acac)(C$_5$H$_4$N-C^4)(PPh$_3$)] (**5c1**), [Pd(tfac)(C$_5$H$_4$N-C^4)(PPh$_3$)] (**5c2**), and [Pd(hfac)(C$_5$H$_4$N-C^4)(PPh$_3$)] (**5c3**)*: The 4-pyridyl complexes were obtained in 63.9, 63.0, and 63.3% yields by methods C, B, and B, respectively.

*[Pd(acac)(C$_5$H$_3$(6-Cl)N-C^2)(PPh$_3$)] (**5d1**), [Pd(tfac)(C$_5$H$_3$(6-Cl)N-C^2)(PPh$_3$)] (**5d2**), [Pd(hfac)(C$_5$H$_3$(6-Cl)N-C^2)(PPh$_3$)] (**5d3**)*: Methods C, C, and B were used to prepare these complexes in 84.0, 78.4, and 65.8% yields, respectively.

*[Pd(acac)(C$_5$H$_4$ N-C^2)]$_2$ (**6a1**), [Pd(tfac)(C$_5$H$_4$N-C^2)]$_2$ (**6a2**)*, and *[Pd(acac)(C$_5$H$_3$(6-Cl)N-C^2)]$_2$ (**6d1**)*: To a suspension of complex **5a1** (0.356 g, 0.652 mmol) in acetone (10 cm^3) was added 2 cm^3 of aqueous hydrogen peroxide solution (10%, 5.8 mmol) and the mixture was stirred at room temperature for 2 h. A yellow precipitate of **6a1** was filtered, washed with diethyl ether and dried *in vacuo*. The yield was 0.147 g (76.2%). Complexes **6a2** and **6d1** were similarly prepared from **5a2** and **5d1** in 43.6% (0.103 g) and 28.1% (0.120 g) yields, respectively.

*[Pd(acac)(C$_5$H$_3$(6-Cl)N-C^2)(PEt$_3$)] (**7d1**)*: Triethylphosphine (0.115 cm^3, 0.788 mmol) was added to a suspension of **6d1** (0.249 g, 0.392 mmol) in dichloromethane (5 cm^3) and the mixture was stirred at room temperature for 1 h. After evaporation of the solvent, the oily residue was treated with diethyl ether and the extract was concentrated to dryness. The yield was 0.198 g (57.9%).

Measurements. Infrared spectra were recorded in Nujol mull on a JASCO DS 701G spectrophotometer. The NMR spectra were taken with JEOL JNM-MH100 (for ^{1}H) and FX 60Q (for ^{13}C) spectrometers. The molecular weight was determined by vapor pressure osmometry with an instrument manufactured by Knauer in West Berlin, West Germany.

The ^{1}H NMR line shape simulation was carried out with a FACOM 230-60 computer according to the Nakagawa's equation.[6]

Results and Discussion

Synthesis. The 2-, 3-, and 4-pyridyl complexes [PdBr(C$_5$H$_4$N-*C*^{2})(PPh$_3$)]$_2$ (**3a**), [PdBr(C$_5$H$_4$N-*C*^{3})(PPh$_3$)$_2$] (**2b**), [PdBr(C$_5$H$_4$(N-*C*^{4})(PPh$_3$)$_2$] (**2c**), and [PdBr(C$_5$H$_3$(6-Cl)N-*C*^{2})(PPh$_3$)$_2$] (**2d**) were used as the starting materials for the present synthetic work, and the reaction sequences from **2b** and **2c** and also from **2d** are illustrated in Figs. 1 and 2, respectively. Hydrogen peroxide treatment of the mononuclear complexes **2b**, **2c**, and **2d** eliminated one of the two PPh$_3$ ligands in each complex to result in [PdBr(C$_5$H$_4$N-*C*^{3})(PPh$_3$)]$_n$ (**3b**), [PdBr(C$_5$H$_4$N-*C*^{4})(PPh$_3$)]$_n$ (**3c**), and [PdCl(C$_5$H$_3$(6-Cl)N-*C*^{2})(PPh$_3$)]$_2$ (**3d**), respectively. The analytical and molecular weight data of **3d** indicate that the yellow complex is dinuclear. It may have the pyridyl-bridged dinuclear structure similar to that of **3a**.[2,3] Complexes **3b** and **3c** are white and insoluble in usual organic solvents, suggesting that they may have polynuclear structures.

The halide ligands in dinuclear complexes **3a** and **3d** were substituted by the perchlorate ion to result in **4a**

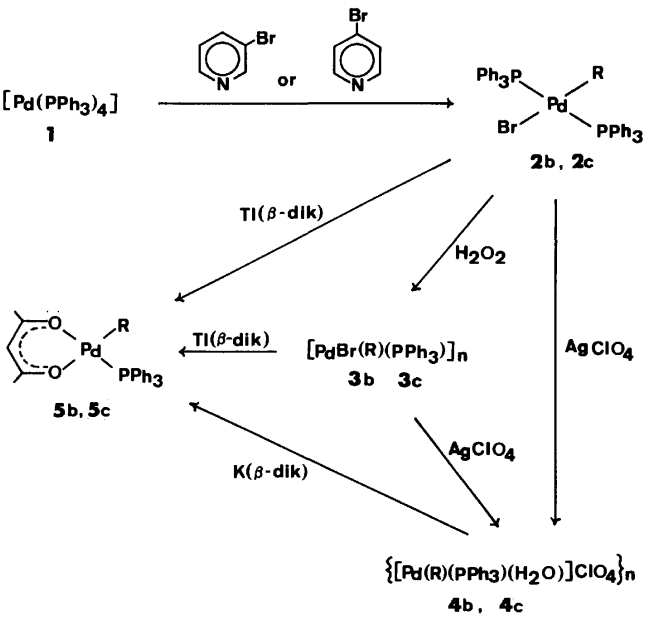

Fig. 1. Reaction sequence for the 3- and 4-pyridyl complexes. R=C$_5$H$_4$N-*C*^{3} and C$_5$H$_4$N-*C*^{4} for complexes b and c, respectively.

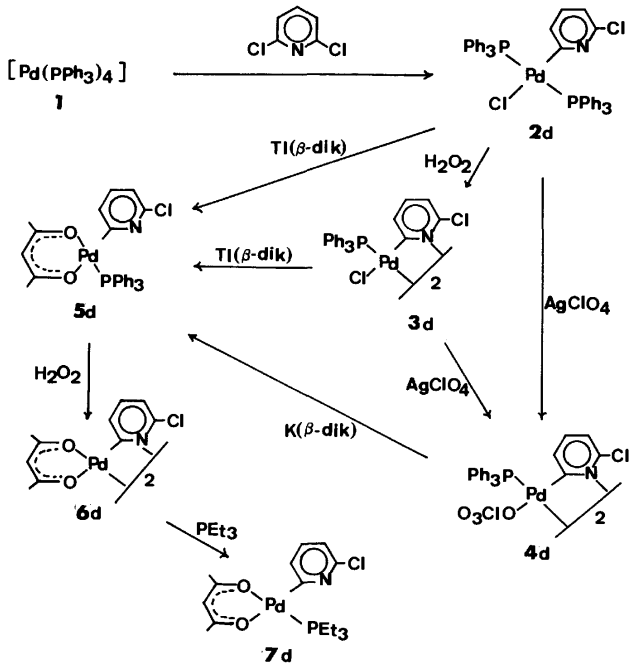

Fig. 2. Reaction sequence for the 6-chloro-2-pyridyl complexes.

and **4d**, respectively, which are yellow and retain the dinuclear structures as evidenced by the analytical and molecular weight data. Although silver perchlorate was again effective in displacing the bromide ligand from **3b** and **3c**, the perchlorate anion was not bound to the metal in these cases, but remained in the outer sphere and instead a water molecule contained in the organic solvents was accepted as a ligand. Silver perchlorate also reacted with mononuclear complexes **2b**, **2c**, and **2d** to remove not only the halide ion but also one phosphine molecule in either case and give rise to **4b**, **4c**, and **4d**, respectively. The molecular weights of **4b** and **4c** determined in dichloromethane at 27°C are 2090 and 1500, respectively, and are much larger than the formula weight (548.2) calculated for the tight ion pair $[Pd(C_5H_4N)(PPh_3)(H_2O)]ClO_4$, indicating that **4b** and **4c** are polynuclear.

The tendency of the σ-carbon-bonded pyridyl ligands to bridge two metal atoms stems from the enhanced basicity of pyridine bound to palladium at either the C^2, C^3, or C^4 position.[4] It seems reasonable on the steric consideration that the 3- and 4-pyridyl ligands favor the polynuclear structure, while the 2-pyridyl ligand stabilizes the dinuclear form. However, it can not be readily rationalized why the perchlorate ion serves as a ligand in the dinuclear 2-pyridyl complexs but not in the polynuclear 3- and 4-pyridyl complexes. It is worth noting that **4a** and **4d** reacted with pyridine to give mononuclear complexes as exemplified by Eq. 1.

$$\underset{\textbf{4a}}{[PdClO_4(C_5H_4N\text{-}C^2)(PPh_3)]_2} + 2py \longrightarrow 2[PdClO_4(C_5H_4N\text{-}C^2)(PPh_3)(py)] \quad (1)$$

Pyridine did not replace the perchlorate ligand, but cleaved the 2-pyridyl bridge. On the other hand, pyridine and even much more basic 4-dimethylaminopyridine in large excess did not split the polynuclear chain in **4b** and **4c**, but merely replaced the aqua ligand (Eq. 2).

$$\underset{\textbf{4b}\quad\textbf{4c}}{\{[Pd(C_5H_4N\text{-}C^3 \text{ or } \text{-}C^4)(PPh_3)(H_2O)]ClO_4\}_n} + n\text{L(py or 4-Me}_2\text{N-py)} \longrightarrow \{[Pd(C_5H_4N\text{-}C^3 \text{ or } \text{-}C^4)(PPh_3)L]ClO_4\}_n + nH_2O \quad (2)$$

However, bidentate β-diketonate anions readily cleaved not only the dinuclear bridge in **4a** and **4d**, but also the polynuclear bridge in **4b** and **4c** to afford the mononuclear type-**5** complexes [Pd(β-dik)(pyridyl)-(PPh_3)], of which the analytical and molecular weight data are listed in Table 1 together with those for complexes **3** and **4**. The type-**5** complexes were also derived by the reactions with thallium(I) β-diketonates from the halogeno complexes **2b**, **2c**, **2d**, **3a**, **3b**, **3c**, and **3d** irrespective of their nuclearity (Figs.1 and 2).

Of the type-**5** complexes, **5a1**, **5a2**, and **5d1** gave the dinuclear complexes **6a1**, **6a2**, and **6d1**, respectively, on

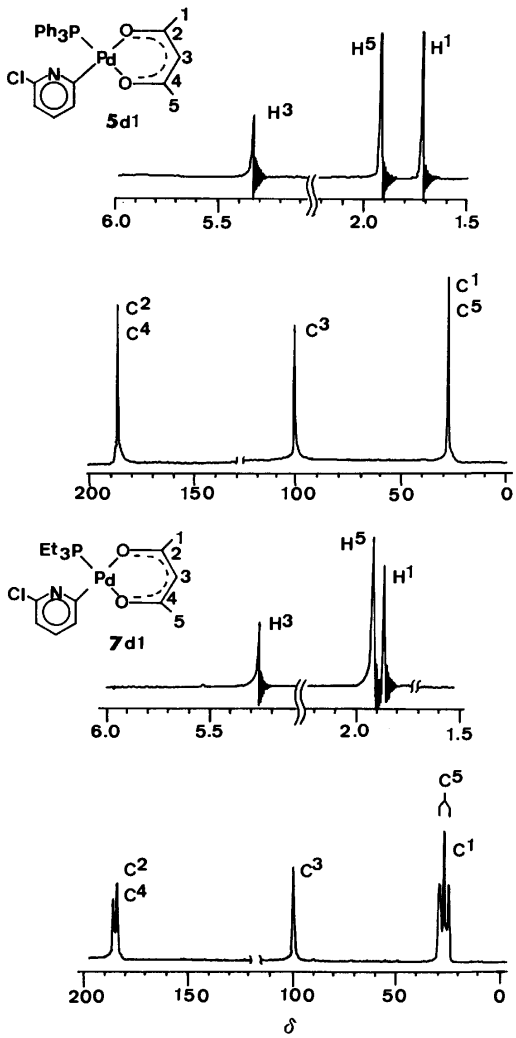

Fig. 3. ^1H and $^{13}C\{^1H\}$ NMR signals from the acetylacetonate ligand in $[Pd(acac)(C_5H_3(6\text{-Cl})N\text{-}C^2)(PPh_3)]$ (**5d1**) and $[Pd(acac)(C_5H_3(6\text{-Cl})N\text{-}C^2)(PEt_3)]$ (**7d1**) in $CDCl_3$ at room temperature. Chemical shifts are shown in ppm from internal Me_4Si.

TABLE 1. ANALYTICAL DATA FOR THE $[PdBr(pyridyl)(PPh_3)]_n$ (**3b** AND **3c**), $[PdCl(pyridyl)(PPh_3)]_2$ (**3d**), $[PdClO_4(pyridyl)(PPh_3)]_2$ (**4a** AND **4d**), $\{[Pd(pyridyl)(PPh_3)(H_2O)]ClO_4\}_n$ (**4b** AND **4c**), $[Pd(\beta\text{-dik})(pyridyl)(PPh_3)]$ (**5**), $[Pd(\beta\text{-dik})(pyridyl)]_2$ (**6**), AND $[Pd(\beta\text{-dik})(pyridyl)(PEt_3)]$ (**7**) COMPLEXES

Compd	β-dik	Pyridyl	Found (Calcd)			
			C(%)	H(%)	N(%)	Mol wt[a]
3b		C_5H_4N-C^3	51.96(52.45)	3.68(3.64)	2.65(2.66)	b)
3c		C_5H_4N-C^4	52.64(52.45)	3.59(3.64)	2.66(2.66)	b)
3d		C_5H_3(6-Cl)N-C^2	53.72(53.47)	3.55(3.51)	2.75(2.71)	1023(1033)
4a		C_5H_4N-C^2	50.75(50.75)	3.62(3.51)	2.57(2.56)	1058(1092)
4b		C_5H_4N-C^3	48.79(48.96)	3.87(3.75)	2.35(2.48)	2090(548.2)
4c		C_5H_4N-C^4	50.03(48.96)	3.98(3.75)	2.35(2.48)	1500(548.2)
4d		C_5H_3(6-Cl)N-C^2	47.50(47.57)	3.14(3.12)	2.40(2.41)	1119(1161)
5a1	acac	C_5H_4N-C^2	61.01(61.61)	4.83(4.80)	2.57(2.57)	535(545.9)
5a2	tfac	C_5H_4N-C^2	55.50(56.06)	3.98(3.86)	2.26(2.33)	600(599.9)
5a3	hfac	C_5H_4N-C^2	50.99(51.44)	3.07(3.08)	2.13(2.14)	620(653.8)
5b1	acac	C_5H_4N-C^3	61.42(61.61)	4.81(4.80)	2.56(2.57)	540(545.9)
5b2	tfac	C_5H_4N-C^3	55.15(56.06)	3.86(3.86)	2.11(2.33)	543(599.9)
5b3	hfac	C_5H_4N-C^3	51.73(51.44)	3.11(3.08)	2.11(2.14)	595(653.8)
5c1	acac	C_5H_4N-C^4	60.81(61.61)	4.81(4.80)	2.49(2.57)	538(545.9)
5c2	tfac	C_5H_4N-C^4	57.37(56.06)	3.98(3.86)	1.92(2.33)	535(599.9)
5c3	hfac	C_5H_4N-C^4	51.84(51.44)	3.09(3.08)	2.12(2.14)	634(653.8)
5d1	acac	C_5H_3(6-Cl)N-C^2	58.07(57.95)	4.35(4.34)	2.86(2.41)	580(580.3)
5d2	tfac	C_5H_3(6-Cl)N-C^2	52.75(53.02)	3.47(3.50)	2.33(2.21)	648(634.3)
5d3	hfac	C_5H_3(6-Cl)N-C^2	47.00(48.86)	2.66(2.64)	1.85(2.04)	692(688.3)
6a1	acac	C_5H_4N-C^2	42.32(42.35)	3.91(3.91)	4.96(4.94)	572(567.2)
6a2	tfac	C_5H_4N-C^2	35.86(35.58)	2.42(2.39)	4.11(4.15)	682(675.1)
6d1	acac	C_5H_3(6-Cl)N-C^2	37.76(37.76)	3.17(3.17)	4.39(4.40)	642(636.1)
7d1	acac	C_5H_3(6-Cl)N-C^2	44.56(44.06)	5.77(5.78)	3.35(3.21)	408(436.2)

a) Determined in dichloromethane at 27 °C. b) Insoluble in organic solvents.

TABLE 2. ^1H NMR SIGNALS FROM THE β-DIKETONATE LIGAND IN THE $[Pd(\beta\text{-dik})(pyridyl)(PPh_3)]$ (**5**) AND $[Pd(\beta\text{-dik})(pyridyl)]_2$ (**6**) COMPLEXES AND $[Pd(acac)(C_5H_3(6\text{-Cl})\text{-}N\text{-}C^2)(PEt_3)]$ (**7d1**)[a]

Compd	CH_3	CH
5a1	1.82, 2.02, 2.05	5.30
5b1	1.82	5.41
5c1	1.82	5.36
5d1	1.70, 1.92	5.33
5d2	1.87, 2.07	5.72
6a1	2.02, 2.05	5.44
6d1	1.94, 2.03	5.44
7d1	1.87, 1.91	5.27

a) Chemical shifts in ppm from internal Me_4Si in $CDCl_3$ at room temperature.

being treated with hydrogen peroxide. Isolation of similar products from the other 2-pyridyl complexes **5a3**, **5d2**, and **5d3** was unsuccessful. The reactions of type-**5** complexes containing the 3- and 4-pyridyl ligands with hydrogen peroxide resulted in decomposition of complexes. Complexes **6** may return to **5** by virtue of the bridge-splitting reactions with triphenylphosphine, and will also react with other Lewis bases to afford similar mononuclear complexes. Table 1 includes the analytical data for one of these complexes $[Pd(acac)(C_5H_3(6\text{-Cl})N\text{-}C^2)(PEt_3)]$ (**7d1**) following those for type-**6** complexes.

NMR Spectra. The ^1H NMR signals from the β-diketonate ligands in the $[Pd(\beta\text{-dik})(pyridyl)(PPh_3)]$ (**5**) and $[Pd(\beta\text{-dik})(pyridyl)]_2$ (**6**) complexes as well as $[Pd(acac)(C_5H_3(6\text{-Cl})N\text{-}C^2)(PEt_3)]$ (**7d1**) are collected in Table 2, and the ^{13}C NMR data for complexes **5d1**, **5d2**, **5d3**, and **7d1** are listed in Table 3. Figure 3 also compares the ^1H and $^{13}C\{^1H\}$ NMR signals from the acac ligand in **5d1** and **7d1**. Complex **5d1** exhibits two methyl proton signals at δ 1.72 and 1.92 reflecting unequal environments of the two methyl groups. The higher-field signal is assigned to the methyl group which is positioned cis to triphenylphosphine and experiences the anisotropic shielding effect of the phenyl ring.[7] In the case of complex **7d1** two methyl signals lie close to each other, of which the lower-field one (δ 1.91) coincides with that from **5d1** and is assigned to the methyl group trans to the phosphine. Methyl protons situated cis to PEt_3 resonate in much lower field than those cis to PPh_3 in **5d1**.

Complex **5d1** shows only three ^{13}C signals at δ 27.7, 99.6, and 186.7 which are assigned to the CH_3, CH, and CO carbons of the acac ligand, respectively, indicating similarity in the magnetic influences of the 6-chloro-2-pyridyl and PPh_3 ligands on both halves of acac. On the other hand, the pyridyl and PEt_3 ligands in **7d1** exert slightly different influences on the carbonyl carbons, exhibiting two signals at δ 186.7 and 186.9 which can not be separately assigned. Both of the methyl carbons in **7d1** resonate at δ 28.0, one as a singlet and the other as a doublet (J(P-C)=6 Hz). The latter is attributed to C^5 positioned trans to PEt_3.

As is seen in Fig. 4, methyl protons of the tfac ligand

Table 3. $^{13}C\{^1H\}$ NMR Data for the 6-chloro-2-pyridyl complexes, [Pd(β-dik)(R)(PPh_3)] (**5**) and [Pd(acac)(R)(PEt_3)] (**7dl**) in $CDCl_3$ at room temperature[a)]

Complex	β-dik					R=C_5H_3(6-Cl)N-C^2					PPh_3 or PEt_3			
	CH_3	CF_3	CH	$CH_3\underline{C}O$	$CF_3\underline{C}O$	C^2	C^3	C^4	C^5	C^6	C^1	C^2	C^3	C^4
5dl	27.7		99.6	186.7		174.4 br	129.5 (4)	134.4	117.5	147.4	131.0 (21)	134.2 (12)	127.9 (11)	130.1
5d2	29.0	118.6 [284]	95.0	194.5	167.9 [33]	171.9 br	129.2 br	134.8	118.1	147.4	130.1 (29)	134.1 (12)	128.0 (10)	130.5
5d3		117.7 [286]	89.7		175.2 [34]	168.1 br	126.9 br	135.0	118.8	147.5	130.0 (21)	134.1 (12)	128.4 (12)	130.9
7dl	28.0		99.6	186.7		174.2 (4)	129.9 (5)	134.6	118.0	148.0	14.2 (31)	7.9 (3)		
	28.0 (6)			186.9										

a) β-dik=acac, tfac, and hfac for complexes **1**, **2**, and **3**, respectively. Chemical shifts are given in ppm from internal Me_4Si. Figures in parentheses and brackets give J(C-P) and J(C-F) in Hz.

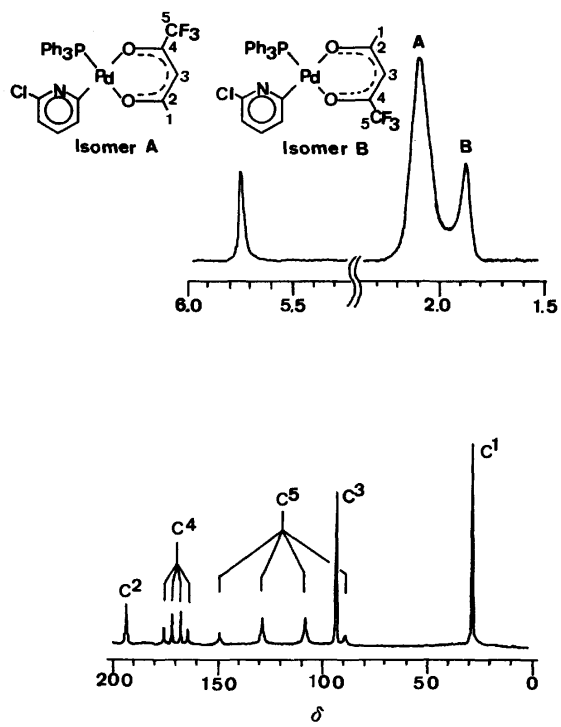

Fig. 4. ^1H and $^{13}C\{^1H\}$ NMR signals from the trifluoroacetylacetonate ligand in [Pd(tfac)(C_5H_3(6-Cl)N-C^2)(PPh_3)] (**5d2**) in $CDCl_3$ at room temperature. Chemical shifts are shown in ppm from internal Me_4Si.

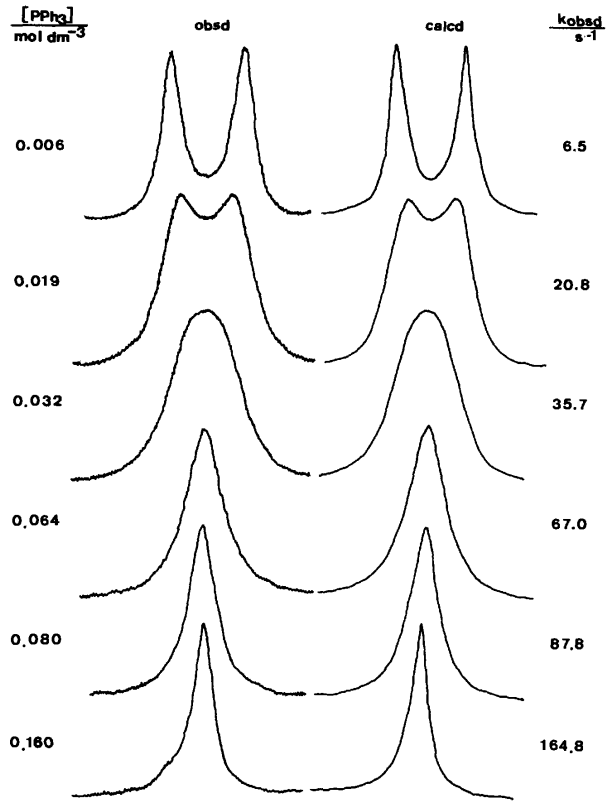

Fig. 5. Methyl proton signals from [Pd(acac)(C_5H_3(6-Cl)N-C^2)(PPh_3)] (**5dl**) in the presence of various concentrations of triphenylphosphine in dichloromethane at −80 °C. [Complex]=0.1 mol dm^{-3}.

in **5d2** exhibit two very broad signals at δ 1.87 and 2.07 with the area ratio of 1:3. There seems to exist two geometrical isomers in solution (Eq. 3) and the minor higher-field signal is assigned to the isomer **B**, in which the methyl group lies at the position cis to PPh_3, and the major one to the other isomer **A**. Similarly to the case of complex **5dl** (Fig. 3), the ^{13}C NMR spectrum of **5d2** involves only one set of signals attributable to the tfac carbons, indicating again that the 6-chloro-2-pyridyl and PPh_3 ligands exert similar trans influences. The hfac ligand in complex **5d3** also shows one set of ^{13}C signals (Table 3).

Coordination-site Exchange Reaction of [Pd(acac)(C_5H_3(6-Cl)N-C^2)(PPh_3)] (5dl) Catalyzed by Lewis Bases. As mentioned already, the acac ligand in complex **5dl** exhibits two sharp methyl signals at δ 1.70 and 1.92 in $CDCl_3$ at room temperature. When an increasing amount of Lewis base such as triphenylphosphine, tri-*o*-tolylphosphine, pyridine, and 2,6-lutidine is added to the solution, these signals become progressively broader to merge into a sharp singlet at δ 1.82. On decreasing temperature of the

solution in dichloromethane, the signal again becomes broader and broader to split into two signals. During these events ^1H signals other than those from the acac-methyls remain unaltered except appearance of peaks due to the added base. These results indicate that **5dl** is stereochemically rigid in noncoordinating solvents but undergoes the coordination-site exchange as shown by Eq. 3 (X=Cl) catalyzed by Lewis bases (L)

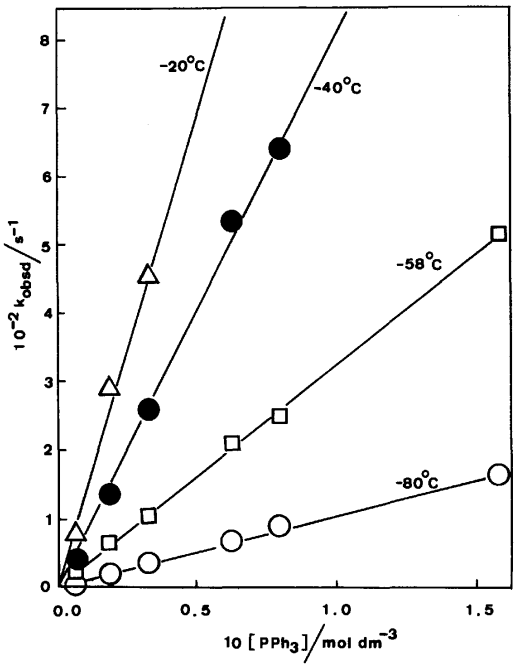

Fig. 6. Pseudo first order rate constant for the coordination-site exchange reaction of complex **5dl** in $CDCl_3$ as a function of triphenylphosphine concentration.

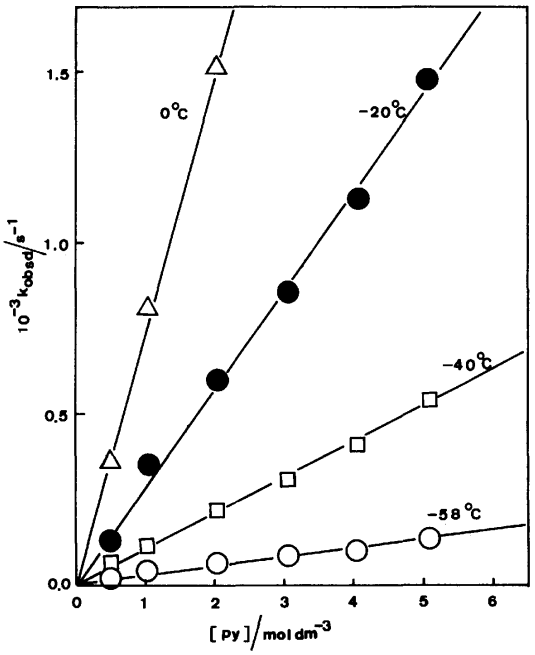

Fig. 7. Pseudo first order rate constant for the coordination-site exchange reaction of complex **5dl** in $CDCl_3$ as a function of pyridine concentration.

and that the fluxional motion is depressed at lower temperatures.

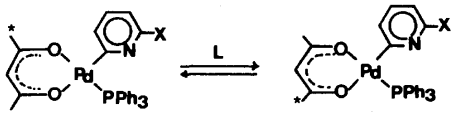

(3)

Pyridine or triphenylphosphine was added in various amounts to a solution (0.1 mol dm^{-3}) of **5dl** in dichloromethane and the rate of coordination-site exchange was determined at 0°C and lower temperatures by means of the line-shape simulation method. Figure 5 exemplifies the change of methyl signals with the concentration of added triphenylphosphine at −80°C. The values of cal-

Table 4. The second order rate constants and activation parameters for the coordination-site exchange reaction of [Pd(acac)(C_5H_3(6-Cl)N-C^2)-(PPh_3)](**5dl**) catalyzed by pyridine and triphenylphosphine

	$\frac{T}{°C}$	py	PPh_3
$10^{-2}k$ / dm^{3}mol^{-1}s^{-1}	0	8.05±0.17	
	−20	2.83±0.08	158±2
	−40	1.03±0.03	82.5±0.6
	−58	0.23±0.02	32.1±0.3
	−80		10.3±0.2
$\Delta H^{\neq}$/kJ mol^{-1}		25.6±0.8	16.8±0.6
$\Delta S^{\neq}$/J K^{-1} mol^{-1}		−94.9±3.0	−96.2±2.4

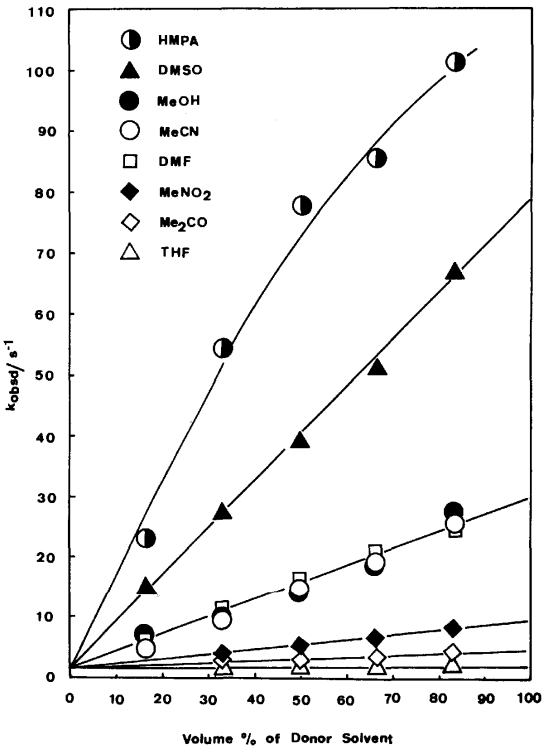

Fig. 8 Pseudo first order rate constant for the coordination-site exchange reaction of complex **5dl** in a mixture of $CDCl_3$ and a donor solvent at 50°C.

culated pseudo first order rate constant k_{obsd} are also included. As is seen in Fig. 6, the plots of k_{obsd} obtained at several temperatures against the concentration of triphenylphosphine afford straight lines passing through the origin. Similar plots in Fig. 7 show the results obtained with pyridine as a catalyst. Slopes of these straight lines gave the second order rate constants which are listed in Table 4. The activation parameters calculated from the Eyring plots are also included in the table. The catalyzed coordination-site exchange reaction has a rather small $\Delta H^{\neq}$ and a large negative $\Delta S^{\neq}$ in either case, suggesting the associative nature of reaction mechanism as is the case for the ligand substitution reactions of square planer complexes.[8] Triphenylphosphine is much more effective as a catalyst than pyridine, the second order rate constants differing by two orders of magnitude.

Various coordinating solvents were also found to stimulate the coordination-site exchange of **5d1** although their catalytic activities are much weaker than those of pyridine and triphenylphosphine. The following eight solvents were examined: hexamethylphosphoric triamide (HMPA), dimethyl sulfoxide (DMSO), methanol, acetonitrile, *N,N*-dimethylformamide (DMF), nitromethane, acetone, and tetrahydrofuran (THF). The pseudo first order rate constant was determined at 50°C by the same way in a mixture of $CDCl_3$ and a perdeuterated donor solvent containing **5d1** at a constant concentration (0.06 mol dm^{-3}). Complex **5d1** is hardly soluble in these solvents and k_{obsd}'s determined in mixed solvents were plotted against the volume percent of donor solvent (Fig. 8). Fortunately all data except those for HMPA lie on straight lines, giving a common intercept at $k_0=2.0\,s^{-1}$. Extrapolation of these lines to 100% gives rates (k_1) in neat donor solvents which can not be determined directly. Tetrahydrofuran is practically ineffective and the rate value 2.0 s^{-1} given by the intercept corresponds to an intrinsic reaction which is not assisted by donor solvents. It is not certain whether the reaction proceeds truly noncatalytically or is promoted by a trace of triphenylphosphine liberated by reaction 4 (X=Cl). It should be noted that straight lines in Figs. 6 and 7

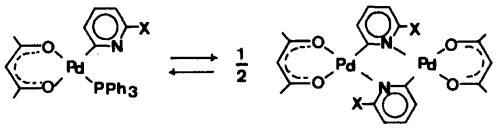

(4)

which show the catalytic effects of pyridine and triphenylphosphine, respectively, do not give intercepts, but go through the origin. Reaction 4 might be endothermic and liberate a trace amount of the phosphine at 50°C (*vide infra*), although the possibility may not be excluded that some other unimolecular mechanism (*e.g.* transformation *via* a tetrahedral transition state), which is not effective below 0°C, makes the observed minor contribution at 50 °C.

The k_1 values (s^{-1}) decreases in the sequence, HMPA (109.5)>DMSO (78.0)>MeOH (30.3)≈MeCN (29.8)≈DMF (29.1)>$MeNO_2$ (8.8)>Me_2CO (4.9). The tendency may be related to the coordination ability of the solvent. In fact the plot of log k_1 against the donor number[9] of solvent gave a straight line although a few data lie far from this line (Fig. 9).

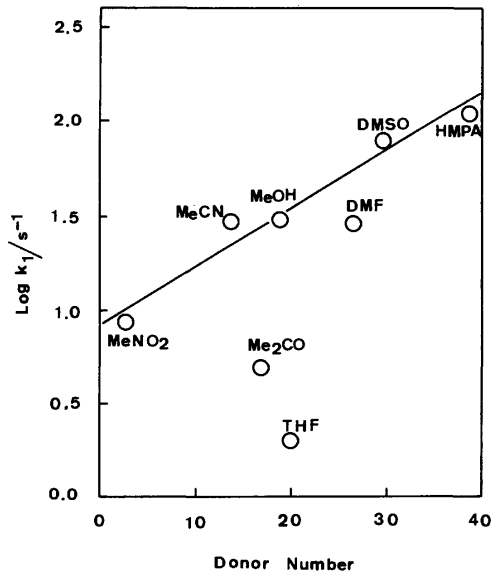

Fig. 9. Relation between the estimated pseudo first order rate constants for the coordination-site exchange reaction of complex **5d1** and donor number of solvents.

Geometrical isomerization of square-planar complexes has been the subject of extensive investigations.[10] Although some complexes such as *cis*-[PtCl(aryl)$(PEt_3)_2$] isomerize spontaneously in polar solvents,[11] most of the isomerization reactions proceed in the presence of neutral or ionic free ligands as catalysts,[12] and two mechanisms, consecutive displacement and intramolecular rearrangement of five-coordinate intermediates, are well documented.[10] Although the catalytic role of a solvent molecule coordinated to a complex as the fifth ligand has been suggested in some cases,[13] no conclusive evidence for solvent catalysis has yet been reported.

The consecutive displacement mechanism is not applicable to the present reaction, since a readily removable unidentate ligand such as halide is not contained in **5d1** and dissociation of the acetylacetonate ligand to give rise to [Pd(pyridyl)$(PPh_3)L_2$](acac) is not conceivable. By the analogy with the case of five-coordinate square-pyramidal complexes [M$(hfac)_2(PR_3)$] ($M=Pd^{II}$ and Pt^{II}, R=*o*-tolyl and cyclohexyl),[14] the intramolecular rearrangement such as illustrated by Eq. 5 is proposed, where R and P denote the pyridyl and phosphine ligands, respectively, and the trigonal-bipyramidal transition state involved in each step is omitted for the sake of brevity.

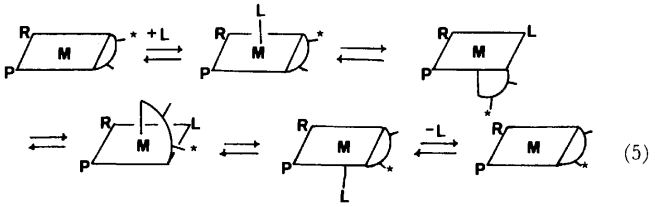

(5)

If the addition reaction to form the five-coordinate

intermediate, **5d1**+L$\overset{K}{\rightleftharpoons}$[Pd(acac)(R)($PPh_3$)L], attains equilibrium rapidly and the following intramolecular transformation is the rate-determining step (k_{tr}), the observed first order rate constant should be expressed by Eq. 6.

$$k_{obsd} = \frac{k_{tr}K[L]}{1+K[L]} \quad (6)$$

The linear dependence of k_{obsd} on the fraction of a donor solvent other than HMPA (Fig. 8) indicates that the equilibrium constants are very small for these solvent molecules even in the neat state. The second order rate law also holds for the reaction catalyzed by pyridine and triphenylphosphine, indicating that K[L] in the denominator of Eq. 6 is much smaller than one even for these strong ligands in the concentration regions examined, [py]<5.0 mol dm^{-3} and [PPh_3]<0.15 mol dm^{-3} against [**5d1**]=0.1 mol dm^{-3}. Although K and k_{tr} cannot be estimated separately at the present stage of investigation, the nature of L may influence not only on K but also on k_{tr}, since k_{obsd} spans over many orders of magnitude.

Coordination-site Exchange Reactions of Acetylacetonate Complexes Containing the 2-, 3-, or 4-Pyridyl Ligand. Methyl protons of the acetylacetonate ligand in the 2-pyridyl complex **5a1** show a singlet at δ 1.82 accompanied by two minor signals at δ 2.02 and 2.05. The chemical shifts of the latter signals exactly coincide with those from the dinuclear complex **6a1**, suggesting attainment of the equilibrium shown by Eq. 4 (X=H). Liberated triphenylphosphine may serve as a catalyst for the coordination-site exchange of **5a1** as expressed by Eq. 3 (X=H), exhibiting a single methyl-proton resonance at δ 1.82. This effect may be called autocatalysis, since the catalyzing species is produced by the reacting species. The δ 1.82 signal becomes broader with decreasing temperature, collapses at −20 °C and gives rise to two signals at −60 °C.

The equilibrium constant of Eq. 4 (X=H) was determined to be 0.01 mol dm^{-3} at 37 °C based on the relative intensities of signals from **5a1** and **6a1**. Oxidation of liberated triphenylphosphine with hydrogen peroxide shifts the equilibrium completely to right and the δ 1.82 signal disappears. On the other hand, the ^1H NMR spectrum of **5d1** shows no sign of coexistence of **6d1**, indicating that the dinuclear bridging is less favorable for the 6-chloro-2-pyridyl ligand than for the 2-pyridyl group. However, treatment of **5d1** with hydrogen peroxide yields **6d1** under the preparative condition, supporting existence of the equilibrium, Eq.4 (X=Cl). It is worth noting that 2,6-dichloropyridine does not catalyze the coordination-site exchange of **5d1** (Eq. 3) although 2,6-dimethylpyridine is effective as a catalyst. The steric requirements of the chloro and methyl substituents are quite similar, and their electronic effects may be responsible for the difference in basicities. Similarly the weaker basicity of the 6-chloro-2-pyridyl ligand than that of the 2-pyridyl ligand seems to make the dinuclear structue in **6d1** less favorable than that in **6a1**.

Each of complexes **5b1** and **5c1** containing the 3- and 4-pyridyl ligands, respectively, shows a broad methyl singlet at δ 1.82 in $CDCl_3$ at room temperature. The signal becomes broader with decreasing concentration and temperature, and is converted into two broad signals at δ 1.74 and 1.92 at −60 °C. Thus the singlet at room temperature seems to be caused by the rapid coordination-site exchange catalyzed by some species. No spectroscopic evidence is observed which suggests liberation of triphenylphosphine to form the dinuclear species from **5b1** and **5c1**. Treatment of these complexes with hydrogen peroxide do not afford type-**6** complexes.

These observations allow the presumption that when two molecules of the reacting species encounter with each other, one is coordinated with the metal atom of the other *via* the nitrogen atom of the pyridyl ligand, forming a five-coordinate intermediate which undergoes the coordination-site exchange. Such a catalysis has no precedent and may be termed "self-catalysis" or "mutual catalysis", since molecules of the reacting species mutually serve as the catalyst. Complexes **5b1** and **5c1** are also effective as catalysts for the coordination-site exchange reaction of **5d1**. The carbon-bonded pyridyl ligand shows higher basicity than free pyridine[4] and tends to interact with another metal atom, stabilizing the dinuclear structure of the 2-pyridyl complexes and the polynuclear linkage in the 3- and 4-pyridyl complexes. The enhanced basicity of the pyridyl ligand is origin of the self-catalysis.

We wish to thank Professor Toshio Tanaka (Osaka University) for his helpful advices on the program of ^1H NMR line shape simulation, and also Mr. Junichi Gohda for elemental analyses.

References

1) K. Isobe and S. Kawaguchi, *Heterocycles*, **16**, 1603 (1981).
2) K. Isobe, K. Nanjo, Y. Nakamura, S. Kawaguchi, K. Kinoshita, and K. Nakatsu, to be published in *Bull. Chem. Soc. Jpn.*
3) K. Nakatsu, K. Kinoshita, H. Kanda, K. Isobe, Y. Nakamura, and S. Kawaguchi, *Chem. Lett.*, **1980**, 913.
4) K. Isobe, E. Kai, Y. Nakamura, K. Nishimoto, T. Miwa, S. Kawaguchi, K. Kinoshita, and K. Nakatsu, *J. Am. Chem. Soc.*, **102**, 2745 (1980); to be published in *Bull. Chem. Soc. Jpn.*
5) Short communications appeared in H. Tanaka, K. Isobe, and S. Kawaguchi, *Chem. Lett.*, **1981**, 769, and *Inorg. Chim. Acta*, **54**, L201 (1981).
6) T. Nakagawa, *Bull. Chem. Soc. Jpn.*, **39**, 1006 (1966).
7) S. Baba, T. Ogura, and S. Kawaguchi, *Bull. Chem. Soc. Jpn.*, **47**, 665 (1974).
8) F. Basolo and R. G. Pearson, "Mechanisms of Inorganic Reactions," 2nd ed, Wiley, New York (1967), Chap. 5.
9) V. Gutman and R. Schmid., *Coord. Chem. Rev.*, **12**, 263 (1974).
10) G. K. Anderson and R. J. Cross, *Chem. Soc. Rev.*, **9**, 185 (1980).
11) R. Romes, D. Minniti, and S. Lanza, *Inorg. Chem.*, **18**, 2362 (1979); **19**, 3663 (1980); H. Kelm, W. J. Louw, and D. A. Palmer, *ibid.*, **19**, 843 (1980); W. J. Louw, R. van Eldik, and H. Kelm, *ibid.*, **19**, 2878 (1980); R. van Eldik, D. A. Palmer, H. Kelm, and W. J. Louw, *ibid.*, **19**, 3551 (1980); W. J. Louw and R. van Eldik, *ibid.*, **20**, 1939 (1981).
12) R. Favez, R, Roulet, A. A. Pinkerton, and D.

Schwarzenbach, *Inorg. Chem.*, **19**, 1356 (1980).
13) D. A. Redfield, J. H. Nelson, R. A. Henry, D. W. Moore, and H. B. Jonassen, *J. Am. Chem. Soc.*, **96**, 6298 (1974); A. W. Verstuyft, L W. Cary, and J. H. Nelson, *Inorg. Chem.*, **14**, 1495 (1975).
14) S. Okeya, T. Miyamoto, S. Ooi, Y. Nakamura, and S. Kawaguchi, *Inorg. Chim. Acta*, **45**, L135 (1980); *Bull. Chem. Soc. Jpn.*, **57**, 395 (1984).

A Study of Inorganic Ion-exchangers. VIII.[1] The Synthesis of the Crystalline $Zr(RNH)_xH_{2-x}(PO_4)_2 \cdot yH_2O$ and Their Characteristics ($R=(C_nH_{2n+1})_3$ and C_5H_5, $n=1—6$)

Etsuro KOBAYASHI* and Shigemitsu SHIN
National Chemical Laboratory for Industry, Yatabemachi, Tsukuba-gun, Ibaraki 305
(Received May 2, 1983)

The synthesis of microcrystalline compounds with the formula of $Zr(RNH)_xH_{2-x}(PO_4)_2 \cdot yH_2O$ ($R=(C_nH_{2n+1})_3$, C_5H_5, $n=1—6$, $x=0.1—0.6$, $y=1—3$) and their characteristics have been investigated. The compounds were formed by means of a hydrothermal reaction between $RNH \cdot H_2PO_4$ and $ZrOCl_2$ in the mole ratio of 4:1 at 130—180 °C. The layer-spacings of the trimethyl-, triethyl-, tripropyl-, tributyl-, tripentyl-, trihexylamine, and pyridine phosphates were 9.9, 13.0, 13.6, 17.0, 16.5, 18.4, and 10.9 Å respectively. In the thermal decomposition of each phosphate, the water of crystallization was eliminated at 105—130 °C. The organic base group in the alkylamine phosphates was burned in the presence of air at 330—360 °C, but this combustion was imperfect in the case of pyridine phosphate. The phosphates condensed at 400—450 °C. $Zr(RNH)_xH_{2-x}(PO_4)_2 \cdot yH_2O$ was also obtained by means of an ion-exchange reaction between γ-$Zr(HPO_4)_2 \cdot 2H_2O$ and the corresponding tertiary amine. In these products, the layer-spacings of the trimethyl-, triethyl-, tripropyl-, tributyl-, tripentyl-, and trihexylamine phosphates were 17.6, 16.4, 16.7, 21.0, 21.5, and 23.2 Å respectively, while those of pyridine and piperidine phosphates were 12.4 and 18.4 Å respectively. The layer-spacings of the products increased roughly with the size of the guest molecules. When $Zr(RNH)_xH_{2-x}(PO_4)_2 \cdot yH_2O$ was treated with HCl, the products from the hydrothermal reaction changed to α-$Zr(HPO_4)_2 \cdot H_2O$, while the products from the ion-exchange reaction returned to γ-$Zr(HPO_4)_2 \cdot 2H_2O$ the raw material.

Recently, inorganic layer structure compounds have been considered to be materials with specific functions. Titanium and zirconium phosphates are useful compounds for ion-exchange, though a compound with a large layer-spacing can not be obtained as a result of the use of hydrogen and exchanged metal ions which are small in radius. The large layer-spacing compounds performing a chemical embellishment are promising as materials with specific functions as catalysers. Zirconium phosphates containing an organic radical have been obtained by means of ion-exchange reactions between α-,β-zirconium(IV) bis(hydrogenorthophosphate) and pyridine,[2] or butylamine.[3] The organo-derivatives of zirconium phosphate with a P-O-P ester bond were obtained by the reactions of γ-$Zr(HPO_4)_2 \cdot 2H_2O$ with ethylene oxide[4] or propylene oxide.[5] By another method, microcrystalline compounds with the $Zr(HOCH_2PO_3)_2 \cdot H_2O$, $Zr(C_6H_5PO_3)_2$, and $Zr(C_2H_5OPO_3)_2$ formulae were formed by slowly decomposing the fluorozirconium complex in the presence of $HOCH_2PO(OH)_2$, $C_6H_5PO(OH)_2$, and $PO(OC_2H_5)_2$.[6]

To develop an inorganic ion-exchanger, we synthesized γ-zirconium phosphate by means of a hydrothermal reaction between $ZrOCl_2$ and MH_2PO_4 (M=Na, K, NH_4).[1] For the present studies, $RNH \cdot H_2PO_4$ ($R=(C_nH_{2n+1})_3$, C_5H_5, $n=1—6$) was prepared by the reaction of phosphoric acid with tertiary amine, while $Zr(RNH)_xH_{2-x}(PO_4)_2$, with a larger layer-spacing than γ-$Zr(HPO_4)_2 \cdot H_2O$, was formed by a hydrothermal reaction between $RNH \cdot H_2PO_4$ and $ZrOCl_2$ in an autoclave. The synthesis conditions were determined, and the characteristics of the product were investigated and compared with those of a product obtained by the ion-exchange between γ-$Zr(HPO_4)_2 \cdot 2H_2O$ and the corresponding tertiary amine.

Experimental

Direct Method Synthesizing $Zr(RNH)_xH_{2-x}(PO_4)_2$. By refluxing between 1 mol of reagent-grade tertiary amine, 1 mol of 85% phosphoric acid, and a little water, an oily tertiary amine phosphate, $RNH \cdot H_2PO_4$ ($R=(C_nH_{2n+1})_3$, C_5H_5, $n=1—6$), was prepared beforehand for the following purpose.

In a 20 cm^3-hard glass tube, 1.61 g of $ZrOCl_2 \cdot 8H_2O$, 2—12 g of $RNH \cdot H_2PO_4$, and 5 cm^3 of water were taken. The contents were then thoroughly mixed, and the tube was sealed. 1—4 sealed tubes thus prepared under varying conditions were placed in a 200-cm^3 stainless steel autoclave with 80 cm^3 of water to prevent the rupture of the glass tubes. The autoclave was then heated at 120—180 °C. The products in the tube were separated from the mother liquors, washed with water, and then dried at 20 °C in a relative humidity (R.H.) of 75%. In direct synthesis by means of a 300-cm^3 autoclave lined with Hastelloy-B, 5—20 times as much of the raw materials were used, and the products were obtained with the above methods.

Formation of $Zr(RNH)_xH_{2-x}(PO_4)_2$ by Means of the Ion-exchange Method. In a 200-cm^3 Erlenmeyer flask, one gram of γ-$Zr(HPO_4)_2 \cdot 2H_2O$ 0.91—8.07 g of tertiary amine and 100 dm^3 of water were mixed and stirred for 24 h at 50 °C; the product thus obtained was separated, washed by means of a centrifugal separator, and finally dried.

Analysis. The P_2O_5 and ZrO_2 as components of the reaction product were determined according to the previously reported methods.[1] H_2O was obtained by deducting the weight of the Tertiary amine from the weight loss of the sample heated at 800 °C. Tertiary amine was obtained by the ammonia-distillation method.

The X-ray diffraction was performed with a Shimadzu Seisakusho diffractometor, using Ni filtered Cu $K\alpha$ radiation at 30 KVP and 20 mA. A Rigaku Denki micro-thermal analyzer with 100 μV of DTA sensibility and 20 mg of TG sensibility was used for the thermal analysis.

Results and Discussion

Reactions of $ZrOCl_2$ with $RNH \cdot H_2PO_4$ (Direct-synthesizing Method). The conditions for the synthesis of $Zr(RNH)_xH_{2-x}(PO_4)_2$ and the analytical data of the products are shown in Table 1.

The influence of the $RNH \cdot H_2PO_4/Zr$ mole ratios on the hydrothermal reaction between $(C_2H_5)_3NH \cdot H_2PO_4$

TABLE 1. SYNTHESIS OF $Zr(RNH)_xH_{2-x}(PO_4)_2$ AND THEIR ANALYSIS (R=(C_nH_{2n+1}), C_5H_5, n=1—6)

No.	Reaction conditions: $ZrOCl_2 \cdot 8H_2O$ (g)	$RNH \cdot H_2PO_4$: Tertiary amine	(%)	(g)	H_2O (ml)	$RNH \cdot H_2PO_4$/Zr (mole ratio)	Temp °C	Time h	Mother liquor (pH)	Reaction products: ZrO_2 (%)	P_2O_5 (%)	Tertiary amine (%)	H_2O (%)	ZrO_2 : P_2O_5 : Tertiary amine : H_2O (mole ratio)
1	1.61	$(C_2H_5)_3N$	83.6	2.38	5	2.0	150	120	1.96	35.5	40.8	3.45	20.4	1.0 : 1.0 : 0.12 : 4.0
2	1.61	$(C_2H_5)_3N$	83.6	3.57	5	3.0	150	120	2.13	34.9	40.2	11.7	13.2	1.0 : 1.0 : 0.41 : 2.6
3	1.61	$(C_2H_5)_3N$	83.6	4.76	5	4.0	150	120	2.23	33.5	38.5	14.8	12.0	1.0 : 1.0 : 0.58 : 2.5
4	3.88	$(C_2H_5)_3N$	99.0	12.3	5	5.14	150	120	2.41	33.2	38.3	15.7	12.3	1.0 : 1.0 : 0.57 : 2.5
5	1.61	$(C_2H_5)_3N$	99.0	9.52	5	8.0	150	120	2.74	33.1	38.1	16.5	12.3	1.0 : 1.0 : 0.60 : 2.5
6	1.61	$(C_2H_5)_3N$	83.6	4.76	5	4.0	130	120	2.26	33.2	38.3	16.6	12.0	1.0 : 1.0 : 0.60 : 2.5
7	1.61	$(n\text{-}C_3H_7)_3N$	99.0	4.75	5	4.0	130	120	2.04	35.5	40.9	7.36	16.3	1.0 : 1.0 : 0.18 : 3.1
8	1.61	$(n\text{-}C_4H_9)_3N$	99.0	5.67	5	4.0	130	120	1.95	31.4	35.5	19.0	14.3	1.0 : 1.0 : 0.40 : 3.1
9	1.61	C_5H_5N	91.3	3.89	5	4.0	130	120	2.42	34.7	40.1	4.46	21.1	1.0 : 1.0 : 0.20 : 4.1
10	1.61	$(C_2H_5)_3N$	83.6	4.76	5	4.0	160	96	2.42	33.8	39.0	14.9	12.3	1.0 : 1.0 : 0.54 : 2.5
11	1.61	$(n\text{-}C_3H_7)_3N$	99.0	4.75	5	4.0	160	96	2.12	36.2	41.8	5.81	16.1	1.0 : 1.0 : 0.14 : 3.0
12	1.61	$(n\text{-}C_4H_9)_3N$	99.0	5.67	5	4.0	160	96	2.51	34.6	39.8	12.9	12.7	1.0 : 1.0 : 0.25 : 2.5
13	1.61	C_5H_5N	91.0	3.89	5	4.0	160	96	2.23	34.9	40.2	5.13	19.8	1.0 : 1.0 : 0.23 : 3.9
14	1.61	$(C_2H_5)_3N$	83.6	4.76	5	4.0	180	96	2.38	32.9	37.8	15.4	13.9	1.0 : 1.0 : 0.58 : 2.9
15	1.61	$(n\text{-}C_3H_5)_3N$	99.0	4.75	5	4.0	180	96	2.25	37.9	43.6	3.98	14.5	1.0 : 1.0 : 0.091 2.6
16	1.61	$(n\text{-}C_4H_9)_3N$	99.0	5.67	5	4.0	180	96	2.26	33.6	38.7	15.0	12.7	1.0 : 1.0 : 0.29 : 2.6
17	1.61	C_5H_5N	91.0	3.89	5	4.0	180	96	2.31	34.9	40.2	5.52	19.2	1.0 : 1.0 : 0.25 : 3.7
18	16.1	$(CH_3)_3N$	57.0	35.1	10	4.0	150	24	2.60	36.9	42.5	9.2	11.4	1.0 : 1.0 : 0.51 : 2.1
19	16.1	$(C_2H_5)_3N$	83.6	47.6	45	4.0	140	24	2.65	35.6	41.1	15.2	8.1	1.0 : 1.0 : 0.51 : 1.5
20	32.2	$(n\text{-}C_3H_7)_3N$	86.7	109.8	40	4.0	140	24	2.14	35.8	41.2	9.0	14.0	1.0 : 1.0 : 0.21 : 2.6
21	16.1	$(n\text{-}C_4H_9)_3N$	80.0	70.9	40	4.0	140	24	2.67	32.1	36.9	23.0	8.0	1.0 : 1.0 : 0.47 : 1.7
22	8.05	$(n\text{-}C_5H_{11})_3N$	60.0	54.2	21	4.0	150	24	2.32	36.6	45.9	8.1	7.0	1.0 : 1.0 : 0.10 : 1.2
23	8.05	$(n\text{-}C_6H_{13})_3N$	90.2	39.9	30	4.0	150	24	2.10	33.6	29.2	32.8	4.4	1.0 : 1.0 : 0.51 : 1.0
24	32.2	C_5H_5N	91.3	77.8	50	4.0	140	24	3.01	39.9	45.9	5.0	9.2	1.0 : 1.0 : 0.20 : 1.6

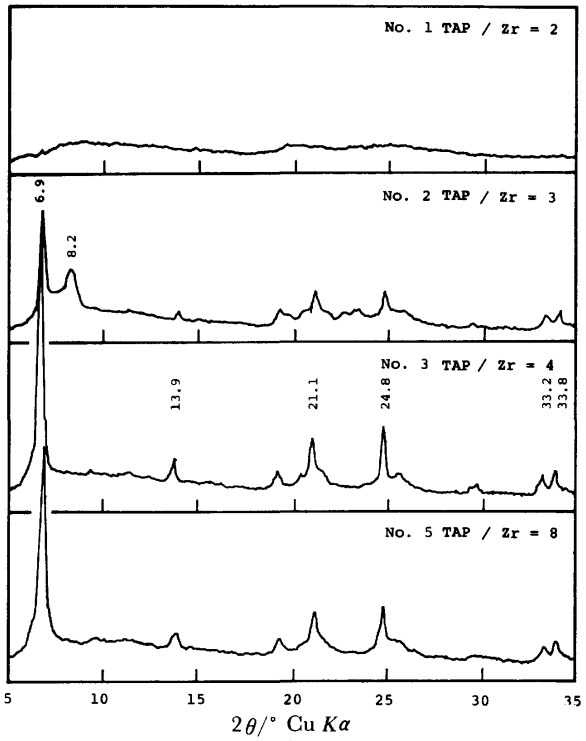

Fig. 1. X-Ray diffraction patterns of $Zr[(C_2H_5)_3NH]_xH_{2-x}(PO_4)_2$. (Influence of mole ratios of $(C_2H_5)_3NH \cdot H_2PO_4$/$ZrOCl_2$).
Numerals on the peaks indicate 2θ/°

and $ZrOCl_2$ were examined in Nos. 1—5 of Table 1; the X-ray diffraction patterns of the reaction products are shown in Fig. 1.

In the $RNH \cdot H_2PO_4$/Zr mole ratio of 2 (No. 1), an amorphous product was formed, though in the X-ray diffraction pattern of the product in the $RNH \cdot H_2PO_4$/Zr mole ratio of 3, the peaks appeared at 6.9 and 8.2°. In the products of the $RNH \cdot H_2PO_4$/Zr mole ratios of 4 (No. 3) and 8 (No. 5), the peak intensity of 6.9° increased and the peak of 8.2° disappeared completely. In Nos. 3, 4, and 5, crystalline products with roughly regular components were obtained. It is considered, therefore, that $RNH \cdot H_2PO_4$/Zr mole ratios of 4 or more are suitable for the synthesis of $Zr(RNH)_xH_{2-x}(PO_4)_2$, which can be written as follows;

$$ZrOCl_2 + 2RNH\,H_2PO_4 \longrightarrow Zr(RNH)_xH_{2-x}(PO_4)_2 + 2\text{-}x\,RNHCl + x\,HCl + H_2O.$$

In the hydrothermal synthesis of γ-$ZrNH_4H(PO_4)_2$,[1] the pH values of the reaction solution were in the range of 2.15—3.56; we are also shown as 2—3 in the formation of $Zr(RNH)_xH_{2-x}(PO_4)_2$.

Influence of Reaction Temperatures: An amorphous product was formed in the mother liquor at temperatures lower than 100 °C. The product crystallized above 120 °C, and the crystallinity was augmented with the elevation of the reaction temperature. The product was red-browned by the thermal decomposition of tertiary amine at 180 °C or higher. In an X-ray diffraction pattern of the reaction product at 250 °C, the diffraction peak-characterized product decreased in intensity; however, the X-ray diffraction peaks of the α-$Zr(HPO_4)_2 \cdot H_2O$ formed as a result of the decomposition of the product appeared anew. It may be concluded, therefore, that heating at 130—180 °C is suitable for the synthesis of $Zr(RNH)_xH_{2-x}(PO_4)_2$.

Composition of Reaction Products: Examples of various reaction conditions are shown in Nos. 6—24 of Table 1.

From the analytical data, the chemical formulae of the products dried in R.H. 75% can be written as follows: $Zr[(CH_3)_3NH]_{0.5}H_{1.5}(PO_4)_2 \cdot 2H_2O$, $Zr[(C_2H_5)_3NH]_{0.5}H_{1.5}(PO_4)_2 \cdot 1.5$—$2.0H_2O$ (No. 19 Product dried in R.H. 0%; 0.5 hydrate), $Zr[(C_3H_7)_3NH]_{0.1-0.2}H_{1.9-1.8}(PO_4)_2 \cdot 1.5$—$2.0H_2O$, (No. 20 Product dried in R.H.

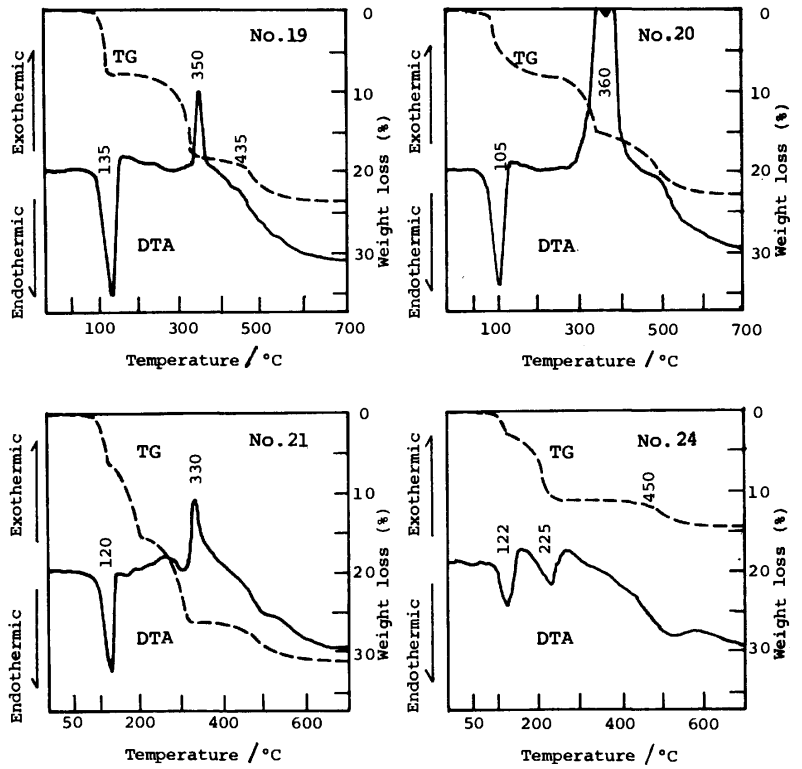

Fig. 2. DTA and TG curves of $ZrRNH_xH_{2-x}(PO_4)_2$ (R= $(C_2H_5)_3$, $(C_3H_7)_3$, $(C_4H_9)_3$, C_5H_5).
No. 19: $Zr[(C_2H_5)_3NH]_{0.5}H_{1.5}(PO_4)_2 \cdot 0.5H_2O$, No. 20: $Zr[(C_3H_7)_3 \cdot NH]_{0.2}H_{1.8}(PO_4)_2 \cdot 1.6H_2O$, No. 21: $Zr[(C_4H_9)_3NH]_{0.5}H_{1.5}(PO_4)_2 \cdot 0.7H_2O$, No. 24: $Zr(C_5H_5NH)_{0.2}H_{1.8}(PO_4)_2 \cdot 0.6H_2O$

Table 2. Formation and analysis of reaction products between γ-$Zr(HPO_4)_2 \cdot 2H_2O$ and tertiary amine

No.	Reaction conditions							Reaction products							
	γ-$Zr(HPO_4)_2 \cdot 2H_2O$ (g)	Tertiary amine Compound	(g)	H_2O (C_2H_5OH) (ml)	Tertiary amine / Zr (mole ratio)	Temp °C	Time h	Dry (temp./°C R.H./%)	ZrO_2 (%)	P_2O_5 (%)	Tertiary amine (%)	H_2O (%)	ZrO_2 : P_2O_5 : Tertiary amine (mole ratio)		
1	1.00	$(CH_3)_3N$	1.86 (57%)	100	3.0	25	30	20, 75	34.6	39.8	12.8	12.9	1.0 : 1.0 : 0.77		2.56
2	1.00	$(C_2H_5)_3N$	0.91	100	3.0	50	24	20, 75	39.1	33.9	16.5	10.5	1.0 : 1.0 : 0.59		2.12
3	1.00	$(n\text{-}C_3H_7)_3N$	4.29	100	9.5	50	24	20, 0	41.1	35.6	13.1	10.3	1.0 : 1.0 : 0.31		1.98
4	1.00	$(n\text{-}C_4H_9)_3N$	5.59	100	9.5	50	24	20, 75	35.2	30.6	21.0	13.2	1.0 : 1.0 : 0.45		2.95
5	1.00	$(n\text{-}C_5H_{11})_3N$	6.82	5 (95)	9.5	25	30	20, 0	32.4	37.3	30.8	0.0	1.0 : 1.0 : 0.52		0.0
6	1.00	$(n\text{-}C_6H_{13})_3N$	8.07	5 (95)	9.5	25	30	20, 0	30.1	34.7	32.8	2.4	1.0 : 1.0 : 0.49		0.56
7	1.00	C_5H_5N	2.22	100	9.5	45	24	20, 75	44.7	38.8	8.39	8.0	1.0 : 1.0 : 0.54		3.18
8	1.00	$C_5H_{11}N$	2.55	100	9.5	25	30	20, 75	32.8	37.7	16.4	13.1	1.0 : 1.0 : 0.72		2.73

0%; 0.7 hydrate), $Zr[(C_4H_9)_3NH]_{0.3-0.5} \cdot H_{1.7-1.5}(PO_4)_2 \cdot 1.5$—$2.0H_2O$ (No. 21 Product dried R.H. 0%; 0.7 hydrate). $Zr(C_5H_5NH)_{0.2-0.25}H_{1.8-1.75}(PO_4)_2 \cdot 2.5$—$3.0H_2O$ (No. 24 Product dried R.H. 0%; 0.6 hydrate). The mole ratios of tertiary amine/P_2O_5 in the product showed the following order: methylamine=ethylamine > butylamine > pyridine > propylamine phosphates. It is considered that the order is influence by the basicity, size, and structure of the tertiary amines.

Behavior of Thermal Decomposition: The DTA and TG curves of $Zr(RNH)_xH_{2-x}(PO_4)_2 \cdot yH_2O$ are shown in Fig. 2.

The products released the water of crystallization at 105—135 °C, and an endothermic peak appeared on the TG curve. In the trialkylamine phosphates of Nos. 19—21, an exothermic peak owing to the combustion of the amine radical appeared at 330—360 °C, but the exothermic peak could not be recognized because of the incomplete combustion of the aromatic radical in the pyridine phosphate of No. 24.

The formation of pyrophosphate attributable to the condensation of orthophosphate occured at 400—450 °C. This temperature was higher than that of γ-$Zr(HPO_4)_2 \cdot 2H_2O$. Therefore, the $Zr(RNH)_xH_{2-x}(PO_4)_2$, which preserved its layer structure until 400 °C, can be considered to be a catalytic functional material.

Ion-exchange between γ-$Zr(HPO_4)_2 \cdot 2H_2O$ and Tertiary Amines. The conditions for the formation of $Zr(RNH)_xH_{2-x}(PO_4)_2$ and the analytical data of the products are shown in Table 2.

We are afraid that, as $(CH_3)_3N$ and $(C_2H_5)_3N$ have a stronger basicity than the other tertiary amines, γ-

$Zr(HPO_4)_2 \cdot 2H_2O$ as a acid salt was dissolved in the solution of the excess amine. Consequently, the amounts of $(CH_3)_3N$ and $(C_2H_5)_3N$ used were 1/3 equivalents as compared with those of the other tertiary amines. The P_2O_5 contents were about the same as those in the corresponding products obtained by the direct synthesizing method, while the tertiary-amine contents in the trimethylamine, tripropylamine, and pyridine phosphates were larger than in the products of the direct-synthesizing method. The tertiary-amine contents in the tripropylamine phosphates obtained by both methods were less than in the other phosphates. All the products dried in 75 % R.H. at 20 °C have 1—2 mol of the water of crystallization. It can be expected that one molecular layer of water is held between the upper and lower phosphate layers.

Layer-spacing and Orientation of Tertiary Amines. The layer-spacing was determined from a first d value (002) of the X-ray diffraction pattern. The layer-spacings of the trimethylamine, triethylamine, tripropylamine, tributylamine, tripentylamine, trihexylamine, and pyridine phosphates obtained by the direct-synthesizing method were 9.9, 13.0, 13.6, 17.0, 16.5, 18.4, and 10.9 Å, (Å=10^{-10} m) respectively. On the other hand, the layer-spacings of trimethylamine, triethylamine, tripropylamine, tributylamine, pyridine, and piperidine phosphates were 17.66, 16.4, 16.7, 21.0, 21.5, 23.2 12.4, and 18.4 Å respectively.

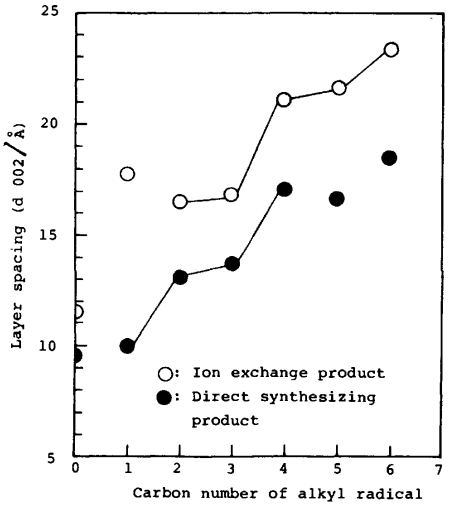

Fig. 3. Relation between layer spacing of product and carbon number of alkyl radical.
○: Ion exchange product of ZrP with NH_4OH. ●: Hydrothermal reaction product of $ZrOCl_2$ with $NH_4H_2PO_4$.

The relation between the layer-spacing of the product and the carbon number of the alkyl group is plotted in Fig 3. In this diagram, the two points at carbon number=0 indicate the layer-spacing of the ion-exchange product between γ-$Zr(HPO_4)_2 \cdot 2H_2O$ with aqueous ammonia and that of the hydrothermal reaction product of $ZrOCl_2$ with $NH_4H_2PO_4$ respectively. The layer-spacing increased with an increase in the carbon numbers of the alkyl group, with the exceptions of the trimethylamine phosphate produced by the ion-exchange and the tripentylamine phosphate produced by the direct method. However, the values of layer-spacing in the cases of n=odd number approximated to that in the cases of $n-1$. The upper and the lower phosphate layers were each connected with the tertiary amines which were sandwiched in the layers. Moreover the C_nH_{2n+1} molecules are considered to be oriented in a step-by-step manner, as is in Fig. 4.

The analytical data in Table 1 show tertiary amine/ZrO_2=0.5 in the products of $n \leqslant 2$ and tertiary amine/ZrO_2=0.1—0.5 in the products of $n \geqslant 3$. If the

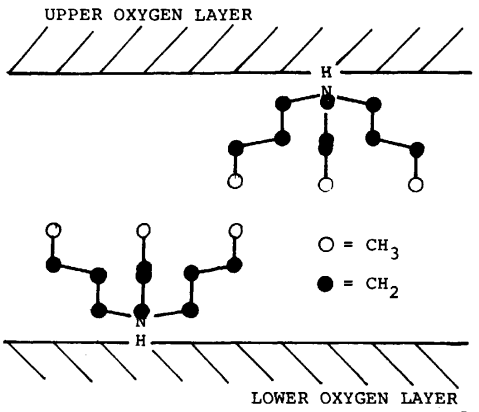

Fig. 4. Interlayer model of $Zr(C_3H_7)_3NH_xH_{2-x}(PO_4)_2$.

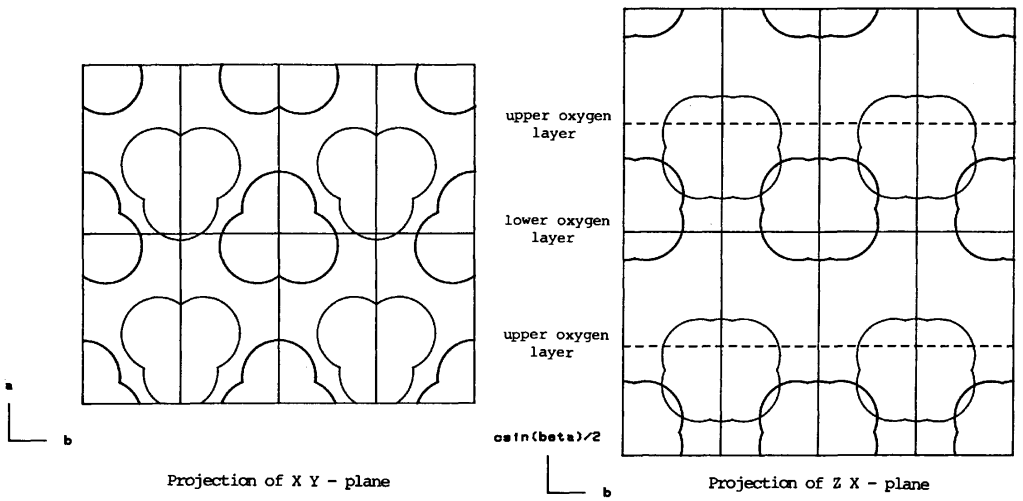

Fig. 5. Configuration of $(C_2H_5)_3N$ in layer spacing of α-$Zr(HPO_4)_2 \cdot H_2O$.

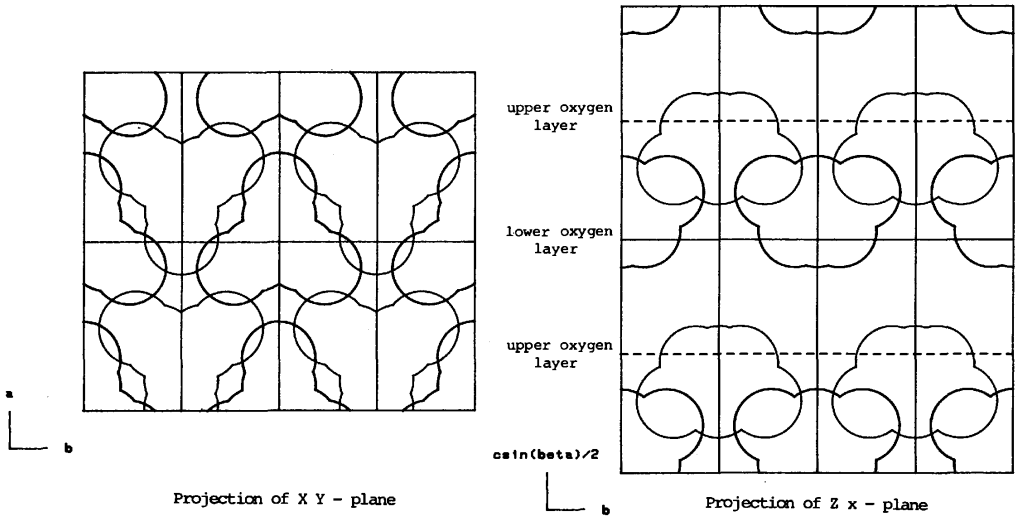

Fig 6. Configuration of $(C_3H_7)_3N$ in layer spacing of α-$Zr(HPO_4)_2$.

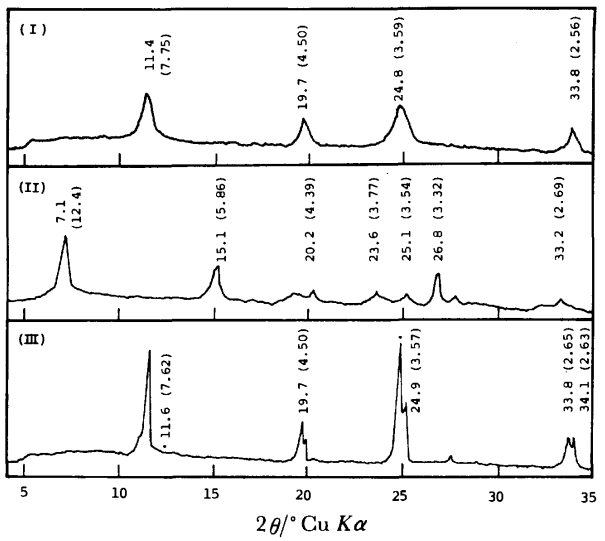

Fig. 7. X-Ray diffraction patterns of zirconium(VI)-bis(hydrogenphosphate).
I: Reaction product between $Zr[(C_4H_9)_3NH]_{0.5}H_{1.5}(PO_4)_2 \cdot 0.7H_2O$ (No. 21) and HCl. II: Reaction product between $Zr[(C_4H_9)_3NH]_{0.5}H_{1.5}(PO_4)_2 \cdot 1.5H_2O$ (Table 2, No. 3) and HCl. III: α-$Zr(HPO_4)_2 \cdot H_2O$. Numerals on the peaks indicate $2\theta/°$ and lattice distances.

value of tertiary amine/ZrO_2 is 0.5, and if the van der Waals radii of CH_2 and CH_3 in the alkyl group are 2 Å, then the arrangement of alkyl groups between the layers of α-$Zr(HPO_4)_2 \cdot H_2O$ may be as projected in Fig. 5 (triethylamine phosphate) and in Fig. 6 (tripropylamine phosphate). If $n \leqslant 2$, the amine molecules between layers of α-$Zr(HPO_4)_2 \cdot H_2O$ are not adjacent to each other and are arranged in a packed state. However ,if $n \geqslant 3$, the products actually have the tertiary amine/ZrO_2 values are 0.1—0.5; consequently, the amine molecules are oriented so as to avoid contact with each other.

Acid Salts of $Zr(RNH)_xH_{2-x}(PO_4)_2$. The X-ray diffraction patterns of the acid salts which are obtained by a hydrochloric acid treatment of the direct-synthesizing and ion-exchange products, and that of α-$Zr(HPO_4)_2 \cdot H_2O$ are shown in Fig. 7.

The direct-synthesizing method is similar to the preparation of $ZrNH_4H(PO_4)_2$[1] as a raw material of γ-$Zr(HPO_4)_2 \cdot 2H_2O$ and the layer-spacing of tributylamine phosphate obtained by the direct-synthesizing method shows a large 17 Å value. It can be simply expected, therefore, that the tributylamine phosphate has the γ-form. Howevere, the X-ray diffraction pattern (I) of the acid-treatment salt of the tributylamine phosphate agreed with that (III) of α-$Zr(HPO_4)_2 \cdot H_2O$. This fact was observed in the acid-treatment salts of the triethylamine, tripropylamine and pyridine phosphates, while the X-ray diffraction pattern (II) of the acid-treatment salt of the tributylamine phosphate obtained by the ion-exchange agreed with that of γ-$Zr(HPO_4)_2 \cdot 2H_2O$ the raw material. A similar phenomenon was also observed in the acid-treatment salts of other $Zr(RNH)_xH_{2-x}(PO_4)_2$ (R=Et, Pr, C_5H_5).

References

1) a) Presented at the 47th National Meeting of the Chemical Society of Japan, Kyoto, April 1983; b) Part VII of this series: E. Kobayashi, *Bull. Chem. Soc. Jpn.*, **56**, 3756 (1983).
2) S. Yamanaka, Y. Horibe, and M. Tanaka, *J. Inorg. Nucl. Chem.*, **38**, 324 (1976).
3) T. Kijima, 45th National Meeting of the Chemical Society of Japan, Tokyo, April 1982, Abstr. I, p. 486.
4) S. Yamanaka, *J. Inorg. Nucl. Chem.*, **41**, 1187 (1979).
5) S. Yamanaka, M. Tsujimoto, and M. Tanaka, *J. Inorg. Nucl. Chem.*, **41**, 606 (1979).
6) G. Alberti and U. Constantino, *J. Inorg. Nucl. Chem.* **40**, 1113 (1978).

Synthesis and Stereoisomerization of Intra- and Intermolecularly Bridged Indigo

Yoshimori OMOTE,* Atsushi TOMOTAKE, Hiromu AOYAMA, Takehiko NISHIO, and Choji KASHIMA
Department of Chemistry, University of Tsukuba, Sakura-mura, Niihari-gun, Ibaraki 305
(Received August 1, 1983)

The intramolecularly bridged *N,N'*-azelaoylindigo (**3**) and *N,N'*-sebacoylindigo (**4**) have been synthesized from indigo and the corresponding dichloride. The intermolecularly bridged *N',N''*-sebacoylbis(*N*-acetylindigo) (**5**) has been synthesized from *N*-acetylindigo and sebacoyl dichloride. The relative rates of the cis-to-trans thermal isomerization of **3**, **4**, and **5**, compared with that of *N,N'*-diacetylindigo (**1c**), were as follows: **3**, 0.77; **4**, 3.9; **5**, 1.4; **1c**, 1.0.

Trichochromes, which were isolated from the red feathers of New Hampshire chickens[1] and human red hair,[2] are low molecular melanin pigments, and are unique in exhibiting photochromism. During the course of an investigation of melanins, we have been interested in indigoid pigments as model compounds of trichochromes.

Indigo (**1a**), an indigoid pigment, exists in trans-form and cannot be isomerized into the corresponding cis-isomer even by irradiation,[3] owing to their photostability caused by a hydrogen-bonding[4] and/or a fast proton transfer in the excited state.[5] Therefore, *N,N'*-dimethyl-(**1b**)[6,7] and *N,N'*-diacetylindigo (**1c**)[3,8] show phototropic behavior, and the stereoisomerization of some *N,N'*-diacylindigo was described in our preceeding report.[9]

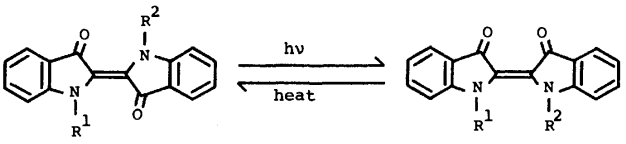

1a : $R^1 = R^2 = H$
1b : $R^1 = R^2 = CH_3$
1c : $R^1 = R^2 = COCH_3$

2 : $R^1 = R^2 = COCO$

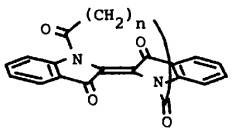

3 : n = 7
4 : n = 8

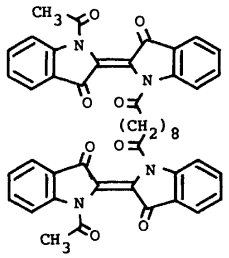

5

On the other hand, *N,N'*-oxalylindigo (**2**), which is an intramolecularly bridged indigo, exists only in the cis-form because of its conformational restriction.[8] Insertion of methylene groups between the two carbonyl carbons of the oxalyl group was expected to cause a relaxation of the restriction. Hence, the synthesis of *N,N'*-azelaoylindigo (**3**), *N,N'*-sebacoylindigo (**4**), and *N',N''*-sebacoylbis(*N*-acetylindigo) (**5**) were carried out, and the cis-to-trans thermal isomerization of these intra- and intermolecularly bridged indigos was investigated.

Results and Discussion

Synthesis of Intra- and Intermolecularly Bridged Indigo. By the reported method,[8] *N,N'*-oxalylindigo (**2**) was synthesized from indigo and oxalyl dichloride in nitrobenzene under mild conditions. Attempted synthesis of compound **3** or **4** by this method failed. These compounds were synthesized by the improved method of Posner.[10]

The structure of *N,N'*-azelaoylindigo (**3**) was confirmed by the IR spectrum which showed two characteristic carbonyl bands at 1670 and 1700 cm^{-1}, by the NMR spectrum which showed the peaks of the methylenic protons at δ=1.3—3.7 and peaks of the aromatic protons at δ=7.4—8.5 and by the elemental analysis. The visible spectrum showed that the absorption maximum of **3** was very similar to that of *N,N'*-diacetylindigo (**1c**) which existed in the trans-form rather than that of *N,N'*-oxalylindigo (**2**) which existed in the cis-form. Therefore the configuration of **3** was assumed to be the trans-form. Similarly the structure and configuration of *N,N'*-sebacoylindigo (**4**) was confirmed by its physical properties in Table 1.

The intermolecularly bridged *N'*, *N''*-sebacoylbis-(*N*-acetylindigo) (**5**) was synthesized from *N*-acetyl

TABLE 1. PHYSICAL PROPERTIES OF INTRA- AND INTERMOLECULARLY BRIDGED INDIGO

Compound	ν^{KBr}/cm^{-1} (C=O)	δ^{CDCl_3}	λ_{max}^{xylene}/nm (ε)
3	1670, 1700	1.3—3.7 (m, 14H), 7.4—8.5 (m, 8H)	569 (6490)
4	1670, 1700	1.1—3.5 (m, 16H), 7.2—8.3 (m, 8H)	572 (7700)
5	1680, 1690, 1710	0.7—3.0 (m, 16H), 2.5 (s, 6H), 7.1—8.5 (m, 16H)	566 (12500)
2	1660, 1695, 1710		439 (8590)
1c	1680, 1700		562 (6630)

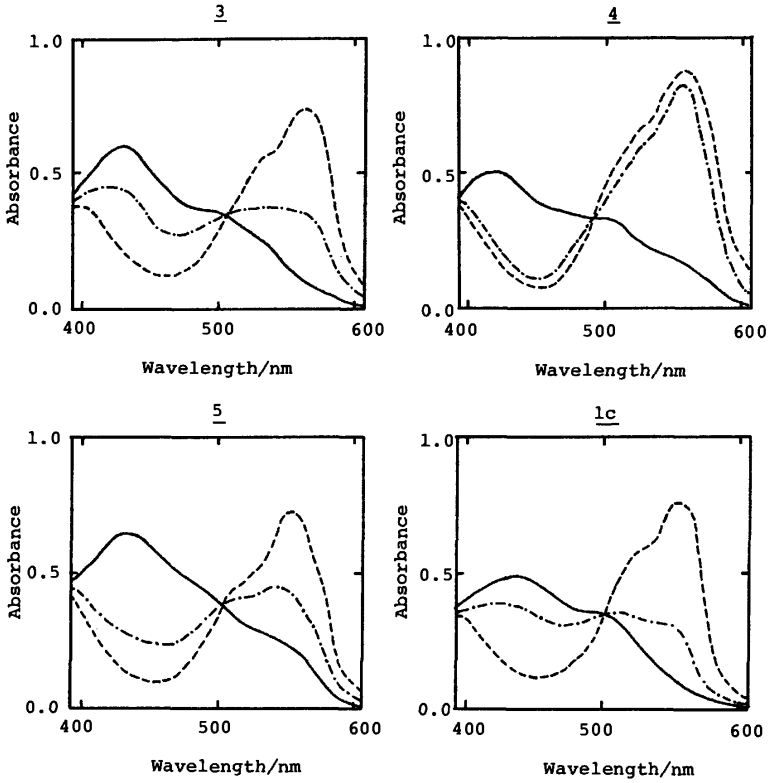

Fig. 1. The cis-to-trans change of the visible spectrum of **3**, **4**, and **5**. Compared with **1c**, after heating at 81.1 °C for 0 min, ——, 1.5 min, -·-·-, 5 min, ----.

Table 2. The cis-to-trans thermal isomerization rate constants (k) and relative rates (k_{rel})

Compound	k/s^{-1} a)	k_{rel} b)
3	1.1×10^{-3}	0.77
4	5.5×10^{-3}	3.9
5	1.8×10^{-3}	1.4
1c	1.4×10^{-3}	1.0

a) Measured in xylene at 81.8 °C. b) Compared with **1c**.

indigo[11] and sebacoyl dichloride.

Thermal cis-to-trans Isomerization of Intra- or Intermolecularly Bridged Indigo. The intramolecularly bridged indigo, **3** or **4**, and the intermolecularly bridged indigo, **5**, were dissolved in xylene and irradiated by a mercury lamp using a filter solution which cuts off the wavelength shorter than 550 nm. The color of the solution changed from red to yellow, accompanied by disappearance of the peak of the trans-form near 570 nm, and appearance of the peak of the cis-form near 440 nm. The change of the visible spectrum was measured as shown in Fig. 1, where the solution was heated, and the thermal cis-to-trans isomerization rates were measured at several wavelengths characteristic to the trans-isomer. The rate constants and the relative rates were calculated and are shown in Table 2.

From Fig. 1 and Table 2, the following facts can be pointed out: i) In the case of intramolecularly bridged indigo, the azelaoyl group neither accelerates nor decelerates the isomerization so much, compared with the acetyl group; ii) The sebacoyl group accelerates the isomerization extremely; iii) In the case of intermolecularly bridged indigo, the bridged sebacoyl substituent neither accelerates nor decelerates the isomerization.

It is of interest that a great difference between the isomerization rate of the two intramolecularly bridged indigo, **3** and **4**, was observed. This can be explained by the instability of **4** in the cis-form because of the strain caused by the highly populated methylene chain.

Also, in the intermolecularly bridged indigo **5**, the bridged substituent did not change the stability because there is no steric restriction.

Experimental

Melting points were measured by Micro Melting Point Apparatus (Yanagimoto Seisakusho) and uncorrected. The IR spectra were recorded on JASCO IRA-1 IR Spectrophotometer. The ^{1}H-NMR spectra were determined with Hitachi R-24 NMR Spectrometer. The visible spectra were recorded on a Shimadzu UV-365 UV-VIS-NIR Recording Spectrophotometer.

N,N′-*Diacetylindigo (1c).* Prepared by the method of Blanc and Ross.[12]

N,N′-*Oxalylindigo (2).* Prepared by the method of Wyman and Zenhäusern.[8]

N,N′-*Azelaoylindigo (3).* Indigo (262 mg) and azelaoyl dichloride (0.6 ml) were dissolved in an anhydrous pyridine (100 ml) and the mixture was heated in a sealed tube at 200 °C for 1 h. The reaction mixture was poured into hydrochloric acid (100 ml and water 300 ml) and extracted with dichloromethane. The organic layer was evaporated and purified first with benzene–ethyl acetate (10:1) on silica-gel column chromatography, and then with hexane–dichloro-

methane–acetonitrile (7:2:1) on silica gel (20×20 cm). The product was recrystallized from benzene–hexane to give purple plates. Yield 10%. Mp 228—230 °C. Found: C, 72.74; H, 5.61; N, 6.40%. Calcd for $C_{25}H_{22}N_2O_4$: C, 72.44; H, 5.35; N, 6.75%.

N,N′-*Sebacoylindigo (4).* Prepared from indigo (262 mg) and sebacoyl dichloride (0.8 ml). Yield 19%. Mp 262—264 °C. Found: C, 72.56; H, 5.68; N, 6.41%. Calcd for $C_{26}H_{24}N_2O_4$: C, 72.88; H, 5.64; N, 6.53%.

N-*Acetylindigo.* Prepared by the method previously reported.[11]

N′,N″-*Sebacoylbis(N-acetylindigo) (5).* A solution of *N*-acetylindigo (246 mg) was heated under reflux with stirring in an anhydrous pyridine (15 ml) and sebacoyl dichloride (193 mg) for 10 min. The reaction mixture was treated in the same manner in **3**. Yield 3%. Mp 120—121 °C. Found: C, 72.05; H, 5.10; N, 6.58%. Calcd for $C_{46}H_{38}N_4O_8$: C, 71.30; H, 4.94; N, 7.23%. It was difficult to remove the solvent from the specimen; calculation was taken into account of the solvent for $C_{46}H_{38}N_4O_8 \cdot 0.5\ C_6H_6$: C, 72.31; H, 5.08; N, 6.88%.

Thermal cis-to-trans Isomerization. The compound, **3**, **4**, **5**, or **1c** was dissolved in distilled xylene, the concentration being in the order of 10^{-4} mol/l. The solution was sealed in several ampoules, and was irradiated by a mercury lamp using a filter solution which cuts off the wavelength shorter than 550 nm until the solution reached a photostationary state, and kept in the dark at 81.8 °C. After 1.5 and 5 min., the solution was quenched in a dry ice–methanol mixture at −78 °C. The change of the visible spectrum in thermal cis-to-trans isomerization was recorded between 350 and 650 nm, by JASCO UVIDEC-1 UV and VIS Absorption Spectrometer. Furthermore, the increase of absorption at 560, 570, and 580 nm was recorded by the improved spectrophotometer (JASCO UVIDEC-100 III) and the rate constants were calculated.

References

1) R. A. Nicolaus, G. Prota, C. Santacroce, G. Scherillo, and D. Sica, *Gazz. Chim. Ital.*, **99**, 323 (1969); G. Prota, A. Suarato, and R. A. Nicolaus, *Experientia*, **27**, 1381 (1971); F. Giordano, L. Mazzarella, G. Prota, C. Santacroce, and D. Sica, *J. Chem. Soc., C*, **1971**, 2610.

2) R. A. Thomson, *Angew. Chem.*, **86**, 355 (1974).

3) W. R. Brode, E. G. Pearson, and G. M. Wyman, *J. Am. Chem. Soc.*, **76**, 1034 (1954).

4) W. Lüttke and M. Klessinger, *Chem. Ber.*, **97**, 2342 (1964).

5) G. M. Wyman, *J. Chem. Soc., Chem. Commun.*, **1971**, 1332; G. M. Wyman and B. M. Zarnegar, *J. Phys. Chem.*, **77**, 1204 (1973); G. M. Wyman and W. R. Brode, *J. Am. Chem. Soc.*, **73**, 1487 (1951); D. A. Rogers, J. D. Margerum, and G. M. Wyman, *ibid.*, **79**, 2464 (1957).

6) J. Weinstein and G. M. Wyman, *J. Am. Chem. Soc.*, **78**, 4007 (1956).

7) C. R. Giuliano, L. D. Hess, and J. D. Margerum, *J. Am. Chem. Soc.*, **90**, 586 (1968).

8) G. M. Wyman and A. F. Zenhäusern, *J. Org. Chem.*, **30**, 2349 (1965).

9) Y. Omote, S. Imada, R. Matsuzaki, K. Fujiki, T. Nishio, and C. Kashima, *Bull. Chem. Soc. Jpn.*, **52**, 3397 (1979).

10) T. Posner, *Ber. B*, **59**, 1977 (1926).

11) Y. Omote, K. Fujiki, H. Awano, I. Kubota, T. Nishio, and H. Aoyama, *Bull. Chem. Soc. Jpn.*, **54**, 627 (1981).

12) J. Blanc and D. L. Ross, *J. Phys. Chem.*, **72**, 2818 (1968).

 © 1984 The Chemical Society of Japan Bull. Chem. Soc. Jpn., 57, 473—479 (1984)

The Substituent Effects in Thiophene Compounds. III.[1] ^{1}H NMR and IR Studies in Methyl [*trans*-β-(Substituted 2-thienyl)acrylate]s

Hajime SATONAKA

Industrial Research Institute of Kanagawa Prefecture, 3173, Showa-machi, Kanazawa-ku, Yokohama 236

(Received August 2, 1983)

The ^{1}H NMR spectra and IR C=O stretching frequencies of methyl [*trans*-β-(3-, 4-, and 5-substituted 2-thienyl)acrylate]s are reported. The chemical shifts of the ring protons in methyl [*trans*-β-(4- and 5-substituted 2-thienyl)acrylate]s are correlated linearly with those of the corresponding protons in substituted thiophenes and methyl (substituted 2-thiophenecarboxylate)s. The substituent effects on the chemical shifts of α-protons in methyl [*trans*-β-(3- and 5-substituted 2-thienyl)acrylate]s have been interpreted by the mesomeric effect of the substituentes. The plots of the coupling constants in methyl [*trans*-β-(substituted 2-thienyl)acrylate]s against those in substituted thiophenes and methyl (substituted 2-thiophenecarboxylate)s gave good linear correlations. The IR C=O stretching wave numbers showed a narrow range of variation. The coupling constants in methyl [*trans*-β-(substituted 2-thienyl)acrylate]s were found to vary linearly with the electronegativity of the substituents.

In previous investigations,[1,2] the ^{1}H NMR spectra of 2- and 3-substituted thiophenes (**1** and **2**), and methyl (3-, 4-, and 5-substituted 2-thiophenecarboxylate)s (**3**—**5**), and methyl (2-, 4-, and 5-substituted 3-thiophenecarboxylate)s (**6**—**8**) were measured, and the effects of the substituents were discussed.

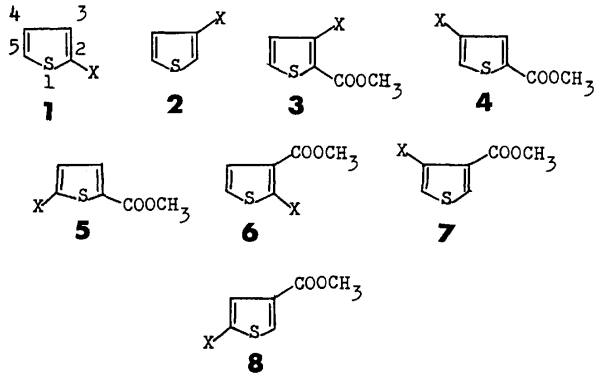

The investigation has been extended to the substituent effects in methyl [*trans*-β-(3-, 4-, and 5-substituted 2-thienyl)acrylate]s (**9**—**11**). The characteris-

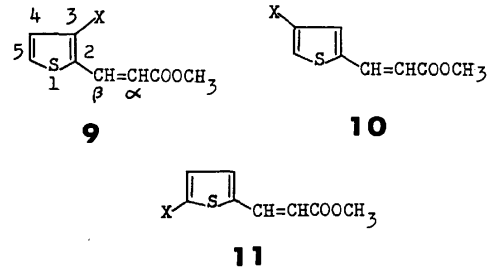

tics of the ^{1}H NMR spectra of methyl [*trans*-β-(substituted 2-thienyl)acrylate]s, and the correlations of the chemical shifts and of the coupling constants between these compounds and substituted thiophenes and methyl (substituted 2-thiophenecarboxylate)s have been discussed in this paper. The coupling constants of methyl [*trans*-β-(substituted 2-thienyl)acrylate]s are correlated with the electronegativities of the substituents. The IR C=O stretching frequencies of methyl [*trans*-β-(substituted 2-thienyl)acrylate]s were measured and compared with those of methyl (substituted 2-thiophenecarboxylate)s.

Results and Discussion

The ^{1}H NMR spectra of methyl [*trans*-β-(3-, 4-, and 5-substituted 2-thienyl)acrylate]s were measured in deuteriochloroform at 25 °C. For convenience, the author used the notations H(2), H(3), H(4), H(5), H(α), and H(β) for the 2-, 3-, 4-, 5-, α-, and β-protons of methyl [*trans*-β-(substituted 2-thienyl)acrylate]s, and *cc*, *p*, *i*, and *s* for the correlation coefficient, slope, intercept, and standard deviation in the least-squares analysis. The ^{1}H NMR spectrum of methyl *trans*-β-(3-chloro-2-thienyl)acrylate (**9**, X=Cl) showed signals of (*ortho*-coupling) ring protons at δ 6.96 and 7.33, of (*trans*-coupling) olefinic protons at δ 7.86 and 6.27, and of methyl protons at δ 3.80. From the detailed analysis of the spectrum, the long-range couplings have been observed between H(5) and H(β) or H(α). It is noteworthy that the long-range coupling is observed between H(5) and H(α), because the interacting

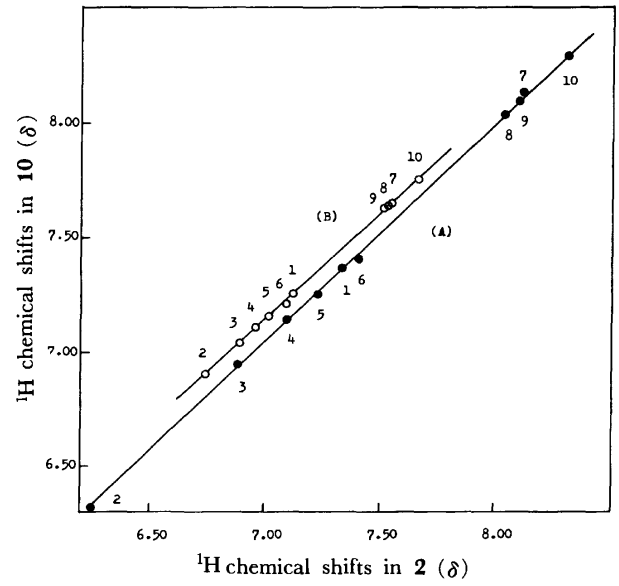

Fig. 1. Correlation between ^{1}H chemical shifts in **10** and **2**; numbering as in Table 2. A, δ_5(**10**) *vs.* δ_2(**2**). B, δ_3(**10**) *vs.* δ_4(**2**).

hydrogen nuclei in this compound are more separated than those in Zig-Zag[3-6] and W-letter couplings.[7,8] The spectra of other methyl [*trans*-β-(substituted 2-thienyl)acrylate]s are similar to this spectrum. In the series of compounds **10** and **11**, the long-range couplings were also found between hydrogens in thiophene ring and those in the side chain. In the series of **10**, both H(3) and H(5) couple with H(α) and H(β), but in the series of **11**, only H(3) with H(α) and H(β). It is found that H(4) in **9** does not couple with any hydrogen in the side chain, whereas H(4) in **11** couples with H(β) in methoxycarbonyl and nitro derivatives (J=0.20 Hz, in both cases). The spectra were assigned on the basis of chemical shifts and characteristic ring and long-range coupling constants. The refined chemical shifts and coupling constants were obtained

TABLE 1. ^{1}H NMR CHEMICAL SHIFTS AND COUPLING CONSTANTS OF METHYL [*trans*-β-(3-SUBSTITUTED 2-THIENYL)ACRYLATE]S (SERIES **9**)

		Chemical shifts (δ)						Coupling constants/Hz					
No.	X	H(4)	H(5)	H(β)	H(α)	$COOCH_3$	Others	J_{45}	$J_{5\beta}$	$J_{5\alpha}$	$J_{\beta\alpha}$	Others	
1	H	7.05	7.37	7.79	6.24	3.79	7.29[H(3)]	5.05	0.75	0.40	15.60	3.65(J_{34})	1.15(J_{35})
												0.65($J_{3\beta}$)	0.45($J_{3\alpha}$)
2	OCH_3	6.82	7.27	7.83	6.15	3.77	3.91(OCH_3)	5.50	0.65	0.35	15.75		
3	CH_3	6.85	7.24	7.85	6.17	3.79	2.34(CH_3)	5.10	0.85	—	15.50	0.40($J_{CH_3\text{-}4}$)	0.40($J_{CH_3\text{-}5}$)
4	Cl	6.96	7.33	7.86	6.27	3.80		5.35	0.85	0.30	15.80		
5	Br	7.03	7.33	7.83	6.30	3.81		5.35	0.90	0.30	15.80		
6	I	7.12	7.32	7.76	6.32	3.81		5.15	1.00	0.30	15.65		
7	CHO	7.49	7.34	8.38	6.44	3.83	10.20(CHO)	5.30	0.75	0.25	15.65	0.30($J_{CHO\text{-}4}$)	0.55($J_{CHO\text{-}5}$)
												0.30($J_{CHO\text{-}\beta}$)	
8	$COCH_3$	7.41	7.29	8.53	6.35	3.80	2.55($COCH_3$)	5.30	0.75	0.30	15.90		
9	$COOCH_3$	7.48	7.26	8.61	6.36	3.81	3.91($COOCH_3$)	5.30	0.80	0.30	15.95		

TABLE 2. ^{1}H NMR CHEMICAL SHIFTS AND COUPLING CONSTANTS OF METHYL [*trans*-β-(4-SUBSTITUTED 2-THIENYL)ACRYLATE]S (SERIES **10**)

		Chemical shifts (δ)						Coupling constants/Hz						
No.	X	H(3)	H(5)	H(β)	H(α)	$COOCH_3$	Others	J_{35}	$J_{3\beta}$	$J_{3\alpha}$	$J_{5\beta}$	$J_{5\alpha}$	$J_{\beta\alpha}$	Others
1	H	7.25	7.37	7.79	6.24	3.79	7.05[H(4)]	1.15	0.65	0.45	0.75	0.40	15.60	3.65(J_{34})
														5.05(J_{45})
2	OCH_3	6.90	6.31	7.64	6.21	3.78	3.80(OCH_3)	1.70	0.60	0.40	0.60	0.40	15.60	
3	CH_3	7.04	6.94	7.71	6.19	3.78	2.24(CH_3)	1.35	0.65	0.40	0.65	0.35	15.60	0.40($J_{CH_3\text{-}3}$)
														1.10($J_{CH_3\text{-}5}$)
4	Cl	7.11	7.14	7.66	6.24	3.80		1.50	0.55	0.45	0.60	0.35	15.70	
5	Br	7.15	7.25	7.67	6.24	3.79		1.40	0.65	0.40	0.65	0.35	15.65	
6	I	7.21	7.41	7.69	6.24	3.79		1.30	0.70	0.40	0.70	0.40	15.65	
7	CHO	7.64	8.12	7.74	6.30	3.81	9.87(CHO)	1.35	0.70	0.45	0.75	0.30	15.70	0.35($J_{CHO\text{-}3}$)
8	$COCH_3$	7.64	8.03	7.73	6.27	3.80	2.52($COCH_3$)	1.35	0.65	0.40	0.75	0.30	15.60	
9	$COOCH_3$	7.63	8.09	7.73	6.26	3.80	3.87($COOCH_3$)	1.30	0.70	0.45	0.85	0.35	15.70	
10	NO_2	7.75	8.29	7.69	6.34	3.82		1.50	0.70	0.40	0.75	0.30	15.70	

TABLE 3. ^{1}H NMR CHEMICAL SHIFTS AND COUPLING CONSTANTS OF METHYL [*trans*-β-(5-SUBSTITUTED 2-THIENYL)ACRYLATE]S (SERIES **11**)

		Chemical shifts (δ)						Coupling constants/Hz					
No.	X	H(3)	H(4)	H(β)	H(α)	$COOCH_3$	Others	J_{34}	$J_{3\beta}$	$J_{3\alpha}$	$J_{\beta\alpha}$	Others	
1	H	7.25	7.05	7.79	6.24	3.79	7.37[H(5)]	3.65	0.65	0.45	15.60	1.15(J_{35})	5.05(J_{45})
												0.75($J_{5\beta}$)	0.40($J_{5\alpha}$)
2	OCH_3	6.93	6.15	7.64	5.94	3.76	3.92(OCH_3)	4.05	0.65	0.55	15.60		
3	CH_3	7.04	6.70	7.70	6.10	3.77	2.49(CH_3)	3.60	0.65	0.50	15.60	0.55($J_{CH_3\text{-}3}$)	1.00($J_{CH_3\text{-}4}$)
												0.30($J_{CH_3\text{-}\beta}$)	
4	Cl	7.02	6.87	7.63	6.11	3.78		3.90	0.65	0.55	15.65		
5	Br	6.99	7.01	7.65	6.13	3.78		3.80	0.60	0.55	15.65		
6	I	6.89	7.20	7.69	6.15	3.78		3.80	0.60	0.50	15.70		
7	CHO	7.32	7.70	7.75	6.43	3.82	9.91(CHO)	3.95	0.60	0.40	15.75		
8	$COCH_3$	7.24	7.60	7.72	6.38	3.81	2.56($COCH_3$)	4.00	0.60	0.40	15.70		
9	$COOCH_3$	7.22	7.70	7.72	6.35	3.81	3.90($COOCH_3$)	3.95	0.60	0.40	15.70	0.20($J_{4\beta}$)	
10	NO_2	7.18	7.85	7.67	6.42	3.83		4.30	0.60	0.40	15.85	0.20($J_{4\beta}$)	

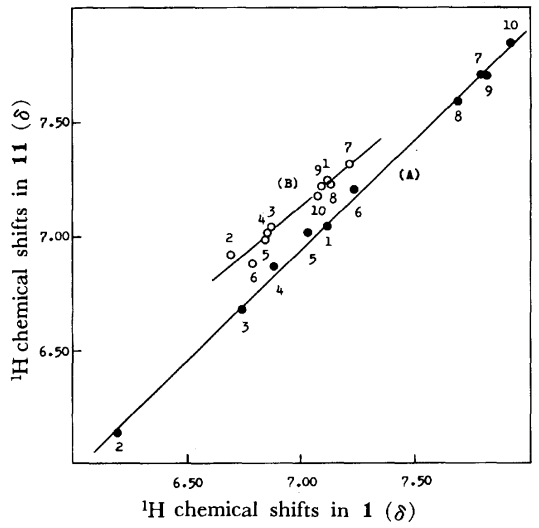

Fig. 2. Correlation between ^{1}H chemical shifts in **11** and **1**; numbering as in Table 3. A, δ_4(**11**) *vs.* δ_3(**1**). B, δ_3(**11**) *vs.* δ_4(**1**).

iteratively using LAOCN 3.[9] The results are given in Tables 1-3. The δ_5 (**10**)[10] *vs.* δ_2 (**2**), and δ_3 (**10**) *vs.* δ_4 (**2**) plots gave excellent correlations, as shown in Fig. 1 (A and B, respectively). Furthermore, the chemical shifts of ring protons in the series of compounds **10** were compared with those in the series of compounds **4**, and good correlations were observed between δ_5(**10**) and δ_5(**4**), and between δ_3(**10**) and δ_3(**4**). These data show that the ^{1}H chemical shifts of 5- and 3-positions in the thiophene ring have the same sensitivity for the substituent effects in both **10** and **4**, and suggest the possibility to estimate empirically with accuracy the ^{1}H chemical shifts of thiophene ring in other 2,4-disubstituted thiophene series. The chemical shifts of H(β) and H(α) in the series of compounds **10** show a narrow range of variation, as expected from those of H(5) in **2**. The effect of a substituent on the 4-position is considered to be transmitted mainly by the inductive effect to δ_β(**10**) and δ_α(**10**). The correlation between δ_α(**10**) and δ_5(**2**) gives a larger *cc* and a steeper *p* than that between δ_β(**10**) and δ_5(**2**).

As shown in Fig. 2, good correlations were obtained between δ_4(**11**) and δ_3(**1**) (A), and between δ_3(**11**) and δ_4(**1**) (B). The chemical shifts of **11** were compared with those of **5**, and better correlations were obtained between δ_4(**11**) and δ_4(**5**), and between δ_3(**11**) and δ_3(**5**). These results also suggest the possibility to estimate the ^{1}H chemical shifts of the thiophene ring in other 2,5-disubstituted thiophene series as in 2,4-disubstituted thiophene series. Quite similarly to the series of compounds **10**, the chemical shifts of H(β) is scarcely affected by the substituent at the 5-position, while that of H(α) considerably by the same substituent. The correlation between δ_α(**11**) and δ_5(**1**) also gives a larger correlation coefficient and a steeper slope than that between δ_β(**11**) and δ_5(**1**). The effect of the substituent on the 5-position is transmitted more strongly to H(α) than H(β) by a factor of about 5. This reason may be ascribed to the resonance effects as shown below. The shift of H(α) is presumed to be caused by a sizable contribution of the resonance structure **c**, which gives the charge delocalization on the α-carbon.

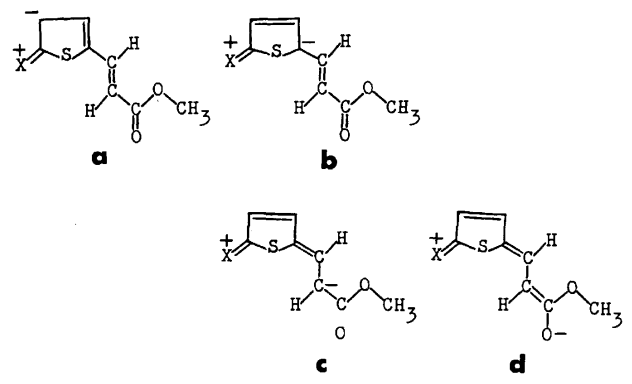

Figure 3 shows a close correlation between the effects of substituents on δ_4(**9**) and δ_4(**2**)(A), and a loose correlation between those on δ_5(**9**) and δ_5(**2**)(B). The chemical shifts of **9** were compared with those of **3**, and a good correlation was obtained between δ_4(**9**) and δ_4(**3**), and a fairly good correlation between δ_5(**9**) and δ_5(**3**). As shown in Table 1, formyl acetyl, and methoxycarbonyl groups cause significantly low field shifts of H(β) signal. These results may be interpreted by the preferred conformation **e**, in which the carbonyl group located very close to H(β) may form an intramolecular

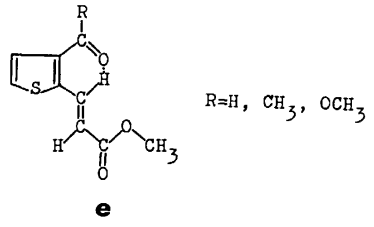

hydrogen bonding. This conformation may rationalize the facts that the chemical shift of the formyl proton in methyl *trans*-β-(3-formyl-2-thienyl)acrylate is shifted considerably towards a lower field than that of the 4-formyl derivative, and also that the former shows the carbonyl band at 1687 cm^{-1}, but the latter at 1701 and 1697 cm^{-1}. The large standard deviation of δ_β(**9**) *vs.* δ_2(**2**) plot may be caused by the complex influence due to neighboring anisotropy, intramolecular hydrogen bonding, inductive, mesomeric, and steric hindrance effects. The resonance contribution (**f**, **g**, **h**) similar to the case of 5-substituted derivatives is again expected with methyl [*trans*-β-(3-substituted 2-thienyl)acrylate]s.

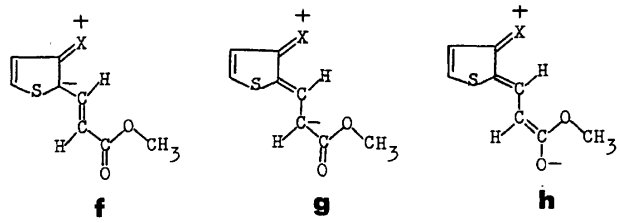

The δ_α(**9**) value is considered to show a narrower range of variation than that of δ_α(**11**) due to the restricted contribution of mesomeric effect by steric hindrance of the 2-substituent. The correlation between δ_α(**9**) and δ_2(**2**) gives a larger *cc* and a lesser *p*. For this reason the substituent effect on the chemical shift of H(α) by the 5-position is more sensitive than that by the 3-position by a factor of about 1.5.

Methyl proton chemical shifts of methyl [*trans*-β-(substituted-2-thienyl)acrylate]s are much less affected by the substituents on the ring, and the substituent effects on these chemical shifts are attenuated to approximately half of those of methyl (substituted 2-thiophenecarboxylate)s. Contrary to the correlation between δ_α(**9**) and δ_α(**11**), the δ_{COOCH_3}(**9**) *vs.* δ_{COOCH_3}(**11**) plot shows that the substituents on the 3-position affect the chemical shift of $COOCH_3$ more remarkably than those on the 5-position. The results of these comparisons are shown in Table 4.

The chemical shifts of the ring protons of methyl

TABLE 4. CORRELATIONS OF CHEMICAL SHIFTS OF SUBSTITUTED THIOPHENES, METHYL (SUBSTITUTED 2-THIOPHENECARBOXYLATE)S, AND METHYL [*trans*-β-(SUBSTITUTED 2-THIENYL)ACRYLATE]S

Series	Proton	Series	Proton	*cc*[a]	*p*[b]	*i*[c]	*s*[d]	*n*[e]
2	H(2)	**10**	H(5)	1.000	0.955	0.353	0.008	10
2	H(4)	**10**	H(3)	1.000	0.924	0.672	0.008	10
1	H(3)	**11**	H(4)	1.000	0.960	0.226	0.017	10
1	H(4)	**11**	H(3)	0.980	0.857	1.14	0.030	10
2	H(4)	**9**	H(4)	0.988	0.848	1.06	0.038	9[f]
2	H(5)	**9**	H(5)	0.538	0.326	4.91	0.044	9[f]
4	H(5)	**10**	H(5)	1.000	1.02	−0.317	0.007	10
4	H(3)	**10**	H(3)	0.999	1.02	−0.655	0.014	10
5	H(4)	**11**	H(4)	1.000	1.03	−0.241	0.004	10
5	H(3)	**11**	H(3)	0.989	1.13	−1.55	0.023	10
3	H(4)	**9**	H(4)	0.988	0.981	0.081	0.037	9[f]
3	H(5)	**9**	H(5)	0.642	0.229	5.59	0.038	9[f]
2	H(2)	**9**	H(β)	0.801	0.446	4.76	0.197	9[f]
2	H(2)	**9**	H(α)	0.915	0.136	5.29	0.035	9[f]
2	H(2)	**9**	$COOCH_3$	0.763	0.022	3.64	0.010	9[f]
2	H(5)	**10**	H(β)	0.604	0.357	5.10	0.035	10
2	H(5)	**10**	H(α)	0.818	0.473	2.81	0.024	10
2	H(5)	**10**	$COOCH_3$	0.801	0.151	2.70	0.007	10
1	H(5)	**11**	H(β)	0.578	0.083	7.09	0.039	10
1	H(5)	**11**	H(α)	0.950	0.433	3.06	0.049	10
1	H(5)	**11**	$COOCH_3$	0.868	0.057	3.38	0.010	10
9	H(β)	**11**	H(β)	0.365	0.056	7.25	0.047	9[f]
9	H(α)	**11**	H(α)	0.864	1.48	−3.09	0.076	9[f]
9	$COOCH_3$	**11**	$COOCH_3$	0.755	0.882	0.344	0.094	9[f]
3	$COOCH_3$	**9**	$COOCH_3$	0.927	0.416	2.15	0.028	9[f]
4	$COOCH_3$	**10**	$COOCH_3$	0.928	0.483	1.90	0.010	10
5	$COOCH_3$	**11**	$COOCH_3$	0.988	0.591	1.50	0.010	10

a) Correlation coefficient. b) Slope. c) Intercept. d) Standard deviation. e) Number of compounds used in correlation. f) NO_2 is excluded.

TABLE 5. FREQUENCIES OF C=O STRETCHINC VIBRATIONS OF METHYL [*trans*-β-(SUBSTITUTED2-THIENYL)ACRYLATE]S

		$\nu_{C=O}$/cm^{-1}									
		Series **9**			Series **10**				Series **11**		
		Ester		Others	Ester		Others		Ester		Others
No.	X	*anti*[a]	*syn*[b]		*anti*	*syn*			*anti*	*syn*	
1	H	1715*	1725		1715*	1725			1715*	1725	
2	OCH_3	1706*	1720		1712*	1725			1708*	1721	
3	CH_3	1707*	1722		1711*	1725			1708*	1723	
4	Cl	1712*	1726		1715*	1728			1708*	1725	
5	Br	1712*	1726		1718*	1728			1710*	1725	
6	I	1712*	1727		1718*	1727			1709*	1725	
7	CHO	1717*	1728	1687	1719*	1727	1697	1701*	1718*	1729	1683
8	$COCH_3$	1715*	1725	1684	1719*	1728	1689		1718*	1728	1672
9	$COOCH_3$		1724			1728			1720*	1726	
10	NO_2				1714*	1729			1720*	1731	

a) *anti-s-trans* form. b) *syn-s-trans* form. * Shoulder.

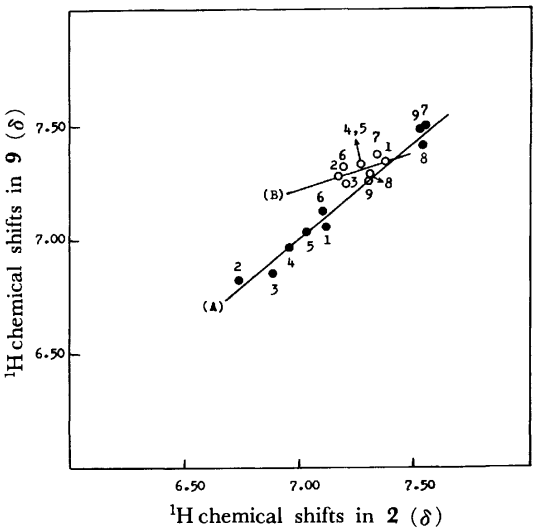

Fig. 3. Correlation between ^{1}H chemical shifts in **9** and **2**; numbering as in Table 1. A, δ_4(**9**) *vs.* δ_4(**2**). B, δ_5(**9**) *vs.* δ_5(**2**).

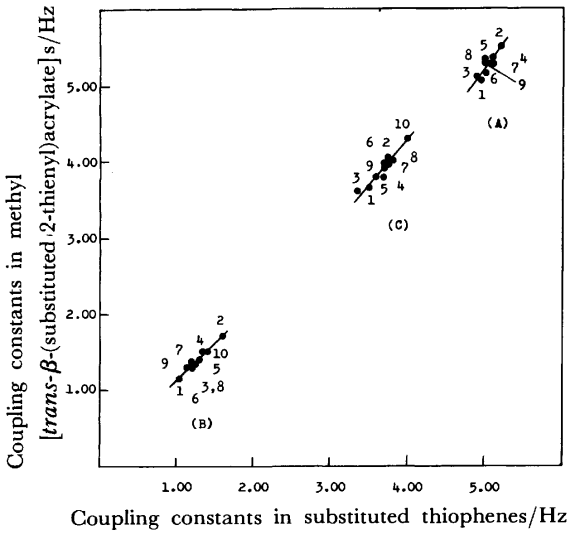

Fig. 4. Correlation between coupling constants in methyl [*trans*-β-(substituted 2-thienyl)acrylate]s and substituted thiophenes; numbering as in Table 1. A, J_{45}(**9**) *vs.* J_{45}(**2**). B, J_{35}(**10**) *vs.* J_{24}(**2**). C, J_{34}(**11**) *vs.* J_{34}(**1**).

Table 6. Correlations of C=O stretchinc vibration frequencies of methyl [*trans*-β-(substituted 2-thienyl)-acrylate]s against methyl (substituted 2-thiophenecarboxylate)s

Series	Series	cc[a]	p[b]	i[c]	s[d]	n[e]
3	**9**	0.784	3.71	1107.7	85.1	6[f]
4	**10**	0.544	1.48	1422.2	48.7	9[g]
5	**11**	0.905	5.45	698.2	86.5	9[g]

a), d), and e) as in Table 4. f) CHO, $COCH_3$, $COOCH_3$, and NO_2 are excluded. g) $COOCH_3$ is excluded.

[*trans*-β-(substituted 2-thienyl)acrylate]s were calculated by making use of those of 2- and 3-substituted thiophenes. Excluding the chemical shift of H(4) of methyl *trans*-β-(3-methoxy-2-thienyl)acrylate, the observed chemical shifts agree with the calculated values within 0.1 ppm in three cases. These results seem to suggest that the additivity rule which is based on substituted thiophenes, is also applicable to the chemical shifts of the ring protons in methyl [*trans*-β-(substituted 2-thienyl)acrylate]s. It is noteworthy that the chemical shifts of the ring protons in the carbonyl derivatives of **9** are in good agreement with the calculated values, although those of **3** differ from the calculated values, which have been stated in the preceding paper.[2] Since the predominant conformations of carbonyl groups are thought to be the *syn* form in **2**, and the *anti* form in **9**, the chemical shifts of the ring protons in the latter are expected to disagree with the calculated values. Nevertheless, the observed values are in good agreement with the calculated. The unexpected agreement is probably due to the accidental compensation caused by the additional effect of the carbonyl group interacting with the CH group in its proximity.

The wave numbers of the C=O stretching vibrations of the series of methyl [*trans*-β-(substituted 2-thienyl)-acrylate]s were measured in CCl_4. The results are given in Table 5. Although two separated C=O stretching bands of the ester group have been observed in some of methyl (substituted 2-thiophenecarboxylate)s,[2] a peak with a shoulder is usually observed in the series of compounds **9**, **10**, and **11**. The main peak at the higher frequency is assignable to the *syn-s-trans* form, and the shoulder to the *anti-s-trans* form. The C=O stretching wave numbers of *syn-s-trans* form show narrow ranges of variation, being 8 cm^{-1} for **9**, 4 cm^{-1} for **10**, and 10 cm^{-1} for **11**. These ranges are about half as wide as those for methyl (substituted 2-thiophenecarboxylate)s. The correlations between the C=O streching frequencies of methyl [*trans*-β-(substituted 2-thienyl)acrylate]s and those of methyl (substituted 2-thiophenecarboxylate)s are shown in Table 6. A good correlation was observed between $\nu_{C=O}$(**11**)[11] and $\nu_{C=O}$(**5**), and fair correlations between $\nu_{C=O}$(**9**) and $\nu_{C=O}$(**3**), and between $\nu_{C=O}$(**10**) and $\nu_{C=O}$(**4**). The substituent effects to the C=O band by positions 5, 3, and 4 of methyl [*trans*-β-(substituted 2-thienyl)acrylate]s and of methyl (substituted 2-thiophenecarboxylate)s show a considerably similar trend. It is interesting that the substituent effect in **4** is transmitted strongly to the C=O stretching frequency of methoxycarbonyl group, but the effect in **10** very weakly.

Plots of the proton-proton coupling constants in methyl [*trans*-β-(substituted 2-thienyl)acrylate]s against the corresponding coupling constants in substituted thio-

phenes gave good correlations as shown in Fig. 4. Moreover, good linear correlations were observed between the coupling constants for methyl [*trans*-β-(substituted 2-thienyl)acrylate]s and methyl (substituted 2-thiophenecarboxylate)s.

For methyl [*trans*-β-(substituted 2-thienyl)acrylate]s as well as for methyl (substituted 2-thiophenecarboxylate)s,[2] relationships were examined between the coupling constants and the sum of the electronegativities of substituents including 2-(methoxycarbonyl)vinyl group. Good correlations were found for J_{35}(**10**)[12] and J_{45}(**9**), but not for other coupling constants.

Experimental

The ^{1}H NMR spectra of the compounds were obtained at 100 MHz on a JEOL PS-100 spectrometer. The chemical shifts were determined with an accuracy of ±0.005 ppm relative to TMS as an internal standard, and the coupling constants were determined with an accuracy of ±0.02 Hz. The concentrations of the substrates were adjusted approximately to 0.3 mol dm^{-3}. The IR spectra were recorded on a Perkin-Elmer 257 spectrometer.

Methyl *trans*-β-(2-thienyl)acrylate and methyl [*trans*-β-(5-bromo-, 5-formyl-, and 5-nitro-2-thienyl)acrylate]s were prepared according to the reported procedures.[13-16]

Methyl trans-β-*(4-Nitro-2-thienyl)acrylate.* This material was prepared by esterification of the corresponding acid,[17] mp 142°C. Found: C, 45.27; H, 3.20; N, 6.70; S, 15.00%. Calcd for $C_8H_7NO_4S$: C, 45.07; H, 3.31; N, 6.57; S, 15.04%. IR(KBr, cm^{-1}): 3100(=C-H); 1718(C=O); 1634(C=C); 967(*trans* CH=CH); 1535, 1433, 723(thiophene ring).

The following esters were prepared by the condensation of methyl acetate with the corresponding aldehydes[18-31] according to the procedure by Gilman and coworkers.[32]

Methyl trans-β-*(3-Methoxy-2-thienyl)acrylate.* Mp 52°C. Found: C, 54.72; H, 4.95; S, 15.98%. Calcd for $C_9H_{10}O_3S$: C, 54.53; H, 5.08; S, 16.17%. IR (KBr, cm^{-1}): 3090 (=C-H); 1706 (C=O); 1618 (C=C); 970 (*trans* CH=CH); 1537, 1428, 727 (thiophene ring).

Methyl trans-β-*(3-Methyl-2-thienyl)acrylate.* Bp 113—113.5°C/2 mmHg (1 mmHg≈133.322 Pa). Found: C, 59.20; H, 5.66; S, 17.49%. Calcd for $C_9H_{10}O_2S$: C, 59.32; H, 5.53; S, 17.59%. IR (neat, cm^{-1}): 3100 (=C-H); 1715 (C=O); 1622 (C=C); 968 (*trans* CH=CH); 1532, 1438, 713 (thiophene ring).

Methyl trans-β-*(3-Chloro-2-thienyl)acrylate.* Mp 69°C. Found: C, 47.55; H, 3.40; Cl, 17.31; S, 15.63%. Calcd for $C_8H_7ClO_2S$: C, 47.41; H, 3.48; Cl, 17.49; S, 15.82%. IR (KBr, cm^{-1}): 3130 (=C-H); 1721 (C=O); 1630 (C=C); 962 (*trans* CH=CH); 1508, 1422, 708 (thiophene ring).

Methyl trans-β-*(3-Bromo-2-thienyl)acrylate.* Mp 76°C. Found: C, 38.75; H, 2.95; Br, 32.50; S, 13.11%. Calcd for $C_8H_7BrO_2S$: C, 38.88; H, 2.86; Br, 32.33; S, 12.98%. IR (KBr, cm^{-1}): 3130 (=C-H); 1720 (C=O); 1628 (C=C); 962 (*trans* CH=CH); 1503, 1422, 707 (thiophene ring).

Methyl trans-β-*(3-Iodo-2-thienyl)acrylate.* Mp 78°C. Found: C, 32.58; H, 2.60; I, 43.07; S, 10.78%. Calcd for $C_8H_7IO_2S$: C, 32.67; H, 2.40; I, 43.15; S, 10.90%. IR (KBr, cm^{-1}): 3090 (=C-H); 1695 (C=O); 1622 (C=C); 960 (*trans* CH=CH); 1488, 1419, 709 (thiophene ring).

Methyl trans-β-*(3-Formyl-2-thienyl)acrylate.* Mp 112°C. Found: C, 55.17; H, 4.00; S, 16.56%. Calcd for $C_8H_8O_3S$: C, 55.09; H, 4.11; S, 16.34%. IR (KBr, cm^{-1}): 3110, 3090 (=C-H); 1719, 1673 (C=O); 1633 (C=C); 961 (*trans* CH=CH); 1520, 1437, 718 (thiophene ring).

Methyl trans-β-*(3-Acetyl-2-thienyl)acrylate.* Mp 82°C. Found: C, 57.15; H, 4.88; S, 15.38%. Calcd for $C_{10}H_{10}O_3S$: C, 57.13; H, 4.79; S, 15.25%. IR (KBr, cm^{-1}): 3120, 3080 (=C-H); 1698, 1678 (C=O); 1615 (C=C); 978 (*trans* CH=CH); 1503, 1438, 1423, 722 (thiophene ring).

Methyl trans-β-*(4-Methoxy-2-thienyl)acrylate.* Mp 73°C. Found: C, 54.70; H, 5.02; S, 16.29%. Calcd for $C_9H_{10}O_3S$: C, 54.53; H, 5.08; S, 16.17%. IR (KBr, cm^{-1}): 3090 (=C-H); 1706 (C=O); 1629 (C=C); 967 (*trans* CH=CH); 1551, 1430, 720 (thiophene ring).

Methyl trans-β-*(4-Methyl-2-thienyl)acrylate.* Bp 122—124°C/3 mmHg. Found: C, 59.55; H, 5.80; S, 17.65%. Calcd for $C_9H_{10}O_2S$: C, 59.32; H, 5.53; S, 17.59%. IR (neat, cm^{-1}): 3100 (=C-H); 1717 (C=O); 1616 (C=C); 967 (*trans* CH=CH); 1542, 1438, 1427, 721 (thiophene ring).

Methyl trans-β-*(4-Chloro-2-thienyl)acrylate.* Mp 80°C. Found: C, 47.64; H, 3.52; Cl, 17.33; S, 15.65%. Calcd for $C_8H_7ClO_2S$: C, 47.41; H, 3.48; Cl, 17.49; S, 15.82%. IR (KBr, cm^{-1}): 3110 (=C-H); 1710 (C=O); 1633 (C=C); 959 (*trans* CH=CH); 1519, 1438, 1421, 719 (thiophene ring).

Methyl trans-β-*(4-Bromo-2-thienyl)acrylate.* Mp 75°C. Found: C, 38.92; H, 2.80; Br, 32.58; S, 12.91%. Calcd for $C_8H_7BrO_2S$: C, 38.89; H, 2.86; Br, 32.33; S, 12.98%. IR (KBr, cm^{-1}): 3110 (=C-H); 1710 (C=O); 1633 (C=C); 959 (*trans* CH=CH); 1511, 1434, 1418, 718 (thiophene ring).

Methyl trans-β-*(4-Iodo-2-thienyl)acrylate.* Mp 44°C. Found: C, 32.44; H, 2.35; I, 43.36, S, 11.02%. Calcd for $C_8H_7IO_2S$: C, 32.67; H, 2.40; I, 43.15; S, 10.90%. IR (KBr, cm^{-1}): 3080 (=C-H); 1703 (C=O); 1627 (C=C); 964 (*trans* CH=CH); 1500, 1438, 718 (thiophene ring).

Methyl trans-β-*(4-Formyl-2-thienyl)acrylate.* Mp 96°C. Found: C, 54.98; H, 4.15; S, 16.18%. Calcd for $C_9H_8O_3S$: C, 55.09; H, 4.11; S, 16.34%. IR (KBr, cm^{-1}): 3080 (=C-H); 1709, 1672 (C=O); 1633(C=C); 978 (*trans* CH=CH); 1528, 1435, 721 (thiophene ring).

Methyl trans-β-*(4-Acetyl-2-thienyl)acrylate.* Mp 86°C. Found: C, 57.08; H, 4.83; S, 15.09%. Calcd for $C_{10}H_{10}O_3S$: C, 57.13; H, 4.79; S, 15.25%. IR (KBr, cm^{-1}): 3080 (=C-H); 1708, 1668 (C=O); 1631 (C=C); 988 (*trans* CH=CH); 1527, 1408, 728 (thiophene ring).

Methyl trans-β-*(5-Methoxy-2-thienyl)acrylate.* Mp 56°C. Found: C, 54.68; H, 4.82; S, 16.38%. Calcd for $C_9H_{10}O_3S$: C, 54.53; H, 5.08; S, 16.17%. IR (KBr, cm^{-1}): 3090 (=C-H); 1707 (C=O); 1616 (C=C); 973 (*trans* CH=CH); 1538, 1423, 703 (thiophene ring).

Methyl trans-β-*(5-Methyl-2-thienyl)acrylate.* Mp 55°C. Found: C, 59.48; H, 5.31; S, 17.75%. Calcd for $C_9H_{10}O_2S$: C, 59.32; H, 5.53; S, 17.59%. IR (KBr, cm^{-1}): 3080 (=C-H); 1708 (C=O); 1620 (C=C); 992 (*trans* CH=CH); 1536, 1435, 720 (thiophene ring).

Methyl trans-β-*(5-Chloro-2-thienyl)acrylate.* Mp 53°C. Found: C, 47.62; H, 3.42; Cl, 17.23; S, 15.80%. Calcd for $C_8H_7ClO_2S$: C, 47.41; H, 3.48; Cl, 17.49; S, 15.82%. IR (KBr, cm^{-1}): 3060 (=C-H); 1719 (C=O); 1626 (C=C); 969 (*trans* CH=CH); 1524, 1422, 721 (thiophene ring).

Methyl trans-β-*(5-Iodo-2-thienyl)acrylate.* Mp 88°C. Found: C, 32.81; H, 2.55; I, 43.02; S, 11.12%. Calcd for $C_8H_7IO_2S$: C, 32.67; H, 2.40; I, 43.15; S, 10.90%. IR (KBr, cm^{-1}): 3050 (=C-H); 1708 (C=O); 1623 (C=C); 9.71 (*trans* CH=CH); 1519, 1417, 717 (thiophene ring).

Methyl trans-β-*(5-Acetyl-2-thienyl)acrylate.* Mp 147°C. Found: C, 57.48; H, 4.58; S, 15.23%. Calcd for $C_{10}H_{10}O_3S$: C, 57.13; H, 4.79; S, 15.25%. IR (KBr, cm^{-1}): 3080 (=C-H); 1711, 1657 (C=O); 1627 (C=C); 987 (*trans* CH=CH); 1519, 1449, 731 (thiophene ring).

Methyl [*trans*-β-(3-, 4-, and 5-methoxycarbonyl-2-thienyl)-acrylate]s were prepared by the oxidation of the corresponding methyl [*trans*-β-(formyl-2-thienyl)acrylate]s followed by the esterification.

Methyl trans-β-*(3-Methoxycarbonyl-2-thienyl)acrylate.* Mp 82°C. Found: C, 52.95; H, 4.58; S, 14.28%. Calcd for

$C_{10}H_{10}O_4S$: C, 53.09; H, 4.46; S, 14.17%. IR (KBr, cm^{-1}): 3110, 3080 (=C-H); 1719, 1708 (C=O); 1621 (C=C); 978 (*trans* CH=CH); 1518, 1438, 1429, 719 (thiophene ring).

Methyl trans-β-*(4-Methoxycarbonyl-2-thienyl)acrylate.* Mp 89°C. Found: C, 52.98; H, 4.43; S, 14.06%. Calcd for $C_{10}H_{10}O_4S$: C, 53.09; H, 4.46; S, 14.17%. IR (KBr, cm^{-1}): 3100 (=C-H); 1718, (C=O); 1630 (C=C); 982 (*trans* CH=CH); 1533, 1431, 722 (thiophene ring).

Methyl trans-β-*(5-Methoxycarbonyl-2-thienyl)acrylate.* Mp 97°C. Found: C, 53.31; H, 4.25; S, 14.28%. Calcd for $C_{10}H_{10}O_4S$: C, 53.09; H, 4.46; S, 14.17%. IR (KBr, cm^{-1}): 3070, (=C-H); 1719 (C=O); 1633 (C=C); 963 (*trans* CH=CH); 1529, 1432, 731 (thiophene ring).

The author wishes to thank to Professor Minoru Hirota of Yokohama National University for his kind suggestions and encouragement, to Dr. Hiroshi Ozawa of the University of Tokyo for his permission to use the Computation Program LAOCN 3, and to Mr. Takayoshi Ozawa for the elemental analyses.

References

1) Part II: H. Satonaka, *Bull. Chem. Soc. Jpn.*, **56**, 3337 (1983).
2) H. Satonaka, *Bull. Chem. Soc. Jpn.*, **56**, 2463 (1983).
3) F. A. L. Anet, *J. Chem. Phys.*, **32**, 1274 (1960).
4) H. S. Gutowsky and A.L. Porte, *J. Chem. Phys.*, **35**, 839 (1961)
5) C. N. Banwel and N. Sheppard, *Discuss. Faraday Soc.*, **34**, 115 (1962).
6) T. Schaefer, *J. Chem. Phys.*, **36**, 2235 (1962).
7) J. Meinwald and A. Lewis, *J. Am. Chem. Soc.*, **83**, 2769 (1961).
8) J. Musher, *Mol. Phys.*, **6**, 93 (1963).
9) S. M. Castellano and A. A. Bothner-By, *J. Chem. Phys.*, **41**, 3863 (1964).
10) The notation δ_r(**N**) is hereafter used for the chemical shift for the *r*th(position)-proton on thiophene ring of the series of compounds **N**.
11) The notation $\nu_{C=O}$(**N**) is hereafter used for the carbonyl stretching frequency of the series of compounds **N**.
12) The notation J_{rs}(**N**) is hereafter used for the spin-spin coupling constant between *r*th- and *s*th-protons of the series of compounds **N**.
13) H. Wynberg, A. Logothetis, and D. Ver Proeg, *J. Am. Chem. Soc.*, **79**, 1972 (1957).
14) G. Pappalardo, *Gazz. Chim. Ital.*, **89**, 540 (1959).
15) C. H. Fawcett, D. M. Spencer, R. L. Wain, A. G Fallis, E. R. H. Jones, M. Le Quan, C. B. Page, V. Thaller, D. C. Shubrook, and P. M. Whitham, *J. Chem. Soc., C*, **1968**, 2455.
16) R. Kimura, T. Yabuuchi, and M. Hisaki, *Chem. Pharm. Bull.*, **10**, 1232 (1962).
17) P. Fournari and J. P. Chane, *Bull. Soc. Chim. Fr.*, **1963**, 479.
18) In the preparation of methyl [*trans*-β-(3- and 4-formyl-2-thienyl)acrylate]s, (3- and 4-diethoxymethyl 2-thiophenecarbaldehyde)s were used, respectively.
19) In the preparation of methyl [*trans*-β-(acetyl 2-thienyl)acrylate]s, [(2-methyl-1,3-dioxolan-2-yl)-2-thiophenecarbaldehyde]s were used.
20) 4-Methoxy-2-thiophenecarbaldehyde (bp 104°C/4 mmHg) is a new compound, and was prepared from 2-(4-iodo-3-thienyl)-1,3-dioxolane by the copper-promoted reaction with sodium methoxide followed by hydrolysis.
21) S. Gronowitz and B. Jagestern, *Ark. Kemi*, **18**, 213 (1961).
22) E. Campaigne and W. L. Archers, *J. Am. Chem. Soc.*, **75**, 989 (1953).
23) E. Profft and G. Solf, *J. Prakt. Chem.*, **24**, 38 (1964).
24) S. Gronowitz, P. Moes, A. Hornfeldt, and R. Hakansson, *Ark. Kemi.*, **17**, 165 (1961).
25) R. Guilard, P. Fournari, and M. Person, *Bull. Soc. Chim. Fr.*, **1967**, 4121.
26) P. Pastour, P. Savalle, and P. Eymery, *C. R. Akad. Sci., Paris*, **260**, 6130 (1965).
27) M. Robba, B. Roques, and M. M. Bonhomme, *Bull. Soc. Chim. Fr.*, **1967**, 2495.
28) J. Iriarte, E. Martinez, and J. M. Muchowski, *J. Heterocycl. Chem.*, **13**, 393 (1976).
29) L. I. Belen'kii, G. P. Gromova, and Ya. L. Gol'dfarb, *Izv. Akad. Nauk. SSSR, Ser. Khim.*, **1971**, 1228.
30) Ya. L. Gol'dfarb, Yu. B. Vol'kenshtein, and V. Lopatin, *Zh. Obshch. Khim.*, **34**, 969 (1964).
31) J. Sice, *J. Am. Chem. Soc.*, **75**, 3697 (1953).
32) H. Gilman, R. E. Brown, and H. L. Jones, *Iowa State College J. Sci.*, **2**, 317 (1928); *Chem. Abstr.*, **22**, 4525 (1928).

Regioselective Homo- and Codimerization of 1-Alkynes Leading to 2,4-Disubstituted 1-Buten-3-ynes by Catalysis of a $(\eta^5\text{-}C_5Me_5)_2TiCl_2$/RMgX System

Munetaka AKITA, Hajime YASUDA, and Akira NAKAMURA*
Department of Macromolecular Science, Faculty of Science, Osaka University, Toyonaka, Osaka 560
(Received August 3, 1983)

A series of 1-alkynes (RC≡CH where R=Et, *n*-Pr, *n*-Bu, *n*-C_6H_{13}, cyclohexyl, Ph, Me_3Si, Me_3SiCH_2, and Me_3SiOCH_2) was found to dimerize regioselectively (>99%) to 2,4-disubstituted 1-buten-3-ynes in 92—99% yields by catalysis of $(\eta^5\text{-}C_5Me_5)_2TiCl_2$/*i*-PrMgBr at 30 °C in 1—3 h. The catalyst system is also effective for the regioselective codimerization of various 1-alkynes with 1-ethynylcyclohexene or ethynylbenzene.

Linear- and cyclo-oligomerizations of 1-alkynes have been extensively studied with a variety of transition metal catalysts. Organometallic complexes of Ni,[1a] Co,[1b] Pd,[1c] and Ti[1d] are known as efficient catalysts for cyclooligomerization of alkynes converting them to substituted or unsubstituted benzenes, cyclooctatetraenes, *etc.* For linear dimerization of 1-alkynes, three different modes are possible as illustrated in Eq. 1.

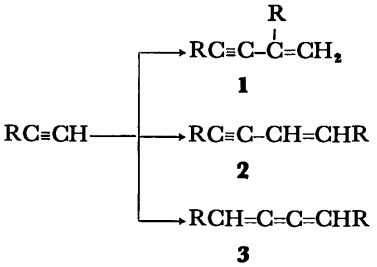

(1)

Only a few catalyst systems have been known for this type of dimerization. $[Cr(O\text{-}n\text{-}Bu)_4]/ZnEt_2$[2] and $[RhCl(PPh_3)_3]$[3] are representative catalysts for the head-to-tail dimerization of 1-alkynes to convert them to 2,4-disubstituted 1-buten-3-ynes (**1**), and some copper salts are known to be catalytically active for the head-to-head dimerization leading to 1,4-disubstituted 1-buten-3-ynes (**2**).[4] $[RuH_2(CO)(PPh_3)_3]$ is the unique catalyst to convert 1-alkynes to cumulene derivatives **3**.[5]

We wish to report herein a novel catalyst system, $(\eta^5\text{-}C_5Me_5)_2TiCl_2$/*i*-PrMgBr, which shows exceedingly high catalytic activities for the linear dimerization of various 1-alkynes to give the head-to-tail bound dimers **1** regioselectively. The present catalyst system is superior to the known catalysts with respect to regioselectivity, yield, reproducibility and broad applicability. Even more important is the experimental simplicity and the mild reaction conditions of our new process. It should be noted here that the formation of higher oligomers are negligible in the present system. This ambient catalyst system is also effective for the regioselective codimerization of two different 1-alkynes, which provides a variety of novel 2,4-disubstituted 1-buten-3-ynes.

Results and Discussion

Regioselective Dimerization of 1-Alkynes. In the preceding paper, we have reported the exceptionally high catalytic activity of $(\eta^5\text{-}C_5Me_5)_2TiCl_2$/RMgX or $(\eta^5\text{-}C_5Me_5)_2TiCl_2/NaC_{10}H_8$ toward the selective isomerization of 1-alkenes to (*E*)-2-alkenes.[6] In our continuing investigations on titanocene species, we have found that "$(\eta^5\text{-}C_5Me_5)_2TiH$" species generated by reduction of $(\eta^5\text{-}C_5Me_5)_2TiCl_2$ with two equivalents of *i*-PrMgBr behaves as an efficient catalyst for the regioselective dimerization of 1-alkynes to lead to **1**. When a mixture of $(\eta^5\text{-}C_5Me_5)_2TiCl_2$/*i*-PrMgBr (2 mol % of $(\eta^5\text{-}C_5Me_5)_2TiCl_2$ based on 1-alkyne was used) and 1-butyne, 1-pentyne, 1-hexyne, or 1-octyne was stirred for 1—3 h at 30 °C in diethyl ether, the highly regioselective dimerization (>99%) occurred to give the corresponding dimers **1a—d** in 92—97% yields. The

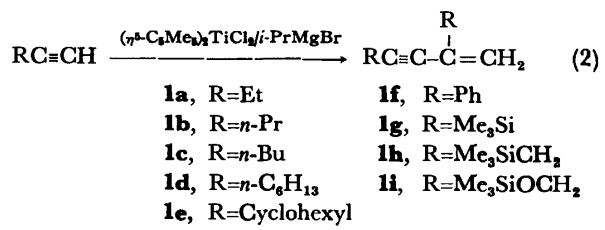

(2)

results are given in Table 1. The maximum turnover number for 1-hexyne was 2.0 (mol/mol min) in diethyl ether and 4.5 (mol/mol min) in THF. The corresponding reactions were examined with $(\eta^5\text{-}C_5Me_5)_2TiCl_2/NaC_{10}H_8$ to find a significantly lower activity (turnover number was 0.24 mol/mol min in THF). Though normal and secondary alkyl-substituted acetylenes readily dimerize at ambient temperature, *t*-butylacetylene (3,3-dimethyl-1-butyne) was completely inert to both catalysts even at 60 °C and was recovered quantitatively. The present catalyst system is active also for 1-alkynes containing Me_3Si group, a leaving group useful for organic synthesis, but inactive for 1-alkynes substituted with an electron donating group such as EtO, EtS, or Et_2N. The greater reactivity of $Me_3SiC{\equiv}CH$ compared to *t*-BuC≡CH may be ascribed to the smaller cone angle and higher acidity of the former. The use of bulky $\eta^5\text{-}C_5Me_5$ ligand is essential to perform the present type dimerization. The $(\eta^5\text{-}C_5H_5)_2TiCl_2$/*i*-PrMgBr catalyst system with a less bulky ligand has practically no catalysis and preferred the oligomerization of 1-alkynes.

Regioselective Codimerization of 1-Alkynes. The successful regioselective dimerization of 1-alkynes prompted us to examine the codimerization between

Table 1. Homodimerization of 1-alkynes (RC≡CH) to 2,4-disubstituted 1-buten-3-ynes with $(C_5Me_5)_2TiCi_2/i$-PrMgBr(1:2) catalyst system[a)]

R	Products	GC yield/% (Isolated yield/%)
Et	**1a**	95 (91)
n-Pr	**1b**	97 (92)
n-Bu	**1c**	97 (91)
n-C_6H_{13}	**1d**	94 (90)
Cyclohexyl	**1e**	96 (90)
Ph	**1f**	92 (78)
Me_3Si	**1g**	95 (93)
Me_3SiCH_2	**1h**	96 (92)
Me_3SiOCH_2	**1i**	94 (90)
t-Bu		0
1-Cyclohexenyl		0
EtO		0
EtS		0
Et_2N		0

a) The reactions were carried out in diethyl ether at 30 °C for 1 h. Concentration of catalyst; 2 mol%. (Ratio of $(C_5Me_5)_2TiCl_2$/1-alkyne=1/50(mol/mol)).

two different ethynyl compounds which have normal, secondary or tertiary alkyl substituents. The following four isomers **1**, **4**, **5**, and **1′** are possible for the codimerization between RC≡CH and R′C≡CH. When the codimerization was carried out using a 1 : 1 mixture of two different normal alkyl-substituted acetylenes (R=Et and *n*-Bu), the four isomers were obtained with the

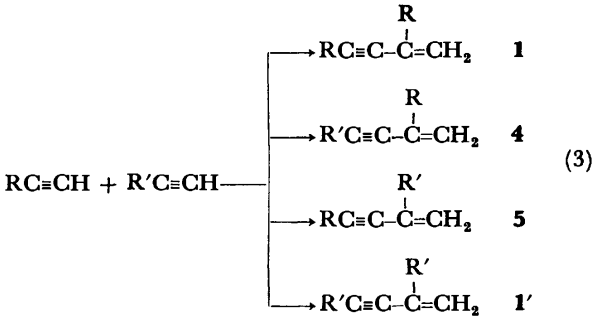

(3)

modest level of selectivities (entry 1 in Table 2). The yields of the respective isomers (**1**, **1′**, **4**, and **5**) are nearly equal. However, when the reactions of normal alkylacetylenes (RC≡CH) were conducted with second-

Table 2. Distributions and total yields of 2,4-disubstituted 1-buten-3-ynes obtained from a mixture of RC≡CH and R′C≡CH[a)]

Entry	R	R′	Reaction time/h	Distribution of the dimer/%				Total yield/%
				1	**4**	**5**	**1′**	
1	Et	*n*-Bu	1	28(**1a**)	27(**4a**)	27(**5a**)	18(**1c**)	86
2	*n*-Bu	Cyclohexyl	1	28(**1c**)	50(**4b**)	8	14(**1e**)	86
3	*n*-Bu	*t*-Bu	3	38(**1c**)	62(**4c**)	0	0	68
4	*n*-Bu	Me_3Si	1	6(**1c**)	92(**4d**)	0	2(**1g**)	92
5	Cyclohexyl	*t*-Bu	3	42(**1e**)	58(**4e**)	0	0	66
6	*n*-Bu	Me_3SiCH_2	1	31(**1d**)	43(**4f**)	7	19(**1h**)	86
7	Me_3SiCH_2	Me_3Si	1	10(**1h**)	82(**4g**)	0	8(**1g**)	96
8	Me_3SiOCH_2	*n*-Bu(1:1)	1	33(**1i**)	65(**4h**)	0	2(**1c**)	67
9	Me_3SiOCH_2	*n*-Bu(1:2)	1	15(**1i**)	83(**4h**)	0	2(**1c**)	65
10	Me_3SiOCH_2	*t*-Bu	3	48(**1i**)	52(**4i**)	0	0	63

a) Yield is expressed by (% conversion of RC≡CH+R′C≡CH)/2 and was determined by the gas chromatographic analysis. Reaction conditions; catalyst concentration, 2 mol% to the sum of RC≡CH and R′C≡CH; temperature, 30 °C in diethyl ether.

Table 3. Regioselective codimerization of ethynyl-1-cyclohexene or ethynylbenzene (R′C≡CH) with less acidic 1-alkynes (RC≡CH)[a)]

Entry	R	R′	Reaction time/h	Distribution of the dimer/%				Total yield/%[b)]
				1	**4**	**5**	**1′**	
11	*n*-Bu	1-Cyclohexenyl	1	0	99(**4j**)	0	1	91
12	Me_3SiCH_2	1-Cyclohexenyl	1	7(**1h**)	93(**4k**)	0	0	86
13	Me_3SiOCH_2	1-Cyclohexenyl	1	4(**1i**)	96(**4l**)	0	0	92
14	Me_3Si	1-Cyclohexenyl	1	21(**1g**)	79(**4m**)	0	0	80
15	Cyclohexyl	1-Cyclohexenyl	1	2(**1e**)	98(**4n**)	0	0	91
16	Ph	1-Cyclohexenyl	1	100(**1f**)	0	0	0	50
17	*t*-Bu	1-Cyclohexenyl	1	0	0	0	0	0
18	*n*-Bu	Ph	1	1(**1c**)	98(**4o**)	0	1(**1f**)	91
19	Me_3SiCH_2	Ph	1	12(**1h**)	76(**4p**)	0	12(**1f**)	89
20	Me_3SiOCH_2	Ph	1	1(**1i**)	97(**4q**)	0	2(**1f**)	93
21	Me_3Si	Ph	1	18(**1g**)	63(**4r**)	0	19(**1f**)	88
22	Cyclohexyl	Ph	1	0	93(**4s**)	0	7(**1f**)	89
23	*t*-Bu	Ph	1	0	0	0	100(**1f**)	49

a) Reactions were carried out at 30 °C in diethyl ether with 2 mol% of catalyst. b) Total yield is expressed by (sum of conversion for RC≡CH and R′C≡CH)/2.

ary or tertiary alkylacetylenes (R'C≡CH), the codimers were obtained with moderate regioselectivity (entries 2 and 3). The formation of **4** exceeded over that of the codimer **5** and homodimers **1** and **1'**. Similar trend was observed also in the reaction of ethynylcyclohexane with *t*-butylacetylene (entry 5) or in the reaction shown in entries 4, 6, and 7.

Thus, the more bulky alkyl groups are always introduced to the terminal position (C_4-carbon) of the 1-buten-3-ynes in preference to the internal position (C_2-carbon). In some favorable cases (entries 3, 4, 5, and 7), the formation of the dimers of the type **5** was completely suppressed. These results are reasonably interpreted by the steric effect of alkyl groups. Especially noteworthy is that the present catalyst system showed no catalysis toward the homo-dimerization of *t*-BuC≡CH while it showed exceedingly high activity toward the codimerization of *t*-BuC≡CH with normal or secondary alkyl-substituted acetylenes. Rather exceptional is the behavior of 3-trimethylsiloxy-1-propyne. Though the bulkiness of Me_3SiOCH_2 is nearly equal to that of *n*-Bu group and the acidity of $Me_3SiOCH_2C{\equiv}CH$ is a little higher than that of 1-hexyne as described later, the formation of **5** was completely suppressed. Since oxygen atom has a good affinity toward Ti atom, the observed enhanced regioselectivity is supposed to be the result of the interaction between the oxygen atom of $Me_3SiOCH_2C{\equiv}CH$ and the metal center.

To evaluate the electronic effect of substituent, the codimerization of ethynylcyclohexane with 1-ethynylcyclohexene or ethynylbenzene was tried (entries 15 and 22 in Table 3). Though the bulkiness of these three substituents is nearly the same, the regioisomers, 4-(1-cyclohexenyl)-2-cyclohexyl-1-buten-3-yne (**4n**) and 2-cyclohexyl-4-phenyl-1-buten-3-yne (**4s**), were formed with an extremely high selectivity. This result may be interpreted primarily by electronic effect or acidity of 1-alkynes. The R'C≡C unit of the product is generally derived from the 1-alkynes of higher acidity and the $-C(R){=}CH_2$ unit is from less acidic 1-alkyne. The relative acidity strength of the 1-alkynes was estimated from the ^{1}H-NMR chemical shift values (Table 4) of the CH proton of 1-alkynes as PhC≡CH>1-ethynylcyclohexene >$Me_3SiC{\equiv}CH{\simeq}Me_3SiOCH_2C{\equiv}CH$>*t*-BuC≡CH≃ethynylcyclohexane≃*n*-BuC≡CH>$Me_3SiCH_2C{\equiv}CH$. The CH signal appeared at lower field with increasing the acidity of 1-alkynes.[7] The ^{13}C-NMR chemical shift values also showed the similar relationship. The C≡C and CH frequencies in their IR spectra are useless to estimate the relative acidity strength because the difference is too small. The reactions of 1-hexyne, 3-trimethylsiloxy-1-propyne or 3-trimethylsilyl-1-propyne with 1-ethynylcyclohexene or ethynylbenzene (entries 11—13, 18—20) also showed the highly regioselective formation of **4**. The good selectivity observed in the reaction of $Me_3SiC{\equiv}CH$ with *n*-BuC≡CH or $Me_3SiCH_2C{\equiv}CH$ (entries 4 and 7 in Table 2) also may be interpreted by the relatively high acidity of $Me_3SiC{\equiv}CH$. However, in the reaction of 3,3-dimethyl-1-butyne with 1-ethynylcyclohexene or with ethynylbenzene, no reaction occurred. This is presumably due to the steric reasons as described later in the discussion. The structures of the resulting dimers and codimers were analyzed by the ^{1}H-NMR (see Experimental section) and ^{13}C-NMR (Table 5) with reference to the chemical shift values of starting 1-alkynes and related 1-alkenes.[8] In cases of $CH_2{=}C(CH_2OSiMe_3)C{\equiv}C$-*n*-Bu and $CH_2{=}C(n\text{-Bu})C{\equiv}CPh$, the structures were identified after hydrogenation to $CH_3CH(CH_2OH)C_6H_{13}$ and $CH_3CH(n\text{-Bu})CH_2CH_2Ph$, respectively, by comparison with authentic samples. Thus, the present catalyst provides 1-buten-3-ynes bearing two different substituents on the C-2 and C-4 atom, most of which are not yet synthesized even in combination of conventional organic reactions.[9]

$$RC{\equiv}CH + R'C{\equiv}CH \xrightarrow{(\eta^5\text{-}C_5Me_5)_2TiCl_2/i\text{-}PrMgBr} R'C{\equiv}C\text{-}\underset{\displaystyle R}{\overset{\displaystyle |}{C}}{=}CH_2 \quad (4)$$

4

R'C≡CH : bulky or acidic 1-alkyne
RC≡CH : less bulky or less acidic 1-alkyne

4a, R=Et, R'=*n*-Bu
4b, R=*n*-Bu, R'=cyclohexyl
4c, R=*n*-Bu, R'=*t*-Bu
4d, R=*n*-Bu, R'=Me_3Si
4e, R=cyclohexyl, R'=*t*-Bu
4f, R=*n*-C_6H_{13}, R'=Me_3SiCH_2
4g, R=Me_3SiCH_2, R'=Me_3Si
4h, R=Me_3SiOCH_2, R'=*n*-Bu
4i, R=Me_3SiOCH_2, R'=*t*-Bu
4j, R=*n*-Bu,
4k, R=Me_3SiCH_2
4l, R=Me_3SiOCH_2
4m, R=Me_3Si
4n, R=cyclohexyl
} R'=1-cyclohexenyl
4o, R=*n*-Bu
4p, R=Me_3SiCH_2
4q, R=Me_3SiOCH_2
4r, R=Me_3Si
4s, R=cyclohexyl
} R'=Ph

TABLE 4. ^{1}H- AND ^{13}C-NMR CHEMICAL SHIFT VALUES FOR 1-ALKYNES[a]

R in RC≡CH	^{1}H (δ) HC≡C-	^{13}C (δ) C^1	^{13}C (δ) C^2
Me_3SiCH_2	1.85	66.81	82.14
n-Bu	1.90	68.12	84.14
Cyclohexyl	2.01	67.93	88.68
t-Bu	2.05	66.64	92.65
Me_3SiOCH_2	2.34	72.93	82.08
Me_3Si	2.35	93.24	89.83
1-Cyclohexenyl	2.78	74.28	85.39
Ph	3.03	77.32	83.71

a) Measured in $CDCl_3$ at 30 °C at 100 MHz for the ^{1}H NMR and 22.5 MHz for the ^{13}C NMR spectra. Assignment of $RC^2{\equiv}C^1H$ was made from the non-decoupled spectra.

TABLE 5. ^{13}C-NMR CHEMICAL SHIFT VALUES (δ) FOR 2,4-DISUBSTITUTED 1-BUTEN-3-YNES AND THE DEVIATION FROM THE MEAN VALUE (PARENTHESES)[a]

R	C-1	C-2	C-3	C-4	C-5	C-6	Compd[b] (A)	Compd[b] (B)
Et	111.8(5)	132.6(2)	80.5(2)	91.3(1)	30.9(2)	14.0(0)	2	2
n-Pr	119.5	132.2	81.3	89.8	39.8	22.4	1	1
n-Bu	120.3(14)	132.3(3)	81.4(9)	90.8(8)	37.1(3)	31.0(2)	7	4
n-C_6H_{13}	118.8(4)	132.8(2)	81.2	90.1	37.8(2)	31.5	2	1
Cyclohexyl	118.0(10)	137.8(3)	80.8(5)	94.5(4)	45.4(3)	29.6(1)	5	2
t-Bu			79.2(4)	99.2(4)	—	—	0	3
Me_3SiCH_2	118.1(17)	129.4(5)	81.0(9)	87.5(4)	28.5(2)	7.9(1)	4	2
Me_3SiOCH_2	118.9(9)	131.0(5)	83.2	88.6	64.9(3)	51.5	5	1
Me_3Si	133.5(11)	134.6(5)	95.8(28)	106.8(8)	—	—	3	3
Cyclohexenyl			87.0(21)	93.2(28)	—	—	0	5
Ph	120.7	137.7	89.2(12)	91.9(21)	—	—	1	6

a) Numbering system follows $C^1{=}C^2(R^5)C^3{\equiv}C^4R^6$. The C-5 and C-6 express the carbons in R^5 and R^6 directly bonded to C-2 and C-4 atoms, respectively. The values were obtained by averaging the observed chemical shift values for **1a—i** and **4a—s** (deviation from the mean was shown in parentheses). b) The number of compounds used for the data collection regarding (A) C-1, C-2 and C-5 atoms and (B) C-3, C-4 and C-6 moiety.

By taking advantage of the ease of substitution of

$$RC{\equiv}C\text{–}\underset{\displaystyle CH_2OSiMe_3}{\overset{\displaystyle |}{C}}{=}CH_2 \xrightarrow{i\text{-PrMgBr}} RC{\equiv}C\text{–}\underset{\displaystyle CH_2CH(CH_3)_2}{\overset{\displaystyle |}{C}}{=}CH_2 \quad (5)$$

4t(R = Ph)

Me_3SiO group, the Me_3SiO group was transformed to *i*-Pr group by reaction with *i*-PrMgBr (Eq. 5). Similar exchange of the Me_3SiO group with an alkyl group is already known for the Ni- or Pd-catalyzed reaction of 3-trialkylsiloxy-1-butenes with PhMgX.[10] The present sequence of reactions provides a useful route to introduce various kinds of alkyl groups into the C-2 atom of the 1-buten-3-ynes.

Reaction Pathway for the Codimerization of 1-Alkynes. A possible mechanism for the selective codimerization of 1-alkynes catalyzed by (η^5-$C_5Me_5)_2$-$TiCl_2$/*i*-PrMgBr is shown in Scheme 1. Reduction of (η^5-$C_5Me_5)_2TiCl_2$ with *i*-PrMgBr will generate low-valent (η^5-$C_5Me_5)_2TiH$ species. The generation of similar species, (η^5-$C_5H_5)_2TiH$, has been suggested by Martin and Sato in the hydrotitanation of conjugated dienes with (η^5-$C_5H_5)_2TiCl_2$/RMgX[11] and in the titanium-assisted hydromagnesiation of disubstituted acetylenes[12] and carbonyl compounds.[13] Hydrotitanation of alkenes with (η^5-$C_5H_5)_2TiH$[14] and hydrozirconation of alkenes or alkynes with (η^5-$C_5H_5)_2$-$ZrHCl$[15] are already known. Formation of the low-valent (η^5-$C_5Me_5)_2Ti$ species may be ruled out because such species generally gives catalytically inactive titana-2,4-cyclopentadienes when it was reacted with 1-alkynes.[16] The reactive species, (η^5-$C_5Me_5)_2TiH$, will readily react with 1-alkynes to give (η^5-$C_5Me_5)_2$-$TiCH{=}CHR'$. Since (η^5-$C_5H_5)_2ZrMe_2$ is known to be cleaved with 1-alkynes (RC≡CH) to give CH_4 and (η^5-$C_5H_5)_2Zr(C{\equiv}CR)_2$,[17] it seems most likely that (η^5-$C_5Me_5)_2TiCH{=}CHR'$ reacts with R'C≡CH to produce (η^5-$C_5Me_5)_2TiC{\equiv}CR'$ (step a). When two different 1-alkynes are present in the system, the more acidic 1-alkyne (R'C≡CH) will cleave the Ti-C bond in preference to the attack of a less acidic alkyne (RC≡CH) to result in the formation of (η^5-$C_5Me_5)_2$-$TiC{\equiv}CR'$. Isolation of (η^5-$C_5Me_5)_2TiC{\equiv}CR$ or (η^5-$C_5H_5)_2TiC{\equiv}CR$ has not been achieved because of its thermal instability. In the case of (η^5-$C_5H_4Me)_2TiC{\equiv}$CPh, spontaneous dimerization to catalytically inactive (η^5-$C_5H_4Me)_4Ti_2$[μ-(1-3-η^2-, 2-4-η^2-1,4-diphenylbutadiene)] occurs when free PhC≡CH is absent in the reaction system.[18] However, we found that when (η^5-$C_5Me_5)_2TiC{\equiv}CPh$ was prepared *in situ* by reaction of (η^5-$C_5Me_5)_2TiCl$ with LiC≡CPh in the presence of excess ethynylbenzene and 1-hexyne (1 : 1 mixture), the catalytic codimerization occurred successfully. The turnover number for this catalyst system (1.8 mol/mol min) is nearly equal to 2.0 mol/mol min for the (η^5-$C_5Me_5)_2TiCl_2$/*i*-PrMgBr system. This finding supports the above reaction pathway through (η^5-$C_5Me_5)_2TiC{\equiv}CR'$ species. Thus, the acidic 1-alkyne forms the (η^5-$C_5Me_5)_2TiC{\equiv}CR'$ at first and then insertion of less acidic 1-alkyne follows (step c) *via* an intermediate coordinated with RC≡CH (step b). The subsequent Ti-C bond fission of the resulting (η^5-$C_5Me_5)_2TiCH{=}C(R)C{\equiv}CR'$ may be done with the

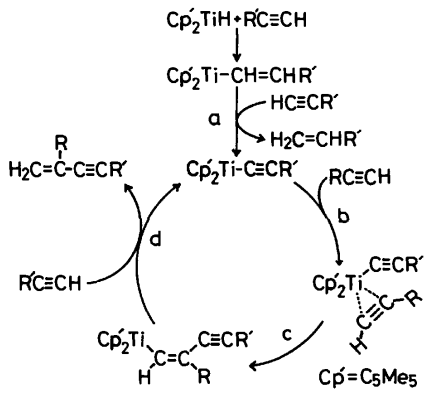

Scheme 1.

acidic R'C≡CH to release CH_2=C(R)C≡CR' and to regenerate (η^5-$C_5Me_5)_2$TiC≡CR' to complete the catalytic cycle. The direction of the alkynyl transfer is assumed to be controlled in the step b by steric repulsion between η^5-C_5Me_5 ligand and alkyl group of 1-alkynes. Coordination of RC≡CH in the opposite direction is sterically improbable. Insertion of RC≡CH to TiC≡CR' bond will occur in the cis-fashion on a plane containing the Ti-C≡CR' bond as predicted by the EH-MO calculation.[19] To verify this postulation, codimerization using PhC≡CD or *n*-BuC≡CD was examined. The 1 : 1 reaction of PhC≡CD with *n*-BuC≡CH in the presence of the catalyst gave (*Z*)-**4o**-1*d* in 98% selectivity (Eq. 6) while 1 : 1 mixture of PhC≡CH and *n*-BuC≡CD gave (*E*)-**4o**-1*d* in 97% selectivity (Eq. 7). The assignment of the structure was made with reference to the ^{1}H-NMR data for butadiene,[20] 1,3-pentadiene,[21] and ethenylbenzene[22] together with the NOE measurement (5—8%) in $CDCl_3$ and C_6D_6. Thus the cis-addition of less acidic 1-alkyne was verified in support of the above mechanism. Similar cis-addition of 1-alkynes is widely observed in the

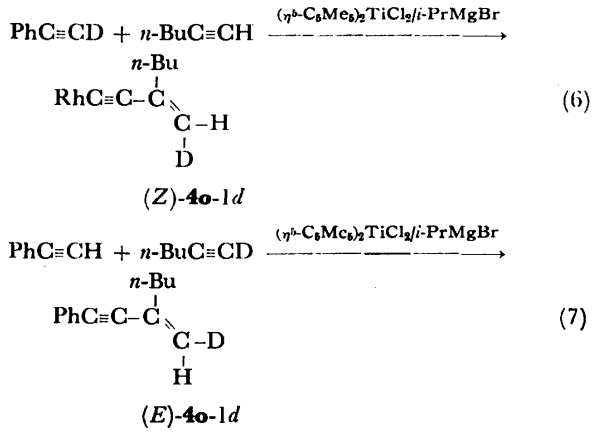

(6)

(*Z*)-**4o**-1*d*

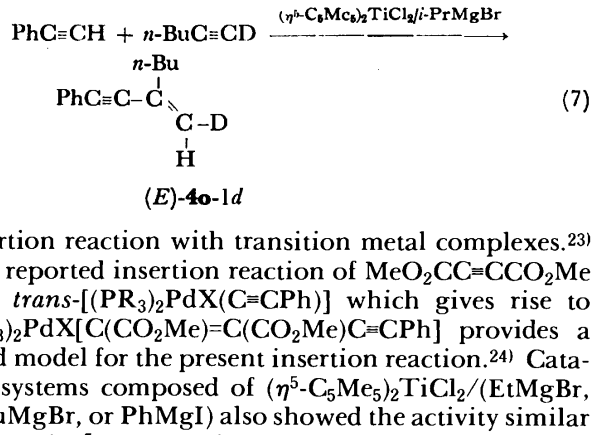

(7)

(*E*)-**4o**-1*d*

insertion reaction with transition metal complexes.[23] The reported insertion reaction of MeO_2CC≡CCO_2Me into *trans*-[$(PR_3)_2$PdX(C≡CPh)] which gives rise to $(PR_3)_2$PdX[C(CO_2Me)=C(CO_2Me)C≡CPh] provides a good model for the present insertion reaction.[24] Catalyst systems composed of (η^5-$C_5Me_5)_2TiCl_2$/(EtMgBr, *n*-BuMgBr, or PhMgI) also showed the activity similar to that of (η^5-$C_5Me_5)_2TiCl_2$/*i*-PrMgBr for the codimerization of PhC≡CH and *n*-BuC≡CH, suggesting that the resulted Ti-R(R=Et, *n*-Bu, Ph) bond is cleaved by RC≡CH to generate the catalytically active (η^5-$C_5Me_5)_2$TiC≡CR species. The isolation of (η^5-$C_5Me_5)_2$-TiC≡CR (R=*t*-Bu, 1-cyclohexenyl) and its stoichiometric reaction with various 1-alkynes are now in progress to get more evidence to verify the proposed mechanism.

Experimental

General Procedure. All operations were conducted with Schlenk technique under an argon atmosphere. 1-Butyne, 1-pentyne, 1-hexyne, 1-octyne, ethynylbenzene, and 3-oxa-1-pentyne were obtained commercially (Tokyo Kasei Co.), and 3,3-dimethyl-1-butyne,[25] ethynylcyclohexane,[26] 1-ethynylcyclohexene,[27] 3-trimethylsilyl-1-propyne,[28] *N*,*N*-diethylethynylamine,[29] and 3-thia-1-pentyne[30] were prepared by the reported methods. 3-Trimethylsiloxy-1-propyne was prepared from 2-propyn-1-ol and chlorotrimethylsilane. Ethynyltrimethylsilane was prepared from chlorotrimethylsilane and sodium ethynide (suspended in xylene) in DMF. All the ethynyl compounds were purified by distillation after drying over calcium hydride. (η^5-$C_5H_5)_2TiCl_2$[31] and (η^5-$C_5Me_5)_2TiCl_2$[32] were prepared referring to literatures. The GLC analyses were carried out with a Yanagimoto Model G-80 gas chromatograph using a column packed with Celite-Silicone DC-550, and the separation of products were done with a Varian-Aerograph Model 700 gas chromatograph using a column packed with DEGS. ^{1}H- and ^{13}C-NMR spectra were recorded on a Varian XL-100 and a JEOL 90Q instruments, respectively. IR spectra were obtained on a Hitachi EPI-2 spectrometer. Mass spectra were recorded on a JEOL JMS-OISG-2 spectrometer.

Dimerization of 1-Alkynes. To a stirred suspension of dichlorobis(η^5-pentamethylcyclopentadienyl)titanum (39 mg, 0.1 mmol) in diethyl ether (1 cm^3) was added a diethyl ether solution of isopropylmagnesium bromide (*f*=0.97, 0.21 cm^3, 0.2 mmol). The color of the solution immediately turned into deep blue. After stirring the mixture for 10 min at 0 °C, 1-alkyne (5.0 mmol) was added to the resulting catalyst system over a 1 min period. The mixture was allowed to warm to 30 °C, magnetically stirred for 1—3 h, and then quenched with a small portion of 1 mol dm^{-3} aq HCl. The product was distilled and separated into the individual isomers on a preparative gas chromatograph when the separation was necessitated. Characterization of the product was made in terms of the ^{1}H-NMR (100 MHz), mass, IR spectra, and elemental analysis together with the ^{13}C-NMR (22.5 MHz) spectrum (Table 5).

2-Ethyl-1-hexen-3-yne (1a): ^{1}H NMR($CDCl_3$) δ=1.10 (3H, t, *J*=8.0 Hz, $C\underline{H}_3CH_2C$≡C), 1.17 (3H, t, *J*=8.0 Hz, $C\underline{H}_3CH_2C$≡C), 2.16 (2H, q, *J*=8.0 Hz, CH_2C≡C), 2.32 (2H, q, *J*=8.0 Hz, CH_2C≡C), 5.13, 5.18 (2H, m, C=CH_2). IR (neat) 3100, 2970, 2940, 2884, 2860 (CH), 2235 (C≡C), 1613 (C=C), 1462, 1377, 1326, 1289, 1243, 894 (C=CH_2) cm^{-1}. MS (70 eV, EI) *m*/*z* (rel intensity), 108 (M^+, 1), 93 (0.7), 91 (1.1), 79 (0.9), 77 (1.7). Found: C, 88.82; H, 11.18%. Calcd for C_8H_{12}: C, 88.81; H, 11.19%.

2-Propyl-1-hepten-3-yne (1b): ^{1}H NMR ($CDCl_3$) δ=0.90 (3H, t, *J*=6.0 Hz, $C\underline{H}_3(CH_2)_2C$≡C), 1.00 (3H, t, *J*=7.0 Hz, $C\underline{H}_3(CH_2)_2C$≡C), 1.34—1.78 (4H, m, CH_2), 2.11 (2H, t, *J*=7.0 Hz, -$C\underline{H}_2C$=CH_2), 2.88 (2H, t, *J*=7.0 Hz, CH_2C≡C), 5.11, 5.20 (2H, m, C=CH_2). IR (neat) 3090, 2960, 2930, 2880, 2230, 1612, 1462, 1382, 1339, 1287, 893 cm^{-1}. MS (70 eV) *m*/*z* (rel intensity), 136 (M^+, 1), 109 (1.5), 94 (2.0), 92 (1.1), 77 (1.5). Found: C, 87.88; H, 11.81%. Calcd for $C_{10}H_{16}$: C, 88.16, H, 11.83%.

2-Butyl-1-octen-3-yne (1c): ^{1}H NMR ($CDCl_3$) δ=0.91, 0.92 (6H, t, *J*=7.0 Hz, CH_3), 1.1—1.7 (8H, m, CH_2CH_2), 2.14 (2H, t, *J*=7.0 Hz, CH_2C=C), 2.32 (2H, t, *J*=7.0 Hz, CH_2C≡C), 5.12, 5.19 (2H, m, C=CH_2). IR (neat) 3100, 2960, 2935, 2880, 2870, 2740, 1612, 1467, 1382, 1331, 1107, 892 cm^{-1}. MS (70 eV) *m*/*z* (rel intensity), 164 (M^+, 1), 122 (5.8), 107 (6.1). Found: C, 87.53; H, 12.30%. Calcd for $C_{12}H_{20}$: C, 87.73; H, 12.27%.

2-Hexyl-1-decen-3-yne (1d): ^{1}H NMR ($CDCl_3$) δ=0.90 (6H, t, *J*=6.0 Hz, CH_3), 1.1—1.7 (16H, m, $(CH_2)_4$), 2.13 (2H, t, *J*=7.0 Hz, CH_2C=C), 2.30 (2H, t, *J*=7.0 Hz, CH_2C≡C), 5.11, 5.19 (2H, m, C=CH_2). IR (neat) 3090, 2960, 2930, 2860, 2730, 1612, 1466, 892 cm^{-1}. MS (70 eV) *m*/*z* (rel intensity) 220 (M^+, 1), 205 (0.5), 191 (0.9). Found: C, 87.13, H, 12.86%. Calcd for $C_{16}H_{28}$: C, 87.20; H, 12.80%.

2,4-Dicyclohexyl-1-buten-3-yne (1e): ^{1}H NMR ($CDCl_3$) δ=1.0—2.1 (20H, m, cyclohexyl), 1.9—2.2 (1H, m, $(CH_2)_5C\underline{H}C$=C), 2.3—2.7 (1H, m, $(CH_2)_5C\underline{H}C$≡C), 5.11, 5.17 (2H, m, C=CH_2). IR (neat) 3090, 2930, 2860, 2220, 1607, 1450, 888 cm^{-1}. MS (70 eV) *m*/*z* (rel intensity), 216 (M^+, 1), 201 (0.2), 187 (0.3), 173 (0.5). Found: C, 88.49; H, 11.31%. Calcd for $C_{16}H_{24}$: C, 88.82; H, 11.18%.

2,4-Diphenyl-1-buten-3-yne (1f): ^{1}H NMR ($CDCl_3$) δ=5.74, 5.95 (2H, d, J=8.0 Hz, C=CH_2), 7.10—7.80 (10H, m, Ph). IR (neat) 3060, 3035, 2210, 1589, 1572, 1492, 1445, 1338, 1071, 1027, 897, 776, 760, 695 cm^{-1}. MS (70 eV) m/z (rel intensity), 204 (M^+, 1), 203 (0.7), 202 (0.6). Found: C, 93.60; H, 5.96%. Calcd for $C_{16}H_{12}$: C, 94.08; H, 5.92%.

2,4-Bis(trimethylsilyl)-1-buten-3-yne (1g): ^{1}H NMR ($CDCl_3$) δ=0.15 (9H, s, Me_3SiC=C), 0.19 (9H, s, Me_3SiC≡C), 5.68 (1H, d, J=3.0 Hz, C=CH), 6.10 (1H, d, J=3.0 Hz, C=CH). IR (neat) 3075, 2965, 2905, 2135, 1245, 973, 926, 840, 760, 698 cm^{-1}. MS (70 eV) m/z (rel intensity), 196 (M^+, 1), 181 (2.1), 155 (2.5). Found: C, 61.06; H, 10.25%. Calcd for $C_{10}H_{20}Si_2$: C, 61.14; H, 10.26%.

5-Trimethylsilyl-2-trimethylsilylmethyl-1-penten-3-yne (1h): ^{1}H NMR ($CDCl_3$) δ=0.03 (9H, s, $\underline{Me_3}SiCH_2C$=C), 0.10 (9H, s, $\underline{Me_3}SiCH_2C$≡C), 1.57 (2H, s, CH_2C≡C), 1.73 (2H, m, CH_2C=C), 4.86, 5.03 (2H, m, C=CH_2). IR (neat) 3100, 2960, 2900, 2230, 1595, 1292, 1245, 1158, 932, 850, 765, 698 cm^{-1}. MS (70 eV) m/z (rel intensity), 224 (M^+, 1), 209 (0.7), 136 (2.0). Found: C, 64.12; H, 10.75%. Calcd for $C_{12}H_{24}Si_2$: C, 64.20; H, 10.78%.

2-Trimethylsiloxymethyl-4-trimethylsiloxy-1-penten-3-yne (1i): ^{1}H NMR ($CDCl_3$) δ=0.14 (9H, s, $\underline{Me_3}SiOCH_2C$=C), 0.19 (9H, s, $\underline{Me_3}SiOCH_2C$≡C), 4.11 (2H, t, J=2.0 Hz, OCH_2C=C), 4.41 (2H, s, OCH_2C≡C), 5.45, 5.55 (2H, m, C=CH_2). IR (neat) 2960, 2860, 1621, 1372, 1248, 1119, 1097, 1037, 872, 844, 756cm^{-1}. MS (70 eV) m/z (rel intensity), 256 (M^+, 1), 255 (1.1), 241 (1.9), 177 (2.4), 147 (5.6). Found: C, 56.42; H, 9.42%. Calcd for $C_{12}H_{24}O_2Si_2$: C, 56.19; H, 9.43%.

Codimerization of RC≡CH with R'C≡CH. The procedure is essentially the same as that described for the homodimerization of 1-alkynes. For a typical example, a mixture of 1-hexyne (205 mg, 2.5 mmol) and ethynylbenzene (255 mg, 2.5 mmol) was added to the catalyst system, (η^5-$C_5Me_5)_2TiCl_2$/i-PrMgBr (0.1 mmol/0.2 mmol), in diethyl ether (0.3 cm^3) at 0 °C and the mixture was stirred for a fixed time (1—3 h) at 30 °C. After the addition of 1 mol dm^{-3} aq HCl (0.3 cm^3), the organic layer was distilled to give 2-butyl-4-phenyl-1-buten-3-yne (**4o**) in 98% GC yield (90% isolated yield). This procedure was applied for the codimerization of other 1-alkynes and the separation of the isomers was made on a preparative gas chromatograph. The ^{1}H NMR, mass, and IR spectral data for the major products were given below. Elemental analysis agreed well with the calculated values.

2-Ethyl-1-octen-3-yne (4a): ^{1}H NMR ($CDCl_3$) δ=0.92 (3H, t, J=8.0 Hz, CH_3), 1.08 (3H, t, J=8.0 Hz, CH_3), 1.20—1.70 (4H, m, CH_2CH_2), 2.16 (2H, q, J=8.0 Hz, CH_2C=C), 2.31 (2H, t, J=7.2 Hz, CH_2C≡C), 5.12, 5.19 (2H, m, C=CH_2). IR (neat) 3100, 2240, 1615, 893 cm^{-1}. MS (70 eV) m/z (rel intensity) 136 (1), 121 (0.9), 107 (1.9).

2-Butyl-1-hexen-3-yne (5a): ^{1}H NMR ($CDCl_3$) δ=0.91 (3H, t, J=8.0 Hz, CH_3), 1.16 (3H, t, J=8.0 Hz, CH_3), 1.2—1.7 (4H, m, CH_2CH_2), 2.12 (2H, t, J=7.0 Hz, CH_2C=C), 2.31 (2H, q, J=8.0 Hz, CH_2C≡C), 5.12, 5.19 (2H, m, C=CH_2). IR (neat) 3100, 2240, 1615, 890 cm^{-1}. MS, m/z (rel intensity), 136, 121.

2-Butyl-4-cyclohexyl-1-buten-3-yne (4b): ^{1}H NMR ($CDCl_3$) δ=0.90 (3H, t, J=7.2 Hz, CH_3), 1.1—2.0 (14H, m, CH_2CH_2 and C_6H_{11}), 2.13 (2H, t, J=7.0 Hz, CH_2C=C), 2.30—2.70 (1H, m, CH in C_6H_{11}), 5.12, 5.20 (2H, m, C=CH_2). IR (neat) 3090, 2225, 1610, 889 cm^{-1}. MS, m/z (rel intensity), 190 (1), 175 (0.2), 161 (1.3), 148 (1.8).

2-Butyl-5,5-dimethyl-1-hexen-3-yne (4c): ^{1}H NMR($CDCl_3$) δ=0.92 (3H, t, J=7.1 Hz, CH_3), 1.25 (9H, s, $C(CH_3)_3$), 1.25—1.66 (4H, m, CH_2), 2.30 (2H, t, J=7.0 Hz, CH_2C=C), 5.10, 5.19 (2H, m, C=CH_2). IR (neat) 3100, 2225, 1612, 892 cm^{-1}. MS, m/z (rel intensity), 164 (1), 149 (1.2), 122 (3.1), 107 (18).

2-Butyl-4-trimethylsilyl-1-buten-3-yne (4d): ^{1}H NMR ($CDCl_3$) δ=0.18 (9H, s, Me_3Si), 0.91 (3H, t, J=7.0 Hz, CH_3), 1.12—1.72 (4H, m, CH_2), 2.14 (2H, t, J=7.0 Hz, CH_2C=C), 5.21, 5.33 (2H, m, C=CH_2). IR (neat) 3100, 2155, 1605 cm^{-1}. MS, m/z (rel intensity), 180 (1), 165 (4.8), 138 (2.9).

2-Cyclohexyl-5,5-dimethyl-1-hexen-3-yne (4e): ^{1}H NMR ($CDCl_3$) δ=1.0—1.5 (6H, m, CH_2), 1.26 (9H, s, $C(CH_3)_3$), 1.5—1.9 (4H, m, CH_2), 1.9—2.2 (1H, m, CH in C_6H_{11}), 5.08, 5.15 (2H, m, C=CH_2). IR (neat) 3090, 2215, 1607 cm^{-1}. MS, m/z (rel intensity), 190 (1), 175 (0.8), 161 (0.5), 147 (0.6).

2-Hexyl-5-trimethylsilyl-1-penten-3-yne (4f): ^{1}H NMR ($CDCl_3$) δ=0.12 (9H, s, Me_3Si), 0.89 (3H, t, J=6.3 Hz, CH_3), 1.20—1.58 (8H, m, CH_2) 1.60 (2H, s, CH_2C≡C), 2.12 (2H, t, J=7.0 Hz, CH_2C=C), 5.07, 5.14 (2H, m, C=CH_2). IR (neat) 3095, 2230, 1612 cm^{-1}. MS, m/z (rel intensity), 222 (1), 207 (1.0), 193 (0.7), 179 (1.0).

4-Trimethylsilyl-2-trimethylsilylmethyl-1-buten-3-yne (4g): ^{1}H NMR ($CDCl_3$) δ=0.05 (9H, s, $\underline{Me_3}SiCH_2$), 0.15 (9H, s, Me_3SiC≡C), 1.65 (2H, m, $SiCH_2C$=C), 5.01, 5.21 (2H, m, C=CH_2). IR (neat) 3100, 2150, 1595 cm^{-1}. MS, m/z (rel intensity), 210 (1), 195 (0.7), 155 (1.3).

2-Trimethylsiloxymethyl-1-octen-3-yne (4h): ^{1}H NMR ($CDCl_3$) δ=0.14 (9H, s, Me_3Si), 0.93 (3H, t, J=7.1 Hz, CH_3), 2.22—2.72 (4H, m, CH_2), 2.31 (2H, t, J=7.0 Hz, CH_2C≡C), 4.09 (2H, t, J=2.0 Hz, OCH_2C=C), 5.34, 5.46 (2H, m, C=CH_2). IR (neat) 2235, 1620 cm^{-1}. MS, m/z (rel intensity), 210 (1), 195 (1.8), 137 (12).

5,5-Dimethyl-2-trimethylsiloxymethyl-1-hexen-3-yne (4i): ^{1}H NMR ($CDCl_3$) δ=0.12 (9H, s, Me_3Si), 1.23 (9H, s, $(CH_3)_3C$), 4.06 (2H, t, J=2.0 Hz, OCH_2C=C), 5.31, 5.43 (2H, m, C=CH_2). IR (neat) 2225, 1620, 878 cm^{-1}. MS, m/z (rel intensity), 210 (1), 195 (1.4), 153 (0.3).

2-Butyl-4-(1-cyclohexenyl)-1-buten-3-yne (4j): ^{1}H NMR ($CDCl_3$) δ=0.91 (3H, t, J=7.2 Hz, CH_3), 1.14—1.85 (8H, m, CH_2), 1.94—2.35 (6H, m, CH_2C=C), 5.16, 5.25 (2H, m, C=CH_2), 6.0—6.2 (1H, m, CH=C). IR (neat) 3100, 2205, 1605 cm^{-1}. MS, m/z (rel intensity), 188 (1), 173 (0.1), 159 (0.1), 146 (2.4).

4-(1-Cyclohexenyl)-2-trimethylsilylmethyl-1-buten-3-yne (4k): ^{1}H NMR ($CDCl_3$) δ=0.08 (9H, s, Me_3Si), 1.45—1.85 (4H, m, CH_2), 1.69 (2H, m, $SiCH_2C$=C), 1.90—2.32 (4H, m, CH_2C=C), 4.97, 5.14 (2H, m, C=CH_2), 6.00—6.18 (1H, m, CH=C). IR (neat) 3095, 2200, 1592 cm^{-1}. MS, m/z (rel intensity), 218 (1), 203 (0.5), 190 (0.2), 175 (0.3).

4-(1-Cyclohexenyl)-2-trimethylsiloxymethyl-1-buten-3-yne (4l): ^{1}H NMR ($CDCl_3$) δ=0.8 (9H, s, Me_3Si), 1.40—1.72 (4H, m, CH_2), 4.06 (2H, m, OCH_2C=C), 1.86—2.24 (4H, m, CH_2C=C), 5.33, 5.44 (2H, m, C=CH_2), 6.00 —6.18 (1H, m, CH=C). IR (neat) 3095, 2205, 1610 cm^{-1}. MS, m/z (rel intensity), 234 (1), 219 (0.8), 206 (0.2).

4-(1-Cyclohexenyl)-2-trimethylsilyl-1-buten-3-yne (4m): ^{1}H NMR ($CDCl_3$) δ=0.15 (9H, s, Me_3Si), 1.44—1.80 (4H, m, CH_2), 1.96—2.38 (4H, m, CH_2C=C), 5.64 (1H, d, J=3.0 Hz, CH=C), 6.00 (1H, d, J=3.0 Hz, CH=C), 6.03—6.15 (1H, m, CH=C in C_6H_9). IR (neat) 3065, 2180 cm^{-1}. MS, m/z (rel intensity), 204 (1), 189 (0.3), 176 (0.1), 163 (0.7).

4-(1-Cyclohexenyl)-2-cyclohexyl-1-buten-3-yne (4n): ^{1}H NMR ($CDCl_3$) δ=1.0—1.95 (14H, CH_2), 1.95—2.30 (5H, m, CH in C_6H_{11} and CH_2C=C), 5.15, 5.20 (2H, m, C=CH_2), 5.98—6.18 (1H, m, CH=C). IR (neat) 3090, 2200, 1600, 888 cm^{-1}. MS, m/z (rel intensity), 214 (1), 199 (0.3), 185 (0.5), 171 (0.4).

2-Butyl-4-phenyl-1-buten-3-yne (4o): ^{1}H NMR ($CDCl_3$) δ=0.95 (3H, t, J=7.0 Hz, CH_3), 1.20—1.75 (4H, m, CH_2), 2.27 (2H, t, J=7.5 Hz, CH_2C=C), 5.28, 5.41 (2H, m, C=CH_2), 7.16—7.56 (5H, m, Ph). IR (neat) 2960, 2935, 2880, 1609, 1490, 1443, 897 cm^{-1}. MS, m/z (rel intensity), 184 (1), 142 (7.6), 141 (5.4), 127 (2.5).

4-Phenyl-2-trimethylsilylmethyl-1-buten-3-yne (4p): ^{1}H NMR ($CDCl_3$) δ=0.11 (9H, s, Me_3Si), 1.77 (2H, m, $SiCH_2C$=C), 5.08, 5.28 (2H, m, C=CH_2), 7.16—7.50 (5H, m, Ph). IR (neat) 2220, 1600, 870 cm^{-1}. MS, m/z (rel intensity), 214 (1), 199

(0.5), 159 (3.1).

4-Phenyl-2-trimethylsiloxymethyl-1-buten-3-yne (4q): ^{1}H NMR ($CDCl_3$) δ=0.19 (9H, s, Me_3Si), 4.24 (2H, t, J=2.0 Hz, $OCH_2C{\equiv}C$), 5.48, 5.54 (2H, m, $C{=}CH_2$), 7.18—7.56 (5H, m, Ph). IR (neat) 3080, 2218, 1613 cm^{-1}. MS, m/z (rel intensity), 230 (1), 215 (1.1), 159 (0.5), 141 (1.2).

4-Phenyl-2-trimethylsilyl-1-buten-3-yne (4r): ^{1}H NMR ($CDCl_3$) δ=0.21 (9H, s, Me_3Si), 5.74 (1H, d, J=3.5 Hz, C=CH), 6.16 (1H, d, J=3.5 Hz, C=CH), 7.20—7.52(5H, m, Ph). IR (neat) 3080, 2190, 1596, 840 cm^{-1}. MS, m/z (rel intensity), 200 (1), 185 (0.6), 159 (1.0).

2-Cyclohexyl-4-phenyl-1-buten-3-yne(4s): ^{1}H NMR ($CDCl_3$) δ=1.1—1.9 (10H, m, CH_2), 2.1—2.3 (1H, m, CH in C_6H_{11}), 5.27, 5.38 (2H, m, $C{=}CH_2$), 7.12—7.56 (5H, m, Ph). IR (neat) 1607, 892 cm^{-1}. MS, m/z (rel intensity), 210 (1), 195 (0.3), 181 (0.7), 167 (0.6).

Identification of 2-Butyl-4-phenyl-1-buten-3-yne (4o): The structure of the sample was identified with authentic samples after converting it to (3-methylheptyl)benzene by hydrogenation on Pd-charcoal. The authentic sample was prepared from the reaction of phenethylmagnesium bromide with 2-hexanone followed by hydrolysis, dehydration with *p*-toluenesulfonic acid and hydrogenation on Pd-charcoal.

(3-Methylheptyl)benzene: ^{1}H NMR ($CDCl_3$) δ=0.76—1.05 (6H, m, CH_3), 1.07—1.80 (9H, m, CH_2), 2.36—2.80 (2H, m, $C\underline{H}_2Ph$), 7.00—7.42 (5H, m, Ph). IR (neat) 3025, 2940, 2925, 2880, 2860, 1604, 1455, 747, 700 cm^{-1}

Identification of 2-Trimethylsiloxymethyl-1-octen-3-yne (4h). A pure sample of the dimer (700 mg, 3.3 mmol) was treated with 0.1 mol dm^{-3} aq NaOH (1 cm^3) in 5 cm^3 methanol to give 2-hydroxymethyl-1-octen-3-yne in 83% yield which was then converted to a 1:1 mixture of 2-methyl-1-octanol and 2-methyloctanal by hydrogenation on Pd-C. The structure of these two products was identified with authentic samples in terms of the ^{1}H NMR and IR spectra, and gas chromatographic analysis. 2-Methyl-1-octanol was prepared by the literature procedure[33] and was converted to 2-methyloctanal by reaction with pyridinium chlorochromate[34] in CH_2Cl_2.

Analysis of Codimers Obtained from Monodeuterio-1-alkynes. PhC≡CD and *n*-BuC≡CD were prepared by deuteration of PhC≡CMgBr or *n*-BuC≡CMgBr with D_2O (99.5% purity) and were reacted with *n*-BuC≡CH and PhC≡CH, respectively, under the same reaction conditions as described above.

(E)-*2-Butyl-4-phenyl-1-buten-3-yne-1*d ((E)-*4o-1*d): ^{1}H NMR ($CDCl_3$) δ=0.95 (3H, t, CH_3), 1.21—1.74 (4H, m, CH_2), 2.28 (2H, t, $CH_2C{\equiv}C$), 5.41 (1H, m, C=CHD) 7.2—7.5 (5H, m, Ph). IR (neat) 2960, 2940, 2880, 2860, 2260, 2220, 1598, 1580, 1490, 1445, 849 cm^{-1}. MS (70 eV) m/z (rel intensity), 185 (M^+).

(Z)-*2-Butyl-4-phenyl-1-buten-3-yne-1*d ((Z)-*4o-1*d): ^{1}H NMR ($CDCl_3$) δ= 0.95 (3H, t, CH_3), 1.21—1.74 (4H, m, CH_2), 2.28 (2H, t, $CH_2C{\equiv}C$), 5.28 (1H, m, C=CHD) 7.1—7.4 (5H, m, Ph). IR (neat) 2960, 2940, 2880, 2860, 2280, 2240, 1598, 1583, 1490, 1445, 842 cm^{-1}. MS (70 eV) m/z (rel intensity), 185 (M^+).

Preparation of 2-(2-methylpropyl)-4-phenyl-1-buten-3-yne (4t). After treating (η^5-$C_5Me_5)_2TiCl_2$ (39 mg, 0.1 mmol) with isopropylmagnesium bromide (f=0.97, 3.1 cm^3, 3.0 mmol) in diethyl ether (1 cm^3), an equimolar mixture of ethynylbenzene (2.5 mmol) and 3-trimethylsiloxy-1-propyne (2.5 mmol) was added to the resulting solution. The mixture was stirred at 30 °C for 3 h and then quenched with aq HCl. Fractional distillation gave **4t** in 83% yield. ^{1}H NMR ($CDCl_3$) δ=0.97 (6H, d, J=6.0 Hz, $(C\underline{H}_3)_2CH$), 1.80—2.20 (3H, m, $(CH_3)_2C\underline{H}C\underline{H}_2$), 5.27, 5.45 (2H, m, $C{=}CH_2$), 7.20—7.56 (5H, m, Ph). IR (neat) 2960, 2930, 2880, 2220, 1609, 1466, 1443, 1386, 1370, 1315, 901, 758, 695 cm^{-1}. MS, m/z (rel intensity), 184 (1), 169 (1.0), 142 (2.0), 141 (1.4).

We thank Shin-etsu Chemical Industrial Co., Ltd. for supplying sodium ethynide.

References

1) a) P. W. Jolly and G. Wilke, "The Organic Chemistry of Nickel," Academic Press, New York (1975), Vol. 2, pp. 94—105; b) K. P. C. Vollhardt, *Acc. Chem. Res.*, **10**, 1 (1977); Y. Wakatsuki and H. Yamazaki, *J. Chem. Soc., Chem. Commun.*, **1973**, 280; c) J. P. Collman and L. S. Hegedus, "Principles and Applications of Organotransition Metal Chemistry," University Science Books, Mill Valley (1980), pp. 636—639; d) E. F. Lutz, *J. Am. Chem. Soc.*, **83**, 2551 (1961).

2) N. Hagihara, M. Tamura, H. Yamazaki, and M. Fujiwara, *Bull. Chem. Soc. Jpn.*, **34**, 892 (1961).

3) L. Carlton and G. Read, *J. Chem. Soc., Perkin Trans.*, **1978**, 1631; S. Yoshikawa, J. Kiji, and J. Furukawa, *Macromol. Chem.*, **178**, 1077 (1977).

4) E. V. Dehmlow, *Z. Naturforsch., B*, **1966**, 815.

5) H. Yamazaki, *J. Chem. Soc., Chem. Commun.*, **1976**, 841.

6) M. Akita, H. Yasuda, K. Nagasuna and A. Nakamura, *Bull. Chem. Soc. Jpn.*, **56**, 554 (1983).

7) A. C. Hopkinson, "The Chemistry of Carbon-Carbon Triple Bond," ed by S. Patai, John Wiley & Sons, New York (1978), Part 1, pp. 75—136.

8) E. Breitmaier, G. Haas, and W. Voelter, "Atlas of Carbon-13 NMR Data," Plenum, New York (1976), Vols. 1 and 2.

9) B. V. Ioffe, Yu. P. Artsybasheva, and B. L. Andondonskaya, *Zh. Org. Khim.*, **4**, 1752 (1968); M. S. Sargsyan and Sh. O. Badonyan, *Arm. Khim. Zh.*, **29**, 167 (1976).

10) T. Hayashi, M. Konishi, K. Yokota, and M. Kumada, *J. Chem. Soc., Chem. Commun.*, **1981**, 313.

11) H. A. Martin and F. Jellinek, *J. Organomet. Chem.*, **12**, 149 (1968).

12) F. Sato, H. Ishikawa, and M. Sato, *Tetrahedron Lett.*, **22**, 85 (1981).

13) F. Sato, T. Jimbo, and M. Sato, *Tetrahedron Lett.*, **21**, 2171 and 2175 (1980).

14) W. D. Bonds, Jr., C. H. Brubaker, Jr., E. S. Chandrasekaran, C. Gibbons, R. H. Grubbs, and L. C. Kroll, *J. Am. Chem. Soc.*, **97**, 2128 (1975); D. E. Bergbreiter and G. L. Parsons, *J. Organomet. Chem.*, **208**, 47 (1981).

15) J. Schwartz and J. A. Labinger, *Angew. Chem., Int. Ed. Engl.*, **15**, 333 (1976).

16) K. Sonogashira and N. Hagihara, *Bull. Chem. Soc. Jpn.*, **39**, 1178 (1966).

17) D. J. Cardin, M. F. Lappert, C. L. Raston, and P. I. Riley, "Comprehensive Organometallic Chemistry," ed by G. Wilkinson, Pergamon Press, Oxford (1982), Vol. 3, p. 584.

18) D. G. Sekutowski and G. D. Stucky, *J. Am. Chem. Soc.*, **98**, 1376 (1976); J. H. Teuben and H. J. de Liefde Meijer, *J. Organomet. Chem.*, **17**, 87 (1969).

19) J. W. Lauher and R. Hoffmann, *J. Am. Chem. Soc.*, **98**, 1729 (1976).

20) A. L. Segre, L. Zetta, and A. Di Corato, *J. Mol. Spectrosc.*, **32**, 296 (1969).

21) P. Albriktsen, A. V. Cunliffe, and R. K. Harris, *J. Magn. Reson.*, **2**, 150 (1970).

22) C. N. Banwell and N. Sheppard, *Mol. Phys.*, **3**, 351 (1960).

23) S. Otsuka and A. Nakamura, *Adv. Organomet. Chem.*, **14**, 245 (1976).

24) Y. Tohda, K. Sonogashira, and N. Hagihara, *J. Chem. Soc., Chem. Commun.*, **1975**, 54.

25) P. J. Kocienski, *J. Org. Chem.*, **39**, 3285 (1974).

26) G. Darzens, *C. R. Acad. Sci., Ser. D*, **149**, 681 (1909).
27) R. W. Hasbrouck and A. D. A. Kiessling, *J. Org. Chem.*, **38**, 2103 (1973).
28) J. Slutsky and H. Kwart, *J. Am. Chem. Soc.*, **95**, 8678 (1973).
29) J. Ficini and C. Barbara, *Bull. Soc. Chim. Fr.*, **1965**, 2787.
30) J. F. Arens and T. Doornbos, *Recl. Trav. Chim. Pays-Bas*, **75**, 481 (1956).
31) G. Wilkinson and J. M. Birmingham, *J. Am. Chem. Soc.*, **76**, 4281 (1954).
32) J. E. Bercaw, *J. Am. Chem. Soc.*, **96**, 5087 (1974).
33) A. P. Mathers and M. J. Pro, *J. Am. Chem. Soc.*, **76**, 1182 (1954).
34) E. J. Corey and J. W. Suggs, *Tetrahedron Lett.*, **1975**, 2647.

Selective Hydrogenation of Cyclopentadiene to Cyclopentene Using Colloidal Palladium Supported on Chelate Resin

Hidefumi HIRAI,* Shigeru KOMATSUZAKI, and Naoki TOSHIMA

Department of Industrial Chemistry, Faculty of Engineering, The University of Tokyo, Hongo, Bunkyo-ku, Tokyo 113

(Received August 3, 1983)

Cyclopentadiene was hydrogenated to cyclopentene selectively by using colloidal palladium supported on chelate resin with iminodiacetic acid moieties as a catalyst. The catalyst, containing metal particles of 1—6 nm in diameter, was prepared by reduction of the palladium(II)-chelate resin complex with methanol. Cyclopentene was produced in 97.1% yield at 100% conversion of cyclopentadiene at 30 °C under 1 atm of hydrogen. This value in yield was also achieved on repeated uses of the catalyst. The hydrogenation rate was correlated to the polarity parameter, $E_T(30)$ values, of the solvents used in the reaction, except in the case of dimethyl sulfoxide. The hydrogenation rates of cyclopentadiene (R_D) and cyclopentene (R_E) were expressed as $R_D=k_D[H_2][\text{catalyst}]$ and $R_E=k_E[H_2][\text{cyclopentene}][\text{catalyst}]$, respectively, where k_D and k_E are the rate constants. The equilibrium constant for complex formation between cyclopentadiene and the catalyst, K_D, was estimated to be over 400 times larger than that between cyclopentene and the catalyst, K_E. A mechanism, including the coordination of olefins to the catalyst and the subsequent hydrogenation of the coordinated complexes, was proposed.

Much attention has been paid for heterogenized transition-metal complex catalysts, since recovering and reusing of catalysts are indispensable in practical use of expensive noble metals.[1-4] The heterogenized homogeneous catalysts on organic or inorganic supports often have efficient catalytic properties of homogeneous analogs. Furthermore, the heterogenized catalysts sometimes have advantages in catalyst stability and reaction selectivity. Metal complexes in the heterogenized catalysts have various structures, *e.g.*, chelated structures, dimeric structures, and metal cluster structures, according to the preparative conditions.

We have already shown that finely dispersed colloidal transition metals were obtained by reduction of metal salts with alcohols in the presence of vinyl polymer with polar groups.[5-7] The particle sizes of these colloidal metals were below several nm in diameter, and were distributed in narrow ranges. Some of them exhibited specific selectivities as hydrogenation catalysts for olefins.[8,9] Chini[10] has pointed out that large metal carbonyl clusters could be applied to the chemistry of small metal particles (0.5—3 nm). Finely dispersed colloidal metals supported on polymers could be regarded as macromolecular complexes of metal clusters. Recently, we have reported on the preparation and the characterization of colloidal palladium catalysts supported on chelate resins with iminodiacetic acid moieties.[11] The chelate resin-supported catalysts were composed of small palladium metal particles and palladium complexes with iminodiacetic acid moieties. The sizes of metal particles were distributed from 1 to 6 nm and mainly from 1 to 2 nm. The metal particles in the resin-supported catalyst had catalytic activities for selective hydrogenation of diene to monoenes. The selective hydrogenation of cyclopentadiene is a significant process for utilization of the C_5 fraction of naphtha cracking products.[12,13] Furthermore, cyclopentadiene is one of the simplest dienes as a substrate for partial hydrogenation, since cyclopentadiene and cyclopentene have no isomers, respectively.

In the present paper the selective hydrogenation of cyclopentadiene to cyclopentene using the resin-supported colloidal palladium will be reported in detail with attention to the swelling effect of the polymer matrix on the catalytic properties.

Experimental

Materials. A chelate resin with iminodiacetic acid moieties attached to a styrene-divinylbenzene copolymer matrix, Diaion CR10 (Mitsubishi Chemical Ind. Co. Ltd., the size of the resin bead ranged from 0.3 to 1.2 mm in diameter in the swelled state) was used as a supporting polymer. The resin-supported colloidal palladium was prepared as follows: Palladium(II) chloride (Kojima Chemical Co. Ltd.) and the chelate resin were kept under stirring in water (pH 3) at room temperature for 1 h to form the palladium complex of the chelate resin, and the resulting complex was kept under refluxing in methanol-water (1:1)(pH 11) for 6 h as described previously.[11] The catalyst was preserved in methanol. One cubic centimeter of the resin-supported Pd catalyst swelled in methanol contained 18.5 μg-atom of palladium. The charged molar ratio of iminodiacetic acid moiety to palladium atom was 75.

Cyclopentadiene was obtained by pyrolysis of dicyclopentadiene (Yoneyama Chemical Co. Ltd.), and was purified by distillation under argon before use. Cyclopentene and cyclopentane were obtained from Tokyo Chemical Ind. Co. Ltd. and were distilled under argon.

Commercial guaranteed reagent grade methanol was used after distillation under argon. Ethanol, benzene, hexane, ethyl methyl ketone, ethyl acetate, *N*,*N*-dimethylformamide, and dimethyl sulfoxide at guaranteed reagent grade were used after removal of oxygen. *N*-Benzyliminodiacetic acid was obtained from Aldrich Chemical Co. Inc. Five percent Pd on charcoal was obtained from Nippon Engelhard Ltd.

Commercial pure grade hydrogen (Nippon Oxygen Ltd., 99.99999% of purity) was passed through a Deoxo column (Nippon Engelhard Ltd.) before use to remove trace amounts of oxygen.

Hydrogenation in Methanol. The measured volume (0—2.69 cm^3) of resin-supported Pd catalyst in methanol was put in a 100 cm^3 flask which was attached to the shaker with thermostat (Tokyo Rikakikai Co. Ltd.). After the atmosphere in the flask was replaced with hydrogen, methanol [$(20-x-y)$ cm^3] was added into the flask and the flask was shaken for 1 h. A methanol solution (x cm^3) of cyclopentadiene or cyclopentene (2 mol/dm^3 each) and a methanol solution (y cm^3) of cyclopentane (2 mol/dm^3) were added into the flask, and the flask was shaken vigorously to start the reaction keeping the total pressure in the flask at 1 atm.

The rates of the hydrogenations were determined by the initial rates of the hydrogen uptake.

For the discussion on kinetics, the initial rates with the fresh catalysts were used. The dependence of the rate on hydrogen partial pressure was measured by using the mixed gases of hydrogen and nitrogen. The mixed gases were prepared by adding each gas into a high pressure vessel of stainless steel in different fixed ratios.

Hydrogenation in Other Solvents. Resin-supported Pd catalyst (2.69 cm^3) separated from methanol was washed with a solvent which should be used for the hydrogenation reaction, and kept in the solvent for more than 1 h. After removal of the solvent, the flask containing the catalyst was mounted in the thermostated shaker. The atmosphere in the flask was replaced with hydrogen, and the solvent (19.7 cm^3) was added. After the flask was shaken for 1 h, cyclopentadiene (0.33 cm^3, 4 mmol) was added into the flask, which was shaken vigorously to start the reaction keeping the total pressure at 1 atm.

Analysis of the Products. The products were analyzed with GLPC by using a glass capillary column of Silicone OV-101 (0.28 mmϕ×30 m) at 20 °C with a flame ionization detector. In the present paper, the selectivity (S%) is defined by the yield of cyclopentene at the point of complete disappearance of cyclopentadiene in the reaction mixtures.

Reaction in Gas-phase Using a Closed Circulation System. Resin-supported Pd catalyst (2.69 cm^3) separated from methanol was supported with glass wool in a reactor. Hydrogen, cyclopentadiene, and methanol were introduced into a circulation system from respective vessels by means of the pressure difference. All parts of the reactor system were composed of either Pyrex glass or Teflon, and the volume of the reaction circuit was 940 cm^3. The reaction was started by connecting the circulation system with the reactor. Gaseous mixtures in the reactor were analyzed periodically with GLPC.

Results

Hydrogenation of Cyclopentadiene in Methanol. Selective hydrogneation of cyclopentadiene to cyclopentene took place by using resin-supported Pd catalyst in methanol at 30 °C under an atmospheric pressure of hydrogen. The volume of hydrogen taken up increased proportionally to the reaction time up to the amount equimolar with cyclopentadiene as indicated in Fig. 1 (No. 1). As shown in the preceding paper,[11] the active species of resin-supported Pd catalyst is metallic palladium. The amount of the metallic palladium is 5% of the charged amount of palladium, *i.e.*, 0.93 μg-atom Pd per 1 cm^3 of the resin catalyst. Hydrogenation rates were represented as rates of hydrogen uptake divided by the amount of metallic palladium in the catalyst. The hydrogenation rate decreases to about one-fifth of the initial rate after the conversion of cyclopentadiene reaches 100% as shown in Fig. 1. This decrease of the rate facilitates the isolation of cyclopentene in a high yield because of the minimum subsequent hydrogenation of cyclopentene. The composition of the products was followed by gas chromatographic analyses. The results are presented by circles in Fig. 2. Cyclopentene was obtained in 97.1% yield at complete conversion of cyclopentadiene by using the fresh resin-supported Pd catalyst.

The catalyst can be separated from the reaction mixtures and can be used again as a catalyst. The initial rate of hydrogen uptake and the selectivity for cyclopentene by using fresh and recovered resin-supported Pd catalysts are summarized in Table 1 as well as those with reference catalysts. When palladium on charcoal is used as a catalyst, cyclopentene is obtained in 88.4% yield. The addition of 75-fold molar amount of *N*-benzyliminodiacetic acid disodium salt to the palladium on charcoal results in 93.2% yield of cyclopen-

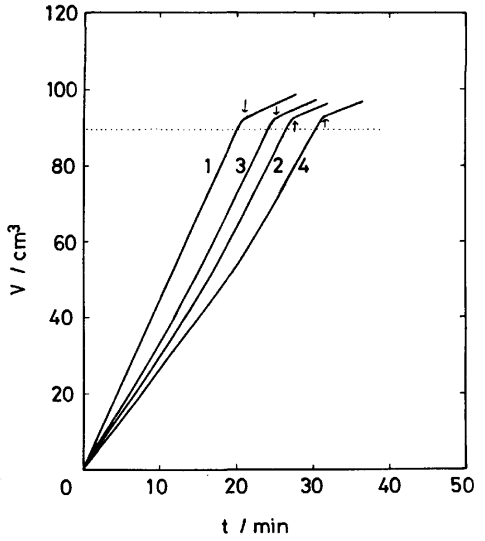

Fig. 1. Hydrogen uptakes (V) against reaction time in the hydrogenation of cyclopentadiene with the fresh (1), reused (2, 3), and pretreated (4) resin-supported Pd catalyst at 30 °C under an atmospheric hydrogen pressure. The dotted line shows the amount equimolar with cyclopentadiene. The arrows represent the points at which 100% conversion of cyclopentadiene was achieved.

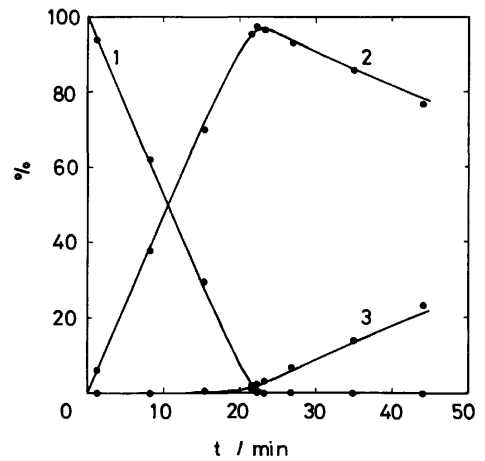

Fig. 2. Experimental and calculated composition (%) of the substrate and products in the hydrogenation of cyclopentadiene. Circles show the experimental values of composition of cyclopentadiene, cyclopentene, and cyclopentane under the conditions [metallic Pd]=0.125 (mol/dm^3), initial concentration of cyclopentadiene=0.2 (mol/dm^3), and $[H_2]$=0.003 (mol/dm^3). The curves are calculated for cyclopentadiene (1), cyclopentene (2), and cyclopentane (3) by assuming k_2=440 (dm^3/mol s), k_4=1000 (dm^3/mol s), m=200 (dm^3/mol) and n=0.5 (dm^3/mol).

Table 1. Hydrogenation of cyclopentadiene[a)]

Run	Catalyst	$r/10^{-1}\,s^{-1}$[b)]	S (%)[c)]
1	Fresh resin-supported Pd	13.4	97.1
2	Recovered resin-supported Pd from run 1	8.2	97.3
3	Recovered resin-supported Pd from run 2	9.4	96.7
4	Resin-supported Pd pretreated with cyclopentane[d)]	7.2	96.6
5	Resin-supported Pd stored in methanol[e)]	13.4	96.7
6	Resin-supported Pd stored in water[e)]	13.6	97.0
7	Commercial Pd on charcoal (5%)	36.0	88.4
8	Pd on charcoal with NBIDA[f)]	37.1	93.2
9	Recovered Pd on charcoal from Run 8[g)]	—	88.9

a) Conditions: 30 °C; H_2, 580 Torr; solvent, methanol; [cyclopentadiene]=0.20 mol/dm^3. b) The initial rate of hydrogen uptake (mol/s) per one g-atom of metallic Pd in the catalyst. c) The selectivity; the yield of cyclopentene at 100% conversion of cyclopentadiene. d) Resin-supported Pd pretreated with methanol containing cyclopentane (0.2 mol/dm^3) for 1 h. e) Under air for 30 d. f) Five percent palladium on charcoal (2.13 mg containing 1 μg-atom of Pd) was used in the presence of *N*-benzyliminodiacetic acid disodium salt (NBIDA) (75 μmol) in methanol (20 cm^3). g) Palladium on charcoal recovered from the reaction mixture in run 8 by decantation was used. Since some of the catalyst was lost in the decantation procedure, the catalytic activity per Pd g-atom was not known exactly.

Table 2. Hydrogenation of cyclopentadiene in various solvents[a)]

Solvent	$r/10^{-1}\,s^{-1}$[b)]	S (%)[c)]	$E_T(30)$/kcal$_{th}$ mol^{-1}[d)]
Methanol	13.4	97.1	55.5
Ethanol	8.0	94.8	51.9
Dimethyl sulfoxide	0.06	—	45.0
N,*N*-Dimethylformamide	7.4	95.6	43.8
Ethyl methyl ketone	4.6	95.1	41.3
Ethyl acetate	5.8	93.6	38.1
Benzene	4.4	94.7	34.5
Hexane	0.62	—	30.9

a) Conditions: 30 °C; H_2 pressure=760 Torr—(vapor pressure of solvent media); catalyst, resin-supported Pd catalyst (2.69 cm^3); solvent, 20 cm^3; [cyclopentadiene]=0.2 mol/dm^3. b) The initial rate of hydrogen uptake (mol/s) per one g-atom of metallic Pd in the catalyst. c) The yield of cyclopentene at 100% conversion of cyclopentadiene. d) From Ref. 22.

tene (run 8). This value is slightly inferior to that with resin-supported Pd, but the yield is reduced to 88.9% by a repeated use of the catalyst (run 9).

After the reaction, the catalyst was separated from the reaction mixture, washed with methanol several times, kept in fresh methanol for 1 h, and then reused. The initial rate (run 2 in Table 1) with the reused resin-supported Pd catalyst is two-thirds of that with the fresh catalyst. But the rate gradually increased with reaction time and recovered to the original value near the hydrogen-uptake equimolar with the charged cyclopentadiene (run 2 in Fig. 1). The yield of cyclopentene at complete conversion of cyclopentadiene is the same as that with the fresh catalyst. When the reused resin-supported Pd catalyst is used again (run 3), the catalytic behavior is similar to that of run 2. To compare with this result, the fresh resin-supported Pd catalyst was kept in methanol containing cyclopentane (0.2 mol/dm^3) for 1 h, washed with methanol and then used as a catalyst. The results were similar to those of the catalyst in the repeated use, as shown at run 4 in Table 1 and Fig. 1.

When resin-supported Pd catalyst was stored in methanol or water under air for 30 d, no difference in the catalytic behavior was observed as shown at runs 5 and 6 in Table 1.

Hydrogenation of Cyclopentadiene in Various Solvents. Hydrogenations of cyclopentadiene in the presence of the resin-supported Pd catalyst were carried out in various solvents at 30 °C under an atmospheric pressure of hydrogen. The results are shown in Table 2 and Fig. 3. The highest activity and selectivity are achieved in methanol among the solvents examined. The hydrogen uptake curves in Fig. 3 are almost linear up to the point where the hydrogen-uptake is equimolar with the charged cyclopentadiene, and the slopes decrease gradually after the equimolar points. The decreasing extents of the rates near the equimolar points are different from each other. When methanol was used as a solvent, the decreasing extent is largest.

Kinetics for Hydrogenation of Cyclopentadiene in Methanol. The dependences of the initial rate on the concentration of cyclopentadiene, the amount of the catalyst, and the pressure of hydrogen were investigated.

Dependence upon Concentration of Cyclopentadiene: The rates of hydrogen uptake are plotted against the concentration (below 0.4 mol/dm^3) of cyclopentadiene in methanol with open circles in Fig. 4. The rate somewhat decreases with increase of the cyclopentadiene concentration. The initial rates were also measured under the condition that the sum of the respective concentrations of cyclopentadiene and cyclopentane was a constant value, 0.4 mol/dm^3, by adding

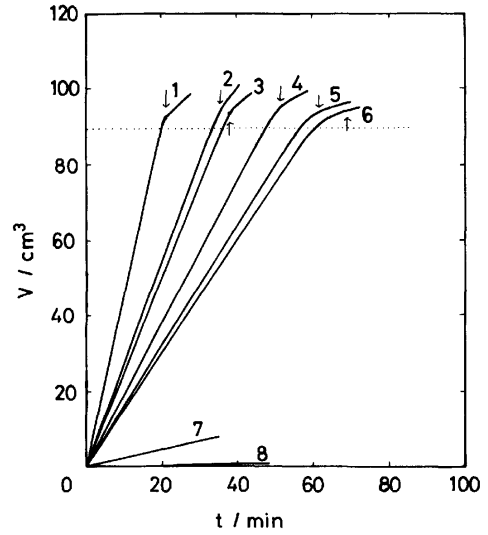

Fig. 3. Hydrogen uptakes (V) against reaction time in the hydrogenation of cyclopentadiene with the resin-supported Pd catalyst at 30 °C under an atmospheric hydrogen pressure in methanol (1), ethanol (2), *N*,*N*-dimethylformamide (3), ethyl acetate (4), ethyl methyl ketone (5), benzene (6), hexane (7), and dimethyl sulfoxide (8). The dotted line shows the amount equimolar with cyclopentadiene. The arrows represent the points at which 100% conversion of cyclopentadiene was achieved.

the appropriate amount of cyclopentane simultaneously at the addition of cyclopentadiene. The results are shown with closed circles in Fig. 4. The dependence of the rates upon the concentration of cyclopentadiene was essentially zero order.

Dependence upon Pressure of Hydrogen: The initial rates of hydrogenation of cyclopentadiene in methanol were measured under partial pressure of hydrogen below 580 Torr (1 Torr≈133.322 Pa). Dependence of the rate upon hydrogen pressure was the first order.

Dependence upon Amount of Catalyst: From the results with various amounts of the catalyst below 1.61 cm^3 in 20 cm^3 of methanol, dependence of the rate upon the amount of the catalyst was the first order.

Kinetic Expression: The kinetic experiments indicate that the rate of hydrogenation of cyclopentadiene, R_D, can be represented by the following Eq. 1, where k_D is a rate constant.

$$R_D=k_D[H_2][\text{catalyst}] \quad (1)$$

The constant k_D was determined at different temperature. The relationship of k_D with temperature is indicated in the Arrhenius plot in Fig. 5. The activation energy is calculated to be 8.0 $kcal_{th}$/mol (1 cal_{th}≈4.184 J) for the hydrogenation of cyclopentadiene.

Kinetics for the Hydrogenation of Cyclopentene in Methanol. Initial rates of the hydrogenation of cyclopentene catalyzed by resin-supported Pd were measured in methanol. Dependence of the rate upon the concentration of cyclopentene, the amount of the catalyst, and the partial pressure of hydrogen were determined.

Results under various cyclopentene concentrations below 0.4 mol/dm^3 are shown with open circles in Fig.

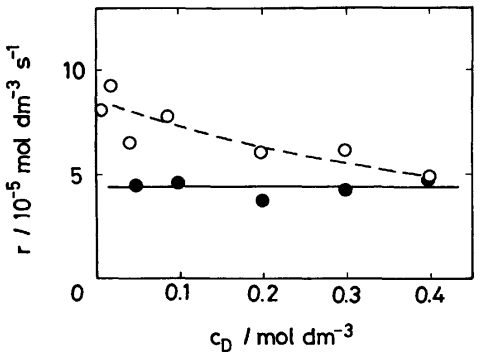

Fig. 4. Dependence of hydrogen uptake rate (r) on cyclopentadiene concentration (c_D) in methanol (20 cm^3) at 30 °C under 580 Torr of hydrogen with the resin-supported Pd catalyst (metallic Pd, 1 μg-atom) without (○) and with addition (●) of cyclopentane ([cyclopentadiene]+[cyclopentane]=0.4 mol/dm^3).

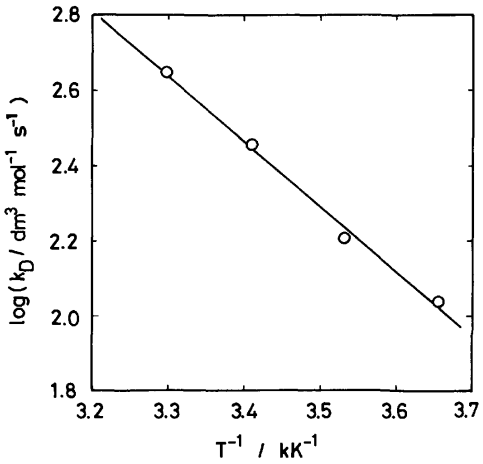

Fig. 5. Arrhenius plot for the rate constant in hydrogenation of cyclopentadiene in methanol.

6. The initial rates of hydrogenation were also measured under the condition that the sum of the respective concentrations of cyclopentene and cyclopentane was a constant value, 0.4 mol/dm^3, by adding the appropriate amount of cyclopentane simultaneously at the addition of cyclopentene. These results are shown with closed circles in Fig. 6, indicating that the dependence upon the cyclopentene concentration is the first order. The hydrogenation rates were measured under various hydrogen pressures below 580 Torr, and the dependence upon the hydrogen pressure was the first order. The rates with various amounts of the catalyst below 1.61 cm^3 in 20 cm^3 of methanol were measured, and the dependence of the rate upon the amount of the catalyst was the first order.

These kinetic experiments indicate that the rate of hydrogenation of cyclopentene, R_E, can be represented by Eq. 2, where k_E is a rate constant.

$$R_E=k_E[H_2][\text{cyclopentene}][\text{catalyst}] \quad (2)$$

Hydrogenation in Gas-phase. Hydrogenations of cyclopentadiene in gas-phase were carried out using a closed circulation system. When the methanol-swelled resin-supported Pd catalyst containing 2.5 μg-atom of metallic palladium was used, the hydrogena-

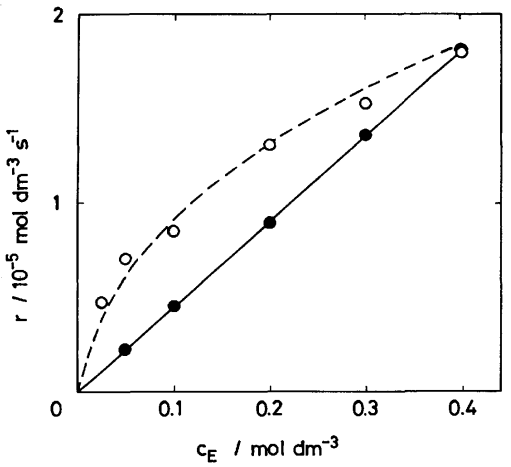

Fig. 6. Dependence of hydrogen uptake rate (r) on cyclopentene concentration (c_E) in methanol (20 cm³) at 30 °C under 580 Torr of hydrogen with the resin-supported Pd catalyst (metallic Pd, 1 μg-atom) without (○) and with addition (●) of cyclopentane ([cyclopentene]+[cyclopentane]=0.4 mol/dm³).

tion proceeded at 25 °C under 280, 70, and 70 Torr of initial partial pressures of hydrogen, cyclopentadiene, and methanol, respectively. After 104 min, the conversion of cyclopentadiene was 14% and the selectivity to cyclopentene was 96%. When the reaction was carried out at 50 °C, the hydrogenation was faster than that at 25 °C by the factor of 9 and the selectivity to cyclopentene at 14% conversion of cyclopentadiene was 90%. When the same gaseous mixture was circulated over the non-swelled resin-supported Pd catalyst (dried at 50 °C for 5 min under vacuum), no hydrogenation products were detected even after 100 min at 50 °C.

Discussion

Kinetics of Hydrogenation of Cyclopentadiene and Cyclopentene. When cyclopentadiene and cyclopentene are hydrogenated independently over the resin-supported Pd catalyst, Eqs. 1 and 2 represent the initial rates of each reaction. For example, the initial rate for cyclopentene is about one tenth of that for cyclopentadiene at 0.1 mol/dm³ of the substrates. When cyclopentadiene is present, however, cyclopentene is not hydrogenated so fast. Thus, cyclopentadiene reacts predominantly and the highly selective hydrogenation of cyclopentadiene to cyclopentene takes place as shown in Table 1 and Fig. 2. In this case, the rate for cyclopentadiene does not change with the reaction time, but the hydrogenation of cyclopentene is suppressed to a very low rate. Indeed, at the reaction time of 10 min in Fig. 2 the hydrogenation rate of cyclopentadiene is almost the same as the initial rate, but that of cyclopentene is nearly equal to zero, although each concentration of cyclopentadiene and cyclopentene is about 0.1 mol/dm³ at this point. This fact suggests that the coordination process of the substrate to the active species of the catalyst is important for the hydrogenation of cyclopentadiene and cyclopentene. Therefore, Eqs. 3—6 are proposed as a scheme, which includes the coordination processes, *i.e.*, the substrate forms an intermediate with the catalyst at first by coordination and then the intermediate reacts with hydrogen to give the product.

$$\text{cyclopentadiene} + \text{catalyst} \underset{k_{-1}}{\overset{k_1}{\rightleftharpoons}} \text{cyclopentadiene - catalyst} \quad (3)$$

$$\text{cyclopentadiene - catalyst} + H_2 \xrightarrow{k_2} \text{cyclopentene} + \text{catalyst} \quad (4)$$

$$\text{cyclopentene} + \text{catalyst} \underset{k_{-3}}{\overset{k_3}{\rightleftharpoons}} \text{cyclopentene - catalyst} \quad (5)$$

$$\text{cyclopentene - catalyst} + H_2 \xrightarrow{k_4} \text{cyclopentane} + \text{catalyst} \quad (6)$$

Similar schemes have been proposed for the hydrogenations of alkynes and alkenes using palladium metal catalysts on vitreous supports.[14] Since the active species, the small Pd metal particle, is fixed to the cross-linked polymer matrix, it is assumed that the active species do not affect each other.[15] So the amount of metallic Pd per unit volume of solvent can be used as the catalyst concentration in kinetic studies. The total concentrations of the catalyst, C, cyclopentadiene, D, and cyclopentene, E, are defined in the following equations, respectively:

$$[C] = [\text{catalyst}] + [\text{cyclopentadiene - catalyst}] + [\text{cyclopentene - catalyst}], \quad (7)$$

$$[D] = [\text{cyclopentadiene}] + [\text{cyclopentadiene - catalyst}], \quad (8)$$

$$[E] = [\text{cyclopentene}] + [\text{cyclopentene - catalyst}]. \quad (9)$$

Assuming the steady state (d[cyclopentadiene—catalyst]/dt=0, d[cyclopentene—catalyst]/dt=0) and the negligibly small concentration of the catalyst compared with substrates, Eqs. 10—12 are derived from Eqs. 3—9:

$$-\frac{d[D]}{dt} = [C][H_2]\frac{\dfrac{k_1k_2[D]}{k_{-1}+k_2[H_2]}}{1+\dfrac{k_1[D]}{k_{-1}+k_2[H_2]}+\dfrac{k_3[E]}{k_{-3}+k_4[H_2]}}, \quad (10)$$

$$\frac{d[E]}{dt} = [C][H_2]\frac{\dfrac{k_1k_2[D]}{k_{-1}+k_2[H_2]}-\dfrac{k_3k_4[E]}{k_{-3}+k_4[H_2]}}{1+\dfrac{k_1[D]}{k_{-1}+k_2[H_2]}+\dfrac{k_3[E]}{k_{-3}+k_4[H_2]}}, \quad (11)$$

$$\frac{d[A]}{dt} = [C][H_2]\frac{\dfrac{k_3k_4[E]}{k_{-3}+k_4[H_2]}}{1+\dfrac{k_1[D]}{k_{-1}+k_2[H_2]}+\dfrac{k_3[E]}{k_{-3}+k_4[H_2]}}, \quad (12)$$

where [A] is the concentration of cyclopentane.

When [E] equals to zero in Eq. 10,

$$-\frac{d[D]}{dt} = \frac{k_1k_2[D][C][H_2]}{k_1[D]+k_{-1}+k_2[H_2]}. \quad (13)$$

And when [D] equals to zero in Eq. 11,

$$\frac{d[E]}{dt} = \frac{-k_3k_4[E][C][H_2]}{k_3[E]+k_{-3}+k_4[H_2]}. \quad (14)$$

The initial rate for the hydrogenation of cyclopentadiene alone is expressed by Eq. 13. Since cyclopentadiene has large coordinating ability owing to its con-

jugated double bond,[16] it can be postulated for Eq. 13 that $k_1[D]$ is much larger than $(k_{-1}+k_2[H_2])$. Then Eq. 13 is simplified to Eq. 15:

$$-\frac{d[D]}{dt} = k_2[C][H_2]. \quad (15)$$

Eq. 15 agrees with the experimental result represented by Eq. 1. The rate constant k_2 $(=k_D)$ is calculated to be 440 (dm^3/mol s) from the experimental results. The activation energy (8.0 $kcal_{th}$/mol) obtained from the Arrhenius plot for k_D in the present reaction is comparable with that in the hydrogenation of 1,3-cyclooctadiene with polymer-bound palladium(II) complex catalyst.[17]

The initial rate for the hydrogenation of cyclopentene alone is expressed by Eq. 14 in the above scheme. It is necessary that k_{-3} is large enough comparing with $(k_3[E]+k_4[H_2])$ for Eq. 14 to be simplified to the experimental expression, Eq. 2. This will be discussed in the next section.

Selectivity in the Hydrogenation of Cyclopentadiene to Cyclopentene. The amounts of cyclopentadiene and cyclopentene at a certain reaction time in the hydrogenation of cyclopentadiene can be calculated by integrating Eqs. 10 and 11 numerically. Equations 10 and 11 can be rewritten by using factors m and n as following expressions:

$$-\frac{d[D]}{dt} = [C][H_2]\frac{k_2m[D]}{1+m[D]+n[E]}, \quad (16)$$

$$\frac{d[E]}{dt} = [C][H_2]\frac{k_2m[D]-k_4n[E]}{1+m[D]+n[E]}, \quad (17)$$

where

$$m = \frac{k_1}{k_{-1}+k_2[H_2]}, \quad n = \frac{k_3}{k_{-3}+k_4[H_2]}. \quad (18)$$

The simultaneous differential Eqs. 16 and 17 were solved numerically with a Runge-Kutta method[18] by substituting various values into the factors m, n, and k_4, respectively. When m=200 (dm^3/mol), $n \leq 0.5$ (dm^3/mol), and $k_4 \geq 1000$ (dm^3/mol s) were assumed, the best agreement of the calculated result with the experimental one was obtained. The compositions of each product were calculated by assuming m=200 (dm^3/mol), k_2=440 (dm^3/mol s), n=0.5 (dm^3/mol), and k_4=1000 (dm^3/mol s), and are drawn as curves in Fig. 2. The experimental data are plotted with circles in Fig. 2. K_D and K_E are defined as equilibrium constants of Eqs. 3 and 5, respectively, *i.e.*, $k_1/k_{-1}=K_D$, and $k_3/k_{-3}=K_E$. Since m=200 (dm^3/mol) and $1/m=(1/K_D)+(k_2[H_2]/k_1)$ (from definition), we have obtained $K_D \geq 200$ (dm^3/mol).

In order to make the theoretical expression (Eq. 14) in good agreement with the experimental expression (Eq. 2) within experimental errors, it is necessary that k_{-3} is at least 5 times larger than the sum of $k_3[E]$ and $k_4[H_2]$. From the experimental conditions, the concentration of cyclopentene [E] is less than 0.4 (mol/dm^3) and that of hydrogen [H_2] equals to 0.003 (mol/dm^3) from the solubility of hydrogen in methanol.[19] These experimental data and the value of k_4 ($\geq$1000 dm^3/mol s) lead the conclusion that $K_E \leq 0.5$ (dm^3/mol) and $k_{-3} \geq 15$ (s^{-1}). Thus, since $K_D \geq 200$, K_D is at least 400 times larger than K_E. On the other hand, k_2 is less than a half of k_4 since k_2=440 and $k_4 \geq 1000$. Therefore, the large K_D/K_E ratio is considered to cause the high selectivity for the hydrogenation of cyclopentadiene to cyclopentene.

Since particle size of palladium metal is very small in the present Pd catalyst,[11] the state of active species is supposed to have some properties of metal complexes or metal clusters.[10,20] This would result in the large K_D/K_E ratio for cyclopentadiene and cyclopentene. Since the selectivity with palladium on charcoal increases with the addition of *N*-benzyliminodiacetic acid disodium salt, the iminodiacetic acid moiety in the resin-supported Pd catalyst possibly causes the increase of the selectivity. The increase of selectivity in the successive catalytic reaction by the presence of foreign substances is known, *e.g.*, in the case of Lindlar catalyst modified by quinoline.[21] The iminodiacetic acid moiety in the resin is not lost in repeated uses of the resin-supported Pd catalyst, though *N*-benzyliminodiacetic acid disodium salt is gradually removed in repeated uses of the palladium-on-charcoal catalyst modified with *N*-benzyliminodiacetic acid disodium salt. So the effect of iminodiacetic acid moiety can be emphasized in the repeated uses of the resin-supported catalyst.

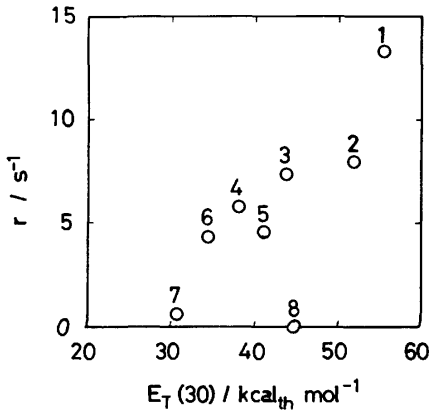

Fig. 7. Correlation of the hydrogenation rate (r) with $E_T(30)$ value of the solvent: 1, methanol; 2, ethanol; 3, *N*,*N*-dimethylformamide; 4, ethyl acetate; 5, ethyl methyl ketone; 6, benzene; 7, hexane; 8, dimethyl sulfoxide. r is the rate of molar hydrogen uptake in a second per molar metallic Pd as catalyst.

Behavior of the Catalyst in Various Reaction Conditions. The hydrogenation rates of cyclopentadiene in various solvents are plotted against the E_T (30) value[22] in Fig. 7. A considerable correlation between the E_T (30) value and the hydrogenation rate is observed, suggesting that the polarity of the solvent affects the rate of hydrogenation. This solvent effect on the rate is supposed to be based on the swelling degree of the resin and on the so-called polar effect which is generally observed in the catalytic hydrogenation of olefins.[23] When dimethyl sulfoxide was used as a solvent, a very low rate was observed compared with that expected from the E_T (30) value. This inhibitory effect of dimethyl sulfoxide on the catalytic activity may be caused by strong coordinating ability of the solvent to the

active species, as the similar effect has been reported in the hydrogenation reaction of dienes by a polymer-bound palladium(II) complex catalyst.[17] In the kinetic measurement the rate in methanol somewhat decreased with the increasing concentration of cyclopentane which was added to make the sum of the concentrations of the substrate and cyclopentane constant. This result may be ascribed to the polarity change of the reaction field by adding cyclopentane, since a very low rate was observed in hexane in contrast with a high rate in methanol. To eliminate the effect of solvent polarity change from kinetic results, the rates were measured in the presence of appropriate amount of cyclopentane as mentioned in the rate dependence on the concentration of cyclopentadiene (Fig. 4).

When the resin-supported Pd catalyst was reused after recovering by filtration from the reaction mixture, the lower initial rate was observed than that with a fresh catalyst. This is probably due to the contact of the catalyst with hydrophobic compounds such as cyclopentane before the start of the reaction, since a similar behavior was observed in the reaction by the catalyst pretreated with methanol containing cyclopentane for 1 h. From the elemental analyses of carbon and nitrogen in the supporting resin, about two-thirds of benzene rings in the resin are considered to have iminodiacetic acid moieties. So the resin consists of the hydrophobic parts like styrene residues and the hydrophilic parts like iminodiacetic acid moieties. The hydrophobicity of the cyclic C_5 compound increases in the order: cyclopentadiene<cyclopentene<cyclopentane.[24] Therefore, when more hydrophobic compound like cyclopentane contacts with the resin-supported Pd catalyst, some cyclopentane would interact with the hydrophobic parts and would remain in the region even after washing with methanol. The hydrophobic parts may surround the active site of the catalyst. Thus in the repeated use, cyclopentadiene might be prevented to approach to the active species of the catalyst by cyclopentene and cyclopentane fixed in the matrix. But, in the steady state of the hydrogenation of cyclopentadiene, the active species is also surrounded by the appropriate amount of cyclopentadiene corresponding to its concentration in the solution. Therefore, it should take a time for the environmental conditions of the active species to achieve the steady state.

The results using a closed circulation reactor indicate that the swelling of the resin with methanol is necessary for resin-supported Pd catalyst to function effectively. In the dry state the resin is shrunk to prevent the substrate from approaching to the active species. When the catalyst was used in the swelled state under the existence of methanol vapor in the gas-phase, the selective hydrogenation of cyclopentadiene was observed to proceed by using a closed circulation reactor.

The authors would like to express their acknowledgment to Mr. Kazuo Seino at the Research Institute for Catalysis, Hokkaido University for his provision of a gas circulating pump for the closed circulation system. The present work was partially supported by a Grant-in-Aid for Developmental Scientific Research No. 485220 from the Ministry of Education, Science, and Culture.

References

1) R. H. Grubbs, *CHEMTECH*, **7**, 512 (1977).
2) D. D. Whitehurst, *CHEMTECH*, **10**, 44 (1980).
3) "Kobunshi Sakutai Shokubai," ed by H. Hirai and N. Toshima, Japan Scientific Societies Press, Tokyo (1982).
4) J. Lieto, D. Milstein, R. L. Albright, J. V. Minkiewicz, and B. C. Gates, *CHEMTECH*, **13**, 46 (1983).
5) H. Hirai, Y. Nakao, and N. Toshima, *J. Macromol. Sci.-Chem.*, **A12**, 1117 (1978).
6) H. Hirai, *J. Macromol. Sci.-Chem.*, **A13**, 633 (1979).
7) H. Hirai, Y. Nakao, and N. Toshima, *J. Macromol. Sci.-Chem.*, **A13**, 727 (1979).
8) H. Hirai, Y. Nakao, and N. Toshima, *Chem. Lett.*, **1978**, 545.
9) H. Hirai, H. Chawanya, and N. Toshima, *Macromol. Chem., Rapid Commun.*, **2**, 99 (1980).
10) P. Chini, *J. Organomet. Chem.*, **200**, 37 (1980).
11) H. Hirai, S. Komatsuzaki, and N. Toshima, *J. Macromol. Sci.-Chem.*, in press.
12) N. Calderon and R. L. Hinrichs, *CHEMTECH*, **4**, 627 (1974).
13) a) Goodyear Tire and Rubber, U. S. Patent, 3751499 (1973); 3819734 (1974); 3915891 (1975); 4131627 (1978); b) Gulf Res. Dev., U. S. Patent, 4062902 (1977); c) Kanegafuchi Chem. Ind., Japan Kokai, 49-31642; 50-14657; d) Nissan Chem. Ind., Japan Kokai, 49-35358; e) Sakai Chem., Japan Kokai, 49-125340; f) Shell. Inst. Res., Ger. Offen., 2127625 (1971).
14) G. Carturan, G. Facchin, G. Cocco, S. Enzo, and G. Navazio, *J. Catal.*, **76**, 405 (1982).
15) T. H. Kim and H. F. Rase, *Ind. Eng. Chem., Prod. Res. Dev.*, **15**, 249 (1976).
16) G. Henrici-Olivé and S. Olivé, "Coordination and Catalysis," Verlag Chemie, Weinheim, New York (1977), p. 211.
17) M. Terasawa, K. Kaneda, T. Imanaka, and S. Teranisi, *J. Catal.*, **51**, 406 (1978).
18) F. B. Hildebrand, "Advanced Calculus for Applications," 2nd ed, Prentice-Hall, New Jersey (1976), p.102.
19) W. F. Linke, "Solubilities of Inorganic and Metal Organic Compounds," 4th ed , D. VanNostrand Co., Inc., Princeton (1958), Vol. 1, p. 1086.
20) E. L. Muetterties,, *Chem. Eng. News*, **60** (No.35), 28 (1982).
21) H. Lindlar, *Helv. Chim. Acta*, **35**, 446 (1952).
22) C. Reichardt, "Solvent Effect in Organic Chemistry," Verlag Chemie, Weinheim, New York (1979), p. 241.
23) H. O. House, "Modern Synthetic Reactions," 2nd ed , W. A. Benjamin, Inc., Menlo Park, California (1972), p. 3.
24) "Kobunshi Shuugotai (Macromolecular Assembly)," ed by E. Tsuchida, K. Horie, and Y. Abe, Japan Scientific Societies Press, Tokyo (1983), p. 7.

 © 1984 The Chemical Society of Japan Bull. Chem. Soc. Jpn., 57, 495—499 (1984)

N-Hydroxy Amides. I. Synthesis of *N*-Benzyloxy and *N*-Hydroxy Peptides *via* Polymerization of *N*-Benzyloxy DL-α-Amino Acid *N*-Carboxy Anhydrides

Kazuyuki SHIMIZU, Masayoshi HASEGAWA, and Masayasu AKIYAMA*
Department of Applied Chemistry for Resources, Tokyo University of Agriculture and Technology, Koganei, Tokyo 184
(Received August 11, 1983)

Polymerization of *N*-benzyloxy DL-α-amino acid *N*-carboxy anhydrides (*N*-benzyloxy-NCAs) has been carried out in benzene for 30 d with cyclohexylamine as initiator. The N-benzyloxy-NCAs of glycine, alanine, 2-aminobutyric acid, and leucine give the corresponding polymers in good yields, while the starting material is recovered from those of valine and phenylalanine. The different behavior in the polymerization is discussed in terms of steric crowding. Catalytic hydrogenation of the *N*-benzyloxy polymers produces poly(*N*-hydroxy peptide)s. Complex formation of these polymers with iron(III) has been examined. Among the polymers, poly(*N*-hydroxyalanine) is further converted into poly(*N*-acetoxyalanine), which acts as an acyl active polymer. Treatment of poly(*N*-benzyloxyalanine) with $B(CF_3CO_2)_3$ gives 1,4-dihydroxy-3,6-dimethyl-2,5-piperazinedione.

A number of hydroxamic acid derivatives have been found in nature. These natural hydroxamic acids show unique biological activities, including microbial iron transport (siderophore).[1-3] It is worthwhile to synthesize *N*-hydroxy peptides which have hydroxamic acid functions in their peptide backbone. Several simple *N*-hydroxy peptides have already been prepared by a few procedures,[4-7] and studies in this field have become increasingly active.[8-11] In a preliminary letter, we have shown a stepwise synthesis of an alternating *N*-hydroxy peptide by use of *N*-benzyloxy DL-α-amino acid *N*-carboxy anhydrides (*N*-benzyloxy-NCAs).[8] The synthesis was successful because of the slowness of the NCA polymerization. In an attempt to obtain homodetic poly(*N*-hydroxy peptide)s, a prototype of *N*-hydroxy peptides, we felt it necessary to examine polymerization of these new NCAs. This paper describes polymerization of these NCAs and subsequent removal of the benzyl group in the polymers, which will lead to hitherto unknown poly(*N*-hydroxy peptide)s.

Results and Discussion

Scheme 1 depicts the outline of the reactions. *N*-Benzyloxy DL-α-amino acids (**1a—f**) were obtained by reaction of α-bromoalkanoic acids with *O*-benzylhydroxylamine.[12] Their amino group has a low pK_a due to the inductive effect of the oxygen. Phosgenation of **1a—f** in benzene–THF gave *N*-benzyloxy-NCAs (**2a—f**) in good yields.

It is known that NCAs having bulky substituents seldom polymerize, and successful examples are limited to certain polymers, polyproline, poly(*N*-methylalanine), and a few poly(*N*-substituted glycines).[13-16] Preliminary experiments did show, however, that some of the present NCAs can be polymerized into peptide derivatives under well-chosen conditions. The first-order plots of the reactions show a small upward break, familiar in the usual NCA (Fig. 1). They indicate a slow reaction.

Accordingly, polymerization of **2a—f** was performed in benzene at 40 °C for 30 d using cyclohexylamine as an initiator. Water also proved to be an efficient initiator. Typical polymerization results are summarized in Table 1. **2a—d** afforded polymerization products (**3a—d**), although **3d** was a glassy solid and showed a slight deviation in elemental analysis. The starting material was recovered from **2e** and **2f**, and even more forcing conditions failed to give a polymer from **2e**. The degree of polymerization (DP) for polymers obtained is smaller than the value expected from the ratio of NCA

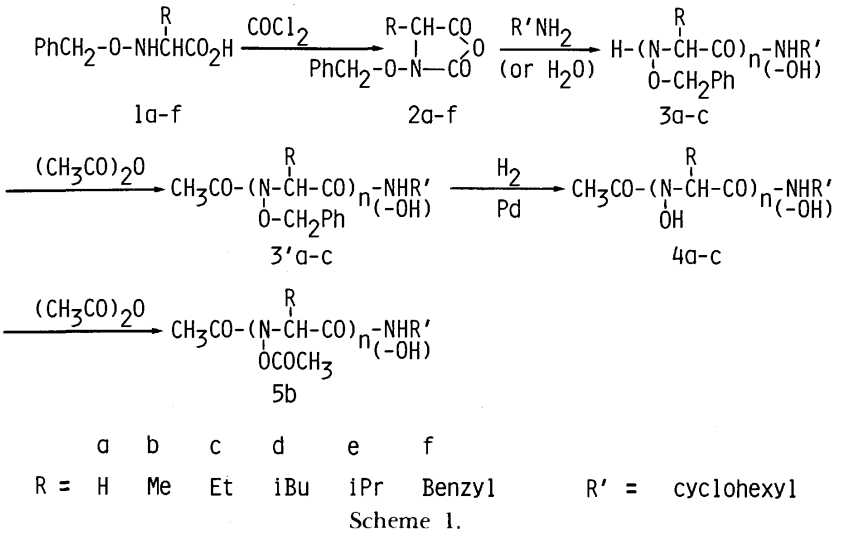

Scheme 1.

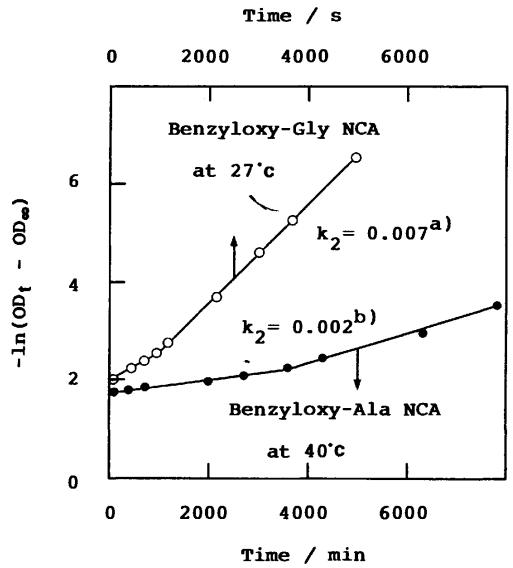

Fig. 1. Pseudo-first-order plots for cyclohexylamine initiated polymerization of *N*-benzyloxy-NCAs of glycine and alanine, as followed by the optical density difference, (OD_t—OD_∞), of the anhydride carbonyl group at 1860 cm^{-1}. [NCA]/[amine]=10. The corresponding second-order rate constants (k_2) appear along with linear portions of the plots: a) 1 $mol^{-1}s^{-1}$: b) 1 $mol^{-1}min^{-1}$.

TABLE 1. POLYMERIZATION OF *N*-BENZYLOXY-NCAs[a]

NCA	R	Yield %	Product	Mol wt (DP)[b]
2a	H	99	**3a**	2350 (14)
2b	Me	99	**3b**	2300 (13)
		95	**3b**	5500 (30)[c]
2c	Et	83	**3c**	1290 (7)
2d	*i*-Bu	96	**3d**	1280 (6)
2e	*i*-Pr		No polymer[d]	
2f	Benzyl		No polymer[d]	

a) Carried out in benzene at 40 °C for 30 d in the presence of cyclohexylamine with a ratio of [NCA]/[amine]=25. b) Degree of polymerization. c) [NCA]/[cyclohexylamine]=50. d) Most of the NCA was recovered unchanged.

to initiator, and a decrease in DP with increasing bulkiness of α-substituents, is also noted. These results indicate that there is a boundary line between α-substituents, *i*-Bu and *i*-Pr, as to polymerizability of these NCAs. The fact that DP is low while the yield is high suggests a concurrent initiation other than that caused by the initiator amine.[17] Initiation by water is most plausible for the present system.

A key factor for the polymerization seems to be steric bulk rather than basicity, since the *N*-benzyloxyamino group has much weaker basicity than the *N*-alkylamino group. Compare, for example, *N*-benzyloxyalanine with *N*-benzylalanine. The NCA of the latter does not polymerize.[15] The former has a less hindered environment around the nitrogen than the latter; there are only two unshared electron pairs and one methylene group on the oxygen adjacent to the nitrogen in the former, while two hydrogens and one phenyl group exist on the adjacent carbon atom in the latter. The failure of **2e** and **2f** in the polymerization is ascribed to a combined steric hindrance of *N*- and C^α-substituents.[18]

In the IR spectra poly(*N*-benzyloxy peptide)s show an amide I band at slightly higher wave number (1670 cm^{-1}) than those of *N*-alkyl substituted polypeptides[15] (1635—1639 cm^{-1}). ^{1}HNMR peaks correspond to protons of the expected structures for the polymers; common peaks observed are around δ=5.0 for $PhCH_2O$-, 5.4 for α-CH, and 7—7.5 for C_6H_5. A molecular formula for each polymer is provided by adequately adding fractions of a water molecule on the basis of observed DP and the initiator used. The detailed data for polymer characterization are presented in the experimental section.

For conversion of poly(*N*-benzyloxy peptide)s into poly(*N*-hydroxy peptide)s several debenzylation procedures were attempted. Treatment of poly(*N*-benzyloxyalanine) (**3b**) with $B(CF_3CO_2)_3$[7] in CF_3CO_2H gave the cyclic dimer of *N*-hydroxy-DL-alanine in 68% yield. The product was identified on the basis of IR, NMR and mass spectral data. The preferential cyclodimerization seemed to occur through fragmentation from a formed *N*-hydroxy peptide *N*-terminus, since no decrease in DP was observed when **3b** was dissolved in CF_3CO_2H for the same period. Hydrogenolysis with Pd catalysts gave partially debenzylated products, or extensively hydrolyzed products when subjected to a prolonged reaction. Hydrolysis in this case is considered to take place on the catalyst surface by the action of water which is generated from occluded oxygen.[19]

Hydrogenolysis was accomplished by reducing *N*-terminal-acetylated polymers (**3′**) with $Pd(AcO)_2$, giving the desired poly(*N*-hydroxy peptide)s (**4**). The catalyst was effective because $Pd(AcO)_2$ is soluble and can penetrate into the polymer entanglement at the outset of the reaction. Typical results are summarized in Table 2. Times required for the reaction apparently depend on the size of the α-substituents. Decrease in DP during the hydrogenolysis was inevitable with **4a**. Polymers (**4a—c**) show ^{1}HNMR signals which correspond to the expected structure; common signals are at δ=2.0 for CH_3CO, 5.3 for α-CH, and 9.2 for HO-N. IR spectra show a broad and strong band in the carbonyl region (1650 cm^{-1}) and new peaks at 3200 and 1180 cm^{-1} due to the *N*-OH moiety.

Hydroxamic acid polymers **4a—c** when mixed with $FeCl_3$ gave an intense violet color characteristic of the complex with $FeCl_3$. The absorbancy of the complex with increasing amounts of iron (III) is shown for poly(*N*-hydroxyalanine) as a representative example (Fig. 2). For comparison, the complex formation

TABLE 2. DEBENZYLATION OF POLYMERS (**3**) BY HYDROGENOLYSIS[a]

Polymer used	(mg)	(DP)	Solvent	Temp °C	Time h		Yield mg	(DP)
3a′	350	(14)	TFA	35	1	**4a**	175	(8)
3b′	350	(30)	DMF	30	4	**4b**	189	(30)
3c′	350	(7)	DMF	40	40	**4c**	167	(7)

a) Under atmospheric pressure with 500 mg of $Pd(CH_3COO)_2$.

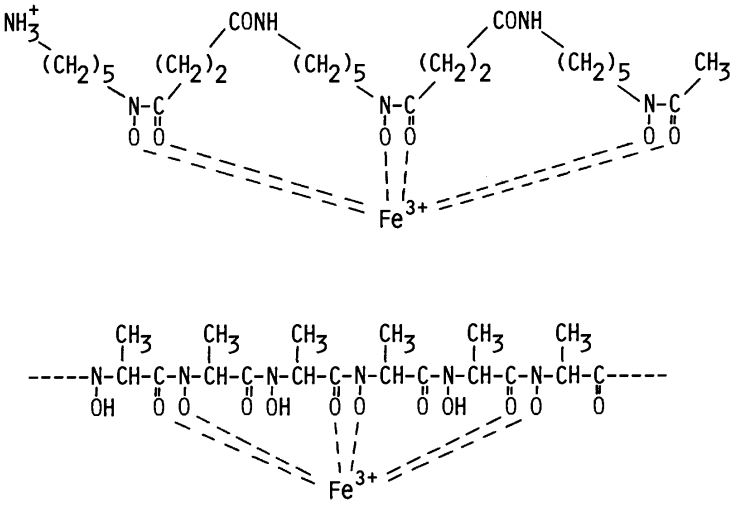

Scheme 2.

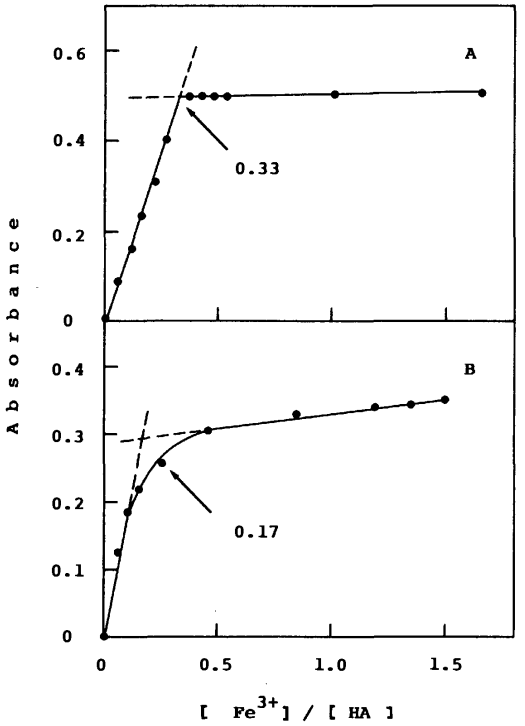

Fig. 2. Plot of absorbance *vs.* the ratio of iron(III) to the hydroxamic acid units; A: DFO and B: poly(*N*-hydroxyalanine) as a representative of these poly(*N*-hydroxy peptide)s. Absorbance at 430—450 nm in A and 450—470 nm in B, in 50% aqueous DMF, pH=3, ionic strength=0.1 (KNO_3).

of a typical trihydroxamic acid, desferrioxamine B (DFO),[20] was measured under similar conditions. An intersection of the dashed lines corresponds to an average molar ratio between Fe^{3+} and the hydroxamic acid groups. DFO gives a sharp inflection, while the polymer reveals considerable curvature. Compared with the ratio of DFO (0.33), values of the ratio for polymers decreased gradually from **4a** to **4c**; 0.26 for **4a**, 0.17 for **4b**, and 0.15 for **4c**. The absorbance of the complex is larger for DFO than that for the polymers under these conditions. These differences clearly indicate that for effective iron binding, considerable chain spacing is necessary between hydroxamic acid groups, while bulky α-substituents in the polymers are unfavorable for formation of stable iron complexes.

By acylation with acetic anhydride, polymer **4b** gave poly(*N*-acetoxyalanine) (**5b**). Strong carbonyl absorptions are observed for **5b** at 1800 (N-O-$COCH_3$) and 1670 (N-CO-) cm^{-1}, the latter amide band being shifted again close to that of the poly(*N*-benzyloxy peptide)s. As expected from the structure, **5b** was able to acetylate cyclohexylamine readily at room temperature.

Experimental

All melting points are uncorrected. IR spectra were taken with a JASCO model DS 403G infrared spectrophotometer. ^{1}HNMR spectra were recorded on a JEOL FX 200 spectrometer with Me_4Si as internal standard. Visible spectra were obtained on a Hitachi 320 spectrophotometer. Elemental analyses was performed by the analytical section, Institute of Physical and Chemical Research, Saitama. *N*-Benzyloxy α-amino-acids were prepared by the reported procedure with slight modifications.[12] Methanesulfonate salt of desferrioxamine B (Desferal) was obtained through Ciba-Geigy, Japan.

N-Benzyloxy α-Amino Acid N-Carboxy Anhydrides (2). *N*-Benzyloxy α-amino acid (0.10 mol) was suspended in a benzene-THF mixture (70 ml, 1:1 v/v). Phosgene from trichloromethyl chloroformate (24 ml, 0.20 mol) was bubbled to the suspension at 40 °C for 1 h, the clear solution which resulted was concentrated before the addition of THF (30 ml). The THF solution was treated with triethylamine (5 g, 0.05 mol) with stirring at −5—−10 °C for 1 h. After filtration of triethylammonium chloride and evaporation of the solvent, the residue was dissolved in diethyl ether and hexane was added. The mixture was kept at −20 °C until crystallization was completed. The crystals were collected and dried in a desiccator over P_2O_5. *N-Benzyloxyglycine NCA (2a)*: Mp 70—71 °C (lit,[8] 63—64 °C) (Found: C, 58.28; H, 4.39; N, 6.86%. Calcd for $C_{10}H_9NO_4$: C, 57.96; H, 4.39, N, 6.76%). *N-Benzyloxy-DL-alanine NCA (2b)*: Mp 71—72 °C (lit,[8] 71—72 °C). (Found: C, 59.67; H, 4.97; N, 6.30%. Calcd for $C_{11}H_{11}NO_4$: C, 59.72; H, 5.01; N, 6.33%). *N-Benzyloxy-DL-α-aminobutyric Acid NCA (2c)*: Mp 67—68 °C (lit,[8] 65—66 °C) (Found: C, 61.58; H, 5.73; N, 6.96%. Calcd for $C_{12}H_{13}NO_4$: C, 61.28; H, 5.53; N, 6.96%). *N-Benzyloxy-DL-leucine NCA (2d)*: Oil, (Found: C 3.92; H, 6.56; N, 5.40%.

Calcd for $C_{13}H_{17}NO_2$: C, 63.86; H, 6.51; N, 5.32%). *N-Benzyloxy-DL-valine NCA (2e)*: Mp 51—52°C (lit,[8] 50—51 °C) (Found: C, 62.71; H. 6.03; H, 5.38%. Calcd for $C_{13}H_{15}NO_4$: C, 62.64; H, 6.07; N, 5.62%). *N-Benzyloxy-DL-phenylalanine NCA (2f)*: Mp 147—148°C (lit,[8] 147—148°C) (Found: C, 68.45; H, 5.12; N, 4.68%. Calcd for $C_{17}H_{15}NO_4$ C, 68.67; H, 5.08; N, 4.71%). These NCAs were stable for several months in the refrigerator. For polymerization they were recrystallized (or reprecipitated) twice from diethyl ether–hexane.

Kinetics by IR. Polymerization of NCAs (**2a** and **2b**) in benzene was initiated with [NCA]/[cyclohexylamine]=10. For **2a**, a portion of the mixture was transferred to the IR cell and spectra of the mixture were taken at appropriate time intervals through a range of 1900—1600 cm^{-1}. The temperature of the cell was 27±1°C. For **2b**, aliquots were transferred at intervals from a polymerization solution maintained at 40± 0.1°C to the IR cell, and the spectra were taken as above.

Polymerizaion. To a solution of the NCA (**2**) (2—3 g, 9.45 mmol) in benzene (19 ml) was added 3.0 ml solution of cyclohexylamine (0.312 g, 3.15 mmol) in benzene (25 ml). The mixture was cooled, degassed, and sealed off under vacuum; it was kept at 40°C for one month. After the tube was opened and the solvent was evaporated, the residue was washed with diethyl ether on a glass filter. The product was dissolved in benzene (**3a** in dioxane) and precipitated into hexane.

Poly(N-benzyloxyglycine) (3a): Mp 164—167°C; IR 1665 cm^{-1} (C=O); ^{1}HNMR ($C_4D_8O_2$) δ=0.8—1.3 (weak m, cyclohexyl), 4.4—4.7 (2H, m, NCH_2), 4.83 (2H, br s, OCH_2), and 7.1—7.6 (5H, m, phenyl). Found: C, 66.23; H, 5.95; N, 8.51%. Calcd for $(C_9H_9NO_2)_{14}\cdot C_6H_{13}N\cdot(11/14)H_2O$: C, 66.18; H, 5.76; N, 8.68%.

Poly(N-benzyloxy-DL-alanine) (3b): Mp 119—121°C; IR 1665 cm^{-1} (C=O); ^{1}H NMR ($C_4D_8O_2$) δ=1.2—1.5 (3H, m, Me), 4.9—5.1 (2H, m, OCH_2), 5.4 (1H, br s, α-H), and 7.1—7.5 (5H, br s, phenyl). Found: C, 67.77; H, 6.57; N, 8.11%. Calcd for $(C_{10}H_{11}NO_2)_{13}\cdot C_6H_{13}N\cdot(12/13)H_2O$: C, 67.62; H, 6.42; N, 8.01%.

Poly(N-benzyloxy-DL-α-aminobutyric acid) (3c): Mp 106—109°C; IR 1655 cm^{-1} (C=O); ^{1}H NMR ($C_4D_8O_2$) δ=0.5—0.9 (3H, m, Me), 1.8—2.2 (2H, br d, C-CH_2), 4.9—5.5 (3H, m, OCH_2 and α-H), and 7.1—7.5 (5H, m, phenyl). Found: C, 68.70; H, 7.10; N, 7.70%. Calcd for $(C_{11}H_{13}NO_2)_7\cdot C_6H_{13}N\cdot(18/7)H_2O$: C, 68.59; H, 7.05; 7.44%.

Poly(N-benzyloxy-DL-leucine) (3d): A glassy solid, IR 1655 cm^{-1} (C=O); ^{1}H NMR ($C_4D_8O_2$) δ=0.4—1.1 (6H, m, 2Me), 1.1—2.2 (3H, m, CH-CH_2), 4.7—5.8 (3H, m, OCH_2 and α-H), and 7.1—7.6 (5H, m, phenyl). Found: C, 70.19; H, 7.94; N, 7.03%. Calcd for $(C_{13}H_{17}NO_2)_6\cdot C_6H_{13}N\cdot H_2O$: C, 70.46; H, 8.23; N, 6.89%.

None of the following solvents gave better polymerization results than benzene; acetonitrile, dichloromethane, dioxane, THF, and toluene.

Debenzylation. *(a) With $B(CF_3CO_2)_3$*: To a solution of the *N*-benzyloxyalanine polymer (**3b**) (400 mg, 2.2 mmol) in trifluoroacetic acid (5 ml) was added $B(CF_3CO_2)_3$ (7.9 g, 22.5 mmol) and stirred for 48 h at room temperauture. The acid was evaporated and methanol was added to the residue. Evaporation and addition of methanol were repeated three times. After filtration of the orthoboric acid derivative and concentration to 3 ml, the solution was introduced into an LH-20 Sephadex column and eluted with methanol. Evaporation of the main fraction gave a crystalline compound (132 mg): yield 68%; mp 212°C (decomp); R_f 0.66 (*n*-BuOH:AcOH:H_2O 4:1:1); IR 1670 cm^{-1} (C=O); ^{1}H NMR (D_2O) δ=1.46 (6H, d, Me), 4.30 (2H, q, α-H). Found: C, 41.33; H, 5.82; N, 15.70%; M^+, 174. Calcd for $C_6H_{10}N_2O_4$: C, 41.60; H, 5.85; N, 15.66%; M^+, 174.

(b) Hydrogenolysis: Before hydrogenolysis, *N*-terminal acetylation was performed by heating the polymers (**3a—c**) (800 mg) with Ac_2O (10 ml) in dioxane (10 ml) at 80°C for 1 h, to give acetylated polymers (**3a′—c′**) (778 mg). A solution of **3a′** (350 mg) and $Pd(AcO)_2$ (500 mg) in trifluoroacetic acid (20 ml), or **3b′** or **3c′** (350 mg) in DMF (20 ml), was reduced with H_2 under atmospheric pressure until Pd metal separated from the solution. After removal of the Pd catalyst and evaporation of the solvent, the residues were washed with Et_2O and dried under vacuum to give white powders (**4a—c**) (Table 2).

Poly(N-hydroxyglycine) (4a): Mp 169—173°C (decomp); ^{1}H NMR (Me_2SO-d_6 at 80°C) δ=1.5 (br, C_6H_{11}-), 2.0 (s, CH_3CO-), 4.5 (2H, CH_2), and 9.5 (1H, HO-N). Found: C, 34.37; H, 4.64; N, 16.98%. Calcd for $(8/14)CH_3CO(6/14)H\text{-}(C_2H_3NO_2)_8\cdot(8/25)C_6H_{12}N\cdot(17/25)OH+H_2O$: C, 34.15; H, 4.87; N, 17.39%.

Poly(N-hydroxy-DL-alanine) (4b): Mp 139—142°C; ^{1}H NMR (Me_2SO-d_6 at 80°C) δ=1.35 (3H, CH_3), 1.7 (br, C_6H_{13}), 2.0 (CH_3CO), 5.3(1H, α-H), and 9.2 (1H, HO-N). Found: C, 42.48; H, 6.33; N, 15.33%. Calcd for $CH_3CO(C_3H_5NO_2)_{30}\cdot(30/50)C_6H_{12}N\cdot(20/50)OH$: C, 42.18; H, 5.98; N, 15.75%.

Poly(N-hydroxy-DL-α-aminobutyric acid) (4c): Mp 161—163 °C; ^{1}H NMR (Me_2SO-d_6 at 80°C) δ=0.85 (3H, CH_3), 1.85 (2H, -CH_2), 2.1 (CH_3CO), 5.3 (1H, α-H), and 9.1 (1H, HO-N). Found: C, 46.81; H, 7.09; N, 13.25%. Calcd for $CH_3CO(C_4H_7NO_2)_7\cdot(7/25)C_6H_{12}N\cdot(18/25)OH+H_2O$: C, 47.07; H, 7.19; N, 12.62%.

Poly(N-acetoxy-DL-alanine) (5b) and Its Use as an Acyl Active Polymer. *(a) Acetylation*: To a suspension of **4b** (135 mg) in THF (10 ml) was added acetic anhydride (5 ml) in THF (10 ml); the mixture was heated at 50°C for 1 h. The resulting solution was concentrated under vacuum and the residue was washed with Et_2O to give a white product. The product was precipitated from THF into Et_2O and dried under vacuum to give **5b** (161 mg, 80%). Mp 154—157°C, IR 1800 (N-O-$COCH_3$) and 1670 (N-CO-) cm^{-1}. Found: C, 46.22; H, 5.59; N, 10.64%. Calcd for $CH_3CO(C_5H_7NO_3)_{30}\cdot(30/50)C_6H_{12}N\cdot(20/50)OH$: C, 46.93; H, 5.54; N, 10.79%.

(b) Acylation with 5b: To a solution of **5b** (95 mg, 0.74 mmol) in THF (10 ml) was added cyclohexylamine (65.6 mg, 0.66 mmol) in THF (10 ml). After the mixture was kept at 25°C for 30 h, the solution was concentrated to dryness and the residue was extracted with Et_2O. Evaporation of the combined ethereal solution gave a crude product (86 mg, 92%) of mp 99—101°C (*N*-cyclohexylacetamide, mp 104°C).

Molecular Weight Determination. The degree of polymerization (DP) was determined by measuring the number average molecular weight of the products (**3a—c** and **4a—c**) with a Hitachi vapour pressure osmometer, model 117. A calibration line was made with benzil as a reference compound. Measurement was performed using dioxane for **3a** at 35°C, benzene for **3b—c** at 40°C, and DMF for **4a—c** at 55°C, respectively. The values are accurate within±5% errors.

Molar Ratio Determination for Iron(III) Complexes. DMF stock solutions of samples were prepared at concentrations of 0.002 hydroxamic acid equiv/l. Aqueous ferric nitrate solutions of approximately 0.003 mol/l were prepared and standardized with EDTA (bismuth method). Aliquots (1 ml) of the sample solution were placed in each of a series of 10 ml volumetric flasks, and varying amounts of iron solution were added. The resulting solutions were diluted to 10 ml, so as to become aqueous 50% DMF solution of ionic strength of 0.1 (KNO_3). The pH of the solutions was made 3.0 with diluted nitric acid. The absorbance of each solution was measured at λ_{max} (450—470 nm).

We thank Messrs. Hiroshi Shimizu, Haruyuki Takeuchi, and Koji Morisada, and Miss Chika

Tsuchiya for performing some of the experiments.

References

1) J. B. Neilands, *Science*, **156**, 1443 (1967); "Microbial Iron Metabolism," Academic Press, New York (1974); "Inorganic Biochemistry," ed by G. L. Eichhorn, Elsevier, Amsterdam (1973), p. 167.
2) H. Maehr, *Pure Appl. Chem.*, **28**, 603 (1971).
3) K. N. Raymond and C. J. Carrano, *Acc. Chem. Res.*, **12**, 183 (1979).
4) A. H. Cook and C. A. Slater, *J. Chem. Soc.*, **1956**, 4133; C. Shin, K. Nanjo, M. Kato, and J. Yoshimura, *Bull. Chem. Soc. Jpn.*, **48**, 2584 (1975).
5) O. Neunhoeffer, G. Lehmann, D. Haberer, and G. Steinle, *Justus Liebigs Ann. Chem.*, **712**, 208 (1968).
6) G. Zvilichovsky and L. Heller, *Tetrahedron Lett.*, **1969**, 1159.
7) T. Kolasa and A. Chimiak, *Tetrahedron*, **33**, 3285 (1977).
8) M. Akiyama, M. Hasegawa, H. Takeuchi, and K. Shimizu, *Tetrahedron Lett.*, **1979**, 2599.
9) A. Chimiak and T. Polonski, *J. Prakt. Chem.*, **322**, 669 (1980).
10) J. D. M. Herscheid, R. J. F. Nivard, M. W. Tijhuis, H. P. H. Scholten, and H. C. J. Ottenheijm, *J. Org. Chem.*, **45**, 1880 (1980).
11) J. D. M. Herscheid, J. H. Colstee, and H. C. J. Ottenheijm, *J. Org. Chem.*, **46**, 3346 (1981).
12) T. Kolasa and A. Chimiak, *Tetrahedron*, **30**, 3591, (1974).
13) C. H. Bamford and H. Block, "Polyamino Acids, Peptides and Proteins," ed by M. A. Stahman, Univ. of Winsconsin Press (1962), p. 65.
14) M. Goodman and M. Fried, *J. Am. Chem. Soc.*, **89**, 1264 (1967).
15) A. Cosani, M. Palumbo, M, Terbojevich, and E. Peggion, *Macromolecules*, **11**, 1041 (1978).
16) M. Sisido, Y. Imanishi and S. Okamura, *Biopolymers*, **7**, 937 (1969).
17) H. Sekiguchi, *Pure Appl. Chem.*, **53**, 1689 (1981).
18) D. G. H. Ballard and C. H. Bamford, *J. Chem. Soc.*, **1958**, 355.
19) S. Nishimura and T. Itaya, *J. Chem. Soc., Chem. Commun.*, **1967**, 422.
20) A. Winston and E. T. Mazza, *J. Polym. Sci., Polym. Chem. Ed.*, **13**, 2019 (1975).

Influence of Boric Acid on the Hydrolysis Rate of a Hydroxy Schiff Base

Hiroshi MATSUDA, Hiroaki NAGAMATSU, Tadashi OKUYAMA,* and Takayuki FUENO
Faculty of Engineering Science, Osaka University, Toyonaka, Osaka 560
(Received August 13, 1983)

Effects of boric acid on the rate of hydrolysis of a Schiff base derived from α-hydroxyisobutyrophenone and 2-methoxyethylamine were examined in the pH range 4.2—10.4 at 30 °C. The rate increased above pH 7 but decreased below pH 7 with increasing borate concentration following a saturation curve. This is consistent with a reaction sequence involving a preequilibrium formation of a borate-substrate complex followed by its rate-determining decay to the hydrolysis products. The formation constant of the complex showed a bell-shaped change with pH but the rate constant for the complex decay was constant above pH 7, a small change being observed at lower pH. A mechanism involving an intramolecular transfer of the boron-coordinated hydroxide ion to the imine carbon within the complex is presented. Hydrazone formation from the hydroxy ketone was also examined in the presence of boric acid.

Hydrolyses of some hydroxy esters[1,2] and imines[3,4] have been found to be accelerated remarkably by boric acid in aqueous solutions. The reactions undoubtedly proceed through a borate-substrate complex similar to the one formed from diol and boric acid.[5,6] Although detailed mechanisms of the catalytic actions of boric acid are yet to be solved, they are of great interest in view of their similarity to the enzyme catalysis.[2,7]

We previously studied the borate-catalyzed hydrolysis of a hydroxy thiocarboxylic *S*-ester[2] and demonstrated that the catalysis occurs through a mechanism involving an intramolecular transfer of a boron-coordinated hydroxide ion within a borate-substrate complex. In the present investigation are examined effects of added boric acid on the rate of hydrolysis of a Schiff base derived from α-hydroxyisobutyrophenone **1**. It has been found that the hydrolysis is accelerated above pH 7 but the reaction is contrastingly decelerated below pH 7 by boric acid. A mechanism of the borate action on the hydrolysis is proposed.

$CH_3OCH_2CH_2N{=}C\begin{matrix}\diagup C_6H_5\\ \diagdown C(CH_3)_2OH\end{matrix}$

1

Results

Hydrolysis of the hydroxy Schiff base **1** was studied in aqueous solutions of ionic strength of 0.5 (KCl) at 30 °C. The reaction was monitored by following spectrophotometrically the formation of the product ketone at 245 nm. The rates were first measured without any added boric acid in usual buffer solutions of carboxylates, phosphate, tertiary and secondary amines, carbonate, and 2,2,2-trifluoroethanol as well as in HCl solutions in the pH range 0—12. Buffer effects were observed below pH 9.3 but not examined in detail here. The logarithms of the observed rate constants k_0 extrapolated to zero buffer concentration are plotted against pH in Fig. 1.

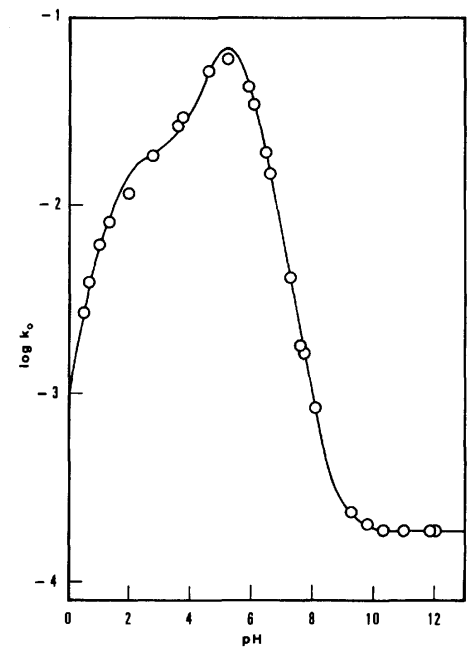

Fig. 1. pH-rate profile for the hydrolysis of the Schiff base **1** at 30 °C. The curve was calculated according to Scheme 1 and parameters given in Table 1.

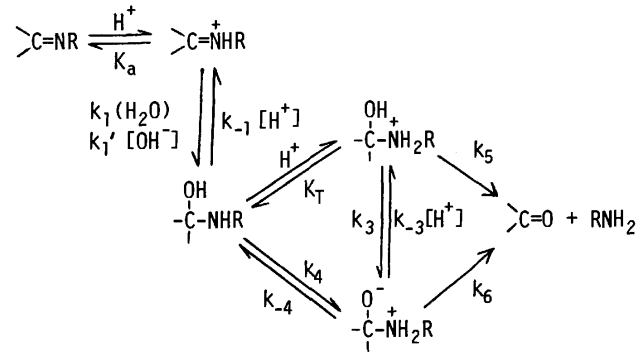

Scheme 1.

The pH rate profile is quite similar to that observed for a benzophenone Schiff base[8a] and may be interpreted in the same way (Scheme 1). This mechanism is analogous to that proposed by Kayser and Pollack;[8b] it involves changes in the rate-determining step of the decay of a carbinolamine (α-amino alcohol) intermediate in a low pH region in addition to the changeover of the slow step from the formation (pH>6) to the decay of the carbinolamine (pH<6). Kinetic parameters (defined in Scheme 1) are summarized in Table 1. The value of pK_a for the protonated Schiff base $\mathbf{1H^+}$ was estimated also from the bell-shaped correlation of pH

Table 1. Kinetic parameters for the hydrolysis of the Schiff base 1[a]

pK_a	5.75
k_1/s^{-1}	1.22×10^{-1}
$k_1'/M^{-1}\ s^{-1}$	2.30×10^{4}
$(K_1k_3/K_T)/s^{-1}$	2.2×10^{-2}
$K_1k_4/M^{-1}\ s^{-1}$	2×10^{-6}
$K_1K_4k_6/M^{-1}\ s^{-1}$	9.0×10^{-4}
K_c/M^{-1}	4.35×10^{2}
$(k_7/K_3)/M^{-1}\ s^{-1}$	$\approx10^{3}$
k_8/s^{-1}	9.9×10^{-3}
$k_8'/M^{-1}\ s^{-1}$	$<10^{2}$

a) 30 °C, μ=0.50 (KCl).

with the equilibrium constant K_{app} for the borate complexation (see below). A solid curve of Fig. 1 is a theoretical one based on the parameters given in Table 1.

When a small amount of boric acid was added to the reaction mixture, the hydrolysis was markedly accelerated at high pH but inhibited at low pH. The spectra of the product solutions were the same as those found in the absence of boric acid. Induction periods were not observed in any kinetic runs.

The dependence of hydrolysis rate on boric acid concentrations was examined at constant pH maintained with a second buffer. The rate increased at pH>7 while it decreased at pH<7 with increasing total borate concentration $[B]_t$, following the saturation curve expressed by Eq. 1 (Fig. 2).

$$k_{obsd} = (k_{obsd}^{0} + k_{\infty}K_{app}[B]_t)/(1+K_{app}[B]_t) \quad (1)$$

where k_{obsd}^{0} is the rate constant observed in the absence of boric acid. Borate is known to associate by itself at higher concentrations especially in the pH range 8—9;[5,9] this may diminish the activity of boric acid. To avoid this effect borate concentrations were kept low

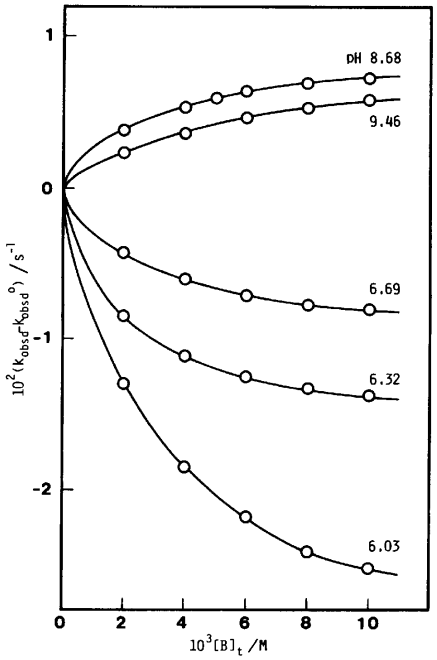

Fig. 2. Dependence of the hydrolysis rate of 1 on the borate concentration at pH indicated (30 °C, μ=0.50).

Table 2. Kinetic parameters for the hydrolysis of the Schiff base 1 in the presence of boric acid[a]

pH[b]	Added buffer (concn/M)	K_{app}/M^{-1}	$10^3k_{\infty}/s^{-1}$
4.21	Acetate (0.10)	12.2±0.5	8.6±2.4
4.62	Acetate (0.10)	23.7±0.7	8.60±1.08
4.90	Acetate (0.10)	40.9±0.4	9.76±0.34
5.20	Acetate (0.10)	82.2±1.3	10.19±0.49
5.24	Acetate (0.08)	90.0±3.2	9.91±0.29
5.45	Acetate (0.10)	149±2	10.60±0.48
5.65	Phosphate (0.10)	195±8	11.40±1.23
5.79	Phosphate (0.10)	235±13	10.31±1.60
5.86	Phosphate (0.10)	263±11	11.56±1.56
6.03	Phosphate (0.10)	321±7	12.1±0.3
6.04	Phosphate (0.08)	301±7	9.77±0.75
6.16	Phosphate (0.10)	332±24	10.51±2.13
6.32	Phosphate (0.10)	345±19	9.73±1.42
6.58	Phosphate (0.10)	366±28	9.32±2.23
7.27	Phosphate (0.05)	422±20	9.76±0.78
7.40	*N*-Methylmorph. (0.08)	412±9	9.83±0.35
7.70	*N*-Methylmorph. (0.10)	416±11	9.73±0.42
8.05	*N*-Methylmorph. (0.10)	405±12	9.88±0.48
8.30	*N*-Methylmorph. (0.10)	384±10	9.50±0.40
8.52	Morpholine (0.10)	365±26	9.48±1.07
8.68	Morpholine (0.10)	346±13	9.72±0.58
8.97	Morpholine (0.10)	269±4	9.89±0.36
9.08	Morpholine (0.10)	243±5	9.86±0.30
9.30	Carbonate (0.10)	213±4	9.92±0.29
9.46	Carbonate (0.10)	148±5	10.06±0.46
9.88	Carbonate (0.10)	65.7±2.8	10.18±0.63
10.40[c]	Carbonate (0.05)	26.7±1.8	9.05±0.92

a) 30 °C, μ=0.50 (KCl). b) Deviations are greater than ±0.02 unless stated otherwise. c) ±0.05.

enough ($[B]_t$ <0.01 M (mol dm^{-3}) at pH 6.5—9.5 and <0.2 M at other pH); so the observed curvatures are not affected by the association.

The curved rate dependence of Eq. 1 is consistent with the reaction sequence involving an equilibrium formation of a borate-substrate complex followed by its breakdown to give the hydrolysis products (Eq. 2), where K_{app} and k_∞ stand for the equilibrium constant for the complexation and the rate constant for the decay of the complex, respectively. Constants K_{app} and k_∞ were calculated by a least-squares treatment of the data according to Eq. 4 which is derived from Eq. 1.

$$\mathbf{1} + \text{borate} \overset{K_{app}}{\rightleftharpoons} \text{complex} \overset{k_\infty}{\longrightarrow} \text{products} \quad (2)$$

$$K_{app} = [\text{complex}]/[\mathbf{1}][B]_t \quad (3)$$

$$(k_{obsd} - k_{obsd}^0)/[B]_t = K_{app}k_\infty - K_{app}k_{obsd} \quad (4)$$

Since the substrate concentration ($[\mathbf{1}] \simeq 10^{-4}$ M) is significantly smaller than $[B]_t$ ($>10^{-3}$ M), initial borate concentrations were used for $[B]_t$. The constants K_{app} and k_∞ in various buffer solutions are summarized in Table 2 and plotted against pH in Fig. 3.

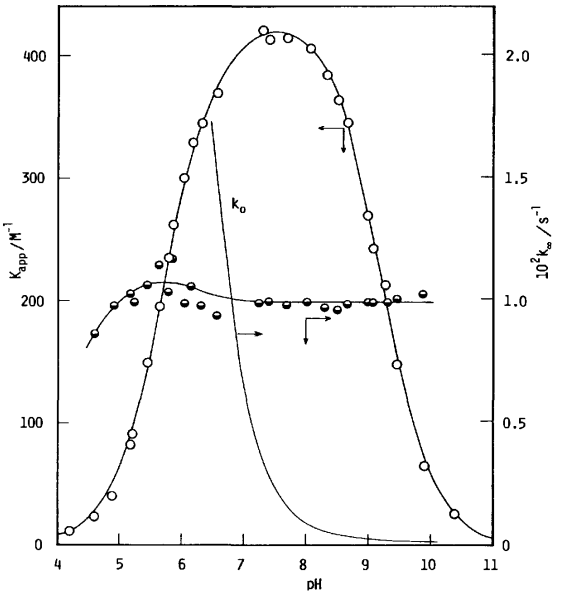

Fig. 3. Correlations of K_{app} (○) and k_∞ (●) with pH. The curves are theoretical (Eq. 8 and 10). Hydrolysis rate k_0 is partly shown.

Possible buffer effects have to be taken into account in two ways. Although borate definitely exerts specific effects on the hydrolysis rate of **1**, potential general base catalytic acceleration must be subtracted, if any, from the observed effects of borate in order to evaluate quantitatively its specific effects. The catalytic constant for such catalysis by borate can be estimated to be $k_B \simeq 5$ $M^{-1}s^{-1}$ from k_1 (for H_2O) and approximate k_B values for phosphate and *N*-methylmorpholine (1 and 1.5 $M^{-1}s^{-1}$, respectively). The apparent catalytic constant k_{Bt}, referring to total borate concentration, is proportional to both conjugate base fraction of borate and acid fraction of the substrate $\mathbf{1}H^+$ (Eq. 5), and the k_{Bt} value is at its maximum at pH≃7.5, where $k_{Bt} \simeq 1.8 \times 10^{-3}$ M^{-1} s^{-1}.

$$k_{Bt} = k_B\left(\frac{[H^+]}{K_a + [H^+]}\right)\left(\frac{K_{BH}}{K_{BH} + [H^+]}\right) \quad (5)$$

Table 3. Effects of added buffers on the borate-assisted hydrolysis of the Schiff base **1** at 30 °C

[Buffer]/M	K_{app}/M^{-1}	$10^3k_\infty/s^{-1}$
Acetate pH 5.24±0.02		
0[a]	91.1±0.9	9.81±0.41
0.02	91.9±2.8	9.76±1.03
0.04	90.0±1.1	10.10±0.51
0.06	93.0±2.7	10.16±1.04
0.08	90.0±3.2	9.41±0.29
Phosphate pH 6.03±0.02		
0[a]	312±13	8.94±1.01
0.02	309±12	9.19±0.94
0.04	308±9	9.48±0.57
0.06	294±7	9.66±0.66
0.08	301±7	9.77±0.75
0.10	321±7	12.1±0.3
N-Methylmorpholine pH 7.40±0.02		
0[a]	413±9	9.85±0.30
0.08	412±9	9.83±0.35
0.12	437±16	9.68±0.32
0.16	431±12	9.63±0.44
0.20	415±8	9.76±0.40

a) Calculated from k_{obsd} extrapolated to zero buffer concentration.

From these evaluations, a general-base catalytic contribution is less than 1/10^3 of the observed effects of borate over the whole pH range examined.

Secondly, the borate reaction which is responsible for the specific effects may be subject to the general catalysis by a second buffer added to keep pH constant. Buffer effects were, however, not detected in morpholine (pH 8.1) nor in carbonate buffers (pH 9.3) at borate concentration of 0.01 M. Detailed analyses according to Eq.1 were carried out at varying concentrations of 3 typical buffers and the results are given in Table 3. Both K_{app} and k_∞ are independent of buffer concentrations of acetate (pH 5.24) and *N*-methylmorpholine (pH 7.4) within experimental uncertainties, but k_∞ slightly increases with buffer concentration in phosphate buffer solutions of pH 6.0.

A kinetic investigation of hydrazinolysis of the Schiff base **1** was also attempted to know if boric acid influences the rate, but the attempts were unsuccessful because of a very small spectral change due to the reaction.

The effects of added boric acid on the hydrazone formation from α-hydroxyisobutyrophenone (**2**) were examined briefly as a reverse reaction of the Schiff base hydrolysis. Reactions were carried out in hydrazine buffers (pH 8—9) with or without added boric acid. For runs at pH 7.1 and above pH 9.3, low concentrations of phosphate and carbonate buffers were used to maintain constant pH. A possible initial drop of ketone absorption due to carbinolamine formation was not observed in the absence nor in the presence of boric acid. Observed pseudo-first-order rate constants k_{obsd}' were obtained from the decrease in the ketone absorption (245 nm) and divided by concentrations of neutral hydrazine [Hy] to give rate constants for the hydrazone formation.[10] The rate was linearly increased with

$$k_{obsd}' = k_{Hy}[Hy] \quad (6)$$

$$k_{Hy} = k_{Hy}^0 + k_{Hy}^B[B]_t \quad (7)$$

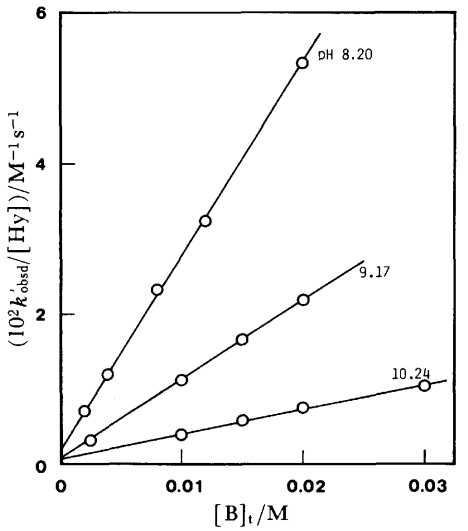

Fig. 4. Dependence of rate for the hydrazone formation from **2** on the borate concentration at pH indicated (30 °C, μ=0.50).

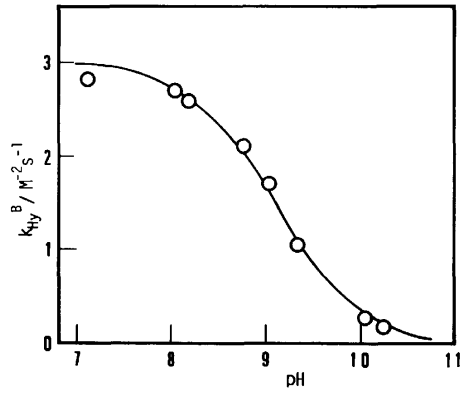

Fig. 5. Plot of k_{Hy}^{B} against pH.

increasing concentration of boric acid $[B]_t$ as shown in Fig. 4. The slopes k_{Hy}^{B} are much greater than those expected for the general catalysis.[11] General catalysis by hydrazine (second-order terms) and borate may be small enough to be neglected under the reaction conditions employed ($[Hy]_t \leq 0.125$ M, $[B]_t \leq 0.03$ M). Plots of the catalytic constants k_{Hy}^{B} *vs.* pH fit a sigmoid curve with $pK_a = 9.2$ (Fig. 5). Boric acid involved in the catalysis is its acid form, a limiting value of the catalytic constant k_{Hy}^{B} at lower pH being 2.9 M^{-2} s^{-1}.

Discussion

Hydrolysis of the Schiff base **1** derived from the α-hydroxy ketone **2** takes place in a usual way in well-behaved buffer solutions, exhibiting a pH-rate profile typical of the hydrolysis (Fig. 1).[8] On the other hand, borate buffer has never shown any unusual effects on the hydrolysis of Schiff bases except for those derived from *o*-hydroxybenzaldehyde.[3,4]

The specific effects of boric acid observed here must arise from the interaction of the hydroxyl group of **1** with boric acid and the associated borate function may facilitate the hydrolysis. In fact the observed rate constants change with borate concentration according to Eq. 1 which is based on the mechanism involving equilibrium formation of a borate-substrate complex. The complex formation must be very rapid as compared with its decay because no induction period was observed in spite of a large extent of complexation during the borate reaction.

The apparent equilibrium constants K_{app} for the complexation show a bell-shaped change with pH as seen in Fig. 3. The bell-shaped pH-K_{app} curve fits well Eq. 8, where $K_c = 435$ M^{-1}, $pK_a = 5.75$, and $pK_{BH} = 9.2$.

$$K_{app} = K_c\left(\frac{K_a}{K_a+[H^+]}\right)\left(\frac{[H^+]}{K_{BH}+[H^+]}\right) \quad (8)$$

$$K_c = [\mathbf{3}]/[\mathbf{1}][B(OH)_3] \quad (9)$$

The parameters are defined in Scheme 2 which presents possible reaction sequences. A main form of the complex present must consist of the neutral form of the substrate **1** and boric acid (acid form), and the formation constant K_c is as great as 435 M^{-1}; a probable structure **3** is presented in Scheme 2. In this complex **3** a borate group associated with the α-hydroxyl group coordinates on the imine nitrogen in a Lewis acid-base fashion forming a five-membered ring. Salicylaldehyde oxime was reported to form a stable complex with boric acid, the formation constant being about 300 M^{-1} (pH 9.2).[12] Salicylamide was also found to form a borate complex of six-membered ring involving nitrogen.[5] On the other hand, well-known complexations between boric acid and 1,2-diols usually give formation constants of 1—10 M^{-1}.[6] The formation constant K_c observed here is too large to be ascribed to a diol complex, carbinolamine-borate complex like **4**.

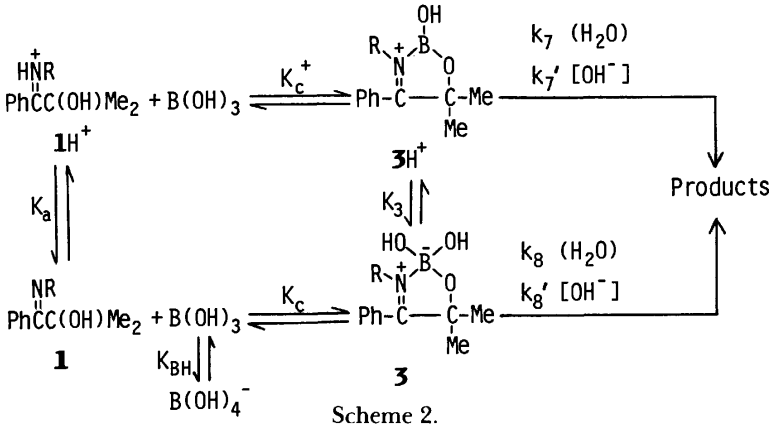

Scheme 2.

Furthermore, formation of the carbinolamine intermediate is not always rapid enough. The complex **4** is unlikely and the structure **3** is most probable. The complex **3** may equilibrate with a cationic form $3H^+$ at low pH but its contribution to the kinetics is small even at pH 4; the acid dissociation constant of $3H^+$ is thus estimated to be greater than 10^{-4} ($pK_3<4$).

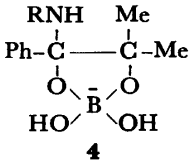

4

The limiting rate constant k_∞ extrapolated to the infinite concentration of borate refers to the breakdown of the complex to give the hydrolysis products. The k_∞ value does not change greatly over the pH range 5—10, showing only a slight increase at pH about 6 and a tendency to decrease below pH 5. The Schiff base hydrolysis takes place through a nucleophilic reaction of water with the protonated substrate. The borate complexes with Lewis acid-type boron coordination at the imine nitrogen (**3** and $3H^+$) are structurally similar to the protonated Schiff base and may be subject to the nucleophilic attack by water and hydroxide ion.

In analogy to the usual mechanism of the Schiff base hydrolysis (Scheme 1), the decrease in k_∞ at low pH (<5) must be due to the changeover of the rate-determining step from the formation to the breakdown of the (complexed) carbinolamine intermediate.

Above pH 5 nucleophilic attacks by water and hydroxide ion on the complexes **3** and $3H^+$ to form carbinolamine species would be rate determining and k_∞ is described by Eq. 10 using rate constants given in Scheme 2.

$$k_\infty = (k_7/K_3)[H^+] + k_7'K_w/K_3 + k_8 + k_8'[OH^-] \quad (10)$$

Since the k_∞ value is constant over pH 7—10, the hydroxide-ion catalysis is negligible ($k_8'<10^2\ M^{-1}\ s^{-1}$). The uncatalyzed term consists of two terms due to the hydroxide ion reaction of $3H^+$ and the water reaction of **3** ($k_7'K_w/K_3+k_8=9.9\times10^{-3}\ s^{-1}$). If the former term mainly contributed to k_∞, $k_7'>10^8\ M^{-1}\ s^{-1}$: This value is too large as compared to the rate constant for the hydroxide reaction of $1H^+$ ($k_1'=2.30\times10^4\ M^{-1}\ s^{-1}$). Thus the main reaction here must be the water reaction of **3**: $k_8=9.9\times10^{-3}\ s^{-1}$, which is about 1/10 of k_1 for $1H^+$. If the water reaction of **3** were mechanistically similar to that of $1H^+$, *i. e.* a simple nucleophilic reaction, the reactivity difference between **3** and $1H^+$ would allow to estimate the rate constant for the hydroxide reaction k_8' from k_1'. Since the reactivity difference is usually smaller toward hydroxide ion than toward water,[8] k_8' must be greater than $10^3\ M^{-1}\ s^{-1}$. This is too large as compared with the observed value ($<10^2\ M^{-1}\ s^{-1}$). That is, a simple water reaction of **3** is unlikely. Observed lack of general base catalysis of the k_∞ reaction in this pH region is also incompatible with the rate-determining water attack on **3**.

An alternative mechanism kinetically equivalent to this process may involve the rearrangement of **3** to an

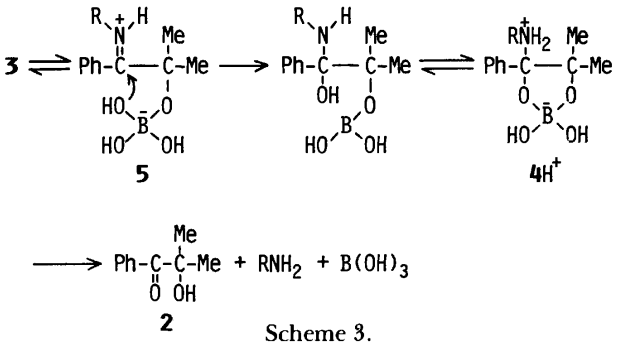

Scheme 3.

open-type complex like **5** followed by an intramolecular transfer of a hydroxide ion coordinated to the boron atom (Scheme 3). This process does not require any general catalysis and may be more effective than the hydroxide reaction k_8' up to pH 10. Furthermore, this mechanism closely resembles that proposed for the borate catalysis of hydrolysis of a hydroxy thiocarboxylic *S*-ester.[2]

In the pH region near **6**, scattering of plots of k_∞ is rather large because of experimental limitations due to a small rate change caused by boric acid but a small increase in k_∞ seems to be real. This may be attributed to the water reaction of $3H^+$; $k_7/k_3\simeq10^3\ M^{-1}\ s^{-1}$ and $k_7>10^{-1}\ s^{-1}$. The k_7 value is near or greater than k_1, which may not be unreasonable. In accord with the mechanism, general catalysis of the k_∞ process was observed at pH 6.0.

The apparent effect of added boric acid was acceleration of the hydrolysis up to 50-fold at high pH while the deceleration below pH 7. This arises from the smaller reactivity of the complexed substrate **3** than the protonated Schiff base $1H^+$ and the large formation constant K_c of the complex **3**. At higher pH equilibrium concentration of **3** is much greater than that of $1H^+$, which results in acceleration. At lower pH, where the concentration of $1H^+$ is large enough for the hydrolysis to be rapid, added boric acid converts $1H^+$ into less reactive complex **3** to inhibit the hydrolysis. Similar effects of boric acid on the Schiff base hydrolysis were previously examined with *N*-salicylideneaniline.[3] It was noted that the hydrolysis rate increased linearly with boric acid concentration, suggesting that the formation constant of the complex is small in this case. Deceleration has never been observed. The proposed mechanism involving a reaction of a cationic complex (similar to $3H^+$) with hydroxide ion[3] is however very unlikely in view of the present observations.

Hydrazone formation from the hydroxy ketone **2**, a reverse of the hydrolysis, was found to be accelerated by boric acid in the pH range 7—10. The rate increased linearly with borate concentration. A mechanism for the borate catalysis in this pH region is considered, as a microscopic reverse of the hydrolysis, to involve rate-determining formation of a stable borate-hydrazone complex from a borate-carbinolamine adduct. The formation constant for the borate-carbinolamine adduct (similar to **4**) must be small to allow linear dependence of the rate on borate concentration as observed. The key step of the reaction may be an intramolecular hydroxide transfer from the carbon to

the boron atom in accord with the mechanism of the borate-assisted hydrolysis.

Experimental

Materials. α-Hydroxyisobutyrophenone **2** was prepared from α-bromoisobutyrophenone[13] according to the literature.[14] The Schiff base **1** was prepared from **2** and 2-methoxyethylamine in a usual way[15] and recrystallized from ligroine, mp 53.8—54.4 °C. Found: C, 70.26; H, 8.59; N, 6.37%. Calcd for $C_{13}H_{19}NO_2$: C, 70.56; H, 8.65; N, 6.33%.

Other chemicals were obtained as before.[2,7] Glass-distilled water was used throughout.

Kinetic Measurements. All the aqueous solution containing appropriate amounts of boric acid, hydrazine, and other buffers were prepared in a volumetric flask at room temperature and adjusted to ionic strength of 0.5 with KCl. Stock solutions of the substrates were obtained as an acetonitrile solution of about 10^{-2} M. Reactions were started by adding 0.03 cm^3 of the substrate stock solution from a microsyringe into a 3-cm^3 buffer solution equilibrated at 30.0±0.1 °C in a stoppered quartz cuvette inserted in a water-jacketed cell holder. The reaction was followed by the increase (hydrolysis) or the decrease (hydrazone formation) in the absorption of the ketone **2** at 245 nm on a Shimadzu UV 200 or UV 140 spectrophotometer. Pseudo-first-order rate constants were calculated by a modified Guggenheim method.[16] Infinity absorbances calculated coinside well with those observed. pH of buffer and reaction solutions were measured by a Hitachi-Horiba F7 pH meter.

References

1) B. Capon and B. Ch. Ghosh, *J. Chem. Soc., B*, **1966**, 472.
2) T. Okuyama, H. Nagamatsu, and T. Fueno, *J. Org. Chem.*, **46**, 1336 (1981).
3) J. Hoffmann and V. Šterba, *Collect. Czech. Chem. Commun.*, **37**, 2043 (1972).
4) J. J. Charette and E. de Hoffmann, *J. Org. Chem.*, **44**, 2256 (1979).
5) D. W. Tanner and T. C. Bruice, *J. Am. Chem. Soc.*, **89**, 6954 (1967).
6) J. Boeseken, *Adv. Carbohydr. Chem.*, **4**, 189 (1949); G. L. Roy, A. L. Laferriere, and J. O. Edwards, *J. Inorg. Nucl. Chem.*, **4**, 106 (1957).
7) W. P. Jencks "Catalysis in Chemistry and Enzymology," McGraw-Hill New York, N. Y. (1969), pp. 30—32.
8) a) T. Okuyama, H. Shibuya, and T. Fueno, *J. Am. Chem. Soc.*, **104**, 730 (1982); b) R. H. Kayser and R. M. Pollack, *ibid.*, **99**, 3379 (1977).
9) N. Ingri, G. Lagerstrom, M. Frydman, and L. G. Sillén, *Acta Chem. Scand.*, **11**, 1034 (1957); N. Ingri, *ibid.*, **16**, 439 (1962); **17**, 573, 681 (1963).
10) Effects of second buffers (phosphate at pH 7.1 and carbonate at pH>9.3) were eliminated by extrapolating k_{obsd}' to zero buffer concentration.
11) J. M. Sayer, M. Peskin, and W. P. Jencks, *J. Am. Chem. Soc.*, **95**, 4277 (1973).
12) R. Ripan, G. Kiss-Imreh, and Z. Székely, *Rev. Roum. Chim.*, **10**, 965 (1965).
13) C. H. DePuy and R. J. Van Lanen, *J. Org. Chem.*, **39**, 3360 (1974).
14) K. v. Auers, H. Ludewig, and A. Müller, *Justus Liebigs Ann. Chem.*, **526**, 143 (1936).
15) C. L. Stevens, P. Blumberg, and M. Munk, *J. Org. Chem.*, **28**, 331 (1963).
16) E. S. Swinbourne, *J. Chem. Soc.*, **1960**, 2371.

NAD(P)$^+$-NAD(P)H Model. 47. Mechanism of the Formation of 1,4-Dihydronicotinamide in the Reaction of Pyridinium Salt and Amine

Atsuyoshi OHNO,* Satoshi USHIDA, and Shinzaburo OKA
Institute for Chemical Research, Kyoto University, Uji, Kyoto 611
(Received August 17, 1983)

An amine reduces 1-benzyl-3-carbamoylpyridinium ion (BNA$^+$) into 1-benzyl-1,4-dihydronicotinamide (BNAH) in aqueous solution. The mechanism of reduction has been elucidated. The covalently bound adduct of the amine and BNA$^+$ at the 6-position is found to be the true reductant. The reduction with formate proceeds through the direct "hydride-transfer" mechanism. Selectivity of nucleophilic attack on the 4- and 6-positions of BNA$^+$ is discussed in terms of hard-soft-acid-base (HSAB) principle.

The biological reduction of NAD$^+$ coupled with oxidation of substrates such as alcohols and amines takes place smoothly. On the other hand, only a few results on the non-enzymic reduction of pyridinium salts, model compounds for NAD$^+$, by organic substrates have been accumulated. As a model for an alcohol dehydrogenase, Ohnishi and Kitami reported the reduction of pyridinium salts by alkoxides.[1] However, the mechanism of the reaction seems to be different from that of the dehydrogenase, because, in their investigation, a direct hydrogen-transfer from an alkoxide to pyridinium salt was not observed. Recently we reported that 1-benzyl-1,4-dihydronicotinamide (BNAH) is produced[2] by the reaction of 1-benzyl-3-carbamoylpyridinium ion (BNA$^+$) with α-ketols such as glyceraldehyde and glycolaldehyde and that the mechanism is different from that suggested for the reaction catalyzed by glyceraldehyde 3-phosphate dehydrogenase.[3] In the reduction of BNA$^+$ with glycolaldehyde, addition of glycolaldehyde to the 4-positon of BNA$^+$ takes place initially, and the adduct acts as the real reductant for another molecule of BNA$^+$.[3]

By using a variety of amines and ammonia, Ohnishi reported the formation of BNAH from BNA$^+$.[4] The mechanism of the reduction, however, has remained unclear. In enzymic systems, the reduction of NAD$^+$ by amine is found in the reaction catalyzed by glutamate dehydrogenase,[5] where, according to the suggested mechanism, glutamate is oxidized to 2-iminoglutarate with simultaneous formation of NADH.[6]

$$\mathrm{NAD^+ + HOOCCH_2CH_2\underset{\displaystyle NH_2}{\underset{|}{C}}HCOOH \longrightarrow NADH + HOOCCH_2CH_2\overset{\displaystyle NH}{\overset{\|}{C}}COOH} \quad (1)$$

It is interesting to compare the mechanism of non-enzymic formation of 1,4-dihydropyridine by amines with that of enzymic process, not only from the view point of a simple comparison of the two systems but also from that for understanding biochemical reactions as well as to extend biomimetic reactions. We now report a mechanism of the formation of BNAH in the reaction of BNA$^+$ with amines.

Results and Discussion

According to a literature reported by Ohnishi,[4]

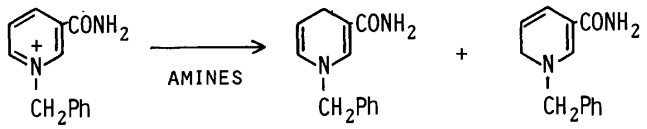

BNA$^+$ BNAH (2)

Table 1. Reaction of BNA$^+$ and amines[a]

BNA$^+$/M	Amine/M	Solvent	Reaction time/h	Yield of BNAH/%[g]
0.50[b]	1.60 (AE[d])	H_2O[f]	12	10
0.22[b]	1.88 (DA[e])	H_2O-MeOH	22	8
0.22[b]	1.88 (AE)	H_2O-MeOH	22	9
0.22[c]	1.88 (DA)	CH_3CN	50	18

a) At room temperature in the dark. b) Counter anion is Cl^-. c) Counter anion is ClO_4^-. d) 2-Aminoethanol. e) Diethylamine. f) In the presence of CH_2Cl_2 (bi-phase system). g) Yields based on BNA$^+$ were determined on NMR using *p*-nitrotoluene as an internal standard.

BNAH is formed in the reaction of BNA$^+$ and excess of amine in a yield of 18% in acetonitrile and 5% in water, respectively. We re-examined the reaction under similar conditions and obtained the results listed in Table 1. The reduction products were confirmed with an NMR spectrum to be almost consisted of the 1,4-dihydro isomer (more than 90%) with contamination of small amount of the 1,6-dihydro derivative.

Among informations to elucidate the mechanism, the most important one is that which clarifies the

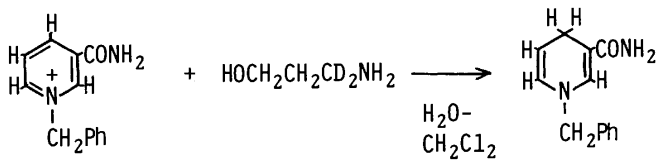

BNA$^+$ (3)

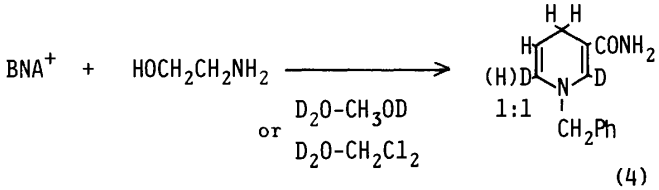

(4)

origin of hydrogen at the 4-position of BNAH produced. First of all, the reactions with 3-amino-1-propanol-3,3-d_2 and 2-aminoethanol in D_2O–CH_3OD (50/50 v/v) were carried out.[7] As shown in Eqs. 3 and 4, both hydrogens at the 4-position of the BNAH were "H", which indicates that the hydrogen comes neither from the substrate nor from the solvent. The latter reaction yields BNAH-2,6-d_2. The contamination of deuteriums in BNAH is due to H–D exchange in BNA$^+$.[8] The H–D exchanges at the 2- and 6-positions of BNA$^+$ was confirmed by the observation of disappearance of NMR signals from the protons at 2- and 6-positions of BNA$^+$ in an alkaline buffer solution. Roberts and his co-workers have claimed, in a recent papaer,[9] partial incorporation of deuterium at the 2-position of BNAH in the reduction by sodium dithionite in D_2O suggesting bimolecular isomerization and reisomerization between BNA$^+$ and BNAH. However, it should be noted that BNAH-2-*d* is formed without isomerization.

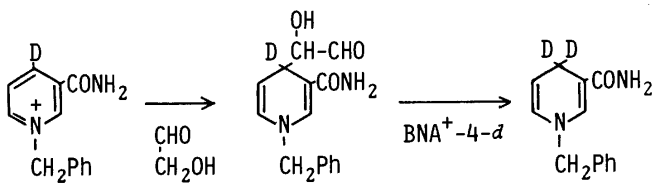

BNA$^+$-4-*d* BNAH-4,4-d_2

(5)

It is well known that nucleophiles attack easily the pyridinium salt to afford adducts that have dihydropyridine structure.[10] Such adducts sometimes have abilities to reduce pyridinium salt. For example, the adduct of BNA$^+$ and glycolaldehyde reduces BNA$^+$ to form BNAH.[3] The mechanism of this reaction was confirmed by the finding that BNAH-4,4-d_2 was formed from BNA$^+$-4-*d* with glycolaldehyde in protic solvents. The reaction with amine may undergo with the same mechanism and we examined the possibility. When BNA$^+$-4-*d* was reacted with 2-aminoethanol in H_2O–CH_3OH the obtained dihydropyridine was an about 1:1 mixture of BNAH-4-*d* and BNAH-4,4-d_2

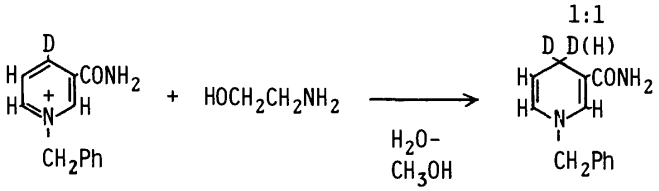

BNA$^+$-4-*d*

(6)

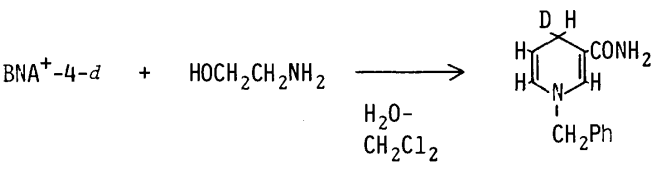

BNAH-4-*d*

(7)

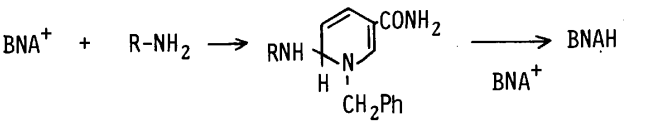

1

(8)

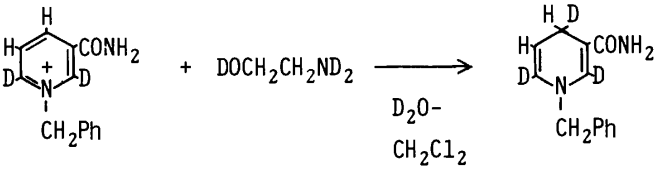

BNA$^+$-2,6-d_2

(9)

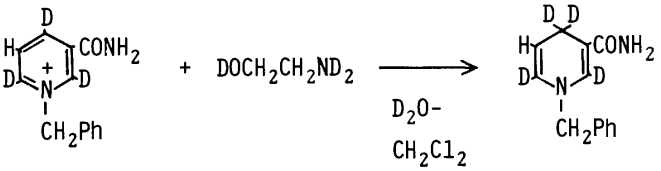

BNA$^+$-2,4,6-d_3

(10)

(Eq. 6). On the other hand, when the reaction was carried out in H_2O in the presence of CH_2Cl_2 (bi-phase reaction), the product obtained from the organic layer was BNAH-4-*d* (Eq. 7). If the reductant were the adduct at the 4-position of BNA$^+$, the product should be BNAH-4,4-d_2. Therefore, the above result is inconsistent with the mechanism for the reduction with glycolaldehyde. Because a large amount of absorption at around 350 nm due to the dihydropyridine structure was observed during the reaction, we assumed that the hydrogen transfered from the 6-position of BNA$^+$ through an adduct (**1**) (Eq. 8). Similar idea has appeared in a literature.[11] In order to ascertain the hypothesis, BNA$^+$-2,6-d_2 and BNA$^+$-2,4,6-d_3 were reacted with $DOCH_2CH_2ND_2$ in D_2O in the presence of CH_2Cl_2 (Eqs. 9 and 10). In both cases, incorporated hydrogens at the 4-position were deuterium. Since it has been confirmed that these hydrogens do not come from the solvent, the result clearly indicates that the origin of the hydrogen at the 4-position of BNAH is the 2- or 6-position of BNA$^+$. Whereas the hydrogen at the 2-position of BNA$^+$ can easily be exchanged by deuterium in D_2O under the basic conditions, the exchange at the 6-position is rather slow.[8] On the basis of the result from the reaction in D_2O (Eq. 4) that no deuterium incorporation took place within the limitation of NMR spectroscopy, the possibility of the transfer from the 2-position is excluded or is estimated to be a very minor path, if any. That is, only from the 6-position, the hydrogen-transfer is expected.

In spite that the hydrogen at the 6-position of BNA$^+$ exchanges with a proton from solvent, no deuterium incorporation onto the 4-position was observed in the reaction shown in Eq. 4. This result stems from the fact that the proton exchange and the reaction of **1** with BNA$^+$ proceeds comparably in rate so that the

amount of **1**-6-*d* is not so large. Even though the **1**-6-*d* is produced in certain amount, kinetic isotope effect[11] prefers the "H"-transfer from **1** than "D"-transfer from **1**-6-*d*.

In the reaction described in Eq. 6, the product was a mixture of BNAH-4-*d* and BNAH-4,4-d_2. The result is accounted for by transhydrogenation between initially produced BNAH-4-*d* and BNA^+-4-*d*. The isotope effect of 6[12] suggests that hydrogen dissociates six times as selectively as deuterium does from the 4-positions of BNAH-4-*d* and BNAH-4,4-d_2 accumulating BNAH-4,4-d_2 after repetition of bimolecular isomerization. The easiness of transhydrogenation was ascertained by an experiment; when BNAH-4-*d* was reacted with about tenfold excess of BNA^+-4-*d* for 16 h, the recovered dihydropyridine was found to be solely composed of BNAH-4,4-d_2.

Therefore, it is concluded that the adduct of amine at the 6-position of BNA^+ (**1**) reduces another molecule of BNA^+ to afford BNAH as shown in Eq. 8. The conclusion shows an interesting contrast between the reactions of α-ketols and those of amines. The result also discards the possibility of direct hydrogen-transfer from amines.

Adduct formation from pyridinium salts with many kinds of nucleophiles such as cyanide,[13] thiols,[14] and enolates[15] have been reported.[10] The attack by these nucleophiles is generally thought to occur at the 4-position.[10,16] In contrast, the additions by amine and hydroxide ion[17] take place at the 6-position. Similar reaction centers[18] are, thus, selectively discriminated by nucleophiles depending on their own property. The selectivity can be interpreted in terms of the hard-soft-acid-base (HSAB) principle.[19] Because of adjcent cationic center, the 6-position is harder center than the 4-position for the nucleophilic attack.

In the present system the product had mainly (more than 90%) 1,4-dihydro structure. It is reported[20] that a small amount of pyridinium salt catalyzes the equilibrium between 1,4- and 1,6-isomers with large predominance of the 1,4-isomer. Therefore, it is reasonable that the reaction in an aqueous medium produces an equilibrium mixture containing a large excess of the 1,4-isomer. However, even when the reaction proceeded in a bi-phase system, where the dihydropyridine produced was extracted immediately into organic phase, the predominant product was the 1,4-isomer (more than 97%). Moreover, in the reaction of BNA^+-4-*d* in the bi-phase system, in which there takes place no equilibration between BNA^+ and BNAH, the extracted dihydropyridine was BNAH-4-*d* with 1,4-selectivity. These results indicate that the selectivity for the 1,4-isomer is not due to thermodynamic control but to the kinetic preference of transhydrogenation from **1** to the 4-position of BNA^+. Thus, based on the HSAB principle discussed above, the transferring "hydride" might be a soft species.

Most substrates that reduce NAD^+ in enzymic systems are nucleophiles. As mentioned above, such nucleophiles attack the pyridinium ion to form covalently bound adducts in organic reaction systems. The formation of these adducts seems to be one of the major reasons for the difficulty to achieve the biomimetic reduction of pyridinium ion by a direct hydrogen-transfer from organic substrates.

Although the formation of 1,4-dihydropyridine derivative was observed in the reactions of α-ketols and amines, it has been elucidated that the mechanism is different from that proposed for enzymic reactions. Only one example for direct hydrogen-transfer from a substrate to NAD^+-models was observed in the reduction with formate. Gizzi and Joullie reported a direct deuterium-transfer to 1-(*p*-fluorobenzyl)-3-carbamoylquinolinium chloride in the reduction with DCOOH.[21] We also confirmed the deuterium-transfer in the reduction of BNA^+ with DCOOK[22] under the conditions reported by Ohnishi and Tanimoto.[23]

In the active site of enzymes, the formation of covalently bound adduct between NAD^+ and a substrate is prohibited because of proper orientation of two reactants. Even though the adduct is formed, it cannot be a reductant for another molecule of NAD^+ because of the interference of the enzyme wall. Therefore, in the model system for the reduction of pyridinium salt, the reactants should be designed to suppress the adduct formation as well as the transhydrogenation from the adduct. Facile reductions coupled with oxidation of alcohols or amines have been performed in the case of pyrido[2,3-*d*:6,5-*d'*]dipyrimidine,[24] hydroxyacridinium salt,[25] and deazaflavines.[26] The reason for the facility is thought to be based on the ring structure that have an ability to accept a "hydride" compared to the attack by a nucleophile. In fact, in a certain case,[27] the desired reaction is suppressed by adduct formation, which shows the importance of proper design for model molecules. Unfortunately, these compounds are not direct models for NAD^+ where pyridinium ion participates. Further investigations for the simulation of reduction of NAD^+ by the use of pyridinium salts are desired.

Experimental

Instruments. UV and NMR spectra were obtained on a Union Giken SM-401 and a JEOL JNMFX-100, respectively.

Materials. 3-Amino-1-propanol-3,3-d_2 was prepared from 3-hydroxypropionitrile by the reduction with lithium aluminum deuteride in tetrahydrofuran. ^1H NMR ($CDCl_3$; δ from TMS): 1.70 (t, 2H), 2.70 (bs, 3H), and 3.77 (t, 2H).

BNA^+-4-*d* was prepared from BNA^+ by repetition of reduction by sodium dithionite in D_2O and oxidation by Malachite Green[28] for three times. Deuterium content at the 4-position was more than 97%. BNA^+-2,6-d_2 and BNA^+-2,4,6-d_3 were prepared as follows: The solution of 100 mg of BNA^+ (or BNA^+-4-*d*) and 100 mg of anhydrous sodium tetraborate in 1 cm^3 of D_2O was placed at 60 °C until the NMR signals from the protons at the 2- and 6-positions disappeared. It took about an hour for the disappearance of the proton at the 2-position and about several hours for the one at the 6-position. Water was removed by evaporation and obtained solid was washed with dichloromethane for three times. BNA^+-2,6-d_2 (or BNA^+-2,4,6-d_2) was extracted with methanol from the solid and used without further purification.

Reaction of BNA^+ and Amine. A Typical Procedure: To the solution of BNA^+ (41.5 mg) in a 1:1 (v/v) mixture of H_2O–CH_3OH (0.75 cm^3) 87×10^{-6} cm^3 of 2-

aminoethanol was added. Methanol was added to keep the solution homogeneous. The solution was stirred for 20 h at room temperature in the dark. Reduced products were extracted by 10 cm^3 of ether for three times and collected by removing the solvent. The NMR signals from the product were identical with those from the authentic sample of BNAH. The yield of BNAH was measured on an NMR spectrometer using *p*-nitrotoluene as an internal standard. NMR signals from the products obtained under various conditions are listed in Table 2. Oxidized **1** or decomposed products from BNA$^+$ could not be isolated because of complication.

Table 2. Type of coupling and amount of protons attached to the dihydropyridine ring in ^{1}H NMR spectra of the products

No. of Eq.	Position of the proton[a)]			
	4- (3.16)	5- (4.75)	6- (5.75)	2- (7.16)
3	m (2H)	dt (1H)	d (1H)	s (1H)
4	dd (2H)	m (1H)	m (0.5H)	—
7	d (1H)	dd (1H)	d (1H)	s (1H)
9	d (1H)	d (1H)	—	—
10	—	s (1H)	—	—

a) Chemical shifts (δ from TMS in $CDCl_3$) of each position are represented in parentheses. Each product shows other signals at δ=4.25 (s, 2H), 5.3—5.6 (bs, 2H), and 7.28 (s, 5H). dd: double doublet, dt: double triplet.

For the reaction in bi-phase system, dichloromethane as a solvent for extraction was added to an aqueous solution of BNA$^+$ and the amine.

References

1) Y. Ohnishi and M. Kitami, *Tetrahedron Lett.*, **1978**, 4035.

2) A. Ohno, S. Ushida, and S. Oka, *Tetrahedron Lett.*, **23**, 2487 (1982).

3) A. Ohno, S. Ushida, and S. Oka, *Bull. Chem. Soc. Jpn.*, **56**, 1822 (1983).

4) Y. Ohnishi, *Tetrahedron Lett.*, **1977**, 2109.

5) E. L. Smith, B. A. Austen, K. M. Blumenthal, and J. F. Nyc, "The Enzymes," 3rd ed, ed by P. D. Boyer, Academic Press, London (1975), Vol. 11, pp. 293—367.

6) J. E. Rife and W. W. Cleland, *Biochemistry*, **19**, 2328 (1980).

7) The reaction in bi-phase system in the presence of dichloromethane gave the same result.

8) B. Nowak-Wydra and M. Szafran, *J. Org. Chem.*, **48**, 2327 (1983). The H-D exchange proceeds much faster than the reduction to BNAH.

9) R. M. G. Roberts, D. Ostović, and M. M. Kreevoy, *J. Org. Chem.*, **48**, 2053 (1983).

10) T. C. Bruice and S. J. Benkovic, in "Bioorganic Mechanism," W. A. Benjamin, New York, N. Y. (1966), Vol. 2, pp. 301—349.

11) K. Kano and T. Matsuo, *Tetrahedron Lett.*, **1975**, 1389.

12) P. van Eikeren and G. L. Grier, *J. Am. Chem. Soc.*, **99**, 8057 (1977).

13) S. P. Colowick, N. O. Kaplan, and M. M. Ciotti, *J. Biol. Chem.*, **191**, 447 (1951).

14) J. van Eys and N. O. Kaplan, *J. Biol. Chem.*, **228**, 305 (1957); O. Piepers and R. M. Kellogg, *J. Chem. Soc., Chem. Commun.*, **1980**, 1147.

15) W. von E. Doering and W. E. McEwen, *J. Am. Chem. Soc.*, **73**, 2104 (1951).

16) S. L. Johnson and K. W. Smith, *J. Org. Chem.*, **42**, 2580 (1979).

17) F. M. Moracci, A. Casini, F. Liberatore, and V. Carelli, *Tetrahedron Lett.*, **1976**, 3723; K. Wallenfels and W. Hanstein, *Angew. Chem., Int. Ed. Engl.*, **4**, 869 (1965).

18) Molecular orbital calculations on the charge densities at the 4- and 6-positions predicted that they are almost equivalnt. *Cf.* B. Pullman and A. Pullman, *Proc. Natl. Acad. Sci.*, **45**, *136 (1959)*; F. Yoneda, K. Mori, S. Matsuo, Y. Kadokawa, and Y. Sakuma, *J. Chem. Soc., Perkin Trans. 1*, **1981**, 1836.

19) T. Ho, in "Hard and Soft Acids and Bases Principle in Organic Chemistry," Academic Press, London (1977), pp. 78—80.

20) T. J. van Bergen, T. Mulder, and R. M. Kellogg, *J. Am. Chem. Soc.*, **98**, 1960 (1976); H. Minato, T. Ito, and M. Kobayasi, *Chem. Lett.*, **1977**, 13.

21) L. R. Gizzi and M. M. Joullie, *Tetrahedron Lett.*, **1969**, 3117.

22) Unpublished result from our laboratory (1983).

23) Y. Ohnishi and S. Tanimoto, *Tetrahedron Lett.*, **1977**, 1909.

24) F. Yoneda, H. Yamato, and M. Ono, *J. Am. Chem. Soc.*, **103**, 5943 (1981).

25) S. Shinkai, H. Hamada, H. Kuroda, and O. Manabe, *Chem. Lett.*, **1980**, 1235.

26) F. Yoneda, Y. Sakuma, and P. Hemmerich, *J. Chem. Soc., Chem. Commun.*, **1977**, 825; F. Yoneda, Y. Sakuma, Y. Kadokawa, and A. Koshiro, *Chem. Lett.*, **1979**, 1467.

27) F. Yoneda and K. Nakagawa, *J. Chem. Soc., Chem. Commun.*, **1980**, 878; T. Nagamatsu, Y. Hashiguchi, Y. Sakuma, and F. Yoneda, *Chem. Lett.*, **1982**, 1309.

28) D. Mauzerall and F. H. Westheimer, *J. Org. Chem.*, **36**, 3553 (1971).

The Carbon-13 NMR Spectra and Electronic Structure of 3*H*-Phenothiazin-3-one and Its Methyl Derivatives

Kan-ichi HASEGAWA* and Yoshio UENO†

Department of Natural Science, Nagoya University of Arts, Shikatsu-cho, Nishikasugai-gun 481

†*Department of Industrial Chemistry, Nagoya Institute of Technology, Gokiso-cho, Showa-ku, Nagoya 466*

(Received August 19, 1983)

The ^{13}C NMR chemical shifts of 3*H*-phenothiazin-3-one (**1**) and eleven of its methyl derivatives are reported. The effect of including sulfur 3d orbitals is discussed in relation to the ^{13}C chemical shifts. The chemical shifts of **1** can be explained in terms of both the successive polarization of the long π-conjugated framework promoted by the carbonyl group and the contribution of the sulfur d-orbitals. The ^{13}C chemical shifts gave a better correlation with the CNDO/2 π- and total electron densities calculated by means of the *sp*-basis set than by means of the *spd*-basis set, but an improved correlation was obtained by reducing the extent of d-orbital participation on sulfur. From the correlation of the ^{13}C chemical shifts with the CNDO/2 *sp* π- and the total electron densities of all the carbons of **1** and monomethyl derivatives, the proportionality constants of −300 and −180 ppm/e respectively were obtained.

There have been extensive studies of phenothiazines in connection with medical chemistry, with particular reference to the correlation of the psychopharmacological activities with the molecular structures such as the electronic and steric properties of substituents and the conformational change in the parent molecule.[1] It is well known that phenothiazines can be used as neuroleptics and that they depress the vital function of the dopamine receptor in the central nervous system.[2] Although phenothiazine itself is not an effective neuroleptic, its pharmacological activity is increased by the introduction of both electron-withdrawing group such as Cl or CF_3 at the 2-position and the *N*-side chain such as *N*-[3-(dimethylamino)propyl], *N*-[3-(4-methyl-1-piperazinyl)propyl], or *N*-[3-[4-(2-hydroxyethyl)-1-piperazinyl]propyl] group (for example, trifluoperazine, chlorpromazine, fluphenazine, and perphenazine).[1a,c]

From X-ray analysis[3–9] and the determination of the dipole moment and the molar Kerr constant,[10] phenothiazines are known to have a folded structure about the N–S axis and a quasi-equatorial substituent on the nitrogen. The dihedral angles between the two planes of the benzenoid rings of phenothiazines in a solid vary from 134.4° for thioridazine to 158.5° for orthorhombic phenothiazine.[3] In a solution, however, *N*- and ring inversions take place with butterflylike flapping motion, and the population of the *N*-quasi-axial substituent seems to increase with an increase in the bulkiness of the *N*-substituent.[11]

Although phenothiazin-3-ones have been used as enzyme inhibitors, anthelmintics, stabilizers, antioxidants, dyestuffs, and indicators,[12–22] their relative difficulty of preparation has limited the number of compounds examined. 3*H*-Phenothiazin-3-one (**1**) inhibits the activities of succinoxidase, cytochrome oxidase, and glyoxalase as well as phenothiazine.[13] On the other hand, 3*H*-phenoxazin-3-one is well known to be the chromophore part of actinomycin D, which binds to double-helical DNA and specifically inhibits RNA synthesis.[23]

Whereas many papers have been devoted to the study of the electronic and conformational properties of phenothiazines by means of the ^{13}C NMR[11] and ^{1}H NMR[24–28] chemical shifts, the dipole moments,[10] the molar Kerr constants,[10] the EPR and polarographic oxidation potentials,[29] X-ray crystal analyses,[3–9] and molecular orbital calculations,[11,29] there have been few corresponding data on **1** and its derivatives.

This paper will deal with the ^{13}C NMR spectra of **1** and eleven of its methyl derivatives in order to elucidate how the presence of *p*-benzoquinone monoimine type and the methyl group influences the electronic properties of phenothiazines. The ^{13}C chemical shifts of 3*H*-phenothiazin-3-ones give an index of the electronic densities of their carbons for the ground state and would seem to be useful for any future discussion of their pharmacological properties and reactivities.

Experimental

Materials. **1** was synthesized by the cyclization of *o*-aminothiophenol with *p*-benzoquinone according to the method of Bodea and Raileanu;[30] mp 162—163 °C (lit, 161—162 °C). The monomethyl-3*H*-phenothiazin-3-ones were prepared by the method of Terdic:[31] 1-methyl-(**2**), mp 146—148 °C (lit, 145—147 °C); 2-methyl- (**3**), mp 182—183 °C (lit, 181—183 °C); 4-methyl- (**4**), mp 142—143 °C (lit, 141—143 °C); 6-methyl- (**5**), mp 192—193 °C (lit, 190—192 °C); 7-methyl- (**6**), mp 210—211 °C (lit, 208 °C); 8-methyl- (**7**), mp 181—182 °C (lit, 180—182 °C); 9-methyl- (**8**), mp 179—180 °C (lit, 171—173 °C). Dimethyl- and trimethyl-3*H*-phenothiazin-3-ones were synthesized from *o*-aminothiophenol and the corresponding methyl derivatives of *p*-benzoquinone; 1,2-dimethyl- (**9**), mp 191—192 °C; 1,4-dimethyl- (**10**), mp 146—148 °C; 2,4-dimethyl- (**11**), mp 164—165 °C; 1,2,4-trimethyl- (**12**), mp 160—161 °C. Found for **10**: C, 69.33; H, 4.54; N, 5.97%. Calcd for $C_{14}H_{11}NOS$: C, 69.68; H, 4.59; N, 5.80%. Found for **11**: C, 69.50; H, 4.32; N, 5.65%. Found for **12**: C, 70.43; H, 5.08; N, 5.42%. Calcd for $C_{15}H_{13}NOS$: C, 70.56; H, 5.13; N, 5.49%. All the compounds were purified by TLC and column chromatography and checked by means of their IR and ^{1}H NMR spectra. The *N*-chloro-*p*-benzoquinone monoimine was commercially obtained (guaranteed reagent) and used without further purification.

Procedures. The ^{13}C NMR spectra were recorded on a JEOL FX-100 Fourier-transform spectrometer at room temperature at 25.00 MHz, using a deuterium lock. Samples were prepared in the 9:1 $CDCl_3$–CD_3OD solvent system, with tetramethylsilane as an internal reference, in 5-mm spinning tubes because these compounds were not soluble enough in $CDCl_3$. The melting points were determined on a

Yanagimoto micromelting apparatus and are uncorrected.

Theoretical

The quantum chemical calculations were carried out by the CNDO/2 method[32] and using parametrizations without further modification. The convergence was judged from the electron-density criterion of 10^{-4} in the density matrix. The CNDO/2 program suppled by QCPE[33] Program No. 141 was modified to accommodate atomic orbital matrices greater than seventy. The dihedral angles associated with the inner thiazine ring of **1** in the butterfly structure were calculated by using QCPE[33] Program No. 397. Computations were carried out on a HITAC M-200H computer at the Computer Center of the Institute for Molecular Science.

For Runs 2, 4—13, and 19 in the CNDO calculations of **1** shown in Table 3, the X-ray data for the bond lengths and bond angles of the benzenoid ring and the *p*-benzoquinone imine portion of the actinomycin D obtained from light-atom analysis were used to those for the corresponding bond lengths and bond angles of **1**, except that the bond length of C-6—C-7 was 1.41 Å; for the other runs, their bond angles were assumed to be 120°. For the hydrogen bonding of the carbonyl group of **1** with methanol, the atomic distance between the carbonyl oxygen and the alcoholic hydrogen was presumed to be 1.61 Å, and the hydroxyl group was arranged on the extension line of the carbonyl bond. The geometry of **1** has been transferred to the monomethyl derivatives. The atomic coordinates of the methyl group and methanol were determined from the following bond distances and bond angles: C–C (methyl), 1.51 Å; C–O, 1.43 Å; olefinic (or aromatic) C–H, 1.08 Å; methyl C–H, 1.09 Å; O–H, 1.02 Å; ∠COH, 110°; ∠OCH=∠CCH=109.5°. The bond lengths and angles of planar *N*-chloro-*p*-benzoquinone monoimine were: C=O, 1.23 Å; C=N, 1.33 Å; C=C, 1.32 Å; C–C, 1.49 Å, N–Cl, 1.75 Å; C–H, 1.08 Å; ∠C–C–C, 116°; ∠C=C–C, 122°; ∠C=N–Cl= ∠C=C–H =120°.

Results and Discussion

^{13}C Chemical Shifts of 3H-Phenothiazin-3-one. A reasonably self-consistent set of assignments for the chemical shifts of the 3*H*-phenothiazin-3-ones and the substituent-induced chemical shifts (SCS) of the methyl group are summarized in Tables 1 and 2 respectively. The carbon resonances of **1** can be assigned not directly, but on the basis of the off-resonance decoupling technique and the methyl-substituent effects on benzenes[34] and olefins.[35]

The signal for the carbonyl nuclei in **1** appeared at 183 ppm; it is shifted to a magnetic field higher by 4 ppm relative to those (187.0 and 186.5 ppm, respectively) in *p*-benzoquinone[36] and *N*-chloro-*p*-benzoquinone monoimine.[37] The chemical shifts of carbonyl carbons increase in the order of: **1**

Table 1. ^{13}C NMR chemical shifts of 3*H*-phenothiazin-3-one and its methyl derivatives

Substituent	Chemical shift, δ												
	C-1	C-2	C-3	C-4	C-4a	C-5a	C-6	C-7	C-8	C-9	C-9a	C-10a	Me
Nil (**1**)	139.9	134.9	182.6	119.6	135.8	123.8	125.1	131.3	128.2	134.0	139.1	146.1	
1-Me[a] (**2**)	[147.9][b]	132.9	182.5	118.9	135.7	123.9	124.7	131.0	127.8	134.1	138.5	145.8	18.4
2-Me (**3**)	136.5	[144.2]	182.8	119.5	134.9	123.4	125.0	130.6	127.9	133.7	139.2	146.4	16.5
4-Me (**4**)	139.8	134.3	181.7	[127.4]	131.3	124.6	125.4	130.8	128.1	133.7	138.8	146.7	16.5
6-Me (**5**)	139.9	135.0	182.9	119.8	136.1	123.3	[133.7]	132.2	127.5	132.7	139.3	145.6	18.7
7-Me (**6**)	140.1	134.6	182.8	119.3	136.0	124.0	125.1	[143.0]	129.7	133.9	137.4	145.1	21.8
8-Me (**7**)	139.9	134.8	182.5	119.2	136.0	120.7	124.7	132.7	[138.6]	134.0	139.0	145.9	20.9
9-Me (**8**)	140.2	134.4	182.6	118.8	135.9	123.8	122.7	131.0	129.5	[142.8]	137.4	144.4	18.1
1,2-Me$_2$ (**9**)	[142.9]	[140.1]	182.2	118.6	134.9	123.5	124.7	130.4	127.6	134.0	138.8	145.9	14.3(1-Me), 13.0(2-Me)
1,4-Me$_2$ (**10**)	[147.4]	132.2	181.3	[126.2]	130.9	124.4	124.8	130.4	127.6	133.7	137.9	146.1	18.2(1-Me), 11.9(4-Me)
2,4-Me$_2$ (**11**)	136.3	[143.2]	181.7	[127.0]	130.5	124.1	125.3	130.2	127.8	133.2	138.8	146.4	16.8(2-Me), 12.6(4-Me)
1,2,4-Me$_3$ (**12**)	[145.8]	[139.1]	181.1	[125.8]	130.1	124.2	124.8	129.8	128.4	133.5	138.5	142.5	14.2(1-Me), 13.3(2-Me), 12.5(4-Me)

a) Methyl group. b) Square brackets denote positions of methyl substituents.

Table 2. Effect of methyl substitution of 3*H*-phenothiazin-3-one

Substituent	Methyl substituent-induced chemical shift[a]/ppm											
	C-1	C-2	C-3	C-4	C-4a	C-5a	C-6	C-7	C-8	C-9	C-9a	C-10a
1-Me[b] (**2**)	[8.0][c]	−2.0	−0.1	−0.7	−0.1	0.1	−0.4	−0.3	−0.4	0.1	−0.6	−0.3
2-Me (**3**)	−3.4	[9.3]	0.2	−0.1	−0.9	−0.4	−0.1	−0.7	−0.3	−0.3	0.1	0.3
4-Me (**4**)	−0.1	−0.6	−0.9	[7.8]	−4.5	0.8	0.3	−0.5	−0.1	−0.3	−0.3	0.6
6-Me (**5**)	0.0	0.1	0.3	0.2	0.3	−0.5	[8.6]	0.9	−0.7	−1.3	0.2	−0.5
7-Me (**6**)	0.2	−0.3	0.2	−0.3	0.2	0.2	0.0	[11.7]	1.5	−0.1	−1.7	−1.0
8-Me (**7**)	0.0	−0.1	−0.1	−0.4	0.2	−3.1	−0.4	1.4	[10.4]	0.0	−0.1	−0.2
9-Me (**8**)	0.3	−0.5	0.0	−0.8	0.1	0.0	−2.4	−0.3	1.3	[8.8]	−1.7	−1.7
1,2-Me$_2$ (**9**)	[3.0]	[5.2]	−0.4	−1.0	−0.9	−0.3	−0.4	−0.9	−0.6	0.0	−0.3	−0.2
1,4-Me$_2$ (**10**)	[7.5]	−2.7	−1.3	[6.6]	−4.9	0.6	−0.3	−0.9	−0.6	−0.3	−1.2	0.0
2,4-Me$_2$ (**11**)	−3.6	[8.3]	−0.9	[7.4]	−5.3	0.3	0.2	−1.1	−0.4	−0.8	−0.3	0.3
1,2,4-Me$_3$ (**12**)	[3.6]	[4.2]	−1.5	[6.2]	−5.7	0.4	−0.3	−1.5	−0.8	−0.5	−0.6	−0.3

a) Relative to parent. b) Methyl group. c) Substituted carbons indicated by square brackets.

(182.6)<1,4-naphthoquinone (184.7)[38]<*p*-benzoquinone (187.0)[36] <cyclohexenone (198.9)[39]<cyclohexanone (208.8).[40] This order suggests that the upfield shift is closely associated with the delocalization of the partial possitive charge of the carbonyl carbon so long as the steric perturbation is negligible.

The chemical shifts of C-1 and C-2 in **1** move 3—4 ppm to a lower field than those of the corresponding carbons of *N*-chloro-*p*-benzoquinone monoimine. In the *p*-benzoquinone imine framework of **1**, the fact that the signal for the C-4a is more shielded than that for the C-1, in spite of the replacement of sulfur atom more electronegative than hydrogen, may be explained in terms of the normal character of phenyl vinyl sulfides and/or the contribution of the d-orbitals of the sulfur atom. The chemical shifts of the C-4 and C-4a in **1** moved downfield by 4—5 ppm in comparison with those of the corresponding vinyl group of phenyl vinyl sulfide.[41] This deshielding effect may be due to the change in the vinyl group to the olefinic double bond of a cyclic compound because the difference in chemical shifts between ethylene and the olefinic carbons of cyclohexene[42] was observed to be 5 ppm. As will be shown below, the CNDO/2 calculation of **1** suggests that the participation of sulfur d-orbitals results in the enhancement and lowering of the total electron densities of the odd-numbered carbons except for the C-9a and the even-numbered carbons except for the C-4a respectively; especially, the increased total electron densities of C-4a and C-5a adjacent to the sulfur atom are mainly based on the remarkably increased $2p_x$ orbital densities of their carbons.

The biggest differences between the benzenoid carbon shieldings of **1** and phenothiazine are the chemical shifts of C-7 and C-9. The C-7 and C-9 nuclei in the former are more deshielded than those for the corresponding carbon nuclei in the latter by 10 and 20 ppm respectively. As the C-7 and C-9 carbons are meta-carbons relative to the sulfur atom, their chemical shifts are strongly affected not by the sulfur atom, but the polar and electron-withdrawing characteristics of the imino group, promoted by the powerful polarizing carbonyl group, even if the internal olefinic double bond attenuates the transmission effect. The deshielding of C-7 and C-9 reflects the relative importance of the polar canonical forms, 1C and 1D, which have the partial positive charge on the 7 and 9 positions of the aromatic ring attributable to the electron-withdrawing carbonyl group. As a result, the signals for the C-7 and C-9 shifted to a lower field because of their positions para and ortho respectively relative to the imino group.

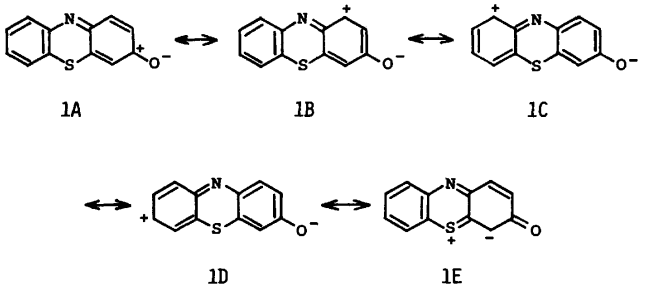

1A 1B 1C

1D 1E

The nitrogen atom of phenothiazine forms the apex of a flattened pyramid, with the two ipso carbons of the benzenoid moiety and hydrogen as the base. According to the classical resonance theory, a hybrid orbital containing the lone-pair electrons of the nitrogen atom has a perpendicular orientation on the base plane of the pyramid; this orientation is convenient for overlapping the $2p_\pi$ orbitals of the aromatic ring because their orbitals are relatively parallel. Therefore, a part of the lone-pair electrons flows the ortho- and para-carbons of the benzenoid ring through the π-conjugation. In the case of **1**, however, the sp^2 hybrid orbital of the lone-pair electrons is almost perpendicular to the $2p_\pi$ orbitals of the benzenoid ring. Therefore, the delocalization of lone-pair electrons is very poor. The electron-attracting nature of the imino group is facilitated by a fair overlapping between the $2p_\pi$ orbitals of nitrogen and benzenoid carbons, since the C–N bond length of the 3*H*-phenoxazin-3-one skeleton of actinomycin D has been found to be 1.36 Å; this value is smaller than that (1.399 Å) of phenothiazine.[3] The relatively high shielding of C-5a, the bridgehead quaternary carbon linking to the sulfur atom, may be due to the d-orbital contribution of the sulfur atom.

Methyl-subsituent Effect. The methyl substitution on the aromatic ring caused a shift of the ipso carbon downfield by 9—12 ppm and a shift of the para benzenoid carbon upfield by 1—3 ppm. The ortho carbon farther from the thiazine ring shifted downfield by 0.9—1.5 ppm, and another ortho carbon, upfield by 0.0—1.7 ppm. The introduction of the methyl group resulted in an upfield shift of the meta carbon, making it remoter from the thiazine ring, by 0.1—0.7 ppm, but the nearer meta carbon was only slightly affected in the range of −0.1—0.2 ppm. The upfield shift of para carbon induced by methyl substitution was enhanced as the para position approached the sulfur atom.

When a methyl group is introduced on any of the aromatic moiety except for the C-6, the signals for the 2, 4, and 10a carbons, *i.e.*, the even-numbered carbons, in the quinone imine ring shift to a field higher by 0.1—1.7 ppm, while the shielding of the other carbons, *i.e.*, the odd-numbered carbons and the C-4a, in the quinonoid ring is either unaffected or moved only slightly downfield; the substituent effect is transmitted mainly through its π-conjugated framework by means of alternation.

The replacement of the hydrogen of quinone imine by a methyl group caused a deshielding of α-carbon by 8—9 ppm and a shielding of olefinic β-carbon by 2—4.5 ppm, but the chemical shift of β-carbonyl carbon was almost unaffected. The carbonyl carbons of **1** and eleven of its methyl derivatives absorb over a fairly narrow range, *ca.* 2 ppm, or from δ_C=181 to 183. This remarkable insensitivity of carbonyl carbons to substituents has also been observed in methyl-*p*-benzoquinones[36] and 3-substituted and 2-cyclohexenones.[39] The magnitude of the β-effect of methyl group bonded to the 4-position carbon was larger than that of the other monomethyl-3*H*-phenothiazin-3-ones. The magnitude for the β-effect of the 2-methyl group is similar to that of 2-methyl-*p*-benzoquinone.[36]

The chemical shift of methyl carbon increased in the following sequence: 4-methyl=2-methyl< 9-methyl<1-methyl<6-methyl<8-methyl<7-methyl. This order suggests that the shielding of methyl carbon increases when the methyl carbon is spatially near to the more electronegative heteroatom. The electrostatic interaction between the heteroatom and the nearest hydrogen of the methyl group enhances the polarization of the methyl $C^{\delta-}$–$H^{\delta+}$ bond and the resulting higher shielding of methyl carbon. As the methyl group can be treated as a pseudo-π-electron system, the polarization of the C–H bond of the methyl group affects the chemical shifts of α- or ipso carbon as an inductive effect through the σ-bond and those of β- or ortho and para carbons as a resonance effect through the π-bond. The magnitudes of the C_α- and C_{ipso}-SCS of the methyl group decrease with an increase in the shielding of the methyl carbon, except for the methyl C_α-SCS greater than that expected at the C-2; this trend suggests that the α-effect of the methyl group is attenuated by the dispersion of the partially negative charge on the methyl carbon through the C–C σ bond. The deviation of the methyl C_α-SCS on the C-2 may be due to the more important contribution of the π-electron delocalization.

The chemical shifts of dimethyl- and trimethyl-3*H*-phenothiazin-3-ones agreed roughly with the values estimated from the data of monomethyl derivatives by using the additivity relationship, except that those of the C-1 and the C-2 in 1,2-dimethyl- and 1,2,4-trimethyl-3*H*-phenothiazin-3-ones appeared at a field higher by 2 ppm than the estimated values. The magnitude of the difference is responsible for the steric compression effects, which have been found in the chemical shifts of spatially crowded carbons, such as *o*-xylene[34,43] and 1,2- and 2,3-dimethylindoles.[44] Similarly, the chemical shift of methyl carbons is upfield in the sterically more compressed form.

TABLE 3. TOTAL ENERGIES AND DIPOLE MOMENTS OF 3*H*-PHENOTHIAZIN-3-ONE IN VARIOUS CONFORMATIONS[a)]

Run	Bond length /Å								Fashion	Total energy/a.u.		Dipole moment/D	
	C–N	C=N	C=O	C-4a–S	C-5a–S	Aromatic	Quinone			*spd*	*sp*	*spd*	*sp*
							C–C	C=C					
1	1.40	1.37	1.24	1.76	1.76	1.39	1.49	1.32	Planar(120°, 125°, 125°, 126°)[b)]	−131.42$_0$	−131.11	3.34	4.10
2	1.36	1.34	1.24	1.76	1.661	1.39—1.43	1.42—1.36		Planar(120°, 124°, 126°, 124°)[c)]	−131.42$_1$	−131.07	3.58	5.26
3	1.36	1.36	1.15	1.71	1.66	1.39	1.40	1.38	Planar(116°, 120°, 120°, 120°)[b)]	−131.33		2.83	
4	1.36	1.34	1.24	1.55	1.563	1.39—1.43	1.42—1.36		Planar(120°, 124°, 126°, 124°)[b)]	−131.34		5.34	
5	1.36	1.34	1.24	1.76	1.76	1.39—1.43	1.42—1.36		Planar except for S(ψ_1=−20.85°)[d)]	−131.41	−131.09$_5$	3.60	4.88
6	1.36	1.34	1.24	1.78	1.76	1.39—1.43	1.42—1.36		Planar except for S(ψ_1=−20.88°)[d)]	−131.41	−131.09$_9$	3.63	4.84
7	1.36	1.34	1.24	1.669	1.76	1.39—1.43	1.42—1.36		Twisted[e)] (ψ_2=5°)[d)]	−131.42$_1$	−131.07	3.57	5.22
8	1.36	1.34	1.24	1.76	1.76	1.39—1.43	1.42—1.36		Twisted[f)] (ψ_2=15°)[d)]	−131.41	−131.09$_5$	3.75	4.78
9	1.36	1.34	1.24	1.74	1.76	1.39—1.43	1.42—1.36		Twisted[f)] (ψ_2=17.8°)[d)]		−131.08$_6$		4.75
10	1.36	1.34	1.24	1.76	1.76	1.39—1.43	1.42—1.36		Twisted[e)] (ψ_2=18.59°)[d)]	−131.41	−131.08	3.41	4.81
11	1.36	1.34	1.24	1.71	1.751	1.39—1.43	1.42—1.36		Twisted[f)] (ψ_2=19°)[d)]	−131.40	−131.06	3.75	4.78
12	1.36	1.34	1.24	1.76	1.766	1.39—1.43	1.42—1.36		Twisted[f)] (ψ_3=155°)[d)]	−131.40	−131.07	3.89	4.41
13	1.36	1.34	1.24	1.76	1.702	1.39—1.43	1.42—1.36		Twisted[f)] (ψ_3=160°)[d)]	−131.41		4.19	
14	1.38	1.34	1.15	1.76	1.76	1.39	1.44	1.34	Butterfly(116°, 52.90°; 120°, −49.85°; 120°, 35.56°; 100°, −19.31°; 120°, 21.84°; 120°, −40.24°)[g)]	−131.31		2.34	
15	1.35	1.35	1.15	1.71	1.71	1.39	1.40	1.38	Butterfly(120°, 25.15°; 120°, −26.69°; 120°, −16.88°; 92°, 47.05°; 120°, −48.71°; 120°, 19.95°)[g)]	−131.32		3.17	
16	1.36	1.36	1.15	1.76	1.76	1.39	1.43	1.34	Butterfly(116°, 56.15°; 120°, −45.63°; 120°, 3.13°; 100°, 23.51°; 120°, −15.13°; 120°, −21.20°)[g)]	−131.33		2.98	
17	1.40	1.38	1.15	1.76	1.76	1.39	1.44	1.34	Butterfly(116°, 56.70°; 120°, −36.24°; 120°, −7.88°; 100°, 29.22°; 120°, −12.23°; 120°, −27.13°)[g)]	−131.34		2.93	
18	1.43	1.34	1.23	1.76	1.76	1.39	1.49	1.32	Butterfly(116°, 50.16°; 120°, −46.66°; 120°, 36.69°; 100°, −23.82°; 120°, 26.78°; 120° −42.52°)[g)]	−131.39		3.22	
19	1.36	1.34	1.24	1.76	1.76	1.39—1.43	1.42—1.36		Butterfly(118°, 30.31°; 123°, −41.02°; 123°, 19.03°; 98°, 8.64°; 123°, −17.60°; 123°, 1.02°)[g)]	Not converged(both *spd* and *sp*)			

a) More detailed information on molecular geometries are described in the Theoretical section. b) Bond angles of N, C-10a, C-4a, and C-9a. c) Bond angles of N, C-10a, C-5a, and C-9a. d) The bond angles of N, C-4a, C-10a, and C-9a, except for C-5a instead of C-4a for Runs 7 and 9, are equal to the corresponding data for Run 4. ψ_1 represents the dihedral angle between the N—C-10a and the C-4a—S bonds; ψ_2, that between the C-9a—N and the C-10a—C-4a bonds, and ψ_3, that between the N—C-10a and the C-9a—C-5a bonds. e) Sulfur coplanar to the benzenoid ring. f) Sulfur coplanar to the quinonoid ring. g) The bond angles and the approximate dihedral angles of atoms varying from N to C-9a in a clockwise direction on the inner thiazine ring. The angles are defined as shown in Fig. 1 of Ref. 50.

CNDO/2 Calculation of 3H-Phenothiazin-3-ones. None of the crystal structures of **1** have been reported in spite of a detailed clarification of the medicinally more important phenothiazine and its derivatives. On the other hand, in the case of 3*H*-phenoxazin-3-one, the molecular geometry can be presumed from that of actinomycin D, about which detailed stereochemical information with the DNA helix served to clarify the cancer-inhibiting mechanism.[23] X-ray crystal analysis showed the quinonoid portion of the 3*H*-phenoxazin-3-one ring system to be slightly twisted in a propeller-like fashion with respect to the aromatic portion of the chromophore.

In general, the C–S bond is longer than the C–O bond, whereas the interior angle of C–S–C is smaller than that of C–O–C.[45] If the inside thiazine ring of **1** is a planar structure in order to enhance the resonance stabilization between the benzene and the quinone rings, the bond lengths and/or bond angles among C, N, and S atoms must, at least in part, lie outside normal ranges.

There are various possible conformations of **1**, for example; (i) a planar structure, (ii) a twisted quinone fashion, and (iii) a butterfly structure such as phenothiazine. Therefore, CNDO/2 calculations of the above possible molecular structures were carried out in order to obtain information on the conformation with the lowest total energy, the correlation of the ^{13}C chemical shifts with CNDO/2 charge densities, and the magnitude of the sulfur-d-orbital contribution.

Table 3 lists the CNDO/2 total energies and dipole moments of various molecular geometries of **1**. In the *spd* approximation, the total electronic energies of **1** for the (i), (ii), and (iii) structures varied from −552.7 to −566.3 a.u., whereas the total energy for those structures changed only slightly between −131.3 and −131.4 a.u. The inclusion of d-orbitals on the sulfur atom in **1** resulted in a lowering of the total energy of 0.3—0.4 a.u. and of the dipole moment of 0.5—1.6 debye in comparison with the case of the exclusion of d-orbitals. The sulfur 3d orbitals reduce the dipole moment by introducing a *pd* polarization in the opposite sense to the *sp* polarization. The *sp* and *spd* calculations for **1** suggest that Runs 1 and 7 have the lowest total energies, −131.1133 and −131.4210 a.u. respectively; generally, (i) and (ii) are more stable than (iii) unless the repulsion of the cores increases abnormally because of the shorter bond length. The molecular geometry for Run 1 is the ideal geometry considered to maintain the planarity of the inner thiazine ring having the C–S bond length of 1.76 Å observed in phenothiazine[3] under the normal geometries of benzene and *p*-benzoquinone[46] frameworks. Run 7 is responsible for the slightly twisted, semiactual but ideal structure between the benzene and the *p*-quinone imine rings, whose bond lengths and angles are referred to the corresponding data of the 3*H*-phenoxazin-3-one geometry of actinomycin D.

Table 4 shows the CNDO/2 π and total electron densities of **1** and its methyl derivatives for the planar and twisted structures. The ^{13}C chemical shifts gave a better correlation with the π- or total ($\sigma+\pi$) electron densities calculated by the *sp*-basis set rather than the *spd*-basis set except for the α-carbons of the sulfur atom. As Table 4 shows, the *spd* approximation underestimated the total density on the C-4 and results

TABLE 4. CNDO/2 π AND TOTAL ELECTRON DENSITIES OF 3*H*-PHENOTHIAZIN-3-ONE AND ITS METHYL DERIVATIVES[a]

Substituent	Fashion	C-1	C-2	C-3	C-4	C-4a	C-5a	C-6	C-7	C-8	C-9	C-9a	C-10a
Nil (**1**)	Planar[b]	3.9874	4.0423	3.7631	4.0748	3.9314	3.9568	4.0053	3.9876	3.9983	4.0055	3.9133	3.9148
		π 0.9702	1.0044	0.8583	1.0574	0.9521	1.0020	1.0138	0.9921	1.0057	1.0012	1.0067	0.9746
Nil (**1**)[c]	Planar	3.9925	4.0379	3.7721	4.0268	3.9853	4.0106	3.9673	4.0021	3.9820	4.0185	3.8779	3.8901
		π 0.9691	1.0019	0.8650	1.0052	0.9529	1.0077	0.9801	1.0090	0.9808	1.0132	0.9722	0.9545
Nil (**1**)[d]	Planar	3.9817	4.0474	3.7476	4.0806	3.9273	3.9553	4.0060	3.9855	3.9985	4.0027	3.9140	3.9221
		π 0.9612	1.0122	0.8351	1.0663	0.9430	0.9999	1.0145	0.9884	1.0059	0.9976	1.0101	0.9858
1-Me (**2**)	Planar	3.9478	4.0663	3.7655	4.0743	3.9336	3.9569	4.0057	3.9875	3.9986	4.0054	3.9132	3.9240
		π 0.9417	1.0431	0.8555	1.0538	0.9557	1.0003	1.0141	0.9917	1.0064	1.0011	1.0074	0.9805
2-Me (**3**)	Planar	4.0151	3.9961	3.7708	4.0772	3.9317	3.9584	4.0051	3.9896	3.9979	4.0071	3.9117	3.9136
		π 1.0131	0.9707	0.8611	1.0605	0.9487	1.0057	1.0132	0.9955	1.0049	1.0039	1.0025	0.9651
4-Me (**4**)	Planar	3.9871	4.0446	3.7705	4.0272	3.9575	3.9591	4.0055	3.9892	3.9983	4.0068	3.9116	3.9142
		π 0.9670	1.0075	0.8615	1.0238	0.9954	1.0031	1.0139	0.9946	1.0057	1.0032	1.0035	0.9677
6-Me (**5**)	Planar	3.9880	4.0419	3.7634	4.0748	3.9356	3.9747	3.9661	4.0062	3.9924	4.0158	3.9080	3.9128
		π 0.9703	1.0039	0.8579	1.0582	0.9500	1.0305	0.9821	1.0186	0.9934	1.0177	0.9952	0.9707
7-Me (**6**)	Planar	3.9865	4.0445	3.7629	4.0767	3.9305	3.9507	4.0242	3.9490	4.0167	3.9988	3.9230	3.9208
		π 0.9688	1.0076	0.8573	1.0600	0.9512	0.9881	1.0406	0.9600	1.0313	0.9876	1.0228	0.9844
8-Me (**7**)	Planar	3.9879	4.0420	3.7633	4.0751	3.9317	3.9652	3.9997	4.0054	3.9605	4.0241	3.9089	3.9135
		0.9704	1.0039	0.8581	1.0581	0.9512	1.0182	1.0018	1.0171	0.9754	1.0281	0.9956	0.9718
9-Me (**8**)	Planar	3.9872	4.0433	3.7632	4.0761	3.9308	3.9506	4.0157	3.9814	4.0169	3.9647	3.9318	3.9172
		0.9697	1.0059	0.8574	1.0593	0.9510	0.9904	1.0304	0.9788	1.0323	0.9687	1.0326	0.9794
Nil (**1**)	Twisted[e]	3.9960	4.0433	3.7565	4.0797	3.9263	3.9669	4.0050	3.9868	3.9932	4.0085	3.9127	3.9018
Nil (**1**)[c]	Twisted	3.9997	4.0391	3.7648	4.0286	3.9849	4.0256	3.9666	4.0015	3.9769	4.0222	3.8771	3.8744
Nil (**1**)[d]	Twisted	3.9882	4.0508	3.7392	4.0876	3.9191	3.9631	4.0062	3.9823	3.9944	4.0038	3.9163	3.9096
1-Me (**2**)	Twisted	3.9546	4.0690	3.7569	4.0789	3.9277	3.9666	4.0052	3.9867	3.9936	4.0088	3.9131	3.9103
2-Me (**3**)	Twisted	4.0251	3.9968	3.7633	4.0833	3.9255	3.9693	4.0044	3.9897	3.9924	4.0113	3.9101	3.8978
4-Me (**4**)	Twisted	3.9948	4.0468	3.7635	4.0301	3.9544	3.9696	4.0051	3.9891	3.9930	4.0109	3.9103	3.8981
6-Me (**5**)	Twisted	3.9964	4.0430	3.7567	4.0802	3.9286	3.9863	3.9629	4.0070	3.9869	4.0189	3.9074	3.9001
7-Me (**6**)	Twisted	3.9944	4.0464	3.7555	4.0823	3.9243	3.9595	4.0248	3.9464	4.0121	4.0011	3.9238	3.9080
8-Me (**7**)	Twisted	3.9965	4.0428	3.7568	4.0798	3.9269	3.9751	3.9999	4.0039	3.9568	4.0277	3.9078	3.9000
9-Me (**8**)	Twisted	3.9946	4.0459	3.7558	4.0822	3.9242	3.9597	4.0164	3.9800	4.0141	3.9636	3.9316	3.9055
Nil (**1**)	Planar except	3.9945	4.0443	3.7570	4.0750	3.9285	3.9596	4.0089	3.9856	3.9956	4.0066	3.9155	3.9019
	for S[f]	π 0.9751	1.0052	0.8678	1.0521	0.9513	0.9893	1.0077	0.9853	1.0086	0.9952	1.0139	0.9888
Nil (**1**)[c]	Planar except	3.9985	4.0397	3.7646	4.0254	3.9905	4.0213	3.9701	4.0004	3.9785	4.0211	3.8816	3.8751
	for S	π 0.9711	1.0033	0.8747	0.9970	0.9454	0.9964	0.9707	1.0041	0.9833	1.0084	0.9771	0.9647

a) Calculated by *sp* approximation. b) Molecular geometry referred to Run 1. c) *Spd* calculation. d) Hydrogen bonding of the carbonyl group to methanol. e) Geometry associated with Run 8. f) Molecular structure in connection with Run 6.

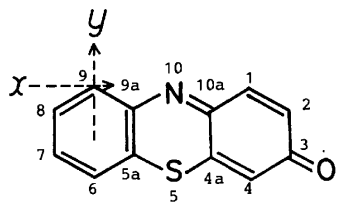

Fig 1. Numbering and coordinate systems for **1**. The *z* axis is perpendicular to this paper.

generally in a lowering of the total electron densities on the β- and δ-carbons numbered from the sulfur atom, and the enhancement of those on the α- and the γ-carbons; the former is mainly attributable to the decreased π-electron density, and the latter, to increases in the σ-electron density and the π-electron density. As has been described above, in the ^{13}C NMR spectrum of **1**, the signal of the C-4 appeared in the highest magnetic field; this trend is in agreement with the theoretical data calculated by means of the *sp* approximation; in the *spd* calculation, the most electron-rich carbon is not the C-4, but the C-2.

The values of the correlation coefficient, *r*, between the ^{13}C chemical shifts of all the carbons in **1** and their total electron densities, calculated in Runs 1, 5, 6, 8, and 10 by means of *sp*- and *spd*-basis sets, are 0.88 and 0.85—0.86 respectively. If it is reasonable that the linear relationship holds between the electron densities calculated by means of the *sp*- and *spd*-basis sets, the value of *r* is enhanced up to 0.89 by evaluating the degree of sulfur-d-orbital participation as 28—36%. From the linear correlation of the ^{13}C chemical shifts with the π-electron densities of the over-all carbons of interest, the best value of *r* is 0.94 for Run 1 when the *spd* contributions are somewhere between 43 and 44%, and a proportionality constant of -350.8 ± 39.6 ppm/e was obtained for the π-electron system composed of *sp* 56% and *spd* 44%.

In the *sp* calculation of **1** in a twisted form, it is the most stable structure that the quinonoid portion is twisted at a torsional angle of 15° with respect to the aromatic ring, where the X-ray-diffraction data of actinomycin D were adopted for the bond lengths and bond angles of these rings. In this case, the value of *r* for their total electron densities is equal to 0.884, enhanced to 0.887 when the carbonyl group is weakly bonded to the solvent by means of hydrogen bonding.

From the linear relationship between the ^{13}C chemical shifts of all the carbons of **1** and its monomethyl derivatives, except for methyl carbons and their CNDO/2 *sp* electron densities in the case of a planar structure carried out in Run 1, the proportionality constants of -297.6 ± 13.8 ppm/e ($r=0.912$) and -179.5 ± 10.2 ppm/e ($r=0.875$) were obtained for the π- and the total electron systems respectively. Improved correlations could be obtained for only quinonoid carbons: -300.7 ± 15.5 ppm/e ($r=0.944$) for the π-system and -181.5 ± 9.6 ppm/e ($r=0.941$) for the total electron system. Similar *sp* calculations on the twisted structure with the torsional angle of 15° gave a

Table 5. Charge distribution in the atomic orbitals of 3*H*-phenothiazin-3-one[a)]

Atom	Atomic orbital	Run 1 Planar		Run 6 Planar except for S		Run 8 Twisted	
		spd	*sp*	*spd*	*sp*	*spd*	*sp*
C-4	2s	1.0198	1.0209	1.0135	1.0152	1.0130	1.0141
	$2p_x$	1.2036	1.0203	1.0360	1.0311	1.0334	1.0306
	$2p_y$	0.9783	0.9762	0.9789	0.9767	0.9814	0.9801
	$2p_z$	1.0052	1.0574	0.9970	1.0521	1.0008	1.0549
C-4a	2s	1.0340	1.0398	1.0343	1.0415	1.0291	1.0379
	$2p_x$	1.0263	0.9873	1.0331	0.9783	1.0261	0.9762
	$2p_y$	0.9721	0.9522	0.9776	0.9574	0.9738	0.9581
	$2p_z$	0.9529	0.9521	0.9454	0.9513	0.9559	0.9541
S	3s	1.7991	1.7886	1.8149	1.8074	1.8079	1.7995
	$3p_x$	0.8242	1.1465	0.8295	1.2126	0.8664	1.2183
	$3p_y$	1.0920	1.2187	1.2346	1.3202	1.2816	1.3701
	$3p_z$	1.9174	1.9163	1.7165	1.7435	1.6474	1.6887
	$3d_{z^2}$	0.0481		0.0636		0.0721	
	$3d_{xz}$	0.0793		0.1011		0.1070	
	$3d_{yz}$	0.0472		0.0555		0.0508	
	$3d_{x^2-y^2}$	0.1004		0.0977		0.0975	
	$3d_{xy}$	0.1811		0.1695		0.1587	
C-5a	2s	1.0241	1.0312	1.0396	1.0463	1.0428	1.0497
	$2p_x$	0.9951	0.9411	1.0115	0.9495	1.0144	0.9531
	$2p_y$	0.9837	0.9824	0.9738	0.9746	0.9795	0.9881
	$2p_z$	1.0077	1.0020	0.9964	0.9893	0.9890	0.9830
C-6	2s	1.0031	1.0067	1.0097	1.0129	1.0092	1.0126
	$2p_x$	1.0135	1.0167	1.0201	1.0205	1.0192	1.0206
	$2p_y$	0.9706	0.9681	0.9697	0.9678	0.9701	0.9680
	$2p_z$	0.9801	1.0138	0.9707	1.0077	0.9681	1.0039

a) *z* axis is perpendicular to the benzenoid plane.

slightly less good correlation of -170.8 ± 9.9 ppm/e ($r=0.931$) for the total electron system.

In the case of phenothiazine, the fair linear relationship between the ^{13}C chemical shifts and the CNDO/2 total electron densities gave a proportionality constant of -127.7 ± 7.1 ppm/e ($r=0.985$).[47] A slope of -171.1 ± 25.0 ppm/e ($r=0.908$) was obtained for the π-electron system;[47] this value is approximately equal to the generally accepted value of -160 ppm/e for the π-electron of aromatics.[48,49] The correlation of the ^{13}C chemical shifts of the *N*-chloro-*p*-benzoquinone monoimine used as a reference compound for the quinone portion of **1** with their charge densities was also examined. An excellent correlation with the experimental results was obtained; the proportionality constants for the π- and total electrons were -458.2 ± 36.1 ppm/e ($r=0.988$) and -224.8 ± 5.3 ppm/e ($r=0.999$) respectively. These results indicate that the proportionality constants of **1** are close to the arithmetic mean values between those of *N*-chloro-*p*-benzoquinone monoimine and phenothiazine in the cases of both π- and total electrons.

Table 5 shows the distribution of charges among the atomic orbitals from the C-4 to the C-6 of **1** in the planar and twisted fashions. The sulfur total electron densities of **1** were evaluated to be 6.05—6.08 and 6.09—6.11 by means of the *sp* and *spd* approximations respectively. The summation of the electron densities of the five d-orbitals calculated varies from 0.46 to 0.53 and decreases as the distance of the C–S bond becomes longer and/or the conformation of **1** approaches the planar structure. The participation of the 3d orbital in bonding brings about a remarkable decrease in the electron density of sulfur $3p_\sigma$ orbitals, chiefly the $3p_x$ orbital; the reverse was found for the $3p_x$ orbitals of C-4a and C-5a adjacent to the sulfur atom. The perturbation of the charge densities of even-numbered carbons non-adjacent to the sulfur by the d-orbitals occurs through the $2p_\pi$ orbitals, as can be clear in Tables 4 and 5. In particular, the $2p_\pi$ electron density on the non-nearest-neighbor carbon, C-4, is strikingly decreased. As has been described above, however, the electron densities calculated by the *spd*-basis set did not fit the observed values of the ^{13}C chemical shifts well. A significantly improved correlation was obtained by reducing the extent of sulfur d-orbital participation to less than 50%.

Thanks are due to the Computer Center of the Institute for Molecular Science for its assistance in the CNDO/2 calculations.

References

1) For reviews, see: a) J. J. H. McDowell, "The Phenothiazines and Structurally Related Drugs," ed by I. S. Forrest, C. J. Carr, and E. Usdin, Raven Press, New York (1974); b) C. Bodea and I. Silberg, "Advances in Heterocyclic Chemistry," ed by A. R. Katrit and A. J. Boulton, Academic Press, New York (1968), Vol. 9, p. 321; c) A. Goth, "Medical Pharmacology," 9th ed, C. V. Mosby Co., St. Louis (1978), Chap. 19; d) J. K. Landquist, "Six-membered Ring Systems," in "Comprehensive Organic Chemistry, Heterocyclic Compounds," ed by P. G. Sammes, Pergamon Press, Oxford (1979), Vol. 4.

2) A. Carlsson, T. Persson, B.-E. Roos, and J. Walinder, *J. Neural Transm.*, **33**, 83 (1972).

3) J. J. H. McDowell, *Acta Crystallogr., Sect. B*, **32**, 5 (1976); **31**, 2256 (1975); **26**, 954 (1970); **25**, 2175 (1969).

4) J. D. Bell, J. F. Blount, O. V. Briscoe, and H. C. Freeman, *Chem. Commun.*, **1968**, 1656.

5) P. Marsau, *Acta Crystallogr., Sect. B*, **27**, 42 (1971).

6) P. Marsau and B. Busetta, *Acta Crystallogr., Sect. B*, **29**, 986 (1973).

7) P. Marsau and M.-R. Calas, *Acta Crystallogr., Sect. B*, **27**, 2058 (1971).

8) P. Marsau and Y. Cam, *Acta Crystallogr., Sect. B*, **29**, 980 (1973).

9) P. Marsau and J. Gauthier, *Acta Crystallogr., Sect. B*, **29**, 992 (1973).

10) M. J. Aroney, G. M. Hoskins, and R. J. W. le Fèvre, *J. Chem. Soc., B*, **1968**, 1206.

11) G. Fronza, R. Mondelli, G. Scapini, G. Ronsisvalle, and F. Vittorio, *J. Magn. Reson.*, **23**, 437 (1976).

12) H. B. Collier and D. E. Allen, *Can. J. Res.*, **20B**, 284 (1942).

13) H. B. Collier and G. M. Allenby, *Can. J. Med. Sci.*, **30**, 443 (1952).

14) H. B. Collier and S. C. Mcrae, *Can. J. Med. Sci.*, **31**, 195 (1953).

15) I. Ghizdavu, C. Bodea, and L. Ghizdavu, *Bull. Inst. Agron. Cluj-Napoca*, **31**, 65 (1977).

16) M. Ashikaga, *Okayama Igakkai Zasshi*, **66**, 977 (1954).

17) R. Yamamoto and T. Hiroyoshi, Japanese Patent 4148 (1956); *Chem. Abstr.*, **51**, 13324g (1957).

18) T. Takahashi and T. Takahashi, Japanese Patent 7301586, 18 Jan. (1973); *Chem. Abstr.*, **80**, 19541a (1974).

19) C. R. Thompson, *Ind. Eng. Chem.*, **42**, 922 (1950).

20) S. Kikkawa, Y. Shimizu, and K. Hatanaka, *Nippon Kagaku Kaishi*, **1977**, 695.

21) S. Kikkawa, Y. Shimizu, and T. Fukui, *Nippon Kagaku Kaishi*, **1979**, 656.

22) E. Ruzicka and J. Adamek, *Z. Anal. Chem.*, **195**, 411 (1963).

23) S. C. Jain and H. M. Sobell, *J. Mol. Biol.*, **68**, 1 (1972).

24) D. A. Simov, L. L. Kamenov, and S. T. Stoyanov, *C. R. Acad. Bulg. Sci.*, **24**, 1035 (1971).

25) I. C. Calder, R. B. Johns, and J. M. Desmarchelier, *Aust. J. Chem.*, **24**, 325 (1971).

26) N. S. Angermann and S. S. Danyluk, *Org. Magn. Reson.*, **4**, 895 (1972).

27) M. Rouillard, N. Giulieri, and M. Azzaro, *Bull. Soc. Chim. Fr.*, **1974**, 2141.

28) L. S. Israndt, R. K. Jensen, and L. Petrakis, *J. Magn. Reson.*, **12**, 143 (1973).

29) J. P. Malrieu and B. Pullman, *Theor. Chim. Acta*, **2**, 293 (1964).

30) C. Bodea and M. Raileanu, *Acad. Repub. Pop. Rom. Fil. Cluj, Stud. Cercet. Chim.*, **11**, 325 (1960); *Chem. Abstr.*, **58**, 3420b (1964).

31) M. Terdic, *Ann. Chem.*, **746**, 200 (1971).

32) J. A. Pople and D. L. Beveridge, "Approximate Molecular Orbital Theory," McGraw-Hill, New York, N.Y. (1970); J. A. Pople and G. A. Segal, *J. Chem. Phys.*, **44**, 3289 (1966); D. P. Santry and G. A. Segal, *ibid.*, **47**, 158 (1967).

33) Quantum Chemistry Program Exchange, Chemistry Department, Indiana University, Bloomington, Ind. 47001.

34) W. R. Woolfenden and D. M. Grant, *J. Am. Chem. Soc.*, **88**, 1496 (1966).

35) J. B. Stothers, "Carbon-13 NMR Spectroscopy," Academic Press, New York (1972), p. 75.

36) St. Berger and A. Rieker, *Tetrahedron*, **28**, 3123 (1972).

37) When the carbons of *N*-chloro-*p*-benzoquinone monoimine are numbered as:

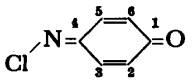

the ^{13}C chemical shifts, δ, of their carbons in $CDCl_3$ are as follows: C-1, 186.5; C-2, 127.2; C-3, 134.6; C-4, 167.2; C-5, 137.4; C-6, 130.8. The CNDO/2 *spd* π- and total electron densities of their carbons are as follows: C-1, 0.8699, 3.7689; C-2, 0.9863, 4.0274; C-3, 0.9770, 3.9948; C-4, 0.8981, 3.8559; C-5, 0.9841, 3.9905; C-6, 0.9818, 4.0246.

38) G. Höfle, *Tetrahedron*, **33**, 1963 (1977).

39) G. R. Bedford and P. J. Taylor, *Org. Magn. Reson.*, **9**, 49 (1977).

40) F. J. Weigert and J. D. Roberts, *J. Am. Chem. Soc.*, **92**, 1347 (1970).

41) W. F. Reynolds and R. A. McClelland, *Can. J. Chem.*, **55**, 536 (1977).

42) B. L. Shapiro and M. D. Johnston, Jr., *J. Magn. Reson.*, **12**, 199 (1973).

43) D. M. Grant and B. V. Cheney, *J. Am. Chem. Soc.*, **89**, 5315 (1968).

44) R. G. Parker and J. D. Roberts, *J. Org. Chem.*, **35**, 996 (1970).

45) L. E. Sutton, "Tables of Interatomic Distances," ed by the Chemical Society, London (1958).

46) a) J. M. Robertson, *Nature*, **134**, 138 (1934); *Proc. R. Soc. London, Ser. A*, **150**, 106 (1935); b) S. M. Swingle, *J. Am. Chem. Soc.*, **76**, 1409 (1954); c) M. Kimura and S. Shibata, *Bull. Chem. Soc. Jpn.*, **27**, 163 (1954).

47) Data calculated from Tables 3 and 5 in Ref. 11 using the least-squares method.

48) H. Spiesecke and W. G. Schneider, *Tetrahedron Lett.*, **1961**, 468.

49) G. A. Olah and G. D. Matescu, *J. Am. Chem. Soc.*, **92**, 1430 (1970).

50) N. Go and H. A. Scheraga, *Macromolecules*, **3**, 178 (1970).

Preparation of *S,S*-Diphenylsulfilimines, -sulfoximines, and -*N*-(*p*-tolylsulfonyl)sulfonediimines *N*-Substituted with Sulfur Groups of Different Oxidation States

Kunihiko Akutagawa, Naomichi Furukawa,* and Shigeru Oae*,†
Department of Chemistry, University of Tsukuba, Sakura-mura, Niihari-gun, Ibaraki 305
(Received September 9, 1983)

S,S-Diphenyl-*N*-(*p*-tolylthio)-, -*N*-(*p*-tolylsulfinyl)-, -*N*-(*p*-toluenesulfinimidoyl)-, -*N*-(*p*-tolylsulfonyl)-, and -*N*-(*p*-toluenesulfonimidoyl)sulfoximines have been synthesized either by sulfenylation, sulfinylation, sulfinimidoylation, sulfonylation, and sulfonimidoylation or by oxidation of the *N*-substituted sulfoximines with sulfur groups of lower oxidation states, *i.e.*, the *N*-sulfenylated sulfoximine. Similar attempts have been made on similarly substituted sulfonediimines. Sulfenylation and sulfonylation of *N*-unsubstituted *N*-(*p*-tolylsulfonyl)sulfonediimine were unsuccessful but its sulfinylation underwent nicely. An attempt to disulfonylation of the *N,N'*-unsubstituted sulfonediimine ended up in the monosulfonylation. *N,N'*-bis(*p*-Tolylsulfonyl)sulfonediimine was successfully prepared by oxidation of the *N*-(*p*-tolylsulfinyl)-*N'*-(*p*-tolylsulfonyl)sulfonediimine with *m*-chloroperbenzoic acid.

Numerous *N*-substituted sulfilimines,[1] sulfoximines,[2] and *N'*-*p*-tolylsulfonylsulfonediimines,[3] such as *N*-alkyl, *N*-aryl-, *N*-sulfonyl, *N*-acyl-, *N*-silyl, and *N*-phosphoryl derivatives, have been prepared. In general, these compounds are fairly stable. Whereas, only a few *N*-substituted derivatives having a heteroatom with lone-pair electrons directly attached to the imino nitrogen atom of sulfilimine have been known. Furthermore, very little of the chemistry of these compounds has been explored. The compounds actually isolated are *N*-chloro-,[4] *N*-bromo-,[4] *N*-iodo-,[4] *N*-sulfenyl-,[5] *N,N*-phthaloyl-,[6] *N*-aryl-[7] derivatives which are in general thermally unstable as compared to other *N*-substituted derivatives having an atom with no electron pair in the *N*-substituent directly combined to the imino nitrogen atom. These sulfilimines bearing *N*-substituents of heteroatoms possessing lone-pair electrons, are generally quite reactive and readily decompose *via* the initial S–N bond fission. These reactive derivatives, upon activation by addition of a suitable electrophile such as sulfenyl chloride, undergo facile cleavage of the S–N linkage. For example, the *N*-chlorosulfilimine readily decomposes even at room temperature to afford the corresponding sulfide and the sulfonium salt ($Ph_2S{=}\overset{+}{N}{=}SPh_2\ Cl^-$) and the decomposition is accelerated further by addition of Brönsted acids. The structures of these activated derivatives formed by addition of an electrophile are considered to be analogous to that of the persulfoxide,[8] or that of the intermediates formed in the treatment of dimethyl sulfoxide with primary or secondary alcohols to afford aldehydes or ketones,[9] or those of the reactions of sulfoxides,[10] sulfilimines,[11] sulfonium ylides,[12] and sulfoximines[13] with carbenes or nitrenes, to afford eventually the reduction products (Eq. 1).

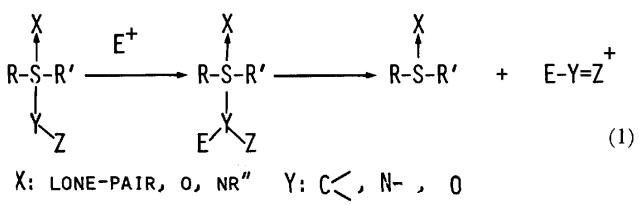

(1)

The repulsive interaction between lone-pair electrons of the imino nitrogen and the adjacent heteroatom is considered to weaken the S–N linkage for facile cleavage. Meanwhile, the sulfilimines having either *N*-aryl, or *N*-phthalimido-substituent attached to the imino nitrogen are relatively stable thermally because the repulsive interactions of lone-pair electrons between the nitrogen atom and the adjacent sulfur atom is relieved considerably in these compounds. Similarly, the *N*-chlororsulfoximine, in which the repulsive interaction between two adjacent heteroatoms is reduced, undergoes degradation to afford the corresponding sulfoxide only at an elevated temperature, *e.g.*, 200 °C.

In order to explore the rough correlation between the nature of the S–N linkage and the stability of the sulfilimine derivatives, various *S,S*-diaryl-*N*-substituted sulfilimines (**1**), -*N*-substituted sulfoximines (**2**), and *N'*-substituted-*N*-(*p*-tolylsulfonyl)sulfonediimines (**3**) containing an S–N group, *e.g.*, *N*-(*p*-tolylthio)-, *N*-(*p*-tolylsulfinyl)-, *N*-(*p*-toluenesulfinimidoyl)-, and *N*-(diphenylsulfonio)sulfonium derivatives have been synthesized and their chemical properties have been examined.

Definition of Abbreviation for the Compounds. The following numbering and abbreviation for the *S,S*-diphenyl sulfur compounds are used through this paper.

Ph–S(NR)–Ph: *N*-*R*-Substituted-*S,S*-diphenylsulfilimines (**1**),
Ph–S(O)(NR)–Ph: *N*-*R*-Substituted-*S,S*-diphenylsulfoximines (**2**),
Ph–S(NR)(NR')–Ph: *N,N'*-*R,R'*-Disubstituted-*S,S*-diphenylsulfonediimines (**3**),
R or R' groups:
R (or R'); H, *N*-unsubstituted- (**a**),
; –STol(*p*-), *N*-(*p*-tolylthio)- (**b**),
; –S(O)Tol(*p*-), *N*-(*p*-tolylsulfinyl)- (**c**),

† Present address; Okayama University of Science, Ridai-cho 1-1, Okayama 700.

; $-S(NTs)Tol(p-)$, *N*-(*p*-toluenesulfinimidoyl)- (**d**),
; $-S(O)_2Tol(p-)$, *N*-(*p*-tolylsulfonyl)- (**e**),
; $-S(O)(p\text{-}TolN)Ph$, *N*-(*p*-toluenesulfonimidoyl)- (**f**),
; $-S(Ph)_2$, *N*-(diphenylsulfo)- (**g**).

other derivatives are shown by their *N*-substituent and numbering of the compounds *e.g.*, *N*-chloro-(**1**). Therefore, for expample, **1b** and **3ab** indicate *N*-(*p*-tolylthio)-*S,S*-diphenylsulfilimine and *N'*-unsubstituted *N*-(*p*-tolylthio)-*S,S*-diphenylsulfonediimine respectively.

Results and Discussion

N-Substituted S,S-Diphenylsulfilimines (1). Treatment of *N*-unsubstituted sulfilimines with *p*-toluenesulfonyl chloride gave the corresponding thermally extremely stable compounds, *N*-(*p*-toylsulfonyl)-sulfilimines. However, *N*-(*p*-tolylthio)-(**1b**), *N*-(*p*-toylsulfinyl)-(**1c**), *N*-(*p*-toluenesulfinimidoyl)-(**1d**), or *N*-(*p*-toluenesulfonimidoyl)sulfilimines (**1f**) have not been reported in the literature. Preparations of **1b—d** have been attempted, by treating *N*-unsubstituted sulfilimine (**1a**) with *p*-toluenesulfenyl chloride, *p*-toluenesulfinyl chloride, or *p*-toluenesulfinimidoyl chloride in the presence of triethylamine, however only the corresponding reduction product, the sulfide, was obtained (Eq. 2).

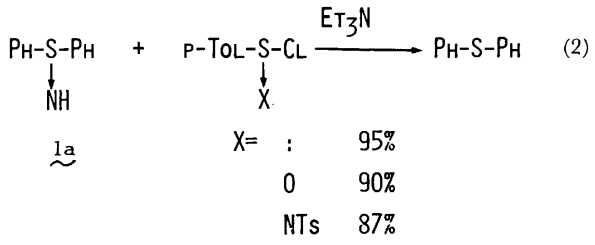

(2)

Finally, diphenyl *N*-(benzenesulfonimidoyl)sulfilimine (**1f**) was prepared by treating **1a** with *N*-benzenesulfonimidoyl chloride in the presence of triethylamine in 89% yield.

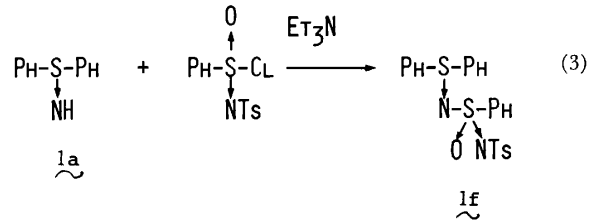

(3)

N-Substituted S,S-Diphenylsulfoximines (2). Conversion of *N*-unsubstituted sulfoximines into the corresponding *N*-(*p*-tolylsufonyl)sulfoximines and the desulfonylation of the latter compound are well known. Thus, *N*-unsubstituted *S,S*-diphenylsulfoximine (**2a**) was shown to react with *p*-toluenesulfonyl chloride in pyridine affording quantitatively the corresponding **2e**, which can reproduce **2a** by treating with concentrated sulfuric acid[14] or sodium in liquid ammonia.[15] However, nothing is known about *N*-substituted sulfoximines (**2b**, **2c**, **2d**, and **2f**). In the course of our systematic study of sulfilimines and their derivatives, especially the bonding nature of the semipolar S–N linkage in sulfilimines, sulfoximines and sulfondiimines, these compounds have been prepared in order to compare the characteristic properties of these bonds with those of known *N*-unsubstituted sulfoximines or *N*-(*p*-toylsulfonyl)sulfoximines. **2b** was prepared by treating *N*-sodium salt of the sulfoximine with *p*-toluenesulfenyl chloride or by treatment of two equivalents of **2a** with *p*-toluenesulfenyl chloride. Other bases such as pyridine or triethylamine gave no good result. The sulfoximines, **2c**, **2d**, and **2f** were prepared by treating the *N*-sodium salt of the sulfoximine with *p*-toluenesulfinyl chloride, *p*-toluenesulfinimidoyl chloride, and *p*-toluenesulfonimidoyl chloride, respectively, in good yields. These compounds were able to be prepared using other bases such as pyridine or triethylamine in good yields.

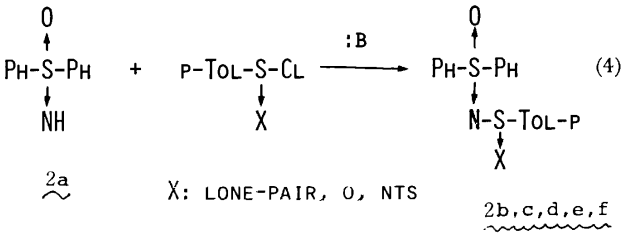

(4)

Another route to prepare **2c**, **2d**, and **2f** has been examined, using **2b** as the key starting material, which was converted to other *N*-substituted **2** by oxidation with such oxidizing reagents, as *m*-chloroperbenzoic acid (**mCPBA**) and sodium salt of *N*-chloro-*p*-toluenesulfonamide (chloramine-*T*). **2b** was oxidized readily with one equivalent of sodium periodate in aqueous acetonitrile or **mCPBA** in dichloromethane to **2c** (Eq. 5).

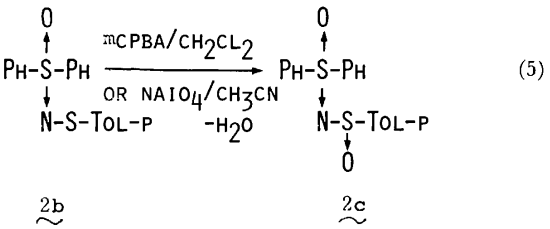

(5)

Meanwhile, **2b** reacts with chloramine-*T* to afford **2d** in a good yield in chloroform–methanol solution (Eq. 6).

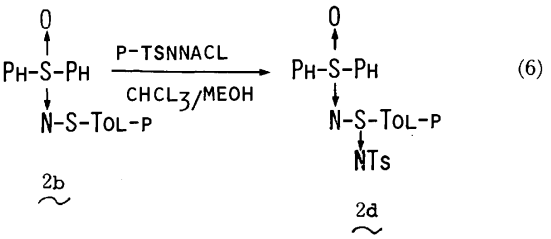

(6)

The use of two-fold excess of **mCPBA** in dichloromethane converted **2a** to **2e**, while the use of one equivalent of **mCPBA** oxidized **2c** to **2e**. Thus, these oxidation reactions of **2b** or **2c** should be another convenient way to prepare **2e**. In the same way, **2d** was nicely converted to **2f** by treating with **mCPBA** in dichloromethane in a good yield. Thus, **2b** is a good starting material for preparation of various other *N*-substituted sulfoximine derivatives. **2g** was also prepared by the

reaction of the *N*-chloro-**2** with the sulfide, according to the method reported earlier[16] (Eq. 7).

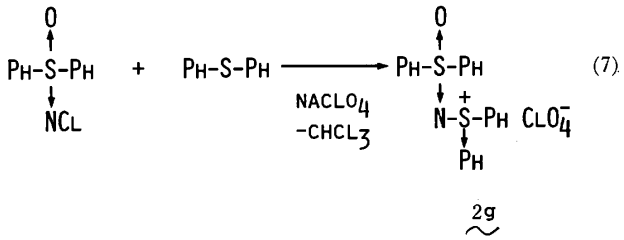

Thus, one can prepare all kinds of *N*-substituted sulfoximines, **2b—g**. The results are summarized in Scheme 1 and Tables 1 and 2.

Preparation of N'-*Substituted* S,S-*Diphenyl*-N-*(*p-*tolylsulfonyl)sulfonediimines (3).* Treatment of *N'*-unsubstituted *S,S*-diphenyl-*N*-(*p*-tolylsulfonyl)sulfonediimines (**3ae**) with *p*-toluenesulfenyl chloride at −20 °C in the presence of bases, *e.g.*, pyridine, triethylamine or **3ae**, did not afford the corresponding **3be** at all, but the reduction product, **1e** was obtained in a high yield (Eq. 8).

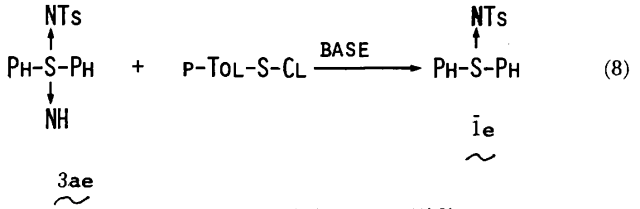

Base: NaH, Et_3N, pyridine, γ-collidine, **3ae**.

Table 1. Preparation of *N*-substituted-sulfoximines

Ph-S(O)-Ph, N-X, X	Condition	Yield/%[a]
S-Tol-*p*	*p*-TolSCl, NaH/PhH	92
(**b**)	*p*-TolSCl, Ph-S(O)-Ph/Et_2O, NH	81
	p-TolSCl, py/Et_2O	8
	p-TolSCl Et_3N/Et_2O	10
S-C_6H_4-NO_2-*o*	*o*-$NO_2C_6H_4SCl$, NaH/PhH	98
	o-$NO_2C_6H_4SCl$, Ph-S(O)-Ph/Et_2O, NH	95
S-Tol-*p*, O	*p*-TolS(O)Cl, NaH/PhH	95
	p-TolS(O)Cl, Et_3N/Et_2O	92
(**c**)	*p*-TolS(O)Cl, py/Et_2O	90
	*m*CPBA/CH_2Cl_2, Ph-S(O)-Ph, N-S-Tol-*p*	85

a) Isolated yield.

However, the reaction of **3ae** with *p*-toluenesulfinyl chloride at −20 °C in the presence of bases, *e.g.*, pyridine or triethylamine proceeded nicely (Eq. 9)

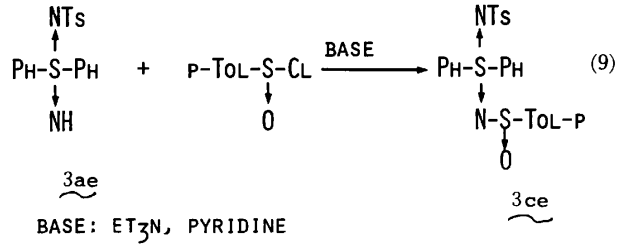

Furthermore, treatment of **3aa** with an equimolar amount of *p*-toluenesulfonyl chloride gave only **3ae**, monosulfonylated product. Disulfonylation of **3aa** was attempted by treating **3ae** with *p*-toluenesulfonyl chloride under various conditions and failed, recovering only **3ae** quantitatively. However, interestingly, **3ee**, *N,N'*-bis(*p*-tolylsulfonyl)sulfonediimine, was obtained in a quantitative yield when **3ce** was oxidized with 1 equiv of **mCPBA** (Eq. 10).

Table 2. Preparation of *N*-substituted-sulfoximines (**2**)

X	Condition	Yield/%[a]
S-Tol-*p*, O	$NaIO_4$/70% CH_3CN, Ph-S(O)-Ph, N-S-Tol-*p*	96
(**c**)		
S-Tol-*p*, NTs	*p*-TolS(NTs)Cl, NaH/PhH	75
(**d**)	*p*-TsNNaCl/$CHCl_3$/MeOH, Ph-S(O)-Ph, N-S-Tol-*p*	87
	p-TsNNaCl/CH_3CN, Ph-S(O)-Ph, N-S-Tol-*p*	90
$OClO_3^-$, S^+-Ph, Ph	PhSPh, PhSPh, $NaOClO_3$/$CHCl_3$, N-Cl	80
(**g**)	(2 equiv)*m*CPBA/CH_2Cl_2, Ph-S(O)-Ph, N-S-Tol-*p*	99
O, S-Tol-*p*, O	*m*CPBA/CH_2Cl_2, Ph-S(O)-Ph, N-S(O)-Tol-*p*	95
O, S-Tol-*p*, NTs	*p*-TolSCl, NaH/PhH	53
(**f**)	*m*CPBA/CH_2Cl_2, Ph-S(O)-Ph, N-S-Tol-*p*, NTs	79

a) Isolated yield.

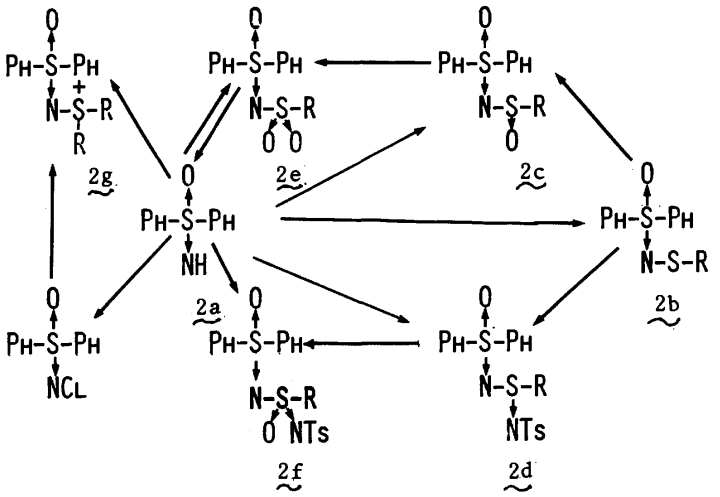

Scheme 1. Diagram of *N*-substituted sulfoximine starting from unsubstituted sulfoximine.

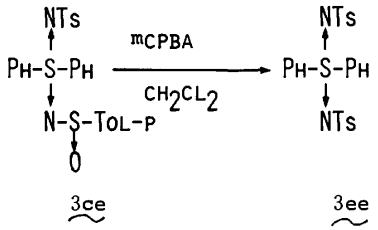

(10)

The lack of reactivity of **3ae** toward the sulfonyl chloride and the facile reaction of **3ce** with **mCPBA** may be reasonably rationalized in the following manner.

Namely, in the former reaction, the nucleophilicity of the imino nitrogen of **3ae** is considerably diminished while the sterically bulky sulfonyl group attached to the imino group would hinder the second sulfonylation of the imino nitrogen; whereas in the latter reaction, no matter whether the oxidation is caused by electrophilic attack of **mCPBA** or nucleophilic attack of the perbenzoate anion, the approach of the oxygen atom of **mCPBA** toward the sulfinyl sulfur atom should not be hindered both sterically and electronically.

These new derivatives of sulfonediimines thus obtained were identified by both spectroscopic and elemental analyses. This is the first and perhaps the best method to prepare *S,S*-diaryl-*N,N'*-bis(*p*-tolylsulfonyl)sulfonediimine. These results are listed in Table 3.

Table 3. Preparation of *N*-substituted-*N'*-*p*-toluenesulfonylsulfonediimines (**3**)

Ph-S(NTs)-Ph, N-X (**3**), X	Condition	Yield/%[a]
S-Tol-*p*	*p*-TolSCl, NaH/PhH	0
(b)	*p*-TolSCl, Ph-S(NTs)-Ph/CH_2Cl_2	0
	p-TolSCl, NH	
	p-TolSCl, py/CH_2Cl_2	0
	p-TolSCl, γ-collidine/CH_2Cl_2	0
	P-TolSCl, Et_3N/CH_2Cl_2	0
S-Tol-*p*	*p*-TolS(O)Cl, Et_3N/CH_2Cl_2	85
O	*p*-TolS(O)Cl, py/CH_2Cl_2	80
(c)		
O	*p*-$TolSO_2Cl$, NaH/PhH	0
S-Tol-*p*		
O	*p*-$TolSO_2Cl$, Et_3N/CH_2Cl_2	0
(e)	*p*-$TolSO_2Cl$, py/CH_2Cl_2	0
	p-$TolSO_2Cl$, γ-collidine/CH_2Cl_2	0
	*m*CPBA/CH_2Cl_2, Ph-S(NTs)-Ph, N-S-Tol-*p* (O)	94

a) Isolated yield.

Experimental

General. Melting points of the products were measured by Yanaco instrument and were uncorrected. IR spectra were obtained using a Hitachi 215 spectrophotometer. ^1H NMR spectra of the all compounds were obtained with a Hitachi Perkin-Elmer R-20 spectrometer in 20% solutions in deuteriochloroform using tetramethylsilane as an internal standard. Mass spectra were recorded on a Hitachi RMU-6MG mass spectrometer with a direct inlet system. Liquid chromatographs were obtained by Yanaco L-1030 instrument using methanol as an eluent. Thin-layer chromatographies were carried out with Merck DC-Plastikofolien Kieselgel 60 F 254 Art 5735 with fluorescent indicator using various solvents and mixed solvents. Development was followed by UV light or by coloring with iodine. Silica gel used for column chromatography was either of Wako or of Merck chromatographic grade. Elemental analyses were carried out at the Chemical Analysis Center of this University. Oxidizing agents, **mCPBA**, sodium periodate and chloramine-*T* were obtained from Wako Pure Chemicals. Anhydrous dichloromethane and ether were obtained by the usual procedures.[17] Other chemicals were of reagent grade.

p-Toluenesulfenyl Chloride. *p*-Toluenesulfenyl chloride was prepared by treating the corresponding disulfide with gaseous chlorine in dichloromethane at 5 °C, accord-

ing to the known method,[18,19] and purified by distillation under reduced pressure. Bp 76.0—78.0 °C/2.5 mmHg (1 mmHg≈133.322 Pa),[18] (77.5—78.2 °C/2.5 mmHg).

o-Nitrobenenesulfenyl Chloride. Mp 74.0—75.0 °C (from tetrachloromethane), (lit, 75 °C[19]).

p-Toluenesulfinyl Chloride. *p*-Toluenesulfinyl chloride was obtained by treatment of *p*-toluenethiol with gaseous chlorine in anhydrous acetic anhydride at 10 °C, in the usual manner.[20] Bp 107.0—109.5 °C/2.5 mmHg, (lit, 92—102 °C/0.5 mmHg).[20]

p-Toluenesulfinimidoyl Chloride. *p*-Toluenesulfinimidoyl chloride was prepared by the reaction of *p*-toluenesulfenyl chloride with anhydrous chloramine-*T* in benzene, according to the previously reported method.[21] Mp 141.5—142.5 °C, (lit, 141.5—142.5 °C).[21]

N-(p-Tolylulfonyl)-p-toluenesulfonimidoyl Chloride. *p*-Toluenesulfonimidoyl chloride was prepared by the reaction of *p*-toluenesulfinyl chloride with commercially available chloramine-*T* in benzene, according to the method reported earlier.[22] Mp 76.5—77.5 °C, (lit, 76—78 °C).[22]

Preparation of 1a, 2a, 3ae. **1a**,[23] **2a**,[24] and **3ae**[25] were prepared by the method reported earlier.

Preparation of 1a, 2a, 3ae. **1a**,[23] **2a**,[24] and **3ae**[25] were prepared by the method reported earlier.

Preparation of N-Chlorosulfoximine. **3a** (2.0 g, 9.2 mmol) was dissolved in 10 mL of acetonitrile. This solution was added to a stirred solution of 15 mL of cold sodium hypochlorite solution. The reaction mixture was stirred for 15 min before the starting sulfoximine disappeared upon checking the TLC or HPLC. The solution was extracted with chloroform, which was dried, filtrated and evaporated. The purification was performed on recrystallization from benzene. Yield was 1.85 g (80%), colorless crystals, mp 150.0—151.0 °C.

Preparation of 1f. To a mixture of **1a** (200 mg, 0.91 mmol) and triethylamine (138 mg) in chloroform, a chloroform solution of *N*-(*p*-tolylsulfonyl)benzenesulfonimidoyl chloride (300 mg, 0.91 mmol) was added. After stirring the reaction mixture for 30 min at 25 °C, solid precipitates were washed with dilute aqueous hydrochloric acid solution, water, and dried over magnesium sulfate. After the solvent was removed, the crude product was purified by column chromatography. The crystals were recrystallized from ethanol. Yield was 401 mg (89%), mp 139.5 °C; IR(KBr) 1315(SO_2), 1305(SO_2), 1240(O=S=N-), 1150(SO_2), 1100(O=S=N-), 1060(O=S=N-), 1035, 1021, and 995 cm^{-1}; ^1H NMR ($CDCl_3$) δ=2.32 (3H, s, -$SO_2C_6H_4CH_3$-*p*), 7.00—7.90 (19H, m, aromatic protons); MS (20 eV) *m/z* (rel intensity) (M^+; 0.3), 292(7), 248(36), 186([PhSPh]$^+$; 100), 171(84), 170(81), 155(5), 125(11), 109(13), 90(23), and 77(18). Found: C, 60.70; H, 4.27; N, 5.50%. Calcd for $C_{25}H_{22}N_2O_3S_3$: C, 60.70; H, 4.48; N, 5.66%.

Preparation of 2b. To the ethereal solution of **2a** (10 g, 46 mmol) was added *p*-toluenesulfenyl chloride (3.5 g, 22 mmol) in ether solution under cooling with a Dry Ice-acetone bath with stirring. The reaction mixture was kept at −70 °C for 10 min and the cooling bath was removed and the heterogeneous reaction mixture was stirred until the solution reached at room temperature. The precipitates formed were filtered off after stirring the solution at 25 °C for 20 min. The solvent was evaporated. The crude product was purified through column chromatography and crystals thus obtained were recrystallized from dichloromethane-pentane. Yield was 6.1 g, 81%, mp 110 °C. Sodium salt of *S,S*-diphenylsulfoximine, which was prepared from **2a** and sodium hydride in benzene, also afforded **2b** by the reaction with *p*-toluenesulfenyl chloride in 92% yield. Colorless crystals; mp 110 °C; IR(KBr) 1220(O=S=N-), 1085(O=S=N-), and 980(O=S=N-); ^1H NMR ($CDCl_3$) δ=2.26 (3H, s, -$C_6H_4CH_3$-*p*), 6.96—8.09 (14H, m, aromatic protons); MS (20 eV) *m/z* (rel intensity) 339(M^+; 7), 246(50), 202([PhS(O)Ph]$^+$; 100), 186(75), 174(22), 154(77), 136(22), 123(61), 97(31), 90(31), and 77(17). Found: C, 67.11; H, 4.86; N, 4.15%. Calcd for $C_{19}H_{17}NOS_2$: C, 67.22; H, 5.04; N, 4.12%.

Preparation of S,S-Diphenyl-N-(o-nitrophenylthio)sulfoximine. Yield was 95—98%; colorless crystals; mp 161.0—162.0 °C; IR (KBr) 1210 (O=S=N-), 1090 (O=S=N-), 1005, and 985 (-S=N-); ^1H NMR ($CDCl_3$) δ=6.87—8.17 (14H, m, aromatic protons); Found: C, 58.29; H, 3.81; N, 7.45%. Calcd for $C_{18}H_{14}N_2O_3S_2$: C, 58.36; H, 3.80; N, 7.56%.

Preparation of 2c. This compound was prepared by either one of the following two processes.

Method A: **2a** (3.0 g, 13.8 mmol) and triethylamine (1.7 g, 16.6 mmol) were dissolved in ether. Under stirring and cooling with a Dry Ice-acetone bath, and ethereal solution of *p*-toluenesulfinyl chloride (2.5 g, 14.3 mmol) was added dropwise. After warming at 25 °C for 20 min the precipitates were separated by filtration. Ether was removed, the crude crystals thus obtained were recrystallized from dichloromethane-pentane. Yield was 4.5 g, 92%; mp 192.5—193.0 °C; colorless crystals.

Method B: **2b** (300 mg, 0.88 mmol) was oxidized with **mCPBA** (152 mg) at 25 °C for 15 min. The usual work-up process afforded **2c**. Yield was 267 mg, 85%; IR(KBr) 1235(O=S=N-), 1105(O=S=N-), 1090(O=S=N-), 1075(-S=O), 1040, 1020, and 995(-S-N=); ^1H NMR ($CDCl_3$) δ=2.35 (3H, s, -$C_6H_4CH_3$-*p*), 7.22—8.23 (14H, m, aromatic protons); MS (20 eV) *m/z* (rel intensity) 355(M^+; 9), 264(56), 202([PhSPh]$^+$; 100), 186(14), 174(10), 154(36), 138(11), 124(8), and 109(22). Found: C, 64.55; H, 4.76; N, 3.98%. Calcd for $C_{19}H_{17}NO_2S_2$: C, 64.19; H, 4.82; N, 3.98%.

Preparation of 2d. **2b** (600 mg, 1.77 mmol) was dissolved in chloroform. To this solution was added chloramine-*T* (75 mg) in methanol. After stirring the mixture for 30 min at 25 °C, the solvent was removed *in vacuo*, the crude product was separated through column chromatography using chloroform as eluent. The yield was 782 mg, 87% (recrystallized from ethanol). This sulfoximine was also prepared by the reaction of sodium salt of *S,S*-diphenylsulfoximine with *N*-(*p*-tolylsulfonyl)-*p*-toluenesulfinimidoyl chloride in benzene. Yield was 75% (colorless crystals). Mp 118.0—118.5 C; IR(KBr) 1290(O=S=O), 1280 (O=S=O), 1230(O=S=N-), 1140(O=S=O), 1095(O=S=N-), 1085 (O=S=N-), 1035 and 955 (S(IV)-N); ^1H NMR ($CDCl_3$) δ= 2.34 (3H, s, -$C_6H_4CH_3$-*p*), 2.34 (3H, s, -$SO_2C_6H_4CH_3$-*p*), 7.10—8.12 (18H, m, aromatic protons); MS (20 eV) *m/z* (rel intensity) 508 (M^+; 2), 369 ([PhS(O) (NS(N)$C_6H_4CH_3$-*p*)]$^+$; 100), 339(8), 202(60), 186(28), 169(12), 155(17), 137(40), 125(39), 124(28), 123(28), 109(18), 91(77), 90(62), and 77(16). Found: C, 61.23; H, 4.66; N, 5.41%. Calcd for $C_{26}H_{24}N_2O_3S_3$: C, 61.39; H, 4.75; N, 5.50%.

Preparation of 2g. *S,S*-Diphenyl-*N*-chlorosulfoximine which was prepared by the reaction of **2a** with sodium hypochlorite in aqueous acetonitrile, was dissolved into chloroform at 25 °C. To this solution was added diphenyl sulfide in chloroform with stirring at 25 °C for 30 min. The mixture was washed with an aqueous solution of sodium perchlorate, with water and dried over magnesium sulfate. Chloroform was removed *in vacuo* and the product was separated by column chromatography using chloroform-methanol (9 : 1) as an eluent. Recrystallization of this product was performed from ethanol. Yield was 80%; colorless crystals; mp 155.5—156.0 °C. IR(KBr) 1235(O=S=N-), 1100(O=S=N-), 1090($OClO_3$), 1030, and 985(-S-N=); ^1H NMR ($CDCl_3$) δ=7.23—7.97 (20H, m, aromatic protons). Found: C, 57.49; H, 4.02; N, 2.84%. Calcd for $C_{24}H_{20}NO_5S_2Cl$: C, 57.42; H, 4.01; N, 2.79%.

Preparation of 2e. The sulfonylation of **2a** was

reported earlier.[14] **2c** (300 mg, 0.85 mmol) was dissolved in dichloromethane. To this solution was added a solution of **mCPBA** (220 mg) in dichloromethane. After 2 h of stirring the usual work-up gave the crude product upon column chromatography using chloroform as an eluent. Further purification was carried out by recrystallization from ethanol. Yield was 297 mg, 95%; colorless crystals; mp 137.5 °C.

This sulfoximine was also obtained from the corresponding **2b** by oxidation with 2 equiv of **mCPBA** in dichloromethane. Yield was 99%; IR(KBr) 1295(O=S=O), 1240 (O=S=N-), 1150(O=S=O), 1100(O=S=N-), 1065, 1020, and 995(O=S=N-); ^{1}H NMR ($CDCl_3$) $\delta=2.38$ (3H, s, -$C_6H_4CH_3$-*p*), 7.13—8.06 (14H, m, aromatic protons); MS (20 eV) *m/z* (rel intensity) 371(M^+; 12), 294(2), 278(29), 139([PhS(O)N]$^+$; 100), and 125(45).

Preparation of 2f. To a dichloromethane solution of **2d** (200 mg, 0.39 mmol) was added a dichloromethane solution of **mCPBA** (9 mg). After 8 h, the reaction mixture was washed with water, aqueous sodium carbonate solution and then washed with water. Dichloromethane solution was dried over magnesium sulfate and the solvent was removed under reduced pressure. The solid obtained was purified through column chromatography using chloroform as an eluent. Further purification was accomplished by recrystallization from ethanol. Yield was 163 mg, 79%; colorless crystals; mp 198.0—198.5 °C; IR(KBr) 1300(O=S=O), 1250(O=S=N-), 1235(O=S=N-), 1140(O=S=N-), 1100(O=S=N-), 1060, 1035, 1005, and 990 (-S=N-); ^{1}H NMR ($CDCl_3$) $\delta=2.33$ (3H, s, -$C_6H_4CH_3$-*p*), 2.33 (3H, s, -$SO_2C_6H_4CH_3$-*p*), 7.05—7.95 (18H, m, aromatic protons; MS (20 eV) *m/z* (rel intensity) 524(M^+; 0.9), 447(0.9), 417(1), 385(8), 308(l), 278(11), 264([Ph_2S(O)NSO]$^+$; 100), 246(8), 202(6), 200(13), 139(89), 125(27), and 109(2). Found: C, 59.28; H, 4.41; N, 5.20%. Calcd for $C_{26}H_{24}N_2O_4S_3$: C, 59.52; H, 4.61; N, 5.33(%).

Reaction of 3ae with p-Toluenesulfenyl Chloride. **3ae** (700 mg, 1.9 mmol) and triethylamine (230 mg, 2.3 mmol) were dissolved into dichloromethane (20 mL). To this solution was added dropwise *p*-toluenesulfenyl chloride (300 mg, 1.9 mmol) in dichloromethane (10 mL) at −20 °C under stirring. After the solution was kept for 10 min at −20 °C, the cooling bath was removed and heterogeneous reaction mixture was stirred until the solution was reached at room temperature. After the usual work-up, **1e** (578 mg) was obtained in 86% yield. **3be** was not obtianed.

Preparation of 3ce. **3ae** (3.0 g, 8.1 mmol) was dissolved in 30 mL of dichloromethane. To this solution was added dropwise *p*-toluenesulfinyl chloride (1.5 g) and triethylamine (1.1 g) with stirring at −70 °C under cooling with Dry Ice-acetone bath. After stirring for 20 min at 25 °C, the precipitates were filtrated off. The organic solution was washed with water and dried over magnesium sulfate. The crude product thus obtained was recrystallized from dichloromethane-pentane. Yield was 3.5 g (85%); colorless crystals; mp 143.0—144.0 °C; IR(KBr) 1320 (O=SO), 1305(O=S=O), 1185(O=S=O), 1160(-N=S=N-), 1105(-N=S=N-), 1060(-N=S=N-), and 985(-S-N=); ^{1}H NMR ($CDCl_3$) $\delta=2.34$ (3H, s, -S(O)$C_6H_4CH_3$-*p*), 2.44 (3H, s, -$SO_2C_6H_4C_6H_4CH_3$-*p*), and 7.05—8.27 (18H, m, aromatic protons); MS (20 eV) *m/z* (rel intensity) 354(1), 278(1), 214(1), 200([Ph_2S-N]$^+$; 100), 186(10), 139(1), and 123(6). Found: C, 61.56; H, 4.65; N, 5.47%. Calcd for $C_{26}H_{24}N_2O_3S_3$: C, 61.39; H, 4.75; N, 5.50%.

Preparation of 3ee. Sulfonylation of **3ae** with *p*-toluenesulfonyl chloride in the presence of various bases, such as triethylamine or 2,2,6-trimethylpyridine was not successful, and the original sulfonediimine was recovered nearly quantitatively. However, **3ee** was obtained by another way. To a dichloromethane solution of **3ce** (500 mg, 0.98 mmol) was added a dichloromethane solution of **mCPBA** (2-fold excess) under cooling at 0 °C with an ice-water bath with stirring. After removing the precipitated *m*-chlorobenzoic acid, the solution was washed with aqueous sodium carbonate, water and dried over magnesium sulfate. The solvent was removed by evaporation, the crude crystals were obtained. Purification was achieved by recrystallization from ethanol. Yield was 485 mg, 94%; colorless crystals, mp 213.5 °C; IR(KBr) 1330(O=S=O), 1165(-N=S=N-), 1080 (-N=S=N-), 1050(-N=S=N-), and 995(-S-N=); ^{1}H NMR ($CDCl_3$) $\delta=2.40$ (3H, s, -$NSO_2C_6H_4CH_3$-*p*), 2.40 (3H, s, -$NSO_2C_6H_4CH_3$-*p*), and 7.11—8.02 (18H, m, aromatic protons). MS (20 eV) *m/z* (rel intensity) 370(5), 306(12), 279(42), 265(47), 215(10), 201(66), 186(78), 171(6), 155(23), 139(15), 119(73), and 91([Tol]$^+$; 100). Found: C, 59.97; H, 4.54; N, 5.20%. Calcd for $C_{26}H_{24}N_2O_4S_3$: C, 59.52; H, 4.61; N, 5.33%.

References

1) T. L. Gilchrist and C. J. Moody, *Chem. Rev.*, **77**, 409 (1977).

2) P. D. Kennewell and J. B. Taylor, *Chem. Soc. Rev.*, **1975**, 189; C. R. Johnson, *Acc. Chem. Res.*, **6**, 341 (1973); S. L. Huang and D. Swern, *Phosphorus and Sulfur*, **1**, 309 (1976); W. E. Truce, T. C. Klinger, and W. W. Brand, "Organic Chemistry of Sulfur," ed by S. Oae, Plenum Press, New York, London (1977), p. 527.

3) M. Haake, "Topics in Sulfur Chemistry," ed by A. Senning, George Thieme Verlag, Stuttgart (1976), Vol. 1, p. 187.

4) N. Furukawa, T. Yoshimura, and S. Oae, *Tetrahedron Lett.*, **1973**, 2113.

5) S. Oae, K. Iida, and T. Takata, *Tetrahedron Lett.*, **22**, 573 (1981); *Phosphorus and Sulfur*, **12**, 103 (1981).

6) D. J. Anderson, T. L. Gilchrist, D. C. Horwell, and C. W. Rees, *J. Chem. Soc., Chem. Commun.*, **1969**, 146; S. Colonna and C. J. M. Stirling, *ibid.*, **1971**, 1591; C. W. Rees and M. Yelland, *J. Chem. Soc., Perkin Trans. 1*, **1972**, 77; D. J. Anderson, D. J. Horwell, E. Stanton, T. L. Gilchrist, and C. W. Rees, *ibid.*, **1972**, 1317.

7) R. H. Heintzelman, R. B. Bailey, and D. Swern, *J. Org. Chem.*, **41**, 2207 (1967).

8) C. S. Foote and J. W. Peters, *J. Am. Chem. Soc.*, **93**, 3795 (1971); L. D. Martin and J. C. Martin, *ibid.*, **99**, 3511 (1977).

9) K. E. Pfitzner and J. G. Moffatt, *J. Am. Chem. Soc.*, **85**, 3027 (1963); **87**, 5661, 5670 (1965); **88**, 1762 (1966).

10) H. S. D. Soya and W. P. Weber, *Tetrahedron Lett.*, **1978**, 1969.

11) S. Oae, "Yuuki Iou Kagaku (Organic Sulfur Chemistry)," Kagaku Dojin, Kyoto (1982), Chap. 7.

12) A. Wm. Johnson and R. T. Amel, *Tetrahedron Lett.*, **1966**, 819.

13) N. Furukawa, F. Takahashi, T. Yoshimura, and S. Oae, *Tetrahedron Lett.*, **1977**, 3633; *Tetrahedron*, **35**, 317 (1978).

14) H. R. Bentley and J. K. Whitehead, *J. Chem. Soc.*, **1950**, 2081; D. J. Cram, J. Day, D. R. Rayner, D. M. von Schriltz, D. J. Duchamp, and D. G. Garwood, *J. Am. Chem. Soc.*, **92**, 7369 (1970); H. S. Veale, J. Levin, and D. Swern, *Tetrahedron Lett.*, **1978**, 503.

15) R. B. Greenwald and D. H. Evans, *Synthesis*, **1977**, 650.

16) R. Appel, H. W. Fehlhaber, D. Haenssgen, and T. Schoellhorn., *Chem. Ber.*, **99**, 3108 (1966).

17) A. I. J. Vogel, *J. Chem. Soc.*, **1948**, 616.

18) F. Montanari, *Gazz, Chim. Ital.*, **86**, 406 (1956).

19) M. H. Hubacker, *Org. Synth.*, Col. Vol. II, 455 (1943).

20) F. Kurzer, *J. Chem. Soc.*, **1953**, 549.

21) T. R. Williams, A. Nudelman, R. E. Booms, and D. J.

Cram, *J. Am. Chem. Soc.*, **94**, 4684 (1972).
22) E. S. Levchenko, N. Ya Derkach, and A. V. Kirsanov., *Zh. Obshch. Khim.*, **31**, 1971 (1961).
23) N. Furukawa, T. Omata, T. Aida, and S. Oae, *Tetrahedron Lett.*, **1972**, 1619; T. Yoshimura, T. Omata, N. Furukawa, and S. Oae, *J. Org. Chem.*, **41**, 1728 (1976).
24) N. Furukawa, K. Akutagawa, T. Yoshimura, and S. Oae, *Synthesis*, **1982**, 77.
25) N. Furukawa, K. Akutagawa, T. Yoshimura, T. Akasaka, and S. Oae, *Synthesis*, **1979**, 289.

 © 1984 The Chemical Society of Japan Bull. Chem. Soc. Jpn., 57, 525—528 (1984)

Reactivities of Stable Rotamers. XII. Reactions of 9-(2-Bromomethyl-6-methylphenyl)fluorene Rotamers with Nucleophiles[1,2]

Shigeru MURATA, Seiichiro KANNO, Yo TANABE, Mikio NAKAMURA, and Michinori ŌKI*
Department of Chemistry, Faculty of Science, The University of Tokyo, Bunkyo-ku, Tokyo 113
(Received September 19, 1983)

Rates of some substitution reactions of 9-(2-bromomethyl-6-methylphenyl)fluorene rotamers with nucleophiles are compared. Methanolysis of the rotamers proceeded smoothly in the *sp* form but was sluggish in the *ap*. Reactions of the *sp* form with sodium methoxide afforded 6-methylspiro[benzocyclobutene-1(2*H*), 9'-[9*H*]fluorene] and *sp*-9-(2-methoxymethyl-6-methylphenyl)fluorene, the former being a minor product. In addition to these, isomerization to the *ap* was detected. In contrast, the *ap* form afforded the spiro compound as a major product and the *ap* form of the methoxy compound as a minor product. Menschutkin reactions with pyridine bases were much faster in the *sp* form than in the *ap*. These results are attributed to the steric effect in the transition states of the reactions: the *sp* form reacts much faster than the *ap* because of the presence of the fluorene moiety in proximity of the reaction site in the latter.

Understanding of reactivities of rotational isomers is essential, if we wish to improve the selectivity of a reaction which is carried out at a low temperature, where conformations are frozen. To achieve this end, we have been studying the reactivities of stable rotamers since the success in isolating atropisomers at room temperature.[3,4] In a previous paper,[5] we gave a full account of the research on ionization reactions of 9-(2-bromomethyl-6-methylphenyl)fluorene (**1**) rotamers and a general conclusion is that, if the transition state for a reaction is space-demanding, the reaction is very slow in the *ap* form relative to that in the *sp* form. Similar conclusions were reached in related compounds.[1,6]

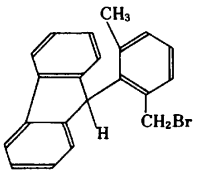

sp-1

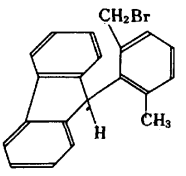

ap-1

This paper reports the results of investigations on the reactivities of *sp*-**1** and *ap*-**1** with some nucleophiles. Since S_N2 type reactions are space-demanding in their transition states, the relative reactivities (k_{sp}/k_{ap}) are expected to be large in these reactions and the expectation is proved to be true.

Results and Discussion

Main reactions investigated in this work are summarized in the following chart, together with a related reaction.

Methanolysis of alkyl halides is known to be autocatalytic. Therefore, only the initial reaction rates are valid, if we wish to discuss the results quantitatively.[7] Alternatively, a base which shows proton affinity but no affinity to other acids may be added to obtain reliable data. Furthermore, it was pointed out that benzyl halides react in both S_N1 and S_N2 fashions in solvolytic reactions.[8]

Heating a rotamer of **1** in methanol containing *ca.* 2 (v/v)% of chloroform, which was necessary for facile

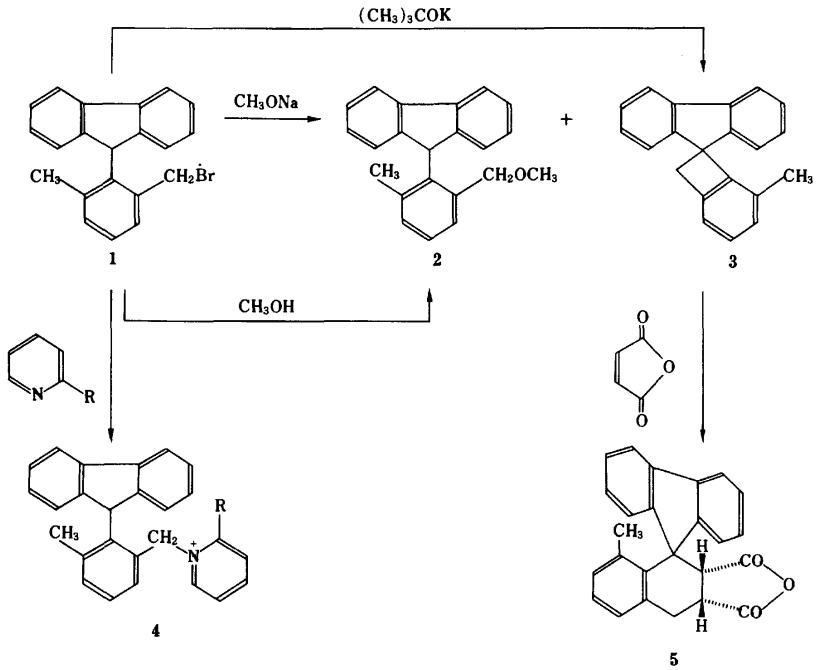

Table 1. Conditions and products of reactions of 1 with sodium methoxide in methanol

Temp/°C	Time/min	Substrate	Conversion	Products (%)[a]			
				Isomerization	*sp*-2	*ap*-2	3
25	500	*sp*-1	72	4	78	Trace	19
		ap-1	58	8	6	Trace	86
50	80	*sp*-1	94	0	72	7	20
		ap-1	88	0	5	Trace	95

a) Normalized to 100%.

dissolution, at 52 °C afforded methanolysis products, *sp*- and *ap*-9-(2-methoxymethyl-6-methylphenyl)fluorene (**2**). The reaction obeyed the pseudo-first order rate law until 20—30% completion. The rate constants were obtained as follows: $k_{sp}=5.5\times10^{-3}\,min^{-1}$, $k_{ap}=1.9\times10^{-4}\,min^{-1}$. *Under competitive conditions,* k_{sp}/k_{ap} was *ca.* 29 which is in good agreement with the data of the individual constants.[9]

The data allured us to investigate the methanolysis of 9-[2,6-bis(bromomethyl)phenyl]fluorene (**6**).[5] This compound possesses a diastereotopic pair of bromomethyl groups but thier reactivities should be different to a great extent. Indeed, methanolysis of **6** afforded *ap*-9-(2-bromomethyl-6-methoxymethylphenyl)-fluorene (**7**) as a sole product.

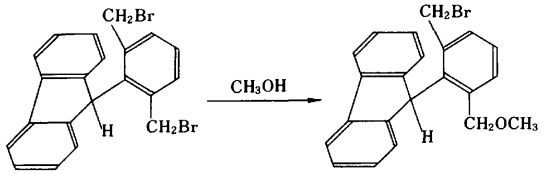

6 7

Using a strong base as a nucleophile should erase the effect of proton which is produced by the reaction but may cause deprotonation at the 9-position of fluorene. We have experiences of base-catalyzed isomerization of rotamers of 9-arylfluorenes.[6] Thus the use of a strong base should materialize the competitive reactions between deprotonation from the 9-position of fluorene and nucleophilic substitution at the CH_2Br group in **1**. As such a base, we examined the case of methoxide. This reaction afforded a mixture of 9-(2-methoxymethyl-6-methylphenyl)fluorene (**2**) and a spiro compound, 6-methylspiro[benzocyclobutene-1(2*H*),9′-[9*H*]fluorene] (**3**), which was also prepared by treating either *sp*-**1** or *ap*-**1** with sodium hydride. The reaction conditions and product distributions are summarized in Table 1.

Isomerization of *sp*-**1** to the *ap* form and the reverse are observed at 25 °C to a small extent. Since the formation of **3** must proceed *via* deprotonation at the 9-position followed by an intramolecular S_N2 reaction, the observation of the isomerization suggests that the intramolecular S_N2 reaction is slower than the deprotonation. Nonexistence of the isomerization of **1** in the reactions at 50 °C may mean that the rate of the cyclization is comparable with that of the deprotonation at this temperature. The mechanism of the formation of the isomerized methoxycompound (**2**) is not clear, since **2** can be formed either by isomerization of **1** or that of **2**. Probably the both mechanisms are involved. The most interesting point here is that, in *sp*-**1**, the substitution to produce *sp*-**2** is a main reaction, whereas, in *ap*-**1**, the deprotonation is main. Apparently the S_N2 type substitution is faster than the deprotonation in *sp*-**1**, but the S_N2 type reaction is so slow in the *ap* that the deprotonation becomes the main reaction.

According to the idea discussed above, the reaction of **1** with *t*-butoxide should produce **3** as a sole product, since S_N2 reactions of *t*-butoxide is known to be unimportant.[10] Indeed, treatment of either *sp*-**1** or *ap*-**1** with potassium *t*-butoxide in *t*-butyl alcohol produced the spiro compound (**3**) as a sole product. The relative reactivity (k_{sp}/k_{ap}) was 1.4. The cause for this difference in the reactivities of the rotamers is probably ligation between the cation and the bromine atom in the 2-substituent, which is close to the reaction site in the *sp* form. Since potassium *t*-butoxide exists most probably as ion pairs in *t*-butyl alcohol which has a low dielectric constant,[11] ligation of the bromine to potassium ion should reduce the effective size of the alkoxide to some extent. Such an example of assistance in deprotonation has been reported.[12]

The facile formation of the spiro compound (**3**) was a surprise for us because it contained a benzocyclobutene moiety; benzocyclobutenes are usually prepared by special techniques. In order to confirm the structure, we have carried out a reaction. Benzocyclobutenes are known to be pyrolyzed to produce *o*-quinone dimethides which can be trapped by a dienophile.[13] This reaction is used even for syntheses of natural products.[14] Heating a solution of **3** in toluene with maleic anhydride at 135 °C, we were able to isolate an adduct (**5**). Thus the structure of **3** is supported by a chemical means.

Pyridine bases are known to undergo pure S_N2 reactions with benzyl chloride.[15] Since their basicities are not high, their activity for deprotonation may not be very high as well. Thus it is hopeful that we examine pure S_N2 reactions of **1** without isomerization and formation of **3**, if we use a pyridine base. The results are summarized in Table 2. Compound *sp*-**1** reacts 35 times faster with 2-methylpyridine and 22 times faster with pyridine than *ap*-**1**.

Under the same conditions utilized for the reaction of **1** with 2-methylpyridine, benzyl bromide reacted with the

Table 2. Rates of menschutkin reactions of 1 with pyridine bases

		Pyridine	2-Methylpyridine
Temp/°C		35	34
k_2/L mol^{-1} s^{-1}	*sp*-1	8.5×10^{-4}	2.3×10^{-4}
	ap-1	3.9×10^{-5}	6.7×10^{-6}
k_{sp}/k_{ap}		22	35

base with a rate constant of 3.8×10^{-5} L mol^{-1} s^{-1}. The rate constant is in good agreement with that reported.[16] Thus benzyl bromide is about 6 times more reactive than *ap*-**1** but is less reactive than *sp*-**1** by a factor of *ca.* 6. The tendency of enhancement of the reaction rate by substitution of the ortho position of benzyl halides is known.[17] The explanation of the enhancement by the van der Waals interaction[18] may be valid in this case as well.

If we summarize the results presented above, the S_N2 type reactions are, without exception, slow in *ap*-**1** relative to *sp*-**1**. This is reasonable, from the experiences we have had before,[1,6] since S_N2 type reactions take space-demanding transition states which require high energy state in the *ap* because of the steric effect. The decrease in the difference in reactivities of the rotamers by going from 2-methylpyridine to pyridine is a reflection of the steric effect. It is also interesting to note that the relative reactivity of the bromomethyl group in the rotamers is not dependent on the nucleophilicity[19] of the nucleophiles: steric effects are the controlling factor in determining the relative reactivity because 2-methylpyridine which is rather a strong nucleophile exhibited the highest selectivity.

Experimental

9-(2-Methoxymethyl-6-methylphenyl)fluorene (2). A solution of 29 mg of *sp*-**1** in 3 mL of chloroform and 20 mL of methanol was heated at 50—60 °C for 24 h and then was poured into water. The mixture was extracted with ether and the extract was dried over magnesium sulfate. After evaporation of the solvent, the residue was submitted to silica-gel TLC (1:2 hexane–benzene) to afford *ca.* 95% *sp*-**2**, oil, which gave identical ^{1}H NMR spectrum with an authentic sample.[5]

Similar treatment of *ap*-**1** in methanol showed the presence of the starting material (35%) as well as *ap*-**2** (55%), of which ^{1}H NMR spectrum was identical with that of an authentic sample,[5] after 70 h heating.

ap-*9-(2-Bromomethyl-6-methoxymethylphenyl)fluorene (7).* A solution of 46 mg of **6**[5] in 0.5 mL of chloroform and 30 mL of methanol was heated at 50—60 °C for 7 h and the solvent was evaporaed. The residue was submitted to silica-gel TLC (3:1 hexane–benzene) to give 6 mg of the recovered material and 25 mg (58%) of the desired product. Recrystallization from hexane gave a pure sample, mp 91—92 °C Found: C, 69.43; H, 4.99; Br, 21.34%. Calcd for $C_{22}H_{19}BrO$: C, 69.67; H, 5.05; Br, 21.07%. ^{1}H NMR ($CDCl_3$, δ): 3.38 (2H, s), 3.44 (3H, s), 4.73 (2H, s), 5.57 (1H, s), 7.1—8.0 (11H, m).

6-Methylspiro[benzocyclobutene-1(2H),9′-[9H] fluorene] (3). A solution of 140 mg (0.40 mmol) of a *ca.* 1:1 mixture of *sp*-**1** and *ap*-**1** in 3.5 mL of tetrahydrofuran was mixed with a suspension of 60 mg (2.5 mmol) of sodium hydride in 3.5 mL of tetrahydrofuran. To the mixture was added 0.7 mL of *N,N*-dimethylformamide and the whole was stirred for 3 h at 55—60 °C under a nitrogen atmosphere. After being cooled, the mixture was treated with 7 mL of ether containing 1.4 mL of methanol. Water was added and the organic layer was separated. The organic layer and ether extracts of the aqueous layer were combined, and washed successively with dilute hydrochloric acid and aqueous sodium hydrogencarbonate. The combined solution was dried and evaporated. The residue was purified by TLC (4:1 hexane–benzene) to give 80 mg (75%) of the desired product. Recrystallization of the product from ethanol–pentane gave a pure sample, mp 93 °C. Found: C, 94.28; H, 5.83%. Calcd for $C_{21}H_{16}$: C, 93.99; H, 6.01%. MS showed an M^+ peak at *m/z* 268 while the calculated value is 268. ^{1}H NMR ($CDCl_3$, δ): 1.49 (3H, s), 3.65 (2H, s), 6.9—7.9 (11H, m).

8′-Methyl-3′,4′-dihydrospiro[9H-fluorene-9,1′(2′H)-naphthalene]-cis-2′,3′-dicarboxylic Anhydride (5). A solution of 85 mg (0.32 mmol) of **3** and 40 mg (0.41 mmol) of maleic anhydride in 0.5 mL of toluene was sealed in a tube under a nitrogen atmosphre and heated in a boiling xylene bath for 2 d. The reaction mixture was cooled and the precipitate was collected. Washing the crystals with benzene afforded 45 mg of the desired product whereas the mother liquor afforded 25 mg of the starting material after evaporation followed by TLC on silica gel (3:1 hexane–benzene). The yield was 55%. A pure sample of **5**, mp 235—236 °C, was obtained by recrystallization of the crude product from benzene. Found: C, 82.04; H, 4.69%. Calcd for $C_{25}H_{18}O_3$: C, 81.95; H, 4.95%. MS (M^+): 366. ^{1}H NMR (DMSO-d_6, δ): 1.02 (3H, s), 3.4—4.4 (4H, m), 6.9—8.1 (11H, m). IR (KBr disk): 1860, 1780 cm^{-1}.

1-[2-(9-Fluorenyl)-3-methylbenzyl]-2-methylpyridinium Bromide (4: R=CH$_3$). A solution of 20 mg (57 μmol) of *sp*-**1** in 0.3 mL of acetone containing 50 μL (510 μmol) of 2-methylpyridine. The mixture was stirred for 2 h at 35 °C. The precipitate was collected and was washed with acetone to give 12 mg (48%) of the desired compound. Recrystallization of the product from methanol–ethanol–hexane afforded a pure sample, mp 227 °C (decomp). Found:, 73.30; H, 5.18; N, 3.33; Br, 18.21%. Calcd for $C_{27}H_{24}NBr$: C, 73.30; H, 5.47, N, 3.18; Br, 18.06%. ^{1}H NMR (DMSO-d_6, δ): 1.12 (3H, s), 2.96 (3H, s), 5.50 (1H, s), 6.39 (2H, s), 6.7—9.2 (15H, m).

Similar reaction of *ap*-**1** carried out for 3 d under a nitrogen atmosphere afforded colorless crystals, mp 210 °C (decomp), after recrystallization from acetone–hexane. Found: C, 71.59; H, 5.42; N, 3.11; Br, 17.87%. Calcd for $C_{27}H_{24}NBr\cdot 1/2H_2O$: C, 71.84; H, 5.58; N, 3.10; Br, 17.70%. ^{1}H NMR (DMSO-d_6, δ): 1.81 (3H, s), 2.83 (3H, s), 4.40 (2H, s), 5.77 (1H, s), 6.6—8.5 (15H, m). ^{1}H NMR ($CDCl_3$, δ): 2.04 (3H, s), 2.79 (3H, s), 4.75 (2H, s), 5.62 (1H, s), 7.1—8.3 (15H, m). The *ap*-**4** (R=CH$_3$) was much more soluble in various solvents than *sp*-**4** (R=CH$_3$).

1-[2-(9-Fluorenyl)-3-methylbenzyl]pyridinium Bromide (4: R=H). The reaction of **1** with pyridine was carried out similarly as described for the reaction of 2-methylpyridine.

sp-**4** (R=H), mp 216 °C (decomp). Found: C, 73.40; H, 5.25; N, 3.32; Br, 18.90%. Calcd for $C_{26}H_{22}NBr$: C, 72.90; H, 5.18; N, 3.27; Br, 18.65%. ^{1}H NMR (DMSO-d_6, δ): 1.04 (3H, s), 5.46 (1H, s), 6.38 (2H, s), 6.7—9.2 (16H, m).

ap-**4** (R=H), mp 189 °C (decomp). Found: C, 71.02; H, 4.92; N, 3.14; Br, 18.22%. Calcd for $C_{26}H_{22}NBr\cdot 1/2H_2O$: C, 71.40; H, 5.30; N, 3.20; Br, 18.27%. ^{1}H NMR ($CDCl_3$, δ): 2.79 (3H s) 5.05 (2H, s), 5.60 (1H, s), 7.0—8.2 (16H, m).

Reaction of 1 with Sodium Methoxide. To a solution of 20 mg (57 μmol) of *sp*-**1** or *ap*-**1** and 15 mg of 2-methylnaphthalene, which served as an internal reference in the subsequent analysis, in 0.4 mL of chloroform and 28.6 mL of methanol, was added 1 mL of a methanolic solution of sodium methoxide, which was prepared by adding 0.13 g of sodium to 10.0 mL of methanol. After the solution was heated at appropriate temperatures for given times, the conversion ratio was checked by means of HPLC (a Waters M-6000 instrument) with a UV detecter. The reaction mixture was cooled and diluted with chilled water. The mixture was acidified with dilute hydrochloric acid and was extracted with dichloromethane. The organic layer was washed, dried, and evaporated. The residue in chloroform-*d* showed the presence of the spiro compound (**3**) and the methoxy compound (**2**) in addition to others. The results are summarized in Table 1.

Reaction of 1 with Potassium t-Butoxide. To a solution of 5 mg (14 μmol) each of *sp*-**1** and *ap*-**1** in 14 mL of *t*-butyl alcohol containing 3 mg of 2-methylnaphthalene, was added 1 mL of a solution of potassium *t*-butoxide (280 μmol) in

t-butyl alcohol, of which concentration was determined by titration. After 30 min, the reaction mixture was treated in a usual manner and the products were checked with ^{1}H NMR, HPLC, and/or TLC. No products other than the spiro compound (**3**) were detected.

Determinaion of Rates of Reactions. Methanolysis: A solution of 6.0 mg (17 μmol) each of *sp*-**1** and *ap*-**1** and 2.9 mg of fluorene in 0.4 mL of chloroform and 20 mL of methanol was heated at 52 °C. The aliquot was syringed out at appropriate intervals and the materials were analyzed with the use of HPLC, using the fluorene as an internal standard. The data satisfied the pseudo-first order rate law until 20—30% completion.

Menshutkin Reactions. To a solution of 12.5 mg (36 μmol) of *sp*-**1** or *ap*-**1** in 0.18 mL of dry acetone containing a small amount of dichloromethane or 1,2-dichloroethane in an NMR tube, was added 0.18 mL of a solution (0.190 mol/L) of pyridine and the tube was placed in an NMR probe at 35 °C. The decrease in the amount of the halide (**1**) was measured by taking the signal intensity of the added dichloromethane or 1,2-dichloroethane as an internal standard. The reaction obeyed the second-order rate law until 15—20% completion.

The reaction of **1** with 2-methylpyridine was monitored similarly except that the excess of an acetone solution (1.0 mol/L) of the base was used. Pseudo-first order rate constants thus obtained gave the second-order rate constants.

Competitive Reactions. Methanolysis was carried out as described in the section of rates of methanolysis except that 6.0 mg each of *sp*-**1** and *ap*-**1** were dissolved at the beginning. The relative reactivity was calculated by the following equation, where subscript 0 denotes the initial state.

$$k_{sp}/k_{ap} = \log \frac{[sp]}{[sp]_0} \Big/ \log \frac{[ap]}{[ap]_0}$$

Reaction with potassium *t*-butoxide was carried out similarly using 2-methylnaphthalene as an internal standard.

This work was supported by a Grant for a Special Project Research of the Ministry of Education, Science and Culture, to which the authors thanks are due.

References

1) Part XI: R. Saito and M. Ōki, *Bull. Chem. Soc. Jpn.*, **55**, 3273 (1982).
2) A preliminary note of this work was published: S. Murata, S. Kanno, Y. Tanabe, M. Nakamura, and M. Ōki, *Angew. Chem., Int. Ed. Engl.*, **20**, 606 (1981).
3) M. Ōki, *Angew. Chem., Int. Ed. Engl.*, **15**, 87 (1976).
4) M. Ōki, *Top. Stereochem.*, **14**, 1 (1983).
5) S. Murata, S. Kanno, Y. Tanabe, M. Nakamura, and M. Ōki, *Bull. Chem. Soc. Jpn.*, **55**, 1522 (1982).
6) R. Saito and M. Ōki, *Bull. Chem. Soc. Jpn.*, **55**, 3267 (1982).
7) E. Grunwald and S. Winstein, *J. Am. Chem. Soc.*, **69**, 2051 (1947).
8) S. Winstein, E. Grunwald, and H. W. Jones, *J. Am. Chem. Soc.*, **73**, 2700 (1951).
9) If this is a purely unimolecular reaction, a much smaller ratio is expected since other ionizing reactions give smaller k_{sp}/k_{ap} ratios. See Ref. 5.
10) H. C. Brown and I. Moritani, *J. Am. Chem. Soc.*, **76**, 455 (1954).
11) M. Szwarc, "Concept of Ion Pairs" in "Ions and Ion Pairs in Organic Chemistry" ed by M. Szwarc, Wiley-Interscience, New York (1972), Vol. 1, pp. 1—26.
12) M. Nakamura and M. Ōki, *Chem. Lett.*, **1975**, 671.
13) F. R. Jensen, W. E. Coleman, and A. J. Berlin, *Tetrahedron Lett.*, **1962**, 15; R. Huisgen and H. Seidl, *ibid.*, **1964**, 3381: B. J. Arnold, P. G. Sammes, and T. W. Wallace, *J. Chem. Soc., Perkin Trans. 1*, **1974**, 415.
14) For example, see T. Kametani, H. Matsumoto, T. Honda, and K. Fukumoto, *Tetrahedron Lett.*, **1981**, 2379.
15) J. W. Baker, *J. Chem. Soc.*, **1934**, 987.
16) J. W. Baker and W. S. Nathan, *J. Chem. Soc.*, **1935**, 519.
17) J. C. Charlton and E. D. Hughes, *J. Chem. Soc.*, **1956**, 855.
18) J. F. Bunnett and J. D. Reinheimer, *J. Am. Chem. Soc.*, **84**, 3284 (1962).
19) R. G. Pearson, H. Sobel, and J. Songstadt, *J. Am. Chem. Soc.*, **90**, 319 (1968).

Total Synthesis of Aminoglycoside Antibiotics, Apramycin and Saccharocin (KA-5685)

Kuniaki TATSUTA,* Kohji AKIMOTO, Hideaki TAKAHASHI, Takao HAMATSU, Masahiko ANNAKA, and Mitsuhiro KINOSHITA

Department of Applied Chemistry, Faculty of Science and Technology, Keio University, Hiyoshi, Kohoku-ku, Yokohama 223

(Received September 24, 1983)

Apramycin and saccharocin (KA-5685) have been synthesized from previously synthesized neamine (**3**). Addition of allylmagnesium chloride to 4-*O*-[3′,4′-*O*-cyclohexylidene-2′-deoxy-2′-(tosylamino)-α-D-*gluco*-hexodialdo-1′,5′-pyranosyl]-5,6-*O*-cyclohexylidene-1,3-di-*N*-tosyl-2-deoxystreptamine which was derived from **3** through the 6′-*N*-oxide, gave 4-*O*-[3′,4′-*O*-cyclohexylidene-2′,7′,8′,9′-tetradeoxy-2′-(tosylamino)-L-*glycero*- and D-*glycero*-α-D-*gluco*-non-8′-enopyranosyl]-5,6-*O*-cyclohexylidene-1,3-di-*N*-tosyl-2-deoxystreptamines which were in turn converted into 4-*O*-[(8′*S*)-7′-*N*,6′-*O*-carbonyl-2′,3′,7′-trideoxy-8′-*O*-methyl-7′-(methylamino)-2′-(tosylamino)-D-*glycero*-α-D-*allo*-octodialdo-1′,5′:8′,4′-dipyranos-1′-yl]-5,6-*O*-cyclohexylidene-1,3-di-*N*-tosyl-2-deoxystreptamine (**25**), *via* azidonitration of 1-*N*-acetyl-4-*O*-[3′,6′-di-*O*-acetyl-4′,8′-anhydro-2′,7′-dideoxy-2′-(tosylamino)-L-*glycero*-α-D-*gluco*-oct-7′-enopyranos-1′-yl]-5,6-*O*-cyclohexylidene-1,3-di-*N*-tosyl-2-deoxystreptamine and epimerization of the 6′-hydroxyl group. Successive deprotection of **25** afforded aprosamine, from which 1,2′,3,7′-tetrakis(*N*-benzyloxycarbonyl)aprosamine (**28**) was prepared, and glycosidation of **28** with 4-azido-2,3,6-tri-*O*-benzyl-4-deoxy-β-D-glucopyranosyl fluoride or 2,3,4,6-tetra-*O*-benzyl-β-D-glucopyranosyl fluoride, followed by hydrogenolysis, completed the total synthesis.

Apramycin[1] (**1**) and saccharocin[2a] (**2**: antibiotic KA-5685 [2b]) are aminoglycoside antibiotics active against Gram-positive and Gram-negative bacteria including resistant strains of other aminoglycoside antibiotics. Apramycin (**1**) was isolated in 1967 as nebramycin component 2 from fermentation broths of *Streptomyces tenebrarius*,[1a] and saccharocin and KA-5685 (**2**), which were found to be identical with each other later on, were independently reported in 1983 as metabolites of *Saccharopolyspora sp.* by two Japanese groups.[2] Structural studies have revealed that antibiotics **1**[1b] and **2**[2] contain the unusual bicyclic aminooctodialdose and 2-deoxystreptamine units as common structures, and, in addition, 4-amino-4-deoxy-D-glucose and D-glucose units respectively. The unique structural features as well as the opportunity to develop synthetic strategy for the construction of more diverse analogs of these interesting antibiotics have prompted substantial recent synthesis efforts.[3,4] Very recently, the first total synthesis of **1** was disclosed in our laboratories.[5]

Herein we describe in detail, the first total synthesis of apramycin (**1**) and saccharocin (**2**: KA-5685).

Our point of departure is the known aminoglycoside antibiotic, neamine (**3**), which has already been synthesized by one of us[6] and Umezawa.[7] Neamine (**3**) was successively converted into 6′-*N*-(benzyloxycarbonyl)-3′,4′:5,6-di-*O*-cyclohexylidene-1,2′,3-tri-*N*-tosylneamine (**4**) by preferential *N*-benzyloxycarbonylation,[8] *N*-tosylation and *O*-cyclohexylidenation[9] in a 79% overall yield. Saponification of **4** with potassium *t*-butoxide followed by treatment of the resulting 6′-amino compound with 30% aqueous formaldehyde and $NaBH_3CN$[10] afforded the 6′-dimethylamino compound, which after oxidation with *m*-chloroperbenzoic acid gave the *N*-oxide **5** in an 83% overall yield. Treatment of **5** with benzoyl chloride and *N*,*N*-diisopropylethylamine produced the aldehyde, 4-*O*-[3′,4′-*O*-cyclohexylidene-2′-deoxy-2′-(tosylamino)-α-D-*gluco*-hexodialdo-1′,5′-pyranosyl]-5,6-*O*-cyclohexylidene-1,3-di-*N*-tosyl-2-deoxystreptamine (**6**) in a 75% yield, suggesting that the procedure would be useful for the preparation of the aldehydes from the primary amines.[11] Other couples of reagents (acetic anhydride, α-toluenesulfonyl chloride, trifluoroacetic anhydride, mesyl chloride, methanesulfonic anhydride, and tosyl chloride) and bases (*N*,*N*-diisopropylethylamine, 4-dimethylaminopyridine, *N*-methylmorpholine, and pyridine, *etc.*) were investigated, but gave **6** in lower yields.

Addition of allylmagnesium chloride to **6** gave a mixture of the (6′*S*)- and (6′*R*)-alcohols,[3a,12] 4-*O*-[3′,4′-*O*-cyclohexylidene-2′,7′,8′,9′-tetradeoxy-2′-(tosylamino)-L-*glycero*- and D-*glycero*-α-D-*gluco*-non-8′-enopyranosyl]-5,6-*O*-cyclohexylidene-1,3-di-*N*-tosyl-2-deoxystreptamines (**7** and **8**) in 37 and 41% yields, respectively. Reaction with allyltributyltin[13] also gave the similar ratio of the products with that by the Grignard reagent, but allyllithium[13] did not. The stereochemistry

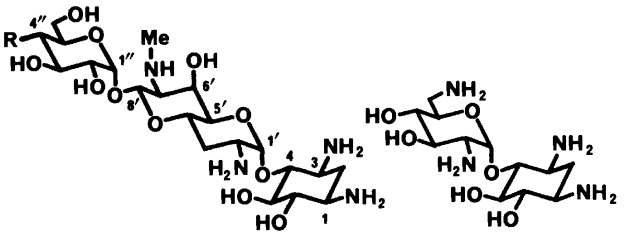

1 (Apramycin): R = NH_2 **3** (Neamine)

2 (Saccharocin): R = OH

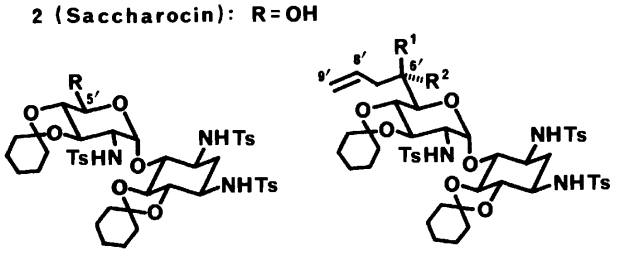

4: R = CH_2NHZ **7**: R^1 = H, R^2 = OH

5: R = $CH_2N(O)Me_2$ **8**: R^1 = OH, R^2 = H

6: R = CHO **16**: R^1 = H, R^2 = OAc

Chart 1.

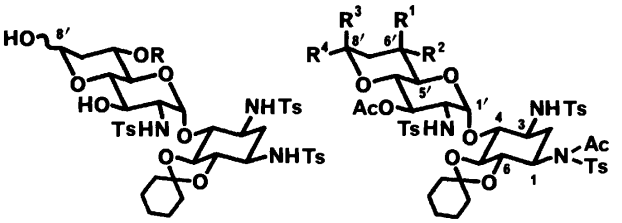

9 : R = H
17 : R = Ac

10a : $R^1=R^4=H$, $R^2=R^3=OAc$
10b : $R^1=R^3=H$, $R^2=R^4=OAc$
11 : $R^1=R^4=OAc$, $R^2=R^3=H$

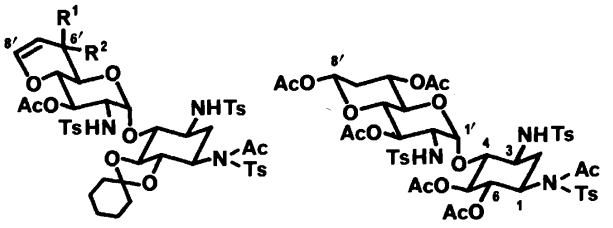

13 : $R^1=H$, $R^2=OAc$
14 : $R^1=OAc$, $R^2=H$

12

Chart 2.

at C-6′ in **7** and **8** was reasonably clarified by ^{1}H-NMR of the derivatives **10a, b** and **11** as follows. Oxidative cleavage of the olefin group of **7** with osmium tetraoxide and then sodium periodate to give the aldehyde, followed by selective removal of the cyclohexylidene group by aqueous acetic acid, afforded the octodialdose[3a] derivative **9** in a 60% yield. Acetylation of **9** with acetic anhydride and pyridine at 40 °C gave a mixture of the 1-*N*-acetyl-α- and β-acetates, 1-*N*-acetyl-4-*O*-[(8′*S*)- and (8′*R*)-3′,6′,8′-tri-*O*-acetyl-2′,7′-dideoxy-2′-(tosylamino)-L-*glycero*-α-D-*gluco*-octodialdo-1′,5′:8′,4′-dipyranos-1′-yl]-5,6-*O*-cyclohexylidene-1,3-di-*N*-tosyl-2-deoxystreptamines (**10a** and **10b**) in 34 and 37% yields. Similarly, **8** was transformed into a single β-acetate **11**. Their ^{1}H-NMR decoupling revealed the H-6′ methine protons in **10** and **11** to be axial ($J_{5',6'}$=10 Hz) and equatorial ($J_{5',6'}$=2.5 Hz), respectively, assigning the stereochemistry of **7** and **8**. Also, the 1-*N*-acetyl structures of **10** and **11** were deduced by the ^{1}H-NMR spectrum of the 1-*N*-acetyl-3′,5,6,6′,8′-penta-*O*-acetyl derivative **12**, which was formed by removal of the cyclic acetal of **10b** followed by acetylation. All methine protons of the 2-deoxystreptamine moiety were completely assigned in **12**, and the significant downfield shift was observed for the H-1 signal (δ 4.34) in comparison with the H-3 signal (δ 3.40).

The aforesaid intermediate **9** was converted by our method[14] using tosyl chloride and triethylamine, and acetylation into the acetyl glycal, 1-*N*-acetyl-4-*O*-[3′,6′-di-*O*-acetyl-4′,8′-anhydro-2′,7′-dideoxy-2′-(tosylamino)-L-*glycero*-α-D-*gluco*-oct-7′-enopyranos-1′-yl]-5,6-*O*-cyclohexylidene-1,3-di-*N*-tosyl-2-deoxystreptamine (**13**) in a 52% overall yield. The glycal **13** was treated with 0.5 M† hydrochloric acid, followed by acetylation to give **12** as one of the anomeric acetates, supporting the 1-*N*-acetyl structure. Though **13** possessed an acetoxyl group at C-6′ having the (*S*)-configuration which was incompatible with the natural stereochemistry, it was clear that **13** could be a useful intermediate provided that a cis cyclic carbamate formation could be achieved with the appropriate S_N2 inversion at the later stage (for an example: **24**→**25**). On the other hand, the glycal **14**, which was similarly derived from the other alcohol **8**, possessed the natural (*R*)-configuration at C-6′, but, on azidonitration[15] with sodium azide and ammonium ceric nitrate, gave a single (7′*R*,8′*R*)-product **15** with the undesired axial azido group owing to the sizeable steric interactions of the C-6′ axial acetoxyl group. Then, **8** was efficiently transformed into the glycal **13** through the inversion of the 6′-hydroxyl group. Mesylation of **8** followed by displacement reaction with potassium acetate gave the corresponding acetate **16** in an 85% yield, which was identical with the acetate of **7**. As described above, oxidative cleavage of the olefin group and selective hydrolysis of **16** afforded the octodialdose derivative **17**, which was in turn led to the key glycal **13** in a 55% yield.

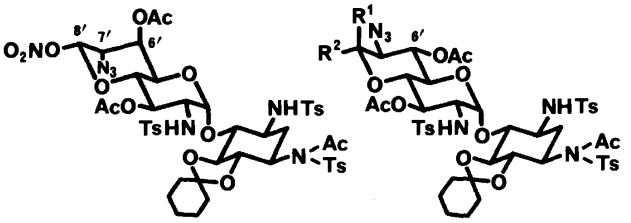

15

18 : $R^1=ONO_2$, $R^2=H$
19 : $R^1=H$, $R^2=ONO_2$

Chart 3.

Azidonitration[15] of **13** gave two major azidoglycosyl nitrates **18** and **19** having the (7′*S*,8′*S*)- and (7′*S*,8′*R*)-configurations in 63 and 14% yields. The stereochemistry was defined by their ^{1}H-NMR spectra. Remarkably, the addition was effectively stereoselective, generating only one of the two possible configurations at C-7′. Treatment of either **18** or **19** with barium hydroxide in methanol afforded the corresponding deacetylated methyl β-glycoside, 4-*O*-[(8′*S*)-7′-azido-2′,7′-dideoxy-8′-*O*-methyl-2′-(tosylamino)-D-*thereo*-α-D-*gluco*-octodialdo-1′,5′:8′,4′-dipyranos-1′-yl]-5,6-*O*-cyclohexylidene-1,3-di-*N*-tosyl-2-deoxystreptamine (**20**) in 71% or 40% yield, along with less than 7% yield of the α-glycoside. In a straightforward fashion **20** was transformed in a 61% overall yield into the 7′-[*N*-(benzyloxycarbonyl)-methylamino] derivative **22** through **21** *via* a four-step process: catalytic reduction, *N*-benzyloxycarbonylation, hydride reduction and again *N*-benzyloxycarbonylation.

Mesylation of **22** afforded quantitatively the labile dimesylate **23**, the C-3′ position of which was selectively chlorinated to form the 3′-chloro compound, by analogy with the results obtained by Umezawa and co-workers.[16] Dechlorination of the intermediate with tributylstannane gave the 3′-deoxy compound, 4-*O*-{(8′*S*)-7′-[*N*-(benzyloxycarbonyl)methylamino]-2′,3′,7′-trideoxy-6′-*O*-mesyl-8′-*O*-methyl-2′-(tosylamino)-D-*glycero*-β-L-*talo*-octodialdo-1′,5′:8′,4′-dipyranos-1′-yl}-5,6-

† 1 M=1 mol dm^{-3}.

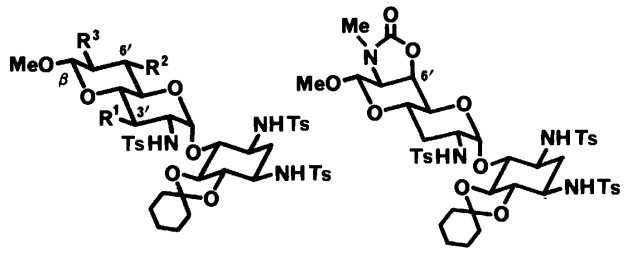

20: $R^1=R^2=OH$, $R^3=N_3$ **25**

21: $R^1=R^2=OH$, $R^3=NHZ$

22: $R^1=R^2=OH$, $R^3=N<^{Z}_{Me}$

23: $R^1=R^2=OMs$, $R^3=N<^{Z}_{Me}$

24: $R^1=H$, $R^2=OMs$, $R^3=N<^{Z}_{Me}$

Chart 4.

O-cyclohexylidene-1,3-di-*N*-tosyl-2-deoxystreptamine (**24**) in an 81% yield from **23**. All attempts[17] to form a cis cyclic carbamate failed, except for epimerization[18] of the 6′-hydroxyl group by heating **24** with sodium acetate trihydrate in 2-methoxyethanol, which yielded only 4-*O*-[(8′*S*)-7′-*N*,6′-*O*-carbonyl-2′,3′,7′-trideoxy-8′-*O*-methyl-7′-(methylamino)-2′-(tosylamino)-D-*glycero*-α-D-*allo*-octodialdo-1′,5′:8′,4′-dipyranos-1′-yl]-5,6-*O*-cyclohexylidene-1,3-di-*N*-tosyl-2-deoxystreptamine (**25**) needed for the apramycin skeleton. The stereochemistry was also confirmed by the ^{1}H-NMR and IR spectra.[17,18]

De-*N*-tosylation of **25** with sodium metal in liquid ammonia followed by alkaline hydrolysis to remove the *N*,*O*-carbonyl group and subsequent acidic hydrolysis to remove the cyclohexlidene group afforded the aminooctodialdose derivative, methyl β-aprosaminide[1b] (**26**) in a 65% overall yield, which was further hydrolyzed with 4M hydrochloric acid to give aprosamine[1b,4] (**27**). Both **26** and **27** were identical in all respects with the naturally derived products, thus setting the stage for introduction of the 4-amino-4-deoxy-D-glucose or D-glucose unit.

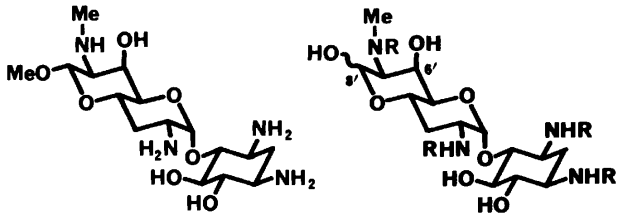

26 (Methyl β-aprosaminide) **27** (Aprosamine): R=H

28: R=Z

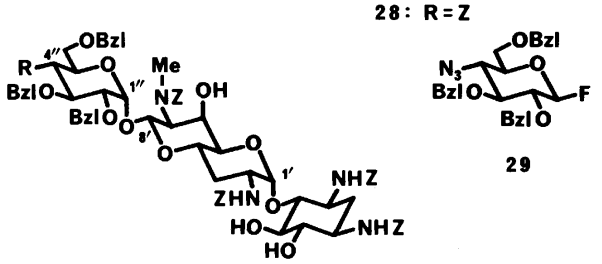

29

30: $R=N_3$

31: R=OBzl

Chart 5.

N-Benzyloxycarbonylation of **27** generated the key intermediate for the following glycosidation, 1,2′,3,7′-tetrakis(*N*-benzyloxycarbonyl)aprosamine[4] (**28**) in a 77% yield.

Methanolysis of **28** with a methanolic hydrogen chloride solution or methylation with methyl iodide and silver oxide, to give the corresponding methyl glycoside, followed by catalytic reduction gave the aforesaid methyl β-aprosaminide (**26**) in a fairly good yield (81% or 70%). The findings suggested that the 1,3-diaxial interaction between C-6′- and C-8′- substituents would then lead to the less sterically encumbered transition state and thus to the exclusive formation of the β-glycoside even under acidic conditions, where the anomeric effect could be predominant.[19] Further, reaction of *O*-benzylglycosyl halides with alcohols are known to yield exclusively the corresponding α-glycosides owing to the anomeric effect as commonly seen in carbohydrates.[19-22] Consequently, it was expected that reaction of the appropriate *O*-benzylglycosyl halides with **28** would produce the desired α-glycosyl-β-aprosaminides in reasonable yields. In the glycosidation studies on **28**, a large number of variables including catalyst and temperature were assayed.[20-22] The best result was realized under modified Mukaiyama conditions[20] by using 4-azido-2,3,6-tri-*O*-benzyl-4-deoxy-β-D-glucopyranosyl fluoride (**29**), which was prepared from the corresponding α-D-glycosyl chloride,[22] to give two major products having R_f 0.48 and 0.44 on thin-layer chromatography. The R_f 0.44-substance, which was found to be the desired glycoside **30** by the following chemical and physical evidence, could be isolated by silica-gel column chromatography in a modest yield (40% yield based on unrecovered alcohol **28**). It should be noted, however, that the glycosidation was achieved without protection of the C-5, 6, and 6′ hydroxyl groups. Hydrogenolysis of **30** furnished apramycin (**1**) in a 74% yield, which was identical with the natural antibiotic in all respects including antibacterial activity, but the R_f 0.48-substance did not give **1**.

Similarly, glycosidation of the key alcohol **28** employing 2,3,4,6-tetra-*O*-benzyl-β-D-glucopyranosyl fluoride[20] provided the expected glycoside **31** in a 24% yield (42% yield based on unrecovered **28**) after column chromatography. Hydrogenolysis of **31** completed the synthesis, giving saccharocin (**2**: KA-5685) identical with the natural antibiotic in all respects.

The antibacterial activities of **1**, **2**, **26**, and **27**, which are shown in Table 1, were identical with those of the natural products and their derivatives.

The application of this synthetic strategy for the construction of other related antibiotics as well as some of their potentially therapeutically interesting analogs is an exciting prospect.

Experimental

Melting points were determined on a micro hot-stage Yanaco MP-S3 and were uncorrected. IR and Mass spectra were recorded on Hitachi Perkin-Elmer 225 and Hitachi M-80H (SIMS) spectromters, respectively, and ^{1}H-NMR spectra with TMS as internal standard on a Varian EM-390 (90 MHz) or a Bruker WM 250 spectromter (250 MHz). Optical rotations were measured on a Carl Zeiss photoelectric polar-

TABLE 1. MINIMAL INHIBITORY CONCENTRATION (mcg/ml) OF **1**, **2**, **26**, AND **27**

	1	**2**	**26**	**27**
Staphylococcus aureus FDA 209P	1.56	6.25	12.5	12.5
Klebsiella pneumoniae PCI 602	3.12	6.25	12.5	25
Salmonella typhi T-63	1.56	3.12	6.25	12.5
Escherichia coli K-12 ML 1629	1.56	12.5	12.5	25
Escherichia coli K-12 C600 R135	3.12	6.25	6.25	12.5
Escherichia coli JR66/W677	3.12	12.5	6.25	25
Pseudomonas aeruginosa A3	0.78	1.56	3.12	6.25
Pseudomonas aeruginosa NO. 12	12.5	25	100	50

imeter. Silica-gel TLC and column chromatography were performed on Merck TLC 60F-254 and Wakogel C-200 or Kieselgel 60. In general, organic solvents were purified and dried by the appropriate procedures, and evaporation and concentration were carried out under reduced pressure below 30 °C.

6′-N-(Benzyloxycarbonyl)-3′,4′:5,6-di-O-cyclohexylidene-1,2′,3-tri-N-tosylneamine (4). To a solution of neamine (**3**: 50 g) in 50% aqueous methanol (500 ml) containing triethylamine (23.8 ml) was added *N*-(benzyloxycarbonyloxy)-5-norbornene-2,3-dicarboximide[8] (53.4 g), and the solution was stirred at room temperature for 5 h. After addition of 28% aqueous ammonia (110 ml), the solution was evaporated to a residue of the 6′-*N*-benzyloxycarbonyl derivative. A solution of the residue in 70% aqueous 1,4-dioxane (1 l) was stirred with tosyl chloride (106.4 g) and Na_2CO_3 (61.1 g) at room temperature for 5 h. After filtration, the filtrate was concentrated to give gummy precipitates, which were washed with water and then dried to give a solid of the tri-*N*-tosyl derivative (166 g). To a solution of the solid in DMF (1.66 *l*) were added 1,1-dimethoxycyclohexane (187 ml) and anhydrous TsOH (2.67 g), and the solution was stirred at 50 °C for 1 d under reduced pressure (≃25 Torr††). After further addition of 1,1-dimethoxycyclohexane (187 ml), the reaction was continued at the same conditions for another 2 d. After addition of triethylamine (2.16 ml) and $NaHCO_3$ (6.51 g), the mixture was evaporated to a residue, which was chromatographed on silica gel (2 kg) with 2:1 toluene-ethyl acetate to give a solid of **4** (132.2 g, 79% from **3**): R_f 0.64 (20:1 $CHCl_3$-MeOH); mp 139—142 °C; $[\alpha]_D^{23}$ −38° (*c* 1.0, $CHCl_3$); IR (KBr): 1700 (NH-CO), and 1160 cm^{-1} (SO_2); ^{1}H-NMR (acetone-d_6): δ=2.39, 2.40, and 2.43 (each 3H, s, Ts), 5.06 (2H, s, CH_2 of Z), and 5.30 (1H, d, H-1′, $J_{1',2'}$=3.5 Hz).

Found: C, 58.76; H, 6.19; N, 5.34; S, 8.59% Calcd for $C_{53}H_{66}N_4O_{14}S_3$: C, 58.98; H, 6.16; N, 5.19; S, 8.91%.

3′,4′:5,6-Di-O-cyclohexylidene-6′,6′-di-N-methyl-1,2′,3-tri-N-tosylneamine 6′-N-oxide (5). A solution of **4** (60.8 g) in *t*-butyl alcohol (1830 ml) containing water (3.10 ml) and potassium *t*-butoxide (63.2 g) was stirred at 70 °C for 1 h. The reaction solution diluted with ethyl acetate (1000 ml) was neutralized with 0.1 M HCl (2100 ml), and the organic layer was washed with a saturated aqueous NaCl solution, dried, and then evaporated to give a solid of the 6′-amino compound (56 g).

To a stirred and ice-cooled solution of the solid in acetonitrile (1030 ml) were added 30% aqueous formaldehyde (52.0 ml), $NaBH_3CN$ (10.6 g), and acetic acid (32.0 ml), and stirring was continued at room temperature for 1 h. The reaction mixture neutralized with a saturated aqueous $NaHCO_3$ solution was extracted with ethyl acetate (400 ml×3). The combined extracts were washed with a saturated aqueous NaCl solution, dried, and evaporated to a residue of the dimethylamino compound (60 g): R_f 0.47 (10:1 $CHCl_3$-MeOH).

A solution of the residue in chloroform (1120 ml) was stirred with *m*-chloroperbenzoic acid (9.80 g) at room temperature for 1 h. The solution diluted with chloroform (500 ml) was washed successively with saturated aqueous $NaHCO_3$ and NaCl solutions, dried, and then evaporated to a residue, which was chromatographed on silica gel (500 g) with 10:1→8:1 chloroform-methanol to give a solid of the monohydrate of **5** (47.1 g, 83% from **4**): R_f 0.36 (10:1 $CHCl_3$-MeOH); mp 175—179 °C; $[\alpha]_D^{23}$ −23° (*c* 1.0, $CHCl_3$); ^{1}H-NMR ($CDCl_3$): δ=2.42 (9H, s, Ts), 3.24 and 3.31 (each 3H, s, NMe_2), and 5.45 (1H, d, H-1′, $J_{1',2'}$=3.0 Hz).

Found: C, 55.78; H, 6.42; N, 5.40%. Calcd for $C_{47}H_{64}N_4O_{13}S_3 \cdot H_2O$: C, 56.05; H, 6.60; N, 5.56%.

4-O-[3′,4′-O-Cyclohexylidene-2′-deoxy-2′-(tosylamino)-α-D-gluco-hexodialdo-1′,5′-pyranosyl]-5,6-O-cyclohexylidene-1,3-di-N-tosyl-2-deoxystreptamine (6). To a stirred and ice-cooled solution of **5** (11.5 g) in acetone (115 ml) were added *N,N*-diisopropylethylamine (3.99 ml) and benzoyl chloride (2.66 ml), and stirring was continued at room temperature for 3 min and then at 40 °C for 10 min. The resulting solution diluted with chloroform (250 ml) was washed successively with saturated aqueous $NaHCO_3$ and NaCl solutions, dried, and evaporated to a residue, which was chromatographed on silica gel (600 g) with 3:1→2:1 chloroform-acetone to give a solid of the monohydrate of **6** (8.24 g, 75%): R_f 0.38 (20:1 $CHCl_3$-MeOH); mp 144—148 °C; $[\alpha]_D^{23}$ −15° (*c* 1.0, $CHCl_3$); IR (KBr): 1735 (CHO), and 1160 cm^{-1} (SO_2); ^{1}H-NMR ($CDCl_3$+D_2O): δ=2.41 (9H, s, Ts×3), and 9.67 (1H, s, CHO).

Found: C, 56.41; H, 6.18; N, 4.21%. Calcd for $C_{45}H_{57}N_3O_{13}S_3 \cdot H_2O$: C, 56.18; H, 6.18; N, 4.37%.

4-O-[3′,4′-O-Cyclohexylidene-2′,7′,8′,9′-tetradeoxy-2′-(tosylamino)-L-glycero- and D-glycero-α-D-gluco-non-8′-enopyranosyl]-5,6-O-cyclohexylidene-1,3-di-N-tosyl-2-deoxystreptamines (7 and 8). To an allylmagnesium chloride solution prepared *in situ* from magnesium (2.39 g), allyl chloride (3.21 ml), and iodine (0.05 g) in THF (120 ml) was added dropwise with stirring at 5 °C under argon, a solution of **6** (6.20 g) and allyl chloride (4.82 ml) in THF (186 ml), and stirring was continued at room temperature for 15 min and then at 60 °C for 30 min. After the reaction was quenched with a saturated aqueous NH_4Cl solution, the reaction mixture was extracted with ethyl acetate (200 ml×3). The combined extracts were washed with a saturated aqueous NaCl solution, dried, and evaporated to a residue, which was chromatographed on silica gel (600 g) with 40:1:1 chloroform-acetone-methanol to give **7** (2.35 g, 37%) and **8** (2.61 g, 41%) having the R_f-values of 0.48 and 0.43 (20:1 $CHCl_3$-MeOH) respectively.

7: Mp 134—137 °C; $[\alpha]_D^{23}$ −20° (*c* 1.0, $CHCl_3$); ^{1}H-NMR ($CDCl_3$+D_2O): δ=3.97 (1H, dd, H-5′, $J_{4',5'}$=9.5 Hz, $J_{5',6'}$=7.0 Hz), 5.11 (1H, dd, H-9′a, $J_{7',9'a}$=2.0 Hz, $J_{8',9'a}$=10 Hz), 5.14 (1H, dd, H-9′b, $J_{7',9'b}$=2.0 Hz, $J_{8',9'b}$=17.5 Hz), 5.34 (1H, d, H-1′, $J_{1',2'}$= 3.0 Hz), and 5.90 (1H, ddt, H-8′, $J_{7',8'}$=7 Hz).

Found: C, 58.67; H, 6.58; N, 4.14; S, 9.49%. Calcd for $C_{48}H_{63}N_3O_{13}S_3$: C, 58.46; H, 6.44; N, 4.26; S, 9.75%.

8: Mp 131—133 °C; $[\alpha]_D^{23}$ −5° (*c* 1.0, $CHCl_3$); ^{1}H-NMR ($CDCl_3$+D_2O): δ=3.94 (1H, m, H-6′), 4.12 (1H, dd, H-5′, $J_{4',5'}$=10 Hz, $J_{5',6'}$=3.5 Hz), 5.09 (1H, dd, H-9′a, $J_{7',9'a}$≈1.5 Hz, $J_{8',9'a}$=10 Hz), 5.14 (1H, dd, H-9′b, $J_{7',9'b}$≈2.0 Hz, $J_{8',9'b}$=16.5 Hz), 5.31 (1H, d, H-1′, $J_{1',2'}$=2.5 Hz), and 5.88 (1H, ddt, H-8′, $J_{7',8'}$=7 Hz).

††1 Torr≈133.322 Pa.

Found: C, 58.57; H, 6.58; N, 4.02; S, 9.48%. Calcd for $C_{48}H_{63}N_3O_{13}S_3$: C, 58.46; H, 6.44; N, 4.26; S. 9.75%.

5,6-O-Cyclohexylidene-4-O-[(8'RS)-2',7'-dideoxy-2'-(tosylamino)-L-glycero-α-D-gluco-*octodialdo-1',5':8',4'-dipyranos-1'-yl]-1,3-di*-N-*tosyl-2-deoxystreptamine (9).* A solution of **7** (3.2g) in 75% aqueous 1,4-dioxane (128ml) was stirred with OsO_4 (41mg) at room temperature. After 30min, to the stirred solution was added portionwise $NaIO_4$ (2.94g), and stirring was continued at room temperature for 1h. The resulting solution diluted with ethyl acetate was washed with a saturated aqueous NaCl solution (50ml) containing $NaHSO_3$ (17mg), dried, and evaporated to a residue of the aldehyde (3.2g): R_f 0.44 (15:1 $CHCl_3$-MeOH); ^{1}H-NMR ($CDCl_3+D_2O$): δ=2.40 (9H, broad s, Ts×3), and 9.79 (1H, broad s, CHO).

A solution of the residue in a 2:1:1 mixture (64ml) of acetic acid, 1,4-dioxane and water was stirred at room temperature for 1.5h. The mixture was poured into a saturated aqueous $NaHCO_3$ solution, and extracted with ethyl acetate (100ml×3). The combined extracts were washed with a saturated aqueous NaCl solution, dried, and evaporated to a residue, which was chromatographed on silica gel (150g) with 3:1→2:1 chloroform-acetone to give a solid of the monohydrate of **9** (1.80g, 60% from **7**): R_f 0.17 (15:1 $CHCl_3$-MeOH); mp 180—183°C; $[\alpha]_D^{23}$ −13° (*c* 1.0, MeOH); ^{1}H-NMR (CD_3CN+D_2O): δ=3.88 (1H, ddd, H-6' $J_{5',6'}$=9.5 Hz, $J_{6',7'ax}$=11.5 Hz, $J_{6',7'eq}$=5.0 Hz), 4.69 (0.5H, dd, H-8'ax, $J_{7'ax,8'ax}$=10 Hz, $J_{7'eq,8'ax}$=2.0 Hz), 5.08 and 5.09 (1H in total, each d, H-1', $J_{1',2'}$=4.0 Hz and 3.5 Hz respectively), and 5.21 (0.5H, dull d, H-8'eq, $J_{7',8'eq}\approx$3 Hz).

Found: C, 52.98; H, 5.75; N, 4.75%. Calcd for $C_{41}H_{53}N_3O_{14}S_3\cdot H_2O$: C, 53.17; H, 5.99; N, 4.54%.

1-N-Acetyl-4-O-[(8'S)- and (8'R)-3',6',8'-tri-O-acetyl-2',7'-dideoxy-2'-(tosylamino)-L-glycero-α-D-gluco-*octodialdo-1',5':8',4'-dipyranos-1'-yl]-5,6-O-cyclohexylidene-1,3-di-N-tosyl-2-deoxystreptamines (**10a** and **10b**).* A solution of **9** (5.6mg) and acetic anhydride (0.06ml) in pyridine (0.11ml) was stirred at 40°C for 16h. The mixture diluted with ethyl acetate was washed with a saturated aqueous $NaHCO_3$ solution, dried, and evaporated to a residue, which was chromatographed on silica gel (1g) with 4:1 benzene-ethyl acetate to give **10a** (2.4mg, 37%) and **10b** (2.2mg, 34%) having the R_f-values of 0.33 and 0.38 (2:1 benzene-ethyl acetate) respectively.

10a: Mp 160—162°C; $[\alpha]_D^{23}$ +18° (*c*1.0, $CHCl_3$); ^{1}H-NMR ($CDCl_3$): δ=1.61, 2.12, 2.16, and 2.23 (each 3H, s, Ac), 1.80 (1H, ddd, H-7'ax, $J_{6',7'ax}$=11.5 Hz, J_{gem}=13.5 Hz, $J_{7'ax,8'}$=3.8 Hz) , 3.48 (1H, dt, H-2', $J_{1',2'}$=3.8 Hz, $J_{2',NH}=J_{2',3'}$=10 Hz), 3.62 (1H, t, H-4', $J_{3',4'}=J_{4',5'}$=10 Hz), 3.95 (1H, t, H-5', $J_{5',6'}$=10 Hz), 4.38 (1H, dd, H-6, $J_{1,6}$=10.5 Hz, $J_{5,6}$=9 Hz), 4.53 (1H, dt, H-1, $J_{1,2ax}$=10.5 Hz, $J_{1,2eq}$=4.5 Hz), 4.94 (1H, t, H-3'), and 6.07 (1H, dull d, H-8').

Found: C, 54.54; H, 5.89; N, 3.86%. Calcd for $C_{49}H_{61}N_3O_{18}S_3$: C, 54.69; H, 5.71; N, 3.90%.

10b: Mp 164—168°C; $[\alpha]_D^{23}$ +60° (*c* 1.0, $CHCl_3$); ^{1}H-NMR ($CDCl_3+D_2O$): δ=1.55, 2.07, 2.15, and 2.22 (each 3H, s, Ac), 3.22 (1H, t, H-4', $J_{3',4'}=J_{4',5'}$=10 Hz), 3.42 (1H, dd, H-2', $J_{1',2'}$=3.5 Hz, $J_{2',3'}$=10 Hz), 3.48 (1H, t, H-5, $J_{4,5}=J_{5,6}$=9.5 Hz), 3.71 (1H, t, H-4, $J_{3,4}$=9.5 Hz), 3.83 (1H, t, H-5', $J_{5',6'}$=10 Hz), 4.38 (1H, dd, H-6, $J_{1,6}$=10.5 Hz, $J_{5,6}$=9.5 Hz), 4.54 (1H, dt, H-1, $J_{1,2ax}=J_{1,6}$= 10.5 Hz, $J_{1,2eq}$=4 Hz), 4.92 (1H, t, H-3'), 4.95 (1H, ddd, H-6', $J_{6',7'ax}$= 10.5 Hz, $J_{6',7'eq}$=5 Hz), 5.28 (1H, d, H-1'), and 5.60 (1H, dd, H-8', $J_{7'ax,8'}$=10 Hz, $J_{7'eq,8'}$=2.0 Hz).

Found: C, 54.78; H, 5.82; N, 3.65%. Calcd for $C_{49}H_{61}N_3O_{18}S_3$: C, 54.69; H, 5.71; N, 3.90%.

1-N-Acetyl-4-O-[(8'R)-3',6',8'-tri-O-acetyl-2',7'-dideoxy-2'-(tosylamino)-D-glycero-α-D-gluco-*octodialdo-1',5':8',4'-dipyranos-1'-yl]-5,6-O-cyclohexylidene-1,3-di-N-tosyl-2-deoxystreptamine (**11**).* A sample of **8** (315mg) was treated with OsO_4 and $NaIO_4$ followed by hydrolysis with acetic acid by the procedure described in the preparation of **9**, and then acetylated as described for **10a,b** to give a solid of **11** (154mg, 45%): R_f 0.43 (2:1 benzene-ethyl acetate); mp 164—169°C; $[\alpha]_D^{23}$ +30° (*c* 1.0, $CHCl_3$); IR (KBr): 1750 (ester), and 1160 cm^{-1} (SO_2); ^{1}H-NMR ($CDCl_3$): δ=1.60, 2.05, 2.14, and 2.18 (each 3H, s, Ac), 3.79 (1H, t, H-4', $J_{3',4'}=J_{4',5'}$=10 Hz), 4.36 (1H, dd, H-5', $J_{5',6'}$=2.5 Hz), 5.12 (1H, d, H-1', $J_{1',2'}$=3.5 Hz), 5.59 (1H, m, H-6'), and 5.85 (1H, dd, H-8', $J_{7'ax,8'}$=9.5 Hz, $J_{7'eq,8'}$=3.0 Hz).

Found: C, 54.57; H, 5.78; N, 3.68; S, 8.90%. Calcd for $C_{49}H_{61}N_3O_{18}S_3$: C, 54.69; H, 5.71; N, 3.90; S, 8.94%.

1-N-Acetyl-5,6-di-O-acetyl-4-O-[(8'R)-3',6',8'-tri-O-acetyl-2',7'-dideoxy-2'-(tosylamino)-L-glycero-α-D-gluco-*octodialdo-1',5':8'4'-dipyranos-1'-yl]-1,3-di-N-tosyl-2-deoxystreptamine (**12**).*

*A) From **10b***: A solution of **10b** (23 mg) in a 2:1:1 mixture (0.5ml) of acetic acid, 1,4-dioxane and water was warmed at 50°C for 1d. The resulting solution diluted with ethyl acetate was washed with a saturated aqueous $NaHCO_3$ solution, dried, and evaporated to give a residue: R_f 0.28 (1:1 benzene-ethyl acetate).

A solution of the decyclohexylidenated product in pyridine (0.5ml) was stirred with acetic anhydride (0.3ml) at 40°C overnight. After addition of a few drops of ethanol, the solution was evaporated to a residue, which was partitioned between ethyl acetate and a saturated aqueous $NaHCO_3$ solution. The organic layer was dried and evaporated to a residue, which was chromatographed on silica gel (2g) with 5:2 benzene-ethyl acetate to give a solid of **12** (13mg, 56% from **10b**): R_f 0.50 (1:1 benzene-ethyl acetate); mp 161—164°C; $[\alpha]_D^{23}$ +58° (*c* 1.0, $CHCl_3$); IR (KBr): 1750 (ester), and 1160 cm^{-1} (SO_2); ^{1}H-NMR ($CDCl_3+D_2O$): δ=1.34, 1.80, 2.06, 2.11, 2.15, and 2.25 (each 3H, s, Ac), 2.40, 2.41, and 2.47 (each 3H, s, Ts), 3.19 (1H, t, H-4', $J_{3',4'}=J_{4',5'}$=9.8 Hz), 3.40 (1H, m, H-3), 3.46 (1H, dd, H-2', $J_{1',2'}$=3.8 Hz, $J_{2',3'}$=10.8 Hz), 3.80 (1H, t, H-4, $J_{3,4}=J_{4,5}$= 9.5 Hz), 4.13 (1H, t, H-5', $J_{5',6'}\approx$9.5 Hz), 4.34 (1H, m, H-1), 4.80 (1H, dd, H-3'), 4.94 (1H, dt, H-6', $J_{6',7'ax}$=9.5 Hz, $J_{6',7'eq}$=5.5 Hz), 5.18 (1H, d, H-1'), 5.22 (1H, t, H-5, $J_{5,6}$=9.5 Hz), 5.56 (1H, dd, H-8', $J_{7'ax,8'}$=10.5 Hz, $J_{7'eq,8'}$=2.5 Hz), and 5.65 (1H, dull t, H-6, $J_{1,6}$=10 Hz).

Found: C, 52.21; H, 5.40; N, 3.88; S, 8.65%. Calcd for $C_{47}H_{57}N_3O_{20}S_3$: C, 52.26; H, 5.32; N, 3.89; S, 8.90%.

*B) From **13***: A solution of **13** (7.7mg) in a 1:1 mixture (0.15ml) of 0.5M HCl and 1,4-dioxane was warmed at 50°C for 2d, and then evaporated to a residue of the octodialdose derivative. The residue was acetylated with acetic anhydride (0.2ml) in pyridine (0.4ml) at 40°C for 13h, and worked up as described above to give two products having R_f-values of 0.50 and 0.45 (1:1 benzene-ethyl acetate). The R_f 0.50-substance (2.5mg, 31%) was identical with **12** in all respects. The R_f 0.45-substance (2.8mg) seemed to be the corresponding (8'*S*)-isomer, but was not further investigated.

1-N-Acetyl-4-O-[3',6'-di-O-acetyl-4',8'-anhydro-2',7'-dideoxy-2'-(tosylamino)-L-glycero-α-D-gluco-*oct-7'-enopyranos-1'-yl]-5,6-O-cyclohexylidene-1,3-di-N-tosyl-2-deoxystreptamine (**13**).*

A)[14] *From **9***: To a stirred and ice-cooled solution of **9** (1.27g) in acetonitrile (25.4ml) were added triethylamine (1.17ml) and tosyl chloride (0.8g), and stirring was continued at room temperature for 12h. After addition of ethanol (0.16ml) and a saturated aqueous $NaHCO_3$ solution (0.3ml), the mixture was evaporated to a residue. The residue was partitioned between chloroform and a saturated aqueous $NaHCO_3$ solution, and the combined organic layers were evaporated to give a solid of the glycal (1.4g): R_f 0.39 (15:1 $CHCl_3$-MeOH).

A solution of the solid in pyridine (28ml) was stirred with acetic anhydride (14ml) at 40°C for 19h. After addition of ethanol (8.6 ml), the resulting solution was neutralized with a saturated aqueous $NaHCO_3$ solution and extracted with

ethyl acetate. The combined extracts were washed with a saturated aqueous NaCl solution, dried, and evaporated to a residue, which was chromatographed on silica gel (60g) with 2:1→3:2 hexane-ethyl acetate to give a solid of **13** (0.73g, 53%): R_f 0.86 (1:1 benzene-EtOAc); R_f 0.40 (3:1 benzene-EtOAc); mp 161—164°C;$[\alpha]_D^{23}$ +98° (*c* 1.0, $CHCl_3$); IR (KBr): 1745 cm^{-1} (ester), ^{1}H-NMR ($CDCl_3$): δ=1.58, 2.20, and 2.23 (each 3H, s, Ac), 3.59 (1H, dd, H-4′, $J_{3',4'}$=9.0 Hz, $J_{4',5'}$=10.5 Hz), 3.91 (1H, dd, H-5′ $J_{5',6'}$=8.0 Hz), 4.74 (1H, dd, H-3′, $J_{2',3'}$=10.5 Hz), 4.84 (1H, dd, H-7′, $J_{6',7'}$=2.3 Hz, $J_{7',8'}$=6.0 Hz), 5.20 (1H, d, H-1′, $J_{1',2'}$=4.0 Hz), 5.32 (1H, m, H-6′), and 6.29 (1H, dd, H-8′, $J_{6',8'}$=1.5 Hz).

Found: C, 55.63; H, 5.68; N, 3.86; S, 9.48%. Calcd for $C_{47}H_{57}N_3O_{16}S_3$: C, 55.55; H, 5.65; N, 4.14; S, 9.47%.

B) From 17: **17** (0.6g) was treated with triethylamine and tosyl chloride in acetonitrile, followed by acetylation, as described above, to give a solid of **13** (0.35g, 55%).

*1-N-Acetyl-4-O-[3′,6′-di-O-acetyl-4′,8′-anhydro-2′,7′-dideoxy-2′-(tosylamino)-*D*-glycero-α-*D*-gluco-oct-7′-enopyranos-1′-yl]-5,6-O-cyclohexylidene-1,3-di-N-tosyl-2-deoxystreptamine (14).* A sample of **8** (400mg) was treated by the procedure described in the preparation of **13** through **9**, and then worked up to give, after reprecipitation from benzene-hexane, a solid of **14** (95mg, 23%): R_f 0.33 (3:1 benzene-EtOAc); mp 142—145°C; $[\alpha]_D^{23}$ −35° (*c* 1.0, $CHCl_3$): IR (KBr): 1745 cm^{-1} (ester); ^{1}H-NMR ($CDCl_3+D_2O$): δ=1.69, 2.09, and 2.17 (each 3H, s, Ac), 3.83 (1H, dd, H-4′, $J_{3',4'}$=9.5 Hz, $J_{4',5'}$=11 Hz), 4.46 (1H, dd, H-5′, $J_{5',6'}$=4.0 Hz), 4.98 (1H, t, H-7′, $J_{6',7'}=J_{7',8'}$=6.0 HZ), 5.13 (1H, d, H-1′, $J_{1',2'}$=3.5 Hz), 5.24 (1H, dd, H-3′, $J_{2',3'}$=11 Hz), 5.49 (1H, dd, H-6′), and 6.43 (1H, d, H-8′).

Found: C, 55.59; H, 5.62; N, 4.10%. Calcd for $C_{47}H_{57}N_3O_{16}S_3$: C, 55.55; H, 5.65; N, 4.14%.

*1-N-Acetyl-4-O-[(8′R)-3′,6′-di-O-acetyl-7′-azido-2′,7′-dideoxy-8′-O-nitro-2′-(tosylamino)-*L*-threo-α-*D*-gluco-octodialdo-1′,5′:8′,4′-dipyranos-1′-yl]-5,6-O-cyclohexylidene-1,3-di-N-tosyl-2-deoxystreptamine (15).* To a solution of **14** (246mg) in acetonitrile (4.9ml) were added sodium azide (24mg) and ammonium ceric nitrate (400mg) at −10°C under argon, and the mixture was stirred at this temperature for 3h. After further addition of ammonium ceric nitrate (270mg), stirring was continued for another 3h. The reaction mixture diluted with ice-cooled chloroform was washed sequentially with saturated aqueous NaCl and $NaHCO_3$ solutions under ice-cooling, dried, and evaporated to a residue, which was chromatographed on silica gel (30g) with 6:1→5:1 benzene-ethyl acetate to give a solid of **15** (163mg, 60%): R_f 0.45 (3:1 benzene-EtOAc); mp 160—163°C; $[\alpha]_D^{23}$ −7.5°(*c* 1.0, $CHCl_3$); IR (KBr): 2120 (azide), 1655 and 1290 cm^{-1} (ONO_2), ^{1}H-NMR ($CDCl_3+D_2O$): δ=1.68 (3H, s, Ac), 2.18 (6H, s, Ac×2), 2.43 (6H, s, Ts×2), 2.45 (3H, s, Ts), 4.08 (1H, t, H-4′, $J_{3',4'}=J_{4',5'}$=10.5 Hz), 4.09 (1H, dd, H-7′, $J_{6',7'}$=3.0 Hz, $J_{7',8'}\simeq$0.5 Hz), 4.50 (1H, dd, H-5′, $J_{5',6'}$=3.0 Hz), 5.07 (1H, d, H-1′, $J_{1',2'}$=3.5 Hz), 5.21 (1H, t, H-3′, $J_{2',3'}\simeq$10 Hz), 5.41 (1H, t, H-6′), and 6.04 (1H, apparently s, H-8′).

Found: C, 50.54; H, 5.09; N, 8.52%. Calcd for $C_{47}H_{57}N_7O_{19}S_3$: C, 50.40; H, 5.13; N, 8.75%.

*4-O-[6′-O-Acetyl-3′,4′-O-cyclohexylidene-2′,7′,8′,9′-tetradeoxy-2′-(tosylamino)-*L*-glycero-α-*D*-gluco-non-8′-enopyranosyl]-5,6-O-cyclohexylidene-1,3-di-N-tosyl-2-deoxystreptamine (16).* *A) From 8*: To a stirred and ice-cooled solution of **8** (1.64g) in pyridine was added mesyl chloride (0.26ml), and stirring was continued at room temperature for 2.5h. After addition of ethanol (0.39ml), the resulting solution was neutralized with a saturated aqueous $NaHCO_3$ solution and extracted with ethyl acetate. The extracts were washed with a saturated aqueous NaCl solution, dried, and evaporated to a residue, which was chromatographed on silica gel (60g) with 3:1 benzene-ethyl acetate to give a solid of the mesylate (1.70g): R_f 0.21 (3:1 benzene-EtOAc).

A solution of the solid (2.29g) in DMSO (22.9ml) was stirred with potassium acetate (1.26g) at 78°C for 18h. The solution diluted with ethyl acetate was washed with a saturated aqueous NaCl solution, dried, and evaporated to a residue,which was chromatographed on silica gel (100g) with 4:1→3:1 benzene-ethyl acetate to give a solid of **16** (1.96g, 85% from **8**): R_f 0.35 (3:1 benzene-EtOAc); R_f 0.69 (15:1 $CHCl_3$-MeOH); mp 136—138°C; $[\alpha]_D^{23}$ −33° (*c* 1.0, $CHCl_3$); IR (KBr): 1735, 1720 (ester), and 1160 cm^{-1} (SO_2); ^{1}H-NMR ($CDCl_3+D_2O$): δ=2.07 (3H, s, Ac), 4.16 (1H, dd, H-2′, $J_{1',2'}$=3.5 Hz, $J_{2',3'}$=9.5 Hz), 5.02 (1H, m, H-6′), 5.07 (1H, dd, H-9′a, $J_{7',9'a}$=2.0 Hz, $J_{8',9'a}$=10 Hz), 5.12 (1H, dd, H-9′b, $J_{7',9'b}$=2.0 Hz, $J_{8',9'b}$=16 Hz`[illegible]47 (1H, d, H-1′), and 5.79 (1H, m, H-8′).

Found: C, 58.26; H, 6.39; N, 3 Calcd for $C_{50}H_{65}N_3O_{14}S_3$: C, 58.40; H, 6.37; N, [illegible] %.

B) From 7: A solution of **7** (10mg) in pyridine (0.25ml) was stirred with acetic anhydride (0.10ml) at room temperature for 3h. After addition of a few drops of ethanol, the resulting solution was evaporated to a residue, which was chromatographed on silica gel (1g) with 3:1 benzene-ethyl acetate to give a solid of **16** (9.8mg, 94%).

*4-O-[(8′RS)-6′-O-Acetyl-2′,7′-dideoxy-2′-(tosylamino)-*L*-glycero-α-*D*-gluco-octodialdo-1′,5′:8′,4′-dipyranos-1′-yl]-5,6-O-cyclohexylidene-1,3-di-N-tosyl-2-deoxystreptamine (17).* A sample of **16** (1.24g) was treated by the procedure described in the preparation of **9** and then worked up to give, through the aldehyde: R_f 0.67 (1:1 benzene-EtOAc); ^{1}H-NMR ($CDCl_3+D_2O$): δ=2.09 (3H, s, Ac) and 9.77 (1H, broad s, CHO), a solid of **17** (0.94g, 82%): R_f 0.15 (1:1 benzene-EtOAc); R_f 0.28 (15:1 $CHCl_3$-MeOH); mp 164—166°C; $[\alpha]_D^{23}$ +2.5° (*c* 1.0, $CHCl_3$); IR (KBr): 1730 (ester), and 1160 cm^{-1} (SO_2); ^{1}H-NMR ($CDCl_3+D_2O$): δ=1.98 (3H, s, Ac), 2.35 (3H, s, Ts), and 2.41 (6H, s, Ts×2).

Found: C, 54.15; H, 5.88; N, 4.15%. Calcd for $C_{43}H_{55}N_3O_{15}S_3$: C, 54.40; H, 5.83; N, 4.42%.

*1-N-Acetyl-4-O-[(8′S)- and (8′R)-3′,6′-di-O-acetyl-7′-azido-2′,7′-dideoxy-8′-O-nitro-2′-(tosylamino)-*D*-threo-α-*D*-gluco-octodialdo-1′,5′:8′,4′-dipyranos-1′-yl]-5,6-O-cyclohexylidene-1,3-di-N-tosyl-2-deoxystreptamines (18 and 19).* To a solution of **13** (262mg) in acetonitrile (5.2ml) were added sodium azide (25mg) and ammonium ceric nitrate (424mg) at −17°C under argon, and the mixture was stirred at this temperature for 1.5h. After further addition of ammonium ceric nitrate (140mg), stirring was continued for another 1h. The reaction mixture was worked up as described for **15** to give **18** (182mg, 63%) and **19** (41mg, 14%) having the R_f-values of 0.44 and 0.50 (3:1 benzene-ethyl acetate) respectively.

18: Mp 158—161°C; $[\alpha]_D^{23}$ −13° (*c* 1.0, $CHCl_3$); IR (KBr): 2115 (azide), 1750 (ester), 1650 and 1280 cm^{-1} (ONO_2); ^{1}H-NMR ($CDCl_3$): δ=1.57, 2.19, and 2.20 (each 3H, s, Ac), 3.76 (1H, t, H-4′, $J_{3',4'}=J_{4',5'}$=10 Hz), 3.94 (1H, dd, H-7′, $J_{6',7'}$=10.5 Hz, $J_{7',8'}$=4 Hz), 4.44 (1H, t, H-5′, $J_{5',6'}$=10 Hz), 5.40 (1H, dull t, H-6′), and 6.20 (1H, d, H-8′).

Found: C, 50.63; H, 5.25; N, 8.55; S, 8.28%. Calcd for $C_{47}H_{57}N_7O_{19}S_3$: C, 50.40; H, 5.13; N, 8.75; S, 8.59%.

19: Mp 153—157°C; $[\alpha]_D^{23}$ +25° (*c* 1.0, $CHCl_3$); IR (KBr): 2115 (azide), 1750 (ester), 1660 and 1285 cm^{-1} (ONO_2); ^{1}H-NMR ($CDCl_3+D_2O$): δ=1.62, 2.22, and 2.24 (each 3H, s, Ac), 3.34 (1H, t, H-4′, $J_{3',4'}=J_{4',5'}$=10 Hz), 3.43 (1H, dd, H-2′,$J_{1',2'}$= 3.5 Hz, $J_{2',3'}$=10.5 Hz), 3.50 (1H, dd, H-7′, $J_{6',7'}$=10 Hz, $J_{7',8'}$= 9.0 Hz), 4.12 (1H, t, H-5′, $J_{5',6'}$=10 Hz), 4.48 (1H, m, H-1), 5.13 (1H, t, H-6′), 5.14 (1H, dd, H-3′), 5.32 (1H, d, H-1′), and 5.43 (1H, d, H-8′).

Found: C, 50.50; H, 5.23; N, 8.62%. Calcd for $C_{47}H_{57}N_7O_{19}S_3$: C, 50.40; H, 5.13; N, 8.75%.

*4-O-[(8′S)-7′-Azido-2′,7′-dideoxy-8′-O-methyl-2′-(tosylamino)-*D*-threo-α-*D*-gluco-octodialdo-1′,5′:8′,4′-dipyranos-1′-yl]-5,6-O-cyclohexylidene-1,3-di-N-tosyl-2-deoxystreptamine (20).* *A)*

From 18: A solution of **18** (177.5 mg) in methanol (5.4 ml) was stirred with $Ba(OH)_2 \cdot 8H_2O$ (100 mg) at 60 °C for 25 min. The mixture diluted with methanol was neutralized with Dry Ice, and then evaporated to a residue, which was chromatographed on silica gel (17 g) with 3:1 chloroform–acetone to give a solid of **20** (108 mg, 71%): R_f 0.44 (15:1 $CHCl_3$–MeOH); mp 157—160 °C ; $[\alpha]_D^{23}$ +5° (*c* 1.0, MeOH); IR (KBr): 2115 (azide), and 1160 cm^{-1} (SO_2); ^{1}H-NMR (acetone-d_6+D_2O): δ=2.41, 2.43, and 2.44 (each 3H, s, Ts), 2.98 (1H, dd, H-3′, $J_{2',3'}$=9.8 Hz, $J_{3',4'}$=9.5 Hz), 3.23 (1H, dd, H-2′, $J_{1',2'}$=3.5 Hz), 3.47 (1H, t, H-6′, $J_{5',6'}$=$J_{6',7'}$=9.5 Hz), 3.53 (3H, s, OMe), 3.79 and 3.80 (each 1H, t, H-4′, and H-5′, $J_{4',5'}$=9.5 Hz), 4.21 (1H, d, H-8′, $J_{7',8'}$=8.0 Hz), and 5.34 (1H, d, H-1′).

Found: C, 52.20; H, 5.62; N, 8.45%. Calcd for $C_{42}H_{54}N_6O_{14}S_3$: C, 52.38; H, 5.65; N, 8.73%.

B) From 19: A solution of **19** (177 mg) was treated with $Ba(OH)_2 \cdot 8H_2O$ in methanol as described above to give a solid of **20** (61 mg, 40%) having R_f 0.44 (15:1 $CHCl_3$–MeOH) and another solid (11 mg) having R_f 0.47. The latter solid, probably the (8′*R*)-isomer, was not further investigated.

4-O-[(8′S)-7′-(Benzyloxycarbonylamino)-2′,7′-dideoxy-8′-O-methyl-2′-(tosylamino)-D-threo-α-D-gluco-*octodialdo-1′,5′:8′,4′-dipyranos-1′-yl]-5,6-O-cyclohexylidene-1,3-di-*N-*tosyl-2-deoxystreptamine (21).* A solution of **20** (45.6 mg) in methanol (0.91 ml) was shaken with platinum black and 3-atm hydrogen at room temperature for 2 h, filtered and evaporated to give a solid of the amino compound (46 mg): R_f 0.07 (10:1 $CHCl_3$–MeOH).

To a stirred and ice-cooled solution of the solid in 75% aqueous acetone (1.9 ml) were added Na_2CO_3 (6.3 mg) and benzyloxycarbonyl chloride (0.0085 ml), and stirring was continued at room temperature for 10 min. The reaction mixture diluted with ethyl acetate was washed with a saturated aqueous NaCl solution, dried, and evaporated to a residue, which was chromatographed on silica gel (4 g) with 5:2 chloroform–acetone to give a solid of **21** (38.7 mg, 76.3%): R_f 0.49 (10:1 $CHCl_3$–MeOH); mp 160—164 °C ; $[\alpha]_D^{28}$ −10° (*c* 1.0, $CHCl_3$); ^{1}H-NMR ($CDCl_3$+D_2O): δ=3.47 (3H, s, OMe), 4.94 and 5.18 (each 1H, d, J_{AB}=12.5 Hz, CH_2Ph), and 5.05 (1H, d, $J_{1',2'}$=4.0 Hz, H-1′).

Found: C, 55.87; H, 5.83; N, 5.14%. Calcd for $C_{50}H_{62}N_4O_{16}S_3$: C, 56.06; H, 5.83; N, 5.23%.

4-O-{(8′S)-7′-[N-(Benzyloxycarbonyl)methylamino-2′,-7′-dideoxy-8′-O-methyl-2′-(tosylamino)-D-threo-α-D-gluco-*octodialdo-1′,5′:8′,4′-dipyranos-1′-yl}-5,6-O-cyclohexylidene-1,3-di-*N-*tosyl-2-deoxystreptamine (22).* A solution of **21** (38.1 mg) in THF (1.2 ml) was stirred with $LiAlH_4$ (13.5 mg) at 80 °C for 3 h. After quenching with $Na_2SO_4 \cdot 10H_2O$, the reaction mixture diluted with ethyl methyl ketone was washed with a saturated aqueous NaCl solution, dried and evaporated to a residue of the methylamino compound (40 mg): R_f 0.09 (10:1 $CHCl_3$–MeOH).

The residue was again *N*-benzyloxycarbonylated as described above to give, after column chromatography on silica gel (4 g) with 5:2 chloroform–acetone, a solid of **22** (31.3 mg, 81%): R_f 0.51 (10:1 $CHCl_3$–MeOH); mp 163—167 °C ; $[\alpha]_D^{23}$ −44° (*c* 1.0, $CHCl_3$); IR ($CHCl_3$) 1675 (NH-CO), and 1155 cm^{-1} (SO_2); ^{1}H-NMR ($CDCl_3$+D_2O): δ=2.98 (1H, t, H-4′, $J_{3',4'}$=$J_{4',5'}$=9.5 Hz), 3.03 (1H, t, H-7′, $J_{6',7'}$=$J_{7',8'}$=9.5 Hz), 3.13 (1H, dd, H-2′, $J_{1',2'}$=4 Hz, $J_{2',3'}$=9.5 Hz), 3.22 (3H, s, NMe), 3.32 (1H, t, H-6′, $J_{5',6'}$=9.5 Hz), 3.50 (3H, s, OMe), 3.91 (1H, t, H-3′), 3.98 (1H, t, H-5′), 4.93 (1H, d, H-1′), and 4.93 (1H, d, H-8′).

Found: C, 56.25; H, 6.11; N, 5.02; S, 8.69%. Calcd for $C_{51}H_{64}N_4O_{16}S_3$: C, 56.44; H, 5.94; N, 5.16; S, 8.86%.

4-O-{(8′S)-7′-[N-(Benzyloxycarbonyl)methylamino]-2′,7′-dideoxy-3′,6′-di-O-mesyl-8′-O-methyl-2′-(tosylamino)-D-threo-α-D-gluco-*octodialdo-1′,5′:8′,4′-dipyranos-1′-yl}-5,6-O-cyclohexylidene-1,3-di-*N-*tosyl-2-deoxystreptamine (23).* A solution of **22** (14.3 mg) in pyridine (0.29 ml) was stirred with mesyl chloride (0.004 ml) at 8 °C for 11 h. After further addition of mesyl chloride (0.002 ml), stirring was continued at 8 °C for 15 h and then at room temperature for 5 h. After addition of a few drops of water, the resulting solution was evaporated to a residue, which was partitioned between ethyl acetate and a saturated aqueous $NaHCO_3$ solution. The combined organic layers were evaporated to a residue, which was chromatographed on silica gel (1.4 g) with 2:1 benzene–ethyl acetate to give quantitatively a solid of **23** (16.3 mg): R_f 0.56 (4:3 benzene–ethyl acetate); mp 161—164 °C ; $[\alpha]_D^{23}$ +2.5° (*c* 1.0, $CHCl_3$), IR ($CHCl_3$): 1695 (NH-CO), 1175 and 1160 cm^{-1} (SO_2); ^{1}H-NMR ($CDCl_3$); δ=2.42, 2.44, and 2.48 (each 3H, s, Ts), 2.80 and 2.96 (each 3H, s, Ms), 3.00 (3H, s, NMe), and 3.45 (3H, s, OMe).

Found: C, 51.22; H, 5.46; N, 4.40; S, 12.67%. Calcd for $C_{53}H_{68}N_4O_{20}S_5$: C, 51.28; H, 5.52; N, 4.51; S, 12.91%.

4-O-{(8′S)-7′-[N-(Benzyloxycarbonyl)methylamino]-2′,3′,7′-trideoxy-6′-O-mesyl-8′-O-methyl-2′-(tosylamino)-D-glycero-β-L-talo-*octodialdo-1′,5′:8′,4′-dipyranos-1′-yl}-5,6-O-cyclohexylidene-1,3-di-*N-*tosyl-2-deoxystreptamine (24).* A solution of **23** (9.1 mg) in DMF (0.27 ml) was stirred with LiCl (6.2 mg) at 100 °C for 2 h under argon. The solution diluted with ethyl acetate was washed with a saturated aqueous $NaHCO_3$ solution, dried, and evaporated to a residue, which was chromatographed on silica gel (1 g) with 3:1 benzene–ethyl acetate to give a solid of the chloro compound (7.8 mg, 90%): R_f 0.64 (4:3 benzene–ethyl acetate); positive Beilstein test.

To a solution of the solid (6.9 mg) in 1,4-dioxane (0.21 ml) were added tributylstannane (0.0138 ml) and α,α′-azobis-(isobutyronitrile) (0.7 mg), and the reaction mixture was heated at 80 °C for 1.5 h under argon. The resulting solution was partitioned between acetonitrile (1 ml) and hexane (0.2 ml×3). The acetonitrile layer was evaporated to a residue, which was chromatographed on silica gel (1 g) with 2:1 benzene–ethyl acetate to give a solid of **24** (6.0 mg, 90%): R_f 0.58 (4:3 benzene–EtOAc); mp 162—168 °C ; $[\alpha]_D^{23}$ +13° (*c* 1.0, $CHCl_3$); ^{1}H-NMR (50 °C, $CDCl_3$+D_2O): δ=2.44 (9H, s, Ts×3), 2.76 (3H, s, OMs), 3.00 (3H, s, NMe), and 3.44 (3H, s, OMe).

Found: C, 54.47; H, 5.90; N, 4.64; S, 10.97%. Calcd for $C_{52}H_{66}N_4O_{17}S_4$: C, 54.44; H, 5.80; N, 4.88; S, 11.18%.

4-O-[(8′S)-7′-N,6′-O-Carbonyl-2′,3′,7′-trideoxy-8′-O-methyl-7′-(methylamino)-2′-(tosylamino)-D-glycero-α-D-allo-*octodialdo-1′,5′:8′,4′-dipyranos-1′-yl]-5,6-O-cyclohexylidene-1,3-di-*N-*tosyl-2-deoxystreptamine (25).* A solution of **24** (5.4 mg) in 2-methoxyethanol (0.22 ml) was heated with sodium acetate trihydrate (5.4 mg) at 130 °C for 2 d. The reaction mixture was partitioned between ethyl acetate and a saturated aqueous NaCl solution, and the organic layer dried and then evaporated to a residue, which was chromatographed on silica gel (0.5 g) with 2:3 benzene–ethyl acetate to give a solid of **25** (3.6 mg, 78%): R_f 0.12 (4:3 benzene–ethyl acetate); mp 159—162 °C ; $[\alpha]_D^{23}$ −25° (*c* 1.0, $CHCl_3$); IR ($CHCl_3$): 1750—1745 (cis cyclic carbamate),[17,18] and 1160 cm^{-1} (SO_2); ^{1}H-NMR (CD_3CN+D_2O): δ=2.83 (3H, s, NMe), 3.42 (3H, s, OMe), 3.52 (1H, dd, H-7′, $J_{6',7'}$=7.0 Hz, $J_{7',8'}$=6.0 Hz), 4.22 (1H, dd, H-5′, $J_{4',5'}$=10.5 Hz, $J_{5',6'}$=3.8 Hz), 4.42 (1H, d, H-8′), 4.71 (1H, dd, H-6′), and 4.93 (1H, d, H-1′, $J_{1',2'}$=3.5 Hz).

Found: C, 54.97; H, 5.74; N, 5.64%. Calcd for $C_{44}H_{56}N_4O_{14}S_3$: C, 54.99; H, 5.87; N, 5.83%.

Methyl β-Aprosaminide (26). *A) From 25*: To a solution of **25** (19.8 mg) in liquid ammonia (≃6 ml) at −35 °C was added sodium metal (25 mg×3) with stirring, and the resulting deep-blue solution was kept at −35 °C for 15 min. After evaporation of ammonia at room temperature, methanol (0.2 ml) and water (1.8 ml) were added, and the

resulting solution of the detosylated intermediate was heated at 100 °C for 5 h to hydrolyze the cyclic carbamate. To the solution was added Dowex 50WX2 resin (H form, 200—400 mesh, 6.0 ml), and the mixture was allowed to stand overnight at room temperature in order to remove the cyclohexylidene group. The resin was packed in a column, washed with water, and then treated with 1 M aqueous ammonia. The ninhydrin-positive fractions were collected and evaporated to give a solid, which was purified by chromatography over CG-50 resin (NH_4 form, 0→0.2 M aqueous ammonia) to yield a solid of the monohydrate of **26** (5.3 mg, 65%): R_f 0.62 (1 : 3 : 2 $CHCl_3$–MeOH–17% aqueous NH_3); mp 141—143 °C; $[\alpha]_D^{23}$ +108° (*c* 0.6, water)[lit,[1b] $[\alpha]_D^{27}$ +104° (*c* 1.1, water)]; MS (SIMS): *m/z* 393 (M^++1); ^{1}H-NMR (5% ND_3 in D_2O): δ=1.20 (1H, q, H-2ax, *J*=13 Hz), 1.65 (1H, q, H-3′ax, *J*=12 Hz), 1.97 (1H, dt, H-2eq, $J_{1,2eq}=J_{2eq,3}$=3.5 HZ, J_{gem}=13 Hz), 2.12 (1H, m, H-3′eq), 2.35 (3H, s, NMe), 2.46 (1H, dd, H-7′, $J_{6',7'}$=3.0 Hz, $J_{7',8'}$=8.5 Hz), 2.70 and 2.86 (each 1H, m, H-1 and H-3, *vice versa*), 3.01 (1H, dt, H-2′, $J_{1',2'}=J_{2',3'eq}$= 3.5 Hz, $J_{2',3'ax}$=12.5 Hz), 3.14, 3.30, and 3.49 (each 1H, t, H-4, H-5, or H-6, *J*≃9.5 Hz), 3.64 (1H, dd, H-5′, $J_{4',5'}$=10 Hz, $J_{5',6'}$=2.5 Hz), 3.78 (1H, m, H-4′), 4.26 (1H, t, H-6′, *J*≃3 Hz), 4.52 (1H, d, H-8′), 5.14 (1H, d, H-1′). This spectrum was superimposable on that of the naturally derived **26** and the reported spectrum.[1b]

Found: C, 46.59; H, 8.10; N, 13.47%. Calcd for $C_{16}H_{32}N_4O_7\cdot H_2O$: C, 46.82; H, 8.35; N, 13.65%.

B) From 28 by Methanolysis: A solution of **28** (5.0 mg) in 1.2% methanolic hydrogen chloride solution (0.33 ml) was heated in a sealed tube at 73 °C for 5 h, and evaporated to a residue, which was chromatographed on silica gel (1.5 g) with 3 : 2 chloroform–acetone to give a solid of the methyl glycoside (4.5 mg): R_f 0.44 (12 : 1 $CHCl_3$–MeOH); ^{1}H-NMR (50 °C, $CDCl_3$): δ=2.98 (3H, s, NMe), 3.46 (3H, s, OMe).

A solution of the solid in 67% aqueous 1,4-dioxane (0.35 ml) was shaken with palladium black and 3-atm hydrogen at room temperature for 4.5 h, filtered and evaporated to a residue. The residue was purified by chromatography over CG-50 resin (NH_4 form, 0→0.2 M aqueous ammonia) to give a solid of the monohydrate of **26** (1.8 mg, 81% from **28**).

C) From 28 by Methylation: To a stirred solution of **28** (4.5 mg) in acetonitrile (0.011 ml) were added methyl iodide (0.045 ml) and Ag_2O (9.0 mg), and stirring was continued at room temperature for 1 h. After filtration, the filtrate was evaporated to give a solid of the methyl glycoside. The solid was hydrogenated as described above to give a solid of the monohydrate of **26** (1.4 mg, 70% from **28**).

Aprosamine (27). *A) From 26*: A solution of the monohydrate of **26** (20.5 mg) in 4 M HCl (1.3 ml) was heated in a sealed tube at 95 °C for 3 d. The brown solution was evaporated and co-evaporated with toluene to give a residue which was purified by chromatography over CG-50 resin (NH_4 form, 0→0.2 M aqueous ammonia) to give a solid of the free base of **27**. The solid was dissolved in 0.5 M HCl and evaporated to a residue, which was reprecipitated from water–acetone to give a solid of the tetrahydrochloride trihydrate of **27** (20 mg, 70%): R_f 0.46 (1 : 3 : 2 $CHCl_3$–MeOH–17% aqueous NH_3); mp 176—180 °C (decomp); $[\alpha]_D^{25}$ +44° (*c* 1.0, water) [lit, $[\alpha]_D^{25}$ +21.6° (*c* 1.27, water);[1b] $[\alpha]_D^{22}$ +53° (*c* 1.075, water)[4]]; MS (SIMS): *m/z* 379 (M^++1); ^{1}H-NMR (D_2O): δ=1.92 (1H, q, H-2ax, *J*=12.5 Hz), 2.04 (1H, m, H-3′ax), 2.35 (1H, m, H-2eq), 2.55 (1H, dt, H-3′eq, J_{gem}=12.5 Hz, $J_{2',3'eq}=J_{3'eq,4'}$=4 Hz,), 2.81 and 2.82 (3H in total, each s, NMe), 4.51 and 4.58 (1H in total, each t, H-6′, *J*≃3), 5.20 and 5.47 (1H in total, each d, $J_{7',8'ax}$=9.0 Hz, $J_{7',8'eq}$=4.0 Hz, H-8′ax and H-8′eq respectively), 5.75 and 5.77 (1H in total, each d, H-1′, $J_{1',2'}$=3.0 Hz and 3.5 Hz, respectively). This ^{1}H-NMR spectrum was found to be superimposable on that of the naturally derived aprosamine and the reported spectrum.[1b]

Found: C, 30.92; H, 6.87; N, 9.47%. Calcd for $C_{15}H_{30}N_4O_7\cdot 4HCl\cdot 3H_2O$: C, 31.15; H, 6.97; N, 9.69%.

B) From Natural Apramycin (1): A solution of apramycin (**1** : 9.9 mg) in 4 M HCl (0.1 ml) was heated at 95 °C for 7 h. The solution was evaporated and co-evaporated with toluene to a residue, which was purified as described above to give a solid of the tetrahydrochloride trihydrate of **27** (8.6 mg, 81%). The solid was identical with the aforeside synthetic aprosamine in all respects.

*1,2′,3,7′-Tetrakis(*N*-benzyloxycarbonyl) aprosamine (28).* To a stirred and ice-cooled solution of the free base of **27** (12.8 mg) in 80% aqueous acetone (0.48 ml) were added Na_2CO_3 (18 mg), 1 M NaOH (0.04 ml) and benzyl chloroformate (0.023 ml), and stirring was continued at room temperature for 2 h. After filtration, the filtrate was agitated with CG-50 resin (H-form) and again filtrated. The filtrate was neutralized with triethylamine (0.023 ml) and then evaporated to a residue, which was chromatographed on silica gel (1 g) with 15 : 1 chloroform–methanol to give a solid: mp 196—198 °C (decomp). Reprecipitation from ethanol–ether yielded the monohydrate of **28** (24 mg, 77%): R_f 0.38 (15 : 1 $CHCl_3$–MeOH); mp 188—190 °C (decomp); $[\alpha]_D^{23}$ +43° (*c* 1.0, MeOH) [lit,[4] prisms of **28**: mp 233—234.5 °C; $[\alpha]_D^{22}$ +48.8° (*c* 1.005, DMF)]; IR (KBr): 1710—1670 (NH-CO); ^{1}H-NMR (CD_3CN+D_2O): δ=3.00 (3H, s, NMe), and 4.21 (1H, broad s, H-6′).

Found: C, 60.44; H, 5.95; N, 5.94%. Calcd for $C_{47}H_{54}N_4O_{15}\cdot H_2O$: C, 60.51; H, 6.05; N, 6.01%.

*4-Azido-2,3,6-tri-*O*-benzyl-4-deoxy-β-*D*-glucopyranosyl Fluoride (29).* To a stirred solution of 4-azido-2,3,6-tri-*O*-benzyl-4-deoxy-α-D-glucopyranosyl chloride[22] (130 mg) in acetonitrile (0.65 ml) was added AgF (130 mg), and stirring was continued at room temperature for 22 h under protection from light. The reaction mixture was filtered and a saturated aqueous NaCl solution was added to precipitate any silver ions from solution. The mixture was again filtered and evaporated to a residue, which was partitioned between chloroform and water. The organic layer was dried and evaporated to a residue, which was chromatographed on silica gel (4 g) with 4 : 1 benzene–ethyl acetate to give a syrup of **29** (122 mg, 97%): R_f 0.41 (benzene); $[\alpha]_D^{23}$ +108° (*c* 1.0, $CHCl_3$); IR ($CHCl_3$): 2120 cm^{-1} (azide); ^{1}H-NMR ($CDCl_3$): δ=5.19 (1H, dd, H-1, $J_{1,2}$=6.4 Hz, $J_{1,F}$=52 Hz, apparently two doublets at δ=5.06 and 5.32).

Found: C, 67.69; H, 5.98; N, 8.87%. Calcd for $C_{27}H_{28}N_3O_4F$: C, 67.91; H, 5.91; N, 8.80%.

*4-O-[(8′*R*)-2′-Amino-8′-O-(4″-azido-2″,3″,6″-tri-O-benzyl-4″-deoxy-α-D-glucopyranosyl)-2′,7′-bis(*N*-benzyloxycarbonyl)-2′,3′,7′-trideoxy-7′-(methylamino)-D-glycero-α-D-allo-octodialdo-1′,5′ : 8′,4′-dipyranos-1′-yl]-1,3-bis(*N*-benzyloxycarbonyl)-2-deoxystreptamine (30).* Before coupling, **28** was dried overnight at 50 °C under reduced pressure. To a mixture of **28** (12.6 mg, 0.0137 mmol), **29** (7.9 mg, 0.0165 mmol), $SnCl_2$ (5.5 mg, 0.029 mmol), $AgClO_4$ (5.7 mg, 0.027 mmol), and Molecular Sieves 4A (12.6 mg) was added a 4 : 1 mixture (0.189 ml) of 1,4-dioxane–benzene at 0 °C, and the mixture was stirred at this temperature for 24 h. After further addition of the same amounts of **29**, $SnCl_2$, $AgClO_4$ and Molecular Sieves 4A as described above, stirring was continued at 0 °C for another 24 h. The reaction mixture was filtered and the filtrate evaporated to give a residue. The residue was chromatographed on silica gel (1.5 g) with 20 : 1 chloroform–methanol to give two products having R_f-values of 0.44 and 0.48 (15 : 1 chloroform–methanol) with recovery of the unreacted **28** (5.4 mg) having R_f 0.38. The R_f 0.44-substance was the desired glycoside **30** as described below.

30 (R_f 0.44-substance): 4.3 mg (23% from **28**; 40% yield based on the unrecovered **28**); mp 89—92 °C; $[\alpha]_D^{23}$ +63° (*c* 0.5, $CHCl_3$); ^{1}H-NMR (50 °C, CD_3CN+D_2O): δ=3.00

(3H, s, NMe), 3.73 (1H, dt, H-2′, $J_{1',2'}=J_{2',3'eq}=4.0$ Hz, $J_{2',3'ax}=13$ Hz), 4.13 (1H, m, H-7′), 4.27 (1H, dull t, H-6′), 5.24 (1H, d, H-1′), 5.27 (1H, d, H-8′, $J_{7',8'}=9.5$ Hz), and 5.41 (1H, d, H-1″, $J_{1'',2''}=3.0$ Hz).

Found: C, 64.57; H, 6.19; N, 6.96%. Calcd for $C_{74}H_{81}N_7O_{19}$: C, 64.76; H, 5.95; N, 7.14%.

R_f 0.48-substance: 2.1 mg; mp 89—92 °C ; $[\alpha]_D^{28}$ +62° (*c* 0.85, $CHCl_3$); IR ($CHCl_3$): 2115 cm^{-1} (azide); ^{1}H-NMR (50 °C, $CDCl_3+D_2O$): $\delta=2.98$ and 3.02 (3H in total, each s, NMe), and 7.1—7.4 (35H, m, Ph×7).

By catalytic reduction, the R_f 0.44-substance (**30**) yielded apramycin (**1**) as described below, while the R_f 0.48-substance did not give apramycin but gave another product (R_f 0.43 on TLC with 1 : 3 : 2 $CHCl_3$-MeOH-17% aqueous NH_3; apramycin:R_f 0.35). Therefore, the R_f 0.48-substance was not further investigated.

Apramycin (1). A solution of **30** (10 mg) in a 3 : 1 : 1 mixture (0.5 ml) of 1,4-dioxane, acetic acid and water was shaken with palladium black and 3-atm hydrogen at room temperature for 2 h, filtered and evaporated to give a residue. The residue was purified by chromatography over CG-50 resin (NH_4 form, 0→0.1 M aqueous ammonia) to give a solid of the monocarbonate monohydrate of **1** (3.4 mg, 74%): R_f 0.35 (1 : 3 : 2 $CHCl_3$-MeOH-17% aqueous NH_3); mp 237—240 °C (decomp); $[\alpha]_D^{23}$ +162° (*c* 0.94, water) [lit,[1] monohydrate: mp 245—247 °C; $[\alpha]_D^{25}$ +162.5° (water)]; MS (SIMS): *m/z* 540 (M^++1); ^{1}H-NMR (5% ND_3 in D_2O): $\delta=1.18$ (1H, m, H-2ax), 1.68 (1H, q, H-3′ax, $J=12$ Hz), 2.03 (1H, m, H-2eq), 2.14 (1H, m, H-3′eq), 2.39 (3H, s, NMe), 2.69 (1H,dd, H-7′, $J_{6',7'}=2.5$ Hz, $J_{7',8'}=8.5$ Hz), 3.03 (1H, dull dt, H-2′, $J_{2',3'ax}=12.5$ Hz), 4.29 (1H, broad s, H-6′), 4.92 (1H, d, H-8′), 5.15 (1H, d, H-1′, $J_{1',2'}=3.5$ Hz), and 5.37 (1H,d, H-1″, $J_{1'',2''}=3.5$ Hz). This spectrum was superimposable on that of the authentic sample of apramycin and the reported spctrum.[1b]

Found: C, 42.57; H, 7.29; N, 11.45%. Calcd for $C_{21}H_{41}N_5O_{11}\cdot H_2CO_3\cdot H_2O$: C, 42.65; H, 7.32; N, 11.30%.

*4-O-[(8′*R*)-2′-Amino-8′-O-(2″,3″,4″,6″-tetra-O-benzyl-α-*D*-glucopyranosyl)-2′,7′-bis(*N*-benzyloxycarbonyl)-2′,3′,7′-trideoxy-7′-(methylamino)-*D*-glycero-α-*D*-allo-octodialdo-1′,5′ : 8′,4′-dipyranos-1′-yl]-1,3-bis(*N*-benzyloxycarbonyl)-2-deoxystreptamine (31).* Following the procedure described for **30**, a sample of **28** (12.6 mg) was treated with 2,3,4,6-tetra-*O*-benzyl-β-D-glucopyranosyl fluoride[20] (9.0 mg×2), $SnCl_2$ (5.5 mg×2), $AgClO_4$ (5.7 mg×2), and Molecular Sieves 4A (12.6 mg×2) in a 4 : 1 mixture (0.189 ml) of 1,4-dioxane and benzene, and then worked up. Column chromatography on silica gel (1.5 g) with 20 : 1 chloroform–methanol gave two products (4.7 mg and 1.7 mg) having R_f-values of 0.43 and 0.48 (15 : 1 chloroform–methanol) with recovery of the unreacted **28** (5.5 mg). The R_f 0.43-substance was the desired glycoside **31** as described below.

31 (R_f 0.43-substance): 4.7 mg (24% from **28**; 42% yield based on the unrecovered **28**); mp 94—97 °C; $[\alpha]_D^{23}$ +48° (*c* 0.80, $CHCl_3$); ^{1}H-NMR (50 °C, $CDCl_3+D_2O$): $\delta=2.97$ (3H, s, NMe), 3.52 (1H, dd, H-2″, $J_{1'',2''}=4.0$ Hz, $J_{2'',3''}=9.5$ Hz), and 5.28 (1H, d, H-1″).

Found: C, 67.44; H, 6.40; N, 3.81%. Calcd for $C_{81}H_{88}N_4O_{20}$: C, 67.67; H, 6.17; N, 3.90%.

R_f 0.48-substance: 1.7 mg; mp 97—101 °C ; $[\alpha]_D^{23}$ +57° (*c* 0.41, $CHCl_3$): IR ($CHCl_3$): 2110 cm^{-1} (azide); ^{1}H-NMR (50 °C, $CDCl_3+D_2O$): $\delta=3.02$ and 3.05 (3H in total, each broad s, NMe), and 7.1—7.4 (40H, m, Ph×8).

By catalytic reduction, the R_f 0.43-substance (**31**) yielded saccharocin (**2**) as described below, while the R_f 0.48-substance gave another product (R_f 0.46 on TLC with 1 : 3 : 2 $CHCl_3$-MeOH-17% aqueous NH_3; saccharocin: R_f 0.38). Therefore, the R_f 0.48-substance was not further investigated.

Saccharocin (2: KA-5685). A sample of **31** (8 mg) was hydrogenated and then purified as described for apramycin (**1**) to give a solid of the monocarbonate monohydrate of **2** (2.7 mg, 78%): R_f 0.38 (1 : 3 : 2 $CHCl_3$-MeOH-17% aqueous NH_3); mp 187—190 °C (decomp); $[\alpha]_D^{23}$ +175° (*c* 0.5, water) [lit, dihydrate:[2a] mp 188—190 °C; $[\alpha]_D^{24}$ +163.5° (*c* 1.0, water); KA-5685:[2b] $[\alpha]_D^{25}$ +124° (*c* 0.5, H_2O)]; MS (SIMS): *m/z* 541 (M^++1); ^{1}H-NMR (5% ND_3 in D_2O): $\delta=1.21$ (1H, q, H-2ax, $J=12.5$ Hz), 1.67 (1H, q, H-3′ax, $J=11.5$ Hz), 1.98 (1H, dt, H-2eq, $J_{1,2eq}=J_{2eq,3}=4.0$ Hz, $J_{gem}=13$ Hz), 2.12 (1H, dt, H-3′eq, $J_{2',3'eq}=J_{3'eq,4'}=4.0$ Hz, $J_{gem}=11.5$ Hz), 2.39 (3H, s, NMe), 2.68 (1H, dd, H-7′, $J_{6',7'}=2.5$ Hz, $J_{7',8'}=8.5$ Hz), 2.70 and 2.87 (each 1H, m, H-1 and H-3, *vice versa*), 3.01 (1H, m, H-2′), 3.61 (1H, dd, H-2″, $J_{1'',2''}\simeq 4$ Hz, $J_{2'',3''}=10$ Hz), 4.29 (1H, t, H-6′), 4.93 (1H, d, H-8′), 5.15 (1H, d, H-1′, $J_{1',2'}=3.5$ Hz), and 5.35 (1H, d, H-1″). This spectrum was superimposable on that of the authentic antibiotic **2** and the reported spectra.[2]

Found: C, 42.73; H, 7.36; N, 9.29%. Calcd for $C_{21}H_{40}N_4O_{12}\cdot H_2CO_3\cdot H_2O$: C, 42.58; H, 7.15; N, 9.03%.

We are grateful to Prof. Sumio Umezawa, Institute of Bioorganic Chemistry, and Prof. Hamao Umezawa, Institute of Microbial Chemistry, for their generous support of our program. We also thank Drs. Shinichi Kondo of the Institute, Hideo Sakakibara[2a] and Toshihito Mori[2b] for their generous gifts of natural apramycin, saccharocin and KA-5685, and are indebted to Mr. S. Nakada for elemental analyses and Miss Y. Suzuki for 250 MHz NMR analyses.

References

1) a) R. Q. Thompson and E. A. Presti, *Antimicrob. Ag. Chemother.-1967*, 332 (1968); b) S. O'Connor, L. K. T. Lam, N. D. Jones, and M. O. Chaney, *J. Org. Chem.*, **41**, 2087 (1976).

2) a) M. Awata, S. Satoi, N. Muto, M. Hayashi, H. Sagai, and H. Sakakibara, *J. Antibiot.*, **36**, 651 (1983); b) K. Kamiya, T. Deushi, A. Iwasaki, I. Watanabe, H. Itoh, and T. Mori, *ibid.*, **36**, 738 (1983).

3) a) H. C. Jarrell and W. A. Szarek, *Carbohydr. Res.*, **67**, 43 (1978); *Can. J. Chem.*, **57**, 924 (1979); W. A. Szarek and O. R. Martin, 183rd National Meeting of the American Chemical Society, Las Vegas, March 1982, Abstr., No. CARB-5; b) H. A. Kirst, B. A. Truedell, and J. E. Toth, *Tetrahedron Lett.*, **22**, 295 (1981).

4) K. Igarashi and T. Honma, Belg. Patent BE-890873 (1982); Japan Patent 57-75994 (1982); *Chem. Abstr.*, **97**, 24167p (1982).

5) K. Tatsuta, K. Akimoto, H. Takahashi, T. Hamatsu, M. Annaka, and M. Kinoshita, *Tetrahedron Lett.*, **24**, 4867 (1983).

6) K. Tatsuta, E. Kitazawa, and S. Umezawa, *Bull. Chem. Soc. Jpn.*, **40**, 2371 (1967).

7) A. Harayama, T. Tsuchiya, and S. Umezawa, *Bull. Chem. Soc. Jpn.*, **52**, 3626 (1979).

8) T. Naito, S. Nakagawa, Y. Narita, and H. Kawaguchi, *J. Antibiot.*, **29**, 1286 (1976).

9) F. H. Bissett, M. E. Evans, and F. W. Parrish, *Carbohydr. Res.*, **5**, 184 (1967).

10) R. F. Borch and A. I. Hassid, *J. Org. Chem.*, **37**, 1673 (1972).

11) The similar strategy was independently reported for preparation of 2-alkenals from the *N,N*-dialkyl-2-alkenylamines *via* the Polonovsky reaction: K. Takabe, T. Yamada, and T. Katagiri, *Chem. Lett.*, **1982**, 1987; K. Takabe and T. Yamada, *Chem. Ind.*, **1982**, 959.

12) D. A. Evans, J. V. Nelson, and T. R. Taber, *Top. Stereochem.*, **13**, 1 (1982).

13) D. Seyferth and M. A. Weiner, *J. Org. Chem.*, **26**, 4797 (1961).
14) K. Tatsuta, K. Fujimoto, M. Kinoshita, and S. Umezawa, *Carbohydr. Res.*, **54**, 85 (1977).
15) R. U. Lemieux and R. M. Ratcliffe, *Can. J. Chem.*, **57**, 1244 (1979).
16) T. Miyake, Y. Takahashi, T. Tsuchiya, S. Umezawa, and H. Umezawa, *Nippon Kagaku Kaishi*, **1982**, 1706.
17) For examples: T. Tsuchiya and T. Shitara, *Carbohydr. Res.*, **109**, 59 (1982); T. Tsuchiya, S. Sakamoto, T. Yamazaki, S. Umezawa, and H. Umezawa, *J. Antibiot.*, **35**, 639 (1982).
18) H. Sano, T. Tsuchiya, S. Kobayashi, H. Umezawa, and S. Umezawa, *Bull. Chem. Soc. Jpn.*, **50**, 975 (1977); L. Goodman, *Adv. Carbohydr. Chem.*, **22**, 109 (1967).
19) R. U. Lemieux, "Molecular Rearrangement Part II," ed by P. de Mayo, Interscience, New York (1963), p. 709.
20) T. Mukaiyama, Y. Murai, and S. Shoda, *Chem. Lett.*, **1981**, 431.
21) K. C. Nicolaou, S. P. Seitz, and D. P. Papahatjis, *J. Am. Chem. Soc.*, **105**, 2430 (1983) and references cited therein.
22) Y. Takagi, T. Tsuchiya, and S. Umezawa, *Bull. Chem. Soc. Jpn.*, **46**, 1261 (1973); Y. Nishimura, T. Tsuchiya, and S. Umezawa, *ibid.*, **46**, 1263 (1973).

N-(Phenylsulfonyl)- and *N*-Methyl-*N*-(phenylsulfonyl)benzohydrazonoyl Azides. Thermally Induced Cyclization to Tetrazoles and Decomposition to Benzonitriles[1)]

Suketaka Ito,* Yumo Tanaka, and Akikazu Kakehi
Department of Industrial Chemistry, Faculty of Engineering, Shinshu University, Wakasato, Nagano 380
(Received September 24, 1983)

N-(Phenylsulfonyl)- and *N*-methyl-*N*-(phenylsulfonyl)benzohydrazonoyl azides, prepared from the corresponding hydrazonoyl chlorides and sodium azide, undergo the cyclization to 5-phenyl-1-(phenylsulfonylamino)-1*H*-tetrazoles together with the competitive decomposition to benzonitriles and the Curtius-type rearrangement leading to semicarbazides when heated in benzene under reflux. The tetrazole formation of hydrazonoyl azides may be characteristic of such hydrazonoyl azides as those carrying an *N*-sulfonyl substituent, the strong electron-withdrawing nature of which probably promotes the cyclization.

Imidoyl azides are well known, in general, to cyclize to tetrazoles which are more stable than the azides themselves in many cases.[2)] However, according to Hergarty *et al.*,[3)] *N*-arylbenzohydrazonoyl azides, a class of imidoyl azides, do not undergo this type of cyclization under a variety of conditions in spite of the fact that the corresponding tetrazoles have been obtained from hydrazidines on treatment with nitrous acid:[4)] the hydrazonoyl azides give only semicarbazides *via* an acid-induced Curtius-type rearrangement.

In the course of our investigation of arylsulfonylhydrazine derivatives, we found that the title hydrazonoyl azides undergo the cyclization to 1,5-disubstituted tetrazoles along with the competitive decomposition to benzonitriles. In the present paper, these characteristic behavior of *N*-(phenylsulfonyl)- (**1**) and *N*-methyl-*N*-(phenylsulfonyl)benzohydrazonoyl azides (**2**) are described.

Results and Discussion

Preparation of N-*Methyl*-N-*(phenylsulfonyl)benzohydrazonoyl Chlorides.* *N*-Methyl-*N*-(phenylsulfonyl)benzohydrazonoyl chlorides (**3b—f**), the starting materials for preparing hydrazonoyl azides **2**, were obtained by the *N*-methylation of *N*-(phenylsulfonyl)benzohydrazonoyl chlorides (**4**)[5)] with diazomethane according to the method previously reported for **3a**.[6)] The yields and physical data of **3b—f** are listed in Table 1.

Preparation of N-*(Phenylsulfonyl)- (1) and* N-*Methyl*-N-*(phenylsulfonyl)benzohydrazonoyl Azides (2).* Hydrazonoyl azides **1** and **2** were prepared by the reaction of the corresponding hydrazonoyl chlorides (**4** and **3**) with sodium azide. Azides **1** could be obtained in good yields by using aqueous dioxane as the solvent. The use of DMF or DMSO as the solvent caused the formation of considerable amounts of benzonitriles together with evolution of nitrogen even under cooling. On the other hand, azides **2** could be obtained in satisfactory yields when the reaction was carried out in DMSO at room temperature; and on treatment in aqueous dioxane, no formation of **2** was observed. The results are summarized in Scheme 1 and Table 2.

In the IR spectra of **2a—f**, the azide ν_{as} band (near 2100 cm^{-1}) was observed to split into three peaks. 13-C NMR studies showed that compounds **2** exist in a single geometric isomer; thus, the ternary splits of azide

Table 1. Preparation of *N*-methyl-*N*-(phenysufonyl)benzohydrazonoyl chlorides (**3**), X-C(Cl)=N-N(Me)-SO_2Ph

3	(X)	Yield[a)] %	Mp θ_m/°C (Solvent)[b)]	IR (KBr) $\nu_{C=N}$ cm^{-1}	IR (KBr) ν_{SO_2} cm^{-1}	NMR[c)] N-CH_3[d)]	Formula	Found (Calcd) (%) C	H	N
3b	(Me)	76	101—103 (B)	1592	1348, 1165	3.03	$C_{15}H_{15}N_2O_2SCl$	55.97 (55.81)	4.76 (4.68)	8.46 (8.68)
3c	(OMe)	79	116—118 (B)	1603	1350, 1175	3.00	$C_{15}H_{15}N_2O_3SCl$	53.38 (53.18)	4.52 (4.46)	8.08 (8.27)
3d	(Cl)	76	111—112 (B)	1579	1340, 1153	3.06	$C_{14}H_{12}N_2O_2SCl_2$	48.74 (48.99)	3.40 (3.52)	7.91 (8.16)
3e	(CN)	74	135—137 (T—H)	1593	1362, 1173	3.14	$C_{15}H_{12}N_3O_2SCl$	53.98 (54.13)	3.62 (3.62)	12.59 (12.68)
3f	(NO_2)	76	140—141 (T—H)	1579	1327, 1155		$C_{14}H_{12}N_3O_4SCl$	47.73 (47.53)	3.40 (3.42)	11.96 (11.88)

a) Yield after recrystallization. b) Solvent for recrystallization; B: benzene, T-H: THF-hexane. c) Data in $CDCl_3$ (δ) with TMS as an internal standard. Compound **3f** is almost insoluble in $CDCl_3$. d) Singlet.

Table 2. *N*-(Phenylsulfonyl)-(**1**) and *N*-methyl-*N*-(phenylsulfonyl)benzohydrazonoyl azides (**2**)

Azide	Yield/%	Mp (decomp) θ_m/°C	IR (KBr)/cm^{-1} ν_{NH} cm^{-1}	IR (KBr)/cm^{-1} assym. ν_{N_3}[a] cm^{-1}	IR (KBr)/cm^{-1} ν_{SO_2} cm^{-1}		NMR ($CDCl_3$) δ[b,c) N-H	N-CH_3	Aromatic H		Found (Calcd) (%) C	H	N
1a	90	118—120	3164	2130	1307	1160	8.29		7.40—8.23	$C_{13}H_{11}N_5O_2S$	51.64 (51.82	3.64 3.68	23.35 23.24)
1b	84	117—118	3180	2140	1303	1165	8.17		7.04—8.20	$C_{14}H_{13}N_5O_2S$	53.07 (53.32	4.09 4.15	22.45 22.21)
1c	93	131—132	3175	2150	1305	1165	8.11		6.78—8.20	$C_{14}H_{13}N_5O_3S$	50.74 (50.75	3.97 3.95	21.35 21.14)
1d	93	142—143	3180	2145	1307	1170	8.33		7.36—8.26	$C_{13}H_{10}N_5O_2SCl$	46.61 (46.50	2.99 3.00	20.56 20.86)
1e	80	133—134	3180	2140	1304	1168	8.39		7.40—8.64	$C_{14}H_{10}N_6O_2S$	51.42 (51.53	2.98 3.09	26.00 25.75)
1f	86	140—141	3170	2160	1315	1167	8.29		7.35—8.50	$C_{13}H_{10}N_6O_4S$	44.97 (45.09	3.01 2.91	24.01 24.27)
2a	93	77—78		2140 (2180, 2080)	1305	1158		2.93	7.25—8.15	$C_{14}H_{13}N_5O_2S$	53.37 (53.32	4.14 4.15	22.45 22.21)
2b	95	100—102		2145 (2195, 2095)	1305	1178		2.91	7.00—8.16	$C_{15}H_{15}N_5O_2S$	54.76 (54.70	4.58 4.95	20.98 21.26)
2c	91	110—112		2145 (2195, 2095)	1307	1160		2.91	6.70—8.15	$C_{15}H_{15}N_5O_3S$	52.30 (52.17	4.35 4.38	19.97 20.28)
2d	96	120—121		2145 (2195, 2090)	1315	1165		2.72	7.21—8.32	$C_{14}H_{12}N_5O_2SCl$	48.00 (48.07	3.46 3.46	19.98 20.02)
2e	94	100—102		2140 (2195, 2085)	1310	1174		3.04	7.28—8.15	$C_{15}H_{12}N_6O_2S$	53.18 (52.93	3.57 3.55	24.29 24.69)
2f	96	115—116		2140 (2195, 2085)	1310	1168		3.29	7.15—8.53	$C_{14}H_{12}N_6O_4S$	46.65 (46.66	3.30 3.36	23.04 23.32)

a) Minor peakes due to Fermi resonance are shown in parentheses. b) Signal patterns are as follows: N-H, broad siglet; N-CH_3, singlet; aromatic H, multiplet. c) Other signals are as follows: **1b**, 2.40, s, *p*-CH_3; **1c**, 3.86, s, *p*-OCH_3 ; **2b**, 2.40, s, *p*-CH_3 ; **2c**, 3.87, s, *p*-OCH_3.

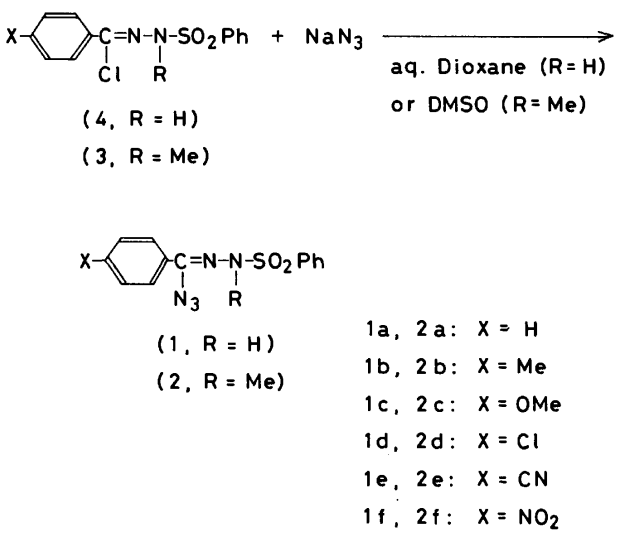

Scheme 1.

ν_{as} band should be attributed to Fermi resonance. This type of Fermi resonance has been reported as regards some organic azides.[7]

Azides **2** and azides **1** carrying an electron-donating group in the *C*-aryl group such as **1b** and **1c** are somewhat thermolabile, and **1e** and **1f** are comparatively stable.

Thermolyses of Hydrazonoyl Azides 1 and 2. Hydrazonoyl azide **1a** was heated for 10 h in dry benzene under reflux. Work-up gave 5-phenyl-1-(phenylsulfonylamino)-1*H*-tetrazole (**5a**, 14%), 4-phenyl-1-(phenylsulfonyl)semicarbazide (**6a**, 36%), and benzonitrile (**7a**, 28%). In Tables 3, 4, and 5, the results are summarized along with those obtained from **1b—f** which were treated under the same reaction conditions. In these reactions, small amounts of diphenyl disulfide and *S*-phenyl benzenethiosulfonate were also obtained.

Table 3. Thermolyses of hydrazonoyl azides (**1** and **2**)

Azide	Products[a] and yields/%[b,c) **5** (**8**)	**6** (**9**)	**7**
1a (**2a**)	14 (12)	36 (16)	28 (45)
1b (**2b**)	6 (6)	24 (23)	47 (48)
1c (**2c**)	— (—)	15 (15)	35 (31)
1d (**2d**)	13 (14)	29 (13)	56 (48)
1e (**2e**)	15 (16)	30 (10)	30 (64)
1f (**2f**)	13 (15)	34 (20)	23 (64)

a) The *p*-substituent of 5-aryl group of **5** (**8**), 4-aryl group of **6** (**9**), or compound **7** corresponds to that of *C*-aryl group of the respective reactant, **1a** (**2a**) to **1f** (**2f**). b) Data in parentheses are those of thermolyses of **2**. c) Isolated Yield except those of **7a** and **7b** which were detected by GLC.

On a similar treatment, hydrazonoyl azides **2** underwent the same type of reaction as those of **1** (Tables 3, 4, and 5). Methyl benzenesulfinate and benzenesulfonate were also detected besides *S*-phenyl benzenethiosulfonate in these cases.

The structure assignment of the tetrazoles and semicarbazides obtained was done on the basis of their analytical and spectral data, and the confirmation of the known compounds was made also by direct comparison with authentic specimens.

The present reactions can be explained by the following routes (Scheme 2).

S-Phenyl benzenethiosulfonate would be generated from benzensulfinic acid *via* its disproportionation:[8] benzenesulfinic acid and methyl benzenesulfinate may be formed from the possible *N*-nitrene[9] or azo sulfone[10] intermediate (Scheme 2).

TABLE 4. PHYSICAL[a] AND ANALYTICAL DATA OF TETRAZOLES,

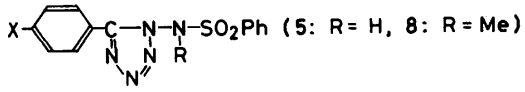

5 or 8	X	Mp θ_m/°C	IR (KBr) ν_{NH} cm^{-1}	IR (KBr) ν_{SO_2} cm^{-1}	IR (KBr) $\nu_{CN,ring}$ cm^{-1}	Formula	Found (Calcd) (%) C	H	N
5a	H	179—180	3062	1362 1175	1265, 1087 983	$C_{13}H_{11}N_5O_2S$	51.83 (51.82	3.68 3.68	23.19 23.24)
5b	Me	188—189	3160	1357 1170	1275, 1085 995	$C_{14}H_{13}N_5O_2S$	53.65 (53.32	4.26 4.15	22.11 22.21)
5d	Cl	199—200	3190	1365 1170	1285, 1090 980	$C_{13}H_{10}N_5O_2SCl$	46.51 (46.50	3.02 3.00	21.03 20.86)
5e	CN	192—193	3200	1364 1170	1280, 1088 980	$C_{14}H_{10}N_6O_2S$	51.43 (51.53	3.00 3.09	25.92 25.75)
5f	NO_2	206—207	3190	1365 1168	1280, 1085 995	$C_{13}H_{10}N_6O_4S$	45.19 (45.09	2.90 2.91	24.04 24.27)
8a	H	186—187		1378 1170	1272, 1088 977	$C_{14}H_{13}N_5O_2S$	53.41 (53.32	4.20 4.15	22.48 22.21)
8b	Me	174—175		1373 1168	1271, 1086 974	$C_{15}H_{15}N_5O_2S$	54.35 (54.70	4.58 4.59	21.62 21.26)
8d	Cl	173—175		1378 1168	1270, 1100 979	$C_{14}H_{12}N_5O_2SCl$	48.06 (48.07	3.40 3.46	19.91 20.02)
8e	CN	185—187		1375 1177	1275, 1095 1005	$C_{15}H_{12}N_6O_2S$	53.02 (52.94	3.57 3.55	24.87 24.70)
8f	NO_2	199—202		1371 1167	1278, 1085 1000	$C_{14}H_{12}N_6O_4S$	46.64 (46.66	3.30 3.36	23.38 23.32)

a) NMR signals ($CDCl_3/\delta$) of N-CH_3 in **8a**, **8b**, **8d**, and **8e** are 3.44, 3.41, 3.44, and 3.47 (singlet), respectively. Compound **8f** is almost insoluble in $CDCl_3$. Signals of N-H in compounds **5a—f** are comsealed by those of aromatic protons.

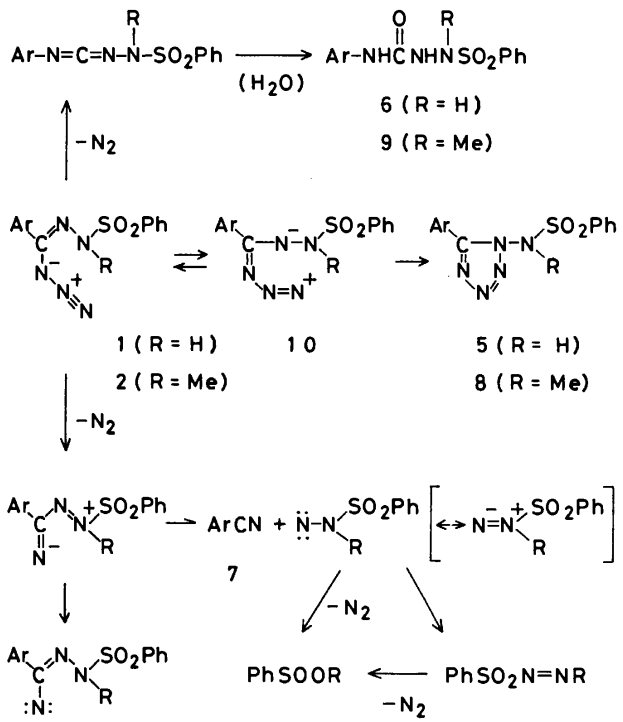

Scheme 2.

Since the disproportionation of benzenesulfinic acid gives also benzenesulfonic acid, the reaction medium should be acidic to a certain extent. Thus, the Curtius-type rearrangement of **1** and **2** leading to **6** and **9** may be acid-induced. Indeed, when **1a** was heated in benzene in the presence of pyridine, **6a** was obtained in a diminished yield (3%) and an increase in the yield of **5a** was observed (14→40%). Methyl benzenesulfonate detected in the reaction of **2** may result from the ester interchange between methyl benzenesulfinate and benzenesulfonic acid.

The tetrazole formation is one of the 1,5-dipolar cyclization. The present reaction is the first example of this type of cyclization of hydrazonoyl azides. The strong electron-withdrawing nature of benzenesulfonyl group probably accelerates the cyclization; that is, the 1,5-dipole structure, **10**, may be stabilized owing to the reduced electron density at the amino nitrogn. This type of contribution can not be expected for *N*-arylbenzohydrazonoyl azides which do not undergo tetrazole formation.

As shown in Table 3, hydrazonoyl azides **1c** and **2c** gave no tetrazoles, which can be explained on the basis of the electron-donating effect of *p*-methoxyl group attached to the *C*-aryl group. That is to say, the electron-donating group may prevent the transformation of azide forms (**1** and **2**) to the 1,5-dipole structure (**10**).

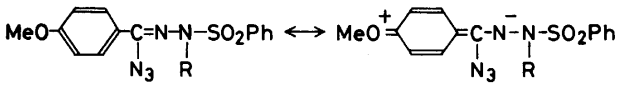

The lower yields of **5b** and **8b** may be also due to the electron-donating effect of *p*-methyl group.

Table 5. Physical and Analytical Data of Semicarbazides,

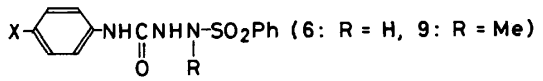

6 or 9	X	Mp θ_m/°C	IR (KBr) ν_{NH} cm^{-1}	IR (KBr) ν_{CO} cm^{-1}	IR (KBr) ν_{SO_2} cm^{-1}	Formula	Found (Calcd) (%) C	H	N
6a	H	204—206a)	3389, 3200 3100	1642	1347 1169	$C_{13}H_{13}N_3O_3S$	53.50 (53.60	4.69 4.50	14.62 14.42)
6b	Me	222—223	3409, 3202 3120	1649	1354 1176	$C_{14}H_{15}N_3O_3S$	55.10 (55.25	4.98 4.97	13.90 13.81)
6c	MeO	202—203	3400, 3200 3110	1644	1349 1171	$C_{14}H_{15}N_3O_4S$	52.30 (52.49	4.73 4.72	13.10 13.12)
6d	Cl	240—241	3316, 3275 3194	1674	1334 1164	$C_{13}H_{12}N_3O_3SCl$	47.87 (47.93	3.70 3.71	12.85 12.90)
6e	CN	234—236	3290, 3255 3190	1683	1325 1165	$C_{14}H_{12}N_4O_3S$	52.95 (53.16	3.75 3.82	17.93 17.71)
6f	NO_2	205—206	3311, 3247 3110	1692	1333 1161	$C_{13}H_{12}N_4O_5S$	46.21 (46.43	3.54 3.60	16.72 16.66)
9a	H	192—194	3302, 3210	1688	1349 1163	$C_{14}H_{15}N_3O_3S$	55.11 (55.07	4.89 4.95	13.75 13.76)
9b	Me	162—164	3361, 3097	1687	1360 1178	$C_{15}H_{17}N_3O_3S$	56.67 (56.41	5.40 5.36	13.19 13.16)
9c	MeO	188—189	3341, 3108	1697	1368 1177	$C_{15}H_{17}N_3O_4S$	53.58 (53.73	5.42 5.11	12.23 12.53)
9d	Cl	207—208	3305, 3092	1695	1355 1170	$C_{14}H_{14}N_3O_3S$	49.55 (49.49	4.09 4.15	12.60 12.37)
9e	CN	227—228	3323, 3280	1700	1360 1168	$C_{15}H_{14}N_4O_3S$	54.42 (54.54	4.24 4.27	17.00 16.96)
9f	NO_2	233—234	3307, 3097	1697	1330 1169	$C_{14}H_{14}N_4O_5S$	47.75 (48.00	3.85 4.03	15.94 15.99)

a) Lit, mp 228 °C: P. Grammaticakis, *Bull. Soc. Chim. Fr.*, **1953**, 86.

Experimental

Melting points were determined with a Yanagimoto MP-S3 micromelting point apparatus, and are uncorrected. The microanalysis was performed on a Perkin-Elmer 240 elemental analyzer. The IR and NMR spectra were recorded with a Hitachi 260-10 and a Varian EM-360A spectrometer, respectively.

Preparation of N-*Methyl*-N-*(phenylsulfonyl)benzohydrazonoyl Chlorides (3). General Procedure*: To a solution of *N*-(phenylsulfonyl)benzohydrazonoyl chloride[5] (**4**, 10 mmol) in THF (30 ml), slightly excess amounts of an ethereal solution of diazomethane was added by portions. The reaction completed almost immediately with evolution of nitrogen. The removal of solvent gave practically pure **3** (yield: nearly quantitative), which was recrystallized from an appropriate solvent. The results are summarized in Table 1.

Preparation of N-*(Phenylsulfonyl)benzohydrazonoyl Azides (1). General Procedure*: To a homogeneous aqueous dioxane solution of hydrazonoyl chloride **4**, prepared by adding water (10 ml) to a solution of **4** (10 mmol) in dioxane (40 ml), a solution of sodium azide (11 mmol) in water (5 ml) was added at room temperature. The mixture turned pale yellow immediately. After standing for a few minutes, 300 ml of ice water was added to the reaction mixture; and then, the mixture was ice-cooled for 10—15 min. The product separated was purified by crystallization from acetone–hexane. The results are summarized in Table 2.

Preparation of N-*Methyl*-N-*(phenylsulfonyl)benzohydrazonoyl Azides (2). General Procedure*: A mixture of hydrazonoyl chloride **3** (10 mmol), sodium azide (12 mmol), and DMSO (60 ml) was stirred for 10—15 h at room temperature. To the reaction mixture, ice water was added by portions, and the resulting precipitates of hydrazonoyl azide were filtered, dried, and then crystallized from acetone–methanol. The results are summarized in Table 2.

Thermolyses of Hydrazonoyl Azides 1. Typical Procedure: A solution of **1a** (1.505 g, 5 mmol) in dry benzene (30 ml) was refluxed for 10 h. The progress of reaction was checked by means of TLC. The reaction mixture was cooled and filtered to give 4-phenyl-1-(phenylsulfonyl)semicarbazide (**6a**; 498 mg, 34%) as a benzene-insoluble substance, which was purified by crystallization from ethanol. The filtrate was concentrated to about 5 ml by fractional distillation, and then chromatographed on a silica-gel column (20 cm-d, 15 cm-h; eluents: hexane, benzene, benzene–diethyl ether, and benzene–ethanol) to give a benzonitrile fraction, diphenyl disulfide (22 mg, 2%), *S*-phenyl benzenethiosulfonate (203 mg, 16%), 5-phenyl-1-(phenylsulfonylamino)-1*H*-tetrazole (**5a**; 210 mg, 14%; purified by crystallization from ethanol–hexane), **6a** (29 mg, 2%), and an undeterminable mixture (202 mg). From the benzonitrile fraction, **7a** (144 mg, 28%) was detected by GLC (Silicone grease DC-550/celite 545, 2 m; 130 °C). The results are summarized in Tables 3, 4, and 5.

Thermolysis of Ia in the Presence of Pyridine: A solution of **1a** (1.505 g, 5 mmol) and pyridine (0.4 g, 5 mmol) in dry benzene (30 ml) was refluxed for 10 h. A similar work-up of the reaction mixture gave **5a** (596 mg, 40%), **6a** (48 mg, 3%), and **7a** (171 mg, 33%) together with *S*-phenyl benzenethiosulfonate (132 mg, 11%) and trace amounts of diphenyl disulfide.

Thermolyses of Hydrazonoyl Azides **2**. *Typical Procedure*: A solution of **2a** (1.575 g, 5 mmol) in dry benzene (30 ml) was refluxed for 3 h. The reaction mixture was treated in a manner similar to those mentioned above to afford **7a** (232 mg, 45%), **8a** (189 mg, 12%), and **9a** (245 mg, 16%) along with *S*-phenyl benzenethiosulfonate (62 mg), methyl benzenesulfinate (197 mg), methyl benzenesulfonate (141 mg), and an undeterminable mixture (73 mg). The results are summarized in Tables 3, 4, and 5.

References

1) A preliminary communication of parts of this study has appeared: S. Ito, Y. Tanaka, and A. Kakehi, *Chem. Lett.*, **1982**, 59.

2) W. Lwowsky, "The Chemistry of the Azido Group" ed by S. Patai, Interscience, London (1971), p. 510.

3) A. F. Hegarty, J. B. Aylward, and F. L. Scott, *Tetrahedron Lett.*, **1967**, 1259; *J. Chem. Soc., C*, **1967**, 2587.

4) J. M. Burgess and M. S. Gibson, *Tetrahedron*, **18**, 1001 (1962).

5) S. Ito, Y. Tanaka, and A. Kakehi, *Bull. Chem. Soc. Jpn.*, **49**, 762 (1976).

6) S. Ito, Y. Tanaka, A. Kakehi, T. Fukuyama, N. Osawa, and N. Sayo, *Bull. Chem. Soc. Jpn.*, **56**, 545 (1983).

7) E. Lieber, C. N. R. Rao, A. E. Thomas, E. Oftedahl, R. Minnis, and C. V. N. Nambury, *Spectrochim. Acta*, **19**, 1135 (1963), and references cited therein.

8) E. Vinkler, F. Klivengi, and J. Szabo, *Acta Chim. Acad. Sci. Hung.*, **15**, 384 (1958); J. L. Kice and K. W. Bowers, *J. Am. Chem. Soc.*, **84**, 605 (1962).

9) For a reference for the chemistry of *N*-nitrenes, see D. M. Lemal, "Aminonitrenes," ed by W. Lwowski, Interscience, New York (1970), p. 345.

10) The thermal decomposition of azo sulfones in nonpolar solvents such as benzene generates sulfinic acids together with other products; see J. L. Kice and R. S. Gabrielsen, *J. Org. Chem.*, **35**, 1004, 1010 (1970).

Base-induced Dehydrosulfinatocyclization of *N*-Alkyl-*N*-phenylsulfonyl-*N*″-arylbenzamidrazones to 3,4-Diaryl-4*H*-1,2,4-triazoles

Suketaka Ito,* Yumo Tanaka, and Akikazu Kakehi
Department of Industrial Chemistry, Faculty of Engineering, Shinshu University, Wakasato, Nagano 380
(Received October 3, 1983)

3,4-Diaryl-4*H*-1,2,4-triazoles were obtained in good to comparable yields by the reaction of *N*-alkyl-*N*-phenylsulfonyl-*N*″-arylbenzamidrazones with sodium hydride. The reaction probably proceeds *via* the elimination of benzenesulfinic acid and the oxidative cyclization of *N*-alkylidene-*N*″-arylbenzamidrazones generated by the base-catalyzed isomerization of azo intermediates.

As the McFadyen-Stevens[1] and the Bamford-Stevens reactions,[2] such reactions of arylsulfonylhydrazine derivatives involving the elimination of arenesulfonyl group as arenesulfinate anion may be attractive from synthetic aspects.

In a previous paper,[3] we reported a preparative method of 3-aryl-1,2,4-benzotriazines by the mercury(II) oxide-oxidation of *N*-phenylsulfonyl-*N*″-arylbenzamidrazones (**1**). This reaction has been postulated to proceed *via* diazonium benzenesulfinates generaed from intermediate azo sulfones (**2**), the oxidizing producs of the benzamidrazones.

Ar–C(=N–Ar′)–N=N–Z

2 (Z=PhSO$_2$)

3 (Z=Alkyl)

N,*N*-Disubstituted amidrazones such as the title amidrazones (**4**) cannot undergo this type of oxidation leading to the formation of **2**, as a matter of course. However, as has been seen in some reactions of arylsulfonylhydrazines (carrying a free hydrogen at the 2-position) with a base,[4] the base-induced 1,2- (or 1,4-) elimintion of arenesulfinic acid can be expected for the title amidrazones, which would result in the formation of 1,2,4-triazabutadiene intermediates (**3**). The present paper deals with the formation of 3,4-diaryl-4*H*-1,2,4-triazoles (**5**) from *N*-alkyl-*N*-phenylsulfonyl-*N*″-arylbenzamidrazones (**4**) *via* the elimination of benzenesulfinic acid by the action of sodium hydride.

Results and Discussion

Preparation of N-*Alkyl*-N-*phenylsulfonyl*-N″-*arylbenzamidrazones (4).* Amidrazones **4** were prepared by the reaction of anilines with *N*-alkyl-*N*-(phenylsulfonyl)benzohydrazonoyl chlorides (**6**), readily obtainable from *N*-(phenylsulfonyl)benzohydrazonoyl chlorides or *N*-alkyl-*N*-(phenylsulfonyl)benzohydrazides[5] (Scheme 1).

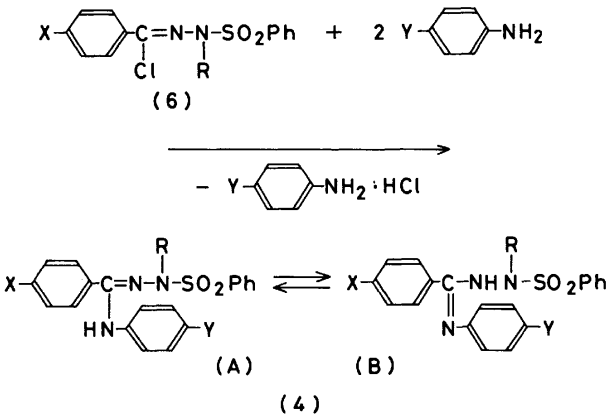

Scheme 1.

TABLE 1. *N*-ALKYL-*N*-PHENYLSULFONYL-*N*″-ARYLBENZAMIDRAZONES (**4**),

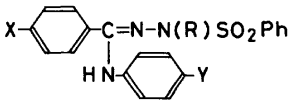

	Amidrazone			Yield/%[a]	Mp θ_m/°C	Formula	Found (%)			Calcd (%)		
	X	Y	R				C	H	N	C	H	N
4a	H	H	Me	70	154—156	$C_{20}H_{19}N_3O_2S$	65.70	5.24	11.50	65.78	5.25	11.63
4b	H	Me	Me	56	165—167	$C_{21}H_{21}N_3O_2S$	66.14	5.68	11.06	66.47	5.58	11.07
4c	H	MeO	Me	50	172—174	$C_{21}H_{21}N_3O_3S$	63.82	5.56	10.21	63.82	5.35	10.63
4d	H	Cl	Me	62	161—162	$C_{20}H_{18}N_3O_2SCl$	59.45	4.63	10.70	60.07	4.54	10.51
4e	Me	H	Me	79	152—154	$C_{21}H_{21}N_3O_2S$	66.41	5.54	10.86	66.47	5.58	11.07
4f	Me	Me	Me	61	167—168	$C_{22}H_{23}N_3O_2S$	67.07	5.81	10.64	67.15	5.89	10.68
4g	Me	Cl	Me	69	172—173	$C_{21}H_{20}N_3O_2SCl$	60.97	4.85	10.05	60.94	4.87	10.15
4h	Cl	H	Me	71	148—150	$C_{20}H_{18}N_3O_2SCl$	59.89	4.50	10.40	60.07	4.54	10.51
4i	Cl	Me	Me	68	173—175	$C_{21}H_{20}N_3O_2SCl$	60.70	4.86	10.25	60.94	4.87	10.15
4j	Cl	Cl	Me	77	194—196	$C_{20}H_{17}N_3O_2SCl_2$	55.23	3.93	9.65	55.31	3.95	9.67
4k	H	H	Et	76	140—142	$C_{21}H_{21}N_3O_2S$	66.29	5.51	10.71	66.47	5.58	11.07
4l	H	Cl	Et	87	146—148	$C_{21}H_{20}N_3O_2SCl$	61.15	4.76	10.03	60.94	4.87	11.15

a) Isolated yield.

Table 2. Spectral data of amidrazones (**4**)

Amidrazone	IR (KBr)[a]				NMR ($CDCl_3$) δ[b,c]		
	ν_{NH}	$\nu_{C=N}$	as. ν_{SO_2}	sym. ν_{SO_2}	N-H	N-CH_3 (-CH_2CH_3)	Aromatic H
	cm^{-1}	cm^{-1}	cm^{-1}	cm^{-1}			
4a	3300	1590s	1390m 1343s	1167m 1158s	8.23brs	2.92s	6.60—8.12m
4b	3280	1598s	1383m 1348s	1170w 1165s	7.98brs	2.92s	6.50—8.20m
4c	3280	1595s	1390m 1335s	1175m 1156s	8.08brs	2.91s	6.40—8.20m
4d	3295	1590s	1375m 1344s	1175w 1157s	8.19brs	2.91s	6.50—8.10m
4e	3350	1598s	1395m 1350s	1185m 1163s	8.47brs	2.90s	6.55—8.40m
4f	3295	1600s	1391m 1339s	1184m 1162s	8.07brs	2.90s	6.50—8.30m
4g	3285	1605s	1388m 1340s	1180m 1160s	8.15brs	2.90s	6.50—8.30m
4h	3260	1582s	1362m 1330s	1163sh 1147s	7.93brs	2.90s	6.65—8.08m
4i	3265	1583s	1361w 1330s	1162w 1150s	8.18brs	2.90s	6.50—8.10m
4j	3260	1600s	1360w 1332s	1172w 1148s	8.47brs	2.90s	6.50—8.10m
4k	3290	1595s	1382m 1340s	1154m 1167s	8.30brs	3.23q, 1.18t (J=7.2, 7.2 Hz)	6.60—8.15m
4l	3290	1590s	1382m 1340s	1155sh 1166s	8.23brs	3.24q, 1.15t (J=7.2, 7.2 Hz)	6.55—8.10m

a) Abbreviations are as follows: m, medium; s, strong; w, weak; sh, shoulder. b) Abbreviations are as follows: brs, broad singlet; s, singlet; q, quartet; t, triplet. c) Other signals are as follows: **4b**, 2.24s, *p*-CH_3 (Y); **4c**, 3.71s, *p*-OCH_3 (Y); **4e**, 2.31s, *p*-CH_3 (X), **4f**, 2.31s, *p*-CH_3 (X) and 2.25s, *p*-CH_3 (Y); **4g**, 2.33s, *p*-CH_3 (X); **4i**, 2.27s, *p*-CH_3 (Y).

On heating in refluxing dioxane, hydrazonoyl chlorides **6** and anilines afforded amidrazones **4** only in poor yields (for example, *N*-methyl-*N*-(phenylsulfonyl)-benzohydrazonoyl chloride and aniline gave the corresponding amidrazone in an 18% yield after refluxing for 24 h). However, when chlorides **6** were fused with anilines at 105—110 °C for 3—4 h under an atmosphere of nitrogen, compounds **4** were obtained in good yields. Small amounts of *N*-methyl-*N*-(phenylsulfonyl)benzohydrazide, hydrolyzed products of **6**, were also obtained. The results are summarized in Tables 1 and 2.

Interestingly, when a fusion of compounds **6** with anilines was conducted at higher temperature, the yields of amidrazones decreased remarkably and the formation of 3-aryl-1,2,4-benzotriazines was observed. For example, *N*-methyl-*N*-(phenylsulfony)-*p*-methylbenzohydrazonoyl chloride gave **4g** in a 19% yield and 7-chloro-3-*p*-tolyl-1,2,4-benzotriazine in a 17% yield on heating with *p*-chloroaniline at 120 °C for 1.5 h, and 7-chloro-3-phenyl-1,2,4-benzotriazine (21%) was obtained by the fusion of *N*-methyl-*N*-(phenylsulfonyl)benzohydrazonoyl chloride with *p*-chloroaniline at 150 °C for 1.5 h. In the latter case, no amidrazone could be detected.

For these benzotriazine formations, the *N*-alkyl group of **4** must be eliminated. Since hydrogen chloride exists in the reaction medium, the reaction may proceed *via* a route which involves the protonation of initially formed amidrazones and the subsequent nucleophilic attack of chloride ion. The resulting *N*-dealkylated amidrazones (**1**) probably undergo air oxidation leading to the formation of benzotriazines *via* **2** (Scheme 2).

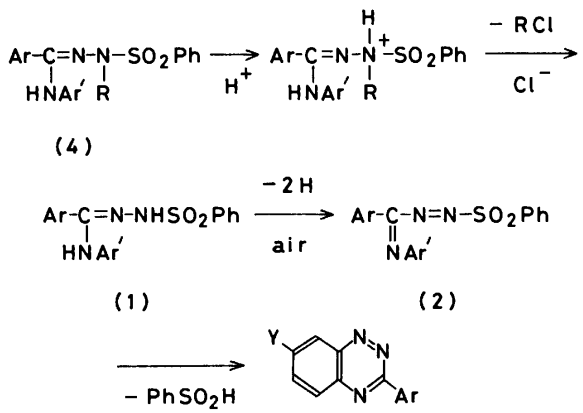

Scheme 2.

N-Alkylaion of *N*-phenylsulfonyl-*N''*-arylbenzamidrazone (**1**) with diazoalkane or alkyl iodide may be available for preparing **4**. For example, **4a** was obtained in a good yield by these methods (Scheme 3).

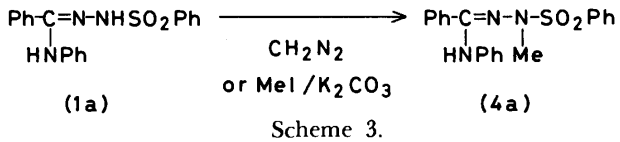

Scheme 3.

For the amidrazones, two tautomeric structures, **4**(A) and **4**(B), are possible. The IR spectra of **4** are far simple in the N-H absorption region (>3000 cm^{-1}) as compared with those of *N*-phenylsulfonyl-*N*″-arylbenzamidrazones. According to Walter and Weiss,[6] *N*,*N*-disubstituted *N*″-arylbenzamidrazones prefer to an amide hydrazone form which is stabilized by intramolecular hydrogen bonding. Thus, amidrazones **4** also may take the amide hydrazone structure, **4**(A). The duality of as. ν_{SO_2} and sym. ν_{SO_2} absorptions may be due to Fermi resonance.

Reactions of Amidrazones 4 with Sodium Hydride. Amidrazones **4** were allowed to react with small excess amounts of sodium hydride dispersion in dioxane under reflux.[7] With the progress of reaction, precipitation of sodium benzenesulfinate was observed. The reaction went essentially to completion after about 20 h of refluxing. After removal of the precipitated sodium benzenesulfinate, the reaction mixtures were chromatographed to give 3,4-diaryl-4*H*-1,2,4-triazoles in good to comparable yields along with small amounts of undeterminable oils. The results are summarized in Tables 3 and 4.

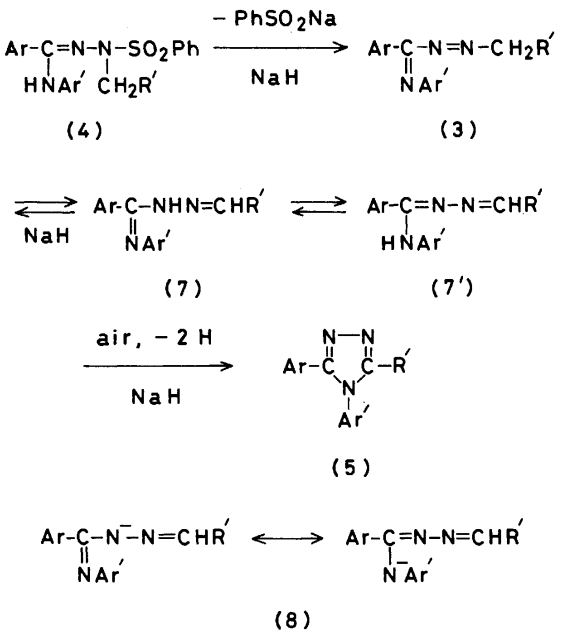

Scheme 4.

Table 3. 3,4-Diaryl-4*H*-1,2,4-triazoles (**5**) from amidrazones **4**

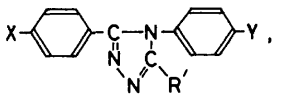

	Triazole			Yield/%[a]	Mp θ_m/°C	Formula	Found (%)			Calcd (%)		
	X	Y	R′				C	H	N	C	H	N
5a	H	H	H	78	139—140[b]	$C_{14}H_{11}N_3$	75.79	5.12	18.42	75.60	5.01	18.99
5b	H	Me	H	57	149—151	$C_{15}H_{13}N_3$	76.47	5.67	18.07	76.57	5.57	17.86
5c	H	MeO	H	63	121—122	$C_{15}H_{13}N_3O$	71.65	5.16	16.88	71.70	5.21	16.72
5d	H	Cl	H	80	189—190	$C_{14}H_{10}N_3Cl$	65.31	3.90	16.49	65.76	3.94	16.43
5e	Me	H	H	46	165—166	$C_{15}H_{13}N_3$	76.41	5.58	17.64	76.57	5.57	17.86
5f	Me	Me	H	34	192—194	$C_{16}H_{15}N_3$	77.10	6.02	17.02	77.08	6.06	16.85
5g	Me	Cl	H	57	201—203	$C_{15}H_{12}N_3Cl$	66.93	4.53	15.71	66.79	4.48	15.58
5h	Cl	H	H	36	174—175	$C_{14}H_{10}N_3Cl$	65.98	3.95	16.20	65.76	3.94	16.43
5i	Cl	Me	H	40	174—176	$C_{15}H_{12}N_3Cl$	66.76	4.43	15.67	66.79	4.48	15.58
5j	Cl	Cl	H	40	184—186	$C_{14}H_{10}N_3Cl_2$	57.66	3.07	14.38	57.95	3.13	14.48
5k	H	H	Me	90	161—163[c]	$C_{15}H_{13}N_3$	76.72	5.64	17.90	76.57	5.57	17.86
5l	H	Cl	Me	63	160—162	$C_{15}H_{12}N_3Cl$	66.88	4.57	15.75	66.79	4.48	15.58

a) Isolated yield. b) Lit, mp 140 °C: R. Fusco and S. Rossi, *Ann. Chim.*, **50**, 277 (1960). c) Lit, mp 158.0—160.5 °C: Ref. 11.

Table 4. Spectral data of triazoles (**5**)

Triazole	IR (KBr) ν/cm^{-1}			NMR ($CDCl_3$) δ				
	1,2,4-triazole ring			5-H	5-CH_3	*p*-CH_3	(-OCH_3)	Aromatic H
5a	1598	1070	1016	8.35s				7.00—7.70m
5b	1600	1070	1010	8.31s		2.45s	(Y=Me)	7.00—7.70m
5c	1610	1070	1017	8.29s		3.87s	(Y=OMe)	6.80—7.68m
5d	1575	1073	1013	8.32s				6.80—7.68m
5e	1596	1090	1012	8.32s		2.34s	(X=Me)	6.90—7.70m
5f	1612	1089	1010	8.29s		2.35s	(X=Me)	6.85—7.53m
						2.43s	(Y=Me)	
5g	1620	1089	1018	8.28s		2.33s	(X=Me)	6.95—7.67m
5h	1584	1073	1007	8.36s				7.00—7.60m
5i	1599	1082	1003	8.32s		2.46	(Y=Me)	7.00—7.60m
5j	1595	1080	1004	8.33s				7.00—7.60m
5k	1596	1073	1012		2.34s			7.00—7.70m
5l	1597	1075	1010		2.37s			7.00—7.70m

The triazoles obtained were confirmed by their analytical and spectral data, and the idetification of known compounds was made by direct comparison with authentic specimens. The absorptions at near 1600, 1080, and 1010 cm^{-1} in the IR spectra can be attributed to the 1,2,4-triazole ring vibrations.[8]

The present triazole formation can be explained by the following route, which involves the 1,4-elimination of benzenesulfinic acid[9] and the base-catalyzed tautomerization[10] of **3** to *N*-alkylidene-*N*''-arylbenzamidrazones (**7** or **7**') followed by oxidative cyclization to 1,2,4-triazoles (Scheme 4).

In view of the acidity of the amino hydrogen of **4**, **4** should generae initially **3**, from which **7** or **7**' may be formed. The cyclization of *N*-arylmethylene-*N*''-arylbenzamidrazones to 3,4,5-trisubstituted 4-*H*-triazoles by mercury(II) oxide-oxidation has been reported by Spassov *et al.*[11] For the oxidative cyclization step, **7** or **7**' to **5**, the anionic 6π-electrocyclic process or intramolecular nucleophilic process of **8** and the subsequent aromatization to **5** may be conceivable.

Experimental

Melting points were determined with a Yanagimoto MP-S3 micromelting point apparatus, and are uncorrected. The microanalysis was performed on a Perkin-Elmer 240 elemen tal analyzer. The IR and NMR spectra were recorded with a Hitachi 260-10 and a Varian EM-360A spectrometers, respectively. *N*-Methyl-*N*-(phenylsulfonyl)benzohydrazonoyl chlorides were prepared by the method previously reported.[5]

Preparation of N-*Ethyl*-N-*(phenylsulfonyl)benzohydrazonoyl Chloride.* To a solution of 1-benzoyl-2-phenylsulfonylhydrazine (5.52 g, 20 mmol) in DMF (50 ml), a 0.58 g-portion (net 24 mmol) of sodium hydride dispersion (70% in liquid paraffin) was added under external cooling. After the cease of gas evolution (a few minutes), ethyl iodide (3.43 g, 22 mmol) was added to the mixture. After stirring for 1 h at room temperature, the DMF solution was poured into water to separate 1-benzoyl-2-ethyl-2-phenylsulfonylhydrazine, which was purified by crystallization from ethanol (yield: 4.95 g, 82%). Mp 162—164 °C; IR(KBr, cm^{-1}): 3210 (NH), 1673 (C=O), 1353, and 1163, (SO_2); NMR ($CDCl_3$), δ=3.73 (2H q, N-$C\underline{H}_2CH_3$, J=7.2 Hz), 1.25 (3H t, N-$CH_2C\underline{H}_3$, J=7.2 Hz), and 7.20—8.20 (11H m, 2Ph and NH). Found: C, 59.35; H, 5.46; N, 9.18%. Calcd for $C_{15}H_{16}N_2O_3S$: C, 59.19; H, 5.30; N, 9.20%.

A mixture of 2-ethylated hydrazine thus obtained (4.53 g, 15 mmol) and 30 ml of thionyl chloride was refluxed for 3 h. After removal of excess thionyl chloride *in vacuo*, the oily residue was chromatographed on a silica-gel column (2.5 cm-d, 15 cm-h; eluent: benzene) to give *N*-ethyl-*N*-(phenylsulfonyl)benzohydrazonoyl chloride (3.49 g, 72%), which was crystallized from benzene-hexane. Mp 63—65 °C; IR (KBr, cm^{-1}): 1591 (C=O), 1350, and 1168 (SO_2); NMR ($CDCl_3$), δ=3.41 (2H q, N-$C\underline{H}_2CH_3$, J=7.0 Hz), 1.07 (3H t, N-$CH_2C\underline{H}_3$, J=7.0 Hz), and 7.30—8.20 (10H m, 2Ph). Found: C, 55.76; H, 4.71; N, 8.70%. Calcd for $C_{15}H_{15}N_2O_2SCl$: C, 55.81; H, 4.68; N, 8.68%.

Preparaton of Amidrazones **4**. *General Procedure*: A mixture of **6** (10 mmol) and aniline (22 mmol) was heated in an oil bath at 105—110 °C for 3—4 h under nitrogen atmosphere. After being cooled, the reaction mixture was extracted with water and chloroform. The chloroform layer was washed and dried, and then concentrated. The chloroform extract was chromatographed on a silica-gel column (2.5 cm-d, 10 cm-h; eluent: benzene–ethanol) to give **4**, which was recrystallized from benzene. The results were summarized in Tables 1 and 2.

Fusion of **6** *with Anilines at a Higher Temperature. A Typical Example*: A mixture of *N*-methyl-*N*-(phenylsulfonyl)-*p*-methylbenzohydrazonoyl chloride (2.582 g, 8 mmol) and *p*-chloroaniline (2.245 g, 17.6 mmol) was heated at 120 °C for 1.5 h in a similar manner. Chloroform extraction followed by chromatography gave amidrazone **4g** (0.569 g, 19%) and 7-chloro-3-*p*-toly-1,2,4-benztoriazine[3] (mp 175—177 °C, 0.342 g, 17%) from the reaction mixture.

N-*Methyltion of* N-*Phenylsulfonyl*-N''-*phenylbenzamidrazone (***1a***). *With Methyl Iodide and Potassium Carbonate*: A mixture of **1a** (703 mg, 2 mmol) and methyl iodide (430 mg, 3 mmol) in THF (30 ml) was stirred with potassium carbonate (420 mg, 3 mmol) for 18 h at room temperature. The reaction mixture was poured into water (150 ml) to give precipitates, which were purified by column chromatography to give **4a** (557 mg, 76%).

With diazomethane: To a solution of **1a** (352 mg, 1 mmol) in THF (15 ml), slightly excess amounts of an ethereal solution of diazomethane was added by portions. After removal of solvent, the residue was chromatographed to give **4a** (313 mg, 89%).

The Reaction of Amidrazones **4** *with Sodium Hydride. General Procedure*: A mixture of **4** (1 mmol) and sodium hydride dispersion (net 1.5 mmol) in dry dioxane (30 ml) was refluxed for 20 h under nitrogen atmosphere. After removal of separated sodium benzenesulfinate by filtration, the reaction mixture was concentrated and chromatographed on a silica-gel column (2.0 cm-d, 10 cm-h; eluent: benzene–ethanol) to give **5**, which was recrystallized from benzene–hexane. The results were summarized in Tables 3 and 4.

The sodium benzenesulfinate above obtained (crude yield: nearly quantitative) was allowed to react with benzyl chloride in ethanol to give phenyl benzyl sulfone, mp 147—148 °C (ethanol), the IR spectrum of which was spectroscopically identical with that of an authentic sample.

References

1) J. S. McFadyen and T. S. Stevens, *J. Chem. Soc.*, **1936**, 584.
2) W. R. Bamford and T. S. Stevens, *J. Chem. Soc.*, **1952**, 4735.
3) S. Ito, Y. Tanaka, and A. Kakehi, *Bull. Chem. Soc. Jpn.*, **55**, 859 (1982).
4) The McFadyen-Stevens reaction falls within these types of reactions. The formation of diimide by the reaction of *p*-tolylsulfonylhydrazine with sodium hydroxide (R. S. Dewey and E. E. van Tamelen, *J. Am. Chem. Soc.*, **83**, 3729 (1961)) may be the simplest type in these reactions.
5) S. Ito, Y. Tanaka, A. Kakehi, T. Fukuyama, N. Osawa, and N. Sayo, *Bull. Chem. Soc. Jpn.*, **56**, 545 (1983); S. Ito, Y. Tanaka, and A. Kakehi, *ibid.*, **57**, 539 (1984).
6) W. Walter and H. Weiss, *Justus Liebigs Ann. Chem.*, **758**, 162 (1972).
7) When compounds **4** were stirred with potassium carbonate at room temperature, no reactions were observed.
8) For a reference to IR spectra of 1,2,4-triazoles, see E. Lieber, D. R. Levering, and L. J. Patterson, *Anal. Chem.*, **23**, 1594 (1951).
9) The 1,4-elimination of benzenesulfinic acid has been observed in the reaction of acetophenone *N*-(phenylsulfonyl)phenylhydrazone with sodium isopropoxide, for example: D. Y. Curtin and E. W. Tristram, *J. Am. Chem. Soc.*, **72**, 5238 (1950).
10) For a reference to the azo-hydrazone tautomerism, see J. Buckingham, *Quart. Rev.*, **23**, 37 (1969).
11) A. Spassov, E. Golovinsky, and G. Russev, *Chem. Ber.*, **96**, 2996 (1963).

Preparation of New Nitrogen-bridged Heterocycles. 8.[1] Syntheses of Some Fused Indolizine Derivatives *via* the Acid-catalyzed Cyclizations of Functionalized 1- and 3-Vinylindolizines

Akikazu KAKEHI,* Suketaka ITO, Shinji MURAKAMI, and Hiroaki SANO
Department of Industrial Chemistry, Faculty of Engineering, Shinshu University, Wakasato, Nagano 380
(Received October 1, 1983)

Pyrano[3,2-*a*] and pyrano[2,3-*b*]indolizin-2-one derivatives were prepared in 12—86% yields by the acid-catalyzed deacetylation-cyclization of 2-acetoxy-1- and 3-[2-(ethoxycarbonyl)vinyl]indolizines with concentrated sulfuric acid at room temperature. On the other hand, similar reactions of 2-acetoxy-3-[1,2-bis(methoxycarbonyl)vinyl]indolizines did not give the initially expected pyrano[2,3-*b*]indolizinones at all, but, instead of them, afforded 3-(methoxycarbonylmethylene)furo[2,3-*b*]indolizin-2-one derivatives in fair yields. Formation mechanisms and some physical properties are also discussed.

In our pevious paper, we reported the direct formation of ethyl 2-oxo-2*H*-pyrano[2,3-*b*]indolizine-3-carboxylates by the reactions of 1-(ethoxycarbonylmethyl)-2-methylpyridinium bromides with diethyl (ethoxymethylene)malonate, in which we proposed the presence of 3-[2,2-bis(ethoxycarbonyl)vinyl]-2-indolizinols as the key intermeiates.[2] More recently, it was found that these 2-indolizinol intermediates could be trapped smoothly with various acylating and alkylating agents to give the corresponding esters and ethers,[3] and that an acetate, 2-acetoxy-[2,2-bis(ethoxycarbonyl)vinyl]-5-methylindolizine, in these compounds was converted slowly to the corresponding pyranoindolizinone in various solvents. These findings focused our attention to the syntheses of fused indolizines starting from readily available 2-acetoxy-3-vinylindolizine derivatives. In this paper, we wish to report the preparations of some 2*H*-pyrano[3,2-*a*] and [2,3-*b*]indolizin-2-one and 3-methylene-2*H*-furo[2,3-*b*]indolizin-2-one derivatives from the reactions of functionalized 2-acetoxy-1- or 3-vinylindolizines with concentrated sulfuric acid.

Results and Discussion

Preparations of 2H-Pyrano[2,3-b]indolizin-2-one Derivatives. Since the spontaneous deacetylation-cyclization of these 2-acetoxy-3-vinylindolizine derivatives could not be actually observed in various solvents except only one example described above, we examined the possibility of this process under various acidic and basic conditions[4] and found a method in which concentrated sulfuric acid was employed as a catalyst. Treatment of 2-acetoxy-3-[2,2-bis(ethoxycarbonyl)vinyl]indolizines (**1**—**4**) with a small amount of concentrated sulfuric acid (1 ml per 1 mmol indolizine) at room temperature gave the expected ethyl 2-oxo-2*H*-pyrano[2,3-*b*]indolizine-3-carboxylates (**5**—**8**) in 41—86% yields as strongly fluorescent orange crystals. Similar treatment of 3-[2-acetyl-2-(ethoxycarbonyl)vinyl]indolizines (**9**—**12**) (cis-trans mixtures) afforded the corresponding 3-acetyl derivatives (**13**—**16**), but the yields were lower (12—54%) than those of **5**—**8**. On the other hand, the reactions of 3-[2-cyano-2-(ethoxycarbonyl)vinyl]indolizines (**17** and **19**) with sulfuric acid at room temperature afforded only undeterminable insoluble substances but those of **17**—**20** at 80—95 °C gave 3-unsubstituted 2*H*-pyranoindolizinones (**21**—**24**) in variable yields (0—50%) (Scheme 2). Several attempts to prepare **23** from indolizine (**19**) and ethyl 2-oxo-2*H*-pyranoindolizine-3-carboxylate (**7**) under various conditions were unsuccessful.

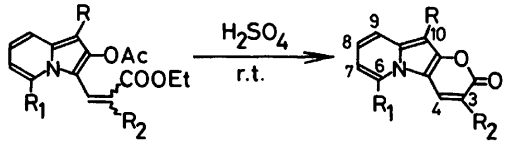

1-4,9-12

	R	R_1	R_2
1	Me	H	COOEt
2	Et	H	COOEt
3	Ph	H	COOEt
4	H	Me	COOEt
9	Me	H	Ac
10	Et	H	Ac
11	Ph	H	Ac
12	H	Me	Ac

5-8,13-16

	R	R_1	R_2
5	Me	H	COOEt
6	Et	H	COOEt
7	Ph	H	COOEt
8	H	Me	COOEt
13	Me	H	Ac
14	Et	H	Ac
15	Ph	H	Ac
16	H	Me	Ac

Scheme 1.

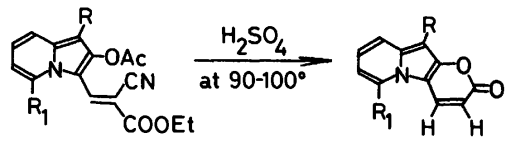

17-20

	R	R_1
17	Me	H
18	Et	H
19	Ph	H
20	H	Me

21-24

	R	R_1
21	Me	H
22	Et	H
(23)	Ph	H
24	H	Me

Scheme 2.

The structures of pyranoindolizinones (**5**—**8**, **13**—**16**, **21**, **22**, and **24**) were determined by their NMR spectral inspection and partly by the comparisons of **5**, **7**, and **8** with authentic samples prepared previously by us.[2] In particular, the structures of 3-unsubstituted pyranoindolizinones (**21**, **22**, and **24**) were determined by the presence of a AB type proton signals at near δ 5.9 and 8.0 with the coupling constant of 9.5 Hz together with other signals due to the indolizine moiety in their NMR spectra (see Table 1).

TABLE 1. SOME DATA OF FUNCTIONALIZED 1- AND 3-VINYLINDOLIZINES

Compd No.	Yield %	Mp θ_m/°C	$\nu_{C=O}^{KBr}$/cm^{-1}			δ (vinyl proton)	Formula	Calcd(%)			Found(%)		
								C	H	N	C	H	N
2	59	99—100	1771	1718	1700	7.93	$C_{20}H_{23}NO_6$	64.33	6.21	3.75	64.29	5.98	3.80
4	67	113—115	1755	1705	1695	8.41	$C_{19}H_{21}NO_6$	63.50	5.89	3.90	63.62	5.78	3.89
9[a]	68	105—106	1769	1716		7.93 and 7.98[b]	$C_{18}H_{19}NO_5$	65.64	5.82	4.25	65.69	5.61	4.39
10[a]	69	65—67	1770	1701		7.92 and 7.95[b]	$C_{19}H_{21}NO_5$	66.46	6.16	4.08	66.19	6.02	3.87
11[a]	58	123—125	1770	1700		7.98 and 8.03[b]	$C_{23}H_{21}NO_5$	70.58	5.41	3.58	70.67	5.61	3.29
12[a]	30	112—115	1760	1683		8.43[c]	$C_{18}H_{19}NO_5$	65.64	5.82	4.25	65.53	5.80	4.38
26	60	100—102	1769	1721	1702	4.13	$C_{18}H_{19}NO_6$	62.60	5.55	4.06	62.45	5.49	3.98
28	53	84—85	1760	1712		4.52	$C_{17}H_{17}NO_6$	61.63	5.17	4.23	61.88	5.19	4.39
34	49	86—87	1724	1714		6.18	$C_{16}H_{17}NO_5$	63.36	5.65	4.62	63.18	5.64	4.63
35	61	105—106	1751	1709	1673	8.06	$C_{18}H_{19}NO_5$	65.64	5.82	4.25	65.56	5.82	4.28
36	45	110—111	1755	1693	1681	8.10	$C_{19}H_{21}NO_5$	66.46	6.16	4.08	66.49	6.15	4.07

a) This compound is a cis-trans mixture, but its ratio could not be calculated because of the absence of definitely separated signals in the NMR spectrim. b) The peak of major isomer. c) Both vinyl proton signals of cis and trans isomers were overlapped.

Preparations of 3-Methylene-2H-furo[2,3-b]indolizines. When the acidic treatment of 2-acetoxy-3-[1,2-bis(methoxycarbonyl)vinyl]indolizines (**25—27**) at room temperature were carried out, the initially expected 2-oxo-2*H*-pyranoindolizine-4-carboxylates such as **29** could not be obtained at all, but, instead of them, reddish crystalline substances **30—32** were obtained in 51—68% yields (Scheme 3). Although various reaction conditions such as the quantity and the concentration of sulfuric acid, the reaction time, and the reaction temperature, were tested in the case of 5-methylindolizine (**28**), no furoindolizine (**33**) could be isolated and only a small amount of 2-methoxy-3-vinylindolizine (**34**) could be always obtained.

The structural assignment of 3-methylenefuroindolizinones (**30—32**) was accomplished mainly by their physical and spectral means. The facts that these compounds have not any strong fluorescence characteristics of pyranoindolizinone as seen in **5—8**, **13—16**, **21**, **22**, and **24** and that their NMR spectra were very similar to those of the starting materials **25—27** except the loss of an acetoxyl and a methoxyl proton signals supported clearly these structures fused with a nonaromatic furan ring. The cis configuration of the exo-methylene group in **30—32** was decided by the similarity of the chemical shifts (δ 6.2—6.4) due to the olefinic proton with those (δ 6.1—6.3) of **25—27**. On the other hand, an abnormal product **34** from the reaction of 5-methyl-3-vinylindolizine (**28**) was concluded to be 3-[1,2-bis(methoxycarbonyl)vinyl]-2-methoxy-5-methylindolizine by its NMR inspecion and an unequivocal synthesis (see Experimental section).

Preparations of 2H-Pyrano[3,2-a]indolizines. Similar reaction of 2-acetoxy-1-[2-acetyl-2-(ethoxycarbonyl)vinyl]-5-methylindolizine (**35**) at room temperature gave the corresponding 3-acetyl-8-methyl-2*H*-pyrano[3,2-*a*]indolizin-2-one (**37**) and an unexpected 1-vinyl-2(3*H*)-indolizinone (**38**) in 12 and 87% yields. The major product **38** was obtained also from the reaction using 2-propionyloxyindolizine deriva-

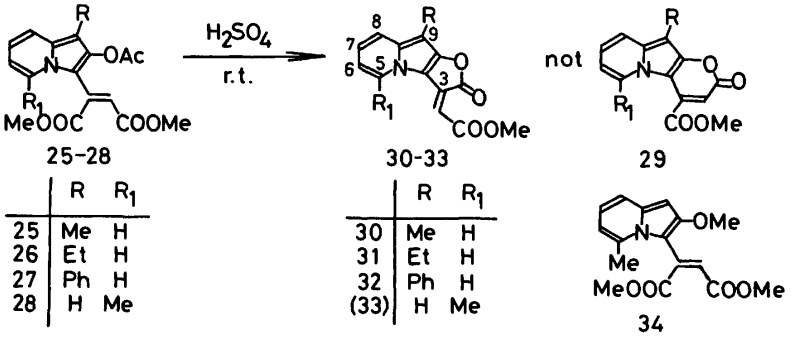

Scheme 3.

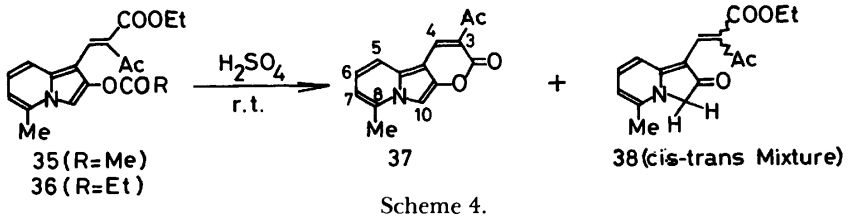

Scheme 4.

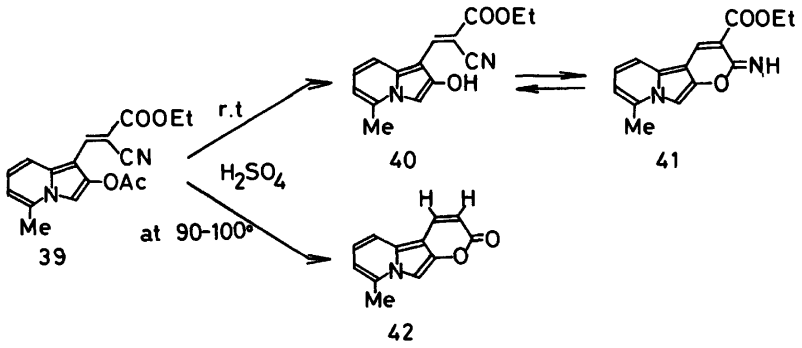

Scheme 5.

tive (**36**) in 89% yield (Scheme 4). Similar reaction of 1-[2-cyano-2-(ethoxycarbonyl)vinyl] derivative (**39**) gave 1-vinyl-2-indolizinol (**40**) and/or pyranoindolizin-2-imine (**41**) in 95% yield. On the other hand, the reaction of **39** under heating conditions afforded the corresponding 3-unsubstituted 8-methyl-2*H*-pyrano[3,2-*a*]indolizin-2-one (**42**) in 41% yield (Scheme 5).

The structures of pyrano[3,2-*a*]indolizinones (**37** and **42**) were determined by the comparisons of their physical and spectral data with those of pyrano[2,3-*b*]indolizinone derivatives. On the other hand, the structure of 1-vinyl-2(3*H*)-indolizinone (**38**) was decided by its NMR inspection and its chemical conversion to acetate 43. Since this compound **38** was a cis-trans mixture (cis:trans=3:4),[5] the NMR spectrum showed multiple complex signals due to the two sets of protons, but a two proton singlet attributable to the 3-methylene group was appeared clearly at δ 4.30. Furthermore, the fact that this group is an active methylene was also indicated by the disappearance of the proton signal with deuterium oxide as seen in known 2(3*H*)-indolizinones.[2] The acetate **43** obtained from **38** was same with compound **35** in the IR spectra, but an another set of proton signals were also appeared in the NMR spectrum of **43** and the melting point (102—104°C) was lower than that (mp 105—106°C) of **35**. Thus, we concluded compound **43** to be a cis-trans mixture[6] of 2-acetoxy-1-[2-acetyl-2-(ethoxycarbonyl) vinyl]-5-methylindolizin (**35**). The structure of product from the reaction of **39** at room temperature was tentatively assigned to be an equilibrium mixture of 1-vinyl-2-indolizinol (**40**) and pyranoindolizin-2-imine (**41**), because this compound has a very strong fluoresence similar to that of tricyclic pyranoindolizinones and extremely low solubility in contract with bicyclic vinylindolizines and vinylindolizinone, and its IR spectrum exhibited a weak cyano absorption band at 2198 cm^{-1}.[7] On the other hand, an alternative possibility of the presence of its 3-cyanopyranoindolizinone derivative was neglected clearly by its elementary analysis, by which the composition of the product was completely in accord with the structure possessing an ethoxycarbonyl group.[8]

Reaction Mechanisms. The formation reaction of 2*H*-pyrano[2,3-*b*]indolizin-2-ones (**5**—**8** and **13**—**16**) and 3-methylenefuro[2,3-*b*]indolizin-2-ones (**30**—**32**) can be explain reasonably by considering the intermediacy of 3-vinyl-2-indolizinol intermediate **44** or **46** from the acetates (**1**—**4**, **9**—**12**, and **25**—**28**) and subsequent intramolecular nucleophilic reactions between the hydroxyl and the ester carbonyl group in the

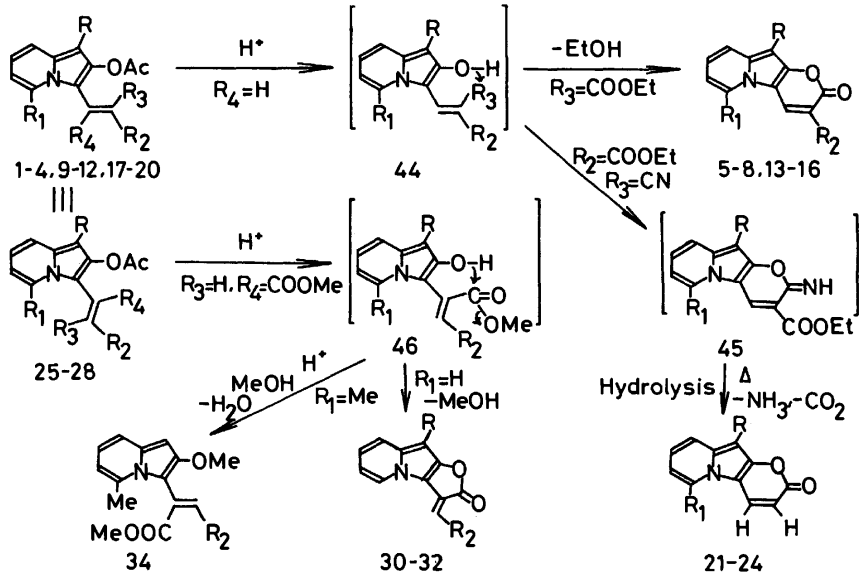

Scheme 6.

six- or five-membered transition states. Similarly, 3-unsubstituted pyrano[2,3-*b*]indolizin-2-ones (**21**—**24**) must be formed *via* the nucleophilic attack of the hydroxyl group onto the cyano group in **44** followed by the acid hydrolysis and then decarboxylation of the resulting 2*H*-pyrano[2,3-*b*]indolizin-2-imine (**45**). Furthermore, the acid-catalyzed dehydration from indolizinol (**46**) and a methanol generated by the hydro lysis of the methoxycarbonyl group may afford 2-methoxyindolizine (**34**). These mechanisms are summarized in Scheme 6. The fact that no 2-oxopyranoindolizine-4-carboxylate such as **29** could be obtained in the reactions of indolizines (**25**—**28**) may suggest the cis character of the two ester groups in **25**—**28** and the difficulty of the cis-trans isomerization of the vinyl group under reaction conditions employed here. We described previously the cis configuration of this group in **25** and **27**[3] and, here, observed the cis character of the exocyclic 3-methylene group in **30**—**32** and the more diminished yields of 3-acetylpyranoindolizinones (**13**—**16**) compared with those of 2-oxopyranoindolizine-3-carboxylate (**5**—**8**). In the reaction of 5-methylindolizine (**28**), the fact that no tricyclic product such as **29** and **32** was obtained seems to indicate the loss of requisite of planarity for the transition states in such cyclizations owing to the steric repulsion between the 5-methyl and the 3-[1-(methoxycarbonyl)] group, and, thus, to lead to the formation of an ethereal product (**34**) from 2-indolizinol (**46**).

The formation mechanisms of 2*H*-pyrano[3,2-*a*]-indolizinone derivatives (**37**, **41** (or **40**), and **42**) can be also considered by similar manners described above in the cases of 2-acetoxy-3-vinylindolizines, while 1-vinyl-2(3*H*)-indolizinone (**38**) is simply a keto-isomer of 1-vinyl-2-indolizinol intermediate.

Experimental

Melting points were measured with a Yanagimoto micro-melting point apparatus and are uncorrected. Microanalyses were carried out on a Perkin-Elmer 240 Elemental Analyzer. The NMR spectra were determined with a Varian EM360A Spectrometer in deuteriochloroform with tetramethylsilane as an internal standard. .The chemical shifts are expressed in δ values. The IR spectra were taken with a Hitachi 260-10 Infrared Spectrophotometer.

Preparations of 1- and 3-Vinylindolizine Derivatives. These functionalized 2-acetoxy-3-vinylindolizines (**1**—**4**), (**9**—**12**), (**17**—**20**), and (**25**—**28**) and 2-methoxy-5-methyl-3-vinylindolizine (**34**) were obtained as red prisms by the 2(3*H*)-indolizinone route[3] and 2-acetoxy-1-vinylindolizine derivatives (**35**, **36**, and **39**) were given as orange needles by the 2-allylidene-1,2-dihydropyridine route appeared in our previous papers.[9,10] These results and some physical data of new 1- and 3-vinylindolizine derivatives (**2**, **4**, **9**—**12**, **26**, **28**, and **34**—**36**) are summarized in Table 1.

Reactions of 1- and 3-Vinylindolizines with Sulfuric Acid. *Method A*: To 1 mmol of 2-acetoxy-1- or 3-vinylindolizine derivative 1 ml of concentrated sulfuric acid was added and the resulting mixture was kept overnight at room temperature. The reaction solution was poured slowly into a 20 ml of ice-water, neutralized carefully with aqueous potassium carbonate under stirring, and extracted twice with 50 ml portions of chloroform. After the combined extract was filtered through a phase-separating filter paper, the filtrate was concentrated at reduced pressure and the residue was separated by column chromatography (alumina) using ether and then chloroform as eluents. Recrystallization of the crude products from chloroform or ethanol gave the corresponding pyranoindolizinones (**5**—**8** and **13**—**16**) as yellow to orange needles and methylenefuroindolizinones (**30**—**32**) as red prisms.

Method B: The similar mixture of vinylindolizine and concentrated sulfuric acid was heated in a sealed tube at 90—100°C for 1—2 h. The usual work-ups of the resulting solutions gave the corresponding 3-unsubstituted pyranoindolizinones (**21**, **22**, **24**, and **42**) as yellow needles.

Table 2. NMR spectral data of pyrano-[2,3-*b*]indolizin-2-ones

Compd[a]	C-3		C-4	C-6	C-7	C-8	C-9	R	
5	1.41 t	4.42 q	8.78 s	8.38 br d	6.93 dt	7.30 br t	7.59 br d	2.31 s	
6	1.38 t	4.37 q	8.74 s	8.26 br d	6.83 dt	7.18 br t	7.48 br d	1.27 t	2.79 q
7	1.41 t	4.45 q	8.97 s	8.45 br d	7.02 dt	b)	b)	7.2—8.1 m	
8	1.40 t	4.38 q	8.91 s	2.88 s	6.76 br d	7.26 q	7.45 dd	6.37 s	
13	2.71 s		8.83 s	8.35 br d	6.88 dt	7.28 br t	7.49 br d	2.32 s	
14	2.72 s		8.88 s	8.38 br d	6.90 dt	7.28 br t	7.54 br d	1.30 t	2.83 q
15	2.77 s		8.94 s	c)	c)	c)	c)	6.9—8.1 m	
16	2.70 s		8.97 s	2.91 s	6.78 br d	7.28 q	7.50 dd	6.42 s	
21	5.97 d		7.88 d	8.10 br d	6.73 dt	7.00 br t	7.46 br d	2.34 s	
22	5.96 d		7.90 d	8.11 br d	6.72 dt	7.02 br t	7.48 br d	1.30 t	2.87 q
24	5.91 d		8.17 d	2.82 s	6.59 br d	7.04 q	7.45 dd	6.44 s	

a) These coupling constants are as follows: $J_{6,7}=J_{7,8}=7.0$, $J_{3,4}=J_{8,9}=9.0$, $J_{7,9}=1.5$, $J_{Et}=7.0$ Hz. b) Overlapped with the phenyl signals. c) These proton signals could not be determined by its low solubility in deuteriochloroform.

Table 3. NMR spectral data of methylenefuro-[2,3-*b*]indolizin-2-ones and pyrano-[3,2-*a*]indolizin-2-ones

Compd[a]	C-5	C-6	C-7	C-8	R		3(1)-H	COOMe
30	8.79 br d	6.62 dt	7.00 br t	7.38 br d	2.30 s		6.25 s	4.00 s
31	8.78 br d	6.63 dt	7.00 br t	7.43 br d	1.27 t	2.43 q	6.27 s	4.03 s
32	8.87 br d	6.74 dt	7.09 br t	b)	7.2—8.0 m		6.37 s	4.05 s

Compd[c]	C-3	C-4	C-5	C-6	C-7	C-8	C-10
37	2.72 s	8.95 s	7.75 dd	7.28 q	6.87 br d	2.63 s	7.14 s
42	6.98 d	7.94 d	7.54 dd	7.09 q	6.71 br d	2.58 s	7.13 s

a) $J_{5,6}=J_{6,7}=7.0$, $J_{7,8}=9.0$, $J_{6,8}=1.5$, $J_{Et}=7.0$ Hz. b) Overlapped with the phenyl signals. c) $J_{5,6}=9.0$, $J_{6,7}=7.0$, $J_{5,7}=1.5$ Hz.

TABLE 4. SOME DATA OF FUSED INDOLIZINE DERIVATIVES

React. No.	Prod. No.	Method	Yield %	Mp θ_m/°C	$\nu_{C=O}^{KBr}$/cm^{-1}		Formula	Calcd(%) C	H	N	Found(%) C	H	N
1	**5**	A	75	239—241	a)								
2	**6**	A	80	202—203	1735	1685	$C_{16}H_{15}NO_4$	67.35	5.29	4.90	67.31	5.31	4.94
3	**7**	A	86	212—213	a)								
4	**8**	A	41	190—192	a)								
9	**13**	A	24	292—293	1715		$C_{14}H_{11}NO_3$	69.70	4.60	5.81	69.71	4.66	5.74
10	**14**	A	54	255—256	1708		$C_{15}H_{13}NO_3$	70.58	5.13	5.49	70.80	5.07	5.23
11	**15**	A	49	>300	1715		$C_{19}H_{13}NO_3$	75.24	4.32	4.62	74.95	4.30	4.92
12	**16**	A	12	247—250	1700		$C_{14}H_{11}NO_3$	69.70	4.60	5.81	69.91	4.62	5.57
17	**21**	B	8	191—193	1705		$C_{12}H_9NO_2$	72.35	4.55	7.03	72.05	4.75	7.12
18	**22**	B	50	185—186	1690		$C_{13}H_{11}NO_2$	73.23	5.20	6.57	73.27	5.24	6.36
19	**23**	B	0										
20	**24**	B	Trace	b)									
25	**30**	A	51	196—197	1715	1700	$C_{14}H_{11}NO_4$	65.37	4.31	5.45	65.49	4.31	5.46
26	**31**	A	68	149—151	1722	1708	$C_{15}H_{13}NO_4$	66.41	4.83	5.16	66.48	4.88	5.05
27	**32**	A	67	201—203	1717	1700	$C_{19}H_{13}NO_4$	71.47	4.10	4.39	71.43	4.17	4.36
28	**34(33)**	A	7(0)	86—87	1724	1714	$C_{16}H_{17}NO_5$	63.36	5.65	4.62	63.18	5.64	4.63
35	**37**	A	12	264—266	1700	1656	$C_{14}H_{11}NO_3$	69.70	4.60	5.81	69.53	4.61	5.97
	38		87	161—162	1705	1663	$C_{16}H_{17}NO_4$	66.89	5.96	4.88	67.07	5.89	4.76
36	**38**	A	89										
39	**40/41**	A	95	237—244	1700	2198[c)]	$C_{15}H_{14}N_2O_3$	66.65	5.22	10.37	66.51	5.26	10.16
39	**42**	B	41	174—176	1700		$C_{12}H_9NO_2$	72.35	4.55	7.03	72.62	4.65	7.21

a) Known compound, see Ref. 2. b) The preparation of the analytical sample was unsuccessful because of its low yield. c) Cyano band.

The reactions of vinylindolizine (**19**) and ethyl 2-oxo-2*H*-pyranoindolizine-3-carboxylate (**7**) with sulfuric acid were examined in detail under various conditions, but the synthesis of the corresponding 10-phenylpyranoindolizinone (**23**) was not unsuccessful. In the similar reaction (Method A) of **28**, the initially expected pyranoindolizinone such as **29** and methylenefuroindolizinone (**33**) were not obtained at all, but 2-methoxy-3-vinylindolizine (**34**) was isolated in only 7% yield. This compound (**34**) was completely in accord with authentic sample prepared above in all respects. These results and some properties of products are listed in Tables 2—4.

Acetylation of 1-Vinyl-2(3H)-indolizinone (38). A mixture of indolizinone **38** (144 mg, 0.5 mmol), acetic anhydride (1 ml), and pyridine (3 ml) was heated at 70—80 °C in a water bath for 2 h. The unreacted anhydride and pyridine was then removed at reduced pressure and the residual oil was separated by column chromatography (alumina) using hexane and then ether as eluents. The ether layer was collected and concentrated at reduced pressure. Recrystallization from ethanol gave pure 2-acetoxy-1-vinylindolizine (**43**), 118 mg, 72%, orange needles, mp 102—104 °C, ν (KBr) 1751, 1709, and 1673 cm^{-1} (CO), δ ($CDCl_3$)[11] 1.19 (3H, t, J=7.0 Hz, $CH_2\underline{CH_3}$), 2.33, 2.42 (each 3H, s, 2Ac), 2.53 (3H, s, 5-Me), 4.25 (2H, q, J=7.0 Hz, $O\underline{CH_2}CH_3$), 6.61 (1H, br d, J=7.0 Hz, 6-H), 7.03 (1H, q, J=9.0 and 7.0 Hz, 7-H), 7.49 (1H, br d, J=9.0 Hz, 8-H), 7.53 (1H, s, 3-H), and 8.05 (1H, s, vinyl-H). Found: C, 65.89; H, 5.83; N, 4.26%. Calcd for $C_{18}H_{19}NO_5$: C, 65.64; H, 5.82; N, 4.25%.

The NMR signals due to the main isomer in **43** were completely in accord with those of **35**.

References

1) For part 7 of this series, see A. Kakehi, S. Ito, and B. Wada, this Bulletin, in press.

2) A. Kakehi, S. Ito, K. Watanabe, M. Kitagawa, S. Takeuchi, and T. Hashimoto, *J. Org. Chem.*, **45**, 5100 (1980).

3) A. Kakehi, S. Ito, B. Wada, K. Watanabe, K. Nishimura, and A. Kumagai, *Bull. Chem. Soc. Jpn.*, **55**, 3590 (1982).

4) The reaction conditions in which acidic and basic media such as hydrochloric acid, sulfuric acid, sodium ethoxide, potassium t-butoxide, sodium hydroxide, and po tassium carbonate were employed in various solvents were examined.

5) Or cis:trans=4:3. The NMR spectrum of **38** is as follows: Major isomer, δ ($CDCl_3$) 1.37 (3H, t, J=7.0 Hz, $OCH_2\underline{CH_3}$) 2.36 (3H, s, Ac), 2.48 (3H, s, 5-Me), 4.30 (2H, s, methylene, disappeared with deuterium oxide), 4.43 (2H, q, J=7.0 Hz, $O\underline{CH_2}CH_3$), 6.60 (1H, br d, J=7.0 Hz, 6-H), 7.42 (1H, s, vinyl-H), and 6.9—7.9 (2H, m, 7- and 8-H). Minor isomer, δ ($CDCl_3$) 1.34 (3H, t, J=7.0 Hz, $OCH_2\underline{CH_3}$), and 7.37 (1H, s, vinyl-H). The other proton signals due to the minor product were overlapped with those of major isomer.

6) The cis-trans ratio could not be calculated because of the absence of definitely separated signals in its NMR spectrum, but isomer **35** was major.

7) The presence of a strong interaction between these groups in a similar system was reported. See K. Kurita, H. Awaya, Y. Tominaga, Y. Matsuda, and G. Kobayashi, *Yakugaku Zasshi*, **101**, 980 (1981).

8) Because of its extremely low solubility, our attempts to obtain further structural information were unsuccessful.

9) A. Kakehi, S. Ito, T. Maeda, R. Takeda, M. Nishimura, M. Tamashima, and T. Yamaguchi, *J. Org. chem.*, **43**, 4837 (1978).

10) The trans configuration of the 1-vinyl group in **35** and **36** was assigned tentatively from the reasons that the vinyl proton of the trans isomer may appear in lower magnetic field than that of the cis one and that the corresponding pyrano[3,2-*a*]indolizinone (**37**) was formed only in very low yield.

11) This is major compound (**35**). The NMR data of minor compound are as follows: δ ($CDCl_3$) 1.32 (3H, t, J=7.0 Hz, $OCH_2\underline{CH_3}$), 2.33 and 2.38 (each 3H, s, 2Ac), 2.53 (3H, s, 5-Me), and 8.03 (1H, s, vinyl-H). The other signals were overlapped with those of major isomer (**35**).

Reactions of 2,3,5-Tri-*O*-benzoyl-D-ribofuranosyl Acetate with Enol Silyl Ethers Catalyzed by Tin(IV) Chloride. Regiochemical Features[1)]

Yayoi S. YOKOYAMA, Tan INOUE, and Isao KUWAJIMA*
Department of Chemistry, Tokyo Institute of Technology, Meguro-ku, Tokyo 152
(Received October 5, 1983)

In condensation reactions of 2,3,5-tri-*O*-benzoyl-D-ribofuranosyl acetate with various kinds of enol silyl ethers in the presence of tin(IV) chloride, the acetate behaves as an ambident electrophile to give two types of products arising from nucleophilic attack of the enol ether on C-1 carbon of the ribose derivative and on carbonyl carbon of 2-benzoyloxyl group, depending remarkably on the enol silyl ethers.

Much attention has recently been attracted on *C*-glycosyl nucleosides because of their important antibiotic properties and potent anticancer and antiviral activities.[2)] It is quite important and valuable to prepare them and their structural analogues easily, from the viewpoint to research for higher bioactive compounds. Some of synthetic studies have already been described on formycin,[3)] showdomycin,[4)] pyrazomycin,[5)] and their analogues.[6)] Although they had few synthetic relation to each other, most of these syntheses have a common strategy which involves an introduction of a cyano, aryl, or other nucleophilic moieties to C-1 position of 1-halo- or 1-acetoxy-β-D-ribofuranose derivatives to construct appropriate heterocycles. From this viewpoint, a key reaction is to make the new carbon-carbon bond between C-1 carbon of ribose and various nucleophilic reagents. It has been well documented that 2,3,5-tri-*O*-benzoyl-D-ribofuranosyl acetate (**1**), an easily accessible material, generates an electrophilic species, 1,2-*O*-benzylidene oxonium ion (**2**), by the aid of either appropriate bases or acids through neighboring participation of C-2 benzoyloxyl group. The resulting electrophile **2** has two reaction sites for nucleophiles; C-1 carbon and carbonyl carbon of 2-benzoyloxyl group. Under basic conditions C–C bond formation between **2** and nucleophiles takes place at C-1 and/or 2-benzoyloxyl carbonyl,[6c,7)] whereas reactions with olefins including 1-trimethylsiloxycyclohexene have been reported to proceed selectively on C-1 position in the presence of Lewis acid.[8)]

Based on such feature, we previously examined the use of a enol silyl ether for such purpose and reported synthesis of showdomycin which includes the C–C bond formation between **1** and 1,2-bis(trimethylsiloxy)-cyclobutene as a key step.[4a)] However, it has not been systematically studied what kind of enol silyl ethers react to form desired carbon-carbon linkages. In this paper we describe regiochemical features of the reaction between 2,3,5-tri-*O*-benzoyl-D-ribofuranosyl acetate (**1**) and various kinds of enol silyl ethers, which disclose the scope and limitations to use enol silyl ethers for synthesis of *C*-nucleosides and their analogues.

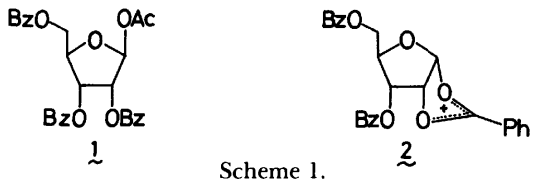

1 **2**

Scheme 1.

Enol silyl ethers **3a—g** have been chosen as typical nucleophiles and their reactions with **1** have been studied under the influence of 1 equiv of tin(IV) chloride in dichloromethane at room temperature. On contrary to our expectation, the condensation reaction at C-1 position of **1** is not a general phenomenum even on using enol silyl ethers; some of them (**3e—g**) give the desired C-1 condensation products **4e—g**, whereas others (**3a—d**) are found to yield the products **5a—d** selectively arising from their nucleophilic attack on carbonyl carbon of 2-benzoyloxyl group[9)] under same reaction conditions.

As shown in the table, regiochemical results of the reaction are definitely determined by the kind of enol silyl ethers used and no regio-isomer could be detected in every case. According to these results, enol silyl

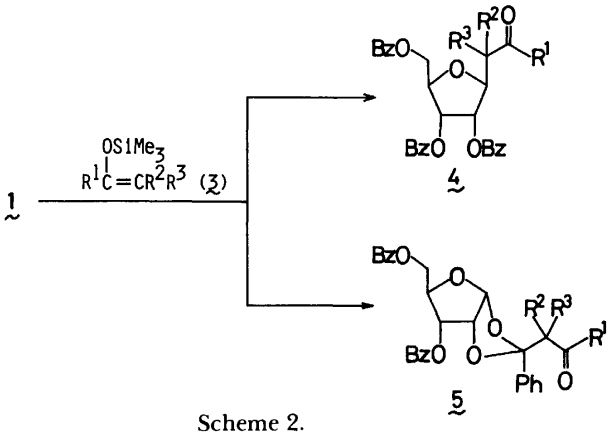

1 **4** **5**

Scheme 2.

TABLE 1. REACTIONS OF 2,3,5-TRI-*O*-BENZOYL-D-RIBOFURANOSYL ACETATE **1** WITH ENOL SILYL ETHERS (**3**)

	Enol silyl ethers (**3**)			Reaction period/h	Yield/%[a)]	
	R^1	R^2	R^3		**4**	**5**
a	C_2H_5	H	CH_3	1.5	—	88
b	$(CH_3)_3C$	H	H	16	—	55
c[b)]	C_2H_5O	H	H	1	—	32
d	C_2H_5O	H	C_6H_5S	2	—	82
e	CH_3	H	C_6H_5S	1	83	—
f	$(CH_3)_3C$	H	C_6H_5S	2	45	—
g[c)]	$-(CH_2)_2-$		Me_3SiO	2	95	—
h[d)]	$-(CH_2)_4-$		H	1	95	—

a) Isolated yield. b) *t*-Butyldimethylsilyl ether was used. c) Taken from Ref 4a. d) Taken from Ref 8.

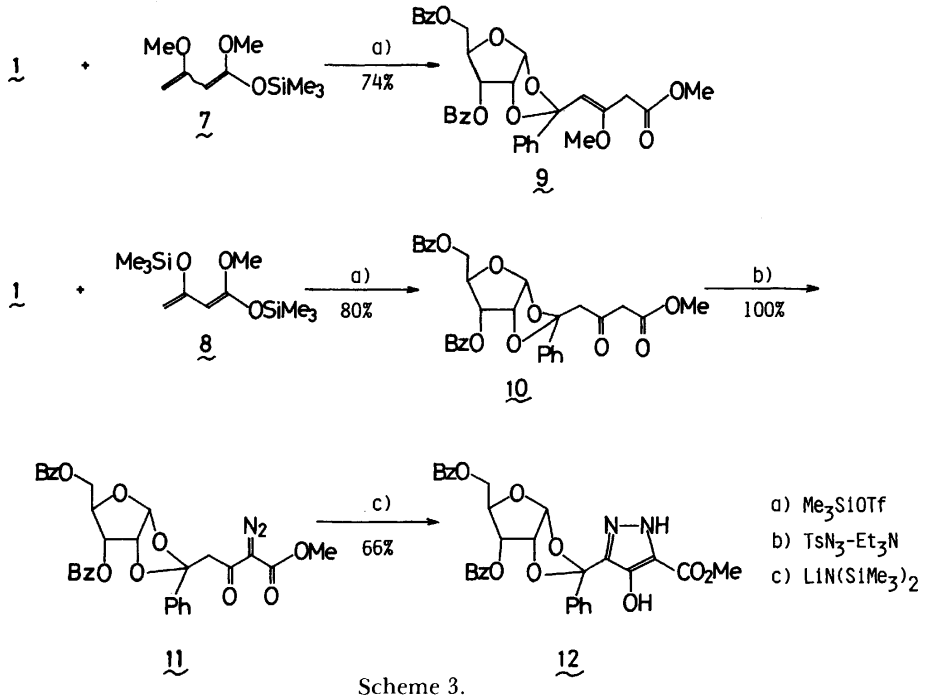

Scheme 3.

ethers seem to be classified into the following two categories. Those of usual acyclic ketones (**3a** and **3b**) and of esters (**3c** and **3d**) generally react on carbonyl carbon of 2-benzoyloxyl group to give the products of type **5**. On the other hand, in the case of enol ethers of ketones having α-hetero substituents (**3e**, **3f**, and **3g**), the reaction takes place selectively on C-1 site of **1** to afford the desired products **4e—g**. Thus, a site-determining influence of α-hetero substituent has now become very important from synthetic viewpoints of *C*-nucleosides. Enol silyl ethers of ketones bearing α-phenylthio group are quite useful for the introduction of 2-oxoalkyl group on C-1 position of **1** because the phenylthio group is easily removable by reduction. For example, α-phenylthio ketone (**4e**) gave the desulfurization product **6** in 70% yield on treatment with Raney nickel in boiling ethanol.

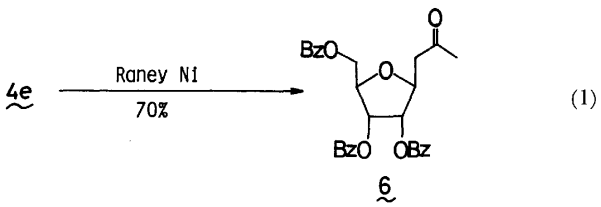

(1)

These regiochemical features have aroused a question whether there are any differences in actual nucleophilic species between these two types of enol silyl ethers. As reported already, tin(IV) chloride readily reacts with usual enol silyl ethers to afford the corresponding α-trichlorostannyl ketones,[10] which might act as real nucleophilic species in this case. In order to clarify such possibility, tin(IV) chloride was treated with **3a** in deuterochloroform at room temperature, and an immediate formation of the corresponding α-trichlorostannyl ketone was confirmed by ^1H NMR analysis of the reaction mixture. Further, treatment of the resulting solution with **1** led to the formation of **5a**.

In the cases of enol silyl ethers (**3e—g**), on the other hand, α-subsituents seem to prevent silyl/stannyl exchange, and the silyl ethers remain unchanged on exposure to tin(IV) chloride.

On the basis of these results, we wish to suggest the following points on the different behaviors observed here. On treatment with **1** in the presence of tin(IV) chloride, enol silyl ethers of usual acyclic ketones and of esters, *e.g.* **3a—d**, undergo silyl/stannyl exchange with tin(IV) chloride initially to yield α-stannyl ketones. Then, the resulting α-stannyl ketones act as nucleophiles to **1** to afford the corresponding **5a—d**. On the other hand, **3e—g** react as olefinic[8] or aromatic nucleophiles[11] in a usual Friedel-Crafts like manner to yield the desired C-1 condensation products **4e—g**.

However, other uncertain site-determining factors might also be involved in this type of reaction, considering an anomolous behavior of 1-trimethylsiloxycyclohexene which affords the condensation product of type **4**[8] irrespective of its facile silyl/stannyl exchange reaction with tin(IV) chloride.

Finally, in order to explore a simple synthetic route to pyrazomycin, we also examined the introduction of an acetoacetic ester moiety on C-1 position by using dienal ethers **7** or **8**. In the presence of trimethylsilyl triflate,[12,13] however, they react on C-2 benzoyloxyl group exclusively to yield **9** or **10**, although construction of requisite pyrazole ring can be efficiently performed through its diazo compound as shown in Scheme 3.

Experimental

General Procedures. IR spectra were taken on a Hitachi 260-10 spectrometer; absorptions are given in reciprocal centimeters. ^1H NMR spectra were recorded on a Hitachi R-24B (60 MHz) or a Varian EM-390 (90 MHz) spectrometer; chemical shifts (δ) are expressed in parts per million down-

field from internal tetramethylilane.

Column chromatography was performed on Wakogel C-200 or Florisil (mesh 100—200). All the reactions were carried out in an glass sealed tube with magnetic stirring bar under dry nitrogen.

Materials. Tetrahydrofuran (THF) was distilled from sodium-benzophenone ketyl in a recycling still immediately before use. Chlorotrimethylsilane, triethylamine, and hexamethylphosphoric triamide (HMPA) were distilled from calcium hydride. Acetonitrile and dichloromethane were distilled successively from phosphorus pentaoxide and potassium carbonate under nitrogen. 3-Trimetylsiloxy-2-pentene (**3a**), 3,3-dimethyl-2-trimethylsiloxy-1-butene (**3b**), 1-phenylthio-2-trimethylsiloxy-1-propene (**3e**), and 3,3-dimethyl-1-phenylthio-2-trimethylsiloxy-1-butene (**3f**) were prepared by the method of House.[14] 1-Ethoxy-1-(*t*-butyldimethylsiloxy)ethylene (**3c**)[15] and 1,3-bis(trimethylsiloxy)-1-methoxy-1,3-butadiene **8**[16] were prepared according to the reported procedure. 1-Ethoxy 2-phenylthio-1-trimethylsiloxyethylene (**3d**) and 1,3-dimethoxy-1-trimethylsiloxy-1,3-butadiene (**7**) were prepared by using THF instead of DME as a solvent in the method of House.[14]

Condensation of 2,3,5-Tri-O-benzoyl-D-ribofuranosyl Acetate (1) with Enol Silyl Ethers (3). 3-Trimethylsiloxy-2-pentene (3a): A mixture of the acetate **1** (75.1 mg, 0.15 mmol) and tin(IV) chloride (0.18 mmol) in dichloromethane (2 ml) was stirred for 5 min at room temperature, and the enol silyl ether **3a** (0.18 mmol) was added to the resulting solution. After stirring for 1.5 h, aq K_2CO_3 solution was added to the reaction mixture and was extracted with ether repeatedly. Organic layer was washed with satd. aq NaCl, dried over anhyd. Na_2SO_4, and concentrated to give an oil, which was separated by silica-gel column chromatography to give **5a** (95.3 mg, 88%) as an oil. Calcd for $C_{31}H_{30}O_8$: C, 70.18; H, 5.70%. Found: C, 69.72; H, 5.70%. **5a** could be separated into diastereomers **5a**$_1$ and **5a**$_2$ by column chromatography **5a**$_1$: IR (neat) 1730, 1715 cm^{-1}; NMR (60 MHz) (CCl_4) δ=0.87 (t, J=7 Hz, 3H), 0.99 (d, J=7 Hz, 3H), 2.21 (q, J=7 Hz, 2H), 2.93 (q, J=7 Hz, 1H), 3.40 (m, 1H), 4.17 (m, 2H), 4.76 (dd, J=9 and 5 Hz, 1H), 5.10 (dd, J=5 and 4 Hz, 1H), 5.90 (d, J=4 Hz, 1H), 7.30 (m, 11H), 7.84 (m, 4H). **5a**$_2$: IR(neat) 1730, 1715 cm^{-1}; NMR (60 MHz) (CCl_4) δ=0.94 (d, J=7 Hz, 3H), 0.97 (t, J=7 Hz, 3H), 2.36 (q, J=7 Hz, 2H), 2.90 (q, J=7 Hz, 1H), 3.45 (m, 1H), 4.18 (m, 2H), 4.70 (m, 2H), 6.05 (d, J=4 Hz, 1H), 7.30 (m, 11H), 7.78 (m, 4H).

In a similar manner, 3,3-dimethyl-2-trimethylsiloxy-1-butene (**3b**), 1-ethoxy-1-(*t*-butyldimethylsiloxy)ethylene (**3c**), and 1-ethoxy-2-phenylthio-1-trimethylsiloxyethylene (**3d**) gave the corresponding condensation products **5b—d**, and 1-phenylthio-2-trimethylsiloxy-1-propen (**3e**) and 3,3-dimethyl-1-phenylthio-2-trimethylsiloxy-1-butene (**3f**) gave **4e** and **4f**, respectively. **5b**: An amorphous oil; IR (Nujol) 1730, 1720 cm^{-1}; NMR(60 MHz) (CCl_4) δ=1.06 (s-like, 9H), 2.86 (s-like, 2H), 6.05 (d, J=4 Hz, 1H), 7.32 (m, 11H), 7.85 (m, 4H); Calcd for $C_{32}H_{32}O_8$: C, 70.58; H, 5.92%. Found: C, 70.74; H, 6.17%. **5c**: An amorphous oil: IR (Nujol) 1720 cm^{-1}; NMR (60 MHz) (CCl_4) δ=1.24 (t, J=7 Hz, 3H), 2.74 (s-like, 2H), 3.56 (m, 1H), 4.04 (q, J=7 Hz, 2H), 4.22 (m, 2H), 4.78 (dd, J=9 and 5 Hz, 1H), 5.20 (dd, J=5 and 4 Hz, 1H), 6.10 (d, J=4 Hz, 1H), 7.30 (m, 11H), 7.85 (m, 4H). **5d**: An amorphous oil: IR (Nujol) 1730, 1720 cm^{-1}; NMR (60 MHz) (CCl_4) δ=1.03 (t, J=7 Hz, 3×1/2H), 1.07 (t, J=7 Hz, 3×1/2H), 3.90 (q, J=7 Hz, 2×1/2H), 3.96 (q, J=7 Hz, 2×1/2H), 4.23 (m, 2H), 4.67 (s, 1×1/2H), 4.78 (s, 1×1/2H), 5.00 (m, 2H), 6.10 (d, J=4 Hz, 1×1/2H), 6.19 (d, J=4 Hz, 1×1/2H), 7.25 (m, 16H), 7.80 (m, 4H); Calcd for $C_{36}H_{32}O_9S$: C, 67.49; H, 5.03; S, 5.00%. Found: C, 67.40; H, 5.05; S, 4.91%. **4e**: An amorphous oil: IR (Nujol) 1730, 1715 cm^{-1}; NMR (60 MHz) (CCl_4) δ=2.17 (s, 3×5/9H), 2.27 (s, 3×4/9H), 3.75 (d, J=8 Hz, 1×4/9H), 3.92 (d, J=4 Hz, 1×5/9H), 4.50 (m, 4H), 5.68 (m, 2H), 7.25 (m, 14H), 7.85 (m, 6H); Calcd for $C_{35}H_{30}O_8S$: C, 68.84; H, 4.95; S, 5.25%. Found: C, 68.89; H, 5.15; S, 5.51%. **4f**: An amorphous oil: IR (Nujol) 1730, 1720 cm^{-1}; NMR (60 MHz) (CCl_4) δ=1.10 (m, 9H), 3.55 (m, 1H), 4.50 (m, 4H), 5.65 (m, 2H). 7.30; (m, 14H), 7.85 (m, 6H); Calcd for $C_{38}H_{36}O_8S$: C, 69.92; H, 5.56; S, 4.91%. Found: C, 70.03; H, 5.16; S, 5.15%.

Desulfuriztion of 4e. Raney nickel (W-2; 1.5 g) was added to a solution of **4e** (105.5 mg, 0.17 mmol) in ethanol (10 ml) and it was heated to reflux for 1 h. Filtration of the reaction mixture through Celite followed by removal of the solvent gave an oil, which was purified by column chromatography on silica gel to afford the desulfurization product **6** (61.6 mg, 70%). IR (Nujol) 1720 cm^{-1}; NMR (60 MHz) (CCl_4) δ=2.10 (s, 3H), 2.79 (d, J=7 Hz, 2H), 4.50 (m, 4H), 5.52 (m, 2H), 7.37 (m, 9H), 7.93 (m, 6H).

The Reaction of 1 with 1,3-Bis(trimethylsiloxy)-1-methoxy-1,3-butadiene (8). The acetate **1** (320.1 mg, 0.63 mmol) was dissoled in dichloromethane (2 ml) and trimethylsilyl triflate (0.80 mmol) was added to this solution at room temperature. After stirring for 5 min, the enol silyl ether **8** (1.0 mmol) was added. The mixture was stirred for 1.5 h at room temperature. The reaction mixture was quenched with satd. aq K_2CO_3 and was extracted several times with ether. The combined organic extracts were washed with satd. aq NaCl and dried over anhyd. Na_2SO_4. Removal of the solvent followed by column chromatography on silica-gel afforded **10** (282.1 mg, 80%) as an oil. IR (neat) 1730 cm^{-1}; NMR(90 MHz) ($CDCl_3$) δ=3.06 (s-like, 2H), 3.41 (s-like, 2H), 3.61 (m, 1H), 3.64 (s, 3H), 4.22 (dd, J=12 and 5 Hz, 1H), 4.45 (dd, J=12 and 4 Hz, 1H), 4.92 (dd, J=9 and 5 Hz, 1H), 5.26 (dd, J=5 and 4.5 Hz, 1H), 6.18 (d, J=4.5 Hz, 1H), 7.38 (m, 11H), 7.93 (m, 4H); Calcd for $C_{31}H_{28}O_{10}$: C, 66.42; H, 5.03%. Found: C, 66.31; H, 5.32%.

In a similar manner, 1,3-dimethoxy-1-trimethylsiloxy-1,3-butadiene (**7**)[17] gave the corresponding **9** as an oil in 74% yield. IR (neat) 1730 cm^{-1}; NMR (60 MHz) (CCl_4) δ=3.32 (s-like, 2H), 3.36 (s, 3H), 3.52 (s, 3H), 3.70 (m, 1H), 4.24 (m, 2H), 4.70 (dd, J=9 and 5 Hz, 1H), 4.86 (s, 1H), 5.02 (dd, J=7 and 6 Hz, 1H), 5.93 (d, J=4 Hz, 1H), 7.27 (m, 11H), 7.83 (m, 4H); Calcd for $C_{32}H_{30}O_{10}$: C, 66.89; H, 5.26%. Found: C, 66.95; H, 5.50%.

Diazo Compound 11 from Diketone 10. To a solution of diketone **10** (923.9 mg, 1.65 mmol) in acetonitrile (5 ml) was added triethylamine (0.3 ml, 2.14 mmol) and *p*-toluenesulfonyl azide (345.2 mg, 1.75 mmol) at room temperature. The mixture was stirred for 1.5 h at that temperature, and the solvent was removed under reduced pressure. The residue was dissolved in ether, washed successively with dil. aq NaOH and satd. aq NaCl, and dried over anhyd. Na_2SO_4. Removal of the solvent followed by column chromatography on Florisil afforded the diazo compound **11** (966.8 mg, 100%). IR (neat) 2150, 1730 cm^{-1}; NMR (90 MHz) ($CDCl_3$) δ=3.45 (s-like, 2H), 3.74 (s, 3H), 3.67 (m, 1H), 4.18 (dd, J=12 and 5 Hz, 1H), 4.42 (dd, J=12 and 4 Hz, 1H), 4.88 (dd, J=9 and 5 Hz, 1H), 5.22 (dd, J=5 and 5 Hz, 1H), 6.15 (d, J=5 Hz, 1H), 7.45 (m, 11H), 7.95 (m, 4H); Calcd for $C_{31}H_{26}O_{10}N_2$: C, 63.48; H, 4.47; N, 4.78%. Found: C, 63.78; H, 4.66; N, 4.66%.

Cyclizatio of Diazo Compound 11. Lithium hexamethyldisilazanide (1.6 ml of 0.58 M THF solution, 0.92 mmol) was added to the diazo compound **11** (253 mg, 0.43 mmol) in a mixture of THF (0.5 ml) and HMPA (0.25 ml) at −78 °C. Then it was warmed up to −20 °C and stirred for 1 h at that temperature. The reaction mixture was poured into buffered solution and extracted several times with ether. The organic layer was washed with satd. aq NaCl and dried over anhyd. Na_2SO_4. Removal of the solvent followed by column chromatography on Florisil afforded the pyrazole **12** (188.5 mg,

66%). IR (neat) 1730cm^{-1}; NMR (90MHz) ($CDCl_3$) δ= 3.83 (s, 3H), 4.14 (quint, J=4.5 Hz, 1H), 4.32 (dd, J=12 and 5 Hz, 1H), 4.56 (dd, J=12 and 4 Hz, 1H), 5.02 (dd, J=9 and 5 Hz, 1H), 5.27 (dd, J=5 and 5 Hz, 1H), 6.29 (d, J=5 Hz, 1H), 6.75 (br s, 1H), 7.43 (m, 11H), 7.95 (m, 4H); Calcd for $C_{31}H_{26}O_{10}N_2$: C, 63.48; H, 4.47; N, 4.78%. Found: C, 63.19; H, 4.60; N, 4.68%.

References

1) A preliminary report dealing with certain aspects of this work has been published; Y. S. Yokoyama, M. R. H. Elmoghayar, and I. Kuwajima, *Tetrahedron Lett.*, **23**, 2673 (1982).

2) R. H. Suhadolnik, "Nucleoside Antibiotics," Wiley-Interscience, New York, (1970), p. 354—404; G. D. Davis, Jr., and C. C. Cheng, *Prog. Med. Chem.*, **13**, 303 (1976).

3) a) R. M. Acton, K. J. Pyran, D. W. Henry, and L. Goodman, *J. Chem. Soc., Chem. Commun.*, **1981**, 986; b) J. G. Buchnan, A. R. Edger, R. J. Hutchson, A. S. Stobie, and R. H. Wightman, *ibid.*, **1980**, 237.

4) a) T. Inoue and I. Kuwajima, *J. Chem. Soc., Chem. Commun.*, **1980**, 251; b) L. Kalvoda, J. Farkas, and F. Sorm, *Tetrahedron Lett.*, **1970**, 2297; c) G. Trummlitz and J. G. Moffatt, *J. Org. Chem.*, **38**, 1841 (1973); d) R. Noyori, T. Sato, and Y. Hayakawa, *J. Am. Chem. Soc.*, **100**, 2561 (1978); e) J. G. Buchnan, A. R. Edger, M. J. Power, and C. T. Shanks, *J. Chem. Soc., Perkin Trans. 1*, **1979**, 225; f) A. P. Kozikowski and A. Ames, *J. Am. Chem. Soc.*, **103**, 3923 (1981); g) Y. Ito, T. Shibata, M. Arita, H. Sawai, and M. Ohno, *ibid.*, **103**, 6739 (1981).

5) a) J. Farkas, Z. Flegelova, and F. Sorm, *Tetrahedron Lett.*, **1972**, 2279; b) S. D. Bernardo and M. Weigele, *J. Org. Chem.*, **41**, 287 (1976); c) M. Sprinzl, J. Farkas, and F. Sorm, *Tetrahedron Lett.*, **1969**, 289.

6) a) G. Just and G. Reader, *Tetrahedron Lett.*, **1973**, 1521, 1525; G. Just and B. Chalard-Faure, *Can. J. Chem.*, **54**, 861 (1976); b) J. Farkas and F. Sorm, *Coll. Czech. Chem. Commun.*, **37**, 2799 (1972); c) H. P. Albrecht, D. B. Repke, and J. G. Moffatt, *J. Org. Chem.*, **39**, 2176 (1974); d) A. K. Sakasena and A. K. Ganguly, *Tetrahedron Lett.*, **22**, 5227 (1981); e) M. Bober, J. Farkas, and F. Sorm, *ibid.*, **1970**, 4611.

7) a) S. Hanessian and A. G. Pernet, *Can. J. Chem.*, **52**, 1280 (1974); b) P. S. Klein, M. P. Kotick, K. A. Watanabe, and J. J. Fox, *J. Org. Chem.*, **36**, 4113 (1971); c) K. Arakawa, T. Miyashita, and N. Hamamichi, *Chem. Lett.*, 1305 (1974).

8) T. Ogawa, A. G. Pernet, and S. Hanessian, *Tetrahedron Lett.*, **1973**, 3543.

9) Supports of these assignment come from spectroscopic studies. ^{1}H NMR spectra of these products are consistent with that of 3,5-di-*O*-benzoyl-1,2-[α-[2-(methoxycarbonyl)-ethenyl]benzylidene]-α-D-ribofuranose.[6c] In the case having the asymmetric carbon atom bearing α-substituent, two diastereomers were detected by ^{1}H NMR. These diastereomers could not be separated except **5a**.

10) E. Nakamura and I. Kuwajima, *Chem. Lett.*, **1983**, 59.

11) L. Kalavoda, *Coll. Czech. Chem. Commun.*, **38**, 1679 (1973).

12) Using tin(IV) chloride as a catalyst in stead of trimethylsilyl triflate, the reaction gave a complex mixture.

13) H. F. Vorbruggen, U. Niedballa, K. Krolikiewicz, and B. Bennua, "Chemistry and Biology of Nucleosides and Nucleotides," ed by R. H. Harmon, R. K. Robins, and L. B. Townsend, Academic Press, New York (1978), p. 251—265.

14) H. O. House, L. J. Czuba, M. Gall, and H. D. Olmstead, *J. Org. Chem.*, **34**, 2324 (1968).

15) M. W. Rathke and D. F. Sullivan, *Tetrahedron Lett.*, **1973**, 1279.

16) K. Yamamoto, S. Suzuki, and J. Tsuji, *Chem. Lett.*, **1978**, 649; T. H. Chan and P. Brownbridge, *J. Chem. Soc., Chem. Commun.*, **1979**, 578.

17) Enol silyl ether **7** (bp 67—69 °C/4.5 mmHg, 1 mmHg= 133.322 Pa) was prepared from methyl 3-methoxycrotonate.[18]

18) A. Michael, *J. Am. Chem. Soc.*, **57**, 159 (1935).

 © 1984 The Chemical Society of Japan Bull. Chem. Soc. Jpn., 57, 557—560 (1984)

Studies on Salt Hydrates for Latent Heat Storage. V. Preheating Effect on Crystallization of Sodium Acetate Trihydrate from Aqueous Solution with a Small Amount of Sodium Pyrophosphate Decahydrate

Takahiro WADA,* Koji MATSUNAGA, and Yoshihiro MATSUO
Central Research Laboratory, Matsushita Electric Industrial Co., Ltd., 1006 Kadoma, Osaka 571
(Received June 6, 1983)

Influences of preheating temperature and time were studied on the crystallization of $CH_3CO_2Na \cdot 3H_2O$ from three kinds of CH_3CO_2Na aqueous solutions, whose concentrations were 58.0, 60.3, and 62.8 wt% and which contained a small amount of crystal nucleation catalyst, $Na_4P_2O_7 \cdot 10H_2O$. In 60.3 wt% aqueous solution ($CH_3CO_2Na \cdot 3H_2O$), the nucleation catalyst begins to get deactivated by preheating at about 81 °C, higher by 23 °C than the melting point of $CH_3CO_2Na \cdot 3H_2O$. The temperature at which the catalyst begins to get deactivated is raised with increasing CH_3CO_2Na concentration of the solution; thus, in 62.8 wt% CH_3CO_2Na aqueous solution, the catalyst begins to get deactivated at 85 °C. One hundred samples, each consisting of 8 g of 60.3 wt% CH_3CO_2Na aqueous solution and 0.16 g of $Na_4P_2O_7 \cdot 10H_2O$, all crystallized on cooling to 40 °C, even after they had been preheated at 80 °C for 39 h. These results are explained on the basis of the crystalline adsorption model proposed by Richards.

Sodium Acetate Trihydrate ($CH_3CO_2Na \cdot 3H_2O$) has recently attracted attention as a useful heat storage material because of its large latent heat of fusion (264 J/g).[1,2] $CH_3CO_2Na \cdot 3H_2O$ melt tends to supercool even if cooled considerably below its melting point (58.4 °C).[3,4] Its practical application has been impaired by this supercooling phenomenon.[5] Wada and Yamamoto,[6] in search for a crystal nucleation catalyst, have found that addition of $Na_4P_2O_7 \cdot 10H_2O$ is very effective for preventing the supercooling.

A phase diagram of binary system CH_3CO_2Na–H_2O, based on data from Seidell's compilation,[7] is shown in Fig. 1. The dashed line is the liquidus line for metastable CH_3GO_2Na. It is clear that $CH_3CO_2Na \cdot 3H_2O$ melts incongruently to a 58.0 wt% CH_3CO_2Na aqueous solution in equilibrium with the residual solid, anhydrous CH_3CO_2Na, and that anhydrous CH_3CO_2Na dissolves entirely in its water of crystallization at about 78 °C.

Ternary system CH_3CO_2Na–$Na_4P_2O_7$–H_2O has been investigated between 38 and 85 °C.[9] No double salt formation occurs in this temperature range. Saturation concentrations of $Na_4P_2O_7$ in saturated CH_3CO_2Na solutions are 0.08 wt% at 38 °C, 0.06 wt% at 50 °C, 0.02 wt% at 62 °C, 0.02 wt% at 75 °C, and 0.02 wt% at 85 °C. The lowest formation temperature of anhydrous $Na_4P_2O_7$ is about 47 °C.

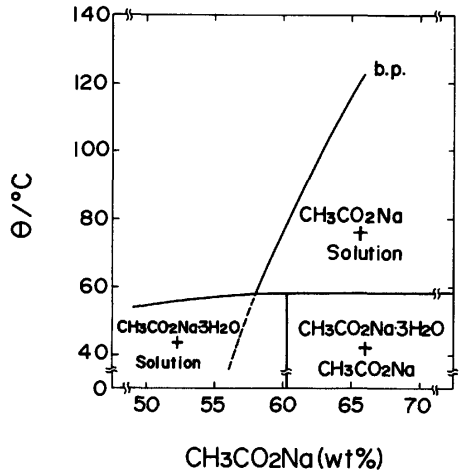

Fig. 1. Phase diagram of the binary system CH_3CO_2Na–H_2O.[8]

The crystallization tendency of the liquid is diminished with increasing preheating temperature.[10,11] Richards[12] studied the preheating effect on crystallization of $CH_3CO_2Na \cdot 3H_2O$ from aqueous solution. He used 20 sealed tubes each containing 3 g of 12 M (1 M= 1 mol dm^{-3}), about 50 wt%, CH_3CO_2Na aqueous solution and kept them at room temperature during intervals between preheating treatments. He reported that $CH_3CO_2Na \cdot 3H_2O$, when preheated at a temperature 2, 3.5, or 7 °C above its melting point, was allowed to crystallize in 100, 35, or 5% of the sample tubes, respectively.

A number of explanations are applicable to the above behavior. Richards[12] proposed the crystalline adsorption model that a crystal form may persist above its melting point if some adsorbent present in a sample binds the crystalline adsorbate more strongly than the liquid adsorbate, that is, if the heat of adsorption of the crystalline adsorbate onto the adsorbent is higher than that of the liquid adsorbate. This crystalline adsorption model is illustrated in Fig. 6. This model is characteristically capable of explaining the fact that reactivation of a deactivated nucleation catalyst can be effected by forced crystallization of the liquid containing that catalyst.

This paper reports influences of preheating temperature and time on crystallization of $CH_3CO_2Na \cdot 3H_2O$ from three kinds of CH_3CO_2Na aqueous solutions, whose concentrations are 58.0, 60.3, and 62.8 wt% and which have a small amount of $Na_4P_2O_7 \cdot 10H_2O$ added. For the system to be useful as a latent heat storage material, the temperature at which the crystal nucleation catalyst begins to get deactivated is very important. Results obtained are explained on the basis of the crystalline adsorption model.

Experimental

$CH_3CO_2Na \cdot 3H_2O$, CH_3CO_2Na, and $Na_4P_2O_7 \cdot 10H_2O$ were guaranteed grade reagents from Wako Pure Chemical Industries, Ltd. Eight grams of CH_3CO_2Na aqueous solu-

tion and 0.16 g of $Na_4P_2O_7 \cdot 10H_2O$ were placed in a tube, which was afterwards sealed. The concentration of the CH_3CO_2Na aqueous solution prepared was 58.0 wt% (peritectic composition), 60.3 wt% ($CH_3CO_2Na \cdot 3H_2O$), or 62.8 wt%. The sealed tubes were put into a water bath equipped with a gently-vibrating rack. Before subsequent steps, all aqueous solutions with a smal amount of $Na_4P_2O_7 \cdot 10H_2O$ added were heated at 70 °C for 1 h and then cooled to room temperature in order to force $CH_3CO_2Na \cdot 3H_2O$ to crystallize, with shaking if necessary.

Experiment 1. One hundred sealed tubes each containing a 60.3 wt% CH_3CO_2Na aqueous solution were heated to a predetermined temperature above the melting point of $CH_3CO_2Na \cdot 3H_2O$, kept there for 3 h, and then cooled to 40 °C at a rate of 5 °C/h. This process was repeated with the preheating temperature raised stepwise. In some of the 100 tubes preheated at a certain temperature, $CH_3CO_2Na \cdot 3H_2O$ failed to crystallize on cooling to 40 °C. Such tubes were excluded because the nucleation catalyst in the tube must have heen deactivatd. This deactivation possibility was supported by the observation that $CH_3CO_2Na \cdot 3H_2O$ scarcely crystallized in the excluded tubes during similar heating and cooling tests as mentioned above. The other two aqueous solutions were examined in the same manner as above. Thus, the influence of preheating temperature on the crystallization of $CH_3CO_2Na \cdot 3H_2O$ from aqueous solution was studied. The percentage of the tubes in which the nucleation catalyst was deactivated was plotted against the temperature difference between the preheating temperature and the melting point to get Fig. 2.

Experiment 2. Experimental procedures were similar to those in *Experiment 1* except that the preheating temperature was kept constant. One hundred tubes were heated to a preheating temperature, kept there for 3 h, and then cooled to 40 °C at a rate of 5 °C/h. In some of the 100 tubes preheated for a certain time, $CH_3CO_2Na \cdot 3H_2O$ failed to crystallize on cooling to 40 °C. Such tubes were excluded for the same reason as in *Experiment 1*. Similar experiments were conducted with a variation of preheating temperature. The influence of preheating time on the crystallization of $CH_3CO_2Na \cdot 3H_2O$ from 60.3 and 58.0 wt% CH_3CO_2Na aqueous solutions was studied by finally plotting the percentage of the tubes in which the catalyst was deactivated against the preheating time to get Figs. 3 and 4, respectively.

Experiment 3. Experimental procedures were similar to those adopted in *Experiment 2* except that, when in some tubes $CH_3CO_2Na \cdot 3H_2O$ failed to crystallize on cooling to 40 °C, these tubes were cooled to room temperature to force $CH_3CO_2Na \cdot 3H_2O$ to crystallize, with shaking if necessary, and returned to subsequent steps. This experiment was conducted on the 58.0 wt% CH_3CO_2Na aqueous solution. The percentage of the tubes in which the catalyst was deactivated was plotted against the preheating time to get Fig. 5.

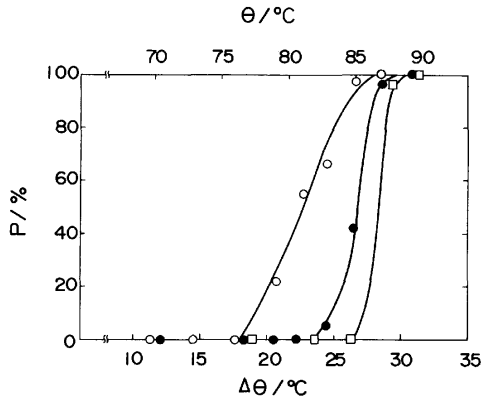

Fig. 2. The influence of preheating temperature on the crystallizaion of $CH_3CO_2Na \cdot 3H_2O$ from the three kinds of aqueous solution with a small amount of $Na_4P_2O_7 \cdot 10H_2O$.
○: 58.0 wt% CH_3CO_2Na aqueous solution, ●: 60.3 wt% CH_3CO_2Na squeous solution, □: 62.8 wt% CH_3CO_2Na aqueous solution.

Results

It is clear from Fig. 2 that under the conditions of *Experiment 1*, the nucleation catalysts in the 60.3 wt% CH_3CO_2Na aqueous solutions begin to get deactivated at 81 °C, higher by 23 °C than the melting point of $CH_3CO_2Na \cdot 3H_2O$ until all of them were deactivated at about 89 °C and that those in the 58.0 and 62.8 wt% solutions begin to get deactivated at 77 and 85 °C until all were deactivated at 85 and 89 °C, respectively. In the 100 tubes each containing 8 g of 60.3 wt% CH_3CO_2Na aqueous solution with no nucleation catalyst added, the cooling to 40 °C preceded by the preheating at 60 °C for 3 h caused no $CH_3CO_2Na \cdot 3H_2O$ to crystallize at all. The present CH_3CO_2Na aqueous solutions with no nucleation catalyst begin to get deactivated at a temperature lower than in the Richards experiment. This may be caused not only by differences in the CH_3CO_2Na concentration and experimental conditions but also by the difference in purity of reagents used. It is evident that the addition of $Na_4P_2O_7 \cdot 10H_2O$ to the CH_3CO_2Na aqueous solution is very effective for preserving the crystal nucleation ability above the melting point of $CH_3CO_2Na \cdot 3H_2O$.

It is understood from Fig. 2 that the temperature at which the catalyst begins to get deactivated is raised with increasing CH_3CO_2Na concentration of the solution containing that catalyst. The amount of the $Na_4P_2O_7 \cdot 10H_2O$ added is so small and the solubility of $Na_4P_2O_7$ in the $CH_3CO_2Na \cdot 3H_2O$ melt is so low[9] that the liquidus lines for $CH_3CO_2Na \cdot 3H_2O$ and CH_3CO_2Na may be considered to be scarcely influenced by the addition of $Na_4P_2O_7 \cdot 10H_2O$ to the CH_3CO_2Na aqueous solution. Figure indicates that the anhydrous CH_3CO_2Na in the 58 wt% aqueous solution is unstable above 58.4 °C, the one in the 60.3 wt% solution is unstable above 78 °C, and that the one in the 62.8 wt% solution is unstable above 97 °C. The deactivation of the nucleation catalyst depends on the CH_3CO_2Na concentration of the solution containing that catalyst, but is not directly related to the existence of anhydrous CH_3CO_2Na in the solution, although Kimura[13] has pointed out that the existence of anhydrous CH_3CO_2Na plays an important role in the crystallization of $CH_3CO_2Na \cdot 3H_2O$ from the solution.

It can be seen from Fig. 3 that in the 100 tubes each containing 8 g of 60.3 wt% CH_3CO_2Na aqueous solution with 0.16 g $Na_4P_2O_7 \cdot 10H_2O$ added, the nucleation catalysts were all caused to deactivate by preheating at 85 °C for 10 h, at 86 °C for 8 h or at 87 °C for 4 h. The preheating time that results in deactivation of all the catalysts is shortened with incressing preheating temperature. As is also seen from Fig. 3, even the preheating of the solutions at 80 °C for 39 h leads in any cases to crystallization on cooling to

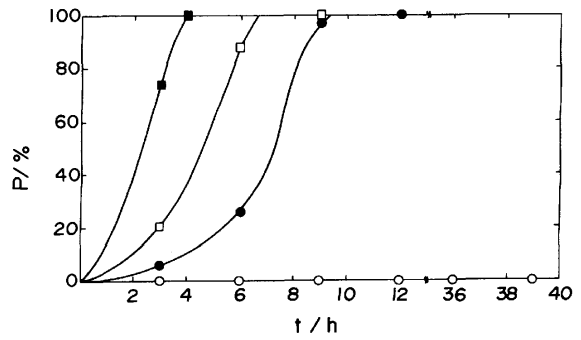

Fig. 3. The influence of preheating time on the crystallization of $CH_3CO_2Na \cdot 3H_2O$ from the 60.3 wt% CH_3CO_2Na aqueous solution.
○: Preheated at 80 °C, ●: preheated at 85 °C, □: preheated at 86 °C, ■: preheated at 87 °C.

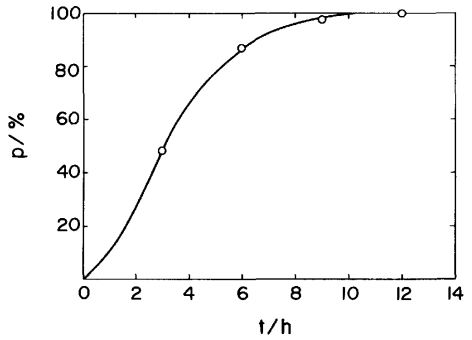

Fig. 4. The influence of preheating time on the crystallization of $CH_3CO_2Na \cdot 3H_2O$ from the 58.0 wt% CH_3CO_2Na aqueous solution preheated at 83 °C.

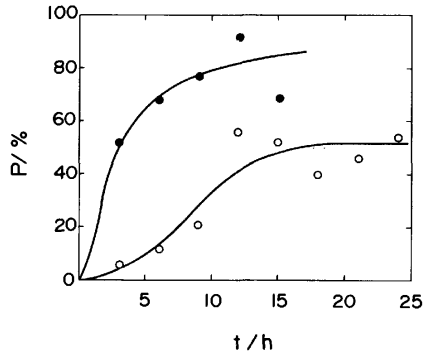

Fig. 5. The influence of preheating time on the crystallization of $CH_3CO_2Na \cdot 3H_2O$ from the 58.0 wt% CH_3CO_2Na aqueous solution under the *Experiment 3* conditions.
○: Preheated at 80 °C, ●: preheated at 83 °C.

40 °C. Thus it is deduced that the nucleation catalysts will not be caused to deactivate at all, no matter how long the solutions containing them are preheated below 80 °C. This is a very important finding from the standpoint of practical application.

It is seen from Fig. 4 that in the 100 tubes each containing a 58.0 wt% CH_3CO_2Na aqueous solution with the catalyst added, the catalysts were all deactivated when preheated at 83 °C for 10 h. The curve in Fig. 4 is similar to those in Fig. 3, so that the preheating time at which the catalysts were all caused to deactivate is supposed to be shorter than 10 h when the preheating temperature is above 83 °C.

In Fig. 5, the percentage of the tubes containing deactivated catalysts seems to approach a constant value, not 100%, with increasing preheating time. When 58.0 wt% CH_3CO_2Na aqueous solutions are preheated at 80 °C under the conditions of *Experiment 3*, the constant value is about 50%, and when they are preheated at 83 °C, it is about 90%. Compared with Fig. 3, it is evident that deactivated catalysts may be reactivated by forced crystallization of $CH_3CO_2Na \cdot 3H_2O$ from solutions containing them.

In 20 tubes each containing 8g of 58 wt% CH_3CO_2Na aqueous solution with 0.0001, 0.0005, or 0.001 g $Na_4P_2O_7 \cdot 10H_2O$ added, $CH_3CO_2Na \cdot 3H_2O$ hardly crystallized on cooling to 40 °C after the $Na_4P_2O_7 \cdot 10H_2O$ had been dissolved entirely in the CH_3CO_2Na solution by preheating at 70 °C. It is understood from this experiment and the phase equilibria of ternary system CH_3CO_2Na–$Na_4P_2O_7$–H_2O that anhydrous $Na_4P_2O_7$ solid is required for the crystallization of $CH_3CO_2Na \cdot 3H_2O$ to occur from the solution near the transition temperature.

Discussion

The results obtained from the present experiments will be discussed on the basis of the crystalline adsorption model proposed by Richards, which is illustrated in Fig. 6. According to this model, the $Na_4P_2O_7 \cdot 10H_2O$ added to a CH_3CO_2Na aqueous solution offers an adsorbent for which the heat of adsorption of crystalline $CH_3CO_2Na \cdot 3H_2O$ is higher than that of liquid adsorbate. The adsorbent is considered to be anhydrous $Na_4P_2O_7$ from the phase equilibria of ternary system CH_3CO_2Na–$Na_4P_2O_7$–H_2O,[9] although Wada and Yamamoto[6] discussed the crystal nucleation catalytic effect from the similarity of crystallographic data between $CH_3CO_2Na \cdot 3H_2O$ and $Na_4P_2O_7 \cdot 10H_2O$. The crystalline $CH_3CO_2Na \cdot 3H_2O$ adsorbed on the adsorbent is not allowed to fuse at its ordinary melting

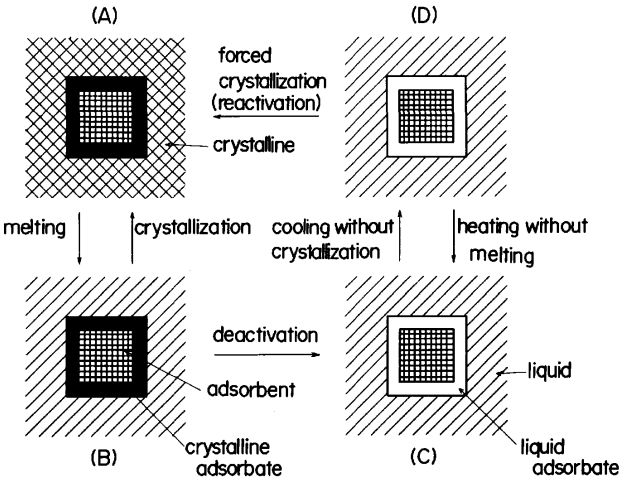

Fig. 6. The crystalline adsorption model proposed by Richards.[11]
(A): Crystalline state, (B): melting state with crystalline adsorbate, (C): melting state with liquid adsorbate, (D): supercooled state.

point but preserves its crystal nucleation ability above its melting point. This condition is shown in Figs. 6(A) snd (B). When the crystalline $CH_3CO_2Na \cdot 3H_2O$ adsorbate is fused entirely at an elevated temperature, $CH_3CO_2Na \cdot 3H_2O$ hardly crystallizes from the solution. This is also shown in Figs. 6(C) and (D). However, even if the crystalline adsorbate has been fused entirely, it is again formed by a forced crystallization of $CH_3CO_2Na \cdot 3H_2O$ from the solution containing the adsorbent. This is shown in Figs. 6(D) and (A). This expectation is compatible with the result obtained from *Experiment 3.*

It is understood on the basis of the concept of adsorption that the melting temperature of crystalline $CH_3CO_2Na \cdot 3H_2O$ adsorbed on the adsorbent depends not only on the difference in the heat of adsorption for the adsorbent between the crystalline $CH_3CO_2Na \cdot 3H_2O$ and the CH_3CO_2Na aqueous solution but also on the CH_3CO_2Na concentration of the solution. The temperatre is lowered with decreasing CH_3CO_2Na concentration of the slution. This is compatible with the result obtained from *Experiment 1.*

It is also plausible that the crystalline $CH_3CO_2Na \cdot 3H_2O$ adsorbate melts faster at higher temperatures. Therefore, the preheating time which results in complete catalyst deactivaion is expected to be shortened with increasing preheatig temperature. This expectation is also compatible with the result obtained in *Experiment 2.*

It is also found that when a small amount of glycine ($H_2NCH_2CO_2H$) or calcium tartrate tetrahydrate ($C_4H_4O_6Ca \cdot 4H_2O$) is added to a CH_3CO_2Na aqueous solution containing with a small amount of $Na_4P_2O_7 \cdot 10H_2O$ the crystal nucleation catalyst is caused to deactivate by heating and cooling cycles, even if the heating is conducted at 75 °C. That is to say, $H_2NCH_2CO_2H$ or $C_4H_4O_6Ca \cdot 4H_2O$ acts as a catalytic poison for the nucleation catalyst $Na_4P_2O_7 \cdot 10H_2O$. This fact is also explained satisfactorily on the basis of the crystalline adsorption model. If these compounds adsorb on the surface of adsorbent more strongly than the crystalline $CH_3CO_2Na \cdot 3H_2O$ adsorbate, that is, the heats of adsorption of these compounds for the adsorbent are higher than that of the crystalline adsorbate, these compounds will adsorb on the surface of adsorbent through displacement of the crystalline $CH_3CO_2Na \cdot 3H_2O$ adsorbate during heating and cooling cycles. Therefore, the crystal nucleation catalysts are caused to deactivate by the thermal cycling.

Thus, the results obtained have all been explained satisfactorily on the basis of the crystalline adsorption model. However, these explanations are qualitative and the existence of crystalline adsorbate above its ordinary melting point has not yet been confirmed. Therefore, quantitative explanations of these behavior are future problems.

The authors wish to express their thanks to Dr. Ryoichi Kiriyama for his helpful discussions and to Drs. Tsuneharu Nitta, Eiichi Hirota, and Masanari Mikoda for their continuous encouragements. They are also grateful to Dr. Ryoichi Yamamoto for his discussion throughout this work.

References

1) M. Telkes, "Solar Materials Science," ed by L. E. Murr, Academic Press, New York (1980), Chap. 11.
2) A. Pebler, *Thermochim. Acta*, **13**, 109 (1975).
3) F. de Winter, *Solar Energy*, **17**, 379 (1975).
4) K. Narita and J. Kai, *J. Inst. Electr. Eng. Jpn.*, **101**, 15 (1981).
5) M. Telkes, *Ind. Eng. Chem.*, **44**, 1308 (1952).
6) T. Wada and R. Yamamoto, *Bull. Chem. Soc. Jpn.*, **55**, 3603 (1982).
7) A. Seidell, "Solubility of Inorganic and Metal Organic Compounds," 4th ed, Academic Press, New York (1965), Vol. 2, p. 854.
8) W. F. Green, *J. Phys. Chem.*, **12**, 655 (1908).
9) T. Wada, F. Yokotani, and Y. Matsuo, *Bull. Chem. Soc. Jpn.*, in press.
10) P. Othmer *Z. Anorg. Chem.*, **91**, 209 (1915).
11) C. N. Hinshelwood and H. Hartley, *Philos. Mag.*, **43**, 78 (1922).
12) W. T. Richards, *J. Am. Chem. Soc.*, **54**, 478 (1932).
13) H. Kimura, *J. Jpn. Assoc. Cryst. Growth*, **9**, No. 3, 73 (1982).

 © 1984 The Chemical Society of Japan Bull. Chem. Soc. Jpn., 57, 561—563 (1984)

Studies on Salt Hydrates for Latent Heat Storge. VI. Preheating Effect on Crystallization of Sodium Acetate Trihydrate from Aqueous Solution with a Small Amount of Disodium Hydrogenphosphate

Takahiro WADA* and Yoshihiro MATSUO

Central Research Laboratory, Matsushita Electric Industrial Co., Ltd., 1006 Kadoma, Osaka 571

(Received July 14, 1983)

With particular reference to the use of Na_2HPO_4 as nucleation catalyst for crystallization of $CH_3CO_2Na \cdot 3H_2O$, influences of preheating temperature and time were studied on the crystallization of $CH_3CO_2Na \cdot 3H_2O$ from three kinds of CH_3CO_2Na aqueous solutions, whose concentrations were 58.0, 60.3, and 62.8 wt%. In 60.3 wt% aqueous solution ($CH_3CO_2Na \cdot 3H_2O$), the nucleation catalyst begins to get deactivated by preheating at 81 °C. The temperature at which the catalyst begins to get deactivated is slightly raised with increasing CH_3CO_2Na concentration of the solution. The results obtained are compared with those previously reported on the use of $Na_4P_2O_7 \cdot 10H_2O$ as nucleation catalyst, and are discussed on the basis of the crystalline adsorption model.

Sodium Acetate Trihydrate ($CH_3CO_2Na \cdot 3H_2O$) has recently attracted attention as a useful heat storage material because of its large latent heat of fusion (264 J/g).[1,2] Pure $CH_3CO_2Na \cdot 3H_2O$ melt supercools at condiserably lower temperatures than its melting point (58.4 °C).[3,4] Its practical application has been impaired by this supercooling phenomenon.[5] Wada and Yamamoto[6] found that addition of $Na_4P_2O_7 \cdot 10H_2O$ is very effective for preventing the supercooling. Afterward, Kimura[7] found that addition of a mixture of Na_2HPO_4 and anhydrous CH_3CO_2Na is also effective for the prevention.

Ternary system CH_3CO_2Na–Na_2HPO_4–H_2O has been investigated between 38 and 75 °C.[8] No double salt formation occurs in this temperature range. The saturation concentrations of Na_2HPO_4 in saturated CH_3CO_2Na solutions are 1.5 wt% at 50 °C, 0.7 wt% at 62 °C, and 0.6 wt% at 75 °C. The lowest formation temperature of anhydrous Na_2HPO_4 is about 57 °C.

Recently, Wada *et al.*[9] studied the influence of preheating on the crystallization of $CH_3CO_2Na \cdot 3H_2O$ from aqueous solutions containing $Na_4P_2O_7 \cdot 10H_2O$ as nucleation catalyst and obtained results that the nucleation catalyst $Na_4P_2O_7 \cdot 10H_2O$ begins to get degraded in its nucleation ability by preheating at about 81 °C and that the temperature (T_c) at which the catalyst begins to get degraded in its nucleation ability is raised with increasing CH_3CO_2Na concentration of the solution. Such results have been explained in detail on the basis of the crystaline adsorption model[9] proposed by Richards.[10] This model is illustrated in Fig. 1.

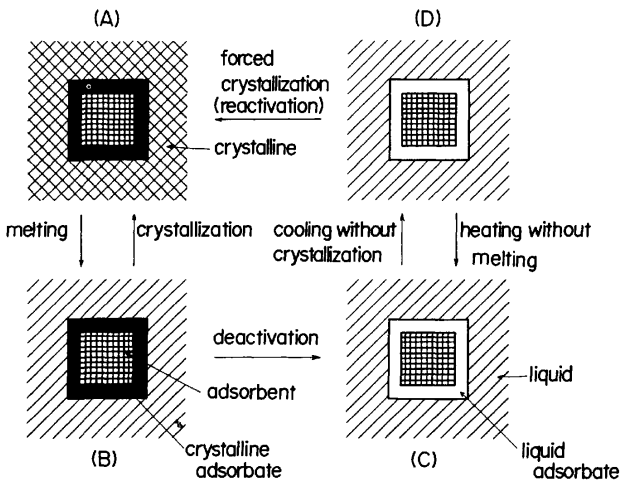

Fig. 1. The crystalline adsorption model for crystal nucleation.
(A): Crystalline state, (B): melting state with crystalline adsorbate, (C): melting state with liquid adsorbate, (D): supercooled state.

It can be seen from Fig. 1 that the crystalline $CH_3CO_2Na \cdot 3H_2O$ adsorbed on the adsorbent ($Na_4P_2O_7$) is not allowed to fuse at its ordinary melting point, preserving its crystal nucleation ability even above its melting point. The heat of adsorption of crystalline $CH_3CO_2Na \cdot 3H_2O$ onto the adsorbet is higher than that of liquid adsorbate. When crystalline $CH_3CO_2Na \cdot 3H_2O$ adsorbate has been fused entirely at an elevated temperature, $CH_3CO_2Na \cdot 3H_2O$ hardly crystallizes from the solution. However, even if the crystalline adsorbate has entirely been fused, it will again be formed during the cooling process becsuse of forced crystallization of $CH_3CO_2Na \cdot 3H_2O$ from the solution containing the nucleation catalyst.

This paper reports influences of preheating temperature and time on the crystal nucleation of $CH_3CO_2Na \cdot 3H_2O$ from sodium acetate solutions containing a small amount of Na_2HPO_4 added. Results obtained are compared with those in the case of solutions containing $Na_4P_2O_7 \cdot 10H_2O$ as nucleation catalyst and subjected to a discussion on the basis of the crystalline adsorpton model.

Experimental

$CH_3CO_2Na \cdot 3H_2O$, CH_3CO_2Na, and Na_2HPO_4 were guaranteed grade reagents from Wako Pure Chemical Industries, Ltd. Experimental procedures are similar to those reported in the preceding paper.[9] Eight grams of CH_3CO_2Na aqueous solution and 0.16 g of Na_2HPO_4 were placed in a tube, which was afterwards sealed. The sealed tubes were put into a water bath equipped with a gently-vibrating rack. Before subsequent steps, all aqueous solutions with a small amount of Na_2HPO_4 added were heated at 70 °C for 1 h and then cooled to room temperature in order to force $CH_3CO_2Na \cdot$

$3H_2O$ to crystallize. Then, the tubes were shaked if necessary.

Experiment 1. One hundred sealed tubes, each containing a CH_3CO_2Na aqueous solution at a concentration of 58.0, 60.3, or 62.8 wt% and a small amount of nucleation catalyst added, were heated to a predetermined temperature, kept there for 3 h and then cooled to 40 °C at a rate of 5 °C/h. This process was repeated with the preheating temperature raised stepwise. In some of the 100 tubes preheated at a certain temperature, $CH_3CO_2Na \cdot 3H_2O$ failed to crystallize on cooling to 40 °C. Such tubes were excluded because the nucleation catalyst in the tube must have been deactivated or degraded in its nucleation ability. This deactivation possibility was supported by the observation that $CH_3CO_2Na \cdot 3H_2O$ scarcely crystallized in the excluded tubes during similar heating and cooling tests as mentioned above. The percentage of the tubes having deactivated nucleation catalysts over the total tubes was plotted against the temperature difference between the preheating temperature and the melting point (58.4 °C) to get Fig. 2.

Experiment 2. One hundred tubes, each containing a 58 wt% aqueous solution and a small amount of nucleation catalyst added, were heated to a constant preheating temperature, kept there for 3 h, and then cooled to 40 °C at a rate of 5 °C/h. This procedure was applied to several preheating temperatures. In some of the 100 tubes preheated for a certain time, $CH_3CO_2Na \cdot 3H_2O$ failed to crystallize on cooling to 40 °C. Such tubes were excluded for the same reason as in *Experiment 1.* The percentage of the tubes in which the nucleation catalyst was deactivated over the total tubes was plotted against the preheating time to get Fig. 3.

Experiment 3. Experimental procedures were similar to those in *Experiment 2* except that those tubes in which $CH_3CO_2Na \cdot 3H_2O$ had failed to crystallize on cooling to 40 °C were not excluded but cooled to room temperature to force $CH_3CO_2Na \cdot 3H_2O$ to crystallize; they were then subjected to sequentially succeeding heating and cooling tests. The percentage of the tubes in which the nucleation catalyst was deactivated over the total tubes was plotted against the preheatng time to get Fig. 4.

Results and Discussion

It is clear from Fig. 2 that, under the conditions of *Experiment 1,* the nucleation catalysts in the 60.3 wt% CH_3CO_2Na aqueous solutions begin to get deactivated at 81 °C, higher by 23 °C than the melting point of $CH_3CO_2Na \cdot 3H_2O$ until all of them were deactivated at about 88 °C. These temperatures are in good agreement with the data obtained when $Na_4P_2O_7 \cdot 10H_2O$ was used as nucleation catalyst. In 58.0 and 62.8 wt% solutios, the nucleation catalysts begin to get deactivated at 81 and 82 °C, until all were deactivated at 88 and 89 °C, respectively. In 100 tubes each containing 8 g of 60.3 wt% aqueous solution with no nucleation catalyst, the cooling to 40 °C preceded by preheating at 60 °C for 3 h caused no $CH_3CO_2Na \cdot 3H_2O$ to crystallize. It is evident that the addition of Na_2HPO_4 is very effective for preserving the crystal nucleation ability above the melting point of $CH_3CO_2Na \cdot 3H_2O$. It is understood from Fig. 2 that T_c is slightly raised with increasing CH_3CO_2Na concentration of the solution. Such a phenomenon is qualitatively similar to one observed in the case of solutions with $Na_4P_2O_7 \cdot 10H_2O$ added as nucleation catalyst; the degree of concentration dependence of T_c is appreciably lower than in the previous case.

It can be seen from Fig. 3 that under the conditions of *Experiment 2,* in the 100 tubes each containing 8 g of 58.0 wt% CH_3CO_2Na aqueous solution and 0.16 g of

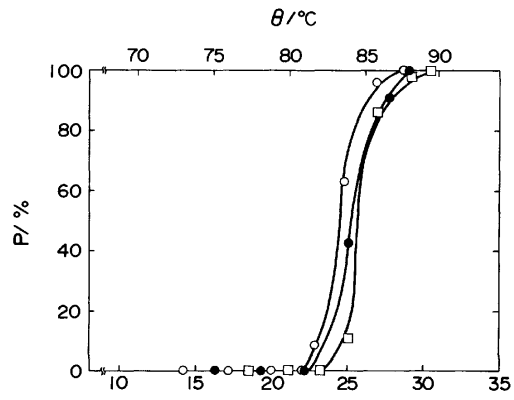

Fig. 2. The influence of preheating temperature on the crystallization of $CH_3CO_2Na \cdot 3H_2O$ from the three aqueous solutions in use of a small amount of Na_2HPO_4 as a nucleation catalyst.
○: 58.0 wt% CH_3CO_2Na aqueous solution, ●: 60.3 wt% CH_3CO_2Na aqueous solution, □: 62.8 wt% CH_3CO_2Na aqueous solution.

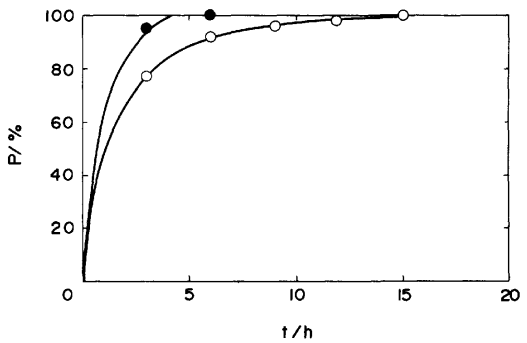

Fig. 3. The influence of preheating time on the crystallization of $CH_3CO_2Na \cdot 3H_2O$ from the 58.0 wt% aqueous solution in use of Na_2HPO_4 as a nucleation catalyst under the conditions of *Experiment 2.*
○: Preheated at 84 °C, ●: preheated at 85 °C.

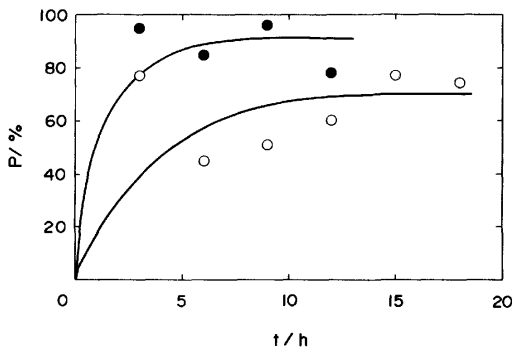

Fig. 4. The influence of preheating time on the crystallization of $CH_3CO_2Na \cdot 3H_2O$ from the 58.0 wt% aqueous solution in use of Na_2HPO_4 as a nucleation catalyst under the conditions of *Experiment 3.*
○: Preheated at 84 °C, ●: preheated at 85 °C.

Na_2HPO_4, $CH_3CO_2Na \cdot 3H_2O$ did not crystallize at all after the tubes had been preheated at 84 °C for 15 h and at 85 °C for 6 h. The preheating time that results in deactivation of all the catalysts is shortened with increasing preheating temperature. This result is similar to the case of $Na_4P_2O_7 \cdot 10H_2O$.

It is seen from Fig. 4 that under the conditions of *Experiment 3,* in some of the 100 pieces of tubes each containing 8 g of 58.0 wt% CH_3CO_2Na aqueous solution and 0.16 g of Na_2HPO_4, $CH_3CO_2Na \cdot 3H_2O$ crystallized even after they had been preheated at 84 °C for 15 h and at 85 °C for 6 h. The percentages of the tubes with deactivated nucleation catalysts seem to approach constant values with increasing preheating time, though with a wide variation; the preheating at 84 or 85 °C corresponds to about 70 or 90%, respectively. Compared with Fig. 3, it is evident that deactivated nucleation catalysts may be reactivated by forced crystallization of $CH_3CO_2Na \cdot 3H_2O$ from solutions containing the crystal nucleation catalyst. The same phenomenon was observed in the case of CH_3CO_2Na aqueous solution with $Na_4P_2O_7 \cdot 10H_2O$ added.

In 20 pieces of tubes each containing 8 g of 58 wt% CH_3CO_2Na aqueous solution with 0.001, 0.01 or 0.04 g Na_2HPO_4 added, $CH_3CO_2Na \cdot 3H_2O$ hardly crystallized on cooling after the Na_2HPO_4 had been dissolved entirely in the CH_3CO_2Na solution by the preheating at 70 °C. It is understood from this experiment and the phase equilibria of ternary system CH_3CO_2Na–Na_2HPO_4–H_2O that the anhydrous Na_2HPO_4 solid in the solution is required for the crystallization of $CH_3CO_2Na \cdot 3H_2O$ to occur from the solution near the transition temperature. A similar conclusion was drawn in our preceding investigation using $Na_4P_2O_7 \cdot 10H_2O$ as crystal nucleation catalyst.

The results obtained from the present experiments will be discussed on the basis of the crystalline adsorption model proposed by Richards, which is illustrated in Fig. 1. According to this model, the Na_2HPO_4 added to a CH_3CO_2Na aqueous solution offers an adsorbent for which the heat of adsorption of crystalline $CH_3CO_2Na \cdot 3H_2O$ is higher than that of liquid adsorbate. From the phase equilibria of ternary system CH_3CO_2Na–Na_2HPO_4–H_2O the adsorbent is considered to be anhydrous Na_2HPO_4.

It is understood on the basis of the concept of adsorption that the melting temperature of crystalline $CH_3CO_2Na \cdot 3H_2O$ adsorbed on the adsorbent is raised with increasing CH_3CO_2Na concentration of the solution. Therefore, T_c is expected to be raised with increasing CH_3CO_2Na concentration. This expectation is compatible with the result shown in Fig. 2.

It is also plausible that the crystalline $CH_3CO_2Na \cdot 3H_2O$ adsorbate melts faster at higher temperatures than T_c. Therefore, the preheating time which results in complete catalyst deactivation is expected to be shortened with increasing preheating temperature. This expectation is also compatible with the result shown in Fig. 3.

According to the crystalline adsorption model a satisfactory, though qualitative, explanation has been given the reactivation of a deactivated nucleation catalyst which is effected by forced crystallization of $CH_3CO_2Na \cdot 3H_2O$ from the solution containing that nucleation catalyst; some quantitative explanation of these crystal nucleation catalytic actions remains to be given.

The authors wish to express their thanks to Dr. Ryoichi Kiriyama for his useful discussions and to Drs. Tsuneharu Nitta, Eiichi Hirota, and Masanari Mikoda for their continuous encouragements. They are also grateful to Dr. Ryoichi Yamanoto for his discussions throughout this work.

References

1) M. Telkes, "Solar Materials Science," ed by L. E. Murr, Academic Press, New York (1980), Chap. 11.
2) A. Pebler, *Thermochim. Acta,* **13**, 109 (1975).
3) F. de Winter, *Solar Energy,* **17**, 379 (1975).
4) T. Wada, F. Kimura, and Y. Matsuo, *Bull. Chem. Soc. Jpn.*, **56**, 3827 (1983).
5) M. Telkes, *Ind. Eng. Chem.*, **44**, 1308 (1952).
6) T. Wada and R. Yamamoto, *Bull. Chem. Soc. Jpn.*, **55**, 3603 (1982).
7) H. Kimura, *J. Jpn. Assoc. Cryst. Growth,* **9**, No. 3, 73 (1982).
8) T. Wada, F. Yokotani, and Y. Matsuo, *Bull. Chem. Soc. Jpn.*, in press.
9) T. Wada, K. Matsunaga, and Y. Matsuo, *Bull. Chem. Soc. Jpn.*, **57**, 557 (1984).
10) W. T. Richards, *J. Am. Chem. Soc.*, **54**, 478 (1932).

Kinetics of Ligand Substitution Reaction between Cyanide Ion and NiL_2 (L=4-(2-Pyridylazo)resorcinol, Diethylenetriamine, and Ethylenediamine)

Hari Chand BAJAJ, Madhu PHULL, and Prem Chandra NIGAM*

Department of Chemistry, Indian Institute of Technology, Kanpur-208016, U.P., India

(Received February 4, 1983)

The kinetics of substitution reaction of cyanide ion with some bis complexes $[NiL_2]^{2-2n}$, where L^{n-} is 4-(2-pyridylazo)resorcinolate, diethylenetriamine, or ethylenediamine, to form the square planar complex $[Ni(CN)_4]^{2-}$ has been studied spectrophotometrically in aqueous solutions. The rate expression has the form: rate $=\{k_d^{NiL_2}+k'[CN^-]\}[NiL_2^{2-2n}]$, where k' is a composite rate constant in case of par and dien and is equal to $k_{CN}^{NiL_2}$ in case of en. These results indicate that these bis complexes are not directly converted into $[Ni(CN)_4]^{2-}$ but first lose one ligand molecule and cyanide assists this loss. The backward reaction between $[Ni(CN)_4]^{2-}$ and L is first order in each reactant and inverse first order in cyanide. Though the mechanism for the reactions appears to be same, there are kinetic differences in the behaviour of en and the other two chelates. The rate determining step for the three reactions have been identified. The activation parameters for the forward reaction have been evaluated to support the proposed mechanism. The temperature dependence of backward reaction has also been given.

The mechanism of formation and dissociation reactions of some complexes of polyamines with nickel(II) has been investigated previously.[1-5] Ligand exchange reactions involving complexes of polyamines and nickel (II) with amine-*N*-acetic acids,[6] 2,2′-bipyridyl, 1,10-phenanthroline, and 2,2″,6′,2″-terpyridyl[7] have been studied extensively. A considerable work has been reported on the formation of $[Ni(CN)_4]^{2-}$ from nickel complexes of amine-*N*-acetic acids,[8] polyamines,[9] 1, 10-phenanthroline,[10] and from $Ni^{2+}_{(aq)}$.[11,12] Crouse and Margerum[13] have studied the reactions of $[Ni(CN)_4]^{2-}$ with various ligands in the presence and the absence of iodine as a scavanger for cyanide ion.

Previously we reported the formation of $[Ni(CN)_4]^{2-}$ from binuclear complexes Ni_2L, where L is ttha[14,15] and dtpa.[15] In the present paper, the kinetics of reactions of NiL_2^{2-2n} with CN^- is reported (Eq. 1).

$$NiL_2^{2-2n} + 4CN^- \underset{k_b}{\overset{k_f}{\rightleftharpoons}} [Ni(CN)_4]^{2-} + 2L^{n-} \quad (1)$$

where L^{n-} indicates 4-(2-pyridylazo)resorcinolate (par), diethylenetriamine (dien), or ethylenediamine (en), and k_f and k_b are the overall rate constants for forward and backward reactions.

Experimental

Diethylenetriamine, obtained from Eastman Kodak Co., (U.S.A.) and ethylenediamine (BDH) were purified by distillation at 45 °C under reduced pressure and stored in amber coloured bottles. The monosodium salt of par was obtained from Riedel (Germany) and was used after recrystallization. Sodium perchlorate (AR) was used to maintain ionic strength (I). All other chemicals used were of AR grade. Complex species $[Ni(dien)_2]^{2+}$, $[Ni(en)_2]^{2+}$, $[Ni(par)_2]^{2-2n}$, and $[Ni(CN)_4]^{2-}$ were prepared by mixing stoichiometric amounts of aqueous nickel(II) ion and ligand at appropriate pH. Sodium cyanide and nickel(II) perchlorate solutions were standardized as reported earlier.[8] A borate buffer was used wherever mentioned, otherwise sodium hydroxide and perchloric acid were used to maintain pH.

A stopped-flow spectrophotometer model SF-3A from Hitech, England and an ECIL storage oscilloscope model OS-7865 equipped with a Polaroid camera were used for measuring rates of rapid reactions. Details of apparatus used for the study of slow reactions and pH measurements were reported previously.[8]

Kinetic Measurements

The ligand exchange reactions of $[Ni(dien)_2]^{2+}$ and $[Ni(en)_2]^{2+}$ with cyanide ion were followed at 267 nm (λ_{max} of $[Ni(CN)_4]^{2-}$, $\varepsilon=1.16\times10^4$ dm^3 mol^{-1} cm^{-1}) or 285 nm ($\varepsilon=4.63\times10^3$ dm^3 mol^{-1} cm^{-1}) where the absorbances of the other species were negligible under the present conditions. The forward reactions were run in excess cyanide. The results gave pseudo first order plots, and the rate expression is given by

$$\frac{d[Ni(CN)_4]^{2-}}{dt} = k_{obsd}[NiL_m]_T,$$

where $[NiL_m]_T$ indicates the total concentration of nickel(II) complexes with L^{n-}, which contains mixed cyanide complexes of the type $NiL(CN)_x$. The forward and backward reactions in case of $Ni(par)_2$ were followed at 494 nm (λ_{max} of NiL_2, $\varepsilon=8.2\times10^4$ dm^3 mol^{-1} cm^{-1}) by monitoring disappearance or appearance of $Ni(par)_2$.

The absorbances of par and $[Ni(par)_2]$ remained constant for a pH range of 8—9.5. Considering the protonation constants $\log K_{H_2L}^{H_2L}=2.6$, $\log K_{H_2L}^{HL}=5.5$ and $\log K_{HL}^{H}=12.5$,[16] at higher pH the dominant species of par is the monoprotonated one. The absorption of par increases above pH 9.5 and hence all the reactions were studied at a pH of 9.0±0.1. The reaction of NiL complex with cyanide was also studied at 494 nm ($\varepsilon_{NiL}=3.63\times10^4$ dm^3 mol^{-1} cm^{-1}) by monitoring its disappearance. At the working pH, percentage of NiL was calculated[17] to be 80%.

For the study of reaction of $[Ni(CN)_4]^{2-}$ with par, solutions of par higher than 1.0×10^{-4} mol dm^{-3} could not be used because they do not obey Lambert-Beer law above this concentration. The reaction could not be followed at 267 or 285 nm (absorption maxima of $[Ni(CN)_4)^{2-}]$ because NiL_2 and par also absorb appreciably at these wave lengths ($\varepsilon_{NiL_2}=1.15\times10^4$ dm^3 mol^{-1} cm^{-1}, $\varepsilon_{par}=2.75\times10^3$ dm^3 mol^{-1} cm^{-1} at 267 nm).

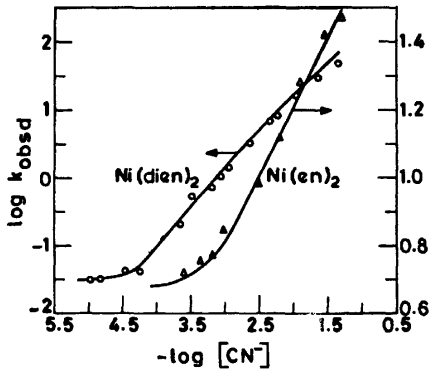

Fig. 1. Cyanide dependence of the observed forward rate constants in the reaction of $[Ni(dien)_2]^{2+}$ and $[Ni(en)_2]^{2+}$ with cyanide ion. pH 11.0, 25 °C and $I=0.1$ mol dm^{-3}.

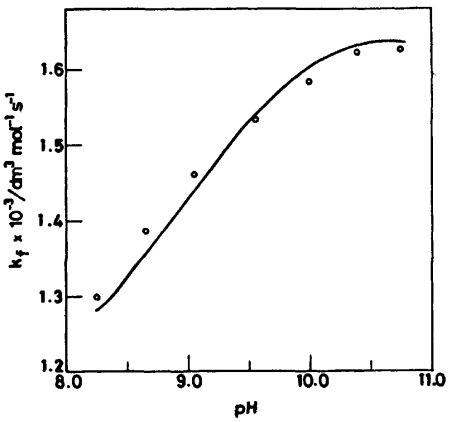

Fig. 2. Effect of pH on the reaction of $[Ni(dien)_2]^{2+}$ with cyanide at 25 °C and $I=0.1$ mol dm^{-3}.

Results

I. Reaction of $Ni(dien)_2$ with Cyanide. The rate of formation of $[Ni(CN)_4]^{2-}$ is first order each in $[Ni(dien)_2]^{2+}$ and CN^- at pH 11.0 where cyanide is present in large excess. The effect of cyanide can be seen in Fig. 1 where the slope of log k_{obsd} *vs.* log [CN$^-$] plot gives the order of reaction in cyanide. The order in cyanide varies from zero at low cyanide concentration to one at higher cyanide concentration. A similar observation was also reported by Coombs and Margerum[18] while studying the reaction of cyanide ion with bis complexes of nickel(II) with imino-*N*-diacetate (ida) and methylimino-*N*-diacetate (mida). The observed zero order dependence in cyanide indicates a slow dissociation step according to Eq. 3 followed by further reaction of NiL with cyanide to give $[Ni(CN)_4]^{2-}$

$$NiL_2 \xrightarrow{k_d^{NiL_2}} NiL + L. \qquad (3)$$

Thus k_{obsd} can be expressed by Eq. 4

$$k_{obsd} = k_d^{NiL_2} + k_3[CN^-]_T. \qquad (4)$$

The values of $k_d^{NiL_2}=3.85\times10^{-2}$ s^{-1} and $k_3=1.34\times10^3$ dm^3 mol^{-1} s^{-1} at 25 °C and $I=0.1$ mol dm^{-3} ($NaClO_4$).

Dependence of k_f on pH: The pH was varied from 8.2 to 11.0 and it was found that the reaction rate increases with an increase of pH and then levels at pH higher than 9.5 (Fig. 2). The difference in reactivities of CN^- and HCN can be resolved using Eq. 5.

$$k_f\frac{[CN]_T}{[CN^-]} = k_{CN} + k_{HCN}K_{HCN}[H^+], \qquad (5)$$

where

$$\frac{[CN]_T}{[CN^-]} = 1 + K_{HCN}[H^+],$$

and K_{HCN} is the protonation constant of cyanide ion (log $K_{HCN}=9.0$ at 25 °C and $I=0.1$). Thus a plot of left hand side of Eq. 5 *vs.* $[H^+]$ gives a straight line (Fig. 3). The values of k_{HCN} and k_{CN} are 1.25×10^3 and 1.65×10^3 dm^3 mol^{-1} s^{-1}, respectively.

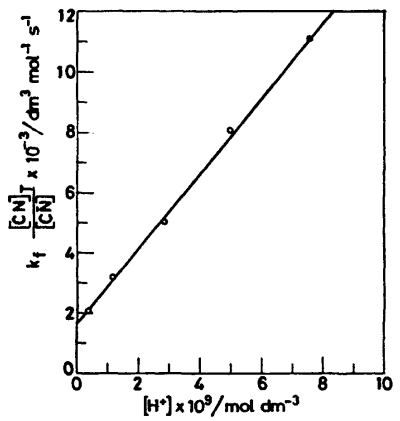

Fig. 3. Resolution of rate constants for the reaction of $[Ni(dien)_2]^{2+}$ with cyanide ion.

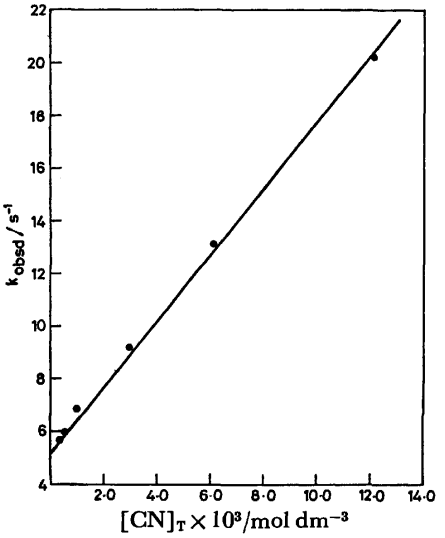

Fig. 4. Plot of k_{obsd} *vs.* $[CN]_T$ for the reaction of $[Ni(en)_2]^{2+}$ with cyanide ion.

II. Reaction of $[Ni(en)_2]^{2+}$ with Cyanide Ion. The rate of reaction of $[Ni(en)_2]^{2+}$ with cyanide is first order in $[Ni(en)_2]^{2+}$ and the rate increases with an increase in cyanide ion concentration (Fig. 1). The nature of dependence on cyanide concentration shows that the bis complex dissociates and the mono-complex formed reacts rapidly with CN^- through the formation of mixed ligand complexes finally giving

TABLE 1. KINETICS OF THE DECOMPOSITION OF $Ni(CN)_4^{2-}$ IN ITS REACTION WITH dien, en, AND par

A. dien: $[Ni(CN)_4^{2-}]_i = 2.6\times10^{-5}$ mol dm^{-3}, pH 11.0, I=0.1 mol dm^{-3}, 25 °C.

$[dien]_T$/mol dm^{-3}	$10^9\times k'_{obsd}$/mol dm^{-3} s^{-1}	$10^6\times k_b$/s^{-1}
1.45×10^{-3}	6.90	4.76
1.09×10^{-3}	5.28	4.84
0.73×10^{-3}	3.61	4.95

B. en: $[Ni(CN)_4^{2-}]_i = 1.65\times10^{-5}$ mol dm^{-3}, pH 10.5, I=0.5 mol dm^{-3}, 25 °C.

$[en]_T$/mol dm^{-3}	$10^5\times k'_{obsd}$/mol dm^{-3} s^{-1}	$10^4\times k_b$/s^{-1}
0.18	5.8	3.2
0.20	7.4	3.7
0.25	8.5	3.4
0.30	9.6	3.2

C. par: $[Ni(CN)_4^{2-}]_i = 4.0\times10^{-6}$ mol dm^{-3}, pH 9.0, I=0.15, 30 °C.

$[par]_T$/mol dm^{-3}	$10^{10}\times k'_{obsd}$/mol dm^{-3} s^{-1}	$10^6\times k_b$/s^{-1}
4.0×10^{-5}	3.45	8.62
6.0×10^{-5}	4.75	7.92
8.0×10^{-5}	6.48	8.10
10.0×10^{-5}	8.24	8.24

$[Ni(CN)_4]^{2-}$. In this case, if first order dependence in cyanide is assumed,

$$k_{obsd} = k_d^{NiL_2} + k'[CN^-]. \quad (6)$$

So a plot of k_{obsd} *vs.* $[CN^-]$ should be a straight line, which is found to be the case for $[CN^-]>10^{-3}$ mol dm^{-3} (Fig. 4). The values of $k_d^{NiL_2}$ and k' obtained from Fig. 4 are 5.1 s^{-1} and 1.3×10^3 dm^3 mol^{-1} s^{-1}, respectively. The value of $k_d^{NiL_2}$ for ethylenediamine is much larger than that for dien. This accounts for the slope being different from the expected value of one (Fig. 1).

Kinetics of Reactions of $[Ni(CN)_4]^{2-}$ with dien and en: The dissociation of $[Ni(CN)_4]^{2-}$ is greatly accelerated by the presence of polyamines in comparison to the much slower reaction of $[Ni(CN)_4]^{2-}$ with amine-*N*-acetic acids[8] or perchloric acid. The reaction is first order each in $[Ni(CN)_4]^{2-}$ and polyamine. A notable feature of these backward reactions is an inverse first order dependence in cyanide and the integrated rate expression has the form

$$(A_i - A_t) + A_i \ln\frac{A_t}{A_i} = -\frac{\varepsilon l}{4}k'_{obsd}t. \quad (7)$$

The terms used in Eq. 7 have their usual meaning as described earlier.[8] The values of $k'_{obsd}$and k_b are given in Table 1.

III. Reaction of $Ni(par)_2$ and $Ni(par)$ with Cyanide. The stability constant of $Ni(par)_2$ is fairly large (log β_2=22.2)[19] and a slow exchange reaction was observed for this system. As in the case of $[Ni(dien)_2]^{2+}$ and $[Ni(en)_2]^{2+}$, a cyanide free path was also observed at $[CN^-]$ less than 10^{-3} mol dm^{-3} (Fig. 5) which indicates the dissociation of bis complex in addition to the cyanide assisted dissociation of $Ni(par)_2$ and

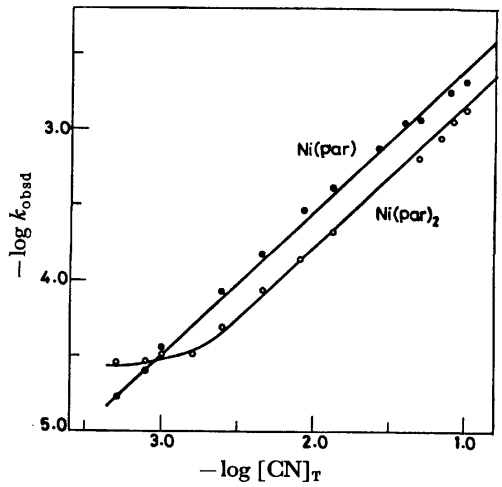

Fig. 5. Effect of cyanide ion concentration on the reaction of $[Ni(par)_2]^{2-}$ and [Ni(par)]. pH 9.0, 30 °C and I=0.15 mol dm^{-3}.

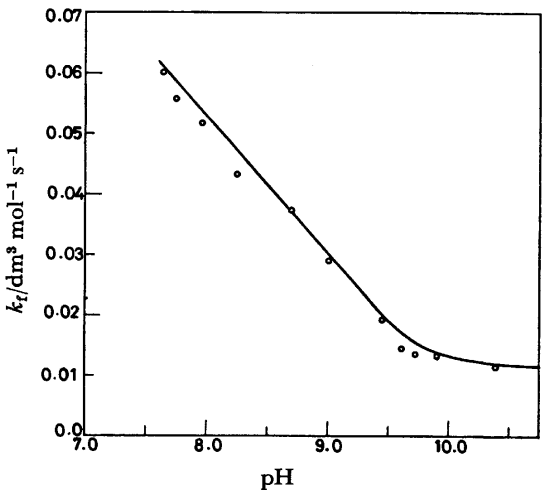

Fig. 6. Effect of hydrogen ion concentration on the reaction of [Ni(par)] with cyanide ion at 30 °C, and I=0.1 mol dm^{-3}.

formation of mixed ligand complexes of type Ni(par)$(CN)_x$ and finally $[Ni(CN)_4]^{2-}$.

The rate of the substitution reaction of monocomplex, [Ni(par)] was found to be first order with respect to cyanide over a wide range of cyanide concentration (Fig. 5). The rate constants are comparable with those of substitution reaction of the biscomplex (Fig. 5). This leads to a conclusion that the rate-determining step is the same in both reactions of Ni(par) and $(Ni(par)_2$ with cyanide ion.

Effect of pH on k_f: The rate of the forward reaction decreased with increase of pH (Fig. 6). This observation can be explained on the basis of labilities and structures[19] of the protonated forms of $Ni(par)_2$. It is also observed that reactions of Ni(par) and $Ni(par)_2$ with cyanide give similar rate constants on variation of pH.

A rate expression consistent with these observations is written below (Eq. 8).

$$k_{obsd} = k_f[CN]_T = \{k_{CN} + k_{HCN}K_{HCN}[H^+] + k'_{CN}K_{NiHL}^{NiL}[H^+] + k'_{HCN}K_{HCN}K_{NiHL}^{NiL}[H^+]^2\}[CN^-], \quad (8)$$

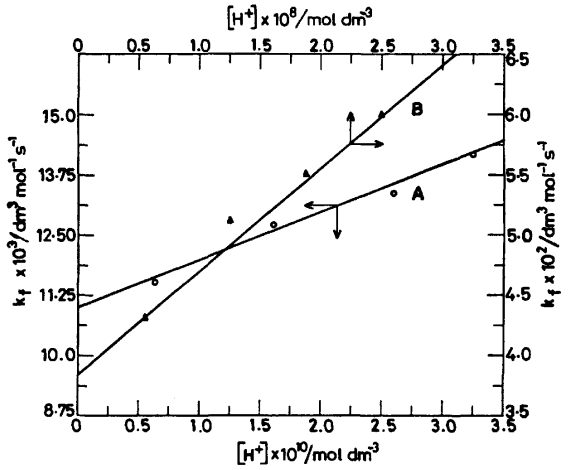

Fig. 7. Resolution of rate constants for the forward reaction of [Ni(par)] with cyanide ion.

where k_{CN} and k_{HCN} are the rate constants for the reaction of Ni(par) with CN^- and HCN while k'_{CN} and k'_{HCN} are rate constants for the reaction of Ni (Hpar) with CN^- and HCN respectively. K^{NiL}_{NiHL} is the protonation constant of Ni(par).

In high pH range, the terms containing protonated form of the complex can be neglected ($K^{NiHPar}_{NiPar}=10^{7.7}$ [20]) in 50% dioxane, the value in aqueous solution is not known). Considering $1 \gg K_{HCN}[H^+]$ at pH>9.5, Eq. 8 under assumption of $[CN]_T \approx [CN^-]$ is transformed to

$$k_f = k_{CN} + k_{HCN}K_{HCN}[H^+]. \quad (9)$$

The value of k_{CN} and k_{HCN} can be evaluated by plotting k_f *vs.* $[H^+]$ (Fig. 7), and are 1.11×10^{-2} and 1.01×10^{-2} $dm^3\ mol^{-1}\ s^{-1}$ respectively.

On the other hand, in lower pH range, the rate expression can be rearranged, assuming that $K_{HCN}[H^+] \gg 1$ and $[CN]_T \approx [HCN]$, to

$$k_f = k'_{CN}\frac{K^{NiL}_{NiHL}}{K_{HCN}[H^+]} + k'_{HCN}K^{NiL}_{NiHL}[H^+]. \quad (10)$$

A plot of k_f *vs.* $[H^+]$ gave a straight line (Fig. 7). The slope and intercept of this line give the values of product of k'_{HCN} and k'_{CN} with K^{NiL}_{NiHL}, and these are 8.36×10^5 and 3.90×10^7 $dm^3\ mol^{-1}\ s^{-1}$ respectively. The solid line in Fig. 6 shows the curve calculated from the various resolved rate constants.

IV. Kinetics of Reaction of $[Ni(CN)_4]^{2-}$ with par. The stability constant of tetracyanonickelate(II) is much greater than those of Ni(par) and $Ni(par)_2$ ($\log\beta_4=30.5$[12], $\log K_{Ni(par)}=17.8$, and $\log\beta_2=22.2$).[19] By using very dilute solution of $[Ni(CN)_4]^{2-}$ ($\approx10^{-6}$ mol dm^{-3}) and a moderately high concentration of par ($\approx10^{-4}$ mol dm^{-3}), it is possible to force the backward reaction. An excellent fit to the data was obtained by assuming a first order dependence in $[Ni(CN)_4]^{2-}$ and par and an inverse first order dependence in cyanide. The rate equation is formulated as given in Eq. 11, assuming that the change in absorbance of par during the course of reaction is negligible due to its high concentration compared to $[Ni(CN)_4]^{2-}$.

$$(A_t-A_0) + (A_\infty-A_0)\ln\frac{A_\infty-A_t}{A_\infty-A_0} = -\frac{\varepsilon l}{4}k'_{obsd}t, \quad (11)$$

where A_0 is the initial absorbance due to par, (A_t and A_∞ are the absorbances at time t and after completion of reaction, ε is the molar absorption coefficient of $Ni(par)_2$ and l is the light path length. Plots of left hand side of Eq. 11 *vs.* t, were linear (Fig. 8). From the plots, k'_{obsd} can be calculated and hence k_b ($k_b=k'_{obsd}/[par]_T$). The values are given in Table 1.

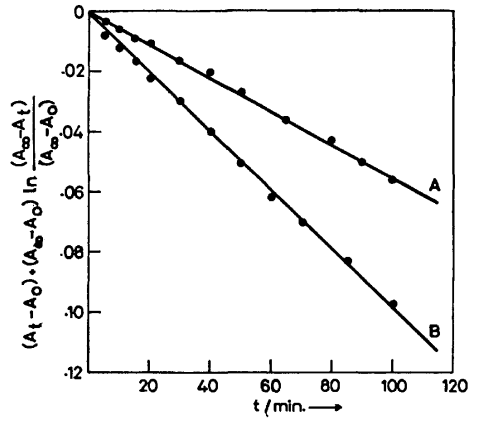

Fig. 8. Inverse first order plots for reaction of $[Ni(CN)_4]^{2-}$ with par at 30 °C, pH 9.0 and $I=0.15$ mol dm^{-3}, using Eq. 11. $[Ni(CN)_4]^{2-}=4\times10^{-6}$ mol dm^{-3}; (A) $[par]=6\times10^{-5}$ mol dm^{-3}, (B) $[par]=1\times10^{-4}$ mol dm^{-3}.

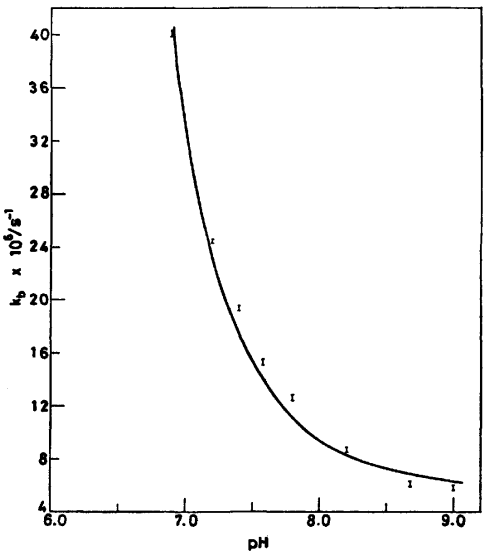

Fig. 9. Effect of pH on the backward reaction between $[Ni(CN)_4]^{2-}$ and par at 30 °C and $I=0.15$ mol dm^{-3}.

Effect of pH on the Reaction of $[Ni(CN)_4]^{2-}$ with par: The reaction was studied in the pH range 6.5—9.5 and the rate increased with decrease of pH (Fig. 9). $[Ni(CN)_4]^{2-}$ is known to be protonated only at pH below 5.0.[12] Therefore, the above behaviour can be explained on the basis of reactivities of the protonated forms of par *viz.* H_2par and Hpar. A rate law expressing the behaviour over the whole pH range investigated can be written as Eq. 12,

$$k_b\frac{[par]_T}{[par^{2-}]}\cdot\frac{1}{[H^+]} = k_{Hpar}K_{Hpar} + k_{H_2par}K_{H_2par}K_{Hpar}[H^+], \quad (12)$$

where

TABLE 2. TEMPERATURE DEPENDENCE OF FORWARD REACTION

A: Cyanide independent path, $k_d^{NiL_2}$. A′: Cyanide dependent path, k_3 or $k_{CN}^{NiL_2}$.

Temp/°C	$Ni(par)_2$–$CN^{a,a')}$		$Ni(dien)_2$–$CN^{b,b')}$		$Ni(en)_2$–$CN^{c')}$
	A $10^5\times k_d^{NiL_2}/s^{-1}$	A′ $10^2\times k_3/dm^3\ mol^{-1}\ s^{-1}$	A $10^2\times k_d^{NiL_2}/s^{-1}$	A′ $10^{-3}\times k_3/dm^3\ mol^{-1}\ s^{-1}$	A′ $10^{-3}\times k_{CN}^{NiL_2}/dm^3\ mol^{-1}\ s^{-1}$
25	—	—	3.57±0.07	1.30±0.03	1.52±0.05
30	3.02±0.07	1.30±0.03	6.96±0.10	2.10±0.04	2.10±0.04
35	4.78±0.03	1.78±0.06	9.67±0.06	2.70±0.05	2.65±0.03
40	7.48±0.05	2.41±0.04	17.62±0.12	3.40±0.05	3.55±0.05
45	11.50±0.06	3.25±0.05	—	—	—
E_a/kJ mol^{-1}	71.1	49	77.4	39.7	44.7
ΔS^*/K^{-1} J mol^{-1}	−106	−162	−25	−60.7	−79.4

a) $[CN^-]=8\times10^{-4}$ mol dm^{-3}; pH 10.0; $I=0.15$ mol dm^{-3}, a′) $[CN^-]=5\times10^{-2}$ mol dm^{-3}; pH, I same as in a. b) $[CN^-]=6\times10^{-5}$ mol dm^{-3}; pH 11.0; $I=0.1$ mol dm^{-3}, b′) $[CN^-]=2.2\times10^{-3}$ mol dm^{-3}; pH, I same as in b. c′) $[CN^-]=1.22\times10^{-2}$ mol dm^{-3}; pH 11.0, $I=0.1$ mol dm^{-3}.

TABLE 3. TEMPERATURE DEPENDENCE OF BACKWARD REACTION ($k_b=K_4^{-1}k_{-3}$)

Temp/°C	$[Ni(CN)_4]^{2-}$–par$^{a)}$ $10^5\times k_b/s^{-1}$	$[Ni(CN)_4]^{2-}$–dien$^{b)}$ $10^6\times k_b/s^{-1}$	$[Ni(CN)_4]^{2-}$–en$^{c)}$ $10^4\times k_b/s^{-1}$
25	—	4.76±0.05	3.20±0.03
30	0.83±0.01	8.05±0.07	5.03±0.04
35	1.32±0.02	13.1 ±0.04	7.96±0.07
40	2.06±0.04	21.6 ±0.06	12.29±0.05
45	3.18±0.03	—	—

a) $[Ni(CN)_4]^{2-}=4.6\times10^{-6}$ mol dm^{-3}; [par] $=1\times10^{-4}$ mol dm^{-3}; pH 9.0, $I=0.15$ mol dm^{-3}. b) $[Ni(CN)_4]^{2-}=2.6\times10^{-5}$ mol dm^{-3}; [dien] $=1.45\times10^{-3}$ mol dm^{-3}; pH 11.0; $I=0.1$ mol dm^{-3}. c) $[Ni(CN)_4]^{2-}=1.65\times10^{-5}$ mol dm^{-3}; [en] $=0.18$ mol dm^{-3}; pH 11.0; $I=0.1$ mol dm^{-3}.

$$\frac{[par]_T}{[par]^{2-}} = 1 + K_{Hpar}[H^+] + K_{H_2par}K_{Hpar}[H^+]^2 + K_{H_3par}K_{H_2par}K_{Hpar}[H^+]^3.$$

From plots of left-hand side of Eq. 12 *vs.* [H$^+$], k_{HL} and k_{H_2L} were calculated to be 6.35×10^{-10} s^{-1} and 3.98×10^{-8} s^{-1}, respectively. Using these values, k_b was calculated for the whole range of pH. A good agreement between the calculated curve and the experimental points (Fig. 9) justifies the assumptions made in deriving the above rate equation.

V. Effect of Temperature on All Three Reactions. The forward reactions were studied in temperature range 25—45 °C at two different cyanide concentrations *i.e.* where order with respect to cyanide is zero and one respectively. The rate constants obeyed the Arrhenius equation. The activation parameters were calculated and are given in Table 2. The high energy of activation at low [CN$^-$] (cyanide independent path) indicates rupture of metal–ligand bond accompanied by a less negative entropy change as compared to cyanide dependent path of high [CN$^-$]. The backward reaction rates ($k_b=K_4^{-1}k_{-3}$) for all the three reactions in this temperature range are given in Table 3. Although these are composite rate constants, they also obeyed the Arrhenius equation.

Discussion

A detailed study of forward and backward reaction (Eq. 1) reveals that the substitution of polydentate ligands in octahedral bis complexes of Ni(II) proceeds by an associative mechanism. A mechanism consistent with experimental observation can now be written (Eqs. 13—17).

$$NiL_2 \xrightarrow{k_d^{NiL_2}} NiL + L, \qquad (13)$$

$$NiL_2 + CN^- \underset{k_{-1}'}{\overset{k_1'}{\rightleftharpoons}} NiL(CN) + L \quad \text{fast}, \qquad (14)$$

$$NiL(CN) + CN^- \underset{}{\overset{K_2}{\rightleftharpoons}} NiL(CN)_2 \quad \text{fast}, \qquad (15)$$

$$NiL(CN)_2 + CN^- \underset{k_{-3}}{\overset{k_3}{\rightleftharpoons}} NiL(CN)_3 \quad \text{rds}, \qquad (16)$$

$$NiL(CN)_3 + CN^- \underset{}{\overset{K_4}{\rightleftharpoons}} Ni(CN)_4^{2-} + L \quad \text{fast}. \qquad (17)$$

The bis complexes do not convert directly to $[Ni(CN)_4]^{2-}$ but lose one of the ligands before the rate determining step (Eqs. 13 and 14), and mixed ligand complexes of type $NiL(CN)_x$ ($x=1$ or 2) are formed rapidly. Addition of third cyanide (Eq. 16) is rate determining.

The observed first order dependence in cyanide leads to a conclusion that either $k_{CN}^{NiL_2}$ or k_3 may be the slowest step. The average value of $k_{CN}^{NiL_2}$ ($=6.8\times10^4$ dm^3 mol^{-1} s^{-1}) obtained under the condition $[Ni(dien)_2^{2+}]>[CN^-]$ is higher than the observed value of k_3 ($=1.34\times10^3$ dm^3 mol^{-1} s^{-1}) at higher cyanide concentration (Tables 4 and 6) indicating that $k_{CN}^{NiL_2}$ is not the rate determing step for $[Ni(dien)_2]^{2+}$–CN$^-$ reaction system.

However, mono and bis complexes of nickel(II)

Table 4. Forward rate constants in presence of excess or comparable

$[Ni(dien)_2]^{2+}$ at 25 °C, pH 11.0 and $I=0.1$ mol dm^{-3}
$[Ni(dien)_2^{2+}]=3.6\times10^{-3}$ mol dm^{-3}

$[CN]_T$/mol dm^{-3}	$k_{CN}^{NiL_2}$/dm^3 mol^{-1} s^{-1}
3.55×10^{-3}	$(6.6\pm0.6)\times10^4$
3.33×10^{-3}	$(7.1\pm0.7)\times10^4$
1.06×10^{-4}	$(6.9\pm1.0)\times10^4$

Table 5. Effect of ionic strength on the observed pseudo first order rate constant for the reaction of $[Ni(en)_2]^{2+}$ with cyanide ion

$[Ni(en)_2]_T=9.2\times10^{-5}$ mol dm^{-3}, $[CN]_T=4.0\times10^{-3}$ mol dm^{-3}, pH 11.0, 25 °C.

$I(NaClO_4)$/mol dm^{-3}	k_{obsd}/s^{-1}
0.1	12.5
0.2	8.8
0.3	7.7
0.3	7.7
0.45	7.0

and par react with cyanide at similar rates (Fig. 6) under similar conditions. This fact suggests that the rate determining step may be same for both reactions. Based on our earlier studies on reactions of mono complexes[8] of nickel(II) with amine-*N*-acetic acids, this would in all probability be the addition of third cyanide. The observed inverse first order dependence in cyanide for the backward reaction further supports the supposition that the step shown in Eq. 16 is rate determining.

For quantitative conversion to $NiL(CN)_2$ which is the reactive species for forward reaction in presence of moderate or high concentration of cyanide, the stability of the same must be quite high. Values of K_1K_2 (or β_2) can be calculated from an expression derived by us earlier and given in Eq. 18.

$$K_1K_2=\frac{K_4^{-1}k_{-3}\beta_4}{k_3K_{NiL}}, \qquad (18)$$

where the symbols used have their usual meanings.[8] These values, given in Table 6, suggest that rapid conversion of NiL_2 to $NiL(CN)_2$ can be expected. For $[Ni(en)_2]^{2+}$ reaction with cyanide, the value of K_1K_2 ($=1.6\times10^{16}$) is many orders of magnitude higher than the maximum possible value ($=3\times10^{11}$)[12] estimated for $Ni(CN)_2\cdot4H_2O$.[12] The magnitude of stability constant of the ternary complex will be equal to or less than that of $Ni(en)_2\cdot4H_2O$.[12] The large difference in stabilities calculated for $Ni(en)(CN)_2$ shows that Eq. 18, which has been derived on the supposition that addition of third cyanide is rate determining, is not applicable in the case of ethylenediamine complex though it is applicable to $[Ni(dien)_2]^{2+}$ and $[Ni(par)_2]^{2-}$ reaction. It seems that $k_{CN}^{NiL_2}$ for $[Ni(en)_2]^{2+}$ system is smaller than k_3 and the addition of first cyanide is slower than the addition of third cyanide. The observation of a negative salt effect (Table 5) further supports this proposition. A similar conclusion was made earlier by Coombs and Margerum[18] for reactions of $[Ni(ida)_2]$ and $[Ni(mida)_2]$ with cyanide.

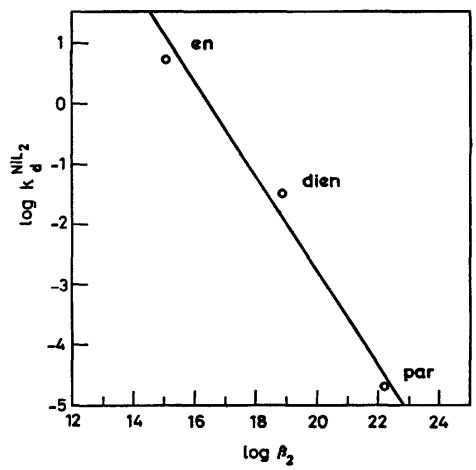

Fig. 10. A Linear Free Energy Relationship (LFER); a plot of $\log k_d^{NiL_2}$ *vs.* $\log\beta_2$.

The different kinetic behaviour of $[Ni(en)_2]^{2+}$ may be due to bidentate nature of ethylenediamine and presence of water molecules in cis positions.[21] Water molecules in cis position are known to be less labile than the ones in trans location.[22] The substitution of cis water by first cyanide is expected to be slower than the substitution, possibly of trans water, during the addition of third cyanide. In case of $[Ni(dien)_2]$ and $[Ni(par)_2]$, on the other hand, no water molecules are present due to tridentate ligands. The order of reactivity of bis complexes is reverse of the order of their stabilities. The dissociation rate constants $k_{CN}^{NiL_2}$ are also directly related to their overall stability constants β_2's. This free energy relationship is shown in

Table 6. Summary of the rate and equilibrium constants obtained at 25 °C and $I=0.1$ mol dm^{-3} ($NaClO_4$)

Constant	dien	en	par
K_{NiL}^{Ni}	5.0×10^{10}	4.0×10^7	6.3×10^{17}
$\beta_{NiL_2}^{Ni}$	7.94×10^{18}	1.26×10^{15}	1.58×10^{22}
$k_d^{NiL_2}$/s^{-1}	3.85×10^{-2}	5.1	1.86×10^{-5}
K_1K_2/dm^6 mol^{-2}	9.5×10^{10}	—	1.0×10^{11}
k_3/dm^3 mol^{-1} s^{-1}	$(1.34\pm0.2)\times10^3$	—	1.4×10^{-2}
k_{CN}/dm^3 mol^{-1} s^{-1}	1.65×10^3	—	1.11×10^{-2}
k_{HCN}/dm^3 mol^{-1} s^{-1}	1.25×10^3	—	1.01×10^{-2}
$k_{CN}^{NiL_2}$/dm^3 mol^{-1} s^{-1}	$(6.8\pm0.7)\times10^4$	$(1.3\pm0.2)\times10^3$	—
$K_4^{-1}k_{-3}$/s^{-1}	4.85×10^{-6}	3.38×10^{-4}	4.4×10^{-6}

Fig. 10. Table 6 summarises the various equilibrium and rate constant data obtained in this investigation.

One of the authors (Ms. M. Phull) is grateful to the University Grants Commission and a second (H.C. Bajaj) to the Council of Scientific and Industrial Research, for award of their respective fellowships by these bodies.

References

1) A. K. S. Ahmad and R. G. Wilkins, *J. Chem. Soc.*, **1959**, 3700; 2895, 2901 (1960).
2) G. A. Melson and R. G. Wilkins, *J. Chem. Soc.*, **1963**, 2662.
3) D. W. Margerum, D. B. Rorabacher, and J. F. G. Clarks, Jr., *Inorg. Chem.*, **2**, 66 (1963).
4) J. P. Jones and D. W. Margerum, *J. Am. Chem. Soc.*, **92**, 470 (1970).
5) R. G. Wilkins, *Acc. Chem. Res.*, **3**, 408 (1970).
6) H. C. Bajaj, K. Kumar, and P. C. Nigam, *Indian J. Chem.*, **20A**, 1070 (1981) and references contained therein.
7) M. S. Melvin, D. P. Rablen, and G. Gordon, *Inorg. Chem.*, **11**, 488 (1972).
8) K. Kumar and P. C. Nigam, *J. Phys. Chem.*, **84**, 140 (1980) and references contained therein.
9) G. B. Kolski and D. W. Margerum, *Inorg. Chem.*, **8**, 1125 (1969).
10) L. P. Morgenthaler and D. W. Margerum, *J. Am. Chem. Soc.*, **84**, 710 (1962).
11) H. Person and C. G. Ekstrom, *Acta Chem. Scand., Ser. A*, **30**, 31, 39 (1976).
12) G. B. Kolski and D. W. Margerum, *Inorg. Chem.*, **7**, 2239 (1968).
13) W. C. Crouse and D. W. Margerum, *Inorg. Chem.*, **13**, 1437 (1974).
14) K. Kumar and P. C. Nigam, *J. Phys. Chem.*, **84**, 1867 (1980).
15) K. Kumar, H. C. Bajaj, and P. C. Nigam, *J. Phys. Chem.*, **84**, 2351 (1980).
16) W. J. Geary, G. Nickless, and F. H. Pollard, *Anal. Chim. Acta*, **27**, 71 (1962).
17) D. D. Perrin and I. G. Sayce, *Talanta*, **14**, 833 (1967).
18) L. C. Coombs and D. W. Margerum, *Inorg. Chem.*, **9**, 1711 (1970).
19) H. Hoshina, T. Yotsuyanaji, and K. Aomhra, *Anal. Chim. Acta*, **83**, 317 (1976).
20) L. G. Sillen and A. E. Martell, "Stability Constants of Metal-Ion Complexes," Chem. Soc., Spcl. Publ. No. 25 (1971), Supp. I.
21) C. K. Jorgenson, *Acta Chem. Scand.*, **10**, 887 (1956).
22) M. A. Cobb and D. N. Hague, *J. Chem. Soc., Faraday Trans. 1*, **5**, 932 (1972).

The Catalytic Isomerization of Butenes over a Graphite Oxide

Susumu TSUCHIYA,* Masahiro MIKAMI, and Hayao IMAMURA
Department of Industrial Chemistry, Faculty of Engineering, Yamaguchi University, Ube, Yamaguchi 755
(Received June 10, 1983)

Synopsis. The relative rate constants and the activation energies of the isomerization of butenes over a graphite oxide have been measured, The reactivity of butenes and the selectivity ratios are in agreement with the characteristics of acid catalysts. The reaction profile shown on the triangular graph is of the rake-type.

Much attention has been paid to the characteristic properties of graphite oxide since Brodie first synthesized the compound.[1,2] Scarecely no study of its catalytic properties has, however, been reported so far. In this study, the isomerization of butenes, employed as a model reaction, has been investigated in order to explore its catalytic characteristics.

Experimental

Materials. The graphite oxide samples used as catalysts were prepared in a manner similar to that decribed previously.[3] The X-ray-diffraction data and the IR spectroscopic data of the sample formed agreed quite well with those reported by Alexanian.[4] The sample was dark brown.

The 1-butene, *cis*-, and *trans*-2-butene used as the reactans were obtained from the Tokyo Kasei Kogyo Co., Ltd.; their purity was confirmed by gas chromatography to be more than 99%. The nitrogen (99.99%) was obtained from the Seitetsu Kagaku Co., Ltd.

Procedure. A usual flow-type system with a by-pass at atmospheric pressure was employed to follow the reaction, nitrogen being used as the diluent. The graphite oxide, the catalyst, the BET surface area of which was 36 m^2/g, had been prepared beforehand; it was fixed in the system. The nitrogen stream with one of the butene isomers as a reactant was flowing only through the by-pass in the meantime; then it was diverted to flow through the reactor. The flowing rate of the nitrogen was *ca.* 15 cm^3/min, the amount of catalyst used being 0.39 g for each run. The [a butene isomer]/[nitrogen] ratio was 1/49. The reaction mixtures were analyzed by means of gas chromatography, with a column packing of 2,4-dimethylsulfolane on Uniport C. Before each run, the catalyst was evacuated at 353 K for 14 h. The experimental results were well reproducible.

Results and Discussion

The double-bond migration and the cis-trans isomerization of butenes took place over graphite oxide. The skeletal isomerization could not be observed. No gaseous hydrocarbon other than the butenes could be detected in the reaction mixtures under the present experimental conditions. The graphite does not show any catalytic activity for a reaction under the same experimental conditions. In the initial stage the activity of a fresh catalyst was very high (the per-pass conversion was 85% at 323 K), but it decreased with time on stream. After about 200 min, the conversion became steady-state (with a per-pass conversion of *ca.* 8% at 323 K). Since the steady state continued a rather long time, all the kinetic studies were carried out in this state.

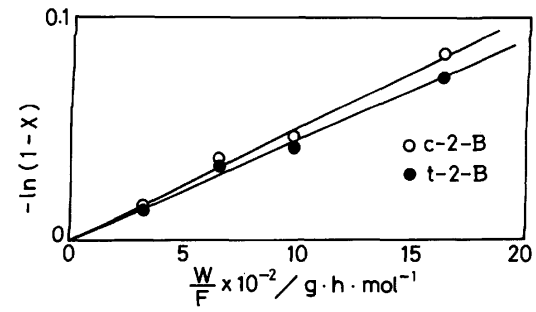

Fig. 1. First-order plots of isomerization of 1-butene over graphite oxide at 328 K.

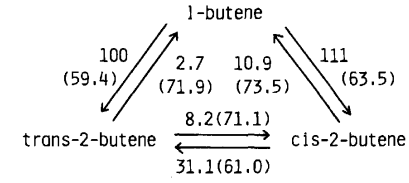

Fig. 2. Relative rate constants at 328 K and activation energies (kJ/mol) bracketed.

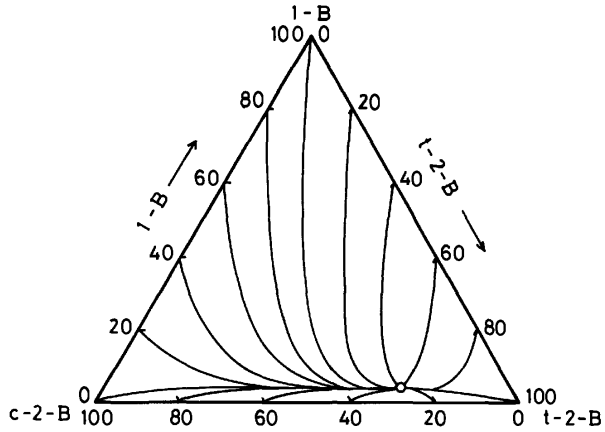

Fig. 3. Reaction profile of isomerization of butenes over graphite oxide at 328 K.

Figure 1 shows the first-order plots of the isomerization of 1-butene. From the rates of reaction and the selectivity ratios at different temperatures, all six of the relative rate constants and the activation energies of the reaction were determined in a manner similar to that described previously.[5] The results are shown in Fig. 2.

When the isomerization of butenes proceeds, the composition of the butenes in the gas phase may vary with the reaction time. The mol% of 1-butene, *cis*-, and *trans*-2-butene corresponding to the reaction time can be calculated from the relative rate constants, k_{ij}.[5-7] Figure 3 shows the reaction paths calculated at 328 K. The triangular graph thus represents one of the catalytic characteristics of graphite oxide for the isomerization of butenes. The time variable, t, is eliminated in

the graph. When the reactants initially contain much more 1-butene than *cis*- or *trans*-2-butene, the curves corresponding to the reaction paths go downwards in an almost straight manner. This profile may be named the "rake-type," which is entirely different from that obtained in the isomerization over KC_8.[5]

Graphite oxide is often called graphitic acid because of its acid character.[10] The acid properties are caused by the acid-hydroxyl groups between the graphite layers, which can be observed by IR spectroscopy. The active sites of graphite oxide for the isomerization of butenes may therefore, have acid properties.

The following mechanisms for the isomerization of butenes have been proposed for different catalytic systems:[6] (1) a hydride-addition mechanism for metals, (2) a carbenium-ion mechanism for acid catalysts, and (3) an allylic mechanism for basic catalysts. When the isomerization takes place with a carbenium-ion mechanism, (1) the order of the relative rate constants of the isomerization is 1-butene>*cis*-2-butene>*trans*-2-butene, and (2) the selectivity ratio, *cis*/*trans*, is about unity, while 1/*cis*-2- and 1/*trans*-2- are less than 3.0, usually less than 1.0.[8-9] The reactivity of butenes as well as the selectivity ratios obtained in the present study are in agreement with a carbenium-ion mechanism for acid catalysts.

A large pulse of 1-butene (50 ml) was introduced into the flow system, where only carrier gas was flowing. The effluent stream was monitored by means of gas chromatography. The graphite-oxide catalyst (0.45 g) employed was at the steady state, as has been mentioned above. The flowing rate of the carrier gas was 8.6 cm^3/min. A large peak with tailing was observed, as is shown in the upper part in Fig. 4; the abscissa is the effluent time. The tailing continued more than 1 h. Since the active sites of graphite oxide may be the hydroxyl groups between the graphite layers, the reactant molecules must get into the space between the graphite layers and chemisorb on the sites for isomerization. The product admolecules then desorb from the sites and crawl out of the layer space. The tailing may correspond to the crawling-out-process.

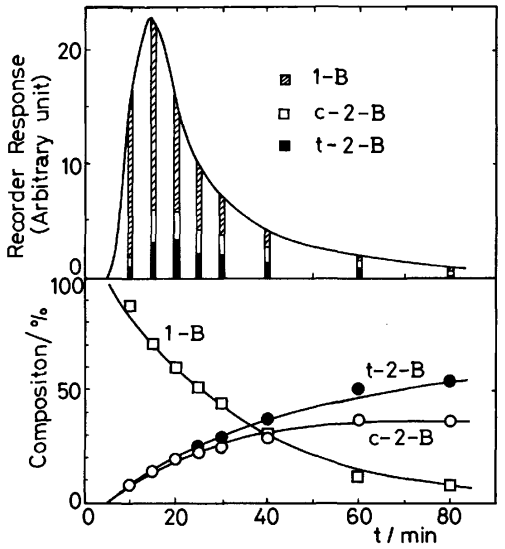

Fig. 4. Effluent peak and composition.
1-Butene (50 ml) was introduced over graphite oxide (0.45 g) at 298 K. Flowing rate of carrier gas was 8.6 cm^3/min.

The composition of the effluent gas was analyzed by means of gas chromatography. The analytical samples were taken out from the effluent at suitable time intervals. The results are shown in Fig. 4; the amounts of the individual butene isomers are shown in the upper part, while the compositions are shown in the lower part. In this case, the reaction time, the contact time, may correspond to the effluent time. The solid lines in the lower part represent the curves calculated from the relative first-order rate constants and the activation energies, the reaction time being assumed to be the effluent time. The points which represent the compositions experimentally obtained fall on the solid lines quite well. These results also support the idea that the isomerization reaction takes place between the graphite layers and proceeds by means of first-order kinetics.

It is, accordingly, concluded that the graphite oxide is a solid-acid catalyst and that it shows the rake-type profile for the isometization of butenes, which takes place between the graphite layers.

This work was supported by a Grant-in-Aid for Scientific Research from the Ministry of Education, Science and Culture, to which the authers' thanks are due.

References

1) B. C. Brodie, *Phil. Trans. R. Soc. London*, **149**, 249 (1859).
2) B. C. Brodie, *Ann. Chim. Phys.*, **45**, 351 (1986).
3) W. S. Hummers, Jr., and R. E. Offeman, *J. Am. Chem. Soc.*, **80**, 1339 (1958).
4) C. Alexanian, *J. Chim. Phys.*, **58**, 133 (1961).
5) S. Tsuchiya, T. Misumi, N. Ohuye, and H. Imamura, *Bull. Chem. Soc. Jpn.*, **55**, 3089 (1982).
6) J. Wei and C. D. Prater, "Adv. Catal.," ed by D. D. Eley, P. W. Selwood, and P. B. Weisz, Academic Press, New York (1962), Vol. 13, p. 203.
7) W. O. Haag and H. Pines, *J. Am. Chem. Soc.*, **82**, 387, 2488 (1960).
8) J. Goldwasser and W. K. Hall, *J. Catal.*, **71**, 53 (1981).
9) H. Hattori, N. Yoshii, and K. Tanabe, *Proc. 5th Int. Congr. Catal. (Miami)*, **10**, 233 (1973).
10) H. P. Boehm, A. Clauss, and U. Hofmann, *J. Chim. Phys.*, **58**, 141 (1961).

Linear Dependence of ODMR Transition Frequency on $T_1 \rightarrow S_0$ Transition Energy. *p*-Dichlorobenzene in Various Matrices

Noriko IWASAKI and Minoru KINOSHITA*

The Institute for Solid State Physics, The University of Tokyo, Roppongi, Minato-ku, Tokyo 106

(Received June 29, 1983)

Synopsis. The linear dependence of ODMR transition frequency on the $T_1 \rightarrow S_0$ transition energy of *p*-dichlorobenzene in various matrices was interpreted with the spin-orbit couplings of the lowest triplet state with the triplet and singlet manifold, by assuming that the matrix dependent shifts in the triplet and singlet state energy are correlated with each other.

Lemaistre and Zewail have explained the origin of the difference in the linewidth between ODMR (optically detected magnetic resonance) and optical transitions, by considering selective spin-orbit coupling (SOC) between singlet and triplet states.[1-3] Their theory has also provided an explanation for the linear dependence of the ODMR transition frequency on the optical transition energy in a system where the ODMR and optical transitions show inhomogeneous broadening.[4] On the other hand, Egmond *et al.* have explained the linear relation of these two transitions by the interaction between triplet states.[5]

Recently we have found a linear correlation between the ODMR transition and the $T_1 \rightarrow S_0$ transition energy of *p*-dichlorobenzene (*p*-DCB) in various matrices,[6] but the origin for the correlation has not yet been clarified. In this note, we apply their methods to the systems of *p*-DCB in various matrices, and show that the SOC with a higher triplet and a singlet state can provide a possible explanation for the correlation between the ODMR transition frequency and the $T_1 \rightarrow S_0$ transition energy rather than the vibronic coupling between triplet states.

At first we apply Zewail's method to a compound which has different electronic energies in various matrices. We assume that the contribution of the solvent to the spin-orbit matrix element is very small, and only the difference of the electronic energies between a perturbing state and the T_1 state has an influence on the ODMR transition energy. We neglect the inhomogeneous broadening in a matrix. The full widths at half maxima (fwhm) of the 0,0 bands of the phosphorescence spectra of *p*-DCB in the matrices are 3—4 cm^{-1} except for fwhm of 20 cm^{-1} in benzene. Therefore, the inhomogeneous broadening effect in the $T_1 \rightarrow S_0$ and ODMR transitions discussed by them is rather small in the case of *p*-DCB and may be neglected compared to the variation of the transition energies with matrix. We thus consider, instead of inhomogeneous broadening, the matrix dependence of the electronic and ODMR transition energies in terms of their method. The electronic energy shifts of the singlet and triplet excited states in various matrices may be written as

$$E^r = E_0^r + \delta_M^r, \tag{1}$$

where r denotes the singlet (S) or the triplel (T) state, E_0^r is the electronic energy of the molecule in a certain standard matrix (M_0) and δ_M^r denotes the energy shift of the molecule in a matrix (M) from E_0^r. We assume that only one magnetic sublevel (say T_y) of its lowest triplet state effectively couples with a particular singlet state through SOC (mechanism 1). According to their method,[2] the total energy for each sublevel is given by

$$E_z^T = E_0^T + Z + \delta_M^T, \tag{2-a}$$

$$E_y^T = E_0^T + Y + \delta_M^T - |\tau^y|^2/[(E_0^S + \delta_M^S) - (E_T^0 + \delta_M^T + Y)], \tag{2-b}$$

$$E_x^T = E_0^T + X + \delta_M^T, \tag{2-c}$$

where X, Y, and Z denote the zero-order energies of the sublevels of the triplet state in zero-magnetic field and τ^y is the SOC matrix element between the perturbing singlet state and the T_y sublevel. The sublevel order of *p*-DCB is $T_y > T_z > T_x$ in energy. The shift of the ODMR transition frequency between the spin-orbitally active magnetic sublevel (T_y) and the inactive sublevel (T_x) is

$$\Delta\hbar\omega_{yx} = -|\tau^y|^2/(\Delta_{ST} - Y + \delta_M^S - \delta_M^T), \tag{3}$$

where $\Delta_{ST} = E_0^S - E_0^T$ is the singlet and triplet energy separation of the molecule in the standard matrix (M_0). Since $\Delta_{ST} \gg Y$, $(\Delta_{ST} - Y) \sim \Delta_{ST}$. In the case of *p*-DCB, the magnitude of Δ_{ST} is larger at least by a factor of about 10^2 than δ_M^T. Although we have not measured δ_M^S, δ_M^S is expected to be comparable with δ_M^T. Therefore, we may expand the denominator in Eq. 3 as

$$\Delta\hbar\omega_{yx} = |\tau^y|^2(\delta_M^S - \delta_M^T)/(\Delta_{ST})^2, \tag{4}$$

where we have omitted the term $-|\tau^y|^2/\Delta_{ST}$ which does not depend on matrices. Assuming that the energy shifts of the singlet and triplet states are correlated as $\delta_M^S = \alpha\delta_M^T$, we obtain

$$\Delta\hbar\omega_{yx} = |\tau^y|^2(\alpha - 1)\delta_M^T/(\Delta_{ST})^2. \tag{5}$$

Equation 5 shows that the ODMR microwave transition frequency depends linearly on the energy shift of the 0,0 band in the phosphorescence spectrum except for the case of $\alpha = 1$. In the case of $\alpha > 1$, *i.e.*, the shift of the singlet energy being larger than that of triplet one, the slope of a plot of $\Delta\hbar\omega_{yx}$ *vs.* δ_M^T becomes positive.

Next we consider the SOC between triplet states (mechanism 2). We assume the two magnetic sublevels (say T_z and T_x) effectively couple with each other. The shifts of the ODMR microwave transitions are given by

$$\Delta\hbar\omega_{zx} = 2|\tau_{j1}^{xz}|^2\varepsilon(\alpha - 1)\delta_M^1/(\Delta_{j1})^3, \tag{6}$$

$$\Delta\hbar\omega_{yx} = -|\tau_{j1}^{xz}|^2(\alpha - 1)\delta_M^1/(\Delta_{j1})^2, \tag{7}$$

where $\varepsilon = (Z_j - X_j) + (Z_1 - X_1)$ is the sum of the $T_z - T_x$ transition energies of the interacting triplet states, and $\alpha\delta_M^1 = \delta_M^1$. Note the negative sign of Eq. 7, which is opposite to Eq. 5.

Finally, we consider an interaction with a higher triplet state, T_j. If V is the operator for the perturbation which does not include spin, for example, one for the vibronic coupling or one for the solvent field perturbation (mechanism 3),[5] the perturbation matrix elemenls are given by

$$<T_i\tau_r|V|T_j\tau_s> = V_{ij}\delta_{rs}. \quad (8)$$

The shift of the energy of the T_{1x} state becomes

$$\Delta E_{1x} = -|V_{j1}|^2/(E_0^j + X_j - E_0^1 - X_1), \quad (9)$$

where the super- or subscripts 1 and j denote the lowest and j-th triplet states, respectively. The shift of the ODMR microwave transition frequency between two sublevels (say, T_z and T_x) is

$$\Delta\hbar\omega_{zx} = -|V_{j1}|^2\varepsilon'/(\Delta_{j1})^2, \quad (10)$$

where $\Delta_{j1}=E_0^j-E_0^1$ is the energy separation of two triplet states, and $\varepsilon'=(Z_j-X_j)-(Z_1-X_1)$ is the energy difference between the $T_z - T_x$ transitions in the lowest and j-th triplet states. We have used the relation $\Delta_{j1} \gg Z_1$, X_1, Z_j, and X_j. Using the equation for the shift of the phosphorescence S,

$$S = -|V_{j1}|^2/\Delta_{j1}, \quad (11)$$

we obtain

$$\Delta\hbar\omega_{zx} = \varepsilon' S/\Delta_{j1}. \quad (12)$$

It may be noted in this case that the perturbation which shifts the phosphorescence origin is the same as that on the ZFS parameters.

The ODMR transition energies are plotted against the $T_1 \rightarrow S_0$ transition energies in various matrices[6,7] in Fig. 1. Only the $T_1 \rightarrow S_0$ transition energy in p-xylene is deviated far apart from that in the other matrices. The ODMR transitions related to the T_y sublevel show the wavelength dependence, while the $T_z - T_x$ transition does not. The slopes of the lines for the $T_y - T_x$ and $T_y - T_z$ transitions are found to be 2.7×10^{-5}, and 3.1×10^{-5}, respectively.

Mechanism 3 can provide an explanation for the linear dependence of the $T_y - T_x$ and $T_y - T_z$ transitions, but is not to give the explanation for the $T_z - T_x$ transition. Independence of the microwave transition from the $T_1 \rightarrow S_0$ transition energy means $\varepsilon'=0$. This may not be acceptable, since we can not expect the same microwave transition energy in different electronic states.

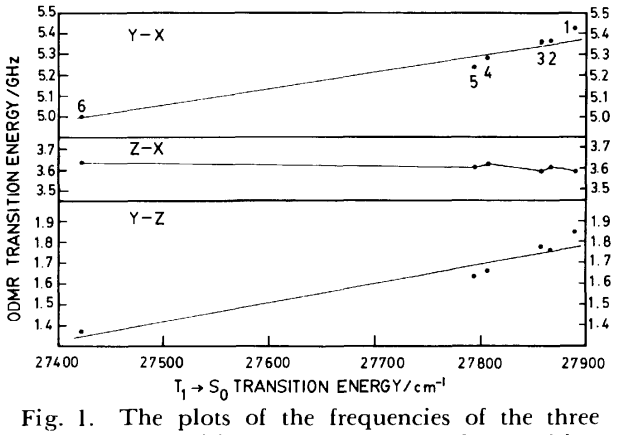

Fig. 1. The plots of the frequencies of the three sublevel transitions *versus* the $T_1 \rightarrow S_0$ transition energy of p-dichlorobenzene in various matrices: 1; in p-dichlorobenzene-d_4, 2; trap 1 in the neat crystal, 3; in p-dibromobenzene, 4; trap 2 in the neat crystal, 5; in benzene, 6; in p-xylene.

We apply mechanism 1 to the system of p-DCB. The triplet state ($^3B_{1u}$) of p-DCB directly couples with the singlet state ($^1B_{3u}$) through the top sublevel, T_y by SOC. This mechanism expects the linear dependence of the $T_y - T_x$ and $T_y - T_z$ transition energies on the $T_1 \rightarrow S_0$ transition energy, and independence of the $T_z - T_x$ transition. This is just the case we have observed in p-DCB. If we assume $\alpha - 1 \sim 1$ and $\tau^y = 63\,cm^{-1}$ for p-DCB, the latter being the value for 1,2,4,5-tetrachlorobenzene,[8] we get $\Delta_{ST} \approx 10^4\,cm^{-1}$. This value seems to be plausible.

The T_z and T_x sublevels of the lowest triplet state of p-DCB couple with the $^3B_{3u}$ by SOC, and mechanism 2 would also explain the experimental results. The shift of the $T_x - T_z$ transition is smaller by a factor of $\varepsilon/\Delta_{j1} \approx 10^{-5} - 10^{-6}$ than that of the other two transitions, as shown in Eqs. 6 and 7. The slope is opposite to the case of mechanism 1.

The magnitude of τ, α, and Δ determines which mechanism, 1 or 2, is dominant. As both α and τ are expected to be comparable for the triplet and singlet B_{3u} states and may be used commonly, the shift of the microwave transition may be written as

$$\Delta\hbar\omega_{yx} = |\tau|^2(\alpha-1)\delta\left(\frac{1}{(\Delta_{ST})^2} - \frac{1}{(\Delta_{j1})^2}\right). \quad (13)$$

Since Δ_{j1} is smaller than Δ_{ST}, the second term in Eq. 13 surpasses the first term. The slopes of microwave transitions are found to be positive, and we expect $\alpha < 1$ in p-DCB. We have neglected completely the spin-distribution change in the triplet state with varying matrices. Especially, the values in p-xylene are very far away from those in the other systems. Therefore, we might have to consider the spin-distribution change of p-DCB in p-xylene. However, the linear dependence of the ODMR microwave transition energy on the $T_1 \rightarrow S_0$ transition energy is well explained by the mechanisms 1 and 2, namely by the SOC's with the triplet and singlet manifolds, with an assumption that the matrix dependent shifts in the triplet and singlet energy are correlated with each other.

Since Δ_{j1} is smaller than Δ_{ST}, the second term in Eq. 13

We are greatly thankful for the referee's important suggestion.

References

1) A. H. Zewail, *J. Chem. Phys.*, **70**, 5759 (1979).
2) J. P. Lemaistre and A. H. Zewail, *Chem. Phys. Lett.*, **68**, 296 (1979).
3) J. P. Lemaistre and A. H. Zewail, *Chem. Phys. Lett.*, **68**, 302 (1979).
4) J. U. von Schütz, J. Zuclich, and A. H. Maki, *J. Am. Chem. Soc.*, **96**, 714 (1974).
5) J. van Egmond, B. E. Kohler, and I. Y. Chan, *Chem. Phys. Lett.*, **34**, 423 (1975).
6) M. Kinoshita, N. Goto, and N. Iwasaki, *Bull. Chem. Soc. Jpn.*, **56**, 2591 (1983).
7) M. J. Buckley and C. B. Harris, *J. Chem. Phys.*, **56**, 137 (1972).
8) J. P. Lemaistre and A. H. Zewail, *J. Chem. Phys.*, **72**, 1055 (1980).

Kinetic Studies of the Polyiodide Complex Formation in the Iodine-Iodide Solutions

Takayuki SANO, Hiroka HORI, Masako YAMAMOTO,† and Tatsuya YASUNAGA*
Department of Chemistry, Faculty of Science, Hiroshima University, Hiroshima 730
†Department of Home Economics, Hiroshima Women's University, Hiroshima 734
(Received July 4, 1983)

Synopsis. A relaxation obviously different from that due to the triiodide complex formation was observed by the temperature-jump experiments in the iodine-iodide solution. On the basis of the dependences of the relaxation time on the concentration of iodine and iodide and on the temperature, the relaxation was assigned to the complex formation of I_6^{2-}. The rate constants of the reaction were estimated to be 2.2×10^5 M^{-1} ††s^{-1} and 5.3×10^5 s^{-1} for forward and backward processes, respectively.

The iodine-iodide system has been subjected to extensive studies[1-4] in connection with not only the electron-transfer reaction but also the well known "blue starch-iodine" reaction. However the reactions proceeding in this system are complicated depending on the conditions of solution and their mechanisms are still obscure. In the course of our temperature-jump experiments in the cyclodextrin, iodine, and iodide system as a model system of the amylose-iodine solution, we observed a relaxation at micro second region in the iodine-iodide solution. The behavior of the relaxation phenomenon was obviously different from those reported for the hydrolysis of iodine[5] and the triiodide formation reaction.[6] This fact motivated us to clarify the origin of the observed relaxation in the iodine-iodide solution prior to the kinetic investigations on the cyclodextrin-iodide interaction.

In this paper, the observed relaxation will be discussed on the basis of the complex formation reactions proposed for the iodine-iodide system by the spectrophotometric experiments.

Experimental

The kinetic measurements were performed with a Joule heating temperature-jump apparatus equipped with a coaxial cable as a capacitor. Temperature jumps of about 2 °C was attained within 0.7 μs by matching the impedance of sample cell to that of coaxial cable. The temperature of sample solution in the cell was controlled to ±0.5 °C by circulating water from an external thermostat. In order to prevent cavitation by the intense electric current, the sample cell was maintained at constant pressure of 7 atm with nitrogen gas. The details of the apparatus has been described elsewhere.[7] To obtain a rectangular current pulse the ionic strength of solution was adjusted to be 0.023 M by an addition of KI for almost all experiments and of KCl in the case of the experiments changing the iodide concentration. The standardized thiosulfate was used for the determination of the iodine concentration. All chemicals were of reagent grade and used as be received.

Results and Discussion

A typical relaxation curve observed at 500 nm which corresponds to the absorption band of iodine is shown in Fig. 1. The relaxation curve could be analyzed as two relaxations; one has a much faster relaxation time than the resolution time (0.7 μs) of the present apparatus (fast relaxation), and the other has a relaxation time around 2 μs (slow relaxation). The directions of the both relaxation signals indicate the decrease of transmittance. Meanwhile, the relaxation curve observed at 350 nm which is absorption band of triiodide also consists of two relaxations in accordance

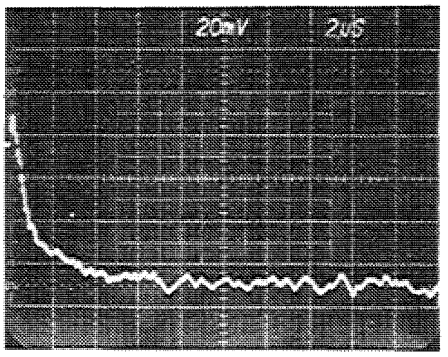

Fig. 1. Typical relaxation curve for the solution of 2.3×10^{-2}M potassium iodide and 5.0×10^{-2}M iodine at 25 °C; sweep=2 μs/division, and λ=500 nm.

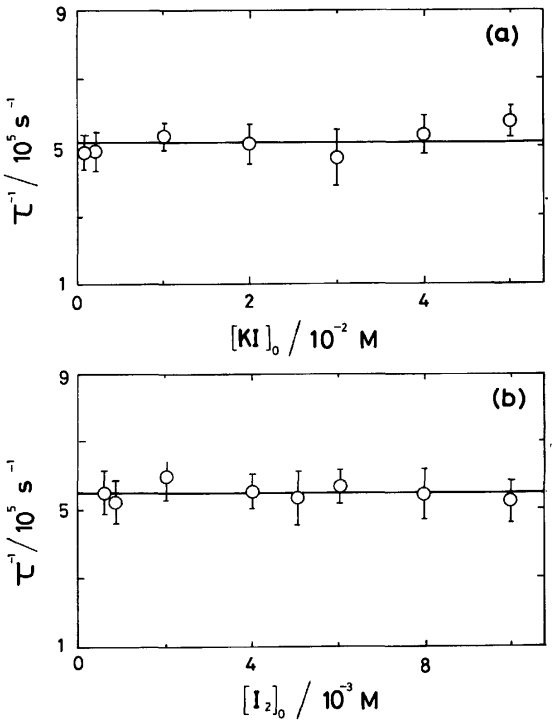

Fig. 2. Dependence of the reciprocal relaxation time on the iodide concentration at constant $[I_2]$ of 5.0×10^{-3}M (a) and on the iodine concentration at constant [KI] of 2.3×10^{-2}M (b) at 25 °C.

†† $1\ M^{-1}=1\ dm^3\ mol^{-1}$.

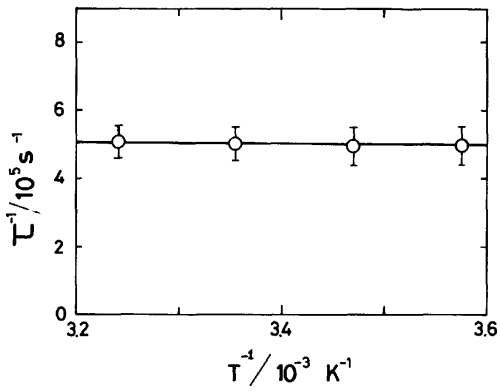

Fig. 3. Dependence of the reciprocal relaxation time on the temperature in the solution of 2.3×10^{-2}M potassium iodide and 4.0×10^{-3}M iodine.

with those observed at 500 nm; the relaxation time as well as the direction of the relaxation signal of the slow process is the same as that obtained from the experiments at 500 nm but the direction of the fast relaxation signal is opposite to that observed at 500 nm. The slow relaxation was examined quantitatively in the present study. The concentration dependence of the reciprocal relaxation time is shown in Fig. 2. The relaxation time is obviously independent of both iodine and iodide concentrations. Further, the relaxation time is insensitive to temperature as can be seen in Fig. 3.

In the system of iodine and iodide, following complex formation have been proposed from the spectrophotometric experiments.[1-6]

$$I^- + I_2 \rightleftharpoons I_3^- \quad (1)$$

$$I^- + I_3^- \rightleftharpoons I_4^{2-} \quad (2)$$

$$I_2 + I_3^- \rightleftharpoons I_5^- \quad (3)$$

$$2\,I_3^- \rightleftharpoons I_6^{2-} \quad (4)$$

Among these four reactions, the triiodide complex formation of Reaction 1 is most well known, and has been studied kinetically by several kinds of methods.[2,4,6] According to these studies, the relaxation due to this reaction is much faster than the resolution time of the present apparatus. In practice, the rapid increase of iodine and decrease of triiodie within 0.7 μs were observed at 550 and 350 nm, respectively, which indicates Reaction 1 is responsible for the fast process. Reaction 2 occurs predominantly at considerably high ionic strength of 2.0 M,[4] and then can be discared in the present system of low ionic strength (I=0.023 M). Reaction 3 is also eliminated from the possible origin of the relaxation because of the positive value of the enthalpy change reported for Reaction 3[3] ($\Delta H_3 \simeq 12$ kcal/mol) resulting in the decrease of iodine concentration with the temperature rise. Finally, Reaction 4 is remained as a plausible mechanism. The relaxation time for the Reaction 4 which is coupled with the fast reaction of triiodide complex formation, can be written as

$$\tau^{-1} = k_{-4}\left\{1+\frac{4K_1K_4(I_2+I^-)I_3^-}{1+K_1(I_2+I^-)}\right\}. \quad (5)$$

In this equation, the second term which can be calculated by using the values of K_1=732 M^{-1} [3] and K_4= 0.42 M^{-1} [1] is far smaller than unity. Thus, Eq. (5) can be transformed to

$$\tau^{-1} = k_{-4}. \quad (6)$$

Firstly, this equation implies that the relaxation time is independent of the concentration of any reaction species, satisfying the present experimental results in Fig. 2. Secondly, the insensitive temperature dependence of the relaxation time in Fig. 3 is consistent with the small and negative value of the enthalpy change (ΔH_4 = −0.77 kcal/mol)[1] for Reaction 4.[8] Thirdly, the increase of both iodine and triiodide concentrations during the relaxation is also consistent with the negative value of ΔH_4. These facts finally enable us to assign the observed relaxation to Reaction 4, and an application of Eq. (6) to the present data gives the values of k_4 and k_{-4} to be 2.2×10^5 M^{-1} s^{-1} and 5.3×10^5 s^{-1} respectively. The obviously small value of binding rate constant k_4 compared with that of the diffusion controlled process suggests the existence of further elementary steps in Reaction 4, but the detailed discussion on the elementary process can not be advanced at the moment.

In conclusion, the relaxation phenomenon observed in the iodine-iodide solutions was assigned to the polyiodide complex formation of I_6^{2-} among the several kinds of complex formations proposed from the spectrophotometric studies. The kinetic studies of the interaction between cyclodextrin and iodide will be reported in a subsequent paper by taking into consideration the polyiodide complex formation.

References

1) M. Davies and E. Gwynne, *J. Am. Chem. Soc.*, **74**, 2748 (1952).
2) O. E. Meyers, *J. Chem. Phys.*, **28**, 1027 (1958).
3) R. W. Ramet and R. W. Sandford, Jr., *J. Am. Chem. Soc.*, **87**, 5001 (1965).
4) E. E. Genser and R. E. Connick, *J. Chem. Phys.*, **58**, 990 (1973).
5) M. Eigen and K. Kustin, *J. Am. Chem. Soc.*, **84**, 1335 (1962).
6) D. H. Turner, G. W. Flynn, N. Sutin, and J. Beitz, *J. Am. Chem. Soc.*, **94**, 1554 (1972).
7) T. Sano, J. Ishibashi, N. Ikeda, and T. Yasunaga, *Biopolymers*, **20**, 187 (1981).
8) In the case of negative value of ΔH_4, the activation enthalpy of backward $\Delta H^{\ddagger}_{-4}$ should be greater than $|\Delta H_4|$. Accordingly, the enthalpy change ΔH_4 less than −2.0 kcal/mol gives rise to the temperature dependence of relaxation time beyond the experimental errors of about 10%.

Behavior of Amine in Rhodium Complex-Tertiary Amine Catalyst System Active for Hydrogenation of Aldehyde under Oxo Reaction Conditions

Tsutomu MIZOROKI, Mamoru KIOKA, Masayasu SUZUKI, Shiro SAKATANI, Atsushi OKUMURA, and Ken-ichi MARUYA*

Research Laboratory of Resources Utilization, Tokyo Institute of Technology, 4259 Nagatsuta, Midori-ku, Yokohama 227

(Received July 11, 1983)

Synopsis. The title reaction was investigated to elucidate the reported disagreements on the kinetics. The concentration and the coordination stability of amine were found to affect the optimum pressure of carbon monoxide and the kinetics, and were suggested to control the reaction mechanism.

Rhodium complex is very active for the hydroformylation of olefin,[1-3] but not so effective for the hydrogenation of aldehyde under the hydroformylation conditions.[3,4] The addition of tertiary amine to the rhodium catalyst, however, markedly facilitates the hydrogenation to make possible one step synthesis of oxo alcohol.[5] With the system of rhodium complex and tertiary amine, the hydroformylation of olefin,[5-7] the hydrogenation of aldehyde,[6,7] and the selective hydrogenation of α,β-unsaturated aldehyde to alcohol[8,9] have been studied, but different optimum pressures of carbon monoxide,[5,9] and linear[6,7] and nonlinear[5,9] dependences on the pressure have been reported. It is accepted that anionic clusters of rhodium are formed in the presence of amine,[7] but the interaction of amine with the rhodium complex is not clear. In this paper we wish to clarify the behavior of amine in the system of rhodium complex and tertiary amine, and to describe a cause of disagreement on the effect of carbon monoxide.

Experimental

$[Rh_2Cl_2(CO)_4]$[10] and $[Rh(acac)(CO)_2]$[11] were prepared according to the procedures in the literatures. Amines were, on occasion, distilled from CaH_2, but typically used without further purification. Aminated polystyrene (Found: H; 9.0, C; 84.4, N; 5.5, Cl; 0.0%) was prepared as described in a previous paper.[9] Other reagents of guaranteed grade were used without further purification. The reactions of hydrogention and hydroformylation, and the reaction of $[Rh_2Cl_2(CO)_4]$ with aminated polystyrene were carried out as described in a previous paper.[9]

Results and Discussion

Figure 1 shows the dependence of the yield of heptanol in the hydroformylation on the content of 1-hexene. The obvious inhibition by olefin is seen on the hydrogenation, but not the hydroformylation. The similar inhibition by carbon monoxide is seen in Fig. 2. Since the yield of alcohol is independent of the concentration of aldehyde in spite of the high pressure of carbon monoxide as shown in Fig. 3, these inhibitions seem to indicate the competitive coordination of olefin and carbon monoxide with amine rather than aldehyde. The optimum pressure of carbon monoxide, P_{CO}(Max), where the highest yield of alcohol is

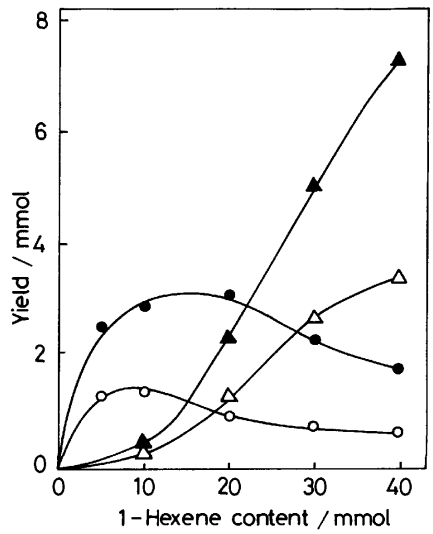

Fig. 1. Dependence of alcohol yields on 1-hexene content in hydroformylation of 1-hexene with $Rh_2Cl_2(CO)_4$ (0.05 mmol) and *N*-methylpyrrolidine (20 mmol) in benzene (20 ml) at 60 kg/cm^2 (P_{H_2}/P_{CO}=1) and 80 °C for 20 min.
▲: Heptanal, △: 2-methylhexanal, ●: 1-heptanol, ○: 2-methyl-1-hexanol.

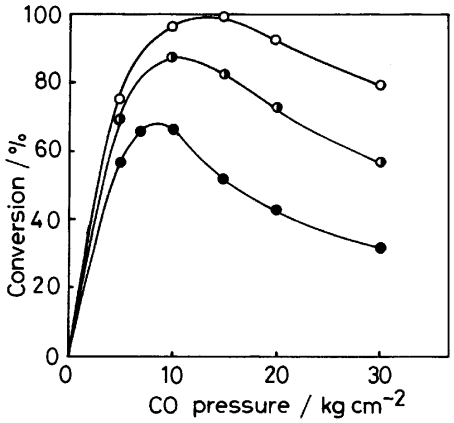

Fig. 2. Dependence of benzaldehyde conversion on pressure of carbon monoxide with $Rh_2Cl_2(CO)_4$ (0.05 mmol) and *N*-methylpyrrolidine in benzene (20 ml) at 30 kg/cm^2 (P_{H_2}) and 80 °C for 20 min.
N-Methylpyrrolidine; ●: 2.5 mmol, ◑: 5 mmol, ○: 10 mmol.

obtained, seems to increase with an increase in the concentrtion of amine (Fig. 2). Figure 4 shows a good correlation between P_{CO}(Max) and the concentration of amine, including reported P_{CO}(Max)s.[5,9] This indicates that the coordination of amine on the rhodium complex is competitive with carbon monoxide, although Jurewicz *et al.*[7] proposed an equilibrum

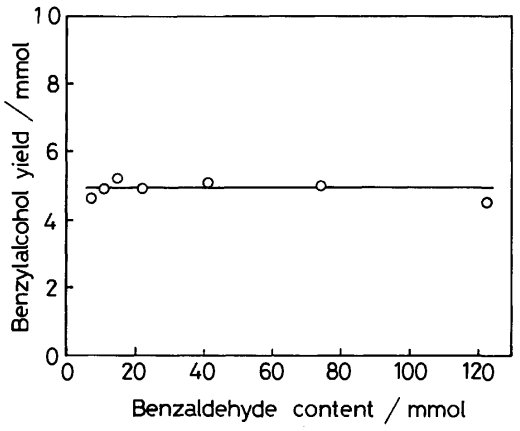

Fig. 3. Dependence of benzyl alcohol yield on content of benzaldehyde in hydrogenation of benzaldehyde with $Rh(acac)(CO)_2$ (0.05 mmol) and *N*-methylpyrrolidine (10 mmol) in benzene (20 ml) at 40 kg/cm^2 (P_{CO}) and 30 kg/cm^2 (P_{H_2}) and 60 °C for 30 min.

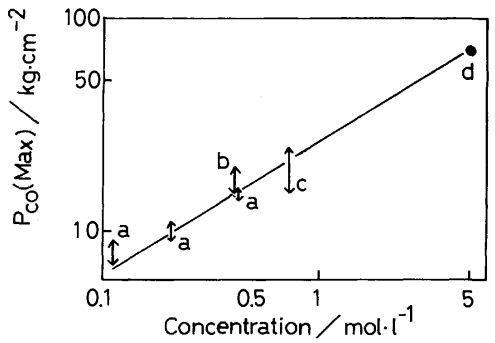

Fig. 4. Dependence of P_{CO}(Max) on concentration of *N*-methylpyrrolidine.
a) Hydrogenation of benzaldehyde at 30 kg/cm^2 (P_{H_2}) and 80 °C. b) Hydrogenation of benzaldehyde at 30 kg/cm^2 (P_{H_2}) and 60 °C. c) Hydrogenation of cinnamaldehyde at 40 kg/cm^2 (P_{H_2}) and 80 °C (Ref. 8). d) Hydroformylation of 1-hexene at 75 kg/cm^2 (P_{H_2}) and 90 °C (Ref. 5).

between $[HRh_x(CO)_y(NR_3)]$ and $[HNR_3^{\ddagger}\cdot Rh_x(CO)_y^{-}]$. Thus, it is concluded that the reported difference of P_{CO}(Max)s[5,9] is because of the different concentrations of amine. In the presence of carbon monoxide and amine, rhodium carbonyl complexes easily transform into anionic clusters,[7,13,14] suggesting that the interacton of amine with rhodium complex may be written as Eq. 1,

$$Rh_x(CO)_{y+1}^{n-} \underset{CO}{\overset{NR_3}{\rightleftharpoons}} Rh_x(NR_3)(CO)_y^{n-} \underset{NR_3}{\overset{olefin}{\rightleftharpoons}} Rh_x(olefin)(CO)_y^{n-}, \quad (1)$$

where $[Rh_x(NR_3)(CO)_y^{n-}]$ and $[Rh_x(olefin)(CO)_y^{n-}]$ may be active for the hydrogenation of aldehyde and the hydroformylation of olefin, respectively.

The results with the catalyst system of polymer amine are different from that of monomer amine. The hydroformylation of 1-hexene (10 mmol) in benzene (20 ml) at 80 °C and 60 kg/cm^2 ($P_{CO}/P_{H_2}=1$) for 60 min with $[Rh_2Cl_2(CO)_4]$ (0.05 mmol) and aminated polystyrene (0.75 matom-N) gave 1.0 mmol of heptanal, 0.9 mmol of 2-methylhexanal, 3.0 mmol of 1-heptanol, and 1.7 mmol of 2-methyl-1-hexanol. Further addition of the polymer (5 matom-N) resulted in no further increase in the yields. These results contrast with the cases of monomer amine where large amounts of amine are used.[5,7-9] It is known that $[Rh_2Cl_2(CO)_4]$ firmly interacts with aminated polystyrne.[6,7,9] $[Rh_2Cl_2(CO)_4]$ (0.05 mmol) was treated with aminated polystyrene (0.5 matom-N) in toluene (20 ml) to give colorless solution and brown polymer while evolving carbon monoxide. In N/Rh>10 the polymer-anchored rhodium complex showed no absorption band in ν(CO) region, while in N/Rh<5 three bands at 2060 (w), 1985 (s), and *ca.* 1800 cm^{-1} (w, broad) due to ν(CO)[9] were observed. These results indicate that polymer amine strongly interacts with rhodium complex to exclude carbon monoxide ligand, leading to a first order dependence on carbon monoxide.[6,7] Thus, it can be concluded that the kinetic disagreement of polymer amine system with monomer one comes from the difference of their coordination stability, though Jurewicz *et al.*[7] attributed the disagreement to the difference of reaction conditions.

The difference between polymer and monomer amines seems to bring about the different dependence on the concentration of aldehyde, *i.e.*, zero order with monomer amine system (Fig. 3) and first order with polymer one.[6] These kinetic difference might suggest different reaction mechanisms. Taking into account the first order dependence on the pressure of hydrogen,[5,6,9] the formation of rhodium hydride with monomer amine system may be a slow step followed by a fast reaction of the hydride with aldehyde, while the coordination of aldehyde or the reaction of a hydride with aldehyde on polymer-anchored rhodium complex may be slow.

References

1) P. Pino, F. Piacenti, and M. Bianchi, "Organic Syntheses *via* Metal Carbonyls," ed by I. Wender and P. Pino, Wiley-Interscience, New York (1977), Vol. 2, p. 43.
2) B. Cornils, "New Syntheses with Carbon Monoxide," ed by J. Falbe, Springer-Verlag, New York (1980), p. 1.
3) B. Heil and L. Marko, *Chem. Ber.*, **99**, 1086 (1966).
4) B. Heil and L. Marko, *Acta Chim. Acad. Sci. Hung.*, **55**, 105 (1968).
5) B. Fell and A. Guerts, *Chem. Ing. Tech.*, **44**, 708 (1972).
6) W. O. Haag and D. D. Whitehurst, Int. Congr. Catal. 5th, Palm Beach, Fla. Aug. (1972), No. 29.
7) A. T. Jurewicz, L. D. Rollmann, and D. D. Whitehurst, "Homogeneous Catalysis II," ed by D. Forster and J. F. Roth, Am. Chem. Soc. Washington, D. C. (1974) p. 240.
8) S. Meguro, T. Mizoroki, and A. Ozaki, *Chem. Lett.*, **1975**, 943.
9) T. Mizoroki, K. Seki, S. Meguro, and A. Ozaki, *Bull. Chem. Soc. Jpn.*, **50**, 2148 (1977).
10) J. McLeverty and G. Wilkinson, *Inorg. Synth.*, **8**, 211 (1966).
11) F. Bonati and G. Wilkinson, *J. Chem. Soc.*, **1964**, 3156.
12) P. Chini and S. Martinengo, *Inorg. Chim. Acta*, **3**, 315 (1972).
13) S. Martinengo and P. Chini, *Gazz. Chim. Ital.*, **102**, 344 (1972).
14) L. D. Rollmann, *Inorg. Chim. Acta*, **6**, 137 (1972).

A Study of the Thermal Decomposition of Ruthenium Ammine Zeolites

Takashi TATSUMI,* Wataru MAEKAWA, and Hiro-o TOMINAGA
Departmet of Synthetic Chemistry, Faculty of Engineering, The University of Tokyo, Hongo, Bunkyo-ku, Tokyo 113
(Received July 16, 1983)

Synopsis. Treatment of Ru(II) ammine-NaY under nitrogen at 100 and 300 °C leads to formation of $[Ru(NH_3)_5N_2]^{2+}$-NaY and metallic Ru-N_2, respectively. The effect of atmosphere and the type of Ru ammine complexes and zeolites on the decomposition behavior is discussed.

Metal ions can be introduced into zeolites by cation exchange. This ion exchange procedure is expected to give metal catalysts with a highly dispersed metal phase with superior properties to catalysts prepared by impregnation with simple metal halide salts.[1] Recently much attention is being devoted to the catalytic activity of zeolite-supported Ru,[2-5] since Ru has been shown to be one of the best catalysts for the hydrogenation of CO.[10] The preparation of Ru-containing zeolites *via* ammine complexes has been successful and shows promise as an advantageous route to industrially important catalysts.[4-9] Ruthenium is also known to be a highly effective metal for the activation of nitrogen and adsorbs a significant amount of nitrogen during ammonia synthesis, when K is added. Adsorbed or coordinated nitrogen is infrared active in the $\approx 2000\,cm^{-1}$ region of the spectrum.[11] In this paper we describe the IR results of zeolite-supported Ru ammine complexes during heating processes under a nitrogen atmosphere.

Experimental

$[Ru(NH_3)_6]Cl_2$ was prepared by the method of Allen and Senoff.[12] $[Ru(NH_3)_6]Cl_3$ was purchased from Strem Chemicals. The $[Ru(NH_3)_6]^{2+}$ cation was exchanged into the zeolite NaY (Ru content *ca.* 4 wt%) in deoxygenated water under a nitrogen atmosphere. The pH of the exchanged solution was adjusted to 4.5 by the addition of hydrochloric acid. $[Ru(NH_3)_6]^{3+}$ cation was exchanged into the NaY or HY zeolite (Ru *ca.* 4 wt%). In this case no attempt was made to control the pH of the solution. The zeolites were filtered, washed with water and then with ethanol, and dried under vacuum at room temperature for 2 d. Samples for IR investigations were prepared in the form of wafers having a diameter of 20 mm and weights between 25 and 35 mg. IR spectra were recorded on a Nihon Bunko IRA-2 grating spectrophotometer. The wafers were heated to desired temperature in a stream of nitrogen or helium, maintained at that temperature for 30 min, and then subjected to IR analysis at room temperature.

Results and Discussion

The ammine complex $[Ru(NH_3)_6]^{2+}$ was exchanged into the Na-Y zeolite and the zeolite obtained was degassed for 2 d at room temperature. The IR spectrum of the fresh zeolite sample (Fig. 1a) showed three significant bands assigned as follows: $1640\,cm^{-1}$ (very strong, $\delta_d(NH_3)$ in conjunction with adsorbed water), $1450\,cm^{-1}$ (weak, $\delta_d(NH_4)$) and $1320\,cm^{-1}$ (strong, $\delta_s(NH_3)$). The $\delta_s(NH_3)$ band at $1220\,cm^{-1}$ which is characteristic of the original $[Ru(NH_3)_6]Cl_2$ complex,[12] has been shifted by $100\,cm^{-1}$ to higher wavenumber upon exchange into the zeolite. When the pale yellow $[Ru(NH_3)_6]^{2+}$-NaY zeolite sample was kept for a few days under an inert atmosphere, the zeolite turned purple and the band at $1450\,cm^{-1}$ increased in intensity, while the band at $1320\,cm^{-1}$ was shifted to $1340\,cm^{-1}$ and weakened (Fig. 1b). This finding indicates a part of Ru(II) ions has undergone the hydrolysis as follows:

$$[Ru^{II}(NH_3)_6]^{2+}\text{-NaY} + H_2O \longrightarrow [Ru^{III}(NH_3)_5OH]^{2+}\text{-NaY} + NH_4^+.$$

This reaction is closely similar to that proposed by Laing *et al.* to account for the color change of $[Ru(NH_3)_5N_2]^{2+}$-NaY upon storage.[8] This purple zeolite designated as RuNaY was used for the subsequent experiment.

As shown in Fig. 2a, the IR spectrum of the freshly prepared $[Ru(NH_3)_6]^{3+}$-HY sample displayed two intense bands at $1640\,cm^{-1}$ ($\delta_d(NH_3)$ plus $\delta_d(H_2O)$) and $1440\,cm^{-1}$ ($\delta_d(NH_4)$). The band around $1350\,cm^{-1}$ which is typical of deformation band of coordinated NH_3 of $[Ru(NH_3)_6]^{3+}$ was not observed.[12] This fact suggess that the NH_3 ligands which had been present in the coordination sphere of Ru migrated to Brønsted acid site of the zeolite. This is contrasted with the results obtained with the fresh $[Ru(NH_3)_6]^{3+}$-NaY zeolite, which showed an intense band at $1340\,cm^{-1}$ ($\delta_s(NH_3)$) and a very weak NH_4 deformation band.[9]

Figure 1c shows the IR spectrum of RuNaY when

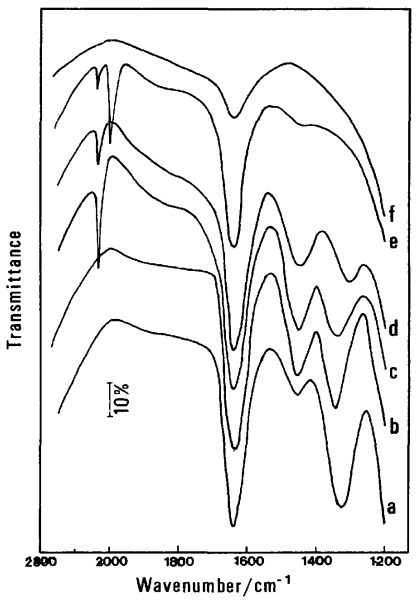

Fig. 1. Variation of infrared spectra of $[Ru(NH_3)_6]^{2+}$-NaY under N_2.
a): Fresh, b): on storage under N_2 for 2 weeks, c): 100 °C, d): 200 °C, e) 300 °C, f): 350 °C.

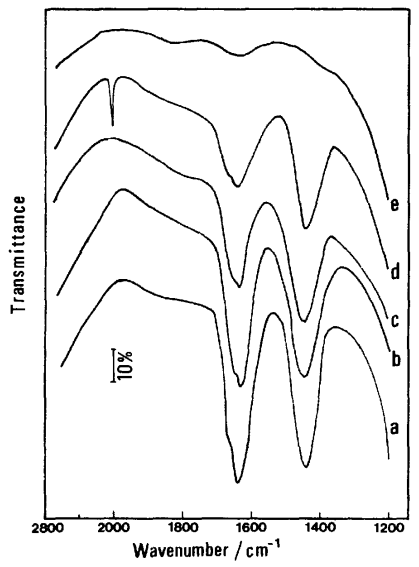

Fig. 2. Variation of infrared spectra of $[Ru(NH_3)_6]^{3+}$–HY under N_2.
a): Fresh, b): 100 °C, c): 200 °C, d): 300 °C, e) 400 °C.

heated under N_2 at 100 °C. The band at 1340 cm^{-1} was attenuated and the strong band developed at 2135 cm^{-1}. The latter may be assigned to the stretching frequency of a coordinated nitrogen molecule and suggested the formation of $[Ru(NH_3)_5N_2]^{2+}$–NaY which was first prepared by Laing *et al.* by the addition of hydrazine to $[Ru(NH_3)_5NO]^{3+}$–NaY.[8] Atmospheric nitrogen seems to have substituted one NH_3 ligand from the residual $[Ru(NH_3)_6]^{2+}$ ion in RuNaY, although this type of simple displacement reaction in solution has not been reported. A similar treatment of RuNaY under helium at 100 °C resulting in the spectrum lacking the band around 2135 cm^{-1}. Recently Aika *et al.* found that N_2 is adsorbed on a support with K[13] or a basic support such as CaO and MgO_2.[14] Thus the band at 2135 cm^{-1} might be due to a N_2 species adsorbed on the NaY support. No band corresponding to the adsorbed N_2 species was found over NaY. It is well known that transition metals which bind nitrogen molecules are in low oxidation states;[15,16] no nitrogen complex of Ru(III) has been reported. As we would expect, treatment of $[Ru(NH_3)_6]^{3+}$–NaY or HY with N_2 at 100 °C afforded a spectrum with no N–N band. From these results we assumed that N_2 is coordinated to a Ru(II) species encaged in NaY.

When RuNaY was subsequently heated at 200 °C, the band at 2135 cm^{-1} was weakened and the band at 1340 cm^{-1} was shifted to 1295 cm^{-1} (Fig. 1d). Subsequent heating at 300 °C resulted in a new band at 2000 cm^{-1} (Fig. 1e). Since its frequency is too low to regard as that arising from ionic Ru species,[15,16] the band is attributable to ν(NN) of a nitrogen molecule chemisorbed to Ru(0) (presumably metallic ruthenium in view of the absence of the band at 1295 cm^{-1}). An almost identical spectrum resulted from the treatment of $[Ru(NH_3)_6]^{3+}$–NaY with N_2 at 300 °C. Heating the samples at 350 °C resulted in the removal of the bands at 2000 and 1450 cm^{-1}, as shown in Fig. 1f. It should be noted that Laing *et al.* have observed a band at 2000 cm^{-1} on the reaction of $[Ru(NH_3)_x(NO)]Y$ with NH_3 at 150 °C.[8] Treatment of RuNaY under helium at 300 °C resulted in only a weak band at 2000 cm^{-1}; the presence of N_2 greatly enhanced the intensity of the ν(NN) band. The nitrogen molecule observed in the case of the treatment under a helium flow is ascribed to the decompsition of the NH_3 ligands. Verdonck *et al.* have shown that on degassing $[Ru(NH_3)_6]^{3+}$–NaY the complex is reduced to the metallic state accompanied by the liberation of N_2.[6]

Treatment of $[Ru(NH_3)_6]^{3+}$–HY with N_2 at 300 °C yielded a band at 2025 cm^{-1}, as shown in Fig. 2d. The difference in wavenumber between the ν(NN) bands in the two zeolites should be accounted for in terms of electron defficiency in the metal on HY. The electron-acceptor strength of the zeolite is expected to increase in the direction NaY<HY. The electron concentration in the metal would decrease accordingly, thus decreasing electron donation to N_2. The bands might be due to N_2 species adsorbed on the zeolite supports but they were observed for neither NaY nor HY without Ru. The acidic property of the HY zeolite is also responsible for the persistence of the $\delta_d(NH_4)$ band during the heating process (Fig. 2d). After the treatment at 300 °C, the $\delta_d(NH_4)$ band was scarcely observed with the RuNaY zeolite, while the $[Ru(NH_3)_6]^{3+}$–HY sample still retained 40—50% of its NH_4^+ (as estimated from the intensity of $\delta_d(NH_4)$).

References

1) For example, see T. Kubo, H. Arai, H. Tominaga, and T. Kunugi, *Bull. Chem. Soc. Jpn.*, **45**, 607 (1972).
2) T. Yashima, Y. Ushida, M. Ebisawa, and N. Hara, *J. Catal.*, **36**, 320 (1975).
3) D. Couglan, S. Narayanan, W. A. McCann, and W. M. Caroll, *J. Catal.*, **49**, 97 (1977).
4) N. M. Gupta, V. S. Kamble, K. A. Rao, and K. M. Iyer, *J. Catal.*, **60**, 57 (1979).
5) H. H. Nijs and P. A. Jacobs, *J. Catal.*, **66**, 40 (1980); H. Nijs, P. A. Jacobs, and J. B. Uytterhoeven, *J. Chem. Soc., Chem. Commum.*, **1979**, 180, 1095; J. Verdonck, P. A. Jacobs, and J. B. Uytterhoeven, *ibid.*, **1979**, 181.
6) J. J. Verdonck, P. A. Jacobs, M. Genet, and G. Poncelet, *J. Chem. Soc., Faraday Trans. 1*, **76**, 403 (1980).
7) J. G. Goodwin, Jr., and G. Naccache, *J. Catal.*, **64**, 482 (1980).
8) K. R. Laing, R. L. Leubner, and J. H. Lunsford, *Inorg. Chem.*, **14**, 1400 (1975).
9) J. R. Pearce, B. L. Gustafson, and J. H. Lunsford, *Inorg. Chem.*, **20**, 2957 (1981).
10) M. A. Vannice, *J. Catal.*, **37**, 449 (1975).
11) M. Oh-kita, K. Aika, K. Urabe, and A. Ozaki, *J. Catal.*, **44**, 460 (1976) and references therein.
12) A. D. Allen and C. V. Senoff, *Can. J. Chem.*, **45**, 1337 (1967).
13) K. Aika, H. Midorikawa, and A. Ozaki, *J. Phys, Chem.*, **86**, 3263 (1982).
14) K. Aika, H. Midorikawa, and A. Ozaki, *J. Catal.*, **78**, 147 (1982).
15) K. Nakamoto, "Infrared Spectra of Inorganic and Coordination Compounds," John Wiley and Sons, Inc., New York (1963), pp. 146, 200.
16) J. Chatt, J. R. Dilworth, and R. Richards, *Chem. Rev.*, **78**, 589 (1978).

Determination of the Vapor Pressures of Cesium Fluoride and Cesium Chloride by Means of Surface Ionization

Hiroyuki KAWANO,* Tsutomu KENPŌ, and Yoshiaki HIDAKA
Department of Chemistry, Faculty of Science, Ehime University, 2-5, Bunkyō-chō, Matsuyama 790
(Received August 3, 1983)

Synopsis. A molecular beam of CsF or CsCl effusing from a Knudsen cell was detected with a heated rhenium filament, and the vapor pressure P (in atm) of each halide at a temperature T (in K) was found to be expressed by $\log_{10} P(\mathrm{CsF})=(7.239\pm0.072)-(9883\pm72)/T$ for 630—830 K, $\log_{10} P(\mathrm{CsCl})=(7.269\pm0.064)-(10054\pm66)/T$ for 640—820 K.

When a beam intensity of molecules (MX) effusing from a Knudsen cell at a given temperature is evaluated thermodynamically, it is necessary to know the accurate value of the vapor pressure (P(MX)) at the temperature. Literature values of P(MX), however, are generally in poor agreement with each other. For example, P(CsF) changes from literature to literature by up to ≈6 times. This fact suggests that further investigations should be made with many samples in order to obtain reliable data on the pressure.

From the viewpoint mentioned above, the present authors have tried to measure accurately the pressures of CsF and CsCl using a positive surface ionization technique developed in their laboratory and also to determine the entropy and enthalpy changes due to molecular sublimation. The results thus obtained are summarized together with literature values, thereby indicating that the present method is quite useful for pressure measurements.

Experimental

Sectional views of the present instrument are shown in Fig. 1, where F is the ionizing filament (0.013 cm in diameter) made of rhenium; B the stainless steel box; R the rotatable shutter; P the shield plate; K the Knudsen cell made of stainless steel; H the molybdenum wire heater; W the pipe for cooling water; A_1 and A_2 the calibrated alumel-chromel thermocouples; and C the Faraday cup. A molecular beam of cesium halide (CsX) effusing from the exit slit S_1 (0.12 cm in diameter) impinged upon F after passing through the inlet slit S_2 (0.17 cm in diameter). The ion-extraction voltage applied to F was usually 50 V. A part of the positive ions (Cs^+) emitted from F was collected with C, and the ion current ($i^+(Cs^+)$) was measured with a vibrating reed electrometer. The collection efficiency of the ions was 1.45 ± 0.03%, which was determined in a separate experiment by simultaneous measurement of the ion currents collected by B and C. Accordingly, the total ion current ($I^+(Cs^+)$) is equal to $i^+(Cs^+)/0.0145$. The residual gas pressure inside the vacuum vessel containing the above system was usually $\approx2\times10^{-7}$ Torr (1 Torr≈133.322 Pa). The temperatures (T and T_F) of the cell and the filament were determined with A_1 and an optical pyrometer, respectively. The temperature measured with A_1 was always higher by up to ≈3K than that with A_2. The samples (CsF and CsCl) of optical grade were obtained from Aldrich Chem. Co., Inc., and Wako Pure Chem. Ind., Ltd., respectively.

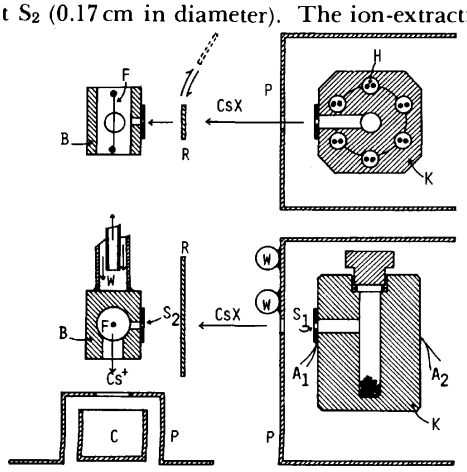

Fig. 1. Horizontal and vertical sectional views of the instrument employed in this work.

Results and Discussion

When the cell containing CsF was heated to 824 K, for example, $I^+(Cs^+)$ was constant at $(4.50\pm0.21)\times10^{-8}$ A without depending upon the filament temperature so long as T_F was higher than ≈1300 K. In this range, therefore, the ionization efficiency of the molecules incident upon F may be concluded to be essentially 100%. A similar result was obtained with CsCl, too. These results may be natural because the first ionization energy (≈3.9 eV) of Cs is much smaller than the effective work function (≈5.4 eV) of Re for positive ion production.[1]

Consideration of the present experimental method and of gas kinetics[2] leads to the following equations:

$$P(\mathrm{CsX}) = \frac{\pi L^2[2\pi M(\mathrm{CsX})RT]^{1/2}}{1.013\times10^6 N_A S_C} N(\mathrm{CsX}), \quad (1)$$

$$N(\mathrm{CsX}) = \frac{I^+(Cs^+)}{e S_F}. \quad (2)$$

Here, P(CsX) is the vapor pressure (in atm) in the cell; L the distance (6.5 cm) between the cell orifice and the ionizing filament; M(CsX) the molecular weight of CsX; R the gas constant; N_A the Avogadro's number; S_C the effusing slit area (1.13×10^{-2} cm^2) of the cell; N(CsX) the flux of sample molecules (in cm^{-2} s^{-1}) at L; e the elementary electric charge; and S_F the sectional area (2.16×10^{-3} cm^2) of the filament intercepting the molecular beam. Consequently, we obtain the relation:

$$P(\mathrm{CsX}) = 1.27[M(\mathrm{CsX})T]^{1/2} I^+(Cs^+), \quad (3)$$

where $I^+(Cs^+)$ is expressed in ampere.

A typical result obtained by the present authors is shown, together with results by other workers,[3-5] in Fig. 2, which leads to a general expression as follows:

$$\log_{10} P(\mathrm{CsX}) = A - B/T. \quad (4)$$

The values of both A and B determined in this work and also cited from literatures[3-8] are summarized in Table 1, where the pressures at three selected tempera-

TABLE 1. SUMMARY OF THE EXPERIMENTAL DATA OBTAINED BY THE PRESENT AND OTHER WORKERS

Sample	T_R / K	$\bar{T}$ / K	A	B / K	P(CsX)/μatm 700 K	800 K	900 K	$\Delta S(\bar{T})$ cal[a] mol^{-1} K^{-1}	$\Delta H(\bar{T})$ kcal mol^{-1}	$\Delta H(300)$ kcal mol^{-1}	Ref.
CsF	677—878	778	7.708	10140	0.167	10.8	276	35.3	46.4	48.6	3
	753—856	805	7.556	10208	0.0940	6.25	164	34.6	46.7	49.1	4
	838—919	879	6.458±0.037	9783±47	0.0304	1.70	38.7	29.6±0.2	44.8±0.2	47.5±0.2	5
	644—821	733	7.419±0.079	9989±78	0.141	8.58	209	33.9±0.4	45.7±0.4	47.7±0.4	This work (a)
	685—834	760	7.229±0.079	9878±85	0.131	7.61	179	33.1±0.4	45.2±0.4	47.3±0.4	This work (b)
	634—823	729	7.050±0.117	9767±117	0.125	6.93	157	32.3±0.5	44.7±0.5	46.7±0.6	This work (c)
	634—834	734	7.239±0.072	9883±72	0.132	7.68	181	33.1±0.3	45.2±0.3	47.2±0.3	This work (A)
CsCl	720—892	806	7.534	10198	0.0923	6.11	160	34.5	46.7	49.1	3
	793—893	843	6.424	9670	0.0408	2.17	47.9	29.4	44.2	46.9	6
	784—905	845	6.854±0.041	9806±50	0.0701	3.95	90.8	31.4±0.2	44.9±0.2	47.5±0.2	7
	690—891	791	7.649±0.058	10230±59	0.108	7.29	192	35.0±0.3	46.8±0.3	49.2±0.3	8
	638—819	729	7.329±0.093	10109±95	0.0772	4.93	125	33.5±0.4	46.3±0.4	48.4±0.5	This work (d)
	639—820	730	7.229±0.057	10013±57	0.0841	5.16	127	33.1±0.3	45.8±0.3	47.9±0.3	This work (e)
	638—820	729	7.269±0.064	10054±66	0.0806	5.03	125	33.3±0.3	46.0±0.3	48.1±0.3	This work (B)

a) 1 cal=4.184 J.

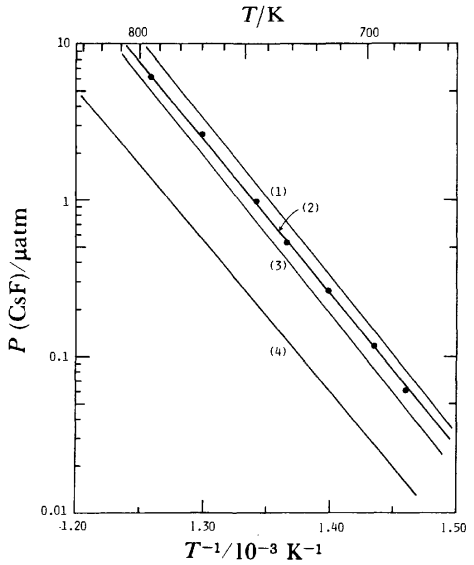

Fig. 2. Temperature dependence of the vapor pressure observed with CsF. (1): Ref. 3, (2): this work at T_F=1600 K, (3): Ref. 4, (4): Ref. 5.

tures are evaluated by substituting the respective values of A and B in Eq. 4. The entropy change due to sublimation ($\Delta S(\bar{T})$) and the heat of sublimation ($\Delta H(\bar{T})$) at the mean temperature ($\bar{T}$) in the range (T_R) covered in each measurement are evaluated from Eqs. 5 and 6, respectively, where 1 cal is equal to 4.184 J.

$$\Delta S(\bar{T}) = (\ln 10)\, R\, A \equiv 4.575\, A \quad \text{cal mol}^{-1}\,\text{K}^{-1}. \tag{5}$$

$$\Delta H(\bar{T}) = (\ln 10)\, R\, B \equiv 4.575 \times 10^{-3}\, B \quad \text{kcal mol}^{-1}. \tag{6}$$

The heat of sublimation at 300 K is given by

$$\Delta H(300) = \Delta H(\bar{T}) + \int_{300}^{\bar{T}} [C_P(\text{c}) - C_P(\text{g})]\,dT, \tag{7}$$

$$\simeq \Delta H(\bar{T}) + a\, R\, (\bar{T} - 300). \tag{8}$$

Here, C_P(c) and C_P(g) are the specific heats of CsX at crystalline and gaseous states, respectively. According to data compiled in Ref. 9, Eq. 7 may be approximated by Eq. 8, where the values of a in the range 300—800 K are taken as 2.34 and 2.47 for CsF and CsCl, respectively.

The temperatures of the ionizing filament in the cases (a)—(e) indicated in the last column in Table 1 were 1910, 1600, 1450, 2108, and 2215 K, respectively. The data (A) and (B) are the mean values of those (a)—(c) and those (d)—(e), respectively. In the case of CsF, the values in Refs. 3 and 4 and Ref. 5 are close to and apart from those in this work, respectively, as may be seen in Fig. 2 and Table 1. Our data on CsCl fall between those in Ref. 3 and those in Ref. 7, and most deviate from those in Ref. 6. Consequently, the data in Refs. 5 and 6 seem to be less accurate probably because of a systematic error.

Conclusion

The positive surface ionization method is quite useful for determining the vapor pressure of cesium halide without citing any thermochemical value from literatures, and hence for checking the accuracy of published data on the pressure. Since the effective work function of an oxygenated tungsten wire for positive ion production is ≈6.7 eV,[1] the ionization efficiency of element having the ionization energy less than ≈6 eV is generally expected to be essentially unity when the wire at a suitable temperature is employed as a beam detector. Therefore, the present method may also be applicable to those salts which include a readily ionized element[1] such as alkali metal, alkaline earth, actinoid, or lanthanoid.

References

1) H. Kawano and F. M. Page, *Int. J. Mass Spectrom. Ion Phys.*, **50**, 1 (1983).
2) H. Kawano, Y. Hidaka, and F. M. Page, *Int. J. Mass Spectrom. Ion Phys.*, **50**, 35 (1983).
3) M. D. Scheer and J. Fine, *J. Chem. Phys.*, **36**, 1647 (1962).
4) A. C. P. Pugh and R. F. Barrow, *Trans. Faraday Soc.*, **54**, 671 (1958).
5) M. Eisenstadt, G. M. Rothberg, and P. Kush, *J. Chem. Phys.*, **29**, 797 (1958).
6) K. Niwa, *J. Fac. Sci. Hokkaido Imp. Univ., Ser. III*, **2**, 201 (1938).
7) W. D. Treadwell and W. Werner, *Helv. Chim. Acta*, **36**, 1436 (1953).
8) G. E. Cogin and G. E. Kimball, *J. Chem. Phys.*, **16**, 1035 (1948).
9) D. R. Stull and H. Prophet, "JANAF Thermochemical Tables," 2nd ed, Natl. Bur. Stand., Washington (1971).

On the Reduction Products of Carbon Dioxide at a p-Type Gallium Phosphide Photocathode in Aqueous Electrolytes

Kaname Ito,* Shoichiro Ikeda, Makoto Yoshida, Soji Ohta, and Takaya Iida
Department of Synthetic Chemistry, Nagoya Institute of Technology, Gokiso-cho, Showa-ku, Nagoya 466
(Received August 22, 1983)

Synopsis. Formic acid, formaldehyde, and methanol, previously reported as photoelectrochemical reduction products of CO_2, were observed to be obtained also by photolysis of cell materials such as electrolytes and epoxy resin. The reduction product of CO_2 at a p-GaP photocathode in aqueous electrolytes was experimentally confirmed to be mainly formic acid.

Halmann[1] observed formic acid, formaldehyde, and methanol as reduction products of CO_2 at a p-type gallium phosphide (p-GaP) photocathode in aqueous lithium carbonate electrolyte. Tamura *et al.*[2] reported that their yield increased with addition of crown ether to the electrolyte. In our similar experiments[3] oxalic acid, glycolic acid, ethanol, and acetaldehyde were also observed.

Here, similar organic compounds will be shown to be produced also by photolysis of cell materials such as electrolytes and epoxy resin. When experimental conditions were improved so as to produce no organic compound as a photolytic product, the products obtained by photoelectrochemical reduction of CO_2 in aqueous electrolytes were mainly formic acid.

Experimental

The photoelectrochemical cell with a quartz window was made of Teflon. The structure was designed to separate the cathode chamber from the anode chamber by an ion-exchange membrane, Nafion-315, and to allow operation with a small volume of catholyte of *ca.* 5 ml for easy determination of the products.

The photocathode was prepared by molding p-GaP wafer of *ca.* 1 cm^2 with epoxy resin; it was etched in aqua regia for 1 min before use. The photocathode set in the cell was illuminated through the quartz window and aqueous electrolytes by a 300 W Xenon lamp (Varian). The platinum plate served as an anode and the silver–silver chloride electrode as a reference electrode.

The electrolytes used were 0.1 mol dm^{-3} aqueous solutions of Li_2CO_3, $(C_2H_5)_4NClO_4$ (TEAP), $(C_2H_5)_4NBr$ (TEABr), $(n\text{-}C_4H_9)_4NBr$ (TBABr), and Li_2CO_3 plus 15-crown-5.

The products were detected and determined by high performance liquid chromatography on a column of Shodex HC-125S for carboxylic acids and by steam chromatography on a column of Chromosorb 101 for alcohols and aldehydes.

Results and Discussion

Photoelectolysis as a blank test of the present experiment was performed by bubbling N_2 gas instead of CO_2 to Li_2CO_3 or TEAP solution in the above mentioned cell and by illuminating the p-GaP photocathode with the Xenon lamp. The results are shown in Table 1, in which the results previously reported as photoelectrochemical reduction products of CO_2 are also listed for comparison. The products in N_2 and in CO_2 atmospheres are quite similar, so that they are assumed to be produced by photolysis of cell materials such as electrolytes and epoxy resin.

In order to determine the photolytic products from various electrolytes, they were individually illuminated in quartz test tubes by a 300 W Xenon lamp alone or with the UV-37 filter, Toshiba, to cut off light of wavelength shorter than 370 nm. The results, as summarized in Table 2, show that the photolysis of the electrolytes by illumination of the Xenon lamp alone produces acetaldehyde from TEABr and TEAP, acetaldehyde and ethanol from TBABr, and many kinds of products from 15-crown-5, and also that the photolysis of them by the Xenon lamp with the filter does not produce any organic compounds from TEABr, TEAP, and TBABr, but a large amount of formic acid and a small amount of oxalic acid from 15-crown-5.

The comparison of the results shown in Tables 1 and 2 suggests that formic, oxalic and glycolic acids are produced by photolysis of epoxy resin used for mount-

Table 1. Photoelectrolytic products under N_2 and CO_2 atmospheres in the cell with various electrolytes and a p-GaP photocathode molded by epoxy resin

Photoelectrolysis was performed up to 10 C at −1.2 V *vs.* Ag/AgCl electrode by illuminationg with a 300 W Xenon lamp alone.

Atmosphere	Electrolyte	n/μmol					
		HCOOH	CH_3OH+HCHO[a]	$(COOH)_2$	$HOCH_2COOH$	CH_3CHO	C_2H_5OH
N_2	Li_2CO_3	1.5	0.04	0.1	2.1	0.02	0.02
	TEAP	1.3	0.03	t	1.3	0.36	0.06
CO_2	TEABr	2.3	0.12	0.28	4.8	0.9	t
	TBABr	1.9	t[b]	0.18	1.9	0.17	t
	15-Crown-5	6.5	t	0.25	1.5	0.29	t

a) Methanol and formaldehyde were represented as CH_3OH+HCHO in the present paper because they were not able to be separated by the steam chromatographic technique; the amount of product was calculated as an amount of methanol. b) t; Trace amount of product.

Table 2. Photolytic products of various electrolytes in quartz test tube illuminated by a 300 W Xenon lamp alone or with the filter, Toshiba UV-37, under N_2 atmosphere

Filter of Xe lamp	Time h	Electrolyte	n/μmol					
			HCOOH	CH_3OH+HCHO	$(COOH)_2$	$HOCH_2COOH$	CH_3CHO	C_2H_5OH
Not used	25	Li_2CO_3	n[a]	n	n	n	n	n
	28	TEAP	n	n	n	n	0.24	n
	24	TEABr	n	n	n	n	0.28	n
	26	TBABr	n	n	n	n	0.21	0.14
	29	15-Crown-5	16.7	0.55	0.22	n	0.07	1.01
Used	24	TEAP	n	n	n	n	n	n
	26	TEABr	n	n	n	n	n	n
	24	15-Crown-5	13.1	n	0.22	n	n	n

a) n: No product.

Table 3. Photolytic products in the catholyte of the Teflon cell with various electrolytes, a p-GaP photocathode and an ion-exchange memberane, when the epoxy resin region of the photocathode was shielded by a Pt foil and the illumination was carried out by a 300 W Xenon lamp with UV-37 filter under N_2 atmosphere

Time h	Electrolyte	n/μmol					
		HCOOH	CH_3OH+HCHO	$(COOH)_2$	$HOCH_2COOH$	CH_3CHO	C_2H_5OH
24	TEAP	n[a]	n	n	n	n	n
48	TEAP	n	n	n	n	n	n
48	TEABr	n	n	n	n	n	n
48	TBABr	n	n	n	n	n	n
24	15-Crown-5 +Li_2CO_3	11.6	n	0.16	n	n	n

a) n: No product.

Table 4. Photoelectrochemical reduction products of CO_2 under the improved exprimental conditions

Photoelectrolysis was performed up to 100 C at −1.5 V *vs.* Ag/AgCl electrode.

Electrolyte	HCOOH	CH_3OH+HCHO
	n/μmol(cur. eff. %)	n/μmol
TEAP	25.0 (4.8)	t[a]
TEABr	18.0 (3.5)	t
TBABr	22.0 (4.3)	n[b]
Li_2CO_3	2.0 (0.4)	n

a) t: Trace amount of product. b) n: No product.

ing of a p-GaP electrode. This was experimentally confirmed, although the results are not shown in the present paper.

However, the photolysis of the electrolytes and epoxy resin as cell materials could be prevented, as shown in Tables 3, when the epoxy resin region of a p-GaP electrode was shielded by a platinum foil, the UV-37 filter was set in front of the Xenon lamp to cut off ultraviolet rays, and TEABr, TEAP, or TBABr (except 15-crown-5) was used as an electrolyte.

Under such improved experimental conditions, the photoeletrochemical reduction of CO_2 was carried out up to 100 C at −1.5 V *vs.* Ag/AgCl electrode. The products, as shown in Table 4, were mainly formic acid and sometimes a trace amount of formaldehyde plus methanol.

Accordingly, it may be concluded that the photoelectrochemical reduction products of CO_2 at a p-GaP electrode in aqueous electrolytes are mainly formic acid and the many kinds of products involving large part of formic acid in the previous papers[1-3] are due to photolysis of cell materials. This conclusion coincides with the previously reported fact that only formic acid is mainly produced by electrochemical reduction of CO_2 in aqueous electrolytes.[4,5]

The present work was partially supported by Grant-in-Aid for Energy Research (No. 57045052) from the Ministry of Education, Science and Culture.

References

1) M. Halmann, *Nature*, **275**, 115 (1978).
2) Y. Taniguchi, H. Yoneyama, and H. Tamura, *Bull. Chem. Soc. Jpn.*, **55**, 2034 (1982).
3) K. Ito, S. Ohta, S. Ikeda, and T. Iida, Extended Abstract at the 49th Meeting of the Electrochemical Soc. Jpn., 71, (1982).
4) K. Ito, S. Ikeda, and M. Okabe, *Denki Kagaku*, **48**, 247 (1980).
5) K. Ito, S. Ikeda, T.Iida, and H. Niwa, *Denki Kagaku*, **49**, 106 (1981).

The Sensitization Effect in the Laser-induced Infrared Fluorescence Spectroscopy by Addition of a Second Component. III

Seiichiro HIGUCHI,* Yasuhiro KAGAWA, and Shigeyuki TANAKA

Departmet of Industrial Chemistry, Faculty of Engineering, The University of Tokyo, Hongo, Bunkyo-ku, Tokyo 113

(Received February 25, 1983)

Synopsis. The sensitization effect in the infrared fluorescence spectra for diethyl ether–alkene systems has been examined in terms of the quantity and the kind of alkenes added as sensitizers. The sensitivity seems to be determined by the molar ratios between diethyl ether and alkenes, and the sensitization degree lowers in an orderly fashion as the alkene molecules become larger.

In the previous papers,[1,2] we examined the sensitization effect in the laser-induced infrared fluorescence (IR-F) spectroscopy, which was realized when some alkene compounds were added as second components. The degree of sensitization was examined quantitatively in terms of the concentrations of diethyl ether as an objective sample. In the present investigation, we have examined this sensitization effect for the same sample in view of the influence of the quantity and the kind of alkene compounds as the sensitizer.

Experimental

The experimental arrangement for the measurement of IR-F spectra is the same as that described in the previous papers.[1,2] The samples are vibrationally excited with the irradiation of the 10.6 μm lines from a CO_2 laser (output power: 3 W), and the emitted light from samples is spectrally measured. Diethyl ether was used as a sample, and the alkenes such as ethylene, propylene, 1-butene, 1-pentene, and 1-hexene were added as the sensitizing agents. The 8.7 μm band (C–O–C stretching vibration band) of diethyl ether was used as a key band. The measurements were all made for samples in the gaseous state.

Results and Discussion

The Relation between the Degree of Sensitization and the Quantity of a Sensitizing Agent. It was reported in the previous paper[2] that the degree of sensitization increases to a great extent as the concentrations of diethyl ether become lower. It will be reasonable to consider that the sensitivity depends also on the quantity of sensitizing agents. Thus, we have examined the influence of the partial pressure of added alkenes on the sensitized IR-F intensities of the 8.7 μm band of diethyl ether. In Fig.1 are plotted the values of $H_{8.7}/P_E$ ($H_{8.7}$: the peak intensity of the 8.7 μm band of diethyl ether, P_E: the partial pressure of diethyl ether) against the partial pressure of propylene, P_P. $H_{8.7}/P_E$ can be regarded as the intensity per unit concentration of diethyl ether, and therefore, this variable is considered to be a measure of the spectral sensitivity. It is seen that the sensitivity clearly depends on P_P, though the changes of $H_{8.7}/P_E$ with P_P are more gentle than the dependence of $H_{8.7}/P_E$ on P_E.[2] It appears that there is an optimum range of P_P to give the maximum degree of sensitization.

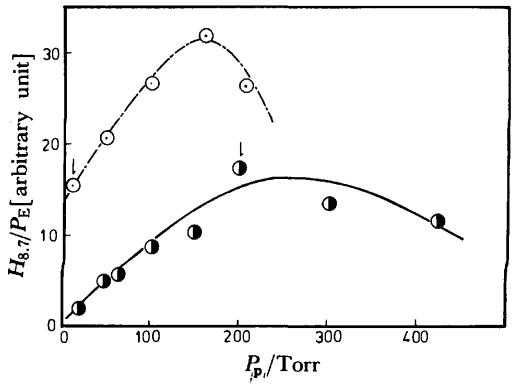

Fig. 1. Plots of values of $H_{8.7}/P_E$ *vs.* P_P on diethyl ether–propylene mixed sample.
$H_{8.7}$: Peak height of 8.7 μm band of diethyl ether, P_E: partial pressure of diethyl ether, P_P: partial pressure of propylene. ◑: P_E=20 Torr, ⊙: P_E=1 Torr. The data marked with arrows correspond to molar ratio of 1:1 (diethyl ether:propylene).

We examined the fashion of the curves in Fig. 1 in view of the kinetics of the energy transfers relating to the infrared emissions in question. We assume that five vibrationally excited energy levels are involved in the kinetics of the energy transfers. One of them is a level of propylene which is responsible for the absorption of the exciting laser light, and the others are those of diethyl ether. Three of the latter four levels yield the infrared emission bands, and the remaining one is representative of all other levels. Moreover, we assume that the sample system is in the stationary state. Under these conditions, the following expression is derived for the population of the emitting energy levels, *i.e.*,

$$X_i = \frac{A_iP_S^5+B_iP_S^4+C_iP_S^3+D_iP_S^2+E_iP_S+F_i}{P_S^5+G_iP_S^4+H_iP_S^3+I_iP_S^2+J_iP_S+K_i}, \quad (1)$$

where X_i is the population of the i-th energy level of the objective sample molecule, resulting from the energy transfers, P_S is the partial pressure of the sensitizer (in this case, P_P), and A_i, B_i, *etc.*, are the constants related to the rate constants for various energy transfers. Formula (1) predicts that when P_S becomes greater, the fashion of the change of X_i (consequently, the fashion of the intensity change of the i-th emission band) becomes gradually flat, converging ultimately to a constant, A_i. This partly explains the fashion of the curves in Fig.1.

Concerning the reason why the sensitivity lowers when P_P becomes greater than a certain magnitude, the following considerations may be possible. The first is the lowering of the effective absorption coefficient of propylene at 10.6μm because of the pressure broadening of rotational lines responsible for the absorption. The second is the weakening of the intensity of the exciting laser light due to the absorption of the added component. The third is that when the number of propylene molecules becomes much larger than that of diethyl ether, the energy first absorbed by propylene molecules may be transferred mainly to the same molecules rather than to diethyl ether. Of course, these are only speculations, and it is highly probable that some other factors play essential roles in the experimental results in question. The problem is related to the mechanism of the

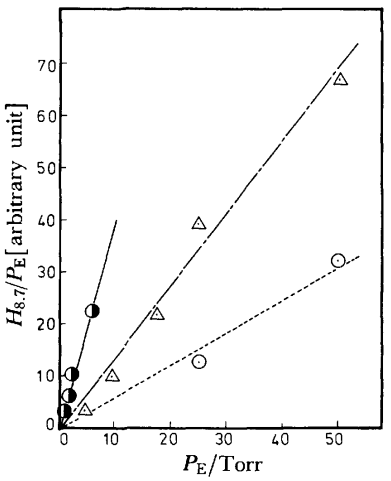

Fig. 2. Effect of molar ratios of diethyl ether to ethylene on the relations between IR-F intensities of 8.7 μm band of diethyl ether and P_E.
◑: 1:100 (diethyl ether:ethylene), △: 1:5, ⊙: 1:1. The points in the case of the molar ratio of 1:1 are only a part of the data up to P_E=100 Torr, which fit well to the straight line shown in the figure.

sensitization effect, and we are not in a position to make further mention of it in the present note.

It is noteworthy that the optimum range of P_p in the case of both P_E=20 Torr (1 Torr≈133.322 Pa.) and P_E=1 Torr seems to be not so different. This fact can be favourably utilized when the effect in question is made use of in analytical applications. Furthermore, it is also noticeable that the values of $H_{8.7}/P_E$ corresponding to the equal molar ratio between diethyl ether and propylene appear to be constant.

Therefore, we have examined the IR-F intensities in terms of the molar ratios between diethyl ether and a sensitizing agent. Figure 2 shows the result for diethyl ether–ethylene system. In this figure are shown the relations between $H_{8.7}$ and P_E for the individual constant molar ratios. From these results, it was proved that the slopes of the straight lines, *i.e.*, $H_{8.7}/P_E$, are kept constant for each of the molar ratios, and that the sensitivity of IR-F becomes rapidly greater when the quantities of ethylene increase relative to those of diethyl ether. The latter result is consistent with the phenomena that $H_{8.7}/P_E$ increases rapidly with lowering P_E under the constant partial pressure of ethylene. To sum up, the IR-F sensitivity changes not only with the quantity of diethyl ether but also with that of sensitizing agents, and the sensitivity is not influenced independently by the two quantities but by the relative magnitudes of them.

The Influence of the Kind of Alkenes on the Degree of Sensitization. We have examined the difference in degree of sensitization due to the kind of alkenes. In Fig. 3 are shown the IR-F spectra for the mixed samples which consist of 50 Torr of diethyl ether and 50 Torr of various alkenes. It is clear that the IR-F intensities of the 8.7 μm band of diethyl ether are markedly different according to the kind of alkenes. Figure 4 shows graphically the dependence of the intensities of the 8.7 and 7.1 μm band of diethyl ether on the kind of sensitizing compounds. It is seen that as the alkene molecules become larger, the sensitized IR-F intensities lower in an orderly fashion. Although any definite interpretation for this result can not be given at present, it can be supposed that the factors which may be related to the phenomenon are the

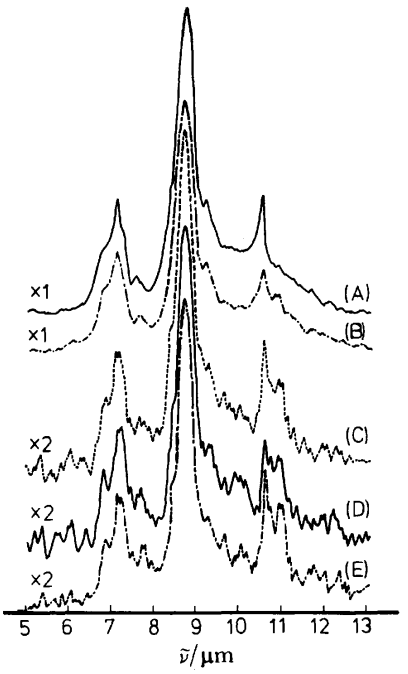

Fig. 3. Effect of the kind of alkenes on IR-F spectra of diethyl ether–alkene mixed samples. (A) ethylene, (B) propylene, (C) 1-butene, (D) 1-pentene, (E) 1-hexene. The instrumental sensitivity for the spectra (C), (D) and (E) is set twice higher than that for (A) and (B).

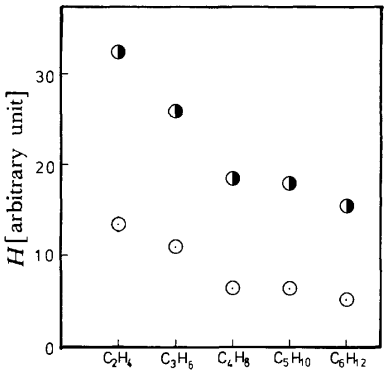

Fig. 4. Effect of the kind of alkenes on IR-F intensities of 8.7 and 7.1 μm bands of diethyl ether.
◑: 8.7 μm band, ⊙: 7.1 μm band.

following, *i.e.*, the characteristics and the number of vibrational levels of the alkenes involved, the intensities of the absorption at 10.6 μm and the agreement of the wavelengths of excitation laser lines with the rotational absorption lines of the alkenes, *etc.*

It can be concluded that though there remain many problems unsolved, the present experimental results give useful guide for the analytical and structural applications of the IR-F spectra sensitized by addition of the alkenes.

References

1) S. Higuchi, N. Kihara, H. Waki, and S. Tanaka, *Chem. Lett.*, **1981**, 609.
2) Y. Kagawa, S. Higuchi, and S. Tanaka, *Bull. Chem. Soc. Jpn.*, **55**, 1437 (1982).

Immunoassay Using a Metal-complex Compound as a Chemiluminescent Catalyst. III. Flow-through Analysis of a Labeled Antigen Bound by Immune Reaction

Tadashi HARA,* Motohiro TORIYAMA, and Kazuhiko TSUKAGOSHI
Department of Chemical Engineering, Faculty of Engineering, Doshisha University, Karasuma Imadegawa, Kamigyo-ku, Kyoto 602
(Received May 26, 1983)

Synopsis. By measuring the chemiluminescence intensity by the flow-through method rather than the conventional batchwise method, the sensitivity and precision of immunoassay and the time required for the measurement of the chemiluminescence intensity were improved as follows: 20 ng—50 μg of human albumin per tube, 5.8—7.2% (n=9) coefficient of variation, and 4 min measuring time.

Studies on automatic and continuous immunoassay have been made for non-labeled immunoassays such as laser nephelometry[1-3] and latex-photometric immunoassay,[4] but few such attempts have been made for a labeled immunoassay like enzyme immunoassay (EIA), because the enzyme as a labeling reagent is more unstable than an ordinary chemical reagent and requires some reaction time.

Chemiluminescence complex catalyst immunoassay(CLCCIA), in which a synthesized metal-complex compound acting as a labeling reagent, was reported by the authors for the determination of human serum albumin(HSA) as a model compound for the protein.[5] CLCCIA was also shown to provide the sensitivity necessary for practical immunoassay.[6] Moreover, CLCCIA has the following advantages in comparison with EIA: 1) The labeling reagent, that is, the metal-complex compound is more stable. 2) The analysis utilizing chemiluminescence reaction is more rapid. Judging from these advantages, CLCCIA is suitable for automatic and continuous immunoassay. As the first step for determining such a procedure, a flow-through apparatus by which the chemiluminescence intensity(CL intensity) could be continuously measured was set up and its performance was investigated.

The present method was superior to the previous batchwise method in the following points: 1) The time necessary for the measurement of the CL intensity was reduced to about one-tenth. 2) The limit of detection was also reduced to about one-half. And 3) the coefficient of variation for the measurement was smaller.

Experimental

The following procedures were done as explained in the previous paper:[6] synthesis of iron(III) 4,11,18,25-tetrakis-(chlorocarbonyl)phthalocyanine (TCCP-Fe(III)) as a labeling reagent, labeling of TCCP-Fe(III) to the HSA chosen as an analyte model, preparation of glass beads immobilized with antibodies(Ab-bead), and the competitive immune reaction between labeled HSA and HSA.

A schematic flow diagram of the apparatus used for the measurement of the CL intensity is shown in Fig. 1. Each bottle was filled with (a) a 1.0×10^{-3} mol/dm^3 5-amino-2,3-dihydro-1,4-phthalazinedione (luminol) solution (pH 11.4, a 0.014 mol/dm^3 disodium tetraborate–0.03 mol/dm^3 sodium hydroxide buffer solution (BS-I)), (b) BS-I as a liberating solution, (c) a washing solution (pH 7.2, a 0.0072 mol/dm^3 disodium hydrogenphosphate buffer solution (BS-II)), and (d) a 7.5×10^{-3} mol/dm^3 hydrogen peroxide (H_2O_2) solution.

Each solution was fed at the flow rate of 2.5 cm^3/min by means of pump (e) (ATTO, Perista Mini-pump SJ1211). The CL intensity at the flow-cell (i), which was obtained by winding spirally a 40 cm×0.8 mm diam. transparent poly(vinyl chloride) tube, was measured by means of a photon counter(k)(high voltage=−900 V, gate time=0.1 s, discriminator=330 mV) (Hamamatsu TV, C1230) equipped with a photomultiplier(j) (Hamamatsu TV, R464). The output was recorded with a recorder(l) (Matsushita Communication Industrial, VP6521A).

The CL intensity was measured as follows: 1) The Ab-bead (g) which had been washed with BS-II after the immune reaction was put into a sampler (f) and washed with a washing solution (c) for 2 min. 2) A liberating solution was sent onto an Ab-bead in a sampler from (b) by operating a six-way cock (h) and some labeled antigen was liberated from an immune complex. The liberated HSA and labeled HSA were both introduced into a flow-cell (i), and the chemiluminescence of luminol, which was based on the catalytic action of TCCP-Fe(III) on a labeled HSA, was measured. The maximum CL intensity was obtained in about 30 s after operating a six-way cock, and a standard curve of HSA was obtained from the maximum CL intensity. 3) The inside of the sampler was washed for 1 min with a washing solution by operating again a six-way cock 1 min after its first operation. The Ab-bead in the sampler was replaced by a new Ab-bead and the same procedure was repeated.

Results and Discussion

An immune complex dissociates in a strongly acidic or basic solution as well as a high concentration of salt solution. In order to examine the liberation of antigen from an immune complex, each Ab-bead after immune reaction was washed for 3 min with each pH of solution and the CL intensity due to the labeled HSA on an

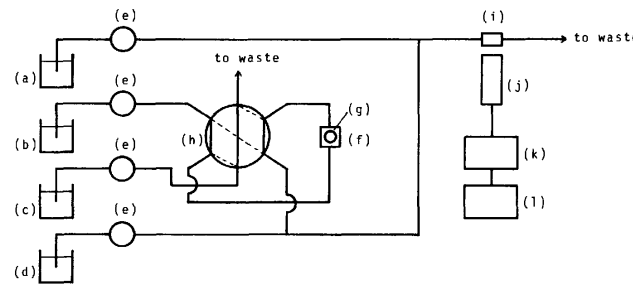

Fig. 1. Schematic flow diagram.
a: Luminol solution (pH 11.4), b: liberating solution (pH 11.4), c: washing solution (pH 7.2), d: H_2O_2 solution, e: pump, f: sampler, g: Ab-bead, h: six-way cock, i: flow-cell, j: photomultiplier, k: photon counter, and l: recorder.

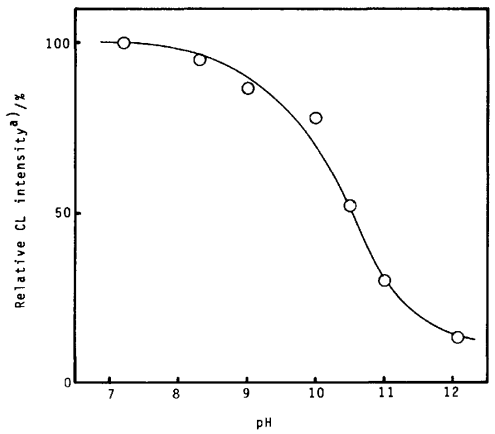

Fig. 2. Effect of pH of a washing solution on the CL intensity.
a) CL intensity at pH 7.2 of a washing solution was normalized to 100%.

Ab-bead was measured by the previous batchwise method (Fig. 2).

As shown in Fig. 2, the CL intensity decreased with an increasing pH value and this decrease corresponded to the amount of labeled HSA which was lost during washing. Most of the immune complex was found to dissociated only by putting an Ab-bead into a washing solution having pH value over 11. On the basis of this result, we achieved a rapid and accurate immunoassay, in which an antigen was liberated from an Ab-bead after the immune reaction and in which the catalytic effect of TCCP-Fe(III) in a liberated antigen solution on the chemiluminescence between luminol and H_2O_2 was measured.

A flow-through apparatus was set up to measure the CL intensity (Fig. 1). Both a luminol solution(a) and a liberating solution(b), shown in Fig. 1, were held at the same pH value and their pH values were changed simultaneously. This change was followed by measuring the CL intensity (Fig. 3). As can be seen from Fig. 3, the CL intensity increased with an increasing pH value of a luminol solution and a liberating solution, and gave a constant value in the vicinity of pH 12. By taking the large background of chemiluminescence at high pH into account, pH 11.4 was chosen as both the luminol solution and the liberating solution in the following experiments.

The relationship between the CL intensity and washing time of an Ab-bead with washing solution(c) shown in Fig. 1 was examined. No change in the CL intensity was observed in 1 to 10 min of washing time; so 2 min washing was recommended.

A standard curve of HSA was obtained under the above-mentioned optimum conditions (Fig. 4). According to the present method, up to 50 μg/tube HSA can be estimated with a limit of detection of 20 ng/tube

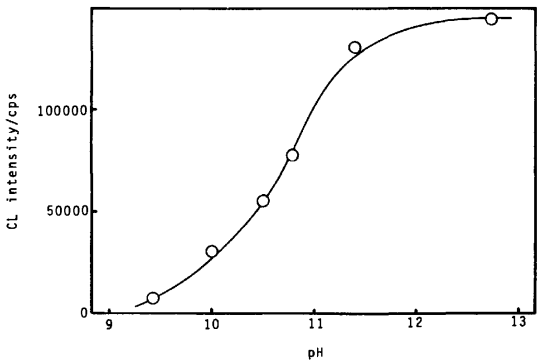

Fig. 3. Effect of pH of a luminol solution and a liberating solution on the CL intensity.

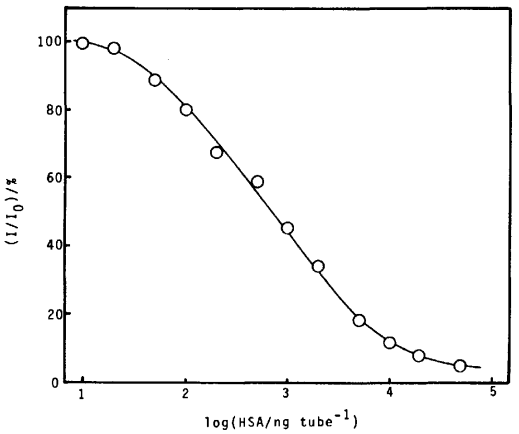

Fig. 4. Standard curve for HSA.
I, I_0: The CL intensity of the sample in the presence or absence of HSA.

and with coefficient of variation 5.8—7.2% for 9 analyses. The present method was superior to the previous batchwise method (limit of detection 50 ng/tube HSA and coefficient of variation 6—16%). The time necessary for analysis of a sample after immune reaction could be reduced to 4 min from 35 min in the previous batchwise method.

References

1) R. J. Cohen and G. B. Benedek, *Immunochemistry*, **12**, 349 (1975).
2) P. J. Wyatt, *Appl. Optics*, **7**, 1879 (1968).
3) P. J. Wyatt, *J. Colloid Interface Sci.*, **39**, 479 (1972).
4) H. Kakishima, K. Umezawa, N. Kubota, I. Oka, N. Tsubota, K. Morita, T. Kurozumi, Y. Takahashi, and S. Matsuzaki, *Nippon Rinshou Kensa Jidouka Gakkai Kaishi*, **8**, 156 (1983).
5) T. Hara, M. Toriyama, and K. Tsukagoshi, *Bull. Chem. Soc. Jpn.*, **56**, 2267 (1983).
6) T. Hara, M. Toriyama, and K. Tsukagoshi, *Bull. Chem. Soc. Jpn.*, **56**, 2965 (1983).

Polarographic Minimum Wave of Tetraiodocadmate(II) Complex in Acetonitrile

Yukio NAGAOSA* and Isao TANAKA
Faculty of Engineering, Fukui University, 3-chome Bunkyo, Fukui 910
(Received June 13, 1983)

Synopsis. Tetraiodocadmate(II) anion gives a polarographic minimum wave at potentials above −1.1 V *vs.* Ag/AgCl, when tetrabutylammonium iodide is used as a supporting electrolyte. The experimental results show that the minimum wave appears as a result of electrostatic repulsion between the cadmate(II) anion and the negatively charged mercury surface.

It is well-known that a normal polarographic wave is produced for metal complexes in acetonitrile of an inert aprotic solvent.[1-3] A polarographic minimum wave was observed for tetraiodocadmate(II) anion over the potential range from −1.1 to −1.5 V, when it was extracted into an acetonitrile phase containing 0.1 mol dm^{-3} tetrabutylammonium iodide as the supporting electrolyte and as the extracting agent. An electrochemical interpretation is attempted on the minimum wave in the presence of quaternary ammonium salts, based on the experimental evidence of the electrocapillary curves, the current-time (*i–t*) curves and the effect of different surfactants or inorganic salts. Until now, there has been little reported on the minimum wave in acetonitrile in contrast with the aqueous solutions.[4,5] Further, we should pay attention to the choice of supporting electrolytes in the anodic stripping analysis,[6] because the pre-electrodeposition efficiency is decreased at the potential range inducing such a minimum wave.

Experimental

Cadmium(II) in aqueous solution (20.0 cm^3) is quantitatively extracted into the aqueous phase (10.0 cm^3) containing 0.1 mol dm^{-3} quaternary ammonium iodide, when 10.0 g of ammonium sulfate and a small amount of ascorbic acid were added. A Yanako P-8 polarograph was used for all polarographic work. The electrochemical cell was equipped with a silver-silver chloride reference electrode, a platinum wire counter electrode and the dropping mercury electrode which had the capillary characteristics: m= 0.932 mg s^{-1} and t=6.01 s at an open circuit in acetonitrile. A Watanabe Sokki WTR-2C oscillograph linear corder was used for measuring *i–t* curves, in which a 1 kΩ resistor was inserted into the platinum counter electrode in a series. The chemicals used were available from Wako Junyaku Co., Ltd. The other experimental procedures were similar to that described earlier.[7]

Results and Discussion

Figure 1 shows d.c. polarograms for the teraiodocadmate(II) ion which was extracted into acetonitrile phases containing different kinds of quaternary ammonium iodide (0.1 mol dm^{-3}). Normal well-defined waves were obtained with tetraethylammonium iodide (TEAI) and tetrapropylammonium iodide (TPrAI) at $E_{1/2}$=−0.77 V *vs.* Ag/AgCl, while polarographic minimum waves appeared from about −1.1 V with tetrabutylammonium iodide (TBAI) and tetrapentylammonium iodide (TPeAI). The limiting current on the four polarographic waves were all diffusion-controlled. To clarify the difference in the polarographic wave, we investigated the electrode reaction between the cadmate(II) ion and the mercury electrode by means of the conventional polarographic analysis.[8] The plots of log $i/(i_d-i)$ *vs.* E for the d.c. waves yield straight lines with reciprocal slopes of 30.9 and 34.1 mV for TEAI and TBAI at 25 °C, respectively. It is obvious that the reversibility of the electrode reaction is lowered for TBAI. The electrocapillary and *i–t* curves were examined to ascertain whether the cadmate(II) ion was adsorbed onto the mercury electrode on electrolysis or not. From the electrocapillary curves

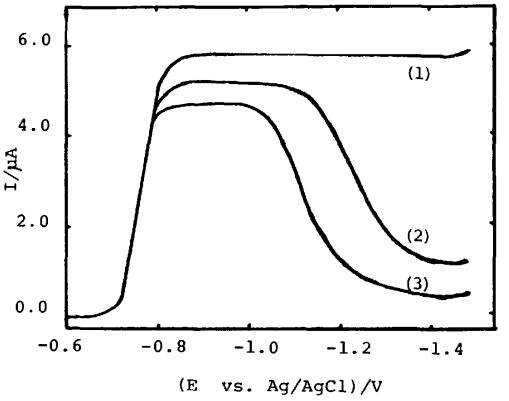

Fig. 1. D.c. polarograms of 8.8×10^{-4} mol dm^{-3} tetraiodocadmate(II) complex in acetonitrile.
Supporting electrolyte: (1) 0.1 mol dm^{-3} TEAI or TPrAI; (2) 0.1 mol dm^{-3} TBAI; (3) 0.1 mol dm^{-3} TPeAI.

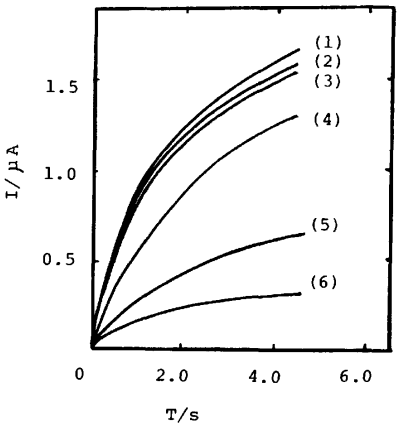

Fig. 2. *i–t* curves for 8.8×10^{-4} mol dm^{-3} tetraiodocadmate(II) complex at various potentials.
(1): 0.1 mol dm^{-3} TEAI at potentials from −1.0 to −1.5 V; (2): 0.1 mol dm^{-3} TBAI at −1.0 V; (3): −1.1 V; (4): −1.2 V; (5): −1.3 V; (6): −1.4 V.

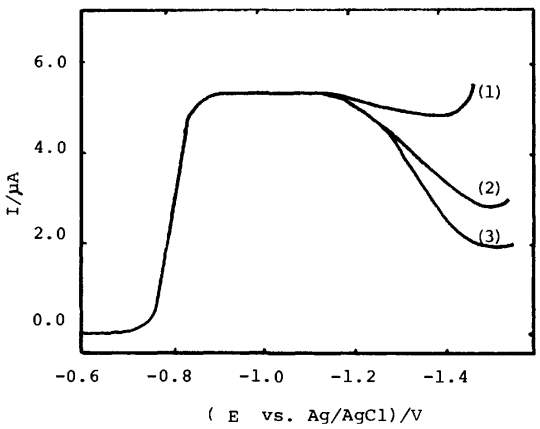

Fig. 3. Effect of inorganic salts on d.c. polarogram of 8.8×10^{-4} mol dm^{-3} tetraiodocamate(II) complex in acetonitrile containing 0.1 mol dm^{-3} TBAI. (1): 0.08 mol dm^{-3} $Al(ClO_4)_3$, (2): 0.07 mol dm^{-3} $LiClO_4$, (3): 0.04 mol dm^{-3} $LiClO_4$.

obtained, it was found that the drop-time was gradually decreased at the potential range from −0.8 to −1.5 V, and that no sharp decrease of drop-time was observed in both cases of TEAI and TBAI. The *i–t* curves shown as in Fig. 2 indicate that the current is almost proportional to $t^{1/6}$ at all potentials investigated, even above −1.1 V for TBAI. These results reveal that no adsorption of the ionic species onto the mercury electrode occurs. There seems to be other reasons for the appearance of the polarographic minimum wave in acetonitrile containing 0.1 mol dm^{-3} TBAI.

The effect of various surfactants and inorganic salts on the minimum wave was investigated for TBAI. It was observed that the addition of triton X-100 and hexadecyltrimethylammonium chloride to the acetonitrile solution recovered the diminution of the reduction current for the cadmate(II) ion at potentials above −1.1 V, but that of sodium dodecylbenzenesulfonate does not. It is interesting to note from Fig. 3 that more positive effect of recovering the minimum wave was obtained with the addition of cations of higher valency ($Al^{3+}>Li^+$). It is also noted that the degree of depression on the minimum wave was decreased as the concentration of salts added was increased.

Y. Umezawa *et al.* have discussed the polarographic behavior of minimum waves for inorganic anions in aqueous medium, based on the quantum mechanical effect and the electrostatic one.[9] In the present study, the appearance of the minimum wave can merely be explained in terms of the electrostatic model:[10] the minimum wave takes place with the electrostatic repulsion between the cadmate(II) anion and the negatively charged mercury surface. This is because the presence of cationic substances gives rise to normal reduction waves. When the large TBA^+ ion was exchanged with a small cation near the mercury electrode, the cadmate(II) ion is possible to approach to the electrode where as a result the electron transfer occurs to a more greater extent. We also consider that the large TBA^+ ion interfere sterically with the approach of the cadmate(II) ion to the electrode. It seems that a slightly negative shift of $E_{1/2}$ by addition of Li^+ or Al^{3+} is attributed to the ion-pair formation with the cadmate(II) ion, or to the salt effect due to increasing supporting electrolyte.[11]

References

1) I. M. Kolthoff, *J. Polarogr. Soc.*, **10**, 22 (1965).
2) R. Takahashi, *Talanta*, **12**, 1211 (1965).
3) C. K. Mann, "Electroanalytical Chemistry," ed by A. J. Bard, Marcel Dekker, New York, (1969), Vol. 3.
4) A. N. Frumkin, *Z. Electrochem.*, **59**, 807 (1955).
5) I. M. Kolthoff and C. S. Miller, *J. Am. Chem. Soc.*, **63**, 1405 (1941).
6) Y. Nagaosa, unpublished results.
7) T. Fujinaga and Y. Nagaosa, *Bull. Chem. Soc. Jpn.*, **53**, 416 (1980).
8) I. M. Kolthoff and J. J. Lingane, "Polarography," Interscience, New York, (1952).
9) Y. Umezawa, M. Hirota, and S. Fujiwara, *Bull. Chem. Soc. Jpn.*, **47**, 1181 (1974).
10) A. N. Frumkin, *Trans. Faraday Soc.*, **55**, 156 (1959).
11) T. Fujinaga and I. Sakamoto, *J. Electroanal. Chem.*, **67**, 201 (1976).

Sodium Dibutyldiselenocarbamate. Analytical Application to the Extraction Spectrophotometry of Heavy Metals

Takaharu HONJO

Department of Chemistry, Faculty of Science, Kanazawa University, Kanazawa 920

(Received June 13, 1983)

Synopsis. Sodium dibutyldiselenocarbamate is soluble in water, and the form of its dibutyldiselenocarbamic acid is extractable by methylene dichloride; more than 99% of the reagent exists in the methylene dichloride phase in the pH region of 4—10. The reagent readily forms extractable chelates with Au^{III}, Co^{II}, Cu^{II}, Hg^{II}, Ni^{II}, Pd^{II}, and Zn^{II} while it gives considerable white precipitates with Ag^{I} and Hg^{II} in the pH region of 1—7. Each chelate in methylene dichloride absorbs at wavelengths lower than 400 nm. The peak of the copper(II) chelate with the molar absorbtivity of 1.50×10^4 at 442 nm is not affected by the spectra of the reagent and other metal chelates, and it can be used for the selective spectrophotometric determination of copper(II) up to 0—10 μg/cm³.

It is well known that heavy-transition metals form more stable complexes with chelating ligands which have π-acceptor donor atoms with unfilled pπ or dπ orbitals, like sulfur and selenium elements. However, scarcely no information on the solvent-extraction reagents with a selenium donor atom has been reported.[1,2] In a previous paper, the present author reported the synthesis of new monoseleno analogs of β-diketone, 1,1,1-trifluoro-4-(2-thienyl)-4-hydroseleno-3-buten-2-one and its analytical utility as an extraction-spectrohotometric reagent for heavy metals.[3] Now that author has investigated a selenium containing a chelating reagent of dithiocarbamate, sodium dibutyldiselenocarbamate, in the anticipation of enhanced stability and selectivity in reactions with heavy-transition metals; the investigation has been undertaken with analytical applications in view

Experimental

Apparatus. A model 323 Hitachi Recording Spectrophotometer; a model 239 Hitachi Digital Spectrophotometer; a Hitachi-Horiba glass electrode pH meter ,model M-5; an Iwaki shaking machine, model KM; a Kubota centrifuge machine, and a Yanagimoto Micro Melting-point Apparatus, Model MP-J2, were used.

Preparation of Metal Solution. The solution of the copper(II) ion was prepared by dissolving $CuSO_4 \cdot 5H_2O$ of a guaranteed-grade reagent in a slightly acidic hydrochloric acid solution to make a 10^{-1} M† aqueous solution. The concentration of the copper(II) ion was standardized complexometrically, and the solution was diluted as required with distilled water. The other guaranteed-grade metal salts of Ag^{I}, Au^{III}, Bi^{III}, Cd^{II}, Co^{II}, Cu^{II}, $Fe^{II,III}$, Hg^{II}, In^{III}, Ir^{III}, Mn^{II}, Ni^{II}, Pb^{II}, Pd^{II}, Pt^{II}, Rh^{III}, Sn^{II}, Tl^{I}, UO_2^{II}, VO_2^{I}, and Zn^{II} were also dissolved in distilled water or in an acidic hydrochloric or nitric acid solution to make a 10^{-1} M aqueous stock solution of each metal ion.

Synthesis of Sodium Dibutyldiselenocarbamate. Carbon diselenide was synthesized by the similar method of Barnard and Woodbridge.[4] It turns from a clear lemon-yellow color to orange within a couple of weeks and finally to black as solid-carbon diselenide polymers form; it is used as soon as possible for the synthesis of sodium dibutyldiselenocarbamate. Sodium dibutyldiselenocarbamate was synthesized by a slight modification of the method of Barnard and Woodbridge.[4]

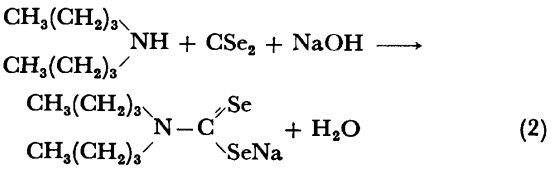

(2)

Carbon diselenide (2.11 g, 0.0124 M) in dioxane (20 cm³) was added to a solution of sodium hydroxide (0.5 g, 0.0124 M) and dibutylamine (1.6 g, 0.0124 M) in water (20 cm³) at −10 °C for 30 min while being stirred in an atmosphere of nitrogen. In order to avoid possible insoluble impurities coming from the polymerization of carbon diselenide, the solution was filtered once, and the sodium salt of dibutyldiselenocarbamate thus prepared was separated by extraction with methylene dichloride. The methylene dichloride solution was dried over anhydrous sodium sulfate, and the product was recovered by the evaporation of the excess solvent under low pressure. The sodium dibutyldiselenocarbamate thus obtained was an orange-red oily substance, which showed a melting point of 50—60 °C. The reagent was sealed in a brown-colored bottle in a nitrogen atmosphere and stored in a refrigerator kept at 5 °C.

Extraction Procedure. To an aqueous solution containing 10^{-6}—10^{-2} M metal ions we added 10^{-2} M acetic acid (in the pH region of 0—7) or 10^{-2} M boric acid (in the pH region of 7—13); its pH was adjusted to the desired value by means of a 0.1—1 M sodium hydroxide or hydrochloric acid solution. Ten cm³ of this solution and 10 cm³ of 3×10^{-5} M sodium dibutyldiselenocarbamate in methylene dichloride were then introduced into a 50-cm³ glass-stoppered centrifuge tube; the mixture was equilibrated for 1—30 min, after which the phases were separated by centrifugation. Metal complexes of dibutyldiselenocarbamate are also readily extractable in such organic solvents as chloroform, benzene, carbon tetrachloride, and isobutyl methyl ketone. In general, halogen-substituted hydrocarbons with large dielectric constants are superior for the extraction of metal complexes.

Results and Discussion

Sodium dibutyldiselenocarbamate is soluble in water to give a pH of 11.30 and is extractable with methylene dichloride; it is, in fact, remarkably stable in this solvent. However, sodium dibutyldiselenocarbamate is unstable in an acid medium, and the decomposition of the reagent gradually proceeds below pH 4. From the experimental results on the variation of the percentage of the extraction of sodium dibutyldiselenocarbamate (2×10^{-5} M) from an aqueous solution into methylene dichloride as a function of the pH, it was found that more than 99% of the reagent was in the

† 1 M = 1 mol dm⁻³.

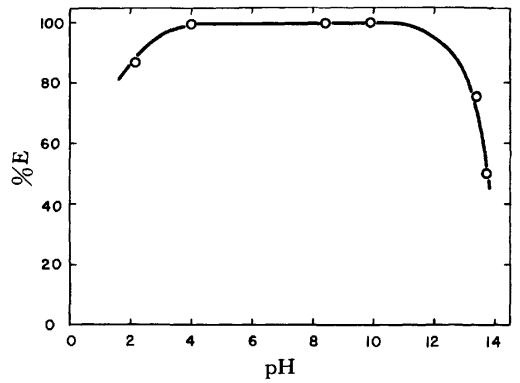

Fig. 1. Variation in the percentage extraction of 2×10^{-5} M dibutyldiselenocarbamic acid from an aqueous solution into methylene dichloride as a function of pH.

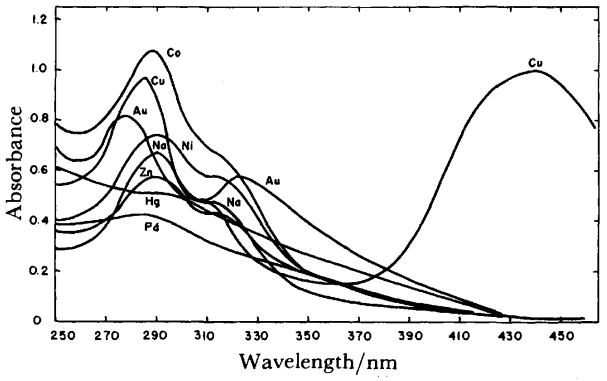

Fig. 2. Absorption spectra of 3×10^{-5} M sodium dibutyldiselenocarbamate and of 1.5×10^{-5} M its metal chelates in methylene dichloride.

methylene dichloride phase in the pH region of 4—10 within 5 min (Fig. 1). The pH value of an aqueous phase corresponding to a 50% extraction of the ligand was 13.7. The sodium dibutyldiselenocarbamate (10^{-3} M) readily forms extractable chelates into methylene dichloride with many metals (trace—10^{-2} M), such as Au^{III}, Co^{II}, Cu^{II}, Hg^{II}, Ni^{II}, Pd^{II}, and Zn^{II}, in the pH region of 1—7 within 30 min. Each metal chelate in methylene dichloride absorbs at wavelengths lower than 400 nm (Fig. 2), shows its own specific color, and has absorption maxima (λ_{max}/nm), as is shown in Table 1, together with the results for dibutyldithiocarbamate. The electronic spectra of metal complexes of dibutyldiselenocarbamate closely resemble those of the corresponding dibutyldithiocarbamate in intensity and position, except for a general red shift, that is, a slight shift to longer wavelengths. Ag^{I} and Hg^{II} give white precipitates. The reaction of the sodium dibutyldiselenocarbamate with Bi^{III}, Cd^{II}, $Fe^{II,III}$, In^{III}, Ir^{III}, Mn^{II}, Pb^{II}, Pt^{II}, Rh^{III}, Sn^{II}, UO_2^{II}, VO_2^{I}, and Tl^{I} is not observed distinctly. The molar absorptivity at the λ_{max} of sodium dibutyldiselenocarbamate and its copper(II) chelate, expressed in cm^2 l mol^{-1}, is 2.37×10^4 (288.5 nm) and 1.69×10^4 (311 nm) for the ligand and 6.66×10^4 (283.2 nm), 3.00×10^4 (308 nm), and 1.50×10^4 (440 nm) for the complex respectively. The peak of the copper chelate at 442 nm is not affected by the spectra of the ligand and other metal chelates, is stable at least for several hours, and can be used for the selective-extraction spectrophotometric determination of copper(II) up to 0—10 μg/cm^3 without such treatment as masking the foreign cations. The results reveal that dibutyldiselenocarbamate has analytical potentiality as diethyldithiocarbamate, one of the most useful agents.[2,7]

Table 1. Extraction of metals with sodium dibutyldiselenocarbamate in methylene dichloride in the pH region of 1—7

Metal[a]	Color	λ_{max}/nm	Remarks
Na^{I}	Colorless	288.5, 311[b] (281)	
Ag^{I}	Colorless		ppt.
Au^{III}	Bright-brown	275.5, 319.8[b] (275, 319)	
Co^{II}	Bright-brown	288.5, 315[b] (259, 285)	
Cu^{II}	Yellow-green	283.2, 308,[b] 440 (273, 287,[b] 430)	
Hg^{II}	Colorless	290[b] (252, 276)	ppt.
Ni^{II}	Yellow	289.5, 311.5[b] (261, 280)	
Pd^{II}	Orange-brown	283.0 (275)	
Zn^{II}	Yellow	288.5, 313.0[b] (266, 282[b])	

a) The reaction of sodium dibutyldiselenocarbamate with Bi^{III}, Cd^{II}, $Fe^{II,III}$, In^{III}, Ir^{III}, Mn^{II}, Pb^{II}, Pt^{II}, Rh^{III}, Sn^{II}, Tl^{I}, UO_2^{II}, and VO_2^{I} was not observed distinctly. b) Shoulder.
The values in brackets are the absorption maxima of metal dibutyldithiocarbamates. Sodium dibutyldithiocarbamate (mp 33—34 °C) was synthesized by using the method of Klapping and Van der Kerk.[5,6]

References

1) T. Honjo and T. Kiba, *Bunseki Kagaku*, **21**, 676 (1972).
2) K. Burger, "Organic Reagents in Metal Analysis," Pergamon Press, Oxford (1973).
3) T Honjo, *Chem Lett.*, **1974**, 481.
4) D. Barnard and D. T. Woodbridge, *J. Chem. Soc.*, **1966**, 2922.
5) H. L. Klöpping and G. J. M. Van der Kerk, *Recl. Trav. Chim. Pays-Bas*, **70**, 917 (1951).
6) T. Honjo, H. Imura, S. Shima, and T. Kiba, *Anal. Chem.*, **50**, 1545 (1978).
7) T. Honjo and H. Imura, *Bull. Chem. Soc. Jpn.*, **53**, 1753 (1980).

The Crystal Structure of Calcium Sulfite Tetrahydrate. Interatomic Distances and Angles

Takashi MATSUNO,* Hiroaki TAKAYANAGI,† Kimio FURUHATA,† Masumi KOISHI,†† and Haruo OGURA,†

School of Medicine, Kitasato University, Kitasato, Sagamihara 228

†*School of Pharmaceutical Sciences, Kitasato University, Shirokane, Minato-ku, Tokyo 108*

††*Faculty of Pharmaceutical Sciences, Science University of Tokyo, and Institute of Colloid and Interface Science, Ichigaya, Funagawaramachi, Shinjuku-ku, Tokyo 162*

(Received June 16, 1983)

Synopsis. Detailed geometries of the sulfite ions and of the oxygen-coordinations around the calcium ions in calcium sulfite tetrahydrate were determined based on the results of the X-ray analysis. It was revealed that the structure consists of two alternating layers, one consisting of calcium ions and water molecules, and the other consisting of sulfite ions and water molecules.

In a previous paper[1] we reported the preparation, the solution and refinement of the crystal structure and the mode of disorder of a sulfite ion of calcium sulfite tetrahydrate. The interatomic distances and angles of the hydrates and anhydride of calcium sulfate were reported in detail.[2-7] But no study has been reported on geometries of the sulfite ions and of the oxygen neighbors of the calcium ions in calcium sulfites. This note reports the interatomic distances and angles and the characteristic layer structure of calcium sulfite tetrahydrate.†††

The atomic coordinates used for the present calculations are the same as in the previous paper.[1]

Results and Discussion

A projection of a part of the structure along the c axis and numbering of the atoms are shown in Fig. 1. The $S(2)O_3^{2-}$ ion is in a disordered state.[1] It can be presumed that the low thermostability of the tetrahydrate is caused by the $S(2)O_3^{2-}$ ion in the disordered state.

The interatomic distances and angles are given in Tables 1 and 2. The S–O and O–O interatomic distances and O–S–O bond angles in the $S(1)O_3^{2-}$ ion are 1.52(2)—1.53(3) Å, 2.37(1)—2.39(1) Å, and 102.2(3)—102.9(4)°, respectively. The corresponding distances and angles in the $S(2)O_3^{2-}$ ion are 1.43(3)—1.44(5) Å, 2.19(4)—2.45(5) Å, and 98.9(14)—117.2(10)°, respectively. These values show that the degree of symmetry of the $S(2)O_3^{2-}$ ion is lower than that of the $S(1)O_3^{2-}$ ion. The average S(2)–O bond distance of 1.44 Å is approximately the same as the S–O bond distances in SO_4^{2-} ions (calcium sulfate dihydrate 1.459 Å,[2-4] calcium sulfate anhydride 1.44 Å[5-7]), but is considerably short-

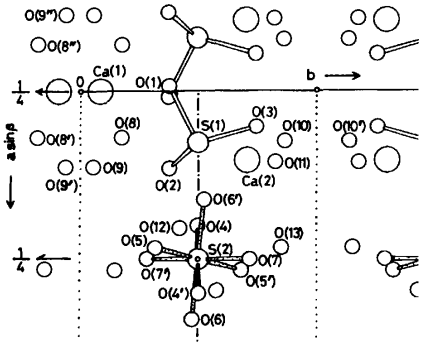

Fig. 1. Projection of the structure along the c axis and numbering of the atoms.

TABLE 1. INTERATOMIC DISTANCES (l/Å) AND THEIR ESTIMATED STANDARD DEVIATIONS

Ca(1)-O(1)	2.53(1)	S(1)-O(3)	1.53(1)
Ca(1)-O(2)	2.53(7)	O(1)-O(2)	2.39(1)
Ca(1)-O(8')	2.38(5)	O(1)-O(3)	2.38(1)
Ca(1)-O(9')	2.45(1)	O(2)-O(3)	2.37(1)
Ca(1)-O(8")	2.38(5)	S(2)-O(4)	1.44(5)
Ca(1)-O(9")	2.45(1)	S(2)-O(5)	1.43(3)
Ca(2)-O(2)	2.52(1)	S(2)-O(6)	1.44(4)
Ca(2)-O(3)	2.52(3)	S(2)-O(7)	1.44(2)
Ca(2)-O(10')	2.45(1)	O(4)-O(5)	2.44(4)
Ca(2)-O(11)	2.38(1)	O(4)-O(6)	2.43(11)
Ca(2)-O(12)	2.45(1)	O(4)-O(7)	2.45(5)
Ca(2)-O(13)	2.38(9)	O(5)-O(6)	2.22(4)
Sulfite ion		O(5)-O(7)	2.25(3)
S(1)-O(1)	1.53(3)	O(6)-O(7)	2.19(4)
S(1)-O(2)	1.52(2)		

TABLE 2. BOND ANGLES (ϕ/°) AND THEIR ESTIMATED STANDARD DEVIATIONS

O(1)-Ca(1)-O(2)	56.4(2)	O(13)-Ca(2)-O(3)	85.1(3)
O(1)-Ca(1)-O(9")	74.4(2)	O(13)-Ca(2)-O(12)	77.1(3)
O(9")-Ca(1)-O(8")	78.8(3)	O(13)-Ca(2)-O(11)	103.2(3)
O(8")-Ca(1)-O(9')	77.1(3)	O(13)-Ca(2)-O(10')	79.2(2)
O(9')-Ca(1)-O(2)	78.8(2)	Ca(1)-O(2)-Ca(2)	104.6(2)
O(8')-Ca(1)-O(1)	87.0(3)	Sulfite ion	
O(8')-Ca(1)-O(2)	85.1(2)	O(1)-S(1)-O(2)	102.9(4)
O(8')-Ca(1)-O(9")	77.1(3)	O(1)-S(1)-O(3)	102.2(3)
O(8')-Ca(1)-O(8")	102.5(3)	O(2)-S(1)-O(3)	102.3(4)
O(8')-Ca(1)-O(9')	78.8(3)	O(4)-S(2)-O(5)	117.2(10)
O(2)-Ca(2)-O(3)	56.3(2)	O(4)-S(2)-O(6)	115.7(13)
O(12)-Ca(2)-O(2)	74.7(3)	O(4)-S(2)-O(7)	117.1(10)
O(11)-Ca(2)-O(12)	78.8(3)	O(5)-S(2)-O(6)	102.0(14)
O(10')-Ca(2)-O(11)	77.1(3)	O(5)-S(2)-O(7)	103.2(15)
O(3)-Ca(2)-O(10')	78.9(3)	O(6)-S(2)-O(7)	98.9(14)
O(13)-Ca(2)-O(2)	86.5(2)		

††† The anisotropic temperature factors and the complete F_o—F_c data are deposited as Document No. 8405 at the Office of the Editor of Bull. Chem. Soc. Jpn.

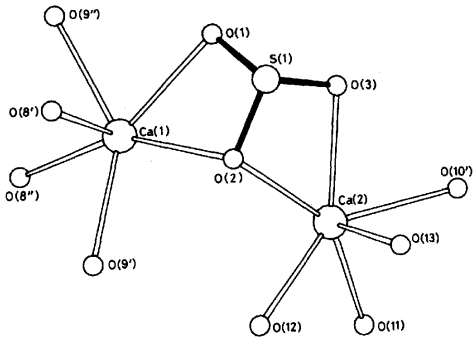

Fig. 2. Environment of the calcium ions.

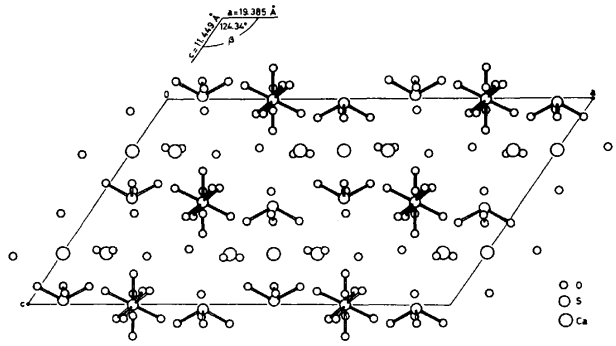

Fig. 3. Projection of the structure along the b axis.

er than 1.53 Å in the $S(1)O_3^{2-}$ ion. One of the reasons for the difference of the S–O bond distances between $S(1)O_3^{2-}$ and $S(2)O_3^{2-}$ may be that only the O atoms of the $S(1)O_3^{2-}$ ion coordinate to the Ca^{2+} ions (*cf.* Fig. 2). Another reason may be that, in many cases, the interatomic distances and angles calculated from the coordinates of the atoms which are in a disordered state give rise to apparent deviations from the usual values.

The coordinations of the O atoms around the Ca^{2+} ions are shown in Fig. 2. Both Ca(1) and Ca(2) are coordinated by six O atoms in distorted octahedral arrangements: two O atoms originate from the $S(1)O_3^{2-}$ ion, and the other four from water molecules. The Ca(1)–O(1) distance is almost the same as the Ca(1)–O(2) distance. The Ca(1)–O(9′) and Ca(1)–O(9″), and the Ca(1)–O(8′) and Ca(1)–O(8″) distances are the same, respectively. The Ca(2)–O distances are similar to the Ca(1)–O distances; the average values are both 2.45 Å. These Ca–O distances are close to those (2.378—2.544 Å) in calcium sulfate dihydrate.[2-4] The O–Ca(2)–O bond angles are also similar to the corresponding O–Ca(1)–O angles. Thus, the geometries of the Ca(1)–O and Ca(2)–O coordinations resemble each other very closely.

The crystal structure viewed along the b axis is shown in Fig. 3. It is observed that two layers, one consisting of the Ca^{2+} ions and water molecules, and the other consisting of the SO_3^{2-} ions and water molecules, arrange alternately parallel to the (001) plane.

References

1) T. Matsuno, H. Takayanagi, K. Furuhata, M. Koishi, and H. Ogura, *Chem. Lett.*, **1983**, 459.
2) W. F. Cole and C. J. Lancucki, *Acta Crystallogr., Sect. B*, **30**, 921 (1974).
3) W. F. Cole and C. J. Lancucki, *Nature, Phys. Sci.*, **240**, 48 (1972).
4) W. F. Cole and C. J. Lancucki, *Nature, Phys. Sci.*, **242**, 104 (1973).
5) W. H. Baur, *Trans. Am. Cryst. Assoc.*, **6**, 192 (1970).
6) G. Ferraris and M. Catti, *Acta Crystallogr., Sect. B*, **29**, 2006 (1973).
7) J. A. McGinnety, *Acta Crystallogr., Sect. B*, **28**, 2845 (1972).

Preparation and Characterization of (L-Histidinato)-(L-methioninato)cobalt(III) Bromide

Ken-ichi OKAMOTO,* Hiroko MAKI, and Jinsai HIDAKA
Department of Chemistry, University of Tsukuba, Sakura, Ibaraki 305
(Received, June 24, 1983)

Synopsis. The (L-histidinato)(L-methioninato)cobalt(III) complex was prepared and separated into three geometrical isomers by ion-exchange chromatography. The isomers were characterized from their absorption, ^{1}H NMR, and CD spectra.

Some cobalt(III) complexes with terdentate amino carboxylates, such as L-methioninate, L-histidinate, and L-2,4-diaminobutyrate, have been investigated.[1-8] However, the stereochemical property of the thioether type sulfur atom of the L-met has not been clarified yet.[1,7] The coordinated L-met has a flexible conformation for the six-membered N–S chelate ring, while the L-his takes a rigid conformation for the six-membered N–N chelate ring. This rigidity of the L-his chelate ring is favorable for the investigation of the stereochemical property of the coordinated L-met. This note presents the preparation and separation of (L-histidinato)(L-methioninato)cobalt(III). The isomers obtained are characterized from their absorption, ^{1}H NMR and CD spectra and by comparison with those of $[Co(L\text{-met})_2]^+$[1] and $[Co(L\text{-his})_2]^+$.[2,3]

Experimental

[Co(L-his)(L-met)]Br. A solution of 2.4 g of $CoCl_2 \cdot 6H_2O$ in 5 cm^3 of water was added to a solution containing 1.5 g of L-Hhis and 1.5 g of L-Hmet in 25 cm^3 of water. To the solution 0.75 g of activated charcoal and 3 g of PbO_2 were gradually added and the mixture was then stirred at 60 °C for 40 min. The reaction mixture was filtered in order to remove the excess of PbO_2 and activated charcoal after cooling to room temperature. The filtrate was poured onto a column of Dowex 50W-X8 (Na^+ form, 4 cm×70 cm). After the column had been swept with water, the adsorbed band was eluted with 0.1 mol dm^{-3} aqueous solution of ammonium bromide. Nine colored bands, F1—F9, were eluted in succession. The F3 and F4 eluates or the F6 and F7 ones partially overlapped. Their absorption and CD spectral measurements showed that the F1, F6, and F8 eluates contained the isomers of $[Co(L\text{-his})_2]^+$[2,3] and the F2, F3, and F5 ones were the isomers of $[Co(L\text{-met})_2]^+$.[1] The F4 (violet), F7 (dark violet), and F9 (brown red) eluates, of which the formation ratio was *ca.* F4:F7:F9=2:2:1, were separately concentrated to about 10 cm^3 with a rotary evaporator below 30 °C. The deposited NH_4Br was filtered off and the filtrate was treated with a gel filtration chromatography (Sephadex G-10 resin). The resulting aqueous solution was concentrated with a rotary evaporator again. The crystals of each isomer were obtained by adding ethanol and then ether to the concentrated solution. Found for F4: C, 30.85; H, 4.30; N, 12.57%. Calcd for $[Co(L\text{-his})(L\text{-met})]Br=CoC_{11}H_{18}N_4O_4SBr$: C, 29.94; H, 4.11; N, 12.96%. Found for F7: C, 27.31; H, 4.29; N, 13.41%. Calcd for $[Co(L\text{-his})(L\text{-met})]Br \cdot 0.5NH_4Br$: C, 26.95; H, 4.11; N, 12.85%. Found for F9: C, 14.28; H, 4.11; N, 13.30%. Calcd for $[Co(L\text{-his})(L\text{-met})]Br \cdot 5NH_4Br$: C, 14.19; H, 4.11; N, 13.54%.

Measurements. Electronic absorption spectra were recorded with a JASCO UVIDEC-1 spectrophotometer and CD spectra with a JASCO J-20 spectropolarimeter. ^{1}H NMR spectra were recorded on a JEOL JNM-MH-100 NMR spectrometer in D_2O. Sodium 2,2-dimethyl-2-silapentane-5-sulfonate (DSS) was used as an internal reference. All the measurements were carried out at room temperature.

Results and Discussion

Three geometrical isomers were isolated for $[Co(L\text{-his})(L\text{-met})]^+$ (Fig. 1), and their absorption and CD spectra are shown in Fig. 2. Splitting pattern of the first absorption band is expected to reflect the geometry of each of the three isomers, as in the case of $[Co(L\text{-met})_2]^+$[1] and $[Co(L\text{-his})_2]^+$.[2,3] Namely, F4, F7, and F9 are assigned to *trans*(N_iS), *trans*(N_iO), and *trans*(N_iN), respectively, where N_i denotes an imidazole nitrogen atom in the L-his, in accordance with the expected

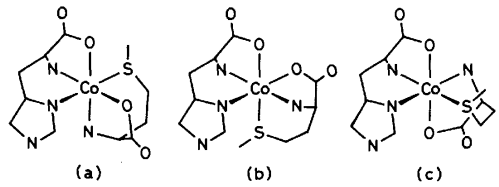

Fig. 1. Three possible isomers of $[Co(L\text{-his})(L\text{-met})]^+$; (a) *trans*($N_iS$), (b) *trans*($N_iO$), and (c) *trans*($N_iN$).

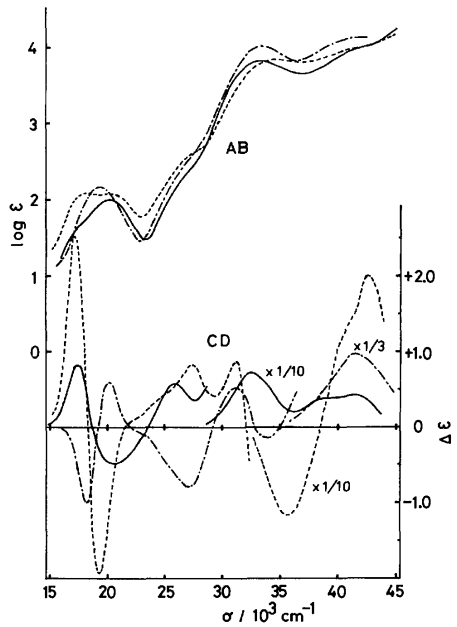

Fig. 2. Absorption and CD spectra of $[Co(L\text{-his})(L\text{-met})]^+$; *trans*($N_iS$) (-·-·-), *trans*($N_iO$) (——), and *trans*($N_iN$) (----).

Table 1. ^{1}H NMR spectral data of [Co(L-his) (L-met)]$^+$

	S-CH_3	H(C_2)[b]	H(C_5)[b]
trans (N_iS)	2.03[a]	7.78	7.24
trans (N_iO)	1.86	7.88	7.18
	2.12	8.22	7.26
trans (N_iN)	2.29	8.40	7.30

a) Ppm from DSS. b) H(C_2) and H(C_5) denote the 2-proton and 5-proton of imidazole, respectively.

splittigs which were estimated semiempirically.[1-7] As is shown in Table 1, the *S*-methyl proton signals of the *trans*(N_iS) and *trans*(N_iN) isomers appear in lower field than those of the *trans*(N_iO) one. This is in line with the ^{1}H NMR spectral behavior of the cobalt(III) complexes with D- or L-aspartate and L-methioninate;[7,8] namely, this result suggests that the imidazole and amino nitrogen atoms occupy the trans position to the sulfur atoms of the *trans*(N_iS) and *trans*(N_iN) isomers and the oxygen atom occupies the trans position to the sulfur atom of the *trans*(N_iO) one.[9,10] The information from the ^{1}H NMR spectra of the three isomers supports the assignment based on the absorption spectra. When the sulfur, oxygen or nitrogen atom occupies the trans position to the imidazole nitrogen atom, the resonance line of the C_2 proton (near 8 ppm) on the imidazole moiety shifts to the higher field in the order of *S*, *O*, and *N*.

The *R*(*S*) or *S*(*S*) configuration is expected for the coordinated sulfur atom of each isomer. The *trans*-(N_iO) isomer shows two signals due to the *S*-methyl protons and two sets of signals for each of the C_2 and C_5 protons of the imidazole moiety of the L-his (Table 1).[3,5,6] These facts indicate that the *trans*(N_iO) isomer is a mixture of *R*(*S*) and *S*(*S*) configurations. On the other hand, only one signal of the *S*-methyl protons and one set of signals due to the imidazole moiety are observed for the *trans*(N_iS) and *trans*(N_iN) isomers (Table 1). These suggest that the *trans*(N_iS) and *trans*-(N_iN) isomers selectively take the *R*(*S*) or *S*(*S*) configuration. Model construction reveals that the *S*(*S*) configuration is more probable for the *trans*(N_iS) isomer. The *trans*(N_iN) isomer has the *R*(*S*) configuration because the *S*(*S*) configuration is rejected by the striking repulsion between the *S*-methyl group and imidazole ring. The chromatographic separation was repeated for the F7 eluate which contained the *trans*-(N_iO) isomer, but all of its fractionated eluates showed quite similar CD spectra.

The *trans*(N_iS)- and *trans*(N_iN)-[Co(L-his)(L-met)]$^+$ isomers are quasi-antipodal in framework and show almost enantiomeric CD spectra in the first and second absorption band region (Fig. 2). In the region of (30—45)$\times 10^3$ cm^{-1}, however, the *trans*(N_iS) and *trans*(N_iN) isomers show similar CD patterns. The CD spectral behavior in the region of (30—45)$\times 10^3$ cm^{-1} depends mainly on the absolute configuration of the coordinated L-met and/or L-his, as in the case of the cobalt(III) complexes with *S*-methyl-L-cysteinate and *S*-methyl-L-penicillaminate.[11,12] In the first absorption band region, the *trans*(N_iN)-[Co(L-his)(L-met)]$^+$ isomer whose coordinated sulfur atom is regulated to the *R*(*S*) configuration shows a similar CD pattern and a similar intensity to those of the *trans*(*O*)-[Co(L-met)$_2$]$^+$[1] and *trans*(*O*)-[Co(L-his)$_2$]$^+$[2,3] whose frameworks are similar to that of the mixed complex. Some differences are observed for the other isomers of [Co(L-his)-(L-met)]$^+$, [Co(L-met)$_2$]$^+$, and [Co(L-his)$_2$]$^+$.[1-3] In the first absorption band region, the *trans*(N_iO)-[Co(L-his)(L-met)]$^+$ isomer shows two CD bands weaker than those of the *trans*(*N*)-[Co(L-met)$_2$]$^+$ and *trans*(*N*)-[Co(L-his)$_2$]$^+$ isomers, though the CD components in the higher energy side of the three isomers align at *ca.* 20×10^3 cm^{-1}.[1-3] A similar trend is observed for the *trans*(N_iS)-[Co(L-his)(L-met)]$^+$, *trans*(*S*)-[Co(L-met)$_2$]$^+$, and *trans*(N_i)-[Co(L-his)$_2$]$^+$, namely, the negative CD bands at *ca.* 18×10^3 cm^{-1} weaken gradually and shift to the lower energy in the order of the *trans*(N_i), *trans*-(N_iS) and *trans*(*S*) isomers.[1-3] These results suggest that the CD bands in the first absorption band region are contributed from the flexibility of the conformation of the six-membered N-S chelate ring in the L-methioninate.

References

1) J. Hidaka, S. Yamada, and Y. Shimura, *Chem. Lett.*, **1974**, 1487.
2) L. J. Zompa, *J. Chem. Soc., Chem. Commun.*, **1969**, 783.
3) S. Bagger, K. Gibson, and C. S. Sørgensen, *Acta Chem. Scand.*, **26**, 2503 (1972).
4) W. A. Freeman and C. F. Liu, *Inorg. Chem.*, **9**, 1191 (1973).
5) M. Watabe, H. Yano, and S. Yoshikawa, *Bull. Chem. Soc. Jpn.*, **52**, 61 (1979).
6) M. Watabe, M. Zama, and S. Yoshikawa, *Bull. Chem. Soc. Jpn.*, **51**, 1354 (1978).
7) T. Isago, K. Igi, and J. Hidaka, *Bull. Chem. Soc. Jpn.*, **52**, 407 (1978).
8) M. Watabe, K. Onuki, and S. Yoshikawa, *Bull. Chem. Soc. Jpn.*, **48**, 687 (1975).
9) U. Sakaguchi, S. Yamazaki, and H. Yoneda, *Bull. Chem. Soc. Jpn.*, **49**, 402 (1976).
10) Y. Nakashima, U. Sakaguchi, and H. Yoneda, *Bull. Chem. Soc. Jpn.*, **48**, 762 (1975).
11) K. Okamoto, K. Wakayama, H. Einaga, S. Yamada, and J. Hidaka, *Bull. Chem. Soc. Jpn.*, **56**, 165 (1983).
12) K. Wakayama, K. Okamoto, H. Einaga, and J. Hidaka, *Bull. Chem. Soc. Jpn.*, **56**, 1995 (1983).

Catalytic Effects of Chlorate Ions on the Electrode Reaction Processes of 12-Molybdophosphate and 12-Molybdosilicate

Kei UNOURA,* Atuko IWASHITA,† Eiki ITABASHI,*,† and Nobuyuki TANAKA††
Department of Chemistry, Faculty of Science, Yamagata University, Kojirakawa-machi, Yamagata 990
†*Department of Chemistry, Miyagi University of Education, Aoba, Aramaki, Sendai 980*
††*Department of Chemistry, Faculty of Science, Tohoku University, Aoba, Aramaki, Sendai 980*
(Received June 24, 1983)

Synopsis. The third cathodic waves corresponding to the reduction processes from the four-electron to the six-electron reduction products of both 12-molybdophosphate and 12-molybdosilicate are catalytic in nature in the presence of chlorate ions. The six-electron reduction product of 12-molybdophosphate is oxidized by chlorate ions more rapidly than that of 12-molybdosilicate.

It is well known that the reduction products of 12-heteropoly molybdates show a deep blue color, which are often called heteropoly molybdenum blue compounds, and that many workers applied the formation of heteropoly molybdenum blue compounds to the determination of traces of P^{V}, As^{V}, or Si^{IV} without the clarification of the properties of the heteropoly molybdenum blue compounds in detail.

The physicochemical properties of the heteropoly molybdenum blue compounds have been recently clarified by several workers by using various techniques.[1-4] On the other hand, the informations about the chemical reactivities of the heteropoly molybdenum blue compounds are still in scarcity, although such informations seem to be important to the application of the compounds as catalysis.

The authors, therefore, studied recently the electrochemical behaviors of 12-molybdophosphate and 12-molybdosilicate in water–dioxane mixed solutions, and found that the six-electron reduction product of the 12-molybdophosphate is more reactive for a homogeneous electron transfer reaction than that of 12-molybdosilicate.[5,6]

In the present paper are presented the results of a study of the effects of some inorganic anions on the electrode reaction processes of 12-molybdophosphate and 12-molybdosilicate at a thin-layer electrode cell.

Experimental

Materials. Sodium salts of 12-molybdosilicate and 12-molybdophosphate were obtained from Climax Molybdenum Co. and Wako Pure Chemical Ind., respectively. Other chemicals used were of analytical reagent grade. All solutions were prepared with twice-distilled water and deaerated with high-purity nitrogen.

Measurement. Voltammetric experiments were performed with a potentiostat (Hokuto Denko Co., HA 501) in connection with a function generator (Hokuto Denko Co., HB 104).

The thin-layer electrode was constructed by sandwiching a gold-minigrid (500 mesh; Buckbee-Mears Co.) between two glass slides. The electrochemical cell volume was 41.4 μl.

Standard procedures were used for a thin-layer voltammetric experiment.[7]

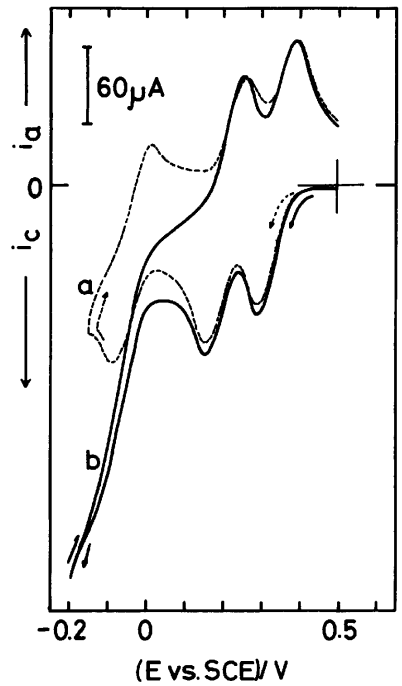

Fig. 1. Thin-layer cyclic voltammograms of 1.0×10^{-3} M 12-molybdophosphate in 50%(v/v) dioxane–water solutions containing 0.5 M H_2SO_4 at 22°C. [$NaClO_3$]: (a) 0, (b) 0.05 M. Scan rate 2 mV s^{-1}; initial potential +0.500 V *vs.* SCE.

Results and Discussion

Typical thin-layer cyclic voltammograms of 12-molybdophosphate are given in Fig. 1. In the absence of chlorate ions, 12-molybdophosphate in 50% (v/v) dioxane–water solutions containing sulfuric acid exhibits three consecutive two-electron reversible waves in agreement with the results of the voltammetric studies at a platinum electrode.[8]

Most of the previous electrochemical investigations of heteropoly molybdates were carried out with sulfuric acid or hydrochloric acid as a supporting electrolyte. Nitrate and perchlorate were little used as a supporting electrolyte. This might be resulted from the consideration of the fact that nitrate and perchlorate oxidized the reduction products of some molybdenum(VI) complexes.[9,10] However, this study has shown that neither nitrate nor perchlorate ions do exhibit a catalytic effect on the electrode reaction processes of 12-molybdophosphate; the cathodic waves of 12-molybdophosphate was found to be little affected by the addition of nitrate or perchlorate ions.

On the other hand, chlorate ions gave a remarkable

influence on the third cathodic wave, although the first two cathodic waves remained almost unchanged upon the addition of chlorate ions. In the presence of chlorate ions, the third cathodic wave exhibited a plateau rather than a peak and increased in height with an increase of chlorate ion concentrations. Moreover, the third anodic peak corresponding to the reoxidation of the six-electron reduction product disappears completely. These indicate that the third reduction wave of 12-molybdophosphate is catalytic in nature in the presence of chlorate ions.

The mechanism of this catalytic wave involves apparently regeneration of the four-electron reduction product of 12-molybdophosphate, which is supported by the disappearance of the third anodic peak. The controlled potential electrolysis was performed at the potential at which the catalytic current was observed in the presence of chlorate ions. The solution subjected to the electrolysis reacted with silver nitrate to yield the precipitates of silver chloride. This indicates that chlorate ions are reduced to chloride ions by the six-electron reduction product of 12-molybdophosphate.

According to these results, this catalytic wave can be explained by the sequence of the following reactions:

$$PMo^{V}_{4}Mo^{VI}_{8}O_{40}^{7-} + 2e^{-} \underset{\text{fast}}{\rightleftharpoons} PMo^{V}_{6}Mo^{VI}_{6}O_{40}^{9-} \quad (1)$$

$$3PMo^{V}_{6}Mo^{VI}_{6}O_{40}^{9-} + ClO_{3}^{-} + 6H^{+} \longrightarrow 3PMo^{V}_{4}Mo^{VI}_{8}O_{40}^{7-} + Cl^{-} + 3H_{2}O \quad (2)$$

The cyclic regeneration of the electroactive four-electron reduction product of 12-molybdophosphate accounts for the enchancement of the reduction current.

The third cathodic wave of the cyclic voltammogram of 12-molybdophosphate in the presence of chlorate ions at a glassy carbon electrode was found also catalytic in nature. At scan rates larger than 20 mV s^{-1}, however, the third cathodic wave depended on the scan rate and the anodic wave corresponding to the third cathodic wave appears on the anodic scan. This indicates that the chemical reaction (Eq. 2) is relatively slow.

The same set of experiments was performed for 12-molybdosilicate. Typical cyclic voltammograms of 12-molybdosilicate are shown in Fig. 2. In the absence of chlorate ions, 12-molybdosilicate in 50% (v/v) dioxane–water solutions containing sulfuric acid also gave three two-electron reversible waves. Neither nitrate nor perchlorate ions exhibited a catalytic activity for the electroreduced 12-molybdosilicate.

In the presence of chlorate ions, the third reduction wave of 12-molybdosilicate, as shown by curve b in Fig. 2, was found to be catalytic in nature. However, it still exhibits a peak rather than a plateau. This appearance of peak may be due to a slow chemical reaction of the six-electron reduction product of 12-molybdosilicate and chlorate ions; chlorate ions can oxidize the six-electron reduction product of 12-molybdosilicate, but more slowly than that of 12-molybdophosphate.

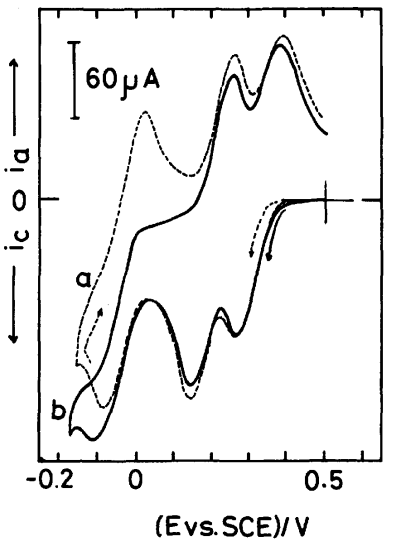

Fig. 2. Thin-layer cyclic voltammograms of 1.0×10^{-3} M 12-molybdosilicate in 50%(v/v) dioxane–water solutions containing 0.5 M H_2SO_4 at 22 °C. [$NaClO_3$]: (a) 0, (b) 0.05 M. Scan rate 2 mV s^{-1}; initial potential +0.500 V *vs.* SCE.

It is interesting to note that the reaction rate of the six-electron reduction product of 12-molybdosilicate for chlorate ions is slower than that of 12-molybdophosphate for chlorate ions. This could support the fact that the six-electron reduction product of 12-molybdophosphate is more reactive for a homogeneous electron transfer reaction than that of 12-molybdosilicate.[6]

This study was supported in part by Science Research Grants nos. 56104001, 56540334, and 57540343, for which the authors thank the Ministry of Education, Science and Culture.

References

1) H. So and M. T. Pope, *Inorg. Chem.*, **11**, 1441 (1972).
2) R. A. Prados, P. T. Meikeljohn, and M. T. Pope, *J. Am. Chem. Soc.*, **96**, 1261 (1974).
3) E. Papaconstantinou and M. T. Pope, *Inorg. Chem.*, **9**, 667 (1970).
4) E. Papaconstantinou and M. Z. Hoffman, *Inorg. Chem.*, **21**, 2087 (1982).
5) N. Tanaka, K. Unoura, and E. Itabashi, *Inorg. Chem.*, **21**, 1662 (1982).
6) K. Unoura and N. Tanaka, *Inorg. Chem.*, **22**, 2963 (1983).
7) T. P. DeAngelis and W. R. Heineman, *J. Chem. Educ.*, **53**, 594 (1976).
8) G. A. Tsigdinos, *Climax Molybdenum Co. Bull.*, **Cdb-15**, 1971.
9) M. Lamache and P. Souchay, *J. Chim. Phys.*, **2**, 384 (1973).
(10) C. D. Garner, M. R. Hyde, F. E. Mabbs, and V. I. Routledge, *J. Chem. Soc., Dalton Trans.*, **1975**, 1175; 1180.

The Incorporation of Dicarboxylates into Octacalcium Bis(hydrogenphosphate) Tetrakis(phosphate) Pentahydrate

Hideki MONMA

National Institute for Research in Inorganic Materials, 1-1 Namiki, Sakura-mura, Niihari-gun, Ibaraki 305

(Received July 28, 1983)

Synopsis. Octacalcium bis(hydrogenphosphate) tetrakis(phosphate) pentahydrate (OCP) has been found to complex with saturated aliphatic dicarboxylate ions, $C_nH_{2n}C_2O_4^{2-}$; n=1—6. These organic substances were incorporated, instead of HPO_4^{2-}, into the "B-layer" of the OCP structure. The incorporation caused expansion in the basal spacing (d_{100}) of OCP from 18.7 Å to 19.6—26.1 Å. A possible structural model is proposed for the incorporation.

Octacalcium bis(hydrogenphosphate) tetrakis(phosphate) pentahydrate ($Ca_8(HPO_4)_2(PO_4)_4\cdot 5H_2O$; OCP), which has a structural similarity to hydroxyapatite, has become of biological and bio-material interest. The structure of OCP, as shown in Fig. 1, is composed of alternative stackings of "apatitic layers" (A-layers) similar to the apatite structure and "hydrated layers" (B-layers) corresponding to the composition of brushite ($CaHPO_4\cdot 2H_2O$).[1-3] In the preceding paper,[4] it was pointed out as a feature of the OCP structure that the B-layers contained +Ca-HPO_4-Ca+ pillars. It was claimed that succinate ions ($C_2H_4C_2O_4^{2-}$) were able to replace the HPO_4^{2-} in the pillar, which resulted in an expansion of the basal spacing (d_{100}) of OCP. In the present work, a series of saturated aliphatic dicarboxylate ions were investigated to determined whether the ions were able to be incorporated into OCP or not.

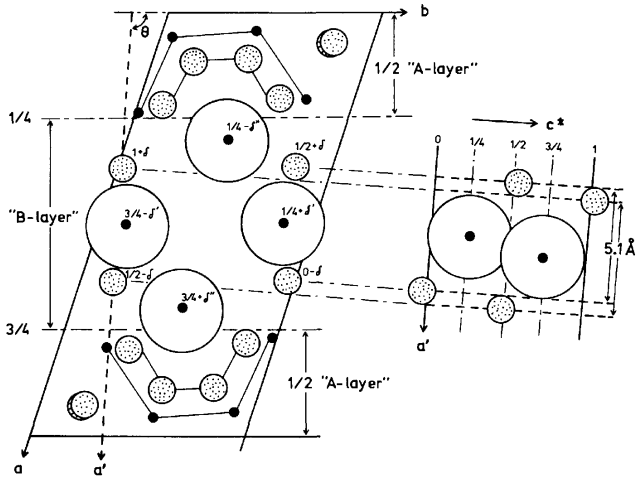

Fig. 1. Simplified OCP structure projected on the a-b plane and +Ca-HPO_4-Ca+ pillars projeted on the a'-c* plane, where ●: P, ⊙: HPO_4, ◎: Ca, c*: vertical to the a-b plane, δ: 0.0313, δ': 0.0168, δ'': 0.0045, θ: 94.1°, the corners of the larger and smaller half hexagons: P and Ca sites in hydroxyapatite, respectively. The illustration was based on the Ref. 1).

Experimental

Powdery α-tricalcium bis(phosphate) (α-$Ca_3(PO_4)_2$) synthesized by solid state reaction[4] was heated in aqueous solutions containing dicarboxylate ions ($C_nH_{2n}C_2O_4^{2-}$; n=0—6) at 40 °C for 3 h. All reactant solutions were prepared at a concentration of 0.25 mol dm^{-3} from chemical reagents of dicarboxylic acids and distilled water. Initial pH's were adjusted to 6.4 ± 0.1 for malonic acid (n=1) and 6.0 ± 0.1 for the other acids (n=0,2—6) with ammonia water. The resulting solid products were examined with respect to product phase and interplanar spacings of OCP by X-ray diffraction, and Ca/P ratio by chemical analyses. The chemical composition of OCP phase was estimated by distributing the residual amount on quantitative analyses of Ca and PO_4 among the other components (H, $C_nH_{2n}C_2O_4$, and H_2O), using the Ca/P ratio of products (OCP+ unreacted α-$Ca_3(PO_4)_2$), conversion of α-$Ca_3(PO_4)_2$ into OCP, and a general formula of dicarboxylate-complexed OCP determined in this work.[4]

Results and Discussion

In the case of the oxalate solution (n=0), α-$Ca_3(PO_4)_2$ was converted completely into calcium oxalate without formation of OCP. OCP was formed from the other reactant solutions (n=1—6). Table 1 lists interplanar spacings and chemical compositions of OCP, Ca/P ratios of products and some reference data. It was clear that the organic substances caused expansions of the basal spacing (d_{100}) of OCP and increases in the Ca/P ratio. Here, adopting the same structural consideration introduced in the preceding paper, dicarboxylate ions incorporated as +Ca-$C_nH_{2n}C_2O_4$-Ca+ instead of +Ca-HPO_4-Ca+ can be illustrated as shown in Fig. 2. The structures of the dicarboxylate ions were taken from those of corresponding acids,[5] and the arrangements and numerals were determined graphically using the radii of $r_{Ca^{2+}}$= 0.99 Å, r_C=0.77 Å, and r_O≈1 Å. The r_O of carboxyl oxygen was estimated from bond lengths of C-O and O-Ca in calcium carboxylate crystals, *e.g.*, calcium

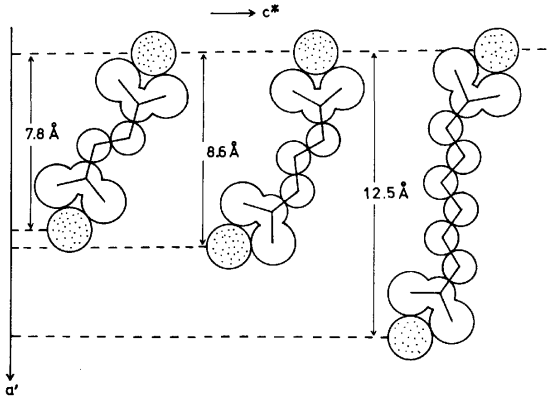

Fig. 2. Examples of the structural model for +Ca-$C_nH_{2n}C_2O_4$-Ca+pillars (N=2, 3, 6) projected on the a'-c* plane.

TABLE 1. DICARBOXYLATE-COMPLEXED OCP

Incorporated ion		OCP formed					Ca/P of product[d]	Conversion[e]/%
Name	n[b]	Interplanar spacing/Å			Formula[c]			
		d_{100}	d_{010}	d_{002}	z	m		
None[a]	—	18.7	9.36	3.42	0	5.1	1.34	100
Malonate	1	19.6	—	3.43	0.42	≈5	1.47	≈45
Succinate	2	21.4	9.39	3.42	0.83	5.5	1.55	100
Glutarate	3	22.3	9.37	3.43	0.35	≈5	1.45	≈60
Adipate	4	23.6	9.41	3.42	0.45	6.6	1.44	100
Pimelate	5	24.4	9.36	3.42	0.22	≈6	1.41	≈80
Suberate	6	26.1	9.38	3.42	0.92	7.6	1.55	≈70

a) Pure OCP.[4] b) $C_nH_{2n}C_2O_4^{2-}$. The case of n=0 (oxalate) formed calcium oxalate. c) $Ca_8(HPO_4)_{2-z}(PO_4)_4(C_nH_{2n}C_2O_4)_z \cdot mH_2O$. d) Mole ratio of OCP+unreacted α-$Ca_3(PO_4)_2$. e) Conversion of α-$Ca_3(PO_4)_2$ into OCP.

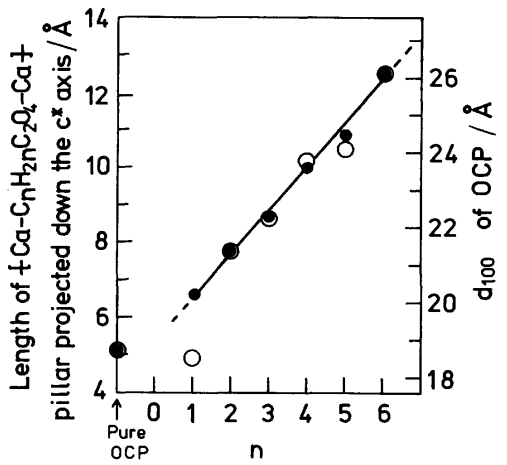

Fig. 3. Pillar lengths and basal spacings of dicarboxylate-complexed OCP.
●: Experimentally obtained, ○: graphically obtained.

formate and calcium oxalate.[5] In addition, we assumed there were no changes in the b and c* directions on the basis of the very small changes in d_{010} and d_{002}, *i.e.*, the b and c directions. Figure 3 shows plots of the lengths of +Ca-$C_nH_2C_{2n}O_4$-Ca+ pillars and d_{100} values *vs.* n, where $[d_{100}(\text{graphic})] \approx [d_{100}(\text{experimental}) - \text{pillar length down the c*}]_{\text{pure OCP}} + [\text{pillar length down the c*}]_{\text{dicarboxylate-complexed OCP}}$, because $\sin\theta \approx 1$ (refer to Fig. 1). The experimental data showed a good linearity, and supported the graphic data approximately. However, departures of graphic data for n=1 and n=5 from the line left an uncertainty about the structural model. The data given in Fig. 3 were considered to confirm the previous claim about succinate-complexed OCP.[4] A general formula would be apparently $Ca_8(HPO_4)_{2-z}(PO_4)_4(C_nH_{2n}C_2O_4)_z \cdot mH_2O$; $0 \leq z \leq 1$, $m \gtrsim 5$, n=1—6 in analogy with that of the succinate-complexed OCP.

References

1) W. E. Brown, *Nature*, **196**, 1048 (1962).
2) W. E. Brown, M. S. Tung, and L. C. Chow, *Proc. 2nd Int. Congr. Phosphorus Compd.*, **1981**, 59.
3) H. Monma, *Sekko To Sekkai*, No.166, 33 (1980).
4) H. Monma and M. Goto, *Bull. Chem. Soc. Jpn.*, **56**, 3843 (1983).
5) R. W. G. Wyckoff, "Crystal Structures," 2nd ed, Interscience, New York (1966), Vol. 5, pp. 126—128, 415—416, 558—573.

Acid Catalysis of the Denitrosation of *N*-Methyl-*N'*-cyclohexyl-*N*-nitrosothiourea

Masayoshi ISOBE

Department of Chemistry, Saitama Medical School, Moroyama, Saitama 350-04

(Received February 2, 1983)

Synopsis. The kinetics of denitrosation of *N*-methyl-*N'*-cyclohexyl-*N*-nitrosothiourea has been studied in the range of pH 3.45—3.73 using four organic acids; acetic acid, formic acid, chloroacetic acid, and cyanoacetic acid. Analyses of the kinetic data including the Brönsted plots have shown that the reaction is subject to a general acid catalysis.

It has been observed that many aliphatic nitroso compounds can act as nitrosating agents of naturally existing amines under conditions analogous to those found in the rat or human stomach (pH 1.7—3.6 with thiocyanate or other nucleophiles as catalyst).[1] Certain aromatic *N*-nitroso compounds have also long been known to be good transnitrosating agents.[2] In addition to above substances, *N*-methyl-*N'*-cyclohexyl-*N*-nitrosothiourea(**1**) was found to undergo denitrosation under nearly neutral conditions (pH 6.7). To investigate acid catalysis of the denitrosation of **1**, the buffer dilution study was performed in the range of pH 3.45—3.73.

Results and Discussion

Pseudo first-order rate constants were measured in a series of buffer solutions of four carboxylic acids at different buffer concentration. The results are summarized in Table 1. The plots of k_{obsd} *vs.* $[buffer]_T$ (total concentration of buffer) are shown in Fig. 1. Since the denitrosation of **1** is catalyzed by buffer and H_3O^+, the k_{obsd} is given by Eq. 1,

$$k_{obsd} = k_H{}^+[H_3O^+] + k_{HA}'[HA] \quad (1)$$

where k_{HA}' and k_{H^+} are second-order rate constants for the buffer catalysis and the hydronium-ion catalysis, respectively. Therefore, the slope and the intercept in Fig. 1 correspond to k_{HA}' and $k_H{}^+[H_3O^+]$, respectively. The slopes and the intercepts were calculated by least squares computation. The k_{H^+} values were obtained from the intercepts. Since the true buffer catalysis is associated with the concentration of acid form of buffer, true second-order rate constants for the general acid catalysis (k_{HA}) are equal to $k_{HA}'/1-\alpha'$ (α'; dissociated fraction of acid). The k_{H^+} and k_{HA} determined are summarized in Table 2. From the data of Table 2, the average k_{H^+} value of **1** for all buffers determined at pH 3.45—3.73 was calculated to be 4.85 ± 0.93. The lowest k_{H^+} value for cyanoacetic acid buffer among those for other acids may be caused by somewhat hindered approach of hydronium ion to the amino nitrogen atom of **1** due to the interaction between hydronium ion and the resonance-stabilized anion partly formed by the abstraction of the α-hydrogen of the parent acid. This anion must be analogous to that formed from mandelonitrile by the attack of base. This average k_{H^+} value was 45 times greater than k_{HA} value for cyanoacetic acid and about 260 times greater than that for acetic acid, respectively. The former value was almost the same with that of acid catalysis in ether hydrolysis (*ca.* 40)[3] and the latter was about 1.7 times greater than that of acid catalysis in hydrolysis of 1,1-dimethoxy-2-phenylethene (*ca.* 160).[4]

The Brönsted plots of pK_a *vs.* log k_{HA} provided the linear relationship (r=0.998, slope($-\alpha$)=−0.38) presented by Eq. 2, as shown in Fig. 2.

$$\log k_{HA} = 0.006 - 0.38\,pK_a \quad (2)$$

This indicates that the denitrosation of **1** is a general acid catalysis. The higher general acid catalysis by the acids possessing electron-withdrawing substituent at the α position suggests that the acid-catalyzed denitrosation of **1** would occur through rate-determining protonation (Scheme 1). The rate of denitrosation at 36.9 °C was measured in CH_3COOD/D_2O to evaluate the solvent deuterium isotope effect. The results at the same buffer concentration (0.05 M, $[HA(DA)]/[A^-]$=0.42, μ=0.2) also showed that denitrosation of **1** involves rate-determining protonation ($k(CH_3COOH/H_2O)/k(CH_3COOD/D_2O)$=1.36, $k(CH_3COOH/$

TABLE 1. DENITROSATION RATE CONSTANTS OF *N*-METHYL-*N'*-CYCLOHEXYL-*N*-NITROSOTHIOUREA[a] AT 36.9 °C

Buffer	pH	[Buffer]/M	$10^3 \times k/s^{-1}$[b]
$NCCH_2COOH$	3.45	0.01	1.33±0.02
		0.02	1.46±0.01
		0.04	1.64±0.03
$ClCH_2COOH$	3.73	0.01	1.12±0.03
		0.02	1.27±0.02
		0.04	1.45±0.01
HCOOH	3.58	0.01	1.56±0.02
		0.02	1.76±0.02
		0.03	1.93±0.05
CH_3COOH	3.54	0.01	1.63±0.01
		0.02	1.94±0.03
		0.04	2.18±0.01

a) 8.28×10^{-5} M, μ=0.2(NaCl). b) The errors are deviation from the average of two runs.

TABLE 2. SECOND-ORDER RATE CONSTANTS FOR GENERAL ACID CATALYSIS

Catalyst	pK_a[a]	Reaction pH	α′	Slope$((1-\alpha')k_{HA})$ / $M^{-1}\,s^{-1}$	$k_{HA}/M^{-1}\,s^{-1}$
$NCCH_2COOH$	2.47	3.45	0.904	$(1.02\pm0.04)\times10^{-2}$	0.107 ±0.005
$ClCH_2COOH$	2.87	3.73	0.878	$(1.08\pm0.06)\times10^{-2}$	0.0888±0.0053
HCOOH	3.75	3.58	0.403	$(1.81\pm0.15)\times10^{-2}$	0.0304±0.0025
CH_3COOH	4.76	3.54	0.056	$(1.76\pm0.01)\times10^{-2}$	0.0186±0.0001
H_3O^+	−1.74				3.46±0.03[b]
					5.48±0.19[c]
					5.27±0.00[d]
					5.18±0.07[e]

a) Ref. 3. b —e) From the intercept of [Buffer] dependence: b) cyanoacetic acid; c) chloroacetic acid; d) formic acid; e) acetic acid.

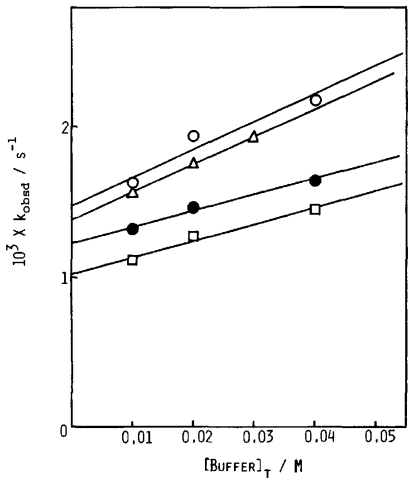

Fig. 1. Plots of k_{obsd} *vs.* buffer concentration (cyanoacetic acid (●), chloroacetic acid (□), formic acid (△), and acetic acid (○)) for **1**.

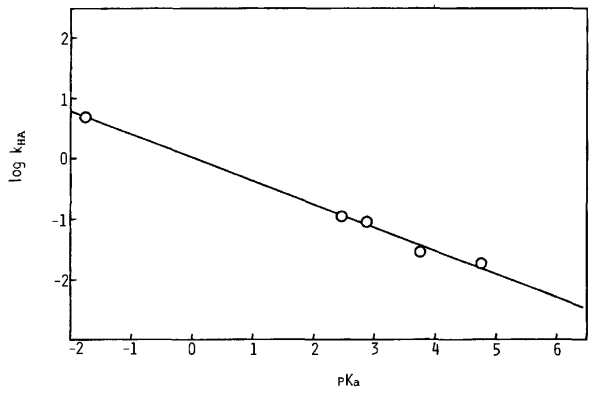

Fig. 2. The Brönsted plots for denitrosation of **1**.

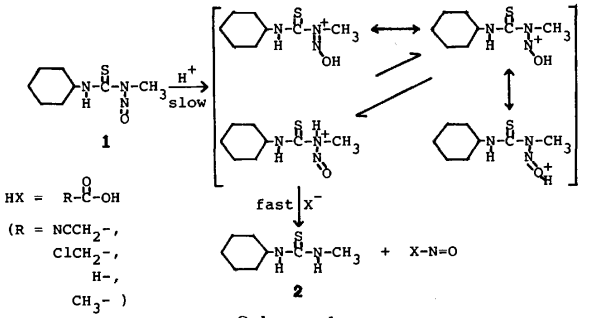

Scheme 1.

H_2O)=1.38×10^{-3} s^{-1}, $k(CH_3COOD/D_2O)$=1.01×10^{-3} s^{-1}). The analogous general acid-catalyzed denitrosation has also been observed in decomposition of *N*-*n*-butyl-*N*-nitrosoacetamide[5] or *N*-nitroso-2-pyrrolidone.[6] The latter showed the Brönsted relationship with a slope(α) of 0.64. Since the rate of protonation of **1** is influenced by the reduced basicity of the amino nitrogen atom due to electron-withdrawing property of the nitroso-substituent, which may also be true for the protonation of *N*-nitroso-2-pyrrolidone, the difference in α between **1** (α=0.38) and *N*-nitroso-2-pyrrolidone (α=0.64) must be caused by the basicity difference of the amino nitrogen atom which is affected by the thiocarbonyl group in **1** or the carbonyl group in the latter. These results suggest that **1** would also be subject to general acid catalysis by carboxylic acid residue of an enzyme under acidic conditions.

Experimental

N-Methyl-N'-cyclohexyl-N-nitrosothiourea (1). *N*-Methyl-*N'*-cyclohexylthiourea (**2**) (0.6 g, 3.48 mmol), which was obtained from the reaction of cyclohexylamine and methyl isothiocyanate in acetone at room temperature (18 h), was treated with sodium nitrite (0.36 g, 5.23 mmol) in acetic acid (5 ml)-acetic anhydride (20 ml) at 0 °C (1 h). The reaction mixture was poured in ice-water and extracted with ether (80 ml) three times. The ethereal solution was washed with 5% Na_2CO_3 solution (4 times), 5% $NaHCO_3$ solution (3 times), saturated NaCl solution, dried ($MgSO_4$), and evaporated to give an orange liquid, which upon trituration with pentane gave yellow crystals of **1** (0.39 g, 56%). **1**: Mp 44.5—45.5 °C (lit,[7] mp 35—36 °C); IR (KBr) 3310 (NH), 2930, 2860, 1515, 1495, 1407, 1175, 1000, 965, 910, and 790 cm^{-1}; NMR (CCl_4) δ 8.36 (1H, br, NH), 4.34 (1H, m, methine), 3.43 (3H, s, $-CH_3$), 2.40—1.00 (10H, m, $-CH_2-$). Found: C, 47.63; H, 7.46; N, 21.20; S, 15.90%. Calcd for $C_8H_{15}ON_3S$: C, 47.73; H, 7.51; N, 20.88; S, 15.93%. **2**: Mp 163—164 °C (lit,[7] mp 165—166 °C).

Product Analysis. A solution of *N*-methyl-*N'*-cyclohexyl-*N*-nitrosothiourea(**1**)(150 mg, 0.745 mmol in 5 ml of methanol was added to 150 ml of Tris buffer solution (pH 6.70, 0.05 M, μ=0.2 with NaCl) and stirred for 5 h at 37 °C. After cooling, the contents were saturated with NaCl and extracted with ether (80 ml×3) and the combined extracts were washed with saturated NaCl solution, dried ($MgSO_4$), and evaporated to give a solid and yellow liquid. The product was separated with pentane to **2** (white solid, 53 mg, 41%) insoluble in pentane and cyclohexyl isothiocyanate (**3**, yellow liquid, 45 mg, 43%) soluble in pentane. **3**: IR(neat) 2950, 2870, 2110(N=C=S), 1450, 1360, and 1307 cm^{-1}; NMR (CCl_4) δ 3.85—3.45 (1H, m, methine), 2.25—1.20 (10H, m, $-CH_2-$).

Kinetic Measurements. The kinetic measurements of the denitrosation of **1** were carried out at 36.9±0.3 °C in a thermostated UV cell. The appropriate buffer solution (3 ml) was transferred into each cell with a pipet, and after standing for thermal equilibration, the reaction was initiated by adding 20 μl of the substrate solution (1 mg/0.4 ml-MeOH) with the aid of a microsyringe. The progress of the reaction was monitored spectrophotometrically by following the disappearance of the absorption maximum at 270 nm. The reaction followed pseudo first-order kinetics; infinity readings were obtained after 8—10 half lives.

References

1) S. S. Singer, W. Lijinsky, and G. M. Singer, *Tetrahedron Lett.*, **1977**, 1613; S. S. Singer, *J. Org. Chem.*, **43**, 4612 (1978); S. S. Singer, G. M. Singer, and B. B. Cole, *ibid.*, **45**, 4931 (1980).

2) C. L. Baumgardner, K. A. MaCallum, and J. P. Freeman, *J. Am. Chem. Soc.*, **83**, 4417 (1961); H. Sieper, *Chem. Ber.*, **100**, 1646 (1967).

3) A. J. Kresge and Y. Chiang, *J. Am. Chem. Soc.*, **95**, 803 (1973).

4) T. Okuyama, S. Kawano, and T. Fueno, *J. Org. Chem.*, **46**, 4372 (1981).

5) C. N. Berry and B. C. Challis, *J. Chem. Soc., Perkin Trans. 2*, **1974**, 1638.

6) B. C. Challis and S. P. Jones, *J. Chem. Soc., Perkin Trans. 2*, **1975**, 153.

7) J. W. Lown and S. M. S. Chauhan, *J. Org. Chem.*, **48**, 507 (1983).

Ozonation of Xanthene

Masaki MATSUI,* Yoshihiko MIYAMOTO, Katsuyoshi SHIBATA, and Yoshimi TAKASE
Department of Industrial Chemistry, Faculty of Engineering, Gifu University, Yanagido, Gifu 501-11
(Received April 5, 1983)

Synopsis. The ozonation of xanthene was studied using an oxygen stream. Ozone attacks the methylene group of xanthene *via* a 1,3-dipolar insertion reaction to give the hydrotrioxide intermediate, followed by a loss of singlet oxygen to form xanthydrol. The ozonation of xanthydrol gave singlet oxygen, water and xanthone accompanied by autoxidation.

Methylene group ozonation gives the corresponding carbonyl group. In 1949, Cavill *et al.* reported that xanthene ozonation gave xanthyldrol and xanthone.[1] However, a detailed study of this mechanism has not been reported. In this paper, the authors discuss the ozonation mechanism of xanthene which may possibly produce intermediates capable of giving off singlet oxygen.

Experimental

General. Liquid chromatography was performed with a Jasco Twincle liquid chromatography. Mass spectra were obtained with a Hitachi M-52 spectrometer. Gas chromatography was performed with a Shimadzu 4C-PF gas chromatograph. Melting points were measured with a Yanagimoto micro melting point apparatus and are uncorrected. Ozone was generated by a Nihon Ozon 0-1-2 type ozonizer.

Materials. Xanthene (Nakarai Kagaku Yakuhin Co.) was recrystallized from ethanol. Mp 100.4 °C (lit, 100.5 °C);[2] NMR (CCl_4) δ=4.02 (2H, s) and 6.8—7.3 (8H, m); MS (70 eV) *m/e* (rel intensity) 182(56), 181(100), 152(44), and 76(23). Xanthydrol was synthesized according to the literature.[3] Mp 121.1 °C (lit, 121—123 °C); NMR ($CDCl_3$) δ=2.24 (1H, s), 5.75 (1H, s) and 6.9—7.6 (8H, m); MS (70 eV) *m/e* (rel intensity) 198(16), 197(25), 181(100), and 153(89); IR (KBr disk) 3300 cm^{-1} (OH). Xanthone (Nakarai Kagaku Yakuhin Co.) was recrystallized from ethanol. Mp 175.1 °C (lit, 173.5 °C);[4] MS (70 eV) *m/e* (rel intensity) 196(100), 168(52), and 139(21); IR (KBr disk) 1655 cm^{-1} (C=O).

Ozonation Reaction. Ozonations in all cases were carried out with ozone-oxygen mixtures (ozone: 9.4 mg/min, oxygen: 200 ml/min) on 0.27 mmol of xanthene and xanthydrol in 20 ml of solvent. Products determination was made immediately by liquid chromatography and xanthone was isolated by liquid chromatography. The mass spectra, IR spectra, and mp of xanthone were compared with those of an authentic sample. Though xanthydrol could not be isolated, the NMR and LC analysis of the ozonated solution showed the formation of xanthydrol. Yields were determined by comparison with standard solution of known compounds. The conditions in the liquid chromatography were as follows: column: SS-10, mobile phase: chloroform: hexane= 5:1, detector 254 nm. And the conditions in the gas chromatography for the identification of *o*-dibenzoylbenzene and (*Z*)-α,β-dibenzoylstilbene were as follows: column: 3ϕ×1 m, 2% OV-1, on Gas Chrom Q, injection temp: 280 °C, detector temp: 280 °C, column temp: 130—240 °C, 10 °C/min, detector: FID.

Results and Discussion

Xanthene reacts with ozone to give water, xanthydrol and xanthone. The results of the reactions are shown in Table 1. It was found that 1.2—1.4 molar equivalents of ozone were consumed in reacting with xanthene, indicating that oxidation of xanthene to xanthone does not proceed only with ozone. The greater the polarity of the solvent, the greater is the conversion of xanthene, suggesting a 1,3-dipolar insertion of ozone to the methylene group. The carbonium ion character of the intermediate should be stabilized by the resonance effect from oxygen at the 10-position. In the case of xanthydrol ozonation, from the facts that (1) only 0.2—0.3 molar equivalent of ozone was consumed in reacting with xanthydrol, (2) the rate of the reaction did not depend on the solvent as in the case of xanthene, and (3) when the xanthydrol solution was allowed to stand, xanthone was formed by autoxidation, it is considered that the role of ozone in the ozonation of xanthydrol to xanthone is not particularly significant compared with that of ozone to oxidize xanthene to xanthydrol. On the other hand, it is of interest to identify molecular oxygen by decomposition of the hydrotrioxides. Stary and Kovač reported that the decomposition of aldehyde- and acetal-hydrotrioxides gave singlet oxygen.[5,6] The ozonation of

TABLE 1. OZONATION OF XANTHENE AND XANTHYDROL[a]

Run	Substrate	Solvent	Conversion %	Ozone (10^{-4} mol)	Ozone/Substrate reacting ratio[b]	Yield[c]/% Xanthydrol	Yield[c]/% Xanthone
1	Xanthene[d]	CH_2Cl_2	98	3.6	1.4	4	74
2	Xanthene[d]	$CHCl_3$	94	3.6	1.4	3	57
3	Xanthene[d]	CCl_4	59	3.0	1.9	8	30
4	Xanthydrol[e]	CH_2Cl_2	58	0.9	0.2	—	45
5	Xanthydrol[e]	$CHCl_3$	50	0.5	0.2	—	41
6	Xanthydrol[e]	CCl_4	42	0.8	0.3	—	37

a) Ozonation was carried out with ozone-oxygen mixtures (ozone: 9.4 mg/min, oxgen: 200 ml/min) on 0.27 mmol of xanthene and xanthydrol in 20 ml of solvent at 0 °C. b) The molar ratio of ozone to the substrate reacting. c) Yields were based on the substrate reacting with ozone. d) Ozonation was carried out for 4 min. e) Ozonation was carried out for 1.5 min.

TABLE 2. SINGLET OXYGEN DETERMINATION IN THE OZONATION OF XANTHENE AND XANTHYDROL[a)]

Run	Substrate	Singlet oxygen acceptor	Conversion	Yield[b)]/%			
			%	Xanthydrol	Xanthone	*o*-Dibenzoylbenzene	(*Z*)-α,β-Dibenzoylstilbene
1	Xanthene	1,3-Diphenylisobenzofuran	94	4	63	26	—
2	Xanthene	Tetraphenylcyclopentadienone	95	4	61	—	5
3	Xanthydrol	1,3-Diphenylisobenzofuran	62	—	77	16	—
4	Xanthydrol	Tetraphenylcyclopentadienone	87	—	75	—	2

a) The substrates (2.7 mmol) were ozonized in dichloromethane (20 ml) at −78 °C. Singlet oxygen acceptor (0.37 mmol) was then added to the ozonized solutions and allowed to warm to −20 °C. b) Yields were based on the substrates reacting.

TABLE 3. THE DISTRIBUTION OF SINGLET OXYGEN PRODUCTS IN THE OXIDATION OF 1,2-DIMETHYLCYCLOHEXENE

Method	Product distributions/%	
	1-Methyl-2-methylenecyclohexanol	1,2-Dimethylcyclohex-2-en-1-ol
Xanthene-hydrotrioxide decomposition[a)]	93	7
Photooxidation[b)]	89	11
Hydrochlorite-hydrogen peroxide method[b)]	91	9

a) Xanthene (1.1 mmol) was ozonized in dichloromethane (20 ml) at −78 °C. 1, 2-Dimethylcyclohexene (1.9 mmol) was then added to the ozonized solution and allowed to warm to −20 °C. The hydrotrioxide products were reduced to the corresponding alcohols by sodium borohydride and analyzed by GLC. b) Ref. 7.

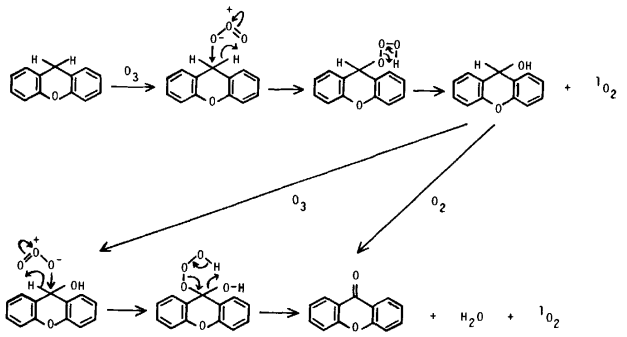

Scheme 1.

xanthene and xanthydrol was carried out at −78°C and then the excess ozone was removed. 1,3-Diphenylisobenzofuran and tetraphenylcyclopentadienone, singlet oxygen acceptors, were added to the ozonated solution which was then allowed to warm to −20°C. As expected, *o*-dibenzoylbenzene and (*Z*)-α,β-dibenzoylstilbene were detected. The results are shown in Table 2. The product yields were low because of the instability of the hydrotrioxides. In order to obtain further evidence that decomposition of xanthene-hydrotrioxide gives singlet oxygen, the technique of Foote *et al.* was also used.[7] The result is shown in Table 3. The products distribution by decomposition of xanthene-hydrotrioxide was the same as that by the sensitized photooxidation and hydrochlorite-hydrogen peroxide method. The probable reaction mechanism of xanthene ozonation is shown in Scheme 1.

The authors thank Prof. Teijiro Kitao of University of Osaka Prefecture for a useful discussion.

References

1) G. W. K. Cavill, A. Robertson, and W. B. Whalley, *J. Chem. Soc.*, **1949**, 1567.
2) V. Merz and W. Weith, *Ber.*, **14**, 187 (1881).
3) A. F. Holleman, *Org. Synth.*, Coll. Vol. I, 554 (1956).
4) W. H. Perkin, *Ber.*, **16**, 339 (1883).
5) F. E. Stary, D. E. Emge, and R. W. Murray, *J. Am. Chem. Soc.*, **98**, 1880 (1976).
6) F. Kovač and B. Plesničar, *J. Am. Chem. Soc.*, **101**, 2677 (1979).
7) C. S. Foote, *Acc. Chem. Res.*, **1**, 104 (1968).

The Reaction of 3,5-Diphenyl-1,2,4-dithiazol-1-ium Perchlorate with Active Methylene Compounds

Isao SHIBUYA
National Chemical Laboratory for Industry, Yatabe, Ibaraki 305
(Received June 1, 1983)

Synopsis. The reaction of 3,5-diphenyl-1,2,4-dithiazol-1-ium perchlorate with several kinds of active methylenes gives a number of heterocycles, such as 4-hydroxy and 4-mercaptopyrimidine, pyrimidinone, and thiazole derivatives. On treatment with hydroxylamine-*O*-sulfonic acid, the 4-mercaptopyrimidines lead to the aminothio compounds or the isothiazolo[5,4-*d*]pyrimidine.

Some heteroaromatic cationic species have high reactivity against nucleophiles, such as amino compounds and various kinds of carbanions.[1] The reactivities of heteroaromatic cations are essentially similar, but, strictly speaking, they react with a nucleophile in slightly different fashions to lead to various types of derivatives.[2] 3,5-Diphenyl-1,2-dithiol-1-ium cation was found to react with active methylenes to produce a number of derivatives.[3] It can therefore be assumed that 3,5-diphenyl-1,2,4-dithiazol-1-ium cation, the *N*-analog of the corresponding dithiolium cation, would afford several derivatives by treatment with active methylenes. In the present study, the reaction of 3,5-diphenyl-1,2,4-dithiazol-1-ium perchlorate (**1**) with several active methylene compounds was carried out in order to survey its reactivity.

The starting material, **1**, was obtained by treating thiobenzamide with thiobenzanilide *S*-oxide in acetic anhydride–perchloric acid.[4]

When cyanoacetamide, benzoylacetamide, and benzoylacetoanilide were heated to reflux with **1** in MeO-Na–MeOH, **2**, **3**, and **4** were afforded in 92, 38, and 44% yields respectively. These were same compounds given by the reaction of 2,4,6-triphenyl-1,3,5-thiadiazin-1-ium salt with these reagents,[5] so that **2**, **3**, and **4** were identified to be 5-cyano- and 5-benzoyl-4-hydroxy-2,6-diphenylpyrimidine, and 5-benzoyl-2,3,6-triphenyl-4(3*H*)-pyrimidinone. 3,5-Diphenyl-1,2-dithiol-1-ium salt similarly reacted with these reagents to afford the corresponding pyridines and pyridinone,[3] and consequently the behavior of **1** and the corresponding dithiolium salt toward these reagents was assumed to be the same.

Malononitrile, ethyl cyanoacetate, and diethylcarbamoylacetonitrile were heated to reflux with **1** in presence of sodium hydride, and then treated with hydrochloric acid to afford yellow powders of **5**, **6**, and **7** in 92, 42, and 47% yields respectively. Compounds **5** and **6** were confirmed to be 5-cyno- and 5-ethoxycarbonyl-4-mercapto-2,6-diphenylpyrimidine which are given by the reaction of 2,4,6-triphenyl-1,3,5-thiadiazin-1-ium salt with the two reagents.[5] The UV and IR spectra of **7** were similar to those of **5** and **6**. Its MS data and analytical results supported the conclusion that **7** is 5-diethylcarbamoyl-4-mercapto-2,6-diphenylpyrimidine.

On the other hand, benzoylacetonitrile and phenylsulfonylacetonitrile gave a common product, **8**, in 42 and 53% yields, respectively, when treated with **1** in the presence of sodium hydride. Its IR spectrum had an absorption assignable to a cyano group, but neither a benzoyl nor a phenylsulfonyl group. The molecular weight of **8** was determined by its MS data to be 262. These spectral data and the analytical results supported the assignment that **8** is 5-cyano-2,4-diphenylthiazole.

The reaction of the corresponding dithiolium salt with active methylene possessing ester groups gives a number of 2*H*-thiopyran-2-ones,[3] while the reaction of **1** with diethyl malonate and ethyl benzoylacetate did not give 6*H*-1,3-thiazin-6-ones. This fact suggested that **1** has no reaction mode in which an ester group of these reagents participates.

The results of forming **2**—**8** are summarized in Scheme 1.

When treated with hydroxylamine-*O*-sulfonic acid in the presence of sodium hydroxide, **5** and **7** gave white powders of **9** and **11** in good yields. Their IR spectra have two absorptions assignable to the N–H stretching in the range of 3376—3244 cm^{-1} and an absorption of a pyrimidine ring at around 1525 cm^{-1}. Their molecular weights were determined by their MS data to be 304 and 378. These spectral data suggested that **9** and **11** are 4-(aminthio)-5-cyano- and 4-(aminothio)-5-diethylcarbamoyl-2,6-diphenylpyrimidines respectively. Their analytical results also supported the structure assignments. On treatment with hydroxyamine-*O*-sulfonic acid under the same conditions as the above, however, **6** did not give the corresponding aminothiopyrimidine, **10**, but another product, **12**, was obtained. The spectrum of **12** had no absorption assignable to an ester group (*ca.* 1750 cm^{-1}). The molecular weight was determined to be 305. The structure of **12** was thus confirmed by these spectral and the analytical data to be 3-hydroxy-4,6-diphenylisothiazolo[5,4-*d*]pyrimidine. The reaction could be assumed to proceed as follows: **6** leads to **10** in the same fashion as do the other two mercaptopyrimidines (**5** and **7**); however, **6** further cyclizes to form **12** together with the elimination of ethanol (Scheme 2). This process could be regarded as analogous to that forming 3-amino-4,6-dimethylisothiazolo[5,4-*b*]-pyridine.[6]

Experimental

Reactions of 1 with Cyanoacetamide, Benzoylacetamide, and Benzoylacetanilide. Into a solution of cyanoacetamide, benzoylacetamide, or benzoylacetanilide (1.5 mmol) in 1 mol dm^{-3} MeONa–MeOH (3 ml), **1** (0.36 g, 1.0 mmol) was added with stirring in small portions, and then heated to reflux for 1 h. The reaction mixture was poured into dilute hydrochloric acid. The resulting precipitate was filtered off and recrystallized from acetonitrile to afford 5-cyano- or 5-benzoyl-4-hydroxy-2,6-diphenylpyrimidine (**2**, **3**), or 5-benzoyl-2,3,6-triphenyl-4(3*H*)-pyrimidinone (**4**) in 92, 38, 44% yield. Their IR spectra could be completely superimposed on those of the authentic samples.[5]

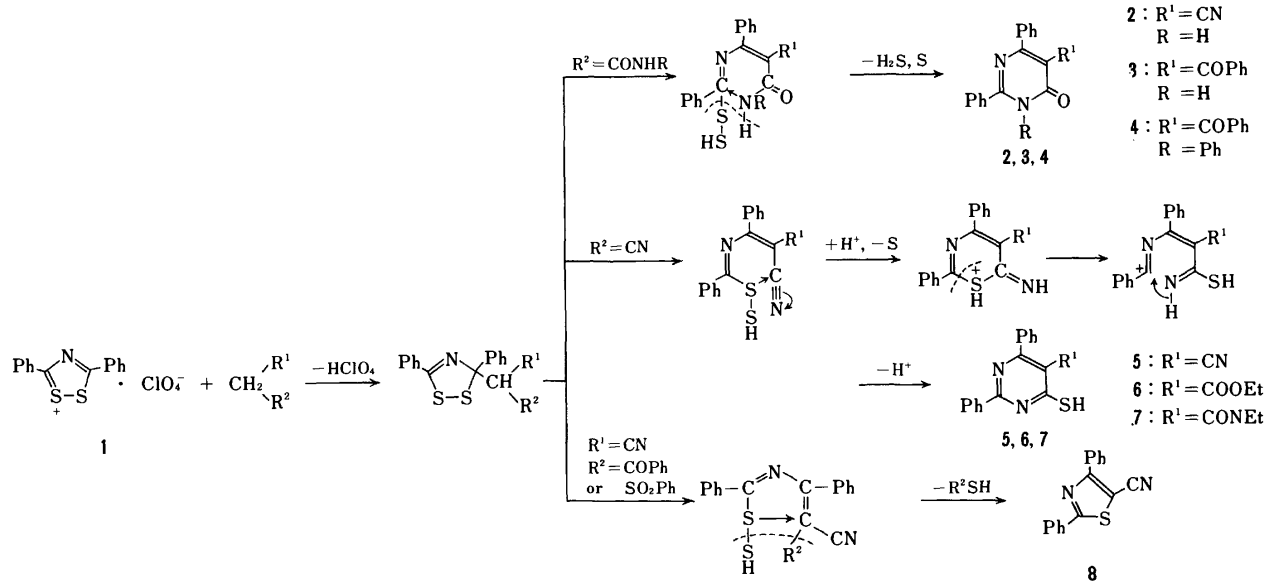

Scheme 1.

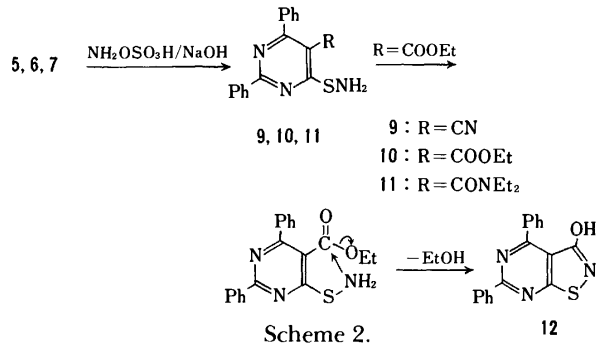

Scheme 2.

Reaction of 1 with Malononitrile, Ethyl Cyanoacetate, and Diethylcarbamoylacetonitrile. Into a solution of malononitrile ethyl cyanoacetate, or diethylcarbamoylacetonitrile (1.5 mmol) and sodium hydride (0.10 g, 4.2 mmol) in THF (3 ml), **1** (0.36 g, 1.0 mmol) was added with stirring in small portions, and heated to reflux for 1 h. The reaction mixture was poured into dilute hydrochloric acid. The precipitate was separated by decantation, and dissolved again in 2 mol dm^{-3} HCl–EtOH (3 ml); the resulting mixture was allowed to stand overnight. The solution was poured into an excess amount of water. The resulting precipitate was recrystallized from acetonitrile (**5**, **6**) or ethanol (**7**) to give 5-cyano-, 5-ethoxycarbonyl-, or 5-diethylcarbamoyl-4-mercapto-2,6-diphenylpyrimidine (**5**, **6**, or **7**) in 92, 42, or 47% yield. The IR spectra and the melting points of **5** and **6** agreed with those of their authentic samples.[5] The data of 7 are presented below.

Mp, 266 °C; IR (KBr), 3058—2872, 1609, 1552, 1496, and 1235 cm^{-1}. UV_{max} (EtOH), 256 (ε 25400), 314 (12600), and 381 nm (4100); MS *m/e*, (rel intensity) 364 (M^+, 11.5), 330 (M^+-SH, 20.5), 291 (M^+-NEt_2, 20.5), 264 (13.1), 104 (72.3), and 72 (Et_2N^+, 100). Found: C, 69.14; H, 5.80; N, 11.57; S, 8.53%. Calcd for $C_{21}H_{21}N_3SO$: C, 69.39; H, 5.82; N, 11.56; S, 8.82%.

5-Cyano-2,4-diphenylthiazole (8). Into a solution of benzoylacetonitrile (0.22 g, 1.5 mmol) and sodium hydride (0.10 g, 4.2 mmol) in THF (3 ml), **1** (0.36 g, 1.0 mmol) was added with stirring in small portions, heated to reflux for 1 h. The reaction mixture was poured into dilute hydrochloric acid, and the precipitate was recrystallized from cyclohexane to give 0.11 g (42%) or 0.14 g (53%) of **8**; m, 132 °C. MS *m/e*, (rel intensity) 262 (M^+, 50.7), 159 (M^+-PhCN, 100), 115 (Ph_2N^+, 23.6). UV_{max} (EtOH), 266 (ε 31000) and 318 nm (12100). Found: C, 73.50; H, 3.67; N, 10.60; S, 12.56%. Calcd for $C_{16}H_{10}N_2S$: C, 73.26; H, 3.84; N, 10.68; S, 12.72%.

4-(Aminothio)-5-cyano- and 4-(Aminothio)-5-diethylcarbamoyl-2,6-dipenylpyrimidine (9 and 11). Into a solution of hydroxylamine-*O*-sulfonic acid (0.50 g, 4.4 mmol) in 2 M NaOH (10 ml), **5** (0.29 g, 1.0 mmol) or **7** (0.37 g, 1.0 mmol) was added with stirring in small portions at 0—5 °C, and then allowed to stand at room temperature overnight. The resulting white powders were filtered off and recrystallized from ethanol to give **9** (0.22 g, 72%) or **11** (0.24 g, 63%).

9: Mp, 147 °C; IR (KBr), 3376, 3288, 2216, 1525, 1491, 1442, and 1379 cm^{-1}. UV_{max} (EtOH), 279 nm (ε 42800); MS *m/e*, (rel intensity) 304 (M^+, 75.1), 303 (M^+-1, 100), 153 (51.0), and 77 (39.7). Found: C, 67.23; H, 4.04; N, 18.16; S, 10.57%. Calcd for $C_{17}H_{12}N_4S$: C, 67.08; H, 3.98; N, 18.16; S, 10.57%.

11: Mp, 179 °C; IR (KBr), 3344, 3244, 2984, 2940, 1621, 1525, 1496, 1446, and 1383 cm^{-1}. UV_{max} (EtOH), 262 nm (ε 36500). MS *m/e*, (rel intensity) 378 (M^+, 28.9), 306 (M^+-NEt_2, 82.5), 100 (Et_2NCO^+, 38.8). Found: C, 66.47; H, 5.86; N, 14.80; S, 8.47%. Calcd for $C_{21}H_{22}N_4SO$: C, 66.64; H, 5.86; N, 14.77; S, 8.67%.

3-Hydroxy-4,6-diphenylisothiazolo[5,4-d]pyrimidine (12). **6** was treated with hydroxylamine-*O*-sulfonic acid as the same conditions as described above. The reaction mixture was poured into dilute hydrochloric acid and the resulting precipitate was recrystallized from acetonitrile to give **12** (0.16 g, 53%). Mp, 297 °C; IR (KBr), 3054, 2922, 2710, 1657, 1524, 1493, 1449, and 1395 cm^{-1}. UV_{max} (EtOH), 276 nm (ε 36500); MS *m/e*, (rel intensitey) 305 (M^+, 85.5), 272 (M^+-SH, 7.0), 202 (M^+-PhCN, 11.2), 159 (11.9), 152.5 ($M^+/2$, 14.1), 128 (PhC_3NH^+, 100). Found: C, 67.08; H, 3.52; N, 13.76; S, 10.50%. Calcd for $C_{17}H_{11}N_3SO$: C, 66.87; H, 3.63; N, 13.77; S, 10.28%.

References

1) K. Dimroth and K. Wolf, *Angew. Chem.*, **72**, 777 (1960); R. Schmidt, *Synthesis*, **1972**, 333.
2) I. Shibuya, *Technocrat*, **16**, 27 (1983).
3) I. Shibuya, *Bull. Chem. Soc. Jpn.*, **52**, 1235 (1979).
4) I. Shibuya, *Nippon Kagaku Kaishi*, **1982**, 1518.
5) I. Shibuya, *Bull. Chem. Soc. Jpn.*, **55**, 2158 (1982).
6) K. Gewald, U. Schlegel, and H. Schäfer, *J. Prakt. Chem.*, **317**, 959 (1975).

Catalytic Conversion of Allylic Esters to Corresponding Allylic Silanes with Hexamethyldisilane and Palladium(0) or Rhodium(I) Complexes

Hisao URATA, Hiroharu SUZUKI,* Yoshihiko MORO-OKA,* and Tsuneo IKAWA
Research Laboratory of Resources Utilization, Tokyo Institute of Technology, 4259 Nagatsuta-cho, Midori-ku, Yokohama 227
(Received June 20, 1983)

Synopsis. Treatment of allylic esters ($R^1CH=CR^2CH_2OCOR^3$: R^1=H, Ar; R^2=H, alkyl; and R^3=Me, Ph) with hexamethyldisilane in the presence of catalytic amounts of PdL_4 (L=PPh_3 or $P(OPh)_3$) or $RhCl(PPh_3)_3$ gives the corresponding allylic silanes in the excellent yield.

Synthetic utility of disilanes ($Cl_nMe_{6-n}Si_2$: n=0—6) have recently been developed. Monosilylation[1] and disilylaion ("double silylation")[2] of many classes of organic substrates have been achieved *via* the cleavage of Si-Si bond catalyzed by transition metal complexes. Disilane can also be used in the Pd(0)-catalyzed reductive dehalogenation of α-halogenated carbonyl and cyano compounds.[3] We report herein a simple preparative method of allylic silances, **3**, from allylic esters, **1**, and hexamethyldisilane, **2**, by using PdL_4 (L=PPh_3 or $P(OPh)_3$) or $RhCl(PPh_3)_3$ as catalyst.

Results and Discussion

Treatment of allylic acetates or benzoates, **1**, with hexamethyldisilane, **2**, in the presence of catalytic amounts of Pd(0) or Rh(I) complex at 140—160°C in sealed tube gave the corresponding allylic silanes, **3** (Eq. 1). Trimethylsilyl acetate[4] or benzoate,[5] **4**, was also formed in this reaction. The products were separated by column chromatography on silica gel and were identified and quantified by means of ^{1}H-NMR and GLC. Gaseous by-products were also identified and quantified by use of GLC. The results of the Pd(0) and Rh(I)-catalyzed conversion of allylic esters to allylic

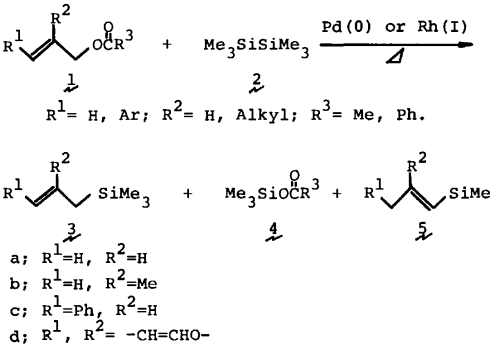

(1)

silanes are summarized in Table 1.

As shown in Table 1, β-methallyl acetate, β-methallyl benzoate, cinnamyl acetate, and furfuryl acetate were efficiently converted to the corresponding allylic silanes. Trimethylsilyl group was regioselectively introduced into the α-position of cinnamyl group to give (*E*)-cinnamyltrimethylsilane,[6] **3c** (entries 12 and 13).

Tetrakis(triphenylphosphite)palladium(0) effectively catalyzed the reaction of allyl acetate or benzoate with hexamethyldisilane to give allyltrimethylsilane,[6] **3a**, in an excellent yield whereas tetrakis(triphenylphosphine)palladium(0) and chlorotris(triphenylphosphine)rhodium(I) caused side reaction to afford propylene and (*E*)-1-propenyltrimethylsilane,[7] **5**, the double bond migration product of **3a**. The isomerization of allyltrimethylsilane, **3a**, to (*E*)-1-propenyltrimethylsilane, **5**, was examined under the various

Table 1. Conversion of allylic esters to allylic silanes catalyzed by Pd(0) or Rh(I) complexes

Entry	Allylic ester(1)			Cat[1]	[Cat]	Temp	Time	Yield/%		
	R^1	R^2	R^3		[1]	°C	h	**3**	**4**	**5**
1[2]	H	H	Me	A	1/204	180	2	**a**; 48	100	48
2				B	1/90	160	4	**a**;100	100	0
3[2]				C	1/106	160	24	**a**; 19	69	10
4[2]	H	H	Ph	A	1/73	160	3	**a**; 41	100	41
5				B	1/71	160	3	**a**; 82	84	0
6	H	Me	Me	A	1/101	150	10	**b**;100[3]	100	0
7				B	1/65	160	3	**b**;100	100	0
8				C	1/98	160	24	**b**; 31	31	0
9	H	Me	Ph	A	1/81	160	5	**b**; 75	99	0
10				B	1/98	160	24	**b**; 66	84	0
11[4]				C	1/80	160	5	**b**; 33	100	0
12	Ph	H	Me	A	1/91	160	10	**c**; 79	95	0
13				B	1/90	160	10	**c**; 60	50	0
14[5]				C	1/77	160	10	**c**; 42	42	0
15	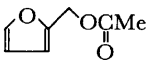			A	1/83	140	2	**d**; 37[6]	—	0

1) A: $Pd(PPh_3)_4$, B: $Pd[P(OPh)_3]_4$, C: $RhCl(PPh_3)_3$. 2) Propylene was detected as a by-product. 3) Ref. 11. 4) 2,5-Dimethyl-1,5-hexadiene was obtained in a 17% yield. 5) β-Methylstyrene was obtained in a 40% yield. 6) Furfuryltrimethylsilane was obtained. Ref. 12.

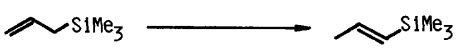

Conditions
A) 150 °C-2 h (no reaction)
B) $Pd(PPh_3)_4$—150 °C-2 h (no reaction) (2)
C) $Pd(PPh_3)_4$-AcOH—160 °C-2 h (20%)

conditions (Eq. 2).

Allyltrimethylsilane, **3a**, was isomerized to (*E*)-1-propenyltrimethylsilane, **5**, in a 20% conversion under the conditions C where palladium hydride was an actual active species.[8] This suggests the double bond migration of **3a** to **5** occurs by way of the addition-elimination of Pd–H formed by β-elimination from intermediary Pd–$SiMe_3$ species.

The applicability of the present method is however limited to the allylic esters having no *primary* or *secondary* alkyl group at the γ-position of allylic moiety. When R^1 was *primary* or *secondary* alkyl group, treatment of **1** with Pd(0) or Rh(I) complex gave the conjugated diene even in the presence of excess amounts of hexamethyldisilane. These results well agreed with those reported by Tsuji *et al.*[9]

From the results mentioned above, the following mechanism would be proposed for the conversion of allylic esters to the allylic silanes catalyzed by Pd(0) complex (Scheme 1).

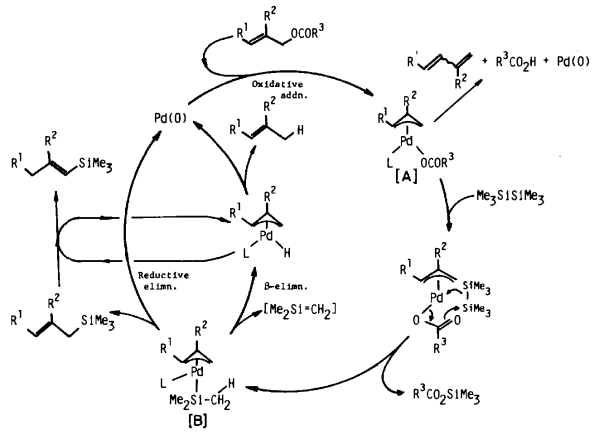

Scheme 1.

Allylic ester oxidatively adds to palladium(0) complex to give a π-allylpalladium carboxylate complex [**A**][10] followed by a nucleophilic attack of disilane to form a trimethylsilyl-π-allylpalladium species [**B**] and trimethylsilyl ester. The reductive elimination from [**B**] affords allylic silane and Pd(0) complex. The Pd–H species formed *via* the β-elimination from [**B**] promotes the double bond migration of the allylic silane to the vinylic one and ultimately turns to Pd(0) with formation of the alkene such as propylene or β-methylstyrene.

Experimental

All reactions were conducted in Pyrex sealed tubes under nitrogen atmosphere.

Synthesis of (E)-*Cinnamyltrimethylsilane (entry 12).* Tetrakis(triphenylphosphine)palladium (62.8 mg, 0.054 mmol) was placed in a Pyrex tube equipped with a three-way stopcock. After the atmosphere was replaced with nitrogen, hexamethyldisilane (0.70 g, 4.78 mmol) and cinnamyl acetate (0.87 g, 4.94 mmol) were added. Then the tube was sealed and heated at 160 °C for 10 h. Bulb to bulb distillation of the resultant mixture gave trimethylsilyl acetate[4] (0.60 g, 95%), ^{1}H-NMR (CCl_4) δ=0.20 (9H, s), 1.97 (3H, s). Purification of the residue by column chromatography (silica gel, benzene) afforded (*E*)-cinnamyltrimethylsilane[6] (0.72 g, 79%), bp 234 °C; IR (CCl_4) 960 cm^{-1} (*trans* CH=CH); ^{1}H-NMR (CCl_4) δ=0.05 (9H, s), 1.63 (2H, m), 6.10 (2H, m), 7.11 (5H, bs).

Synthesis of Allyltrimethylsilane and (E)-*1-Propenyltrimethylsilane (entry 1).* $Pd(PPh_3)_4$ (57.6 mg, 0.05 mmol), hexamethyldisilane (1.44 g, 10.05 mmol), and allyl acetate (1.02 g, 10.22 mmol) were placed in a Pyrex tube under N_2. After the tube was sealed and heated at 180 °C for 2 h, bulb to bulb distillation of the resultant mixture gave a mixture (2.40 g) of trimethylsilyl acetate[4] (100%), allyltrimethylsilane[6] (48%), and (*E*)-1-propenyltrimethylsilane[7] (48%), IR (CCl_4) 982 cm^{-1} (*trans* CH=CH); ^{1}H-NMR (CCl_4) δ=0.02 (9H, s), 1.80 (3H, d, *J*=5 Hz), 5.44 (1H, d, *J*=19 Hz), 6.06 (1H, dq, *J*=19 and 5 Hz). Propylene was also detected from gas phase by GLC analysis in a 2% yield.

Isomerization of Allyltrimethylsilane to (E)-*1-Propenyltrimethylsilane.* To a benzene solution (1 ml) of $Pd(PPh_3)_4$ (66.2 mg, 0.057 mmol) and acetic acid (3 μl) was added allyltrimethylsilane (0.77 g, 6.75 mmol). After the mixture was heated at 160 °C for 2 h in a Pyrex sealed tube, ^{1}H-NMR measurement of the reaction mixture showed a 20% conversion of (*E*)-1-propenyltrimethylsilane.

The authors are grateful to the Toshiba Silicon Co. Ltd. for a generous gift of disilane residue in the direct synthesis.

References

1) For eample, H. Matsumoto, S. Nagashima, T. Kato, and Y. Nagai, *Angew. Chem., Int. Ed. Engl.*, **17**, 279 (1978); K. Yamamoto, S. Suzuki, and J. Tsuji, *Tetrahedron Lett.*, **21**, 1653 (1980); M. Lefort, C. Simmonet, M. Birot, G. Deleris, J. Donogues, and R. Calas, *ibid.*, **21**, 1857 (1980); H. Matsumoto, K. Shono, and Y. Nagai, *J. Organomet. Chem.*, **208**, 145 (1981).

2) For example, H. Sakurai, Y. Kamiyama, and Y. Nakadaira, *Chem. Lett.*, **1975**, 887; H. Okinoshima, K. Yamamoto, and M. Kumada, *J. Organomet. Chem.*, **86**, C27 (1975); K. Tamao, T. Hayashi, and M. Kumada, *ibid.*, **114**, C19 (1976); K. Tamao, S. Okazaki, and M. Kumada, *ibid.*, **146**, 87 (1978); H. Watanabe, M. Kobayashi, K. Higuchi, and Y. Nagai, *ibid.*, **186**, 51 (1980).

3) H. Urata, H. Suzuki, Y. Moro-oka, and T. Ikawa, *J. Organomet. Chem.*, **234**, 367 (1982).

4) Yves Étienne, *C. R. Acad. Sci.*, **235**, 966 (1952).

5) N. E. Hoffman, A. Milling, Jr., and P. Parmelee, *Anal. Biochem.*, **32**, 386 (1969).

6) J. Slutsky and H. Kwart, *J. Am. Chem. Soc.*, **95**, 8678 (1973).

7) T. H. Chan and I. Fleming, *Synthesis*, **1979**, 761.

8) V. H. Hey and H. J. Arpe, *Angew. Chem.*, **85**, 968 (1973).

9) J. Tsuji, T. Yamakawa, M. Kaito, and T. Mandai, *Tetrahedron Lett.*, **1978**, 2075.

10) T. Yamamoto, O. Saito, and A. Yamamoto, *J. Am. Chem. Soc.*, **103**, 5600 (1981).

11) H. Matsumoto, T. Yako, S. Nagashima, T. Motegi, and Y. Nagai, *J. Organomet. Chem.*, **148**, 97 (1978).

12) Furfuryltrimethylsilane: Bp 149 °C. Found: C, 62.36; H, 9.03%. Calcd for $C_8H_{14}OSi$: C, 62.28; H, 9.15%. ^{1}H-NMR (CCl_4) δ=0.05 (9H, s), 2.03 (2H, s), 5.68 (1H, m), 6.10 (1H, m), 7.10 (1H, m).

A Convenient Synthesis of 3-Aminotropolone and Its Reactions with Orthoesters. Formation of 8*H*-Cyclohept[*d*]oxazol-8-ones

Kimiaki IMAFUKU,* Miki FURUYA,† and Zhong-Tian JIN††
Department of Chemistry, Faculty of Science, Kumamoto University, Kurokami, Kumamoto 860
††*Department of Chemistry, Yanbian University, Yanji, Jilin Province, People's Republic of China*
(Received June 21, 1983)

Synopsis. Schmidt reaction of 3-acetyltropolone gave 3-acetamidotropolone, which was hydrolyzed to afford 3-aminotropolone (**3**). The compound **3** reacted with orthoformate, orthoacetate, orthopropionate, and orthobenzoate to give the corresponding 2-substituted 8*H*-cyclohept[*d*]oxazole-8-one derivatives.

Recently, we found and reviewed that 3-acetyltropolone is very useful as starting material for the synthesis of heterocycle-condensed troponoid compounds.[1] In this series, we reported that 3-acetyltropolone and its methyl ethers reacted with hydroxylamine to afford 8*H*-cyclohept[*d*]isoxazol-8-one and 8*H*-cyclohept[*c*]isoxazol-8-one as a major and minor product, respectively.[2] It is also known that 3-aminotropolone reacted with formamide, acetic anhydride, or *p*-nitrobenzaldehyde to give 8*H*-cyclohept[*d*]oxazol-8-ones,[3,4] while 2-amino-3-hydroxytropone reacted with acetic anhydride to give 4*H*-cyclohept[*d*]oxazol-4-one.[5,6] The 1,3-dipolar addition of arenecarbonitrile oxide to tropone gave 4*H*-cyclohept[*d*]isoxazol-4-one derivatives.[7]

Previously, 3-aminotropolone was prepared from 3-nitrotropolone[8] or 3-bromotropolone.[9] On the other hand, it was reported that Schmidt reaction of 4-acetyltropolone afforded 4-aminotropolone.[10]

In a series of 3-acetyltropolone chemistry, we wish to report the convenient synthesis of 3-aminotropolone by Schmidt reaction of 3-acetyltropolone and its conversion to 8*H*-cyclohept[*d*]oxazole-8-ones by reactions with orthoesters.

Results and Discussion

When we applied the Schmidt reaction to 3-acetyltropolone(**1**),[11] 3-acetamidotropolone(**2**)[3] was isolated. The compound **2** was readily hydrolyzed to give 3-aminotropolone(**3**), whose averall yield based on **1** was 56%.

A mixture of 3-aminotropolone (**3**) and triethyl orthoformate or triethyl orthoacetate was heated under reflux to afford respectively 8*H*-cyclohept[*d*]oxazole-8-one (**4a**)[4] (44%) and its 2-methyl derivative (**4b**)[3] (73%). In the NMR spectrum of the compound **4a**, the H-2 proton in the oxazole ring is observed at lower magnetic field (δ=8.21) than the H-2 proton in oxazole ring (δ=7.95).[12] In a similar manner, the reaction with triethyl orthopropionate and trimethy orthobenzoate gave 2-ethyl- and 2-phenyl-8*H*-cyclohept[*d*]oxazol-8-ones (**4c** and **4d**) in 80 and 10% yields, respectively.

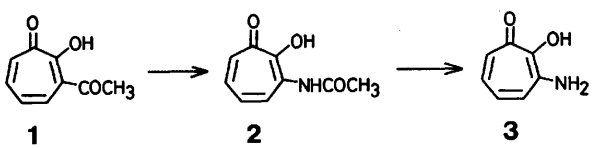

1 2 3

Scheme 1.

Experimental

Measurements. The melting points were determined with a Yanagimoto MP-S2 melting point-measuring apparatus and are uncorrected. The IR spectra were taken on a JASCO IRA-1 spectrophotometer, and the UV spectra on a Hitachi EPS-3T spectrophotometer. The NMR spectra were recorded with a Hitachi R-24 spectrometer (60 MHz).

3-Acetamidotropolone (2). Sodium azide (2.60 g, 40 mmol) was added to a solution of 3-acetyltropolone (**1**) (3.28 g, 20 mmol) in chloroform (40 ml). Concentrated sulfuric acid (10 ml) was carefully dropped into the mixture in an ice-cooled bath under stirring. After stirring for 2 h at room temperature, the chloroform was removed by decantation. After cold water (80 ml) was added to the residue, a precipitate was collected and recrystallized from methanol to give 2.3 g (66%) of 3-acetamidotropolone (**2**) as colorless needles: mp 119—120 °C (lit,[3] 107—108 °C); IR ($CHCl_3$) 3315 (NH), 1702 cm^{-1} (C=O); NMR ($CDCl_3$) δ=2.30 (3H, s, CH_3), 7.0—7.6 (3H, m), 9.1—9.4 (1H, m, NH).

3-Aminotropolone (3). 3-Acetamidotropolone (**2**) (2.0 g) in 50% sulfuric acid (22 ml) was heated on a water bath for 1 h. The mixture was neutralized with sodium hydrogencarbonate solution, acidified slightly with 30% acetic acid, and extracted with chloroform. The evaporation residue from the extract was recrystallized from benzene–petroleum ether to give 1.3 g (85%) of 3-aminotropolone (**3**) as yellow needles: mp 86 °C (lit,[8] 86 °C); NMR ($CDCl_3$) δ=5.6—6.7 (2H, br, NH_2), 6.6—7.5 (m, 4H).

Reaction of 3-Aminotropolone (3) with Triethyl Orthoformate. A mixture of 3-aminotropolone (**3**) (137 mg, 1.0 mmol) and triethyl orthoformate (2 ml) was refluxed for 2 h. After cooling, the precipitate was collected and recrystallized from benzene–hexane to give 65 mg (44%) of 8*H*-cyclohept[*d*]oxazol-8-one (**4a**) as pale yellow needles: mp 149—150 °C (lit,[4] 150—151 °C); IR ($CHCl_3$) 1625 cm^{-1} (C=O); UV (CH_3OH) 237 (log ε 4.56), 310 nm (3.94); NMR ($CDCl_3$) δ=6.8—8.0 (4H, m), 8.21 (1H, s, H-2).

Reaction of 3 with Triethyl Orthoacetate. A mixture of **3** (274 mg, 2.0 mmol) and triethyl orthoacetate (2 ml) was refluxed for 2 h. The reaction mixture was dissolved in chloroform and twice washed with water. After removal of the solvent, the residue was recrystallized from benzene–hex-

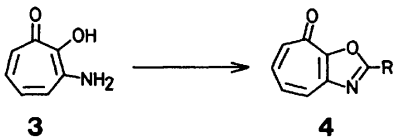

3 4

a R = H
b R = CH_3
c R = CH_2CH_3
d R = Ph

Scheme 2.

† Present address: Hirata Industrial Machineries Co., Ltd., Myotaiji-machi, Kumamoto 860.

ane to give 234 mg (73%) of 2-methyl-8*H*-cyclohept[*d*]oxazol-8-one (**4b**) as pale yellow needles: mp 150—151 °C (lit,[3] 144—145 °C); IR ($CHCl_3$) 1640 cm^{-1} (C=O); UV (CH_3OH) 243 (log ε 4.44), 312 nm (3.68); NMR ($CDCl_3$) δ=2.67 (3H, s, CH_3), 6.9—7.8 (4H, m).

Reaction of 3 with Triethyl Orthopropionate. A mixture of **3** (274 mg, 2.0 mmol) and triethyl orthopropionate (2 ml) was refluxed for 2 h and worked up, as mentioned above, to afford 280 mg (80%) of 2-ethyl-8*H*-cyclohept[*d*]oxazol-8-one (**4c**) as pale yellow needles: mp 92—93 °C (from benzene–hexane); IR ($CHCl_3$) 1640 cm^{-1} (C=O); UV (CH_3OH) 245 (log ε 4.49), 312 nm (3.83); NMR ($CDCl_3$) δ=1.50 (3H, t, J=7 Hz, CH_3), 3.03 (2H, q, J=7 Hz, CH_2), 6.9—7.8 (4H, m). Found: C, 68.51; H, 5.21; N, 7.92%. Calcd for $C_{10}H_9NO_2$: C, 68.56; H, 5.18; N, 8.00%.

Reaction of 3 with Trimethyl Orthobenzoate. A solution of **3** (137 mg, 1.0 mmol) and trimethyl orthobenzoate (182 mg, 1.0 mmol) in chloroform (2 ml) was refluxed for 2 h. After removal of the solvent, the residue was chromatographed on a Wakogel B-10 plate (30×30 cm^2) with ethyl acetate to give 23 mg (10%) of 2-phenyl-8*H*-cyclohept-[*d*]oxazol-8-one (**4d**) as pale yellow needles: mp 149—150 °C (from benzene–hexane); IR ($CHCl_3$) 1640 cm^{-1} (C=O); UV (CH_3OH) 275 (log ε 4.42), 349 (sh, 3.84), 365 nm (sh, 3.63); NMR ($CDCl_3$) δ=7.0—7.8 (7H, m,), 8.1—8.5 (2H, m, H-2′, 6′). Found: C, 75.32; H, 4.06; N, 6.28%. Calcd for $C_{14}H_9NO_2$: C, 75.50; H, 3.96; N, 6.26%.

References

1) K. Imafuku and Z.-T. Jin, *Yanbian Daxue Xuebao*, **1983** (1), 35.
2) Y. Sudoh, Z. -T. Jin, K. Imafuku, and H. Matsumura, *J. Heterocycl. Chem.*, **19**, 525 (1982).
3) Y. Kitahara, *Sci. Repts. Tohoku Univ., I*, **40**, 83 (1956).
4) T. Nozoe, K. Doi, and Y. Kitahara, *Bull. Chem. Soc. Jpn.*, **34**, 312 (1961).
5) A. W. Johnson and M. Tisler, *J. Chem. Soc.*, **1955**, 1841.
6) M. Tisler, *Univ. Ljubljiani Tehniska Fak. Acta Tech., Ser. Chem.*, No. 2, 40 (1956); *Chem. Abstr.*, **53**, 18927 (1959).
7) C. De Micheli, R. Gandolfi, and P. Grunager, *Tetrahedron*, **30**, 3765 (1974).
8) J. W. Cook, J. D. Hobson, and D. K. Steel, *J. Chem. Soc.*, **1954**, 530.
9) T. Nozoe and Y. Kitahara, *Proc. Jpn. Acad.*, **30**, 204 (1954).
10) K. Doi, *Bull. Chem. Soc. Jpn.*, **34**, 501 (1961).
11) A. Yamane, M. Nagayoshi, K. Imafuku, and H. Matsumura, *Bull. Chem. Soc. Jpn.*, **52**, 1972 (1979).
12) E. Pretsch, T. Clerc, J. Seibl, and W. Simon, "Tabellen zur Strukturaufklarung organischer Verbindungen mit spektropishen Methoden," 2nd ed, Springer Verlag, Berlin (1981), p. H270.

Electrochemical Carboxylation of α,β-Unsaturated Ketones with Carbon Dioxide

Junji HARADA, Yoshihisa SAKAKIBARA, Atsutaka KUNAI,* and Kazuo SASAKI
Department of Applied Chemistry, Faculty of Engineering, Hiroshima University, Shitami, Saijou, Higashi Hiroshima 724
(Received June 25, 1983)

Synopsis. Several aromatic and aliphatic α,β-unsaturated ketones were converted to the corresponding γ-keto acids by the electrochemical reduction in acetonitrile in the presence of CO_2. The yields of the keto acid were 73—82% when the enones have at least one aromatic substituent. In the case of aliphatic enones, the yields of the carboxylation reaction were 67% for 2-cyclohexen-1-one and 44% for 3-buten-2-one.

γ-Keto acids or γ-keto esters are useful intermediates for γ-lactones, cyclopentenones, butenolides, 1,3-cyclopentanediones and heterocyclic compounds. Available synthetic methods of γ-keto acid or γ-keto esters usually need multi-stage reactions.[1a-g] In recent years, electrochemical carboxylation of various unsaturated compounds has received considerable attention from synthetic and mechanistic point of views. Among these, reductive carboxylation of α,β-unsaturated ketones has been reported,[2-4] where γ-keto acids were produced. However, the yields were not satisfactory in the earlier works because of the formation of dimeric and polymeric products.

We would like to report the effective transformation of aromatic and aliphatic α,β-unsaturated ketones into γ-keto acid by electrochemical carboxylation with CO_2 in acetonitrile under the controlled potential conditions.

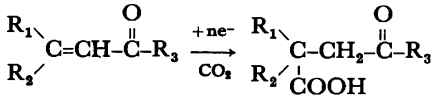

1 R_1=H, R_2=Ph, R_3=Me
2 R_1=H, R_2=Ph, R_3=Ph
3 R_1=Ph, R_2=Ph, R_3=Ph
4 R_1=H, R_2R_3=-$(CH_2)_3$-
5 R_1=Me, R_2R_3=-$(CH_2)_3$-
6 R_1=H, R_2=H, R_3=Me

Results and Discussion

The α,β-unsaturated ketones, 4-phenyl-3-buten-2-one (**1**), 1,3-diphenyl-2-propen-1-one (**2**), 1,3,3-triphenyl-2-propen-1-one (**3**), 2-cyclohexen-1-one (**4**), 3-methyl-2-cyclohexen-1-one (**5**), and 3-buten-2-one (**6**) were used for starting materials. The polarographic half-wave potential in each case is summarized in Table 1. The aromatic enones **1**—**3** showed two one-electron reduction waves, while the aliphatic enones **4**—**6** exhibited only a single one-electron wave. For all of the compounds studied, the half-wave potentials of both the first and second waves are more positive than that of carbon dioxide (*ca.* −2.5 V).

When carbon dioxide was introduced into the solution of the aromatic enone **2**, the first wave grew as CO_2 concentration increased and the final height of it became approximately two times of that of the original first wave. A similar phenomenon was observed for the aliphatic enone **4**. These facts suggest that at the first wave potential the ECE reaction of an anion radical with CO_2 proposed by Wawzonek[2] may operate to afford the carboxylated product.

When preparative electrolysis of the aromatic enone **2** was carried out at the potential of the first wave, at which the anion radical species is formed, the carboxylated product was obtained less selectively (35%), and considerable amounts of dimeric and polymeric materials were formed, in accordance with the results shown by Wawzonek. When the electrolysis of the enone **2** was made at the potential of the second wave, 2,4-diphenyl-4-oxobutanoic acid was produced in 77% yield (run 2 in Table 1). In this case, by-products were a minor amount of a dihydro compound, 1,3-diphenyl-1-propanone, and traces amounts of dimeric and polymeric materials. Similar results were also obtained with the aromatic enones **1** and **3** (runs 1 and 3). Here, it is worth noting that an introduction of bulky phenyl groups into the enone moiety does not hinder the efficiency of the carboxylation reaction. This is the marked difference from the cases of aliphatic enones. The fact that more selective transformation of the enone **2** into the γ-keto acid was achieved at the second wave potential, at which dianion species is formed, suggests that a pathway arising from the reaction of the dianion with CO_2 is more effective to the carboxylation reaction.

On the other hand, the second reduction waves were not observed for the aliphatic enones **4**—**6**. When the electrolysis of **4** was carried out at −2.40 V, the yield of the keto acid was 43% and considerable amounts of dimeric products of cyclohexenone were formed (50%, run 4). When a methyl group was attached to the 3-position of cyclohexenone ring, the yield of γ-keto acid decreased to 10% (run 10). With the enone **5**, the carboxylation reaction became rather a minor path and a large amount of a mixture of dimeric compounds was obtained in 80% yields. In order to examine the effect of the anion radical concentration on the electrode surface on the competitive pathways of carboxylation and dimerization, we carried out a series of controlled current experiments with 2-cyclohexen-1-one (**4**) (runs 5—9). When the current density, which should relate to the radical concentration on the electrode surface, was chosen to be 20 A dm^{-2}, the yield of the keto acid was only 18% (run 9). By lowering the current density, the yields were definitely improved up to 67% (run 6). With 2-buten-1-one (**6**), the carboxylation also occurred in moderate yield (run 12), but a detailed study has not been done in this case.

Table 1. Electrolyses of α,β-unsaturated ketones with CO_2 in acetonitrile

Run	Starting materials (mmol)	Half wave potential / V	Conditions[a] / V or A dm^{-2}	Conversion / %	Yield of the products[b]/% γ-Keto acid	Saturated ketone	Dimeric products	Current[c] efficiency / %
1	**1** (7.0)	−1.73 & −2.25	−2.40 V	100	82	Trace	Trace	82
2	**2** (7.0)	−1.50 & −2.10	−2.20 V	92	77	18	Trace	71
3	**3** (7.0)	−1.62 & −1.96	−2.10 V	95	73	5	Trace	70
4	**4** (7.0)	−2.20	−2.40 V	100	43	4	50	43
5	**4** (1.0)		7.3 A dm^{-2}	97	58	Trace	12	55
6	**4** (1.0)		11.0 A dm^{-2}	95	67	Trace	16	64
7	**4** (1.0)		14.7 A dm^{-2}	100	38	Trace	31	38
8	**4** (1.0)		17.0 A dm^{-2}	100	26	Trace	30	26
9	**4** (1.0)		20.6 A dm^{-2}	100	18	Trace	18	18
10	**5** (7.0)	−2.32	−2.50 V	64	10	—	80	6
11	**6** (1.0)	−2.00	3.7 A dm^{-2}	—	35	—	—	35
12	**6** (1.0)		3.7 A dm^{-2}	—	44	—	—	22

a) Electricity was 2.0 F mol^{-1} for runs 1—11, and 4.0 F mol^{-1} for run 12. b) Based on reacted ketones. c) Current efficiency of carboxylation.

Experimental

General. Guaranteed grade enones were purified by distillation or recrystallization before use. Acetonitrile was purified in the usual way.[5] The base solution used for polarographic measurements and preparative electrolyses was always acetonitrile containig 0.1 mol dm^{-3} tetraethylammonium perchlorate. All the potential values cited are referred to a saturated calomel electrode using acetonitrile as the solvent.[6] Preparative electrolyses were carried out in a divided cell with a mercury pool cathode at 5—10°C under the controlled potential conditions. A solution of a enone (10 mmol dm^{-3}) was placed into the cathode compartment and saturated with bubbling CO_2. In some experiments, the electrolyses were made under the controlled current. The electrolyzed solution was evaporated to remove the solvent and the residue was taken into a small amount of water, acidified, and extracted with ether throughly. The condensed extract was subjected to product analyses. The γ-keto acids were isolated by silica-gel column chromatography or preparative GLC after esterifications. Reaction conditions and results are summarized in Table 1. All the spectroscopic data, melting points, and elemental analyses agreed with those of the authentic samples.

References

1) a) A. Takeda, K. Takahashi, S. Torii, and T. Moriwake, *J. Org. Chem.* **31**, 616 (1966); b) P. A. Wehrli and V. Chu, *ibid.*, **38**, 3436 (1973); c) C. G. Chavdarian and C. H. Heathcock, *J. Am. Chem. Soc.*, **97**, 3822 (1975); d) A. R. B. Manas and R. A. J. Smith, *J. Chem. Soc., Chem. Commun.*, **1975**, 216; e) H. Stetter, M. Schreckenberg, and K. Wiemann, *Chem. Ber.*, **109**, 541 (1976); f) E. Nakamura, K. Hashimoto, and I. Kuwajima, *J. Org. Chem.*, **42**, 4166 (1977); g) M. Miyashita, T. Kumazawa, and A. Yoshikoshi, *Chem. Lett.*, **1980**, 1043.

2) S. Wawzonek and A. Gundersen, *J. Electrochem. Soc.*, **111**, 324 (1964).

3) E. Lamy and L. Nadjo, *Nuovo J. Chim.*, **3**, 21 (1979).

4) D. A. Tyssee, J. H. Wagenknecht, M. M. Baizer, and J. L. Chruma, *Tetrahedron Lett.*, **1972**, 4809.

5) I. M. Kolthoff, M. K. Chantooni, Jr., and H. Smagowski, *Anal. Chem.*, **42**, 1622 (1970).

6) O. Bravo and R. T. Iwamoto, *J. Electroanal. Chem. Interfacial Electrochem.*, **23**, 419 (1969).

A Simple and Convenient Method for the Synthesis of Sulfones Using Polyethylene Glycols or Their Dialkyl Ethers as Solvents or Catalysts

Kazuaki SUKATA
Nihon Tokushu Kagaku Kogyo Co., Ltd., 3-36, Tohda-cho, Moriguchi, Osaka 570
(Received June 2, 1983)

Synopsis. Various alkyl *p*-tolyl sulfones were prepared in good yields under mild conditions in the presence of polyethyene glycols or their dialkyl ethers as solvents or catalysts.

It has been reported[1] that the alkylation of sodium *p*-toluenesulfinate in methanol (MeOH) or *N*, *N*-dimethylformamide gives both the *p*-toluenesulfinic ester and the sulfone, and alkylation with hard alkylating agents gives predominantly the ester, whereas a soft alkylating agent gives predominantly the sulfone. This alkylation usually gives the sulfone only in moderate yields.[1]

$$R-SO_2^- + R'X \longrightarrow R-\overset{\overset{O}{\uparrow}}{\underset{\underset{O}{\downarrow}}{S}}-R' + S-\overset{\overset{O}{\uparrow}}{S}-OR' + X^-$$

Recently, Veenstra and Zwanenburg[2] have reported the reaction of tetrabutylammonium *p*-toluenesulfinate with alkyl halides as an improved method for the synthesis of sulfones. More recently, Manescalchi *et al.*[3] have reported a similar method using Amberlyst A-26, a macroreticular anion-exchange resin. In these methods, however, the tedious preparation of tetrabutylammonium *p*-toluenesulfinate or the sulfinate form of Amberlyst A-26 is required before reaction with the alkyl halide.

In this paper, a simpler and more convenient method for the synthesis of sulfones using polyethylene glycols (PEG) or their diethyl ethers is reported.

The reactions were carried out with sodium *p*-toluensulfinate monohydrate and various alkyl halides in PEG having an average molecular weight of 400 (PEG-400), PEG-400 diethyl ether (PEG-400-Et_2), or MeOH containing PEG-1000 or PEG-1000-Et_2 as a catalyst. Table 1 shows the results. In all cases, the sulfones were obtained in good to excellent yields. When PEG-400 was employed as a solvent, GLC showed that the product was almost entirely the sulfone because of the rapid hydrolysis of the ester. In the case of PEG-400-Et_2 or MeOH with a catalytic amount of PEG-1000 or PEG-1000-Et_2, however, GLC showed that a small amount of the ester remained under the experimental conditions used. These facts indicate that PEG is a good solvent for the alkylation of sulfinate anion to yield sulfones.

Table 1. Reaction of $C_7H_7SO_2Na \cdot H_2O$ with alkyl halides[a]

Alkyl halide	Solvent	Catalyst[b]	Time / h	Temp / °C	Yield[c] / %	Mp θ_m or Bp θ_b/°C (mmHg)	Lit Mp θ_m or Bp θ_b/°C (mmHg)
C_2H_5Br	PEG-400	—	3	60	89		
	PEG-400-Et_2	—	4	60	89	53—55	55—56[5]
	MeOH	A	7	reflux	80[d]	151—152(3)	
	MeOH	—	7	reflux	64[e]		
n-C_4H_9Br	PEG-400	—	3	60	90		
	PEG-400-Et_2	—	9	60	82[d]	143—144(1)	175—177(4)[6]
	MeOH	A	7	60	83[d]		
	MeOH	—	7	60	61[e]		
n-$C_8H_{17}Br$	PEG-400	—	4	60	94		
	PEG-400-Et_2	—	12	60	59[d]	40.0—40.5	[f]
	MeOH	A	7	60	80	150—151(0.12)	
	MeOH	—	7	60	56[d]		
CH_2=$CHCH_2Br$	PEG-400	—	1.5	60	95		
	PEG-400-Et_2	—	3	60	95	51—52	52—53[7]
	MeOH	A	3	60	89[d]	137(1)	
$PhCH_2Cl$[g]	PEG-400	—	2	60	94		
	MeOH	A	4	60	90	144—145	144—145[8]
$ClCH_2CN$	PEG-400	—	2	60	93		
	MeOH	B	4	60	83	147—148	145—146[10]
$BrCH_2Br$	PEG-400	—	6	60	73		
	PEG-400	—	4	80	89	87—88	90—92[9]

a) All reactions were carried out with $C_7H_7SO_2Na \cdot H_2O$ (0.05 mol) and alkyl halide (0.075 mol) in a solvent (20 ml) with or without a catalyst (0.005 mol). b) A: PEG-1000-Et_2, B: PEG-1000. c) Isolated yields. Unless otherwise noted, purities were >99% by GLC. d) Purities were 98% by GLC. e) Purities were 97% by GLC. f) See Experimental section. g) Forty milliliters of solvent were used.

Experimental

Materials. Methanol and PEG-400 (reagent grade, Kishida Kagaku Co., Ltd.) were dried with molecular sieves 4A. PEG-1000 (reagent grade, Kishida Kagaku Co., Ltd.) was used without further purification. PEG-400-Et_2 and PEG-1000-Et_2 were prepared according to the method previously reported.[4] Sodium *p*-toluenesulfinate ($C_7H_7SO_2Na$ nH_2O, $n\approx1$) (reagent grade, Tokyo Kasei Kogyo Co., Ltd.) was used as obtained. The physical properties (bp or mp) of ethyl *p*-tolyl sulfone,[5] butyl *p*-tolyl sulfone,[6] allyl *p*-tolyl sulfone,[2,7] benzyl *p*-tolyl sulfone,[8] cyanomethyl *p*-tolyl sulfone,[2,10] and bromometyl *p*-tolyl sulfone[2,9] were in good agreement with those reported in the literature (Table 1) and satisfactory IR spectra for these compounds were obtained.

Typical Procedure for the Reaction of Sodium p-*Toluenesulfinate Monohydrate with Alkyl Halides. Bromomethyl* p-*Tolyl Sulfone*: A mixture of powdered sodium *p*-toluenesulfinate monohydrate (9.8 g, 0.05 mol) and dibromomethane (13.0 g, 0.075 mol) was stirred at 80 °C for 4 h in PEG-400 (20 ml). After removal of the excess dibromomethane, the reaction mixture was poured into water (300 ml). The precipitated white solid was collected and recrystallized from ethanol–water, giving 11.1 g (89%) of bromomethyl *p*-tolyl sulfone, mp 87—88 °C (lit,[9] mp 90—92 °C).

Butyl p-*Tolyl Sulfone*: A mixture of powdered sodium *p*-toluenesulfinate monohydrate (9.8 g, 0.05 mol), butyl bromide (10.3 g, 0.075 mol), MeOH (20 ml), and PEG-1000-Et_2 (5.3 g, 0.005 mol) was stirred at 60 °C for 7 h. The reaction mixture was diluted with water (200 ml) and extracted with benzene (20 ml×3). The benzene layers were combined, washed with water, and dried. After removal of the benzene, the residual oil was distilled under reduced pressure, giving 8.8 g (83%) of butyl *p*-tolyl sulfone, bp 137—142 °C/1 mmHg (1 mmHg=133.322 Pa) (lit,[6] bp 175—177 °C/4 mmHg). The purity was 98% by GLC.

Octyl p-*Tolyl Sulfone*: A mixture of powdered sodium *p*-toluenesulfinate monohydrate (9.8 g, 0.05 mol), octyl bromide (14.5 g, 0.075 mol), and PEG-400 (20 ml) was stirred at 60 °C for 3 h. After the reaction mixture had been treated according to the method for butyl *p*-tolyl sulfone, the residual oil was distilled under reduced pressure, giving 12.6 g (94%) of octyl *p*-tolyl sulfone (>99% pure), bp 175—178 °C/0.5 mmHg. Redistillation of the product gave pure octyl *p*-tolyl sulfone having bp 150—151 °C/0.12 mmHg, mp 40.0—40.5 °C; IR (neat) 1310, 1140 cm^{-1} ($-SO_2-$). Found: C, 66.90; H, 9.07; S, 11.93%. Calcd for $C_{15}H_{24}O_2S$: C, 67.12; H, 9.01; S, 11.94%.

The author thanks Nihon Tokushu Kagaku Kogyo Co., Ltd. for permission to publish this article, and also Dr. Nobuaki Wada for useful suggestions during this work.

References

1) J. S. Meek and J. S. Fowler, *J. Org. Chem.*, **33**, 3422 (1968)
2) G. H. Veenstra and B. Zwanenburg, *Synthesis*, **1975**, 519.
3) F. Manescalchi, M.Orena, and D. Savoia, *Synthesis*, **1979**, 445.
4) K. Sukasa, *Yuki Gosei Kagaku Kyokai Shi*, **39**, 86 (1981).
5) R. Otto, *Ber.*, **13**, 1277 (1880).
6) H. Gilman and N. J. Beaber, *J. Am. Chem. Soc.*, **47**, 1450 (1925).
7) R. Otto, *Justus Liebigs Ann. Chem.*, **283**, 184 (1894).
8) R. Otto, *Ber.*, **13**, 1278 (1880).
9) R. Otto, *J. Prakt. Chem.*, [2], **40**, 544 (1889).
10) J. Tröger and W. Hille, *J. Prakt. Chem.* [2], **71**, 226 (1905)

Generation and Reactions of 5,6-Dimethylene-2-cyclohexene-1,4-diones. A New Synthesis of Polycyclic 1,4-Benzoquinones

Yoshinori KANAO† and Masaji ODA*

Department of Chemistry, Faculty of Science, Osaka University, Toyonaka, Osaka 560
†*Department of Chemistry, Faculty of Science, Tohoku University, Aobayama, Sendai 980*

(Received July 4, 1983)

Synopsis. 1,2,3,6-Tetrahydrobenzocyclobutene-3,6-dione underwent thermal ring opening of the four-membered ring at 140°C to generate 5,6-dimethylene-2-cyclohexene-1,4-dione. This is a highly reactive substance and was trapped as dimers or Diels-Alder adducts giving polycyclic 1,4-benzoquinones. Intramolecular rearrangements preferably took place in some derivatves.

5,6-Dimethylene-1,3-cyclohexadienes (*o*-quinodimethanes) have proved to be useful intermediates in organic syntheses by virtue of their high reactivity in cycloaddition reactions.[1] Accordingly, 5,6-dimethylene-2-cyclohexene-1,4-dione (**1**) is an interesting compound, since its Diels-Alder reactions with dienophiles would afford polycyclic 1,4-benzoquinones in a single step. Although the intermediary formation and some reactions of 2,3-dimethyl and benzo derivative of **1** have been reported,[2,3] the parent compound **1** remains unknown. We have recently reported the synthesis of 1,2,3,6-tetrahydrobenzocyclobutene-3,6-dione (**2**) which is considered to be a promising precursor for **1**.[4] This paper describes the results of thermolysis of **2** and some derivatives in the absence or presence of trapping agents.

Thermal electrocyclic ring opening of the cyclobutene of **2** readily took place at about 140°C. This temperature is considerably lower than that required for the ring opening of 1,2-dihydrobenzocyclobutene, which ring-opens at about 200°C,[1a] probably because there is no loss of aromatic stabilization in the ring opening of **2**. In a typical experiment, heating of a 0.05 M solution of **2** in xylene under reflux for 2 h gave dimers **3** and **4** in 11% and 39% yield, respectively. The ^{1}H NMR spectrum of **3** shows the presence of six olefinic protons including two exocyclic methylene protons and the absence of symmetry, whereas that of **4** shows the presence of four olefinic protons and a mirror plane, supporting the assigned structures. Dimer **3** is thus a Diels-Alder adduct of two molecules of **1**, and dimer **4** is that of **1** and **2**. The predominant formation of **4** is in accord with the high dienophilicity of the strained internal double bond of **2** as previously observed in its Diels-Alder reactions.[5] As might be expected, **2** gave only **3** under conditions of flash vacuum thermolysis at 350°C where **2** would rapidly open to **1**.

In the presence of excess of dienophiles (5 equiv.) such as *N*-phenylmaleimide (**5a**), dimethyl fumarate (**5b**), 1,4-naphthoquinone (**5c**), and acenaphthylene (**5d**) **1** could form adduct **6a** (29%), **6b** (47%), **6c** (11%), and **6d** (28%), respectively. The yields were, however, poor to moderate due to the competition of the dimerization forming **4**. In the case of **5c**, the primary Diels-Alder adduct was apparently further oxidized to **6c** under the reaction conditions. Although hydrocarbon **5d** could form adduct **6d**, other simple olefins such as indene and cyclooctene failed to form adducts giving only the dimers.

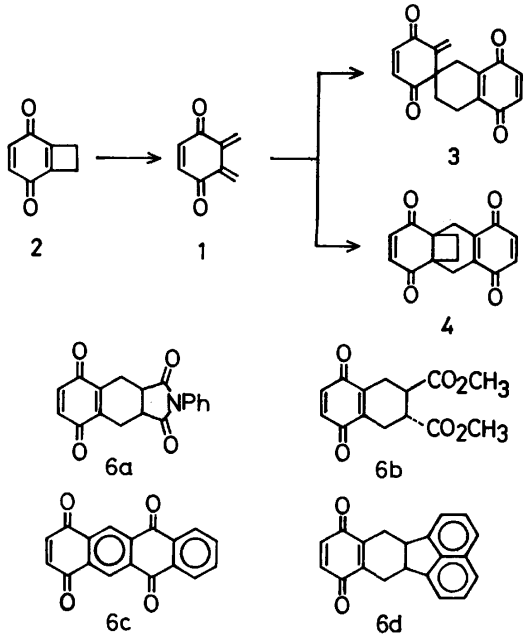

When alkyl groups are present on the four-membered ring, intramolecular rearrangements become feasible in the ring-opened form and were actually observed to take place. Thermolysis of 1,4,4b,5,6,7,8,8a-octahydrobiphenylene-1,4-dione (**7**) at 140°C gave 1,4,7,8,9,10-hexahydrobenzocyclooctene-1,4-dione (**9**) in 72% yield. The rearrangement can be accounted for in terms of conrotatory ring opening to a (*E,Z*)-cyclooctadiene **8** followed by [1,5] sigmatropic hydrogen shift. A molecular model of **8** suggests the favorable spatial location of a methylene proton for the hydrogen shift. On the other hand, 1,1,2,2-tetramethyl derivative **10** gave 2,3-diisopropenylhydroquinone (**12**) in 51% yield. The formation of **12** can be rationalized by a double [1,5] sigmatropic hydrogen shift involving the carbonyl groups in the ring-opened form **11**.

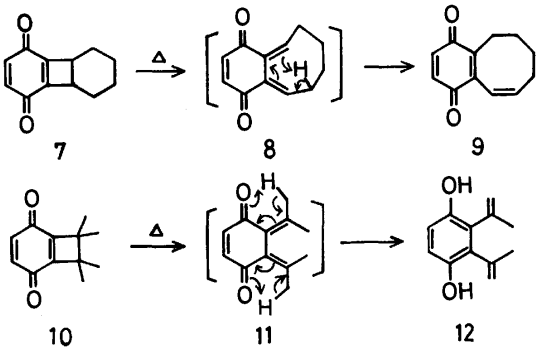

Experimental

All the melting points were determined on either a Yamato MP-21 or a Mettler FP-2 apparatus and are uncorrected. Infrared spectra were recorded with a Hitachi 215 grating spectrophotometer, and electronic absorption spectra with a Hitachi 323 spectrophotometer. ^{1}H NMR spectra were obtained with either a JNM-PMX 60 or a JNM-FX90Q spectrometer using $(CH_3)_4Si$ as an internal standard. Mass spectra were measured with a Hitachi M-52 mass spectrometer. Merck Kieselgel 60 was used for column chromatography.

Thermolysis of 1,2,3,6-Tetrahydrobenzocyclobutene-3,6-dione (2) in the Absence of Trapping Agent. A solution of **2** (268 mg, 2 mmol) in xylene (10 ml) was heated under reflux under a nitrogen atmosphere for 2 h. After evaporation of the solvent, the residue was chromatographed on silica gel (50 g) and eluted with benzene–ethyl acetate (95:5). The first yellow band gave **3** (31 mg, 11.5%) and the second yellow band **4** (150 mg, 39%). **3**: Yellow crystals from dichloromethane–hexane, mp 147—149 °C. MS *m/z* (rel intensity) 268 (M^+; 100), 240 (61); IR (KBr)1684, 1670, 1640, 1598 cm^{-1}; UV (EtOH) λ_{max} 240 (log ε 4.32), 338 nm (2.97); ^{1}H NMR ($CDCl_3$) δ 1.95 (2H, dd, J=6, 7 Hz), 2.47 (2H, m), 2.86 (1H, m), 3.20 (1H, m), 5.29 (1H, s), 6.18 (1H, s), 6.78 (2H, s), 6.79 (1H, d, J=10.4 Hz), 6.97 (1H, d, J=10.4 Hz); Found: C, 71.25; H, 4.52%. Calcd for $C_{16}H_{12}O_4$: C, 71,63; H, 4.51%. **4**: Yellow crystals from dichloromethane–hexane, mp 204—205 °C; MS *m/z* 268 (M^+, 13), 240 (100); IR (KBr) 1662, 1648, 1600, 1292, 824 cm^{-1}; UV (EtOH) λ_{max}=225 (log ε 4.22), 240 (4.19), 248 (4.19), 340 nm (2.88); ^{1}H NMR ($CDCl_3$) δ=2.13 (4H, m), 2.36 (2H, d, J=16.4 Hz), 3.37 (2H, d, J=16.4 Hz), 6.87 (2H, s), 6.91 (2H, s); Found: C, 71.57; H, 4.46%. Calcd for $C_{16}H_{12}O_4$: C, 71.63; H, 4.51%.

Flash Vacuum Thermolysis of 2. Sublimatively vapourized **2** (51 mg) was passed through a preheated quartz column (15×200 mm) packed with Pyrex glass chips at 350 °C at 0.5 mmHg. The pyrolysate was led into a receiver cooled at 0 °C, but yellow solids condensed on the inside of the wall of the column just out the electronic furnace. After cooling to room temperature the condensate was washed out with dichloromethane into the receiver. The solvent was evaporated and the residue chromatographed on silica gel to give **3** (14 mg, 27%).

General Procedure for the Trapping Experiments with Dienophiles. Solutions of **2** (134 mg, 1 mmol) and a dienophile (5 mmol) in xylene (10 ml) were heated under reflux under a nitrogen atmosphere for 2 h. After evaporation of the solvent the residue was chromatographed on silica gel and eluted with benzene–ethyl acetate.

(a) With N-Phenylmaleimide: Unreacted *N*-phenylmaleimide (742 mg), dimer **4** (32 mg, 24%), and adduct **6a** (90 mg, 29%) were obtained. **6a**: Yellow crystals from benzene–dichloromethane, mp 243—244 °C; IR (KBr) 1700, 1644, 1590, 1386, 1180 cm^{-1}; ^{1}H NMR ($CDCl_3$–CD_3SOCD_3) δ=2.7—3.2 (4H, m), 3.3—3.6 (2H, m), 6.87 (2H, s), 7.1—7.6 (5H, m); Found: C, 70.16; H, 4.12; N, 4.49%. Calcd for $C_{18}H_{13}NO_4$: C, 70.35; H, 4.26; N, 4.56%.

(b) With Dimethyl Fumarate: Unreacted dimethyl fumarate (580 mg), adduct **6b** (130 mg, 47%), and dimer **4** (30 mg, 22%) were obtained. **6b**: Yellow crystals from dichloromethane–hexane, mp 91—92 °C; IR (KBr) 1730, 1655, 1600, 1305, 1232 cm^{-1}; ^{1}H NMR ($CDCl_3$) δ=2.6—3.3 (6H, m), 3.77 (6H, s), 6.78 (2H, s); Found: C, 60.37; H, 5.13%. Calcd for $C_{14}H_{14}O_6$: C, 60.43; H, 5.07%.

(c) With 1,4-Naphthoquinone: Unreacted naphthoquinone (686 mg) and adduct **6c** (30.5 mg, 11%) were obtained. **6c**: Deep yellow crystals from benzene–dichloromethane, mp 261—262 °C (lit.[6] 262 °C).

(d) With Acenaphthylene: Unreacted acenaphthylene, adduct **6d** (79 mg, 28%), and dimer **4** (15 mg, 11%) were obtained. **6d**: Yellow crystals from dichloromethane, mp 176—177 °C; IR (KBr) 1645, 1590, 1325, 1290, 783 cm^{-1}; ^{1}H NMR ($CDCl_3$) δ=2.6—3.4 (4H, m), 4.10 (2H, m), 6.61 (2H, s), 7.2—7.8 (6H, m); Found: C, 83.88; H, 4.77%. Calcd for $C_{20}H_{14}O_2$: C, 83.90; H, 4.93%.

Thermal Rearrangement of 1,4,4b,5,6,7,8,8a-Octahydrobiphenylene-1,4-dione (7): A solution of **7** (90 mg) in xylene (10 ml) was heated under reflux under a nitrogen atmosphere for 5 h. After evaporation of the solvent, the residue was chromatographed on silica gel (3 g) and eluted with hexane–ethyl acetate (9:1) to give **9** (65 mg, 72%); yellow crystals from dichloromethane–hexane, mp 59—60 °C; IR (KBr) 1650 1590, 1300, 855 cm^{-1}; UV (cyclohexane) λ_{max}=249 (log ε 4.20), 368 (3.25), 439 sh (2.34), 460 sh (2.09), 492 sh nm (1.64); ^{1}H NMR ($CDCl_3$) δ=1.60 (4H, m), 2.21 (2H, m), 2.63 (2H, m), 6.02 (1H, dd, J=12.0, 5.4 Hz), 6.26 (1H, d, J=12.0 Hz), 6.71 (2H, s); Found: C, 76.72; H, 6.51%. Calcd for $C_{12}H_{12}O_2$: C, 76.57; H, 6.43%.

Thermal Rearrangement of 1,1,2,2-Tetramethyl-1,2,3,6-tetrahydrobenzocyclobutene-3,6-dione (10): A solution of **10** (150 mg) in xylene (10 ml) was heated under reflux under a nitrogen atmosphere for 1 h. After evaporation of the solvent the residue was chromatographed on silica gel (15 g) and eluted with hexane–ethyl acetate (92:8) to give **12** (112 mg, 74.5%); colorless crystals from hexane–ethyl acetate, mp 119—121 °C; IR (KBr) 3240, 1640, 1610, 1340, 1290, 878, 809 cm^{-1}; ^{1}H NMR ($CDCl_3$–CD_3OD) δ=2.04 (6H, s), 4.97 (2H, br. s), 5.35 (2H, br. s), 6.70 (2H, s); Found: C, 75.49; H, 7.52%. Calcd for $C_{12}H_{14}O_2$: C, 75.76: H, 7.42%.

References

1) For reviews, see; a) W. Oppolzer, *Synthesis*, 793 (1978); b) T. Kametani, "New Synthetic and Biological Active Substances," ed by Z. Yoshida, Kodansha, Tokyo (1981), p. 113; c) Y. Ito, *Yuki Gosei Kagaku Kyokai Shi*, **40**, 559 (1982).

2) A. J. Lin and A. C. Satorelli, *J. Org. Chem.*, **38**, 813 (1973).

3) M. P. Cava and P. I. Shirley, *J. Org. Chem.*, **26**, 2212 (1961).

4) M. Oda and Y. Kanao, *Chem. Lett.*, **1981**, 37.

5) M. Oda and Y. Kanao, *Chem. Lett.*, **1981**, 1547.

6) J. Laduranty, L. Lepage, and Y. Lepage, *Can. J. Chem.*, **58**, 1161 (1980).

Acylations of 2-Isopropenyl-2,3-dihydrobenzofurans

Seiji YAMAGUCHI, Aiko MIYATA, Mariko UENO, Takayuki HASE, Kenichi YAMAMOTO, and Yoshiyuki KAWASE*

Department of Chemistry, Faculty of Science, Toyama University, Gofuku, Toyama 930

(Received July 11, 1983)

Synopsis. Methoxy-substituted 2-isopropenyl-2,3-dihydrobenzofurans were prepared from methoxy-substituted phenols and 1,4-dibromo-2-methyl-2-butene in one-step reactions. Their acylations with acetic acid-trifluoroacetic anhydride or *N*-methylformanilide-phosphoryl chloride were studied.

In our previous paper, we reported a new preparative method of 2-isopropenyl-2,3-dihydrobenzofuran (**1**) from phenol and 1,4-dibromo-2-methyl-2-butene and its acylations with acetic acid-trifluoroacetic anhydride (acetylation) or with *N*-methylformanilide-phosphoryl chloride (formylation).[1] Some naturally occurring hydroxy or methoxy-substituted 2-isopropenyl-2,3-dihydrobenzofuran derivatives having an acetyl group in 5 or 7 position have been reported.[2-8] Now, we report the preparation of methoxy-substituted 2-isopropenyl-2,3-dihydrobenzofurans and their acylations.

By the method used before, 2-isopropenyl-5-methoxy-2,3-dihydrobenzofuran (**3**) was obtained from *p*-methoxyphenol and 1,4-dibromo-2-methyl-2-butene. From *m*-methoxyphenol, a mixture of 4-methoxy **2** and 6-methoxy derivative **4** was obtained. But 7-methoxy derivative **5** was not obtained by this method, it was prepared by dehydration of 2-(1-hydroxy-1-methylethyl)-7-methoxy-2,3-dihydrobenzofuran with phenyl isocyanate.

Acetylations were run with acetic acid-trifluoroacetic anhydride at room temp for 3 h and formylations were run with *N*-methylformanilide-phosphoryl chloride at 90 °C for 1 h. Thier yields are summarized in Table 1. Phosphoryl chloride which used in formylations is a weaker acid than trifluoroacetic acid which derived from trifluoroacetic anhydride in the acetylations. Therefore, formylations can run at higher temp than acetylations, and the former showed better yields than the latter. In all 2-isopropenyl-2,3-dihydrobenzofurans, the position 5 was the most reactive. In 5-methoxy derivative **3**, formylation at 90 °C afforded 6-formyl compound **9b**, but acetylation at room temp could not afford any acetylated compound.

TABLE 1. ACYLATIONS OF 2-ISOPROPENYL-2,3-DIHYDROBENZOFURANS

2-Isopropenyl-2,3-dihydrobenzofuran	Acylated position	Yield/%	
		Acetylation[a]	Formylation[b]
1	5	45.9[c]	20.9[c]
2	5	14.5[d]	27.9[d]
	7	21.7[d]	55.7[d]
3	6	0	24.8
4	5	32.0	46.7
5	5	12.8	64.1

a) With acetic acid-trifluoroacetic anhydride at room temp for 6 h (**1**) or 3 h (**2**—**5**). b) With *N*-methylformanilide-phosphoryl chloride at 90 °C for 1 h. c) Reported in our previous paper.[1] d) Calcd by the methoxy signal ratio in the ^{1}H-NMR spectra.

The structure of the acyl compounds were determined by the coupling constants among aromatic hydrogens in their ^{1}H-NMR spectra. The yields of **7a, b** and **8a, b** were calculated by methoxy signal ratio in their ^{1}H-NMR spectra. By addition of europium tris-dipivaloylmethanate, the methoxy signal of 5-acyl compound **7a, b** shifted to a low field than that of 7-acyl compound **8a, b**, perhaps because they have different chelating structures.

The spectral data of **11a** agreed with the data of the natural compound reported by Bohlmann *et al.*[3]

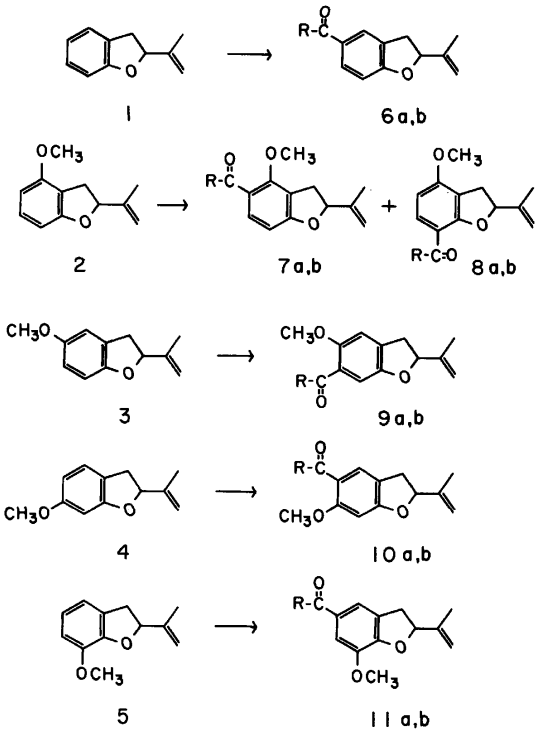

Experimental

The boiling points and melting points were uncorrected (in boiling points: 1 mmHg=133.322 Pa); the IR spectra were measured on a Hitachi EPI-S2 spectrophotometer, and the ^{1}H-NMR spectra, on a JEOL JNM-MH-60 spectrometer.

Preparation of Methoxy-substituted Dihydrobenzofurans (2—8). By the method described in our previous paper,[1] **3** was obtained from *p*-methoxyphenol and a mixture of **2** and **4** was obtained from *m*-methoxyphenol. The mixture was separated on silica gel with cyclohexane. **2**. Yield: 2.4%; ^{1}H-NMR (CCl_4): δ=1.8 (3H, s), 2.8 (1H, dd, J=16+9 Hz), 3.2 (1H, dd, J=16+9 Hz), 3.8 (3H,s), 4.8 (1H, broad s), 5.0 (1H, broad s), 5.1 (1H, t, J=9 Hz), 6.2 (1H, d, J=9 Hz), 6.3 (1H, d, J=9 Hz), 6.9 (1H, t, J=9 Hz); Found: C, 75.96; H, 7.19%. Calcd for $C_{12}H_{14}O_2$: C, 75.76;H, 7.42%. **3**. Yield: 59.3%; bp 110—117 °C (2 mmHg); ^{1}H-NMR (CCl_4): δ=1.8

(3H, s), 3.0 (1H, dd, J=16+9 Hz), 3.3 (1H, dd, J=16+9 Hz), 3.8 (3H, s), 4.9 (1H, broad s), 5.1 (1H, broad s), 5.1 (1H, t, J=9 Hz), 6.6— 6.8 (3H,m); Found: C, 75.76; H, 7.69%. Calcd for $C_{12}H_{14}O_2$: C, 75.76; H, 7.42%. **4**. Yield: 13.8%; ^{1}H-NMR (CCl_4) : δ=1.8 (3H, s), 2.9 (1H, dd, J=16+9 Hz), 3.2 (1H, dd, J=16+9 Hz), 3.7 (3H, s), 4.8 (1H, broad s), 5.0 (1H, broad s), 5.1 (1H,t,J=9 Hz), 6.2 (1H, d, J=2 Hz), 6.2 (1H, dd, J=9+2 Hz), 6.9 (1H, d, J=9 Hz); Found: C, 75.65; H, 7.33%. Calcd for $C_{12}H_{14}O_2$: C, 75.76; H, 7.42%.

Dehydrative Preparation of 5. By the method similar to that described in our previous paper,[1] 7-methoxy-2,3-dihydrobenzofuran-2-carboxylic acid[9] gave methyl 7-methoxy-2,3-dihydrobenzofuran-2-carboxylate: yield, 86.6%; bp 172—173.5 °C (17 mmHg); IR (neat): 1760 cm^{-1}; ^{1}H-NMR (CCl_4): δ=3.3 (1H, dd, J=16+8 Hz), 3.4 (1H, dd, J=16+9 Hz), 3.7 (3H, s), 3.8 (3H, s), 5.1 (1H, dd, J=9+8 Hz), 6.6 (3H, s); Found: C, 63.50; H, 5.91%. Calcd for $C_{11}H_{12}O_4$: C, 63.45; H, 5.81%. The product was converted to 2-(1-hydroxy-1-methylethyl)-7-methoxy-2,3-dihydrobenzofuran: yield, 53.0%; IR (neat) 3400 cm^{-1}; ^{1}H-NMR (CCl_4): δ=1.2 (3H, s), 1.3 (3H,s), 2.2 (1H, broad s), 3.1 (1H, dd, J=16+9 Hz), 3.2(1H, dd, J=16+8 Hz), 3.8 (3H, s), 4.6 (1H, dd, J=9+8 Hz), 6.7 (3H, s); Found: C, 68.99; H, 7.90%. Calcd for $C_{12}H_{16}O_3$: C, 69.21; H, 7.74%. A mixture of 2-(1-hydroxy-1-methylethyl)-7-methoxy-2,3-dihydrobenzofuran (1.02 g, 4.90 mmol) and phenyl isocyanate (5.85 g, 4.90 mmol) was refluxed for 10 h.[10] After the reaction, the mixture was distilled. The fraction boiling at 118—136 °C (2 mmHg) (0.679 g, 72.9%) showed two peaks (5:1) in GLC. The mixture was separated into components by silica gel chromatography. The fractions eluted with 1:4 benzene–hexane gave 2-isopropyl-7-methoxybenzofuran (101 mg, 10.8%); ^{1}H-NMR (CCl_4): δ=1.4 (6H, d, J=7 Hz), 3.1 (1H, m, J=7 Hz), 3.9 (3H, s), 6.2 (1H, s), 6.6 (1H, t, J=5 Hz), 6.9 (2H, d, J=5 Hz); Found: C, 75.47;H, 7.14%. Calcd for $C_{12}H_{14}O_2$: C, 75.76; H, 7.42%. The fractions eluted with 2:3 benzene–hexane gave 2-isopropenyl-7-methoxy-2,3-dihydrobenzofuran (**5**) (258 mg, 27.7%); ^{1}H-NMR (CCl_4): δ=1.8 (3H, s), 3.0 (1H, dd, J=15+9 Hz), 3.2 (1H, dd, J=15+9 Hz), 3.8 (3H, s), 4.8 (1H, broad s), 5.1 (1H, broad s), 5.1 (1H, t, J=9 Hz), 6.6 (3H, s); Found: C, 75.74; H, 7.12%. Calcd for $C_{12}H_{14}O_2$: C, 75.76; H, 7.42%.

Acylations of Methoxy-substituted Dihydrobenzofurans 2—5. By a method similar to that described in our previous paper,[1] dihydrobenzofuran **2—5** was acetylated with acetic acid and trifluoroacetic anhydride for 3 h at room temp, and was formylated with *N*-methylformanilide and phosphoryl chloride for 1 h at 90 °C. In case of the acylations of **2**, mixtures were obtained; the spectrum of the acetylated compounds showed two methoxy signals at 3.85 (**8a**) and 3.88 ppm (**7a**) (relative intensity 3:2), which shifted to 3.87 and 4.03 ppm by the addition of europium trisdipivaloylmethanate, and the spectrum of the formylated compounds showed signals at 3.84 (**8b**) and 3.93 ppm(**7b**) (relative intensity 2:1), which shifted to 3.90 and 4.06 ppm by similar treatment. Their yields were calculated by the methoxy signal ratio in their ^{1}H-NMR spectra.

The yields of acyl dihydrobenzofurans **7a**, **b**—**11a**,**b** are summarized in Table 1. And their physical data are listed below.

Mixture of **7a** and **8a**; bp 225—240 °C (14.5 mmHg) (bath temp); IR (neat): 1670 cm^{-1}; ^{1}H-NMR (CCl_4): δ=1.8 (s, **7a** and **8a**), 2.45 (s, **7a**), 2.48 (s, **8a**), 3.0 (dd, J=16+10 Hz, **7a** and **8a**), 3.4 (dd, J=16+10 Hz, **7a** and **8a**), 3.85 (s, **8a**) 3.88 (s, **7a**), 4.95 (broad s, **7a** and **8a**), 5.1 (broad s, **7a** and **8a**), 5.3 (t, J=10 Hz, **7a** and **8a**), 6.43 (d, J=10 Hz, **8a**), 6.55 (d, J=10 Hz, **7a**), 7.65 (d, J=10 Hz, **7a**), 7.75 (d, J=10 Hz, **8a**); Found: C, 72.22; H, 6.99%. Calcd for $C_{14}H_{16}O_3$: C, 72.39; H, 6.94%. **10a**; mp 111— 112 °C (recrystallized from cyclohexane); IR (KBr disk): 1650 cm^{-1}; ^{1}H-NMR (CCl_4): δ=1.8 (3H, s), 2.6 (3H, s), 3.0 (1H, dd, J=16+9 Hz), 3.2 (1H, dd, J=16+9 Hz), 3.8 (3H, s), 4.9 (1H, broad s), 5.1 (1H, broad s), 5.2 (1H, t, J=9 Hz), 6.4 (1H, s), 7.7 (1H, s); Found: C, 72.23; H, 7.08%. Calcd for $C_{14}H_{16}O_3$: C, 72.39; H, 6.94%. **11a**: bp 230—255 °C (15 mmHg); IR (neat): 1670 cm^{-1}; ^{1}H-NMR (CCl_4): δ=1.8 (3H, s), 2.4 (3H, s), 3.0 (1H, dd, J=16+9 Hz), 3.3 (1H, dd, J=16+9 Hz), 3.9 (3H, s), 4.9 (1H, broad s), 5.1(1H, broad s), 5.2 (1H, t, J=9 Hz), 7.3 (2H, s); Found: C, 72.23; H, 7.08%. Calcd for $C_{14}H_{16}O_3$: C, 72.39; H, 6.94%. Mixture of **7b** and **8b**; bp 220—265 °C (14.5 mmHg); IR (neat): 1635 cm^{-1}; ^{1}H-NMR (CCl_4): δ=1.8 (s, **7b** and **8b**), 3.0 (dd, J=16+8 Hz, **7b** and **8b**), 3.3 (dd, J= 16+8 Hz, **7b** and **8b**), 3.84 (s, **8b**), 3.93 (s, **7b**), 4.9 (s, **7b** and **8b**), 6.39 (d, J=9 Hz, **8b**), 6.51 (d, J=9 Hz, **7b**), 7.53 (d, J=9 Hz, **8b**), 7.63 (d, J=9 Hz, **7b**), 10.08 (s, **8b**), 10.14 (s,**7b**); Found: C, 71.15; H,6.50%. Calcd for $C_{13}H_{14}O_3$: C, 71.54; H, 6.47%. **9b**; mp 64—66 °C (recrystallized from cyclohexane); IR (KBr disk): 1670 cm^{-1}; ^{1}H-NMR (CCl_4): δ=1.7 (3H, s), 3.0 (1H, dd, J=16+8 Hz), 3.3 (1H, dd, J=16+8 Hz), 3.7 (3H, s), 4.8 (1H, broad s), 5.0(1H, broad s), 5.1 (1H, t, J=8 Hz), 6.7 (1H, s), 6.9 (1H, s), 10.2 (1H, s); Found: C, 71.62; H, 6.70%. Calcd for $C_{13}H_{14}O_3$: C, 71.54; H, 6.47%. **10b**; mp 97—99 °C (recrystallized from cyclohexane); IR (KBr disk): 1680 cm^{-1}; ^{1}H-NMR (CCl_4): δ=1.7 (3H, s), 3.0 (1H, dd, J=16+9 Hz), 3.2 (1H, dd, J=16+9 Hz), 3.9 (3H, s), 4.9 (1H, broad s), 5.0 (1H, broad s), 5.2 (1H, t, J=9 Hz), 6.3 (1H, s), 7.5 (1H, s), 10.1 (1H, s); Found: C, 71.32; H, 6.35%. Calcd for $C_{13}H_{14}O_3$: C, 71.54; H, 6.47%. **11b**;Benzene eluted oil; IR (neat): 1690 cm^{-1}; ^{1}H-NMR (CCl_4): δ=1.8 (3H, s), 3.1 (1H, dd, J=16+9 Hz), 3.3 (1H, dd, J=16+9 Hz), 3.8 (3H, s), 4.9 (1H, broad s), 5.1 (1H, broad s), 5.2 (1H, t, J=9 Hz), 7.1 (2H, s), 9.7 (1H, s); Found: C, 71.30; H, 6.43%. Calcd for $C_{13}H_{14}O_3$: C, 71.54; H, 6.47%.

References

1) S. Yamaguchi, S. Kondo, K. Shimokawa, O. Inoue, M. Sannomiya, and Y. Kawase, *Bull. Chem. Soc. Jpn.*, **55**, 2500 (1982).

2) W. A. Bonner and J. I. DeGraw, Jr., *Tetrahedron*, **18**, 1295 (1962).

3) F. Bohlmann and M. Grenz, *Chem. Ber.*, **103**, 90 (1970).

4) M. Hirotani, J. O'Reilly, and D. M. X. Donnell, *Tetrahedron Lett.*, **1977**, 651.

5) R. D. Allan, R. L. Correll, and R. J. Wells, *Tetrahedron Lett.*, **1969**, 4673.

6) R. D. Allan, R. J. Wells, and J. K. MacLeod, *Tetrahedron Lett.*, **1970**, 3945.

7) F. Bohlmann, J. Jakupovic, A. Schuster, R. M. King, and H. Robinson, *Phytochemistry*, **21**, 161 (1982).

8) J. I. DeGraw, Jr., D. M. Bowen, and W. A. Bonner, *Tetrahedron*, **19**, 19 (1963).

9) B. Libis and E. Habicht, Ger. Offen., 1927393 (1970); *Chem. Abstr.*, **72**, P43426x (1970).

10) Refluxing for 5 h gave a mixture of 7-methoxy-2-isopropenyl-2,3-dihydrobenzofuran (21.9%) and 7-methoxy-2-isopropylbenzofuran (9.3%); longer refluxing caused an isomerization of the dihydrobenzofuran **5** to the benzofuran.

Synthetic Photochemistry. XXVII.[1] An Efficient Synthesis of Deoxytrisporone by Photocycloaddition

Hitoshi TAKESHITA,* Seiji HATTA, and Toshihide HATSUI
Research Institute of Industrial Science, 86, Kyushu University, Sakamoto, Kasuga, Fukuoka 816
(Received July 11, 1983)

Synopsis. Deoxytrisporone was synthesized from isobutene and methyl 2,4-dioxohexanoate to show the utility of the regioselective photocycloaddition of β-diketone for construction of polysubstituted cyclohexenones.

Deoxytrisporone (**1**)[2,3] is a fundamental trimethylcyclohexene derivative. We have accomplished its facile total synthesis by photocycloaddition of 2-methylpropene (**2**) with methyl 2,4-dioxohexanoate (**3**)[4] followed by a series of chemical conversions which will be described herein.

Photocycloaddition of **2** with **3** gave a single 1:1-adduct (**4**) in 56% yield. The structure of **4** was shown to be methyl 3,3-dimethyl-2,6-dioxooctanoate, on the basis of its NMR spectroscopic analysis[5] as well as its chemical conversion: Treatment of **4** with *p*-toluenesulfonic acid (TsOH) gave an α,β-unsaturated ketone, methyl 3-oxo-β-cyclogeranate (2,6,6-trimethyl-3-oxo-1-cyclohexene-1-carboxylate, **5**), which upon borohydride reduction yielded a dihydro derivative (**6**).[6]

The keto ester (**5**) was converted to the 3,3-ethylenedithio derivative (**7**) of β-cyclocitral *via* corresponding derivatives (**8**, **9**) of methyl β-cyclogeranate and β-cyclogeraniol by consecutive reactions with 1,2-ethanedithiol and boron trifluoride, lithium aluminum hydride (LAH), and the Collins reagent. The dianionic species[7] generated from 3-methyl-2-butenoic acid (**10**) and lithium diisopropylamide (LDA) was treated at −30°C with **7** to give 1:1-condensates from which, a crystalline δ-lactone (**11**) has been isolated in 74% yield. A mild sodium methoxide treatment of **11** quantitatively gave the (2*Z*,4*E*)-trienic acid (**12**) whose methyl ester (**13**) can be equilibrated to a 2:3-mixture with the (2*E*,4*E*)-ester (**14**) iodine in benzene.[8] Isolation of **14**, a colorless oil, from the mixture was accomplished by high-pressure liquid chromatography (HPLC).

The LAH-reduction of **14** quantitatively gave the colorless oily alcohol (**15**) which was immediately treated with silver nitrate[9] to form a colorless oil whose identity with **1** was confirmed by comparison of the H-NMR spectrum taken in a carbon tetrachloride solution.[2]

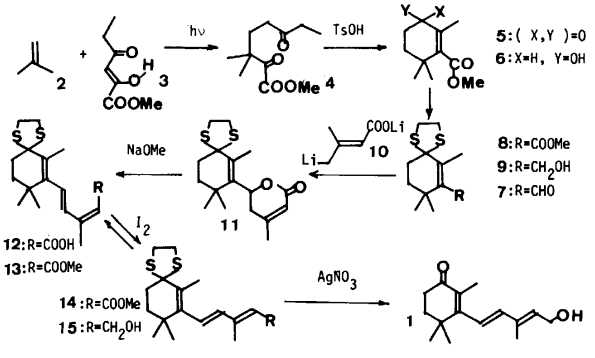

Consequently, the alternative synthesis of **1** has been completed.

Experimental

Photocycloaddition of 2 with 3. Formation of 4: In ethyl acetate (30 cm³), **2** (*ca.* 20 cm³), and **3** (10.0 g) were internally irradiated by means of a 100-W high-pressure mercury lamp at −50 to −60°C under N_2 atmosphere for 37 h. Silica-gel chromatography of the mixture from hexane-ethyl acetate (9:1) eluted a colorless oil, 6.7 g (56%) [Found: C, 61.76; H, 8.59%. Calcd for $C_{11}H_{18}O_4$: C, 61.66; H, 8.47%. δ=1.02 (3H, t, *J*=8 Hz), 1.21 (6H, s), 1.92 (2H, m), 2.36 (2H, m), 2.42 (2H, q, *J*=8 Hz), and 3.83 (3H, s). δ(C)=7.9, 23.5 (2C), 32.5, 35.9, 37.5, 45.5, 52.3, 164.0, 201.1, and 210.0. ν: 1715, 1740 cm⁻¹].

Dehydration of 4 to 5. A mixture of **4** (4.00 g) and TsOH (30 mg) was refluxed in benzene (20 cm³) for 17 h. Subsequent silica-gel chromatography gave, from hexane-ethyl acetate (4:1), a colorless liquid (**5**), 3.3 g (90%) [Found: C, 66.93; H, 8.28%. M. W., 196.1119. Calcd for $C_{11}H_{16}O_3$: C, 67.32; H, 8.22%; M. W., 196.1099. δ=1.24 (6H, s), 1.70 (3H, s), 1.90 (2H, m), 2.52 (2H, m), and 3.80 (3H, s). δ(C)=13.0, 26.8 (2C), 34.1, 34.2, 37.5, 51.6, 130.9, 154.7, 168.5, 198.3. ν: 1715, 1665 cm⁻¹].

$NaBH_4$-reduction of 5. In methanol (4.5 cm³), **5** (1.00 g) was reduced with $NaBH_4$ (300 mg) for 1 h at 15—20°C to give a colorless liquid (**6**), 920 mg (91%) [δ=1.06 (3H, s), 1.09 (3H, s), 1.2—2.0 (4H, m), 1.73 (3H, s), 2.73 (1H, br), 3.72 (3H, s), and 3.94 (1H, t, *J*=5 Hz)].

The Reaction of 5 with 1,2-Ethanedithiol. In anhydrous CH_2Cl_2 (5 cm³), **5** (500 mg) and BF_3-etherate (1 cm³) were kept at 15—20°C for 35 h. The mixture was washed with 5% NaOH and then with water, and the solvent was removed to leave colorless needles (**8**), mp 89—91°C, 700 mg (≈100%) [Found: M. W., 272.0878. Calcd for $C_{13}H_{20}O_2S_2$: 272.0904. δ=1.05 (6H, s), 1.65 (3H, m), 1.88 (3H, s), 2.28 (2H, m), 3.28 (4H, s), and 3.71 (3H, s). δ(C)=17.4, 28.0 (2C), 33.1, 38.0, 40.0, 40.6 (2C), 51.2, 69.6, 133.4, 139.3, 170.1. ν: 2900, 1725 cm⁻¹].

The LAH-reduction of 8. In anhydrous ether (50 cm³), **8** (700 mg) was reduced with LAH (400 mg) at 15—20°C for 3 h to give colorless needles (**9**), mp 88—89°C, 625 mg (≈100%) [Found, M. W., 244.0951. Calcd for $C_{12}H_{20}OS_2$: 244.0952. δ=1.04 (6H, s), 1.37 (1H, br. s), 1.65 (2H, m), 2.04 (3H, s), 2.22 (2H, m), 3.31 (4H, s), and 4.08 (2H, s). δ(C)=16.0, 27.9 (2C), 34.0, 38.4, 40.1, 40.4 (2C), 59.1, 71.5, 133.9, 142.2. ν: 3300 cm⁻¹].

Oxidation of 9. A mixture of **9** (600 mg) with Collins reagent (3 g, 5 equiv.) in CH_2Cl_2 (5 cm³) was kept at 15—20°C for 3.5 h with stirring. Then, the mixture was chromatographed on a silica-gel column to give a colorless oil (**7**), 430 mg (72%) [Found: M. W., 242.0808. Calcd for $C_{12}H_{18}OS_2$: 242.0798. δ=1.18 (6H, s), 1.62 (2H, m), 2.24 (2H, m), 2.32 (3H, s), 3.37 (4H, s), and 10.06 (1H, s). δ(C)=16.1, 27.6 (2C), 33.1, 39.5, 39.6, 41.1 (2C), 71.9, 142.3, 152.5, and 193.9. ν: 1675 cm⁻¹].

Reaction of 7 with 10 and LDA. To tetrahydrofuran (THF, 1 cm³) containing diisopropylamine (12 mg), commercially available *n*-BuLi (1.8 cm³ of 1 M solution) was added at −45°C, and kept stirring for 1 h, while the temperature

was gradually raised to 18°C. After cooling the mixture to −40°C, **10** (120 mg) was added to the mixture in a 1-h period, and maintained at 15—20°C for 1 h. To the mixture, **7** (120 mg) was introduced at −30°C and was kept under stirring for 9 h, then the temperature was gradually raised to 15°C. The mixture was treated with 10% HCl, and extracted with ether. The ethereal extract was washed with aqueous $NaHCO_3$, and chromatographed on a silica-gel column to give colorless needles (**11**), mp 153—154.5°C, 119 mg (74%) [Found: M. W., 324.1220. Calcd for $C_{17}H_{24}O_2S_2$: 324.1218. δ=1.00 (3H, s), 1.12 (3H, s), 1.67 (2H, m), 1.98 (3H, br. s), 2.05 (3H, s), 2.22 (2H, m), 3.30 (4H, s), 4.96 (1H, dd, *J*=13, 5 Hz), and 5.79 (1H, br. s). δ(C)=17.6, 22.9, 27.3, 28.3, 34.4, 34.6, 38.6, 39.8, 40.4, 40.7, 72.2, 75.6, 116.3, 136.0, 139.0, 157.3, and 165.2. ν: 2925, 1705 cm^{-1}].

NaOMe-treatment of 11. In methanol (1 cm^3), **11** (40 mg) and NaOMe (8 mg) were kept at 15—20°C for 6.5 h. After acidification with 10% HCl, the mixture was extracted with ether; removal of the organic layer left the carboxylic acid (**12**), which was immediately esterified with diazomethane, and chromatgraphed on a silica-gel column to give a colorless oil (**13**), 38 mg (91%) [Found: M. W., 338.1376. Calcd for $C_{18}H_{26}O_2S_2$: 338.1373. δ=1.05 (6H, s), 1.65 (2H, m), 1.98 (3H, d, *J*=1 Hz), 2.04 (3H, d, *J*=1 Hz), 2.25 (2H, m), 3.32 (4H, s), 3.68 (3H, s), 5.66 (1H, br. s), 6.48 (1H, d, *J*=18 Hz), and 7.58 (1H, d, *J*=18 Hz). δ(C)=18.4, 20.8, 28.6 (2C), 34.4, 38.9, 40.1, 40.7 (2C), 50.9, 71.9, 116.9, 131.4, 131.9, 134.8, 142.1, 151.1, and 166.7. ν: 2900, 1715, 1620, 1450, 1435 cm^{-1}].

Treatment of 13 with Iodine. In anhydrous benzene-ether (1:1, 1 cm^3), and **13** (10 mg) and I_2 (2 mg) were kept at 15—20°C for 72 h. After washings with $Na_2S_2O_3$, the mixture was separated by HPLC on μ-Polasil with hexane–ethyl acetate (80:1); less polar fractions yielded colorless needles, mp 115—116°C (**14**), 4.8 mg (48%) [Found: C, 63.96; H, 7.76%. M. W., 338.1378. Calcd for $C_{18}H_{26}O_2S_2$: C, 63.86; H, 7.76%. M. W., 338.1373. δ=1.00 (6H, s), 1.68 (2H, m), 1.91 (3H, d, *J*=1 Hz), 2.26 (2H, m), 2.31 (3H, d, *J*=1 Hz), 3.31 (4H, s), 3.70 (3H, s), 5.75 (1H, br. s), 6.08 (1H, d, *J*=16, and 6.48 (1H, d, *J*=16 Hz). δ(C)=13.5, 18.2, 28.5 (2C), 34.4, 38.4, 40.0, 40.5 (2C), 50.9, 71.6, 118.6, 131.0, 133.5, 137.4, 142.0, 152.1, and 167.2. ν: 1715, 1420, 1230, 1150, 980, 875, 840 cm^{-1}]. The more polar fractions yielded recovered **13**, 3.2 mg (32%).

LAH-reduction and Hydrolysis of 14 (as a Mixture with 13) to 1. To the above mixture of **13** and **14** (10 mg) in anhydrous ether (5 cm^3), LAH (3 mg) was added and kept at 15—20°C for 1 h; the mixture was then extracted with benzene and water, and chromatographed on a silica-gel column to give a colorless liquid, **15**, 5.1 mg (54%) [Found: *m/e*, 310 (M^+). δ=1.00 (6H, s), 1.6—1.75 (2H, m), 1.89 (3H, s), 1.94 (3H, s), 2.2—2.3 (2H, m), 3.32 (4H, s), 4.28 (2H, d, *J*=8 Hz), 5.55 (1H, t, *J*=8 Hz), 6.12 (1H, d, *J*=16 Hz), and 6.34 (1H, d, *J*=16 Hz) together with 1.82 (3H, s), 5.62 (1H, t, *J*=8 Hz), and 6.04 (1H, s) of the contaminated *Z,E*-isomer]. This was dissolved in ether (1.5 cm^3), and hydrolyzed with aqueous $AgNO_3$ (5 mg) at −5°C for 2 h. The mixture was then washed with aqueous NH_4Cl, and chromatographed on a silica-gel column; the eluant from ethyl acetate–hexane (1:9) gave a colorless liquid, 3.7 mg (98%), whose NMR figures [δ^{CCl_4}=1.17 (6H, s), 1.76 (3H, s). 1.85 (3H, s), 2.40 (2H, m), 4.22 (2H, d, *J*=7 Hz), 5.75 (1H, br. t, *J*=7 Hz), and 6.15 (1H, s). ν: 1665 cm^{-1}] were in accord to those reported of **1**.[9]

References

1) Part XXVI: A. Mori and H. Takeshita, *Kyushu Daigaku Sogo Rikogaku Kenkyuka Hokoku*, **3**, 125 (1981).

2) P.Graselli and A. Selva, *Chim. Ind. (Milan)*, **52**, 584 (1970).

3) K. Uneyama and S. Torii, *Tetrahedron Lett.*, **1976**, 443.

4) For a use of **3** as the cycloaddend, see H. Takeshita and K. Komiyama, *Kyushu Daigaku Seisan Kagaku Kenkyusho Hokoku*, **73**, 25 (1982).

5) The NMR spectra were measured, by use of an FX-100 Model (JEOL, Tokyo) spectrometer, in $CDCl_3$ solutions otherwise stated, and the chemical shifts were expressed in the δ unit from internal Me_4Si.

6) This was identical with the sample prepared by epoxidation and subsequent base treatment of methyl α-cyclogeranate.

7) G. Cardelli, G. Cardello, M. Contento, G. Trapani, and A. U.-Ronci, *J. Chem. Soc., Perkin Trans. 1*, **1973**, 440.

8) J. S. Baran, *J. Org. Chem.*, **30**, 3564 (1965).

9) C. A. Rees, J. O. Rodin, R. G. Brounlee, W. G. Duncan, and R. M. Silverstein, *Tetrahedron*, **24**, 4249 (1968).

The 2*H*-Cyclohepta[*b*]furan-2-one Formation from 2,4-Dichloro-5-methoxytropone with Dimethyl Malonate and Methyl Acetoacetate

Hitoshi TAKESHITA,* Akira MORI, and Tomoyoshi MINAMI
Research Institute of Industrial Science, 86, Kyushu University, Sakamoto, Kasuga, Fukuoka 816
(Received August 3, 1983)

Synopsis. 2,4-Dichloro-5-methoxytropone afforded 3,5,6-trisubstituted 2*H*-cyclohepta[*b*]furan-2-one derivatives by condensation with dimethyl malonate and methyl acetoacetate in an exclusive *ciné*-condensation mode in various solvents.

Recently, we have reported[1] a solvent effect on the condensation of 2,5-disubstituted tropones with dimethyl malonate (DM); a concomitant formation of *ciné*- and normal condensates in the 2*H*-cyclohepta[*b*]furan-2-one (oxazulanone) formation from 5-chloro-2-methoxytropone (**A**) was a characteristic feature. In connection to our recent synthesis of the 1*H*-cyclohepta[1,2-*d*;3,4-*d'*]- and 1*H*-cyclohepta[1,2-*d*;4,5-*d'*]diimidazoles,[2] same ring systems to unique metabolites from marine organisms, paragracine[3] and zoanthoxanthins,[4] from 2,4-dichloro-5-methoxytropone (**1**), we thought it would be worthwhile to examine the further cyclohepta[*b*]furanone formation by condensation of **1**[5] with active methylene derivatives.[6] Since the intermediates possess the two leaving groups in the conjugated positions, two different products could be formed by the *ciné*-condensation reaction. In this paper, we wish to describe the results.

When **1** was allowed to react with DM in methanol, a rapid reaction occurred at 15 °C to give two products, **2** and **3**, both yellow crystals, in sum of *ca.* 50 to 60% yields. The major product, **3**, was shown to be a secondary product derived from **2** and sodium methylate. The NMR of **2** showed a small but characteristic long-range coupling between the methoxyl signal at δ[7]= 4.13 and an aromatic proton signal at δ=8.55, but other than this, no spin-spin interaction was detectable for this signal. Since these cycloheptafuranones exhibited a clear meta-coupling between H_4–H_6 in the 5-substituted derivatives,[1] the chlorine must be located on C-6. The J_{vic} value of the other two aromatic protons, 10.5 Hz, is compatible to that of H_7–H_8 in view of the bond alternation in this conjugated system. Therefore, **2** is 6-chloro-5-methoxy-3-methoxycarbonyl-2*H*-cyclohepta[*b*]furan-2-one, and not the alternative, **2a**, 7-chloro-6-methoxy-3-methoxycarbonyl derivative.[1] On the other hand, the NMR spectrum of **3** showed a close resemblance to that of **2**. Both methoxyl signals revealed a long-range spin-spin splitting with the protons on the seven-membered ring. The condensation of **1** with DM for a prolonged time afforded another product, **4**, which was independently prepared by further reactions of **2** or **3** with DM. The malonyl group of **4** was deduced to be at C-6; the NMR signal of C-4 proton at δ=8.48 resembled those at 8.55 and 8.58 of **2** and **3**, while the *AB*-doublets were moved to δ=7.16 and 7.46 (J=10 Hz) from 6.79 and 7.20 (J=10.5Hz) in **3**. As expected, **3** was undetectable in the reaction of **1** in benzene. The yields of **2** were most satisfactory in dimethyl sulfoxide (DMSO).

Similarly, **1** was treated with methyl acetoacetate (MA) in methanol at 15 °C; the products were again the *ciné*-products, 6-chloro-5-methoxy derivative (**5**) and 5,6-dimethoxy derivative (**6**). According to the NMR analysis, the position of the methoxy group of **5** was at C-5, because the same long-range splitting behavior was found. A further treatment of **5** under the reaction conditions gave **6**. The reaction features in the different solvents of **1** with MA was parallel to those of **1** with DM.

It has been noted that, in the cyclohepta[*d*]imidazole formation,[2] the introduction of substituents, such as halogens or methoxy group, on the seven-membered ring caused a diminishment of the reactivity toward nucleophilic attack; the present results however disagree for **1** gave the condensates in good yields.

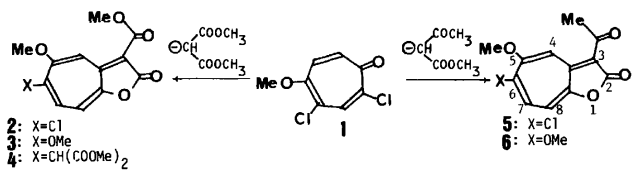

Scheme 1.

Experimental

The Condensation of 1 and Dimethyl Malonate with NaOMe. a): To an anhydrous MeOH solution (8 cm³) of DM (160 mg) containing NaOMe (55 mg), **1** (60 mg) was added in dropwise at 10—15 °C. Instantly, dark yellow color developed in the solution. After 2 h, the mixture was poured into ice-water, acidified with dil HCl, and extracted with $CHCl_3$. The major product, **2**, obtained by silica gel column chromatography (hexane:ethyl acetate, 9:1) was further purified by fractional recrystallizations from benzene to give yellow needles, mp 249—250 °C (decomp), 29 mg (55%) [Found: C, 53.64; H, 3.37%. Calcd for $C_{12}H_9O_5Cl$: C, 53.65; H, 3.38%. δ=3.92 (3H, s), 4.13 (3H, br. s), 7.04 (1H, d, J=10.5 Hz), 7.72 (1H, d, J=10.5 Hz), and 8.55 (1H, br. s). ν: 1755, 1683, 1580, 1520, 1242, 895, 790, 760 cm^{-1}. λ_{max}^{MeOH}: 294 nm (ε=25000), 306 (25000), 402 (19000)], together with a trace amount of **3**, yellow needles, mp 259—260 °C (from benzene) [Found: C, 58.85; H, 4.47%. Calcd for $C_{13}H_{12}O_6$: C, 59.09; H, 4.58%. δ=3.92 (3H, s), 3.98 (3H, s), 4.12 (3H, br. s), 6.79 (1H, d, J=10.5 Hz), 7.20 (1H, d, J=10.5 Hz), and 8.58 (1H, br. s). ν: 1743, 1675, 1583, 1538, 1470, 1240, 695 cm^{-1}. λ_{max}^{MeOH}: 278 nm (ε=23000), 294 (21000), 402 (18000)]. The recovered **1**, 14 mg (24%), was obtained from the fractions eluted by hexane: ethyl acetate (1:1).

b): Similarly, **1** (30 mg) was allowed to react with DM (80 mg) and NaOMe (25 mg) in methanol (4 cm³) for 22 h. Similar work-up yielded **2**, 22%, and **3**, 28%, together with some of the recovered **1**.

c): To an anhydrous benzene dispersion (10 cm³) of DM (130 mg) and NaOMe (45 mg), **1** (50 mg) was added under stirring for 20 min at 10—15 °C. The mixture was then diluted with water, acidified with dil HCl, and was $CHCl_3$ extracted. Purification by silica gel column chromatography

of the extracts yielded **2**, 32.5 mg (61.5%), and the recovered **1**, 4.3 mg (8.6%).

d): Similarly, **1** (50 mg) was treated with DM (130 mg) and NaOMe (45 mg) in benzene (10 cm^3) at 10—15 °C for 20 min. The products were isolated by silica-gel column chromatography to give **2**, 36.7 mg (61.3%).

e): Similarly, a mixture of **1** (50 mg), DM (130 mg), and NaOMe (40 mg) in benzene (10 cm^3) was kept at 10—15 °C for 2 d. The mixture was chromatographed on a silica-gel column; the yield of **2** has dropped to 2 mg (3%) and another product, **4**, pale yellow needles, mp 209.5—210 °C (from benzene) [Found: C, 55.82; H, 4.38%. Calcd for $C_{17}H_{16}O_9$: C, 56.04; H, 4.43%. δ=3.77 (6H, s), 3.92 (3H, s), 4.05 (3H, s), 5.09 (1H, s), 7.16 (1H, d, J=10 Hz), 7.46 (1H, d, J=10 Hz), and 8.48 (1H, s). ν: 1758, 1680, 1590, 1518, 1470, 1405, 1250, 890, 765 cm^{-1}. λ_{max}^{MeOH}: 283 nm (ε=25000), 294 (25000), 393 (19000)] was obtained, 16 mg (18%).

f): To anhydrous DMSO solution (10 cm^3) of DM (1.05 g) and NaOMe (400 mg), **1** (220 mg) was added. After 40 min, the mixture was diluted with water, and extracted by $CHCl_3$. Silica-gel chromatography gave yellow crystals, **2**, 231 mg (92%), together with the recovered **1** (25 mg, 12%).

The Reaction of 2 with Dimethyl Malonate. To an anhydrous MeOH solution (4 cm^3) of DM (100 mg) and NaOMe (20 mg), **2** (20 mg) was added at 15 °C and kept 12 h. The mixture was diluted with ice-water, extracted with $CHCl_3$, and purified on a silica-gel column to give **4**, 20 mg (74%).

The Reaction of 3 with Dimethyl Malonate. Similarly, **3** (20 mg) was mixed with DM (100 mg) and NaOMe (15 mg) in a MeOH (4 cm^3) solution at 15 °C. A similar work-up after 12 h yielded **4**, 15 mg (54%).

The NaOMe-catalyzed Reaction of 1 with Methyl Acetoacetate. *a)*: To an anhydrous MeOH solution (8 cm^3) of MA (160 mg) and NaOMe (55 mg), **1** (60 mg) was added under stirring at 10—15 °C. After 5 min, the separated crystals were collected by filtration. After fractional recrystallizations from benzene, **5**, yellow needles, mp 235—236 °C, 45 mg (74%) [Found: C, 56.96; H, 3.60%. Calcd for $C_{13}H_9O_4$: C, 57.05; H, 3.59%. δ=2.61 (3H, s), 4.14 (3H, br. s), 7.11 (1H, d, J=11.5 Hz), 7.78 (1H, d, J=11.5 Hz), and 9.00 (1H, br. s). ν: 1743, 1638, 1515, 1450, 1240 cm^{-1}. λ_{max}^{MeOH}: 239 nm (ε=22000), 305 (23000), 410 (20000)], was obtained together with the recovered **1**, 3 mg (5%).

b): Anhydrous benzene dispersion (10 cm^3) of MA (160 mg) and NaOMe (55 mg) was mixed with **1** (60 mg) and kept at 10—15 °C for 2 h. Then the mixture was diluted with water and extracted with $CHCl_3$. Silica gel chromatography of the product gave **5**, 54 mg (84%).

c): To an anhydrous DMSO solution (3 cm^3) of MA (160 mg) and NaOMe (55 mg), **1** (60 mg) was added, the mixture was kept at 10—15 °C After 5 min, it was chromatographed on a silica-gel column to give **5**, 64 mg (quantitative yield).

The Conversion of 5 to 6. **5** (27 mg) was dissolved in a mixture of MeOH (1 cm^3) and benzene (7 cm^3) containing NaOMe (10 mg) at 15—20 °C for 2 d. Then the mixture was poured into water, and extracted with $CHCl_3$. Silica-gel chromatography of the extracts gave yellow needles, mp 244—245 °C (from benzene), **6**, 22 mg (80%) [Found: C, 63.50; H, 4.94%. Calcd for $C_{13}H_{12}O_5$: C, 62.90; H, 4.87%. δ=2.60 (3H, s), 3.98 (3H, s), 4.12 (3H, s), 6.85 (1H, d, J=11 Hz), 7.26 (1H, d, J=11 Hz), and 9.00 (1H, br. s). ν: 1722, 1640, 1623, 1588, 1460, 1243 cm^{-1}. λ_{max}^{MeOH}: 285 nm (ε=19000), 301 (20000), 414 (19000)].

References

1) T. Nozoe, H. Takeshita, and K. Tajiri, *Bull. Chem. Soc. Jpn.*, **56**, 3679 (1983).

2) H. Takeshita, A. Mori, T. Minami, and H. Kondo, *Heterocycles*, **14**, 793 (1980).

3) Y. Komoda, S. Kaneko, M. Yamamoto, M. Ishikawa, A. Itai, and Y. Iitaka, *Chem. Pharm. Bull.*, **23**, 2464 (1975).

4) L. Cariello, S. Crescenzi, G. Prota, F. Giordano, and L. Mazzarella, *J. Chem. Soc., Chem. Commun.*, **1973**, 99.

5) As a 2-chlorotropone derivative, occurrence of the *ciné*-condensates from **1** is predictable.

6) T. Nozoe, S. Seto, and S. Matsumra, *Proc. Jpn. Acad.*, **28**, 483 (1952).

7) The NMR spectra were measured in $CDCl_3$ solutions, and the chemical shifts were expressed in δ units from the internal Me_4Si.

Reactions of 3-Acetyltropolone Methyl Ethers with 1,2-Cyclohexanediamine

Yasunori SUDOH† and Kimiaki IMAFUKU*

Department of Chemistry, Faculty of Science, Kumamoto Universuty, Kurokami, Kumamoto 860

(Received July 25, 1983)

Synopsis. 3-Acetyl-2-methoxytropone reacted with 1,2-cyclohexanediamine (**2**) (a mixture of *cis* 60% and *trans* 40%) to give four *cis-trans* pairs of 6-acetyl-5*H*-1,2,3,4,4a,11a-hexahydrocyclohepta[*b*]quinoxaline (**3**), 6-acetyl-9-formyl-1,2,3,4,4a,5,10,10a-octahydrophenazine (**4**), 6-acetyl-1,2,3,4,-4a,5,10,10a-octahydrophenazine (**5**), and 1-methyl-6*H*-6a,7,8,-9,10,10a-hexahydropyrrolo[3,2,1-*de*]phenazine (**6**). The reaction of 2-acetyl-7-methoxytropone with **2** gave *cis*- and *trans*-*N,N'*-bis(6-acetyl-7-oxo-1,3,5-cycloheptatrienyl)-1,2-cyclohexanediamine, besides the above products. The *cis*- and *trans*-isomers of **4**, **5**, and **6** were secondary products from the *cis*- and *trans*-isomers of **3**, respectively.

Recently, we found and reviewed that 3-acetyltropolone and its methyl ethers reacted with a variety of nucleophilic reagents having two functional groups to give heterocycle-fused troponoid compounds.[1] On the extension of this series, we carried out the reactions with 1,2-alkanediamines in order to obtain diazaheptalene derivatives.[2] However, the desired compounds were not isolated, but 1*H*-2,3-dihydrocyclohepta[*b*]pyrazine derivatives and some rearrangement products were obtained.[2] In this paper, we describe the reactions of 3-acetyltropolone methyl ethers with 1,2-cyclohexanediamine.

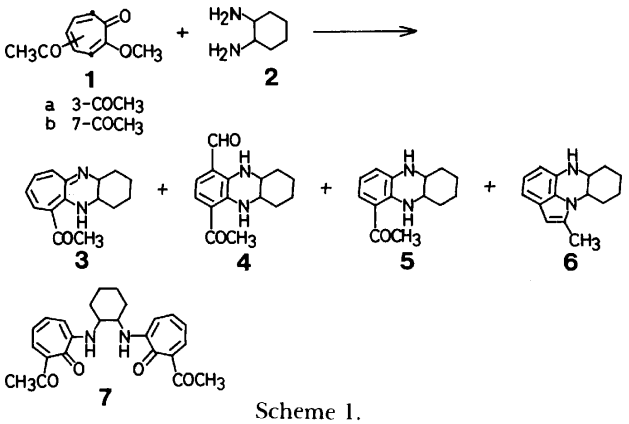

Scheme 1.

A solution of 3-acetyl-2-methoxytropone (**1a**) and an equimolar amount of 1,2-cyclohexanediamine (**2**) (a mixture of *cis* 60% and *trans* 40%) in methanol was refluxed for 2 h to afford *cis*- and *trans*-6-acetyl-5*H*-1,2,3,4,4a,11a-hexahydrocyclohepta[*b*]quinoxaline [**3a** (44%) and **3b** (27%)], *cis*- and *trans*-6-acetyl-9-formyl-1,2,3,4,4a,5,10,10a-octahydrophenazine [**4a** and **4b** (mix. 1%)], *cis*- and *trans*-6-acetyl-1,2,3,4,4a,5,10,10a-octahydrophenazine [**5a** and **5b** (mix. 1%)], and *cis*- and *trans*-1-methyl-6*H*-6a,7,8,9,10,10a-hexahydropyrrolo[3,2,1-*de*]phenazine [**6a** (5%) and **6b** (3%)]. The structures were determined by their elemental analyses and spectral data, which were analogous with those of previously reported compounds.[2]

Refluxing of **1a** with five molar amounts of the diamine (**2**) caused remarkable decreases of the yields of **3a** (19%) and **3b** (3%). Instead, the yields of the by-products increased [**4a** (8%), **4b** (5%), **5a** (3%), **5b** (2%), **6a** (12%), and **6b** (7%)]. This result suggested that the compounds (**4a**, **4b**, **5a**, **5b**, **6a**, and **6b**) were secondary products from the compounds (**3a** and **3b**).

A solution of **3a** in methanol was refluxed for 21 h in the presence of the diamine (**2**) gave **4a** (26%), **5a** (7%), and **6a** (36%). The same treatment of **3b** with the diamine (**2**) also gave **4b** (16%), **5b** (10%), and **6b** (24%).

When a mixture of 2-acetyl-7-methoxytropone (**1b**) and an equimolar amount of **2** was refluxed for 2 h, dimeric products—*cis*- and *trans*-*N,N'*-bis(6-acetyl-7-oxo-1,3,5-cycloheptatrienyl)-1,2-cyclohexanediamine (**7a** and **7b**) were obtained in 10 and 7% yields, respectively, besides **3a** (13%) and **3b** (10%). Furtheremore, the prolonged reaction (24 h) gave five pairs of *cis*- and *trans*-isomers [**3a** (55%), **3b** (15%), **4a** and **4b** (mix. 2%), **5a** and **5b** (mix. trace), **6a** (1%), and **6b** (0.5%)].

Experimental

Measurements. The melting points were determined with a Yanagimoto MP-S2 apparatus and are uncorrected. The HPLC separations were performed on an Altex 330/110A/153 apparatus with a HY-ODS column. The IR and UV spectra were taken on a JASCO IRA-1 and a Hitachi EPS-3T spectrophotometer, respectively. The ^{1}H NMR spectra were recorded with a Hitachi-Perkin-Elmer R-24 spectrometer (60 MHz). The high-resolution mass spectra were obtained with a JEOL JMS-DX-300 apparatus.

Material. 1,2-Cyclohexanediamine (purchased from Tokyo Kasei Co., Ltd.) is a mixture of approximately 60% of *cis*- and 40% of *trans*-isomer.

Reaction of 3-Acetyl-2-methoxytropone (1a) with 1,2-Cyclohexanediamine (2). A mixture of 3-acetyl-2-methoxytropone (**1a**) (178 mg, 1.0 mmol) and 1,2-cyclohexanediamine (**2**) (0.1 ml, 1.0 mmol) in methanol (10 ml) was refluxed for 2 h. After removal of the solvent, the residue was four times chromatographed on a Wakogel B-10 plate (30×30 cm^2) with benzene. The first fraction was collected and recrystallized from hexane to give 12 mg (5%) of *cis*-1-methyl-6*H*-6a,7,8,9,10,10a-hexahydropyrrolo[3,2,4-*de*]-phenazine (**6a**) as colorless plates; mp 149—150°C; IR ($CHCl_3$) 3380 cm^{-1} (NH); UV (CH_3OH) 226 (log ε 4.47), 283 (3.94), 295 nm (sh, 3.91); NMR ($CDCl_3$) δ=1.1—2.2 (8H, m, $CH_2\times4$), 2.37 (3H, s, CH_3), 3.20 (1H, br, NH), 3.5—3.8 (1H, m, CH), 3.8—4.4 (1H, m, CH), 6.02 (1H, s, H-2), 6.18 (1H, dd, J=6, 3 Hz, H-5), 6.78 (1H, dd, J=8, 6 Hz, H-4), 6.84 (1H, dd, J=8, 3 Hz, H-3). Found: *m/e* 226.1446 (M$^+$). Calcd for $C_{15}H_{18}N_2$: M, 226.1470. The third fraction was recrystallized from hexane to give 8 mg (3%) of *trans*-1-methyl-6*H*-6a,7,8,9,10,10a-hexahydropyrrolo[3,2,1-*de*]phenazine (**6b**) as colorless prisms; mp 195—196°C; IR ($CHCl_3$) 3370 cm^{-1} (NH); UV (CH_3OH) 227 (log ε 4.41), 280 nm (3.91); NMR ($CDCl_3$) δ=1.1—2.2 (8H, m, $CH_2\times4$), 2.43 (3H, s, CH_3), 2.6—3.4 (1H, m, CH), 3.45 (1H, br, NH), 3.4—4.1 (1H, m, CH), 6.07 (1H, s, H-2), 6.23 (1H, dd, J=5, 3 Hz, H-5), 6.82 (1H, dd, J=8.5, 5 Hz, H-4), 6.87 (1H, dd, J=8.5, 3 Hz, H-3). Found: *m/e* 226.1458 (M$^+$). Calcd for $C_{15}H_{18}N_2$: M,

† Present address: Taiho Pharamaceutical Co., Ltd., Kawauchi-machi, Tokushima 771-01.

226.1470. The second fraction gave 3 mg (1%) of a mixture of *cis*- and *trans*-6-acetyl-9-formyl-1,2,3,4,4a,5,10,10a-octahydrophenazine (**4a** and **4b**), which was separated by the HPLC method (eluent: 70% methanol) to *cis*- and *trans*-isomers (**4a**:**4b**=5:3). **4a**: Red needles (from methanol-water); mp 103—104.5 °C; IR ($CHCl_3$) 3280 (NH), 1655 (acetyl C=O), 1640 cm^{-1} (formyl C=O); UV (CH_3OH) 241 (log ε 4.24), 272 (sh, 3.96), 339 (4.05), 492 nm (3.78); NMR ($CDCl_3$) δ=1.1—2.2 (8H, m, $CH_2\times4$), 2.50 (3H, s, CH_3), 3.3—3.8 (2H, m, $CH\times2$), 6.64 (1H, d, J=8.5 Hz, H-7), 6.90 (1H, d, J=8.5 Hz, H-8), 8.54 (1H, br, NH-10), 9.03 (1H, br, NH-5), 9.73 (1H, s, CHO). Found: *m/e* 258.1363 (M^+). Calcd for $C_{15}H_{18}N_2O_2$: M, 258.1368. **4b**: Red needles (from methanol-water); mp 88—90 °C; IR ($CHCl_3$) 3280 (NH), 1655 (acetyl C=O), 1640 cm^{-1} (formyl C=O); UV (CH_3OH) 240 (log ε 4.21), 274 (3.96), 327 (3.99), 488 nm (3.72); NMR ($CDCl_3$) δ=1.0—2.3 (8H, m, $CH_2\times4$), 2.54 (3H, s, CH_3), 2.7—3.2 (2H, m, $CH\times2$), 6.70 (1H, d, J=8.5 Hz, H-7), 6.96 (1H, d, J=8.5 Hz, H-8), 8.42 (1H, br, NH-10), 8.94 (1H, br, NH-5), 9.73 (1H, s, CHO). Found: *m/e* 258.1389 (M^+). Calcd for $C_{15}H_{18}N_2O_2$: M, 258.1368. The fourth fraction gave 3 mg (1%) of a mixture of *cis*- and *trans*-6-acetyl-1,2,3,4,-4a,5,10,10a-octahydrophenazine (**5a** and **5b**), which was separated on a TLC plate with benzene to *cis*- and *trans*-isomers, (**5a**:**5b**=2:1). **5a**: A yellow oil; IR ($CHCl_3$) 3300 (NH), 1635 cm^{-1} (C=O); UV (CH_3OH) 264 (log ε 3.90), 422 nm (3.58); NMR ($CDCl_3$) δ=1.1—2.2 (8H, m, $CH_2\times4$), 2.51 (3H, s, CH_3), 3.40 (1H, br, NH-5), 3.2—3.8 (2H, m, $CH\times2$), 6.37 (1H, dd, J=8, 8 Hz, H-8), 6.50 (1H, dd, J=8, 2 Hz, H-9), 7.14 (1H, dd, J=8, 2 Hz, H-7), 8.75 (1H, br, NH-10). Found: *m/e* 230.1471 (M^+). Calcd for $C_{14}H_{18}N_2O$: M, 230.1419. **5b**: Yellow needles (from hexane); mp 95—96 °C; IR ($CHCl_3$) 3300 (NH), 1635 cm^{-1} (C=O); UV (CH_3OH) 262 (log ε 4.06), 417 nm (3.74); NMR ($CDCl_3$) δ=0.8—3.4 (10H, m, $CH_2\times4+CH\times2$), 2.51 (3H, s, CH_3), 3.50 (1H, br, NH-5), 6.37 (1H, dd, J=8, 8 Hz, H-8), 6.52 (1H, dd, J=8, 2.5 Hz, H-9), 7.15 (1H, dd, J=8, 2.5 Hz, H-7), 8.58 (1H, br, NH-10). Found: C, 72.95; H, 8.07; N, 12.21%. Calcd for $C_{14}H_{18}N_2O$: C, 73.01; H, 7.88; N, 12.16%. The fifth fraction was collected and rechromatographed on a TLC palte to give *cis*- and *trans*-6-acetyl-5*H*-1,2,3,4,4a, 11a-hexahydrocyclohepta[*b*]quinoxaline [**3a** (106 mg, 44%) and **3b** (66 mg, 27%)]. **3a**: Yellow prisms (from benzene-hexane); mp 117-119 °C; IR ($CHCl_3$) 3160 (NH), 1600 cm^{-1} (C=O); UV (CH_3OH) 255 (log ε 4.30), 390 (3.83), 454 nm (4.03): NMR ($CDCl_3$) δ=1.0—2.1 (8H, m, $CH_2\times4$), 2.48 (3H, s, CH_3), 3.3—4.0 (2H, m, $CH\times2$), 5.81 (1H, ddd, J=11, 5.5, 3 Hz, H-8), 6.2—6.8 (2H, m, H-9, 10), 6.90 (1H, d, J=11 Hz, H-7), 12.2 (1H, br, NH). Found: C, 74.54; H, 7.44; N, 11.68%. Calcd for $C_{15}H_{18}N_2O$: C, 74.35; H, 7.49; N, 11.56%. **3b**: A yellow semisolid; IR ($CHCl_3$) 3160 (NH), 1600 cm^{-1} (C=O); UV (CH_3OH) 255 (log ε 4.11), 390 (3.65), 448 nm (3.81); NMR ($CDCl_3$) δ=0.9—3.3 (10H, m, $CH_2\times4+CH\times2$), 2.42 (3H, s, CH_3), 5.87 (1H, ddd, J=11, 6, 2.5 Hz, H-8), 6.2—6.8 (2H, m, H-9,10), 6.89 (1H, d, J=11 Hz, H-7), 11.9 (1H, br, NH). Picrate: Mp 182—183 °C. Found: C, 53.89; H, 4.52; N, 14.82%. Calcd for $C_{21}H_{21}N_5O_8$: C, 53.50; H, 4.49; N, 14.86%.

*Reaction of 2-Acetyl-7-methoxytropone (**1b**) with 1,2-Cyclohexanediamine (**2**).* A solution of 2-acetyl-7-methoxytropone (**1b**) (178 mg, 1.0 mmol) and 1,2-cyclohexanediamine (**2**) (0.1 ml, 1.0 mmol) in methanol (10 ml) was refluxed for 2 h. After removal of the solvent, the residue was chromatographed on a Wakogel B-10 plate (30×30 cm^2) with ethyl acetate. The first fraction gave 70 mg of *cis*- and *trans*-*N,N'*-bis(6-acetyl-7-oxo-1,3,5-cycloheptatrienyl)-1,2-cyclohexanediamine (**7a** and **7b**), which was separated by the HPLC method (eluent: 60% methanol) to *cis* and *trans*-isomers (**7a**:**7b**=7:5). **7a**: A yellow oil; IR ($CHCl_3$) 3250 (NH), 1695 (acetyl C=O), 1595 cm^{-1} (tropone C=O); UV (CH_3OH) 248 (log ε 4.43), 355 (4.05), 421 nm (4.21); NMR ($CDCl_3$) δ=1.3—2.2 (8H, m, $CH_2\times4$), 2.48 (6H, s, $CH_3\times2$), 3.9—4.4 (2H, m, $CH\times2$), 6.4—7.7 (8H, m, aromatic H), 7.76 (2H, br. d, J=8 Hz, $NH\times2$). Found: *m/e* 406.1883 (M^+). Calcd for $C_{24}H_{26}N_2O_4$: M, 406.1893. **7b**: Yellow brown crystals (from benzene-hexane); mp 111-113 °C; IR ($CHCl_3$) 3240 (NH), 1695 (acetyl C=O), 1595 cm^{-1} (tropone C=O); UV (CH_3OH) 249 (log ε 4.46), 358 (4.06), 421 nm (4.20); NMR ($CDCl_3$) δ =1.1—2.4 (8H, m, $CH_2\times4$), 2.44 (6H, s, $CH_3\times2$), 3.5—4.1 (2H, m, $CH\times2$), 6.3—7.6 (8H, m, aromatic H), 7.70 (2H, br. d, J=6 Hz, $NH\times2$). Found: *m/e* 406.1869 (M^+). Calcd for $C_{24}H_{26}N_2O_4$: M, 406.1893. The second and third fractions gave **3b** (23 mg, 10%) and **3a** (32 mg, 13%), respectively.

We wish to thank Dr. Tetsuo Nozoe, Professor Emeritus of Tohoku University, for his continuous encouragement. We also thank Mr. Masanori Tsumura of Ichikawa Chemical Laboratories, Higashi-Osaka, for his kind measurements of the high-resolution mass spectra.

References

1) K. Imafuku and Z.-T. Jin, *Yanbian Daxue Xuebao*, **1983** (1), 35.

2) Y. Sudoh, K. Onitsuka, K. Imafuku, and H. Matsumura, *Bull. Chem. Soc. Jpn.*, **56**, 3358 (1983).

The Preparation of 1-Carbamoyl-3-cyanoguanidine and 1-Cyanobiuret from Cyanourea[1)]

Kokoro Iio

Industrial Products Research Institute, Yatabe-machi Higashi, Tsukuba-gun, Ibaraki 305

(Received September 7, 1983)

Synopsis. Cyanourea in an aqueous or organic solution which was allowed to stand at room temperature gave 1-carbamoyl-3-cyanoguanidine and 1-cyanobiuret. The reaction was promoted by a mixture of cyanourea and its alkali salt. 1-Cyanobiuret was also obtained quantitatively by the reaction of cyanourea with alkali cyanate.

It has previously been reported[2,3)] that 1-carbamoyl-3-cyanoguanidine (**1**) was obtained by the reaction of 2-methyl-1-carbamoylisourea with cyanamide, while 1-cyanobiuret (**2**) was obtained by the reaction of *S*-methyl 1-thioallophanate with cyanamide.

In this paper, the author will describe convenient methods of synthesizing **1** and **2** from cyanourea (**3**).

When **3** in a crystalline state had been kept for a long time in the atmosphere, the IR spectrum of **3** showed new absorptions at 2200 and 740 cm^{-1}. This fact was explained by the formation of **1**. Potassium, sodium, or copper(II) salt of **3** in the crystalline state, however, could be kept under the same conditions without any transformation. On the other hand, the formation of **1** was found in an aqueous solution of **3** or its alkali salt. The yield of **1** was enhanced by mixing **3** with its alkali salt; especially when their molar ratio was 3/1, **1** and alkali salt of **2** were obtained in 80 and 1% yields respectively when the solution was kept at 35 °C for a week. A similar reaction was also observed in organic solutions. Even if **3** and its alkali salt were slightly soluble in ethanol, dioxane and acetonitrile, **1** and the alkali salt of **2** were obtained in low yields. The yield of the alkali salt of **2** was enhanced by using DMF or sulfolane as a solvent. Only **3** in sulfolane, however, gave **1** and ammelide, which was the cyclic compound of **2**, in 11 and 14% yields respectively. This fact suggests that the free state of **2** was unstable and cyclized to ammelide, while the alkali salt of **2** was stable. **1**, the alkali salt of **2**, and ammelide were confirmed by comparing their IR spectrum and melting points with those of an authentic sample.[2,3)] These results are summarized in Table 1.

TABLE 1. PREPARATION OF 1 AND 2 FROM 3

3		Solvent	Products (Yield/%[b)])	
Free[a)]	K salt[a)]		1	2[c)]
1	0	H_2O	6	0
0	1	H_2O	11	0
1	1	H_2O	68	1
3	1	H_2O	80	1
1	1	EtOH	9	1
1	1	Dioxane	24	3
1	1	CH_3CN	22	4
1	1	DMF	28	30
1	1	Sulfolane	22	38
3	1	Sulfolane	31	27
1	0	Sulfolane	11	14[d)]

a) Molar ratio. b) Yield based on 2 **3**→**1**+**2**. c) Yield of K salt of **2**. d) Yield of ammelide.

Though **1** could be constituted by the addition of cyanamide to **3**, cyanamide was not detected in any case and did not react with **3**. On the other hand, **2** was obtained quantitatively by the reaction of **3** with alkali cyanate in water, DMF, and sulfolane at room temperature. Ammonia was detected in the aqueous solution, but was not detected in organic solutions. It may be suggested that the decomposition of cyanic acid to ammonia and carbon dioxide caused the low yield of **2** in the aqueous solution.

These results suggest that **3** was dimerized to the labile intermediate (**4**), that **1** was formed by the elimination of cyanic acid from **4**, and that then cyanic acid reacted with the remaining **3** to form **2**.

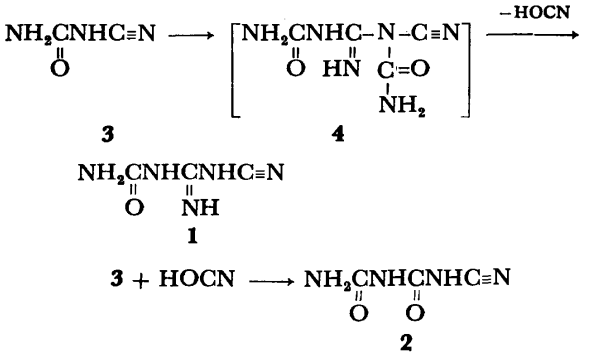

Experimental

The melting points are uncorrected. The IR spectra were taken with a Hitachi EPI-2 spectrometer.

Materials. The **3** was prepared by the alkali hydrolysis of cyanoguanidine.[4)] The other reagents were commercially available and were used after purification if necessary.

Reaction of 3 in an Aqueous Solution. A mixture of **3** (1.70 g) and its potassium salt (2.46g) in water (10ml) was allowed to stand for a week at 35 °C. The precipitate was then filtered off and washed with a small amount of water to give 1.72 g (68%) of **1**;[2)] mp>360 °C. IR (KBr) 2200, 2100, 1700, 1650, 1595, 770, and 740 cm^{-1}. After the pH had been made 3.5—4.0 with 6 mol dm^{-3} of nitric acid, the filtrate was evaporated and extracted with DMF. The residue was dissolved in water, and copper(II) chloride was added to form copper(II) salt of **2** (0.1 g, 1%);[3)] mp>360 °C. Found: N, 28.41%. Calcd for $C_6H_6N_8O_4Cu \cdot 4H_2O$: N, 28.75%.

In the cases of ethanol, dioxane, and acetonitrile solutions, the method was similar to that described above.

Reaction of 3 in DMF Solution. A mixture of **3** (1.70 g) and its potassium salt (2.46 g) in DMF (10 ml) was allowed to stand for a week at 35 °C. The precipitate, potassium salt of **2**, was then filtered off and washed with methanol. The yield was 1.98 g (30%). The filtrate was evaporated under reduced pressure. The residue was dissolved in water, and the insoluble crystals, **1**, were filtered off. The yield was 0.70 g (28%).

In the case of the sulfolane solution, the method was similar to that described above.

Reaction of 3 with Potassium Cyanate. **3** (2.55g) and potassium cyanate (3.05g, as the purity was 80%) were dissolved in water (10ml). The reaction mixture was then kept at room temperature for 24 h. Potassium salt of **2** was subsequently deposited by the addition of 2-propanol. The yield was 4.46g (90%).

In the case of DMF and sulfolane, potassium salt of **2** was deposited quantitatively from the solution.

The author is indebted to Dr. Eiichi Ichikawa of the Tokyo Institute of Technology for his kind suggestions.

References

1) "Studies of Cyanamide Derivatives." Part CXI.
2) K. Iio, E. Ichikawa, and K. Odo, *Yuki Gosei Kagaku Kyokai Shi*, **32**, 513 (1974).
3) K. Iio, E. Ichikawa, and K. Odo, *Yuki Gosei Kagaku Kyokai Shi*, **33**, 184 (1975).
4) F. Hallwachs, *Justus Liebigs Ann. Chem.*, **153**, 293 (1870); H. Bieling, P. Barth, and H. Beyer, *Z. Chem.*, **4**, 146 (1964).

The Intermolecular Interaction of Tetrathiafulvalene and Bis(ethylenedithio)-tetrathiafulvalene in Organic Metals. Calculation of Orbital Overlaps and Models of Energy-band Structures

Takehiko MORI,* Akiko KOBAYASHI, Yukiyoshi SASAKI, Hayao KOBAYASHI,† Gunzi SAITO,†† and Hiroo INOKUCHI††

Department of Chemistry, Faculty of Science, The University of Tokyo, Hongo, Bunkyo-ku, Tokyo 113

†*Department of Chemistry, Faculty of Science, Toho University, Funabashi, Chiba 274*

††*Institute for Molecular Science, Okazaki 444*

(Received May 12, 1983)

Based on the extended Hückel molecular orbital calculations, the relation between the anisotropy of the band structure and the arrangement of the organic molecules is investigated for two organic donors, tetrathiafulvalene (TTF) and bis(ethylenedithio)tetrathiafulvalene (BEDT-TTF). The intermolecular overlaps of their HOMO are calculated while the intermolecular arrangements are varied. The maps of the overlaps thus obtained are then used to estimate the band-structure parameters of $(TMTTF)_2X$ and $(BEDT\text{-}TTF)_2ClO_4(C_2H_3Cl_3)_{0.5}$. The Fermi surface of $(TMTTF)_2X$ is quasi-one-dimensional and not closed. On the contrary, $(BEDT\text{-}TTF)_2ClO_4(C_2H_3Cl_3)_{0.5}$ is regarded as a two-dimensional semimetal.

It has been widely believed that a face-to-face stacking of planar molecules is an indispensable requirement of organic metals and that most of organic metals are quasi-one-dimensional conductors. In these compounds, the intermolecular π-π interaction is responsible for their one-dimensional energy band. However, charge- and spin-density-wave instabilities inherent in one-dimensional metals tend to destroy the metallic states. In the organic superconductors $(TMTSF)_2X$ (TMTSF; tetramethyltetraselenafulvalene, X=PF_6, AsF_6, SbF_6, ClO_4, *etc.*), however, it has been pointed out that the metallic states are stabilized by the relatively large transverse interaction.[1,2] Molecular orbital calculations using seiempirical parameters (extended Hückel method) have been performed by different authors for the $(TMTSF)_2X$ series compounds. Whangbo *et al.*,[3] Grant,[4] and the present authors[5] obtained a quasi-one-dimensional Fermi surface, at least when selenium 4 d orbitals were not included in the calculation. In these calculations, the ratio of the transverse and the longitudinal transfer integrals t_b/t_a was about 0.1. Including selenium 4d orbitals, Whangbo *et al.* noticed a large enhancement of the transverse dispersion leading to a closed Fermi surface on the a* b* plane. However, we found that the change in t_b/t_a was too small to close the Fermi surface. Minot and Louie obtained a complicated semimetallic band structure, with closed Fermi surfaces, by using 'swelled' selenium 4p orbitals, but no 4d orbital.[6] We obtained a similar result when the ionization potential of selenium 4d atomic orbitals was chosen close to the energy level of the highest occupied molecular orbital (HOMO).

On the other hand, increasing interest has been taken in the cation radical salts of BEDT-TTF (4,5-4',5'-bis(ethylenedithio)tetrathiafulvalene). Saito *et al.* reported that the conductivity of $(BEDT\text{-}TTF)_2ClO_4(C_2H_3Cl_3)_{0.5}$ is metallic down to 16 K; below this temperature it decreases slightly, but remains high ($670\ \Omega^{-1}\ cm^{-1}$) even at 1.4 K.[7] The X-ray structure analysis showed that this compound does not have the column structure characteristic of one-dimensional organic conductors.[8] We have calculated the intermolecular overlap integrals of this compound and showed the importance of the transverse interactions.[9] Recently it has also been observed that, in β-$(BEDT\text{-}TTF)_2PF_6$, which shows metal-insulator transition at 297 K, the most conducting axis is parallel to the molecular plane.[10] These results suggest that, in BEDT-TTF compounds, the transverse interaction is more important than, or at least is similar in importance to, the longitudinal interaction.

The present investigation is intended to clarify the relation between the anisotropy (dimensionality) of the band structure and the mode of the intermolecular arrangement of organic molecules. In the calculation, the methyl groups of TMTSF can be replaced by hydrogens (TSF; tetraselenafulvalene) without any significant change in the molecular orbitals. However, if its selenium atoms are replaced by sulfur (TTF; tetrathiafulvalene), the subsequent significant contraction of the atomic orbitals influences the molecular orbitals. In the present investigation, the calculation is performed for two organic donors, TTF and BEDT-TTF.

In order to discuss the physical properties on the basis of quantum-chemical calculations, it is necessary to

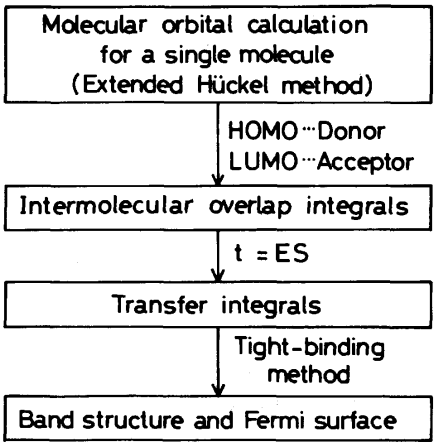

Scheme

carry out an energy-band calculation which takes the three-dimensional periodicity of the crystal into consideration. However, it is not easy to calculate the energy-band structure considering all electrons because of the large size of the organic molecules and because of the complicated crystal structures. Since the anisotropy of the physical properties mainly reflects the shape of the Fermi surface, we may neglect the levels other than the conduction level. Our procedure of the approximate band-structure calculation is thus (Scheme);

(1) Since the size of the organic molecules is very large, the molecular orbitals of a single molecule are calculated by means of the extended Hückel method.

(2) In the case of donor molecules, the intermolecular overlap S of the HOMO is calculated.

(3) Transfer integrals t are estimated using the relation $t=ES$, where E is a constant of the order of energy of the HOMO. This relation is the same as that generally used in the extended Hückel method to obtain resonance integrals.

(4) Using the standard tight-binding approximation, the band structure of the conduction band and the shape of the Fermi surface are obtained.

Alternatively, the transfer integrals can be obtained by calculating the molecular orbitals of a dimer. Unlike this method, our approximation completely neglects the polarization of the molecular orbitals caused by the interaction with other molecules. However, the simplicity of the calculation is more efficient in comparing a number of different intermolecular arrangements. In the present investigation, the intermolecular overlaps of the HOMO are calculated while the molecular arrangements are varied. Using the maps of the intermolecular overlaps thus obtained, the band-structure parameters of $(TMTTF)_2X$ and $(BEDT\text{-}TTF)_2ClO_4(C_2H_3Cl_3)_{0.5}$ are estimated, and the shape of their Firmi surface is discussed. In addition, the characteristic side-by-side arrangement of BEDT-TTF molecules in $(BEDT\text{-}TTF)_2ClO_4(C_2H_3Cl_3)_{0.5}$ is interpreted in view of the electronic stabilization due to the maximum overlap of the conduction orbitals.

Molecular Orbital Calculation

The molecular structures of TTF and BEDT-TTF were idealized so as to have a D_{2h} symmetry, based on the crystal structures of TTF-TCNQ and $(BEDT\text{-}TTF)_2ClO_4(C_2H_3Cl_3)_{0.5}$ (Fig. 1).[8,11] All the atoms except the hydrogens in BEDT-TTF were put on the xy-plane, and the x-axis was placed so as to correspond with the long axis of the molecule. The C-H bond lengths were assumed to be 1 Å.

Since the large size of the molecules prevented us from adopting *ab initio* calculations, the simple extended Hückel method was used. The parameters (Table 1) were taken from Ref. 12.

The coefficients of the HOMO are shown in Table 2. The HOMO of BEDT-TTF as well as that of TTF has a π-character with B_{1u} symmetry (in the D_{2h} point group) and has nodes on all the C-S bonds. The electron density is largest on the inner sulfur atom, S_1. The fact that the charge density on the outer sulfur atom, S_2, of BEDT-TTF is larger than the charge on the C_2 of TTF, shows the considerable expansion of the HOMO of BEDT-TTF in comparison with TTF.

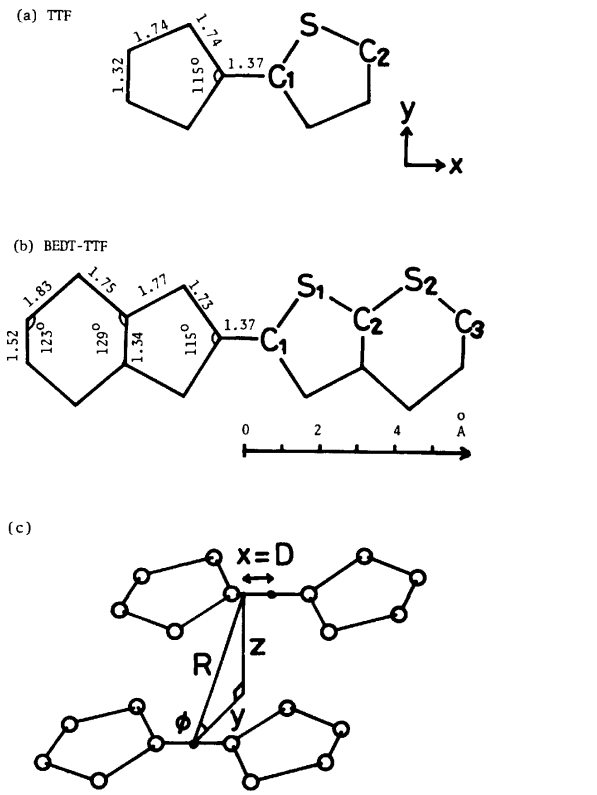

Fig. 1. Molecular structures of (a) TTF and (b) BEDT-TTF. Bond lengths in Å. (c) Relative orientation of a molecular dimer. D represents the molecular slipping along the long axis, R stands for the distance between the long axes of the two molecules, and ϕ is changed from 0° (the side-by-side arrangement) to 90° (the face-to-face stacking).

Table 1. The exponents ζ and the ionization energies ε (eV) for atomic orbitals

Atomic	Orbitals	ζ	ε
S	3 s	2.122	−20.0
	3 p	1.827	−11.0
	3 d	1.5	−5.44
C	2 s	1.625	−21.4
	2 p	1.625	−11.4
H	1 s	1.0	−13.6

Intermolecular Overlaps

Since, both in the $(TMTTF)_2X$ analogs and in many BEDT-TTF salts, molecules are arranged so as to keep their long axes and their molecular planes parallel to each other, we did not consider the relative rotation of the molecules. The relative arrangement of two molecules is represented by a set of cylindrical coordinates

Table 2. Coefficients of the highest occupied orbitals

TTF			BEDT-TTF		
C_1	$2p_z$	−0.26614	C_1	$2p_z$	−0.23510
S	$3p_z$	0.45070	S_1	$3p_z$	0.41358
	$3d_{yz}$	0.12960		$3d_{yz}$	0.12596
	$3d_{xy}$	−0.00412		$3d_{xy}$	−0.00498
C_2	$2p_z$	−0.13851	C_2	$2p_z$	−0.15968
			S_2	$3p_z$	0.16581
				$3d_{yz}$	0.06339
				$3d_{xy}$	0.01547
			C_3	$2p_z$	−0.01877
			H	1 s	0.00927

(D, R, ϕ), as is shown in Fig. 1 (c).

The molecular orbital calculation of a dimer when ϕ=90° has been repeatedly carried out for TCNQ and TTF as a function of D, in which attention has been paid to the most favored slipping D of the stacked molecules.[13] The total energy of a dimer may be divided into the core repulsion and the electronic bonding energy. In the case of TCNQ, the core repulsion is a flat function of D over a wide range of D, and the maximum of the overlap of the lowest unoccupied molecular orbitals (LUMO) corresponds with the minimum of the total energy and also agrees with the slipping in the actual crystals.[13,14] On the contrary, in the case of TTF, the actual slipping corresponds with the minimum of the core repulsion, and the overlap of the HOMO has a *minimum* near this slipping. The applica-

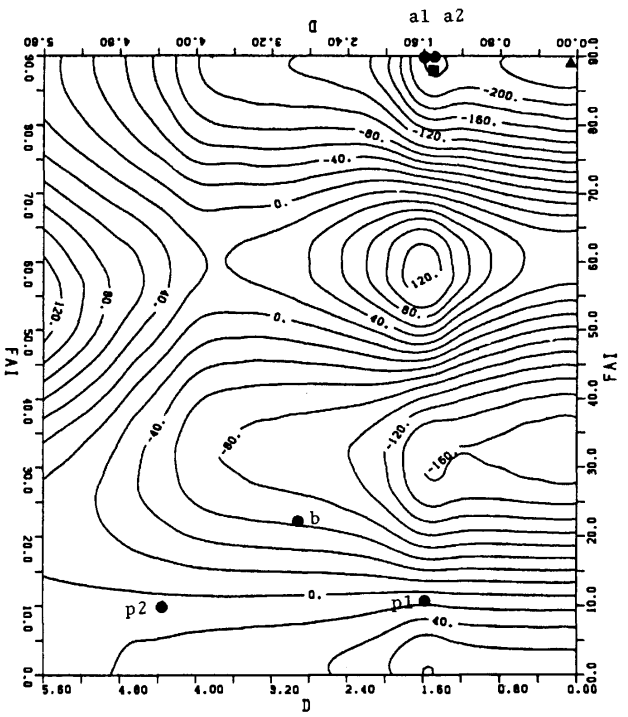

Fig. 2. Overlap integral ($\times 10^{-4}$) of the HOMO between two TTF molecules as a function of the slipping D and the relative angle ϕ (FAI) (see Fig. 1(c)). The triangle designates the stacking mode in TTF-$I_{0.72}$ or TTF-$SCN_{0.58}$. The aquare shows the slipping in the TTF-TCNQ analogs. The other symbols correspond to the interactions in $(TMTTF)_2X$ shown in Fig. 5.

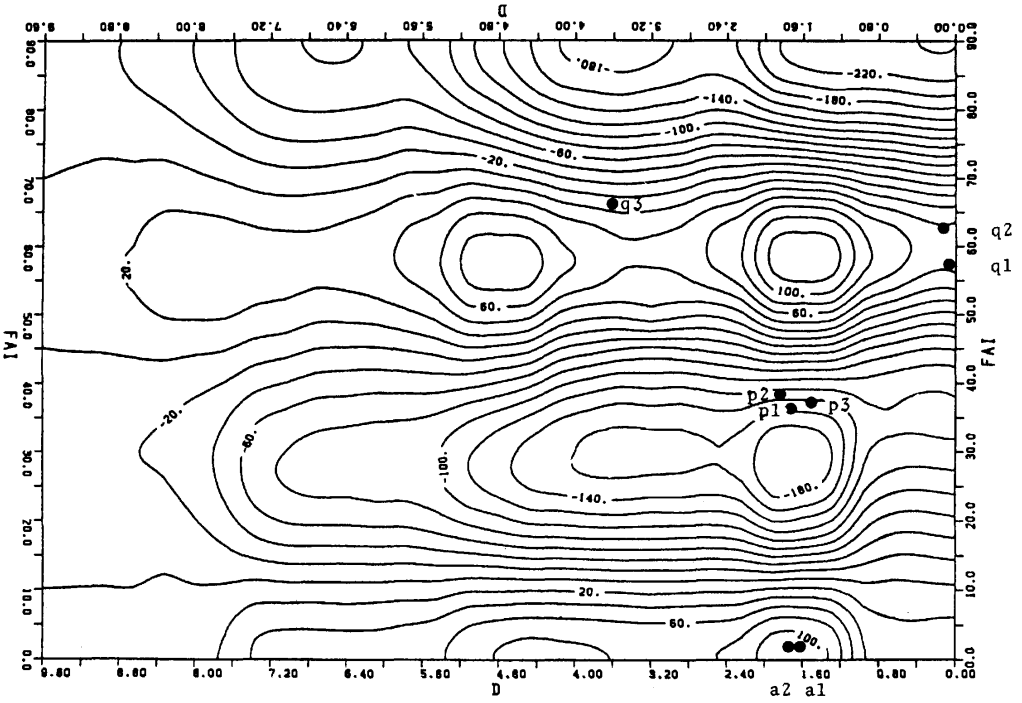

Fig. 3. Overlap integral ($\times 10^{-4}$) of the HOMO between two BEDT-TTF molecules as a function of the slipping D and the relative angle ϕ(FAI).
The symbols a1, a2, *etc.* correspond to the interactions in $(BEDT\text{-}TTF)_2ClO_4$ $(C_2H_3Cl_3)_{0.5}$ shown in Fig. 6.

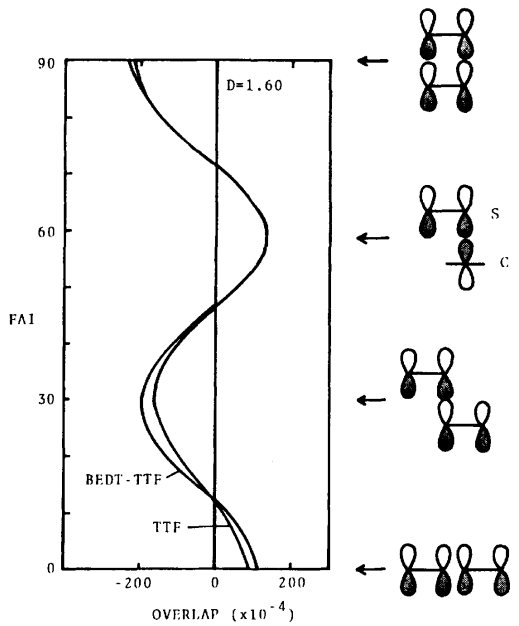

Fig. 4. Cross section of Figs. 2 and 3 at $D=1.60$ Å. In the right hand, the HOMO viewed along the long axes of the molecules are shown.

tion of the local-density-functional theory also suggests the importance of the core repulsion.[15] These results are not surprising, for the van der Waals radius of sulfur is considerably larger than those of carbon and nitrogen. In order to eliminate the effect of this core repulsion, we restricted our calculation to the plane of a crumpled cylinder where the shortest sulfur-to-sulfur distance was arbitrarily fixed as 3.80 Å. The effect of changing the sulfur-to-sulfur distance will be discussed later. By this 'rigid-body approximation,' the coordinate R is given as a function of the other two coordinates, D and ϕ.

In Figs. 2 and 3, the intermolecular overlap integrals are shown as a function of D and ϕ. Figure 4 shows the cross-section of Figs. 2 and 3 at $D=1.60$ Å. The largest overlap at $\phi=90°$ corresponds to the normal face-to-face stacking. The interaction at $\phi=0°$ is the π-like interaction of the p_z (and d) orbitals. The peak around $\phi=30°$ corresponds to the σ-like interaction. In these contexts, σ-like and π-like represent the overlaps which mainly come from the components of the p_z orbitals projected parallel to and perpendicular to the bonding direction respectively. The peak at $\phi=60°$, $D=1.60$ Å, mainly comes from the overlap between the central carbon, C_1, and the sulfur.

The interactions of the TMTTF molecules in $(TMTTF)_2Br$ are shown in Fig. 2 by five symbols, a_1, a_2, p_1, p_2, and b, which correspond to the interactions designated in Fig. 5.[16] Other $(TMTTF)_2X$ type compounds are isostructural to $(TMTTF)_2Br$, regardless of X. The longitudinal interactions, a_1 and a_2, are the same as that of TTF in TTF-TCNQ (the square in Fig. 2). Though the shortest sulfur-to-sulfur distance is found in p_1 and p_2, these interactions ($\phi=10°$) are located nearly midway between the σ-like and the π-like overlaps of the p_z orbitals. As a consequence, these interactions are

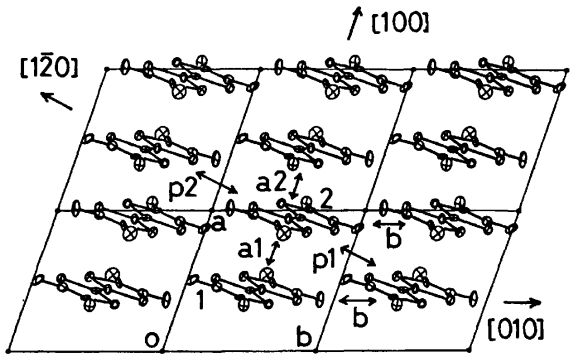

Fig. 5. Intermolecular interactions in $(TMTTF)_2X$.

smaller than the oblique interaction, b, which is close to the peak of the σ-like interaction. Near the region where the overlap crosses zero, the magnitude of the overlap is sensitive to a small variation in the crystal structures. This is also valid for $(TMTSF)_2X$, which is isostructural to $(TMTTF)_2X$. This is the reason why Grant found that the magnitudes of p_1 and p_2 were very sensitive to the kinds of anions, but that other interactions were hardly changed by the anions.[4] The large aniotropy which all the $(TMTSF)_2X$ series compounds show, comes from the large longitudinal interactions, a_1 and a_2, which are scarcely changed by the anions. On the contrary, the difference in the anions, X, causes a small structural variation, which gives rise to the sensitive change of p_1 and p_2, and influences the distortion of the Fermi surface. Therefore, it is possible that the onset of spin-density waves and other instabilities are influenced by the small variation in the crystal structure produced by the anions.

The map of BEDT-TTF in Fig. 3 resembles that of TTF. Figure 4 shows that, in BEDT-TTF, the transverse interactions at $\phi=0°$ and 30° are somewhat enhanced in comparison with those in TTF. The three symbols, a, p, and q, stand for the interactions along [100], [$\bar{1}$02], and [102] respectively in $(BEDT\text{-}TTF)_2ClO_4(C_2H_3Cl_3)_{0.5}$ (Fig. 6). It is worth noting that the overlap along the $\phi=90°$ direction, which exists universally in TTF salts, is not observed in this crystal. As is shown in Fig. 3, p and a are close to the peaks at $\phi=30°$ and $\phi=0°$ respectively. However, q_1, q_2, and q_3 are apart from the peak at $\phi=60°$, $D=1.60$ Å, and are smaller than the other interactions, a and p.

Models of the Energy-band Structures

In actual crystals, the sulfur-to-sulfur distances, $R_{S\text{-}S}$ are not always $R_0=3.80$ Å. However, as is shown in Fig. 7, the overlap integrals change similarly in all the directions as a function of the sufur-to-sulfur distance. Therefore one can estimate the intermolecular overlaps in the actual crystals by using Fig. 7 together with Figs. 2 and 3. The transfer integrals, t, can then be obtained from the relation; $t=E\,S$. Though the best choice of the E value depends on the parameters used for the molecular orbital calculation, we ordinarily use $E=-10$ eV, because it has given realistic values of the transfer integrals for a number of com-

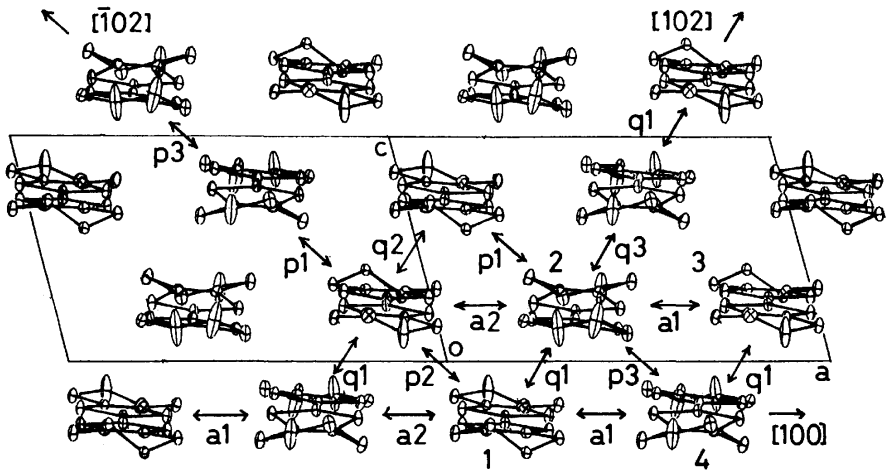

Fig. 6. Intermolecular interactions in $(BEDT\text{-}TTF)_2ClO_4(C_2H_3Cl_3)_{0.5}$.

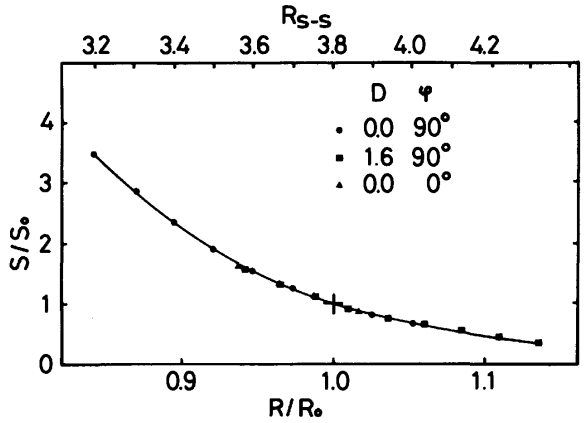

Fig. 7. Relative change of the overlap S as a function of the intermolecular sulfur-to-sulfur distance R, compared with the overlap S_0 at R_0=3.80 Å.

pounds.[9,14,17] When the transfer integrals are estimated, it is easy to obtain the conduction-band structure by the use of the standard tight-binding theory.

From Figs. 2 and 7, the transfer integrals of $(TMTTF)_2X$ were estimated (Table 3(a)). From the standard tight-binding approximation, the matrix elements of the secular equation were;[18]

$$H_{11} = H_{12} = 2t_b \cos kb,$$

$$H_{12} = H_{21}^* = t_{a1} + t_{a2}e^{-ika} + t_{p1}e^{-ikb} + t_{p2}e^{i(kb-ka)}.$$

Solving the resulting quadratic equation, the following dispersion relation was obtained;

$$\varepsilon = 2t_b \cos kb + \Delta^{1/2},$$

$$\Delta = [(t_{a1}+t_{a2})\cos(ka/2) + (t_{p1}+t_{p2})\cos(ka/2-kb)]^2 + [(t_{a1}-t_{a2})\sin(ka/2) + (t_{p1}-t_{p2})\sin(ka/2-kb)]^2.$$

Using this relation, the energy-band structure and the Fermi surface were numerically calculated (Fig. 8). From the stoichiometry, the upper band is exactly half-filled, and the Fermi surface is a plane located around $k_F=\pi/2a$. The deviation from the averaged k_F is about 0.15 π/a. Since, in such a half-filled band, a closed orbit

Table 3. Estimated transfer integrals (in eV)

(a) $(TMTTF)_2X$			(b) $(BEDT\text{-}TTF)_2ClO_4(C_2H_3Cl_3)_{0.5}$		
[100]	t_{a1}	−0.20	[100]	t_{a1}	0.045
	t_{a2}	−0.23		t_{a2}	0.045
[010]	t_b	−0.035	[1̄02]	t_{p1}	−0.060
[12̄0]	t_{p1}	0.020		t_{p2}	−0.060
	t_{p2}	0.007		t_{p3}	−0.060
			[102]	t_{q1}	0.015
				t_{q2}	0.015
				t_{q3}	0.015

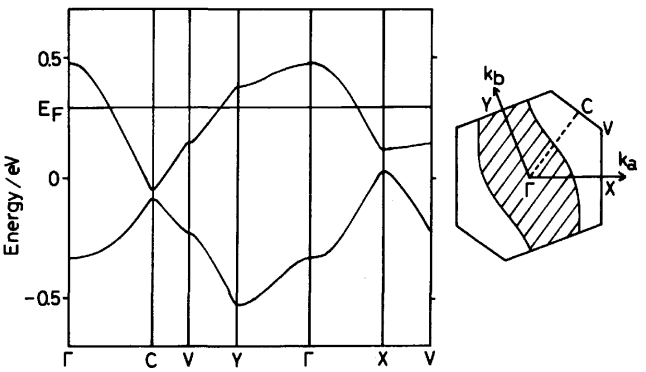

Fig. 8. Band structure and Fermi surface of $(TMTTF)_2X$ calculated by using the transfer integrals in Table 3(a).

arises only at t_a/t_b=1.0,[19] one may safely conclude that the Fermi surface is a plane.

Table 3(b) shows the band parameters of $(BEDT\text{-}TTF)_2ClO_4(C_2H_3Cl_3)_{0.5}$ estimated similarly from Figs. 3 and 7. The matrix elements of the secular equation were obtained by reference to Fig. 6;

$$H_{11} = H_{22} = H_{33} = H_{44} = 0,$$

$$H_{12} = H_{21}^* = H_{34}^* = H_{43} = t_{q1} + t_{p1}e^{-ikc},$$

$$H_{13} = H_{31}^* = t_{p2}e^{-ika} + t_{q2}e^{-i(ka+kc)},$$

$$H_{14} = H_{41}^* = H_{23} = H_{32}^* = t_{a1} + t_{a2}e^{-ika},$$

$$H_{24} = H_{42}^* = t_{p3} + t_{q3}e^{ikc}.$$

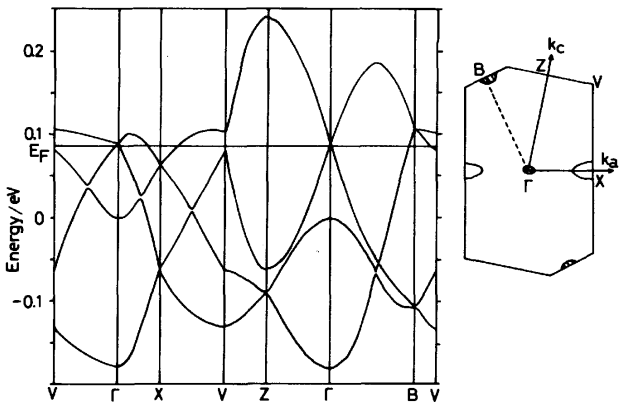

Fig. 9. Band strure and Fermi surface of (BEDT-TTF)$_2$ClO$_4$(C$_2$H$_3$Cl$_3$)$_{0.5}$ calculated by using the transfer integrals in Table 3(b). The shaded region indicates hole-like part.

By solving the secular equation, the band structure and the Fermi surface were found to be as is shown in Fig. 9. From the stoichiometry of the complex, the conduction band is three-quarters filled. Since the unit cell contains four molecules, the conduction level splits into four bands. Because the alignments along p and q have a fourfold periodicity, if the difference of the overlaps belonging to the same direction, p and q, is very large, the energy gap which is opened between the third and the fourth levels makes the compounds semiconductive. However, since the small difference in the calculated overlaps was not regarded as meaningful because of the qualitative nature of the calculation, the interactions belonging to the same direction were averaged in the model in Table 3(b). Consequently, the resulting band structure is two-dimensional and semimetallic. These results agree with the obwervation of the conductivity and the Drude-like optical reflectance along the two directions.[7,23]

Discussion

The organic superconductors (TMTSF)$_2X$ are isostructural to (TMTTF)$_2$Br. In the present investigation, we did not deal with the calculation of selenium analogs. However, as has already been reported,[10] the band structure of (TMTSF)$_2X$ is qualitatively similar to that of (TMTTF)$_2X$. One of the central points of interest with regard to the band structure of (TMTSF)$_2X$ is whether or not there exists a closed Fermi surface. The only experimental evidence of the closed orbit so far is the observation of the Shubnikov-de Haas resistance.[20] However, as was discussed by Horovitz *et al.*,[21] this observation can be interpreted in terms of the semimetallic electronic states under the spin-density-wave states. Since the large calculated anisotropy agreed with the anisotropy of the conductivity (σ_a/σ_b=300)[22] and the analysis of the optical reflectance (t_b=0.14 eV),[24] we conclude that the Fermi surface at high temperatures is a distorted plane, as is shown in Fig. 8.

Another open question is by what mechanism organic molecules are made to be aligned in the transverse directions, as is found in the actual crystals. Considering a chain of organic donors, the bottom of the conduction band corresponds to the bonding alignment of the element orbitals (HOMO), while the top has an antibonding nature. If this band is partially filled, the wider the band splits (or the stronger the interaction is), the more stable the system becomes by means of the intermolecular bonding, compared with the independent molecules. If the core repulsion is not as dominant as this electrical bonding energy, the orientation giving the maximum of the overlap of the HOMO can be expected to correspond with the most stable molecular alignment. In (BEDT-TTF)$_2$ClO$_4$-(C$_2$H$_3$Cl$_3$)$_{0.5}$, the interactions, a and p, are close to the peaks of the overlap in Fig. 3. Therefore, the alignment of the molecules along these directions is favorable because of the intermolecular bonding interaction of the HOMO. The absence of the ϕ=90° interaction is probably due to the large core repulsion of the out-of-plane ethylene groups.

The authors wish to thank Dr. Imoto for a part of the program and to Mr. Tajima for his valuable discussions on the band structures. The computations are carried out partly on the HITAC M-200H computer system at the Institute for Molecular Science and partly on the HITAC M-280H computer system at the Computer Center of the University of Tokyo.

References

1) N. Thorup, G. Rindrof, H. Solig, and K. Bechgaard, *Acta Crystallogr., Sect. B*, **37**, 1236 (1981).
2) H. Kobayashi, A. Kobayashi, G. Saito, and H. Inokuchi, *Chem. Lett.*, **1982**, 245.
3) M. -H. Whangbo, W. M. Walsh, Jr., R. C. Haddon, and F. Wudl, *Solid State Commun.*, **43**, 637 (1982).
4) P. M. Grant, *Phys. Rev. B*, **26**, 6888 (1982).
5) T. Mori, A. Kobayashi, Y. Sasaki, and H. Kobayashi, *Chem. Lett.*, **1982**, 1923.
6) C. Minot and S. G. Louie, *Phys. Rev. B*, **26**, 4793 (1982).
7) G. Saito, T. Enoki, K. Toriumi, and H. Inokuchi, *Solid State Commun.*, **42**, 557, (1982).
8) H. Kobayashi, A. Kobayashi, Y. Sasaki, G. Saito, T. Enoki, and H. inokuchi, *J. Am. Chem. Soc.*, **105**, 297 (1983).
9) T. Mori, A. Kobayashi, Y. Sasaki, H. Kobayashi, G. Saito, and H. Inokuchi, *Chem. Lett.*, **1982**, 1963.
10) H. Kobayashi, T. Mori, R. Kato, A. Kobayashi, Y. Sasaki, G. Saito, and H. Inokuchi, *Chem. Lett.*, **1983**, 581.
11) T. J. Kistenmacher, T. E. Phillips, and D. O. Cowan, *Acta Crystallogr., Sect. B*, **30**, 763 (1974).
12) A. J. Berlinsky, J. F. Carolan, and L. Weiler, *Solid State Commun.*, **15**, 795 (1974).
13) J. P. Lowe, *J. Am. Chem. Soc.*,**102**, 1262 (1980), and the references cited therein.
14) T. Mori, unpublished results.
15) B. D. Silverman, *J. Chem. Phys.*, **72**, 5501 (1980).
16) J. L. Gailigne. B. Liautard, S. Peytavin, G. Brun, J. M. Farbe, E. Torreilles, and L. Grial, *Acta Crystallogr., Sect. B*, **34**, 620 (1978).
17) T. Mori, A. Kobayashi, Y. Sasaki, and H. Kobayashi, *Bull. Chem. Soc. Jpn.*, **56**, 3376 (1983).
18) There is some arbitrariness in the choice of the phase factor of the 'basis functions,' which consist of the HOMO on each molecule in a unit cell. In our notation, the origins of all

the MO are taken in common, but conventionally the origins are taken at the center of each molecule. Our notation can easily be transformed to the conventional notation by multiplying a phase factor, for example, $e^{ika/2}$, by the MO of the second molecule in $(TMTTF)_2X$.

19) In a half-filled band, the area of the occupied region is equal to that of the unoccupied region in the first Brillouin zone.

20) J. F. Kwak, J. E. Schirber, R. L. Greene, and E. M. Engler, *Phys. Rev. Lett.*, **46**, 1296 (1981).

21) B. Horovitz, H. Gutfreunt, and M. Weger, *Solid State Commun.*, **39**, 541 (1981).

22) K. Bechgaard, C. S. Jacobsen, K. Mortensen, H. J. Pedersen, and N. Thorup, *Solid State Commun.*, **33**, 1119 (1980).

23) H. Tajima K. Yakushi, H. Kuroda, G. Saito, and H. Inokuchi, *Solid State Commun.*, to be published.

24) J. F. Kwak, *Phys. Rev. B*, **26**. 4789 (1982).

Plastic Phase of Formylferrocene Studied by X-Ray Diffraction and Mössbauer Spectroscopy

Kumiko SATO,* Makoto IWAI, Hirotoshi SANO, and Michiko KONNO†
Department of Chemistry, Faculty of Science, Tokyo Metropolitan University, Fukasawa, Setagaya-ku, Tokyo 158
†*The Institute for Solid State Physics, The University of Tokyo, Roppongi-7, Minato-ku, Tokyo 106*
(Received June 7, 1983)

The structures of both the crystal and the plastic phases of formylferrocene have been determined to be orthorhombic by single-crystal X-ray diffraction. The structural change proposes a mechanism of the transition that postulates the translational molecular motion along the a-axis. Mössbauer spectra observed in the plastic phase show little fluctuation of the electric field gradient ascribed to the orientational disorder between x, y, and z axes of the molecule.

It is known that organometallic compounds, such as ferrocene derivatives, exhibit various kinds of mesophase transitions. Malthete and Billard have reported that ferrocene derivatives of *N*-(*p*-benzoyloxybenzylidene)aniline exhibit mesomeric properties.[1] The plastic crystal (PC) phases of formyl- and polychloroferrocenes were studied and the former especially has been widely investigated by Daniel *et al.*[2-4] Although the structure of the ordered low-temperature phase of formylferrocene was determined to be orthorhombic (space group $P2_12_12_1$; Z=4, a=7.635, b=10.520, c=11.281 Å) by using a single crystal, the structure of the PC phase was assinged to a simple face-centered cubic (f.c.c.) lattice with a unit-cell parameter a=9.99 Å accompanied by orientational disorder based on a Debye-Scherrer pattern.

In the present paper the plastic phase transition in formylferrocene has been studied by means of single crystal X-ray diffraction and Mössbauer spectroscopy. Although the present X-ray diffraction data determined at room temperature agreed essentially with those reported by Daniel *et al.*, the results obtained for the PC phase determined by oscillation and Weissenberg photographs were found to be orthorhombic, with a'=11.9, b'=16.4, c'=7.0 Å at 50 °C. The temperature dependence of the Mössbauer spectra was determined in order to confirm dynamic molecular motion.

Experimental

Formylferrocene was synthesized by acylation of ferrocene with *N*,*N*-dimethylformamide. The products were separated by column chromatography on an alumina and purified by recrystallization and sublimation. The purity was checked by melting point and elemental analysis. The thermal properties of formylferrocene were determined by a Rigaku Thermoflex Differential Scanning Calorimeter (DSC). The thermal parameters at transition and melting points were found to be ΔH=12.09±0.04 and 2.184±0.008 kJ mol^{-1} and ΔS=38.37±0.12 and 5.82±0.04 J mol^{-1} deg^{-1}, respectively, which agreed with the values reported in the previous paper.[2]

Mössbauer spectra were determined by using an Austin Science Associated Mössbauer spectrometer. Velocity calibration was carried out based on the room-temperature spectra of metallic iron. By fitting the resonance line with a Lorentzian function, the Mössbauer parameters were extracted. A high-temperature apparatus was constructed with a heater in a vacuum furnace. The sample was sealed to suppress sublimation. Temperature was checked by using a CA thermocouple with a precision of about ±0.05°.

Because our results on the structural analysis of the PC phase of formylferrocene contradicted those reported by Daniel *et al.*, the crystal structure of this compound at room temperature was determined in order to confirm that the compound used here has the same crystal structure in the crystal phase as the one used by them.

Single crystals suitable for X-ray study were obtained by a slow sublimation method. A crystal specimen with approximate dimensions of 0.28×0.25×0.23 mm was used, kept in a Lindemann-glass capillary filled with nitrogen gas. Intensity data were collected on a four-circle diffractometer with Mo $K\alpha$ radiation monochromated by a graphite plate.

The crystals are orthorhombic with space group $P2_12_12_1$, a=10.525(9), b=11.294(10), c=7.639(5) Å, V=908.1(13) Å^3 and Z=4 at room temperature. The details of the basic crystal data have been omitted in the present paper as the results obtained at room temperature agree essentially with those reported by Daniel *et al.* in 1981.[3] There are, however, some comments in connection with the crystal structure. The positions of hydrogen atoms could be determined and are shown in Table 1. In refinement, incorporating the model with two-fold disorder, the cyclopentadienyl rings are found to be twisted approximately by 36° around the molecular axis with respect to one another, as shown by the solid circles in Fig. 1. The disordered model involves two alternative ring orientations in a ratio of occupancy of 0.85:0.15. A composite structure, which attempts to model the disorder, gives R=3.72% over 1001 independent reflections with $|F_o|>3\sigma(|F_o|)$ up to 2θ=60°.†† The disordered structure at room temperature provides a useful clue to understanding the molecular motion of this compound at the transition point as described later.

Results and Discussion

Crystal Structure. Formylferrocene exists approximately on the a and c plane and a prominent feature of the molecular structure is the layer structure along b axis. There exist the 020 reflections with a significant intensity characteristic of a layer structure.

The molecules occupying in the ratio of 0.85 exhibit an appreciable interaction between neigh-

†† The complete F_o—F_c data are deposited as Document No. 8401 at the Office of the Editor of the Bulletin of the Chemical Society of Japan.

Table 1. Fractional atomic coordinates ($\times 10^3$) and equivalent isotropic thermal parameters

	x	y	z	U_{eq}/10 Å
H(1)	−90(6)	366(6)	228(10)	97(23)
H(2)	−122(5)	88(5)	233(8)	60(18)
H(3)	38(5)	28(5)	463(8)	52(19)
H(4)	146(6)	204(6)	561(8)	71(21)
H(5)	64(6)	436(6)	426(9)	80(24)
H(6)	115(6)	302(6)	−78(8)	83(22)
H(7)	91(7)	63(6)	−89(10)	104(28)
H(8)	268(8)	−2(8)	179(10)	104(28)
H(9)	354(6)	152(5)	234(9)	73(21)
H(11)	224(7)	470(6)	43(10)	82(25)

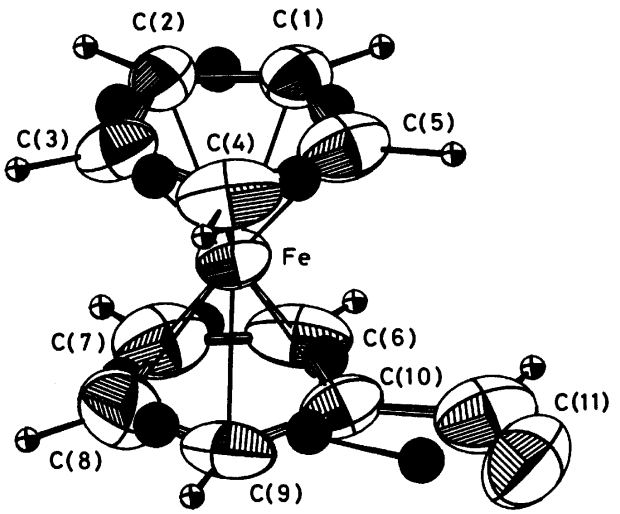

Fig. 1. View of the compound. Solid circles refer to disordered molecule.

bouring molecules along the b axis. The nearest distance between O(1) and H(5) is estimated to be 2.53 Å and the C(5)-H(5)···O′(1) bond angle 128°. The H(11)-O′(1) distance is estimated to be 2.84 Å, the O(1)-H(11)···O′(1) bond angle 148° and the H(2)-O′(1) distance 2.81 Å the C(2)-H(2)···O′(1) bond angle 132°. There is a network of intermolecular interaction along c axis as shown by broken lines in Fig. 2.

The molecules occupying in the ratio of 0.15 are twisted approximately by 36° around the molecular axis and too far separated to form an intermolecular bonding network. At room temperature the probability of molecules sitting in the disordered positions is about 15% and the possibility may increase with increasing temperature.

Plastic Crystalline Structure. The crystal specimen was heated by electrically heated air, controlled with a precision of about ±0.25°. In the PC phase, oscillation and Weissenberg photographs were taken at temperatures from 45 to 70 °C. After the transition at 43.5 °C, there remained only five independent reflections with significant intensity, 111, 210, 030, 121, and 220. Oscillation and Weissenberg photographs indicate that the PC phase is orthorhombic, $a'=11.9$, $b'=16.4$ ($b'=3/2b$, where b stands for the lattice

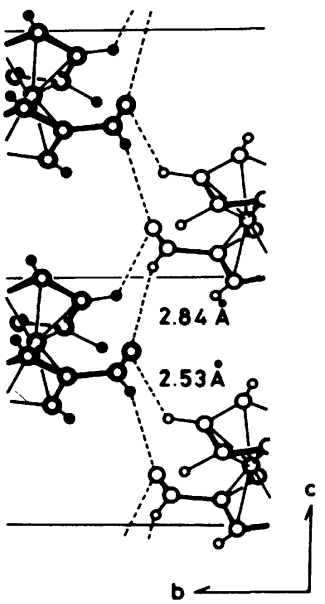

Fig. 2. The conformation of the network of weak intermolecular bonding along c axis. The intermolecular bonding C(5)-H(5)···O′(1) and O(1)-H(11)···O′(1) are indicated by broken lines.

constant at room temperature), $c'=7.0$ Å at 50 °C. The lattice constant exhibits no serious change up to 70 °C.

These results contradict the f.c.c. structure with the lattice constant 9.99 Å concluded by Daniel *et al.*,[3] since the observed reflections cannot be interpreted by the f.c.c. structure. The X-ray powder pattern at 50 °C exhibits two characteristic reflections with very strong intensity. Although these reflections seem to correspond to 111 and 200 in f.c.c. lattice, they consist of five overlapped reflections, *i.e.*, 111, 210, 030, 121, and 220 in the orthorhombic lattice. The results indicate that the PC phase of formylferrocene is explained not by f.c.c. but by an orthorhombic structure, although there are few reports suggesting any orthorhombic PC phase.

Phase Transition Model. The PC phase yeilds only a few diffracted X-ray reflections at low Bragg angles, as a consequence of the very high Debye-Waller factors owing to orientationally disordered molecules, but a detailed comparison of the structural data of the crystal phase with those of the PC phase permit a hypothetical structure for the PC phase.

A structural model of the PC phase may be proposed based on the structure determined at room temperature having six molecules in a unit-cell as shown in Fig. 3. The iron atoms lie in the mirror planes at $Z'=0$ and 1/2 as illustrated with open and solid circles, respectively. There exist four crystallographically independent molecules, I, II, III, and IV, in the unit cell. Furthermore, molecules III and IV are located in the mirror planes both at $y'=1/2$ and there is a two fold axis along a′. Although the space group could not be unequivocally determined, the PC phase exhibits an increase in symmetry compared to the crystal phase.

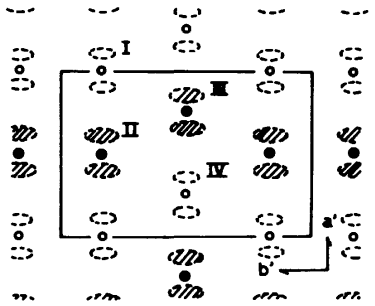

Fig. 3. A proposed structure of the PC phase projected along c' axis. Open circles refer to iron atoms in each molecule lying on the mirror plane at $z=0$. Solid circles refer to iron atoms in each molecule lying on the mirror plane at $z=1/2$.

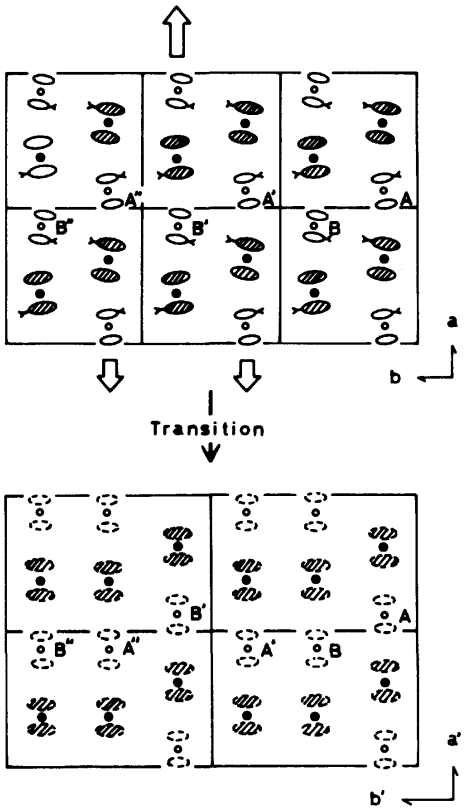

Fig. 4. The upper part shows schematically the crystal structure at room temperature and the lower part the proposed PC phase structure (a triad structure).

The structure proposed for the PC phase dose not give rise to any essential deviations of molecular positions from the crystal structure in the crystal state at room temperature.

The projections of the structures of modifications viewed along the c axis of the crystal phase and the c' axis of the PC phase are given in the upper and lower parts of Fig. 4, respectively. Bragg reflections observed in the PC phase have little contribution from carbon and oxygen atoms, because of the large Debye-Waller factors ascribed to the large thermal motion of cyclopentadienyl rings and the formyl groups which make their scattering factors much

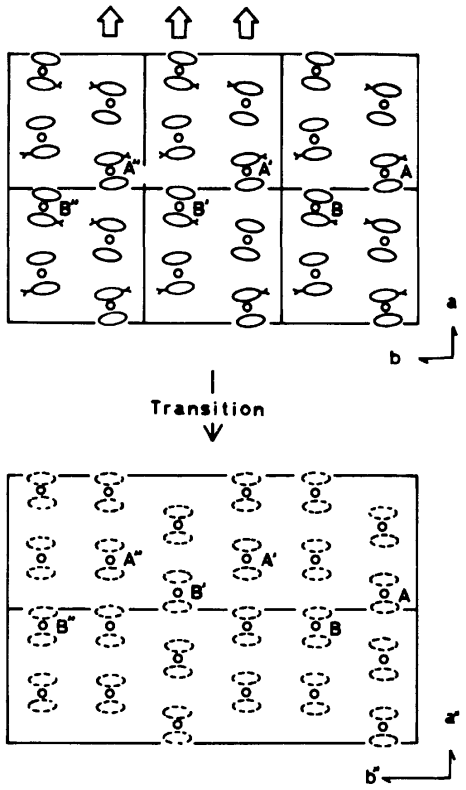

Fig. 5. The upper part shows schematically the crystal structure at room temperature and the lower part the proposed PC phase structure (a hexa-periodical structure).

weaker compared with that of iron atoms.

The 030 reflections with significant intensities indicate a triad structure for the PC phase. The lattice constant of the b' axis in the PC phase *vs.* that of b axis in the crystal phase gives a ratio of 3:2. The structural change which accounts for the different lattice suggests a cooperative slide of the layer consisting of molecules on the a and c planes along the a axis. As shown in Fig. 4, in the crystal phase, the molecules A, A', and A'' are equivalent in each cell separated by translating molecules to the nearest molecular position along the b axis. In the PC phase, the molecule B' will probably be equivalent with the molecule A because of the reason described above. The molecules A, A', A'', B, B', and B'' in the crystal phase correspond to those in the PC phase, respectively. There is an indication that the iron atoms cooperatively slide along the a axis at the phase transition point. The schematic features of the phase transition are indicated by downward and upward arrows in Fig. 4, although the model described above seems to overestimate the sliding motion up and down along the a axis.

An alternative model is shown in Fig. 5, where the PC phase is considered to have a hexa-periodical structure. The 030 reflections with significant intensities are regarded as the 060 reflections. As shown in Fig. 5, in the PC phase the molecule A can be described as equivalent to the molecule A in the adjacent unit-cell repeatedly appearing along the b' axis. This model requires that all the molecules slide upward along the a axis as

shown by the arrows in Fig. 5. In this case, the positional deviation from the original molecular position in the crystal phase is also considered to occur in the direction of the c axis, causing the change of molecular positions undetectable by X-ray analysis.

Although it remains undetermined whether a triad or a hexa-periodical structure is to be prefered for the PC phase, it is concluded that formylferrocene acquires a considerable degree of translational freedom in the direction of the a axis above the transition point.

When the plastic crystalline molecules are almost spherical, the entropy of melting is expected to be close to the value of $3R/2$ which is expected for molecules possessing freedom in three dimensional translation based on the classic theory. Because each molecule can rotate without significant translational motion of the centers of gravity in the crystal phase, the molecule may have as much rotational entropy in the plastic crystal as in the liquid phase. On the other hand, formylferrocene with the first-order transition has an entropy of melting of 1.39 entropy units which is less than $3R/2$. Molecules that have anisotropic structures may need translation of the center of gravity, such as the translational motion to the adjacent position, so that they can start rotating and a kind of cooperative motion, making the transition first order at the transition point from crystal to PC phase. Since a part of the translational entropy has already been consumed below the melting point, the entropy of melting is interpreted to be less than $3R/2$.

There exists no significant change of the lattice constant between 50 °C and room temperature, except that the b axis in the PC phase *vs.* the b′ axis in the crystal phase is in the ratio of 3:2, and the PC phase remains orthorhombic. This is one of strong pieces of evidence supporting the anisotropic molecular rotation in the PC phase. The a axis in the PC phase lengthens by *ca.* 13%, while the c and b axes become shortened by *ca.* 8 and 3% of each axis in the crystal phase at room temperature. It has generally been known that the lattice constant in the PC phase is larger than that in the crystal phase. The present data, which indicate an anisotropic expansion, also suggest an anisotropic orientation such as a partial rotation around the molecular axis. The results of the crystal structure in the crystal phase, involving occupancy of two alternative ring orientations in the ratio of 0.85:0.15 provide us with additional evidence supporting rotational motion around the molecular axis. The orientational disorder in the PC phase may have the effect of deteriorating a weak intermolecular bonding network found along the b and c axes in the crystal phase at room temperature. This model provides a possible explanation for the contraction of the b and c axes, although further investigations should be carried out for more detailed discussions.

Mössbauer Spectra. The values of the isomer shift and quadrupole splitting are 0.43 and 2.23 mm s^{-1} at room temperature, respectively, and the electronic state of the iron atom is found to be divalent with a low-spin state. The characteristically large quadrupole splitting is attributed to the large electric field gradient: that is, a larger population of electrons in the x, y directions than in the z direction for iron atoms.

In the Mössbauer spectra there exists no serious difference between the crystal and the plastic crystal phase, as shown in Fig. 6. If there is any fluctuation of the electric field gradient owing the orientational disorder between x, y, and z axes, one can expect a change in the spectral line shape. In the case of acetylferrocene, an orientational phase transition was observed at a temperature a few degrees below the melting point in X-ray diffraction. The temperature dependence of the recoil-free fraction in the Mössbauer spectra of acetylferrocene was ascribed to the quadrupole relaxation effect caused by the orientational disorder.[5] In the PC phase of formylferrocene, the unchanged line-width indicates either that there may be little orientational disorder around x or y axes of the molecule or that the quadrupole relaxation time may be very long.

Mössbauer spectra cannot be detected above 85 °C

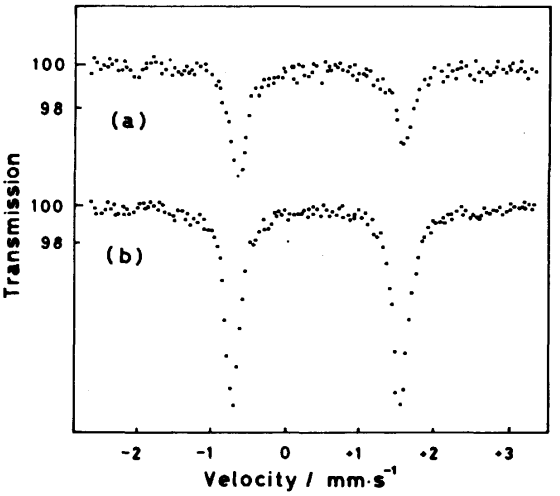

Fig. 6. (a) Mössbauer spectrum of the PC phase at 75 °C, which indicates an asymmetric quadrupole split line. (b) Mössbauer spectrum of the crystal phase at room temperature.

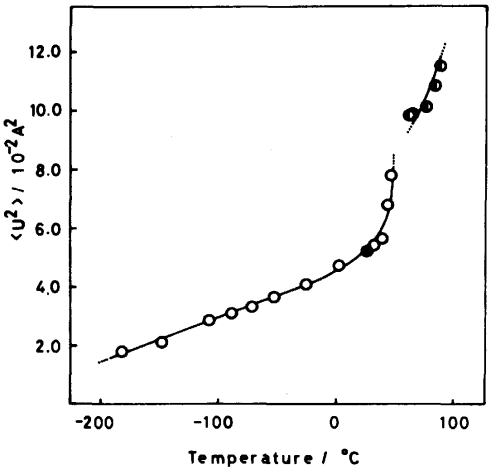

Fig. 7. The temperature dependence of the mean-square amplitude. The solid circle shows the value estimated from the thermal factor based on the X-ray study.

because of a rapid decrease of the recoil-free fraction in the higher temperature phase. The areal intensity of the Mössbauer spectrum abruptly decreases at the transition point, as shown in Fig. 7, and is related to the mean-square amplitude of Mössbauer atoms $<U^2>$ as follows:

$$A \propto f = \exp\left[-\frac{4\pi^2}{\lambda_\gamma^2}\langle U^2\rangle\right],$$

where λ_γ is the wavelength of the Mössbauer γ-ray and f is the recoil-free fraction. In the high-temperature approximation, $<U^2>$ can be estimated from the areal intensity. The solid circle in Fig. 7 is the value of the isotropic mean-square amplitude estimated from the thermal factor determined by the X-ray analysis for the crystal phase at room temperature, which agrees with the value obtained by the Mössbauer spectrum.

The mean-square amplitude shows a linear temperature dependence in the temperature range from about -200 °C to 0 °C, indicating an harmonic lattice vibration, but a significant deviation is found near the transition temperature, *e.g.*, an abruptly increased value, 0.07 $Å^{-2}$, is given before the transition. This indicates a substantial modification in the lattice characteristics of the solid. Although a thin sample, 32.8 mg cm^{-2}, shows no detectable spectra after the transition, because of the decreasing spectral intensity, definite spectra are successfully obtained with a thick sample, 97.5 mg cm^{-2}. The percent effects of the spectrum cannot precisely be normalized with those obtained for the thin sample because of a saturation effect. Therefore, the mean-square amplitude in the PC phase shown in Fig. 7 may be underestimated.

The PC phase of formylferrocene is characterized by the abnormally large translation similar to that expected in the liquid phase. The ratio, δ, between the mean square-root amplitude and the mean intermolecular distance has been used as an estimation of lattice vibrations in metallic solids and crystals of metal halides.[6] The value of δ is estimated at approximately 5% for formylferrocene at temperatures from 50 °C to 85 °C below the melting point, 123.5 °C, while other ferrocene derivatives, mono- and diacetylferrocene and ferrocenemono- and dicarboxylic acid, reveal the values of 2 to 3% even near the melting points. The anomalous value of δ for formylferrocene in the PC phase below the melting point suggests an unusual lattice vibration in the crystal phase. There may exist an anisotropic translation of molecules in the PC phase as was proposed for the transition in the previous section.

The authors wish to thank Prof. Yoshihiko Saito for his helpful discussions concerning the crystallographic aspects of this work.

References

1) J. Malthete and J. Billard, *Mol. Cryst. Liq. Cryst.*, **34**. 117 (1976).
2) M. F. Daniel, A. J. Leadbetter, R. E. Meads, and W. G. Parker, *J. Chem. Soc., Faraday Trans. 2*, **74**, 456 (1978).
3) M. F. Daniel, A. J. Leadbetter, and M. A. Mazid, *J. Chem. Soc., Faraday Trans. 2*, **77**, 1863 (1981).
4) M. F. Daniel, A. J. Leadbetter, and R. M. Richardson, *J. Chem. Soc., Faraday Trans. 2*, **77**, 1851 (1981).
5) K. Sato, M. Konno, and H. Sano, *Chem. Lett.*, **1982**, 817.
6) F. Lindemann, *Phys. Z.*, **11**, 609 (1910).

 © 1984 The Chemical Society of Japan Bull. Chem. Soc. Jpn., 57, 639—643 (1984)

Nonisothermal Kinetics of Crystal Growth from Preexisting Nuclei

Takeo Ozawa
Electrotechnical Laboratory, Sakura-mura, Niihari-gun, Ibaraki 305
(Received June 22, 1983)

Fundamental kinetic equations for nonisothermal crystal growth from preexisting nuclei are derived, by introducing a concept of reduced time. A method of kinetic analysis of thermoanalytical data of these processes is proposed, and all kinetic parameters can be estimated by the method, so that the process proceeding under various temperature changes can also be predicted.

It is well known that crystalline nuclei form first in supercooled liquids and amorphous solids, and then they grow to crystallites. Some solid reactions also proceed in a similar way to this nucleation-and-growth process. When they occur isothermally, these processes follow Avrami's equation;

$$-\ln(1-C) = Zt^n, \quad (1)$$

where C, Z, t, and n are respectively the conversion, a constant, the time, and an integer dependent on the mechanism of the process.[1-3] Evans[4] derived this equation in an ingenious way, in which the nuclei are compared to rain-drops falling down on a pond and the fronts of the crystal growth are compared to the traversing wave fronts caused by the rain drops. He calculated expectancy of the number of the wave fronts passing over a particular point, and the unconverted fraction can be calculated by using the expectancy thus calculated and Poisson's distribution.

In 1971 the present author set forth theoretical considerations of nonisothermal kinetics of the processes by extending Evans' way to nonisothermal conditions. A method for kinetic analysis of thermoanalytical data of the processes proceeding at a linear rate of heating or cooling was also derived, and the method was applied to crystallization of poly(ethylene terephthalate) observed at linear cooling rates by differential scanning calorimetry (DSC).[5]

Recently various amorphous materials, such as amorphous magnetic materials and amorphous silicon for solar photovoltaic cells, are under extensive research and development, and to evaluate their thermal stability, crystallization behaviors of these materials are investigated by differential thermal analysis and DSC. To estimate the kinetic parameters for predicting the crystallization behavior is also important in research of latent heat thermal energy storage materials, especially of the materials containing nucleating agent. The kinetic analysis is also useful for inorganic glasses. For analyzing thermoanalytical data of crystallization of inorganic glasses and amorphous materials, mainly Kissinger plot[6] proposed for usual chemical reactions has been applied to the data. Therefore, it is erroneous to apply the plot to the crystallization processes for estimating the activation energy, as was already pointed out by Matusita and Sakka,[7] though the plot is rigorously applicable to first order reactions and approximately applicable to reactions of the other orders.[8]

Matusita and Sakka[7] derived a theory and an analytical method of the processes, in which the random nucleation occurs in lower temperature range and prior to the growth, which proceeds separately after the nucleation. They applied their method to crystallization of inorganic oxide glasses. However, they derived the theory roughly, neglecting the rigorous theoretical derivations of nonisothermal relations for crystallization[5] and chemical reactions,[8] so that "modified Ozawa plot" proposed by them should be corrected by rigorous theoretical considerations. To derive rigorous nonisothermal equations, isothermal equations for each unit process should be expanded separately to nonisothermal equations, because the expansion of isothermal kinetic equations as a whole may lead to erronous results.[5]

Moreover, their method does not have any means to check the applicability of the method in itself. In other words, there is no means to confirm certain applicability of the method by observing consistency between the observed process and the model on which the theory and method are based. Therefore, we can not deny possibility that the method may be applied outside of its applicability. A method to estimate the kinetic parameter, n, is also not included in their method, so that n may be determined inaccurately. By the method, the activation energy can only be estimated, and the other kinetic parameters can not be obtained. Therefore, the crystallization behavior of the materials under various conditions can not be predicted for assessing thermal stability of the materials, though Matusita and Sakka clearly and exactly criticized the arbitrary and unsupported application of the Kissinger plot.

The present author's theory and the method for kinetic analysis of the thermoanalytical data cover more general cases, in which the random nucleation and the growth occur either concurrently or separately.[5] However, the applicability of these theory and method is limited in the cases of linear heating or cooling. For the cases, in which the nucleation occurs separately in the lower temperature range prior to the growth, a simple, but rigorous, theory and method can be derived, and they are applicable to more general cases of temperature change. One can overcome the above-mentioned drawbacks by the present author's method for kinetic analysis based on this rigorous theory, and one can also predict the process proceeding under various types of temperature changes using the kinetic parameters thus obtained. In this paper, the theory and the method are reported.

Models

There are two models for the case of crystal growth

from preexisting nuclei with negligible concurrent random nucleation. The first model is the crystal growth from impurity or nucleating agent, as is the case for latent heat thermal energy storage materials containing nucleating agent, and the number of the nuclei is independent on the thermal history of the materials. The second case is that the temperature range for random nucleation is much lower than that for the crystal growth, and the two temperature ranges are separated clearly, so that the number of the nuclei existing in the beginning of the growth is constant during the growth but dependent on the thermal history in the nucleation temperature range. For the crystal growth there are three cases, *i.e.*, one-dimensional growth, two-dimensional growth and three-dimensional growth.

Method for Deriving the Kinetic Equation

As mentioned before, the excellent and elegant way of Evans[4] is adopted and extended in this paper. First, let us consider the case in which many stones fall on the pond at the same time t_1. The stones are compared to the nuclei, and the wave fronts caused by the stones are compared to the front of the crystal growth. The expectancy, E, of the number of the wave fronts passing over a particular point until the time t_2 is equal to the number of the stones falling in a circle, the radius of which is the distance the wave fronts traversed from t_1 to t_2. It is given as follows:

$$E = \pi NR^2, \tag{2}$$

where N and R are the number of stones falling in a unit area and the distance which the wave fronts traversed from t_1 to t_2, respectively, and R is given below.

$$R = \int_{t_1}^{t_2} v\mathrm{d}t, \tag{3}$$

where v is the linear velocity of the wave fronts.

Because the fronts of crystal growth pass over a particular point only once in contrast with the wave fronts on the pond, the part of the pond, over which the wave fronts have not yet passed, has real physical meaning in crystallization, and it is the fraction of unconverted portion. The conversion of the crystallization can thus be expressed by applying Poisson's distribution as follows:

$$1 - C = \exp(-E), \tag{4}$$

or

$$-\ln(1-C) = E. \tag{5}$$

By applying this derivation to the nonisothermal conditions, we can obtain the fundamental equation for nonisothermal crystallization from preexisting nuclei.

Fundamental Equation for Nonisothermal Crystallization from Preexisting Nuclei

The number of preexisting nuclei per unit volume is dependent on the above-mentioned models. For the first model, the number of the nuclei, N, is a constant.

$$N = \text{constant} \tag{6}$$

On the other hand, N is given below for random nucleation for the second model as follows:

$$N = \int_0^{t_1} \nu(T)\mathrm{d}t, \tag{7}$$

where $\nu(T)$ is a nucleation rate per unit volume as a function of the temperature, T, and as is assumed in the model, the nucleation does not occur after the time t_1.

The expectancy, E, can be derived, taking into accounts of the dimension of the growth. For the one-dimensional growth,

$$E = dNR, \tag{8}$$

where d is the cross section of the needle-like crystallites. For the two-dimensional growth,

$$E = \pi dNR^2, \tag{9}$$

where d is the thickness of the disk-like crystallites. For the three-dimensional growth,

$$E = \frac{4\pi}{3} NR^3. \tag{10}$$

Taking account of the temperature dependence of the linear growth velocity, *i.e.*,

$$v(T) = v_0 f(T), \tag{11}$$

let us introduce a concept, reduced time, θ, namely[8,9]

$$\theta = \int f(T)\mathrm{d}t, \tag{12}$$

and

$$R = v_0\theta. \tag{13}$$

Thus, the fundamental equation is given as follows:

$$-\ln(1-C) = Z_0\theta^m, \tag{14}$$

where Z_0 equals to gNv_0^m and g and m are a constant and the number of the growth dimension, respectively. The constant, g, is equal to d, πd and $4\pi/3$ respectively for the one-dimensional growth, the two-dimensional growth and the three-dimensional growth. The integer, n, in Eq. 1 is equal to the number of growth dimension, m, for the isothermal crystallization from the preexisting nuclei without the concurrent random nucleation, while n is equal to $(m+1)$ for the isothermal crystallization with the concurrent random nucleation. The constant, Z, in Eq. 1 is equal to $gN\{v(T)\}^m$. We also get the next equation for the crystallization rate per unit reduced time,

$$\frac{\mathrm{d}C}{\mathrm{d}\theta} = mZ_0(1-C)\theta^{m-1}, \tag{15}$$

and the crystallization rate per unit real time is given below:

$$\frac{\mathrm{d}C}{\mathrm{d}t} = \frac{\mathrm{d}C}{\mathrm{d}\theta}\frac{\mathrm{d}\theta}{\mathrm{d}t} = mZ_1(1-C)\theta^{m-1}, \tag{16}$$

where Z_1 is $gNv_0^{m-1}v(T)$.

Equations for Linear Heating and Cooling

First, we will consider N for the second model. When the melt is cooled at a linear rate, ϕ_1, to the temperature

where the nucleation does not occur and heated again at a linear rate, ϕ_2, to the temperature at which the crystal growth begins, N is given according to Eq. 7 as follows:

$$N = \left\{\frac{1}{\phi_1}+\frac{1}{\phi_2}\right\}\int_{T_1}^{T_2} v(T)\mathrm{d}T, \tag{17}$$

where T_1 and T_2 are the minimum and maximum temperatures of the nucleation, and the integral in Eq. 17 is a constant. Expressing this constant to be N_0 we get

$$N = N_0\left\{\frac{1}{\phi_1}+\frac{1}{\phi_2}\right\}. \tag{18}$$

When the materials are, then, heated up at a linear heating rate, ϕ_3, in the temperature range of the crystal growth, R is given as follows:

$$R(T) = \frac{1}{\phi_3}\int_{T_3}^{T} v(T)\mathrm{d}T, \tag{19}$$

where T_3 is the minimum temperature for the crystal growth.

Combining these relations, we get the equation for the first model:

$$-\ln(1-C) = \frac{Z_0}{\phi_3{}^m}\{F(T)\}^m, \tag{20}$$

where

$$F(T) = \int_{T_3}^{T} f(T)\mathrm{d}T. \tag{21}$$

For the second model, we get

$$-\ln(1-C) = \frac{Z_0{}'}{\phi_3{}^m}\{F(T)\}^m\left\{\frac{1}{\phi_1}+\frac{1}{\phi_2}\right\}, \tag{22}$$

where Z_0' is $gN_0v_0{}^m$.

For the crstallization rate per unit real time, we get following two equations for the first and second models:

$$\frac{\mathrm{d}C}{\mathrm{d}t} = \frac{mZ_1}{\phi_3{}^{m-1}}(1-C)\{F(T)\}^{m-1}, \tag{23}$$

$$\frac{\mathrm{d}C}{\mathrm{d}t} = \frac{mZ_1{}'}{\phi_3{}^{m-1}}(1-C)\{F(T)\}^{m-1}\left\{\frac{1}{\phi_1}+\frac{1}{\phi_2}\right\}, \tag{24}$$

where Z_1' is $gN_0v_0{}^{m-1}v(T)$.

If the temperature dependence of the linear crystal growth rate follows Arrhenius law, namely

$$f(T) = \exp\left(-\frac{\Delta E}{\mathbf{R}T}\right), \tag{25}$$

where ΔE and $\mathbf{R}$ are the activation energy and the gas constant, respectively, we obtain the next equation for the reduced time:

$$\theta = \frac{\Delta E}{\phi_3\mathbf{R}}\mathrm{p}\left(\frac{\Delta E}{\mathbf{R}T}\right), \tag{26}$$

where p is the p function proposed by Doyle[10] and $v(T)$ is assumed to be negligibly small at T_3. The p function is given as follows:

$$\mathrm{p}(y) = \frac{\exp(-y)}{y} - \mathrm{Ei}(-y), \tag{27}$$

where Ei is the exponential integral function. Therefore,

$$E(T) = \frac{\Delta E}{\mathbf{R}}\mathrm{p}\left(\frac{\Delta E}{\mathbf{R}T}\right). \tag{28}$$

Thus, we get the fundamental equations for the first and second models:

$$-\ln(1-C) = \frac{Z_0\Delta E^m}{\phi_3{}^m\mathbf{R}^m}\left\{\mathrm{p}\left(\frac{\Delta E}{\mathbf{R}T}\right)\right\}^m, \tag{29}$$

$$-\ln(1-C) = \frac{Z_0{}'\Delta E^m}{\phi_3{}^m\mathbf{R}^m}\left\{\mathrm{p}\left(\frac{\Delta E}{\mathbf{R}T}\right)\right\}^m\left\{\frac{1}{\phi_1}+\frac{1}{\phi_2}\right\}, \tag{30}$$

and the crystallization rate is given as follows:

$$\frac{\mathrm{d}C}{\mathrm{d}t} = \frac{mZ_1\Delta E^{m-1}}{\phi_3{}^{m-1}\mathbf{R}^{m-1}}(1-C)\left\{\mathrm{p}\left(\frac{\Delta E}{\mathbf{R}T}\right)\right\}^{m-1}, \tag{31}$$

$$\frac{\mathrm{d}C}{\mathrm{d}t} = \frac{mZ_1{}'\Delta E^{m-1}}{\phi_3{}^{m-1}\mathbf{R}^{m-1}}(1-C)\left\{\mathrm{p}\left(\frac{\Delta E}{\mathbf{R}T}\right)\right\}^{m-1}\left\{\frac{1}{\phi_1}+\frac{1}{\phi_2}\right\}. \tag{32}$$

At the maximum rate of crystallization,

$$\frac{\mathrm{d}^2C}{\mathrm{d}t^2} = 0. \tag{33}$$

On the other hand, we have the next two relations;

$$\frac{\mathrm{d}C}{\mathrm{d}t} = \frac{\mathrm{d}C}{\mathrm{d}\theta}\frac{\mathrm{d}\theta}{\mathrm{d}t} = \exp\left(-\frac{\Delta E}{\mathbf{R}T}\right)\frac{\mathrm{d}C}{\mathrm{d}\theta}, \tag{34}$$

and

$$\frac{\mathrm{d}^2C}{\mathrm{d}t^2} = \exp\left(-\frac{2\Delta E}{\mathbf{R}T}\right)\frac{\mathrm{d}^2C}{\mathrm{d}\theta^2} + \frac{\phi_3\Delta E}{\mathbf{R}T^2}\exp\left(-\frac{\Delta E}{\mathbf{R}T}\right)\frac{\mathrm{d}C}{\mathrm{d}\theta}. \tag{35}$$

The above-mentioned p function can also be approximated as follows:

$$\mathrm{p}(y) \approx \frac{\exp(-y)}{y^2} \qquad (20\leqq y\leqq 50). \tag{36}$$

By applying this approximation and combining Eqs. 33 and 35, we get

$$\frac{\mathrm{d}C}{\mathrm{d}\theta} + \theta\frac{\mathrm{d}^2C}{\mathrm{d}\theta^2} = 0. \tag{37}$$

The same relation was also found previously for the usual chemical reactions.[8,9] By applying Eq. 5, the right hand side of Eq. 14 is found to be unity, so that the conversion at the maximum rate, C_m, is given as follows;

$$-\ln(1-C_m) = 1, \tag{38}$$

then

$$C_m = 1 - \frac{1}{\mathrm{e}}. \tag{39}$$

Namely, the conversion at the maximum rate is about 63.2%, which is equal to that for the first order reaction.[11]

For nonisothermal crystallization in cooling mode, we drive the same equations as Eqs. 14, 16, 20 and 23, in which the lower limits of the integrals of $R(T)$, $F(T)$ and θ are the melting temperature or its time.

Methods for Kinetic Analysis of Thermoanalytical Data

First of all, we should ascertain whether the process under measurement is the first model or the second one. It is useful for this purpose to observe the effect of the

thermal history in the nucleation temperature range, for instance by changing ϕ_1 and/or ϕ_2 in wide range. Then, the value of m can be determined by using Eqs. 20 and 22, namely for the first model,

$$\log(-\ln(1-C)) = \log[Z_0\{F(T)\}^m] - m\log\phi_3, \quad (40)$$

and for the second model cooled and heated at the same rate ($\phi_1=\phi_2=\phi_3$),

$$\log(-\ln(1-C)) = \log[2Z_0'\{F(T)\}^m] - (m+1)\log\phi_3. \quad (41)$$

When we observe the process at different rates of heating and cooling and plot $\log(-\ln(1-C))$ against $\log\phi_3$ at the same temperature, we get linear plots, and the slopes of the plots are equal to $-m$ or $-(m+1)$, because the first term in the right hand side of the above equations is constant at the same temperature. When we use the specimens of the second model obtained by quenching and observed the crystal growth at different heating rates ($\phi_1 \gg \phi_2=\phi_3$), the slopes of the plots are also equal to $-(m+1)$, because $1/\phi_1$ is negligibly small and

$$\log\{-\ln(1-C)\} = \log[Z_0\{F(T)\}^m] - (m+1)\log\phi_3. \quad (42)$$

From the intercept of these plots, we get the first terms in Eqs. 40, 41, and 42, and they are the temperature integral of Z or $gN_0\{v(T)\}^m$. These plots are essentially the same as those proposed for more general cases by the present author previously.[5] As pointed out previously, we can predict the crystallization behavior at linear rates by using the kinetic parameters thus obtained.

For the case that m equals to unity, *i.e.*, the one-dimensional growth, a simple relation can be applied to the data. From Eqs. 23 and 24, we get for the first model

$$\frac{dC}{dt} = Z(1-C), \quad (43)$$

where Z is $gNv(T)$.
and for the second model

$$\frac{dC}{dt} = Z'(1-C)\left\{\frac{1}{\phi_1}+\frac{1}{\phi_2}\right\}, \quad (44)$$

where Z' is $gN_0v(T)$. When both the conversion and the rate of conversion are obtained, we can directly estimate Z or Z' as a function of the temperature by using the above relation. The temperature dependence of the linear growth rate can also be obtained by comparing the rate of conversion observed at different heating rates at a given conversion, as is seen in Eqs. 23 and 24. However, the obtained values are somewhat complicated for the case that m is not equal to unity.

If the temperature dependence of the crystal growth rate follows the Arrhenius law, further kinetic analysis can be done by using the data obtained at different heating rates, because the p function can be approximated as follows, and this is much better approximation than Eq. 36;[10]

$$\log p(y) \approx 2.315 - 0.4567y \quad (20 \leqq y \leqq 60). \quad (45)$$

We get the next equations at a given conversion from Eqs. 29, 30, and 45; for the first model,

$$\log\phi_3 + 0.4567\frac{\Delta E}{RT} = \text{constant}, \quad (46)$$

and for the second model ($\phi_1=\phi_2=\phi_3$, or common ϕ_1 but different $\phi_2=\phi_3$),

$$\log\phi_3 + 0.4567\frac{m\Delta E}{(m+1)RT} = \text{constant}. \quad (47)$$

Thus, when we plot the logarithm of the heating rate against the reciprocal absolute temperature at a given conversion, we obtain linear plots and we can estimate the activation energy from the slope as is described in Eqs. 46 and 47. This relation is also applicable to the maximum rates, such as the peaks in DSC curves, because the conversions at the maximum rates are equal to each other, as is shown in Eq. 39. The above procedure to estimate the activation energy is similar to, but somewhat different in its coefficient from, so-called "modified Ozawa plot" proposed by Matusita and Sakka,[7] and it is essentially the same as the procedure for usual chemical reactions.[8]

By applying rougher approximation, *i.e.*, Eq. 36, we get the next equations at a given conversion and also at the maximum rate; for the first model

$$\frac{\Delta E^m}{\phi_3{}^m R^m}\left\{\exp\left(-\frac{\Delta E}{RT}\right)\Big/\frac{\Delta E^2}{R^2T^2}\right\}^m = \text{constant}, \quad (48)$$

and for the second model

$$\frac{\Delta E^m}{\phi_3{}^{m+1}R^m}\left\{\exp\left(-\frac{\Delta E}{RT}\right)\Big/\frac{\Delta E^2}{R^2T^2}\right\}^m = \text{constant}. \quad (49)$$

Therefore, for the first model

$$\ln\frac{\phi_2}{T^2} + \frac{\Delta E}{RT} = \text{constant}, \quad (50)$$

and for the second model

$$\ln\frac{\phi_3{}^{m+1}}{T^{2m}} + \frac{\Delta E}{RT} = \text{constant}. \quad (51)$$

The activation energy can also be estimated by the similar plots of $\ln\phi_3/T^2$ or $\ln\phi_3{}^{m+1}/T^{2m}$ against the reciprocal absolute temperature. Kissinger plot mentioned in the introduction is the same plot as Eq. 50 applied to the maximum rate, but modification such as shown in Eq. 51 should be made. Moreover, these plots are applicable to a given conversion. Matusita and Sakka[7] derived an equation similar to, but different in its exponent from, Eq. 51. These plots are not preferable to the plots by Eqs. 46 and 47, because they are based on the rough approximation of Eq. 36 and the terms are complicated, so that much error may be involved in actual applications. Recently, it was pointed out from experimental evaluation for usual chemical reactions that Kissinger plot has no practical advantages over Ozawa plot and that the conversion at the peak of heat-flux DSC curve is not practically a constant due to instrumental effect and heat transfer within the sample, while uniform temperature within the sample is implicitly assumed in all theoretical considerations.[12]

When the linear plots obtained at different conversions are not parallel to each other and the activation energies estimated vary along the conversion, the observed process is inconsistent with

the model from which the theory and the method are derived, and we should abandon the kinetic analysis. When we get the constant activation energy, we can calculate the reduced time at different conversions by using the activation energy and Eq. 26, so that we can draw the curve of the conversion versus the reduced time, which is the experimental master curve. Because the reduced time is proportional to the real time in isothermal cases and also equal to the real time at infinite temperature, the methods for analyzing isothermal data can be applied to this experimental master curve. For example, when we plot $\log(-\ln(1-C))$ against $\log\theta$, we get a linear line with the slope of m and, when we plot $-\ln(1-C)$ against θ^m, we get also a linear line. In both plots for the second model, both ϕ_1 and ϕ_2 should be constant and common, otherwise they should be reduced taking into account of their effect in Eqs. 14 and 30.

The linearity of these master lines can be used to ascertain the consistency between the observed process and the model on which the theory and the method are based. We can also calculate the reduced time for various temperature changes by using the activation energy, and, thus, we can predict the crystallization behavior for the various types of temperature changes.

Concluding Remarks

The nonisothermal kinetic models in this paper are those of the special cases dealt with in the previous paper.[5] However, because the random nucleation does not occur concurrently with the crystal growth in the present cases, the more generally applicable equations are derived here than in the previous paper. The relations described previously for the general model[5] are limited for the case of the linear cooling and heating. On the other hand, the relations applicable to various types of temperature changes are presented in the present paper.

The concept of the reduced time can be introduced in the more complicated process than the usual chemical reactions[8] and diffusions,[9] and it is also clearly shown that the concept of the reduced time is very useful and effective in nonisothermal kinetics. As is seen in Eqs. 14 and 15, the real time, t, in the isothermal kinetic equations can be replaced by the generalized time, *i.e.*, the reduced time, and this generalized nonisothermal kinetic equations are applicable both to nonisothermal cases and to isothermal cases, where θ is equal to $tf(T)$ and Z is replaced by Z_0.

The conversion at the maximum rate for the linearly heated process in which Arrhenius law holds is revealed to be constant even in the complicated processes such as the crystal growth, and it is interesting to note that this constancy is also found in the usual chemical reactions and diffusion in which Arrhenius law holds,[11] so that it seems to be generally true that the conversion at the maximum rate for the linear heating is constant for the process in which only a single unit process proceeds and Arrhenius law holds for the rate constant.

References

1) M. J. Avrami, *J. Chem. Phys.*, **7**, 1103 (1939); **8**, 212 (1940); **9**, 177 (1941).
2) F. von Goler and G. Z. Sachs, *Z. Phys.*, **77**, 281 (1932).
3) W. A. Johnson and R. F. Mehl, *Tras. Am. Inst. Min. Metall. Eng.*, **135**, 416 (1939).
4) U. R. Evans, *Trans. Faraday Soc.*, **41**, 365 (1945).
5) T. Ozawa, *Polymer*, **12**, 150 (1971).
6) H. E. Kissinger, *Anal. Chem.*, **29**, 1702 (1957); *J. Res. Natl. Bur. Std.*, **57**, 217 (1956).
7) K. Matusita and S. Sakka, *Phys. Chem. Glasses*, **20**, 81 (1979); *Bull. Inst. Chem. Res., Kyoto Univ.*, **59**, 159 (1981).
8) T. Ozawa, *Bull. Chem. Soc. Jpn.*, **38**, 1881 (1965); *J. Therm. Anal.*, **2**, 301 (1970).
9) T. Ozawa, *J. Therm. Anal.*, **5**, 563 (1973).
10) C. D. Doyle, *Nature*, **207**, 290 (1965).
11) T. Ozawa, *J. Therm. Anal.*, **6**, 401 (1974).
12) A. A. van Dooren and B. W. Muller, *Thermochim. Acta*, **65**, 257 (1983).

The Structure of Liquid Alcohols by Neutron Diffraction. I. Molecular Structure of Methyl Alcohol

Yukio TANAKA,† Norio OHTOMO,† and Kiyoshi ARAKAWA*
Research Institute of Applied Electricity, Hokkaido University, Sapporo 060
†Faculty of Engineering, Hokkaido University, Sapporo 060
(Received June 25, 1983)

The structure factor $S_m(Q)$ for liquid methyl alcohol (CD_3OD) at room temperature was obtained by means of the LINAC-TOF neutron diffraction method. An analysis of the diffraction data was carried out, and the molecular structure of CD_3OD in liquid phase was determined as: the O-D, C-O, and C-D bond lengths are 0.990±0.010, 1.435±0.005, and 1.085±0.005 Å, respectively. The O-D and C-D lengths were found to be longer than those values determined in gaseous phase.

The usefulness of the LINAC-TOF neutron diffraction method for the structure analysis of liquid systems has recently become progressively evident. Its merit in comparison with usual X-ray analysis is especially clear for the structure analysis of liquids composed of molecules including hydrogen atoms. In the preceding papers,[1,2] the structure of liquid water (D_2O) was determined to contain hydrogen-bonded tetrahedral pentamers as a main constituent. Here we extend our study of liquid structures to the next example of hydrogen-bonded liquids, *i.e.*, liquid methyl alcohol. Then, the present study aims first to determine the structure of methyl alcohol molecules in liquid phase.

By using microwave[3-5] and electron diffraction techniques,[6] several authors have performed studies of gaseous methyl alcohol and its molecular geometry in gaseous phase has been elucidated. However, studies of the molecular structure in its liquid phase are very few. From a great deal of spectroscopic data, the hydroxyl groups in liquid methyl alcohol are known to be concerned with hydrogen bonding.[7,8] The molecules are supposed to make up an aggregate by hydrogen bonding in the liquid. It is expected, for example, that, as well as in the case of water, the O–H bond length of methyl alcohol molecules is strongly influenced by the existence of hydrogen bonding in the liquid phase. Thus, the determination of the molecular geometry of liquid methyl alcohol is required as the starting point of a detailed investigation of its properties, and also the variation in the molecular structure from gaseous to liquid phases is very interesting.

Recently, Montague *et al.*[9] performed a neutron diffraction study of liquid CD_3OD by means of the reactor conventional method. However, as described in later sections, their results are considered to contain important implausible aspects, showing the restriction in the conventional method. Then, we have carried out a LINAC-TOF neutron diffraction measurement on methyl alcohol and have made an analysis of the data to determine its molecular structure.

Experimental

The experiment was performed by means of the TOF neutron diffraction method, using pulsed neutrons produced by electron LINAC at Hokkaido University. As the sample, deuterated methyl alcohol CD_3OD (purity of deuteration 99.5%, Commisariat à l'Energie Atomique (CEA), France) was used. Measurements were carried out at room temperature at five different scattering angles: 2θ=32.0°, 42.0°, 66.5°, and 90.5° at 10.0±0.5 °C, and, 2θ=140.7° at 16.5±0.5°C.

Corrections for background, absorption, multiple scattering, inelastic scattering, and incoherent scattering were performed in the usual manner.[2,10,11] Absolute normalization of data was carried out by using the scattering data from a polycrystalline vanadium rod as an isotropic and incoherent scatterer. The structure factors $S_m(Q)$ thus determined after all corrections and calibrations of Q-scale are shown in Fig. 1 for five scattering angles. The coincidence of the values from different angles in each overlapping region of Q is quite well as seen in Fig. 1, and, combining these data sets, we obtained the final $S_m(Q)$ values of wide Q range as given in Table 1. The statistical error for values of the $S_m(Q)$ is smaller than 1.0%, and the resolving power $\Delta Q/Q$ less than a few % in the whole range of Q.[11]

Procedures of Analysis

The structure factor $S_m(Q)$ for molecular liquids consists of an intramolecular structure factor $f_1(Q)$ and

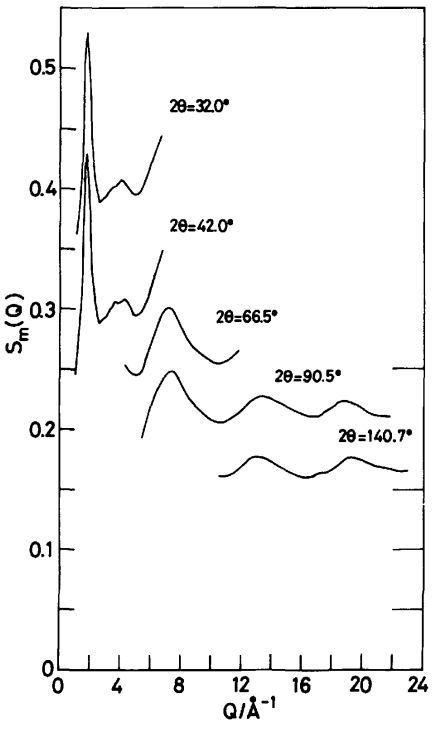

Fig. 1. Observed neutron structure factors $S_m(Q)$ for deuterated methyl alcohol at various scattering angles.

Table 1. The observed absolute neutron scattering factor $S_m(Q)$ as a function of scattering vector Q/Å^{-1} for deuterated methyl alcohol

Q/Å^{-1}	$S_m(Q)$	Q/Å^{-1}	$S_m(Q)$	Q/Å^{-1}	$S_m(Q)$	Q/Å^{-1}	$S_m(Q)$
1.00	0.113	4.90	0.144	10.00	0.156	15.10	0.166
1.05	0.113	5.00	0.145	10.10	0.155	15.20	0.166
1.10	0.114	5.10	0.145	10.20	0.155	15.30	0.165
1.15	0.116	5.20	0.146	10.30	0.154	15.40	0.164
1.20	0.126	5.30	0.147	10.40	0.154	15.50	0.164
1.25	0.132	5.40	0.149	10.50	0.154	15.60	0.163
1.30	0.144	5.50	0.151	10.60	0.154	15.70	0.163
1.35	0.155	5.60	0.152	10.70	0.154	15.80	0.162
1.40	0.170	5.70	0.155	10.80	0.155	15.90	0.161
1.45	0.189	5.80	0.159	10.90	0.155	16.00	0.161
1.50	0.210	5.90	0.163	11.00	0.156	16.10	0.161
1.55	0.224	6.00	0.167	11.10	0.157	16.20	0.161
1.60	0.244	6.10	0.171	11.20	0.157	16.30	0.161
1.65	0.262	6.20	0.176	11.30	0.158	16.40	0.161
1.70	0.271	6.30	0.181	11.40	0.158	16.50	0.160
1.75	0.274	6.40	0.186	11.50	0.159	16.60	0.160
1.80	0.271	6.50	0.189	11.60	0.160	16.70	0.160
1.85	0.259	6.60	0.192	11.70	0.161	16.80	0.159
1.90	0.245	6.70	0.195	11.80	0.162	16.90	0.159
1.95	0.230	6.80	0.196	11.90	0.163	17.00	0.158
2.00	0.213	6.90	0.197	12.00	0.164	17.10	0.159
2.05	0.199	7.00	0.199	12.10	0.166	17.20	0.160
2.10	0.186	7.10	0.199	12.20	0.167	17.30	0.161
2.15	0.169	7.20	0.199	12.30	0.168	17.40	0.162
2.20	0.159	7.30	0.198	12.40	0.170	17.50	0.163
2.30	0.147	7.40	0.196	12.50	0.171	17.60	0.164
2.40	0.141	7.50	0.195	12.60	0.172	17.70	0.164
2.50	0.140	7.60	0.193	12.70	0.173	17.80	0.164
2.60	0.138	7.70	0.191	12.80	0.174	17.90	0.165
2.70	0.139	7.80	0.189	12.90	0.174	18.00	0.166
2.80	0.141	7.90	0.186	13.00	0.175	18.10	0.167
2.90	0.142	8.00	0.183	13.10	0.175	18.20	0.168
3.00	0.142	8.10	0.181	13.20	0.176	18.30	0.169
3.10	0.144	8.20	0.178	13.30	0.176	18.40	0.169
3.20	0.146	8.30	0.176	13.40	0.176	18.50	0.171
3.30	0.149	8.40	0.174	13.50	0.176	18.60	0.172
3.40	0.151	8.50	0.172	13.60	0.175	18.70	0.174
3.50	0.154	8.60	0.170	13.70	0.175	18.80	0.175
3.60	0.154	8.70	0.168	13.80	0.175	18.90	0.175
3.70	0.154	8.80	0.167	13.90	0.174	19.00	0.175
3.80	0.153	8.90	0.166	14.00	0.174	19.10	0.176
3.90	0.154	9.00	0.165	14.10	0.173	19.20	0.175
4.00	0.155	9.10	0.164	14.20	0.173	19.30	0.174
4.10	0.157	9.20	0.163	14.30	0.172	19.40	0.174
4.20	0.157	9.30	0.162	14.40	0.172	19.50	0.173
4.30	0.156	9.40	0.161	14.50	0.170	19.60	0.172
4.40	0.154	9.50	0.160	14.60	0.169	19.70	0.171
4.50	0.152	9.60	0.159	14.70	0.168	19.80	0.170
4.60	0.150	9.70	0.158	14.80	0.168	19.90	0.169
4.70	0.147	9.80	0.158	14.90	0.167	20.00	0.168
4.80	0.146	9.90	0.157	15.00	0.167		

intermolecular one. The $S_m(Q)$ for a higher Q region is characteristic of the intramolecular structure ($S_m(Q) \rightarrow f_1(Q)$ for high Q). The $f_1(Q)$ is written as

$$f_1(Q) = (\sum_i b_i)^{-2} \sum_{ij} b_i b_j j_0(Q r_{ij}) \exp(-\gamma_{ij} Q^2), \quad (1)$$

where b_i is the coherent scattering length of i-th nucleus in the molecule, r_{ij} the distance between i-th and j-th nucleus, $2\gamma_{ij}$ the mean square variation to the distance r_{ij} and $j_0(x)=\sin x/x$ a zeroth order spherical Bessel function. $\sum$ is over all the nuclei in the molecule. With respect to γ_{ij}, we assume that $\gamma_{ij}=1/2D_{ij}^2 r_{ij}$, where D_{ij} is estimated to be 0.06 Å$^{1/2}$ per Å for all distances in the same molecule.[1,2,6,12]

In the observed $S_m(Q)$ curves marked features are found as follows: the height of the first peak at *ca.* Q=1.8 Å^{-1}, a doublet of the hump at *ca.* 4 Å^{-1}, a shape of the second peak at *ca.* 7 Å^{-1}, and the peaks at *ca.* 13 and 19 Å^{-1}. With reference to the higher Q region ($Q \gtrsim 6$ Å^{-1} in the present study), being compared with the case of water,[1,2] the intensity of the second peak ($Q \simeq 7$ Å^{-1}) and the bent of the curve at *ca.* Q=8 Å^{-1} are distinctive. Then, for determining the intramolecular structure, reproduction of those features of $Q \gtrsim 6$ Å^{-1} is required in our calculation of $f_1(Q)$.

The structure of methyl alcohol molecule CD_3OD is shown schematically in Fig. 2. With respect to the intramolecular parameters, it is assumed that deute-

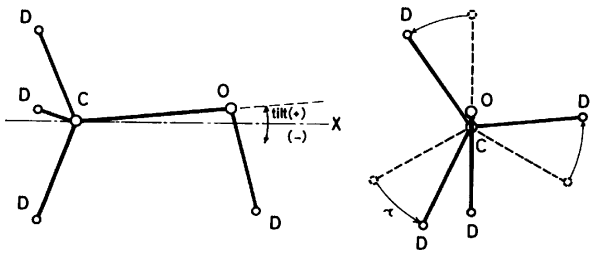

Fig. 2. The structure of deuterated methyl alcohol (CD_3OD) molecule.

Table 2. Range of parameters

Parameter	Range	Interval of variation
r_{CO}/Å	1.420—1.450	0.005
r_{OD}/Å	0.950—1.010	0.005
r_{CD}/Å	1.070—1.100	0.005
DCD/°	105.0—115.0	1.0
COD/°	100.0—125.0	1.0
tilt/°	0.0—3.27	3.27
τ/°	0.0—60.0	2.0

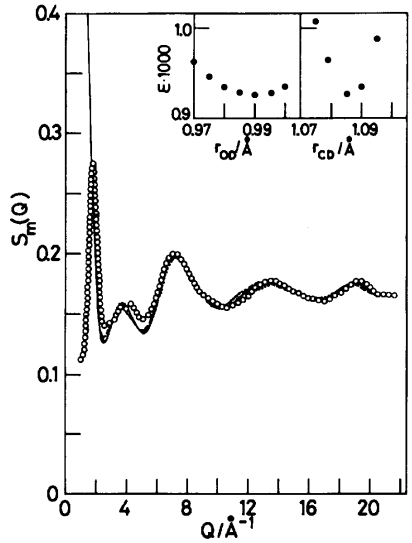

Fig. 3. Observed neutron structure factor $S_m(Q)$ for deuterated methyl alcohol and calculated $f_1(Q)$ curves. ○: Observed $S_m(Q)$, ——: calculated $f_1(Q)$ for the model with fixed methyl group (All parameters used are given in the upper row in Table 3.), (ε=0.9282×10^{-3}), – – –: calculated $f_1(Q)$ curves for the model with freely rotating methyl group (All parameters used are given in the lower row in Table 3.), (ε=0.9880×10^{-3}), ……: calculated $f_1(Q)$ curves for the Lees and Baker model[3] (ε=1.3213×10^{-3}). ε is a measure for indicating the deviations of $f_1(Q)$ from the experimental data, and is expressed as

$$\varepsilon = (\sum_i^N \{S_m(Q)_{obsd} - f_1(Q)_{calcd}\}^2)^{1/2} / \sum_i^N S_m(Q)_{obsd},$$

where N is the number of data points in the fitting range of Q, 6—18 Å^{-1}. Variation of ε with distances r_{OD} and r_{CD} is shown in the insets.

rium atoms in the methyl group rotate about the methyl axis (defined as C-X axis in Fig. 2), and that the three C-D bonds in the methyl group are equivalent as well as the three DCD angles. Then, we characterize the molecular structure by seven structural parameters, *i.e.* the bond lengths r_{OD}, r_{CO}, r_{CD}, the DCD angle in the methyl group, the hydroxyl angle COD, the tilt angle and the methyl rotation angle τ (Fig. 2). In order to determine the molecular parameters, $f_1(Q)$ were calculated for more than 12000 models by using Eq. 1 and the curves obtained were compared with the observed $S_m(Q)$ data in the higher Q region ($Q \gtrsim 6$ Å^{-1}). The magnitudes of the parameters were varied in reference to the values given in Table 2.

Results and Discussion

Determination of Intramolecular Parameters for Liquid Methyl Alcohol. By making the calculated $f_1(Q)$ curves fit with the observed $S_m(Q)$ data, we have determined the best structural model for liquid methyl alcohol as follows: $r_{OD}=0.990\pm0.010$ Å, $r_{CO}=1.435\pm0.005$ Å, $r_{CD}=1.085\pm0.005$ Å, DCD=109.5±0.5°, COD=112.0±3.0° and tilt=0.0±3.0°.

Concerning the best structural model, slight arbitrariness still remains in its detailed structure. The methyl rotation angle τ was not decided uniquely in the present study, and the following two models remains undiscriminated as the best ones (Fig. 3): the one is that with $\tau=15.0\pm3.0°$ and the other that with free rotation of methyl group (Table 3). Taking account of the symmetry of the arrangement of deuterium atoms in the methyl group, the two models are regarded as effectively identical with each other. As seen in Table 3, the molecular parameters of the two best models are essentially in good agreement on the whole, though slight discrepancy is observed for the COD angle (and, of course, for the methyl rotation angle τ). The best fit $f_1(Q)$ curves with the experimental data are shown in Fig. 3, including the curve calculated by using Lees and Baker's parameters for gaseous molecules[3] for comparison. Variations of ε with the C-D and O-D bond lengths for the model of fixed methyl group ($\tau=15.0°$) are also shown in Fig. 3.

The best structural parameters determined are tabulated in Table 4, together with those by Montague *et al.*[9] and by Magini *et al.*,[12] where the values also determined in gaseous and crystalline states are shown.

Variation of the Structure of Molecules in Liquid State from that in Gaseous State. The $f_1(Q)$ curve calculated by using the molecular parameters given by Lees and Baker[3] (microwave spectroscopy) is shown in

Table 3. Molecular parameters determined by neutron diffraction method

r_{CO}/Å	r_{OD}/Å	r_{CD}/Å	DCD/°	COD/°	tilt/°	τ/°	$\varepsilon\times10^3$
1.435	0.990	1.085	109.5	109.5	0	15.0	0.9282
1.440	0.985	1.090	109.5	115.0	0	free	0.9880

With respect to ε, see Fig. 3.

Table 4. Comparison of intramolecular parameters obtained for methyl alcohol molecule in the present study with those obtained by other workers

	r_{CO}/Å	r_{OD}/Å	r_{CD}/Å	COD/°	DCD/°	tilt/°	τ/°
Liquid							
Present	1.435±0.005	0.990±0.010	1.085±0.005	112.0±3.0°	109.5±0.5°	0±3.0°	15.0±3.0°, free
Montague *et al.*[a]							
$\lambda=0.5$ Å	1.411±0.009	1.030±0.011	1.070±0.004	99.7±2.2°	(108°38′)	(3°16′)	—
$\lambda=0.7$ Å	1.424±0.004	1.027±0.008	1.062±0.002	103.4±1.2°	(108°38′)	(3°16′)	—
Magini *et al.*[b]	1.437						
Gas							
Lees and Baker[c]	1.4246 ±0.0024	0.9451 ±0.0034	1.0936 ±0.0032	108°32′ ±29′	108°38′ ±42′	3°16′ ±11′	— —
Kimura and Kubo[d]	1.428±0.003	0.960±0.05	1.095±0.010	109°±3°	(109°28′)	—	—
Nishikawa[e]	1.427	0.953	1.096	108°24′	109°04′	3°18′	—
Venkateswarlu and Gordy[f]	1.427±0.007	0.956±0.015	1.096±0.01	108°52′±2°	109°02′±45′	3°20′	—
Crystal							
Tauer and Lipscomb[g]	1.42 at −110 °C 1.44 at −160 °C						

a) Neutron diffraction at reactor, Ref. 9. b) X-Ray diffraction, Ref. 12. c) Microwave, Ref. 3. d) Electron diffraction, Ref. 6. e) Microwave, Ref. 4. f) Microwave, Ref. 5. g) X-Ray diffraction, K. J. Tauer and W. N. Lipscomb, *Acta Crystallogr.*, **5**, 606 (1952). The values in parentheses were assumed.

Fig. 3, together with the present $S_m(Q)$ data in liquid phase. In the range of $Q \gtrsim 6$ Å^{-1}, a significant disagreement is seen between the present $S_m(Q)$ curve and Lees and Baker's one. This is ascribed to the variation of the intramolecular structure of molecules within liquids in comparison with that in gaseous state, as seen in Table 4.

The most remarkable change of intramolecular parameters from liquid to gaseous state is that in the O–D distance. As seen in Table 4, the O–D distance determined in the present study is 0.990±0.010 Å, and a stretching of the bond length compared with that in gaseous phase, 0.945—0.960 Å,[3-6] is obvious. The magnitude of this stretch is found to be similar to the case in water: from 0.96 Å in gaseous state to 0.98 Å in liquid state.[1,2] With respect to the nearest intermolecular O···O distance, Magini *et al.*[12] reported recently the value of about 2.8 Å from the result by their X-ray diffraction experiment on liquid methyl alcohol. The value is nearly identical with the nearest O···O distance in liquid water.[1,2] These all results support an idea that, concerning the distances, r_{OD} and $r_{O\cdots O}$, the situations in hydrogen bonded state are quite similar between the two liquids, methyl alcohol and water.

With respect to other molecular parameters (C–O distance, C–D distance, DCD angle and tilt angle), the following features are pointed out. The present value of C–O distance is 1.435±0.005 Å. This is in good agreement with the value given by Magini *et al.* (1.437 Å) in liquid phase,[12] and is longer than that in gaseous systems, 1.425—1.428 Å.[3-6] Concerning the methyl group, a slight shortening of the C–D distance and a slight increase of the DCD angles are observed in comparison with those in gaseous state. As described in the preceding item, it is found that the tilt angle becomes zero in liquid state. On the other hand, the angle is observed to be 3°09′—3°30′ in gaseous phase.[3-5]

In a recent neutron diffraction study on liquid CD_3OD by means of the reactor conventional method, Montague *et al.*[9] have reported a result on the structure analysis of the liquid, and the molecular parameters determined are listed up together in Table 4 for comparison. Noticeable discrepancies between the present results and theirs are found, especially with respect to the O–D distance. The O–D distance assigned by Montague *et al.*, 1.03 Å, is fairly longer than that for heavy water, 0.98 Å, and still longer than that in heavy ice-I (1.01 Å).[13] This is clearly unreasonable.

Concluding Remarks

A neutron diffraction study of liquid methyl alcohol (CD_3OD) by means of the LINAC-TOF method was performed, and the geometry of molecules within the liquids was determined. The present study has made it clear that the LINAC-TOF neutron diffraction method is useful in determining the molecular structure in liquid state. And then, due to a series of recent successful results on D_2O,[1,2] CD_3COCl,[10] and CD_3OD *etc.* by our group, the present LINAC-TOF neutron diffraction method may be said to have been established as a means for the structure analysis of molecular fluids.

References

1) N. Ohtomo, K. Tokiwano, and K. Arakawa, *Bull. Chem. Soc. Jpn.*, **54**, 1802 (1981).
2) N. Ohtomo, K. Tokiwano, and K. Arakawa, *Bull. Chem. Soc. Jpn.*, **55**, 2788 (1982).
3) R. M. Lees and J. G. Baker, *J. Chem. Phys.*, **48**, 5299 (1968).
4) T. Nishikawa, *J. Phys. Soc. Jpn.*, **11**, 781 (1956).
5) P. Venkateswarlu and W. Gordy, *J. Chem. Phys.*, **23**, 1200 (1955).
6) K. Kimura and M. Kubo, *J. Chem. Phys.*,**30**, 151 (1959).
7) W. A. P. Luck, *Discuss. Faraday Soc.*, **43**, 115 (1967).
8) W. A. P. Luck, "Water," ed by F. Franks, Plenum, New York (1973) Vol. 2, Chap. 4.
9) D. G. Montague, I. P. Gibson, and J. C. Dore, *Mol. Phys.*, **44**, 1355 (1981).
10) N. Ohtomo and K. Arakawa, *Bull. Chem. Soc. Jpn.*, **53**, 1510 (1980).
11) N. Ohtomo, Y. Tanaka, and K. Arakawa, *Bull. Faculty Eng. Hokkaido Univ.*, **109**, 43 (1982).
12) M. Magini, G. Paschina, and G. Piccaluga, *J. Chem. Phys.*, **77**, 2051 (1982).
13) E. Whalley, *Mol. Phys.*, **28**, 1105 (1974).

Effect of Temperature on the Polarographic Catalytic Current Produced by Proteins in the Presence of Cobalt Salts

Kenji KANO,† Ichiro TOKIMITSU,†† Tokuji IKEDA, and Mitsugi SENDA*
Department of Agricultural Chemistry, Faculty of Agriculture, Kyoto University, Sakyo-ku, Kyoto 606
(Received July 5, 1983)

The effect of temperature on the polarographic catalytic hydrogen evolution current (Brdička current) produced by ribonuclease-A in an ammoniacal buffer containing cobalt salt has been studied using the theoretical equation of Brdička current. With increasing temperature, the Brdička current at −1.3 V increased between 10 and 30 °C then fell off above 30 °C, whereas the currents at −1.4 and −1.5 V decreased continuously. Analysis showed that the initial increase of the Brdička current at −1.3 V was only apparent and that the Brdička current constant, k_B, which represents the catalytic activity of the protein, always decreased with increasing temperature in the potential range of −1.3 to −1.5 V. Further analysis has revealed that the intrinsic catalytic activity of the protein–cobalt(0) complex, which is transiently formed on the electrode surface and which catalyzes the hydrogen evolution, increases with increasing temperature whereas the life time of the complex decreases and the latter decrease cancels the former increase, resulting in the decrease of the k_B value with increasing temperature.

The Brdička current, or polarographic catalytic hydrogen evolution current produced by proteins containing so-called Brdička-active groups, such as SH- and/or SS-groups[1] and others,[2,3] in the presence of cobalt salt, has found a variety of applications in structure analysis as well as trace analysis of proteins (see Ref. 4—6 for review). The effect of temperature on the Brdička current has been studied by many investigators,[5—11] but these studies have remained qualitative or at most semiquantitative. This is probably due to the lack of a suitable theoretical equation to predict the Brdička current in a quantitative way. In previous papers,[6,12] we have presented a theoretical equation for the Brdička current, in which it is expressed as a function of the surface concentration of protein, the bulk concentration of cobalt ion and two parameters representing the properties of the protein–cobalt(0) complex which catalyzes the hydrogen evolution. In this study, the effect of temperature on the Brdička current has been analyzed by the theoretical equation presented in the previous papers.

Experimental

Bovine pancreas ribonuclease-A (Type-A, Sigma Chemical Co., lot No. 58C-0116) was obtained commercially and used as received. All other chemicals were of reagent grade quality. The apparatus for the electrochemical measurements has been described in a previous paper.[12] Potentials were measured against a saturated calomel electrode (SCE). All measurements were made in a thermostat which was controlled within ±0.5 °C.

Results and Discussion

Figure 1 shows d.c. polarograms of ribonuclease-A (RNase) at 10, 25, and 40 °C in a base solution (0.1 mol dm^{-3} ammonia, 0.1 mol dm^{-3} ammonium chloride, and 0.1 mol dm^{-3} potassium chloride, pH 9.5 at 25 °C) containing 2×10^{-4} mol dm^{-3} hexaamine cobalt(III) chloride, Co(III). The Brdička current of RNase showed a typtical double-step wave with two maxima. With increasing temperature, the height of the first wave at −1.35 V (so-called Brdička first wave) increased, whereas that of the second wave at −1.55 V (so-called Brdička second wave) decreased, and the second maximum disappeared at increased temperature. The reduction waves of cobalt(II) to cobalt(0) shifted to less negative potential with increasing temperature both in the presence and in the absence of RNase. The limiting diffusion current of cobalt ion also increased with increasing temperature.

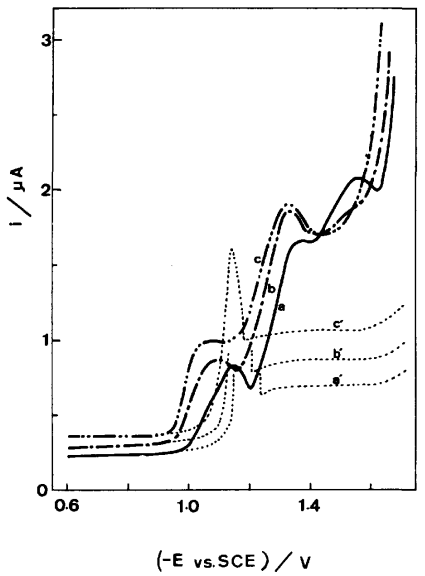

Fig. 1. D.c. polarograms of 4 μg cm^{-3} RNase at a) 10, b) 25, and c) 40 °C in the base solution containing 2×10^{-4} mol dm^{-3} Co(III). The broken lines represent d.c. polarograms in the absence of RNase at a') 10, b') 25, and c') 40 °C.

Many previous authors[7—11] have measured the maximum heights of the first and second waves of Brdička current to study the effect of temperature on the Brdička current. However, as the temperature and other experimental conditions change, the maxima are not always

† Present address: Gifu College of Pharmacy, Mitahora-higashi 5-6-1, Gifu 502.

†† Present address: Tokyo Research Laboratories, Kao Soap Co., Ltd., Bunka 2-1-3, Sumida-ku, Tokyo 131.

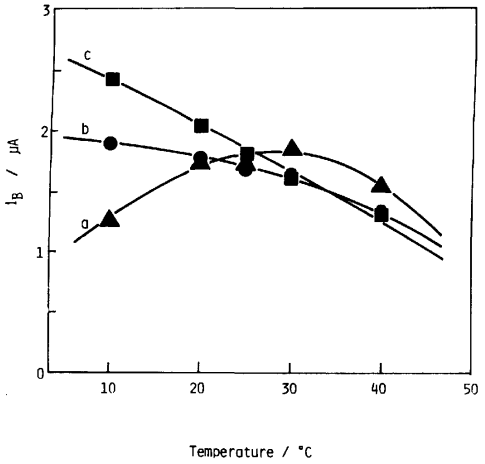

Fig. 2. Temperature dependence of the Brdička currents of 4 μg cm^{-3} RNase at a) −1.3, b) −1.4, and c) −1.5 V in the base solution containing 2×10^{-4} mol dm^{-3} Co(III).

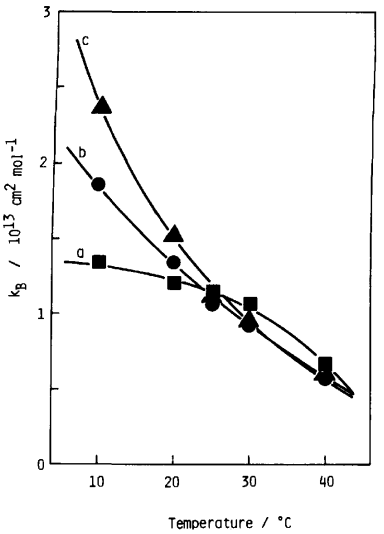

Fig. 3. Temperature dependence of the k_B values of RNase at a) −1.3, b) −1.4, and c) −1.5 V in the base solution.

well-defined and the potential of the maxima also shifts as shown in Fig. 1. Accordingly we have measured the heights of the Brdička current at three fixed potentials, *i.e.* −1.3, −1.4, and −1.5 V, as a function of temperature. In measuring the current with a dropping mercury elecrode (DME), the current intensity at the maximum growth of each mercury drop was taken and the net Brdička current, i_B, was obtained by correcting for the diffusion current of cobalt ion, i_{Co}. Figure 2 shows i_B at −1.3, −1.4, and −1.5 V plotted against temperature. With increasing temperature, i_B at −1.3 V increased initially from 10 °C to 30 °C, then decreased, whereas at −1.4 and −1.5 V, i_B decreased continuously.

It has been shown[6,12] that the Brdička current observed in the presence of Co(III) at low concentration, usually less than 2×10^{-4} mol dm^{-3}, can be expressed by

$$i_B = FAk_B\Gamma f_{Co}, \quad (1)$$

where F is Faraday, A the surface area of mercury electrode, k_B the Brdička current constant representing the catalytic activity of the protein, Γ the surface concentration of the protein adsorbed on the electrode surface, and f_{Co} the flux of cobalt ion at the electrode surface. In Eq. 1, f_{Co} and Γ as well as k_B depend on temperature. f_{Co} at a given temperature can be estimated from i_{Co} (broken lines in Fig. 1) according to the Ilkovič equation; $f_{Co}=i_{Co}/nFA=(7D_{Co}/3\pi t)^{1/2}C_{Co}$ at DME, where n is the number of electrons involved (here $n=3$), D_{Co} the diffusion coefficient of the cobalt ion, C_{Co} the bulk concentration of the cobalt ion and t the drop time. It has been shown[6,12] that Γ is given by the Koryta equation,[13] $\Gamma=(12D_pt/7\pi)^{1/2}C_p$ at DME in good approximation, for the Brdička current of RNase at the potential $E\geqq-1.5$ V and $C_p\leqq4$ μg ml^{-1} under the usual DME conditions, where D_p and C_p are the diffusion coefficient and the bulk concentration of the protein, respectively. The values of D_p at different temperatures were estimated by $D_p=(\text{const.})T/\eta$,[14] where $D_p=13.1\times10^{-7}$ cm^2 s^{-1} at 20 °C,[15] T; the absolute temperature, and η; the viscosity of water at each temperature,[16] respectively. Thus f_{Co} and Γ for a given temperature were calculated and k_B's at three different potentials were determined by Eq. 1. The results are plotted against temperature in Fig. 3. Note that k_B decreased continuously with increasing temperature at all potentials.

The negative temperature coefficient of the Brdička current has been pointed out by many previous authors,[7-11] who have interpreted this phenomenon by the decreased adsorption of protein on the electrode surface at increased temperature. The present result clearly indicates that the negative temperature coefficient of the Brdička current is due to the negative temperature coefficient of k_B, and is not attributable to the decreased adsorption of protein. Also it is clear that the initial increase of i_B at −1.3 V (the Brdička first wave, curve a in Fig. 2) is due to the increase in Γ and f_{Co}, and does not indicate any increase in the catalytic activity itself of the protein with increasing temperature, as Březina and Gultajaj[7] have suggested.

The mechanism of the Brdička current is not yet fully understood, but it is now generally accepted[5,6,17] that zero-valent cobalt, Co(0), which is liganded to a Brdička active group of protein to form a protein-Co(0) complex on the electrode surface, may catalyze the hydrogen evolution before the complex is decomposed into Co(0)-amalgam. The proposed mechanism has led to a theoretical equation for the Brdička current,[6,12]

$$i_B = H_1C_{Co}/[H_2+C_{Co}], \quad (2)$$

with

$$H_1 = FAn_ck_c\Gamma, \quad (3)$$

$$H_2 = (k_d/k_f)C_{Co}/f_{Co}, \quad (4)$$

where k_c is the constant representing the intrinsic cata-

lytic activity of the protein-Co(0) complex, n_c the number of sites where the protein-Co(0) complex can be formed per protein molecule, and k_f and k_d the rate constants of formation and decomposition of the protein-Co(0) complex, *i.e.* k_f/k_d represents the stability or life time of the complex. Equation 2 also predicts that $n_c k_c(k_f/k_d)=k_B$ in Eq. 1, which is valid for $f_{Co}(k_f/k_d)\ll 1$ or at sufficiently low value of C_{Co}, usually[12] less than 2×10^{-4} mol dm^{-3}. Thus, the dependence of i_B on C_{Co} was analyzed using Eqs. 2—4 in the C_{Co} range between 5×10^{-5} and 2×10^{-3} mol dm^{-3} at different temperatures to give the $n_c k_c$ and k_f/k_d values as functions of temperature. The results are shown in Figs. 4 and 5.

As seen in Fig. 4, $n_c k_c$ increases with increasing temperature at all potentials, except at -1.5 V where $n_c k_c$ tends to decrease slightly. The decreasing tendency of $n_c k_c$ at -1.5 V is probably due to overestimation of Γ at such a negative potential. The adsorption of protein is usually weaker,[18] so that the Koryta equation is not valid, but gives an overestimated value of Γ, *i.e.* $\Gamma<(12D_p t/7\pi)^{1/2}C_p$, and the weaker the adsorption, the lower is Γ. On the other hand, k_f/k_d always decreases with temperature (Fig. 5). Thus the decrease in the stability or life time of the protein-Co(0) complex cancels the increase in the intrinsic catalytic activity of the complex, resulting in the decrease in the over-all catalytic activity of the protein, *i.e.* the k_B value, with increasing temperature. In the above discussion, the change of the pH with temperature is not taken into account; this is calculated to be from 9.95 to 9.05 for the temperature change from 10 to 40 °C in ammoniacal buffer.[19] It has been shown[20] that both $n_c k_c$ and k_f/k_d decrease with decreasing pH. This implies that the "true" temperature coefficient should be larger for $n_c k_c$ and smaller for k_f/k_d. However this correction for pH change can be shown to be not sufficiently significant to modify the above conclusion.

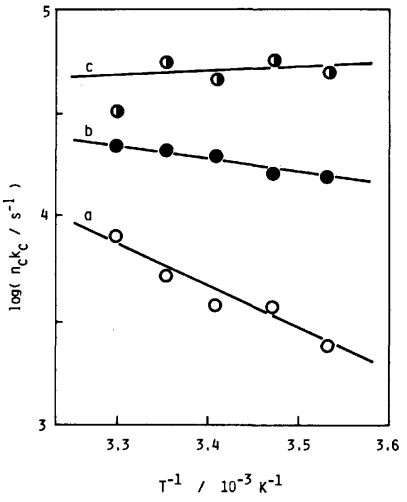

Fig. 4. Temperature dependence of the $n_c k_c$ values of RNase at a) -1.3, b) -1.4, and c) -1.5 V in the base solution.

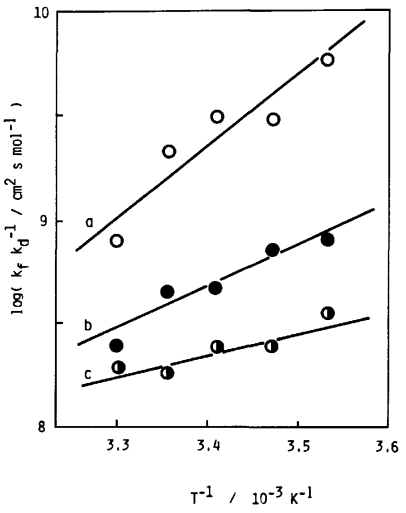

Fig. 5. Temperature dependence of the $k_f k_d$ values of RNase at a) -1.3, b) -1.4, and c) -1.5 V in the base solution.

The slopes of the linear plots in Fig. 4 give the apparent activation energy of the catalytic hydrogen evolution on the electrode surface, which was calculated to be 37 kJ mol^{-1} at -1.3 V, 17 kJ mol^{-1} at -1.4 V (and -1 kJ mol^{-1} at -1.5 V). Also, the plots in Fig. 5 give the difference between the apparent activation energies of the formation and the decomposition of the protein-Co(0) complex, which was calculated to be -64 kJ mol^{-1} at -1.3 V, -36 kJ mol^{-1} at -1.4 V and -20 kJ mol^{-1} at -1.5 V. The potential dependence of these energy values may be associated with the conformational change of the protein absorbed on the electrode surface.

References

1) R. Brdička, *Collect. Czech. Chem. Commun.*, **5**, 112, 148 (1933).
2) T. Ikeda, H. Kinoshita, Y. Yamane, and M. Senda, *Bull. Chem. Soc. Jpn.*, **53**, 112 (1980).
3) H. Kinoshita, T. Ikeda, Y. Yamane, and M. Senda, *Agric. Biol. Chem.*, **44**, 2337 (1980).
4) O. H. Muller, "Methods of Biochemical Analysis," ed by D. Glick, John Wiley & Sons, New York, London (1963), Vol. 11, p. 329.
5) S. G. Mairanovskii, "Catalytic and Kinetic Waves in Polarography," trans. by B. M. Fabuss and P. Zuman, Plenum Press, N. Y. (1968), p. 269.
6) M. Senda, T. Ikeda, T. Kakutani, K. Kano, and H. Kinoshita, *Bioelectrochem. Bioenerg.*, **8**, 151 (1981).
7) M. Březina and V. Gultjaj, *Collect. Czech. Chem. Commun.*, **28**, 181 (1963).
8) Y. Weber, J. Koutecký, and J. Koryta, *Z. Electrochem.*, **63**, 583 (1959).
9) B. Alexandrov, M. Březina, and V. Kalous, *Collect. Czech. Chem. Commun.*, **28**, 210 (1963).
10) I. M. Kolthoff, K. Yamashita, Tan Boen Hie, and A. Kanbe, *J. Electroanal. Chem.*, **53**,417 (1974).
11) I. M. Kolthoff and S. Kihara, *Collect. Czech. Chem. Commun.*, **45**, 669 (1980).
12) M. Senda, T. Ikeda, K. Kano, and I. Tokimitsu, *Bioelectrochem. Bioenerg.*, **9**, 253 (1982).
13) J. Koryta, *Collect. Czech. Chem. Commun.*, **18**, 206 (1953).

14) C. Tanford, "Physical Chemistry of Macromolecules," John Wiley & Sons, New York, London (1961), p. 367.
15) "CRC Handbook of Biochemistry," ed by H. A. Sober and R. A. Harte, CRC Press, Florida (1968), C-10.
16) "CRC Handbook of Chemistry and Physics," ed by R. C. Weast and M. J. Astile, 60th ed, CRC Press, Florida (1979), F-51.
17) I. M. Kolthoff, K. Yamashita, Tan Boen Hie, and A. Kanbe, *Proc. Natl. Acad. Sci. U. S. A.*, **70**, 2020 (1970).
18) M. Senda, T. Ikeda, and H. Kinoshita, *Bioelectrochem. Bioenerg.*, **3**, 253 (1976).
19) R. G. Bates, "Electrometric pH Determination," John Wiley & Sons, New York, London (1964), P. 108.
20) I. Tokimitsu, K. Kano, T. Ikeda, and M. Senda, Paper presented at the 27th Annual Meeting of Polarography in Yokohama, Oct. 17—18th, 1981; Abstract, *Rev. Polarogr. (Kyoto)*, **27**, 84 (1981).

Electrical Relaxations in Mixtures of Lithium Chloride and Glycerol[1)]

F. Scott HOWELL,* Cornelius T. MOYNIHAN,† and Pedro B. MACEDO††
Department of Chemistry, Faculty of Science and Technology, Sophia University, Kioicho 7-1, Chiyoda-ku, Tokyo 102
††*Vitreous State Laboratory, Department of Chemical Engineering and Materials Science, The Catholic University of America, Washington, D.C. 20064, U.S.A.*
(Received July 22, 1983)

The dielectric constant ε' and the electrical conductivity σ were measured as a function of frequency (0.1—2 MHz) and temperature for an electrolyte-polar solvent system: lithium chloride in glycerol. Mole fractions of LiCl were 0, 1, 2, 5, 10, 20, and 33.3%. Data were analysed in terms of an inverse complex permittivity (electrical modulus). At lower mole fractions, two separate modulus relaxations were observed, one due to the ionic diffusion and the other to the dipole reorientation. These two relaxation processes converged with increasing LiCl mole fraction and were not distinguishable at 20%. The moduli isotherms at 33.3% were characteristic of a fused salt. Average relaxation times and distributions for both processes were determined by computer fits to a Gaussian distribution in the logarithms of these times. Their temperature and mole fraction dependences are discussed. The conductivity relaxations became slightly broader than single at 10%; this shows the influence of the charge concentration on the structural relaxation process.

Numerous studies have been conducted on dielectric relaxation in solutions of electrolytes in polar solvents. Some of these have been limited because the frequency, temperature, and/or concentration ranges studied were narrow. We report here a study of electrical relaxations in mixtures of LiCl in glycerol[2)] covering the 0—33.3 mol% LiCl range, i.e., from the dilute solution to the solvated melt where the number of solvent molecules is sufficient to fill more than the first solvation sphere of the ions.[3)] These solutions are highly viscous and supercool readily, so a wide range of temperature can be investigated over a wide frequency range in which accurate complex permittivity measurements can be made by conventional audio bridge techniques. The purpose of this work was to determine as a function of composition the relative contributions of ionic transport and reorientation of polar solvent molecules to the electric field relaxation in the mixture.

Experimental

Materials. A stock solution of lithium chloride in glycerol, containing nominally 33.3 mol% LiCl, was prepared by weight from Fisher Certified Reagent grade LiCl and Fisher Reagent grade glycerol. The salt was placed in a flask and dried to constant weight in an oven at 160 °C before the glycerol was added. The mixture, in a tightly-capped flask, was then heated and stirred on a hot-plate magnetic stirrer to bring the salt into solution. This 33.3% solution was too viscous to flow readily at room temperature and could be poured only when hot. The lower mole fraction mixtures (approximately 20, 10, 5, 2, and 1%) were formed by dilution of the 33.3 mol% mixture with glycerol. The pure glycerol and all mixtures were stored in tightly-capped flasks in a dessicator.

All the solutions were analyzed by titration of chlorine ions with a silver nitrate solution using the absorption indicator method. The density measurements for glycerol agreed with Bosart and Snoddy's results.[4)] The kinematic viscosity of the pure glycerol, measured at (20.0±0.1) °C with a factory-calibrated Cannon-Fenske capillary viscometer, was 0.0014 $m^2 s^{-1}$ (14 St), which corresponds to a glycerol–water solution of 0.998 mass fraction.[5)]

Apparatus and Procedures. Glass transition temperatures for glycerol and the mixtures were measured on a Perkin-Elmer differential scanning calorimeter (DSC-1B) at a heating rate of twenty degrees per minute. T_g was taken as the extrapolated point at which the heat capacity curve begins to rise rapidly.[6)]

The cell was described previously.[7,8)] Its vacuum capacitance was measured before each sample was poured in. This C_0 value changed slightly whenever the cell was disassembled for cleaning and then reassembled; it ranged from 0.81 to 0.90 pF.

Measurements of the equivalent parallel capacitance C and the conductance G were carried out over the frequency range 0.1 Hz to 2 MHz. We used a modified Cole-Berberian[9)] bridge (0.1 Hz to 500 Hz), a General Radio 1615A bridge (500 Hz to 100 kHz), and a Wayne-Kerr B601 bridge (15 kHz to 2 MHz). Electronic frequency counters (Hewlett-Packard 522B or 3734-A) were used to assure frequency accuracy wthin 0.2%.

The LiCl–glycerol mixtures were thermostated in a Tenney Jr. Environmental Chamber. The temperature range from −85 to −20 °C was sufficient to cover the relaxations studied. Chamber temperatures were determined with an accuracy of 0.1 °C by calibrated copper-constantin thermocouples located at the cell.

Densities of three of the mixtures were measured at 0 °C and at room temperature with a dilatometer.

Results and Discussion

Solution Properties. Table 1 compares the result of the composition analysis with the mixture compositions calculated from the reagent masses used. The densities and the glass transition temperatures are also listed.

The T_g measured for glycerol (192.8 K) does not agree with the value reported by Matheson *et al.* ((186.0 ±2) K).[10)] They used a DTA technique with a scanning rate of two degrees per minute. The discrepancy may be resolved by the difference in scanning rates (20 *vs.* 2 K min^{-1}), by uncertainties in our DSC temperature scale, or by differences in the water content of the glycerol samples studied.

† Present address: Rensselaer Polytechnic Institute, Troy, New York 12181, U.S.A.

TABLE 1. LiCl IN GLYCEROL: ANALYTICAL RESULTS

Nominal[a] content LiCl/mol%	Nominal content LiCl/wt%	Analysed content LiCl/wt%	Density[b] g cm^{-3}	T_g[c] K
Glycerol	0		1.275	192.8
1	0.462	0.474		191.9
2	0.931	0.926		
5	2.364	2.378		195.6
10	4.87	4.86	1.299	200.1
20	10.32	10.29	1.323	208.6
33.3	18.71	18.68		229.5

a) Calculated by assuming that the glycerol was 100% pure. b) At 0 °C; the changes in density per degree were -6.0×10^{-4} g cm^{-3} K^{-1}. c) Uncertainty: ±2 K.

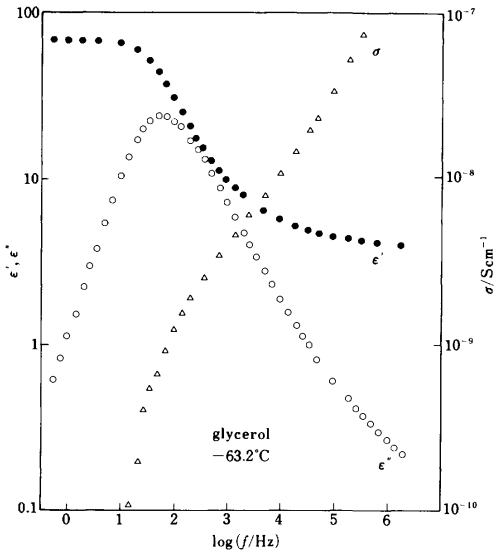

Fig. 1. Frequency dependence of conductivity △ and complex permittivity, ε': ● and ε'' :○, for glycerol at −63.2 °C. Left-side scale for permittivity, right-side scale for conductivity.

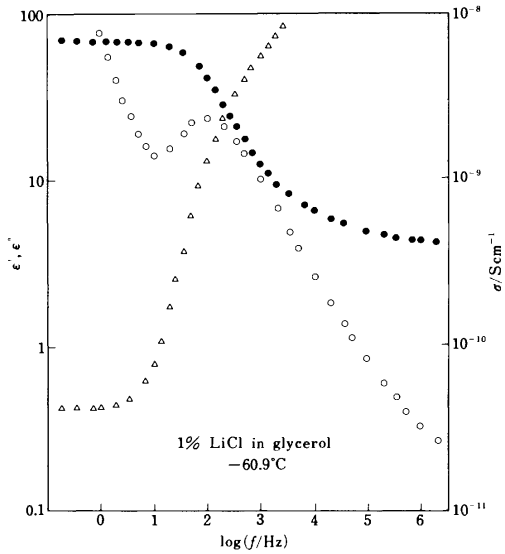

Fig. 2. Frequency dependence of conductivity and complex permittivity for 1 mol% LiCl in glycerol at −60.9 °C. Symbols and scales in Fig. 1.

Conductivities σ and dielectric constants (real parts of the complex relative permittivities) ε' were calculated from the experimental parallel G and C values *via* these equations:

$$\sigma = \varepsilon_0 G/C_0, \quad \varepsilon' = C/C_0, \tag{1}$$

where ε_0 is the permittivity of free space. Complete tables of σ and ε' values as functions of temperature and frequency are available.[1] In Figs. 1—4, experimental values of σ, ε', and $\varepsilon''=G/2\pi fC_0$ are plotted as a function of the logarithm of the measurement frequency f for glycerol and three mole fractions of LiCl in glycerol. At the temperatures selected, the complete relaxation could be seen within the experimentally available frequency range.

At low frequencies, the conductivity of the salt-glycerol mixtures becomes frequency-independent at the value σ_0. For glycerol this value is apparently much lower than the values available in these experiments.

The real part of the complex permittivity exhibits a frequency-independent shoulder (typically one decade wide) at low frequencies. This value is designated as ε_g

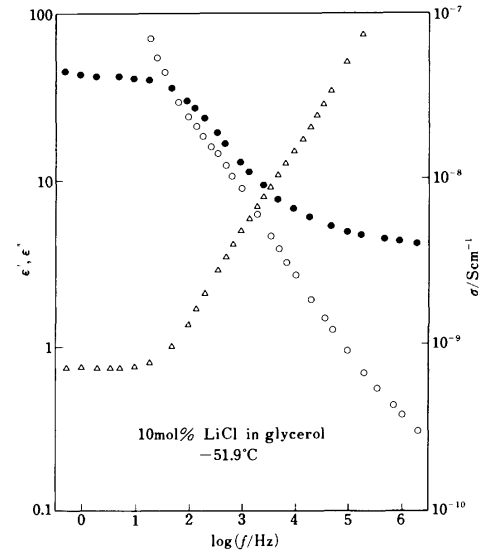

Fig. 3. Frequency dependence of conductivity and complex permittivity for 10 mol% LiCl in glycerol at −51.9 °C. Symbols and scales in Fig. 1.

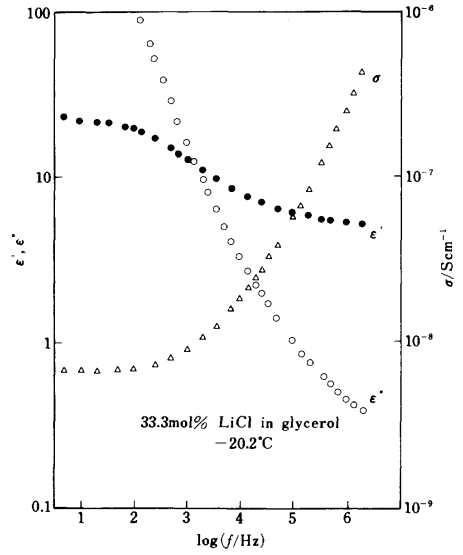

Fig. 4. Frequency dependence of conductivity and complex permittivity for 33.3 mol% LiCl in glycerol at −20.2 °C. Symbols and scales in Fig. 1.

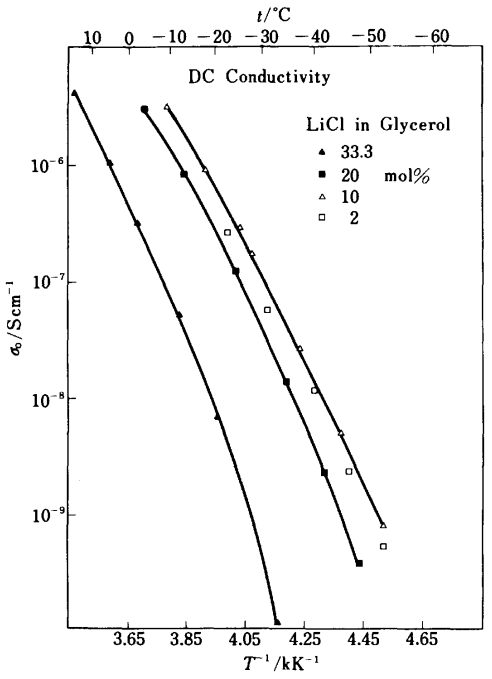

Fig. 5. Arrhenius plots of d.c. conductivity: 2, 10, 20, and 33.3 mol% LiCl in glycerol.

for glycerol and as ε_{LCg} for the salt-glycerol mixtures. The very rapid rise in ε' at still lower frequencies (beginning, for example, in Fig. 3 below 1 Hz and in Fig. 4 below 10 Hz) is due to electrode polarization and related sample-electrode interface effects which have been dealt with extensively in earlier papers.[7,11,12] These demonstrate that the frequency dependences of σ and ε' at frequencies higher than the frequency at which electrode-related effects are seen can be associated with the Li^+ ionic conductivity mechanism and with the glycerol dipole dielectric relaxation.

Figure 5 shows Arrhenius plots of the d.c. conductivity for the 2, 10, 20, and 33.3 mol% mixtures of LiCl. The 1% data fell slightly below the 2% points. The 5% data almost overlapped the line connecting the 10% points; the latter show a slightly higher activation energy. At a given temperature, the magnitudes of the d.c. conductivities occur in the following order: 33.3%≪20%≅1%<2%<5%≅10%.

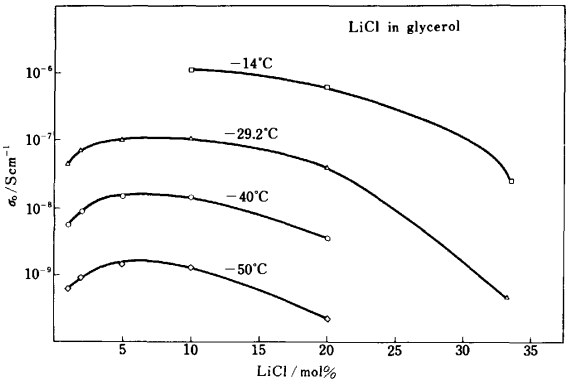

Fig. 6. Mole fraction dependence of d.c. conductivity for mixtures of LiCl in glycerol at various temperatures.

Figure 6 shows the d.c. conductivity as a function of mole fraction for various temperatures. A maximum in isothermal conductivity is seen between 5% and 10% mole fraction of LiCl. A similar maximum was reported by Bressel[13] for aqueous LiCl solutions and by Kartzmark *et al.*[14] for aqueous $LiNO_3$ solutions. The values of the molar conductivity, $\Lambda = \sigma_0/c$, where c is the amount-of-substance concentration, decrease monotonically with increasing mole fraction of LiCl and do not exhibit a minimum.

This maximum found in σ_0 can be explained by the mole fraction dependences of the different components of the conductivity. The value of the conductivity is given by $\sigma_0 = \sum N_i z_i \mu_i$, where N_i is the number of i-type ions per unit volume, z_i is the charge number of the ith ion, and μ_i is the electric mobility of the ith ion. N_i increases with increasing mole fractions of salt ions, but these additional ions introduce stronger electrical forces into the mixture and increase the viscosity and internal pressure. The total ionic diffusion mobility μ_i is inversely proportional to the average dielectric relaxation time, which is approximately the time for the mixture's local structure to break up. The ions will move as soon as the solvent structure opens to allow diffusive motion. This average dielectric relaxation time, in turn, is proportional to viscosity, by Debye's relation and McDuffie's results.[15] Thus the maximum found in σ_0 is due to the fact that the ionic electrical mobilities decrease much faster with increasing mole fraction of salt than the number of ions per unit volume increases.

Bartoli *et al.*[2] suggested that ion-pairing, which would decrease the N_i contribution to σ_0 at higher mole fractions, was responsible for the leveling out of σ_0 as a function of mole fraction. But this proposal neglects the mole fraction dependence of the ionic mobilities and does not easily explain the sharp decrease in σ_0 beyond 10 mol%. Nor is other evidence for ion-

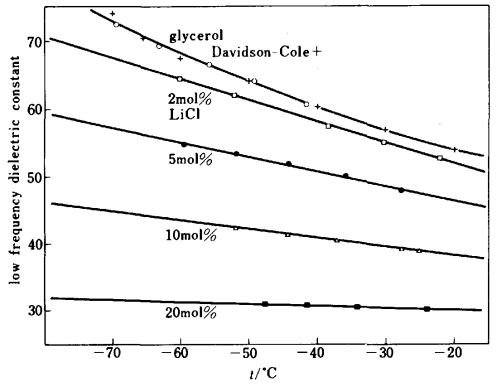

Fig. 7. Temperaure dependence of the low frequency dielectric constant for mixtures of LiCl in glycerol and for glycerol.

pairing available.

Figure 7 shows the low frequency limit of the real part of the complex permittivity as a function of temperature for glycerol and four mole fractions of salt in glycerol. The glycerol data of Davidson and Cole are included in the figure; the agreement is excellent.[16]

Within experimental error, the ε_{LCg} values for the 1% mole fraction were the same or slightly higher than the ε_g values and so have been omitted from Fig. 7.

The decrease of ε_g and ε_{LCg} with increasing temperature is due to the increasing thermal energy in the liquid mixture; this increased energy opposes the forces due to the external field, which tend to align the glycerol dipoles. Pottel has reported a similar temperature dependence for 1 mol dm^{-3} aqueous solutions of divalent sulfate salts.[17]

Modulus Data. Figures 8 and 9 show the low frequency dependences of the real and imaginary parts of the inverse complex relative permittivity, or complex electrical modulus, for each mole fraction of LiCl in glycerol at a selected temperature. The temperatures were chosen so that the entire electrical relaxation fell with the frequency ranges of the modified Cole-Berberian and General Radio bridges. In these figures, some data sets at higher mole fractions were shifted along the horizontal frequency axis by the number of decades indicated in the legend. At the lowest frequencies both M' and M'' decrease to zero. The zero lines are stepped up by the vertical scale shifts indicated in the legends. The 2% data for M'' at frequencies above 100 Hz overlap the 1% data and are omitted from the figure for convenience. Higher mole fraction data sets of M'' also have high frequency points which would appear on the figure beyond the peak; these have also been omitted.

Figure 10 shows the real and imaginary parts of the complex modulus for pure glycerol at −63.2 °C. Notice that the low frequency value of M' levels out at a non-zero value.

The complex modulus M^* is a function of angular frequency:

$$M^* = M' + iM'' = (\varepsilon^*)^{-1} = \varepsilon'/(\varepsilon'^2+\varepsilon''^2) + i\varepsilon''/(\varepsilon'^2+\varepsilon''^2). \quad (2)$$

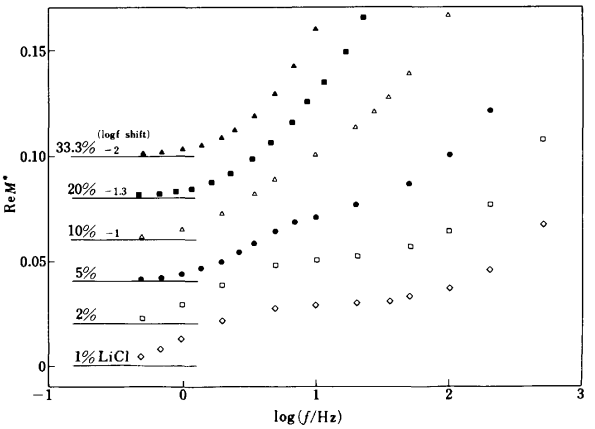

Fig. 8. Low frequency dependence of the real part of the complex modulus (M') of various mole fractions of LiCl in glycerol at typical temperatures. Vertical scale is labeled for 1 mol% data and should be stepped by 0.02 for each higher mole fraction. Horizontal scale is correct for 1, 2, and 5 mol% data; higher mole fraction data are shifted left as noted to avoid data overlap. Temperatures: 1 mol%, −60.9 °C; 2 mol%, −60.1 °C; 5 mol%, −51.8 °C; 10 mol%, −51.9 °C, frequency shifted by one decade; 20 mol%, −41.6 °C, frequency shifted by 1.3 decades; 33.3 mol%, −20.2 °C, frequency shifted by 2 decades.

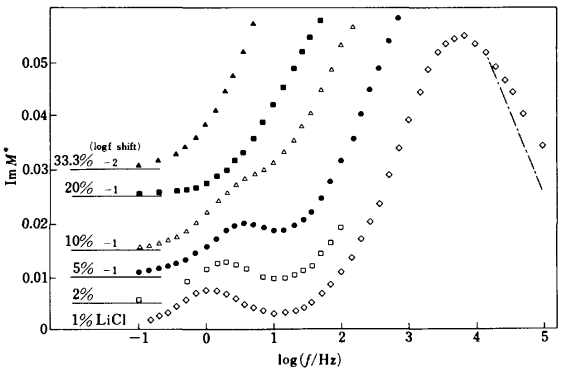

Fig. 9. Low frequency dependence of the imaginary part of the complex modulus (M'') of various mole fractions of LiCl in glycerol at typical temperatures, as listed in caption for Fig. 8. Vertical scale is labeled for 1 mol% data and should be stepped by 0.005 each for 2, 5, and 10 mol% data, by 0.01 for 20 mol% data, and again by 0.005 for 33.3 mol% data. Horizontal scale is correct for 1 and 2 mol% data; it should be shifted left by one decade for 5, 10, and 20 mol% data and by two decades for the 33.3 mol% data.

This formalism was first suggested in 1967 by McCrum *et al.*[18] and has been employed to describe electrical relaxations by analogy with the well-known compressional and shear moduli for viscoelastic flow.[11] The complex electrical modulus has been helpfully explained in terms of the more usual admittance, impedance, and permittivity formalisms by Hodge *et al.*[19] The mathematics of this M^* formalism has been developed in several reports.[7,8,12,19-21] The present case, in which a conducting dielectric

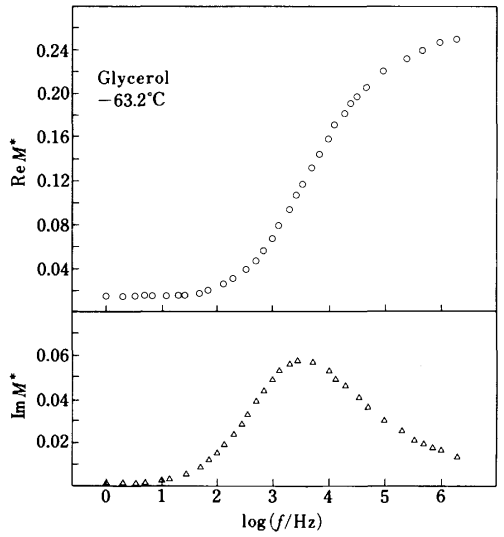

Fig. 10. Frequency dependence of the real (M') and imaginary (M'') parts of the complex modulus of glycerol at −63.2 °C.

undergoes a relaxation involving molecular mechanisms which do not contribute to the long-range conduction process, has been discussed in detail (see Eq. 15 in Refs. 7 and 21).

The complex modulus can be decomposed into two additive terms, which represent the conductivity relaxation (at lower frequencies) and the dielectric relaxation (at higher ones). If both these relaxations occurred at single relaxation times, the complex modulus equation would be

$$M^*(\omega) = M_s i\omega\tau_\sigma/(1+i\omega\tau_\sigma) + (M_\infty - M_s)i\omega\tau_D/(1+i\omega\tau_D). \quad (3)$$

Here M_s is the reciprocal of ε_s, the frequency-independent value of the dielectric constant at low frequency; M_∞ is the reciprocal of the high frequency value, ε_∞. τ_σ is the conductivity relaxation time. τ_D is the dielectric relaxation time at constant displacement vector and is related to the conventional dielectric relaxation time for constant electric field, τ_E, by $\tau_D=(M_s/M_\infty)\tau_E$.

One or both of the terms in Eq. 3 may need to be modified to allow for a distribution of relaxation times. In this work a log gaussian distribution of times[22-23] was used to generate best-fit curves to the M^* data at each temperature and concentration.

$$M^* = M_s\int_{-\infty}^{\infty} g_\sigma\left(\ln\frac{\tau_\sigma}{\tau'_\sigma}\right)\left[\frac{(\omega\tau_\sigma)^2+i\omega\tau_\sigma}{1+(\omega\tau_\sigma)^2}\right] d\ln\frac{\tau_\sigma}{\tau'_\sigma} + (M_\infty - M_s)\int_{-\infty}^{\infty} g_D\left(\ln\frac{\tau_D}{\tau'_D}\right)\left[\frac{(\omega\tau_D)^2+i\omega\tau_D}{1+(\omega\tau_D)^2}\right] \times d\ln\frac{\tau_D}{\tau'_D}. \quad (4)$$

The log gaussian distribution functions are the subscripted g's:

$$g_\sigma(\ln\tau_\sigma/\tau'_\sigma) = b_\sigma(\pi)^{-1/2}\exp(-b_\sigma^2\ln^2(\tau_\sigma/\tau'_\sigma)),$$
$$g_D(\ln\tau_D/\tau'_D) = b_D(\pi)^{-1/2}\exp(-b_D^2\ln^2(\tau_D/\tau'_D)). \quad (5)$$

Table 2. Gaussian fit parameters for glycerol

Temp °C	M_s	$M_\infty - M_s$	b_D	τ'_D μs
−41.7	0.0166	0.210	0.442	0.216
−49.1	0.0157	0.205	0.446	1.21
−55.8	0.0151	0.206	0.425	6.17
−63.2	0.0145	0.205	0.414	43.9
−69.4	0.0138	0.203	0.403	527.
−77.7	0.0132[a]	0.201	0.396	22800

Standard deviations: 0.0002—0.00057. a) Estimated.

The primed *tau*'s are the most probable relaxation times for the respective distribution functions; the b values are inversely proportional to the widths of the distributions. A b value greater than 2.5 is considered equivalent to a delta function distribution, *i.e.* a single relaxation time. Fit parameters obtained at each temperature and concentration are given in Tables 2—5.

The M' data sets for glycerol level out at the expected non-zero $M_s=1/\varepsilon_s$ values at low frequencies. The fits shown in Table 2 were performed for data up to the peak in the M'' values.

For the dilute and moderately concentrated mixtures (1, 2, 5, 10 mol%), each conductivity and dielectric wave (in M') and peak (in M'') was fit separately to a log gaussian distribution. If sufficient data were available to show both peaks, a six-parameter function, the sum of two log gaussian distributions, was fit to the entire spectrum up to the top of the dielectric peak; this procedure reproduces Eq. 4. The 20 mol% data fits are discussed below. The 33.3 mol% data were fit to one broad log gaussian distribution; Table 5 shows the results.

For all cases, the data at frequencies beyond the maximum value of M'' were excluded when the least-squares fit was performed. No attempt was made to introduce a low, broad function centered a decade or so higher in frequency than the M'' maximum, a procedure which would probably have reproduced the high frequency shape of the data more adequately than the one we used. The high-frequency asymmetry in the M^* data which other authors[24] and ourselves[8,21] have reported was thus ignored. The generated fits fall inside the data points for frequencies beyond the dielectric M'' peak, as the dotted line for the 1 mol% data in Fig. 9 shows. All fits have an overall accuracy of about 3%; as might be expected, the fit is usually worst in the M'' valley between the conductivity peak and the dielectric peak.

The fit reported in Table 4 for the 20 mol% data was not acceptable. We believe that the conduction and the dipole reorientation processes contribute almost equally to the observed spectra. Extrapolation of the ratios of the average times (see below) as a function of concentration to the 20 mol% case indicated that the two peaks would be within a factor of ten in center frequencies. The six-parameter sum of two log gaussian distributions, however, was unable to separate the two presumed processes: the central

times could not be well-specified. Thus the fits shown in Table 4 are from a log gaussian distribution using three parameters which fortunately converged. This fit was in error by 100% for the data in the lowest decade of frequency, but it did match the data near the M'' maximum sufficiently closely for the fit program to converge.

Average Times. The average relaxation times

Table 3. Gaussian fit parameters for 1—10 mol% LiCl in glycerol

Temp °C	Conductivity fit			Dielectric fit			Ratio of average times
	M_s	b_σ	τ'_σ ms	$M_\infty - M_s$	b_D	τ'_D μs	
			— 1 mol% —				
−21.2	0.0189	1.90	0.0258				
−28.7	0.0180	1.80	0.0969				
−36.8	0.0165	single	0.495	0.204	0.433	0.0965	1432
−46.6	0.0157	single	4.16	0.194	0.441	0.812	1425
−52.9	0.0149	single	20.7	0.201	0.412	3.57	1327
−60.9	0.0144	single	140.	0.196	0.411	25.8	1239
−66.2	0.014[a]			0.192	0.403	260.	
−74.8	0.014[a]			0.189	0.397	9580	
			— 2 mol% —				
−22.0	0.0196	2.38	0.0143				
−30.3	0.0192	2.17	0.0748				
−38.5	0.0184	2.20	0.377				
−45.8	0.0176	2.41	1.96				
−52.1	0.0159	single	10.2	0.211	0.401	3.48	618
−60.1	0.0154	single	93.0	0.202	0.402	36.9	538
−66.9	0.015[a]			0.203	0.391	392.	
−75.3	0.015[a]			0.195	0.397	16200	
			— 5 mol% —				
−21.0	0.0245	1.33	0.00660				
−27.6	0.0241	1.19	0.0198				
−35.8	0.0188	single	0.122	0.209	0.416	0.147	196
−44.2	0.0181	single	0.777	0.207	0.404	0.930	181
−51.8	0.0171	single	5.33	0.208	0.388	6.27	162
−59.5	0.0162	2.18	50.3	0.206	0.376	66.3	136
−66.9	0.016[a]			0.202	0.374	806.	
−73.1	0.016[a]			0.196	0.386	19500	
			— 10 mol% —				
−37.1	0.0198	2.24	0.141	0.205	0.382	0.494	54
−44.4	0.0179	2.30	0.788	0.212	0.354	2.61	43
−51.9	0.0168	1.87	5.15	0.206	0.353	20.9	36
−60.6	0.0137	2.25	57.9	0.207	0.340	296.	24
−65.0	0.013[a]			0.196	0.358	3030	
−73.7	0.013[a]			0.188	0.406	247000	

a) Estimated.

Table 4. Compromise gaussian fit parameters for 20 mol% LiCl in glycerol

Temp °C	M_s	b	τ' μs
−13.3	0.191	0.290	0.0671
−24.1	0.196	0.289	0.441
−41.6	0.169	0.357	50.7
−47.8	0.162	0.396	402.
−55.4	0.153	0.466	7900

Standard deviations: 5.4×10^{-4}—1.2×10^{-3}.

Table 5. Gaussian fit parameters for 33.3 mol% LiCl in glycerol

Temp °C	M_s	b_σ	τ'_σ μs
−11.4	0.138	0.547	5.93
−20.3	0.142	0.566	45.1
−29.05	0.140	0.610	620
−33.8	0.144	0.609	2930
−39.6	0.145	0.633	34200

Standard deviations: $(4.8—6.6)\times10^{-4}$.

for each process can be calculated from the fit parameters. For a logarithmic gaussian distribution:[23]

$$\langle\tau\rangle = \tau' \exp(-1/4b^2). \quad (6)$$

The τ' and b are to be subscripted for either conductivity relaxation or dielectric relaxation at constant displacement vector (σ or D).

For the 20% data, the average time which this procedure generates is a compromise between $\langle\tau_\sigma\rangle$ and $\langle\tau_D\rangle$. A rough extrapolation of the ratios of the average times as a function of mole fraction indicated that the two times were within a factor of ten of each other when the LiCl mole fraction was about 20%.

The procedure of omitting from the fit the M^* data at frequencies beyond the dielectric M'' maximum had no significant effect on either of the average times calculated from the fit parameters.

Dielectric Times: Figure 11 shows the Arrhenius plots of the logarithms of the average dielectric relaxation times (at constant displacement vector) for glycerol and for the 1, 2, 5, and 10% LiCl mixtures with glycerol. At a given temperature, the increase in the magnitude of the logarithm of $\langle\tau_D\rangle$ from one to ten per cent was found to be linear with the mole fraction.

A wide distribution of dielectric relaxation times is observed. The cooperative aspects of the structural break-up are thus reflected in the dielectric behavior. The dielectric width parameter b_D decreases slightly with increasing concentration. Harris and O'Konski report a similar broadening for aqueous 1:1 electrolyte solutions.[25] They suggest that two processes are responsible for increasing the relaxation times of the polar solvent molecules. First, because more of the solvent molecules are bound in complexes with the cations at higher concentrations, there are fewer available to reorient freely with the applied electric field. Secondly, more of these free solvent molecules are in the second coordination shells of the solvated ions and are thus somewhat hindered in following the electric field.

At each concentration the dielectric width parameter b_D tends to increase with increasing temperature. This corresponds to a narrowing of the peak; Bartoli *et al.* found a similar narrowing in NaCl-glycerol mixtures.[2] As the temperature is increased, the amount of bonding in the liquid is lowered as the liquid structure becomes more randomized by the increased thermal energy of the individual molecules or complexes. The environmental relaxation model[26] had predicted such a temperature behavior of the width parameter associated with the structural rearrangement.

Conduction Times: Figure 12 shows the Arrhenius plots of the logarithms of the average conductivity relaxation times for all six mole fractions of LiCl in glycerol. $\langle\tau_\sigma\rangle$ decreases with increasing mole fraction for 1, 2, and 5 mol% LiCl. As the salt concentration in the sample increases, the conductivity increases; consequently, the electric field decays with a shorter time constant.

The 5 and 10 mol% values of $\langle\tau_\sigma\rangle$ are indistinguishable; the same line is used for both sets of data. These time values reflect the reversal in the concentration dependence of the d.c. conductivity in Fig. 6.

Distribution of Conduction Times: The dilute salt-glycerol mixtures show a single relaxation time for the conductivity relaxation at those temperatures at which sufficient data are available for a six-parameter sum of two log gaussian functions to be fit. When

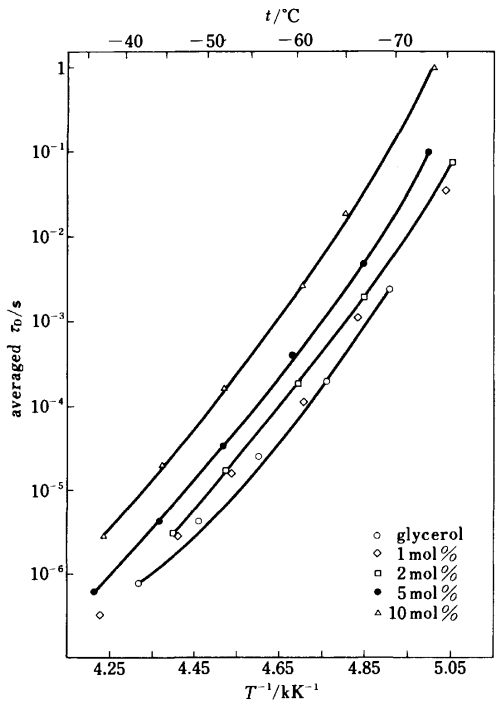

Fig. 11. Arrhenius plots of the average dielectric relaxation times at constant displacement vector for glycerol and for mixtures of 1, 2, 5, and 10 mol% LiCl in glycerol.

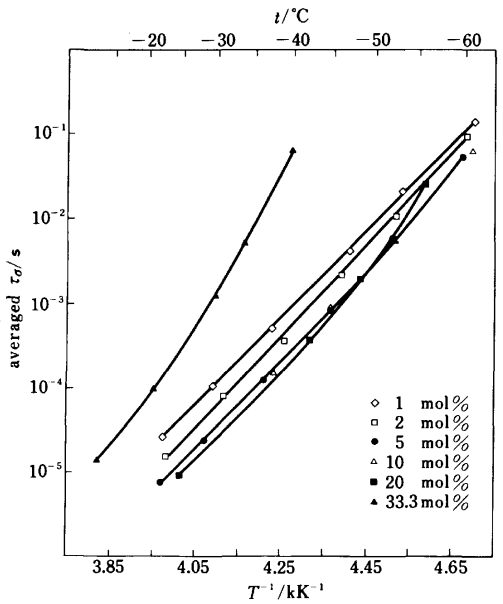

Fig. 12. Arrhenius plots of the average conductivity relaxation times for mixtures of 1, 2, 5, 10, 20, and 33.3 mol% LiCl in glycerol.

a 'single' relaxation is reported in the tables, b converged to a value greater than 2.5. Thus $\tau_\sigma' = \langle \tau_\sigma \rangle$. This result was confirmed by calculating the average relaxation times from the d.c. conductivity and the low-frequency frequency-independent value of ε', using $\langle \tau_\sigma \rangle = \varepsilon_0 \varepsilon_s / \sigma_0$.[11] These independent calculations gave times which agreed with the fit values.

At the higher temperatures studied for these dilute salt-glycerol mixtures, only enough data was available to characterize the conductivity relaxation. Values of b_σ slightly lower than 2.5 were obtained, but these are an artifact of the fit procedure for the log gaussian function; this procedure included some of the data points beyond the M'' conductivity peak and thus some contribution from the beginnings of the dielectric relaxation. Single relaxation times were always achieved when both peaks were available for fitting.

Some structural considerations which could explain these results are given below. Besides these, the low concentration of charge carriers would give rise to long-range ionic conduction with little or no dispersion in ε' and σ at frequencies near the M'' conduction peak. This has been found to be the case in vitreous ionic conductors, specifically Phasil glass[27] and GeO_2,[28] as well as in ionically conducting single crystals which contain only a small concentration of charge carriers, such as NaCl crystals doped with divalent chlorides.[29]

The 10 mol% LiCl mixture shows a distribution of conduction relaxation times which is slightly broader than single. The average b_σ value is 2.17. At this moderate mole fraction, the number of charge carriers and the structural details of the glycerol reorientations are beginning to influence the conduction process. Part of the measured dispersion in ε' is thus due to the conductivity relaxation: this conclusion was impossible to draw using the complex permittivity data representation.[2]

Structural Consideration: This distribution of relaxation times which appears in the conduction modulus with increasing mole fraction of salt can be explained in terms of the interaction of the structural break-up process and the ionic diffusion process and by the increasingly cooperative character of the ionic conduction as the mole fraction of salt increases. We assume with Litovitz and McDuffie that the rate of an electrical relaxation is determined by the time in which a cooperative break-up occurs in the local structure of the liquid. Such a structural time would ordinarily be determined by an ultrasonic measurement, but it is reasonable to use the average dielectric relaxation time for constant displacement vector in place of the structural relaxation time for glycerol, since the ratio of the structural time and the usual dielectric relaxation time τ_E is only 1.5.[15,30]

If the characteristic time for structural relaxations is comparable to an electrical relaxation time, a distribution of electrical times is observed: this is the case for the dielectric relaxations reported here at all mole fractions. If, however, this structural time is much shorter than an electrical time, then the process will show a single electrical relaxation time, as is the case for the conductivity relaxations here at very low mole fractions.

When the mole fraction of ions is very low, the few ions present have to execute a large number of jumps in order to relax the electric field. If the ionic jump time is denoted as t_j, then we have $\tau_\sigma \gg t_j$ for the dilute cases. This also means that the field-biased ionic jumps are uncorrelated: the occurrence of a jump by a given ion does not bias the probability or direction of subsequent jumps by that ion or by other ions in its vicinity. At low concentrations, the details of the structural process are averaged out before the electric field decays, and thus the decay is seen as occurring with a single relaxation time.

When the mole fraction is increased to 10 mol%, however, it takes a much shorter time, that is, fewer jumps by a larger number of ions, before the field decays to zero. τ_σ becomes more comparable to t_j in this case. As the ionic concentration becomes higher, the average distance of ionic separation becomes smaller; thus the interionic coulombic interaction begins to become significant. The movement of an ion from one site to another will perturb the electrical potential in its vicinity; at a moderate mole fraction, other ions will be in the region of perturbed potential and their future motions will be biased. This cooperative motion of the ions will lead to a non-exponential decay function[24] and to dispersions in ε' and σ associated with long-range ionic migration.

Earlier reports[11,12] on alkali silicate glasses have followed Stevels,[31] Taylor,[32] and Isard[33] in suggesting that the dispersion in the complex permittivity would be accounted for by the lack of translational invariance of the free energy barriers impeding ionic diffusion in a vitreous quasi-lattice. These reports postulated that materials with a long-range lattice structure, such as ionic crystals, would have free energy barriers against ionic diffusion which would be regularly spaced and of equal height. For such equivalent lattice sites it was asserted that, on the average, the ions would spend the same duration of time at each site during the conduction process and that the long-range diffusion process would thus exhibit a single relaxation time. But recent experimental results for single crystals which contain a high concentration of charge carriers, $LiGaO_2$[34] and beta-alumina,[35] have shown a distribution of conductivity relaxation times when analysed in the complex modulus representation. These results underline the need in future theoretical work to pay more attention to the concentration of charge carriers. Not only a distribution of microscopic conductivities but also a moderate mole fraction of charge carriers, as in our 10 mol% LiCl mixture, can give rise to a distribution of conductivity relaxation times.

Jonscher[36] has advanced a model based on relaxation of screening charge about an ion following a jump, to account for the high frequency dispersion of the conductivity of dielectric materials. He had in mind producing an explanation only for the very high frequency losses due to localized motions, which are observed in all types of amorphous systems (insulators, ionic conductors, and electronic conductors), but his

model involves cooperative motion *via* interionic interactions and seems capable of expansion to the present system.

Higher Concentration Times: The 33.3 mol% average conduction times shown in Fig. 12 are much longer than the times for any of the other concentrations. This reflects the increase in viscosity and the sharp rise in the glass transition temperature for this concentration.

The 20 mol% average times are also displayed in Fig. 12 as if they were average conduction times, although we think that these apparent fit times are some compromise values between the dielectric reorientation time and the ionic conductivity time. The curvature in the Arrhenius plot is much different from that seen for the lower concentration data, especially at the lowest temperatures. The curve for the 20 mol% average times bends away from the slopes of the lower concentrations and towards the slope of the 33.3 mol% average conductivity times.

Distributions at Higher Concentrations: The 33.3 mol% data exhibit a wide conductivity relaxation. The magnitude of b_σ decreases by about 10% as the temperature increases. The modulus wave and peak broaden with increasing temperature in a way similar to the highly viscous liquid behavior of the glass-forming nitrate mixture studied earlier.[8] This similarity is another indication that the 33.3 mol% LiCl glycerol mixture should be considered a quasi-fused-salt.

The 20 mol% data show a wide distribution of relaxation times similar to that for the 33.3 mol% results. Over a temperature increase of about 40 K, the width parameter broadens from 0.466 to 0.290. This temperature dependence of the width parameter at least suggests the onset of fused salt behavior, even when it is remembered that the fit is only apparent (since the two times have moved so close together that the fit functions cannot separate them).

Ratios of Average Electrical Times: The ratio of the average conductivity relaxation time to the average dielectric relaxation time at constant displacement vector is given in Table 3, for those temperatures at which both relaxations could be adequately fit by the six-parameter sum of two gaussian functions. This ratio is a strong function of concentration, dropping from an average value of 1400 at 1 mol% LiCl to 580 at 2 mol%, 170 at 5 mol%, and about 40 at 10 mol%. This decrease in the $\langle\tau_\sigma\rangle/\langle\tau_D\rangle$ ratio with increasing concentration is due to the facts that $\langle\tau_\sigma\rangle$ decreases with concentration, remaining constant between 5 and 10 mol%, while $\langle\tau_D\rangle$ increases with concentration. The extrapolation of this dependence to 20 mol% LiCl yields a ratio of about six, while further extension to the 33.3 mol% case yields a value of less than one.

At a given concentration, an increase in temperature increases the magnitude of the ratio of electrical times. Over the temperature range −61 °C to −37 °C, the ratio increases by more than 15% for the 1 mol% mixture, while for the 10 mol% mixture the ratio more than doubles. Only when the ratio is less than 100 does the conductivity relaxation show a distribution of relaxation times.

The authors are grateful to M. Samanta and Dr. Regan Howard for their assistance with the chemical analyses and the DSC measurements. They are especially grateful to Dr. William Stamm for measuring the 2 mol% data. This research was partially supported by the United States Office of Naval Research. One of us (FSH) acknowledges with gratitude the Traineeship provided by the United States National Aeronautics and Space Administration.

References

1) F. S. Howell, Ph. D. Thesis, The Catholic University of America, Washington, D. C. (1972), Chap. 5; University Microfilms order number 72-22591.
2) F. J. Bartoli, J. N. Birch, N-H. Toan, and G. E. McDuffie, *J. Chem. Phys.*, **49**, 1916 (1968).
3) J. O'M. Bockris and A. K. N. Reddy, "Modern Electrochemistry," Plenum Press, New York (1974), pp. 76—80. The treatment is for water molecules.
4) L. W. Bosart and A. O. Snoddy, *Ind. Eng. Chem.*, **19**, 506 (1927).
5) M. L. Sheehy, *Ind. Eng. Chem.*, **24**, 1060 (1932).
6) C. A. Angell and E. J. Sare, *J. Chem. Phys.*, **52**, 1058 (1970).
7) J. H. Ambrus, C. T. Moynihan, and P. B. Macedo, *J. Phys. Chem.*, **76**, 3287 (1972).
8) F. S. Howell, R. A. Bose, P. B. Macedo, and C. T. Moynihan, *J. Phys. Chem.*, **78**, 639 (1974).
9) J. G. Berberian and R. H. Cole, *Rev. Sci. Instrum.*, **40**, 811 (1969).
10) M. R. Carpenter, D. B. Davies, and A. J. Matheson, *J. Chem. Phys.*, **46**, 2451 (1967).
11) P. B. Macedo, C. T. Moynihan, and R. Bose, *Phys. Chem. Glasses*, **13**, 171 (1972).
12) V. Provenzano, L. P. Boesch, V. Volterra, C. T. Moynihan, and P. B. Macedo, *J. Am. Ceram. Soc.*, **55**,492 (1972).
13) R. D. Bressel, Ph. D. Thesis, Purdue University, Lafayette, Indiana (1972); University Microfilms order number 72-21164. *Cf.* p. 102 and Fig. 42.
14) A. N. Campbell, G. H. Debus, and E. M. Kartzmark, *Can. J. Chem.*, **33**, 1508 (1955).
15) G. E. McDuffie, Jr., R. G. Quinn, and T. A. Litovitz, *J. Chem. Phys.*, **37**, 239 (1962); G. E. McDuffie, Jr., and T. A. Litovitz, *ibid.*, **37**, 1699 (1962); T. A. Litovitz and G. E. McDuffie, Jr., *ibid.*, **39**, 729 (1963).
16) D. W. Davidson and R. H. Cole, *J. Chem. Phys.*, **19**, 1484 (1951).
17) R. Pottel, "Chemical Physics of Ionic Solutions," ed by B. E. Conway and R. G. Barradas, Wiley, New York (1966), pp. 581—589.
18) N. G. McCrum, B. E. Read, and G. Williams, "Anelastic and Dielectric Effects in Polymeric Solids," Wiley, New York (1967), p. 110.
19) I. M. Hodge, M. D. Ingram, and A. R. West, *J. Electroanal. Chem. Interfacial Electrochem.*, **74**, 125 (1976).
20) C. T. Moynihan, R. D. Bressel, and C. A. Angell, *J. Chem. Phys.*, **55**, 4414 (1971).
21) C. T. Moynihan, L. P. Boesch, and N. L. Laberge, *Phys. Chem. Glasses*, **14**, 122 (1973).
22) T. A. Litovitz and C. M. Davis, "Physical Acoustics," ed by W. P. Mason, Academic Press, New York (1965), Vol. IIA, pp. 281—349.
23) W. A. Yager, *Physics*, **7**, 434 (1936).
24) G. Williams and D. C. Watts, *Trans. Faraday Soc.*, **66**, 80 (1970); G. Williams and P. J. Hains, *Faraday Symp. Chem. Soc.*, **6**, 14 (1972).

25) F. A. Harris and C. T. O'Konski, *J. Phys. Chem.*, **61**, 310 (1957).
26) H. Tweer, J. H. Simmons, and P. B. Macedo, *J. Chem. Phys.*, **54**, 1952 (1971).
27) C. T. Moynihan, J. H. Simmons, and P. B. Elterman, Glass Division Meeting, American Ceramic Society, Bedford, PA, October 14, 1976; Abstract in *Bull. Am. Ceram. Soc.*, **55**, 745 (1976).
28) H. Bohm, *J. Appl. Phys.*, **43**, 1103 (1972).
29) Y. Haven, *J. Chem. Phys.*, **21**, 171 (1953).
30) C. J. Montrose and T. A. Litovitz, "Neutron Inelastic Scattering," I. A. T. A., Vienna (1968), Vol. 1, pp. 623—637.
31) J. M. Stevels, "Handbuch der Physik," Springer-Verlag, Berlin (1957), Vol. 20, pp. 372—379.
32) H. E. Taylor, *J. Soc. Glass Technol.*, **41**, 350T (1957); **43**, 124T (1959).
33) J. O. Isard, *Proc. Inst. Elec. Engrs. (London)*, **109B**, Supplement 22, 440 (1962); *J. Non-Cryst. Solids*, **4**, 357 (1970).
34) R. J. Grant, I. M. Hodge, M. D. Ingram, and A. R. West, *J. Am. Ceram. Soc.*, **60**, 226 (1977).
35) R. J. Grant, I. M. Hodge, M. D. Ingram, and A. R. West, *Nature*, **226**, 42 (1977).
36) A. K. Jonscher, *Nature*, **253**, 717 (1975).

Volume and Adiabatic Compressibility of Amino Acids in Urea-Water Mixtures

Toshio Ogawa,* Motoo Yasuda, and Kiyoshi Mizutani
Department of Chemistry, College of General Education, Nagoya University, Chikusa-ku, Nagoya 464
(Received August 2, 1983)

Apparent molal volumes (ϕ_V) and apparent molal adiabatic compressibilities (ϕ_{KS}) at 25 °C have been obtained for the following amino acids in water and in urea-water mixtures (up to 8 mol kg^{-1} urea for ϕ_V and at 3 mol kg^{-1} for ϕ_{KS}) from measurements of density and ultrasonic velocity: glycine, L-alanine, β-alanine, α-aminoisobutyric acid, L-valine, L-serine, and L-threonine. The limiting values ϕ_V° and ϕ_{KS}° were calculated by a linear extrapolation using the least-squares method. These data were used to derive the volumes of transfer and the adiabatic compressibilities of transfer of the amino acids from water to aqueous urea solutions. Both of these transfer functions were positive. The results were interpreted in terms of structure-breaking interaction of urea upon water.

In recent years, mixed aqueous solvents are used extensively in chemistry and other fields to control factors, *e.g.*, solubility, reactivity, and stability of systems. Due to the high solubility of urea in water and its protein-denaturing ability in aqueous solutions urea-water mixtures have been employed as the solvents for extensive experimental investigations. The theoretical treatment of the mixtures also has been carried out by Frank and Franks.[1] It is generally accepted that urea does not appreciably interact with either hydrophobic or hydrophilic molecules or groups, and acts mainly to disrupt hydrogen bonding among water molecules in aqueous medium. Thus, as noted by Mathieson and Conway, thermodynamic and transport properties of aqueous urea solutions with added electrolytes or nonelectrolytes have been interpreted in terms of nonspecific interaction of urea with the solute.[2] The values of the thermodynamic functions are consistent with the hypothesis that urea solutions are similar to water but with less structure.

For a better understanding of an increased interest in the states of water in the living cells it will be necessary to carry out systematic investigations of model systems under various conditions. In the present work densities and ultrasonic velocities were measured at 25 °C for aqueous amino acid solutions and for amino acid-urea-water ternary systems at various concentrations. Apparent molal volumes and apparent molal adiabatic compressibilities and their limiting values were calculated from these data.

Experimental

The amino acids and urea used in this study were guaranteed reagents from Wako Chemical Industries, Ltd., and were used without further purification. As seen later, their limiting apparent molal volumes in aqueous solutions measured here were all in good agreement with the values reported recently by other workers, except α-aminoisobutyric acid, for which there is no previous value reported. The densities of the amino acids solutions were measured in water and in 1, 3, 5, and 8 mol kg^{-1} aqueous urea solutions and the ultrasonic velocities in water and in 3 mol kg^{-1} urea solution.

All solutions were prepared by weight in the concentration range 0.2—1 mol kg^{-1} (the number of moles of amino acid per kg of mixed solvent whenever the mixed solvent was used); the highest concentration depends on the solubility of the amino acids. The experimental errors were greatly reduced by employing the rather high amino acid concentration range.[3-5] Fresh stock solutions of urea were prepared for each series of measurements; the densities and ultrasonic velocities were determined for each stock solution.

The densities were measured to $\pm 2\times10^{-6}$ g cm^{-3} with an Anton Paar DMA 02D Densimeter. The system was calibrated with dry air and distilled water; their densities were taken from the literatures.[6,7]

The ultrasonic velocities were measured at 5 MHz to a precision of ±0.1 m s^{-1} using an improved ultrasonic interferometer designed by Nomura and Kawaizumi,[8] and the principle of the system is identical with the one used by Nomura *et al.*[5] Since there is an error due to the temperature variation, a relative error is estimated to be $\delta u/u = \pm 1.0\times10^{-4}$. The temperature control of the thermostated bath systems regulating the densimeter and ultrasonic interferometer was better than ±0.005 °C.

Results

The densities and ultrasonic velocities were determined at 25 °C for the following amino acids; glycine (Gly), L-alanine (Ala); β-alanine (β-Ala), α-aminoisobutyric acid (Me-ala), L-valine (Val), L-serine (Ser), and L-threonine (Thr). The apparent molal volumes were calculated from the relation:

$$\phi_V = \frac{M}{d} + \frac{1000(d_0 - d)}{m d_0 d}, \quad (1)$$

where d_0 and d are the densities of a solvent and a solution respectively and m is the molal concentration; M, the molecular weight of the amino acid. The adiabatic compressibilities β_S and the apparent molal adiabatic compressibilities ϕ_{KS} were calculated using Eqs. 2 and 3 respectively, where β_S is expressed in bar^{-1}.

$$\beta_S = \frac{100}{du^2}, \quad (2)$$

$$\phi_{KS} = \frac{\beta_S M}{d} + \frac{1000(\beta_S d_0 - \beta_S^\circ d)}{m d_0 d}, \quad (3)$$

where u is the velocity of sound (m s^{-1}) and β_S° is the adiabatic compressibility of the solvent. The limiting values ϕ_V° and ϕ_{KS}° were obtained by linear extrapolation using the least-squares fit to the equations:

Table 1. Limiting apparent molal volumes of amino acids in water

Amino acid	ϕ_V° / cm^3 mol^{-1}	S_V / cm^3 mol^{-2} kg	σ[a] / cm^3 mol^{-1}	ϕ_V° / cm^3 mol^{-1}
Glycine	43.23	0.82	0.01	43.19[b]
L-Alanine	60.50	0.59	0.02	60.47[b]
β-Alanine	58.25	0.95	0.02	58.28[c]
α-Aminoisobutyric acid	77.54	0.21	0.01	—
L-Valine	90.78	0.16	0.01	90.78[b]
L-Serine	60.72	1.14	0.02	60.62[d]
L-Threonine	76.94	0.89	0.01	76.83[e]

a) Standard deviation. b) Ref. 9. c) Ref. 11. d) Ref. 12. e) Ref. 13.

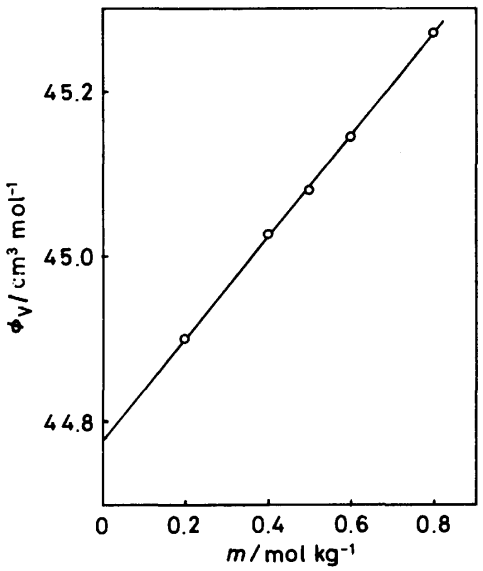

Fig. 1. Plot of ϕ_V *vs.* m for glycine in 3 mol kg^{-1} urea solution.

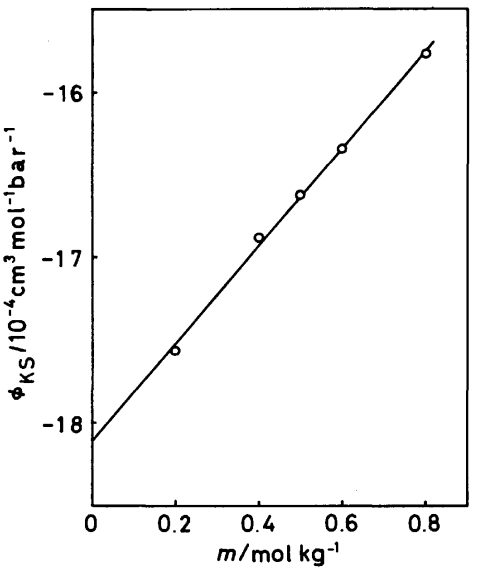

Fig. 2. Plot of ϕ_{KS} *vs.* m for glycine in 3 mol kg^{-1} urea solution.

$$\phi_V = \phi_V^\circ + S_V m, \tag{4}$$

and

$$\phi_{KS} = \phi_{KS}^\circ + S_K m, \tag{5}$$

where $\phi_V^\circ = \overline{V}^\circ$ and $\phi_{KS}^\circ = \overline{K}^\circ$ are the infinite dilution partial molal volume and partial molal adiabatic compressibility, respectively, and S_V and S_K are the experimental slopes. The ϕ_V and ϕ_{KS} of glycine in 3 mol kg^{-1} aqueous urea solutions are plotted against the amino acid molality in Figs. 1 and 2 respectively. The values of ϕ_V°, S_V, and standard deviations, σ, obtained in water are listed in Table 1 along with literature values reported recently. The apparent molal volumes at infinite dilution in 1, 3, 5, and 8 mol kg^{-1} aqueous urea solutions are given in Table 2, and the apparent molal adiabatic compressibilities at infinite dilution and standard deviations, σ, in water and in 3 mol kg^{-1} aqueous urea solutions are given in Table 3.

As seen from Table 1, our results are in good agreement with the literature values. As with the apparent molal adiabatic compressibilities our results are in good agreement with the values reported by Millero *et al.*,[9] but Cabani *et al.* obtained rather larger (less negative) values.[10] For example, the $10^4 \times \phi_{KS}^\circ$ value of glycine is reported as −27.00 by Millero *et al.* and as −25.0 by Cabani *et al.* The main reason for the discrepancy is probably due to the difference in the extrapolation procedure, thus Cabani *et al.* fitted to the equation

$$\phi_{KS} = \phi_{KS}^\circ + Bm + Cm^2. \tag{6}$$

Table 2. Limiting apparent molal volumes of amino acids in urea-water mixtures

Amino acid	ϕ_V° / cm^3 mol^{-1}			
	1[a]	3[a]	5[a]	8[a]
Glycine	43.92	44.78	45.39	46.08
L-Alanine	60.90	61.75	62.33	63.10
β-Alanine	58.77	59.65	60.28	60.89
α-Aminoisobutyric acid	77.92	78.50	78.99	79.80
L-Valine	91.03	91.94	92.47	93.08
L-Serine	61.37	62.41	63.05	64.06
L-Threonine	77.46	78.38	79.06	79.79

a) Urea concentration in mol kg^{-1}.

Table 3. Limiting apparent molal adiabatic compressibilities

Amino acid	Water		Urea-Water[a)]	
	ϕ_{KS}° / 10^{-4} cm^3 mol^{-1} bar^{-1}	σ / 10^{-4} cm^3 mol^{-1} bar^{-1}	ϕ_{KS}° / 10^{-4} cm^3 mol^{-1} bar^{-1}	σ / 10^{-4} cm^3 mol^{-1} bar^{-1}
Gly	−27.16	0.36	−18.11	0.05
Ala	−24.74	0.18	−15.30	0.14
β-Ala	−26.36	0.11	−16.67	0.09
Mc-ala	−23.46	0.27	−12.55	0.10
Val	−30.43	0.10	−15.91	0.45
Ser	−29.88	0.10	−19.49	0.16
Thr	−31.23	0.10	−19.01	0.18

a) Urea concentration is 3 mol kg^{-1}.

In our experiment no systematic deviations at higher concentrations from the straight line expressed by Eq. 5 were observed up to the highest concentration studied, and so our data were extrapolated using Eq. 5 following Millero *et al.*[9)]

Discussion

The volume and compressibility behaviour of solutes in solution can provide information concerning solute-solvent and solute-solute interactions. The infinite dilution partial molal volumes and adiabatic compressibilities are, by definition, independent of solute-solute interactions and thus determined only by the respective intrinsic value and the solute-solvent interactions. Accordingly, they can be used to examine solute-solvent interactions. The slopes, S_V and S_K, can be assumed to be an indication of solute-solute interactions. The volumes of transfer, $\Delta\overline{V}_{tr}^{\circ}=\overline{V}^{\circ}$(urea)$-\overline{V}^{\circ}$(water), for some amino acids studied are plotted *versus* the urea concentration (Fig. 3). The magnitudes of the transfer functions increase continuously with the urea concentration. The same trend was observed by Enea *et al.*[14)] for the transfer functions of the heat capacities and volumes of three amino acids (Gly, Ala, and Ser) and several oligopeptides in urea-water systems. Detailed results are, however, presented only for 7 mol dm^{-3} urea concentration, and we cannot compare our volume data with their data directly, though the sequence of increment of $\Delta\overline{V}_{tr}^{\circ}$ for these three amino acids are identical with ours. Desrosiers *et al.*[15)] also observed the same trend for the transfer functions of the volume, expansibility, compressibility and heat capacity of alkali halides in urea-water mixtures. The transfer functions of volume for Ala and β-Ala are very similar up to 8 mol kg^{-1} urea concentration, though their $\overline{V}^{\circ}$ values differ by *ca.* 2 cm^3 mol^{-1} in urea-water mixtures as well as in water. This fact indicates the more effective hydration of β-Ala in aqueous urea solutions in comparison with Ala to almost the same amount as in water. In Fig. 4 $\overline{V}^{\circ}$'s are plotted *versus* V_W; V_W is the van der Waals volume, which was calculated using the data reported by Bondi[16)] and by Edward.[17)] As seen from Fig. 4, the amino acids having no OH group lie almost on a straight line both in water and in 8 mol kg^{-1} urea. Positions of

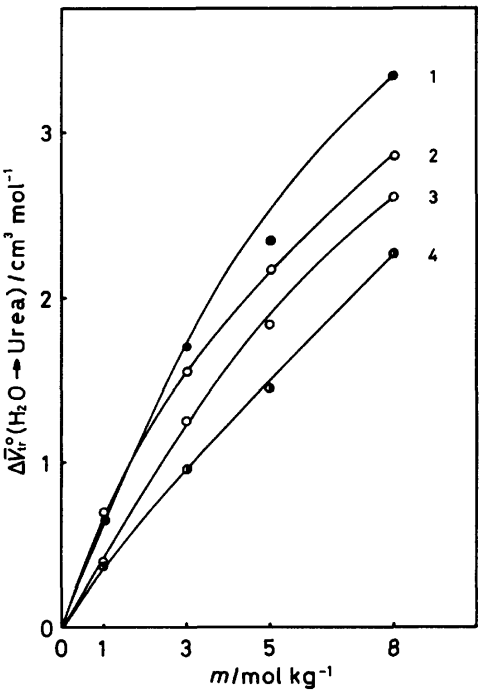

Fig. 3. Plot of $\Delta\overline{V}_{tr}^{\circ}$ *vs.* urea concentration.
(1) Ser, (2) Gly, (3) Ala, (4) Me-ala.

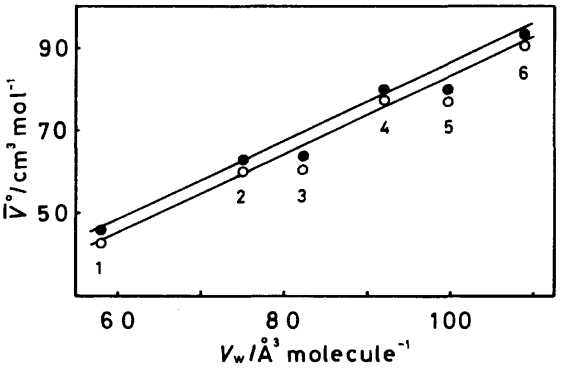

Fig. 4. Plot of $\overline{V}^{\circ}$ of α-amino acids *vs.* van der Waals volume.
(1) Gly, (2) Ala, (3) Ser, (4) Me-ala, (5) Thr, (6) Val.
○: in water, ●: in 8 mol kg^{-1} urea.

serine and threonine which have OH groups are below the straight line in urea solution as in water. This fact shows that even in 8 mol kg^{-1} urea solution there is a rather large volume decrease brought about by hydrogen bonding of the OH group with water.

Millero *et al.*[9] estimated the intrinsic partial molal volume $\overline{V}°$(int) of amino acids from the crystal volume and also from the partial molal volume of uncharged isomers. The intrinsic volume is made up of two terms, the van der Waals volume and the volume due to packing effects. They obtained the electrostriction partial molal volume, $\overline{V}°$(elect), due to the hydration of amino acid from the experimentaly measured $\overline{V}°$ and the reasonably estimated $\overline{V}°$(int):

$$\overline{V}°(\text{elect}) = \overline{V}° - \overline{V}°(\text{int}). \quad (7)$$

Using the corresponding equation for the adiabatic compressibility

$$\overline{K}°(\text{elect}) = \overline{K}° - \overline{K}°(\text{int}), \quad (8)$$

they also estimated the electrostriction partial molal compressibilities of the amino acids. From both $\overline{V}°$(elect) and $\overline{K}°$(elect) they estimated the number of water molecules hydrated to the amino acids as 4.1±0.4. Recently, Shahidi and Farrell[13] also calculated the electrostriction volumes and the number of hydrated water for the amino acids from a somewhat different standpoint using Eq. 9 and consideration of the branching effects

$$\overline{V}° = 4\pi(r_w + 0.57)^3 N_A/3 - \sum_{i=1}^{m} n_i\sigma_i - E, \quad (9)$$

where r_W is the van der Waals radius of the amino acid, n_i is the number of interacting groups of type i in the solute, which contains m different interacting groups with the solvent; σ_i is the volume decrease due to the specific group-solvent interaction (*e.g.*, hydrogen-bonding),[18] and N_A is the Avogadro constant. The van der Waals radius is calculated from the van der Waals volume V_W assuming the amino acid to be spherical *i.e.*, $r_W=(3V_W/4\pi)^{1/3}$. The value 0.57 in Eq. 9 is added to the van der Waals radius because there is an empty volume between the solute and the solvent, which is assumed to be a spherical shell of constant thickness of 0.57 Å. An average of 13.0±1.2 cm^3 mol^{-1} was obtained for the electrostriction E for the α-amino acids. Since the volume of water is decreased by 3 cm^3 per mole when taken from the bulk phase to the region near the amino acid,[9] the number of water molecules involved in hydration of the α-amino acid is calculated as to be 4.33±0.39.

As noted by Millero *et al.*,[9] $\overline{K}°$(int) is small and as a first approximation one can assume $\overline{K}°$(int)=0. This makes $\overline{K}°=\overline{K}°$(elect). Thus the adiabatic compressibilities are the better measure for the hydration of the solute. The partial molal adiabatic compressibilities of the seven amino acids studied increase (*i.e.*, less negative) in the following order in water:

Thr<Val<Ser<Gly<β-Ala<Ala<Me-ala,

and in the following order in 3 mol kg^{-1} urea solution:

Ser<Thr<Gly<β-Ala<Val<Ala<Me-ala.

From these two series it is seen that the most hydrophobic solute studied, valine, is most affected by the transfer from water to 3 mol kg^{-1} urea solution. Of the solutes having an OH group threonine is more hydrophobic than serine and has a larger value of $\Delta\overline{K}_{tr}°$. The sequence Gly<β-Ala<Ala<Me-ala is the same both in water and in urea solution. By the introduction of the methyl group in glycine, *i.e.*, Gly→Ala and Ala→Me-ala, cospheres of the hydrophilic COO^- and NH_3^+ groups overlap with that of the hydrophobic group, thus decreasing their hydration ability in that order both in water and in aqueous urea solution. The decrease in hydration is reflected in the increase in compressibility. Concerning alanines, β-alanine with a larger charge separation has a larger negative value of adiabatic compressibility, indicating that β-alanine has a larger number of hydrated water molecules. According to Millero *et al.*[9] the number of water molecules hydrated to the amino acid, n_H, is given by

$$n_H = -\overline{K}°(\text{elect})/\beta_B°\overline{V}_B°, \quad (10)$$

where $\beta_B°$ is the compressibility of bulk water and $\overline{V}_B°$ is the molar volume of bulk water. As shown by Desrosiers *et al.*,[15] $\beta_B°$ and $\overline{V}_B°$ values in 3 mol kg^{-1} urea solution differ only slightly from those in pure water. Thus the ratio $\overline{K}°$(urea)/$\overline{K}°$(water) represents the ratio of hydration number of the solute in aqueous urea solution to that in water. The ratios for valine and α-aminoisobutyric acid are 0.52 and 0.53 respectively and those for the other amino acids studied are 0.61—0.67. The results show that more hydrophobic amino acids undergo more dehydration effect of urea.

As noted by Enea and Jolicoeur,[14] urea-water mixtures exhibit a dielectric constant similar to water (8% higher at 3 mol dm^{-3} urea), so the electrostatic hydration effects of amino acids should be comparable in both solvents; further, it may be improbable that the pK values of amino acids in urea-water mixtures differ appreciably from those in pure water. The pH values of 0.3 mol kg^{-1} amino acid aqueous solutions studied here, *e.g.*, glycine; 6.0, β-alanine: 6.8, were very close to the isoelectric point of the respective amino acid. Those of the corresponding aqueous urea solutions were only *ca.* 0.4 pH unit higher than those in water, *e.g.*, glycine: 6.4, β-alanine: 7.2. Accordingly, all amino acid molecules can be considered to exist virtually as zwitter ions in both solvents; hence, association or dissociation effects of ionic groups to $\phi_V°$ or $\phi_{KS}°$ must be trivial for water→aqueous urea transfer.

As noted above, the amino acids have *ca.* 4 molecules of hydrated water on an average, then how many water molecules hydrate the amino acids in 3 mol kg^{-1} urea-water mixtures? Since, for example, the value of $\overline{K}°$(urea)/$\overline{K}°$(water) for alanine is 0.6, it is estimated that it has 2.4 hydrated water molecules in the solvent. On the other hand, the value of $\Delta\overline{V}_{tr}°$ of alanine from water to the solvent was 1.25 cm^3 mol^{-1}; if it is supposed that this increment of volume is entirely due to the decrease in hydration in the solvent, the decrease in hydrated water molecules is 1.25/3=0.42, thus the alanine molecule has 3.6 water molecules in the solvent. Accordingly, the compressibility data gave the smaller hydration number than that derived from the vol-

ume data. Of these two values, 2.4 and 3.6, we consider that the former may be more correct, because the compressibility data are more directly related to hydration; the same relationship as for alanine was seen for the other amino acids studied. Thus, using the compressibility data as a measure of hydration, we tried to estimate the thickness of the empty volume between the amino acid and the solvent in 3 mol kg^{-1} urea solution, which is 0.57 Å in aqueous solution, from Eq. 9. The decrease in the thickness brings about the decrease in $\Delta\overline{V}_{tr}^{\circ}$, so seemingly the increase in hydration number in the solvent. The electrostriction E in Eq. 9 was modified by a factor $\overline{K}^{\circ}$(urea)/$\overline{K}^{\circ}$(water) of respective amino acid; the resulting electrostriction E' was used, together with σ_i and $\overline{V}^{\circ}$(urea), to calculate the thickness for each amino acid in the mixed solvent. As with σ_i values, the hydrogen-bonding effect of OH group of serine and threonine is still apparent in even 8 mol kg^{-1} urea solution as seen from Fig. 4, so the values in water were used. The results show that the thickness is 0.54±0.02 Å instead of 0.57 Å in water. Though more experimental studies must be necessary to draw a firm conclusion, the decrease in thickness by 0.03 Å on the average might be due to the lower structure in the mixed solvent broken by the presence of urea. In order to clarify the thermodynamics of amino acid solutions, similar studies in other mixed solvent media are in progress.

The authors wish to express their thanks to Professor Hiroyasu Nomura and Dr. Fumio Kawaizumi of Nagoya University for their helpful suggestion on making the improved ultrasonic interferometer.

References

1) H. S. Frank and F. Franks, *J. Chem. Phys.*, **48**, 4764 (1968).
2) J. G. Mathieson and B. E. Conway, *J. Solution Chem.*, **3**, 781 (1974).
3) F. Franks and H. T. Smith, *Trans. Faraday Soc.*, **63**, 2586 (1967).
4) J. G. Mathieson and B. E. Conway, *J. Solution Chem.*, **3**, 455 (1974).
5) H. Nomura and R. E. Verrall, *J. Phys. Chem.*, **85**, 1042 (1981).
6) "CRC Hand Book of Chemistry and Physics," 61st ed, CRC Press, Boca Raton, Florida (1980), p. F-11.
7) "Kagaku Binran (Handbook of Chemistry)," 2nd ed, ed by the Chemical Society of Japan, Maruzen, Tokyo (1975), p. 667.
8) Private communication. For details see Ref. 5.
9) F. J. Millero, A. Lo Surdo, and C. Shin, *J. Phys. Chem.*, **82**, 784 (1978).
10) S. Cabani, G. Conti, E. Matteoli, and M. R. Tiné, *J. Chem. Soc., Faraday Trans. 1*, **77**, 2385 (1981).
11) J. C. Ahluwalia, C. Ostiguy, G. Perron, and J. E. Desnoyers, *Can. J. Chem.*, **55**, 3364 (1977).
12) C. Jolicoeur and J. Boileau, *Can. J. Chem.*, **56**, 2707 (1978).
13) F. Shahidi and P. G. Farrell, *J. Chem. Soc., Faraday Trans. 1*, **77**, 963 (1977).
14) O. Enea and C. Jolicoeur, *J. Phys. Chem.*, **86**, 3870 (1982).
15) N. Desrosiers, G. Perron, J. G. Mathieson, B. E. Conway, and J. E. Desnoyers, *J. Solution Chem.*, **3**, 789 (1974).
16) A. Bondi, *J. Phys. Chem.*, **68**, 441 (1964).
17) J. T. Edward, *J. Chem. Educ.*, **47**, 261 (1970).
18) F. Shahidi, P. G. Farrell, and J. T. Edward, *J. Chem. Soc., Faraday Trans. 1*, **73**, 715 (1977).

 © 1984 The Chemical Society of Japan Bull. Chem. Soc. Jpn., 57, 667—672 (1984)

Kinetic and Mechanistic Studies on the Kölbel-Engelhardt Reaction over an Iron Oxide Catalyst

Yasushi MIYATA, Masamichi AKIMOTO,* Nobukazu OOBA, and Etsuro ECHIGOYA
Department of Chemical Engineering, Tokyo Institute of Technology, Ookayama, Meguro-ku, Tokyo 152
(Received August 2, 1983)

The yield and selectivity to hydrocarbons in the Kölbel-Engelhardt (KE) reaction over a Fe_2O_3 catalyst at 548—593 K under atmospheric pressure were as low as 0.6—2.2% and 2.0—3.8%, respectively, but the observed four characteristic features of the reaction, *i.e.*, the distribution of produced hydrocarbons following the Schulz-Flory plot, the decrease in propagation probability with increasing reaction temperature, nearly the same value of propagation probability irrespective of a great change in contact time of the reaction, and the remarkable decrease in the yield ratio of olefins to paraffins with increasing contact time of the reaction agreed with the common features of the synthesis of hydrocarbons by the Fischer-Tropsch reaction. The catalyst was composed of Fe_3O_4 with a low concentration of χ-type carbide (Fe_5C_2) during the KE reaction, and the results of the effect of contact time on the reaction revealed that formation of hydrocarbons took place following the water-gas shift (WGS) reaction. Furthermore, both the rates of formation of hydrocarbons in the reactions of carbided iron catalyst (Fe_5C_2) with H_2O and with H_2 at 573 K were smaller by a factor of >5 than the rate of formation of hydrocarbons in the KE reaction at a steady state at 573 K. Thus, it is concluded that a much greater portion of hydrocarbons produced in the KE reaction was *via* a sequential reaction pathway involving the WGS reaction followed by the Fischer-Tropsch reaction, not *via* the decomposition of carbided iron catalyst with H_2O and its reduction with H_2. Based on the observed increase in the catalytic activity of Fe_2O_3 upon addition of a small amount of such metal oxides as Cu, Pt, Co, Ni, and Rh oxides, the mechanical mixture of a WGS reaction catalyst and a Fischer-Tropsch reaction catalyst is proposed to be an effective catalyst for the production of hydrocarbons and one illustration of this view is presented.

The catalytic reaction of CO with H_2O to produce hydrocarbons and CO_2 is known as the Kölbel-Engelhardt (KE) reaction.[1] Recently, the KE reaction has received a great deal of attention as a process for the production of hydrocarbons from CO-rich synthesis gas, and the catalytic activity of Fe and Fe-based catalysts,[2-4] a RuY-zeolite catalyst[5] and supported Rh catalysts[6] has been investigated. However, the mechanism of the KE reaction has not been firmly established. There are two possible pathways by which the reaction may proceed. The first pathway involves the coupling of a WGS reaction and a Fischer-Tropsch reaction. The second possibility involves a reaction of H_2O with metal carbide or surface carbons to form hydrocarbons. Gustafson and Lunsford[5] indicated that the KE reaction over a RuY-zeolite catalyst by which only CH_4, CO_2, and H_2 were produced proceeds *via* a sequential reaction pathway involving the WGS reaction followed by the methanation reaction. While the first pathway is thus generally acceptable there are reports[7,8] which suggest that H_2O may react with metal carbide to form hydrocarbons in the KE reaction over Fe-based catalysts.

In the present work, we have mechanistically investigated the KE reaction over a Fe_2O_3 catalyst and have then discussed the promotional effects of Cu, Pt, Co, Ni, Cr, Rh, Ru, and Pd oxides on the catalytic activity of Fe_2O_3 in relation to the mechanism of the KE reaction.

Experimental

Reaction and Analysis The catalytic reaction of CO with H_2O was carried out at 548—593 K with a conventional flow fixed-bed reactor at atmospheric pressure. The reactor system comprised a 18-mm-i.d. Pyrex tube, 350 mm long, and a concentric thermowell. The reactor was heated with a cylindrical electric furnace. The catalyst was of powder-type, and Rasching rings (3×3 mm) were added above and below the catalyst bed. Research grade CO–Ar mixed gas (CO 90.2 vol%, Japan Oxygen Company, Ltd.) was used. It was fed into the reactor after bubbling through a H_2O-saturator held at a controlled temperature. The standard feed rate of the CO–Ar gas was 20 NTP cm^3 min^{-1} and the feed molar ratio of CO to H_2O was always 3. Purchased He and H_2 of greater than 99.99% purity were used without further purification. All reaction products were analyzed by gas chromatography. Two columns in series, 2.0 m of Porapak Q(383 K) and 1.5 m of Molecular sieve 5A(308 K), and hydrogen as the carrier gas were used for the analysis of CO, CO_2, Ar, and H_2O. Hydrogen, CH_4, and CO were analyzed by means of 2.0 m of Molecular Sieve 5A (323 K) with Ar as the carrier gas, and hydrocarbons were analyzed with a temperature-programmed FID system (Shimadzu GC-MINI 2, 333→473 K, Chromosorb 102 3.0 m).

Catalyst. A Fe_2O_3 catalyst was prepared following the method reported[9]: the $Fe(OH)_3$ cake obtained was dried at *ca.* 380 K in an electric oven for 24 h and was then calcined at 673 K in air for 6 h. X-Ray powder diffraction analysis revealed that Fe_2O_3 thus prepared was of α-type (hematite).[10] Its surface area determined by the conventional B.E.T. method was 28 m^2 g^{-1}. We also prepared metal oxide-promoted Fe_2O_3 catalysts and SiO_2-and Al_2O_3-supported metal oxide catalysts using an impregnation method. Metal oxide-promoted Fe_2O_3 catalysts were prepared by use of the Fe_2O_3 catalyst prepared above. Al_2O_3 employed as a carrier was JRC-ALO-4(60—80 mesh, 166—174 m^2g^{-1}), one of the referenced Al_2O_3 catalysts in the Catalysis Society of Japan.[11] SiO_2(32—60 mesh) as a carrier had a B. E. T. surface area of 200 m^2 g^{-1}. Metal nitrates were used as a catalyst resource for Cu, Co, Ni, and Cr oxides whereas metal chlorides were used similarly for Ru, Rh, and Pd oxides. These impregnated catalysts were then calcined at 673 K in air for 3 h. Supported Pt oxide catalysts were similarly prepared by use of $H_2PtCl_6 \cdot 6H_2O$. A CuO-ZnO catalyst (24 m^2 g^{-1}), a commercial catalyst for the WGS reaction, was prepared following the

method reported.[12]

Results

KE Reaction over Fe_2O_3. The characteristic feature of the KE reaction over Fe_2O_3 was first investigated. Non-pretreated Fe_2O_3 catalyst (15.0 g) was packed in the reactor and was heated to the reaction temperature after complete purging of air from the reactor with He at room temperature. Table 1 summarizes the steady-state catalytic activities of Fe_2O_3 in the KE reaction at 548, 573, and 593 K. These catalytic activities were obtained after a preliminary period of 4—5 h and the conversion of H_2O was always nearly 100% at these three reaction temperatures. The main products in the reaction were CO_2 and H_2, as reported previously.[2-4] The conversion of CO and the yield of hydrocarbons were 30.5 and 0.6% at 548 K, and the conversion increased to 45.2 and 67.5% with increasing reaction temperature from 548 K to 573 and 593 K but the yield of hydrocarbons still remained to be as low as 1.7% (selectivity=3.8%) and 2.2% (3.2%) at 573 and 593 K, respectively (Table 1). The equilibrium conversion of CO due to the WGS reaction calculated on the basis of thermodynamic data[13] is 32.7% at a (CO/H_2O) feed molar ratio of 3 at 600 K. Hence, the relatively great values of the conversion of CO, 45.2 and 67.5%, found at 573 and 593 K (Table 1) are probably caused by the occurrence of the Boudouard reaction($2CO \rightarrow CO_2+C$). On the other hand, the distribution of hydrocarbons produced by the KE reaction at these three reaction temperatures followed the Schulz-Flory plot† (Fig. 1, at 573 K). The values of propagation probability obtained are also summarized in Table 1. The propagation probability decreased with increasing reaction temperature (Table 1).

Table 1. Summary of the steady-state catalytic activity of Fe_2O_3 for the KE reaction[a]

Reaction temp/K	548	573	593
Conversion of CO/%	30.5	45.2	67.5
Yield of H.C.[b]/%	0.6	1.7	2.2
Selectivity to H.C.[b]/%	2.0	3.8	3.2
Hydrocarbon	Distribution/carbon wt%		
C_1	15	24	35
C_2'	10	14	18
C_2	10	14	11
C_3'	19	22	18
C_3	1	3	2
C_4	13	8	6
C_5	12	7	4
C_6	9	4	3
C_7	9	2	1
C_{8+}[c]	1	2	3
Propagation probability/—	0.66	0.48	0.38

a) Catalyst: Fe_2O_3 15.0 g, non-pretreated. Contact time: 311 g-catalyst·h·mol CO^{-1}. CO/H_2O feed molar ratio: 3. b) Hydrocarbons. C_2'=ethylene, C_2=ethane, C_3'=propylene, C_3=propane, C_n($n \geq 4$)=hydrocarbons having n carbon atoms in a molecule. c) Hydrocarbons having eight and more than eight carbon atoms in a molecule.

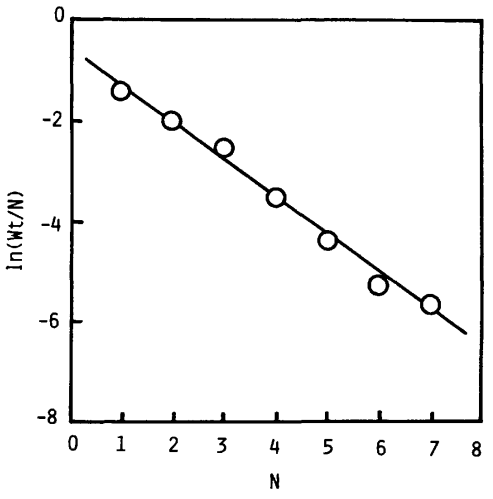

Fig. 1. Schulz-Flory plot for the hydrocarbons obtained at a steady state in the KE reaction at 573 K. Catalyst: Fe_2O_3 15.0 g, non-pretreated. Contact time: 311 g-catalyst·h·mol CO^{-1}. CO/H_2O feed molar ratio: 3.

The steady state of Fe_2O_3 during the KE reaction at a (CO/H_2O) feed molar ratio of 3 at 573 K was quenched by flushing the reactor with He. The result of X-ray powder diffraction analysis revealed that the quenched catalyst was composed of Fe_3O_4 (magnetite)[14] and Fe_5C_2 (χ-type carbide)[15] with a ratio of the strongest diffraction peak of 100:5.

Effect of Contact Time. Figure 2 shows the effect of contact time on the KE reaction over Fe_2O_3 at 573 K. At a contact time of 18.7 g-catalyst·h·mol CO^{-1} the yield of hydrocarbons was negligible although the conversion of CO was as high as 18.0%: both the yields of CO_2 and H_2 were nearly the same as the conversion of CO. However, formation of hydrocarbons was seen at 29.4 g-catalyst·h·mol CO^{-1} and the yield of hydrocarbons then increased with increasing contact time of the reaction to reach 2.8% at 562 g-catalyst·h·mol CO^{-1} (Fig. 2). The propagation probability calculated on the basis of the Schulz-Flory plot remained nearly constant at 0.47—0.49 at 573 K although the contact time changed greatly between 29.4 and 562 g-catalyst·h·mol CO^{-1}. In contrast, the ratio of the combined yield of $C_2H_4+C_3H_6$ to that of $C_2H_6+C_3H_8$ was 25.9, 9.4, and 0.5 at 29.4, 141, and 562 g-catalyst·h·mol CO^{-1}, respectively. Thus the ratio of the yield of olefins to that of paraffins decreased markedly with increasing contact time of the reaction.

Reaction of H_2O with Carbided Iron Catalyst. The reaction of H_2O with Fe_5C_2 was studied at 573 K. The

† Schulz-Flory plot

$$\ln \frac{W_t}{N} = N \ln P + \ln \frac{(1-P)^2}{P},$$

where N, P, and W_t are number of carbon atom in hydrocarbon molecule produced, propagation probability, and distribution (carbon weight fraction) of hydrocarbon molecule having N carbon atoms, respectively.

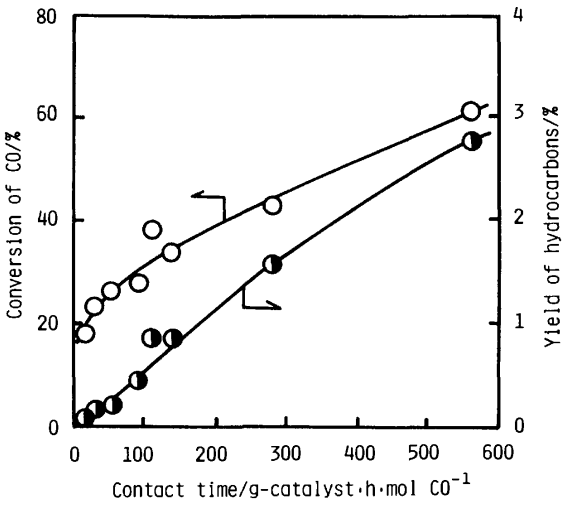

Fig. 2. Effect of contact time on the KE reaction at 573 K.
Catalyst: Fe_2O_3, non-pretreated. CO/H_2O feed molar ratio: 3.
○: Conversion of CO, ◑: Yield of hydrocarbons.

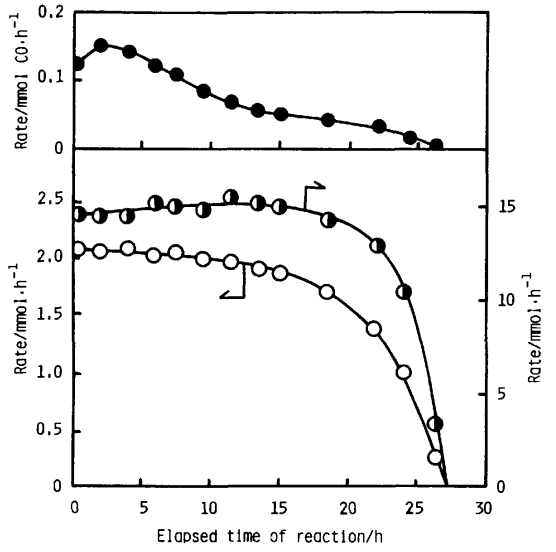

Fig. 3. Variation in the rates of H_2, CO_2, and hydrocarbon formations during the reaction of H_2O with carbided iron catalyst at 573 K.
Catalyst pretreatment: Fe_2O_3 (15.0 g) was carbided in a stream of CO-Ar(CO 90.2 vol%, 60 NTP cm^3 min^{-1}) at 573 K for 22 h.
Reaction with H_2O: Ar/H_2O feed molar ratio=3, Ar 20 NTP cm^3 min^{-1}.
○: Rate of CO_2 formation, ◑: rate of H_2 formation, ●: rate of hydrocarbon formation.

Fe_2O_3 catalyst (15.0 g) had been carbided in a stream of CO-Ar (CO 90.2 vol%, 60 NTP cm^3 min^{-1}) at 573 K for 22 h. The result of X-ray powder diffraction analysis revealed that the Fe_2O_3 catalyst was completely carbided to Fe_5C_2[15] by the above pretreatment. Figure 3 shows variation in the rates of formation of H_2, CO_2, and hydrocarbons with time during the reaction of H_2O with the carbided iron catalyst at 573 K. The rate of formation of hydrocarbons showed the maximum value (0.15 mmol $CO \cdot h^{-1}$) at 45 min, but it then decreased with time and reached negligible values within 27 h. The rates of formation of CO_2 and H_2 also showed a similar behavior (Fig. 3). Thus, the decomposition of Fe_5C_2 with H_2O at 573 K was completed within 27 h. It should be noted that the maximum rate of formation of hydrocarbons obtained in the reaction of H_2O with the carbided iron catalyst at 573 K was smaller by a factor of five than the rate of formation of hydrocarbons at a steady state in the KE reaction at 573 K (0.816 mmol $CO \cdot h^{-1}$, Table 1). The hydrocarbons formed in the reaction had the distributions similar to those of hydrocarbons produced in the KE reaction (Table 1) although the distribution of CH_4 in the former reaction was fairly greater than that in the latter reaction and although the yield of higher hydrocarbons was negligible in the former reaction (*i.e.*, C_1 47 wt%, C_2' 12 wt%, C_2 9 wt%, C_3' 16 wt%, C_3 7 w%, and C_4 9 wt% at 18 h). The result of X-ray powder diffraction analysis revealed that the carbided iron catalyst completely changed to Fe_2O_3 after the reaction with H_2O at 573 K for 27 h.

Table 2. Material balance for the reaction of H_2O with carbided iron catalyst at 573 K for 27 h[a]

Reactants and products	Amount/mol
H_2O fed	0.42
H_2O reacted	0.38
H_2 evolved	0.37
CO_2 evolved	0.061
Hydrocarbons formed	0.002[b]
Carbon in carbided iron catalyst	0.075[c]

a) Reaction conditions: see Fig. 3. b) Carbon atoms converted to hydrocarbons. c) Calculated as Fe_5C_2 in atom unit.

The material balance for the reaction of H_2O with the carbided iron catalyst at 573 K for 27 h (Fig. 3) is presented in Table 2. The amount of oxygen caught by the carbided iron catalyst was 0.38—0.061×2=0.26 atoms, which is nearly equal to the amount of oxygen contained in 15.0 g of Fe_2O_3 (0.28 atoms). Similarly, the amount of CO_2 evolved (0.061 mol) was nearly equal to that of carbon previously existed in the Fe_5C_2 (0.075 atoms), and the ratio of the amount of H_2 evolved to that of CO_2 evolved was 0.37/0.061=6.0. The total yield of hydrocarbons was as low as (0.002/0.075)×100 =3% (Table 2).

Reduction of Carbided Iron Catalyst with H_2. The Fe_2O_3 catalyst (15.0 g) had similarly been carbided in a stream of CO-Ar at 573 K for 22 h, and the carbided iron catalyst obtained was then reduced at 573 K in a stream of H_2-Ar (H_2 33.3 vol%, 30 NTP cm^3 min^{-1}). The main product in the reaction was CH_4. Although formation of C_2H_4, C_2H_6, and C_3H_6 was seen at the initial stages of the reaction, the yield of these hydrocarbons was as low as 0.05, 0.5, and 0.6%, respectively, of the yield of CH_4. The rate of formation of hydrocarbons in the reduction experiment at 573 K was 0.22,

0.19, and 0.12 mmol $CO \cdot h^{-1}$ at 10, 30, and 60 min, respectively. These three values were much smaller than the rate of formation of hydrocarbons observed in the KE reaction at a steady state at 573 K (0.816 mmol $CO \cdot h^{-1}$, Table 1).

Effect of Pretreatment of Catalyst. The effect of pretreatment of Fe_2O_3 on its catalytic activity for the KE reaction was studied. When the catalyst had been reduced at 573 K in a stream of CO–Ar (CO 90.2 vol%, 60 NTP $cm^3\ min^{-1}$) for 23 h, the conversion of CO, the yield and selectivity to hydrocarbons were 64.4, 3.1, and 4.8%, respectively, at 30 min (Table 3). These values are clearly greater than those observed at a steady state in the KE reaction over the non-pretreated Fe_2O_3 catalyst (Table 1). The decrease in catalytic activity of the prereduced Fe_2O_3 with time (Table 3) was probably caused by the reoxidation of the catalyst with H_2O. Similarly, the catalytic activity of Fe_2O_3 was much more greatly enhanced by the pretreatment with CO and H_2 (Table 3). The X-ray diffraction pattern of the catalyst prereduced with CO and H_2 could not be measured because the reoxidation took place in atmosphere.

Promotional Effect of Metal Oxides. The activity of metal oxide-promoted Fe_2O_3 catalysts for the KE reaction was monitored at 573 K (Table 4). When the Fe_2O_3 catalyst had been promoted by oxides of Cu, Pt, Co, and Ni, the conversion of CO, the yield and selectivity to hydrocarbons fairly increased although the distribution of hydrocarbons formed remained nearly unchanged. In contrast, the catalytic activity of Fe_2O_3 rather decreased when it had been promoted by oxides of Cr, Rh, Ru, and Pd. Unlike Cr, Ru, and Pd oxides, however, Rh oxide was able to enhance the yield and selectivity to hydrocarbons markedly (Table 4). Since the Fe_2O_3 catalyst impregnated with HCl (0.7 wt%) showed a negligible activity for the KE reaction at 573 K (conversion of CO=1.6%, yield of hydrocarbons =0%), the extremely low catalytic activity of the Fe_2O_3 promoted by oxides of Rh, Ru, and Pd (Table 4) can be attributed to the presence of Cl^- in these catalysts (See preparation of catalyst).

The catalytic activity of SiO_2-supported Cu, Pt, Co, Ni, Cr, Rh, Ru, and Pd oxides for the KE reaction was similarly monitored at 573 K (Table 5). The catalysts had been reduced at 573 K in a stream of H_2 (20 NTP $cm^3\ min^{-1}$) for 3 h because the metal oxide-promoted Fe_2O_3 catalysts were exposed to H_2 at 573 K formed via the WGS reaction during the KE reaction. The main products in the reaction were CO_2 and H_2, and with the exception of the catalytic results for the supported Co and Ni oxides both the yields of CO_2 and H_2 were nearly equal to the conversion of CO. Thus, only the supported Co and Ni oxide catalysts were able to produce hydrocarbons whereas the other supported metal oxide catalysts promoted

Table 3. Effect of various pretreatments on the catalytic activity of Fe_2O_3 in the KE reaction at 573 K[a]

Pretreatment	CO[b]		CO and H_2[c]	
	At 30 min	At 10 h	At 30 min	At 10 h
Conversion of CO/%	64.4	43.7	96.1	43.6
Yield of H.C.[d]/%	3.1	1.7	7.9	1.7
Selectivity to H.C.[d]/%	4.8	3.9	8.3	3.9

a) Catalyst: Fe_2O_3 15.0 g. Contact time: 311 g-catalyst·h·mol CO^{-1}. CO/H_2O feed molar ratio: 3. b) The catalyst was previously reduced at 573 K in a steam of CO–Ar (CO 90.2 vol%, 60 NTP $cm^3\ min^{-1}$) for 23 h. c) The catalyst was previously reduced at 573 K in a stream of CO–Ar (CO 90.2 vol%, 40 NTP $cm^3\ min^{-1}$) for 30 h and was then reduced at 573 K in a stream of H_2 (20 NTP $cm^3\ min^{-1}$) for 30 h. d) Hydrocarbons.

Table 4. Summary of the activity of metal oxide-promoted Fe_2O_3 catalysts in the KE reaction at 573 K[a]

Metal	Conversion of CO/%	Yield of H.C.[b]/%	Selectivity to H.C.[b]/%	Distribution of hydrocarbons/carbon wt%									
				C_1	C_2'	C_2	C_3'	C_3	C_4	C_5	C_6	C_7	C_{8+}
None	45.2	1.7	3.8	24	14	14	22	3	8	7	4	2	3
Pt	47.3	1.9	4.1	22	9	18	19	5	12	7	4	2	2
Cu	57.4	2.9	5.0	23	8	18	20	5	12	6	4	2	2
Co	53.2	2.6	4.8	24	10	16	21	4	12	6	4	1	2
Ni	52.9	3.4	6.3	27	6	20	16	7	11	6	3	2	2
Cr	38.3	0.7	1.7	22	18	11	20	1	13	8	4	1	3
Rh	18.5	2.1	13.8	29	5	9	23	4	13	12	4	2	0
Ru	3.9	0.01	0.3	40	60	0	0	0	0	0	0	0	0
Pd	4.9	0	0	—	—	—	—	—	—	—	—	—	—

a) Catalyst: M_xO_y–Fe_2O_3 (M/Fe_2O_3=0.2 wt%) 15.0 g, non-pretreated. Contact time: 311 g-catalyst·h·mol CO^{-1}. CO/H_2O feed molar ratio: 3. The catalytic activity was determined after a preliminary period of 5 h. b) Hydrocarbons.

Table 5. Summary of the catalytic activity of SiO_2-supported metal oxides for the KE reaction at 573 K[a)]

Catalyst	Conversion of CO/%	Yield of H.C.[b)]/%
0.4 wt% Pt	21.0	0
2.0 wt% Cu	33.0	0
2.0 wt% Co	23.1	1.2
2.0 wt% Ni	51.0	10.7
2.0 wt% Cr	1.7	0
0.4 wt% Rh	0.4	0
1.6 wt% Ru	3.8	0
0.4 wt% Pd	4.7	0

a) Catalyst: M_xO_y-SiO_2 15.0 g, previously reduced in a stream of H_2 (20 NTP cm^3 min^{-1}) at 573 K for 3 h. Contact time: 311 g-catalyst·h·mol CO^{-1}. CO/H_2O feed molar ratio: 3. The catalytic activity was determined after a preliminary period of 20 min. b) Hydrocarbons. The other products were CO_2 and H_2.

only the WGS reaction (Table 5). The observation of the relatively great catalytic activities of the supported Pt and Cu oxide catalysts for the WGS reaction agrees with the previous results reported.[16] Hence, one could say that Pt and Cu oxides have a relatively great ability to catalyze the WGS reaction whereas Co and Ni oxides are able to catalyze both the WGS and the KE reactions. No formation of hydrocarbons over the SiO_2-supported Rh oxide catalyst is attributable to its fairly low catalytic activity for the WGS reaction as seen in the extremely low conversion of CO (Table 5).

Discussion

We first discuss the mechanism of the KE reaction over iron-based catalysts. Although the yield and selectivity to hydrocarbons in the KE reaction at 548—593 K were as low as 0.6—2.2% and 2.0—3.8%, respectively (Table 1), the observed four characteristic features of the reaction, *i.e.*, the distribution of produced hydrocarbons following the Schulz-Flory plot, the decrease in propagation probability with increasing reaction temperature, nearly the same value of propagation probability irrespective of the great change in contact time of the reaction, and the remarkable decrease in the yield ratio of olefins to paraffins with increasing contact time of the reaction (Table 1, Figs. 1 and 2) well agree with the common features of the synthesis of hydrocarbons by the Fischer-Tropsch reaction reported. The findings that only the WGS reaction took place at sufficiently small contact times of the KE reaction and that formation of hydrocarbons became to be observable at a relatively great contact time of the reaction (Fig. 2) suggest that the KE reaction over Fe_2O_3 proceeds *via* a sequential reaction pathway involving the WGS reaction followed by the hydrogenation of CO to hydrocarbons.

Formation of hydrocarbons by the reaction of carbided iron catalysts with H_2O was already found.[7,8] Based on this finding the mechanism of the KE reaction over iron oxide catalysts was proposed in which hydrocarbons are formed via a direct reaction of H_2O with iron carbide.[7] However, the two findings made in the present work, *i.e.*, the low rate of formation of hydrocarbons in the reaction of H_2O with carbided iron catalyst at 573 K as compared with the rate of formation of hydrocarbons in the KE reaction over Fe_2O_3 at a steady state at 573 K (Fig. 3) and the very low concentration of Fe_5C_2 in the catalyst during the KE reaction at 573 K (See Results section) do not support the mechanism of the KE reaction reported.[7] Since the ratio of the total yield of H_2 to that of CO_2 in the reaction of the carbided iron catalyst with H_2O at 573 K was 6.0 and since the total yield of hydrocarbons in the reaction was as low as 3% of the amount of carbon existed in the carbided iron catalyst (Table 2), we believe that the reaction of the carbided iron catalyst (Fe_5C_2) with H_2O proceeds preferentially in the following reaction scheme:

$$2Fe_5C_2 + 23H_2O \longrightarrow 5Fe_2O_3 + 23H_2 + 4CO_2. \quad (1)$$

On the other hand, both the selective formation of CH_4 in the reduction of the carbided iron catalyst with H_2 at 573 K and the low rate of CH_4 formation as compared with the rate of formation of hydrocarbons observed in the KE reaction at a steady state at 573 K (See Results section) do not support the view that the C_2 and higher hydrocarbons obtained in the KE reaction were produced *via* a reduction of the carbided iron catalyst with H_2 formed by the WGS reaction. Although a very little portion of hydrocarbons produced in the KE reaction was caused by the decomposition of Fe_5C_2 by H_2O and by the hydrogenation of Fe_5C_2 and/or carbons[6,17] deposited on the catalyst surface, we may conclude that a much greater portion of hydrocarbons produced in the KE reaction was via a sequential reaction pathway involving the WGS reaction followed by the Fischer-Tropsch reaction. This mechanism of the KE reaction over Fe_2O_3 agrees with that reported for a RuY-zeolite catalyst.[5] The observed increase in the yield of hydrocarbons with increasing the degree of reduction of Fe_2O_3 (Table 3) suggests the role as the active sites played by the zerovalent iron atoms and/or metallic irons for the catalytic hydrogenation of CO to hydrocarbons. Based on these findings made in the present work, we propose the following catalytic cycle during the course of the KE reaction over Fe_2O_3.

$$Fe_3O_4 + 4CO \longrightarrow 3Fe + 4CO_2 \quad (2)$$

$$3Fe + 4H_2O \longrightarrow Fe_3O_4 + 4H_2 \quad (3)$$

$$5Fe + 4CO \longrightarrow Fe_5C_2 + 2CO_2 \quad (4)$$

$$3F_5C_2 + 32H_2O \longrightarrow 5Fe_3O_4 + 6CO_2 + 32H_2 \quad (5)$$

$$n\mathrm{CO} + 2n\mathrm{H_2} \xrightarrow{\mathrm{Fe}} -(\mathrm{CH_2})_n- + n\mathrm{H_2O} \quad (6)$$

We now discuss the promotional effect of metal oxides on the catalytic activity of Fe_2O_3 in the KE reaction. The observed increase in the yield and selectivity to hydrocarbons upon addition of Cu and Pt oxides to Fe_2O_3 which were able to catalyze the WGS reaction (Tables 4 and 5) supports the mechanism of the KE reaction over Fe_2O_3 proposed in the present work. Since the cat-

Table 6. Summary of the catalytic results for the KE reaction over mechanically admixed catalysts at 573 K[a)]

Catalyst	CuO-ZnO(3.0 g) +5 wt% Ni-Al_2O_3(7.0 g)	CuO-ZnO(3.0 g) +5 wt% Co-SiO_2(7.0 g)
Conversion of CO/%	59.2	40.9
Yield of H.C.[b)]/%	13.8	3.2
Selectivity to H.C.[b)]/%	24.1	8.1
Hydrocarbon	Distribution/carbon wt%	
C_1	77	31
C_1'	0.2	13
C_2	10	5
C_2'	2	23
C_3	6	0
C_4	3	12
C_5	1	7
C_6	0.4	4
C_7	0.1	4
C_{8+}	0	1

a) Catalyst: non-pretreated. Contact time: 207 g-catalyst·h·mol CO^{-1}. CO/H_2O feed molar ratio: 3. The catalytic activity was determined after a preliminary period of 30 min. b) Hydrocarbons.

alytic activity and selectivity of Fe_2O_3 for the KE reaction were also enhanced by the addition of Co, Ni, and Rh oxides which were able to catalyze the hydrogenation of CO to hydrocarbons (Tables 4 and 5), one could say that the mechanical mixture of two catalysts one of which has an ability to promote the WGS reaction and the another has an ability to promote the hydrogenation of CO to hydrocarbons is an effective catalyst for the production of hydrocarbons by the KE reaction. One illustration of this view is presented in Table 6. Here, CuO-ZnO was used as a catalyst for the WGS reaction whereas Al_2O_3-supported Ni (5 wt%) and SiO_2-supported Co (5 wt%) were used as catalysts for the hydrogenation of CO to hydrocarbons. In the case of CuO-ZnO+Ni-Al_2O_3 catalyst, the yield and selectivity to hydrocarbons at 573 K, 13.8 and 24.1%, are much greater than those observed over Fe_2O_3 at 573 K (Table 1) although the distribution of CH_4 in the hydrocarbons produced was as high as 77 wt% and that of C_2H_4 was only 0.2 wt%. A similar increase in the yield and selectivity to hydrocarbons was also seen in the case of CuO-ZnO+Co-SiO_2 catalyst (Table 6).

References

1) H. Kölbel and F. Engelhardt, *Erdöl u. Kohle*, **2**, 529 (1949) and **5**, 1 (1952); *Chem. Ind. Tech.*, **32**, 97 (1950); *Angew. Chem.*, **64**,54(1952); *Brenstoff Chem.*, **33**, 13 (1952).
2) Y. Maekawa, S. Chakrabartty, and N. Berkowitz, Preprint of the 5th Canadian Symposium on Catalysis, Calgary, Alberta, 1977, p. 2.
3) E. Kikuchi, H. Wada, and Y. Morita, Preprint of the llth Annual Meeting of the Petroleum Society of Japan, Okayama, 1981, p. 94.
4) K. Ejima, K. Fujimoto, and H. Tominaga, Preprint of the 50th Annual Meeting of the Catalysis Society of Japan, Niigata, 1982, p. 361.
5) B. L. Gustafson and J. H. Lunsford, *J. Catal.*, **74**, 393 (1982).
6) M. Niwa and J. H. Lunsford, *J. Catal.*, **75**, 302 (1982).
7) T. Kotanigawa, S. Chakrabartty, and N. Berkowitz, *Fuel Processing Tech.*, **5**, 79 (1981).
8) T. Kotanigawa, K. Shimokawa, and M. Yamamoto, *J. Chem. Soc., Chem. Comm.*, **1982**, 29.
9) Y. Kunugi, T. Sakai, H. Oose, and M. Hamada, *Kōgyō Kagaku Zasshi*, **69**, 2244 (1966).
10) ASTM Card No. 13-534.
11) *Shokubai (Catalyst)*, **22**, 115 (1980).
12) M. Ozaki *et al.*, "Shokubai Chōsei Kagaku," Kōdansha, Tokyo (1980), p. 244.
13) D. R. Stull, E. F. Westrum, Jr., and G. C. Sinke, "The Chemical Thermodynamics of Organic Compounds," John Wiley & Sons, New York (1969), pp. 219, 220, and 229.
14) ASTM Card No. 19-629.
15) ASTM Card No. 20-509.
16) D. C. Grenoble, M. M. Estadt, and D. F. Ollis, *J. Catal.*, **67**, 90 (1981).
17) J. G. McCarty and H. Wise, *J. Catal.*, **57**, 406 (1979).

 © 1984 The Chemical Society of Japan Bull. Chem. Soc. Jpn., 57, 673—677 (1984)

ENDOR Study of Benzothiazolone Azine Cation Radicals by Means of a TM_{110} Mode Cavity

Javier LOPEZ,† Jun YAMAUCHI,* Keiichi OKADA, and Yasuo DEGUCHI
College of Liberal Arts and Sciences, Kyoto University, Sakyo-ku, Kyoto 606
(Received August 3, 1983)

The electron nuclear double resonance (ENDOR) spectra of benzothiazolone azine cation radicals were observed by means of an ENDOR spectrometer equipped with a TM_{110} mode cavity. Highly diluted solutions of the radicals and a high radiofrequency power of 300 W facilitated the ENDOR observation. The obtained ENDOR values are different from the previously published results determined only from the ESR data, especially for the substituted alkyl groups. The assignment of the hyperfine coupling constants was made on the basis of the molecular orbital calculations as well as the re-examination of the ESR spectrum simulation. Good agreement between the calculated and the measured spectra is obtained if one assumes that the hyperfine coupling constants of the two different sets of nitrogen nuclei are equal as has been pointed out earlier.

Benzothiazolone azine and similar systems are well-known as two-step redox systems.[1] One can see easily from Fig. 1 that the intermediate compound B is a radical species. Hünig *et al.*[2] tried to observe ESR spectra of the benzothiazolone azine cation radicals, but no well-resolved ESR spectra could be obtained. As far as we know, no further ESR experiments have been performed to obtain more knowledge about spin density distributions in these systems. Recently well-resolved ESR spectra were obtained by means of a cylindrical TE_{011} mode cavity and spectral simulations were carried out.[3] No ENDOR spectra, however, could be observed successfully with the same type of ENDOR cavity. The nitrogen nucleus causes a short relaxation time due to the quadrupole moment. It is, therefore, very difficult to saturate the ESR transition of the radical containing the nitrogen nucleus although this is needed for performing ENDOR spectroscopy.

Möbius *et al.*[4] developed a TM_{110} mode cavity several years ago. The TM_{110} mode cavity allows one to apply higher radiofrequency power than the TE_{011} mode cavity does. In addition, the direction of the magnetic field of the radiofrequency is the same as that of the sample tube. The TM_{110} mode cavity, therefore, is more appropriate for the application of the ENDOR spectroscopy to systems which become saturated only with difficulty, like benzothiazolone azine cation radicals. This advantage was utilized for ^{14}N ENDOR observation of di-*t*-butyl nitroxide, which is not saturated easily, presumably because of a quadrupole moment and high freedom of molecular motions.[5]

The assignment and analysis of the coupling constants and ESR spectra in the work published previously[3] were mainly performed by means of MO calculations: Hückel and McLachlan method.[6,7] As is mentioned in that work, the obtained results are not necessarily final and conclusive ones. Successful application of ENDOR spectroscopy can help to confirm the calculated data and the conclusions in the published work.

Experimental

The synthesis of 2(3-alkyl)-benzothiazolone azine is described elsewhere.[1,3] The cation radicals of $\mathbf{1}^{+}$, $\mathbf{2}^{+}$, and $\mathbf{3}^{+}$ (Fig. 2) can be obtained by oxidation of the neutral compound with lead tetraacetate in various kinds of solvents. In our case, the oxidation of the neutral precursor was performed in an evacuated sealed sample tube using dichloromethane as a solvent. The previously published ESR spectra were observed in acetone at 295 K. Acetone was found to be inappropriate for ENDOR observation since it has a higher polarity than dichloromethane. Polar solvents can be disadvantageous for the ENDOR spectroscopy, since they cause lower *Q*-values for the cavity.

The ESR spectra of $\mathbf{1}^{+}$, $\mathbf{2}^{+}$, and $\mathbf{3}^{+}$ were recorded with a JEOL ES-EDX2, FE 3X spectrometer equipped with a cylindrical TE_{011} mode cavity. The observed ESR spectra show an observable temperature dependence, which is probably caused by the molecular motions of the benzothiazolone groups with respect to the inter-nitrogen bond as well as those of methyl and ethyl groups attached to the nitrogen atoms. The anisotropic effects of the nitrogen and the sulfur atoms may also be responsible. The ESR spectrum of $\mathbf{1}^{+}$ is not perfectly symmetric around the center. This is also attributed to the molecular motions and the anisotropic effects. The displayed ESR spectra in Figs. 3—5 were observed in an extremely diluted acetone solution

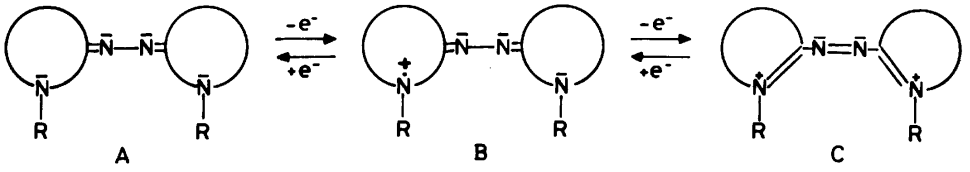

Fig. 1. A two-step redox system. The three oxidation levels are called reduced from (A), semiquinone (B), and oxidized form (C).

† Physikalisch-Chemisches Institut der Universität Basel, 4056 Basel, Switzerland.

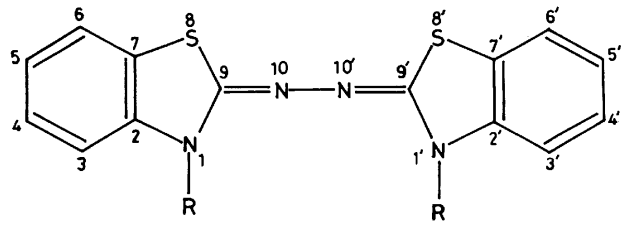

1: R=CH_3
2: R=CD_3
3: R=CH_2CH_3

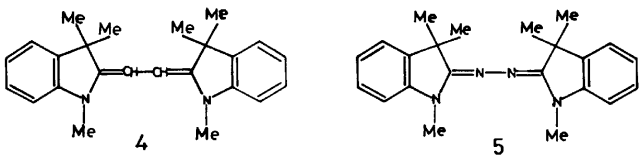

4 5

Fig. 2. The molecular structures **1**, **2**, and **3** studied in this work and similar systems **4** and **5**.

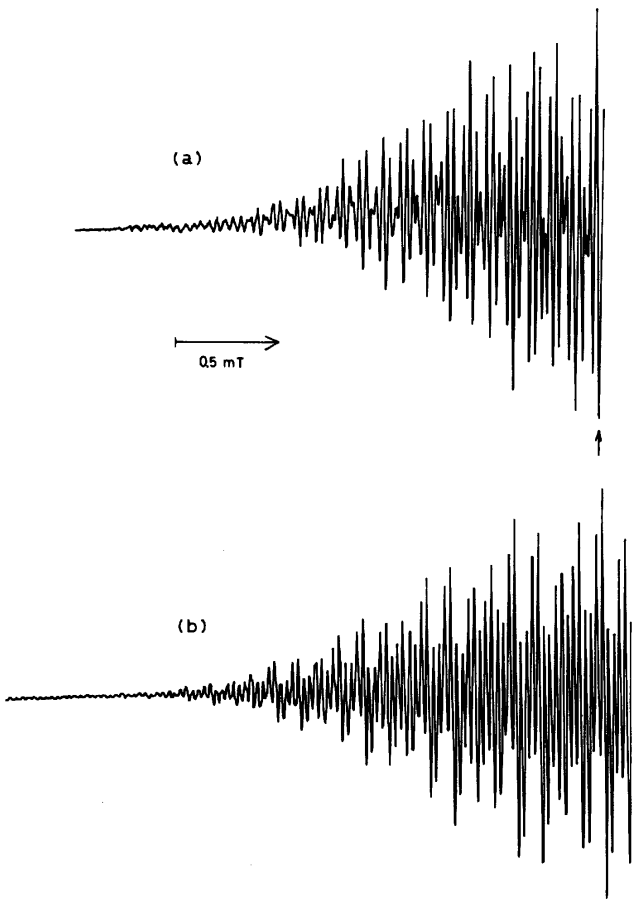

Fig. 3. The ESR and the simulated spectra of $\mathbf{1}^{+}$. The ESR spectrum (a) is recorded in acetone at 295 K.

of the corresponding cation radicals, which had been isolated and purified several times. The ESR spectra when ENDOR was observed were rather less resolved because the oxidation reaction was performed in the sample tube under high vacuum and because ESR observation was made

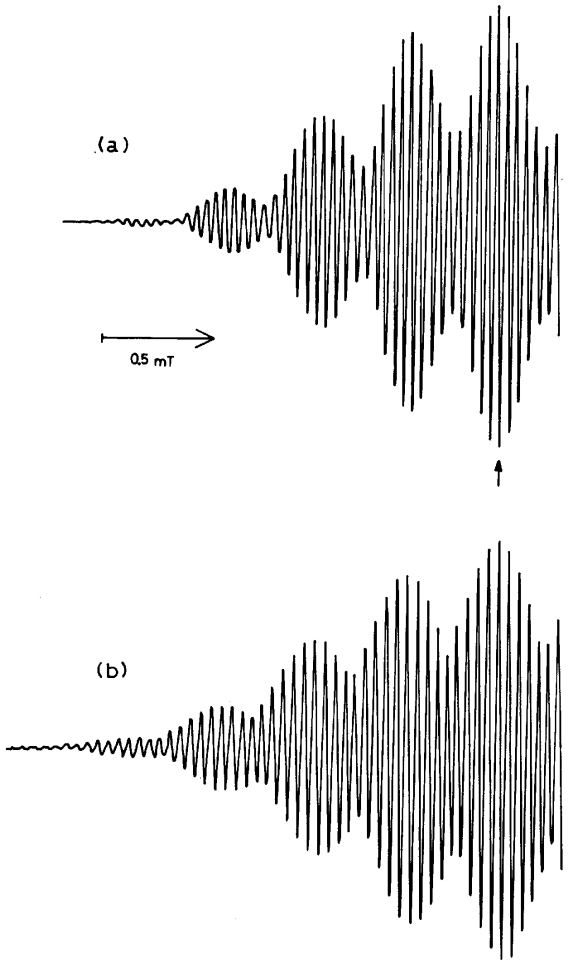

Fig. 4. The ESR and the simulated spectra of $\mathbf{2}^{+}$. The ESR spectrum (a) is recorded in acetone at 295 K.

with an 80 Hz field modulation in a cylindrical TM_{110} mode cavity. Good agreement of the calculated and the original spectra were obtained for $\mathbf{1}^{+}$, $\mathbf{2}^{+}$, and $\mathbf{3}^{+}$ on the basis of the MO data and the hyperfine coupling constans determined from the ENDOR, as is shown in Figs. 3—5. The hyperfine coupling constants were calibrated by using an alkaline solution of a nitrosyl bis(sulfate) ion. The original ESR spectra were recorded with a 100 kHz field modulation in acetone at 295 K, whereas in ENDOR an 80 Hz field modulation was employed.

The ENDOR spectra (Fig. 6) were observed by means of the TM_{110} mode cavity under the following conditions: microwave power 50 mW, radiofrequency power 300 W (ENI-type A300 power amplifier), field modulation 80 Hz, modulation amplitude 0.1 mT, and FM modulation of radiofrequency 2.5 kHz. For the ENDOR spectroscopy, a more diluted (nearly colorless) solution than that for the ESR spectroscopy had to be used. No ENDOR spectra could be obtained in the same concentration which produced the best ESR. The best ENDOR spectra were observed at 223 K. In Table 1 the hyperfine coupling constants of $\mathbf{1}^{+}$,$\mathbf{2}^{+}$, and $\mathbf{3}^{+}$ are listed.

Discussion

One can see from the ENDOR values in Table 1 that the hyperfine coupling constants of $\mathbf{1}^{+}$, $\mathbf{2}^{+}$, and $\mathbf{3}^{+}$

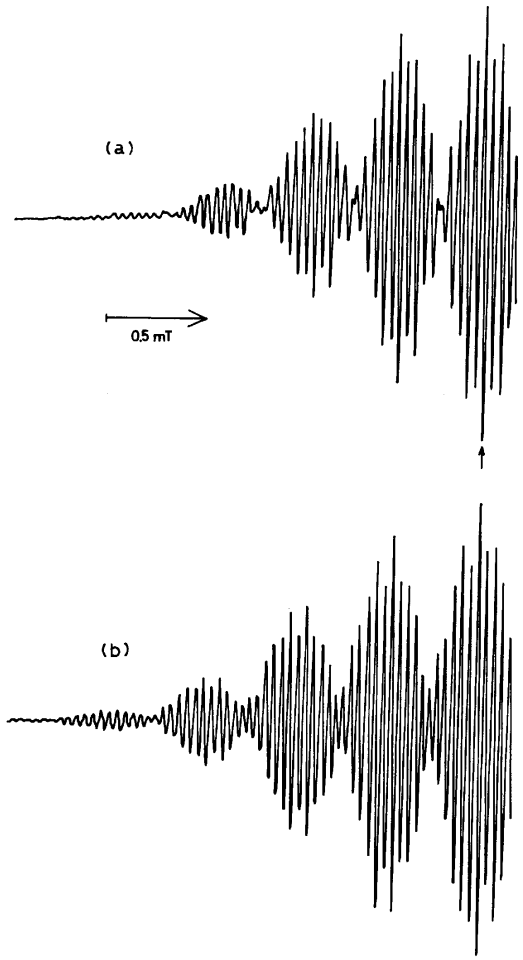

Fig. 5. The ESR and the simulated spectra of $\mathbf{3}^{\dagger}$. The ESR spectrum (a) is recorded in acetone at 295 K.

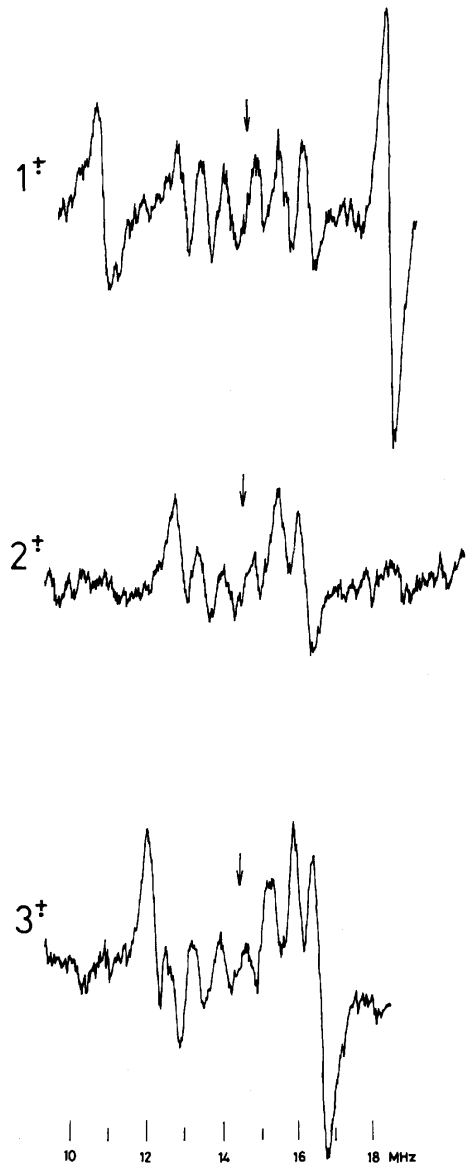

Fig. 6. The ENDOR spectra obtained in dichloromethane at 223 K. The arrow indicates the free proton frequency.

are very similar, except for the biggest value due to the protons of the alkyl substituent. This means that these coupling constants are very weakly influenced by the different alkyl substituents. The following procedure was chosen for the assignment of the coupling constants. The hyperfine coupling constants of the methyl protons in $\mathbf{1}^{\dagger}$ can be easily assigned, since the ENDOR signals in the spectrum of $\mathbf{1}^{\dagger}$ at 10.63 and 18.18 MHz disappear in the spectrum of $\mathbf{2}^{\dagger}$. These signals also do not appear in the spectrum of $\mathbf{3}^{\dagger}$ in which another pair of absorption lines appears instead. Thus, the biggest proton coupling constants 0.268 and 0.154 mT can be assigned to the methyl protons and the methylene protons of the ethyl groups, respectively. Then, the remanining coupling constants must be assigned to the ring protons of the two benzo moieties. There are four different sets of the ring protons, but the recorded ENDOR spectra for all systems show only three different values for the ring protons. One can, therefore, conclude either that the missing coupling constant must be less than the line width (*ca.* 0.015 mT) or that two coupling constants have similar values so that their absorption lines are not resolved. The best calculated spectra are obtained if one assumes that the missing coupling constant is almost the same as the smallest of the three. Hückel and McLachlan methods for the calculation of spin density, as is discussed later, predict the same conclusion. This is also compatible with the ESR simulation. Thus, the smallest coupling may be assigned to two kinds of equivalent protons, so that one has three different sets of the ring protons out of four equivalent proton groups.

The assignment of the coupling constants to the ring protons was made on the basis of the MO data obtained from the Hückel and McLachlan methods. The π-electron MO calculation of benzothiazolone azine framework was discussed in detail in the previous paper.[3] We employed the same MO parameters and no further modification was made. The results are shown in Table 1, where the proton hyperfine coupling constants are also estimated using the

Table 1. Hyperfine coupling constants and MO results for the radicals 1^+, 2^+, and 3^+ in 10^{-4} T units

Radical Position		1^+ ESR	1^+ ENDOR	2^+ ESR	2^+ ENDOR	3^+ ESR	3^+ ENDOR	McLachlan Spin density	McLachlan Coupling constant
1,1′	(2N)[a]	4.09	—	3.91	—	4.09	—	0.2025	—
10,10′	(2N)	4.09	—	3.91	—	4.09	—	0.2006	—
3,3′	(2H)	1.12	1.14	1.34	1.14	1.19	1.19	0.0540	1.13
4,4′	(2H)	0.33_5	0.29	0.43_5	0.26	0.40	0.24	−0.0201	0.42
5,5′	(2H)	0.86_5	0.74	0.87	0.74	0.80	0.74	0.0502	1.05
6,6′	(2H)	0.33_5	0.29	0.43_5	0.26	0.40	0.24	−0.0194	0.40
$R=CH_3$	(6H)	2.97	2.68	—	—	—	—	—	—
$R=CD_3$	(6D)	—	—	0.43_5	—	—	—	—	—
$R=CH_2$[b]	(4H)	—	—	—	—	1.58	1.54	—	—

a) Number of the equivalent nuclei, N, H, or D. b) Methylene protons of the ethyl group, $R=CH_2CH_3$.

McConnell equation[8] with a proportionality constant $|Q|=2.1$ mT. By comparing the ENDOR results with those arrived at previously from the ESR study,[3] the following conspicuous facts are revealed: 1) the alkyl protons have much larger coupling constants (almost two times bigger) than those from the ESR data[3]; 2) ENDOR shows slightly bigger coupling constants of the ortho protons ($H_{3,3'}$) of the two benzo moieties and slightly smaller ones of the two meta protons ($H_{4,4'}$ and $H_{6,6'}$), while in the para protons ($H_{5,5'}$) the constants have almost the same value; 3) in conjunction with fact 1), one has to take into account the deuteron hyperfine coupling constant, which was neglected in the previous work.[3] After we consider the reliability of proton ENDOR, we re-examined the spectral simulation of the ESR on the basis of the coupling constants determined from the ENDOR. First, the big nitrogen hyperfine coupling constants are again confirmed: these constitute the fundamental group pattern of the ESR spectra, as is discussed in the literature.[3] Next, by changing the proton coupling constants little by little from the ENDOR values, as well as changing the deuteron coupling constant starting from 0.041 mT predicted from $A_D/A_H=1/6.51437$[9] where $A_H=0.268$ mT of the methyl protons, an acceptable set of the hyperfine coupling constants for each compound is obtained; these are shown in Table 1. Figures 3—5 are comparisons between the experimental and the simulated spectra. The newly determined values do not deviate from the ENDOR values as much as 0.03 mT. Such agreement is rather satisfactory, considering the fact that the ESR spectra were recorded under different conditions (*e.g.* different temperature and solvent) for the best resolution.

The ESR simulations in this paper are more reliable than the previous ones, because the ENDOR results are taken into account this time. Again, the equivalent hyperfine coupling constants could be assigned to the thiazolone and the bridged nitrogen atoms. This may support the validity of the choice of the MO parameters in the previous paper.[3] Agreement between the experimental and the theoretical proton hyperfine coupling constants at the ring positions are also excellent, except for the para positions ($H_{5,5'}$). The McLachlan calculation predicts a quite small difference between the ortho ($H_{3,3'}$) and para ($H_{5,5'}$) protons. The deuteron coupling constants is taken into consideration this time and found to be 0.0435 mT, giving $A_D/A_H=1/6.8$. From the methyl coupling constant 0.298 mT, 0.0456 mT is expected theoretically.[9]

Next, we comment about the R-substitution effect. The alkyl substitution never has a severe effect on the unpaired electron distribution, as was said in the first section of this discussion. However, the spectrum itself is influenced dramatically because of the big spin density at the nitrogen atoms to which the alkyl groups are attached. There are a lot of data for the nitrogen and the methyl or ethyl proton hyperfine coupling constants where the alkyl groups are attached directly to the nitrogen atom.[10-12] For the nitrogen and methyl protons, the same order of magnitude of the couplings are commonly observed.[12] In this work, however, the methyl hyperfine coupling constant is reduced to 75%, as compared to the nitrogen value. This may be caused by the deformed bond angle around the nitrogen atom in the thiazolone ring. On the other hand, the relation in magnitude between the methyl and the ethyl coupling constants is as usual, *i.e.* the methylene protons of the ethyl have sometimes *ca.* 50% of the methyl coupling constants.[12]

Two similar systems (**4** and **5** in Fig. 2) were investigated some years ago.[2] They do not contain sulfur but non-π part, $>C(CH_3)_2$, is introduced in the sulfur position of the compounds **1**—**3**. Therefore, the π-system does not extend over the five-membered rings, as in **1**—**3**. The ESR spectrum of 5^+ could not be analyzed, since it showed a poor resolution. A comparison of the calculations for 1^+-3^+ and 4^+-5^+ shows a similar behavior. The large spin densities are greatly delocalized in the ortho and para, and less delocalized in the meta positions, both for 1^+, 2^+, 3^+, and for 4^+, 5^+. The Hückel and McLachlan methods give inequivalent spin densities for the two different sets of nitrogen nuclei in 5^+, $A_{N1}/A_{N10}=1.4$.[3] This is also the case for 1^+, 2^+, and 3^+ when the proposed set of the MO parameters is used. In 4^+ the nitro-

gen and the vinyl protons have the same coupling constant. This, however, does not mean that the same spin densities are located on these nuclei. The nitrogen coupling constant in $\mathbf{4}^{\dagger}$ differs only by 0.021 mT from that in $\mathbf{1}^{\dagger}$, $\mathbf{2}^{\dagger}$, $\mathbf{3}^{\dagger}$. Nevertheless, the coupling constants of the methyl protons do not have similar values. These inconsistencies certainly suggest the necessity of the ENDOR experiments in the two above-mentioned systems. A common feature of all systems ($\mathbf{1}^{\dagger}$ through $\mathbf{5}^{\dagger}$) is that about 70% of the spin density is located on the atom sequence >N-C=N-N=C-N< and only a small amount is located on the two benzo moieties.

Some concluding remarks should be made about the TM_{110} mode cavity. The application of this cavity has not yet been widely extended after its development.[4] The collected experience with this cavity shows that it offers a better resolution in the ENDOR spectroscopy than the TE_{011} mode cavity and it also allows one to observe much more easily nitrogen ENDOR.[5] However, we did not succeed till now in detecting the nitrogen ENDOR for the present series of compounds. This may be due to the properties of the bobbin with which the radiofrequency signal is transmitted to the cavity.

References

1) S. Hünig, *Pure Appl. Chem.*, **15**, 109 (1967). S. Hünig, H. Balli, H. Conrad, and Schott, *Justus Liebigs Ann. Chem.*, **676**, 36 (1964).
2) S. Hünig, F. Linhart, and D. Scheutzow, *Ann. Chem.*, 2102 (1975).
3) K. Okada, J. Yamauchi, and Y. Deguchi, *J. Heterocycl. Chem.*, **20**, 723 (1983).
4) K. Möbius and R. Biehl, "Multiple Electron Resonance Spectroscopy," ed by M. M. Dorio and J. H. Freed, Plenum Press, New York (1979) Chap. 14.
5) J. Yamauchi and Y. Deguchi, *Chem. Lett.*, **1983**, 257.
6) A. Streitwieser, Jr., "Molecular Orbital Theory for Organic Chemists," John Wiley & Sons, New York (1961).
7) A. D. McLachlan, *Mol. Phys.*, **3**, 233 (1960).
8) H. M. McConnell, *J. Chem. Phys.*, **24**, 764 (1956).
9) R. G. Lawler and G. K. Fraenkel, *J. Chem. Phys.*, **49**, 1126 (1968).
10) A. R. Forrester, J. M. Hay, and R. H. Thomson, "Organic Chemistry of Stable Free Radicals," Academic Press, London (1968).
11) G. Vincow, "Radical Ions," ed by E. T. Kaiser and L. Kevan, John Wiley & Sons, New York (1968), Chap. 4.
12) H. Fujita and J. Yamauchi, *J. Heterocycl. Chem.*, **17**, 1053 (1980).

Kinetic Studies of the Complex Formation in the System of Cyclodextrin, Iodine, and Iodide

Takayuki SANO, Masako YAMAMOTO,† Hiroka HORI, and Tatsuya YASUNAGA*
Department of Chemistry, Faculty of Science, Hiroshima University, Hiroshima 730
†Department of Home Economics, Hiroshima Women's University, Hiroshima 734
(Received August 4, 1983)

Kinetic studies of complex formation in the system consisting of cyclodextrin, iodine, and iodide have been made by the temperature-jump method. By addition of α-cyclodextrin to the iodine–iodide solution, a new relaxation in addition to that due to I_6^{2-}, formation was observed, but not in the case of addition of β-cyclodextrin. The reciprocal relaxation time is independent of the iodine concentration, but increases with increase of both iodide and α-cyclodextrin concentration, with a tendency to reach a constant value at their high concentrations. From these concentration dependences of the relaxation time, the observed relaxation was assigned to the conformational change of the complex between α-cyclodextrin and iodide ion, and the rate constants were estimated to be 5.9×10^5 and 1.2×10^5 s^{-1} for the forward and backward processes, respectively. A rationalization for the difference between α-cyclodextrin and β-cyclodextrin in this complex formation is proposed in terms of the molecular structure of cyclodextrin.

The cyclodextrins are well known for their ability to form inclusion complexes with a variety of guests,[1–3] and the main driving forces of the complex formation have been attributed to hydrogen bonding,[4] hydrophobic interaction,[5] and van der Waals forces[6] depending on the nature of the guest molecules. Kinetic studies[7–9] of the inclusion complex formation of cyclodextrin have revealed the importance of the conformational change of cyclodextrin and the breakdown of the water structure around guest substances. However, the details of the reaction mechanism are still obscure especially with respect to the effect of the structure of cyclodextrin.

Meanwhile, Noltmeyer and Saenger[10] have reported that the α-cyclodextrin–iodine complex has the same structure as the amylose–iodine complex. This fact motivated us to start some kinetic studies of the complex formation of the cyclodextrin with iodine in connection with our previous studies on the amylose–iodine complex formation.[11] In the preliminary temperature-jump experiment, an addition of α-cyclodextrin to the iodine–iodide solution gives rise to new relaxation besides that which was observable without cyclodextrin.[12] The present work was undertaken to clarify the mechanism of the new relaxation with use of both α- and β-cyclodextrins.

Experimental

Materials. The α- and β-cyclodextrins were purchased from Nakarai Co., and used as received. Iodine and potassium iodide were of reagent grade and used without further purification.

Measurements. Kinetic measurements were carried out by a temperature-jump method[13] with detection of transmittance at 500 nm which corresponds to the absorption band of iodine. The ionic strength of the solution was kept at 0.023 M†† to attain a rapid temperature rise within 0.75 μs. Spectrophotometric measurements were made on a Union Giken SM-401 spectrophotometer. All the experiments were carried out at 25 °C.

†† 1 M=1 mol dm^{-3}.

Results and Discussion

A typical relaxation curve observed in a solution containing α-cyclodextrin, iodine, and iodide is shown in Fig. 1. This relaxation becomes predominant with increase of α-cyclodextrin concentration, and is obviously different from that observed in the iodine–iodide solution in both the relaxation time and the direction of the relaxation signal.[12] The present relaxation spectra show a decrease of iodine concentration and was characterized by a single relaxation. In order to simplify the analysis, the kinetic experiments were undertaken by changing the concentration of one species while keeping those of the other two constant. The plots of the reciprocal relaxation time, τ^{-1} against the total concentration of α-cyclodextrin, iodine, and iodide are shown in Figs. 2, 3, and 4. As shown in these figures, the value of τ^{-1} increases with concentration of α-cyclodextrin and iodine, showing a trend to level off at high concentration, but it is independent of that of iodine. In contrast to the α-cyclodextrin, the addition of β-cyclodextrin to the iodine–iodide solution did not give rise to any new re-

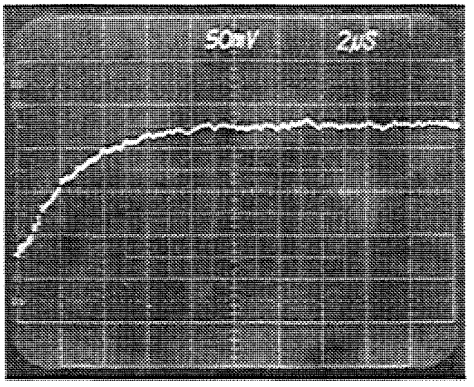

Fig. 1. Typical relaxation curve for the solution containing α-cyclodextrin, potassium iodide, and iodine at 25 °C; $[\alpha\text{-CD}]=6.0\times10^{-3}$ M, $[KI]=2.3\times10^{-2}$ M, $[I_2]=6.0\times10^{-3}$ M; sweep 2 μs/division and $\lambda=500$ nm.

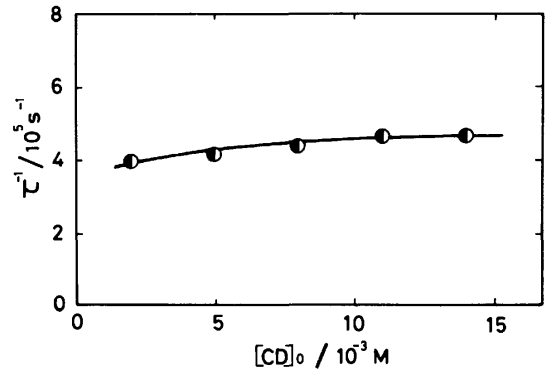

Fig. 2. Dependence of the reciprocal relaxation time on the α-cyclodextrin concentration at constant $[I_2]=5.0\times10^{-3}$ M and $[KI]=2.3\times10^{-2}$ M at 25 °C.

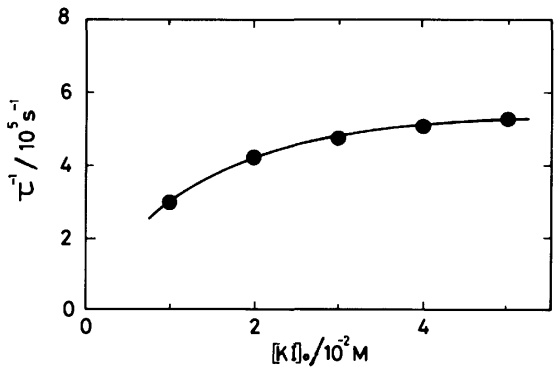

Fig. 3. Dependence of the reciprocal relaxation time on the potassium iodide concentration at constant $[I_2]=5.0\times10^{-3}$ and $[\alpha\text{-CD}]=5.0\times10^{-3}$ M at 25 °C.

laxation, which is indicative of the specificity of the present relaxation to α-cyclodextrin.

In the solution containing the α-cyclodextrin, iodine, and iodide, according to the investigations reported so far,[7,13-15] the following reactions are at least expected to proceed,

$$I^- + I_2 \rightleftharpoons I_3^- \qquad K_I, \qquad (I)$$

$$2I_3^- \rightleftharpoons I_6^{2-} \qquad K_{II}, \qquad (II)$$

$$CD + I^- \rightleftharpoons CDI \qquad K_{III}, \qquad (III)$$

where CD and CDI denote the free α-cyclodextrin and the complex of α-cyclodextrin and iodide, respectively. Among these three reactions, the relaxations due to the reactions I and II, which are much faster than the present relaxation, have been already investigated kinetically by the temperature-jump method.[13,14] As for the reaction III, the kinetic studies have not been performed successfully because of the existence of relaxation due to the conformational change of α-cyclodextrin.[7] Accordingly, we first examined reaction III, and also the complex formations of α-cyclodextrin with I_2, I_3^-, or I_6^{2-} as origin of the present relaxation, but failed to explain all the concentration dependences of the relaxation time in Figs. 2, 3, and 4. By reference to the concentration dependence of relaxation time in Figs. 2 and 3 specific to the intramolecular process following the fast binding pro-

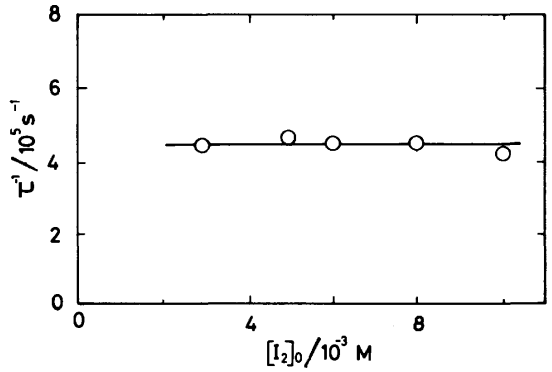

Fig. 4. Dependence of the reciprocal relaxation time on the iodine concentration at constant $[KI]=2.3\times10^{-2}$ M and $[\alpha\text{-CD}]=4.0\times10^{-3}$ M at 25 °C.

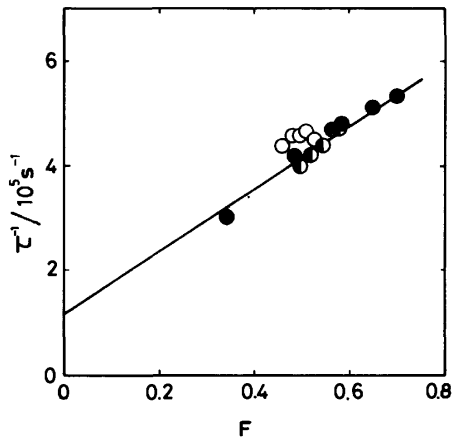

Fig. 5. Plots of τ^{-1} *vs.* the concentration term F in the Eq. (1). The circles correspond to those in Figs. 2, 3, and 4.

cess, we analyzed the kinetic data with the reaction scheme as follows:

$$CD + I^- \overset{K_1}{\rightleftharpoons} CDI' \underset{k_{-2}}{\overset{k_2}{\rightleftharpoons}} CDI''. \qquad (IV)$$

This reaction is a modification of reaction III and the binding process of iodide ion to α-cyclodextrin is followed by the intramolecular process of the complex. If the reactions I and II and the first step of reaction IV are faster than the second step, the relaxation time for the second step can be finally represented by

$$\tau^{-1} = k_2F + k_{-2}, \qquad (1)$$

with

$$F = \frac{K_1[CD + I^-(1 + K_1(I^- + I_2 + CD))]}{K_1[CD + I^-(1 + K_1(I^- + I_2 + CD))] + 1}. \qquad (2)$$

The derivation of this equation will be described in the appendix section. The value of K_1, 2.1±0.3 M^{-1}, was determined so as to obtain a best linear relationship between the observed τ^{-1} and the concentration term F, in the Eq. 1. The final results are shown in Fig. 5. The values of k_2, $(5.9\pm0.5)\times10^5$ s^{-1}, and k_{-2}, $(1.2\pm0.5)\times10^5$ s^{-1}, were obtained from the slope and intercept of the straight line, respectively. Using

these values of K_1 and $K_2=k_2/k_{-2}$, the overall binding constant of reaction IV, $K_{IV}=K_1(1+K_2)$, was found to be 13±2 M^{-1}. The good agreement of this value with the binding constant obtained statically by the conductometric method (12.4 M^{-1})[15] gives proof of the validity of an assignment of the present relaxation to reaction IV. Furthermore, it was recognized from the spectrophotometric experiments that the addition of α-cyclodextrin to the iodine–iodide solution results in the increase in I_2 concentration and the decrease in I_3^- concentration in solution. This spectrophotometric result implies the complex formation of α-cyclodextrin with I^- rather than I_2, I_3^-, and I_6^{2-}, supporting the present assignment of the kinetic data.

The apparent difference in the kinetic behavior observed in the present studies for the α-cyclodextrin and β-cyclodextrin can be discussed from the viewpoint of the molecular structure of cyclodextrin. For α-cyclodextrin, a conformational change in the inclusion complex formation was proposed by X-ray crystallographic studies,[16] while there is no evidence of such conformational change for the β-cyclodextrin. Accordingly, at the present stage, the second process of reaction IV can be ascribed to a conformational change resulting from the "strained"[16] structure of α-cyclodextrin.

In conclusion, the present work clarifies that, in contrast to the polyiodide chain structure proposed by Noltemeyer and Saenger[10] for the α-cyclodextrin–iodine complex in the solid state, α-cyclodextrin binds predominantly with I^- rather than I_2, I_3^-, or I_6^{2-} in solution. Furthermore, the difference observed in the present kinetic experiments on the α- and β-cyclodextrins was ascribed to the "strained" conformation of α-cyclodextrin.

Appendix

If reactions I, II, and the first step in IV in the text are much faster than the second step of reaction IV, the following relationships can be derived from the mass balance and the mass conservation laws;

$$K_1(I^-\Delta I_2+I_2\Delta I^-) = \Delta I_3^-, \tag{A1}$$

$$2K_{II}I_3^-\Delta I_3^- = \Delta I_6^{2-}, \tag{A2}$$

$$K_1(I^-\Delta CD+CD\Delta I^-) = \Delta CDI', \tag{A3}$$

$$\Delta I^- + \Delta I_3^- + 2\Delta I_6^{2-} + \Delta CDI' + \Delta CDI'' = 0, \tag{A4}$$

$$\Delta I_2 + \Delta I_3^- + 2\Delta I_6^{2-} = 0, \tag{A5}$$

$$\Delta CD + \Delta CDI' + \Delta CDI'' = 0. \tag{A6}$$

The rate equation for the second step of reaction IV is

$$\frac{d\Delta CDI''}{dt} = k_2\Delta CDI' - k_{-2}\Delta CDI'', \tag{A7}$$

Combining the Eqs. A1—A6, the Eq. A7 is converted into the next equation

$$\frac{d\Delta CDI''}{dt} = -(k_2F+k_{-2})\Delta CDI'', \tag{A8}$$

with

$$F = \frac{K_1(I^-+CD)+(1+4K_{II}I_3^-)K_IK_1I^-(I^-+I_2+CD)}{1+K_1(I^-+CD)+K_IK_1I^-(I^-+I_2+CD)(1+4K_{II}I_3^-)}. \tag{A9}$$

Accordingly, the relaxation time can be represented by

$$\tau^{-1} = k_2F + k_{-2}.$$

Under the present experimental conditions, Eq. A10 can be rewritten in good approximation as

$$\tau^{-1} = k_2\frac{K_1\{CD+I^-(1+K_I(I^-+I_2+CD))\}}{1+K_1\{CD+I^-(1+K_I(I^-+I_2+CD))\}} + k_{-2}. \tag{A11}$$

References

1) D. W. Griffiths and M. L. Bender, *Acd. Catal.*, **23**, 209 (1973); R. K. McMullan, W. Saenger, J. Fayos, and D. Moots, *Carbohydr. Res.*, **31**, 37, 211 (1973).

2) F. Cramer, W. Saenger, and H. -ch. Spatz, *J. Am. Chem. Soc.*, **89**, 14 (1967).

3) E. A. Lewis and L. D. Hansen, *J. Chem. Soc., Perkin Trans. 2*, **1973**, 2081.

4) F. Cramer and W. Kampe, *J. Am. Chem. Soc.*, **87**, 1115 (1965).

5) G. Nemethy and H. A. Scheraga, *J. Chem. Phys.*, **36**, 3401 (1962).

6) D. French, *Adv. Carbohydr. Chem.*, **12**, 250 (1957).

7) R. P. Rohrbach, L. J. Rodriguez, E. M. Eyring, and J. F. Wojcik, *J. Phys. Chem.*, **81**, 944 (1977).

8) W. P. Jencks, "Catalysis in Chemistry and Enzymology," McGraw-Hill, New York (1969), p. 409.

9) L. Bender and M. Komiyama, "Cyclodextrin Chemistry," Springer-Verlag, Berlin (1978).

10) M. Noltemeyer and W. Saenger, *Nature*, **259**, 629 (1976).

11) M. Yamamoto, T. Sano, and T. Yasunaga, *Bull. Chem. Soc. Jpn.*, **55**, 1186, 3702 (1982).

12) T. Sano, H. Hori, M. Yamamoto, and T. Yasunaga, *Bull. Chem. Soc. Jpn.*, in press.

13) T. Sano, J. Ishibashi, N. Ikeda, and T. Yasunaga, *Biopolymers*, **20**, 187 (1981).

14) D. H. Turner, G. W. Flynn, N. Sutin, and J. Beitz, *J. Am. Chem. Soc.*, **94**, 155 (1972).

15) J. F. Wojcik and R. P. Rohrbach, *J. Phys. Chem.*, **79**, 2251 (1975).

16) P. C. Manor and W. Saenger, *J. Am. Chem. Soc.*, **96**, 3630 (1974).

17) D. W. Griffiths and M. L. Bender, "Starch Chemistry and Technology," Academic Press, New York (1965), p. 209.

Competition between Hydrogen Fluoride and Hydrogen Chloride Molecular Elimination Channels in the Infrared Multiple-photon Decomposition of 1,2-Dichloro-1,1-difluoroethane

Yo-ichi ISHIKAWA* and Shigeyoshi ARAI
The Institute of Physical and Chemical Research, Wako, Saitama 351
(Received August 25, 1983)

Time-resolved infrared emission spectra have been measured in the infrared multiple-photon decomposition of $CClF_2CH_2Cl$. The spectra were composed of emissions attributable to vibrationally excited HF* and HCl*. The emission yield of HF* increased rapidly with an increase in the fluence, while the yield of HCl* showed a maximum at 20 J cm^{-2}. These results suggest that the HF and HCl molecular elimination channels compete with each other in the unimolecular decomposition of highly vibrationally excited parent molecules. The stochastic trajectory calculations provided a satisfactory description of the fluence dependences of the HF and HCl yields observed here for $CClF_2CH_2Cl$ and previously for CHClFCHClF.

The infrared multiple-photon decomposition (IRMPD) of large molecules frequently shows more than one reaction channel, leading to a variety of products.[1] For the occurrence of a particular reaction channel, the parent molecules must be excited to levels above the threshold energy of the corresponding channel in the multiple-photon excitation process. The branching ratio among the channels can be interpreted in terms of the distribution of excited molecules with respect to the internal energy and the kinetic parameters of excited molecules as a function of the internal energy. Although there are several quantitative methods of determining product yields in the IRMPD of large molecules, the energy distribution and kinetic parameters have been studied to only a limited extent.

The effects of the laser fluence (J cm^{-2}) and the intensity (W cm^{-2}) on the IRMPD of large molecules have been reported extensively in recent publications.[1,2] It is generally accepted that an increase in the fluence significantly increases product yields, while, in contrast, a change in the intensity slightly affects the IRMPD. However, the laser intensity is directly proportional to the rates of optical absorption and stimulated emission for molecules in an intense laser field. The energy distribution should depend on the rates of these optical processes as well as on the rates of the decomposition of excited molecules.

West *et al.* have investigated the fluence dependences of HF and HCl molecular elimination channels in the IRMPD of $CClF_2CH_3$ using an infrared emission spectroscopic technique.[3] Krajnovich *et al.* have studied the fluence dependences of Cl atomic elimination and C-C bond rupture in the IRMPD of C_2F_5Cl by the use of a molecular-beam technique.[4] These experiments have, in principle, two advantages. One is that there is no complication caused by the subsequent reactions of initial intermediate products; another is that the fluence variation within the reaction zone is relatively small. Since IRMPD usually requires high fluences, the laser beam is tightly focussed in a reaction cell. Therefore, the resulting inhomogeneity of the fluence must be considered carefully in the analysis of the data. In infrared-emission and molecular-beam experiments, it is possible to detect emitting species and fragment species produced in a small reaction zone, where the fluence variation is somewhat limited.

In this study we have examined the IRMPD of $CClF_2CH_2Cl$ using a time-resolved infrared-emission spectroscopic technique. The experimental results show that HF and HCl molecular-elimination reactions occur competitively in the decomposition of highly vibrationally excited parent molecules. In addition, the fluence dependences of the channels are quite different from each other. These findings are similar to those obtained with the IRMPD of CHClFCHClF in a previous study.[5] The stochastic trajectory calculations can satisfactorily explain the observed fluence dependences in both studies on a reasonable assumption of kinetic parameters.

Experimental

The experimental apparatus used here is essentially the same as in a previous study.[6] The details have been described elsewhere.[7] The pulsed beam from a Lumonics TEA 103 CO_2 laser was truncated by an iris with a diameter of 9.9 mm and focussed in an irradiation cell by means of a BaF_2 lens with a focal length of 20 cm. The pulse profile was a spike of 80-ns fwhm without any tail. The laser was tuned to the R(20) line of the 9.6-μm CO_2 band at 1078.59 cm^{-1} and operated at a repetition rate of 0.7 Hz. The intensity distribution across the laser beam after passing through the iris was nearly flat; the deviation from the mean value was less than 15%. The beam area at focus was estimated to be 5×10^{-3} cm^2 from the beam divergence of 2 mrad. The laser fluence at focus was calculated from the beam area and the laser energy. The length of the reaction zone inside the cell was 2 cm along the laser beam, and the focal point was in the middle. The fluence at each end was estimated to be 60% of that at focus. In addition, the optical system was arranged so that the emission at focus could be monitored most efficiently during the observation. An InSb detector was set behind the exit slit of a Ritsu Kogaku MC-20L monochromator. Raw signals from the detector were first amplified by means of a PAR model 115 preamplifier. Then, the amplified signals were treated with a PAR model 162 boxcar averager and PAR model 155 gated integrator for the spectrum measurements, and with a Biomation 8100 transient digitizer and Keisoku Giken model 8100 signal averager for the time-resolved intensity measurements. The aperture duration, τ_g, and the aperture delay, τ_d, used for the boxcar averager were 10 and 3 μs respectively. The laser pulse picked up with a photon-drag detector (Hamamatsu TV, model B749) was used as a trigger signal of the detection system. The overall rise time was about 2 μs.

The flow rate of a reactant gas in the cell was 10 Torr

$cm^3\,min^{-1}$ (1 Torr≈133.3 Pa),[8] and the pressure was measured with a MKS Baratron model 220 BH manometer (10 Torr pressure range). The reactant gas, $CClF_2CH_2Cl$, was purchased from PCR Research Chemicals and was purified by trap-to-trap distillation before use.

Results and Discussion

First of all, the final products in the IRMPD of $CClF_2CH_2Cl$ were examined using infrared-absorption spectroscopic analysis. A special cell with a KBr window at each end (10 cm in length and 1.5 cm in inner diameter) was filled with 5-Torr $CClF_2CH_2Cl$. The laser beam was tightly focussed by means of a 7.5-cm focal length BaF_2 lens. The pulse energy and the focus fluence were 0.20 J and 280 J cm^{-2} respectively. The infrared-absorption spectrum was measured after irradiation using a JASCO type A-102 infrared spectrometer. The products assigned in the infrared spectrum are HCl (ν_1=2900 cm^{-1}), SiF_4 (ν=1030 cm^{-1}),[9] CF_2CHCl (ν_1=3130 cm^{-1}; ν_2=1740 cm^{-1}; ν_3=1330 cm^{-1}; ν_4=1200 cm^{-1}; ν_5=970 cm^{-1}),[10] and CClFCHCl (ν_3 for cis- and/or trans-form=1650 cm^{-1}; ν_6 for trans-form=850 cm^{-1}).[11] The formation of SiF_4 is explained by the secondary reaction of the primary product, HF, with the glass wall. These products suggest that the α,β-molecular elimination of HF and HCl occurs in the IRMPD of $CClF_2CH_2Cl$:

$$CClF_2CH_2Cl + mh\nu \rightarrow CF_2CHCl + HCl, \quad (1)$$

and:

$$CClF_2CH_2Cl + nh\nu \rightarrow CClFCHCl + HF. \quad (2)$$

Figure 1 presents the fluence effects on the infrared emission spectra for 1-Torr $CClF_2CH_2Cl$ irradiated at 1078.59 cm^{-1} in a flow system. The fluences at focus are indicated in the same figure. The slit function, with 0.056 μm fwhm, is also illustrated at the top of the figure. The emission with two peaks in the wavelength region from 3.1 to 4.2 μm is due to highly vibrationally excited HCl*, while the emission in the region from 2.2 to 3.1 μm is due to HF*. The spectral simulation based on the spectroscopic constants of HCl and HF supports the above assignments.[5,6] We could not detect any meaningful emission in the same wavelength region when the empty cell was irradiated at a fluence of 53 J cm^{-2}, as is shown in Fig. 1f. Since all the spectra have been measured under the same conditions except for the fluence, the intensities of the HF* and HCl* emissions can be said to be proportional to the yields of HF* and HCl* respectively among the spectra. As the fluence is increased, the intensity of HF*(I_{HF^*}) grows much more rapidly than the intensity of HCl*(I_{HCl^*}). The ratio of I_{HF^*} to I_{HCl^*} changes from 0.4 at 11 J cm^{-2} to 2.5 at 43 J cm^{-2}, where HF* and HCl* emission intensities are monitored at the wavelengths of about 2.8 and 3.8 μm respectively.

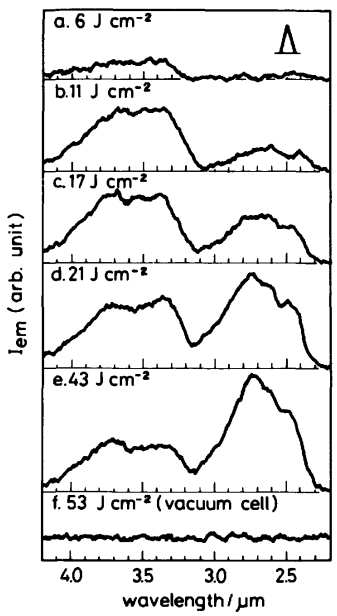

Fig. 1. Infrared fluorescence spectra observed for 1-Torr $CClF_2$-CH_2Cl irradiated with CO_2 TEA laser. Laser wavenumber, 1078.59 cm^{-1}.

Setser and his co-workers have examined the HF(DF) and HCl(DCl) elimination reactions of highly vibrationally excited haloethanes prepared in radical combination reactions.[12,13] They estimated that α,α-elimination contributes approximately 10% to the total molecular elimination in CHF_2CH_3. We have measured the fluorescence spectrum in the IRMPD of $CHCl_2CF_3$, where the α,α- and α,β-elimination channels were expected to give HCl* and HF* respectively. There appears to be no contribution of HCl* emission to the observed spectrum in Fig. 2. These facts suggest that α,α-elimination is a minor process in the decomposition of vibrationallly excited haloethanes.

Figure 3 presents the time dependences of the emission intensities observed at 2.4, 2.8, 3.0, 3.4, and 3.8 μm for 1-Torr $CClF_2CH_2Cl$. The fluence was 29 J cm^{-2}. The spectrum simulation suggests that the emission at 2.4 μm mainly corresponds to the R-branch of the HF* (v'=1)→HF(v''=0) transition, and those at 2.8 and 3.0 μm, to several transitions (Δv=1) originating from HF* at various vibrational levels. Similarly, the emissions at 3.4 and 3.8 μm are due to several transitions (Δv=1) of vibrationally excited HCl*. The emission profiles show a rapid initial rise and then a rapid

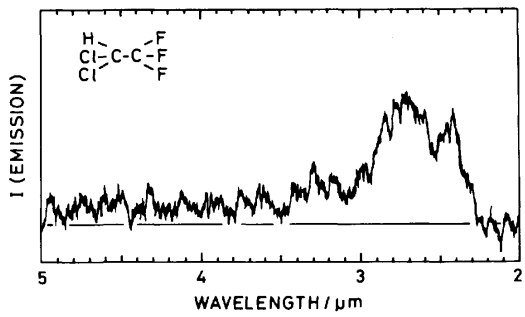

Fig. 2. Infrared fluorescence spectra observed for 5-Torr $CHCl_2CF_3$ irradiated with CO_2 TEA laser. Laser wavenumber, 1078.59 cm^{-1}; fluence, 40 J cm^{-2}; wavelength resolution, 0.068 μm fwhm.

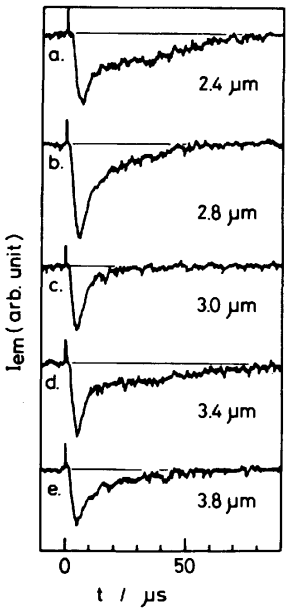

Fig. 3. Typical HF* and HCl* fluoresence signals observed for 1.0-Torr $CClF_2CH_2Cl$. Laser fluence, 29 J cm^{-2}; emission measurement wavelength, 3.8 and 3.4 μm for HCl* and 3.0, 2.8, and 2.4 μm for HF*; wavelength resolution, 0.056 μm fwhm; laser wavenumber, 1078.59 cm^{-1}.

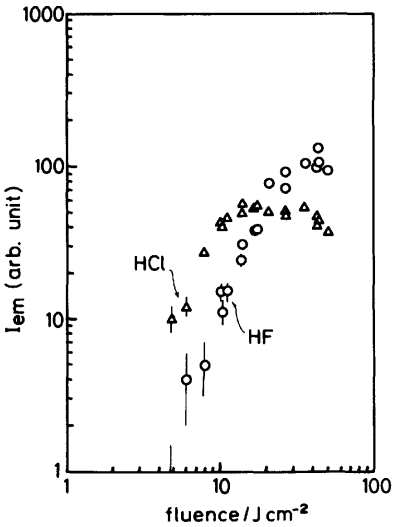

Fig. 4. Peak emission intensities of HCl* (triangles, at 3.8 μm) and HF* (circles, at 2.8 μm) *vs.* laser fluence observed for IRMPD of $CClF_2CH_2Cl$. Laser wavenumber, 1078.59 cm^{-1}.

decay, followed by a slower decay. Although the slow-decay component is relatively small in the emission at 3.0 μm, there is no essential difference in dynamic behavior between the two emitting species, HF* and HCl*. Both may be produced by a similar process, *i.e.*, molecular elimination from highly vibrationally excited $CClF_2CH_2Cl$*. The considerably different fluence dependences observed for HF* and HCl* seem to exclude the possibility that the initial molecular elimination to form HCl* and $CHClCF_2$ is followed by the subsequent elimination of HF* from $CHClCF_2$.

The rate constants for the quenching of vibrationally excited HF* and HCl* by some simple molecules have been determined in laser-induced infrared fluorescence experiments.[14,15] On the assumption that the quenching-rate constants of HF* and HCl* by $CClF_2CH_2Cl$ are approximately the same as those by CH_4, the lifetimes of HF* and HCl* are estimated to be a few microseconds in 1-Torr $CClF_2CH_2Cl$. Since these lifetimes are much shorter than the spontaneous fluorescence lifetimes of HF* and HCl*,[16] these excited molecules can be said to be mainly deactivated in collisions. We propose that large fractions of HF* and HCl* are produced during the laser pulse by means of Reactions 1 and 2. These fractions are responsible for the initial emission spikes in Fig. 3. The rise time of the spike corresponds to the response time of the detection system, while the rapid decay is due to the collisional deactivation of HF* and HCl*. On the other hand, HF* and HCl* are also produced in the collision-induced excitation of $CClF_2CH_2Cl$, followed by immediate decomposition:

$$CClF_2CH_2Cl'' + CClF_2CH_2Cl'' \rightarrow CClF_2CH_2Cl^{\dagger} + CClF_2CH_2Cl', \quad (3)$$

and:

$$CClF_2CH_2Cl^{\dagger} \rightarrow CF_2CHCl + HCl^* \rightarrow CClFCHCl + HF^*, \quad (4)$$

where $CClF_2CH_2Cl^{\dagger}$ represents a reactant molecule excited to a level beyond the decomposition threshold. $CClF_2CH_2Cl''$ is excited below or just above the threshold. Its lifetime is as long as several dozen microseconds. $CClF_2CH_2Cl'$ is a deactivated molecule. The collision-induced processes cause a delayed fluorescences of HF* and HCl* lasting for about 80 μs.

The emission intensities of HF* and HCl* are plotted against the laser fluence in Fig. 4, where I_{HF^*} and I_{HCl^*} are measured at 2.8 and 3.8 μm respectively. The Einstein coefficient of HF* is about five times larger than that of HCl*.[17] Therefore, I_{HF^*} divided by a factor of five and I_{HCl^*} are proportional to the yields of HF* and HCl* on the same scale, if the quenching rate of HF* is equal to that of HCl*. West *et al.* have measured the fluence dependences of the HF* and HCl* emission intensities in the IRMPD of $CClF_2CH_3$.[3] In their measurements, both intensities were found to increase almost linearly with an increase in the fluence. They reported that the calculated RRKM curves for k(HF) and k(HCl) *vs.* the internal energy are virtually parallel over a wide range. This result leads to the constant HF*/HCl* ratio in the corresponding range. In our study of $CClF_2CH_2Cl$, however, the HF*/HCl* ratio clearly depends on the laser fluence. The emission due to HCl* is much stronger than that due to HF* at lower fluences, while I_{HF^*}/I_{HCl^*} is about three at 50 J cm^{-2}. This fact suggests that highly vibrationally excited $CClF_2CH_2Cl$ decomposes competitively *via* HF and HCl molecular-elimination channels and that the branching ratio changes depending on the internal energy of the excited parent molecule. We also observed similar fluence dependences of I_{HF^*} and I_{HCl^*} for a mixture of 0.2-Torr $CClF_2CH_2Cl$ and 4-Torr Ar when

it was irradiated in the fluence region from 30 to 43 J cm^{-2}. Krajnovich *et al.* have examined the IRMPD of C_2F_5Cl in a molecular beam. Cl atomic elimination was dominant at lower fluences. As the fluence was increased, however, the atomic elimination approached saturation, and the C-C bond scission became more eminent.[4] The fluence dependences seem to be consistent with the present study.

The infrared fluorescence experiment can not provide any information concerning the production of HF and HCl in a ground vibrational state. In comparing the observed results with the calculated ones, we assume that the emission intensities of HF* and HCl* are proportional to the total yields of HF and HCl respectively. We simply use the peak emission intensities monitored at 2.8 and 3.8 μm in place of the integrated emission intensities, because a change in fluence does not appreciably affect the shapes of the fluorescence spectra due to HF* and HCl*. It is extremely difficult to separate the HF* and HCl* produced directly in the IRMPD from those produced in collision-induced processes. Therefore, I_{HF^*} and I_{HCl^*} probably correspond to the emissions of HF* and HCl* arising from the IRMPD, not only within the laser pulse, but also after the pulse.

Barker proposed an exact stochastic method based on an energy-grained master equation for the theoretical interpretation of IRMPD.[18] The method has been further applied to consecutive and competitive IRMPD.[19] The details will not be given here. Although there has been no kinetic or thermodynamic study of the two elimination channels of $CClF_2CH_2Cl$ itself, the Arrhenius parameters of HF and HCl elimination reactions have been reported on a number of halogenated hydrocarbons: log A=13—14 and E_0=55—70 kcal mol^{-1} (1 cal=4.184 J) for HF elimination; log A=11—14 and E_0=50—60 kcal mol^{-1} for HCl elimination.[20] The numerical values and assumptions employed for the present calculations are as follows: (a) σ_0 (infrared absorption cross-section of $CClF_2CH_2Cl$ in a ground vibrational state)=1.3×10^{-19} cm^2; (b) the fundamental vibrational frequencies of the $-CH_2Cl$ group in the CH_3CH_2Cl and the $-CClF_2$ group in CF_3CClF_2[21] were used for those of the $-CH_2Cl$ and $-CClF_2$ groups in $CClF_2CH_2Cl$; (c) the laser pulse was assumed to have a 80-ns duration and a constant intensity; (d) parent molecules excited to levels higher than threshold energies were assumed to undergo competitively three processes: collisional deactivation (k_d=1×10^6 s^{-1}), HF elimination, and HCl elimination. The cross-section was determined from the absorption measurement at 1078.59 cm^{-1}. The fundamental vibration frequencies are tabulated in Table 1. The weights of the three reaction processes depend on their rates. The number of trajectories is 1000 in the present calculation.

The simulation of the fluence dependences shown in Fig. 4 was performed for various Arrhenius parameters of the two reaction channels. The absorption cross-section was assumed to have the following form with respect to a given energy level n: $\sigma_n=\sigma_0/(n+1)^\alpha$, where α can be regarded as a parameter. The following set of numerical values gave the best-fitting simulation: log A=12 and E_0=50 kcal mol^{-1} for HCl elimination; log A=14 and E_0=68 kcal mol^{-1} for HF elimination; α=0.2. Table 2 shows the calculated results of the IRMPD of $CClF_2CH_2Cl$ at various fluences using the above-mentioned parameters. The decomposition within the laser pulse becomes more important with an increase in the fluence. In the intermediate fluence region of 10—20 J cm^{-2}, however, the decomposition after the end of the pulse contributes significantly to the total production of HCl,[23] where HCl elimination has a lower threshold energy. The typical energy distributions $P(n)$, *i.e.*, the fraction of molecules at a given energy level n, are illustrated in Fig. 5, where $CClF_2CH_2Cl$ is supposed to be irradiated at six different fluences. The cross-hatched and filled areas correspond to the fractions of the HCl (F_{total}(HCl)) and HF(F_{total}(HF)) elimination channels respectively in the figure. As the degree of vibration freedom s is as large as 18 in $CClF_2CH_2Cl$, the unimolecular decomposition rates calculated for molecules at levels a little higher than the threshold energies, *i.e.*, n=17—23 for HCl elimination and n=23—27 for HF elimination, are smaller than the assumed quenching rate. The k_{HCl} (n) and k_{HF} (n) are about equal to the quenching rate k_d at n=24 and 28 respectively. The two rate constants are roughly equal to each other at n=35; the value is 2.0×10^8 s^{-1}. When the laser fluence is 20 J cm^{-2}, the absorption rate for the molecule at n=50 is five times less than k_{HCl} and 30 times less than k_{HF}. Therefore, it is hard to excite molecules to such high energy levels.

The calculated fluence dependences of the HCl elimination and HF elimination are shown in Fig. 6, where the decomposition after the end of the pulse

Table 1. Fundamental vibration frequencies of $CClF_2CH_2Cl$ and CHClFCHClF used in the calculations

$CClF_2CH_2Cl$		CHClFCHClF	
Vibration[a]	Frequency ν/cm^{-1}	Vibration[a]	Frequency ν/cm^{-1}
CH_2 a-stretch.	3000	CH a-stretch.	2983
CH_2 s-stretch.	3000	CH s-stretch.	2850
CH_2 scis.	1430	CH op-bend.	1439
CH_2 wag.	1300		1357
CH_2 twist.	1240	CH ip-bend.	1297
CF_2 a-stretch.	1185		1239
CF_2 s-stretch.	1110	CF a-stretch.	1188
CC stretch.	1030	CF s-stretch.	1105
CH_2 rock.	820	CC stretch.	1032
CCl a-stretch.	770	CCl a-stretch.	794
CCl s-stretch.	660	CCl s-stretch.	753
CF_2Cl deform.	454	CFCl a-deform.	700
CF_2Cl deform.	441	CFCl s-deform.	628
CCCl a-deform.	336	CCFCl deform.	462
CCCl s-deform.	330		452
CF_2Cl deform.	315		236
Torsion.	251		236
CF_2Cl deform.	186	Torsion.	160

a) See Ref. 22 for abbreviation.

TABLE 2. IRMPD OF $CClF_2CH_2Cl$

ϕ / J cm^{-2}	$\bar{n}$[a]	n[b]	Within pulse			After pulse		Total R[f]	Pg[g]
			F(HCl)[c]	F(HF)[c]	R[d]	F(HCl)[e]	F(HF)[e]		
4	12.7	17.2	0.001	0	—	0.002	0	—	0.003
6	16.8	24.4	0	0	—	0.058	0.001	58	0.059
8	19.9	31.0	0.025	0.003	8.3	0.180	0.006	22.8	0.214
10	23.1	37.2	0.062	0.018	4.8	0.348	0.022	10.3	0.451
12	25.4	42.6	0.167	0.052	3.2	0.375	0.029	6.7	0.423
14	27.5	47.0	0.283	0.109	2.6	0.332	0.036	4.2	0.760
16	29.1	51.2	0.367	0.156	2.4	0.286	0.038	3.4	0.846
18	30.3	54.0	0.462	0.209	2.2	0.204	0.034	2.7	0.909
20	31.1	55.8	0.531	0.241	2.2	0.151	0.024	2.6	0.947
25	32.5	59.7	0.589	0.318	1.9	0.062	0.013	2.0	0.982
30	33.2	62.0	0.618	0.342	1.8	0.024	0.007	1.8	0.991
35	33.6	62.9	0.607	0.382	1.6	0.008	0.002	1.6	0.999
40	33.9	63.5	0.578	0.417	1.4	0.004	0.001	1.4	1.0
45	34.1	64.8	0.588	0.409	1.4	0.002	0	1.4	1.0
50	34.5	65.6	0.556	0.444	1.3	0	0	1.3	1.0
55	34.6	66.0	0.537	0.463	1.2	0	0	1.2	1.0
60	34.8	66.0	0.543	0.457	1.2	0	0	1.2	1.0
65	34.9	66.3	0.516	0.484	1.1	0	0	1.1	1.0
70	35.2	66.4	0.530	0.470	1.1	0	0	1.1	1.0

a) Average number of photons contained in a molecule at end of laser pulse. b) Average number of photons absorbed per molecule at end of laser pulse. c) Fraction of reaction within laser pulse. d) F(HCl)/F(HF). e) Fraction of reaction after pulse. f) F(HCl)/F(HF), where collisions are taken into consideration. g) Reaction probability.

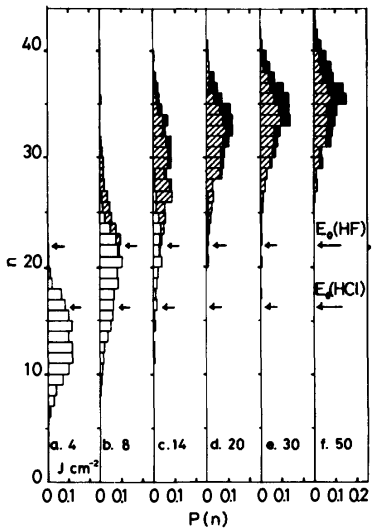

Fig. 5. Typical vibrational population distributions for $CClF_2CH_2Cl$ irradiated at various fluences. Cross-hatched and filled areas indicate the extents of HCl and HF elimination reactions, respectively. $\sigma_n = \sigma_0/(n+1)^{0.2}$ cm^2. The postirradiation decomposition was taken into consideration.

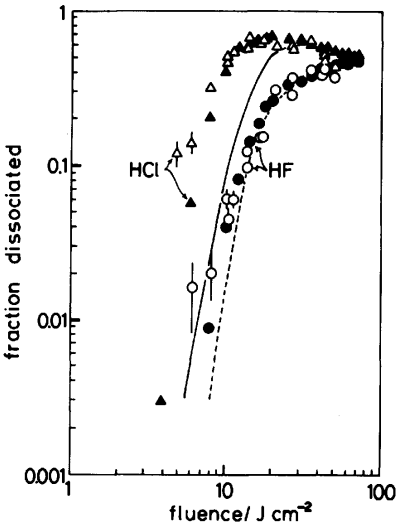

Fig. 6. Comparison of calculated yields of HCl and HF to observed ones in IRMPD of 1-Torr $CClF_2CH_2Cl$ at various fluences. Filled triangles, calculated yields of HCl; triangles, observed yields of HCl; filled circles, calculated yields of HF; circles, observed yields of HF. Solid and dotted curves show the calculated fractions of HF and HCl produced within the pulse.

has been taken into consideration. The filled triangles and filled circles present F_{total}(HCl) and F_{total}(HF) respectively. The same figure also shows the fluence dependences of the observed I_{HCl^*} (open triangles) and I_{HF^*} (open circles) values, where the scales have been chosen arbitrarily so that the experimental data fit the calculated ones. The I_{HF^*}/F_{total} (HF) ratio was found to be approximately three times larger than the I_{HCl^*}/F_{total} (HCl) ratio. From the emission efficiencies of HCl* and HF*, the factor can be expected to be five if these molecules are in the $v'=1$ state.[17] The solid and dotted curves in Fig. 6 present the fractions of HCl and HF respectively which are produced within the pulse.

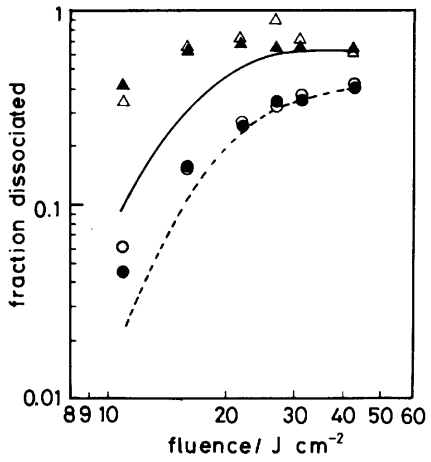

Fig. 7. Comparison of calculated yields of HCl and HF to observed ones in IRMPD of 2-Torr CHClFCHClF at various fluences. Filled triangles, calculated yields of HCl; triangles, observed yields of HCl; filled circles, calculated yields of HF; circles, observed yields of HF. Solid and dotted curves show the calculated fractions of HF and HCl produced within the pulse.

Our previous paper has reported the fluence dependences of I_{HF^*} and I_{HCl^*} in the IRMPD of CHClFCHClF using the same experimental technique.[5] By applying the stochastic trajectory calculation to the compound, we obtained the results in Fig. 7. The fundamental vibration frequencies are also tabulated in Table 1. The kinetic parameters for the HF and HCl elimination reactions are the same as $CClF_2CH_2Cl$. The α parameter is changed into 0.3, which seems to give a better fit. I_{HF^*}/F_{total} (HF) is four times larger than I_{HCl^*}/F_{total} (HCl).

At present, the calculations seems to have a somewhat unavoidable uncertainty because of the lack of the kinetic parameters of $CClF_2CH_2Cl$ and CHClFCHClF, together with incomplete understanding of the multiple-photon absorption process. However, the calculated results satisfactorily describe the fluence dependences of I_{HF^*} and I_{HCl^*} for the IRMPD of $CClF_2CH_2Cl$ and CHClFCHClF. It is interesting that the IRMPD is able to induce the reaction channel with a higher threshold energy, rather than the channel with the lowest threshold energy, under some selected experimental conditions.

The authors wish to express their thanks to Miss Kyoko Sugita for the computer calculations. They also wish to express their thanks to Dr. Takashi Igarashi for the assignments of the fundamental vibration frequencies of haloethanes.

References

1) W. C. Danen and J. C. Jang, "Multiphoton Infrared Excitation and Reaction of Organic Compounds," in "Laser-Induced Chemical Processes," ed by J. I. Steinfeld, Plenum Press, New York (1981), Chap. 2, p. 63.
2) J. B. Black, P. Kolodner, M. J. Shultz, E. Yablonovitch, and N. Bloembergen, *Phys. Rev., A*, **19**, 704 (1979); J. C. Stephenson and D. S. King, *J. Chem. Phys.*, **78**, 186 (1983).
3) G. A. West, R. E. Weston, Jr., and G. W. Flynn, *Chem. Phys.*, **35**, 275 (1978).
4) D. J. Krajnovich, A. Giardini-Guidoni, Aa. S. Sudbo, P. A. Schultz, Y. R. Shen, and Y. T. Lee, "Crossed Laser and Molecular Beam Study of Multiphoton Dissociation of C_2F_5Cl," in "Laser-Induced Processes in Molecules," ed by K. L. Kompa and S. D. Smith, Springer-Verlag, Berlin (1979), p. 176.
5) Y. Ishikawa and S. Arai, *Chem. Phys. Lett.*, **103**, 68 (1983).
6) C. R. Quick, Jr., and C. Wittig, *J. Chem. Phys.*, **72**, 1694 (1980).
7) Y. Ishikawa, T. Yamazaki, Y. Hama, and S. Arai, *Appl. Phys., B*, **32**, 85 (1983).
8) No change could be observed in the ratio of I_{HCl^*} to I_{HF^*}, even at a fast flow rate of 200 Torr cm^3 min^{-1}. This fact indicates that the secondary reactions involving stable products, $CClF_2CH_2Cl^*+HCl(HF)\rightarrow CClF_2CH_2Cl+HCl^*(HF^*)$ and $CF_2CHCl+nh\nu\rightarrow CFCCl+HF^*$, do not occur appreciably at the slow flow rate, *i.e.*, 10 Torr cm^3 min^{-1}, used here.
9) E. A. Jones, J. S. Kirby-Smith, P. L. H. Woltz, and A. H. Nielsen, *J. Chem. Phys.*, **19**, 242 (1950).
10) J. R. Nielsen, C. Y. Liang, and D. C. Smith, *J. Chem. Phys.*, **20**, 1090 (1952).
11) N. C. Craig, G. Y. Lo, C. D. Needham, and J. Overend, *J. Am. Chem. Soc.*, **86**, 3232 (1964).
12) K. C. Kim and D. W. Setser, *J. Phys. Chem.*, **76**, 283 (1972).
13) K. C. Kim, D. W. Setser, and B. E. Holmes, *J. Phys. Chem.*, **77**, 725 (1973).
14) H. L. Chen and C. B. Moore, *J. Chem. Phys.*, **54**, 4080 (1971).
15) J. K. Hancock and W. H. Green, *J. Chem. Phys.*, **59**, 6350 (1973).
16) J. T. Yardley, "Introduction to Molecular Energy Transfer," Academic Press, New York (1980), p. 58.
17) J. M. Herbelin and G. Emanuel, *J. Chem. Phys.*, **60**, 689 (1974).
18) J. R. Barker, *J. Chem. Phys.*, **72**, 3686 (1980).
19) R. E. Weston, Jr., *J. Phys. Chem.*, **86**, 4864 (1982).
20) P. J. Robinson and K. A. Holbrook, "Unimolecular Reactions," Wiley-Interscience, London (1972), p. 221.
21) J. R. Nielsen, C. Y. Liang, R. M. Smith, and D. C. Smith, *J. Chem. Phys.*, **21**, 383 (1953).
22) T. Shimanouchi, "Tables of Molecular Vibrational Frequencies," NSRDS-NBS, 39 (1972), Consolidated Vol. 1, p. 104.
23) Y. Ishikawa, H. Kasugai, T. Ishii, and S. Arai, to be published.

Sodium Sulfate Doped with Sodium Vanadate and Rare Earth Sulfate as a Solid Electrolyte for a Sulfur Dioxide Gas Detector

Nobuhito IMANAKA, Gin-ya ADACHI,* and Jiro SHIOKAWA
Department of Applied Chemistry, Faculty of Engineering, Osaka University, Yamadaoka, Suita, Osaka 565
(Received August 31, 1983)

Sodium sulfate doped with $NaVO_3$ and $Ln_2(SO_4)_3$ (Ln=Eu, Pr, and Y) show higher electrical conductivity for Na^+ ions and maintains a high temperature phase, Na_2SO_4-I, without showing phase transformation. The electromotive force (EMF) using solid solutions, Na_2SO_4-$NaVO_3$-$Ln_2(SO_4)_3$ (Ln=Pr and Y), as solid electrolytes exhibits good agreement with the calculated value, the temperature as low as 673 K which is approximately 300 K lower than pure sodium sulfate can be.

Influence of sulfur dioxide exhausted from coal power plants and automobiles to the environment has been taking place and becoming a serious problem. Especially, acid rain resulting from the absorption of sulfur dioxide and nitrogen dioxide by water is considerably affecting the surroundings in North America and some other countries.

Recently, some attempts have been made to utilize sodium sulfate as a solid electrolyte for a SO_2 gas sensor.[1-4] However, in practical use, a phase transformation from Na_2SO_4-III (a low temperature phase) to Na_2SO_4-I (a high temperature phase)[5-21] is a serious obstacle. In addition, other disadvantages in using sodium sulfate alone as an electrolyte are its lower electrical conductivity and the difficulty in obtaining a SO_2-SO_3 equilibrium on the surface of the electrolyte. Mono-, di-, and trivalent cations have been doped in order to improve their electrical and thermodynamic properties.[22-26] In our previous study,[27] sodium sulfate doped with $NaVO_3$ and $Ln_2(SO_4)_3$ (Ln=Eu and Pr) has been found to show no phase transformation, to maintain a Na_2SO_4-I-similar phase, and to increase the electrical conductivity.

In the present study, effects of doping with rare earth sulfates and sodium vanadate into sodium sulfate on the electrical conductivity and on the phase transformation of the solid solutions are examined, and also EMF measurements by applying Na_2SO_4-$NaVO_3$-$Ln_2(SO_4)_3$ (Ln=Pr and Y) as an electrolyte for a SO_2 gas concentration cell are to be discussed.

Experimental

Materials. Rare earth sulfate was prepared by adding concentrated H_2SO_4 into rare earth oxide. Sodium vanadate was synthesized by heating the mixture of Na_2CO_3 and NH_4VO_3 (by molar ratio 1:2) at 823 K for 5 h in air. A mixture of appropriate amount of Na_2SO_4 and $Ln_2(SO_4)_3$ (Ln=Eu, Pr, and Y) were pelletatized and heated at 1073 K for 3 h in air. In Na_2SO_4-$NaVO_3$-$Ln_2(SO_4)_3$ (Ln=Eu, Pr, and Y) systems, the heated pellets were ground, remade into pellets and sintered 3 h at 1073 K in air.

Measurements. Phases and thermal properties were measured with X-ray diffraction method and thermal analysis. Electrical conductivity measurements were carried out by a complex impedance method[28] using a Hewlett Packard vector impedance meter 4800 A. The apparatus for the electrical conductivity measurements is shown in Fig. 1. EMF measurements were performed by constructing a SO_2 gas concentration cell which is depicted in Fig. 2. The inner quartz tube compartment was separated by spring loading the electrolyte with a quartz rod. A gold O-ring was used in order to separate the test and the reference SO_2 gas completely. The SO_2 gas concentration was regulated by changing SO_2 and O_2 gas flow rate. A Pt net was applied as an electrode so that the electrolyte could maintain good contact with the SO_2 gas. EMF measurements were performed with a Takeda Riken Digital Multimeter TR-6855. The response time, which is here defined as the time required from the test gas arrival at the electrolyte to the attainment of about 96% of the calculated EMF, was also measured.

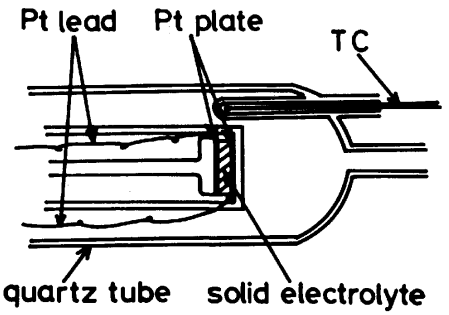

Fig. 1. The apparatus for the electrical conductivity measurements.

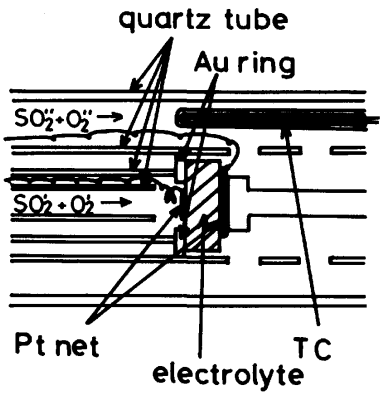

Fig. 2. The apparatus for the electromotive force (EMF) measurements.

Results and Discussion

Electrical Conductivity, Phases, and Thermal Properties. The Na_2SO_4-$Ln_2(SO_4)_3$ (Ln=Eu, Pr, and Y): Sodium sulfate doped with $Ln_2(SO_4)_3$ (Ln=Eu, Pr, and Y) ex-

Table 1. The phases and thermal properties of Na_2SO_4-$Pr_2(SO_4)_3$

Sample No.	Na_2SO_4 (mol%)	$Pr_2(SO_4)_3$ (mol%)	Phases	DTA peaks T/K
1	99.1	0.9	α+Na_2SO_4-V	573
2	98.4	1.6	α+Na_2SO_4-V	573
3	95.2	4.8	γ	573
4	90.7	9.3	γ	853

α phase is similar to phase Na_2SO_4-III.[18,19] γ phase is different from any Na_2SO_4 phase.

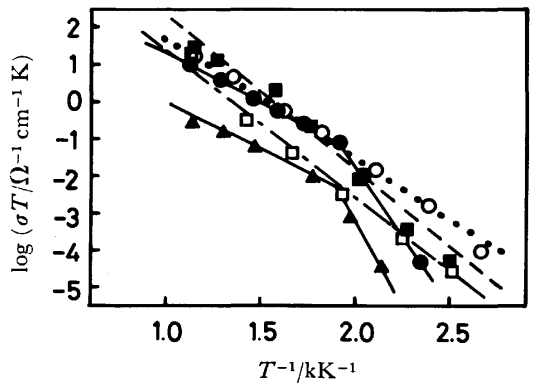

Fig. 3. Temperature dependences of electrical conductivities for the Na_2SO_4-$Pr_2(SO_4)_3$.
—□— Na_2SO_4 : $Pr_2(SO_4)_3$=90.7 : 9.3, —■— Na_2SO_4 : $Pr_2(SO_4)_3$=95.2 : 4.8, ···○··· Na_2SO_4 : $Pr_2(SO_4)_3$=98.4 : 1.6, —●— Na_2SO_4 : $Pr_2(SO_4)_3$= 99.1 : 0.9, —▲— Na_2SO_4.

hibits almost the same electrical conductivity, phases, and thermal properties with one another.

The representative results of Na_2SO_4-$Pr_2(SO_4)_3$ are listed in Table 1. Sodium sulfate doped with 0.9 mol% or 1.6 mol% $Pr_2(SO_4)_3$ exhibits phase α which is similar to the Na_2SO_4-III phase [18,19] including a starting material (Na_2SO_4-V phase). The other two samples show phase γ which is different from any Na_2SO_4 phase. All samples exhibit an endothermal peak in DTA curves, indicating that the phase transformation still exists.

Electrical conductivity measurements in the systems of Na_2SO_4-$Pr_2(SO_4)_3$ are shown in Fig. 3. Doping $Pr_2(SO_4)_3$ into Na_2SO_4 increases the concentration of cation vacancies of the sulfate, and then the electrical conductivity enhances. A break or bend in $\log(\sigma T)$ *vs.* $1/T$ curves is due to the phase transformation in the sulfate. The solid solution of sodium sulfate doped with 1.6 mol% $Pr_2(SO_4)_3$ did not exhibit any break. The III-I phase transformation appeared to be fairly suppressed. However, the phase transformation was found to still remain on DTA measurement. The sulfate doped with 4.8 mol% $Pr_2(SO_4)_3$ gives the highest electrical conductivity (from 571 K to 873 K) in the Na_2SO_4-$Pr_2(SO_4)_3$ systems.

This fact means that the number of cation vacancies which is effective for cation conduction becomes a maximum with the doping. By doping $Pr_2(SO_4)_3$ more than 4.8 mol%, cation vacancies appear to make clusters and then the electrical conductivity in Na_2SO_4-$Pr_2(SO_4)_3$ systems rather decreases.

Table 2. The phases and thermal properties of Na_2SO_4-$NaVO_3$-$Y_2(SO_4)_3$

Sample No.	Na_2SO_4 (mol%)	$NaVO_3$ (mol%)	$Y_2(SO_4)_3$ (mol%)	Phases	DTA peaks T/K
1	98.3	0.7	1.0	α	485
2	96.9	1.1	2.0	α	408, 463
3	95.7	1.3	3.0	β	—
4	93.6	2.4	4.0	β	—
5	91.4	3.6	5.0	β	573 (very small)

α phase is similar to phase Na_2SO_4-III.[18,19] β phase is similar to phase Na_2SO_4-I.[18,19]

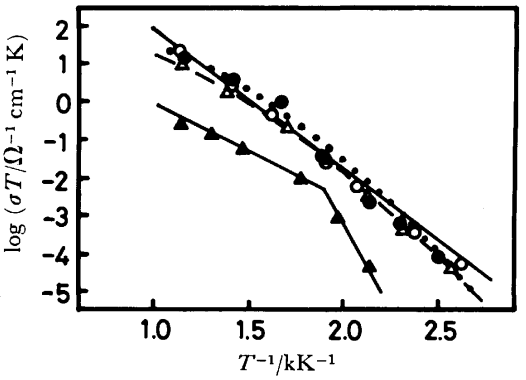

Fig. 4. Temperature dependences of electrical conductivities for the Na_2SO_4-$NaVO_3$-$Y_2(SO_4)_3$ which exhibit β phase.
—○— Na_2SO_4 : $NaVO_3$: $Y_2(SO_4)_3$ = 91.4 : 3.6 : 5.0, ···●··· Na_2SO_4 : $NaVO_3$: $Y_2(SO_4)_3$ = 93.6 : 2.4 : 4.0, —△— Na_2SO_4 : $NaVO_3$: $Y_2(SO_4)_3$ = 95.7 : 1.3 : 3.0, —▲— Na_2SO_4.

Although the electrical conductivities of the sulfates increase with the $Ln_2(SO_4)_3$ (Ln=Eu, Pr, and Y) doping, the phase transformation still remains. Therefore, the bicomponent solid solutions do not seem to be appropriate as solid electrolytes for a SO_2 gas detector.

The Na_2SO_4-$NaVO_3$-$Ln_2(SO_4)_3$(Ln=Eu, Pr, and Y) Systems: The phases and thermal properties of sodium sulfate doped with $NaVO_3$ and $Ln_2(SO_4)_3$ (Ln=Eu, Pr, and Y) are all similar.

A typical behavior (Na_2SO_4-$NaVO_3$-$Y_2(SO_4)_3$) is presented in Table 2. Samples No. 1 and 2 show phase α which is similar to the phase Na_2SO_4-III.[18,19] On the other hand, samples No. 3, 4, and 5 show phase β which resembles the phase Na_2SO_4-I.[18,19] From DTA measurements, the samples which show phase α exhibit endothermal peaks, that is, a phase transformation still remains. The samples which exhibit phase β show no endothermal peak, indicating that no phase transformation occurs.

The plots of $\log(\sigma T)$ *vs.* $1/T$ for sodium sulfate doped with $NaVO_3$ and $Y_2(SO_4)_3$(phase β) are given in Fig. 4. The slope of the Na_2SO_4-$NaVO_3$-$Y_2(SO_4)_3$ curves closely approaches that of Na_2SO_4-I (a high

temperature phase). The electrical conductivity of Na_2SO_4-$NaVO_3$-$Y_2(SO_4)_3$ systems is increased with doping $Y_2(SO_4)_3$ because of the increase in cation vacancies. In addition, the Na_2SO_4-$NaVO_3$-$Y_2(SO_4)_3$ systems maintain a Na_2SO_4-I-like phase (phase β) which is excellent in Na^+ ion conduction.

As mentioned above, the conductivity of Na_2SO_4-I is considerably high and the three component systems also support the similar structure with the Na_2SO_4-I phase. Therefore, the conductivity of the solid solution is also high. The Na_2SO_4-$NaVO_3$-$Y_2(SO_4)_3$ systems are considered to be very good ionic conductors. In this system, sodium sulfate doped with 3.6 mol% $NaVO_3$ and 5.0 mol% $Y_2(SO_4)_3$ shows the best linearity in the three $\log(\sigma T)-1/T$ curves. The three component systems, including rare earth sulfates other than $Y_2(SO_4)_3$ also give the similar optimum composition of 91:4:5.

EMF Measurements. The EMF measurements were performed with Na_2SO_4-$NaVO_3$-$Ln_2(SO_4)_3$ (Ln=Eu, Pr, and Y) (91:4:5) as solid electrolytes. Temperature dependences of measured EMF/calculated EMF ratio with a fixed SO_2 gas concentration are shown in Fig. 5.

The measured EMF for pure Na_2SO_4 and Na_2SO_4-$Ln_2(SO_4)_3$ (Ln=Eu, Pr, and Y) solid solutions were less than half of calculated EMF. The measured value for sodium sulfate doped with 4.0 mol% $NaVO_3$ and 5.0 mol% $Eu_2(SO_4)_3$ is consistent with that calculated at 623 K and appears to be an appropriate electrolyte. However, the measured value of the EMF has exceeded that calculated at 673 K. This appears to have resulted because Eu^{3+} ions in the systems are easily reduced to a divalent state with SO_2 gas and change in free energies for the reduction might have been added to the calculated EMF value. Thus, the solid solution of Na_2SO_4-$NaVO_3$-$Eu_2(SO_4)_3$ is not appropriate for the electrolyte.

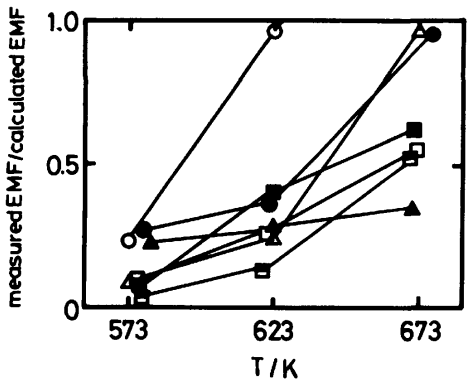

Fig. 5. The ratio of measured EMF/calculated EMF for Na_2SO_4, Na_2SO_4-$Ln_2(SO_4)_3$, Na_2SO_4-$NaVO_3$-$Ln_2(SO_4)_3$ (Ln=Eu, Pr, and Y) with initial SO_2 gas composition, approximately 24 and 8 vol%.
—○— Na_2SO_4 : $NaVO_3$: $Eu_2(SO_4)_3$=91.0 : 4.0 : 5.0, —●— Na_2SO_4 : $NaVO_3$: $Pr_2(SO_4)_3$=91.1 : 3.9 : 5.0, —△— Na_2SO_4 : $NaVO_3$: $Y_2(SO_4)_3$ = 91.4 : 3.6 : 5.0, —□— Na_2SO_4 : $Eu_2(SO_4)_3$=95.9 : 4.1, —■— Na_2SO_4 : $Pr_2(SO_4)_3$=95.2 : 4.8, —▬— Na_2SO_4 : $Y_2(SO_4)_3$ =95.0 : 5.0, —▲— Na_2SO_4.

The systems of Na_2SO_4-$NaVO_3$-$Ln_2(SO_4)_3$ (Ln= Pr and Y) give almost the same EMF as calculated one at 673 K. In the temperature range higher than 673 K, the electrolytes became soft because of $NaVO_3$. The EMF measurements in variation of the test SO_2 gas concentration were conducted with the Na_2SO_4-$NaVO_3$-$Ln_2(SO_4)_3$ (Ln=Pr and Y) systems as solid electrolytes at 673 K.

Results of the EMF measurements with the Na_2SO_4-$NaVO_3$-$Pr_2(SO_4)_3$ electrolyte are presented in Fig. 6. The calculated EMF is cited from theoretical one of Jacob and Rao.[2] The measured EMF shows good

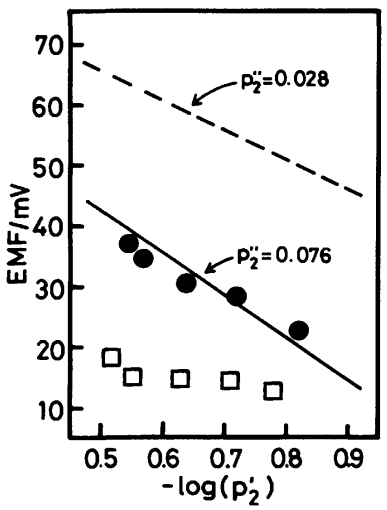

Fig. 6. Variation of the EMF for the concentration cell; $Pt|O_2(p_1'), SO_2(p_2')|Na_2SO_4$ (3.9 mol% $NaVO_3$, 5.0 mol% $Pr_2(SO_4)_3)|O_2(p_1''), SO_2(p_2'')|Pt$, with p_1''= 0.924, p_2''=0.076 (●) and p_1''=0.972, p_2''=0.028 (□) at 673 K.
—— and —— are calculated EMF,[2] respectively.

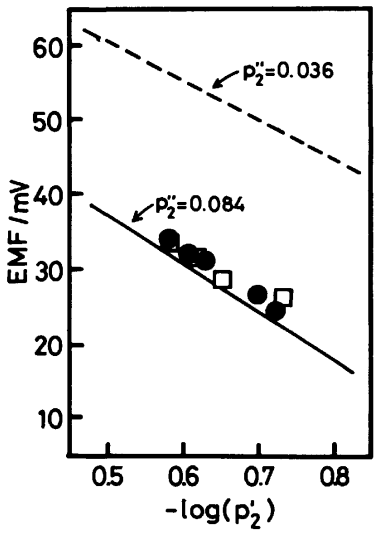

Fig. 7. Variation of the EMF for the concentration cell; $Pt|O_2(p_1'), SO_2(p_2')|Na_2SO_4$ (3.6 mol% $NaVO_3$, 5.0 mol% $Y_2(SO_4)_3)|O_2(p_1''), SO_2(p_2'')|Pt$, with p_1''= 0.916, p_2''=0.084 (●) and p_1''=0.964, p_2''=0.036 (□) at 673 K.
—— and —— are calculated EMF,[2] respectively.

accordance with the calculation in which the initial reference SO_2 gas concentration is 7.6 vol%. Sodium sulfate doped with $NaVO_3$ and $Pr_2(SO_4)_3$ is able to use for a solid electrolyte, a temperature as low as 673 K which is approximately 300 K lower than pure sodium sulfate can be operative. In the case that the initial reference SO_2 gas concentration is 2.8 vol%, the measured EMF is appreciably smaller than the calculated EMF. The EMF results for the Na_2SO_4-$NaVO_3$-$Y_2(SO_4)_3$ electrolyte are also presented in Fig. 7. The measured EMF also shows good agreement with the calculated EMF if the initial reference SO_2 gas concentration is 8.4 vol%. The difference between the measured and the calculated EMF also becomes larger when the initial reference SO_2 gas concentration is 3.6 vol%.

Dependence of the initial reference SO_2 gas concentration on the measured EMF/calculated EMF ratios at 673 K for the Na_2SO_4-$NaVO_3$-$Ln_2(SO_4)_3$ (Ln= Pr and Y) electrolytes are shown in Fig. 8. The measured EMF/calculated EMF ratio abruptly decreases

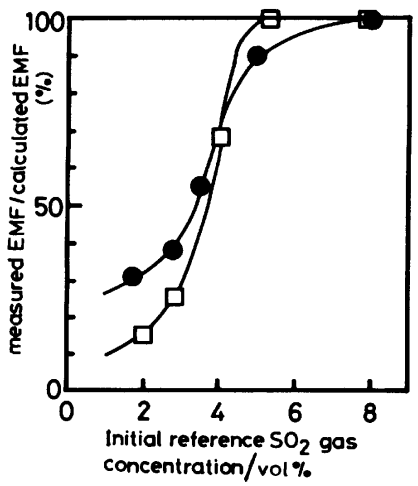

Fig. 8. Dependences of initial SO_2 gas concentration for reference on measured EMF/calculated EMF at 673 K.
□ Na_2SO_4 : $NaVO_3$: $Pr_2(SO_4)_3$=91.1 : 3.9 : 5.0,
● Na_2SO_4 : $NaVO_3$: $Y_2(SO_4)_3$=91.4 : 3.6 : 5.0.

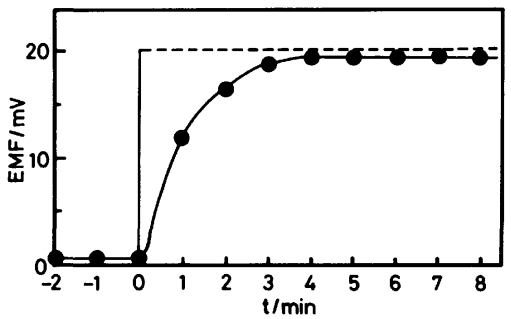

Fig. 9. A typical EMF response for the Na_2SO_4-$NaVO_3$-$Y_2(SO_4)_3$(91.4 : 3.6 : 5.0) electrolyte at 673 K.
The test and the reference SO_2 gas concentration are 20.5 and 9.7 vol%, respectively.
—— is calculated EMF.[2]

when the initial reference SO_2 gas concentration becomes less than 5 vol%. The electrolyte can not detect SO_2 gas accurately because the SO_2 gas concentration on the surface for the reference electrode is smaller than 5 vol% and the electrical conductivity of the electrolyte is appreciably low because the operating temperature is as low as 673 K.

A typical EMF response for the Na_2SO_4-$NaVO_3$-$Y_2(SO_4)_3$ electrolyte at 673 K is presented in Fig. 9. The EMF increases immediately when the test SO_2 gas reaches the surface of the electrolyte. However, about 4 min are necessary for the EMF to attain 96% of the calculated EMF. Jacob and Rao[2] have described that approximately 4 min are required to attain 98% of the calculated EMF when pure sodium sulfate is used as a solid electrolyte at 973 K. The response time in our measurement coincides with their results. However, operating temperature of ours is approximately 300 K lower than theirs.

In conclusion, sodium sulfate doped with $NaVO_3$ and $Ln_2(SO_4)_3$ (Ln=Pr and Y) has suitable properties for the solid electrolyte because the solid solution shows considerably high electrical conductivity. The sulfate can be utilized as the solid electrolyte for a SO_2 gas sensor even at 673 K which is approximately 300 K lower than pure sodium sulfate can be used. The doping of sodium vanadate as well as rare earth sulfates makes considerable progress in the improvement of the electrolyte.

References

1) L. G. Boxall and K. E. Johnson, *J. Electrochem. Soc.*, **118**, 885 (1971).
2) K. T. Jacob and D. B. Rao, *J. Electrochem. Soc.*, **126**, 1842 (1979).
3) N. Imanaka, G. Adachi, and J. Shiokawa, *Chem. Lett.*, **1983**, 287.
4) N. Imanaka, G. Adachi, and J. Shiokawa, *Denki Kagaku*, **51**, 93 (1983).
5) J. P. Coughlin, *J. Am. Chem. Soc.*, **77**, 868 (1955).
6) Y. A. Badr, F. El-Kabbany, and M. Tosson, *Phys. Status Solidi A*, **53**, K51 (1979).
7) F. El-Kabbany, Y. Badr, and M. Tosson, *Phys. Status Solidi A*, **63**, 699 (1981).
8) Q. R. Goyal, V. V. Deshpande, and M. D. Karkhanavala, *Indian J. Chem.*, **9**, 1006 (1971).
9) J. E. D. Davies and W. F. Sandford, *J. Chem. Soc., Dalton Trans.*, **1975**, 1912.
10) B. N. Mehrotra, Th. Hahn, H. Arnold, and W. Eysel, *Acta Crystallogr., Sect. A*, **31**, S79 (1975).
11) V. Amirthalingam, M. D. Karkhanavala, and U. R. K. Rao, *Acta Crystallogr., Sect. A*, **33**, 522 (1977).
12) C. A. Cody, L. Dicarlo, and R. K. Darlington, *J. Inorg. Nucl. Chem.*, **43**, 398 (1981).
13) F. C. Kracek, *J. Phys. Chem.*, **33**, 1281 (1929).
14) F. C. Kracek and R. E. Gibson, *J. Phys. Chem.*, **33**, 1304 (1929).
15) F. C. Kracek and R. E. Gibson, *J. Phys. Chem.*, **34**, 188 (1930).
16) F. C. Kracek and C. J. Ksanda, *J. Phys. Chem.*, **34**, 1741 (1930).
17) G. E. Brodale and W. F. Giauque, *J. Phys. Chem.*, **76**, 737 (1972).
18) E. L. Kreidl and Ivan Simon, *Nature*, **181**, 1529 (1958).

19) Y. Saito, K. Kobayashi, and T. Maruyama, *Thermochim. Acta*, **53**, 289 (1982).
20) K. Kobayashi and Y. Saito, *Thermochim. Acta*, **53**, 299 (1982).
21) Y. Saito, K. Kobayashi, and T. Maruyama, *Solid State Ionics*, **1981**, 393.
22) H. H. Höfer, W. Eysel, and U. v. Alpen, *J. Solid State Chem.*, **36**, 365 (1981).
23) H.H. Höfer, W. Eysel, and U. v. Alpen, *Mater. Res. Bull.*, **13**, 265 (1978).
24) R. M. Mupray and E. A. Secco, *Can. J. Chem.*, **56**, 2616 (1978).
25) K. L. Keester, W. Eysel, and Th. Hahn, *Acta Crystallogr., Sect. A*, **31**, S79 (1975).
26) H. H. Hofer, U. v. Alpen, and W. Eysel, *Acta Crystallogr., Sect. A*, **34**, S358 (1978).
27) N. Imanaka, G. Adachi, and J. Shiokawa, *Can. J. Chem.*, in press.
28) J. E. Bauerle, *J. Phys. Chem. Solids*, **30**, 2657 (1969).

Kinetics of the Conformational Change and Subunit Dissociation of Aldolase

Yoko OHGA, Mamoru NAKANISHI, and Masamichi TSUBOI*
Faculty of Pharmaceutical Sciences, The University of Tokyo, Hongo, Bunkyo-ku, Tokyo 113
(Received September 8, 1983)

The kinetics of acid denaturation of muscle aldolase were examined by stopped-flow fluorescence and stopped-flow light scattering measurements. The denaturation reaction was found to consist of three distinguishable steps—step I with fluorescence increase only, step II with both fluorescence increase and light scattering decrease, and step III with fluorescence decrease alone. Circular dichroism and sedimentation equilibrium measurements were also made at different pH's in the course of the acid denaturation. It was concluded that in the acid denaturation of this enzyme a rearrangement of the secondary or tertiary structures takes place rapidly (4 s^{-1} at 21.5 °C and at pH 3.4), and then the subunit dissociation occurs more slowly (0.04 s^{-1} at 21.5 °C and at pH 3.4), with further conformational change. The subunit dissociation was found to be caused by two H^+ per tetramer.

We have recently proposed a new method of characterizing the subunit-structure of a macromolecule.[1] The method consists of the use of a stopped-flow light scattering measurement in combination with a stopped-flow fluorescence measurement. By this combination, one can establish a sequence of *cause and effect* between an inter-subunit dissociation reaction and an intra-subunit conformation change in the macromolecule in question. The method was once applied to the subunit structure of concanavalin A and *Limulus* haemocyanin.[1] Practically the same method was followed by Tashiro *et al.*[2] with bovine liver glutamate dehydrogenase. In this paper, we examine the applicability of this method with a slightly more complex example, namely aldolase.

Rabbit muscle aldolase is an enzyme which splits fructose 1,6-diphosphate to yield glyceraldehyde 3-phosphate and dihydroxyacetone phosphate in the second stage of glycolysis.[3] The enzyme is tetramer with each subunit having a molecular weight of 40 000.[4] Kawahara and Tanford showed that the four-subunit structure of the enzyme is dissociated into monomers by guanidine hydrochloride.[5] The enzyme is also dissociated by urea or acid.[6,7] The subunit reassociation and reactivation of denatured aldolase were found to be slow processes (3 h at 0 °C), and the kinetics of these processes were once examined by Teipel.[8] The kinetics of unfolding and subunit dissociation of the enzyme, however, have not been examined so far.

Experimental

Aldolase. Rabbit muscle aldolase was purchased from Sigma as a crystalline suspension in 3.2 M† ammonium sulfate. After centrifugation of the suspension the enzyme solution was obtained by dialyzing it against 0.01 M sodium citrate buffer (pH 5.4) for a few days at 4 °C. Protein concentrations were determined spectrophotometrically using the value of $E^{1\%}_{1\,cm}$=9.1 at 280 nm.[9] Buffer systems used are: citric acid+sodium citrate buffer (in the pH 6—3 range) and sodium citrate+HCl buffer (in the pH 2—2.7 range). The enzyme solution was filtered everytime before the light scattering measurement through a 0.45 μm Millipore type HA filter.

Fluorescence Measurements. Fluorescence spectra were observed by a Hitachi Fluorescence Spectrophotometer model 650-10S with circulating water to maintain the temperature of the cell at 25 °C.

Circular Dichroism Measurements. Circular dichroism spectra were measured by a JASCO CD Spectrometer J 20 at room temperature. All the measurements were made with a 1 mm path length quartz cell.

Stopped-flow Measurements. The rate of fluorescence and light scattering changes (in intesity) were examined with a Union Giken stopped-flow spectrophotometer RA-401 in combinaton with a microcomputer RA-450 system.[10] We used a Hoya UV 33 cut filter (which allows the emitted light of wavelength longer than 330 nm to come into the detector) in the fluorescence measurements. For the light scattering measurements a 4 mW He-Ne laser was used. For introducing the laser beam into the cell window, an optical fiber was used. This makes it easier to guide the beam and to adjust the position and direction of the light path than a convensional mirror system. All scattering measurements were made at the angle of 90° to the incident beam, since the dimension of the protein molecule was small relative to the wavelength of the light.

Results

Fluorescence Spectra. We first observed the fluorescence spectra of rabbit muscle aldolase at several pH values and the results are shown in Fig. 1. As is seen in the figure, the emission maximum is shifted towards longer wavelength on going from pH 4.4 to pH 3.4. The pH dependence of the wavelength (λ_{max}) of the emission maximum and the intensity are shown in Fig. 2. From this figure it is suggested that the enzyme is denatured in acidic pH and the denaturation point is around pH 3.7. This value is in agreement with the previously proposed denaturation point.[6]

Circular Dichroism. The observed molecular ellipticity [θ] of this enzyme at 225 nm was plotted against pH as shown in Fig. 2 (c). In the acid denaturation a loss of gross secondary or tertiary structure is seen from the figure.

Sedimentation Equilibrium. Dissociation of aldolase into dimer and monomer has next been examined at acidic pH. According to the results of sedimen-

† 1M=1 mol dm^{-3}.

tation equilibrium measurements (see Table 1) aldolase is considered to be tetramer at pH 5.4, a mixture of dimer and monomer at pH 3.5, and monomer at pH 2.7.

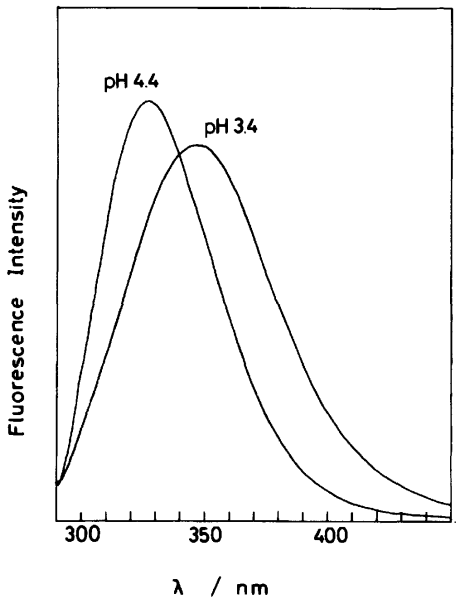

Fig. 1. Fluorescence spectra of aldolase (0.13 mg ml^{-1}), excited at 280 nm. Solvents, 0.1 M citrate buffer. Temperature, 25 °C.

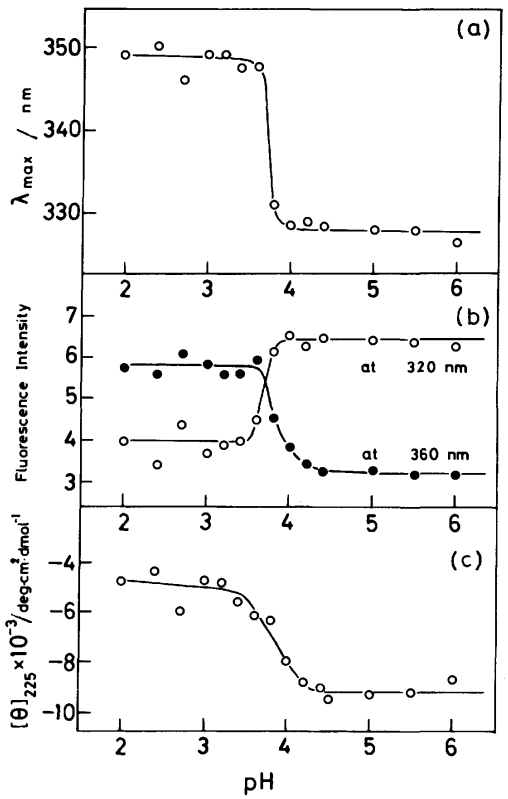

Fig. 2. Effects of pH on (a) the fluorescence peak position, (b) fluorescence intensities, (c) circular dichroism of aldolase. For the fluorescence measurements, the protein concentration was 0.13 mg ml^{-1}, and for the circular dichroism measurements 1.3 mg ml^{-1}. For both measurements, the solvents were 0.1 M citrate buffer. Temperature, 25 °C.

This conclusion is consistent with the previous results.[4]

Kinetic Measurements. After a rapid change of pH from 5.4 to 3.4 of aldolase solution, time-dependent fluorescence and light scattering measurements were made. As may be seen in Fig. 3 (a) and (b), the fluorescence increase (excited at 280 nm and observed all the

Table 1. Apparent molecular weights of aldolase determined by sedimentation equilibrium measurements[a] at different pH's

pH 5.4	174 000± 3 600
pH 3.5	59 800—87 200[b]
pH 2.7	50 300± 400

a) All the experiments were made with aldolase solutions of 0.44 mg ml^{-1} in 0.1 M sodium citrate buffer. b) At pH 3.5, log c *versus* r^2 relation (where c is the concentration and r the distance from the axis of rotation) was not found to be linear, showing that the molecules are not homogeneous.

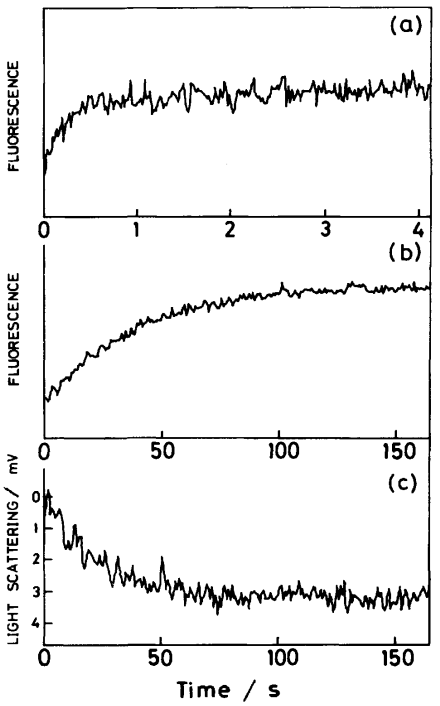

Fig. 3. The time dependence of the increase in the fluorescence intensity (a) and (b) and of decrease in the light scattering intensity (c), of aldolase solution on pH=5.4→3.4 jump. In each experiment, aldolase solution of 3.2 mg ml^{-1} in 0.01 M citrate buffer (pH 5.4) was rapidly mixed with an equal volume of 0.2 M citrate buffer (pH 3.4) at time zero with a stopped-flow device. The final pH was found to be 3.4 and the final concentration of aldolase was 1.6 mg ml^{-1}. Temperature, 21.5 °C. The fluorescence was excited at 280 nm and observed with a cut-filter of 330 nm. The light scattering was observed at 632.8 nm. The ordinate scale (read in mV) is arbitrary but should be taken as equal to that of Fig. 4(c), because all the experimental conditions were the same for these two recordings.

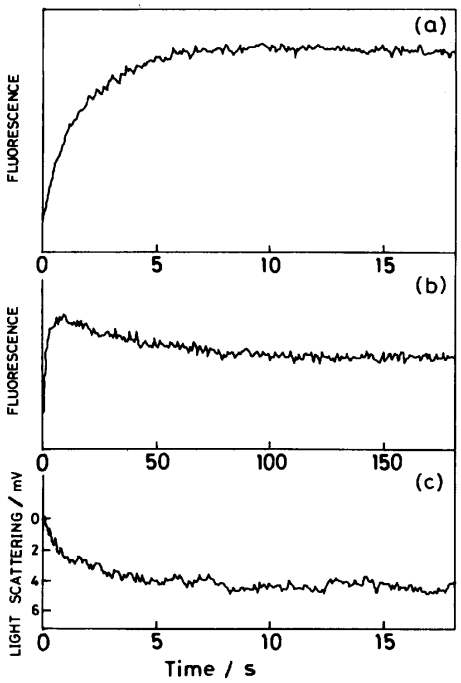

Fig. 4. The time dependent changes in fluorescence intensity ((a) and (b)) and in the light scattering intensity (c) of aldolase solution on pH=5.4→2.7 jump. In each experiment, aldolase solution of 3.2 mg ml^{-1} in 0.01 M citrate buffer (pH 5.4) was rapidly mixed with an equal volume of 0.2 M citrate buffer (pH 2.7) at time zero with the stopped-flow device. The final pH was found to be 2.7 and the final concentration of aldolase was 1.6 mg ml^{-1}. Temperature, 21.5 °C. The fluorescence was excited at 280 nm and observed with a cut-filter of 330 nm. The light scattering was observed at 632.8 nm. The ordinate scale (read in mV) is arbitrary but should be taken as equal to that of Fig. 3(c), because all the experimental conditions were the same for these two recordings.

emitted light of wavelength longer than 330 nm) takes place in two steps. In both steps the fluorescence intensity was found to increase as nearly first-order process with rate constants of 4.0 and 0.03 s^{-1} at 21.5 °C. In the course of these processes, however, the light scattering intensity (at 632.8 nm) was found to decrease in only one step. Its rate constant is nearly equal to that of the second step of the fluorescence increase (step II). Similar experiments were made with different final pH's (to which pH jumps were made from pH 5.4). An example (pH=5.4→2.7 jump) is shown in Fig. 4. The rate constants of the light scattering and fluorescence change were both found to be dependent on the final pH of the solution. As may be seen in Fig. 5, the rate constant of the second-step reaction (step II) is nearly proportional to square of the H^+ concentration, $[H^+]^2$. The rate constant of the first-step (step I) would probably be also proportional to $[H^+]^2$, but it could not be confirmed because the reaction was found too fast to be observed for pH≦3.2 (see Fig. 5). At pH lower than 3.2, on the other hand, even slower reaction (let us call it step III) came out, which could be monitored by a very slow fluorescence decrease. This is seen in Fig. 4 (b). Its rate

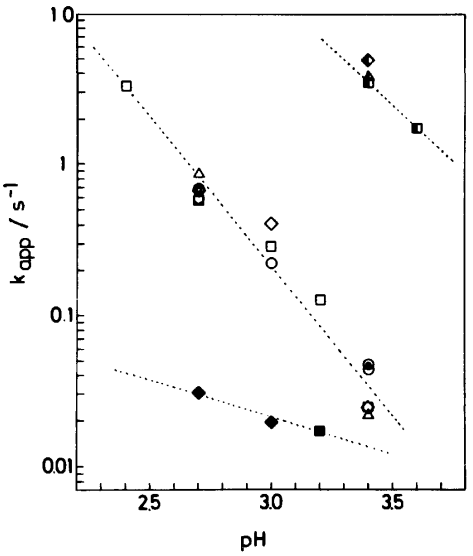

Fig. 5. Observed rate constants of the fluorescence and light scattering changes plotted against the pH values to which the pH jumps (from pH=5.4) were made at 21.5 °C.
◭ △ Fluorescence changes observed with aldolase concentration 6.2 mg/ml. ◐ ◇ ◆ Fluorescence changes, at 1.6 mg ml^{-1}. ◧ □ ■ Fluorescence changes, at 0.67 mg ml^{-1}. ◎ Light scattering changes, at 6.2 mg ml^{-1}. ○ Light scattering changes, at 1.6 mg ml^{-1}.

constants are plotted in Fig. 5 with black squares. The kinetic measurements were also done at different aldolase concentrations, 0.67—6.2 mg/ml. The rate constants of both fluorescence and light scattering changes, however, were found to be independent of the protein concentration (see Fig. 5).

Discussion

Present experimental results indicate that the acid denaturation of rabbit muscle aldolase consists of three distinguishable steps. Step I is a fast reaction in which fluorescence increases but no change in the light scattering takes place. Step II is a slow reaction in which a fluorescence increase and a light scattering lowering take place simultaneously. Step III is a further slower reaction in which fluorescence decreases and no light scattering change occurs. An interpretation of this set of steps is schematically represented in Fig. 6.

Apparently, the subunit dissociation takes place in step II. The rate constant of this dissociation reaction is about 0.04 s^{-1} at pH 3.4 but 0.6 s^{-1} at pH 2.7. The amplitude of the light scattering change is greater at pH 2.7 than that at pH 3.4 (see Figs. 3(c) and 4(c)). These facts may be interpreted by taking into account the finding (by sedimentation equilibrium measurements) that at pH 3.4 aldolase tetramer dissociates only into dimer-monomer mixture, whereas at pH 2.7 completely into monomer (Table 1). The rate of light scattering decrease was found to be independent of the protein concentration. This fact is explained if we assume (i) that tetramer←dimer back reaction is very slow (≈10^{-3} s^{-1}),[8] and (ii) that dimer⇄monomer equilibrium takes place very fast (>1 s^{-1}). In order to explain

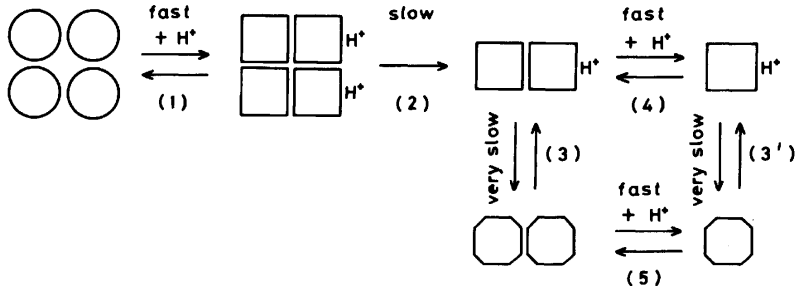

Fig. 6. Schematic representation of the proposed mechanism of acid denaturation of aldolase. We speculate that the observed step I corresponds to the process (1), the observed step II to the processes (2)+(4), and the observed step III to the processes (3)+(3') or (3)+(3')+(5).

the fact that this rate is proportional to $[H^+]^2$ we have to assume, in addition, (iii) that every tetramer has two sites of H^+ binding, which are essential to cause the tetramer→dimer dissociation. Because the step II fluorescence increase takes place simultaneously with the molecular weight change, it is likely (iv) that this fluorescence change is caused merely by a new exposure of some tyrosine or tryptophan groups located on the dimer surface, rather than an intra-dimer or intra-monomer conformation change.

The fluorescence change of step I (fast) must be attributed to an intra-tetramer, intra-dimer, or intra-monomer conformational change, because it is not accompanied by any molecular weight change. This fast conformational change seems to prepare for a two-site H^+ binding to cause the subunit dissociation. The fluorescence change of step III must be ascribed to an intra-monomer (intra-subunit) conformational change. This seems to be a final adjustment to reach a stable conformation of the monomer (or dimer) in acidic pH.

We thank Dr. A. Ikai and Dr. M. Kikuchi for the sedimentation equilibrium measurement. We also thank Dr. K. Watanabe for the circular dichroism measurement and Dr. A. Y. Hirakawa and Dr. H. Todoriki for the use of an optical fiber. This work was supported in part by a grant from Ministry of Education, Science and Culture.

References

1) Y. Ohga, M. Nakanishi, and M. Tsuboi, *Biochim. Biophys. Acta*, **670**, 298 (1981).
2) R. Tashiro, T. Inoue, and R. Shimozawa, *Biochim. Biophys. Acta*, **706**, 129 (1982).
3) B. L. Horecker, O. Tsolas, and C. Y. Lai, "The Enzymes," ed by P. D. Boyer, Academic Press, New York (1972), Vol. 7, pp. 213—258.
4) E. Penhoet, M. Kochman, R. Valentine and W. J. Rutter, *Biochemistry*, **6**, 2940 (1967).
5) K. Kawahara and C. Tanford, *Biochemistry*, **5**, 1578 (1966).
6) E. Stellwagen and H. K. Schachman, *Biochemistry*, **1**, 1056 (1962).
7) W. C. Deal, W. J. Rutter, and K. E. Van Holde, *Biochemistry*, **2**, 246 (1963).
8) J. W. Teipel, *Biochemistry*, **11**, 4100 (1972).
9) K. Kabashi, C. Y. Lai, and B. L. Horecker, *Arch. Biochem. Biophys.*, **117**, 437 (1966).
10) M. Nakanishi and M. Tsuboi, *J. Am. Chem. Soc.*, **100**, 1273 (1978).

Note added in proof. It is speculated that the two sites of proton binding, which are essential to cause the tetramer →dimer dissociation, are Asp 358 of the two β-subunits. In the α-subunits, this is replaced by Asn358 (This is the only difference in the amino acid sequences of α and β subunits; C. Y. Lai, *Arch. Biochem. Biophys.*, **166**, 358 (1975)), and cannot be protonated. Therefore, it is understandable that the effective protonation sites are only two, instead of four, per tetramer.

Induction of the β-Form of Poly(*S*-carboxymethyl-L-cysteine) and Poly[*S*-(2-carboxyethyl)-L-cysteine] by Chromium(III), Iron(III), and Lanthanum(III) Chlorides

Kazuki OKA, Hiroshi MAEDA,* and Shoichi IKEDA*
Department of Chemistry, Faculty of Science, Nagoya University, Chikusa-ku, Nagoya 464
(Received October 7, 1983)

The β-form was induced by the addition of $CrCl_3$, $FeCl_3$, and $LaCl_3$ to the salt-free solutions of fully ionized poly(*S*-carboxymethyl-L-cysteine) (poly[Cys(CH_2COOH)]) and poly[*S*-(2-carboxyethyl)-L-cysteine] (poly[Cys(CH_2CH_2COOH)]). The induction occurred below the equivalent point in both polypeptides. The inducing powers of the three trivalent cations were rather similar. They were weaker than Cu^{2+} ions in the case of poly[Cys(CH_2COOH)], while they were comparable with Cd^{2+} ions in the case of poly[Cys(C_2H_4COOH)]. Cu^{2+} and Cd^{2+} ions were the most effective species among divalent cations in the induction of the β-form of poly[Cys(CH_2COOH)] and Poly[Cys(C_2H_4COOH)], respectively.

Recently, the effects of various divalent metal ions on the conformation of poly[Cys(CH_2COOH)][1] and poly[Cys(C_2H_4COOH)][2] were studied. Transition metal ions, such as Cu^{2+}, Cd^{2+}, Zn^{2+}, and Ni^{2+}, effectively induced the β-form of these two polypeptides, while alkaline earth ions (Mg^{2+}, Ca^{2+}, and Ba^{2+}) were not effective inducers. Based on these results, it is likely that the β-form of these polypeptides is induced *in solution* only when their negative charges are annihilated by the redistribution of charges between the side chains and bound cations. In the present study, the effects of three kinds of trivalent metal chlorides, $CrCl_3$, $FeCl_3$, and $LaCl_3$, on the conformation of both polypeptides are examined in the fully ionized state.

Experimental

Poly[Cys(CH_2COOH)] (Lot No. KO125W; M_W=12 000, Dp=75) and poly[Cys(CH_2CH_2COOH)] (Lot No. H920WR; M_W=16 000, Dp=92) were the same samples as used in the previous studies.[1,2] Here M_W and Dp represent the molecular weight and the degree of polymerization, respectively. Reagent grade $CrCl_3 \cdot 6H_2O$, $FeCl_3 \cdot 6H_2O$, and $LaCl_3 \cdot 7H_2O$ were purchased from Nakarai Chemicals Ltd. (Kyoto) and used without further purification. Doubly distilled water was used to prepare the solutions.

Circular dichroism (CD) spectra were taken on a JASCO J-40 A circular dichrograph using a cell of 1 mm path length. Measurements of pH were carried out on a Hitachi-Horiba F-7 ss pH meter. These measurements were carried out at 25±2 °C. The polymer concentration C_p is expressed in the residue molarity, mol dm^{-3} (M), which is kept constant at 1.0×10^{-3} M in the present study. Metal concentration C_M is expressed in molarity (M), mol dm^{-3}. To compare the effects of trivalent ions with those of divalent ions, the metal concentrations are also expressed in normality (equiv dm^{-3}) and designated as C_s. Stock solutions of metal chlorides were used within half an hour after their preparation. After metal solutions were added to the polypeptide solutions, the mixtures were incubated for at least 24 h before the measurements, unless otherwise stated.

Results

In Figs. 1(a) and (b), the CD spectra of poly[Cys(CH_2COOH)] (a) and poly[Cys(C_2H_4COOH)] (b) are shown when various amounts of $CrCl_3$ are added. When $CrCl_3$ is not added, the CD spectra indicate the random coil state of respective polypeptides.[3] The CD spectra change with the addition of $CrCl_3$; the residue ellipticity around 200 nm, $[\theta]_{200}$, changes from negative to positive and reaches as large as about 4×10^4 and 2×10^4 in the case of poly[Cys(CH_2COOH)] and poly[Cys(C_2H_4COOH)], respectively. The CD spectra at large values of C_M/C_p resemble those of the β-form in the case of poly[Cys(C_2H_4COOH)].[3] In the case of poly[Cys(CH_2COOH)], however, the negative band around 225 nm shifts to 230 nm as C_M/C_p increases from 0.202 to 0.253. This shift of band position as well as a large residue ellipticity at 200 nm suggest a possible contribution from some electronic transition involving Cr^{3+} ions.

A charge transfer from a sulfur to Cr atom has been reported to exist around 240—260 nm.[4-6] Peerce *et al.* reported an absorption band around 195 nm for a complex of Cr(III) with a ligand containing sulfur and nitrogen atoms.[6] When a sulfur atom was substituted by a methylene group, this absorption was not found any more.[6] It is likely that an electronic transition involving a thioether and Cr is present in this wavelength region. All these results suggest that the CD spectra of both polypeptides should be carefully interpreted when Cr^{3+} ions are bound to them.

Contrary to the case of $CrCl_3$, normal CD pattern is obtained for the β-forms induced by $FeCl_3$ or $LaCl_3$. The CD spectra in the presence of $FeCl_3$ are shown in Figs. 2(a) and (b).

In Figs. 3 and 4, the residue ellipticities at 200 nm are plotted against the mixing ratio for poly[Cys(CH_2COOH)] and poly[Cys(C_2H_4COOH)], respectively. As a comparison, the results obtained on Cu^{2+} ions in the case of poly[Cys(CH_2COOH)] and Cd^{2+} ions in the case of poly[Cys(C_2H_4COOH)] are also shown in these figures. These ions are the most effective species among divalent metal cations in the induction of the β-form of each polypeptide. To facilitate the comparison, the abscissa is expressed as C_s/C_p instead of C_M/C_p, where C_s represents the normality of various metal ions. The equivalent point is thus located at C_s/C_p=1, irrespective of the valences of ions. In the case of poly[Cys(CH_2COOH)], both Fe^{3+} and La^{3+} ions are less effective to induce the β-form than Cu^{2+}

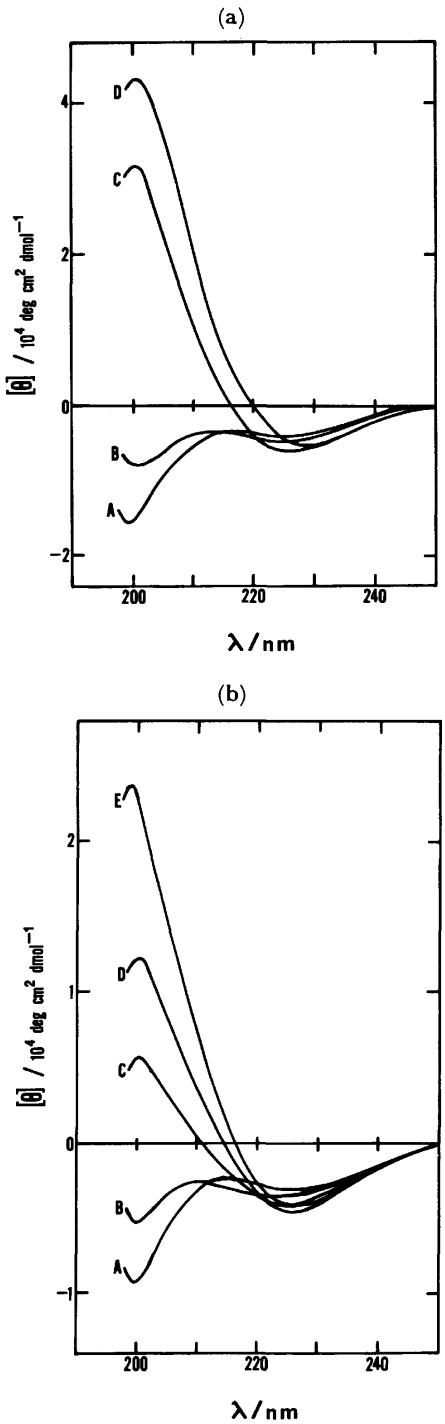

Fig. 1. CD spectra of the polypeptides in the presence of $CrCl_3$.
$C_p = 1 \times 10^{-3}$ M. (a) Poly[Cys(CH_2COOH)], C_M/C_p: (A) 0, (B) 0.101, (C) 0.202, (D) 0.253. (b) Poly-[Cys(C_2H_4COOH)], C_M/C_p: (A) 0, (B) 0.101, (C) 0.202, (D) 0.253, (E) 0.303.

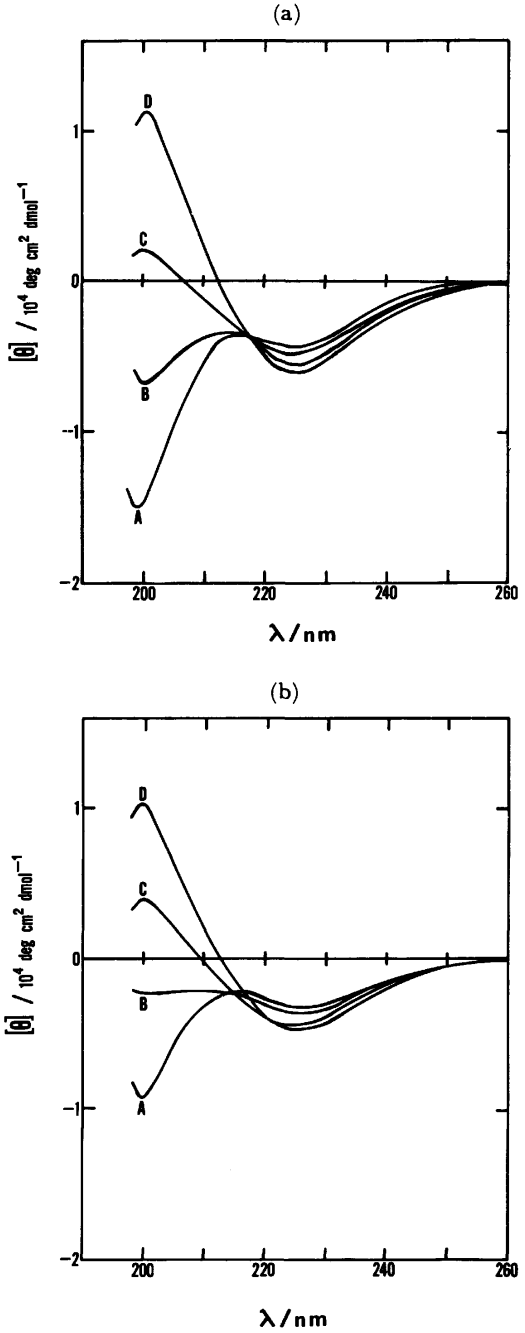

Fig. 2. CD spectra of the polypeptides in the presence of $FeCl_3$.
$C_p = 1 \times 10^{-3}$ M. (a) Poly[Cys(CH_2COOH)], C_M/C_p: (A) 0, (B) 0.100, (C) 0.200, (D) 0.299. (b) Poly-[Cys(C_2H_4COOH)], C_M/C_p: (A) 0, (B) 0.100, (C) 0.200, (D) 0.301.

ions. In the case of poly[Cys(C_2H_4COOH)] both Fe^{3+} and La^{3+} ions have a comparable power to or even stronger power than Cd^{2+} ions.

In Figs. 5(a) and (b), the state of poly[Cys(CH_2-COOH)] solutions at various values of C_M/C_p is diagramatically shown, at 1 h (a) and 48 h (b) after the addition of metal chlorides. In Figs. 6(a) and (b), corresponding results on poly[Cys(C_2H_4COOH)] are given. Slow precipitation occurs for $CrCl_3$ and $LaCl_3$ in the case of poly[Cys(CH_2COOH)], while it occurs only for $CrCl_3$ in the case of poly[Cys(C_2H_4COOH)]. Among three metal chlorides, the least solubility is found in $LaCl_3$ solutions for both polypeptides. In $CrCl_3$ and $LaCl_3$ solutions, poly[Cys(C_2H_4COOH)] is more soluble than poly[Cys(CH_2COOH)]. As discussed previ-

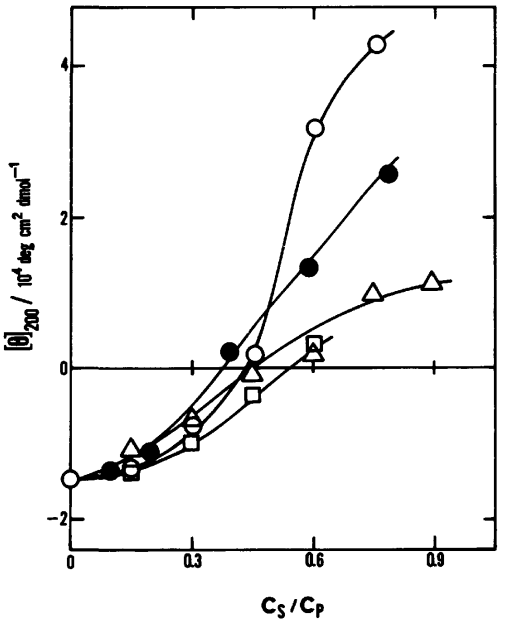

Fig. 3. Residue ellipticity of poly[Cys(CH_2COOH)] at 200 nm, $[\theta]_{200}$, as functions of metal chloride concentrations C_s.
$C_p = 1 \times 10^{-3}$ M. C_s is expressed in equiv dm^{-3}. (○) $CrCl_3$, (△) $FeCl_3$, and (□) $LaCl_3$. Previous results on $CuCl_2$ are shown by filled circles (●).

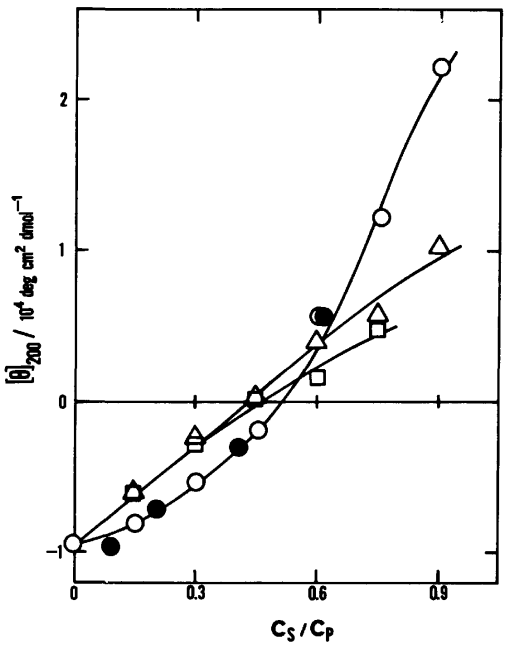

Fig. 4. Residue ellipticity of poly[C_2H_4COOH)] at 200 nm, $[\theta]_{200}$, as functions of metal chloride concentrations C_s.
$C_p = 1 \times 10^{-3}$ M. C_s is expressed in equiv dm^{-3}. (○) $CrCl_3$, (△) $FeCl_3$, and (□) $LaCl_3$. Previous results on $CdCl_2$ are shown by filled circles (●).

ously,[2] the β-form of poly[Cys(C_2H_4COOH)] is always less soluble than that of poly[Cys(CH_2COOH)] when induced by the binding of proton or divalent cations. In this context, the reverse situation found in

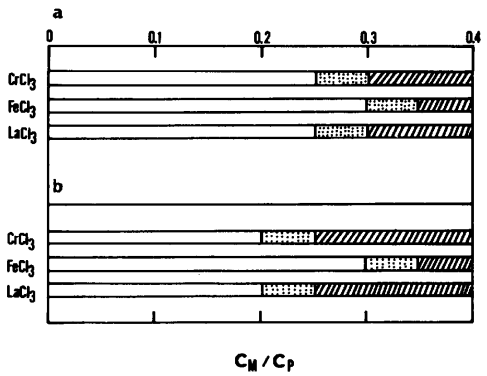

Fig. 5. Precipitation diagrams for aqueous solutions of poly[Cys(CH_2COOH)] in the presence of different metal chlorides.
$C_p = 1 \times 10^{-3}$ M. Blank region: clear solution. Dotted region: unspecified region. Shaded region: precipitation. (a) 1 h after preparation, and (b) 48 after preparation.

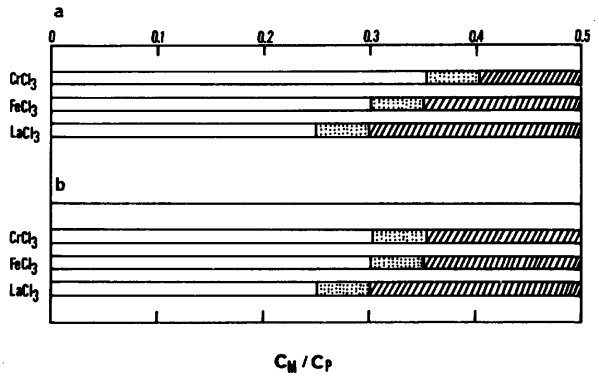

Fig. 6. Precipitation diagrams for aqueous solutions of poly[Cys(C_2H_4COOH)] in the presence of different metal chlorides.
$C_p = 1 \times 10^{-3}$ M. Blank region: clear solution. Dotted region: unspecified region. Shaded region: precipitation. (a) 1 h after preparation, and (b) 48 h after preparation.

the present study on $CrCl_3$ and $LaCl_3$ is interesting but puzzling.

Values of pH of the solutions of both polypeptides in the presence of the metal chlorides are shown in Fig. 7. The changes of pH are rather similar among three metal chlorides. This is in contrast to the result shown in Figs. 3 and 4, where a marked increase of $[\theta]_{200}$ is observed only for $CrCl_3$. The observed pH change supports the suggested interpretation that some contribution other than the conformational change is involved in the CD spectra of the solutions containing $CrCl_3$.

In Fig. 7, changes of pH take place at higher metal concentrations C_M in the case of poly[Cys(C_2H_4-COOH)] as compared with the case of poly[Cys(CH_2-COOH)]. This result implies that the binding of cations is stronger in poly[Cys(CH_2COOH)] than in poly[Cys(C_2H_4COOH)].

In Fig. 7, values of pH of the solutions of poly-[Cys(C_2H_4COOH)] are higher by approximately one

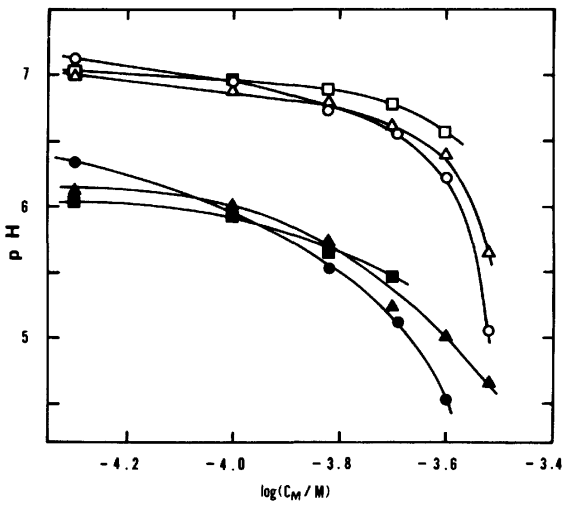

Fig. 7. Variation of pH with the logarithm of metal concentration C_M.
$C_p = 1 \times 10^{-3}$ M. Filled symbols refer to poly[Cys(CH_2COOH)] and open symbols refer to poly[Cys(C_2H_4COOH)]. $CrCl_3$ (●, ○), $FeCl_3$ (▲, △), and $LaCl_3$ (■, □).

pH unit than those of poly[Cys(CH_2COOH)]. This simply stems from different intrinsic dissociation constants K_0 of the carboxyl groups of the two polypeptides; pK_0=3.25 for poly[Cys(CH_2COOH)][7] and pK_0=4.00 for poly[Cys(C_2H_4COOH)].[8]

Time courses of $[\theta]_{200}$ after the addition of metal chlorides are shown in Figs. 8(a) and (d) for poly[Cys(CH_2COOH)] and poly[Cys(C_2H_4COOH)], respectively. As shown in these figures, stationary values are reached within 5—6 h. Based on these results, all the data presented in the preceding sections were taken at 24 h (or longer) after the addition of metal chlorides, to confirm the equilibrium values.

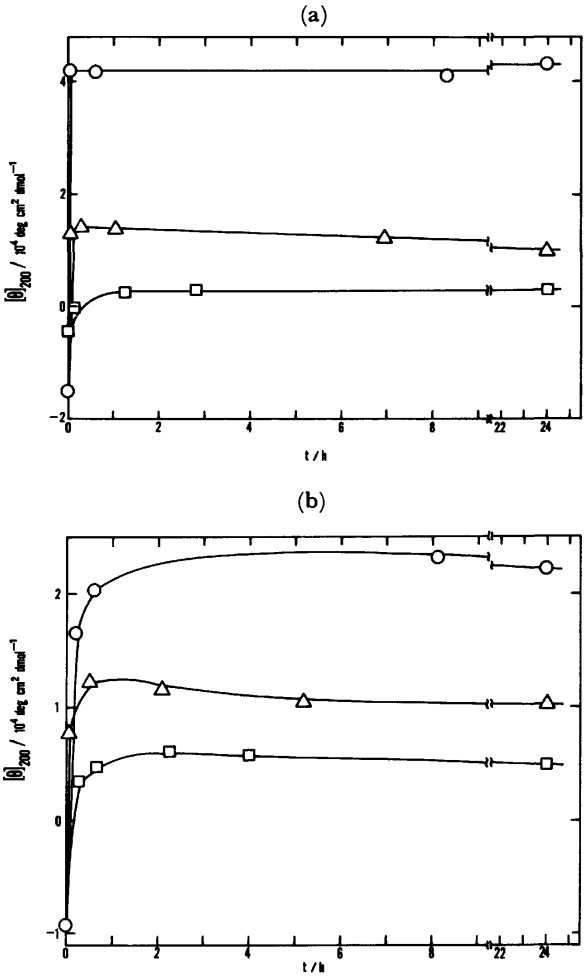

Fig. 8. Changes of the residue ellipticity at 200 nm, $[\theta]_{200}$, with time.
$C_p = 1 \times 10^{-3}$ M. (a) Poly[Cys(CH_2COOH)]; (○) $CrCl_3$, C_M/C_p=0.253: (△) $FeCl_3$, C_M/C_p=0.250: (□) $LaCl_3$, C_M/C_p=0.201. (b) Poly[Cys(C_2H_4COOH)]; (○) $CrCl_3$, C_M/C_p=0.303: (△) $FeCl_3$, C_M/C_p=0.301: (□) $LaCl_3$, C_M/C_p=0.250.

Discussion

Comparison of the Extents of the β-Form Induction between the Two Polypeptides. The total change of $[\theta]_{200}$ associated with the complete conversion is undoubtedly larger for poly[Cys(CH_2COOH)] than for poly[Cys(C_2H_4COOH)].[3,9] However, the magnitude of the total change has been definitely evaluated for none of these two polypeptides. This is one of the problems of comparing the extent of the β-form induction between these two polypeptides, which was discussed previously.[2] In the present study, however some conclusion can be derived on the effect of trivalent cations. Comparison of Fig. 3 with Fig. 4 shows that the values of $[\theta]_{200}$ of the two polypeptides are very similar at the same mixing ratio C_s/C_p for $FeCl_3$ and $LaCl_3$. The result suggests that the induction of the β-form occurs more extensively for poly[Cys(C_2H_4COOH)] than for poly[Cys(CH_2COOH)] at the same value of C_s/C_p. On the other hand, the binding of counterions is suggested to occur more strongly for poly[Cys(CH_2COOH)] than for poly[(Cys(C_2H_4COOH)] from the pH changes. When these two results are combined, it is likely that the β-form is induced more effectively in the case of poly[Cys(C_2H_4COOH)] than poly[Cys(CH_2COOH)], if compared at the same bound fraction of counterions. This situation is the same as that found for proton binding.[7]

Comparison of the Effect of the Trivalent Ions with That of the Divalent Ions. In the present study, all three kinds of trivalent ions induce the β-form of poly[Cys(CH_2COOH)] and poly[Cys(C_2H_4COOH)] to approximately comparable extents with those found in the case of effective divalent cations. Counterion condensation of trivalent ions occurs more predominantly over divalent ions.[10] However, this cannot explain the effectiveness of the trivalent ions in the induction of the β-form. As described in the introduction part, the induction of the β-form occurs as a result of the annihilation of negative charges on the polypeptides by bound cations. However, the situation at the equivalent point is not uniquely determined but depends on the valency of bound counterions. A complete cancellation of charges takes place in the case of monovalent and diva-

lent cations such as protons or Cu^{2+} ions. In contrast to these cases, complete cancellation between opposite charges cannot be expected in the case of trivalent ions, since a bound trivalent ion interacts most likely with two (or perhaps four) side chains, leaving a positive (or negative) charge. Under this situation, there would be a distribution of positive and negative charges on the pleated sheets, their sum being zero at the equivalent point. This supposed unique situation of trivalent ions would provide additional stability which is lacking in the case of monovalent and divalent counterions. Effective but rather nonspecific induction of the β-form found in the present study may be ascribed to this unique stabilization factor of trivalent ions.

The specificity of counterion species is expected to originate from the specificity involved in the interaction of carboxyl group with bound counterions. The precipitation of poly(acrylic acid) by various metal cations provides an interesting example. The effect of $LaCl_3$ on the precipitation of poly(acrylic acid) was similar to that of $MgCl_2$, $CaCl_2$, and $BaCl_2$ (designated as type L precipitation).[11] This behavior of $LaCl_3$ is in marked contrast with the present result. In the present study, $LaCl_3$ behaves like $CrCl_3$ and $FeCl_3$, quite differently from alkaline earth divalent cations, in the induction of the β-form of the polypeptides carrying carboxyl groups.

References

1) H. Maeda, J. Nakajima, K. Oka, K. Ooi, and S. Ikeda, *Int. J. Biol. Macromol.*, **4**, 352 (1982).
2) K. Oka, H. Maeda, and S. Ikeda, *Int. J. Biol. Macromol.*, **5**, 342 (1983).
3) S. Ikeda, A. Fukutome, T. Imae, and T. Yoshida, *Biopolymers*, **18**, 335 (1979).
4) C. J. Weschler and E. Deutsch, *Inorg. Chem.*, **12**, 2682 (1973).
5) R. H. Lane, F. A. Sedor, M. J. Gilroy, and L. E. Bennett, *Inorg. Chem.*, **16**, 102 (1977).
6) P. J. Peerce, H. B. Gray, and F. C. Anson, *Inorg. Chem.*, **18**, 2593 (1979).
7) H. Maeda and S. Ikeda, *Biopolymers*, **14**, 1623 (1975).
8) H. Maeda and S. Ikeda, *Biopolymers*, **10**, 2525 (1971).
9) H. Maeda and K. Ooi, *Biopolymers*, **20**, 1549 (1981).
10) F. Oosawa, "Polyelectrolytes," Marcel Dekker, New York (1971), Chap. 4.
11) A. Ikegami and N. Imai, *J. Polym. Sci.*, **56**,133 (1962).

 © 1984 The Chemical Society of Japan Bull. Chem. Soc. Jpn., 57, 701—705 (1984)

Preparation of Graphite Fluoride by Vertical Vibrating Reactor

Nobuatsu WATANABE,* Saburo KATOH, and Tsuyoshi NAKAJIMA
Department of Industrial Chemistry, Faculty of Engineering, Kyoto University, Sakyo-ku, Kyoto 606
(Received July 20, 1983)

A study was made of the yield and crystallinity of graphite fluoride using a vertical vibrating reactor, which made it possible to prepare much graphite fluoride. The yield of graphite fluoride decreased beyond 500 °C for natural graphite and petroleum coke heat-treated at 2800 °C, and beyond 300 °C for calcined petroleum coke. The crystallinity of graphite fluoride was improved through the decomposition and refluorination process in these temperature ranges where the yield decreased. It was found that a sublimative solid by-product was formed together with gaseous fluorocarbons. It was a white solid fluorocarbon with 5—9 cyclohexane rings.

There are two kinds of stable graphite fluorides, $(CF)_n$ and $(C_2F)_n$, prepared by a high temperature reaction between a carbon material and fluorine gas. Their formation and yield depend on the crystallinity of the starting carbon material, on reaction temperature, and on fluorine pressure. When natural graphite is used as a raw material, $(CF)_n$ and $(C_2F)_n$ are formed at *ca.* 600 °C and 350—400 °C, respectively.[1] Between these temperatures, a mixture of $(CF)_n$ and $(C_2F)_n$ is obtained.

As the rotary reactor[1] previously reported produces only 1—2 g of graphite fluoride, it is not suitable for the evaluation of the yield of the graphite fluoride. In this study, the yield and crystallinity of graphite fluoride were investigated using a vertical vibrating reactor which made it possible to prepare 5—40 g of graphite fluoride. It has been said that the decrease in the yield of graphite fluoride is due to the formation of gaseous fluorocarbons such as CF_4 and C_2F_6. However, it was found in the present study that solid fluorocarbons with molecular weights of 798—2016 were formed together with the gaseous compounds. The structure of these solid fluorocarbons was also studied.

Experimental

Samples. Starting carbon materials were natural graphite (290—833 and 61—74 μm) and petroleum coke (original and heat-treated at 2800 °C). Fluorine gas of purity, 99.4—99.7% was used for the fluorination of carbon materials. Most of the impurity contained in fluorine gas was nitrogen.

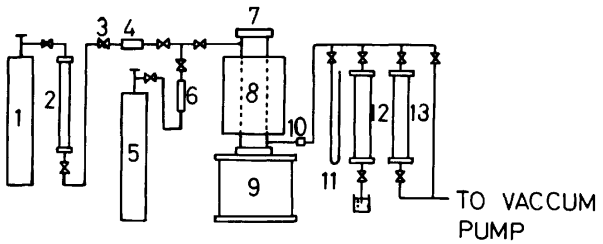

Fig. 1-a. Schematic diagram of vertical vibrating reactor.
1: F_2 cylinder, 2: HF absorber (NaF pellets heated at 110 °C), 3: control valve, 4: mass flowmeter for F_2, 5: Ar gas, 6: flowmeter for Ar, 7: reaction tube, 8: electric furnace, 9: Uras vibrator, 10: safety valve, 11: Hg manometer, 12, 13: F_2 absorber (soda lime pellets).

Vertical Vibrating Reactor. Figure 1-a is the schematic diagram of the vertical vibrating reactor for the production of 5—40 g of graphite fluoride. This vibration system was adopted to achieve the continuous mixing of a carbon material. When the mixing of carbon is insufficient, the explosive decomposition of formed graphite fluoride sometimes occurs due to the lack of supply of fluorine gas. The mixing of

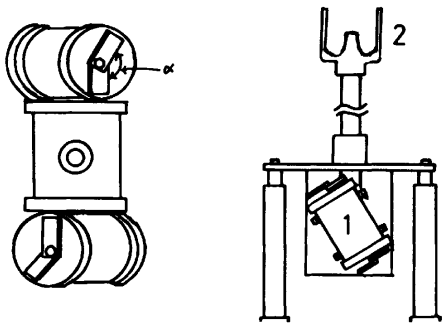

Fig. 1-b. Uras vibrator.
1: Uras vibrator, 2: reaction vessel.

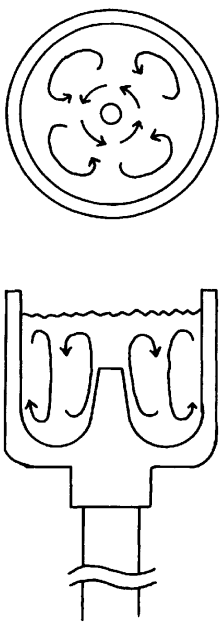

Fig. 1-c. Aspect of movement of carbon material by vibration.

carbon is therefore very important for the fluorination of large amounts of carbon. Vibration caused by a Uras vibrator (Fig. 1-b) installed at the bottom of the nickel reactor is transmitted through a nickel rod to a reaction vessel. The adjustment of vibration is made by changing the angle (α) between two unbalanced weights attached to the Uras vibrator. The aspect of movement of a carbon material in the reactor is schematically shown in Fig. 1-c.

Fluorination Reaction and Analyses of the Product. After pumping at room temperature, the reactor containing the starting carbon material was heated to a temperature between 300 and 600 °C; this was followed by further pumping for several hours. The reactor was then filled by argon gas at 1 atm, and a mixture of argon and fluorine gases was supplied to the reaction system (gas flow rate, F_2: 80 ml/min for natural graphite or 60 ml/min for petroleum coke, Ar: 70 ml/min). Unreacted fluorine gas was made to react with soda lime. After fluorination, the graphite fluoride prepared was analyzed by X-ray diffractometry (by Cu $K\alpha$) and elemental analysis. In addition to these analytical methods, the structure of the solid by-product was investigated by IR, ^{19}F-NMR, ESCA, and mass spectroscopies.

Results and Discussion

Yield of Graphite Fluoride. Figure 2 shows the yield of $(CF)_n$ and the time required for the completion of fluorination reaction as a function of the amount of each carbon material. The yield was decreased with increasing amounts of natural graphite, because it took a much longer time for fluorination with any increase in raw material and the decomposition of graphite fluoride to gaseous fluorocarbons occurred at the same time.

Figure 3 is the change of yield for the fluorination of a fixed amount of natural graphite as a function of reaction time and temperature. No unreacted graphite was detected under any condition. As seen in the figure, the yield decreased with increasing time and temperature. The decrease in yield started at *ca.* 500 °C for natural graphite and at *ca.* 300 °C for the original petroleum coke. The remarkable decrease in yield was observed especially in the latter case.

Composition and Crystallinity of Graphite Fluoride Prepared from Natural Graphite. Figure 4 is the composition and crystallinity of $(CF)_n$ prepared from natural graphite at 600 °C. The interlayer spacing and half width of the (001) diffraction line (d_{001}, β_{001}) decreased with increasing time, which means the improvement of crystallinity of graphite fluoride, while the chemical composition, F/C was almost unchanged. The improvement of crystallinity would be attained by eliminating the disordered parts among crystallites of graphite or $(CF)_n$. The disordered parts are easily attacked by fluorine gas to give gaseous fluorocarbons such as CF_4 and C_2F_6.[1,2]

The change in composition and cystallinity of graphite fluoride prepared from the flaky natural graphite

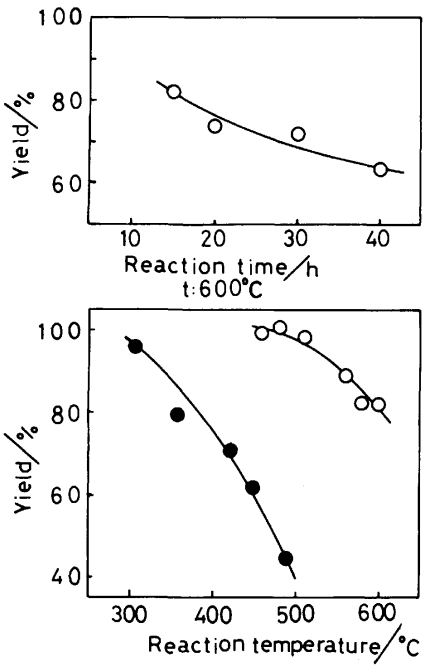

Fig. 3. Dependence of yield of graphite fluoride on reaction time and temperature.
○: Natural graphite (290—833 μm, 20 g), ●: petroleum coke (10 g).

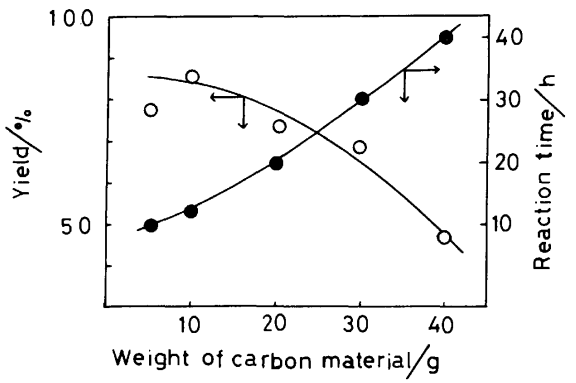

Fig. 2. Dependence of yield of $(CF)_n$ and reaction time on weight of starting carbon material.
Carbon material: natural graphite (290—833 μm).
Reaction temperature: 600 °C.

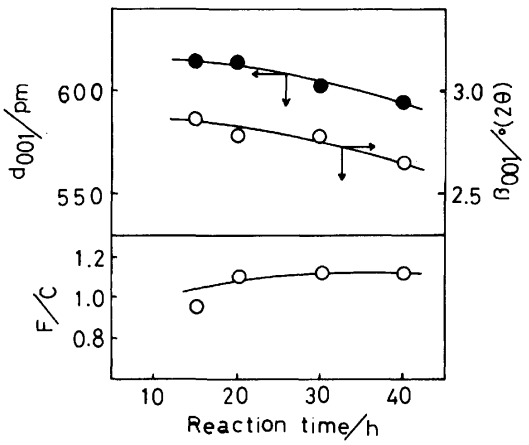

Fig. 4. Dependence of crystallinity and composition of $(CF)_n$ on reaction time.
Carbon material: natural graphite (290—833 μm).
Reaction temperature: 600 °C.

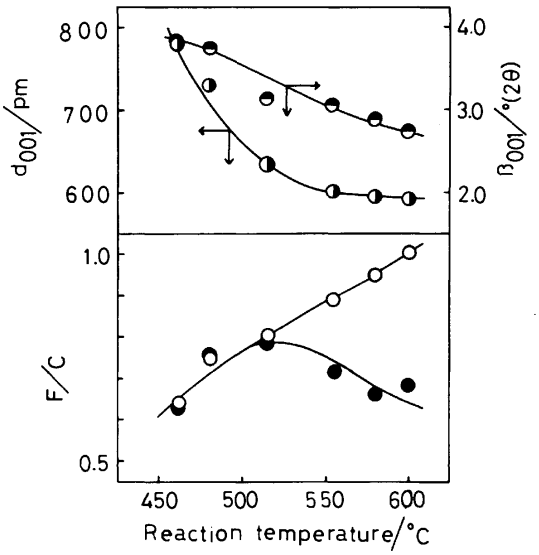

Fig. 5. Dependence of crystallinity and composition of graphite fluoride on reaction temperature.
Carbon material: natural graphite (61—74 μm), F/C: ○; from elemental analysis, ●; from weight increase.

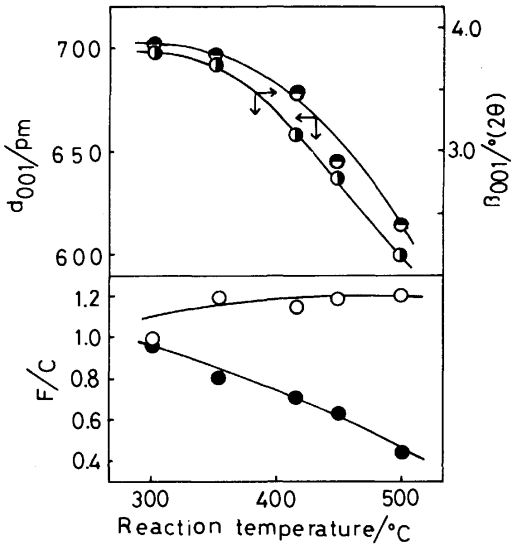

Fig. 6. Dependence of crystallinity and composition of $(CF)_n$ on reaction temperature.
Carbon material: petroleum coke.
F/C: ○; from elemental analysis, ●; from weight increase.

is shown in Fig. 5 as a function of temperature. $(CF)_n$ was prepared at around 600 °C with d_{001} of 585—590 pm and F/C of 1. An F/C value of more than unity is attributable to CF_2 and CF_3 groups at the edge of the crystallite. As $(C_2F)_n$ was mainly formed at 450—500 °C, the d_{001} and F/C approached 900 pm and 0.5, respectively, with decreasing temperature. As shown in the lower part of Fig. 5, the F/C calculated from the weight increase of a carbon material started to deviate from that obtained by elemental analysis at around 500 °C, and their difference was caused by the decomposition of graphite fluoride to gaseous fluorocarbons. No decomposition of graphite fluoride occurred in the temperature regions where $(C_2F)_n$ was preferentially formed.

Composition and Crystallinity of Graphite Fluoride Prepared from Petroleum Coke. When graphite fluoride was prepared from the original petroleum coke, the d_{001} and β_{001} decreased remarkably in a temperature range higher than 350 °C, while the F/C was between 1.1 and 1.2 at 350—500 °C (Fig. 6). Graphite fluoride prepared at 300—500 °C had larger d_{001} and β_{001} values than $(CF)_n$ prepared from the natural graphite. This is not because of the simultaneous formation of $(C_2F)_n$ but is attributed to the formation of $(CF)_n$ with low crystallinity. It is known that only $(CF)_n$ is formed from a carbon material with low crystallinity under any condition and F/C is much greater than unity because of CF_2 and CF_3 groups on the surface.[2] The crystallinity of graphite fluoride has also a close relation with that of a raw material. With increasing temperature, the crystallinity of $(CF)_n$ was remarkably improved by the decomposition of amorphous parts to gaseous fluorocarbons, the d_{001} and β_{001} approaching those of $(CF)_n$ prepared from natural graphite. The F/C obtained from weight increase decreased monotonously with increasing temperature, corresponding to the decrease in the yield.

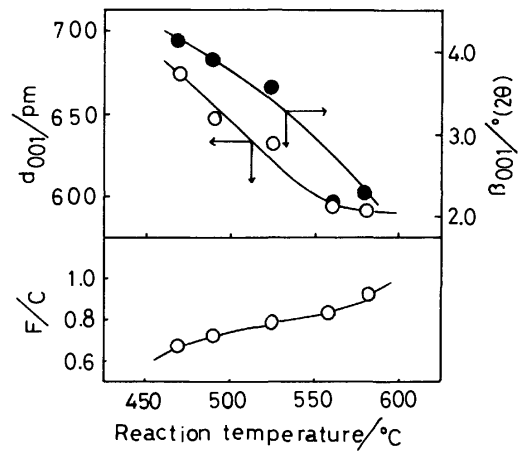

Fig. 7. Dependence of crystallinity and composition of graphite fluoride on reaction temperature.
Carbon material: petroleum coke heat-treated at 2800 °C.

The temperature dependences of the composition and crystallinity of graphite fluoride prepared from the petroleum coke heat-treated at 2800 °C were similar to those from the natural graphite (Fig. 7). The yield started to decrease at 500 °C as in the case of the natural graphite, but, the rate of decrease was larger than that in the natural graphite. The F/C value was much smaller than unity since $(C_2F)_n$ was formed from the graphitized carbon. The d_{001} and β_{001} approached those of $(CF)_n$ with increasing temperature, and only $(CF)_n$ was prepared at 580 °C.

Structure of Solid By-product. It was found that a white solid by-product was formed in the upper part of the reactor when the fluorination of a carbon material was made at a temperature where the yield of graphite fluoride largely decreased. In addition to gaseous

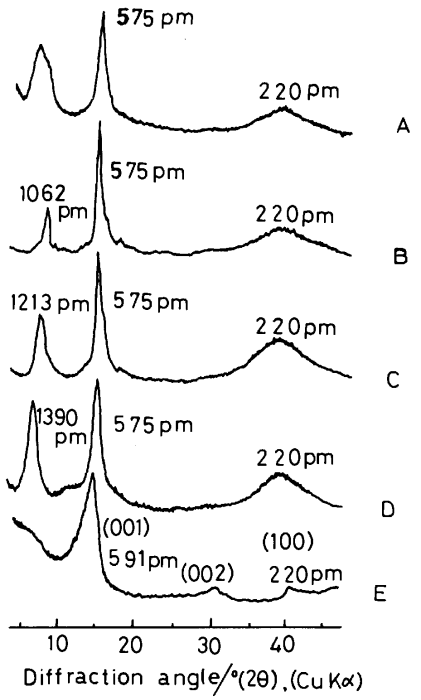

Fig. 8. X-Ray diffraction patterns of by product.
A: Original by-product, B: sublimated at 150 °C, C: sublimated between 200 and 250 °C, D: residue on sublimation at 300 °C, E: graphite fluoride, $(CF)_n$.

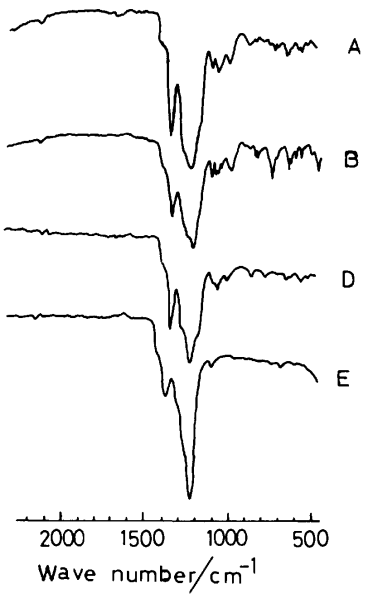

Fig. 9. IR spectra of by-product.
A: Original by-product, B: sublimated at 150 °C, D: residue on sublimation at 300 °C, E: graphite fluoride, $(CF)_n$.

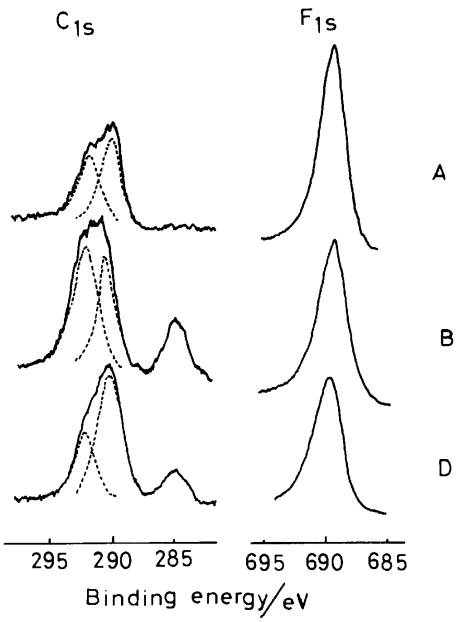

Fig. 10. ESCA spectra of by-product.
A: Original by-product, B: sublimated at 150 °C, D: residue on sublimation at 300 °C.

fluorocarbons, this solid by-product would also cause the decrease in the yield. In this section, the structure of solid by-product was described.

a) X-Ray Diffraction Patterns: Figure 8 is the X-ray diffraction patterns of the by-product. The by-product obtained gave the pattern A, which has nearly the same peaks as (001) and (100) diffraction lines of $(CF)_n$ except for a broad one at 6—9° in 2θ (Cu $K\alpha$). By sublimation at several temperatures, this by-product was separated into three groups, giving the pattern B (sublimated at 150 °C), C (sublimated at 200—250 °C), and D (residue on sublimation at 300 °C). As seen in B, C, and D, the broad diffraction line at 6—9° was separated into three different peaks. With increasing the sublimation temperature, the separated peak was shifted to a lower angle, corresponding to a larger d spacing.

b) ^{19}F-NMR Spectra: The 2nd moment obtained from the absorption derivative of the by-product was 10.1 G^2; this value is very near that of $(CF)_n$, 10.6 G^2.[1] Poly(tetrafluoroethylene) (Teflon) had the value, 5.0 G^2, which is different from the by-product value. This suggests that the unit structure in the by-product is the same as that for $(CF)_n$.

c) IR Spectra: Figure 9 is the IR spectra measured by the KBr method. The spectra of the by-product was very similar to that of $(CF)_n$. The absorption at 1215 cm^{-1} was ascribed to the CF stretching vibration and those at 1380 and 1110 cm^{-1} were due to the symmetric and asymmetric stretching vibrations of CF_2 bonds, respectively.[3] The latter two absorptions were larger in the by-product than in $(CF)_n$, which indicates that the by-product contains more CF_2 groups than $(CF)_n$ does. It is known from the spectra of Teflon that the absorptions due to the bending vibration of CF_2 appear between 500 and 900 cm^{-1},[4] where many small absorptions were also observed in the by-product.

d) ESCA Spectra: In the C_{1s} spectra of the by-products, two peaks corresponding to CF and CF_2 covalent bonds were observed at 290.5 and 292.4 eV, respectively.[1] These two chemical bonds between carbon and fluorine are the same as those of $(CF)_n$. In $(CF)_n$ powder, a small peak due to CF_3 group is observed at 294 eV in addition to the above two peaks. However, the by-products had only two peaks corresponding to CF

Table 1. Elemental analysis of by-product

Sample	F(wt%)	C(wt%)
A	67.66	31.66
B	66.60	31.25
C	70.75	29.88
D	66.86	33.92

Table 2. Composition and molecular weight of by-product by mass spectra

Sample	Composition	Molecular weight	Number of cyclohexane ring
B	$C_{19}F_{30}$-$C_{25}F_{38}$	798—1022	5—7
C	$C_{24}F_{36}$-$C_{40}F_{56}$	972—1544	7—13
D	$C_{43}F_{60}$-$C_{54}F_{72}$	1656—2016	14—19

and CF_2 groups and the ratio of CF_2/CF for the by-product was much larger than that of $(CF)_n$. This tendency was more distinctive in the by-products sublimated at a lower temperature.

e) Chemical Analysis and Mass Spectra: The results of chemical analysis are shown in Table 1. Though the fluorine content in a single crystal of $(CF)_n$ is 61.3 wt%, analyzed values are often larger than 61.3 wt% owing to the CF_2 and CF_3 groups on the surface. The highest value hitherto found is 65 wt%. However, the fluorine content in the by-product was 66—70 wt%, much higher than in $(CF)_n$. This is consistent with the presence of more CF_2 groups on the surface of the by-product than there were CF groups in the bulk. Mass spectra revealed that samples B, C, and D separated by sublimation were not a single compound but a mixture of those with different compositions. From the analytical results obtained in the previous sections, the by-product would have a structure in which some cyclohexane rings to which fluorines are bonded are linked with each other. Based on this model, the molecular weight and number of cyclohexane ring were calculated from the result of mass spectra. As shown in Table 2, the raw by-product would be a mixture of fluorocarbons consisting of 5—19 cyclohexane rings with molecular weight of 798—2016. The molecular weight increased in the order of B, C, and D, which is consistent with the fact that the sublimation temperature and *d* spacing obtained from X-ray diffraction pattern increased in the same order.

The analytical results are summarized as follows.

(1) All the by-products separated by sublimation had the same two peaks as (001) and (100) diffraction lines of ideal $(CF)_n$ crystal. The diffraction line at 6—9° in 2θ gave a larger *d* spacing for the sample separated at a higher temperature.

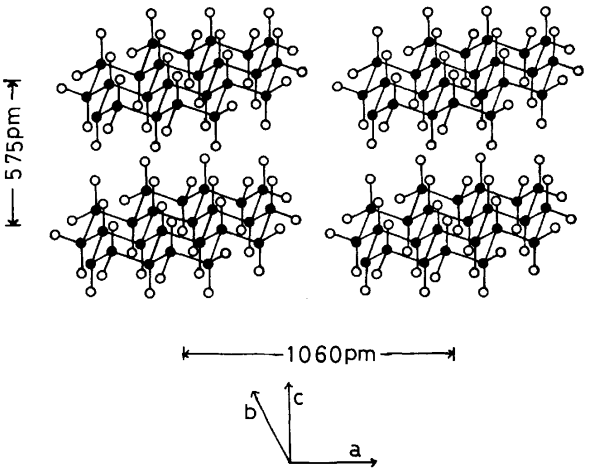

Fig. 11. Crystal structure of $C_{24}F_{36}$.
○: F, ●: C.

(2) IR and ESCA spectra showed that the by-product had the same CF and CF_2 groups as $(CF)_n$ and the ratio of CF_2/CF was much larger in the by-product than in $(CF)_n$.

(3) ^{19}F-NMR spectrum indicated that the unit structure of the by-product was the same as that of $(CF)_n$.

(4) Molecular weight was between 798 and 2016, corresponding to fluorocarbon compounds with 5—19 cyclohexane rings.

From these results, the by-product is regarded as a mixture of low molecular weight fluorocarbons having the same structural unit as that of $(CF)_n$. As an example, the crystal structure of $C_{24}F_{36}$ molecule with 7 cyclohexane rings is shown in Fig. 11, where each molecule is arranged in cubic system. The *d* spacing along the c-axis is 575 pm and the lattice parameter along the a and b-axis is almost the same as that of the diameter of a circular molecule.

References

1) Y. Kita, N. Watanabe, and Y. Fujii, *J. Am. Chem. Soc.*, **101**, 3822 (1979).
2) N. Watanabe, Y. Ashida, and T. Nakajima, *Bull. Chem. Soc. Jpn.*, **55**, 3197 (1982).
3) R. J. Lagow, R. B. Badachhape, J. L. Wood, and J. L. Margrave, *J. Chem. Soc., Dalton Trans.*, **1974**, 1268.
4) C. Y. Liang and S. Krimm, *J. Chem. Phys.*, **25**, 563 (1956).

Response Time Curves of Neutral Carrier Membrane Electrode of Tubular Shape

Hisao DEGAWA,* Noriko SHINOZUKA, and Shigeo HAYANO
Institute of Industrial Science, The University of Tokyo, 7-22-1 Roppongi, Minato-ku, Tokyo 106
(Received July 22, 1983)

A tubular flow-through electrode system for measuring the response time curves under the step change of concentration using an ammonium ion-selective poly(vinyl chloride) membrane electrode was described. The response time data are analyzed by the curve fitting method using two theoretical equations, which are an exponential type equation based on an assumption of the film diffusion and a square root type one based on that of the diffusion within the membrane, and a semiempirical equation of hyperbolic type. A method of curve fitting in which the equilibrium potential is regarded as an unknown parameter was described in detail. The initial part of the response time curves, where the potential change is large, was fitted by the exponential type equation, while the following part close to the equilibrium potential was fitted by the square root type one. The semiempirical equation could also be fitted to the wide range of the curves. The dependence of the time constant of the exponential type equation upon the flow rate of sample solution is examined; the results firmly supports both the film diffusion as a determining process for the initial part of the curve and the reliability of the present experimental system.

The discovery of the electrically neutral carrier antibiotics which show the selective complexation behavior toward alkali cations, and the synthesis of the macrocyclic polyethers which show the same behavior as the antibiotics have yielded a large number of ion-selective membrane electrodes of practical use. Among the performance characteristics of these electrodes, the dynamic response behavior is not satisfactorily characterized compared with the selectivity behavior. This is mainly due to the difficulties in obtaining the reproducible data of response times under the step change of concentration. Response time curves (potential *vs.* time curves), particularly of the order of a few tenths of milliseconds to some seconds, are greatly dependent on the flowing conditions of the bathing solution and are subject to electrical noise. The precise characterization of the response time of ion-selective electrodes is prerequisite for the monitorings in continuous flow-through systems and for the measurements during chemical reactions. Moreover, it is supposed that the investigation of the rate determining processes in the dynamic response of ion-selective electrodes can contribute to the understanding of the electrode response mechanism. Usually the investigation can be done by the curve fitting method using the theoretical equations which predict the response time curves.

In general, to precisely measure response time curves of ion-selective electrodes, it is necessary to control the thickness of the stagnant (adhering) film of the conditioning solution. This is achieved by using simple electrode configurations where the thickness of the stagnant film is straightforward function of the flow rate of the bathing solution. To satisfy this requirement, three geometric types are considered; these are the rotating disk electrode, the so-called wall-jet electrode, and the tubular electrode. Oosterhuis *et al.*[1] applied a rotating disk electrode system to an amperometric flow cell detector for HPLC and continuous flow analysis because the system provided a high sensitivity by controlling the rotation speed. However, to the best of our experience, an application of the rotating disk electrode to the concentration step was unsuccessful, since the sufficiently fast step change was not attained and the measured potential was distorted by electrical noise. Lindner and coworkers[2–5] studied the dynamic chracteristics of precipitate-based electrodes and neutral carrier electrodes using an elaborate apparatus mounted with the solution jets perpendicular to the electrode surface; their apparatus corresponds to the wall-jet electrode system. Akiyama *et al.*[6] also examined the factors affecting the transient response properties of the valinomycin based potassium ion-selective electrode using a wall-jet system, and concluded that the diffusion through a stagnant solution layer was rate controlling. Quite recently, we reported a tubular flow-through electrode system for measuring the response time curves of an ammonium selective poly(vinyl chloride) (PVC) membrane electrode.[7] In the report, we attempted curve fittings using two theoretical equations described by Morf *et al.*[8] The theoretical equations are an exponential type one that based on the assumption of the adhering film diffusion and a square root type one based on that of the diffusion within the membrane. According to Morf *et al.*,[8] the square root type equation essentially explains the dynamic response of carrier membranes. The study by Akiyama *et al.*[6] and our preliminary results,[7] however, suggest that the square root type equation do not always cover the dynamic response behavior of the eletrodes.

The present paper gives a more detailed report dealing with examinations of the curve fitting method and with discussion on the rate determining processes of the dynamic response of the electrode.

Experimental

Chemicals and Membrane Electrode. Macrotetrolide actin mixture (tetranactin 65%, trinactin 30%, dinactin 5%) was kindly supplied by Research Laboratories, Chugai Pharmaceutical Co., Ltd. and was used as ion-selective ligand.[9] The electrode membrane consisted of ligand (5%), dibutyl sebacate (70%, Tokyo Kasei Kogyo Co., Ltd.), and PVC (25%, HS-589, Toyo Soda Manufacturing Co., Ltd.). The tubular

flow-through electrode unit was prepared in the manner mainly after Fraticelli and Meyerhoff.[10] Tygon tubing of internal diameter 0.8 mm was employed as a main part of the tubular electrode. The mixture containing membrane components was cast into a cut opening (*ca.* 2 mm diameter) of the side of the tubing, within which a syringe needle was inserted as a mandrel. Thus the membrane having a smooth cylindrical surface inside the tube was formed.

Apparatus and Procedure. Figure 1 schematically illustrates an experimental set-up for the response time measurement. The tubular membrane electrode (12 in Fig. 1) was attached to the flow system. A silver wire coated with silver chloride (10) was immersed in inner reference solution (11). A conventional silver-silver chloride electrode was placed in the reference electrode compartment (13) containing the waste solution. To eliminate electrical noise, particularly arising from the source of 50 Hz line, a stainless steel pipe (9) was inserted in the upper stream of the tubular electrode, and was connected to the ground terminal of a home made differential impedance converter (5); the terminal was also connected to a shield box made of aluminum chassis which covered the tubular electrode and the reference electrode compartments. A digital storage device (1 on the right in Fig. 1, Auto Digitizer Model 210, Autnics Co., Ltd) provides the resolution of 12-bit, the maximum sampling speed of 1 μs/word, and the storage capacity of 4 Kword. For the acquisition and processing of data, a microcomputer (PC-8801, CPU: μPD780C-1 (Z-80A compatible), 4 MHz, Nippon Electric Co., Ltd.) was used with programmable interfaces μPD8255AC-5 (NEC).

A Liquid drive syringe unit was constructed by attaching a commercial glass syringe (10 ml) to Union Giken Sample Mixing Device MX-7 and connecting Gas Drive Unit-A; a total distance of displacement of the syringe plunger was 40 mm. A linear potentiometer (2 in Fig. 1, Model LP-100F, Midori Precisions Co., Ltd.) was attached to the syringe unit to measure the flow rate of the bathing solution. Another digital storage device with an 8-bit resolution (1 on the left in Fig. 1, Wave Memory Model WM-841, NF Circuit Design Block Co., Ltd.) linked the linear potentiometer to the microcomputer. To interchange the bathing solution, a T-joint for use in HPLC (8) was set as shown in Fig. 1.

In all measurements, 0.1 mol dm^{-3} lithium chloride was used as supporting electrolyte of the bathing solution to eliminate streaming potential between the tubular electrode and the reference electrode compartment. The reason for the use of lithium chloride is that the selectivity coefficient of lithium ion is sufficiently low. Step changes in solution concentrations were attained by closing a cock (6), opening a cook (7), and triggering the gas drive unit to inject new solution into the tubular electrode which had already been exposed to conditioning solution. All measurements were made at room temperature (*ca.* 20 °C).

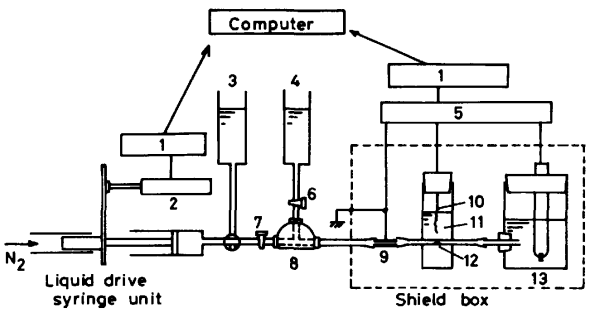

Fig. 1. Experimental set-up for the fast response time measurement.
1: Digital storage device, 2: linear potentiometer, 3: injection solution, 4: conditioning solution, 5: differential impedance converter, 6, 7: two-way stop cocks, 8: T-joint, 9: stainless steel pipe, 10: inner reference electrode (Ag/AgCl), 11: inner solution (NH_4Cl), 12: ion sensitive membrane, 13: reference electrode compartment.

Results and Discussion

As mentioned above, to investigate the rate determining processes in the dynamic response of the ammonium ion-selective electrodes, two theoretical models[8] containing the intrinsic parameters were used for the curve fitting. Additionally, to sufficiently describe the experimental curves, a semiempirical equation was also applied to the curve fitting. The semiempirical equation will be introduced in the following context.

Theoretical Equations. An exponential type equation which is based on the assumption that the diffusion of fresh electrolyte into the static layer controls the response time is as follows:

$$E(t) = E(\infty) + s\log\left[1-\left(1-\frac{a_i^\circ}{a_i}\right)\exp\left(-\frac{t}{\tau'}\right)\right], \quad (1)$$

$$\tau' \approx \frac{\delta^2}{2D'}, \quad (2)$$

where $E(t)$ is the potential measured at the time t, $E(\infty)$ is the final potential after the activity step, s is the slope of the calibration graph, a_i° is the activity of the conditioning solution, a_i is the activity of the newly injected solution, δ is the thickness of the aqueous adhering layer, and D' is the diffusion coefficient of ion within the adhering layer. Another is a square root type equation derived from the assumption that the diffusion process within the membrane is regarded as rate controlling:[8]

$$E(t) = E(\infty) = s\log\left[1-\left(1-\frac{a_i^\circ}{a_i}\right)\frac{1}{(t/\tau)^{1/2}+1}\right], \quad (3)$$

$$\tau = \frac{DK^2\delta^2}{\pi D'^2}, \quad (4)$$

where D is the mean diffusion coefficient of electrolyte within the membrane and K is the salt distribution constant.

Curve Fitting Procedure. This paragraph describes a procedure of curve fitting using the exponential type equation; the same procedure can also be applied to the other equations. Our treatment of the least-squares estimate is on the basis of Wentworth's Papers[11,12] and Deming's book[13] dealing with the method of curve fitting applicable to some nonlinear equations. For curve fitting, we rewrite Eq. 1:

$$E(t) = E(\infty) + s\log\left[1-\left(1-\frac{a_i^\circ}{a_i}\right)\exp\left(-\frac{t-\theta}{\tau'}\right)\right], \quad (5)$$

where θ is an time adjustable parameter additionally introduced in order to allow the situation that the theoretical curve do not necessarily pass through the origin of E *vs.* t relationship. In this equation, the unknown parameter to be determined are $E(\infty)$, τ', and θ (but in our previous paper,[7] $E(\infty)$ was regarded as an

experimentally measurable quantity).

The least-squares problem is to determine the three parameters so as to obtain a minimization of the sum of the squares of the residuals:

$$\Sigma[\{E_i(t) - \bar{E}_i(t)\}^2] = \text{minimum}, \tag{6}$$

under the restriction that the condition equations

$$F_i(\bar{t}_i,\ \bar{E}_i(t),\ E(\infty),\ \tau',\ \theta) = \bar{E}_i(t) - E(\infty) - s\log\left[1-\left(1-\frac{a_i^\circ}{a_i}\right)\exp\left(-\frac{\bar{t}_i-\theta}{\tau'}\right)\right] = 0, \tag{7}$$

$$(i = 1,\ 2,\ \cdots\ n)$$

be satisfied. The symbol n is the number of the observed points, $E_i(t)$ is the observed value of the potential, and $\bar{E}_i(t)$ is the adjusted or calculated value of the potential. The weighting factor is treated as equal for all the points. It is assumed that the condition equations are linear with respect to t_i, $E_i(t)$, $E(\infty)$, τ', θ; Eq. 7 are expanded to the first order terms in a Taylor's Series about the point $(t_i, E_i(t), E^\circ(\infty), \tau'^\circ, \theta^\circ)$, where $E^\circ(\infty)$, τ'°, θ° are values of the first approximations. The Taylar's Series expansion and Eq. 6 yield normal equations:

$$\left.\begin{aligned}
&\Sigma\frac{\partial F_i}{\partial E(\infty)}\frac{\partial F_i}{\partial E(\infty)}\Delta E(\infty) + \Sigma\frac{\partial F_i}{\partial E(\infty)}\frac{\partial F_i}{\partial \tau'}\Delta\tau' + \Sigma\frac{\partial F_i}{\partial E(\infty)}\frac{\partial F_i}{\partial \theta}\Delta\theta = \Sigma\frac{\partial F_i}{\partial E(\infty)}F_i^\circ\\
&\Sigma\frac{\partial F_i}{\partial \tau'}\frac{\partial F_i}{\partial E(\infty)}\Delta E(\infty) + \Sigma\frac{\partial F_i}{\partial \tau'}\frac{\partial F_i}{\partial \tau'}\Delta\tau' + \Sigma\frac{\partial F_i}{\partial \tau'}\frac{\partial F_i}{\partial \theta}\Delta\theta = \Sigma\frac{\partial F_i}{\partial \tau'}F_i^\circ\\
&\Sigma\frac{\partial F_i}{\partial \theta}\frac{\partial F_i}{\partial E(\infty)}\Delta E(\infty) + \Sigma\frac{\partial F_i}{\partial \theta}\frac{\partial F_i}{\partial \tau'}\Delta\tau' + \Sigma\frac{\partial F_i}{\partial \theta}\frac{\partial F_i}{\partial \theta}\Delta\theta = \Sigma\frac{\partial F_i}{\partial \theta}F_i^\circ
\end{aligned}\right\} \tag{8}$$

where assuming $\partial F_i/\partial t_i=0$ and $\Delta E(\infty)=E^\circ(\infty)-E(\infty)$, $\Delta\tau'=\tau'^\circ-\tau'$, $\Delta\theta=\theta^\circ-\theta$. This equations can be solved for $\Delta E(\infty)$, $\Delta\tau'$, $\Delta\theta$; the least-square estimates of the parameters $E(\infty)$, τ', θ are calculated. It is usual to repeat the computations using the new $E(\infty)$, τ', θ as the first approximations; setting $E^\circ(\infty)=E(\infty)$, $\tau'^\circ=\tau'$, $\theta^\circ=\theta$, the normal equations 8 are iteratively solved. As a measure of fit, the variance σ^2 is employed:

$$\sigma^2 = \frac{\Sigma\{E_i(t)-\bar{E}_i(t)\}^2}{n-m}, \tag{9}$$

where m is the number of the unknown parameters. Using the new parameters, the variance or the standard error can be calculated. If the iterative procedure results in a satisfactory convergence of the variance, the three parameters are finally determined. Practically, the iterative computations are continued untill the change in σ^2 for successive iterations, $\Delta\sigma^2$, becomes less than a criterion which is previously evaluated by the estimated error in the experiments or some other convenience.

To determine the first approximate values $E^\circ(\infty)$, τ'°, θ°, the following procedure was carried out. The potential at the nearly equilibrium part (*i.e.* at 5 s) on E-t curve was employed as the $E^\circ(\infty)$, with which the plot of the left hand function *vs.* t of the linearized equation (from Ep. 5)

$$\ln\frac{1-a_i^\circ/a_i}{1-10^{\{E(t)-E^\circ(\infty)\}/s}} = \frac{1}{\tau'^\circ}t - \frac{\theta^\circ}{\tau'^\circ}, \tag{10}$$

yields the parameters τ'° and θ°.

Results of Curve Fitting. A typical response time curve of the ammonium ion-selective electrode for the concentration change from 1×10^{-4} to 1×10^{-3} mol dm^{-3} ammonium chloride is shown in Fig. 2. The linearized plot of Eq. 10 using 56.1 mV as $E^\circ(\infty)$ is illustrated in Fig. 3. In this example, a straight line is fitted in a range of 60 to 460 ms; the range corresponds to the potential level of 25.9% to 96.8% of the $E^\circ(\infty)$. The correlation coefficient is 0.997.. The lower limit of the range was determined at a flection point of the response time curve; the occurrence of the flection point may due to the unavoidable marginal zone between the conditioning solution and the injection solution. Beyond the range, a deviation notably occurs. The reciprocal slope and the intercept of the fitted straight line determined the values τ'°=158 ms and θ°=40 ms. A result of the iterative procedure with these values is shown in Table 1. As a criterion of $\Delta\sigma^2$, 0.25 (mV)^2 was employed. The $E(\infty)$ gradually approaches the potential of Nernstian response as the successive iteration is continued. Correspondently it is observed that τ' and θ slightly change. The facts that the $E(\infty)$ becomes a reasonable value and that the standard error is sufficiently small (σ=0.8 mV) indicate that this procedure of curve fitting is appropriate for the estimation of the parameters $E(\infty)$, τ', θ. The resultant value τ' will be tried to confirm by examining the flow rate dependence of τ' in the following

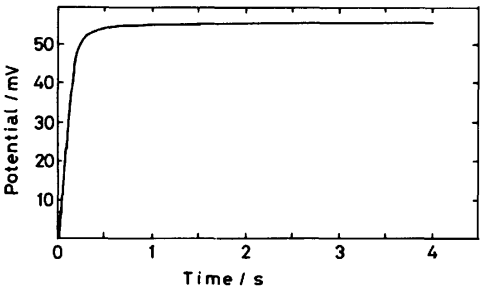

Fig. 2. Typical response time curve for 1×10^{-4} to 1×10^{-3} mol dm^{-3} NH_4Cl. Flow rate is 1.2 m s^{-1}.

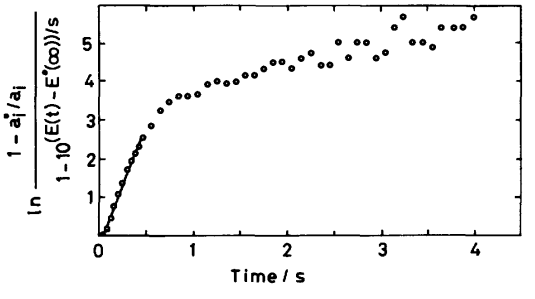

Fig. 3. Linearized plot of the Eq. 10 using the data of Fig. 2. Straight line is fitted in a range of time from 60 to 460 ms.

Table 1. Least-squares adjustment[a] of three parameters of the exponential type equation 5

No.[b]	$E(\infty)$ / mV	τ' / ms	θ / ms	σ^2 [c] / $(mV)^2$	$\Delta\sigma^2$ [d] / $(mV)^2$	σ [e] / mV
0	56.1	158	40	2.5	—	1.6
1	56.4	158	43	1.2	−1.3	1.1
2	56.5	158	45	0.7	−0.4	0.9
3	56.5	159	46	0.6	−0.1	0.8

a) Regression range: 60—460 ms. b) Number of iteration. c) Variance. d) The change in σ^2 for successive iterations. e) Standard error.

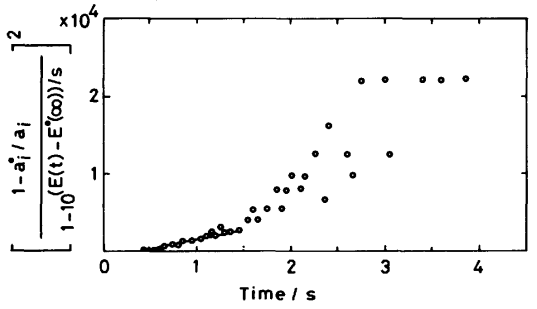

Fig. 4. Linearized plot derived from the square root type Eq. 3 using the data of Fig. 2. Straight line is fitted in a range of time from 480 to 1450 ms.

paragraph. The value θ can be regarded as a time lag due to the marginal zone of the flowing solution.

On the other hand, the linearized plot derived from the square root type equation 3 is shown in Fig. 4. In pratice, we determined the range of regression so that the range should be as wide as possible under the restriction that the correlation coefficient is more than 0.97 for example. The plot is fitted in a range of time from 480 to 1450 ms; the range corresponds to the potential level of 97.3% to 99.3% of the $E°(\infty)$. The correlation coefficient is 0.970. From this linearized plot, $\tau°$ and $\theta°$ were estimated at 0.33 ms and 457 ms respectively ($E°(\infty)$=56.1 mV). In this case, the iterative computation was carried out only once because the variance immediately converged. As the result, the three parameters were obtained: $E(\infty)$=56.1 mV, τ=0.38 ms, θ=448 ms. The standard error was 0.1 mV. The fact that the lower limit of the fitted range of Eq. 3 is close to the upper limit of the range of the exponential type equation means that the square root time dependence specific to the neutral carrier membrane becomes apparent after the outside equilibration is attained. In this case, the ratio of $\tau'/\tau(\approx D'/(DK^2))$ was about 400. For useful electrode systems, K must be sufficiently less than 1. Accordingly, it seems that the yielded ratio $\tau'/\tau(\approx 400)$ is a reasonable value. If we knew the numerical values D and K in this experimental system, the confirmation of the meaning of τ would be attained. At the present speaking, however, this cannot be done. In the literature,[8] concerning the potassium ion-selective membrane electrode in a fast stirring condition (so-called immersion technique), τ is reported to be 2 ms. Additionally, it is also described that for silcone rubber

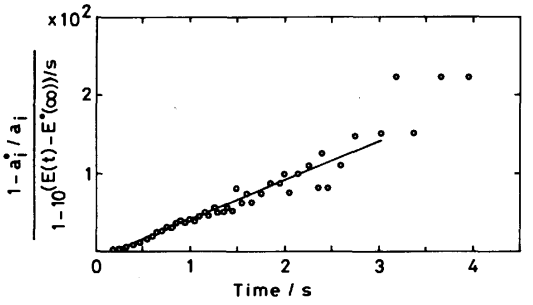

Fig. 5. Linearized plot of the semi-empirical equation using the data of Fig. 2. Straight line is fitted in a range of time from 200 to 3050 ms.

membrane in a rapid flow-through system, τ of down to 1 ms is observed. Under the circumstances, our result of τ=0.38 ms may not be unreasonable. The result of θ=448 ms and upper limit 460 ms of the range of Eq. 1 slightly overlap. In authers' opinion, as mentioned above, the diffusion process within the membrane equivalently begins at the time θ=448 ms. Practically, best fitting by Eq. 1 up to 97% potential completion means the response rate of the electrode is considerably fast. The more precise measurements with this electrode, however, is rather difficult for the diffusion within the membrane.

A Semi-empirical Equation. It seems that a parabola can be fitted to the plot in Fig. 4. This means that instead of Eq. 3 the following equation can be applied to the curve fitting.

$$E(t) = E(\infty) + s\log\left[1-\left(1-\frac{a_i^\circ}{a_i}\right)\frac{1}{t/\tau+1}\right], \qquad (11)$$

Accordingly a plotting shown in Fig. 5 was attempted. A straight line can be fitted to the plot in a range of time from 200 to 3050 ms; the range corresponds to the potential level of 83.8% to 99.7% of the $E°(\infty)$. The correlation coefficient is 0.947. The iterative computation yielded the following values: $E(\infty)$=56.2 mV, τ=27.3 ms, θ=165 ms, σ=0.4 ms. As a matter of fact, Eq. 11 can also be derived from the principle of second-order kinetics described by Morf[14] or Buffle and Parthasarathy.[15] According to Morf,[14] the time constant τ of Eq. 11 is equal to $1/(|a_i-a_i^\circ|k)$, where k is the rate constant of an kinetic equation of ion transfer reaction

$$\frac{d}{dt}\Delta a_i(t) = -k[\Delta a_i(t)]^2, \qquad (12)$$

$$(\Delta a_i(t) = |a_i'(t)-a_i|).$$

When the potential change is sufficiently small, the logarithmic function in Eq. 11 can be linearized:

$$E(t) = E(\infty) - \frac{1}{At+B}, \qquad (13)$$

where A and B are constants. This hyperbolic type expression is equivalent to Müller's equation.[16,17] However, Eq. 11 or 13 is rationalized not for neutral carrier membrane electrodes but for solid-state membrane electrodes (*e.g.* chloride electrode). Therefore the measured time constant τ=27.3 ms is not necessarily to be interpreted by the second-order kinetics mentioned

above.

We cannot theoretically explain why Eq. 11 is more fitted to the data than Eq. 3 is. Qualitatively, the exponential type curve is fast to approach the equilibrium potential, while the square root type curve is slow to do; the hyperbolic type curve has a medium property between the other two equations. In authors' opinion, the setting of $E°(\infty)$ is just appropriate to the curve fitting with Eq. 11. In our treatment, the potential at 5 s was employed as $E°(\infty)$ and the range of observation was restricted up to 4 s. If the Eq. 3 is forced to be fitted to the potential at about 4 s, the equilibrium potential should be higher than the potential at 5 s. At present, we can only say that the semi-empirical equation (Eq. 11) is apparently fitted to the data if the potential at several seconds is taken as equilibrium potential.

Effect of Flow Rate. A remarkable character of our apparatus is that the thickness of the adhering layer can be controlled by varying the flow rate. The flow rate was varied from 1.1 to 2.6 m s^{-1}. This corresponds to the Reynolds number from 860 to 2040. The flow of fluid in a smooth pipe at Reynolds numbers up to about 2000 is always laminar. If the wall of our tubular electrodes, however, have rough surface, the turbulent flow may occurs. Therefore we must examine both the cases of the laminar flow and the turbulent flow. For the turbulent flow in a smooth pipe, the thickness of adhering layer δ is expressed as a function of the flow rate of sample solution:[18]

$$\delta = (\text{const})v^{-7/8}, \tag{14}$$

where v is the linear flow rate and (const) is a lumped constant. By eliminating δ from Eqs. 2 and 14, a theoretical relationship between τ' and v is derived:

$$\tau' = (\text{const})'v^{-7/4}, \tag{15}$$

where (const)' is a lumped constant. On the other hand, assuming the laminar flow, $\tau' \propto v^{-2/3}$. Figure 6 shows a log-log plot of τ' against v using the data for concentration change from 1×10^{-4} to 1×10^{-3} mol dm^{-3} NH_4Cl. In this case, every upper limit of the range of regression is fixed on 97% of completion of potential response. The slope of the straight line drawn through the experimental points is -1.3; the correlation coefficient is 0.973. A series of the experimental data is located between the turbulent domain and the laminar domain, but is rather close to the turbulent one. In this paragraph, the flow rate dependence of the time constants are discussed; but the absolute values of the time constants are not confirmed yet. The facts that the initial part of the response time data was best fitted by Eq. 1 and that the flow rate dependence of the time constants was approximately agree with the expectation assuming the turbulent flow, however, support the assumption that the initial part of the response time data is due to the film diffusion.

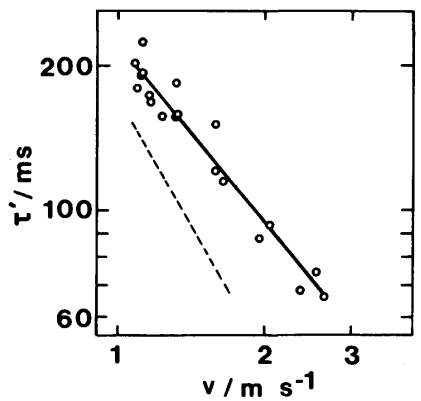

Fig. 6. Log-log plot of the time constant τ'(in Eq. 15) against the linear flow rate v using the data for concn change from 1×10^{-4} to 1×10^{-3} mol dm^{-3} NH_4Cl. The full line is drawn through the points; the slope is -1.3. The broken line represents a theoretical slope (-1.75). Every upper limit of the range of regression is 97% of completion of potential response.

Theoretically the dependence of the square root type equation (Eq. 3) upon the flow rate is the same with that of the exponential type one (refer to Eqs. 2 and 4). Actually, the slope of log-log plot of τ in Eq. 3 against v using the same data that was described above was also close to the theoretical one. The range of regression was from 97% to 99%. But the correlation coefficient was considerably less than that of Fig. 6. This is due to the fact that the effect of experimental error becomes relatively large because of the slightly variation in potential.

Conclusion

An application of tubular flow-through electrode to the measurement of the response time curve yields reproducible data which could be analyzed by the curve fitting method. For the curve fitting, two theoretical equations and a semi-empirical equation were used. A method of curve fitting in which the equilibrium potential was regarded as an unknown parameter provided reasonable results concerning the time constant, the equilibrium potential, and the adjustable parameter of time. On the response time curves, the first part where the potential change is large was fitted by the theoretical equation based on the film diffusion, while the next part close to the equilibrium potential was fitted by that based on the diffusion process within membrane. On the other hand, a semi-empirical equation of hyperbolic type could also be fitted to the wide range of the response time curves.

The fact that the dependence of the time constant of the exponential type equation upon the flow rate was fairly consistent with the theoretical expectation supports both the explanation of the first part of the response time curves by means of the film diffusion and the reliablity of the present experimental system.

The authors are grateful to Chugai Pharmaceutical Co., Ltd. for a gift of polynactin.

Reference

1) B. Oosterhuis, K. Brunt, B. H. C. Westerink, and D. A. Doornbos, *Anal. Chem.*, **52**, 203 (1980).
2) E. Lindner, K. Tóth, and E. Pungor, *Anal. Chem.*, **48**,

1071 (1976).
3) E. Lindner, K. Tóth, W. E. Morf, and W. Simon, *Anal. Chem.*, **50**, 1627 (1978).
4) E. Lindner, K. Tóth, and E. Pungor, *Anal. Chem.*, **54**, 72 (1982).
5) E. Lindner, K. Tóth, and E. Pungor, *Anal. Chem.*, **54**, 202 (1982).
6) T. Akiyama, K. Kinoshita, Y. Horita, and E. Niki, *Nippon Kagaku Kaishi*, **1980**, 1431.
7) H. Degawa, N. Shinozuka, and S. Hayano, *Chem. Lett.*, **1983**, 25.
8) W. E. Morf, E. Lindner, and W. Simon, *Anal. Chem.*, **47**, 1596 (1975).
9) H. Degawa, N. Shinozuka, and S. Hayano, *Nippon Kagaku Kaishi*, **1980**, 1462.
10) Y. M. Fraticelli and M. E. Meyerhoff, *Anal. Chem.*, **53**, 992 (1981).
11) W. E. Wentworth, *J. Chem. Educ.*, **42**, 96 (1965).
12) W. E. Wentworth, *J. Chem. Educ.*, **42**, 162 (1965).
13) W. E. Deming, "Statistical Adjustment of Data," Willy, New York (1943); translated by S. Moriguchi, "Suikeigaku Ni Yoru Deta No Matomekata," Iwanami shoten, Tokyo (1950).
14) W. E. Morf, "Studies in Analytical Chemistry, Vol. 2; The Principles of Ion-Selective Electrodes and of Membrane Transport," Elsevier, Amsterdam (1981), Chap. 14.
15) J. Buffle and N. Parthasarathy, *Anal. Chim. Acta.*, **93**, 111 (1977).
16) R. H. Müller, *Anal. Chem.*, **41** (12), 113A (1969).
17) J. Mertens, P. Van den Winkel, and D. L. Massart, *Anal. Chem.* **48**, 272 (1976).
18) J. T. Davies, "Turbulence Phenomena," Academic Press, New York (1972), Chap. 3.

The Sodium Isotopic Exchange Rate between High-temperature Phases of Disodium Zirconium(IV) Bis(orthophosphate) and Aqueous Solutions

Yasushi INOUE* and Yoshimune YAMADA
Department of Nuclear Engineering, Faculty of Engineering, Tohoku University, Aramaki-aza-Aoba, Sendai 980
(Received July 25, 1983)

A monohydrate (Phase II) and three anhydrous phases prepared by the thermal treatment (at 250, 700, and 900 °C respectively for Phases III, IV, and V) of disodium zirconium(IV) bis(orthophosphate) trihydrate were studied from the sodium isotopic exchange rate between them and aqueous solutions. In Phases III and IV, which had been sufficiently adapted in water in advance, the rate was found to be controlled by the diffusion of sodium ions along the direction perpendicular to the layers consisting of zirconium atoms and the diffusion constants, and their activation energies (for Phases III and IV, 57 and 52 kJ/mol) were evaluated. When these phases were used as dried, the rate was governed by the irreversible dissociation of sodium in the solid phases. In Phase II, used as dried, and in Phase V, used as dried and wetted, the rate was controlled by neither particle diffusion, film diffusion, nor chemical reaction alone. This behavior was attributed to the complex behavior of phase transformation as the isotopic exchange proceeded.

The dehydration of the disodium zirconium(IV) bis(orthophosphate) trihydrate (hereafter this material will be referred to as Phase I) obtained from the zirconium(IV) bis(hydrogenphosphate) monohydrate prepared by the direct precipitation method[1] was found to give a monohydrate and three anhydrous phases, depending on the temperature of thermal treatment and on the surrounding humidity. The most suitable conditions for the preparation and for the storage of these five phases, including Phase I, were also established in addition to the examination of phase transformation brought about by immersing them in aqueous solutions.[2]

As Phase I is the most stable of them at room temperatures, it was at first used for the study of the sodium isotopic-exchange rate to provide fundamental data which would be useful for elucidating ion-exchange kinetics. It was concluded that the rate was controlled by the particle diffusion along the direction perpendicular to the layers of crystals; the diffusion constants and their activation energies were obtained as has previously been described.[3]

Since this type of material, known as "crystalline zirconium phosphate", can be used as an ion exchanger at high temperatures, the study of ion-exchange kinetics for its high-temperature phases is interesting. The rate for them acquires additional interest from the facts that their structures differ in different phases and that the capillary water introduced by placing them in contact with aqueous solutions plays an important role in the rate of the exchange.

This paper will deal with the radiochemical experiments performed to measure the isotopic-exchange rate of sodium ions between $Na_2Zr(PO_4)_2 \cdot nH_2O$($n$=0, 1) and concentrated sodium nitrate solutions and will discuss the results with reference to their phase stability in aqueous solutions.[2]

Experimental

Preparation of the Materials Spiked with ^{22}Na. Phase I labeled with ^{22}Na at about 40 μCi/g(1 Ci=3.7×10^{10} Bq), with uniform crystal sizes, was prepared by the procedure reported previously.[3] Its average size is given in Table 1. The radiochemical purity of ^{22}Na was confirmed by gamma-ray spectrometry. The monohydrate (Phase II) was obtained by drying Phase I over P_2O_5 for three weeks, while the anhydrous phases, phases III, IV, and V, were formed by heating Phase I at 250, 700, and 900 °C respectively for 4 d.[2] They were stored *in vacuo* over P_2O_5 and used for the rate measurement (as a dried system). In addition, parts of them were immersed in water for a definite period of time (Phases III and IV, 1 d; Phase V, one week) to adapt them to aqueous solutions and then also used for the experiments (wet system).

TABLE 1. PARTICLE SIZE OF THE SAMPLES

No.	Mean crystal size/μm		
	Length	Width	Thickness
1	286±44	238±32	16±3
2	190±24	159±15	16±2

The Measurement of the Isotopic-exchange Rate. All the experiments were performed in a nitrogen atmosphere. The rate was measured by using the same apparatus as before.[3] A 400-mg portion of the sample was placed in the cage and immersed in 200 cm^3 of a 5-mol dm^{-3} sodium nitrate solution, whose pH was adjusted to 11 by sodium hydroxide, while the cage was rotated at a rate of 1200 min^{-1}. The solution had been adjusted in advance to a constant temperature within ±0.1 °C. Aliquots of the solution (about 0.2 cm^3) were taken out at appropriate time intervals in order to measure the radioactivity with a well-type NaI(Tl) scintillation counter. The time of contact of the solution with the exchanger was taken as the time which elapsed between the immersion of the cage and the withdrawal of an aliquot of the solution.

The fractional attainment of equilibrium, $F=C_t/C_\infty$, was calculated from these results; here, C_t is the total radioactivity of the solution at time t and C_∞ at $t=\infty$. C_∞ was calculated by means of this equation; $C_\infty=CM/(M+m)$, where C is the initial total radioactivity of the exchanger and where m and M are the total amounts of Na^+ ions in the exchanger and in the solution respectively. After the experiments were finished, it was confirmed microscopically that the particles did not break down at all during this series of procedures.

The other materials, apparatus, and experimental proce-

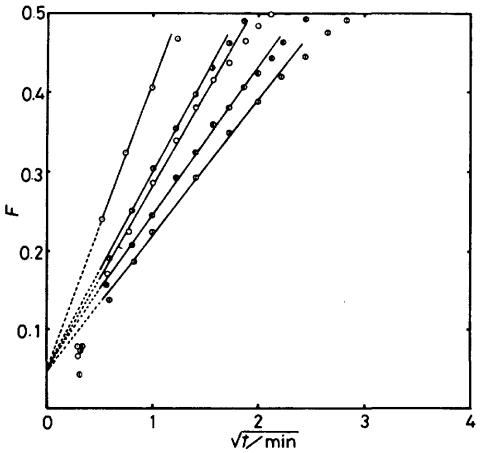

Fig. 1. Isotopic exchange rate for Phase III(wet system).
pH 11, 5 mol dm^{-3} $NaNO_3$.
⊙: 19.6 °C, sample 2, ◑: 12.5 °C, sample 1, ○: 9.5 °C, sample 2, ◐: 5.0 °C, sample 2, ⓘ: 1.3 °C, sample 1.

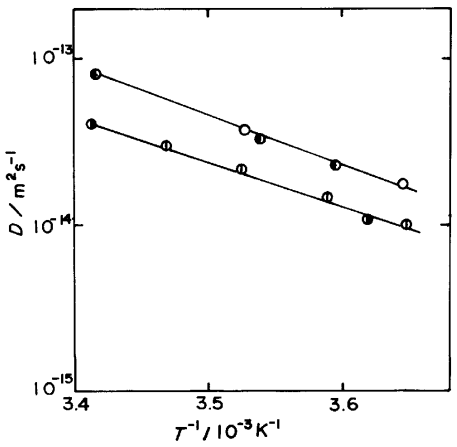

Fig. 2. Arrhenius plot of D for Phases III and IV(wet system).
pH 11, 5 mol dm^{-3} $NaNO_3$.
○: Phase III, sample 1, ◐: Phase III, sample 2, ◑: Phase IV, sample 1, ⓘ: Phase IV, sample 2.

dures were the same as had been described previously,[3] except as otherwise noted.

Results and Discussion

The sodium isotopic-exchange rate was measured with two types of samples: (a) dried and (b) wet. The results for each type of experiment will be described separately for convenience.

Wet System. The fractional attainment of equilibrium, F, against the square root of the time needed for Phase III is shown in Fig. 1. For Phase IV, curves similar to Fig. 1 were also obtained, though the rate was slower for Phase IV than for III. This figure clearly indicates that a linear relation held between F and $\sqrt{t}$ in the F range smaller than about 0.4 except for the initial portion of these plots. The curves also reveal that the rate was independent of the particle size. In this manner, the dependence of the rate on various experimental factors for Phases III and IV is similar to that for Phase I; hence, we can analyze the data by applying the same assumptions made for Phase I, that is, the rapid attainment of exchange equilibrium on the surface of the crystals, followed by a slow diffusion into the bulk of them, a diffusion along the direction perpendicular to the layers consisting of zirconium atoms. The diffusion constant, D, can, therefore, be obtained from F by means of this equation;

$$F = \frac{2}{\pi^{1/2}}\sqrt{\beta t}.$$

where $\beta = D/l$, and l is the half-thickness of the crystals.[3] For calculating D, a revised value of l was used in place of that presented in Table 1. When Phase I is transformed to Phase III, the interlayer distance decreases from 0.983 to 0.839 nm.[2] This inevitably shortens the thickness of the crystals to 0.839/0.983×16=13.7 nm. When log D was plotted against $1/T$, a good linearity was obtained, as is shown in Fig. 2. From the Arrhenius equation, $D = D_0\exp(E_a/RT)$, the activation energy and the constant, D_0, were evaluated. The values of D_0 for Phases III and IV respectively were 1.1×10^{-3} and 9.5×10^{-5} m^2/s, while those of E_a were 57±3 and 52±5 kJ/mol. It is not strange that the diffusion constants and their activation energies for these phases are about the same, for Phase IV is transformed to Phase III immediately after being immersed in water.[2] The slightly higher activation energy for Phase III than for IV can be explained in terms of the lower diffusion barrier in the latter, since the latter has more crystal defects than the former.[2] The exchange rate is much faster for Phases III and IV than for Phase I, and the activation energy of particle diffusion in these anhydrous phases has values about half that in Phase I (101 kJ/mol).[3] These differences cannot be attributed to the difference in the size of the openings, which interconnect the layers and which have a diameter of 0.24 nm at the largest, large enough to allow sodium ions to diffuse across the layers. Phase I contains three molecules of water of crystallization per formula, while the anhydrous phase has only a small amount of capillary water. Phase I, therefore, requires sodium ions to travel as large hydrated ions instead of free sodium ions, the species participating in the diffusion in the anhydrous phases. The difference between the trihydrate and anhydrous phases, therefore, results from the difference in the size of the ions traveling through the layers.

The F *vs.* $\sqrt{t}$ plots for Phase V are shown in Fig. 3, which indicates that no linearity held and that the rate slowed down abruptly after 60 min. This relation cannot be explained by the diffusion mechanism alone, but it might be due to the slow transformation of the crystals as the exchange proceeds.

Dried System. Contrary to the rate for the wet system, Phases III and IV when dried did not show a linear relation between F *vs.* $\sqrt{t}$, but they did show one between $-\log(1-F)$ and t, as is shown in Figs. 4 and 5. This means that the exchange rate is not controlled by the particle diffusion, but by either film diffusion or a chemical reaction. The film diffusion, however, does not appear to control the rate under the conditions adopted in the present experiments, *i.e.*, a high sodium-

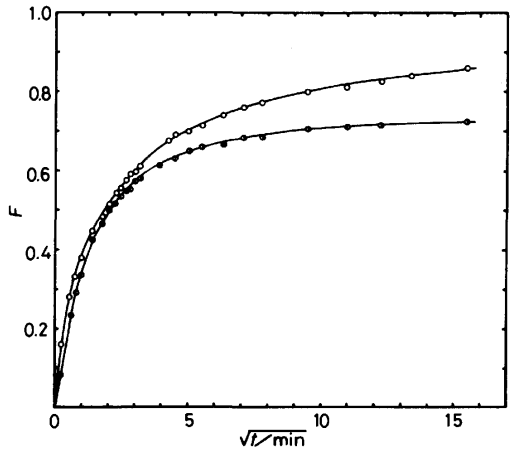

Fig. 3. Isotopic exchange rate for Phase V(wet system).
pH 11, 5 mol dm^{-3} $NaNO_3$, sample 2.
○: 17.4 °C, ⓘ: 4.5 °C.

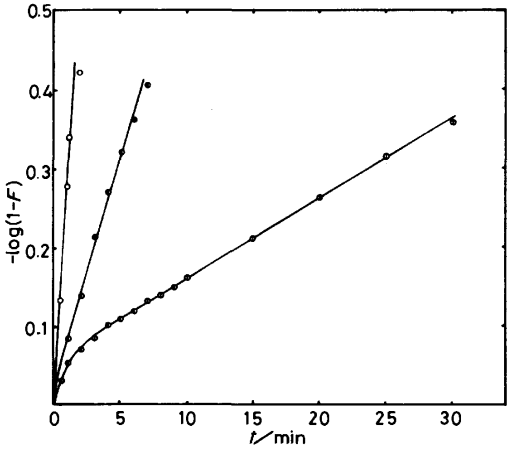

Fig. 4 Isotopic exchange rate for Phase III (dried system).
pH 11, 5 mol dm^{-3} $NaNO_3$, sample 2.
○: 44.7 °C, ◐: 24.9 °C, ⓘ: 5.9 °C.

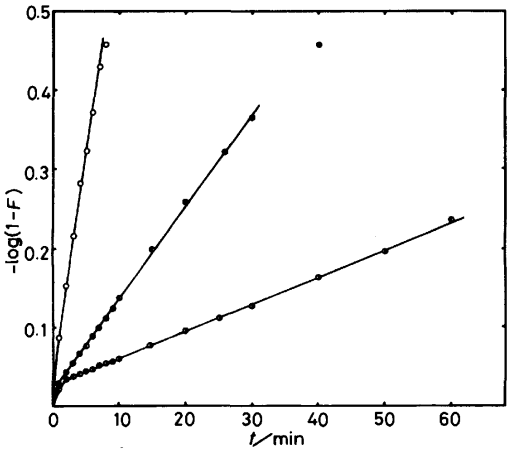

Fig. 5. Isotopic exchange rate for Phase IV (dried system).
pH 11, 5 mol dm^{-3} $NaNO_3$, sample 2.
○: 41.0 °C, ◐: 18.7 °C, ⓘ: 4.5 °C.

ion concentration and a high stirring speed in the range where it does not affect the exchange rate. Moreover, if the rate is controlled by the film diffusion, it must be faster for a dried than for a wet system. The experimental data, however, do not support this assumption. From these considerations, it can reasonably be assumed that the rates for the dried Phases III and IV are governed by a chemical reaction. The sodium in completely dried samples is considered to be strongly bonded with phosphate groups and not to be dissociated. As an ion-exchange reaction occurs between dissociated ions in the crystals and those present in the solution, sodium must be dissociated before the ion-exchange reaction commences.

If sodium is dissociated irreversibly with the rate constant, k, and if the sodium ions thus formed participate in the isotopic exchange reaction, that is,

$$\overline{RA} \xrightarrow{k} \overline{R} + \overline{A^+}$$

$$\overline{A^+} + B^+ \underset{}{\overset{K}{\rightleftarrows}} A^+ + \overline{B^+}$$

$$K = \frac{m_B C_A}{m_A C_B}.$$

From the material balance,

$$m_{RA} + m_R = E,$$

$$m_R = m_A + m_B,$$

where R^- is the matrix of the exchanger; K, the equilibrium constant of the exchange reaction; m, the amount of designated species in the exchanger; E, the specific ion-exchange capacity, and C, the concentration of designated species in the solution, and where a bar refers to the solid phase.

From the experimental conditions, C_A/C_B is always unity. Thus,

$$m_{RA} = E - m_A - m_B = E - \frac{1+K}{K} m_B.$$

The rate of increase of m_B can be written by;

$$\frac{dm_B}{dt} = K\frac{dm_A}{dt} Kkm_{RA} = KkE - k(1+K)m_B. \quad (1)$$

By integrating Eq. 1, we obtain:

$$m_B = \frac{1}{k(1+K)} [KkE - \exp\{-k(1+K)t+g\}], \quad (2)$$

where g is the integration constant.

By applying the initial conditions, $t=0$, and $m_B=0$, Eq. 2 becomes;

$$Q = m_B = \frac{KkE}{k(1+K)}[1-\exp\{-k(1+K)t\}], \quad (3)$$

$$Q_\infty = \frac{KkE}{k(1+K)}.$$

When we set $Q/Q_\infty=F$, we obtain:

$$\log(1-F) = -\frac{k}{2.303}(1+K)t.$$

In the isotopic exchange, $K=1$; therefore,

$$\log(1-F) = -\frac{2k}{2.303}t. \quad (4)$$

Equation 4 agrees with the results of the experiments.

Even when the dissociation reaction proceeds reversibly, Eq. 4 is valid. If we consider that the dissociation

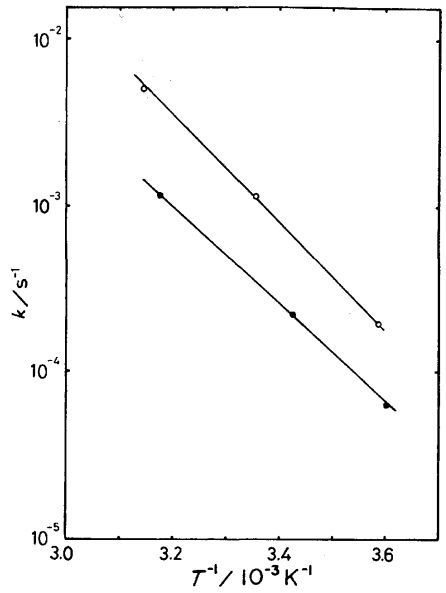

Fig. 6. Arrhenius plot of k for Phasses III and IV (dried system).
pH 11, 5 mol dm^{-3} $NaNO_3$, sample 2.
○: Phase III, ●: Phase IV.

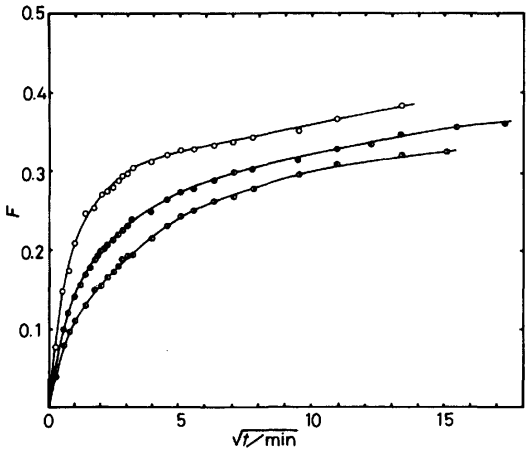

Fig. 7. Isotopic exchange rate for Phase II (dried system).
pH 11, 5 mol dm^{-3} $NaNO_3$, sample 2.
○: 44.3 °C, ◐: 18.7 °C, ⓘ: 4.9 °C.

reaction is reversible, the same relation must hold for a wet system. However, as the isotopic-exchange reaction for a wet system is much faster than this and is controlled by the particle diffusion, the reversible dissociation cannot be rate controlling. Accordingly, when the completely dried Phases III and IV are in contact with the solution without having been wet in advance, the rate of exchange reaction is controlled by the irreversible dissociation of sodium in the exchanger, which is much slower than the particle diffusion.

The reaction rate constants, k, were obtained from the slopes of the straight lines in Figs. 4 and 5; they are plotted against $1/T$ in Fig. 6. The activation energies of

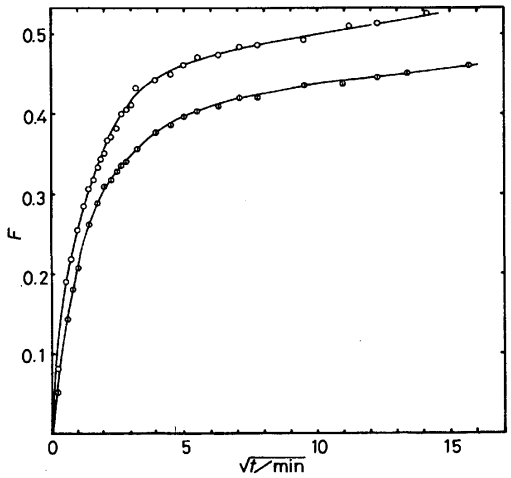

Fig. 8. Isotopic exchange rate for Phase V (dried system).
pH 11, 5 mol dm^{-3} $NaNO_3$, sample 2.
○: 18.4 °C, ⓘ: 5.4 °C.

the dissociation reaction for Phases III and IV were 63±2 and 56±2 kJ/mol respectively, while the frequency factors of the Arrhenius equation, k_0, are 1.2×10^8 and 2.6×10^6 s^{-1}. The faster reaction rate for Phase III than for IV can be ascribed to the lower temperature of the thermal treatment of the former.

The plots of F against $\sqrt{t}$ for Phases II and V are shown in Figs. 7 and 8. Contrary to Phases III and IV, neither these plots nor the plots of $-\log(1-F)$ *vs.* t are straight lines; hence, the rate is governed by neither film diffusion, particle diffusion, nor a chemical reaction alone.

In the case of Phase II, the rate slowed down markedly with the progress of the exchange. The rate will be controlled at first by the faster diffusion in Phase II, followed by the slower diffusion in Phase I, which is formed as the exchange reaction proceeds.[2] In other words, the curves may result from a complicated combination of the transformation rate of the crystals and the diffusion of ions in them.

Figure 8 indicates that the isotopic-exchange rate for Phase V behaved similarly to that for Phase II and was slower than that for a wet system. The reason for this rather complicated behavior is not clear, but it may be due to the complex behavior of the transformation of this phase.[2]

Further investigations must be undertaken before the kinetics of the sodium isotopic-exchange reaction for Phases II and V can be unambiguously determined.

References

1) Y. Inoue and Y. Yamada, *Bull. Chem. Soc. Jpn.*, **52**, 3528 (1979).
2) Y. Inoue and Y. Yamada, *Bull. Chem. Soc. Jpn.*, **55**, 792 (1982).
3) Y. Inoue and Y. Yamada, *Bull. Chem. Soc. Jpn.*, **56**, 705 (1983).

Stability Constants of Scandium Complexes. I. Monocarboxylate Complexes Species

Hisako Itoh, Naomi Itoh, and Yasuo Suzuki*
Department of Industrial Chemistry, Faculty of Engineering, Meiji University, Higashi-mita, Tama-ku, Kawasaki 214
(Received August 26, 1983)

The stability constants of scandium complexes with some carboxylate ligands were determined potentiometrically at 25.0 and 40.0 °C and at an ionic strength of 0.10 with potassium nitrate as supporting electrolyte. The constants of the scandium complexes were appreciably greater than those of the corresponding lanthanoid complexes, as expected. The changes in free energy, enthalpy, and entropy for the formation of the scandium complexes were calculated from the stability constants at two temperatures.

Since scandium has a similar outer electron shell configuration to the trivalent lanthanoids, the chemical properties of scandium are close to those of the trivalent lanthanoids. The stability constants of various lanthanoid complexes have been determined by many investigators,[1] however, only a few investigations of scandium complexes have been reported so far. Trivalent scandium, which is the only oxidation state for scandium in solution, has a smaller ionic radius than any of the lanthanoids but is larger than that of aluminium.[2] Thus scandium(III) should form more stable complexes with both anionic and neutral ligands than the lanthanoids,[3] although it undergoes extensive hydrolysis in aqueous solution. In the present study, the stability constants of scandium complexes with some monobasic carboxylic acids were determined and compared with those of the corresponding lanthanoid complexes.

The method employed for determining constants was based on conventional potentiometry as developed by Bjerrum,[4] Sonesson,[5] and others, and has been used in the previous work[6,7] by one of the authours.

Experimental

Reagents. Scandium nitrate stock solution was prepared by dissolving scandium oxide of 99.9% purity in nitric acid and diluting to a definite volume with water. The concentration of excess nitric acid was as high as 0.035 mol dm^{-3} to prevent hydrolysis. The potasium nitrate stock solution was prepared from the purified salt. The buffer solution of each ligand acid was prepared by half neutralization of the acid solution with an appropriate amount of carbonate-free standard sodium hydroxide.

Apparatus. The pH of the sample solution was measured with an Orion model 701A digital pH/mV meter equipped with Orion Ross 810100 pH and 800500 double-junction reference electrodes. The instrument is capable of measuring pH of a solution with an accuracy of 0.001 unit.

Procedures. An aliquot portion of scandium nitrate solution was added to a volumetric flask together with a carboxylate buffer solution and potassium nitrate to bring the final solution to an ionic strength of 0.10. The flask was brought to the mark with water then suspended in a constant temperature bath set at 25.0 °C for 24 h. The sample solutions used in measuring acid dissociation constants were prepared in the same way as the sample solutions described above, but without scandium nitrate.

Results and Discussion

There have been no previous reports on the stability constants of scandium complexes with the ligand acids used in the present study, except for acetylacetone,[8] acetic acid,[9] and D-gluconic acid.[10] The stability constants of the scandium complexes obtained are shown in Table 1, along with the values from the previous work. The stability constants obtained are in good agreement with those of the previous work.

The relation between basicity of ligands and the stability constants of complexes has been extensively discussed.[11–16] The ligands of stronger basicity produce more stable complexes, in other words, ligands which strongly combine with protons form stable complexes with metal ions. The linear correlations between the basicity of a series of ligands and the stability constants of complexes have been reported.[11–16] The relation

Table 1. Logarithms of stability constants and thermodynamic data of scandium complexes at 25.0 °C and at I=0.10 (KNO_3)

Ligand acid	This work	Previous work	$-\Delta G$ / kJ mol^{-1}	$-\Delta H$ / kJ mol^{-1}	$T\Delta S$ / kJ mol^{-1}
α-Hydroxyisobutyric acid	4.84	—	27.6	115	−87.0
Isobutyric acid	4.47	—	25.5	90.1	−64.6
Glycolic acid	4.40	—	25.5	121	−96.2
Acetic acid	3.48	3.16[8]	19.6	1.25	18.8
Propionic acid	3.77	—	21.3	8.78	12.5
Mandelic acid	2.91	—	16.7	−5.43	22.1
D-Gluconic acid	4.21	3.92[9]	23.8	−52.3	76.5
Acetylacetone	7.77	8.88[7]	44.3	388	−344

between the stability constants of the scandium complexes and the basicity of the ligand acids used here is shown in Fig. 1. Isobutyric, acetic, and propionic acids do not have an alcoholic OH group, whereas α-hydroxyisobutyric, glycolic, mandelic, and D-gluconic acids have OH. In the latter acids, the OH group apparently contributes to form five-membered rings, consequently the stability constants are greater than those of the former.

In considering the ionic radius, it is expected that the greater the charge and smaller the ionic radius, the greater will be the stability of the complexes, since the energy of an ionic bond corresponds to the electrostatic work to bring metal ions close to ligands. The relationship to the stability constants of α-hydroxyisobutyrato, glycolato, gluconato, and mandelato complexes against ionic radius is shown in Fig. 2. The stability constants of scandium complexes are on the extrapolated lines of those of the lanthanoid complexes. In the case of the mandelato complexes, the gradient of the line is smaller than the others, possibly due to steric hindrance. The relations between the stability constants of isobutyrato, acetato, and propionato complexes and ionic radius are shown in Fig. 3. The scandium complexes are on the extrapolated lines of the lighter rare earth complexes rather than the heavier rare earth complexes. The previous investigations[17-21] indicated that the relation between the stability constants and ionic radii was remarkably different for each of the ligands studied, and that the trends in the stability of the rare earth complexes were dependent on the changes in the coordinating characteristics of the ligands as well as on the changes in the degree of cationic hydration. Therefore, the scandium complexes are thought to be similar to the lighter rare earth complexes with regard to the coordinating characteristics and the degree of cationic hydration.

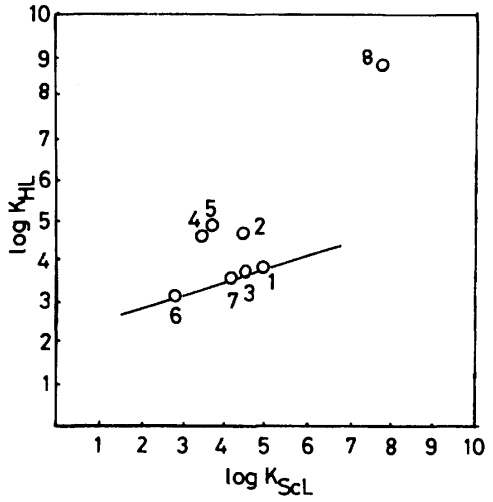

Fig. 1. Relation between stability constants of scandium complexes and basicity of ligands.
1: α-Hydroxyisobutyric acid, 2: isobutyric acid, 3: glycolic acid, 4: acetic acid, 5: propionic acid, 6: mandelic acid, 7: D-gluconic acid, 8: acetylacetone.

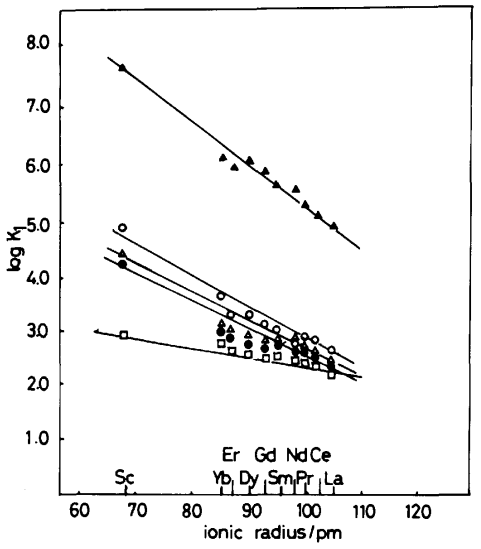

Fig. 2. Logarithms of stability constants of rare earth complexes. I.
○: α-Hydroxyisobutyrate, ●: D-gluconate, △: glycolate, ▲: acetylacetonate, □: mandelate.

The relation betweeen the stability constants of α-hydroxyisobutyrates and glycolates and ionization enthalpies of the rare earth elements are shown in Fig. 4. A straight line through yttrium, lanthanum, lutetium, and scandium, which have no d- and f-electrons, was obtained. Since electronegativity or ionization enthalpy is a measure of attracting electrons from the donor atoms of ligands, the linear relationships between the stability constants and the ionization enthalpy is reasonable. However, such lines were not obtained for isobutyrato, acetato, propionato, mandelato, gluconato, and acetylacetonato complexes.

The calculated values of the change in free energy, enthalpy, and entropy for the formation of the scandium complexes are shown in Table 1. Thermody-

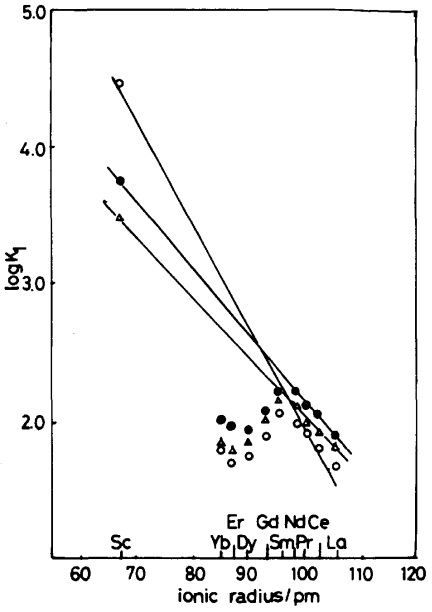

Fig. 3. Logarithms of stability constants of rare earth complexes. II.
○: Isobutyrate, ●: propionate, △: acetate.

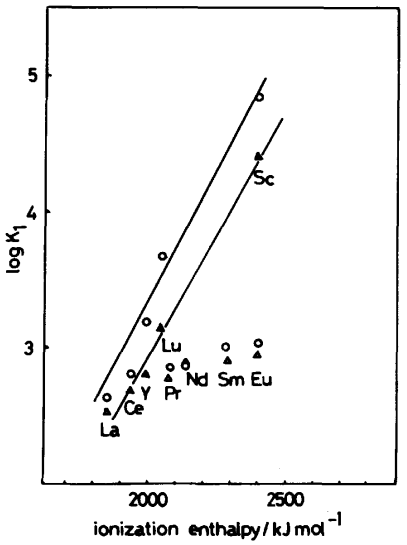

Fig. 4. Logarithms of stability constants of α-hydroxyisobutyrate and glycolate complex species *versus* ionization enthalpy.
○: α-Hydroxyisobutyrate, △: glycolate.

namic data on the scandium complexes indicate that $-\Delta H$ values are larger than $T\Delta S$ values for the α-hydroxyisobutyrate, isobutyrate, glycolate, and acetylacetonate systems. However, the entropy terms are larger than the enthalpy terms for acetato, propionato, mandelato, and gluconato complexes. The formation reactions of mandelato, and gluconato complexes are endothermic and the existence of the complexes is due to favorable entropy change. The increase in ΔS would be due to the increase in steric hindrance, thereby loosening the bond and increasing the configurational entropy of ligands such as mandelic and D-gluconic acids.

References

1) T. Moeller, D. F. Martin, L. C. Thompson, R. Ferrús, G. R. Feistel, and W. J. Randall, *Chem. Rev.*, **65**, 1 (1965).
2) R. D. Shannon and C. T. Prewitt, *Acta Crystallogr., Sect. B*, **25**, 925 (1969).
3) G. A. Melson and P. W. Stotz, *Coord. Chem. Rev.*, **7**, 133 (1971).
4) J. Bjerrum, "Metal Ammine Formation in Aqueous Solution," P. Hasse and Son, Copenhagen (1957).
5) A. Sonesson, *Acta Chem. Scand.*, **12**, 165 (1958).
6) Y. Suzuki and J. E. Powell, *Bull. Chem. Soc. Jpn.*, **49**, 2327 (1976).
7) Y. Suzuki, S. Yokoi, M. Katoh, and N. Takizawa, "Stability Constants of Rare Earth Complexes with Some Organic Ligands," in "The Rare Earths in Modern Science and Technology," ed by G. J. McCarthy, J. J. Rhyne, and H. B. Silber, Plenum, New York (1980), Vol. 2, pp. 121—126.
8) R. M. Izatt, W. C. Fernelius, C. G. Haas, and B. P. Block, *J. Phys. Chem.*, **59**, 170 (1955).
9) F. Vesely, F. Petru, and K. Mader, *Chem. Zvesti*, **20**, 792 (1966).
10) N. A. Kostromine and E. D. Romanenko, *Ukr. Khim. Zh.*, **31**, 332 (1965).
11) J. Bjerrum, *Chem. Rev.*, **46**, 381 (1950).
12) M. Calvin and K. W. Wilson, *J. Am. Chem. Soc.*, **67**, 2003 (1945).
13) H. K. J. Powell and N. F. Curtis, *J. Chem. Soc., A*, **1967**, 1441.
14) G. Schwarzenbach, H. Ackermann, and P. Ruckstuhl, *Helv. Chim. Acta*, **32**, 1175 (1949).
15) M. Yasuda, K. Suzuki, and K. Yamasaki, *J. Phys. Chem.*, **60**, 1649 (1956).
16) G. Schwarzenbach, A. Willi, and R. O. Bach, *Helv. Chim. Acta*, **30**, 1303 (1947).
17) F. H. Spedding and G. Atkinson, "Properties of Rare Earth Salts in Electrolytic Solutions" in "The Structure of Electrolytic Solutions" ed by W. J. Hamer, John Wiley and Sons, New York (1959), pp. 319—339.
18) F. H. Spedding, D. A. Csejka, and C. W. DeKock, *J. Phys. Chem.*, **70**, 2423 (1966).
19) F. H. Spedding and M. J. Pikal, *J. Phys. Chem.*, **70**, 2430 (1966).
20) F. H. Spedding, M. J. Pikal, and B. O. Ayers, *J. Phys. Chem.*, **70**, 2440 (1966).
21) F. H. Spedding and K. C. Jones, *J. Phys. Chem.*, **70**, 2450 (1966).

Synthesis of [3](1,1′)[3](3,3′)- and [4](1,1′)[4](3,3′)Ruthenocenophanes

Shin-ichi KAMIYAMA* and Akira KASAHARA†
Government Industrial Research Institute, Tohoku, 115-10 Ishiyose, Minaminome, Haranomachi, Sendai 983
†*Department of Applied Chemistry, Faculty of Engineering, Yamagata University, Yonezawa 992*
(Received March 22, 1983)

[3](1,1′)[3](3,3′)- and [4](1,1′)[4](3,3′)Ruthenocenophanes were synthesized *via* cyclization of the propionic acid derivatives of [3](1,1′)- and [4](1,1′)ruthenocenophanes with polyphosphoric acid or trifluoroacetic anhydride, respectively. The ^{1}H NMR, IR, and electronic spectra of these dibridged ruthenocenes were measured and compared with those of monobridged ruthenocenes.

There have been a large number of studies[1–19] on heteroannularly multibridged ferrocenes including tri-, tetra-, and pentamethylene chains, because their unusual chemical and physical properties can be compared with those of cyclophanes.[20] However, no synthetic work on multibridged ruthenocenes has been found in the literature. Studies on the bridged ruthenocenes include our previous description of the synthesis and properties of [3](1,1′)- and [4](1,1′)ruthenocenophanes.[21] The synthesis of [5](1,1′)ruthenocenophanes[22] with substituents in their chains has been reported by Nesmeyanov *et al.* The precise structures of [3](1,1′)- and [4](1,1′)ruthenocenophanes have been uncovered by X-ray crystal analysis.[23] Since the distance between two cyclopentadienyl (Cp) rings in ruthenocene[24] is longer than that in ferrocene,[25] the steric strain in ruthenocenophanes can be expected to be larger than that in the corresponding ferrocenophanes. In this paper, we wish to describe the synthesis and spectral properties of [3](1,1′)[3](3,3′)- and [4](1,1′)[4](3,3′)ruthenocenophanes[26] and compare these results with those of the corresponding monobridged ruthenocenes.

Results and Discussion

[3][3]- and [4][4]Ferrocenophanes can be prepared *via* a stepwise cyclization and/or bridge enlargement in more advantageous yields than a one-step process.[2,7] Accordingly, we synthesized [3](1,1′)[3](3,3′)- and [4](1,1′)[4](3,3′)ruthenocenophanes (**6** and **15**) from the corresponding monobridged compounds.

Synthesis of [3][3]Ruthenocenophanes. 6-Formyl[3](1,1′)ruthenocenophane (**2**) was synthesized in 52% yield by formylation of [3](1,1′)ruthenocenophane (**1**) with *N*-methylformanilide and $POCl_3$ without any solvent.[21] A small amount of the isomer, 5-formyl[3](1,1′)ruthenocenophane, which was not isolated in pure state, was also produced. Condensation of **2** with malonic acid in the presence of piperidine gave 6-(2-carboxyvinyl)[3](1,1′)ruthenocenophane (**3**) in good yield, and the subsequent hydrogenation of **3** over PtO_2 afforded 6-(2-carboxyethyl)[3](1,1′)ruthenocenophane (**4**). Cyclization of **4** with polyphosphoric acid gave [3](1,1′)[3](3,3′)ruthenocenophan-1-one (**5**) in 54% yield, while the reaction of **4** with trifluoroacetic anhydride did not produce **5**. [3](1,1′)[3](3,3′)Ruthenocenophane (**6**) was obtained by reduction of **5** with lithium aluminum hydride–aluminum trichloride in the usual manner (Scheme 1).

Synthesis of [4][3]- and [4][4]Ruthenocenophanes. Formylation of [4](1,1′)ruthenocenophane (**7**) with *N*-methylformanilide and $POCl_3$ without any solvent afforded 6-formyl- and 7-formyl[4](1,1′)ruthenocenophanes (**8** and **9**) in 12 and 79% yields, respectively. 7-(2-Carboxyethyl)[4](1,1′)ruthenocenophane (**11**) was prepared from **9** in good yield, in a manner similar to the one utilized in the preparation of **4**. Cyclization of **11** with trifluoroacetic anhydride in refluxing cyclohexane for 2 weeks[21] gave [4](1,1′)[3](3,3′)ruthenocenophan-16-one (**12**) in 80% yield. Bridge enlargement of **12** with diazomethane led to formation of [4](1,1′)-[4](3,3′)ruthenocenophan-2-one (**14**) in 83% yield, accompanied by a small amount of the isomer, [4](1,1′)-[4](3,3′)ruthenocenophan-1-one, which was not isolated in pure state. Reduction of **12** and **14** with lithium aluminum hydride–aluminum trichloride in the usual manner gave good yields of [4](1,1′)[3](3,3′)- and [4](1,1′)[4](3,3′)ruthenocenophanes (**13** and **15**), respectively (Scheme 2).

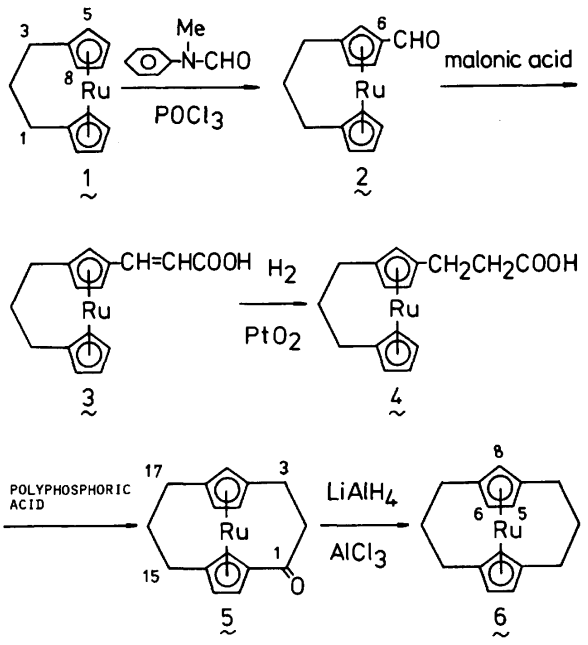

Scheme 1. Synthesis of [3][3]ruthenocenophanes.

^1H NMR Spectra. The chemical shifts of Cp ring protons in [*m*](1,1′)- and [*m*](1,1′)[*n*](3,3′)ruthenocenophanes (*m*, *n*=3, 4), together with those of the corresponding ferrocenophanes, are listed in Table 1. The signals observed in the ^1H NMR spectra of these ruthenocenophanes are assigned on the basis of the analogy to those of the corresponding ferrocenophanes and tri- and tetrabridged ferrocenes. The Cp ring protons of dibridged ruthenocenes **6** and **15** shift to lower fields than those of the corresponding ferrocenophanes **6′** and **15′**. These results are in accordance with those of ruthenocene and ferrocene.[27]

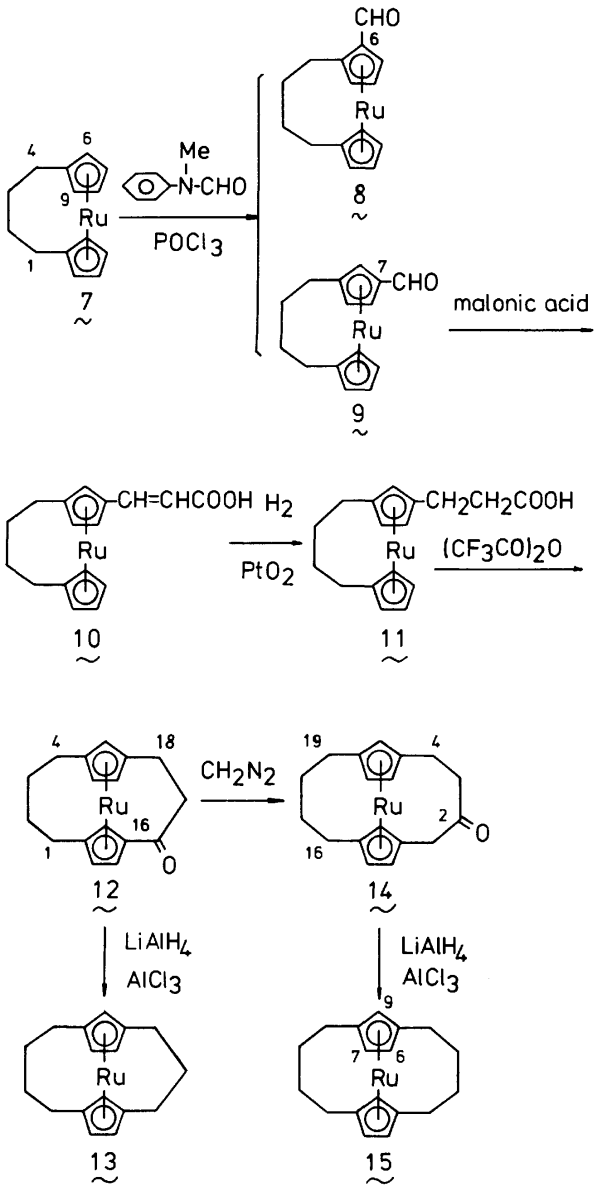

Scheme 2. Synthesis of [4][3]- and [4][4]Ruthenocenophanes.

The inductive effects of the methyl and ethyl groups have been reported to influence the chemical shifts of Cp ring protons only to a small extent in the ^1H NMR spectra of alkylferrocenes.[28] The differences in the chemical shifts of dimethyl and diethyl 1,1′-ruthenocenes are 0.05[29] and 0.04 ppm, respectively (Table 2). Accordingly, the nonequivalence of the Cp ring protons in ruthenocenophanes and ferrocenophanes cannot be due to the inductive effects of methylene bridges.

The difference in chemical shifts of Cp ring protons of monobridged ruthenocenes **1** and **7** are 0.23 and 0.14 ppm, respectively. We have previously discussed these chemical shifts and splittings of Cp ring protons in **1** and **7**, and have proposed that the nonequivalent shielding of Cp rings from their original parallel geometry.[21] Such a shift difference seems to be closely related to the dihedral angles of two Cp rings in **1** and **7**; these dihedral angles are found to be *ca.* 15° and 2°, respectively.[23]

On the other hand, the difference in the chemical shifts of the Cp ring protons of [3](1,1′)ferrocenophane (**1′**) and of [4](1,1′)ferrocenophane (**7′**) is 0.04 ppm; the corresponding difference for [3](1,1′)[3](3,3′)ferrocenophane (**6′**) is 0.05 and for [4](1,1′)[4](3,3′)ferrocenophane (**15′**) is 0.08 ppm. Hisatome *et al.* have not given clear-cut explanations of these results.[15] Simple molecular models for **1′** and **7′** suggest that the dihedral angles for the two Cp rings in **1′** and **7′** are *ca.* 0°. It has been reported that the dihedral angle of two Cp rings in **6′** is 9°.[30] Again, a simple molecular model for **15′** suggests that the dihedral angle in **15′** is *ca.* 0°.

Such a correlation between shift difference in Cp ring protons and the dihedral angle of two Cp rings in the monobridged systems is not found in the dibridged systems. In ruthenocenophane system, the difference in the chemical shifts of Cp ring protons of **6** is 0.12 and that of **15** is 0.21 ppm. The distance between two Cp rings in ruthenocene[24] is longer than

TABLE 1. CHEMICAL SHIFTS OF Cp RING PROTONS IN RUTHENOCENOPHANES AND FERROCENOPHANES (δ)[a]

Compound	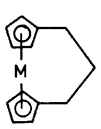		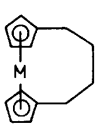		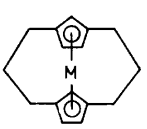		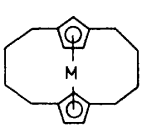	
M	M=Ru, **1**; M=Fe, **1′**		M=Ru, **7**; M=Fe, **7′**		M=Ru, **6**; M=Fe, **6′**		M=Ru, **15**; M=Fe, **15′**	
	H(5, 8)	H(6, 7)	H(6, 9)	H(7, 8)	H(5, 6)	H(8)	H(6, 7)	H(9)
Ru	4.42	4.65	4.58	4.44	4.43	4.31	4.47	4.68
Fe[b]	3.98	4.02	4.14 4.13	4.10	3.89	3.84	3.96	4.04

a) In $CDCl_3$. b) Ref. 15.

TABLE 2. CHEMICAL SHIFTS OF Cp RING PROTONS IN DIALKYL 1,1′-RUTHENOCENES (δ)

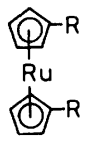

	H (2, 5)	H (3, 4)	R	
R = Me[a]	4.34	4.29	-Me	1.89
R = Et[b]	4.44	4.40	-Me	1.07(t, J=7.4 Hz)
			$-CH_2-$	2.91(q, J=7.4 Hz)

a) Ref. 29 in CCl_4. b) This work in $CDCl_3$.

TABLE 3. CHEMICAL SHIFTS OF METHYLENE PROTONS OF BRIDGES IN RUTHENOCENOPHANES AND FERROCENOPHANES (δ)[a]

Compound	Methylene protons of bridges
1	1.76 (bs)[c,e]
7	1.3—1.8 (m)[d,e] 2.1—2.6 (m)
6	1.72 (bs) 2.22 (bs)
15	1.4—1.6 (m) 2.1—2.3 (m)
1′	1.95 (s)[b,f]
7′	1.4—1.5 (m)[f] 2.0—2.2 (m)
6′	0.9—1.3 (m)[g]
15′	1.60—1.90 (m)[h] 2.20—2.55 (m)

a) In $CDCl_3$. b) Singlet. c) Broad singlet. d) Multiplet. e) Ref. 21. f) This work. g) Ref. 33. h) Ref. 7.

that in ferrocene[25] by 0.36 Å. Accordingly, the dihedral angle in **6** may be more than 9°, which may be larger than that in **15**. On the basis of molecular model examinations, the considerable strain in **6** and **15** might result in the deviations of two Cp rings from their original sp^2 planes. This might affect the chemical shifts and splittings of the Cp ring protons in **6** and **15**. Such an assumption would be confirmed by X-ray crystal analysis.

The chemical shifts of methylene protons of bridges in [*m*](1,1′)- and [*m*](1,1′)[*n*](3,3′)ruthenocenophanes (*m*, *n*=3, 4), together with those of the corresponding ferrocenophanes, are summarized in Table 3. The methylene protons of **7** and **15** with one and two tetramethylene bridges show two multiplets. However, methylene protons of **1** with one trimethylene bridge show one broad singlet, while those of **6** with two trimethylene bridges show two broad singlets. This seems to suggest that **6** has a more rigid structure than **1**, in contrast to the systems of **7** and **15**. On the other hand, **6′** shows one multiplet, in contrast to **6**. Although **15′** shows two multiplets, similar to **15**, the widths of the multiplets in **15′** are larger than those in **15**. These results suggest that the ruthenocenophanes **6** and **15** have more rigid structures than those of the corresponding ferrocenophanes **6′** and **15′**, and that **6** has the most rigid structure among these phane compounds.

IR Spectra. The frequencies of carbonyl-stretching absorptions in [*m*](1,1′)- and [*m*](1,1′)[*n*](3,3′)-ruthenocenophanones (*m*, *n*=3, 4), together with those of the corresponding ferrocenophanones, are listed in Table 4. In our previous paper,[21] the carbonyl-stretching vibrations have suggested that the π-orbitals of the carbonyl group effectively conjugate with the π-systems of the adjacent Cp ring in [3](1,1′)-ruthenocenophan-1-one (1656 cm^{-1}), as in acetylruthenocene (1658 cm^{-1}). The dihedral angle between the plane of the carbonyl group and the plane of the adjacent Cp ring has been considered to become smaller when two Cp rings are tilted to a greater extent. We have confirmed this assumption from the ^{13}C NMR measurements of several ruthenocenophanones and ferrocene homologs.[31] The carbonyl group in the ruthenocenophanone **5** with two trimethylene bridges is located at higher frequency (1686 cm^{-1}) than that in [3](1,1′)ruthenocenophan-1-one with one trimethylene bridge. A similar trend is observed in ferrocene homologs; [3](1,1′)ferrocenophan-1-one (1658 cm^{-1}) and [3](1,1′)[3](3,3′)ferrocenophan-1-one (1665 cm^{-1}). Owing to an additional trimethylene bridge, therefore, the dihedral angles between the carbonyl group and the adjacent Cp ring in **5** and the corresponding ferrocenophanone might be larger than those in [3](1,1′)ruthenocenophan-1-one and the corresponding ferrocenophanone.

Electronic Spectra. The spectra of trimethylene bridged ruthenocenes **6** and **1** and tetramethylene bridged ruthenocenes **15** and **7** are shown in Figs. 1 and 2, respectively. The intensities of the charge transfer band in the 230—260 nm region and the spin-allowed d-d band in 310—340 nm region of the dibridged ruthenocene **6** increase as compared with those of the monobridged ruthenocene **1** (Fig. 1). In the spectrum of the dibridged ruthenocene **15**, again, the intensity of the charge transfer band increases, while the intensity of spin-allowed d-d band decreases relative to that for the monobridged ruthenocene **7** (Fig. 2). We have previously reported that the ring-tilting would increase the intensity of the spin-allowed d-d band in the electronic spectra of **1** and **7**.[21] Recently, the dihedral angles of two Cp rings in **1** and **7** have been found to be *ca.* 15° and 2°, respectively.[23] These results suggest that the intensity of the spin-allowed d-d band might be affected by the steric strain at the Ru atom, and that **6** might be the most compressed among [*m*](1,1′)- and [*m*](1,1′)[*n*](3,3′)ruthenocenophanes (*m*, *n*=3, 4).

TABLE 4. CARBONYL-STRETCHING FREQUENCIES IN RUTHENOCENOPHANONES AND FERROCENOPHANONES (cm^{-1})[a]

Compound / M	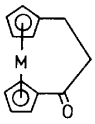	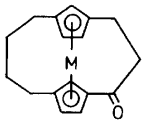	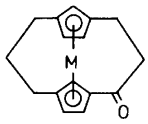	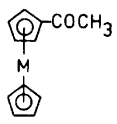
Ru	1656[b]	1652	1686	1658[c]
Fe	1681[d] 1658[g]	1662[e]	1665[f]	1658[e]

a) In KBr pellets. b) Ref. 21. c) Ref. 32. d) Ref. 33. e) Ref. 7. f) Ref. 2. g) This work.

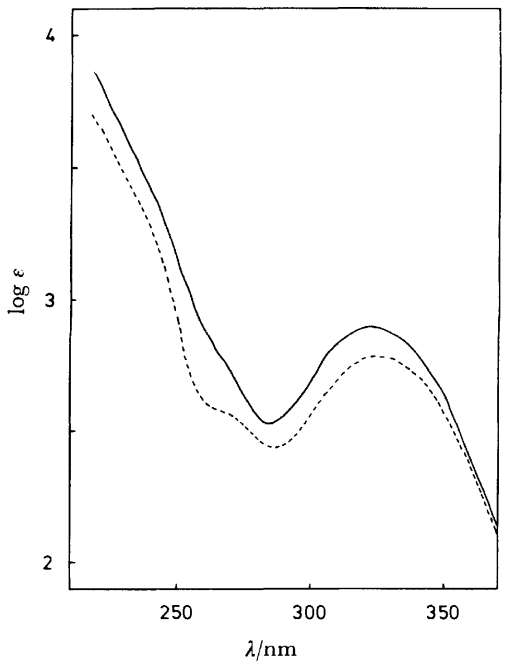

Fig. 1. Electronic spectra in abs EtOH: (——) [3](1,1′)-[3](3,3′)ruthenocenophane (**6**) and (----) [3](1,1′)-ruthenocenophane (**1**).

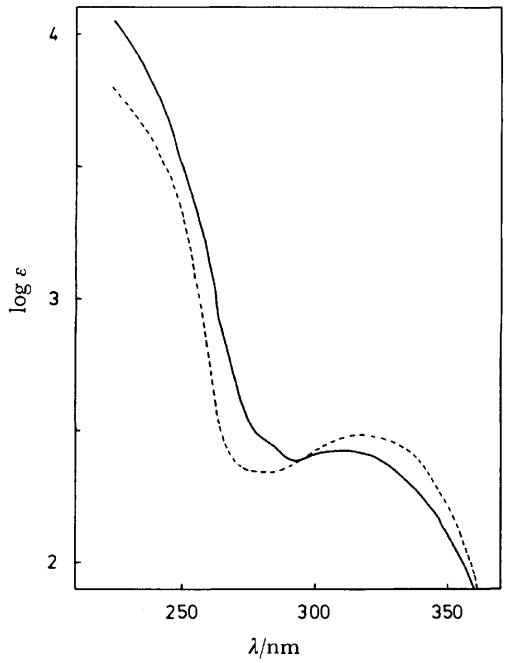

Fig. 2. Electronic spectra in abs EtOH: (—) [4](1,1′)-[4](3,3′)ruthenocenophane (**15**) and (----) [4](1,1′)-ruthenocenophane (**7**).

Experimental

Measurements. All the melting points are uncorrected. The ^1H NMR spectra were obtained in $CDCl_3$ with a JEOL JNM-FX 100 spectrometer (100 MHz) at room temperature. All the chemical shifts are expressed in δ (ppm; downfield from internal Me_4Si). The IR spectra were measured in KBr pellets with a Hitachi Model 285 infrared spectrometer. All IR spectral data are expressed in cm^{-1}. The electronic spectra were recorded in abs EtOH with a Hitachi Model 100—60 double beam spectrophotometer at room temperature. All absorption frequencies are given in λ (nm). The mass spectra were obtained with a JEOL JMS-DX 300 mass spectrometer using a direct insertion probe at 70 eV ionizing energy.

Materials. [3](1,1′)- and [4](1,1′)Ruthenocenophanes (**1** and **7**) were prepared according to the method in the literature.[21] Column chromatographic separations were carried out with Merck Kieselgel 60 (70—230 mesh), Wakogel C-200 (200 mesh), Mallinckrodt silicic acid (100 mesh) or Kanto Kagaku silica gel (100 mesh). All the synthetic reactions were performed under a N_2 atmosphere.

6-Formyl[3](1,1′)ruthenocenophane (2). A mixture of [3](1,1′)ruthenocenophane (**1**) (3.0 g, 11 mmol), *N*-methylformanilide (1.7 g, 13 mmol) and $POCl_3$ (3.7 g, 24 mmol) was vigorously stirred at 70 °C for 4 h. After the addition of sodium acetate trihydrate (16.5 g) in water (100 ml), the solution was stirred at 70 °C for 2 h, and then extracted with ether. The residue was chromatographed over silica gel with benzene–ethyl acetate as eluent. The first band eluted with benzene yielded a small amount of 5-formyl[3](1,1′)-ruthenocenophane, which was not isolated in pure state.

The second band eluted with benzene–ethyl acetate (40:1) yielded **2** (1.7 g, 52%), pale orange prisms, mp 90—91 °C (hexane–ethyl acetate). ^1H NMR: δ=1.76 (4H, bs, bridged $-CH_2-$), 1.84(2H, bs, bridged $-CH_2-$), 4.39 (1H, dd, J=1.3 and 3.1 Hz, Cp), 4.57 (1H, dd, J=1.5 and 2.9 Hz, Cp), 4.75 (3H, m, Cp), 4.95 (1H, t, J=1.2 Hz, Cp), 5.05 (1H, dd, J=1.2 and 2.4 Hz, Cp) and 9.65 (1H, s, −CHO). IR: 1650 (C=O). Electronic spectrum ($\lambda_{max}(\varepsilon)$): 253 (10500) and 345 (2960). MS (*m/z*): 299 (M^+, 71) and 270 ([M−CHO]$^+$, 100). Found: C, 55.93; H, 4.62%. Calcd for $C_{14}H_{14}ORu$: C, 56.18; H, 4.71%.

6-(2-Carboxyvinyl)[3](1,1′)ruthenocenophane (3). A solution of **2** (1.0 g, 3.3 mmol), malonic acid (0.69 g, 6.6 mmol) and piperidine (0.24 g) in dry pyridine (15 ml) was stirred at 100 °C for 3 h. The cooled solution was diluted with water and extracted with chloroform. The extract was washed with dil HCl and water, and then extracted with a 2 M NaOH solution (1 M=1 mol dm^{-3}). The aqueous layer

was acidified with dil HCl, and placed in a refrigerator overnight. The precipitates were found to be **3** (0.95 g, 84%), orange plates, mp 205—206 °C (EtOH). ^{1}H NMR: δ=1.74 (4H, bs, bridged -CH_2-), 1.89 (2H, bs, bridged -CH_2-), 4.34 (1H, m, Cp), 4.56 (3H, m, Cp), 4.74 (2H, m, Cp), 4.89 (1H, m, Cp), 5.90 and 7.53 (2H, an AX system, J=15.5 Hz, *trans* olefinic protons). IR: 1665 (C=O) and 1605 (C=C). $\lambda_{max}(\varepsilon)$: 275 (17600) and 365 (714). MS: 341 (M^+, 100), 296([M−CO_2-H]$^+$, 87) and 270 ([M−CH=CHCO_2H]$^+$, 11). Found: C, 56.43; H, 5.16%. Calcd for $C_{16}H_{16}O_2Ru$: C, 56.30; H, 4.72%.

6-(2-Carboxyethyl)[3](1,1′)ruthenocenophane (4). A solution of **3** (4.0 g, 12 mmol) in ethanol (500 ml) was hydrogenated over PtO_2 (50 mg) at room temperature for 20 h under H_2 1 atm to give **4** (4.0 g, 99%), yellow needles, mp 131—132 °C (EtOH). ^{1}H NMR: δ=1.73 (6H, bs, bridged -CH_2-), 2.50 (4H, s, -CH_2- of -$CH_2CH_2CO_2H$), 4.32 (1H, m, Cp), 4.36 (2H, m, Cp), 4.44 (1H, m, Cp), 4.54 (2H, m, Cp), and 4.63 (1H, m, Cp). IR: 1686 (C=O). $\lambda_{max}(\varepsilon)$: 270^{sh} (646) and 324 (898). MS: 343 (M^+, 75) and 284 ([M−CH_2CO_2-H]$^+$, 100). Found: C, 56.01; H, 5.24%. Calcd for $C_{16}H_{18}$-O_2Ru: C, 55.97; H, 5.28%.

[3](1,1′)[3](3,3′)Ruthenocenophan-1-one (5). A suspension of **4** (0.80 g, 2.3 mmol) and polyphosphoric acid (400 g) was vigorously stirred at 100 °C for 24 h. The cooled solution was poured into ice-cold water, and extracted with chloroform. The residue was chromatographed over silica gel with benzene-ethyl acetate (5:1) to give **5** (0.40 g, 54%), deep yellow needles, mp 150—151 °C (hexane-ethyl acetate). ^{1}H NMR: δ=1.69 (4H, bs, bridged -CH_2-), 1.78 (2H, bs, bridged -CH_2-), 2.4—3.2 (4H, m, H(2) and H(3) of bridged -CH_2-), 4.4—4.5 (2H, m, Cp), 4.5—4.6 (1H, m, Cp), 4.6—4.7 (1H, m, Cp), 4.78 (1H, s, Cp), and 4.82 (1H, s, Cp). $\lambda_{max}(\varepsilon)$: 254 (5830), 340^{sh} (1160), and 372 (1320). MS: 325 (M^+, 100), 297 ([M−CO]$^+$, 70), 283 ([M−CH_2CO]$^+$, 11), and 269 ([M−CH_2CH_2CO]$^+$,9). Found: C, 59.23; H, 5.11%. Calcd for $C_{16}H_{16}ORu$: C, 59.06; H, 4.96%.

[3](1,1′)[3](3,3′)Ruthenocenophane (6). A solution of **5** (0.40 g, 1.2 mmol) in dry ether (50 ml) was added dropwise to a suspension of $LiAlH_4$ (0.60 g, 16 mmol) and $AlCl_3$ (3.2 g, 24 mmol) in dry ether (50 ml). After refluxing for 4 h, the reaction mixtures were extracted with ether. The residue was chromatographed over silica gel with benzene to yield **6** (0.30 g, 78%), pale yellow needles, mp 114—115 °C (ethyl acetate). $\lambda_{max}(\varepsilon)$: 272^{sh} (481) and 322 (778). MS: 311 (M^+, 100), 297([M−CH_2]$^+$, 16), and 283([M-CH_2CH_2]$^+$, 7). Found: C, 62.01; H, 5.40%. Calcd for $C_{16}H_{18}Ru$: C, 61.72; H, 5.83%.

6-Formyl- and 7-formyl[4](1,1′)ruthenocenophanes (8 and 9). [4](1,1′)Ruthenocenophane (**7**) (1.5 g, 5.3 mmol), *N*-methylformanilide (0.78 g, 5.8 mmol), and $POCl_3$ (0.89 g, 5.8 mmol) were stirred at 70 °C for 4 h. After the addition of sodium acetate trihydrate (7.2 g) in water (50 ml), the solution was stirred at 70 °C for 2 h. The residue was separated into two bands by chromatography over silica gel with hexane-ethyl acetate as eluent. The first band eluted with hexane-ethyl acetate (20:1) yielded **8** (0.20 g, 12%), deep yellow prisms, mp 144—145 °C (hexane-ethyl acetate). ^{1}H NMR: δ=1.5—1.7 (4H, m, H(2) and H(3) of bridged -CH_2-), 2.2—2.5 (4H, m, H(1) and H(4) of bridged -CH_2-), 4.45 (1H, m, Cp), 4.58 (2H, t, J=2.2 Hz, Cp), and 4.66 (1H, m, Cp), 4.74(1H, d, J=2.9 Hz, Cp), 4.92 (2H, m, Cp), and 9.97 (1H, s, -CHO). IR: 1669 (C=O). $\lambda_{max}(\varepsilon)$: 248 (10400) and 351 (1090). MS: 313 (M^+, 57), 284 ([M−CHO]$^+$, 100), 270 ([M−CH_2CHO]$^+$, 22), and 256 ([M−CH_2CH_2CHO]$^+$, 33). Found: C, 57.13; H, 5.10%. Calcd for $C_{15}H_{16}ORu$: C, 57.49; H, 5.15%.

The second band eluted with hexane-ethyl acetate (5:1) yielded **9** (1.3 g, 79%), deep yellow needles, mp 90—91 °C (hexane-ethyl acetate). ^{1}H NMR: δ=1.5—1.7 (4H, m, H(2) and H(3) of bridged -CH_2-), 2,2—2.5 (4H, m, H(1) and H(4) of bridged -CH_2-), 4.59 (3H, m, Cp), 4.74(1H, m, Cp), 4.90, (1H, m, Cp), 4.96 (1H, m, Cp), 5.14 (1H, s, Cp), and 9.63 (1H, s, -CHO). IR: 1669 (C=O). $\lambda_{max}(\varepsilon)$: 257 (13300) and 359 (2060). MS: (M^+, 91), 284 ([M−CHO]$^+$, 100), 270 ([M−CH_2CHO]$^+$, 16), and 256 ([M−CH_2CH_2CHO]$^+$, 31). Found: C, 57.75; H, 5.20%. Calcd for $C_{15}H_{16}ORu$: C, 57.49; H, 5.15%.

7-(2-Carboxyvinyl)[4](1,1′)ruthenocenophane (10). The aldehyde **9** (1.9 g, 6.1 mmol) was treated with malonic acid (1.3 g, 12 mmol) and piperidine (0.27 g) in dry pyridine (30 ml) at 100 °C for 3 h. The cooled solution was extracted with chloroform. The extract was washed with dil HCl and water, and then extracted with a 2 M NaOH solution. Acidification of the aqueous layer with dil HCl gave the precipitate of **10** (1.9 g, 88%), pale orange prisms, mp 189—190 °C (EtOH). ^{1}H NMR: δ=1.4—1.7 (4H, m, H(2) and H(3) of bridged -CH_2-), 2.2—2.4 (4H, m, H(1) and H(4) of bridged -CH_2-), 4.29 (1H, m, Cp), 4.56 (2H, m, Cp), 4.71 (1H, m, Cp), 4.76 (2H, d, J=1.0 Hz, Cp), 4.93 (1H, s, Cp), 5.90 and 7.50 (2H, an AX system, J=15.6 Hz, *trans* olefinic protons). IR: 1666 (C=O) and 1611 (C=C). $\lambda_{max}(\varepsilon)$: 287 (18800) and 354 (4800). MS: 355 (M^+, 100), 310 ([M−CO_2-H]$^+$, 45), and 284 ([M−CH=CHCO_2H]$^+$, 39). Found: C, 57.37; H, 5.59%. Calcd for $C_{17}H_{18}O_2Ru$: C, 57.45; H, 5.10%.

7-(2-Carboxyethyl)[4](1,1′)ruthenocenophane (11). Hydrogenation of **10** (4.0 g, 11 mmol) over PtO_2 (50 mg) in ethanol (500 ml) gave **11** (4.0 g, 99%), pale yellow prisms, mp 128—129 °C (EtOH). ^{1}H NMR: δ=1.4—1.6 (4H, m, H(2) and H(3) of bridged -CH_2-), 2.2—2.4 (4H, m, H(1) and H(4) of bridged -CH_2-), 2.49(4H, s, -CH_2- of -CH_2CH_2-CO_2H), 4.31 (1H, m, Cp), 4.42 (1H, m, Cp), 4.5—4.6 (4H, m, Cp), and 4.63 (1H, m, Cp). IR: 1701 (C=O). $\lambda_{max}(\varepsilon)$: 313 (312). MS: 357 ($M^+$, 14), 312([M−$CO_2H$]$^+$, 41), 298 ([M−$CH_2CO_2H$]$^+$, 83), and 284 ([M−$CH_2CH_2CO_2H$]$^+$, 100). Found: C, 56.80; H, 5.67%. Calcd for $C_{17}H_{20}O_2Ru$: C, 57.13; H, 5.64%.

[4](1,1′)[3](3,3′)Ruthenocenophan-16-one (12). A mixture of **11** (5.0 g, 14 mmol) and $(CF_3CO)_2O$ (15 g, 0.70 mol) in dry cyclohexane (500 ml) was refluxed for 2 weeks. The cooled mixture was poured into saturated aq $NaHCO_3$ and extracted with ether. The residue was chromatographed over silica gel with benzene-ethyl acetate(1:1) to give **12** (3.8 g, 80%), yellow prisms, mp 139—140 °C (hexane-ethyl acetate). ^{1}H NMR: δ=1.4—1.6 (4H, m, H(2) and H(3) of bridged -CH_2-), 2.1—2.4 (4H, m, H(1) and H(4) of bridged -CH_2-), 2.87 (4H, bs, H(17) and H(18) of bridged -CH_2-), 4.57 (1H, dd, J=1.2 and 2.0 Hz, Cp), 4.82 (1H, dd, J=1.2 and 2.1 Hz, Cp), 4.93 (1H, dd, J=2.4 and 4.9 Hz, Cp), 4.94 (1H, dd, J=2.4 and 4.8 Hz, Cp), 5.20 (1H, t, J=1.0 Hz, Cp), and 5.28 (1H, t, J=1.1 Hz, Cp). $\lambda_{max}(\varepsilon)$: 259 (4840) and 333^{sh} (787). MS: 339 (M^+, 100), 311 ([M−CO]$^+$, 100), 297 ([M−CH_2-CO]$^+$, 48), and 283 ([M−CH_2CH_2CO]$^+$, 69). Found: C, 60.00; H, 5.24%. Calcd for $C_{17}H_{18}ORu$: C, 60.16; H, 5.35%.

[4](1,1′)[3](3,3′)Ruthenocenophane (13). A suspension of **12** (0.50 g, 1.5 mmol), $LiAlH_4$ (0.17 g, 4.4 mmol), and $AlCl_3$ (0.88 g, 6.64 mmol) in dry THF (50 ml) was refluxed for 3 h. After the excess reagent was decomposed with moist THF and water, the products were extracted with ether. The residue was chromatographed over silica gel with benzene to yield **13** (0.35 g, 72%), pale yellow needles, mp 40—41 °C (benzene). ^{1}H NMR: δ=1.3—1.7 (10H, m, bridged -CH_2-), 1.8—2.3 (4H, m, bridged -CH_2-), 4.33 (2H, dd, J=1.2 and 2.0 Hz, Cp), 4.52 (2H, s, H(9) and H(15) of Cp), and 4.68 (2H, dd, J=1.2 and 2.1 Hz, Cp). $\lambda_{max}(\varepsilon)$: 266^{sh} (645) and 319 (606). MS: 325 (M^+, 100) and 297 ([M−CH_2CH_2]$^+$, 87). Found: C, 62.43; H, 6.16%. Calcd for $C_{17}H_{20}Ru$: C, 62.75; H, 6.19%.

[4](1,1′)[4](3,3′)Ruthenocenophan-2-one (14). To a solution of **12** (2.5 g, 7.4 mmol) in methanol (100 ml) and ether (150 ml), CH_2N_2 (0.37 mol) in ether (500 ml) was

added. The resulting solution was stirred at 0 °C for 10 h in the dark, and then evaporated. The residue was chromatographed over silica gel with benzene-ethyl acetate as eluent. The first band eluted with benzene-ethyl acetate (10:1) yielded **14** (2.2 g, 83%), pale orange prisms, mp 118—119 °C (hexane-ethyl acetate). ^{1}H NMR: δ=1.4—1.6 (4H, m, H(17) and H(18) of bridged -CH_2-), 2.1—2.3 (4H, m, H(16) and H(19) of bridged -CH_2-), 2.5—2.6 (2H, m, H(4) of bridged -CH_2-), 2.7—2.9 (2H, m, H(3) of bridged -CH_2-), 3.16 (2H, s, H(1) of bridged -CH_2-), 4.50 (2H, dd, J=1.2 and 2.3 Hz, Cp), 4.58 (2H, dd, J=1.2 and 2.3 Hz, Cp), and 4.78 (2H, s, H(9) and H(15) of Cp). IR: 1686 (C=O). $\lambda_{max}(\varepsilon)$: 280^{sh} (1490). MS: 353 (M^+, 98), 325 ([M−CO]$^+$, 100), 311 [M−CH_2CO]$^+$, 47), and 297 ([M−CH_2CH_2CO]$^+$, 85). Found: C, 61.43; H, 5.79%. Calcd for $C_{18}H_{20}ORu$: C, 61.17; H, 5.70%.

The second band eluted with benzene-ethyl acetate (1:20) yielded a small amount of [4](1,1′)[4](3,3′)ruthenocenophan-1-one, which was not isolated in the pure state.

[4](1,1′)[4](3,3′)Ruthenocenophane (15). A mixture of **14** (1.0 g, 2.8 mmol), $LiAlH_4$ (0.32 g, 8.4 mmol), and $AlCl_3$ (1.7 g, 13 mmol) in dry THF (100 ml) was refluxed for 5 h, and then extracted with ether. The residue was chromatographed over silica gel with benzene-ethyl acetate (20:1) to yield **15** (0.72 g, 75%), pale yellow needles, mp 94—95 °C (petroleum ether). $\lambda_{max}(\varepsilon)$: 280^{sh} (292) and 309 (260). MS: 339 (M^+, 100) and 311 ([M−CH_2CH_2]$^+$, 66). Found: C, 63.76; H, 6.58%. Calcd for $C_{18}H_{22}Ru$: C, 63.69; H, 6.53%.

References

1) K. Schlögl and M. Peterlik, *Tetrahedron Lett.*, **1962**, 573; *Monatsch. Chem.*, **93**, 1328 (1962).

2) K. L. Rinehart, Jr., D. E. Bublitz, and D. H. Gustafson, *J. Am. Chem. Soc.*, **85**, 970 (1963).

3) D. E. Bublitz and K. L. Rinehart, Jr., *Tetrahedron Lett.*, **1964**, 827.

4) F. M. Vigo, Ph. D. Thesis, University of Illinois, Urbana, Illinois (1969).

5) A. D. Brown, Jr., and J. A. Winstead, *J. Org. Chem.*, **36**, 2832 (1971).

6) D. Astruc, R. Dabard, M. Martin, P. Batail, and D. Grandjean, *Tetrahedron Lett.*, **1976**, 829.

7) M. Hisatome, T. Sakamoto, and K. Yamakawa, *J. Organomet. Chem.*, **107**, 87 (1976).

8) A. Nagy, I. Dezsi, and M. Hillman, *J. Organomet. Chem.*, **117**, 55 (1976).

9) A. N. Nesmeyanov, M. I. Rybinskaya, G. B. Schul'pin, and M. V. Tolystaya, *Dokl. Akad. Nauk SSSR*, **229**, 1124 (1976).

10) M. Hisatome, N. Watanabe, T. Sakamoto, and K. Yamakawa, *J. Organomet. Chem.*, **125**, 79 (1977).

11) M. Hisatome, Y. Kawajiri, K. Yamakawa, and Y. Iitaka, *Tetrahedron Lett.*, **1979**, 1777.

12) M. Hillman, B. Gordon, A. J. Weiss, and A. P. Guzikowski, *J. Organomet. Chem.*, **155**, 77 (1978).

13) M. Hillman and E. Fujita, *J. Organomet. Chem.*, **155**, 87 and 99 (1978).

14) L. D. Spaulding, M. Hillman, and G. J. B. Williams, *J. Organomet. Chem.*, **155**, 109 (1978).

15) M. Hisatome and M. Hillman, *J. Organomet. Chem.*, **212**, 217 (1981).

16) M. Hisatome, Y. Kawajiri, K. Yamakawa, Y. Harada, and Y. Iitaka, *Tetrahedron Lett.*, **23**, 1713 (1982).

17) M. Hisatome, Y. Kawajiri, and K. Yamakawa, *J. Organomet. Chem.*, **226**, 71 (1982).

18) M. Hisatome, Y. Kawajiri, and K. Yamakawa, *J. Organomet. Chem.*, **236**, 359 (1982).

19 M. Hisatome, Y. Kawajiri, K. Yamakawa, K. Mamiya, Y. Harada, and Y. Iitaka, *Inorg.Chem.*, **21**, 1345 (1982).

20) S. Misumi and T. Otsubo, *Acc. Chem. Res.*, **11**, 251 (1978); F. Vögtle and L. Rossa, *Angew. Chem., Int. Ed. Engl.*, **18**, 515 (1979) and references cited therein.

21) S. Kamiyama, T. M. Suzuki, T. Kimura, and A. Kasahara, *Bull. Chem. Soc. Jpn.*, **51**, 909 (1978).

22) A. N. Nesmeyanov, G. B. Schul'pin, D. V. Zagorevskii, and M. I. Rybinskaya, *Dokl. Akad. Nauk SSSR*, **229**, 881 (1976).

23) Dr. S. Ohba and Professor Y. Saito of Keio University, private communication.

24) G. L. Hardgrove and D. H. Templeton, *Acta Crystallogr.*, **12**, 28 (1959).

25) E. A. Siebold and L. E. Sutton, *J. Chem. Phys.*, **23**, 1967 (1955); J. D. Dunitz, L. E. Orgel, and A. Rich, *Acta Crystallogr.*, **9**, 373 (1956).

26) For nomenclature, see F. Vögtle and P. Neumann, *Tetrahedron*, **26**, 5847 (1970).

27) M. D. Rausch and V. Mark, *J. Org. Chem.*, **28**, 3225 (1963).

28) D. W. Slocum, W. E. Jones, and C. R. Ernst, *J. Org. Chem.*, **37**, 4278 (1972).

29) O. Hofer and K. Schlögl, *J. Organomet. Chem.*, **13**, 443 (1968).

30) I. C. Paul, *J. Chem. Soc., Chem. Commun.*, **1966**, 377.

31) Y. Senda, S. Kamiyama, A. Kasahara, T. Izumi, and S. Murakami, *Bull. Chem. Soc. Jpn.*, **53**, 3381 (1980).

32) M. D. Rausch, E. O. Fischer, and H. Grubert, *J. Am. Chem. Soc.*, **82**, 76 (1960).

33) M. Rosenblum, A. K. Banerjee, N. Danieli, R. W. Fish, and V. Schlatter, *J. Am. Chem. Soc.*, **85**, 316 (1963).

 © 1984 The Chemical Society of Japan Bull. Chem. Soc. Jpn., 57, 725—728 (1984)

Catalytic Reduction of 4*H*-Cyclopenta[*def*]phenanthrene under Mild Conditions

Masahiro MINABE,* Yōji YAMAMOTO,† Masaaki YOSHIDA, Katsuko NAKADA, and Kazuo SUZUKI**

Department of Industrial Chemistry, Faculty of Engineering, Utsunomiya University, Ishiicho, Utsunomiya 321

†*Department of Agricultural Chemistry, Faculty of Agriculture, The University of Tokyo, Bunkyo-ku, Tokyo 113*

(Received April 22, 1983)

The catalytic hydrogenation of 4*H*-cyclopenta[*def*]phenanthrene over Raney nickel afforded 8,9-dihydro-4*H*-cyclopenta[*def*]phenanthrene and 1,2,3,3a-tetrahydro derivative. Under these conditions, di- and tetrahydro compounds were reduced into two diastereomers, *cis*-3a-*cis*-9a- and *trans*-3a-*cis*-9a-1,2,3,3a,8,9,9a,9b-octahydro-4*H*-cyclopenta[*def*]phenanthrene. The reduction over palladium gave a dihydro compound and a platinum catalyst provided products analogous with those obtained over Raney nickel.

One of polynuclear aromatic hydrocarbons, 4*H*-cyclopenta[*def*]phenanthrene (**1**), is made up of one five-membered and three six-membered rings, and is of interest for its the carcinogenic property.[1] The reactivity of **1** with electrophiles has been found to differ from those of phenanthrene, fluorene, and pyrene.[2] The C_8–C_9 bond of **1** shows the double bond character. For example, **1** was converted into the stable C_8–C_9 ozonide[3] and into the 8,9-diketone.[4,5]

Catalytic hydrogenation of **1** has been reported to give only 8,9-dihydro-4*H*-cyclopenta[*def*]phenanthrene (**2**) when it is carried out using copper chromite at 160 °C[6] or over palladium-on-charcoal at room temperature.[7] The reactivity of C_8–C_9 bond of **1** would seem to be preferable to that of C_9–C_{10} bond of phenanthrene, and may be ascribed to the distorted phenanthrene moiety of **1** by the central methylene bridge.

Our present interest is whether the hydrogenation of **1** proceeds regiospecifically. For example, reduction of benz[*a*]anthracene using a Pd/C catalyst took place at the K-region to give 5,6-dihydro compound in a predominant yield, while an analogous reaction in the presence of a Pt catalyst occurred regiospecifically to afford 8,9,10,11-tetrahydro compound.[8]

The present paper deals with the detailed investigation on the catalytic reduction of **1** in order to clarify the reactivity of **1** and the related derivatives. This may give information on the hydrogenation of other aromatic hydrocarbons.

Results and Discussion

The catalytic hydrogenation of **1** was carried out at room temperature under an atmospheric pressure of

TABLE 1. CATALYTIC HYDROGENATION OF 4*H*-CYCLOPENTA[*def*]PHENANTHRENES

Reactant	Catalyst (m/g)	Time h	Proportions/%					
			1	**2**	**3**	**4a**	**4b**	**5**
1	R-Ni(W-7) (2.0)	1/2	Trace	72	2	12	14	0
		7	0	Trace	0	43	57	0
1	R-Ni(W-7) (1.0)	3/4	8	73	3	7	9	0
2	R-Ni(W-7) (2.0)	1/2		78		8	14	0
		8		Trace		36	64	0
3	R-Ni(W-7) (1.0)	1/2			20	46	34	0
		1			0	55	45	0
1	R-Ni(W-4) (2.0)	1/3	0	82	Trace	8	10	0
		6	0	0	0	41	59	0
		21	0	0	0	33	54	13
1	Pd/C(5%) (2.0)	1	71	25	<1	<1	4	0
		24	<1	92	Trace	2	6	0
1	PtO_2(0.05)	1/2	76	5	1	5	6	7
		7	15	21	Trace	24	30	11
		24	0	0	0	11	47	42
1[a]	PtO_2(0.05)	1	46	15	<1	12	18	8
		3	13	20	Trace	24	31	12
2	PtO_2(0.05)	1/2		72		5	15	8
		7		Trace		5	69	26
3	PtO_2(0.024)	1/2			79	13	8	0
		5			0	55	32	13

a) Under a pressure of 5 kg cm^{-2}.

** Present address: Akita Technical College, Iijimabunkyocho, Akita 011.

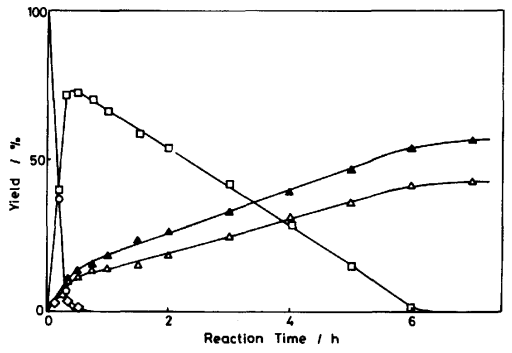

Fig. 1. Typical process of hydrogenation of **1** over R–Ni (**1**, 1 mmol; R–Ni, W-7, 2.0 g).
—○—: **1**, —□—: **2**, —◇—: **3**, —△—: **4a**, —▲—: **4b**.

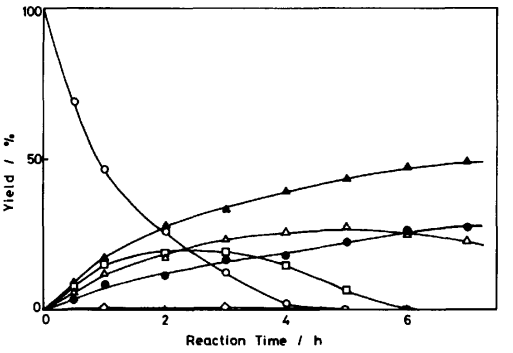

Fig. 2. Typical process of hydrogenation of **1** over PtO_2 (**1**, 1 mmol; PtO_2, 50 mg; 5 kg cm^{-2}).
—○—: **1**, —□—: **2**, —◇—: **3**, —△—: **4a**, —▲—: **4b**, —●—: **5**.

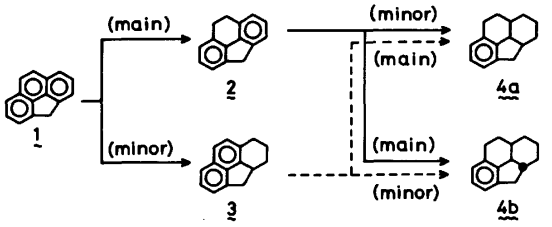

Scheme 1. Diagram of hydrogenation of **1**.

hydrogen, as is summarized in Table 1. These conditions are controllable and practical for preparation of hydroarenes.

Figure 1 shows a typical process of the reaction of **1** using a Raney nickel catalyst (W-7). The hydrocarbon **1** was easily converted into **2** (max. yield 75%) and 1,2,3,3a-tetrahydro-4*H*-cyclopenta[*def*]phenanthrene (**3**)[9] (max. yield 5%) in an earlier stage. Dihydro compound **2** was gradually hydrogenated under these conditions to afford two diastereomeric 1,2,3,3a,8,9,9a,9b-octahydro-4*H*-cyclopenta[*def*]phenanthrenes having melting points of 53—55 °C (**4a**) and of 63—65 °C (**4b**). On the other hand, tetrahydro compound **3** was smoothly reduced into **4a** and **4b**. Further hydrogenations of **4a** and **4b** to perhydro derivatives (**5**)[10] did not proceed under the same conditions. The amount of catalyst affected only the progress of hydrogenation, but not the proportion of the products in the range of 0.2 g to 2.0 g of catalyst per 1 mmol of **1**.

The hydrogenation of **1** over a neutral nickel catalyst (W-4) afforded, **2**, **3**, **4a**, and **4b**, similar to the case of W-7. Minor but significant differences due to the catalytic species could be detected: one of these is that the reaction was accelerated by W-4 catalyst. Second, about 13% of **5** was formed after 21 h, different from the instance of W-7.

Hydrogenation of **1** over a palladium-on-charcoal (5%) was substantially slow and furnished predominantly **2**. Reduction of **2** was scarcely possible, since more than 88% of **2** remained intact after a period of 48 h.

Figure 2 shows a typical pattern of the hydrogenation of **1** in the presence of a platinum oxide catalyst. Arene **1** was reduced to **2** and **3**, as was the case over Raney nickel, but those di- and tetrahydroarenes were again converted into **4a** and **4b**. Hydrogenation of **4a** was faster than that of **4b** under these conditions.

Four kinds of diastereomers in 1,2,3,3a,8,9,9a,9b-octahydro derivatives of **1** may exist, namely (i) *cis*-3a-*cis*-9a, (ii) *trans*-3a-*cis*-9a, (iii) *trans*-3a-*trans*-9a, and (iv) *cis*-3a-*trans*-9a. However, the former two structures are possible and the latter two are impossible, judging from the consideration that the catalytic hydrogenation would proceed *via* cis-addition and that **3** gave both **4a** and **4b**. The first suggestion on the assignment is ascribed to the findings that the non-planar **3** afforded **4a** more predominantly than **4b** over a nickel catalyst, due to the catalytic hindrance. One of the diastereomers, **4a** may be assigned to be *cis*-3a-*cis*-9a. Isomeric **4b** (*trans*-3a-*cis*-9a), whose protons at both 9a- and 9b-positions are located *trans* with respect to 3a-hydrogen, would thermodynamically be more stable than **4a**. The boiling point of **4a** seems to be higher than that of **4b**, based on the GLPC using a nonpolar liquid phase.

The yield of **4b** is more than that of **4a** in reduction of the planar molecule **2**. This would seem to disagree with the general finding that the hydrogenation of aromatics is controlled kinetically to afford all-*cis* compound under the conditions of relatively low temperature using nickel or platinum catalyst. The internal strain of **4a** may be significant due to the *cis-cis* configuration of the *peri*-condensed skeleton, differing from the case of hydrogenated phenanthrene. Consequently, the hydrogenation of **2** could be controlled thermodynamically.

In an earlier stage of the reduction of **3** using a platinum oxide, the ratio of **4a**/(**4a**+**4b**) is larger than the case over a nickel catalyst; this accords with the von Auwers-Skita rule. The decrease of the ratio, **4a**/(**4a**+**4b**), with the extension of the reaction time would be ascribed to the fact that unstable **4a** rather than stable **4b** is easily reduced to perhydro compound 5.

The relative intensity of the molecular ion to the total ion intensity of **4b** is greater than the case of **4a**. This is consistent with the assignment of **4a** and **4b**, since $M^{\cdot+}$ of *trans*- or *exo*-form isomer is generally more intense than that of *cis*- or *endo*-isomer.[11] The fragmentations of **4a** and **4b** show remarkable differences. The relative intensities at *m/z* 170 and *m/z* 169 are 62 and 80% for **4a** and 88 and 8% for **4b** to each

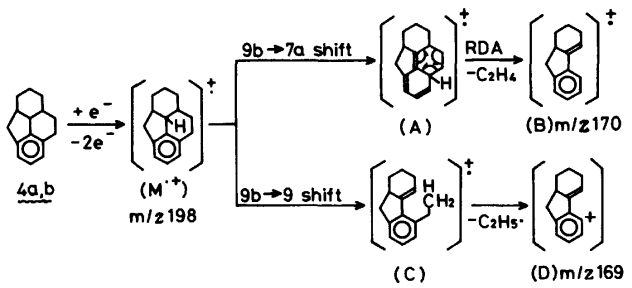

Scheme 2. Speculation on fragmentation pathways of **4a** and **4b**.

molecular ion intensity.

The ion (B) at *m/z* 170 is speculated to form through the 1,3-hydrogen shift of H_{9b} of $M^{\cdot+}$ to C_{7a} to give ion (A), followed by retro-Diels-Alder reaction (RDA) with *cis*-elimination of ethylene under the electron-impact conditions, as is shown in Scheme 2. The generation of ion (D) at *m/z* 169 is considered to be mainly due to the 1,3-hydrogen shift of H_{9b} to C_9 to yield ion (C) and the elimination of ethyl radical from (C). Ions (B) plus (D) from **4a** (1.4 times of $M^{\cdot+}$) are more intense than those from **4b**; this would be due to the stabilities of **4a** and **4b** under the conditions used.[11,12] Isomer **4a** may be less stable thermodynamically than **4b** due to the distorted configuration, and readily undergoes dissociation to ions (A) and (C).

The migration of hydrogen during the hydrogenation is interesting. 9,10-Dihydrophenanthrene has been found to be converted to phenanthrene and tetrahydrophenanthrene under vigorous conditions (100—140 atom, 250 °C).[13] The conversion of **2** to **3** is neglected because that no **3** was detected in the reduction of **2** in all cases examined here. This suggests that **2** and **3** are independently formed by different attacks on the 8,9-positions and on the 1,2,3,3a-positions, respectively. Preferential formation of **2** may be due to the high double bond character at the C_8–C_9 bond.

In the catalytic reduction of **1** under mild conditions, the palladium catalyst seems useful for the preparation of **2**: this accords with the suggestion by Fu, Lee, and Harvey.[8] Raney nickel is available for the synthesis of octahydro compounds **4a** and **4b**, and a platinum catalyst affords further hydrogenated arenes such as **5**. The order of reactivity agrees only with that of the activity of catalyst (Pt>Ni>Pd) used as evaporated metallic films on deuteration of benzene.[14]

Experimental

All the melting points are uncorrected. The ^{1}H NMR, ^{13}C NMR, IR, and UV data were recorded on a JNM-C-60HL (JEOL, 60 MHz, using Me_4Si in $CDCl_3$), a JNM-FX-100 (JEOL, 25 MHz, from Me_4Si in $CDCl_3$), an IR-G (JASCO, as KBr-disk), and a UV-180 (Shimadzu, in cyclohexane) spectrometers, respectively. The mass spectra were measured (direct inlet) at 70 eV on an M-80 GC-MS apparatus (Hitachi) with an M-003 computer data system. An equimolar mixture of **4a** and **4b** was submitted to GC-MS (column: Silicone OV-1, 10%, 1 m, 160 °C) at 20 eV to compare the relative intensities of $M^{\cdot+}$; 32.1% of $\sum_{18}$ in **4a** and 35.7% of $\sum_{18}$ in **4b** were observed.

The GLPC data were obtained with a JGC-1100FP gaschromatograph (JEOL) equipped with a column (3 mmϕ, 0.2 m) containing PEGA (10%) on Diasolid (80—100 mesh) at 145 °C under 0.59 kg cm^{-2} of nitrogen, by means of comparison of each peak area using a TR-2217 automatic integrator (Takeda Riken).

The Raney nickel catalysts (W-4 and W-7) were prepared by standard procedure using nickel-aluminium alloy (48% of nickel): the quantity of catalyst was indicated as weight of the alloy. The palladium-on-charcoal (5%) was also prepared by a known method. The Adams platinum oxide was purchased from Kawaken Fine Chemical Co.

In Table 1, the amount of catalyst means the weight based on 1 mmol of reactant in HOEt (50 ml) over nickel catalyst or in EtOAc (50 ml) over Pd-C or PtO_2. Docosane was added as an internal reference for quantitative treatment.

Hydrogenation of 1 over R-Ni (W-7). To a mixture of **1** (190 mg, 1 mmol) in HOEt (30 ml) placed in the Paal-type hydrogenation flask (so-called "Magen"), R-Ni catalyst was added to HOEt (20 ml) (time, 0 h). Upon substitution of air with hydrogen (4 times), the flask was shaken at room temperature under an atmosphere of hydrogen. In order to follow the sequence of reduction, a small amount of reaction mixture (*ca.* 0.2 ml) was taken out *via* Teflon septum by an injector, filtered and submitted to GLPC after each 1/6, 1/3, 1/2, 3/4, 1, 3/2, 2 h and additionally every 1 h.

Hydrogenation of 1 over Adams PtO_2. Platinum oxide (25.4 mg) was added with 10 ml of EtOAc into a solution of **1** (95.1 mg, 0.5 mmol) in EtOAc (15 ml) placed in a stainless steel autoclave. After 4 purges with hydrogen, the mixture was stirred at room temperature under a hydrogen pressure of 5.0 kg cm^{-2}. After each prescribed time, the proportion of mixture was measured by GLPC.

Hydrogenation of 3 over R-Ni (W-7). Tetrahydro compound **3** (97.1 mg, 0.5 mmol) was treated with R-Ni (W-7, 0.5 g) in HOEt (25 ml) for 2 h. The reaction mixture was filtered and the residue was extracted with HOEt (100 ml). The filtrate and extract were combined and evaporated to dryness. The residue was extracted with cyclohexane (10 ml), and the solution was chromatographed on a column (17 mmϕ; 85 cm) of silica gel with petroleum ether (bp 50—65 °C) as eluent. The rate of effusion was *ca.* 0.65 ml/min. The eluate, which ranged from 287 ml to 333 ml, gave 39.2 mg (40%) of **4b**, mp 63—65 °C, by recrystallization from petroleum ether: retention time, 12.8 min (on a GLPC with a column containing Silicone SE-30, 120 °C). IR: 3050, 2970, 2880, 1604, 1482, 1443, 1329, 1152, 1083, 944, 842, 807, and 762 cm^{-1}. UV_{max}: 220 (log ε 3.91), 268 (2.86), and 276 nm (2.86). ^{1}H NMR: δ=0.73—3.14 (m, 15H) and 6.80—7.05 (m, 3H). ^{13}C NMR: δ=22.8, 24.6, 25.1, 27.3, 28.6, 32.4, 38.9, 41.0, 44.2, 122.4, 124.8, 126.2, 133.9, 141.3, and 142.9. MS *m/z* ($\sum_1$): 199 (4.2), 198 (25.9, $M^{\cdot+}$), 197 (7.6, $M^{\cdot+}-1$), 171 (3.3), 170 (22.9, $C_{13}H_{14}$), 169 (2.1, $C_{13}H_{13}$), 156 (1.4, $C_{12}H_{12}$), 155 (3.6, $C_{12}H_{11}$), 142 (5.0, $C_{11}H_{10}$), 129 (3.5, $C_{10}H_9$), 128 (1.2, $C_{10}H_8$), and 28 (0.5, C_2H_4). Found: C, 90.67; H, 9.08%. Calcd for $C_{15}H_{18}$: C, 90.85; H, 9.15%.

The fraction from 333 ml to 352 ml was a mixture (17.6 mg) of **4a** and **4b**.

In addition, 36.4 mg (37%) of **4a**, mp 53—55 °C (from hexane), was afforded from the eluate, which ranged from 352 ml to 404 ml: retention time, 16.8 min (SE-30, 120 °C). IR: 3050, 2970, 2870, 1603, 1492, 1450, 1332, 843, and 787 cm^{-1}. UV_{max}: 212 (log ε 4.14) and 266 nm (2.69). ^{1}H NMR: δ=0.77—3.05 (m, 15H) and 6.82 (3H, s). ^{13}C NMR: δ=24.0, 26.1, 29.2, 41.4, 44.4, 125.9, 131.1, and 144.3. MS *m/z* ($\sum_1$): 199 (4.2), 198 (25.1, $M^{\cdot+}$), 197 (2.1, $M^{\cdot+}-1$), 171 (2.1), 170 (15.6, $C_{13}H_{14}$), 169 (20.0, $C_{13}H_{13}$), 156 (7.8, $C_{12}H_{12}$), 155 (4.9, $C_{12}H_{11}$), 142 (3.7, $C_{11}H_{10}$), 129 (1.0, $C_{10}H_9$), 128 (0.6, $C_{10}H_8$), and 28 (0.5, C_2H_4). Found: C, 90.92; H, 9.32%. Calcd

for $C_{15}H_{18}$: C, 90.85; H, 9.15%.

References

1) D. P. Griswold, Jr., A. E. Casey, E. K. Weisburger, J. H. Weisburger, and F. M. Schabel, Jr., *Cancer Res.*, **26A**, 619 (1966).

2) For example: M. Yoshida, M. Kobayashi, M. Minabe, and K. Suzuki, *Bull. Chem. Soc. Jpn.*, **54**, 1159 (1981).

3) M. Yoshida, A. Kadokura, M. Minabe, and K. Suzuki, *Tetrahedron*, **35**, 2237 (1979).

4) B. M. Trost and P. L. Kinson, *J. Am. Chem. Soc.*, **97**, 2438 (1975).

5) M. Yoshida, A. Kadokura, M. Minabe, and K. Suzuki, *Bull. Chem. Soc. Jpn.*, **53**, 1179 (1980).

6) L. F. Fieser and J. Cason, *J. Am. Chem. Soc.*, **62**, 1293 (1940).

7) T. Horaguchi, R. Yamazaki, and T. Abe, *Bull. Chem. Soc. Jpn.*, **53**, 494 (1980): 89% of **2** was isolated from **1** (1 mmol) using Pd-C (8%, 170 mg) for 20 h.

8) P. P. Fu, H. M. Lee, and R. G. Harvey, *J. Org. Chem.*, **45**, 2797 (1980).

9) W. E. Bachmann and J. C. Sheehan, *J. Am. Chem. Soc.*, **63**, 204 (1941).

10) Some kinds of isomers were detected by GLPC; however, these were not studied further.

11) A. Mandelbaum, "Stereochemistry," ed by H. B. Kagan, Georg Thieme Publishers, Stuttgart (1977), Vol. 1, p. 148.

12) H. Budzikiewicz and C. Djerassi, *J. Am. Chem. Soc.*, **84**, 1430 (1962).

13) J. R. Durland and H. Adkins, *J. Am. Chem. Soc.*, **60**, 1501 (1938). Also, in anthracene series: E. A. Garlock, Jr., and E. Mosettig, *ibid.*, **67**, 2255 (1945).

14) J. R. Anderson and C. Kemball, *Adv. Catal.*, **9**, 51 (1957).

 © 1984 The Chemical Society of Japan Bull. Chem. Soc. Jpn., 57, 729—733 (1984)

Conversion of 2-Sulfinylated 2-Alkenoate Esters to (2*E*,4*E*)-2,4-Alkadienoate Esters by Pyrolysis

Rikuhei TANIKAGA,* Yoshihito NOZAKI, Masaharu NISHIDA, and Aritsune KAJI
Department of Chemistry, Faculty of Science, Kyoto University Sakyo-ku, Kyoto 606
(Received July 1, 1983)

Thermal reaction of ethyl (2*E*)-2-phenylsulfinyl-2-alkenoates (*E*-**2**) prepared from aldehydes and ethyl 2-phenylsulfinylacetate have been investigated. Refluxing of *E*-**2** or their *Z*-isomers in xylene resulted in the formation of ethyl (2*E*,4*E*)-2,4-alkadienoates accompanied by ethyl (2*E*)-4-hydroxy-2-alkenoates. Ethyl 2-cycloalkylidene-2-phenylsulfinylacetates were found to be more susceptible to pyrolysis. The enoate esters (**2**) undergo migration of their carbon-carbon double bond and then [2,3]sigmatropic rearrangement to benzenesulfenate esters, followed by thermolytic extrusion of a benzenesulfenic acid probably *via* ethyl (2*E*)-4-phenylsulfinyl-2-alkenoates to afford ethyl (2*E*,4*E*)-2,4-alkadienoates.

(2*E*,4*E*)-2,4-Alkadienoate esters (**1**) are versatile synthetic intermediates for naturally occurring compounds.[1-3] A number of syntheses of (2*E*,4*E*)-*N*-isobutyl-2,4-decadienamide (pellitorine) have been accomplished by the pathway *via* decadienoic acid or its esters,[1,4,5] which in turn were prepared by a number of routes.[6-11] We previously reported that pyrolysis of 2-phenylsulfinyl-2-alkenoate esters (**2**) led to the formation of **1**.[7]

Saturatd sulfoxides with one or more β-hydrogen atoms are known to undergo readily syn elimination on pyrolysis to form olefins by way of a concerted five-membered cyclic pathway.[12,13] This reaction is of great value for making carbon-carbon double bonds and introducing unsaturation at the α-position of esters, ketones and aldehydes,[14] but the corresponding thermal reaction of α,β- and β,γ-unsaturated sulfoxides had scarecely been investigated.[15] Cookson and Parsons reported the formation of 2-methyl-1,3-nonadien-5-one from 2-methyl-4-phenylsulfinyl-2-nonen-5-one, but no explanation of this observation was given.[16] Recently Nokami *et al.* prepared butyl 2,4-decadienoate by pyrolysis of butyl 2-phenylsulfinyl-2-decenoate and proposed an attractive mechanism involving a flexible seven-membered cyclic transition state.[9] It seems interesting to clarify whether this mechanism is operative or not. The present report aims at elucidating the mechanism of this novel conversion of **2** to **1**.

Results and Discussion

Ethyl (2*E*)-2-phenylsulfinyl-2-alkenoates (*E*-**2**) were easily prepared by treatment of aldehydes with ethyl 2-phenylsulfinylacetate and a catalytic amount of piperidine.[17] Their configurations were assigned by the comparison of δ values for olefinic protons (-CH=) in ^{1}H-NMR spectra of the corresponding sulfides (**3**). For example, the olefinic proton of ethyl (2*E*)-2-phenylthio-2-hexenoate (*E*-**3a**) appeared at δ 6.41, whereas that of its *Z*-isomer (*Z*-**3a**) at δ 7.36. It seems reasonable to conclude that the chemical shift of the proton cis to the carbonyl group must show up at a lower field than that cis to the sulfenyl group.

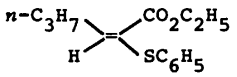

E-3a

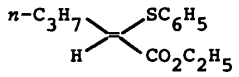

Z-3a

When ethyl (2*E*)-2-phenylsulfinyl-2-hexenoate (*E*-**2a**) was refluxed for 4 h in xylene containing anhydrous potassium carbonate ethyl (2*E*,4*E*)-2,4-hexadienoate (**1a**) and ethyl (2*E*)-4-hydroxy-2-hexenoate (**4a**) were formed, but (2*E*,4*Z*)-, (2*Z*,4*E*)-, and (2*Z*,4*Z*)-2,4-hexadienoate esters were scarecely found (GLPC).

The results obtained in the thermolysis of *E*-**2a**—**g** are summarized in Table 1.

The carbon-carbon double bonds of α,β-unsaturated sulfoxides and sulfilimines are known to migrate under basic conditions.[18,19] O'Connor established that base-catalyzed equilibriation between α,β- and β,γ-unsaturated sulfoxides greatly favored the latter ones.[18] Therefore, **2** may at first undergo migration of their double bonds to yield ethyl 2-phenylsulfinyl-3-alkenoates (**5**), which may produce **1** and **4** with loss of the sulfenic acid group. This assumption appears to be consistent with the findings that both *E*-**2a** and *Z*-**2a** gave **1a** and **4a** in the same ratio.

In order to study the validity of the seven-membered transition state for the diene formation (Ei mechanism; Fig. 1),[9] pyrolysis of ethyl 2-cyclopentylidene-2-

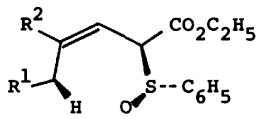

Fig. 1.

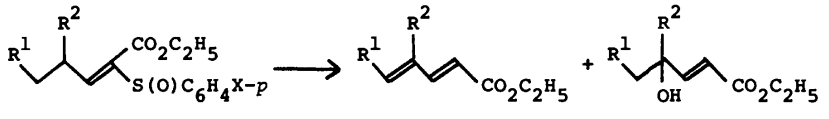

E-2 1 4

TABLE 1. PYROLYSIS OF ETHYL (2*E*)-2-PHENYLSULFINYL-2-ALKENOATES (*E*-**2**)

	R^1	R^2	X	Reaction time/h	Yield[a] of **1**/%	(2*E*, 4*E*)/ other isomers[b]	Yield[a] of **4**/%
a	CH_3	H	H	4	59	91/9	12
b	CH_3	H	Cl	4	30	92/8	27
c	*n*-C_3H_7	H	H	4	55	93/7	10
d	*n*-C_5H_{11}	H	H	4	60	94/6	8
e	*n*-C_5H_{11}	H	Cl	4	25	93/7	25
f	*n*-C_7H_{15}	H	H	4	58	93/7	9
g	$-(CH_2)_4-$		H	15	46(68[c])	97/3	5

a) Isolated yield. b) Determined by GLPC with a 30 m glass capillary column. c) Yield was based on the consumed **2g**.

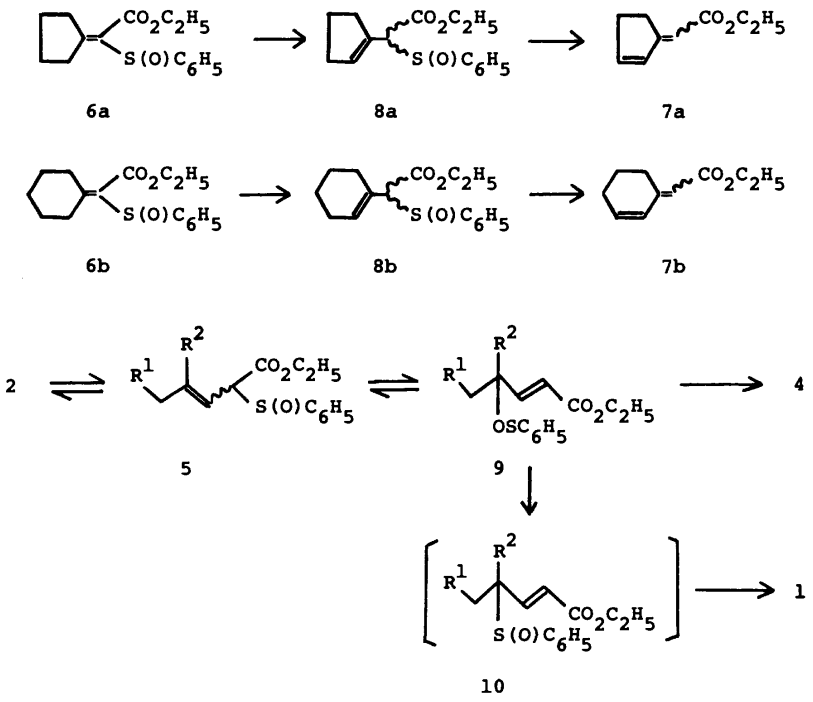

Scheme 1.

phenylsulfinylacetate (**6a**) and ethyl 2-cyclohexylidene-2-phenylsulfinylacetate (**6b**) was then investigated. Refluxing of **6a** and **6b** in xylene afforded ethyl 2-(2-cyclopentenylidene)acetate (**7a**) and ethyl 2-(2-cyclohexenylidene)acetate (**7b**) in 59 and 51% yields, respectively. The yields were moderate because **7** were somewhat unstable at high temperature. The α,β-unsaturated sulfoxides **6a**, **6b**, and **2a** were found to be labile to pyrolysis in that order. If the seven-membered transition state were operative, neither **6a** nor **6b** might show high reactivities because the hydrogen atom at δ position is located too far (3.5—4.0 Å) from the sulfinyl oxygen atom in the intermediary β,γ-unsaturated sulfoxides **8a** and **8b**.[20]

On the basis of these findings, the mechanism shown in Scheme 1 seems to be more reasonable than the Ei mechanism.

In the present transformation, it is assumed that the [2,3]sigmatropic rearrangement of **5** would take place in the first step to yield the sulfenate esters **9**, which produce **1** probably *via* the sulfoxides **10**. The rapid [2,3]sigmatropic rearrangement of **5** may be supported by the observations that the treatment of **2** with an equimolar amount of piperidine in acetonitrile resulted in the formation of **4**, the hydrolysis products of **9**, in high yields,[21] and in the attempted preparation of **8a** the oxidation of the corresponding sulfide, ethyl 2-(1-cyclopentenyl)-2-(phenylthio)acetate, with *m*-chloroperbenzoic acid at 0 °C gave ethyl (2*E*)-2-(2-hydroxycyclopentylidene)acetate, but did not allow the isolation of **8a**. Since it is known that the introduction of an electron-withdrawing group at the phenyl group of sulfoxides brings about the acceleration of thermolysis,[22] the *p*-chloro derivatives, **2b** and **2e**, were examined. The yields of **1** were rather low, however, probably owing to the ready hydrolysis of **9**.

Although the thermal rearrangement of sulfenates to sulfoxides is known to occur in benzylic derivatives,[23] we could not rigorously prove, at the present time, that the thermal reaction of **2** proceeds through ethyl (2*E*)-4-

phenylsulfinyl-2-alkenoates (**10**). However, it shoud be pointed out that **10a**, prepared from the corresponding sulfide by oxidation, produced **1a** upon heating in xylene.[24] In addition it was observed that the attempted isolation of **9a** from the reaction mixture of benzenesulfenyl chloride with sodium salt of **4a** was unsuccessful, but **1a** was detected in the pyrolysis product of that mixture. The predominant formation of the (2*E*,4*E*)-isomers of **1** might also be in accordance with the mechanism shown in Scheme 1.

Experimental

NMR spectra were recorded with a JEOL JNM-PS-100 or a Hitachi R-24B spectrometer in $CDCl_3$ using TMS as an internal standard. IR spectra were taken on a Hitachi 215 spectrometer. Mass spectra were determined with a Hitachi M-52 spectrometer. GLPC analysis was performed with a Varian 920 using a glass column (1 m×6 mm) packed with 20% silicone DC-550 or a Shimadzu GC-6AM using a SS-4 glass capillary column (30 m×0.3 mm). Column chromatography was performed using Wakogel 200 silica gel.

Materials. All aldehydes were commercially available and purified by distillation before use. Commercial acetonitrile and piperidine were used without purification. Xylene and tetrahydrofuran (THF) were distilled over CaH_2 prior to use.

*Ethyl 2-(Phenylthio)acetate (**11a**).* To a solution of sodium ethoxide prepared by dissolving Na (11.5 g, 0.5 mol) in ethanol (300 ml), benzenethiol (55.1 g, 0.5 mol) was added at room temperature. To the stirred solution was added dropwise a solution of ethyl bromoacetate (83.5 g, 0.5 mol) in ethanol (50 ml) at 0 °C. The reaction mixture was refluxed for 1 h, diluted with water (500 ml), and extracted with chloroform (300 ml). The chloroform solution was washed with water and dried over anhydrous Na_2SO_4. After removal of chloroform **11a** was obtained as a colorless liquid by distillation *in vacuo*: yield 88.0 g (90%); bp 101—104 °C/0.4 mmHg (1 mmHg≈133.322 Pa).[25]

Ethyl 2-(*p*-chlorophenylthio)acetate (**11b**) was obtained as a colorless liquid by the similar method: yield 85%; bp 130—133 °C/1.8 mmHg.[26]

*Ethyl 2-Phenylsulfinylacetate (**12a**).* A solution of **11a** (88.0 g, 0.45 mol) and $NaIO_4$ (115 g, 0.54 mol) in water (400 ml) and methanol (100 ml) was kept stirring at room temperature for 1 d, and filtered. The filtrate was extracted with chloroform (300 ml). The chloroform layer was washed with water, dried over anhydrous Na_2SO_4, and concentrated to afford **12a** as a colorless liquid: yield 94.2 g (99%); NMR ($CDCl_3$) δ=1.19 (3H, t), 3.62 (1H, d), 3.82 (1H, d), 4.09 (2H, q), and 7.4—7.8 (5H, m).[27]

Ethyl 2-(*p*-chlorophenylsulfinyl)acetate (**12b**) was similarly prepared by oxidation of **11b**: yield 96%; colorless solid; mp 43 °C; NMR ($CDCl_3$) δ=1.20 (3H t, J=7 Hz), 3.64 (1H, d, J=12 Hz), 3.82 (1H, d, J=12 Hz), 4.10 (2H, q, J=7 Hz), 7.44 (2H, d, J=8 Hz), and 7.60 (2H, d, J=8 Hz); IR (Nujol) 1725, 1270, and 1050 cm^{-1}. Found: C, 48.70; H, 4.55%. Calcd for $C_{10}H_{11}ClO_3S$: C, 48.67; H, 4.50%.

*Ethyl (2E)-2-Phenylsulfinyl-2-hexenoate (E-**2a**).* A solution of **12a** (2.12 g, 10 mmol), butanal (1.08 g, 15 mmol), and piperidine (0.08 g, 1 mmol) in acetonitrile (30 ml) was allowed to stand at 0 °C for 2 d. After removal of acetonitrile the residue was chromatographed on a silica-gel column with a chloroform eluent to give *E*-**2a** (1.46 g, 55%) and **12a** (0.7 g, recovery 33%). *E*-**2a**: viscous colorless oil; NMR ($CDCl_3$) δ=0.98 (3H, t, J=7 Hz), 1.14 (3H, t,J=7 Hz), 1.4—1.8 (2H, m), 2.73 (2H, q, J=7 Hz), 4.06 (2H, q, J=7 Hz), 7.12 (1H, t, J=7 Hz), and 7.3—7.7 (5H, m); IR (neat) 1720, 1200, and 1050 cm^{-1}; MS m/z 266 (M^+). Found: C, 63.34; H, 6.91%. Calcd for $C_{14}H_{18}O_3S$: C, 63.13; H, 6.81%.

Other ethyl (2*E*)-2-phenylsulfinyl-2-alkenoates (*E*-**2b—g**) were obtained by similar treatment of **12a** or **12b** (10 mmol) with aldehydes (15 mmol) and piperidine (1 mmol).

*Ethyl (2E)-2-(p-Chlorophenylsulfinyl)-2-hexenoate (E-**2b**)*: Viscous colorless oil; yield 68%, NMR ($CDCl_3$) δ=0.96 (3H, t, J=7 Hz), 1.14 (3H, t, J=7 Hz), 1.4—1.8 (2H, m), 2.70 (2H, q, J=7 Hz), 4.06 (2H, q, J=7 Hz), 7.11 (1H, t, J=7 Hz), 7.34 (2H, d, J=8 Hz), and 7.53 (2H, d, J=8 Hz); IR (neat) 1725, 1210, and 1055 cm^{-1}; MS m/z 301 (M^+). Found: C, 56.10; H, 5.89%. Calcd for $C_{14}H_{17}ClO_3S$: C, 55.89; H, 5.70%.

*Ethyl (2E)-2-Phenylsulfinyl-2-octenoate (E-**2c**)*: Viscous colorless oil; yield 51%; NMR ($CDCl_3$) δ=0.90 (3H, t, J=7 Hz), 1.15 (3H, t, J=7 Hz), 1.0—1.8 (8H, br), 4.06(2H, q, J=7 Hz), 7.13 (1H, t, J=7 Hz), and 7.3—7.7 (5H, m); IR (neat) 1720, 1210, and 1050 cm^{-1}: MS m/z 294 (M^+). Found: C, 65.50: H, 7.59%. Calcd for $C_{16}H_{22}O_3S$: C, 65.27; H, 7.53%.

*Ethyl (2E)-2-Phenylsulfinyl-2-decenoate (E-**2d**)*: Viscous colorless oil; yield 50%; NMR ($CDCl_3$) δ=0.87 (3H, t, J=7 Hz), 1.14 (3H, t, J=7 Hz), 1.0—1.8 (12H, br), 4.06 (2H, q, J=7 Hz), 7.14 (1H, t, J=7 Hz), and 7.3—7.7 (5H, m); IR (neat) 1720, 1210, and 1050 cm^{-1}; MS m/z 322 (M^+). Found: C, 67.31; H, 8.02%. Calcd for $C_{18}H_{26}O_3S$: C, 67.04; H, 8.13%.

*Ethyl (2E)-2-(p-Chlorophenylsulfinyl)-2-decenoate (E-**2e**)*: Viscous colorless oil; yield 77%; NMR ($CDCl_3$) δ=0.87 (3H, t, J=7 Hz), 1.14 (3H, t, J=7 Hz), 1.0—1.8 (12H, br), 4.06 (2H, q, J=7 Hz), 7.10 (1H, t, J=7 Hz), 7.34 (2H, d, J=8 Hz), and 7.54 (2H, d, J=8 Hz); IR (neat) 1725, 1210, and 1055 cm^{-1}; MS m/z 357 (M^+). Found: C, 60.62; H, 7.34%. Calcd for $C_{18}H_{25}ClO_3S$: C, 60.62: H, 7.06%.

*Ethyl (2E)-2-Phenylsulfinyl-2-dodecenoate (E-**2f**)*: Viscous colorless oil; yield 53%; NMR ($CDCl_3$) δ=0.87 (3H, t, J=7 Hz), 1.14 (3H, t, J=7 Hz), 1.0—1.8 (16H, br), 4.06 (2H, q, J=7 Hz), 7.13 (1H, t, J=7 Hz), and 7.3—7.7 (5H, m); IR (neat) 1720, 1210, and 1050 cm^{-1}; MS m/z 350 (M^+). Found; C, 68.50; H, 8.75%. Calcd for $C_{20}H_{30}O_3S$: C, 68.53; H, 8.63%.

*Ethyl (2E)-2-Phenylsulfinyl-3-cyclohexyl-2-propenoate (E-**2g**)*: Viscous colorless oil; yield 71%; NMR ($CDCl_3$) δ=1.14 (3H, t, J=7 Hz), 1.0—1.9 (10H, br), 3.0—3.4 (1H, m), 4.06 (2H, q, J=7 Hz), 6.98 (1H, d, J=9 Hz), and 7.3—7.7 (5H, m); IR (neat) 1720, 1210, and 1050 cm^{-1}; MS m/z 306 (M^+). Found: C, 66.91; H, 7.41%. Calcd for $C_{17}H_{22}O_3S$: C, 66.63; H, 7.24%.

*Ethyl (2E)-2-Phenylthio-2-hexenoate (E-**3a**).* Trifluoroacetic anhydride (0.63 g, 3 mmol) was added to a stirred solution of *E*-**2a** (0.53 g, 2 mmol) and NaI (0.75 g, 5 mmol) in acetone (30 ml) at 0 °C.[28] The mixture was stirred for 2 min, diluted with benzene (100 ml), and washed with water, aq $NaHCO_3$, aq $Na_2S_2O_3$, and then water. After drying over anhydrous Na_2SO_4 the solvent was evaporated to give *E*-**3a** in a quantitative yield; yellowish liquid; NMR ($CDCl_3$) δ=0.96 (3H, t, J=7 Hz), 1.09 (3H, t, J=7 Hz), 1.4—1.7 (2H, m), 2.53 (2H, q, J=7 Hz), 4.11 (2H, q, J=7 Hz), 6.41 (1H, t, J=7 Hz), and 7.2—7.5 (5H, m); IR (neat) 1720 cm^{-1}; MS m/z 250 (M^+). Found: C, 67.06; H, 7.23%. Calcd for $C_{14}H_{18}O_2S$: C, 67.16; H, 7.25%.

*Ethyl (2Z)-2-Phenylthio-2-hexenoate (Z-**3a**).* Similar reduction of ethyl (2*Z*)-2-phenylsulfinyl-2-hexenoate (*Z*-**2a**)[7] gave *Z*-**3a** in a quantitative yield; yellowish liquid; NMR ($CDCl_3$) δ=0.98 (3H, t, J=7 Hz), 1.09 (3H, t,J=7 Hz), 1.4—1.7 (2H, m), 2.54 (2H, q, J=7 Hz), 4.11 (2H, q, J=7 Hz), 7.36 (1H, t, J=7 Hz), and 7.2—7.5 (5H, m); IR (neat) 1720 cm^{-1}; MS m/z 250 (M^+). Found: C, 67.03; H, 7.21%. Calcd for $C_{14}H_{18}O_3S$: C, 67.16; H, 7.25%.

*Ethyl 2-(1-Hydroxycyclopentyl)-2-phenylsulfinylacetate (**13a**).* A solution of ethyl 2-phenylsulfinylacetate (7.29 g, 44 mmol) in anhydrous THF (15 ml) was added under argon

atomosphere at −78 °C to a stirred solution of lithium diisopropylamide (44 mmol) prepared from diisopropylamine (6.16 ml) and butyllithium (29.0 ml, 1.55 M solution in hexane) in anhydrous THF (30 ml), and stirring was continued for 1 h at −60 °C. A solution of cyclopentanone (3.80 ml, 43 mmol) in anhydrous THF (10 ml) was added dropwise. The resultant solution was stirred for 1.5 h at −60 °C, quenched with aq NH_4Cl, and diluted with ether (300 ml). The ethereal solution was washed with 10% HCl and aq saturated NaCl, dried over anhydrous Na_2SO_4, and evaporated. The residue was chromatographed on silica gel with a benzene eluent to give **13a** (8.75 g, 78%) as a yellowish liquid; NMR (CCl_4) δ=1.22 (3H, t, J=7 Hz), 0.9-2.3 (10H, m) 3.00 (1H, s), 3.52 (1H, s), 4.01 (2H, q, J=7 Hz), and 7.0—7.4 (5H, m).[29]

Ethyl 2-Cyclopentylidene-2-(phenylthio)acetate (14a). A solution of **13a** (3.65 g, 13 mmol) in acetic anhydride (10 ml) was refluxed for 3 h, cooled to room temperature, neutralized with 30% aq NaOH, and diluted with ether (200 ml). The ethereal solution was washed with water, dried over anhydrous Na_2SO_4 and evaporated. The residue was dissolved in anhydrous THF (5 ml), and the resultant solution was added to a solution of lithium diisopropylamide (14.4 mmol) in anhydrous THF (30 ml) at −10 °C. The mixture was stirred at room temperature for 2 h, quenched with aq NH_4Cl, and extracted with ether (200 ml). The ethereal extract was washed with 10% HCl and aq saturated NaCl, dried over anhydrous Na_2SO_4, and evaporated. The product **14a** was separated by chromatography on a silica-gel column using a hexane–benzene mixture (v/v=1/1); yellowish liquid; yield 1.17 g (50%); NMR (CCl_4) δ=1.00 (3H, t, J=7 Hz), 1.5—2.0 (4H, m), 2.4—2.9 (4H, m), 3.95 (2H, q, J=7 Hz), and 6.9—7.4 (5H, m); IR (neat) 1705 cm^{-1}; MS m/z 262 (M^+).[29]

Ethyl 2-Cyclopentylidene-2-phenylsulfinylacetate (6a). To a solution of **14a** (4.07 g, 15.5 mmol) in dichloromethane (100 ml) was added a solution of *m*-chloroperbenzoic acid (3.68 g, 17 mmol) in dichloromethane (50 ml) at 0 °C. The reaction mixture was stirred at 0 °C for 1 h and neutralized with aq $NaHCO_3$. The organic layer was washed with aq saturated NaCl, dried over anhydrous Na_2SO_4, and evaporated. The residual crude **6a** was purified by chromatography on silica gel using chloroform; colorless liquid; yield 2.74 g (64%); NMR ($CDCl_3$) δ=1.03 (3H, t, J=7 Hz), 1.7—2.0 (4H, m), 2.8—3.1 (4H, m), 3.98 (2H, q, J=7 Hz), and 7.3—7.7 (5H, m); IR (neat) 1710 and 1045 cm^{-1}; MS m/z 278 (M^+). Found: C, 64.92; H, 6.61%. Calcd for $C_{15}H_{18}O_3S$: C, 64.72; H, 6.52%.

Ethyl 2-Cyclohexylidene-2-phenylsulfinylacetate (6b). Similar treatment of cyclohexanone with lithium enolate of **12a**, followed by elimination and oxidation procedures as described above, yielded **6b** as a colorless liquid; overall yield 27%; NMR ($CDCl_3$) δ=1.02 (3H, t, J=7 Hz), 1.5—2.0 (6H, m), 2.3—2.9 (4H, m), 3.92 (2H, q, J=7 Hz), and 7.3—7.7 (5H, m); IR (neat) 1720 and 1047 cm^{-1}; MS m/z 292 (M^+). Found: C, 65.93; H, 6.91%. Calcd for $C_{16}H_{20}O_3S$: C, 65.72; H, 6.89%.

General Pyrolysis of Ethyl 2-Phenylsulfinyl-2-alkenoates (2). A mixture of **2** (10 mmol) and anhydrous K_2CO_3 (12 mmol) in xylene was refluxed while the reaction was monitored by TLC and GLPC. The reaction completed after 4 h in the cases of *E*-**2a**—**f** and *Z*-**2a**, but *E*-**2g** remained unreacted after 15 h. After cooling K_2CO_3 and xylene were removed by filtration and evaporation. The residue was separated through silica-gel column chromatography with a hexane–benzene mixture (v/v=1/1) and then chloroform to afforded **1** and **4**.[21] The ratio of (2*E*,4*E*)/(2*E*,4*Z*)+(2*Z*,4*E*)+(2*Z*,4*Z*) was determined by GLPC analysis using a capillary column. The configuration of **1** was determined by comparison of NMR spectra of authentic **1a** (=**1b**), **1c**[30], and **1d** (=**1e**).[31,32] Physical data of **1e** and **1g** are as follows.

Ethyl (2E,4E)-2,4-Dodecadienoate (1f): Colorless liquid; NMR(CCl_4) δ=0.88 (3H, t, J=7 Hz), 1.25 (3H, t, J=7 Hz), 1.0—1.7 (10H, m) 2.0—2.4 (2H, m), 4.07 (2H, q, J=7 Hz), 5.64 (1H, d, J=15 Hz), 5.8—6.3 (2H, m), and 7.0—7.4 (1H, m); IR (neat) 1720, 1640, and 1620 cm^{-1}; MS m/z 224 (M^+). Found: C, 74.90; H, 10.71%; Calcd for $C_{14}H_{24}O_2$: C, 74.95; H, 10.78%.

Ethyl (2E)-3-(1-Cyclohexenyl)-2-propenoate (1g): Colorless liquid; NMR (CCl_4) δ=1.25 (3H, t, J=7 Hz), 1.4—2.4 (8H, br), 4.07 (2H, q, J=7 Hz), 5.58 (1H, d, J=15 Hz), 5.23 (1H, m), and 7.1—7.6 (1H, m); IR (neat) 1720 and 1630 cm^{-1}; MS m/z 180 (M^+). Found: C, 73.35; H, 9.03%. Calcd for $C_{11}H_{16}O_2$: C, 73.30; H, 8.95%.

Pyrolysis of Ethyl 2-Cyclopentylidene-2-phenylsulfinylacetate (6a). A mixture of **6a** (1.39 g, 5 mmol) and anhydrous K_2CO_3 (0.83 g, 6 mmol) in xylene (6 ml) was refluxed monitoring with TLC and GLPC. The reaction was completed within 20 min. After removal of K_2CO_3 and xylene chromatograpy on silica gel with hexane–benzene (v/v=1/1) as an eluent gave ethyl 2-(2-cyclopentenylidene)acetate (**7a**) as a colorless liquid; yield 0.45 g (59%); *E*/*Z*=54/46; NMR ($CDCl_3$) δ=1.27 (3H, t, J=7 Hz), 2.4—3.1 (4H, m), 4.13 (2H, t, J=7 Hz), 5.56 (s, =CHCO, *Z*-isomer), 5.70 (s, =CHCO, *E*-isomer), and 6.1—6.7 (2H, m); IR (neat) 1700 cm^{-1}; MS m/z 152 (M^+). Found: C, 71.23; H, 7.92%. Calcd for $C_9H_{12}O_2$: C, 71.02; H, 7.95%.

Pyrolysis of Ethyl 2-Cyclohexylidene-2-phenylsulfinylacetate (6b). A mixture of **6b** and anhydrous K_2CO_3 was similarly refluxed for 1 h. Chromatography on silica gel with hexane–benzene as an eluent afforded ethyl 2-(2-cyclohexenylidene)acetate (**7b**) as a colorless liquid; yield 51%; *E*/*Z*=51/49; NMR ($CDCl_3$) δ=1.24 (3H, t, J=7 Hz), 1.5—1.9 (2H, m), 2.1—2.5 (3H, m), 2.8—3.0 (1H, m), 4.11 (2H, q, J=7 Hz), 5.41 (s, =CHCO, *Z*-isomer), 5.50 (s, =CHCO, *E*-isomer), and 5.9—6.3 (2H, m); IR (neat) 1705 cm^{-1}; MS m/z 166 (M^+). Found: C, 72.45; H, 8.51%. Calcd for $C_{10}H_{14}O_2$: C, 72.26; H, 8.49%.

Oxidation of Ethyl 2-(1-Cyclopentenyl)-2-(phenylthio)acetate (15a). To a stirred solution of **15a**[20] (2.62 g, 10 mmol) in dichloromethane (100 ml) was added dropwise a solution of *m*-chloroperbenzoic acid (2.37 g, 11 mmol) in dichloromethane (50 ml) at 0 °C, and the resultant mixture was stirred for 30 min at 0 °C. During the oxidation ethyl (2*E*)-2-(2-hydroxycyclopentylidene)acetate (**16a**) and diphenyldisulfide were gradually formed (TLC and GLPC). The reaction mixture was neutralized with aq $NaHCO_3$, washed with aq saturated NaCl, and dried over anhydrous Na_2SO_4. After evaporation of the solvent the residue was chromatographed on a silica-gel column successively using hexane–benzene (v/v=2/1), benzene and chloroform to give diphenyldisulfide (0.32 g), *S*-phenyl benzenethiosulfonate (*ca.* 0.1 g), **15a** (1.23 g, 47% recovery), **16a** (0.76 g, 45%), and some unidentified compounds. **16a**: colorless liquid; NMR ($CDCl_3$) δ=1.1—2.2 (4H, m), 1.24 (3H, t), 2.6—3.0 (2H, m), 3.8 (1H, s), 4.10 (2H, q), 4.51 (1H, m), and 5.93 (1H, q, J=2 Hz).[20]

References

1) L. Crombie, *J. Chem. Soc.*, **1955**, 999, 1007.
2) C. A. Henrick, *Tetrahedron*, **33**, 1845.
3) D. F. Taber. *J. Am. Chem. Soc.*, **99**, 3513 (1977).
4) T. Mandai, J. Gotoh, J. Otera, and M. Kawada, *Chem. Lett.*, **1980**, 313.
5) K. Tanaka, M. Terauchi, and A. Kaji, *Chem. Lett.*, **1981**, 315 and references therein.
6) J. Tsuji, H. Nagashima, T. Takahashi, and K. Masaoka, *Tetrehedron Lett.*, **1977**, 1917.
7) R. Tanikaga, M. Nishida, N. Ono, and A. Kaji, *Chem. Lett.*, **1980**, 781.

8) N. Ono, M. Miyake, Y. Tanabe, K. Tanaka, and A. Kaji, *Chem. Lett.*, **1980**, 1365.
9) J. Nokami, K. Nishiuchi, S. Wakabayashi, and R. Okawara, *Tetrahedron Lett.*, **21**, 4455 (1980).
10) T. Nakai, K. Mikami, S. Taya, Y. Kimura, and T. Mimura, *Tetrahedron Lett.*, **22**, 69 (1981).
11) Y. Tamura, H. D. Choi, H. Maeda, and H. Ishibashi, *Tetrahedron Lett.*, **22**, 1343 (1981).
12) C. A. Kingsbury and D. J. Cram, *J. Am. Chem. Soc.*, **82**, 1810 (1960).
13) H. Kwart, T. J. George, R. Louw, and W. Ultee, *J. Am. Chem. Soc.*, **100**, 3927 (1978).
14) B. M. Trost, *Acc. Chem. Res.*, **11**, 453 (1978) and references therein.
15) W. Ando, T. Oikawa, K. Kishi, T. Saiki, and T. Migita, *J. Chem. Soc., Chem. Commun.*, **1975**, 704.
16) R. C. Cookson and P. J. Parsons, *J. Chem. Soc., Chem. Commun.*, **1978**, 821.
17) The more detailed discussion on this Knoevenagel reaction will be given subsequently.
18) D. E. O'Connor and C. D. Broaddus, *J. Am. Chem. Soc.*, **86**, 2267 (1964).
19) M. Kakimoto, T. Yamamoto, and M. Okawara, *Tetrahedron Lett.*, **1979**, 623.
20) S. Yamagiwa, H. Sato, N. Hoshi, H. Kosugi, and H. Uda, *J. Chem. Soc., Perkin Trans. 1*, **1979**, 570.
21) R. Tanikaga, Y. Nozaki, T. Tamura, and A. Kaji, *Synthesis*, **1983**, 134.
22) J. R. Shelton and K. E. Davis, *Int. J. Sulfur Chem.*, **8**, 197 (1973).
23) E. G. Miller, D. R. Rayner, H. T. Thomas, and K. Mislow, *J. Am. Chem. Soc.*, **90**, 4861 (1968).
24) R. Tanikaga, Y. Nozaki, K. Tanaka, and A. Kaji, *Chem. Lett.*, **1982**, 1703.
25) E. Müller and A. Freytag, *J. Prakt. Chem.*, **146**, 56 (1936).
26) B. Roth and G. H. Hitchings, *J. Org. Chem.*, **26**, 2770 (1961).
27) N. Kunieda, J. Nokami, and M. Kinoshita, *Tetrahedron Lett.*, **1974**, 3997.
28) J. Drabowicz and S. Oae, *Synthesis*, **1977**, 404.
29) Physical data for the methyl ester are available in Ref. 20.
30) T. Sakai, K. Seko, A. Tsuji, M. Utaka, and A. Takeda, *J. Org. Chem.*, **47**, 1101 (1982).
31) G. Ohloff and M. Pawlak, *Helv. Chim. Acta*, **56**, 1176 (1973).
32) G. Rickards and L. Weiler, *J. Org. Chem.*, **43**, 3607 (1976).

The Reaction of Cyclic 1,3-Diketones with Alkylthiocyclopropenium Ions to Yield 2-Alkylthio-substituted 2*H*-Pyrans

Hiroshi YOSHIDA,* Mikito NAKAJIMA, Tsuyoshi OGATA, and Kiyoshi MATSUMOTO†

Department of Applied Chemistry, Faculty of Engineering, Shizuoka University, Hamamatsu 432

†*College of Liberal Arts and Sciences, Kyoto University, Sakyo-ku, Kyoto 606*

(Received August 29, 1983)

This study treats the reactions of methylthio-, ethylthio-, or benzylthiodiphenylcyclopropenium ion (**1**) with 5-, 6-, and 7-membered cyclic 1,3-diketones, giving either 2-alkylthio-2*H*-pyrans or dienone derivarives. Treatment of **1** with 1,3-cyclopentanedione, 1,3-cyclohexanedione, 5,5-dimethyl-1,3-cyclohexanedione, 4-hydroxy-6-methyl-2-pyrone, 4-hydroxycoumarin, and 1,3-cycloheptanedione in the presence of triethylamine afforded 2-alkylthio-2*H*-pyrans. The structure of the products was elucidated on the basis of their elemental analyses, IR, ^{1}H-NMR, ^{13}C-NMR, and mass spectroscopic data, as well as chemical transformations. 2-Alkylthio-2*H*-pyrans with mercury(II) chloride in an alcohol underwent conversion to the corresponding 2-alkoxy-2*H*-pyrans. The ^{1}H- and ^{13}C-NMR data of these compounds clearly show that the equilibrium lies completely on the side of the 2*H*-pyran. In contrast, the reaction of **1** with 1,3-indandione yielded the ring-opened dienone derivative as a mixture of *E* and *Z* isomers.

2*H*-Pyrans are apparently not well known.[1] Electrocyclic ring openings of 2*H*-pyrans and ring closures of dienones have been of considerable interest in view of the yet unresolved questions of how the presence of heteroatoms in a conjugated chain exerts influence on the electrocyclic process.[2] Although some synthetic routes to the stable 2*H*-pyrans like halogen-substituted 2*H*-pyrans have been developed,[2] neither physical nor chemical properties of sulfur-containing 2*H*-pyrans have been reported. Quite recently, we have communicated[3] the reaction of alkylthiodiphenylcyclopropenium salts **1** which acyclic 1,3-diketones to give the cyclopentadienol derivatives. Here we describe a novel cyclization reaction of **1** with cyclic 1,3-diketones to produce 2-alkylthio-substituted 2*H*-pyrans.

Methylthio-, ethylthio-, and benzylthiodiphenylcyclopropenium salts **1a—c** were prepared by the previously reported method.[3] A mixture of **1**, cyclic 1,3-diketone, and triethylamine in a molar ratio of 1:1:2 was stirred in dry benzene at room temperature for 15 min. The product was then purified by recrystallization or by column chromatography. Cyclic 1,3-diketones such as 5,5-dimethyl-1,3-cyclohexanedione (**2**), 1,3-cyclopentanedione (**3**), 1,3-cyclohexanedione (**4**), 4-hydroxy-6-methyl-2-pyrone(**5**), 4-hydroxycoumarin (**6**) and 1,3-cycloheptanedione (**7**) gave the corresponding 2-alkylthio-2*H*-pyrans **8—13** in good yield as shown in Table 1. Treatment of the compounds with mercury (II) chloride in an alcohol yielded the corresponding desulfurization products: 2-alkoxy-2*H*-pyrans **14—19**.

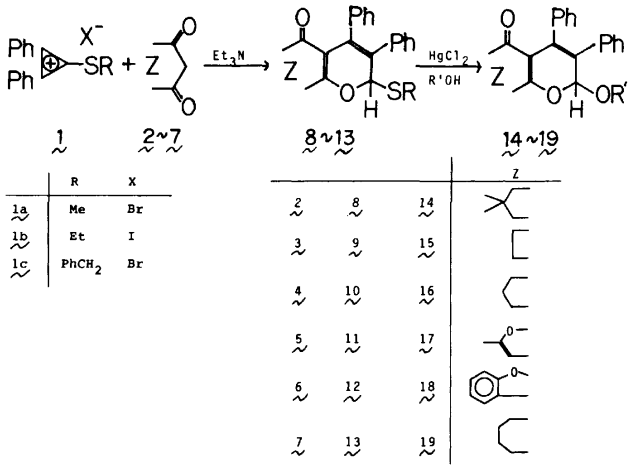

Scheme 1.

The 2-alkylthio- and 2-alkoxy-2*H*-pyran structures of the products **8—19** were elucidated on the basis of elemental analyses, MS, ^{1}H- and ^{13}C-NMR spectroscopic studies. For example, the ^{1}H- and ^{13}C-NMR spectrum of **8a** showed a singlet at δ=6.03 for one hydrogen and an sp^3 carbon bonded to one hydrogen at δ=88.3.

TABLE 1. ALKYLTHIO- AND ALKOXY-2*H*-PYRAN DERIVATIVES

Reactant		Product	Yield/%
1a	**2**	**8a**(R=Me)	84
1b	**2**	**8b**(R=Et)	58
1c	**2**	**8c**(R=PhCH$_2$)	67
1a	**3**	**9**(R=Me)	89
1a	**4**	**10**(R=Me)	74
1a	**5**	**11**(R=Me)	90
1a	**6**	**12**(R=Me)	84
1a	**7**	**13**(R=Me)	63
8a	MeOH	**14a**(R′=Me)	93
8a	EtOH	**14b**(R′=Et)	78
8a	*i*-PrOH	**14c**(R′=*i*-Pr)	80
8b	MeOH	**14a**(R′=Me)	83
9	MeOH	**15a**(R′=Me)	87
9	EtOH	**15b**(R′=Et)	81
10	MeOH	**16**(R′=Me)	74
11	EtOH	**17**(R′=Et)	89
12	EtOH	**18**(R′=Et)	65
13	EtOH	**19**(R′=Et)	61

Coupling constants were $^{1}J_{C^3H}$=170 Hz and $^{3}J_{C^3SC^1'H}$=$^{3}J_{HC^3SC^1'}$=3 Hz, thus indicating the framework:

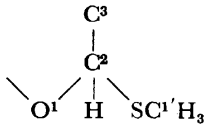

On treatment with mercury(II) acetate in acetic acid 2-alkylthio-2*H*-pyrans **8a** and **8b** gave 2-hydroxy-2*H*-pyran (**20**). The ^{1}H-NMR spectroscopic studies of **20** were interesting. A chloroform-*d* solution of **20** which showed a singlet at δ=5.76 due to the C-2 hydrogen, gave two new singlets at 9.22 (D_2O exchangeable, OH) and 9.80 (HC=O) on addition of a small amount of triethylamine to the solution. Attempt at isolation of the expected α,β-unsaturated aldehyde **22** failed, and **20** was recovered from the solution. However, treatment of a solution with *p*-toluenesulfonohydrazide in ethanol containing 10% of triethylamine yielded the corresponding *p*-tolylsulfonyl hydrazone **23** in 38% yield. The unsaturated aldehyde **22** must be stabilized as enolate anion, since **20** was soluble in aqueous sodium hydroxide and acidification of the solution with phosphoric acid yielded **20**. These results indicate that 2-hydroxy-2*H*-pyran **20** is not stable in a basic solvent, but under acidic or neutral conditions the equilibrium lies completely on the side of 2*H*-

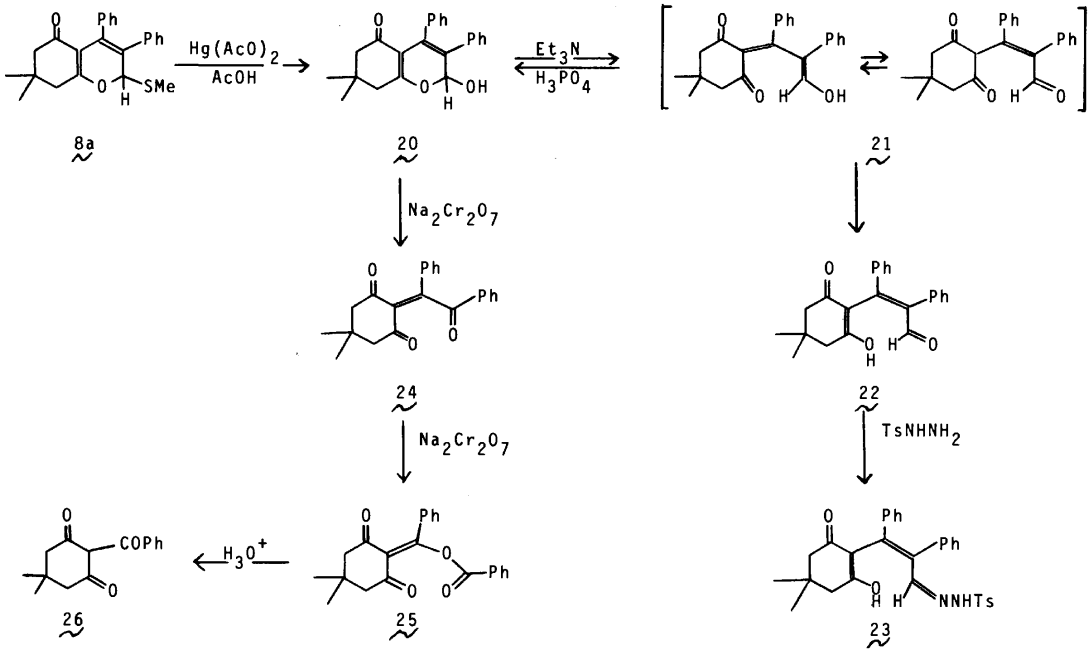

Scheme 2.

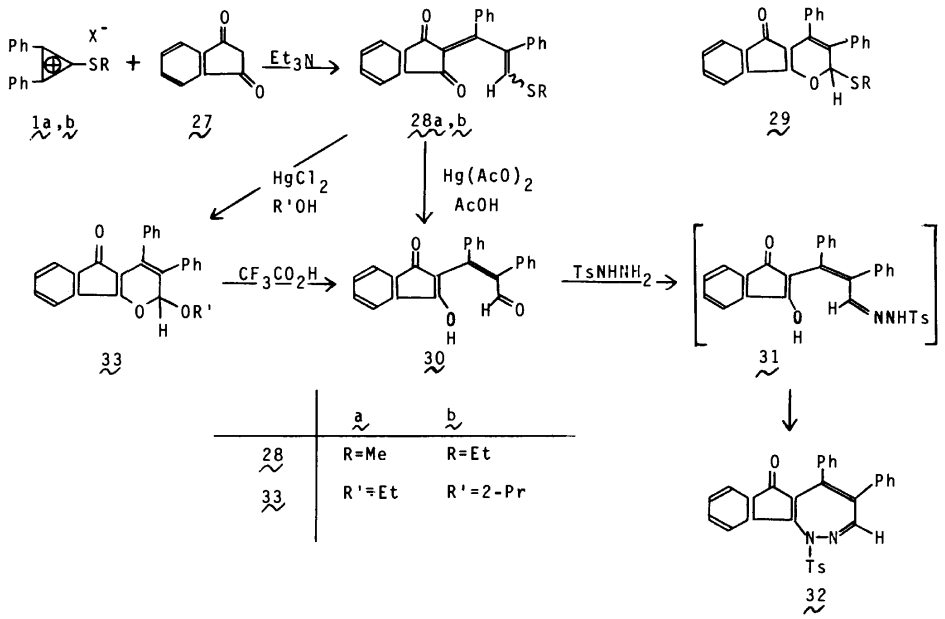

Scheme 3.

pyran **20**. The aldehyde **22** may be formed *via* either isomerization of **20** or electrocyclic ring opening of **20** to give **21**, followed by keto-enol isomerization.

Oxidation of **20** with sodium dichromate in acetic acid yielded the benzoylphenylmethylene derivative **24** as an initial oxidation product in 45% yield; further oxidation under the same reaction conditions gave **25** in 24% yield. The latter product **25** produced the known 2-benzoyl-5,5-dimethyl-1,3-cyclohexanedione (**26**)[4] on hydrolysis in an acidic medium (Scheme 2).

A spontaneous reaction took place between **1a** (or **1b**) and 1,3-indandione (**27**) in the presence of triethylamine. In contrast to the reactions of 1,3-diketones **2**—**7**, the product isolated by column chromatography showed no peak corresponding to the 2*H*-pyran structure **29** in ^{1}H- and ^{13}C-NMR spectra. The product is most likely to be an *E,Z*-isomer mixture of the dienone **28**, since the ^{1}H-NMR spectrum gave olefinic protons at δ=6.60 and 6.71 in a 1:2 ratio.

Treatment of **28** with mercury(II) acetate in acetic acid yielded a resinous crystalline mass, the structure of which was establised to be the ring-opened vinyl aldehyde **30**. The ^{1}H-NMR spectrum of **30** showed two singlets at δ=4.44 (OH) and 9.59 (HC=O). The aldehyde **30** was converted by *p*-toluenesulfonohydrazide to the diazepine **32**[5] *via* the *p*-tolylsulfonylhydrazone **31** intermediate. In contrast, the reaction of **28a** with mercury(II) chloride in an alcohol afforded 2-alkoxy-2*H*-pyran **33** (the C-2 hydrogen as a singlet at around δ=6.0). Addition of a small amount of trifluoroacetic acid to a solution of **33** in $CDCl_3$ yielded a ^{1}H-NMR spectrum in agreement with the structure **30**.

The reaction mechanism shown in Scheme 4 is proposed. The initial step involves a nucleophilic attack of the carbanion generated from 1,3-diketone on the cyclopropene ring of **1**. Subsequent elimination of the acidic methine hydrogen and ring opening gives either a conjugated betaine or a dienone intermediate, followed by intramolecular cyclization leading to the 2-alkylthio-2*H*-pyran. A cyclic 1,3-diketone like 1,3-indandione (**27**), which has little flexibility, gave no cyclization product, while 5-, 6-, and 7-membered flexible 1,3-diketones **2**—**7** yielded only 2-alkylthio-2*H*-pyran derivatives.

Experimental

General. Melting points are uncorrected. The ^{13}C FT NMR spectra were recorded on a JEOL JNM FX-60 spectrometer (15.04 MHz), and ^{1}H-NMR spectra, on a Hitachi-Perkin-Elmer R-24 (60 MHz). The IR spectra were recorded on a JASCO A-3 spectrometer, and mass spectra on a Hitachi RMU-7M mass spectrometer.

Alkylthiodiphenylcyclopropenium Ions ***1a—c.*** Methylthio-, ethylthio-, and benzylthiodiphenylcyclopropenium ions **1a**—**c** were prepared as previously described.[3]

The Reaction of Alkylthiodiphenylcyclopropenium Salts ***1a—c*** *with Cyclic 1,3-Diketones* ***2—7.*** *(a) The Reaction of* ***1a*** *with* ***2***: A mixture of **1a** (1 mmol), **2** (1 mmol), and triethylamine (2 mmol) in dry benzene (15 cm^3) was stirred for 20 min at room temperature. After the separation of the precipitate, the benzene solution was condensed and chromatographed over silica gel (chloroform) to give colorless crystals of 7,7-dimethyl-3,4-diphenyl-2-methylthio-5,6,7,8-tetrahydro-2*H*-1-benzopyran-5-one (**8a**) in 84% yield. **8a**: mp 190—192 °C: IR (KBr) 1670 and 1630 cm^{-1}: ^{1}H-NMR ($CDCl_3$) δ=1.16 (3H, s, Me), 1.21 (3H, s, Me), 2.30 (5H, s, MeS and CH_2), 2.48(2H, s, CH_2), 6.03(1H, s, CH), and 6.9—7.2 (10H, m, 2Ph); ^{13}C-NMR ($CDCl_3$) δ=13.9 (q, MeS), 27.3 and 29.4 (q, 2Me), 31.8 (s), 42.9 (t), 51.7 (t), 88.3 (d), 116.5 (s), 123.4 (s), 126.6 (d), 127.0 (d), 127.4 (d), 127.8 (d), 129.2 (d), 132.4 (s), 136.9 (s), 137.8 (s), 168.5 (s), and 193.5 (s): MS (*m/z*) 376 (M^+). Found: C, 76.33; H, 6.44%. Calcd for $C_{24}H_{24}O_2S$: C, 76.56; H, 6.42%. *(b) The Reaction of* ***1b*** *with* ***2***: A similar reaction of **1b** with **2** yielded 7,7-dimethyl-3,4-diphenyl-2-ethylthio-5,6,7,8-tetrahydro-2*H*-1-benzopyran-5-one (**8b**) in 58%. **8b**: mp 152—154 °C; IR (KBr) 1650 and 1620 cm^{-1}; ^{1}H-NMR ($CDCl_3$) δ=1.17 (3H, s, Me), 1.22 (3H, s, Me), 1.37 (3H, t, *J*=7.5 Hz, MeCH_2), 2.28 (2H, s, CH_2CO), 2.48 (2H, s, CH_2C=C), 2.77 (2H, q, CH_2S), 6.16 (1H, s, CH), and 6.8—7.4 (10H, m, 2Ph); MS (*m/z*) 390 (M^+). Found: C, 77.02; H, 6.79%. Calcd for $C_{25}H_{26}O_2S$: C, 76.89; H. 6.71%. *(c) The Reaction of* ***1c*** *with* ***2***: Similar reaction of **1c** with **2** yielded 2-benzylthio-7,7-dimethyl-3,4-diphenyl-5,6,7,8-tetrahydro-2*H*-1-benzopyran-5-one (**8c**) in 67% yield. **8c**: mp 157—159 °C; IR (KBr) 1665, 1650, and 1620 cm^{-1}; ^{1}H-NMR ($CDCl_3$) δ=1.11 (3H, s, Me), 1.18 (3H, s, Me), 2.25 (2H, s, CH_2C=C), 2.29 (2H, CH_2CO), 3.94 (2H, dd, *J*=2.5 and 14.5 Hz, PhCH_2S), 6.06 (1H, s, CH), and 6.8—7.4 (15H, m, 3Ph); MS (*m/z*) 452 (M^+). Found: C, 79.37; H, 6.14%. Calcd for $C_{30}H_{28}O_2S$: C, 79.61;

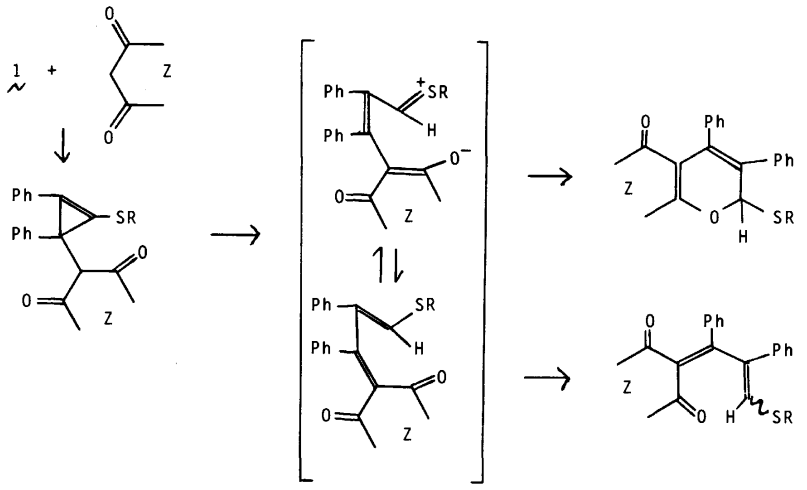

Scheme 4.

H, 6.24%. *(d) The Reacion of* ***1a*** *with* ***3***: Similar treatment of **1a** with **3** afforded 3,4-diphenyl-2-methylthio-6,7-dihydrocyclopenta[*b*]pyran-5(2*H*)-one (**9**) in 89%. **9**: mp 175 °C; IR(KBr) 1670 and 1620 cm^{-1}; ^{1}H-NMR ($CDCl_3$) δ=2.32 (3H, s, MeS), 2.4—2.9 (4H, m, CH_2CH_2), 6.35 (1H, s, CH), 6.8—7.6 (10H, m, 2Ph); ^{13}C-NMR ($CDCl_3$) δ=13.8 (q, MeS), 25.9 (t), 34.6 (t), 91.3 (d), 117.5 (s),123.2 (s), 127.4 (d), 128.0 (d), 129.5 (d), 130.0 (d), 131.6 (s), 134.0 (s), 136.3 (s), 183.1 (s), and 198.3 (s); MS (*m/z*) 334 (M^+). Found: C, 75.15; H, 5.63%. Calcd for $C_{21}H_{18}O_2S$: C, 75.42; H, 5.43%. *(e) The Reaction of* ***1a*** *with* ***4***: Similar treatment of **1a** with **4** yielded 3,4-diphenyl-2-methylthio-5,6,7,8-tetrahydro-2*H*-1-benzopyran-5-one (**10**) in 74% yield. **10**: mp 174—176 °C; IR (KBr) 1660 and 1640 cm^{-1}; ^{1}H-NMR ($CDCl_3$) δ=1.8—2.8 (6H, m, $CH_2CH_2CH_2$), 2.28 (3H, s, MeS), 6.04 (1H, s, CH), and 6.8—7.6(10H, m, 2Ph); ^{13}C-NMR ($CDCl_3$) δ=14.0 (q, MeS), 20.0 (t), 29.4 (t), 37.8 (t), 88.2 (d), 117.7 (s), 123.5 (s), 126.6 (d), 127.1 (d), 127.4 (d), 127.8 (d), 128.3 (d), 129.3 (d), 132.5(s), 137.0 (s), 137.9 (s), 169.9 (s), and 193.5 (s); MS (*m/z*) 348 (M^+). Found: C, 75.68; H, 5.84%. Calcd for $C_{22}H_{20}O_2S$: C, 75.83; H, 5.79%. *(f) The Reaction of* ***1a*** *with* ***5***: Similar treatment of **1a** with **5** yielded **11** in 90%. **11**; mp 162—164 °C; IR (KBr) 1700 and 1640 cm^{-1}; ^{1}H-NMR ($CDCl_3$) δ=2.20 (3H, s, MeC=C), 2.23 (3H, s, MeS), 5.92 (1H, s, HC-SMe), 6.06 (1H, s, HC=C), and 6.8—7.3 (10H, m, 2Ph); ^{13}C-NMR($CDCl_3$) δ=14.1 (q, MeS), 20.2 (q), 88.0 (d), 100.2 (d), 103.4 (s), 125.2 (s), 127.1 (d), 127.2 (d), 127.5 (d), 127.8 (d), 128.2 (d), 129.2 (d), 129.4 (d), 132.0 (s), 136.1 (s), 136.7 (s), 163.0 (s), and 163.8 (s); MS (*m/z*) 315 (M^+—SMe). Found: C, 72.99; H, 5.25%. Calcd for $C_{22}H_{18}O_3S$: C, 72.91; H, 5.04%. *(g) The Reaction of* ***1a*** *with* ***6***: Similar treatment of **1a** with **6** yield **12** in 84% yield. **12**: mp 204 °C; IR (KBr) 1720 and 1610 cm^{-1}; ^{1}H-NMR ($CDCl_3$) δ=2.27 (3H, s, MeS), 6.29 (1H, s, CH), and 6.7—8.1 (14H, m, Arom); ^{13}C-NMR ($CDCl_3$) δ=13.8 (q, MeS), 88.4 (d, MeSC H), 105.6 (s), 115.6 (s), 116.6 (d), 122.6 (d), 124.0 (d), 126.8 (s), 127.2 (d), 127.5 (d), 127.6 (d), 127.9 (d), 129.2 (d), 129.4 (d), 132.3 (s), 132.4 (d), 136.2 (s), 136.5 (s), 153.5 (s), 157.8 (s), and 158.2 (s); MS (*m/z*) 351 (M^+—SMe). Found: C, 75.63; H, 4.72%. Calcd for $C_{25}H_{18}O_3S$: C, 75.63; H, 4.55%. *(h) The Reaction of* ***1a*** *with* ***7***: Similarly **13** was obtained in 63% yield. **13**: mp 138—140 °C; IR (KBr) 1660 cm^{-1}; ^{1}H-NMR ($CDCl_3$) δ=1.5—2.1 (4H, m, $COCH_2CH_2CH_2CH_2$), 2.24 (3H, s, MeS), 2.3—2.9 (4H, m, $COCH_2CH_2CH_2CH_2$), 6.00 (1H, s, CH), and 6.7—7.4 (10H, m, 2Ph); ^{13}C-NMR ($CDCl_3$) δ=13.8 (q), 21.7 (t), 22.9 (t), 32.3 (t), 42.9 (t), 87.8 (d), 121.2 (s), 122.9 (s), 126.6 (d), 126.9 (d), 127.5 (d), 127.7 (d), 129.1 (d), 134.3 (s), 137.0 (s), 138.1 (s), 163.5 (s), and 199.9 (s); MS (*m/z*) 315 (M^+—SMe). Found: C, 76.34; H, 6.19%. Calcd for $C_{23}H_{22}O_2S$: C, 76.21; H, 6.12%.

Desulfurization of ***8—13*** *with Mercury(II) Chloride. (a) The Reaction of* ***8a*** *in Methanol*: A mixture of **8a** (0.5 mmol) mercury(II) chloride (0.55 mmol), methanol (5 cm^3), and dichloromethane (10 cm^3) was stirred for 2 h to give a clear solution. The solution was quenched in water and extracted with chloroform. The chloroform extract was evaporated *in vacuo* to give colorless crystals (98%), and recrystallization from chloroform-hexane yielded 7,7-dimethyl-3,4-diphenyl-2-methoxy-5,6,7,8-tetrahydro-2*H*-1-benzopyran-5-one (**14a**) in 93% yield. **14a**: mp 175—177 °C; IR (KBr) 1670 and 1630 cm^{-1}: ^{1}H-NMR ($CDCl_3$) δ=1.11 (3H, s, Me), 1.20 (3H, s, Me), 2.26 (2H, s, CH_2), 2.58 (2H, s, CH_2), 3.59 (3H, s, MeO), 5.56 (1H, s, CH), and 6.8—7.7 (10H, m, 2Ph); ^{13}C-NMR ($CDCl_3$) δ=27.3 (q), 29.3 (q), 31.7 (s), 42.6 (t), 51.8 (t), 55.3 (q), 101.4 (d), 113.9 (s), 123.5 (s), 126.5 (d), 126.7 (d), 127.7 (d), 129.2 (d), 129.3 (d), 132.0 (s), 137.1 (s), 138.0 (s), 167.2 (s), and 193.6 (s); MS (*m/z*) 360 (M^+). Found: C, 79.88; H, 6.54%. Calcd for $C_{24}H_{24}O_3$: C, 79.97; H, 6.71%. *(b) The Reaction of* ***8a*** *in Ethanol*: Similar treatment of **8a** in ethanol afforded 7,7-dimethyl-3,4-diphenyl-2-ethoxy-5,6,7,8-tetrahydro-2*H*-1-benzopyran-5-one (**14b**) in 78% yield. **14b**: mp 116—118 °C; IR (KBr) 1660 and 1620 cm^{-1}; ^{1}H-NMR ($CDCl_3$) δ=1.13 (3H, s, Me), 1.22 (3H, s, Me), 1.32 (3H, t, *J*= 7 Hz, CH_3CH_2), 2.25 (2H, s, CH_2), 2.53 (2H, s, CH_2), 3.88 (2H, dd, *J*=6 and 7 Hz, CH_2O), 5.63 (1H, s, CH), and 6.5—7.5 (10H, m, 2Ph); MS(*m/z*) 374 (M^+). Found: C, 80.11; H, 7.06%. Calcd for $C_{25}H_{26}O_3$: C, 80.18; H, 7.00%. Similar treatment of **8b** in ethanol yielded **14b** in 82% yield. *(c) The Reaction of* ***8a*** *in 2-Propanol*: Similarly **14c** was obtained in 80% yield. **14c**: mp 163—164 °C; IR(KBr) 1660 cm^{-1}; ^{1}H-NMR ($CDCl_3$) δ=1.07 and 1.16 (6H, s, CMe_2), 1.25 (6H, d, *J*=7 Hz, $CHMe_2$), 2.21 and 2.49 (4H, s, $CH_2CMe_2CH_2$), 4.21 (1H, sept, $CHMe_2$), 5.65 (1H, s, OCHO), and 6.7—7.4 (10H, m, 2Ph); MS (*m/z*) 345 (M^+—$CHMe_2$) and 329 (M^+—$OCHMe_2$). Found: C, 80.20; H, 7.36%. Calcd for $C_{26}H_{28}O_3$: C, 80.38; h, 7.26%. *(d) The Reaction of* ***9*** *in methanol* yielded 3,4-diphenyl-2-methoxy-6,7-dihydrocyclopenta-[*b*]pyran-5(2*H*)-one (**15a**) in 87% yield. **15a**: mp 130—133 °C; IR (KBr) 1690 and 1630 cm^{-1}; ^{1}H-NMR ($CDCl_3$) δ= 2.3—3.0 (4H, m, CH_2CH_2), 3.63 (3H, s, MeO), 5.83 (1H, s, CH), and 6.5—7.6 (10H, m, 2Ph); MS (*m/z*) 318 (M^+). Found: C, 79.11; H, 5.82%. Calcd for $C_{21}H_{18}O_3$; C, 79.23; H, 5.70%. *(e) The reaction of* ***9*** *in ethanol* yielded **15b** in 81% yield. **15b**: mp 157—158 °C; IR (KBr) 1680 and 1620 cm^{-1}: ^{1}H-NMR ($CDCl_3$) δ=1.26 (3H, t, *J*=7 Hz, CH_3CH_2), 2.3—2.9 (4H, m, $COCH_2CH_2$), 3.5—4.2 (2H, m, CH_2O), 5.84 (1H, s, CH), and 6.7—7.3 (10H, m, 2Ph); MS (*m/z*) 332 (M^+). Found: C, 79.30; H 6.09%. Calcd for $C_{22}H_{20}O_3$: C, 79.49; H, 6.06%. *(f) The reaction of* ***10*** *in methanol* yielded 3,4-diphenyl-2-methoxy-5,6,7,8-tetrahydro-2*H*-1-benzopyran-5-one (**16**) in 79% yield. **16**: mp 175—177 °C; IR(KBr) 1660 and 1620 cm^{-1}; ^{1}H-NMR ($CDCl_3$) δ=1.7—2.8 (6H, m, $-(CH_2)_3-$), 3.53 (3H, s, MeO), 5.49 (1H, s, CH), and 6.5—7.5 (10H, m, 2Ph); MS (*m/z*) 318 (M^+); Found: C, 76.62; H, 6.06%. Calcd for $C_{22}H_{20}O_3$: C, 79.50; H, 6.06%. *(g) The reaction of* ***11*** *in ethanol* yielded **17** in 65% yield. **17**: mp 202—205 °C: IR (KBr) 1710, 1640, and 1620 cm^{-1}; ^{1}H-NMR ($CDCl_3$) δ=1.29 (3H, t, *J*=7 Hz, CH_3CH_2), 2.22 (3H, s, MeC=C), 3.5—4.2 (2H, m, CH_2O), 5.68 (1H, s, CH), 5.99 (1H, s, CH), and 6.8—7.4 (10H, m, 2Ph); ^{13}C-NMR ($CDCl_3$) δ= 15.3 (q), 20.2 (q), 64.6 (t), 100.0 (d), 100.2 (d), 101.5 (s), 125.5 (s), 127.0 (d), 127.5 (d), 127.8 (d), 129.3 (d), 129.6 (d), 131.5 (s), 136.5 (s), 137.1 (s), 160.1 (s), 162.2 (s), and 163.1 (s); MS (*m/z*) 360 (M^+). Found: C, 76.38; H, 5.49%. Calcd for $C_{23}H_{20}O_4$: C, 76.65; H, 5.59%. *(h) The reaction of* ***12*** *in ethanol* yielded **18** in 89% yield. **18**: mp 172—174 °C; IR (KBr) 1720, 1630, and 1610 cm^{-1}; ^{1}H-NMR ($CDCl_3$) δ=1.26 (3H, t, *J*= 7 Hz, CH_3CH_2), 3.5—4.3 (2H, m, CH_2), 5.89 (1H, s, CH), and 6.8—8.2 (10H, m, Arom); ^{13}C-NMR ($CDCl_3$) δ=15.4 (q), 64.6 (t), 100.4 (d), 104.4 (s), 115.5 (s), 116.6 (d), 122.6 (d), 124.0 (d), 126.9 (s), 127.1 (d), 127.2 (d), 127.6 (d), 127.9 (d), 129.2 (d), 129.5 (d), 131.6 (s), 132.2 (d), 136.6 (s), 136.9 (s), 153.4 (s), 157.0 (s), and 158.6 (s); MS (*m/z*) 395 (M^+—1). Found: C, 78.96; H, 4.92. Calcd for $C_{26}H_{20}O_4$: C, 78.77; H, 5.08%. *(i) The reaction of* ***13*** *in ethanol* yielded **19** in 61% yield. **19**: mp 120—122 °C; IR (KBr) 1650 and 1630 cm^{-1}; ^{1}H-NMR ($CDCl_3$) δ=1.25 (3H, t, *J*=7 Hz, CH_3), 1.6—2.2 (4H, m, $COCH_2(CH_2)_2$), 2.3—2.9 (4H, m, $COCH_2(CH_2)_2CH_2$), 3.5—4.1 (2H, m, CH_3CH_2), 5.56 (1H, s, CH), and 6.7—7.3 (10H, m, 2Ph); ^{13}C-NMR($CDCl_3$) δ=15.4 (q), 21.6 (t), 22.9 (t), 31.8 (t), 42.7 (t), 63.6 (t), 99.8 (d), 118.6 (s), 123.0 (s), 126.4 (d), 126.5 (d), 127.4 (d), 127.5 (d), 129.1 (d), 133.4 (s), 137.4 (s), 138.2 (s), 161.8 (s), and 200.8 (s); MS (*m/z*) 315 (M^+—EtO). Found: C, 80.22; H, 6.66%. Calcd for $C_{24}H_{24}O_3$: C, 79.97; H, 6.71%.

The Reaction of ***8a*** *in Acetic Acid.* A mixture of **8a** (0.5 mmol) and mercury(II) acetate (0.55 mmol) in acetic acid (5 cm^3) was stirred at room temperature for 2 h to give a clear solution. The solution was poured into water and extracted with chloroform. The extract was treated with aqueous sodium hydroxide (5%, 20 cm^3) and aqueous layer was sep-

arated. Acidification of the aqueous extract with phosphoric acid, extraction with chloroform, and condensation of the chloroform extract under reduced pressure yielded a resinous mass (86%). Crystallization from benzene and petroleum ether yielded scales, 7,7-dimethyl-3,4-diphenyl-2-hydroxy-5,6,7,8-tetrahydro-2*H*-1-benzopyran-5-one (**20**) in 57%. **20**: mp 105—107 °C; IR (KBr) 3300 (OH), 1640, and 1620 cm^{-1}; ^{1}H-NMR($CDCl_3$) δ=1.09 (3H, s, Me), 1.11 (3H, s, Me), 2.23 (2H, s,CH_2), 2.26 (2H, s, CH_2), 5.76 (1H, s, CH), and 6.6—7.6 (10H, m, 2Ph); ^{13}C-NMR($CDCl_3$) δ=26.9 (q), 29.7 (q), 31.4 (s), 42.9 (t), 51.3 (t), 95.0 (d), 113.6 (s), 125.5 (s), 126.7 (d), 126.9 (d), 127.5 (d), 127.7 (d), 128.3 (d), 129.3 (d), 130.5 (s), 136.7 (s), 137.6 (s), 168.2 (s), and 194.8 (s); MS (*m/z*) 328 (M^+−18). Found: C, 79.94; H, 6.74%. Calcd for $C_{23}H_{22}O_3$: C, 79.74; H, 6.40%.

The ^{1}H-NMR spectrum of **20** in $CDCl_3$-Et_3N(100:3, v/v) showed δ=1.05 (6H, br, s, Me_2), 2.25 (4H, br, s, CH_2CH_2), 6.8—7.5 (10H, m, 2Ph), 9.22 (1H, s, exchangeable with D_2O) and 9.80 (1H, s, CH) indicating the structure to be the unsaturated aldehyde **22**. The reaction of **22** with *p*-toluenesulfonohydrazide was carried out as follows. A solution of **20** (0.5 mmol), *p*-toluenesulfonohydrazide (1 mmol), triethylamine (3 mmol) in ethanol (3 cm^3) was allowed at room temperature for 2 d. The precipitated needles were collected and recrystallized from ethanol to give the hydrazone **23** in 38%. **23**: mp 125—127 °C; IR (KBr) 3400 and 1710 cm^{-1}; ^{1}H-NMR($CDCl_3$) δ=0.91 (6H, s, Me_2), 2.30 (3H, s, $\underline{CH}_3C_6H_4$), 2.41 (2H, s, CH_2), 3.21 (2H, s, CH_2), 6.6—7.8 (15H, m, 2Ph, C_6H_4, and NH), and 8.59 (1H, s, CH=N); MS (*m/z*) 497 (M^+−OH). Found: C, 69.78; H, 5.87; N, 5.42%. Calcd for $C_{30}H_{30}N_2O_4S$: C, 70.02; H, 5.88; N, 5.44%.

*Oxidation of **20** with Sodium Dichromate. (a)*: A mixture of **20** in acetic acid (1 mmol in 5 cm^3) and sodium dichromate in water (1 mmol in 2 cm^3) was stirred for 10 min. The resulting solution was diluted with water and extracted with chloroform. The chloroform extract was condensed and chromatographed over silica gel (chloroform, petroleum ether, and ethyl acetate in 4:4:1, v/v). 2-(Benzoylphenylmethylene)-5,5-dimethyl-1,3-cyclohexanedione (**24**) was obtained in 45% yield. **24**: mp 156—157 °C; IR (KBr) 1710 and 1670 cm^{-1}; ^{1}H-NMR ($CDCl_3$) δ=1.12 (6H, s, Me_2), 2.57 (2H, s, CH_2), 2.63 (2H, s, CH_2), and 7.0—7.9 (10H, m, 2Ph); ^{13}C-NMR ($CDCl_3$) δ=28.5 (q), 29.9 (s), 53.1 (t), 54.5 (t), 128.2 (d), 128.3 (d), 128.7 (d), 129.0 (d), 129.8 (d), 133.2 (d), 133.3 (s), 133.6 (s), 134.8 (s), 161.9 (s), 194.7 (s), 196.6 (s), and 197.6 (s); MS (*m/z*) 332 (M^+). Found: C, 79.28; H, 6.07. Calcd for $C_{22}H_{20}O_3$: C, 79.50; H, 6.06. *(b)*: Further oxidation of **24** was carried out as follows. A mixture of **24** (1 mmol) and sodium dichromate (2 mmol) in acetic acid (20 cm^3) was stirred at room temperature for 5 h. The resulting solution was treated as above to yield 2-[α-(benzoyloxy)benzylidene]-5,5-dimethyl-1,3-cyclohexanedione (**25**) in 24% yield. **25**: mp 146—148 °C; IR(KBr) 1730, 1680, and 1660 cm^{-1}; ^{1}H-NMR ($CDCl_3$) δ=1.25 (6H, s, Me_2), 2.46 (2H, s, CH_2), 2.78 (2H, s, CH_2), and 6.9—8.1 (10H, m, 2Ph); ^{13}C-NMR ($CDCl_3$) δ=28.2 (q), 33.1 (s), 42.2 (t), 51.0 (t), 127.7 (s), 128.3 (s), 128.5 (d), 128.9 (d) 130.0 (d), 133.6 (d), 134.1 (d), 136.6 (s), 162.8 (s), 166.3 (s), 192.1 (s), and 196.4 (s); MS (*m/z*) 348 (M^+). Found: C, 75.82; H, 5.66%. Calcd for $C_{22}H_{20}O_4$: C, 75.84; H, 5.79%.

*Hydrolysis of **25**.* In a mixture of concd HCl (1 cm^3) and 20% aqueous ethanol (20 cm^3), some **25** (0.3 mmol) was kept for 2 d. The resulting solution was quenched in water and extracted with chloroform. The chloroform extract was condensed under reduced pressure and then dissolved in 30 cm^3 of ether. The solution was shaken with an aqueous saturated solution of copper(II) acetate (0.3 mmol) and the resulting precipitate was separated. The precipitate was treated with 3 M hydrochloric acid (1 M=1 mol dm^{-3}) to give colorless crystals. The crystals were collected and recrystallized from petroleum ether to yield the known 2-benzoyl-5,5-dimethyl-1,3-cyclohexanedione **26** in 36% yield. **26**: mp 120—121 °C (lit,[4] mp 120—122 °C); ^{1}H-NMR ($CDCl_3$) δ=1.08 (6H, s, Me_2), 2.24 (2H, s, CH_2), 2.49 (2H, s, CH_2), and 7.1—7.5 (5H, br s, Ph); MS (*m/z*) 244(M^+).

*The Reaction of **1a** or **1b** with 1,3-Indandione **27**.* The reaction was carried out as was described in the reaction of **1a** with **2**. The salt **1a** gave **28a** in 41% yield. **28a**: mp 190—191 °C; IR (KBr) 1690 cm^{-1}; ^{1}H-NMR ($CDCl_3$) δ=2.18 (3H, s, MeS), 6.60 and 6.71 (1H, s, 1:2, C=CH), and 6.8—8.1 (14H, m, Arom); MS(*m/z*) 381 (M^+−1). Found:C, 78.22; H, 4.66%. Calcd for $C_{25}H_{18}O_2S$: C, 78.50; H, 4.74%. The salt **1b** yielded **28b** in 37% yield. **28b**: mp 134—136 °C; IR (KBr) 1650 cm^{-1}; ^{1}H-NMR ($CDCl_3$) δ=1.11 (3H, t, *J*=7 Hz, CH_3), 2.54 (2H, q, CH_2), 6.49 and 6.58 (1H, s, 1:2, C=CH), and 6.8—8.0 (14H, m, Arom); MS (*m/z*) 396 (M^+). Found: C, 78.43; H, 4.96%. Calcd for $C_{26}H_{20}O_2S$: C, 78.76; H, 5.08%.

*The Reaction of **28a** with Mercury(II) Acetate in Acetic Acid.* The compound **28a** was treated in a way similar to that described in the reaction of **8a** with mercury(II) acetate in acetic acid; **30** was obtained in 50% yield. **30**: resinous; IR (KBr) 3400, 1700, and 1680 cm^{-1}; ^{1}H-NMR ($CDCl_3$) δ= 4.44 (1H, s, exchangeable with D_2O, OH), 6.4—8.3 (14H, m, Arom), and 9.59 (1H, s, CHO); MS (*m/z*) 352 (M^+). Found: C, 81.66; H, 4.67%. Calcd for $C_{24}H_{16}O_3$:C, 81.80; H, 4.57%.

The reaction of 30 with *p*-toluenesulfonohydrazide in ethanol at room temperature for 2 d yielded the corresponding diazepine **32** in 44% yield. **32**: mp 280—281 °C; IR (KBr) 1730 cm^{-1}; ^{1}H-NMR ($CDCl_3$) δ=2.30 (3H, s, CH_3), 6.5—9.1 (18H, m, Arom), and 8.38 (1H, s, N=CH); MS (*m/z*) 502 (M^+). Found: C, 74.06; H, 4.50; N, 5.70%. Calcd for **31**, $C_{31}H_{24}N_2O_4S$:C, 71.52; H, 4.65; N, 5.38% and for **32**, $C_{31}H_{22}N_2O_3S$: C, 74.08; H, 4.41; N, 5.57%.

*The Reaction of **28a** with Alcohol in the Presence of Mercury(II) Chloride.* The compound **28a** was treated as described in the reaction of **8a**. The reaction of **28a** in ethanol yielded **33a** in 84%. **33a**: mp 133—134 °C; IR (KBr) 1690 cm^{-1}; ^{1}H-NMR ($CDCl_3$) δ=1.23 (3H, t, *J*=7 Hz, CH_3), 3.82 (2H, q, CH_2), 5.93 (1H, s, CH), and 6.6—7.7 (14H, m, Arom); MS (*m/z*) 380 (M^+). Found: C, 82.01; H, 5.27%. Calcd for $C_{26}H_{20}O_3$: C, 82.08; H, 5.29%.

The reaction of **28a** in 2-propanol gave **33b** in 63% yield. **33b**: mp 135—136 °C; IR (KBr) 1700 cm^{-1}; ^{1}H-NMR ($CDCl_3$) δ=1.26 (6H, d, *J*=7Hz, Me_2), 4.24 (1H, sept, $O\underline{CH}Me_2$), 6.13 (1H, s, CH), and 6.9—7.4 (14H, m, Arom); ^{13}C-NMR ($CDCl_3$) δ=23.2 (q), 73.2 (d, $CHMe_2$), 106.1 (d, CH), 118.3 (d), 121.7 (d), 122.4 (s), 126.9 (d), 127.4 (s and d), 127.6 (s), 127.8 (d), 129.5 (d), 130.2 (d), 130.3 (d), 131.0 (d), 132.6 (d), 134.5 (s), 135.0 (s), 137.0 (s), 188.8 (s); MS (*m/z*) 394 (M^+). Found: C, 82.34; H, 5.55%. Calcd for $C_{27}H_{22}O_3$: C, 82.21; H, 5.62%.

References

1) R. M. Acheson, "An Introduction to the Chemistry of Heterocyclic Compounds," 3rd ed, John Wiley & Sons, New York (1977).

2) E. N. Marvel, "Thermal Electrocyclic Reactions," Academic Press, New York (1980).

3) H. Yoshida, M. Nakajima, T. Ogata, K. Matsumoto, R. M. Acheson, and J. D. Wallis, *Chem. Lett.*, **1983**, 155; *Bull. Chem. Soc. Jpn.*, **56**, 3015 (1983).

4) W. Kirokor and J. Baranowicz, *Lodz. Towarz. Nauk. Wydzial III, Acta Chim.*, **8**, 69 (1962); *Chem. Abstr.*, **59**, 7415d (1963).

5) The assignment of the structure **32** was tentative. Attempted conversion of **23** to the corresponding 1*H*-1,2-diazepine was unsuccessful, even on refluxing in toluene or on treating with trifluoroacetic acid in benzene, presumably because of steric repulsion between toluenesulfonyl and two methyl groups.

 © 1984 The Chemical Society of Japan Bull. Chem. Soc. Jpn., 57, 739—746 (1984)

Asymmetric Hydrogenation with Rhodium(I)-Chiral Diphosphinites. The Effect of the Dimethylamino Group of the Ligand on the Asymmetric Induction

Masanobu YATAGAI, Masanobu ZAMA, Takamichi YAMAGISHI,* and Mitsuhiko HIDA

Department of Industrial Chemistry, Faculty of Technology, Tokyo Metropolitan University, Fukasawa, Setagaya-ku, Tokyo 158

(Received September 5, 1983)

New chiral diphosphinites were prepared starting from (+)-diethyl tartrate. The asymmetric hydrogenation of dehydroamino acids, itaconic acid and dehydrodipeptides was studied using Rh(I)–diphosphinite catalysts. In the hydrogenation of dehydroamino acid derivatives, an introducion of ω-(dimethylamino)alkyl group in the ligands did not raise the optical yield. By the use of Rh(I)–diphosphinite having 3-(dimethylamino)propyl group, the inversion of the preferred product was observed. Itaconic acid can be hydrogenated in a good optical yield (76% e.e.) by use of the diphosphinite having 2-(dimethylamino)ethyl group. The diphosphinites having ω-dimethylamino group gave high optical yields in the case of dehydrodipeptides with a chiral center. Especially Rh(I)-catalysts coordinated by diphosphinites with 4-methyl or 4-methoxyl group on the phenyl ring of the ligand gave excellent stereoselectivities (more than 98% d.e.) in the case of Ac-ΔPhe-(*S*)-Phe-OH. The effect of these new chiral diphosphinites on the asymmetric hydrogenation of dehydroamino acids, itaconic acid and dehydrodipeptides was discussed in terms of the stereocontrol induced by electrostatic interaction between the dimethylamino group of the ligand and the substrate and by the steric interaction between the ligand and the substrate.

Recently, asymmetric hydrogenation of prochiral olefins has been studied very actively using many chiral ligands. In the hydrogenation of dehydroamino acid derivatives, several ligands could give high enough optical yields to be practically applied for amino acid production.[1]

Since most of these ligands were designed to control the asymmetric induction only by the steric interaction between the substrate and phenyl groups on phosphorus atoms of the ligand,[2] the efficiency of these ligands seems to depend strongly on the structure of olefins.[3]

We intended to introduce both electrostatic and steric effects into the asymmetric hydrogenation of olefinic compounds. The electrostatic interaction between ligand and olefin will serve more significantly to discriminate the prochiral face of the substrate. So we prepared new chiral diphosphinites with pyrrolidine moiety, some of them having ω-(dimethylamino)alkyl substituent on the pyrrolidine ring. The dimethylamino group is expected to interact with a carboxyl group of prochiral olefins. These diphosphinites were used for asymmetric hydrogenation of dehydroamino acid derivatives, itaconic acid and dehydrodipeptides.[4] The result of itaconic acid and dehydrodipeptides strongly suggested that an electrostatic effect contributed to the stereoselection (Scheme 1).

Result and Discussion

The preparative route to the diphosphinites (**1**—**5**) is shown in Scheme 2. 1,4-Di-*O*-tosyl-L-threitol was induced from (+)-diethyl tartrate by conventional method.[5] *N*-Substituted (*S,S*)-3,4-pyrrolidinediols were obtained by the reaction of the corresponding amine and 1,4-di-*O*-tosyl-L-threitol. These diols were easily converted to the diphosphinites (**1**—**5**) by the reaction with chlorodiarylphosphine in the presence of triethylamine.[6] Diphosphinite (**1**) is a carbon analog of **2** and is expected to show a similar steric effect to that of **2**.

The result of asymmetric hydrogenation of dehydroamino acid derivatives with Rh(I)–diphosphinite (**1**—**3**) catalysts are summarized in Table 1. Rh(I)–diphosphinite (**1**—**3**) catalysts gave low optical yields. In

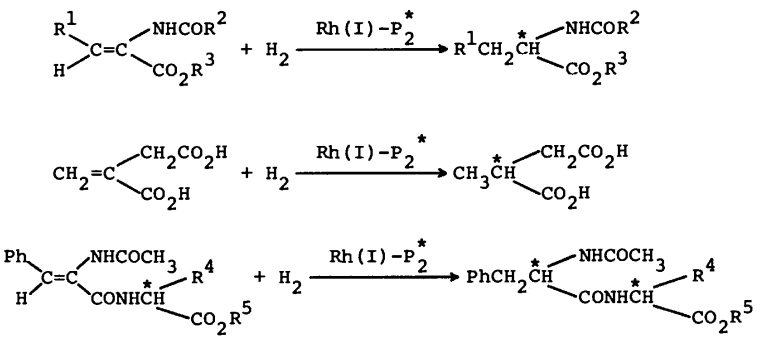

Scheme 1.

the hydrogenation of α-acetamidocinnamic acid, diphosphinite (**1**) without dimethylamino group, gave (*S*)-product in a higher optical yield than that with **2** (29% e.e. and 16% e.e., respectively). In the case of other *N*-acyl dehydroamino acids, diphosphinite (**1**) also gave (*S*)-product in higher optical yields than those with diphosphinite (**2**). It is noted that diphosphinite (**3**), which has a longer aminoalkyl group than **2**, gave (*R*)-product although the absolute configrations of the diphosphinites (**1**—**3**) are the same. The inversion of

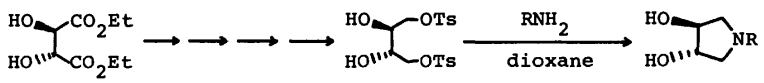

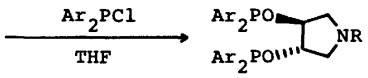

diphosphinite	Ar	R
1	Ph	$CH_2CH_2CH(CH_3)_2$
2	Ph	$CH_2CH_2N(CH_3)_2$
3	Ph	$CH_2CH_2CH_2N(CH_3)_2$
4		$CH_2CH_2N(CH_3)_2$
5	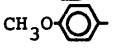	$CH_2CH_2N(CH_3)_2$

Scheme 2.

TABLE 1. ASYMMETRIC HYDROGENATION OF DEHYDROAMINO ACID DERIVATIVES USING Rh(I)-DIPHOSPHINITE (**1**—**3**) CATALYSTS[a]

Substrate[b]	Diphosphinite[c]	Time / min	Conversion / %	% e.e.	Configuration
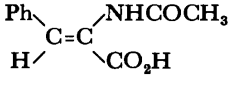	**1**	20	100	29	*S*
	1	50	100	5	*S*[e]
	2	720	100	16	*S*
	2	90	100	4	*S*[e]
	3	60	100	13	*R*
	3	90	100	10	*R*[e]
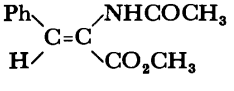	**1**	20	100	27	*S*
	2	very slow		—	—
	3	600	100	35	*R*
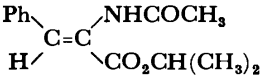	**1**	11	100	3	*S*
	3	1500	65	2	*R*
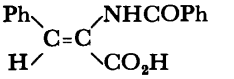	**1**	40	100	40	*S*
	2	720	100	19	*S*
	3	180	100	1	*R*
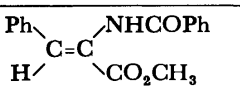	**1**	50	100	28	*S*
	3	120	100	4	*R*
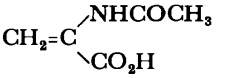	**1**	10	100	19	*S*
	2	90	100	6	*S*
	3	70	100	9	*R*

a) Hydrogenations were performed in ethanol-benzene (2/1) under atmospheric hydrogen pressure at 20 °C. b) Substrate/Rh=100. c) Diphosphinite/Rh=1.5. d) Optical yields (% e.e.) were calculated from the specific rotation of the product and that of optically pure substance: *N*-acetyl-(*S*)-phenylalanine, $[\alpha]_D^{26}$ +46.0° (*c* 1.0, EtOH);[1a] *N*-acetyl-(*S*)-phenylalanine methyl ester, $[\alpha]_D^{25}$ +15.9° (*c* 2.0, MeOH);[13] *N*-acetyl-(*S*)-phenylalanine isopropyl ester, $[\alpha]_D^{25}$ +76.1° (*c* 1.0, $CHCl_3$);[13] *N*-benzoyl-(*S*)-phenylalanine, $[\alpha]_D^{27}$ −40.3° (*c* 1.0, MeOH);[1a] *N*-benzoyl-(*S*)-phenylalanine methyl ester, $[\alpha]_D^{25}$ −45.3° (*c* 1.3, 95% EtOH);[18] *N*-acetyl-(*R*)-alanine, $[\alpha]_D^{26}$ +66.3° (*c* 2.0, H_2O).[1a] e) Addition of triethylamine (NEt_3/Rh=10).

the preferred product using diphosphinite (**3**) was also observed in the reaction of esters. This inversion in the system of **3** is considered to arise mainly from the change of the conformation of phenyl group on phosphorus atoms by the steric repulsion between the dimethylamino group and the phenyl groups. The results obtained indicate that the diphosphinite with a longer aminoalkyl group lowered the (*S*)-selectivity in the reaction of dehydroamino acid derivatives.

The rate of the hydrogenation with Rh(I)-diphosphinite (**2** or **3**) catalyst was much slower than that with Rh(I)-diphosphinite (**1**) catalyst, especially for dehydroamino acid esters. The suppression of the hydrogenation of esters would be ascribed to the coordination of the dimethylamino group onto rhodium and the weaker coordination ability of esters onto rhodium than that of carboxylic acids. The reaction was also suppressed by the presence of bulky alkyl substituent in the dehydroamino acid ester. The results of the hydrogenation of dehydroamino acids make it unlikely that any electrostatic interaction exists between carboxyl group of the substrate and the dimethylamino group of the ligand in the rhodium complex.

The low stereoselectivity by Rh(I)-diphosphinite (**1**—**3**) catalysts can be explained by the presence of several kinds of Rh(I) species in the reaction systems. ^{31}P NMR spectra of Rh(I)-diphosphinite (**2** or **3**)-α-acetamidocinnamic acid systems showed the presence of several Rh(I) species in the solution (Fig. 1). The different ^{31}P NMR patterns of the two systems (**2** and **3**), as well as CD spectra (*vide infra*), suggest the presence of different rhodium species in each system which has a different stereoselectivity.

Triethylamine addition into rhodium-chiral diphosphine systems increased the optical yields of hydrogenation of *N*-acyl dehydroamino acids.[7] It is thought that triethylamine deprotonates a carboxyl group of the substrate on rhodium. In our diphosphinite (**1**—**3**) systems, however, the addition of triethylamine lowered the optical yield of the hydrogenation of α-acetamidocinnamic acid (Table 1). Amine addition increased the intensity of the absorptions corresponding to d-d transition and CT transition of the rhodium complex for both systems (**2** and **3**). The intensity of the CD spectrum was reduced by the amine addition in the system of Rh(I)-(**2**)-α-acetamidocinnamic acid while the intensity was increased by the additive amine in the system of **3** (Fig. 2). The different effect of the additive amine on the CD spectra of the two systems would indicate that the main Rh(I) species have different coordination manners for these two diphosphinite systems.

We applied the diphosphinite (**1**—**3**) catalysts to itaconic acid (α-methylenesuccinic acid) which has a structure similar to α-acetamidoacrylic acid. Itaconic acid is considered to be more suitable to examine the effect of electrostatic interaction because of the presence of two carboxyl groups in the molecule. The dimethylamino group of **2** and **3** may interact electrostatically with β-carboxyl group of itaconic acid to enable the three points' recognition of the prochiral face of itaconic acid. As shown in Table 2, Rh(I)-diphosphinite (**2** and **3**) catalysts gave much higher optical yields for itaconic acid than those of α-acetamidoacrylic acid. It is noted that diphosphinite (**2**) gave the highest optical yield (66% e. e.) among the ligands examined; the optical yield increased to 76% e.e. by lowering the reaction temperature (−20 °C).[8] Since the catalyst of **1**, sterically similar to **2**, gave a lower optical yield (42% e. e.) than the catalyst of **2**, the above results would indicate the enhancement of the stereoselectivity by the dimethylamino group of **2** in the reaction of itaconic acid. The

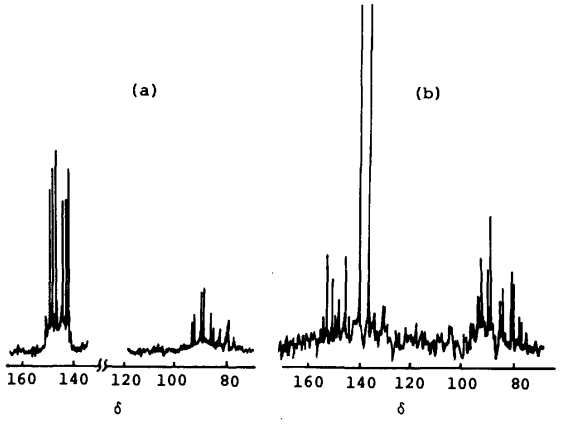

Fig. 1. ^{31}P NMR spectra of Rh(I)-diphosphinite (**2**)- or (**3**)-α-acetamidocinnamic acid systems in methanol solution.

(a): $[Rh(\begin{smallmatrix}Ph\\H\end{smallmatrix}\!\!>\!C\!=\!C\!<\!\begin{smallmatrix}NHCOCH_3\\CO_2H\end{smallmatrix})(\mathbf{2})]^+BF_4^-$,

(b): $[Rh(\begin{smallmatrix}Ph\\H\end{smallmatrix}\!\!>\!C\!=\!C\!<\!\begin{smallmatrix}NHCOCH_3\\CO_2H\end{smallmatrix})(\mathbf{3})]^+BF_4^-$.

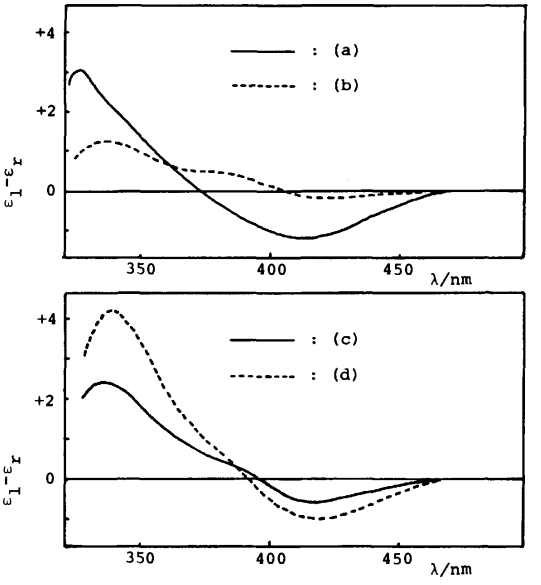

Fig. 2. CD spectra of Rh(I)-diphosphinite (**2**)- or (**3**)-α-acetamidocinnamic acid systems in methanol solution.

(a): $[Rh(\begin{smallmatrix}Ph\\H\end{smallmatrix}\!\!>\!C\!=\!C\!<\!\begin{smallmatrix}NHCOCH_3\\CO_2H\end{smallmatrix})(\mathbf{2})]^+BF_4^-$,

(b): (a)+NEt_3,

(c): $[Rh(\begin{smallmatrix}Ph\\H\end{smallmatrix}\!\!>\!C\!=\!C\!<\!\begin{smallmatrix}NHCOCH_3\\CO_2H\end{smallmatrix})(\mathbf{3})]^+BF_4^-$,

(d): (c)+NEt_3.

TABLE 2. ASYMMETRIC HYDROGENATION OF ITACONIC ACID USING Rh(I)-DIPHOSPHINITE (**1**—**3**) CATALYSTS[a]

Diphosphinite[b]	Temp °C	Time min	Conversion %	% e.e.[c]	Configuration
1	0	12	100	42	*R*
1	0	36	100	29	*R*[d]
1	−20	180	100	52	*R*
2	0	9	100	66	*R*
2	0	26	100	25	*R*[d]
2	−20	180	100	76	*R*
3	0	30	100	45	*R*
3	0	18	100	14	*R*[d]

a) Hydrogenations were performed in ethanol under atmospheric hydrogen pressure. Itaconic acid/Rh = 100. b) Diphosphinite/Rh = 1.5. c) Optical yields (% e.e.) were calculated from the specific rotation of the product and that of optically pure (*R*)-3-methylsuccinic acid: $[\alpha]_D^{31}$ +16.88° (*c* 2.16, EtOH).[19] d) Addition of triethylamine (NEt_3/Rh = 10).

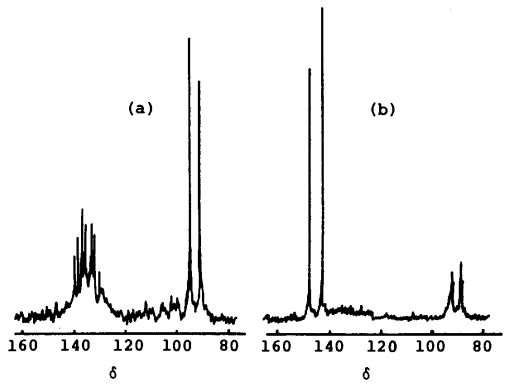

Fig. 3. ^{31}P NMR spectra of Rh(I)-diphosphinite (**2**)-itaconic acid systems in methanol solution.
(a): $[Rh(CH_2{=}C(CH_2CO_2H)CO_2H)(\mathbf{2})]^+BF_4^-$,
(b): (a) + NEt_3.

catalyst of **3** gave lower optical yield (45% e. e.). This decrease in the (*S*)-selectivity is in accord with the results of the hydrogenation of dehydroamino acid derivatives in the system of **3**.

In the reaction of itaconic acid, addition of triethylamine (NEt_3/Rh=10) lowered drastically the optical yield. The ^{31}P NMR spectrum of Rh(I)-diphosphinite (**2**)-itaconic acid system showed the presence of several Rh(I) species in the solution, but the addition of amine simplified the spectrum and no P-P coupling was observed (Fig. 3). These are explained by the competitive coordination between the diphosphinite and amine onto rhodium. Amine addition increased the intensity of absorption spectra in the systems of **1** and **2**, and the intensity of CD spectra also increased in both systems (Fig. 4). These would correspond to the competitive coordination between the diphosphinite and amine. Thus the addition of triethylamine weakened the stereocontrol by the diphosphinite to result in the decrease of the optical yield. On the other hand, it is also possible that triethylamine deprotonates the carboxyl

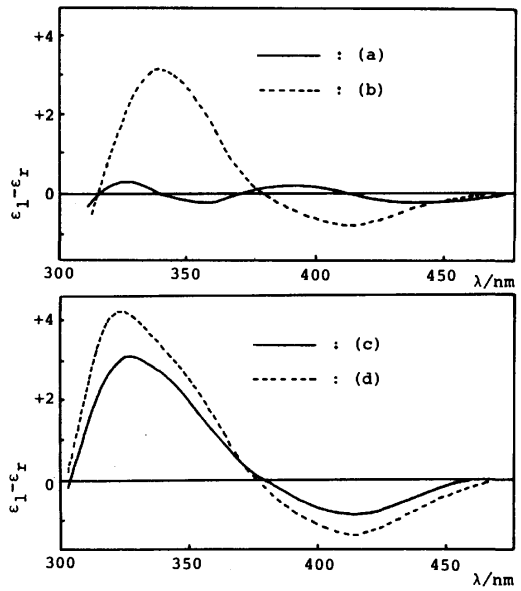

Fig. 4. CD spectra of Rh(I)-diphosphinite (**1**)- or (**2**)-itaconic acid systems in methanol solution.
(a): $[Rh(CH_2{=}C(CH_2CO_2H)CO_2H)(\mathbf{1})]^+BF_4^-$,
(b): (a) + NEt_3,
(c): $[Rh(CH_2{=}C(CH_2CO_2H)CO_2H)(\mathbf{2})]^+BF_4^-$,
(d): (c) + NEt_3.

group of itaconic acid, as is supposed in the hydrogenation of dehydroamino acid.[7] The reaction of monosodium salt of itaconic acid gave lower optical yield in methanol than the reaction of itaconic acid in the absence of amine in methanol (25% e. e. and 51% e. e., respectively). Therefore, the presence of itaconate anion does not serve to raise the optical yield unless the interaction exists between itaconate anion and the ligand.

As mentioned previously, several Rh(I) species are present in the solution to lower the optical yield. In order to decrease the number of Rh(I) species in the solution, the following diphosphinites (**4** and **5**) were examined. They have an electron-donating group (4-methyl or 4-methoxyl group) on the phenyl group on phosphorus atom and are expected to coordinate more strongly onto rhodium. As shown in Table 3, the reaction rate increased strikingly in the case of α-acetamidocinnamic acid by the introduction of the electron-donating substituent on the phenyl group, though the optical yield did not change so much. On the other hand, the reaction rate in the hydrogenation of itaconic acid was almost unchanged, but the optical yield slightly decreased as the coordination of diphosphinites onto rhodium became stronger. This different behavior seems to indicate that the coordination mode of the substrates was different between itaconic acid[9] and dehydroamino acid.

The electrostatic interaction between diphosphinite (**2**) and itaconic acid was expected, but considered to be not strong enough to allow the precise discrimination of the prochiral face of itaconic acid. In the case of dehydrodipeptides,[10] the carboxyl group of the sub-

Table 3. Asymmetric hydrogenation of α-acetamidocinnamic acid and itaconic acid using Rh(I)-diphosphinite (**2**, **4**, and **5**) catalysts

Substrate	Diphosphinite	Solvent	Temp °C	Time min	Conversion %	% e.e.	Configuration
Ph, $NHCOCH_3$; $C=C$; H, CO_2H	**2**	EtOH/Bz(2/1)	20	720	100	16	*S*
	4	EtOH/Bz(2/1)	20	120	100	16	*S*
	5	EtOH/Bz(2/1)	20	9	100	22	*S*
$CH_2=C$; CH_2CO_2H; CO_2H	**2**	EtOH	0	9	100	66	*R*
	4	EtOH	0	12	100	63	*R*
	5	EtOH	0	11	100	53	*R*

Table 4. Asymmetric hydrogenation of dehydrodipeptides using Rh(I)-diphosphinite (**1**—**5**) catalysts[a]

Dihydrodipeptide[b]	Diphosphinite[c]	Temp °C	Time min	Conversion %	(*S*)/(*R*) or (*S*,*S*)/(*R*,*S*)	% e.e. or % d.e.
Ph, $NHCOCH_3$; $C=C$; H, $CONHCH_2CO_2H$ (Ac-⊿Phe-Gly-OH)	**1**	20	20	100	74/26	48
	2	20	30	100	67/33	34
	3	20	20	100	58/42	16
Ph, $NHCOCH_3$; $C=C$; H, $CONHCH(CH_2Ph)CO_2H$ (Ac-⊿Phe-(*S*)-Phe-OH)	**1**	20	120	92	79/21	58
	2	20	180	71	95/ 5	90
	3	20	120	91	93/ 7	86
	4	20	45	100	>99/<1	>98
	5	20	15	100	>99/<1	>98
Ph, $NHCOCH_3$; $C=C$; H, $CONHCH(CH_3)CO_2H$ (Ac-⊿Phe-(*S*)-Ala-OH)	**1**	20	20	100	68/32	36
	2	20	30	100	94/ 6	88
	3	20	30	100	91/ 9	82
	5	20	30	100	98/ 2	96
Ph, $NHCOCH_3$; $C=C$; H, $CONHCH(CH_2Ph)CO_2CH_3$ (S) (Ac-⊿Phe-(*S*)-Phe-OMe)	**1**	20	180	100	51/49	2
	2	40	50 h	0	—	—
	3	40	30 h	20	—	—
	5	40	8 h	0	—	—

a) Hydrogenations were performed in ethanol under atmospheric hydrogen pressure. b) Dehydrodipeptide/Rh = 50. c) Diphosphinite/Rh = 1.5.

strate is expected to interact more easily with the dimethylamino group of the ligands. Accordingly, our diphosphinite catalysts were applied to the asymmetric hydrogenation of dehydrodipeptides (Table 4). The reaction of Ac-⊿Phe-Gly-OH, using diphosphinite (**2** and **3**) catalysts, having the dimethylamino group, proceeded as rapidly as the reaction with diphosphinite (**1**). These results present an interesting contrast with the reaction of dehydroamino acid derivatives using diphosphinites with the dimethylamino group. Diphosphinites (**2** and **3**) gave (*S*,*S*)-products with high stereoselectivity in the reaction of Ac-⊿Phe-(*S*)-Phe-OH (90% d.e. and 86% d.e., respectively), while diphosphinite (**1**) gave the product with much lower stereoselectivity (58% d.e.). These results indicate the effect of the dimethylamino group on the asymmetric induction. Introduction of the electron-donating substituent on the phenyl group of the diphosphinite (**2**) increased the reactivity and gave an extremely high stereoselectivity (more than 98% d. e. with both **4** and **5**). The presence of the dimethylamino group in the ligand induced also high stereoselectivity (96% d. e. with **5**) in the reaction of Ac-⊿Phe-(*S*)-Ala-OH, while diphosphinite (**1**) gave only low stereoselectivity (36% d. e.). In the case of Ac-⊿Phe-(*S*)-Phe-OMe, the reactivity was extremely low using diphosphinites (**2** and **5**) with the dimethylamino group, as was observed in the reaction of dehydroamino acid esters. Hydrogenation took place smoothly using diphosphinite (**1**) without dimethylamino group, but the stereoselectivity was very low. This striking difference between the reaction of Ac-⊿Phe-(*S*)-Phe-OH and that of Ac-⊿Phe-(*S*)-Phe-OMe will further support the electrostatic interaction between the carboxyl group of the dipeptide and the dimethylamino group of the ligand.

These results indicate the importance of the chiral center in the substrate, as well as the dimethylamino group of the ligand for asymmetric induction (Scheme 3). The electrostatic interaction between the dimethylamino group of the ligand and the carboxyl group of the dipeptide will play a role to fix the substrate onto rhodium. In the case of dehydrodipeptide with a chiral center, coordination of the substrate onto rhodium by the ($C_\alpha$si, $C_\beta$re) face of the double bond is unfavorable because of the steric repulsion between the substituent on the chiral carbon of the substrate and the phenyl

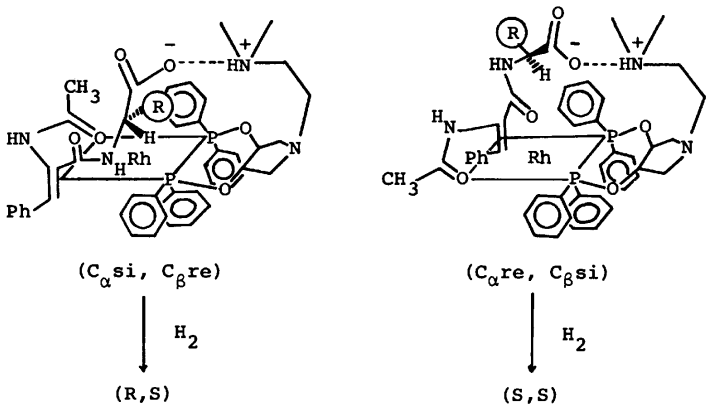

Scheme 3.

group of the ligand. So the coordination by the (Cαre, Cβsi) face becomes favorable, resulting in the predominant (*S*, *S*)-product formation. That is to say, the electrostatic interaction emphasized the steric effect of the chiral center of the dipeptide, resulting in the high stereoselective induction.

For dehydrodipeptides with (*R*)-chiral center, (*R*, *R*)-product was formed in a high stereoselectivity instead of (*S*, *R*)-isomer.[11]

In the case of dehydroamino acids, the dimethylamino group in the ligand and the carboxyl group of the substrate are too distant to interact strongly enough to increase the optical yield. On the other hand, in the case of itaconic acid, the carboxyl group of the substrate would interact with the dimethylamino group of the ligand to give high optical yield. Furthermore, in the case of dehydrodipeptides with a chiral center, the electrostatic interaction fixed the substrate onto rhodium to induce excellent stereoselectivity by emphasizing the steric effect. The detailed study of the asymmetric hydrogenations of dehydrodipeptides and dehydrooligopeptides is in progress using diphosphinite systems. Our ligand with the dimethylamino group will be applied for more complex substrates with many functional groups.

Experimental

^{1}H NMR spectra were recorded on Hitachi R-24 High Resolution NMR spectrometer (60 MHz) with tetramethylsilane as internal standard. ^{31}P NMR spectra were recorded on a JEOL JNM-FX60Q spectrometer with triphenylphosphine as external standard (6.2 ppm). CD spectra were recorded on a JASCO J-40A spectropolarimeter. Optical rotations were measured with a UNION PM101 automatic digital polarimeter.

Materials. α-Acetamidocinnamic acid, α-acetamidoacrylic acid, and itaconic acid were purchased as commercial products. α-Benzoylaminocinnamic acid,[12] methyl α-acetamidocinnamate,[13] isopropyl α-acetamidocinnamate,[13] methyl α-benzoylaminocinnamate,[13] *N*-acetyl dehydrophenylalanylglycine,[14] *N*-acetyl dehydrophenylalanyl-(*S*)-phenylalanine,[14] *N*-acetyl dehydrophenylalanyl-(*S*)-alanine,[14] and *N*-acetyl dehydrophenylalanyl-(*S*)-phenylalanine methyl ester[10c] were prepared by the conventional methods. All substrates except α-acetamidoacrylic acid and itaconic acid were purified by repeated recrystallization.

Ethanol and methanol were dried and distilled over magnesium and stored under nitrogen. Tetrahydrofuran, diethyl ether, dioxane, triethylamine, and benzene were dried and distilled over sodium and stored under nitrogen. 1,4-Di-*O*-tosyl-L-threitol was prepared through four steps from (+)-diethyl tartrate.[5] Chlorodi-*p*-tolylphosphine and chlorobis(4-methoxyphenyl)phosphine were prepared by the reaction of corresponding Grignard reagent and sodium diethyl phosphite followed by hydrolysis and chlorination with phosphorus trichloride.[15]

$[Rh(cod)_2]^+BF_4^-$(cod: 1,5-cyclooctadiene) was prepared by a conventional method and stored under nitrogen.[16]

Preparation of Diphosphinites. (3S,4S)-N-Isopentyl-3,4-pyrrolidinediol (6): Isopentylamine (4 cm^3, 3.4×10^{-2} mol) and 1,4-di-*O*-tosyl-L-threitol (4.8 g, 1.1×10^{-2} mol) were reacted in dioxane (6 cm^3) under reflux with stirring for 20 h under nitrogen. The reaction mixture was evaporated under reduced pressure, and the residual solid was extracted with THF in an ice-water bath. The extract was evaporated to dryness under reduced pressure. Recrystallization of the residue from diethyl ether with hexane gave 650 mg of pale yellow crystals containing a small amount of ammonium salt and unchanged amine. (85 mol% purity, 34% yield) This diol was used for the preparation of diphosphinite (**1**) without further purification. ^{1}H NMR ($CDCl_3$) δ=0.87 (6H, d, H^a), 1.38 (3H, br m, H^b, H^c), 2.33—3.11 (6H, m, H^d, H^e), 4.11 (2H, br t, H^f), 4.87 (2H, s, H^g).

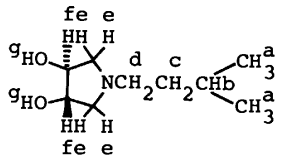

6

(3S,4S)-N-[2(Dimethylamino)ethyl]-3,4-pyrrolidinediol (7): *N*,*N*-Dimethylethylenediamine (18.2 g, 2.1×10^{-1} mol) and 1,4-di-*O*-tosyl-L-threitol (30 g, 6.9×10^{-2} mol) were reacted in dioxane and the product was treated in the manner described above. The crude diol was purified by short column chromatography of neutral alumina (ethanol eluent) and recrystallization from THF. In this way, the diol was obtained as white crystals. (2.4 g, 20% yield) $[\alpha]_D^{25}$ +2.9° (*c* 0.90, $CHCl_3$); ^{1}H NMR ($CDCl_3$) δ=2.22 (6H, s, H^a), 2.43—3.10 (8H, m, H^b, H^c, H^d), 4.02 (2H, br t, H^e), 4.87 (2H, s, H^f).

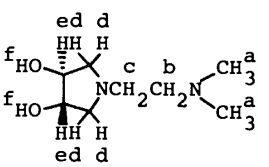

7

(3S,4S)-N-[3-(Dimethylamino)propyl]-3,4-pyrrolidinediol (8): *N,N*-Dimethyl-1,3-propanediamine (4.2 cm³, 3.3×10⁻² mol) and 1,4-di-*O*-tosyl-L-threitol (4.8 g, 1.1×10⁻² mol) were reacted in dioxane and the product was treated in the manner described previously. The crude diol was obtained as oily material containing a small amount of ammonium salt and unchanged amine (530 mg, 93 mol% purity, 25% yield); this diol was used without further purification in the preparation of the diphosphinite (**3**). ^{1}H NMR ($CDCl_3$) δ= 1.66 (2H, br m, H^c), 2.20 (6H, s, H^a), 2.20—3.08 (8H, m, H^b, H^d, H^e), 4.07 (2H, br t, H^f), 4.97 (2H, s, H^g).

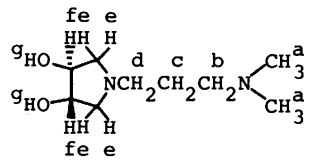

8

(3S,4S)-N-Isopentyl-3,4-bis(diphenylphosphinooxy)pyrrolidine (1): The phosphinitation of the diol (**6**) was performed in 2 steps because of the contamination by impurities (ammonium salt and amine). To the solution of the diol (**6**) (490 mg, 2.82×10⁻³ mol) and triethylamine (1.3 cm³, 9.3×10⁻³ mol) in THF (30 cm³), chlorodiphenylphosphine (0.6 cm³, 3.3×10⁻³ mol) in THF (5 cm³) was added dropwise in 3 h with stirring in an ice-water bath. After the addition, the mixture was stirred for 1.5 h at 0 °C. The white precipitate was filtered off and the filtrate was evaporated to dryness under reduced pressure. ^{1}H NMR of the oily residue indicated the formation of monophosphinite and diphosphinite (**1**). This oily product was further phosphinitated and treated as before. The resulting oily product was extracted with ether, and the ether extract was concentrated. Addition of hexane to the ether solution gave white precipitate of diphosphinite (**1**) at −50 °C. Repeated recrystallization from ether-hexane gave pure diphosphinite (**1**) as white crystals. (1.05 g, 68% yield) mp 54.5—57.2 °C (corr); $[\alpha]_D^{25}$ +59.8° (*c* 0.48, C_6H_6); ^{1}H NMR ($CDCl_3$) δ=0.86 (6H, d, H^a), 1.34 (3H, br m, H^b, H^c), 2.31—3.13 (6H, m, H^d, H^e), 4.65 (2H, br m, H^f), 7.40 (20H, m, H^g). Found: C, 72.66; H, 6.86; N, 2.62; P, 11.61. Calcd for $C_{33}H_{38}NP_2O_2$: C, 73.18; H, 6.88; N, 2.58; P, 11.43.

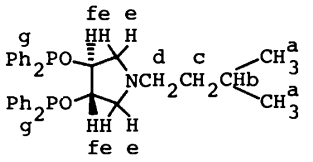

1

(3S,4S)-N-[2-(Dimethylamino)ethyl]-3,4-bis(diphenylphosphinooxy)pyrrolidine (2): Chlorodiphenylphosphine (0.65 cm³, 3.6×10⁻³ mol) in THF (3 cm³) was added dropwise to the solution of the diol (**7**) (310 mg, 1.7×10⁻³ mol) and triethylamine (0.5 cm³, 3.6×10⁻³ mol) in THF (20 cm³) in 30 min with stirring in an ice-water bath. After the addition, the mixture was stirred for 3 h at 0 °C. The white precipitate was filtered off and the filtrate was evaporated to dryness under reduced pressure. The oily residue was purified by recrystallization from ether-hexane, and the pure diphosphinite was obtained as white crystals having a melting point near the r.t. (610 mg, 63% yield) $[\alpha]_D^{25}$ +55.4° (*c* 0.97, C_6H_6); ^{1}H NMR ($CDCl_3$) δ=2.22 (6H, s, H^a), 2.41—3.17 (8H, m, H^b, H^c, H^d), 4.64 (2H, br m, H^e), 7.41 (20H, m, H^f).

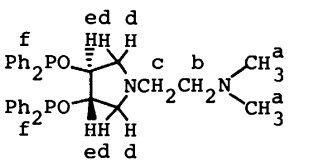

2

Found: C, 70.70; H, 6.94; N, 5.25; P, 11.59. Calcd for $C_{32}H_{36}N_2P_2O_2$: C, 70.83; H, 6.68; N, 5.16; P, 11.41.

(3S,4S)-N-[3-(Dimethylamino)propyl]-3,4-bis(diphenylphosphinooxy)pyrrolidine (3): The phosphinitation of the diol (**8**) was performed in 2 steps. To the solution of the diol (**8**) (530 mg, 2.8×10⁻³ mol) and triethylamine (1.2 cm³, 8.6×10⁻³ mol) in THF (30 cm³), chlorodiphenylphosphine (0.5 cm³, 2.8×10⁻³ mol) in THF (5 cm³) was added dropwise in 30 min with stirring in an ice-water bath. The resulting mixture was further stirred for 30 min at 0 °C. Filtration of the reaction mixture followed by evaporation of the filtrate gave oily monophosphinite. The monophosphinite was further phosphinitated with 0.5 cm³ of chlorodiphenylphosphine and 1.2 cm³ of triethylamine, and treated as before. The oily product was purified by recrystallization from ether-hexane and pure diphosphinite (**3**) was obtained as a colorless oil. (800 mg, 57% yield) $[\alpha]_D^{25}$ +56.0° (*c* 0.31, C_6H_6); ^{1}H NMR ($CDCl_3$) δ=1.61 (2H, m, H^c), 2.17 (6H, s, H^a), 2.17—3.13 (8H, m, H^b, H^d, H^e), 4.64 (2H, br, m, H^f), 7.44 (20H, m, H^g).

Found: C, 71.20; H, 6.98; N, 4.91; P, 11.08. Calcd for $C_{33}H_{38}N_2P_2O_2$: C, 71.20; H, 6.88; N, 5.30; P, 11.12.

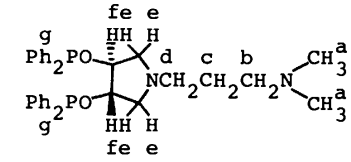

3

(3S,4S)-N-[2-(Dimethylamino)ethyl]-3,4-bis(di-p-tolylphosphinooxy)pyrrolidine (4): To the solution of the diol (**7**) (500 mg, 2.9×10⁻³ mol) and triethylamine (2.8 cm³, 20×10⁻³ mol) in THF (50 cm³), chlorodi-*p*-tolylphosphine (1.9 g, 7.6×10⁻³ mol) in THF (15 cm³) was added dropwise in 2 h with stirring at −30 °C. The mixture was further stirred for 2 h at 0 °C. Similar treatment of the reaction mixture to the case of (**2**) and recrystallization of the product from ether-hexane gave pure diphosphinite (**4**) as white needles. (780 mg, 45% yield) mp 74.5—76.5 °C (corr); $[\alpha]_D^{25}$ +60.4° (*c* 0.51, C_6H_6); ^{1}H NMR ($CDCl_3$) δ=2.18—3.09 (26H, m, H^a, H^b, H^c, H^d), 4.52 (2H, br m, H^e), 6.96—7.44 (16H, m, H^f).

Found: C, 72.48; H, 7.59; N, 4.57; P, 10.16. Calcd for $C_{36}H_{44}N_2P_2O_2$: C, 72.22, H, 7.40; N, 4.67; P, 10.34.

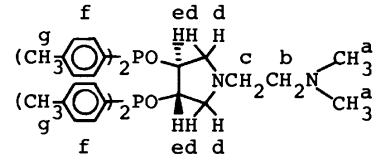

4

(3S,4S)-N-[2-(Dimethylamino)ethyl]-3,4-bis[bis(4-methoxyphenyl)phosphinooxy]pyrrolidine (5): To the solution of the diol (**7**) (600 mg, 3.4×10⁻³ mol) and triethylamine (5.5 cm³, 40×10⁻³ mol) in THF (50 cm³), chlorobis(4-methoxyphenyl)phosphine (2.2 g, 7.8×10⁻³ mol) in THF (15 cm³) was added dropwise in 2 h with stirring at −30 °C. The mixture was further stirred for 30 min at 0 °C. Similar treatment of the reaction mixture to the case of **2** and recrystallization of the product from ether-hexane gave pure diphosphinite (**5**) as white crystals. (1.67 g, 47% yield) mp 62.8—65.7 °C (corr); $[\alpha]_D^{25}$ +58.9° (*c* 0.95, C_6H_6); ^{1}H NMR ($CDCl_3$) δ=2.17 (6H, s, H^a) 2.33—3.06 (8H, M, H^b, H^c, H^d), 3.72 (12H, s, H^g), 4.43

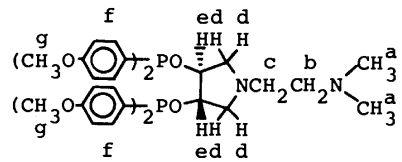

5

(2H, br, m, H^e), 6.57—7.48 (16H, m, H^f).

Found: C, 65.27; H, 6.77; N, 4.03; P, 9.16. Calcd for $C_{36}H_{44}N_2P_2O_6$: C, 65.24; H, 6.96; N, 4.22; P, 9.36.

Hydrogenation Procedure. Dehydroamino Acid Derivatives and Itaconic Acid: Typically, $[Rh(cod)_2]^+BF_4^-$ (4.1 mg, 1.0×10^{-5} mol) and a diphosphinite (1.5×10^{-5} mol) were dissolved in a solvent (3 cm^3) under nitrogen and the solution was stirred at r.t. for 5 min. This catalyst solution was transferred into the hydrogenation flask containing the substrate (1.0×10^{-3} mol) and a solvent (7 cm^3) by a narrow stainless steel tube under nitrogen. After the solution was stirred for 1 h at r. t. under nitrogen, degassing under reduced pressure and filling the flask with hydrogen were repeated several times, quickly. The resultant solution was stirred vigorously until the required amount of hydrogen had been absorbed. The reaction mixture was worked up by the conventional method[17] and the optical yield was determined polarimetrically. In the case of itaconic acid, hydrogen was introduced after stirring of the mixture for 5 min under nitrogen.

Dehydrodipeptides: $[Rh(cod)_2]^+BF_4^-$ (4.1 mg, 1.0×10^{-5} mol) and a diphosphinite (1.5×10^{-5} mol) were dissolved in ethanol (2 cm^3) under nitrogen and the solution was stirred at r. t. for 5 min. This catalyst solution was transferred into the hydrogenation flask containing a dehydrodipeptide (5.0×10^{-4} mol) and ethanol (3 cm^3) by a narrow stainless steel tube under nitrogen, and the hydrogenation procedure described above was carried out. The reaction mixture was worked up by the conventional method[10] and the optical yield was determined by ^1H NMR usig a shift reagent ($Eu(tfc)_3$).

^{31}P NMR Spectra. The Typical Procedure for Preparation of the Sample: The solution of $[Rh(cod)_2]^+BF_4^-$ (37 mg, 9.1×10^{-5} mol) and a diphosphinite (9.1×10^{-5} mol) in methanol (1 cm^3) containing 10% of an internal lock (CD_3OD or C_6D_6) in a Schlenk tube was degassed by a freeze and thaw cycle. Hydrogen was introduced and the solution was stirred at r. t. for the time necessary for removing the coordinated cod. Then the solution was evacuated by three freeze and thaw cycles and transferred into a Schlenk tube containing a substrate (1.8×10^{-3} mol) with a narrow stainless steel tube under nitrogen, further degassed by the above procedure, and stirred at r. t. for 30 min. Finally, the solution was transferred into a NMR tube and the tube was sealed under nitrogen.

CD Spectra. The Typical Procedure for Preparation of the Sample: The stock solution of $[Rh(cod)_2]^+BF_4^-$ (8.1 mg, 2.0×10^{-5} mol) and a diphosphinite (2.4×10^{-5} mol) in methanol (20 cm^3) was evacuated by two freeze and thaw cycles. The solution (2.5 cm^3) was treated as described above and transferred into a Schlenk tube containing the methanol solution of a substrate (2.5×10^{-5} mol, 2.5cm^3), further degassed, and stirred at r. t. for 30 min. The resultant solution was transferred into a 10 mm cell under nitrogen.

The authors express their gratitude to Professor A. Yamamoto and Dr. F. Ozawa, Tokyo Institute of Technology, for ^{31}P NMR spectroscopy, and to Professor M. Kobayashi, Tokyo Metropolitan University, for CD spectroscopy.

References

1) a) M. D. Fryzuk and B. Bosnich, *J. Am. Chem. Soc.*, **99**, 6262 (1977); b) I. Ojima and T. Kogure, *Chem. Lett.*, **1979**, 641; c) A. Miyashita, A. Yasuda, H. Takaya, K. Toriumi, T. Ito, T. Souchi, and R. Noyori, *J. Am. Chem. Soc.*, **102**, 7932 (1980); d) H. Brunner, W. P. Ronzuk, B. Schönhammer, K. Streng, I. Bernal, and J. Korp, *Chem. Ber.*, **144**, 1137 (1981); e) O. Samuel, R. Coufingnal, M. Lauer, S. Y. Zhang, and H. B. Kagan, *Nouv. J. Chim.*, **5**, 151 (1981).

2) W. S. Knowles, B. D. Vineyard, M. J. Sabacky, and B. R. Stults, "Fundamental Research in Homogeneous Catalysis," ed by M. Tsutsui, Plenum, New York (1979), Vol. 3, p. 537.

3) B. D. Vineyard, W. S. Knowles, M. J. Sabacky, G. L. Bachman, and D. J. Weinkauff, *J. Am. Chem. Soc.*, **99**, 5946 (1977); K. Yamamoto, J. Wakatsuki, and R. Sugimoto, *Bull. Chem. Soc. Jpn.*, **53**, 1132 (1980).

4) M. Yatagai, M. Zama, T. Yamagishi, and M. Hida, *Chem. Lett.*, **1983**, 1203.

5) W. Dumont, J. C. Poulin, T. P. Dang, and H. B. Kagan, *J. Am. Chem. Soc.*, **95**, 8295 (1973).

6) G. M. Kosolapoff and L. Maier, "Organic Phosphorus Compounds," Wiley-Interscience, New York (1972), Vol. 4, pp. 473—475.

7) K. Achiwa, *J. Am. Chem. Soc.*, **98**, 8265 (1976); G. Descotes, D. Lafont, and D. Sinou, *J. Organomet. Chem.*, **150**, C14 (1978).

8) Rh(I)-diphosphinite (**2**) catalyst possessed very low reactivities for the hydrogenations of mesaconic acid and citraconic acid as isomers of itaconic acid. These results indicate that in the asymmetric hydrogenation of itaconic acid the isomerisation of the substrate did not take place.

9) J. M. Brown, P. A. Chaloner, and D. Parker, *Nouv. J. Chim.*, **5**, 167 (1981).

10) a) I. Ojima and T. Suzuki, *Tetrahedron Lett.*, **1980**, 1239; b) I. Ojima, T. Kogure, N. Yoda, T. Suzuki, M. Yatabe, and T. Tanaka, *J. Org. Chem.*, **47**, 1329 (1982); c) D. Meyer, J. C. Poulin, and H. B. Kagan, *ibid.*, **45**, 4680 (1980); d) K. Onuma, T. Ito, and A. Nakamura, *Chem. Lett.*, **1980**, 481.

11) M. Yatagai, T. Yamagishi, and M. Hida, *Bull. Chem. Soc. Jpn.*, **57**, (1984), in press.

12) R. M. Herbst and D. S. Shemin, *Org. Synth.*, Coll. Vol. II, 1, 406 (1943).

13) R. Glaser and B. Vainas, *J. Organomet. Chem.*, **121**, 249 (1976).

14) D. G. Doherty, J. E. Tietzman, and M. Bergmann, *J. Biol. Chem.*, **147**, 617 (1943).

15) B. B. Hunt and B. C. Saunders, *J. Chem. Soc.*, **1957**, 2413.

16) M. Green, T. A. Kuc, and S. H. Taylor, *J. Chem. Soc., A*, **1971**, 2334.

17) I. Ojima, T. Kogure, and N. Yoda, *J. Org. Chem.*, **45**, 4728 (1980).

18) R. Glaser and S. Geresh, *Tetrahedron*, **35**, 2381 (1979).

19) E. Berner and R. Leonardsen, *Justus Liebigs Ann. Chem.*, **538**, 1 (1939).

 © 1984 The Chemical Society of Japan Bull. Chem. Soc. Jpn., 57, 747—751 (1984)

The Synthesis of Coleon B Tri-*O*-methyl Ether

Takashi MATSUMOTO,* Sachihiko IMAI, Katsumi NISHIZAKI, Fumio KURIHARA, and Fumitaka GOTO

Department of Chemistry, Faculty of Science, Hiroshima University, Higashisenda-machi, Naka-ku, Hiroshima 730

(Received September 12, 1983)

Methyl (+)-12-benzoyloxy-11,14-dioxo-8,12-abietadien-18-oate was converted into methyl 11,12,14-trimethoxy-8,11,13-abietatrien-18-oate (**8**). The Grignard reaction of **8** with phenylmagnesium bromide, followed by oxidation with lead tetraacetate, afforded 11,12,14-trimethoxy-19-norabieta-4(18),8,11,13-tetraene. This was then converted into 3α-bromo-11,12,14-trimethoxy-18-norabieta-8,11,13-trien-2-one (**15**) by a series of reactions: selenium dioxide oxidation, catalytic hydrogenation, dehydration, hydroxybromination, and Jones oxidation. Acetalization of **15** with 1,2-ethanediol, followed by oxidation with Jones reagent and then with oxygen in the presence of potassium *t*-butoxide, afforded 3-bromo-2,2-ethylenedioxy-6-hydroxy-11,12,14-trimethoxy-18-norabieta-5,8,11,13-tetraen-7-one, which was converted into (−)-coleon B tri-*O*-methyl ether (**4**) by hydrolysis and dehydrobromination. Another conversion of **15** into **4** was also achieved by a series of reactions: debromination, acetalization, Collins oxidation, oxygen oxidation, hydrolysis, and dehydrogenation.

Coleon B (**1**), a highly oxygenated tricyclic norditerpene phenol, has been isolated from the leaves of *Coleus igniarius* Schweinf. (Labiatae) by Eugster *et al.*[1] Recently, the synthesis of coleon B tetra-*O*-methyl ether (**2**) was reported by Burnell *et al.*[2] In the previous paper,[3] we also reported the synthesis of an A and B ring analog of coleon B, (−)-6-hydroxy-19-norabieta-3,5,8,11,13-pentaene-2,7-dione (**3**). As an extension of the previous work,[3] we here describe the successful synthesis of (−)-coleon B tri-*O*-methyl ether (**4**), starting from methyl (+)-12-benzoyloxy-11,14-dioxo-8,12-abietadien-18-oate (**5**)[4] which was prepared from (+)-dehydroabietic acid (**6**).

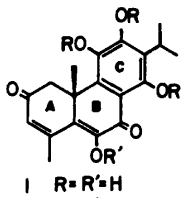

1 R=R'=H
2 R=R'=Me
4 R=Me, R'=H

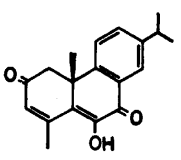

3

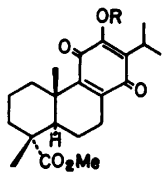

5 R=COPh

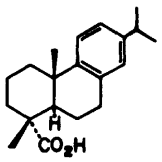

6

The 11,14-dioxo compound **5** was reduced with sodium dithionite in aqueous acetic acid at 80—95 °C or with zinc powder and dilute hydrochloric acid in benzene at 55—60 °C. The resulting phenol was methylated with methyl iodide in the presence of anhydrous potassium carbonate in refluxing ethyl methyl ketone to afford methyl 12-benzoyloxy-11,14-dimethoxy-8,11,13-abietatrien-18-oate (**7**) in 87.1% or 78.0% yield. The dimethoxy compound **7** was then converted into methyl 11,12,14-trimethoxy-8,11,13-abietatrien-18-oate (**8**: 82.4%) by alkaline hydrolysis and subsequent methylation. The Grignard reaction of **8** with phenylmagnesium bromide at 95—105 °C afforded a diphenylmethanol derivative (**9**: 71.3%). This was treated with lead tetraacetate and calcium carbonate in refluxing benzene to give 11,12,14-trimethoxy-19-norabieta-4(18),8,11,13-tetraene (**10**: 57.5%). The presence of an *exo*-methylene group at C-4 in **10** was supported by its ^{1}H NMR spectrum, which showed two broad singlet signals at δ 4.53 and 4.78 due to two olefinic protons. The tetraene **10** was oxidized with selenium dioxide in refluxing aqueous ethanol to yield 11,12,14-trimethoxy-19-norabieta-4(18),8,11,13-tetraen-3α-ol (**11**: 56.6%). The stereochemistry of the hydroxyl group at C-3 in **11** was assigned to be α-configuration from its ^{1}H NMR spectrum, which showed a broad signal due to the C-3 proton at δ 4.21 with half-height width of 5.4 Hz, suggesting the presence of an equatorial β proton. Catalytic hydrogenation of **11** in ethyl acetate over PtO_2 at room temperature afforded 11,12,14-trimethoxy-18-norabieta-8,11,13-trien-3α-ol[5] (**12**: 97.4%) which was dehydrated with phosphoryl chloride in refluxing pyridine to give 11,12,14-trimethoxy-18-norabieta-2,8,11,13-tetraene (**13**) in quantitative yield. The ^{1}H NMR spectrum of **13** showed doublet signals at δ 1.06 due to the C-4 methyl group and at δ 5.59 due to two olefinic protons. The tetraene **13** was treated with *N*-bromosuccinimide[6] in dimethyl sulfoxide containing a small quantity of water at room temperature under a stream of nitrogen to give a bromohydrin (**14**), which was used without purification in the next reaction. In the ^{1}H NMR spectrum of **14**, the down field shift of the signal (δ 1.38) due to the methyl group at C-10 relative to the corresponding signals for **12** (δ 1.28) and **13** (δ 1.26) suggested a 1,3-diaxial-*cis*-relationship between the methyl group and the new hydroxyl group. From the above spectral data and a well-documented mechanistic pathway (*trans*-diaxial addition),[7] the structure of **14** was assigned to be 3α-bromo-11,12,14-trimethoxy-18-norabieta-8,11,13-trien-2β-ol. Oxidation of the crude **14** in acetone with Jones reagent afforded 3α-bromo-11,12,14-trimethoxy-18-norabieta-8,11,13-trien-2-one (**15**) in 62.4% yield from **13**. To protect the carbonyl group as ethylene acetal, the

ketone **15** was refluxed with 1,2-ethanediol and *p*-toluenesulfonic acid in benzene to give a mixture of the C-3 epimeric acetals (**16**: 88.2%). Oxidation of the mixture (**16**) in acetone with Jones reagent afforded a mixture of the corresponding 7-oxo compounds (**17**: 81.8%[8]). This was then treated with oxygen in *t*-butyl alcohol in the presence of potassium *t*-butoxide to give a diosphenol derivative (**18**: 27.7%). The stereochemistry of the bromine atom at C-3 remains unsettled. Hydrolysis of **18** with dilute hydrochloric acid in refluxing acetic acid afforded a bromo ketone, which was immediately refluxed with pyridine to give the desired (−)-6-hydroxy-11,12,14-trimethoxy-19-norabieta-3,5,8,11,13-pentaene-2,7-dione (coleon B tri-*O*-methyl ether) (**4**) in 36.2% yield.

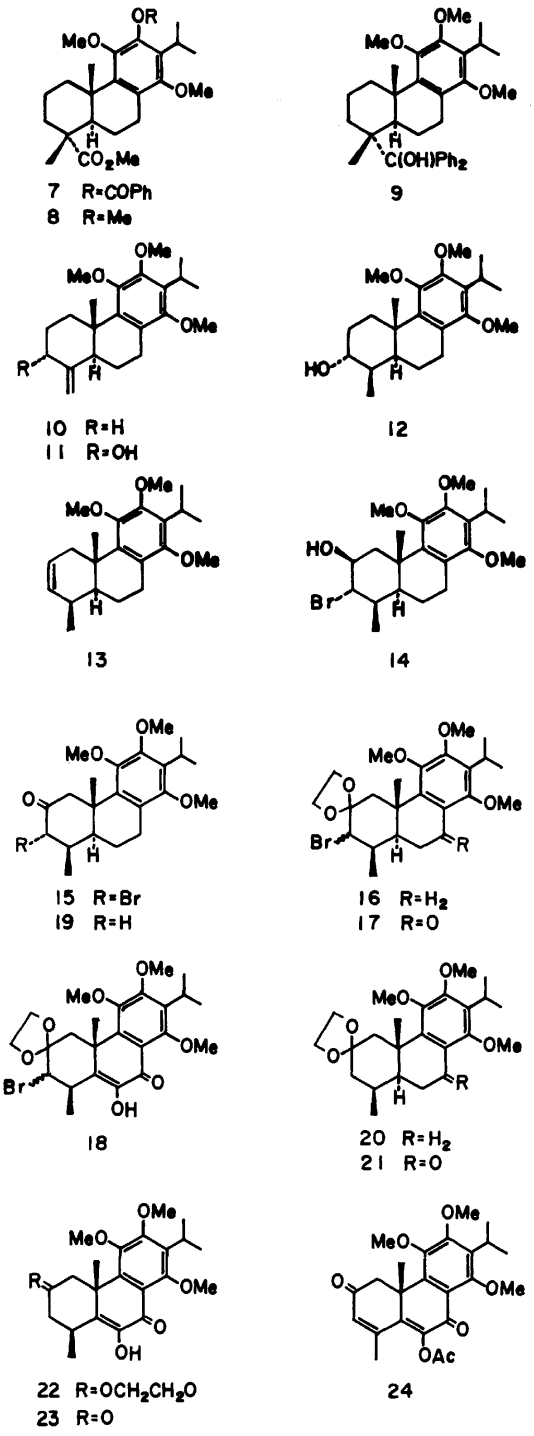

Subsequently, another conversion of **15** into **4** was also carried out as follows. Debromination of **15** with sodium iodide and chlorotrimethylsilane in refluxing acetonitrile[9] afforded 11,12,14-trimethoxy-18-norabieta-8,11,13-trien-2-one (**19**: 90.0%). The ketone **19** was treated with 1,2-ethanediol and *p*-toluenesulfonic acid in refluxing benzene to give an acetal (**20**: 93.0%). Oxidation of **20** with Collins reagent[10] in dichloromethane at room temperature afforded the corresponding 7-oxo compound (**21**: 41.4%). This was further oxidized with oxygen in *t*-butyl alcohol in the presence of potassium *t*-butoxide to give a diosphenol derivative (**22**: 86.9%). Hydrolysis of **22** with dilute hydrochloric acid at room temperature afforded 6-hydroxy-11,12,14-trimethoxy-18-norabieta-5,8,11,13-tetraene-2,7-dione (**23**: 96.7%). Dehydrogenation of **23** with 2,3-dichloro-5,6-dicyano-*p*-benzoquinone and acetic acid in refluxing benzene under a stream of nitrogen produced **4** (*ca.* 59%).[8]

In the present study, the latter route for the synthesis of **4** from **15** was superior to the former one.

Experimental

All melting points are uncorrected. The IR spectra and optical rotations were measured in chloroform, and the ^{1}H NMR spectra in carbon tetrachloride at 60 MHz, with tetramethylsilane as an internal standard, unless otherwise stated; s: singlet, bs: broad singlet, d: doublet, bd: broad doublet, m: multiplet. The column chromatography was performed using Merck silica gel (0.063 mm).

Methyl 12-Benzoyloxy-11,14-dimethoxy-8,11,13-abietatrien-18-oate (7). *a)*: A solution of sodium dithionite (11 g) in water (30 ml) was added dropwise at 80—95 °C to a stirred solution of methyl (+)-12-benzoyloxy-11,14-dioxo-8,12-abietadien-18-oate (**5**)[4] (550 mg) in acetic acid (30 ml). The mixture was stirred at this temperature for 15 min, cooled, and extracted with ether. The ether extract was washed successively with water, aqueous sodium hydrogencarbonate, and water. The solution was dried over sodium sulfate and evaporated *in vacuo* to give a crude phenol.

A stirred solution of the above crude phenol in ethyl methyl ketone (25 ml) was refluxed for 13 h with methyl iodide (3.0 ml) and anhydrous potassium carbonate (5.0 g). The mixture was cooled, diluted with water, and extracted with ether. The ether extract was washed successively with water, aqueous sodium thiosulfate, and water. The dried solution was evaporated *in vacuo*. The residue was recrystallized from methanol containing a small amount of acetone to give **7** (430 mg: 73.4%), mp 192.5—196 °C, $[\alpha]_D$+70.9°(*c* 1.27); IR: 1730, 1720 cm^{-1}; ^{1}H NMR: δ=3.53 and 3.60 (3H, each s, $-OCH_3$),[11] 3.66 (3H, s) and 3.73 (3H, s) ($-CO_2CH_3$ and $-OCH_3$), 7.43—7.7 (3H, m) and 8.08—8.3 (2H, m) ($-C_6H_5$). Found: C, 72.63; H, 7.85%. Calcd for $C_{30}H_{38}O_6$: C, 72.85; H, 7.74%. The mother liquor of recrystallization was evaporated *in vacuo*. The residue was chromatographed on silica gel (30 g), using ether–benzene (1:99) as the eluent, to give some additional **7** (80 mg after recrystallization: 13.7%).

b): A solution of **5** (5.080 g) in benzene (50 ml) was stirred at 55—60 °C for 30 min with a mixture of zinc powder (12 g) and dilute hydrochloric acid (10%:120 ml). After cooling, the benzene solution was separated. This was washed with water, dried over sodium sulfate, and evaporated *in vacuo* to give a

crude phenol. The crude phenol was immediately methylated for 14 h with methyl iodide (7.0 ml) and anhydrous potassium carbonate (25 g) in refluxing ethyl methyl ketone (70 ml). After the work-up as described in *a*), the crude product was purified by recrystallization and column chromatography to give **7** (4.174 g: 78.0%).

Methyl 11,12,14-Trimethoxy-8,11,13-abietatrien-18-oate (8). A mixture of **7** (14.482 g) and aqueous sodium hydroxide (10%: 72 ml) in ethanol (600 ml) was refluxed for 4 h. The mixture was concentrated *in vacuo*, acidified with dilute hydrochloric acid, and extracted with ether. The ether extract was washed successively with aqueous sodium hydrogencarbonate and brine, dried over sodium sulfate, and evaporated *in vacuo* to give a crude phenol.

A stirred solution of the above crude phenol in ethyl methyl ketone (150 ml) was refluxed for 16 h with methyl iodide (35 ml) and anhydrous potassium carbonate (50 g). The mixture was cooled, diluted with water, and extracted with ether. The ether extract was washed successively with aqueous sodium thiosulfate and brine, dried over sodium sulfate, and evaporated *in vacuo*. The residue was chromatographed on silica gel (800 g: 70—230 mesh), using ether—benzene (1:99) as the eluent, to give **8** (9.763 g: 82.4%). This was recrystallized from methanol, mp 96—97 °C, $[\alpha]_D$+97.4°(*c* 2.84), IR:1715 cm^{-1}; ^1H NMR:δ=1.25 (3H, s, C_4-CH_3), 1.30 (3H, s, C_{10}-CH_3), 1.30 (6H, d, J=7 Hz, -CH($C\underline{H}_3$)$_2$), 3.58, 3.62, 3.70, and 3.73 (each 3H and s, -CO_2CH_3 and 3-OCH_3). Found: C, 71.00; H, 9.06%. Calcd for $C_{24}H_{36}O_5$· $\frac{1}{2}$, 71.25; H, 8.97%.

Grignard Reaction of 8 with Phenylmagnesium Bromide. A solution of **8** (2.908 g) in dry ether (13 ml) was added to a refluxing ether solution of phenylmagnesium bromide prepared from magnesium turnings (0.699 g) and bromobenzene (3.0 ml) in dry ether (10 ml). The mixture was refluxed for 1 h and the ether was removed. The viscous residue was heated at 95—105 °C for 8 h. After cooling, the mass was carefully hydrolyzed with a mixture of dilute hydrochloric acid and ice, and then extracted with ether. The ether extract was washed successively with aqueous sodium thiosulfate and brine, dried over sodium sulfate, and evaporated *in vacuo*. The residue was chromatographed on silica gel (200 g: 70—230 mesh), using benzene as the eluent, to give a diphenylmethanol derivative **9** (2.710 g: 71.3%), $[\alpha]_D$ +89.8°(*c* 2.25), IR: 3587 cm^{-1}; ^1H NMR: δ=1.34 (6H, s, C_4-CH_3 and C_{10}-CH_3), 2.43 (1H, bs, -OH), 3.30 (3H, s) and 3.72 (6H, s) (3-OCH_3), 7.03—8.0 (10H, m, 2-C_6H_5). Found: C, 79.65; H, 8.57%. Calcd for $C_{35}H_{44}O_4$: C, 79.51; H, 8.39%.

11,12,14-Trimethoxy-19-norabieta-4(18),8,11,13-tetraene (10). A solution of **9** (166.3 mg) in dry benzene (2.0 ml) was added to a stirred suspension of lead tetraacetate (87%: 167.4 mg) and calcium carbonate (188.7 mg) in dry benzene (1.0 ml). The mixture was refluxed for 5 h, cooled, and then filtered. The filtrate was diluted with ether and the solution was washed successively with aqueous potassium iodide, aqueous sodium thiosulfate, aqueous sodium hydrogencarbonate, and brine. The dried solution was evaporated *in vacuo*. The residue was chromatographed on silica gel (15 g), using hexane-benzene (7:3) as the eluent, to give **10** (62.3 mg: 57.5%), $[\alpha]_D$ +176°(*c* 3.15), IR: 1644 cm^{-1}; ^1H NMR: δ=1.10 (3H, s, C_{10}-CH_3), 1.30 (6H, d, J=7 Hz, -CH($C\underline{H}_3$)$_2$), 3.60 (3H, s) and 3.76 (6H, s) (3-OCH_3), 4.53 and 4.78 (each 1H and bs, -$\underline{C}$=CH_2). Found: C, 76.60; H, 9.64%. Calcd for $C_{22}H_{32}O_3$; C, 76.70; H, 9.36%.

11,12,14-Trimethoxy-19-norabieta-4(18),8,11,13-tetraen-3α-ol (11). Selenium dioxide (96%: 0.505 g) was added to a stirred solution of **10** (3.011 g) in ethanol (56.0 ml) and water (3.2 ml). The mixture was refluxed for 4 h, cooled, and then filtered. The filtrate was evaporated *in vacuo*. The residue was chromatographed on aluminium oxide (Merck activ. II—III: 180 g), using ether-benzene (2:8 and then 4:6) as the eluent, to give **11** (1.785 g: 56.6%). This was recrystallized from hexane, mp 141.5—142.5 °C, $[\alpha]_D$ +153° (*c* 1.91); IR: 3605, 3450 cm^{-1}; ^1H NMR: δ=1.05 (3H, s, C_{10}-CH_3), 1.30 (6H, d, J=7 Hz, -CH($C\underline{H}_3$)$_2$), 1.63 (1H, s, -OH), 3.61 (3H, s) and 3.76 (6H, s) (3-OCH_3), 4.21 (1H, bs, $W_{1/2}$=5.4 Hz, $C_{3\beta}$-H), 4.62 and 4.97 (each 1H and bs, -$\underline{C}$=CH_2). Found: C, 73.26; H, 9.22%. Calcd for $C_{22}H_{32}O_4$: C, 73.30; H, 8.95%.

11,12,14-Trimethoxy-18-norabieta-8,11,13-trien-3α-ol (12). A solution of **11** (285 mg) in ethyl acetate (10.0 ml) was hydrogenated at room temperature for 3 h in an atmosphere of hydrogen using PtO_2 (60 mg). After the usual work-up, the crude product was chromatographed on silica gel (20 g), using ether-benzene (3:97) as the eluent, to give **12** (279 mg: 97.4%). This was recrystallized from acetone-hexane, mp 176—177 °C, $[\alpha]_D$ +103° (*c* 1.55); IR: 3613, 3462 cm^{-1}; ^1H NMR ($CDCl_3$): δ=1.01 (3H, d, J=7 Hz, C_4-CH_3), 1.28 (3H, s, C_{10}-CH_3), 1.33 (6H, d, J=7 Hz, -CH($C\underline{H}_3$)$_2$), 1.61 (1H, s, -OH), 3.65 (3H, s) and 3.80 (6H, s) (3-OCH_3). Found: C, 72.95; H, 9.71%. Calcd for $C_{22}H_{34}O_4$: C, 72.89; H, 9.45%.

11,12,14-Trimethoxy-18-norabieta-2,8,11,13-tetraene (13). A mixture of **12** (2.210 g), phosphoryl chloride (2.96 ml), and pyridine (28.0 ml) was refluxed for 1 h, cooled, and then poured into ice-dilute hydrochloric acid. The mixture was extracted with ether. The ether extract was washed with brine, dried over sodium sulfate, and evaporated *in vacuo*. The crude product was chromatographed on silica gel (110 g), using hexane-benzene (7:3) as the eluent, to give **13** (2.100 g: 100%), $[\alpha]_D$+292° (*c* 1.74), IR: 1646 cm^{-1}; ^1H NMR: δ=1.06 (3H, d, J=7.5 Hz, C_4-CH_3), 1.26 (3H, s, C_{10}-CH_3), 1.31 (6H, d, J=7 Hz, -CH($C\underline{H}_3$)$_2$), 3.59, 3.76, and 3.79 (each 3H and s, 3-OCH_3), 5.59 (2H, bd, J=3 Hz, C_2-H and C_3-H). Found: C, 76.96; H, 9.64%. Calcd for $C_{22}H_{32}O_3$: C, 76.70; H, 9.36%.

3α-Bromo-11,12,14-trimethoxy-18-norabieta-8,11,13-trien-2-one (15). A solution of **13** (1.076 g) in dimethyl sulfoxide (12.0 ml) containing a small quantity of water (0.17 ml) was stirred with *N*-bromosuccinimide (1.668 g) at room temperature for 2 h under a stream of nitrogen. The stirred mixture was cooled in an ice-water bath and aqueous sodium hydrogencarbonate was added. The mixture was extracted with ether. The ether extract was washed with brine, dried over sodium sulfate, and evaporated *in vacuo* to give the crude 3α-bromo-11,12,14-trimethoxy-18-norabieta-8,11,13-trien-2β-ol (**14**); IR: 3560, 3440 cm^{-1}; ^1H NMR: δ=1.31 (9H, d, J=7 Hz, C_4-CH_3 and -CH($C\underline{H}_3$)$_2$), 1.38 (3H, s, C_{10}-CH_3), 3.58, 3.74, and 3.83 (each 3H and s, 3-OCH_3).

The above crude bromohydrin (**14**) in acetone (12.0 ml) was oxidized with Jones reagent [2.5 M (1 M=1 mol dm^{-3}): 3.50 ml] at 0—5 °C for 5 min. The mixture was diluted with water and extracted with ether. The ether extract was washed with brine, dried over sodium sulfate, and evaporated *in vacuo*. The residue was chromatographed on silica gel (80 g), using benzene as the eluent, to give **15** (856 mg: 62.4%), $[\alpha]_D$ +153° (*c* 1.57), IR: 1706 cm^{-1}; ^1H NMR: δ=1.06 (3H, d, J=7 Hz, C_4-CH_3), 1.26 (3H, s, C_{10}-CH_3), 1.31 (6H, d, J=7 Hz, -CH($C\underline{H}_3$)$_2$), 3.62, 3.74, and 3.82 (each 3H and s, 3-OCH_3), 4.06 (1H, bs, $C_{3\beta}$-H); MS (*m/z*): 440 (M^++2), 438 (M^+).

3-Bromo-2,2-ethylenedioxy-11,12,14-trimethoxy-18-norabieta-8,11,13-triene (16). A mixture of **15** (405 mg), 1,2-ethanediol (1.14 ml), *p*-toluenesulfonic acid (200 mg), and dry benzene (20.0 ml) was refluxed for 8 h with a water separator containing 4 Å Molecular Sieves. The mixture was washed successively with aqueous sodium hydrogencarbonate and brine, dried over sodium sulfate, and evaporated *in vacuo*. The residue was chromatographed on silica gel (20 g), using hexane-benzene (2:8) as the eluent, to give a mixture of the C-3 epimers (**16**) (394 mg: 88.2%). MS (*m/z*): 484

(M⁺+2), 482 (M⁺).

3-Bromo-2,2-ethylenedioxy-11,12,14-trimethoxy-18-norabieta-8,11,13-trien-7-one (17). A solution of **16** (109.0 mg) in acetone (3.0 ml) was oxidized with Jones reagent (2.5 M: 0.32 ml) at 0—10 °C for 35 min and then at room temperature for 1.5 h. The mixture was diluted with water and extracted with ether. The ether extract was washed with brine, dried over sodium sulfate, and evaporated *in vacuo*. The residue was chromatographed on silica gel (10 g), using hexane–benzene (1:9) as the eluent, to give the starting **16** (45.5 mg: 41.7%). Further elution with ether–benzene (5:95) gave **17** (53.5 mg: 47.7%, 81.8%[a]), IR: 1673 cm⁻¹; MS (*m/z*): 498 (M⁺+2), 496 (M⁺).

3-Bromo-2,2-ethylenedioxy-6-hydroxy-11,12,14-trimethoxy-18-norabieta-5,8,11,13-tetraen-7-one (18). A stream of oxygen was bubbled in a stirred solution of **17** (171.5 mg) and potassium *t*-butoxide (433.2 mg) in *t*-butyl alcohol (8.0 ml) at 35 °C for 35 min. The mixture was diluted with water and extracted with ether. The ether extract was washed with brine, dried over sodium sulfate, and evaporated *in vacuo*. The residue was chromatographed on silica gel (10 g), using ether–benzene (1:99) as the eluent, to give **18** (48.9 mg: 27.7%). This was recrystallized from acetone–hexane, mp 173—174 °C, $[\alpha]_D$ +67.2° (*c* 0.625); IR: 3394, 1686, 1627 cm⁻¹; ¹H NMR (90 MHz): δ=1.33 (6H, d, *J*=7 Hz, -CH(C<u>H</u>₃)₂), 1.49 (3H, d, *J*=7 Hz, C_4-CH_3), 1.63 (3H, s, C_{10}-CH_3), 2.10 (1H, d, *J*=14 Hz) and 2.80 (1H, d, *J*=14 Hz) (C_1-H_2), 3.73, 3.84, and 3.88 (each 3H and s, 3-OCH_3), 3.89—4.2 (4H, m, -OCH_2-CH_2O-), 4.33 (1H, d, *J*=11 Hz, C_3-H), 6.93 (1H, s, -OH). Found: C, 56.31; H, 6.18%. Calcd for $C_{24}H_{31}O_7Br$: C, 56.36; H, 6.11%.

6-Hydroxy-11,12,14-trimethoxy-19-norabieta-3,5,8,11,13-pentaene-2,7-dione (Coleon B Tri-O-methyl Ether) (4). A solution of **18** (13.9 mg) and dilute hydrochloric acid (10%: 0.1 ml) in acetic acid (2.0 ml) was refluxed for 1 h. The solution was concentrated *in vacuo*, diluted with water, and extracted with ether. The ether extract was successively washed with aqueous sodium hydrogencarbonate and brine, dried over sodium sulfate, and evaporated *in vacuo* to give a crude bromo ketone (11.0 mg), which was used without purification in the next reaction.

A solution of the above crude bromo ketone (11.0 mg) in pyridine (2.0 ml) was refluxed for 3 h. The solution was cooled, poured into dilute hydrochloric acid, and extracted with ether. The ether extract was washed successively with aqueous sodium thiosulfate and brine, dried over sodium sulfate, and evaporated *in vacuo*. The residue was chromatographed on silica gel (5.0 g), using ether–benzene (1:99) as the eluent, to give **4** (3.8 mg: 36.2%), $[\alpha]_D$ −52.8° (*c* 0.625); IR: 3325, 1651, 1626 cm⁻¹; ¹H NMR (90 MHz): δ=1.35 (6H, d, *J*=6.5 Hz, -CH(C<u>H</u>₃)₂), 1.63 (3H, s, C_{10}-CH_3), 2.47 (3H, d, *J*=2 Hz, C_4-CH_3), 2.23 (1H, d, *J*=16 Hz) and 3.62 (1H, d, *J*=16 Hz) (C_1-H_2), 3.74, 3.89, and 3.93 (each 3H and s, 3-OCH_3), 5.98 (1H, bs, C_3-H), 7.89 (1H, s, -OH); MS (*m/z*): 386 (M⁺).

11,12,14-Trimethoxy-18-norabieta-8,11,13-trien-2-one (19). A mixture of **15** (308.6 mg) and sodium iodide (316.0 mg) in acetonitrile (5.0 ml) was stirred at room temperature for 5 min. A solution of chlorotrimethylsilane (98%: 0.27 ml) in acetonitrile (5.0 ml) was then added to the above mixture, and this was refluxed for 2 h. The mixture was cooled, diluted with water, and extracted with ether. The ether extract was washed successively with aqueous sodium thiosulfate and brine, dried over sodium sulfate,and evaporated *in vacuo*. The residue was chromatographed on silica gel (20 g), using ether–benzene (3:97) as the eluent, to give **19** (228.7 mg: 90.0%). This was recrystallized from hexane, mp 111.5—112.5 °C, $[\alpha]_D$ +111° (*c* 0.820) (lit,[b] mp 111.5—113°C, $[\alpha]_D$ +98°), IR: 1697 cm⁻¹; ¹H NMR: δ=1.07 (3H, d, *J*=7 Hz, C_4-CH_3), 1.29 (3H, s, C_{10}-CH_3), 1.30 (6H, d, *J*=7 Hz, -CH(C<u>H</u>₃)₂), 3.60, 3.74, and 3.81 (each 3H and s, 3-OCH_3). Found: C, 73.05; H, 8.94%. Calcd for $C_{22}H_{32}O_4$: C, 73.30; H, 8.95%.

2,2-Ethylenedioxy-11,12,14-trimethoxy-18-norabieta-8,11,13-triene (20). A mixture of **19** (55.2 mg), 1,2-ethanediol (0.2 ml), and *p*-toluenesulfonic acid (60 mg) in dry benzene (10.0 ml) was refluxed for 16 h with a water separator containing 4 Å Molecular Sieves. After the work-up as described for the preparation of **16**, the crude product was chromatographed on silica gel (10 g), using ether–benzene (1:99) as the eluent, to give **20** (57.6 mg: 93.0%). This was recrystallized from hexane, mp 123—125.5 °C, $[\alpha]_D$ +70.6° (*c* 1.105); ¹H NMR: δ=1.11 (3H, d, *J*=7 Hz, C_4-CH_3), 1.30 (6H, d, *J*=7 Hz, -CH(C<u>H</u>₃)₂), 1.37 (3H, s, C_{10}-CH_3), 3.58, 3.75, and 3.78 (each 3H and s, 3-OCH_3), 3.75—4.0 (4H, m, overlap,-OCH_2-CH_2O-). Found: C, 71.05; H, 8.78%. Calcd for $C_{24}H_{36}O_5$: C, 71.25; H, 8.97%.

2,2-Ethylenedioxy-11,12-14-trimethoxy-18-norabieta-8,11,13-trien-7-one (21). Chromium trioxide (700 mg) was added to a stirred solution of **20** (122.5 mg) and pyridine (1.13 ml) in dichloromethane (7.0 ml). The mixture was stirred at room temperature for 23 h, diluted with water, and extracted with ether. The ether extract was washed successively with aqueous sodium hydroxide, water, dilute hydrochloric acid, and brine. The dried solution was evaporated *in vacuo*. The residue was chromatographed on silica gel (10 g), using ether–benzene (5:95) as the eluent, to give **21** (52.5 mg: 41.4%). This was recrystallized from acetone–hexane, mp 151.5—152.5 °C, $[\alpha]_D$ +145° (*c* 0.415), IR: 1670 cm⁻¹; ¹H NMR: δ=1.28 (6H, d, *J*=7 Hz, -CH(C<u>H</u>₃)₂), 1.44 (3H, s, C_{10}-CH_3), 3.66 (3H, s),and 3.80 (6H, s) (3-OCH_3). Found: C, 68.57; H, 8.43%. Calcd for $C_{24}H_{34}O_6$: C, 68.87; H, 8.19%.

2,2-Ethylenedioxy-6-hydroxy-11,12,14-trimethoxy-18-norabieta-5,8,11,13-tetraen-7-one (22). A stream of oxygen was bubbled in a stirred solution of **21** (22.2 mg) and potassium *t*-butoxide (66.6 mg) in *t*-butyl alcohol (3.5 ml) at 35—40 °C for 100 min. After the work-up as described for the preparation of **18**, the crude product was chromatographed on silica gel (10 g), using ether–benzene (5:95) as the eluent, to give **22** (18.4 mg: 86.9%). This was recrystallized from acetone–hexane, mp 216—217 °C, $[\alpha]_D$ +40.0°(*c* 0.475); IR: 3394, 1684, 1625 cm⁻¹; ¹H NMR (90 MHz): δ=1.32, 1.34, and 1.36 (each 3H, d, and *J*=7 Hz, C_4-CH_3 and -CH(C<u>H</u>₃)₂), 1.65 (3H, s, C_{10}-CH_3), 1.81 (1H, d, *J*=14 Hz) and 2.90 (1H, d, *J*=14 Hz) (C_1-H_2), 3.72, 3.86, and 3.88 (each 3H and s, 3-OCH_3), 6.92 (1H, s, -OH); MS (*m/z*): 432 (M⁺).

6-Hydroxy-11,12,14-trimethoxy-18-norabieta-5,8,11,13-tetraene-2,7-dione (23). A solution of **22** (33.5 mg) and dilute hydrochloric acid (10%: 0.75 ml) in tetrahydrofuran (3.0 ml) was stirred at room temperature for 20 h. The solution was diluted with ether. The ether solution was washed with brine, dried over sodium sulfate, and evaporated *in vacuo*. The residue was chromatographed on silica gel (10 g), using ether–benzene (5:95) as the eluent, to give **23** (29.1 mg: 96.7%). This was recrystallized from acetone–hexane, mp 169—170 °C, $[\alpha]_D$ +61.5° (*c* 0.390); IR: 3397, 1705, 1628 cm⁻¹; ¹H NMR (90 MHz): δ=1.34 (6H, d, *J*=7 Hz, -CH(C<u>H</u>₃)₂), 1.44 (3H, d, *J*=7 Hz, C_4-CH_3), 1.72 (3H, s, C_{10}-CH_3), 2.20 (1H, d, *J*=16 Hz) and 3.57 (1H, d, *J*=16 Hz) (C_1-H_2), 3.72, 3.86, and 3.90 (each 3H and s, 3-OCH_3), 7.06 (1H, s, -OH); MS (*m/z*): 388 (M⁺).

Dehydrogenation of 23. A stirred mixture of **23** (10.0 mg), 2,3-dichloro-5,6-dicyano-*p*-benzoquinone (98%: 6.5 mg), and acetic acid (0.15 ml) in dry benzene (3.0 ml) was refluxed for 37 h under a stream of nitrogen. The mixture was cooled and then filtered. The filtrate was washed successively with sodium hydrogencarbonate and brine, dried over sodium sulfate, and evaporated *in vacuo*. The residue

was chromatographed on silica gel (10 g), using ether–benzene (5:95) as the eluent, to give the starting **23** (2.2 mg: 22%). Further elution gave a mixture (5.3 mg) of **4** and **23**. The ^{1}H NMR spectrum of the mixture indicated that it was composed of approximately 3.5 mg (35%, 59%[8]) of **4** and 1.8 mg (18%) of **23**.

The above mixture of **4** and **23** was acetylated at 80—85 °C for 1 h with acetic anhydride (0.2 ml) in pyridine (0.4 ml). After the usual work-up, the crude product was chromatographed on silica gel (10 g), using ether–benzene (1:9) as the eluent, to give 6-acetoxy-11,12,14-trimethoxy-19-norabieta-3,5,8,11,13-pentaene-2,7-dione (**24**) (3.3 mg). IR: 1765, 1655 cm^{-1}; ^{1}H NMR (90 MHz): δ=1.32 (6H, d, J=7 Hz, $-CH(CH_3)_2$), 1.68 (3H, s, C_{10}–CH_3), 2.31 (3H, d, J=1.8 Hz, C_4–CH_3), 2.32 (3H, s, $-OCOCH_3$), 3.68, 3.84, and 3.92 (each 3H and s, 3-OCH_3), 6.06 (1H, bs, C_3-H); MS (m/z): 428 (M^+).

Hydrolysis of **24** with dilute hydrochloric acid in refluxing ethanol afforded **4**.

References

1) M. Ribi, A. C. Sin-Ren, H. P. Küng, and C. H. Eugster, *Helv. Chim. Acta*, **52**, 1685 (1969).

2) R. H. Burnell, M. Leroux, M. Jean, and S. Savard, *Synth. Commun.*, **12**, 423 (1982).

3) T. Matsumoto, K. Iyo, and S. Miuchi, *Bull. Chem. Soc. Jpn.*, **55**, 3831 (1982).

4) T. Matsumoto, Y. Ohsuga, S. Harada, and K. Fukui, *Bull. Chem. Soc. Jpn.*, **50**, 266 (1977).

5) The β-configuration of the C-4 methyl group was supported by conversion of 18-norabieta-8,11,13-trien-3α-ol[3] into **12**. The results will be described elsewhere.

6) D. R. Dalton, J. B. Hendrickson, and D. Jones, *J. Chem. Soc., Chem. Commun.*, **1966**, 591.

7) G. J. Matthews and A. Hassner, "Organic Reaction in Steroid Chemistry," ed by J. Fried and J. A. Edwards, Van Nostrand Reinhold, New York (1972), Vol. 2, p. 15; J. Fried and E. F. Sabo, *J. Am. Chem. Soc.*, **79**, 1130 (1957).

8) Yields are based on the starting material consumed.

9) G. A. Olah, M. Arvanaghi, and Y. D. Vanker, *J. Org. Chem.*, **45**, 3531 (1980).

10) R. Ratcliffe and R. Rodehorst, *J. Org. Chem.*, **35**, 4000 (1970).

11) These signals arose from rotation isomers due to a methoxyl group, whose free rotation was restricted by the bulky benzoyloxyl group.

Palladium Catalyzed C-C Coupling for Synthesis of π-Conjugated Polymers Composed of Arylene and Ethynylene Units

Kenichi SANECHIKA, Takakazu YAMAMOTO,* and Akio YAMAMOTO
Research Laboratory of Resources Utilization, Tokyo Institute of Technology, 4259 Nagatsuta, Midori-ku, Yokohama 227
(Received October 11, 1983)

Palladium compounds such as $Pd(PPh_3)_4$ and $Pd(OAc)_2$ catalyze polycondensation between dihalo aromatic compounds, X-Ar-X (Ar=*p*-phenylene, 2,5-thiophenediyl, 9,10-anthracenediyl, 2,6-pyridinediyl, *p*-benzenedicarbonyl, *p*-xylene-α,α′-diyl), and acetylenic compounds (*p*-$C_6H_4(C{\equiv}CH)_2$ or *p*-$C_6H_4(C{\equiv}CMgBr)_2$). The polymers obtained have high thermal stabilities and most of them show fluorescence. One of the polymers is converted into semiconductors by doping with electron acceptors.

Preparation of π-conjugated polymers and studying their electric conducting properties are the subject of recent interest.[1-5] We have reported preparation of several π-conjugated, thermostable polymers such as poly(thienylene),[6] poly(phenylene),[7] and poly(1,1′-ferrocenediyl),[8] which are converted into semiconductors on doping with electron acceptors. We now report two new methods for preparation of π-conjugated polymers composed of arylene and ethynylene units.

Method I.

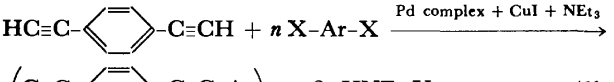

$$n\,HC{\equiv}C\text{-}Ar\text{-}C{\equiv}CH + n\,X\text{-}Ar\text{-}X \xrightarrow{\text{Pd complex + CuI + NEt}_3} \{C{\equiv}C\text{-}Ar\text{-}C{\equiv}C\text{-}Ar\}_n + 2n\,HNEt_3X \quad (1)$$

Method II.

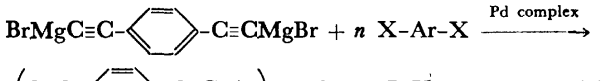

$$n\,BrMgC{\equiv}C\text{-}Ar\text{-}C{\equiv}CMgBr + n\,X\text{-}Ar\text{-}X \xrightarrow{\text{Pd complex}} \{C{\equiv}C\text{-}Ar\text{-}C{\equiv}C\text{-}Ar\}_n + 2n\,MgBrX \quad (2)$$

Both the methods utilize Pd-catalyzed C-C coupling reactions. The basic reaction for Method I,

$$RC{\equiv}CH + R'X + Et_2NH \xrightarrow{\text{Pd complex}} RC{\equiv}CR' + Et_2NH_2X \quad (3)$$

was developed by Hagihara and his coworkers.[9] They utilized a similar reaction to synthesize Pt-, Pd-, or Ni-containing polyynes.[10] The basic reaction for Method II,

$$RhC{\equiv}CMgBr + PhI \xrightarrow{\text{Pd complex}} PhC{\equiv}CPh + MgBrI \quad (4)$$

was developed by Sekiya and Ishikawa.[11] Polymers containing C≡C bonds in their main chains have been recently prepared by several research groups.[10,12,13] A part of results given in this paper was reported elsewhere.[14]

Results and Discussion

We first examined applicability of the Pd-catalyzed coupling reactions (3) and (4), which have been mainly developed for monohaloaromatic compounds, to condensation of two acetylene units with dihaloaromatic compounds (Eqs. 5 and 6).

$$X\text{-}Ar\text{-}X + 2PhC{\equiv}CH \xrightarrow{\text{Pd}} PhC{\equiv}C\text{-}Ar\text{-}C{\equiv}CPh \quad (5)$$

$$X\text{-}Ar\text{-}X + 2PhC{\equiv}CMgBr \xrightarrow{\text{Pd}} PhC{\equiv}C\text{-}Ar\text{-}C{\equiv}CPh \quad (6)$$

As shown in Table 1, $Pd(PPh_3)_4$ and $Pd(OAc)_2$ serve as good catalysts for the coupling reactions between dihaloaromatic compounds and the acetylenic compounds when used with an appropriate co-catalyst and/or base, whereas $PdCl_2$, $FeCl_2$, $FeCl_3$, $NiCl_2$, and $NiCl_2$(bpy) were not effective for the C-C coupling reaction. Use of pyridine, instead of NEt_3, did not give the product, either. The products were characterized by elemental analysis and IR spectroscopy. The products, except for 1,4-bis(phenylethynylcarbonyl)benzene obtained in Nos. 2 and 3, fluoresce by visible light strongly when irradiated by UV light. Fluorescence of 9,10-bis(phenylethynyl)anthracene (product in No. 1) pre-

Table 1. Pd-catalyzed coupling reactions between X-Ar-X and PhC≡CH (A) or PhC≡CMgBr (B)

No.	Acetylenic compound[a]	X-Ar-X[b]	Catalyst[c]	Base	Solvent	Temp °C	Time h	Yield[d] %	Product[e] Color	Product[e] Fluorescence
1	A (2)	$C_{14}H_8Br_2$	$Pd(PPh_3)_4$ + 2 CuI	NEt_3	None	89	3	100	Brown	Green
2	A (2)	$C_6H_4(COCl)_2$	$Pd(PPh_3)_4$	NEt_3	None	89	0.1	92	White	None
3	A (2)	$C_6H_4(COCl)_2$	$Pd(OAc)_2$ + 2 PPh_3	NEt_3	None	89	0.1	85		
4	A (2)	$C_6H_4I_2$	$Pd(PPh_3)_4$ + 2 CuI	NEt_3	None	89	0.05	100		
5	B (4)	$C_6H_4Br_2$	$Pd(OAc)_2$ + 2 PPh_3	None	THF	66	2	92	White	Bluish purple
6	B (2)	$C_6H_4Br_2$	$Pd(OAc)_2$ + 2 PPh_3	None	THF	66	3	79		
7	B (2)	$C_6H_4I_2$	$Pd(OAc)_2$ + 2 PPh_3	None	THF	66	2	73		
8	B (2)	$C_4H_2SBr_2$	$Pd(OAc)_2$ + 2 PPh_3	None	THF	66	2	76	Yellow	Bluish purple

a) Molar ratios to X-Ar-X are given in the parentheses. b) $C_{14}H_8Br_2$=9,10-Dibromoanthracene. $C_6H_4(COCl)_2$=*p*-Benzenedicarbonyl dichloride. $C_6H_4X_2$=*p*-Dihalobenzene. $C_4H_2SBr_2$=2,5-Dibromothiophene. c) About 1 mol% of the Pd catalyst per mol of X-Ar-X was added. d) Yield of $(PhC{\equiv}C)_2Ar$ based on X-Ar-X. e) Color and fluorescing color of the product are shown.

Table 2. Pd-catalyzed polycondensation between X-Ar-X and p-$C_6H_4(C{\equiv}CH)_2$ (A) or p-$C_6H_4(C{\equiv}CMgBr)_2$ (B)

Run	X-Ar-X[b]	Catalyst	Time / h	Yield[c] / %	Polymer obtained
Route I: Diacetylenic compound = A[a]					
1	$C_6H_4Br_2$	$Pd(PPh_3)_4+2$ CuI	2	79	**1**
2	$C_6H_4I_2$	$Pd(PPh_3)_4+2$ CuI	2	97	**1**
3	$C_4H_2SBr_2$	$Pd(PPh_3)_4+2$ CuI	2	84	**2**
4	$C_{14}H_8Br_2$	$Pd(PPh_3)_4+2$ CuI	2	93	**3**
5	$C_5H_3NBr_2$	$Pd(PPh_3)_4+2$ CuI	2	95	**4**
6	$C_6H_4(COCl)_2$	$Pd(PPh_3)_4+2$ CuI	3	64	**5**
Route II: Diacetylenic compound = B[d]					
7	$C_6H_4I_2$	$Pd(PPh_3)_4$	2	97	**1**
8	$C_4H_2SBr_2$	$Pd(OAc)_2+2$ PPh_3	3	82	**2**
9	$C_6H_4(CH_2Cl)_2$	$Pd(OAc)_2+2$ PPh_3	3	72	**6**

a) Excess NEt_3 was added. In toluene under reflux. Amount of Pd catalyst = 0.01 mol per mol of X-Ar-X. b) $C_5H_3NBr_2$ = 2,6-Dibromopyridine. $C_6H_4(CH_2Cl)_2$ = p-Bis(chloromethyl)benzene. c) Yield based on the weight of carbon in the polymer (calculated from the weight and carbon content of polymer). Yield after removing toluene extractable fraction (see Experimental). d) In THF under reflux. Amount of Pd catalyst = 0.01 per mol of X-Ar-X.

pared through an independent reaction route have been extensively studied.[15] Recently Marvel and his coworkers reported preparation of 1,4-bis(phenylethynyl)benzene by a similar Pd-catalyzed coupling reaction.[16] 1,4-Bis(phenylethynylcarbonyl)-benzene and 2,5-bis(phenylethynyl)thiophene prepared in Nos. 2 (or 3) and 8, respectively, are new compounds.

Based on the results shown in Table 1, we have carried out the polycondensation expressed by Eqs. 1 and 2. Table 2 shows the results. The repeating units of the new polymers thus obtained are shown below.

	Color	Fluorescence
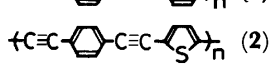 (1)	Yellow	Bluish purple
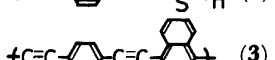 (2)	Yellow	Bluish purple
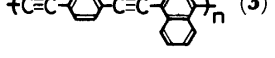 (3)	Red	Green
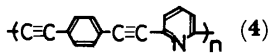 (4)	Light yellow	Purple
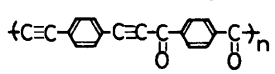 (5)	White	None
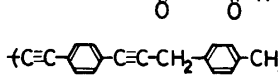 (6)	Yellow	Purple

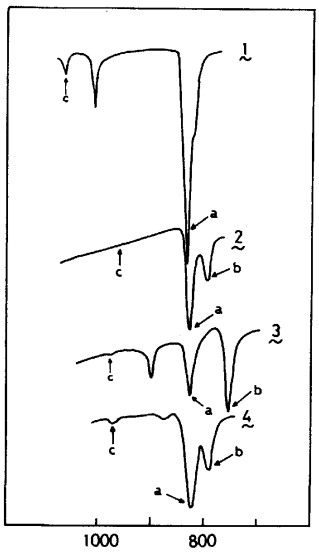

Fig. 1. IR spectra (in the range of 1100—700 cm^{-1}) of **1**—**4** obtained in Runs 1, 3, 4, and 5 (Table 2). Arrows a, b, and c show δ(C-H) of p-phenylene unit, δ(C-H) of other arylene unit, and position of ν(C-Br) of the terminal -Ar-Br group, respectively.

As shown in Table 2, yields of polymers attained by using Method I and Method II are comparable. Since Method II requires precaution to remove water from the reaction system, we consider that Method I is suprior to Method II in preparing the polymers.

The polymers, except for **5**, show strong fluorescence when irradiated by UV light. The polymers have low solubility in solvents. TGA curves of **1**, **2**, and **3** indicate that these polymers have high thermal stabilities. Degradation of these polymers starts at about 380 °C under N_2, and the TGA curves show residual weight of 70—85% at 800 °C. IR spectra of **1**—**6** are consistent with the structures described above, showing ν(C≡C) bands at about 2200 cm^{-1}, δ(C-H) of the phenylene unit at 830—835 cm^{-1}, and δ (C-H) of other arylene units, Ar, (*e.g.*, *cf.* Fig. 1). The IR spectrum of **5** shows a strong ν(C=O) band at 1630 cm^{-1}. IR spectra of **1**, **4**, and **6** show weak ν(C-halogen) bands of terminal groups of the polymers but ν(C-H) of terminal -C≡CH group is not observable in the IR spectra.[17] Since the ν(C-H) absorption band of -C≡CH generally has an absorption coefficient comparable to that of the ν(C-halogen) absorption band, the IR data indicate that most of terminal groups of the polymers are consisted of the halogenated group, -Ar-X. The low solubility of the polymers prevented measuring molecular weights of

the polymers by usual methods. However, if we assume that the both polymer ends have halogen, the molecular weights of the polymers are calculated from their halogen contents. The molecular weights of **1**, **2**, **3**, and **4** prepared by Method I thus calculated are 1400(Run 1)—1690(Run 2), 4000, 1760, 1550, respectively. Polymers **1** and **2** prepared by Method II have comparable molecular weights to those of **1** and **2** prepared by Method I. Deposition of the polymers from the polymerization solvent seems to prevent further elongation of the polymer chain by the polycondensation. The molecular weight of some polymers can be roughly estimated also by comparing the strength of ν(C–halogen) absorption band with that of δ(C–H) of the phenylene and arylene unit in IR spectra of the polymers. The molecular weights thus estimated roughly agree with the molecular weights calculated from the halogen content. Powder X-ray diffraction patterns of the polymers show sharp diffraction bands, indicating high crystallinity of the polymers.

Polymers **1**—**6** are insulators having electric conductivity (σ) of below 10^{-12} S cm^{-1}. Polymers **1**, **2**, and **4** showed no apparent interaction with I_2, whereas **3** and **5** showed interaction with I_2 (gas). Polymer **3** showed electric conductivity of $\sigma=4\times10^{-5}$ S cm^{-1} after exposure to vapor of I_2 for 18 h at room temperature, but the iodine adduct of **5** (iodine: 24 wt% per **5**) remained as an insulator. Polymer **3** showed certain electric conductivity ($\sigma=6.6\times10^{-8}$ S cm^{-1} at 247 K) after exposure to vapor of AsF_5, whereas it did not interact with tetracyanoethylene and tetracyanoquinodimethane as proved by no change in IR spectrum after dipping **3** in solutions of these electron acceptors.

Experimental

Materials, Analysis, and Manipulation. $Pd(PPh_3)_4$ was prepared according to literature.[18] $Pd(OAc)_2$, CuI, PPh_3, NEt_3, and crystalline dihaloaromatic compounds were used as purchased from Tokyo Kasei Kogyo Co., Ltd. or Kanto Chemical Co., Inc. 2,5-Dibromothiophene was recrystallized from hexane at 78 °C. PhC≡CMgBr was prepared *in situ* by a reaction of PhC≡CH with EtMgBr in a 1:1 ratio. 1,4-Diethynylbenzene was prepared according to literature,[19] and purified by sublimation: mp 96 °C (lit, 96.5 °C). Solvents were dried over CaH_2 or Na, distilled under N_2, and stored under N_2. Microanalysis of C, H, and N was performed with a Yanagimoto CHN Autocorder MT-2, and that of halogen with a Yazawa halogen analyzer. IR spectra were recorded on a Hitachi 295 spectrometer. Thermogravimetric analysis was performed with a Shimadzu thermoanalyzer DT-30. Powder X-ray diffraction patterns were obtained with Phillips PW-1051. Electric conductivity was measured wth a Takeda Riken TR-8651 electrometer. The powdery polymer–electron acceptor adduct was molded into a pellet (diameter=1.3 cm) by pressing it at 600 kg/cm^2. From the pellet a bar was obtained by cutting off other parts of the pellet and the electric conductivity was measured with the bar using the four-point method. Reactions listed in Tables 1 and 2 were carried out under nitrogen or argon by using Schlenk type tubes.

Coupling Reactions between X-R-X and PhC≡CH or PhC≡CMgBr (cf. Table 1).

No. 1: $Pd(PPh_3)_4$ (36 mg, 0.031 mmol) and CuI (12 mg, 0.062 mmol) were added to a mixture of 9,10-dibromoanthracene (1.06 g, 3.15 mmol), PhC≡CH (0.645 g, 6.32 mmol), and NEt_3 (1.6 cm^3, 15 mmol). The reaction mixture was stirred for 3 h under reflux. Then, it was poured into an excess amount of methanol after cooling to room temperature. The light precipitate was collected by filtration and recrystallized to yield 0.72 g (1.9 mmol) of known 9,10-bis(phenylethynyl)anthracene.[15] Condensation of the methanol solution gave another crop (9.59 g, 1.3 mmol) of 9,10-bis(phenylethynyl)anthracene. Found: C, 95.4; H, 4.6%. Calcd for $C_{30}H_{18}$: C, 95.2; H, 4.8%.

Nos. 2—4 were carried out analogously. *p*-$(PhC{\equiv}CCO)_2C_6H_4$ was characterized by IR and elemental analysis. Found: C, 86.2; H, 4.2%. Calcd for $C_{24}H_{14}O_2$: C, 86.2; H, 4.2; mp 185 °C. IR(KBr): 2200s, 1640s, 1320m, 1205m, 1030m, 750s, 695m, 680m. 1,4-bis(phenylethynyl)benzene was characterized by IR and mp, 182 °C (lit,[19] 180—183 °C).

No. 5: A THF (11 cm^3) solution of C_2H_5MgBr (13.6 mmol) was added to a THF solution of PhC≡CH (1.39 g, 13.6 mmol) at room temperature, and the mixture was stirred for 2 h. To this mixture were added 0.80 g (3.4 mmol) of *p*-dibromobenzene, 10 mg of $Pd(OAc)_2$ and 34 mg of PPh_3. After the reaction mixture was stirred for 2 h under reflux, it was cooled to room temperature. Excess of dil. aqueous HCl solution was added to the reaction mixture. Extraction of the product with benzene, drying the benzene solution with $MgSO_4$, purification by column chromatography (Al_2O_3, benzene), and evaporation of benzene gave crystals of 1,4-bis(phenylethynyl)benzene: yield=0.87 g (92%), after recrystallization from toluene. Reactions shown by Nos. 6 and 7 were carried out analogously.

No. 8: A THF (14 cm^3) solution of C_2H_5MgBr (24.2 mmol) was added to 2.48 g (24.2 mmol) of phenylacetylene. After stirring for 1.5 h at room temperature, 2,5-dibromothiophene (2.93 g, 12 mmol), $Pd(OAc)_2$ (39 mg, 0.12 mmol), and PPh_3 (100 mg, 0.24 mmol) were added to the reaction mixture. After stirring the reaction mixture for 2 h under reflux, it was cooled to room temperature. An excess amount of dil aqueous HCl solution was added to the reaction mixture. Extraction of the product with benzene, drying the benzene solution with $MgSO_4$, purification by the column chromatography, and recrystallization from methanol gave 2.61 g (76%) of brown 2,5-bis(phenylethynyl)thiophene, which was characterized by IR and elemental analysis; mp 85 °C. Found, 83.8; H, 4.3; S, 10.7%. Calcd. for $C_{20}H_{12}S$: C, 84.5; H, 4.3; S, 11.3%. IR(KBr disk): 1590m, 1480m, 1440m, 800s, 750s, and 680s.

Polycondensation (cf. Table 2). Run 1: $Pd(PPh_3)_4$ (27 mg, 0.023 mmol) and CuI (8 mg, 0.04 mmol) were added to a mixture of *p*-diethynylbenzene (300 mg, 2.38 mmol), *p*-dibromobenzene (562 mg, 2.38 mmol), and NEt_3 (2 cm^3) in toluene (39 cm^3). After stirring for 2 h under reflux, the reaction mixture was poured into excess methyl alcohol. The precipitate obtained was separated by filtration, washed repeatedly with methyl alcohol, and dried under vacuum to obtain 510 mg of **1**. After removing a toluene-soluble fraction of **1** by extraction with hot toluene using a Soxhlet extractor, the yellow solid was dried under vacuum to yield 0.43 g of **1**. Found: C, 83.5; H, 3.7; Br, 11.4%. From the toluene extract we obtained 80 mg of low molecular weight **1**. Polymerization in Run 2 was carried out analogously.

Run 3: $Pd(PPh_3)_4$ (45 mg, 0.039 mmol) and CuI (15 mg, 0.080 mmol) were added to a mixture of *p*-diethynylbenzene (514 mg, 4.07 mmol), 2,5-dibromothiophene (985 mg, 4.07 mmol), and NEt_3 (3 cm^3) in toluene (50 cm^3). After stirring for 2 h under reflux, the polymer obtained was treated as in the case of Run 1 to obtain 810 mg of crude **2**, from which 710 mg of toluene-unextractable **2** was obtained. Found: C, 80.2; H, 2.9; Br, 4.0%.

Runs 4—6 were carried out analogously. Analytical data of **3**, **4**, and **5** are as follows. **3**: Found: C, 87.3; H, 3.8; Br, 9.1%. **4**: C, 80.7; H, 3.2; N, 6.1; Br, 10.3%. **5**:C, 77.4; H, 3.7; Br, 4.4%.

Run 7: When a THF (9.2 cm^3) solution of C_2H_5MgBr

(15.6 mmol) was added into a Schlenk tube containing 986 mg (7.82 mmol) of 1,4-diethynylbenzene at room temperature, vigorous evolution of ethane was observed. After addition of 7 cm^3 of THF and stirring the reaction mixture for 5 h at room temperature, 2.58 g (7.82 mmol) of *p*-diiodobenzene in 5 cm^3 of THF, 18 mg (0.080 mmol) of $Pd(OAc)_2$, and 42 mg (9.16 mmol) of PPh_3 were added. This reaction mixture was stirred for 2 h under reflux. After cooling to room temperature, the reaction mixture was poured into an HCl–methyl alcohol mixture (150 cm^3). This light yellow precipitate was collected by filtration, washed with methyl alcohol, and dried under vacuum to obtain 920 mg of crude **1**. Removing a toluene-soluble fraction (by Soxhlet technique) gave 800 mg of **1**. Found: C, 80.4; H, 3.0; I, 15.7%.

Runs 8 and 9 were carried out analogously. **6**: C, 90.9; H, 4.7; Br, 1.2%.

References

1) H. Shirakawa and T. Yamabe, "Synthetic Metals," Kagaku-Dojin, Kyoto (1980).

2) Y. W. Park, A. J. Heeger, M. A. Druy, and A. G. MacDiarmid, *J. Chem. Phys.*, **73**,946 (1980); H. Shirakawa, E. J. Louis, A. G. MacDiarmid, C. K. Chiang, and A. J. Heeger, *J. Chem. Soc., Chem. Commun.*, **1977**, 578.

3) D. M. Ivory, G. G. Miller, J. M. Sowa, L. W. Shacklette, R. R. Chance, and R. H. Baughmann, *J. Chem. Phys.*, **71**, 1506 (1979).

4) A. F. Diaz, K. K. Kanazawa, and G. P. Gardini, *J. Chem. Soc., Chem. Commun.*, **1979**, 653.

5) J. F. Rabolt, T. C. Clarke, K. K. Kanazawa, J. R. Reynolds, and G. B. Street, *J. Chem. Soc., Chem. Commun.*, **1980**, 347.

6) T. Yamamoto, K. Sanechika, and A. Yamamoto, *Bull. Chem. Soc. Jpn.*, **56**, 1503 (1983).

7) T. Yamamoto, Y. Hayashi, and A. Yamamoto, *Bull. Chem. Soc. Jpn.*, **51**, 2091 (1978).

8) K. Sanechika, T. Yamamoto, and A. Yamamoto, *Polym. J.*, **13**, 255 (1981).

9) Y. Tohda, K. Sonogashira, and N. Hagihara, *Synthesis*, **1977**, 777; K. Sonogashira, Y. Tohda, and N. Hagihara, *Tetrahedron Lett.*, **1975**, 4467.

10) K. Sonogashira, S. Takahashi, and N. Hagihara, *Macromolecules*, **10**, 879 (1977); S. Takahashi, M. Kariya, T. Yatake, and K. Sonogashira, *ibid.*, **11**, 1063 (1978); K. Sonogashira and S. Takahashi, "Organometallic Polymers," ed by N. Hagihara and A. Nakamura, Gakkai Shuppan Center, Tokyo (1982) P. 175.

11) A. Sekiya and N. Ishikawa, *J. Organomet. Chem.*, **118**, 349 (1976).

12) A. S. Hay, *J. Polym. Sci., A-1*, **7**, 1625 (1969).

13) G. N. Patel, E. N. Duesler, D. Y. Curtin, and I. C. Paul, *J. Am. Chem. Soc.*, **102**, 461 (1980).

14) K. Sanechika, T. Yamamoto, and A. Yamamoto, *Polym. Prepr.*, **30**, 3B27 (1981).

15) e.g., C. A. Heller, R. A. Henry, B. A. LcLaughin, and D. E. Bliss, *J. Chem. Eng. Data*, **19**, 214 (1974).

16) S. Havens, C. C. Yu, D. Draney, and C. S. Marvel, *J. Polym. Sci., Polym. Chem. Ed.*, **19**, 1349 (1981).

17) The IR spectra of toluene-extractable, low molecular weight fractions obtained during work-up of the polymers (see Experimental), show stronger ν(C–halogen) bands. However, the ν(C–H) band of the –C≡CH group is not observable or very weak.

18) A. S. Hay, *J. Org. Chem.*, **25**, 637 (1960).

19) A. M. Sladkov, L. Yu. Ukhim, and V. V. Korshak, *Izv. Acad. Nauk SSSR, Ser. Khim.*, **1963**, 2213.

ESR in Mercury(II) Iodide Thiocyanate

Kunio TAKEI,* Kazuo SUGIHARA, Hitoshi HAGIWARA, and Seisuke NAKAMURA
Department of Industrial Chemistry, Faculty of Engineering, Miyazaki University, Kirishima, Miyazaki 880
(Received August 2, 1982)

Powder of mercury(II) iodide thiocyanate (HgISCN) gives a weak electron spin resonance (ESR) signal at $g=2.003$ in the dark. When the powder is irradiated, the ESR-signal intensity increases during the exposure. When the light is turned off, the intensity decreases. The ESR-signal may be due to electrons trapped by lattice defects.

Mercury(II) iodide thiocyanate (HgISCN), was prepared for the first time by Rao and Watson[1] in order to study the photochromism of this compound, but its crystal structure was not investigated. In recent years,[2,3] though, the photochromic process of HgISCN has been studied in our laboratory by the use of the radioisotopic tracer technique. When powder of labeled HgISCN with radioactive tracers is exposed to sunlight, it immediately turns from orange yellow to black, and ^{203}Hg, ^{35}S and ^{131}I atoms diffuse toward the crystal surface and escape into atmosphere. On the other hand, the ^{14}C atom does not move. The black color of this powder is somewhat bleached by keeping it in the dark at room temperature for several months. These results suggest that the electrons belonging to $(SCN)^-$ or I^- may be optically excited to the conduction band and may be trapped by the lattice defects or impurity levels. These trapped electrons must show an ESR-signal. It was found that HgISCN is, optically, a very sensitive compound, showing the ESR-signal during irradiation with light, and thermally it is an unstable compound, decomposing at 165 °C. HgISCN seems to be a molecular compound between mercury(II) iodide and mercury(II) thiocyanate. The present paper will present the results of our ESR experiments.

Experimental

Materials. The powder of mercury(II) iodide thiocyanate was prepared as reported in a previous paper.[2,3] The chemical analysis with an atomic-absorption apparatus exhibited this Hg content for HgISCN: calcd 52.02%, obsd 53%, while the chemical analysis by a fused method[4] exhibited this S content for HgISCN: calcd 8.32%, obsd 8.0%. This powder shows photochromic behavior.

ESR. ESR measurements were made in the dark by the use of ESR equipment [JEOL, X-band] at a field of 3250 ± 250 G (1 G=10^{-4} T). Then, the HgISCN powder was irradiated at room temperature with a tungsten lamp of 150 W through the window of the cavity of the ESR equipment for the appropriate length of times. The ESR-signal intensity of the powder rapidly grew and then gradually approached saturation after 30 min irradiation. When the light was switched off after saturation has been reached, the ESR-signal decayed rapidly. The excitation intensity in front of the window of the cavity was measured as 7000 lx with a Toshiba luxmeter. The rise-and-decay ESR experiments were repeated at various temperatures (*cf.* Fig. 2). The temperature was controlled at about 60, 25, −10, and −50 °C by flowing through nitrogen gas, warmed with a heater or cooled with liquid nitrogen, into the cavity: it was measured by means of a copper-constantan thermocouple.

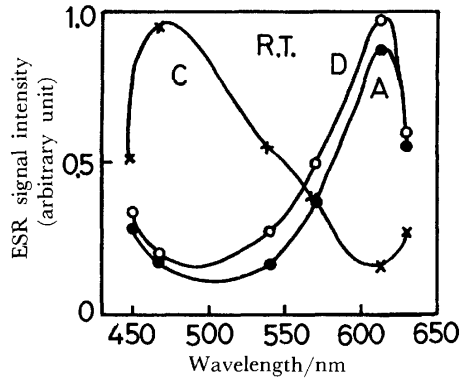

Fig. 1. Excitation spectra of the ESR signal intensity for A, C, and D. A: powder of HgISCN, C: one of the thermal decomposition products of $Hg(SCN)_2$, D: powder of $Hg(SCN)_2$ which was heated up to 155—158 °C.

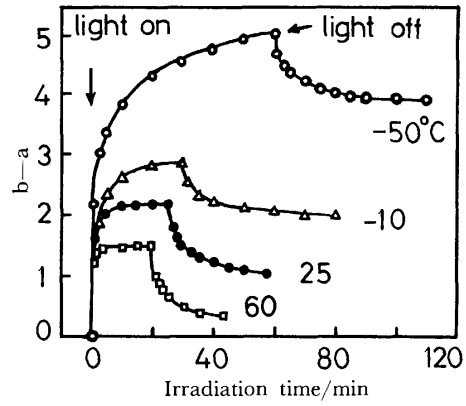

Fig. 2. The relationship between b—a and irradiation time at various temperatures. a is the ESR signal intensity of a nonirradiated HgISCN powder normalized to that of MnO. b is the ESR signal intensity of an irradiated HgISCN powder normalized to that of MnO.

Excitation Spectra of ESR-signal. Monochromatic light was obtained by the use of six filters made by the Shimadzu Co. The radiation from the tungsten lamp was selected with filters and was focussed on a capillary glass tube containing HgISCN powder (*cf.* Fig. 1).

Results and Discussion

ESR-signal of Nonirradiated Powder of HgISCN. A weak signal for the nonirradiated orange yellow powder of HgISCN, which is conveniently denoted by A, was observed at $g=2.003$. The observed ESR-signal

of A is ascribed not to an impurity, but to a defect in A. This can be explained as follows. A was formed when a mixture of mercury(II) iodide and mercury(II) thiocyanate was heated at 162°C. The mixture heated only to 150°C gave no ESR-signal at all. When heated up to 155—158°C, though, the mixture begins to show the ESR-signal (g=2.003). This signal may be due to mercury(II) thiocyanate, because mercury(II) thiocyanate heated to 155—158°C, denoted by D, gives a weak ESR-signal at g=2.003, while mercury(II) iodide heated to the same temperature shows no ESR-signal. Mercury(II) thiocyanate decomposes at 165°C into a black powder, denoted by B, and into a yellow powder, denoted by C. B and C gave weak signals at g=2.003. The signal intensity of B was not sensitive to light, but that of C was sensitive to light. B was removed from A by washing with concentrated hydrochloric acid containing pottasium chlorate. The X-ray diffraction pattern of A was different from those of B, C, and D. The patterns of B and D were similar to those of cubic mercury(II) sulfide and of mercury(I) thiocyanate respectively, while the pattern of C showed that C is a nearly amorphous material. In order to make clear the origin of the ESR-signal of A, the excitation spectra of the ESR-signal was measured. The spectra of A and D were similar to each other, while the spectrum of C was entirely different from that of A or D (*cf.* Fig. 1). Consequently, when the mixture is heated to 155—158°C, the mixture may begin to form a structure of A, although its fraction may be small. In order to form A, the mixture must be heated to 162°C. It is not clear, however, whether the observed ESR-signal of A is attributed to the lattice defects which are formed in A in the 155—162°C range or to the signal of D, which exists in A as an impurity. This problem was solved by the following experiment. If A contains a small quantity of D as an impurity, the ESR-signal intensity of a mixture of A and D must become stronger than that of A when a small quantity of D is added to A. Various quantities of D were added to A, and the ESR-signals of these mixtures were measured at room temperature. Quantities of mixtures in the quartz-glass capillary tube were kept constant in order to keep the quality factor in the cavity constant. The experimental results show that the ESR-signal intensities of A containing D at 4.17, 8.30, or 12.5 wt% of D are smaller than the intensity of alone A and that they gradually decrease according to the increase in the content of D (*cf.* Fig. 3). This fact shows that the signal of A is attributed not to the signal of D in A as an impurity, but to the lattice defects in A.

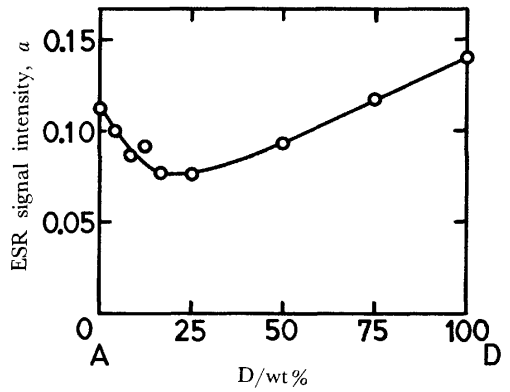

Fig. 3. The relationship between the ESR signal intensity in the dark of A containing D at various weight percents and the weight percent of D. The ESR signal intensities are normalized to that of MnO.

ESR-signal of Irradiated HgISCN. A quartz-glass capillary tube containing MnO powder was put into the cavity. The ESR of MnO was then measured as a standard of the ESR-signal at the same time as the ESR of A put into another quartz-glass capillary tube was measured. When A was irradiated with a tungsten lamp, MnO powder was irradiated at the same time. The ESR-signal intensity of MnO during the exposure did not change from that of MnO in the dark. When a is the signal intensity of A in the dark normalized to that of MnO, and b is the signal intensity of an irradiated A normalized to that of MnO, b—a means the increase in the signal intensity during exposure to the light. Figure 2 shows the b—a relationships and the irradiation times at various temperatures. The rising curves of the ESR-signal intensity during the irradiation show the speed at which the traps are filled with excited electrons. The saturation value of b—a was reached after about 10 min under the irradiation at 60°C, but the saturation was not reached even after 60 min under the irradiation at −50°C. The decay curves of the ESR-signal intensity show the detrapping speed of electrons from the traps. When the light was switched off at the saturation of b—a at 60°C, the value of b—a decreased rapidly; it approached a zero value after 20 min. When the light was switched off after saturation had been reached at −50°C, the value of b—a decreased slowly, but it was still somewhat big even after 60 min. It takes a long time at −50°C before the value of b—a reaches zero.

Under constant excitation with light, the rising-and-decay curves of the ESR-signal intensity may be discussed by the use of a simple electron-trapping model in terms of a simple first-order reaction equation. If F is the number of photons absorbed per unit of volume per unit of time, the number of optically excited electrons may be proportional to F. It is assumed that the θ fraction of mF, where m is the proportional constant, is trapped by trap and that the $(1-\theta)$ fraction of mF is consumed by recombination or fluorescence. If p is the probability of an electron escaping from a trap with a depth of E and a cross-section for the capture of an electron, S, at a certain temperature T, the filling speed of an electron into a trap may be given by $dn/dt=\theta mF-np$, where n is number of trapped electrons and $p=Nv S\cdot\exp(-E/kT)$.[5] N is the effective density of states in the conduction band, v is the thermal velocity of an electron, and k is the Boltzmann constant. At saturation with a value of b—a, $dn/dt=0$ and $\theta mF=n_0 p$, where n_0 is the value of n at the saturation. Then, $dn/dt=p(n_0-n)$. The solution of this equation is:

$$n = n_0(1-e^{-pt}). \quad (1)$$

The rate of change of the number of trapped electrons during the decay is $-dn/dt=np$. The solution of this equation is:

$$n = n_0 e^{-pt}. \quad (2)$$

The rising-and-decay curves of the ESR-signal intensity are shown by Eqs. 1 and 2 respectively. These equations contain the term of $1/e^{E/kT}$. At some time t, a value of $1/e^{pt}$ at a higher temperature may become smaller than those at a lower temperature if N, v, S, and E are independent of the temperature in the range of 60—−50°C. Therefore, it is expected that, at 60°C, n may rapidly increase and n_0 may be reached rapidly after irradiation. At −50°C, n may slowly increase, and n_0 may be reached slowly after irradiation. Similarly, the decay rate may be effected to be big at 60°C and small at −50°C. The value of n_0 at −50°C in Fig.2 is bigger than that at 60°C. This comes from the fact that the lower the temperature, the greater the number of the trapped electrons. The results in Fig.2 nearly satisfy these expectations. The actual filling and detrapping speeds may be a mean of the individual speeds for the individual traps with a given depth E, because there are a number of traps with various depths.

Excitation Spectra of ESR-signal. The excitation spectra of the ESR-signal of HgISCN at room temperature are shown in Fig. 1. The most sensitive wavelength of the ESR-signal is located at about 620 nm.

The authors wish to thank Dr. S. Fujiwara for his many helpful discussions and suggestions during this work.

References

1) S. V. Raghava Rao and H. E. Watson, *J. Phys. Chem.*, **32**, 1354 (1938).
2) K. Takei, H. Kichikawa, and H. Hagiwara, *Radioisotopes*, **27**, 80 (1978).
3) K. Takei, H. Hagiwara, and S. Nakamura, *Radioisotopes*, **31**, 6 (1982).
4) K. Kato, "Hyojun Teiryobunsekiho," Maruzen, Tokyo (1944), p. 704.
5) R. H. Bube, "Photoconductivity of Solids," John Wiley and Sons, New York and London (1960), p. 278.

 © 1984 The Chemical Society of Japan Bull. Chem. Soc. Jpn., 57, 759—762 (1984)

An Electrochemical Study on Anion Doping-Undoping Process of Polyacetylene by Means of FFT Impedance Measurement

Tetsuya OSAKA* and Takashi KITAI

Department of Applied Chemistry, School of Science and Engineering, Waseda University, Okubo, Shinjuku-ku, Tokyo 160

(Received June 27, 1983)

An electrochemical anion doping-undoping process of *cis*-polyacetylene, $(CH)_x$, was investigated in 1 mol dm^{-3} $LiClO_4$ or $LiBF_4$ in propylene carbonate by the FFT impedance measurement. This could be applied to the system with time-variation because of its high speed measuring duration. The doping-undoping process of the anion was represented by the Randles-type equivalent circuit, considering the corrective term concerned with surface roughness. The impedance behavior of the doping-undoping process was pursued by the variation of resistive component, *Rr*. The value of *Rr* was mainly reflected by the dopant concentration at the surface. The variation of *Rr* indicated that rapid or strong-drive doping produces non-uniformity of dopant distribution in the film and high dopant concentration at the surface.

A conduction polymer has recently been developed as a new electrode material for high-density batteries. Polyacetylene, $(CH)_x$, is very suitable as a new electrode material, since its conductivity can be varied over twelve orders of magnitude depending on the dopant concentration[1] and it can be easily synthesized. Polyacetylene can be electrochemically doped as either n-type or p-type to induce semiconducting and ultimately metallic conditions with a variety of species.[2,3] Accordingly, some attempts have been made to use polyacetylene as an electrode material in lightweight rechargeable storage batteries.[4,5] Studies of the electrochemical characteristics of polyacetylene, however, are recent and so far there have been only a few reports on the analysis of the electrochemical doping or undoping process of polyacetylene.[6] In this paper, we report the electrochemical doping-undoping process of polyacetylene as a cathode by means of electrochemical measurements, especially the FFT impedance method.[7] The FFT impedance method has an advantage of rapid measurement for the frequency-dispersion within a very short time-duration. Phenomena with time-variation such as the doping-undoping process may be analyzed easily by this method.

Experimental

The *cis*-polyacetylene films with 0.3 mm thickness were prepared by the Shirakawa method.[8] The working electrode consisted of a single circular film of 8 mmϕ of the *cis*-$(CH)_x$ (weight density 0.44 g cm^{-3}), attached to a platinum plate as a current collector. A circular platinum or lithium mounted on platinum counter electrode was placed opposite to the *cis*-$(CH)_x$ working electrode in a Teflon or glass cell. A Li/Li^+, reference electrode was set at the mid point between the working and counter electrodes, and the potential was referred to the Li/Li^+ in the same solution. The electrolyte solution was 1.0 mol dm^{-3} $LiClO_4$ or 1.0 mol dm^{-3} $LiBF_4$ in propylene carbonate (PC). The solvent and electrolyte were purified and handled in the usual method.[4,9] Electrochemical measurements were performed by voltammetry and the FFT impedance method with frequency range between 0.01 and 2.5 kHz. The system and method for the FFT impedance measurements were the same as described in the previous paper.[7] All experiments were carried out in a dry and inert Ar gas atmosphere.

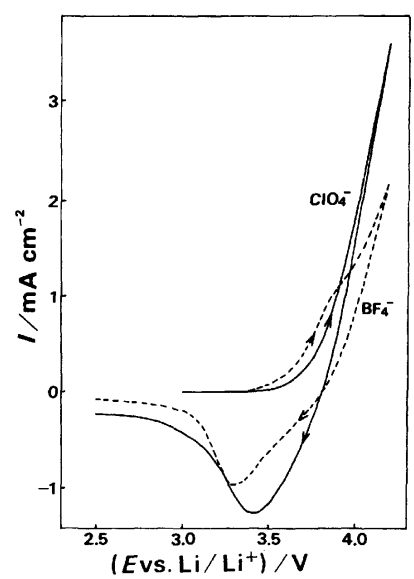

Fig. 1. Current *vs.* potential curves of $(CH)_x$ electrode at anion doping-undoping process in various solutions at 1 mV s^{-1} at Ar atmosphere.
——: 1 mol dm^{-3} $LiClO_4$/PC, ----: 1 mol dm^{-3} $LiBF_4$/PC.

Results and Discussion

Current vs. *Potential Curves of $(CH)_x$ Electrode.* Figure 1 shows the typical current *vs.* potential curves of the $(CH)_x$ electrode at the third time scan for the anion doping-undoping process in 1 mol dm^{-3} $LiClO_4$/PC and 1 mol dm^{-3} $LiBF_4$/PC using a scan rate of 1 mV s^{-1}, since the behavior of current *vs.* potential curves with 1 mV s^{-1} becomes steady-state from the third time scan. The first time scan showed the greatest difference from the steady-state of the current *vs.* potential curve, *i.e.*, the doping at the first time scan was small. In Fig. 1, the anodic current indicates anion doping into $(CH)_x$ and the cathodic current indicates anion undoping from doped $(CH)_x$, respectively. The electrochemical doping reaction involves the partial oxidation of $(CH)_x$ as shown in Eq. 1.[3,5]

$$(CH)_x + xyClO_4^- \longrightarrow [(CH^{+y})(ClO_4)_y^-]_x + xye. \quad (1)$$

The $(CH)_x$ film is doped readily to the composition of $[CH(ClO_4)_y]_x$ or $[CH(BF_4)_y]_x$ from approximately the

same potential around 3.4 V in each electrolyte solution. The anodic doping current increases more rapidly for ClO_4^- doping than for BF_4^- doping, though at the initial doping potential the increase for BF_4^- anion is greater than that for ClO_4^- anion. In Fig. 1, the charging ratio from anodic scan until the anodic current becoming zero at cathodic scan was 1.47% for ClO_4^- and 0.72% for BF_4^-, respectively.† At the cathodic scan, the cathodic currents for the undoping process show a peak at 3.4 V for ClO_4^- undoping and at 3.3 V for BF_4^- undoping. It is assumed from the behavior of the current-potential curves that ClO_4^- anion doping-undoping occurs easier than BF_4^- anion doping-undoping. The doping process as seen in Eq. 1 shows that the doped polymer is utilized as a cathode material, and the characteristics of doping-undoping process for ClO_4^- may be superior to that for BF_4^-, thus the polyacetylene doped ClO_4^- anion might be a superior cathode for a high power density battery of $(CH)_x$.

Impedance Measurements of the $(CH)_x$ Electrode. Figures 2(a) and 2(b) show the impedance of the $(CH)_x$ electrode at various potentials in 1 mol dm^{-3} $LiBF_4$/PC during anodic and cathodic scans, respectively, at 1 mV s^{-1}. At the anodic scan in Fig. 2(a), the impedance plots are semi-circles, and their diameters decrease with the doping process. The behavior of the cathodic scan for the undoping process is also similar to that of the anodic scan as seen in Fig. 2(b), and the diameters increase with the undoping process. Figure 3 shows the impedance representation of $(CH)_x$ in 1 mol dm^{-3} $LiClO_4$/PC at various doping levels using

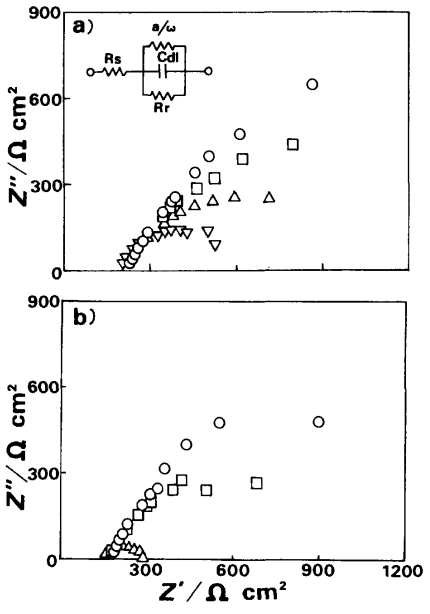

Fig. 2. Impedance representations of $(CH)_x$ electrode at anion doping-undoping process with using potential-sweep at 1 mV s^{-1} in 1 mol dm^{-3} $LiBF_4$/PC at Ar atmosphere.
a) Doping process measured at various potentials; ○: 3.5 V, □: 3.6 V, △: 3.7 V, ▽: 3.8 V. b) Undoping process measured at various potentials; ○: 3.0 V, □: 3.15 V, △: 3.3 V.

† Here, 1% doping corresponds to 278 mC.

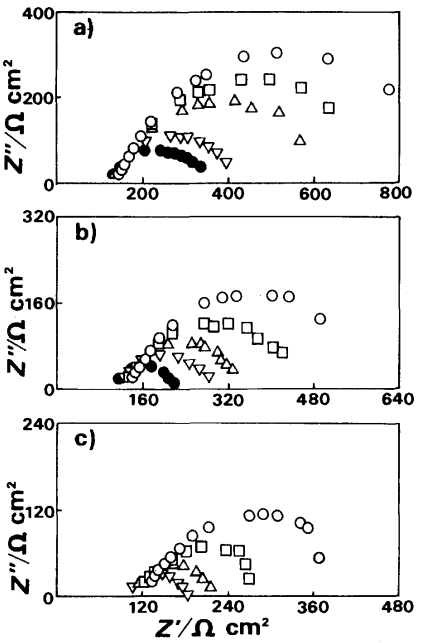

Fig. 3. Impedance representations of $(CH)_x$ electrode at anion doping process with using potential-step in 1 mol dm^{-3} $LiBF_4$/PC at Ar atmosphere.
a) Doping at constant potential of 3.6 V at various charges; ○: 0.2 mC, □: 3.4 mC, △: 10.4 mC, ▽: 44.0 mC, ●: 70.0 mC. b) Doping at constant potential of 3.8 V at various charges; ○: 0.4 mC, □: 11.0 mC, △: 30.0 mC, ▽: 50.0 mC, ●: 90.0 mC. c) Doping at constant potential of 4.0 V at various charges; ○: 1.2 mC, □: 19.6 mC, △: 56.6 mC, ▽: 96.0 mC.

potential-step doping. The doping potentials for *p*-$(CH)_x$ are 3.6, 3.8, and 4.0 V for Figs. 3(a)—(c), respectively. The behavior shown in Fig. 3 is similar to that in Fig. 2(a) for the potential-scaning doping process. However, the greater the anodic potential of the doping level becomes, the earlier the diameter of semi-circle becomes small, namely, the diameter of semi-circle is shorter even at the same charging value when the doping is performed at the more anodic potential. This behavior is shown more clearly in Fig. 5. The impedance representation of $(CH)_x$ for ClO_4^- anion doping-undoping process is similar to that for BF_4^-.

The theoretical equivalent circuit for the analysis and the interpretation of the experimental data shown in Fig. 2 are described as follows. The doping-undoping results are interpreted by the Randles-type equivalent circuit shown in Fig. 2(a), which displays a semi-circle in the impedance representation. The components of *Rs*, *Rr*, *Cdl*, and $a\,\omega^{-1}$, (ω: angular frequency) are the solution resistance, the resistive component due to the electrode reaction, the double-layer capacitance, and the corrective term concerned with surface roughness.[10] The surface of polyacetylene film may be porous because of it being composed of a fibril unit, thus the term concerned with the roughness, $a\,\omega^{-1}$, should be added into the circuit. If porous states are assumed, the double-layer capacitance, *Cdl*, means the total value of each pore's double-layer capacitance. The resistive component, *Rr*, arises

mainly from two factors of the partial oxidation or reduction (*i.e.*, doping-undoping) reaction and of the film resistivity itself. The diffusion of the anion into the film (or diffusion of anion from exterior to interior of fibrils) is not directly detected between these frequency regions as seen in Fig. 2. The double-layer capacitance, *Cdl*, of $(CH)_x$ shows the same value of *ca.* 8.0 μF cm^{-2} as that of the platinum electrode and also the value of *Cdl* is scarcely changed by the doping-undoping process. The value of the term '*a*' is very large and it is scarcely changed by the doping-undoping process. This means that the semi-circle is hardly inclined from the real component axis as is seen in Fig. 2. Accordingly, the information from the values of *Cdl* and '*a*' suggests that the surface porosity scarcely influences the impedance behavior of the polyacetylene film. This conclusion may be due to the very fine porosity of the $(CH)_x$ film (of the order of ten nm) formed by the fibril unit. A slight variation of *Rs* was observed in Figs. 2 and 3; this can be caused by the swelling of the $(CH)_x$ film on doping, which causes a decrease of the distance between the electrodes.[††] The value of *Rr*, which corresponds to the diameter of the semi-circle, changes greatly during the doping-undoping process. The value of *Rr* decreases with doping, while it increases with undoping. Consequently, the values of *Rs*, *Cdl*, and '*a*' are scarcely changed by the doping-undoping process but the opposite is true for *Rr*. Accordingly, there is a high possibility that the doping-undoping process of $(CH)_x$ is associated with the variation of *Rr*.

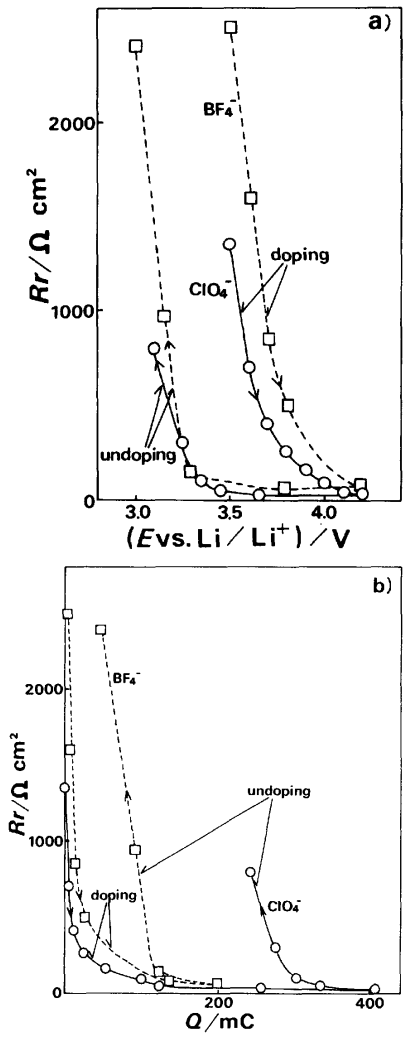

Fig. 4. Variation of resistive component, *Rr*, in equivalent circuit as a function of potential, *E*, (Fig. 4(a)) or amount of charge, *Q*, (Fig. 4(b)) of $(CH)_x$ electrode at anion doping-undoping process with using scaning at 1 mV s^{-1} in various solutions.
○: 1 mol dm^{-3} $LiClO_4$/PC, □: 1 mol dm^{-3} $LiBF_4$/PC.

Variation of Rr Value of $(CH)_x$ at Doping-Undoping Process. Figure 4(a) shows the variation of the *Rr* value of the $(CH)_x$ electrode as a function of the potential during the potential-sweep doping-undoping process with 1 mV s^{-1} in the two kinds of solution. In both solutions of $LiClO_4$ and $LiBF_4$ in propylene carbonate, the value of *Rr* greatly decreases at the initial doping potential and finally reaches a small constant value. During the undoping scan, the value of *Rr* increases with the undoping process. The decrease of *Rr* for ClO_4^- ion is larger than that for BF_4^- ion at the same doping potential. At the beginning of the cathodic scan, an anodic current is observed until 3.8 V in the current *vs.* potential curves in Fig. 1. From the potential of 3.8 V during cathodic scan, anion undoping starts to occur and the values of *Rr* begins to increase abruptly at *ca.* 3.3 V after sufficient undoping process. A similar variation of *Rr* is observed in both scans and in both solutions, but during the anion doping process, the value of *Rr* for ClO_4^- doping is always smaller than that of BF_4^- doping at the same potential. This indicates that a greater amount of ClO_4^- anion is doped at the same potential and that the ClO_4^- anion can be doped more easily than the BF_4^- anion.** Since the measured impedance reflects the value not at the whole impedance of polyacetylene film electrode but at the interface between film electrode and solution, the variation of *Rr* is assumed to correspond to that at the surface region of $(CH)_x$ and the electrode reaction at the interface. The value of *Rr* is considered to contain two factors (i) the reaction resistance for the doping-undoping process at the interface as shown in Eq. 1 and (ii) the film resistivity of the $(CH)_x$ film itself at the actual surface region. The main factor related to the abrupt variation of *Rr* is more probably the latter than the former, because the former is usually not more than one hundred ohms. The variation of *Rr* can also be represented as a function of the amount of charge doped as seen in Fig. 4(b). In Fig. 4(b), the value of *Rr* decreases abruptly with the increase in the amount of charge, *Q*, especially at the beginning of the doping process, and it becomes constant after 100 mC.

[††] The cell used has the volume of 0.283 cm^3 for electrolyte solution and the distance between working and reference electrodes is 0.58 cm. The swelling of $(CH)_x$ film is observed *ca.* 0.2 cm at the most, which may cause the decrease of *Rs ca.* 30%.

** The Stokes' radii of ClO_4^- and BF_4^- ions in PC were reported as 0.31 and 0.28 nm, respectively.[11] Thus, the above results cannot simply be explained by the radii of ions. The ease of doping in the $(CH)_x$ film might be discussed by considering the interaction between the dopant ions and $(CH)_x$ or other factors.

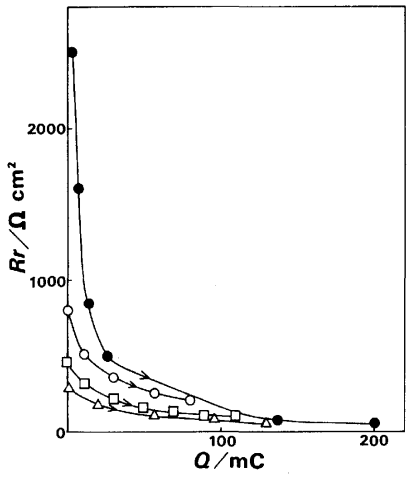

Fig. 5. Variation of resistive component, *Rr*, in equivalent circuit as a function of amount of charge of $(CH)_x$ electrode at anion doping-undoping process with using potential-step at various potentials in 1 mol dm^{-3} $LiClO_4$/PC.
○: 3.6V, □: 3.8V, △: 4.0V, ●: potential-sweep doping at 1 mV s^{-1}.

On the other hand, the value of *Rr* increases with the decrease in *Q*, and the abrupt increase starts from a different point of the fairly doped amount of charge. This can be explained by the fact that the dopant anions entered deeply into the fibrils from the film surface but can not get out of them so easily. These results also strongly indicate that the variation of *Rr* does not reflect the total dopant concentration but only the dopant concentration at the surface of the $(CH)_x$ film. The hysteresis in the potential *vs.* charge relation similar to that in Fig. 4(b) has already been noted and discussed.[5,12,13] The hysteresis can be explained more readily by the variation of *Rr* as seen in Fig. 4(b).

Figure 5 shows the relationship between *Rr* and *Q* for the anion doping process by various doping methods in 1 mol dm^{-3} $LiBF_4$/PC In Fig. 5, the value of *Rr* at the potential-sweep doping with 1 mV s^{-1} is always larger than that at the potential-step doping. During the potential-step doping the value of *Rr* is decreased to less values by the very small charge of several mC's at the initial doping stage as compared with that during the potential-sweep doping. Moreover, the decrease of *Rr* occurs earlier at more anodic potential doping even for the same amount of charge doped. In the case of the potential-sweep doping with 1 mV s^{-1}, the doping rate is slower as compared with that of the potential-step doping. Then, the anion dopant diffuses more readily into the interior of the polyacetylene film. It is expected that the dopant concentration at the surface of the film is higher for the faster or stronger doping process. This assumption can readily explain the different variation of *Rr* by the different doping method. A similar behavior was observed also in 1 mol dm^{-3} $LiClO_4$/PC.

In conclusion, the resistive component, *Rr*, in the equivalent circuit reflects the dopant concentration at the surface of the film and the doped conditions can be detected by the variation of *Rr*. Rapid doping produces non-uniform dopant conditions of the surface concentration of dopant being very high. These non-uniformed states of the dopant cause the decrease of *Rr* and they tend to make the film potential more anodic.

The authors are indebted to Mr. Yoshimitsu Sawada, Showa Denko Co. Ltd., for providing polyacetylene samples and for helpful discussion.

References

1) C. K. Chiang, S. C. Gau, C. R. Fincher Jr., Y. W. Park, A. G. MacDiarmid, and A. J. Heeger, *Appl. Phys. Lett.*, **33**, 18 (1978).
2) P. J. Nigrey, A. G. MacDiarmid, and A. J. Heeger, *J. Chem. Soc., Chem. Commun.*, **1979**, 594.
3) D. MacInnes Jr., M. A. Druy, P. J. Nigrey, D. P. Nairns, A. G. MacDiarmid, and A. J. Heeger, *J. Chem. Soc., Chem. Commun.*, **1981**, 317.
4) P. J. Nigrey, D. MacInnes Jr., D. P. Nairns, and A. G. MacDiarmid, *J. Electrochem. Soc.*, **128**, 1651 (1981).
5) K. Kaneto, M. Maxfield, D. P. Nairns, and A. G. MacDiarmid, *J. Chem. Soc., Faraday Trans. 1*, **78**, 3417 (1982).
6) M. Aizawa, H. Shinohara, and H. Shirakawa, *Polym. Prepr. Jpn*, **31**, 2815 (1982); M. Aizawa, H. Shinohara, and S. Watanabe, 46th National Meeting of the Chem. Soc. Jpn., Niigata, October 1982, Abstract, p. 132; M. Aizawa, H. Shinohara, S. Watanabe, and H. Shirakawa, 49th Conference of Electrochem. Soc. Jpn., Extended Abstract, p. 155 (1982).
7) T. Osaka, and K. Naoi, *Bull. Chem. Soc. Jpn.*, **55**, 36 (1982).
8) T. Ito, H. Shirakawa, and S. Ikeda, *J. Polym. Sci.*, **12**, 11 (1974).
9) Y. Matsuda, *Denki Kagaku*, **48**, 665 (1980).
10) R. J. Brodd, *J. Res. Natl. Bur. Stand., Sect. A*: **65**, 275 (1961).
11) Y. Matsuda, H. Nakashima, M. Morita. and Y. Takasu, *J . Electrochem. Soc.*, **128**, 2552 (1981).
12) A. Feldblum, J. H. Kaufman, S. Etemad, A. J. Heeger, T. C. Chung, and A. G. MacDiarmid, *Phys. Rev. B*, **26**, 815 (1982).
13) J. H. Kaufman, J. W. Kaufer, A. J. Heeger, R. Kaner, and A. G. MacDiarmid, *Phys. Rev. B.*, **26**, 2327 (1982).

Oxidation Potential of Intramolecular Exciplex on a Vinyl Copolymer as Estimated by Electron-transfer Quenching Reactions

Kaoru IWAI,* Fukuo TAKEMURA, Masaoki FURUE,† and Shun-ichi NOZAKURA†
Department of Chemistry, Faculty of Science, Nara Women's University, Nara 630
†*Department of Macromolecular Science, Faculty of Science, Osaka University, Toyonaka, Osaka 560*
(Received August 11, 1983)

In the electron-transfer reaction from the fluorescent intramolecular exciplexes of a copolymer containing phenanthrene and *N,N*-dimethylaniline moieties, and of a model compound to electron acceptors, the reactivity of the exciplexes was studied kinetically in polar and nonpolar media. The copolymer was poly(9-vinylphenanthrene-co-*p*-dimethylaminostyrene) and the model compound was *N,N*-dimethyl-4-[3-(9-phenanthryl)propyl]aniline. The oxidation potential of the exciplex was evaluated by the relation of the exciplex-quenching rate constants to the reduction potentials of electron-accepting quenchers according to the equations of Rehm and Weller. It was found that the electron-donating ability of these intramolecular exciplexes resembled with each other and was larger than that of excited phenanthrene. In polar media the donating ability was very close to that of the phenanthrene anion radical.

Much attention has been given to exciplexes as reaction intermediates in photoinduced electron-transfer and photochemical reactions. In the field of polymer chemistry, several papers have been published dealing with exciplex-forming polymers in recent years.[1-4] In a previous paper[2] we reported the intramolecular exciplex formation in 9-vinylphenanthrene–*p*-dimethylaminostyrene copolymers, P(VPh–co-DMAS), and photoinduced electron transfer from the copolymer to *p*-dicyanobenzene. The *p*-dicyanobenzene anion radical was concluded to be generated by both the electron-transfer process *via* exciplex and the direct electron-transfer process from the excited phenanthrene unit in the copolymer.

We now want to estimate the reactivity of the exciplex in the electron-transfer reaction between an exciplex and other molecules. The electron-donating ability of an exciplex can be estimated from the relation between exciplex-quenching rate constants by electron acceptors and reduction potentials of the acceptors applying the equations of Rehm and Weller.[5,6] Such a reaction between an exciplex and other molecules has been studied recently and a few papers on exciplex-quenching reactions have appeared in the field of low-molecular-weight compound.[7-11]

In this paper the reactivity of the fluorescent exciplex formed on P(VPh–co-DMAS) is estimated kinetically in polar and nonpolar media, and compared with that of the model compound *N,N*-dimethyl-4-[3-(9-phenanthryl)propyl]aniline, Ph$\{CH_2\}_3$DMA.

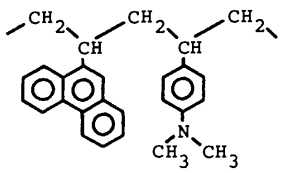

P(VPh-co-DMAS)

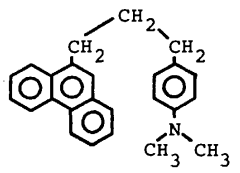

Ph$\{CH_2\}_3$DMA

Experimental

Materials. P(VPh–co-DMAS), which has 59 mol% of the VPh unit, was described in the literature.[2] Ph$\{CH_2\}_3$DMA[12] was synthesized according to the method of Thomas and coworkers who prepared *N,N*-dimethyl-4-[3-(1-pyrenyl)-propyl]aniline.[13] Phenanthrene used for measurements was zone-refined reagent (Tokyo Chemical Ind. Co.). *N,N*-dimethylformamide (DMF) was obtained by removing water as benzene azeotrope, followed by fractional distillation after drying over CaH_2. CH_3CN was Dotite Spectrosol Grade and was used without further purification. 1,4-Dioxane was refluxed over sodium and then distilled through a Vigreux column. *p*-Dicyanobenzene was sublimed under reduced pressure and recrystallized from acetone. Benzonitrile was purified by fractional distillation after drying over P_2O_5. Pyridine, acrylonitrile, and cinnamonitrile were purified by fractional distillation. Biphenyl and naphthalene were recrystallized from methanol and tetrahydrofuran, respectively. Fumaronitrile (Tokyo Chemical Ind. Co.) was used without purification. Another electron-accepting quenchers (Guaranteed Reagent, Nakarai Chemicals, LTD) were used without further purification.

Measurements. Fluorescence spectra were recorded by a Shimadzu RF-502A spectrofluorometer at 25 °C. Solution samples were made free from oxygen by freeze-pump-thaw cycles on a vacuum line. Fluorescence lifetime was measured by the pulse method with a small Blumlein-type nitrogen gas laser as described in the literature.[2] A sample solution was sealed in a 3 mm Pyrex glass capillary tube after degassed by four freeze-pump-thaw cycles on a vacuum line. Fluorescence was detected through appropriate cutoff filters and a monochrometer (Union FS-401) by a photomultiplier (Hamamatsu TV 1P28) and an oscilloscope (Tektronix 485). The exciplex fluorescence was monitored at 440 nm in dioxane and at 460 nm in CH_3CN and in DMF. Phenanthrene fluorescence was monitored at 370 nm both in dioxane and CH_3CN.

Results and Discussion

In Fig. 1 are shown the fluorescence spectra of P(VPh–co-DMAS) containing 59 mol % of the VPh unit and Ph$\{CH_2\}_3$DMA in dioxane. They are found to exhibit an intense and broad intramolecular exciplex fluorescence at *ca.* 440 nm. These exciplex fluorescence are observed in a longer wavelength region in a polar solvent DMF also as shown in Fig. 1. We have determined the quenching rate constants of these two kinds of (Ph–DMA) intramolecular exciplexes with a number of electron acceptors. In general, a fluorescence-quenching rate constant can be determined by either a fluorescence intensity measurement or a fluorescence

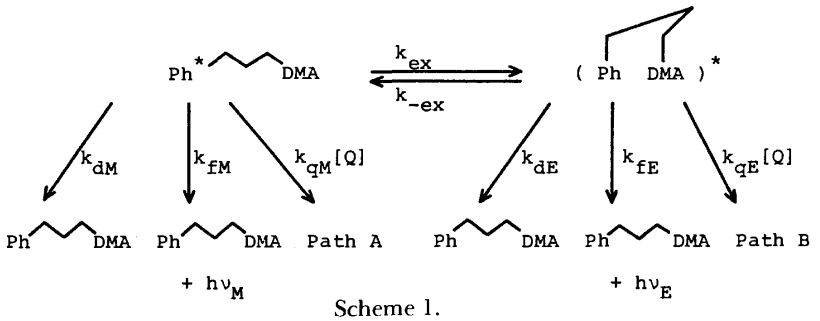

Scheme 1.

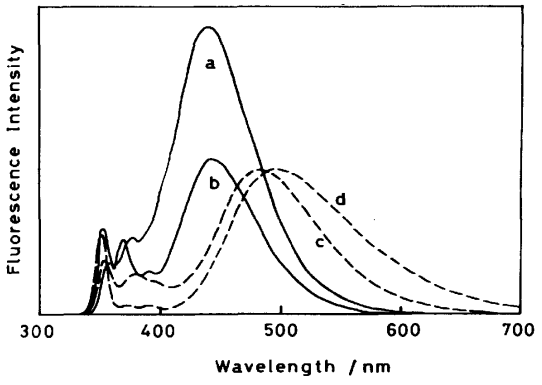

Fig. 1. Fluorescence spectra of P(VPh-co-DMAS) and Ph{CH_2}$_3$DMA: P(VPh-co-DMAS) in (a) dioxane and in (c) DMF, [VPh unit]=3×10^{-4} mol dm^{-3}, excitation at 352 nm; Ph{CH_2}$_3$DMA in (b) dioxane and in (d) DMF, [Ph{CH_2}$_3$DMA]= 2×10^{-4} mol dm^{-3}, excitation at 350 nm. Fluorescence intensities were normalized at Ph monomer fluorescence part [(a) and (b)] or at exciplex fluorescence part [(c) and (d)].

lifetime measurement. In this paper the exciplex-quenching rate constant, k_{qE}, was obtained from exciplex fluorescence lifetime data but not from exciplex fluorescence intensity quenching data by the following reasons. As shown in Scheme 1 some electron acceptors, Q, can quench an excited phenanthrene portion, Ph*, (Path A) as well as the exciplex (Path B). In such a case, the quantum yields of the exciplex and Ph* monomer fluorescence under stationary conditions are presented by the following equations 1—4.

$$\Phi_E^\circ = \frac{k_{ex}k_{fE}}{(k_{fM}+k_{dM}+k_{ex})(k_{fE}+k_{dE}+k_{-ex})-k_{ex}k_{-ex}}, \quad (1)$$

$$\Phi_E = \frac{k_{ex}k_{fE}}{(k_{fM}+k_{dM}+k_{ex}+k_{qM}[Q])(k_{fE}+k_{dE}+k_{-ex}+k_{qE}[Q])-k_{ex}k_{-ex}}, \quad (2)$$

$$\Phi_M^\circ = \frac{k_{fM}(k_{fE}+k_{dE}+k_{-ex})}{(k_{fM}+k_{dM}+k_{ex})(k_{fE}+k_{dE}+k_{-ex})-k_{ex}k_{-ex}}, \quad (3)$$

$$\Phi_M = \frac{k_{fM}(k_{fE}+k_{dE}+k_{-ex}+k_{qE}[Q])}{(k_{fM}+k_{dM}+k_{ex}+k_{qM}[Q])(k_{fE}+k_{dE}+k_{-ex}+k_{qE}[Q])-k_{ex}k_{-ex}}, \quad (4)$$

where Φ_E° and Φ_E are the exciplex fluorescence quantum yields in the absence and presence of Q, Φ_M° and Φ_M are the Ph* monomer fluorescence quantum yields in the absence and presence of Q, respectively, k_{ex} and k_{-ex} are the rate constants of the exciplex formation and dissociation processes, respectively, k_{dM}, k_{fM}, and k_{qM} are the rate constants of radiationless deactivation, fluorescence and quenching of the excited phenanthrene part, respectively, and k_{dE}, k_{fE}, and k_{qE}, are the corresponding rate constants of the exciplex. The value of I_E°/I_E ratio can be expressed by Eq. 5,

$$I_E^\circ/I_E = \Phi_E^\circ/\Phi_E = \frac{\Phi_M^\circ}{\Phi_M}\times\left(\frac{k_{qE}[Q]}{k_{fE}+k_{dE}+k_{-ex}}+1\right) = \frac{I_M^\circ}{I_M}\times(1+k_{qE}\tau_E^\circ[Q]), \quad (5)$$

where I_E° and I_E are the exciplex fluorescence intensity in the absence and presence of Q, I_M° and I_M are the Ph* monomer fluorescence intensity in the absence and presence of Q, and τ_E° is lifetime of the exciplex fluorescence in the absence of Q, respectively. Therefore k_{qE} cannot be determined from the measurement of exciplex fluorescence intensity only. On the other hand, as the exciplex fluorescence lifetime depends only on its decay processes, the value of τ_E°/τ_E can be expressed by Stern-Volmer equation 6. Typical examples of exciplex

$$\tau_E^\circ/\tau_E = 1 + k_{qE}\tau_E^\circ[Q], \quad (6)$$

fluorescence lifetime measurements for P(VPh-co-DMAS) - and Ph{CH_2}$_3$DMA - acceptor systems are shown in Figs. 2 and 3, respectively. It has been reported that in such intramolecular excited complex systems, especially in polymer systems, the accurate fluorescence decay seemed to be multicomponent decay.[14] However, the observed exciplex fluorescence decay curves could be analyzed by a single exponential kinetics as shown in Figs. 2 and 3.

The phenanthrene fluorescence-quenching rate constant, k_{qPh}, for phenanthrene-acceptor systems and k_{qE} for (Ph-DMA) intramolecular exciplexes-acceptor systems by Eq. 6 are listed in Table 1 together with the reduction half-wave potentials[15] of electron-accepting quenchers, $E_{1/2}$. Phenanthrene has a unique redox potential in the sense that the electron-donating ability of the phenanthrene anion radical [$E_{1/2}(Ph/Ph^-)$= -2.5 V[16]] is larger than that of excited phenanthrene [$E_{1/2}(Ph^+/Ph^*)=-2.1$ V[15]] (Scheme 2). In this respect the quenchers are classified into three groups in Table 1. As shown in Scheme 2, Q_c is a strong electron acceptor which can accept an electron from both the phenanthrene anion radical and excited phenanthrene, Q_b is a moderate one which can accept only from the phenanthrene anion radical, and Q_a is a weak one which cannot accept from either.

TABLE 1. EXCIPLEX AND PHENANTHRENE FLUORESCENCE QUENCHING RATE CONSTANTS MEASURED IN POLAR SOLVENTS

Quencher	$E_{1/2}$[b]/V		k_q[a]/mol^{-1} dm^3 s^{-1}		
			Phenanthrene	Ph{CH$_2$}$_3$DMA	P(VPh-co-DMAS)
Biphenyl	−2.70[e]	Q_a			9.8×10^6
Naphthalene	−2.63[d]			1.5×10^8	3.0×10^7
Pyridine	−2.62[d]		*6.8×10^5		
Benzonitrile	−2.44[c]	Q_b	*1.2×10^6	5.0×10^9	2.0×10^9
Methyl benzoate	−2.32[c]			4.2×10^9	2.3×10^9
Acrylonitrile	−2.17[c]			3.8×10^9	2.0×10^9
Ethyl benzoate	−2.14[e]			4.8×10^9	1.8×10^9
Cinnamonitrile	−1.99[c]	Q_c	*3.0×10^9	6.3×10^9	4.2×10^9
p-Dicyanobenzene	−1.67[c]		*9.3×10^9	7.3×10^9	4.7×10^9
Fumaronitrile	−1.36[c]		*1.2×10^{10}	7.1×10^9	5.7×10^9
Maleic anhydride	−0.85[d]		*1.6×10^{10}	7.3×10^9	5.6×10^9

a) Fluorescence-quenching rate constants k_q were determined in DMF and CH_3CN(*). b) $E_{1/2}$ (V *vs.* SCE). c) In DMF. d) In CH_3CN. e) In 75% aqueous dioxane.

In simple fluorescer-quencher systems, fluorescence-quenching rate constants k_q are correlated to the free energy change for the reaction ΔG and the free energy change of activation ΔG^* by Eq. 7,[5,6]

$$k_q = \frac{2.0 \times 10^{10}}{1 + 0.25\left[\exp\left(\frac{\Delta G^*}{RT}\right) + \exp\left(\frac{\Delta G}{RT}\right)\right]}, \quad (7)$$

$$\Delta G = 23.06\,[E_{1/2}(D^+/D) - E_{1/2}(A/A^-) - e_0^2/\varepsilon a] - \Delta E_{0,0},$$

$$\Delta G^* = \left[\left(\frac{\Delta G}{2}\right)^2 + (\Delta G^*(0))^2\right]^{1/2} + \frac{\Delta G}{2},$$

where $\Delta G^*(0)$ is ΔG^* at $\Delta G=0$, and is assumed to be 2.4 kcal mol^{-1},[6] $\Delta E_{0,0}$ is the 0-0 excitation energy of fluorophore, and the term $e_0^2/\varepsilon a$ is the Coulomb attraction energy and is *ca.* 0.06 V in CH_3CN solution (calculated with the values of dielectric constant ε=37.5

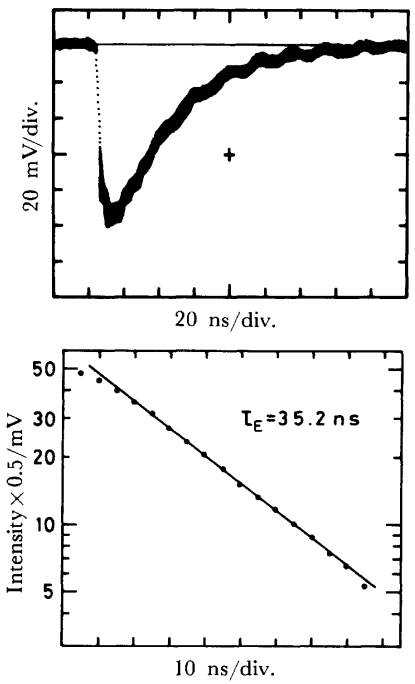

Fig. 2. Typical exciplex fluorescence decay curve and its semilogarithmic plot of P(VPh-co-DMAS)-maleic anhydride system in dioxane: [VPh unit]= 1.4×10^{-3} mol dm^{-3}, [maleic anhydride]=2.23×10^{-3} mol dm^{-3}. Monitored at 440 nm.

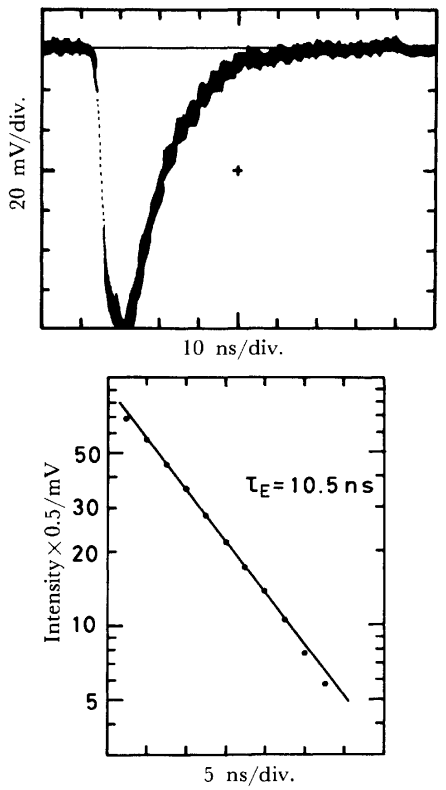

Fig. 3. Typical exciplex fluorescence decay curve and its semilogarithmic plot of Ph{CH$_2$}$_3$DMA-maleic anhydride system in CH_3CN:[Ph{CH$_2$}$_3$DMA]= 1.4×10^{-3} mol dm^{-3}, [maleic anhydride]=3.34×10^{-3} mol dm^{-3}. Monitored at 460 nm.

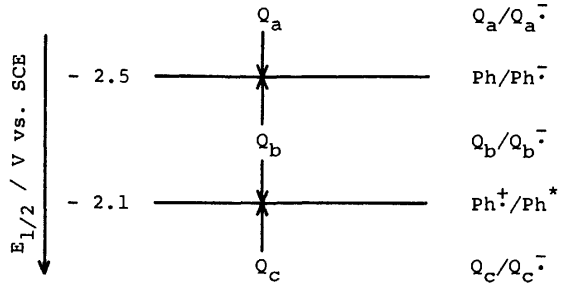

Scheme 2. Redox potential diagram.

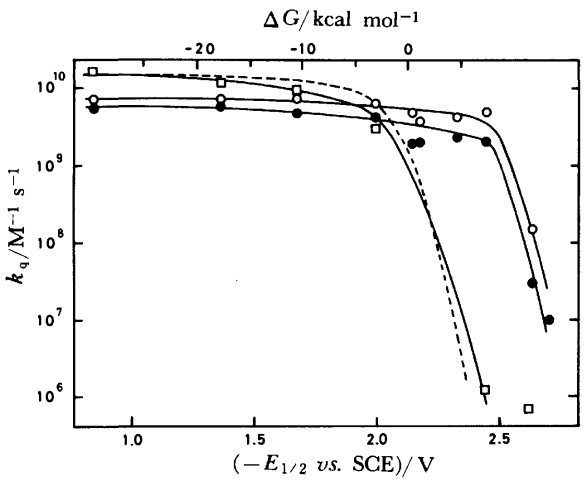

Fig. 4. Quenching of (Ph-DMA) intramolecular exciplexes by electron acceptors in polar solvents. Plots of log k_q *vs.* $E_{1/2}$ of the quenchers: (●) P(VPh-co-DMAS) in DMF, (○) Ph{CH_2}$_3$DMA in DMF, (□) phenanthrene in CH_3CN, the dotted line was calculated from the Eq. 7 for the phenanthrene-acceptor system.

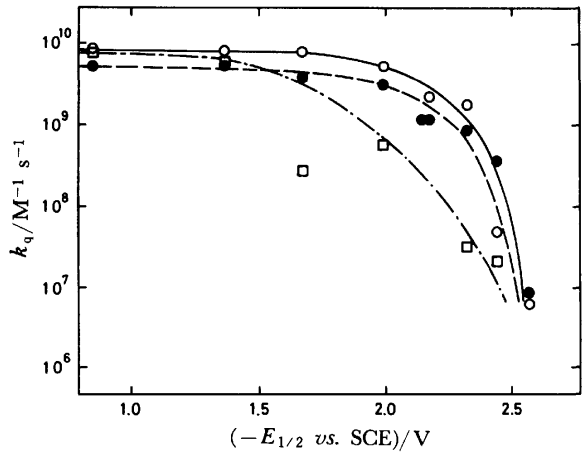

Fig. 5. Quenching of (Ph-DMA) intramolecular exciplexes by electron acceptors in nonpolar solvent(dioxane). Plots of log k_q *vs.* $E_{1/2}$ of the quenchers: (●) P(VPh-co-DMAS), (○) Ph{CH_2}$_3$DMA, (□) phenanthrene.

and distance between ion radicals a=7 Å). Figure 4 illustrates the plots of log k_{qPh} *vs.* ΔG for the excited phenanthrene-acceptor system in CH_3CN. The experimental values of k_{qPh} are in fair agreement with the calculated dotted line by equation 7. Similar relation can be expected for two (Ph-DMA) intramolecular exciplexes-acceptor systems in DMF. The determined k_{qE} values are plotted for $E_{1/2}$ values also in Fig. 4. The tendency of k_{qE} for two intramolecular exciplex systems is similar to each other. In the phenanthrene system, k_{qPh} has diffusion-controlled values only for strong quenchers Q_c and decreases with decreasing reduction potentials of quenchers, whereas in these intramolecular exciplex systems the quenching reactions for Q_c and moderate quenchers Q_b are found to proceed at nearly diffusion-controlled rates and for weak quenchers Q_a smaller values of k_{qE} are obtained. Therefore the electron-donating ability of these intramolecular exciplexes resembles with each other and can be larger than that of excited phenanthrene. That is, the oxidation potentials of the exciplexes can be located in between the two observed points —2.44 V of benzonitrile and —2.63 V of naphthalene, where a large decrease in the quenching rate constant k_{qE} was observed. Although the experimental data points at low $E_{1/2}$ region were not sufficient, we estimated the oxidation potentials of the exciplexes. From Eq. 7 it can be seen that a plot of log k_q *vs.* ΔG (or $E_{1/2}$) should approach a constant limiting value at large negative ΔG (or higher $E_{1/2}$), be linear at large positive ΔG (or low $E_{1/2}$) with a slope of $-(1/2.303\,RT)$, and have an intermediate region (centered at ΔG=0[17]). For very small values of $\Delta G^*(0)$ the intermediate region is very small and the connection between the limiting value and the limiting slope takes place in a very narrow ΔG range. These two lines intersect at *ca.* ΔG=0[18] ultimately. The constant limiting value at higher $E_{1/2}$ and the limiting slope at low $E_{1/2}$ intersect at the oxidation potentials of exciplexes, yielding $E_{1/2}$ values of *ca.* —2.5 V[19] for two kinds of intramolecular exciplexes. This value —2.5 V happens to be very close to the reduction potential of phenanthrene.

One can conclude from the results in polar media that the electron-donating ability of the intramolecular exciplex on P(VPh-co-DMAS) is similar to that of Ph{CH_2}$_3$DMA, is larger than that of excited phenanthrene, and is very close to that of the phenanthrene anion radical.

In nonpolar solvent dioxane k_{qE} and k_{qPh} are also similarly determined and plotted for $E_{1/2}$ in Fig. 5. The estimation of electron-donating ability of (Ph-DMA) intramolcular exciplexes was not feasible because $E_{1/2}$ measured in polar media was used instead of one in dioxane. It can be seen, nevertheless, that the behavior of k_{qE} of two exciplex systems was similar to each other and the exciplexes were better donors than excited phenanthrene.

As a photosensitizer excited phenanthrene cannot donate an electron to moderate electron acceptors, Q_b, but the (Ph-DMA) intramolecular exciplexes can. P(VPh-co-DMAS) may act as a photosensitizer in the case of the electron-transfer reactions to moderate electron acceptors because in this copolymer the efficient energy migration can take place from an excited phenanthrene unit to an exciplex-forming site on the polymer chain.[2]

References

1) K. Iwai, M. Furue, S. Nozakura, Y. Shirota, and H. Mikawa, *Polym. J.*, **12**, 97 (1980).
2) K. Iwai, Y. Itoh, M. Furue, and S. Nozakura, *J. Polym. Sci., Polym. Chem. Ed.*, **21**, 2439 (1983).
3) Y. Itaya and S. Tazuke, *Macromolecules*, **15**, 396 (1982) and references therein.
4) S. Tazuke and H. L. Yuan, *J. Phys. Chem.*, **86**, 1250 (1982).
5) D. Rehm and A. Weller, *Ber. Bunsenges. Phys. Chem.*, **73**, 834 (1969).
6) D. Rehm and A. Weller, *Isr. J. Chem.*, **8**, 259 (1970).
7) R. A. Caldwell, D. Creed, D. C. DeMarco, L. A. Melton, H. Ohta, and P. H. Wine, *J. Am. Chem. Soc.*, **102**, 2369

(1980) and references cited therein.
8) M. Itoh, N. Takita, and M. Matsumoto, *J. Am. Chem. Soc.*, **101**, 7363 (1979).
9) C. Pac and H. Sakurai, *Chem. Lett.*, **1976**, 1067.
10) M. G. Kuzmin, N. A. Sadovskii, and I. V. Soboleva, *Chem. Phys. Lett.*, **71**, 232 (1980).
11) S. Tazuke and K. Sato, *J. Phys. Chem.*, **80**, 1727 (1976).
12) K. Iwai, F. Takemura, M. Furue, and S. Nozakura, to be published.
13) B. Katusin-Razem, M. Wong, and J. K. Thomas, *J. Am. Chem. Soc.*, **100**, 1679 (1978).
14) A. J. Roberts, D. V. O'Connor, and D. Phillips, *Ann. N. Y. Acad. Sci.*, **366**, 109 (1981) and references therein.
15) N. L. Weinberg, "Techniques of Chemistry," ed by A. Weissberger, A Wiley-Interscience Publication, John Wiley & Sons, New York (1975), Vol. 8, Part 2, Appendix. The reduction half-wave potentials $E_{1/2}$ of electron-accepting quenchers refer to those *vs.* SCE in DMF or CH_3CN solutions. We do not distinguish between them as $E_{1/2}$ values measured in DMF and CH_3CN were in fair agreement with each other (*ca.* $\pm$0.05 V).
16) H. Beens and A. Weller, *Acta Phys. Pol.*, **34**, 593 (1968).
17) F. Scandola, V. Balzani, and G. B. Schuster, *J. Am. Chem. Soc.*, **103**, 2519 (1981).
18) For phenanthrene–acceptor system the intersection of these two lines was calculated to be at ΔG=0.6 kcal mol^{-1} (0.026 V) from the equations of Rehm and Weller and their experimental data.
19) In DMF solution the Coulomb attraction energy is *ca.* 0.06 V (ε=36.7 and a=7 Å) and is negligible for the estimation of the oxidation potential.

Initial Process of Photo-oxidation of Ethanol by Uranyl Ions in the Rigid Matrix at 77 K

Toshie HARAZONO, Shin SATO, and Hiroshi FUKUTOMI*

Research Laboratory for Nuclear Reactors, Tokyo Institute of Technology, Ookayama, Meguro-ku, Tokyo 152

(Received September 2, 1983)

ESR spectra of radicals produced in the uranyl ion-photosensitized decomposition of ethanol have been measured in the rigid matrix at 77 K. At high concentrations of uranyl ions (>1 mol dm^{-3}), methyl radicals were observed. With decreasing concentrations of uranyl ions, $CH_3\dot{C}HOH$ radicals became important, as expected from the previous studies. This result suggests that the charge transfer mechanism is important in the ethanol rigid matrix, although the hydrogen atom abstraction mechanism is accepted as the main initial process.

The photochemistry of uranyl ions has been extensively investigated during the last fifty years.[1] In aqueous solutions, the quenching processes of the luminescence from excited uranyl ions by a variety of substrates were studied and several mechanisms have been proposed. In the case of alcohols, the quenching process is believed to occur through the intermolecular abstraction of a hydrogen atom by excited uranyl ions from a C–H bond of the hydroxylated carbon atom of alcohols.[2]

Liquid phase ESR studies using the spin-trapping method supported this mechanism.[3] All normal alcohol (RCH_2OH) used as substrates gave the alcohol radicals ($R\dot{C}HOH$) spin-trapped. In the case of secondary alcohols, the radicals produced by the loss of a hydrogen atom from the weakest C–H bond were observed; *i.e.*, $(CH_3)_2CHCH_2OH$ gave $(CH_3)_2\dot{C}CH_2OH$ and 2-propanol gave $(CH_3)_2\dot{C}OH$.

One exception was found with methanol. In this case, the principal radical spin-trapped was $CH_3O\cdot$ but not $\dot{C}H_2OH$. This reaction was classified as an exception due to an atypical behavior of methanol to uranyl ions.[1]

In the rigid matrix at low temperatures, a C–C bond cleavage was observed with secondary and tertiary alcohols.[4] For example, the photolysis of uranyl ions in a *t*-butyl alcohol glass gave the ESR spectrum of methyl radicals. This reaction was tentatively explained in terms of the charge transfer mechanism followed by the C–C bond cleavage:

$$(CH_3)_3COH + (UO_2^{2+})^* \rightarrow (CH_3)_3CO\cdot + UO_2^+ + H^+$$
$$(CH_3)_3CO\cdot \rightarrow (CH_3)_2CO + \cdot CH_3.$$

A similar observation was made with 1-propanol, for which ethyl radicals were found to be formed:

$$CH_3CH_2CH_2OH + (UO_2^{2+})^* \rightarrow CH_3CH_2CH_2O\cdot + UO_2^+ + H^+$$
$$CH_3CH_2CH_2O\cdot \rightarrow CH_2O + CH_3CH_2\cdot.$$

On the other hand, in the ethanol rigid matrix at 77K, the observed radicals were reported to be only $CH_3\dot{C}HOH$, suggesting that the abstraction of a hydrogen atom by excited uranyl ions from a C–H bond is the main process even in the matrix of ethanol as was found in the liquid phase.

Obviously there is some controversy in the mechanism of the photo-oxidation of alcohols by uranyl ions in the rigid matrix. We, therefore, have studied this reaction in some detail.

Experimental

The yellow crystalline powder of uranyl perchlorate, $UO_2(ClO_4)_2\cdot 7H_2O$, was prepared by the recrystallization from the perchloric acid solution of uranium trioxide, which was obtained by heating analytical grade $UO_2(NO_3)_2\cdot 6H_2O$ at 400 °C. Water, which was distilled after having been passed through an ion exchange resin column, was further refluxed with potassium permanganate and distilled twice. Ethanol (Wako Co.) was of guaranteed grade and used without further purification.

The observation of ESR spectra was made by means of a JEOL JES-FX3 spectrometer. A sample used for the ESR measurement was prepared by dissolving the $UO_2(ClO_4)_2\cdot 7H_2O$ powder in the known amount of ethanol or the mixture of the alcohol and water,and degassed under vacuum at the liquid nitrogen temperature. The yellow rigid glass thus obtained was irradiated with the light from a high-pressure mercury lamp (Ushio Electric Co.) through a filter (Corning 052) which cut off the wavelengths shorter than 365 nm. The ESR measurement was carried out during the light irradiation.

Results

When a 0.1 M (M=mol dm^{-3}) ethanol solution of $UO_2(ClO_4)_2\cdot 7H_2O$ was irradiated, the ESR spectrum, which appeared initially, was that of No. 5 spectrum shown in Fig. 1, and after a long irradiation, the spectrum changed to that of No. 6, together with an increase in the total intensity. This spectral change suggests that there are two kinds of radicals produced initially and their stabilities are not equal. Therefore, we measured the ESR spectra initially observed with the samples of various concentrations of $UO_2(ClO_4)_2\cdot 7H_2O$.

Figure 1 shows the results, where the numbers from 1 to 6 indicate the difference of the concentration of uranyl ions. All the spectra were obtained at 10 min from the start of light irradiation. No spectral change except the total intensity could be recognized during the first 10 min. The No. 1 spectrum clearly shows the presence of methyl radicals, while the No. 6 spectrum may be assigned to that of ethanol radicals ($CH_3\dot{C}HOH$).[5]

In order to investigate the stabilities of these radicals, the signal intensities were measured by turning off the lamp after a 30 min-irradiation. The intensity of the spectrum due to methyl radicals decayed to half in about 14 min, while the spectrum of $CH_3\dot{C}HOH$ radicals did not decay at all. This decay process

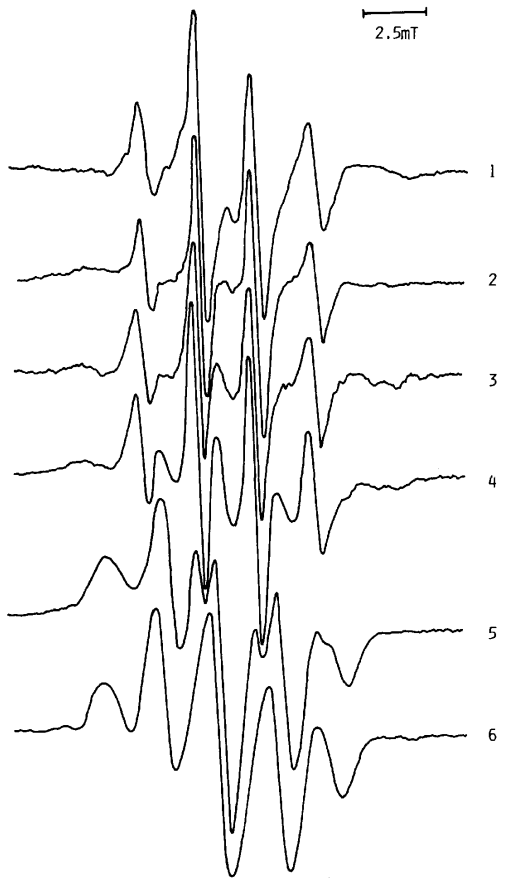

Fig. 1. ESR spectra of radicals initially produced in the uranyl ion-photosensitized decomposition of ethanol in the rigid matrix at 77 K. The numbers indicate the concentration of $UO_2(ClO_4)_2 \cdot 7H_2O$ in the matrix: 1, 2.5 M; 2, 1.8 M; 3, 1.0 M; 4, 0.5 M; 5, 0.1 M; 6, 0.04 M. Relative ESR intensities are arbitrarily adjusted.

was independent of both of the concentration of uranyl ions and the irradiation time.

Figure 2 shows the effect of the addition of water to the ethanol solution, where the concentration of uranyl ions was kept constant at 0.1 M (1 M=1 mol dm^{-3}). With the increase of water content, the ESR spectrum due to methyl radicals became more prominent than that due to $CH_3\dot{C}HOH$ radicals.

Discussion

According to the previous measurement on the ESR spectrum of the photolysis of uranyl ions in an ethanol rigid matrix, only $CH_3\dot{C}HOH$ radicals were observed,[4] but this measurement was carried out at low concentrations of uranyl ions (0.05—0.1 M); therefore, it is possible to overlook the spectrum due to methyl radicals initially produced. The present experiments clearly showed that methyl radicals are produced at the beginning of light irradiation.

The formation of methyl radicals may be explained in terms of the charge transfer mechanism followed by the C–C bond cleavage:

$$CH_3CH_2OH + (UO_2^{2+})^* \rightarrow CH_3CH_2O\cdot + UO_2^+ + H^+, \quad (1)$$

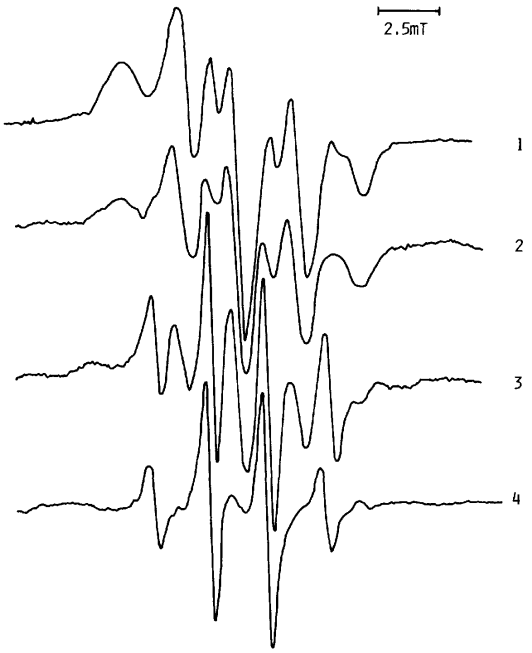

Fig. 2. ESR spectra of radicals produced in the uranyl ion-photosensitized decomposition of ethanol in the rigid matrix at 77 K. The numbers indicate the content of water: 1, no water added; 2, 20 volume % of water; 3, 50%; 4, 95%. The concentration of uranyl ions is kept constant at 0.1 M.

$$CH_3CH_2O\cdot \rightarrow \cdot CH_3 + CH_2O. \quad (2)$$

This is consistent with the mechanism proposed for the photosensitized decomposition of 1-propanol and secondary and tertiary alcohols in the rigid matrix at 77K.

For the formation of ethanol radicals ($CH_3\dot{C}HOH$) at lower concentrations of uranyl ions, we can consider three mechanisms: 1) the abstraction of a hydrogen atom by excited uranyl ions, 2) the abstraction of a hydrogen atom by ethoxyl radicals produced in Reaction 1 from the surrounding ethanol, and 3) the hydrogen atom abstraction by methyl radicals produced in Reaction 2.

The first mechanism may be discarded because, if this mechanism is operative, the formation of $CH_3\dot{C}HOH$ radicals should have been observed even at higher concentrations of uranyl ions. The third mechanism may also be disregarded since, if this is the case, the increase of $CH_3\dot{C}HOH$ radicals should have been observed with the decay of methyl radicals after the light irradiation was turned off.

It is well known that alkoxyl radicals are so reactive that the ESR spectra cannot easily be observed in the rigid matrix at 77 K;[6,7] therefore, if ethoxyl radicals are surrounded by ethanol, the abstraction of a hydrogen atom, Reaction 3, will occur immediately after the formation of ethoxyl radicals.

$$CH_5CH_2O\cdot + CH_3CH_2OH \rightarrow CH_3CH_2OH + CH_3\dot{C}HOH. \quad (3)$$

With the increase of uranyl ions, the concentration of free ethanol molecules from which the hydrogen atom is abstracted by ethoxyl radicals is concomitantly re-

duced, and Reaction 2 becomes more prominent than Reaction 3.

The decay of methyl radicals observed in the present experiments is probably due to the back reaction of UO_2^+ ions:

$$\cdot CH_3 + H^+ + UO_2^+ \rightarrow CH_4 + UO_2^+.$$

The Difference in Quenching Mechanism between Rigid Matrix and Liquid Phase. As has been discussed above, in the rigid matrices of alcohols at 77 K, the charge transfer mechanism seems to be the main process for the quenching of excited uranyl ions. On the other hand, the hydrogen atom abstraction mechanism is believed to be operative in the liquid phase photochemistry of uranyl ions.[1,8]

In the liquid phase, ethanol molecules surround an uranyl ion as shown in Fig. 3, and because of the

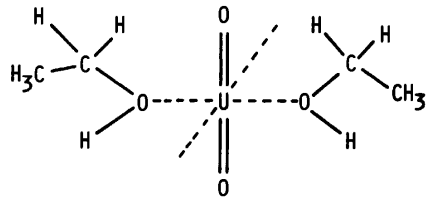

Fig. 3. The configuration of ethanol molecules around a uranyl ion in the liquid phase.

thermal vibration, an oxygen atom of the uranyl ion and a hydrogen atom of the C–H bond may occasionally approach each other very closely; therefore, when the excitation of uranyl ions occurs, the abstraction of a hydrogen atom may easily take place. On the other hand, in the rigid matrix at low temperatures, the ligand molecules will be mainly water, if $UO_2(ClO_4)_2 \cdot 7H_2O$ is used as the source of uranyl ions, since the heat of coordination is larger for water than for ethanol.[9] Consequently, the quenching of excited uranyl ions probably occurs through the hydrogen bond attached to an oxygen atom of the uranyl ion (Fig. 4). This process may be one detail of the charge transfer mechanism. A different approach is obviously necessary to establish these detailed mechanisms.

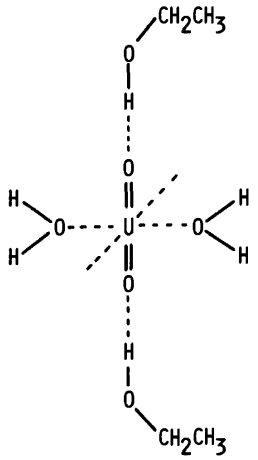

Fig. 4. The configuration of ethanol and water molecules around a uranyl ion in the rigid matrix at low temperatures.

The present work was partially supported by a Grant-in-Aid for Scientific Research No. 57470035 from the Ministry of Education, Science and Culture.

References

1) H. D. Burrows and T. J. Kemp, *Chem. Soc. Rev.*, **1974**, 139.
2) R. J. Hill, T. J. Kemp, D. M. Allen, and A. Cox, *J. Chem. Soc., Faraday Trans. 1*, **68**, 847 (1972).
3) A. Ledwith, P. J. Russel, and L. H. Sutcliffe, *Proc. R. Soc. London, Ser. A*, **332**, 151 (1973).
4) D. Greatorex, R. J. Hill, T. J. Kemp, and T. J. Stone, *J. Chem. Soc., Faraday Trans. 1*, **68**, 2059 (1972).
5) D. Greatorex and T. J. Kemp, *Trans. Faraday Soc.*, **67**, 56 (1971).
6) W. A. Bernhard and D. M. Close, *J. Chem. Phys.*, **67**, 1211 (1977).
7) M. Iwasaki and K. Toriyama, *J. Am. Chem. Soc.*, **100**, 1964 (1978).
8) S. Sakuraba and M. Matsushima, *Bull. Chem. Soc. Jpn.*, **43**, 2359 (1970).
9) V. Gutman and R. Schmid, *Coord. Chem. Rev.*, **12**, 236 (1979).

 © 1984 The Chemical Society of Japan Bull. Chem. Soc. Jpn., 57, 771—775 (1984)

The Laser-flash Photolysis of Propanone, Butanone, and 2-Pentanone. Study of Triplet Decay Processes in Aliphatic Carbonyl Compounds

Ikuo NAITO* and Wolfram SCHNABEL†

Department of Photography, Kyushu Sangyo University, Matsugadai, Higashi-ku, Fukuoka 813
†*Hahn-Meitner Institute für Kernforschung Berlin, Bereich Strahlenchemie, Glienicker Str. 100, D-1000 Berlin 39, Fed. Rep. of Germany*

(Received February 7, 1983)

The laser-flash photolysis of propanone, butanone, and 2-pentanone were carried out in dichloromethane (265 nm, 15 ns flash duration). The emission spectra (fluorescence, phosphorescence, and P-type delayed fluorescence) and the transient absorption spectra (triplet state and acetyl radical) were recorded. From the decays of the emission and the absorption, the unimolecular (triplet decay) and bimolecular (T-T annihilation and self quenching) reaction-rate constants were determined. Oxygen quenched the triplet states with a diffusion-controlled rate constant (k_{O_2}=*ca.* $3\times10\,dm^3\,mol^{-1}\,s^{-1}$).

Photochemical processes induced by stationary irradiation of aliphatic carbonyl compounds have been studied before in the absence and presence of quenchers.

Recently, the triplet state of propanone was investigated in detail by the use of tetramethyl-1,2-dioxetane (Chemiluminescence technique).[1]

In the flash photolysis studies of propanone, triplet-triplet absorption and phosphorescence spectra were recorded at wavelengths longer than λ=300 nm by Porter *et al.*[2] In these studies the ketyl radical formed from the triplet propanone was also detected.[3]

In the laser-flash photolysis of 2-hexanone, 5-methyl-2-hexanone, and poly(3-buten-2-one), triplet 1,4-biradical intermediates produced by a Norrish Type II reaction were detected recently.[4] In the photolysis of 3,3-dimethyl-2-butanone, poly(4,4-dimethyl-1-penten-3-one), and poly(3-methyl-3-buten-2-one), on the other hand, only radicals produced by α-cleavage in a Type I reaction were detected.[4] The triplet lifetimes of propanone, butanone, and 2-pentanone were reported to be relatively long [τ_T=47 μs,[4] 0.94 μs,[5] (propanone), 13 μs, (butanone in gas phase),[6] 77 ns,[7] and 240 ns (in the gas phase)[8] (2-pentanone)].

This paper reports on studies concerning the 265 nm laser-flash photolysis of propanone, butanone, and 2-pentanone carried out in dichloromethane solution in order to elucidate the physical and chemical deactivation processes of the triplet aliphatic carbonyl compounds.

Experimental

Materials. The propanone, butanone, and 2-pentanone were dried on sodium sulfate and distilled twice using a split-tube column.

The dichloromethane (for fluorescence spectroscopy) was washed five times with a 5% sodium carbonate solution and five times with distilled water. After drying on anhydrous calcium chloride, the dichloromethane was distilled twice using the split-tube column.

The acetonitrile (for spectroscopy) was refluxed five times on diphosphorus pentaoxide and distilled twice using the split-tube column.

The hexane (for fluorescence spectroscopy) was washed five times with sulfuric acid and five times with distilled water. After drying on anhydrous calcium chloride and calcium hydride, the solvent was distilled twice using the split-tube column.

The methanol (for spectroscopy) was refluxed with magnesium methoxide for eight hours and distilled twice using the split-tube column.

Apparatus. The flash photolysis system consisting of a Nd-laser has been described before (265 nm, 15 ns flash length).[9] The output of the laser and the intensity of the incident laser light were determined by means of the cycloreversion reaction of *r*-1,*t*-2,*t*-3,*c*-4-tetraphenylcyclobutane in 1-chlorobutane (ϕ=0.34).[10] The transient absorptions were measured using a pulsed Xenon lamp (Osram XBO 450 W). For the emission measurements a gating system was used.[11] This system protected the highly sensitive photomultiplier (RCA 78-35) from the strong emission during and immediately after the flash. The gating times of 1—2 μs (propanone) and 100—200 ns (butanone and pentanone) were applied. At the wavelengths longer than λ=400 nm, filters (Schott, BG 23, GG 455, *etc.*) were used. By choosing an appropriate concentration of the solute (3×10^{-2} mol dm^{-3}), the absorbance at λ=265 nm was kept at 0.5. After the solutions were filled in rectangular cells (optical length: 1.0×10^{-2} m) they were saturated with purified argon and, then, the laser-flash photolyis was carried out. The O_2 impurity of the argon gas was estimated to be less than 1×10^{-1}%. The emission and the absorption spectra were normalized with respect to an incident intensity of 2.0×10^{-8} einstein per flash.

Results and Discussion

1. Emission Spectra. During and immediately after the flash, a strong emission was detected in the wavelength range of 300—500 nm. The spectrum exhibited an emission maximum at λ=400 nm which agrees with the reported maximum of the fluorescence spectrum.[12]

Figure 1 shows time-resolved emission spectra monitored several microseconds after the flash by using the gating system [monitored at 6, 8, and 10 μs (propanone), 1.0, 1.5, 2.0, and 2.5 μs (butanone), 0.8, 1.0, 1.2, and 1.6 μs (2-pentanone)]. The emission spectrum, first-recorded, possesed the maximum in the wavelenth range of 410—430 nm. The maximum shifted to longer wavelengths with the lapse of the time after the flash. The spectra of butanone recorded at 2.0 μs and of 2-pentanone recorded at 1.2 μs at after the flash had two maxima, at λ=410 and 445 nm. Since the excited singlet lifetimes of these compounds have been reported to be much shorter than the time range investi-

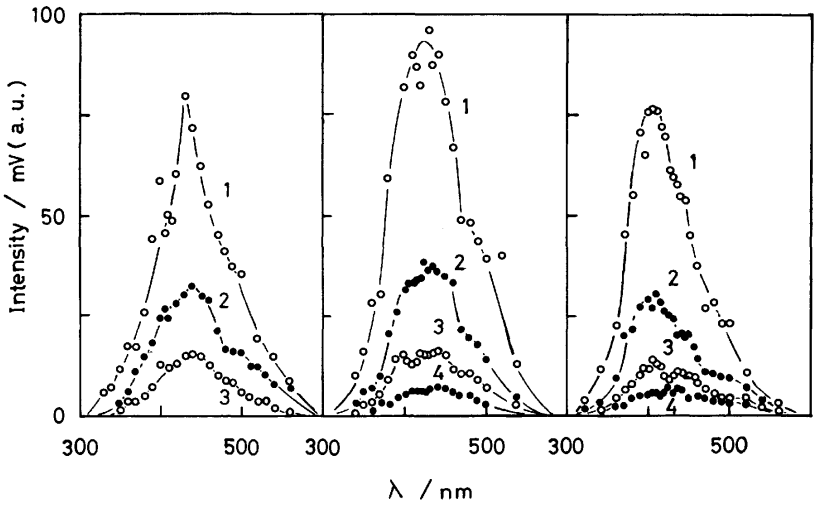

Fig. 1. Time-resolved emission spectra of propanone, butanone, and 2-pentanone in dichloromethane (3.0×10^{-2} mol dm^{-3}) recorded with the aid of a gating system. Time of recording: a) (propanone) 6 (1), 8 (2), and 10 (3) μs; b) (butanone) 1.0 (1), 1.5 (2), 2.0 (3), and 2.5 (4) μs; c) (2-pentanone) 0.8 (1), 1.0 (2), 1.2 (3), and 1.6 μs after the flash. The spectra were normalized with respect to an incident intensity of 2×10^{-8} einstein per flash.

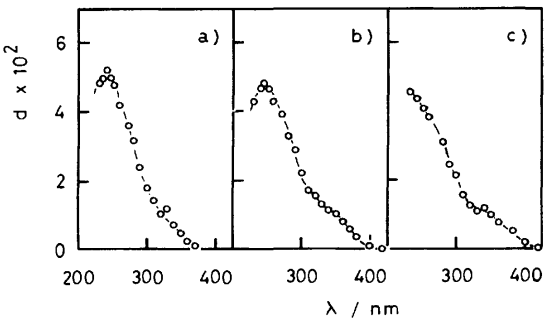

Fig. 2. Transient absorption spectra of propanone, butanone, and 2-pentanone monitored immediately after the flash in dichloromethane solution (3.2×10^{-2} mol dm^{-3}). a: propanone; b: butanone; c: 2-pentanone. The spectra were normalize with respect to an incident intensity of 2×10^{-8} einstein per flash.

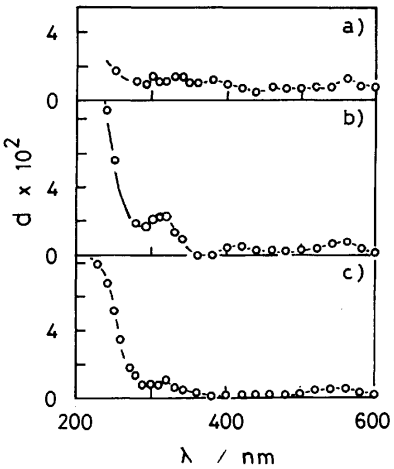

Fig. 3. Transient absorption spectra of the long-lived species of propanone (a), butanone (b), and 2-pentanone (c) in dichloromethane solution (3.2×10^{-2} mol dm^{-3}) recorded at 14(a), 7(b), and 2(c) μs after the flash. The spectra were normalized with respect to an incident intensity of 2×10^{-8} einstein per flash.

gated here,[13] it seems that the observed emission is due to the P-type delayed fluorescence and the phosphorescence. On this basis, the spectra recorded latest are attributed to the phosphorescence. Indeed, they agree with the phosphorescence spectra reported in the literature.[14]

2. Absorption Spectra of the Transient Species. The absorption spectra of transient species monitored immediately after the flash are shown in Fig. 2. The spectra exhibit an absorption maximum at λ=240 nm (propanone), at λ=245 nm (butanone), and at a wavelength shorter than 240 nm (2-pentanone). These transient absorption spectra are assigned to triplet-triplet absorption on the basis of the decay rate, which corresponds to the rate of the decay of the long-lived emission (*vide ante*).

Figure 3 presents absorption spectra of long-lived species, recorded at 14 μs (propanone), 7 μs (butanone), and 2 μs (2-pentanone). The spectra which have maxima around 320 nm and at λ=560 nm resemble strongly the spectrum of the acetyl radical reported by Noda *et al.*[15] Therefore, they are assigned to acetyl radicals. The generation of acetyl radical is feasible, in the present case, in terms of the generally accepted mechanism that the α-cleavage reaction is an important route in the deactivation of the triplet states of the carbonyl compounds.

3. Decay of the Transient Absorption and Emission. Figure 4 presents oscilloscope traces depicting the decay. The decays of both the absorption and the emission obeyed first-order kinetics. Whereas the decay rate ($k_{meas.}$) of the transient absorption was constant at all wavelengths monitored, the $k_{meas.}$ value of the emission depended on the wavelength. Figure 5 shows the effect of the laser light intensity on the $k_{meas.}$ value, obtained by means of the decay of the absorption at λ=250 nm and those of the emissions at λ=360 and

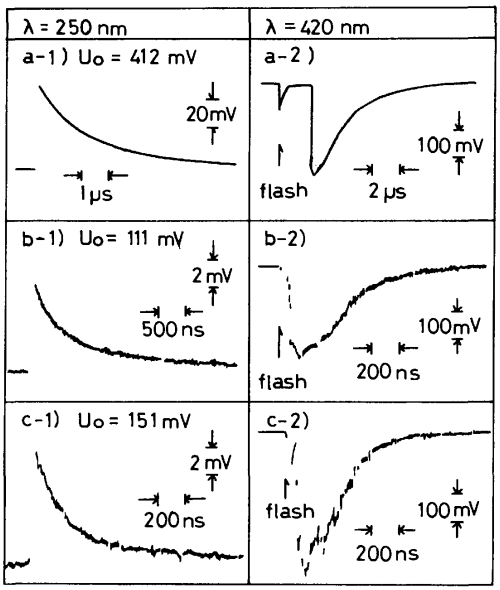

Fig. 4. Typical oscilloscope traces illustrating changes of the absorption (1) and the emission (2) of propanone (a), butanone (b), and 2-pentanone (c) in dichloromethane solution (3.0×10^{-2} mol dm^{-3}). Monitored at wavelength: λ=250 nm (absorption) and 420 nm (emission), flashed photons (10^{-8} einstein per flash): 2.0 (a-1), 2.2 (a-2), 1.0 (b-1), 1.4 (b-2), 0.8 (c-1), and 1.0 (c-2).

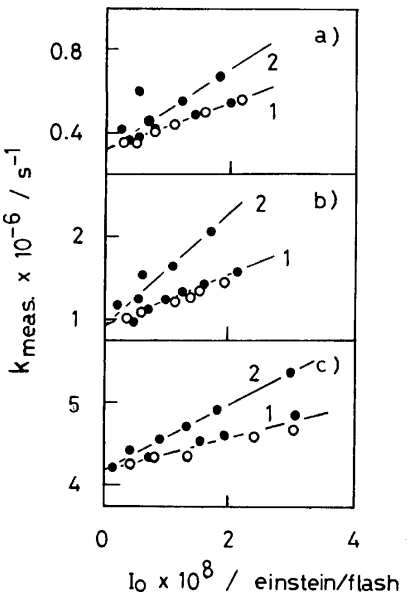

Fig. 5. The plot of the $k_{meas.}$ values as a function of the flashed photons. a: propanone; b: butanone; c: 2-pentanone in dichloromethane solution (3×10^{-2} mol dm^{-3}). Curve 1: absorption at λ= 250 nm and emission at λ=500 nm. Curve 2: emission at λ=360 nm.

500 nm. The two emission wavelengths were chosen with the intention to discriminate, possibly, delayed fluorescence from phosphorescence. It can be seen from Fig. 5, $k_{meas.}$ value increased linearly with the incident intensity, I_0, which is proportional to the quantity of the absorbed photons. This behavior is indicative for triplet-triplet annihilation. Actually, the same linear relationship between the $k_{meas.}$ value an I_0 was found for the decay of the absorption at all wavelengths and the decay of the emission at λ=500 nm (straight line 1, in Fig. 5). On the other hand, a slope about twice that of straight line 1 was found for straight line 2, obtained by monitoring the decay of the delayed fluorescence at λ=360 nm. As a matter of fact, the decay rate constant of the P-type delayed fluorescence should be twice as large as the triplet decay rate constant. These results confirm the assumed attribution of the transient absorption spectrum recorded immediately at the end of the flash to the triplet states.

4. Dependence of the Triplet Decay Rate on the Absorbed Photons. In a simplified way, the triplet decay can be considered being due to two Reactions, 1 and 2;

$$T_1 \xrightarrow{\Sigma k'} S_0, \quad (1)$$

$$T_1 + T_1 \xrightarrow{k'_{T-T}} 2\,S_0, \quad (2)$$

where $\Sigma k'$, and k'_{T-T} are the apparent rate constants of all first order (including self-quenching) and second-order (T-T annihilation) processes respectively. The rate of the triplet decay is given by Eq. 3:

$$-\frac{d[T]}{dt} = \Sigma k'[T] + k'_{T-T}[T]^2, \quad (3)$$

By dividing both sides of Eq. 3 by [T], the triplet concentration, Eq. 4 is obtained:

$$-\frac{d[T]}{[T]dt} = \Sigma k' + k'_{T-T}[T]. \quad (4)$$

The left side of Eq. 4 can be transformed into $[-d(\ln[T])/dt\ (\equiv k_{meas.})]$. Figure 5 shows that the $k_{meas.}$ values is directly proportional to I_0. The initial triplet concentration, $[T]_0$, is obtained from I_0 using a quantum yield of the intersystem crossing, $\phi_{ic}=1.0$ (propanone[5] and butanone[6]) and 0.63 (2-pentanone).[7]

The experimental decay rate constant, $k_{meas.}$ is expressed by Eq. 5:

$$k_{meas.} = \Sigma k' + k'_{T-T}[T]_0. \quad (5)$$

Figure 6 shows the plots of the $k_{meas.}$ values, determined by the absorption measurements at various initial concentrations of the carbonyl compounds ($[S_0]$), *vs.* $I_{abs.}$, which is proportional to $[T]_0$. For all initial concentrations of the carbonyl compound, the plots yielded straight lines being parallel to each other.

As far as the T-T annihilation is concerned, it has to be taken into account that two pathes are possible as is shown below;

$$T_1 + T_1 \xrightarrow{\alpha} S_1^* + S_0, \quad (6a)$$

$$T_1 + T_1 \xrightarrow{(1-\alpha)} 2\,S_0. \quad (6b)$$

Here, α denotes the portion of the triplet states reacting accordig to Reaction 6a which regenerates the triplet state *via* the intersystem crossing ($S_1^* \rightarrow T_1$). This process occurs rather rapidly, *i.e.* the singlet lifetime (∠10 ns[13]) is much shorter than the triplet lifetime. Consequently, the apparent rate constant, k'_{T-T}, is related to the rate constant of the T-T annihilation, k_{T-T}, according to Eq. 7:

Table 1. Triplet decay rate constants $\sum k_T$, and rate constants of triplet-triplet annihilation. k_{T-T}, and self-quenching $k_{self.}$

Compound	$\sum k_T \times 10^{-6}$	$k'_{T-T} \times 10^{-9}$	$k_{self.} \times 10^{-6}$
	s^{-1}	$dm^3\ mol^{-1}$	s^{-1}
Propanone	0.16	3	3
Butanone	0.73	7	6
2-Pentanone	3.8	6	6

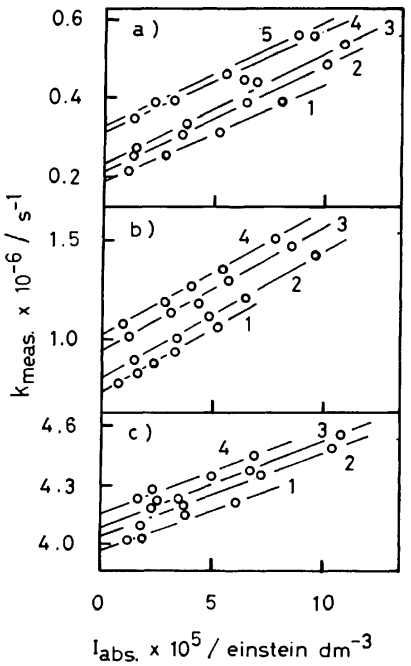

Fig. 6. The triplet decay rate, $k_{meas.}$, as a function of the absorbed photons per flash observed with the ketone solutions of various concentration in dichloromethane. a: [propanone]=1.3 (1) 2.0 (2), 2.6 (3), 5.2 (4), and 6.5 (6)$\times 10^{-2}$ mol dm^{-3}; b: [butanone]= 0.7 (1), 2.1 (2), 4.2 (3), and 5.6 (4)$\times 10^{-2}$ mol dm^{-3}; c: [2-pentanone]=0.7 (1), 1.4 (2), 2.0 (3), and 3.4 (4)$\times 10^{-2}$ mol dm^{-3}.

$$k'_{T-T} = (1-\alpha\,\phi_{ic}/2)\,k_{T-T}. \quad (7)$$

The values of k'_{T-T}, obtained from the slope of the straight lines in Fig. 6, are listed in Table 1. Because α is not known, the values of k_{T-T}, could not be calculated.

5. Self-quenching. The intercept of the straight lines in Fig. 6 corresponds to the values of $\sum k'$, in Eq. 5. The plots of $\sum k'$, obtained with the three carbonyl compounds, *vs.* the carbonyl concentration are shown in Fig. 7. The straight lines observed reflect the dependence of $\sum k'$, on the carbonyl concentration according to Eq. 8;

$$\sum k' = \sum k_T + k_{self.}[S_0], \quad (8)$$

where $k_{self.}$ is the rate constant of the self-quenching reaction: $S_0 + T_1 \rightarrow S_0 + S_0$ and $\sum k_T$ is the sum of all the first-order rate constants. The values of $\sum k_T$ and $k_{self.}$ obtained from the intercept and the slope of the straight lines in Fig. 7 are given in Table 1. The $\sum k_T$ values found with propanone and butanone are

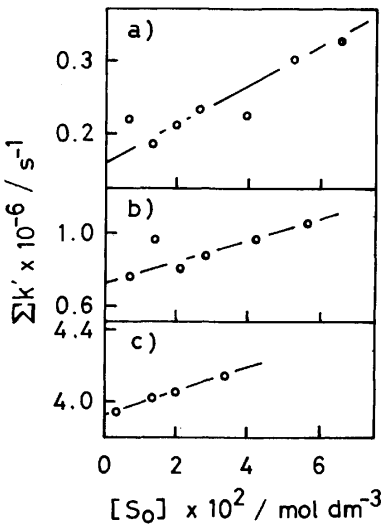

Fig. 7. Plots of the k', values *vs.* the initial carbonyl concentrations. a: propanone; b: butanone; and c: 2-pentanone.

Table 2. Decay rate constants of the triplet states in various solvents and quenching-rate constant of oxygen

Compound	Solvent	$k_{meas.} \times 10^{-6}$ a)	$k_{meas.O_2} \times 10^{-7}$ a)	$[O_2] \times 10^3$	$k_{O_2} \times 10^{-10}$
		s^{-1}		mol dm^{-3}	$dm^3\ mol^{-1}\ s^{-1}$
Propanone	CH_2Cl_2	0.55	6.0	*ca.* 2 b)	*ca.* 3
	CH_3CN	0.41	7.0	1.3 c)	5.4 ?
	CH_3OH	0.37	8.8	2.1 d)	4.2
	C_6H_{14}	1.2	7.9	3.1 d)	2.5
Butanone	CH_2Cl_2	2.0	5.9	*ca.* 2 b)	*ca.* 3
	CH_3CN	2.0	5.8	1.3 c)	4.3 ?
	CH_3OH	2.0	6.1	2.1 d)	2.8
	C_6H_{14}	3.5	*ca.* 11	3.1 d)	3.4
2-Pentanone	CH_2Cl_2	4.5	5.7	*ca.* 2 b)	*ca.* 3
	CH_3CN	4.2	4.6	1.3 c)	3.2
	CH_3OH	4.1	6.4	2.1 d)	2.9
	C_6H_{14}	—	*ca.* 11	3.1 d)	3.4

Concentrations of carbonyl compounds: 3.0×10^{-2} mol dm^{-3}. Flashed photons: 2.0×10^{-8} einstein per flash, a) pseudo first order rate constants (error limit: ±20%), b) Ref. 17, c) Ref. 18, d) Ref. 19.

greater than the values previously reported [$\sum k_T = 2.1 \times 10^4$ s^{-1} (propanone in acetonitrile)[2] and 7.7×10^4 s^{-1} (butanone in the gas phase)[6]]. The $k_{self.}$ value is in the order of 10^6 dm^3 mol^{-1} s^{-1}.

6. Reaction of Triplets with Molecular Oxygen. Oxygen was found to quench the triplet states very effectively. Rate constants, k_{O_2}, were determined by measuring the triplet decay rate in O_2-saturated solution ($k_{meas.O_2}$) by using Eq. 9:

$$k_{meas.O_2} = k_{meas.} + k_{O_2}[O_2]. \quad (9)$$

As can be seen from Table 2, $k_{O_2} = (3.0 \pm 1.5) \times 10^{10}$ dm^3 mol^{-1} s^{-1} was found, *i.e.* the reaction of O_2 with the triplet states of the carbonyl compounds under investigation is encounter-controlled.

7. Solvent Effects. Three additional solvents were used in this work besides dichloromethane; acetonitrile, methanol, and hexane. As can be seen from Table 2, $k_{meas.}$ value is the same within the error limit, except for hexane. The hydrogen abstraction reaction, presumable, becomes important in hexane and thus leads to faster triplet decay rates.

Conclusion

Propanone, butanone, and 2-pentanone were irradiated in dilute solution at room temperature with 15 ns flashes of 265 nm light. The absorption and emission measurements were carried out. The T–T absorption, prompt and the P-type delayed fluorescence, and the phosphorescence were observed. The rate constants of the T–T annihilation and the self-quenching were measured. The k'_{T-T} (*ca.* 5×10^9 dm^3 mol^{-1} s^{-1}) was found to be about four times lower than in the case of benzophenone.[20] This difference might be indicative for the fact that a significant portion of the T–T annihilation reactions regenerate the triplet states *via* $T_1 + T_1 \rightarrow S_1^* + S_0$, following by $S_1^* \rightarrow S_0$. The self-quenching rate constans are much higher than the value reported for propanone (10^3 dm^3 mol^{-1} s^{-1}).[21] Actually, the present values lie in the range of 10^5 to 10^7 dm^3 mol^{-1} s^{-1} pertaining to aromatic carbonyl compounds such as acetophenone and benzophenone.[20]

It appears, that in the case of propanone and butanone the α-cleavage reaction is the most important chemical deactivation process for the triplet states. The same holds for 2-pentanone, despite the fact that the α-hydrogen abstraction leading to the triplet 1,4-biradicals is feasible in this case.

The authors wish to thank Professor Setsuo Takamuku of Osaka University and Assistant Professor Kazuyuki Horie of the University of Tokyo for their useful discussions, and Dr. G. Beck of Hahn-Meitner-Institut für Kernforschung Berlin for his assistance in running the laser flash photolysis apparatus.

References

1) N. J. Turro, "Modern Molecular Photochemistry," The Benjamin/Cumming Publishing Co. Menlo Park, Calif. (1978) p. 599.
2) G. Porter, R. W. Yip, J. M. Dunston, A. J. Cessna, and S. E. Sugamori, *Trans. Faraday Soc.*, **67**, 3149 (1971).
3) G. Porter, S. K. Dogra, R. O. Loutfy, S. E. Sugamori, and R. W. Yip, *J. Chem. Soc., Faraday Trans. 1*, **69**, 1462 (1973).
4) I. Naito, *Bull. Chem. Soc. Jpn.*, **56**, 2851 (1983); I. Naito and W. Schnabel, *Polym. J.*, in press.
5) S. L. Murov, "Handbook of Photochemistry," Marcel Dekker, New York (1973) p. 3.
6) E. A. Lissi, E. Abuin, and M. V. Encinas, *J. Photochem.*, **2**, 377 (1973/74).
7) P. J. Wagner, *Acc. Chem. Res.*, **4**, 168 (1971).
8) H. E. O'Neal, R. G. Miller, and E. Gunderson, *J. Am. Chem. Soc.*, **96**, 3351 (1974).
9) S. Takamuku, G. Beck, and W. Schnabel, *J. Photochem.*, **11**, 49 (1979).
10) The quantum yield of the *trans*-stilbene formation in the photolysis of *r*-1,*t*-2,*t*-3,*c*-4-tetraphenylcyclobutane in 1-chlorobutane by 254 nm irradiation was determined to be 0.68.
11) H. Ushiki, K. Horie, A. Okamoto, and I. Mita, *Polym. J.*, **13**, 191 (1981).
12) M. O'Sullivan and A. C. Testa, *J. Am. Chem. Soc.*, **92**, 5842 (1970).
13) A. C. Somersall and J. E. Guillet, *Macromolecules*, **5**, 410 (1970).
14) M. O'Sullivan and A. C. Testa, *J. Am. Chem. Soc.*, **92**, 258 (1970).
15) S. Noda, K. Fueki, and Z. Kuri, *J. Chem. Phys.*, **49**, 3287 (1968).
16) "Advances of Photochemistry," ed by C. A. Parker, W. Noyes, Jr., G. S. Hammond, and N. J. Pitts, Jr., Interscience New York (1964), Vol. 2, p. 305.
17) This value was estimated in Ref. 4.
18) U. Gröllmann and W. Schnabel, private communication.
19) S. L. Murov, "Handbook of Photochemistry," Marcel Dekker, New York (1973), p. 89.
20) R. E. Brown, L. A. Singer, and G. A. Davis, *J. Am. Chem. Soc.*, **94**, 8584 (1972); L. A. Singer, R. E. Brown, and G. A. Brown, *ibid.*, **95**, 8038 (1973); T. S. Fang, R. Funda, R. E. Brown, and L. A. Singer, *J. Chem. Phys.*, **82**, 246 (1978).
21) G. Schuster and N. J. Turro, *Tetrahedron Lett.*, **1975**, 2261.

Oxygen- and Carbon Monoxide-binding Affinity of the Liposomal Heme under Semiphysiological Conditions

Eishun TSUCHIDA,* Hiroyuki NISHIDE, Makoto YUASA, and Mikiya SEKINE
Department of Polymer Chemistry, Waseda University, Shinjuku-ku, Tokyo 160
(Received June 9, 1983)

Oxygen- and carbon monoxide-binding affinity ($P_{1/2}$) of the [α,α,α,α-*meso*-tetrakis(*o*-pivalamidophenyl)-porphinato]iron(II)-mono(1-dodecyl-2-methylimidazole) complex incorporated in liposome of phosphatidylcholine (abbreviated as liposomal heme) were measured in pH 7.0 aqueous solution at 15—37 °C. The $P_{1/2}(O_2)$ and $P_{1/2}(CO)$ values at 37 °C were 49 and 0.02 mmHg,† respectively. Enthalpy and entropy changes for the reversible bindings were similar to those of hemoglobin. The relationship between temperature and $P_{1/2}$ for the dimyristoylphosphatidylcholine-liposomal heme had a breaking point at *ca.* 24 °C, which agreed with the phase transition temperature of the liposomal heme.

Much effort has been made to mimic natural oxygen carriers like hemoglobin by using modified synthetic iron-porphyrin derivatives.[1-6] Success was reported in oxygen-binding in aprotic and organic solvents but not in aqueous media.

The authors have recently found that the [α,α,α,α-*meso*-tetrakis(*o*-pivalamidophenyl)porphinato]iron(II) (abbreviated as heme) complex of mono(1-dodecyl-2-methylimidazole) incorporated in liposome of phosphatidylcholine (abbreviated as "liposomal heme") binds molecular oxygen reversibly under semiphysiological conditions (in pH 7.0 aqueous media at 37 °C).[7] It was considered that the iron porphyrin complex was embedded in a bilayer of liposome and that the hydrophobic environment of the inner region of liposome protected the oxygen adduct from its proton-driven oxidation.[8] The oxygen-binding and -dissociation proceeded very rapid, and their kinetic constants were comparable to those of hemoglobin (Hb).[9] Oxygen-binding affinity ($P_{1/2}(O_2)$: oxygen pressure at half oxygen-binding) was also preliminarily reported to be similar to that of Hb in blood.[10]

The present paper describes the oxygen- and carbon monoxide-binding affinity ($P_{1/2}(O_2)$ and $P_{1/2}(CO)$) for the liposomal heme composed of dimyristoylphosphatidylcholine (DMPC), dipalmitoylphosphatidylcholine (DPPC), and egg yolk lecithin (EYL) in pH 7.0 phosphate buffer solution at 15—37 °C. The binding-affinity was discussed in connection with the phase state of phospholipid, which was estimated by differential scanning calorimetry (DSC) and the fluorescence polarization method.

Experimental

Preparation of Liposomal Hemes. [α,α,α,α-*meso*-Tetrakis(*o*-pivalamidophenyl)porphinato]iron(III) bromide was prepared as reported.[11,12] 1-Dodecyl-2-methylimidazole (DMI) was prepared by the reaction of dodecyl bromide with 2-methylimidazole at 200 °C: bp 150 °C/1.5 mmHg; Found: C, 76.1; H, 12.9; N, 11.0%; C/N, 6.91, Calcd for $C_{16}H_{30}N_2$: C, 76.8; H, 12.0; N, 11.2%; C/N, 6.86; NMR ($CDCl_3$) δ=0.95 (3H, dodecyl-CH_3), 1.30—1.85 (20H, dodecyl-$(CH_2)_{10}$-), 2.30 (s, 3H, imidazole 2-CH_3), 3.90 (t, 2H, Im-CH_2-), 6.90 (d, 1H, imidazole 4 or 5-CH), 6.95 (d, 1H, imidazole 4 or 5-CH) ppm.

Dimyristoylphosphatidylcholine (DMPC) and dipalmitoylphosphatidylcholine (DPPC) were purchased from Sigma Co. (special grade). Egg yolk lecithin (EYL) was obtained and purified by the reported method.[13]

The iron porphyrin (1 μmol), 1-dodecyl-2-methylimidazole (50 μmol) and phosphatidylcholine (200 μmol) were mixed in dichloromethane. By evaporating the solution under reduced pressure, a thin film was prepared on the glass wall of a round flask. Oxygen-free pH 7.0 M/15 phosphate buffer solution (20 cm^3) was added, and the mixture was ultrasonicated and homogenized in an ice-water bath. Then a small excess of L-ascorbic acid (20-fold mol of the iron(III)) was added to the solution under nitrogen atmosphere, and the mixture was incubated at room temperature for 2 h. The red transparent solution showed the ultraviolet (UV) and visible absorption spectrum with maxima at 438, 535, and 562 nm, which agreed with the pentacoordinate deoxy complex of the liposomal heme.[7]

Oxygen-binding Equilibrium Curve. An oxygen adduct (λ_{max}=422 and 546 nm) of the liposomal heme was formed by bubbling oxygen gas through the solution. The spectral change in visible region was measured with a spectrophotometer (Hitachi Co., UV-320) and the oxygen concentration in the solution was monitored with an oxygen probe (Yellow Springs Instrument Co., YSI 5331) at the same time, after equilibrium was reached. Equilibrium between the deoxy heme and the oxygen adduct was shown in Fig. 1 (a); the visible absorption spectrum changes through isosbestic points at 520, 536, 552, and 589 nm by bubbling oxygen and nitrogen gas. The percentage of oxygen-binding was calculated from the differential absorbance at 562 nm.

For reference, the red blood cell suspension was prepared by the method of Imai.[14] The oxygen-binding equilibrium curve of the red blood cell suspension was measured with the above-mentioned apparatus; it was consistent with the curve reported.[14,15] This result supports the validity of the measurements in the present experiment.

Carbon Monoxide-binding Equilibrium Curve. The carbon monoxide adduct (λ_{max}=423 and 540 nm) was formed by bubbling the mixture gas of carbon monoxide and nitrogen; the carbon monoxide concentration was determined by infrared spectroscopy. Equilibrium between the deoxy heme and the carbon monoxide adduct was shown in Fig. 1(b); the UV (Soret band) absorption spectrum was changed through isosbestic points at 403, 431, and 464 nm. The percentage of carbon monoxide-binding was calculated from the differential absorbance at 438 nm after equilibrium was reached.

Differential Scanning Calorimetry (DSC) Measurement. The liposome solution of DMPC(2.5 mmol dm^{-3}) and the DMPC-liposomal heme solution were prepared in the same manner as above. The DSC thermogram of these samples were measured with a differential scanning calorimeter (Seiko Co., SSC-560U).

† 1 mmHg≈133.3 Pa.

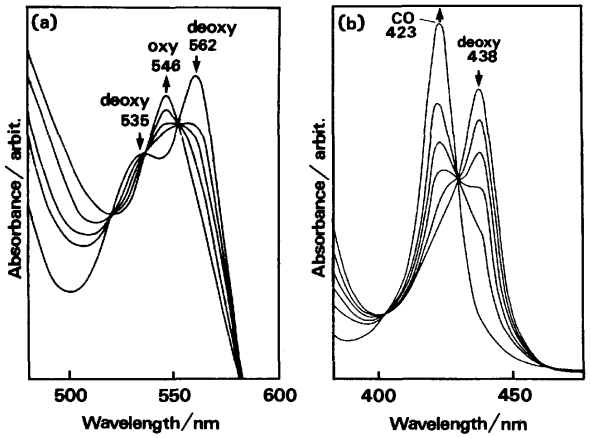

Fig. 1. Visible spectra of the DMPC-liposomal deoxy-heme and its oxygen adduct (a) and ultraviolet spectra of the DMPC-liposomal deoxy-heme and its carbon monoxide adduct (b) in pH 7.0 phosphate buffer solution at 37°C.
[heme]=0.05 mmol dm^{-3}. After bubbling oxygen: $P(O_2)$=0, 25, 50, 100, 760 mmHg (a); after bubbling carbon monoxide: $P(CO)$=0, 0.0034, 0.0071, 0.014, 0.034, 760 mmHg (b).

Fluorescence Measurement. Fluorescent compounds, 1,6-diphenyl-1,3,5-hexatriene (DPH) and 8-anilino-1-naphthalenesulfonic acid (ANS), were used as probes for monitoring fluidity in the liposome lipid layers. A thin film composed of heme (0.075 μmol), DMI (3.76 μmol), and DMPC (15 μmol) was prepared according to the above mentioned method. For labelling, DPH (0.05 μmol) or ANS (0.5 μmol) and phosphate buffer solution (5 cm^3) were added and the mixture was ultrasonicated and homogenized in an ice-water bath. In a similar manner, the fluorescent probe-labelled liposome of DMPC was prepared. Fluorescence intensity was measured by fluorescence polarimeter (Japan Spectroscopic Co., JASCO FP-550). The lights at 360 and 366 nm were used for excitation of liposome-incorporated DPH and ANS , respectively. Fluorescence intensities (I) were measured at 433 nm for DPH and 480 nm for ANS, respectively. Fluorescence polarization (P) was calculated by the equation: $P=(I_{\parallel}-I_{\perp})/(I_{\parallel}+I_{\perp})$, where $I_{\parallel}$ and $I_{\perp}$ are the fluorescence intensities polarized parallel and perpendicular to the direction of polarization of the excitation beam, respectively, and simultaneously measured.

Results and Discussion

The oxygen-binding equilibrium curve of the DMPC-liposomal heme was shown in Fig. 2. Deviation of the oxygen-dissociation curve from this oxygen-binding curve was within 5%; the former was obtained by measuring the oxygen-binding % from the oxygen adduct to the deoxy state by bubbling nitrogen gas and the latter from the deoxy state to the oxygen adduct by bubbling oxygen gas. Figure 2 shows that oxygen-binding equilibrium curve is hyperbolic like that of myoglobin (Mb). ($P_{1/2}(O_2)$) of the DMPC liposomal heme is 49 and 22 mmHg at 37 and 25°C, respectively. The ($P_{1/2}(O_2)$) value at 25°C is comparable with the previously reported ($P_{1/2}(O_2)$) value (=38 mmHg at 25°C) of the heme complex with 1,2-dimethylimidazole in toluene.[16,17] Figure 2 also means that the ($P_{1/2}(O_2)$) value of the liposomal heme in aqueous medium is close to $P_{1/2}$ (*ca.* 27 mmHg at 37°C) of Hb in blood[18] but is fairly far from that (0.9 mmHg at 37°C) of Mb.[19] This suggests that the liposomal heme has a potential to act as an oxygen carrier, under physiological conditions, which transports oxygen from the lung ($P(O_2)$=*ca.* 110 mmHg) to Mb in muscle tissue as Hb does.

The carbon monoxide-binding equilibrium curve (Fig. 3) of the DMPC-liposomal heme is also hyperbolic like that of Mb. The $P_{1/2}$ (CO) value is 0.020 and 0.0075 mmHg at 37 and 25°C, respectively. The latter value agrees with the $P_{1/2}$ (0.0089 mmHg at

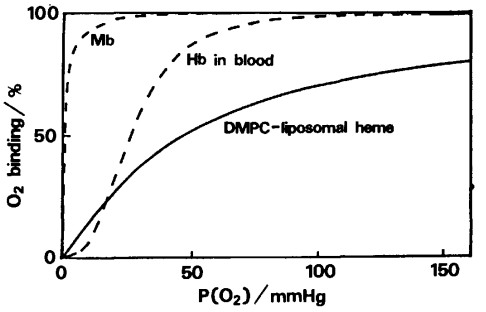

Fig. 2. Oxygen-binding equilibrium curve for the DMPC-liposomal heme in pH 7.0 phosphate buffer solution at 37°C.
[heme]=0.05 mmol dm^{-3}.

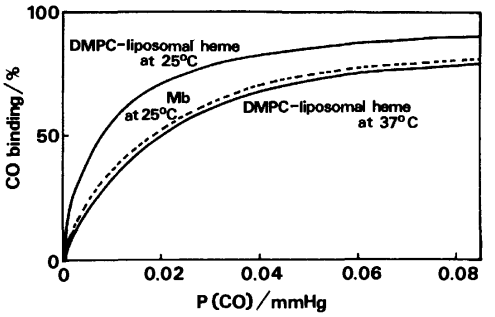

Fig. 3. Carbon monoxide-binding equilibrium curve for the DMPC-liposomal heme in pH 7.0 phosphate buffer solution.
[heme]=0.01 mmol dm^{-3}.

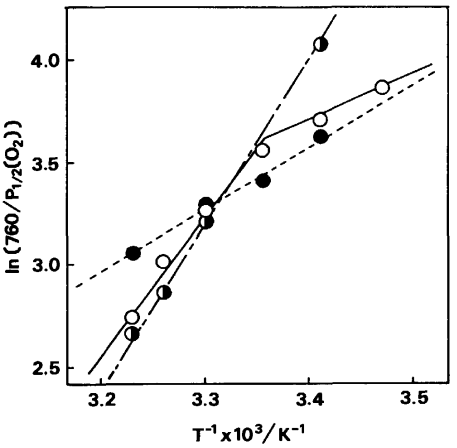

Fig. 4. van't Hoff plots for the oxygen-binding of the liposomal hemes in pH 7.0 phosphate buffer solution.
[heme]=0.05 mmol dm^{-3}. The liposomal heme composed of DMPC; ○, DPPC; ●, EYL; ◑.

TABLE 1. $P_{1/2}$ VALUES AND THERMODYNAMIC PARAMETERS

Iron porphyrin	O_2				CO			
	$P_{1/2}$		ΔH	ΔS	$P_{1/2}$		ΔH	ΔS
	mmHg[a]		kcal mol^{-1}	eu[b]	mmHg		kcal mol^{-1}	eu
	at 37 °C	at 25 °C			at 37 °C	at 25 °C		
Liposomal heme								
DMPC[c] (below T_c)	—	—	- 4.3	- 7.2	—	—	- 8.3	- 4.9
(above T_c)	49	22	-14	-41	0.020	0.0075	-17	-33
DPPC[c]	35	—	- 5.9	-14	—	—	—	—
EYL[c]	51	—	-16	-46	—	—	—	—
Heme-M_2I/Tol[d]	—	38	-14	-41	—	0.0089	—	—
Chelated heme[e]	—	—	-14	-35	—	—	-18	-34
Hemoglobin[f]	27	—	-14—-15	—	0.35	0.10—0.28	-17	—
Myoglobin[g]	0.9	—	-14—-21	—	—	0.012—0.028	—	—

a) 1 mmHg≈133.3 Pa. b) 1 eu=1 cal mol^{-1} K^{-1}. c) The liposomal heme composed of DMPC; dimyristoylphosphatidylcholine, DPPC; dipalmitoylphosphatidylcholine, EYL; egg yolk lecithin. d) [α,α,α,α-*meso*-tetrakis(*o*-pivalamidophenyl)porphinato]iron(II)-mono(1,2-dimethylimidazole) complex in toluene. Taken from Refs. 16, 17, 20. e) Iron(II)protoporphyrin *IX* *N*-[3-(1-imidazolyl)propyl]amide methyl ester in 2% aqueous myristyltrimethylammonium bromide suspension at pH 7.3. Taken from Ref. 23. f) Taken from Refs. 18, 19, 20. g) Taken from Refs. 19, 20.

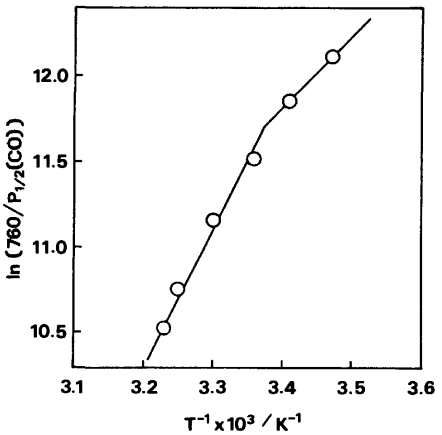

Fig. 5. van't Hoff plots for the carbon monoxide-binding of the DMPC-liposomal heme in pH 7:0 phosphate buffer solution.
[heme]=0.01 mmol dm^{-3}.

25 °C) of the corresponding heme complex in toluene.[20] These gaseous molecule-binding affinities of the liposomal heme suggest that the heme complex behaves as in toluene, although it is solubilized in the aqueous medium.

The oxygen-binding and -dissociation behaviors of the DPPC- and EYL-liposomal hemes were the same as that of the DMPC-liposomal heme except for the $P_{1/2}$ (O_2) of the DPPC-liposomal heme at 37 °C.

Temperature (T)-dependence of $P_{1/2}(O_2)$ and $P_{1/2}$(CO), *i.e. van't Hoff plots*; *ln* $(760/P_{1/2})$ vs. $1/T$, were shown in Figs. 4 and 5. The van't Hoff plots for the oxygen binding of the DPPC- and EYL-liposomal heme give linear relationships. On the other hand, the temperature dependences of oxygen- and carbon monoxide-binding for the DMPC-liposomal heme have breaking points at *ca.* 24 °C. Enthalpy change (ΔH) and entropy change (ΔS) for the oxygen- and carbon monoxide-binding equilibrium were determined and were given in Table 1. $\Delta H(O_2)$ and $\Delta S(O_2)$ for the oxygen-binding of the EYL-liposomal heme and the DMPC-liposomal heme (above 24 °C) were estimated to be *ca.* −15 kcal mol^{-1} and *ca.* −45 eu†, respectively. These values are comparable to those of the corresponding heme complex in toluene[17] and those of Hb[19,21] and Mb.[19,22] They are also comparable to those of iron(II) protoporphyrin *IX* N-[3-(1-imidazoryl)propyl]amide, which was previously evaluated with kinetic methods in aqueous medium.[23] This result indicates that the oxygen- and carbon monoxide-binding by the EYL-liposomal heme and DMPC-liposomal heme (above 24 °C) proceed in the same way as do the bindings by Hb, Mb and iron porphyrin complexes.

On the contrary, both $\Delta H(O_2)$ and $\Delta S(O_2)$ values for the DPPC-liposomal heme and the DMPC-liposomal heme (below 24 °C) are much larger than those of the others (Table 1). The phospholipid environment gives a large effect on the oxygen-binding affinity of the heme through its enthalpy contribution. ΔH(CO) and ΔS(CO) for the DMPC-liposomal heme (below 24 °C) are also much larger than those above 24 °C. One can say that the gaseous molecule-binding affinity is relatively decreased for the DPPC-liposomal heme and the DMPC-liposomal heme (below 24 °C) because the enthalpy gain in the binding equilibrium is much reduced (*ca.* 10 kcal mol^{-1}).

The liposome of DPPC has its transition temperature (T_c) between gel and liquid crystal phase of phospholipid at 41 °C, and the liposome of EYL has it at −15—−7 °C.[24] It is reasonable to assume that the DPPC-liposomal heme is situated below its T_c and the EYL-liposomal heme is above its T_c under these experimental conditions. The liposome of DMPC has its T_c at 23 °C[24]; T_c of the DMPC-liposomal heme was measured as described below.

DSC thermograms are shown in Fig. 6. The DMPC-liposome gives T_c at 24 °C, which agrees with the literature datum.[24] For the DMPC-liposomal

† 1 eu=1 cal mol^{-1} K^{-1}.

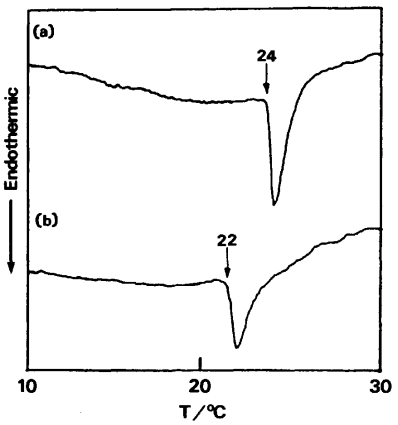

Fig. 6. DSC thermograms of the DMPC-liposome (a) and the DMPC-liposomal heme (b). [DMPC]=2.5 mmol dm^{-3}.

heme, the endothermic peak is brodened and shifted to the lower temperature at 22 °C. This means that incorporation of the heme complex into the phospholipid bilayer causes partial disorder in the alkyl chain orientation of phospholipid molecules.

Fluorescence measurement on the liposomal heme was carried out to monitor fluidity in the liposome lipid layers by using DPH and ANS. DPH is known as the probe embedded in the hydrophobic region of the liposome,[25] and ANS is the probe in the hydrophilic region.[26] The reciprocal of the degree of fluorescence polarization ($1/P$) is a parameter to represent the fluidity in the liposome lipid layers; values are given in Fig. 7. Figure 7(a) shows T_c obserbed at 24 °C for the DMPC-liposome and the DMPC-liposomal heme, and Fig. 7(b) shows values at 24 °C for the former and at 21 °C for the latter. From these data, one can say at least that the DMPC-liposomal heme has its T_c at *ca.* 24 °C.

Thus T_c of the DMPC-liposomal heme agrees with the breaking point of the temperature dependence of oxygen- and carbon monoxide-binding by the DMPC-liposomal heme. The oxygen- and carbon

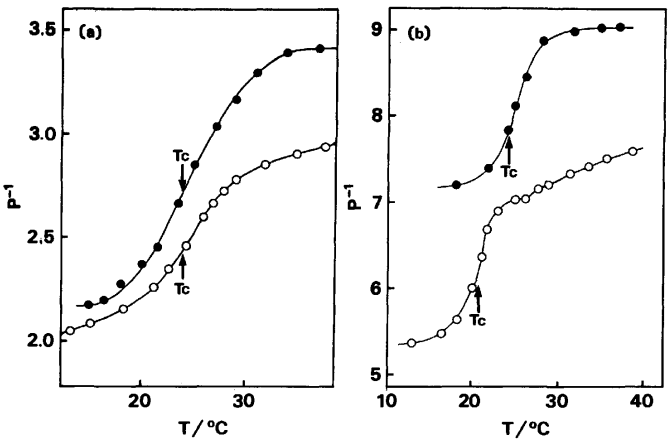

Fig. 7. Membrane fluidity of the DMPC-liposome and the DMPC-liposomal heme by using DPH (a) and ANS (b) in pH 7.0 phosphate buffer solution. [heme]=0.0015 mmol dm^{-3}. [DPH]=0.0015 mmol dm^{-3}. DPH; *Ex.* 366 nm, *Em.* 433 nm. [ANS]= 0.0010 mmol dm^{-3}. ANS; *Ex.* 360 nm, *Em.* 480 nm.

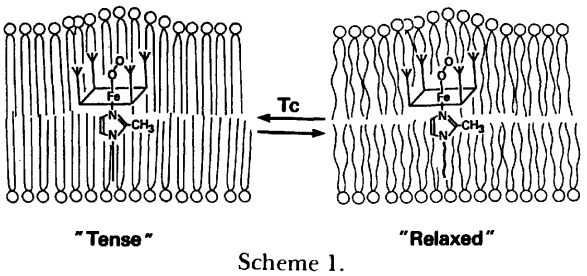

Scheme 1.

monoxide-binding affinity of the liposomal heme is dependent on the phase state of the phospholipid.

The solubility of oxygen in a DPPC-liposome has been previously reported;[27] it was slightly affected by the phase state of the phospholipid. Thus the dependence of gaseous molecule-binding affinity on T_c can not be explained only by the solubility of oxygen in the liposome phospholipid layer.

The gaseous molecule-binding affinity of the liposomal heme may be explained by using Scheme 1 as follows. Above T_c, phospholipid molecules are in the liquid crystal state, which provides an environment just like organic solvents such as toluene around heme; the heme complex is in a "*relaxed*" state, and the gaseous molecule-binding affinity and the ΔH values are comparable with those of the corresponding heme complex in toluene and with those of Hb and Mb. On the other hand, below T_c, phospholipid molecules are in the crystal state which causes an orientation of the DMI ligand; this is supported by the existence of the phase transition for the liposomal heme as well as the liposome without the heme complex (see the results by the DSC and fluorescence measurements). The orientation of the DMI ligand probably causes a structural distortion of the heme complex, because the bulky heme molecule is embedded in the phospholipid-DMI bilayer in the crystal state. The heme complex is in a "*tense*" state, and this may be one of the reasons for the low oxygen-binding affinity of the DMPC-liposomal heme (below T_c) and the DPPC-liposomal heme. The "*tense*" and "*relaxed*" states of the heme complex for the liposomal heme are not the same ones as the tense(T)- and relaxed(R)-states for Hb; The latter are caused by globin protein. But the gaseous molecule-binding phenomenon of the liposomal heme resembles that of Hb.

This work was partially supported by a Grant-in-Aid for Special Project Research (Design of Multiphase Biomedical Materials, No. 57219016) from the Ministry of Education, Science and Culture.

References

1) Reviewed by R. D. Jones, D. A. Summerville, and F. Basolo, *Chem. Rev.*, **79**, 139 (1979).

2) Reviewed by J. P. Collman, *Acc. Chem. Res.*, **10**, 265 (1977).

3) Reviewed by T. G. Traylor and P. S. Traylor, *Ann. Rev. Biophys. Bioeng.*, **11**, 105 (1982).

4) Reviewed by E. Tsuchida, *J. Macromol. Sci.*, **A13**, 545 (1979).

5) H. Ogoshi, H. Sugimoto, and Z. Yoshida, *Tetrahedron Lett,*. **55**, 1515 (1977) and references therein.
6) I. Tabushi and T. Sasaki, *Tetrahedron Lett.*, **23**, 1913 (1982) and references therein.
7) E. Hasegawa, Y. Matsushita, M. Kaneda, K. Eshima, and E. Tsuchida, *Biochem. Biophys. Res. Commun.*, **105**, 1416 (1982).
8) E. Tsuchida, M. Sekine, H. Nishide, and H. Ohno, *Nippon Kagaku Kaishi*, **1983**, 255.
9) E. Tsuchida, H. Nishide, M. Sekine, M. Yuasa, T. Iizuka, and Y. Ishimura, *Biochem.Biophys. Res. Commun.*, **109**, 858 (1982).
10) E. Tsuchida, H. Nishide, M. Yuasa, and M. Sekine, *Chem. Lett.*, **1983**, 473.
11) J. P. Collman, R. R. Gagne, C. A. Reed, T. R. Halbert, G. Lang, and W. T. Robinson, *J. Am. Chem. Soc.*, **97**, 1427 (1975).
12) T. N. Sorrell, *Inorg. Synth.*, **20**, 161 (1980).
13) S. L. Regen, A. Singh, G. Oehme, and M. Singh, *J. Am. Chem. Soc.*, **104**, 791 (1982).
14) K. Imai, H. Morimoto, M. Kotani, H. Watari, W. Hirata, and M. Kuroda, *Biochim. Biophys. Acta*, **200**, 189 (1970).
15) K. Imai, "Method in Enzymology," ed by E. Antonini, L. R. -Bernardi, and E. Chiancone, Academic Press, New York (1981).
16) J. P. Collman and K. S. Suslick, *Pure Appl. Chem.*, **50**, 951 (1978).
17) J. P. Collman, J. I. Brauman, K. M. Doxsee, T. R. Halbert, and K. S. Suslick, *Proc. Natl. Acad. Sci. U.S.A.*, **75**, 564 (1978).
18) J. W. Severinghaus, *J. Appl. Physiol.*, **21**, 1108 (1966).
19) E. Antonini and M. Brunori, "Hemoglobin and Myoglobin in their Reaction with Ligands," North-Holland Pub., Amsterdam (1970).
20) J. P. Collman, J. I. Brauman, and K. M. Doxsee, *Proc. Natl. Acad. Sci. U.S.A.*, **76**, 6035 (1979).
21) H. T. Gaud, B. G. Barisas, and S. J. Gill, *Biochem. Biophys. Res. Commun.*, **59**, 1389 (1974).
22) M. R. Wang, B. M. Hoffman, S. J. Shire, and F. R. N. Gurd, *J. Am. Chem. Soc.*, **101**, 7394 (1979).
23) T. G. Traylor and A. P. Berzinis, *Proc. Natl. Acad. Sci. U.S.A.*, **77**, 3175 (1980).
24) D. Chapman, "Form and Function of Phospholipids," ed by G. B. Ansell, R. M. C. Damson, and J. N. Hamthorne, Elsevier, Amsterdam (1973).
25) M. Shinitzky and M. Inbar, *J. Mol. Biol.*, **85**, 603 (1974).
26) D. H. Haynes and H. Staerk, *J. Membr. Biol.*, **17**, 313 (1974).
27) R. Kimmich, A. Peters, and K.-H. Spohn, *J. Membr. Sci.*, **9**, 313 (1981).

 © 1984 The Chemical Society of Japan Bull. Chem. Soc. Jpn., 57, 781—786 (1984)

A New and Effective Synthetic Method for the Preparation of the Esters, Peptides, and Lactones Using 3-(5-Nitro-2-oxo-1,2-dihydro-1-pyridyl)-1,2-benzisothiazole 1,1-Dioxide. Synthesis of (±)-(*E*)-8-Dodecen-11-olide, Recifeiolide

Alauddin AHMED, Nagahiro TANIGUCHI, Hirohiko FUKUDA, Hideki KINOSHITA,* Katsuhiko INOMATA, and Hiroshi KOTAKE

Department of Chemistry, Faculty of Science, Kanazawa University, Kanazawa 920

(Received July 8, 1983)

3-(5-Nitro-2-oxo-1,2-dihydro-1-pyridyl)-1,2-benzisothiazole 1,1-dioxide (BID-NPy), readily prepared from 3-chloro-1,2-benzisothiazole 1,1-dioxide and 5-nitro-2-pyridone, proved to be a very useful condensing reagent. A variety of esters, dipeptides, and lactones were obtained in excellent yields. Furthermore, BID-NPy was successfully employed for the lactonization step in a new synthesis of a naturally occurring (±)-(*E*)-8-dodecen-11-olide, recifeiolide.

Saccharin is a commercially available industrial product. Its derivative, 3-chloro-1,2-benzisothiazole 1,1-dioxide (BID-Cl) was found to have reactivities as a condensing reagent and has been utilized in the preparation of some peptides.[1] However, the yields were not so good and BID-Cl was found to be very unstable to moisture and could not be stored for a long time. Therefore, we tried to prepare various saccharin derivatives, which are generally stable crystalline compounds,[2] and found that 3-(5-nitro-2-oxo-1,2-dihydro-1-pyridyl)-1,2-benzisothiazole 1,1-dioxide (BID-NPy) (**1**) was a new condensing reagent for the preparation of esters, peptides, and lactones.

BID-NPy was easily prepared by the reaction of BID-Cl and 5-nitropyridone in dry CH_3CN in the presence of triethylamine (TEA). The structure of **1** was confirmed by elemental analysis. The IR spectrum cleanly showed the presence of the carbonyl group at 1670 cm^{-1}. This compound was quite stable on storage.

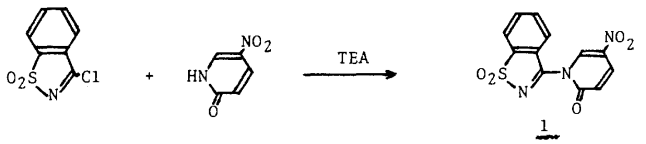

1

TABLE 1. PREPARATION OF ESTERS

$$\text{BID-NPy}+\text{R}^1\text{COOH}+\text{R}^2\text{OH} \xrightarrow[\text{overnight}]{\text{Et}_3\text{N in CH}_2\text{Cl}_2,\ -10\,^\circ\text{C to r.t.}} \text{R}^1\text{COOR}^2$$

R^1CO_2H	R^2OH	Yield/%	$\nu_{C=O}/cm^{-1}$
$PhCH{=}CHCO_2H$	$PhCH_2OH$	92	1710
$PhCH_2CO_2H$	$PhCH_2OH$	95	1735
$PhCH_2CO_2H$	$O_2NC_6H_4OH$	96	1760
$PhCH_2CO_2H$	CCl_3CH_2OH	93	1760
$PhCO_2H$	$O_2NC_6H_4OH$	88	1735
$PhCO_2H$	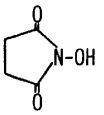	93	1765, 1735
$PhCO_2H$	C_6Cl_5OH	93	1745

TABLE 2. PREPARATION OF PROTECTED DIPEPTIDE ESTERS

$$\text{BID-NPy}+\text{Y-A.A.-OH}^{a)}+\text{Et}_3\text{N} \xrightarrow[\text{in CH}_2\text{Cl}_2]{-10\,^\circ\text{C to }0\,^\circ\text{C, 2 h}} \xrightarrow[\text{overnight}]{\text{H-A.A-OR, r.t.}} \text{Y-dipeptid-OR}$$

Product	Yield/%	Mp θ_m/°C(lit)	$[\alpha]_D$/°(*c*, solvent) (lit)	Ref.
Z-Val-Gly-OEt	86	163—164 (162—164)	-27.0 (0.77, EtOH) (-27.0)	12
Z-Ala-Gly-OEt	87	98—99 (99—100)	-21.8 (3.60, EtOH) (-22.2)	12
Z-Met-Gly-OEt	85	94—95 (94—96)	-19.6 (3.50, EtOH) (-19.8)	11
Z-Cys(Bzl)-Gly-OEt	Quant.	97—98 (97—99)	-28.6 (5.86, AcOEt) (-27.0)	11
Boc-Phe-Val-OMe	84	115—117 (118—119)	-11.2 (1.99, DMF) (-11.6)	13
Boc-Leu-Leu-OMe	73	134—135 (132—133)	-50.2 (0.41, MeOH) (-50.4)	14
Boc-Ala-Val-OMe	85	66—67 (63—64)	-49.4 (0.36, MeOH) (-49.5)	15
Boc-Leu-Val-OMe	83	143—145 (144—147)	-41.0 (0.52, MeOH) (-41.1)	16

a) This means *N*-protected amino acids (Y=Z or Boc).

First, **1** was allowed to react with a carboxylic acid in order to check its reactivity. A suspension of equimolar amount of phenylacetic acid, benzyl alcohol, and **1** in dichloromethane was treated with 1 equiv of TEA at −10°C to room temperature under N_2 to give the expected benzyl phenylacetate in 95% yield. In a similar manner, a variety of esters were obtained in excellent yields, as shown in Table 1. BID-NPy also proved to be an excellent reagent for synthesizing various protected dipeptide esters. The results are shown in Table 2.

The probable course of the reactions of **1** with acids is illustrated in Scheme 1. Formation of the activated ester (**3**, R′= CH_2Ph) could be actually isolated.

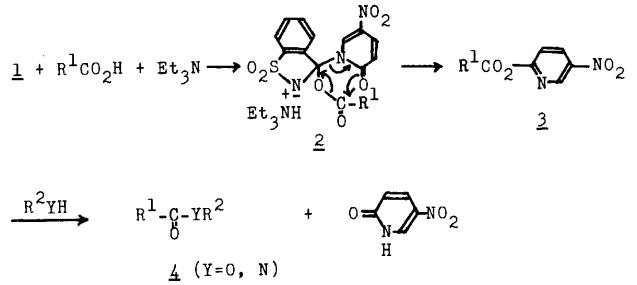

Scheme 1.

The preliminary results of ester and amide bond formation with BID-NPy encouraged us to use it to make macrolide. Initially, when TEA was added to a suspension of ω-hydroxy carboxylic acid and **1** (equimolar amount) in dichloromethane at room temperature under N_2 and the reaction mixture was stirred overnight, the yields of the corresponding lactones were not satisfactory. Many attempts to improve the yields under various conditions were unsuccessful. However, when a catalytic amount of *p*-toluenesulfonic acid (TsOH) was added to the reaction mixture, the yield of lactone was increased. Thus, the active ester prepared by the addition of equimolar amount of TEA to a suspension of carboxylic acids **5a—g** and **1** in 1,2-dichloroethane was added dropwise to a refluxing 1,2-dichloroethane containing 2 equiv of TsOH in a period of 6 h using a mechanically driven syringe. The usual work-up of the reaction mixture gave monolides in quite high yields with a small amount of diolides. Such an effect of the acid catalyst seems to be due to the activation of the intermediary active ester, as shown in 7. The results are listed in Table 3.

TABLE 3 LACTONIZATION OF ω-HYDROXY CARBOXYLIC ACIDS

	Hydroxy acids	Lactones(**6a—g**) Ring size	Yield/%
5a	$HO(CH_2)_{10}CO_2H$	12	72
5b	$HO(CH_2)_{11}CO_2H$	13	71
5c	$HO(CH_2)_{12}CO_2H$	14	86
5d	$HO(CH_2)_{14}CO_2H$	16	88
5e	$HO(CH_2)_{15}CO_2H$	17	81
5f	$CH_3(CH_2)_5CH(OH)(CH_2)_{10}CO_2H$	13	86
5g	$CH_3(CH_2)_5CH(OH)CH_2$-Z-$CH{=}CH(CH_2)_7CO_2H$	13	68

The yields of the monolides from ω-hydroxy carboxylic acids (**5a—g**) are comparable to those obtained by any existing methods.[3]

The starting materials (**5a**, **5c**, and **5d**) have been effectively made by modified Baeyer-Villiger oxidation[4] of the corresponding ketones. It was found that the addition of boron trifluoride etherate was quite effective for the oxidation of the ketones with *m*-chloroperbenzoic acid (MCPBA) in chloroform. The resulting lactones were directly saponified to give the corresponding ω-hydroxy carboxylic acids **5a**, **5c**, and **5d**, in 69, 78, and 82% yields, respectively.

Based on these results, we examined how to apply **1** to the synthesis of a naturally occurring macrolide, (±)-recifeiolide (**16**) isolated from *fungus Cephalosponim recifei*,[5] by the cyclization of (±)-11-hydroxy-(*E*)-8-dodecenoic acid (**15**).[6]

In the synthesis of **15**, one of the important points is the creation of the carbon-carbon double bond at C-8 of the chain with *E*-stereochemistry. In this regard, recently a convenient method for the preparation of allylic sulfones from the corresponding allylic acetate has been invented in our laboratory.[7] The stereochemistry of the double bond in the resulting allylic sulfones was completely *E*-form. Based on this finding, the synthesis of **16** was carried out according to

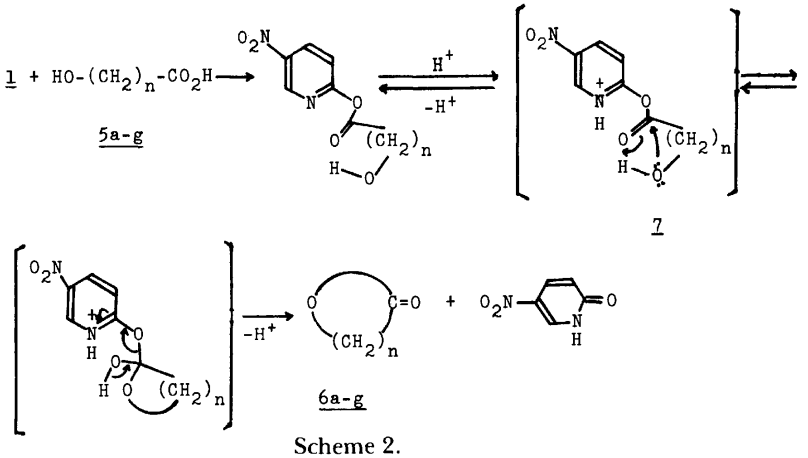

Scheme 2.

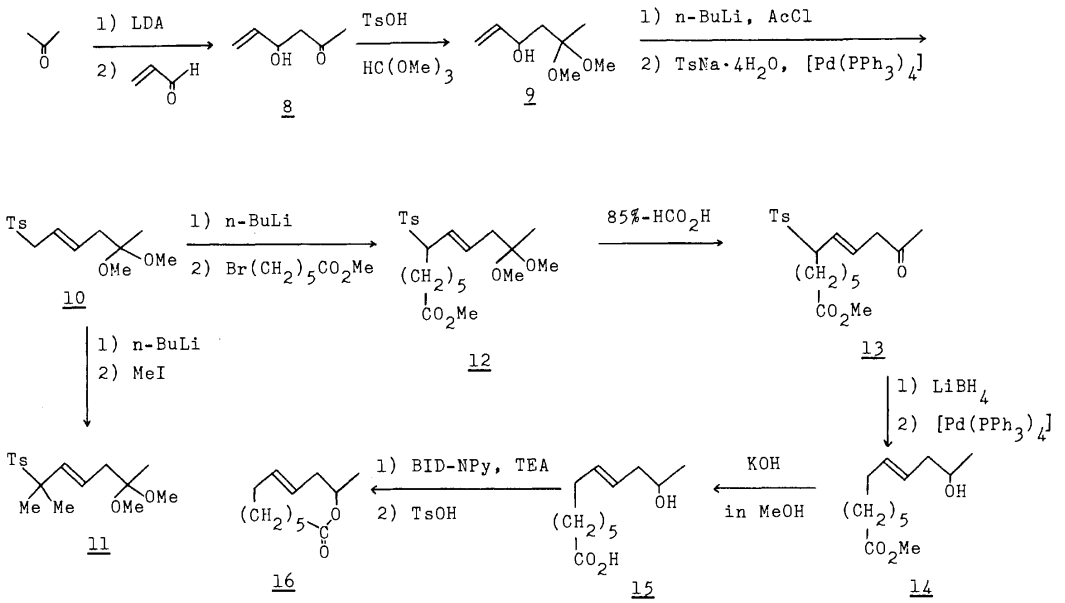

Scheme 3.

Scheme 3.

The reaction of acrylaldehyde with lithiated acetone in THF at −78°C gave the hydroxy ketone (**8**) in 89% yield. Acetalization of the carbonyl group of **8** by the use of 3 equiv of methyl orthoformate gave the compound (**9**) in 82% yield. The hydroxyl group of **9** was acetylated with *n*-BuLi and acetyl chloride. The crude acetate was converted to the corresponding sulfone (**10**) using a catalytic amount of $[Pd(PPh_3)_4]$ (5 mol%) and sodium *p*-toluenesulfinate in THF–MeOH in 78% yield from **9**. Stereochemistry[7,8] of the double bond in **10** was confirmed to be *E*-form by NMR spectrum of its dimethyl product (**11**), that is, the coupling constant between the two olefinic protons was 15.2 Hz. Treatment of the compound (**10**) with *n*-BuLi in the presence of HMPA, followed by the addition of 1.1 equiv of methyl 6-bromohexanoate, gave the alkylated product (**12**) in 90% yield. Deprotection of the acetal group of **12** by the treatment with 85% formic acid for 1 min at room temperature gave the keto ester (**13**) in 95% yield. Reduction of the carbonyl group to the alcohol and the subsequent detosylation[9] were accomplished in one-pot as follows: A solution of **13** in THF was treated with $LiBH_4$ at −10°C for 5 min and then $[Pd(PPh_3)_4]$ (6 mol%) was added. The mixture was allowed to stand for 1.5 h at room temperature to yield the hydroxy ester (**14**) in 72% yield. Its NMR and IR spectra were completely in accordance with the reported ones.[6] Hydrolysis of **14** with 40%-methanolic KOH solution gave the hydroxy acid (**15**) as a precursor of recifeiolide in 97% yield. It was lactonized using BID–NPy by high dilution method. The active ester derived from the reaction of **15** with **1** in 1,2-dichloroethane at −5°C was added slowly to a refluxing 1,2-dichloroethane containing 2 equiv of TsOH in a period of 15 h under N_2. The desired product (**16**) was separated in 81% yield with a preparative TLC.

As mentioned above, BID–NPy was found to be a versatile condensing reagent for the preparation of esters, peptides, and macrolides.

Experimental

All the melting points were determined with a micro melting apparatus (Yanagimoto-Seisakusho) and were uncorrected. The ^{1}H-NMR and IR spectra were recorded on JEOL JNM-PMX-60 and JASCO IRA-1 diffraction grating infrared spectrometer, respectively. The chemical shifts are recorded in the δ scale relative to TMS as an internal standard. For the reactions requiring slow addition, a Natume syringe pump, model KN-202, was used.

Materials. All the solvents were distilled and stored over a drying agent. Thin-layer chromatography (TLC) was performed on Merck's silica gel 60 PF_{254} (Art. 7749).

Preparation of BID-Cl. A mixture of $SOCl_2$ (10.62 g, 90 mmol) and saccharin (5.50 g, 30 mmol) was refluxed for 15 h in dioxane (100 ml) in the presence of active charcoal (0.8 g) and a catalytic amount of DMF (0.19 g, 2.6 mmol). The hot reaction mixture was filtered through celite to remove the charcoal. After evaporation of the solvent *in vacuo*, the resulting product was recrystallized from dry benzene. Yield, 4.60 g, 76%. Mp 145—147°C (lit, 143—145°C).[10] This BID-Cl was found to be unstable to moisture and thus was kept under vaccum.

Preparation of BID-NPy (1). To a suspension of BID-Cl (2.02 g, 10 mmol) and 5-nitro-2-pyridone (1.12 g, 8 mmol) in dry CH_3CN (25 ml) was added TEA (0.81 g, 8 mmol) at 0°C. A yellowish white crystalline precipitate started to separate almost immediately. After the suspension was stirred for 2 h at room temperature, the precipitate was filtered, washed with chloroform to remove triethylammonium chloride and recrystallized from CH_3CN to give pure BID-NPy (**1**) in 77% yield. 1.89 g, mp 239—241°C; IR (KBr) 3100, 1670, 1605, 1560, 1350, 1180 cm^{-1}; Found: C, 47.24; H, 2.18; N, 13.54%. Calcd for $C_{12}H_7N_3O_5S$: C, 47.22; H, 2.31; N, 13.77%.

Preparation of Esters from Carboxylic Acids and Alcohols. To a mixed suspension of **1** (152 mg, 0.5 mmol), phenylacetic acid (68 mg, 0.5 mmol), and benzyl alcohol (54 mg, 0.5 mmol) in CH_2Cl_2 (3 ml) was added a solution of TEA (51 mg, 0.5 mmol) in CH_2Cl_2 (2 ml) at −10°C under N_2. The suspension became clear after a few minutes as the slightly soluble **1** was consumed in the progress of the reaction. The reaction mixture was gradually raised to room temperature.

After stirring overnight, the solvent was evaporated *in vacuo* and the resulting residue was taken up in AcOEt (30 ml). This was then washed successively with a saturated solution of $NaHCO_3$, with 1 mol dm^{-3} HCl, and with brine. The resulting residue was then subjected to preparative TLC (solvent; benzene: AcOEt=5:1, v/v) to afford 112 mg of benzyl phenylacetate, (95% yield). An oil.[17] IR (neat) 1735 cm^{-1}; NMR ($CDCl_3$) δ=3.50 (s, 2H), 4.98 (s, 2H), 7.13 (s, 5H), 7.15 (s, 5H).

The other esters shown in Table 1 were prepared in a similar manner.

Benzyl Cinnamate: IR (neat) 1710,1630, 1160 cm^{-1}; NMR ($CDCl_3$) δ=5.09 (s, 2H), 6.29 (d, J=17 Hz, 1H), 7.22 (m, 10H). p-*Nitrophenyl Phenylacetate*: Mp 61—63 °C (lit, 62—63 °C).[18] 2,2,2-*Trichloroethyl Benzoate*: IR (neat) 1735, 1235, 1138 cm^{-1}; NMR ($CDCl_3$) δ=4.92 (s, 2H), 7.42—7.62 (m, 3H), 8.0—8.13 (m, 2H).[19] *Pentachlorophenyl Benzoate*: Mp 159—161 °C (lit, 159—160 °C).[19] p-*Nitrophenyl Benzoate*: Mp 142—144 °C (lit, 142 °C).[19] N-*(Benzoyloxy) Succinimide*: Mp 137—139 °C (lit, 139—140 °C).[17]

Preparation of Benzyloxycarbonyl Dipeptide Esters. Z--Cys(Bzl)-Gly-OEt: To a mixed suspension of **1** (152 mg, 0.5 mmol) and Z-Cys(Bzl)-OH (173 mg, 0.5 mmol) in CH_2Cl_2 (3 ml) was added a solution of TEA (51 mg, 0.5 mmol) in CH_2Cl_2 (2 ml) dropwise at −10 °C under N_2. After stirring for 2 h at −10 °C, H-Gly-OEt·HCl (70 mg, 0.5 mmol) and a solution of TEA (51 mg, 0.5 mmol) in CH_2Cl_2 (2 ml) were successively added to the reaction mixture. The solution was stirred at 0 °C for 2 h and stirring was continued overnight at room temperature. The solvent was evaporated *in vacuo* and the resulting residue was taken up in AcOEt (30 ml). This was then successively washed with a saturated solution of $NaHCO_3$, with 1 mol dm^{-3} HCl, and with brine, dried over Na_2SO_4, and evaporated to dryness *in vacuo*. The resulting residue was subjected to preparative TLC (solvent; benzene: AcOEt=1:1, v/v) to separate the desired product. Recrystallization from benzene-hexane gave the product, Z-Cys(Bzl)-Gly-OEt, in quantitative yield (208 mg).

In a similar manner, various benzyloxycarbonyl dipeptide esters were prepared, as shown in Table 2.

*Lactonization of ω-Hydroxy Carboxylic Acids. 12-Dodecanolide (**6b**)*: To a suspension of **5b** (43 mg, 0.2 mmol) and **1** (61 mg, 0.2 mmol) in 1,2-dichloroethane (95 ml) was added a solution of TEA (21 mg, 0.2 mmol) in 1,2-dichloroethane (5 ml) dropwise at −0 °C in a period of 10 min under N_2. After about 30 min the initial suspension became a clear yellowish solution. Stirring was continued for about 1 h to complete the formation of the active ester. The resulting reaction mixture containing the active ester was added slowly to a refluxing dry 1,2-dichloroethane (50 ml) containing anhydrous TsOH (76 mg, 0.4 mmol) with a mechanically driven syringe in a period of 6 h. After the addition, it was further refluxed for 2 h. The solvent was evaporated *in vacuo* and the resulting residue was partitioned between water and AcOEt. The AcOEt layer was successively washed with 10% $NaHCO_3$, 1 mol dm^{-3} HCl, and brine. The solution was dried over Na_2SO_4 and was evaporated *in vacuo*. The resulting residue was subjected to preparative TLC (solvent; hexane:ether=10:1, v/v). Two fractions were obtained. From the first fraction (R_f=0.64), monolide was obtained as an oil (28 mg, 71%). Its spectral data (IR, NMR), behavior on TLC, and GLC were identical with the authentic sample. MS m/z 198 (M^+); IR (neat) 1735, 1245 cm^{-1}; NMR ($CDCl_3$) δ=1.1—2.0 (m, 18H), 2.35 (t, J=6 Hz, 2H), 4.15 (t, J=6 Hz, 2H). The crystalline substance obtained from the second fraction (R_f=0.52) was found to be the dimeric lactone by comparison with the authentic sample. 7 mg, 18%; mp 102—103 °C (lit, 103—104 °C).[3b]

Other ω-hydroxy carboxylic acids (**5a**, **5c—g**) were cyclized in a similar manner.

6a: An oil, MS m/z 184 (M^+); IR (neat) 2930, 2870, 1738, 1465, 1440, 1350, 1245, 1170, 1140, 1090 cm^{-1}; NMR ($CDCl_3$) δ=1.15—1.84 (m, 16H), 2.31 (t, J=6 Hz, 2H), 4.01 (t, J=6 Hz, 2H).

6c: An oil, MS m/z 212 (M^+); IR (neat) 2930, 2845, 1730, 1460, 1370, 1285, 1258, 1225, 1170, 1100 cm^{-1}; NMR ($CDCl_3$) δ=1.06—1.83 (m, 20H), 2.30 (t, J=6 Hz, 2H), 4.13 (t, J=6 Hz, 2H).

6d: Mp 35—36 °C (lit, 34 °C).

6e: After the addtion of the active ester, the reaction mixture was further refluxed for 10 h. MS m/z 254 (M^+); IR (neat) 2940, 2845, 1730, 1460, 1380, 1350, 1250, 1160 cm^{-1}; NMR ($CDCl_3$) δ=1.16—1.83 (m, 26H), 2.30 (t, J=6 Hz, 2H), 4.15 (t, J=6 Hz, 2H).

6f: An oil, MS m/z 282(M^+); IR (neat) 2920, 2860, 1725, 1470, 1370, 1320, 1245, 1170, 1138 cm^{-1}; NMR ($CDCl_3$) δ= 0.93 (t, J=7 Hz, 3H), 1.03—1.86 (m, 28), 2.35 (t, J=6 Hz, 2H), 4.70—5.00 (m, 1H).

6g: An oil, MS m/z 280 (M^+); IR (neat) 2920, 2850, 1720, 1640, 1440, 1360, 1230, 1170 cm^{-1}; NMR ($CDCl_3$) δ=0.93—1.01 (t, J=7 Hz, 3H), 1.02—1.93 (bm, 24H), 2.10—2.46 (bt, 2H), 3.50—4.01 (bm, 1H), 5.35—5.56 (m, 2H).

*Preparation of ω-Hydroxy Carboxylic Acids (**5a**, **5c**, and **5d**). 13-Hydroxytridecanoic Acid (**5c**)*: A solution of cyclotridecanone (0.98 g, 5 mmol) in CH_2Cl_2 (30 ml) was treated with freshly distilled boron trifluoride etherate (0.85 g, 6 mmol) for 15 min. To the reaction mixture was added MCPBA (purity 70%, 2.59 g, 15 mmol) in a period of about 20 min and the reaction mixture was stirred for 15 h at 40 °C. The mixture was cooled and water was added to it. The excess peroxy acid was destroyed by the dropwise addition of 10% solution of Na_2SO_3 and then the layers were separated. The aqueous portion was extracted with CH_2Cl_2 three times. The combined organic extracts were washed with water, dried over Na_2SO_4, and evaporated to dryness *in vacuo*. The crude lactone thus obtained was directly subjected to alkaline hydrolysis with 1 mol dm^{-3} NaOH in methanol and water (4:1). The solution was heated at 60 °C for 1 h. After cooling, the mixture was concentrated to half the volume, diluted with water, and washed with chloroform. The aqueous layer was acidified with 1 mol dm^{-3} HCl (pH=3) at 0 °C to give a crystalline substance. After standing for about 1 h, the precipitate was filtered and recrystallized from 1,2-dichloroethane to give **15c** (0.90 g, 78%). Mp 78—79 °C (lit, 79 °C).[20]

In a similar manner, other carboxylic acids were prepared from the corresponding cycloalkanones.

*11-Hydroxyundecanoic Acid (**5a**)*: 69%, mp 65—67 °C (lit, 66 °C).[21]

*15-Hydroxypentadecanoic Acid(**5d**)*: 82%, mp 80 °C (lit, 82—84 °C).[19]

Preparation of Methyl 6-Bromohexanoate: 6-Bromohexanoic acid prepared by the reported method[19] was treated with diazomethane in ether. Distillation of the crude product gave pure oily product: Bp 72—78 °C/1 Torr: IR (neat) 2950, 1730, 1432, 1251, 1200,1168 cm^{-1}; NMR ($CDCl_3$) δ=1.30—2.13 (m, 6H), 2.30 (t, J=6 Hz, 2H), 3.37 (t, J=6 Hz, 2H), 3.63 (s, 3H).

*4-Hydroxy-5-hexen-2-one (**8**)*. To a solution of diisopropylamine (1.11 g, 11 mmol) in THF (15 ml) was slowly added a solution of *n*-BuLi (*ca.* 15% in hexane, 6.68 ml, 10 mmol) dropwise at −50 °C under N_2. After stirring for about 1 h at −50 °C to −30 °C, the reaction mixture was cooled to −78 °C and a solution of acetone (5.80 g, 10 mmol) in THF (5 ml) was slowly added to the reaction mixture during 1 h. The reaction mixture was stirred for about 30 min at −78 °C to −30 °C and again the temperature was cooled to −78 °C. A solution of acrylaldehyde

(6.72 g, 12 mmol) in THF (2 ml) was added all at once. After 5 min, the reaction mixture was quenched with CH_3OH–HCl. The solution was evaporated to dryness and the residue was partitioned between ether and water. The resulting mixture of products was separated by column chromatography (silica gel, solvent; benzene: AcOEt=3:1 v/v). The desired product was obtained in 89% yield (1.02 g). IR (neat) 3400, 2980, 2930, 1700, 1640, 1420, 1365, 1160, 1120, 1060, 990, 925 cm^{-1}; NMR ($CDCl_3$) δ=2.20 (s, 3H), 2.63 (d, J=6 Hz, 2H), 3.50 (s, 1H), 4.33—4.70 (bm, 1H), 4.94—6.21 (bm, 3H).

5,5-Dimethoxy-1-hexen-3-ol (9). To a solution of **8** (342 mg, 3 mmol) in MeOH (15 ml) in the presence of Molecular Sieves (4A, 1/16, 3 g) was added trimethyl orthoformate (1.32 ml, 12 mmol) at room temperature under N_2. A catalytic amount of TsOH (68 mg, 12 mol%) was added to the reaction mixture and, after stirring for 3 h, it was made slightly basic (pH=8) by adding a saturated solution of Na_2CO_3. The MeOH was removed *in vacuo* and the resulting residue was taken up in chloroform (40 ml). The organic layer was washed with water three times, dried over Na_2SO_4, and evaporated. The resulting residue was subjected to preparative TLC (solvent; benzene: AcOEt=2:1, v/v) to give 393 mg of the desired product (82%). IR (neat) 3460, 3080, 2960, 2840, 1640, 1450, 1420, 1370, 1265, 1220, 1140, 1040, 985, 920 cm^{-1}; NMR ($CDCl_3$) δ=1.26 (s, 3H), 1.80 (bm, 2H), 3.01 (s, 6H), 3.63 (s,1H), 4.13—4.53 (bm, 1H), 4.90—6.20 (bm, 3H).

5,5-Dimethoxy-1-tosyl-2-hexene (10). n-BuLi (3 mmol) was added dropwise to a solution of **9** (480 mg, 3 mmol) in THF (6 ml) at −78 °C under N_2. The mixture was stirred for about 30 min. To the reaction mixture was added a solution of acetyl chloride (273 mg, 3.5 mmol) at −78 °C. After 10 min, the reaction was found to be complete and the mixture was quenched with a buffer solution of K_2HPO_4–NaOH (pH=7). The solvent was evaporated and the residue was taken up in chloroform. The chloroform solution was washed with a small amount of water, dried, and evaporated. The crude product was obtained in quantitative yield and used in the subsequent reaction. IR (neat) 2940, 2840, 1738, 1640, 1420, 1370, 1240, 1040, 925, 845, 800 cm^{-1}; NMR ($CDCl_3$) δ=1.33 (s, 3H), 2.08 (s, 3H) 1.95—2.35 (bm, 2H), 3.20 (s, 6H), 4.95—6.10 (bm, 5H).

Sodium p-Toluenesulfinate Tetrahydrate (0.8 g, 3.2 mmol) was dissolved in MeOH (2 ml) and THF (4 ml) at room temperature under N_2. The crude acetylated compound obtained above (*ca.* 3 mmol) in THF (2 ml) was added to it. A solution of $[Pd(PPh_3)_4]$ (174 mg, 0.15 mmol) in THF (2 ml) was added to the reaction mixture. After 30 min, the clear brownish solution changed to light yellow, accompanied by precipitation, and gradually it turned lemon yellow. After stirring overnight, KCN (36 mg) dissolved in a minimum amount of water was added to the reaction mixture. The solution became colorless. The solvent was evaporated *in vacuo* and the resulting residue was dissolved in CH_2Cl_2 (40 ml) and the insoluble materials were filtered. The filtrate was dried over Na_2SO_4. After removal of the solvent, the residual oil was subjected to preparative TLC (solvent; hexane: AcOEt=2:1, v/v) to give the desired product (**10**) (698 mg, 78%) from **9**. MS m/z 267 (M^+—OMe); IR (neat) 2960, 1735, 1595, 1380, 1360, 1310, 1295, 1280, 1230, 1138, 1080, 1030, 960, 805, 725 cm^{-1}; NMR ($CDCl_3$) δ=1.06 (s, 3H), 2.20—2.40 (bm, 2H), 2.46 (s, 3H), 3.10 (s, 6H), 3.76 (d, J=6 Hz, 2H), 5.30—5.67 (bm, 2H), 7.20 (d, J=8 Hz, 2H), 7.60 (d, J=8 Hz, 2H).

6,6-Dimethoxy-2-methyl-2-tosyl-3-heptene (11). To a solution of **10** (100 mg, 0.34 mmol) in THF (4 ml) was added one equiv of n-BuLi (0.34 mmol) dropwise at −78 °C under N_2. After 10 min, hexamethylphosphoric triamide (HMPA) (0.4 ml) was added and then after 1 h, a solution of CH_3I (53 mg, 0.37 mmol) in THF (1.5 ml) was dropwise added. The reaction mixture was stirred for 2 h at −78 °C, warmed to room temperature, and then cooled down at −78 °C again. This alkylation procedure was repeated once again. The crude material was purified by preparative TLC (solvent; hexane:AcOEt=2:1, v/v) to afford **11** in 53% yield. MS m/z 295(M^+—OMe); IR (neat) 2940, 1590, 1292, 1170, 1150, 1120, 972, 810 cm^{-1}; NMR ($CDCl_3$) δ=1.13 (s, 3H), 1.43 (s, 6H), 2.35 (d, J=7 Hz, 2H), 2.42 (s, 3H), 3.14 (s, 6H), 5.27 (dd, J=7, 15.2 Hz, 1H), 5.60 (d, J=15.2 Hz, 1H), 7.23 (d, J=8 Hz, 2H), 7.57 (d, J=8 Hz, 2H).

Methyl (E)-11,11-Dimethoxy-7-tosyl-8-dodecenoate (12). To a solution of **10** (570 mg, 1.91 mmol) in THF (10 ml) was added 1.1 equiv of n-BuLi at −78 °C under N_2, followed by the addition of HMPA (2 ml) after 20 min. After 1 h, a solution of methyl 6-bromohexanoate (439 mg, 2.10 mmol) in THF (5 ml) was dropwise added in a period of 20 min at −78 °C. The reaction mixture was allowed to stand overnight at room temperature. The usual work-up gave an oily crude product which was purified by preparative TLC (solvent; hexane:AcOEt=2:1, v/v). Yield was 90% (an oil, 737 mg). MS m/z 395 (M^+—OMe); IR (neat) 2950, 1729, 1590, 1295, 1140, 1080, 1045, 968, 805, 750 cm^{-1}; NMR ($CDCl_3$) δ=1.10 (s, 3H), 1.13—2.50 (m, 12H), 2.40 (s, 3H), 3.10 (s, 6H), 3.20—3.53 (m, 1H), 3.60 (s, 3H), 5.17—5.47 (m, 2H), 7.27 (d, J=8 Hz, 2H), 7.56 (d, J=8 Hz, 2H).

Methyl (E)-11-Hydroxy-8-dodecenoate (14). The compound(**12**) (616 mg, 1.45 mmol) was dissolved in 85% formic acid (4.5 ml). The formic acid was immediately removed *in vacuo* to give a residue which was taken up in AcOEt. The organic solution was washed with 10% $NaHCO_3$, brine, and dried over $MgSO_4$. Removal of the solvent gave an oily keto ester (**13**) in 95% yield, which was used in the subsequent reaction without further purification. IR (neat) 2930, 1722, 1710, 1595, 1295, 1135, 1080, 965, 810 cm^{-1}; NMR ($CDCl_3$) δ=1.03—2.37 (m, 12H), 2.03 (s, 3H), 2.43 (s, 3H), 3.08 (d, J=6 Hz, 2H), 3.23—3.57 (m, 1H), 3.63 (s, 3H), 5.27—5.60 (m, 2H), 7.34 (d, J=8 Hz, 2H), 7.59 (d, J=8 Hz, 2H).

To a solution of **13** (86 mg, 0.23 mmol) in THF (2 ml) was added $LiBH_4$ (910 mg, 0.5 mmol) in one portion at −10 °C under N_2. After 5 min, 6 mol% of $[Pd(PPh_3)_4]$ (16 mg) dissolved in THF (2 ml) was added to the reaction mixture at −10 °C. The reaction mixture was stirred for 1.5 h at room temperature. The color of the solution gradually changed into dark brown. The reaction mixture was quenched with water. The THF was removed *in vacuo* to give a residue which was taken up in AcOEt. The AcOEt solution was washed with brine and dried over $MgSO_4$. The solvent was removed under reduced pressure. The residue was subjected to preparative TLC (solvent; hexane:AcOEt=4:1, v/v) to give the desired product (**14**) in 72% yield (37 mg) from **13**. Its IR and NMR data were in accord with the reported ones.[6b] CI-MS m/z 229 (M^++1); IR (neat) 1730, 962 cm^{-1}; NMR ($CDCl_3$) δ=1.07—1.77 (d, J=6 Hz, 3H), 1.17 (d, J=6 Hz, 3H), 1.77—2.47 (m, 6H), 3.43—4.02 (m, 1H), 3.60 (s, 3H), 5.13—5.47 (m, 2H).

(±)-(E)-11-Hydroxy-8-dodecanoic Acid (15). To **14** (424 mg, 1.86 mmol) was added 6 mol dm^{-3} methanolic KOH solution (3.8 ml) at room temperature. Water (2 ml) was added to the solution and the reaction mixture was stirred for 1 h at room temperature and extracted with ether three times. The aqueous layer was acidified with 6 mol dm^{-3} HCl. The separated oil was extracted with chloroform. The organic solution was washed with brine and dried over $MgSO_4$. Removal of the solvent afforded **15** in 97% yield (386 mg). IR and NMR data of **15** thus obtained were in good agreement with the reported ones.[6a] IR (neat) 1700, 965 cm^{-1}; NMR ($CDCl_3$) δ=1.00—1.80 (m, 8H), 1.17 (d, J=6 Hz, 3H), 1.80—

2.53 (m, 6H), 3.50—4.10 (m, 1H), 5.20—5.43 (m, 2H), 6.93 (bs, 2H).

(±)-(E)-8-Dodecen-11-olide, Recifeiolide (16). To a suspension of **15** (50 mg, 0.23 mmol) and **1** (78 mg, 0.25 mmol) in 1,2-dichloroethane (180 ml) was added a solution of TEA (24 mg, 0.23 mmol) in 1,2-dichloroethane (5 ml) dropwise at −5 °C. After about half an hour, the initial suspension became a clear yellowish solution. It was diluted with 1,2-dichloroethane (60 ml). The reaction mixture was added slowly to a refluxing 1,2-dichloroethane containing anhydrous TsOH (88 mg, 0.46 mmol) with a mechanically driven syringe under N_2. After completion of the addition, it was further refluxed for 2 h. The solvent was evaporated and the resulting residue was partitioned between AcOEt and water. The AcOEt portion was washed successively with 10% $NaHCO_3$ and brine. After drying, the resulting residue was subjected to preparative TLC (solvent; hexane: AcOEt=8:1, v/v) to give the desired product (**16**) (37 mg, 81%). Its spectral data were completely in accordance with the reported values.[6] An oil; CI-MS *m/z* 197(M^++1); IR (neat) 1720, 1245, 965 cm^{-1}; NMR ($CDCl_3$) δ=1.23 (d, J=6 Hz, 3H), 1.10—1.90 (m, 8H), 1.90—2.77 (m, 6H), 4.60—5.00 (m, 1H), 5.00—5.50 (m, 2H).

References

1) F. Micheel and M. Lorenz, *Tetrahedron Lett.*, **1963**, 2119.

2) a) K. Inomata, H. Kinoshita, H. Fukuda, O. Miyano, Y. Yamashiro, and H. Kotake, *Chem. Lett.*, **1979**, 1265; b) A. Ahmed, H. Fukuda, K. Inomata, and H. Kotake, *ibid.*, **1980**, 1161.

3) a) T. Mukaiyama, R. Matsueda, and M. Suzuki, *Tetrahedron Lett.*, **1970**, 1901; b) E. J. Corey and K. C. Nicolou, *J. Am. Chem. Soc.*, **96**, 5614 (1974); c) S. Masamune, S. Kamata, and W. Schilling, *ibid.*, **97**, 3515 (1975); d) H. Gerlach and A. Thalmann, *Helv. Chim. Acta*, **57**, 2661 (1974); e) T. Kurihara, Y. Nakajima, and O. Mitsunobu, *Tetrahedron Lett.*, **1976**, 2455.

4) B. D. Mookherjee, R. W. Trenkle, and R. R. Patel, *J. Org. Chem.*, **37**, 3846 (1972).

5) R. F. Vesonder, F. H. Stodola, L. J. Wickerham, J. J. Ellis, and W. K. Rohwedder, *Can. J. Chem.*, **49**, 2029 (1971).

6) a) E. J. Corey, P. Ulrich, and J. M. Fitzpatrick, *J. Am. Chem. Soc.*, **98**, 222 (1976); b) H. Gerlach, K. Oertle, and A. Thalmann, *Helv. Chim. Acta*, **59**, 755 (1976); c) K. Narasaka, M. Yamaguchi, and T. Mukaiyama, *Chem. Lett.*, **1977**, 959.

7) K. Inomata, T. Yamamoto, and H. Kotake, *Chem. Lett.*, **1981**, 1357.

8) It is known that the stereochemistry of olefinic bond of allylic sulfone is not changed during aklylation with its lithium salt: P. A. Grieco and Y. Masaki, *J. Org. Chem.*, **39**, 2135 (1974).

9) H. Kotake, T. Yamamoto, and H. Kinoshita, *Chem. Lett.*, **1982**, 1331.

10) Deutchen Chemischen Gesellshaft, "Beilsteins Handbuch der Organischen Chemie," Springer-Verlag. Berlin (1942), Vol. 27, p. 39.

11) T. Mukaiyama, M. Ueki, R. Matsueda, and K. Goto, "Proceedings of the 7th Symposium on Peptide Chemistry," ed by S. Akabori, Protein Research Foundation, Osaka (1969), p. 25.

12) M. Miyoshi and Y. Tamura, "Proceedings of the 8th Symposium on Peptide Chemistry," ed by T. Kaneko, Protein Research foundation, Osaka (1970), p. 36.

13) J. E. Schields, S. T. McDowell, J. Pavlos, and G. R. Gray, *J. Am. Chem. Soc.*, **90**, 3549 (1968).

14) D. E. Nitecki, B. Halpern, and J. W. Westly, *J. Org. Chem.*, **33**, 864 (1968).

15) H. Kinoshita, K. Inomata, O. Miyano, and H. Kotake, *Bull. Chem. Soc. Jpn.*, **52**, 2619 (1979).

16) D. A. Laufer and E. R. Blout, *J. Am. Chem. Soc.*, **89**, 1246 (1967).

17) K. Inomata, H. Kinoshita, H. Fukuda, K. Tanabe, and H. Kotake, *Bull. Chem. Soc. Jpn.*, **51**, 1866 (1978).

18) K. Kanaoka, K. Tanizawa, E. Sato, O. Yonemitsu, and Y. Ban, *Chem. Pharm. Bull.*, **15**, 593 (1976).

19) "Dictionary of Organic Compounds," ed by J. R. A. Pollock and R. Stevens, Maruzen, Tokyo (1965).

20) K. Saotome, H. Komoto, and T. Yamazaki, *Bull. Chem. Soc. Jpn.*, **39**, 480 (1966).

21) S. Kamei, K. Wakabayashi, and N. Shimazono, *J. Biochem.*, **56**, 72 (1964).

 © 1984 The Chemical Society of Japan Bull. Chem. Soc. Jpn., 57, 787—790 (1984)

The Reaction of *N*-Aryl-*C*-ethoxycarbonylnitrilimine with Olefins[1]

Tomio SHIMIZU,* Yoshiyuki HAYASHI, Toshiyuki NISHIO, and Kazuhiro TERAMURA
Department of Color Chemistry and Technology, Faculty of Industrial Arts, Kyoto Technical University, Matsugasaki, Sakyo-ku, Kyoto 606
(Received August 1, 1983)

C-Ethoxycarbonylnitrilimines treated with monosubstituted olefins predominantly gave 5-substituted 3-ethoxycarbonyl-2-pyrazolines. From the analysis of the relative rate and regioselectivity of a variety of monosubstituted olefins for the cycloaddition, the nitrilimine is shown to have reactivity and regioselectivity similar to the throughly studied diphenylnitrilimine. The cycloaddition regioselectivity is discussed in terms of frontier orbital energies and coefficients.

Nitrilimines have been widely investigated and are one of the most versatile 1,3-dipoles for cycloaddition. *C*-Ethoxycarbonylnitrilimines especially have led to the synthesis of functional heterocyclic compounds. The reactivity of 1,3-dipolar cycloaddition reactions has been explained by frontier molecular orbital (FMO) theory,[2] but only a qualitative prediction has been made for the reactivity of nitrilimines. Recently, diphenylnitrilimine was identified at 85 K.[3] But the structural data of the nitrilimine can not be applied to the prediction of reactivity of the nitrilimine at ambient temperature. Some 1,3-dipoles react with monosubstituted electron-rich olefins to form products predicted by dipole-LUMO control. However for conjugated and electron-deficient dipolarophiles the regiochemistry of the reaction depends on which frontier orbital interaction (dipole-HOMO/dipolarophile-LUMO or dipole-LUMO/dipolarophile-HOMO) is dominant.[2] The reaction of diphenylnitrilimine with monosubstituted olefins gives predominantly 5-substituted 2-pyrazolines[4] and the orientation phenomena can be explained more or less satisfactorily by electronic effects alone. Dipole-LUMO/dipolarophile-HOMO interaction only controls the reaction of *N*-phenylsulfonylnitrilimine.[5] While the preparation and reaction of *C*-ethoxycarbonylnitrilimines have been the subject of intensive study,[6,7] a systematic investigation of the reactivity has not been carried out. Recently, 4-substituted 2-pyrazolines were claimed to be the exclusive products of the reaction of *C*-ethoxycarbonyl-*N*-arylnitrilimines with acrylic acid derivatives,[7] although the structure was assigned tentatively on the

TABLE 1. YIELDS, MELTING POINTS, AND ANALYTICAL DATA OF **2**

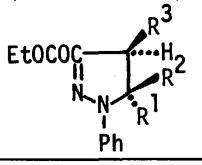

2

	R^1	R^2	R^3	Yield %	Mp θ_m/°C	Found(Calcd) (%) C	H	N
2a	Ph	H	H	85[d]	86—87	73.62 (73.45	6.15 6.16	9.55 9.52)
2b	CO_2Me	H	H	80[d]	83—84	60.71 (60.86	5.79 5.84	10.02 10.14)
2c	CN	H	H	70[d]	98—100	64.45 (64.18	5.41 5.39	17.38 17.28)
2d	$CONH_2$	H	H	81[d]	212—213	59.70 (59.76	5.77 5.79	16.05 16.08)
2e	*n*-Bu	H	H	80[e]				
2f	OBu-*n*	H	H	100[e]				
2g	CO_2Et	H	CH_3	100[e]				
2h	CO_2Me	CH_3	H	78[d]	100—101	62.25 (62.05	6.27 6.25	9.65 9.65)
2i[a]	H	$-C_5H_8-$		100[d]	82—83	71.85 (71.80	7.06 7.09	9.85 9.85)
2j	CO_2Me	H	CO_2Me	100[d]	78—80	57.23 (57.48	5.48 5.43	8.39 8.38)
2k[b]	H	$-C_4H_8-$		85[e]				
2m[c]	COPh	H	Ph	43[c]	133—138[c]	74.64 (74.59	5.73 5.74	7.22 7.25)
2n[c]	Ph	H	COPh	29[c]				

a) Cycloadduct of norbornene. b) Cycloadduct of cyclohexene. c) The mixture of **2m** and **2n** was obtained from the reaction with chalcone, and the ratio was determined by NMR. d) Isolated yields. e) Estimated from NMR.

basis of FMO theory only. We have investigated the reactivity and regioselectivity of *C*-ethoxycarbonyl-*N*-arylnitrilimines toward olefins.

Results and Discussion

Cycloadducts (**2**) were obtained when the reaction of olefins with ethyl chloroglyoxylate arylhydrazones (**1**) was carried out in the presence of triethylamine (Table 1). NMR analysis of the reaction mixture showed that the cycloadducts were formed quantitatively but an attempt to isolate pure material from liquid product (**2i**) by distillation failed because of decomposition to 3-ethoxycarbonyl-1-phenylpyrazole (**4**), which was also obtained in high yield by distillation of the reaction mixture of **1** with vinyl acetate. The structure of the cycloadducts was identified on the basis of elemental analysis and of their characteristic IR and NMR spectra. Both electron-rich and electron-deficient monosubstituted olefins gave exclusively one of two possible isomers, 5-substituted 2-pyrazolines. A distinction between the two isomers was made on the basis of the chemical shift of the methylene and methine hydrogens on the pyrazoline ring in the NMR spectra (Table 2). The three hydrogens show ABX or A_2X patterns depending on the substituent. Methylene chemical shifts at both 4- and 5-positions would be expected to be approximately same and in our cases the appearance of the methylene protones at δ 2.6—3.7 is compatible with both assignment. The methine chemical shift at the 5-position would be expected to appear at lower field than that at the 4-position,[8] although the chemical shift data for CH are much less abundant and less reliable than those for $-CH_2-$. The methine chemical shift at δ 4.0—5.8 was too low to be assigned to CH at the 4-position. Several attempts to prepare an authentic 4-substituted 2-pyrazoline failed, and therefore, we compared the chemical shifts with those of the thoroughly studied diphnylnitrilimine cycloadducts(**3**)[9a] (Table 2). Both substituents, phenyl and ethoxycarbonyl at 3-position, would have roughly the same effects on the chemical shift of methylene protones at the 4-position. Between the cycloadducts (**2** and **3**) having the same substituent at the 5-position each of methine and metylene protons shows comparable chemical shifts. Tewari *et al.*[7a] and Padwa *et al.*[7b] assigned 4-substituted 2-pyrazoline structures to the reaction products from *C*-ethoxycarbonyl-*N*-arylnitrilimines and acrylamide or methyl acrylate, respectively, on the basis of orbital interaction as discussed later. We confirmed these reactions but the chemical shifts of the products showed comparable δ values to ours. Thus, it seems reasonable to assume that all *C*-ethocycarbonylnitrilimines prepared so far give 5-substituted 2-pyrazolines almost exclusively, when reacted with monosubstituted olefins.

Table 2. NMR spectral data of **2** and **3**[a]

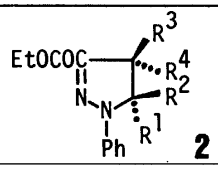

2

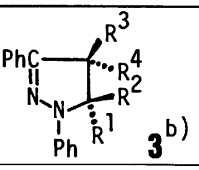

3[b]

	R^2(5-H)	R^3(4-H)	R^4(4-H)	R^2(5-H)	R^3(4-H)	R^4(4-H)
a	5.33(dd) J=8 and 13 Hz,	3.67(dd) J=13 and 18 Hz,	2.95(dd) J=8 and 18 Hz,	5.19(dd) J=8 and 12.1 Hz,	3.75(dd) J=12.1 and 16 Hz,	3.06(dd) J=8 and 16 Hz
b	4.90(dd) J=8 and 11 Hz,	3.20(dd) J=8 and 18 Hz,	3.57(dd) J=11 and 18 Hz,	4.62(dd) J=8 and 11 Hz,	3.20(dd) J=11 and 17 Hz,	3.38(dd) J=8 and 17 Hz
c	5.04(t) J=9 Hz	3.50(d) J=9 Hz		4.88(t)	3.55(d)	
d	4.90(dd) J=8 and 13 Hz,	2.97(dd) J=8 and 18 Hz,	3.54(dd) J=13 and 18 Hz	----------		
e	4.2—4.5(m)	3.25(dd) J=10 and 18 Hz,	2.80(dd) J=7 and 18 Hz,	4.02(m)	3.25(dd) J=11 and 17 Hz,	2.83(dd) J=6 and 17 Hz
f	5.73(t) J=6 Hz,	3.07(d) J=6 Hz		----------		
g	4.47(d) J=5 Hz,	—	3.60(dq) J=5 and 7 Hz,	4.43(d) J=4 Hz,	—	3.73(m)
h	—	3.10(d) J=18 Hz,	3.58(d) J=18 Hz,	—	3.15(d) J=17 Hz,	3.57(d) J=17 Hz
i	4.08(d) J=10 Hz,	3.28(d) J=10 Hz,	—	4.02(d) J=10 Hz,	3.44(d) J=10 Hz,	—
j	5.15(d) J=6 Hz,	—	4.37(d) J=6 Hz,	5.17(d) J=5 Hz,	—	4.57(d) J=5 Hz
k	4.0—4.5(m)	2.7—3.6(m)	—	----------		
m	5.77(d) J=5 Hz,	—	4.43(d) J=5 Hz,	5.61(d) J=5 Hz,	—	4.61(d) J=5 Hz
n	5.47(d) J=7 Hz,	—	5.07(d) J=7 Hz,	----------		

a) **2d** was dissolved in DMSO-d_6, the others were dissolved in $CDCl_3$. b) Data were cited from Ref. 9a and 11.

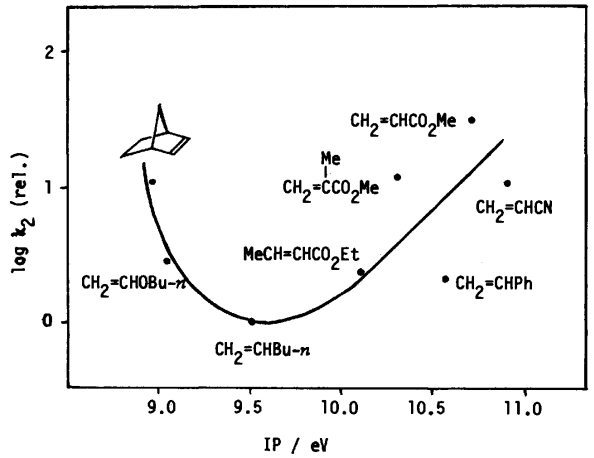

Fig. 1. The relative reaction rates and the ionic potentials of the dipolarophiles.

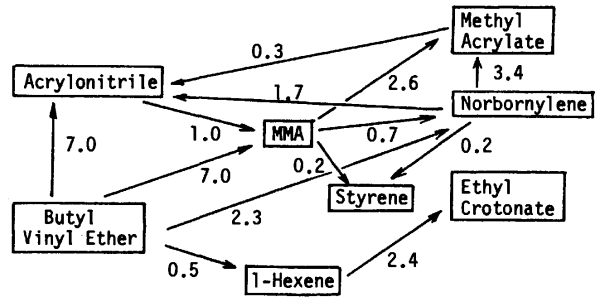

Fig. 2. The relative reaction rates of the diporaro-philes.
The numbers show relative reaction rates, x, where $x=k_B/k_A$ in the presence of both dipolarophiles, A and B. (B is shown after the arrow.)

In order to obtain additional criteria for the reactivity of the nitrilimine, competitive reactions of **1** were carried out between a variety of pairs of dipolarophiles (Fig. 2.). Relative rates in reference to 1-hexene are shown in Fig 1. These results clearly indicate that *C*-ethoxycarbonylnitrilimine is similar in reactivity to diphenylnitrilimine[9b] except for a lower reactivity toward electron-poor dipolaropiles.

The interpretation of the reactivity and regioselectivity of cycloadditions of the nitrilimine with electron-rich or conjugated olefins is fully in agreement with the prediction[2] that dipole-LUMO/dipolarophile-HOMO interaction is important and 5-substituted 2-pyrazolines are favored. On the other hand, it should be expected that the reaction of electron-deficient dipolarophiles and nitrilimines having relatively high HOMO energy is controlled by dipole-HOMO/dipolarophile-LUMO interaction. It is erroneously accepted that the coefficient of the nitrogen atom in HOMO of diphenylnitrilimine is much larger than that of the carbon atom. Consequently, the 4-substituted 2-pyrazolines are favored or the predominant formation of 5-substituted 2-pyrazolines with electron-deficent dipolarophiles can be only explained by an energetically unfavorable dipole-LUMO/dipolarophile-HOMO interaction [see interaction (a) in Fig. 3] based on the erroneous assumption.[2a] Recently, Houk and Caramella on the basis of *ab initio* molecular orbital calculations argued that in the non-planar most stable conformation of H-C≡$\overset{+}{N}$-$\overset{-}{N}$-H the biggest HOMO coefficient is to be found on the carbon atom[10] and this is also the case in diphenylnitrilimine.[11] Therefore the formation of 5-substituted 2-pyrazolines can be explained satisfactorily on the basis of dipole-HOMO control [see interaction (c) in Fig. 3] by assuming that the coefficient of carbon atom in HOMO of diphenyl- or *C*-ethoxycarbonyl-*N*-phenylnitrilimine is much larger than that of nitrogen atom.

Experimintal

Measurements. All the melting and boiling points are uncorrected. The IR spectra were determined on a Hitachi 215 Infrared Spectrophotometer. The ^{1}H NMR spectra were measured on a Varian T-60A instrument with TMS as an internal standard.

Materials. Ethyl chloroglyoxalate phenylhydrazone (**1**)[12] was prepared according to the method described in the literature. All the olefins are commercially available and

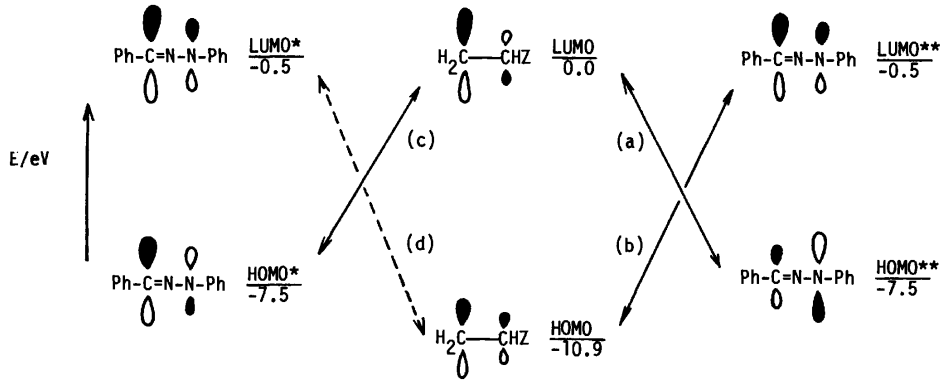

Fig. 3. Frontier orbital interactions (a—d) of diphenylnitrilimine and electron-deficient olefins.
* Magnitude of the coefficients is estimated from the calculation based on *ab initio* molecular orbital method.[10,11]
** Magnitude of the coefficients is estimated from the calculation based on CNDO/2 molecular orbital method.[2a]

were used after fractional distillation under nitrogen.

Reaction of 1 with Olefins. General Method: To a stirred chloroform (100 ml) solution of triethylamine (2.7 g, 26.4 mmol) and olefin (40 ml), was added a chloroform (20 ml) solution of ethyl chloroglyoxalate phenylhydrazone (3.0 g, 13.2 mml) at room temperature. After refluxing the chloroform solution for 2 h, the reaction mixture was cooled, washed with water several times. The chloroform solution was dried over sodium sulfate and the solvent and an excess amount of olefin were evaporated in a rotary evaporator at up to 60 °C *in vacuo*, giving crystals (**2a—d**, **2h—j**, **2m**, and **2n**), which were recrystallized from ethanol. Analysis of the residue by NMR after the evaporation gave aproximate yields of the other oily products as shown in Table 1. Distillation of the reaction mixture of **1** and butyl vinyl ether *in vacuo* gave 3-ethoxycarbonyl-1-phenylpyrazole (**4**) quantitatively; bp 180—185 °C/2 mmHg (1 mmHg≈133.322 Pa). NMR ($CDCl_3$) δ=1.33 (t, 3H, J=7 Hz), 4.37 (q, 2H, J=7 Hz), 6.95 (d, 1H, J=2 Hz), 7.0—7.85 (m, 5H), and 8.0 (d, 1H, J=2Hz).

Relative Reaction Rate of Dipolarophiles in Cycloaddition of C-Ethoxycarbonyl-N-phenylnitrilimine. This measurement was carried out according to the method described in the literature.[9b] To a refluxing chloroform solution (100 ml) of ten molar equivalents (0.13 mol) of two kind of dipolarophile and triethylamine (0.13 mol), was added dropwise a chloroform solution (20 ml) of ethyl chloroglyoxalate phenylhydrazone (3.0 g, 13 mmol) over a period of 1 h. After cooled to room temperature, the mixture was washed with water several times, dried (Na_2SO_4) and the solvent and the excess of the dipolarophiles was evaporated *in vacuo* at up to 60 °C. The residue was analysed by NMR in deuteriochloroform and the ratio of the competitive reaction products between dipolarophiles were estimated from the integration of each characteristic peaks. The results of the measurements are shown in Fig. 2.

References

1) Presented in part at the 42nd National Meeting of the Chemical Society of Japan, Sendai, September 1980, Abstr. Vol. II, p 537.

2) a) K. N. Houk, J. Sims, C, R. Watts, and L. J. Luskus, *J. Am. Chem. Soc.*, **95**, 7301 (1973); b) G. Bianchi, C. De Micheli, and R. Gandolfi, "1,3-Dipolar Cycloadditions Involving X=Y Groups" in "Supplement A: The Chemistry of Double-bonded Functional Groups, Part 1," ed by S. Patai, John Wiley & Sons, New York (1977), Chap. 6, pp. 369—532.

3) N. H. Toubro and A. Holm, *J. Am. Chem. Soc.*, **102**, 2093 (1980).

4) R. Huisgen, *Angew, Chem., Int. Ed. Engl.*, **2**, 565 (1963).

5) T. Sasaki, S. Ito, A. Kakehi, and T. Matsumoto, *Chem. Lett.*, **1979**, 733.

6) a) L. Garanti, A. Sala, and G. Zecchi, *J. Org. Chem.*, **42**, 1389 (1977); R. Fusco, L. Garanti, and G. Zecchi, *Tetrahedron Lett.*, **1974**, 269; b) A. S. Shawali and C. Parkanyi, *J. Heterocycl. Chem.*, **17**, 833 (1980) and references cited therein.

7) a) R. S. Tewari and P. Parihar, *Tetrahedron*, **39**, 129 (1983); b) A. Padwa and S. Nahm *J. Org. Chem.*, **46**, 1402 (1981).

8) N. F. Chamberlain, "The Practice of NMR Spectroscopy, "Plenum, New York (1974), p. 149.

9) a) R. Huisgen, H. Knupfer, R. Sustmann, G. Wallbillich, and V. Weberndörfer, *Chem. Ber.*, **100**, 1580 (1967); R. Sustmann, R. Huisgen, and H. Huber, *ibid.*, **100**, 1802 (1967); b) K. Bast, M. Christl, R. Huisgen, and W. Mack, *ibid.*, **106**, 3312 (1973).

10) P. Caramella and K. N. Houk, *J. Am. Chem. Soc.*, **98**, 6397 (1976).

11) G. Bianchi, R. Gandolfi, and C. De Micheli, *J. Chem. Res., (S)* **1981**, 6; *(M)* **1981**, 0135.

12) L. Garanti and G. Zecchi, *J. Chem. Soc., Perkin Trans. 1*, **1977**, 2092.

 © 1984 The Chemical Society of Japan Bull. Chem. Soc. Jpn., 57, 791—795 (1984)

Intramolecular Cycloaddition of Two Acyl-1,4-benzoquinone Moieties on Photolysis

Yo MIYAGI,* Kazuhiro MARUYAMA,† Nobuo TANAKA,†† Mamoru SATO,†† Toshinori TOMIZU, Yasuhiro ISOGAWA, and Hisae KASHIWANO

Faculty of Education, Kanazawa University, Kanazawa, 920

†*Department of Chemistry, Faculty of Science, Kyoto University, Sakyo-ku, Kyoto 606*

††*Institute for Protein Research, Osaka University, Suita, Osaka 565*

(Received August 15, 1983)

Upon irradiation a regio- and stereoselective cycloaddition occurred intramolecularly between two acyl-1,4-benzoquinone moieties connected by a polymethylene bridge. The regio- and stereoselectivities are different from those of the corresponding intermolecular cycloaddition; this was interpreted in terms of the Diels-Alder reaction between an acyl-1,4-benzoquinone moiety and a photochemically produced dienol.

In 1979 we reported[1] that 2-alkanoyl-1,4-benzoquinones (**1**) underwent a regio- and stereoselective dimerization on photolysis to give racemic 4aα-acyl-10β-alkyl-5,8-dihydroxy-4aα,10aα-dihydro-1,4,9(10*H*)-phenanthrenetriones (**2**).[2] We are interested

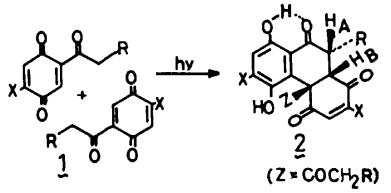

in whether a similar cycloaddition can occur intramolecularly between two acylquinone moieties. If such reactions could proceed, we might obtain, by a simple procedure, a group of compounds which have characteristic structures and properties. Actually the substrates, 2,2′-(α,ω-dioxo-α,ω-alkanediyl)bis(1,4-benzoquinone)s (**5a—d**)[3] prepared by the processs given in Scheme underwent the expected cycloaddition. When a degassed solution of **5** in acetonitrile[4] (0.05 mol dm^{-3}) was irradiated through Pyrex filter by a high pressure mercury-arc lamp, an intramolecular addition product of the substrate was obtained as the sole product in the yield of 25—30%. The yield of the product raised to 54% when the lower initial concentration of **5c** (0.002 mol dm^{-3}) was used.[5] Without light, a degassed solution of **5** had remained unchanged on standing at room temperature over a week.

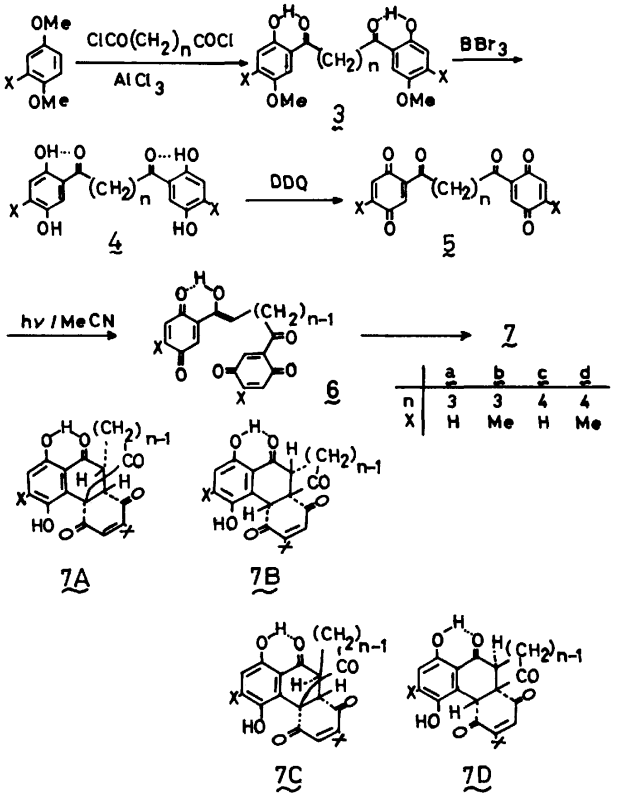

Scheme 1.

TABLE 1. ^{1}H NMR DATA OF **7B** (THE PHOTO-PRODUCT DERIVED FROM **5**): δ (acetone-d_6)

7B	OH[a]	OH	H_D	$H_{D'}$	H_C	$H_{C'}$	H_B	H_A	Me_D	Me_C	$-(CH_2)_{\overline{n-1}}$
a[b]	11.83	9.69	7.02 (ABq, 9.3 Hz)	6.78[c]	6.43 (ABq, 10.6 Hz)	6.97[d]	4.27 (s[e])	3.67 (m)	—	—	i
b	12.02	7.49	6.73 (s)	—	6.24 (q, 1.5 Hz)	—	4.32 (s)	3.53 (m)	2.01 (s)	2.24 (d, 1.5 Hz)	2.3—2.6 (m)
c	12.13	8.22	7.25 (ABq, 8.8 Hz)	6.65[d]	6.29 (ABq, 10.2 Hz)	6.97[d]	4.58 (dd[f])	3.27 (dd[g])	—	—	2.3—2.7 (m)
d	12.11	7.50	6.75 (s)	—	6.40 (q, 1.5 Hz)	—	4.68 (s)	3.22 (dd[h])	2.20 (s)	1.99 (d, 1.5 Hz)	2.3—2.6 (m)

a) Chelated. b) In DMSO-d_6. c) The half wing of the AB quartet broadened by coupling with H_B. d) The each signal of the half wing of the AB quartet spiked to a doublet in coupling with H_B; J=1.8 (H_C′: **a**), 1.4 (H_C′: **c**), and 1.2 Hz (H_D′: **c**). e) A broad singlet; see footnote c and d. f) J=1.4 and 1.2 Hz; see footnote d. g) J=4.9 and 10.7 Hz. h) J=4.9 and 11.2 Hz. i) Behind the signals of residual protons of DMSO.

	a	b	c	d
Y	$H_{C'}$	Me_C	$H_{C'}$	Me_C
Z	$H_{D'}$	Me_D	$H_{D'}$	Me_D
n	3	3	4	4

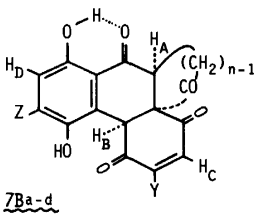

7Ba-d

The ^{1}H NMR data of the products (Table 1) were similar to those of **2**, suggesting a compound either of the structures **7A—D**.[6] While the signals of **2** at about δ 4.1 due to H_B were doublets ($J\simeq4$ Hz), the corresponding signals of the products derived from **5a**,[7] **5b**, and **5d** were singlets and that of the product from **5c** was a double doublet (J=1—2 Hz). The double resonance technique revealed that the atoms coupling with the atom giving the double doublet were an olefinic and an aromatic protons,[8] but not the proton corresponding to H_A of **2**. This fact exclude the possibilities of **7A** and **7C**, which should show a doublet due to the atom corresponding to H_B of **2**. The structure of the product derived from **5d** was unequivocally established as (4a*RS*,-8a*SR*,13b*SR*)-10,13-dihydroxy-2,12-dimethyl-6,7,8,8a-tetrahydro-1,4,5,9(13b*H*)-benz[*e*]anthracenetetrone (**7Bd**) by the X-ray structural analysis. The perspective view of a molecule of **7Bd** is given in Fig. 1.

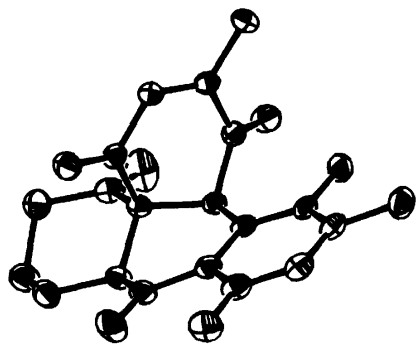

Fig. 1. Perspective view of (4a*R*,8a*S*,13b*S*)-10,13-dihydroxy-2,12-dimethyl-6,7,8,8a-tetrahydro-1,4,5,9-(13b*H*)benz[*e*]anthracenetetraone (**7Bd**).

The above finding indicates that the regio- and stereoselectivities of the intramolecular addition are different from those of the intermolecular one. The stereochemistry of the reactions is explicable in terms of the Diels-Alder reaction between an acylquinone moiety and a photochemically produced dienol moiety. For the intramolecular addition reaction, four orientations, **8A-D** corresponding to **7A-D**, may be possible. In **8C** and **8D** the access of two molecular planes is sterically hindered by the polymethylene chain existing inside the *cis*-dienol form. Such hindrance may not be exerted either in **8A** nor in **8B**. Though **8B** may be less favorable than **8A** because of steric hindrance caused by folding the polymethylene chain of **8B**, the chain (n=3 and 4) is not long enough to construct **8A**. Consequently the reaction to give **7B** may proceed preferentially. Second, for the intermolecular addition of **1** with the dienol **9**, orientations **10A—D** can be drawn. In **10C, D** the access of the molecular planes are hindered by a process similar to that explained for **8C, D**. **10B** is sterically hindered by the overlapping of the alkyl and acyl groups. Because of the least steric hindrance of **10A**, the selective formation of **2** is feasible.

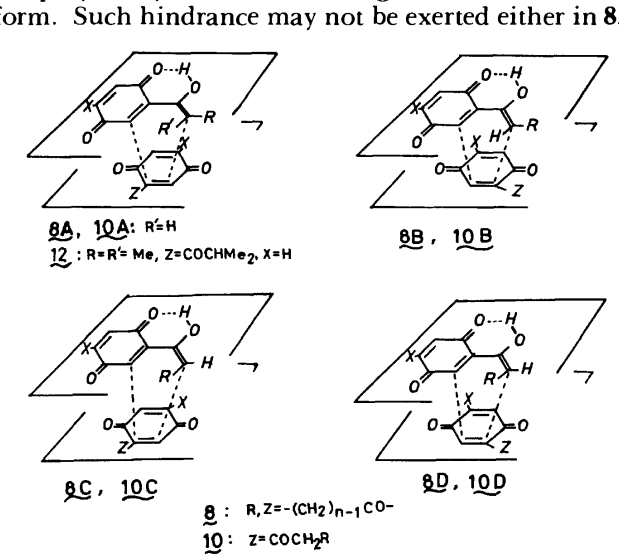

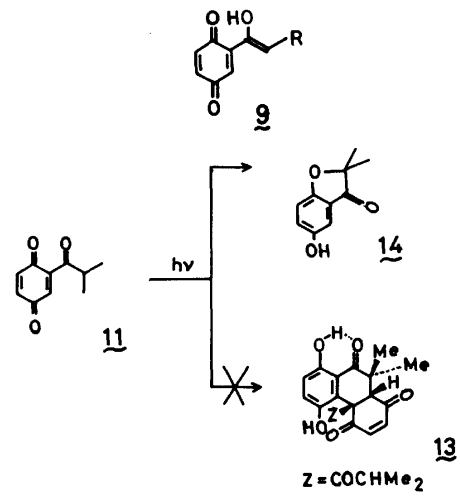

TABLE 2. FINAL ATOMIC COORDINATES ($\times10^4$) OF THE NON-HYDROGEN ATOMS OF **7Bd** WITH THEIR ESTIMATED STANDARD DEVIATIONS IN PARENTHESES[12]

C(1)	1300(3)	1101(5)	5321(5)
C(2)	1757(3)	2110(5)	4701(5)
C(3)	2121(3)	3004(5)	5410(4)
C(4)	2059(3)	3068(5)	6805(5)
C(4a)	1635(3)	1972(5)	7464(4)
C(5)	2210(3)	878(5)	7745(5)
C(6)	2811(3)	1137(6)	8798(6)
C(7)	2390(4)	1469(7)	10033(6)
C(8)	1884(3)	2653(6)	9825(5)
C(8a)	1294(3)	2417(5)	8739(5)
C(9)	780(3)	3550(5)	8499(5)
C(9a)	291(3)	3549(5)	7317(5)
C(10)	-273(3)	4501(5)	7136(5)
C(11)	-766(3)	4466(6)	6071(6)
C(12)	-694(3)	3488(5)	5196(5)
C(13)	-144(3)	2538(5)	5379(5)
C(13a)	357(3)	2547(4)	6412(4)
C(13b)	966(3)	1485(5)	6589(4)
C(2-Me)	1803(3)	2040(6)	3273(5)
C(12-Me)	-1221(3)	3438(7)	4004(6)
O(1)	1229(2)	30(3)	4869(4)
O(4)	2340(2)	3954(4)	7388(3)
O(5)	2164(3)	-130(4)	7192(5)
O(9)	742(3)	4443(4)	9260(4)
O(10)	-370(2)	5471(4)	7969(4)
O(13)	-83(2)	1569(4)	4491(3)

To examine the above steric effect towards the access of the molecular planes, we investigated the photolysis of 2-isobutyryl-1,4-benzoquinone (**11**). The cycloaddition through the corresponding orientation, **12**, may be unfavorable because a methyl group locates inside the *s-cis* dienol form. On irradiation, **11** did not afford the corresponding dimer **13**, but gave 2,2-dimethyl-5-hydroxy-3(2*H*)-benzofuranone (**14**), an intramolecularly cyclized product in 20% yield.

If the above cycloadditions proceed through the dienols, **6** and **9**,[9] they should be trapped with another dienophile present in the reaction solution. As stated previously,[1] however, no such adducts were obtained and **2** was still the only isolable product when the photolysis of **1** was effected in the presence of maleic anhydride, *N*-phenylmaleimide, or dimethyl acetylenedicarboxylate. A similar result was obtained for the intramolecular reaction. When a solution of **5c** in acetonitrile (0.002 mol dm^{-3}) was irradiated in the presence of maleic anhydride (0.2 mol dm^{-3}), no adducts between them were obtained and **7Bc** was isolated in a yield of 57%, a comparable yield with the reaction in the absence of maleic anhydride (*vide supra*).

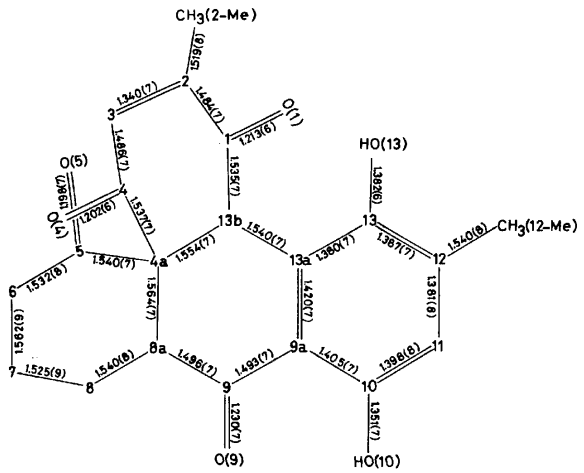

Fig. 2. Bond distances (*l*/Å) and atomic labelling numbers of **7Bd**.

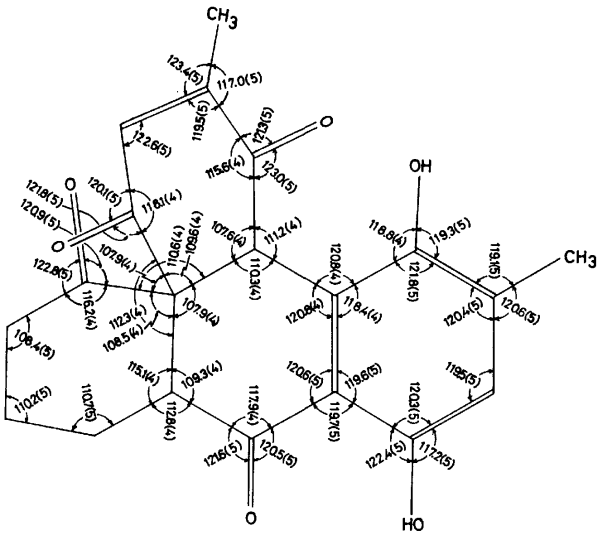

Fig. 3. Bond angles (ϕ/°) of **7Bd**.

Experimental

All new compounds gave satisfactory results in mass spectrometry. ^{1}H NMR spectra were measured by a JEOL JNM FX-100 and FX-90Q spectrometers.

α,ω-Bis(2,5-dihydroxyphenyl)-α,ω-alkanediones (4).[10] Glutaryl or adipoyl dichloride (0.05 mol) was added dropwise to a suspension of $AlCl_3$ (0.1 mol) in a solution of *p*-dimethoxybenzene or 2,5-dimethoxytoluene (0.1 mol) in 1,2-dichloroethane (100 cm^3) with stirring. After further stirring under refluxing for 8 h and subsequent addition of ice water and concentrated hydrochloric acid (10 cm^3), the reaction mixture was extracted with diethyl ether. The concentrated residue of the extract gave, after recrystallization from ethanol, a yellow solid of α,ω-bis(2-hydroxy-5-methoxyphenyl)-α,ω-alkanedione (**3**), which contained a small amount of α,ω-bis(2,5-dimethoxyphenyl)-α,ω-alkanedione. This crude product was treated with BBr_3 in dichloromethane in the usual manner to give a yellow solid of α,ω-bis(2,5-dihydroxyphenyl)-α,ω-alkanedione (**4**), which was recrystallized from ethanol.

1,5-Bis(2,5-dihydroxyphenyl)-1,5-pentanedione (4a). Yield 80%. Mp 211—213 °C. Found: C, 64.31; H, 5.10%. Calcd for $C_{17}H_{16}O_6$: C, 64.55; H, 5.10%.

1,5-Bis(2,5-dihydroxy-4-methylphenyl)-1,5-pentanedione (4b). Yield 80%. Mp 202—203 °C. Found: C, 66.49; H, 5.90%. Calcd for $C_{19}H_{20}O_6$: C, 66.27 H, 5.85%.

1,6-Bis(2,5-dihydroxyphenyl)-1,6-hexanedione (4c). Yield 85%. Mp 236—238 °C. Found: C, 65.25; H, 5.55%. Calcd for $C_{18}H_{18}O_6$: C, 65.44; H, 5.49%.

1,6-Bis(2,5-dihydroxy-4-methylphenyl)-1,6-hexanedione (4d). Yield 85%. Mp 137—139 °C (recrystallized from EtOH–THF (1:1)). Found: C, 67.08; H, 6.19%. Calcd for $C_{20}H_{22}O_6$: C, 67.02; H, 6.19%.

The ^{1}H NMR and IR data of **4** are presented for **4d**; δ (acetone-d_6)=1.81 (4H, m, $(-COCH_2\underline{CH_2})_2$, 2.23 (6H, broad s, 2ArMe), 3.05 (4H, m, $(-COC\underline{H_2}CH_2)_2$), 6.72 (2H, broad s, 2ArH), 7.31 (2H, s, 2ArH), 7.97 (2H, s, 2OH), 11.85 (2H, s, 2 chelated OH); ν (KBr) 3480 (broad and strong), 3080, 2980, 2920, 2880, 1660, 1610, 1600 cm^{-1}.

2,2'-(1,5-Dioxo-1,5-pentanediyl)bis(1,4-benzoquinone) (5a) and 2,2'-(1,5-Dioxo-1,5-pentanediyl)bis(5-methyl-1,4-benzoquinone) (5b). A solution of DDQ (4 mmol) in dry acetone (5 cm^3) was added to a solution of **4a** or **4b** (2 mmol) in dry acetone (30 cm^3) under a dry atmosphere. After about 0.5 h the solvent was evaporated under 10^{-4} mmHg (1 mmHg=133.322 Pa). The solid residue was extracted with hot benzene. The crystals which deposited on cooling were recrystallized from benzene.

5a: Mp 108—110 °C, Yield 80%. Found: C, 65.28; H, 3.81%. Calcd for $C_{17}H_{12}O_6$: C, 65.38; H, 3.87%. ^{1}H NMR ($CDCl_3$): δ=2.04 (2H, quintet, *J*=7.0 Hz, $(-COCH_2)_2C\underline{H_2}$), 2.96 (4H, t, *J*=7.0 Hz, $(-COC\underline{H_2})_2CH_2$), 6.8—7.0 (6H, m, ArH). IR (KBr): ν 3060, 2960, 2920, 2880, 1700, 1660, 1610 cm^{-1}. UV (MeCN): λ_{max} (ε) 246 (3.64×10^4), 300 (980) (sh), 450 (73) nm.

5b: Mp 148—150 °C, Yield 80%. Found: C, 66.92; H, 4.74%. Calcd for $C_{19}H_{16}O_6$: C, 67.05; H, 4.75%. ^{1}H NMR ($CDCl_3$): δ= 1.98 (2H, quint, *J*=7.0 Hz, $(-COCH_2)_2C\underline{H_2}$), 2.07 (6H, t, *J*= 1.0 Hz, 2ArMe), 2.93 (4H, t, *J*=7.0 Hz, $(-COC\underline{H_2})_2CH_2$), 6.57 (2H, q, *J*=1.0 Hz, 2ArH), 6.88 (2H, s, 2ArH). IR (KBr): ν 3060, 2980, 2910, 2890, 1710, 1660, 1605 cm^{-1}. UV (MeCN): λ_{max} (ε) 250 (3.50×10^4), 314 (1.30×10^3) (sh), 450 (100) nm.

2,2'-(1,6-Dioxo-1,6-hexanediyl)bis(1,4-benzoquinone) (5c) and 2,2'-(1,6-Dioxo-1,6-hexanediyl)bis(5-methyl-1,4-benzoquinone) (5d). A solution of **4c** or **4d** and DDQ was prepared as above. On standing for about 0.5 h a yellow solid crystallized out; this was recrystallized from dry acetone, with care taken to avoid contact with moisture.

5c: Mp 146—151 °C, Yield 70%. Found: C, 66.34; H, 4.36%.

Calcd for $C_{18}H_{14}O_6$: C, 66.25; H, 4.32%. ^{1}H NMR ($CDCl_3$): δ=1.71 (4H, m, (-$COCH_2\underline{CH_2}$-)$_2$), 2.90 (4H, m, (-$COCH_2$-$\underline{CH_2}$-)$_2$), 6.8—6.9 (6H, m, ArH). IR (KBr): ν 3060, 2960, 2920, 2880, 1700, 1650, 1610 cm^{-1}. UV (MeCN): 246 (3.29×10^4), 300 (960) (sh), 445 (67) nm.

5d: Mp 145—149 °C, Yield 75%. Found: C, 67.75; H, 5.05%. Calcd for $C_{20}H_{18}O_6$: C, 67.79; H, 5.12%. ^{1}H NMR ($CDCl_3$): δ=1.62 (4H, m, (-$COCH_2\underline{CH_2}$-)$_2$, 2.08 (6H, d, J=1.5 Hz, 2ArMe), 2.90 (4H, m, (-$COCH_2\underline{CH_2}$-)$_2$), 6.61 (2H, q, J=1.5 Hz, 2ArH), 6.93 (2H, s, 2ArH). IR (KBr): ν 3050, 2960, 2910, 2880, 1710, 1660, 1610 cm^{-1}. UV (MeCN): λ_{max} (ε) 250 (3.55×10^4), 315 (1.24×10^3) (sh), 435 (75) nm.

Photolysis of 5. A Pyrex glass tube containing a dry acetonitrile solution of **5** (0.05 or 0.002 mol dm^{-3}) was sealed after having been degassed by the thaw-freeze-pump method and irradiated by a 300 W high pressure mercury-arc lamp for 5 h (the yield of **7B** was not increased by prolonged irradiation). Because **7B** was decomposed by silica gel, its isolation and purification could not be performed by column chromatography, but were effected as described in the following to give **7B** in the yield of 25—30%. The yields did not seem to vary much with **5** but did depend on the isolation, because it was decomposed with a trace amount of water contained in solution and sometimes even with moisture in the isolation procedure. No other products except tar were found. Remaining **5** could not be recovered (it was also decomposed by silica gel and water).

The concentrated residue of the irradiated solution of **5a** was washed with ethyl acetate and dissolved in hot dry acetone. Yellow crystals of **7Ba** were obtained by allowing the solution to stand after addition of petroleum ether.

The concentrated residue of the irradiated solution of **5c** was repeatedly extracted with hot benzene. The concentrated residue of the combined extract was recrystallized from dry acetone to give yellow needles of **7Bc**, which contained acetone as crystal-solvent. These were dried at about 60 °C under 10^{-4} mmHg.

The concentrated residue of the irradiated solutions of **5b** and **5d** were repeatedly extracted with hot benzene. The concentrated residues of the extract were dissolved in a small amount of hot benzene. Yellow crystals of **7Bb** and **7Bd** were obtained by allowing the solutions to stand after an addition of petroleum ether. The crystals of **7Bd** containing benzene as crystal-solvent were dried at about 60 °C under 10^{-4} mmHg.

*(4a*RS,*7a*SR,*12b*SR*)-9,12-Dihydroxy-6,7-dihydro-1,4,5,8(7a*H,*12b*H*)-cyclopenta*[k]*phenanthrenetetrone (7Ba).* Decomposed at *ca.* 207 °C. Found: C, 65.29; H, 3.84%. Calcd for $C_{17}H_{12}O_6$: C, 65.38; H, 3.87%. IR (KBr): ν 3400, 3060, 2980, 2910, 2880, 1755, 1720, 1685, 1660, 1620, 1600 cm^{-1}. UV (MeCN): λ_{max} (ε) <220, 260 (7.00×10^3) (sh), 373 (5.05×10^3) nm.

*(4a*RS,*7a*SR,*12b*SR*)-9,12-Dihydroxy-2,11-dimethyl-6,7-dihydro-1,4,5,8,(7a*H,*12b*H*)-cyclopenta*[k]*phenanthrenetetrone (7Bb).* Mp 212—217 °C. Found: C, 66.81; H, 4.69%. Calcd for $C_{19}H_{16}O_6$: C, 67.05; H, 4.75%. IR (KBr): ν 3410, 3080, 3000, 2970, 2930, 2840, 1745, 1710, 1670, 1640, 1580 cm^{-1}. UV (MeCN): λ_{max} (ε) 234 (2.07×10^4), 268 (7.07×10^3) (sh), 361 (4.97×10^3) nm.

*(4a*RS,*8a*SR,*13b*SR*)-10,13-Dihydroxy-6,7,8,8a-tetrahydro-1,4,5,9-(13b*H*)-benz*[e]*anthracenetetrone (7Bc).* Mp 189—192 °C. Found: C, 66.43; H, 4.23%. Calcd for $C_{18}H_{14}O_6$: C, 66.25; H, 4.32%. IR (KBr): ν 3420, 3080, 2970, 2880, 2860, 1735, 1705, 1680, 1650, 1620, 1600 cm^{-1}. UV (MeCN): λ_{max} (ε) <220, 257 (5.49×10^3) (sh), 371 (4.88×10^3) nm.

*(4a*RS,*8a*SR,*13b*SR*)-10,13-Dihydroxy-2,12-dimethyl-6,7,8,8a-tetrahydro-1,4,5,9(13b*H*)-benz*[e]*anthracenetetrone (7Bd).* Mp 214—216 °C. Found: C, 67.95; H, 5.18%. Calcd for $C_{20}H_{18}O_6$: C, 67.79; H, 5.12%. IR (KBr): ν 3450, 3040, 2980, 2950, 2920, 2860, 2850, 1720, 1670, 1640, 1610, 1580 cm^{-1}. UV (MeCN): λ_{max} (ε) 236 (1.97×10^4), 255 (7.12×10^3) (sh), 363 (5.46×10^3) nm.

Isobutyryl-1,4-benzoquinone (11). A mixture of *p*-dimethoxybenzene (5 g), isobutyric acid (5 g), and polyphosphoric acid (70 g) was stirred for 5 h at 60 °C. The reaction mixture was diluted with excess water and extracted with diethyl ether. The concentrated residue of the washed and dried extract was distilled under reduced pressure to give 2′, 5′-dimethoxyisobutyrophenone in the yield of 55%. Bp 120—121 °C/2 mmHg. Found: C, 69.08; H, 7.61%. Calcd for $C_{12}H_{16}O_3$: C, 69.21; H, 7.74%. ^{1}H NMR ($CDCl_3$): δ=1.10 (6H, d, J=6.7 Hz, CH$\underline{Me}_2$), 3.40 (1H, hept, J=6.7 Hz, C$\underline{H}$Me$_2$), 3.67 (3H, s, OMe), 3.72 (3H, s, OMe), 6.7—6.9 (3H, m, ArH).

The treatment of 2′,5′-dimethoxyisobutyrophenone with BBr_3 in the usual manner gave a yellow liquid of isobutyryl hydroquinone in the yield of 80%. Bp 137—138 °C/2 mmHg. Found: C, 66.81; H, 6.84%. Calcd for $C_{10}H_{12}O_3$: C, 66.65; H, 6.71%. ^{1}H NMR (acetone-d_6): δ=1.15 (6H, d, J=6.5 Hz, CH$\underline{Me}_2$), 3.37 (1H, hept, J=6.5 Hz, C$\underline{H}$Me$_2$), 6.7—7.1 (3H, m, ArH), 8.90 (1H, s, OH), 11.85 (1H, s, chelate OH). A solution of isobutyrylhydroquinone in benzene was stirred with an excess of Ag_2O and $MgSO_4$ for 0.5 h.[10] The concentrated residue of the filtered solution was sublimed *in vacuo* to give a yellow solid of isobutyryl-1,4-benzoquinone (**11**) in the yield of 70%. Mp 27—28 °C. Found: C, 67.21; H, 5.72%. Calcd for $C_{10}H_{10}O_3$: C, 67.40; H, 5.66%. ^{1}H NMR ($CDCl_3$): δ=1.10 (6H, d, J=6.8 Hz, CH$\underline{Me}_2$), 3.11 (1H, hept, J=6.8 Hz, C$\underline{H}$Me$_2$), 6.67 (3H, s, ArH). IR (KBr): ν 3060, 3000, 2960, 2920, 2880, 1700, 1670, 1600 cm^{-1}. UV (MeCN): λ_{max} (ε) 246 (1.90×10^4), 300 (461) (sh), 450 (30) nm.

Photolysis of 11. A solution of **11** in actonitrile (0.1 mol dm^{-3}) was irradiated in degassed condition by a 300 W high pressure mercury-arc lamp for 10 h. The concentrated residue of the solution was submitted to column chromatography on silica gel with an eluent of petroleum ether–diethyl ether (2 : 1) to give 2,2-dimethyl-5-hydroxy-3(2*H*)-benzofuranone (**14**) in the yield of 20%. No other products except tar were found and no unreacted **11** was recovered. **14**: Mp 158—159 °C (recrystallized from benzene). Found: C, 67.24; H, 5.72%. Calcd for $C_{10}H_{10}O_3$: C, 67.40; H, 5.66%. ^{1}H NMR ($CDCl_3$): δ=1.45 (6H, s, 2Me), 6.20 (1H, s, OH), 6.9—7.3 (3H, m, ArH). IR (KBr): ν 3280 (broad and strong), 3020, 2980, 2920, 1710, 1630 cm^{-1}. UV (EtOH): λ_{max} (ε) 253 (7.67×10^3), 370 (4.48×10^3) nm.

X-Ray Structural Analysis. The compound of **7Bd** was crystallized from toluene to give crystals containing solvent molecules. A single crystal of an approximate size, $0.1\times0.5\times0.8$ mm, was used for the intensity measurement. The crystal data were: monoclinic, $P2_1/a$, a=17.537(1), b=10.358(1), c=10.588(1) Å, β=91.942(7)°, V=1922.2(2) Å^3, Z=4, D_m=1.378 g cm^{-3} (by floatation method with petroleum ether–carbon tetrachloride solution), D_c=1.382 as $C_{20}H_{18}O_6\cdot1/2(C_6H_5CH_3)$. The unit-cell dimensions were obtained by means of the least-squares technique with the values of 35 reflections. The intensities of 2543 independent reflections were collected in the range of $\sin\theta/\lambda\leqq0.65$ by a θ—2θ scan mode (2°/min) on a Rigaku four-circle diffractometer with Ni-filtered Mo $K\alpha$ radiation. The crystal structure was solved by MULTAN. Refinement was effected by the constraint full matrix least-squares method[11] because of the disorder of solvent molecule. The difference Fourier synthesis after the anisotropic refinement of the nonhydrogen atoms revealed all the hydrogen atoms except the methyl and hydroxyl hydrogen atoms. The final refinement, including the contribution of hydrogen atoms, reduced the R factor to 0.088 without $|F_{obsd}|$=0. The final atomic parameters[12] are given in Table 2. The bond distances and bond angles are shown in Figs. 2 and 3 respectively.

We wish to thank Dr. Yoshitaka Itatani, Faculty of Pharmacutical Sciences, Kanazawa University, for the NMR measurements and for his valuable discussion. The calculations of the X-ray structural analysis were done on an ACOS 700S computer at the Crystallographic Research Center, Institute for Protein Research, Osaka University.

References

1) Y. Miyagi, K. Maruyama, H. Ishii, S. Mizuno, M. Kakudo, N. Tanaka, Y. Matsuura, and S. Harada, *Bull. Chem. Soc. Jpn.*, **52**, 3019 (1879).

2) A enantiomer, **2**, is shown for the convenience of drawing the corresponding intermediate, **10**.

3) The UV spectra of **5** were similar to that of 1,4-benzoquinone (see Experimental section).

4) When benzene was used as solvent, **7B** was obtained in a similar yield as in acetonitrile.

5) The increased yield of **7Bc** in a reaction using a lower initial concentrationof **5c** suggests that polymeric compounds may be formed by intermolecular reactions between **5c**.

6) A enantiomer of each pair is shown.

7) A broad singlet. See footnote e in Table 1.

8) See footnotes d and f in Table 1. This fact is indicative of a W-letter arrangement of H_B and $H_{C'}$.

9) No direct evidences for the intervention of the dienols, **6** and **9**, could be obtained by following the reactions with ^1H NMR and IR spectroscopic methods. In frozen 2-MeTHF, **1** showed a complexed fluorescence spectrum, which could not be straightfowardly interpreted because **2** showed a complexed one. **5** showed no fluorescent bands in frozen 2-MeTHF.

10) **3** was prepared by following the method described for the synthesis of 1,16-bis(2,5-dimethoxyphenyl)-1,16-hexadecanedione; K. Yoshihira, S. Sasaki, H. Ogawa, S. Natori, *Chem. Pharm. Bull.*, **16**, 2383 (1968).

11) W. R. Busing, K. O. Martin, and H. A. Levy, "ORXFLS4: Crystallographic Structure-factor Least-squares Program," Oak Ridge National Laboratory, Tenessee (1978).

12) Table of the anisotropic thermal factors of non-hydrogen atoms are kept at the Chemical Society of Japan. Document No. 8411.

Conformational Studies of Neopentyl- and Trimethylsilylmethyl-substituted Germyl Radicals by Electron Spin Resonance

Kunio MOCHIDA

Department of Chemistry, Faculty of Sciences, Gakushuin University, 1-5-1 Mejiro, Toshima-ku, Tokyo 171

(Received August 30, 1983)

Conformational analyses of a series of neopentyl- and trimethylsilylmethyl-substituted germyl radicals by electron spin resonance (ESR) were investigated on the basis of the modified $\cos^2\theta$ rule. Dimethylneopentylgermyl radical has the conformations with the neopentyl group rotating freely. On the other hand, dimethyl(trimethylsilylmethyl)germyl radical has the preferred conformations with trimethylsilylmethyl group eclipsing with the singly occupied orbital on a germanium atom. The ESR spectra of dineopentylmethylgermyl and bis(trimethylsilylmethyl)methylgermyl radicals showed the existence of two kinds of methylene protons due to the nonplanar geometries and the slow inversion of these germyl radicals. Conformations of trineopentylgermyl and tris(trimethylsilylmethyl)germyl radicals are also discussed.

In connection with stabilization of the radicals and stereoselectivity in homolytic reactions, the structures and conformations of alkyl radicals have been widely studied by ESR.[1] Substituents located in the β position of group 4B-centered radicals also stabilize the radicals and exert stereochemical effects in group 4B-centered radical reactions.[2] However, there are few reports on the structures and conformations of β-substituted 4B-centered radicals by ESR.[3-6]

We have previously reported on the ESR spectra of benzyl-substituted germyl radicals.[5,6] Benzyl-substituted germyl radicals have nonplanar configurations and the preferred conformations of these germyl radicals are those with the phenyl ring of the benzyl group eclipsing the singly occupied orbital on a germanium atom on the basis of the values of the hyperfine splitting constants (hfsc) of the benzylic protons and the marked temperature dependence. Such preferred conformations of benzyl-substituted germyl radicals are due to the interaction between a singly occupied orbital on a germanium atom and the phenyl π orbitals.

In this paper, the ESR spectra of neopentyl- and trimethylsilylmethyl-substituted germyl radicals are reported. Neopentyl and trimethylsilylmethyl groups are more hindered sterically and interacted less electronically with a singly occupied orbital on a germanium atom than a benzyl group. Therefore, the conformations of neopentyl- and trimethylsilylmethyl-substituted germyl radicals are expected to be different from those of benzyl-substituted germyl radicals.

Results and Discussion

Neopentyl- and trimethylsilylmethyl-substituted germyl radicals were generated by abstraction of hydrogen from the corresponding hydrogermanes using photochemically generated *t*-butoxyl radicals.[7,8]

$$(CH_3)_3CO\text{-}OC(CH_3)_3 \xrightarrow{h\nu} 2(CH_3)_3CO\cdot \quad (1)$$

$$R_nMe_{3-n}GeH + (CH_3)_3CO\cdot \longrightarrow R_nMe_{3-n}Ge\cdot + (CH_3)_3COH \quad (2)$$

$$R = CH_2C(CH_3)_3,\ CH_2Si(CH_3)_3$$

$$n = 1-3$$

The *g* factors and hfsc's of a series of neopentyl- and trimethylsilylmethyl-substituted germyl radicals at various temperatures are summarized in Table 1.

ESR Spectra of Neopentyl-substituted Germyl Radicals. Figure 1 shows the ESR spectrum of dimethylneopentylgermyl radical at −100°C. It consists of a nonet arising from the circumstance that the magnitude of the coupling constant of the methyl protons is the same as that of the methylene protons. The line intensities of this germyl radical are satisfactorily reproduced by computer simulation. The outermost lines of the

TABLE 1 THE *g* FACTORS AND HYPERFINE SPLITTING CONSTANTS OF NEOPENTHYL- AND TRIMETHYSIL YLMETHYL-SUBSTITUTED GERMYL RADICALS

Radicals	Temp/°C	*g* factors	Hfsc/G		
			$a(CH_3)$	$a(CH_2)$	Others
$Me_2\dot{G}eCH_2Bu^t$	−70	2.0107	5.45	5.45	
	−135		5.46	5.46	
$Me\dot{G}e(CH_2Bu^t)_2$	20		5.49	6.65, 3.58	
	−60	2.0106	5.54	6.68, 3.67	
	−120		5.49	6.51, 3.83	
$\dot{G}e(CH_2Bu^t)_3$	50	2.0107		4.96	
	−120			5.14	
$Me_2\dot{G}eCH_2SiMe_3$	−60	2.0100	5.35	4.18	
	−140		5.38	3.27	
$Me\dot{G}e(CH_2SiMe_3)_2$	10		5.34	6.11, 3.95	
	−60	2.0098	5.35	5.98, 3.63	
$\dot{G}e(CH_2SiMe_3)_3$	40			5.07	$a(^{29}Si)$=5.0
	−90	2.0094		5.07	

nonet are lost in the noise. The spectrum of dimethylneopentylgermyl radical was measured over a temperature range between −70 and −135°C. As shown in Table 1, the methylene and methyl protons hfsc's are equivalent and there is no temperature dependence with experimental error over the investigated temperature range.

Figure 2 shows the ESR spectrum of dineopentylmethylgermyl radical at −60°C. It consists of a quartet due to 3 methyl protons further split into two sets of triplets (6.68 and 3.67 G, 1 G=10^{-4} T), indicative of the existence of two kinds of methylene protons. The hfsc's of the two sets of triplets showed small temperature dependence, while the methyl proton hfsc was almost constant. The experimental spectra of dineopentylmethylgermyl radical were reproduced by computer simulation with the listed hfsc's.

Figure 3 shows the ESR spectrum of trineopentylgermyl radical at −60°C which consists of a septet due to 6 equiv methylene protons. The methylene protons hfsc's showed small negative temperature dependence.

ESR Spectra of Trimethylsilylmethyl-substituted Germyl Radicals. Figure 4 shows the ESR spectrum of dimethyl(trimethylsilylmethyl)germyl radical at −120°C which consists of a septet due to 6 methyl protons split further into a triplet due to 2 methylene protons. As shown in Table 1, the methylene proton hfsc's were temperature dependent while the methyl proton hfsc's were almost constant over the investigated temperature range. The methylene proton hfsc's decreased without selective line broadening as the temperature was lowered.

Figure 5 shows the ESR spectrum of bis(trimethylsilylmethyl)methylgermyl radical at −40°C which consists of a quartet due to 3 methyl protons further split into two sets of triplets (5.98 and 3.63 G), indicative of the existence of two kinds of methylene protons. The hfsc's of two sets of triplets showed small temperature dependence, while the methyl proton hfsc was almost constant. The experimental spectra of this germyl rad-

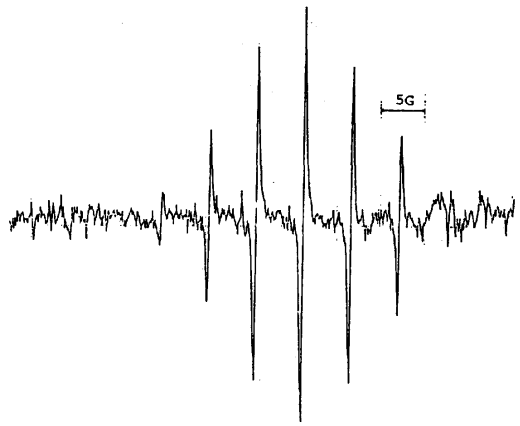

Fig. 1. ESR spectrum of dimethylneopentylgermyl radical at −100°C.

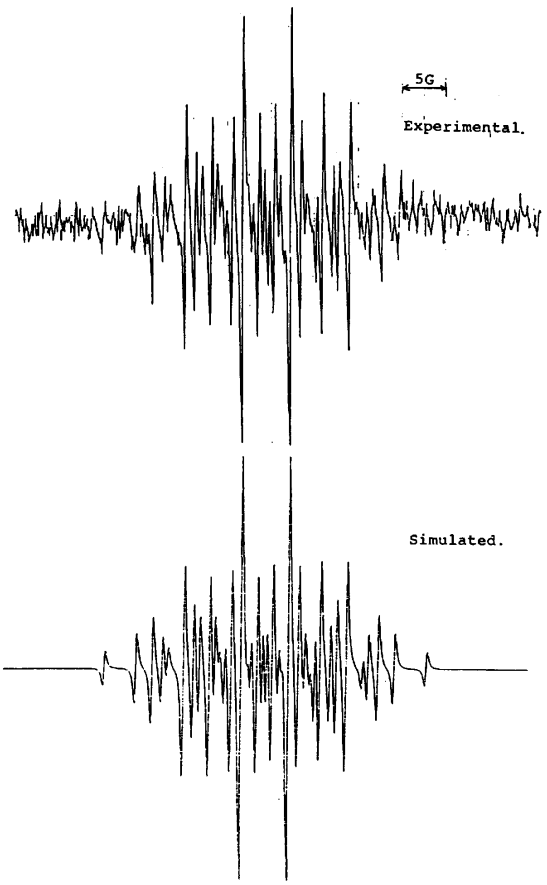

Fig. 2. ESR spectrum of dineopentylmethylgermyl radical at −60°C.

Fig. 3. ESR spectrum of trineopentylgermyl radical at −60°C.

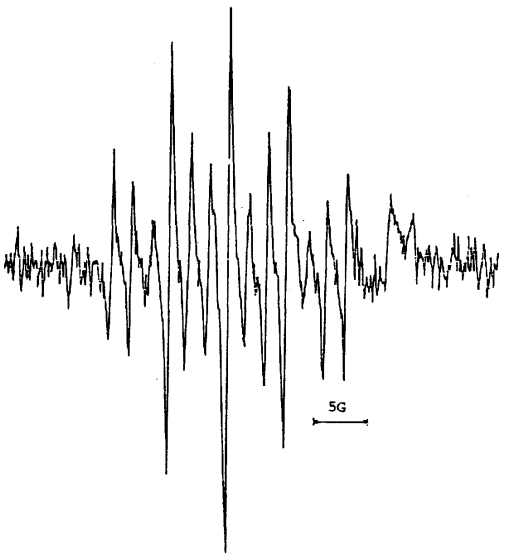

Fig. 4. ESR spectrum of dimethyl(trimethylsilylmethyl)germyl radical at −120°C.

ical were well reproduced by computer simulation with the listed hfsc's.

Figure 6 shows the ESR spectrum of tris(trimethylsilylmethyl)germyl radical at −60 °C which consists of a septet due to 6 equiv methylene protons. The ^{29}Si species (^{29}Si natural abundance=4.7%) attributed to the principal radical was observed as shown in Fig. 6. The methylene proton hfsc's showed no temperature dependence.

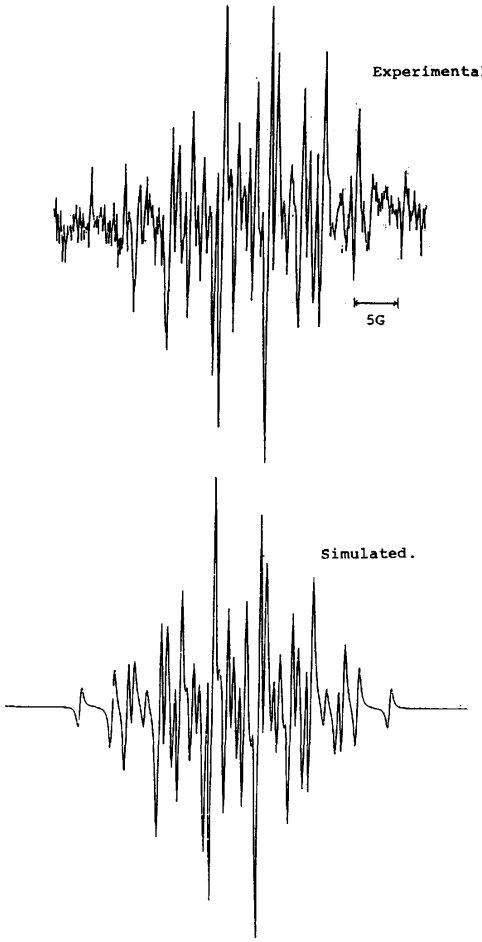

Fig. 5. ESR spectrum of bis(trimethylsilylmethyl)-methylgermyl radical at −40 °C.

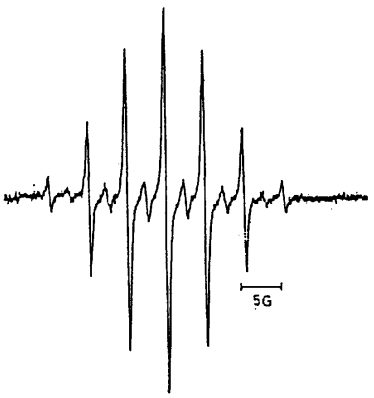

Fig. 6. ESR spectrum of tris(trimethylsilylmethyl)-germyl radical at −60 °C.

Conformations of Neopentyl- and Trimethylsilylmethyl-substituted Germyl Radicals. Organogermyl radicals are inferred to have nonplanar configurations on the basis of the ESR parameters,[9] the IR data,[10] and the stereochemistry of a chlorine-abstraction from carbon tetrachloride with a chiral germyl radical.[11] Therefore, it is reasonable to discuss the conformations of neopentyl- and trimethylsilylmethyl-substituted germyl radicals by the modified $\cos^2\theta$ rule by Eqs. 3 and 4, where θ is the dihedral angle between the β carbon–hydrogen bond and the p orbital at the radical center.[6b,12]

$$a(\beta\text{-H}) = B\cos^2\theta \quad (0°<\theta<90°) \tag{3}$$

$$a(\beta\text{-H}) = B'\cos^2\theta \quad (90°<\theta<180°) \tag{4}$$

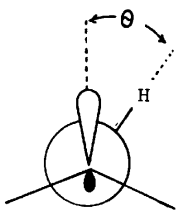

Constants B and B', depend on whether or not the β-proton is placed on the same side of the larger lobe of the singly occupied orbital. Since freely rotating methyl protons ($<\cos^2\theta>=1/2$) showed hfsc's around 5.4 G for organogermyl radicals studied here, $(B+B')/2$ may be estimated roughly as 10.8 G. Constants B and B' may depend highly on the extent of the pyramidality of the radical center. Constants B and B' are taken roughly as 5 and 15 G, respectively, when the pyramidality of the germyl radicals may be supposed to be similar to that of 1,1-difluoroalkyl radicals where B/B' is estimated to be *ca.* 0.31 by INDO calculation.[12a]

Conformations of Dimethylneopentylgermyl and Dimethyl(trimethylsilylmethyl)germyl Radicals. Equilibrium conformations, **1**—**12**, for the methylene protons in the germyl radicals and the corresponding phases for angular dependence are illustrated as Fig. 7. Values of the methylene protons hfsc's are calculated in Table 2.

Taking into consideration that the freely rotating methylene proton hfsc's for equilibrium conformations as shown in Fig. 7 are estimated as around 5.4 G, for radicals with conformations, **1**, **6**, **7**, or **8** (R^1=R^2=Me), the methylene proton hfsc is expected to decrease as the temperature is lowered. On the other hand, for radicals with conformations, **3**, **4**, **10**, or **11** (R^1=R^2=Me), the methylene proton hfsc is expected to increase as the temperature is lowered.

The temperature dependences of the methylene proton hfsc's of dimethylneopentylgermyl and dimethyl(trimethylsilylmethyl)germyl radicals are shown graphically in Fig. 8. It is seen that the magnitude of

Table 2. Values of the methylene protons Hfsc's for conformations, **1**—**12**

	1	**2**	**3**	**4**	**5**	**6**	**7**	**8**	**9**	**10**	**11**	**12**
$a(\beta\text{-H}^1)$	3.75	11.25	15	11.25	3.75	0	1.25	3.75	5	3.75	1.25	0
$a(\beta\text{-H}^2)$	3.75	0	1.25	3.75	5	3.75	1.25	0	3.75	11.25	15	11.25

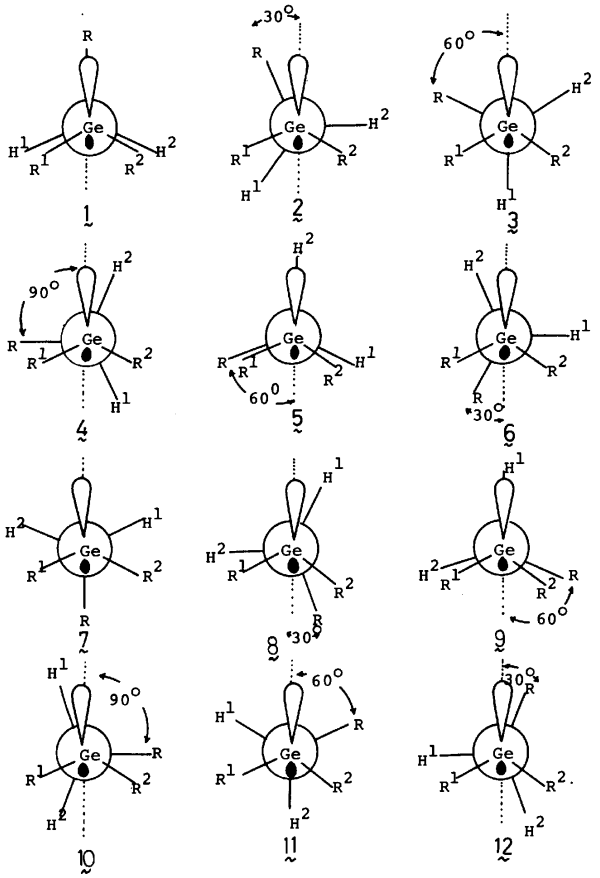

Fig. 7. Equilibrium conformations for the methylene protons in the germyl radicals and the corresponding phases for angular dependence.

the methylene proton hfsc's of dimethylneopentylgermyl radical is almost the same as that of the methyl proton hfsc's and the methylene proton hfsc's showed no temperature dependence with experimental errors. Therefore, the dimethylneopentylgermyl radical has the conformation with the neopentyl group rotating freely in the investigated temperature range.

On the other hand, the methylene protons hfsc's of dimethyl(trimethylsilylmethyl)germyl radical decreased as the temperature was lowered. Therefore, this germyl radical has the preferred conformations, **1**, **6**, **7**, or **8**; the trimethylsilylmethyl group eclipsing or nearly so with the singly occupied orbital on a germanium atom. For favoring such conformations, the odd electron is delocalized onto the carbon-silicon bond hyperconjugatively as well as onto d orbitals of the silicon atom (*p—d*) homoconjugatively.[13]

Conformations of Dineopentylmethylgermyl and Bis(trimethylsilylmethyl)methylgermyl Radicals. The ESR spectra of dineopentylmethylgermyl and bis(trimethylsilylmethyl)methylgermyl radicals showed the existence of two kinds of the methylene proton hfsc's without significant temperature dependence.

Recently, the activation barrier for inversion of a pyramidal germyl radical is estimated to be about 7.0 kcal mol^{-1} (1cal=4.184 J).[14] On the other hand, the barrier for rotation about the Ge-C bond is smaller than that about the C-C bond due to the longer Ge-C bond length (2.00 Å) compared to the C-C bond length

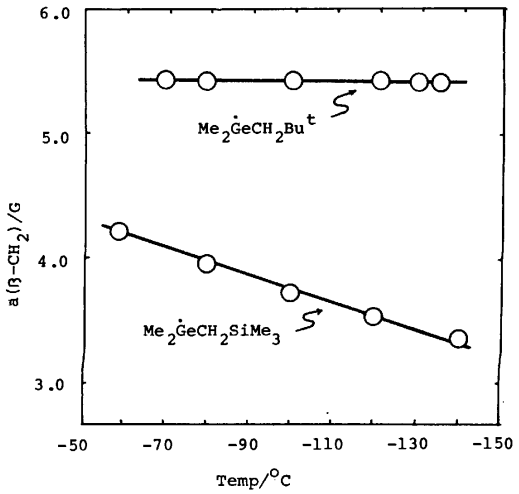

Fig. 8. Temperature dependence of a(β-CH_2) of $Me_2\dot{G}eCH_2Bu^t$ and $Me_2\dot{G}eCH_2SiMe_3$.

(1.54 Å). Therefore, the existence of two kinds of methylene proton hfsc's of dineopentylmethylgermyl and bis(trimethylsilylmethyl)methylgermyl radicals can be explained reasonably by assuming that the configurations of these germyl radicals are fixed to nonplanar geometry and the inversion rates of these germyl radicals are much smaller than those of rotation of substituents about the Ge-C bond.

Typical equilibrium conformations of dineopentylmethylgermyl and bis(trimethylsilylmethyl)methylgermyl radicals are shown in Fig. 7 (R^1=Me, R^2=CH_2R, R=Bu^t or $SiMe_3$). Conformations, **8**, **9**, **10**, and **11** may be eliminated due to steric repulsion between R-substituted methyl groups (R=Bu^t or $SiMe_3$) on a Ge atom and R groups on $a\beta$-C atom. The potential energies in the various conformations as shown in Fig. 7 are not taken into consideration. However, $a(\beta$-$H^1)$ and $a(\beta$-$H^2)$ in conformations, **1**—**12** except for **8**, **9**, **10**, and **11**, average roughly 5.8 and 3.3 G, respectively, with listed hfsc's in Table 2. These values reproduce experimental data of two kinds of methylene proton hfsc's of dineopentylmethylgermyl and bis(trimethylsilylmethyl)methylgermyl radicals.

Conformations of Trineopentylgermyl and Tris(trimethylsilylmethyl)germyl Radicals. Taking into consideration the steric hindrance of *t*-butyl or trimethylsilyl groups, the conformation **1**, **2**, or **12** as shown in Fig. 7 (R^1, R^2=CH_2R, R=Bu^t or $SiMe_3$) may be selected as a candidate for the preferred conformation of trineopentylgermyl or tris(trimethylsilylmethyl)germyl radical. For example, the conformation **1** for these germyl radicals are shown in the following to minimize the steric repulsion of the substituents.

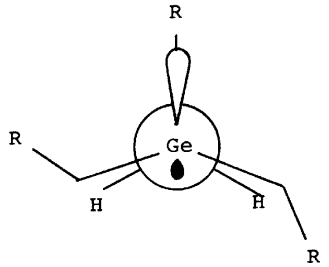

Fast rotational interconversion among three individual conformations, **1**, **2**, and **12** as shown in Fig. 7 (R^1, R^2=CH_2R, R=Bu^t or $SiMe_3$), of equal probability 1/3 will make the 6 methylene protons epuivalent. Such a correlated interconversion for tris(trimethylsilylmethyl)aminium ion radical has been reported.[15]

Experimental

ESR Measurements. The Varian X band spectrometer, light sources, and sample tubes are as described previously.[16]

The field sweep of the spectrometer was calibrated with an aqueous solution of Fremy's salt (a_N=13.07 G). The *g* factors were determined by reference to that of the anthracene cation radical (*g*=2.002565) with a dual cavity.

All samples were throughly degassed using a freeze-pump-thaw cycle.

Materials. Di-*t*-butyl peroxide (DTBP) was distilled prior to use. Dimethyldichlorogermane, bp 121—122 °C,[17] dimethylphenylchlorogermane, bp 113 °C/17 mmHg (1 mmHg≈133.322 Pa),[18] methylphenyldibromogermane, bp 139—140 °C/15 mmHg,[19] and (chloromethyl)trimethylsilane, bp 98 °C[20] were prepared as described literatures.

Preparation of Dimethylneopentylchlorogermane. Neopentylmagnesium chloride was prepared (5.3 g, 0.22 mol) in THF (100 ml). The Grignard reagent was added to dimethyldichlorogermane (30.0 g, 0.17 mol) in ether (400 ml). After the mixture was stirred under gentle reflux for 2 h, the resulting salt was filtered off and the solvent was removed. Fractional distillation gave dimethylneopentylchlorogermane (6.5 g, 0.03 mol, 17.6%), bp 70.0—72.5 °C/16 mmHg.

Preparation of Dimethylneopentylgermane. A mixture of dimethylneopentylchlorogermane (6.5 g, 0.03 mol) and lithium aluminum hydride (1.4 g, 36.4 mmol) in ether (200 ml) was stirred with reflux for 2 h. After hydrolysis with water, the organic layer was dried over calcium chloride. The solvent was removed and then fractional distillation gave dimethylneopentylgermane (4.5 g, 25.8 mmol, 82.8%), bp 122.0—122.5 °C. n^{20} 1.4302; IR (cm^{-1}, neat) 2020 (Ge-H), 1240 (Ge-Me); NMR ($CDCl_3$) δ=0.21 (d, *J*=4.0 Hz, 6H), 0.92 (d, *J*=4.0 Hz, 2H) 0.97 (s, 9H), 3.89 (*m*, 1H). Found: C, 47.91; H, 10.46%, Calcd for $C_7H_{18}Ge$: C, 48.10; H, 10.38%.

Preparation of Dineopentylmethylphenylgermane. Neopentylmagnesium chloride was prepared from neopentyl chloride (46.0 g, 0.43 mol) and magnesium (10.5 g, 0.43 mol) in THF (300 ml). To this Grignard reagent, methylphenyldibromogermane (19.0 g, 0.06 mol) was added. The mixture was stirred with reflux for 10 h. After hydrolysis with water, the organic layer was extracted and dried over sodium sulfate. The solvent was removed and then fractional distillation gave dineopentylmethylphenylgermane (14.0 g, 0.05 mol, 84.6%), bp 92.5—93.0 °C/0.15 mmHg. NMR ($CDCl_3$) δ=0.63 (s, 3H), 0.91 (s, 18H), 1.14 (s, 4H), 7.37 (m, 5H); IR (cm^{-1}, neat) 1240 (Ge-Me).

Preparation of Dineopentylmethylchlorogermane. Iodine monochloide (7.4 g, 45.6 mmol) in dichloromethane (10 ml) was added to dineopentylmethylphenylgermane (13.5 g, 44.0 mmol) in dichloromethane (50 ml). The mixture was stirred at room temperatre for 5 h. After the solvent was removed, fractional distillation gave dineopentylmethylchlorogermane (8.1 g, 30.5 mmol, 69.3%), bp 102—103 °C/9 mmHg. NMR ($CDCl_3$) δ=0.87 (s, 3H), 1.04 (s, 18H), 1.34 (s, 4H).

Preparation of Dineopentylmethylgermane. A mixture of dineopentylmethylchlorogermane (7.3 g, 27.5 mmol) and lithium aluminum hydride (1.2 g, 30.4 mmol) in ether (200 ml) was stirred with reflux for 2 h. After hydrolysis with water, the organic layer was dried over calcium chloride. The solvent was removed and then fractional distillation gave dineopentylmethylgermane (6.0 g, 26.0 mmol, 94.5%), bp 83.0—84.0 °C/19 mmHg. n^{20}1.4420; IR (cm^{-1}, neat) 2040 (Ge-H), 1240 (Ge-Me); NMR ($CDCl_3$) δ=0.25 (d, *J*=4.0 Hz, 3H), 0.94 (d, *J*=4.0 Hz, 4H), 0.97 (s, 18H), 4.02 (m, 1H). Found: C, 56.92; H, 11.52%. Calcd for $C_{11}H_{26}Ge$: C, 57.22; H, 11.35%.

Preparation of Trineopentylgermane. Neopentylmagnesium bromide was prepared from neopentyl bromide (24.2 g, 0.16 mol) and magnesium (4.0 g, 0.16 mol) in THF (200 ml). To this Grignard reagent, tetrachlorogermane (10.0 g, 0.05 mol) in ether (50 ml) was added. The mixture was stirred with reflux for 10 h. The resulting salt was filtered off and the solvent was removed. The crude trineopentylchlorogermane was added to lithium aluminum hydride (4.0 g, 0.10 mol) in ether (200 ml) and then stirred with reflux for 5 h. After hydrolysis with water, the organic layer was dried over sodium sulfate. The solvent was removed and then fractional distillation gave trineopentylgermane, bp 140 °C/16 mmHg. IR (cm^{-1}, neat) 2040 (Ge-H); NMR ($CDCl_3$) δ=0.94 (d, *J*=4.0 Hz, 6H), 0.97 (s, 27H), 4.03 (m, 1H). For ESR measurements, the sample was purified by preparative GLC (SE30 20% 2 m).

Preparation of Dimethylphenyl(trimethylsilylmethyl)germane. (Lithiomethyl)trimethylsilane was prepared from (chloromethyl)trimethylsilane (12.3 g, 0.10 mol) and dispersed lithium (2.8 g, 0.4 mol) in ether (200 ml) at −10 °C. To this ether solution, dimethylphenylchlorogermane (8.0 g, 0.04 mol) in ether (50 ml) was added over a period of 30 min while the temperature was maintained below 10 °C. After addition was completed, the mixture was stirred with reflux for 5 h. Methanol was added to this solution and then the mixture was hydrolyzed with water. The solution was extracted with ether and the ether solution was dried over calcium chloride. Fractional distillation gave dimethylphenyl(trimethylsilylmethyl)germane (6.8 g, 25 mmol, 63.7%), bp 115 °C/15 mmHg.

Preparation of Dimethyl(trimethylsilylmethyl)germane. Iodine monochloride (3.2 g, 0.02 mol) in dichloromethane (10 ml) was added to dimethylphenyl(trimethylsilylmethyl)-germane (5.0 g, 0.02 mol) in dichloromethane (50 ml). The mixture was stirred at room temperature for 5 h. After the solvent was removed, the crude dimethyl(trimethylsilylmethyl)chlorogermane was added to lithium aluminum hydride (1.0 g, 25 mmol) in ether (100 ml). The mixture was stirred with reflux for 5 h. After hydrolysis with water, the organic layer was extracted with ether and the ether solution was dried over calcium chloride. The solvent was removed and then fractional distillation gave dimethyl(trimethylsilylmethyl)germane, bp 121 °C. n^{20} 1.4440; IR (cm^{-1}, neat) 2020 (Ge-H), 1225 (Ge-Me); NMR ($CDCl_3$) δ=−0.18 (d, *J*=4.0 Hz, 2H), 0 (s, 9H), 0.19 (d, *J*=4.0 Hz, 6H), 3.82 (m, 1H). Found: C, 37.16; H, 9.39%. Calcd for $C_6H_{18}SiGe$: C, 37.75; H, 9.51%.

Preparation of Bis(trimethylsilylmethyl)methylphenylgermane. (Lithiomethyl)trimethylsilane was prepared from (chloromethyl)trimethylsilane (12.3 g, 0.10 mol) and dispersed lithium (2.8 g, 0.40 mol) in ether (200 ml) at −10 °C. To this ether solution, methylphenyldibromogermane (6.0 g, 0.02 mol) in ether (50 ml) was added over a period of 30 min while the temperature was maintained below 10 °C. After addition was completed, the mixture was stirred with reflux for 5 h. Methanol was added to this solution and then the mixture was hydrolyzed with water. The solution was extracted with ether and the ether solution was dried over calcium chloride. Fractional distillation gave bis(trimethylsilylmethyl)methylphenylgermane, bp 105 °C/4.0 mmHg.

Preparation of Bis(trimethylsilylmethyl)methylchlorogermane. Iodine monochloride (1.6 g, 0.01 mol) in dichloromethane (20 ml) was added to bis(trimethylsilylmethyl)methylphenylgermane (30 g, 8.8 mmol) in dichloromethane (10 ml). The mixture was stirred at room temperature for 5 h. After the solvent was removed, fractional distillation gave bis(trimethylsilylmethyl)methylchlorogermane, bp 98—103 °C/12 mmHg.

Preparation of Bis(trimethylsilylmethyl)methylgermane. A mixture of bis(trimethylsilylmethyl)methylchlorogermane (2.0 g, 6.7 mmol) and lithium aluminum hydride (1.0 g, 25.0 mmol) in ether (200 ml) was stirred with reflux for 2 h. After hydrolysis with water, the organic layer was extracted with ether. The ether solution was dried over calcium chloride. The solvent was removed and then fractional distillation gave bis(trimethylsilylmethyl)methylgermane (1.2 g, 4.6 mmol, 68.7%), bp 89 °C/30 mmHg. n^{25} 1.4627; IR (cm^{-1}, neat) 2020 (Ge-H), 1250 (Ge-Me,Si-Me); NMR ($CDCl_3$) δ=—0.16 (d, J=4.0 Hz, 4H), 0 (s, 18H), 0.22 (d, J=4.0 Hz, 3H), 3.91 (m, 1H). Found: C, 41.19; H, 9.70%. Calcd for $C_9H_{26}Si_2Ge$: C, 41.09; H 9.96%.

Preparation of Tetrakis(trimethylsilylmethyl)germane. (Lithiomethyl)trimethylsilane was prepared from (chloromethyl)trimethylsilane (61.3 g, 0.5 mol) and dispersed lithium (13.9 g, 2.0 mol) in ether (300 ml) at —10 °C. To this ether solution, tetrachlorogermane (21.4 g, 0.10 mol) in ether (50 ml) was added over a period of 30 min while the temperature was maintained below 10 °C. After the addition was completed, the mixture was stirred with reflux for 10 h. Methanol was added to this solution and the mixture was hydrolyzed with water. The solution was extracted with ether and the ether solution was dried over calcium chloride. Fractional distillation gave tetrakis(trimethylsilylmethyl)germane (14.0 g, 33 mmol, 33.0%), bp 127—130 °C/5 mmHg. n^{16} 1.4725; IR (cm^{-1}, neat) 1240 (Si-Me); NMR ($CDCl_3$) δ=—0.13_5 (s, 2H), —0.04 (s, 9H). Found: C, 45.17; H, 10.03%. Calcd for $C_{16}H_{44}Si_4Ge$: C, 45.60; H, 10.52%.

Preparation of Tris(trimethylsilylmethyl)bromogermane. Tris(trimethylsilylmethyl)bromogermane was prepared by bromination of tetrakis(trimethylsilylmethyl)germane (10.0 g, 23 mmol) with an equivalent amount of bromine (4.0 g, 24 mmol) in 50 ml of refuxing 1,2-dibromoethane for 30 min. The solvent was removed under reduced pressure, leaving about 10 ml of residue. Fractional distillation gave crude tris(triethylsilylmethyl)bromogermane (7.5 g, 18 mmol, 78.7%), bp 125—126 °C/5 mmHg. NMR (CCl_4) δ=—0.02_3 (s, 2H), 0.05 (s, 9H).

Preparation of Tris(trimethylsilylmethyl)germane. A mixture of tris(trimethylsilylmethyl)bromogermane (7.5 g, 18 mmol) and lithium aluminum hydride (3.0 g, 79.2 mmol) in ether (200 ml) was stirred with reflux for 3 h. After hydrolysis with water, the organic layer was dried over calcium chloride. The solvent was removed and then fractional distillation gave tris(triethylsilylmethyl)germane (4.3 g, 13 mmol, 71.3%), bp 117—118 °C/18 mmHg. n^{16}1.4620; IR (cm^{-1}, neat) 1985 (Ge-H), 1235 (Si-Me); NMR (CCl_4) δ=—0.19 (d, J=3.8 Hz, 6H), —0.05 (s, 27H), 4.00 (sept., J=3.8 Hz, 1H). Found: C, 43.03; H, 10.09%. Calcd for $C_{12}H_{34}Si_3Ge$: C, 42.99; H, 10.22%.

The author is grateful to Professor Hideki Sakurai and Dr. Mitsuo Kira of Tohoku University for their interests, encouragements, and computer simulation of ESR spectra. I also thank Professor Tadashi Suehiro of Gakushuin University for accomodation of a Varian E-9 ESR spectrometer and Mr. Isoo Miyagawa for preparation of dimethylneopentylgermane and dineopentylmethylgermane.

References

1) For examples: P. S. Skell, "Free Radicals," ed by J. K. Kochi, Wiley-Interscience, New York, N. Y. (1973), Vol. 2, Chap. 26; L. Kaplan, "Bridged Free Radicals," Marcel Dekker, New York, N. Y. (1972); A. L. J. Beckwith and K. U. Ingold, "Rearrangement in Ground and Excited States," ed by P. de Mayo, Academic Press, New York, N. Y. (1973), Vol. 1, Essay 4.

2) H. Sakurai, "Free Radicals," ed by J. K. Kochi, Wiley-Interscience, New York, N. Y. (1973), Vol. 2, Chap. 25.

3) P. J. Krusic and J. K. Kochi, *J. Am. Chem. Soc.*, **91**, 6161 (1969).

4) H. Sakurai, M. Kira, and M. Sato, *Chem. Lett.*, **1974**, 1323.

5) K. Mochida, M. Kira, and H. Sakurai, *Chem. Lett.*, **1981**, 645.

6) a) K. Mochida, M. Kira, and H. Sakurai, 20th ESR Symposium, Osaka, October 1981, Abstr., p. 118; b) K. Mochida, I. Miyagawa, M. Kira, and H. Sakurai, 21st ESR Symposium, Tsukuba, October 1982, Abstr., p. 164.

7) P. J. Krusic and J. K. Kochi, *J. Am. Chem. Soc.*, **90**, 7155 (1968).

8) A. Hudson and H. A. Hussain, *Mol. Phys.*, **16**, 199 (1969).

9) R. L. Morehouse, J. J. Christiansen, and W. Gordy, *J. Chem. Phys.*, **45**, 1751 (1966); G. S. Jackel, J. J. Christiansen, and W. Gordy, *ibid.*, **47**, 4274 (1967); J. Roncin and R. Debuyst, *ibid.*, **51**, 577 (1969); R. V. Lloyd and Max T. Rogers, *J. Am. Chem. Soc.*, **95**, 2459 (1973); M. Geoffroy, L. Ginet, and E. A. C. Lucken, *Chem. Phys. Lett.*, **38**, 321 (1976).

10) L. Andrews and D. L. Fredrick, *J. Am. Chem. Soc.*, **92**, 775 (1970); R. J. Isabel and W. A. Guillory, *J. Chem. Phys.*, **55**, 1197 (1971); **57**, 1116 (1972); W. A. Guillory and E. C. Smith, *ibid.*, **56**, 1661 (1972); G. R. Smith and W. A. Guillory, *ibid.*, **56**, 1423 (1972).

11) H. Sakurai and K. Mochida, *Chem. Commun.*, **1971**, 1581.

12) Following papers contain material relevant to the modified $\cos^2\theta$ rule; a) K. S. Chen, D. Y. H. Tang, L. K. Montgomery, and J. K. Kochi, *J. Am. Chem. Soc.*, **96**, 2201 (1974); b) R. V. Lloyd and D. E. Wood, *ibid.*, **97**, 5986 (1975); c) T. Kawamura, M. Matsunaga, and T. Yonezawa, *ibid.*, **100**, 92 (1978).

13) T. Kawamura and J. K. Kochi, *J. Am. Chem. Soc.*, **94**, 648 (1972)..

14) H. Hayashi and K. Mochida, *Chem. Phys. Lett.*, **101**, 307 (1983); K. U. Ingold, J. Lusztyk, and J. C. Scaiano, *J. Am. Chem. Soc.*, to be published.

15) H. Bock, W. Kaim, M. Kira, H. Osawa, and H. Sakurai, *J. Organomet. Chem.*, **164**, 295 (1979).

16) H. Sakurai, K. Mochida, and M. Kira, *J. Organomet. Chem.*, **124**, 235 (1977).

17) A. E. Finholt, *Nucl. Sci. Abstr.*, **6**, 617 (1957).

18) M. Kumada, S. Sakamoto, and M. Ishikawa, *J. Organomet. Chem.*, **17**, 235 (1969).

19) A. G. Brook and G. J. D. Peddle, *J. Am. Chem. Soc.*, **85**, 1869 (1963).

20) F. C. Whitemore and L. H. Sommer, *J. Am. Chem. Soc.*, **68**, 481 (1946).

A Convenient Synthesis of 4-(2,2-Dichloroethenyl)-5,5-dimethyltetrahydro-2-furanone Derivatives, a Key Intermediate of Permethrinic Acid[1)]

Sadao Tsuboi, Eiichiro Amano, and Akira Takeda*
Department of Synthetic Chemistry, School of Engineering, Okayama University, Tsushima, Okayama 700
(Received September 5, 1983)

A key intermediate of 2-(2,2-dichloroethenyl)-3,3-dimethylcyclopropanecarboxylic acid, 3-alkoxycarbonyl-(or acyl)-4-(2,2-dichloroethenyl)-5,5-dimethyltetrahydro-2-furanone was prepared by the base-catalyzed condensation of 2-methyl-3,5,5-trichloro-4-penten-2-ol with acetate derivatives such as malonic esters, acetoacetic esters, and benzoylacetate. The reactivity of 3-acetyl-4-(2,2-dichloroethenyl)-5,5-dimethyltetrahydro-2-furanone to an excess amount of thionyl chloride in ethanol was also examined. An analog, 5-butyl-4-(2,2-dichloroethenyl)-3-ethoxycarbonyl-5-methyltetrahydro-2-furanone was also prepared in 31% yield.

A large number of synthetic methods of permethrinic acid [2-(2,2-dichloroethenyl)-3,3-dimethylcyclopropanecarboxylic acid] (**1a**, R=H), the acid moiety of the insecticide Permethrin (NRDC 143)[2b)], have been reported since the first synthesis by Farkas *et al.*[2,3)] Klemmensen *et al.*[4)] have reported a convenient synthesis of ethyl ester **1b** (R=Et) of permethrinic acid

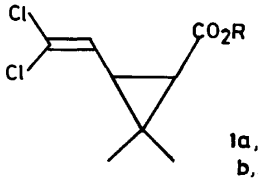

1a, R = H
b, R = Et

from 4-(2,2-dichloroethenyl)-3-methoxycarbonyl-5,5-dimethyltetrahydro-2-furanone (**3a**), which was derived from the reaction of 1,1-dichloro-3,4-epoxy-4-methyl-1-pentene (**2**)[5)] with dimethyl malonate in the presence of base. We had reported a facile synthesis of **2** by dehydrochlorination of 3,5,5-trichloro-2-methyl-4-penten-2-ol (**5**),[5)] which was readily prepared by the Grignard reaction of 5,5,5-trichloro-3-penten-2-one (**4**)[6)] with methylmagnesium iodide.

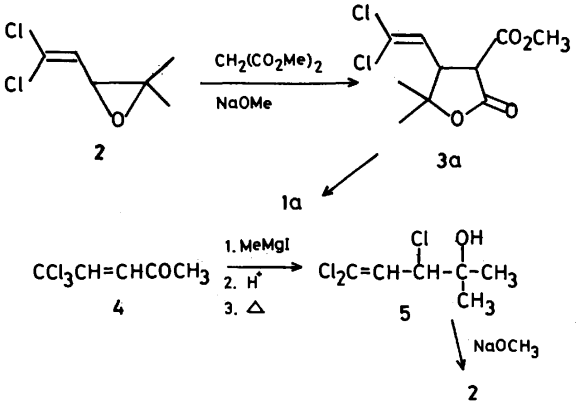

Recently we found that the chlorohydrin **5** reacts with methyl sodiomalonate to give the lactone **3a**. As an extension of the previous work[5,6)] and to establish the generality of this reaction we investigated in detail the base-catalyzed condensation of **5** with acetate derivatives such as malonic esters and acetoacetic esters. This paper will describe and discuss the results of these reactions.

Chlorohydrin **5** reacted with sodiomalonic esters at room temperature to give the lactones **3a** and **3b** in 30%

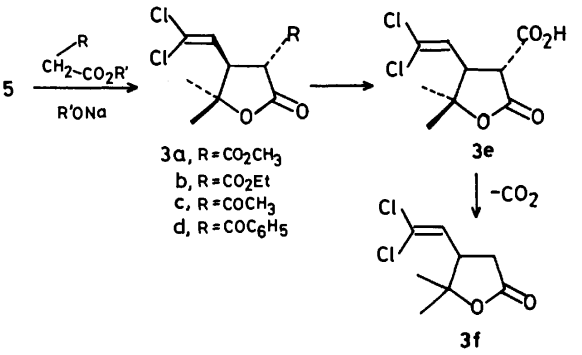

(52%)[7)] and 41% (49%)[7)] yields, respectively. Hydrolyses of **3a** and **3b** gave the corresponding lactone acid **3e**, which released carbon dioxide to yield **3f**[4)] when heated. Reaction of methyl acetoacetate with **5** in the presence of sodium methoxide gave 3-acetyl-4-(2,2-dichloroethenyl)-5,5-dimethyltetrahydro-2-furanone (**3c**) in 50% yield. However, the reaction of ethyl benzoylacetate with **5** in the presence of sodium ethoxide afforded only the poor yield (7%, 24%[7)]) of 3-benzoyl-4-(2,2-dichloroethenyl)-5,5-dimethyltetrahydro-2-furanone (**3d**) along with a mixture of unidentified products and the starting materials. The lactones **3c** and **3d** can be easily converted to **3f** by the deacylation with sodium ethoxide or aqueous sodium hydroxide.[8,9)]

Lactones **3** obtained in the present reactions were characterized by analytical and spectroscopic data, and by comparison with literature data[4)] in the case of the known lactones (**3a** and **3f**). The physical properties and analyses of lactones **3** are listed in Table 1. IR spectra of **3** showed characteristic strong peaks at around 1770 cm^{-1} due to the carbonyl groups of lactone rings. When the olefinic proton of **3a** at the ^1H NMR measurement was irradiated, the coupling constant between C_3–H and C_4–H was observed to be 12.1 Hz. This suggests that the configuration between R and dichloroethenyl group is *trans*.[10)] The best evidence that the lactones **3** have no isomers comes from the clear ^{13}C-NMR spectra which were summarized in Table 2. The signals due to lactone carbonyls exhibit upfieid-shifts of *ca.* 8 ppm from that of unsubstituted γ-butyrolactone.[11)]

Conversion of lactone **3c** to chloroester **6** was attempted by means of the procedure used for the ring opening of pyrocin (**7**).[8)] Treatment of **3c** with a ten-

TABLE 1. PHYSICAL PROPERTIES AND ANALYSES OF LACTONES **3**

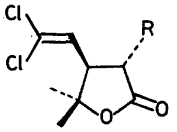

3

Compd	R	Bp θ_b/°C (Torr) [Mp θ_m/°C]	Found (Calcd) (%) C	Found (Calcd) (%) H	IR ν/cm^{-1}	^{1}H NMR δ
3b	CO_2Et		47.07 (47.00)	5.14 (5.02)	1775 1735 1620	1.32(t, 3, J=8 Hz, OCH_2CH_3), 1.32(s, 3, C_5-CH_3), 1.55(s, 3, C_5-CH_3), 3.54(d, 1, J=12 Hz, C_3-H), 3.84(dd, 1, J=10 and 12 Hz, C_4-H), 4.30(q, 2, J=8 Hz, OCH_2CH_3), 5.80(d, 1, J=10 Hz, =CH-)
3c	$COCH_3$	112(0.07)	57.27 (57.40)	4.66 (4.82)	1765 1735 1645 1625	1.31(s, 3, C_5-CH_3), 1.50(s, 3, C_5-CH_3), 3.60—3.96(m, 2, C_3-H, C_4-H), 5.70(d, 1, J=8 Hz, =CH-)
3d	COC_6H_5	180—210(0.1)	57.45 (57.53)	4.58 (4.51)	1780 1680 1625 1600	1.41(s, 3, C_5-CH_3), 1.60(s, 3, C_5-CH_3), 4.0—4.4(m, 1, C_4-H), 4.62(d, 1, J=10 Hz, C_3-H), 5.82(d, 1, J=10 Hz, =CH-), 7.2—8.2 (m, 5, C_6H_5)
3e	CO_2H	[128—129]	42.85 (42.71)	4.16 (3.98)	2650 1800 1625	1.34(s, 3, CH_3), 1.55(s, 3, CH_3), 3.57(d, 1, J=12 Hz, C_3-H), 3.80(dd, 1, J=8 and 12 Hz, C_4-H), 5.77(d, 1, J=8 Hz, =CH-), 7.46 (s, 1, CO_2H)

TABLE 2. ^{13}C NMR SPECTRA OF LACTONES **3**[a)]

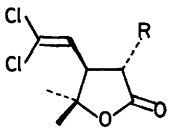

3

Compd	R	^{13}C NMR (δ) C_2	C_3	C_4	C_5	Cl_2C=	CH=	CH_3	CH_3	R
3a	CO_2CH_3	169.2	50.0	52.0	85.4	126.1	124.2	23.1	27.3	53.2 (q), 167.1 (s)
3c[b)]	$COCH_3$	169.6 (58.0)	58.7 (47.9)	47.4 (85.7)	85.1	125.5	124.8 (124.9)	23.7	27.6	30.1 (q), 199.0 (s) (29.5)
3d	COC_6H_5	169.7	53.9	48.5	85.3	128.3	124.5	23.9	27.6	128.8 (d), 129.5 (d), 134.2 (d), 135.7 (s), 193.5 (s)
3e	CO_2H	169.7*	50.0	51.9	86.1	126.8	124.1	23.3	27.6	170.2* (s)
3f	H	169.8	34.5	46.0	86.3	124.1	126.4	22.8	27.7	

a) Measured in $CDCl_3$. Assignments are consistent with the multiplicities observed in off-resonance decoupled spectra unless otherwise indicated. b) Signals in parenthesis seem to be those of an enol isomer (22%). * Assignment may be interchangeable.

fold excess of thionyl chloride in ethanol resulted in the formation of 4-(2,2-dichloroethenyl)-3-ethoxycarbonyl-2,5,5-trimethyl-4,5-dihydrofuran (**8**) in 79% yield. Dihydrofuran **8** is thought to have been derived from **6** by the spontaneous dehydrochlorination.

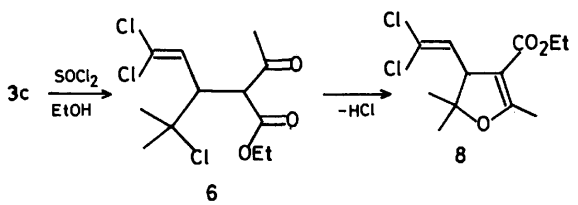

6 **8**

An analog of the lactone **3** was prepared by the adaptation of the method described above. Reaction of **4** with butylmagnesium bromide gave 1,1,3-trichloro-4-methyl-1-octen-4-ol (**9**) in 64% yield. ^{1}H NMR analysis showed that the alcohol **9** exists in two diastereomeric forms, *dl-erythro* and *dl-threo* (3 : 2). Condensation of **9** with diethyl sodiomalonate afforded the dehydrochlorination product of **9**, 1,1-dichloro-3,4-epoxy-4-methyl-1-octene (**10**) (30% yield) and a 3 : 2 diastereomeric mixture of 5-butyl-4-(2,2-dichloroethenyl)-3-ethoxycarbonyl-5-methyltetrahydro-2-furanones (**11a, b**) [31% (45%)[12)] yield]. The epoxide **10**, which was identified by the independent synthesis from **9**, was a mixture of *cis* and *trans* isomers (2 : 3). It has been shown in the previous paper that the *erythro* alcohol is cyclized to the *trans* epoxide and the *threo* alcohol to the *cis* epoxide, respectively.[5)] The stereochemistry of **11a** and **11b** was determined by a detailed study of their proton and ^{13}C NMR spectra. The chemical shift of

methyl carbon of C_5 in **11b** was considerably upfieid from that of methyl carbon of C_5 in **11a**.[13] In addition, the chemical shift of C_1 of butyl group in **11a** was upfield from that of C_1 of butyl group in **11b**. This showed that the methyl group of C_5 and dichloroethenyl group in **11b** was *cis*.[13] This was further confirmed by the observation of 18% NOE between the olefin proton and the methyl protons of C_5 in **11b**.

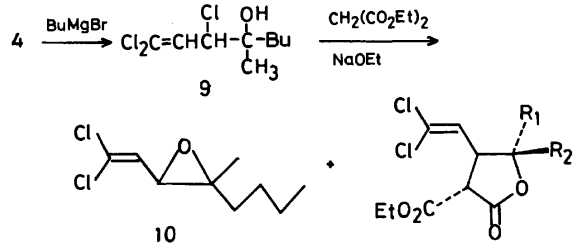

11a, $R_1=CH_3$; $R_2=Bu$
b, $R_1=Bu$; $R_2=CH_3$

The reaction mechanism on the present reaction is discussed as follows. In the reaction of chlorohydrin **5** with malonic ester and acylacetate under the basic conditions, one can imagine that the initially formed product would be most likely epoxide **2**, which is subsequently attacked by the carbanion of esters to afford the corresponding lactones **3**. This prospect seemed to be valid because both reactions of sodiomalonate with chlorohydrin **5** and with epoxide **2**[4,14] yielded the lactones **3**. However, attempted reactions of acetoacetic esters with **2** resulted in the recovery of the starting materials, while the reactions of acetoacetic esters with **5** gave lactones **3** in reasonable yields, as described above. A number of experiments between acetoacetic esters and **2** were conducted under various conditions, using alcohols, tetrahydrofuran (THF), and *N,N*-dimethylformamide (DMF) as a solvent, in the presence of equimolar or excess amount of base (NaOR and NaH), but the desired product **3** could not be isolated. This result strongly suggests that the present reaction between **5** and acetate derivatives proceeds *via* not the epoxide **2** but an S_N2 substitution product **12** as an intermediate.

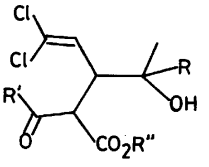

12, $R=CH_3$, Bu; $R'=CH_3$, C_6H_5; $R''=CH_3$, C_2H_5

Experimental

The melting points and boiling points are uncorrected. Elemental analyses were carrried out by Mr. Eiichiro Amano. Analytical determinations by GLPC were performed on a Hitachi Model K-53 gas chromatograph filled with 10% Apiezon Grease L on Chromosorb W (3 mm o.d. × 1 m). High-performance liquid chromatography (HPLC) was performed with Yanagimoto components consisting of a PN-101 pump and R-203 differential refractometer. Infrared spectra were determined with a JASCO A-102 diffraction grating infrared spectrophotometer. ^1H NMR spectra (60 MHz) were recorded with a Hitachi Model R-24 apparatus. ^{13}C NMR spectra were obtained with a JEOL LTD, JNM-FX100 apparatus. Chemical shifts were measured using TMS as an internal standard and are given in terms of δ (ppm).

The synthesis of *2-methyl-3,5,5-trichloro-4-penten-2-ol (5)* was described in the previous paper.[5]

4-(2,2-Dichloroethenyl)-3-methoxycarbonyl-5,5-dimethyltetrahydro-2-furanone (3a). Sodium (0.2 g, 8.8 mmol) was dissolved in 50 ml of dry methanol. To the solution was added 1.16g (8.8mmol) of dimethyl malonate. After the mixture was stirred at room temperature for 1 h, **5** (1.62 g, 8 mmol) was added. The mixture was stirred for 1 d, and then condensed *in vacuo*. The residual oil was poured into water, acidified with 10% HCl, and the organic material was extracted with ether. The ethereal layer was washed with water and dried over $MgSO_4$. Removal of the solvent gave a mixture of an oil and crystals. The filtration afforded 0.638 g (30%, 52%[7]) of **3a**: mp 102—103 °C (lit,[4] mp 100—102 °C). IR and ^1H NMR data were identical with those of the authentic sample.[4] The filtrate (1.09 g) was a mixture of **5** and dimethyl malonate (1:1 1.09g by ^1H NMR).

4-(2,2-Dichloroethenyl)-5,5-dimethyl-3-ethoxycarbonyltetrahydro-2-furanone (3b) was prepared in 41% (49%)[8] yield from 0.813 g (4 mmol) of **5** and 0.705 g (4.4 mmol) of diethyl malonate, as described above. The physical properties and analytical data are shown in Table 1.

4-(2,2-Dichloroethenyl)-5,5-dimethyl-2-oxotetrahydro-3-furancarboxylic Acid (3e). The mixed solution of 0.5 g (1.87 mmol) of **3a** and 40 ml of 2 M NaOH (1 M=1 mol dm^{-3}) was stirred at room temperature for 16 h. The mixture was extracted with ether. The organic layer, after being dried over $MgSO_4$, was condensed to leave 0.421 g (89%) of **3e**: mp 128—129 °C (from benzene). The physical data and analyses are shown in Table 1.

3-Acetyl-4-(2,2-dichloroethenyl)-5,5-dimethyltetrahydro-2-furanone (3c). Sodium (0.247 g, 10.7 mmol) was dissolved in 20 ml of dry methanol. Methyl acetoacetate (1.24 g, 10.7 mmol) was added, and the mixture was stirred at 50 °C for 1 h. To the solution was added slowly 2.14 g (10.7 mmol) of **5** under reflux. The mixture was stirred at the reflux temperature for 24 h. After being cooled, the mixture was condensed *in vacuo*, and neutralized with 50% CH_3CO_2H. The organic layer was extracted with ether, and dried over $MgSO_4$. After removal of the solvent, the residual oil was distilled *in vacuo*. The first fraction (1.2 g) was distilled at 110 °C/24 Torr (1 Torr≈ 133.322 Pa). GLPC analysis showed it consists of a 1:1 mixture of the starting materials. The second fraction was collected at 112 °C/0.07 Torr to give 1.33 g (50%, 76%[7]) of **3c**: on TLC analysis (silica gel, 3:1 hexane:acetone), one spot at R_f 0.35. Spectral data and analysis are shown in Table 1.

3-Benzoyl-4-(2,2-dichloroethenyl)-5,5-dimethyltetrahydro-2-furanone (3d). From a mixture of **5** (2.03 g, 10 mmol), ethyl benzoylacetate (1.92 g, 10 mmol), sodium (0.23 g, 10 mmol), and dry ethanol (20 ml), 3.2 g of an oil was obtained by the same treatment as described in the preparation of **3c**. The distillation gave 1.95 g of the first fraction at bp 125 °C/15 Torr, consisting of a 71:29 mixture of ethyl benzoylacetate and **5**, and 0.377 g of the second fraction distilling at bp 180—210 °C/0.1 Torr. TLC analysis (silica gel, 3:1 hexane: acetone) of the second fraction gave two spots at R_f 0.45 and 0.33. The component at R_f 0.33 was collected by preparative TLC to give 0.206 g (7%, 24%[7]) of **3d**. Physical properties and analyses are shown in Tables 1 and 2.

4-(2,2-Dichloroethenyl)-3-ethoxycarbonyl-2,5,5-trimethyl-4,5-dihydrofuran (8). To a solution of **3c** (0.502 g, 2 mmol) in 20 ml of dry ethanol was slowly added 1.4 ml (20 mmol) of thionyl chloride. The solution was heated at 70 °C for 6 h. After being cooled, the mixture was condensed *in vacuo* to give 0.56 g (79%) of **8**: one spot at R_f 0.79 on TLC analysis (silica gel, 3:1 hexane: acetone); IR (neat) 1705 (ester C=O), 1645, 1625 cm^{-1} (C=C); NMR ($CDCl_3$) δ=1.08 (t, 3H,

OCH_2CH_3), 1.12 (s, 3H, C_5-CH_3), 1.22 (s, 3H, C_5-CH_3), 1.98 (s, 3H, =C-CH_3), 3.57 (d, 1H, J=10 Hz, C_4-H), 3.92 (q, 2H, OCH_2CH_3), 5.49 (d, 1H, J=10 Hz, =CH). Found: C, 51.77; H, 5.85%. Calcd for $C_{12}H_{16}Cl_2O_3$: C, 51.63; H, 5.78%.

Reaction of **2** *with Acetoacetic Esters in the Presence of Base.* Reactions of **2** with sodioacetoacetic esters prepared by dissolving acetoacetic esters in the solvents in the presence of NaOR or NaH were carried out under following conditions: (a) **2** (0.5 g, 2.9 mmol), methyl acetoacetate (0.349 g, 2.9 mmol), $NaOCH_3$ (5.0 mmol), MeOH (4.5 ml), at room temperature for 2.5 h and at reflux temperature for 1 h; (b) **2** (1.0 g, 5.9 mmol), ethyl acetoacetate (0.858 g, 6.6 mmol), EtOH (7 ml), at room temperature for 12 h, and at reflux temperature for 6 h; (c) **2** (1.0 g, 5.9 mmol), methyl acetoacetate (0.767 g, 6.6 mmol), NaH (7.2 mmol), THF (10 ml), at room temperature for 22 h and at reflux temperature for 20 min; (d) **2** (1.0 g, 5.9 mmol), methyl acetoacetate (1.56 g, 12 mmol), NaH (18 mmol), THF (5 ml), at reflux temperature for 16 h; (e) **2** (1.0 g, 5.9 mmol), ethyl acetoacetate (0.858 g, 6.6 mmol), NaH (7.9 mmol), DMF (6 ml), at 70—75 °C for 10 h. After the usual work-up, the starting materials were recovered for all procedures.

The Epimeric Mixture (3:2 erythro: threo*) of 1,1,3-Trichloro-4-methyl-1-octen-4-ol (9).* An ethereal solution of *n*-BuMgBr (0.10 mol) in dry ether (50 ml) was added dropwise to a solution of **4** (15 g, 0.08 mol) in 50 ml of dry ether at −30 °C during a period of 2 h. After being stirred at −20 — −10 °C for an additional 4 h, the mixture was acidified with 10% HCl. The usual work-up gave an oil, which was distilled to give 12.5 g of **9**, yield 64%: bp 95—102 °C (2 mm); IR (neat) 3350 (OH), 1620 (C=C), 872, 746 cm^{-1}; ^1H NMR ($CDCl_3$) δ=0.90 (broad t, 3H, $CH_3(CH_2)_3$), 1.21—1.71 (m, 9H, $CH_3(CH_2)_3C$-CH_3), 3.74 (broad s, 1H, OH), 4.67 (d, 1H, J=10 Hz, $\rangle$CHCl), 6.16 (d, 0.6H, J=10 Hz, *erythro* =CH-), 6.18 (d, 0.4H, J=10 Hz, *threo* =CH-). Found: C, 43.83; H, 5.92%. Calcd for $C_9H_{15}Cl_3O$: C, 44.02; H, 6.16%.

The Epimeric Mixture (2:3 cis: trans*) of 1,1-Dichloro-3,4-epoxy-4-methyloctene (10).* To a stirred solution of **9** (4.9 g, 0.02 mol) in 40 ml of dry ether was added sodium methoxide (2.38 g, 44 mmol) in several portions at −5 °C. The mixture was stirred at room temperature for 6 h, and then acidified with 10% HCl with cooling. The organic layer was extracted with ether, and the ethereal extract was dried over $MgSO_4$. After removal of the solvent, the residual oil was distilled to give 2.5 g of **10**, yield 60%: bp 124—129 °C (20 mm); IR (neat) 1614 (C=C), 930, 895, 860 cm^{-1}; ^1H NMR ($CDCl_3$) δ=0.9 (broad t, 3H, $CH_3(CH_2)_3$), 1.28 (s, 1.8H, *trans* O-C-CH_3), 1.34 (s, 1.2 H, *cis* O-C-CH_3), 1.1—1.7 (m, 6H, $CH_3(CH_2)_3$), 3.44 (d, 1H, J=8 Hz, $\rangle$CH-CH=), 5.75 (d, 1H, J=8 Hz, =CH-). Found: C, 51.46; H, 6.48%. Calcd for $C_9H_{14}Cl_2O$: C, 51.69; H, 6.75%.

Reaction of **9** *with Diethyl Malonate in the Presence of Sodium Ethoxide.* A mixture of chlorohydrin **9** (2.76 g, 11.2 mmol) and diethyl sodiomalonate prepared from sodium (0.284 g, 12.3 mg-atom) and diethyl malonate (1.97 g, 12.3 mmol) in dry ethanol (10 ml) was heated at reflux temperature for 24 h. After removal of the solvent, the residue was poured into water. The mixture was acidified with dilute acetic acid and the organic layer was extracted with ether. The ethereal layer was washed with water, and dried over $MgSO_4$. After removal of the solvent, the residual oil was distilled *in vacuo*. The first fraction at bp 140 °C/2 Torr. gave 1.4 g of **10** (28% yield) and diethyl malonate (47:53 by ^1H NMR). Column chromatography (silica gel, 3:1 hexane: acetone) of the residual oil (1.74 g) gave 42 mg (2%) of **10**, 0.168 g of diethyl malonate, and 1.12 g (31%, 45%[12]) of a diastereomeric mixture of *5-butyl-4-(2,2-dichloroethenyl)-3-ethoxycarbonyl-5-methyltetrahydro-2-furanone (11)* as an oil. HPLC analysis (Yanapak SA-I, 6×250 mm; 10:1 hexane: ethyl acetate, 1.7 ml/min) showed two peaks at retention times (integrated percentages) of 10.8 (60%) and 15.2 min (40%). Each component was isolated by preparative HPLC. The first fraction yielded t-*5-butyl*-t-*4-(2,2-dichloroethenyl)*-r-*3-ethoxycarbonyl*-c-*5-methyltetrahydro-2-furanone (11a)*: an oil; IR (neat) 1790 (lactone C=O), 1742 (ester C=O), 1626 (C=C); ^1H NMR ($CDCl_3$) δ=0.92 (broad t, 3H, $CH_3(CH_2)_3$-), 1.32 (t, J=7.5 Hz, 3H, $CO_2CH_2CH_3$), 1.52 (s, 3H, C_5-CH_3), 1.1—1.6 (m, 6H, $CH_3(CH_2)_3$-), 3.56 (d, J=12 Hz, 1H, C_3-H), 3.87 (q, J=10 and 12Hz, 1H, C_4-H), 4.30 (q, J=7 Hz, 2H, $CO_2CH_2CH_3$), 5.85 (d, J=10 Hz, 1H, -CH=): ^{13}C NMR ($CDCl_3$) δ=13.9 (q, $CH_3(CH_2)_3$-), 14.0 (q, $CO_2CH_2CH_3$), 23.0 (t, $CH_3CH_2CH_2CH_2$), 25.0 (q, C_5-CH_3), 25.4 (t, $CH_3CH_2CH_2CH_2$-), 36.3 (t, $CH_3CH_2CH_2CH_2CH_2$-), 50.8 (d, C_4), 52.3 (d, C_3), 62.4 (t, $CO_2CH_2CH_3$), 87.4 (s, C_5), 124.0 (d, -CH=), 125.9 (s, Cl_2C=), 166.5 (s, CO_2Et), 169.3 (s, lactone C=O). Found: C, 52.19; H, 6.33%. Calcd for $C_{14}H_{20}Cl_2O_4$: C, 52.02; H, 6.24%. The second fraction gave c-*5-butyl*-t-*4-(2,2-dichloroethenyl)*-r-*3-ethoxycarbonyl*-t-*5-methyltetrahydro-2-furanone (11b)*: an oil; IR (neat) 1788 (lactone C=O), 1740 (ester C=O), 1625 (C=C); ^1H NMR ($CDCl_3$) δ=0.94 (broad t, 3H, $CH_3(CH_2)_3$-), 1.32 (s, 3H, C_5-CH_3), 1.34 (t, J=7 Hz, 3H, $CO_2CH_2CH_3$), 1.1—1.6 (m, 6H, $CH_3(CH_2)_3$-), 3.56 (d, J=12 Hz, 1H, C_3-H), 3.91 (q, J=10 and 12 Hz, 1H, C_4-H), 4.31 (q, J=7 Hz, 2H, $CO_2CH_2CH_3$), 5.85 (d, J=10 Hz, 1H, -CH=); ^{13}C NMR ($CDCl_3$) δ=13.8 (q, $CH_3(CH_2)_3$-), 14.0 (q, $CO_2CH_2CH_3$), 21.6 (q, C_5-CH_3), 22.7 (t, $CH_3CH_2CH_2CH_2$-), 25.3 (t, $CH_3CH_2CH_2CH_2$-), 39.8 (t, $CH_3CH_2CH_2CH_2$-), 48.3 (d, C_4), 52.1 (d, C_3), 62.4 (t, $CO_2CH_2CH_3$), 87.2 (s, C_5), 124.4 (d, -CH=), 125.8 (s, Cl_2C=), 166.4 (s, CO_2Et), 169.1 (s, lactone C=O). Found: C, 52.24; H, 6.27%. Calcd for $C_{14}H_{20}Cl_2O_4$: C, 52 .02; H, 6.24%.

References

1) Presented in part at the 38th National Meeting of the Chemical Society of Japan, Nagoya, October 1978, Lecture No. 2K28.

2) For early syntheses, see: a) J. Farkas, P. Kouriim, and F. Sorm, *Chem. Listy*, **52**, 688 (1958); b) M. Elliott, A. W. Farnham, H. F. Janes, P. H. Needham, E. A. Pulman, and J. H. Stevenson, *Nature (London)*, **246**, 169 (1973); c) K. Kondo and K. Matsui, Japan. Kokai, 51—41316 (1976).

3) For reviews, see: a) M. Elliot, "Synthetic Pyrethroids," ed by American Chemical Society, ACS Symp. Ser. (1977), P. 42; b) H. Yoshioka and S. Miyamoto, *Kagaku To Seibutsu*, **14**, 427, 549 (1976).

4) P. D. Klemmensen, H. Kolind-Andersen, H. B. Madsen, and A. Svendsen, *J. Org. Chem.*, **44**, 416 (1979).

5) A. Takeda, S Tsuboi, T. Moriwake, and E. Hirata, *Bull. Chem. Soc. Jpn.*, **45**, 3685 (1972).

6) S. Tsuboi, T. Uno, and A. Takeda, *Chem. Lett.*, **1978**, 1325.

7) Estimated from the consumed **5**.

8) A. Takeda, T. Sakai, S. Shinohara, and S. Tsuboi, *Bull. Chem. Soc. Jpn.*, **50**, 1133 (1977).

9) A. Takeda, S. Tsuboi, and T. Sakai, *J. Org. Chem.*, **39**, 2601 (1974).

10) M. Petrzilka, D. Felix, and A. Eschenmoser, *Helv. Chim. Acta*, **56**, 2950 (1973).

11) J. B. Stothers and P. C. Lanterour, *Can. J. Chem.*, **42**, 1563 (1964).

12) Estimated from the consumed diethyl malonate.

13) The chemical shifts of sterically perturbed carbon atoms are generally found at higher magnetic fields than for similar carbons which are not spatially crowded: D. M. Grant and B. V. Cheney, *J. Am. Chem. Soc.*, **89**, 5315 (1967); D. E. Dorman, M. Jautelat, and J. D. Roberts, *J. Org. Chem.*, **36**, 2757 (1971).

14) We reinvestigated the reaction of **2** with methyl malonate in the presence of sodium methoxide to give **3a** in 76% yield.

A Synthetic Route to the Morphan Ring System by Skeletal Transformation of Norbornadiene[1)]

Hiroo INOUE,* Toshiki ORIGUCHI, and Katsumi UMANO
Department of Applied Chemistry, College of Engineering, University of Osaka Prefecture, Sakai, Osaka 591
(Received September 8, 1983)

The morphan skeleton was prepared from 2-phenylsulfonyl-2-azabicyclo[3.2.1]oct-6-ene (**2**), derived from norbornadiene, through the addition of dichlorocarbene to the monoene **2** and the subsequent thermal isomerization of the adduct obtained. The isomerization products, 2-phenylsulfonyl-6,7-dichloro-2-azabicyclo-[3.3.1]non-7-ene and 2-phenylsulfonyl-7,8-dichloro-2-azabicyclo[3.3.1]non-6-ene, which are mutually convertible in the presence of lithium chloride, were converted into various morphans by reductive dechlorination and alkylation. Furthermore, the 6,7-pyridazino-annelated morphan was synthesized by the cycloaddition of dimethyl 1,2,4,5-tetrazine-3,6-dicarboxylate to 2-phenylsulfonyl-2-azabicyclo[3.3.1]non-6-ene.

In the course of our studies on the reactivity of the methano-bridged azabicyclic molecules,[2)] we took an interest in the morphan ring system having pharmacological activity.[3)] The morphan ring system has been synthesized by using mostly intramolecular cyclization reactions starting from an appropriate material.[3,4)] We planned to construct the morphan skeleton by an alternative route, utilizing skeletal transformation of available bicyclic molecule such as norbornadiene (**1**). The transformation of the diene **1** to 2-phenylsulfonyl-2-azabicyclo[3.2.1]oct-6-ene (**2**) through ring expansion has already been reported.[5,6)] We examined to transform the monoene **2** to the morphan ring system and now wish to report a novel synthetic route to various morphans starting from the diene **1**.

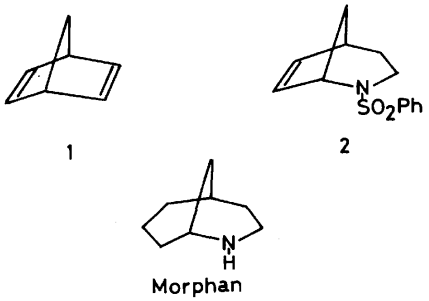

Results and Discussion

Ring Expansion of the Monoene 2 to the Morphan Ring System. On the basis of the fact that the dichlorocarbene adduct to norbornene readily undergoes ring expansion,[7)] the ring expansion of the monoene **2** was carried out using the dichlorocarbene adduct to the monoene **2**. The cheletropic addition of dichlorocarbene to the monoene **2**, using hexadecyltrimethylammonium bromide as the phase-transfer catalyst, gave 2-phenylsulfonyl-7,7-dichloro-2-azatricyclo-[3.2.1.0.^{6,8exo}]nonane (**3**) in 56% yield (Scheme 1). During this reaction, no rearrangement occurred. The exo configuration of the adduct **3** was determined by the absence of the coupling between 1-H and 8-H. The thermal isomerization of the adduct **3** was achieved successfully by heating the adduct **3** at 130—135 °C in the absence or presence of the solvent, thus giving rise to 2-phenylsulfonyl-6,7-dichloro-2-azabicyclo[3.3.1]-

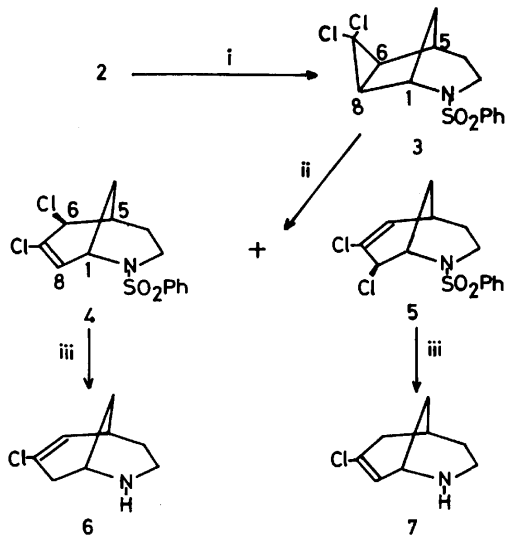

Scheme 1. i) $|CCl_2$, r.t., 48 h; ii) 130—135 ℃, 1.5 h; iii) $LiAlH_4$, THF, r.t., 30 h.

non-7-ene (**4**) and its positional isomer (**5**) which can be separated readily by silica-gel chromatography (Scheme 1). The position of the double bond of **4** and **5** was determined by the fact that the doublet absorptions of vinyl protons at δ=5.37 (**4**) and 5.94 (**5**) collapse to singlet by double irradiation of 1-H of **4** and 5-H of **5** respectively. The absence of the coupling between 5-H and 6-H for **4** and between 1-H and 8-H for **5** indicated the configuration of endo 6-H for **4** and endo 8-H for **5**. The yields of **4** and **5** are shown in Table 1. The polar solvent was favorable for isomerization, although no significant solvent effect on the isomer ratio was observed. Furthermore, we found that the treatment of **4** or **5** with lithium chloride in *N*, *N*-dimethylformamide (DMF) at 50 °C for 7 h results in the migration of the double bond to give the equilibrium mixture of **4** and **5** in the ratio of 65:35, although no allylic rearrangement occurs in the absence of lithium chloride under similar conditions (Table 2). The reaction is considered to proceed through the intermediate A to give **4** and **5**.

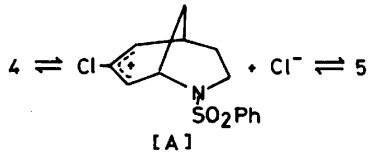

Table 1. The yields of **4** and **5** in the thermal isomerization of **3**[a)]

Solvent	Time/h	Yield/%		Recov./%
		4	**5**	**3**
None	1.5	54	43	0
m-Xylene	3.0	18	9	72
Chlorobenzene	1.5	65	33	0
DMF	1.5	56	41	0

a) Temperature: 130—135 °C.

Table 2. The allylic rearrangement of **4** and **5** in the presence of lithium chloride[a)]

Substrate	Temp/°C	Time/h	Yield/%	
			4	**5**
4	50	1	84	16
4	50	3	68	32
4	50	7	65	35
4	80	15	64	35
5	50	3	58	42
5	50	7	63	37

a) Solvent: DMF.

Reductive Dechlorination of Compounds 4 and 5. The reductive cleavage of the C_6–Cl bond of **4** with lithium aluminium hydride in tetrahydrofuran (THF) at room temperature for 30 h proceeded by the S_N2' process, accompanied by the cleavage of the N–S bond, to give 7-chloro-2-azabicyclo[3.3.1]non-6-ene (**6**) in 80% yield (Scheme 1). Next, compound **6** was treated with sodium in liquid ammonia for 40 min to give 2-azabicyclo[3.3.1]non-6-ene (**8a**) in 78% yield. Attempts to undergo one-step dechlorination of **4** with sodium in liquid ammonia failed because of the destruction of the morphan skeleton. Compound **8a** was alkylated with methyl iodide and benzyl bromide to give **8b** and **8c** in 52 and 77% yields respectively.

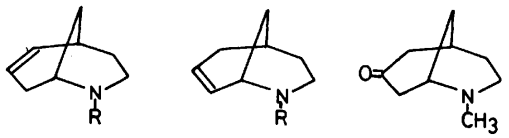

8 9 10

(a; R=H, b; R=CH_3, c; R=$PhCH_2$)

Compound **5** also was converted into **9a—c** by the steps shown in the case of **4**. The yields in the conversion of **5** into **7**, **7** into **9a**, and **9a** into **9b**, **c** were 76, 52, 36, and 70% respectively. The structure of **8b** and **9b** was established by the fact that the melting points and NMR spectra of picrates of **8b** and **9b** prepared here are identical to those of two isomers (**8b** and **9b**) prepared by an alternative route[8)] starting from 2-methyl-2-azabicyclo[3.3.1]nonan-7-one (**10**) [**8b** picrate: δ 5.84 (single multiplet, 2H, 6- and 7-H); **9b** picrate: δ 6.45 (a doublet of triplets, 1H, 7-H) and δ 5.82 (poorly resolved triplet, 1H, 8-H)].[8)] Thus, it was established that the morphan derivatives having a double bond at 6- or 7-position are synthesized from the diene **1** by skeletal transformation.

Annelation of Pyridazine Ring onto the Morphan Ring. We attempted to annelate a heterocyclic ring instead of the benzene ring of 6,7-benzomorphans. Previously it has been reported that 1,2,4,5-tetrazines undergo cycloaddition to various dienophiles to form pyridazines.[9)] To annelate a pyridazine ring onto the 6,7-position of the morphan ring, we carried out the cycloaddition of dimethyl 1,2,4,5-tetrazine-3,6-dicarboxylate (**12**) to 2-phenylsulfonyl-2-azabicyclo-[3.3.1]non-6-ene (**11**). When a solution of a 1:2 mixture of **11** and **12** in chloroform was stirred at 50 °C for 15 h, the reaction proceeded with the evolution of nitrogen gas to give 2-phenylsulfonyl-3′,6′-bis(methoxycarbonyl)-6,7-(4′,5′-pyridazino)-2-azabicyclo[3.3.1]non-6-ene (**14**) in a quantitative yield, together with dimethyl 1H,4H-1,2,4,5-tetrazine-3,6-dicarboxylate (**15**) in nearly equimolar amounts with those of **14**. In equimolar solution of **11** and **12** in chloroform, the reaction gave **14** and **15** in 31 and 36% yields respectively. These facts indicate that the reaction proceeds by the cycloaddition of **12** to **11** to give the intermediate dihydropyridazine adduct (**13**) by release of nitrogen, followed by the dehydrogenation of **13** with **12** to give **14**, as shown in Scheme 2.

Next, we carried out the cycloaddition of **12** to 2-phenylsulfonyl-7-chloro-2-azabicyclo[3.3.1]non-6-ene (**16**) under conditions similar to those described above. The reaction proceeded through the evolution of nitrogen gas and then the dehydrochlorination of the intermediate adduct to give **14** in 37% yield. Thus, it was established that the pyridazine ring is annelated onto the morphan ring.

The above results provide a new route for the preparation of the morphan ring system from readily available diene **1**.

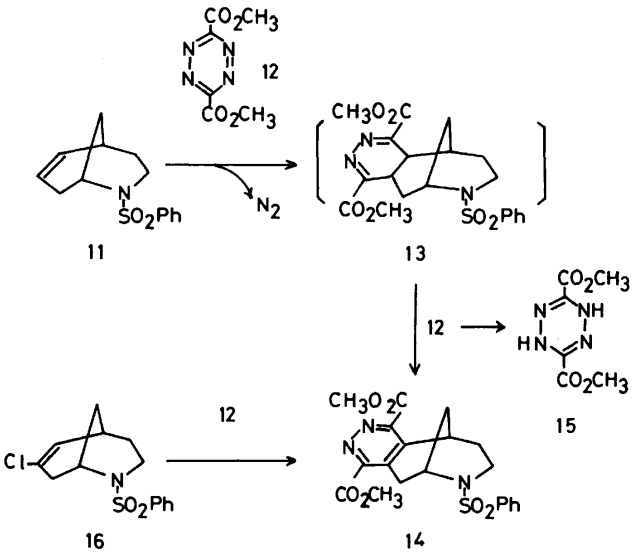

11 13 15 16 14

Scheme 2.

Experimental

The ^1H NMR spectra were determined on a Hitachi R-24A NMR spectrometer at room temperature with $CDCl_3$ as a solvent, using tetramethylsilane as the internal standard. The ^{13}C NMR and IR spectra were measured with a JEOL FX 90Q

Fourier transformation NMR spectrometer and a Hitachi 215 grating infrared spectrometer, respectively. All melting points were uncorrected. Compound **1** was obtained commercially and compound **2** was synthesized by the modification of the methods described in the literature.[5,6]

2-Phenylsulfonyl-7,7-dichloro-2-azatricyclo[3.2.1.0.^{6,8exo}]nonane (**3**). A 50% aqueous sodium hydroxide solution(73 g) was stirred, drop by drop, into a solution of **2** (6.6 g, 27 mmol) in chloroform (115 g) with hexadecyltrimethylammonium bromide (0.98 g) for 1 h at room temperature. After stirring for 2 d, the reaction mixture was extracted with chloroform. The chloroform solution was washed with water and dried over anhydrous magnesium sulfate. After removal of the chloroform *in vacuo*, the residue was chromatographed with a silica-gel column [chloroform–hexane (10:1) as an eluant] to give **3** (5 g, 56%), which was recrystallized from ethanol: mp 113—115 °C; IR (KBr) 1350 and 1170 cm^{-1} (SO_2); ^{1}H NMR δ=1.15—2.32 (m, 6H, 4-CH_2, 6-H, 8-H, and 9-CH_2), 2.51 (m, 1H, 5-H), 2.72—3.87 (m, 2H, 3-CH_2), 4.50 (d, 1H, J=4.7 Hz, 1-H), and 7.20—8.05 (m, 5H, aromatic). Found: C, 50.80; H, 4.62; N, 4.46%. Calcd for $C_{14}H_{15}NO_2SCl_2$: C, 50.60; H, 4.56; N, 4.22%.

Ring Expansion of **3**. In the Absence of Solvent. Compound **3** (3 g, 9 mmol) was placed in a test tube and heated at 130—135 °C for 1.5 h. The mixture was cooled and chromatographed with a silica-gel column (benzene as an eluant) to give 1.62 g (54%) of **4** and 1.29 g (43%) of **5**. Compounds **4** and **5** were recrystallized from ethanol. **4**: mp 136.5—138.5 °C; IR (KBr) 1350 and 1165 cm^{-1} (SO_2); ^{1}H NMR δ=1.40—2.30 (m, 4H, 4-CH_2 and 9-CH_2), 2.45 (m, 1H, 5-H), 2.82 (m, 1H, 3-$H_{exo\ or\ endo}$), 3.60 (m, 1H, 3-$H_{exo\ or\ endo}$), 4.18 (s, 1H, 6-H), 4.48 (m, 1H, 1-H), 5.37 (d, 1H, J=6.3 Hz, 8-H), and 7.18—8.02 (m, 5H, aromatic). Found: C, 50.61; H, 4.61; N, 4.27%. Calcd for $C_{14}H_{15}NO_2SCl_2$; C, 50.60; H, 4.56; N, 4.22%. **5**: mp 108—109 °C; IR (KBr) 1340 and 1165 cm^{-1} (SO_2); ^{1}H NMR δ=1.10—2.42 (m, 4H, 4-CH_2 and 9-CH_2), 2.60 (m, 1H, 5-H), 3.00 (m, 1H, 3-$H_{exo\ or\ endo}$), 3.70 (m, 1H, 3-$H_{exo\ or\ endo}$), 3.97 (s, 1H, 8-H), 4.42 (m, 1H, 1-H), 5.94 (d, 1H, J=6.3 Hz, 6-H), and 7.25—8.00 (m, 5-H, aromatic). Found: C, 50.58; H, 4.72; N, 4.31%. Calcd for $C_{14}H_{15}NO_2SCl_2$: C, 50.60; H, 4.56; N, 4.22%.

In the Presence of Solvent. A solution of **3** (3 g, 9 mmol) in *m*-xylene, chlorobenzene, or DMF (10 cm^3) was refluxed for 1.5 h. After the removal of the solvent, the mixture was worked up as described above.

Conversion of **5** *into* **4**. A solution of a mixture of **5** (1 g, 3 mmol) and lithium chloride (0.63 g, 15 mmol) in DMF (40 cm^3) was stirred at 50 °C for 7 h. After the removal of DMF *in vacuo*, water (20 cm^3) was added and the mixture was extracted with chloroform. The chloroform solution was washed with water, dried over anhydrous magnesium sulfate, and the solvent was removed *in vacuo*. The residue was chromatographed with a silica-gel column (benzene as an eluant) to give **4** (0.63 g, 63%) with recovery of **5** (0.37 g, 37%).

7-Chloro-2-azabicyclo[3.3.1]non-6-ene (**6**). A solution of **4** (1.25 g, 3.8 mmol) in THF (17 cm^3) was added, drop by drop, to a suspension of lithium aluminium hydride (0.6 g, 16 mmol) in THF (43 cm^3) at room temperature. The mixture was stirred for 30 h at room temperature and water was added. After filtration of the mixture, the filtrate was extracted with chloroform. The chloroform solution was washed with water and dried over anhydrous magnesium sulfate. The removal of the solvent *in vacuo* gave **6** (0.48 g, 80%): IR (KBr) 3250 cm^{-1} (NH) and 1645 cm^{-1} (C=C); ^{1}H NMR δ=1.10—1.85 (m, 4H, 4-CH_2 and 9-CH_2), 1.90 (s, 1H, NH), 2.20—3.11 (m, 4H, 3-CH_2 and 8-CH_2), 2.55 (m, 1H, 5-H), 3.25 (m, 1H, 1-H), and 5.78 (d, 1H, J=6.7 Hz, 6-H). The treatment of **6** with hydrogen chloride in ether gave HCl salt of **6** which was recrystallized from acetonitrile: mp 216—218 °C; Found: C, 49.50; H, 6.68; N, 7.37%. Calcd for $C_8H_{13}NCl_2$: C, 49.50; H, 6.76; N, 7.22%.

7-Chloro-2-azabicyclo[3.3.1]non-7-ene (**7**) was prepared from **5** in 76% yield by procedures similar to those in the case of **6**. **7**: IR (KBr) 3250 cm^{-1} (NH) and 1645 cm^{-1} (C=C): ^{1}H NMR δ=1.10—2.10 (m, 4H, 4-CH_2 and 9-CH_2), 2.20 (s, 1H, NH), 2.20—3.20 (m, 5H, 3-CH_2, 5-H, and 6-CH_2), 3.45 (m, 1H, 1-H), and 5.66 (d, 1H, J=6.7 Hz, 8-H). HCl salt of **7**: mp 216.5—218 °C; Found: C, 49.54; H, 7.00; N, 7.21%. Calcd for $C_8H_{13}NCl_2$: C, 49.50; H, 6.76; N, 7.22%.

2-Azabicyclo[3.3.1]non-6-ene (**8a**). A piece of sodium was added under stirring to a solution of **6** (0.6 g, 3.8 mmol) in ether (10 cm^3) and liquid ammonia (25 cm^3) at −78 °C until the solution kept the dark blue color for about 5 min. After stirring for 40 min, ammonia was removed, methanol was added, and the resulting solution extracted with ether. The ether solution was washed with water and dried over anhydrous sodium sulfate. The removal of ether gave **8a** (0.36 g, 78%): IR (KBr) 3270 cm^{-1} (NH) and 1645 cm^{-1} (C=C); ^{1}H NMR δ=1.00—3.00 (m, 9H, 3-CH_2, 4-CH_2, 5-H, 8-CH_2, and 9-CH_2), 2.10 (s, 1H, NH), 3.10 (m, 1H, 1-H), and 5.77 (m, 2H, 6-H and 7-H). HCl salt of **8a** was recrystallized from acetonitrile: mp 278—279 °C; Found: C, 60.26; H, 9.15; N, 8.80%. Calcd for $C_8H_{14}NCl$: C, 60.17; H, 8.86; N, 8.77%.

2-Azabicyco[3.3.1]non-7-ene (**9a**) was prepared from **7** in 52% yield by the procedures being similar to those in the case of **8a**. **9a**: IR (KBr) 3260 cm^{-1} (NH) and 1615 cm^{-1} (C=C); ^{1}H NMR δ=1.20—3.10 (m, 9H, 3-CH_2, 4-CH_2, 5-H, 6-CH_2, and 9-CH_2), 2.07 (s, 1H, NH), 3.32 (m, 1H, 1-H), 5.50 (dd, 1H, J=9.7, 6.0 Hz, 8—H),and 5.97 (dt, 1H, J=9.7, 4.0 Hz, 7-H). $(COOH)_2$ salt of **9a**: mp 210.5—212 °C; Found: C, 64.26; H, 8.59; N, 8.41%. Calcd for $C_{18}H_{28}N_2O_4$: C, 64.25; H, 8.33; N, 8.33%.

Alkylation of **8a** *and* **9a**. *With Methyl Iodide*: Sodium hydride (0.16 g, 3.2 mmol) was added to a solution of **8a** or **9a** (0.2 g, 1.6 mmol) in dimethyl sulfoxide (10 cm^3) and the mixture was stirred at 45 °C for 20 min. A solution of methyl iodide (0.71 g, 5 mmol) in dimethyl sulfoxide (5 cm^3) was added to the resulting solution. After stirring for 10 min, the mixture was poured into water (80 cm^3) and extracted with ether. The ether solution was washed with water and dried over anhydrous sodium sulfate. The removal of ether gave **8b** and **9b** in 52 and 36% yields, respectively. The melting points and NMR spectra of picrates of **8b** and **9b** were identical to those described in the literature.[9]

With Benzyl Bromide: A mixture of **8a** (0.28 g, 2.3 mmol), benzyl bromide (0.39 g, 2.3 mmol), sodium hydrogencarbonate (0.33 g, 3.9 mmol), and DMF (30 cm^3) was refluxed for 4 h. After filtration of the reaction mixture, the filtrate was evaporated and the residue was extracted with ether. The ether solution was washed with water and dried over anhydrous sodium sulfate. The removal of ether gave **8c** (0.38 g, 77%): ^{1}H NMR δ=1.50—2.05 (m, 4H, 4-CH_2 and 9-CH_2), 2.17 (m, 1H, 5-H), 2.25—2.67 (m, 4H, 3-CH_2 and 8-CH_2), 2.92 (m, 1H, 1-H), 3.49 (s, 2H, -C$\underline{H}_2$Ph), 5.72 (m, 2H, 6-H and 7-H), and 7.16 (s, 5H, aromatic). $(COOH)_2$ salt of **8c**: mp 177.5—180 °C; Found: C, 67.27; H, 7.12; N, 4.79%. Calcd for $C_{17}H_{21}NO_4$: C, 67.33; H, 6.93; N, 4.62%. Compound **9c** was prepared by the procedures being similar to those in the case of **8c**. **9c** (70% yield): ^{1}H NMR δ=1.15—2.80 (m, 9H, 3-CH_2, 4-CH_2, 5-H, 6-CH_2, and 9-CH_2), 3.12 (m, 1H, 1-H), 3.49 (s, 2H, -C$\underline{H}_2$Ph), 5.55 (m, 1H, 8-H), 6.03 (m, 1H, 7-H), and 7.18 (s, 5H, aromatic). $(COOH)_2$ salt of **9c**: mp 183—184.5 °C; Found: C, 67.18; H, 6.96; N, 4.55%. Calcd for $C_{17}H_{21}NO_4$: C, 67.33; H, 6.93; N, 4.62%.

2-Phenylsulfonyl-2-azabicyclo[3.3.1]non-6-ene (**11**). Benzenesulfonyl chloride (0.28 g, 1.6 mmol) was added gradually to a solution of **8a** (0.16 g, 1.3 mmol) in 2 M† sodium hydroxide (11 cm^3) and the mixture was stirred at room temperature for 5 h. The resulting solution was extracted

† 1 M=1 mol dm^{-3}.

with chloroform, and the chloroform solution was washed with water and dried over anhydrous sodium sulfate. After the removal of chloroform *in vacuo*, the residue was chromatographed on a silica-gel column using benzene as the eluant to give 0.32 g (91%) of **11**, which was recrystallized from ethanol: mp 108.5—110.5 °C; IR (KBr) 1310 and 1155 cm^{-1}(SO_2); ^1H NMR δ=1.31—1.76 (m, 4H, 4-CH_2 and 9-CH_2), 1.76—2.56 (m, 3H, 5-H and 8-CH_2), 3.06 (m, 1H, 3-$H_{exo\ or\ endo}$), 3.66 (m, 1H, 3-$H_{exo\ or\ endo}$), 4.21 (m, 1H, 1-H), 5.58 (m, 2H, 6-H and 7-H), and 7.26—7.86 (m, 5H, aromatic). Found: C, 63.77; H, 6.80; N, 5.29%. Calcd for $C_{14}H_{17}NO_2S$: C, 63.84; H, 6.52; N, 5.32%.

2-Phenylsulfonyl-7-chloro-2-azabicyclo[3.3.1]non-6-ene (16) was prepared from **6** by procedures similar to those used in the case of **11**. **16**: mp 124—126 °C; IR (KBr) 1350 and 1170 cm^{-1} (SO_2); ^1H NMR δ=1.40—2.05 (m, 4H, 4-CH_2 and 9-CH_2), 2.05—2.95 (m, 3H, 5-H and 8-CH_2), 3.03 (m, 1H, 3-$H_{exo\ or\ endo}$), 3.72 (m, 1H, 3-$H_{exo\ or\ endo}$), 4.33 (m, 1H, 1-H), 5.76 (d, 1H, J= 6.0 Hz, 6-H), and 7.30—7.95 (m, 5H, aromatic). Found: C, 56.22; H, 5.40; N, 4.79%. Calcd for $C_{14}H_{16}NO_2ClS$: C, 56.46; H, 5.43; N, 4.70%.

2-Phenylsulfonyl-3',6'-bis(methoxycarbonyl)-6,7-(4',5'-pyridazino)-2-azabicyclo[3.3.1]non-6-ene (14). A solution of a mixture of **11** (0.1 g, 0.38 mmol) and **12** (0.15 g, 0.76 mmol) in chloroform (10 cm^3) was stirred at 50 °C for 15 h. After the removal of chloroform *in vacuo*, the residue was chromatographed on a silica-gel column using chloroform as the eluant to give **14** (0.18 g, 91%) and **15** (0.11 g, 57%). Compound **14** was recrystallized from chloroform–benzene and **15** from chloroform–hexane. **14**: mp 197—199 °C; IR (KBr) 1735 cm^{-1} (CO); ^1H NMR δ=1.50—3.70 (m, 9H, 3-CH_2, 4-CH_2, 5-H, 8-CH_2, and 9-CH_2), 3.86 (s, 3H, -CO_2Me), 3.92 (s, 3H, -CO_2Me), 4.52 (m, 1H, 1-H), and 7.30—7.85 (m, 5H, aromatic); ^{13}C NMR δ=27.1, 29, 29.8, and 30.3 (4-, 5-, 8-, and 9-C), 37.7 (t, 3-C), 45.7 (d, 1-C), 53.1 and 53.3 (OMe), 127, 129.3, and 132.7 (aromatic), 137.6 and 140 (s, 6- and 7-C), 151.2 and 152 (s, 3'- and 6'-C), and 164.5 and 164.7 (s, CO). Found: C, 55.38; H, 4.77; N, 9.70%. Calcd for $C_{20}H_{21}N_3O_6S$: C, 55.67; H, 4.92; N, 9.74%. **15**: mp 174.5—175.5 °C; IR (KBr) 1728 cm^{-1} (CO); ^1H NMR 3.83 (s, 6H, -CO_2Me), and 7.42 (brs, 2H, NH). Found: C, 35.99; H, 4.04; N, 27.99%. Calcd for $C_6H_8N_4O_4$: C, 36.08; H, 4.00; N, 27.75%.

Reaction of 16 with 12. A solution of a mixture of **16** (0.1 g, 0.34 mmol) and **12** (0.13 g, 0.68 mmol) in chloroform (5 cm^3) was stirred at 50 °C for 15 h. The reaction mixture was worked up as described in the case of **11**.

References

1) H. Inoue, T. Origuchi, and K. Umano, The Ninth International Congress of Heterocyclic Chemistry, Tokyo, August 1983, Abstr., No. P-74.

2) K. Umano, H. Taniguchi, H. Inoue, and E. Imoto, *Tetrahedron Lett.*, **1979**, 247; K. Umano, S. Mizone, K. Tokisato, and H. Inoue, *ibid.*, **1981**, 73; K. Umano, H. Koura, and H. Inoue, *Bull. Chem. Soc. Jpn.*, **54**, 2827 (1981); H. Inoue, K. Tokisato, and K. Umano, *ibid.*, **55**, 1661 (1982).

3) D. C. Palmer and M. J. Strauss, *Chem. Rev.*, **77**, 1 (1977).

4) J. A. Bartrop, *J. Chem. Soc.*, **1947**, 399; E. L. May and J. G. Murphy, *J. Org. Chem.*, **19**, 618 (1954); **20**, 1197 (1955); F. Ramirez and J. W. Sargent, *J. Am. Chem. Soc.*, **77**, 6297 (1955); P. G. Gassman and J. H. Dygos, *Tetrahedron Lett.*, **1970**, 4749; M. Markotoff and R. C. Cavestri, *J. Org. Chem.*, **39**, 409 (1974); D. A. Evans, C. H. Mitch, R. C. Thomas, D. M. Zimmerman, and R. L. Robey, *J. Am. Chem. Soc.*, **102**, 5955 (1980); A. Manmade, J. L. Marshall, R. A. Minns, H. Dalzell, and R. K. Razdan, *J. Org. Chem.*, **47**, 1717 (1982) and references cited therein.

5) A. C. Oehlschlager and L. H. Zalkow, *J. Org. Chem.*, **30**, 4205 (1965).

6) P. Barraclough, S. Bilgic, and D. W. Young, *Tetrahedron*, **35**, 91 (1979).

7) R. C. De Selms and C. M. Combs, *J. Org. Chem.*, **28**, 2206 (1963); C. W. Jefford, V. de los Heros, and U. Burger, *Tetrahedron Lett.*, **1976**, 703; P. M. Kwantes and G. W. Klumpp, *ibid.*, **1976**, 707.

8) R. C. Cavestri and M. Mokotoff, *J. Med. Chem.*, **20**, 1493 (1977).

9) M. Tisler and B. Stanovnik, "Recent Advances in Pyridazine Chemistry," in "Advances in Heterocyclic Chemistry," ed by A. R. Katritzky and A. J. Boulton, Academic Press, New York, San Francisco, London (1979), Vol. 24, pp. 363—456; T. Wagner-Jauregg, *Synthesis*, **1980**, 165.

Syntheses of Aryl Glyoxylate. I. The Reaction of Alkyl Dichloro(alkoxy)acetates with Aromatics in the Presence of Lewis Acid

Osamu ITOH,* Takayoshi NAGATA, Isamu NOMURA, Tetsuya TAKANAGA, Toshio SUGITA, and Katsuhiko ICHIKAWA

Department of Hydrocarbon Chemistry, Faculty of Engineering, Kyoto University, Yoshida, Sakyo-ku, Kyoto 606

(Received September 19, 1983)

Ethyl dichloro(ethoxy)acetate (**1**) and methyl dichloro(methoxy)acetate (**2**) were characterized. The reaction of **1** and **2** with aromatics in the presence of $AlCl_3$ gave a considerable yield of aromatic α-keto ester. The aromatics included mono- and polymethylbenzene and anisol. The reaction was studied under various conditions and the results were compared with the acylation by ethoxalyl or methoxalyl chloride. The reaction mechanism was also discussed.

The chemical properties of ethyl dichloro(ethoxy)-acetate (**1**) and methyl dichloro(methoxy)acetate (**2**) which are prepared by the reactions of dialkyl oxalate and phosphorus pentachloride[1] appear to have not been fully studied, in spite of their potential wide usability in organic synthesis.

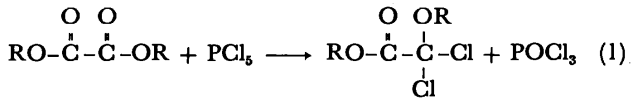

(1)

1: R=Et, **2**: R=Me

In this paper we wish to report the syntheses of aromatic α-keto esters by the reactions of **1** and **2** with aromatics in the presence of Lewis acids.

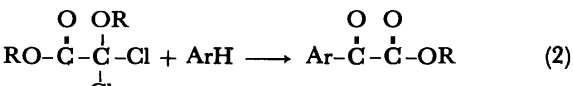

(2)

3: R=Et, **4**: R=Me

Needless to say, aromatic α-keto esters can be prepared by the Friedel-Crafts acylation of aromatics with ethoxalyl chloride.[2]

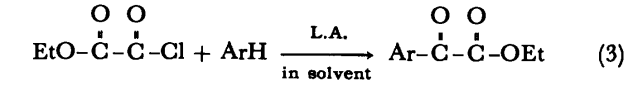

(3)

3

Ethoxalyl chloride is usualy prepared by two-step reactions of diethyl oxalate with phosphorus pentachloride.[3]

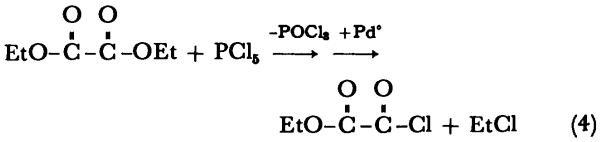

(4)

However the reaction intermediate should be one of the titled compounds. The reaction mixture of Eq. 1 or Eq. 4 (for 4 d at 95—100 °C) was subjected to a fractional distillation and the higher boiling fractions were found to be a mixture of **1** and diethyl oxalate. One more careful fractional distillation gave the fraction which consisted of 80% of **1** and 20% of diethyl oxalate. It was very difficult to obtain a fraction of more than 95% in purity. This fraction was heated at 180—200 °C for 6 h and then pure ethoxalyl chloride was obtained in 58% (corr. value; 70%). The conversion of **1** to ethoxalyl chloride was followed by GLC and ^{13}C NMR spectra. The evolved gas was partially trapped by Dry Ice–methanol and was identified to be ethyl chloride by ^1H NMR (CH_3: 3.55, CH_2: 1.50 in $CDCl_3$ *cf.* CH_3: 3.57. CH_2: 1.48 in CCl_4).

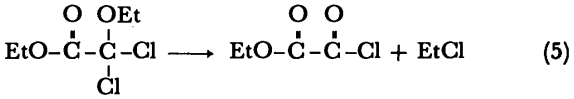

(5)

1 could not be purified to 100%, but the analogue, methyl dichloro(methoxy)acetate (**2**) was purified by two fractional distillations. The elemental analysis of the most purified fraction coincided with the calculated value for $C_4H_6O_3Cl_2$.

Syntheses of Aromatic α-Keto Esters. Compounds **1** and **2** in $CHCl_3$ reacted with the aromatics (ArH) in the precence of $AlCl_3$, $FeCl_3$, and $TiCl_4$ to form aromatic α-keto esters. To the $CHCl_3$ solution of an equivalent mole of **1** and ArH, powdered $AlCl_3$ (2 equiv mol) was added in parts with constant stirring, keeping the temperature under 5 °C (Method A). After 2 h, the reaction mixture was poured into ice water. The products were distilled out and analyzed by GLC, ^1H and ^{13}C NMR. Once **1** and **2** were treated with $AlCl_3$ or $FeCl_3$, **1** and **2** could not be recovered, and then the end point of the reaction could not precisely be detected. Although these reactions were very rapid, 2 h were too short to complete the reaction. However the isolated yields under such reaction conditions were fairly good; they are shown in the first column of Table 1.

The numbers of the yields could indicate a relative rate of the reaction, from the point of view as mentioned above, though the reaction mixture was heterogeneous. The numbers within parentheses were corrected values based on the purity of **1**, and the contaminated diethyl oxalate had no effect on the reaction.

In the reaction of **1** with benzene at bp of $CHCl_3$, ethyl phenylglyoxylate (20%) and a little (3.6%) ethyl *p*-ethylphenylglyoxylate were obtained. The latter was obtained through a fast ethylation of benzene with ethyl chloride and $AlCl_3$, followed by acylation of ethylbenzene. When **1** was treated with $AlCl_3$ or $FeCl_3$ at bp of CH_2Cl_2 or $CHCl_3$, it rapidly decomposed to eliminate ethyl chloride gas. So **1** reacted in two ways: the acylation of ArH and the decomposition, depending upon the reaction conditions. At a lower temperature, the rate of the decomposition might be much slower than that of the acylation. These reactions were

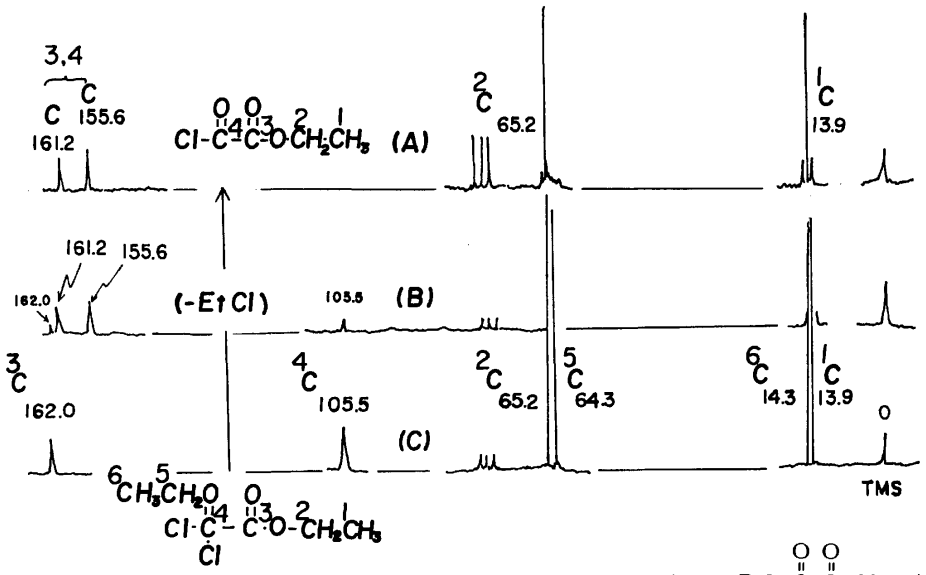

Fig. 1. C-13 NMR spectral change in the decomposition of **2** to EtO-C(=O)-C(=O)-Cl. (A) After 2 h at 200 °C, spectrum of EtO-C(=O)-C(=O)-Cl. (B) Spectrum of mixtures. (C) Spectrum of **2**; before heating.

Table 1. Yields of substituted phenylglyoxylates[a)]

Starting materials	3	Column No. Products Substituents	1 **1** (%) (Corr. value)	2 **1** or **11** (%) Max. value	3 Ethoxalyl chloride (%)	4 (%)
Mesitylene	**3a**	2, 4, 6-Me_3	53.0 (74)	90[b)] (**4a**)	47.9	—
o-xylene	**3b**	3, 4-Me_2	57.0 (88)	—	76	—
m-xylene	**3c**	2, 4-Me_2	50	—	56	—
p-xylene	**3d**	2, 5-Me_2	41 (61)	—	48.3	—
Toluene	**3e**	2-or 4-Me	43.2 (64.5) *o*/*p*=0.09	50[c)] (**4e**) *o*/*p*=0.18	31.6 *o*/*p*=0.01	79[g)]
Anisole	**3f**	2-or 4-MeO	27 (32) only *p*-	65[d)] *o*/*p*=0.23	63.4	79[g)]
Benzene	**3g**	H	—	20[e)]+3.6[f)]	13.6	50[h)]

a) All compounds recorded in this table gave satisfactory analysis. Isolated yields in all cases. Method A: ArH (0.05 mol) and **1** (0.05 mol) were dissolved in 100 ml of $CHCl_3$ at 0—5 °C. Powdered $AlCl_3$ (0.1 mol) was added into the well-stirring reaction mixture for 20—40 min. The reaction time is 80—120 min. b) CH_2Cl_2 solvent; mesitylene (0.50 mol), $AlCl_3$ (0.10 mol), **2** (0.05 mol). c) Reaction time is 1 day at r.t. d) **1** was added to the CH_2Cl_2 solution. e) Benzene (0.24 mol), $AlCl_3$ (0.2 mol), **1** (0.1 mol). f) Another compound=ethyl *p*-ethylphenylglyoxylate. g)Ref. 2; solvent is $C_6H_5NO_2$. h) Ref. 2; solvent is C_6H_6. In our case (Table 2), the yields is 47%.

dependent on the following three factors: the solvents, the catalysts, and the reagent ratio. 1) The best solvent is CH_2Cl_2. Other usable solvents are $CHCl_3$ and CH_3NO_2, but CS_2, Et_2O, and $C_6H_5NO_2$ are not good solvents. 2) The best catalysts are $AlCl_3$, $TiCl_4$, and $SnCl_4$. When $TiCl_4$ was used, the reaction worked well in a homogeneous state. This reaction will be reported in future. 3) The reagent ratio of ArH, $AlCl_3$, and **1** or **2** must be the most suitable value in response to the reactivity of ArH; the ratios of 1:2:1 and 10:2:1 were generally used.

In the cases of mesitylene, toluene, benzene, and anisol, the reactions under the optimum conditions were tried; the maximum yields are shown in the second column of Table 1.

The configuration of the Aromatic α-Keto Esters. The aromatic α-keto esters (**3e—g**) were identified with the authentic samples obtained by the known methods as mentioned above Eq. 3 and in Ref. 3 (*cf.* footnote of Table 1). By using ^1H and ^{13}C NMR spectra of each compound, we were able to assign their configurations.

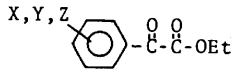

3a; 2,4,6-Me_3
3b; 3,4-Me_2
3c; 2,4-Me_2
3d; 2,5-Me_2
3e; 2-or 4-Me
3f; 2-or 4-MeO

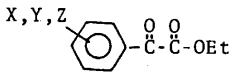

3g; unsubstituted

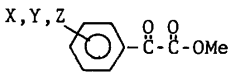

4

There were many other compounds (**3a—d**) which could not be found in the literature, but these configurations were determined by ^{13}C NMR spectra. The observed chemical shifts were compared with the calculated values; the values almost coincided.

In the case of toluene, the product was a mixture whose composition were variable with the reaction conditions; it always included two compounds. The C, H analysis of the mixture coincided with the calculated values for $C_{11}H_{12}O_3$. The isolation of one of the mixtures was very difficult. From the reaction of toluene with methoxalyl chloride (*cf*; Table 2), an almost pure compound (95%), one of the two compounds, was obtained; its configuration was determined to be methyl *p*-methylphenylglyoxylate. The other compound, therefore, was deduced to be methyl *o*-methylphenylglyoxylate.

In the case of anisole, the same method was applied.

Table 2. Yields of substituted phenylglyoxylates[a)]

Starting materials		Column 1 Reagent **2**	Column 2 Reagent MeO-C(=O)-C(=O)-Cl
Mesitylene	**4a**	15	18
Toluene	**4e**	0[b)]	50 (*o*/*p*=0.05)
Anisole	**4f**	0[c)]	50 (*o*-: trace)
Benzene	**4g**	38 and 47[d)]	62

a) Method B: mole ratio of ArH: $AlCl_3$: **2** or MeO-C(=O)-C(=O)-Cl was about 30:2:1. An acylating reagent was added at the end. b) No distillable product was obtained. c) Some other product was obtained. d) To the cooled mixture of ArH and an acylating reagent, $AlCl_3$ was added.

The Reaction of Ethoxalyl Chloride with ArH in $CHCl_3$. The yields of classical Friedel-Crafts reaction using ethoxalyl chloride as an acylating reagent are shown in column 4. These values were very large, in comparison with our data, although the reaction conditions were very severe, at higher temperature for longer reaction time in CH_2Cl_2 or in nitrobenzene. We also reexamined this reaction under our reaction conditions (0 °C, 80 min, in $CHCl_3$); the available data are tabulated in the column 3.

These values in the columns 1 and 3 show only small differences. However, under the reaction without solvents, great diffrences were observed between the reaction of **2** with ArH and that of methoxalyl chloride with ArH (Columns 1 and 2 in Table 2).

*The Reaction of **2** and Methoxalyl Chloride with ArH without a Solvent.* Compounds **2** was a little more stable under these reaction conditions than **1** was, although **2** decomposed to eliminate methyl chloride under more severe conditions (*e.g.*, at bp of CH_2Cl_2). The reaction of **2** with ArH at 0 °C was studied in detail. To an aromatic hydrocarbon containing 2 equivs of $AlCl_3$, 1 equiv of **2** was added with good stirring and cooling with ice. The results with respect to mesitylene, toluene, anisole, and benzene are shown in the first column of Table 2. In the second column, the yields of aromatic α-keto esters obtained by the reaction of methoxalyl chloride with ArH without solvent are shown. The yield of the reaction of **2** with mesitylene decreased from 53% (in the case of **1**) to 15%. In the case of anisole, an aromatic α-keto ester was not obtained, but some other compound[4)] was obtained. In the case of toluene, none of the product could be distilled out. Only when $AlCl_3$ was added to the toluene solution of **2**, a little amount of α-keto ester and some other product happened to be obtained. We can not yet explain why the reaction in toluene did not work well.

In contrast to this reaction, the reaction of methoxyalyl chloride with ArH was a normal reaction and the yields increased except only the case of mesitylene.

The Reaction Mechnism. An analogous reaction to this was reported earlier by Riech and Gross:[5)] the formylation of ArH by dichloro(methoxy)methane in the presence of $AlCl_3$, $TiCl_4$, and $SnCl_4$ (Eq. 6). They explained the reaction route through the parenthesized intermediate.

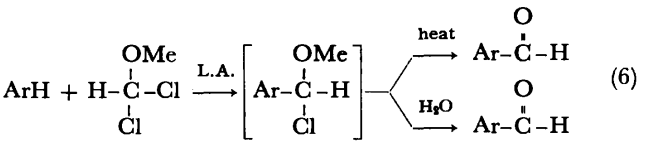

(6)

The parenthesized compound was not the final product, but the reaction product, which was labile to heat or to work-up condition.

The same mechanism was most probable for the aromatic α-keto ester reaction.

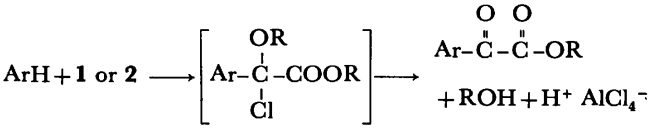

In the case of **1**, another mechanism could be as follows:

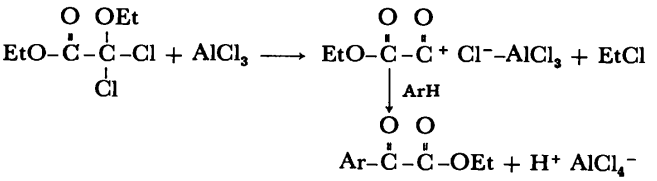

When ArH was added after the treatment of **1** or **2** with $AlCl_3$ in a solvent, the yield of the product greatly decreased or reduced to zero. Thus, the latter mechanism is not probable. The parenthesized compound of this reaction Ar-C(OR)(Cl)-C(=O)-OR, is more stable than Ar-C(OMe)(Cl)-H, that of the formylation reaction. The parenthesized compound was the reaction product, and then it changed to aromatic α-keto esters under work-up.

Aromatic α-keto esters were generally synthesized through the oxidation of mandelic acid derivatives,[6)] but the yield of oxidation was generally low. Recently a new synthesis of α-keto esters and acids was reported by Mosher and *et al.*[7)] The acylating reagents was

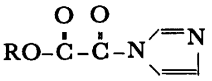 , which was prepared by the reaction between ethoxalyl chloride and imidazole. This method is the best method on laboratory scale. In comparison to these methods, **1** and **2** are easily prepared in large scale and the cost to prepare **1** and **2** is most inexpensive. In addition, **1** and **2** have other usabilities in organic synthesis. The other kinds of aromatic α-keto esters could be synthesized using **1**, **2**, ethoxalyl and methoxalyl chloride. The application of this reaction to halobenzenes, biphenyl, and naphthalene will be reported in future.

Experimental

Measuremets. Melting and boiling points were uncorrected. ^{1}H NMR spectra were measured on a JEOL-60 (60 MHz) spectrometer with tetramethylsilane as an internal standard, and IR spectra on a Hitachi EPI-G_2 infrared spectrometer.^{13}C NMR spectra were measured on a JEOL-PFT-100 spectrometer.

Materials. The following materials were synthesized according to the reported method[1] and an improved one.

1. An equivalent mole of diethyl oxalate (2mol) and PCl_5 (2mol) were mixed and then heated at 105—115 °C for 6—10 h. The reaction mixture was distilled through a Vigrew column by a water pump. The amounts of the third, fourth and fifth fraction (bp of them, 80—92 °C/18 mmHg, 92—98 °C/18mmHg and 99 °C/18mmHg—104 °C/24mmHg) were 79, 44, and 194 g; their purities were 76, 88, and 95%. These fractions was further subjected to efficient fractional distillation. The total yield amounted to 67% (1.35 mol), as found by GLC analyses.

2. Dimethyl oxalate (236 g, 2.0 mol) and PCl_5 (417 g, 2.0 mol) were mixed in a solid state and heated at 110 ± 5 °C for 10—15 h. An aliquot was analyzed by GLC. After dimethyl oxalate of more than 80% converted to **2**, oxyphosphoryl chloride and then **2** were distilled off from the reaction mixture. The first fraction (bp 35 °C/49 mmHg) and the second fraction (bp 44 °C/36 mmHg—50 °C/36 mmHg) were composed of oxyphosphoryl chloride and a little dimethyl oxalate. The third fraction (bp 77 °C/34 mmHg—87 °C/32 mmHg) was composed of 60% of **2** and 40% of dimethyl oxalate. The GLC analysis gave the total yield as 190 g, 55%. The third and fourth fractions were combined and this was subjected to efficient distillation. The fraction of constant bp, 80 °C/22 mmHg (98 g, 28%) was analyzed as shown below. Calcd for $C_4H_6O_3Cl_2$: C, 27.77; H, 3.49; Cl, 40.98%. Found: C, 27.96; H, 3.42; Cl, 40.83%. ^{1}H NMR δ=3.82 (s, 3H) 3.93 (s, 3H). IR: $\nu_{C=O}$ 1770 cm^{-1}: $\delta_{C=O\ or\ C=O}$ 1285, 1200, and 1150 cm^{-1}: ν_{C-Cl} 660 cm^{-1}.

Reaction of Substituted Benzene with 1 or 2 in $CHCl_3$. The substituted benzene (0.05 mol) and **1** or **2** (0.05 mol) were dissolved in 100 ml of $CHCl_3$ and kept at 0—5 °C on the ice bath. Powdered $AlCl_3$ (0.1 mol) was added into the well-stirred reaction mixture for 20—40 min. Then it was kept at 0—5 °C for 80 min. The reaction mixture was

Table 3. C and H Analyses of Substituted Phenylglyoxylates

Products	Bp θ_b/°C(mmHg) Mp θ_m/°C	Obsd (Calcd) (%) C	H
4a	129—131(3)	69.87(69.89)	7.00(6.84)
3e	148—149(10)[a]	68.46(68.43)	6.26(6.29)
4e	122(5)[a]	67.68(67.41)	5.66(5.66)
3f	140(5)[a]	63.44(63.45)	5.99(5.81)
4f	150(4)[a]	61.97(61.85)	5.14(5.19)
3g	—	—	—
4g	120—123(6)[b]	65.96(65.84)	4.92(4.92)
3b	140(4)	69.74(69.89)	7.12(6.84)
3c	53	69.61(69.89)	6.78(6.84)
3d	135(5)	70.11(69.89)	6.88(6.84)
3h[c]	122(5)	69.96(69.89)	6.93(6.84)

a) Bp of a mixture of *o*- and *p*-isomer. b) 250—255 °C/760 mmHg; R.B.Corson *et al. Org. Synth.* Coll. Vol. I, 241 (1955). c) **3h**=Ethyl *p*-ethylphenylglyoxylate prepared by Eq. 3.

Table 4. Carbon-13 NMR chemical shifts of **3** and **4**[a]

Substituents		C_1	C_2	C_3	C_4	C=O	O-C=O	$-CH_2$	$-CH_3$	Me *et al.*
2, 4, 6-Me_3	**3a**	133.0	136.2	129.0	141.0	191.9	162.8			^{2,6}(19.6, ^{4}21.1)
	4a	133.0	136.2	129.0	141.0	191.4	163.6		52.9	
4-Me	**3e**	129.7	(129.8,	129.6)[b]	146.3	185.8	164.3			
	4e									
4-MeO	**3f**	125.4	132.4	114.4	165.2	185.1	164.4	62.1	14.1	
	4f	125.4	132.6	114.2	165.0	184.4	164.3		52.6	$^{MeO-}$55.7
H	**3g**	132.5	129.9	128.9	134.9	186.5	164.0	62.3	14.1	
	4g	132.4	130.0	128.8	134.9	186.0	164.0		52.7	
		C_1	C_2	C_3	C_4	C_5	C_6	C=O	O-C=O	Me *et al.*
3, 4-Me_2	**3b**	130.3	130.1	137.4	145.0	130.7	127.8	186.3	164.2	^{3}19.6, ^{4}20.1
2, 4-Me_2	**3c**	128.4	141.1	133.3	144.9	126.7	132.7	188.5	165.0	^{2,4}21.5
2, 5-Me_2	**3d**	131.0	138.0	132.2	134.5	135.5	132.6	188.9	164.7	^{2,5}20.7, 20.8

a) Samples were 5—10% w/v. Solvent is $CDCl_3$. b) Similar values in paretheses may be interchanged.

Numbering of C:

Upper: 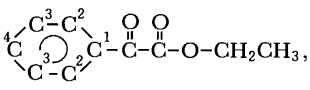 , Bottom: 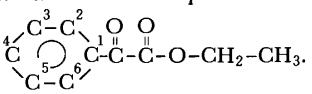 .

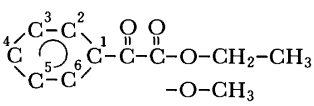

-O-CH_3 : 4

poured into ice water and then $CHCl_3$ was added; this mixture was extracted two times and the $CHCl_3$ solution was washed with a 10% solution of sodium hydrogencarbonate and then with water and dried with $MgSO_4$. After distilling off $CHCl_3$, the residue was distilled by an oil pump. The distillates were analyzed by GLC, IR, and NMR. The chemical shift of ^{13}C NMR was compared with the calculated value. The elemental analyses of all of the products showed that the structures were right (see Table 3).

The Reaction of Ethoxalyl Chloride with Aromatics in $CHCl_3$. These reactions were carried out in the same way as above.

The Reaction of **2** *or Methoxalyl Chloride with ArH without Solvents.* Powdered $AlCl_3$ (0.05 mol) was suspended in the cooled aromatics (1.5 mol). Compound **2** or methoxalyl chloride (0.025 mol) was added to the cooled mixture for about 10—25 min. After 2 h the organic layer was washed with 10% sodium hydrogen-carbonate solution and water, and was dried with $MgSO_4$. After distilling off $CHCl_3$, the residue was distilled by an oil pump. All products gave satisfactory analyses of C and H.

^{13}C NMR Spectra of **3** *and* **4**. The chemical shifts of a series of **3** and **4** in $CDCl_3$ solution using TMS as a standard, are summarized in Table 4. The assignments were made with the help of off-resonance decoupling, the comparison of the signal intensity, and the use of the long range coupling constants. Furthermore, the observed chemical shifts were compared with the calculated values. Each signal were reasonably assigned to be due to the corresponding carbon, on the basis of the signals of ethyl phenylglyoxylate and methyl phenylglyoxylate.

References

1) R. Anschutz, *Ann.*, **254**, 1 (1889).
2) L. Bouveault, *Bull. Chem. Soc. Fr.*, **15**, 1014 (1896); **17**, 363, 366, 940, 943, and 947 (1898).
3) K. Kindler, W. Metzendorf and Dschi-yin-Kwok, *Ber.*, **70**, 308 (1943).
4) A further reaction occurred, which will be reported in future.
5) A. Rieche, H. Gross, and E. Hoeft, *Org. Synth.* Coll. Vol. V, p. 49 and 365 (1973).
6) B. B. Corson, Ruth A. Dodge, S. A. Harris, and R. K. Hazen, *Org. Synth.* Coll. Vol. I, p. 241 (1967).
7) J. S. Nimitz and H. S. Mosher, *J. Org. Chem.*, **46**, 211 (1981).

Studies of Bitter Peptides from Casein Hydrolyzate. IX.[1] Syntheses and Bitter Taste of Bitter Peptide BPIa Dimer, (Arg-Gly-Pro-Pro-Phe-Ile-Val)$_2$, and Gly-Gly BPIa Derivatives[2]

Ichizo MIYAKE, Katsushige KOUGE, Hidenori KANEHISA, and Hideo OKAI*
Department of Fermentation Technology, Faculty of Engineering, Hiroshima University, Shitami, Saijo-cho, Higashihiroshima 724
(Received October 1, 1983)

In order to elucidate the relationship between taste exhibition and chemical structure of bitter peptide BPIa, di-BPIa, Gly-Gly-BPIa, BPIa-Gly-Gly, and Gly-Gly-BPIa-Gly-Gly were synthesized. All of the peptides possessed a strong bitter taste of the same level as that of BPIa. In addition, the CD curves of the peptides were similar to that of BPIa. The results suggested that their spatial structures are essentially similar and that the whole molecular shape of BPIa contributes to its bitterness.

Minamiura *et al.* isolated a bitter heptapeptide named BPIa from cow milk casein hydrolyzate by bacterial proteinase and determined its amino acid sequence to be H-Arg-Gly-Pro-Pro-Phe-Ile-Val-OH.[3] We synthesized it and confirmed that synthetic BPIa was identical to Minamiura's natural one.[4] Synthetic BPIa possessed an extremely bitter taste, with a threshold value of 0.05 mM (1 M=1 mol dm^{-3}). To elucidate the relationship between chemical structure and bitterness of BPIa, various fragments and analogs which possessed several characteristic features of BPIa have been prepared in our laboratory. N-Terminal hexapeptide (des-Val^7-BPIa) exhibited the same bitterness as BPIa, whereas the bitterness of des-Arg^1-BPIa and of N-terminal pentapeptide fragment were much weaker than that of BPIa.[5] These results indicated that both arginine residue in the N-terminal position and hydrophobic amino acids in the C-terminal moiety are necessary for the intense bitter taste of BPIa. This finding was favored by the bitterness exhibited by both Arg^1- and C-terminal tripeptide-substituted analogs of BPIa.[6,7] On the other hand, the analogs in which prolylproline resiude was substituted for glycylglycine or D-prolyl-D-proline residues exhibited a weaker bitterness than BPIa, and their CD curves measured in water were different from that of BPIa.[8] The results suggested that the spatial structure of BPIa molecule attributed to prolylproline in the center also contributes to its bitter taste. In addition, retro-BPIa, which has the reverse sequence of BPIa, exhibited a strong bitter taste of the same level as that of BPIa. This indicated that it is possible for the N-terminal basic amino acid residue and C-terminal hydrophobic amino acids moiety in BPIa to change places with each other.[9] In the previous paper,[1] we reported that *cyclo*-BPIa, in which N-terminal arginine and C-terminal valine residues were combined, possessed the same bitternss as BPIa and that its CD curve measured in water was similar to that of BPIa. The findings of *cyclo*-BPIa suggested that the two bitter functional groups of both terminals of BPIa are situated close together in the molecule and that the bitterness of BPIa is caused by its characteristic spatial structure which is analogous to that of *cyclo*-BPIa.

The next subject in the investigations of BPIa is to examine the relationship of molecular size to bitter taste. We prepared a dimerized BPIa (di-BPIa, **1**) and ascertained whether or not the synergistic effect by molecular size for bitter taste was produced.

The synthesis of di-BPIa was carried out according to Fig. 1. Boc-Arg(NO_2)-Gly-OH was coupled with H-Pro-Pro-Phe-Ile-Val-OBzl·HCl, which was an intermediate in the synthesis of BPIa,[4] by the mixed anhydride method to yield the protected BPIa derivative (**12**). It was converted to the corresponding heptapeptide ester hydrochloride (**13**) by the action of hydrogen chloride in formic acid. Then **13** was coupled with the acid (**14**) derived from another intermediate in the synthesis of BPIa, Z-Arg(NO_2)-Gly-Pro-Pro-Phe-Ile-Val-OBzl, by the dicyclohexylcarbodiimide-1-hydroxybenzotriazole (DCC-HOBt) method to yield acyltetradecapeptide ester (**15**). The catalytic hydrogenation of **15** gave di-BPIa (**1**). The purity of final product and its intermediates was confirmed by thin-layer chromatography on two solvent systems and by elemental analyses.

Taste of peptides was organoleptically determined by panel evaluation employing five people. Di-BPIa

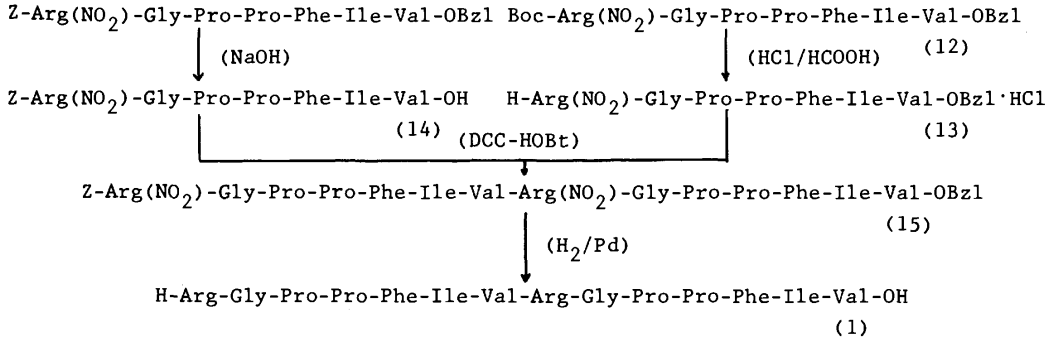

Fig. 1. Synthesis of di-BPIa.

TABLE 1. THE THRESHOLD VALUE FOR BITTER TASTE OF BPIa AND ITS DERIVATIVES

Compound	Threshold value for bitter taste/mM
BPIa	0.05
di-BPIa (**1**)	0.04
Gly-Gly-BPIa (**2**)	0.08
BPIa-Gly-Gly (**3**)	0.05
Gly-Gly-BPIa-Gly-Gly (**4**)	0.04

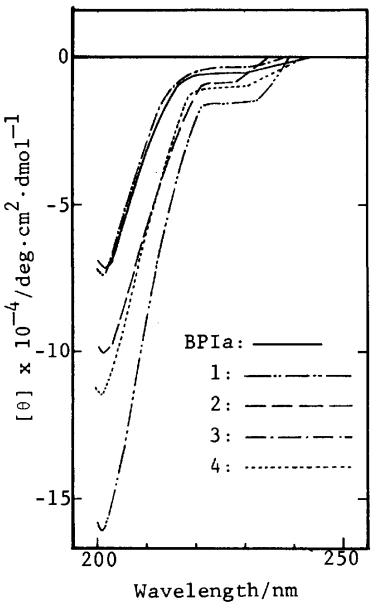

Fig. 2. CD curves of BPIa and its derivatives in water.

exhibited a strong bitter taste. Although we at first expected that di-BPIa would exhibit much stronger bitterness than BPIa, actually its threshold value was nearly equal to that of BPIa, as shown in the Table. This suggested that the bitterness of di-BPIa is caused by one of a pair of BPIa molecules and that the size of BPIa molecule is fit for a receptor of bitter taste in a taste bud. CD curves of di-BPIa and BPIa measured in water are presented in Fig. 2. The pattern of di-BPIa is similar to that of BPIa. It seems that the spatial structure of BPIa, which is important for showing the strong bitter taste, is kept in di-BPIa.

To further ascertain the relationship of the molecular shape of BPIa to its bitter taste, we prepared Gly-Gly-BPIa (**2**), BPIa-Gly-Gly (**3**), and Gly-Gly-BPIa-Gly-Gly (**4**), in which a tasteless glycylglycine was coupled to either the N-terminal or the C-terminal or both terminals of BPIa and examined whether both the strong bitter taste and CD pattern of BPIa were maintained in those BPIa derivatives in spite of the introduction of glycylglycine residue.

The sequence of reactions employed for the synthesis of Gly-Gly-BPIa is shown in Fig. 3. Condensation of Z-Gly-Gly-OH with H-Arg(NO_2)-Gly-OBzl·HCl by the 1-ethyl-3-(3-dimethylaminopropyl)carbodiimide (EDC) method gave Z-Gly-Gly-Arg(NO_2)-Gly-OBzl (**5**). Saponification of **5** gave the corresponding acid (**6**). Then **6** was coupled with H-Pro-Pro-Phe-Ile-Val-OBzl·HCl by DCC-HOBt method to yield acylnonapeptide ester (**7**). It was hydrogenated in the

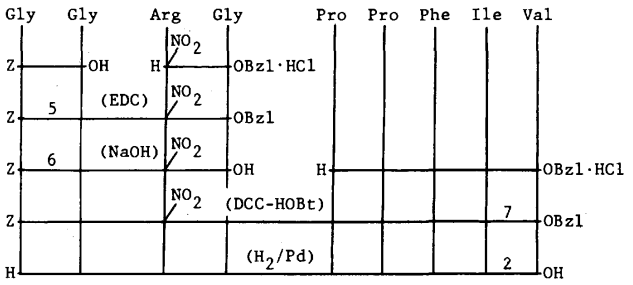

Fig. 3. Synthesis of Gly-Gly-BPIa.

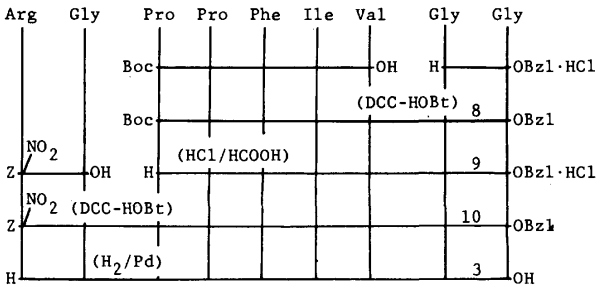

Fig. 4. Synthesis of BPIa-Gly-Gly.

presence of palladium black to yield Gly-Gly-BPIa (**2**).

The synthetic route for BPIa-Gly-Gly is shown in Fig. 4. Boc-Pro-Pro-Phe-Ile-Val-OH, which was an intermediate in the synthesis of *cyclo*-BPIa,[1] was coupled with H-Gly-Gly-OBzl·HCl by DCC-HOBt method to yield the protected heptapeptide (**8**). It was converted to the corresponding heptapeptide ester hydrochoride (**9**) by the action of hydrogen chloride in formic acid. Condensation of Z-Arg(NO_2)-Gly-OH with **9** by DCC-HOBt method afforded the fully protected BPIa-Gly-Gly (**10**). The catalytic hydrogenation of **10** yielded BPIa-Gly-Gly (**3**). Gly-Gly-BPIa-Gly-Gly (**4**) was yielded by hydrogenation of Z-Gly-Gly-Arg(NO_2)-Gly-Pro-Pro-Phe-Ile-Val-Gly-Gly-OBzl (**11**) derived from **6** and **9** by DCC-HOBt method.

The results of sensory tests are listed in the Table. All the Gly-Gly introduced BPIa derivatives possessed a strong bitter taste of the same level as BPIa. The results indicated that glycylglycine residue coupled not only to the N-termial but also to the C-terminal of BPIa did not affect the bitterness of BPIa. The CD curves of these peptides in water are shown in Fig. 2. These indicated similarly shaped curves with nagative troughs at 202 nm to that of BPIa. The results of CD measurements indicated that the spatial structure of BPIa is kept in those BPIa derivatives and that the structure causes the bitterness of BPIa.

Experimental

All the melting points are uncorrected. Thin-layer chromatography was carried out on Merck silica gel G with the solvent systems: R_f^1, 1-butanol-acetic acid-pyridine-water (4:1:1:2, v/v); R_f^2, chloroform-methanol (5:1, v/v). Spots of materials possessing a free amino group on a thin layer plate were detected by spraying ninhydrin, and those of amino group blocked materials by spraying 25% hydrogen bromide in acetic acid and then ninhydrin. The optical

rotations were measured on a Union PM-101 polarimeter. Amino acid analyses in acid hydrolyzate with 6 M hydrochloric acid at 110°C for 72 h were performed with a Hitachi amino acid analyzer, KLA-5 type. Prior to analyses, the compounds were dried over phosphorus pentaoxide at 66°C and 2 mmHg (1 mmHg≈133.332 Pa) for 2 h.

Z-Gly-Gly-Arg(NO_2)-Gly-OBzl (5). To a solution of Z-Gly-Gly-OH[10] (2.66 g, 10 mmol), H-Arg(NO_2)-Gly-OBzl·HCl[1] (4.0 g, 10 mmol), and NMM (1.1 ml, 10 mmol) in DMF (20 ml), EDC (2.12 ml, 15 mmol) was added at 0°C with stirring. The reaction mixture was stirred for 3 h at 0°C, then at room temperature overnight. A large amount of water was poured into the mixture. The obtained precipitate was filtered, and washed with 4% sodium hydrogencarbonate, 0.5 M hydrochloric acid, and water successively. It was recrystallized from hot methanol: yield 4.68 g (76%); mp 101—103°C; $[\alpha]_D^{20}$ −8° (*c* 2, DMF); R_f^1 0.86 and R_f^2 0.57.

Found: C, 51.00; H, 5.54; N, 17.85%. Calcd for $C_{27}H_{34}O_9N_8 \cdot H_2O$: C, 51.25; H, 5.74; N, 17.71%.

Z-Gly-Gly-Arg(NO_2)-Gly-OH (6). Compound **5** (1.83 g, 3 mmol) was saponified with 1 M sodium hydroxide (3.6 ml, 3.6 mmol) in methanol (15 ml) for 1.5 h at room temperature. After evaporation, the aqueous solution was acidified to pH 3 with 1 M hydrochloric acid, and extracted with 1-butanol. The extract was washed with water and dried over anhydrous sodium sulfate. The filtrate was evaporated *in vacuo* and the residue was crystallized with ether. It was recrystallized from methanol-ether: yield 0.94 g (60%); mp 139°C; $[\alpha]_D^{20}$ −15° (*c* 1, DMF); R_f^1 0.62 and R_f^2 0.07.

Found: C, 45.70; H, 5.35; N, 21.59%. Calcd for $C_{20}H_{28}O_9N_8$: C, 45.80; H, 5.38; N, 21.37%.

Z-Gly-Gly-Arg(NO_2)-Gly-Pro-Pro-Phe-Ile-Val-OBzl (7). To a solution of **6** (0.53 g, 1 mmol) and H-Pro-Pro-Phe-Ile-Val-OBzl·HCl[4] (0.70 g, 1 mmol) and NMM (0.11 ml, 1 mmol) in DMF (8 ml), HOBt (0.15 g, 1.1 mmol), and DCC (0.25 g, 1.2 mmol) were added at 0°C with stirring. The reaction mixture was stirred for 3 h at 0°C and then at room temperature overnight. DCUrea was filtered off and the filtrate was dissolved in 1-butanol. The solution was washed with 4% sodium hydrogencarbonate, 0.5 M hydrochloric acid, and water successively, then dried over anhydrous sodium sulfate. The filtrate was evaporated *in vacuo* and the residue was crystallized with ether. It was recrystllized from methanol-ether: yield 0.78 g (67%); mp 125°C (decomp); $[\alpha]_D^{20}$ −51° (*c* 1, DMF); R_f^1 0.81 and R_f^2 0.70.

Found: C, 56.98; H, 6.79; N, 15.17%. Calcd for $C_{57}H_{77}O_{14}N_{13} \cdot 2H_2O$: C, 56.86; H, 6.78; N, 15.12%.

H-Gly-Gly-Arg-Gly-Pro-Pro-Phe-Ile-Val-OH·AcOH (2). Compound **7** (0.47 g, 0.4 mmol) was dissolved in a mixture of methanol (5 ml) and acetic acid (5 ml), and hydrogenated in the presence of palladium black for 24 h at room temperature. The filtrate from catalyst was evaporated *in vacuo* and the residual oil was solidified by the aid of acetone. It was recrystallized from methanol-ether: yield 0.31 g (80%); $[\alpha]_D^{20}$ −122° (*c* 0.5, H_2O); R_f^1 0.65 and R_f^2 0.00. Amino acid ratios in acid hydrolyzate: Arg 0.90, Gly 2.65, Pro 2.03, Phe 1.07, Ile 1.00, Val 1.00.

Found: C, 53.42; H, 7.42; N, 16.54%. Calcd for $C_{42}H_{66}O_{10}N_{12} \cdot CH_3COOH \cdot 2H_2O$: C, 53.10; H, 7.50; N, 16.89%.

Boc-Pro-Pro-Phe-Ile-Val-Gly-Gly-OBzl (8). To a solution of Boc-Pro-Pro-Phe-Ile-Val-OH[1] (2.02 g, 3 mmol), H-Gly-Gly-OBzl·HCl[11] (1.16 g, 4.5 mmol) and NMM (0.50 ml, 4.5 mmol) in DMF (10 ml), HOBt (0.61 g, 4.5 mmol) and DCC (0.93 g, 4.5 mmol) were added at 0°C with stirring. The reaction mixture was stirred for 3 h at 0°C and kept in a refrigerator overnight. DCUrea was filtered off and the filtrate was dissolved in 1-butanol. The solution was washed with 4% sodium hydrogencarbonate, 4% citric acid, and water successively, then dried over anhydrous sodium sulfate. The filtrate was evaporated *in vacuo* and the residue was crystallized with ether: yield 2.45 g (93%); mp 193—196°C; $[\alpha]_D^{20}$ −36° (*c* 1, DMF); R_f^1 0.86 and R_f^2 0.76.

Found: C, 62.87; H, 7.86; N, 11.28%. Calcd for $C_{46}H_{65}O_{10}N_7$: C, 63.06; H, 7.50; N, 11.19%.

H-Pro-Pro-Phe-Ile-Val-Gly-Gly-OBzl·HCl (9). Compond **8** (1.75 g, 2 mmol) was dissolved in 98% formic acid (5 ml) and 3.5 M hydrogen chloride in dioxane (10 ml) at 0°C. After 30 min, the solvent was removed by evaporation and the oily residue was solidified by the aid of ether: yield 1.60 g (98%); mp 160—162°C; $[\alpha]_D^{20}$ −39° (*c* ,1 DMF); R_f^2 0.77 and R_f^2 0.44.

Found: C, 58.12; H, 7.17; N, 11.69%. Calcd for $C_{41}H_{57}O_8N_7 \cdot 2H_2O$: C, 58.04; H, 7.37; N, 11.56%.

Z-Arg(NO_2)-Gly-Pro-Pro-Phe-Ile-Val-Gly-Gly-OBzl (10). This compound was prepared from Z-Arg(NO_2)-Gly-OH[4] (0.50 g, 1 mmol) and **9** (0.81 g, 1 mmol) as described for the preparation of **7**: yield 0.97 g (83%); mp 145°C (decomp); $[\alpha]_D^{20}$ −41° (*c* 1, DMF); R_f^1 0.84 and R_f^2 0.70.

Found: C, 58.80; H, 6.70; N, 15.35%. Calcd for $C_{57}H_{77}O_{14}N_{13}$: C, 58.60; H, 6.64; N, 15.59%.

H-Arg-Gly-Pro-Pro-Phe-Ile-Val-Gly-Gly-OH·AcOH (3). Compound **10** (0.47 g, 0.4 mmol) was treated with hydrogen as described for the preparation of **2**: yield 0.32 g (83%); $[\alpha]_D^{20}$ −90° (*c* 0.5, H_2O); R_f^1 0.62 and R_f^2 0.00. Amino acid ratios in acid hydrolyzate: Arg 0.95, Gly 3.38, Pro 1.84, Phe 1.04, Ile 1.00, Val 0.94.

Found: C, 52.78; H, 7.36; N, 16.83%. Calcd for $C_{42}H_{66}O_{10}N_{12} \cdot CH_3COOH \cdot 2H_2O$: C, 53.10; H, 7.50; N, 16.89%.

Z-Gly-Gly-Arg(NO_2)-Gly-Pro-Pro-Phe-Ile-Val-Gly-Gly-OBzl (11). This compound was prepared from **6** (0.53 g, 1 mmol) and **9** (0.81 g, 1 mmol) as described for the preparation of **7**: yield 0.96 g (75%); mp 149°C (decomp); $[\alpha]_D^{20}$ −41° (*c* 1, DMF); R_f^1 0.85 and R_f^2 0.59.

Found: C, 57.18; H, 6.64; N, 16.54%. Calcd for $C_{61}H_{83}O_{16}N_{15}$: C, 57.13; H, 6.52; N, 16.38%.

H-Gly-Gly-Arg-Gly-Pro-Pro-Phe-Ile-Val-Gly-Gly-OH·AcOH (4). Compound **11** (0.39 g, 0.3 mmol) was hydrogenated as described for the preparation of **2**: yield 0.23 g (71%); $[\alpha]_D^{20}$ −100° (*c* 0.5, H_2O); R_f^1 0.59 and R_f^2 0.00. Amino acid ratios in acid hydrolyzate: Arg 1.15, Gly 5.28, Pro 2.02, Phe 1.02, Ile 1.00, Val 0.95.

Found: C, 53.16; H, 7.42; N, 17.84%. Calcd for $C_{46}H_{72}O_{12}N_{14} \cdot CH_3COOH \cdot H_2O$: C, 52.83; H, 7.12; N, 17.97%.

Boc-Arg(NO_2)-Gly-Pro-Pro-Phe-Ile-Val-OBzl (12). Boc-Arg(NO_2)-Gly-OBzl[1] (1.41 g, 3 mmol) was saponified with 1 M sodium hydroxide (3.6 ml, 3.6 mmol), as described for the preparation of **6**, except for acidification. Aqueous 10% citric acid solution was used instead of 1 M hydrochloric acid: yield of hygroscopic Boc-Arg(NO_2)-Gly-OH, 0.74 g (67%); R_f^1 0.69 and R_f^2 0.08. Then this compound was coupled with H-Pro-Pro-Phe-Ile-Val-OBzl·HCl[4] to yield **12**. To a solution of Boc-Arg(NO_2)-Gly-OH (0.74 g, 2 mmol) and NMM (0.22 ml, 2 mmol) in DMF (6 ml), ethyl chloroformate (0.2 ml, 2 mmol) was added at −5°C with stirring. After 10 min, a precooled solution of H-Pro-Pro-Phe-Ile-Val-OBzl·HCl[4] (1.40 g, 2 mmol) and NMM (0.22 ml, 2 mmol) in chloroform (4 ml) was added to it. The reaction mixture was stored in an ice bath for 1 h, then at room temperature overnight. The mixture was evaporated *in vacuo* and the residue was dissolved in ethyl acetate. The solution was washed with 4% sodium hydrogencarbonate, 4% citric acid, and water successively, then dried over anhydrous sodium sulfate. The filtrate was evaporated *in vacuo* and the residual oil was crystallized with ether; yield 1.45 g (71%); mp 130°C (decomp); $[\alpha]_D^{20}$ −49° (*c* 1, DMF); R_f^1 0.86 and R_f^2 0.69.

Found: C, 58.66; H, 7.27; N, 15.25%. Calcd for $C_{50}H_{73}O_{12}N_{11}$: C, 58.86; H, 7.21; N, 15.10%.

H-Arg(NO_2)-Gly-Pro-Pro-Phe-Ile-Val-OBzl·HCl (13). Compound **12** (1.02 g, 1 mmol) was treated with hydrogen

chlorid as described for the preparation of **9**: yield 0.84 g (88%); mp 157—160°C; $[\alpha]_D^{20}$ −47° (*c* 1, DMF); R_f^1 0.78 and R_f^2 0.31.

Found: C, 55.32; H, 6.89; N, 15.60%. Calcd for $C_{45}H_{66}O_{10}N_{11}Cl \cdot H_2O$: C, 55.46; H, 7.03; N, 15.81%.

Z-Arg(NO$_2$)-Gly-Pro-Pro-Phe-Ile-Val-OH (14). To a solution of Z-Arg(NO$_2$)-Gly-Pro-Pro-Phe-Ile-Val-OBzl[4] (1.05 g, 1 mmol) in methanol (5 ml), 1 M sodium hydroxide (2 ml, 2 mmol) was added. After 6 h at room temperature, the mixture was evaporated *in vacuo* and diluted with water. The solution was extracted with ethyl acetate. The aqueous layer was acidified to pH 3 with 1 M hydrochloric acid and extracted with 1-butanol. The extract was washed with water and dried over anhydrous sodium sulfate. The filtrate was evaporated *in vacuo* and the product was crystallized with ether. It was recrystllized from methanol-ether: yield 0.81 g (84%); mp 185°C (decomp); $[\alpha]_D^{20}$ −43° (*c* 1, DMF); R_f^1 0.69 and R_f^2 0.18.

Found: C, 56.98; H, 6.61; N, 16.04%. Calcd for $C_{46}H_{65}O_{12}N_{11}$: C, 57.30; H, 6.80; N, 15.98%.

Z-Arg(NO$_2$)-Gly-Pro-Pro-Phe-Ile-Val-Arg(NO$_2$)-Gly-Pro-Pro-Phe-Ile-Val-OBzl (15). This compound was prepared from **13** (0.57 g, 0.6 mmol) and **14** (0.58 g, 0.6 mmol) as described for the preparation of **7**: yield 0.84 g (75%); mp 158°C (decomp); $[\alpha]_D^{20}$ −59° (*c* 1, DMF); R_f^1 0.82 and R_f^2 0.58.

Found: C, 61.88; H, 6.99; N, 16.49%. Calcd for $C_{98}H_{134}O_{21}N_{22} \cdot H_2O$: C, 61.88; H, 7.31; N, 16.20%.

H-Arg-Gly-Pro-Pro-Phe-Ile-Val-Arg-Gly-Pro-Pro-Phe-Ile Val-OH·2AcOH (1). Compound **15** (0.37 g, 0.2 mmol) was treated with hydrogen for 48 h as described for the preparation of **2**: yield 0.30 g (90%); $[\alpha]_D^{20}$ −84° (*c* 1, methanol); R_f^1 0.44 and R_f^2 0.00. Amino acid ratios in acid hydrolyzate: Arg 1.67, Gly 2.00, Pro 3.97, Phe 2.32, Ile 2.19, Val 2.07.

Found: C, 54.62; H, 7.40; N, 16.06%. Calcd for $C_{76}H_{118}O_{15}N_{20} \cdot 2CH_3COOH \cdot 5H_2O$: C, 54.53; H, 7.78; N, 15.90%.

The air-dried product lost 4.9% of its weight after drying or 2 h at 110°C and 2 mmHg. Calcd for $5H_2O$: 5.1%.

CD Measurement. This was performed with a JASCO J-20A. A cell of path length 0.2 mm was used and runs were made at ambient temperature. Patterns in water are presented in Fig. 2.

Sensory Test. Taste of the peptides was organoleptically determined by panel evaluation employing four people. A series of solutions of decreasing concentration, each half as strong as the preceding one, were prepared. Before tasting the sample, the mouth was thoroughly rinsed with deionized water. The sample solution was held in the mouth for *ca.* 10 s and then spit out, and the threshold value was determined. The results are listed in the Table.

The authors wish to express their thanks to Associate Professor Michio Kondo of Saga University for the CD measurements. Thanks are also due to Dr. Shinji Okumura of Ajinomoto Co. Inc., for supplying some amino acids.

References

1) Part VIII. I. Miyake, K. Kouge, H. Kanehisa, and H. Okai, *Bull. Chem. Soc. Jpn.*, in press.

2) Theabbreviations recommended by the IUPAC-IUB commission of Biochemical Nomenclature (*J. Biol. Chem.*, **247**, 977 (1972)) have been used. Amino acid symbols except glycine denote L-configuation. Additional abbreviations: DCC, dicycloheylcarbodiimide; DCUrea, *N,N'*-dicyclohexylurea; DMF, *N,N*-dimethylformamide; EDC, 1-ethyl-3-(3-dimethylaminopropyl)carbodiimide; HOBt, 1-hydroxyenzotriazole; NMM, *N*-methylmorpholine.

3) N. Minamiura, Y. Matsumura, J. Fukumoto, and T. Yamamoto, *Agric. Biol. Chem.*, **36**, 588 (1972).

4) H. Fukui, H. Kanehisa, N. Ishibashi, I. Miyake, and H. Okai, *Bull. Chem. Soc. Jpn.*, **56**, 766 (1983).

5) K. Otagiri, I. Miyake, N. Ishibashi, H. Fukui, H. Kanehisa, and H. Okai, *Bull. Chem. Soc. Jpn.*, **56**, 1116 (1983).

6) H. Kanehisa and H. Okai, *Bull. Chem. Soc. Jpn.*, **57**, 301 (1984).

7) K. Otagiri, T. Shigenaga, H. Kanehisa, and H. Okai, *Bull. Chem Soc. Jpn.*, **57**, 90 (1984).

8) I. Miyake, K. Kouge, H. Kanehisa, and H. Okai, *Bull. Chem. Soc. Jpn.*, **56**, 1678 (1983).

9) T. Shigenaga, K. Otagiri, H. Kanehisa, and H. Okai, *Bull. Chem. Soc. Jpn.*, **57**, 103 (1984).

10) F. Weygand and W. Steglich, *Chem. Ber.*, **93**, 2983 (1960).

11) L. Zervas and D. M. Theodoropoulos, *J. Am. Chem. Soc.*, **78**, 1359 (1956).

Studies of Bitter Peptides from Casein Hydrolyzate. X.[1] Synthesis and Bitter Taste of H-Arg-Gly-Pro-Phe-Pro-Ile-Ile-Val-OH Corresponding to C-Terminal Portion of β-Casein[2]

Hidenori KANEHISA,† Ichizo MIYAKE, Hideo OKAI,* Haruhiko AOYAGI,†† and Nobuo IZUMIYA††

Department of Fermentation Technology, Faculty of Engineering, Hiroshima University, Shitami, Saijo-cho, Higashihiroshima 724

††*Laboratory of Biochemistry, Faculty of Science, Kyushu University, Higashi-ku, Fukuoka 812*

(Received October 1, 1983)

In order to ascertain the validity of the structure of bitter peptide BPIa (H-Arg-Gly-Pro-Pro-Phe-Ile-Val-OH) isolated from casein hydrolyzate by Minamiura *et al.*, the C-terminal octapeptide of β-casein (H-Arg-Gly-Pro-Phe-Pro-Ile-Ile-Val-OH) determined by Ribadeau Dumas *et al.*, which is assumed to correspond to BPIa, was synthesized and compared with the synthetic BPIa which was confirmed to be identical with the natural one. The two synthesized peptides, however, did not match on thin-layer chromatography. The result indicates that the structure of BPIa need not be converted to Ribadeau Dumas' formula. The octapeptide possessed an extremely bitter taste, with a threshold value of 0.004 mM (1 M=1 mol dm^{-3}). It is the most bitter peptide.

Many bitter peptides have been found in the proteolytic hydrolyzates of casein. Minamiura *et al.* isolated a bitter heptapeptide named BPIa from cow milk casein hydrolyzate by alkaline proteinase of *Bacillus subtilis*, and determined its amino acid sequence to be H-Arg-Gly-Pro-Pro-Phe-Ile-Val-OH.[3] In this series of studies of bitter peptides, we previously described the synthetic identification of BPIa.[4] Synthetic BPIa was indistinguishable from Minamiura's natural one when thin-layer chromatography, paper electrophoresis, and carboxymethylcellulose column chromatography were used. We also found that the synthetic BPIa possessed an extremely bitter taste, whose threshold value was 0.05 mM. Ribadeau Dumas *et al.* determined the whole primary structure of bovine β-casein which contains the partial sequence of -Arg^{202}-Gly-Pro-Phe-Pro-Ile-Ile-Val^{209}-OH in the C-terminal portion.[5] Although the sequence of BPIa can not be found in the structure of Ribadeau Dumas' formula, it is similar to the C-terminal of the formula. Aoyagi and Izumiya synthesized a hexapeptide, H-Arg-Gly-Pro-Phe-Pro-Ile-OH (**1**), corresponding to the C-terminal portion (202—207) of β-casein and suggested that BPIa is to be changed so as to correspond to the C-terminal portion of Ribadeau Dumas' formula from the result that the synthetic hexapeptide possessed a bitter taste, with its threshold value of 0.13—0.25 mM.[6] They also synthesized a heptapeptide, H-Gly-Pro-Phe-Pro-Ile-Ile-Val-OH (**2**), corresponding to the C-terminal portion (203—209) and compared it with the natural peptide isolated from tryptic hydrolyzate of casein.[7] They reported that the two peptides matched each other closely and that the treshold value of bitter taste of the two peptides was 0.17—0.34 mM, and supported Ribadeau Dumas' formula.

In order to ascertain the validity of the structure of BPIa, it becomes necessary to compare BPIa with the C-terminal octapeptide (202—209) of Ribadeau Dumas' formula. In the present paper, we describe the synthesis of the octapeptide, H-Arg-Gly-Pro-Phe-Pro-Ile-Ile-Val-OH (**3**), the measurement of its threshold value of bitter taste, and the comparison between sythetic BPIa and **3**. Further, this paper deals with the synthesis of a heptapeptide, H-Arg-Gly-Pro-Phe-Pro-Ile-Val-OH (**4**), in which an isoleucine residue of **3** is missing.

The sequence of reactions employed for the synthesis of **3** is shown in Fig. 1. The syntheses of the intermediates (**5**, **6**, **15**, and **16**) had been performed and was described in the previou paper.[4] Compound **6** was coupled with Boc-Ile-OH by the mixed anhydride (MA) method to yield Boc-Ile-Ile-Val-OBzl (**7**). Removal of Boc group from **7** with hydrogen chloride in dioxane afforded the corresponding tripeptide ester hydrochloride (**8**). Compound **8** was coupled with Boc-Pro-OH by MA method to yield Boc-Pro-Ile-Ile-Val-OBzl (**9**). This was converted to the corresponding tetrapeptide ester hydrochloride (**10**) by the action of hydrogen chloride in dioxane. Compound **10** was coupled with Boc-Phe-OH by MA method to form Boc-Phe-Pro-Ile-Ile-Val-OBzl (**11**). After the treatment of **11** with hydrogen chloride in dioxane, the resulting pentapeptide ester hydrochloride (**12**) was coupled with Boc-Pro-OH by MA method to yield Boc-Pro-Phe-Pro-Ile-Ile-Val-OBzl (**13**). It was converted to the corresponding hexapeptide ester hydrochloride (**14**) by the action of hydrogen chloride in dioxane. Then compound **14** was coupled with Z-Arg(NO_2)-Gly-OH (**16**) by the dicyclohexylcarbodiimide (DCC) method to yield the protected octapepide (**17**). Catalytic hydrogenation of **17** gave the desired product (**3**).

The synthetic route for heptapeptide **4** is shown in Fig. 2. MA and DCC methods were used for the coupling reactions. The removal of Boc groups of the intermediates was performed by the action of hydrogen chloride in dioxane. The protected heptapetide (**24**) derived from Z-Arg(NO_2)-Gly-OH (**16**) and H-Pro-Phe-Pro-Ile-Val-OBzl·HCl (**23**) was hydrogenated in the presence of palladium black to yield the heptapeptide **4**. The homogeneity of final products was confirmed by thin-layer chromatgraphy, paper electrophoresis, amino acid analysis, and elemental analysis.

The taste of **3** and **4** was organoleptically determined by a panel evaluation employing four persons. The

†Present address: Research and Development Division, Sunstar Inc., Asahi-cho, Takatsuki, Osaka 569.

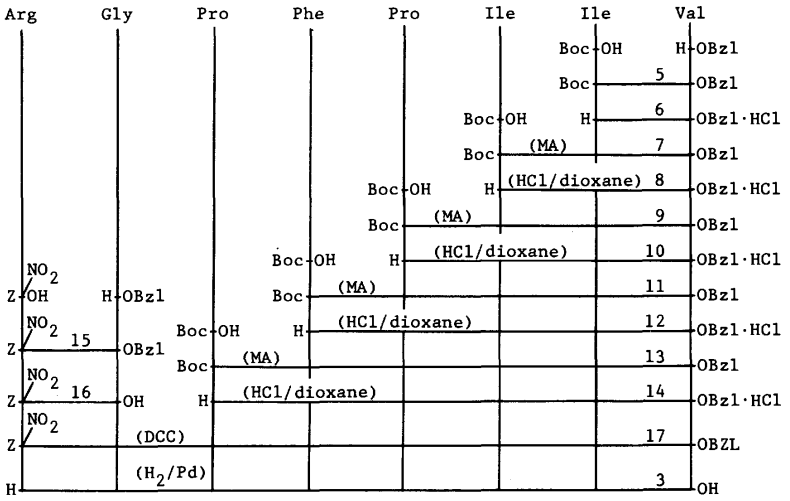

Fig. 1. Synthesis of the octapeptide **3**.

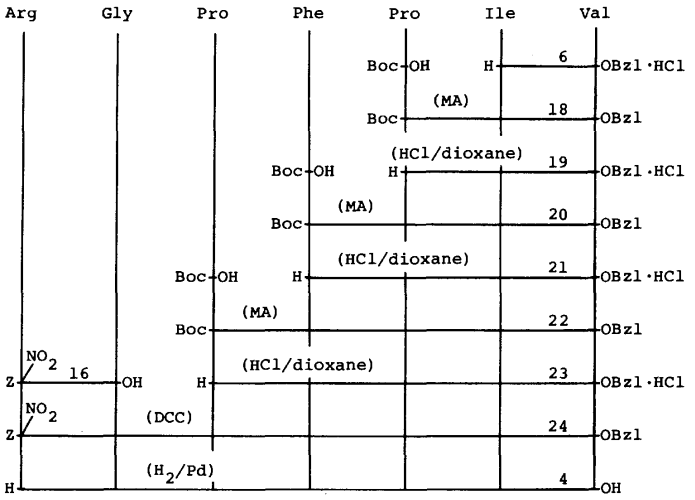

Fig. 2. Synthesis of the heptapeptide **4**.

TABLE 1. THE THRESHOLD VALUES FOR BITTER TASTE OF SYNTHESIZED PEPTIDES AND TYPICAL BITTER SUBSTANCES

Compound	Threshold value for bitter taste/mM
Arg-Gly-Pro-Phe-Pro-Ile (**1**)	0.13—0.25
Gly-Pro-Phe-Pro-Ile-Ile-Val (**2**)	0.17—0.34
Arg-Gly-Pro-Phe-Pro-Ile-Ile-Val (**3**)	0.004
Arg-Gly-Pro-Phe-Pro-Ile-Val (**4**)	0.11
Arg-Gly-Pro-Pro-Phe-Ile-Val (BPIa)	0.05
Caffeine	1.0
Strychnine	0.003
Brucine	0.0008

results are listed in Table 1. The synthesized peptides possessed a strong bitter taste. The threshold value of **3** was 0.004 mM; this is the most bitter among the peptides as far as we know. By comparison with some alkaloids known to have strong bitterness, the potency of **3** corresponds to 250 times that of caffeine and is nearly equal to that of strychnine. In this connection, the threshold value of brucine, which is an alkaloid and the most bitter substance known, is 0.0008 mM. The cause of the strong bitterness of this peptide can be shown by comparing the bitterness of **3** with that of **1** and **4**. It is obvious that **3** became the most bitter one due to the increase of the number of hydrophobic amino acids in the C-terminal moiety. Further, the difference in potency between **2** and **3** indicates that N-terminal arginine residue is indispensable for the extremely bitter taste observed in **3**. These findings agree with those obtained in our previous investigations of bitterness in BPIa.

The CD curves of **3**, **4**, and BPIa are presented in Fig. 3. These peptides showed similarly shaped curves. It seems that the whole molecular shape is also important for showing the strong bitter taste in peptides which are related to BPIa, in addition to the presence of both basic and hydrophobic amino acids.

In addition, electrophoretic tests of the octapeptide **3**, the heptapeptide **4**, and the synthetic BPIa, which was confirmed to be identical with the natural one,[4] were carried out. The mobilities of both **3** and **4** were indistinguishable from that of BPIa on paper electrophoresis. However, on thin-layer chromatography, by using the solvent system, 1-butanol–acetic acid–pyidine–water (4:1:1:2, v/v), the R_f value of BPIa was not identical with that of **3**, but nearly equal to that of **4**. These results indicate that BPIa does not correspond to the C-termial portion of β-casein

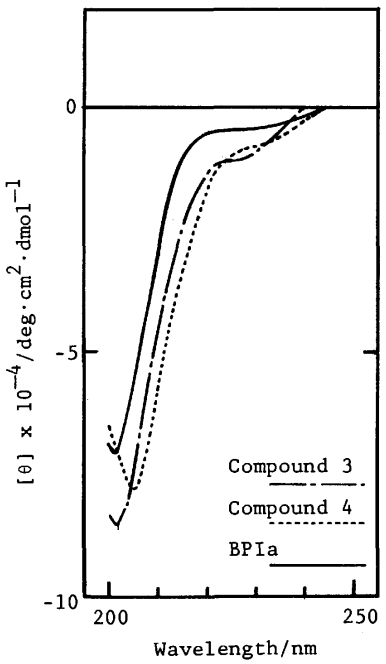

Fig. 3. CD curves of **3**, **4**, and BPIa.

determined by Ribadeau Dumas *et al.* One possible explanation for our finding is that there are other kinds of variants in β-casein, perhaps due to differeces between the cattle species throughout the world, a possibility of gene mutation among the same species, and other factors besides those known at the present.

Experimental

All the melting points are uncorrected. Thin-layer chromatography was carried out on Merck silica gel G with the solvent systems: R_f^1, 1-butanol-acetic acid-pyridine-water (4:1:1:2, v/v); R_f^2, chloroform-methanol (5:1, v/v). Spots of materials possessing a free amino group on a thin layer plate were detected by spraying ninhydrin, and those of amino group blocked materials by spraying 25% hydrogen bromide in acetic acid and then ninhydrin. The optical rotations were measured on a Union PM-101 polarimeter. Amino acid analyses in acid hydrolyzate with 6 M hydrochloric acid at 110 °C for 72 h were performed with a Hitachi amino acid analyzer, KLA-5 type. Prior to analyses, the compounds were dried over phosphorus pentaoxide at 66 °C and 2 mmHg (1 mmHg≈133.332 Pa) for 2 h, except in the case of compound **22**.

Boc-Ile-Ile-Val-OBzl (7). Boc-Ile-OH·DCHA (9.08 g, 22 mmol) was dissolved in ethyl acetate (150 ml), and 1 M sulfuric acid (50 ml) was added to the mixture with stirring. The organic layer was washed with water and dried over anhydrous sodium sulfate. The solution was concentrated to dryness *in vacuo*, and the oily residue was dissolved in THF (40 ml) and NMM (2.2 ml, 20 mmol). ECF (2.0 ml, 20 mmol) was added to the mixture at −5 °C with stirring. After 10 min, a precooled solution of H-Ile-Val-OBzl·HCl[4] (7.14 g, 20 mmol) and NMM (2.2 ml, 20 mmol) in chloroform (40 ml) was added to it. The reaction mixture was stored in an ice bath for 1 h and then at room temperature overnight. The mixture was evaporated *in vacuo* and the oily residue was dissolved in ethyl acetate. The solution was washed successively with 4% sodium hydrogencarbonate, 4% citric acid, and water, and then dried over anhydrous sodium sulfate. The filtrate was evaporated *in vacuo* and the oily residue was crystallized with ether-petroleum ether: yield 8.86 g (83%); mp 173—175 °C (lit,[7] 173—174 °C): $[\alpha]_D^{20}$ −75° (*c* 1, ethanol) (lit,[7] −77° (*c* 2.2, ethanol)); R_f^1 0.98 and R_f^2 0.72.

Found: C, 65.30; H, 8.98; N, 7.75%. Calcd for $C_{29}H_{47}O_6N_3$: C, 65.26; H, 8.88; N, 7.87%.

H-Ile-Ile-Val-OBzl·HCl (8). Compound **7** (5.34 g, 10 mmol) was dissolved in 4.1 M hydrogen chloride in dioxane (50 ml). The solution was allowed to stand for 2 h at room temperature and then evaporated *in vacuo*. The oily residue was solidified by the aid of ether: yield 4.52 g (96%); mp 240 °C; $[\alpha]_D^{20}$ −39° (*c* 1, methanol); R_f^1 0.92 and R_f^2 0.64.

Found: C, 61.13; H, 8.67; N, 9.05%. Calcd for $C_{24}H_{40}O_4N_3Cl$: C, 61.32; H, 8.58; N, 8.94%.

Boc-Pro-Ile-Ile-Val-OBzl (9). To a chilled solution of Boc-Pro-OH (1.05 g, 5 mmol) and NMM (0.55 ml, 5 mmol) in THF (10 ml), ECF (0.5 ml, 5 mmol) was added at −5 °C with stirring. After 10 min, a precooled solution of **8** (2.35 g, 5 mmol) and NMM (0.55 ml, 5 mmol) in DMF (10 ml) was added to it. The reaction mixture was stored in an ice bath for 1 h and then at room temperature overnight. The mixture was diluted with ethyl acetate and the solution was washed successively with 4% sodium hydrogencarbonate, 4% citric acid, and water, and then dried over anhydrous sodium sulfate. The filtrate was evaporated *in vacuo* and the residue was crystallized with ether-petroleum ether: yield 2.74 g (87%); mp 192—194 °C (lit,[7] 191—193 °C); $[\alpha]_D^{20}$ −100° (*c* 1, ethanol) (lit,[7] −82° (*c* 1.1, ethanol)); R_f^1 0.98 and R_f^2 0.78.

Found: C, 64.55; H, 8.80; N, 8.88%. Calcd for $C_{34}H_{54}O_7N_4$: C, 64.73; H, 8.63; N, 8.88%.

H-Pro-Ile-Ile-Val-OBzl·HCl (10). Compound **5** (3.15 g, 5 mmol) was treated with hydrogen chloride as described for the preparation of **8**: yield 2.69 g (95%); mp 240 °C<; $[\alpha]_D^{20}$ −91° (*c* 1, methanol); R_f^1 0.90 and R_f^2 0.55.

Found: C, 61.13; H, 8.34; N, 10.03%. Calcd for $C_{29}H_{47}O_5N_4Cl$: C, 61.41; H, 8.35; N, 9.88%.

Boc-Phe-Pro-Ile-Ile-Val-OBzl (11). This was prepared from Boc-Phe-OH·DCHA (1.56 g, 3.5 mmol) and **10** (1.70 g, 3 mmol) in the same way as described for the preparation of **7**: yield 2.06 g (88%); mp 163—165 °C (lit,[7] 165—166 °C); $[\alpha]_D^{20}$ −84° (*c* 1, ethanol) (lit,[7] −81° (*c* 2.0, ethanol)); R_f^1 0.98 and R_f^2 0.71.

Found: C, 66.54; H, 8.02; N, 8.89%. Calcd for $C_{43}H_{63}O_8N_5$: C, 66.38; H, 8.16: N, 9.00%.

H-Phe-Pro-Ile-Ile-Val-OBzl·HCl (12). Compound **11** (2.34 g, 3 mmol) was treated with hydrogen chloride, as described for the preparation of **8**: yield 2.09 g (97%); mp 160—162 °C; $[\alpha]_D^{20}$ −80° (*c* 1, methanol); R_f^1 0.90 and R_f^2 0.64.

Found: C, 63.25; H, 7.77; N, 9.81%. Calcd for $C_{38}H_{56}O_6N_5 \cdot 1/2H_2O$: C, 63.10; H, 7.94; N, 9.68%.

Boc-Pro-Phe-Pro-Ile-Ile-Val-OBzl (13). This was prepare from Boc-Pro-OH (0.65 g, 3 mmol) and **12** (2.14 g, 3 mmol), as described for the preparation of **9**: yield 2.33 g (89%); mp 131—134 °C; $[\alpha]_D^{20}$ −114° (*c* 1, methanol); R_f^1 0.97 and R_f^2 0.80.

Found: C, 65.59; H, 8.36; N, 9.50%. Calcd for $C_{48}H_{70}O_9N_6$: C, 65.88; H, 8.06; N, 9.60%.

H-Pro-Phe-Pro-Ile-Ile-Val-OBzl·HCl (14). Compound **13** (1.65 g, 2 mmol) was treated with hydrogen chloride, as describd for the preparation of **8**: yield 1.49 g (92%); mp 157—159 °C; $[\alpha]_D^{20}$ −95° (*c* 1, methanol); R_f^1 0.87 and R_f^2 0.60.

Found: C, 63.44; H, 7.91; N, 10.79%. Calcd for $C_{43}H_{63}O_7N_6Cl$: C, 63.64; H, 7.83; N, 10.36%.

Z-Arg(NO$_2$)-Gly-Pro-Phe-Pro-Ile-Ile-Val-OBzl (17). To a solution of Z-Arg(NO$_2$)-Gly-OH[4] (0.68 g, 1.65 mmol) in DMF (3 ml), DCC (0.34 g, 1.65 mmol) was added at 0 °C with stirring. After 20 min, a precooled solution of **14** (1.22 g, 1.5 mmol) and NMM (0.17 ml, 1.5 mmol) in chloroform (3 ml) was added to it. The reaction mixture was stirred for 3 h at 0 °C and then at room temperature overnight. DCUrea was filtered off and the filtrate was diluted with ethyl acetate.

The solution was washed successively with 4% sodium hydrogencarbonate, 0.5 M hydrochloric acid, and water, and then dried over anhydrous sodium sulfate. The filtrate was evaporated *in vacuo* and the residue was collected by the aid of ether. It was recrystallized from methanol-ether: yield 1.36 g (78%); mp 129—132 °C; $[\alpha]_D^{20}$ −103° (*c* 1, methanol); R_f^1 0.95 and R_f^2 0.59.

Found: C, 60.22; H, 7.33; N, 13.90%. Calcd for $C_{59}H_{82}O_{13}N_{12}\cdot 1/2H_2O$: C, 60.23; H, 7.11; N, 14.29%.

H-Arg-Gly-Pro-Phe-Pro-Ile-Ile-Val-OH·HCl (3). Compound **17** (0.47 g, 0.4 mmol) was dissolved in a mixture of methanol (3 ml) and acetic acid (3 ml) and hydrogenated in the presence of palladium black for 23 h at room temperature. The filtrate from catalyst was evaporated *in vacuo* and the residual oil was solidified by the aid of ether to give 0.31 g (81%) of **3** as a hygroscopic acetate form. It was dissolved in methanol (3 ml) and 4.1 M hydrogen chloride in dioxane (1 ml) was added to it. The solution was evaporated *in vacuo* and the residue was crystallized from acetone and ether: yield 0.29 g (76%); $[\alpha]_D^{20}$ −108° (*c* 0.5, H_2O); R_f^1 0.65 and R_f^2 0.00. Amino acid ratios in acid hydrolyzate: Arg 0.88, Gly 1.02, Pro 1.97, Phe 1.01, Ile 1.89, Val 1.00.

Found: C, 52.62; H, 7.80; N, 14.92%. Calcd for $C_{44}H_{72}O_9N_{11}Cl\cdot 4H_2O$: C, 52.50; H, 8.01; N, 15.31%.

Boc-Pro-Ile-Val-OBzl (18). This was prepared from Boc-Pro-OH (2.15 g, 10 mmol) and H-Ile-Val-OBzl·HCl[4] (3.57 g, 10 mmol), as described for the preparation of **9**: yield 4.47 g (86%); mp 102—103 °C; $[\alpha]_D^{20}$ −94° (*c* 1, methanol); R_f^1 0.94 and R_f^2 0.69.

Found: C, 64.78; H, 8.50; N, 8.23%. Calcd for $C_{28}H_{43}O_6N_3$: C, 64.96; H, 8.37; N, 8.12%.

H-Pro-Ile-Val-OBzl·HCl (19). Compound **18** (1.04 g, 2 mmol) was dissolved in 4.1 M hydrogen chloride in dioxane (10 ml). The solution was allowed to stand for 1 h at room temperature and then evaporated *in vacuo*. The residual syrup was washed three times with ether by decantation, and dried in a vacuum desiccater: yield 0.91 g (100%); R_f^1 0.82 and R_f^2 0.48.

BoC-Phe-Pro-Ile-Val-OBzl (20). This was prepared from Boc-Phe-OH·DCHA (0.98 g, 2.2 mmol) and **19** (0.91 g, 2 mmol), as described for the preparation of **7**. The product was obtained as an oly form: yield 1.12 g (84%); R_f^1 0.98 and R_f^2 0.70.

H-Phe-Pro-Ile-Val-OBzl·HCl (21). Compound **20** (1.12 g, 1.68 mmol) was treated with hydrogen chloride, as described for the preparation of **8**. The product was obtained as a hygroscopic solid: yield 0.93 g (92%); R_f^1 0.87 and R_f^2 0.63.

Boc-Pro-Phe-Pro-Ile-Val-OBzl (22). This was prepared from Boc-Pro-OH (0.33 g, 1.55 mmol) and **21** (0.93 g, 1.55 mmol), as described for the preparation of **9**: yield 0.84 g (71%); mp 61—63 °C; $[\alpha]_D^{20}$ −113° (*c* 1, methanol); R_f^1 0.93 and R_f^2 0.69.

Found: C, 65.84; H, 7.90; N, 8.93%. Calcd for $C_{42}H_{59}O_8N_5$: C, 66.20; H, 7.81; N, 9.19%.

H-Pro-Phe-Pro-Ile-Val-OBzl·HCl (23). This was prepared from **22** (0.76 g, 1 mmol), as described for the preparation of **8**. The product was obtained as a hygroscopic solid: yield 0.57 g (81%); R_f^1 0.79 and R_f^2 0.55.

Z-Arg(NO₂)-Gly-Pro-Phe-Pro-Ile-Val-OBzl (24). To a solution of Z-Arg(NO_2)-Gly-OH[4] (0.41 g, 1 mmol) and **23** (0.59 g, 0.81 mmol) and NMM (0.09 ml, 0.81 mmol) in DMF (4 ml), DCC (0.21 g, 1 mmol) was added at 0 °C with stirring. The reaction mixture was stirred for 3 h at 0 °C and then at room temperature overnight. DCUrea was filtered off and the filtrate was diluted with ethyl acetate. The solution was washed successively with 4% sodium hydrogencarbonate, 0.5 M hydrochoric acid, and water, and then dried over anhydrous sodium sulfate. The filtrate was evaporated *in vacuo* and the residue was solidified with ether. It was recrystallized from methanol-ether: yield 0.67 g (79%); mp 93—94 °C; $[\alpha]_D^{20}$ −90° (*c* 1, mthanol); R_f^1 0.83 and R_f^2 0.66.

Found: C, 59.48; H, 6.98; N, 14.46%. Calcd for $C_{53}H_{71}O_{12}N_{11}\cdot H_2O$: C, 59.37; H, 6.86; N, 14.37%.

H-Arg-Gly-Pro-Phe-Pro-Ile-Val-OH·AcOH (4). A solution of **24** (0.32 g, 0.3 mmol) in methanol-acetic acid (1:1, 6 ml) was hydrogenated in the presence of palladium black for 23 h at room temperature. The catalyst was removed by filtration and the filtrate was evaporated *in vacuo*. The residue was crystallized by the aid of acetone. It was recrystallized from methanol-ether: yield 0.17 g (67%); $[\alpha]_D^{20}$ −110° (*c* 0.5, H_2O); R_f^1 0.57 and R_f^2 0.00. Amino acid ratios in acid hydrolyate: Arg 0.91, Gly 1.01, Pro 1.88, Phe 1.09, Ile 1.00, Val, 0.98.

Found: C, 56.05; H, 7.84; N, 16.30%. Calcd for $C_{38}H_{60}O_8N_{10}\cdot CH_3COOH\cdot 1/2H_2O$: C, 56.35; H, 7.75; N, 16.40%.

Paper Electrophoresis. This was carried out under the following conditions: paper, Toyo Roshi No. 51A chromatography paper; solvent, pyridine-acetic acid-water (10:0.4:90, v/v) (pH 6.4): voltage gradient, 15 V/cm; charge period, 2.5 h. Electrophoretic mobilities were recorded as R_{Arg}, the ratio of the distance the compounds moved to that which a standard arginine spot moved on the same electrophoreogram. The compounds (**3** and **4**) and BPIa migrated toward the cathode and revealed a single spot after being sprayed with Sakaguchi reagent; ninhydrin gave the same result. The R_{Arg} value of both **3** and **4** was 0.72; BPIa gave the same R_{Arg} value.

CD Measurement. This was performed with a JASCO J-20A. A cell of path length 0.2 mm was used and runs were made at ambient temperature. Patterns in water are shown in Fig. 3.

Sensory Test. Taste of the synthesized peptides was organoleptically determined by panel evaluation employing four persons. A series of solutions of decreasing concentration, each half as strong as the preceding one, were prepared. Before tasting the sample, the mouth was thoroughly rinsed with deionized water. The sample solution was held in the mouth for *ca.* 10 s and then spit out, and then the threshold value was determined. The results are listed in the Table.

The authors wish to express their thanks to Associate Professor Michio Kondo of Saga University for the CD measurements. Thanks are also due to Dr. Shinji Okumura of Ajinomoto Co., Inc., for supplying some amino acids.

References

1) Part IX. I. Miyake, K. Kouge, H. Kanehisa, and H. Okai, *Bull. Chem. Soc. Jpn.*, **57**, 815 (1984).

2) The abbreviations recommended by IUPAC-IUB commission of Biochemical Nomenclature (*J. Biol. Chem.*, **247**, 977 (1972)) have been used. Amino acid symbols except glycine denoted L-configuration. Additional abbreviations: AcOH, acetic acid; DCC, dicyclohexylcarbodiimide; DCHA, dicyclohexylamine; DCUrea, *N,N'*-dicyclohexylurea; DMF, *N,N*-dimethylformamide; ECF, ethyl chloroformate; NMM, *N*-methylmorpholine; THF, tetrahydrofuran.

3) N. Minamiura, Y. Matsumura, J. Fukumoto, and T. Yamamoto, *Agric. Biol. Chem.*, **36**, 588 (1972).

4) Part I. H. Fukui, H. Kanehisa, N. Ishibashi, I. Miyake, and H. Okai, *Bull. Chem. Soc. Jpn.*, **56**, 766 (1983).

5) B. Ribadeau Dumas, C. Brignon, F. Grosclade, and J. C. Mercier, *Eur. J. Biochem.*, **25**, 505 (1972).

6) H. Aoyagi and N. Izumiya, *Bull. Chem. Soc. Jpn.*, **50**, 2387 (1977).

7) A. Hashimoto, H. Aoyagi, and N. Izumiya, *Bull. Chem. Soc. Jpn.*, **53**, 2926 (1980).

 © 1984 The Chemical Society of Japan Bull. Chem. Soc. Jpn., 57, 823—826 (1984)

Asymmetric Hydrogenation of Dehydrodipeptides with Rhodium(I)-Chiral Diphosphinites. Selective (*S,S*)- and (*R,R*)-Product Formation by Double Asymmetric Induction

Masanobu YATAGAI, Takamichi YAMAGISHI,* and Mitsuhiko HIDA
Department of Industrial Chemistry, Faculty of Technology, Tokyo Metropolitan University, Fukasawa, Setagaya-ku, Tokyo 158
(Received October 6, 1983)

In the hydrogenation of dehydrodipeptides, the effect of chiral center of the substrate ((*S*) or (*R*)) on the asymmetric induction was examined using the catalysts of Rh(I)-chiral diphosphinite containing pyrrolidine moiety (POP). The catalysts with POP's having the ω-(dimethylamino)alkyl group indicated an extremely large double asymmetric induction to give (*S,S*)- or (*R,R*)-product in high stereoselectivities, depending on the chiral center of the substrates. This result was ascribed to the electrostatic interaction between the ligand and substrate. POP's without ω-(dimethylamino)alkyl group gave (*R,R*)-product for (*R*)-substrate in a high stereoselectivity by the steric effect between the ligand and substrate, while for (*S*)-substrate, (*S,S*)-product was obtained in a low stereoselectivity.

In the catalytic asymmetric hydrogenation with Rh(I) catalysts, asymmetric induction is generally caused by the steric interaction between the ligand and the substrate on the rhodium species.[1] If the electrostatic interaction between the ligand and the substrate intensifies the stereocontrol, the chiral catalyst will be more widely applied to the asymmetric reactions.

The authors prepared new chiral diphosphinites with pyrrolidine moiety (POP's) from (+)-diethyl tartrate, which are listed in Table 1. Some of them have ω-(dimethylamino)alkyl substituent, which is expected to interact electrostatically with a carboxyl group of the substrate. They were applied to the asymmetric hydrogenation of olefinic compounds with a carboxyl group and proved to be very effective for the hydrogenation of dehydrodipeptides with (*S*)-chiral center.[2,3] In the reaction of dehydrodipeptides, the carboxyl group can approach the dimethylamino group of the ligand on rhodium species, causing a strong electrostatic interaction. In the reaction of Ac-ΔPhe-Gly-OH without a chiral center, however, only moderate optical yields were obtained.[2,3] This would indicate that the steric effect by the chiral center of the dehydrodipeptides and the electrostatic interaction between the ligand and substrate lead to the high stereoselectivity in the Rh(I)–POP-catalyzed hydrogenation.

In this paper, we will describe how the chiral center ((*S*) and (*R*)) of dehydrodipeptides affects the stereoselectivity, leading to an extremely large double asymmetric induction in the Rh(I)–POP-catalyzed hydrogenation.

TABLE 1. CHIRAL DIPHOSHINITES (POP's)

Diphosphinite[a] 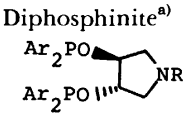	Ar	R
POP-AE	Ph	$CH_2CH_2N(CH_3)_2$
p-Me-POP-AE	CH_3-	$CH_2CH_2N(CH_3)_2$
p-MeO-POP-AE	CH_3O-	$CH_2CH_2N(CH_3)_2$
POP-AP	Ph	$CH_2CH_2CH_2N(CH_3)_2$
POP-IP	Ph	$CH_2CH_2CH(CH_3)_2$
p-MeO-POP-IP	CH_3O-	$CH_2CH_2CH(CH_3)_2$
POP-BZ	Ph	CH_2Ph

a) AE, AP, IP, and BZ represent alkyl group(R) of POP and denote dimethylaminoethyl, dimethylaminopropyl, isopentyl, and benzyl, respectively.

Results and Discussion

The catalysts of the diphosphinites (POP's) were examined for the asymmetric hydrogenation of dehydrodipeptides. POP-AE and POP-AP have ω-(dimethylamino)alkyl groups, which facilitate electrostatic interaction between the ligand and substrate. POP-IP is a carbon analogue of POP-AE, and the isopentyl group will have a similar steric factor to that of the 2-(dimethylamino)ethyl group of POP-AE. For *p*-Me-POP-AE, *p*-MeO-POP-AE, and *p*-MeO-POP-IP, the increasing in the electron density on the phosphorus atoms of the ligands will cause the stronger coordination of them onto rhodium. The results of asymmetric hydrogenations of dehydrodipeptides using Rh(I)–POP catalysts are summarized in Table 2. For the substrates with (*S*)-chiral center, POP's with ω-(dimethylamino)alkyl group showed good to excellent stereoselectivities. For Ac-ΔPhe-(*S*)-Phe-OH, the stereoselectivity with *p*-Me-POP-AE and *p*-MeO-POP-AE was near 100% d.e. POP's without dimethylamino group gave low or moderate optical yields. These results clearly indicated the contribution of the dimethylamino group of POP in the asymmetric induction.

From the hydrogenation of Ac-ΔPhe-Gly-OH and dehydrodipeptides with (*S*)-chiral center, the present POP's were considered to have (*S*)-selectivity.[2,3] Surprisingly, the hydrogenation of dehydrodipeptides with (*R*)-chiral center using POP's with dimethylamino group gave (*R,R*)-product with high optical yields (86—96% d.e.) instead of (*S,R*)-isomer. The reaction of Ac-ΔPhe-(*R*)-Phe-OH was much slower than that of Ac-ΔPhe-(*S*)-Phe-OH. Achiral 1,2-bis-

[bis(4-methoxyphenyl)phosphinooxy]ethane catalyst gave (*S,S*)- or (*R,R*)-product with low optical yields (20% d.e.) for Ac-⊿Phe-(*S*)-Ala-OH and Ac-⊿Phe-(*R*)-Ala-OH, respectively. These results indicate that the POP catalysts caused an excellent double asymmetric induction, leading to high stereoselectivity for both (*S*)- and (*R*)-substrate. This makes a striking contrast to the results reported with chiral diphosphines.[4]

It is further noted that POP's without dimethylamino group gave (*R,R*)-product in fairly high stereoselectivities (68—90% d.e.), though they gave low optical yields for (*S,S*)-isomer from (*S*)-substrates.

[Rh(*p*-MeO-POP-AE)(cod)]$^+BF_4^-$ was treated with an equimolar amount of perchloric acid in ethanol-methanol solution; this resulted in an orange-yellow precipitate. ^1H NMR spectra of this orange-yellow complex (A) in CD_3OD showed that the protonation occurred mainly at the ω-dimethylamino group of *p*-MeO-POP-AE. The hydrogenation with the complex (A) afforded much lower stereoselectivities for Ac-⊿Phe-(*S*)-Ala-OH and Ac-⊿Phe-(*R*)-Ala-OH (62% and 66% d.e., respectively) (Table 3). From these results, it is concluded that the dimethylamino group of POP plays an important role in the asymmetric induction by electrostatic interaction with a carboxyl group of the substrate. The result of the hydrogenation of Ac-⊿Phe-(*S*)-Ala-OMe with POP-AP supports the above conclusion: In the reaction of Ac-⊿Phe-(*S*)-Ala-OMe, Rh(I)-(POP-AP) catalyst gave a very low optical yield ((*S,S*)/(*R,S*)=46/54, 8% d.e.), while the same catalyst afforded a high diastereomeric excess ((*S,S*)/(*R,S*)=91/9, 82% d.e.) in the reaction of Ac-⊿Phe-(*S*)-Ala-OH.

(*R*)-Selectivity observed in the case of Ac-⊿Phe-(*S*)-Ala-OMe by POP-AP was in accord with the reactions of dehydroamino acids using POP-AP where electrostatic interaction is not likely to function.[3]

Tertiary amine moiety of *p*-MeO-POP-IP was also converted to the ammonium type by treating [Rh(*p*-MeO-POP-IP)(cod)]$^+BF_4^-$ with $HClO_4$. The resulting complex (B) gave similar stereoselectivities for both (*S*)- and (*R*)-substrates to that for *p*-MeO-POP-IP complex (Table 3). Therefore, it is unlikely that nitrogen of the pyrrolidine ring contributed to the asymmetric induction. In the case of dehydrodipeptide esters, electrostatic interaction between the substrate and the ligand will be impossible. However, the double asymmetric induction with POP-IP was also observed for the esters with (*R*)-chiral center (Table 4). Therefore, it would be the steric effect of the POP's without dimethylamino group that produced a fairly large double asymmetric induction for (*R,R*)-products from (*R*)-substrates. In the reaction of the substrate with (*R*)-chiral center, methoxyl group on the ligand slightly lowered the (*R,R*)-selectivity, contrary to the results of the (*S*)-substrate (Tables 2 and 4), since strong coordination of the ligand onto rhodium increased (*S*)-selectivity inherent to the ligand.

As shown in Fig. 1, the system of Rh(I)-(*p*-MeO-POP-IP) containing Ac-⊿Phe-Ala-OH gave the same CD spectra irrespective of the chirality in the substrate. On the other hand, CD spectra of the system of Rh(I)-(*p*-MeO-POP-AE) containing Ac-⊿Phe-Ala-OH depended on the chirality of the substrate. This indicates that the substrate with (*S*)-chiral center coordinates onto rhodium in a different mode from that for the substrate with (*R*)-chiral center in the *p*-MeO-POP-AE system. That is to say, the dimethyl-

TABLE 2. ASYMMETRIC HYDROGENATION OF DEHYDRODIPEPTIDES USING THE CATALYSTS OF POP'S[a]

Dehydrodipeptide[b]	Diphosphinite[c]	(*S*) Time	(*S*) Conversion	(*S, S*)/(*R, S*)	% d.e.	(*R*) Time	(*R*) Conversion	(*S, R*)/(*R, R*)	% d.e.
		min	%			min	%		
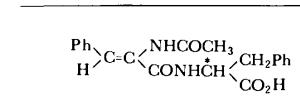 (Ac-⊿Phe-Phe-OH)	POP-AE	180	71	95/5	90				
	p-Me-POP-AE	45	100	>99/<1	>98				
	p-MeO-POP-AE	15	100	>99/<1	>98	16 h	90	7/93	86
	POP-AP	120	91	93/7	86				
	POP-IP	120	92	79/21	58				
	p-MeO-POP-IP	120	84	82/18	64	20 h	76	9/91	82[d]
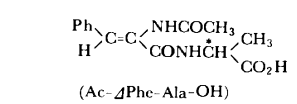 (Ac-⊿Phe-Ala-OH)	POP-AE	30	100	94/6	88	50	100	4/96	92
	p-MeO-POP-AE	30	100	98/2	96	25	100	7/93	86
	POP-AP	30	100	91/9	82	40	73	8/92	84
	POP-IP	20	100	68/32	36	30	100	5/95	90
	p-MeO-POP-IP	25	100	69/31	38	16	100	7/93	86
	POP-BZ	40	100	66/34	32	40	100	16/84	68
	e)	40	100	60/40	20	40	100	40/60	20

a) Hydrogenations were performed in ethanol at 20 °C under atmospheric hydrogen pressure. b) Dehydrodipeptide/Rh=50. c) Diphosphinite/Rh=1.5. d) Reaction temp=40 °C. e) [Rh(1, 2-bis{bis(4-methoxyphenyl)phosphinooxy}ethane) (cod)]$^+BF_4^-$.

TABLE 3. ASYMMETRIC HYDROGENATION OF Ac-⊿Phe-(*S*)-Ala-OH AND Ac-⊿Phe-(*R*)-Ala-OH WITH THE COMPLEX **A** AND **B**[a]

Catalyst[b]	(*S*) Time	(*S*) Conversion	(*S, S*)/(*R, S*)	% d.e.	(*R*) Time	(*R*) Conversion	(*S, R*)/(*R, R*)	% d.e.
	min	%			min	%		
Complex **A**	30	100	81/19	62	30	100	17/83	66
Complex **B**	90	73	70/30	40	40	68	12/88	76

a) Hydrogenations were performed in ethanol at 20 °C under atmospheric hydrogen pressure. b) Ac-⊿Phe-Ala-OH-/Rh=50

TABLE 4. ASYMMETRIC HYDROGENATION OF DEHYDRODIPEPTIDE ESTERS WITH THE CATALYSTS OF POP-IP AND *p*-MeO-POP-IP[a]

Dehydrodipeptide[b]	Diphosphinite[c]	(S) Time	(S) Conversion	(S, S)/(R, S)	% d.e.	(R) Time	(R) Conversion	(S, R)/(R, R)	% d.e.
		min	%			min	%		
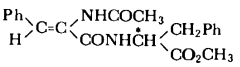 (Ac-⊿Phe-Phe-OMe)	POP-IP	180	100	51/49	2				
	p-MeO-POP-IP	60	100	55/45	10	180	45	35/65	30
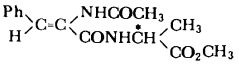 (Ac-⊿Phe-Ala-OMe)	POP-IP	20	100	59/43	16	25	100	17/83	66
	p-MeO-POP-IP					30	100	22/78	56

a) Hydrogenations were performed in ethanol at 20 °C under atmospheric hydrogen pressure. b) Dehydrodipeptide/Rh=50. c) Diphosphinite/Rh=1.5.

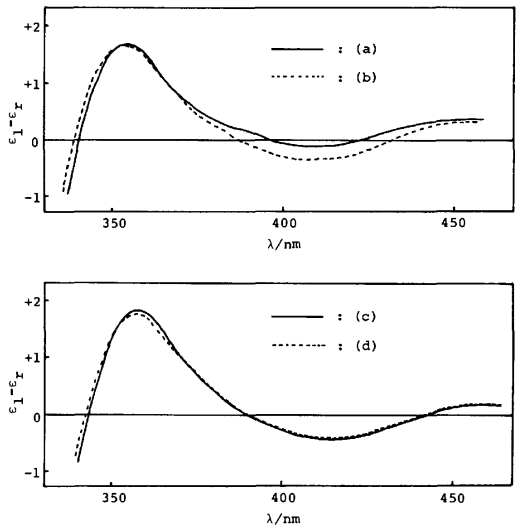

Fig. 1. CD spectra of Rh(I)-(*p*-MeO-POP-AE) and Rh(I)-(*p*-MeO-POP-IP) systems in the presence of Ac-⊿Phe-Ala-OH in methanol solution. ([Rh]= 5.0×10^{-4} mol dm^{-3}, [POP]=6.0×10^{-4} mol dm^{-3}, [Ac-⊿Phe-Ala-OH]=2.5×10^{-3} mol dm^{-3}). (a): Rh(I)-(*p*-MeO-POP-AE)-(Ac-⊿Phe-(*S*)-Ala-OH), (b): Rh(I)-(*p*-MeO-POP-AE)-(Ac-⊿Phe-(*R*)-Ala-OH), (c): Rh(I)-(*p*-MeO-POP-IP)-(Ac-⊿Phe-(*S*)-Ala-OH), (d): Rh(I)-(*p*-MeO-POP-AE)-(Ac-⊿Phe-(*R*)-Ala-OH).

amino group of the ligand could affect the step of prochiral face selection of the substrate by means of the electrostatic interaction with the carboxyl group of the substrate to emphasize the steric effect of the chiral center in the substrate.

In the reaction of Ac-⊿Phe-(*S*)-Ala-OH in ethanol, *p*-MeO-POP-AE afforded much higher optical yield than *p*-MeO-POP-IP, while similar optical yields were obtained by the above two diphosphinites in the reaction of Ac-⊿Phe-(*R*)-Ala-OH in ethanol. The hydrogenation of Ac-⊿Phe-(*R*)-Ala-OH in 2-propanol using *p*-MeO-POP-AE gave higher optical yield than that by *p*-MeO-POP-IP (86% and 78% d.e., respectively). This is because a decrease in the polarity of solvent can emphasize the electrostatic interaction between the ligand and substrate. But the difference in the optical yields between the two diphosphinites in 2-propanol was not large. So it is considered that the contribution of the electrostatic interaction for (*R,R*)-product formation would be smaller than that for (*S,S*)-product formation.

As described so far, the present POP's with the dimethylamino group showed an excellent stereoselectivity in the hydrogenation of dehydrodipeptides with (*S*)- or (*R*)- chiral center by the extremely large double asymmetric induction. These phenomena will be ascribed mainly to the contribution of the electrostatic interaction to emphasize the stereocontrol for asymmetric induction. The steric interaction between the substituent on the chiral center of the substrate and the phenyl group on the phosphorus atom of the ligand evoked by the electrostatic interaction will affect the selection of the prochiral face of the substrate in coordination onto rhodium.[3] On the other hand, POP's without dimethylamino group indicated high (*R*)-selectivity in the reaction of the (*R*)-substrate due to the steric effect of the ligand, though the details of the stereocontrol are not clear in the present stage.

p-MeO-POP-AE and *p*-MeO-POP-IP were applied to the hydrogenation of Ac-⊿Phe-Asp-OH with two carboxyl groups capable of interaction with the ligand. *p*-MeO-POP-AE showed a double asymmetric induction in the case of both Ac-⊿Phe-(*S*)-Asp-OH and Ac-⊿Phe-(*R*)-Asp-OH, while with *p*-MeO-POP-IP the chirality newly formed was the same for both substrates. This would suggest the possibility of selecting the newly formed chirality of the product by utilizing the steric factor and/or electrostatic factor of the present POP catalysts. Furthermore, it will be fruitful to apply the present POP catalysts to other substrates, for example, dehydrodipeptides of Y-AA-⊿AA-OH type, or dehydrooligopeptides.

Experimental

^{1}H NMR spectra were recorded on a HITACHI R-24 High Resolution NMR spectrometer (60 MHz) with tetramethylsilane as internal standard. CD spectra were recorded on a JASCO J-40A spectropolarimeter. Optical rotations were measured with a UNION PM 101 automatic digital polarimeter.

Rh(I) catalysts were prepared *in situ* from $[Rh(cod)_2]^+BF_4^-$ and a diphosphinite (POP). The procedure of asymmetric hydrogenations and determination of the optical yields were the same as described previously.[3] CD spectra were measured by the method described previously.[3]

Materials. All *N*-acetyl dehydrodipeptides were prepared by Bergmann's method.[5] Esterification of *N*-acetyl

dehydrodipeptides was performed by a conventional method.[4c] All solvents were dried, distilled, and stored under nitrogen. $[Rh(cod)_2]^+BF_4^-$ was prepared by a conventional method and stored under nitrogen.[6]

Preparation of Chiral Diphosphinites (POP-BZ and p-MeO-POP-IP). *(3S, 4S)-N-Benzyl-3,4-pyrrolidinediol*: Benzylamine (30 cm³, 27.5×10^{-2} mol) and 1,4-di-*O*-tosyl-L-threitol (24.2 g, 5.6×10^{-2} mol) were reacted in dioxane under nitrogen; the product was treated in the manner described previously.[3] (7.0 g, 64% yield) $[\alpha]_D+8.5°$ (*c* 2.07, $CHCl_3$); ^1H NMR δ=2.45—2.89 (4H, m, H^c), 3.55 (2H, s, H^b), 4.01 (2H, br t, H^d), 4.30 (2H, s, H^e), 7.18(5H, s, H^a).

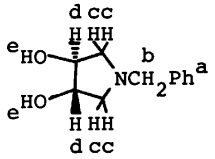

(3S,4S)-N-Benzyl-3,4-bis(diphenylphosphinooxy)pyrrolidine (POP-BZ): The diol (870 mg, 4.5×10^{-3} mol) and chlorodiphenylphosphine (2.2 g, 1.0×10^{-2} mol) were reacted in the presence of triethylamine (1.0 g, 1.0×10^{-2} mol); white crystals of POP-BZ were obtained by the work up described previously.[3] (1.8 g, 90% yield) $[\alpha]_D+50.4°$ (c 1.02, C_6H_6); ^1H NMR ($CDCl_3$) δ=2.53—3.11 (4H, m, H^c), 3.56 (2H, br s, H^b), 4.55 (2H, br m, H^d), 7.20 (25H, s, m, H^a, H^e).

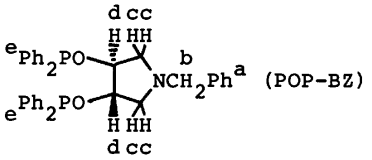

(3S,4S)-N-Isopentyl-3,4-bis[bis(4-methoxyphenyl)phosphinooxy]-pyrrolidine (p-MeO-POP-IP): (3S,4S)-*N*-Isopentyl-3,4-pyrrolidinediol (200 mg, 1.2×10^{-3}mol) and chlorobis(4-methoxyphenyl)phosphine (670 mg, 2.4×10^{-3} mol) were reacted in the presence of triethylamine (720 mg, 7.1×10^{-3} mol); white crystals of *p*-MeO-POP-IP were obtained by the procedure described previously.[3] (310 mg, 40% yield) $[\alpha]_D^{20}$ +53.3° (c 0.27, C_6H_6); ^1H NMR ($CDCl_3$) δ=0.85 (6H, d, H^a), 1.31 (3H, br m, H^b, H^c), 2.24—3.00 (6H, m, H^d, H^e), 3.72 (12H, s, H^h), 4.46 (2H, br m, H^f), 6.75—7.48 (16H, m, H^g).

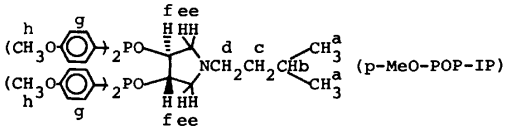

[Rh(1,2-bis{bis(4-methoxyphenyl)phosphinooxy}ethane) (cod)]$^+$ BF_4^-: To the solution of ethylene glycol (250 mg, 4.0×10^{-3} mol) and pyridine (700 mg, 8.8×10^{-3} mol) in THF (10 cm³), chlorobis(4-methoxyphenyl)phosphine (2.4 g, 8.5×10^{-3} mol) was added dropwise in 1.5 h with stirring in an ice-water bath. The resulting mixture was stirred overnight at r.t. Filtration of the reaction mixture, followed by evaporation of the filtrate, gave an oily product containing monophosphinite. This oily product was phosphinitated with 520 mg of chlorobis(4-methoxyphenyl)phosphine and 600 mg of pyridine, and the same work up as above gave an oily product. This oil was purified from diethyl ether–hexane, and crude diphosphinite was obtained. (100 mg, 70 mol% purity) This diphosphinite and $[Rh(cod)_2]^+BF_4^-$ (54 mg, 1.3×10^{-4} mol) are dissolved in CH_2Cl_2 (5 cm³) and the solution was stirred at r.t. for 1 h. Addition of ether (10 cm³) to this solution gave a yellow precipitate, and yellow needles were obtained by recrystallization of this precipitate from CH_2Cl_2–THF–diethyl ether (73 mg, 64% yield). ^1H NMR ($CDCl_3$) δ=3.74 (20H, s, m, H^c, H^e), 4.27 (4H, br, H^a), 6.54—7.70 (20H, br m, H^b, H^d).

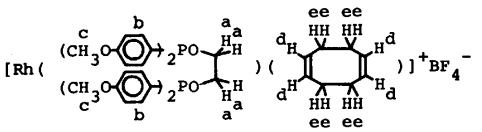

Rh Complex A: To the solution of the *p*-MeO-POP-AE (83 mg, 1.25×10^{-4} mol) and $[Rh(cod)_2]^+BF_4^-$ (47 mg, 1.15×10^{-4} mol) in ethanol (20 cm³) and methanol (5 cm³), $HClO_4$ (1.21×10^{-4} mol) was added as an ethanol solution. This solution was stirred for 15 min at r.t.; orange-yellow crystals precipitated from the solution. This mixture was concentrated by evaporation and filtrated under nitrogen. Yellow-orange crystals of complex **A** were dried under reduced pressure. (56 mg, 48% yield) ^1H NMR (CD_3OD): δ=2.76—3.58 (14H, s, br m, H^a, H^b, H^c, H^d), 3.84 (20H, br m, H^g, H^h), 5.05 (2H, br, H^e), 6.63—7.78 (20H, br m, H^f, H^i).

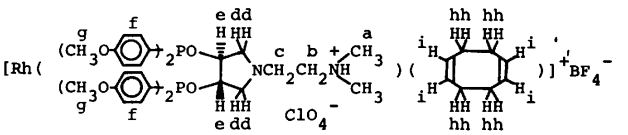

A

Rh Complex B: To the solution of *p*-MeO-POP-IP (70 mg, 1.05×10^{-4} mol) and $[Rh(cod)_2]^+BF_4^-$ (40 mg, 1.0×10^{-4} mol) in ethanol (10 cm³), $HClO_4$ (1.05×10^{-4} mol) was added as an ethanol solution. This solution was stirred for 5 min at 0°C; yellow crystals separated from it. The remaining mixture was cooled to −20°C and filtrated under nitrogen. Crystals of complex **B** were dried under reduced pressure. (73 mg, 69% yield) ^1H NMR (CD_2Cl_2) δ=0.91 (6H, br d, H^a), 1.66 (3H, br, H^b, H^c), 3.74 (26H, br m, H^d, H^e, H^h, H^i, H^j), 4.79 (2H, br, H^f), 6.36—7.70 (20H, br m, H^g, H^i).

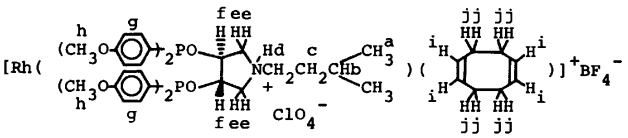

B

The authors express their gratitude to Professor M. Kobayashi and Dr. N. Kamigata, Tokyo Metropolitan University, for CD spectroscopy.

References

1) M. D. Fryzuk and B. Bosnich, *J. Am. Chem. Soc.*, **99**, 6262 (1977); A. Miyashita, A. Yasuda, H. Takaya, K. Toriumi, T. Ito, T. Souchi, and R. Noyori, *ibid.*, **102**, 7932 (1980); H. Brunner, W. P. Ronzuk, B. Schönhammer, K. Streng, I. Bernal, and J. Korp, *Chem. Ber.*, **144**, 1137 (1980); O. Samuel R. Coufingnal, M. Lauer, S. Y. Zhang, and H. B. Kagan, *Nouv. J. Chim.*, **5**, 151 (1981).

2) M. Yatagai, M. Zama, T. Yamagishi, and M. Hida, *Chem. Lett.*, **1983**, 1203.

3) M. Yatagai, M. Zama, T. Yamagishi, and M. Hida, *Bull. Chem. Soc. Jpn.*, **57**, 739 (1984).

4) a) I. Ojima and T. Suzuki, *Tetrahedron Lett.*, **21**, 1239 (1980); b) I. Ojima, T. Kogure, N. Yoda, T. Suzuki, M. Yatabe, and T. Tanaka, *J. Org. Chem.*, **47**, 1329 (1982); c) D. Meyer, J. C. Poulin, and H. B. Kagan, *ibid.*, **45**, 4680 (1980); d) K. Onuma, T. Ito, and A. Nakamura, *Chem. Lett.*, **1980**, 481.

5) D. G. Doherty, J. E. Tietzman, and M. Bergmann, *J. Biol. Chem.*, **147**, 617 (1943).

6) M. Green, T. A. Kuc, and S. H. Taylor *J. Chem. Soc., A*, **1971**, 2334.

Specific Generation of Lithiated 3-Trimethylsiloxy-1,2-propadiene Derivatives from 1-(Trimethylsilyl)propargyl Alcohols

Masahiro KATO and Isao KUWAJIMA*
Department of Chemistry, Tokyo Institute of Technology, Meguro-ku, Tokyo 152
(Received October 19, 1983)

1-(Trimethylsilyl)propargyl alcohols have been prepared by treating acyltrimethylsilanes with magnesium acetylides, and their base-induced reactions involving rearrangement of silyl group have been examined. Treatment of the alcohol with an equimolar amount of butyllithium in hexane followed by addition of tetrahydrofuran has allowed to generate the lithiated 3-trimethylsiloxy-1,2-propadiene, which reacts with an alkyl iodide to afford the alkylated 1-trimethylsiloxy-1,2-propadiene in high yield. Further, a catalytic amount of butyllithium also effects an efficient conversion of the alcohol to the corresponding 1-siloxy-1,2-propadiene through a similar rearrangement process.

Strong affinity of silicon atom to oxide anion has sometimes allowed a facile transfer of trialkylsilyl group from carbon to oxygen. Under basic conditions, 1-(trialkylsilyl)alkanols undergo rearrangement to yield the corresponding alkyl silyl ethers, which is well documented as Brook rearrangement.[1,2] Similar migration of silyl group has also been proposed for Peterson type olefination reaction[2] of 2-(trialkylsilyl)-alkanols under basic conditions.[3] In these rearrangement processes, formation of the corresponding carbanionic species during equilibration with the alkoxides has been assumed or proved in certain cases, but it has been quite difficult to make use such kinds of nucleophilic species for carbon chain homologation because of their high lability under reaction conditions. To control a generation of such carbanionic species effectively through this rearrangement, an additional anion-stabilizing substituent such as phenyl or olefinic group seems to be required, and we have recently reported several synthetic applications of such anionic species generated from 1-(trimethylsilyl)-allylic alcohols[4] and 3-trimethylsilyl-4-penten-1-ol derivative[5] for synthesis of enol silyl ethers and 1,5-heptadien-3-ol, an oxy-Cope rearrangement precursor.

Based on a similar background, 1-(trimethylsilyl)-propargyl alcohols (**1**) have also been expected to undergo silyl group migration to generate anionic species of propargyl silyl ether **3** or 1-trimethylsiloxy-1,2-propadiene derivatives **4** under basic conditions. Different from the precedent cases, an internal coordination of siloxy group to metal which has brought about a thermodynamic stability may be ruled out from these anionic species **3** and **4**, but allenic species **4** is expected to be much more common than **3** judging from literatures dealing with metallated allene derivatives.[6] Resulting nucleophiles **4** seem to be especially useful on synthetic standpoints that selective introduction of various organic substituents may be feasible on both α- and β-carbons of α,β-unsaturated carbonyl compounds (Scheme 1). In this paper we describe full details on the rearragement reactions of the propargyl alcohol **1** to afford siloxy allenes **5** and **6**.[7,8]

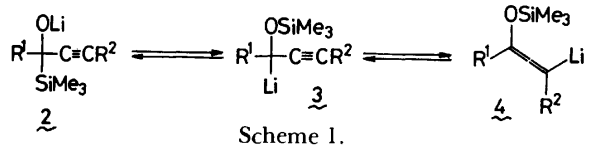

Scheme 1.

The starting materials, 1-(trimethylsilyl)propargyl alcohols (**1**) were easily prepared by treating the corresponding acyltrimethylsilanes[9] with appropriate bromomagnesium acetylides (Eq. 1). A straight-chained acyltrimethylsilane undergoes addition of acetylides quite efficiently in ether to give the corresponding **1** as a sole product, whereas a small amount of rearrangement prouct, propargyl silyl ether, is also formed from the addition reaction of an α-branched acyltrimethylsilane when ether or tetrahydrofuran (THF) is employed as the solvent. In the latter case, use of hexane as the reaction solvent excludes the formation of side-product, and the desired **1** could be obtained in high yield.

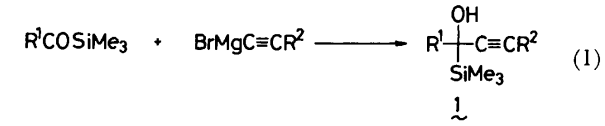

(1)

TABLE 1. PREPARATION OF 1-(TRIMETHYLSILYL)-PROPARGYL ALCOHOLS (**1**)

	R^1	R^2	Yield/% of **1**
a)	C_3H_7	C_6H_5	96
b)	$C_6H_5CH_2CH_2$	C_4H_9	95
c)	$C_6H_5CH_2CH_2$	C_6H_5	99
d)	$C_6H_5CH_2CH_2$	$SiMe_3$	96
e)	$C_6H_5CH_2CH_2$	CH_2OCH_3	94

On lithiation of this alcohol **1** with butyllithium, we have experienced similar difficulties encountered with 1-(trimethylsilyl)allylic alcohols:[4] complete conversion of the alcohol **1** to the lithium alkoxide **2** is quite difficult when tetrahydrofuran is used as the solvent. Formation of complex mixture has usually been observed on treatment of the resulting solution with various electrophiles. This curious result may be explained by assuming that an extremely rapid equilibrium between the lithium alkoxide **2** and the lithiated allenic species **4** has been attained through rearrangement of silyl group from carbon to oxygen before complete formation of **2**. The resulting carbanionic species **4** may be protonated by the remaining alcohol **1**, which leads to fomation of a mixture of siloxyallene **5** and its lithiated one **4** together with the alkoxide **2** and butyllithium (Eq. 2).

However, use of a nonpolar solvent such as hexane has excluded the equilibration between **2** and **4**, and the alcohol **1** can be converted to the corresponding lithium alkoxide **3** almost completely. Further, addition of

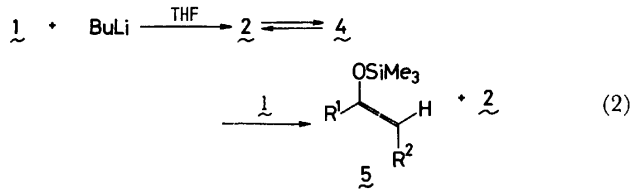

(2)

THF to the resulting hexane solution induces the equilibration to generate **4**. Carbon chain homologation can be achieved efficiently by the *in situ* reaction of this species with appropriate alkyl halides. Although two types of alkylation products may be conceivable during this procedure, the reaction takes place selectively on allenic carbon as expectedly,[6] and the corresponding α,β-unsaturated ketone **7** is obtained in high yield after aqueous work-up of the reaction mixture (see Scheme 2 and Table 2). Only exceptional case is that bearing a leaving group on an appropriate position, which undergoes a facile elimination as shown in the following example.

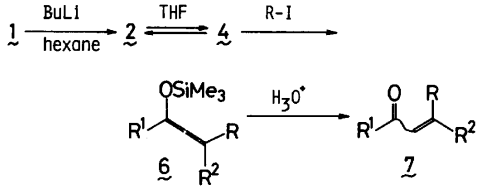

Scheme 2.

TABLE 2. ALKYLATION OF LITHIATED ALLENES **4**

	R^1	R^2	R-I	Yield/% of **7**
a)	C_3H_7	C_6H_5	CH_3-I	92
b)	$C_6H_5CH_2CH_2$	C_4H_9	CH_3-I	94
c)	$C_6H_5CH_2CH_2$	C_6H_5	CH_3-I	92
d)	$C_6H_5CH_2CH_2$	C_6H_5	C_4H_9-I	86
e)	$C_6H_5CH_2CH_2$	$SiMe_3$	CH_3-I	87
f)	$C_6H_5CH_2CH_2$	$(C_2H_4O_2)$-$CHCH_2CH_2$	CH_3-I	82

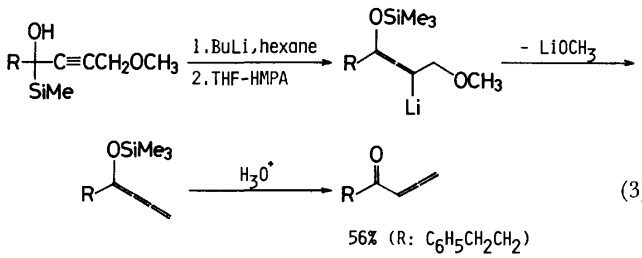

(3)

56% (R: $C_6H_5CH_2CH_2$)

Further, in a similar manner with 1-(trimethylsilyl)-allylic alcohols,[4] the alcohols **1** undergo a specific conversion to the corresponding 1-trimethylsiloxy-1,2-propadienes in excellent yield under the influence of a catalytic amount of butyllithium in THF through the following four steps: (1) formation of the alkoxide **2**, (2) generation of lithiated allenic species **4** *via* equilibration, (3) protonation of **4** with the remaining alcohol, and (4) regeneration of the alkoxide **2**. This transformation has been effected by treating the alcohol **1** with *ca.* 5 mol% of butyllithium in THF at −78 °C followed by warming up to 0 °C.

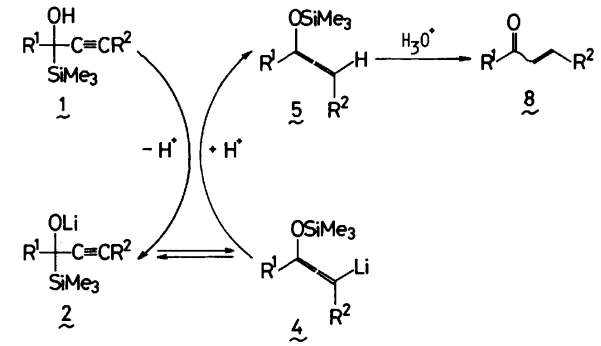

Scheme 3.

In most cases, protonation takes place selectively on terminal allenic carbon to yield **5**, but the alcohol prepared from silylacetylene afforded a mixture of the corresponding **5** (63%) and the propargyl silyl ether (29%).

Unfortunately, on an attempt for purification, the resulting siloxyallenes **5** and **6** are very labile on column chromatography and sometimes on heating for a distillation. Accordingly, the yields of the products were determined on the basis of α,β-unsaturated ketones **8** obtained by aqueous work-up of the reaction mixture. The results are shown in Table 3.

TABLE 3. CATALYTIC CONVERSION OF ALCOHOLS **1** TO **8** *via* **5**

	R^1	R^2	Yield/% of **8**
a)	C_3H_7	C_6H_5	96
b)	$C_6H_5CH_2CH_2$	C_4H_9	97
c)	$C_6H_5CH_2CH_2$	C_6H_5	89
d)	$C_6H_5CH_2CH_2$	$SiMe_3$	63[a]
e)	$C_6H_5CH_2CH_2$	CH_2OCH_3	80

a) The propargyl silyl ether was also formed in 29% yield.

However, the crude products **5** are usually pure enough for further synthetic elaboration without purification. By using the crude 5, several organic substituents can be introduced on the central carbon of the allenic linkages very efficiently under the influence of Lewis acid as shown below. For example, the crude **5** (R^1=C_3H_7, R^2=C_6H_5) obtained from the corresponding alcohol **1** gave the condensation product in 81% overall yield on treating with a benzaldehyde acetal. Thus, starting from the alcohol **1**, this procedure has allowed to effect two types of carbon chain homologation on each α- and β-carbon, respectively, by way of lithiated allenic species **4**.

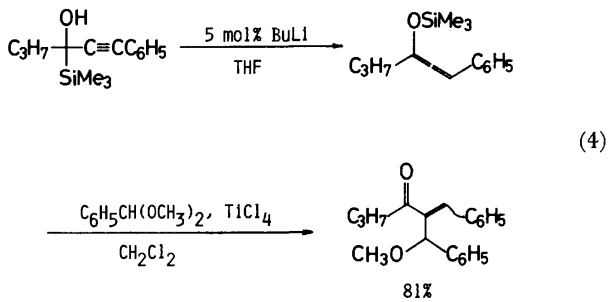

(4)

81%

Experimental

General Methods. Boiling points are uncorrected. Infrared (IR) spectra were recorded on a Hitachi EPI-G3 spectrometer; absorptions are reported in reciprocal centimeters. Proton nuclear magnetic resonance spectra (^{1}H NMR) were obtained on a Hitachi R-24B spectrometer; chemical Shifts (δ) are expressed in part per million downfield from tetramethylsilane. Analytical gas-liquid chromatography (GLC) was performed on a Hitachi 163 instrument with a flame-ionization detector and nitrogen carrier gas (1.0—1.3 kg/cm^2) using a OV-101 fused silica 20 m capillary column (Hitachi Chemi-Column). Microanalysis were performed with a Perkin-Elmer 240 at the Microanalytical Laboratory, Tokyo Institute of Technology.

Reactions involving air- or moisture-sensitive compounds were carried out in appropriate round-bottomed flasks with stirring bars under nitrogen or argon. Bulb-to-bulb distillation was performed with a Buchi Kugelrohr apparatus.

Preparative thin-layer chromatography (TLC) was carried out on glass plates (20×20 cm) coated with Merck silica gel PF 254 (1 mm thick).

Hexane was distilled from sodium. Ether and tetrahydrofuran (THF) were distilled from sodium/benzophenone ketyl immediately before use.

Materials. Acyltrimethylsilanes were prepared from the corresponding enol trimethylsilyl ethers of benzene- or methane-thiol esters according to the procedure developed in our laboratory.[9]

Preparation of 1-(Trimethylsilyl)propargyl Alcohols (1). *General Procedure*: To ethylmagnesium bromide (32 mL of 0.71 M THF solution, 22.5 mmol) diluted with ether (50 mL) was added an ethereal solution (25 mL) of a substituted acetylene (25 mmol) at 0 °C and it kept stirring for 30 min at room temperature. Then, an acyltrimethylsilane (15 mmol) in ether (25 mL) was added to the resulting solution and was stirred further 10 min at 0 °C. The reaction mixture was quenched with satd aq NH_4Cl and was extracted three times with 50 mL portions of ether. The extracts were washed with satd aq NaCl and were dried over anhyd $MgSO_4$. Removal of the solvent from the filtrate followed by distillaion gave the corresponding 1-(trimethylsilyl)propargyl alcohol (**1**).

*1-Phenyl-3-trimethylsilyl-1-hexyn-3-ol (**1a**)*: Bp 101—102 °C/0.05 mmHg;[10] IR (neat) 3400, 2200, 1245, 840 cm^{-1}; NMR (CCl_4) δ=0.16 (s, 9H), 0.80—1.20 (m, 3H), 1.43—1.87 (m, 5H including a singlet of OH at 1.73), 7.03—7.43 (m, 5H); Calcd for $C_{15}H_{22}OSi$: C, 73.10; H, 9.02%. Found: C, 73.21; H, 8.94%.

*1-Phenyl-3-trimethylsilyl-4-nonyn-3-ol (**1b**)*: Bp 118—119 °C/0.025 mmHg; IR (neat) 3430, 1600, 1250, 845 cm^{-1}; NMR (CCl_4) δ=0.12 (s, 9H), 0.73—2.03 (m, 10H including a singlet of OH at 1.55), 2.06—2.47 (m, 2H), 2.67—3.05 (m, 2H), 7.13 (s, 5H); Calcd for $C_{18}H_{28}OSi$: C, 74.94; H, 9.78%. Found: C, 74.81; H, 9.79%.

*1,5-Diphenyl-3-trimethylsilyl-1-pentyn-3-ol (**1c**)*: Bp 146—147 °C/0.037 mmHg; IR (neat) 3410, 1600, 1250, 850 cm^{-1}; NMR (CCl_4) δ=0.18 (s, 9H), 1.76—2.16 (m, 3H including a singlet of OH at 1.91), 2.75—3.16 (m, 2H), 7.00—7.50 (m, 10H).

*5-Phenyl-1,3-bis(trimethylsilyl)-1-pentyn-3-ol (**1d**)*: Bp 104—105 °C/0.025 mmHg; IR (neat) 3400, 2135, 1248, 845 cm^{-1}; NMR (CCl_4) δ=0.12 (s, 9H), 0.19 (s, 9H), 1.62—2.03 (m, 3H including a singlet of OH at 1.67), 2.68—3.03 (m, 2H), 7.16 (s, 5H); Calcd for $C_{17}H_{28}OSi_2$: C, 67.04; H, 9.27%. Found: C, 67.32; H, 9.22%.

*6-Methoxy-1-phenyl-3-trimethylsilyl-4-hexyn-3-ol (**1e**)*: Bp 110—112 °C/0.027 mmHg; IR (neat) 3370, 2200, 1246, 840 cm^{-1}; NMR (CCl_4) δ=0.15 (s, 9H), 1.65—2.08 (m, 2H), 2.37 (s, 1H), 2.68—3.10 (m, 2H), 3.31 (s, 3H), 4.12 (s, 2H), 7.13 (s, 5H); Calcd for $C_{16}H_{24}OSi$: C, 69.52; H, 8.75%. Found: C, 69.20; H, 8.60%.

*Alkylation of a Lithiated Allene **4** Generated from **2**.* *General Procedure*: To a hexane (1 mL) solution of 1-(trimethylsilyl)propargyl alcohol (**1**) (1 mmol) was added butyllithium (0.55 mL of 2.0 M hexane solution, 1.1 mmol) at 0 °C and it was stirred for 30 min. After cooling to −78 °C, THF (5 mL) was added and it was stirred for 10 min at that temperature. Then, an appropriate alkyl iodide (1.2 mmol) in THF (1 mL) was added and the reaction mixture was stirred for 1.5 hr at −40 °C. Hexane (20 mL) precooled to −78 °C was added to the reaction mixture and was poured into a buffer (KH_2PO_4–NaOH) solution. The aqueous layer was extracted twice with 20 mL portions of ether, and the combined extracts were dried over anhyd $MgSO_4$. After removal of the solvent, the crude 1-(trimethylsiloxy)allene (**6**) was dissolved in THF (10 mL) and 3—5 drops of 1M HCl was added. After stirring for 20 min at room temperature, the reaction mixture was treated with aq $NaHCO_3$ and was extracted twice with 20 mL portions of ether. The combined extracts were washed with satd aq NaCl and dried over anhyd $MgSO_4$. Removal of the solvent followed by separation with TLC gave a mixture of the corresponding (*E*)- and (*Z*)-α,β-unsaturated ketone.

*5-Methyl-1-phenyl-3-trimethylsiloxy-3,4-nonadiene (**6a**)*: IR (neat) 1950, 1600, 1250, 850 cm^{-1}; NMR (CCl_4) δ=0.12 (s, 9H), 0.70—2.93 (m, 16H), 7.10 (s, 5H).

*2,6-Diphenyl-4-trimethylsiloxy-2,3-hexadiene (**6c**)*: IR (neat) 1934, 1600, 1250, 845 cm^{-1}; NMR (CCl_4) δ=0.10 (s, 9H), 2.00 (s, 3H), 2.30—3.00 (m, 4H), 7.12 (s, 10H).

(E)-*2-Phenyl-2-hepten-4-one (**7a-(E)**)*: 16%; IR (neat) 1675, 1595 cm^{-1}; NMR (CCl_4) δ=0.95 (t, J=7 Hz, 3H), 1.33—1.93 (m, 2H), 2.43 (t, J=7 Hz, 2H), 2.50 (s, 3H), 6.36 (s, 1H), 7.03—7.63 (m, 5H).

(Z)-*2-Phenyl-2-hepten-4-one (**7a-(Z)**)*: 76%; IR (neat) 1685, 1655, 1610 cm^{-1}; NMR (CCl_4) δ=0.70 (t, J=6 Hz, 3H), 1.03—1.70 (m, 2H), 1.98 (t, J=6 Hz, 2H), 2.11 (s, 3H), 5.99 (s, 1H), 7.00—7.40 (m, 5H).

(E)-*5-Methyl-1-phenyl-4-nonen-3-one (**7b-(E)**)*: 45%; IR (neat) 1676, 1609 cm^{-1}; NMR (CCl_4) δ=0.66—1.67 (m, 7H), 1.76—2.30 (m, 2H), 2.04 (d, J=1 Hz, 3H), 2.40—3.02 (m, 4H), 5.87 (q, J=1 Hz, 1H), 7.04 (s, 5H).

(Z)-*5-Methyl-1-phenyl-4-nonen-3-one (**7b-(Z)**)*: 49%; IR (neat) 1679, 1606 cm^{-1}; NMR (CCl_4) δ=0.68—1.57 (m, 7H), 1.78 (d, J=1 Hz, 3H), 2.34—3.01 (m, 6H), 5.85 (q, J=1 Hz, 1H), 7.01 (s, 5H).

(E)-*1,5-Diphenyl-4-hexen-3-one (**7c-(E)**)*: 28%; IR (neat) 1680, 1600 cm^{-1}; NMR (CCl_4) δ=2.48 (d, J=1.6 Hz, 3H), 2.60—3.06 (m, 4H), 6.32 (q, J=1.6 Hz, 1H), 6.97—7.45 (m, 10H).

(Z)-*1,5-Diphenyl-4-hexen-3-one (**7c-(Z)**)*: 64%; IR (neat) 1685, 1655, 1610 cm^{-1}; NMR (CCl_4) δ=2.13 (d, J=1.4 Hz, 3H), 2.13—2.87 (m, 4H), 5.96 (q, J=1.4 Hz, 1H), 6.65—7.47 (m, 10H).

(E)-*1,5-Diphenyl-4-nonen-3-one (**7d-(E)**)*: 17%; IR (neat) 1668, 1585 cm^{-1}; NMR (CCl_4) δ=0.73—1.57 (m, 7H), 2.67—3.17 (m, 6H), 6.22 (s, 1H), 7.10 (s, 5H).

(Z)-*1,5-Diphenyl-4-nonen-3-one (**7d-(Z)**)*: 69%; IR (neat) 1680, 1650, 1605 cm^{-1}; NMR (CCl_4) δ=0.70—1.57 (m, 7H), 2.07—2.87 (m, 6H), 5.95 (s, 1H), 6.70—7.37 (m, 10H).

(E)-*1-Phenyl-5-trimethylsilyl-4-hexen-3-one (**7e-(E)**)*: 39%; IR (neat) 1675, 1578, 1250, 850 cm^{-1}; NMR (CCl_4) δ=0.11 (s, 9H), 2.12 (d, J=2 Hz, 3H), 2.60—2.98 (m, 4H), 6.25 (q, J=2 Hz, 1H), 7.09 (s, 5H).

(Z)-*1-Phenyl-5-trimethylsilyl-4-hexen-3-one (**7e-(Z)**)*: 48%; IR (neat) 1675, 1570, 1242, 850 cm^{-1}; NMR (CCl_4) δ=0.13 (s, 9H), 1.93 (d, J=1.8 Hz, 3H), 2.60—2.94 (m, 4H), 6.56 (q, J=1.8 Hz, 1H), 7.10 (s, 5H).

(E)- *and* (Z)-*4-Methyl-6-oxo-8-phenyl-4-octenal Ethylene Acetal (7f)*: 82%; IR (neat) 1678, 1610 cm^{-1}; NMR (CCl_4) δ=1.47—3.03 (m, 11H), 3.60—3.91 (m, 4H), 4.71 and 4.78 (t, J=4 Hz, 1H), 5.94 (q, J=1 Hz, 1H), 7.08 (s, 5H).

1-Phenyl-4,5-hexadien-3-one. To a THF (6 mL) solution of 6-methoxy-1-phenyl-3-trimethylsilyl-4-hexyn-3-ol (276 mg, 1.0 mmol) was added butyllithium (0.67 mL of 1.5 M hexane solution, 1.0 mmol) and hexamethylphosphoric triamide (HMPA) successively at −78°C, and it was stirred for 2 h at −40°C. Then, the reaction mixture was worked up in a similar manner as described above to afford the title compound (96 mg, 56%). Bp 90—92°C/0.08 mmHg; IR (neat) 1940, 1915, 1665, 855 cm^{-1}; NMR (CCl_4) δ=2.80 (s, 4H), 5.70 (d, J=6 Hz, 2H), 5.65 (dd, J=6 and 6 Hz, 1H), 7.08 (s, 5H); Calcd for $C_{12}H_{12}O$: C, 83.69; H, 7.02. Found: C, 83.89; H, 7.10%.

Conversion of 1-(Trimethylsilyl)propargyl Alcohol (1) to the 1-Trimethylsiloxy-1,2-propadiene (5) Catalyzed by Butyllithium. General Procedure: Buytllithium (0.04 mL of 1.5 M hexane solution, 0.06 mmol) was added to a THF (5 mL) solution of a 1-(trimethylsilyl)propargyl alcohol (**1**) (1 mmol) at −78°C, and the reaction mixture was warmed up to 0°C during 1 h. After stirring for 20 min at that temperature, the reaction mixture was worked up in a similar manner as described above to give the corresponding **8**.

1-Phenyl-3-trimethylsiloxy-1,2-hexadiene (5a): Bp 88—89°C/0.035 mmHg; IR (neat) 1925, 1250, 850 cm^{-1}; NMR (CCl_4) δ=0.13 (s, 9H), 0.94 (t, J=7 Hz, 3H), 1.71—1.81 (m, 2H), 2.17 (dt, J=7 and 2 Hz, 2H), 6.38 (t, J=2 Hz, 1H), 7.16 (s, 5H).

1,5-Diphenyl-3-trimethylsiloxy-1,2-pentadiene (5c): IR (neat) 1930, 1250, 850 cm^{-1}; NMR (CCl_4) δ=0.14 (s, 9H), 2.40—3.00 (m, 4H), 6.37 (t, J=2 Hz, 1H), 6.90—7.37 (m, 10H).

(E)-*1-Phenyl-1-hexen-3-one (8a-(E))*: 24%; IR (neat) 1675, 1650, 1600 cm^{-1}; NMR (CCl_4) δ=0.95 (t, J=7 Hz, 3H), 1.68 (tq, J=7 and 7 Hz, 2H), 2.55 (t, J=7 Hz, 2H), 6.58 (d, J=16 Hz, 1H), 7.41 (d, J=16 Hz, 1H), 7.15—7.55 (m, 5H).

(Z)-*1-Phenyl-1-hexen-3-one (8a-(Z))*: 72%; IR (neat) 1675, 1590 cm^{-1}; NMR (CCl_4) δ=0.85 (t, J=7 Hz, 3H), 1.56 (tq, J=7 and 7 Hz, 2H), 2.31 (t, J=7 Hz, 2H), 6.01 (d, J=12 Hz, 1H), 6.65 (d, J=12 Hz, 1H), 7.08—7.65 (m, 5H).

(E)-*1-Phenyl-4-nonen-3-one (8b-(E))*: 75%; IR (neat) 1685, 1665, 1620 cm^{-1}; NMR (CCl_4) δ=0.71—1.62 (m, 7H), 1.88—2.38 (m, 2H), 2.63—2.95 (m, 4H), 5.95 (dq, J=16 and 1 Hz, 1H), 6.68 (dt, J=16 and 6 Hz, 1H), 7.09 (s, 5H).

(Z)-*1-Phenyl-4-nonen-3-one (8b-(Z))*: 22%; IR (neat) 1682, 1610 cm^{-1}; NMR (CCl_4) δ=0.68—1.61 (m, 7H), 2.42—3.05 (m, 6H), 5.83—6.12 (m, 2H), 7.10 (s, 5H).

(E)-*1,5-Diphenyl-1-penten-3-one (8c-(E))*: 43%; IR (neat) 1680, 1650, 1600 cm^{-1}; NMR (CCl_4) δ=2.89 (s, 4H), 6.56 (d, J=16 Hz, 1H), 7.41 (d, J=16 Hz, 1H), 6.97—7.50 (m, 10H).

(Z)-*1,5-Diphenyl-1-penten-3-one (8c-(Z))*: 46%; IR (neat) 1678, 1595; NMR (CCl_4) δ=2.40—2.97 (m, 4H), 5.97 (d, J=12 Hz, 1H), 6.63 (d, J=12 Hz, 1H), 6.87—7.60 (m, 10H).

(E)-*5-Phenyl-1-trimethylsilyl-1-penten-3-one (8d-(E))*: 52%; IR (neat) 1670, 1249, 842 cm^{-1}; NMR (CCl_4) δ=0.10 (s, 9H), 2.79 (s, 4H), 6.29 (d, J=19 Hz, 1H), 6.91 (d, J=19 Hz, 1H), 7.05 (s, 5H).

(Z)-*5-Phenyl-1-trimethylsilyl-1-penten-3-one (8d-(Z))*: 11%; IR (neat) 1680, 1240, 845 cm^{-1}; NMR (CCl_4) δ=0.11 (s, 9H), 2.67—2.93 (m, 4H), 6.17 (d, J=14 Hz, 1H), 6.70 (d, J=14 Hz, 1H), 7.02 (s, 5H).

(E)-*6-Methoxy-1-phenyl-4-hexen-3-one (8e-(E))*: 53%; IR (neat) 1680, 1660, 1625 cm^{-1}; NMR (CCl_4) δ=2.79 (s, 4H), 3.27 (s, 3H), 3.93 (dd, J=4 and 1.8 Hz, 1H), 6.16 (dt, J=16 and 1.8 Hz, 1H), 6.67 (dt, J=16 and 4 Hz, 1H). 7.11 (s, 5H).

(Z)-*6-Methoxy-1-phenyl-4-hexen-3-one (8e-(Z))*: 27%; IR (neat) 1680, 1610 cm^{-1}; NMR (CCl_4) δ=2.63—2.90 (m, 4H), 3.28 (s, 3H), 4.35 (d, J=2 Hz, 2H), 6.00—6.18 (m, 2H), 7.10 (s, 5H).

The Reaction of 1-Phenyl-3-trimethylsiloxy-1,2-hexadiene with Benzaldehyde Dimethyl Acetal. 1-Phenyl-3-trimethylsiloxy-1,2-hexadiene was prepared from 1-phenyl-3-trimethylsilyl-1-hexyn-3-ol (246 mg, 1.0 mmol) by procedures described above. The crude diene was dissolved in dichloromethane (4 mL) and was added to a mixture of benzaldehyde dimethyl acetal (152 mg, 1.0 mmol) and titanium tetrachloride (0.11 mL, 1.0 mmol) in dichloromethane (8 mL) at −78°C. After stirring for 1 h at that temperature, the reaction mixture was poured into 0.4 M aq $NaHCO_3$ (20 mL) and was filtered through Celite. The aqueous layer was extracted twice with 20 mL portions of dichloromethane, and the combined extracts were dried over anhyd $MgSO_4$. Removal of the solvent from the filtrate followed by separation with TLC afforded 2-(α-methoxybenzyl)-1-phenyl-1-hexen-3-one (237 mg, 81% based on 1-phenyl-3-trimethylsilyl-1-hexyn-3-ol). Bp 118—119°C/0.024 mmHg; IR (neat) 1680 cm^{-1}; NMR (CCl_4) δ=0.61 (t, J=8 Hz, 3H), 0.91—2.35 (m, 4H), 5.00 (s, 1H), 6.43 and 6.45 (s, 1H), 7.07 (s, 5H), 7.21 (s, 5H); Calcd for $C_{20}H_{22}O_2$: C, 81.60; H, 7.53%. Found: C, 81.84; H, 7.58%.

References

1) A. G. Brook, *Acc. Chem. Res.*, **7**, 77 (1974).
2) E. W. Colvin, "Silicon in Organic Synthesis," Butterworths, London (1981), Chap. 5.
3) See Ref. 2, Chap. 12, and W. P. Weber, "Silicon Reagents for Organic Synthesis," Springer-Verlag, Berlin (1983), Chap. 6.
4) I. Kuwajima and M. Kato, *J. Chem. Soc., Chem. Commun.*, **1979**, 708; *Tetrahedron Lett.*, **21**, 2745 (1980); M. Kato, A. Mori, H. Oshino, J. Enda, K. Kobayashi, and I. Kuwajima, *J. Am. Chem. Soc.*, in press.
5) H. Urabe and I. Kuwajima, *Tetrahedron Lett.*, **24**, 4241 (1983).
6) G. Linstrumelle and D. Michelot, *J. Chem. Soc., Chem. Commun.*, **1975**, 561; D. Michelot and G. Linstrumelle, *Tetrahedron Lett.*, **1976**, 275; J. C. Clinet and G. Linstrumelle, *ibid.*, **1978**, 1137.
7) I. Kuwajima and M. Kato, *Tetrahedron Lett.*, **21**, 623 (1980).
8) Similar results have also been reported by Reich and his collaboraors: H. J. Reich, R. E. Olson, and M. C. Clark, *J. Am. Chem. Soc.*, **102**, 1423 (1980).
9) I. Kuwajima, T. Abe, and N. Minami, *Chem. Lett.*, **1976**, 993; I. Kuwajima, M. Arai, and T. Sato, *J. Am. Chem. Soc.*, **99**, 4181 (1977); I. Kuwajima, M. Kato, and T. Sato, *J. Chem. Soc., Chem. Commun.*, **1978**, 478; I. Kuwajima, A. Mori, and M. Kato, *Bull. Chem. Soc. Jpn.*, **53**, 2368 (1980).
10) 1 mmHg=133.322 Pa.

 © 1984 The Chemical Society of Japan Bull. Chem. Soc. Jpn., 57, 831—835 (1984)

Interactions between Anionic Surfactants and Oil Dyes in the Aqueous Solutions. III. Thermochromism in the Presence of Surfactant Micelle and Dye–Surfactant Complexes

Masahiko ABE,*,†,†† Mitsuo OHSATO,† Nobuyuki SUZUKI,† and Keizo OGINO†,††

†*Faculty of Science and Technology, Science University of Tokyo, Noda, Chiba 278*

††*Institute of Colloid and Interface Science, Science University of Tokyo, 1-3, Kagurazaka, Shinjuku-ku, Tokyo*

(Received July 1, 1983)

The interactions between 4 anionic surfactants and 3 azo oil dyes have been studied by a spectrophotometer. The spectrographic behavior of these solutions was dependent on the kinds of hydrophilic groups in each surfactant and the kind of auxochrome in the azo oil dyes. In particular, a sulfate and two sulfonates including strongly hydrophilic groups interacted strongly with the oil dyes (4-NH_2) which have an amino group at 4-position of naphthalene. At lower concentrations, an isosbestic point was recognized; this occurred because of the formation of the hydrophobic dye-surfactant complex (1:1). In the neighborhood of the cmc region, the spectrum with a peak at 520 nm changed with temperature into another one with a 440 nm band; this is the so-called thermochromism. This may be attributed to the fact that, in the presence of surfactant micelles, the 4-NH_2 exhibits an azo form at higher temperature, but a resonance stabilized azonium form is found at lower temperature.

A number of investigations have been made on the interactions between surfactants and dyes in order to clarify the formation of dye–surfactant complexes.[1-3] In recent years, Nemoto[4] and Kuroiwa[5] have published reviews on interactions between surfactants and dyes. For example, Kuroiwa[6] studied a complex of dispersing dye and anionic surfactant; Nemoto[7] studied that of acid–nonionic surfactant. But few studies have been made on the interactions between oil dyes and surfactants.

The changes of complementary color of the dye solutions include solvatochromism,[8] halochromism,[9] and thermochromism.[10] However, these have not been measured in the presence of surfactant micelles.

We have reported the solubilization of some oil dyes by sodium dodecyl sulfate.[11] We found that the surfactant anion interacted strongly with the oil dye including amino group at 4-position of naphthalene; moreover, the spectrum with a peak at 520 nm changed with temperature into another one with a 440 nm band.

In this paper, we report the interaction between 4 anionic surfactants, which have different hydrophilic groups, and 3 azo oil dyes, which have different functional groups in aqueous solutions by the spectrographic method. We discuss the effect of surfactant micelle structure on the protonation equilibrium of azo oil dyes.

Experimental

Materials. *Anionic Surfactants*: Sodium dodecyl sulfate (SDS) was supplied by Nihon Surfactant Industries, Co., Ltd, Tokyo, Japan; sodium 1-dodecanesulfonate (DSS), sodium dodecylbenzenesulfonate (SDBS), and sodium laurate (SL) were purchased from Tokyo Kasei Kogyo Co., Ltd, Tokyo. They are more than 99.5% pure. All surfactants were extracted with ether and crystallized from ethanol; their purities were ascertained by surface tension measurements and differential thermal analysis. Oil dyes: The details of 4-phenylazo-1-naphthylamine (4-NH_2), 4-phenylazo-1-naphthol (4-OH), and Naphthalene-1-azobenzene (NA) were described in our previous paper.[11]

Methods. *Preparation of Surfactant Solution Including Oil Dye*: Into several 100 ml glass-stoppered Erlenmeyer flasks, 50 ml portions of a given concentration of a surfactant solution were placed; a measured amount of oil dye was added to each. The mixtures were stirred with ultrasonic waves for 5 min, then they were stirred by a shaker (model SS-82 D type of Tokyo Rikakikai Co., Ltd, Tokyo) for 24 h and allowed to stand for 24 h in a thermostat at 30 °C in order to establish a solubilization equilibrium.

Determinaton of Maximal Absorption (λ_{max}) and Optical Density of the Solution Owing to Temperature Change. After equilibrium had been established, these mixtures were centrifuged. Then the supernatant liquids of these solutions were collected. The temperature dependence of each maximal absorption and the optical density of each solution were measured by a double beam spectrophotometer (model UVIDEC 505 of Nihon Bunko Ltd, Tokyo) with a quartz cell (1.0, 10.0, or 20.0 mm in length).

Determinaton of cmc of Surfactant by Dye-solubilization Method. The cmc of surfactants determined by the dye-solubilization method were the same as reported previously.[11]

Determination of cmc of Surfactant Alone. The cmc of surfactants alone were determined by the surface tension method.[12] The surface tensions of the surfactant alone were measured at 30 °C with a Wilhelmy tensiometer (model CBVP-A3 of Kyowa Kagaku Co., Ltd, Tokyo) equipped with a platinum plate.

Determinaton of Binding Molar Ratio of Dye-surfactant Complex. The binding molar ratio of dye-surfactant complex was investigated with the continuous variation in optical density method by Kuroiwa and Ogasawara[13] at 30 and 70 °C.

Results

The cmc Given by Dye-solubilization Method and by Surface Tension Method. The cmc given by dye (4-NH_2) solubilization method (I), and that of the surfactant alone given by surface tension method (II) are shown in Table 1. The spectrographic measurements have been made at the following concentrations: A region (below I), B region (between I and II), and C region (above II).

Thermochromism. Oil dyes used in this study were almost insoluble in water at room temperature, but they dissolved slightly in hot water: the complementary color of the solution was yellowish. The complementary color of 4-NH_2 in SDS, DSS, and

Table 1. Cmc by dye solubilization method (I) and surface tension method (II)

Surfactant	cmc/mol dm^{-3}	
	I	II
SDS	2.1×10^{-3}	8.0×10^{-3}
DSS	2.5×10^{-3}	9.8×10^{-3}
SDBS	1.4×10^{-2}	2.0×10^{-2}
SL	1.8×10^{-2}	3.0×10^{-2}

SDBS micellar solutions changed (reddish→yellowish) with increasing temperature; thus the so-called thermochromism occurred. However, the complementary color of 4-NH_2 in SL micellar solution (yellowish) did not change with increasing temperature. Moreover, in the case of NA, and 4-OH, no thermochromism occurred in any surfactant micellar solution.

The Shift of Maximal Absorption with Increase of Temperature. (1) For SDS-4-NH_2 Systems: (a) Concentration of SDS; (i) A Region. Optical densities for the SDS solutions of 3.2×10^{-4} mol dm^{-3} including 4-NH_2 of 1.6×10^{-4} mol dm^{-3} in the temperature range 30°C to 70°C are plotted against the measuring wavelength in Fig. 1. As can be seen from Fig. 1, the maximal absorption was about 440 nm; this was not dependent on temperature. But the optical density at maximal absorption increased with increasing temperature: the so-called transition of chemical species. An isosbestic point was recognized at higher wavelength (about 520 nm) than that at the maximal absorption (440 nm).

(ii) B Region. Optical densities for the SDS solutions of 5.0×10^{-3} mol dm^{-3} including 4-NH_2 of 1.6×10^{-4} mol dm^{-3} in the temperature range 30°C to 72°C are plotted against the measuring wavelength in Fig. 2. The maximal absorption shifted from longer wavelengths (520 nm) to shorter wavelengths (440 nm) with increase in temperature: the so-called hypsochromic shift.

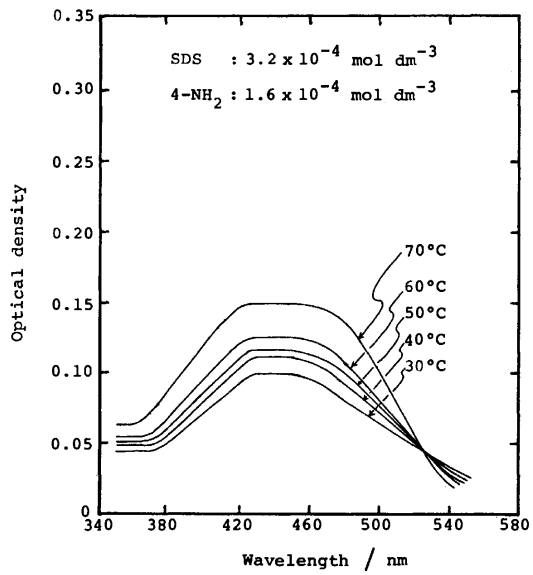

Fig. 1. Effect of temperature on absorption spectra for SDS solution which have dissolved 4-NH_2. (below I: A region)

(iii) C Region. Optical densities for the SDS solutions of 1.6×10^{-2} mol dm^{-3} including 4-NH_2 of 1.6×10^{-4} mol dm^{-3} in the temperature range 30°C to 70°C are plotted against the measuring wavelength in Fig. 3. The maximal absorption was not dependent on temperature; its wavelength was about 520 nm, which was about 80 nm higher than that below the cmc. The optical density at maximal absorption increased with increase in temperature. The maximal absorption caused by the increase of temperature changed considerably in the SDS concentration range 2.2×10^{-3} mol dm^{-3} to 1.0×10^{-2} mol dm^{-3}. The shifting temperature, at which the maximal absorption moved from 520 nm to 440 nm, increased with increasing concentration of SDS at the above-mentioned cmc region (58°C to 70°C).

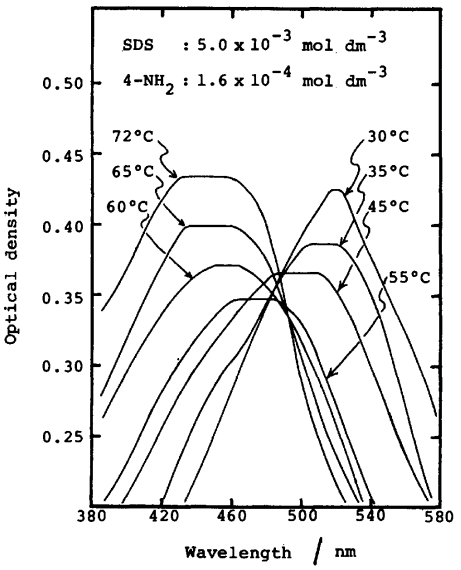

Fig. 2. Effect of temperature on absorption spectra for SDS solution which have dissolved 4-NH_2. (between I and II: B region)

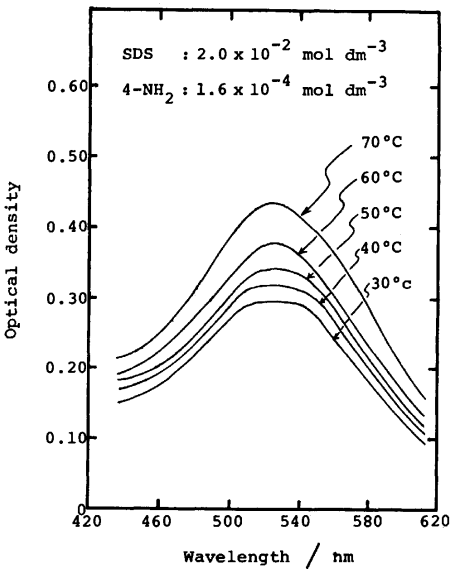

Fig. 3. Effect of temperature on absorption spectra for SDS solution which have dissolved 4-NH_2. (above II: C region)

(b) Concentration of 4-NH_2: As the amounts of 4-NH_2 in each concentration of SDS were considerably higher than the limits of solubilization, thermochromism was not observed. The optimum amount of 4-NH_2 for the observation of thermochromism was just lower than the limit of solubilization.

(2) For SDBS-4-NH_2 Systems: The maximal absorptions of the solutions below the cmc and above the cmc were the same as those of SDS. The change of maximal absorption (520 nm to 440 nm) with increase in temperature was also recognized in the SDBS solutions of 3.0×10^{-2} mol dm^{-3}. Thermochromism also occurred in the SDBS concentration of the cmc range (I, II in Table 1), and for the dye amount just lower than the limit of solubilization as in the case in SDS solutions.

(3) For DSS-4-NH_2 Systems: The maximal absorption of the solutions below the cmc and above the cmc were the same as those of SDS. The change of maximal absorption (520 nm→440 nm) with increase in temperature was also recognized in the DSS solutions of 1.0×10^{-2}mol dm^{-3}. Optical densities for the DSS solutions of 1.0×10^{-2} mol dm^{-3} (at C region) including 4-NH_2 of 1.6×10^{-4} mol dm^{-3} in the temperature range 20°C to 75°C are plotted against the measuring wavelength in Fig.4. In the case of SDS and SDBS, the optical density at about 520 nm decreased with increase in temperature, but in the case of DSS, it increased with increasing temperature until 35°C, and then it decreased for higher temperatures. 4-NH_2 in the DSS solutions was found to undergo both hyperchromic effect and transition of chemical species. Thermochromism also occurred in the SDS concentration of the cmc range (I, II in Table 1) and for the dye amount just lower than the limit of solubilization, as in the case in SDS solutions.

(4) For SL-4-NH_2 Systems: Optical densities for the SL solutions of 5.0×10^{-2} mol dm^{-3} (at B region), including 4-NH_2 of 1.6×10^{-4} mol dm^{-3} in temperature range 30°C to 70°C are plotted against the measuring

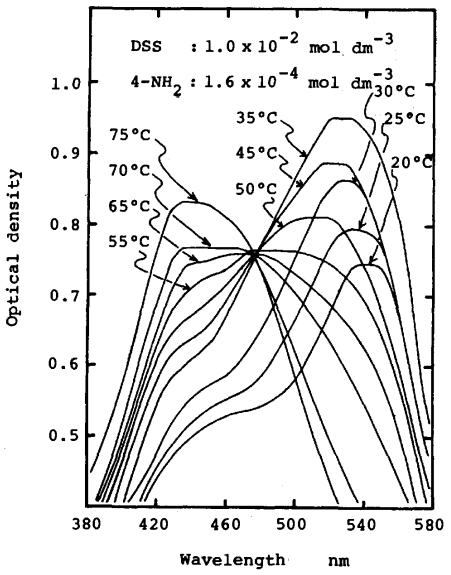

Fig. 4. Effect of temperature on absorption spectra for DSS solution which have dissolved 4-NH_2. (between I and II: B region)

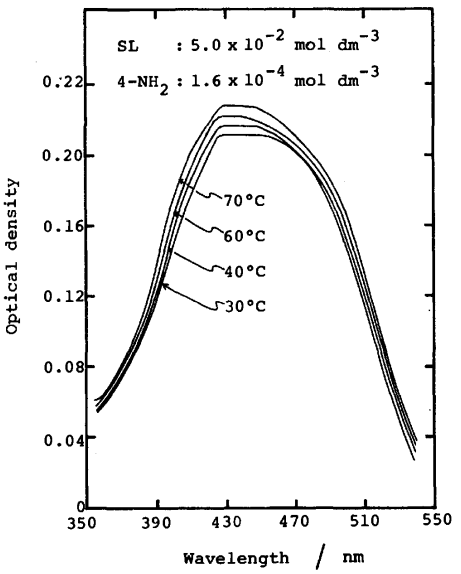

Fig. 5. Effect of temperature on absorption spectra for LS solution which have dissolved 4-NH_2. (regardless of the concentration of LS)

wavelength in Fig. 5. Figure 5 shows that the maximal absorption of SL solutions was independent of temperature. Thus, we found that the concentration of SL is not significant.

(5) For 4-OH and NA: All of the maximal absorptions of the solutions were unchanged with increase in temperature; the values were 480 nm (4-OH) and 380 nm (NA) for all kinds and concentrations of surfactants.

Discussion

The Isosbestic Point at A Region. In the case of 4-NH_2 and anionic surfactants except SL of lower concentration, the isosbestic point was recognized at a 520 nm band, as shown in Fig. 1. Kuroiwa[14] describes how the isosbestic point like this is recognized in SDS (and/or SDBS)-1,4,5,8-tetraaminoanthraquinone system because of the formation of a dye-surfactant complex.

Nemoto *et al.*[15,16] report that the distinction between hydrophilic and hydrophobic complexes can be made by measuring the surface tension of the solution and by extracting the solution from chloroform. In the same manner, we previously confirmed the hydrophobic complex.[11] Except for SL, the formation of hydrophobic complex in the cases of SDBS and DSS was thus established. We adopted the continuous variation method[13] in order to determine the binding molar ratio of these complexes. The results are shown in Table 2. Except for SL, surfactants including strongly polar groups and 4-NH_2 seem to form a hydrophobic complex of 1:1.

TABLE 2. MOLAR RATIO OF COMPOUND FORMED FROM DYE (4-NH_2) AND VARIOUS SURFACTANTS BY CONTINUOUS VARIATION METHOD (λ_{max}=440 nm)

Surfactant	Ratio (S:D)
SDS	1 : 1
DSS	1 : 1
SDBS	1 : 1
SL	—

The Thermochromism at B Region. As can be seen from Figs. 1 and 3, the maximal absorption of 4-NH_2 at A region is at the 440 nm band, while that at C region is at the 520 nm band regardless of temperature: it seems that the maximal absorption at 440 nm band arises from the dispersing state of 4-NH_2 in monomer phase, while that at 520 nm band arises from that solubilized into micellar phase. The maximal absorption at B region, in other words, that at the neighborhood of the cmc, is dependent on temperature. The results can be interpreted as follows. The cmc of anionic surfactants are shifted from lower concentration to higher concentration with increasing temperature.[17] Moreover, it is well known that the amount of solubilization is dependent on the concentration of anionic surfactant.[18,19] Thus, with increasing temperature, the values of the cmc shifted from lower concentration to higher concentration and the number of surfactant micelles decreased; as a result, the 4-NH_2 solubilized in surfactant micelle is released into a monomer phase. Therefore, the complementary color of the solution at B region changed with temperature; the so-called thermochromism occurred.

In the C region, there are many micelles in the solution, so that the increase of the value of cmc is slight and the 4-NH_2 solubilized in micelle does not release into the monomer phase with increasing temperature. Therefore, thermochromism does not occur. In general, a dye including amino group in organic solvent takes the azo form.[20] The spectrum in dodecane provides an absorption band at 440 nm, which is attributed to the azo form. Accordingly, the tautomer of 4-NH_2 at both A region and B region under higher temperature seems to be azo form.

Secondly, we consider the structure of 4-NH_2 in surfactant micellar solutions other than SL. For the location of 4-NH_2 in surfactant micelle, we[21] found that, because the functional group of the dye is fairly strong and dissociates slightly, it thrusts the functional group out of the SDS micelles and its hydrophobic parts penetrate into the palisade layers of SDS micelles. Moreover, because the pH of the SDS solution to which 4-NH_2 was added is larger than that of SDS alone (6.8—7.9), 4-NH_2 is thought to act as a base.

Klotz *et al.*[22] describe the protonation process as follows: the first proton goes to the amino group and then a second proton goes to the azo group with an increase in the hydrogen ion concentration. On the contrary, Tanizaki *et al.*[9] point out that a proton addition to amino group must shift the color band to a shorter wavelength, because the electronic theory insists that the protonated amino group cannot be conjugated with the ring system because of the number of the π-type electrons is too few: the protonation to the β-azo-nitrogen atom of the dye shifts the color band to a longer wavelength than that of azo form. The halochromism of 4-NH_2 is shown in Fig. 6. As can be seen from Fig. 6, the spectrum with a peak at a 440 nm band in an alkaline solution changed into another one (520 nm) with an increase in the hydrogen ion concentration. According to Tanizaki *et al.*,[9] the spectrum with a peak at 520 nm seems to be the protonation to β-azo-nitrogen atom of the dye (in

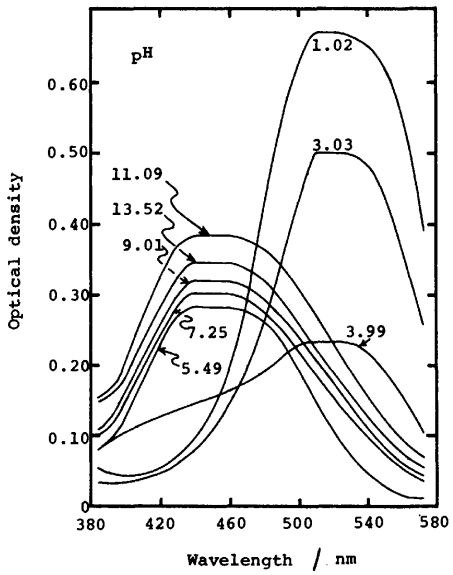

Fig. 6. Effect of pH on absorption spectra for 4-NH_2 aqueous solutions.

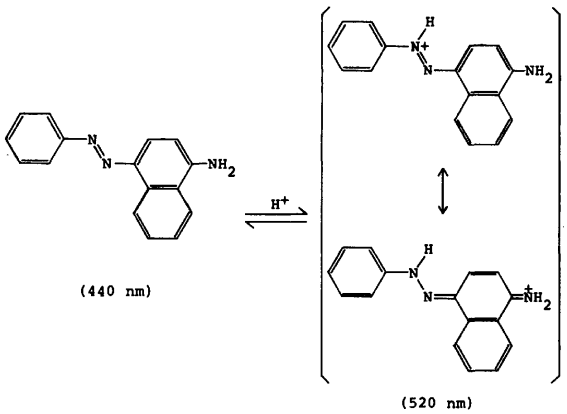

Fig. 7. Relationship between protonation process of dye and λ_{max}.

Fig. 7). However, this study was not made in a higher acid solution but in a neutral solution. From the study of synthesis of oil dye reported previously,[21] we found that the replacement reaction occurred not at the position of azo group, but at the position of amino group. Furthermore, Matsuoka *et al.*[23] suggest that, when the proton goes to β-azo-nitrogen atom, electric charge transfer occurs; as a result a nitrogen atom of amino group becomes positively charged. The 4-NH_2, described previously, was solubilized into SDS micelle as the functional group (amino group) out of the micelle,[21] and then it becomes a counterion for the surface negative charge of the micelle. And so this micelle was stable at room temperature. Therefore, the quinoidal form of 4-NH_2 was stabilized in the SDS micelle at room temperature.

For SL Solutions. As can be seen from Fig. 5, regardless of the concentration of SL and temperature, the maximal absorption was still a peak at 440 nm. SL is mild alkaline, so that the pH value of solution is shifted to basic 8.5, to prevent protonation. In general, an aliphatic soap like SL is partly hydrolyzed in water.[24] It seems that, because the aliphatic acid

produced is preferentially solubilized into SL micelles, the 4-NH_2 is adsorbed on the surface (hydrophilic parts) of the solubilized micelles, as mentioned by Kondo and Meguro.[25] Therefore, 4-NH_2 is always placed in the bulk phase, and the maximal absorption is 440 nm. However, an aliphatic soap like SL does not form a spherical micelle like SDS, but a hexagonal packing of cylindrical micelles,[26] where the insoluble hydrocarbon chains are turned inward, in a neutral particle of soap, and the heavily hydrated carboxylate group is presented to the surrounding water.[27] It seems that the 4-NH_2 exists in the surrounding water, even when the concentration of SL is somewhat above the cmc.

In any event, because the polar nature of SL is weaker than that of SDS, the proton in water is not in contact with the dye; so the protonation to the 4-NH_2 did not occur.

References

1) W. Luck, *Angrew. Chem.*, **72**, 57 (1960); W. Luck, *Melliand Textiller*, **41**, 315 (1960).
2) T. D. Tuong, K.Otsuka, and S. Hayano, *Chem. Lett.*, **1977**, 1319.
3) A. Datyner, *J. Colloid Interface Sci.*, **65**, 527 (1978).
4) Y. Nemoto, *Yukagaku*, **28**, 809 (1979).
5) S. Kuroiwa, *Sen'i Gakkai Shi*, **20**, 52, 183 (1964).
6) S. Kuroiwa, *Sen'i Gakkai Shi*, **36**, 27 (1980).
7) Y. Nemoto, *J. Colloid Interface Sci.*, **79**, 313 (1981).
8) M. Mitsuishi, R. Kamimura, M. Ieda, K. Shinohara, and N. Ishii, *Sen'i Gakkai Shi*, **32**, T-382 (1976).
9) Y. Tanizaki, *Bull. Chem. Soc. Jpn.*, **39**, 558 (1966).
10) S. Tokita, "Color Chemistry," Maruzen, Tokyo (1982), p. 136.
11) M. Abe, N. Suzuki, and K. Ogino, *J. Colloid Interface Sci.*, in press.
12) K. Tajima, *Nippon Kagaku Kaishi*, **1973**, 83.
13) S. Kuroiwa and S. Ogasawara, *Nippon Kagaku Kaishi*, **1976**, 790.
14) S. Kuroiwa and S. Ogasawara, *Sen'i Gakkai Shi*, **24**, 536 (1968).
15) Y. Nemoto and H. Funahashi, *J. Colloid Interface Sci.*, **62**, 95 (1977).
16) Y. Nemoto and H. Funahashi, *Shikizai Kyokai Shi*, **53**, 488 (1980).
17) B. D. Flockhart and A. R. Ubbelohde, *J. Colloid Sci.*, **8**, 428 (1953).
18) K. Ogino, M. Abe, and N. Takeshita, *Bull. Chem. Soc. Jpn.*, **49**, 3679 (1976).
19) K. Ogino, M. Abe, and N. Takeshita, *Bull. Chem. Soc. Jpn.*, **51**, 1880 (1978).
20) K. Konishi and N. Kuroki, "Gousei Senryo No Kagaku," Maki Shyoten, Tokyo (1978), p. 157.
21) M. Abe, N. Suzuki, and K. Ogino, *J. Colloid Interface Sci.*, **93**, 285 (1983).
22) M. I. Klotz, *J. Am. Chem. Soc.*, **76**, 5136 (1954).
23) M. Matsuoka, *Shikizai Kyokai Shi*, **53**, 724 (1980).
24) P. Ekwall, *Kolloid-Z.*, **92**, 144 (1940); S. Miyashita and Y. Uzu, *Yukagaku*, **29**, 350 (1980); H. W. Brouwer and W. Skoda, *Kolloid-Z.*, **234**, 1138 (1969).
25) T. Kondo and K. Meguro, *Bull. Chem. Soc. Jpn.* **32**, 267, 857 (1959).
26) K. L. Mittal and P. Mukerjee, "Micellization, Solubilizaion, and Microemulsions," ed by K. L. Mittal, Plenum Press, New York (1977), Vol. 1, p. 10.
27) J. W. McBain, "Colloid Science," D. C. Heath and Company, Boston (1950), p. 5.

A Consideration on the Structure of the Nascent Fibril Produced by *Acetobacter xylinum*

Akira KAI

Department of Industrial Chemistry, Faculty of Technology, Tokyo Metropolitan University, Fukazawa, Setagaya-ku, Tokyo 158

(Received July 11, 1983)

The structure of the nascent fibril produced by *Acetobacter xylinum* was examined by electron microscopy and resistance to alkali. It was found that the inner part of the fibril after production is stained uniformly with sodium tungstophosphate. This suggests that the nascent fibril is in an amorphous state. Moreover, the fact that in the amorphous fibril microscopic fibrils with closely similar widths always appear in the course of time and that the X-ray diffraction diagram of the never-air-dried fibril treated with 11 wt% aqueous NaOH solution show cellulose I not cellulose II diffraction patterns, indicate that the arrangement of cellulose chains in its cross section can transform easily to that of chains in ellulose I crystalline. For such an arrangement, it must be presumed that in the nascent fibril cellulose chains are in the form of sheets of monomolecular layers corresponding to the $(1\bar{1}0)$ plane of cellulose I crystalline.

The structure of the fibril after production by *Acetobacter xylinum (A. xylinum)* is still unknown. Brown *et al.* suggested initially that a fibril (a microfibril) crystallized simultaneously when it is extruded from a synthesizing site in the envelope of a bacterial cell.[1] But lately, they suggested that a nascent microfibril is composed of bundles of chains in the tactoidal state since the inner part of the fibril from an incubated medium with fluorescent brightener was dyed by the brightener.[2,3] Zaar reported that fibril formation from *A. xylinum* is similar to that described by Brown *et al.* He presumed that the crystallization of a fibril (a microfibril) occurred after extrusion from the synthesizing site.[4,5] Colvin *et al.*, from observation of the freeze-etching of incubated suspension of *A. xylinum* reported that a nascent fibril has a dense core surrounded by a sheath of amorphous gel.[6–8] We suggested, from the negative staining behavior of the nascent fibrils, that they are in a homogeneous amorphous state.[9]

It was found that in the course of time microscopic fibrils with almost the same width of 40—50 Å develop in the amorphous fibril.[10,11] Since the same transformation of the amorphous fibril always occurred, we have presumed that it is composed not of random chains but of chains which retain a specific correlation with each other.

In this paper the structure of the fibril produced by *A. xylinum* was examined with respect to its staining behavior toward sodium tungstophosphate and its resistance to alkali.

Experimental

Culture of Cells and Preparations of the Samples for Electron Microscopy. The methods described previously were followed.[10] Two series of samples were prepared for electron microscopy; one of the series is the fibrils from the glucose medium with sodium tungstophosphate and the other is the fibrils, stained by an aqueous solution of sodium tungstophosphate before drying, from the glucose medium without the staining agent.

Ten ml of *A. xylinum*-preserved culture medium (IFO 13693) was added to 100 ml of complex medium (distilled water: 100 ml, D-glucose: 1 g, peptone: 1 g, yeast extract: 0.3 g, sodium chloride: 0.2 g, disodium hydrogenphosphate (anhydrous): 0.14 g, citric acid: 0.035 g, pH adjusted to 6.8 with 1 M† HCl or NaOH aq) and incubated at 28 °C for 72 h. After being thus cultured, 10 ml of the liquid phase of the starter culture was added to 100 ml of the fresh complex medium, and was incubated at 28 °C for 48 h. Separating the cellulose produced in the incubated medium requried filtration through a membrane filter of 5 μm pore size while cooling the filtrate with ice water. The filtrate was immediately filtered through a membrane filter of 0.45 μm pore size, allowing the cells to collect on the membrane filter. Cells were washed with a buffer solution (pH 6.8, disodium hydrogenphosphate: 0.14 wt%, citric acid: 0.035 wt%, 0 °C) to remove the medium components. They were then suspended in 60 ml of the fresh buffer solution. A 4 ml quantity of 0.2 wt% glucose medium (pH 6.8) with 2 wt% sodium tungstophosphate was added to 36 ml of cellulose-free cell suspension. The final concentrations of glucose and sodium tungstohosphate in the medium were 0.02 and 0.2 wt% respectively. These values were determined for the concentrations easily observable by electron microscopy without washing the fibrils produced. A drop of the culture medium was immediately placed on a sheet mesh covered with a collodion membrane and incubated in a 100%RH atmosphere at 28 °C for a given time. After the fibrils so produced had been allowed to settle on the sheet mesh by removing the medium, they were dried over P_2O_5 at room temperature for more than 24 h, and observed through an electron microscope. Preparations of the sample for the fibrils from 0.02 wt% glucose medium without staining agent are the same as described above except for staining with addition of a drop of 0.5 wt% aqueous sodium tungstophosphate solution for 15 min before drying. In the above incubation procedure, the complex medium was sterilized by autoclaving while the glucose medium was sterilized by filtration.

For electron microscopy, all preparations were examined with a JEOL JEM-100U electron microscope operating at 80 kV.

Measurement of the Linear Growth Rate of a Cellulose Fibril.

The linear growth rate of a cellulose fibril at a given temperature was obtained from the relation between the time of incubation and the mean length of ten fibrils after glucose incubation for a given time at a given temperature. The linear growth rate was constant within the range of the measurable length of a fibril.

Resistance of the Never-air-dried Fibrils to Alkali. Samples: 40 ml of 3 wt% glucose medium (pH 6.8) was added to 200 ml

† 1 M=1 mol dm^{-3}.

of cellulose-free cell suspension and incubated at 28 °C for a given time. Cellulose gels in the incubated mediums were the samples for alkali-treatment.

Alkali-treatment of the Never-air-dried Cellulose Gels: To the incubated medium an equal volume of aqueous NaOH was added dropwise at twice the given concentration. It was kept at 20 °C for 1 h and then 30 vol% aqueous acetic acid solution was added to neutralize. The solution was dialyzed through Cellulose Dialyzer Tubing (Nakarai Chemicals Ltd make, through M.W. cut-off: 8000, diameter: 90 mm, thickness: 0.09 mm) until sodium acetic acid free, and then boiled to collect cellulose. The cellulose collected, before drying, was again boiled in 1 wt% aqueous NaOH solution for 10 h under a nitrogen atmosphere, then neutralized and washed. The wet cellulose was compressed to a disk with the diameter of 1.5 mm and a thickness of about 1 mm for X-ray diffraction photography.

The X-ray diffraction diagram of the cellulose was taken with a flat-film camera with Ni filtered Cu $K\alpha$ radiation (35 kV, 15 mA, time of exposure: about 35 min) at specimen film distance of 50 mm. A Rigaku Denki make, Rota-Unit RU-3v X-ray camera was used.

Results and Discussion

The structure of the cellulose fibril after production by *A. xylinum* may be mainly determined by the mechanism of biogenesis of the fibril. However, it is supposed that if the structure of a fibril after extrusion from a cell is in an amorphous state, it may also be affected by the physicochemical environment, that is, temperature, the elapsed time of an amorphous fibril, the pH of medium and medium components *etc.* Therefore, first, the relation between the linear growth rate of a fibril produced by *A. xylinum* empolyed in this study and the temperature of incubation was examined.

The linear growth rate of a microfibril was maximum at about 28 °C as is evident from Fig. 1. As shown in Fig. 2a, the fibril, with its inner part stained uniformly, was obtained from a medium incubated with sodium tungstophosphate for 30 min at the most suitable temperature, 28 °C for the biogenesis of fibril. Moreover, it was found that the inner part of the fibril obtained from the incubated medium without staining agent at 28 °C for 5 min was uniformly stainable,

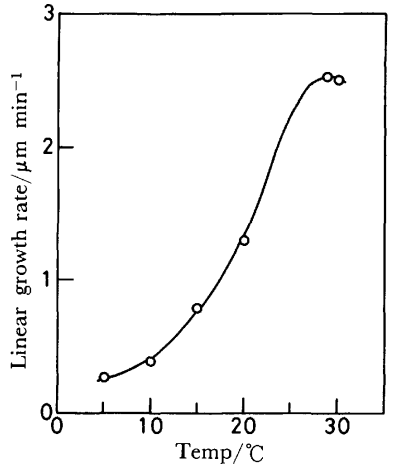

Fig. 1. Influence of temperature on the growth rate of the microfibril in glucose incubation.
Concentration of glucose: 1 wt%, pH of culture medium: 6.8.

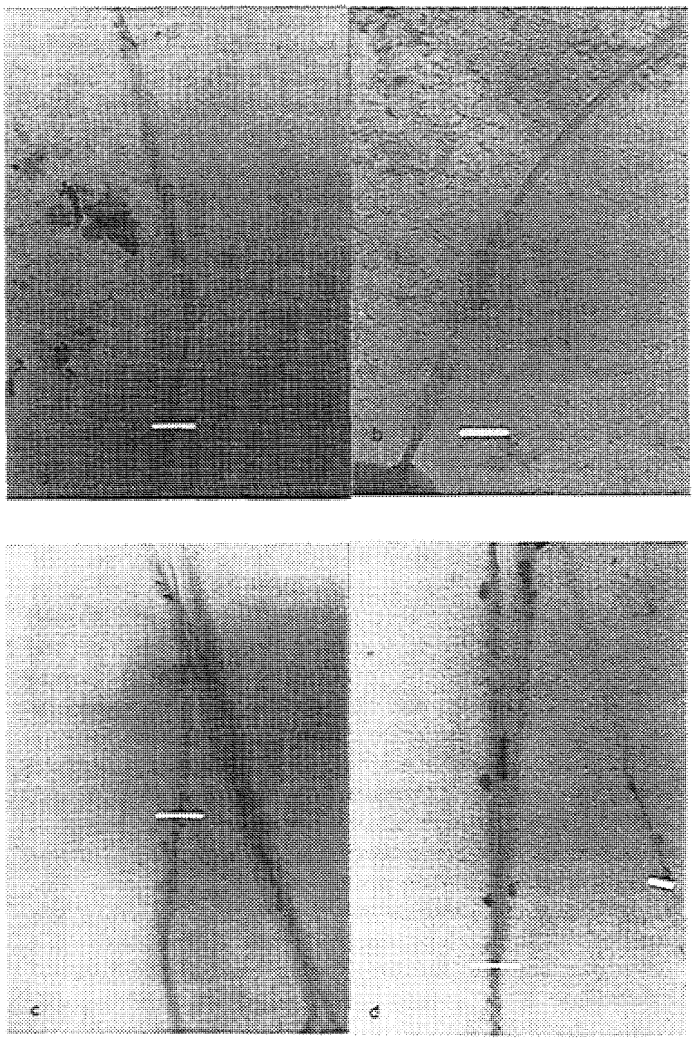

Fig. 2. Electron micrographs of the fibril obtained from 0.02 wt% glucose incubation included 0.2 wt% sodium tungstophosphate (pH 6.8) (a, c, and d) and the fibril obtained from 0.02 wt% glucose incubation (pH 6.8) (b) for a given time at 28 °C. The fibril obtained from the medium without staining agent before drying, was stained with 0.25 wt% aqueous sodium tungstophosphate solution for 15 min at room temperature. Time of incubation; a: 30 min, b: 5 min, c: 1 h, d: 5 h.
Scale bars=0.1 μm.

similar to the fibril obtained from the incubated medium with staining agent (Fig. 2b). The higher electron opacity of the twisted, thickened portions of these fibrils seemed to be the cause of the uniform staining of their inner part. In these fibrils the dense core, as reported by Colvin *et al.*, could not be found. According to the staining behavior of a nascent fibril toward sodium tungstophosphate, the fibril after production seemed to retain an amorphous state for about 30 min. Subsequently unevenness occurred perpendicular to the long axis of the fibril (some striations occurred parallel to the fibril axis) (Fig. 2c). Later microscopic fibrils with similar widths of 40—50 Å appeared simultaneously within the amorphous fibril about 5 h after production (Fig. 2d). Since the same transformation of the amorphous fibril as shown

in Fig. 2 always occurred, we suggested that a nascent fibril is composed not of random chains but of chains keeping specific correlation with each other.

The microscopic fibrils found in this study correspond to the elementary fibril formerly regarded as the fundamental structure of bacterial cellulose.[12-14] Recently, Brown *et al.*[1,2] and Zaar[4,5] pointed out that the synthesizing sites exist in the envelope of the cell and microfibrils (which correspond to the microscopic fibrils named in our paper) with the width of 30 Å are extruded from the synthesizing sites. Their illustrations allow us to understand the reproducibility of the microscopic fibrils in the amorphous fibril. Furthermore, the so-called "microfibril" of the earlier workers are assemblies of microscopic fibrils as shown in Fig. 2d. However, it is not always clear whether the crystallization of microscopic fibrils occurs before assembly or after.

It is considered that the staining agent, sodium tungstophophate does not have affinity towards polysaccharides. If this is true, it is to be assumed that sodium tungstophosphate does not change the structure of the nascent fibril, but is absorbed in it when it is extruded from the cell and is rejected from the stained fibril in the course of crystallization. Indeed, the reproducibility of the width of a microscopic fibril seems to support this process. On the other hand, according to Brown *et al.*[2,3] the cellulose material obtained from the incubated medium with a fluorescent brightener having a vital stain[15] is also in a non-crystalline state because the inner parts of fibril are stained. They also reported that this amorphous cellulose stained by brightener became cellulose I crystalline after drying. Although the microscopic fibrils could not be found in the cellulose material; its crystallinity was reduced, and the width of a crystallite changed from 30 to 28 Å. However, it is noteworthy that the influence of both sodium tungstophosphate and the brightener on the width of a crystallite after drying seems to be little different, although the influences of both on the morphology of the product are different because of their different affinity. This fact suggested that the fibril after production is not a mere bundle of chains but is restorable to the original width of the crystallite even if the product has absorbed the staining agent. For such a structure to be restorable, it must be assumed that in the nascent fibril cellulose chains are in the form of sheets of a monomolecular layer corresponding to the $(1\bar{1}0)$ plane of cellulose I. If the fibril after production has such a structure, the results observed both by Brown *et al.* and in this study can be satisfactorily explained.

It was found that the stainable state of the inner part of a fibril obtained from the incubation at 5 °C was retained for about 3 h (At this temperature the linear growth rate of a fibril is equivalent to about 1/10 of its value at 28 °C. See Fig. 1) as shown in Fig. 3. Although the influence of temperature on the crystallization of the amorphous fibril is unknown, it is apparent that the inner part of a fibril after production is in a stainable state even if the linear growth rate is different, and moreover, the microscopic fibrils after assembly are in an amorphous state.

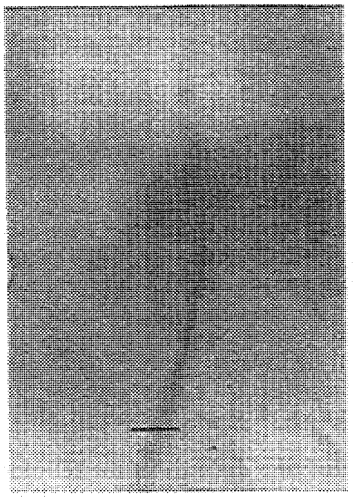

Fig. 3. Electron micrograph of the fibril obtained from 0.02 wt% glucose incubation included 0.2 wt% sodium tungstophosphate (pH 6.8) for 3 h at 5 °C. Scale bar=0.1 μm.

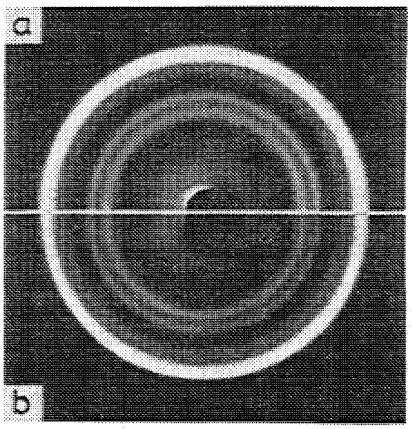

Fig. 4. X-Ray diffraction photograph of the 11 wt% alkali-treated cellulose from the glucose medium incubated for 5 h at 28 °C.
a: Purified and dried cellulose. b: Never-air-dried cellulose was treated in 11 wt% aqueous NaOH solution, then purified and dried.

It is very difficult to determine directly the structure of a fibril after production because the quantities required for usual analytical measurements are not easily obtainable, and even if they can be obtained, the structure of the nascent fibril is very changeable. However, it is supposed that the examination of the resistance of the never-air-dried fibrils to alkali allows us to assume the structure of a fibril after production. From the relation between the yield of cellulose as a function of the incubation time and the progress of the transformation of an amorphous fibril, it is assumed that the never-air-dried cellulose material from the incubated glucose medium at 28 °C for 5 h is composed of 11 wt% of the fibril having the stainable inner part, 60 wt% of the fibrils with staining-unevenness, and 29 wt% of microscopic fibrils.[16] The X-ray diffraction diagram of the never-air-dried cellulose treated with 11 wt% aqueous NaOH solution showed apparently cellulose I as shown in Fig. 4. The diffraction patterns of cellulose II could not be found in the diagram. This result

suggest that not only the microscopic fibrils but also the fibrils with staining unevenness already have the lattice of cellulose I crystalline or a structure able be transform easily to cellulose I crystalline. In spite of the never-air-dried cellulose material containing the amorphous fibrils, the non-occurrence of the diffraction pattern of cellulose II may be due to reject amorphous material by alkali-treatment. But, the weights of the sample treated with 11 wt% alkali and the untreated sample were almost the same. This result shows that the non-occurrence of the diffraction pattern of cellulose II is not because of rejecting the low order region. Accordingly, it is reasonable that the non-occurrence of cellulose II is due to the structure of an amorphous fibril. If an amorphous fibril is composed of some sheets of monomolecular layers corresponding to the $(1\bar{1}0)$ plane of cellulose I as described above, it is supposed that the nascent fibrils may have resistance to 11 wt% alkali, and furthermore, the dehydration of the water contained among the cellulose sheets or the shrinkage of some part of the fibril with alkali-treatment allow the cellulose sheets to bind easily. The structure of the nascent fibril proposed in this paper may also be supported by papers reporting that the swelling of cellulose I with alkali-treatment takes place along the $(1\bar{1}0)$ plane in the first place.[17,18]

References

1) R. M. Brown, J. H. Willson, and C. L. Richardson, *Proc. Natl. Acad. Sci. U.S.A.*, **73**, 4565 (1976).
2) C. H. Haigler, R. M. Brown, and M. Benziman, *Science*, **210**, 903 (1980).
3) M. Benziman, C. H. Haigler, R. M. Brown, A. R. White, and K. M. Cooper, *Proc. Natl. Acad. Sci. U.S.A.*, **77**, 6678 (1980).
4) K. Zaar, *Cytobiologie*, **16**, 1 (1977).
5) K. Zaar, *J. Cell Biol.*, **80**, 773 (1979).
6) G. G. Leppard, L. C. Sowden, and J. R. Colvin, *Science*, **189**, 1094 (1975).
7) J. R. Colvin, M. Takai, and G. G. Leppard, *Naturwissenchaften*, **63**, 297 (1976).
8) J. R. Colvin and G. G. Leppard, *Can. J. Microbiol.*, **23**, 701 (1977).
9) A. Kai, J. Kogusuri, and Y. Kobayashi, *Nippon Kagaku Kaishi*, **1982**, 148.
10) A. Kai, J. Kogusuri, and Y. Kobayashi, *Nippon Kagaku Kaishi*, **1982**, 536.
11) A. Kai, J. Kogusuri, and Y. Kobayashi, *Nippon Kagaku Kaishi*, **1982**, 1934.
12) A. Frey-Wyssling, *Science*, **119**, 80 (1954).
13) I. Ohad, M. D. Danon, and S. Hestrin, *J. Cell Biol.*, **12**, 31 (1962).
14) A. Frey-Wyssling and K. Mühlethaler, *Makromol. Chem.*, **62**, 25 (1963).
15) H. Maeda and N. Ishida, *J. Biochem.*, **62**, 276 (1967).
16) A. Kai, T. Koseki, and Y. Kobayashi, *Nippon Kagaku Kaishi*, **1983**, 719.
17) J. O. Warwicker and A. C. Wright, *J. Appl. Polym. Sci.*, **11**, 659 (1967).
18) R. Jeffries and J. O. Warwicker, *Text. Res. J.*, **39**, 548 (1969).

Structural Characterization of Soluble Products from a Series of Reductively Butylated Coals Prepared in Refluxing Tetrahydrofuran

Mikio MIYAKE,* Masayuki SUKIGARA, Masakatsu NOMURA, and Shōichi KIKKAWA†
Department of Applied Chemistry, Faculty of Engineering, Osaka University, 2-1, Yamada-oka, Suita, Osaka 565
(Received July 15, 1983)

A series of butylated Yūbari coals were prepared by an improved reductive alkylation method, and detailed structural parameters of respective solution products in pentane (PS) and benzene (BS) were estimated; this experimental procedure is likely to offer more insight into chemical structures of products and important factors effective for solubilization than any analyses on a single product. The PS and BS have average molecular weights of 700—800 and 1500—2050 and are composed of about two and more than five structural units, respectively. These values suggest that the BS molecule is quite large compared with the corresponding products obtained by other methods such as hydrocracking. On the other hand, the ring sizes of one structural unit of the respective products are roughly the same (about three rings). The BS materials are coal macromolecules with stackings loosened by introduction of alkyl groups, while the PS materials are products through cleavage of bonds connecting the structural units and through addition of so many alkyl groups as to increase the affinity for the solvent. In addition, an absence of intermolecular hydrogen bonds mainly due to OH groups contributes to quite a high solubility of the alkylated coals. Increase in BS yield accompanies an increase in aliphatic carbon ratio and polymerization degree and a decrease in size of aromatic ring systems. These results may be ascribed to the heterogeneity of coal constituents.

For the purpose of structural analysis of coals, many methods to transform coals to soluble derivatives have been reported. Among them, reductive alkylation proposed by Sternberg *et al.*[1] is accepted to be one of the most promising methods.[2—13] Soluble materials in reductively alkylated coals were analyzed by applying various techniques.[3,5,6,8,11—13] Compounds contained in alkylated coals were identified by gas chromatography–mass spectrometry preceded by mild oxidation.[14] Some information about the reaction mechanism has been obtained by conducting reactions using model compounds[5,15] and various alkyl halides.[10,12] However, effects of change of a series of reaction conditions, such as reaction time, on the structure of soluble products have hardly been reported, since Sternberg's procedure requires a reaction time as long as 2—14 d.[1—13]

In our previous papers[16,17] we have proposed an improved method which has solved the problems of Sternberg's procedure, such as long reaction time[1—13] and contamination of an electron transfer agent, naphthalene.[18,19] It has been demonstrated that almost all carbonaceous matters in Yūbari coal (more than 90 wt%) can be solubilized in hot benzene by only 6 h reaction.[16,17] However, no detailed structural characterization has yet been reported.

The present study aims at a structural characterization of a series of soluble materials from butylated Yūbari coals obtained by varying the reaction conditions of the improved method. Analysis of these products is likely to offer more insight into the chemical structure of reductively alkylated coals than analysis of a single product. Furthermore, information will be obtained about key factors leading to highest solubility and the solubilization mechanism.

Experimental

Reaction Procedures. Yūbari coal (86.0% C) was used as a coal sample, whose proximate and ultimate analyses were described elsewhere.[16,17] Dry pulverized coal (10 g) was allowed to react in a flask with stirring with molten potassium metal (4—12 g) (mp 63 °C) in refluxing tetrahydrofuran, THF, (150 cm³) (bp 66 °C) for 2—12 h. After this anion formation reaction, the flask was cooled to −50 °C and 1 mol of butyl iodide was added dropwise. The stirring was continued at room temperature overnight to alkylate the coal anions and to destroy the excess potassium. The solid product was washed with aqueous ethanol solutions repeatedly until no iodide ion had become detected in the filtrate, and dried under vacuum at 90 °C for 12 h. The alkylated coal samples were extracted with pentane or benzene by using Soxhlet thimbles; a dried extract thus obtained will be termed PS or BS (BS contains the PS fraction), respectively. Detailed procedures were previously described.[16,17]

To investigate the effect of OH groups on the solubilization, methylated or hydrogenated coals also was prepared by adding 1 mol of methyl iodide or ethanol, respectively, to a coal anion suspension which had been prepared by 6 h reaction with 8 g of molten potassium. They were each extracted with benzene to give BS and BI (benzene insoluble). The BS material from the methylated coal was further hydrogenated in a similar manner as described just above.

Analysis of Products. Analytical data of the alkylated coals were reported elsewhere.[16,17] The PS and BS materials were subjected to an ultimate analysis, a ^{1}H NMR spectroscopy, and an average-molecular-weight measurement, as previously conducted.[16,17] The hydrogens in NMR spectra are classified as follows: the hydrogen attached to an aromatic carbon, H'_{ar}; the hydrogen attached to an α carbon to an aromatic ring, H'_{α}; the hydrogen contained in a methylene group at other than α positions, H'_{β}; the hydrogen contained in a methyl group, H'_{γ}.

The amount of OH groups was determined by the acetylation method using pyridine.[20] IR spectra of BS were obtained with hexachlorobutadiene solutions on a Hitachi 260-10 infrared spectrophotometer.

†Present adress: Department of Applied Chemistry, Osaka Institute of Technology, 5-16-1, Ohmiya, Asahi-ku, Osaka 535.

Structural parameters were estimated according to the equations by Ouchi *et al.*[21,22] with a slight modification as follows: The contribution of sulfur atoms and inert oxygen atoms was neglected because the original Yūbari coal contained few sulfur atoms (0.3 wt%) and a relatively small amount of inert ether bonds (less than 40% of the total oxygen atoms) for the present reaction. The latter was determined from the amounts of OH groups before and after the reductive hydrogenation. Tsukashima *et al.*[3] also neglected the effect of sulfur and inert oxygen atoms with regard to structural parameters for reductively methylated Yūbari coals. Therefore, in the present study, all oxygen atoms in soluble products are assumed to be present as group $-O-(CH_2)_3CH_3$ at positions peripheral to aromatic rings. The structural parameters concerned are as follows: The carbon aromaticity, $f_a=(C'-H'_\alpha/2-H'_\beta/2-H'_\gamma/3)/C'$; the degree of aromatic ring condensation, $H'_{au}/C'_a=(H'_{ar}+H'_\alpha/2+O'+2N')/(C'-H'_\alpha/2-H'_\beta/2-H'_\gamma/3)$; the degree of substitution of aromatic nuclei, $\sigma=(H'_\alpha/2+O'+2N')/(H'_{ar}+H'_\alpha/2+O'+2N')$; the degree of aliphatic chain substitution of aromatic nuclei, $\sigma_{al}=(H'_\alpha/2)/(H'_{ar}+H'_\alpha/2+O'+2N')$; the number of aromatic carbons per molecule, $C'_{ar}=C'\cdot f_a$; the number of aliphatic carbons per molecule, $C'_{al}=C'-C'_{ar}$; the number of aromatic carbons per structural unit, $C'_{ar(u.s.)}=3/(H'_{au}/C'_a-1/2)$; the number of structural units per molecule, $n=C'_{ar}/C'_{ar(u.s.)}$; the number of aromatic rings per structural unit, $R_{a(u.s.)}=C'_{ar(u.s.)}(1-H'_{au}/C'_a)/2+1$; the number of aromatic rings per molecule, $R_a=n\cdot R_{a(u.s.)}$; the number of total rings per molecule, $R_t=C'-H'/2+1-C'_{ar}/2$; the number of naphthenic rings per molecule, $R_N=R_t-R_a$; the average number of carbon atoms in side chains, $C'_{side}=C'_{al}-3\cdot R_N$, where C', H', *etc.* denote the numbers of carbon atoms, hydrogen atoms, *etc.* in PS and BS molecules, respectively. Division of each of the above values per molecule by n gives the corresponding value per structural unit.

Results and Discussion

Structural Character of PS and BS. Basic data obtained for PS and BS materials are summarized in Table 1, which contains the items: yields of butylated coals and soluble materials, ultimate analyses, hydrogen distributions, and average molecular weights. The yields of the soluble materials, PS and BS, from raw Yūbari coal are trace and 2 wt%, respectively. The treatment of the coal gave PS and BS in 18—39 and 74—93 wt% yields, respectively. The average molecular weights obtained for the PS and BS are 700—800 and 1520—2050, respectively; the molecular weight of the PS is less than half that of the BS. The average molecular weights, corrected for introduced butyl groups, also are given in Table 1.

In Table 2 are given the number of butyl groups introduced per 100 carbon atoms and the values of f_a, H'_{au}/C'_a, σ σ_{al}, and n for PS and BS materials. The number of introduced butyl groups was estimated in a similar manner as reported conventionally for soluble products;[5,9] that is, it was estimated on the assumption that the change in H/C atomic ratio of products relative to raw coal is due exclusively to the introduction of alkyl groups. The numbers obtained are 9.3—17.7 and 6.1—12.1 for the PS and BS, respectively. It should be noted that the estimated values become uncertain when the soluble products themselves are different in H/C value from the original coal. The high values of σ (0.55—0.64) and σ_{al} (0.39—0.45) for both the PS and BS idicate that the aromatic nuclei have many substituents, especially alkyl side-chains. The PS material show lower f_a and slightly higher σ and σ_{al} values than the BS, suggesting themselves to be abundant in aliphatic carbons and alkyl side-chains. The number of structural units, n, in the BS molecule is more than 5.0, whereas that in the PS is less than 2.6.

The numbers of individual rings and carbons per molecule and per structural unit for the PS and BS materials are shown in Tables 3 and 4, respectively. The BS molecules have high values of R_t, R_a, C'_{ar}, and

TABLE 1. BASIC DATA OBTAINED FOR PS AND BS MATERIALS

Fraction	Reaction time	K/coal	Yield of Bu-coal[a]	Yield of fraction[b]	Ultimate analysis[c]/wt%				Hydrogen distribution				Mol wt	
	h	g/g	wt%	wt%	C	H	N	O[d]	H'_{ar}/H'	H'_α/H'	H'_β/H'	H'_γ/H'	Obsd	Bu-free
PS	2	0.4	129	18	87.2	9.0	1.0	2.8	0.14	0.27	0.32	0.27	780	560
PS	6	0.4	139	30	84.0	9.6	0.9	5.5	0.09	0.22	0.38	0.31	700	450
PS	12	0.8	154	35	84.8	9.6	1.0	4.6	0.11	0.24	0.37	0.28	790	460
PS	6	1.2	152	39	84.1	10.1	0.9	4.9	0.09	0.21	0.41	0.29	800	470
BS	2	0.4	129	74	85.5	8.1	1.3	5.1	0.13	0.29	0.31	0.27	2050	1640
BS	6	0.4	139	81	84.9	8.7	1.3	5.1	0.14	0.26	0.31	0.29	1520	1100
BS	12	0.8	154	91	83.1	8.7	1.3	6.9	0.14	0.27	0.31	0.28	1720	1180
BS	6	1.2	152	93	83.0	9.0	1.2	6.8	0.14	0.26	0.30	0.30	1620	1100

a) Relative to feed coal (dry basis). b) Relative to butylated coal (dry ash free basis). c) Dry ash free basis. d) From difference.

TABLE 2. NUMBER OF BUTYL GROUPS INTRODUCED PER 100 CARBON ATOMS AND STRUCTURAL PARAMETERS OF PS AND BS

Fraction	Yield of fraction	No. of Bu's per 100 C's	Structural parameters				
	wt%		f_a	H'_{au}/C'_a	σ	σ_{al}	n
PS	18	9.3	0.52	0.74	0.55	0.44	2.4
PS	30	14.2	0.45	0.76	0.64	0.45	1.9
PS	35	17.7	0.46	0.81	0.61	0.44	2.6
PS	39	17.7	0.42	0.83	0.62	0.44	2.6
BS	74	6.1	0.56	0.69	0.62	0.43	5.0
BS	81	9.2	0.53	0.76	0.57	0.40	5.0
BS	91	11.8	0.52	0.84	0.61	0.40	7.0
BS	93	12.1	0.50	0.88	0.58	0.39	7.1

C'_{al}, at least higher than twice those for the PS molecules. On the other hand, the ring sizes per structural unit are roughly the same as seen from $R_{t(u.s.)}$, $R_{a(u.s.)}$, and $C'_{ar(u.s.)}$. The number of each of the rings per BS molecule decreases with an increase in the BS yield. The increase in C'_{side} and C'_{al}/C'_{ar} of both the PS and BS molecules is dependent on the increase in the number of butyl groups introduced. It should be noted that, in high yield regions of PS, the number of carbons in side chains exceeds that in aromatic rings, which has resulted from an introduction of many bulky butyl groups.

Factors Governing the Production of PS and BS. For the conventional reductive alkylation, it has been reported[1,5,15] that coals are solubilized by introduction of alkyl groups to their condensed aromatic nuclei to loosen their stacking and by cleavage of ether and some carbon-carbon linkages connecting ring systems.

Two important reaction factors to produce PS from coal or BS are considered: the first is a depolymerization, that is, cleavage of bonds connecting structural units to produce small molecules (molecular weights, 700—800 as observed; 450—560 on butyl-free basis) with about two structural units; the second is an addition of many alkyl groups, as seen from the values of C'_{al}/C'_{ar} and $C'_{side(u.s.)}$, which results in increasing the affinity for the solvent, pentane.

On the other hand, the BS materials are macromolecules (observed molecular weights, 1520—2050; n, 5.0—7.1) with a loosened stacking by introduction of alkyl groups. In addition, the absence of intermolecular hydrogen bonds due to alkylation of polar groups, such as OH group, may contribute to the attainment of quite high BS yields. Effect of this factor is to be discussed in detail in the next section.

With an increase in the BS yield, the values of H'_{au}/C'_a, C'_{side}, and C'_{al}/C'_{ar} increase and those of f_a and total and aromatic rings per molecule and per structural unit decrease. This result may be ascribed to the addition of many butyl groups caused under the severe reaction conditions. However, the value of n increases with an increase in the BS yield, which should have decreased by cleavage of ether and some carbon-carbon bonds when severe reaction conditions were applied. A possible interpretation for these results is that the constituents in coal are heterogeneous, that lowly polymerized materials, which are composed of more developed aromatic ring systems relatively easy to get anionized because of their high electron affinity, will preferentially be converted to BS at an early stage, and that highly polymerized materials with less condensed aromatic ring systems and higher aliphatic carbon ratios will resist the reaction so as to get converted later. This view is in accord with an observation that a BS produced at an early stage has slightly higher σ_{al} and $C'_{side(u.s.)}$ values (*i.e.*, it contains more alkyl groups) than a BS produced later, and also with a report[2,9,23] that the solubility of low rank coals, which may be considered to be composed of similar materials as contained in the BS produced later, is considerably low for the conventional reductive alkylation (or hydrogenation) method.

Effects of OH Groups on Coal Solubilization. Table 5 summarizes the yields of the BS and BI from methylated and hydrogenated coals and from further

TABLE 3. NUMBER OF RINGS IN PS AND BS

Fraction	Yield of fraction	Number of rings					
		per molecule			per structural unit		
	wt%	R_t	R_a	R_N	$R_{t(u.s.)}$	$R_{a(u.s.)}$	$R_{N(u.s.)}$
PS	18	7.7	6.2	1.5	3.2	2.6	0.6
PS	30	5.5	4.5	1.0	2.9	2.4	0.5
PS	35	6.1	5.0	1.1	2.3	1.9	0.4
PS	39	5.0	4.5	0.5	1.9	1.7	0.2
BS	74	23.4	17.8	5.6	4.6	3.5	1.1
BS	81	14.0	11.8	2.2	2.8	2.4	0.4
BS	91	14.5	11.9	2.6	2.1	1.7	0.4
BS	93	11.6	10.5	1.1	1.6	1.5	0.1

TABLE 4. NUMBER OF CARBONS IN PS AND BS

Fraction	Yield of fraction	Number of carbons						
		per molecule				per structural unit		
	wt%	C'_{ar}	C'_{al}	C'_{side}	C'_{al}/C'_{ar}	$C'_{ar(u.s.)}$	$C'_{al(u.s.)}$	$C'_{side(u.s.)}$
PS	18	29	27	23	0.93	12.4	11.5	9.6
PS	30	22	27	24	1.23	11.5	14.2	12.6
PS	35	25	30	27	1.20	9.6	11.6	10.3
PS	39	23	33	31	1.43	9.0	12.6	12.1
BS	74	81	65	48	0.80	16.1	12.8	9.5
BS	81	57	50	44	0.88	11.4	10.1	8.8
BS	91	62	58	50	0.94	8.8	8.3	7.2
BS	93	56	56	52	1.00	7.9	7.9	7.4

TABLE 5. PROPERTIES OF METHYLATED AND HYDROGENATED COALS

Coal	Yield of fraction/wt%		No. of OH's per 100 C's		OH per O/%	
	BS	BI	BS	BI	BS	BI
Me-coal[a)]	84	16	0.4	3.1	7	58
Hy-coal[b)]	18	82	2.6	3.7	47	67
Hy-Me-BS[c)]	50	50[d)]	2.1	3.9	38	48

a) Methylated coal. b) Hydrogenated coal. c) BS from Me-coal was further hydrogenated. d) Starting material contained no BI fraction.

hydrogenated BS of the methylated coal, the amount of OH groups per 100 carbon atoms, and the ratio of OH groups to the total oxygen atoms contained. The number of OH groups per 100 carbon atoms in the original Yūbari coal is estimated to be 3.0.

The yield of BS from the hydrogenated coal is only 18 wt%, extremely low compared with the value of 84 wt% for the methylated coal. The fractions from the hydrogenated coal contain more OH groups than those from the methylated one, since the ether bonds and OH groups in the original coal are converted to $-O-CH_3$ and -OH groups by the methylation and hydrogenation, respectively.[1,3)] The decrease in OH groups caused by the methylation has also been suggested with the conventional procedures.[3)] In all the cases, the OH groups are caused to accumulate in the BI fractions. This suggests that the presence of OH groups in large quantity will hinder the solution probably through formation of hydrogen bonds. When the BS from the methylated coal which has already been released from the stacking is further hydrogenated, the amount of OH groups is increased by a demethylation on $-O-CH_3$ groups[1)] and a large amount of BI (50 wt%) is newly formed, into which the OH groups are also made to accumulate.

IR spectra of various BS's are shown in Fig. 1. The BS materials from the hydrogenated coal and from the further hydrogenaed BS of the methylated coal show absorption bands assignable to intermolecular hydrogen bonds at about 3100—3600 cm^{-1}, whereas the corresponding absorption is hardly observed for the BS from the methylated coal. Hence, it has been demonstrated that the extremely high BS yield from the reductively alkylated coals is due at least to the absence of intermolecular hydrogen bonds.

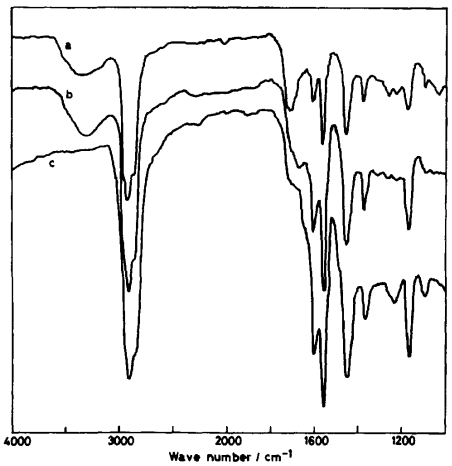

Fig. 1. IR spectra of BS fractions from (a) hydrogenated coal, (b) further hydrogenated BS of methylated coal, and (c) methylated coal.

References

1) H. W. Sternberg, C. L. Delle Donne, P. Pantages, E. C. Moroni, and R. E. Markby, *Fuel*, **50**, 432 (1971).
2) H. W. Sternberg and C. L. Delle Donne, *Fuel*, **53**, 172 (1974).
3) H. Tsukashima, T. Katoh, F. Wakita, T. Kuruma, and N. Nei, *Nenryo Kyokai Shi*, **55**, 254 (1976).
4) B. S. Ignasiak and M. Gawlak, *Fuel*, **56**, 216 (1977).
5) T. Ignasiak, A. V. Kemp-Jones, and O. P. Strausz, *J. Org. Chem.*, **42**, 312 (1977).
6) R. Doğru, G. Erbatur, A. F. Gaines, Y. Yürüm, S. Içli, and T. Wirthlin, *Fuel*, **57**, 399 (1978).
7) B. S. Ignasiak, J. F. Fryer, and P. Jadernik, *Fuel*, **57**, 578 (1978).
8) L. B. Alemany, S. R. King, and L. M. Stock, *Fuel*, **57**, 738 (1978).
9) H. Wachowska, *Fuel*, **58**, 99 (1979).
10) L. B. Alemany, C. I. Handy, and L. M. Stock, *Adv. Chem. Ser.*, **192**, 207 (1981).
11) T. Katoh, S. Hashimoto, and H. Tsukashima, *Nenryo Kyokai Shi*, **60**, 432 (1981).
12) L. B. Alemany and L. M. Stock, *Fuel*, **61**, 250 (1982).
13) L. B. Alemany and L. M. Stock, *Fuel*, **61**, 1088 (1982).
14) R. Doğru, A. Gaines, A. Olcay, T. Tuğrul, *Fuel*, **58**, 823 (1979).
15) L. Lazarov and S. Angelov, *Fuel*, **59**, 55 (1980).
16) M. Miyake, M. Sukigara, M. Nomura, and S. Kikkawa, *Fuel*, **59**, 638 (1980).
17) S. Kikkawa, M. Miyake, M. Sukigara, and M. Nomura, *Nippon Kagaku Kaishi*, **1980**, 939.
18) J. A. Frantz and W. E. Skiens, *Fuel*, **57**, 502 (1978).
19) J. W. Larsen and L. O. Urban, *J. Org. Chem.*, **44**, 3219 (1979).
20) Y. Hasegawa, K. Tokuhashi, and Y. Maekawa, 47th Annual Meeting of Coal Science Jpn., Tokyo, October 1980, Preprints No. 3.
21) N. Kanda, H. Itoh, S. Yokoyama, and K. Ouchi, *Fuel*, **57**, 676 (1978).
22) K. Ouchi, T. Katoh, and H. Itoh, *Fuel*, **60**, 689 (1981).
23) K. Ouchi, Y. Hirao, M. Makabe, and H. Itoh, *Fuel*, **59**, 751 (1980).

Studies on the Electronic Absorption Spectra of Some Selected Furan Derivatives. Molecular Orbital Calculations

Rafie Hassan ABU-EITTAH*,† and Maher Mohamed HAMMED
Department of Chemistry, Faculty of Science, University of Cairo, Giza, Egypt

(Received April 5, 1982)

The electronic absorption spectra of three groups of furan derivatives: 2-formyl, 2-acetylfuran, and 2-furoic acid, *N*-(2-furylmethylene)amines and phenylfurans were investigated. The predominant conformation as well as the polarity of the molecule could be predicted from its spectrum. The investigated molecules were proved to be "all planar" configuration which led to substantial interaction between the electronic states of the subsystems. The preferred conformations of *N*-(2-furylemthylene)methylamine and *N*-(2-furylemthylene)aniline were predicted with the aid of molecular orbital calculations.

The electronic absorption spectra of furan derivatives are rarely found in the literature. Horvath and Kiss[1] attributed the long wavelength absorption of extremely low intensity in the spectrum of furan to a singlet-triplet transition and the main absorption band in the UV region to a singlet $\pi\rightarrow\pi^*$ transition. The triplet states of furan, thiophene, and pyrrole were detected by variable-angle electron impact spectroscopy.[2] In furan, the singlet-triplet transition occurs with maximum intensity at 3.99 and 5.22 eV.

The absorption spectra of numerous furfural acetals[3] and 2-arylfuran[4] have been reported. The conformation of 2-furylphenyl ketone has been investigated by means of spectroscopic methods.[5] It was suggested that furyl conjugation with the carbonyl group is superior to phenyl conjugation with the same group.[5] The absorption spectra of some furylcarbonyl derivatives have been measured, and the band maxima were correlated to the reactivity of the carbonyl group of the compounds.[5] Head and Jones[6] investigated the electronic absorption spectra of some *N*-(2-furylmethylene)arylamines in ethanol. The dipole moments of some furfural derivatives in benzene, dioxane, and CCl_4 were determined from dielectric data.[7,8]

In this work the electronic absorption spectra of three groups of furan derivatives: acylfurans and 2-furoic acid, *N*-(2-furylmethylene)amines, and phenylfurans, have been investigated. The results give much information on the nature of the spectra of furan derivatives as well as on the conformation of the composite furan derivatives. Molecular orbital calculations were performed on representative examples of the compounds studied. The SCF-Cl and the MIM methods were used and proved to be useful for conformational analysis.

Experimental

Methanol, ethanol, and cyclohexane were BDH reagent grade chemicals and were purified by the conventional methods reported.[9]

2-Acetylfuran and furfural (Koch light reagent grade) were used after purification by vacuum distillation. 2-Furoic acid (BDH reagent grade) was purified by crystalization. 2-Phenylfuran was prepared by suspending stabilized benzene diazonium salt (0.1 mol) in furan (150 ml) and vigorously stirring throughout the preparation while adding sodium hydroxide and sodium acetate.[4] After 24 h of stirring, the product was steam distilled. The product was extracted with ether and then vacuum distilled (bp 94 °C/10 mmHg, 1 mmHg≈133.322 Pa). In a similar way 2-(*p*-chlorophenyl)furan was prepared. 2,4-Diphenylfuran was prepared by oxidizing 1,3-diphenyl-2-buten-1-one (0.1 mol) with selenium dioxide (0.05 mol) in dioxane. The product was distilled in a vacuum (200 °C/3 mmHg) and solidified in the side arm. The compound was purified by recrystallization from ethanol (mp 109—110 °C).[11] 2,5-diphenylfuran was prepared by heating 1,4-diphenyl-1,4-butanedione, which was prepared from phenacyl bromide,[12] with concentrated HCl (one part of 1,4-diphenyl-1,4-butanedione to two parts of HCl) at 130—150 °C. The product was precipitated from ice cold water and purified by crystallization from ethanol (mp 91 °C).[13]

N-(2-Furylmethylene) amines were prepared by mixing the stoichiometric amounts of furfural and an appropriate amine in benzene.[6] The temperature of the mixture was kept near 5 °C for 1 h. The benzene solution was dried over magnesium sulfate and evaporated to give the imines that were purified by vacuum distillation or recrystallization. The compounds thus prepared were *N*-(2-furylmethylene)-methylamine, *N*-(2-furylmethylene)aniline, *N*-(2-furylmethylene)-*o*-toluidine, *N*-(2-furylmethylene)-*p*-toluidine, *N*-(2-furylmethylene)-*o*-chloroaniline, *N*-(2-furylmethylene)-*o*-methoxyaniline, *N*-(2-furylmethylene)-*p*-methoxyaniline, *N*-(2-furylmethylene)-*p*-nitroaniline, and *N*-(2-furylmethylene)-2-pyridinamine. Melting points and boiling points agreed with the values reported in the literature.[14—16]

The absorption spectra were measured with a Beckman DK-1 spectrophotometer using 1.0 cm fused silica cells.

Results and Discussion

A. Electronic Absorption Spectra. (I) Carbonyl and Carboxy Derivatives of Furan: Figure 1a shows the electronic absorption spectra of furan, furfural, 2-acetylfuran, and 2-furoic acid in a nonpolar solvent. The spectrum of furan has been investigated.[1,2] Substitution, in the furan nucleus, by a formyl, acetyl or carboxyl group reduced the symmetry from C_{2v} to C_s and perturbed significantly the electronic spectrum of furan (Fig. 1a). At least two $\pi\rightarrow\pi^*$ transitions (280—210 nm) appear in the spectra of substituted compounds in addition to an $n\rightarrow\pi^*$ (≈330 nm) transition. The spectra of the formyl and acetyl derivatives show much similarities but differ basically from that of 2-furoic acid. Such differences are mainly due to the dimerization of the acid, specially in nonpolar solvent. A large increas in intensity of the

† Present address: Chemistry Department, Faculty of Science, King Abdulaziz University, Jeddah, Saudi Arabia.

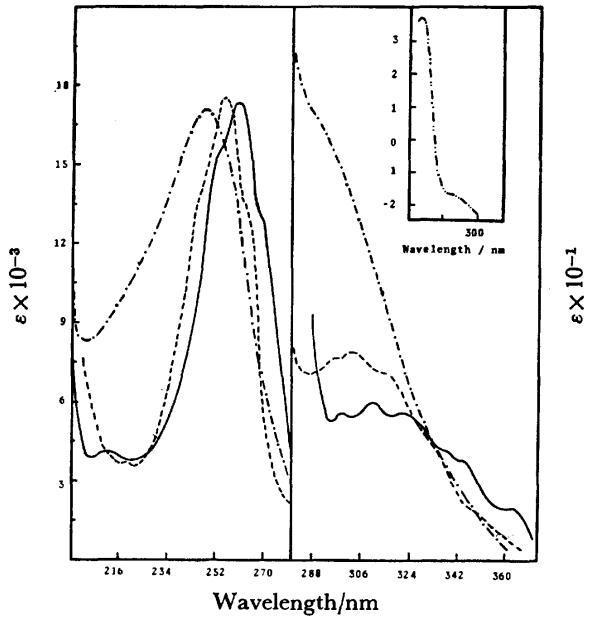

Fig. 1a. Electronic absorption spectra of:
—·—·— furan in hexane, —— furfural in cyclohexane, ---- 2-acetylfuran in cyclohexane, —·—·— 2-furoic acid in cyclohexane.

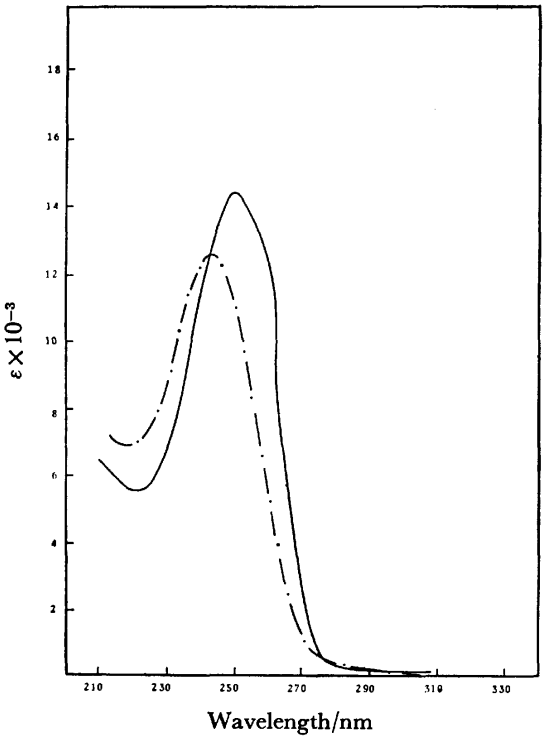

Fig. 1b. Electronic absorption spectra of 2-furoic acid (dil soln).
—— In cyclohexane, —·—·— in methanol.

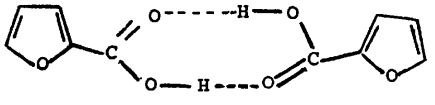

longest wavelength transition of the acid, in nonpolar solvent, suggests that such a transition is not n→π^* but π→π^* of the dimer. The n→π^* band is probably somewhere in the 280 nm region. The spectrum of

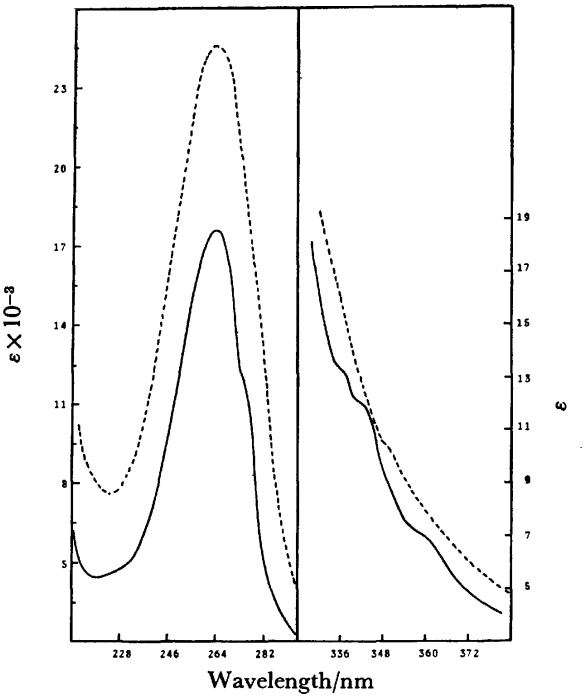

Fig. 2a. Electronic absorption spectra of *N*-(2-furylmethylene)methylamine.
—— In cyclohexane, ---- in ethanol.

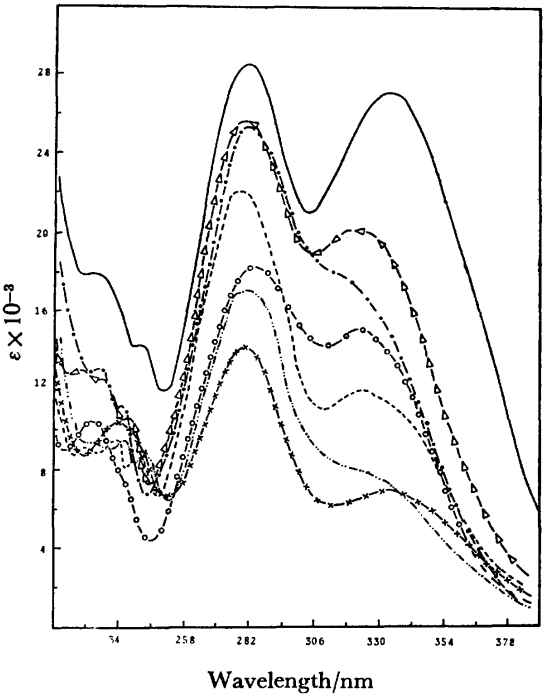

Fig. 2b. Electronic absorption spectra (in cyclohexane) of:
—·—·— *N*-(2-furylmethylene)aniline, ---- *N*-(2-furylmethylene)-*o*-toluidine, —··—··— *N*-(2-furylmethylene)-*o*-chloroaniline, —×—×— *N*-(2-furylmethylene)-*o*-methoxyaniline, ---- *N*-(2-furylmethylene)-*p*-toluidine, —○—○— *N*-(2-furylmethylene)-*p*-chloroaniline, —— *N*-(2-furylmethylene)-*p*-methoxyaniline.

2-furoic acid in methanol is that of a mixture of the monomer and dimer, and the 310 nm band partially comprises an n→π* transition. On dilution, the longest wavelength band disappears and the spectrum obtained is only that of the monomer (Fig. 1b). Table 1 shows the values of band maxima and band intensities of furfural, 2-acetylfuran, and 2-furoic acid.

(II) Furylmethylenes: In a previous study[17] the electronic absorption spectra of *N*-(2-thenylidene) amines were investigated. In this work the spectra of a variety of *N*-(2-furylmethylene) amines were studied (Figs. 2a and 2b). Although *N*-(2-furylmethylene)-methylamine (**a**) and 2-acetylfuran (**b**) are π-isoelectronic and of the same symmetry and their π→π* transitions are of nearly the same energy, the n_N→π* transition being of much lower energy and having lower intensity than the n_O→π* transition (Tables 1 and 2). The spectrum of *N*-(2-furylmethylene)aniline

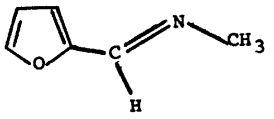

(**a**)

differs basically from that of the methylamine derivative. Figure 2b suggests that the interaction between the subsystems of *N*-(2-furylmethylene)methylamine and benzene is pronounced as will be discussed below. The spectreum of *N*-(2-furylmethylene)aniline provides

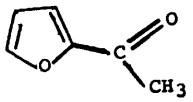

(**b**)

some important information about the conformation of the molecule. If the molecule is a "free rotator"

Table 1. Numerical values of band maxima and band intensities of furfural, 2-acetylfuran and 2-furoic acid in cyclohexane and methanol[a]

Compound	λ_{max}/nm	ε/M^{-1} cm^{-1}	f
Furfural	317 (314)	60 (80)	0.002 (0.002)
	266 (270)	17400 (9400)	0.350 (0.210)
	218 (218)	4240 (3100)	0.100 (0.130)
2-Acetylfuran	309 (307)	79 (95)	0.003 (0.001)
	261 (267)	17500 (18700)	0.350 (0.400)
	(219)	(4600)	(0.260)
2-Furoic acid	294	170	0.005
	255 (240)	17200 (12500)	0.440 (0.330)
	228	11000	0.470

a) Values in parentheses are those when methanol was used as a solvent.

Table 2. Numerical values of band maxima and band intensities of *N*-(2-furylmethylene) amines[a]

Compound	λ_{max}/nm	ε/m^{-1} cm^{-1}	f
N-(2-Furylmethylene)methylamine	360 (354) [b]	7.5 (10.5)	—
	264 (264) [b]	17600 (24, 740)	0.420 (0.667)
N-(2-Furylmethylene)aniline	318 (315)	17500 (27, 200)	0.512 (0.763)
	282 (285)	25150 (27, 600)	0.644 (0.755)
	228 (228)	13200 (13, 900)	0.352 (0.461)
	324 (312)	11840 (12, 200)	0.346 (0.420)
N-(2-Furylmethylene)-*o*-toluidine	279 (285)	22000 (22, 400)	0.615 (0.594)
	234 (231)	9400 (8, 200)	0.259 (0.299)
N-(2-Furylmethylene)-*p*-toluidine	323 (321)	20000 (23, 700)	0.584 (0.640)
	280 (282)	25600 (22, 070)	0.650 (0.565)
	222 (222)	12800 (11, 800)	0.422 (0.454)
N-(2-Furylmethylene)-*o*-chloroaniline	324 (318)	7860 (11, 000)	0.230 (0.303)
	280 (282)	17000 (18, 700)	0.430 (0.457)
	236 (234)	9300 (8, 900)	0.276 (0.272)
N-(2-Furylmethylene)-*p*-chloroaniline	324 (318)	14890 (23, 500)	0.395 (0.692)
	285 (288)	18400 (21, 940)	0.525 (0.638)
	225 (222)	10400 (12, 850)	0.343 (0.508)
N-(2-Furylmethylene)-*o*-methoxyaniline	333 (330)	6910 (8, 910)	0.209 (0.298)
	282 (280)	14140 (15, 300)	0.345 (0.439)
	234 (228)	10340 (11, 250)	0.314 (0.608)
N-(2-Furylmethylene)-*p*-methoxyaniline	335 (333)	26900 (27, 100)	0.730 (0.749)
	282 (282)	28500 (23, 100)	0.896 (0.811)
	225 (220)	17900 (16, 100)	0.533 (0.544)
N-(2-Furylmethylene)-*p*-nitroaniline	323 (341)	14900 (22, 370)	0.587 (0.782)
	218 (218)	9900 (14, 270)	0.466 (0.672)
N-(2-Furylmethylene)-2-pyridineamine	315 (324)	16350 (6, 500)	0.458 (0.147)
	282 (294)	12000 (9, 340)	0.293 (0.302)
	222 (231)	12540 (16, 400)	0.434 (0.385)

a) Values in parentheses are those when methanol was used as a solvent. b) In ethanol.

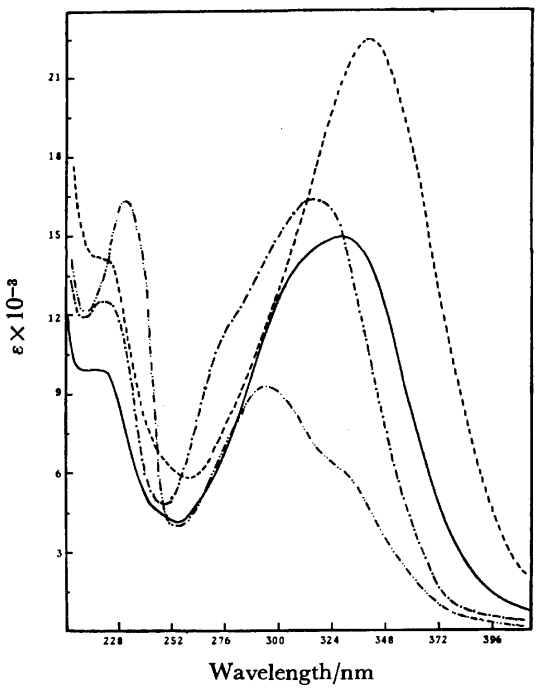

Fig. 3. Electronic absorption spectra of: *N*-(2-furylmethylene)-2-pyridineamine; —·—·— in cyclohexane, —··—··— in methanol, *N*-(2-furylmethylene)-*p*-nitroaniline; —— in cyclohexane, ---- in methanol.

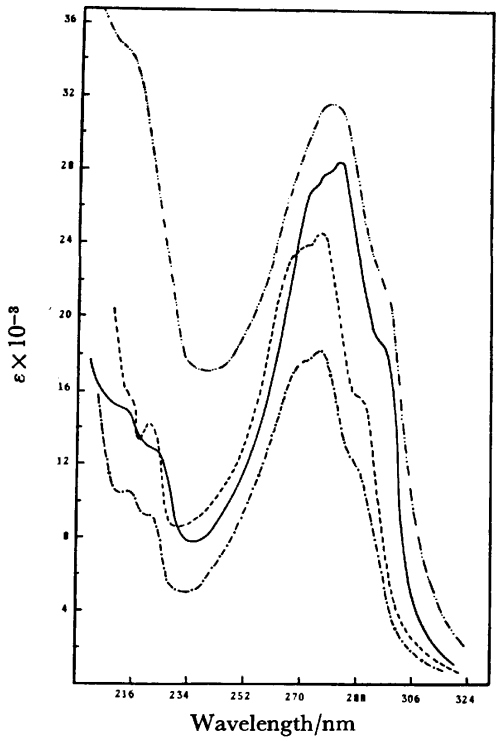

Fig. 4. Electronic absorption spectra of: 2-phenylfuran; ---- in cyclohexane, —·—·— in methanol, 2-(*p*-chlorophenyl)furan; —— in cyclohexane, —··—··— in methanol.

around the single bond (C–C) or (N–C), its spectrum may become superposition of the spectra of its subsystems. On the other and, if the steric factor owing to the H–H repulsion is pronounced, the molecular

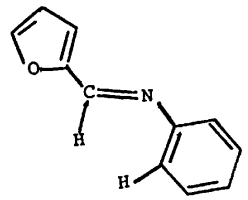

structure would be distorted and the spectrum of the composite molecule would resemble either of the sepectra of its constituents. From the spectrum of the molecule (Fig. 2b), one can predict that the molecule is not a "free rotator" and the molecular structure is not apparently distorted. This will be theoretically confirmed below. The position of the band maxima did not vary on scanning the spectrum in polar solvent. Therefore, it can be said that the molecule has no strong dipole. The feature of the overlap of the transitions is very significant in the spectra of *N*-(2-furylmethylene) amines as in the spectra of the related compounds, *N*-benzylidene-anilines and azobenzenes.

To confirm the relation between the spectra of *N*-(2-furylmethylene) amines and the conformations of these compounds, the spectra of a series of *N*-(2-furylmethylene)anilin derivatives have been investigated (Fig. 2b). An important result is that the feature of the spectra of all derivatives (except the nitro derivatives) is very much similar to that of the parent compound *N*-(2-furylmethylene)aniline. The spectra show three $\pi \rightarrow \pi^*$ electronic transitions with a degree of overlap and intensity depended on the substituents, whose band maxima are not so different from each other. This indicates that planarity of the molecule is pronounced. It is true that, generally, transitions in *N*-(-*o*)-substituted(2-furylmethylene)anilines have lower intensity than those in *p*-substituted furyl isomers.

The spectra of the nitro derivatives (Fig. 3), differ significantly from those of *N*-(2-furylmethylene) amines as a result of the perturbation of a nitro group. From the spectra one can tell that the nitro derivatives have nearly the "all-planar" configuration. If planarity of the molecule is apparently distorted, the spectrum of the composite molecule should be similar to those of the subsystems as stated above. Such behavior is not encountered in the spectra of the compounds studied.

The absorption spectra of *N*-(2-furylmethylene)-2-pyridinamine in cyclohexane and methanol are shown in Fig. 3. The internal rotation of either the furan or the pyridine nucleus seems to be restricted, since the spectrum observed differs significantly from those of the subsystems. The molecule will aquire a quasi-rigid configuration, and the electronic interaction between the two subsystems (pyridine and 2-furylmethylene) is significant. All transitions observed are $\pi \rightarrow \pi^*$, which shift to red in polar media. This suggests that the excited state has a polar structure. Table 2 gives the values of band maxima and intensities of *N*-(2-furylmethylene) amines.

(III) 2-Phenylfurans: An objective of this work is to investigate the extent of mixing of the electronic states of furan with those of other subsystems when

the two chromophores are joined through a single bond. The above section has shown that such interaction is significant when furan nucleus is attached to either a carbonyl group or a benzylimino group. A theoretical treatment of the extent of "state mixing" in phenylfurans and bifurans has been reported.[18] The spectrum of 2-phenylfuran (Fig. 4) consistis of two intense structured band systems (I and II), which are blurred with no shift in band maxima as the solvent is changed from cyclohexane to methanol. The numberical values of band maxima indicate that the bands do not correspond to localized transitions in either the "benzene" or "furan" nucleus. Substitution of a chlorine atom into furan such as 2-(*p*-chlorophenyl) furan did not affect the spectrum significantly. The vibrational components of an electronic transition in a sterically hindered molecule are blurred. This is not to be the case in a non-hindered molecule (compare the spectra of *cis*- and *trans*-stilbenes). Figure 4 indicates clearly the well resolved vibrational components of bands I and II, suggesting that the conformation of 2-phenylfuran is planar or nearly planar. Molecular orbital calculations show that as the angle of twist increases the lowest transition energy increases (reaching to a maximum value when the subsystems are perpendicular).[18] This result is also confirmed when one considers the spectrum of biphenyl.[19]

A comparison of the electronic spectra of 2-phenylfuran with biphenyl is worthwhile. The lowest $\pi \rightarrow \pi^*$ transition (276 nm) for 2-phenylfuran is at longer wavelength than that of biphenyl (247 nm) although one expected the reverse. It was expected that the higher symmetry and larger delocalization energy of biphenyl might give rise to a lower transition energy for biphenyl than that for 2-phenylfuran. However, the release of steric hindrance in 2-phenyl furan results in the transition energy lower than that of biphenyl.

Figure 5a shows the absorption spectra of 2,4-diphenylfuran. The results indicate that planarity of the 2,4-diphenyl derivative is more distorted than that of the monophenyl derivative. The shoulder shown in the spectrum of 2,4-diphenylfuran ($\lambda \approx 300$ nm, $\varepsilon \approx 400$) was not observed in the spectra of the furan derivatives studied. This suggests that the band designated as I corresponds to two overlapping transitions. A confirmation of this suggesstion was obtained from molecular orbital calculation.[18] 2-Phenylfuran had two electronic transitions at 4.33 and 4.92 eV whereas the 3-phenyl derivative had transition energies at 4.58 and 4.98 eV.

The spectra of 2,5-diphenylfuran in cyclohexane and methanol are given in Fig. 5b. The pronounced red shift and intensification of the band corresponding to the lowest energy transition, compared to that of 2,4-diphenylfuran, are evidence of a nearly "all planar" conformation for the 2,5-diphenyl derivative. This result indicates the dependence of the electronic absorption spectrum on the conformation of the molecule. Table 3 shows the values of band maxima and intensities of the studied phenylfurans.

B. Molecular Orbital Calculations. The method of molecule-in-molecule[20] has been very nicely adopted to MO calculations on composite systems such as

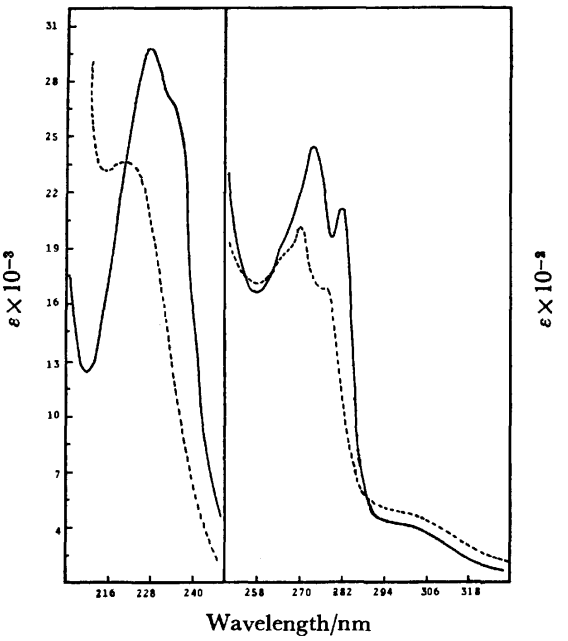

Fig. 5a. Electronic absorption spectra of 2,4-diphenylfuran.
—— In cyclohexane, ---- in methanol.

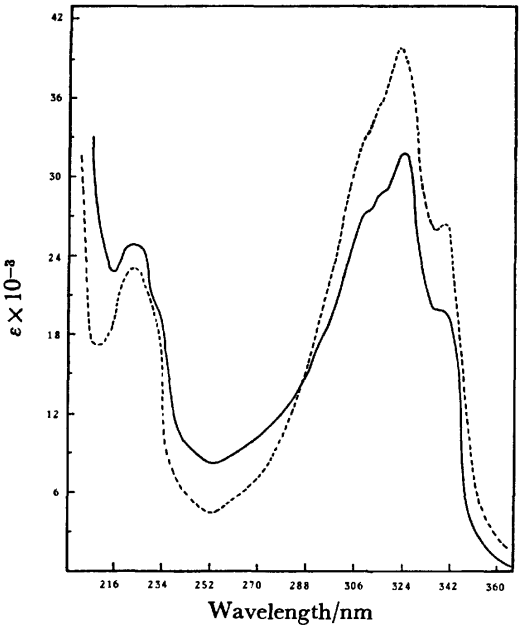

Fig. 5b. Electronic absorption spectra of 2,5-diphenylfuran.
—— In cyclohexane, ---- in ethanol.

phenylthiophenes,[21] bithienyls,[22] and phenylfurans.[18] The results encouraged us to adopt this method for calculations on *N*-(2-furylmethylene)aniline.

The two subsystems of the composite molecule, *N*-(2-furylmethylene)aniline, are 2-furylmethyleneamine (A) and benzene (B). The core of the molecule-in-molecule method is to calculate the interaction between the electronic states of subsystems (A) and (B). The PPP[23] version of the SCF method was applied to the two conformers, Ia and Ib, and the SCF MO's were computed. The CI state functions and the corresponding energies were then calculated. The results

Table 3. Numerical values of band maxima and band intensities of phenylfurans[a)]

Compound	λ_{max}/nm	ε/M^{-1} cm^{-1}	f
2-Phenylfuran	276 (276)	24500 (18260)	0.435 (0.337)
	216 (216)	15680 (10500)	0.362 (0.249)
2-(*p*-Chlorophenyl)furan	282 (282)	28260 (31350)	0.662 (0.936)
	216 (216)	14880 (34000)	0.353 (1.215)
2,4-Diphenylfuran	300 (300)	418 (480)	0.006 (0.013)
	228 (216)	29900 (23600)	0.637 (0.575)
2,5-Diphenylfuran	324 (322)[b)]	32850 (40970)	0.163 (0.935)
	222 (225)[b)]	26050 (24000)	0.868 (0.799)

a) Values in parentheses are when methanol was used as a solvent. b) In ethanol.

Table 4. Configuration interaction state functions and the corresponding energies(eV) of *N*-(2-furylmethylene)methylamine

Cis isomer	
$\psi_{EX.\ I}=0.9424y_4y_5^*-0.0861y_4y_6-0.323y_3y_5-0.0076y_3y_6$	4.94
$\psi_{EX.\ II}=0.3236y_4y_4+0.4675y_4y_6+0.8173y_3y_5+0.0932y_3y_6$	6.21
$\psi_{EX.\ III}=0.8703y_4y_6-0.0829y_4y_5-0.4760y_3y_5+0.0956y_3y_6$	7.63
$\psi_{EX.\ IV}=0.9910y_3y_6-0.0335y_3y_5-0.1286y_4y_6-0.0152y_4y_5$	8.74
Trans isomer[b)]	
$\psi_{EX.\ I}=0.9886y_4y_5-0.0313y_4y_6-0.1464y_3y_5+0.0176y_3y_6$	3.37
$\psi_{EX.\ II}=0.1431y_4y_5+0.4403y_4y_6+0.8823y_3y_5+0.0853y_3y_6$	6.10
$\psi_{EX.\ III}=0.8934y_4y_6-0.0385y_4y_5-0.4446y_3y_5+0.0520y_3y_6$	7.64
$\psi_{EX.\ IV}=0.9948y_3y_6-0.0498y_3y_5-0.0839y_4y_6-0.0279y_4y_5$	8.77

* y_4y_5=Electronic configuration in which an electron transfers from the fourth MO(y_4) to the fifthe MO(y_5).
a) The conformer Ia. b) The conformer Ib.

Table 5. State functions and the corresponding energies of *N*-(2-furylmethylene)aniline[a)]

Cis isomer[b)]	Corresponding energy/eV
$\psi_0=0.9986\Gamma+0.0924CR_1+0.0850CR_3+0.0520CR_2$	−0.13
$\psi_{EX.\ I}=0.6699Y_1+0.7072\theta_\beta-0.1772CR_2+0.1067CR_3$	4.77
$\psi_{EX.\ II}=-0.7072Y_1+0.6922\theta_\beta-0.0569CR_4$	4.96
$\psi_{EX.\ III}=0.1151Y_1-0.5006\theta_\beta-0.2193Y_2-0.1542\theta_\alpha-0.5383CR_3-0.6077CR_4$	5.87
Trans isomer[c)]	
$\psi_0=0.9886\Gamma+0.1009CR_2+0.1039CR_4$	−0.17
$\psi_{EX.\ I}=0.9710Y_1-0.0412\theta_\beta-0.1659CR_1-0.0840CR_2-0.1301CR_4$	3.19
$\psi_{EX.\ II}=-0.9672\theta_\beta+0.1625CR_2-0.1752CR_4$	4.77
$\psi_{EX.\ III}=0.1739Y_1-0.5138Y_2-0.5952\theta_\beta-0.2007\theta_p+0.1206\theta_\alpha-0.3914CR_1-0.2364CR_2-0.2915CR_3$	5.80

a) Γ=Ground configuration, Y_1-Y_4 excited states on subsystem A, θ's excited states on subsystem B, CR's charge resonance functions. b) The conformer IIa. c) The conformer IIb.

are given in Table 4. The electronic states of the planar conformers, IIa and IIb, of *N*-(2-furylmethylene)aniline were calculated by considering the following interactions between (i) the CI state function of subsystems (A) and (B); (ii) the CI state functions of the subsystems and charge transfer configurations

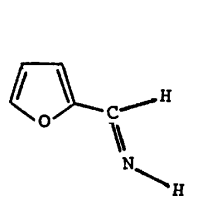

(Ia)

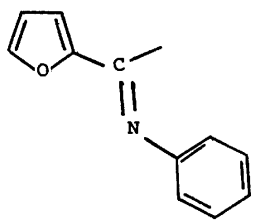

(IIa)

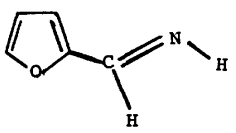

(Ib)

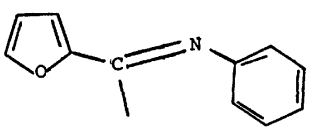

(IIb)

where an electron transfers from (A) to (b) or from (B) to (A); (iii) the ground state and the charge transfer configurations. The results are listed in Table 5.

The oscillator strength was calculated from the equation

$$f = 2.085 \times 10^{-5} M^2 \bar{\nu},$$

where M is the electric dipole transition moment and $\bar{\nu}$(cm^{-1}) is the wave number of the electronic transition. The moment, $\vec{M}$, was calculated from the equation

$$\vec{M} = \langle \psi_0 | \hat{M} | \psi_E \rangle,$$

where ψ_0 and ψ_E are the ground and excited state wave functions respectively. In the molecule-in-molecule procedure the wave functions have the forms:

$$\psi_0 = {}_a\Gamma + \sum_n b_n T_n,$$

$$\psi_E = \sum_n C_n \Lambda_n + \sum_{n'} d_{n'} T_{n'} + e\Gamma,$$

Table 6. Calculated and observed transition energies and oscillator strengths

Compound	Transition energy/eV		Oscillator strength	
	Calcd	Obsd	Calcd	Obsd
cis-*N*-(2-Furylmethylene)-methylamine[a]	4.94		0.15	
	6.21		0.27	
	7.63			
		4.70		0.33
trans-*N*-(2-Furylmethylene)-methylamine[b]	3.37		0.01	
	6.10		0.08	
	7.64			
cis-*N*-(2-Furylmethylene)-aniline[c]	4.90		0.17	
	5.09		0.10	
	6.00			
		3.90		0.51
		4.40		0.64
		5.44		
trans-*N*-(2-Furylmethylene)-aniline[d]	3.36		0.01	
	4.94		0.08	
	5.97			

a) The conformer Ia. b) The conformer Ib. c) The conformer IIa. d) The conformer IIb.

where Λ_n is the nth excited state function of the subsystem and T is the charge transfer state function. In the ZDO approximation

$$\langle\psi_0|\hat{M}|\psi_E\rangle = a\sum_n\langle\Gamma|\hat{M}|\Lambda\rangle+\sum_n\sum_{n'}b_nd_{n'}\langle T_n|\hat{M}|T_{n'}\rangle.$$

The first term was calculated by the usual procedure and the second term was zero unless $n=n'$.

(IV) Comparison with Experimental Results: Table 6 shows comparison of theoretical results with the experimental data. For *N*-(2-furylmethylene)methylamine the correspondence between the theoretical computation using conformer Ia and the experimental results is quite satisfactory. The computed transition energies of 3.36, 4.94, and 5.97 eV favour conformer IIb for *N*-(2-furylmethylene)aniline. Computations on conformer IIa predict the presence of two overlapping transitions in the region of 5.0 eV (at 4.90 and 5.09) and two overlapping transitions in the region of 6.0 eV (at 6.0 and 6.02). Experimentally three transitions were observed at 3.90, 4.40, and 5.44 eV.

Discussion and Conclusion

Many studies have been reported on the electronic structure of the rotational isomers of furfural but none has been reported on *N*-(2-furylmethylene)methylamine. Infrared spectra[24] show the presence of two carbonyl absorption bands corresponding to two conformers. On the other hand dipole moment measurements[8] indicate that at room temperature the mixture of the two conformers contains mainly conformer IIIa. The low temperature NMR spectra[25] indicate that conformer IIIb is energetically favored. The IR spectrum of furfural has been interpreted on the basis that at room temperature conformer IIIa is predominant in carbon tetrachloride.[24] Calculations by the PPP-CI and DelRe method[26] of the dipole moments have provided no reason to conclude, as shown previously,[15,26] that conformer IIIa of furfural is predominant at room temperature.

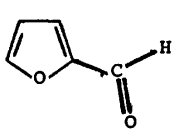

(IIIa)

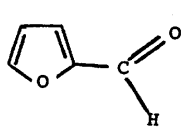

(IIIb)

Molecular orbital calculations performed in this work were not *ab initio*, yet some important results were obtained. It was proved that *N*-(2-furylmethylene)-methylamine exists mainly as conformer Ia (oxygen and nitrogen atoms are in the same side).

Molecular orbital calculations on *N*-(2-furylmethylene)aniline were not yet reported. The calculated spectrum for conformer IIb agrees with the experimental data, rather than that for conformer IIa. Although the molecule is rather large, yet the adopted method was shown to be useful for conformational analysis. Figure 2b shows the electronic absorption spectra of the studied *N*-(2-furylmethylene)arylamines. Table 2 gives the numerical values of band maxima. It can be seen that solvent polarity slightly affects the band maxima indicating that the contribution of charge transfer configuration to the state functions is slight (Table 5). Conformer IIa may have a stronger dipole than IIb. Hence an electronic transition from one subsystem to the other would result in a significant change in dipole moment and consequently an apparent shift in the band maxima with solvent polarity. Such a spectral shift was not observed experimentally. It may be interesting to compare the wave functions of the excited states of conformers IIa and IIb of *N*-(2-furylmethylene)aniline (Table 5). For conformer IIa the form of the wave functions indicates extensive mixing between the states of the subsystems (θ's and Y's) to produce the electronic states of the composite molecule. On the other hand the extent of mixing of the states of the subsystems is slight for conformer IIb. Such situation leads to 'localized' transitions of either of the subsystems of the composite molecule. The interaction between the excited states of the subsystems and the charge transfer configurations lowers the transition energies in the composite molecule relative to those in the isolated subsystems. The results of this work indicate that conformer IIb is predominant for *N*-(2-furylmethylene)aniline.

References

1) G. Horvath and A. I. Kiss, *Spectrochim. Acta, Part A*, **23**, 921 (1967).

2) W. M. Flicker, O. A. Mosher, and A. Kuppermann, *Chem. Phys. Lett.*, **38**, 489 (1976).

3) Z. I. Zolikman, A. I. Supaunova, and V. G. Kul'nevich, *Izv. Vyssh. Uchebn. Zaved., Pishch. Teknol.*, **1968**, 27; *Chem. Abstr.*, **70**, 105735s (1969).

4) D. C. Ayres and J. R. Smith, *J. Chem. Soc., C*, **1968**, 2737.

5) L. Kaper and T. J. De Boer, *Spectrochim. Acta, Part A*, **27**, 261 (1971).

6) R. J. Head and R. A. Jones, *Aust. J. Chem.*, **19**, 1747 (1966).
7) K. N. Kovalenko, V. I. Minkin, Z. N. Nazarova, and D. V. Kazachenke, *Zh. Obshch. Khim.*, **32**, 549 (1962): *Chem. Abstr.*, **58**, 100h (1963).
8) V. N. Sheinker, A. S. Kuzharov, S. B. Bulgarevich, E. G. Derecha, O. A. Osipov, and V. I. Minkin, *Zh. Obshch. Khim.*, **44**, 175 (1974): *Chem. Abstr.*, **80**, 107877v (1974).
9) A. I. Vogel, "Practical Organic Chemistry," 3rd ed, Longmans, London, (1965).
10) N. O. Calloway and L. D. Green, *J. Am. Chem. Soc.*, **59**, 809 (1937).
11) R. C. Fuson C. L. Fleming and R. Johnson, *J. Am. Chem. Soc.*, **60**, 1994 (1938).
12) W. J. Hale and L. Thorp, *J. Am. Chem. Soc.*, **35**, 71 (1913).
13) S. Kapf and C. Paal, *Ber.*, **21**, 3057 (1888).
14) F. M. Litterscheid, *Ann.*, **335**, 371 (1904).
15) G. de Chalmot, *Ann.*, **271**, 13 (1892).
16) I. P. Tsukervanik and S. A. Israilova, *Dokl. Akad. Nauk Uzb. SSR*, **20**, 25 (1963): *Chem. Abstr.*, **59**, 11392b (1963).
17) R. Abu-Eittah and R. Hilal, *Bull. Chem. Soc. Jpn.*, **51**, 2718 (1978).
18) R. Abu-Eittah, R. Hilal, and M. M. Hamed, *Int. J. Quantum Chem.*, **19**, 383 (1981).
19) H. Suzuki, "Electronic Absorption Spectra and Geometry of Organic Molecules," Academic Press, New York (1967), p. 339.
20) H. C. Longuet-Higgins and J. N. Murrel, *Proc. Phys. Soc.*, **A68**, 601 (1955).
21) R. Abu-Eittah and R. Hilal, *Bull. Chem. Soc. Jpn.*, **49**, 2158 (1976).
22) R. Abu-Eittah and F. Al-Sugeir, *Int. J. Quantum Chem.*, **13**, 565 (1978).
23) R. Pariser and R. G. Parr, *J. Chem. Phys.*, **21**, 466, 767 (1953); J. A. Pople, *Trans. Faraday Soc.*, **49**, 1375 (1953).
24) G. Allen and H. J. Bernstein, *Can. J. Chem.*, **33**, 1055 (1955); N. Claverie, C. Garrigou-Lagrange and J. Domingues Dos Santos, *J. Chim. Phys.*, **55**, 1046 (1962).
25) K. I. Dahlqvist and S. Forsen, *J. Phys. Chem.*, **69**, 4062 (1965).
26) I. Juchnovaki and J. Kaneti, *Tetrahedron*, **27**, 4269 (1971).

Studies of Molecular Complexes of Some π Donors with Iodine by Constant Activity Method

Vinay P. SHEDBALKAR and Subray N. BHAT*

Department of Chemistry, North-Eastern Hill University Shillong 793 003, Meghalaya, India

(Received August 27, 1982)

The iodine complexes of benzene, toluene, *o*-, *m*-, *p*-xylene and mesitylenes in cyclohexane are studied by using constant activity method. The association constants and the other thermodynamic parameters of the complexes are determined and the results are compared with those obtained by using conventional spectral methods. The blue shifted iodine band maxima are determined directly.

Although extensive spectrophotometric studies have been made on molecular complexes of iodine with various electron donors, reliable informations are still lacking on thermodynamic and spectral constants, particularly for weak donor–iodine complexes.[1–4] The constant activity method proposed by Childs *et al.*,[5] allows precise determination of the position as well as molar extinction coefficient of the blue-shifted iodine band, ε_{BS}, directly. So recently we have begun the investigations of a number of electron donor–acceptor complexes of iodine by the constant activity method, some of which were studied by the earlier investigators by spectral methods, but whose importance as typical examples is so great that extra efforts to obtain accurate data are justified.[6–7] In the present paper, the studies of iodine complexes of weak donors, namely benzene, toluene, xylenes, and mesitylene by constant activity method, have been reported.

Materials and Method

Solid tetramethylammonium pentaiodide ($TMAI_5$) was prepared as described by Chattaway and Hoyle.[8] All the donors namely benzene, toluene, xylenes, and mesitylene and acceptor, iodine, were purified by the standard procedures. Purified cyclohexane was used as solvent.

The procedure used to obtain the equilibrium constant, K_c, is based on using a mixture of tetramethylammonium polyoidides to maintain a constant activity of iodine, *e.g.*,

$$(CH_3)_4NI_5(s) \rightleftharpoons (CH_3)_4NI_3(s) + I_2.$$

The concentration of iodine is controlled by the temperature of the experiment. Addition of a donor to this system establishes a second equilibrium between donor and iodine,

$$D + I_2 \rightleftharpoons DI_2.$$

The latter equilibrium can be analyzed directly from the increase in absorbance at the isosbestic point of iodine in visible region and the procedure used to obtain the equilibrium constant, K_c, has been described in detail elsewhere.[6,7]

For obtaining isosbestic point, as well as the molar extinction coefficient at the isosbestic point, ε_{isos}, the spectra of pure iodine and complexed iodine in cyclohexane were recorded by keeping the iodine concentration constant (≈0.4 mM†) and varying the donor concentration (1—5 M). Pure $TMAI_5$ was equilibrated with cyclohexane (≈48 h) at constant temperature (in a thermostat) and the spectrum of iodine in the equilibrium solution was recorded. Then a series of several solutions of donors in cyclohexane were similarly equilibrated with $TMAI_5$ (≈150 mg) and spectra were recorded for all those solutions at all constant temperatures.

The spectra were recorded in UV and visible region by Beckmann 26 recording spectrophotometer fitted with a temperature control accessories with a four position manual sample changer. The spectra were recorded at 25, 30, 35, and 40 °C and the temperature of the solution could be controlled within ±0.1 °C. However, for the sake of brievity, the data at only one temperature have been reported.

For locating the blue-shifted iodine band of the donor–iodine complex, the spectrum of the complex was recorded with the donor and the constant activity source of iodine in the sample cell and only the constant activity source of iodine in the reference cell, at constant temperature.

Results and Discussion

Benzene–Iodine System. Figure 1 shows the iso-

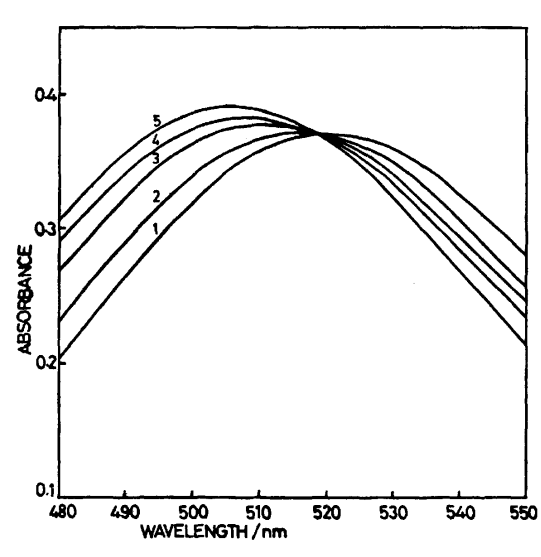

Fig. 1. Isosbestic point of the benzene-iodine complex in cyclohexane at 25 °C, cell path = 1.00 cm.
(1) Iodine alone (4.0×10^{-4} M); (2) I_2 + 1 M benzene; (3) I_2 + 2 M benzene; (4) I_2 + 3 M benzene; (5) I_2 + 4 M benzene.

† 1 M = 1 mol dm^{-3}.

sbestic point of benzene–iodine complex (at 518 nm). The molar extinction coefficient of iodine in cyclohexane at 518 nm is 962 $dm^3\ mol^{-1}\ cm^{-1}$ (Table 1). The isosbestic point does not vary with the concentration of the donor (in the experimental range of concentration of 1 M to 5 M) and the increase in absorbance at the isosbestic point is attributed solely to the formation of the complex. The charge-transfer band appears at 298 nm (Table 2). The equilibrium constants were determined at 25, 30, 35, and 40 °C, but K_c value at only one temperature, *i.e.*, 25 °C has been listed for the sake of brievity (Table 3). Our data agree with those of Plucknett[9] as well as of Childs *et al.*,[5] but differ from those of Keefer[10]. The K_c values obtained by constant activity method *i.e.* K_c^* are generally higher than those obtained by conventional spectral method using Benesi-Hildebrand[11] procedure. The discrepancy is more in weak complexes. In the case of strong complexes like pyridine–iodine, the contribution due to nonspecific interaction between the donor and iodine is around zero and under such circumstances K_c^* will be equal to K^{th} (*i.e.*, corrected equilibrium constant[4,12]). Moreover, the activity coefficient, γ, varies throughout the range of donor concentration and the values of association constant corrected for γ_{I_2} estimated from solubility parameters are comparable to those reported, obtained by B-H method[12]. Trotter and Hanna[13] had suggested a simple model. According to them a molecule of D replaces one of the molecules in the solvent shell surrounding A, and the equilibrium constant is given by

$$K_{exp} = K^* - [S]_0^{-1},$$

where $[S]_0^{-1}$ is the molar volume of the pure solvent and K^* is the true association constant (corresponding to the equilibrium $AS_n + DS_m \rightleftharpoons \overline{AD}SP + qS$). Applying the correction due to this, the corrected values are given in Table 3. Here it must be worth mentioning that the literature data correspond to heptane (as solvent) and our data correspond to cyclohexane. If one carefully goes through the literature data, one finds that $K_{heptane} > K_{cyclohexane}$.

The concentrations of benzene used for obtaining equilibrium constants are from 0.25 M to 1.5 M. We observed ΔA_{CT} (the change in A_{CT}—Absorbence at the charge-transfer band corrected for free iodine band and donor) varies reasonably linearly with ΔA_{isos}, and the linear regression line forced through the origin is used to calculate the limiting slope of the plot. The molar absorptivity of the charge-transfer band is 9450

Table 1. Molar extinction coefficient and isosbestic points of iodine complexes in cyclohexane at 298 K

[I] = 4.0×10^{-4} M; path length = 1.00 cm, [D] = 1.0 to 5 M.

Donor	λ^*_{isos} / nm	A_{isos}	ε^{**}_{isos} / $dm^3\ mol^{-1}\ cm^{-1}$
Benzene	518 (520) a)	0.385	962
Toluene	515 (518) a)	0.383	959
o-Xylene	519 (519) a)	0.388	971
m-Xylene	518 (518) a)	0.389	973
p-Xylene	518 (518) a)	0.392	980
Mesitylene	519 (520)	0.392	980

* ±1 nm, ** ±2.5. a) Childs Ph. D. thesis, Univ. of Oklahoma (Normon, Oklahoma, 1971) as quoted by M. Tamres in "Spectroscopy and Structure of Molecular Complexes".

Table 2. Spectral characteristics of charge-transfer and visible bands of some iodine complexes

Solvent: cyclohexane, temp = 298 K.

Donor	I_D/eV	Charge-transfer band					Visible band				
		λ_{CT} b) / nm	ε_{CT} c) / $dm^3\ mol^{-1}\ cm^{-1}$	$\Delta\bar{\nu}_{1/2}$ d) / cm^{-1}	f e)	$\vec{\mu} \times 10^{30}$ / C m	λ_{max}* / nm	ε_{max} c) / $dm^3\ mol^{-1}\ cm^{-1}$	$\Delta\bar{\nu}_{1/2}$ d) / cm^{-1}	f e)	$\vec{\mu} \times 10^{30}$ / C m
Benzene	9.254	289 (288) a)	9450 (8080) a)	5042	0.206 (0.280) g)	11.8 (13.7) g)	503 (504) a)	1023 (984) a)	3067 (3320) a)	0.0135 (0.0142) a)	4.01 (4.13) a)
Toluene	8.82	301 (300) a)	9472 (6900) a)	6231	0.259	13.6	500 (502) a)	1039 (1020) a)	4126 (3240) a)	0.0185 (0.0143) a)	4.67 (4.13) a)
o-Xylene	8.56	313 (313) a)	8570 (6520) a)	6230	0.231	13.1	500 (501) a)	1093 (1030) a)	3558 (3450) a)	0.0168 (0.0153) a)	4.44 (4.26) a)
m-Xylene	8.50	314 (314) a)	8193 (5719) a)	6390	0.226	12.9	497 (499) a)	1102 (1030) a)	3316 (3430) a)	0.0158 (0.0158) a)	4.30 (4.30) a)
p-Xylene	8.445	303 (303) a)	7733 (6550) a)	9718	0.324	15.24	500 (501) a)	1088 (1060) a)	3414 (3460) a)	0.0160 (0.0153) a)	4.35 (4.26) a)
Mesitylene	8.40	329 (327)	9000 (7730)	9002	0.350	16.49	496 (495) a)	1130 (1110) a)	3500 (3470) a)	0.0170 (0.0169) a)	4.47

a) J. D. Childs, Ph. D. thesis, University of Oklahoma (Normen, Oklahoma, 1971), as reported by M. Tamres in "Spectroscopy and Structure of Molecular Complexes." b) ±1 nm. c) Average error limit = ±100; C: average error limit = ±50. d) Half width, difference in wave number at half the maximum intensity on the high and low energy side of the band, ±40 cm^{-1}. e) Oscillator strength calculated from, $f = 4.42 \times 10^{-9}$. $\varepsilon_{max} \cdot \Delta\bar{\nu}_{1/2}$ ±0.0025. f) Transition moment, calculated from, $\vec{\mu} = 0.0958\left[\frac{\varepsilon_{max} \cdot \Delta\bar{\nu}_{1/2}}{\bar{\nu}_{max}}\right]$. g) B. B. Bhowmik., *Spectrochim. Acta, Part A*, **27**, 321 (1971). *: ±2 nm.

TABLE 3. SUMMARY OF THE THERMODYNAMIC PARAMETERS OF SOME COMPLEXES OF IODINE

Solvent: cyclohexane, temp: 298 K.

Donor	K_c [b]	ε_{CT} [c]	$-\Delta H°$ [d]	$-\Delta S°$
	$dm^3\ mol^{-1}$	$dm^3\ mol^{-1}\ cm^{-1}$	$kJ\ mol^{-1}$	$J\ mol^{-1}$
Benzene	0.365	9450	6.65	30.75
	(0.356) [a]	(8080) [a]	(6.78) [e]	(34.1) [e]
	(0.348) [h]			
Toluene	0.409	9472	8.69	36.29
	(0.500) [a]	(6900) [a]	(7.5) [f]	(35.5) [f]
	(0.382) [h]			
o-Xylene	0.658	8570	8.75	32.8
	(0.641) [a]	(6520) [a]		(36.0)
	(0.640) [h]			
m-Xylene	0.730	8193	8.00	29.51
	(0.698) [a]	(5910) [a]		
	(0.705) [h]			
p-Xylene	0.725	7733	10.10	47.23
	(0.642) [a]	(6550) [a]	(9.12) [g]	(40.2) [g]
	(0.700) [h]			
Mesitylene	0.962	9000	12.00	41.41
	(0.960)	(7730) [a]		(44.7)
	(0.955) [h]			

a) Childs, Ph. D. Thesis, Univ. of Oklahoma (Norman, Oklahoma, 1971) as reported by M. Tamres, in "Spectroscopy and Molecular Structure." b) ±0.005; c) ±100; d) ±0.06. e) Ref. B. B. Bhowmik, *Spectrochim. Acta, Part A*, **27**, 321 (1971); f) Ref. J. A. A. Ketelaar, *J. Phys. Rad. (Paris)*, **15**, 197 (1954). g) Andrews and Keefer, *J. Am. Chem. Soc.*, **74**, 4500 (1952). Keefer and Andrews, *ibid.*, **77**, 2161 (1955); h) Calculated by using Trotter and Hanna's method. Ref. 13.

±100 $dm^3\ mol^{-1}\ cm^{-1}$ which is higher than the reported value. (As the intensity of a CT transition is best measured by its oscillator strength, *f*, or its transition dipole moment, μ_{VN}, the results for alkyl benzenes –iodine complexes are summarised in Table 2) As we do not have any informations regarding the experimental conditions of Childs *et al.*[5] we are unable to comment on this. However, it is worth mentioning that Orgel and Mulliken[14] are of the opinion that approximately, one fourth of the CT band intensity for benzene–iodine interaction in CCl_4 is due to absorption by complex and the remaining results from "donor–acceptor contacts" due to which the molar absorptivity is high. Lane *et al.*,[12] have rightly pointed out in the case of weak molecular complexes (when the donor concentration is high), the value of ε determined using different concentration scales can differ widely (due to $d\gamma_A^*/dC_D \neq 0$). The molar absorptivity of the complex appears to decrease with the increase in temperature which may be due to band broadening.[2,4] The enthalpy, $-\Delta H°$ (6.65 $kJ\ mol^{-1}$), agrees well with the literature value. The heats of complexation must be considered as representing a composite results for benzene–iodine of different aggregation.

The visible spectrum of iodine–benzene system in cyclohexane obtained by the constant activity method has been shown in Fig. 2. The blue-shifted iodine band maximum (λ_{BS}) is at 503±2.0 nm (Table 2). An examination of the spectra at different concentrations of benzene (0.1 M to 1.5 M) shows that the blue-shifted iodine band position slightly shifts to lower wavelengths with the increase in concentration of donor. However, the shift is within the experimental error. Similar observations were made recently for benzene–iodine system from supersonic beam method.[15] Voigt[16] has reported that iodine absorbs at 502 nm in benzene. This change in λ_{BS} (with concentration), may be due to specific and non-specific interaction of iodine with the medium. The so called dielectric theory may successfully correlate the solvent shift of the absorption band to the dielectric media. As the dielectric constant is increased, (concentration of benzene is increased), the absorbance energy increases, *i.e.*, there is a blue shift in the absorption medium.

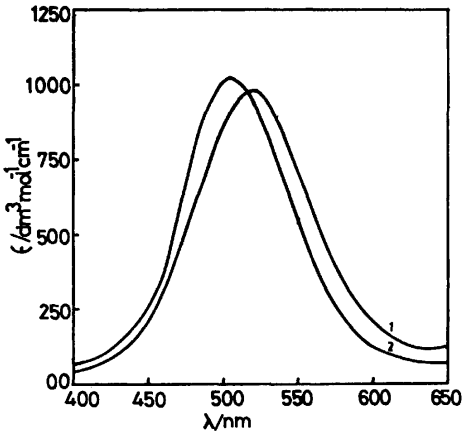

Fig. 2. Visible spectra of benzene–iodine complex in cyclohexane by constant activity method at 25 °C. 1. Free iodine; 2. complexed iodine.

The "blue-shift" of iodine band in polar media is due to perturbation of I_2 by its complexing partner.[1] The B←X electronic transition in I_2 shifts an electron from a π_g to a σ_u antibonding orbital which is spacially larger. So the magnitude of the iodine blue shift should correlate well with the electron donor ability of the bonding solvent molecules. The molar absorptivity of the blue shifted iodine band maximum, ε_{BS}, is 1023±50 $dm^3\ M^{-1}\ cm^{-1}$. The characteristic intensification of the shifted iodine band is explained by increased mixing of the $^3\pi_{o+u}$ state (520 nm band) with either CT the state or with the other excited states (like $^1\Sigma_u^+$ state). The shift and mixing should be greater the stronger the complex, leading to a greater borrowing intensity and therefore a more intense band.[1] The oscillator strength and the transition dipole moments for the blue shifted iodine band are reported in Table 2.

Toluene–Iodine System. The isosbestic point, charge-transfer band, blue-shifted iodine band and the molar extinction coefficients of toluene–iodine system are given in Tables 1—3. It can be seen from the data that the average equilibrium constant at 25 °C is 0.409 $dm^3\ mol^{-1}$ and it is slightly lower than the literature value of 0.500 $dm^3\ mol^{-1}$. The enthalpy is higher than that of benzene–iodine complex which is expected. The molar extinction coefficient of toluene–

iodine complex at CT band (310 nm) is slightly lower than that of benzene–iodine which is not expected (provided the structures are the same). Such discrepancy was reported earlier also. Murakami[17] is of the opinion that since "the degree" of overlapping between orbital functuons which are essential to CT interactions is considerably different for different models, it is reasonable to assume that each configuration has its own molar extinction coefficient. The oscillator strength and transition dipole moments of toluene–iodine are higher compared to those of benzene–iodine complex, which is expected. The blue-shifted iodine band maximum which is slightly concentration dependent of the donor for toluene–iodine appears at 500 nm ($\varepsilon_{BS}=1039$ dm^3 mol^{-1} cm^{-1}). This observation of λ_{BS}, ε_{BS}, f and μ_{VN} data (Table 2) indicate that toluene–iodine is definitely a stronger complex compared to benzene–iodine.

Xylenes–Iodine System. The isosbestic points, charge-transfer bands, blue-shifted iodine bands and their molar extinction coefficients of *o*-, *m*-, and *p*-xylene–iodine complexes are summarised in Tables 1—3. The molar extinction coefficients of the charge-transfer bands are higher than those compiled by Tamres.[18] (In the absence of detailed information in the literature we are not in a position to comment on this) The oscillator strengths and transition dipole moments of CT band indicate that *p*-xylene–iodine complex seems to be stronger compared to the others. These go in parallel with the ionization potentials of the donors. The molar extinction coeffecients, the oscillator strengths and transition dipole moments of visible bands are nearly the same (Table 2). So it is not possible to compare the strength of xylene–iodine complexes from visible absorption band data.

Mesitylene–Iodine System. The spectral and thermodynamic parameters of mesitylene–iodine complexes are reported in Table 1—3. Judging from the position of blue-shifted band and equilibrium constant and other thermodynamic parameters, it is clear that mesitylene–iodine complex is stronger compared to benzene–iodine or xylenes–iodine complexes.

Thus, as shown earlier, our present observations confirm our earlier suggestive evidences that the constant activity method (sometimes known as polyiodide solubility method or simply solubility method) is a convenient alternative to purely spectral methods for determining K_c and ε_{CT} especially for weak molecular complexes of iodine. Secondly the blue shifted iodine band maximum can be obtained precisely and directly. In addition to this, the heat of complexation can be determined by temperature dependence study of the absorbance of the complex using only a single solution of donor with excess of polyiodide.

One of the authors (V.P.S.) is thankful to CSIR, India, for the award of JRF. The authors are thankful to Prof. T.S.B. Narasaraju, Head, Chemistry Department for providing research facilities.

References

1) R. S. Mulliken and W. B. Person, "Molecular Complexes", Wiley Interscience, New York (1969).
2) "Molecular Complexes," ed by R. Foster, Eleck Science, London (1974), Vols. I and II.
3) C. N. R. Rao, S. N. Bhat, and P. C. Dwivedi, *Appl. Spectros. Revs.*, **5**, 1 (1972).
4) M. Tamres "Spectroscopy and Structure of Molecular Complexes," ed by J. Yarwood, Plenum Press, London (1973).
5) a) J. D. Childs, S. D. Christian, J. Grundness, and S. R. Roach, *Acta Chem. Scand.*, **25**, 1679 (1969); b) J. D. Childs, S. D. Christian, and J. Grundness, *J. Am. Chem. Soc.*, **94**, 5657 (1972).
6) J. Grundness, M. Tamres, and S. N. Bhat, *J. Phys. Chem.*, **75**, 3682 (1971).
7) a) M. Tamres and S. N. Bhat, *J. Am. Chem., Soc.* **94**, 2577 (1972); b) R. A. Singh and S. N. Bhat, *Can. J. Chem.*, **59**, 1212 (1981); c) Ph. D. Thesis of R. A. Singh.
8) P. D. Chattaway and G. Hoyle, *J. Chem. Soc.*, **123**, 654 (1923).
9) W. K. Plucknett and H. L. Richards, *J. Chem. Eng. Data*, **8**, 239 (1963).
10) R. M. Keefer and L. J. Andrews, *J. Am. Chem. Soc.*, **77**, 2164 (1955).
11) H. A. Benesi and J. H. Hildebrand, *J. Am. Chem. Soc.*, **71**, 2703 (1949).
12) a) E. H. Lane, S. D. Christian, and J. D. Childs, *J. Am. Chem. Soc.*, **96**, 38 (1974); b) S. D. Christian, J. D. Childs, and E. H. Lane and D. R. Hershbach, *ibid.*, **94**, 6861 (1972).
13) P. J. Trotter and M. W. Hanna, *J. Am. Chem. Soc.*, **88**, 3724 (1966).
14) L. E. Orgel and R. S. Mulliken, *J. Am. Chem. Soc.*, **79**, 4839 (1957).
15) K. L. Saenger, C. M. McClelland, and D. R. Hershbach, *J. Phys. Chem.*, **85**, 3333 (1981).
16) E. M. Voigt, *J. Phys. Chem.*, **72**, 3300 (1968).
17) M. Murakami, *Bull. Chem. Soc. Jpn.*, **26**, 441 (1953).
18) H. C. Tse and M. Tamres, *J. Phys. Chem.*, **81**, 1376 (1977).

The Electronic Structure of Heterotropones. Photoelectron Spectra and Molecular Orbital Calculations

Rolf GLEITER,* Peter BISCHOF, Michael C. BÖHM, Roger GUILARD, and Hiroyuki YAMAGUCHI

Institut für Organische Chemie der Universität, Im Neuenheimer Feld 270, D-6900 Heidelberg, West-Germany

Laboratoire de Synthèse et d'Electrosynthèse organométallique associé au CNRS (LA 33), Faculté des Sciences "Gabriel," 21100 Dijon, France

Department of Chemistry, Faculty of Science, Kumamoto University, Kurokami, Kumamoto 860, Japan

(Received January 24, 1983)

Using a helium discharge lamp with an energy of 21.21 eV ($He(I)_\alpha$ line) the photoelectron (PE) spectra of the heterotropones **1**—**7** have been investigated and compared with the PE spectra of benzologue tropones and with the PE data of thiophene, furan and pyrrole. The first five ionization events in the PE spectra of **1** to **7** could be assigned to electron ejections from $2a_2(\pi)$, $4b_1(\pi)$, $9b_2(n)$, $3b_1(\pi)$, and $1a_2(\pi)$ orbitals. This assignment has been deduced by means of experimental correlation techniques and using ZDO calculations of the LCBO and HMO type as well as semiempirical SCF versions (MINDO/3 and PPP).

The photoelectron (PE) spectra of tropone, benzotropone, naphthotropone and related alkylderivatives have been investigated by several groups[1-3] using an open helium discharge lamp with an energy of 21.21 eV ($He(I)_\alpha$ line). Although the variations due to alkyl substitution and due to hydrocarbon annelation have been studied in great detail,[1] informations concerning the effect of hetero atoms are sparse.

Therefore we felt it of interest to investigate the PE spectra of tropone derivatives with variable hetero fragments. The investigated systems are collected below:

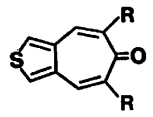

1 R=H
2 R=CH_3

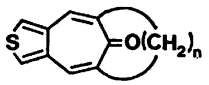

3 n=5
4 n=6

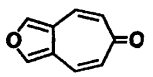

5

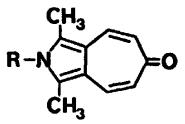

6 R=H
7 R=CH_3

The measured vertical ionization potentials are compared with results of semiempirical MO calculations.

The PE Spectra of Thiophene-fused Propones 1 to 4

The He(I) PE spectra of 6*H*-cyclohepta[*c*]thiophen-6-one (**1**), 5,7-pentamethylene-6*H*-cyclohepta[*c*]thiophen-6-one (**3**), 5,7-hexamethylene-6*H*-cyclohepta[*c*]-thiophen-6-one (**4**), 6*H*-cyclohepta[*c*]furan-6-one (**5**), 1,3-dimethyl-2*H*,6*H*-cyclohepta[*c*]pyrrol-6-one (**6**), and 1,2,3-trimethyl-6*H*-cyclohepta[*c*]pyrrol-6-one (**7**) are shown in Fig. 1 and the measured vertical ionization potentials, $I_{v,j}$, of the first PE bands of **1** to **4** collected in Tables 1 and 2. For the assignment of these data we assume the validity of Koopmans' theorem.[4]

$$I_{v,j} = -\varepsilon_j \quad (1)$$

This approximation relates the vertical ionization potentials to the one-electron energies of canonical molecular orbitals derived for the electronic ground state.

The PE spectrum of **1** shows below 12 eV two band systems with strongly overlapping ionization events. The first peak with approximate maxima at 8.62, 8.77, and 9.09 eV is assigned to three ionization events (bands 1 to 3) while the two maxima at 10.68 and 10.84 eV should correspond to two transitions. This assignment is supported by the comparison with the PE spectra of the alkyl derivatives **2**, **3**, and **4**. In the case of **2** and **3** the alkyl groups yield a definite separation of the first peak into three separated bands. The two latter molecules additionally provide evidence that the second peak between 10 and 11 eV is the result of two transitions (bands 4 and 5) as the small

TABLE 1. COMPARISON BETWEEN MEASURED IONIZATION POTENTIALS $I_{v,j}$ AND CALCULATED ORBITAL ENERGIES OF **1**. ALL VALUES IN eV

Band	$I_{v,j}$	Assignment[a]	LCBO A	LCBO B	MINDO/3[b]	PPP
1	8.62	$2a_2(\pi)$	−8.36	−8.47	−8.68	−9.42
2	8.77	$4b_1(\pi)$	−8.16	−8.75	−8.98	−8.97
3	9.07	$9b_2(n)$			−9.65	
4	10.68	$3b_1(\pi)$	−9.99	−10.59	−10.88	−11.23
5	10.84	$1a_2(\pi)$	−11.29	−11.02	−11.33	−11.76

a) The orbital numbering corresponds to the valence electrons; the core orbitals are neglected. b) Some σ orbitals between the π levels have been omitted.

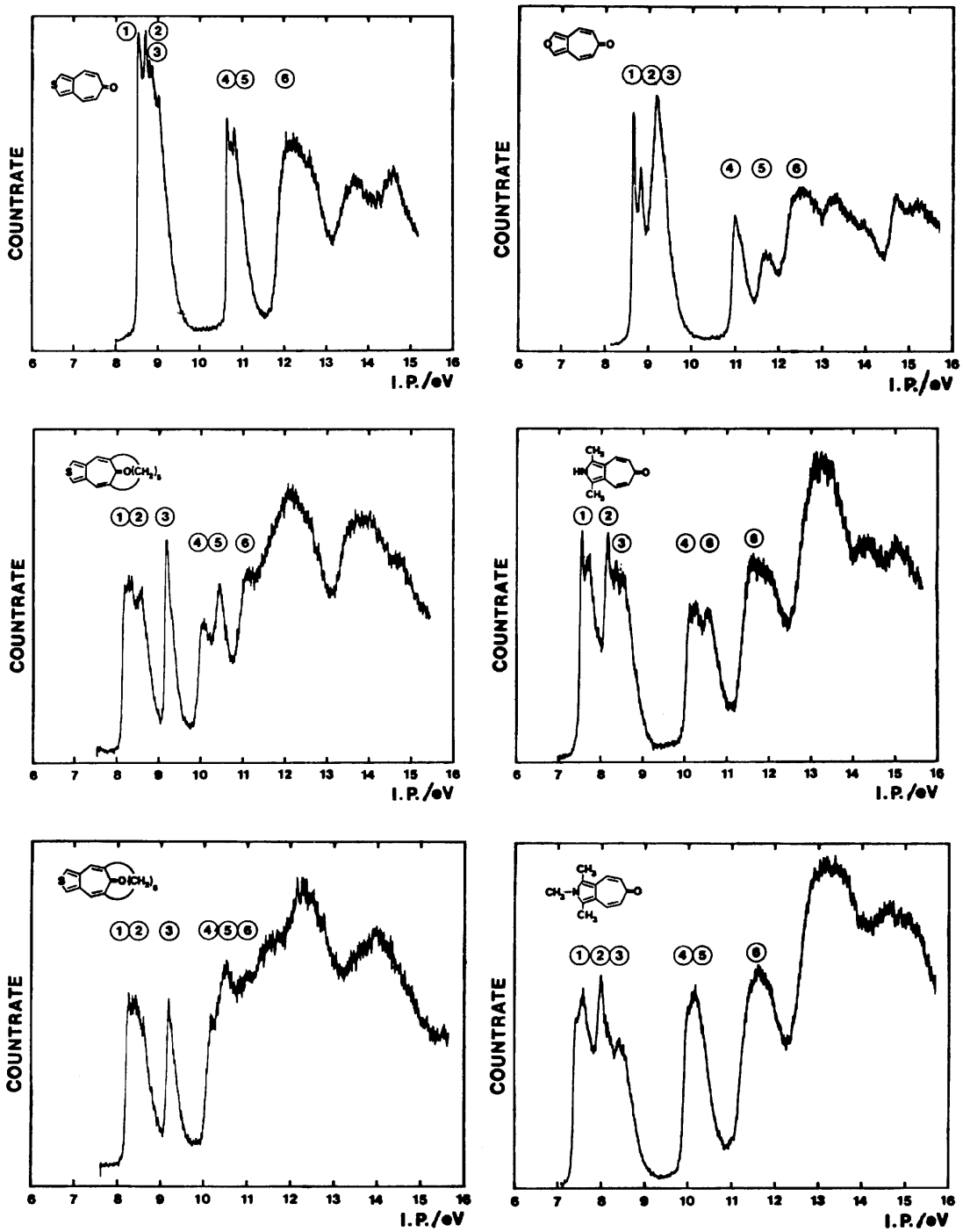

Fig. 1. He(I) PE spectra of **1**, and **3**—**7**.

Table 2. Vertical ionization potentials in the thiophene series **1**, **2**, **3**, and **4** for the first five ionization events. The irreducible representations correspond to the unsubstituted molecule **1**. All values in eV

Peak	Assignment	1	2	3	4
1	$2a_2(\pi)$	8.62	8.40	8.25	8.22
2	$4b_1(\pi)$	8.77	8.59	8.57	8.38
3	$9b_2(n)$	9.07	9.09	9.15	9.14
4	$3b_1(\pi)$	10.68	10.48	10.01	10.11
5	$1a_2(\pi)$	10.84	10.61	10.43	10.48

gap of 0.16 eV in **1** is increased to 0.38 and 0.37 eV in **3** and **4**.

The PE spectra of the four thiopheno-tropones are similar to the PE data obtained for benzotropones with the corresponding substituents (**8** to **11**) as counterparts of **1** to **4**.[1)]

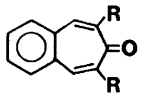

8 R=H
9 R=CH_3

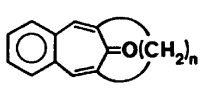

10 n=5
11 n=6

This close resemblence, at least for the first band system is not surprising since the first ionization events in **8** to **11** correspond to MO's predominantly localized in the seven-membered ring. The replacement of one double bond by a sulfur will not cause large variations in the IP's as the electronegativities of carbon and sulfur are of comparable size.[5] The difference between the two types of tropones is caused by the inclusion of a 3p-orbital on the sulfur center only. As a result of this restriction all coefficients in the a_2 orbitals are set to 0 in the hetero position as shown below.

The pairwise analogy between **1/8**, **2/9**, **3/10**, and **4/11** suggests that two bands of the first peak are the result of ionization events out of π orbitals (b_1 and a_2) while the third one is due to the lone pair of the carbonyl group.[1-3] The correspondence between the second band system with two strongly overlapping maxima leads to the assumption that the π-orbitals of b_1 and a_2 symmetry lead to these peaks. To assign the ionization events in the sulfur derivatives explicitly we discuss the sequence of the π-orbitals in the unsubstituted molecule **1** in some detail.

a) ZDO Models: To derive the orbital energies of the π MO's of **1** we make use of the linear combination of bonding orbitals (LCBO)[6] successfully applied in the benzologue tropone series by Heilbronner *et al.*[1] Two alternatives for the construction of the molecular orbitals of **1** are displayed below:

A **B**

In the case of **A** the MO's are constructed from bonding orbitals of C=C and C=O double bond fragments and from the sulfur 3p AO. In the alternative model we couple the orbitals of the thiophene moiety to the remaining bonding fragments. To calculate the orbital energies in the zero differential overlap (ZDO) model we have to estimate the energies of the basis orbitals in **A** and **B**.

For the complete fragmentation scheme **A** one has to know the diagonal elements $A_a=A_e$, $A_b=A_d$, A_f and A_c as well as the interaction parameters $B_{ab}=B_{ed}$, $B_{ef}=B_{af}$, $B_{bc}=B_{dc}$, and B_{bd} respectively. For the fragments of the tropone unit we use the parameters derived by Heilbronner *et al.*:[1]

$$A_a = A_e = -10.64\,\text{eV},$$
$$A_f = -13.70\,\text{eV},$$
$$B_{af} = B_{ef} = -0.9\,\text{eV}.$$

For the double bonds b and d of the thiophene moiety we neglect the inductive effect of the carbonyl group, an approximation which should be allowed due to the remarkable separation between b and d and the carbonyl chromophore. As the electronegativity of C and S are of comparable magnitude we neglect this influence too. These simplifications lead to a basis orbital energy of $A_b=A_d=-10.22$ eV.[1] From our previous experience with thiophene derivatives we choose the following S dependent parameters:[7] $A_c=-9.4$ eV and $B_{bc}=B_{dc}=-1.8$ eV. The interaction integrals that couple the thiophene moiety to the triene fragment once again were taken from Ref. 1 $B_{ab}=B_{ed}=-1.215$ eV. The same value also has been used in the case of B_{bd}.

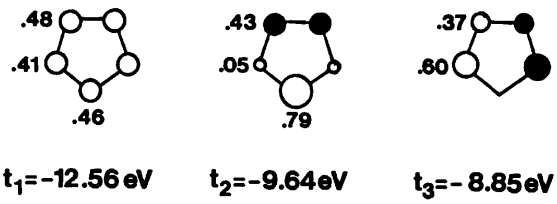

Fig. 2. HMO levels for thiophene.

In the case of **B** one has to determine the LCAO coefficients and the orbital energies of the thiophene fragment, t, which are then coupled to the basis orbital energies and resonance integrals of a, b, and c, the values of which already have been explained. The basis energies for thiophene are taken from experiment:[8] $A_s=-9.4$ eV, $A_c=-7.0$ eV, $B_{cc}=-3.0$ eV, and $B_{cs}=-1.8$ eV. The MO wave functions obtained by the Hückel (HMO) model[9] are displayed in Fig. 2. With these LCAO coefficients it is possible to calculate the B parameters of the second LCBO alternative. The new interaction integrals for the LCBO approach **B** are listed below:

$$B_{at_1} = B_{ct_1} = -0.8188\,\text{eV},$$
$$B_{at_2} = B_{ct_2} = -0.7374\,\text{eV},$$
$$B_{at_3} = -0.6388\,\text{eV}, \qquad B_{ct_3} = +0.6388\,\text{eV}.$$

Solving the secular determinants for the two LCBO models **A** and **B** described above yields the eigenvalues for the π orbital energies given in Table 1. It is seen that both sets are in line with the measured ionization energies. A closer look into the corresponding columns, however, demonstrated that model **B** leads to the better agreement in comparison with the experiment. Thus a more realistic description of the orbitals of **1** is obtained if the thiophene orbitals are coupled to the remaining bonding fragments.

b) Semiempirical MO Calculations on 1: To support the assignment based on the LCBO model we also performed semiempirical calculations using the MINDO/3 method[10] and the PPP-Hamiltonian.[12,13] The results of both approaches are included in Table 1. In the case of the PPP model the canonical orbital energies were corrected according to Eq. 2:[14]

$$\varepsilon_j = 0.168\,\text{eV} + 0.932 \times \varepsilon_j^{PPP} \qquad (2)$$

Thi ₃linear dependence has been obtained earlier and is based on a regression analysis on several thiophene derivatives. The agreement between the measured IP's and the semiempirical calculations is as good as can reasonably be expected. Both types confirm the assignment derived within the LCBO framework and experimentally deduced from the benzologue tropone.

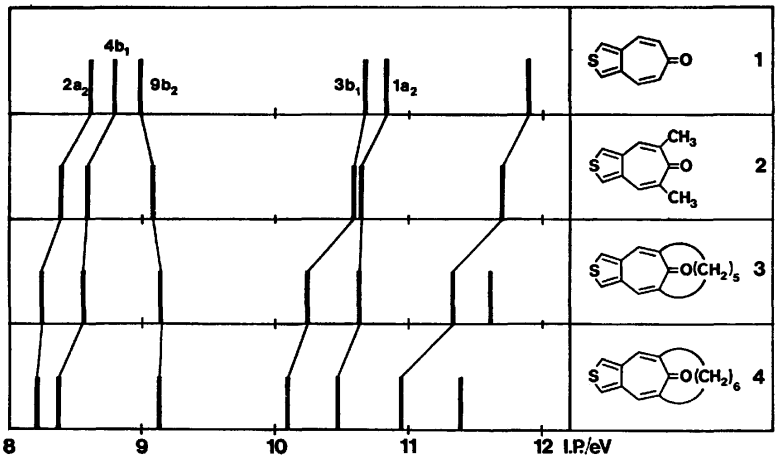

Fig. 3. Correlation between the first bands in the PE spectra of **1**, **2**, **3**, and **4**.

Table 3. Comparison between measured ionization potentials, $I_{v,j}$, and calculated orbital energies of **5**, **6**, and **7**. All values in eV

Compd	Peak	$I_{v,j}$	Assignment[a]	LCBO **B**	HMO	MINDO/3[b]	PPP
5	1	8.65	$2a_2(\pi)$	−8.68	−8.78	−8.50	−9.86
	2	9.17	$4b_1(\pi)$	−8.82	−8.96	−9.26	−9.18
	3		$9b_2(n)$			−9.60	
	4	10.98	$1a_2(\pi)$	−11.03	−10.68	−11.23	−11.99
	5	11.70	$3b_1(\pi)$	−11.50	−11.74	−11.86	−12.20
6 [c]	1	7.55	$2a_2(\pi)$	−7.07	−7.75[d]	−8.14	−9.04[d]
	2	8.16	$4b_1(\pi)$	−7.87	−8.65	−8.57	−8.98
	3	8.50	$9b_2(n)$			−9.33	
	4	10.21	$3b_1(\pi)$	−10.73	−10.75	−10.93	−11.68
	5	10.56	$1a_2(\pi)$	−10.85	−10.38	−10.90	−11.66
7 [c]	1	7.59	$2a_2(\pi)$		−7.75[d]	−8.11	−8.82
	2	8.01	$4b_1(\pi)$		−8.55	−8.43	−8.91
	3	8.44	$9b_2(n)$			−9.30	
	4	10.14	$3b_1(\pi)$		−10.32	−10.66	−11.45
	5		$1a_2(\pi)$		−10.38	−10.87	−11.60

a) The orbital numbering corresponds to the valence electron configuration; the core orbitals are neglected. b) Some σ orbitals between the π levels have been omitted. c) The MO's of the methyl substituents have been neglected in the numbering of the irreducible representations. d) Results obtained by simple perturbation theory (formula 3).

In Table 2 and Fig. 3 we have correlated the different ionization potentials in the thiophene series **1** to **4**.

In analogy to the benzotropones **9** and **10** a remarkable separation between $4b_1$ and $9b_2$ is found for $n=5$ and 6. This observation has been rationalized by the fact that for $n=5/6$ the carbonyl group is strongly bent out of the molecular plane and behaves as a predominantly unconjugated fragment.[1] This PE spectroscopic finding is in line with the results of various physicochemical investigations.[1]

The PE Spectra of 5, 6, and 7

The He(I) PE spectra of the furan derivative **5** and the two pyrrole descendents **6** and **7** are also shown in Fig. 1. The measured vertical ionization potentials are collected in Table 3 together with the results of the already discussed computational procedures. As the LCBO approach **B** gave better results only this model has been used in the case of **5**, **6**, and **7**. Additionally simple HMO results[9] are added in Table 3.

To rationalize the variation of the IP's in **5**, **6**, and **7** in comparison to **1** it is constructive to discuss the shift of the two highest occupied MO's in the series furan, pyrrole and thiophene.[8,15] A schematical representation is given in Fig. 4. A detailed explanation for the observed variations and the unexpected changes in pyrrole have been discussed elsewhere.[8] If we rely on the validity of Koopmans' theorem in the case of the tropone derivatives, we expect for the first two bands of **1** ($2a_2$, $4b_1$) a similar shift by replacing the sulfur atom by oxygen or NR as for the first two bands in the series thiophene, furane and pyrrole. According to Fig. 4 the $2a_2$ MO of the heterotropones should be constant if **1** and **5** are considered and shifted to higher energies if $2a_2$ of **1** is correlated with $2a_2$ of

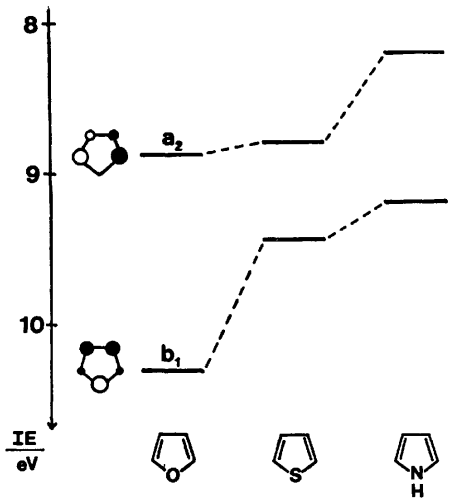

Fig. 4. Correlation of the two lowest ionization energies of furan, thiophene and pyrrole.

the pyrrole derivatives **6** and **7**. For the $4b_1$ MO one expects a stabilization going from **1** to the furane molecule **5** and a lowering if **1** is compared with **6** and **7**. These expectations are fulfilled as displayed in the correlation diagram of Fig. 5. For the comparison of the measured IP's of **5**, **6**, and **7** we follow the lines of the foregoing paragraph.

a) ZDO Models: For **5** and **6** we performed LCBO calculations of the type **B**. HMO data of the furane

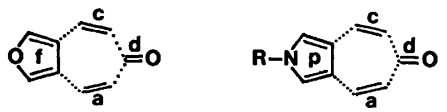

B

moiety were chosen to fit the experimental IP's of furan.[16] With the following parameters ($A_o=-11.0$ eV, $A_c=-7.3$ eV, $A_{c'}=-7.0$ eV, all interaction integrals -3 eV) an almost perfect agreement between HMO energies and measured data is observed:

	$I_{v,j}$	ε_j^{HMO}/eV
$1a_2$	8.88	9.07
$2b_1$	10.31	10.31
$1b_1$	14.40	14.48

The MO coefficients obtained with this approximation are collected in Fig. 6a. The calculation of the unknown interaction integrals in **5** then is straightforward and not explicitly performed in this context. Inspection of the LCBO results in Table 3 demonstrates that the measured ionization energies are reproduced with high accuracy. Also the HMO results on the right hand of the LCBO calculations lead to a satisfactorical description of the ionization energies. The HMO parameters were taken from the literature.[17]

The pyrrole basis orbital energies were calculated with HMO parameters close to Eland's values:[17] $A_{NH}=-9.61$ eV, $A_c=-6.64$ eV, $A_{c'}=-6.37$ eV, all interaction integrals are set to -2.70 eV. The HMO energies are compared below with the measured ionization potentials of pyrrole:[18]

	$I_{v,j}$	ε_j^{HMO}/eV
$1a_2$	8.21	8.24
$2b_1$	9.20	9.24
$1b_1$	13.0	12.93

The HMO wave functions for the LCBO model are given in Fig. 6b. The calculated orbital energies for **6** confirm the qualitative assignment. Furthermore it is seen that also the HMO calculations with the parameters of Ref. 7 are in good agreement with the measured ionization energies. The inductive effect of the methyl groups in **6** and **7** has been taken into account by the simple first order perturbation theory:[9]

$$\delta\varepsilon_j = \sum_\mu c_{j\mu}^2 \delta\alpha_\mu + \sum_\omega c_{j\omega}^2 \delta\alpha_\mu/3. \qquad (3)$$

For the perturbation parameter $\delta\alpha_\mu$ a value of 1.16 eV has been used. The indices ω refer to the position ortho to μ.

*b) Semiempirical MO Calculations on **5**, **6**, and **7***: The results of the semiempirical calculations of the MINDO/3 and PPP type in Table 3 suggest for all three heterotropones **5**, **6**, and **7** the same orbital sequence as in the thiophene derivative **1**. The variation of $2a_2$ and $4b_1$ upon changes of the hetero fragment have already been commended on. It is seen that MINDO/3 leads to the better agreement with the measured data while the PPP model fails to reproduce the sequence $2a_2$ on top of $4b_1$ in the case of **5** and **6**.

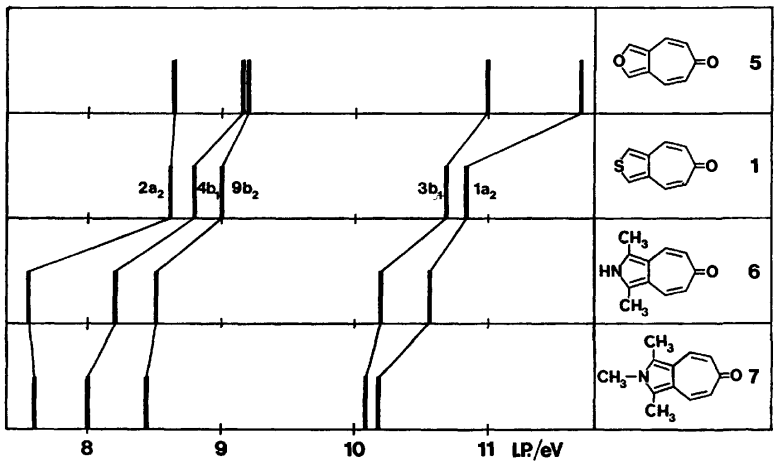

Fig. 5. Correlation between the first bands in the PE spectra of **1**, **5**, **6**, and **7**.

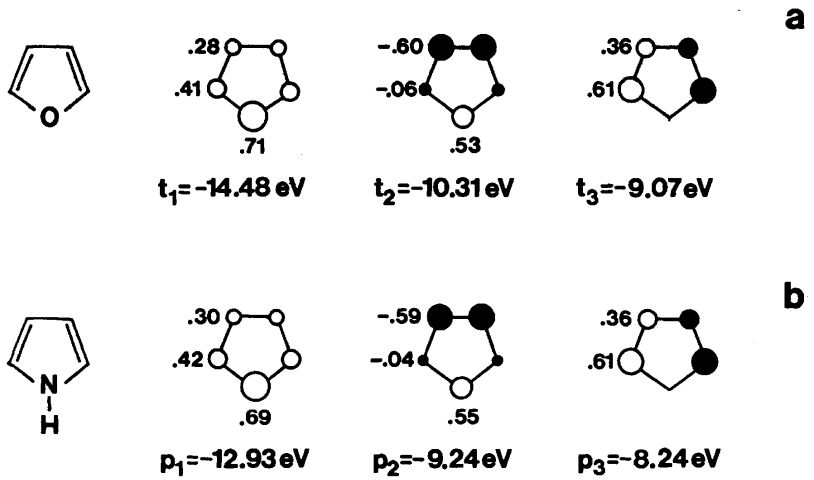

Fig. 6. HMO levels for furan (**a**) and pyrrole (**b**).

Conclusions

In the present publication we have investigated the He(I) PE spectra of seven heterotropones containing sulfur, oxygen and nitrogen as hetero fragment. The sequence of the ionization potentials has been derived by experimental correlation techniques and by simple LCBO considerations based on the validity of Koopmans' theorem. Although it has been demonstrated that ionization events in heterocycles are accompanied by significant reorganization effects of the electrons[19,20] that can be taken into account by sophisticated many-body procedures, our approach is as successful as the LCBO calculation of Heilbronner *et al.*[1] in the benzologue tropones. The comparison between the PE spectra of **1**/**2** with thiophene, of **5** with furane and **6**/**7** with pyrrole lead to an unambigous assignment of the ionization potentials of the tropone derivatives. It has been demonstrated that the variation of the hetero group leads to significant changes in the magnitude of the IP's but the sequence is constant in all investigated compounds.

The investigation of the PE spectra of the tropones **1** to **7** allowed a rationalization of the changes in the electronic structure of these molecules upon variation of the hetero fragment. However, it should be noted that no direct conclusions regarding the "aromaticity" or "reactivity" of these compounds should be drawn from these results.

Experimental

The heterotropones **1** to **5** were prepared according to methods described in the literature.[21] The PE spectra were recorded on a PS 18 spectrometer of Perkin-Elmer Ltd. (Beaconsfield, England) and calibrated with Ar. A resolution of about 20 meV of the Ar line was obtained.

The work in Heidelberg has been supported by the Fonds der Chemischen Industrie and the BASF Aktiengesellschaft in Ludwigshafen. H. Y. is grateful to the Humboldt-Stiftung for a fellowship. We thank Professor R. Kreher for samples of **6** and **7**.

References

1) M. Allan, E. Heilbronner, and E. Kloster-Jensen, *J. Electron Spectrosc.*, **6**, 181 (1975).
2) J. C. Bünzli, D. C. Forst, and L. Weiler, *J. Am. Chem. Soc.*, **96**, 1952 (1974).
3) C. Müller, A. Schweig, and H. Vermeer, *Angew. Chem.*, **86**, 275 (1974).
4) T. Koopmans, *Physica*, **1**, 104 (1934).
5) L. Pauling, "The Nature of the Chemical Bond," Cornell University Press, Ithaca, N. Y. (1960).
6) M. Beez, G. Bieri, H. Bock, and E. Heilbronner, *Helv. Chim. Acta*, **56**, 1028 (1973).
7) R. Gleiter, M. Kobayashi, J. Spanget-Larsen, J. P. Ferraris, A. N. Bloch, K. Bechgaard, and D. O. Cowan, *Ber. Bunsenges. Phys. Chem.*, **79**, 1218 (1975).
8) R. Gleiter, M. Kobayashi, J. Spanget-Larsen, S. Gronowitz, A. Konar, and M. Farnier, *J. Org. Chem.*, **42**, 2230 (1977).
9) E. Heilbronner and H. Bock, "Das HMO Modell und seine Anwendung," Verlag Chemie GmbH, Weinheim (1970); M. J. S. Dewar and R. C. Dougherty, "The PMO theory of organic chemistry," Plenum Press, New York (1975).
10) R. C. Bingham, M. J. S. Dewar, and D. H. Lo, *J. Am. Chem. Soc.*, **97**, 1285 (1975); we actually used a of MINDO/3 written by P. Bischof.[11]
11) P. Bischof, *J. Am. Chem. Soc.*, **98**, 6844 (1976).
12) R. Pariser and R. G. Parr, *J. Chem. Phys.*, **21**, 446, 767 (1953); J. A. Pople, *Trans. Faraday Soc.*, **49**, 1375 (1953).
13) J. Fabian, A. Mehlhorn, and R. Zahradnik, *J. Phys. Chem.*, **72**, 3975 (1968).
14) P. A. Clark, R. Gleiter, and E. Heilbronner, *Tetrahedron*, 29, 3085 (1973).
15) R. Gleiter and J. Spanget-Larsen, *Top. Curr. Chem.*, Springer Verlag, Berlin (1979), Vol. 86.
16) P. J. Derrick, L. Asbrink, O. Edquist, B.-O. Jonsson, and E. Lindholm, *Int. J. Mass. Spectrom., Ion. Phys.*, **6**, 161 (1971).
17) J. H. D. Eland, *Int. J. Mass. Spectrom., Ion. Phys.*, **2**, 471 (1969).
18) P. J. Derrick, L. Asbrink, O. Edquist. B.-O. Jonsson, and E. Lindholm, *Int. J. Mass. Spectrom., Ion. Phys.*, **6**, 191 (1971).
19) W. v. Niessen, W. P. Kraemer, and L. S. Cederbaum, *J. Electron Spectrosc.*, **8**, 179 (1976); W. v. Niessen, L. S. Cederbaum, and G. H. F. Diercksen, *J. Am. Chem. Soc.*, **98**, 2066 (1976).
20) L. S. Cederbaum and W. Domcke, *Adv. Chem. Phys.*, **36**, 205 (1977).
21) R. Guilard and P. Fournari, *Bull. Soc. Chim. Fr.*, **1971**, 1437; **1972**, 4349; M. El Boari, R. Guilard, and P. Foumari, *ibid.*, **1974**, 1383.

Ion Exchange Equilibria between Alkali Metals and Hydrogen Ions on Iron(III) Antimonate, an Inorganic Ion Exchanger

Jagdish Prasad RAWAT* and Balbir SINGH
Department of Chemistry, Aligarh Muslim University, Aligarh-202001 India

(Received July 19, 1982)

Ion exchange equilibria of alkali metal ions (Li^+, Na^+, K^+ and Rb^+)/H^+ systems have been studied at 30, 40, 50, and 60 °C on iron(III) antimonate as a cation exchanger. The exchange isotherms have been measured for both forward and backward reactions with solutions of ionic strength 0.1 by the batch technique. The isotherms showed S-shaped curves for each exchange system except Li^+/H^+. Selectivity coefficients vary with the equivalent fraction ($\bar{X}_M$) of the alkali metal ions in the exchanger and give linear functions against $\bar{X}_M$ in the range from 0—0.40. The selectivity sequence shows $Na^+ < Li^+ < K^+ < Rb^+$. The overall thermodynamic data are evaluated.

Synthetic inorganic ion exchangers have been developed in recent years. The primary aim of most of the studies done in this field has been to achieve the separations. Besides the preparation of new materials and their applications to the separations interest has also been developed towards the study of ion exchange equilibria on these materials. Because of their thermal stability, their rigid structure and consequently negligible swelling, the ion exchange equilibrium studies at different temperatures on these materials will be simpler than on organic ion exchange resins which swell quite appreciably and are prone to thermal instability. The contributions of Larsen Vissers,[1] Ruvarac,[2] Amphlett,[3] Alberti,[4] Nancollas & Dyer[5] are noteworthy in this field. Recently Abe and Sudoh[6,7] described the ion exchange equilibrium studies on antimonic acid for the systems of transition metal ions/H^+ and from these results the appropriate thermodynamic data were derived.

The influence of temperature on the equilibrium between alkaline earth metal ions and hydrogen ion on tantalum arsenate has been described in our earlier paper.[8] Similar studies on the equilibria between alkaline earth metal ions and sodium ion on iron(III) antimonate have also been described.[9] The ion exchange characteristics of iron(III) antimonate are of considerable interest since it behaves as a cation exchanger with different selectivities for cations.[10]

Limiting our attention to series of ions belonging to the same group of the periodic table, that is having the same valency and similar electronic structure, we can study the effects of ion size and hydration upon equilibria eliminating the problem of the influence of eletronic and valency differences. Alkali metal ions can be taken as models for metal ions since they have univalent positive charge. Furthermore, they form inoic bonds and the effect of complex formation can be avoided.

Experimental

The iron(III) antimonate was prepared as described previously.

Determination of Maximum Uptake of Alkali Metal Ions on Iron(III) Antimonate. A 0.1 mol dm^{-3} solution of alkali metal chloride was passed continuously through the iron(III) antimonate column in H^+ form until the change in concentration of the alkali metal ion was negligible between the influent and effluent. The equivalent fraction of H^+ and M^+ in iron(III) antimonate was calculated on the basis of total exchange capacity.

Ion Exchange Equilibria. In the forward reactions the iron(III) antimonate (0.5 g) in H^+ form was immersed in 20 cm^3 of a mixed solution of varying ratio of alkali metal chloride/hydrochloric acid in the conical flasks with intermittent shaking at 30±1, 40±1, 50±1 and 60±1 °C. The ionic strength in the mixed solution was adjusted to 0.1 with hydrochloric acid.

In the reverse reactions the ion exchanger iron(III) antimonate in the respective alkali metal forms corresponding in weight (0.5 g in the hydrogen form) was immersed in the 20 cm^3 of the mixed solution of alkali metal chloride/hydrochloric acid at an ionic strength of 0.1.

Theoretical Aspects. The ion exchange reactions of the univalent alkali metal ions/H^+ exchange systems on iron(III) antimonate can be represented by the following expression:

$$\bar{H}^+ + M^+ \rightleftharpoons \bar{M}^+ + H^+, \quad (1)$$

where the bar refers to iron(III) antimonate phase and M^+ is the alkali metal ion.

The corrected selectivity coefficient of the above reaction can be defined as:

$$K_c = \frac{\bar{X}_M \cdot X_H}{\bar{X}_H \cdot X_M} \frac{\gamma_H}{\gamma_M}, \quad (2)$$

where K_c is the corrected selectivity coefficient, $\bar{X}_M$ and $\bar{X}_H$ are the equivalent fractions of the metal and H^+ in the exchanger phase, respectively. X_H and X_M are the equivalent fractions of exchanging H^+ and M^+ in the solution phase, respectively. γ_H and γ_M the activity coefficients of hydrogen and the metal in solution respectively. For dilute concentrations the contribution of the activity coefficient ratio (γ_H/γ_M) may be taken as unity.

The thermodynamic equilibrium constant K_a can be calculated using the simplified form of the expression given by Gains and Thomas (11):

$$\ln K_a = \int_0^1 \ln K_c d\bar{X}_M. \quad (3)$$

The change in the free energy of the ion exchange reaction, ΔG° was calculated from the thermodynamic equilibrium constant K_a using the expression:

$$\Delta G^\circ = -RT \ln K_a. \quad (4)$$

The standard enthalpy change, ΔH° has been calculated from the plot of $\log K_a$ against $1/T$.

The standard entropy change, ΔS° is then calculated by the relation:

$$\Delta G^\circ = \Delta H^\circ - T\Delta S^\circ. \quad (5)$$

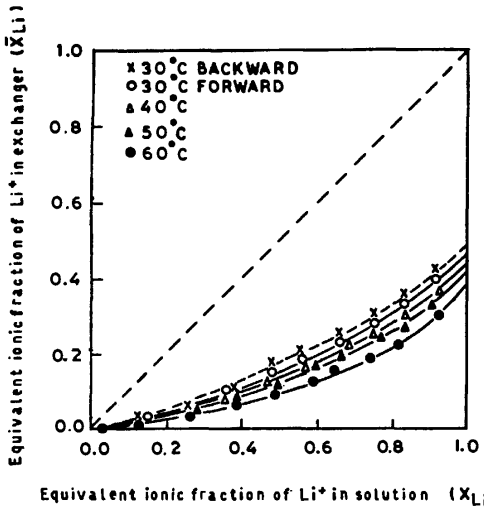

Fig. 1. Ion exchange isotherm of Li^+–H^+ exchange iron(III) antimonate.

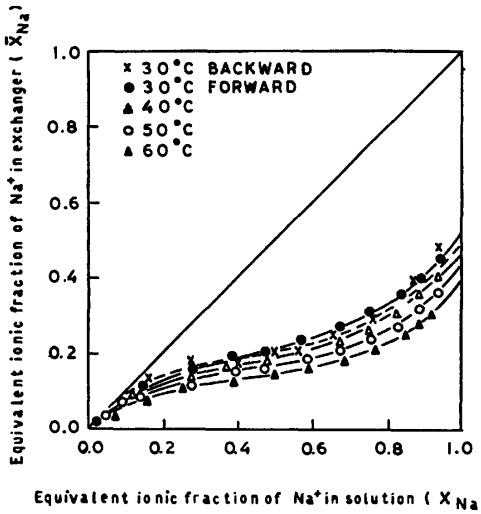

Fig. 2. Ion exchange isotherm of Na^+–H^+ exchange on iron(III) antimonate.

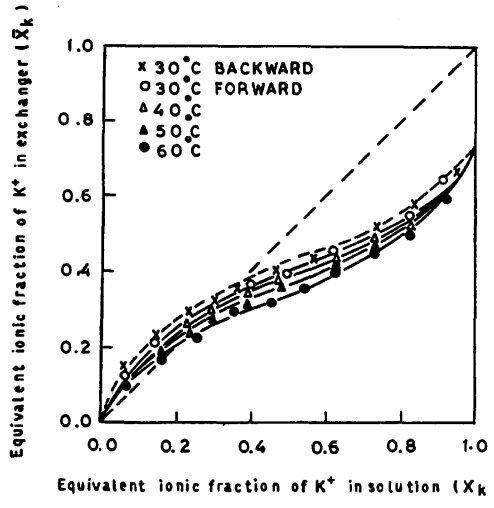

Fig. 3. Ion exchange isotherm of K^+–H^+ exchange on iron(III) antimonate.

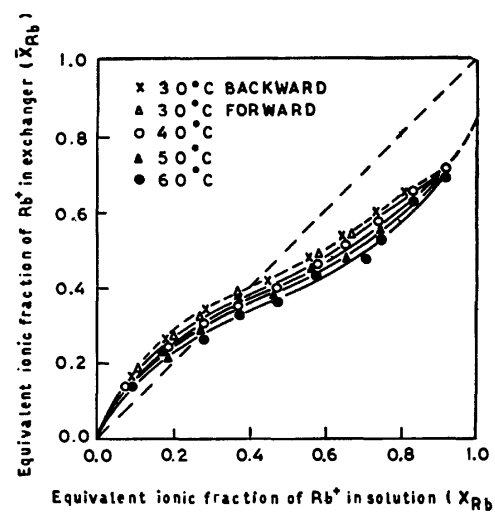

Fig. 4. Ion exchange isotherm of Rb^+–H^+ exchange on iron(III) antimonate.

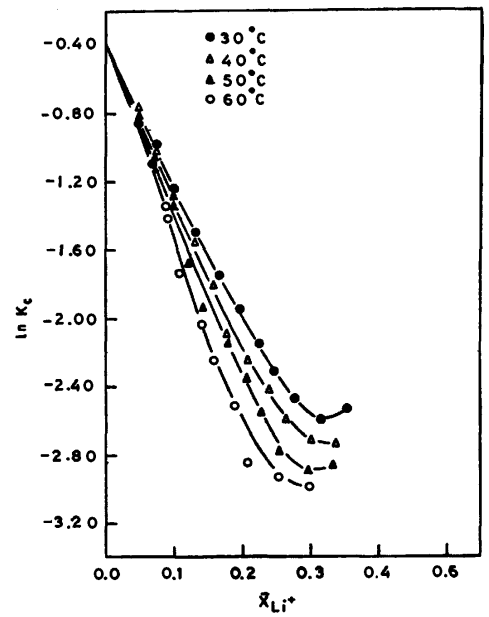

Fig. 5. Logarithms of selectively coefficient *vs.* ionic fractions of Li^+ in exchanger phase.

Results and Discussion

The equilibrium was attained for the forward and backward ion exchange reactions within 6 h shaking. The ion exchange isotherms for the systems Li^+/H^+, Na^+/H^+, K^+/H^+, and Rb^+/H^+ in a temperature range of 30—60 °C are shown in Figs. 1 to 4. Ion exchange isotherms have been used to represent graphically experimental data pertinent to ion competition (at different concentration ratios).

For Li^+/H^+ and Na^+/H^+, the isotherms showed that the exchange does not go to completion although entering cation is initially preferred and the degree of exchange gives a value lower than unity. For K^+/H^+ and Rb^+/H^+ the entering cations show a selectivity reversal with increasing equivalent fraction in the exchanger. The isotherms for the reverse exchange are performed only at 30±1 °C and can be plotted

TABLE 1. THERMODYNAMIC PARAMETERS ON IRON(III) ANTIMONATE AT AN IONIC STRENGTH OF 0.1 AND VARIOUS TEMPERATURES

Alkali metal ion	K_a				$\Delta G°$/kJ equiv^{-1}				$\Delta H°$/kJ equiv^{-1} 30—60 °C	$\Delta S°$/J equiv^{-1} deg^{-1}
	30 °C	40 °C	50 °C	60 °C	30 °C	40 °C	50 °C	60 °C		
Li^+	0.08	0.06	0.05	0.04	6.50	7.20	8.10	8.78	17.06	77.60±0.17
Na^+	0.05	0.04	0.03	0.02	7.69	8.74	9.61	10.66	22.17	98.40±0.35
K^+	0.37	0.30	0.27	0.22	2.56	3.15	3.55	4.18	13.85	54.14±0.18
Rb^+	0.60	0.51	0.45	0.40	1.31	1.74	2.17	2.56	11.09	40.98±0.23

TABLE 2. HYPOTHETICAL THERMODYNAMIC DATA ON "ZERO LOADING" OF THE ION EXCHANGE REACTION AT 30 °C

	Li^+	Na^+	K^+	Rb^+
$\ln K_{c\,\bar{x}_M \to 0}$	−0.35	−1.50	−2.00	−1.25
$\frac{\Delta G°_{\bar{x}_M \to 0}}{\text{kJ equiv}^{-1}}$	0.88	3.79	5.06	3.16
$\Delta H°_{\bar{x}_M \to 0}$	0.00	0.00	0.00	0.00
$\frac{\Delta S°_{\bar{x}_M \to 0}}{\text{J equiv}^{-1}}$	−2.9	−12.5	−16.7	−10.4

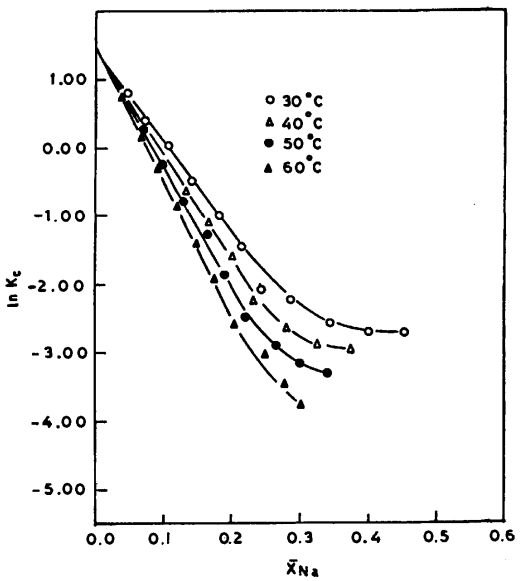

Fig. 6. Logarithms of selectivity coefficient *vs.* ionic fractions Na^+ in exchanger phase.

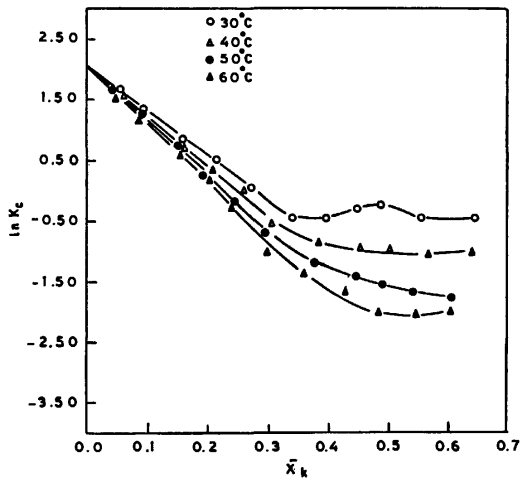

Fig. 7. Logarithms of selectivity coefficients *vs.* ionic fractions of K^+ ions in the exchanger phase.

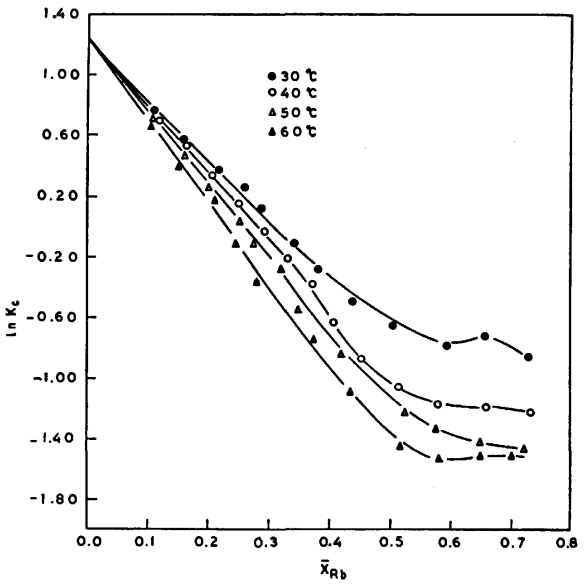

Fig. 8. Logarithms of selectivity coefficients *vs.* ionic fractions of Rb in exchanger ohase.

on the curves of the isotherms for the forwared exchange (Fig. 1 to 4). Thus the ion exchange reactions are reversible throughout the entire range of the compositions studied.

The selectivity of the exchanger can be measured in terms of K_c, which is the quantitative measure of the prefernce of the exchanger for one ion over another in solution with it. The ln K_c *vs.* $\bar{X}_M$ which is referred to as Kielland plot gave fairly straight line for all systems at lower values of $\bar{X}_M$ (Figs. 5 to 8). The linear Kielland plot was also observed for the alkali metal ions/H^+ systems on crystalline antimonic acid.

The thermodynamic equilibrium constant K_a was evaluated from Eg. 3 by assuming that the relation between ln K_c *vs.* $\bar{X}_M$ remains unity over entire range 0 to 1 of X_M. The $\Delta H°$ and $\Delta S°$ showed a corresponding change in their values with the change in temperature since the plots of log K_a *vs.* $1/T$ showed fairly good linearity over the entire range of temperatures studied. The thermodynamic selectivity series was found to be:

$$Na^+ < Li^+ < K^+ < Rb^+.$$

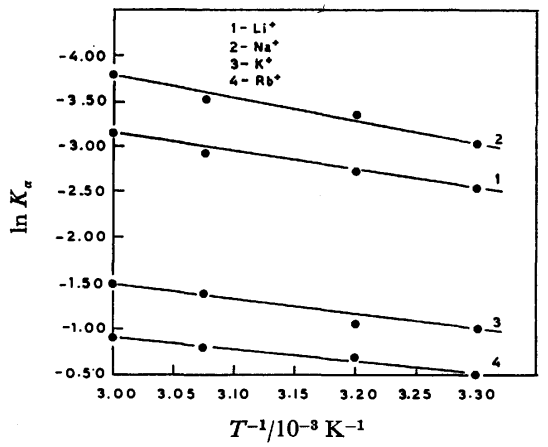

Fig. 9. Temperature dependence of thermodynamic equilibrium constant.

Interpretation of the Selectivity in the Infinitesimal Concentration of the Alkali Metals. The hypothetical thermodynamic data in infinitesimal concentration were calculated for interpretation of the selectivity of the alkali metal in the trace amounts on iron(III) antimonate and for comparison with those data obtained with other exchangers. The values of $(\ln K_c)\overline{X}_M \rightarrow 0$ were obtained by extrapolating to "zero loading" (7) of the alkali metals on Fig. 5—8. From these values the hypothetical thermodynamic data were calculated by the similar treatment as for the overall equilibrium constants. The accuracy of these values may be higher than those of the latter. The calculated $(\Delta H^\circ)\overline{X}_M \rightarrow 0$ values indicate that there is no enthalpy change in the reaction when metal ion concentration in the solid phase approaches to zero over the entire range of temperatures. While the $(\Delta S^\circ)\overline{X}_M \rightarrow 0$ increases with increasing ionic radii of alkali metals except for Rb^+.

The Authors are thankful to Prof. W.Rahman, Head, Department of Chemistry, Aligarh Muslim University, Aligarh. One of the authors (B.S.) is thankful to C.S.I.R., New Delhi for financial assistance.

References

1) E. M. Larsen and D. R. Vissers, *J. Phy. Chem.*, **64**, 1732 (1960).
2) I. Gal and A. Ruvarac, *Bull. Boris Kidric Inst. Nucl. Sci.*, **13**, 1 (1962).
3) C. B. Amphlett, P. Baton, L. A. McDonald and A. J. Miller, *J. Inorg. Nucl. Chem.*, **26**, 297 (1964).
4) G. Alberti and U. Costantino, *J. Inorg. Nucl. Chem.*, **36**, 653 (1974).
5) G. H. Nancollas and B. V. K. R. A. Tillak, *J. Inorg. Nucl. Chem.*, **31**, 3643 (1969).
6) M. Abe and K. Sudoh, *J. Inorg. Nucl. Chem.*, **42**, 1051 (1980).
7) M. Abe and K. Sudoh, *J. Inorg. Nucl. Chem.*, **43**, 2537 (1981).
8) J. P. Rawat and P. S. Thind, *J. Indian Chem. Soc.*, **LVII**, 819 (1980).
9) J. P. Rawat and K. P. S. Muktawat, *J. Inorg. Nucl. Chem.*, **43**, 2121 (1981).
10) J. P. Rawat and D. K. Singh, *Anal. Chim. Acta*, **87**, 157 (1976).
11) G. L. Gains and H. C. Thomas, *J. Chem. Phys.*, **21**, 714 (1953).

Extraction and Spectrophotometric Determination of Iron(III) with N^1-Hydroxy-N^1,N^2-diphenylbenzamidine in Presence of Azide

Ghirma Moges, Demirew Assefa, and Bhagwan Singh Chandravanshi*
Department of Chemistry, Addis Ababa University, P.O. Box 1176, Addis Ababa, Ethiopia
(Received April 11, 1983)

N^1-Hydroxy-N^1,N^2-diphenylbenzamidine (HDPBA) reacts with iron(III) in the presence of azide to give a violet-coloured complex insoluble in water. The mixed ligand complex having a composition of 1:2:2 (Fe: HDPBA:N_3^-) is quantitatively extracted into chloroform at pH 2—5. The violet-coloured complex has an absorption maximum at 530 nm with a molar absorptivity of 4900 l mol^{-1} cm^{-1}. On the basis of this sensitive colour reaction, a highly selective method has been developed for the extraction and spectrophotometric determination of microgram quantities of iron(III). The effect of foreign ions and several experimental variables have been studied. The method is simple, rapid, precise, and free from the regid control of experimental parameters.

N^1-Hydroxy-N^1,N^2-diphenylbenzamidine (HDPBA) and its analogues are typical monobasic and bidentate chelating agents for metal ions.[1—18] These reagents have been used for the spectrophotometric determination of iron(III) in ethanol.[19,20] However, the method is neither sensitive nor selective and suffers from the serious interferences due to many common metal ions. Recently N^1-Hydroxy-N^1,N^2-diarylbenzamidines have been reported[21] as reagents for the extraction and spectrophotometric determination of iron(III) in the presence of azide. This method, though quite selective is relatively less sensitive. Beside these, the method requires a large excess of the reagent for the complete extraction of iron(III) and benzene is used as a solvent which is lighter than water, and in which the reagent is relatively less soluble. Hence, in the present investigation, detailed studies have been made for the extraction of iron(III) with HDPBA and azide in different experimental conditions to overcome these problems. These studies have resulted in the development of simple, rapid, sensitive, and highly selective method for the extraction and photometric determination of iron(III).

The present investigation deals with the extraction and spectrophotometric determination of microgram quantities of iron(III) as a mixed ligand complex with HDPBA and azide. The present method is more sensitive and highly selective than the parent HDPBA method[19] and other methods[21] using HDPBA analogues as reagents. The present paper also describes a new extraction-photometric method for the determination of iron(III) as simple chelate complex with HDPBA in chloroform. However this method is not selective and is relatively less sensitive.

Experimental

Apparatus. A Beckman(R) model 24 UV-VIS spectrophotometer equipped with 1-cm quartz cells was used for absorbance measurements. A Beckman CHEM MATE pH meter was used for the measurements of pH. A Pye Unicam model SP 191 atomic absorption spectrophotometer equipped with a hallow cathode lamp and air-acetylene flame was used for the determination of iron in the aqueous phase.

Standard Iron(III) Solution. A stock solution of iron(III) was prepared by dissolving 4.0402 g of hydrated iron(III) nitrate (BDH, Analar) in 100 ml of 1:5 (v/v) nitric acid and diluted to 1 litre with distilled water. This solution was standardized gravimetrically.[22] A working solution of iron(III) was prepared by diluting a suitable aliquot of stock solution with distilled water to give 0.1 mg of iron(III) per millilitre.

A 1 M (M=mol dm^{-3}) solution of azide was prepared by dissolving sodium azide (BDH, AnalaR) in distilled water. All the other chemicals used were of analytical reagent grade.

Reagent Solutions. The reagent, HDPBA, was prepared by the condensation of *N*-phenylbenzimidoyl chloride with *N*-phenylhydroxylamine in diethyl ether medium at low temperature, mp 163 °C; reported[1,19] 163 °C.

A 0.25% (w/v) solution of the reagent in acetone was used for the formation of simple iron(III)–HDPBA complex and its subsequent extraction into chloroform. A 0.1% (w/v) solution of the reagent in chloroform was used for the extraction of mixed ligand complex.

Procedure for Extraction of Iron(III) as Mixed Ligand Complex. Transfer an aliquot of iron(III) solution containing 30—300 μg of the metal in a 50-ml beaker. To this, add 10 ml of 1 M sodium azide solution and adjust the pH to 2—5 with 2 M hydrochloric acid. Transfer the solution into a 100-ml separatory funnel, wash the beaker with few ml of water, and add the washings to the funnel. Adjust the volume of the aqueous phase to 25 ml and add 10 ml of 0.1% (w/v) solution of reagent in chloroform. Shake the mixture for two min and allow the two phases to separate. Collect the organic phase into a 50-ml beaker containing about 2 g of anhydrous sodium sulfate. Wash the aqueous phase twice with 5 ml of chloroform and add the washing to the main extract. Transfer the coloured extract into a 25-ml volumetric flask and dilute to volume with chloroform. Measure the absorbance at 530 nm against chloroform as a reference.

Procedure for Extraction of Iron(III) as Simple Complex. Transfer an aliquot of iron(III) solution containing 0.05—0.40 mg of the metal in a 50-ml beaker. To this, add 5 ml of 0.25% (w/v) solution of the reagent in acetone and dilute the solution to about 20 ml with water. Adjust the pH of the solution to 8—10 using 1 M ammonia or 1 M hydrochloric acid. Transfer the solution into a 100-ml separatory funnel and wash the beaker with few ml of water and then with chloroform and add the washings to the funnel. Adjust the volumes of aqueous and organic phases to 25 and 10 ml respectively and then proceed as for extraction of mixed ligand complex. Measure the absorbance at 520 nm against chloroform as a reference.

Results and Discussion

Absorption Spectra. The absorption spectra of the reagent (HDPBA), iron(III)–HDPBA complex, and

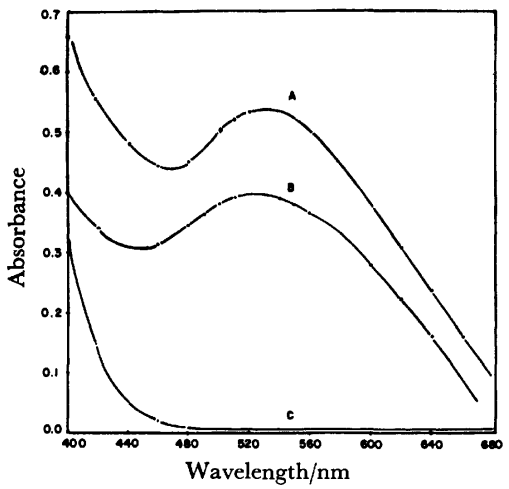

Fig. 1. Absorption spectra of iron(III) complex and reagent.
A: 1.09×10^{-4} M Fe(III) + 1.8×10^{-3} M HDPBA + 0.4 M azide, B: 1.09×10^{-4} M Fe(III) + 1.8×10^{-3} M HDPBA, C: 1.8×10^{-3} M HDPBA in chloroform.

iron(III)–HDPBA–azide complex in chloroform are shown in Fig. 1. The iron(III)–HDPBA–azide complex shows maximum absorption around 530 nm while iron(III)–HDPBA complex shows maximum absorption at 520 nm. Thus, there is a shift in the absorption maximum due to the formation of mixed ligand complex. As the reagent shows negligible absorption in the region of 450—700 nm, the reagent blank can be replaced by chloroform.

Choice of Solvent. Several organic solvents such as benzene, toluene, *o*-xylene, chlorobenzene, *o*-dichlorobenzene, diethyl ether, chloroform, and carbon tetrachloride were found to extract both the simple and the mixed ligand complexes quantitaively. The spectra of both the complexes were found to be similar in all nonpolar organic solvents. However, slight variations in the absorbance values were noticed. Chloroform was found to be the best solvent because the extraction of iron(III)–HDPBA and iron(III)–azide–HDPBA complexes are readily accomplished in it. It was also preferred because of its higher density than water allowing easy separation from the separatory funnel, its low cost, easy to recover and higher solubility of HDPBA in it than in other solvents.

It has also been found that iron(III) as a mixed ligand complex is quantitatively extracted by the chloroform solution of reagent. However, iron(III) as a simple complex can not be quantitatively extracted by the chloroform solution of reagent. Hence, the reagent was introduced in acetone solution to precipitate iron(III) as iron(III)–HDPBA complex and then the complex was quantitatively extracted by chloroform. However, care must be exercised about the amount of acetone in the aqueous phase that it should not exceed more than 50% (v/v). Increasing amount of acetone in the aqueous phase decreases the percent extraction of iron(III) as well as separation of the two phases becomes difficult.

Effect of pH. The optimum pH range for the complete extraction of iron(III)–HDPBA complex was found to be 8—11 while in the presence of azide, the optimum pH range for the complete extraction of iron(III)–HDPBA–azide complex was found to be 2—5. Thus, the pH range for complete extraction of iron(III) has been shifted from basic to the acidic medium due to formation of the mixed ligand complex. It has also been found that there is no formation of mixed ligand complex in the strongly acidic medium as reported by earlier workers.[21]

Effect of Amount of Reagents. A 1:8 molar ratio of iron to HDPBA was found to be adequate for the complete extraction of iron(III)–HDPBA complex while a 1:5 molar ratio of iron to HDPBA was necessary for the complete extraction of azide–iron(III)–HDPBA complex. A large excess of the reagent upto 50-fold had no adverse effect. Thus, the present method has a distinct advantage over the reported method.[21] in which a large excess of reagent (30-fold) is required for the complete extraction.

The optimum concentration range of azide in the aqueous phase for the complete extraction of iron(III) as a mixed ligand complex was found to be 0.25 to 0.50 M. Higher concentration of azide upto 1.0 M did not have any effect on the extraction. It was also found that the extraction of iron(III)–HDPBA–azide complex is dependent on the concentration of azide in the aqueous phase and not simply on the molar ratio of iron(III) to azide as reported in literature.[21]

Effect of Other Variables. Both the simple and mixed ligand complexes were completely extracted into chloroform within 2 min. The chloroform extracts of both the complexes were stable for at least 48 h at 27±2 °C. The volume of the aqueous and organic phases can vary from 1:1 to 5:1 without any adverse effect on the absorbance values or the extraction efficiency of both systems. Variation in temperature of the aqueous phase between 20 and 35 °C did not affect absorbance value of both the systems.

Beer's Law, Optimum Concentration Range, Molar Absorptivity, Sensitivity, and Precision. Beer's law obeys in the concentration ranges 1.8—16 ppm for simple system and 1.2—11.2 ppm of iron(III) for mixed ligand complex system. The optimum concentration ranges for the determination of iron as evaluated from the Ringbom's plot[23] are 3.0—14 ppm and 2.4—10 ppm for simple and mixed ligand complex systems respectively. The molar absorptivities of the Fe(III)–HDPBA and Fe(III)–HDPBA–azide complexes are 3.6×10^{3} and 4.9×10^{3} l mol^{-1} cm^{-1} respectively. The photometric sensitivities[24] of the colour reactions are 0.0155 and 0.0114 μg cm^{-2} of iron(III) for simple and mixed ligand complexes respectively. Thus, the present method is found to be more sensitive than the literature method[21] with similar reagents.

The relative standard deviations for the determination of iron(III) as simple and mixed ligand complexes were found to be ±0.50 and ±0.70% respectively.

Effect of Foreign Ions. The influence of foreign ions was studied by adding known quantities of an ion in question to an aliquot of standard iron(III) solution and determining the iron content according to the procedures described earlier. The tolerence limits of foreign ions (ppm) which causes an error less than

±2% are shown in parentheses.

Mixed Ligand Complex System (pH=3.0, 6 ppm Iron). Chloride, nitrate, sulfate (2000); arsenate, phosphate, borate (400); citrate or tartrate (100); cyanide or thiocyanate (40); ammonium (2000); alkali and alkaline earth metals (1000); Zn^{2+} or Cd^{2+} (800); Cr^{3+} or Mn^{2+} (600); Ti^{4+} or Zr^{4+} (800); Al^{3+} or La^{3+} (400); Ni^{2+} or Co^{2+} (400); Cu^{2+} (200); Hg^{2+} (200); Mo^{6+} (50); U^{6+} (50).

Vanadium(V) interferes with the determination. However, its interference was eliminated by its prior extraction at pH 0.5 and then iron(III) was extracted after raising the pH to 3.0

Simple Complex System (pH=9, 8 ppm Iron). Chloride, nitrate, sulfate (2000); phosphate, arsenate, borate (400); citrate, tartrate (200); alkali and alkaline earth metals (1000); ammonium (1000); Zn^{2+}, Cd^{2+}, Hg^{2+} (200); Al^{3+}, La^{3+} (200); Cr^{3+} (200); Th^{4+} (200); Ti^{4+}, Zr^{4+} (100); W^{6+} (50). Cu^{2+}, Ni^{2+}, Co^{2+}, Mn^{2+}, V^{5+}, Mo^{6+}, and U^{6+} interfere with the determination of iron(III) with HDPBA and the method is not selective.

Thus, there is a great improvement in the selectivity of the method for the determination of iron(III) with HDPBA due to formation of mixed ligand complex in the presence of azide. Furthermore, the sensitivity of the method is also increased considerably.

Composition of Complexes. The composition of both complexes were determined by different methods.[25] The ratio of iron(III) to HDPBA in Fe(III) HDPBA complex was determined by continuous variations[26] and mole ratio[27] methods. The result obtained by both methods indicates the formation of 1:3 (Fe:HDPBA) complex. The ratio of iron(III) to HDPBA in the mixed ligand complex was also determined by continuous variations and mole ratio methods. The concentration of azide was kept constant excess for these experiments. To determine the ratio of iron(III) to azide, the concentration of iron(III) was kept constant and HDPBA was taken in constant excess, and then the concentration of azide was varied. Iron(III) was extracted as a mixed ligand complex into chloroform and determined according to the procedure described earlier. The remaining iron(III) in the aqueous phase was determined by atomic absorption spectroscopy and the distribution ratio, D, of iron(III) was calculated at different concentrations of azide in the aqueous phase. Log D was plotted aqainst log $[N_3^-]$. The slope of the curve gave the number of azide ions in the ternary complex. These results indicated the formation of 1:2:2 (Fe:HDPBA:N_3^-) mixed ligand complex. It may be suggested from the composition and extractability as a neutral complex into chloroform that only one HDPBA molecule is deprotonated in the complex formation. However, the structure of the mixed Ligand complex has not been confirmed.

It can be noted that the earlier workers[21] have reported the composition of the mixed ligand complex as 1:1:2 (Fe:HDPBA:N_3^-). In contrast to that, it has been found to be 1:2:2 (Fe:HDPBA:N_3^-) in the present investigation.

The authors are thankful to the Department of Chemistry, Addis Ababa University, Addis Ababa, Ethiopia for providing research facilities. They are also grateful to the Swedish Agency for Research Cooperation with Developing Countries for the financial assistance.

References

1) K. Satyanarayana and R. K. Mishra, *Anal. Chem.*, **46**, 1609 (1974).
2) K. Satyanarayana and R. K. Mishra, *Indian J. Chem.*, **13**, 295 (1975).
3) K. Satyanarayana and R. K. Mishra, *J. Indian Chem. Soc.*, **53**, 928 (1976).
4) K. S. Patel and R. K. Mishra, *J. Indian Chem. Soc.*, **55**, 462 and 773 (1978).
5) R. S. Kharsan, K. S. Patel, and R. K. Mishra, *Mikrochim. Acta*, **I**, 353 (1979).
6) R. S. Kharsan, K. S. Patel, and R. K. Mishra, *Z. Anal. Chem.*, **297**, 159 (1979); **295**, 415 (1979).
7) K. S. Patel, K. K. Deb, and R. K. Mishra, *Ann. Chim. (Rome)*, **68**, 803 (1978).
8) K. S. Patel, K. K. Deb, and R. K. Mishra, *Sep. Sci. Technol.*, **14**, 333 and 815 (1979).
9) R. S. Kharsan, K. S. Patel, and R. K. Mishra, *J. Less Comm. Metals*, **64**, 155 (1979).
10) K. S. Patel and R. K. Mishra, *Bull. Chem. Soc. Jpn.*, **52**, 592 (1979).
11) R. S. Kharsan, K. S. Patel, and R. K. Mishra, *Talanta*, **26**, 50 and 254 (1979).
12) K. S. Patel, K. K. Deb, and R. K. Mishra, *J. Chinese Chem. Soc.*, **26**, 79 (1979).
13) R. S. Kharsan and R. K. Mishra, *Bull. Chem. Soc. Jpn.*, **53**, 1736 (1980).
14) R. S. Kharsan, K. S. Patel, and R. K. Mishra, *Indian J. Chem.*, **19A**, 499 (1980).
15) R. S. Kharsan, K. S. Patel, R. K. Mishra, and L. R. Malewar, *Proc. Indian Acad. Sci.*, **89**, 411 (1980).
16) K. S. Patel, R. S. Kharsan, and R. K. Mishra, *Proc. Indian Acad. Sci.*, **88 A**, 297 (1979).
17) H. Mohabey and R. K. Mishra, *J. Indian Chem. Soc.*, **57**, 562 (1980).
18) K. S. Patel, R. M. Verma, and R. K. Mishra, *Anal. Chem.*, **54**, 52 (1982).
19) K. Satyanarayana and R. K. Mishra, *J. Indian Chem. Soc.*, **53**, 63 (1976).
20) K. K. Deb and R. K. Mishra, *Curr. Sci.*, **45**, 134 (1976).
21) K. S. Patel, K. K. Deb, and R. K. Mishra, *Bull. Chem. Soc. Jpn.*, **52**, 595 (1979).
22) A. I. Vogel, "A Text Book of Quantitative Inorganic Analysis," Longmans, London (1978), p. 466.
23) A. Ringbom, *Z. Anal. Chem.*, **115**, 332 (1938).
24) E. B. Sandell, "Colorimetric Determination of Traces of Metals," Interscience, New York (1959), p. 83.
25) J. Inczedy, "Analytical Applications of Complex Equilibria," Ellis Horwood, Sussex (1976).
26) P. Job, *Ann. Chim. (Paris)*, **9**, 113 (1928).
27) J. H. Yoe and A. L. Jones, *Ind. Eng. Chem., Anal. Ed.*, **16**, 111 (1944).

© 1984 The Chemical Society of Japan

NOTES

Bull. Chem. Soc. Jpn., 57, 869—870 (1984)

Silent Electric Discharge in the Equimolar Dihydrogen-Carbon Monoxide Mixture

Sintaro HATA, Koji HIRAMOTO, Katsuaki KATOH and Kazuo SASAKI*

Department of Applied Chemistry, Faculty of Engineering, Hiroshima University, Saijo-cho, Higashi-Hiroshima 724

(Received April 11, 1983)

Synopsis. The purpose of this paper is focused on seeking the possibility of utilizing electric discharge in H_2–CO mixtures as a mean of industrial processes. Along this line, the silent discharge in the equimolar mixture of CO and H_2 has been studied as a function of both the flow rate of reacting gas mixture and the length of the discharge tube. The yield of formaldehyde, the main product, increased with increasing flow rate of gas. At a given flow rate, however, the yield increased with increasing tube length indicating that the selectivity of formaldehyde can be increased steadily by increasing the rate of gas flow. The best value of the formaldehyde selectivity was 34% at the shortest residence time (0.25 s). Improvement of this value seems to be promising.

Although recent development of plasma chemistry[1,2] is attracting a growing attention in several special fields, the application of it for the mass production industry seems very limited. However, it is also a fact that the glow discharge has been utilized in ozone production and also in acetylene industry.[3] This shows that there still remain possibilities of utilizing the discharge reaction in some organic raw material industries. We thus attempted to study the reaction occuring in an equimolar mixture of H_2 and CO. There are several papers[4–7] which deal with the same gas system with use of various modes of discharge. Among these, Blaustein and Fu[6] showed that in a microwave discharge in static gas (H_2/CO=5) gave conversion of CO to CH_4 an C_2H_2 of approximately 17 and 22%. No yield of HCHO was reported. Quite recently, the system has been studied by Bauer[7] using several modes of glow discharge (dc, pulsed dc and rf). Reaction products seem a complex mixture and only a few compounds were analyzed quantitatively.

Experimental

An equimolar mixture of H_2–CO was used as the reactant. A 135 VA transformer provided high voltage upto 15 kV. Four discharge tubes having the same dimensions of tube diameters (o.d.=12, i.d.=10 mm) but different in tube length (2, 6, 12, and 24 cm) were used. The reactor circuit was composed of a small diaphragm pump, a rotameter and two-stage gas trap which were placed in series with the discharge tube. A gas burette, which served as the gas reservoir, was connected to the gas circuit. Of the two gas traps, one contained 150 ml of water to trap water soluble products and the other was cooled by Dry Ice–methanol mixture. Total volume of the gas circuit except the gas burette was *ca.* 840 ml. Discharge voltage was fixed at 12 kV throughout the experiments.

The product analyses were carried out separately for the gaseous products and the liquid products. Formaldehyde which was trapped in water was analyzed spectrophotometrically with use of acetylacetone and ammonium acetate. Sampling was made periodically in every 2 h. For the gaseous products, 1 ml of gas was taken with an injection syringe while for formaldehyde 10 ml of trap water was withdrawn for each time. After each time of sampling, 10 ml of fresh water was supplied to the water trap to keep the amount of trapping water constant (150 ml).

Results and Discussion

Experiments were conducted by circulating the reacting gas mixture. The gas flowing out of the discharge tube was first led to the water trap to remove the water soluble products and then to the cold trap to condense components of high boiling point. Actually, however, no detectable amount of condensate was obtained in the cold trap other than water which came from the water trap. A small amount of oily material accumulated gradually on the surface of the discharge tube.

Result of gas phase analysis is listed in Table 1. It is seen that CH_4, CO_2, and C_2H_6 are the major products in the gas phase. It is a marked contrast that no acetylene was detected in our system, while it is dominant in the discharge reaction in low pressure gases.[6,7]

The amount of HCHO trapped in water was analyzed separately. No effort was made for methanol and other alcohols which might be existed in the water trap.

General features of HCHO production can be summarized as follows.

1. In every measurement, regardless of both the tube length and flow rate, the accumulation of HCHO in water trap exhibits a downward convex curve against the reaction time, *i.e.*, the rate is rather dull at the initial stage of reaction but becomes increasingly fast with the elongation of the reaction time. This is a marked contrast to the accumulation of CH_4 in gas phase, where the amount of CH_4 increases almost linearly with the increase of reaction time.

TABLE 1. COMPOSITION OF GAS PHASE PRODUCTS

Compound	Concn/mol%
H_2	49.706
CO	39.551
Air	2.386
CO_2	3.580
CH_4	4.676
C_2H_4	0.094
C_2H_8	0.006
C_4	Trace
C_5	Trace

Tube length: 6 cm. Flow rate: 42 ml min^{-1} Discharge time: 12 h.

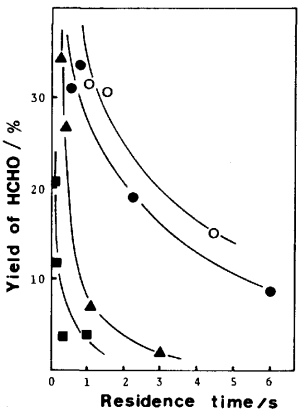

Fig. 1. Percentage yield (selectivity) of formaldehyde after 12 h of reaction as a function of the residence time. Discharge voltage: 12 kV. Curve parameter is the length of tube. ○: 24 cm, ●: 12 cm, ▲: 6 cm, ■: 2 cm.

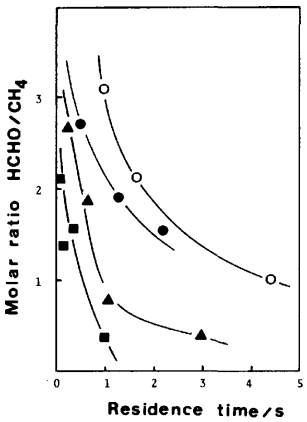

Fig. 2. Molar ratio of formaldehyde to methane against the residence time. Symbols are same as in Fig. 1.

2. The yield of HCHO increases with the increasing flow rate when the tube length is fixed. This effect is, however, only significant at the lower flow rate (*ca.* 300 ml min^{-1}) and becomes insignificant at higher rates. The effect of flow rate on the CH_4 formation seems, on the other hand, to be opposite and the lower flow rate seems to favour the production of CH_4.

3. When the flow rate is fixed, the HCHO yield increases almost linearly with increasing tube length. This applies also to the formation of CH_4.

The downward convex shape observed in the accumulation curve of HCHO seems to suggest that some sort of intermediate(s) is converted gradually to HCHO to enhance the reaction rate. On the other hand, the accumulation of CH_4, being the most dominant gaseous product, increases almost linearly with the reaction time. It is thus more likely that the accumulation of some compounds, which is rather inert against the discharge reaction than H_2 or CO themselves, will act as the energy carrier (sensitizer) as rare gas atoms do. Methane may be a candidate if this is the case.

The percentage yield of HCHO after 12 h. of the discharge reaction is plotted in Fig. 1 against the residence time (τ) of flowing gas molecule in the discharge tube. In this figure, values of percentage yield were calculated on the base of total gas volume decreased and no correction was applied for the volume occupied by gaseous products. Similarly, the molar ratio of $HCHO/CH_4$ in the reaction products is shown in Fig. 2. In these figures, lines were drawn to connect points of the same tube length. Figure 1 indicates clearly that the shorter the residence time the better the yield of HCHO, and that the increase in the tube length favours the formation of HCHO.

As has been described above, the effect of flow rate on the yield of HCHO is insensitive at higher flow rate. This indicates, at least apparently, that the use of an execessive flow rate is meaningless for increasing the yield of HCHO. However, the increase in flow rate results in the diminution of CH_4 yield reflecting upon the steep rise of the selectivity of HCHO as is seen in Figs. 1 and 2.

The rather contradicting findings with respect to the tube length and the residence time tell us that, at a given tube length, the decrease in the residence time improves the product selectivity. Note that the integrated residence time ($N\tau$, N being the number of circulation over the whole reaction time) is unchanged by the change of flow rate when the tube length is fixed. It should be also noted that, when a comparison is made at a fixed residence time, the integrated residence time increases with increasing tube length. This must increase the product yield.

Concluding Remarks

Results obtained can be summarized as follows. The main product of silent discharge reaction occuring in equimolar H_2–CO mixture at atmospheric pressure is formaldehyde, which has never been noticed in the recent works using glow discharge[7] and microwave discharge[6] conducted in low pressure gas mixtures. Although methane is found to be the second dominant product in agreement with these authors, it is contrasting that no acetylene is detectable in our experiment.

Experiments has been conducted (along the line) to increase the selective formation of formaldehyde over many by-products particularly methane. (In order to accomplish this purpose.) It was found essential to shorten the one pass-residence time. For instance, with a Siemens tube of 6 cm length the selectivity of formaldehyde increased steeply from 2.0 to 34.3% by decreasing residence time from 3.0 to 0.25 s, respectively. Corresponding to these figures, molar ratio $HCHO/CH_4$ increased from 0.22 to 2.6.

The linear velocity of flowing gas which employed in the present experiments was in the order of 24 cm s^{-1} at the highest. A hundred times greater velocity can easily be attained. If the length of discharge tube could be elongated to such a degree without purturbing the reaction conditions employed here, a very high selectivity of HCHO production is expected.

The authors are indeed grateful to the reviewer who kindly gave us notice of Bauer's work.[7]

This work has been supported by a grant supplied by Iwatani Naoji Memorial Foundation to which our thanks are due.

References

1) J. R. Hollahon and A. T. Bell, "Techniques and Applications of Plasma Chem.," John Wiley & Sons, (1976).

2) B. D. Blaustein and F. C. Fu, "Organic Reactions in Electrical Discharges," in "Phys. Methods of Chem.," ed by A. Weissberger and B. W. Rossiter, John Wiley & Sons, New York (1972), Vol. 1, Part IIB, P. 91.

3) K. Weissermel and H. J. Arpe, "Industrielle Organische Chemie," Verlag Chem., Weinheim (1976).

4) S. C. Lind and D. C. Bardwell, *J. Am. Chem. Soc.*, **47**, 2675 (1925).

5) A. Caress and E. K. Rideal, *Proc. R. Soc. London, Ser. A.* **120**, 370 (1928).

6) B. D. Blaustein and F. C. Fu, *Adv. Chem. Ser.*, **80**, 259 (1969).

7) G. H. Bauer, R. R. Maly, H. -R. Weiss and W. H. Bloss, Proc. Int. Ion Eng. Congr. Kyoto 1983, p. 1897.

XPS Studies of the Platinum Species Photodeposited on Titania from Aqueous Chloroplatinic Acid

Choi Sungbom,† Maki Kawai,†† and Kazunori Tanaka*
The Institute of Physical and Chemical Research (Riken), Wako, Saitama 351
(Received July 1, 1983)

Synopsis. Several Pt/TiO_2 catalysts were prepared by photodeposition from aqueous H_2PtCl_6 in the presence or absence of a CH_3COOH-CH_3COONa buffer. The examination of these catalysts by X-ray photoelectron spectroscopy (XPS) revealed that the higher the buffer concentration, the more highly reduced the deposited platinum became.

Platinum-loaded titania (Pt/TiO_2) is known as the most active catalyst in a number of photocatalytic processes. As a means of platinum loading, the photodeposition method of Kraeutler and Bard[1] has been widely used. In this method, the platinizing solution contains acetate, which is considered to act as the reducing agent. Although these authors claimed that the platinum deposit is really metallic, Koudelka *et al.*[2] found no perceptible quantities of metallic platinum on their Pt/TiO_2 samples, which had been prepared by a similar method. Lehn *et al.*,[3] on the other hand, photodeposited platinum from aqueous K_2PtCl_4 on $SrTiO_3$ without adding any organic material.

It thus seemed expedient to prepare a series of Pt/TiO_2 catalysts from aqueous H_2PtCl_6 solutions containing different concentrations of a CH_3COOH-CH_3COONa (AH-ANa) buffer and to examine the oxidation state of the platinum deposit. It would also be interesting to see how the platinum oxidation state of these catalysts varies after their use in typical photosynthetic or photocatalytic reactions. Methanol decomposition and benzene oxidation have been chosen for this purpose.

Experimental

Apparatus. The platinum oxidation state of Pt/TiO_2 catalysts was examined by means of a Hewlett-Packard 5950A X-ray photoelectron spectrometer with monochromatized Al $K\alpha$ X-rays (1486.6 eV). Spectra were recorded at 250 K with a flood gun. The binding energies E_b are referred to the $4f_{7/2}$ peak (84.0 eV) of the Au evaporated onto the sample.

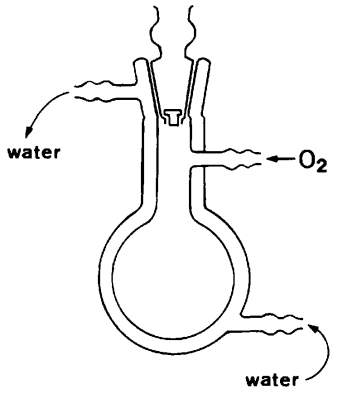

Fig. 1. Reaction vessel II (Water-mantled Pyrex-made).

The lamp-housing quartz reaction vessel (I) used for the platinum photodeposition and methanol decomposition has been described previously.[4] The water-mantled Pyrex reaction vessel (II) used for benzene oxidation is illustrated in Fig. 1. It has a capacity of *ca.* 50 cm^3. The reaction products of the benzene oxidation were analyzed by means of gas chromatography using a 2 m×3 mm i.d. column of 30% PEG 20M on 30—60 mesh chromosorb WAW.

Materials. The rutile-free anatase, with a BET surface area of 11.5 m^2/g, was taken from the same bottle as had been used previously.[4] All the chemicals except for Adams platinum were commercially available and were used as received. The Adams platinum, whose main constituent had been verified to be α-PtO_2 by X-ray powder diffraction, was generously supplied by Professor Takagi of Nihon University.

Catalyst Preparation. The procedure for preparing Pt/TiO_2 catalysts (2.5 wt% Pt) has been presented before.[4] In brief, they were prepared by the photodeposition of platinum on TiO_2 from aqueous TiO_2 suspensions containing H_2PtCl_6 and an AH-ANa buffer (pH 4.07). The buffer concentration was varied from catalyst to catalyst, while the H_2PtCl_6 concentration was fixed so as to give 2.5 wt% of Pt for all catalysts.

Kinetic Procedure. The methanol decomposition was run in reaction vessel I. It was charged with the Pt/TiO_2 catalyst (50 mg), methanol (100 cm^3), and distilled water (100 cm^3). After 30-min N_2 bubbling with magnetic stirring, this reaction mixture was irradiated with a 100-W high-pressure Hg lamp for 1 h at 40 °C, with continued magnetic stirring.

The benzene oxidation was run in reaction vessel II. It was charged with water (10 cm^3), benzene (1 cm^3), and the Pt/TiO_2 catalyst (50 mg), set on a shaker, and connected to an atmospheric O_2 bulb. The reaction mixture was irradiated at 20 °C for 3 h with vigorous shaking with a 500-W Xe lamp, using two filters, UV-33 and IRA-25S, in series. After the reaction, acetic acid (15 cm^3) was added to make the reaction mixture homogeneous, and aliquots were analyzed for phenol.

Results

Oxidation State of the Photodeposited Pt. All of the catalyst samples prepared were examined by means of XPS. The XPS spectra are shown in Fig. 2A. The molar ratios (AH+ANa)/H_2PtCl_6 pertaining to each catalyst preparation are given in Table 1. A comparison of the XPS spectra with these molar ratios reveals that the lower the ratio, the more oxidized state the deposited platinum remains in.

Figure 2B shows the Pt 4f spectra taken with a Pt plate and PtO_2 powders, together with the standard E_b values ($4f_{5/2}$ and $4f_{7/2}$) for Pt^0 and Pt^{IV} determined from these spectra. The corresponding values for Pt^{II} obtained with PtO are 76.6 and 73.4 eV, according to Kim *et al.*[5] Turning back to Fig. 2A, we see that the triplet character (peaks at 73.5, 76.0, and 78.8 eV) of Sample 5 prepared from a buffer-free suspension is

† On leave from Jilin University, Changchun, People's Republic of China.

†† Present address: Government Industrial Research Institute, Osaka; Ikeda, Osaka 563.

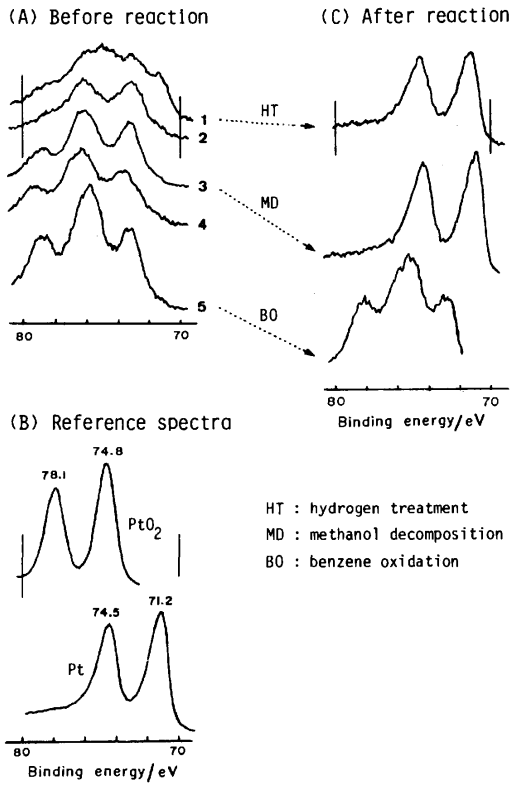

Fig. 2. XPS spectra in the Pt 4f region of Pt/TiO_2 catalysts.

TABLE 1. THE EFFECTS OF THE ACETATE BUFFER-TO-Pt COMPLEX RATIO IN Pt/TiO_2-CATALYST PREPARATION

Sample	$\frac{AH+ANa^{a)}}{H_2PtCl_6}$	MOS[b]	$X^{c)}$ / %
1	30.4	0+II	
1-HT[d]		0	0.69
2	10.1	II	0.17
3	6.1	II+IV	
4	2.0	II+IV	
5	0	II+IV	0.10

a) The molar ratio of acetic acid (AH) plus sodium acetate (ANa) to hexachloroplatinic acid (H_2PtCl_6). AH/ANa=4.56, giving rise to a pH of 4.07. b) The main oxidation states of the deposited platinum, judged from the XPS spectra of Fig. 2. c) Percentage conversion of benzene to phenol. d) Hydrogen-treated sample 1 (*cf.* Fig. 2).

attributable to the partial overlap of the two doublets of the Pt^{II} and Pt^{IV} species; the Pt^{II} $4f_{5/2}$ and Pt^{IV} $4f_{7/2}$ components are superimposed on each other. Upon the addition of an acetate buffer (Sample 3 or 4), the left-wing peak of the triplet became smaller, while the right one was intensified, suggesting the enrichment of the Pt^{II} components. Upon going to a higher buffer concentration (Sample 2), only the Pt^{II} species became predominant. A still further increase in the buffer concentration (Sample 1) resulted in an ill-defined spectrum, which, however, suggests the appearance of Pt^0. The main platinum oxidation states thus estimated from Fig. 2A for each catalyst are listed in Table 1.

The Cl/Pt molar ratio of the photodeposited species was less than 0.7, judging from the area under the Cl 2s peak. This is a much smaller amount of chlorides than would be expected from the $PtCl_6^{2-}$ or $PtCl_4^{2-}$ adsorption; it is in qualitative agreement with the results of Koudelka *et al.*[2], who found a Cl/Pt ratio<1.

Photodeposition Process. From the above results, it may be concluded that the photodeposition from aqueous H_2PtCl_6 on TiO_2 does not yield Pt^0 unless acetate is present in a large excess relative to the platinum complex. Even in a large excess of it, the deposited platinum species tend to remain partially in oxidative states, Pt^{II} and Pt^{IV}. In view of the above-mentioned dearth of chloride, these oxidative species must exist as oxides, hydroxides, or chloride oxides rather than as the tetra- or hexachloroplatinate.

On the basis of these findings, one may speculate that these steps occur in photodeposition: (i) the adsorption of $PtCl_6^{2-}$ and $PtCl_4^{2-}$ ions, (ii) the rapid conversion of these chlorides to the oxides or hydroxides, and (iii) their photo-assisted reduction to Pt^0. The mechanism of each step is not yet clear, however.

Pt Oxidation State after Reactions. Figure 2C shows how the Pt 4f spectra of the Pt/TiO_2 catalysts vary after their use or after hydrogen treatment. A comparison of Fig. 2A with Fig. 2C (Samples 1 and 3) reveals that the oxidized platinum is easily reduced to Pt^0 by either mild hydrogen treatment (1 atm, 1.5 h, 20 °C in water) or subjection to methanol decomposition. The reduction due to methanol decomposition seems reasonable in view of the expected occurrence of hydrogen recombination on the platinum surface:

$$2H^+ + 2e^- \rightarrow H_2. \quad (1)$$

In contrast, the subjection of Catalyst 5 to benzene oxidation did not cause any appreciable change in the XPS spectrum. This intactness might result from a subtle balance between the reductive trend due to the H_2 produced by Reaction 1 and the oxidative trend due to the O_2 or H_2O_2 involved in this reaction:

$$O_2 + 2e^- + 2H^+ \rightarrow H_2O_2. \quad (2)$$

The last column of Table 1 compares the catalytic activities of three different catalyst samples for benzene oxidation. The H_2-treated sample (1-HT) bearing only Pt^0 is prominent, exhibiting an activity which is several times that of the other two. This rather unexpected effect of Pt^0 remains to be elucidated.

We wish to thank Dr. Shousuke Teratani of Riken and Dr. Yuzuru Takagi of Nihon University for their valuable suggestions. It is also a pleasure to acknowledge numerous discussions on the XPS data with Dr. Masayuki Uda of Riken. This work was supported by a grant from the Science and Technology Agency towards the Solar Energy Research Project.

References

1) B. Kraeutler and A. J. Bard, *J. Am. Chem. Soc.*, **100**, 4317 (1978).

2) M. Koudelka, J. Sanchez, and J. Augustynski, *J. Phys. Chem.*, **86**, 4277 (1982).

3) J. -M. Lehn, J. -P. Sauvage, and R. Ziessel, *Nouv. J. Chim.*, **4**, 623 (1980).

4) S. Teratani, J. Nakamichi, K. Taya, and K. Tanaka, *Bull. Chem. Soc. Jpn.*, **55**, 1688 (1982).

5) K. S. Kim, N. Winograd, and R. E. Davis, *J. Am. Chem. Soc.*, **93**, 6296 (1971).

Effect of Urea on Hydrophobic Side Chain Interactions in Polypeptides at the Air-Water Interface

Akira SHIBATA,* Shinsuke YAMASHITA, and Takuya YAMASHITA
Faculty of Pharmaceutical Sciencs, Tokushima University, Shomachi, Tokushima 770
(Received October 6, 1983)

Synopsis The surface activity of urea at the polypeptide monolayer-water interface was investigated by the surface pressure analysis. The expansion of the monolayer is attributed to the penetration of polypeptide monolayer by urea in the subsolution. The hydrophobic side chain interactions in polypeptides are weakened by the action of urea. The surface activity of urea depends on the difference in the chemical composition and the geometrical arrangement of side chains between benzyloxycarbonyl derivatives of basic poly(α-amino acid) and benzyl esters of acidic poly(α-amino acid).

In view of the intense current interest concerning the mode of action of denaturants on biological macromolecules, it seems desirable to advance our understanding of this phenomenon by appropriate experimental studies. Considerable evidence exists from model compound studies to the effect that urea (1) interacts strongly with peptide backbone groups, thus weakening interpeptide hydrogen bonds,[1,2] and (2) enhances the solubility of nonpolar groups, thus reducing hydrophobic interactions.[3] It is difficult to assess the relative significance of such effects in studies with natural biopolymers. Thus far synthetic polypeptides as protein analogs have been provided useful informations concerning protein structure and function.

The purpose of this work is to clarify the effect of urea on the hydrophobic side chain interactions in synthetic polypeptides at the air-water interface.

Experimental

Synthetic polypeptides used here were poly(N^{δ}-benzyloxycarbonyl-L-ornithine) (PLO(Z)), poly(N^{ε}-benzyloxycarbonyl-L-lysine) (PLL(Z)), poly(β-benzyl L-aspartate) (PBLA), and poly(γ-benzyl L-glutamate) (PBLG). The samples and spreading solvents were the same as those used in the preceding work.[4] Urea solutions were treated with activated charcoal in order to remove surface active contaminants. A 10 to 1 compression of the surface of the urea subsolutions, after being left to stand for 20 min, produced less than 0.1 mN m^{-1} film pressure. The surface pressure was measured by the Wilhelmy method at 25±0.5 °C. The films were compressed at a rate of 0.01 nm^2 residue^{-1} min^{-1}.

Results and Discussion

Figure 1 shows the π-A curves for PLO(Z) spread on distilled water, and on 1.0, 2.0, 3.0, and 4.0 M (1 M=1 mol dm^{-3}) urea subsolutions. Plateaux are seen in the curves. The plateau which is characteristic of a number of synthetic polypeptide monolayers is associated with the collapse or transition of the monolayer in the α-helical conformation from a two-dimensional oriented state to a three-dimensional disoriented state.[4,5] The surface tension of water increases with an increase in urea concentration.[6] This is due to the desorption of urea from the subsolution surface. Increasing the concentration of urea in the subsolution progressively expanded the condensed regions of PLO(Z) monolayer (Fig. 1). By measuring the change in surface pressure ($\Delta\pi$) due to the change in mole fraction of urea(Δx) in subsolution, the surface concentration of urea was calculated from:[6,7]

$$(1/RT)(\Delta\pi)/(\Delta x)\,|_A = \Gamma_2/x - \Gamma_1/(x-1) = I/x(1-x), \quad (1)$$

where x is the mole fraction of urea, R is 8.3×10^7 ergs per mole, T is the absolute temperature, Γ_1 is the surface concentration of water, Γ_2 is the surface concentration of urea, A is the area per residue of PLO(Z). I is defined by the expression

$$I = (1-x)\Gamma_2 - x\Gamma_1. \quad (2)$$

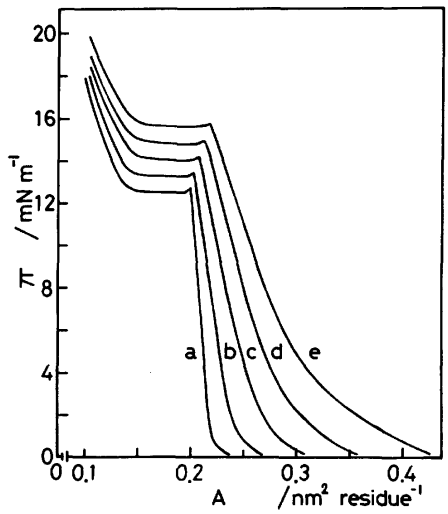

Fig. 1. Surface pressure-area curves for PLO(Z) monolayers on urea subsolutions.
a; Distilled water, b; 1.0 M urea, c; 2.0 M urea, d; 3.0 M urea, e; 4.0 M urea.

TABLE 1. SURFACE CONCENTRATION OF UREA AT FIXED AREA FOR PLO(Z)

Area of PLO(Z) / nm^2 residue^{-1}	x	$I\times10^{10}$ / mol cm^{-2}
0.23	0.018	1.37
0.23	0.035	2.85
0.23	0.051	3.85
0.23	0.067	4.81
0.25	0.035	2.85
0.25	0.051	3.73
0.25	0.067	4.97
0.27	0.051	3.60
0.27	0.067	4.89

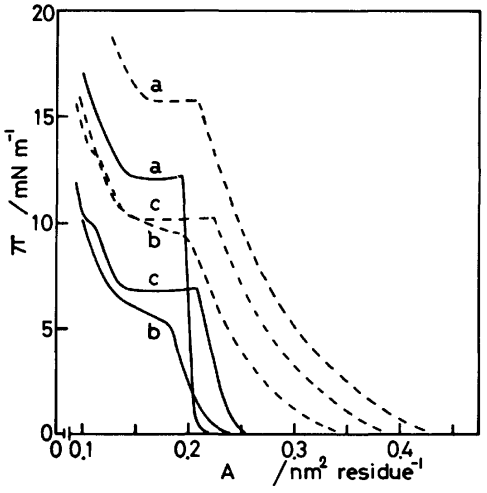

Fig. 2. Surface pressure-area curves for PBLA(a), PBLG(b), and PLL(Z)(c) monolayers on distilled water(——) and 4.0 M urea subsolution(----).

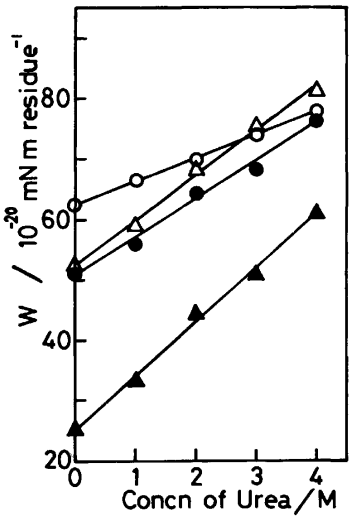

Fig. 3. Work of collapse for PLO(Z)(○), PLL(Z)(●), PBLA(△), and PBLG(▲) monolayers as a function of urea mole fraction.

At the mole fractions of urea used here ($x \leq 0.067$) I is approximately the surface concentration of urea. The results are given in Table 1. When we take the order of magnitude of the effective thickness of the interfacial region to be 10^{-7} cm, for 1, 2, 3, and 4 M bulk concentrations, the concentration of urea in a bulk volume 1 cm×1 cm×10^{-7} cm would be 1×10^{-10}, 2×10^{-10}, 3×10^{-10}, and 4×10^{-10} ml/l, respectively. Therefore, the results indicate that the surface concentration of urea required to provide energy for the observed expansions of the PLO(Z) monolayers is of the same order of magnitude as the bulk concentration of urea (Table 1). There was no surface excess concentration of urea. The film expansion with increase in the concentration of urea can be attributed to the penetration of PLO(Z) monolayer by urea in the subsolution.

Figure 2 shows the π-A curves for PBLA, PBLG, and PLL(Z) spread on distilled water and 4.0 M urea subsolution. The presence of urea brings about the film expansion and the increase in transition pressure for all polymers. The transition pressures were 12.5 mN m^{-1} for PLO(Z), 6.5 mN m^{-1} for PLL(Z), 12.1 mN m^{-1} for PBLA, and 5.3 mN m^{-1} for PBLG, respectively. The addition of one $-CH_2-$ group to the β-C is the direct cause of the lowering of the plateau by 6—7 mN m^{-1}. The lowering of the plateau may arise from the reduction of the adhesion of the polymer to the subsolution by direct hydrophobic interaction with the water, because the methylene side group is close to the backbone.[8]

The work required for collapse of monolayers provides an information concerning the effect of urea on the hydrophobic side chain interactions in polypeptides. The work required for collapse of monolayer, W, is given by

$$W = \pi_{tr} \cdot \Delta A, \tag{3}$$

where π_{tr} is the transition pressure, and ΔA is the difference between initial and final areas of collapse. Figure 3 shows the work of collapse for the monolayers of PLO(Z), PLL(Z), PBLA, and PBLG as a function of urea concentration. The work of collapse for these polymers increases linearly with an increase in concentration of urea, C. The values of dW/dC($\times10^{-20}$ mN m residue^{-1} M^{-1}) were 3.9 for PLO(Z) 6.0 for PLL(Z), 7.6 for PBLA, and 9.0 for PBLG respectively. The addition of one $-CH_2-$ group to the β-C increases the value of dW/dC. This suggests that the hydrophobic side chain interactions in polypeptides are weakened by the action of urea. The obtained values are also larger for benzyl esters of acidic poly(α-amino acid) than for benzyloxycarbonyl derivatives of basic poly(α-amino acid). The surface activity of urea depends on the difference in the chemical composition and geometrical arrangement of side chains between the benzyl esters of acidic poly(α-amino acid) and the benzyloxycarbonyl derivatives of basic poly(α-amino acid).

References

1) Y. Nozaki and C. Tanford, *J. Biol. Chem.*, **238**, 4074 (1963).
2) D. R. Robinson and W. P. Jencks, *J. Am. Chem. Soc.*, **87**, 2462 (1965).
3) D. B. Wetlaufer, S. K. Malik, L. Stoller, and R. L. Coffin, *J. Am. Chem. Soc.*, **86**, 508 (1964).
4) T. Yamashita, A. Shibata, and S. Yamashita, *Bull. Chem. Soc. Jpn.*, **51**, 2751 (1978).
5) B. R. Malcolm, *Prog. Surf. Membr. Sci.*, **7**, 183 (1973).
6) D. F. Sears, *J. Colloid Interface Sci.*, **29**, 288 (1969).
7) E. A. Guggenheim, "Thermodynamics," North-Holland, Amsterdam (1957).
8) B. R. Malcolm, *Biopolymers*, **9**, 911 (1970).

Studies on Lanthanoids-Antimony-Chalcogenides. III. Synthesis and Crystal Data of Nd_3SbS_6, $Ce_6Sb_8S_{21}$, and $Ce_3Sb_3S_{10}$

Jin-zhang GAO,† Izumi NAKAI, and Kozo NAGASHIMA*
Department of Chemistry, The University of Tsukuba, Sakura-mura, Ibaraki 305
(Received August 19, 1983)

Synopsis. Single crystals of three new sulfides were prepared in evacuated silica tubes heated in the temperature range 890—1200 °C. Nd_3SbS_6 is a red transparent crystal. Is is tetragonal, space group $I4_1/acd$ with lattice parameters a=15.54(1) and c=19.52(2) Å. $Ce_6Sb_8S_{21}$ and $Ce_3Sb_3S_{10}$ are isostructural with $La_6Sb_8S_{21}$, and $La_3Sb_3S_{10}$, respectively.

Lanthanoid sulfides have been the subject of intensive investigation for their interesting physical properties such as super-conducting property.[2] However, most of these investigations involved binary sulfides of lanthanoid. There has been little effort to prepare ternary sulfides containing antimony.[3,4] We have started this study to clarify the crystal chemistry of the ternary sulfides.

Recently, we studied a La–Sb–S system and obtained the three new compounds, $LaSbO_2S_2$, $La_6Sb_8S_{21}$, and $La_3Sb_3S_{10}$.[5] In the present work, we have extended our experiment to Ce–Sb–S and Nd–Sb–S systems, and found three more new compounds. This paper reports the synthetic conditions and crystal data of these compounds.

Experimental

The syntheses were made by applying the double silica tube method described in the previous paper.[5] The starting materials were cerium and neodymium metal chips (99.9%), sulfur powder (99.99%), and antimony trisulfide (99.99%). They were mixed in various molar ratios, sealed into an evacuated silica tube, and heated in an electric furnace. Temperature and heating period were decided by a trial and error method.

Reaction products were examined by X-ray powder diffraction patterns using a 114.6 mm Gandolfi camera with Ni-filtered Cu $K\alpha$ radiation. X-Ray single crystal measurements were performed on precession and Weissenberg cameras. The least-squares computer program of Appleman and Evans[6] was used to calculate the lattice parameters. Some of the products were chemically analyzed with an electron microprobe analyzer using an operating voltage of 20 kV, and a probe current of 0.02 μA. The standards used were analyzed monazite (Ce), synthetic $Nd_3Ge_5O_{12}$, (Nd) and Sb_2S_3 (Sb and S).

Results and Discussion

The powder diffraction patterns of the products showed the presence of three unknown compounds: two among the products in the Ce–Sb–S system, and one among those in the Nd–Sb–S system. The former two compounds were proved to be $Ce_6Sb_8S_{21}$ and $Ce_3Sb_3S_{10}$ because they exhibited isostructural powder diffraction patterns with those of $La_6Sb_8S_{21}$ and $La_3Sb_3S_{10}$, respectively.[5] On the other hand, the latter compound gave a powder pattern which has never been reported before. The subsequent electron microprobe analysis has revealed it to be Nd_3SbS_6, which is a new type of compounds in the Ln (lanthanoids)–Sb–S system. Table 1 gives the results of chemical analysis for $Ce_6Sb_8S_{21}$, and Nd_3SbS_6. The powder diffraction patterns for the three new sulfides are listed in Table 2.

Table 1. Electron microprobe chemical analysis of $Ce_6Sb_8S_{21}$ and Nd_3SbS_6

	$Ce_6Sb_8S_{21}$			Nd_3SbS_6	
	wt%	Atomic ratio		wt%	Atomic ratio
Ce	35.59	6.35	Nd	57.86	3.33
Sb	38.97	8	Sb	14.66	1
S	27.03	21.08	S	24.60	6.37
Total	101.59		Total	97.12	

$Ce_6Sb_8S_{21}$. The product is obtained as blackish-red crystals having metallic luster. It is isostructural with $La_6Sb_8S_{21}$:[5] orthorhombic, space group P222. The lattice parameters obtained from the powder data are a=14.27(1), b=15.23(1), and c=8.645(9) Å. These values are slightly smaller than those reported for $La_6Sb_8S_{21}$, a=14.317(2), b=15.239(4), and c=8.685(1) Å. This result is consistent with the lanthanoid contraction. The crystal has plate-like habits with well-developed (010) faces, and elongated along the c axis.

The best crystals were obtained in the following procedures. A mixture of Ce, S, and Sb_2S_3 in a molar ratio 6:9:4, was heated at the reaction temperature of 1000 °C for 1 h and kept at the growth temperature of 900 °C for 1 week. The maximum synthesized crystal is 0.5×0.2×0.1 mm^3 in size.

$Ce_3Sb_3S_{10}$. The crystal is bright red and transparent having the same appearance as $La_3Sb_3S_{10}$.[5] The X-ray single crystal photographs have indicated that $Ce_3Sb_3S_{10}$ and $La_3Sb_3S_{10}$ are isomorphous. It belongs to the monoclinic system. However, as reported for $La_3Sb_3S_{10}$,[5] the presence of very weak superstructure reflections and very diffuse nature of the diffraction spots precluded the determination of the true cell and space group. The lattice parameters of the average lattice were calculated as a=13.15(1), b=14.20(2), c=5.568(6) Å, and β=95.17(8)°, which are slightly smaller than those of $La_3Sb_3S_{10}$: a=13.209(6), b=14.229(6), c=5.583(1) Å, and β=94.54(3)°.[5]

Thin plate crystals of 0.25×0.1×0.02 mm^3 in maximum size were synthesized by heating the mixture of Ce, Sb, and Sb_2S_3 in a molar ratio, 6:9:4. The suitable

† Present address: Department of Chemistry, Northwestern Teachers College, Lanchow, China.

TABLE 2. INDEXED X-RAY POWDER DIFFRACTION DATA FOR THE THREE NEW SULFIDES[a)]

$Ce_6Sb_8S_{21}$				$Ce_3Sb_3S_{10}$				Nd_3SbS_6			
hkl	d_c/Å	d_o/Å	*I*	*hkl*	d_c/Å	d_o/Å	*I*	*hkl*	d_c/Å	d_o/Å	*I*
320	4.034	4.03	vw	$\bar{2}21$	3.760	3.76	m	400	3.885	3.89	vw
140	3.680	3.67	vw	040	3.550	3.54	s	402	3.609	3.60	s
212	3.593	3.60	m	400	3.273	3.27	s	314	3.463	3.48	m
330	3.471	3.46	s	231	3.079	3.09	vw	332	3.429	3.44	m
222	3.326	3.33	m	002	2.773	2.77	s	422	3.273	3.28	vw
420	3.231	3.22	m	500	2.619	2.62	m	431	3.069	3.06	vw
232	2.989	3.00	vw	$\bar{5}11$	2.419	2.43	w	206	3.001	2.99	vw
322	2.949	2.96	w	350	2.380	2.37	w	440	2.747	2.74	vw
142	2.802	2.80	s	302	2.250	2.25	w	523	2.638	2.64	s
332	2.707	2.71	w	$\bar{4}12$	2.190	2.19	m	600	2.590	2.59	vs
242	2.653	2.64	w	$\bar{5}02$	1.996	1.993	w	406	2.494	2.51	w
350	2.566	2.57	w	071	1.905	1.907	vw	336	2.432	2.43	vw
152	2.453	2.45	m	442	1.761	1.759	vw	444	2.394	2.40	w
512	2.353	2.35	m	$\bar{7}31$	1.701	1.700	vw	604	2.288	2.284	w
004	2.161	2.16	m					1.1.10.	1.922	1.926	vw
460	2.069	2.07	w					617	1.884	1.885	m
362	1.989	1.988	m					547	1.831	1.829	m
632	1.928	1.928	m					833	1.752	1.752	w
561	1.853	1.854	w								
712	1.830	1.830	w								
372	1.799	1.800	w								

a) Intensities were visually estimated: vs(very strong) > s > m(medium) > w(weak) > vw.

reaction and growth temperatures were 1200 °C and 1000 °C, respectively. Both $Ce_6Sb_8S_{21}$ and $Ce_3Sb_3S_{10}$ were able to be synthesized from the starting materials of the same composition. It was found that the appearance of each phase largely depends upon the growth temperature.

Nd_3SbS_6. The crystal is red and transparent. It has short prismatic shape with the maximum size of 0.15×0.05×0.05 mm³. The X-ray single crystal photographs have indicated that it belongs to the tetragonal system. The space group was determined as $I4_1/acd$ by the extinction rule. The elongation axis of the crystal is *c*. The indexing of the X-ray powder pattern was made with the aid of the single crystal photographs. As shown in Table 2, they are successfully indexed on the basis of the tetragonal cell. The lattice parameters were calculated as a=15.54(1) and c=19.52(2) Å from the powder data.

The optimum synthetic condition for the preparation of single crystal is as follows. A mixture of Nd, S, and Sb_2S_3 in a molar ratio, 6:9:4, was heated at 1100 °C for 2 h, and the temperature was dropped to 1040 °C. Then, it was slowly lowered to 890 °C at a rate of 6.25 °C/h. The temperature was raised again to 1040 °C, kept for 1 h, and slowly lowered in the same manner. This process was repeated four times in all. The run was terminated by turning off the furnace power to allow natural cooling. Attempts to synthesize at a fixed temperature, *i.e.* 1000 °C, did not yield any good crystals.

The authors wish to thank Mr. Ritsuro Miyawaki of the University of Tsukuba for his kind assistance in the chemical analysis.

References

1) Preliminary part of this work was presented at the Symposium on Rate Earths, Kyoto, March 1983, Abstr. Kidorui (Rare Earths), No. 2, 22 (1983), in Japanese with English summary.

2) R. M. Bozorth, F. Holtzberg, and S. Mathfessel, *Phys. Rev. Lett.*, **14**, 952 (1965).

3) P. Lemoine, D. Carré, and M. Guittard, *Acta Crystallogr., Sect. B*, **37**, 1281 (1981).

4) G. G. Guseinov, F. Kh. Mamedov, I. R. Amiraslanov, and Kh. S. Mamedov, *Sov. Phys. Crystallogr.*, **26**, 470 (1981).

5) J-zh. Gao, I. Nakai, and K. Nagashima, *Bull. Chem. Soc. Jpn.*, **56**, 2615 (1983).

6) D. E. Appleman and H. T. Evans, Jr., *U. S. Department of Commerce, Tech. Inform. Serv.*, PB216188 (1973).

Preparation and Crystal Structure of Bis[(2-aminoethyl)dimethylphosphine][1,2-bis(dimethylphosphino)ethane]cobalt(III) Tribromide Dihydrate, $[Co\{NH_2CH_2CH_2P(CH_3)_2\}_2\{(CH_3)_2PCH_2CH_2P(CH_3)_2\}]Br_3\cdot 2H_2O$

Tomoji OHISHI, Shigeru OHBA,† Kazuo KASHIWABARA, Yoshihiko SAITO,† and Junnosuke FUJITA*

Department of Chemistry, Faculty of Science, Nagoya University, Chikusa-ku, Nagoya 464
†*Department of Chemistry, Faculty of Science and Technology, Keio University, Hiyoshi, Kohoku-ku, Yokohama 223*

(Received August 25, 1983)

Synopsis. The title compound has been prepared and the crystal structure determined by the X-ray diffraction method. The complex ion is the *trans(P, N)* isomer, where one of the N atoms of (2-aminoethyl)dimethylphosphine (edmp) occupies the position trans to the P atom of the other edmp ligand.

In the course of our preparative studies[1,2] of the series-complexes $[Co(en)_x(edmp)_y(dmpe)_z]^{3+}(x+y+z=3)$, where en, edmp, and dmpe denote ethylenediamine, (2-aminoethyl)dimethylphosphine, and 1,2-bis(dimethylphosphino)ethane, respectively, we have obtained $[Co(edmp)_2(dmpe)]Br_3\cdot 2H_2O$ by the reaction of *trans*-$[CoCl_2(edmp)_2]ClO_4$ with dmpe. There are three possible geometrical isomers of the complex ion (Fig. 1). In order to determine the geometrical configuration, crystals of the complex have been subjected to X-ray structure analysis.

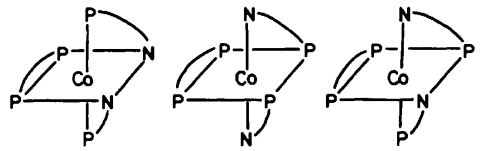

Fig. 1. Three geometrical isomers of $[Co(dmpe)(edmp)_2]^{3+}$.

Experimental

Preparation of the Complex. To an oxygen-free methanol solution (50 cm^3) of *trans*-$[CoCl_2(edmp)_2]ClO_4$[3] (205 mg, 0.467 mmol) was added dropwise an oxygen-free methanol solution (50 cm^3) of dmpe[2] (70 mg, 0.467 mmol) with stirring under an atmosphere of nitrogen at room temperature. After 12 h the resulting yellow solution was filtered to remove yellow precipitate of *fac*-$[Co(edmp)_3]X_3$ ($X=Cl^-$ or ClO_4^-).[1] The filtrate was diluted with water (1 dm^3) and poured on a column (ϕ 3×120 cm) of SP-Sephadex C-25. The adsorbed product was eluted with 0.2 mol dm^{-3} NaCl, giving two main yellow bands with several minor ones. The complex of the second main band was *fac*-$[Co(edmp)_3]^{3+}$. The eluate of the first main band was evaporated to dryness under reduced pressure, and the complex was extracted with a small amount of methanol. The extract was diluted several times with water and rechromatographed in a similar manner using a small column (ϕ 1×10 cm) and 1 mol dm^{-3} NaBr. The yellow eluate was concentrated to a small volume in a desiccator over P_4O_{10} to yield orange yellow crystals. Yield: 13 mg (4%). Most of the reaction product was *fac*-$[Co(edmp)_3]^{3+}$. Found: C, 24.32; H, 6.11, N, 4.07%. Calcd for $C_{14}H_{44}N_2Br_3CoOP_2$=$[Co(edmp)_2(dmpe)]Br_3\cdot 2H_2O$: C, 24.19; H, 6.38; N, 4.03%. The complex is soluble in water and alcohols, but insoluble in nonpolar solvents such as chloroform.

Crystal Structure Determination. Crystals are prismatic b. Crystal data are; monoclinic, $P2_1/a$, a=16.380(5), b=19.845(6), c=9.538(3) Å, β=122.34(2)°, V=2619.4(14) Å^3, Z=4, D_x=1.76, D_m=1.76(2) Mg m^{-3}, MW=695.1, λ(Mo $K\alpha$)=0.70926 Å, μ=5.44 mm^{-1}. The intensity measurements were performed to 2θ=60° ($+h$, $-k$, $\pm l$ set) on a Rigaku AFC-5 four-circle diffractometer with Mo Kα radiation monochromated by a graphite plate and with a crystal of 0.2×0.2×0.2 mm^3 in dimensions. 6613 reflections were measured and 3299 unique ones were obtained. Lorentz, polarization and absorption corrections were applied.[4] The structure was solved by direct methods with MULTAN78.[5] Starting with the positions of the Co and three Br atoms those of the other non-H atoms were determined from electron-density maps and refined by block-diagonal least squares with anisotropic thermal parameters using UNICS III computation program system.[6] The psitions of all the H atoms were calculated except those of water molecules and not refined. Final R was 0.071, wR=0.071, S=2.2 for 3299 unique reflections. Complex neutral-atom scattering factors were taken from International Tables for X-Ray Crystallography.[7]

Results and Discussion

Final atomic parameters of non-H atoms are presented in Table 1 and a perspective drawing of the complex cation in Fig. 2.[8] This is the *trans(P, N)* isomer. Bond lengths and bond angles are listed in Table 2.

TABLE 1. FRACTIONAL COORDINATES AND ISOTROPIC TEMPERATURE FACTORS

Atom	x	y	z	B_{eq}/Å^2
Co	0.2848(1)	0.12353(6)	0.5100(2)	1.2
Br(1)	0.4545(1)	0.12588(7)	0.2550(2)	3.3
Br(2)	0.2767(1)	0.36314(7)	0.0084(2)	3.6
Br(3)	0.4928(1)	0.38548(6)	0.7407(2)	2.9
P(1)	0.1218(2)	0.1358(1)	0.3250(3)	1.7
P(2)	0.2646(2)	0.0326(1)	0.6282(4)	1.7
P(3)	0.2833(2)	0.1996(1)	0.6868(3)	1.6
P(4)	0.4490(2)	0.1314(1)	0.6904(3)	1.6
N(1)	0.2951(6)	0.1915(4)	0.3588(10)	1.7
N(2)	0.2996(6)	0.0544(4)	0.3642(10)	1.8
C(1)	0.1195(7)	0.2023(5)	0.1905(13)	2.0
C(2)	0.2084(9)	0.1964(6)	0.1848(13)	2.8
C(3)	0.2657(10)	-0.0354(6)	0.5002(17)	3.4
C(4)	0.3180(11)	-0.0163(6)	0.4210(16)	3.8
C(5)	0.4078(8)	0.2200(6)	0.8549(13)	2.5
C(6)	0.4742(8)	0.1593(6)	0.8919(13)	2.2
C(7)	0.0367(8)	0.1622(6)	0.3793(15)	2.9
C(8)	0.0555(8)	0.0675(6)	0.1827(13)	2.7
C(9)	0.1525(8)	0.0187(6)	0.6167(13)	2.3
C(10)	0.3524(9)	0.0062(6)	0.8391(15)	3.5
C(11)	0.2344(8)	0.2820(5)	0.6042(14)	2.4
C(12)	0.2267(8)	0.1778(6)	0.7990(14)	2.2
C(13)	0.5075(8)	0.1983(6)	0.6446(13)	2.6
C(14)	0.5279(8)	0.0601(6)	0.7265(14)	2.6
O(1)	0.3168(6)	0.3355(4)	0.3766(10)	3.4
O(2)	0.1867(7)	0.0267(5)	0.0090(10)	4.3

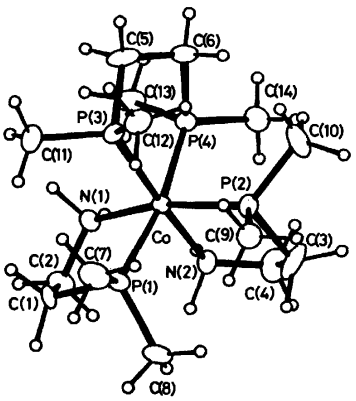

Fig. 2. An ORTEP drawing of the complex cation with thermal ellipsoids scaled at the 50% probability level.[9] H atoms are represented by circles of radius 0.08 Å.

TABLE 2. BOND LENGTHS (l/Å) AND ANGLES (ϕ/°) AND THEIR ESTIMATED STANDARD DEVIATIONS

Co	-P(1)	2.294(3)	P(3)	-C(5)	1.843(10)
Co	-P(2)	2.245(4)	P(3)	-C(11)	1.806(10)
Co	-P(3)	2.273(4)	P(3)	-C(12)	1.803(17)
Co	-P(4)	2.295(3)	P(4)	-C(6)	1.823(13)
Co	-N(1)	2.047(10)	P(4)	-C(13)	1.822(14)
Co	-N(2)	2.058(10)	P(4)	-C(14)	1.820(13)
P(1)	-C(1)	1.827(12)	N(1)	-C(2)	1.503(11)
P(1)	-C(7)	1.804(17)	N(2)	-C(4)	1.476(14)
P(1)	-C(8)	1.811(11)	C(1)	-C(2)	1.49 (2)
P(2)	-C(3)	1.827(16)	C(3)	-C(4)	1.46 (3)
P(2)	-C(9)	1.801(15)	C(5)	-C(6)	1.53 (2)
P(2)	-C(10)	1.815(11)			

P(1)	-Co	-P(2)	92.7(1)	C(3)	-P(2)	-C(9)	102.7(7)
P(1)	-Co	-P(3)	91.7(1)	C(3)	-P(2)	-C(10)	104.0(6)
P(1)	-Co	-P(4)	169.9(1)	C(9)	-P(2)	-C(10)	101.6(6)
P(1)	-Co	-N(1)	83.6(3)	Co	-P(3)	-C(5)	110.2(3)
P(1)	-Co	-N(2)	93.5(3)	Co	-P(3)	-C(11)	117.1(3)
P(2)	-Co	-P(3)	95.6(1)	Co	-P(3)	-C(12)	119.6(5)
P(2)	-Co	-P(4)	96.1(1)	C(5)	-P(3)	-C(11)	101.9(4)
P(2)	-Co	-N(1)	166.9(3)	C(5)	-P(3)	-C(12)	102.6(6)
P(2)	-Co	-N(2)	84.6(3)	C(11)	-P(3)	-C(12)	103.2(6)
P(3)	-Co	-P(4)	82.7(1)	Co	-P(4)	-C(6)	108.9(4)
P(3)	-Co	-N(1)	97.1(3)	Co	-P(4)	-C(13)	115.2(5)
P(3)	-Co	-N(2)	174.8(3)	Co	-P(4)	-C(14)	121.2(4)
P(4)	-Co	-N(1)	88.7(3)	C(6)	-P(4)	-C(13)	100.3(6)
P(4)	-Co	-N(2)	92.1(3)	C(6)	-P(4)	-C(14)	107.4(6)
N(1)	-Co	-N(2)	83.1(4)	C(13)	-P(4)	-C(14)	101.6(6)
Co	-P(1)	-C(1)	101.2(4)	Co	-N(1)	-C(2)	115.8(6)
Co	-P(1)	-C(7)	124.7(5)	Co	-N(2)	-C(4)	117.4(8)
Co	-P(1)	-C(8)	118.8(4)	P(1)	-C(1)	-C(2)	108.4(8)
C(1)	-P(1)	-C(7)	105.2(6)	N(1)	-C(2)	-C(1)	109.2(11)
C(1)	-P(1)	-C(8)	103.6(5)	P(2)	-C(3)	-C(4)	111.8(11)
C(7)	-P(1)	-C(8)	100.8(6)	N(2)	-C(4)	-C(3)	112.0(14)
Co	-P(2)	-C(3)	101.6(5)	P(3)	-C(5)	-C(6)	110.3(8)
Co	-P(2)	-C(9)	120.8(5)	P(4)	-C(6)	-C(5)	105.3(7)
Co	-P(2)	-C(10)	123.1(4)				

Bond length of Co–P(1) is longer than Co–P(2) by 0.049(4) Å, indicating trans influence of the ligating P atoms. A difference of 0.022(4) Å is also found in the bond distances between Co and P atoms of the dmpe ligand, which may be less meaningful since two Co–P bond lengths in $[Co(en)_2(dmpe)]^{3+}$ differ by 0.016(3) Å.[10] The five-membered chelate ring formed by the dmpe ligand takes an envelope conformation as shown in Fig. 3. Conformation of the same ligand in $[Co(en)_2(dmpe)]^{3+}$ is a twisted (gauche) one. The asymmetry of the ring conformation may be caused to release the steric repulsion between two methyl groups, C(9) and C(12) [3.49(2) Å]. The methyl C(13) atom is in close contact with the N(1) atom [3.07(1) Å].

In the *trans(P, P)* isomer, in which the positions of P(1) and N(1) atoms are interchanged, the steric interactions between methyl groups C(9) and C(12) and between C(13) and C(7′) will render the complex unstable. The *trans(N, N)* isomer will also be unstable since it has two pairs of mutually trans P donating atoms as

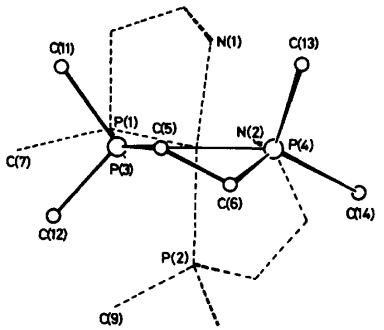

Fig. 3. The dmpe ligand viewed along the line through the Co atom and the midpoint of P(3)–P(4) axis.

exemplified by the elongation of the Co–P(1) bond. This the *trans(P, N)* isomer will be the most stable among the isomers from both steric and electronic factors.

The complex in aqueous solution shows an absorption spectrum very similar to that of $[Co(en)(dmpe)_2]^{3+}$,[2] giving the d-d bands at 24150 cm^{-1} (log ε=2.79) and *ca.* 29000 cm^{-1}(log ε=2.7, shoulder), and the Co–P charge transfer band at 36900 cm^{-1}(log ε=4.42). The thermal stability is also similar to that of $[Co(en)(dmpe)_2]^{3+}$; the complex in water or other solvents is stable at room temperature, but decomposes slowly on heating. The complex in water in the presence of excess NaCl changes to *trans*-$[CoCl_2(edmp$ or $dmpe)_2]^+$ and a small amount of Co(II) species by heating at 60—70 °C for several hours.

This work was supported by the research grant of the Takeda Science Foundation.

References

1) I. Kinoshita, K. Kashiwabara, J. Fujita, K. Matsumoto, and S. Ooi, *Bull. Chem. Soc. Jpn.*, **54**, 2683 (1981).

2) T. Ohishi, K. Kashiwabara, and J. Fujita, *Bull. Chem. Soc. Jpn.*, **56**, 3441 (1983).

3) I. Kinoshita, Y. Yokota, K. Matsumoto, S. Ooi, K. Kashiwabara, and J. Fujita, *Bull. Chem. Soc. Jpn.*, **56**, 1067 (1983).

4) W. R. Busing and H. A. Levy, *Acta Crystallogr.*, **10**, 180 (1957).

5) P. Main, S. E. Hull, L. Lessinger, G. Germain, J. P. Declercq, and M. M. Woolfson (1978). MULTAN78, "A System of Computer Programs for the Automatic Solution of Crystal Structures from X-Ray Diffraction Data," Univs of York, England, and Louvain, Belgium.

6) T. Sakurai and K. Kobayashi, *Rikagaku Kenkyusho Hokoku*, **55**, 69 (1979).

7) "International Tables for X-Ray Crystallography," Kynoch Press, Birmingham (1974), Vol. IV, pp. 71 and 148.

8) Tables of the anisotropic thermal parameters of the non-H atoms, the coordinates of H atoms and observed and calculated structure factors, and a detail of the crystal structure determination are kept as Document No. 8407 at the Chemical Society of Japan.

9) C. K. Johnson (1965). ORTEP. Report ORNL-3794. Oak Ridge National Laboratory, Tennessee.

10) S. Ohba, Y. Saito, T. Ohishi, K. Kashiwabara, and J. Fujita, *Acta Crystallogr., Sect. C*, **39**, 49 (1983).

Pressure and Temperature Effects on Octahedral-Tetrahedral Equilibria in Pyridine Solutions of Some Cobalt(II) Halides. II

Kazuo KOJIMA,* Takeru MIYASHITA, and Jiro MATSUDA
Department of Chemistry, Faculty of Science and Engineering, Ritsumeikan University, Kita-ku, Kyoto 603
(Received September 2, 1983)

Synopsis. Temperature and pressure effects on the configuration equilibrium of cobalt(II) iodide in pyridine solution have been studied spectrophotometrically. High temperature favors the tetrahedral species but high pressure favors the octahedral species, the heat and volume changes being 65.3 kJ mol^{-1} and -6 cm^3 mol^{-1}, respectively. Comparisons among three kinds of halide are also made.

We have reported[1] the ΔH and the ΔV values determined in terms of the shift of the equilibrium $[CoX_2(py)_2]$ (tetrahedral)$+2py \rightleftharpoons [CoX_2(py)_4]$ (octahedral), where X is Cl or Br. This note deals with the case of X= I and discusses the relation among the chloride, the bromide and the iodide complexes.

The experimental details (except that the commercial chemical pure reagent $CoI_2 \cdot 4H_2O$ was used after dehydration in the present study) and the method of determining the values of ΔH and ΔV were the same as previously described.[1]

Results and Discussion

Figure 1 shows the absorption spectra of CoI_2 in pyridine at various temperatures. There found two bands, the one is the T-band due to the tetrahedral species $[CoI_2(py)_2]$ and the other the O-band due to the octahedral species $[CoI_2(py)_4]$. The T-band intensity increases steeply with increasing temperature; two peaks at 658, 685 nm and a shoulder near 626 nm are well-resolved at 74.6 °C. This trend suggests that the equilibrium mentioned above shifts to the tetrahedral-species side with increasing temperature, although the variation of the O-band spectrum with the temperature changes is not found to be clear because of the low molar absorption coefficient of $[CoI_2(py)_4]$.

A plot of the logarithm of A'_{685} *vs.* T^{-1} in Fig. 2 gives a straight line, from the slope of which the ΔH value of 65.3 kJ mol^{-1} is obtained, being comparable with the value of 69.4 kJ mol^{-1}.[2]

The ΔH values increase in the order $Cl^- < Br^- < I^-$, which is consistent with the result of King *et al.*[2] They proposed that this order is ascribed to the degree of contribution of the dative π-bonding to the Co–py bond and that this π-bonding is related to the polarizability of halide ion. By plotting the ΔH values *vs.* the electronic polarizability of halide ions in crystals[3] in Fig. 3, we can find the linear relation between them. Furthermore, we are concerned in the relation between the ΔH values and the electronegativity of halide ions.

Because CoI_2 is less soluble in pyridine (its solubility is the order of one-hundredth of those of the other halides), the intensities of the O- and T-band are weak at room temperature and 1 atm, so that the changes in the absorption spectra with the variation of pressure are not very clear (not shown). However, from the plot of the logarithm of the ratio of the integrated-intensities

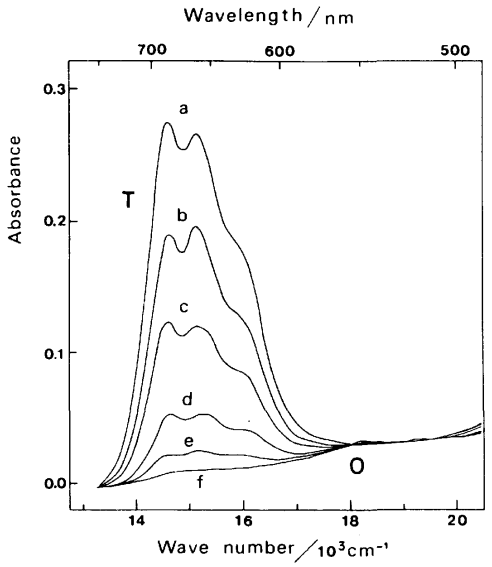

Fig. 1. Absorption spectra of CoI_2 in pyridine at various temperatures (1 atm), uncorrected for the thermal expansion of the solution. Concn: 5.320×10^{-4} mol dm^{-3} (25 °C), optical path length: 0.98 cm.
a: 74.6 °C, b: 62.6 °C, c: 55.0 °C, d: 43.2 °C, e: 34.6 °C, f: 24.4 °C.

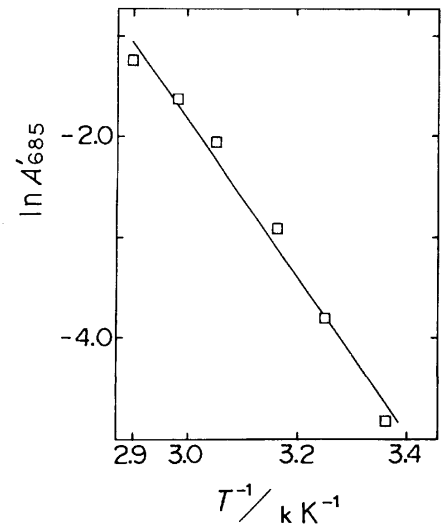

Fig. 2. Logarithm of the corrected absorbance for CoI_2 *vs.* reciprocal of the absolute temperature.
A'_{685} denotes the absorbance at 685 nm corrected by the approximate thermal expansion coefficient of pyridine as in Ref. 1. The line is the least-square fit to the data.

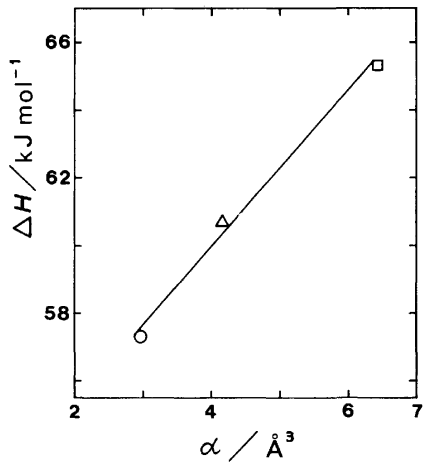

Fig. 3. ΔH *vs.* electronic polarizability of halide ions. ○: Cl^-, △: Br^-, □: I^-. ΔH values for the chloride and bromide are taken from Ref. 1.

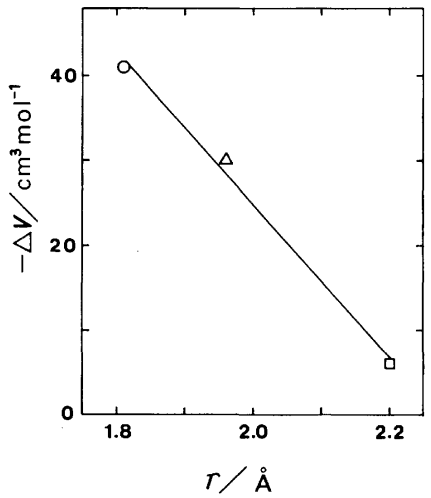

Fig. 4. ΔV at 1 atm *vs.* ionic radii of halide ions. ○: Cl^-, △: Br^-, □: I^-. ΔV values for the chloride and bromide are taken from Ref. 1.

of the O-band to those of the T-band against pressure, we obtain the ΔV value of $-6\ cm^3\ mol^{-1}$ over the pressure range 1 bar to 3 kbar.

The values of ΔV at 1 atm show a linear variation with the ionic radii of the halide ions, as exhibited in Fig. 4. This implies that the larger the ionic radius, the smaller the volume difference between $[CoX_2(py)_4]$ and $[CoX_2(py)_2]$ solvated with two pyridine molecules.

Another effect of pressure on the relation between ΔV and pressure has been described previously.[1] In the present study, the relation for the iodide is found to be the most linear.

References

1) K. Kojima, M. Saida, M. Donoue, and J. Matsuda, *Bull. Chem. Soc. Jpn.*, **56**, 684 (1983).
2) H. C. A. King, E. Körös, and S. M. Nelson, *J. Chem. Soc., A*, **1963**, 5449.
3) J. R. Tessman, A. H. Kahn, and W. Shockley, *Phys. Rev.*, **92**, 890 (1953).

Efficient Synthesis and Structure of Bis[acetonitrile(11,13-dimethyl-1,4,7,10-tetraaza-10,13-cyclotridecadien-12-ylidene)nickel(II)] Perchlorate

Katsura Mochizuki,* Koshiro Toriumi,† and Tasuku Ito†
Department of Chemistry, Yokohama City University, Yokohama 236
†*Institute for Molecular Science, Okazaki 444*
(Received September 20, 1983)

Synopsis. The titled binuclear nickel(II) complex has been synthesized by the oxidation of 11,13-dimethyl-1,4,7,10-tetraaza-10,13-cyclotridecadienatonickel(II) perchlorate with iron(III) perchlorate in deoxygenated CH_3CN in *ca.* 70% yield and its structure has been determined.

Cunninghum *et al.* reported a synthesis of [NiI(Me$_2$[13]dienN$_4$ylidene)]$_2$I$_2$ (**2b**), a dimer of [Ni(Me$_2$[13]dienatoN$_4$)]$^+$ (**1**),[1] though the yield was as low as less than a few percent.[2] In the formation of such a dimer, the combination of radicals formed at the γ-position of the six-membered diiminato chelate ring, *i.e.*, one electron oxidation of the coordinated ligand and the further oxidation of the bridging C–C bond to a C=C double bond should take place.[3] The low yield of the preparation of **2b** by Cunninghum's method is caused by the occurrence of side reactions such as ligand dehydrogenation and ligand oxygenation. Such reactions have been known to take place in the oxidation of **1** with Br_2[4] and in the oxidation of [Co(Me$_2$[14]dieneN$_4$)]$^{2+}$.[5]

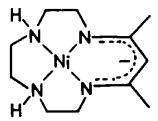

1

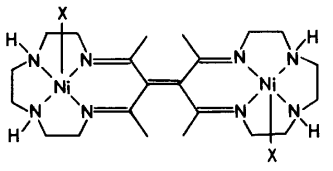

2a: X=CH_3CN Y=ClO_4^- n=4
2b: X=Y=I^- n=2
2c: X=Y=NCS^- n=2

In the present study, the titled nickel(II) complex has been efficiently synthesized by the oxidation of [Ni(Me$_2$[13]dienatoN$_4$)](ClO$_4$) (**1**) in deoxygenated CH_3CN with ion(III) perchlorate, selected as an appropriate and noncoordinating oxydizing agent.[6] In this reaction, the side reactions were suppressed substantially. The dimeric structure of the oxidation product has been confirmed by X-ray analysis as well as a measurement of FD-mass spectra.

To confirm the formation of a radical at the γ-position by the oxidation with ion(III) ions, cyclic voltammograms of [M(Me$_2$[X]dienatoN$_4$)](ClO$_4$) (M=Ni, Cu; X=13, 14) in CH_3CN were measured. Irrespective of kinds of the metal ions, these complexes showed similar irreversible waves with strong anodic peaks (E_{pa}) but did not give corresponding cathodic peaks (i_{pc}=0). Heights and positions of the anodic peaks were scan rate dependent. The electrochemical data were:[7] E_{pa}(M=Ni, X=13)=+0.64 V, E_{pa}(M=Ni, X=14)=+0.64 V, E_{pa}(M=Cu, X=13)=+0.50 V, E_{pa}(M=Cu, X=14)=+0.56 V. These E_{pa} values are in the narrow range of +0.5—+0.7 V and are definitely more negative than $E_{1/2}$ values of Ni^{II}/Ni^{III} couples reported for other macrocyclic nickel(II) complexes (see below).[3,8] A number of tetraaza macrocyclic nickel(II) complexes, which do not have a delocalized six-membered chelate ring, have been known to show quasi-reversible waves ($i_{pc}/i_{pa}\simeq1$) in cyclic voltammograms at $E_{1/2}$=+0.7—+1.3 V in CH_3CN. The waves correspond to Ni^{II}/Ni^{III} couples.[3,8] Furthermore, the constant electrolysis of [Ni(Me$_4$[14]tetraenatoN$_4$)]$^{2+}$, which has the delocalized six-membered rings, at +0.65 V in CH_3CN give the dimeric complex.[9] These facts suggest strongly that the observed waves are attributed to radical formations at the γ-positions. On the basis and from the observed E_{pa} values, we chose Fe(ClO$_4$)$_3$·6H$_2$O ($E_{1/2}$(II)/(III)=+1.1 V *vs.* SCE in CH_3CN[10]) as the oxidizing agent in the preparation of the titled complex.

Figure 1 shows the structure of **2a** and Table 1 lists bond lengths and angles of interest. The complex has an inversion center at midpoint of the C(12)–(12′) bond. The bridge head carbons, C(12) and C(12′), are connected by a double bond to produce a binuclear complex. In the present complex an acetonitrile molecule is coordinated to each nickel(II) ion in five-coordinate fashion. Perchlorates are not involved in coordination. In view of bond lengths and angles, C(12)–C(12′), N(1)–C(13), and N(10)–C(11) are double bonds. Four methyl groups produce large strain to C(12)–C(12′) double bond,[2] so that the double bonds are almost completely localized and the entire complex adopts a chair-like structure as in dodecachloroheptafluvalene.[11] The skeletal structure in **2a** is very similar to that reported for the iodo complex **2b**.[2]

The absorption spectrum of [Ni(CH$_3$CN)(Me$_2$[13]-

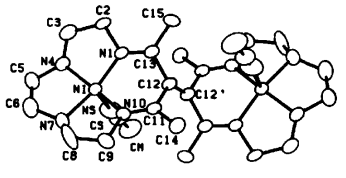

Fig. 1. Structure of [Ni(CH$_3$CN)(Me$_2$[13]dienN$_4$-ylidene)]$_2^{4+}$ (**2a**).

Table 1. Selected bond lengths (l/Å) and angles (ϕ/°)

Ni-N(1)	1.857(6)	C(12)-C(12′)	1.366(12)
Ni-N(4)	1.898(7)	C(13)-N(1)	1.271(9)
Ni-N(7)	1.913(7)	C(11)-N(10)	1.262(9)
Ni-N(10)	1.865(6)	Ni-N(s)	2.510(8)
C(11)-C(12)-C(12′)		119.5(7)	
C(11)-C(12)-C(13)		116.0(7)	
C(13)-C(12)-C(12′)		118.9(7)	

TABLE 2. FRACTIONAL COORDINATES($\times 10^4$)[a]

Atom	x	y	z
Ni	2139(1)	1565(1)	−275(1)
Cl(1)	1359(2)	1269(2)	−3318(2)
Cl(2)	921(2)	4494(2)	2486(2)
N(1)	863(4)	2078(5)	−632(4)
N(4)	2483(6)	3162(6)	−125(8)
N(7)	3524(5)	1214(6)	−176(6)
N(10)	1931(4)	13(5)	−649(4)
C(2)	816(6)	3347(6)	−841(6)
C(3)	1841(9)	3823(9)	−671(12)
C(5)	3550(7)	3326(9)	100(9)
C(6)	4091(8)	2275(9)	−224(10)
C(8)	3686(7)	251(11)	−807(11)
C(9)	2861(6)	−603(8)	−871(7)
C(11)	1100(6)	−483(6)	−775(5)
C(12)	207(6)	168(7)	−432(6)
C(13)	104(6)	1430(6)	−771(5)
C(14)	920(6)	−1685(7)	−1257(7)
C(15)	−877(6)	1825(8)	−1260(7)
O(1)	1521(8)	1326(7)	−4332(5)
O(2)	2131(6)	1700(9)	−2701(6)
O(3)	680(9)	2110(15)	−3171(8)
O(4)	1109(15)	270(9)	−3026(7)
O(5)	702(7)	5619(7)	2852(7)
O(6)	1437(12)	3985(10)	3286(12)
O(7)	1398(18)	4570(15)	1675(13)
O(8)	133(8)	3928(11)	2246(14)
N(S)	1892(7)	1409(9)	1574(6)
C(M)	1492(10)	1170(11)	3431(7)
C(S)	1741(8)	1322(8)	2359(6)

a) Estimated standard deviations are in parentheses.

dienN$_4$ylidene)]$_2$(ClO$_4$)$_4$ in Nujol mull shows a broad band around 500 nm, characteristic of five-coordinate species.

Data of absorption spectra and molar conductivities of **2b** suggest the presence of five-coordinate species in acetonitrile and aqueous solutions.[12]

By using the present synthetic procedures, a relatively large amount of **2a** can be obtained. Iodo and thiocyanato derivatives, **2b** and **2c** were prepared successfully from **2a** and characterized (see Experimental).

Experimental

Materials. [Ni(Me$_2$[13]dienatoN$_4$)](ClO$_4$) (**1**) was synthesized according to the literature.[13]

[Ni(CH$_3$CN)(Me$_2$[13]dienN$_4$ylidene)]$_2$(ClO$_4$)$_4$ (**2a**): Through an acetonitrile solution (50 cm^3) containing 2.0 g of **1** was bubbled a stream of N$_2$ gas for 30 min to remove dissolved oxygen. To the solution was added gradually 2.5 g of Fe(ClO$_4$)$_3$·6H$_2$O dissolved in a small amount of acetonitrile. N$_2$ bubbling was continued for further 30 min. After standing the solution in an open beaker overnight, red brown prismatic crystals formed were filtered and washed with minimum amount of acetonitrile (yield, *ca.* 70%). Found: C, 30.63; H, 4.74; N, 13.63%. Calcd for Ni$_2$C$_{26}$H$_{46}$N$_{10}$O$_{16}$Cl$_4$: C, 30.80; H, 4.57; N, 13.99%. IR (Nujol mull, cm^{-1}) 1651 (C=N); MS (FD), *m/e*, 833 ([Ni(Me$_2$[13]dienN$_4$ylidene)]$_2$(ClO$_4$)$_3^+$). The complex easily releases acetonitriles and absorbs water in the air to produce [Ni(Me$_2$[13]dienN$_4$ylidene)]$_2$(ClO$_4$)$_4$·2H$_2$O. This complex was also prepared in the same manner as described above by use of water (pH=*ca.* 2 with HClO$_4$) in place of acetonitrile. Found: C, 27.32; H, 4.20; N, 11.59%. Calcd for Ni$_2$C$_{22}$H$_{44}$N$_8$O$_{18}$Cl$_4$: C, 27.30; H, 4.58; N, 11.58%. UV$_{max}$(CH$_3$CN) 362 nm (ε 3510) 420 nm (shoulder); Molar conductivity (Ω^{-1} cm^2 mol^{-1}) Λ (H$_2$O, 2.50×10^{-4} mol dm^{-3}, pH 4.7, 25 °C) 476.

[NiX(Me$_2$[13]dienN$_4$ylidene)]$_2$X$_2$ (X=I$^-$(**2b**), NCS$^-$(**2c**)) were prepared by use of anion exchange resin (Amberlite IRA-410) at pH<3. **2b**: Found: C, 25.19; H, 3.97; N, 10.58%. Calcd for Ni$_2$C$_{22}$H$_{40}$N$_8$I$_4$: C, 25.37; H, 3.87; N, 10.76%. IR (Nujol mull, cm^{-1}) 1632 (C=N); UV$_{max}$(CH$_3$CN) 550 nm (broad); Λ (H$_2$O, 2.50×10^{-4} mol dm^{-3}, pH 5.4, 25 °C) 368. **2c**: Found: C, 40.26; H, 5.24; N, 21.58%. Calcd for Ni$_2$C$_{26}$H$_{40}$N$_{12}$S$_4$: C, 40.75; H, 5.26; N, 21.93%. IR (Nujol mull, cm^{-1}) 1651 (C=N), 2075 (N=C=S); Λ (H$_2$O, 2.41×10^{-4} mol dm^{-3}, pH 5.4, 25 °C) 353.

Other materials used were reagent grade.

X-Ray Analysis. The procedures used for data collection (a Rigaku AFC-5 diffractometer, Mo $K\alpha$) as well as the method used in the solution and refinement of the structure were standard and have been described previously.[14] Crystal data: Monoclinic, P2$_1$/n, a=13.533(2), b=11.471(1), c=93.76(1)°, V=2060.2(6) Å^3, z=2, D_x=1.64 g cm^{-3}, R=0.087 for 2857 independent reflections with $F_o > 3\sigma(F_o)$ ($2\theta < 60°$). Table 2 lists atomic coordinates.[15] Hydrogen atoms are not included in the calculation.

Measurements. Absorption spectra were measured with a Hitachi 340 spectrophotometer. A conductometer E518 (Metrohm Herisau) was used. Cyclic voltammograms were recorded with a Yanagimoto Polarographic Analyzer P-1100. Half wave potentials at 25 °C measured with three-electrode system were refered to SCE.

References

1) Ligand abbreviations: Me$_2$[13]dienatoN$_4$=11,13-dimethyl-1,4,7,10-tetraaza-10,13-cyclotridecadienato; Me$_2$[14]dienatoN$_4$=5,7-dimethyl-1,4,8,11-tetraaza-4,7-cyclotetradecadienato; Me$_2$[14]dieneN$_4$=5,7-dimethyl-1,4,8,11-tetraaza-4,7-cyclotetradecadiene; [Me$_2$[13]dienN$_4$ylidene]$_2$=12,12′-bi(11,13-dimethyl-1,4,7,10-tetraaza-10,13-cyclotridecadienylidene); Me$_4$[14]tetraenatoN$_4$=6,8,15,17-tetramethyldibenzo[*b*,*i*][1,4,8,11]tetraaza-5,8,14,17-cyclotetradecatetraenato.

2) J. A. Cunningham and R. E. Sievers, *J. Chem. Soc.*, **95**, 7183 (1973).

3) J. F. Endicott and B. Durham, "Coordination Chemistry of Macrocyclic Compounds," ed by G. A. Melson, Plenum Press, New York (1979), Chap. 6.

4) C. J. Hipp, L. F. Lindoy, and D. H. Busch, *Inorg. Chem.*, **11**, 1988 (1972).

5) J. A. Switzer and J. F. Endicott, *J. Am. Chem. Soc.*, **102**, 1181 (1980); J. A. Switzer, J. F. Endicott, M. A. Kalifa, F. P. Rotzinger, and K. Kumar, *ibid.*, **105**, 56 (1983).

6) Analogous products were obtained by the oxidation of [Ni(Me$_2$[14]dienatoN$_4$)](ClO$_4$) with iron(III) ions in a similar way.

7) The E_{pa} values are given in *vs.* SCE, Et$_4$NClO$_4$=0.1 mol dm^{-3}, scan rate=500 mV s^{-1}, glassy carbon electrode.

8) K. Barefield, F. V. Lovecchio, N. E. Tokel, E. Ochiai, and D. H. Busch, *Inorg. Chem.*, **11**, 283 (1972); D. C. Olson and J. Vasilevskies, *ibid.*, **8**, 1611 (1969); F. V. Lovecchio, E. S. Gore, and D. H. Busch, *J. Am. Chem. Soc.*, **96**, 3109 (1974).

9) F. C. McElroy and J. C. Dabrowiak, *J. Am. Chem. Soc.*, **98**, 7112 (1976).

10) I. M. Kolthoff and J. F. Coetzee, *J. Am. Chem. Soc.*, **79**, 1852, (1957).

11) M. Ishimori, R. West, B. K. Teo, and L. F. Dahl, *J. Am. Cehm. Soc.*, **93**, 7101 (1971).

12) [Ni(Me$_2$[13]dienN$_4$ylidene)]$_2^{4+}$ (**2a**) shows a complicated pH-dependence in aqueous solution.

13) S. C. Cummings and R. E. Sievers, *Inorg. Chem.*, **9**, 1131 (1970).

14) H. Ito, J. Fujita, K. Toriumi, and T. Ito, *Bull. Chem. Soc. Jpn.*, **54**, 2988 (1981).

15) The F_o—F_c data and thermal parameters kept are in the office of the Chemical Society of Japan (Document No. 8410).

^{13}C-NMR Spectra of 2-Aryl-2-(1-azolylmethyl)-4-hydroxymethyl-1,3-dioxolanes and Their Ester and Ether Derivatives

Hiroko SUEZAWA,* Minoru HIROTA, Kazuko YAMAMOTO,†
Isao TAKEUCHI,† and Yoshiki HAMADA†
Department of Applied Chemistry, Faculty of Engineering, Yokohama National University, Tokiwadai, Hodogaya-ku, Yokohama 240
†*Faculty of Pharmacy, Meijo University, Tempakucho, Tempaku-ku, Nagoya 468*
(Received July 29, 1983)

Synopsis. The ^{13}C-NMR spectra of the title compounds were assigned and the substituent effect was discussed briefly. ^{13}C-NMR of 2-aryl-4-benzoyloxymethyl-2-bromomethyl-1,3-dioxolanes provides the way to discriminate the cis and the trans isomers.

4-(Substituted aryl)-2-(1-imidazolyl)-1,3-dioxolanes have been shown to have antifungal activities towards *Microporum canis, Ctenomyces menlagrophytes, Trichophyton rubrum,* and other fungi.[1] These compounds are also active to some gram-negative and gram-positive bacilli. The antifungal and bactericidal activities are known to be sensitive to the stereochemistry of these compounds.

In our recent investigations on a series of the title compounds carrying 1-pyrazolyl, 1-imidazolyl, 1,2,4-triazol-1-yl, and 1-tetrazolyl groups as azolyl group (X in formula I), a number of their derivatives which are analogous to the azolyldioxolanes were synthesized from the corresponding 2-bromomethyl-1,3-dioxolanes.[2] Since the 2- and 4-carbon atoms of the dioxolane ring are asymmetric, two pairs of enantiomers mutually diasteromeric to each other are possible.

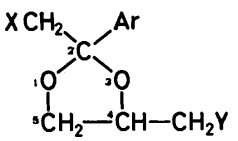

Formula I.

The pharmaceutical activities are strongly dependent on the stereochemistry. *r*-2-(1-Azolylmethyl)-2-(2,4-dichlorophenyl)-*c*-4-hydroxymethyl-1,3-dioxolanes and their derivatives are usually far more active than the other diastereomers, *t*-4-hydroxymethyl compounds.[3]

In this paper, ^{13}C-NMR spectral data of these dioxolanes are reported and their possobility to use for assigning the diastereomers.

Experimental

Preparation of the materials was reported elsehwere.[2,4] NMR spectra were recorded on a JEOL JNM FX-90Q spectrometer usually in chloroform-*d* solutions. The assignment of ^{13}C-NMR spectra were carried out by use of off-resonance technique. Aromatic carbon resonances were estimated by the additivity values[5] and by mutual comparison of the spectra. In some cases, selective decoupling technique was also employed.

Results and Discussion

^{13}C-Chemical shifts of 2-(1-azolylmethyl)-2-(2,4-dichlorophenyl)-4-hydroxymethyl-1,3-dioxolanes, their methanesulfonates, benzoates, and some of their ethers are given in Table 1. The dioxolanes are mostly cis isomers, which are pharmaceutically more active than the corresponding trans isomers. ^{13}C-Chemical shifts of the cis and the trans isomers of 2-aryl-2-bromomethyl-4-benzoloxymethyl-1,3-dioxolanes are also

TABLE 1. ^{13}C-NMR OF 2-ARYL-2-AZOLYLMETHYL-1,3-DIOXOLAN-4-YLMETHANOL AND THEIR DERIVATIVES

No.	X	Ar	Y		X(Azole Ring) 2	3	4	5	Dioxolane Ring 2	4	5	2-CH_2	4-CH_2	Aryl Group (Ar) 1	2	3	4	5	6	Y (or Σ-Ar) Y(Z)	1	2	3	4	5	6
1	pyrazolyl	2,4-$Cl_2C_6H_3$	OH	cis	----	139.8	105.9	131.2	107.9	76.8	65.9	55.9	61.4	135.6	135.1	129.6	133.0	127.0	131.7	OH ----	----	----	----	----	----	----
2			OSO_2CH_3	cis	----	139.4	106.1	131.3	108.9	73.8	68.2	56.0	66.5	135.9	132.4	129.5	133.1	127.2	131.3	CH_3^* 37.6	----	----	----	----	----	----
3			$OCOC_6H_5$	cis	----	139.3	105.7	131.0	108.4	74.1	66.9	56.0	63.9	135.4	134.5	129.6	133.0	126.8	131.0	CO 165.9	131.0	129.6	128.3	133.2	128.3	129.6
4			$OC_6H_3Cl_2$-2,4	cis	----	139.4	105.9	131.3	108.6	74.3	67.4	56.1	68.8	135.7	134.2	129.7	133.2	127.1	131.3	O ----	152.8	123.9	130.1	126.4	127.6	114.5
5	Imidazolyl	2,4-$Cl_2C_6H_3$	OH	cis	139.8	----	128.2	121.3	107.6	77.1	66.9	51.4	61.9	135.9	134.8	129.7	133.0	127.3	131.4	OH ----	----	----	----	----	----	----
6			OSO_2CH_3	cis	138.7	----	128.6	121.2	108.4	73.9	67.7	51.0	66.4	136.1	134.1	129.4	132.9	127.3	131.4	CH_3^* 37.5	----	----	----	----	----	----
7			$OCOC_6H_5$	cis	138.5	----	128.5	120.9	108.1	74.3	67.1	51.5	63.9	135.9	134.2	129.6	132.9	127.2	131.3	CO 166.1	131.3	129.6	128.5	133.3	128.5	129.6
8			$OC_6H_3Cl_2$-2,4	cis	138.9	----	128.6	121.3	108.4	73.9	67.7	51.0	66.4	136.0	134.4	130.1	133.1	127.3	131.5	O ----	152.7	123.7	129.6	126.5	128.6	114.6
9			$SC_6H_3Cl_2$-2,6	cis	138.5	----	128.5	121.0	108.1	76.2	69.4	51.5	36.6	135.7	134.5	129.4	132.9	127.1	131.2	S ----	131.6	141.4	128.7	130.3	128.7	141.4
10	4-NO_2-Im.	2,4-$Cl_2C_6H_3$	OH	cis	138.7	----	146.5	123.2	106.7	76.8	66.9	51.4	61.0	134.8	134.8	130.1	132.5	127.4	130.8	OH ----	----	----	----	----	----	----
11			OSO_2CH_3	cis	137.7	----	147.6	121.4	107.5	74.1	67.1	51.9	66.2	136.7	135.7	129.5	132.9	127.6	131.7	CH_3^* 37.6	----	----	----	----	----	----
12			$OCOC_6H_5$	cis	137.5	----	147.6	121.1	107.3	74.4	66.9	52.1	63.7	136.5	134.4	129.2	133.1	127.5	131.6	CO 166.1	131.6	129.6	128.6	133.4	128.6	129.6
13	2-Me-5-NO_2 -Imid.	2,4-$Cl_2C_6H_3$	OH	cis	144.8	----	123.8	146.4	107.2	76.7	66.8	50.0	61.0	134.9	134.9	130.2	132.5	127.5	130.7	OH ----	----	----	----	----	----	----
14			OSO_2CH_3	cis	146.2	----	122.1	146.7	108.3	74.2	67.1	50.4	60.1	136.8	135.7	129.6	133.1	127.8	131.8	CH_3^* 37.7	----	----	----	----	----	----
15			$OCOC_6H_5$	cis	146.2	----	121.8	146.4	108.0	74.4	66.9	50.7	63.1	136.6	133.6	129.8	133.1	127.7	131.7	CO 166.0	131.7	129.8	128.6	133.4	128.6	129.8
16	Imidazolyl	4-FC_6H_4	$OCOC_6H_5$	trans	138.6	----	128.4	120.9	108.2	74.2	67.0	54.0	64.1	135.0	127.5 127.9	114.9 115.9	157.5 168.6	114.9 115.9	127.5 127.9	CO 166.0	129,7	129.7	128.4	133.3	128.4	129.7
17		4-ClC_6H_4	$OCOC_6H_5$	trans	138.7	----	128.3	120.9	108.5	76.0	66.9	54.7	62.7	134.9	127.1	128.7	138.7	128.7	127.1	CO 166.0	129.7	129.7	128.3	133.3	128.3	129.7
18		4-BrC_6H_4	$OCOC_6H_5$	trans	138.7	----	128.3	120.9	108.5	76.0	66.9	54.6	62.7	138.6	127.3	131.6	123.3	131.6	127.3	CO 166.0	131.6	129.5	128.3	133.3	128.3	129.5
19		4-$CH_3OC_6H_4$	$OCOC_6H_5$	trans	138.7	----	128.5	120.9	108.8	75.7	67.0	54.9	63.2	132.1	126.9	113.8	159.9	113.8	126.9	CO 166.0	132.1	129.6	128.2	133.1	128.2	129.6
20	Triazolyl (1,2,4)	2,4-$Cl_2C_6H_3$	OH	cis	----	151.4	----	145.1	107.2	76.9	66.4	53.5	61.5	135.9	134.2	129.5	132.9	127.3	131.4	OH ----	----	----	----	----	----	----
21			OSO_2CH_3	cis	----	151.4	----	144.9	108.1	73.8	67.6	53.4	66.3	136.2	133.4	129.5	133.0	127.3	131.5	CH_3^* 37.7	----	----	----	----	----	----
22			$OCOC_6H_5$	cis	----	151.4	----	144.7	107.8	74.3	67.0	53.7	63.8	136.0	133.8	129.5	133.0	127.2	131.4	CO 165.9	131.4	129.6	128.5	133.3	128.5	129.6
23			$OC_6H_3Cl_2$-2,4	cis	----	151.3	----	145.0	107.8	74.4	67.4	53.6	68.8	136.2	133.9	129.6	133.2	127.3	131.5	O ----	152.6	123.9	130.1	126.8	127.8	114.7
24			$SC_6H_3Cl_2$-2,6	cis	----	151.5	----	144.9	107.8	76.2	69.4	53.9	37.0	136.0	134.0	129.5	133.2	127.2	131.4	S ----	131.6	141.5	128.9	130.6	128.9	141.5
25	Tetrazolyl (1,2,3,5)	2,4-$Cl_2C_6H_3$	CH_3	cis	----	----	152.6	----	106.5	78.0	69.9	56.9	25.9	135.5	134.5	129.5	133.1	126.9	130.0	CH_3 9.8	----	----	----	----	----	----
26			CH_3	trans	----	----	152.6	----	106.5	79.1	69.6	57.1	25.5	135.7	134.7	129.6	133.2	127.0	131.1	CH_3 9.5	----	----	----	----	----	----
27			OH	cis	----	----	152.8	----	106.9	77.1	66.6	56.7	61.6	135.1	133.9	129.7	133.2	127.2	131.2	OH ----	----	----	----	----	----	----
28			OSO_2CH_3	cis	----	----	152.9	----	107.9	74.0	67.9	56.8	66.3	136.4	134.4	129.6	133.2	127.3	131.5	CH_3^* 37.6	----	----	----	----	----	----
29			$OCOC_6H_5$	cis	----	----	152.7	----	107.4	74.3	67.0	56.7	63.7	135.1	134.1	129.9	133.3	127.0	131.3	CO 165.9	131.3	129.6	128.4	133.3	128.4	129.6

*) Methyl signal of methanesulfonyl group.

TABLE 2. ^{13}C-NMR CHEMICAL SHIFTS OF 2-ARYL-2-BROMOMETHYL-4-BENZOYLOXYMETHYL-1,3-DIOXOLANES (1, X=Br, Y=$OCOC_6H_5$)[b]

No.	Ar		Dioxolane ring					2-Aryl group (Ar)						Benzoyloxyl group (Y)				
			2	4	5	2-CH_2	4-CH_2	1	2	3	4	5	6	CO	1	2	3	4
30	4-FC_6H_4	cis	107.9	74.3	67.5	37.5	64.3	135.9	127.9	114.8	157.6			166.2	129.8	129.8	128.3	133.3
									128.5	115.8	168.5							
31		trans	108.0	76.4	67.3	38.8	63.1	135.9	127.5	114.6	157.3			165.9	129.8	129.5	128.2	133.1
									128.0	115.6	168.4							
32	4-ClC_6H_4	cis	107.7	74.3	67.5	37.2	64.1	134.9	127.5	128.6	139.8			166.1	129.7	129.7	128.4	133.2
33		trans	108.0	76.6	67.4	38.7	63.0	134.8	127.4	128.2	138.7			166.1	130.9	129.5	128.3	133.2
34	4-BrC_6H_4	cis	107.8	74.3	67.5	37.2	64.1	138.4	127.9	131.5	123.3			166.1	131.1	129.7	128.4	133.6
35		trans	108.0	76.5	67.3	38.6	62.8	139.1	127.6	131.4	123.0			165.9	131.4	129.9	128.6	133.4
36	2,4-$Cl_2C_6H_3$	cis	108.0	74.5	67.7	35.4	64.1	135.4	133.2	129.4	133.0	126.9	131.1	166.4	131.3	129.4	128.2	133.2
37		trans	108.0	76.4	67.1	36.1	62.6	135.8	134.6	130.1	133.1	127.1	131.4	165.9	131.4	129.9	128.6	133.4
38	2,4-$Cl_2C_6H_3$[a] (Y=CH_3)	cis	106.7	78.1	70.3	36.0	26.1	136.2	135.1	129.9	132.8	126.7	130.9	(CH_3: 9.9)				
39		trans	106.9	79.9	70.2	36.1	25.5	136.3	135.0	129.8	132.7	126.8	130.7	(CH_3: 10.0)				

a) 2-Bromomethyl-2-(2,4-dichlorophenyl)-4-ethyl-1,3-dioxolane. b) Chemical shifts are given in terms of part per million (ppm) from TMS.

TABLE 3. ^{13}C CHEMICAL SHIFT DIFFERENCES ($\Delta\delta=\delta_{trans}-\delta_{cis}$) OF 2-ARYL-2-BROMOMETHYL-4-BENZOYLOXYMETHYL-1,3-DIOXOLANES

No. of compd		Ar	Carbon atom				
trans	cis		4-CH_2	4	5	2	2-CH_3
31	30	4-FC_6H_4	−1.2	+2.1	−0.2	+0.1	+1.3
33	32	4-ClC_6H_4	−1.1	+2.3	−0.1	+0.3	+1.5
35	34	4-BrC_6H_4	−1.3	+2.0	−0.2	+0.2	+1.4
37	36	2,4-$Cl_2C_6H_3$	−1.5	+1.9	−0.6	0.0	+0.7
39	38	2,4-$Cl_2C_6H_3$ (Y=CH_3)	−0.6	+1.8	−0.1	+0.2	+0.1
26	25	2,4-$Cl_2C_6H_3$ (X=CHN_4) (Y=CH_3)	−0.4	+1.1	−0.3	0.0	+0.2

given in Table 2. These bromides are the intermediates for the syntheses of the compounds in Table 1, and their stereochemistry is very important in the pharmaceutical purpose.

The assignment of the dioxolane spectra in Tables 1 and 2 was carried out according to the method cited in the literatures on simple dioxolanes.[5,6] Quite naturally, the chemical shifts of methylene carbon atom on 4-carbon atom (4-CH_2) are affected predominantly by the oxygen containing substituent (Y) on it and that on 2-carbon atom (2-CH_2) by the nature of the azole moiety. The effect by the substituent Y on 4-CH_2 group is transmitted to the ring carbon atoms in an alternate way. The 4-CH_2 carbon atom attached directly to the substituent Y resonates at the lower field as the substituent becomes more electronegative *i.e.*, in the increasing δ-values in the order of $OH<OCOC_6H_5<OSO_2CH_3$. The sequence of chemical shifts is similar as to the second neighbor carbon atom(C-5), but reversed as to the neighbor carbon atom(C-4). The effect is rather long range, the order of chemical shifts being preserved even on C(2) when compared among the derivatives carrying similar heteroaromatic moiety.

The 2-CH_2 chemical shift is linearly correlated with the N-CH_3 carbon chemical shift of the corresponding *N*-methylazole reported by Roberts and co-workers.[7] The 2-CH_2 chemical shift decreases in the increasing order of acidity.[8]

Signals of azole moiety were assigned without difficulty by comparing with the spectra of the corresponding *N*-methylazoles.[7] Chemical shifts of the carbon atoms in azolyl(X) or 2-aryl group, as well as those of benzoyl or methanesulfonyl group(Y), remain constant irrespective of the substituents in other part of the molecule.

It is important to establish the method to differentiate the cis and the trans isomers of the precursor bromides **30—39**. For this purpose. ^{13}C-NMR spectra of these bromides (in Table 2) were carefully examined. The difference in chemical shifts between the cis and the trans isomers ($\Delta\delta$) is given in Table 3. Without exception, the $\Delta\delta$ value is negative for the 4-CH_2 and positive for 4-carbon atom of the dioxolane ring. The high field shift of the 4-CH_2 chemical shift in the trans isomer is very probably due to the anisotropy effect of the 2-aryl group located just opposite to this methylene group. Another very remarkable difference in $\Delta\delta$ is observed with the 2-CH_2 group of the 4-benzoyloxyl derivatives **30—37**. Since the effect is obscured with the 4-ethyl derivatives (**38** and **39**), the high field shift is supposed to be originated from the anisotropy effect by the benzoyl group. In conclusion, the $\Delta\delta$ values are not large but very consistent in sign, hence usable to discriminate the each diastereoisomer.

References

1) J. Heeres, L. J. J. Backx, J. H. Mostmans, and J. Van Cutsem, *J. Med. Chem.*, **22**, 1003 (1979).

2) Y. Hamada, I. Takeuchi, K. Yamamoto, and R. Uehara, Abstracts of the 102nd Annual Meeting of the Pharmaceutical Society of Japan, Osaka (1982), p. 388.

3) These diastereoisomers are designated as cis when CH_2X and CH_2Y groups are located in the same side in reference to the plane of the dioxolane ring, and as trans when they are located on the other side of the plane.

4) Y. Hamada, I. Takeuchi, K. Yamamoto, M. Hirota, and H. Suezawa, *Chem. Pharm. Bull.*, submitted for publication.

5) G. C. Levy, R. L. Lichter, and G. L. Nelson, "Carbon-13 Nuclear Magnetic Resonance Spectroscopy," 2nd ed, John Wiley & Sons, New York (1980), pp. 102—135.

6) G. Dana and H. Danechpajouh, *Bull. Soc. Chim. Fr.*, **1980**, II-395.

7) J. Elguero, C. Marzin, and J. D. Roberts, *J. Org. Chem.*, **39**, 357 (1974).

8) M. R. Grimmett, "Comprehensive Organic Chemistry," ed by D. Barton and W. D. Ollis, Pergamon Press, Oxford (1979), p. 364.

Photoreductive Dehalogenation of Organic Halides in the Presence of Lithium Aluminum Hydride

Nobujiro SHIMIZU,* Kenji WATANABE, and Yuho TSUNO
Department of Chemistry, Faculty of Science, Kyushu University 33, Higashi-ku, Fukuoka 812
(Received August 11, 1983)

Synopsis Lithium aluminum hydride markedly accelerates photoreductive dehalogenation of cyclopropyl, aromatic, and olefinic halides carried out in ether.

UV irradiation of organic halides in a hydrogen donating solvent often leads reductive dehalogenation.[1] Cyclopropyl bromides are thus obtainable by irradiating the corresponding *gem*-dibromides in ether, although in moderate to low yields.[2] We here report that irradiation in the presence of lithium aluminum hydride (LAH) results in significant improvement in the efficiency and yield of the photoreduction of halides including cyclopropylidene dihalides. Most of the experimental results are summarized in Table 1.

Figure 1 illustrates the photoreduction of 7,7-dibromonorcarane (**1a**) in the presence or absence of LAH carried out at 0 °C under nitrogen with a 100 W mercury lamp using *ca.* 0.02 M (1 M=1 mol dm^{-3}) ethereal solutions. Obviously, LAH exerts a marked rate accelerating effect which increases in keeping with the amount of LAH added. For example, **1a** disappeared practically in 15 min on irradiation in the presence of 2 molar amounts of LAH affording 7-bromonorcarane (**2a**, cis/trans=3.2) as the principal product (75%), whereas in the absence of the hydride, an incomplete photolysis resulted even after prolonged irradiation up to 4 h. LAH also facilitates the

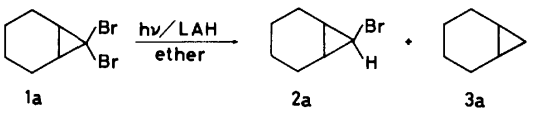

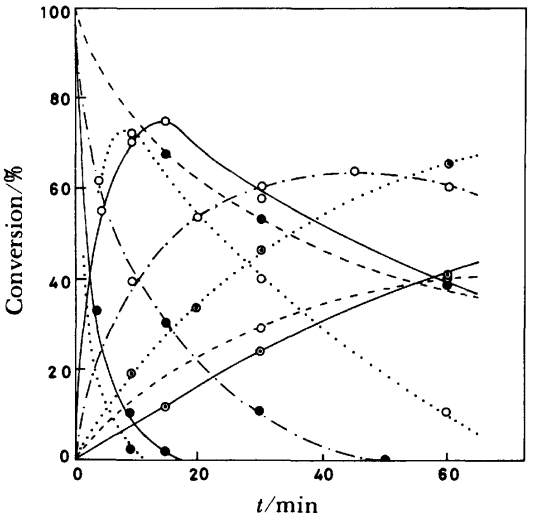

Fig. 1. Photoreduction of **1a** in ether in the presence of LAH.
[LAH]/[**1a**]: 4.0 (·····), 2.0 (——), 1.0 (—·—), and 0 (----). ●: **1a**, ○: **2a**, ⊙: **3a**.

TABLE 1. PHOTOREDUCTIVE DEHALOGENATION IN THE PRESENCE OF LAH[a]

Halide **1**	Conditions		Yield/%[b]	
	[LAH]/[1]	Time/h	**2**[c]	**3** and others
7,7-Dibromonorcarane (**1a**)	2	8[d]	11 (3.0)	≈0 (86)[e]
	0	0.5	27 (3.3)	≈0 (51)[e]
	2	0.5	62 (3.2)	24 (0)[e]
	2	2.5	3 (3.5)	62
	4	0.5	46 (3.3)	44
9,9-Dibromobicyclo[6.1.0]nonane (**1b**)	2	0.5	71 (1.8)	7
7,7-Dichloronorcarane (**1c**)	0	8	19 (1.8)	≈0 (52)[e]
	4	8	77 (2.3)	5 (0)[e]
9,9-Dichlorobicyclo[6.1.0]nonane (**1d**)	4	8	88 (1.8)	7
1,1-Dichloro-2-hexylcyclopropane (**1e**)	4	8	94 (1.4)	5
1,1-Dichloro-2-phenylcyclopropane (**1f**)	4	8	55 (1.5)	5
Chlorobenzene (**1g**)	0	0.5		20 (benzene) (73)[e]
	2	0.5		96 (benzene) (0)[e]
Bromobenzene (**1h**)	2	0.25		95 (benzene)
p-Bromochlorobenzene (**1i**)	2	0.25		77 (**1g**)+18 (benzene)
β-Bromostyrene	2	0.5		55 (styrene)

a) Each halide was irradiated in ether (*ca.* 0.02 M) with a 100 W medium pressure mercury lamp at 0 °C under nitrogen. b) Determined by GLC. c) Isomer ratio (cis/trans) was given in parentheses. d) Dark reaction. e) Recovery of the starting material.

photoreduction of the bromide **2a**; so prolonged irradiation leads to the formation of the fully reduced hydrocarbon **3a** in substantial quantity, especially so when large amounts of LAH are used.[3] LAH itself is capable of reducing most organic halides[4] but the contribution of this thermal process was negligibly small under the present photolysis conditions.

Other halides **1b—j**— they were thermally almost inert toward LAH under the photolysis conditions given in the table for each halide — also underwent rapid reduction on irradiation in the presence of LAH. The reduction proceeded more rapidly for bromides than for chlorides and a selective dehalogenation was feasible for a mixed halide **1i**. For preparative purpose, concentrated solutions could be used as well. For example, **2a** was prepared in 70% isolated yield by irradiating a 0.2 M ethereal solution of **1a** in the presence of 2 molar amounts of LAH (0 °C, 1.5 h).[5]

Two additional observations are worth stating. First, 2,3-diethoxybutane (**4**) was formed in substantial quantity in all LAH-assisted photoreductions. Second, the photolysis of **1a** using lithium aluminum deuteride led no D-incorporation in the products **2a** and **3a**. These results suggest that LAH does not act as a hydrogen donor toward an alkyl (or aryl) radical in contrast to sodium borohydride.[6] Presumably, LAH would

$$\text{R-X} \overset{h\nu}{\rightleftharpoons} \text{R}\cdot + \cdot\text{X} \overset{\text{LAH}}{\longrightarrow} \text{R}\cdot + \text{HX} + \text{LiAlH}_3^{-}\cdot$$

$$\text{R-X} + \text{LiAlH}_3^{-}\cdot \longrightarrow \text{R}\cdot + \text{LiX} + \text{AlH}_3$$

$$\text{R}\cdot + \text{ether} \longrightarrow \text{R-H} + \mathbf{4}$$

depress the recombination between an alkyl and a halogen radicals *vis* efficient capture of the latter. Moreover, aluminum hydride anion radical which would result may induce homolysis of another molecule of a halide. Besides, LAH suppressed the formation of a polymeric material, especially in the photolyses of cyclopropylidene dibromides, and this would also be partly responsible for the observed rate acceleration.

Experimental

Lithium aluminum hydride (Wako Pure Chemical) was used directly as slurries in ethereal solutions. Photolyses were carried out with a 100 W medium pressure mercury lamp (Eikosha Halos PIH-100) at 0 °C under nitrogen. All products **2—4** were characterized by comparison of their spectral data with those reported or those of authentic samples prepared separately. The following photolysis was representative.

Photolysis of 7,7-Dibromonorcarane (1a) in the Presence of LAH. To a cold stirred solution of LAH (965 mg) in ether (500 ml) was added a mixture of **1a** (3.23 g, 12.7 mmol) and tridecane (0.20 ml as an internal standard). The mixture was irradiated with stirring for 30 min at 0 °C and quenched with cold hydrochloric acid. GLC analysis of the crude oil obtained after workup indicated the formation of 7-bromonorcarane (**2a**, cis/trans=3.2) and norcarane (**3a**) in 62 and 24% yields, respectively. The oil was fractionated under reduced pressure to give **2a** (cis/trans=3.35, 1.17 g, 53%), bp 83—85 °C/20 Torr (1 Torr=133.3 Pa) [lit,[7] bp 84—86 °C/23 Torr], together with a low-boiling fraction (760 mg) which was shown to be a mixture of **3a** and 2,3-diethoxybutane (1:1 mixture of two diastereoisomers) in the ratio 1:3.

References

1) J. R. Siegman and J. J. Houser, *J. Org. Chem.*, **47**, 2773 (1982); N. Mitsuo, T. Kunieda, and T. Takizawa, *ibid.*, **38**, 2255 (1972); J. T. Pinhey and R. D. G. Rigby, *Tetrahedron Lett.*, **1969**, 1267.

2) N. Shimizu and S. Nishida, *Chem. Lett.*, **1977**, 839.

3) The isomer ratio of **2a** did not change significantly during the photolysis, suggesting little difference in photochemical behavior between the cis and trans stereoisomers.

4) S. Krishnamurthy and H. C. Brown, *J. Org. Chem.*, **47**, 276 (1982); C. W. Jefford, D. Kirkpatrick, and F. Delay, *J. Am. Chem. Soc.*, **94**, 8905 (1972).

5) The photolysis did not proceed appreciably in the absence of LAH mainly because of the formation of polymeric materials on the surface of the lamp at the very early stage.

6) J. T. Groves and K. W. Ma, *J. Am. Chem. Soc.*, **96**, 6527 (1974); J. A. Barltrop and D. Bradbury, *ibid.*, **95**, 5085 (1973).

7) D. Seyferth, D. L. Lambert, Jr., and M. Massol, *J. Organomet. Chem.*, **88**, 255 (1975).

Ring-contracted Crown Ethers: 14-Crown-5, 17-Crown-6, and Their Sila-analogues. Drastic Decrease in Cation-binding Ability

Mikio Ouchi, Yoshihisa Inoue,* Takashi Kanzaki, and Tadao Hakushi*
Department of Applied Chemistry, Himeji Institute of Technology, 2167 Shosha, Himeji, Hyogo 671-22
(Received August 22, 1983)

Synopsis. As compared with symmetrical 3*m*-crown-*m*, the ring-contracted(3*m*−1)-crown-*m* showed drastic decrease in cation-binding ability, which is attributable not to the diminished cavity size but to the disordered conformation induced by ring contraction.

The control of complexation phenomena has been the major subject of the crown ether chemistry. Recent investigations from this laboratory[1] have shown that the introduction of an extra methylene group into a symmetrical 3*m*-crown-*m* (*m*=4—6) affects remarkably its cation-binding ability toward alkali metal ions; *e.g.* 16-crown-5 derivatives possess much higher Na^+/K^+ selectivity than the parent 15-crown-5. Our subsequent interest in this field is directed toward ring-contracted (3*m*−1)-crown-*m* (*m*=5, 6). Pedersen first reported the effect of ring-contraction upon complex formation,[2] however, no clear-cut discussion was made. In the present study, we report the cation-binding ability of 14-crown-5 (**2**), 17-crown-6 (**5**), and their sila-analogues (**3**, **6**), and the results are discussed in view of the size-fit concept and conformational difference.

In order to evaluate the cation-binding ability, extrations of aqueous alkali metal picrates (Na^+, K^+, Rb^+, and Cs^+) were carried out at 25 °C with dichloromethane solutions of **2**, **3**, **5**, and **6**, and the results were compared with those for the parent 15-crown-5 (**1**) and 18-crown-6 (**4**) and also with those for acyclic analogues, tetraglyme (**8**) and pentaglyme (**9**).

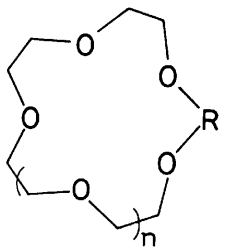

1, *n*=1; R=CH_2CH_2 **5**, *n*=2; R=CH_2
2, *n*=1; R=CH_2 **6**, *n*=2; R=$Si(CH_3)_2$
3, *n*=1; R=$Si(CH_3)_2$ **7**, *n*=1; R=$(CH_2)_4$
4, *n*=2; R=CH_2CH_2

As can be seen from Table 1, the ring-contracted crown ethers **2**, **3**, **5**, and **6** showed extremely low extractabilities as is the case with the open-chain analogues **8** and **9** under the conditions employed,[3] where 15-crown-5 and 18-crown-6 gave moderate extractabilities. It should be noted that, in spite of the longer O-Si-O bond (3.3 Å) than the O–C–O bond (2.8 Å) of **2** and **5**, the sila-crown ethers **3** and **6** show practically the same extractabilities as the corresponding carbon analogues **2** and **5**. This result is very significant in ascertaining the origin of the extremely low extractability for the ring-contracted crown ethers, and may suggest that the reduced cavity size is not the most important factor which is responsible for the low extractability.

Table 1. Extraction of alkali metal picrates[a]

Ligand	Extractability/%[b]			
	Na^+	K^+	Rb^+	Cs^+
15-Crown-5 (**1**)	13.2	14.3	9.6	3.3
14-Crown-5 (**2**)	0.1	0.2	0.2	0.2
Sila-14-crown-5 (**3**)	0.1	0.4	0.5	0.5
Tetraglyme (**8**)	0.1	0.1	0.1	0.1
18-Crown-6 (**4**)	6.3	69.3	57.6	36.7
17-Crown-6 (**5**)	0.8	1.7	1.0	0.7
Sila-17-crown-6 (**6**)	0.3	1.8	1.1	0.7
17-Crown-5 (**7**)	1.8	1.9	0.9	0.7
Pentaglyme (**9**)	0.2	0.7	0.6	0.5

a) Temperature 25.0±0.1 °C; aqueous phase(10 mL): [picrate]=3×10^{-3} M; organic phase(CH_2Cl_2, 10 mL): [ligand]=3×10^{-3} M. b) % Picrate extracted into organic phase.

The drastic decrease in cation-binding ability of **2**, **3**, **5**, and **6** may rather be accounted for in terms of the disordered conformation of crown ether ring. Examinations with CPK molecular model revealed that one of the five or six donor oxygen atoms of **2**, **3**, **5**, and **6** can not be accomodated in the plane which is composed of the rest of the oxygen atoms, while the cavity sizes of the crown ethers do not differ significantly; *ca.* 1.7 Å for **1-3** and 2.5—2.6 Å for **4-6**.

17-Crown-5 (**7**) was synthesized in order to obtain additional support for the above explanation. It was synthesized in 16% yield by the reaction of 1,4-butanediol with tetraethylene glycol ditosylate in tetrahydrofuran in the presence of NaOH as a base.

Definitive evidence arises from the comparison of extractabilities of 17-crown-5 and 17-crown-6. In spite of the reduced number of donor oxygen atoms from six to five, 17-crown-5 still gave comparable extractabilities for all cations. This clearly indicates that one of the formal donor oxygen atoms of 17-crown-6 and probably of 14-crown-5 and their sila-analogues **3** and **6** no longer acts as an effective donor atom due to the conformational disorder of the ring-contracted crown ethers.

Experimental

General. Infrared spectra were obtained on a JASCO A-100 grating spectrophotometer. Mass spectra were measured at 20 eV using Hitachi RM-50GC instrument. ^1H and

^{13}C NMR spectra were obtained in chloroform-*d* solution containing 1% tetramethylsilane as an internal standard, using JEOL PMX-60 and FX-60 spectrometers. UV-VIS spectra were recorded on a Shimiadzu UV-300 spectrophotometer.

Synthesis. 14-Crown-5(**2**) and 17-crown-6 (**5**) were synthesized according to the procedure described in the literature.[4]

1,4,7,10,13-Pentaoxacycloheptadecane (17-Crown-5, 7). 1,4-Butanediol (5.4 g, 0.06 mol) in tetrahydrofuran(THF) (100 mL) was added to a stirred suspension of sodium hydroxide (6.0 g, 0.15 mol) in THF (300 mL) at 66 °C, and the stirring was continued for 1 h at 66 °C. To the mixture was added tetraethylene glycol ditosylate[5] (25.1 g, 0.05 mol) in THF (150 mL) dropwise over 2 h and stirring was continued for 24 h at 66 °C under a nitrogen atmosphere. The solvent was evaporated and the residue was extracted with chloroform. The chloroform extract was dried over magnesium sulfate and the solvent was evaporated. Distillation of the product under a reduced pressure gave 2.0 g (16%) of **7**: bp 105—107 °C/0.13 Torr(1 Torr=133.322 Pa); MS, *m/z* 248 (M^+); ^1H NMR δ=3.63—3.83 (20H, m) and 1.60—1.80 (4H, m); ^{13}C NMR δ=71.8(t), 71.1(t), and 27.5(t, $OCH_2\underline{C}H_2\underline{C}H_2CH_2O$); IR(neat) 2850, 1450, 1350, 1290, 1250, and 1100 cm^{-1}. The ^1H NMR spectrum was in agreement with published data.[6]

2,5,8,11,14,17-Hexaoxaoctadecane (Pentaglyme, 9) was prepared from ethylene glycol monomethyl ether (5.3 g, 0.07 mol) and triethylene glycol ditosylate[5] (13.8 g, 0.03 mol) in the presence of sodium hydroxide in THF according to the procedure described above. Distillation of the product gave 3.7 g (46%) of **9**: bp 100—108 °C/0.27 Torr; MS, *m/z* 266 (M^+); ^1H NMR δ=3.55—3.78 (20H, m) and 3.38 (6H, s); ^{13}C NMR δ=73.0 (t), 71.6 (t), and 59.3 (q, CH_3O); IR (neat) 2800, 1450, 1350, 1290, 1240, and 1110 cm^{-1}; Found: C, 54.19; H, 10.11; Calcd for $C_{12}H_{26}O_6$: C, 54.12; H, 9.84.

Extraction. Sodium, potassium, rubidium, and cesium picrates were prepared according to Wong's method.[7,8] Commercially available 15-crown-5 (Nisso Co.), 18-crown-6 (Nisso Co.), tetraglyme (Nakarai Chemical Co.), and sila crown ethers **3** and **6** (Petrarch Systems Inc.) were used without further purification. The extraction procedures were similar to those reported by Kimura *et al.*[9] Equal volumes (10 mL) of a dichloromethane solution of a ligand (3×10^{-3} M) and of an aqueous alkali metal picrate (3×10^{-3} M) were introduced into an Erlenmeyer flask, which was then stoppered and shaken for 10 min at 25.0±0.1 °C using a TAIYO M100L incubator. The mixture was then allowed to stand for at least 2 h at that temperature in order to complete the phase separation. After the phase separation 2 mL of the dichloromethane phase was withdrawn, to which 2 mL of acetonitrile was added. After further dilution, if necessary, with a 1:1 mixture of dichloromethane and acetonitrile, the picrate concentration in the organic phase was determined from its absorption at 375 nm. The molar extinction coefficients at 375 nm for sodium, potassium, rubidium, and cesium picrates are 18600, 19000, 18800, and 18500 M^{-1} cm^{-1}, respectively.

This work was partially supported by a grant from the Hyogo Foundation for the Promotion of Science and Technology, which is gratefully acknowledged. We thank Prof. T. Shono and Mr. S. Kitazawa of Osaka University for the stimulating discussion on the CPK model.

References

1) M. Ouchi, Y. Inoue, H. Sakamoto, A. Yamahira, M. Yoshinaga, and T. Hakushi, *J. Org. Chem.*, **48**, 3168 (1983).

2) C. J. Pedersen, *J. Am. Chem. Soc.*, **92**, 391 (1970).

3) With **2** and **5**, similar low extractabilities for Li^+, Na^+, and K^+ ions have already been observed under different extraction conditions, where the ratio [ligand]/[picrate] exceeds four; Y. Kawakami, T. Sugiura, and Y. Yamashita, *Bull. Chem. Soc. Jpn.*, **51**, 3053 (1978).

4) Y. Kawakami, J. Suzuki, and Y. Yamashita, *Polym. J.*, **9**, 519 (1977).

5) D. Bailey, D. Tirrell, and O. Vogl, *J. Macromol. Sci. Chem.*, **A12**, 661 (1978).

6) J. G. Kostelc, B. J. Garcia, G. W. Gokel, and L. B. Hendry, *J. Chem. Ecol.*, **5**, 179 (1979).

7) K. H. Wong and H. L. Ng, *J. Coord. Chem.*, **11**, 49 (1981).

8) Caution should be taken in working with the picrate salts since they are heat- and shock-sensitive when dry, as is the picric acid itself.

9) K. Kimura, T. Maeda, and T. Shono, *Talanta*, **26**, 945 (1979).

Mechanochemical Racemization of L-Leucine

Akiko IKEKAWA* and Sohachiro HAYAKAWA†

Faculty of Pharmaceutical Sciences, Showa University, Hatanodai, 1-5-8, Shinagawa-ku, Tokyo 142

†*Department of Applied Physics, Faculty of Science, Tokyo Institute of Technology, Oh-okayama, 2-12-1, Meguro-ku, Tokyo 152*

(Received August 25, 1983)

Synopsis On treating a ball-milled mixture of L-leucine and such diluents as silicone dioxide in hydrochloric acid, a part of L-leucine was transformed into D-leucine.

Racemization of optically active amino acids is of great interest with regard to the origin of optical activity. Mechanochemical racemization has not been reported yet, though several studies have been reported concerning racemization on γ-irradiation,[1] and acid-catalyzed[2,3] or base-catalyzed racemization of α-amino acids[4] under drastic conditions. It is known that little racemization occurs on treating a 6 M hydrochloric acid solution (1M=1 mol dm^{-3}) of α-amino acids at about 100 °C for 20 h.[3] In this paper, racemization of L-leucine on mechanochemical treatment was investigated.

A 10-g portion of a sample was inserted in a stainless-steel mill (in diameter of 10 cm and in capacity of 900 cm^3) containing ten stainless-steel balls (with a density of 8.2 g/cm^3 and in diameter of 2.5 cm) and thirty balls in diameter of 1.9 cm. The mill was rotated at a velocity of 120 min^{-1}. This procedure is called "ball-milling" hereafter. The ball-milled samples were L-leucine, silicone dioxide, talc, alminium oxide, titanium dioxide, microcrystalline cellulose (MCC), ethyl cellulose (EC), and a mixture of L-leucine and one of the other powders (diluents).

After a suspension of various samples containing L-leucine in a 6 M hydrochloric acid solution had been set aside for 30 min at room temperature, the suspension was centrifuged. The degree of optical rotation, $[\alpha]_D$, of the supernatant was measured with a Yanaco automatic polarimeter (Model OR-50).

N-(trifluoroacetyl)leucine isopropyl esters were derived as follows. Approximately 100 mg of leucine obtained by evaporating the supernatant was dissolved in 6.9 cm^3 of a saturated solution of hydrogen chloride in isopropyl alcohol and the solution was heated under reflux for 3 h. The solvent was removed under vacuum with a rotary evaporator. After washed by adding 5 cm^3 of dichloromethane and vacuum evaporating twice, the residue was dissolved in 2 cm^3 of dichloromethane and treated with 3 cm^3 of trifluoroacetic anhydride. The solution was heated under reflux for 15—30 min, and then the solvent was removed under vacuum. The residue was washed twice as before.[5] A dichloromethane solution of these derivatives was analysed by gas chromatography using a 30 m×0.24 mm fused-silica capillary column coated with OA-201 (optically active liquid of Shimadzu Seisakusho) as a stationary phase. This analysis was carried out at 110 °C with an inlet nitrogen pressure of 1 kg/cm^2. The IR spectra were measured by the use of Nujol method with a JASCO diffraction granting infrared spectrophotometer (Model IRA-2).

Results and Discussion

L-Leucine was ball-milled with diluents and treated in hydrochloric acid. The $[\alpha]_D$ value of the supernatant decreased by ball-milling with diluents, though the values for L-leucine ball-milled for 60 h without any diluent (b-L-leucine) or a mixture of b-L-leucine and a diluent ball-milled without leucine (b-diluent) were nearly identical with the value for original L-leucine.

N-(Trifluoroacetyl)leucine isopropyl esters, derived from leucine[5] obtained by evaporating the supernatant, were analyzed by gas chromatography. Hatano *et al.* found that keto acids and ammonia were formed on γ-ray irradiation in aqueous solutions of amino acids or oxidation of them in alkaline solutions.[6] On the other hand, Arakawa *et al.* showed that, on oxidation of amino acids in acidic or neutral solutions, both deamiation and decarboxylation occurred with subsequent formation of the coresponding aldehydes.[7] A large amount of bubbles were generated on treating the mixtures of L-leucine and diluents in hydrochloric acid; from this fact, decarboxylation is suggested to occur. These facts suggest that the peak "P" in Fig. 1 is due to 3-methylbutanal formed by deamination and decarboxylation of leucine. A peak of D-leucine was observed for the ball-milled mixture with talc, silicone dioxide, alminium oxide or titanium dioxide. In contrast, no peak of D-leucine was observed for b-L-leucine, a mixture of b-L-leucine and a b-diluent, or a ball-milled mixture with MCC or EC. Racemization percentage shown in Fig. 2 is twice the percentage of D-leucine in all the leucine, obtained from the peak areas of D- and L-leucine in the chromatogram. After keeping the mixture for some days in a stoppered bottle at room temperature after the end of ball-milling, the racemization percentage was determined. As is shown in Fig. 2, racemization percentage decreased gradually with the lapse of the time after the end of ball-milling. These results show that racemization of L-leucine takes place while the surface of the diluent in the mixture is active.

Figure 3 shows the effect of ball-milling with talc on IR spectra of L-leucine. The spectra of the mixtures of L-leucine and talc were nearly identical with those of

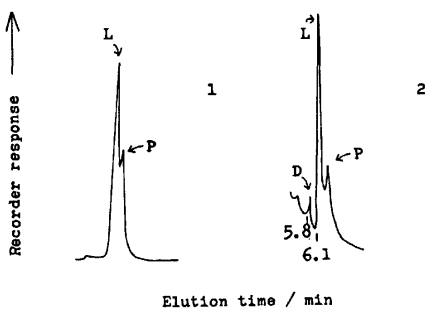

Fig. 1. Gas chromatogram of leucine derivatives. Sample 1: L-leucine, 2: a mixture with silicone dioxide ball-milled together for 18 h. (content of L-leucine; 10 w/w %). P; A peak of a degradation product.

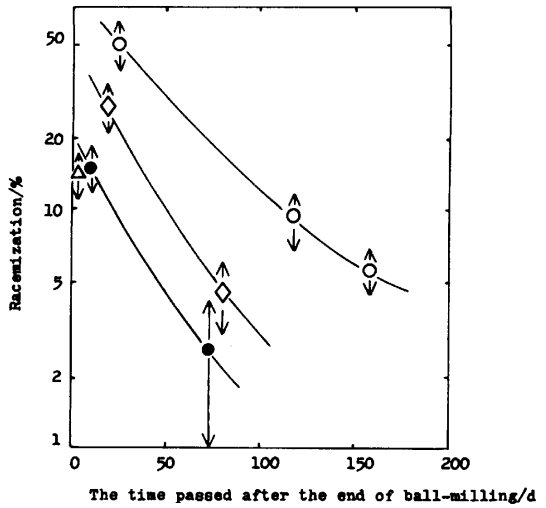

Fig. 2. Decrease in racemization percentage with the lapse of the time after the end of ball-milling.

Ball-milling conditions (content of L-leucine; 10 w/w %).

	diluent	ball-milling time/h
○	talc	60
◇	silicone dioxide	18
●	titanium dioxide	18
△	alminium oxide	3

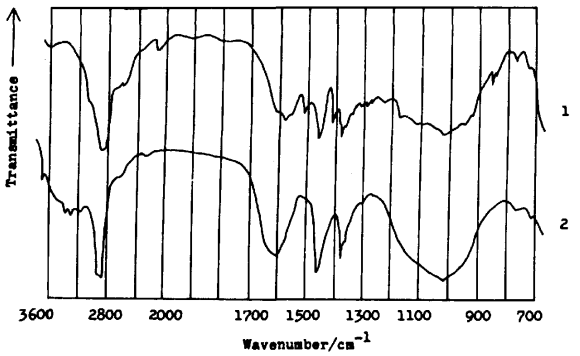

Fig. 3. Influence of ball-milling on IR spectra of the mixtures of L-leucine with talc. Content of L-leucine; 30 w/w %, ball-milling time 1: 0 h, 2: 60 h.

the mixtures of b-L-leucine and b-talc. It is considered from this fact that the changes in the range of 1600—1640 cm^{-1} and 3000—3400 cm^{-1} regions are not due to the adsorption of water. In this case the effect was as follows; (1) the absorbance at 3000—3400 cm^{-1} region (assigned to the NH_2 stretching vibration) increased, (2) the absorbance at 1600—1640 cm^{-1} region (assigned to the COO^- asymmetric stretching vibration) increased, and (3) the band at 1410 cm^{-1} (assigned to the COO^- symmetric stretching vibration) and the band at 1510 cm^{-1} (assigned to the NH_3^+ symmetric stretching vibration) disappeared. The similar effect was also observed upon ball-milling with silicone dioxide, MCC, or EC. Jackovitz and Walter reported an analogous change in the IR spectra of leucine on complexation with such metals as palladium. They considered that leucine in the metal complex was in the state of $NH_2CH(R)COO^-$ ($R=(CH_3)_2CHCH_2-$) where N and O binded with metals,[8] though leucine is in the state of $NH_3^+CH(R)COO^-$ in crystal powders.[9] These facts suggest that leucine in the ball-milled mixture with talc or silicone dioxide is also in the state of $NH_2CH(R)COO^-$ where N and O interact with these diluents. According to Jackovitz and Walter, the band in the range of 1550—1600 cm^{-1} due to the NH_2 scissors vibration is at a higher frequency, when the N-metal bond is stronger. The band in the range of 1570—1640 cm^{-1} due to the COO^- asymmetric stretching vibration is also at a higher frequency, when the O-metal bond is stronger.[8] The IR spectra suggested that the interaction force of L-leucine with talc in the ball-milled mixture was stronger than the force with silicone dioxide. A remarkable change was not observed in the spectra of the mixture with titanium dioxide or alminium oxide. This result shows that leucine in the ball-milled mixture with these diluents is in the state of $NH_3^+CH(R)COO^-$.

Bonner *et al.* found an approximately linear relationship between the extent of racemization and that of degradation upon γ-irradiation for the aqueous sodium salts of leucine.[1] The $[\alpha]_D$ values for the samples within 25 d from the end of ball-milling were nearly identical, and it is not considered from this fact that the degradation percentage for the mixture with talc or silicone dioxide is larger than the percentages for the other mixtures. The racemization percentages within 25 d from the end of ball-milling shown in Fig. 2 are large when leucine is in the state of $NH_2CH(R)COO^-$. It is also shown that racemization of L-leucine takes place more easily when the interaction force with a diluent is stronger. Bonner *et al.* irradiated γ-ray on aqueous solutions of sodium salts or hydrochloride salts of amino acids and found that $NH_2CH(R)COO^-$ suffered 5—11% of racemization and that $NH_3^+CH(R)COOH$ racemized little.[1]

References

1) W. A. Bonner and R. M. Lemmon, *Bioorg. Chem.*, **7**, 175 (1978). W. A. Bonner, N. E. Blair, and R. M. Lemmon, *Origins Life*, **9**, 279 (1979).

2) J. L. O'Brien and C. Niemann, *J. Am. Chem. Soc.*, **73**, 4264 (1951).

3) S. Nakaparksin, E. Gil-Av, and J. Oro, *Anal. Biochem.*, **33**, 374 (1970).

4) M. Sato, T. Tatsuno, and H. Matsuo, *Yakugaku Zasshi*, **90**, 1160 (1970).

5) W. A. Bonner, M. A. Van Dort, and J. J. Flores, *Anal. Chem.*, **46**, 2104 (1974).

6) H. Hatano and S. Rokushika, *Bull. Inst-Chem. Res. Kyoto Univ.*, **41**, 76 (1963); S. K. Upadhyay and M. C. Agrawal, *Indian J. Chem., Sect. A*, **15**, 709 (1977).

7) K. Arakawa, *J. Biochem.*, **44**, 217 (1957); R. S. Verma, M. J. Reddy, and V. S. Shastry, *J. Chem. Soc., Perkin Trans. 1*, **1976**, 469.

8) J. F. Jackovitz and J. L. Walter, *Spectrochim. Acta*, **22**, 1393 (1966).

9) K. Fukushima, T. Onishi, T. Shimanouchi, and S. Mizushima, *Spectrochim. Acta*, **15**, 236 (1959).

Restricted Rotation Involving the Tetrahedral Carbon. LII. Rotational Barriers in 1,2,3,4-Tetrafluoro- and 1,4-Dimethoxy-9-(1-cyano-1-methylethyl)triptycenes[1]

Gaku YAMAMOTO, Akira TANAKA, Masahiko SUZUKI, Yasuji MORITA, and Michinori ŌKI*

Department of Chemistry, Faculty of Science, The University of Tokyo, Bunkyo-ku, Tokyo 113

(Received September 2, 1983)

Synopsis. Kinetic measurements of rotamer isomerization of the title compounds show that the rotational barriers in these compounds are considerably higher than those in the *peri*-unsubstituted and the *peri*-chloro or *peri*-methyl compounds, affording a support to our earlier finding that the rotational barrier increases and then decreases as the *peri*-substituent becomes bulkier in 9-*t*-alkyltriptycenes.

We have shown that introduction of a chloro or a methyl group into a *peri*-position of 9-(1-cyano or methoxycarbonyl-1-methylethyl)triptycene (**1** and **2**) causes a decrease of the energy barrier to rotation about the bridgehead-to-substituent bond relative to the *peri*-unsubstituted compound.[2] A more extensive study on the effect of the *peri*-substituent on the rotational barrier in 9-(1,1-dimethyl-2-phenylethyl)triptycenes (**3**) revealed that a relatively small *peri*-substituent such

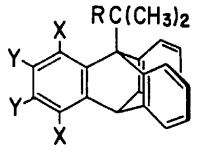

	R
1	CN
2	CO_2CH_3
3	$CH_2C_6H_5$

	X	Y
a	H	Cl
b	F	F
c	OCH_3	H
d	Cl	Cl
e	CH_3	H

as fluoro and methoxyl raises the barrier relative to the *peri*-unsubstituted compound **3a**, while a *peri*-group bulkier than chloro decreases the barrier.[3] Molecular deformation in this highly congested system might partly explain these phenomena.[3] These findings urged us to examine whether a fluoro or a methoxyl group at a *peri*-position raises the rotational barrier in compounds **1** and **2** as well. The results are presented in this note.

Results and Discussion

Reactions of 9-(1-cyano-1-methylethyl)anthracene with tetrafluoro- and 3,6-dimethoxybenzynes gave stereoselectively the ±*sc* atropisomers of **1b** and **1c**, respectively. Kinetic measurements of isomerization were carried out in 1-chloronaphthalene at three to four points of temperature. The equilibrium and rate constants obtained are compiled in Table 1 and the kinetic parameters therefrom are given in Table 2. The rotational barriers in these compounds are actually higher not only than that in the *peri*-unsubstituted derivative **1a** but also than those in the *peri*-chloro (**1d**) and the *peri*-methyl (**1e**) compounds. As shown in Fig. 1, the dependence of the energy barrier upon the *peri*-substituent in compounds **1** is very similar to that found in compounds **3**. This clearly shows that the appearance of the maximal barrier at a relatively small

Table 1. Equilibrium and rate constants

$ap \underset{k_{-1}}{\overset{k_1}{\rightleftharpoons}} \pm sc : K = k_1/k_{-1}$

Compd	Temp / °C	K	k_1 / s^{-1}
1b	240	1.66	1.44×10^{-4}
	211	1.83	1.52×10^{-5}
	196	1.93	4.53×10^{-6}
1c	220	4.11	1.09×10^{-4}
	211	4.39	4.24×10^{-5}
	197	4.73	1.60×10^{-5}
	189	4.36	7.90×10^{-6}

Table 2. Eyring parameters for isomerization[a]

Compd	Process	ΔH^* / kcal mol^{-1}	ΔS^* / cal mol^{-1} K^{-1}	ΔG^*_{473} / kcal mol^{-1}
1b	$ap\rightarrow\pm sc$	36.7±3.6	−5.7±7.3	39.4
	$\pm sc\rightarrow ap$	38.4±2.8	−3.5±5.6	40.0
1c	$ap\rightarrow\pm sc$	36.2±9.9	−4.4±20.8	38.3
	$\pm sc\rightarrow ap$	37.4±11.9	−4.9±24.9	39.7

a) 1 cal=4.184 J.

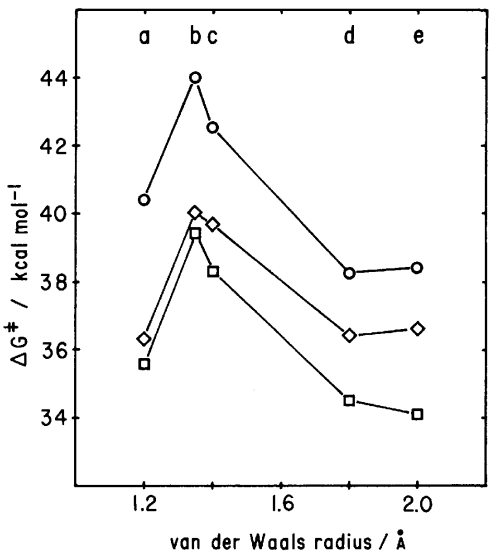

Fig. 1. Dependence of rotational barriers on the bulkiness of the *peri*-substituents.
□: ΔG^*_{473} for $ap\rightarrow\pm sc$ in **1**. ◇: ΔG^*_{473} for $\pm sc\rightarrow ap$ in **1**. ○: ΔG^*_{500} for $ap\rightarrow\pm sc$ in **3**.

peri-substituent is a general phenomenon in 9-*t*-alkyltriptycenes.

The equilibrium constant at 200 °C, K_{473}(±*sc*/*ap*), becomes larger as the *peri*-substituent becomes bulkier with an exception of **1b**:**1a**, 2.3; **1b**, 1.9; **1c**, 4.4; **1d**, 6.8; **1e**, 15. This trend is reasonable from the standpoint of steric effects because methyl is bulkier than cyano. Deviation from the trend by **1b**, where K_{473} is smaller than the statistical value of 2.0, may be ascribed to the electrostatic repulsion between the fluoro and cyano groups overweighing the steric effect.

9-(1-Methoxycarbonyl-1-methylethyl)anthracene failed to react with tetrafluorobenzyne to give **2b**, but reacted with 3,6-dimethoxybenzyne to afford stereoselectively the ±*sc* rotamer of **2c**. Heating a sample of ±*sc*-**2c** in 1-chloronaphthalene for *ca.* 5 h at 189 °C caused the complete equilibration of the rotamers but the equilibrium population of *ap*-**2c** was *ca.* 2-3%, which made the kinetic measurement of isomerization impossible. The overwhelming abundance of the ±*sc* rotamer may be due to the attractive interaction[4] between the methoxycarbonyl and the *peri*-methoxyl groups in ±*sc*-**2c** together with the steric effect also favoring the ±*sc* rotamer.

Experimental

Melting points are not corrected. ^{1}H NMR spectra were recorded on a Varian EM-390 spectrometer at 90 MHz at ambient temperature of *ca.* 35 °C. Experimental procedures of the kinetic measurements were described before.[2,3]

9-(1-Cyano-1-methylethyl)-1,2,3,4-tetrafluorotriptycene (1b). Reaction of 9-(1-cyano-1-methylethyl)anthracene[2] with pentafluorophenyllithium according to the procedure described in the literature[5] followed by column chromatography on silica gel with hexane–benzene as the eluent gave ±*sc*-**1b** in 41% yield, mp 239—240 °C (from tetrahydrofuran–hexane). Found: C, 73.23; H, 3.78; N, 3.66%. Calcd for $C_{24}H_{15}F_4N$: C, 73.28; H, 3.78; N, 3.56%. ^{1}H NMR ($CDCl_3$, δ): 2.39 (3H, d, *J*=7.0 Hz), 2.43 (3H, s), 5.73 (1H, br d, *J*=1.8 Hz), 7.0—7.2 (4H, m), 7.3—7.7 (3H, m), 8.0—8.2 (1H, m). The *ap* rotamer of **1b** was purely isolated from the equilibrated mixture of rotamers by column chromatography on silica gel, mp 231—232 °C (from tetrahydrofuran–hexane). Found: C, 73.11; H, 3.77; N, 3.56%. ^{1}H NMR ($CDCl_3$, δ): 2.41 (6H, d, *J*=6.3 Hz), 5.77 (1H, br d, *J*=1.8 Hz), 7.0—7.2 (4H, m), 7.3—7.6 (2H, m), 7.8—8.1 (2H, m).

9-(1-Cyano-1-methylethyl)-1,4-dimethoxytriptycene (1c). Reaction of 9-(1-cyano-1-methylethyl)anthracene[2] with 3,6-dimethoxyanthranilic acid[6] according to the general procedure described before[3] gave ±*sc*-**1c** in 50% yield, mp 293—296 °C (from tetrahydrofuran–ethanol). Found: C, 81.81; H, 5.83; N, 3.63%. Calcd for $C_{26}H_{23}NO_2$: C, 81.86; H, 6.08; N, 3.67%. ^{1}H NMR ($CDCl_3$, δ): 2.40 (3H, s), 2.42 (3H, s), 3.81 (3H, s), 3.82 (3H, s), 5.85 (1H, s), 6.58 (2H, s), 6.9—7.1 (4H, m), 7.3—7.7 (3H, m) 8.1—8.3 (1H, m). Column chromatography of the equilibrated rotamer mixture on alumina gave *ap*-**1c**, mp 297—298.5 °C (from ethanol). Found: C, 81.64; H,5.92; N, 3.64%. ^{1}NMR ($CDCl_3$, δ): 2.43 (6H, s), 3.72 (3H, s), 3.82 (3H, s), 5.90 (1H, s), 6.58 and 6.67 (2H, AB-q, *J*=9 Hz), 6.9—7.1 (4H, m), 7.3—7.5 (2H, m), 7.9—8.1 (2H, m).

±sc-*1,4-Dimethoxy-9-(1-methoxycarbonyl-1-methylethyl)triptycene (*±sc-*2c),* mp 222—224 °C, was synthesized similarly as ±*sc*-**1c** from 9-(1-methoxycarbonyl-1-methylethyl)anthracene[2] and 3,6-dimethoxyanthranilic acid[6] in 6% yield. Found: C, 78.28; H, 6.38%. Calcd for $C_{27}H_{26}O_4$: C, 78.24; H, 6.32%. ^{1}H NMR ($CDCl_3$, δ): 2.18 (6H, s),[7] 3.59 (3H, s), 3.65 (3H, br s), 3.80 (3H, s), 5.84 (1H, s), 6.48 and 6.59 (2H, AB-q, *J*=9 Hz), 6.7—7.1 (4H, m), 7.2—7.9 (4H, m).

References

1) Part LI: G. Yamamoto, Y. Tanaka, and M. Ōki, *Bull. Chem. Soc. Jpn.*, **56**, 3028 (1983).

2) S. Otsuka, T. Mitsuhashi, and M. Ōki, *Bull. Chem. Soc. Jpn.*, **52**, 3663 (1979); S. Otsuka, G. Yamamoto, T. Mitsuhashi, and M. Ōki, *ibid.*, **53**, 2095 (1980).

Jpn., **52**, 3663 (1979); S. Otsuka, G. Yamamoto, T. Mitsuhashi, and M. Ōki, *ibid.*, **53**, 2095 (1980).

4) M. Ōki, G. Izumi, G. Yamamoto, and N. Nakamura, *Bull. Chem. Soc. Jpn.*, **55**, 159 (1982).

5) J. P. N. Brewer, H. Heaney, S. V. Ley, and T. Ward, *J. Chem. Soc., Perkin Trans. 1*, **1974**, 2688.

6) M. Ōki, Y. Tanaka, G. Yamamoto, and N. Nakamura, *Bull. Chem. Soc. Jpn.*, **56**, 302 (1983).

7) The *gem*-dimethyl protons are accidentally isochronous. In benzene two singlets are observed for them.

Preparation of New Nitrogen-bridged Heterocycles. 7.[1] Reactions of 3-[Bis(methylthio)methylene]-2(3*H*)-indolizinones with Some Pyridinium *N*-Aminides

Akikazu KAKEHI,* Suketaka ITO, and Bunzo WADA
Department of Industrial Chemistry, Faculty of Engineering, Shinshu University, Wakasato, Nagano 380
(Received September 8, 1983)

Synopsis. The reactions of 3-[bis(methylthio)methylene]-2(3*H*)-indolizinones with pyridinium, quinolinium, and isoquinolinium *N*-aminides gave unstable 1,3-dipolar spiro-adducts with the elimination of a methanethiol, and some of these adducts isomerized thermally to afford the corresponding *N*-ylide derivatives.

Ketene dithioacetals are now widely recoginized as versatile intermediates in the syntheses of a variety of organic compounds. In particular, the members conjugated with a vinyl or a keto group serve as carbonyl umpolung reagents,[2] Diels-Alder dienes,[3] and reagents for the preparation of various heterocycles.[4] Recently, we reported the preparation of dihydroaromatic ketene dithioacetals, 3-[bis(methylthio)methylene]-2(3*H*)-indolizinone derivatives, and their transformation into 2*H*-pyrano[2,3-*b*]indolizinones by the reactions with various activated acetates in the presence of alkali.[5] The reaction with actates is the first case in which the high electrophilicity of these α-oxo ketene dithioacetals serves for the syntheses of fused heterocycles. In this note, we wish to report the reactivity of 3-[bis(methylthio)methylene]-2(3*H*)-indolizinones as a dipolarophile and thermal behavior of the resulting 1,3-dipolar spiro-adducts.

When an equimolar mixture of 3-[bis(methylthio)-methylene]-1-methyl-2(3*H*)-indolizinone **1** and 1-aminopyridinium iodide **3** was treated with potassium carbonate in THF at room temperature and then separated carefully by column chromatography, red spiro-adduct **4** was obtained in a quantitative yield. A similar treatment of 1-phenyl derivative **2** and *N*-aminide **3** gave the corresponding compound **5** in a 66% yield. In these reactions, methanethiol was detected by its unpleasant odor. These compounds **4** and **5**, however, were extremely unstable and converted rapidly to intractable tarry materials even at room temperature. So, we next examined the reactions of the stabilized bicyclic *N*-aminides instead of monocyclic one. As might be expected, the reactions of **1** and **2** with 1-aminoquinolinium iodide **6** and 2-aminoisoquinolinium iodide **9** in the presence of alkali afforded relatively stable crystalline spiro-adducts **7**, **8**, **10**, and **11** in 69—100% yields.

Interestingly, compounds **7**, **10**, and **11** isomerized smoothly into the corresponding quinolinium *N*-ylide **12**, and isoquinolinium *N*-ylides **14** and **15** on standing at room temperature or on heating in boiling xylene, while no *N*-ylide **13** could be obtained from the thermolysis of **8** under the same conditions. On the other hand, the reactions of acyclic ketene dithioacetals **16** and **17** with **3** in the presence of alkali afford-

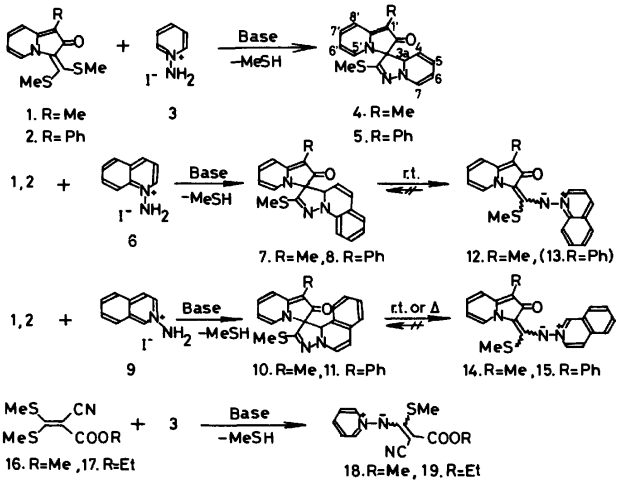

TABLE 1. NMR DATA OF 1,3-DIPOLAR SPIRO-ADDUCTS IN $CDCl_3$

Compd	R	SMe	C-3a	C-4	C-5	C-6	C-6′	C-7, 5′,7′, and 8′
4	1.80	2.48	5.61	4.70	6.08	4.87	6.23	6.70—7.50
	s	s	br s	br d	m	br t	dt	m
	$J_{4,5}$=9.0, $J_{5,6}=J_{6,7}=J_{5',6'}=J_{6',7'}$=7.0, $J_{6',8'}$=1.5 Hz							
5	a)	2.48	5.70	4.77	6.09	4.87	6.30	6.60—7.80
		s	br s	br d	m	br t	m	m
	$J_{4,5}$=9.0, $J_{5,6}=J_{6,7}$=7.0 Hz							
7	1.84	2.57	5.70	5.27	6.60	b)	6.21	6.70—7.70
	s	s	t	dd	dd		dt	m
	$J_{4,5}$=10.0, $J_{4,3a}=J_{5,3a}$=2.5, $J_{5',6'}=J_{6',7'}$=7.0, $J_{6',8'}$=1.5 Hz							
8	c)	2.56	5.73	5.30	6.58	c)	6.23	6.70—7.90
		s	t	dd	dd		m	m
	$J_{4,5}$=10.0, $J_{4,3a}=J_{5,3a}$=2.5 Hz							
10	1.90	2.49	6.11	d)	d)	5.47	6.02	6.80—7.40
	s	s	s			d	dt	m
	$J_{6,7}$=8.0, $J_{5',6'}=J_{6',7'}$=7.0, $J_{6',8'}$=1.5 Hz							
11	e)	2.50	6.17	e)	e)	5.42	6.03	6.80—7.80
		s	s			d)	m	m
	$J_{6,7}$=8.0 Hz							

a) Overlapped with each others at δ 6.60—7.80. b) Overlapped with each others at δ 6.70—7.70. c) Overlapped with each others at δ 6.70—7.90. d) Overlapped with each others at δ 6.80—7.40. e) Overlapped with each others at δ 6.80—7.80.

TABLE 2. PREPARATIONS AND SOME PROPERTIES OF SPIRO-ADDUCTS AND YLIDIC COMPOUNDS

Compd[a] No.	Yield %	Mp θ_m/°C	$\nu_{C=O}^{KBr}$/cm^{-1}	Formula	Calcd(%)			Found(%)		
					C	H	N	C	H	N
4	100	decomp	1602	b)						
5	66	decomp	1610	b)						
7	69	76—79(decomp)	1600	$C_{20}H_{17}N_3OS$	69.14	4.93	12.10	69.11	5.09	11.97
8	100	199—200(decomp)	1600	$C_{25}H_{19}N_3OS$	73.32	4.68	10.26	73.41	4.70	10.16
10	83	106—109	1594	$C_{20}H_{17}N_3OS$	69.14	4.93	12.10	69.00	5.09	12.23
11	100	100(decomp)	1592	$C_{25}H_{19}N_3OS$	73.32	4.68	10.26	73.41	4.73	10.11
12	53	139—140	1600	$C_{20}H_{17}N_3OS$	69.14	4.93	12.10	69.21	4.87	11.96
14	80	156—158	1587	$C_{20}H_{17}N_3OS$	69.14	4.93	12.10	69.12	5.07	11.98
15	80	249—250	1591	$C_{25}H_{19}N_3OS$	73.32	4.68	10.26	73.25	4.73	10.28
18	87	125—127	1662[c]	$C_{11}H_{11}N_3O_2S$	53.00	4.45	16.86	52.98	4.40	16.92
19	97	128—130	1662[d]	$C_{12}H_{13}N_3O_2S$	54.76	4.98	15.96	54.47	4.92	16.02

a) NMR data of ylidic compounds in $CDCl_3$ as follows: **12**, δ 1.89 (3H, s, 1'-Me), 2.68 (3H, s, SMe), and 7.00—8.80 (11H, m, other protons). **14**, δ 1.93 (3H, s, 1'-Me), 2.70 (3H, s, SMe), and 7.00—8.80 (11H, m, other protons). **15**, δ 2.55 (3H, s, SMe) and 6.80—8.70 (16H, m, other protons). **18**, δ 2.47 (3H, s, SMe), 3.51 (3H, s, OMe), and 7.70—8.80 (5H, m, pyridine protons). **19**, δ 1.12 (3H, t, J=7.0 Hz, $CH_2\underline{CH_3}$), 2.47 (3H, s, SMe), 3.98 (2H, q, J=7.0 Hz, $O\underline{CH_2}CH_3$), and 7.70—8.80 (5H, m, pyridine protons). b) The analysis could not be performed because of its thermal instability. c) The cyano absorption band appeared at 2162 cm^{-1}. d) The cyano absorption band appeared at 2178 cm^{-1}.

ed only stable pyridinium *N*-ylides **18** and **19** in good yields, respectively, but did not cycloadducts at all.

Structural elucidation of these spiro-adducts **4**, **5**, **7**, **8**, **10**, and **11** was mainly accomplished by their NMR and IR spectral inspection and partly by their elemental analyses. In particular, their NMR spectra (See Table 1) supported clearly the presences of 2(3*H*)-indolizinone[5] and 3,3a-dihydropyrazolo[1,5-*a*]pyridine moieties.[6] The IR spectra exhibited also the presence of a carbonyl band (near 1600 cm^{-1}) characteristic of 2(3*H*)-indolizinone derivative.[5] Similarly, the structures of *N*-ylides **12**, **14**, **15**, **18**, and **19** were determined by their elemental analyses and by comparison of their spectral data with those of known pyridinium *N*-ylides.[6,7]

The formation of the spiro-adducts **4**, **5**, **7**, **8**, **10**, and **11** may be considered by 1,3-dipolar cycloaddition between ketene dithioacetals **1** and **2** and *N*-amimides **3**, **6**, and **9** followed by the elimination of one molecule of methanethiol from the resulting primary spiro-adducts. Since facile transformations from these spiro-adducts **7**, **10**, and **11** to the corresponding *N*-ylides **12**, **14**, and **15** were observed but the reverse reaction was not, an alternative path *via* 1,5-dipolar cyclization of the *N*-ylides such as **12**—**15** which were formed initially by the nucleophilic substitutions of *N*-aminides onto dithioacetals may be discarded.

Experimental

Melting points were measured with a Yanagimoto micro melting point apparatus and are uncorrected. Microanalyses were carried out on a Perkin-Elmer 240 Elemental Analyzer. The NMR spectra were determined with a Varian EM360A Spectrometer in deuteriochloroform with tetramethylsilane as an internal standard. The chemical shifts are expressed in δ values. The IR spectra were taken with a Hitachi 260-10 Infrared Spectrophotometer.

Reactions of Ketene Dithioacetals with N-*Aminides. General Procedure*: A solution of acetal (*1* or **2**, 1 mmol) and pyridinium salt (1 mmol) in THF (30 mol) was treated with anhydrous potassium carbonate (5 g) under stirring at room temperature for 30 min. Insoluble inorganic substances were filtered and the filtrate was immediately concentrated *in vacuo* at below 10 °C. The residue was separated by column chromatography (alumina) using ether and then chloroform as eluents and the chloroform layer was concentrated carefully by centrifugal freezing dryer (Yamato, RC-11). Recrystallizations from chloroform–hexane at below 5 °C gave pure adducts **7**, **8**, **10**, and **11**, but those of **4** and **5** were unsuccessful because of their thermal instability. On the other hand, only pyridinium *N*-ylides **18** and **19** were formed from the reactions of acyclic acetals **16** and **17** with **3**. The results and data are shown in Tables 1 and 2.

Isomerization of Spiro-adducts to N-*Ylides.* Spiro-adducts **7** and **10** smoothly isomerized to the corresponding *N*-ylides **12** and **14** on standing at room temperature for 3—4 d, but the conversion of **11** to **15** was accomplished by heating for 30 min in boiling xylene. On the other hand, adduct **8** decomposed under above conditions and no ylide could be obtained. The results and data are summarized in Table 2.

References

1) For part 6 of this series, see A. Kakehi, S. Ito, T. Ohizumi, and M. Ito, *Bull. Chem. Soc. Jpn.*, **56**, 1219 (1983).
2) B.-T. Grobel and D. Seebach, *Systhesis*, **1977**, 357.
3) F. A. Carey and A. J. Court, *J. Org. Chem.*, **37**, 4447 (1972).
4) J. P. Marino and J. L. Kostusyk, *Tetrahedron Lett.*, **1979**, 2489, 2493; A. Kumar, V. Aggarwal, H. Ila, and H. Junjappa, *Synthesis*, **1980**, 748; W.-D. Rudorf and M. Augustin, *ibid.*, **1980**, 1022.
5) A. Kakehi, S. Ito, K. Nakanishi, K. Watanabe, and M. Kitagawa, *Bull. Chem. Soc. Jpn.*, **53**, 1115 (1980).
6) T. Sasaki, K. Kanematsu, and A. Kakehi, *J. Org. Chem.*, **37**, 3106 (1972).
7) T. Sasaki, K. Kanematsu, A. Kakehi, I. Ichikawa, and K. Hayakawa, *J. Org. Chem.*, **35**, 426 (1970); T. Sasaki, K. Kanematsu, and A. Kakehi, *Tetrahedron Lett.*, **1972**, 5245; A. Kakehi, S. Ito, K. Uchiyama, Y. Konno, and K. Kondo, *J. Org. Chem.*, **42**, 443 (1977).

A Novel Beckmann Fission Reaction of 2-Aminocyclohexanone Oxime

Haruyo SATO,* Shinzo IMAMURA, and Yukishige KITANO†
Chemicals Research Laboratory, Basic Research Laboratories, Toray Industries, Inc., 9-1, Ooe-cho, Minato-ku, Nagoya 455-91
†*Toray Research Center, Inc., Sonoyama, Ohtsu, 520*
(Received September 16, 1983)

Synopsis. 2-(4-Cyanobutyl)-4,5,6,7-tetrahydrobenzimidazole was obtained by treating 2-aminocyclohexanone oxime with ethyl acetimidate hydrochloride in acetic acid at below 50 °C, though only 2-methyl-4,5,6,7-tetrahydrobenzimidazole was produced by the reaction of 2-aminocyclohexanone oxime and free ethyl acetimidate in neutral solvents. A novel Beckmann fission reaction of dimeric 2-aminocyclohexanone oxime is presumed to participate in the formation of 2-(4-cyanobutyl)-4,5,6,7-tetrahydrobenzimidazole.

2-Aminocyclohexanone oxime (**1**) reveals an electrophilic property at the nitrogen atom of its amino group and a nucleophilic one at the carbon atom bearing hydroxyimino group and thus reacts readily with reagents having reactive functional groups to give various kinds of heterocyclic compounds, such as 2-mercaptoimidazoles,[1] phenazines,[2] and 2-amino-ε-caprolactam.[3] In this study we describe the reactions of **1** with ethyl acetimidate and its hydrochloride, and we continue the structure elucidation.

Results and Discussion

We have obtained **2** as a sole product in 89.2% yield by heating a mixture of **1** and ethyl acetimidate in methanol and/or chloroform under reflux. When we used ethyl acetimidate hydrochloride in chloroform, methanol or a mixture of chloroform and pyridine, only a small amount of 1,2,3,4,6,7,8,9-octahydro phenazine (**4**) was obtained with virtual recovery of the starting materials. When ethyl acetimidate hydrochloride was used in acetic acid at above 80 °C, **4** was obtained as a major product.[2] However, **3** was mainly obtained at below 50 °C.[4] The structure of this new compound **3** has been studied by various means. This material has a molecular formula $C_{12}H_{17}N_3$ and must be formed by the condensation of two molecules of **1** with the elimination of 1 mol of ammonia and 2 mol of water. In the ^{1}H-NMR spectrum, two kinds of 8H multiplets were observed at δ 1.6—2.1 and δ 2.2—2.9, and a 1H doublet, which was replaced by deuterium. oxide, was observed at δ 7.3—8.1. The 1H doublet at low field was assumed to be an imino proton adjacent to olefin or electron-withdrawing groups. The UV spectrum showed an absorption maximum at 226 nm. The MS spectrum showed the parent peak at *m/z* 203 and fragment peaks at 175, 163, 150, 137, 108, 95, and 77, but these peaks are not highly informative. Since constructive structural data were not obtained merely from these data, an X-ray

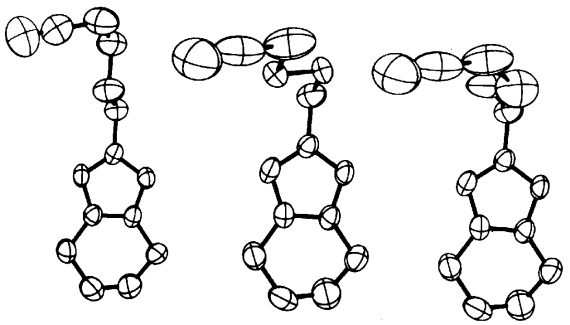

Fig. 1. ORTEP drawings of the molecule **3** determined by X-ray structure analysis.[5] Three conformers of the side chain exist in a monoclinic crystal. The ellipsoids are drawn to enclose 50% probability.

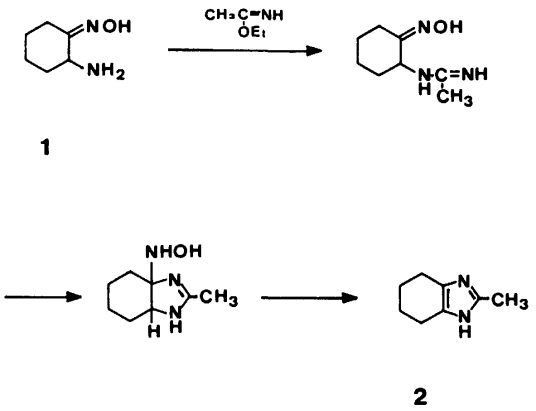

Scheme 1.

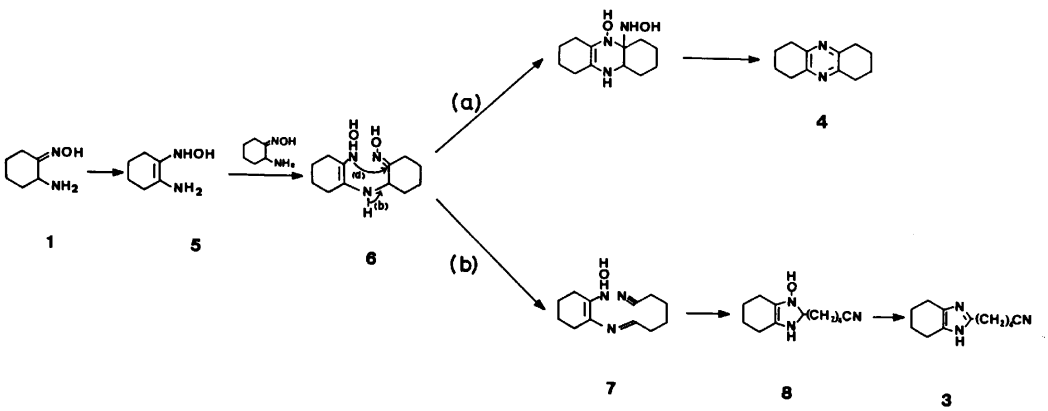

Scheme 2.

crystal structure analysis was then carried out with a single crystal grown from a ethyl acetate solution and the structure was established as **3** (Fig. 1).

The formation of 2-(4-cyanobutyl)-4,5,6,7-tetrahydro benzimidazole from 2 mol of 2-aminocyclohexanone oxime is quite unexpected and unusual. A plausible mechanism to account for its formation is depicted in Schemes 1 an 2.

By treating **1** with ethyl acetimidate in usual solvents such as chloroform and/or methanol, **2** was obtained as the expected product. When ethyl acetimidate hydrochloride was used in acetic acid, the reaction rate became slower and **1** was isomerized to 1-amino-2-(hydroxyamino)cyclohexene (**5**), and **5** reacted with another **1** to give 1-[2-(hydroxyimino)cyclohexylamino]-2-(hydroxyamino)cyclohexene (**6**). At above 80 °C, the carbon atom bearing hydroxyimino group was attacked by the nitrogen of hydroxyamino group to give **4** (path *a* in Scheme 2). When the reaction conditions were milder (at below 50 °C), on the contrary, a Beckmann fission reaction of **6** proceeded to give 1-(6-nitrilohexylideneamino)-2-(hydroxyamino)cyclohexene (**7**), which was converted to **8** by ring closure and finaly to **3** by dehydration (path *b* in Scheme 2).

Although the details of the role of ehtyl acetimidate hydrochloride in this reaction remain to be clarified, no such Beckmann fission reaction has ever been reported to the best of our knowledge.

Experimental

Measurements. The IR, UV, and mass spectra were recorded on Shimadzu IR-40, Shimadzu UV-220, and Hitachi RMU-7M spectrometers respectively. The ^{1}H-NMR spectra were recorded on Hitachi R-24B (60 MHz) spectrometer, using TMS as the internal standard. The X-ray diffraction data were obtained on a Rigaku automated four-circle diffractometer. The details of the crystal structure was reported by a separate cover.[5]

Preparations. 2-Aminocyclohexanone oxime (**1**) was prepared by the method described in the patent.[6]

2-Methyl-4,5,6,7-tetrahydrobenzimidazole (2): To a solution of 2-aminocyclohexanone oxime 64 g (0.5 mol) in methanol (500 ml) was added dropwise an ethyl acetimidate 43.5 g (0.5 mol) in the solution of methanol (50 ml) under reflux during 1 h, and the reaction mixture was heated under reflux for additional 6 h. After the reaction, the solvent was evaporated out, and the crude product was purified by recrystallization from ethyl acetate to give 60.7 g (89.2%) of **2** as a white solid; mp 225—226 °C. ^{1}H-NMR ($CDCl_3$), δ=1.6—2.1 (m, 4H), 2.33 (s, 3H), 2.1—2.8 (m, 4H), 8.7—9.3 (m, 1H); IR (KBr) 3190, 3100, 3000, 2940, 2850, 2760, 1630, 1540, 1460, 1440, 1420, 1240, 1040, 940 cm^{-1}. Found: C, 70.63; H, 8.79; N, 20.50%. Calcd for $C_8H_{12}N_2$: C, 70.55; H, 8.88; N, 20.57%.

2-(4-Cyanobutyl)-4,5,6,7-tetrahydrobenzimidazole (3): A mixture of 2-aminocyclohexanone oxime 12.8 g (0.1 mol), ethyl acetimidate hydrochloride 12.4 g (0.1 mol) and acetic acid 100 ml was heated at 40 °C. After 3 h, acetic acid was removed under reduced pressure, water (30 ml) was added to the residue, and the solution was extracted with benzene (50 ml). The water layer was adjusted to pH 10 with 2 M (1 M=1 mol dm^{-3}) sodium hydroxide solution and the solution was extracted with three 100 ml portions of benzene and then dried over anhydrous magnesium sulfate. After removal of the benzene, the residue was purified by recrystallization from ethyl acetate to give 8.6 g (84.6%) of **3** as a white solid; mp 177—178 °C. ^{1}H-NMR ($CDCl_3$) δ=1.5—2.1 (m, 8H), 2.2—2.8 (m, 8H), 7.3—8.2 (m, 1H); IR (KBr) 3180, 3100, 3020, 2950, 2860, 2770, 2260, 1630, 1440, 1240, 1040 cm^{-1}. Found: C, 70.88; H, 8.49; N, 20.63%. Calcd for $C_{12}H_{17}N_3$: C, 70.90; H, 8.43; N, 20.67%.

References

1) Toray Industries, Inc., Japan Patent Kokai 79-103870 (1979).
2) Toray Industries, Inc., Japan Patent Kokai 83-23679 (1983).
3) Toray Industries, Inc., Japan Patent 66-18087 (1966).
4) In the absence of ethyl acetimidate hydrochloride, **3** was not obtained in acetic acid at 50 °C.
5) Y. Kitano, H. Sato, S. Imamura and T. Ashida, *Acta Crystallogr., Sect. C.* **39**, in press (1983).
6) Toray Industries, Inc., U. S. Patent 3839448 (1974).

Regioselective Hydrogenation of Unsymmetrically Substituted Cyclic Anhydrides Catalyzed by Ruthenium Complexes with Phosphine Ligands

Takao IKARIYA,* Kohtaro OSAKADA, Youichi ISHII, Shoichi OSAWA, Masahiko SABURI, and Sadao YOSHIKAWA

Department of Synthetic Chemistry, Faculty of Engineering, The University of Tokyo, Hongo, Bunkyo-ku, Tokyo 113

(Received September 19, 1983)

Synopsis. Regioselective hydrogenation of unsymmetrically substituted cyclic anhydrides catalyzed by ruthenium complexes with mono-, di-, or triphosphine ligands produced the corresponding two isomeric lactones, where the regioselectivity was influenced by the bulkiness of the substituent(s) on the anhydrides and of the phosphine ligands of catalyst.

We have previously reported that a ruthenium complex having the diop ((−)-2,3-*O*-isopropylidene-1,4-bis(diphenylphosphino)-2,3-butanediol ligand catalyzed stereoselective hydrogenation of prochiral and *meso*-cyclic anhydrides to the corresponding optically active lactones.[1] Such an enantiotopes differentiating reaction is rarely found in the asymmetric reactions catalyzed by transition metal complexes.[2] However, still ambiguous is how the ruthenium complex distinguishes between pro-*R* and pro-*S* groups in a prochiral molecule. In order to obtain more informations about the steric interaction between the cyclic anhydride and the catalyst, the regioselectivity of the hydrogenation of unsymmetrically substituted cyclic anhydrides, which can potentially produce two isomeric lactones **2** and **3**, (Scheme 1), was examined using ruthenium complexes

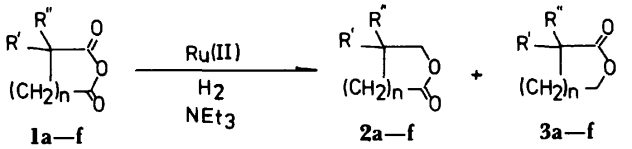

Scheme 1.

having mono-, di-, or triphosphine ligands as catlysts. It was briefly reported that $RuCl_2(PPh_3)_3$ catalyzed hydrogenation of 2,2-dimethylsuccinic anhydride gave preferentially 2,2-dimethyl-γ-butyrolactone.[3] More recently we have shown that the stoichiometric reaction of $RuH_2(PPh_3)_4$ with 2-alkylsuccinic anhydrides afforded two isomeric complexes, in which $RuH(OCOCHRCH_2CHO)(PPh_3)_3$ is the major product.[4] These results promoted us to reinvestigate the systematic study on the catalytic hydrogenation of cyclic anhydrides to reveal the factors which govern the stereo- and regioselectivities for the transformation of cyclic anhydrides to lactones.

Experimental

Ruthenium complexes, $RuCl_2(PPh_3)_3$, $Ru_2Cl_4(dppb)_3$,[5] $Ru_2Cl_4(diop)_3$,[6] and $RuCl_2(ttp)$,[7] (ttp=bis(3-diphenylphosphino)propyl)phenylphosphine) methods in the literatures.

Hydrogenation of Cyclic Anhydrides. A toluene solution containing cyclic anhydride (5 mmol), $MgSO_4$, and triethylamine (0.1 cm^3) was allowed to react with hydrogen gas (10 atom) in the presence of ruthenium complex (0.1—0.2 mmol) at 120 °C for 10—20 h. After being returned to atmospheric pressure, the insoluble materials were separeted by filtration, and the filtrate was evaporated to remove the solvent. The hydrogenated products were isolated by vaccum distillation and identified by ^1H NMR, mass, and IR spectroscopies. The molar ratio of two isomers in each product was determined by GC using acetophenone or propiophenone as an internal standard. Table 1 summerizes the representative results. Hydrogenation of racemic 2-methylsuccinic anhydride using the chiral complex $Ru_2Cl_4(diop)_3$ was carried out in the similar manner to that described above, and the diastereomeric products were isolated by preparative GC (Carbowax 3 m). The optical purities of lactones were determined by measurement of the optical rotation,[8] **2a**; $[\alpha]_D$=+1.3°. 5.9%e.e., **3a**; $[\alpha]_D$=−2.9°, 11.3%e.e.

Results and Discussion

The hydrogenation of cyclic anhydrides **1a—f** catalyzed by ruthenium complexes produces the corresponding isomeric lactones **2a—f** and **3a—f**, where the reaction preferentially occured at the less hindered carbonyl group to give **2a—f** selectively except phenylsuccinic anhydride (**1d**). This is a marked contrast to that the reduction of cyclic anhydrides with $LiAlH_4$ or $NaBH_4$ tends to take place selectively at the more hindered carbonyl group.[9] The regioselectivity increased in the order of 2-methyl<2-isopropyl<2,2-dimethyl-substituted cyclic anhydride, which is the order of the steric bulkiness of the substituent(s). It is possible that the hydrogenation of cyclic anhydrides proceeded *via* an intermediacy ruthenium formyl carboxylate complex formed by the cleavage of one of two C-O bonds on the anhydride.[4] The initial attack of ruthenium to the carbonyl group and succesive C-O fission of one of the C-O bonds should be controlled by the steric hindrance of substituent to give preferentially the formyl carboxylate complex (**II**) as shown in Scheme 2. Thus the carbonyl group adjacent to substituent(s) becomes less reactive. In the case of phenylsuccinic anhydride (**1d**) the more hindered carbonyl group was reduced selectively to some extent. It is obvious that the electron-withdrawing phenyl group weakens the neighboring C-O bond, resulting in the preferable formation of the intermediate complex (**II**) as shown in Scheme 2.

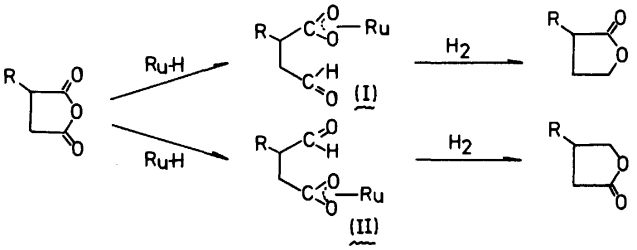

Scheme 2.

Table 1. Regioselective hydrogenation of cyclic anhydrides

Run	Cyclic anhydride		Catalyst[a]	Temp/°C	Time/h	Yield/%	2/3
1	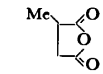		(A)	120	10	48	46/54
2			(B)	120	10	31	35/65
3			(D)	120	20	54	36/64
4		(*RS*)	(C)	120	10	40	30/70
5	(**1a**)	(*R*)	(C)	120	10	34	27/73
6		(*S*)	(C)	120	10	53	32/68
7	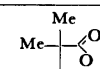		(A)	120	10	52	8/92
8			(B)	120	10	39	2/98
9	(**1b**)		(D)	120	20	13	1/99
10	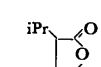		(A)	120	10	51	23/77
11			(B)	120	10	33	20/80
12		(*RS*)	(C)	120	10	40	27/73
13	(**1c**)	(*R*)	(C)	120	10	49	19/81
14		(*S*)	(C)	120	10	46	31/69
15	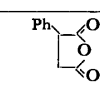		(A)	140	20	31	42/58
16			(B)	140	20	30	44/56
17	(**1d**)		(D)	140	20	62	52/48
18			(A)	120	20	15	28/72
19			(B)	120	20	30	25/75
20	(**1e**)		(D)	120	20	10	23/77
21			(A)	120	20	11	3/97
22			(B)	120	20	20	2/98
23			(D)	120	20	17	0/100
24	(**1f**)		(D)	140	20	29	1/99

a) (A) = $RuCl_2(PPh_3)_3$; (B) = $Ru_2Cl_4(dppb)_3$; (C) = $Ru_2Cl_4(diop)_3$; (D) = $RuCl_2(ttp)$.

To clarify further that the steric interaction between the substituent and ligand controls the selectivity, the hydrogenation of racemic 2-methylsuccinic anhydride (**1a**) with the chiral ruthenium complex $Ru_2Cl_4(diop)_3$ was examined. Of interest is that 2-methyl-γ-butyrolactone (**2a**) obtained from the hydrogenation of racemic **1a** using $Ru_2Cl_4(diop)_3$ was found to contain *R*-isomer in excess (5.9%e.e.), while 3-methyl-γ-butyrolactone (**3a**) obtained as the minor component contained the *S*-isomer in excess (11.3%e.e.).[8] The 2-methylsuccinic anhydride recovered from the reaction mixture exhibited negligible optical activity. These results obviously indicate that the optical activity of the above mentioned lactones could be explained in term of difference in the reactivities between *R*- and *S*-enantiomers toward the chiral complex $Ru_2Cl_4(diop)_3$ caused by the distinctive steric interaction of the chiral phosphine ligand with the substituent on *R*- and *S*-enantiomers. This is supported by the fact that the hydrogenation of (*R*)-2-methylsuccinic anhydride[11] catalyzed by $Ru_2Cl_4(diop)_3$ exhibited the apparently higher regioselectivity than that with *S*-enantiomer as shown in Table 1. The similar difference in the reactivity was observed in the hydrogenation of 2-isopropylsuccinic anhydride (**1c**) catalyzed by $Ru_2Cl_4(diop)_3$.

In conclusion the factor which governs primarily the regio- and stereoselectivities of the ruthenium complex-catalyzed hydrogenation of cyclic anhydrides is the steric interaction between substituent(s) on the substrate and the phosphine ligand. In the case of phenylsuccinic anhydride the electronic effect becomes superior to the effect of the steric demand. With the combination of this hydrogenation of cyclic anhydrides and the dehydrogenation of diols catalyzed by the same complex,[10] the selectivity of the latter being in the opposite direction to the former, the synthetic control of lactone formation can be performed employing the dicarboxylic acids as the starting materials.

This work was supported by a Grant-in-Aid for Developmental Scientific Reseach No. 56850201 from the Ministry of Education, Science and Culture.

References

1) K. Osakada, M. Obana, T. Ikariya, M. Saburi, and S. Yoshikawa, *Tetrahedron Lett.*, **22**, 4297 (1981).

2) T. Hayashi, K. Yamamoto, and M. Kumada, *Tetrahedron Lett.*, **1974**, 331; R. J. Corriu and J. J. E. Moreau, *J. Organomet. Chem.*, **85**, 19 (1975).

3) P. Morand and M. M. Kayser, *J. Chem. Soc., Chem. Commun.*, **1976**, 314.

4) T. Ikariya, K. Osakada, and S. Yoshikawa, *Tetrahedron Lett.*, **1978**, 3749; K. Osakada, T. Ikariya, and S. Yoshikawa, *J. Organomet. Chem.*, **231**, 79 (1982).

5) dppb=1,4-bis(diphenylphosphino)butane, M. Bressan and P. Rigo, *Inorg. Chem.*, **14**, 2286 (1975).

6) B. R. James, D. K. W. Wang, and R. F. Voigt, *J. Chem. Soc., Chem. Commun.*, **1975**, 574.

7) R. Uriarte, T. J. Mazanec, K. D. Tau, and D. W. Meek, *Inorg. Chem.*, **19**, 79 (1980); J. B. Letts, T. J. Mazanec, and D. W. Meek. *J. Am. Chem. Soc.*, **104**, 3898 (1982).

8) Optical purities of these lactones were determined based on the results in the literatures, a) T. Kaneko, K. Wakabayashi, and H. Katsura, *Bull. Chem. Soc. Jpn.*, **35**, 1149 (1962); A. I. Meyers and E. D. Mihelich, *J. Org. Chem.*, **40**, 1186 (1975). b) T. Mukaiyama, K. Fujimoto, T. Kirose, and T. Takeda, *Chem. Lett.*, **1980**, 635.

9) M. M. Kayser and P. Morand, *Can. J. Chem.*, **56**, 1524 (1978); M. M. Kayser, J. Salvator, P. Morand, and H. Gikrishnamurty, *ibid.*, **60**, 1199 (1982); P. Morand, J. Salvator, and M. M. Kayser, *J. Chem. Soc., Chem. Commun.*, **1982**, 458.

10) Y. Ishii, K. Osakada, T. Ikariya, M. Saburi, and S. Yoshikawa, *Tetrahedron Lett.*, **24**, 2677 (1983).

11) A. Landenburg, *Ber.*, **28**, 1170 (1895).

Synthesis of 1,2-Polymethyleneimidazoles Utilizing Intramolecular Ring Transformation

Tadashi SASAKI,* Masatomi OHNO, and Eikoh ITO
Institute of Applied Organic Chemistry, Faculty of Engineering, Nagoya University, Furo-cho, Chikusa-ku, Nagoya 464
(Received October 8, 1983)

Synopsis. Among the intramolecular cyclodehydration of 2-(β-, δ-, and ε-aminoalkyl)oxazoles, 2-(δ-aminoalkyl)oxazoles afforded the desired 1,2-tetramethyleneimidazoles on pyrolysis, while 2-(β- and ε-aminoalkyl)oxazoles unchanged under the same conditions.

We have recently studied[1] an intramolecular cyclodehydration of 2-(γ-aminoalkyl)oxazole affording 1,2-trimethyleneimidazole (*i.e.*, **3**→**8**→**12**) based on the intramolecular ring transformation strategy.[2-4] To apply this method for the synthesis of other 1,2-polymethyleneimidazoles, it is significant to know the effects induced by the number of bridging atoms between an oxazole and an amino function. For this purpose, 2-(β-, δ-, and ε-aminoalkyl)oxazoles were prepared and their pyrolysis was studied.

2-Methyloxazole **1**[5] was lithiated with *n*-BuLi in THF at −78 °C[6] and acylated with ethyl acetate to give β-oxazolyl ketone **2** in 51% yield. The lithiated **1** afforded δ-oxazolyl aldehyde **4** in 65% yield on treatment with bromo acetal **15**[7] followed by hydrolysis of the coupled acetal. δ-Oxazolyl ketone **5** was prepared in 46% yield by the transformation of **4** *via* Grignard reaction followed by the oxidation of the resulting secondary alcohol with pyridinium chlorochromate (PCC). ε-Oxazolyl ketone **6** was similarly prepared in 45% yield from **1** and bromo acetal **16**[8] The carbonyl function of **2**, **4**, **5**, and **6** was indicated by strong absorptions at 1715, 1725, 1715, and 1715 cm^{-1} respectively and their structures were supported by the spectral and elemental analyses. The prepared ketones **2**, **5**, and **6** were reductively aminated to the corresponding amines **7**, **10**, and **11** respectively on treatment with $NaBH_3CN$ in the presence of ammonium acetate. This conversion was indicated by methyl doublets at δ 1.24 (J=6.8 Hz) for **7**, 1.12 (J=6.8 Hz) for **10**, and 1.05 (J=6.8 Hz) for **11** and D_2O-exchangeable N–H signals at δ 1.80 for **7**, 1.90 for **10**, and 1.70 for **11** in the ^1H NMR spectra. Without further purification, δ-oxazolyl amine **10** was directly heated at 280 °C under reduced pressure (5 mmHg, 1 mmHg≈133.322 Pa) to give cyclodehydrated 1,2-tetramethyleneimidazole **14** in 50% overall yield from **5**. In the same manner as for δ-oxazolyl ketone **5**, δ-oxazolyl aldehyde **4** was successfully transformed to **13** in 29% overall yield. The structure of **13** was definitely confirmed by the spectral comparison with an authentic sample reported in the literature,[9] and with the spectral data for **13** in hand, that of **14** was readily determined; ring closure was verified by disappearance of D_2O-exchangeable N–H signal and the chemical shift of ring protons at δ 1.60—2.30 (4H, m, C-6 and C-7 H), 2.70—3.15 (2H, m, C-8 H), and 3.90—4.50 (1H, m, C-5 H). In contrast to the successful ring transformation of **9** and **10**, any attempted pyrolysis of 2-(β- and ε-aminoalkyl)oxazoles **7** and **11** resulted in the recovery of the starting material.

In summary, cyclodehydration of 2-(aminoalkyl)oxazoles was found to be effective for the synthesis of not only 1,2-trimethylene- but also tetramethyleneimidazole ring system. Further application could make this strategy quite capable of providing a number of different fused ring system of interest.

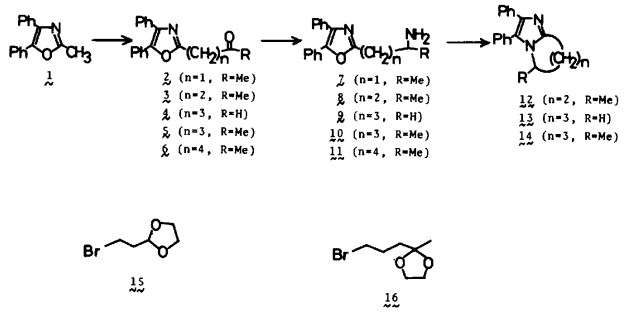

Experimental

Melting points were measured with a Yanagimoto micro-melting point apparatus and are uncorrected. IR spectra were obtained on a JASCO-IRA-1 spectrometer. ^1H NMR spectra were recorded on a JEOL C-60-HL spectrometer and chemical shifts are reported in ppm (δ) relative to Me_4Si as internal standard. Microanalyses were performed with Perkin-Elmer 240B elemental analyzer. Pyrolysis was carried out with a Sibata Glass Tube Oven GTO-250.

2-(2-Oxopropyl)-4,5-diphenyloxazole (2). To a solution of **1**[5] (2.0 g, 8.5 mmol) in dry THF (30 ml) was added a solution of *n*-BuLi in hexane (1.6 M, 6.3 ml, 10.2 mmol) dropwise over 15 min at −78 °C under the current of N_2. After the resulting deep orange-red suspension was stirred at −78 °C for additional 20 min, ethyl acetate (0.95 ml, 9.7 mmol) was added and the mixture was stirred at −78 °C for 30 min. The resulting mixture was then slowly warmed to room temperature and quenched with 30 ml of phosphate buffer (pH 7). The organic layer was extracted with $CHCl_3$ (3×20 ml). The combined $CHCl_3$ solution was washed 3 times with water, dried over $MgSO_4$, and concentrated to leave a yellow oil, which was chromatographed on a silica gel column (AcOEt/hexane 1:2) to give crude **2**. Further purification by recrystallization from ethanol gave 1.2 g (51%) of **2** as yellow crystals; mp 106—108 °C; IR (KBr) 3090, 2910, 1715, 1600, 1570, and 1510 cm^{-1}; ^1H NMR ($CDCl_3$) δ=2.30 (3H, s, CH_3), 3.97 (s, 2H, CH_2), and 7.20—7.80 (10H, m, Ar). Found: C, 77.70; H, 5.72; N, 5.05%. Calcd for $C_{18}H_{15}NO_2$: C, 77.96; H, 5.45; N, 5.05%.

2-(4-Oxobutyl)-4,5-diphenyloxazole (4). To a solution of the lithiated **1** (2.0 g, 8.5 mmol) prepared as above, **15**[7] (1.1 ml, 9.4 mmol) was added and the mixture was stirred at −78 °C for 30 min. The resulting mixture was then slowly warmed to room temperature and quenched with 30 ml of phosphate buffer (pH 7). The organic layer was extracted with $CHCl_3$ (3×30 ml). The combined $CHCl_3$

solution was washed 3 times with water, dried over $MgSO_4$, and concentrated to leave acetal as a yellow oil. A mixture of crude acetal and 0.5 M aqueous HCl (40 ml) was heated under reflux for 1 h. After cooling to room temperature, an orange oil was extracted with $CHCl_3$ (3×30 ml). The combined $CHCl_3$ solution was washed 3 times with water, dried over $MgSO_4$, and concentrated to leave an oil, which was chromatographed on s silica gel column (AcOEt/hexane 1:1) to afford 1.6 g (65%) of **4** as a yellow oil; IR (neat) 3045, 2940, 2810, 2710, 1725, 1600, 1570, and 1500 cm^{-1}; ^1H NMR ($CDCl_3$) δ=2.18 (2H, quintet, J=6.8 Hz, CH_2), 2.50—3.10 (4H, m, CH_2×2), 7.20—7.80 (m, 10H, Ar), and 9.78 (1H, t, J=1.2 Hz, CHO). Found: C, 78.24; H, 6.00; N, 4.78%. Calcd for $C_{19}H_{17}NO_2$: C, 78.33; H, 5.88; N, 4.81%.

2-(4-Oxopentyl)-4,5-diphenyloxazole (5). To a solution of methylmagnesium iodide in ether (6 ml) prepared from magnesium (70 mg, 2.9 mmol) and methyl iodide (0.18 ml, 2.9 mmol), was added a solution of **4** (640 mg, 2.2 mmol) in ether (4 ml) at room temperature. After stirring at room temperature for 1.5 h, the reaction mixture was quenched with saturated aqueous ammonium chloride (20 ml) and extracted with ether (3×15 ml). The combined ether solution was dried over $MgSO_4$ and concentrated to leave crude alcohol as a yellow oil, which was dissolved in CH_2Cl_2 (4 ml). This solution was added to a solution of PCC (630 mg, 2.9 mmol) in CH_2Cl_2 (4 ml) and stirred at room temperature for 17 h. After removal of the solvent, the residue was extracted with ether (3×10 ml). Concentration of the combined ether solution and subsequent chromatography on a silica-gel column (Et_2O/hexane 1:1) gave 320 mg (48%) of **5** as a yellow oil; IR (neat) 3050, 2940, 1715, 1600, 1570, 1500, and 1445 cm^{-1}; ^1H NMR ($CDCl_3$) δ=2.18 (3H, s, CH_3), 2.45—3.08 (6H, m, 3×CH_2), and 7.20—7.80 (10H, m, Ar). Found: C, 78.56; H, 6.32; N, 4.53%. Calcd for $C_{20}H_{19}NO_2$: C, 78.66; H, 6.27; N, 4.59%.

2-(5-Oxohexyl)-4,5-diphenyloxazole (6). By the similar procedure to the preparation of **4**, ε-oxazolyl ketone **6** was prepared by the reaction of the lithiated **1** with bromoacetal **16**[8] at −78 °C, followed by hydrolysis of the resulting acetal with 0.5 M aqueous HCl. Purification was performed on a silica-gel column (Et_2O/hexane 1:1); yield 45; yellow oil; IR (neat) 3050, 2940, 1715, 1600, 1575, 1500, and 1445 cm^{-1}; ^1H NMR ($CDCL_3$) δ=1.50—3.00 (8H, m, 4×CH_2), 2.14 (3H, s, CH_3), and 7.20—7.80 (10H, m, Ar). Found: C, 78.86; H, 6.60; N, 4.63%. Calcd for $C_{21}H_{21}NO_2$: C, 78.97; H, 6.63; N, 4.39%.

2,3-Diphenyl-5,6,7,8-tetrahydroimidazo[1,2-a]pyrdine (13). A solution of **4** (470 mg, 1.6 mmol), $NaBH_3CN$ (710 mg, 11.3 mmol), and ammonium acetate (1.2 g, 15.6 mmol) in dry methanol (16 ml) was heated under reflux for 3 h. The resulting mixture was acidified with concentrated aqueous HCl (pH 2) and then basified with 20% aqueous NaOH (pH 9). After extraction with $CHCl_3$ (3×15 ml), the combined organic layer was dried over $MgSO_4$. Removal of the solvent yielded crude amine **9** as a yellow oil, which was then heated at 280 °C under 5 mmHg for 20 min in a glass tube oven with a trap bulb heated at 200 °C. Tetrahydroimidazopyridine **13** was trapped as a yellow oil, which immediately solidified on cooling; 130 mg (29%); mp 140—142 °C (from AcOEt) (Lit,[9] 137—138 °C). Its spectral data are in good agreement with those reported in the literature.

5-Methyl-2,3-diphenyl-5,6,7,8-tetrahydroimidazo[1,2-a]pyridine (14). In the same way as above, **14** was obtained in 50% yield by the reductive amination of **5**, followed by pyrolysis of the crude 2-(δ-aminoalkyl)oxazole **10**. An analytical sample was obtained by chromatographic purification; mp 116—119 °C; IR (KBr) 3040, 2830, 1600, 1510, 1440, and 1420 cm^{-1}; ^1H NMR ($CDCl_3$) δ=0.98 (3H, d, J=6.8 Hz, CH_3), 1.60—2.30 (4H, m, C-6 and C-7 H), 2.70—3.15 (2H, m, C-8 H), 3.90—4.50 (1H, m, C-5 H), and 7.10—7.60 (10H, m, Ar). Found: C, 83.51; H, 6.81; N, 9.68%. Calcd for $C_{20}H_{20}N_2$: C, 83.30; H, 6.99; N, 9.71%.

References

1) T. Sasaki, M. Ohno, and E. Ito, *J. Chem. Soc., Perkin Trans. 1*, **1983**, 3027.

2) T. Sasaki, E. Ito, and I. Shimizu, *J. Org. Chem.*, **47**, 2757 (1982).

3) T. Sasaki, E. Ito, and I. Shimizu, *Heterocycles*, **19**, 2119 (1982).

4) T. Sasaki, E. Ito, and K. Asai, *Heterocycles*, **20**, 1089 (1983).

5) D. Davidson, M. Weiss, and M. Jelling, *J. Org. Chem.*, **2**, 328 (1937).

6) B. H. Lipshutz and R. W. Hungate, *J. Org. Chem.*, **46**, 1410 (1981).

7) G. Büchi and H. Wüest, *J. Org. Chem.*, **34**, 1122 (1969).

8) C. A. Crob and R. Moesch, *Helv. Chim. Acta*, **42**, 728 (1959).

9) J. H. M. Hill, T. R. Fogg, and H. Guttmann, *J. Org. Chem.*, **40**, 2562 (1975).

Cycloaddition of Vinyl Isocyanate to 1,3-Dipoles

Yoshiki OHSHIRO,* Mitsuo KOMATSU, Aiichiro OKAMURA, and Toshio AGAWA
Department of Applied Chemistry, Faculty of Engineering, Osaka University, Yamada-oka 2-1, Suita, Osaka 565
(Received October 14, 1983)

Synopsis. 1,2-Cycloadditions of 3-methyl-1-(methylthio)-1-butenyl isocyanate with *N*-*t*-butyl-α-toluenimine *N*-oxide and with *in situ*-generated *N*-*t*-butyl-α-methyl-α-lactam afforded an oxadiazolidinone derivative and a hydantoin derivative in 100 and 46% yields, respectively.

Vinyl isocyanates are known to undergo 1,2- and/or 1,4-cycloaddition reactions with several unsaturated compounds and have been often utilized in heterocyclic synthesis.[1,2] Previously we reported synthesis and 1,4-cycloaddition reactions of α-alkylthio(or arylthio)vinyl isocyanates,[3] which are expected to be reagents equivalent to acyl isocyanates[4] because the (alkylthio)vinyl group is easily converted to a carbonyl group.[5] Here we wish to report 1,2-cycloaddition reactions of 1,3-dipoles to the (alkylthio)vinyl isocyanate leading to heterocycles having the (alkylthio)vinyl substituent.

Reaction of (*E*)-3-methyl-1-(methylthio)-1-butenyl isocyanate (**1**) and *N*-*t*-butyl-α-toluenimine *N*-oxide (**2**) in refluxing benzene for 30 h under a nitrogen atmosphere to give 2-*t*-butyl-4-[3-methyl-1-(methylthio)-1-butenyl]-3-phenyl-1,2,4-oxadiazolidin-5-one (**3**) quantitatively.

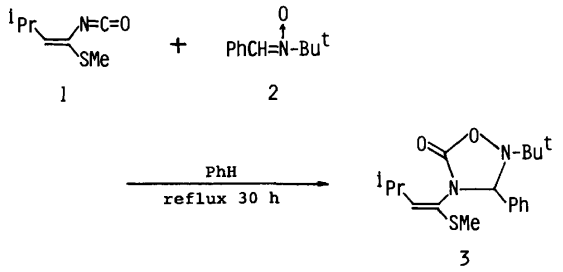

The structure of the oxadiazolidone **3** was determined by spectral data and elemental analysis. The IR spectrum of **3** shows a strong carbonyl absorption at 1740 cm^{-1} as well as a weak one at 1625 cm^{-1} due to the olefinic bond. In the NMR spectrum, two methyl doublets were observed at δ 0.17 and 0.93 (relative area 3H, respectively). These are assignable to the isopropyl group whose methyl groups became nonequivalent by the presence of the asymmetric carbon in the oxadiazolidine ring. The unusual higher shift of one of the methyl signals is due to the deshielding effect by the phenyl ring.

As another candidate for a 1,3-dipole, it is known that an α-halo amide generates an α-lactam and/or a 1,3-dipole such as **5** upon treatment with a strong base.[6] Thus the α-chloropropanamide **4** was reacted with the isocyanate **1** after treatment with butyllithium. 1,2-Cycloadditon again occurred to give the hydantoin derivative **6**. The IR spectrum of **6** showed two carbonyl absorptions at 1770 and 1715 cm^{-1} and a weak one at 1630 cm^{-1} due to the C=C bond. In the NMR spectrum, two doublets of the nonequivalent methyl group of the isopropyl function was observed at δ 0.95 and 1.13. The

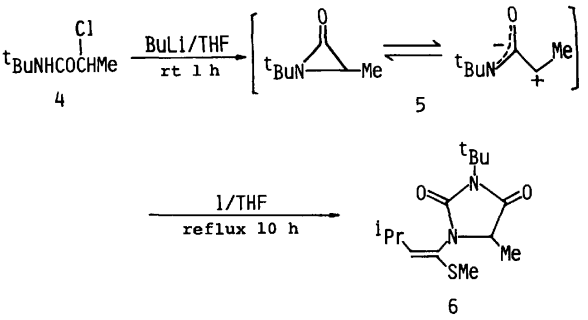

mass spectrum as well as elemental analysis showed good agreement with the structure of the hydantoin **6**.

Thus the two heterocyclic compounds having a thiovinyl substituent were prepared by 1,2-cycloaddition of the (alkylthio)vinyl isocyanate with the 1,3-dipoles. Higher convertibility of the thiovinyl group, as is already mentioned, will enable further conversion of the compounds into various heterocycles and it will increase utility of the (alkylthio)vinyl isocyanates.

Experimental

A melting point was determined on a Yanagimoto micro melting point apparatus and melting and boiling points were uncorrected. ^{1}H-NMR spectra were obtained with a JOEL JNM PMX-60 spectrometer in $CDCl_3$ using TMS as an internal standard. IR spectra were taken on a JASCO IRA-1 spectrophotometer. Mass spectrometry was performed on a Hitachi RMU-6E spectrometer at an ionizing voltage of 70 eV.

Materials. (*E*)-3-Methyl-1-(methylthio)-1-butenyl isocyanate (**1**: bp 31—34 °C/267 Pa) and *N*-*t*-butyl-α-toluenimine *N*-oxide (**2**) were prepared according to the literatures.[3,7] *N*-*t*-Butyl-2-chloropropanamide (**4**) was prepared from *N*-*t*-butylamine and 2-chloropropionyl chloride by the usual manner. Commercially available butyllithium (15% in hexane) was used.

The Reaction of the Isocyanate 1 with the N*-Oxide 2.* A solution of **1** (1.7 g, 10 mmol) and **2** (1.9 g, 10 mmol) in dry benzene (20 ml) was stirred at reflux for 30 h. The reaction mixture was concentrated and chromatographed on a SiO_2 column to give 3.6 g (100%) of 2-*t*-butyl-4-[3-methyl-1-(methylthio)-1-butenyl]-3-phenyl-1,2,4-oxadiazolidin-5-one (**3**): mp 147—148 °C (colorless needles from benzene-hexane); IR (Nujol) 1740 (C=O) and 1625 cm^{-1} (C=C); ^{1}H-NMR δ=0.17 (3H, d, *J*=6.8 Hz, Me), 0.93 (3H, d, *J*=6.4 Hz, Me), 1.18 (9H, s, *t*Bu), 1.8—2.3 (1H, m, CH), 2.30 (3H, s, SMe), 5.57 (1H, d, *J*=10.2 Hz, =CH), 5.83 (1H, s, CH), 7.2—7.7 (5H, m, Ph); MS *m*/*z* 247 (M^+—BuNO). Found: C, 64.71; H, 7.99; N, 8.29%. Calcd for $C_{18}H_{26}N_2O_2S$: C, 64.85; H, 7.84; N, 8.38%.

The Reaction of the Isocyanate 1 with the 1,3-Dipole 5. To a solution of the amide **4** (1.56 g, 9.6 mmol) in THF (20 ml) was added dropwise a solution of butyllithium in hexane (6.4 ml, 9.6 mmol) and the mixture was stirred for 1 h at room temperature. To this mixture was added a solution of the isocyanate **1** (1.5 g, 9.6 mmol) in THF (10 ml) at 0 °C and was stirred for 10 h at reflux. After removal of THF

and addition of cold water, the reaction mixture was extracted (ether), dried (Na_2SO_4), and chromatographed on a SiO_2 column to give 1.3 g (46%) of 1-*t*-butyl-4-methyl-3-[3-methyl-1-(methylthio)-1-butenyl]-2,5-imidazolidinedione (**6**): bp 60 °C (bath temp)/66 Pa by pot distillation; IR (neat) 1770 (C=O), 1715 (C=O), and 1630 cm^{-1} (C=C); ^{1}H-NMR δ=0.95 (3H, d, J=6.2 Hz, Me), 1.13 (3H, d, J=6.2 Hz, Me), 1.37 (3H, d, J=7.0 Hz, Me), 1.62 (9H, s, *t*Bu), 2.12 (3H, s, SMe), 2.2—2.6 (1H, m, CH), 4.17 (1H, q, J=7.0 Hz, CH), 5.72 (1H, d, J=10.0 Hz, =CH); MS *m/z* 284 (M^+). Found: C, 58.83; H, 8.60; N, 9.57; S, 11.22%. Calcd for $C_{14}H_{24}N_2O_2S$: C, 59.13; H, 8.51; N, 9.85; S, 11.26%.

References

1) H. Ulrich, "Cycloaddition Reactions of Heterocumulenes," Academic Press, New York (1967), and references cited therein.

2) L. I. Samaraj, O. W. Wishnewskij, and G. I. Derkatsh, *Angew. Chem.*, **80**, 620 (1968); M. Ohoka, S. Yanagida, and S. Komori, *J. Org. Chem.*, **36**, 3542 (1971); **37**, 3030 (1972).

3) K. Takaki, A. Okamura, Y. Ohshiro, and T. Agawa, *J. Org. Chem.*, **43**, 402 (1978).

4) B. A. Arubzov and N. N. Zoboda, *Synthesis*, 461 (1972).

5) E. J. Corey and J. I. Shulman, *J. Org. Chem.*, **35**, 777 (1970); P. Bakuzis, M. L. F. Bakuzis, C. C. Fortes, and R. Santos, *ibid.*, **41**, 2767 (1976).

6) R. Huisgen, *Angew. Chem.*, **75**, 604 (1963); I. Lengyel and J. C. Sheehan, *ibid.*, **80**, 27 (1968).

7) W. D. Emmons, *J. Am. Chem. Soc.*, **79**, 5739 (1957).

Conformation et Configuration en Solution d'une Serie d'Oxo Aldoximes Aliphatiques

Jean BERNADOU,* Jean Pierre FAYET,† Monique BONNAFOUS, et Pierre MAURET†

Laboratoire de Chimie Therapeutique, Universite Paul Sabatier 31077 TOULOUSE Cedex France

† *Laboratoire de Chimie Organique Structurale, Universite Paul Sabatier 31077 TOULOUSE Cedex France*

(Reçu Mars 10, 1983)

Synopsis. La stéréochimie de cinq α-oxo aldoximes R–CO–CH (NOH) (R=Me **1**, Et **2**, *n*-Pr **3**, *i*-Pr **4**, *t*-Bu **5**) a été étudiée : la configuration connue est E dans tous les cas mais les deux conformères *s*-cis et *s*-trans peuvent exister en différentes proportions lorsque varient la taille de R, la température ou le pH.

Les α-oxo aldoximes R–CO–CH(NOH) constituent une classe importante parmi les antidotes des toxiques organophosphores.[1-4] La géométrie du motif –CO–C(NOH)– est susceptible d'influer sur la réactivité biologique. Il est ainsi important de bien connaitre la stéréochimie de ces composés: la configuration *E* est maintenant bien établie[5-10] mais les conformations en solution ont été peu étudiees[11-14] et sont encore mal connues.

Nous étudions ici, comme nous l'avons déjà fait pour des α-hydroxyimino cétones cyclaniques[15] ou aromatiques,[16] les problèmes conformationnels posés dans la série des α-oxo aldoximes aliphatiques.

Etude dipolemétrique. (Tableau 1) Les valeurs expérimentales permettent par comparaison des valeurs obtenues et théoriques d'éliminer les conformations *c* et *d* mais ne permettent pas de trancher entre les formes *s*-trans *a* et *s*-cis *b*.

Etude par spectrométrie infrarouge. L'étude en solution met en évidence au niveau du groupe carbonyle des dédoublements de bande ou des dissymétries avec ou sans épaulement (Fig. 1). La bande principale est situé dans tous les cas entre 1680 et 1705 cm^{-1}. Cette bande principale peut:

—s'accompagner d'une bande plus faible située à fréquence plus basse (1675 cm^{-1}) et correspondant à une bande CO liée (cas de **1**). Il s'agit alors d'un phénomène d'association qui disparait par dilution suffisante (Fig. 1) et qui correspond à la formation de liaisons hydrogène intermoléculaires entre le groupe carbonyle et l'hydroxyle du groupe oxime.[7]

—s'accompagner d'une bande plus faible située à fréquence plus élevée (1711 cm^{-1}, cas de **5**); cette bande qui persiste malgré la dilution est sensible aux conditions de solvant (augmentation en passsant du CCl_4 au CH_3CN) et pourrait alors correspondre à une bande de Fermi.[17]

—se dédoubler: elle apparait comme un pic dissymétrique pour **1** ou **2**, ou présentant un épaulement pour **3** et **4**, **5** (Fig. 1). Ces dédoublements peuvent être d'origine conformationnelle: l'évolution de la bande CO quand la taille de R augmente peut être raisonnablement attribuée à une modification de l'équilibre conformationnel au profit de la forme *s*-cis:

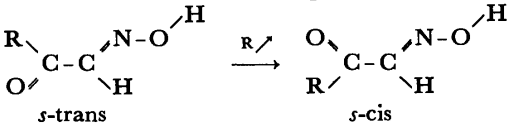

s-trans *s*-cis

Le pic de fréquence la plus élevée correspondrait alors à la vibration du carbonyle de la forme *s*-trans.

—l'enregistrement du spectre de **5** en solution dans CCl_4 à 65° puis à 5 °C montre une légère diminution de la bande à 1687 par rapport à celle à 1680 cm^{-1} confirmant ainsi que la première correspond à la forme *s*-trans, moins stable à basse température, et la deuxième à la forme *s*-cis plus stable.

—l'enregistrement des spectres dans des solvants de polarité variable (CCl_4 et CH_3CN) n'entraine pas de modifications notables à ce niveau; ce résultat s'explique car les polarités théoriques (Tableau 1) des deux isomères conformationnels *a* et *b* sont voisines.

—notons enfin la diminution des fréquences de vibration du carbonyle à la fois pour les isomères *s*-cis et *s*-trans lorsque l'encombrement de R augmente.[18]

	α	β	RM_D	$P_{2\infty}$	μ_D
1	17, 23	−0, 14	20, 51	268, 08	3, 48
2	13, 92	−0, 014	25, 15	259, 72	3, 39
3	12, 40	−0, 19	29, 80	261, 08	3, 36
4	12, 96	+0, 01	29, 80	278, 31	3, 49
5	10, 17	+0, 05	34, 45	254, 30	3, 28

Etude par RMN en variation de température. L'étude dans CH_2Cl_2 entre +80 et −40 °C montre que le signal du proton du groupe –CH= est déplacé vers les champs faibles. Cette variation est la plus im-

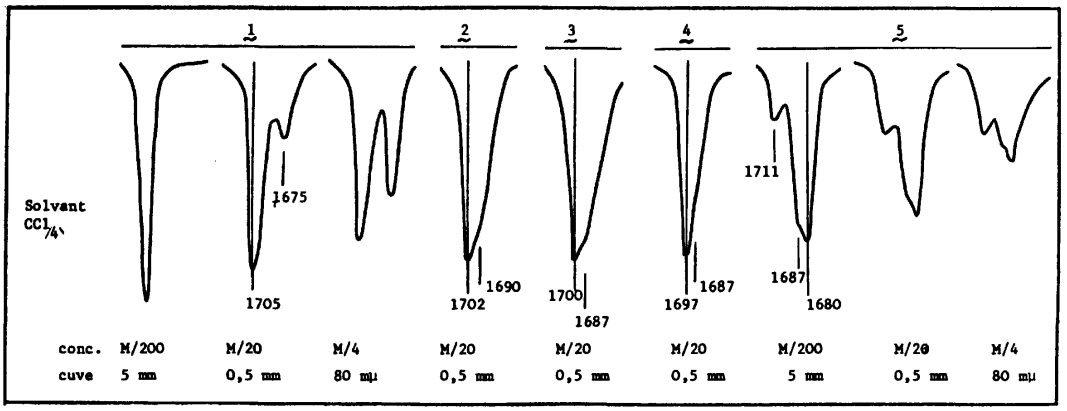

Fig. 1. Etude infra-rouge: bandes d'absorption du groupe carbonyle des α-oxo aldoximes.

TABLEAU 1. DIFFÉRENTES CONFORMATIONS POSSIBLES POUR LES α-OXO ALDOXIMES R-CO-C(NOH)H *E*; VALEURS THÉORIQUES μ_{th} [( )=VALEURS FOURNIES PAR LE 2-MODE DE CALCUL] ET EXPÉRIMENTALES μ_{exp} DES MOMENTS DIPOLAIRES

Conformations					
	s-trans			*s*-cis	
a	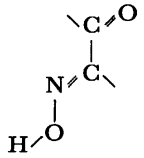	$\mu_{th}=2,56$ (2,68)	b	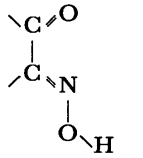	$\mu_{th}=3.04$ (2.79)
c	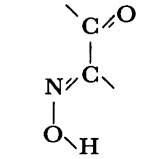	$\mu_{th}=1.08$ (0.30)	d	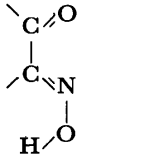	$\mu_{th}=5,56$ (5,48)

R=	Me	Et	Pr	*i*-Pr	*t*-Bu
μ_{exp}=	3,48	3,39	3,36	3,48	3,28

TABLEAU 2. ETUDE RMN: VARIATIONS DU DÉPLACEMENT CHIMIQUE DE -CH=N- EN FONCTION DE LA TEMPÉRTURE ET DU pH (δ/ppm)

Solvant		1	2	3	4	5
CH_2Cl_2	−40 °C	7,65	7,65	7,63	7,64	8,08
	+35 °C	7,55	7,58	7,57	7,56	7,83
	+80 °C	7,51	7,52	7,50	7,49	7,76
D_2O	pH 1—2	7,59	—	—	—	7,64
	pH 13—14	7,95	—	—	—	8,21

portante pour **5** (0,32 ppm) et est plus réduite pour les autres dérivés (0.13 à 0.15 ppm). L'effet du à l'abaissement de température peut être attribué au déplacement de l'équilibre conformationnel vers la forme *s*-cis qui place le proton -CH= dans le cone de déblindage du groupe carbonyle et entraine son déplacement vers les champs faibles. L'effet dû à l'augmentation du volume de R traduit la croissance de l'interaction stérique de ce groupe avec la paire libre de l'azote conduisant à une relative déstabilisation du conformère *s*-trans. L'effet de température, plus fort sur **5** que sur **1—4**, correspond à un déplacement de l'équilibre vers la forme *s*-cis plus facile.

De plus en milieu alcalin on s'attend à voir le signal -CH=, dans l'anion R-CH=NO^-, déplacé vers les champs forts; cependant, comme l'a remarqué Liepin'sh[10] ce déplacement se fait vers les champs faibles (Tableau 2); ceci correspond à un changement de conformation préférentielle de la forme *s*-trans vers *s*-cis;

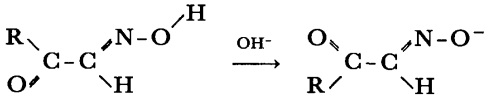

Conclusion. De l'ensemble de ces résultats il ressort que les α-oxo aldoximes étudiées peuvent exister en solution sous deux conformations *s*-trans *a* et *s*-cis *b*; la première est majoritaire pour les composés avec R peu encombré (R=Me, Et, Pr, *i*-Pr) et la deuxième pour le composé **5** (R=*t*-Bu).

Partie experimentale

Synthèse. Les produits étudiés ont été préparés selon des méthodes deja décrites.[2,3]

Etude dipolemétrique. Moments calculés(μ_{calc}): Nous avons obtenu les moments par additivité d'incréments de liaison suivant deux modes de calcul:

- avec les angles CCO, ONC, NCC, HON égaux à 120°
- avec CCO=120°, ONC=111°, NCC=126° HON=103°, valeurs déduites des molécules de formaldoxime[19] et de diméthylglyoxime.[20] Les incréments utilisés sont : (C=N) =1,8 D ; (C=O)=3,0 D; (H-O)=1,5 D; (N-O)=0,3 D;

Moments expérimentaux (μ_{exp}): Les moments ont été mesurés dans le dioxanne à 25 °C, avec des fractions massiques comprises entre 0,0005 et 0,010. Les résultats figurent dans le tableau:

	α	β	RM_D	$P_{2\infty}$	μ_D
1	17,23	−0,14	20,51	268,08	3,48
2	13,92	−0,014	25,15	259,72	3,39
3	12,40	−0,19	29,80	261,08	3,36
4	12,96	+0,01	29,80	278,31	3,49
5	10,17	+0,05	34,45	254,30	3,28

Etude par spectrométrie infrarouge. Les spectres ont été enregistrés sur un spectrophotometre Beckman IR 9; la précision des mesures de réquence d'absorption est ±2 cm^{-1}.

Etude par spectrométrie RMN. Les spectres sont enregistrés sur un spectrophotomètre 90 MHz BRUCKER; les concentrations sont de 0.5 M.

References

1) G. B. Koelle, "Handbook of Experimental Pharmacol. Suppl.," Springer Verlag, Berlin (1963), Vol. 15.

2) J. Bernadou, Thèse Pharmacie, 1975, n° 78, Toulouse (France).

3) J. Bernadou et D. Q. Quan, *Eur. J. Med. Chem.*, **10**, 599 (1975).

4) M. Majewski, et B. Serafin, *Wiad. Chem.*, **33**, 311 (1979); *ibid.*, **33**, 405 (1979).

5) J. P. Guette, J. Armand, et L. Lacombe, *C. R. Acad. Sci.*, **264** 1509 (1967).

6) W. A. Mosher, R. N. Hively, et F. H. Dean, *J. Org. Chem.*, **35**, 3689 (1970).

7) J. Bernadou, J. P. Fayet, M. Bonnafous, et P. Mauret, *Bull. Soc. Chim. Belg.*, **87**, 747 (1978).

8) P. Alderliesten, A. Almenningen, et T. G. Strand, *Acta. Chem. Scand., Ser. B*, **29**, 811 (1975).

9) J. N. Somin, et V. A. Gindin, *Zh Org. Chim.*, **10**, 414 (1974).

10) E. E. Liepin'sh, *Latv. Psr. Zinat. Acad. Vest. Kim. Ser. Sun.*, **3**, 330 (1978).

11) O. Exner, J. Smolikova, V. Jehlicka, et A. S. Shawali, *Collect. Czech. Chem. Commun.*, **44**, 2494 (1979).

12) P. Baas, et H. Cerfontain, *J. Chem. Soc., Perkin Trans. 2*, **1977**, 1351.

13) P. Baas, et H. Cerfontain, *J. Chem. Soc., Perkin Trans. 2*, **1979**, 151.

14) C. L. Raston, R. P. Sharma, B. W. Skelton, et A. M. White, *Aust. J. Chem.*, **31**, 745 (1978).

15) J. Bernadou, et M. Bonnafous, *Bull. Chem. Soc. Jpn.*, **52**, 1535 (1979).

16) J. Bernadou, J. P. Fayet, M. Bonnafous, et P. Mauret, *Bull. Chem. Soc. Jpn.*, **55**, 2309 (1982).

17) M. Oki, et H. Nakanishi, *Bull. Chem. Soc. Jpn.*, **44**, 3144, 3148, et 3197 (1971).

18) A. Gaset, A. Verdier, J. Bonnet, et A. Lattes, *Spectrochim. Acta*, **31A**, 715 (1975).

19) I. N. Levine, *J. Mol. Spectrosc.*, **8**, 279, (1962); *J. Chem. Phys.*, **38**, 2326 (1963).

20) W. C. Hamilton, *Acta Crystallogr.*, **14**, 95 (1961).

The Reaction of 1,1-Dimethyl-1-Phenacylhydrazinium Bromide with Aqueous Sodium Hydroxide

Kunio KANO† and Jean-Pierre ANSELME*

Department of Chemistry, University of Massachusetts at Boston, Harbor Campus, Boston, Massachusetts 02125, U.S.A.

(Received October 26, 1982)

Synopsis. The reaction of 1,1-dimethyl-1-phenacylhydrazinium bromide with 1 M aqueous sodium hydroxide give benzoic acid, 3-phenyl-1-methylpyrazole, 5-benzoyl-3-phenyl-1-methylpyrazole, and benzonitrile as the major components; the expected product, 2-benzoyl-5-phenylimidazole was formed in only small amounts. Mechanisms to rationalize the formation of the major products are discussed.

In contrast to the vigorous conditions usually necessary,[1,2] the Wawzonek rearrangement of 1,1-dimethyl-1-phenacylhydrazinium bromide (**1**) proceeded smoothly upon heating in 1-propanol,[3] to afford 2-benzoyl-5-phenylimidazole (**5**).[4] It thus became of interest to investigate the behavior of **1** in the presence of aqueous alkali.

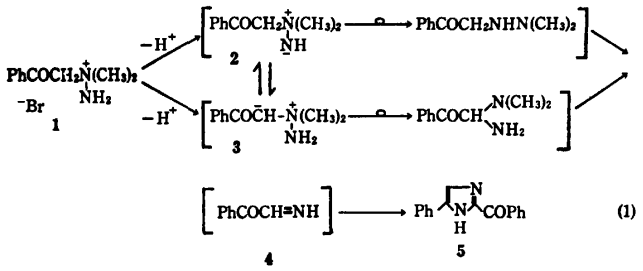

The treatment of 80 mmol of 1,1-dimethyl-1-phenacylhydrazinium bromide (**1**) with 1 M aqueous NaOH gave only trace amounts of 2-benzoyl-5-phenylimidazole (**5**); seven compounds were characterized: benzoic acid (**6**, 24.6 mmol), 3-phenyl-1-methylpyrazole (**7**, 12.2 mmol), 5-benzoyl-3-phenyl-1-methylpyrazole (**8**, 3.3 mmol), benzonitrile (**9**, 2.2 mmol), trace amounts of acetophenone (**10**), acetophenone dimethylhydrazone (**11**) and 3-phenyl-1-methyl-2-pyrazoline (**12**); dimethylamine and trimethylamine were subsequently characterized from the evolved gases.

The formation of benzonitrile can be rationalized *via* an internal nucleophilic attack of the negative nitrogen of the aminimide **2** on the carbonyl group to give the diazetinium ion **13**.[5] Fragmentation of

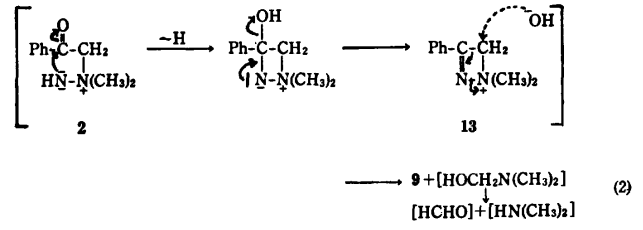

13 or attack of **13** by hydroxide ion (*vide infra*) yields benzonitrile. Support for this mechanism was obtained from the bromination of acetophenone dimethylhydrazone (**11**) with *N*-bromosuccinimide which afforded benzonitrile as one of the products;[6] presumably α-bromination followed by an internal nucleophilic displacement by the sp^3 nitrogen lead to **13**. A Stevens rearrangement of **13** (Eq. 3) can account for the formation of 3-phenyl-1-methyl-2-pyrazoline (**12**). The reaction of **1** with base in the presence of **12** did not result in an increase in the yield of **7** and thus rules **12** out as the source of **7**.[7] An alternate path to **7** involving the condensation of phenylglyoxaldimine (**4**), a probable intermediate in the rearrangement of **1** to **5**,[3] with 1,1-dimethylhydrazine at more reactive *imino* carbon followed by cyclization of the resulting phenylglyoxal dimethylhydrazone (**14**)[6,8] would lead to 4-phenyl-1-methylpyrazole (**15**) and not to **7**. On

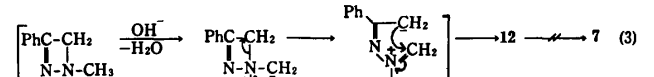

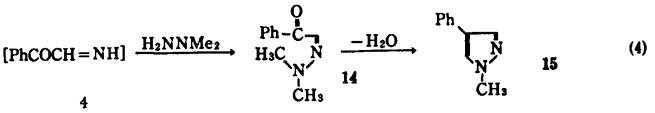

the other hand, attack of 1,1-dimethylhydrazine on **13** (*vide infra*) can lead to an intermediate **16** with the structural features required to undergo cyclization to yield 3-phenyl-1-methylpyrazole (**7**) (Eq. 5). A

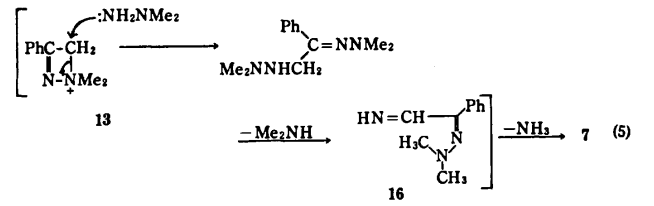

control experiment in which the reaction of **1** with hydroxide ion was carried out in the presence of added 1,1-dimethylhydrazine resulted in a seven-fold increase in the yield of **7** at the expense of benzonitrile.

NMR experiments demonstrated that the CH_2 hydrogens also underwent deuterium exchange and make it likely that ylide **3**, derived from removal of a hydrogen from the CH_2, is also generated.[9] A mechanism proceeding *via* the same intermediate **17** presumably involved in the synthesis of **8** from dibenzoylacetylene and methylhydrazine,[10] explains the formation of **8** (Eq. 6). It is interesting to note that the reaction of **1** with water gave an approximately 1:1 mixture of **2** and **5**.

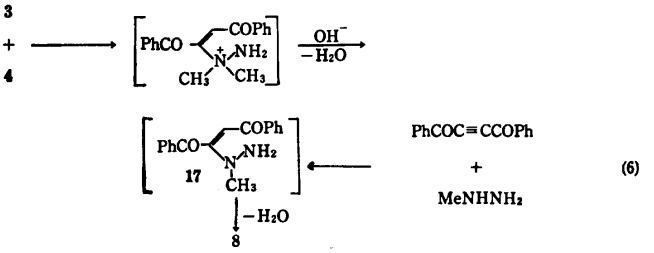

† Taken from the M. S. Thesis of Kunio Kano, University of Massachusetts at Boston, June 1980.

It was initially surmized that *in situ* hydrolysis[11] of benzoyl cyanide (**18**) perhaps generated by air oxidation of phenylglyoxaldimine (**4**), could help account for the formation of benzoic acid. However, the reaction of **1** with hydroxide under *oxygen-free* nitrogen left the yield of benzoic acid unaffected. The hydrazinium salt **1** or more likely the aminimide **2** could act as the oxidizing agent (Eq. 7).[12]

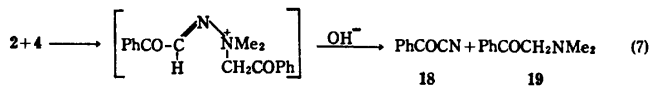

Apparent support for this path came from the reaction of benzaldehyde, *p*-chlorobenzaldehyde and *p*-bromophenylglyoxal with **1** under the same conditions, which gave benzonitrile, *p*-chlorobenzonitrile and *p*-bromobenzoic acid respectively. However, α-dimethylaminoacetophenone (**19**), the expected by-product (Eq. 7) could not be detected by TLC. The reaction of **19** with 1 M sodium hydroxide in the presence of oxygen gave sodium benzoate (60%); the reaction of **1** with hydroxide in the presence of **19** gave 2,3-bis(dimethylamino)-1,4-diphenyl-1,4-butanedione (**20**).[13,14]

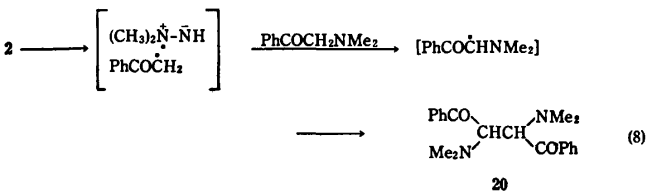

The self-condensation product of **4** which cyclized to **5**,[3] could collapse in an alternate fashion to give benzoyl cyanide and phenacylamine (Eq. 9). Con-

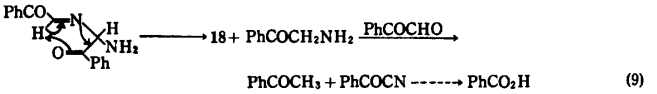

densation of the latter compound with phenylglyoxal hydrate was shown to yield benzoid acid and acetophenone, presumably *via* fragmentation of the intermediate imine, in a fashion analogous to the formation of **18** from phenylglyoxaldoxime with acetyl chloride.[15] Phenacyl alcohol, which might have arisen from attack of hydroxide ion on **1**, was not converted to benzoic acid as expected.[16] Furthermore, the addition of phenacyl alcohol to a reaction of **1** with base resulted in a *decrease* in the yield of benzoic acid.

In view of the failure of these mechanisms, the path involving the direct attack of the hydroxide ion at the carbonyl carbon was reluctantly considered (Eq. 10). Indeed, trimethylhydrazinium iodide under the

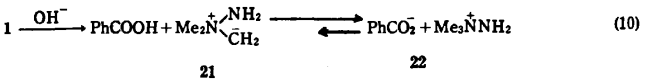

conditions of the reaction gave trimethylamine.[17] Nucleophilic displacement on the methyl group of trimethylhydrazinium ion can lead to methanol and 1,1-dimethylhydrazine, necessary to account for the formation of acetophenone dimethylhydrazone and of the pyrazoles.

Experimental

Elemental analysis were carried out at the Microanalysis Laboratories of the University of Massachusetts at Amherst. Mass spectra were taken at Chemical Spectrometry Laboratory of Massachusetts Institute of Technology and obtained on a Varian Mat 44 mass spectrometer. The infrared spectra were recorded on a Perkin-Elmer model 137B Infrared spectrophotometer and the NMR spectra were determined on a Hitachi Perkin-Elmer R-24 (60 MHz) in deuteriochloroform unless otherwise noted, using tetramethylsilane as internal standard. The vapor phase chromatograms were obtained on a Perkin-Elmer Vapor Fractometer 154D (column: silicone grease).

Reaction of 1,1-Dimethyl-1-phenacylhydrazinium Bromide (1) with 1 M Aqueous Sodium Hydroxide. To 80 mmol of **1** was added 120 ml of 1 M aqueous NaOH, previously degassed for 1 h with purified nitrogen. The reaction mixture was stirred for 24 h at ambient temperature and the reaction flask was protected from light. The reaction mixture was extracted with ether and the ethereal layer was washed with water until it was neutral. The ethereal solution was dried over $MgSO_4$ and evaporated *in vacuo*. The aqueous layer was neutralized with conc. hydrochloric acid, the resulting precipitate was collected, and the filtrate was extracted with ether. The ethereal solution was dried over $MgSO_4$ and evaporated *in vacuo*; the residue and the precipitate obtained from neutralization of the aqueous phase were combined and crystallized from water to give 3.0 g (24.6 mmol) of benzoic acid, mp 121—122 °C.

The IR, NMR, and VPC of the residue obtained from the original ethereal phase were determined. VPC showed a 5.1:1 ratio of 3-phenyl-1-methylpyrazole (**7**)[18] to benzonitrile and trace amounts of acetophenone, acetophenone dimethylhydrazone (**11**) and 3-phenyl-1-methyl-2-pyrazoline (**12**).[19] The mixture was then chromatographed on 50 g of neutral aluminum oxide (powder) using benzene as eluent. The first fraction gave 0.73 g (2.7 mmol) of 5-benzoyl-3-phenyl-1-methylpyrazole (**5**), the second fraction gave 1.9 g of a mixture of **8** and **7** in a ratio of 1:12.1, the third fraction gave 0.175 g (1.07 mmol) of **7**. The total yields of **7** and **8** were 12.2 mmol and 3.3 mmol respectively. The purity and identity of each fraction was checked by TLC and NMR.

In a separate experiment, three picric acid–ethanol traps were attached to the outlet of the reaction vessel; 1.2 g of a mixture of the picrates of dimethylamine and trimethylamine was collected, and its NMR indicated it to be composed of 4 mmol of trimethylamine picrate and 0.7 mmol of dimethylamine picrate.

Reaction of 1 with 1 M NaOH in the Presence of 1,1-Dimethylhydrazine. The reaction of **1** (20 mmol) with 30 ml of 1 M NaOH under nitrogen was carried out and analyzed as described previously, except that 20 mmol of 1,1-dimethylhydrazine was added to the reaction mixture. There was a seven-fold increase in the yield of 3-phenyl-1-methylpyrazole (**7**).

Reaction of 1 in Water. A solution of 5.18 g (20 mmol) of **1** in 100 ml of distilled water was stirred for 5 d at ambient temperature. The precipitate was filtered to give 2 g of a mixture of **5**, **7**, **8**, and the filtrate was extracted with ether. The ethereal layer was dried over $MgSO_4$ and the ether was evaporated to give 0.19 g of a mixture of **5**, **7**, **8**, and other minor products. The aqueous layer was acidified with concd hydrochloric acid and then was extracted with ether. The ethereal solution was dried over $MgSO_4$ and the ether was evaporated to yield 0.10 g (8%) of benzoic acid.

5-Benzoyl-3-phenyl-1-methylpyrazole (**8**) (0.8 g, 31%), mp 65.5—67 °C, was obtained as white crystals from the precipitate after three recrystallizations from ether–pet. ether followed by column chromatography (silica gel).

Reaction of ***1*** *with* p-*Bromophenylglyoxal.* To **1** (1.04 g, 4 mmol) and *p*-bromophenylglyoxal monohydrate (0.92 g, 4 mmol) was added 6 ml of previously degassed 1 M aqueous NaOH and stirred for 24 h. The reaction mixture was acidified with concd HCl; the precipitate was filtered and washed with water. Its IR showed it to be a mixture (0.19 g) of benzoic acid and *p*-bromobenzoic acid.

Reaction of Phenylglyoxal with Phenacylamine. To a suspension of phenylglyoxal monohydrate (2.13 g, 14 mmol) and phenacylamine hydrochloride (2.4 g, 14 mmol)[20] in THF (40 ml) was added triethylamine (1.4 g, 14 mmol) in THF (15 ml); the solution was stirred overnight at room temperature. Triethylamine hydrochloride was filtered and THF was evaporated from the filtrate. The residue was dissolved in 50 ml of ether, then the solution was washed with water, dried over anhydrous $MgSO_4$ and the ether was evaporated. A solution of the residue in toluene (100 ml) was heated to reflux overnight. The cooled reaction mixture was washed with aqueous $NaHCO_3$ and water, dried and the toluene was evaporated. To the residue was added 2,4-dinitrophenylhydrazine solution. The R_f value (silica gel, chloroform) and the IR spectrum of the product were identical with that of authentic acetophenone 2,4-dinitrophenylhydrazone. The sodium bicarbonate solution was neutralized with concd hydrochloric acid to give 0.63 g (37%) of benzoic acid, mp 120—121.5 °C.

Reaction of Trimethylhydrazinium Iodide with 1 M Sodium Hydroxide. To 16.2 g (80 mmol) of trimethylhylhydrazinium iodide in 250 ml three-necked round bottom flask equipped with a 250 ml addition funnel, a nitrogen gas inlet and reflux condenser was added 120 ml of 1 M aqueous NaOH; the condenser was connected to a trap containing 50 ml of a saturated ethanolic solution of picric acid. After the addition, nitrogen gas was bubbled through the reaction flask for 3 d at ambient temperature, The solid which precipitated in the trap was collected, dried and shown to be trimethylamine picrate, mp 221—223 °C, by comparison with an authentic sample.

*2,3-Bis(dimethylamino)-1,4-diphenyl-1,4-butanedione (**20**).* A mixture of 2.70 g (12.5 mmol) of α-dimethylaminoacetophenone in 30 ml of 1 M aqueous NaOH was degassed for 30 min, then added to **1** (5.18 g, 20 mmol). The reaction mixture was treated as described previously in the general procedure. The solid present in the viscous residue which had been left standing, was filtered recrystallized from ether–pet. ether to give pale yellow crystals, mp 136—138 °C. Mass spectrum: *m/e* 324, 162, 105, 77; NMR($CDCl_3$): δ 7.80 (ArH, m, 5H), 4.92 (CH, s, 1H), 2.26 (CH_3, s, 6H); IR: 1680 cm^{-1}.

References

1) W. J. McKillip, E. A. Sedor, B. M. Culbertson, and S. Wawzonek, *Chem. Rev.*, **73**, 255 (1973).

2) H. F. Hodson, P. M. Maytum, and B. R. T. Keene, *Tetrahedron Lett.*, **1972**, 319.

3) M. Koga and J.-P. Anselme, *J. Chem. Soc., Chem. Commun.*, **1973**, 53; M. Koga, A. P. Stamegna, D. J. Burke, and J.-P. Anselme, *J. Chem. Educ.*, **54**, 111 (1977). The rearrangement of **1** to **5** also occurred upon injection in the mass spectrometer, by photolysis in methanol, or upon stirring in DMSO or in water at ambient temperature.

4) The ease of rearrangement of **1** has been ascribed to hydrogen bonding [L. Lessinger, M. K. Killoran, J.-P. Anselme, and T. N. Margulis, *Tetrahedron Lett.*, **1972**, 219].

5) M. A. Battiste and T. J. Barton, *Tetrahedron Lett.*, **1967**, 1227.

6) J.-P. Anselme *et al.*, unpublished results.

7) T. L. Jacobs in "Heterocyclic Compounds," ed by R. C. Elderfield, John Wiley and Sons, New York, N. Y. (1957), Vol. 5, p. 45; A. N. Kost and I. I. Grandberg "Advances in Heterocyclic Chemistry," ed by A. R. Katritzky, Academic Press, New York, N. Y. (1966), Vol. 6, p. 347.

8) N. A. Domnin, V. I. Diurnbaum, and V. A. Cherkasova, *J. Gen. Chem. USSR*, **28**, 1520 (1958).

9) Even under *neutral* conditions, the CH_2 hydrogens undergo deuterium exchange; it is thus probable that the *C*-ylide is generated.

10) H. W. Heine, T. R. Hoye, P. G. Willard, and R. C. Hoye, *J. Org. Chem.*, **38**, 2984 (1973). The structural assignment of these authors has now been confirmed by the synthesis of 3-benzoyl-5-phenyl-1-methylpyrazole by unequivocal route (J.-P. Anselme *et al.*, unpublished results).

11) H. Huber and K. Buchka, *Ber.*, **10**, 479 (1877).

12) I. Ikeda, Y. Machii and M. Okahara, *Synthesis*, **1978**, 301

13) R. E. Lutz, P. S. Bailey, and N. H. Shearer, *J. Am. Chem. Soc.*, **68**, 2224 (1946).

14) A. P. Stamegna, B. A. Thesis, University of Massachusetts at Boston, June 1976.

15) L. Claisen, *Ber.*, **20**. 2194 (1887); **31**, 1023 (1898).

16) C. J. Collins and J. F. Eastham "The Chemistry of the Carbonyl Group," ed by S. Patai, Interscience Publishers, New York, N. Y. (1966), Chap. 15, p. 771.

17) H. H. Sisler, G. M. Omietanski, and B. Budner, *Chem. Rev.*, **57**, 1021 (1957).

18) K. van Auwers and W. Schmidt, *Ber.*, **58**, 528 (1925).

19) C. Mannich and G. Heilner, *Ber.*, **55**, 365 (1922); S. G. Beech, J. H. Turnbull, and W. Wilson, *J. Chem Soc.*, **1952**, 4686.

20) H. Bretschneider and H. Horman, *Monatsh. Chem.*, **84**, 1021 (1953).

Chemical-state Analysis by Means of Soft X-Ray Spectroscopy. I. $L_{2,3}$-Emission Spectra for Phosphorus, Sulfur, and Chlorine in Various Compounds

Kazuo TANIGUCHI

Department of Solid-State Electronics, Osaka Electro-Communication University, 18-8, Hatsucho, Neyagawa, Osaka 572

(Received May 18, 1983)

The phosphorus-, sulfur-, and chlorine-$L_{2,3}$ emission spectra in various compounds are obtained using secondary excitation. The spectra are discussed from the point of view of chemical-state analysis. It should be noted that the spectra of a highly ionic bond reveal scarcely no influence of the cations. However, the spectra with a covalent character are complex as a result of the molecular orbital generated with the covalent bond. The spectral features are influenced by the chemical condition of the surrounding atoms and are sensitive to oxygen and hydrogen.

X-Ray spectroscopy has long been a basic method for studying the elemental compositions of materials and the electronic structures of atoms. It has been known since the 1920's that the X-ray emission spectrum of an element varies according to the state of its chemical combination. However, the effect of chemical combinations on X-ray spectra has been found to be very slight except in the case of a light element. In an earlier work, Lindh and Lundquist[1] were able to observe the chemical-combination effect of X-ray spectra in their studies of the $K\beta$ emission spectra of phosphorus, sulfur, and chlorine compounds. The problems encountered by earlier investigators in X-ray emission spectroscopy were generated mainly by the highly energetic conditions of the direct-electron bombardment of the sample deposited on the anticathode of the X-ray tube. This type of excitation leads to sample oxidation, reduction, decomposition, and other reactions with the anticathode material, which thereby generate a variety of products which add to the complexity to the observed spectra.

The twenty-year period between 1930 and 1950 there were fluorescence X-ray investigations of the $K\beta$ spectra from the point of view of the chemical-state analysis of sulfur, chlorine, and phosphorus in various compounds. The results of these investigations also showed that the effect of chemical bonding had very little influence on an X-ray spectrum.

As was noted earlier,[2] the $K\beta$ emission spectrum is related to the 3p character in the valence band. However, the $L_{2,3}$ emission spectrum is sensitive to the 3s and 3d character of the valence band. For an isolated phosphorus, sulfur, or chlorine in its ground state, the valence-band electrons tend to remain in the 3s and 3p character. In chemical combination, however, some of these valence-band electrons may be partially involved, to a greater or lesser extent, in the 3d orbital and may thereby enhance the 3d character of the molecular orbital structure. In the $L_{2,3}$ emission spectra, therefore, the chemical effect is more extensitive than in the $K\beta$ emission spectra.

Henke and Smith[3] were able to demonstrate the feasibility of obtaining the $L_{2,3}$ spectra of phosphorus, sulfur, and chlorine in various compounds by applying spectrographic techniques of such efficiency as to minimize the effects of radiation decomposition. The $L_{2,3}$ emission spectra of sulfur and chlorine in several compounds have since been more precisely measured and studied from the point of view of the molecular orbital.[2,4–6] However, no sufficiently systematic investigation of the $L_{2,3}$ emission spectra of phosphorus, sulfur, and chlorine in various compounds has been made.

We attempt to describe a chemical-state analysis by means of soft X-ray spectroscopy in this and in companion papers;[7,8] also, in this paper we will try to make clear the relationship between the character of the chemical state and the $L_{2,3}$ emissiom spectra.

Experimental

The high-efficiency techniques which have been developed by Henke *et al.*[9,10] for the secondary excitation of ultrasoft X-ray spectra have made possible the interpretation of the valence-band X-ray spectra for the light element. Ultrasoft X-ray excitation greatly reduces the radiation damage to samples and provides a considerably improved peak-to-background ratio. The basic spectrographic approach that was used in this laboratory is shown in Fig. 1. The X-ray spectrometer is of a vacuum X-ray type provided with a Soller collimator (0.3 mm spacing, 100 mm length). After reflection from the plane crystal, the beam

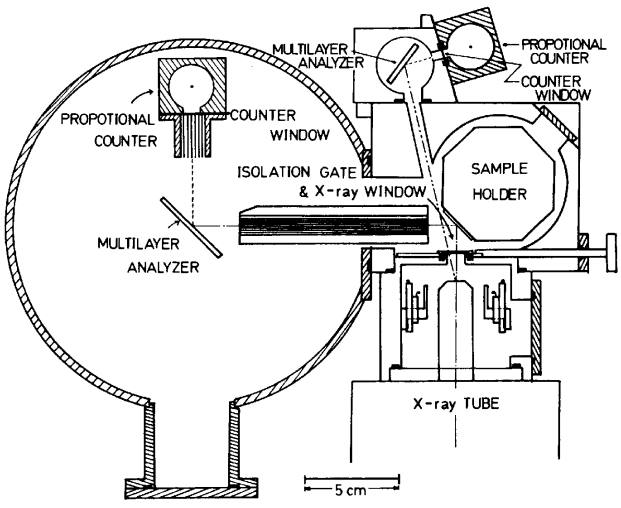

Fig. 1. A single-crystal spectrographic approach for low energy X-ray spectroscopy applying closely coupled demountable X-ray source, the development of large-soap-film crystals, and tuned subatmospheric pressure.

from the fluorescent radiator passes through the Soller collimator (1.0 mm spacing, 20 mm length) before the counter. The most intense and practical line source in the $L_{2,3}$ of phosphorus, sulfur or chlorine is C$K\alpha$ (44.6 Å). It is generated in our demountable source using a copper anode coated with a colloidal graphite. The source is stable for many hours of operation, typically at 8 kV and 150 mA. The X-ray tube window is constructed with a polycarbonate film (Kimfoil) with an aluminum coating a few hundred angstrom thick which has an effective transmission band for the carbon $K\alpha$ (44.6 Å) radiation.

The plane crystal is a specially developed Langmuir-Blodgett-type multilayer[11] analyzer, of lead stearate for chlorine and sulfur compounds or of lead lignocerate for phosphorus compounds, which has $2d$-spacing of 100 Å or 130 Å respectively. Background and impurity lines of a higher order can be reduced by using a gas-flow proportional counter with a pulse-height discriminator. Propane gas at a pressure of 60 mmHg (1 mmHg ≈133.322 Pa) is used as a counting gas and is sealed in the counter with poly(vinyl formal) film (Formver). The solid specimens are prepared by pressing a fine powder into a smooth aluminum ring in order to keep the target sample pure and at a constant pressure. The liquid samples are measured under freezing conditions using the cryostat shown in Fig.2. The spectrum is calibrated by the sharp $M\zeta$ lines of zirconium (81.9 Å) and molybdenum (64.5 Å). A detailed description of these experimental techniques has been reported elsewhere.[10] In order to insure that the radiation decomposition effect upon these measurements would be negligible, the measurement has been done twice for each spectrum with two identical samples. The total counting time is 50 s per point, and the counter is scanned step by step, by 1/10 s or 2/10 degree.

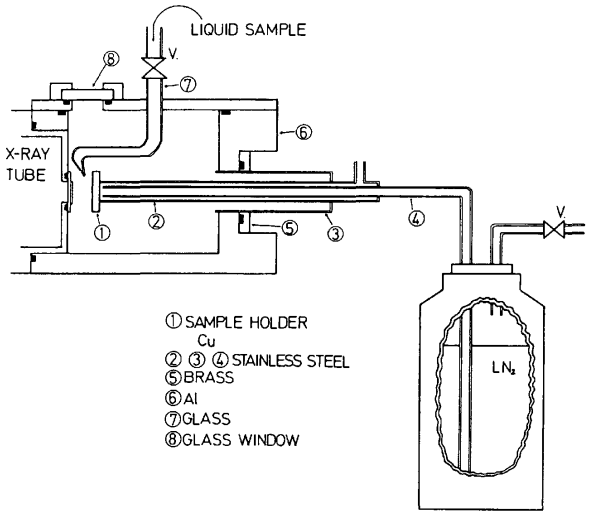

Fig. 2. Sketch of the cryostat for sample holder. The liquid samples were measured at the freezing conditions using the cryostat controlled by liquid nitrogen.

Figure 3 shows schematically a flow- and pressure-regulated system for the counter, and vacuum systems for the sample chamber and the X-ray tube. The optimum pressure in the counter (P.C.) is maintained by the controls with valves (Vl and V2). The gas pressure is indicated by the gauges (P.G.) and the manometer (U.M.M.). The gas is allowed to flow through the flow meter (F.M.) at a rate of 50 cm³/min. The V3 valve is usually closed, but it is opened in order to keep the same pressure in the counter and the spectrometer when the spectrometer is pumped down to a vacuum

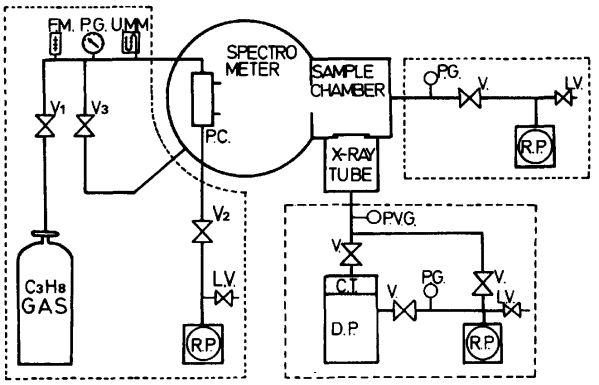

Fig. 3. Schematic diagram of the flow and pressure regulated system for the counter, and vacuum systems for the sample chamber and the X-ray tube.

from the atmosphere. The spectrometer and the sample chamber are pumped to about 10^{-3}'s Torr (1 Torr≈ 33.322 Pa) by means of a rotary pump. The X-ray tube is pumped to about 10^{-6}'s Torr by means of a diffusion pump and rotary pump.

Results and Discussion

In a previous paper,[2] our studies of the sulfur $L_{2,3}$ emission spectra and molecular orbital studies of sulfur compounds were reported. In that paper, the $L_{2,3}$ fluorescence spectra of sulfate ions (SO_4^{2-}) reveal scarcely no influence of the cations of these sulfate compounds. In the case of perchlorate ions (ClO_4^-), the same phenomenon is observed in the $L_{2,3}$ fluorescence spectra. Cl $L_{2,3}$ emission spectra for $LiClO_4$, $NaClO_4$, $KClO_4$, and $AgClO_4$ are shown in Fig. 4. It should be noted that the $L_{2,3}$ fluorescence spectra of perchlorate ions reveal scarcely no influence of the

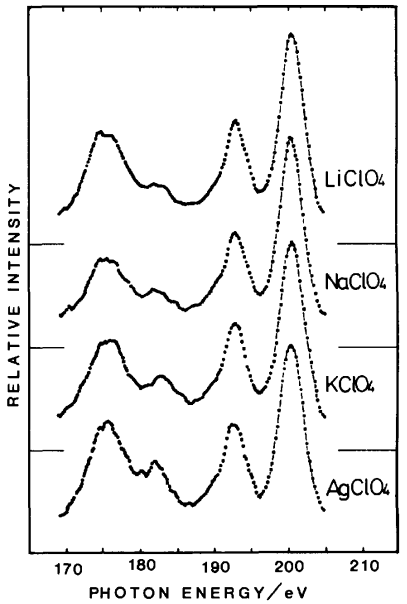

Fig. 4. Chlorine-$L_{2,3}$ emission spectra for $LiClO_4$, $NaClO_4$, $KClO_4$, and $AgClO_4$. Chlorine-$L_{2,3}$ emission spectra have been excited by C$K\alpha$ radiation and analyzed by lead stearate.

cations. This reflects the fact that the covalent interaction between the ions is relatively small, thus accounting for the narrow emission bands, which can be attributed either to the cations or to the anions. With this evidence for strong localization, it seems reasonable to suggest that the crystal effect should be neglected.

In general, there is a similarity in features of the $L_{2,3}$ emission spectra between the molecules with different central atoms, but all with the T_d symmetry, although the energy ranges of the emission spectra are different. A comparison of the features of the $L_{2,3}$ emission spectra for the central atom of the T_d symmetry with Li_3PO_4, Li_2SO_4, and $LiClO_4$ is shown in Fig. 5. There are seven occupied orbitals ($4a_1$, $3t_2$, $5a_1$, $4t_2$, le, $5t_2$, and $1t_1$) in the valence band for these examples of T_d molecular symmetry. Hence, transitions into the 2p-level are allowed only from the a_1, t_1, and e orbitals by the dipole-selection rule. The peaks at lower energy and a middle energy should be assigned to $4a_1$ and $5a_1$ respectively, whose molecular orbitals consist mainly of the 3s population. The main peak at a higher energy has to be assigned to the le and $5t_2$ orbitals with then comparatively high 3d population. The intensity ratios of the peak at a middle energy (from $5a_1$) and at a higher energy (le+$5t_2$) increase with the increase in the atomic number of X for the XO_4^{2-} cluster. It seems reasonable that the 3d population in the valence band increases with a increase in the atomic number of X; therefore, the peak at a higher energy, which is assigned to the le and $5t_2$ orbitals, with then comparatively high 3d population, will increase. In the $LiClO_4$, a small peak appears between $4a_1$ and $5a_1$. This peak should be assigned to $3t_2$, where molecular orbital consists mainly of the 3p and 3d populations of Cl and the 2s population of O. The electron transition involves two excited states, and, as the initial vacancy (core level) has two possible states, $2p_{1/2}$ (L_{II}) and $2p_{3/2}$ (L_{III}), corresponding to the $2p^5$ configuration, the emission component which is due to a transition from a molecular orbital to the 2p levels will result in two emission lines. This spin-orbit separation, however, is about 1.2 eV, and the energy resolution of the spectrometer is about 1 eV for this wavelength region. Therefore, the emission spectra can reflect the structure of the molecular orbital, as the spin-doublet effect need not be so considered.

The phosphorus $L_{2,3}$ fluorescence spectra of Li_3PO_4, K_3PO_4, KH_2PO_4, and H_3PO_4, all of which are composed of the phosphate ion (PO_4^{3-}), are shown in Fig. 6. In this figure, the spectrum of H_3PO_4 differs from that of another phosphate especially in the middle-energy range, though the peak positions on the lower-energy side and the higher-energy side are quite the same. The phosphate anion for strong localization

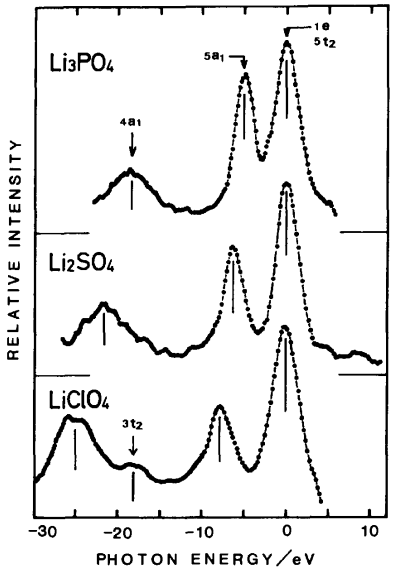

Fig. 5. Comparison of the feature of the $L_{2,3}$ emission spectra of the central atoms of T_d symmetry for Li_3PO_4, Li_2SO_4, and $LiClO_4$. Also shown are the positions of peaks and the molecular orbital assignment for each peak.

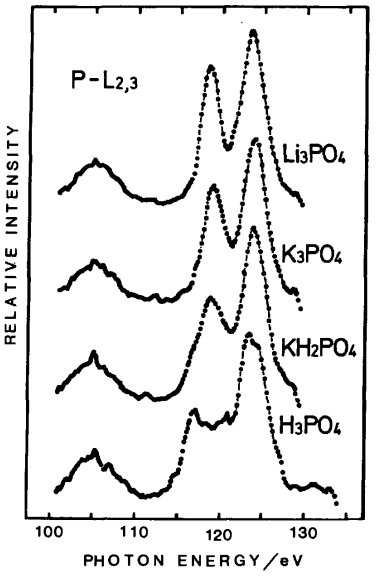

Fig. 6. Comparison of the phosphorus-$L_{2,3}$ emission spectra. Phosphorus-$L_{2,3}$ emission spectra have been excited by $CK\alpha$ radiation and analyzed by lead lignocerate.

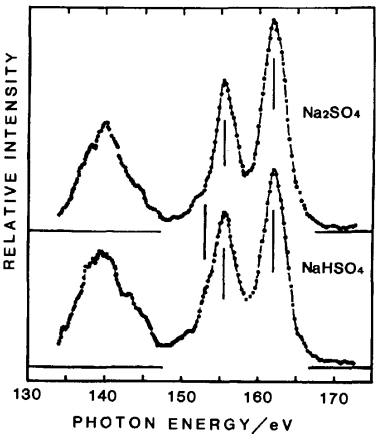

Fig. 7. Sulfur-$L_{2,3}$ emission spectra for Na_2SO_4 and $NaHSO_4$. Sulfur-$L_{2,3}$ emission spectra have been excited by $CK\alpha$ radiation and analyzed by lead stearate.

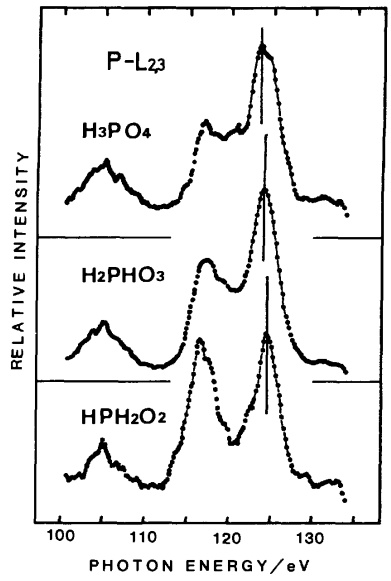

Fig. 8. Comparison of the phosphorus-$L_{2,3}$ emission spectra for phosphoric acid, phosphonic acid, and phosphinic acid. Phosphorus-$L_{2,3}$ emission spectra have been excited by C$K\alpha$ radiation and analyzed by lead lignocerate.

has a tetrahedral symmetry (T_d point group). However, the phosphate anion of H_3PO_4 does not have tetrahedral symmetry because there is not strong localization between PO_4^{3-} and the three H^+. Therefore, in view of the three hydrogens, it seems reasonable that H_3PO_4 has molecular symmetry. If Fig. 6 is looked at carefully, it can be found that the spectral feature of KH_2PO_4 differ just a little from those of other phosphate compounds. The same phenomenon is observed in sulfur compounds. Figure 7 shows a comparison of the sulfur $L_{2,3}$ emission spectra for Na_2SO_4 and $NaHSO_4$. In this case also, there is a hump on the low-energy side of the middle peak in $NaHSO_4$. This may reflect the fact that the structure of the valence band molecular orbital is affected by the H-atom contribution. These facts may suggest that X-ray emission spectra can give information about the chemical bonding of hydrogen; if so, this would be very important.

The P $L_{2,3}$ emission spectra for phosphoric acid (H_3PO_4), phosphonic acid (H_2PHO_3), and phosphinic acid (HPH_2O_2), are compared in Fig. 8. Each spectrum consists of three major peaks, at about 105, 117, and 124 eV. The measured spectra difference depends upon the chemical state. In proportion to the decrease in the number of oxygen atoms, the peak at about 124 eV shifts to the higher-energy side just a little and the peak at about 117 eV increases. The structural formulas for H_3PO_4, H_2PHO_3, and HPH_2O_2 are:

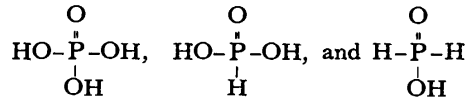

respectively. In the structural formula of H_3PO_4, the central P atom combines with O atoms only. In the H_2PHO_3, the central P atom combines with three O atoms and one H atom. In the HPH_2O_2, however, the central P atom combines with two O atoms and two H atoms. The peak at about 117 eV increases corresponding to the number of direct combinations of the H atom to the P atom. On the other hand, the structural formulas for *cyclo*-triphosphoric acid ($H_3P_3O_9$) and pyrophosphoric acid ($H_4P_2O_7$) are:

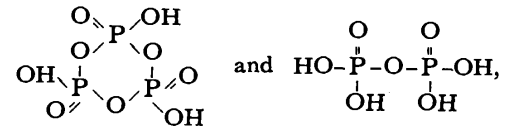

respectively; here, the central P atom combines directly with the O atom, like only H_3PO_4. In this case, the spectral features of these compounds have something in common (Fig. 9). It seems reasonable to consider that the spectral features of these compounds are influenced by the surrounding atoms, but not by the bond conditions.

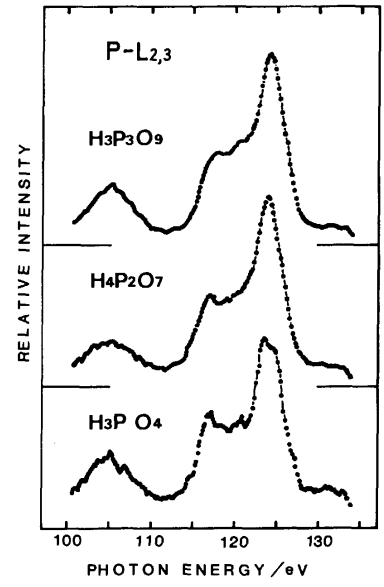

Fig. 9. Comparison of the phosphorus-$L_{2,3}$ emission spectra for phosphoric acid, *cyclo*-triphosphoric acid, and pyrophosphoric acid. Phosphorus-$L_{2,3}$ emission spectra have been excited by C$K\alpha$ radiation and analyzed by lead lignocerate.

The relation between the number of oxygen atoms and the spectral features will be considered. The Cl $L_{2,3}$ emission spectra of NaCl, $NaClO_2$, $NaClO_3$, and $NaClO_4$ are shown in Fig. 10. It is shown that the main peak of the $L_{2,3}$ emission spectra shifts to the higher-energy side and decreases with the increase in the oxidation number. The peak of the higher-energy side appears, and then increases in proportion to the increase in the number of oxygens. It is reasonable to think that the Cl-3d atomic orbital population increases in the valence band according to the increase in the number of oxygens combined to the chlorine atom. Thus, it is found that the 3d atomic orbital plays a very important role in the molecular orbital for the chemical combination of chlorine and oxygens.

Figure 11 shows a comparison of the sulfur $L_{2,3}$ emission spectra for $Na_2S_2O_4$, $Na_2S_2O_5$, $Na_2S_2O_6$, and $Na_2S_2O_7$. These spectra change corresponding to the

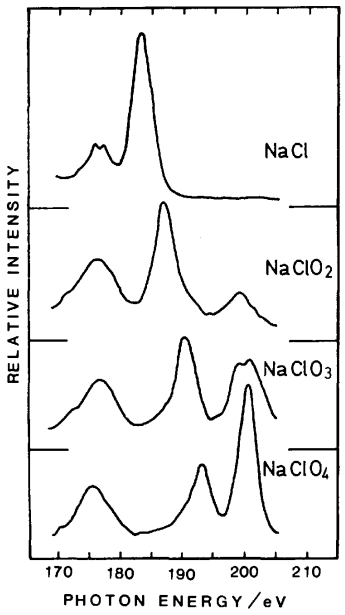

Fig. 10. Chlorine-$L_{2,3}$ emission spectra for NaCl, $NaClO_2$, $NaClO_3$, and $NaClO_4$. Chlorine-$L_{2,3}$ emission spectra have been excited by C$K\alpha$ radiation and analyzed by lead stearate.

chemical-bond state and also with the bonding O atom number. It can thus be thought that the existence of the oxygen atom makes the molecular orbital of the valence band attracted to the O-2p level. In Fig. 11, in proportion to the increase in the quantity of oxygen, the middle peak shifts to the higher-energy side and decreases just a little, while the peak of the higher-energy side increases and shifts just a little to the higher-energy side, but the peak of the lower-energy side does not show any influence of the quantity of oxygen.

Finally, the Cl $L_{2,3}$ emission spectra of LiCl, NaCl, KCl, and AgCl are shown in Fig. 12 in order to make possible a consideration of the relation of the ionic bond and covalent bond to the X-ray spectra. Since these compounds all have highly ionic bonds except for AgCl, the $L_{2,3}$ spectra of these compounds can be expected to be due to the electon transition from the M_1 level to the $L_{2,3}$ levels. However, these spectra have mainly two peak components. Each peak shifts just a little to the higher-energy side according to the order of the increase in the atomic number: Li, Na, and K, but it shifts to the lower-energy side for Ag. The differences in electronegativity between the cation and the anion of the molecule are 2, 2.1, 2.2, and 1.1 for LiCl, NaCl, KCl,and AgCl respectively. Therefore, it seems reasonable that the spectral peaks shift to the higher-energy side with the increase in the ionic character. If these compounds have a highly ionic bond, only the major components in the $L_{2,3}$ spectrum can be expected to fill the $L_{2,3}$ core from the M_1 level. Therefore, it is reasonable to think that the most intense peak is due to the transition from M_1 to $L_{2,3}$.

Cooper and Lavilla[12] interpreted the lower-energy peak in the spectrum of argon as a *'semi-Auger'* process in the $L_{2,3}$ emission, which is a *'shake-up'* process accompanied by the X-ray emission. The final state of

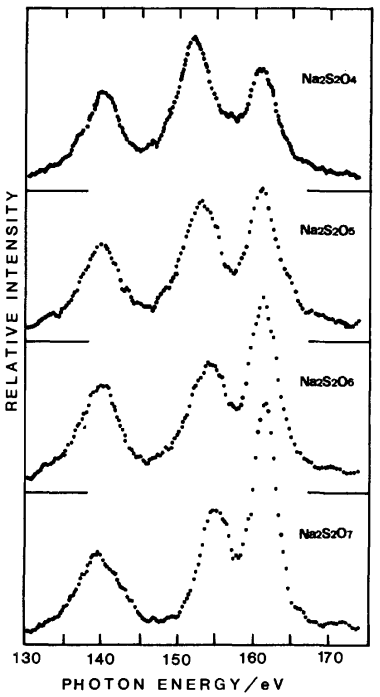

Fig. 11. Sulfur-$L_{2,3}$ emission spectra for $Na_2S_2O_4$, $Na_2S_2O_5$, $Na_2S_2O_6$, and $Na_2S_2O_7$. Sulfur-$L_{2,3}$ emission spectra have been excited by C$K\alpha$ radiation and analyzed by lead stearate.

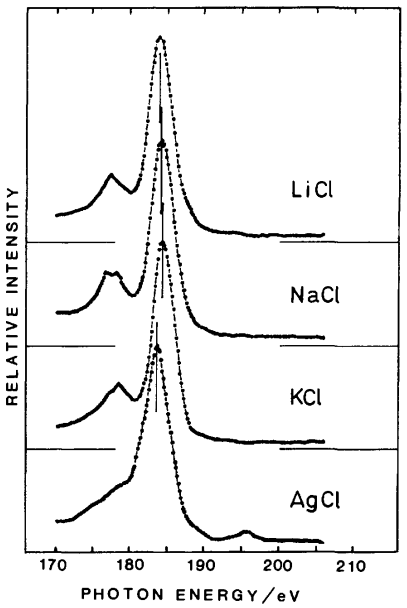

Fig. 12. Chlorine-$L_{2,3}$ emission spectra for LiCl, NaCl, KCl, and AgCl. Chlorine-$L_{2,3}$ emission spectra have been excited by C$K\alpha$ radiation and analyzed by lead stearate.

the X-ray emission can be mixed strongly with states where one of the $M_{2,3}$ electrons is removed and the other is excited, provided that these levels have the same parity. A similar satellite structure is observed in the XPS spectra of argon and alkali halides.[13] A study of the Cl $L_{2,3}$ spectrum clearly indicates that the low-energy tail is due to a series of transitions of this type. The small peak is observed at the higher-energy side in AgCl; this may reflect the fact that this peak is due to a

transition from a molecular orbital in the valence band to the $L_{2,3}$ level, because AgCl has a small ionic character and a strongly covalent character.

Conclusion

In this work, it has been shown that a spectral feature is closely connected with the chemical state and that the $L_{2,3}$ emission spectra are very useful for chemical-state analysis. The following properties have been found:

(1) The $L_{2,3}$ emission spectra of the highly ionic bond scarcely reveals any influence of the cations.

(2) The $L_{2,3}$ emission spectra for the molecular T_d symmetry of different central atoms have similar features.

(3) The peak related to the hydrogen atom is observed on the lower side of the middle peak in the $L_{2,3}$ emission spectra. This is suggests that the X-ray emission spectra give information about the existence of hydrogen in the chemical combination.

(4) In the $L_{2,3}$ emission spectra of the oxyanions, the middle peak shifts to the higher-energy side and its intensity decreases, while the peak of the higher-energy side increases according to the increase in the number of oxidation. It is reasonable to think that the oxygen 2p electron will diffuses into the 3d atomic orbital of the central atom in the valence molecular orbital when the central atom combines with oxygen.

(5) The spectral feature is influenced by the kind of ligand if this atom forms a part of the molecular orbital.

(6) In a highly ionic bond, the spectrum is simple, with two peak components. However, the spectrum is different according to its covalent character.

In this work, we can not interpret the spectra quantitatively as transitions from the molecular orbitals with the help of a molecular orbital calculation. This will remain a subject for future study.

The main program of this work was begun by the author during his stay at the University of Hawaii. The author wishes to express his thanks to Professor B.L.Henke for his kind guidance. We also gratefully acknowledge some very useful discussions with Dr. Sigero Ikeda of Osaka University and Dr. Yōichi Gōshi of Tokyo University, and the invaluable help of the undergraduate students in their laboratories.

Reference

1) A. E. Lindh and O. Lundquest, *Ark. Matem. Astron. Fys.*, **18**, No. 14, 3 (1924); **18**, No. 34, 1 (1924); **18**, No. 35, 1 (1924).

2) K. Taniguchi and B. L. Henke, *J. Chem. Phys.*, **64**, 3021 (1976).

3) B. L. Henke and E. N. Smith, *J. Appl. Phys.*, **37**, 922 (1966).

4) B. L. Henke, R. C. C. Perea, E. N. Gullikson, and M. L. Schattenburg, *J. Appl. Phys.*, **49**, 480 (1978).

5) K. Taniguchi, *Report of O.E.C.U.*, **15**, 1 (1979).

6) K. Taniguchi, "Advances in X-Ray Analysis," Plenum, New York (1980), Vol. 23, p. 193.

7) K. Taniguchi, *Bull. Chem Soc. Jpn.*, **57**, 915 (1984).

8) K. Taniguchi, *Bull. Chem Soc. Jpn.*, **57**,921 (1984).

9) B. L. Henke and M. A. Tester, "Advances in X-Ray Analysis," Plenum, New York (1975), Vol.18, p. 76.

10) B. L. Henke and K. Taniguchi, *J. Appl. Phys.*, **47**, 1027 (1976).

11) K. B. Blodgett and I. Langmuir, *Phys. Rev.*, **51**, 964 (1937).

12) J. W. Cooper and R. E. Lavilla, *Phys. Rev. Lett.*, **25**, 1745 (1970).

13) D. P. Spears, H. J. Fischbeck, and T. A. Carlson, *Phys. Rev. A*, **9**, 1603 (1974).

 © 1984 The Chemical Society of Japan Bull. Chem. Soc. Jpn., 57, 915—920 (1984)

Chemical-state Analysis by Means of Soft X-Ray Spectroscopy. II. $K\beta$ Spectra for Phosphorus, Sulfur, and Chlorine in Various Compounds

Kazuo TANIGUCHI

Department of Solid-State Electronics, Osaka Electro-Communication University, 18-8, Hatsucho, Neyagawa, Osaka 572

(Received May 18, 1983)

The phosphorus-, sulfur- and chlorine-$K\beta$ spectra in various compounds are obtained by means of secondary excitation using a simple quasi-two-crystal X-ray spectrometer. The spectra thus obtained change depending upon the chemical state. The spectra are discussed from the point of view of chemical-state analysis. The spectral features are especially influenced by the hydrogen and oxygen of the ligand. The peak on the lower-energy side appears to be related to the oxygen, and the peak grows with an increase in the oxidation number. The spectrum gives information on the structural formula.

In previous paper[1,2] we have studied the $L_{2,3}$ emission spectra of phosphorus, sulfur, and chlorine in various compounds. As was noted earlier, the $K\beta$ emission spectrum is related to the 3p character of the valence band. The $L_{2,3}$ emission spectrum, however, is sensitive to the 3s and 3d character of the valence band. Therefore, it is well known that the emission spectrum originating from electron transitions between the valence band and the inner shell provides a powerful technique for obtaining information about the electronic structure in the valence band or the chemical-bonding state.

The first evidence in a study of the $K\beta$ emission spectra for phosphorus, sulfur, and chlorine compounds that X-ray spectra were influenced by the chemical combination was reported by Lindh and Lundquest,[3] who worked with direct electron bombardment. Following this discovery, very active investigations were begun to ascertain the effects of chemical combination on the X-ray spectra of many elements using a fluorescent-excitation technique. However, the effects of chemical combination on the X-ray spectra were found to be very slight except in the case of the light elements.

Recently, Takahashi *et al.*[4-6] obtained the $K\beta$ spectra of phosphorus, sulfur, and chlorine compounds and discussed the $K\beta$ spectral profile from the standpoint of chemical-state analysis. However, no sufficient discussion of the peak profile has yet been made because the spectrum is obtained with a single crystal spectrometer. A high-resolution spectrometer is necessary to observe fine splitting structures originating from chemical bonding, as the separation in the energy of the valence-band molecular orbitals is less than several electron volts. Gōshi[7] designed and constructed a simple two-crystal spectrometer in order to obtain highly energy resolved $K\beta$ X-ray emission spectra and then applied it to chemical-state analysis. Whitehead[8] obtained the $K\beta$ spectra of sulfur and chlorine compounds using a double-crystal X-ray spectrometer and discussed the spectra in terms of the molecular-orbital theory. Gōshi *et al.*,[9] in the latest date, constructed a wide-range two-crystal vacuum X-ray spectrometer and showed many possibilities in chemical shift measurement and chemical-state analysis.

There have been many experiments and studies of the $K\beta$ spectra for the third-period elements in various compounds. However, no sufficient and systematic investigation of the $K\beta$ spectra for these compounds, and no systematic studies of chemical-state analysis using these spectra, have yet been done. In this paper, a systematic investigation of the P-, S- and Cl $K\beta$ spectra in various phosphorus, sulfur and chlorine compounds, and a discussion from the point of view of chemical-state analysis, will be done using a simple quasi-two-crystal spectrometer in order to obtain the high-resolution spectra. We have attempted to present the results of chemical-state analysis by means of soft X-ray spectroscopy in this and in companion papers;[10,11] also in this paper we will try to make clear the relationship between the character of the chemical state and the $K\beta$ emission spectra.

Experimental

We designed and constructed a new, simple quasi-two-crystal spectrometer using a commercial single-crystal spectrometer. By rotating the detector arm at $3\Delta\theta$ relative to the rotation angle of the first crystal, (1) the analyzer wavelength can be obtained directly according to Bragg's diffraction law, $2d\sin\theta=n\lambda$, and (2) the scanning range satisfying Bragg's diffraction law is extended.

Figure 1 shows a schematic diagram of the quasi-two-crystal spectrometer in which a two-crystal attachement is added to a commercial single-crystal spectrometer. A parallel-foil collimator, A, limits the divergence of the X-

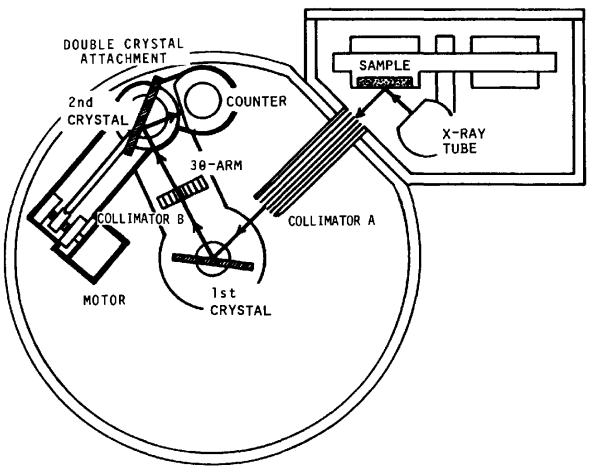

Fig. 1. Schematic diagram of the quasi two-crystal spectrometer.

rays incident on the first crystal, and the collimator, B, between the first- and second-crystals, limits the scattering of the X-rays. An attachment which includes the second crystal and a detector is coupled to the detector arm. The second crystal can be rotated by several degrees for fine adjustment using a bar driven through gears by a small motor. The collimator, A, is 10 cm long with 0.24 mm spacing and with a vertical 1 mm-spacing collimator attached. A flat Ge(110···$2d$=6.532 Å) was used as an analyzer crystal. Background and impurity lines of a higher order can be reduced by using a gas-flow proportional counter with a pulse-height discriminator. P-10 gas is used as the counting gas and is sealed in the counter with a polycarbonate film window (6 μm thick). A Philips PW2188 chromium-target X-ray tube is used and operated at 50 kV and 50 mA. The primary characteristics of this spectrometer are: (1) the intensity and resolution are the same as those of an orthodox two-crystal spectrometer, and (2) it is easy to use and can easily be constructed. A detailed description of this spectrometer has been reported elsewhere.[12]

The solid specimens are prepared by pressing a fine powder into a smooth aluminum ring, thus keeping the target sample pure and at a constant pressure. The liquid samples are measured using a sample holder which is sealed with a polystyrene film window (15 μm thick). The spectrum is calibrated by the sharp Cu$K\beta$ line. In order to insure that the radiation-decomposition effect upon these measurements is negligible, the measurement has been done twice for each spectrum, using two identical samples. The total counting time is 30 s per point, and the counter is scanned, step by step, by 0.01 ° of 3θ.

Results and Discussion

In previous[1] and companion[10] papers, it has been shown that the $L_{2,3}$ fluorescence spectra of sulfate ions (SO_4^{2-}) reveal scarcely no influence of the cations of sulfate compounds. The same phenomenon is expected in the $K\beta$ fluorescence spectra. The S$K\beta$ emission spectra for Na_2SO_4, $CoSO_4$, $NaHSO_4$, $(NH_2)_2H_2SO_4$, and H_2SO_4 are shown in Fig. 2. In the ions of polyatomic compounds, the individual ionic groups, such as SO_4^{2-} in solid Na_2SO_4, K_2SO_4, or $CaSO_4$, are essentially isolated anions, as a whole, and are not signifcantly affected by the cations. In the $K\beta$ spectra from sulfate ions with a T_d symmetry, however, there are two main components. The T_d molecular symmetry has seven occupied orbitals ($4a_1$, $3t_2$, $5a_1$, $4t_2$, $1e$, $5t_2$, and $1t_1$) in the valence band. Hence, transitions into the 1s-level are allowed only from the t_2 orbital by the dipole-selection rule, and it seems that the main peak C, known as $K\beta_{1,3}$, should be a transition from the $4t_2$ orbital, whose molecular orbital consists mainly of the 3p population of sulfur and the 2p population of oxygen. It seems that the position of the main peak C is not influenced by the kind of cation. If the cation of these compounds is replaced by hydrogen, however, the main peak C shifts just a little (≈1 eV). Because X-ray emission involves two levels, the chemical effect is the result of the shift of the core level also and of the structure of the valence band. The effect of the core-level shift is simply to shift the emission spectrum in terms of energy. Therefore, the spectral feature is related to the structure of the valence band. It seems reasonable that the main peak of the $K\beta$ spectra is not shifted by the shift of the core level 1s of sulfur in relation to hydrogen, because the 1s level of hydrogen is separated from the 1s level of sulfur; therefore, the molecular orbital in the valence band is affected in relation to hydrogen. The peak A, known as $K\beta'$ at a lower energy, should be identified as the $3t_2$ orbital, whose molecular orbital consists mainly of the 3p population of sulfur and the 2s population of oxygen. It should be noted that the position of the peak A shows scarcely no influence of the cations; however, the peak A shifts just a little, like peak C, when the cation is replaced by hydrogen. The spectra can be expected to have one more component, as there is the $5t_2$ molecular orbital in the valence band. That is the very small peak D, known as $K\beta''$, because the $5t_2$ orbital consists of the 3d population of sulfur and the 2p population of oxygen. There is a small hump on the lower-energy side of the main peak C. This peak probably originates from the $5a_1$ molecular orbital, whose molecular orbital consists mainly of the 3s population of sulfur and the 2s, 2p population of oxygen. If a symmetry of molecule is distorted and the $5a_1$ molecular orbital contains the 3p population, an electron transition is allowed to the 1s level from $5a_1$, with its 3p population, although transition into the 1s level is not allowed from the a_1 orbital by the dipole-selection rule. It thus seems that the peak B is influenced by the chemical bonding conditions and by the other cations.

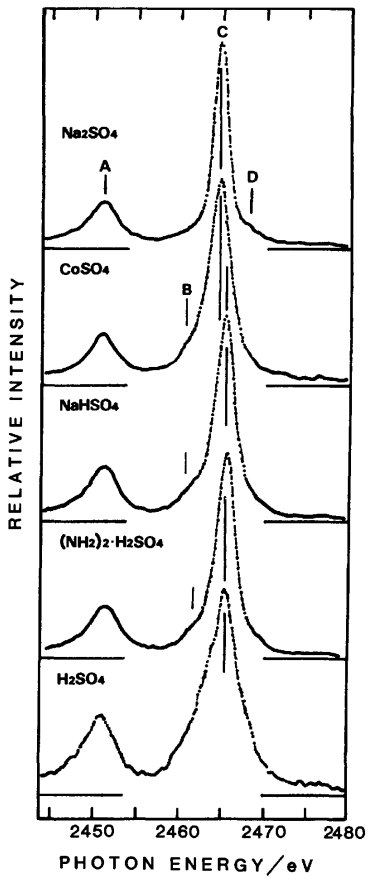

Fig. 2. Comparison of S$K\beta$ spectra of sulfate compounds.

The Cl$K\beta$ spectra for $LiClO_4$, $NaClO_4$, and $KClO_4$ are shown in Fig. 3. It should be noted that the $K\beta$

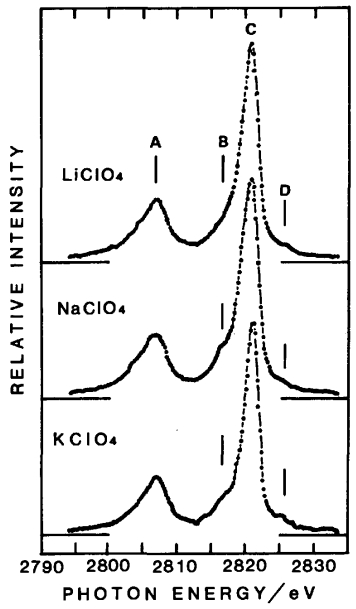

Fig. 3. Comparison of Cl$K\beta$ spectra of perchlorate compounds.

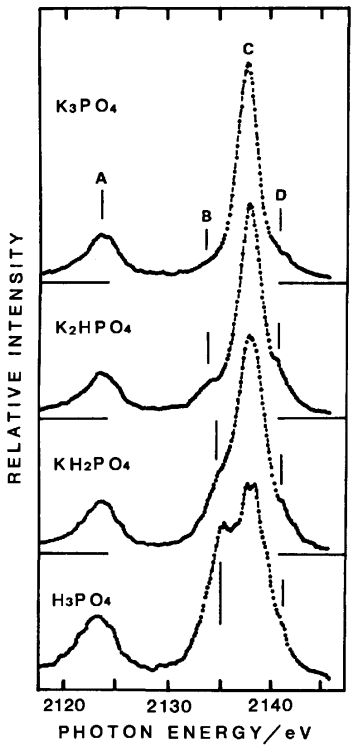

Fig. 4. Comparison of P$K\beta$ spectra of potassium phosphates and phosphoric acid.

spectral profiles of perchlorate ions reveal scarcely no influence of the cation, except for the hump B. The hump B grows up in proportion to the increase in the atomic number of the cation. It seems that the hump B originates from the electron transition from the $5a_1$ molecular orbital of the distorted T_d symmetry to the 1s level, and that the molecular orbital is affected by the interaction between the anion and the cation. If the covalent interaction between the ions is relatively small, it seems that hump B becomes negligibly small.

The P$K\beta$ spectra for K_3PO_4, K_2HPO_4, KH_2PO_4, and H_3PO_4 in each of which the metallic cation is replaced by hydrogen, are compared in Fig. 4. The covalent interaction between PO_4^{3-} and the cations of these compounds is relatively large except in the case of H_3PO_4. No hump B appears in the spectrum in the case of K_3PO_4, but the hump B appears and grows in the cases of K_2HPO_4 and KH_2PO_4, and the hump B grows into a large peak in the case of H_3PO_4. Moreover, the hump B shifts to the higher-energy side according to the contribution of hydrogen. It seems that hydrogen contributes to the hump B and that the intensity of the hump B increases according to the increase in the covalent interaction between the anion and the cation. The main peak C shifts just a little in relation to the hydrogen atom. There is a small component D on the higher-energy side of the main peak.

For a consideration of the contributions of the hydrogen ion or the hydroxide ion in the $K\beta$ spectrum, the P$K\beta$ spectra for phosphinic acid (HPH_2O_2), phosphonic acid (H_2PHO_3), *cyclo*-triphosphoric acid ($H_3P_3O_9$), and pyrophoshoric acid ($H_4P_2O_7$) are compared in Fig. 5. The measured spectra change depending upon the chemical state. The spectra of HPH_2O_2 and H_2PHO_3 have hump B, while $H_3P_3O_9$, $H_4P_2O_7$, and H_3PO_4 have peak B, which is clearly separated from the main peak C. The structural formulas for HPH_2O_2, H_2PHO_3, $H_3P_3O_9$, $H_4P_2O_7$, and H_3PO_4 are:

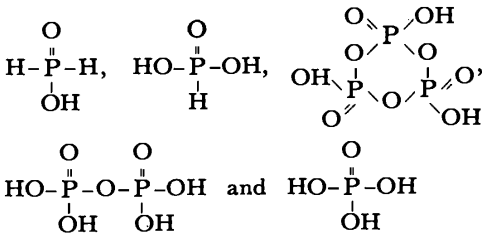

respectively. In the structural formula of HPH_2O_2 or H_2PHO_3, the central P atom combines with O, OH, and H. However, in the case of $H_3P_3O_9$, $H_4P_2O_7$, or H_3PO_4, the central P atom combines with O and OH. In these cases, the $K\beta$ spectral features for these compounds have something in common with each other. However, in the case of the O$K\alpha$ spectrum for these compounds, the spectral features change.[11] It seems reasonable to consider that those spectral features are influenced by the conditions of the surrounding atoms for the observed atom, not by the difference in structure formulas. The same conclusion can be observed for the $L_{2,3}$ emission spectra.[2]

In a companion paper,[10] it will be shown that the main peak of the $L_{2,3}$ emission spectra shifts to the higher-energy side with the increase in the oxidation number. The same phenomenon is observed in the $K\beta$ spectra of oxide compounds. Figure 6 compares the Cl$K\beta$ spectra for NaCl, NaClO, $NaClO_2$, $NaClO_3$, and $NaClO_4$. These spectra change corresponding to the chemical-bond state and also with the number of bonding oxygen atoms. These spectra have fine structures depending upon the chemical state. The main peak C and the small peak D on the higher-energy side shift to higher energy side, but the peak A on the lower-energy side only shifts a little, to higher energy side with the increase in the oxidation number. If

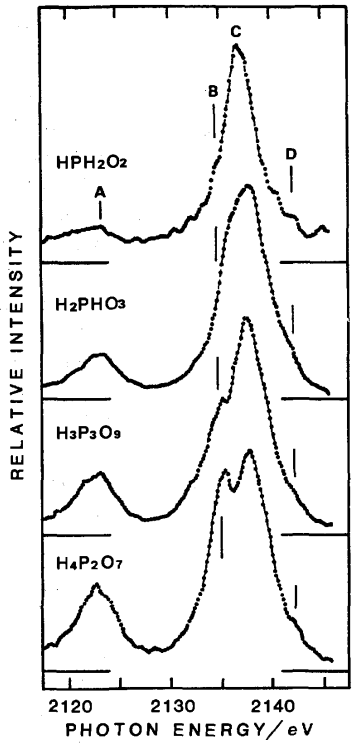

Fig. 5. Comparison of P$K\beta$ spectra of phosphinic acid, phosphonic acid, *cyclo*-triphosphoric acid, and pyrophosphoric acid.

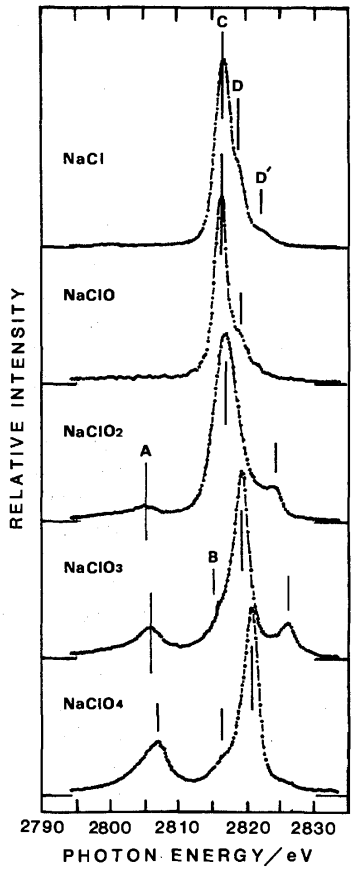

Fig. 6. Comparison of Cl$K\beta$ spectra of NaCl, NaClO, $NaClO_2$, $NaClO_3$, and $NaClO_4$ which are different in the bonding oxygen atom number.

NaCl is of a perfect ionic bond, one can expect that the spectrum will consist of only one component, because there is only the 3p level of the Cl ion which is allowed the transition to the inner ls level. However, the spectrum of NaCl has three components. It seems reasonable to say, therefore, that NaCl involves a partial covalent character. The peak A originates from the transition from the molecular orbitals which consist mainly of the Cl-3p and O-2s populations. Therefore, the peak A grows in proportion to the increase in the number of oxygen. The peak D originates from the transition from the molecular orbitals which consist mainly of the O-2p population, but the molecular orbital involves the Cl-3p or Cl-3d population a little. In the case of ClO_4^-, the peak D is negligibly small, because the ClO_4^- has the oxygen lone pair orbital. However, the peak B on the lower-energy side of the main peak seems to grow with the increase in the oxidation number.

A similar example of the sulfur $K\beta$ spectra for $Na_2S_2O_4$, $Na_2S_2O_5$, $Na_2S_2O_6$, and $Na_2S_2O_7$ is shown in Fig. 7. These spectra consist of five peaks, and they show differences in the chemical-bond state as a function of the number of bonding oxygen atoms. Each peak shifts to the higher-energy side with an increase in the number of oxygen atoms. This fact can be thought to indicate that the initial level (core vacancy) for the electron transition shifts to the higher-energy side according to the increase in the quantity of oxygens combined with the sulfur atom. While the peak A develops with the oxygen atoms, the peak E decays,

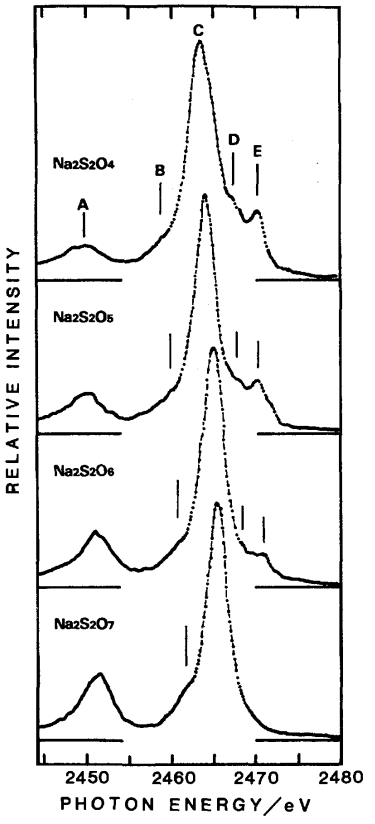

Fig. 7. Comparison of S$K\beta$ spectra of $Na_2S_2O_4$, $Na_2S_2O_5$, $Na_2S_2O_6$, and $Na_2S_2O_7$ which are different in the bonding oxygen atom number.

and it is barely seen in the $Na_2S_2O_7$ spectrum. The peak D is clearly observed in either $Na_2S_2O_4$ or $Na_2S_2O_5$, but not in $Na_2S_2O_6$ or $Na_2S_2O_7$, while in the case of the peak B, the opposite behavior is seen.

We should like to demonstrate another case of the relation between the $K\beta$ spectrum and the chemical-bond-state conditions. Figure 8 shows a comparison of the sulfur $K\beta$ spectra for sodium benzenesulfinate ($C_6H_5SO_2Na$), sodium sulfate (Na_2SO_3), sodium hydrogensulfite ($NaHSO_3$), sodium hydroxymethanesulfinate ($HOCH_2SO_2Na$), and sodium hydroxymethanesulfinate ($HOCH_2SO_3Na$). These compounds contain mainly three or four components in the $K\beta$ spectra. It seems that these spectra all show similar features, but differ from the spectrum of sulfate compounds. However, the intensity ratio of the spectral components of these compounds changes with the chemical state. These compounds contain the $-CSO_2-$ or $-SO_3-$ in their structural formulas. It seems that the main peak B reveals scarcely no influence of the chemical state. However, the peaks A and C change with the chemical state, and it seems that the intensity of the peak C decreases and the position of the peak C shifts to the higher-energy side according to the increase in the peak A. In the case of $NaHSO_4$ in Fig. 2, the small peak B which is contributed by the hydrogen atom appears on the lower-energy side of the main peak of the S $K\beta$ spectra. From these considerations, it seems reasonable that the small peak D of $NaHSO_3$, $HOCH_2SO_3Na$ and $HOCH_2SO_2Na$ is related to the hydrogen atom. In Ref. 5, it is supposed, from an X-ray spectral analysis, that the structural formula for $HOCH_2SO_3Na$ is a sulfone-type structure:

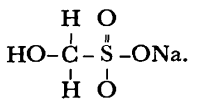

If this conclusion is true, the spectrum of $HOCH_2SO_3Na$ should be classified in the sulfate (SO_4^{2-}) group, as the 2p electrons of carbon play the same role in the valence band as the 2p electron of oxygen in combination with sulfur. However, the spectral profile of $HOCH_2SO_3Na$ seems to be classifiable in the sulfite (SO_3^{2-}) group. Our spectrum analysis suggests that the structural formula for $HOCH_2SO_3Na$ should be given as follows:

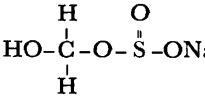

The lowest-energy peak originates from the electron transition from the molecular orbital which consists mainly of the 3p population of sulfur and the 2s population of oxygen. Therefore, if it is no contributed with oxygen atoms, the peak A should not be in the $K\beta$ spectra. The S $K\beta$ spectra for sulfur compounds which contain thiourea or other such substances, but do not contain the oxygen atom, are shown in Fig. 9. These compounds contain mainly two components. The main peak B reveals scarcely no influence, but the intensity and position of peak A are affected by the chemical state. The structural formula for the com-

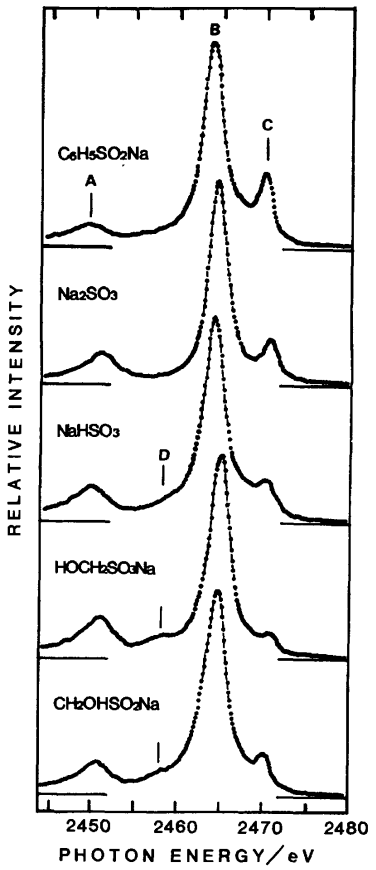

Fig. 8. Comparison of S $K\beta$ spectra of sodium benzenesulfinate, sodium sulfate, sodium hydorgensulfite, sodium hydroxymethanesulfinate, and sodium hydroxymethanesulfonate.

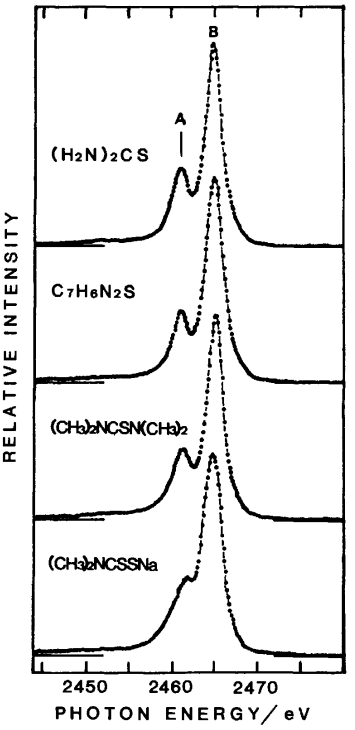

Fig. 9. Comparision of S $K\beta$ spectra of thiourea, 2-mercaptobenzimidazole, tetramethylthiourea, and sodium dimethyldithiocarbamate which do not contain oxygen.

pounds of thiourea has a double bond of carbon and sulfur. The two structural formulas in 2-mercaptobenzimidazole ($C_7H_6N_2S$) may be given as the follows:

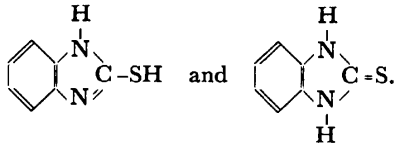

I II

However, in comparing the spectra, it seems reasonable to say that the structural formula for ($C_7H_6N_2S$) has a thiocarbonyl form II. This conclusion is the same as that is given in Ref. 5.

Finally, the Cl $K\beta$ emission spectra of HCl, LiCl, NaCl,and KCl are shown in Fig. 10 in order to consider the relation of the ionic bond and the covalent bond with the $K\beta$ X-ray spectra. These spectra have satellite peaks depending upon the chemical state. Therefore, it should be noted that these compounds have a partial covalent character and that the Cl $K\beta$ spectrum is affected by the kind of cation. If these compounds have a highly ionic bond, these spectra can be expected to have only one peak component, originating from the 3p atomic level. However, one can not discuss the ionic and covalent characters of these compounds from their $K\beta$ spectra alone. Although each peak shifts a little to the higher-energy side according to the atomic-number-increase order: Li, Na, and K, in the Cl $L_{2,3}$ emission spectra, the main peak in the case of the $K\beta$ spectra reveals scarcely no influence of the cations.

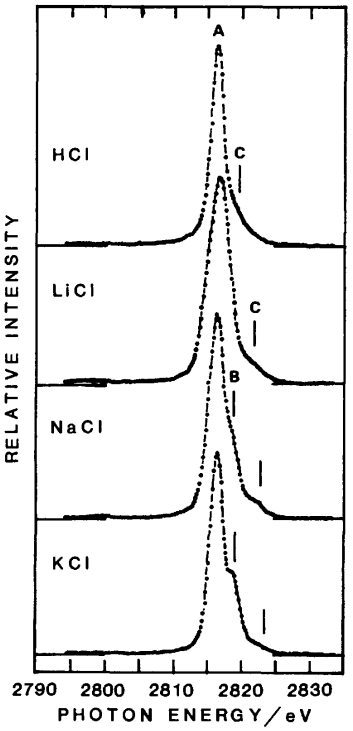

Fig. 10. Comparison of the Cl $K\beta$ spectra of HCl, LiCl, NaCl, and KCl which combine with different cations.

Conclusion

In this paper, we constructed a simple two-crystal spectrometer and showed, using it, that spectra taken with a high resolution spectrometer can give us not only important information for studies of molecular orbitals, but also useful information for application to chemical-state analysis.

We have found the following properties:

(1) Although the $L_{2,3}$ emission spectra of the highly ionic bond reveal scarcely no influence of the cations,[10] the $K\beta$ spectra for phosphorus, sulfur, and chlorine in various compounds are affected by the kind of cation.

(2) The $K\beta$ spectra for the different central atoms of compounds which have T_d molecular symmetry show features similar, as with the $L_{2,3}$ emission spectra.

(3) A peak related to the hydrogen or hydroxyl group is observed on the lower-energy side of the main peak, except in the case of HCl. It seems that the X-ray emission spectra give information about the contribution of hydrogen.

(4) The each peak of the $K\beta$ spectra shifts to the higher-energy side with an increase in the oxidation number.

(5) As the spectral features are sensitive to the chemical condition of the surrounding atoms, one can consider and decide the structural formula from a comparison of the spectra.

In this work, we can not interpret the spectra by the help of a molecular-orbital calculation and can not discuss the spectra quantitatively. This must remain a subject for future study.

We gratefully acknowledge some very useful discussions with Dr. Yōichi Gōshi of Tokyo University and Dr. Sigero Ikeda of Osaka University and invaluable assistance in this work of Mr. Shinji Nagaura of this university.

References

1) K. Taniguchi and B. L. Henke, *J. Chem. Phys.*, **64**, 3021 (1876).
2) K. Taniguchi, "Advances in X-Ray Analysis," Plenum, New York (1980), Vol. 23, p. 193.
3) A. E. Lindh and O. Lundquest, *Ark. Matem. Astron. Pys.*, **18**, No. 14, 3 (1924); **18**, No. 34, 1 (1924); **18**, No. 35, 1 (1924).
4) Y. Takahashi, *Bull. Chem. Soc. Jpn.*, **45**, 4 (1972).
5) Y. Takahashi and Y. Katsumasa, *Bull. Chem. Soc. Jpn.*, **42**, 3064 (1969).
6) Y. Takahashi, *Bull. Chem. Soc. Jpn.*, **44**, 587 (1971).
7) Y. Goshi, "Advances in X-Ray Analysis," Plemum, New York (1969), Vol. 12, p. 518.
8) H. C. Whitehead, Ph. D. Thesis, University of Hawaii, 1973.
9) Y. Goshi, H. Kamada, K. Kohra, T. Utaka, and T. Arai, *Appl. Spectros.*, **36**, 171 (1982).
10) K. Taniguchi, *Bull. Chem. Soc. Jpn.*, **57**, 909 (1984).
11) K. Taniguchi, *Bull. Chem. Soc. Jpn.*, **57**, 921 (1984).
12) K. Taniguchi, *Rev. Sci. Instrum.*, **54**, 559 (1983).

 © 1984 The Chemical Society of Japan Bull. Chem. Soc. Jpn., 57, 921—925 (1984)

Chemical-state Analysis by Means of Soft X-Ray Spectroscopy. III. O$K\alpha$ Emission Spectra for Oxyanions in Different Salts

Kazuo TANIGUCHI

Department of Solid-State Electronics, Osaka Electro-Communication University, 18-8, Hatsucho, Neyagawa, Osaka 572

(Received May 24, 1983)

The oxygen $K\alpha$ spectra of the oxyanions in different salts are obtained by secondary excitation. The obtained spectra are affected by the cations, the central atom, and the chemical-bond condition. Generally, there are four components in the spectra, but one small component may originate from the anomalous reflection of an analyzing crystal. The spectra are discussed from the point of view of chemical-state analysis.

Until a few years ago valence-band spectra originating from the electron transition from the valence-band orbitals to the inner-core level were interpreted by studying the complex interactions involving an isolated atomic model or by using solid-state-band models. Because X-ray emission involves two levels, the chemical effect is the result of the shift of the core level and of the structure of the valence-band orbital levels. Therefore, the X-ray-emission spectra can be directly applied, using standard sample systems, for the identification of an unknown valence state and for investigations of the electronic structures of chemical compounds.

In previous papers[1,2] and companion papers,[3,4] we have studied the valence-band spectra, that is the $L_{2,3}$ emission and $K\beta$ spectra for phosphorus, sulfur, and chlorine, in various compounds and discussed the spectral profile from the point of view of chemical-state analysis. It is concluded that the spectral features of the $K\beta$ or $L_{2,3}$ emission spectra are especially influenced by the oxygen of the ligand. In the ground state, two 2s-electrons and four 2p-electrons are present in the valence band, but they will obviously be directly involved in bonding. The O$K\alpha$ spectrum yields information only about the valence orbitals containing the O-2p population, because the spectra reflect the p-like symmetry on account of the dipole-selection rule. In general, the O-2p electron is related to valence-band orbitals when oxygen combines with another atom. Therefore, one can expect to get information about the electronic structure and be able to apply it to the chemical-state analysis from the results of the analysis of the O$K\alpha$ spectra.

The first evidence in studies of the O$K\alpha$ spectra in various oxide compounds that the X-ray spectra were influenced by the chemical combination was reported on the 1940's;[5,6] using the direct electron bombardment. As samples are decomposed under such electron bombardment, however, fluorescence excitation is frequently used in the region of soft X-rays.[7-11] Recently, O$K\alpha$ spectra have been obtained using low-energy-electron-induced X-ray spectroscopy,[12] a high-resolution concave-grating-grazing incidence spectrometer,[13] synchrotron radiation as a light source for the excitation of substances,[14,15] or the ion-induced X-ray excitation method.[16] Andermann *et al.* have measured the O$K\alpha$ spectra for the oxide compounds with a grating spectrogaph and discussed the C–O bond on the basis of the spectra thus obtained[17] by applying spectral techniques of such efficiency as to minimize the effects of radiation decomposition. Kosuch *et al.* have shown that the comparison of the O$K\alpha$ spectrum with the other X-ray spectra is a useful technique for the investigation of the electronic structures of chemical compounds.[14,15]

In this and in companion papers[3,4] we present the results of chemical-state analysis by means of soft X-ray spectroscopy; in this paper we will also try to make clear the relationship between the character of the chemical state and the O$K\alpha$ emission spectra.

Experimental

Measurements of the oxygen $K\alpha$ spectrum were carried out using the single flat-crystal spectroscopic method with a TAP($2d$=25.8 Å) analyzing crystal. The basic spectrographic approach that is used in this laboratory is shown in Fig. 1. The X-ray spectrometer is a vacuum type equipped with a fine Soller collimator 10 cm long and with 0.08 mm spacing. It has a simple close-coupling of a high-intensity, demountable, low-energy X-ray excitation source. The most intense and practical line source in the oxygen K excitation is Cu$L\alpha$ (13.3 Å). It is generated in a demountable Henke-type tube[18] using a copper anode. The source is stable for many hours of operation, typically at 9 kV and 220 mA. The X-ray tube window is constructed of 6 μm polycarbonate film with an aluminum coating a few hundred angstroms thick. Propane gas at a pressure of 65 mmHg (1 mmHg≈133.322 Pa) is used as the proportional counting gas, and the counting gas in the counter is isolated from the vacuum chamber with poly-(vinyl formal). This spectroscopic approach has been described in detail elsewhere.[18,19] As the oxygen $K\alpha$ emission spectra analyzed with a KAP crystal show a strong anoma-

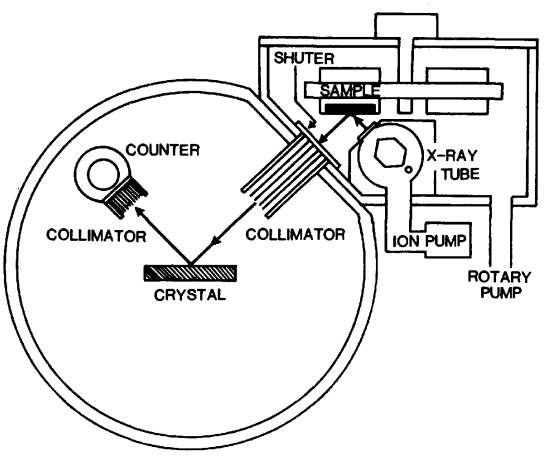

Fig. 1. A single-crystal spectrographic approach for low energy X-ray spectroscopy applying closely coupled demountable X-ray source.

lous peak on the high-energy side of the main peak,[8,20] a flat TAP was used as the analyzer crystal. The solid specimens were prepared by pressing a fine powder into a smooth aluminum ring in order to keep the target sample pure and at a constant pressure. In order to insure that the radiation decomposition effect upon these measurements was negligible, the measurement was done twice for each spectrum with two identical samples. The total counting times were 30 s per point, and the counter was scanned, step by step, by 0.05° of 2θ arm.

Results and Discussion

The spectral features of the O$K\alpha$ spectra for Li_3PO_4, Li_2SO_4, and $LiClO_4$ are compared in Fig. 2. The anions of these compounds all have the T_d molecular symmetry, but with different central atoms. There are mainly four components. These components are probably related to the molecular orbital in the valence band. There are seven occupied orbitals ($4a_1$, $3t_2$, $5a_1$, $4t_2$, 1e, $5t_2$, and $1t_1$) in the valence band for these T_d molecular symmetries. The main peak C originates from the electron transition from the O-2p lone-pair level ($1t_1$) to the O-1s core level. The hump B on the lower-energy side of the main peak probably orignates from the $5t_2$ and 1e molecular orbitals, whose molecular orbitals consist mainly of the oxygen-2p and the central atom-3d population. The peak A on the lower-energy side should be assigned to $4t_2$, with its comparatively high 3p population of the central atom and its relatively poor 2p population of the oxygen. The peak C and the hump B shift to the higher-energy side, and the peak A shifts to the lower-energy side, in proportion to the increase in the atomic number of the central atom with the T_d molecular symmetry. Thus, the domain of the spectra of interest is expanded in proportion to the increase in the atomic number of the central atom.

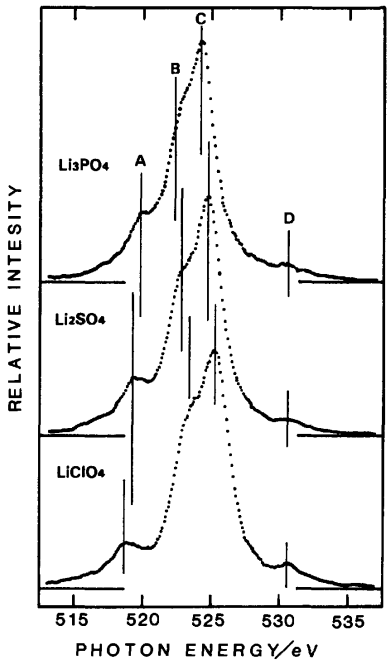

Fig. 2. Comparison of the O$K\alpha$ emission spectra for Li_3PO_4, Li_2SO_4, and $LiClO_4$. O$K\alpha$ spectra have been excited by Cu$L\alpha$ radiation and analyzed by TAP crystal.

In general, there are similar features of the $L_{2,3}$ emission spectra or the $K\beta$ spectra for all anions having the T_d molecular symmetry, though with different central atoms, although the energy ranges of the emission spectra are different,[3,4] and the domain of spectra of interest is expanded in proportion to the increase in the atomic number of the central atom. It should be noted that the peak position of D reveals scarcely no influence of the central atom. It seems reasonable to say that the peak D is due to an enhanced reflectivity of the analyzed crystal with the local continuum background in this energy region.[8]

In companion papers,[3,4] the $L_{2,3}$ emission spectra of the central atom are reported to reveal scarcely no influence of the cations for the phosphate, sulfate, or perchlorate compounds, but the $K\beta$ spectra of the central atom are affected just a little by the cation for these compounds. Kosuch *et al.* conclude that the oxygen $K\alpha$ spectra of oxyanions from different salts do not show any influence of the cation within the limits of accuracy of the measurements.[14] The oxygen $K\alpha$ spectra for lithium sulfate, sodium sulfate, and potassium sulfate are compared in Fig. 3 in order to consider the influences of the cations. Here, the intensity (in arbitrary units) is presented as a function of the 2θ of the Bragg angle θ. Each of the experimental spectra was resolved into its component lines in order to consider

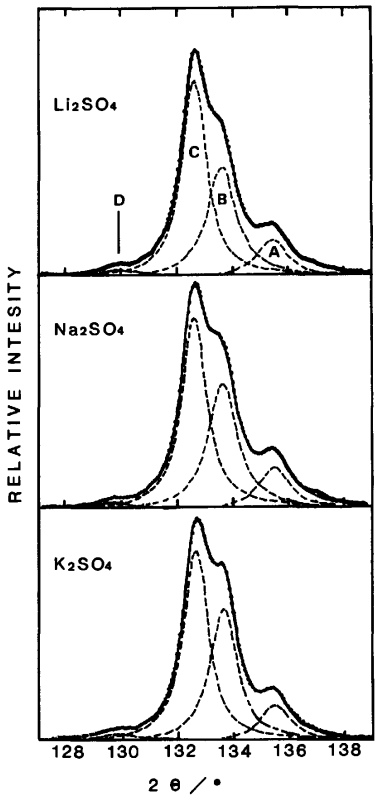

Fig. 3. Comparison of the O$K\alpha$ emission spectra for Li_2SO_4, Na_2SO_4, and K_2SO_4 in order to consider the influences of cations. O$K\alpha$ spectra have been excited by Cu$L\alpha$ radiation and analyzed by TAP crystal. Fit through the experimental points is the sum of convolution function of Lorentzian components with Gaussian function.

it more efficiently. The outmost line is the fitting curve, which is the sum of the emission components, which are also plotted here. Each line component is used as the convolution function, alone the with Lorentzian and Gaussian functions. It can be seen that the peak component B is affected little by the cation. As the main peak C originates from the lone-pair orbital $1t_1$, it seems reasonable to say that the peak C reveals scarcely no influence of the cation. On the other hand, the peak B and the peak A should be affected by the cations, because the oxygen atom is directly related to the cation. It seems that the hump B grows in proportion to the atomic number of the cations. The intensity ratios of the peaks C and B are 0.56, 0.65, and 0.75 for lithium sulfate, sodium sulfate, and potassium sulfate respectively.

The O$K\alpha$ spectra for K_2HPO_4, and KH_2PO_4, in each of which the metallic cation is replaced by hydrogen, are compared with K_3PO_4 in Fig. 4. The spectral features of the O$K\alpha$ spectra for their compounds are especially influenced by hydrogen, as are the $L_{2,3}$ emission spectra (in Ref. 3). The peaks A and B shift to the lower-energy side, and the peak A decreases in proportion to the relation with hydrogen. This phenomenon is very different from the $K\beta$ spectra (in Ref. 4), because the peak on the lower-energy side of the main peak of $K\beta$ shifts to the higher-energy side and increases in proportion to the relation with hydrogen. It can be noted from the $K\beta$ spectra that the molecular level concerning the O–H bond is created on the lower-energy side of the $4t_2$ level, which consists mainly of the 3p population and which is and shifted to near the $4t_2$ level in proportion to the relation with hydrogen. On the other hand, the electron population of oxygen-2p diffuses to lower-energy molecular orbitals with the

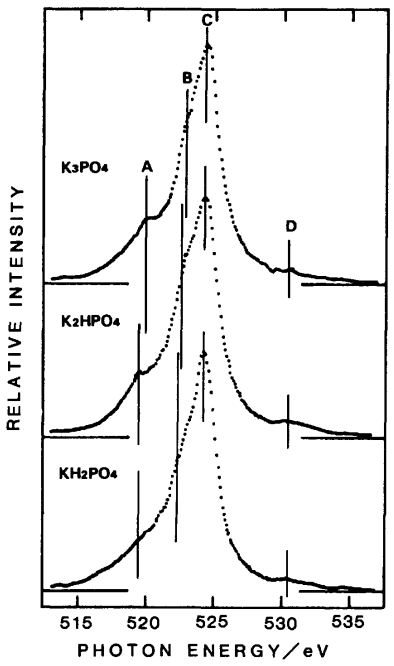

Fig. 4. Comparison of the O$K\alpha$ emission spectra for K_3PO_4, K_2HPO_4, and KH_2PO_4. O$K\alpha$ spectra have been excited by Cu$L\alpha$ radiation and analyzed by TAP crystal.

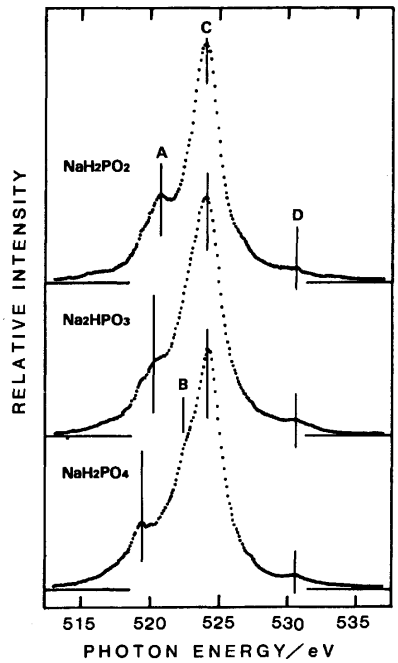

Fig. 5. Comparison of the O$K\alpha$ emission spectra for NaH_2PO_2, Na_2HPO_3, and NaH_2PO_4. O$K\alpha$ spectra have been excited by Cu$L\alpha$ radiation and analyzed by TAP crystal.

relation with hydrogen. Figure 5 shows the same phenomenon in the O$K\alpha$ spectra for NaH_2PO_2, Na_2HPO_3, and $NaHPO_4$. The O$K\alpha$ spectrum for NaH_2PO_4, consists of three components A, B, and C. However, the O$K\alpha$ spectra for NaH_2PO_2 and Na_2HPO_3 consist of only two components, A and C. Moreover, the peak A of NaH_2PO_2 shifts to the higher-energy side as compared with the cases of NaH_2PO_4 and Na_2HPO_3. The structural formulas for $H_2PO_2^-$, HPO_3^{2-}, and $H_2PO_4^-$ are;

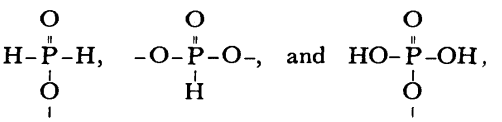

respectively. In the structural formula of $H_2PO_4^-$, the central P atom combines directly with oxygen only, but the partial oxygen atoms combine with hydrogen. In the structural formulas of $H_2PO_2^-$ and HPO_3^{2-}, on the other hand, the central P atom combines directly with oxygen and hydrogen, but the oxygen atom does not combine with hydrogen. In the case of the O$K\alpha$ spectra for NaH_2PO_2, and Na_2HPO_3, the hump B does not appear. Therefore, it seems that the hump B appears when the central atom combines directly with O ions (including OH ions). In the structural formulas of $H_2PO_2^-$ or HPO_3^{2-}, the central P atom combines directly with only two or three oxygen atoms respectively. It may be seen that the peak A is related with the number of the oxygen which is combined with the central atom of the oxyanion, and is shifted to the lower-energy side in proportion to the number of the directly combined oxygen atom with the central atom. Moreover, the peak A for these compounds shifts to the higher-energy side compared with the case of K_3PO_4. It is reasonable that the peak A is related with the

number of oxygen which is combined with the central atom of the oxyanion and is shifted to the lower-energy side in proportion to the number of oxygen.

Figure 6 compares of the $OK\alpha$ spectra for sodium sulfite (Na_2SO_3) and sodium sulfate (Na_2SO_4) with their hydrogensulfite ($NaHSO_3$) and hydrogensulfate ($NaHSO_4$). There are two components in the $OK\alpha$ spectra in the case of SO_3^{2-}, but three components in the case of SO_4^{2-}. The spectral domain of SO_4^{2-} expands compared with that of SO_3^{2-}. The sharpness of the spectra for $NaHSO_3$ or $NaHSO_4$ is inferior to that for Na_2SO_3 or Na_2SO_4 respectively. It seems that the spectral components are broadened a little with the relation to hydrogen.

In Figs. 7 and 8, the relations between the spectral features and the coodination number of oxygen are shown. In both cases, the main peak C shifts to the higher-energy side and the peaks A and B shift to the lower-energy side according to the coodination number of oxygen. However, each peak component shifts to the higher-energy side in the case of the $K\beta$ spectra, and the middle peak only shifts to the higherenergy side, but the higher-energy peak increases in the case of the $L_{2,3}$ emission spectra in proportion to the coordination number of oxygen.

As the chemical effect of the X-ray spectra is the result of the shift of the core level and of the structure of the valence-band orbitals, the variation in the spectral profile will give us information about valence-band orbitals, because the core level is shifted simply with differ chemical states.

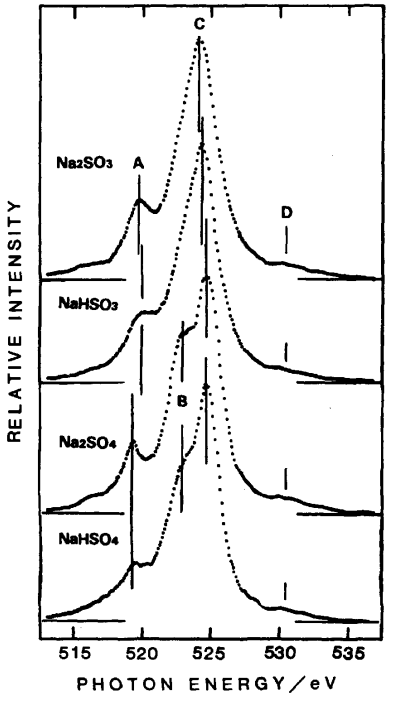

Fig. 6. Comparison of the $OK\alpha$ emission spectra for Na_2SO_3, and Na_2SO_4, with $NaHSO_3$ and $NaHSO_4$. $OK\alpha$ spectra have been excited by Cu$L\alpha$ radiation and analyzed by TAP crystal.

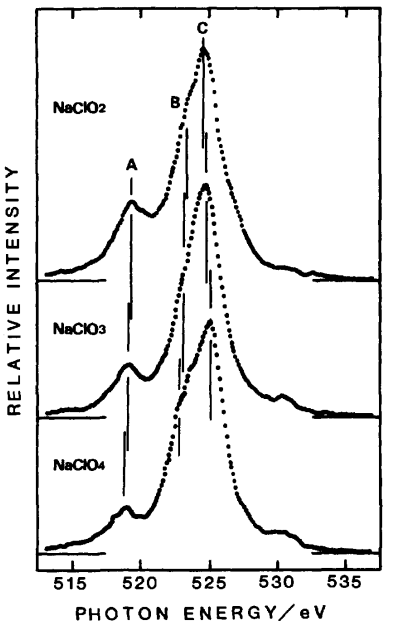

Fig. 7. Comparison of the $OK\alpha$ emission spectra for $NaClO_2$, $NaClO_3$, and $NaClO_4$. $OK\alpha$ spectra have been excited by Cu$L\alpha$ radiation and analyzed by TAP crystal.

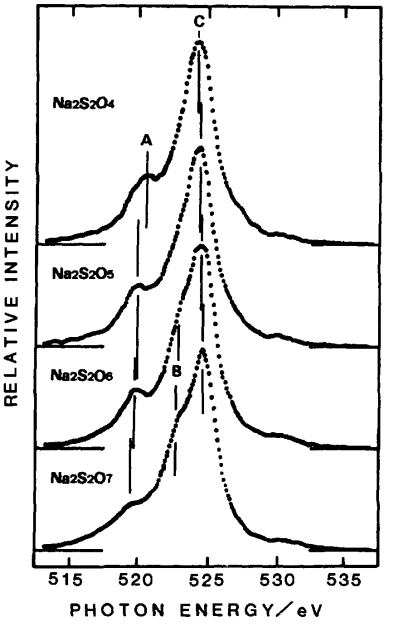

Fig. 8. Comparison of the $OK\alpha$ emission spectra for $Na_2S_2O_4$, $Na_2S_2O_5$, $Na_2S_2O_6$, and $Na_2S_2O_7$. $OK\alpha$ spectra have been excited by Cu$L\alpha$ radiation and analyzed by TAP crystal.

Conclusion

In this work, it has been shown that a spectral feature is closely affected by the chemical state and that the $OK\alpha$ spectra give us not only information for studies of molecular orbitals, but also provide a useful technique for application to chemical-state analysis, because oxygen 2p is related in almost all molecular orbitals of the valence band. The following properties

have been found:

1) The O$K\alpha$ spectra for oxyanions are expanded in proportion to the increase in the atomic mumber of the central atom.

2) The O$K\alpha$ spectra are affected a little by the cations, because oxygen atom is directly related to the cation. This conclusion is very different from that is the case of the $L_{2,3}$ emission spectra for the central atom, and also from the conclusion of Kosuch *et al.* about the O$K\alpha$ spectra.

3) The O$K\alpha$ spectra are especially influenced by hydrogen. It seems that the electron population of oxygen 2p diffuses to the lower-energy molecular orbitals in the relation to the hydrogen.

4) The O$K\alpha$ spectral profile is affected by the quantity of oxygen, the lower-energy peak shifts to the lower-energy side, and the main peak at a higher-energy shifts to the higher-energy side in proportion to the quantity of oxygen, and the hump B appears only when the central atom combines directly with the O (including OH) ions.

In this work, we can not interpret the spectra quantitatively as transitions from the molecular orbital with the help of a molecular orbital calculation. However, it seems that it will be very useful in studying the electronic structure and molecular orbital in chemical compounds in combination with the results of the $L_{2,3}$ emission spectra, the $K\beta$ spectra, and the O$K\alpha$ spectra from various compounds with the help of a molecular orbital calculation. These are subjects for future study in our work.

We gratefully acknowledge some very useful discussions with Dr. Yōichi Gōshi of Tokyo University and Dr. Sigero Ikeda of Osaka University and invaluable assistance in this work of Mr. Masaru Matsuo of this University.

References

1) K. Taniguchi and B. L. Henke, *J. Chem. Phys.*, **64**, 3021 (1976).
2) K. Taniguchi, "Advances in X-Ray Analysis," Plenum, New York (1980), Vol.23, p. 193.
3) K. Taniguchi, *Bull. Chem. Soc. Jpn.*, **57**, 909 (1984).
4) K. Taniguchi, *Bull. Chem. Soc. Jpn.*, **57**, 915 (1984).
5) F. Tyren, *Nova Acta Regiae Soc. Sci. Ups.* **12**, 7 (1940).
6) H. M. O'Bryan and H. W. B. Skinner, *Proc. R. Soc. London, Ser. A*, **176**, 229 (1940).
7) R. A. Mattson and R. C. Enlent, "Advances in X-Ray Analysis," Plenum, New York (1966), Vol. 9, p. 471.
8) B. L. Henke and R. E. Lent. "Advances in X-Ray Analysis," Plenum, New York (1969), Vol. 12, p. 480.
9) D. G. W. Smith, R. K. O'Oions, and K. Norrish, *Spectrochim. Acta, Part B*, **29**, 63 (1974).
10) D. W. Fischer, *J. Phys. Chem. Solids*, **32**, 2455 (1971).
11) A. S. Koster, *J. Phys. Chem. Solids*, **32**, 2685 (1971).
12) R. Bador, "Advances in X-Ray Analysis," Plenum, New York (1981), Vol. 24, p. 351.
13) E. Gilberg, M. J. Hanus, and B. Foltz, *Rev. Sci. Instrum.*, **52**, 662 (1981).
14) N. Kosuch, E. Tegeler, G. Wiech, and A. Faessler, *Chem. Phys. Lett.*, **47**, 96 (1977).
15) N. Kosuch, E. Tegeler, G. Wiech, and A. Faessler, *J. Electron Spectrosc. Relat. Phenom.*, **13**, 263 (1978).
16) K. Kawatsura, K. Ozawa, F. Fujimoto, and M. Terasawa, *Phys. Lett. A*, **58**, 446 (1976).
17) G. Andemann, F. Burkard, F. Fujiwara, and R. Kim, "Inner-Shell and X-Ray Physics of Atomic and Solids 2," Plenum, New York (1981), p. 727.
18) B. L. Henke and M. A. Tester, "Advances in X-Ray Analysis," Plenum, New York (1975), Vol. 18, p. 76.
19) B. L. Henke and K. Taniguchi, *J. Appl. Phys.*, **47**, 1027 (1976).
20) K. Maeda and M. Uda, *Spectrochim. Acta, Part B*, **35**, 561 (1980).

Molecular and Crystal Structures of *endo*- and *exo*-*N*-Methyl-3,7-epoxy-3-methoxy-7-oxo-1,2-benzo-1-cycloheptene-4,5-dicarboximide

Hatsue TAMURA, Toshikazu IBATA, and Kazuhide OGAWA*
College of General Education, Osaka University, Toyonaka, Osaka 560
(Received June 27, 1983)

The crystal structures of *endo*- and *exo*-adducts of 1-methoxy-2-benzopyrylium-4-olate with *N*-methylmaleimide have been determined by means of X-ray analysis. The colorless crystals of the *endo*-adduct are orthorhombic, with the space group $P2_12_12_1$ and with a=14.432(3), b=11.874(2), c=7.762(1) Å, and Z=4. The colorless crystals of the *exo*-adduct are monoclinic, with the space group $P2_1/a$ and with a=13.381(2), b=12.825(1), c=7.4793(4) Å, β=92.13(1)°, and Z=4. The structures were deduced by a direct method and refined by a block-diagonal least-squares technique. The final R values for the *endo*- and *exo*-adducts are 0.047 for 1160 observed reflections and 0.067 for 1986 observed reflections respectively. The configurations of the *endo*- and *exo*-adducts are coincident with those assigned on the basis of the NMR data. The observed values of the ring-current effect on the *N*-methyl chemical shift of the *endo*-adduct and the coupling constants of the vicinal methine protons of both adducts are in good agreement with the ones calculated on the basis of the present X-ray crystal-structure analysis.

The chemistry of carbonyl ylide has received the continuous interest of heterocyclic chemists for the past two decades.[1] One of the present authors (T. I.) has reported the novel formation of carbonyl ylide by the carbene-carbonyl reaction.[2] As an application of this reaction, the $Cu(acac)_2$-catalyzed decomposition of *o*-methoxycarbonyl-α-diazoacetophenone (**1**) was reported to give 1-methoxy-2-benzopyrylium-4-olate (**3**) as a transient species in a high yield *via* an intramolecular carbene-carbonyl reaction of intermediate keto carbene (**2**). The cycloaddition of the pyrylium-4-olate (**3**) to *N*-methylmaleimide gave two adducts: **4a**, mp 210°C; **4b**, 230°C.[3] The reaction procedure is shown in Scheme 1. The two adducts, **4a** and **4b**, were assigned to *endo*- and *exo*-cycloadducts respectively on the basis of their NMR data.[3] In order to confirm the assignment of the structures, an X-ray analysis of the adducts was carried out. Then, using the crystal data thus obtained, the ring-current effect and the coupling constants were calculated according to Farnum-Wilcox's method[4] and Williamson-John's equation[5] respectively.

Experimental

Colorless crystals of the *endo*- and *exo*-adducts were obtained from benzene solutions. The crystal data of the *endo*- and *exo*-adducts, along with the experimental conditions, are listed in Table 1. The X-ray intensity data were measured on a Rigaku four-circle diffractometer with Ni-filtered Cu $K\alpha$ radiation. The numbers of non-zero reflections used in the structure determination were 1160 for the *endo*- and 1986 for the *exo*-adduct. The intensities were corrected for Lorentz and polarization effects.

The NMR spectra of the *endo*- and *exo*-adducts were reexamined on a Hitachi NMR spectrometer, model FT-100, in $CDCl_3$, using TMS as the internal standard, to obtain accurate values of the chemical shifts and coupling constants.

Structure Determination. Using 170 reflections with $|E| \geq 1.39$ for the *endo*-adduct and 170 reflections with $|E| \geq 1.80$ for the *exo*-adduct, the crystal structures were determined by the direct method with the MULTAN 78 program.[6] The *E*-maps computed with the phase sets of the highest combined figure of merit (2.996 for the *endo*-adduct and 3.000 for the *exo*-adduct) revealed the positions of all the non-hydrogen atoms. Several cycles of block-diagonal least-squares refinement with isotropic temperature factors brought the R values to 0.096 for the *endo*-adduct and to 0.121 for the *exo*-adduct. The refinement with anisotropic temperature factors then reduced the R values to 0.061 for the *endo*-adduct and to 0.081 for the *exo*-adduct. At this stage, all the hydrogen atoms except those of the methyl groups were located by means of difference syntheses. After several cycles of block-diagonal least-squares refinement, the R values were reduced to 0.047 for the *endo*-adduct and to 0.067 for the *exo*-adduct. The function minimized was $\sum w(F_o - |F_c|)^2$ with the following weighting scheme: $w = 1/(\sigma(F_o)^2 + 0.0823|F_o| + 0.0013|F_o|^2)$ for the *endo*-adduct and $w = 1/(\sigma(F_o)^2 + 0.0783|F_o| + 0.0028|F_o|^2)$ for the *exo*-adduct.

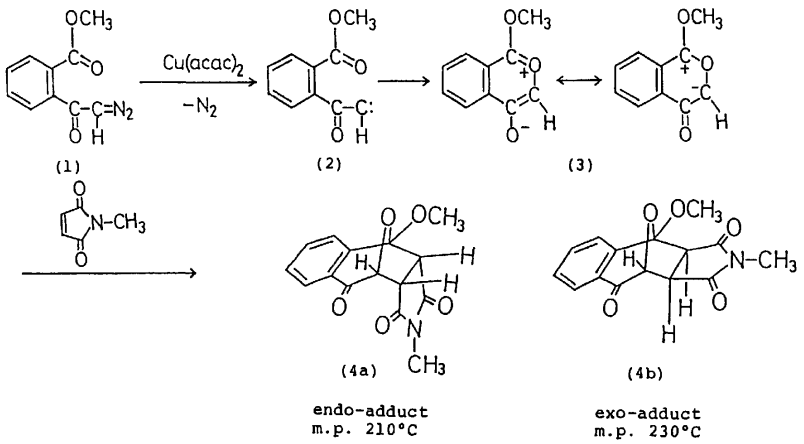

Scheme 1.

TABLE 1. CRYSTAL AND EXPERIMENTAL DATA

	endo-Adduct	*exo*-Adduct
Crystal system	Orthorhombic	Monoclinic
Space group	$P2_12_12_1$	$P2_1/a$
a	14.432(3) Å	13.381 (2) Å
b	11.874(2)	12.825(1)
c	7.762(1)	7.4793(4)
β		92.13(1)°
V	1330.1(3) Å^3	1282.6(2) Å^3
Z	4	4
D_m	1.439 Mg m^{-3}	1.485 Mg m^{-3}
D_x	1.435	1.488
μ(Cu $K\alpha$)	0.93 mm^{-1}	0.96 mm^{-1}
Scan method	θ-2θ	θ-2θ
Scan speed in ω	4°min^{-1}	4°min^{-1}
Scan width	1.2°+0.15° tanθ	1.2°+0.15° tanθ
Background	2×4 s	2×4 s
$2\theta_{max}$(Cu $K\alpha$)	120°	125°
No. of Reflections	1164	2326
	1160(except $\|F_o\|$=0)	1986(except $\|F_o\|$=0)
Crystal size	0.4×0.4×0.3 mm^3	0.2×0.2×0.1 mm^3

TABLE 2(a). ATOMIC POSITIONAL (×10^4) AND THERMAL PARAMETERS FOR *endo*-ADDUCT

Atom	x	y	z	B_{eq}/Å^2
O(1)	-239(1)	3497(1)	3769(3)	2.9
O(2)	-108(1)	1944(1)	2025(3)	3.2
O(3)	663(2)	4231(2)	7679(3)	5.0
O(4)	2380(1)	2145(2)	1427(3)	3.8
O(5)	2430(2)	5073(2)	5184(4)	4.8
N	2595(1)	3533(2)	3451(3)	2.7
C(1)	794(2)	1996(2)	4539(4)	2.7
C(2)	934(2)	2537(2)	6111(4)	2.9
C(3)	660(2)	3737(3)	6305(4)	3.2
C(4)	355(2)	4294(2)	4645(4)	3.0
C(5)	1169(2)	4464(2)	3335(4)	2.5
C(6)	1121(2)	3425(2)	2177(4)	2.3
C(7)	373(2)	2674(2)	3073(4)	2.6
C(8)	1078(2)	882(2)	4336(4)	3.3
C(9)	1495(2)	322(3)	5699(5)	4.1
C(10)	1633(2)	843(3)	7260(5)	4.8
C(11)	1363(3)	1980(3)	7483(4)	4.1
C(12)	2089(2)	2933(2)	2240(4)	2.4
C(13)	2122(2)	4432(2)	4117(4)	2.6
Me(14)	3541(2)	3216(3)	3938(5)	4.3
Me(15)	-690(3)	2462(3)	714(5)	4.4

TABLE 2(b). ATOMIC POSITIONAL (×10^4) AND THERMAL PARAMETERS FOR *exo*-ADDUCT

Atom	x	y	z	B_{eq}/Å^2
O(1)	6925(1)	-630(1)	4150(2)	2.4
O(2)	8161(1)	552(1)	4908(2)	2.8
O(3)	4572(1)	-476(2)	1986(3)	2.7
O(4)	9520(1)	107(2)	2040(3)	4.2
O(5)	7309(2)	-2341(2)	23(4)	5.0
N	8587(2)	-1265(2)	998(3)	2.9
C(1)	6533(2)	1187(2)	3822(3)	2.4
C(2)	5555(2)	900(2)	3294(3)	2.4
C(3)	5381(2)	-171(2)	2591(3)	2.7
C(4)	6297(2)	-859(2)	2621(3)	2.6
C(5)	6959(2)	-575(2)	1028(3)	2.7
C(6)	7690(2)	243(2)	1794(3)	2.5
C(7)	7355(2)	374(2)	3745(3)	2.3
C(8)	6728(2)	2212(2)	4341(4)	3.1
C(9)	5944(2)	2924(2)	4403(4)	3.7
C(10)	4967(2)	2627(2)	3918(4)	3.6
C(11)	4772(2)	1617(2)	3362(4)	3.1
C(12)	8720(2)	-267(2)	1669(3)	2.7
C(13)	7612(2)	-1508(2)	608(4)	3.2
Me(14)	9428(3)	-1977(3)	747(5)	4.3
Me(15)	7952(2)	524(3)	6795(4)	4.1

All the atomic scattering factors were taken from the "International Tables for X-Ray Crystallography."[7] The computations were carried out on an ACOS-S700 computer at the Crystallographic Research Center, Institute for Protein Research Laboratory, Osaka University, using "The Universal Crystallographic Computing System-Osaka."[8] Table 2 lists the final atomic and thermal parameters, along with their estimated standard deviations.[9] The bond distances and angles are given in Fig. 1.

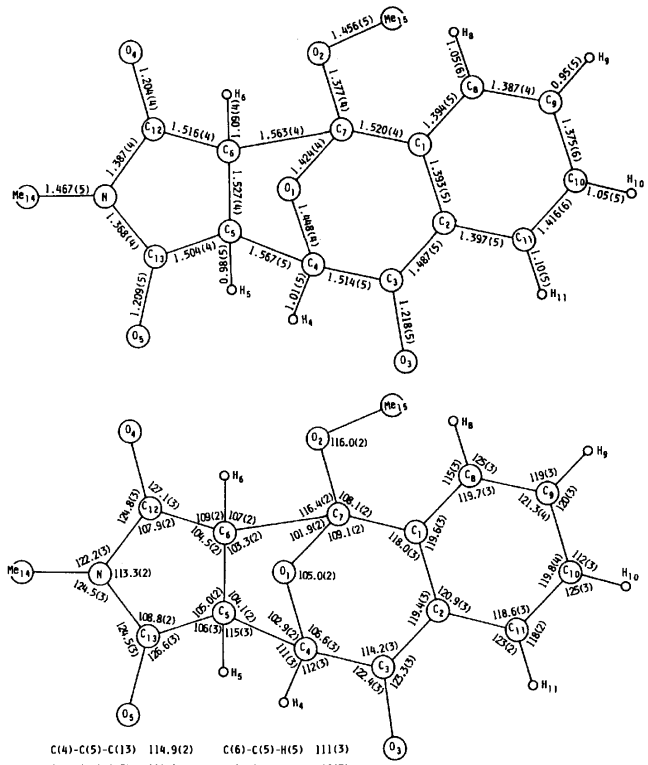

(a)

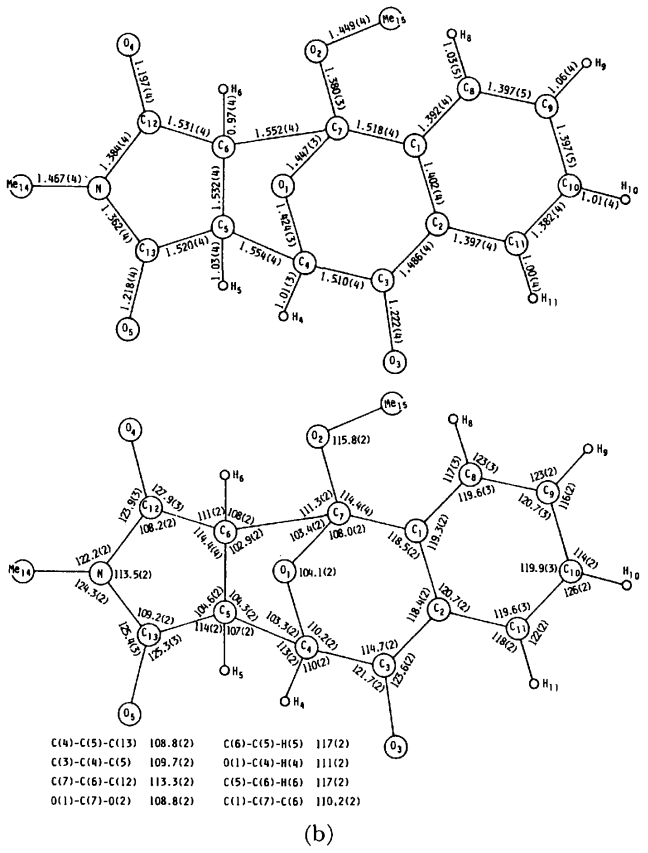

(b)

Fig. 1. (a) Bond distances and angles of the *endo*-adduct. (b) Bond distances and angles of the *exo*-adduct.

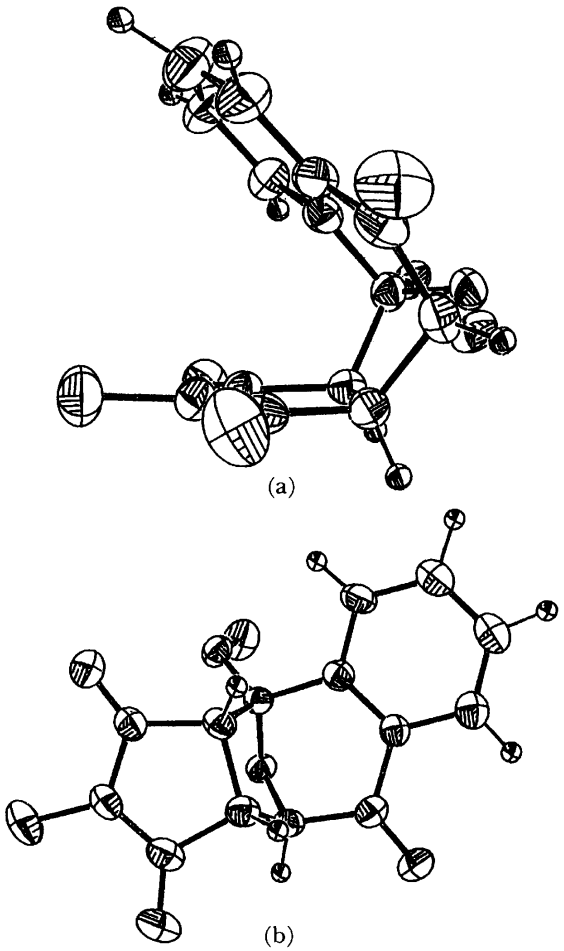

(a)

(b)

Fig. 2. (a) ORTEP view of the *endo*-adduct. (b) ORTEP view of the *exo*-adduct.
The non-hydrogen atoms were drawn at the 50% probability level and the hydrogen atoms were drawn with an arbitrary diameter.

Results and Discussion

Molecular Structure. The molecular structures of the *endo*- and *exo*-adducts are given in Figs. 2(a) and 2(b)[10] respectively. It was confirmed from these structures that the assignment of the configuration to these compounds deduced from the NMR data[3] was correct. The corresponding bond distances and angles in the *endo*- and *exo*-adducts agree fairly well with each other. As is shown in Fig. 1, the N-C, C-O, and C-C bond lengths in the succinimide ring system of both compounds are comparable to those in the derivatives of succinimide.[11-13] The bond lengths between the bridged oxygen atom(O(1)) and the bridgehead carbon atom (C(4) or C(7)) in both compounds are similar to those found in some oxygen-bridged ring compounds.[14] The difference between the O(1)-C(4) and O(1)-C(7) bond distances in the *endo*- or *exo*-adduct can be regarded as significant. The intramolecular distances between O(1) and Me(15) are shorter than the van der Waals' distance; that is, they are 2.749 Å in the *endo*-adduct and 2.792 Å in the *exo*-adduct.

The equations of the best planes through the four selected sets of atoms and the dihedral angles between

TABLE 3(a). BEST PLANES OF THE *endo*-ADDUCT

(a) Equations
The plane equations are of the $AX+BY+CZ+D=0$ form, where X,Y,Z, and D are measured in Å units: $X=ax$, $Y=by$, and $Z=cz$.
Plane(A): N, C(5), C(6), C(12), C(13)
$-0.3225X -0.5818Y +0.7466Z +1.6674=0$
Plane(B): C(4), C(5), C(6), C(7)
$-0.6729X +0.3996Y -0.6225Z +0.5711=0$
Plane(C): O(1), C(4), C(7)
$0.0769X +0.5346Y -0.8416Z +0.2691=0$
Plane(D): C(1), C(2), C(3), C(4), C(7)
$-0.9325X -0.2403Y +0.2694Z +0.6787=0$
(b) Dihedral angles(ϕ/°) between the planes:
(A)-(B) 241.3(or 118.7)
(B)-(C) 46.7
(C)-(D) 115.3
(B)-(D) 68.7

TABLE 3(b). BEST PLANES OF THE *exo*-ADDUCT

(a) Equations
The plane equations are of the $AX+BY+CZ+D=0$ form, where X,Y,Z, and D are measured in Å units: $X=ax+cz\cos\beta$, $Y=by$, and $Z=cz\sin\beta$.
Plane(A): N, C(5), C(6), C(12), C(13)
$-0.1331X -0.3575Y +0.9243Z +0.2541=0$
Plane(B): C(4), C(5), C(6), C(7)
$-0.6336X +0.7171Y -0.2902Z +6.6446=0$
Plane(C): O(1), C(4), C(7)
$-0.7805X +0.4560Y +0.4276Z +6.1845=0$
Plane(D): C(1), C(2), C(3), C(4), C(7)
$0.2170X+0.3004Y-0.9288Z+0.3338=0$
(b) Dihedral angles(ϕ/°) between the planes:
(A)-(B) 116.1(or 243.9)
(B)-(C) 45.8
(C)-(D) 115.4
(B)-(D) 69.7

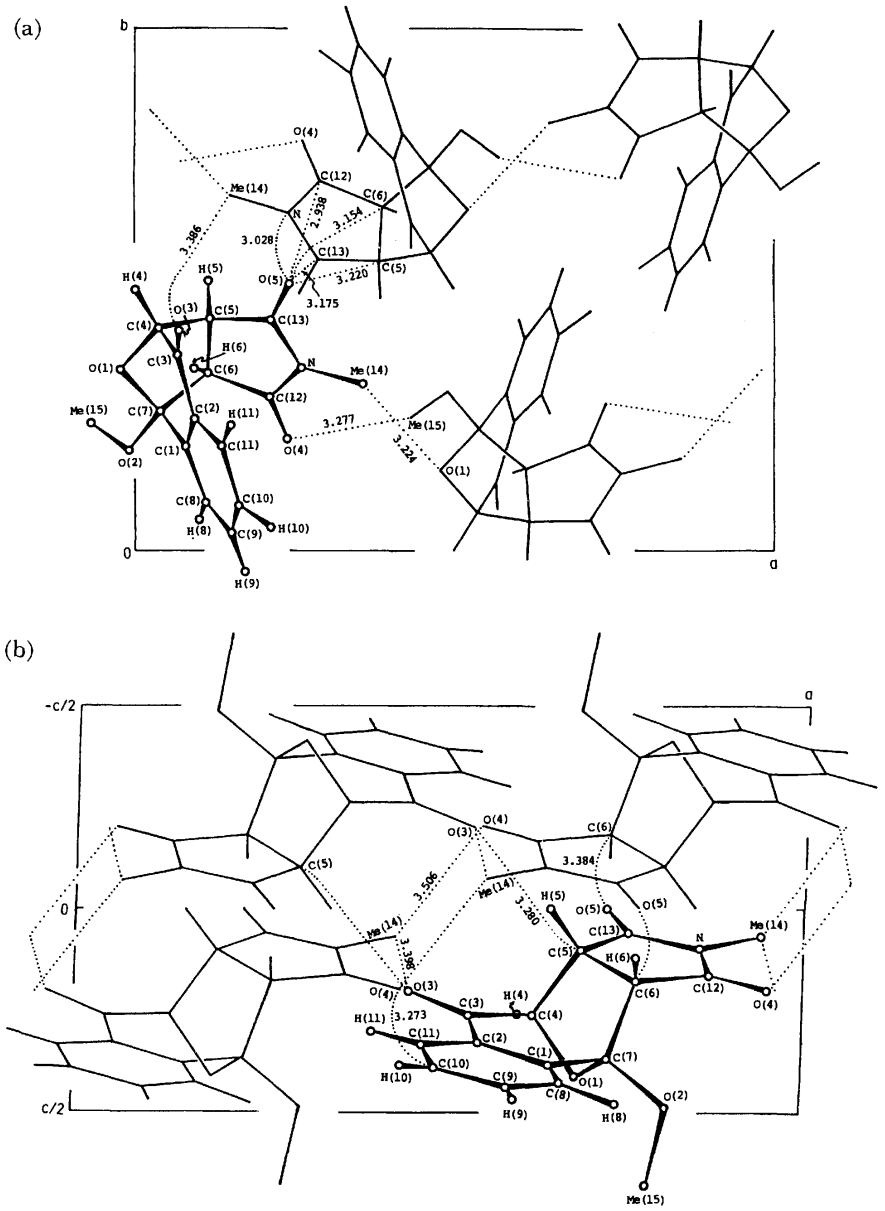

Fig. 3. (a) Crystal structure of the *endo*-adduct projected along the c axis. (b) Crystal structure of the *exo*-adduct projected along the b axis.

them are given in Table 3. The differences between the dihedral angles in the *endo*-adduct and the corresponding ones in the *exo*-adduct are not regarded as significant, but the dihedral angle between the plane (A) and the plane (B) of the *endo*-adduct is opposite to that of the *exo*-adduct in sign, that is, direction. The five-membered ring of the succinimide moiety is planar, with all deviations within ±0.04 Å in the *endo*-adduct and within ±0.02 Å in the *exo*-adduct. The C(3) and O(3) atoms deviate from the plane of the benzene ring by 0.033 Å and by −0.111 Å respectively in the *endo*-adduct, while they deviate by 0.106 and 0.225 Å in the *exo*-adduct.

Crystal Structure. The crystal structure of the *endo*-adduct projected along the c axis is shown in Fig. 3(a) and that of the *exo*-adduct projected along the b axis in Fig. 3(b). Some of the shorter intermolecular contacts are shown by dotted lines.

Ring-current Effect. The ring-current effect on chemical shifts and the values of the coupling constants are usually calculated using the Johnson-Bovey equation[15] and the Karplus equation[16] respectively. However, almost all the present calculations have been based on the values obtained by an inspection of such models as the CPK model or the Dreiding model. In this respect, the molecular model based on the atomic coordinates determined by X-ray analysis is expected to make possible a better interpretation of the NMR data and afford solider grounds for those equations than the above-mentioned models.

The *endo*-adduct showed its *N*-CH_3 signal at 2.37 ppm, and the *exo*-adduct, at 3.08 ppm, which was similar to the value of *N*-methylsuccinimide (2.98 ppm). This high-field shift of the *endo*-adduct by 0.71 ppm was attributed to the ring-current effect by the benzene ring located close to the *N*-CH_3 group. The values of 3.18 as *Z* and 0.50 as *ρ* in Farnum-Wilcox's double-torus model[4] were derived from the molecular structure found in the present X-ray work, as is shown in Fig. 4. The value of the ring-current effect of the *endo*-adduct was estimated from the "isoshielding" lines of the Johnson-Bovey ring-current effect by the use of the values of *Z* and *ρ* obtained above. This calculated value (0.85 ppm) is close to the experimental one (0.71 ppm).

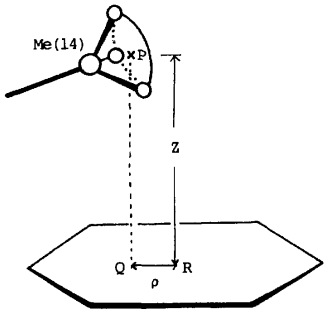

Fig. 4. Configuration of the methyl group (Me(14)) and the benzene ring in the calculation of the ring current effect of the *endo*-adduct.
P: The center of the triangle of the hydrogen atoms, Q: the foot of perpendicular line from P to the plane of the benzene ring, R: the center of the benzene ring. Tetrahedral structure and the C-H bond length of 1.08 Å are assumed for Me(14) radical. The parameters, *Z* and *ρ*, which are used for the estimation of the ring current effect, can be obtained as shown in the figure.

TABLE 4. OBSERVED AND CALCULATED VALUES OF VICINAL COUPLING CONSTANTS

		$J_{5,6}$/Hz	$J_{4,5}$/Hz
endo-Adduct	Obsd	9.5	9.2
	Calcd[a]	9.5	9.1
exo-Adduct	Obsd	7.5	0.0
	Calcd[a]	10.0	0.0

a) Williamson-Johnson's equation:

$$J_{HH} = \begin{cases} 10\cos^2\phi & (0° \leq \phi \leq 90°) \\ 16\cos^2\phi & (90° \leq \phi \leq 180°). \end{cases}$$

Coupling Constant. The observed coupling constants, $J_{5,6}$ and $J_{4,5}$, of both adducts are listed in Table 4. The coupling constants of the vicinal protons depend mainly on the dihedral angle, and they can be calculated by the Karplus method.[16] Of the several modified Karplus equations thus far reported, Williamson-Johnson's equation[5] was found to be most suitable for the ring system in this work. According to the present X-ray crystal-structure analysis, the dihedral angles between the C(5)–C(6)–H(6) plane and the C(6)–C(5)–H(5) plane, and between the C(5)–C(4)–H(4) plane and the C(4)–C(5)–H(5) plane, in the *endo*-adduct were found to be 13° and 17° respectively, while the corresponding dihedral angles in the *exo*-adduct were found to be 1° and 89°. The coupling constants calculated by substituting these dihedral angles (*φ*) in Williamson-Johnson's equation[5] are also shown in Table 4. These calculated values are in good agreement with the observed values obtained on the basis of the NMR spectra.

References

1) R. Huisgen, *Angew. Chem., Int. Ed. Engl.*, **1977**, 572.
2) K. Ueda, T. Ibata, and M. Takebayashi, *Bull. Chem. Soc. Jpn.*, **45**, 2779 (1972).
3) T. Ibata, K. Jitsuhiro, and Y. Tsubokura, *Bull. Chem. Soc. Jpn.*, **54**, 240 (1981).
4) D. G. Farnum, *J. Am. Chem. Soc.*, **89**, 2970 (1967); D. G. Farnum and C. F. Wilcox, *ibid.*, **89**, 5379 (1967).
5) K. L. Williamson and W. S. Johnson, *J. Am. Chem. Soc.*, **83**, 4623 (1961).
6) P. Main, S. E. Hull, L. Lessinger, G. Germain, J-P. Declercq, and M. M. Woolfson, "A System of Computer Programs for the Automatic Solution of Crystal Structures from X-ray Diffraction Data," MULTAN 78, University of York (1978).
7) "International Tables for X-Ray Crystallography," Kynoch Press, Birmingham (1974), Vol. IV, p. 71.
8) T. Ashida, "The Universal Crystallographic Computing System-Osaka, HBLS V," The Computation Center, Osaka University (1979), p. 53; T. Ashida, "The Universal Crystallographic Computing System-Osaka, DAPH," The Computation Center, Osaka University (1979), p. 61.
9) The F_O and F_C tables, anisotropic temperature factors, and hydrogen positional and isotropic thermal parameters are kept as Document No. 8408 at the Chemical Society of

Japan.
10) C. K. Johnson, "ORTEP-II: A FORTRAN Thermal-Ellipsoid Plot Program for Crystal-structure Illustrations, ORNL-5138," March, 1976, Oak Ridge National Laboratory.
11) A. Kirfel, *Acta Crystallogr., Sect.B*, **32**, 1556 (1976).
12) R. Mason, *Acta Crystallogr.*, **14**, 720 (1961).
13) R. N. Brown, *Acta Crystallogr.*, **14**, 711 (1961).
14) E. O. Schlemper, T. Shinmyozu, and J. P. McCormick, *Acta Crystallogr., Sect. B*, **38**, 2981 (1982); B. Berking and N. C. Seeman, *ibid.*, **27**, 1752 (1971); Olga Kennard and D. G. Watson, *ibid.*, **26**, 1038 (1970); E. B. Fleischer and T. S. Srivastava, *ibid., Sect.A*, **25**, S195 (1969); Young Ja Park, H. S. Kim, and G. A. Jeffrey, *ibid., Sect. B*, **27**, 220 (1971); Isabella L. Karle, *ibid.*, **31**, 1519 (1975).
15) C. E. Johnson, Jr., and F. A. Bovey, *J. Chem. Phys.*, **29**, 1012 (1958).
16) M. Karplus, *J. Chem. Phys.*, **30**, 11 (1959).

ESR Studies of Paramagnetic Species Trapped in Single Crystals of Chloro(5,10,15,20-tetraphenylporphyrinato)cobalt(III)

Masahiro KOHNO,* Hiroaki OHYA-NISHIGUCHI,† Kiyoko YAMAMOTO,†† and Tosio SAKURAI††

JEOL Ltd., Akishima, Tokyo 196

†*Department of Chemistry, Faculty of Science, Kyoto University, Sakyo-ku, Kyoto 606*

††*The Institute of Physical and Chemical Research, Wako, Saitama 351*

(Received July 4, 1983)

The ESR spectra of three paramagnetic species trapped in single crystals of chloro(5,10,15,20-tetraphenylporphyrinato)cobalt(III) ($Co^{III}Cl(tpp)$), have been observed at 4.2 K to room temperature. Based on the ESR parameters obtained, the paramagnetic species have been identified as two $Co^{II}(tpp)$ with different axial ligand effects and a previously reported cation radical, $[Co^{III}(tpp)]^{2+\cdot}(Cl^-)_2$. A correlation diagram among *g*, *A*, and axial ligation made from published data of cobalt(II) complexes has been successfully used for identification of the two trapped $Co^{II}(tpp)$ species: one is four-coordinate $Co^{II}(tpp)$ and the other five-coordinate $Co^{II}X(tpp)$ in which X is presumably Cl^-. Their electronic and molecular structures are discussed according to McGarvey's theory. Finally, the formation mechanism of the three paramagnetic species in $Co^{III}Cl(tpp)$ is discussed, based on the results obtained from the single crystalline ESR measurements.

The functional properties of metalloenzymes can often be understood by the study of their prosthetic groups, as has been seen in the famous study of Wang.[1] On the other hand, the study on redox reactions including metalloporphyrin has become increasingly important. In the course of our investigation of chloro(5,10,15,20-tetraphenylporphyrinato)-cobalt(III) ($Co^{III}Cl(tpp)$ (**1**), Fig. 1), we have found by ESR studies[2,3] that in solutions of **1** whose solvents are aromatic or chlorinated hydrocarbons, a π cation radical, $[Co^{III}(tpp)]^{2+\cdot}(Cl^-)_2$, is formed and that the formation of the radical occurs reversibly with small enthalpy change. Subsequent ESR measurements[4] on single crystals of **1** in which the radical is trapped have provided some information about the electronic and molecular structures of the radical and have also shown the existence of two $Co^{II}(tpp)$ species which are influenced by axial ligation. Such co-existence of both oxidation and reduction products in the crystals prepared under ambient conditions and the reversible behavior of the cation radical in the solution are regarded as inherent properties of **1**. These facts can be closely related to the redox reaction of metalloenzyme. We have carried out detailed ESR investigations of the crystals trapping the two $Co^{II}(tpp)$ species. The analysis of the ESR parameters obtained has given useful information for understanding the inherent properties of **1**.

In this paper, we first describe the results obtained from angular dependences of the ESR spectra due to two $Co^{II}(tpp)$ species trapped in the single crystals of **1**.

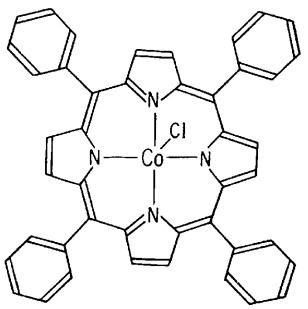

Fig. 1. Chloro(5,10,15,20-tetraphenylporphyrinato)-cobalt(III).

Second, the identification of the two trapped $Co^{II}(tpp)$ species is given using a diagram of correlation among *g*, *A*, and axial ligation made from the published data of many cobalt(II) porphyrins and their related compounds. Third, their electronic and molecular structures are elucidated according to a theoretical treatment reported by McGarvey. Finally, the formation mechanism of the three paramagnetic species in **1** will be presented, based on the results obtained from the single crystalline ESR measurements and those published previously.

Experimental

$Co^{III}Cl(tpp)$ (**1**), was prepared by using a method previously reported.[5] The spontaneous evaporation of the solvent from the solution of **1** gave crystals of various external forms: obelisk, pyramid, prism, and bulky shape. The single crystals doped with 1 mol% of pure $Co^{II}(tpp)$ were also prepared for the comparison with the trapped paramagnetic species. Previously, the X-ray analysis of the obelisk crystals[5] has been reported: **1** is a five-coordinate cobalt(III) complex of tpp which has a square-pyramidal structure with a chlorine atom at the apex. Continuing X-ray analyses[6] for various crystals have shown that the sixth ligand position is completely or partially occupied by water contaminated from the atmosphere. The relationships between the a and b axis and the external forms are illustrated in Fig. 2. The

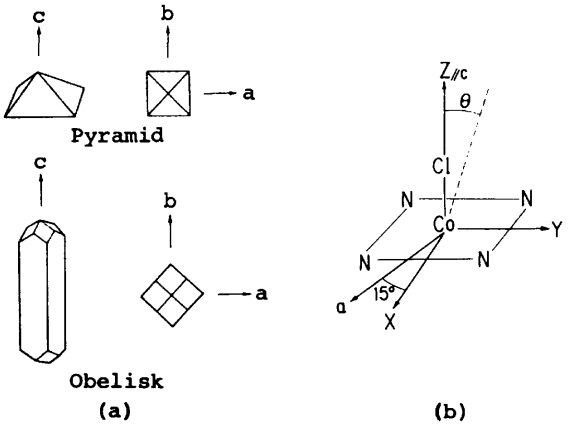

Fig. 2. (a) Crystal axis in pyramid and obelisk type crystals of **1**. (b) Relationship between crystal axes and molecular axes.

Co–Cl bond is parallel to the c axis and the angle between the a axis and one of the Co–N bonds is 15 °. Typical sizes of the obelisk and pyramid crystals used for the measurements were $0.1\times0.1\times0.3$ and $0.2\times0.2\times0.1\,cm^3$, respectively. The ESR spectra were measured at 4.2 K to room temperature with an ESR spectrometer, JEOL FE-3X equipped with 100 kHz magnetic field modulation. The microwave frequency and the magnetic field were directly determined by using a frequency counter, Takeda Riken TR-5211, and a field measurement unit, JEOL ES-FC-4, respectively. ESR parameters were determined by simulation using a JEOL ES-9835 computer system.

Results and Discussion

(1) The ESR Spectra of Paramagnetic Species in the Obelisk and Pyramid Crystals of $Co^{III}Cl(tpp)$. Figure 3 shows the ESR spectra of the paramagnetic species in the pyramid and obelisk type single crystals of **1** with crystal setting of $c\perp H_0$ at 77 K. As can be easily seen from the spectra, three different hyperfine (hf) patterns due to ^{59}Co with $I=7/2$ are clearly distinguished. Hereafter, we call these species α, β, and γ, as is shown in Fig. 3. The saturation behaviors of the three hf patterns were different from one another. The hf pattern due to γ was clearly observed at 4.2 K and

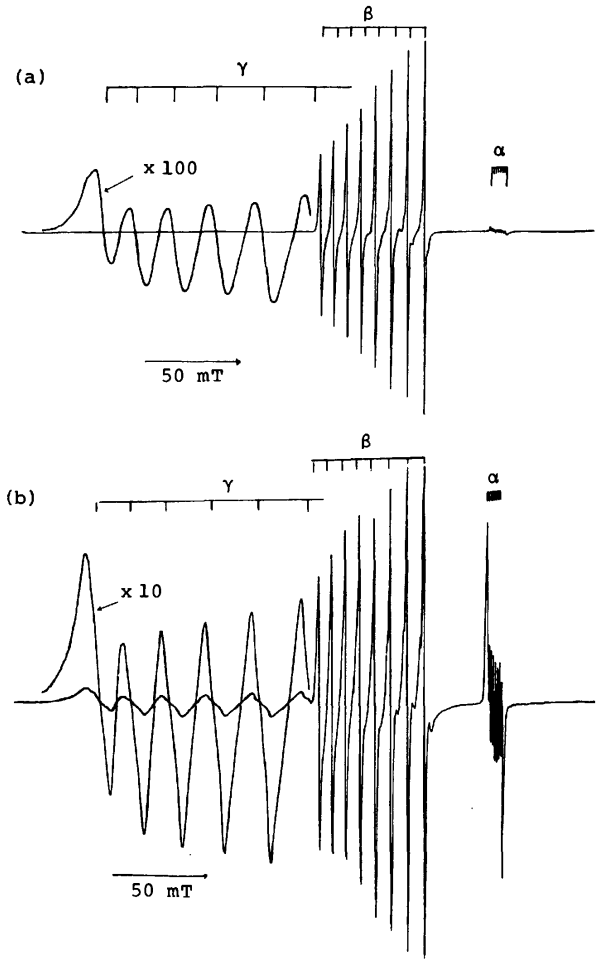

Fig. 3. The ESR spectra of paramagnetic species trapped in (a) obelisk and (b) pyramid type crystals of **1** at 77 K ($c\perp H$). Note that three species, α, β, and γ are clearly distinguished.

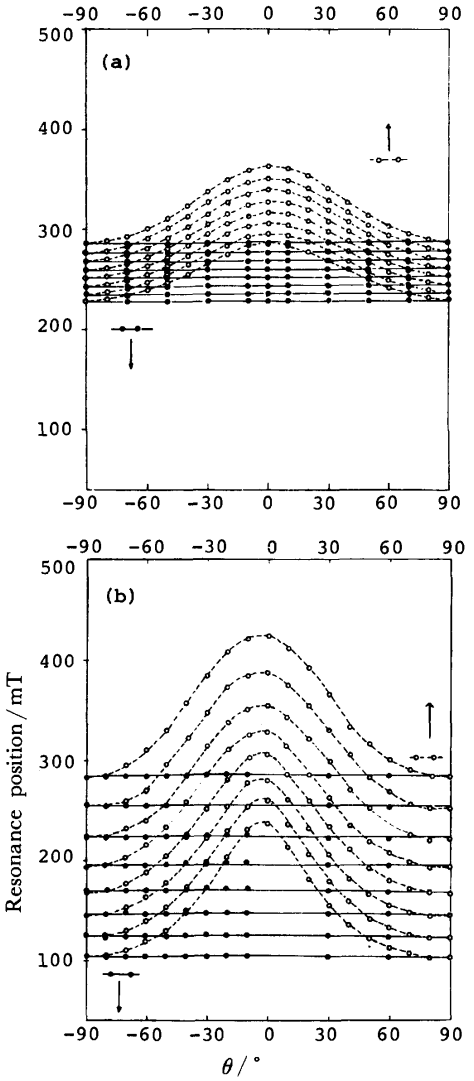

Fig. 4. Angular variations of the ESR positions of (a) β and (b) γ species trapped in **1**.
●: c axis rotation, O: a axis (pyramid) or [110] (obelisk) rotation.

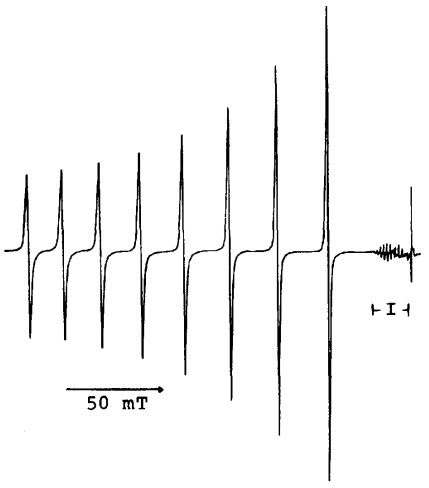

Fig. 5. The ESR spectrum of $Co^{II}(tpp)$ doped in Co^{III}-Cl(tpp) single crystal at 77 K ($c\perp H$). The position marked I in the Figure is due to Cu(tpp) paramagnetic impurity.

disappeared at above 120 K, but those due to α and β were observable even at room temperature. That is, the relaxation time of γ is considerably shorter than those of two others. α[2-4] has previously been identified as a π cation radical, $[Co^{III}(tpp)]^{2+\cdot}(Cl^-)_2$. In order to determine the electronic structures of β and γ, the angular variation of the absorption lines due to these species were measured both for the plane including the c axis and for the ab plane, which are shown in Fig. 4. The measurements show clearly that the g values of both β and γ are minimum at $\theta=0°$ ($g_\parallel$), and maximum at $\theta=90°$ ($g_\perp$). Such angular dependences are characteristic of the d_{z^2} orbital with a configuration of the z axis along the Co–Cl bond. The $g_\parallel$ of β is very close to that of free-electron predicted by first-order perturbation theory.[7] This means that the separations of excited states of β from the ground state are large enough to approximate the system with the first-order

TABLE 1. ESR PARAMETERS ESTIMATED, ENERGY SEPARATIONS ($\Delta(^2B_1)$ AND $\Delta(^4B_1)$), ISOTROPIC HYPERFINE INTERACTION (K) AND DIPOLAR SPLITTING CONSTANT (P) FOR COBALT(II) COMPLEXES OF PORPHYRINS AND THEIR RELATED COMPOUNDS

No.	System[a]	$g_\perp$	$g_\parallel$	$A_\perp$ / cm^{-1}	$A_\parallel$ / cm^{-1}	$\Delta(^2B_1)^0$ / cm^{-1}	$\Delta(^4B_1)^0$ / cm^{-1}	K^0 / 10^{-4} cm^{-1}	P^0 / 10^{-4} cm^{-1}	Ref
1	β species	2.5273 (±0.0003)	1.9964 (±0.0003)	0.0097 (±0.0003)	0.0105 (±0.0003)	4192	3867	77	62.3	This work
2	γ species[b]	3.320 (±0.002)	1.920 (±0.002)	0.0398 (±0.0003)	0.0240 (±0.0003)	1338	1322	145	195	This work
3	δ species	3.0627 (±0.0003)	1.8857 (±0.0003)	0.0306 (±0.0003)	0.0167 (±0.0003)	1773	2976	69.3	237	This work
				Four-coordinate Complex						
4	Co(tpp) in $CHCl_3$	3.330	1.848	0.0380	0.0187	1291	2992	90	243	9
5	Co(tpp) in H_2 (tpp)	3.322	1.798	0.0395	0.0197	1278	1785	122	192	9
6	Co(*p*-OCH_3 tpp) in Ni (*p*-OCH_3 tpp)	3.317	1.75	0.0403	0.0195	1263	2566	102	216	18
7	Co(*p*-OCH_3 tpp) concd polycrystal	3.285	1.79	0.0394	0.0147	1328	2316	144	267	18
8	Co(*p*-OCH_3 tpp) in H_2 (*p*-OCH_3 tpp)	3.264	1.81	0.0374	0.0171	1370	2245	52	255	18
9	Co(tpyp) in H_2 (tpyp)	3.218	1.774	0.0383	0.0213	1423	5997	110	224	10
10	Co(tpp) in $CHCl_3$	3.198	1.848	0.0358	0.0187	1585	2954	61	210	9
11	Co(*p*-OCH_3 (tpp) in H_2 (*p*-CH_3 tpp)	3.193	1.84	0.0352	0.0173	1499	2499	50	228	18
12	Co(omtbp) in (H_2 omtbp)	3.080	1.884	0.0290	0.0123	1736	2793	90	270	12
13	Co(tpp) in $CHCl_3$	3.066	1.848	0.0298	0.0187	1740	8721	90	254	9
14	Co(tbp) in H_2 (tbp)	2.901	1.949	0.0218	0.0128	2227	2713	68	236	10
15	Co(pc) in β-Zn(pc)	2.905	1.91	0.0265	0.0160	2191	6528	11	330	19
16	Co(*o*-CH_3 tpp) concd polycrystal	2.875	1.97	0.0235	0.0139	2328	2385	34.2	267.1	18
17	Co(*p*-OCH_3 tpp) in toluene	2.848	2.006	0.0228	0.0161	2450	2022	25.3	360	18
				Five-coordinate Complex						
18	Co(tpp)[c] in H_2 (tpp)	2.505	2.034	0.0092	0.0115	4517	2407	48.9	158	9
19	Co(oep)[c] in ether	2.44	2.03	0.0050	0.0095	5232	2660	50.0	211	20
20	Co(pc)[c] in α-Zn (pc)	2.422	2.007	0.0066	0.0116	5384	3879	63.5	192	19
21	Co(tpp)[c] in ether	2.395	2.024	0.0056	0.0099	5872	1190	59.1	62.7	20
22	Co(PPIX)ME[d]	2.384	2.018	0.00544	0.00932	6015	3305	32.4	133.4	14
23	Co(PPIX)MTE[d]	2.360	2.016	0.00377	0.00901	6447	3540	16.0	160.6	14
24	Co(cyt c) at pH 0.5	2.359	2.014	0.00388	0.00938	6447	3687	16.7	165.6	14
25	Co(HRP A)	2.34	2.03	0.00115	0.00739	6957	2918	−23.3	217.2	20
26	Co(HRP B, C)	2.33	2.08	0.00125	0.00748	7604	1929	−8.4	198.9	20
27	Co(Mb)[e]	2.327	2.028	0.00055	0.00834	7246	3016	−13.5	189.6	14
28	Co(*p*-OCH_3 tpp)[d] +1 pyridine	2.327	2.025	0.0012	0.00798	7118	3167	−6	185	18
29	Co(*p*-OCH_3 tpp)[d] +1 3-picoline	2.326	2.028	0.0011	0.00787	7266	3033	−7	189	18
30	Co(*p*-OCH_3 tpp)[d] +1 2-picoline	2.324	2.028	0.0011	0.00780	7303	3082	−7	162	18
31	Co(*p*-OCH_3 tpp)[d] +1 n-hexylamine	2.311	2.022	0.0010	0.00782	7604	3381	−3.3	174	18
32	Co(cyt c) at pH 12.9	2.325	2.026	0.0011	0.00757	7273	3110	−6.6	180.4	14
33	Co(tpp) (py)	2.324	2.027	0.0013	0.00789	7307	3082	−4.1	181.5	18
34	Co(Hb)[e]	2.310	2.037	0.0005	0.00790	7760	2728	−10.3	201.6	14
35	Vitamine B_{12r} +1 imidazole	2.27	2.022	—	0.00944	8844	3520	—	—	14

TABLE 1. (Continue)

No.	System[a]	$g_\perp$	$g_\parallel$	$A_\perp$ / cm^{-1}	$A_\parallel$ / cm^{-1}	$\Delta(^2B_1)$[f] / cm^{-1}	$\Delta(^4B_1)$[f] / cm^{-1}	K[f] / 10^{-4} cm^{-1}	P[f] / 10^{-4} cm^{-1}	Ref
					Six-coordinate Complex					
36	Co(PPIX)2(py)[d]	2.247	2.067	−0.00536	0.00647	10443	2147	−49.3	277.6	14
37	Co(*p*-COOH tpp) +2 pyridine	2.236	2.054	−0.0052	0.0053	10743	2394	−52.2	234.9	10
38	Co(*p*-OCH_3 tpp)[d] +2 3-picoline	2.228	2.058	−0.00544	0.0061	11235	2319	−52.0	252.1	18
39	Co(*p*-OCH_3 tpp)[d] +2 4-picoline	2.226	2.060	−0.00500	0.0061	11394	2283	−47.8	244.5	18
40	Co(*p*-OCH_3 tpp)[d] at pH 4-12	2.273	2.035	−0.00517	0.0583	11086	2945	−48.1	228.1	14
41	Co(*p*-OCH_3 tpp)[d] +2 pyridine	2.216	2.047	−0.00570	0.0060	11729	2577	−51.5	244.2	18
42	Co(*p*-OCH_3 tpp)[d] +2 piperidine	2.214	2.054	−0.00538	0.0061	12000	2411	−48.0	241.2	18
43	Co(*p*-OCH_3 tpp)[d] +2 n-hexylamine	2.208	2.067	−0.00618	0.0072	12692	2174	−54.0	284	18

a) Abbreviations: *p*-OCH_3tpp, tetrakis(*p*-methoxyphenyl)porphyrin; tpyp, tetrakis(4-pyridyl)porphyrin; *p*-CH_3tpp, tetrakis(*p*-methylphenyl)porphyrin; omtbp, octamethyltetrabenzoporphyrin; tbp, tetrabenzoporphyrin; pc, phthalocyanine; *o*-CH_3tpp, tetrakis(*o*-methylphenyl)porphyrin; oep, octaethylporphyrin; PPIX, protoporphyrin IX dimethylester; ME, 2-mercaptoethanol; MTE, 2-(methylthio)-ethanol;cyt c, cytochrome c; HPR, horseradish peroxidase; Mb, myoglobin; py, pyridine; Hb, hemoglobin; *p*-COOHtpp, tetrakis(*p*-carboxyphenyl)porphyrin. b) The valies of A, g, $\Delta(^2B_1)$, P, and K are estimated. c) Numbers of ligands are not specified in the references, but these compounds are cited for comparison. d) In toluene. e) Single crystal data. f) The values were estimated from the reported g and A data, except for those in Ref. 14.

perturbation theory. On the other hand, $g_\parallel$ of γ is very small compared with the predicted free-electron value, as will be discussed later.

The concentrations of the paramagnetic species in both pyramid and obelisk crystals were different but their ESR parameters agreed within the experimental errors, which means that the ESR parameters do not depend on the external crystal forms. The ESR parameters of β and γ were estimated by the best fit of the experimental data to an equation derived from the second-order perturbation theory,[8] which are listed in Table 1. The ESR parameters of β and γ are very close to those of two sites of Co^{II}(tpp) diluted in H_2(tpp),[9] respectively.

In order to obtain further information about the electronic environments of β and γ in the crystal of **1**, pure Co^{II}(tpp) (**2**) was doped in **1**. The ESR spectrum of **2** magnetically diluted in **1** is well resolved at 77 K, as is shown in Fig. 5 ($c \perp H_0$). At room temperature, no ESR signal was observed because of a short spin lattice relaxation time just as in the case of γ. It is seen in Fig. 5 that molecules of **2** are properly exchanged with those of **1**. Hereafter this paramagnetic species is called δ. The estimated ESR parameters of the species are also listed in Table 1. The angular dependence of the species also shows the d_{z^2} ground state, but the ESR parameters did not coincide with those of β or γ, nor with those in previous reports.

(2) Correlation Diagram of g, A, *and Axial Ligation.* In order to clarify the electronic and molecular structures of β and γ, correlation among g, A, and axial ligation was examined by using the data of cobalt(II) porphyrins and their related compounds. The data are also listed in Table 1 in order of $g_\perp$ value. A diagram of the correlation is shown in Fig. 6. It is seen from the figure that $g_\perp$ and $g_\parallel$ have linear relationships with $A_\perp$ and $A_\parallel$, respectively. These relationships can be simply expressed as

$$g_\perp = 2.3675 + 20.47A_\perp, \quad (1)$$

$$g_\parallel = 2.1662 - 13.70A_\parallel, \quad (2)$$

with the correlation coefficients 0.82 in Eq. 1 and 0.21 in Eq. 2, respectively. From the diagram the isotropic part of g, g_0, was estimated to be 2.233. The values of $g_\perp$ and $A_\perp$ decrease as the coordination number of Co^{II}(tpp) increases; four-, five-, and six-coordination.

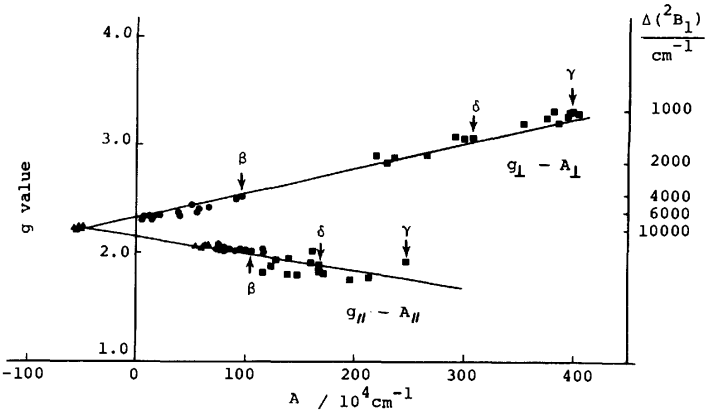

Fig. 6. A correlation diagram among g, A, and axial ligation.
■: Four-coordinate complex, ●: five-coordinate complex, and
▲: six-coordinate complex.

On the other hand, $A_{\parallel}$ decreases with the increase of the coordination number, but $g_{\parallel}$ has a reverse relation. It should be noted here that the sign of $A_{\perp}$ of six-coordinate complexes is minus. This has been already pointed out by Lin.[10] Such a linear relationship between g and A has also been observed in vanadium complexes.[11] In our diagram the relationship between ESR parameters and axial ligation is obvious. That is, the diagram is instructive for assigning the molecular environments of β, γ, and δ. As is shown in Fig. 6, γ resides on the right-end of the four-coordinate complex group and δ is, in the left-hand side of the group. On the other hand, β is on the right-end of five coordinate complex group. This means that β is fundamentally five-coordinate complex and the axial ligand is rather weak, while γ and δ are both four-coordinate complexes. Based on such procedures, γ can be assigned as the square-planar Co^{II}(tpp); on the other hand, β is square-pyramidal Co^{II}(tpp), and also δ is probably tetragonal with a weak axial ligand effect. It is not clear from the results what kind of atom is ligated in the cases of β and δ, but Cl^- in β is most probable as is discussed later.

(3) Theoretical Consideration for the Linear Relationships. The theoretical investigations of cobalt(II) complexes with planar ligands have been carried out by many authors.[12] For the interpretation of the linear relationships, we adopted McGarvey's treatment, which is analytical for the ESR parameters.

McGarvey[13] carried out the third-order perturbation treatment of low spin cobalt complexes with C_2 symmetry including the configurations with excited states $^2B_1$ and $^4B_1$. Dickinson and Chien[14] simplified the treatment and derived the theoretical g values as

$$g_{\perp}=2.0023+2c_3^2-3c_1^2, \quad (3)$$

$$g_{\parallel}=2.0023+2/3c_3^2-6c_1^2+6c_1, \quad (4)$$

where $c_1=\lambda/\Delta(^2B_1)$, $c_3=\lambda/\Delta(^4B_1)$, and λ is the single electron spin-orbit coupling constant, $\Delta(^{2,4}B_1)$ represents energy separation between the ground state $^2A_1$ and the excited state, $^2B_1$ or $^4B_1$. The value of λ for the Co^{2+} ion is 530 cm^{-1},[9] however, as the covalency due to complex formation causes a decrease of 20—40%, we assumed as $\lambda=400\,cm^{-1}$ according to Assour.[9] Energy separations obtained for the cobalt(II) complexes are also given in Table 1. The $\Delta(^2B_1)$ is ranging from 1300 to 13000 cm^{-1}. Introduction of a base along the z axis destabilizes the d_{z^2} orbital relative to the d_{xz} and d_{yz} orbitals, which results in an increase of $\Delta(^2B_1)$. Thus five-coordinate complexes of N_4X type have $\Delta(^2B_1)$ values larger than those of four-coordinate complexes. Those of the N_5 complexes are of the order of 7000 cm^{-1}. Further the separation of the six-coordinate complexes having two bases should be much larger than those of five-coordinate complexes. The relation between $\Delta(^2B_1)$ and $g_{\perp}$ values is also shown in Fig. 6, from which $\Delta(^2B_1)$ can be estimated by substituting the ESR parameters, $g_{\perp}$ or $A_{\perp}$, obtained experimentally.

The principal values of the hyperfine tensor, $A_{\parallel}$ and $A_{\perp}$,[13] are also expressed as functions of c_1 and c_3:

$$A_{//}=K+(P/7)[4-4c_3-6c_1+(2/9)c_3^2+15c_1^2], \quad (5)$$

$$A_{\perp}=K+(P/7)[-2+45c_1+2c_3+(4/3)c_3^2-(57/2)c_1^2], \quad (6)$$

where K is the isotropic Fermi hyperfine interaction parameter, $P=2\beta_e\beta_n\gamma Co(d_{z^2}|r^{-3}|d_{z^2})$ is the dipolar splitting constant, and β_e and β_n are electronic and nuclear magnetons, respectively. The linear relationships of Eqs. 1 and 2 can be derived from Eqs. 3 to 6, if we assume that c_3 is constant and the square terms in Eqs. 3 to 6 are neglected compared with the other terms.[15] The average value of the dipolar splitting constants of cobalt(II) complexes listed in Table 1, P_{av}, is obtained as 0.0219 cm^{-1} which nicely coincides with the value of free Co^{2+} ion ($P=0.0220\,cm^{-1}$);[16] this coincidence means that P_0 should be regarded as a standard value to measure electron density on the $3d_{z^2}$ orbital.

Since P is proportional to the electron density on the $3d_{z^2}$ orbital, the quantity $[(P_0-P)/P_0]$ has often been used as a measure of electron delocalization to the ligands. The value of 0.715 obtained in the case of β is very large compared with those of γ and δ. As can be seen in Table 1, P values of five coordinate complexes are very small compared with those of four- and six-coordinate complexes. This means probably that the spins of five-coordinate complexes including β are delocalized as far as axial ligand. On the other hand, those of γ and δ are not so delocalized.

(4) On the Mechanism of Three Paramagnetic Species Formation in $Co^{III}Cl$(tpp). As described in the previous paper,[2] the π cation radical (α) is formed by thermal activation in chlorinated hydrocarbons. The formation of the species occurs reversibly with small enthalpy change (ΔH). From the ESR measurements described above, it has been found that the crystals grown from the chlorinated solutions trap β and γ in addition to α. The result may indicate an equilibrium between the diamagnetic species **1** and the paramagnetic species (α, β, and γ):

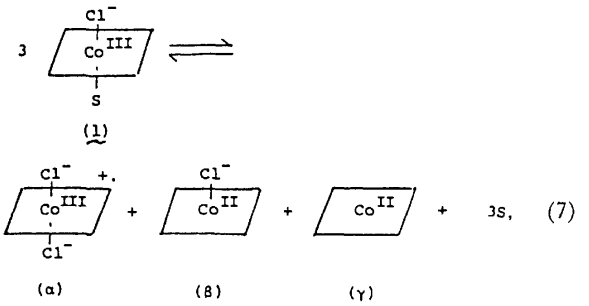

where S means a solvent molecule or a ligand molecule such as water contaminated on crystallization. On the other hand, the crystals doping **2** showed only the formation of δ. This fact excludes the possibility that the formation of β and γ on crystallization originates from free **2**. Therefore, the formation of these species is probably inherent in the solution of **1**.

The detailed examination of Eq. 7 provides several possibilities as the elementary reaction. It was clarified by 400 MHz FT-NMR[17] that **1** in chlorinated hydrocarbons has two axial ligands, one Cl^- and the other water or solvent molecule, at low temperature as low as −60 °C. As the temperature increased, the sixth ligand is removed, which leads to the possibility of a kind of disproportionation expressed by Eq. 8.[2] The temperature dependence of the α concentration shows the appropriateness of this process.

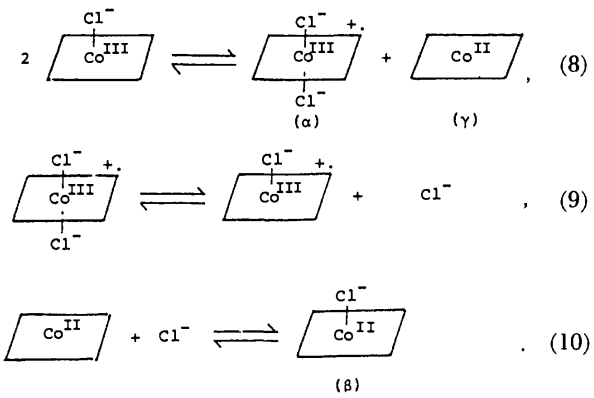

The six-coordinate cation radical formed is also labile for the dissociation into a five-coordinate cation radical and an anion,[3] as is seen in Eq.9. The existence of the five-coordinate $Co^{III}(tpp)$ (β) in the crystal may show the possibility of a recombination reaction of Eq. 10.

In conclusion, **1** is very likely to give the three kinds of paramagnetic species. It should be understood that the observation of these species supports the apparent equilibrium described in Eq. 7 as the results of the several elementary reactions.

References

1) J. H. Wang, A. Nakahara. and E. B. Fleisher, *J. Am. Chem. Soc.*, **80**, 1109 (1958); J. H. Wang, *ibid.* **80**, 3168 (1958).

2) K. Yamamoto, M. Kohno, and H. Ohya-Nishiguchi, *Chem. Lett.*, **1981**, 255.

3) H. Ohya-Nishiguchi, M. Kohno, and K. Yamamoto, *Bull. Chem. Soc. Jpn.*, **54**, 1923 (1981).

4) M. Kohno, H. Ohya-Nishiguchi, and K. Yamamoto, *Bull. Chem. Soc. Jpn.*, **56**, 822 (1983).

5) T. Sakurai, K. Yamamoto, H. Naito, and N. Nakamoto, *Bull. Chem. Soc. Jpn.*, **49**, 3042 (1976).

6) T. Sakurai, Y. Iimura, K. Yamamoto, and H. Honma, Anual Meeting of Crystallographic Society of Japan, Tokyo, November (1982).

7) J. S. Grifith, *Discuss. Faraday Soc.*, **26**, 81 (1958).

8) B. Bleaney, Philos. Mag., **42**, 441 (1951).

9) J. M. Assour, *J. Chem. Phys.*, **43**, 2477 (1965).

10) W. C. Lin, *Mol. Phys.*,**31**, 657 (1976).

11) F. E. Dickson, C. J. Kunesh, E. L. McGinnis, and L. Petrakis, *Anal. Chem.*, **44**, 987 (1972).

12) W. C. Lin, "Electron Resonance and Electronic Structure of Metalloporphyrins," in "The Porphyrins," ed by D. Dolphin, Academic Press, New York and London (1974), Vol. 4, p. 335, and the other references cited therein.

13) B. R. McGarvey, *Can. J. Chem.*, **53**, 2498 (1975).

14) L. C. Dickinson and J. C. W. Chien, *Inorg. Chem.*, **15**, 1111 (1976).

15) The assumption is not so unreasonable. The fluctuation of c_3 in Table 1 is mainly because of the ambiguities encountered on the estimation of ESR parameters. On the other hand, c_1 is estimated from the $g_\perp$ value which is estimated more precisely than that of $g_\parallel$.

16) A. Abragam and M. L. Price, *Proc. R. Soc. London, Ser. A*, **206**, 173 (1951).

17) K. Yamamoto, M. Hoshino, T. Chijimatsu, M. Kohno, and H. Ohya-Nishiguchi, 32nd Symposium of Coordination Chemistry, Nagasaki, October, p. 152 (1982).

18) F. A. Walker, *J. Am. Chem. Soc.*, **92**, 4235 (1970).

19) J. M. Assour and W. K. Kahn, J. Am. Chem. Soc., **87**, 207 (1965).

20) G. C. Wagner, I. C. Gunsalus, M. Y. R. Wang, and B. M. Hoffman, *J. Biol. Chem.*, **256**, 6266 (1981).

Effects of Dispersion in Carbon Monoxide Adsorption and Carbon Monoxide Hydrogenation over Alumina-supported Ruthenium Catalysts

Toshio OKUHARA,* Tomoo KIMURA, Kenji KOBAYASHI,† Makoto MISONO, and Yukio YONEDA
Department of Synthetic Chemistry, Faculty of Engineering, The University of Tokyo, Hongo, Bunkyo-ku, Tokyo 113
(Received July 23, 1983)

Ru/Al_2O_3 catalysts prepared from $[Ru_3(CO)_{12}]$ and from $RuCl_3$ were characterized by chemisorption of H_2 and CO, and by infrared measurement of adsorbed CO. By using these catalysts, the effect of the dispersion on the activity and selectivity in CO hydrogenation was studied. Ru/Al_2O_3 catalysts prepared from $[Ru_3(CO)_{12}]$ showed high dispersions (>80%), and were more active and selective for the production of olefins in the CO hydrogenation than Ru/Al_2O_3 catalysts prepared from $RuCl_3$. However, the distribution of product hydrocarbons was not sensitive to the Ru dispersion. Infrared study of adsorbed CO revealed that twin-type CO ($Ru(CO)_2$) as well as linear-type CO (Ru-CO) was present on each Ru/Al_2O_3. The twin-type CO was more strongly held and was less reactive to hydrogenation. For each series of Ru/Al_2O_3, the turnover frequency increased as the dispersion decreased. This change has been explained by the poisoning effect of the twin-type CO. The higher activity of Ru/Al_2O_3(A) was ascribed to the lower concentration of the twin-type CO on the surface.

In Fisher-Tropsh synthesis, Ru shows high activity and selectivity for the production of long-chain hydrocarbons.[1] The effect of Ru dispersion on the activity of this reaction has been studied by several workers.[2-6] King reported that the turnover frequency (abbreviated as TOF) of both methane formation and CO conversion over supported Ru catalysts declined as the dispersion increased.[2] This is in contrast with the case of Pt or Pd.[7] Kikuchi *et al.* also observed similar changes of TOF with the dispersion over Ru/Al_2O_3 and Ru/V_2O_3. However, TOF over Ru/V_2O_3 was considerably higher than that over Ru/Al_2O_3, indicating that the TOF was dependent not only on the dispersion but also on the nature of the supports.[5] Fujimoto *et al.* reported that the change of TOF with Ru dispersion appeared in a different manner depending on the reaction conditions.[6]

The dispersions of Ru catalysts used in the above studies were limited up to 60%. The authors[8] and Bell *et al.*[4,9] found that Ru/Al_2O_3 prepared from carbonyl complex like $[Ru_3(CO)_{12}]$ or $[Ru_6C(CO)_{17}]$ showed dispersions higher than 60%. As for the highly dispersed Ru/Al_2O_3, Kellner and Bell[4] reported that the TOF decreased as the dispersion increased up to 90%. On the other hand, the authors observed that the TOF for the Ru/Al_2O_3 prepared from $[Ru_3(CO)_{12}]$ was unexpectedly high at high Ru loading levels.[10]

Recently, infrared spectroscopic studies[11-14] have shed light on the surface state of Ru catalysts under reaction conditions. The Ru surface was almost entirely covered by adsorbed CO during the hydrogenation of CO,[11] and the active sites were limited to a small portion of the metal surface.[12] Kellner and Bell,[4,9] and the authors[15] showed that both linear-type CO and twin-type CO (diadsorbed CO) were present on Ru/Al_2O_3. However, there are very few instances in which physical properties and catalysis of highly dispersed Ru catalysts were studied concurrently.

The present study was undertaken to determine the prime factor controlling the change of the TOF with the dispersion of Ru, since, in spite of several efforts, the reason why TOF changes with dispersion has not yet been clarified. The Ru/Al_2O_3 catalysts having a wide range of dispersion were systematically prepared from $RuCl_3$ and $[Ru_3(CO)_{12}]$. By the use of these catalysts, the influences of preparation method and dispersion on the TOF, product distribution and olefin/paraffin ratio were investigated. Moreover, infrared measurement of adsorbed CO was performed to elucidate the strength of adsorption, the reactivity toward hydrogenation and the role of each adsorbed CO in the catalytic reaction.

Experimental

Catalysts. Ru/Al_2O_3 catalysts were prepared using γ-Al_2O_3 (Reference Catalyst of the Catalysis Society of Japan, ALO-4, 170 $m^2\ g^{-1}$) from $[Ru_3(CO)_{12}]$ (Strem Chemical Co.) and $RuCl_3 \cdot 3H_2O$ (Kanto Chemical). $[Ru_3(CO)_{12}]$ was adsorbed from hexane solution at room temperature onto the Al_2O_3 which had been dried in a N_2 flow at 450 °C. Then the solvent was removed in a stream of N_2 at room temperature. The catalysts obtained by the decomposition and reduction with H_2 at 450 °C are designated as Ru/Al_2O_3 (A) hereafter. The second class of Ru/Al_2O_3 catalysts were prepared by incipient wetness impregnation with an aqueous solution of $RuCl_3$ and are designated as Ru/Al_2O_3 (B). The loading amount of Ru metal was altered from 0.9 to 4% for Ru/Al_2O_3 (A) and 0.5 to 5% for Ru/Al_2O_3 (B).

Chemisorption of hydrogen and CO. The pretreatment conditions and procedure have been described in the previous paper.[15] Chemisorption measurement was carried out at room temperature in a conventional static system having a volume of 60 cm^3. Since adsorption of hydrogen to Al_2O_3 alone was negligible, the dispersion of Ru was calculated from the total uptake of hydrogen under an equilibrium pressure of about 60 mmHg. The chemisorption of CO on Ru was calculated from the differences in the uptake of CO between Ru/Al_2O_3 and Al_2O_3 under an equilibrium pressure of about 40 mmHg.

Catalytic Reactions. After the evacuation of the catalyst at 450 °C for 1 h, the catalyst was reduced with H_2 (600 mmHg (1 mmHg≈133.322 Pa)) at 450 °C for 2 h in a closed circulation system having a volume of about 200 cm^3. Then the catalyst was cooled *in vacuo* to 200 °C. Hydrogenation of CO was carried out at 200 °C under the total pressure of about 500 mmHg (H_2/CO=2) in the same system. The reaction was repeated by replacing the reactant gases after a short period of evacuation (≃10 min). The rate and the

†Present address: Nippon Electric Co., Ltd.

distribution of product hydrocarbons were determined at about 10—30% conversion in the second run, in which the reaction proceeded at a steady rate and the selectivity was independent of the conversion in the above conversion range. The product hydrocarbons except for methane were collected in a trap kept at liquid-nitrogen temperature during the reaction to prevent the secondary reactions such as hydrogenation of olefins and hydrogenolysis of products. Actually, when the reaction was carried out without a liquid-nitrogen trap, considerable increases of both methane and paraffin fractions were observed. The column materials used for gas chromatographic analyses consisted of Molecular Sieve 5A (25°C) to separate methane and CO, and Porapak Q (60°C) to separate CO_2, ethylene and ethane. A VZ-7 column (kept at 25°C) was used for C_3 through C_6 hydrocarbons. The formation of methanol and ethanol was checked with Porapak Q (100°C), but was not detected. Hydrogenolysis of ethane was also carried out at 150°C in the same system under the initial pressure of 108 mmHg (H_2/ethane=2) after the same pretreatment as in the case of the hydrogenation of CO.

Infrared Spectroscopy. The procedure has been described in the previous paper.[15] The catalyst was first kept in contact with CO (20 mmHg) at room temperature for 0.5 h. After CO was evacuated at desired temperatures for 1 h, infrared spectra were recorded using a Fourier-transform spectrometer (JEOL JIR 10) at room temperature. The weight of the sample disk was about 60 mg for all catalysts.

Results

Chemisorption of Hydrogen and CO. H/Ru and CO/Ru are summarized in Table 1, where the H/Ru or CO/Ru=number of hydrogen atoms or CO molecules chemisorbed/number of Ru in the catalysts. In the chemisorption of hydrogen, the H/Ru ratio was higher than 0.79 for all Ru/Al_2O_3 (A). The H/Ru for Ru/Al_2O_3 (B) progressively increased as Ru concentration decreased, but they were not more than 0.41. Hereafter, the dispersion of the Ru will be defined as H/Ru×100(%).

The CO/Ru ratio was always greater than the H/Ru. Particularly, in the case of low loading catalysts, *e.g.*, 0.5% Ru/Al_2O_3 (B) and 0.9% Ru/Al_2O_3 (A), high CO/Ru ratios (>1.4) were observed. The CO/H ratio reached 3.6 and 2.7 over 0.5 and 0.9% Ru/Al_2O_3 (B), respectively. The uptakes of H_2 and CO became very small (H/Ru=0.1, CO/Ru=0.1), when 2.5% Ru/Al_2O_3 (A) was pretreated with O_2 (50 mmHg) at 450°C for 4 h followed by reduction with H_2 (600 mmHg) at 450°C for 3 h.

Table 1. Chemisorption of H_2 and CO on ruthenium catalysts

Catalyst	wt%	H/Ru	CO/Ru	CO/H	$\bar{d}$/Å[a]
Ru/Al_2O_3(A)	0.9	0.85	1.41	1.7	(10)
(from[$Ru_3(CO)_{12}$])	2.5	0.82	1.10	1.3	(10)
	4.0	0.79	1.01	1.3	(11)
	2.5[b]	0.10	0.11	1.1	83
Ru/Al_2O_3(B)	0.5	0.41	1.46	3.6	20
(from $RuCl_3$)	0.9	0.38	1.03	2.7	22
	2.5	0.21	0.32	1.5	40
	5.0	0.18	0.26	1.4	46

a) Mean diameter calculated from the adsorption of hydrogen. b) Pre-oxidized sample.

The average particle size was calculated from the hydrogen adsorption as given in Table 1, by assuming that a hydrogen atom is adsorbed on an Ru atom at 1:1 stoichiometry and that the average area of Ru is 8.17 Å^2.[16] The average size of Ru particle on Ru/Al_2O_3 (B) was in the range of 20 to 46 Å, and was less than 10 Å for Ru/Al_2O_3 (A).

Activity and Selectivity. The rates of the CO hydrogenation per gram of Ru are plotted as a function of Ru loading in Fig. 1. The rate for Ru/Al_2O_3 (B) was much less susceptible to the Ru loading levels than that for Ru/Al_2O_3 (A). 4% Ru/Al_2O_3 (A), which was about 30 times more active than 0.9% Ru/Al_2O_3 (A), exhibited the highest activity among the Ru/Al_2O_3 catalysts used.

Figure 2 shows the olefin/paraffin ratio in C_2 through C_4 hydrocarbons as a function of the Ru dispersion. The ratios in these hydrocarbons increased monotonically as the dispersion increased. The selectivity to C_2–C_4 olefins among total hydrocarbons increased from about 40 to 60% in the range of the dispersion from 20 to 85%.

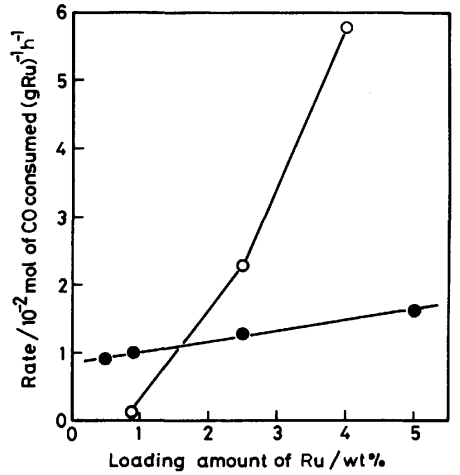

Fig. 1. Rate of the CO hydrogenation as a function of Ru loadings. Total pressure=500 mmHg, H_2/CO=2, 200°C.
○: Ru/Al_2O_3 (A), ●: Ru/Al_2O_3 (B).

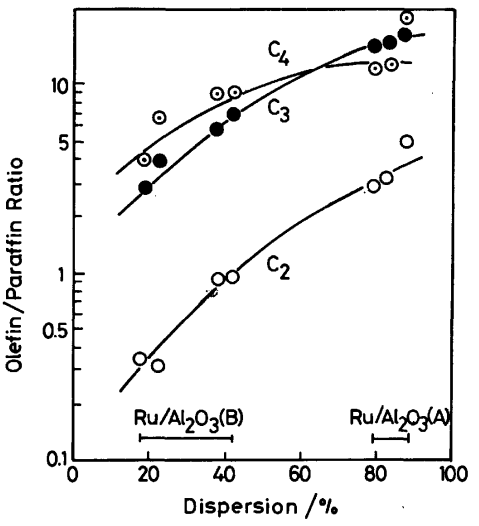

Fig. 2. Effect of Ru dispersion on olefin/paraffin ratio in the CO hydrogenation.

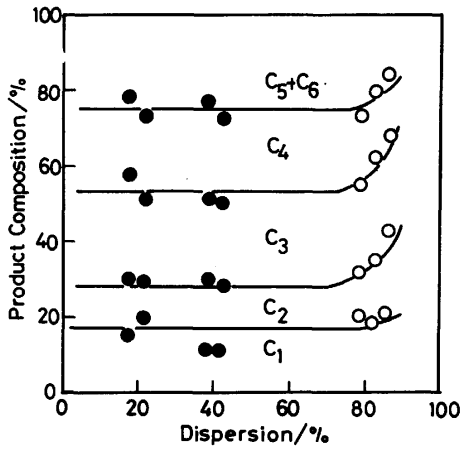

Fig. 3. Effect of Ru dispersion on product composition in the CO hydrogenation.

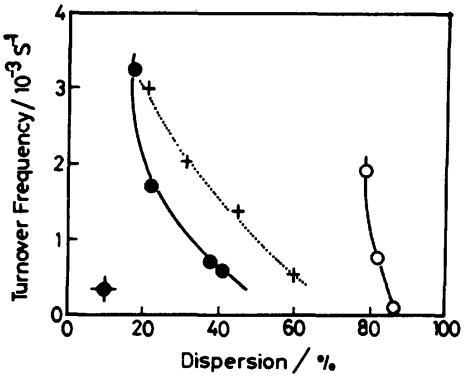

Fig. 4. Change of turnover frequency for the CO hydrogenation as a function of Ru dispersion at 200°C.
○: Ru/Al_2O_3 (A), ●: Ru/Al_2O_3 (B), ◆: Pre-oxidized 2.5% Ru/Al_2O_3 (A), +: King's data.

The influences of the dispersion on the product distribution are shown in Fig. 3. Except for a slight increase in the fraction of C_2 through C_4 hydrocarbons at very high dispersions, the distribution of product hydrocarbons was nearly constant over the wide range of dispersion. The preoxidized 2.5% Ru/Al_2O_3 (A) exhibited an unusual activity and selectivity. The activity for the CO hydrogenation was 1/16 of 2.5% Ru/Al_2O_3 (A) treated ordinarily and methane was the main product (≃70%).

In Fig. 4, the TOF for CO hydrogenation was plotted as a function of the Ru dispersion. King's data for Ru/Al_2O_3,[2] which were adjusted to the present reaction conditions, assuming that the pressure dependence and activation energy were the same as those reported by Vannice,[17] are also shown in Fig. 4. The TOF-dispersion correlation showed two separate lines in Fig. 4. The TOF obtained over Ru/Al_2O_3 (B) is consistent with King's data. On the other hand, with the exception of the dispersion of 85%, the TOF of Ru/Al_2O_3 (A) was appreciably higher than that expected from Ru/Al_2O_3 (B). It is noted that the TOF for the pre-oxidized 2.5% Ru/Al_2O_3 (A) is far below the two lines. In contrast with the CO hydrogenation, the TOF for the hydrogenolysis of ethane was nearly constant, except for 0.9% Ru/Al_2O_3 (A), as shown in Fig. 5.

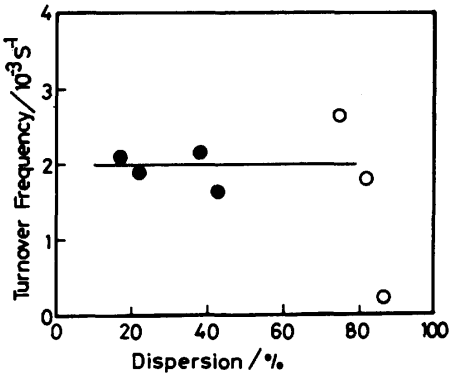

Fig. 5. Change of turnover frequency for the hydrogenolysis of ethane as a function of Ru dispersion at 150°C.
○: Ru/Al_2O_3 (A), ●: Ru/Al_2O_3 (B).

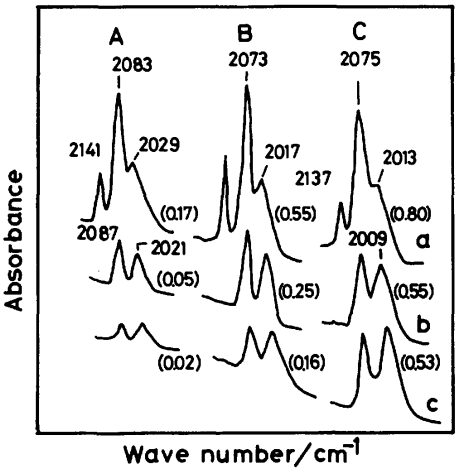

Fig. 6. Changes of infrared spectra of CO adsorbed on Ru/Al_2O_3 (B) by evacuation or hydrogenation: (A) 5 wt%, (B) 2.5 wt%, (C) 0.5 wt%; (a) after evacuation at 25°C, (b) after evacuation at 200°C, (c) after the reaction with H_2 (100 mmHg) at 200°C for 1 h. Figures in parentheses are the integrated intensity of CO(a) per gram of Ru loaded (arbitrary unit).

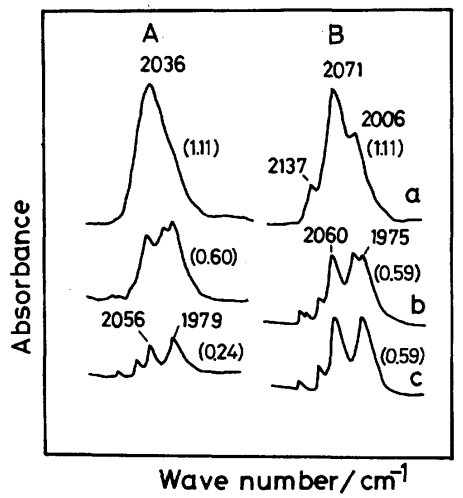

Fig. 7. Changes of infrared spectra of CO adsorbed on Ru/Al_2O_3 (A) by evacuation or hydrogenation: (A) 2.5 wt% (B) 0.9 wt%; (a) after evacuation at 25°C, (b) after evacuation at 200°C, (c) after the reaction with H_2 (100 mmHg) at 200°C, for 1 h.
Figures in parentheses are the integrated intensity of CO(a) per gram of Ru loaded (arbitrary unit).

Infrared Spectra of CO Adsorbed on Ru/Al_2O_3. CO adsorbed is denoted as CO(a) hereafter. Figures 6 and 7 show infrared spectra of CO(a) on Ru/Al_2O_3 (B) and Ru/Al_2O_3 (A), respectively. Spectra a and b in these figures were recorded after evacuation at 25 and 200°C, respectively. Spectra c were taken after the reaction of CO(a) with H_2 (100 mmHg) at 200°C for 1 h. Over Ru/Al_2O_3 (B), three well resolved bands appeared at 2137—2141, 2073—2083, and 2013—2029 cm^{-1} after the evacuation at 25°C (Fig. 6). Both the shape and position of the bands were almost independent of the loading amount of Ru. The evacuation at 200°C caused complete elimination of the highest frequency band and a considerable decrease in the medium frequency band. The remaining CO(a) showed a paired band located at 2075—2087 and 2009—2021 cm^{-1}. As the dispersion increases, the relative intensity of the paired band increases (spectra b in Fig. 6). CO(a) on Ru/Al_2O_3 (A) gave a broad band, as shown in Fig. 7.

Figure 8 shows the relationship between the dispersion and the band intensity of the inactive CO(a). The relative amount of the inactive CO(a) significantly increased as the dispersion increased for each series of Ru/Al_2O_3. Infrared spectra of CO(a) taken under the reaction conditions are shown in Fig. 9. The spectra in the region of CO stretching were essentially unchanged during the reaction for 3 h. Bands attributable to CH_x stretching frequencies observed between 2800 and 3000 cm^{-1} continued to increase with the reaction time, in agreement with the result reported before.[11,13] Over 0.9% Ru/Al_2O_3 (A), two strong bands can be seen at 2056 and 1979 cm^{-1}, while broad bands appeared near 2033 cm^{-1} over 2.5% and 4% Ru/Al_2O_3 (A), and 2.5% Ru/Al_2O_3 (B). The relative amounts of CO(a) per gram of Ru during the reaction, which were estimated from the area of the bands, were fairly consistent with those obtained by chemisorption (CO/Ru in Table 1).

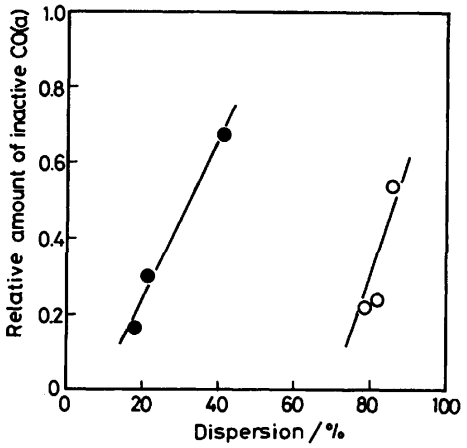

Fig. 8. Relationship between the relative amount of inactive CO(a) and the dispersion:
O: Ru/Al_2O_3 (A), ●: Ru/Al_2O_3 (B).
The ordinate shows the integrated intensity of bands normalized by that of bands obtained after evacuation at 25°C.

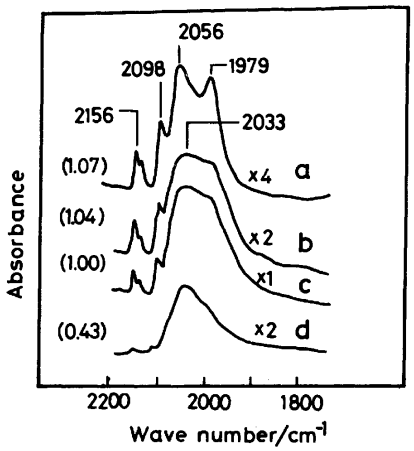

Fig. 9. Infrared spectra obtained under reaction conditions:
(a) 0.9% Ru/Al_2O_3 (A), (b) 2.5% Ru/Al_2O_3 (A), (c) 4% Ru/Al_2O_3 (A), (d) 2.5% Ru/Al_2O_3 (B).
Spectra were taken after 2 h under reaction at 200°C (P_{H_2}=200 mmHg, P_{CO}=60 mmHg).
Figures in parentheses are the integrated intensity of CO(a) per gram of Ru loaded (arbitrary unit).

Discussion

Dispersion and CO Adsorption Data. Chemisorption data in Table 1 demonstrate that the dispersion of Ru/Al_2O_3 (A) is rather high, even at high loading levels, compared with that of Ru/Al_2O_3 (B). Kellner and Bell[4] observed that the dispersion of 1.3% Ru/Al_2O_3, which was prepared from $[Ru_3(CO)_{12}]$, decreased to 60% from 90% during a reaction cycle of CO hydrogenation. They attributed the decrease to the rapid growth of Ru particles, which was accelerated by the temperature rise due to the heat of reaction. However, in the present work the dispersion of 4% Ru/Al_2O_3 (A) decreased from 80% to only 74% after the use for reaction. So, the dispersion of the fresh catalysts may be used as "dispersion" during the reactions carried out in this work.

In chemisorption of CO, the CO/Ru ratio exceeded unity at low loading levels, in agreement with the results of Kobayashi and Shirasaki[18] and Dalla Betta.[19] This suggests that more than two molecules of CO are adsorbed on a single Ru atom, that is, multiple CO adsorption. One hydrogen atom may be considered to be adsorbed on the surface of one Ru atom at 1:1 stoichiometry, since it was reported that the particle size calculated from hydrogen adsorption agreed with that obtained from electron micrographs on Ru/Al_2O_3 and Ru/SiO_2.[16] Accordingly, the ratio in the uptake of CO to hydrogen atom (CO/H) gives the average number of CO molecules attached on each surface Ru atom. The CO/H ratio for Ru/Al_2O_3 (A) was less than 1.65, suggesting that the linear-type CO (Ru–CO) occupied a considerable part of the surface sites. The IR band at about 2036 cm^{-1} for 2.5% Ru/Al_2O_3 (A) (Fig. 7) is assigned to the linear-type CO on the basis of the previous studies.[13,14] As shown in Fig. 7, a considerable amount of linear-type CO is present on 2.5% Ru/Al_2O_3 (A).

The paired IR band observed on these Ru/Al_2O_3 catalysts was quite similar to that of the twin-type CO on Ru/Al_2O_3.[20] It is known that $[Rh_2(CO)_4Cl_2]$ and

$[Ru(CO)_2X_n]$ (X=halogen)[21] shows a paired band associated with the symmetric and assymmetric vibration of the coordinated CO. Accordingly, the paired band observed on Ru/Al_2O_3 can be assigned to the twin-type CO, as reported by Kellner and Bell.[9] In the case of Ru/Al_2O_3 (B), the twin-type CO is the main species on the surface (Fig. 6). However, the CO/H values higher than 3 observed for 0.5% Ru/Al_2O_3 (B) seem to be unusual and the exact structure is not clear. The increase in the CO/H with the Ru dispersion suggests that adsorption sites available for the multiply bonded CO are edge or corner sites of Ru particles. The absence of twin-type CO on a single crystal surface of Ru[22,23] supports the assertion that the twin-type CO is formed on the edge or the corner sites of Ru particles.

Activity, Selectivity vs. *Dispersion.* Although low catalytic activity of low loading Ru/Al_2O_3 (A) is consistent with the result of Kellner and Bell,[4] the high activity of 4% Ru/Al_2O_3 (A) in the CO hydrogenation is a noticeable feature of Ru/Al_2O_3 (A) (Fig. 1). The change of TOF with the dispersion for the CO hydrogenation (Fig. 4) is not so simple as reported by King.[2] One possible reason for the two distinct correlations for Ru/Al_2O_3 (A) and Ru/Al_2O_3 (B) is the effect of the chloride ion remaining on Ru/Al_2O_3 (B) after reduction, but its effect is not known exactly. In any event, Fig. 4 suggests that the TOF for the CO hydrogenation cannot be determined only by the dispersion. Actually, Kikuchi *et al.* showed that the value of the TOF depended on the nature of the supports.[5] Moreover, the pre-oxidized 2.5% Ru/Al_2O_3 (A) showed a rather low TOF in spite of the low dispersion (Fig. 4).

In order to explain the change of the TOF, Kellner and Bell supposed that the electron density was reduced by the interaction with the support as the Ru particle size decreased, and that this led to the weakening of CO adsorption and the reduction of the ability to dissociate CO over highly dispersed catalysts.[4] Contrary to the idea of Kellner and Bell, CO was more strongly adsorbed as the Ru particle size decreases, as shown in Figs. 6 and 7. If the strongly bonded CO dissociates more easily, the TOF would increase with dispersion.

As shown in Figs. 6 and 7, the twin-type CO is more strongly held than the linear-type CO. Comparison of spectra b with c in Figs. 6 and 7 reveals the reactivity of CO(a) toward hydrogenation. Only a small decrease in the band intensity was observed for low loading catalysts after the reaction with H_2 (0.5% Ru/Al_2O_3 (B) and 0.9% Ru/Al_2O_3 (A)), indicating that the twin-type CO was almost inactive for the hydrogenation. It may be emphasized that the relative concentration of inactive twin-type CO increased with the dispersion over each series of Ru/Al_2O_3 (Fig. 8). If one compares these trends with the change of TOF (Fig. 4), it may be stated that the TOF is inversely correlated with the surface concentration of inactive twin-type CO and that the structure-sensitive behavior in the CO hydrogenation is explained by the poisoning effect of the inactive CO. That is, the TOF decreased with the dispersion, since the increasing portion of active sites is occupied by the inactive twin-type CO.

Since the linear-type CO readily reacted with H_2 compared with the twin-type CO (Fig. 7), weakly bonded linear-type CO is probably catalytically active for this reaction. Indeed, only a small amount of linear-type CO is present on the less active 0.9% Ru/Al_2O_3 (A), while other catalysts have a considerable amount of this species under the reaction conditions (Fig. 9). In contrast to the CO hydrogenation, the TOF for the hydrogenolysis of ethane changed little (Fig. 5). This may be explained by the absence of the poisoning materials in this reaction.

Another important feature of Ru/Al_2O_3 (A) is seen in the olefin/paraffin ratio in the product hydrocarbons. As shown in Fig. 2, the ratio in C_2, C_3, and C_4 hydrocarbons increases as the dispersion increases. If the olefin/paraffin ratio is determined by the relative rate of the two processes,[24] *i.e.*, β-elimination of hydrogen from and hydrogen addition to surface alkyl intermediates, the ratio will be controlled by whether the sites adjacent to the alkyl intermediates are empty or occupied by hydrogen atoms. In this case, the olefin/paraffin ratio depends on the ability of hydrogenation under the reaction conditions. It is known that CO(a) acts as a poison for the dissociative adsorption of H_2. Accordingly, the strength of CO(a) would affect the ability of hydrogenation. Since the strength of CO adsorption increased with the Ru dispersion (Figs. 6 and 7), the increase of the olefin/paraffin ratio can be explained in terms of the inhibition of hydrogen-activation by adsorbed CO.

The possibility of the chain growth is essentially independent of the dispersion as shown in Fig. 2, which is consistent with the data of King[2] and Bell *et al.*[4] for supported Ru catalysts. Although a drastic decline in chain growth for higher hydrocarbons was observed in the case of Ru/Y-zeolite,[25] this is probable due to the cage effect of the zeolite and not to the size effect of Ru particles.

The present work partially supported by a Grant-in-Aid for Scientific Research Nos. 56045031 and 57045025 from the Ministry of Education, Science and Culture.

References

1) M. A. Vannice, *J. Catal.*, **37**, 449 (1975).
2) D. L. King, *J. Catal.*, **51**, 386 (1978).
3) R. A. Dalla Betta, A. G. Piken, and M. Shelef, *J. Catal.*, **35**, 54 (1974).
4) C. S. Kellner and A. T. Bell, *J. Catal.*, **75**, 251 (1982).
5) E. Kikuchi, H. Nomura, and Y. Morita, Preprint of the 6th Japan-Soviet Catalysis Seminar, 1981, Osaka, p. 36.
6) T. Fukushima, T. Nobusawa, K. Fujimoto, and H. Tominaga, *Nippon Kagaku Kaishi*, **1982**, 177.
7) M. A. Vannice, *J. Catal.*, **40**, 129 (1975).
8) T. Okuhara, K. Kobayashi, T. Kimura, M. Misono, and Y. Yoneda, *J. Chem. Soc., Chem. Commun.*, **1981**, 1114.
9) C. S. Kellner and A. T. Bell, *J. Catal.*, **71**, 296 (1981).
10) T. Okuhara, T. Kimura, M. Misono, and Y. Yoneda, Preprint of the 6th Japan-Soviet Catalysis Seminar, 1981, Osaka, p. 28.
11) R. A. Dalla Betta and M. Shelef, *J. Catal.*, **48**, 111 (1977).

12) H. Yamasaki, Y. Kobori, S. Naito, T. Onishi, and K. Tamaru, *J. Chem. Soc., Faraday Trans. 1*, **77**, 2913 (1981).
13) D. L. King, *J. Catal.*, **61**, 77 (1980).
14) J. G. Ekerdt and A. T. Bell, *J. Catal.*, **58**, 170 (1979).
15) T. Kimura, T. Okuhara, M. Misono, and Y. Yoneda, *Nippon Kagaku Kaishi*, **1982**, 162.
16) R. A. Dalla Betta, *J. Catal.*, **34**, 57 (1974).
17) M. A. Vannice, *J. Catal.*, **37**, 462 (1975).
18) M. Kobayashi and T. Shirasaki, *J. Catal.*, **28**, 289 (1973).
19) R. A. Dalla Betta, *J. Phys. Chem.*, **79**, 2519 (1975).
20) D. J. C. Yates, L. L. Murrell, and E. B. Prestridge, *J. Catal.*, **57**, 41 (1979).
21) V. L. Kuznetsov and A. T. Bell, *J. Catal.*, **65**, 374 (1980).
22) M. Deeba and B. G. Gates, *J. Catal.*, **67**, 303 (1981).
23) R. A. Dalla Betta, A. G. Piken, and M. Shelef, *J. Catal.*, **35**, 54 (1974).
24) A. T. Bell, *Catal. Rev.*, **23**, 203 (1981).
25) H. H. Nijs, P. A. Jacobs, and J. B. Uytterhoeven, *J. Chem. Soc. Chem. Commun.*, **1979**, 1095.

Studies of Acylamino Acid Monolayers by π-A curves. I. Acylamino Acids with Alkyl Side Chain

Katashi TAKAHASHI,* Fudeko TANAKA, and Kinsi MOTOMURA†
Faculty of Home Life Science, Fukuoka Women's University, Fukuoka 813
†*Department of Chemistry, Faculty of Science, Kyushu University, Fukuoka 812*
(Received September 5, 1983)

In order to obtain some information regarding the behavior of amino acids at interfaces, the monolayers of *N*-acyl L-α-amino acids with alkyl side chains on water have been investigated by measuring the surface pressure *vs.* area curves at various temperatures. It has been found that *N*-octadecanoylglycine and *N*-octadecanoylalanine form the condensed monolayers over the whole surface pressure range measured, *N*-octadecanoylvaline forms the expanded monolayer at a lower surface pressure, and *N*-octadecanoylleucine and *N*-octadecanoylisoleucine collapse at high surface pressures. From the experimental results, it has been concluded that the amino acid residue with a long side chain occupies a large area at the air/water interface and interferes with the condensation of acylamino acid monolayer. It has also been found that the methyl esterification of amino acid residue makes the monolayer state unstable although it produces less significant effect than the increase in the alkyl chain length of amino acid residue.

The behavior of amino acid molecules at interfaces is of great interest from the biological and chemical viewpoints. The conformation of protein molecules is clearly related to the orientation of the side chains of amino acids and the interaction between them. It is noted that surfactants synthesized from amino acids are important in connection with their biode-composition.

Several investigations were carried out for the surface activity of amino acids and their derivatives.[1-4] The critical micelle concentration of mixtures of *N*-lauroyl amino acid sodium salts was also measured.[5] On the other hand, the antibacterial ability of amino acid derivatives was reported by several workers.[6,7] Now it is necessary to investigate systematically the behavior of amino acid molecules at interfaces. For this purpose, insoluble monolayers of acylamino acids on water seem to be appropriate.

In the present paper, *N*-acyl L-α-amino acids with alkyl side chains are used and the surface pressure *vs.* area curves are measured as a function of temperature.

Experimental

Materials. Eight *N*-acyl L-α-amino acids and two *N*-acyl L-α-amino acid methyl esters used in this work are listed with their abbreviations in Table 1. They were prepared from fatty acids and L-α-amino acids. The amino acids (Wako Pure Chemical Industries, Special Grade) were used without further purification. The fatty acids were purified by repeated recrystallizations from ethyl alcohol. Amino acid methyl ester hydrochlorides were first synthesized by the thionyl chloride method.[7] Next, acylamino acid methyl esters were synthesized by making them react with fatty acids in the presence of 1-ethyl-3-[3-(dimethylamino)propyl]carbodiimide hydrochloride in chloroform.[8] Acylamino acids were obtained by the hydrolysis of acylamino acid methyl esters. The acylamino acid methyl esters were purified by repeated recrystallizations from methyl alcohol. The acylamino acids were recrystallized from ethyl alcohol and acetone. Their purity was checked by the elemental analysis and potential difference titration.

TABLE 1. MATERIALS USED

Compound	Abbreviation
Octadecanoylglycine	OcD-Gly
Octadecanoylalanine	OcD-Ala
Octadecanoylvaline	OcD-Val
Octadecanoylleucine	OcD-Leu
Octadecanoylisoleucine	OcD-Ile
Docosanoylvaline	Doc-Val
Docosanoylleucine	Doc-Leu
Docosanoylisoleucine	Doc-Ile
Octadecanoylvaline methylester	OcD-Val-OMe
Docosanoylvaline methylester	Doc-Val-OMe

Procedure. Benzene was used as the spreading solvent; for OcD-Gly, a small amount of ethyl alcohol was added to facilitate its dissolution. The surface pressure was measured by a Wilhelmy type surface balance. The films were compressed at the constant rate of 0.017 $nm^2\ min^{-1}$. The temperature was held constant within 0.1 K.

Results and Discussion

It is reasonably expected that the difference in the interfacial behavior between amino acids is reflected in the surface pressure *vs.* area curves of acylamino acid monolayers. First, the surface pressure π of OcD-Gly, OcD-Ala, OcD-Val, OcD-Leu, and OcD-Ile monolayers on water were measured as a function of area *A* peroctadecanoylamino acid molecule at 298.2 K. The surface pressure *vs.* area curves of acylamino acids are depicted in Fig. 1. It is seen that they differ remarkably with each other and become expanded with increase in the length of the alkyl side chain of amino acid. The π *vs.* *A* curve of OcD-Gly seems to be quite similar to that of octadecanoic acid. This fact indicates that OcD-Gly forms a condensed film. Therefore, we may say that the glycine residue of OcD-Gly is immersed in the substrate and acts as a part of the hydrophilic portion. The OcD-Ala monolayer also seems to form the condensed film, although its limiting area estimated from the π *vs.* *A* curve is larger than that of OcD-Gly. This may be attributable to a bigger side chain of the alanine residue.

On the other hand, it is seen from Fig. 1 that the π *vs.* *A* curves of OcD-Val, OcD-Leu, and OcD-Ile monolayers are significantly different in shape from those of OcD-Gly and OcD-Ala monolayers. The OcD-Val, OcD-Leu, and OcD-Ile monolayers are clearly ex-

panded films in a lower surface pressure region. In a higher surface pressure region, they seem to transform into other states; however, the transformation of OcD-Val is markedly different from those of OcD-Leu and OcD-Ile. In order to clarify this point, the variation of π *vs.* A curve with temperature was investigated.

The π *vs.* A curves of OcD-Val monolayer at 283.2, 288.2, 293.2, 298.2, 300.7, and 303.2 K are shown in Fig. 2. The surface pressure of the break point on the curve is found to increase greatly with increasing temperature. This temperature dependence resembles that of the film-forming substance which transforms from the expanded to the condensed state.[9-11] Furthermore, it turns out that the OcD-Val monolayer forms a condensed film over the whole surface pressure range measured at 283.2 K since its π *vs.* A curve is similar to that of OcD-Ala monolayer shown in Fig. 1. Thus, we can conclude that the OcD-Val monolayer transforms from the expanded to the condensed film at the break of the π *vs.* A curve. Comparing the π *vs.* A curve of OcD-Val monolayer with that of OcD-Ala monolayer, it is noticed that the bigger side chain of valine residue makes its state expanded up to a fairly high surface pressure at 298.2 K.

Similarly, the π *vs.* A curves of OcD-Leu and OcD-Ile, which have longer side chains than OcD-Val, were measured as a function of temperature; their results are illustrated in Figs. 3 and 4, respectively. It is seen that the surface pressure increases slightly with increasing temperature at a large area while it varies irregularly with temperature at a small area. Furthermore, the shape of the curves at the transition region are abnormal. This fact may indicate that the monolayers collapse and change into three-dimensional

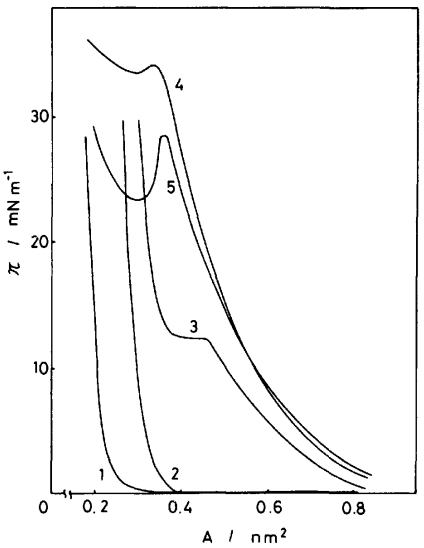

Fig. 1. Surface tension *vs.* area curves of Octadecanoylamino acid monolayers at 298.2 K. 1) OcD-Gly, 2) OcD-Ala, 3) OcD-Val, 4) OcD-Leu, 5) OcD-Ile.

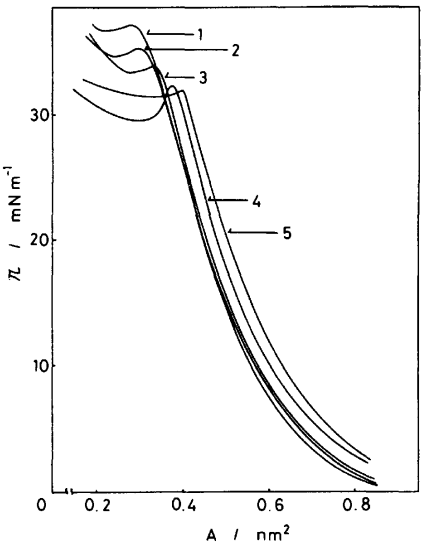

Fig. 3. Surface tension *vs.* area curves of OcD-Leu monolayer. 1) 288.2 K, 2) 293.2 K, 3) 298.2 K, 4) 300.7 K, 5) 303.2 K.

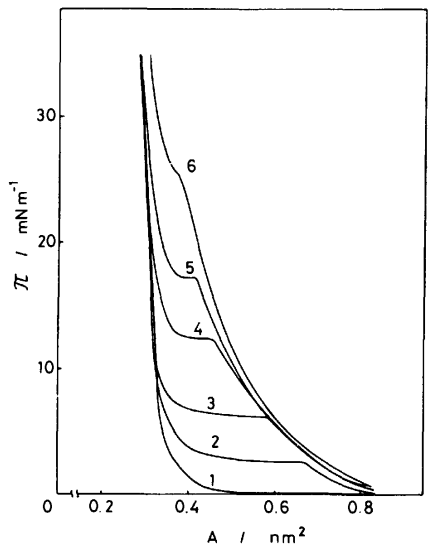

Fig. 2. Surface tension *vs.* area curves of OcD-Val monolayer. 1) 283.2 K, 2) 288.2 K, 3) 293.2 K, 4) 298.2 K, 5) 300.7 K, 6) 303.2 K.

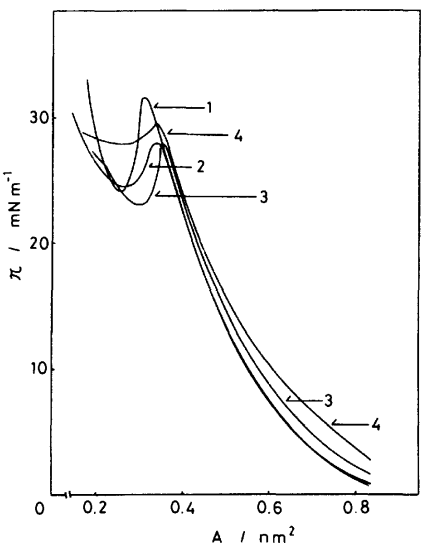

Fig. 4. Surface tension *vs.* area curves of OcD-Ile monolayer. 1) 283.2 K, 2) 293.2 K, 3) 298.2 K, 4) 303.2 K.

bulk phases at high surface pressures. It may be said, therefore, that the intermolecular force between the octadecanoyl groups is not strong enough to make the condensed monolayers of OcD-Leu and OcD-Ile stable. Now measurements seem to be required for acylamino acids having a longer acyl chain.

The π *vs.* A curves of Doc-Leu and Doc-Ile measured at various temperatures are illustrated in Figs. 5 and 6, respectively. It is seen from Fig. 6 that Doc-Ile forms a condensed film of which the limiting area is larger than that of the OcD-Val monolayer at 283.2 K. With an increase in temperature, the Doc-Ile monolayer becomes expanded in a lower surface pressure region. At temperatures above 303.2 K, the curve shows a striking resemblance to that of OcD-Ile given in Fig. 4. In the case of Doc-Leu, the temperature dependence of the π *vs.* A curve is qualitatively similar to that of Doc-Ile, although a typical condensed film is not realized even at the lowest temperature measured. The above results lead us to the conclusion that the amino acid residue with a long side chain occupies a large area at the air/water interface and interferes with the condensation of acylamino acid monolayer. Furthermore, it is noteworthy that the collapse of the expanded films is attended by remarkable super-compression.

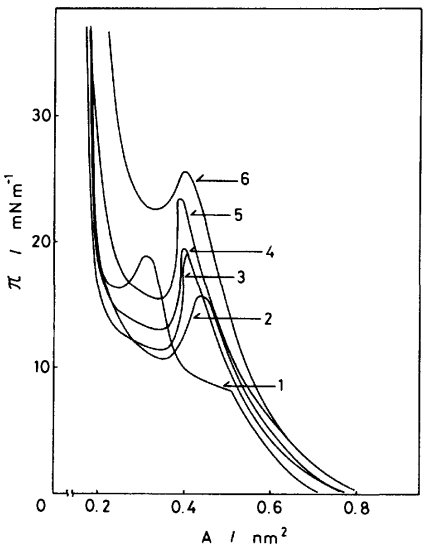

Fig. 5. Surface tension *vs.* area curves of Doc-Leu monolayer. 1) 283.2 K, 2) 288.2 K, 3) 293.2 K, 4) 298.2 K, 5) 303.2 K, 6) 308.2 K.

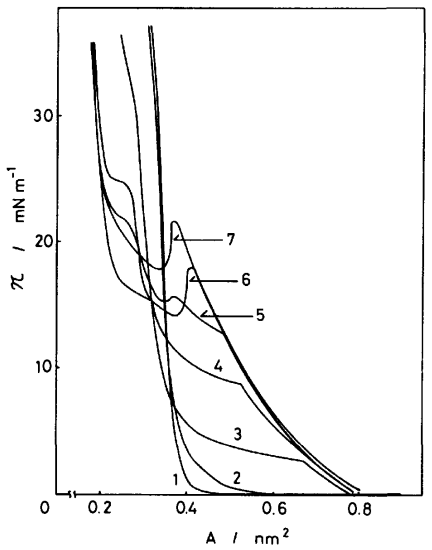

Fig. 6. Surface tension *vs.* area curves of Doc-Ile monolayer. 1) 283.2 K, 2) 288.2 K, 3) 293.2 K, 4) 298.2 K, 5) 300.7 K, 6) 303.2 K, 7) 308.2 K.

It is important to examine the difference between the π *vs.* A curves of *N*-acylleucine and *N*-acylisoleucine which are isomeric with each other. From Figs. 3 and 4, we can see that the OcD-Leu monolayer remains in an expanded state up to a higher surface pressure value than the OcD-Ile monolayer. Comparison between Figs. 5 and 6 tells us that the expanded film of Doc-Leu is hard to transform into the condensed film. Therefore, it can be said that the isobutyl group of *N*-acylleucine forces the monolayer to stay in the expanded state up to a high surface pressure as compared with the s-butyl group of *N*-acylisoleucine.

It is now interesting to investigate the behavior of the monolayer of *N*-acylvaline methyl ester which is an isomer of *N*-acylleucine and *N*-acylisoleucine although different in polar group. In Fig. 7, the π *vs.* A curve of OcD-Val-OMe are drawn at various temperatures. The temperature dependence resembles that of Doc-Leu and Doc-Ile rather than of OcD-Leu and OcD-Ile. It is clear by comparison with Fig. 2 that the methyl esterification makes the monolayer state somewhat unstable. Therefore, Doc-Val-OMe may be expected to form a condensed film at temperatures under consideration by the strong intermolecular interaction between docosanoyl groups. The experimental results for Doc-Val-OMe, which are illustrated in Fig. 8, support the above view. These findings indicate that the increase in the alkyl chain length of the amino acid residue by one carbon atom produces more significant effect on the monolayer behavior than the methyl esterification of the carboxyl group.

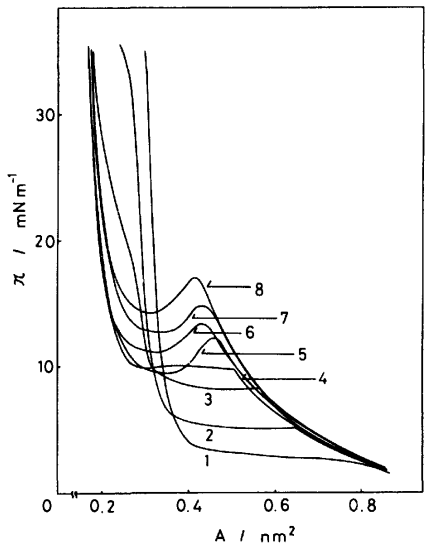

Fig. 7. Surface tension *vs.* area curves of OcD-Val-OMe monolayer. 1) 283.2 K, 2) 288.2 K, 3) 293.2 K, 4) 295.7 K, 5) 298.2 K, 6) 300.7 K, 7) 303.2 K, 8) 308.2 K.

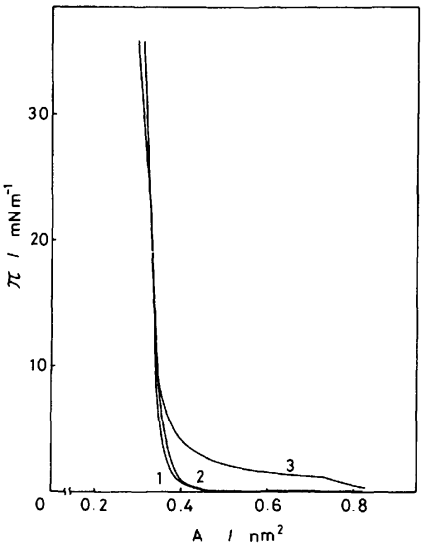

Fig. 8. Surface tension *vs.* area curves of Doc-Val-OMe monolayer. 1) 283.2 K, 2) 303.2 K, 3) 308.2 K.

It has been found from the measurements on the monolayers of acylamino acids that the length and chemical structure of the alkyl side chain of amino acid play a significant role in the monolayer behavior. Further information will be provided by making a similar investigation of amino acids with aromatic or polar side chains.

References

1) M. Takehara, H. Moriyuki, A. Arakawa, I. Yoshimura, and R. Yoshida, *J. Am. Oil. Chem. Soc.*, **50**, 227 (1973).
2) Y. Yoshida, M. Takehara and I. Sakamoto, *Yukagaku*, **25**, 141 (1976).
3) R. Yoshida, M. Yoshimura, Y. Usuba, and A. Shibue, *J. Am. Oil. Chem. Soc.*, **53**, 113 (1976).
4) T. Kida, H. Mizuno, K. Takinami, and S. Matsunaka, *Agric. Biol. Chem.*, **40**, 1551 (1976).
5) B. Yu. Zaslavsky, A. A. Borovskaya, A. Yu. Lisichkin, A. Yu. Davidovich, and S. V. Rogozhin, *Kolloidn. Zh.*, **41**, 553 (1979).
6) K. Ogino, H. Yamauchi, and T. Shibayama, *Yukagaku*, **31**, 37 (1982).
7) N. Izumiya, T. Kato, M. Ohno, and H. Aoyagi, "Pepuchido Gosei," Maruzen, Tokyo (1978), p. 66.
8) J. C. Sheehan, J. Preston, and J. P. Cruickshank, *J. Am. Chem. Soc.*, **87**, 2492 (1965).
9) N. K. Adam, "The Physics and Chemistry of Surfaces," Oxford University Press, London (1941).
10) G. L. Gaines, Jr., "Insoluble Monolayers at Liquid-Gas Interfaces," Wiley-Interscience, New York (1966).
11) K. Motomura, K. Sekita, and R. Matuura, *J. Colloid. Interface Sci.*, **48**, 319 (1974).

A Fluorescence Study of the Adsorption of Water, Methanol, and Acetic Acid on an Activated Europium Ion-exchanged Mordenite

Tsuyoshi ARAKAWA,* Midori TAKAKUWA, and Jiro SHIOKAWA
Department of Applied Chemistry, Faculty of Engineering, Osaka University, 2-1 Yamadaoka, Suita, Osaka 565
(Received September 5, 1983)

The adsorption of water, methanol, and acetic acid on an activated Eu(III) ion-exchanged mordenite(Eu-M) has been studied by the measurement of the fluorescence of the Eu^{2+} ion which was produced by the dehydration at 500 °C. The emission peak of the Eu^{2+} ion sifted to a shorter wavelength on exposure to water and other simple molecules. The magnitude of the shift was correlated to the specific dielectric constant of the adsorbate. The quantum yield for the Eu^{2+} emission band after gas adsorption decreased in all cases. Also, the lifetime in the Eu^{2+}-adsorbate system was shorter than that in an activated Eu-M sample. The rate constants for the radiationless transitions were more sensitive to the nature of the adsorbates, and the order of the quenching power was $H_2O>D_2O>CH_3OH$.

The rare-earth ion-exchanged zeolites are well known as active catalysts for the cracking of fuel oil. The reduction-oxidation of the rare-earth ion in the zeolites, however, has apparently not been studied. We have now studied the fluorescence properties of rare-earth ion-exchanged zeolites in an attempt to clarify the catalytic properties of these compounds. Especially, we have found, from measurements of the fluorescence for europium ions, that Eu(III) is reduced to Eu(II) as Eu(III) ion-exchanged Y type zeolite or mordenite is evacuated at above 300 °C under a pressure of less than 10^{-2} Pa.[1,2]

Physicochemical studies of the synthetic zeolites have been performed by several methods, *i.e.*, X-ray diffraction, electron resonance, infrared spectroscopy, reflectance spectroscopy, Mössbauer spectroscopy, magnetic susceptibility, and X-ray photoelectron spectroscopy, but the interpretation of the results and the establishment of firm conclusions are frequently difficult.[3] Also, there have been a number of studies of the adsorption of various gases on the transition-metal ion-exchanged zeolites. Especially, the formation of a carbonyl, nitrosyl, or ammine complex in the zeolite has been reported on the basis of adsorption measurements and ESR spectroscopy.[4-6] Although fluorescence spectroscopy is by no means a new technique, its application to the study of gas adsorption on rare-earth ion-exchanged zeolites as described here is new. In the case of Eu^{2+}-doped phosphors, it is well known that the emission band for the Eu^{2+} ion changes with the variation in the chemical environment around the Eu^{2+} ion, since the emission for the Eu^{2+} ion is due to a transition between $4f^7$ and $4f^65d$, and so the 5d electron will be most noticeably affected by the crystal field.[7-9] Thus, after gas adsorption on an activated europium ion-exchanged mordenite (Eu-M), the peak position of the emission band for the Eu^{2+} ion can be expected to change with the adsorbates.[10]

In this study, the unique features that have been observed only in an activated Eu-M during the adsorption of water, methanol, and acetic acid are presented.

Experimental

Materials. The Eu-M samples were prepared starting from Na-mordenite, which had been supplied by the Norton Company. The parent mordenite had the following composition; $Na_8(AlO_2)_8\cdot(SiO_2)_{40}\cdot 24H_2O$. This mordenite was ion-exchanged in an excess of a 0.02 M solution containing $EuCl_3$ (pH=4), washed, dried at 100 °C, and calcined in air at 450 °C. The exchanged mordenite was analyzed for europium by means of X-ray fluorometry and for sodium by means of flame photometry. The close correspondence between the decrease in the sodium content and the increase in the europium content indicated that a simple ion-exchange process had occurred. Thus, the exchanged level of the Eu^{3+} ion was 5.8%.

Water, dehydrated methanol, and acetic acid were degassed by the freeze-pump-thaw technique.

Adsorption Measurements. The adsorption experiments were performed on a silica balance, using a sample of 1.0×10^{-4} kg. The sensitivity was 10^{-7} kg. The apparatus of the gravimetric adsorption system, used in connection with a vacuum system, was similar to that described by Boudart *et al.*[11] The pressure was monitored by a digital manometer (Validyne CD-23). The mordenite samples were evacuated for 2 h at room temperature before they were slowly heated at increments of 200 °C/h to 500 °C. The evacuation was then continued at 500 °C for 4 h. The adsorbate was introduced on a dehydrated sample at 25 °C.

Fluorescence and UV Experiments. The emission and excitation spectra were measured using a Shimadzu Recording Absolute Spectrofluorophotometer (RF-502) at room temperature. The UV spectra were taken with a Shimadzu UV-180 apparatus, using MgO as a reference. The particle size of the zeolite was in the 10^{-5}—10^{-4} m range, so that light scattering would be as uniform as possible. The UV spectra in the region from 200 to 400 nm were recorded using a glass filter (UV D-25), since the UV spectra in the region were affected by the fluorescence of a divalent europium ion, as will be described below. Prior to the adsorption, the sample in a quartz cell was dehydrated at 500 °C for 4 h under a pressure of 10^{-5} Torr(1 Torr=133.322 Pa), and then the adsorbate was introduced on dehydrated samples at 25 °C. The inlet adsorbate-gas pressure was the saturated vapor pressure at 25 °C. The quantum yield (Q_0) was decided using the following equation[12];

$$Q_0 = Q_{sample} \times \frac{I_{CaWO_4:Pb}}{I_{sample}}, \quad (1)$$

where Q_{sample} is the photoluminescence outputs (PL) and is comparable to the PL of $CaWO_4$:Pb(NBS 1026), and where I_{sample} and $I_{CaWO_4:Pb}$ are the intensities obtained from the UV spectra.

Lifetime Measurement. The lifetimes were measured using a Nitrogen Laser (337 nm) with a lifetime of less than 5 ns. Also, for the measurement of the lifetimes the monochrometer was used in order to be capable of selecting the

emission wavelength. The lifetimes were determined from the oscilloscope trace as the slope of log I *vs.* t.

Results

Adsorption Measurement. The adsorption of water, methanol, or acetic acid was rapid, and equilibrium was always attained within 1 or 2 h. The adsorption isotherms at 25 °C in Na-M and Eu-M are shown in Fig. 1. The amount of water adsorbed on Eu-M is more than that adsorbed on Na-M. For the adsorption of other species, the difference in the adsorbed amount between Eu-M and Na-M is small. The net amount of adsorption on europium was obtained from the difference between Eu-M and Na-M. In the case of water, this gave a quantity of adsorbed water per europium ion equal to 5.8 when the uptake at 10 Torr was plotted. Since the coordination number of water for the dehydrated europium chloride is 6,[13] the high uptake of water in Eu-M must be mainly due to the formation of the Eu^{2+}-aqua complex. In the case of CH_3OH, the observed CH_3OH/Eu ratio was about unity (1.3). The observed CH_3COOH/Eu ratio was also about unity (1.3). It is considered that, in the system of Eu-CH_3OH or Eu-CH_3COOH, the majority of Eu^{2+} ions exist in a state in which one molecule is coordinated to one Eu^{2+} ion in mordenite.

Fluorescence under Gas Adsorption. The compounds activated with an Eu^{2+} or Eu^{3+} ion generally exhibit fluorescence.[14,15] When Eu-M was degassed at 500 °C, the band emission for the Eu^{2+} ion(peak at 478 nm) and the emission lines for the Eu^{3+} ion, which had peaks at around 570($^5D_0$–$^7F_0$), 590($^5D_0$–$^7F_1$), and 620 nm ($^5D_0$–$^7F_2$), were observed.[2] However, the variation in the fluorescence for the Eu^{3+} ion under gas adsorption is not discussed in this paper, as the relative intensities of the emission lines were much smaller than that of the band emission for Eu^{2+} and the shift of the peak position for the emission band was not observed after the adsorption of gases. On the other hand, the band emission for the Eu^{2+} ion drastically changed after gas adsorption. Some typical excitation and emission spectra for the Eu^{2+} ion in mordenite are shown in Fig. 2. Curve 1 is the band emission for the Eu^{2+} ion which is produced in the course of evacuation at 500 °C. Curve 2 is the emission band when the dehydrated sample is exposed to water. The results of the other adsorbates are summarized in Table 1. The optimum excitation wavelength after gas adsorption was 355 nm in all cases. The emission band thus shifted to a shorter wavelength under gas adsorption.

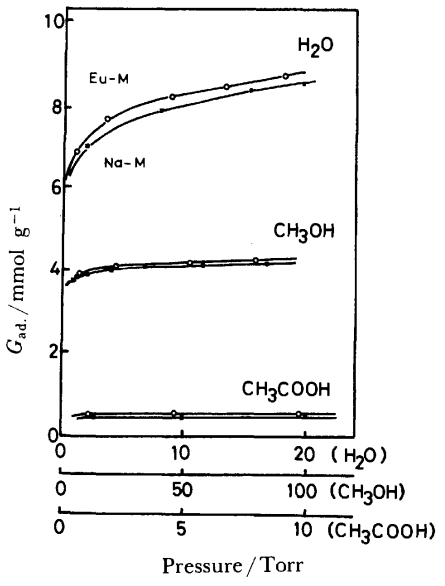

Fig. 1. Adsorption isotherms of water, methanol, and acetic acid in the dehydrated mordenite.

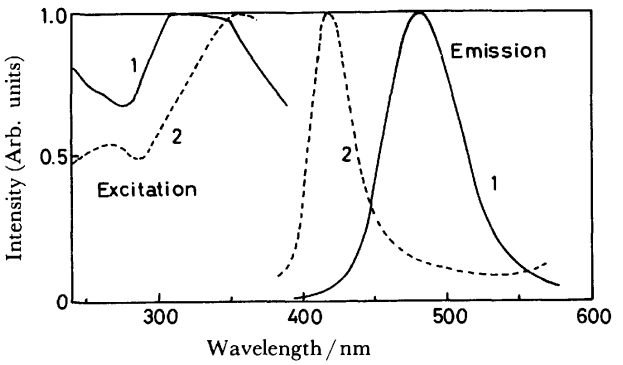

Fig. 2. The emission spectra for Eu^{2+} of Eu-M. (1) Degassed at 500 °C for 4 h and then cooled in vacuum to 25 °C. (2) After the introduction of water to (1).

TABLE 1. THE PEAK POSITION OF THE EMISSION BAND FOR THE Eu^{2+}-ADSORBATE SYSTEM IN MORDENITE

Adsorbate	Peak position (nm)
None	478
H_2O	419
D_2O	419
CH_3OH	418
CH_3COOH	415

UV Spectra. Figure 3 shows some typical absorption spectra before and after the adsorption of water and methanol. Although two bands appear after gas adsorption, the degree of splitting changes almost not at all from Eu-H_2O to Eu-CH_3COOH. On the other hand, the absorption edge of the spectra in the system for all Eu^{2+}-adsorbated molecules, which is the lowest energy edge (or the longest wavelength), almost agreed with the emission peak in Table 1.

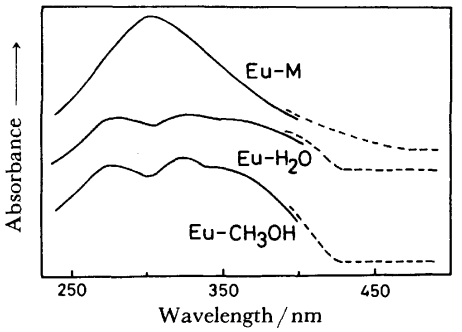

Fig. 3. Absorption spectra of Eu^{2+}-M, Eu^{2+}-H_2O and Eu^{2+}-CH_3OH system. The solid lines are the spectra with a glass filter (UV D-25).

Quantum Yield and Lifetimes. The quantum yield for the Eu^{2+} emission band after gas adsorption under the saturated vapor pressure at 25 °C is summarized in Table 2; it is then compared with the dehydrated sample. The quantum yield after gas adsorption decreases in all cases. That is, H_2O, CH_3OH, and CH_3COOH are quenchers. However, the degree of quenching is dependent on the adsorbates.

Only lifetimes longer than 5 ns could be measured. Thus, the lifetime for the adsorption of CH_3COOH could not be measured. The lifetimes were determined from the oscillograms. Although the oscillogram was composed of two parts (an initial increase in light intensity and then a decay), the results in Table 2 are for only the decreasing part of the picture; the increase was too short to be measured accurately. The decreasing part of the oscillogram represented an exponential decay in the systems of Eu^{2+}–H_2O and Eu^{2+}–D_2O. In an Eu^{2+}–CH_3OH system, although the light intensity decreased exponentially, it was proved that there were two lifetimes from the oscilloscope trace, the slope of log I *vs.* t. In all cases, the lifetime in the Eu^{2+}-adsorbated system is shorter than that in a dehydrated Eu-M. Although the influence of the concentration of an adsorbate on the lifetimes could not be examined as well as in a homogeneous system,[16] the luminescence decay rates in Eu^{2+}–CH_3OH must decrease with the increase in the number of methanol molecules coordinated to the Eu^{2+} ion. Therefore, it would seem that there are two sites where the coordination number of CH_3OH molecules for the Eu^{2+} ion are different from each other. This assumption would be appropriate since the value of CH_3OH/Eu^{2+} is not an integral number as described above.

TABLE 2. LIFETIMES AND QUANTUM YIELDS

Adsorbate	τ/ns	Q_0/%
None	1.1×10^3	0.9
CH_3OH	16,100	0.4
D_2O	7.2	0.2
H_2O	4.8	0.6
CH_3COOH	—	0.08

Discussion

Shift of Emission Peak. The emission for the Eu^{2+} ion is normally associated with the transitions from $4f^65d$ to $4f^7$ where $4f^65d$ is the excited state of Eu^{2+}. Two factors determine the wavelength of the emission band; the splitting of the 5d levels by the crystal field of the surrounding ligand ions and, on the other hand, the energy gap between the 4f ground state and the center of the gravity of 5d excited levels.[7,9] The existence of two peaks in Fig. 3 may be a result of the splitting of the 5d orbitals which increased after gas adsorption. That is, the shift of the emission peak after gas adsorption must be attributed to the fact that the adsorbate molecules are coordinated to an Eu^{2+} ion, as has been described above. Especially, in the Eu^{2+}–H_2O system, it was confirmed that the Eu^{2+}-aqua complex was formed after water adsorption. Moreover, we discussed the shift after gas adsorption. The relationship between the difference in the emission peak before and after gas adsorption and the specific dielectric constant (ε) of adsorbates is shown in Fig. 4. The magnitude of the shift ($\Delta\sigma_F$) is predicted by the approximate equation;[17]

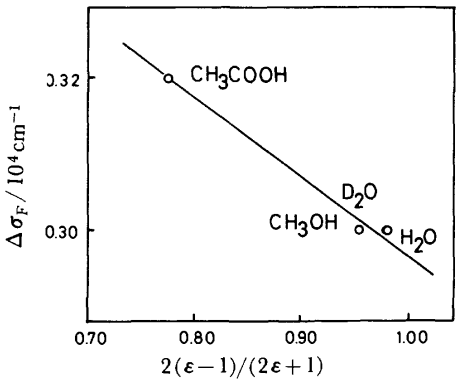

Fig. 4. The relationship between the dielectric constant of adsorbates and the shift of emission peaks for Eu^{2+}-adsorbated molecule in mordenite.

$$\Delta\sigma_F = \frac{2(\varepsilon-1)}{2\varepsilon+1}\alpha, \tag{2}$$

where α is the constant, which is determined by the photoexcited process of the Eu^{2+}-adsorbated molecule. Figure 4 well exhibits the relation of Eq. 2. As can be seen from the finding that the optimum excitation level after the adsorption rarely changed, the variation in the chemical environment around the Eu^{2+} ion under various condition of gas adsorption seems to be relatively unimportant in causing the variation in the excitation process. In Fig. 3, it may be seen that the lowest energy edge (or longest wavelength) almost agrees with the emission peak in Fig. 2. Therefore, it can qualitatively be mentioned that the shifts of the emission peak are dependent on the dielectric constant of the adsorbates, as the adsorbed molecules affect the dipole-dipole interaction Eu^{2+} ion in the dehydrated mordenite.

Rate Constant for Radiative and Radiationless Transitions. The information obtained from the lifetime and quantum-yield measurement enables us to calculate some of the rates of radiationless transitions. The quantum yield may be expressed as;

$$Q_0 = \frac{K_f}{K_f+K_i}, \tag{3}$$

where K_f is the radiative rate constant and K_i is the radiationless rate constant. Also, the observed lifetime, τ, is derived as the following equation;

$$\tau = \frac{1}{K_f+K_i}. \tag{4}$$

From Eqs. 3 and 4, we can calculate K_f and K_i. The results are given in Table 3. The radiationless constant, K_i, increases under the gas adsorption. Comparing the systems of Eu^{2+}–CH_3OH, Eu^{2+}–D_2O, and

TABLE 3. RATE CONSTANTS FOR RADIATIVE (K_f) AND RADIATIONLESS (K_i) TRANSITIONS

Adsorbate	$K_f/10^6\ s^{-1}$	$Q_0/\%$	$K_i/10^6\ s^{-1}$
None	0.09	0.9	0.9
CH_3OH	0.5, ~0	0.4	62, 10
D_2O	0.2	0.2	138
H_2O	1.2	0.6	207

Eu^{2+}–H_2O, the values of K_i are 62, 138, and 207 respectively. That is, the quenching rate constants are more sensitive to the nature of the adsorbates. The order of the quenching power is $H_2O(79)>D_2O(78)>CH_3OH(33)$. The values in parentheses are the dielectric constants. The order associates with the magnitude of the dielectric constant for the adsorbates.

It is considered that the results in this paper lead to a new method for investigating surface characteristics. Further detailed studies to investigate these interesting problems are now in progress.

We are grateful of Prof. H. Mikawa and Dr. Y. Shirota of Osaka University for their support of the measurements of the lifetimes.

References

1) T. Arakawa, T. Takata, G. Adachi, and J. Shiokawa, *J. Chem. Soc., Chem. Commun.*, **1979**, 453; *J. Luminescence*, **20**, 325 (1979).
2) T. Arakawa, T. Takata, M. Takakuwa, G. Adachi, and J. Shiokawa, *Mater. Res. Bull.*, **17**, 171 (1982).
3) For example, T. A. Egerton, A. Hagan, F. S. Stone, and J. C. Vickerman, *J. Chem. Soc., Faraday Trans.* 1, **68**, 723 (1972); K. Klier and M. Ralek, *J. Phys. Chem. Solids*, **29**, 951 (1968); D. H. Olson, *J. Phys. Chem.*, **72**, 4366 (1968).
4) E. F. Vansant and J. H. Lunsford, *J. Phys. Chem.*, **76**, 2860 (1972).
5) Y. Y. Huang, *J. Catal.*, **30**, 187 (1973); *J. Am. Chem. Soc.*, **95**, 6636(1973).
6) Y. Y. Huang and E. F. Vansant, *J. Phys, Chem.*, **77**, 663 (1973).
7) F. M. Ryan, W. Lehmann, D. W. Feldman, and J. Murphy, *J. Electrochem. Soc.*, **121**, 1475 (1974).
8) H. A. Weakliem, *Phys. Rev., B*, **6**, 2743 (1972).
9) D. S. McClure and Z. Kiss, *J. Chem. Phys.*, **39**, 3251 (1963).
10) T. Arakawa, M. Takakuwa, and J. Shiokawa, *Chem. Lett.*, **1982**, 999.
11) Y. Y. Huang, J. E. Benson, and M. Boudart, *Ind. Eng. Chem., Fundam.*, **8**, 346 (1969).
12) J. N. Denas and G. A. Crosby, *J. Phys. Chem.*, **75**, 991 (1971).
13) N. K. Belśkii and Yu. T. Struchkov, *Sov. Phys, Crystallogr.*, **10**, 15 (1965).
14) G. Blasse, W. L. Wanmaker, J. W. terVrugt, and A. Brill, *Philips Res. Reports*, **23**, 189 (1968).
15) G. Blasse and A. Brill, *Philips Tech. Rev.*, **31**, 304 (1970).
16) Y. Hass and G. Stein, *J. Phys. Chem.*, **75**, 3668, 3677 (1979).
17) Y. Ooshika, *J. Phys. Soc. Jpn*, **9**, 594 (1954).

Nonisothermal Crystallization of Poly(tetrafluoroethylene)

Takeo OZAWA
Electrotechnical Laboratory, Sakura-mura, Niihari-gun, Ibaraki 305
(Received September 6, 1983)

Crystallization of poly(tetrafluoroethylene) was observed by differential scanning calorimetry at constant cooling rates. A method for kinetic analysis of thermoanalytical data of nonisothermal crystallization was applied to analyze the data, and it was elucidated that poly(tetrafluoroethylene) crystallizes one-dimensionally from preexisting nuclei, which are presumably impurities. These results are in accordance with electron-microscopic observation of the crystalline morphology of poly(tetrafluoroethylene), which consists of band-like or star-like crystallites. The kinetic parameters, especially the temperature dependence of the linear growth rate, were estimated.

Isothermal crystallization of various polymers has been extensively observed mainly by differential scanning calorimetry (DSC). However, for some polymers such as poly(tetrafluoroethylene) (PTFE), the crystallization is so rapid that one can not observe isothermal crystallization, because it crystallizes in the period during which the sample is cooling to a desired constant temperature. To observe these crystallization behavior, we should observe the process in cooling mode. The present author published a method for analyzing thermoanalytical data of crystallization, and the method was applied to nonisothermal crystallization of poly(ethylene terephthalate) proceeding at constant cooling rates.[1] For more simple crystallization mechanism, *i.e.*, crystallization from preexisting nuclei, another method was devised by the author.[2]

On the other hand, in some actual processes such as fabrication and melt spinning of crystalline polymers, crystallization proceeds nonisothermally, so that nonisothermal observation of crystallization has also actual meaning. Moreover, thermoanalytical observation of crystallization behavior was recently extensively investigated especially for amorphous materials such as amorphous magnetic materials by differential thermal analysis and DSC.

PTFE dealt with in this paper has some unusual features, one of which is its crystalline morphology; the spherulite has not been observed. Bunn *et al.*[3] reported striated band-like structures on fractured surfaces of PTFE. On the other hand, Symons observed dendrites and star-like crystals in the solution-grown crystals[4] and he also observed both the plate-like single crystals of clear hexagonal habit and the striated broad needles.[5] Afterword, Rahl *et al.*[6] observed emulsion-grade PTFE and found ribbon-like and rod-like crystallites; they postulated that these crystallites consist of single crystals of extended chain packing. Thus, it is interesting to know the crystallization kinetics of the polymer, especially the mechanism of the crystal growth. The nonisothermal crystallization was observed with a DSC, and the data were analyzed by the above-mentioned methods. These results are reported in this paper, and the applicability of the method for kinetic analysis of nonisothermal crystallization is illustrated in this report.

Experimental

Teflon No. 5 (E. I. du Pont de Nemours & Co. Inc., bulk polymerized PTFE), Teflon No. 6J (Mitsui Fluorochemicals Co., Ltd., emulsion polymerized PTFE), and Polyflon F-101 (Daikin Co., Ltd., emulsion polymerized PTFE) were used as received. Teflon No. 5 gamma-irradiated by 1 Mrad to decrease the molecular weight was also investigated. A DSC made by Rigaku Denki Co., Ltd. was used; the sample of 10—20 mg was heated in the flow of dry nitrogen up to 350—360 °C and then cooled immediately at a programmed cooling rate of 1, 3 or 5 K/min. Because the temperature of the sample is measured in this apparatus with a thermocouple, a junction of which is located on the bottom of the sample holder, the temperature can be measured precisely even in the cooling mode.

Results and Discussion

As is well known, for isothermal crystallization Avrami's equation holds;

$$-\ln(1-C) = Z t^n, \tag{1}$$

where C, t, Z, and n are the crystallized fraction, the time, a constant and an integer related to the nucleation and the growth dimension, respectively. As was elucidated in the previous paper, the following nonisothermal equation was derived instead of the above Avrami's equation.

$$-\ln(1-C) = \chi_c(T)/\phi^n, \tag{2}$$

or

$$\log(-\ln(1-C)) = \log \chi_c(T) - n \log \phi, \tag{3}$$

where T, ϕ, and $\chi_c(T)$ are respectively the temperature, the cooling rate, and the cooling crystallization function, which is the function characteristic of the sample; this function is dependent on the temperature but independent on the cooling rate. Therefore, the straight line should be obtained by plotting $\log(-\ln(1-C))$ against the logarithms of the cooling rates.

In order to observe this relation, the DSC curves of crystallization were converted to integral type curves of C versus t as is shown in Fig. 1, where C is estimated as follows;

$$C = \int_0^t (dH/dt)\, dt \Big/ \int_0^\infty (dH/dt)\, dt, \tag{4}$$

where dH/dt is the rate of heat evolution due to the exothermic crystallization observed by DSC.

Typical plots of $\log(-\ln(1-C))$ against $\log \phi$ are shown in Fig. 2, where the straight lines of the slope of unity are drawn. As is clearly seen, the crystallization follows Eq. 3 with $n=1$. The values of n obtained by

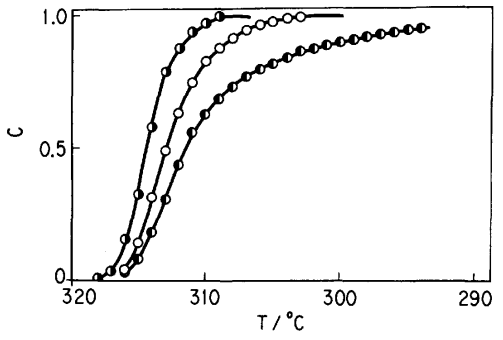

Fig. 1. Relations of crystallized fraction versus temperature obtained at different cooling rates for Teflon No. 5: ◐; 4.5°C/min, O; 2.9°C/min, and ◑; 0.9°C/min.

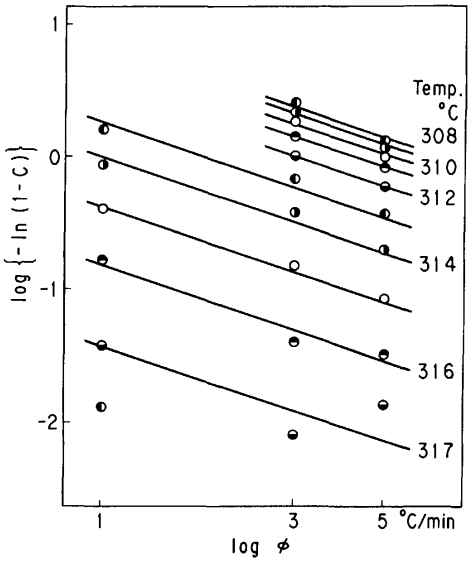

Fig. 2. Plots of $\log(-\ln(1-C))$ *versus* $\log \phi$ at given temperatures for Teflon No. 5. Slopes of straight lines shown are all unity.

TABLE 1. ESTIMATED VALUES OF n

Temerature °C	Teflon No. 5	Teflon No. 5 γ-irradiated	Teflon No. 6J	Polyflon F-101
317	1.0	—	—	—
316	1.0	—	—	—
315	1.0	—	—	—
314	0.9	—	0.8	1.8
313	1.0	0.9	1.1	1.4
312	0.9	1.3	0.8	1.5
311	0.9	1.2	0.7	1.4
310	1.0	1.1	0.7	1.2
309	—	0.9	0.7	1.5
308	—	0.8	0.7	1.1
307	—	—	0.7	0.8
306	—	—	0.7	—
Average	1.0	1.0	0.8	1.3

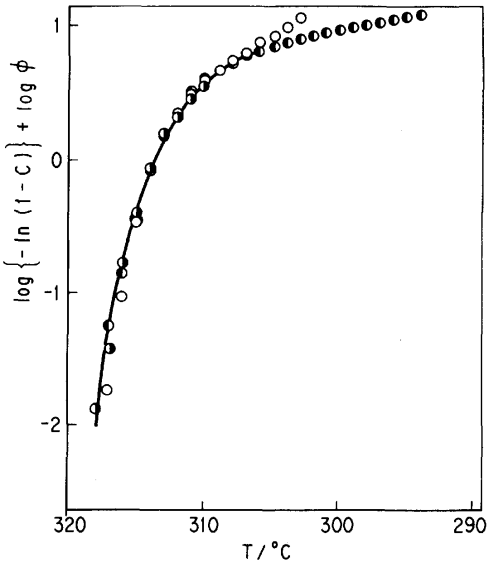

Fig. 3. Experimental master curve reduced to ϕ=1 K/min for Teflon No. 5. The cooling rates are 4.5°C/min (◐), 2.9°C/min (O) and 0.9°C/min (◑).

the similar plots for the other samples are tabulated in Table 1. Although the data are somewhat scattered in a few cases, the values of n are estimated to be approximately unity for all samples by the method of the least square. It can be concluded from these facts that the crystals grow one-dimensionally from preexisting nuclei. However, the origin of the nuclei is not elucidated in this investigation.

This mechanism of one-dimensional growth is in accordance with the above-mentioned report of Bunn *et al.*[3] who observed the fractured surface of the sintered Teflon No. 5 with an electron-microscope and found band-like crystals. The one-dimensional growth is also in accordance with the formation of dendrites and star-shaped crystals in the solution-grown crystallization observed by Symons[4] and with needle-like structure found in sintered deposits by Symons.[5] From the electron-microscopy, the electron-diffraction and the optical observation, Symons proposed a model of a stack of single crystal plate or lamella of hexagonal habit, in which molecular chains are folded and perpendicular to the basal plane.[5] The one-dimensional growth mechanism is also in accordance with the observation of Rahl *et al.*[6] who found ribbon-like and rod-like crystals, and they postulated extended chain structure. According to Symons' models, the value of n obtained in this investigation corresponds to the mechanism of whole process of crystallization and not to the growth of single crystals of hexagonal habit postulated by Symons.[5]

From Eq. 3, another plot can be derived; if one plots $\log(-\ln(1-C))$ against the temperature, the curves of different cooling rates can be superposed on each other by longitudinal shift and an experimental master curve can be obtained. The superposition could not be made, if the slow "secondary" (post-Avrami) crystallization occurs. A typical experimental master curve drawn in this way is shown in Fig. 3. Except the latter part, the curves can be superposed on each other very well, and the discrepancy in the latter part seems to indicate the existence of the secondary crystallization. After the completion of the process, *i.e.*, C=1, the heat of crystallization of the gamma-irradiated sample is measured to be about 50% of the heat of the fusion of the sample by using the peak areas of DSC curves, and that of the Teflon No. 5 is about 30% of the heat of the fusion of the sample. These facts also suggest the

existence of the secondary crystallization, since the crystallinity of the sample sintered ordinarily is higher than those observed in cooling crystallization, and the effect of the secondary crystallization is smaller in the cooling crystallization than in the isothermal run, because the sample is cooled rapidly through the temperature range of the secondary crystallization.

The intercepts of the plots as shown in Fig. 2 give the cooling crystallization function, $\chi_c(T)$. Namely for the crystal growth from preexisting nuclei,[1]

$$\chi_c(T) = gN\int_{T_m}^{T} \{R_c(T) - R_c(\theta)\}^m v(\theta)\, d\theta, \quad (5)$$

where g, N, T_m, θ, $(m+1)$ and $v(\theta)$ are the geometrical factor, the density of the nuclei, the melting temperature, a variable, the growth dimension and the linear growth rate, respectively, and

$$R_c(T) = \int_{T_m}^{T} v(\theta)\, d\theta. \quad (6)$$

For the one-dimensional growth in which m is equal to zero,

$$\chi_c(T) = gN\int_{T_m}^{T} v(\theta)\, d\theta. \quad (7)$$

The values of the function obtained for the samples are plotted in Fig. 4. It is interesting to note that $\chi_c(T)$ for the Teflon No. 5 locates in higher temperature range than the gamma-irradiated Teflon No. 5, though the latter seems to have large tendency to crystallize due to the low molecular weight caused by gamma-irradiation. Since $\chi_c(T)$ represents the nature of crystallization of the sample, it is very interesting to compare $\chi_c(T)$ for Teflon No. 6J with that for polyflon F-101; both samples are polymerized by emulsion-polymerization and used in paste extrusion, and the two curves resemble to each other.

For the one-dimensional growth from the preexisting nuclei, another following simple relation holds from Eq. 2, because $n=1$.

$$\frac{1}{1-C}\frac{dC}{dt} = \frac{d\chi_c(T)}{dT} \quad (8)$$

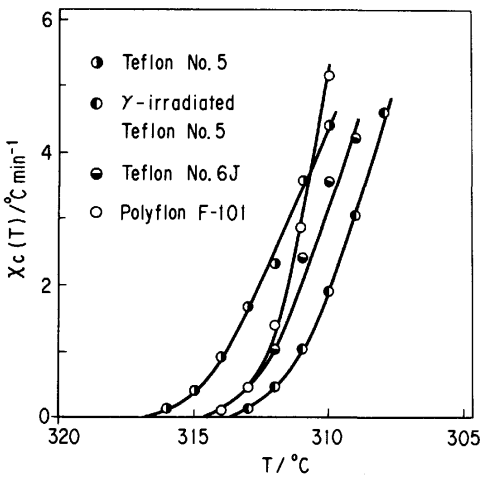

Fig. 4. Cooling crystallization functions for indicated samples.

Because $d\chi_c(T)/dT$ is equal to $gNv(T)$, which is equal to Z in Eq. 1,[2] we can estimate Z directly from the DSC curves by using Eq. 8. The values of Z thus estimated are plotted in Figs. 5 and 6 for Teflon No. 5 and gamma-irradiated Teflon No. 5. As is seen in these figures, the values obtained from the DSC curves at different cooling rates are on the same curve. From these facts the crystallization of Teflon No. 5 and gamma-irradiated Teflon No. 5 is ascertained to follow Avrami's model of the one-dimensional growth from preexisting nuclei. It is interesting that Z of gamma-irradiated Teflon No. 5 is in the lower temperature range, but its maximum is larger than Teflon No. 5. This tendency is in accordance with that of $\chi_c(T)$. On the other hand, the values of Z thus estimated for the other PTFE's are not on the same curve and large scattering of the values is observed. For these

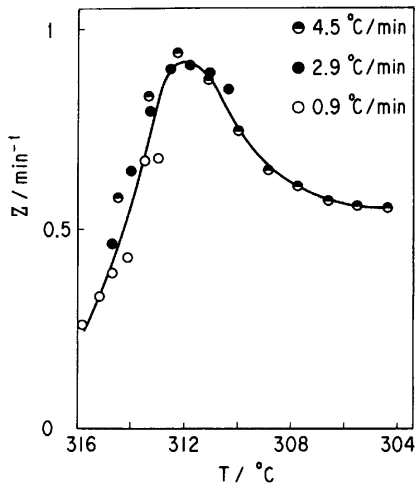

Fig. 5. Temperature dependence of kinetic parameter, Z, for Teflon No. 5. The cooling rates are 4.5°C/min (◓), 2.9°C/min (●), and 0.9°C/min (○).

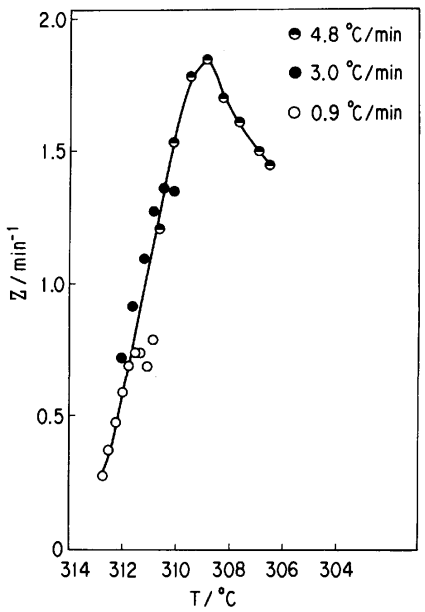

Fig. 6. Temperature dependence of kinetic parameter, Z, for gamma-irradiated Teflon No. 5. The cooling rates are 4.8°C/min (◓), 3.0°C/min (●), and 0.9°C/min (○).

emulsion-polymerized PTFE's, the values of n are also scattered and somewhat different from unity, so that other processes, such as the secondary crystallization, seem to have large effect for these PTFE's.

For poly(vinylidene difluoride), Nakamura *et al.*[7] observed nonisothermal crystallization by DSC and found that $\log(-\ln(1-C))$ is in a linear relation with $\log\phi$ and that the slope is four, which indicates homogeneous random nucleation and three-dimensional growth mechanism. They also observed the crystallization isothermally and elucidated the same mechanism by applying the above-mentioned Avrami's equation. In three examples of nonisothermal crystallization of polymers, *i.e.*, poly(ethylene terephthalate),[1] poly(vinylidene difluoride),[7] and poly(tetrafluoroethylene), the applicability of the present author's theory and method of nonisothermal crystallization is illustrated, and the theory and method are clearly shown to be applicable to other substances, such as amorphous materials and so on.

The author wishes to thank Miss Michiko Osawa for her assistance in the data processing.

References

1) T. Ozawa, *Polymer*, **12**, 150 (1970).
2) T. Ozawa, *Bull. Chem. Soc. Jpn.*, to be published.
3) C. W. Bunn, A. J. Cobbold, and R. P. Palmer, *J. Polym. Sci.*, **28**, 365 (1958).
4) N. K. J. Symons, *J. Polym. Sci.*, **51**, S21 (1961).
5) N. K. J. Symons, *J. Polym. Sci., Part A*, **1**, 2843 (1963).
6) F. J. Rahl, M. A. Evano, R. J. Fredericks, and A. C. Reimschuessel, *J. Polym. Sci., Part A-2*, **10**, 1337 (1972).
7) S. Nakamura, T. Sasaki, J. Funamoto, and K. Matsuzaki, *Makromol. Chem.*, **176**, 3471 (1975).

Optically Active and Racemic Glycerides. II. Thermodynamic Studies on the Polymorphic Transition of (*R*)- and (*RS*)-1,2-Diglycerides

Makio Iwahashi,* Kazuhide Ashizawa,† Miyuki Ashizawa,
Yoshihide Kaneko,†† and Mitsuo Muramatsu†††
Department of Chemistry, Faculty of Science, Tokyo Metropolitan University, Setagaya-ku, Tokyo 158.
(Received September 6, 1983)

The polymorphic relationship between optically active (*R*)- and for racemic (*RS*)-forms of 1,2-distearin and 1,2-dipalmitin were studied by X-ray diffraction, infrared spectrum, and the thermal analysis. These glycerides have two crystalline forms, α and β, wherein α is metastable and β is stable under ordinary conditions. The $\alpha \rightarrow \beta$ transformation for the (*RS*)-1,2-distearin crystal was extremely slow as compared with that for the (*R*)-form crystal, implying that the β-form crystal of (*RS*)-1,2-distearin is an eutectic mixture of small (*R*)- and (*S*)-crystals while the α-form crystal of (*RS*)-1,2-distearin is composed of a replacement type solid solution of (*R*)- and (*S*)-1,2-distearin molecules. Almost the same results were obtained with 1,2-dipalmitin, for which the rate of $\alpha \rightarrow \beta$ transformation is higher than that for the 1,2-distarin, probably because of a higher mobility of this compound.

In the preceding paper[1] on stability of (*S*)- and (*RS*)-α-monostearin crystals, it was pointed out that the (*RS*)- form crystal is a racemic compound, and that the interaction between (*R*)- and (*S*)-molecules in the (*RS*)-crystal is stronger than that between (*S*)- and (*S*)-molecules even above the melting point of the (*RS*)-crystal. Such polymorphic stabilities have been discussed frequently with monoglycerides and triglycerides[2,3] but fewly with 1,2-diglycerides. Thus, the present study deals with the polymorphic relationship of optically active (*R*)- and racemic (*RS*)-forms of 1,2-distearin as well as of 1,2-dipalmitin. Attempts have been made to clarify the mechanism of the extremely slow $\alpha \rightarrow \beta$ transition of (*RS*)-1,2-glycerides as compared with that of (*R*)-1,2-diglycerides by means of X-ray diffraction, infrared spectrum and the thermal analysis for these glycerides. A similar mechanism could be applied to 1,3-diglycerides for which rapid $\alpha \rightarrow \beta$ transformation had been reported.[4-6]

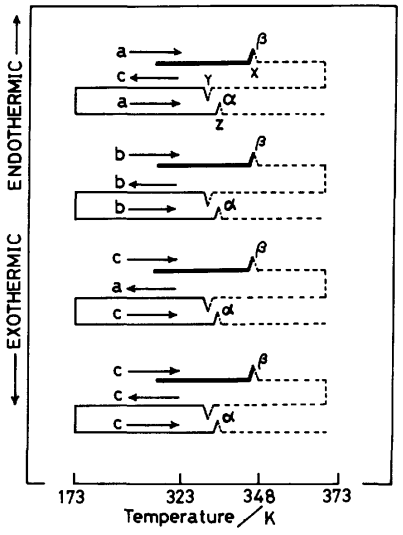

Fig. 1. The DSC performance for (*RS*)-1,2-distearin crystal; a=1 K min^{-1}, b=5 K min^{-1}, and c=10 K min^{-1}. Bold and thin lines express the phases of β- and α-forms, respectively, and dotted lines the liquid state. The enthalpy values for the peaks: X=123.1 kJ mol^{-1}, Y=77.2 kJ mol^{-1}, and Z=76.4 kJ mol^{-1}.

Experimental

Materials. Chemically pure (≥99%) samples of (*R*)- and (*RS*)-1,2-dipalmitins and (*R*)- and (*RS*)-1,2-distearins from Fluka AG (Switzerland) were further purified by repeated recrystallization from hexane to give β-form (stable) crystals of these 1,2-diglycerides. The samples of α-form (metastable) were obtained by rapid cooling of molten samples of the stable glycerides. Melting points of these samples (Table 1) were in good agreement with the reference values.[4,8,9]

Apparatus and Procedures. The calorimetric experiments were carried out with a differential scanning calorimeter (Shimadzu Model DSC-30 equipped with Model LTC-30 cooling unit) in a temperature range from 173 to 473 K (accuracy ±2.5 mJ s^{-1}) by the use of a standard sample of KNO_3[10] for thermal calibration. Identification of the polymorphic

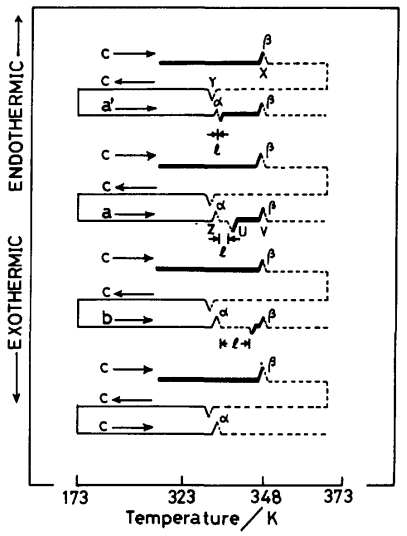

Fig. 2. The DSC performance for (*R*)-1,2-distearin crystal; a'=0.5 K min^{-1}, a=1 K min^{-1}, b=5 K min^{-1}, and c=10 K min^{-1}. Bold and thin lines express the phases of β- and α-forms, respectively, and dotted lines the liquid state. The enthalpy values for the peaks: X=124.0 kJ mol^{-1}, Y=79.4 kJ mol^{-1}, Z=73.3 kJ mol^{-1}, U=121.0 kJ mol^{-1}, and V=120.2 kJ mol^{-1}.

†Present address: Tsukuba Res. Lab., Eizai Co., Ltd., Toyosato Tsukubagun, Ibaragi 305.
††Present address: Shinetsu Polymer Co. Ltd., Omiya.
†††Present address: Dept. of Chem. Faculty of Hygienic Sci., Kitasato Univ., Sagamihara, Kanagawa 228.

crystals was achieved with an X-ray diffraction unit (Rigaku Denki Model 2001), and an IR spectrometer (Hitachi Perkin-Elmer Model 215). For more details, an X-ray small-angle diffraction unit (Rigaku Denki Model 2202E1) was used.

Results and Discussion

In Figs. 1 and 2 which show the DSC performance for (*RS*)- and (*R*)-1,2-distearins, respectively, the first (X) and the second (Z) endothermic peaks are attributable to the fusion of crystals of β- and α-forms, respectively. This was confirmed by the data based on the measurements of X-ray diffraction (Fig. 3), IR spectrum (Fig. 4), melting point and enthalpy of fusion (Table I). The first exothermic peaks (Y), therefore, are attributable to the formation of α-form crystals: The enthalpy amounts calculated from the peaks (Y) were 77.2 and 79.4 kJ mol^{-1} for (*RS*)- and (*R*)-distearins, respectively, in approximate agreement with our observed values (75.8 and 73.3 kJ mol^{-1} for (*RS*)- and (*R*)-forms) for the α-form crystals. This was indeed the case of (*RS*)-distearin for which the DSC performance (Fig. 1) remained unchanged when heating and/or cooling rates were varied.

On the other hand, (*R*)-stearin showed rather peculiar behavior in its performance (Fig. 2); After formation of α-crystal, it was molten (mp of β-form) by re-heating to give an endothermic peak followed by an exothermic one indicative of formation of β-form: The enthalpy value (121.1 kJ mol^{-1}) for the exothermic peak *U*, in good agreement with that (120.0 kJ mol^{-1}) for the endothermic one *V*, agrees well with the enthalpy of fusion (124.0 kJ mol^{-1} from Table 1) for the β-form crystal. It seems that the interval (in temperature scale), *l* in Fig. 2, between the $\alpha \rightarrow$ liquid and liquid $\rightarrow \beta$ transformations is longer for higher

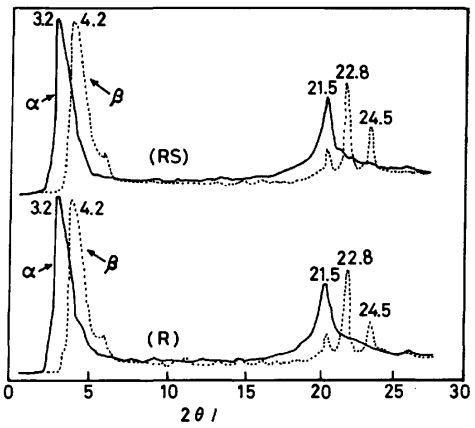

Fig. 3. X-Ray diffraction patterns for (*RS*)-(upper curves) and (*R*)-(bottom) 1,2-distearin crystals in α-(full curves) and β-(dotted) states.

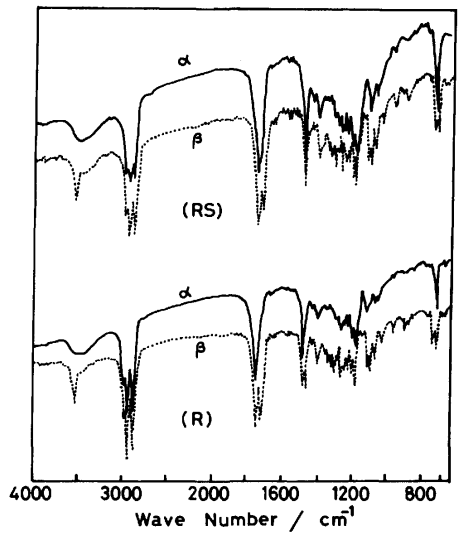

Fig. 4. Infrared spectra for (*RS*)-(upper curvers) and (*R*)-(bottom) 1,2-distearin crystals in α-(full curves) and β-form (dotted).

Table 1.

	1,2-Dipalmitin				1, 2-Distearin			
	(*R*)		(*RS*)		(*R*)		(*RS*)	
	α	β	α	β	α	β	α	β
Mp θ_m/K	322.5	341.1	322.1	336.3	333.1	349.1	332.8	344.9
		341.1 ~ 342.1[8]	323.1[4]	336.6[4]		349.1 ~ 350.1[8]	332.6[4]	344.1[4]
		340.1 ~ 340.6[9]				347.6 ~ 348.1[9]		344.6 ~ 345.6[8]
Enthalpy of fusion / kJ mol^{-1}	52.7[a]	97.2	52.0	98.7	73.3	124.0	75.8	123.1
Entropy of fusion / J K mol^{-1}	163.4	284.9	161.2	293.4	220.0	355.1	227.7	356.9

a) Enthalpy of crystallization: Enthalpy of fusion for α-(*R*)-crystal of 1, 2-dipalmitin could not be obtained for overlaping of the endo-thermic peak due to the fusion of α-crystal with the subsequent peak (exothermic) due to rapid formation of β-crystal.

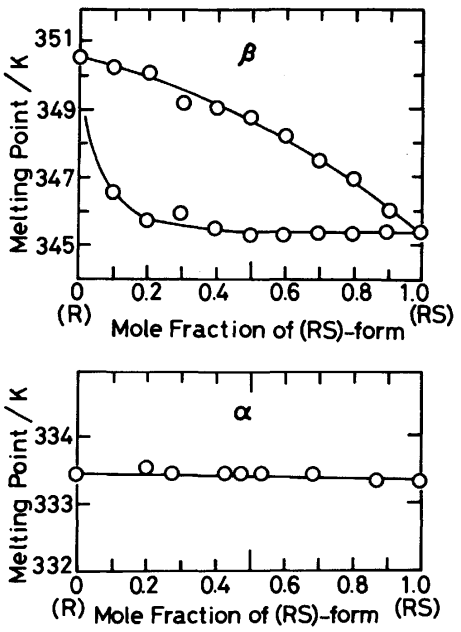

Fig. 5. Melting point-composition diagrams for mixtures of (*R*)- and (*RS*)-1,2-distearins in α-(bottom figure) and β-(upper) forms. Mixture of (*R*)- and (*RS*)-1,2-distearins were prepared by mixing (*R*)- and (*RS*)- forms with hexane and standing overnight *in vacuo* to evaporate the solvent.[1]

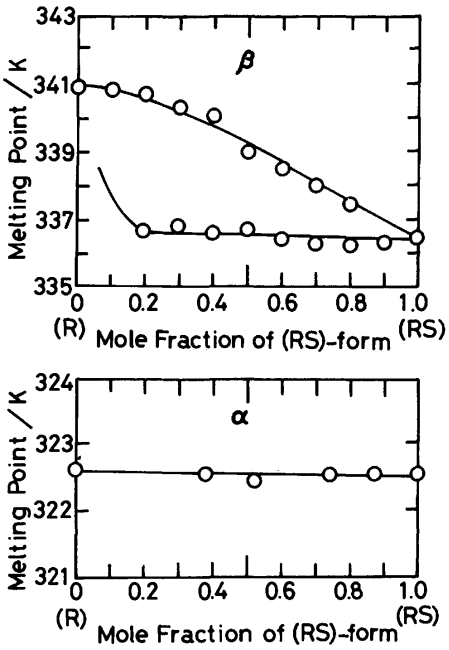

Fig. 6. Melting point-composition diagrams for mixtures of (*R*)- and (*RS*)-1,2-dipalmitins in α-(bottom figure) and β-(upper) forms. Mixture of (*R*)- and (*RS*)-1,2-dipalmitins were prepared by mixing (*R*)- and (*RS*)-forms with hexane and standing overnight *in vacuo* to evaporate the solvent.[1]

the heating rate. Howe and Malkin,[4] and Chapman[11] reported that the formation of the β-form crystal resulted from holding of the α-form crystal of (*RS*)-1,2-distearin for several hours at a temperature slightly below its mp and that both (*R*)- and (*RS*)-1,2-distearins have only two polymorphic forms, α and β, and do not possess a transition temperature between them. Taking account of all these results, we must conclude that the α-form crystal is less stable than the β-form crystal throughout all temperature region; The α- and β-crystals are in monotropic relationship,[12] giving higher stability to the latter. A similar relationship has been observed for the α- and β-crystals of chloramphenicol palmitate.[13]

In order to compare the rate of $\alpha \rightarrow \beta$ transformation between (*R*)- and (*RS*)-1,2-distearins, the DSC scanning for the α-crystals of (*R*)- and (*RS*)-form were carried out, after they had been allowed to stand for three months at room temperature. It was found that the α-(*R*)-crystal was transformed into its β-form, whereas the α-(*RS*)-crystal remained unchanged. Such phenomena could probably suggest that, like the case of (*RS*)-α-monostearin,[1] the (*RS*)-1,2-distearin is composed of a racemic compound. However, both X-ray diffraction patterns (including X-ray small-angle diffraction) and the infrared absorption spectra were almost the same between (*R*)- and (*RS*)-forms irrespective of their crystalline forms (see Figs. 3 and 4). In addition, practically no difference is found in entropy of fusion between (*R*)- and (*RS*)-distearins whatever they are in α- or β-form (see Table 1). Nevertheless, the melting point-composition diagrams (Fig. 5) indicates that the β-(*RS*)-1,2-distearin crystal(upper figure) possesses a minimum melting point at which the crystal seems to be an eutectic mixture of (*R*)- and (*S*)-crystallites in 1:1 molar ratio, whereas the α-crystal (bottom) shows a performance typical to solid solution. There are two types of solid solution, replacement and penetration types.[14] In the former, different kind of molecules freely occupy the lattice points in a crystal, whereas in the latter one kind of molecules can penetrate, with certain limit in its composition, among other kind of molecules occupying their lattice points. The Hume-Rothery rules[14] for the replacement type solid solution can be applicable to the (*R*)- and (*S*)-1,2-distearin molecules which are all the same in their size and attractive force. The $\alpha \rightarrow \beta$ transformation of (*RS*)-1,2-distearins, therefore, must be accompanied by an entropic decrease corresponding to a molecular rearrangement from a solid solution type to an eutectic type, *i.e.*, replacement-type distribution (random) to microcrystallite mixture (microordered).[15] In the case of (*R*)-1,2-distearin, such an entropic decrease is not involved in such transformation. The same is true for 1,3-distearin which has no asymmetric carbon atoms and which is characterized by higher rate of $\alpha \rightarrow \beta$ transformation.[4]

All of the above experimental techniques, DSC scanning, X-ray diffraction, IR spectropy, and the melting point-composition diagrams were applied to α- and β-crystals of (*R*)- and (*RS*)-1,2-dipalmitin, for which essentially the same results were obtained as is summarized in Table 1. A typical example is shown in Fig. 6 which suggests an entropic decrease accompanying the $\alpha \rightarrow \beta$ transformation (random→microordered) of (*RS*)-1,2-dipalmitin. Similarly, the DSC performance was almost the same as that in Fig. 1 from which the enthalpies of fusion for α- and β-forms are tabulated in the 4th and 5th column of Table 1. Only one exception is that the $\alpha \rightarrow \beta$ transformation of (*R*)-

1,2-dipalmitin was so fast that the *l*-value in Fig. 2 was always zero irrespective of the heating rate, *i.e.*, the peaks *Z* and *U* overlap each other. This is evidently attributable to a higher mobility of the C_{16}-compound than that of the C_{18}-glyceride. One, therefore, could not estimate the enthalpy of fusion for α-form but of crystalization (peak *Y*), which is listed in the second column.

The authors wish to express their thanks to Mr. Kazuo Ohbu and Kazuhisa Yoshida of Lion Co. Ltd. (Tokyo) for obtaining the results of the X-ray small angle diffraction.

References

1) M. Iwhahashi, Y. Watanabe, T. Watanabe, and M. Muramatsu, This Journal, submitted for publication.
2) A. W. Ralston, "Fatty Acids and Their Derivertives," John Wiley and Sons, New York (1948), p. 545; D. Chapman, *Chem. Rev.*, **62**, 433 (1962).
3) E. S. Lutton, *J. Am. Oil Chem. Soc.*, **48**, 778 (1971); T. Maruyama, I. Niiya, M. Imamura, M. Okada, and T. Matsumoto, *Yukagaku*, **22**, 85, 141 (1973); T. Maruyama, I. Niiya, M. Imamura, and T. Matsumoto, *ibid.*, **26**, 104 (1977); E. S. Lutton, and F. L. Jackson, *J. Am. Chem. Soc.*, **70**, 2445 (1948).
4) R. J. Howe and T. Malkin, *J. Chem. Soc.*, **1951**, 2663.
5) F. J. Baur, F. L. Jackson, D. G. Kolp, and E. S. Lutton, *J. Am. Chem. Soc.*, **71**, 3363 (1949).
6) D. Chapman, *J. Chem. Soc.*, **1956**, 55.
7) R. Daubert and J. King, *J. Am. Chem. Soc.*, **61**, 3328 (1939).
8) E. Baer and M. Kates, *J. Am. Chem. Soc.*, **72**, 942 (1950).
9) J. C. Sowden and H. O. L. Fisher, *J. Am. Chem. Soc.*, **63**, 3244 (1941)
10) "Kagaku Binran," ed by the Chem. Soc. Jpn., Maruzen, Tokyo (1977), p. 912.
11) D. Chapman, *J. Chem. Soc.*, **1958**, 4680.
12) A. E. Bailey, "Melting and Solidification of Fats," Interscience, New York (1950), p. 32.
13) M. Muramatsu, M. Iwahashi, and K. Masumoto, *J. Chem. Eng. Data*, **20**, 6 (1975).
14) H. Chihara, *Kagaku To Kogyo*, **29**, 96 (1976).
15) Iwase and S. Okamoto, "Standard Phase Diagrams of Two Components Alloys," Nikkan Kogyo Shinbun, Tokyo (1953), p. 7.

Furan Ring Formation in OH-initiated Photooxidation of 1,3-Butadiene and *cis*-1,3-Pentadiene

Tomohiro OHTA

Department of Environmental Sciences, Tokyo Metropolitan Research Laboratory of Public Health, Hyakunincho, Shinjuku-ku, Tokyo 160

(Received September 16, 1983)

Reactions of hydroxyl radicals with 1,3-butadiene and *cis*-1,3-pentadiene in the presence of oxygen were studied in the gas phase. Two OH radical sources were employed; photolysis of H_2O_2 at 254 nm and photolysis of methyl nitrite at 360 nm. In the reaction system for 1,3-butadiene, furan was detected besides acrylaldehyde and in the *cis*-1,3-pentadiene system, 2-methylfuran was detected besides acetaldehyde, acrylaldehyde, and crotonaldehyde by gas chromatographic analysis. Approximate yields of furan and 2-methylfuran were 5.3—6.7% and 6.7—8.4%, respectively, which were sensitive to the conditioning of the surface of reactor but insensitive to hydroxyl radical sources, the surface material of reaction vessel or the surface to volume ratio of reactors. The yields of aldehydes were also measured. Isotopic labeling experiment with $^{18}O_2$ by use of mass spectrometry indicated that abstraction of vinyl-hydrogen from 1,3-butadiene and *cis*-1,3-pentadiene occurred about 3% of the time. Photooxidation of 2,5-dihydrofuran initiated with ·OH radicals was also discussed to explain the increase of furan in the dark after the irradiation.

Atmospheric reactions of ·OH radicals with simple monoolefins are understood to be initiated mainly by ·OH radical addition to double-bond and partly by hydrogen abstraction at allylic position.[1] When a general olefin $R_1R_2C{=}CR_3R_4$ is photooxidized in NO_x-polluted atmosphere, major expected products are $R_1R_2C{=}O$ and $R_3R_4C{=}O$. It is interesting to know whether the general rule is applicable to diolefins. Environmental chamber studies[2,3] have shown that the major initial products of NO_x-air photooxidation of 1,3-butadiene were formaldehyde and acrylaldehyde. *cis*-1,3-Pentadiene is expected analogously to produce formaldehyde, acetaldehyde, acrylaldehyde, and crotonaldehyde in the similar photooxidation process. However, in our previous study[4] on the determination of relative rate constants for the reactions of diolefins with ·OH radicals by photolyzing H_2O_2 in the presence of oxygen and pairs of diolefins, it was found that furan was formed in the reaction of ·OH with 1,3-butadiene and that 2-methylfuran was formed in *cis*-1,3-pentadiene system, in addition to the expected aldehydes. In order to determine the yield of furans and to make an assumption on the mechanism for furan ring formation in the photooxidation of the conjugated diolefins, we carried out several experiments on the system and proposed a mechanism involving abstraction of vinyl-hydrogen by ·OH from conjugated diolefins.

Experimental

Two ·OH radical sources were employed separately; photolysis of hydrogen peroxide (H_2O_2, 90 %) at 254 nm and methyl nitrite (CH_3ONO) at 360 nm. Hydrogen peroxide was used for runs to examine the dependence of the product yield on the initial concentrations of reactants and wall effect. First, 1 Torr (1 Torr=133 Pa) of H_2O_2 (90%) was introduced in a quartz cylindrical reaction cell which was 15 cm in length and 4 cm in diameter (surface to volume ratio, S/V,=1.1 cm^{-1}): this cell was named reactor A for later discussion. Then, diluted 1,3-butadiene or *cis*-1,3-pentadiene in O_2 was added by measuring the pressure with MKS Baratron. Oxygen or nitrogen gas was filled into the cell to pressurize the mixture up to 760 Torr. After allowing the mixture to stand for about 10 min, the cell was irradiated with two 15 W germicide lamps (National GL-15, 254 nm). Products and reactants for 1,3-butadiene system were analyzed by gas chromatography with flame ionization detector by using 1-m glass column of Porapak T operated at 145 °C. For the reaction system of *cis*-1,3-pentadiene, 1-m stainless steel column of Porapak Q was employed. Products of several runs were trapped in a tube filled with small glass beads immersed in liquid oxygen and the solidified fraction was vaporized and, then, analyzed by use of a gas chromatograph-mass spectrometer (LKB 9000) with the same kind of column used for each reaction system. Further identification was made with infrared spectrometer for the effluents from thermal conductivity detector (TCD) corresponding to furan and 2-methylfuran collected repeatedly in the trap cooled with liquid nitrogen by monitoring TCD signal. Carrier gas was helium.

The other ·OH radical source, CH_3ONO, was used for the experiments to carry out the reactions of ·OH with the diolefins in the absence of H_2O_2 and in the presence of NO_x, and also to examine wall effect on the reaction. Atkinson *et al.*[5,6] have shown that CH_3ONO is a good source *via* Reactions 1 to 3.

$$CH_3ONO + h\nu(360\,nm) \rightarrow CH_3O + NO \quad (1)$$

$$CH_3O + O_2 \rightarrow HO_2 + CH_2O \quad (2)$$

$$HO_2 + NO \rightarrow HO + NO_2 \quad (3)$$

Methyl nitrite was prepared from the reaction of methanol, sodium nitrite and sulfuric acid, according to Atkinson *et al.*[5,6] Crude CH_3ONO was vacuum distilled in a greaseless high-vacuum system and stored under vacuum at 77 K in the dark. Procedure for preparing the reaction mixture was similar to the method for the H_2O_2 system. The irradiation source was black light blue fluorescence lamps (Toshiba BLB, λ_{max}=360 nm).

Four more reactors were used besides reactor A, in order to check wall effect: reactor B was 2 l-quartz cylindrical cell (S/V=0.55 cm^{-1}); reactor C was 188 ml-Pyrex cylindrical cell (S/V=1.2 cm^{-1}); reactor D was 94 ml-Pyrex long tube cell (S/V=4.0 cm^{-1}); reactor E consisted of 25.2 l-Pyrex photochemical chamber and 7.57 l-stainless steel optical absorption cell of UV-VIS spectrometer.[7]

The reaction of ·OH with 2,5-dihydrofuran in the presence of oxygen was also studied in reactors A and C with similar methods.

Photolysis of the mixture, $H_2O_2/^{18}O_2/N_2$/diolefin, was carried out several times in reactor A and isotopic product analysis was made by means of GC-MS with the same proce-

dure as for mass spectroscopic identification.

1,3-Butadienen was from Takachiho Kagaku. Acetaldehyde, acrylaldehyde, crotonaldehyde, furan, 2-methylfuran, *cis*-1,3-pentadiene, and 2,5-dihydrofuran were purchased from Tokyo Kasei. They were degassed before use by trap to trap distillation. Heavy oxygen ($^{18}O_2$, 98.6%) was obtained from Merck Frosst Canada and the purity was confirmed by means of mass spectrometer and the detected impurity was only $^{16}O^{18}O$. Research grade N_2 and O_2 were from Nippon Sanso.

Results

Typical gas chromatograms for the products in the photooxidation of either 1,3-butadiene or *cis*-1,3-pentadiene with H_2O_2 are shown in Figs. 1 and 2, respectively, together with identified compounds. It is noteworthy that Porapak Q or R could not separate acrylaldehyde and furan produced in the reaction of 1,3-butadiene. Each peak had GLC elution times, mass spectra, and infrared spectra identical with those of the respective commercial samples. The identified products under our experimental conditions were furan (C_4H_4O), and acrylaldehyde (C_2H_3CHO) in the reaction of 1,3-butadiene (C_4H_6) and 2-methylfuran (C_5H_6O), acetaldehyde (CH_3CHO), acrylaldehyde, and crotonaldehyde (C_3H_5CHO) in the reaction of *cis*-1,3-pentadiene (C_5H_8).

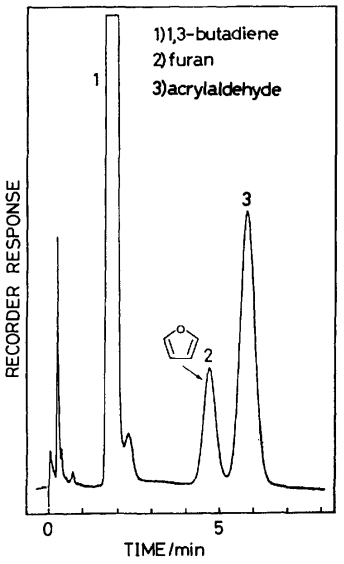

Fig. 1. Typical gas chromatogram of the products in the photolysis of the mixture, H_2O_2[1.0 Torr]/1,3-butadiene[0.4 Torr]/O_2[760 Torr], at 254 nm.

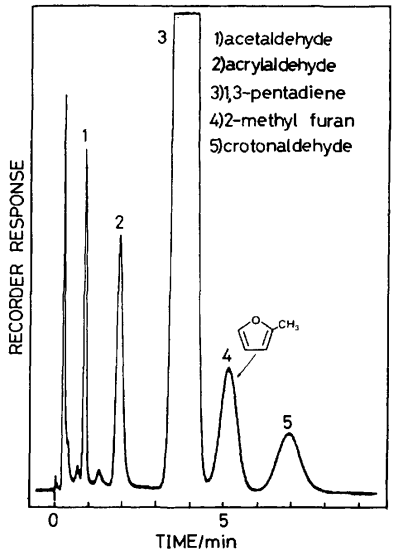

Fig. 2. Typical gas chromatogram of the products in the photolysis of the mixture, H_2O_2[1.0 Torr]/*cis*-1,3-butadiene[0.3 Torr]/O_2[760 Torr], at 254 nm.

For the reaction systems in which H_2O_2 was used as radical source, the reaction cell was kept in the dark after a few minutes irradiation and the concentration of products were measured intermittently. It was observed that furan and 2-methylfuran increased gradually until about 50 min after a few minutes irradiation, while aldehydes remained almost constant (Fig. 3). The yield of furans was determined after the cease of the formation in the dark and the yield of other compounds was determined from the first injection to GC about 30 s after turning off the lamps. For the runs at low pressures, nitrogen was filled upto 760 Torr just after photolysis and gas chromatographic analysis was made. Since it was noticed that furans yield became somewhat larger as the conditioning of the wall surface of reaction cell was improved by repeating the experiments, these series of runs were made after conditioning the surface of the reactor A well. The product yield obtained with various initial conditions is presented in Table 1 for the 1,3-butadiene system and in Table 2 for the *cis*-1,3-pentadiene system. The increase of furan after the photolysis observed for Runs 1 to 6 in Table 1 is shown in Fig. 3. Product yield at 760 Torr total pressure was almost independent of the variation of the initial concentrations of reactants, or of the addition of one of products. But pressure effect was observed: at low total pressure around 2.5 Torr, the yield of furans increased and that of aldehydes decreased (Tables 1 and 2). The difference observed in the pressure effect indicates that some fraction of furan and 2-methylfuran, at least, was not formed *via* initial ·OH addition to the double bonds.

Figure 4 shows the product yield after 1.5 min irradiation of the mixture CH_3ONO [1.0 Torr]/1,3-butadiene [0.27 Torr]/O_2 [760 Torr] in comparison

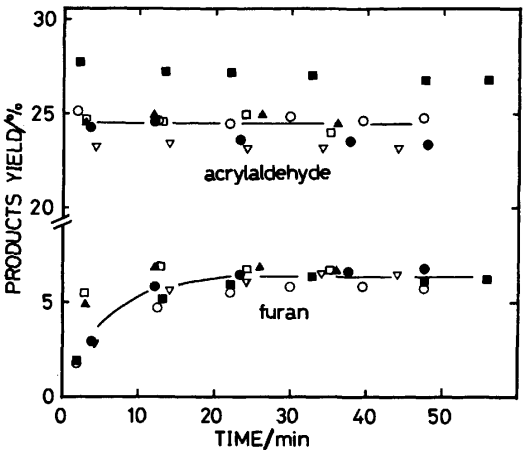

Fig. 3. Dark increase of furan after 1.5—3.0 min irradiation of the mixture H_2O_2/1,3-butadiene/O_2 for Runs 1 to 6 in Table 1.

TABLE 1. PRODUCTS YIELD IN THE PHOTOLYSIS OF H_2O_2/1,3-BUTADIENE/O_2 WITH DIFFERENT INITIAL CONDITIONS

Run	Irrad. time / min	Reactants (Torr)				P_t	Products yield/%	
		C_4H_6	H_2O_2	O_2	Added gas		C_4H_4O	C_2H_3CHO
1	1.5	.407	1.0	1.1	—	760	5.55	25.2
2	1.5	.409	1.0	1.1	—	760	6.18	27.8
3	1.5	.361	1.0	759	—	760	6.59	23.4
4	1.5	.368	1.0	759	—	760	6.68	24.4
5	3.0	1.38	1.0	758	—	760	6.50	23.2
6	3.0	1.39	1.0	758	—	760	6.96	23.5
7	1.5	.404	1.0	1.1	Acrl[a], .341	760	7.19	—
8	1.5	.401	1.0	1.1	Acrl[a], .341	760	7.40	—
9	3.0	.381	.48	1.1	—	760	7.53	29.6
10	3.5	.399	.47	1.1	—	760	7.62	27.9
11	1.5	.306	1.0	1.1	—	2.4	10.5	20.6
12	1.5	.314	1.0	1.1	—	2.4	11.4	21.1

a) Acrylaldehyde.

TABLE 2. PRODUCTS YIELD IN THE PHOTOLYSIS OF H_2O_2/*cis*-1,3-PENTADIENE/O_2 WITH DIFFERENT INITIAL CONDITIONS

Run	Irrad. time / min	Reactants (Torr)					Products yield/%			
		C_5H_8	H_2O_2	O_2	Added gas	P_t	C_5H_6O	CH_3CHO	C_2H_3CHO	C_3H_5CHO
1	2.0	.322	1.0	759	—	760	7.12	13.2	12.2	8.33
2	2.0	.315	1.0	759	—	760	8.45	14.8	13.3	10.1
3	2.0	3.59	1.0	755	—	760	8.11	12.2	13.2	10.3
4	2.0	1.89	1.0	757	—	760	6.84	11.9	12.3	9.87
5	2.0	.340	1.0	9.0	—	760	8.85	15.9	14.6	11.4
6	2.0	.342	1.0	9.0	—	760	9.39	16.4	14.5	11.8
7	3.5	.306	.48	9.0	—	760	9.25	16.7	14.2	9.80
8	3.0	.299	.44	9.0	—	760	9.13	17.4	14.6	11.7
9	2.0	.330	1.0	9.0	Acet,[a] .371	760	13.1	—	14.2	12.4
10	3.0	.330	1.0	9.0	Acet, .428	760	11.4	—	13.0	10.8
11	3.0	.332	1.0	9.0	Acrl, .540	760	9.88	19.2	—	9.12
12	2.5	.336	1.0	9.0	Acrl, .337	760	10.4	17.2	—	9.81
13	3.0	.330	1.0	8.5	Crot, .455	760	11.1	—	16.9	—
14	3.0	.330	1.0	8.5	Crot, .418	760	9.92	—	15.9	—
15	2.0	.367	1.0	1.2	—	2.6	10.3	8.44	8.79	6.54
16	3.0	.367	1.0	1.2	—	2.6	9.71	9.41	9.63	7.33

a) Acet=acetaldehyde, Acrl=acrylaldehyde, Crot=crotonaldehyde.

with the results for the mixture H_2O_2 [1.0 Torr]/1,3-butadiene [0.3 Torr]/O_2 [760 Torr]. It was noticed that the yield of acrylaldehyde was larger and the increase of furan in the dark was faster in the CH_3ONO system than in the H_2O_2 system and that 1,3-butadiene was consumed by NO_2 in the dark. The addition of a proper amount of NO to the CH_3ONO system made the increase of furan in the dark stop and the consumption of 1,3-butadiene in the dark more significant. These facts indicate that some peroxy radicals exist as intermediate compounds to form furan.

In order to examine the wall effect on the reaction, product yield for both ·OH sources in different five reactors were measured and summarized in Tables 3 and 4, for the 1,3-butadiene and for the *cis*-1,3-pentadiene systems, respectively. Irradiation was usually 1 to 2 min for the runs in reactors A to D, and it was 10 to 15 min in reactor E. In the latter case, the yield was corrected by considering the consumption of the diolefins with the dark reactions of NO_2 in CH_3ONO system. The yield of CH_3CHO in CH_3ONO/*cis*-1,3-pentadiene system was lower limit, since the peak of CH_3CHO was on the shoulder of large peak of CH_3ONO in gas chromatogram and the peak height of CH_3CHO was measured from the higher valley rather than ambiguous lower valley. Throughout this series, wall surface was kept rather clean without repeating extra runs. The results showed that the yield of furan and 2-methylfuran was almost independent of the surface material of the reactors or the surface to volume ratio of reactors, or ·OH radical sources, whereas aldehydes yield in the CH_3ONO system was larger than that in the H_2O_2 system. Larger yield of acrylaldehyde in the photolysis of CH_3ONO/1,3-butadiene may be attributed to the faster reaction of NO with peroxy radicals to produce alkoxy radicals which are the precursors of acrylaldehyde than the reactions between some peroxy radicals to lead unspecified products. Since no definite dependence of the yield of furans on S/V of reactors was measured, the discrepancy of the yield in the clean reactor (Tables 3 and 4) and well conditioned reactor (Tables 1 and 2) may be attributed to other reasons: for example, conditioning of the surface would suppress

the wall decay of the intermediate working as reservoir of the precursor radicals of furans.

Results for several isotopic labeling experiments with heavy oxygen are summarized in Tables 5 and 6 for the photolysis of H_2O_2/1,3-butadiene/$^{18}O_2$/N_2 and H_2O_2/*cis*-1,3-pentadiene/$^{18}O_2$/N_2 respectively. Before and after the photolysis, a small fraction of the reaction mixture in the reactor was analyzed by mass spectrometer. Oxygen-16 molecule was not detected in the mixture before the irradiation, and very small amount of $^{16}O_2$ (less than 5%) was detected after the photolysis in some runs. Addition of NO changed the ratio of labeled aldehyde, but the yield for labeled furans was not affected.

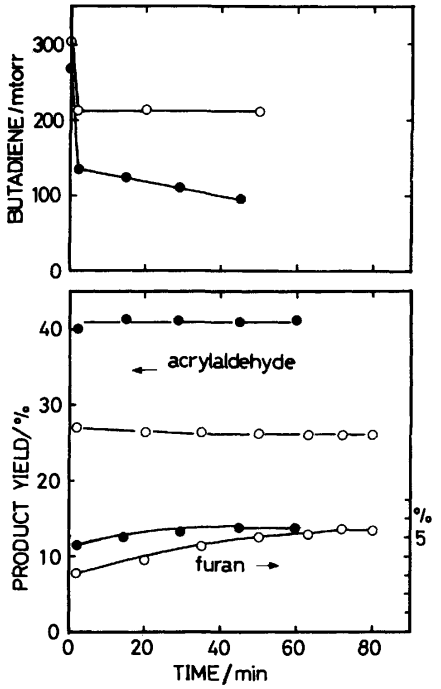

Fig. 4. Difference in the dark reactions after 1.5 min irradiation at 360 nm of the mixture of CH_3ONO[1.0 Torr]/1,3-butadiene[0.27 Torr]/O_2 [760 Torr], (closed circle) and after 1.5 min irradiation at 254 nm of the mixture of H_2O_2[1.0 Torr]/1,3-butadiene[0.30 Torr]/O_2[760 Torr], (open circle).

Discussion

Detection of both ^{18}O-aldehydes and ^{16}O-aldehydes suggests that ·OH addition to nonterminal double-bond carbon atom also occurs as well as to the terminal carbon atom against the assumption of the occurrence of only terminal addition by Maldotti *et al.*[3] In view of the low yield of the detected products, undetected products by our method, such as hydroxy ketones, hydroxy aldehydes and other compounds, might be produced. As an example, possible ·OH addition steps to 1,3-butadiene are shown in Reactions 4 and 5 (O* indicates ^{18}O).

$$C{=}C{-}C{=}C + OH \rightarrow C(OH){-}C{-}C{=}C \xrightarrow{O_2^*} CH_2O + C_2H_3CHO^* \quad (4)$$

$$\rightarrow \text{unspecified products}$$

$$C{-}C(OH){-}C{=}C \xrightarrow{O_2^*} CH_2O^* + C_2H_3CHO \quad (5)$$

$$\rightarrow \text{unspecified products}$$

Table 3. Products yield in the photolysis of OH with 1,3-butadiene in different reactors

Reactor[a]	Reactants[b] (Torr)			Products yield/%	
	C_4H_6	CH_3ONO	H_2O_2	C_4H_4O	C_2H_3CHO
A	.286	.25	—	6.51	41.8
A	.283	.78	—	5.61	38.2
B	.267	.83	—	5.80	42.5
B	.272	.86	—	5.67	39.5
C	.300	.40	—	5.04	37.0
C	.341	.65	—	5.12	32.9
D	.361	.62	—	5.28	33.2
E	.412	.24	—	4.00	32.4
E	.476	.08	—	5.70	54.3
A	.303	—	1.0	5.47	26.1
A	.285	—	1.0	4.91	25.6
B	.302	—	0.9	4.92	23.4
B	.277	—	0.7	5.40	25.2

a) See the Experimental section in the text.
b) Oxygen was added up to 760 Torr.

Table 4. Products yield of the reaction of OH with *cis*-1,3-pentadiene in different reactors

Reactor[a]	Reactants[b] (Torr)			Products yield/%			
	C_5H_8	CH_3ONO	H_2O_2	C_5H_6O	CH_3CHO	C_2H_3CHO	C_3H_5CHO
A	.204	.90	—	6.57	>18.2	17.4	9.89
A	.224	.57	—	7.32	>16.2	17.4	8.27
B	.206	.97	—	7.70	>12.0	19.7	13.5
B	.188	1.6	—	7.57	>16.3	18.5	11.3
C	.226	.55	—	5.62	>14.4	16.2	9.73
C	.261	.65	—	5.89	>15.1	17.2	9.04
D	.271	.67	—	6.01	>11.7	16.0	6.09
E	.340	.07	—	5.04	>18.0	19.2	9.00
E	.501	.27	—	5.50	>20.0	21.0	9.60
A	.291	—	1.0	4.72	14.0	13.0	8.45
A	.309	—	1.0	6.32	15.7	12.9	8.30
B	.321	—	0.8	5.96	14.7	13.2	8.61
B	.347	—	0.8	6.38	15.7	14.2	10.5

a) See the Experimental section in the text. b) Oxygen was added up to 760 Torr.

TABLE 5. ISOTOPIC PRODUCTS ANALYSIS OF THE PHOTOLYSIS OF 1,3-BUTADIENE/H_2O_2/$^{18}O_2$/N_2 AT 760 Torr

Run	Irrad. time / min	Reactants (Torr)				^{18}O-Products ratio/%	
		C_4H_6	H_2O_2	$^{18}O_2$	Added gas	C_4H_4O	C_2H_3CHO
1	27	.217	1.4	9.6	—	32	78
2	25	.180	0.9	>9.0	—	38	83
3	15	1.06	1.0	>8.2	—	37	90
4	20	1.08	1.0	8.0	NO, .262	44	49

a) [^{18}O-product]/([^{18}O-product]+[^{16}O-product])×100.

TABLE 6. ISOTOPIC PRODUCTS ANALYSIS OF THE PHOTOLYIS *cis*-1,3-PENTADIENE/H_2O_2/$^{18}O_2$/N_2 AT 760 Torr

Run	Irrad. time / min	Reactants (Torr)				^{18}O-Products ratio/%[a)]			
		C_5H_8	H_2O_2	$^{18}O_2$	Added gas	C_5H_6O	CH_3CHO	C_2H_3CHO	C_3H_5CHO
1	22	2.03	1.3	9.9	—	42	25	78	80
2	25	0.49	1.0	>8.7	—	48	18	83	80
3	15	0.53	1.0	>8.3	NO, .083	40	19	67	42
4	21	0.36	1.1	8.6	NO, .262	38	9	36	56

a) [^{18}O-product]/([^{18}O-product]+[^{16}O-product])×100.

Formation of ^{16}O-furan and ^{18}O-furan in isotopic labeling experiments suggests that two pathways for the formation of furans at least exist. Furan (C_4H_4O) has two less hydrogen atoms than the parent molecule, 1,3-butadiene(C_4H_6), and also *cis*-1,3-pentadiene (C_5H_8) must lose two hydrogen to form 2-methylfuran (C_5H_6O). The fact that the pressure effect on the formation of furans was observed adversely to the pressure effect on the formation of aldehydes indicates that the ways of initial attack to diolefins by ·OH were different for the two processes. Furthermore, the fact that the addition of NO changed the ratios of ^{18}O labeled aldehydes significantly but did not affect those for furans suggests that the precursors for ^{18}O-furan might be consumed by single pathway without competitive reactions to lead other products. Therefore, it is reasonable to assume that one of the terminal vinyl-hydrogen was abstracted by ·OH radicals in the first step and, then, $^{18}O_2$ added to the unpaired elctron on the radicals and that through some radical-radical reactions, an alkoxy radical, ·R in Scheme 1, was formed. The radical was stabilized by resonance as shown in Scheme 1, and a new bond would be formed between the two radical centers to make furan rings.

Some semi-quantitative discussions on the abstraction pathway in diolefins are tried by comparing with the abstraction pathway in ethylene and benzene. Average yield of furan determined from the runs at 760

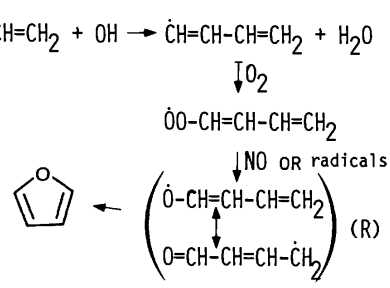

Scheme 1.

Torr without added gas (Runs 1—6 in Table 1) was 6.7% and that of 2-methylfuran was 8.4% from Runs 1—8 in Table 2. And average mixing ratio of labeled furan was 38% from Table 3 and that of labeled 2-methylfuran was 42% from Table 4. Thus, the abstraction of vinyl-hydrogen in 1,3-butadiene occurred 2.5% (=6.7×0.38) of the time and the abstraction in *cis*-1,3-pentadiene occurred 3.5% of the time. This fairy larger contribution of the abstraction pathway to the overall rate constants was surprising. Overall rate constants for the reaction of ·OH with 1,3-butadiene[8] and *cis*-1,3-pentadiene[4] were 68.5×10^{-12}, 103×10^{-12} cm^3 mol^{-1} s^{-1}, respectively. The assigned rate constants for the abstraction of the vinyl-hydrogen were 1.7×10^{-12} (= $68.5\times10^{-12}\times0.025$) and 3.6×10^{-12} cm^3 mol^{-1} s^{-1}, respectively. The contribution of the abstraction of one vinyl-hydrogen in 1,3-butadiene was 4.3×10^{-13} (=$1.7\times10^{-12}/4$) cm^3 mol^{-1} s^{-1}, which is larger than the contribution of the abstraction of a primary C-H bond in alkane by a factor of 6.6,[1] whose bond dissociation energy (BDE) is 98 kcal mol^{-1} (1 cal=4.18 J) and smaller than BDE of C_4H_5-H. Concerning the abstraction of vinyl-hydrogen in ethylene by ·OH, which is exothermic by 11 kcal mol^{-1},[9] two different views have been proposed: BDE(H-C_2H_3)=108, BDE(H-OH) 119 kcal mol^{-1}. Meagher and Heicklen[10] reported that the hydrogen abstraction reaction contributed 26% of the total reaction pathway under their experimental conditions from the analysis of the formic acid yield. However, Atkinson *et al.*[1] concluded that the contribution of the abstraction was very minor in consideration of the comprehensive product study of the reaction of ·OH with propylene by Cevetanovic[11] and the rate constant study of Howard:[12] Howard has shown from a determination of the absolute rate constant for the reaction of ·OH with ethylene over the total pressure range of 0.7—7 Torr of helium, that abstraction of vinyl-hydrogen at room temperature is implied to be negligible, because the rate constant for

ethylene extrapolates to essentially zero at zero pressure. As for hydrogen abstraction by ·OH radicals in benzene, Perry *et al.*[13] reported that the occurrence of the reaction was 1—8% of the time from the study on the temperature dependence of the rate constant. Carbon–hydrogen bond energy in benzene is 110.5 kcal mol^{-1}.[9] If we assume the bond energy of C–H in 1,3-butadiene similar to that in ethylene and benzene, the observed value in 1,3-butadiene appeared to be larger than that expected from the previous works. However, the detection of labeled furans evidently suggests the occurrence of the abstraction of vinyl-hydrogen by ·OH radicals in 1,3-butadiene and *cis*-1,3-pentadiene. But it is obviously necessary to detect directly the abstracted radicals (C_4H_5· and C_5H_7·) by means of more sophisticated techniques, such as flow system coupled to photoionization mass spectrometer.

The mechanism for the formation of ^{16}O-furanes remains unclear in this work. But it is reasonable to assume that ^{16}O came from ·OH radicals and ·OH–diolefin adducts were precursors for furans, since H_2O_2 did not react with the studied conjugated dienes in the dark.

The increase of furans in the dark after irradiation may be attributed to the decomposition of some complexes formed by reversible recombination reactions of peroxy radicals. Benson described[14] that usual alkyl radicals would irreversibly combine with oxygen molecule to become peroxy radicals followed by some reactions to form oxygen containing compound *via* some complexes of peroxy radicals. He also suggested[14] that unsaturated resonance-stabilized radicals, such as allyl and benzyl radicals, would have much smaller equilibrium constant in the combination reaction with O_2, and that back reaction might become important. In the reaction systems studied here, the unsaturated resonance-stabilized radicals, ·R in Scheme 1, and/or other unknown precursors of ^{16}O-furan would combine to form some metastable compound as reserviors for radicals, and, after turning off the lamps, the metastable complex would decompose to produce the initial radicals or the other precursors.

In order to support this assumption, similar size resonance-stabilized radicals were produced and it was examined whether the increase of the products in the dark was observed or not: the reaction of ·OH with 2,5-dihydrofuran (DHF) in the presence of oxygen was studied. DHF has four labil allylic hydrogens for ·OH attack to form radical ·Q in Reaction 6. The radical ·Q is expected to be stabilized by resonance and to lose another hydrogen by O_2 to ultimately form furan (Reaction 7).

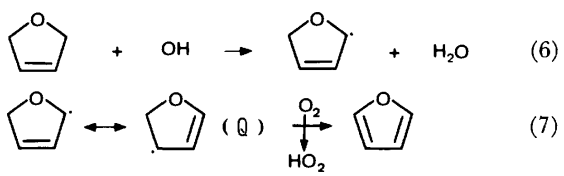

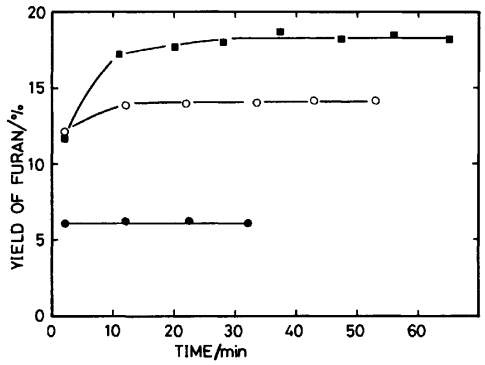

Fig. 5. Dark increase of furan after 1.5 min irradiation of 2,5-dihydrofuran (DHF): initial concentrations (torr): DHF, 0.19; H_2O_2, 1.0; O_2, 760 (closed squares): DHF, 0.32; CH_3ONO, 0.82; O_2, 760 (open circles): DHF, 0.35; CH_3ONO, 0.76; NO, 0.05; O_2, 160; N_2, 600 (closed circle).

By use of a similar procedure used for 1,3-butadiene, the mixture, H_2O_2[1.0 in Torr]/DHF[0.19]/O_2[760], CH_3ONO[0.82]/DHF[0.32]/O_2[760], and NO[0.05]/CH_3ONO[0.76]/DHF[0.35]/O_2[160]/N_2[600], were photolyzed. The detected product under this gas chromatographic condition was only furan. The plots of the yield of furan *vs.* time are shown in Fig. 5. Furan showed increase in the dark after 1.5 min irradiation in the absence of NO, similar to the reactions of the diolefins. However, the addition of NO to the mixture, CH_3ONO/DHF, before the irradiation suppressed the increase of furan in the dark. Thus, the increase of furan in the dark may be explained by the similar assumption that some fraction of ·Q combined with O_2 to form ·QO_2 and that the ·QO_2 radicals were stored as some metastable complexes with fairy large lifetime and, then, the complex decomposed to ·QO_2 and supplied ·Q in the system to form furan even in the dark *via* Reaction 7. Addition of NO to the mixture made ·QO_2 quenched to ·QO to lead other unspecified products. Therefore, it is reasonable to assume that some unsaturated resonance-stabilized radicals consisting of four carbon and an oxygen atom form some metastable compound in the presence of oxygen whose lifetime is in the order of minutes in our reactors. Spectroscopic technique will be able to detect the complexes.

Ring formation from the reaction of 1,3-butadiene with sulfur atoms,[15] and nitrogen atoms[16] were reported. The formation of thiophene was proposed to proceed mainly *via* sulfur atom addition in the 1,2-positions and lose two hydrogens unimoleculary.[15] The formation mechanism of pyrrole was not presented in the paper.[16] Furan was not detected in the reaction of oxygen atoms (^3P) with 1,3-butadiene.[17] There still remain uncertainties in the mechanism for the formation of furan type compound from the reactions of radicals with 1,3-butadiene.

I wish to thank Drs. Hajime Akimoto and Shiro Hatakeyama for very helpful discussions and Dr. Isao Mizoguchi for encouragement.

Reference

1) R. A. Atkinson, K. R. Darnall, A. L. Lloyed, A. M. Winer, and J. N. Pitts, Jr., *Adv. Photochem.*, **11**, 375 (1979).
2) W. A. Glasson and C. S. Tuesday, *Environ. Sci. Technol.*, **4**, 752 (1970).
3) A. Maldotti, C. Chiorboli, C. A. Bignozzi, C. Bartocci, and V. Cardssiti, *Int. J. Chem. Kinet.*, **12**, 905 (1980).
4) T. Ohta, *J. Phys. Chem.*, **87**, 1209 (1983).
5) R. Atkinson, W. P. L. Carter, A. M. Winer, and J. N. Pitts, Jr., *J. Air Poll. Control Assoc.*, **31**, 1090 (1981).
6) R. Atkinson, S. M. Ashmann, A. M. Winer, and J. N. Pitts, Jr., *Int. J. Chem. Kinet.*, **14**, 507 (1982).
7) T. Ohta and I. Mizoguchi, *Environ. Sci. Technol.*, **15**, 1229 (1981).
8) R. Atkinson, R. A. Perry, and J. N. Pitts, Jr., *J. Chem. Phys.*, **67**, 3170 (1977).
9) S. W. Benson, "Thermochemical Kinetics," 2nd ed, Wiley, New York, (1976).
10) J. F. Meagher and J. Heicklen, *J. Phys. Chem.*, **80**, 1645 (1976).
11) R. J. Cvetanovic, 12th Int. Symp. Free Radicals. Laguna Beach, Cali., Jan 4—9 (1976).
12) C. J. Howard, *J. Chem. Phys.*, **65**, 4471 (1976).
13) R. A. Perry, R. A. Atkinson, and J. N. Pitts, Jr. *J. Phys. Chem.*, **81**, 296 (1977).
14) S. W. Benson, *J. Am. Chem. Soc.*, **87**, 972 (1965).
15) K. S. Sidhu, E. M. Lown, O. P. Strausz, and H. E. Gunning, *J. Am. Chem. Soc.*, **88**, 254 (1966).
16) A. Tsukamoto and N. N. Lichitin, *J. Am. Chem. Soc.*, **84**, 1601 (1962).
17) J. J. Havel, and K. H. Chan, *J. Org. Chem.*, **39**, 2439 (1974).

 © 1984 The Chemical Society of Japan Bull. Chem. Soc. Jpn., 57, 967—971 (1984)

Mixed Adsorbed Film of 2-(Octylsulfinyl)ethanol with Decylammonium Chloride at Water/Air Interface

Shozo URYU,† Makoto ARATONO,* Michio YAMANAKA, Kinsi MOTOMURA, and Ryohei MATUURA

Department of Chemistry, Faculty of Science, Kyushu University 33, Higashi-ku, Fukuoka 812

†*Chikushigaoka High School, 2-13-1 Noma, Minami-ku, Fukuoka 815*

(Received November 2, 1983)

The surface tension of the aqueous solution of 2-(octylsulfinyl)ethanol and decylammonium chloride mixture has been measured by changing the total molality and composition of surfactants at 298.15 K under atmospheric pressure. It has been observed that the surface tension decreases with increasing the total molality at a constant composition and with decreasing the composition of decylammonium chloride at a constant total molality. Further the surface tension *vs.* total molality curve has been found to have a break point at a relatively low concentration. The thermodynamic equations have been developed so as to be applicable to the adsorption of nonionic-ionic mixture and used to calculate the surface density and the surface composition. It has been shown that the surface density *vs.* molality curve has the discontinuous change caused by the transition from a gaseous to an expanded film. By drawing the two-dimensional phase diagram and comparing it with the diagrams of the ionic-ionic surfactant mixtures, it has been proved that the shape of the phase diagram is affected greatly by the difference in the surface activity between the two surfactants.

The adsorption at water/air interface in a relatively dilute concentration region has been investigated in our laboratory for various types of surfactants[1,2] and cationic–cationic surfactant mixtures such as dodecylammonium chloride (DAC)–decylammonium chloride (DeAC)[3] and dodecyltrimethylammonium chloride (DTAC)–DeAC.[4] It has been observed that the surface tension *vs.* concentration curve has a break point at which a gaseous and an expanded film coexist in equilibrium. As for the ionic surfactant mixtures, we have derived the relation between compositions of the adsorbed film and the bulk phase and shown that the phase diagrams are useful in describing the miscibility of surfactants and phase transition in the mixed adsorbed films. Some studies on cationic–nonionic surfactant mixtures have been carried out from the viewpoints of their mixed micelle formation[5,6] or of their adsorption at water/air interface.[7] In the present study, 2-(octylsulfinyl)ethanol (OSE) is used as the nonionic surfactant for the following reasons; (a) the synthesis and purification of OSE is relatively easy,[8] (b) the adsorption behavior of OSE in the dilute concentration region has been already reported[2] and (c) information about the solution properties of OSE is available.[9,10] By measuring the surface tension of the aqueous solution of OSE–DeAC mixture and applying the thermodynamic equations, which are developed in the present paper, we consider the adsorption of surfactant mixtures from their aqueous solution at the solution/air interface.

Experimental

2-(Octylsulfinyl)ethanol and decylammonium chloride were synthesized and purified by the methods described previously.[1,11] Their purities were checked by the elementary analysis and guaranteed by the absence of minimum near their critical micelle concentration of the surface tension *vs.* concentration curves at 298.15 K. Water was triply distilled from alkaline permanganate solution. The surface tension was measured by the drop volume technique described in our previous paper.[1] The temperature was kept constant at 298.15 K by immersing the measuring cell in a thermostated water bath. The error estimated for the surface tension value was less than 0.05 mN m^{-1}.

Results and Discussion

It has been shown that the total molality of surfactants m and the composition of the second surfactant X_2 in the aqueous solution are the suitable thermodynamic independent variables to describe the adsorption behavior of surfactant mixture at constant temperature T and pressure p.[3,4] Here m and X_2 are defined as

$$m = m_1 + m_2, \tag{1}$$

and

$$X_2 = m_2/(m_1 + m_2), \tag{2}$$

where the subscripts 1 and 2 refer to 2-(octylsulfinyl)ethanol and decylammonium chloride, respectively. The surface tension γ of the aqueous solution of surfactant mixture was measured as a function of m at various X_2 values at 298.15 K under atmospheric pressure.

Figure 1(a) shows the plot of γ against m at constant X_2. It is seen that each curve has a break point at a relatively high surface tension and a relatively low concentration. It is also found that the m value of the break point increases, while the corresponding γ value decreases, as X_2 increases. The detailed features are given in Fig. 1(b), in which the γ *vs.* m curves are magnified around the break points. It has been already verified that the presence of a break point on the γ *vs.* m curve results from the phase transformation between two states in the adsorbed film.[1–4] Accordingly we can say that the phase transition takes place also in the present nonionic–ionic surfactant system. Taking up the γ values at a given m value from Figs. 1(a) and 1(b), the γ *vs.* X_2 curves are obtained as shown in Fig. 2. It is seen that γ increases with increasing X_2 and some curves have the break points connected by the dotted line. It is clear that the regions above and below the dotted line correspond to

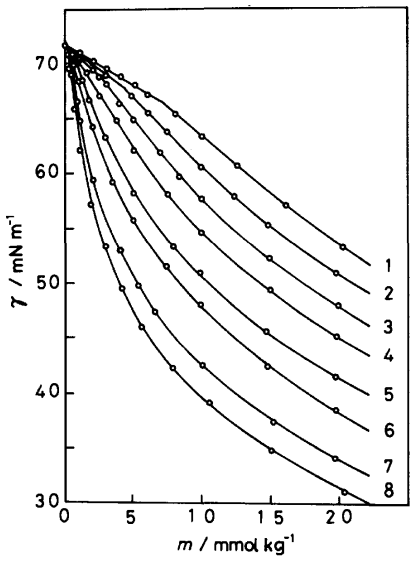

(a)

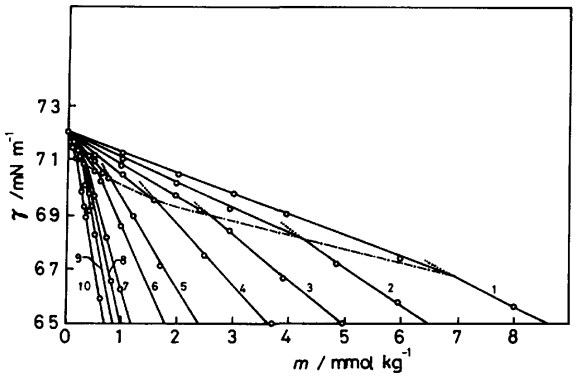

(b)

Fig. 1. (a) Surface tension *vs.* total molality curves at constant bulk composition: (1) X_2=1, (2) 0.979, (3) 0.950, (4) 0.901, (5) 0.801, (6) 0.700, (7) 0.360, (8) 0. (b) Surface tension *vs.* total molality curves at constant bulk composition: (1) X_2=1, (2) 0.979, (3) 0.950, (4) 0.901, (5) 0.801, (6) 0.700, (7) 0.496, (8) 0.360, (9) 0.200, (10) 0.

the different states in the adsorbed films. The surface tension of the phase transition point denoted by γ^{eq} is plotted against X_2 in Fig. 3. The value of γ^{eq} decreases slightly up to about 0.8 and then rapidly with increasing X_2. This behavior is undoubtedly related to the difference in the surface activity between the two surfactants as will be discussed later.

Now let us develop our thermodynamic treatment[3,4,12] so as to be applicable to the nonionic-cationic surfactant mixture. Since decylammonium chloride is a uni-uni valent strong electrolyte and 2-(octylsulfinyl)ethanol is a nonionic surfactant, the surface tension of the aqueous solution is expressed in the differential form as a function of the chemical potential of species at constant temperature and pressure:

$$d\gamma = -\Gamma_1^H d\mu_1 - \Gamma_{2+}^H d\mu_{2+} - \Gamma_{2-}^H d\mu_{2-}, \quad (3)$$

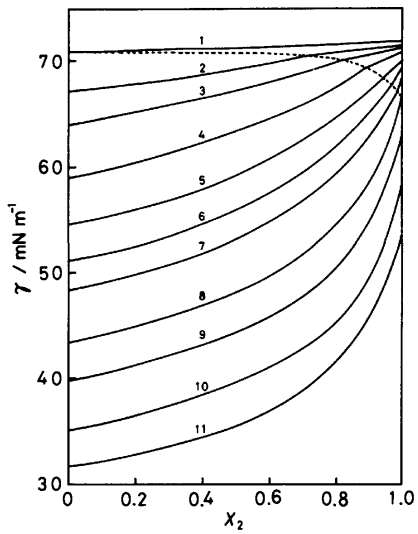

Fig. 2. Surface tension *vs.* bulk composition curves at constant total molality: (1) m=0.2 mmol kg^{-1}, (2) 0.5, (3) 0.8, (4) 1.5, (5) 2.5, (6) 3.5, (7) 4.6, (8) 7.25, (9) 10, (10) 15, (11) 20.

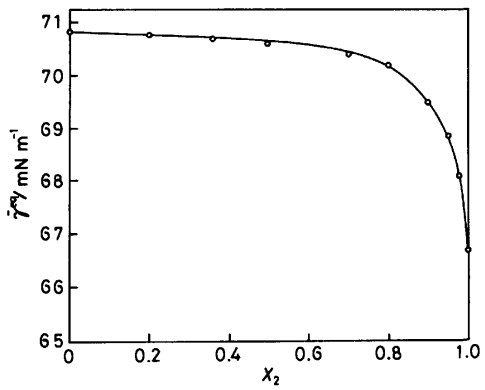

Fig. 3. Equilibrium surface tension *vs.* bulk composition curve.

where Γ_1^H, Γ_{2+}^H, and Γ_{2-}^H are the surface excess numbers of moles per unit surface area of 2-(octylsulfinyl)ethanol, decylammonium ion, and chloride ion, respectively. In Eq. 3, the surface excess quantities are defined with respect to the two dividing planes which make the surface excess numbers of moles of air and water be zero.[1,10] Taking notice that the suitable concentration variables are the total molality m and the composition X_2 defined by Eqs. 1 and 2 and assuming that the solution is ideal, Eq. 3 can be rewritten in the form

$$d\gamma = -RT[(\Gamma_1^H + 2\Gamma_2^H)/m]dm - RT[(2X_1\Gamma_2^H - X_2\Gamma_1^H)/X_1X_2]dX_2, \quad (4)$$

where Γ_2^H is the surface excess number of moles of DeAC defined by

$$\Gamma_2^H = \Gamma_{2+}^H = \Gamma_{2-}^H. \quad (5)$$

By introducing the total surface excess numbers of moles of surfactants defined by

$$\Gamma^{H} = \Gamma_1^{H} + \Gamma_2^{H} \quad (6)$$

and the composition of DeAC in the adsorbed film by

$$X_2^{H} = \Gamma_2^{H}/\Gamma^{H}, \quad (7)$$

Eq. 4 is rearranged to yield

$$d\gamma = -(RT\Gamma^{H}/m)(1+X_2^{H})dm - (RT\Gamma^{H}/X_1X_2)[(2-X_2)X_2^{H} - X_2]dX_2. \quad (8)$$

Thus we can evaluate the surface composition X_2^{H} by applying Eq. 8 to the experimental results:

$$X_2^{H} = [X_2 - (X_1X_2/m)(\partial m/\partial X_2)_{T,p,\tau}]/[(2-X_2) + (X_1X_2/m)(\partial m/\partial X_2)_{T,p,\tau}]. \quad (9)$$

The total surface density Γ^{H}, on the other hand, can be evaluated by

$$\Gamma^{H} = -[m/RT(1+X_2^{H})]/(\partial\gamma/\partial m)_{T,p,X_2}. \quad (10)$$

It should be noted that the value of Γ^{H} cannot be directly calculated from the derivative of γ with respect to m without knowing the values of X_2^{H} given by Eq. 9. This point is essentially different from the adsorption of ionic-ionic surfactant mixtures.

Let us first evaluate the composition of surfactants in the adsorbed film at constant T, p, and γ. Apply ing Eq. 9 to the m *vs.* X_2 curve shown by the full line in Fig. 4, which is obtained from Fig. 1(a), the value of X_2^{H} can be calculated numerically. The resulting m *vs.* X_2^{H} is depicted by the chain line in Fig. 4. Such a diagram gives us the relation between X_2^{H} and X_2 at a given value of γ. It is worth noting that the value of X_2^{H} is always smaller than the corresponding one of X_2. This implies that the difference in the surface activities between surfactants has a great influence on the surface composition. The diagrams 1 and 3, which are the ones for the gaseous and expanded films, respectively, have a shape essentially similar to each other, though the former is a deflated cigar type and the latter a swollen cigar one. When the phase transition takes place in the adsorbed film, the shape becomes more complicated as shown in Fig. 4 (diagram 2); the m *vs.* X_2 curve has a break point indicated by A and correspondingly the m *vs.* X_2^{H} curve changes discontinuously from the value of the gaseous film $X_2^{H,g}$ (point B) to that of the expanded film $X_2^{H,e}$ (point C). It is also seen that $X_2^{H,g}$ has a larger value than $X_2^{H,e}$, which is closely related to the variation of γ^{eq} with X_2 given in Fig. 3.[4] The present results are qualitatively akin to those of our previous ionic-ionic surfactant mixtures, but the diagrams are somewhat swollen compared with those of DAC-DeAC and DTAC-DeAC systems.[3,4] This suggests that OSE is more surface active than DTAC and DAC.

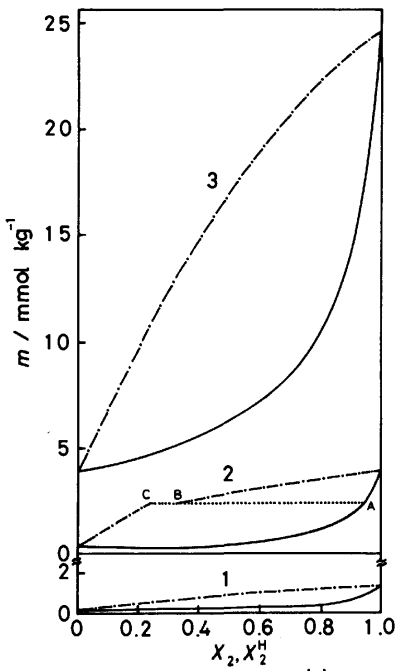

Fig. 4. Total molality *vs.* composition curves at constant surface tension: (1) γ=71 mN m^{-1}, (2) 69, (3) 50; (——) m *vs.* X_2, (-·-) m *vs.* X_2^{H}.

Now the values of Γ^{H} can be evaluated numerically by applying Eq. 10 to the experimental γ *vs.* m curves shown in Fig. 1(a) and using the X_2^{H} values calculated above. In Fig. 5 are drawn the Γ^{H} *vs.* m curves at various X_2 values. As is expected from Fig. 1, the value of Γ^{H} increases monotonously with m and changes discontinuously at the m value corresponding to the break point in Fig. 1. It is seen that the Γ^{H} value of OSE (X_2=0) is fairly large compared with that of DeAC (X_2=1). Taking account of the fact that the hydrocarbon chain length of OSE is shorter than that of DeAC, we can say that the repulsive force among the charged head groups of DeAC considerably diminishes its adsorption. Picking up the values of Γ^{H} at fixed m values in Fig. 5, the Γ^{H} *vs.* X_2 curves are depicted in Fig. 6. It is interesting to note that the variation of Γ^{H} with X_2 is considerably pronounced when X_2 is close to unity. Further, it is seen that the Γ^{H} value is nearly constant up to X_2=*ca.* 0.7 and then decreases suddenly with increase in X_2 at a high total concentration. This fact suggests that the OSE molecules play a predominant role in the adsorption behavior until the value of X_2 becomes considerably large because the surface activity of OSE is fairly high compared with that of DeAC.

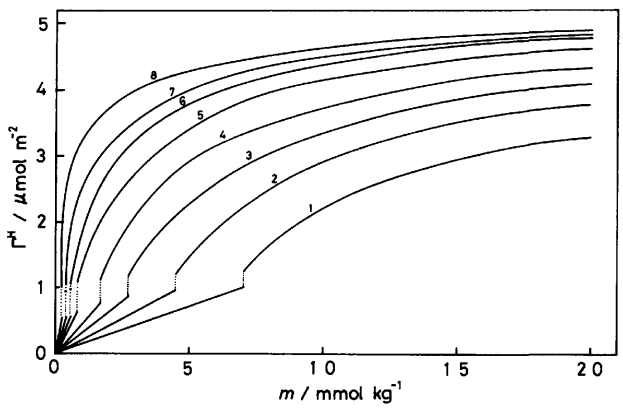

Fig. 5. Total surface density *vs.* total molality curves at constant bulk composition: (1) X_2=1, (2) 0.979, (3) 0.950, (4) 0.901, (5) 0.801, (6) 0.700, (7) 0.496, (8) 0.

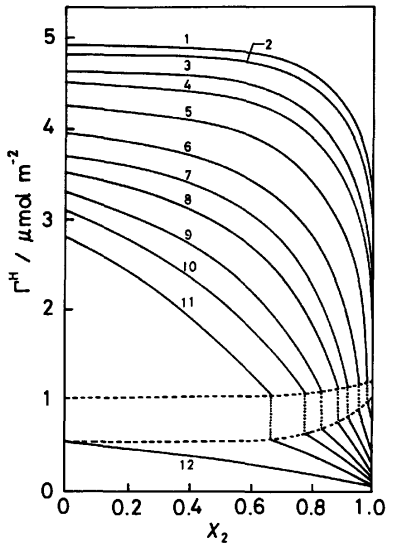

Fig. 6. Total surface density *vs.* bulk composition curves at constant total molality: (1) m=20 mmol kg^{-1}, (2) 15, (3) 10, (4) 8, (5) 5, (6) 3, (7) 2, (8) 1.5, (9) 1, (10) 0.75, (11) 0.5. (12) 0.2.

To make sure that the phase transition of the mixed adsorbed film takes place from a gaseous to an expanded state like those of pure OSE and DeAC films[2] and to get an insight into the film behavior, the surface pressure Π *vs.* the mean area per adsorbed molecule A curves are useful. Π and A are respectively defined by

$$\Pi = \gamma^0 - \gamma, \tag{11}$$

and

$$A = 1/N_A\Gamma^H, \tag{12}$$

where γ^0 is the surface tension of pure water and N_A is the Avogadro's number. By making use of Figs. 1 and 5, the Π *vs.* A curves at constant X_2 in Fig. 7 are obtained. It is seen that the shapes of the curves are similar to each other and vary regularly from the shape of OSE to that of DeAC. This proves that the phase transition of the mixed adsorbed films takes place from the gaseous to the expanded state.

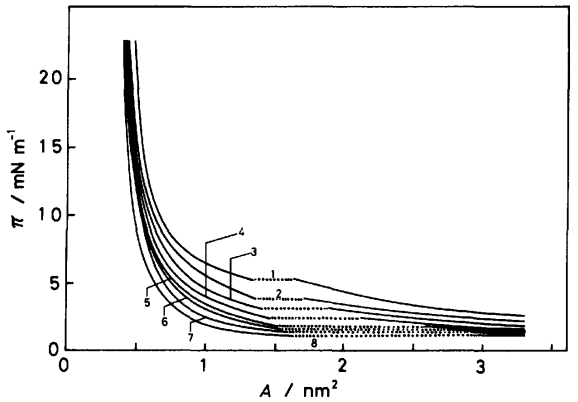

Fig. 7. Surface pressure *vs.* mean area per molecule curves at constant bulk composition: (1) X_2=1, (2) 0.979, (3) 0.950, (4) 0.901, (5) 0.801, (6) 0.700, (7) 0.496, (8) 0.

For mixed insoluble films spread on water, the Π *vs.* A curves are depicted under the condition that the film composition is kept constant. For mixed adsorbed films, the corresponding curves can be drawn; the results are shown in Fig. 8. Comparing Fig. 8 with Fig. 7, we notice that the dependence of the isotherm on the composition is more regular when X_2^H is kept constant. Further it is important to note that the equilibrium transition pressure γ^{eq} between the gaseous and expanded films increases with decreasing A in Fig. 8 while it is constant in Fig. 7.

We have previously shown[3,4] that the phase transition between the gaseous and expanded states of the mixed adsorbed film can be well described by the plots of γ^{eq} against the compositions of the gaseous film $X_2^{H,g}$ and the expanded film $X_2^{H,e}$ corresponding to the two-dimensional phase diagram used commonly in the study of mixed insoluble monolayers.[13] The numerical values of $X_2^{H,g}$ and $X_2^{H,e}$ can be obtained from the diagram 2 in Fig. 4 and the analogous ones at other γ^{eq} values; the phase diagram is illustrated in Fig. 9. The areas above the γ^{eq} *vs.* $X_2^{H,g}$ curve and below the γ^{eq} *vs.* $X_2^{H,e}$ curve correspond to the region of the gaseous and the expanded phase, respectively. It turns out that the value of $X_2^{H,e}$ is smaller than that of $X_2^{H,g}$ over the whole range. This observation is the same as that obtained for the ionic-ionic surfactant

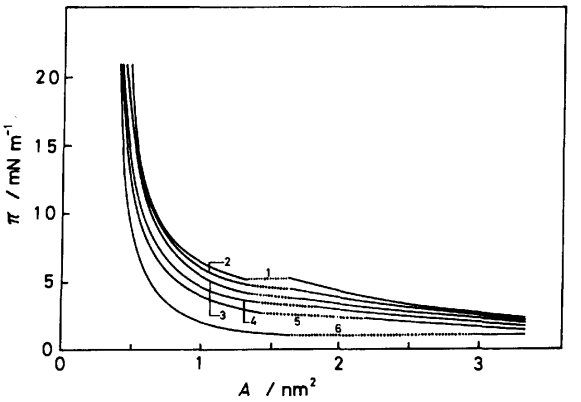

Fig. 8. Surface pressure *vs.* mean area per molecule curves at constant surface composition: (1) X_2^H=1, (2) 0.8, (3) 0.6, (4) 0.4, (5) 0.2, (6) 0.

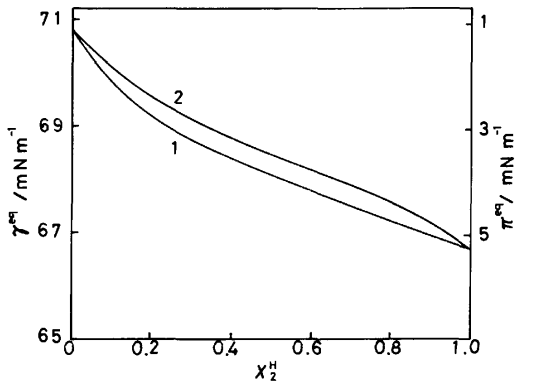

Fig. 9. Equilibrium surface tension (pressure) *vs.* surface composition curves: (1) $\gamma^{eq}(\Pi^{eq})$ *vs.* $X_2^{H,e}$, (2) $\gamma^{eq}(\Pi^{eq})$ *vs.* $X_2^{H,g}$.

mixtures in our previous papers.[3,4] The phase diagrams, however, are different in shape; the present one has a cigar form and the previous ones have crescent shaped forms. This fact indicates that the difference in the surface activity between two surfactants of the present system is larger than DAC–DeAC and DTAC–DeAC systems.

References

1) K. Motomura, S. Iwanaga, Y. Hayami, S. Uryu, and R. Matuura, *J. Colloid Interface Sci.*, **80**, 32 (1981).
2) M. Aratono, S. Uryu, Y. Hayami, K. Motomura, and R. Matuura, *J. Colloid Interface Sci.*, in press.
3) M. Aratono, S. Uryu, Y. Hayami, K. Motomura, and R. Matuura, *J. Colloid Interface Sci.*, **93**, 162 (1983).
4) S. Uryu, M. Aratono, M. Yamanaka, K. Motomura, and R. Matuura, *Bull. Chem. Soc. Jpn.*, **56**, 3219 (1983).
5) D. N. Rubingh, in "Solution Chemistry of Surfactants," ed by K. L. Mittal, Plenum, New York (1979), Vol. 1, p. 337.
6) H. Lange and K.-H. Beck, *Kolloid Z. Z. Polym.*, **243**, 129 (1971).
7) M. J. Rosen and X. Y. Hua, *J. Colloid Interface Sci.*, **86**, 164 (1982).
8) J. M. Corkill, J. F. Goodman, P. Robson, and J. R. Tate, *Trans. Faraday Soc.*, **62**, 987 (1966).
9) J. M. Corkill, J. F. Goodman, and T. Walker, *Trans. Faraday Soc.*, **63**, 759 (1967).
10) J. M. Corkill, J. F. Goodman, and T. Walker, *Trans. Faraday Soc.*, **63**, 768 (1967).
11) K. Motomura, S. Iwanaga, S. Uryu, H. Matsukiyo, M. Yamanaka, and R. Matuura, *Colloids & Surfaces*, **9**, 19 (1984).
12) K. Motomura, *J. Colloid Interface Sci.*, **64**, 348 (1978).
13) K. Motomura, *Adv. Colloid Interface Sci.*, **12**, 1 (1980).

Magnetic Circular Dichroism and Electronic States of Tetrachloroplatinate(II) and Tetrachloropalladate(II) Ions

Kazuhiko NAKAYAMA,* Takashi KOMORITA, and Yoichi SHIMURA
Department of Chemistry, Faculty of Science, Osaka University, Toyonaka, Osaka 560
(Received August 25, 1983)

The magnetic circular dichroism (MCD) spectra of K_2PtCl_4 and K_2PdCl_4 have been carefully remeasured over the visible-near UV region. The examination of the electronic absorption and the MCD spectra together with their Gaussian analyses strongly suggests that the band of K_2PtCl_4 at 30.3×10^3 cm^{-1} contains both $\Gamma_5(^1E_g)$ and $\Gamma_3(^1B_{1g})\leftarrow\Gamma_1(^1A_{1g})$ transitions, and the band of K_2PdCl_4 at 21.1×10^3 cm^{-1} all three spin-allowed d-d transitions. The separation of the $\Gamma_2(^1A_{2g})$ and $\Gamma_5(^1E_g)$ excited states is considerably large with K_2PtCl_4 as compared with K_2PdCl_4. The MCD for the high-intensity absorption bands in K_2PtCl_4 is different from that reported previously. On the basis of new MCD result, the bands at 43.3 and 46.6×10^3 cm^{-1} have been assigned to d-p transitions, $a_{2u}(p_z)\leftarrow a_{1g}(d_{z^2})$ and $e_g(d_{xz,yz})$, respectively.

The solution MCD spectrum of K_2PtCl_4 was obtained firstly by D. S. Martin, Jr. *et al.*[1] for the d-d transition region, and then by McCaffery *et al.*[2] over the visible-near UV spectral region. That of K_2PdCl_4 was measured partly by the latter group. We have reinvestigated the spectra of these two compounds carefully in order to clarify the electronic states of square-planar complexes, providing more reliable spectra over a broader wave number range.

The electronic states of $PtCl_4^{2-}$ and $PdCl_4^{2-}$ have been studied most extensively by solution, single-crystal, and polarized single-crystal absorption spectra, and moreover polarized single-crystal reflection and MCD spectra, as well as ligand field and molecular orbital theories, angular overlap treatments, and so on; then several different spectral assignments have been made (Tables 1 and 2). One of the major problems remaining unsettled is the position of the d_{z^2} metal orbital, and another is the origins of the high-intensity bands of $PtCl_4^{2-}$. This paper intends to throw light on these problems, together with the assignments of the other bands, consistent with many experimental facts given by previous workers.

Experimental

Materials. Potassium tetrachloroplatinate(II) was purchased from Higuchi Chemical Labolatory Ltd., and was recrystallized from an aqueous solution containing hydrochloric acid.

Potassium tetrachloropalladate(II) was prepared from palladium chloride and potassium chloride.

Measurements. Electronic absorption spectra were recorded with a Hitachi 330 spectrophotometer, and MCD spectra with a JASCO MOE-1 spectropolarimeter in a magnetic field of 1.5 T, being remeasured with inversion of magnetic field in order to obtain a greater precision.[30] Spectral measurements of K_2PtCl_4 and K_2PdCl_4 were made in 0.50 M and 2.0 M HCl aqueous solutions, respectively, at room temperature (1 M=1 mol dm^{-3}).

Gaussian Analyses. Gaussian analyses of absorption and MCD curves were performed using a version of program LGNS[31] adapted to the ACOS computer system. In the MCD curve analysis of K_2PtCl_4, the spectrum was divided into two parts (22.0×10^3—26.4×10^3 cm^{-1} and 26.0×10^3—34.2×10^3 cm^{-1}) in order to keep a precision in weak bands. An A term was analyzed as two B terms with opposite signs. All the calculations were carried out at Computation Center, Osaka University.

Results and Discussion

Ligand-field Absorption Bands. In a square-planar d^8 system (D_{4h}) without spin-orbit coupling, the d-d transitions ($d_{x^2-y^2}\leftarrow d_{xy}$, $d_{xz,yz}$, and d_{z^2}) give rise to six excited states: $^{1,3}A_{2g}$, $^{1,3}E_g$, and $^{1,3}B_{1g}$. These states are split and scrambled under spin-orbit coupling into 12 excited states.

$$d_{x^2-y^2}\longleftarrow d_{xy}\quad\begin{cases}^3A_{2g}(\Gamma_1+\Gamma_5)\\ ^1A_{2g}(\Gamma_2)\end{cases},$$

$$d_{x^2-y^2}\longleftarrow d_{xz,yz}\quad\begin{cases}^3E_g(\Gamma_1+\Gamma_2+\Gamma_3+\Gamma_4+\Gamma_5)\\ ^1E_g(\Gamma_5)\end{cases},$$

$$d_{x^2-y^2}\longleftarrow d_{z^2}\quad\begin{cases}^3B_{1g}(\Gamma_4+\Gamma_5)\\ ^1B_{1g}(\Gamma_3)\end{cases}.$$

1) K_2PtCl_4: Absorption and MCD data are given in Fig. 1 and Table 3. The assignment of the band at 25.6×10^3 cm^{-1} has been well established ($\Gamma_2(^1A_{2g})\leftarrow\Gamma_1(^1A_{1g})$) by the polarized absorption spectra.[6-9,28] The band at 30.3×10^3 cm^{-1} has been assigned to $\Gamma_5(^1E_g)\leftarrow\Gamma_1(^1A_{1g})$ by the MCD spectrum[1,2] and the polarization properties[6,9,28] (Table 1). By careful examination of the band shape, it is found to be unsymmetrical (Figs. 1 and 2), which suggests that there is another component in the higher energy side. The MCD spectrum also

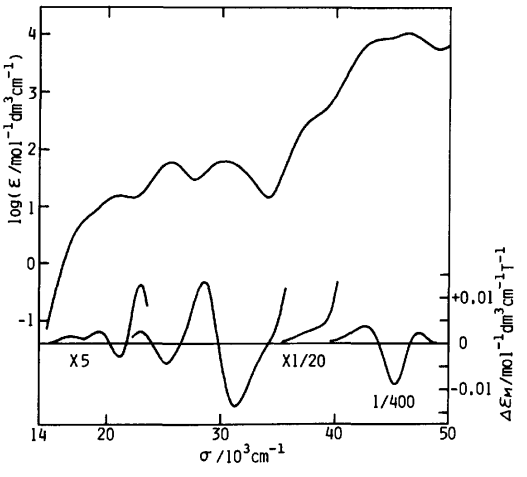

Fig. 1. Absorption and MCD spectra of K_2PtCl_4 in 0.50 M HCl.

TABLE 1. PREVIOUS SPECTRAL ASSIGNMENTS OF K_2PtCl_4 (Wave numbers/10^3 cm^{-1})[a]

Ref. No.[b]	1[c]	2	3	4	5	6	7	8	9	Note
3		17.7 $^3A_{2g}$	21.0 ^3E_g		25.5 $^1A_{2g}$	30.2 ^1E_g	37.9		46 d-p	in 2M HCl
4			[21.6] [22.0] $^3B_{1g}$ $^3A_{2g}$		25.5f $^1A_{2g}$	[29.2] $^1B_{1g}$				LF[d] f: fixed value
5		$^3A_{2g}$	$^1A_{2g}$		$^1B_{1g}$	^1E_g	sfCT[e]		$^1A_{2u}$	MO
6			20.4xy[f] 20.2z $^1B_{1g}$		25.7xy $^1A_{2g}$	28.9xy 29.2z ^1E_g				PAS[g] (r.t.)[h]
7		17.5 17.3xy $^3A_{2g}$	20.4 20.4xy 20.2z $^3E_g/^3B_{1g}$		27.0 26.0xy $^1A_{2g}$	29.0 28.5xy 29.3z $^1E_g/^1B_{1g}$	36.5 $^1B_{1g}/^1E_g$	42.5 $^1A_{2u}$		i) PAS(r.t.)
8	16.9xy 17.2z Γ_1	18.1xy $\Gamma_2+\Gamma_5$	20.8xy 20.7z $\Gamma_3+\Gamma_5$	24.0xy 23.9z $\Gamma_5(^3B_{1g})$	26.1xy $^1A_{2g}$	29.3xy 29.9z $^1B_{1g}$	^1E_g			PAS(5K)
9	17-19z Γ_1	18.0xy $\Gamma_2+\Gamma_5$	20.9xy 20.6z $\Gamma_3+\Gamma_5$	24.0xy 24.1z Γ_1	26.3xy $^1A_{2g}$	29.2xy 29.8z ^1E_g	[36.4] $\Gamma_5(^3B_{1g})$		$^1B_{1g}$	[46.3] PAS(15K) [ ]: LF
1						^1E_g				MCD
10	[15.7-16.8] $\Gamma_1+\Gamma_2+\Gamma_5$ [16.8-17.4] $\Gamma_5+\Gamma_1$	 [18.2] Γ_2	[19.6-22.1] $\Gamma_3+\Gamma_5+\Gamma_1$ [19.6-20.7] $\Gamma_5+\Gamma_3$	[24.2] $\Gamma_5(^3B_{1g})$ [23.7-24.1] $\Gamma_1+\Gamma_5$	[26.4] $^1A_{2g}$ [26.7] $^1A_{2g}$	[29.6] ^1E_g [29.7] [29.9] $^1B_{1g}$ ^1E_g	[35.3] $^1B_{1g}$			A[j] LF B[j]
11					$^1A_{2g}$					induced CD
12		^3E_g	$^3A_{2g}$	$^3B_{1g}$	$^1A_{2g}$	^1E_g	$^1B_{1g}$	$^1A_{2u}+^1E_u(\pi)$		MO
13			[20.2] [21.8] $^1A_{2g}$ ^1E_g			[29.1] $^1B_{1g}$		[40.4] [42.0] $^1B_{1u}{}^p$ $^1E_u{}^p$	[49.2] $^1A_{2u}{}^p$	MO
14		 $^3A_{2g}$	21.0 ^3E_g		25.7 $^1A_{2g}$	30.5 ^1E_g	38.3 ofCT[k]	43.9 $^1A_{2u}+^1E_u(\pi)$	46.5 $^1E_u(\sigma)$	in 2M HCl
15		$^3A_{2g}$	^3E_g	$^3B_{1g}$	$^1A_{2g}$	^1E_g	$^1B_{1g}$		$^1A_{2u}$	l)
16		17.5 ^3E_g	20.2 $^3A_{2g}$		24.8 $^1A_{2g}$	29.5 ^1E_g	37.0 $^1B_{1g}$		44.1 $^1A_{2u}+^1E_u(\pi)$	in CH_3CN (77K)
2					25.5 $^1A_{2g}$	30.3 ^1E_g		43.4 $^1A_{2u}+^1E_u(\pi)$	46.2 $^1A_{2u}{}^p$	in 0.5M HCl MCD
18		$^3A_{2g}$	^3E_g		$^1A_{2g}$	^1E_g	$^1B_{1g}$	$^1A_{2u}+$ $^1E_u(\pi)/^1E_u{}^p$	$^1A_{2u}$ $/^1A_{2u}{}^p$	review
19								$^1A_{2u}{}^p+^1A_{2u}$	$^1E_u{}^p$	MCD calcn
20	17 $\Gamma_5(^3E_g)$	18 $\Gamma_4(^3E_g)$	20.5 $\Gamma_{5,1}(^3A_{2g})$	24.3 $\Gamma_5(^3B_{1g})$	26.3 $^1A_{2g}$	29.6 ^1E_g	>33 $^1B_{1g}$			single crystal (4K)
21							36.5xy 36.5z $^1B_{1g}$			PAS(15K)
22				[23.4-24.2] $^3A_{2g}+^3E_g$	[28.2] [29.1] $^1A_{2g}$ $^3B_{1g}$	[30.7] ^1E_g	[35.5] $^1B_{1g}$	[37.1-38.7] $^1E_u(\pi)+$ $^1A_{2u}$	[44.4] $^1E_u(\sigma)+$ $^1E_u{}^p$	MO

TABLE 1. (Continued)

Ref. No.[b]	1[c]	2	3	4	5	6	7	8	9	Note
23								[43.6] $^1A_{2u}{}^p$	[44.3] ^1E_u	polarized reflection
24					$^1A_{2g}$	^1E_g	$^1B_{1g}$			oscillator strength
27	m)				$^1A_{2g}$	28.5 29.3 $^1B_{1g}$ ^1E_g	$^1B_{1u}{}^p$	$^1E_u{}^p$	$^1A_{2u}{}^p$	ligand substitution and l)
28	17.5z $\Gamma_{4,5}(^3B_{1g})$	18.0xy 20.7z $^1B_{1g}$	20.9xy	24.0xy 24.0z $\Gamma_2+\Gamma_5(^3A_{2g})$	26.2xy $^1A_{2g}$	28.7xy 29.3z ^1E_g				PAS(10K)
29	[17.1] Γ_1	[18.0] $\Gamma_2+\Gamma_5$	[20.8] [21.0] Γ_5 Γ_3	[24.3] $\Gamma_5(^3B_{1g})$	[26.0] $^1A_{2g}$	[30.2] ^1E_g	[34.2] $^1B_{1g}$			AOM

a) Superscripts p's denote d-p transitions; bracketed values represent calculated ones (the remains all experimental ones). b) References are arranged chronologically. c) Band number. d) Ligand field theory. e) A spin-forbidden charge transfer. f) xy: In-plane polarized; z: out-of-plane polarized. g) Polarized single-crystal absorption spectra. h) Room temperature. i) Diffuse reflectance spectrum. j) See Ref. 10. k) An orbitally-forbidden charge transfer. l) Assigned on the basis of experimental facts reported before that time. m) As alternative B in Ref. 10.

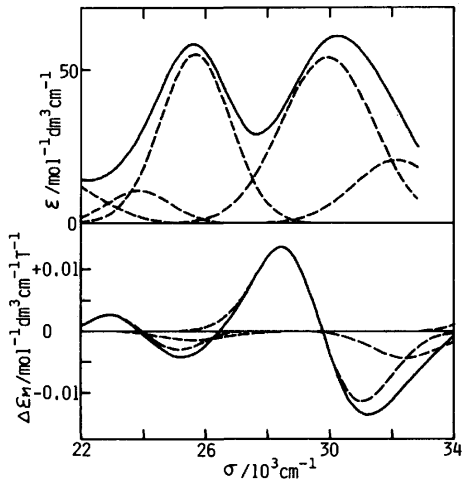

Fig. 2. Gaussian analyses of K_2PtCl_4. ------: Gaussian components and ——: sum of them. The sum fits in very closely with the experimental curve to such an extent that it is impossible to show the difference between them in this figure. An A-term curve is given by a sum of two B terms with opposite signs (See Experimental). Standard deviations are 0.11 $mol^{-1}dm^3cm^{-1}$ for the absorption curve, and 3.4×10^{-5} (in $(22.0—26.4)\times10^3cm^{-1}$) and 1.3×10^{-4} $mol^{-1}dm^3cm^{-1}T^{-1}$ (in $(26.0—34.2)\times10^3$ cm^{-1}) for the MCD one.

suggests the presence of a positive B term for the component. The results of Gaussian analyses for the absorption and MCD curves support this expectation (Fig. 2 and Table 5).[32] It seems reasonable to assign the component to the third spin-allowed d-d transition, $\Gamma_3(^1B_{1g}) \leftarrow \Gamma_1(^1A_{1g})$.

Gaussian analysis of the absorption curve indicates the existence of a minor component under the lower edge of the band at 25.6×10^3 cm^{-1}. This component has been detected in the polarized single-crystal spectra at liquid helium temperature,[8,9,28] and assigned to $\Gamma_5(^3B_{1g}) \leftarrow \Gamma_1(^1A_{1g})$. The MCD exhibits a negative A term in the transition region (Fig. 1), compatible with an assignment to a degenerate excited state; moreover it has the same sign as the A term for the $\Gamma_5(^1E_g)$ state with which the excited state is mixed. This interpretation can explain the MCD band at 22.9×10^3 cm^{-1} near the valley of the absorption spectrum, and leads to the result that the MCD band at 25.2×10^3 cm^{-1} primarily consists of the negative part of the negative A term for $\Gamma_5(^3B_{1g}) \leftarrow \Gamma_1(^1A_{1g})$ rather than the positive B term for $\Gamma_2(^1A_{2g}) \leftarrow \Gamma_1(^1A_{1g})$ as mentioned previously.[2] Thus the latter is considerably smaller than the appearance (Fig. 2 and Table 5). This is consistent with the fact that the MCD under the absorption band at 30.3×10^3 cm^{-1} resembles that in the spin-allowed d-d transition region of K_2PdCl_4, very closely in shape, or the ratio of the positive band to the negative one (*vide infra*, Figs. 1 and 3).

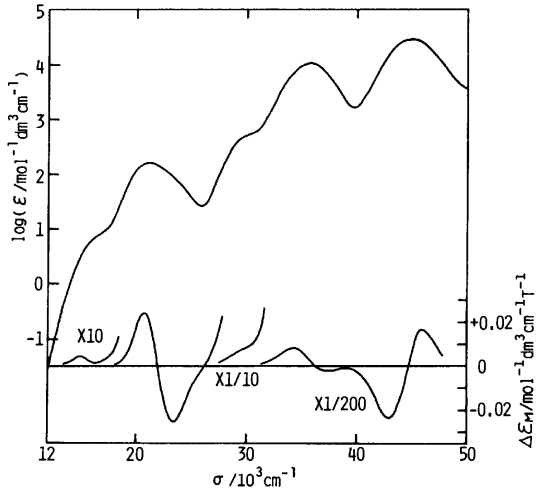

Fig. 3. Absorption and MCD spectra of K_2PdCl_4 in 2.0 M HCl.

TABLE 2. PREVIOUS SPECTRAL ASSIGNMENTS OF K_2PdCl_4 (Wave numbers/10^3 cm^{-1})[a]

Ref. No.[b]	1[c]	2	3	4	5	6	7	8	Note
5		16.7 $^1A_{2g}$	21.5 $^1B_{1g}$	23.3 ^1E_g			36.0 $^1A_{2u}$	44.9 $^1E_u(\pi)$	nujol mull[d] MO
7		18.0 18.0xy[f] 17.0z $^3E_g/^3B_{1g}$	21.5 20.0xy $^1A_{2g}$	22.6xy 23.0z $^1E_g/^1B_{1g}$		31.5 29.5xy $^1B_{1g}/^1E_g$	36.5		i) PAS[g] (r.t.)[h]
12		$^3B_{1g}$	$^1A_{2g}$	^1E_g		$^1B_{1g}$	$^1A_{2u}+^1E_u(\pi)$	$^1E_u(\sigma)$	MO
14		^3E_g	21.0 $^1A_{2g}$	23.7 ^1E_g		30.5 ofCT[k]	35.7 $^1A_{2u}+^1E_u(\pi)$	45.1 $^1E_u(\sigma)$	in 1M HCl
15		^3E_g	$^1A_{2g}$	^1E_g		$^1B_{1g}$	$^1A_{2u}$		l)
2			21.1 ^1E_g			30.2	35.8 $^1A_{2u}+^1E_u(\pi)$	44.9 $^1E_u(\sigma)$	in 2M HCl MCD
17		17.7xy 17.2z $^3A_{2g}+^3E_g$	21.0xy $^1A_{2g}$	22.5xy 23.3z ^1E_g	28.5xy $^3B_{1g}$	33.0xy $^1B_{1g}$	intense xy 37.3z $^1A_{2u}+^1E_u$		PAS (12K)
19								$^1E_u(\pi)$	MCD calcn
22			[20.2] [21.0] $^3A_{2g}$ ^3E_g	[25.8] $^3B_{1g}$	[28.2] $^1A_{2g}+^1E_g$	[34.7] $^1B_{1g}+^1E_u(\pi)$	[37.1] $^1A_{2u}$	[43.6–46.0] $^1E_u(\pi$-s,σ,d-p)[e]	MO
23							36.8 $^1E_u(\pi)$	41.5 $^1E_u(\sigma)$	polarized reflection
25	15.4	17.0 17.7xy 17.0z $^3A_{2g}+^3E_g$	20.8 21.7xy $^1A_{2g}$	22.4 23.2xy 23.2z ^1E_g		30.1 j)	35.7 40.8 intense xy 37.4z $^1E_u(\pi)+^1A_{2u}$	45.0 $^1E_u(\sigma)$	in 2M KCl PAS(15K)
26		17.5 18.9 $\Gamma_1(^3A_{2g})+\Gamma_5(^3B_{1g})$	20.5 21.5 $^1A_{2g}$	23.3 22.5 25.6 ^1E_g j)	28.0 28.9 $^1B_{1g}$		35.8 ^1E_u		single crystal (4K) in Cs_2ZrCl_6 (2K)
27		$^3A_{2g}+^3E_g$	$^1A_{2g}$	22.6 23.0 $^1B_{1g}$ ^1E_g	$^1B_{2g}$(CT)		$^1A_{2u}+^1E_u(\pi)$	$^1E_u(\sigma)$	ligand substitution and l)
28		17.7xy 17.1z $\Gamma_{4,5}(^3B_{1g})$	21.8xy $^1A_{2g}$	23.4xy 23.4z $^1B_{1g}$		^1E_g			PAS(10K)
29		[17.9] $\Gamma_5(^3B_{1g})$	[21.1] $^1A_{2g}$	[23.4] ^1E_g	[26.8] $^1B_{1g}$				AOM

a—c, f—i, k, l) As in Table 1. d) For the bands 7 and 8, in an aqueous solution containing Cl^-. e) π-s: Pd(5s)←Cl(π). j) Not $PdCl_4^{2-}$.

The assignments for the bands at *ca.* 18×10^3 and 21×10^3 cm^{-1} are not straightforward because of many possibilities of spin-triplet excited states, the MCD spectrum also indicating the presence of more than two components in the region. However, it is likely that these bands are tentatively assigned to $\Gamma_1(^3A_{2g}+^3E_g)+\Gamma_2(^3E_g)+\Gamma_5(^3A_{2g}+^3E_g)$ and $\Gamma_3(^3E_g)+\Gamma_5(^3A_{2g}+^3E_g)$ respectively, on the basis of the polarized absorption spectra[9,11] and the available energy calculations.[10,29] (The Γ_4 components arising from $^3B_{1g}$ and ^3E_g are expected to have almost zero intensity since no Γ_4 state is produced from spin- or orbitally-allowed one-electron-transitions with close transition energies).

2) K_2PdCl_4: In general, square-planar palladium(II) complexes have remarkably reduced intensities of the spin-triplet transitions relative to those of the spin-singlet ones, in comparison with the platinum analogs; so, for simplicity we may neglect spin-orbit coupling for palladium(II) complexes in a discussion of the electronic states.

Absorption and MCD data are given in Fig. 3 and Table 4. The shoulder centered at *ca.* 16.9×10^3 cm^{-1} is roughly assigned to the spin-forbidden d-d transitions, $^3A_{2g}$, ^3E_g, and/or $^3B_{1g}\leftarrow{}^1A_{1g}$. Further details of these transitions will not be discussed.

The main band with a peak at 21.1×10^3 cm^{-1} is apparently unsymmetrical, which indicates the presence of transition components more than one. The MCD under the band is very similar to that for the band at 30.3×10^3 cm^{-1} of K_2PtCl_4 as described in the

TABLE 3. ABSORPTION AND MCD DATA OF K_2PtCl_4

σ_{max}	ε	σ_{ext}	$\Delta\varepsilon_M$
$10^3\,cm^{-1}$	$mol^{-1}\,dm^3\,cm^{-1}$	$10^3\,cm^{-1}$	$mol^{-1}\,dm^3\,cm^{-1}\,T^{-1}$
18.5sh[a]	7.2	16.7	+0.0003
		19.3	+0.0005
21.03	15.4	21.1	−0.0006
		22.9	+0.0026
25.62	58.3	25.2	−0.0042
30.31	61.7	28.5	+0.014
		31.2	−0.014
38.4sh	380	38.3sh	+0.06
43.5sh	7600	42.6	+1.5
46.19	10000	45.2	−3.6
		47.3	+0.90

a) sh: shoulder (ε is for the value of σ given).

TABLE 4. ABSORPTION AND MCD DATA OF K_2PdCl_4

σ_{max}	ε	σ_{ext}	$\Delta\varepsilon_M$
$10^3\,cm^{-1}$	$mol^{-1}\,dm^3\,cm^{-1}$	$10^3\,cm^{-1}$	$mol^{-1}\,dm^3\,cm^{-1}\,T^{-1}$
16.8sh[a]	8.7	15.0	+0.0005
		20.7	+0.024
21.11	162	23.3	−0.025
30.0sh[b]	510	29.7sh	+0.075
35.73[c]	10400	34.2	+1.7
		37.3	−0.44
44.92[d]	28000	42.9	−4.7
		45.9	+3.3

a) sh: shoulder (ε is for the value of σ given). b) $^1B_{2g}\leftarrow{}^1A_{1g}$ (CT). c) $^1A_{2u}+{}^1E_u(\pi)\leftarrow{}^1A_{1g}$. d) $^1E_u(\sigma)\leftarrow{}^1A_{1g}$.

previous section. From this observation it is reasonable to consider that the band at 21.1×10^3 cm^{-1} includes the same transition components (^1E_g and $^1B_{1g}\leftarrow{}^1A_{1g}$) as the latter band. The cross point (or zero point) of the apparent A term exists at higher energy than the absorption peak; therefore, it can be predicted that there is another absorption component at lower energy than the cross point. Then the component should correspond to the band at 25.6×10^3 cm^{-1} of K_2PtCl_4, being assigned to the $^1A_{2g}\leftarrow{}^1A_{1g}$ transition. This prediction is supported by the polarized absorption spectra.[17,25] The MCD for the transition is expected to be considerably weak from a comparison between two MCD curves of the Pd and Pt compounds in the spin-allowed d-d transition region.

The absorption band at $21.1\times10^3\,cm^{-1}$ consequently contains all three spin-allowed d-d transitions. On the basis of this conclusion, the Gaussian analyses of the absorption and MCD curves were carried out (Fig. 4), the numerical data being given in Table 5 together with the assignments. These are compatible with the polarized absorption spectra.[17,25]

3) Comparison of Two Compounds: The electronic structures of the two compounds are different in two points. Firstly, the separation of the $\Gamma_2(^1A_{2g})$ and $\Gamma_5(^1E_g)\leftarrow\Gamma_1(^1A_{1g})$ transitions is considerably large with K_2PtCl_4 as compared with K_2PdCl_4. This seems to be primarily due to the high π-bonding character of Pt–Cl over Pd–Cl bonds.[29] Secondly, the electronic spectrum of K_2PtCl_4 exhibits a structure in the region of the spin-triplet transitions, for which the MCD is also complicated. This fact can be attributed to the substantial spin-orbit coupling. In K_2PdCl_4 the electronic and MCD spectra are simplified because of a minor spin-orbit coupling as assumed previously.

Considering the above two points, the absorption and MCD spectra of K_2PdCl_4 can be easily correlated with those of K_2PtCl_4 and in fact they correspond to each other very well. That the $\Gamma_3(^1B_{1g})\leftarrow\Gamma_1(^1A_{1g})$

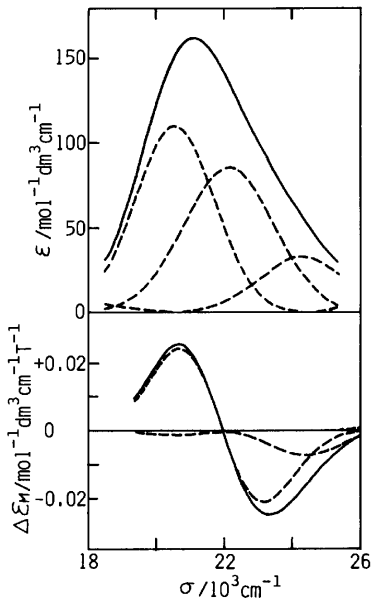

Fig. 4. Gaussian analyses of K_2PdCl_4. See the figure caption of Fig. 2. Standard deviations are 0.27 $mol^{-1}\,dm^3\,cm^{-1}$ and $2.1\times10^{-4}\,mol^{-1}\,dm^3\,cm^{-1}\,T^{-1}$ for the absorption and MCD curves, respectively.

TABLE 5. THE RESULTS OF GAUSSIAN ANALYSES FOR K_2PtCl_4 AND K_2PdCl_4

Absorption				MCD				
σ_{max}	ε	$\Delta\sigma_{1/2}$ [a]	S [b]	σ_{ext}	$\Delta\varepsilon_M$	$\Delta\sigma_{1/2}$	Term	Assignments
10^3 cm^{-1}	mol^{-1} dm^3 cm^{-1}	10^3 cm^{-1}		10^3 cm^{-1}	mol^{-1} dm^3 cm^{-1} T^{-1}	10^3 cm^{-1}		$\leftarrow\Gamma_1(^1A_{1g})$
			K_2PtCl_4					
21.00f [c]	15.2f	3.41	55.1	21.10f	−0.0006	1.39		d)
23.84	10.6	2.38	26.8	22.95 25.15	+0.0027 −0.0030	1.59 1.77	−A	$\Gamma_5(^3B_{1g})$
25.67	55.1	2.68	157	25.67f	−0.0014	2.67	+B	$\Gamma_2(^1A_{2g})$
29.92	54.0	3.49	201	28.64 30.77	+0.0155 −0.0127	2.47 2.69	−A	$\Gamma_5(^1E_{1g})$
32.11	20.5	3.24	70.8	32.41	−0.0042	2.67	+B	$\Gamma_3(^1B_{1g})$
43.28	6330	3.25	21900				−B	$^1A_{2u}$(d-p)
46.54	9470	3.60	36300				+A	^1E_u(d-p)
			K_2PdCl_4					
16.90f	8.1f	3.60	31.0					$^3A_{2g}$, ^3E_g, $^3B_{1g}$
20.55	109.8	2.74	320	20.54	−0.0013	2.27	+B	$^1A_{2g}$
22.14	85.2	3.13	284	20.86 22.97	+0.0283 −0.0233	2.32 2.48	−A	^1E_g
24.27	33.1	2.92	103	24.38	−0.0073	2.33	+B	$^1B_{1g}$

a) Half-value widths. b) Band area=1.0645×(ε_{max}/mol^{-1} dm^3 cm^{-1})×($\Delta\sigma_{1/2}$/10^3 cm^{-1}). c) f: Fixed values. d) See text.

transition has never been evidently identified seems to be ascribed to its low intensity, which is valid for both compounds (Figs. 2 and 4, and Table 5). A combination of this deduction with the data of the polarized single-crystal absorption spectra[9,28] leads to the following result: the low transition-probability with in-plane polarized light is responsible for the low intensity of the $\Gamma_3(^1B_{1g}) \leftarrow \Gamma_1(^1A_{1g})$ transition, at least in K_2PtCl_4. That is to say, the transition does not largely couple with the e_u molecular vibration, but with the b_{2u} one to gain the intensity. This interpretation can also explain the difference in the peak-positions at *ca.* 29—30×10^3 cm^{-1} between the in- and out-of-plane polarized spectra,[8,9,28] which had been a troublesome problem in an assignment of the absorption bands. In brief, the band at 29.2×10^3 cm^{-1} in the in-plane polarized spectrum[9] is composed mainly of the $\Gamma_5(^1E_g) \leftarrow \Gamma_1(^1A_{1g})$ transition, whereas the band at 29.8×10^3 cm^{-1} in the out-of-plane polarized spectrum[9] includes the $\Gamma_3(^1B_{1g}) \leftarrow \Gamma_1(^1A_{1g})$ transition to a considerable extent in addition to the $\Gamma_5(^1E_g) \leftarrow \Gamma_1(^1A_{1g})$ one. As to K_2PdCl_4, a similar discussion cannot be made owing to the smaller splitting between the $^1A_{2g}$ and $^1E_g+{}^1B_{1g} \leftarrow {}^1A_{1g}$ transitions.[17,25]

High-intensity Absorption Bands. *1) K_2PtCl_4*: The MCD above 35×10^3 cm^{-1} is different from that reported by McCaffery *et al.*[2] in two substantial points. First, they had observed a shoulder at *ca.* 44×10^3 cm^{-1}, whereas we have never detected it in spite of careful measurements. Secondly, they had observed a positive B term coinciding with the absorption peak at 46.2×10^3 cm^{-1}; however, we have done a positive A term corresponding to the absorption peak. From the facts that we have measured the MCD spectrum in the same solvent as used by McCaffery *et al.*, and that no difference is found between both absorption spectra; low resolving power of their CD instrument seems to have precluded accurate recordings.

The Gaussian analysis of the absorption curve above 42×10^3 cm^{-1} indicates the presence of absorption components at *ca.* 43.3×10^3 cm^{-1} and 46.5×10^3 cm^{-1} (Table 5). McCaffery *et al.* assigned the 43.3×10^3-cm^{-1} band to $^1A_{2u}+{}^1E_u(\pi) \leftarrow {}^1A_g$ ($b_{1g}(d_{x^2-y^2}) \leftarrow b_{2u}(\pi)+e_u(\pi)$), and the 46.5×$10^3$-cm^{-1} one to $^1A_{2u} \leftarrow {}^1A_{1g}$ ($a_{2u}(p_z) \leftarrow a_{1g}(d_{z^2})$) (Fig. 5). Kroening *et al.*[21] and Elding and Olsson[27] assigned the former band to $^1E_u \leftarrow {}^1A_{1g}$ ($a_{2u}(p_z) \leftarrow e_g(d_{xz,yz})$). Both assignments are based on the MCD result of McCaffery *et al.*; however, these assignments should be reconsidered from the situation described above.

The main band at 46.6×10^3 cm^{-1} shows an A-term MCD, which requires an assignment to a degenerate

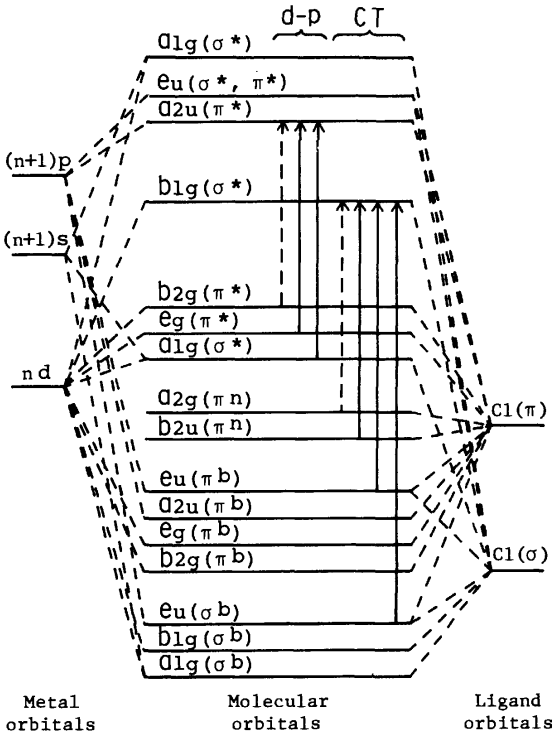

Fig. 5. Relative molecular orbital energy levels for square-planar MCl_4^{2-} complexes (D_{4h}). In a d^8 system, the $b_{2g}(\pi^*)$ and all the orbitals below it are doubly occupied. Transitions to be considered in the assignments of high-intensity bands are shown with full-drawn (for allowed transitions) and dashed (for orbitally-forbidden ones) arrows.

excited state. Considering simply, there are three candidates: $b_{1g}(d_{x^2-y^2}) \leftarrow e_u(\sigma)$, $b_{1g}(d_{x^2-y^2}) \leftarrow e_u(\pi)$, and $a_{2u}(p_z) \leftarrow e_g(d_{xz,yz})$ (Fig. 5). This band is the lowest dipole-allowed transition correlated to a degenerate excited state, and a $b_{1g} \leftarrow e_u(\sigma)$ transition generally occurs in higher energy than the corresponding $b_{1g} \leftarrow e_u(\pi)$ one; therefore the assignment to the former is excluded. In K_2PdCl_4 a negative A term has been observed for the $b_{1g} \leftarrow e_u(\pi)$, transition (*vide infra*). If this is the case with K_2PtCl_4, the assignment to it is also excluded, since the MCD for the band of interest exhibits a positive A term. On the other hand, the band which has been assigned to $a_{2u} \leftarrow e_g$ in $[Pt(NH_3)_4]^{2+}$,[33,34] $[Pt(en)_2]^{2+}$,[34] and $[Pt(tn)_2]^{2+}$,[34] shows a positive A term. Thus, the band at 46.6×10^3 cm^{-1} can be reasonably assigned to the d-p transition, $a_{2u} \leftarrow e_g$ (Fig. 5).

The component at 43.3×10^3 cm^{-1} shows a B-term MCD. Although it is impossible to say definitely that the band exhibits only a B term from the MCD feature alone, the polarized reflection spectra by Anex and Takeuchi[23] indicate the existence of an out-of-plane polarized band with an in-plane polarized one in the region under consideration; therefore, the band should be assigned to a $^1A_{2u} \leftarrow {}^1A_{1g}$ transition. There are two transitions which agree with the excited state: $b_{1g}(d_{x^2-y^2}) \leftarrow b_{2u}(\pi)$ and $a_{2u}(p_z) \leftarrow a_{1g}(d_{z^2})$ (Fig. 5). In K_2PdCl_4 the former transition has a remarkably low intensity as a dipole-allowed transition,[25] as expected for a pure $\sigma^* \leftarrow \pi$ transition by Jørgensen.[35] If this is also the case with K_2PtCl_4, the band at 43.3×10^3 cm^{-1} is too intense to be assigned to $b_{1g} \leftarrow b_{2u}$. The assignment $a_{2u} \leftarrow a_{1g}$, combined with that of the band at $46.6 \times 10^3 cm^{-1}$ seems at a glance to be inconsistent with the corresponding d-d transitions. However, this might be rationalized by the difference in interelectronic repulsion and configuration interaction between the d-d and d-p transitions.[25] Particularly, the $^1A_{2u}(p_z \leftarrow d_{z^2})$ excited state is presumed to be lowered in energy by configuration interaction with the $^1A_{2u}(b_{1g}(d_{x^2-y^2}) \leftarrow b_{2u}(\pi))$ one close to it.[21] Therefore, the band at $43.3 \times 10^3 cm^{-1}$ is also assigned to a d-p transition ($a_{2u} \leftarrow a_{1g}$; Fig. 5).

The above assignments are not in conflict with the experimental results of Anex and Takeuchi,[23] who observed two bands, of which one is out-of-plane and the other is in-plane polarized around 44×10^3 cm^{-1}, the former occurring in lower energy. This order of two components agrees with our assignment. In the previous assignments,[23,27] the 43.3×10^3-cm^{-1} band in solution had been correlated with the higher-energy band (at 44.3×10^3 cm^{-1}) in crystal, and the 46.6×10^3-cm^{-1} band in solution with the lower-energy one (at 43.6×10^3 cm^{-1}) in crystal; then the difference in their relative positions between solution and crystal spectra had been explained by exciton theory.[23] However, our assignment makes the explanation needless.

Finally, the assignment of the shoulder at *ca.* 38×10^3 cm^{-1} remains. Most of the previous workers have assigned it to a d-d transition ($^1B_{1g} \leftarrow {}^1A_{1g}$). On the other hand, Gray and Ballhausen[5] have done it to a spin-forbidden charge-transfer (CT) transition, Ito *et al.*[14] to an orbitally-forbidden d-p one ($a_{2u}(p_z) \leftarrow b_{2g}(d_{xy})$; Fig. 5). In addition to these, there is also a possibility of a spin-forbidden d-p transition. The assignment to a d-d transition is easily excluded on the basis of the discussion made in the previous section. The MCD for the shoulder shows a negative B term, resembling apparently that for the band at *ca.* 29×10^3 cm^{-1} of K_2PdCl_4 (Figs. 1 and 3). However, the shoulder seems to be too remote from a dipole-allowed ligand-to-metal CT band (which is absent below 50×10^3 cm^{-1}) to be assigned to the orbitally-forbidden CT transition ($b_{1g}(d_{x^2-y^2}) \leftarrow a_{2g}(\pi)$) as in K_2PdCl_4 (*vide infra*). A similar difficulty arises for the possible assignment to a spin-forbidden CT transition. The single-crystal polarized spectra by Kroening *et al.*[21] have shown a band at *ca.* $36.5 \times 10^3 cm^{-1}$ in both polarizations. The band has so low intensity that it is not likely to have the same origin as the shoulder at 38×10^3 cm^{-1} in solution. Their data suggest that the neighboring band at higher energy which is presumed to correspond to the shoulder also appears in both polarizations. If the presumption is valid, the assignment to the orbitally-forbidden d-p transition ($a_{2u} \leftarrow b_{2g}$) is unreasonable. It is because that the transition is vibronically allowed by a coupling only with the b_{2g} molecular vibration, being out-of-plane polarized. On the other hand, the assignment to a spin-forbidden d-p transition can be a candidate if spin-orbit coupling is taken into account, although the assignment cannot explain the very simple MCD feature. As has been discussed so far, the assignment of the shoulder at 38×10^3 cm^{-1} is still ambiguous and thus further details will be deferred.

2) K_2PdCl_4: It has been found that both bands at 35.7 and 44.9×10^3 cm^{-1} are in-plane polarized, by the polarized reflection spectra;[23] and that in addition, the former includes a $^1A_{2u}$ component, by the polarized absorption spectra.[17,25] The MCD result is consistent with these facts. Therefore, the lower-energy band can be assigned to $^1A_{2u} + {}^1E_u(\pi) \leftarrow {}^1A_{1g}$ ($b_{1g}(d_{x^2-y^2}) \leftarrow b_{2u}(\pi) + e_u(\pi)$), and the higher-energy one to $^1E_u(\sigma) \leftarrow {}^1A_{1g}$ ($b_{1g} \leftarrow e_u(\sigma)$) (Fig. 5). In view of MCD, the $^1A_{2u}$, $^1E_u(\pi)$, and $^1E_u(\sigma) \leftarrow {}^1A_{1g}$ transitions correspond to a negative B term, a negative A term, and a positive A term, respectively.

The assignments to be considered for the shoulder at *ca.* 29×10^3 cm^{-1} are ones to spin-forbidden and orbitally-forbidden CT transitions.[14,27] In K_2PdBr_4 there is another band, which is assigned to a spin-forbidden CT transition,[25] in addition to the band corresponding to the shoulder of K_2PdCl_4; thus, the former assignment is excluded. The orbitally-forbidden CT transition ($b_{1g} \leftarrow a_{2g}$) is expected to be allowed *via* an e_u vibration, being in-plane polarized. This has been confirmed for the shoulder,[7,17] which supports the latter assignment.

The above all assignments (Tables 4 (footnotes) and 5) have been made on the basis of our MCD data and many experimental ones reported by previous workers. The study on the electronic spectra of square-planar complexes (particularly palladium(II)) with nitrogen and oxygen in addition to chlorine as coordinating atoms will be reported in the near future.

References

1) D. S. Martin, Jr., J. G. Foss, M. E. McCarville, M. A. Tucker, and A. J. Kassman, *Inorg. Chem.*, **5**, 491 (1966).
2) A. J. McCaffery, P. N. Shatz, and P. J. Stephens, *J. Am. Chem. Soc.*, **90**, 5721 (1968).
3) J. Chatt, G. A. Gamlen, and L. E. Orgel, *J. Chem. Soc.*, **1958**, 486.
4) R. F. Fenske, D. S. Martin, Jr., and K. Ruedenberg, *Inorg. Chem.*, **1**, 441 (1962).
5) H. B. Gray and C. J. Ballhausen, *J. Am. Chem. Soc.*, **85**, 260 (1963).
6) D. S. Martin, Jr., and C. J. Lenhardt, *Inorg. Chem.*, **3**, 1368 (1964).
7) P. Day, A. F. Orchard, A. J. Thomson, and R. J. P. Williams, *J. Chem. Phys.*, **42**, 1973 (1965).
8) O. S. Mortensen, *Acta Chem. Scand.*, **19**, 1500 (1965).
9) D. S. Martin, Jr., M. A. Tucker, and A. J. Kassman, *Inorg. Chem.*, **4**, 1682 (1965).
10) D. S. Martin, Jr., M. A. Tucker, and A. J. Kassman, *Inorg. Chem.*, **5**, 1298 (1966).
11) B. Bosnich, *J. Am. Chem. Soc.*, **88**, 2606 (1966).
12) H. Basch and H. B. Gray, *Inorg. Chem.*, **6**, 365 (1967).
13) F. A. Cotton and C. B. Harris, *Inorg. Chem.*, **6**, 369 (1967).
14) H. Ito, J. Fujita, and K. Saito, *Bull. Chem. Soc. Jpn.*, **40**, 2584 (1967).
15) P. Day, M. J. Smith, and R. J. P. Williams, *J. Chem. Soc., A*, **1968**, 668.
16) W. A. Mason, III and H. B. Gray, *J. Am. Chem. Soc.*, **90**, 5721 (1968).
17) E. Francke and C. Moncuit, *C. R. Acad. Sci., Ser. B*, **271**, 741 (1970).
18) D. S. Martin, Jr., *Inorg. Chim. Acta Rev.*, **5**, 107 (1971).
19) H. Kato, *Bull. Chem. Soc. Jpn.*, **45**, 1281 (1972).
20) H. H. Patterson, J. J. Godfrey, and S. M. Khan, *Inorg. Chem.*, **11**, 2872 (1972).
21) R. F. Kroening, R. M. Rush, D. S. Martin, Jr., and J. C. Clardy, *Inorg. Chem.*, **13**, 1366 (1974).
22) R. P. Messmer, L. V. Interrante, and K. H. Johnson, *J. Am. Chem. Soc.*, **96**, 3847 (1974).
23) B. G. Anex and N. Takeuchi, *J. Am. Chem. Soc.*, **96**, 4411 (1974).
24) C. Moncuit, *Theor. Chim. Acta*, **39**, 255 (1975).
25) R. M. Rush, D. S. Martin, Jr., and R. G. Legrand, *Inorg. Chem.*, **14**, 2543 (1975).
26) T. G. Harrison, H. H. Patterson, and J. J. Godfrey, *Inorg. Chem.*, **15**, 1291 (1976).
27) L. I. Elding and L. F. Olsson, *J. Phys. Chem.*, **82**, 69 (1978).
28) W. Tuszynski and G. Gliemann, *Z. Naturforsch., A*, **34**, 211 (1979).
29) L. G. Vanquickenborne and A. Ceulemans, *Inorg. Chem.*, **20**, 796 (1981).
30) H. Kobayashi, M. Shimizu, and Y. Kaizu, *Bull. Chem. Soc. Jpn.*, **43**, 2321 (1970).
31) D. B. Siano and D. E. Metzler, *J. Chem. Phys.*, **51**, 1856 (1969).
32) When the band at 30.3×10^3 cm^{-1} was assumed to consist of only one component, the Gaussian curve did not fit in very closely with the experimental one, and furthermore the half-value width was too wide compared with those of other components.
33) H. Isci and W. R. Mason, *Inorg. Nucl. Chem. Lett.*, **8**, 2321 (1972).
34) K. Nakayama, T. Komorita, and Y. Shimura, unpublished work.
35) C. K. Jørgensen, *Prog. Inorg. Chem.*, **12**, 130 (1970).

Spectrophotometric Determination of Lead, Zinc, and Cadmium after Extraction of Their Diethyldithiocarbamates into Molten Naphthalene and Replacement by Copper

Abdul WASEY, Raj K. BANSAL, Masatada SATAKE,*,† and Bal K. PURI
Department of Chemistry, Indian Institute of Technology, Hauz Khas, New Delhi-110016, India
†*Faculty of Engineering, Fukui University, Fukui 910*
(Received September 10, 1983)

A method is proposed for the extraction of lead, zinc, and cadmium as their diethyldithiocarbamates into molten naphthalene. These complexes are quantitatively extracted into molten naphthalene. After extraction, the solidified naphthalene containing the colorless complex of each of the above metals is dissolved in chloroform and the metal is replaced by copper(II) to develop a yellow color of copper(II) diethyldithiocarbamate. The absorbance is measured at 440 nm. Beer's law is obeyed in the concentration range of 5.0—130.0 μg for lead, 3.0—60.0 μg for zinc, or 5.0—100.0 μg for cadmium in 10 ml of the final solution. The molar absorptivities ($1\ mol^{-1}\ cm^{-1}$) and Sandell sensitivities ($\mu g/cm^2$) for lead, zinc, and cadmium are calculated to be 1.15×10^4, 0.0098, 1.11×10^4, 0.0059, and 1.15×10^4, 0.0098 respectively. Solutions containing 45.0 μg of lead, 40.0 μg of zinc, and 43.0 μg of cadmium separately gave mean absorbances of 0.250, 0.620, and 0.440 with standard deviations of 0.0027, 0.0059, and 0.0038, respectively. Conditions have been decided for the determination of lead, zinc, and cadmium in some alloys and synthetic mixtures.

Sodium diethyldithiocarbamate is one of the most popular and versatile organic reagents, which react with many metal ions.[1] Studies of this reagent for use in solvent extraction have revealed that even with the proper control of pH, this reagent is not selective in extracting specific metals although many masking agents have been used.[2] Liquid-liquid extraction no doubt is an excellent technique for the separation and concentration of metal ions. But it cannot be applied directly for those metal ions which form complexes with the chelating agents only at high temperature and form complexes having low solubilities at room temperatures.[3] In such cases, the metal complex is first precipitated at high temperature and then it is extracted into a suitable organic solvent at room temperature.[3] Thus the method is time consuming. Fujinaga and coworkers have developed a new method of extraction *i.e.* "Solid-liquid separation after liquid-liquid extraction" in which the above mentioned difficulty is overcome.[4,5] The technique is especially useful for the extraction of those metal ions which form complexes with complexing agents at high temperature.[3] In the present communication, conditions have been decided for the extraction of lead, zinc, and cadmium as their diethyldithiocarbamates into molten naphthalene and subsequent spectrophotometric determination after dissolution of the solid naphthalene containing the metal complex in chloroform and replacing the metal by copper(II) to develop a yellow color. The interference of various ions has been studied and the method is applied to the determination of lead, zinc and cadmium in some alloys.

Sodium diethyldithiocarbamate[6] has also been used for the spectrophotometric determination of copper after extraction into molten naphthalene in the pH range of 2.0—8.0. The molar absorptivity was reported to be $1.20\times10^4\ l\ mol^{-1}\ cm^{-1}$. It was compared with the present method.

Experimental

Reagents. Solutions of lead nitrate, zinc sulfate, and cadmium sulfate were prepared in distilled water from their A. R. grade reagents and standardized by the known methods.[7] A 1×10^{-3} M (1 M=1 mol dm^{-3}) solution of sodium diethyldithiocarbamate (Na ddtc) was prepared in distilled water.

Chloroform and naphthalene were tested for impurities spectrophotometrically before use.

Apparatus. An Elico pH meter and a Pye-Unicam SP-700 recording spectrophotometer were used.

General Procedure. An aliquot of each of the metal solution was taken in a beaker and 1 cm^3 of 1.0×10^{-3} M Na ddtc solution was added to it. The pH of the solutions was adjusted to 7.0 for lead, 4.5 for zinc, and 7.5 for cadmium with the buffer solution, perchloric acid (0.2 M) or sodium hydroxide (0.2 M) (Fig. 2). These solutions were transferred to 100 cm^3 round-bottom flasks and warmed in a water-bath at about 60 °C and then naphthalene (2.0 g) was added to each. The flask was stoppered and heating was continued until naphthalene melted. The mixture was stirred vigorously until the naphthalene solidified forming very fine crystals in all the cases. Once more the naphthalene was melted, shaken vigorously, and allowed to stand at room temperature. The naphthalene containing the colorless complex was separated by filtration, dried in the folds of a filter paper, and dissolved in chloroform. In each case, the solution was made exactly to 10 cm^3 in a volumetric flask. This 10 cm^3 extract in chloroform was treated with aqueous copper sulfate solution (10 cm^3 of 1×10^{-3} M) to develop a yellow color in the chloroform layer which was separated and dried with anhydrous sodium sulfate (2.0 g). A portion of this solution was taken in a 1-cm cell and the absorbance was measured at 440 nm in each case against the reagent blank.

Results and Discussion

Absorption Spectra. It has already been established that copper is extracted quantitatively into molten naphthalene as a diethyldithiocarbamate complex in the pH range of 2—11 and has an absorption maximum at 440 nm. The stability constant of copper(II) diethyldithiocarbamate as indicated in the literature is two times more than those of lead, zinc, and cadmium diethyldithiocarbamates.[8] Obviously these metals can be quantitatively replaced by copper from the chloroform layer into the aqueous layer after

their extraction as diethyldithiocarbamates.

The absorption spectra of sodium diethyldithiocarbamate and lead, zinc, and cadmium complexes in naphthalene and chloroform solution were recorded against water and reagent blank after replacing the metal by copper(II). It was observed that copper complex absorbed strongly at 440 nm, where the reagent blank absorbed negligibly (Fig. 1).

Effect of pH. Extractions were carried out at different pH's keeping other conditions constant. It was found that the extractions were quantitative in the pH range of 6.2—8.3 for lead, 4.8—9.3 for zinc, and 6.6—11.5 for cadmium (Fig. 2).

Effect of Reagent Concentration. At optimum pH, extractions were carried out at varying reagent concentrations. It was observed that the extractions were quantitative for 0.5—4.0 cm^3 of the reagent in all the cases (Fig. 3). So 1.0 cm^3 of the reagent was used throughout the experiments in all the cases.

Effect of Electrolytes. Various electrolytes such as sodium chloride, sodium nitrate, sodium acetate, and sodium perchlorate (0.01—1.0 M) caused no improvement in extraction, indicating no salting-out effect.

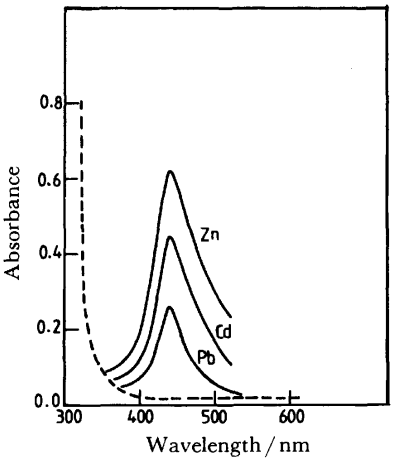

Fig. 1. Absorption spectra of Na ddtc and Cu complex in naphthalene-chloroform solution. Pb: 45.0 mg; Zn: 40.0 mg; Cd: 43.0 mg; Na ddtc (1×10^{-3} M); 2.0 ml in each case; pH: 8.3; naphthalene: 2.0 g. Reference: Water and reagent blank.

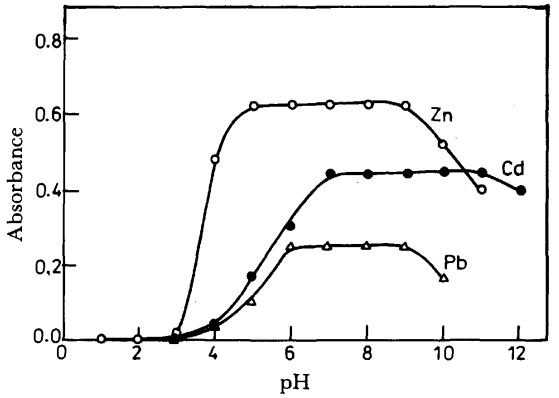

Fig. 2. Effect of pH. Pb: 45.0 mg; Zn: 40.0 mg; Cd: 43.0 mg; Na ddtc (1×10^{-3} M): 2.0 ml in each case; naphthalene: 2.0 g. Wavelength: 440 nm. Reference: Reagent blank.

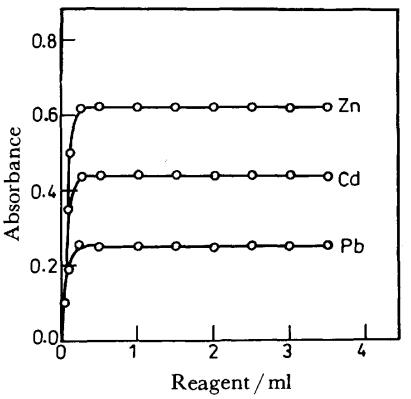

Fig. 3. Effect of reagent concentration. Conditions were same as in Fig. 2. Reference: Reagent blank.

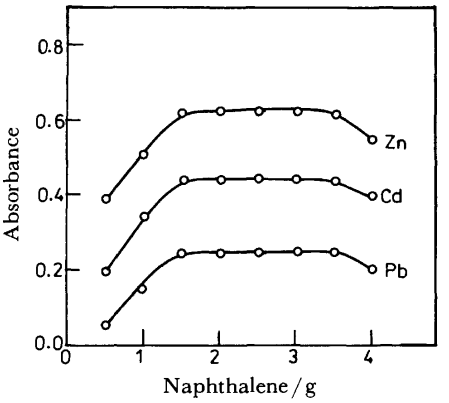

Fig. 4. Effect of amount of naphthalene. Conditions were same as in Fig. 2. Reference: Reagent blank.

Effect of Amount of Naphthalene. The amount of naphthalene was varied from 0.25—4.0 g. The absorbance remained constant when the naphthalene used was in the range of 1.4—3.5 g (Fig. 4).

Effect of Volume of Aqueous Phase. Since the volume of the aqueous phase is very large as compared to that of naphthalene (2.0 g), it was necessary to study the effect of the volume of the aqueous phase on the extraction on these metal ddtc complexes. The volume of the aqueous phase was varied from 10 to 70 cm^3. The extraction was quantitative when the volume of the aqueous phase did not exceed 40 cm^3 for lead and 50 cm^3 for zinc and cadmium. Above these volumes of the aqueous phase the extraction was not quantitative (Fig. 5).

Effect of Digestion and Shaking Times. The complex was digested at high temperature on a boiling water-bath (81 °C) between 1—10 min before extraction into naphthalene. It was observed that the constant absorbance was obtained by digesting between 2—10 min for cadmium, zinc, and lead. Therefore, 5 min of digestion time was selected. The effect of shaking time on the absorbance was also examined. It was observed that the extraction of the complex into molten naphthalene was very fast and no change was seen in the degree of the extraction when shaking time was varied from 1—20 min. Therefore, 2

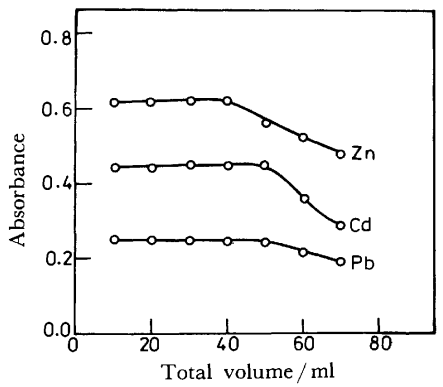

Fig. 5. Effect of volume of aqueous phase. Conditions were same as in Fig. 2. Reference: Reagent blank.

min of shaking time was chosen in all the cases for the further work.

Beer's Law and Sensitivity. Under the optimum conditions described above, calibration curves were constructed at 440 nm in each case. Beer's law held in the concentration range of 5.0—130.0 μg for lead, 3.0—60.0 μg for zinc, and 5.0—100.0 μg for cadmium in 10 cm^3 of the chloroform solution. The molar absorptivities (1 mol^{-1} cm^{-1}) and Sandell sensitivities (μg/cm^2) were calculated to be 1.15×10^4, 0.0098; 1.11×10^4, 0.0059; and 1.15×10^4, 0.0098, respectively (for lead, zinc, and cadmium). Solutions containing 45.0 μg of lead, 40.0 μg of zinc, and 43.0 μg of cadmium gave mean absorbances of 0.250, 0.620, and 0.440 with standard deviations of 0.0027, 0.0059, and 0.0038, respectively. The percentage of the extraction was established in each case by back-extracting the metal from the chloroform layer (before replacing by copper) with 20 cm^3 of 4 M HNO_3 and then determining the metals by atomic absorption spectrophotometry. It was 95.75, 92.40, and 95.80% respectively. These values are consistent with those obtained spectrophotometrically after metal ion exchange with copper(II).

Composition of the Metal Complex. The nature of lead, zinc, and cadmium diethyldithiocarbamates extracted into molten naphthalene was studied by the Job's method of continuous variation and the mole ratio method. A sharp peak at 0.33 mole fraction in Job's curve and a clear break at 1:2 (metal:Na ddtc) ratio in the mole-ratio plot suggested the extraction of $Pb(C_5H_{10}NS_2)_2$, $Zn(C_5H_{10}NS_2)_2$, and $Cd(C_5H_{10}NS_2)_2$ into the molten naphthalene.

Effect of Diverse Ions. The interference of various ions has been studied in detail. Generally, 5.0 mg of the anions and 1.0 mg of the cations were added, individually to the solutions containing 45.0 μg of lead, 40.0 μg of zinc, or 43.0 μg of cadmium before

TABLE 1. EFFECT OF DIVERSE ANIONS
Pb: 45.0 μg, Zn: 40.0 μg, and Cd: 43.0 μg

Alkali salt added	Anion added (mg)	Absorbance at 440 nm		
		Pb	Zn	Cd
—	—	0.250	0.621	0.440
Sodium chloride	5.0	0.250	0.622	0.442
Potassium bromide	5.0	0.245	0.620	0.444
Potassium iodide	5.0	0.200	0.615	0.445
	0.5	0.244	0.620	0.440
Sodium acetate	5.0	0.240	0.620	0.442
Sodium sulfate	5.0	0.100	0.622	0.440
	0.2	0.200	0.620	0.436
	0.1	0.240	0.622	0.440
Sodium perchlorate	5.0	0.250	0.620	0.440
Potassium sodium tartrate	5.0	0.245	0.618	0.440
Sodium citrate	5.0	0.155	0.520	0.390
	0.5	0.240	0.615	0.440
Potassium thiocyanate	5.0	0.250	0.615	0.440
Sodium thiosufate	5.0	0.250	0.615	0.442
EDTA (disodium)	5.0	0.002	0.005	0.003
	0.1	0.014	0.015	0.012

TABLE 2. EFFECT OF DIVERSE CATIONS
Pb: 45.0 μg, Zn: 40.0 μg, and Cd: 43.0 μg

Alkali salt added	Anion added (mg)	Absorbance at 440 nm		
		Pb	Zn	Cd
—	—	0.250	0.621	0.440
Sodium arsenite	1.0	0.250	0.625	0.440
Silver(I) nitrate	1.0	0.240	0.610	0.430
Cobalt(II) chloride	1.0	0.310	0.700	0.520
	0.4	0.255	0.625	0.450
Copper(II) chloride	1.0	0.270[a]	0.650[a]	0.460[a]
	0.5	0.255[a]	0.630[a]	0.445[a]
Chromium(III) nitrate	1.0	0.250	0.620	0.442
Iron(III) chloride	1.0	0.265[b]	0.635[b]	0.460[b]
	0.5	0.252[b]	0.620[b]	0.436[b]
Mercury(II) chloride	1.0	0.245	0.610	0.440
Iridium(III) chloride	1.0	0.255	0.628	0.445
Nickel(II) chloride	1.0	0.290	0.685	0.510
	0.5	0.255	0.620	0.445
Osmium tetraoxide	1.0	0.252	0.624	0.444
Palladium(II) nitrate	1.0	0.340[c]	0.750[c]	0.560[c]
	0.5	0.255[c]	0.640[c]	0.450[c]
Rhodium(III) chloride	1.0	0.250	0.622	0.444
Potassium tellurite	1.0	0.240	0.615	0.430
Ruthenium(III) chloride	1.0	0.254	0.620	0.442
Thallium(I) nitrate	1.0	0.254	0.620	0.442
Sodium tungstate	1.0	0.250	0.622	0.440
Tartar emeric	1.0	0.260	0.624	0.450
Lead(II) nitrate	1.0	—	0.624[d]	0.445[d]
Zinc(II) chloride	1.0	0.256[e]	—	0.650[f]
	0.5	0.254[e]	—	0.580[f]
	0.2	0.252[e]	—	0.550[f]
Cadmium(II) chloride	1.0	0.254[e]	0.757	—
	0.5	0.252[e]	0.680[g]	—
	0.2	0.250[e]	0.680[g]	—
Indium(III) sulfate	1.0	0.260	0.630	0.450

a) Copper was eliminated by preextraction at pH 2.5. b) Interference of iron(III) was eliminated after masking with 10 ml of 5% NaF. c) Extraction of Pb, Zn, and Cd were carried out at pH 9.0 to eliminate Pd. d) Lead was eliminated as lead sulfate. e) Interference of zinc and cadmium was eliminated by masking with 10 ml of 5% NaCN. f) Extraction of cadmium was carried out at pH 11.5 to reduce extraction of zinc up to some extent. g) Extraction of zinc was carried out at pH 4.8 to eliminate cadmium.

TABLE 3. DETERMINATION OF LEAD, ZINC, AND CADMIUM IN ALLOYS AND SYNTHETIC MIXTURES

Alloy/Synthetic mixture	Composition (%)	Metal present (μg)	Metal found (μg)	Average μg	Error %	Metal found by AAS method (μg)
Aluminium brass C NBS-C1120	Cu: 80.1, Zn: 18.1 Al: 1.5	Zn: 18.0	17.8, 17.7, 17.8, 17.8, 17.8	17.78	1.22	18.2
Phosphor bronze NBS-63C	Cu: 80.5, Pb: 9.4 Zn: 9.0, P: 0.2	Pb: 37.6	37.5, 37.0, 37.2, 37.0, 37.2	37.18	1.11	37.5
	As: 0.02	Zn: 36.0	35.5, 35.6, 35.8, 35.7, 35.6	35.62	1.05	35.8
Bronze BCS-182/1	Cu: 84.8, Sn: 5.0, Zn: 5.2, Pb: 3.5,	Pb: 35.0	34.5, 34.4, 34.6, 34.8, 34.7	34.60	1.14	34.8
	P: 0.5, As: 0.14	Zn: 10.4	10.3, 10.3, 10.3, 10.2, 10.3	10.28	1.15	10.5
Gun metal BCS-183/3	Cu: 84.5, Sn: 6.7, Zn: 3.3, Pb: 3.4,	Pb: 34.0	33.8, 33.6, 33.7, 33.6, 33.5	33.64	1.06	34.0
	Ni: 1.5, As: 0.15	Zn: 9.9	9.8, 9.7, 9.8, 9.8, 9.8	9.8	1.01	9.9
Synthetic mixture	Cd: 50.0, Pb: 5.0, Cu: 45.0,	Pb: 50.0	49.5, 49.4, 49.3, 49.4, 49.5	49.42	1.16	49.8
		Cd: 25.0	24.8, 24.7, 24.8, 24.8, 24.6	24.74	1.04	25.0
Synthetic mixture	Pb: 20.0, Cd: 5.0, Ni: 50.0, Co: 25.0	Pb: 40.0	39.5, 39.6, 39.7, 39.5, 39.5	39.52	1.11	40.2
		Cd: 30.0	29.7, 29.8, 29.6, 29.7, 29.7	29.7	1.10	29.9

extraction. Among the anions examined (Table 1), only iodide and sulfate interfered with the determination of lead, but their relatively low concentration can be tolerated. Citrate and Na_2H_2 edta interfered in all the cases, the extraction being impossible in the presence of Na_2H_2 edta in all the cases obviously due to higher stability constant of metal edta complex than that of the metal ddtc complex.[9] Citrate can be tolerated in a relatively low concentration (Table 1). Among the cations examined (Table 2), Fe^{3+}, Co^{2+}, Ni^{2+}, Cu^{2+}, and Pd^{2+} seriously interfered, but Co^{2+} and Ni^{2+} can be tolerated if present in a relatively low concentration. The interference of copper was eliminated by preextraction (chloroform extraction) at pH 2.5 and from the aqueous solution these metal ions (Pb, Zn, and Cd) can be extracted at their respective pH range. To eliminate the effect of palladium the extraction of lead, zinc, and cadmium were carried out at about pH 9 where palladium does not form complexes with Na ddtc. In all the cases Fe^{3+} was masked by adding 10 cm^3 of 5% NaF before extraction. The interference from Cu^{2+}, Co^{2+}, Ni^{2+}, Fe^{3+}, Pd^{2+}, Zn^{2+}, and Cd^{2+} in the determination of lead can also be eliminated by adding 10 cm^2 of 5% NaCN solution before extraction (Table 2).

Determination of Lead, Zinc, and Cadmium in Alloys and Synthetic Mixtures. A Sample of 100 mg of the alloy of known composition was taken in a beaker and 15—20 cm^3 of concentrated nitric acid were added. When the vigorous reaction was over, the solution was evaporated on a hot plate to about 5 cm^3. It was diluted with 50 cm^3 of distilled water, heated again for 20—25 min, filtered through a Whatman No.42 filter paper and the filtrate was collected in a 1 liter volumetric flask. The residue was washed ten times with dilute HNO_3 (1:1000) and the volume was made upto the mark with distilled water. An aliquot of this sample solution was taken and analyzed by the general procedure already stated. Five replicate determinations were made for each sample. The interference of various ions have been eliminated as stated in Table 2.

One of us (A.W.) is grateful to the C.S.I.R., New Delhi, India for financial assistance.

References

1) F. J. Welcher, "Organic Analytical Reagents," D. Van Nostrand Co. Inc., Princeton (1947) Vol. IV.
2) A. K. De, S. M. Khopkar, and R. A. Chalmers, "Solvent Extraction of Metals," Van Nostrand Reinhold, London (1970).
3) H. Bode, *Z. Anal. Chem.*, **144**, 165 (1955).
4) T. Fujinaga, T. Kuwamoto, and E. Nakayama, *Talanta*, **16**, 1225 (1969).
5) B. K. Puri, M. Gautam, and T. Fujinaga, *Bull. Chem. Soc. Jpn.*, **52**, 3415 (1979).
6) A. I. Vogel, "A Text Book of Quantitative Inorganic Analysis," 3rd ed, Longmans Green and Co., London (1969).
7) M. Satake, Y. Yamagishi, and Y. Nagaosa, *Memoirs of the Faculty of Engineering, Fukui University*, **24**, 59 (1976).
8) D. D. Perrin, "Masking and Demasking of Chemical Reactions," Wiley-Interscience, New York (1970).

Syntheses of 2Fe-2S Ferredoxin Model Complexes of Cys-Containing Oligopeptides by Reaction with $Fe_2S_2^{2+}$ Ion or by Sulfide Incorporation

Norikazu UEYAMA, Satoru UENO, Michio NAKATA, and Akira NAKAMURA*
Department of Macromolecular Science, Faculty of Science, Osaka University, Toyonaka, Osaka 560
(Received September 12, 1983)

The 2Fe-2S ferredoxin model complexes of two peptide ligands, Z-L-Ala-L-Cys-OMe (Z=benzyloxycarbonyl) and Z-L-Cys-L-Ala-L-Ala-L-Cys-OMe, were synthesized from $[NMe_4]_2[Fe_2S_2Cl_4]$ by addition of triethylamine. These were characterized by absorption, CD, and MCD spectra in dimethyl sulfoxide or *N,N*-dimethylformamide. Incorporation of inorganic sulfide to the iron(III) complex, $[Fe(Z\text{-cys-Ala-Ala-cys-OMe})_2]^-$ (rubredoxin models), results in the selective formation of a 2Fe-2S cluster by a controlling ability of the peptides.

The 2Fe-2S type of iron-sulfur proteins plays important roles in biochemical reactions, *e.g.* photosynthesis, and have been the subjects of many biological and physicochemical studies.[1] The structure of the active site in oxidized *Spirulina platensis* ferredoxin which is responsible for photosynthetic electron transfer in blue-green algae was confirmed by an X-ray analysis.[2] Three cysteinyl thiolates in one characteristic Cys-A-B-C-D-Cys-X-Y-Cys sequence bind a $[Fe_2S_2]^{2+}$ core.

Structural analogs of 2-Fe ferredoxins, such as $[Fe_2S_2(S_2\text{-}o\text{-xyl})_2]^{2-}$ (S_2-*o*-xyl=*o*-xylene-α,α'-dithiolate) were synthesized and the structure was confirmed crystallographically by Mayerle *et al.*[3] Such analogs have extremely low redox potentials, for example at −1.50 V (*vs.* SCE) in *N,N*-dimethylformamide (DMF) for $[Fe_2S_2(S_2\text{-}o\text{-xyl})_2]^{2-}$,[4] while spinach ferredoxin exhibits one at −0.42 V (*vs.* NHE).[5] The positive shift of the redox potentials of native 2Fe-2S ferredoxins is apparent. Probably the peptide sequence is responsible for this.

An important problem exists in the incorporation of S^{2-} into $[Fe(SR)_4]^-$ to give a 2Fe-2S type, since 2-Fe ferredoxins are formed from 1-Fe iron proteins in nature. Rydon *et al.* reported that the incorporation of S^{2-} and Fe^{3+} in dimethyl sulfoxide (DMSO) into denatured rubredoxin results in the formation of an Fe_4S_4 complex.[6] They also reported the formation of an Fe_4S_4 type complex from Ac-Gly_2-Cys-$(Gly_2\text{-Cys})_n$Gly-NH_2 (n=0—3), iron(III) chloride, and sodium sulfide in DMSO.[7] However, Sugiura *et al.* observed the formation of an Fe_2S_2 complex by the reaction among HS-$(CH_2)_n$SH, iron(III) chloride, and S^{2-}.[8] The difference in these studies is probably attributable to the structure of thiolate ligands; Cys-containing peptide or alkanedithiolate. The Gly-Gly peptide sequence used by Christou *et al.*[6] does not contribute to the bending of the peptide chains which facilitates chelation by the two cysteinyl thiolates. Therefore, we are interested in the synthesis of an Fe_2S_2 complex of Z-Cys-Ala-Ala-Cys-OMe by the reaction of $[Fe_2S_2Cl_4]^{2-}$ with the peptide. The Ala-Ala sequence, interposed between the two cysteinyl residues, promotes the formation of a hairpin turn conformation and enables to chelate to a tetrahedral iron(III) ion. The formation of the tetrapeptide chelate has already been confirmed for palladium(II) and iron(III) ions.[9] We also examined incorporation of S^{2-} into the oxidized rubredoxin analog of a Cys-X-Y-Cys peptide. Recently, Coucouvanis *et al.*[10] reported the synthesis of $[Fe_2S_2\{Ac\text{-}Gly_2\text{-}(cys\text{-}Gly_2)_2NH_2\}]^{2-}$ by the same procedure as mentioned above, but they have not examined the incorporation of S^{2-} into their complexes.

Experimental

All procedures were carried out under argon atmosphere.

Materials. All solvents were purified by distillation before use. The syntheses of Z-Ala-Cys-OMe and Z-Cys-Ala-Ala-Cys-OMe will be reported elsewhere.[11].

Syntheses of $[NMe_4]_2[Fe_2S_2(Z\text{-cys-Ala-Ala-cys-OMe})_2]$ and $[NMe_4]_2[Fe_2S_2(Z\text{-Ala-cys-OMe})_4]$. $[NMe_4]_2[Fe_2S_2Cl_4]$ was prepared by the reaction of $[NMe_4]_2[Fe_2S_2(S_2\text{-}o\text{-xyl})_2]$ (500 mg, 7.6×10^{-4} mol) with PhCOCl (0.46 cm^3, 4×10^{-3} mol) according to the procedure reported by Wong *et al.*[12] The 2Fe-2S complex of Z-Cys-Ala-Ala-Cys-OMe (**1**) was synthesized by the addition of triethylamine (2×10^{-3} cm^3, 1.43×10^{-5} mol) to a solution of $[NMe_4]_2[Fe_2S_2Cl_4]$ (1.7 mg, 3.7×10^{-6} mol) and Z-Cys-Ala-Ala-Cys-OMe (4.2 mg, 8.2×10^{-6} mol) in 2.0 cm^3 of *N,N*-dimethylformamide (DMF). The solution was concentrated *in vacuo* after 5 h. The crude product was washed with methanol and dried *in vacuo*.

$[NMe_4]_2[Fe_2S_2(Z\text{-Ala-cys-OMe})_4]$ (**2**) was synthesized by the reaction of Z-Ala-Cys-OMe (6.6 mg, 1.94×10^{-5} mol) with $[NMe_4]_2[Fe_2S_2Cl_4]$ (2.0 mg, 4.3×10^{-6} mol), followed by the addition of triethylamine (3×10^{-3} cm^3, 2.1×10^{-5} mol) in 2.0 cm^3 of DMF as mentioned above.

Incorporation of S^{2-} to Iron(III) Complex of the Cys-containing Peptides. A solution of $[Fe(Cys\text{-peptide})_4]^-$ was prepared by the same procedure reported previuosly.[13] Iron(III) chloride (3.7 mg, 2.3×10^{-5} mol) and Z-Ala-Cys-OMe (31.7 mg, 9.3×10^{-5} mol) or Z-Cys-Ala-Ala-Cys-OMe (24.2 mg, 4.7×10^{-5} mol) were dissolved in 2 cm^3 of DMSO. The addition of triethylamine (7×10^{-3} cm^3, 5×10^{-5} mol) to the solution gave a deep red-violet solution. Quick addition of Na_2S (1.8 mg, 2.3×10^{-5} mol) resulted in rapid development of a black color. The solution was characterized by absorption, CD, and EPR spectra. The values of ε for absorption and $\Delta\varepsilon$ for CD and MCD are based upon the molar concentration of $Fe_2S_2^{2+}$ ion.

Physical Measurement. Absorption spectra were measured on a JASCO UVIDEC-5A in visible region. CD and MCD spectra were recorded on a JASCO J-40 spectrometer equipped with electromagnets. The magnetic field was calibrated by using a $K_3[Fe(CN)_6]$ aqueous solution, $\Delta\varepsilon_M$ of 3.0 at 420 nm. EPR spectra were obtained at 77 K on a JEOL JESFE1X with 100 kHz magnetic field modulation. The *g*-value (g=1.981) was standardized by using Mn^{2+}. Cyclic voltammetries were measured with a Yanaco-P8-CV equipped with a function generator Yanaco Model FG-1218. Sample solutions were 10^{-3} mol dm^{-3} in DMF containing 0.05

mol dm^{-3} $[N(n\text{-}Bu)_4][ClO_4]$ as a supporting electrolyte. The voltammograms were recorded at 25°C *vs.* a saturated calomel electrode (SCE) as the reference.

Results and Discussion

Syntheses and Spectral Characterization of $[Fe_2S_2(Z\text{-}Ala\text{-}cys\text{-}OMe)_4]^{2-}$ *and* $[Fe_2S_2(Z\text{-}cys\text{-}Ala\text{-}Ala\text{-}cys\text{-}OMe)_2]^{2-}$. The Cys-containing peptide complexes possessing an Fe_2S_2 core were prepared quantitatively by the addition of triethylamine to a solution containing the corresponding peptides and $[Fe_2S_2Cl_4]^{2-}$. An attempt to isolate these complexes as crystals has been unsucessful due to its instability in air. Only a solid material was obtained.

Figure 1 shows the absorption and CD spectra of $[NMe_4]_2[Fe_2S_2(Z\text{-cys-Ala-Ala-cys-OMe})_2]$ (**1**) and $[NMe_4]_2[Fe_2S_2(Z\text{-Ala-cys-OMe})_4]$ (**2**), and the absorption spectra of $[NMe_4]_2[Fe_2S_2Cl_4]$. **1** exhibits three characteristic absorptions due to the core, $Fe_2S_2^{2+}$, at 325 nm (ε:11 100), 414 nm (ε:8 760), and 445 nm (ε:7 150) similar to those of oxidized native 2Fe-2S ferredoxin, while **2** shows only a broad absorption at 450—400 nm. Both complexes provide a strong absorption at 310 nm with similar intensity. Such three characteristic absorptions were reported for native 2Fe-2S ferredoxins and an alkanedithiolate complex. The 2Fe-2S complex of $Ac\text{-}Gly_2\{Cys\text{-}Gly_2\}_2\text{-}NH_2$ was reported to exhibit absorption maxima at 333, 423, and 458 nm.[10] The oxidized native 2Fe-2S ferredoxin was reported to show three absorption maxima at 323—325 nm (ε:12 000—15 000), 423 nm (ε:9 700), and 466 nm (ε: 8 520) in visible region.[14] Absorption maxima at 294 nm (ε:14 500), 338 nm (ε:16 200), 414 nm (ε:17 000), and 590 nm (ε:4 800) with a shoulder at around 455 nm in DMF were observed in the oxidized 2Fe-2S model complex, $[Fe_2S_2(S_2\text{-}o\text{-xyl})_2]^{2-}$.[3,4]

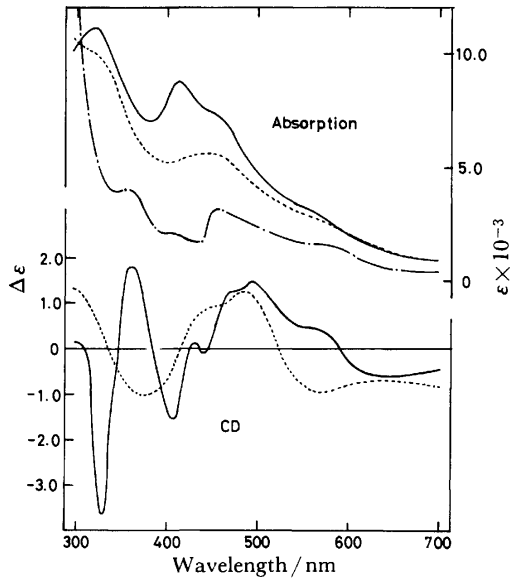

Fig. 1. Absorption and CD spectra of $[Fe_2S_2(Z\text{-Ala-cys-OMe})_4]^{2-}$ ----, $[Fe_2S_2(Z\text{-cys-Ala-Ala-cys-OMe})_2]^{2-}$ ——, $[Fe_2S_2Cl_4]^{2-}$ -·-·- in DMF.

CD spectra of **1** and **2** are quite different from that of the native 2Fe-2S ferredoxin as listed in Table 1. Well-defined troughs at 332, 408, and 660 nm and peaks at 363, 470, and 495 nm were observed in the DMF solution of **1**. The low values of Δε observed for **1** and **2** are distinct from the observed high extrema of native 2Fe-2S ferredoxins with the characteristic peptide sequence. The higher Δε values of **1** at 363 nm (Δε:+1.94) and 332 nm (Δε:−3.61) than those of **2** indicate that chelation by the tetrapeptide leads to the fixation of the peptide conformation where chiral effect of cysteine residues is not averaged.

As listed in Table 2, the MCD spectrum of **1** indicates typical peaks at 486 nm ($\Delta\varepsilon_M$:+0.58) and 526 nm ($\Delta\varepsilon_M$:+0.62) and a broad shoulder at 560 nm ($\Delta\varepsilon_M$:+0.54) of an oxidized 2Fe-2S core reported by Stephens *et al.* for 2Fe-2S ferredoxins of *Spirulina maxima* and putidaredoxin.[14]

Positive MCD transitions at 480 nm ($\Delta\varepsilon_M$:+0.76), and 566 nm ($\Delta\varepsilon_M$:+0.21) in **1** are also observed as well as the oxidized native 2Fe-2S ferredoxin. Unfortunately, assignments of the MCD transitions also in **1** or oxidized native 2Fe-2S ferredoxin were not possible because of the complexity of the energy levels of the Fe_2S_2 core. However, by comparing the native 2Fe-2S ferredoxins with 1Fe or 4Fe-4S ferredoxins, Stephens *et al.* reported that the native 2Fe-2S ferredoxins exhibit a characteristic shape with a positive MCD transition at 486 nm ($\Delta\varepsilon_M$:+0.58).[14] Generally, the MCD spectra of 4Fe-4S ferredoxins have the strongest peak ($\Delta\varepsilon_M$: +1.0—+1.8) at 380—390 nm. However, in the case of the model complex **1**, the MCD peak at 380—385 nm was weak ($\Delta\varepsilon_M$:+0.06) and the strongest MCD peak was observed at 480 nm ($\Delta\varepsilon_M$:+0.76) indicating presence of a 2Fe-2S core.

Table 1. CD spectra of $[Fe_2S_2(Z\text{-cys-Ala-Ala-cys-OMe})_2]^{2-}$, $[Fe_2S_2(Z\text{-Ala-cys-OMe})_4]^{2-}$, and related systems in DMF

Complex	CD extrema λ/nm(Δε)			
$[Fe_2S_2(Z\text{-cys-Ala-Ala-cys-OMe})_2]^{2-}$ (**1**)	660(−0.43)	495(+1.50)	470(+1.23)	448(−0.06)
	433(+0.20)	408(−1.57)	363(+1.94)	332(−3.61)
Fe^{III}/Z-Cys-Ala-Ala-Cys-OMe/Na_2S (1:2:1)[a]	622(−0.63)	563(+0.04)	547(−0.10)	477(+1.39)
	450(+0.62)	444(+0.64)	401(−2.19)	366(+1.14)
	331(−2.71)	303(−0.77)		
$[Fe_2S_2(Z\text{-Ala-cys-OMe})_4]^{2-}$ (**2**)	570(−0.98)	488(+1.30)	450sh(+0.83)	380(−1.03)
Fe^{III}/Z-Ala-Cys-OMe/Na_2S (1:4:1)[a]	526(−0.16)	456(+0.10)	376(−0.35)	318(+0.19)
Native 2Fe-2S ferredoxin[b]	619(−0.05)	602(+0.05)	553(−5.71)	510sh(−2.93)
(*S. maxima*)	429(+19.79)	381(−5.57)	359(+1.93)	344sh(−0.93)

a) In Me_2SO. b) In H_2O.

TABLE 2. CD SPECTRA OF $[Fe_2S_2(Z\text{-cys-Ala-Ala-cys-OMe})_2]^{2-}$, AND RELATED SYSTEMS

Complex	MCD extrema λ/nm(Δε$_M$)			
$[Fe_2S_2(Z\text{-cys-Ala-Ala-cys-OMe})_2]^{2-}$ (**1**)	664(−0.44)	566sh(+0.21)	480(+0.76)	430(−0.18)
	376(+0.32)			
Fe^{III}/Z-Cys-Ala-Ala-Cys-OMe/Na_2S (1:2:1)[a]	685(+0.06)	664(+0.07)	638(+0.05)	561(+0.14)
	544(+0.13)	525sh(+0.16)	508sh(+0.19)	482(+0.23)
	419(+0.03)	400(+0.08)	383sh(+0.07)	362(+0.06)
	332(+0.27)			
Native 2Fe-2S ferredoxin[b]	560sh(+0.54)	526(+0.62)	486(+0.58)	444(−0.08)
(*S.maxima*)	424(+0.20)	377(−0.54)	360(−0.30)	352(−0.31)
	328(+0.23)			

a) In Me_2SO. b) In H_2O.

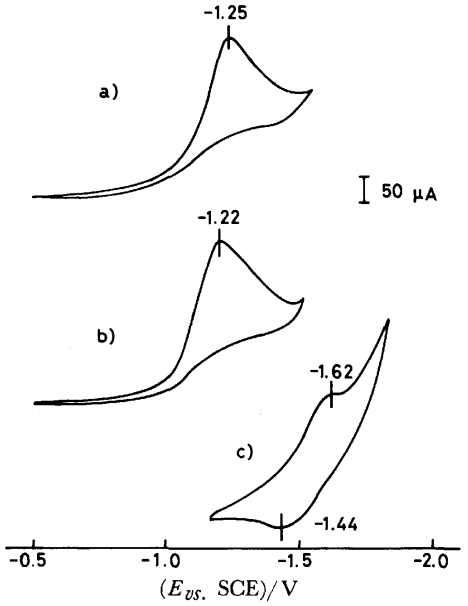

Fig. 2. Cyclic voltammograms of a) $[Fe_2S_2(Z\text{-Ala-cys-OMe})_4]^{2-}$, b) $[Fe_2S_2(Z\text{-cys-Ala-Ala-cys-OMe})_2]^{2-}$, and c) $[Fe_2S_2(S_2\text{-}o\text{-xyl})_2]^{2-}$ in DMF.

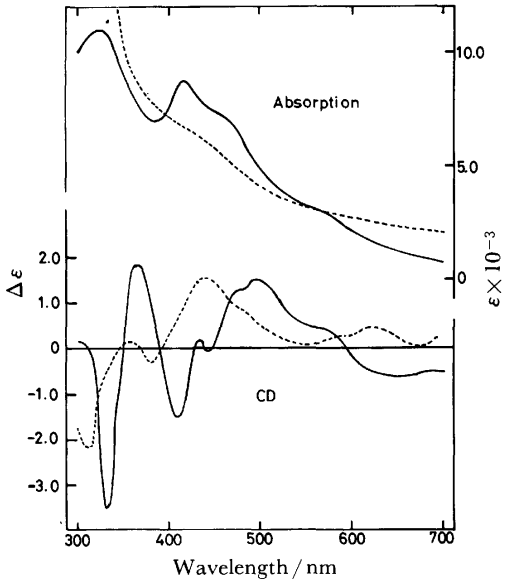

Fig. 3. Absorption and CD spectra of $[Fe_2S_2(Z\text{-cys-Ala-Ala-cys-OMe})_2]^{2-}$ —— and its reduced species with 10 equiv of dithionite complex of 18-crown-6 ---- in DMF.

Electrochemical and Chemical Reduction of $[Fe_2S_2(Z\text{-cys-Ala-Ala-cys-OMe})_2]^{2-}$. Importance of the peptide sequence in the stability of redox couple (2-/3-) was investigated by cyclic voltammetry. Figure 2 shows the cyclic voltammograms of **1** and **2** in DMF at room temperature. Although a reduction peak was observed at −1.22 V(*vs.* SCE) for **1** and −1.25 V(*vs.* SCE) for **2**, no oxidation peak has been recognized. At a low temperature (−12°C), an oxidation peak for **1** was observed ($E_{p,a}$: −1.23 V, $E_{p,c}$: −0.83 V, $i_{p,c}/i_{p,a}$=1/20), while it was undetectable for **2**. The results indicate that both synthetic complexes are readily decomposed by electrochemical reduction and suggest that the chelating peptide such as Z-Cys-Ala-Ala-Cys-OMe has a potential ability to maintain the $[Fe_2S_2]^+$ ion during the redox couple. A stable redox couple of $[Fe_2S_2(S_2\text{-}o\text{-xyl})_2]^{2-}$ in acetonitrile/hexamethylphosphoric triamide(HMPA) (7:3 v/v) was found by Mascharak *et al.*[4] Actually, at the same concentration (10^{-3} mol dm^{-3}) in DMF, a quasi-reversible redox couple ($i_{p,c}/i_{p,a}\simeq 1$) of $[Fe_2S_2(S_2\text{-}o\text{-xyl})_2]^{2-}$ was detected at −1.62 V($E_{p,a}$) and −1.44 V($E_{p,c}$) in fair agreement with their values in the different solvents. **1** or **2** exhibited a positive shift (ΔV=0.37—0.40 V) of the reduction peak in the cyclic voltammogram as compared with the reduction peak of $[Fe_2S_2(S_2\text{-}o\text{-xyl})_2]^{2-}$. Therefore, the reduction of **1** and **2** with $Na_2S_2O_4$ was examined. The reduction of a model complex, $[Fe_2S_2(S_2\text{-}o\text{-xyl})_2]^{2-}$, has been known to require sodium acenaphthylenide in HMPA.[4] Figure 3 shows the visible spectrum of **1** reduced by $Na_2S_2O_4$ complexed with 18-crown-6 in DMF.[15] The spectrum indicates the formation of a $[Fe_4S_4]^{2+}$ core possessing a characteristic absorption maximum at 420 nm (ε: 6 600) in DMF. Also the CD spectrum of the reduced species of **1** exhibits a different pattern from that of **1**. The CD maximum at 440 nm (Δε: +1.57) corresponds to that of $[Fe_4S_4(Z\text{-cys-Gly-Ala-cys-OMe})_2]^{2-}$.[16] The reduction of **2** by $Na_2S_2O_4$ provided the same type of a product having $[Fe_4S_4]^{2+}$ that was detected by an absorption maximum at 420 nm (ε: 4 820). The formation of $[Fe_4S_4X_4]^{2-}$ (X=SR, Cl) by the reduction of $[Fe_2S_2X_4]^{2-}$ was reported by Cambray *et al.*[17] and Wong *et al.*,[12] respectively, except for $[Fe_2S_2(S_2\text{-}o\text{-xyl})_2]^{2-}$. Thus, binuclear-to-tetranuclear conversions have been found to take place by chemical means, which are reflected by the irreversibility of the cyclic voltammograms of **1** and **2** at room temperature. The *o*-xylene-α,α′-dithiolate ligand prevents the $[Fe_2S_2]^+$ core from the reductive conversion to the $[Fe_4S_4]^{2+}$ core. The results suggest that chelation of the

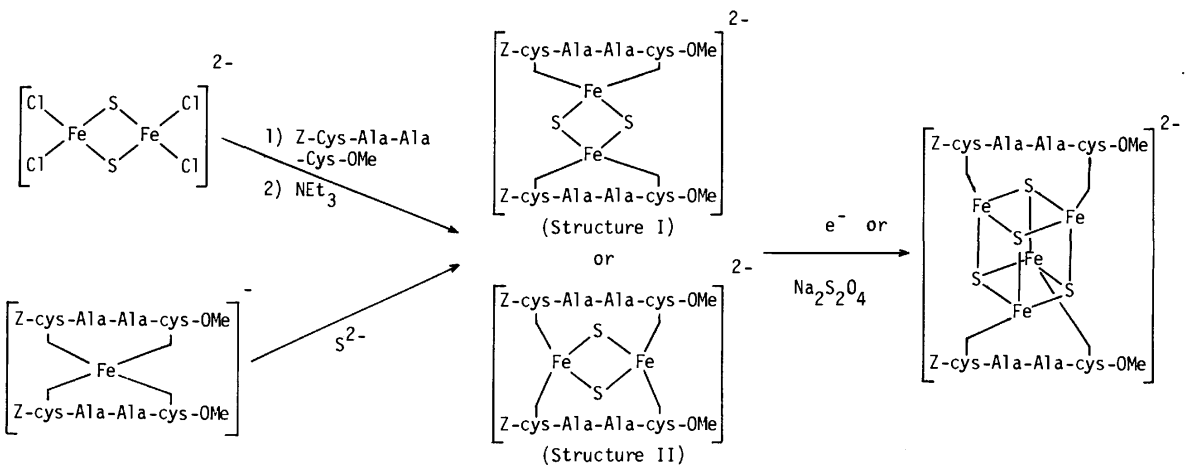

Fig. 4. Syntheses and reactions of the 2Fe-2S complexes of Z-Cys-Ala-Ala-Cys-OMe.

tetrapeptide is involved not for one iron(III) (structure I in Fig. 4) but for two iron(III) ions in a FeS_2Fe system (structure II) and that the alkanedithiolate ligand is more suitable for the chelation to one iron(III) ion. The coordination of Z-Cys-Ala-Ala-Cys-OMe in the structure II corresponds to that of the native Cys-X-Y-Cys sequence as reported with the X-ray analysis.[2] It is plausible that the complex having the structure II easily associates to the 4Fe-4S type by reduction.

Fe^{III}/Cys-containing peptides/S^{2-} Complexes. The formation of iron-sulfur clusters by incorporation of inorganic sulfide(S^{2-}) into Fe^{III}/Cys-containing peptide complexes was studied. On the basis of the investigation on iron-sulfur protein models, Sugiura *et al.*[8] and Cambray *et al.*[17] have found the selective formation of 2Fe-2S complexes from iron(III) complexes of simple thiolate ligands by incorporation of inorganic sulfide. On the other hand, Christou *et al.* reported the formation of a 4Fe-4S complex by the incorporation of inorganic sulfide into iron(III) complexes of Ac-Gly$_2$-(cys-Gly$_2$)$_4$-NH_2.[7] Thus, it is interesting to determine which type of complexes is formed by the incorporation of inorganic sulfide into the present Fe^{III}/peptide complexes. The peptide ligand probably controls the incorporation and the stability of the products.

The addition of an equimolar amount of Na_2S to a solution of Fe^{III}/Cys-containing peptide(1:4) complexes results in the rapid development of black color. We have already established that Fe^{III}/Cys-containing peptide(1:4) complexes provide a Fe(S-Cys)$_4$ core as a model of rubredoxin, especially in the case of macro-ring chelation by Z-Cys-Ala-Ala-Cys-OMe.[18] Tables 1 and 2 list the CD and MCD spectra of the products of the sulfide incorporation, *i.e.* Fe^{III}/Cys-containing peptide/S^{2-} complexes. The absorption spectrum of each of these complexes had maxima at 300 and 415 nm and a weak shoulder around 450 nm, similar to those of **1**. On the other hand, 4Fe-4S ferredoxin model complexes, $[Fe_4S_4(SR)_4]^{2-}$, show two absorption maxima around 300 and 410 nm in DMF or in DMSO/H_2O (8:2 v/v).[19] Sugiura *et al.* reported that the product formed between Fe^{III}/alkanethiolate complexes with inorganic sulfide has absorption maxima at 330, 410, and 450 nm and there is a considerable similarity in spectra between their complexes and the 2Fe-2S ferredoxins.[8] They revealed also that reconstituted adrenodoxins exhibit an absorption maximum at 410 nm with a weak shoulder at 450 nm which is due to a 2Fe-2S cluster.[20] From the comparison of these data with our results, a major component of an iron-sulfur cluster involved in the system, Fe^{III}/peptide complexes/S^{2-}, is suggested to be a 2Fe-2S cluster. The CD (Table 1) and MCD (Table 2) spectra of the Fe^{III}/Cys-containing/S^{2-} system were more highly structured than the corresponding absorption spectra(Table 1) and these are useful for identification of the complexes. In the case of the Fe^{III}/Z-Cys-Ala-Ala-Cys-OMe/S^{2-} system, CD troughs at 331 nm ($\Delta\varepsilon$:−2.71) and 401 nm ($\Delta\varepsilon$:−2.19), and peaks at 366 nm ($\Delta\varepsilon$:+1.14) and 477 nm ($\Delta\varepsilon$:+1.39) were observed, which correspond to those of **1** (Table 1), though the positions of absorption maxima are somewhat ambiguous. In order to compare with the above CD spectrum, $[Fe_4S_4(Z\text{-cys-Ala-Ala-cys-OMe})_2]^{2-}$ was synthesized by a ligand exchange reaction of $[(n\text{-}Bu)_4N]_2[Fe_4S_4(S\text{-}i\text{-}Pr)_4]$ with Z-Cys-Ala-Ala-Cys-OMe in solution.[16] The 4Fe-4S complex in DMF provides two CD troughs at 330 nm ($\Delta\varepsilon$:−0.8) and 400 nm ($\Delta\varepsilon$:−0.7), and two peaks at 360 nm ($\Delta\varepsilon$:+0.2) and 430 nm ($\Delta\varepsilon$:+0.9). The CD spectra of the Fe^{III}/Z-Cys-Ala-Ala-Cys-OMe/Na_2S (1:2:1) system indicate the preferential formation of an 2Fe-2S cluster although being not consistent completely with the CD extrema of **1**. The inconsistency between their CD extrema seems to be caused by the contamination of the 4Fe-4S cluster. The CD spectrum of the Fe^{III}/Z-Ala-Cys-OMe/S^{2-} complex was completely different from that of $[NMe_4]_2[Fe_2S_2(Z\text{-Ala-cys-OMe})_4]$ (Table 1) The low $\Delta\varepsilon$ values suggest that the Fe^{III}/Z-Ala-Cys-OMe/S^{2-} system results in the preferential formation of the 4Fe-4S cluster.

Recently the MCD spectra of ferredoxins of various 2Fe-2S and 4Fe-4S types have been reported in detailed.[11] Those data indicated that the 4Fe-4S ferredoxin in both $Fe_4S_4^{2+}$ and $Fe_4S_4^{+}$ states exhibit only positive MCD bands in all the region from 300 to 2000

nm, whereas the 2Fe–2S ferredoxins show positive and negative bands. The MCD spectra were used to establish whether the structure of the iron-sulfur centers in the peptide complexes is like 2Fe–2S or 4Fe–4S type. The tetrapeptide complex, Fe^{III}/Z-Cys-Ala-Ala-Cys-OMe/S^{2-} (1:2:1), exhibited the strongest peak at 482 nm ($\Delta\varepsilon_M$:+0.23) due to the 2Fe–2S cluster (Table 2). Therefore, the absorption, CD, and MCD results indicate that a 2Fe–2S cluster forms predominantly in the Fe^{III}/tetrapeptide/S^{2-} system and small amounts of other types of clusters are contaminated.

The 2Fe–2S cluster in these peptide complexes was also established by the analysis of the EPR spectra of the Fe^{III}/Cys-containing peptide/S^{2-} system. The EPR signals at g=4.18 of the peptide complexes disappeared completely on the addition of S^{2-} and new signals appeared at g=2.04, 2.00, and 1.98; g_{av}=2.01 for the tetrapeptide complex and at g_{av}=2.06 for the dipeptide complex. Laskowski *et al.* reported that a 4Fe–4S ferredoxin analog, $[Fe_4S_4(SCH_2Ph)_4]^{3-}$, exhibits two EPR signals at g=2.04 and 1.93 in acetonitrile below 15 K.[21] The EPR data of the reduced 2Fe–2S ferredoxin analog are not available at present. From these data and the fact that the EPR signals of the peptide complexes with inorganic sulfide are measurable at 77 K, it is apparent that the tetranuclear cluster are not preferentially formed at least by the simple addition of inorganic sulfide to Fe^{III}/Cys-containing peptide(1:4) complexes.

Thus, a major part of iron-sulfur clusters in the Fe^{III}/Cys-containing peptide/S^{2-} system is the 2Fe–2S type, which is different from the previous study of Rydon *et al.* on iron(III) complexes of sequential oligopeptide, Ac-Gly_2-(Cys-Gly_2)$_n$-NH_2.[7] Probably their peptides, having more than two Cys residues and Gly-Gly residues interposed between the two Cys residues, do not have any controlling power for the selective formation of a 2Fe–2S type ferredoxin core.

We thank Professor Yukio Sugiura for useful discussion on the characterization of 2Fe–2S complexes. The present work was supported by a Grant-in-Aid (No. 56430014) from the Ministry of Education, Science and Culture.

References

1) P. M. Handford and W. K. Lee, "Inorganic Biochemistry," ed by H. A. O. Hill, the Royal Society of Chemistry, Burlington House, London (1979), Vol 2, pp. 84–96.
2) T. Tsukihara, K. Fukuyama, H. Tahara, Y. Katsube, Y. Matsuura, N. Tanaka, M. Kakudo, K. Wada, and H. Matsubara, *J. Biochem.*, **84**, 1645 (1978).
3) J. J. Mayerle, R. B. Frankel, R. H. Holm, J. A. Ibers, W. D. Phillips, and J. F. Weiher, *Proc. Natl. Acad. Sci. U.S.A.*, **70**, 2429 (1973).
4) P. K. Mascharak, G. C. Papaefthymiou, R. B. Frankel, and R. H. Holm, *J. Am. Chem. Soc.*, **103**, 6110 (1981).
5) K. Tagawa, and D. I. Arnon, *Biochim. Biophys. Acta*, **153**, 602 (1968).
6) G. Christou, B. Ridge, and H. N. Rydon, *J. Chem. Soc., Chem. Commun.*, **1979**, 20.
7) G. Christou, B. Ridge, and H. N. Rydon, *J. Chem. Soc., Chem. Commun.*, **1977**, 908.
8) Y. Sugiura, M. Kunishima, and H. Tanaka, *Biochim. Biophys. Res. Commun.*, **48**, 1400 (1972).
9) N. Ueyama, M. Nakata, and A. Nakamura, *Inorg. Chim. Acta*, **55**, L61 (1981).
10) A. Balasukramaniam and D. Coucouvanis, *Inorg. Chim. Acta*, **78**, L35 (1983).
11) N. Ueyama, M. Nakata, and A. Nakamura, in preparation.
12) G. B. Wong, M. A. Bobrik, and R. H. Holm, *Inorg. Chem.*, **17**, 578 (1978).
13) J. J. Mayerle, S. E. Denmark, B. V. Depamphilis, J. A. Ibers, and R. H. Holm, *J. Am. Chem. Soc.*, **97**, 1032 (1975).
14) P. J. Stephens, A. J. Thomson, J. B. R. Dunn, T. A. Keiderling, J. Ramlings, K. K. Rao, and D. O. Hall, *Biochemistry*, **17**, 4770 (1978).
15) T. Mincey and T. G. Traylor, *Bioinorg. Chem.*, **9**, 409 (1978).
16) N. Ueyama, M. Nakata, A. Nakamura, M. Kamata, and S. Otsuka, *Inorg. Chim. Acta*, **80**, 207 (1983).
17) J. Cambray, R. W. Lane, A. G. Wedd, R. W. Johnson, and R. H. Holm, *Inorg. Chem.*, **16**, 2565 (1977).
18) N. Ueyama, M. Nakata, and A. Nakamura, *Bull. Chem. Soc. Jpn.*, **55**, 2364 (1981).
19) C. L. Hill, J. Renaud, R. H. Holm, and L. E. Mortenson, *J. Am. Chem. Soc.*, **99**, 2549 (1977).
20) Y. Sugiura, K. Ishizu, and T. Kimura, *Biochim. Biophys. Res. Commun.*, **60**, 334 (1974).
21) E. J. Laskowski, R. B. Frankel, W. O. Gillum, G. C. Papaefthymiou, J. Renaud, J. A. Ibers, and K. H. Holm, *J. Am. Chem. Soc.*, **100**, 5322 (1978).

 © 1984 The Chemical Society of Japan Bull. Chem. Soc. Jpn., 57, 989—996 (1984)

Preparation and Circular Dichroism Spectra of Cobalt(III) Complexes Containing an Optically Active $NH_2CH_2CH(CH_3)X^-$-*N,X* (X=S or Se) Ligand

Kyoko NAKABAYASHI, Kaoru DOI, Masaaki KOJIMA, and Junnosuke FUJITA*
Department of Chemistry, Faculty of Science, Nagoya University, Chikusa-ku, Nagoya 464
(Received September 24, 1983)

Several cobalt(III) complexes of the $[Co(apS \text{ or } apSe)(N_4)]^{2+}$ type were prepared, where apS and apSe denote chiral 1-amino-2-propanethiolate-*N,S* and 1-amino-2-propaneselenolate-*N,Se* ligands, respectively, and N_4 is (en=ethylenediamine)$_2$, (*R*-chxn=(*R,R*)-1,2-cyclohexanediamine)$_2$, or tren=tris(2-aminoethyl)amine. Their circular dichroism (CD) spectra were compared with one another and with those of complexes containing such ligands as achiral 2-aminoethanethiolate-*N,S*, 2-aminoethaneselenolate-*N,Se*, or chiral 1-amino-2-propanolate-*N,O* (apO). The vicinal CD curves of *S*-apS obtained from CD spectra of the en and *R*-chxn complexes are similar and very large in magnitude in the d-d absorption band region. These curves are very similar to the CD spectrum of $[Co(S\text{-apO})(NH_3)_4]^{2+}$. The vicinal CD curve of *S*-apSe shows a similar pattern, but the magnitude is smaller than those of the *S*-apS and *S*-apO ligands. The vicinal effect of the protonated *S*-apSH ligand is much smaller compared with that of its conjugate base (*S*-apS) ligand. The tren complexes of *S*-apS and *S*-apSe exhibit CD spectra fairly different from the vicinal CD curves of the respective ligands in the d-d absorption band region.

Nishide *et al.*[1] reported that cobalt(III) complexes containing a chiral aminoalkanolate-*N,O* chelate ligand such as *S*-apO (*S*-apOH=(*S*)-1-amino-2-propanol) exhibit exceptionally strong circular dichroism (CD) in the d-d absorption band region, which is attributed to the large vicinal effect of the alcoholate ligand. It is of interest to examine whether the corresponding thiolate-*N,S* and selenolate-*N,Se* chelate ligands give a similar effect. However, complexes with chiral aminoalkanethiolate-*N,S* or the corresponding selenolate-*N,Se* chelate ligands do not seem to be known except for $[Co(R\text{-cys})(en)_2]^+$ and $[Co(S\text{-pen})(en)_2]^+$ (en=ethylenediamine, *R*-cys=(*R*)-cysteinate(2-)-*N,S*, *S*-pen=(*S*)-penicillaminate(2-)-*N,S*).[2,3] The complexes with *R*-cys or *S*-pen will not be suitable for studying the vicinal effect, since the ligands have a carboxylato substituent and the chelate ring formed by *N,S* chelation will be conformationally unstable by forming hydrogen bonds between the carboxylato and other groups. In fact, the *R*-cys chelate ring in *Λ*-$[Co(R\text{-cys})(en)_2]^+$ in crystals forms a *δ* conformer with the axially disposed carboxylato group.[3] It is known that the vicinal effect of a chiral ligand is particularly sensitive to the conformation in a complex.[4]

In the present study, we have prepared complexes of the $[Co(apS \text{ or } apSe)(N_4)]^{2+}$ type, where apS and apSe denote 1-amino-2-propanethiolate-*N,S* and 1-amino-2-propaneselenolate-*N,Se* ligands, respectively, and N_4 is $(en)_2$, (*R*-chxn=(*R,R*)-1,2-cyclohexanediamine)$_2$, or tren=tris(2-aminoethyl)amine, and measured their CD spectra in order to see the vicinal effect of these chiral ligands. To our knowledge, the *S*- or *R*-apSe complexes prepared in this study are the first cobalt(III) complexes containing an optically active selenolate ligand.

Experimental

Ligands. The apSH ligand was prepared by the method of Owen[5] and resolved by the procedure of Piper *et al.*[6] to obtain $(+)_{589}$-apSH·HCl($[\alpha]_{589}$=+34.2° (*c* 1.2, H_2O); lit, $[\alpha]_{589}$=+35.3° (*c* 1.46, H_2O)[6]). The absolute configuration of the $(+)_{589}$-isomer has not been determined yet, but can be assigned to *S* configuration on the basis of the isomer distribution of $[Co(apS)(R\text{-chxn})_2]^{2+}$ and related complexes, and CD spectra of these complexes (*vide infra*). Both *rac*- and $(+)_{589}$-apSH·HCl were oxidized with H_2O_2[7] to give the respective disulfide hydrochlorides $(NH_2CH_2CH(CH_3)S-)_2\cdot 2HCl$ which were used to prepare cobalt(III)–apS complexes.

Racemic 2,2′-diselenodipropylamine dihydrochloride, $(NH_2CH_2CH(CH_3)Se-)_2\cdot 2HCl$ was prepared by the method of Yokoyama *et al.*[8] and used to prepare cobalt(III)–apSe complexes without optical resolution.

Optically active *R*-chxn was obtained by resolving *rac*-chxn (Tokyo Kasei Kogyo Co., Ltd.) according to the method of Treptow,[9] and tren was obtained by separating from crude triethylenetetramine (Tokyo Kasei Co., Ltd.).[10]

Δ(lel$_3$)-[*Co*(R-*apS*)(R-*chxn*)$_2$]*SiF*$_6\cdot 4H_2O$, Δ(oblel$_2$)-[*Co*(S-*apS*)(R-*chxn*)$_2$]*ZnCl*$_4$, Λ(lelob$_2$)-[*Co*(S-*apS*)(R-*chxn*)$_2$]*ZnCl*$_4\cdot H_2O$. An aqueous solution (10 cm^3) containing *R*-chxn·2HCl (3.0 g, 16 mmol) and NaOH (1.28 g, 32 mmol) was deoxygenated by bubbling nitrogen for 15 min, and then was syringed into a deoxygenated, aqueous solution (10 cm^3) of $CoCl_2\cdot 6H_2O$ (1.90 g, 8 mmol) with stirring. The mixture became a pinkish orange suspension. To the mixture was added a deoxygenated aqueous solution (8 cm^3) containing *rac*-$(NH_2CH_2CH(CH_3)S-)_2\cdot 2HCl$ (1.01 g, 4 mmol) and NaOH (0.32 g, 8 mmol). The mixture was stirred under an atmosphere of nitrogen for 3 h at room temperature. The resulting brown solution was filtered to remove a small amount of insoluble material, and the filtrate was passed through a column (ϕ2.7 cm × 5 cm) of SP-Sephadex C-25. The Sephadex charged with the product was placed on the top of a column (ϕ7 cm × 40 cm) of SP-Sephadex C-25, and the product was eluted with 0.1 mol dm^{-3} $Na_2[Sb_2(d\text{-tartrate})_2]$, giving two main brown bands A and B. The first band A contains the *Λ*(*lelob*$_2$), and the second band B a mixture of the *Δ*(*lel*$_3$) and *Δ*(*oblel*$_2$) isomers. The structural assignment for the isomers was made on the basis of the elution order, formation ratio, and CD spectra of the isomers (*vide infra*). No indication of the presence of the *Λ*(*ob*$_3$) isomer was observed in the column chromatography. The eluate of band B was diluted 20 times with water, passed through an SP-Sephadex C-25 column (ϕ2.7 cm × 120 cm), and the complex adsorbed was eluted with 0.15 mol dm^{-3} $(NH_4)_2SO_4$. Bands B-I (*Δ*(*lel*$_3$)) and B-II (*Δ*(*oblel*$_2$)) were eluted separately in this order. Each eluate of bands A, B-I, and B-II was diluted with water and passed again through an SP-Sephadex C-25 column (ϕ1.5 cm × 2 cm). The column charged with A was washed thoroughly with 0.1 mol dm^{-3}

HCl (10 dm^3), and the complex was eluted with 0.8 mol dm^{-3} HCl. The eluate was evaporated to a small volume under reduced pressure. The concentrate was mixed with excess $ZnCl_2$ (0.2 g) in 3 mol dm^{-3} HCl (0.3 cm^3) to precipitate brown tetrachlorozincate of the complex. It was recrystallized from water–ethanol. Found: C, 29.47; H, 6.17; N, 11.52%. Calcd for $C_{15}H_{38}N_5Cl_4CoSZn$: C, 29.89; H, 6.35; N, 11.62%. The complex of B-I was eluted from the column with 0.4 mol dm^{-3} $(NH_4)_2SiF_6$. The eluate was allowed to stand overnight in a refrigerator to give purplish brown needles, which were collected and washed with cold water. Found: C, 30.26; H, 7.66; N, 11.89%. Calcd for $C_{15}H_{44}N_5CoF_6O_4SSi$: C, 30.45; H, 7.50; N, 11.84%. The complex of B-II was isolated as tetrachlorozincate by the same method as that for A. Found: C, 30.82; H, 6.31; N, 11.88%. Calcd for $C_{15}H_{36}N_5Cl_4CoSZn$: C, 30.81; H, 6.21; N, 11.98%. The total yield and the formation ratio, $\Delta(lel_3)$ (B-I): $\Delta(oblel_2)$ (B-II): $\Lambda(lelob_2)$ (A) determined by reference to optical densities of the eluates were *ca.* 80% and 3.6:2.4:1, respectively. The main by-product was Δ-$[Co(R\text{-chxn})_3]^{3+}$.

The same experiment was carried out using the optically active disulfide derived from $(+)_{589}$-apSH·HCl, instead of the racemic one. Two isomers, $\Delta(oblel_2)$ and $\Lambda(lelob_2)$ were formed in the formation ratio of 2.3:1.

Λ- and Δ-[Co(S-apS)(en)$_2$]SiF$_6$·0.5H$_2$O. These complexes were prepared from $Co(ClO_4)_2\cdot 6H_2O$, en, and the optically active disulfide by a method similar to that for $[Co(apS)(R\text{-chxn})_2]^{2+}$. After stirring for 3 h at room temperature, the product was chromatographed by use of an SP-Sephadex C-25 column and an eluent, 0.1 mol dm^{-3} $Na_2[Sb_2(d\text{-tartrate})_2]$. Two brown bands of the Λ- and Δ-isomers were eluted separately, the former being eluted faster. Each eluate was diluted 20 times with water, and passed through a column of SP-Sephadex C-25. The column was washed with 0.02 mol dm^{-3} NH_4Cl (1 dm^3), and the complex was eluted with 0.4 mol dm^{-3} $(NH_4)_2SiF_6$. The eluate was left in a refrigerator to yield brown crystals. Found for the Λ-isomer: C, 19.76; H, 5.87; N, 16.66%. Found for the Δ-isomer: C, 19.94; H, 5.98; N, 16.83%. Calcd for $C_7H_{25}N_5CoF_6O_{0.5}SSi$: C, 20.00; H, 5.99; N, 16.66%. The total yield and the formation ratio, Λ-isomer: Δ-isomer based on optical densities of the eluates were *ca.* 90% and 1.9:1, respectively.

p-[Co(S-apS)(tren)](ClO$_4$)$_2$ and t-[Co(S-apS)(tren)]ZnCl$_4$·0.5ZnCl$_2$.[11] These complexes were prepared from $CoCl_2\cdot 6H_2O$ (8 mmol), tren (8 mmol), and the optically active disulfide (4 mmol), by a method similar to that for $[Co(apS)(R\text{-chxn})_2]^{2+}$. After stirring for 2 d at room temperature, a small portion of the resulting solution was set aside to examine the formation ratio of the isomers, and to the rest was added 4 cm^3 of 60% $HClO_4$. Brown crystals were precipitated, collected, washed with ethanol, and recrystallized from 10^{-3} mol dm^{-3} HCl–60% $HClO_4$. Yield: 2.15 g. The complex was the *p*-isomer as confirmed by column chromatography (Dowex 50W × 2, 2 mol dm^{-3} HCl). Found: C, 21.87; H, 5.37; N, 14.08%. Calcd for $C_9H_{26}N_5Cl_2CoO_8S$: C, 21.87; H, 5.30; N, 14.17%. The filtrate and washings were combined, diluted with water, and passed through a column (ϕ3 cm × 35 cm) of Dowex 50W × 2. By elution with 2 mol dm^{-3} HCl, two bands, T-I (dark brown, *t*-isomer) and T-II (brown, *p*-isomer) appeared separately. The eluate of fast-moving band T-I was collected and evaporated to a small volume under reduced pressure. On addition of $ZnCl_2$ (0.3 g) in 3 mol dm^{-3} HCl (0.4 cm^3) the concentrate gave pink precipitate, which was collected, washed with methanol and acetone, and air-dried. Yield: 0.18 g. Found: C, 18.91; H, 4.53; N, 18.91; Cl, 31.04%. Calcd for $C_9H_{26}Cl_5CoSZn_{1.5}$: C, 18.94; H, 4.60; N, 18.94; Cl, 31.06%. The eluate of band T-II was diluted with water, passed through an SP-Sephadex C-25 column, and the complex was eluted with 0.8 mol dm^{-3} $NaClO_4$. Upon evaporation of the eluate additional 1.3 g of the *p*-isomer perchlorate was obtained. The formation ratio of the *p*- to *t*-isomer contained in the reaction mixture was found to be 15:1 by column chromatography (Dowex 50W × 2, 2 mol dm^{-3} HCl).

[Co(aeS)(en)$_2$]Cl$_2$·H$_2$O and Λ-[Co(aeS)(en)$_2$](ClO$_4$)$_2$ (aeSH=2-aminoethanethiol). The racemic complex was prepared by the method of Lane *et al.*[12] and resolved by column chromatography (SP-Sephadex C-25, 0.1 mol dm^{-3} $Na_2[Sb_2(d\text{-tartrate})_2]$). From the first band the Λ-isomer was isolated as perchlorate. Found: C, 15.87; H, 4.82; N, 15.38%. Calcd for $C_6H_{22}N_5Cl_2CoO_8S$: C, 15.87; H, 4.88; N, 15.42%. The complex has been resolved by fractional crystallization of the diastereomer with $[Sb_2(d\text{-tartrate})_2]^{2-}$.[13]

Δ(lel$_3$)-[Co(R-apSe)(R-chxn)$_2$](ClO$_4$)$_2$·2.5H$_2$O, Δ(oblel$_2$)-[Co(S-apSe)(R-chxn)$_2$](ClO$_4$)$_2$·2.5H$_2$O, and Λ(lelob$_2$)-[Co(S-apSe)(R-chxn)$_2$]$^{2+}$. These complexes were prepared by a method similar to that for the corresponding apS complexes using $CoCl_2\cdot 6H_2O$ (1.19 g, 5 mmol), *R*-chxn·2HCl (1.88 g, 10 mmol), *rac*-$(NH_2CH_2CH(CH_3)Se\text{–})_2\cdot 2HCl$ (0.87 g, 2.5 mmol), and the equivalent amount of NaOH (1.0 g, 15 mol). The mixture was stirred for 3 h at room temperature. The resulting brown solution containing brown precipitate was mixed with water (1 dm^3) and the solution was poured on a column of SP-Sephadex C-25 (ϕ3 cm × 150 cm). By elution with 0.2 mol dm^{-3} Na_2SO_4, the product adsorbed was separated into two brown bands, C and D. The first band C contains the $\Delta(lel_3)$ isomer, and the other D a mixture of the $\Delta(oblel_2)$ and $\Lambda(lelob_2)$ isomers. No band indicative of the $\Lambda(ob_3)$ isomer was observed. The eluate of band D was diluted 20 times with water, poured on a column (ϕ3 cm × 70 cm)of SP-Sephadex C-25, and the complexes adsorbed were eluted with 0.1 mol dm^{-3} $Na_2[Sb_2(d\text{-tartrate})_2]$. Two bands, D-I ($\Lambda(lelob_2)$) and D-II ($\Delta(oblel_2)$) were eluted separately. Each eluate of bands C, D-I, and D-II was diluted with water, poured on a column (ϕ2 cm × 2 cm) of SP-Sephadex C-25, and the complex was eluted with 0.8 mol dm^{-3} $NaClO_4$. The eluate was stored in a refrigerator overnight to yield crystals of the complex perchlorate, which were collected, washed with a small amount of cold water, and air-dried. Yields: $\Delta(lel_3)$-isomer, 530 mg; $\Delta(oblel_2)$-isomer, 65 mg; $\Lambda(lelob_2)$-isomer, 5 mg. The apSe complexes in solution are rather unstable, and decompose during the course of crystallization to decrease the yield extremely. Found for the $\Delta(lel_3)$-isomer: C, 26.98; H, 5.89; N, 10.58%. Found for the $\Delta(oblel_2)$-isomer: C, 27.19; H, 5.94; N, 10.58%. Calcd for $C_{15}H_{41}N_5Cl_2CoO_{10.5}Se$: C, 26.96; H, 6.18; N, 10.48%. The elemental analysis of the $\Lambda(lelob_2)$-isomer was not carried out because of a very low yield, and the complex was assumed to be anhydrous for determining the formation ratio of the isomers by spectrophotometric methods. The formation ratio, $\Delta(lel_3)$ (C): $\Delta(oblel_2)$ (D-II): $\Lambda(lelob_2)$ (D-I), in the reaction mixture was 5.3:3.8:1.

Λ(R)- and Δ(S)-[Co(apSe)(en)$_2$]ZnCl$_4$·H$_2$O and Λ(S)- and Δ(R)-[Co(apSe)(en)$_2$]SiF$_6$·H$_2$O. The racemates of these diastereomers were prepared from $CoCl_2\cdot 6H_2O$ (0.4 g, 1.67 mmol), en (0.2 g, 3.34 mmol), and the diselenide (0.29 g, 0.84 mmol) by a method similar to that for $[Co(apSe)(R\text{-chxn})_2]^{2+}$. The mixture was stirred for 3 h, and then chromatographed by use of an SE-Toyopearl[14] column (ϕ3 cm × 20 cm). By elution with 0.1 mol dm^{-3} Na_2SO_4, two brown bands, E-I and E-II were eluted separately. Bands E-I and E-II contain racemates of the diastereomers, $\Lambda(R)$ and $\Delta(S)$, and $\Lambda(S)$ and $\Delta(R)$, respectively. Each eluate was diluted 20 times with water and passed through an SP-Sephadex C-25 column (ϕ2.7 cm × 120 cm). By elution with 0.1 mol dm^{-3} $Na_2[Sb_2(d\text{-tartrate})_2]$, the band was separated into two. The enantiomers being eluted faster were those of

Λ(R) and *Λ(S)* in E-I and E-II, respectively. The eluate of the *Λ(R)* (or *Λ(S)*) isomer was diluted 20 times with water and poured on an SP-Sephadex C-25 column (φ1.5 cm × 2 cm). The column was washed with 0.01 mol dm^{-3} HCl (8 dm^3), and the complex was eluted with 0.8 mol dm^{-3} HCl. The eluate was evaporated to a small volume under reduced pressure below 35 °C. To the concentrate was added $ZnCl_2$ (0.3 g) in 3 mol dm^{-3} HCl (0.4 cm^3). The solution was mixed with methanol and allowed to cool in a refrigerator overnight to yield brown powder, which was collected, washed with acetone, and air-dried. Found: C, 15.51; H, 4.50; N, 12.91%. Calcd for $C_7H_{26}N_5Cl_4CoSeZn$: C, 15.53; H, 4.84; N, 12.94%. The eluate of the *Λ(S)* (or *Δ(R)*) isomer was diluted 20 times with water and passed through an SP-Sephadex C-25 column (φ1.5 cm × 2 cm). The column was washed thoroughly with 0.01 mol dm^{-3} NH_4Cl (10 dm^3), and the complex was eluted with 0.4 mol dm^{-3} $(NH_4)_2SiF_6$. The eluate was allowed to cool in a refrigerator overnight to yield brown needles, which were collected, washed with cold water, and air-dried. Found: C, 17.75; H, 5.56; N, 14.94%. Calcd for $C_7H_{26}N_5CoF_6OSeSi$: C, 17.65; H, 5.50; N, 14.70%. The formation ratio, *Λ(R)* + *Λ(S)*(E-I):*Λ(S)* + *Δ(R)*(E-II) determined by optical densities of the eluates was 1:4.

(−)$_{589}$-p-[Co(S-apSe)(tren)](ClO$_4$)$_2$ and t-[Co(rac-apSe)(tren)](ClO$_4$)$_2$·H$_2$O. A mixture of racemic *p*- and *t*-[Co(apSe)(tren)]$^{2+}$ was prepared from $CoCl_2 \cdot 6H_2O$ (4 mmol), tren (4 mmol), and the diselenide (2 mmol) by a method similar to that for $[Co(apSe)(R\text{-chxn})_2]^{2+}$. The mixture was stirred for 4 d at room temperature, and then concd HCl was added to make the solution slightly acidic. The solution was chromatographed in a similar manner to that for $[Co(apSe)(R\text{-chxn})_2]^{2+}$. By elution with 0.1 mol dm^{-3} Na_2SO_4 adjusted to pH 2 with HCl, two bands appeared; a fast-moving dark brown band (*p*-isomer) and a slow-moving dark green-brown one (*t*-isomer). The *p*-isomer was isolated as perchlorate by the same method as that for $[Co(apSe)(R\text{-chxn})_2]^{2+}$. Yield: 700 mg. The *t*-isomer was isolated as tetrachlorozincate by the same method as that for *Λ*-$[Co(R\text{-apSe})(en)_2]^{2+}$ and then converted into perchlorate by use of a QAE-Sephadex (ClO_4^- form) column. Yield: 100 mg. Found for the *t*-isomer: C, 19.35; H, 4.58; N, 12.61%. Calcd for $C_9H_{28}N_5Cl_2CoO_9Se$: C, 19.33; H, 5.04; N, 12.52%.

The *p*-isomer was resolved as follows; a mixture of the *p*-isomer perchlorate (0.27 g, 0.5 mmol) and potassium *d*-tartrate hemihydrate (0.117 g, 0.5 mmol) in 10 cm^3 of water was stirred for 30 min. The solution was evaporated to 1.5 cm^3 under reduced pressure below 35 °C and filtered to remove the potassium perchlorate precipitated. The filtrate was mixed with methanol (5 cm^3) and cooled (−10 °C) overnight. Brown granular crystals which formed were collected and recrystallized three times from water–methanol. Yield: 32 mg. No change in the Δε value was observed with further recrystallization. This diastereomer was converted into perchlorate by use of a QAE-Sephadex (ClO_4^- form) column. Found: C, 19.74; H, 4.72; N, 12.93%. Calcd for $C_9H_{26}N_5Cl_2CoO_8Se$: C, 19.97; H, 4.84; N, 12.93%. Attempts to resolve the *t*-isomer by column chromatography and by chemical methods were all unsuccessful.

Λ-[Co(aeSe)(en)$_2$](ClO$_4$)$_2$(aeSeH=2-Aminoethaneselenol). The racemic complex was prepared by the method of Stein *et al.*[15] and resolved by SP-Sephadex C-25 column chromatography using 0.1 mol dm^{-3} $Na_2[Sb_2(d\text{-tartrate})_2]$ as an eluent. The fast-moving *Λ*-isomer was isolated as perchlorate by the same method as that for $[Co(apSe)(R\text{-chxn})_2]^{2+}$. Found: C, 14.23; H, 4.57; N, 13.92%. Calcd for $C_6H_{22}N_5Cl_2CoO_8Se$: C, 14.38; H, 4.43; N, 13.98%. The CD spectrum agreed well with that reported by Konno *et al.*[16] who resolved the complex by fractional crystallization of the diastereomer with $[Sb_2(d\text{-tartrate})_2]^{2-}$.

[Co(S-apOH)(NH$_3$)$_4$]Br$_3$·2.5H$_2$O. This complex was prepared by the method of Nishide *et al.*[1]

Measurements. Absorption and CD spectra were recorded on a Hitachi 323 spectrophotometer and a JASCO J-40 CS spectropolarimeter, respectively. Optical rotations at 589 nm were measured with a JASCO DIP-4 polarimeter.

Results and Discussion

Preparation and Structural Assignment of the Complexes. The present $[Co(apS \text{ or } apSe)(N_4)]^{2+}$-type complexes were prepared by oxidizing Co^{II}-N_4 species with the disulfide or diselenide, $(NH_2CH_2CH(CH_3)X-)_2$ (X=S or Se) according to the method for analogous aminoalkanethiolato-*N,S*[12,17] or selenolato-*N,Se*[15] complexes of cobalt(III). Time required for the oxidation was nearly the same between the apS and apSe complexes, but different between the en and *R*-chxn, and the tren complexes. While the former complexes took a few hours to complete the oxidation, the latter complexes of apS and apSe 2 and 4 d, respectively. Such differences in reactivity seem to be related with reducing strength of Co^{II}-N_4 species toward the disulfide and diselenide. The apS complexes are stable in acidic solution, but slowly decompose in basic solution to give Co^{II} species. The apSe complexes are less stable than the corresponding apS complexes under the same conditions. The *p*-$[Co(apSe)(tren)]^{2+}$ complex in solution is the least stable among the complexes prepared in this study. Thus spectral measurements of the apSe complexes were carried out in 0.01 mol dm^{-3} $HClO_4$ solutions. The lower stability of the apSe complexes might be related to the fact that the complexes exhibit Se-to-Co^{III} charge transfer bands at lower energy (*ca.* 33000 cm^{-1}) than that of the corresponding bands of apS complexes (*ca.* 35000 cm^{-1}); coordinated selenolates are considered to be better reductants than coordinated thiolates.[15]

Except for the pink crystals of *t*-$[Co(apS)(tren)]ZnCl_4 \cdot 0.5ZnCl_2$, all the complexes are brown in the solid state. The pink *t*-$[Co(apS)(tren)]ZnCl_4 \cdot 0.5ZnCl_2$ complex indicates the ligation of the S atom to Zn^{2+} in crystals. Interaction between soft metal ions and thiolato cobalt(III) complexes have been investigated in some detail.[18] For example, a brown solution of $[Co(aeS)(en)_2]^{2+}$ in water turns red upon addition of Ag^+ or $HgCH_3^+$.[18] Since Zn^{2+} is a less soft acid than those ions, it interacts with the S atom of apS only in the solid state of *t*-$[Co(apS)(tren)]ZnCl_4 \cdot 0.5ZnCl_2$. The interaction disappears when the complex is dissolved in water, a brown solution being obtained. The absorption spectrum is identical with that of the corresponding perchlorate which was prepared by use of an anion-exchange resin. Other tetrachlorozincates of the apS and apSe complexes prepared in this study form brown crystals and will involve no interaction between Zn^{2+} and the S or Se atom even in the solid state.

Both chelate rings of *S*(or *R*)-apS and *S*(or *R*)-apSe will be stabilized in the *δ*(or *λ*)-*gauche* conformation with the methyl group disposed equatorially, while the *R*-chxn chelate ring is forced to take the *λ*-*gauche* conformation. Thus there are four possible diaster-

eomers of $[Co(apX)(R\text{-chxn})_2]^{2+}$ (X=S, Se), which can be designated as $lel_3(\Delta(\lambda\lambda\lambda))$, $oblel_2(\Delta(\delta\lambda\lambda))$, $lelob_2(\Lambda(\delta\lambda\lambda))$, and $ob_3(\Lambda(\lambda\lambda\lambda))$. Each of the apS and apSe complexes formed three isomers in the preparation where the *rac*-dicalcogenide was used. The isomers were assigned on the basis of the elution order in column chromatography, the isomer distribution, and the CD spectra. In column chromatography, the lel_3 isomer will be eluted faster by elution with SO_4^{2-}, since its structure is most favorable in forming an ion pair with SO_4^{2-}.[19,20] By elution with $[Sb_2(d\text{-tartrate})_2]^{2-}$, on the other hand, a Λ-isomer is usually eluted faster than a Δ-one.[21] For the isomer distribution, the Δ-isomer will be formed in a larger amount than the Λ-one, since the $lel_2(\Delta(\lambda\lambda))$ structure formed by two *R*-chxn ligands is less crowded than the $ob_2(\Lambda(\lambda\lambda))$ one.[22] For a relation between optical activity and absolute configuration of a complex, it is known that a complex with a positive main CD band in the first absorption band region takes Λ configuration (Figs. 1 and 2).[23] On the basis of these diagnoses, all the isomers of $[Co(apX)(R\text{-chxn})_2]^{2+}$ (X=S, Se) were assigned as given in the experimental section.

In order to assign the absolute configuration of (+)$_{589}$-apSH·HCl, the same bis(*R*-chxn) complex was

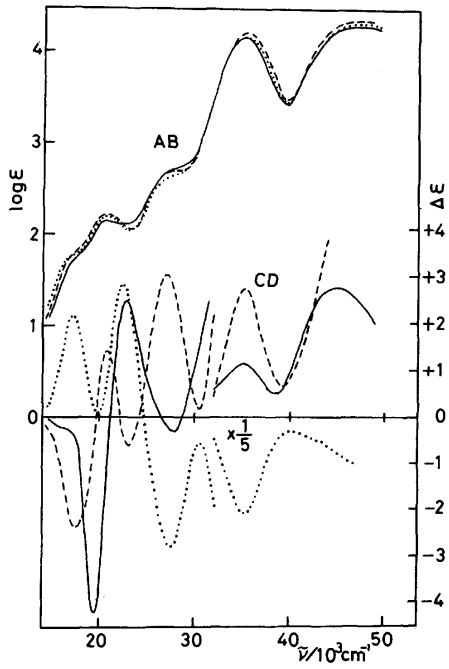

Fig. 1. Absorption and CD spectra of $\Delta(oblel_2)$-$[Co(S\text{-apS})(R\text{-chxn})_2]^{2+}$ (——), $\Delta(lel_3)$-$[Co(R\text{-apS})(R\text{-chxn})_2]^{2+}$ (– – – –), and $\Lambda(lelob_2)$-$[Co(S\text{-apS})(R\text{-chxn})_2]^{2+}$ (·····).

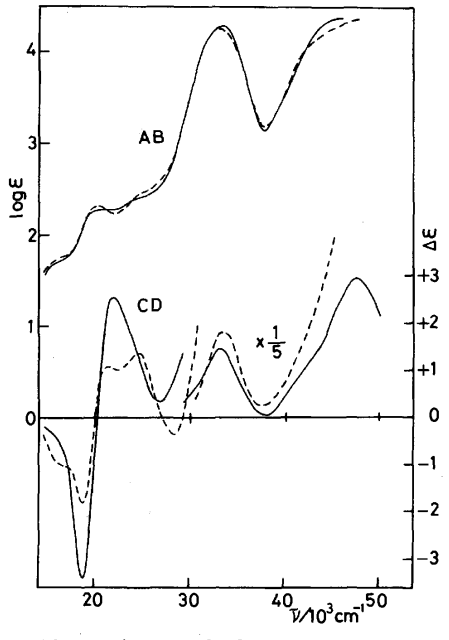

Fig. 2. Absorption and CD spectra of $\Delta(oblel_2)$-$[Co(S\text{-apSe})(R\text{-chxn})_2]^{2+}$ (—) and $\Delta(lel_3)$-$[Co(R\text{-apSe})(R\text{-chxn})_2]^{2+}$ (– – –).

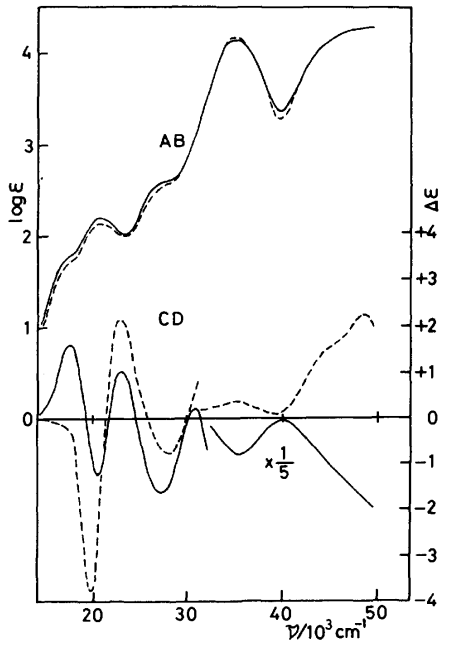

Fig. 3. Absorption and CD spectra of Λ-$[Co(S\text{-apS})(en)_2]^{2+}$ (——) and Δ-$[Co(S\text{-apS})(en)_2]^{2+}$ (– – – –).

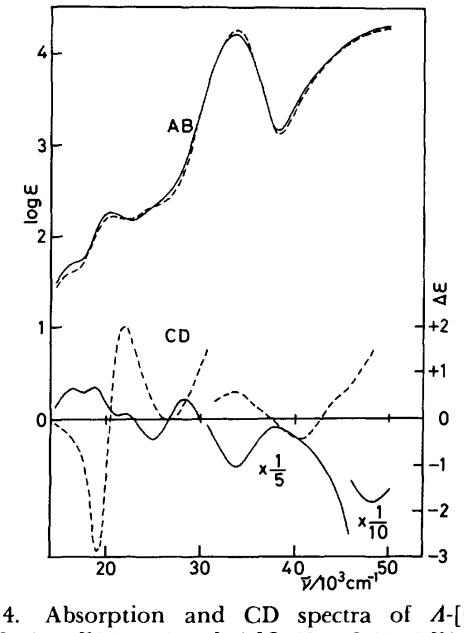

Fig. 4. Absorption and CD spectra of Λ-$[Co(S\text{-apSe})(en)_2]^{2+}$ (——) and Δ-$[Co(S\text{-apSe})(en)_2]^{2+}$ (– – – –).

prepared by use of the optically active disulfide derived from (+)$_{589}$-apSH·HCl. Only two isomers, $\Delta(oblel_2)$($\delta\lambda\lambda$) and $\Lambda(lelob_2)$($\delta\lambda\lambda$) were formed. Thus the absolute configuration of (+)$_{589}$-apSH·HCl can be assigned to *S*, since the *S*-apS chelate ring will be stabilized in the *δ-gauche* conformation as stated previously.

In a similar manner, structures of diastereomeric pairs, Λ- and Δ-[Co(*S*-apS)$(en)_2]^{2+}$, and Λ- and Δ-[Co(*S*-apSe)$(en)_2]^{2+}$ were assigned. The absorption and CD spectra of these complexes are given in Figs. 3 and 4. The [Co(apX)(tren)]$^{2+}$(X=S, Se) complex forms two geometrical isomers, *p* and *t*.[11] The isomers were assigned by comparing the elution order in column chromatography, the formation ratio, and the absorption spectra with those of *p*- and *t*-[Co(aeS)(tren)]$^{2+}$ reported previously.[24] The optically active *p*- and *t*-[Co(*S*-apS)(tren)]$^{2+}$ isomers were prepared by use of the optically active disulfide. The optically active *p*-isomer of apSe was obtained by resolving the racemate with *d*-tartrate ions, but the resolution of the other *t*-isomer was not achieved. The absorption and CD spectra of the tren complexes are given in Figs. 5 and 6. The spectral data of all the complexes are listed in Table 1.

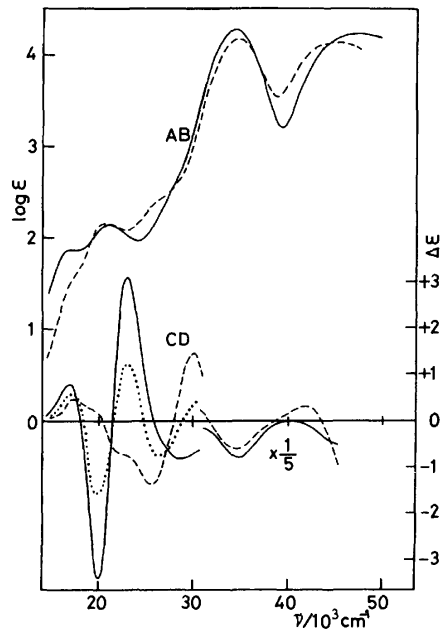

Fig. 5. Absorption and CD spectra of *t*(——) and *p*(----) isomers of [Co(*S*-apS)(tren)]$^{2+}$, and the mean CD curve of the two spectra (·····).

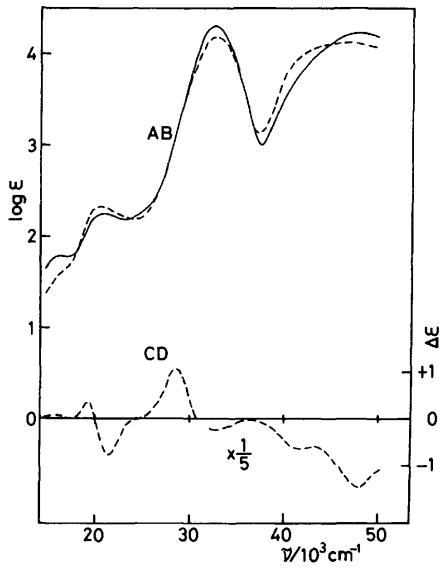

Fig. 6. Absorption spectrum of *t*-[Co(*rac*-apSe)-(tren)]$^{2+}$ (——), and absorption and CD spectra of (−)$_{589}$-*p*-[Co(*S*-apSe)(tren)]$^{2+}$ (----).

Absorption and CD Spectra. All the apS and apSe complexes show absorption spectra similar to one another; the spectra exhibit the split first absorption band, shoulder in the second absorption band region, and the strong X-to-Co^{III} (X=S, Se) and N-to-Co^{III} charge transfer bands in the ultraviolet region. All the bands of apSe complexes shift to the low energy side compared with the corresponding bands of apS complexes. These spectral features are quite similar to those of [Co(aeX)$(en)_2]^{2+}$ (X=S, Se) reported previously.[12,13,15,25] Although spectral differences among the isomers are very small in the *R*-chxn and en complexes of apX (X=S, Se), the spectra of *p*- and *t*-[Co(apX)(tren)]$^{2+}$ (X=S, Se) isomers are fairly different from each other. Some tren complexes with a similar chelate ligand such as aeS[24] or an amino acidate ion[26–28] also show a fairly large difference between the *p*- and *t*-isomers. The *p*- and *t*-isomers are geometrical isomers in which the X atom (X=O, S, Se) occupies the position cis and trans, respectively, to the tertiary amine nitrogen which will exert a weaker ligand field than the primary amine nitrogens. Thus the splitting of the d-d transition components would differ between the geometrical isomers to cause different d-d absorption spectra.[29]

In Fig. 3 are shown CD spectra of Δ- and Λ-[Co(*S*-apS)$(en)_2]^{2+}$. The spectra in the d-d absorption band region are not enantiomeric, but rather similar in pattern. In general, the optical activity of a metal complex is understood as a superposition of the configurational (chiral arrangement of ligands around the metal ion) and the vicinal (chiral ligand) effects. When the optical activity of Δ- and Λ-[Co(*S*-apS)-$(en)_2]^{2+}$ is this case, the spectra suggest that the vicinal effect of *S*-apS is stronger than the configurational effect in these isomers. Figures 7 and 8 show the configurational ($\Delta\varepsilon(\Lambda)=1/2\{\Delta\varepsilon[\Lambda(S)]-\Delta\varepsilon[\Delta(S)]\}$) and vicinal ($\Delta\varepsilon(S)=1/2\{\Delta\varepsilon[\Lambda(S)]+\Delta\varepsilon[\Delta(S)]\}$) effect curves, respectively, obtained from the observed CD spectra. The configurational CD curve for $\Delta\varepsilon(\Lambda)$ is very similar to the observed CD spectrum of Λ-[Co(aeS)-$(en)_2]^{2+}$ indicating that the additivity in CD between the configurational and vicinal effects holds for [Co-(*S*-apS)$(en)_2]^{2+}$. The vicinal CD curve of *S*-apS quite resembles that calculated from the observed CD spectra of $\Delta(\lambda\lambda\lambda)$-[Co(*R*-apS)(*R*-chxn)$_2]^{2+}$ and $\Delta(\delta\lambda\lambda)$-[Co-(*S*-apS)(*R*-chxn)$_2]^{2+}$($1/2\{\Delta\varepsilon[\Delta(\delta\lambda\lambda)]-\Delta\varepsilon[\Delta(\lambda\lambda\lambda)]\}$). Thus it is clear that in the *S*-apS complexes, the vicinal effect is stronger than the configurational effect. The large vicinal effect of *S*-apS corresponds well to those of the structurally similar *S*-apO and related deprotonated aminoalkanolate ligands.[1] In Fig. 8 is given the CD

Table 1. Absorption and CD spectral data of the complexes

Complex	Absorption: $\tilde{\nu}/10^3\,cm^{-1}$ (log ε)	CD: $\tilde{\nu}/10^3\,cm^{-1}$ ($\Delta\varepsilon$)
Δ-[Co(*R*-apS)(*R*-chxn)$_2$]$^{2+}$[a]	17.2(sh, 1.8), 20.5(2.23), 27.5(sh, 2.7) 35.0(4.17), 46.5(4.30)	17.6(−2.37), 20.7(+1.48), 23.2(−0.57) 27.2(+3.09), 35.2(+14.0)
Δ-[Co(*R*-apS)(*R*-chxn)$_2$]$^{2+}$[a]	17.2(sh, 1.7), 20.6(2.16), 27.5(sh, 2.7), 35.1(4.11), 47.0(4.25)	19.6(−4.22), 22.8(+2.53), 27.8(−0.31), 35.1(+5.92), 45.0(+13.8)
Λ-[Co(*R*-apS)(*R*-chxn)$_2$]$^{2+}$[a]	17.2(sh, 1.8), 20.5(2.19), 27.5(sh, 2.6), 35.0(4.13), 47.1(4.26)	17.1(+2.23), 22.3(+2.88), 27.5(−2.80), 35.1(−10.3)
Λ-[Co(*R*-apS)(en)$_2$]$^{2+}$[a]	17.3(sh, 1.7), 20.6(2.17), 27.5(sh, 2.6), 35.3(4.13)	17.5(+1.62), 20.4(−1.21), 23.0(+1.03), 27.1(−1.61), 30.8(+0.23), 35.2(−3.97)
Δ-[Co(*R*-apS)(en)$_2$]$^{2+}$[a]	17.3(sh, 1.7), 20.6(2.11), 27.7(sh, 2.5), 35.1(4.14)	19.7(−3.70), 23.0(+2.16), 28.0(−0.77), 35.1(+1.60)
p-[Co(*R*-apS)(tren)]$^{2+}$[a]	17.2(sh, 1.5), 20.6(2.16), 25.3(sh, 2.3), 34.7(4.14), 45.0(4.11)	17.4(+0.46), 19.2(sh, +0.25), 22.2(sh, −0.7), 25.7(−1.41), 30.2(+1.44), 34.7 (−3.13), 42.1(+1.54)
t-[Co(*R*-apS)(tren)]$^{2+}$[a]	16.9(1.85), 20.9(2.13), 34.3(4.23), 47.2(4.20)	16.9(+0.75), 20.0(−3.45), 23.1(+3.09), 28.9(−0.83), 35.1(−4.18)
Λ-[Co(aeS)(en)$_2$]$^{2+}$[a]	17.0(sh, 1.7), 20.7(2.16), 27.8(sh, 2.5), 35.3(4.14)	17.2(+0.90), 19.2(+1.31), 21.9(−0.32), 26.3(−0.67), 35.3(−5.15), 48.5(−11.3)
Λ-[Co(*S*-apSH)(en)$_2$]$^{3+}$[b]	20.5(2.14), 28.8(2.17), 37.4(3.85), 45.7(4.15)	19.7(+1.94), 22.7(−0.27), 26.5(+0.09), 29.9(+0.18), 40.9(−12.0), 47.6(−12.6)
Λ-[Co(*S*-apSH)(en)$_2$]$^{3+}$[b]	20.4(2.15), 28.8(2.18), 37.5(3.89), 45.7(4.20)	20.2(−2.67), 25.8(−0.07), 28.3(+0.14), 36.0(−2.72), 41.7(+14.6), 46.5(+13.9)
Λ-[Co(aeSH)(en)$_2$]$^{3+}$[b]	20.5(2.16), 29.0(2.37), 37.3(3.84), 46.0(4.15)	19.9(+2.17), 26.5(+0.11), 31.1(+0.20), 35.2(+2.68), 40.2(−5.36)
Δ-[Co(*R*-apSe)(*R*-chxn)$_2$]$^{2+}$[c]	16.5(sh, 1.8), 20.1(2.30), 24.5(sh, 2.4), 33.1(4.22)	16.5(sh, −1.03), 18.7(−1.83), 21.5 (+1.11), 24.4(+1.43), 28.3(−0.33), 33.5(+9.33), 48.0(+30.3)
Δ-[Co(*S*-apSe)(*R*-chxn)$_2$]$^{2+}$[c]	16.5(sh, 1.7), 20.5(2.26), 25.0(sh, 2.4), 33.2(4.24)	18.8(−3.34), 21.9(+2.64), 33.3(+7.56), 47.5(+15.2)
Λ-[Co(*S*-apSe)(en)$_2$]$^{2+}$[c]	16.5(sh, 1.7), 20.2(2.26), 33.4(4.20),	16.5(+0.67), 19.0(+0.70), 22.0(+0.11), 24.9(−0.44), 28.0(+0.40), 33.8(−5.26), 48.0(−18.2)
Δ-[Co(*S*-apSe)(en)$_2$]$^{2+}$[c]	16.5(sh, 1.6), 20.3(2.22), 33.4(4.22)	19.0(−2.84), 22.0(+2.01), 33.6(+3.12), 40.7(−2.03)
p-[Co(*S*-apSe)(tren)]$^{2+}$[c]	16.0(sh, 1.6), 20.4(2.29), 32.8(4.17), 47.0(4.11)	15.5(+0.01), 19.2(+0.37), 21.4(−0.78), 28.5(+1.10), 32.8(−1.10), 41.5(−3.21), 48.0(−7.60)
t-[Co(*rac*-apSe)(tren)]$^{2+}$[c]	16.0(sh, 1.8), 20.6(2.23), 32.6(4.29), 48.0(4.20)	
Λ-[Co(aeSe)(en)$_2$]$^{2+}$[c]	16.5(sh, 1.7), 20.3(2.23), 24.8(sh, 2.3), 33.4(4.22)	16.7(sh, +0.70), 18.9(+1.27), 22.2(sh, −0.45), 24.5(−0.58), 27.9(+0.17), 33.6 (−4.63)

Solvent, a): water. b): concd H_2SO_4, c): 0.01 mol dm^{-3} $HClO_4$.

spectrum of [Co(*S*-apO)$(NH_3)_4$]$^{2+}$ for comparison. The spectrum is similar in both pattern and magnitude to the vicinal CD curve of *S*-apS, although the CD bands shift to the high energy side compared with the corresponding bands of *S*-apS. The result also supports the previous assignment that $(+)_{589}$-apSH·HCl has *S* configuration.

In order to observe the vicinal effect of *S*-apS in the [Co(*S*-apS)(N_4)]$^{2+}$-type complex, it is desirable to prepare [Co(*S*-apS)$(NH_3)_4$]$^{2+}$. However, attempts to prepare this complex have been unsuccessful, and instead we have prepared [Co(*S*-apS)(tren)]$^{2+}$, where no configurational chirality is involved. In Fig. 5 are shown the CD spectra of *p*- and *t*-[Co(*S*-apS)(tren)]$^{2+}$. In the d-d absorption band region, the isomers exhibit CD spectra quite different from each other. The CD pattern of the *t*-isomer resembles the calculated vicinal CD curve of *S*-apS (Fig. 8), but the magnitude is *ca.* 1.5 times as large. Similar differences in CD spectra between *p*- and *t*-isomers have been reported for some tren complexes.[1,32] The tren complex is not suitable for observing the vicinal effect of *S*-apS in the [Co(*S*-apS)(N_4)]$^{2+}$-type complexes. It is interesting to note, however, that the mean curve of the CD spectra of *p*- and *t*-[Co(*S*-apS)(tren)]$^{2+}$ resembles more the calculated curve than the individual CD spectra (Fig. 5).

Nishide *et al.*[1] reported that absorption and CD spectra of S-apO and related aminoalkanolato-*N,O* complexes of cobalt(III) change remarkably with changes in pH of solutions. Similar spectral changes were observed for the *S*-apS complexes. The changes are instantaneous and reversible, and attributed to an acid-base equilibrium of the thiol proton.[33] Figure 9 shows the absorption and CD spectra of Δ- and Λ-[Co(*S*-apSH)$(en)_2$]$^{3+}$ in concd H_2SO_4, where the thiolate chelates will be completely protonated.[33] Both isomers show much more simple absorption and CD patterns than those of their conjugate bases (Fig. 3). In the first absorption band region, the protonated Λ-isomer gives a large positive and a small negative CD

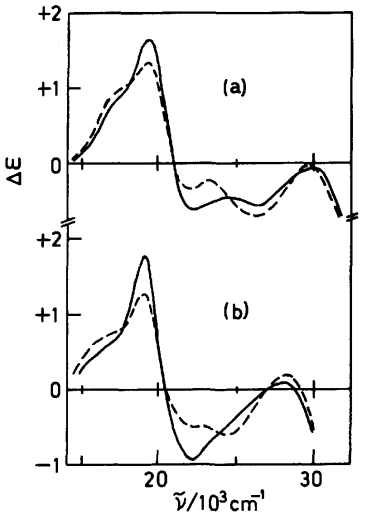

Fig. 7. (a): Configurational effect CD ($\Delta\varepsilon(\Lambda)$) curve of $[Co(S\text{-apS})(en)_2]^{2+}$ (——) and the observed CD spectrum of Λ-$[Co(aeS)(en)_2]^{2+}$ (----). (b): Configurational effect CD ($\Delta\varepsilon)\Lambda$)) curve of $[Co(S\text{-apSe})(en)_2]^{2+}$ (——) and the observed CD spectrum of Λ-$[Co(aeSe)(en)_2]^{2+}$ (----).

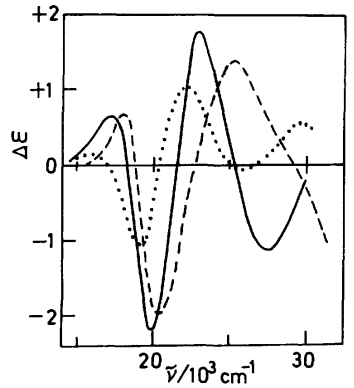

Fig. 8. Vicinal effect CD curves of *S*-apS (——) and *S*-apSe (·····) calculated from Δ- and Λ-$[Co(S\text{-apX})(en)_2]^{2+}$ (X=S, Se), and the observed CD spectrum of $[Co(S\text{-apO})(NH_3)_4]^{2+}$ (----).

band, and the other Δ-isomer only a large negative band. These CD patterns are very similar to those of the corresponding $\Lambda(lel)$- and $\Delta(ob)$-isomers of a bis(en) complex containing a chiral diamine such as (*S*)-1,2-propanediamine.[34] The additivity between the configurational and vicinal effects also holds in the protonated complexes as shown in Fig. 10(a), where the configurational CD curve ($\Delta\varepsilon(\Lambda)$) is compared with the CD spectrum of Λ-$[Co(aeSH)(en)_2]^{3+}$ in concd H_2SO_4. The calculated vicinal CD curve of *S*-apSH shows a single negative band in the first absorption band region, and the magnitude is much smaller than that of the vicinal CD curve of the conjugate base, *S*-apS (Figs. 8 and 10(b)). Very similar CD changes have been observed between the corresponding *S*-apO and *S*-apOH, and between related chiral aminoalkanolato and alcohol complexes. The results together with those described previously lead to the conclusion that aminoalkanethiolato-*N*,*S* cobalt(III) complexes exhibit optical activity very similar to that of the corresponding aminoalkanolato-*N*,*O* complexes in the d-d absorption band region.

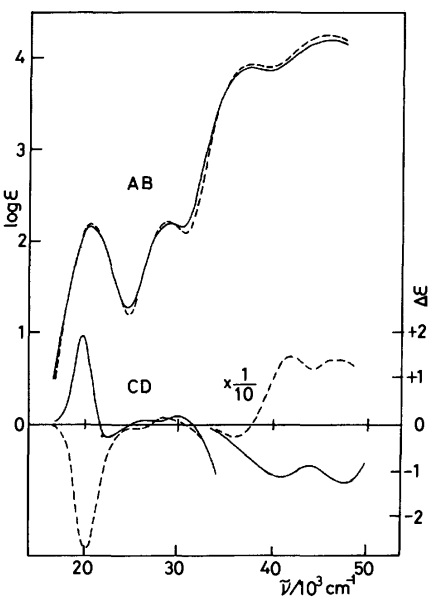

Fig. 9. Absorption and CD spectra of Λ(——) and Δ(----) isomers of $[Co(S\text{-apSH})(en)_2]^{3+}$ in concd H_2SO_4.

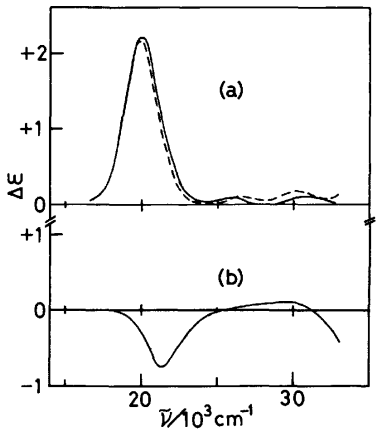

Fig. 10. (a): Configurational effect CD ($\Delta\varepsilon(\Lambda)$) curve of $[Co(S\text{-apSH})(en)_2]^{3+}$(——) and the observed CD spectrum of Λ-$[Co(aeSH)(en)_2]^{3+}$ in concd H_2SO_4 (-----). (b): Vicinal effect CD curve of *S*-apSH (——) calculated from Δ- and Λ-$[Co(S\text{-apSH})(en)_2]^{3+}$.

On the other hand, optical activity of the apSe complexes seems to somewhat differ from that of the apS complexes in the d-d absorption band region. The CD spectra of $\Lambda(lel)$-$[Co(S\text{-apSe})(en)_2]^{2+}$ and $\Delta(lel_3)$-$[Co(R\text{-apSe})(R\text{-chxn})_2]^{2+}$ are fairly different from those of the corresponding isomers of the apS complexes, although other isomers of these en and *R*-chxn complexes show CD patterns similar to those of the corresponding apS complexes (Figs. 1—4). In Figs. 7 and 8 are given the configurational ($\Delta\varepsilon(\Lambda)$) and vicinal ($\Delta\varepsilon(S)$) effect curves, respectively, obtained from the CD spectra of Λ- and Δ-$[Co(S\text{-apSe})(en)_2]^{2+}$. The configurational effect resembles the CD spectrum of Λ-$[Co(aeSe)(en)_2]^{2+}$, and the vicinal effect curve is also similar to that derived from the *R*-chxn complexes. Thus the additivity between the two effects also holds

for the apSe complexes. While the configurational CD curve of [Co(*S*-apSe)(en)$_2$]$^{2+}$ is quite similar to that of the corresponding *S*-apS complex, the vicinal CD curve of *S*-apSe is fairly small in magnitude as compared with those of *S*-apS and *S*-apO, although these curves show a similar pattern, giving (+), (−), and (+) bands from small to large wave numbers in the first absorption band region. Thus it can be concluded that the vicinal effect of the aminoalkaneselenolate-*N*, *Se* chelate ligands is smaller than those of the corresponding thiolate-*N*,*S* and alcoholate-*N*,*O* ligands.

We have shown that the protonated *S*-apSH complexes give absorption and CD spectra quite different from those of the deprotonated ones and similar to those of the corresponding (*S*)-1,2-propanediamine complexes. However, the protonated *S*-apSe complexes were not so stable as to allow the spectral measurements.

Figure 6 shows the CD spectrum of (−)$_{589}$-*p*-[Co(apSe)(tren)]$^{2+}$. The spectrum is quite different from the vicinal CD curve of *S*-apSe obtained from [Co(*S*-apSe)(en)$_2$]$^{2+}$ as has been observed for the corresponding *S*-apS complexes. However, the fact that the CD magnitude is smaller than that of the corresponding *S*-apS complex agrees with the previous result that the vicinal effect of *S*-apSe is smaller than that of *S*-apS. The absolute configuration of apSe in the (−)$_{589}$-isomer may be assigned to *S*, since the CD pattern is rather similar to that of the corresponding *S*-apS complex. All attempts to resolve the *t*-isomer were unsuccessful.

The authors with to thank the Ministry of Education for Scientific Research Grant-in-Aid No. 58470032.

References

1) T. Nishide, K. Ogino, J. Fujita, and K. Saito, *Bull. Chem. Soc.* Jpn., **47**, 3057 (1974).
2) D. L. Herting, C. P. Sloan, A. W. Cabral, and J. H. Krueger, *Inorg. Chem.*, **17**, 1649 (1978).
3) H. C. Freeman, C. T. Moore, W. G. Jackson, and A. M. Sargeson, *Inorg. Chem.*, **17**, 3513 (1978).
4) M. Kojima and J. Fujita, *Bull. Chem. Soc. Jpn.*, **50**, 3237 (1977); M. Kojima, M. Fujita, and J. Fujita, *ibid.*, **50**, 898 (1977).
5) T. C. Owen, *J. Chem. Soc., C*, **1967**, 1374.
6) J. R. Piper and T. P. Johnstone, *J. Org. Chem.*, **29**, 1657 (1964).
7) A. H. Nathan and M. T. Bogert, *J. Am. Chem. Soc.*, **63**, 2361 (1941).
8) A. Yokoyama, H. Sakurai, and T. Tanaka, *Chem. Pharm. Bull.*, **19**, 1089 (1971).
9) R. S. Treptow, *Inorg. Chem.*, **5**, 1593 (1966).
10) H. B. Jonassen and G. T. Strickland, *J. Am. Chem. Soc.*, **80**, 312 (1958).
11) The S (or Se) atoms in the *p*- and *t*-isomers are trans to the primary (*p*) and tertiary (*t*) tren amine nitrogens, respectively.
12) R. H. Lane, F. A. Sedor, M. J. Gilroy, P. F. Eisenhardt, J. P. Bennett, Jr., R. X. Ewall, and L. E. Bennett, *Inorg. Chem.*, **16**, 93 (1977).
13) K. Yamanari, J. Hidaka, and Y. Shimura, *Bull.Chem. Soc. Jpn.*, **50**, 2299 (1977).
14) M. Fujita, Y. Yoshikawa, and H. Yamatera, *Chem. Lett.*, **1982**, 437.
15) C. A. Stein, P. E. Ellis, Jr., R. C. Elder, and E. Deutsch, *Inorg. Chem.*, **15**, 1618 (1976).
16) T. Konno, K. Okamoto, and J. Hidaka, *Chem. Lett.*, **1982**, 535.
17) D. L. Nosco and E. Deutsch, *Inorg. Synth.*, **21**, 19 (1982) and references cited therein.
18) M. J. Heeg, R. C. Elder, and E. Deutsch, *Inorg. Chem.*, **18**, 2036 (1979).
19) Y. Yoshikawa and K. Yamasaki, *Inorg. Nucl. Chem. Lett.*, **6**, 523 (1970).
20) K. Sakakibara, Y. Yoshikawa, and H. Yamatera, *Bull. Chem. Soc. Jpn.*, **52**, 2725 (1979).
21) M. Kojima, H. Yamada, H. Ogino, and J. Fujita, *Bull. Chem. Soc. Jpn.*, **50**, 2325 (1977).
22) S. E. Harnung, B. S. Sϕrensen, I. Creaser, H. Maegaard, U. Pfenninger, and C. E. Schaffer, *Inorg. Chem.*, **15**, 2123 (1976).
23) See for example: C. J. Hawkins, "Absolute Configuration of Metal Complexes," John Wiley & Sons, New York (1971), p. 148.
24) W. G. Jackson and A. M. Sargeson, *Inorg. Chem.*,**17**, 2165 (1978).
25) K. Hori, *Nippon Kagaku Zasshi*, **90**, 561 (1969).
26) E. Kimura, S. A. Yang, and J. P. Collman, *Inorg. Chem.*, **9**, 1183 (1970).
27) Y. Mitsui, J. Watanabe, Y. Harada, T. Sakkamaki, Y.Iitaka, Y. Kushi, and E. Kimura, *J. Chem. Soc., Dalton Trans.*, **1976**, 2095.
28) K. Akamatsu, T. Komorita, and Y. Shimura, *Bull.Chem. Soc. Jpn.*, **54**, 3000 (1981).
29) H. Yamatera, *Bull. Chem. Soc. Jpn.*, **31**, 95 (1958).
30) B. E. Douglas, *Inorg. Chem.*, **4**, 1813 (1965); C. T. Liu and B. E. Douglas, *ibid.*, **3**, 1356 (1964).
31) K. Ogino, K. Murano, and J. Fujita, *Inorg. Nucl. Chem. Lett.*, **4**, 351 (1965).
32) M. Kojima and J. Fujita, *Bull. Chem. Soc. Jpn.*, **56**, 139 (1983).
33) I. K. Adzamli, D. L. Nosco, and E. Deutsch, *J. Inorg. Nucl. Chem.*, **42**, 1364 (1979).
34) A. J. McCaffery, S. F. Mason, B. J. Norman, and A. M. Sargeson, *J. Chem. Soc., A*, **1968**, 1304.

 © 1984 The Chemical Society of Japan Bull. Chem. Soc. Jpn., 57, 997—1002 (1984)

Oxidative Degradation of Monosaccharides by Iron(III) Chlorides with a Near-UV to Visible Light under Aerobic Atmosphere

Koji ARAKI,* Masato SAKUMA, and Shinsaku SHIRAISHI*
Institute of Industrial Science, The University of Tokyo, 7-22-1, Roppongi, Minato-ku, Tokyo 106
(Received October 4, 1983)

Monosaccharides were oxidatively degraded by $FeCl_3$ with irradiation of a near-UV to visible light under aerobic atmosphere. D-Fructose and D-arabinose were degraded to D-erythrose in a yield of more than 80 mol%. D-Glucose and D-mannose were at first degraded to D-arabinose, which was subsequently degraded to D-erythrose. While, D-ribose was directly degraded to D-erythrose and D-glyceraldehyde. The degradation processes were selective, and these reactions were shown to proceed *via* formation of an Fe(III)-monosaccharide complex. The kinetic data and other features of these reactions were also discussed.

Carbohydrate is one of the main components of living organisms bearing variety of functions, and is the most abundant organic resources in nature.[1] Many metal ions are known to form complexes with carbohydrates and other polyhydroxy compounds, and these complexes are the subject of intense studies because of their physiological and clinical importances.[2-8] Among them, an Fe(III)-carbohydrate complex has been studied by several workers in relation to its potential use for the treatment of iron-deficient anemia.[5-8] However, only a little has been known as to the photochemical properties of these complexes.[9]

Photooxidation of organic substrates by an aqueous Fe(III) ion has been studied for long time,[10] and alcohols are known to be oxidized to give the corresponding aldehydes or ketones in high yields.[11,12] The photoreaction was suggested to proceed by radical processes,[13] and, therefore, the reaction was inhibited by the presence of oxygen.[11,12]

In the preceding letter, we reported that photooxidation of D-fructose by $FeCl_3$ gave D-erythrose in a high yield and that the reaction proceeded even under aerobic conditions *via* formation of an Fe(III)-D-fructose complex.[14] Since this finding might imply physiological importance, we further extended this study, and we now wish to report the more detailed studies of the photooxidation of D-fructose and several other monosaccharides by $FeCl_3$ under aerobic conditions.

Experimental

Materials and Photoreactions. D-Erythrose was purchased from Aldrich Chem. Co., and other monosaccharides were obtained from Wako Pure Chem. Ind. Ltd. Other chemicals were also commercial products, and some of them were purified by conventional methods before use.

Sample solutions were prepared freshly with deionized water, and 70 or 500 ml of the solution was irradiated internally under aerobic conditions. For the irradiation under anaerobic conditions, the solution was degassed by three times of freeze-thaw cycles. Light-source was a 100 W high-pressure mercury lamp (Type UM-102, Ushio Electric Inc.) fitted in a Pyrex-made double jacket. The jacket and the reaction vessel were kept at 20 °C by circulating water during irradiation.

For the measurement of quantum yield, a CRM-FA spectroirradiator with a 2 kW Xenon lamp (JASCO) was used. Sample solutions in quartz cells were irradiated by the light of known wavelength and energy at 20 °C.

Analyses. Decrease of pH of a solution during photoirradiation was monitored by a HM-20B pH meter (Toa Electronics Ltd.). The amount of H^+ formed was determined by titration of the irradiated solution with a 0.2 M† NaOH solution. Absorption spectra were recorded by a UVIDEC 505 spectrophotometer (JASCO) at 20 °C, and Fe(III) concentration of a sample solution was determined from the absorbance at 330 nm after 500 times of dilution with a 0.2 M HCl solution.

The irradiated solution was deionized by Amberlite IR-120 (H^+ form) and IRA-410 (HCO_3^- form) (Rohm & Haas Co.), and then water was evaporated to give a colorless syrup. The syrup was analyzed by the following three chromatographic methods; 1) high-performance liquid chromatography (HPLC) (TSK-GEL LS-450NH_2, 300×4 (ID) mm; CH_3CN 85%-H_2O 15%) with a RI-8 refractometer (Toyo Soda Manufacturing Co., Ltd.); 2) gas-liquid chromatography (GLC) after acetylation of the syrup with *N*-methylimidazole-acetic anhydride according to the method of Wachowiak and Connors[15] (Type G-2800 gas chromatograph, Yanaco; Silicone OV-17, 2000×3 (ID) mm); and 3) thin-layer chromatography (TLC) after treating the syrup with 2,4-dinitrophenylhydrazine hydrochloride (DNPH)-1,2-dimethoxyethane (DME) according to the method of Honda *et al.*[16] (Silica Gel 60F_{254}, E. Merck A G.; $CHCl_3$ 80%-CH_3OH 20%). The mass spectrum of the pre-acetylated sample after gas chromatographic separation was recorded by a JMS-DX300 mass spectrometer (JEOL).

Gases evolved from the irradiated solution were analyzed both by gas-solid chromatography (GC-4B gas chromatograph, Shimadzu; Molecular Sieve 5A or Unibeads 1S, 2000×3 (ID) mm) and mass spectrometry (RMU-7M high-resolution mass spectrometer, Hitachi, Ltd.).

Results

Oxidation of D-Fructose. An $FeCl_3$ (0.25 M)-D-fructose (0.5 M) solution (70 ml), pH of which was 1.38, was irradiated for 3 h. The initial brown solution became colorless with considerable pH decrease after irradiation. Absence of Fe(III) and formation of Fe(II) were confirmed by color reactions with potassium thiocyanate and 1,10-phenanthroline, respectively.[17] A colorless syrup obtained from the irradiated solution (yield 95—98 wt% to the initial D-fructose) was subjected to further analyses. HPLC showed the consumption of D-fructose during photoirradiation. Gas chromatogram of the pre-acetylated sample indicated the existence of a single oxidation product, and the retention time of the peak of this product coincided with that of pre-acetylated D-erythrose. Structural information of this product was further derived from

† 1 M=1 mol dm^{-3}.

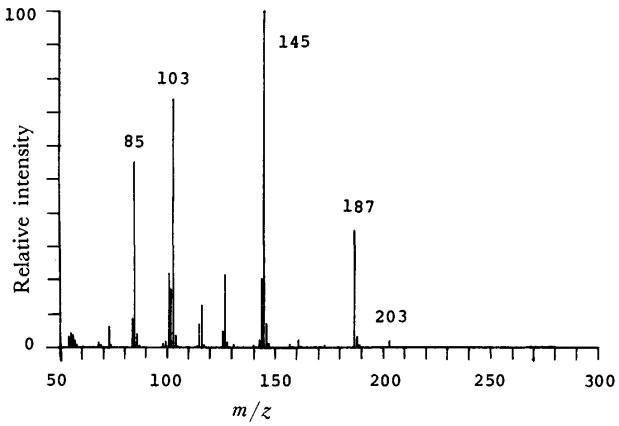

Fig. 1. The mass spectrum of the pre-acetylated oxidation product after gas chromatographic separation (23 eV E. I.).

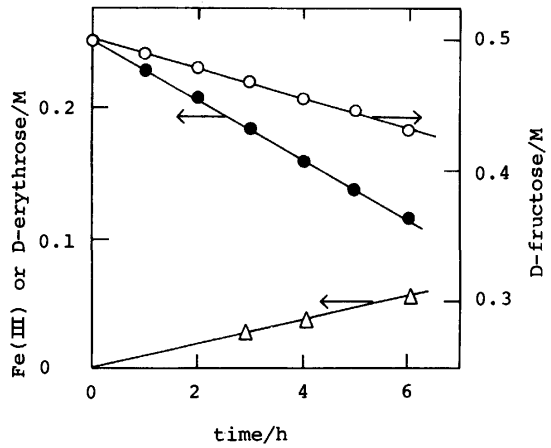

Fig. 2. Photoreaction of the $FeCl_3$ (0.25 M)–D-fructose (0.5 M) solution (500 ml) at 20°C. D-Fructose (○), Fe(III) (●), and D-erythrose (△) concentrations as a function of the irradiation time.

the GC-mass spectrometric analysis. The mass spectrum of the compound shown in Fig. 1 was found to be indistinguishable from that of D-erythrose triacetate (MW 246). Though no molecular ion peak was observed in the spectrum (m/z_{max}=203 at 23 eV E. I.), peracetyl derivatives of monosaccharides have been reported not to exhibit their molecular ion peaks.[18] In addition, the fragmentation pattern of the spectrum could reasonably be interpreted for D-erythrose triacetate based on the fragmentation pattern of other peracetylated monosaccharides.[18,19] Thus, the product was concluded to be D-erythrose. Quantitation of D-erythrose by GLC using dihydroxyacetone and/or caffeine as an internal standard revealed that D-erythrose comprised nearly 90 mol% of D-fructose oxidized, confirming that D-erythrose is the main product of the photooxidation of D-fructose.

Analysis of the syrup after treating with DNPH-DME showed several spots (R_f valuses: 0.39 (major), 0.41 (minor), 0.54 (minor), and 0.81 (minor)) in addition to those corresponding to D-fructose (0.22) and unreacted DNPH (0.62). They were assigned to be due to D-erythrose (0.39 (major) and 0.41 (minor)), D-glyceraldehyde (0.53), and formaldehyde and/or glyoxal (0.80).

A small amount of gas evolution was also observed during photoirradiation. Gases evolved under anaerobic conditions were analyzed only qualitatively by gas chromatography and mass spectrometry, which indicated the formation of CO, CO_2, and H_2.

Based on these results, we concluded that the irradiation of a Pyrex-filtered light to an acidic $FeCl_3$–D-fructose solution induces mainly the oxidative degradation of D-fructose to D-erythrose.

Figure 2 shows the time course of the reaction for a 500 ml of an $FeCl_3$ (0.25 M)–D-fructose (0.5 M) solution irradiated under aerobic atmosphere. The amount of D-fructose and Fe(III) decreased linearly as a function of time with a concomitant linear increase in the formation of D-erythrose. Even when 70 ml of this solution was irradiated under the same conditions, Fe(III) decreased linearly with the same decreasing rate. Therefore, the reaction is dependent on the light intensity under our experimental conditions. No reaction proceeded without irradiation or in the absence of any one of the substrates.

Table 1 summarizes the results of irradiation under different conditions. In all cases, 2 mol of Fe(III) oxidatively degraded 1 mol of D-fructose to give 2 mol of H^+

Table 1. Changes in the solution composition of the Fe(III)-D-fructose solution after irradiation[a]

Initial conditions				Irradiation time/h	Changes after irradiation			
Fructose/M	Fe(III)/M		Atmosphere		Fructose/M	Fe(III)/M	H^+/M	Erythrose/M[b]
0.5	$FeCl_3$	0.25	Anaerobic	2	−0.099	−0.198	+0.196	+0.080 (81%)
0.5	$FeCl_3$	0.25	Aerobic	2	−0.099	−0.199	+0.192	+0.084 (85%)
0.5[c]	$FeCl_3$	0.25	Anaerobic	2.5	−0.112	−0.224	+0.220	+0.092 (82%)
0.5[c]	$FeCl_3$	0.25	Aerobic	2.5	−0.112	−0.226	+0.222	+0.097 (87%)
0.5	$Fe(NO_3)_3$	0.25	Aerobic	2.5	−0.108	−0.222	+0.219	+0.092 (85%)
0.1	$FeCl_3$	0.1	Aerobic	0.5	−0.016	−0.034	+0.034	+0.014 (88%)
0.2	$FeCl_3$	0.1	Aerobic	0.5	−0.019	−0.040	+0.040	+0.016 (84%)
0.2	$FeCl_3$	0.2	Aerobic	0.5	−0.014	−0.030	+0.030	+0.012 (86%)
0.3	$FeCl_3$	0.1	Aerobic	0.5	−0.030	−0.062	+0.062	+0.026 (87%)
0.5	$FeCl_3$	0.1	Aerobic	0.5	−0.038	−0.078	+0.078	+0.033 (87%)
0.5	$FeCl_3$	0.25	Aerobic	0.5	−0.027	−0.055	+0.053	+0.023 (85%)

a) Sample solutions (70 ml) were irradiated internally at 20 °C. b) Conversion based on the D-fructose oxidized (mol%). c) Ref. 14.

according to the Eq. 1, and more than 80 mol% of D-fructose oxidized was converted to D-erythrose. Little

$$\text{D-fructose} + 2\text{Fe(III)} \xrightarrow{h\nu} \text{D-erythrose} + 2\text{Fe(II)} + 2\text{H}^+ \quad (1)$$

difference was observed for the reactions under aerobic and anaerobic atmosphere. These results are in good accordance with the earlier findings.[14] Use of $Fe(NO_3)_3$ instead of $FeCl_3$ did not practically alter the result, excluding the possible participation of counter anions in the reaction. Changes in the initial concentrations of the substrates did not affect the reaction scheme either. However, the reaction rate was sensitive to the initial substrate concentrations, and a higher D-fructose concentration increased the rate, while a higher Fe(III) concentration decreased the rate.

Oxidation of D-Glucose. Addition of D-glucose to an aqueous $FeCl_3$ solution caused the similar changes in color and pH of those observed when D-fructose was added. A brown $FeCl_3$ solution became reddish with a slight decrease in pH, suggesting the formation of an Fe(III)–D-glucose complex. Fig. 3 shows the difference spectrum between before and after addition of D-glucose to the Fe(III) solution, which is thought to represent the absorption due to the complex.

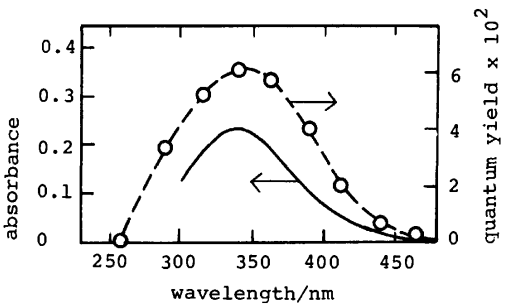

Fig. 3. The difference spectrum between before and after addition of D-glucose (——), and quantum yields of the reduction of Fe(III) (-○-) for the $FeCl_3$ (2×10^{-3} M)–D-glucose (5×10^{-1} M) solution at 20 °C.

Irradiation of a Pyrex-filtered light to an $FeCl_3$–D-glucose solution caused the reduction of Fe(III) with the concomitant consumption of D-glucose under aerobic atmosphere. Quantum yields of the reduction of Fe(III) at different wavelengths were also shown in Fig. 3, and this action spectrum coincided well with the difference spectrum, confirming that the Fe(III)–D-glucose complex is the photoreactive species. These photochemical properties of an $FeCl_3$–D-glucose solution were little different from those of an $FeCl_3$–D-fructose solution.

Colorless syrup was obtained from the irradiated solution (yield 96—100 wt% to the initial D-glucose). Analysis by HPLC and GLC indicated the formation of two products, D-arabinose and D-erythrose, as the main oxidation products. TLC after treating with DNPH also confirmed that these two compounds were the main products (R_f for D-arabinose is 0.30) along with minor spots corresponding to those for D-glyceraldehyde and for formaldehyde and/or glyoxal. Thus, more than 80 mol% of D-glucose oxidized by $FeCl_3$ was found to be degraded to D-arabinose and D-erythrose.

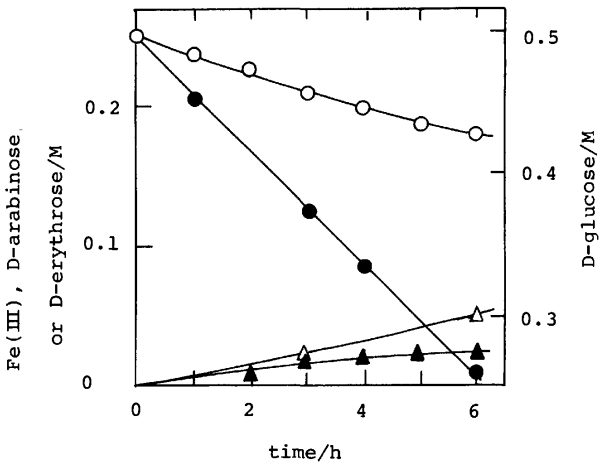

Fig. 4. Photoreaction of the $FeCl_3$ (0.25 M)–D-glucose (0.5 M) solution (500 ml) at 20 °C. D-Glucose (○), Fe(III) (●), D-arabinose (▲), and D-erythrose (△) concentrations as a function of the irradiation time.

The time course of the reaction is shown in Fig. 4, which is somewhat more complex compared to that for the oxidation of D-fructose. Fe(III) concentration decreased linearly as a function of time, indicating that the reaction is light intensity dependent. However, decrease in D-glucose concentration and increase in D-arabinose and D-erythrose concentrations were not linear, suggesting that more than one step may be

Table 2. Changes in the solution composition of D-glucose–$FeCl_3$ solution after irradiation[a]

Initial conditions		Irradiation time/h	Changes after irradiation				
Glucose/M	Fe(III)/M		Glucose/M	Fe(III)/M	H^+/M	Arabinose/M[b]	Erythrose/M[b]
0.5	0.25	3	−0.072	−0.25	+0.248	+0.020(28%)	+0.043(62%)
0.1	0.1	0.5	−0.008	−0.034	+0.034	+0.004(50%)	+0.004(50%)
0.2	0.1	0.5	−0.013	−0.046	+0.046	+0.005(38%)	+0.007(54%)
0.2	0.2	0.5	−0.008	−0.036	+0.036	+0.004(50%)	+0.004(50%)
0.2	0.4	0.5	Trace[c]	−0.016	+0.016	Trace[c]	Trace[c]
0.3	0.1	0.5	−0.016	−0.062	+0.062	+0.005(31%)	+0.010(63%)
0.5	0.1	0.5	−0.025	−0.083	+0.082	+0.007(28%)	+0.017(68%)
0.5	0.25	0.5	−0.018	−0.054	+0.052	+0.006(33%)	+0.009(50%)

a) Sample solutions (70 ml) were irradiated internally at 20 °C under aerobic atmosphere. b) Conversion based on the D-glucose oxidized was given in parenthesis (mol%). c) Changes were too small to be quantitized.

Table 3. Changes of the solution composition of D-arabinose-, D-mannose-, and D-ribose-$FeCl_3$ solutions after irradiation[a)]

Substrate			Product			
Monosaccharide/M		$FeCl_3$/M	H^+/M	Arabinose/M[b)]	Erythrose/M[b)]	Glyceraldehyde/M[b)]
D-Arabinose	−0.124	−0.25	+0.248	—	+0.111(89%)	—
D-Mannose	−0.088	−0.25	+0.246	+0.025(28%)	+0.040(45%)	—
D-Ribose	−0.123	−0.25	+0.248	—	+0.064(52%)	+0.028(23%)

a) Monosaccharide (0.5 M)-$FeCl_3$ (0.25 M) solutions (70 ml) were irradiated internally for 3 h at 20 °C.
b) Conversion based on the substrate oxidized was given in parenthesis (mol%).

involved in the reaction. The results of the irradiation under different conditions are summerized in Table 2. The reaction rate was affected by the initial substrate concentrations, and higher concentration of D-glucose increased the rate, while higher concentration of $FeCl_3$ decreased the rate.

Oxidation of D-Arabinose, D-Mannose, and D-Ribose. Photooxidations of D-arabinose, D-mannose, and D-ribose by $FeCl_3$ were also studied under aerobic atmosphere, and the results are shown in Table 3. All of these monosaccharides were susceptible to the photooxidation. The oxidation product from D-arabinose was identified to be D-erythrose with nearly 90 mol% of yield. D-Mannose yielded D-arabinose and D-erythrose, quite similar to D-glucose. In the case of D-ribose, however, formation of a considerable amount of D-glyceraldehyde in addition to D-erythrose was observed by HPLC and GLC.

Discussion

D-Fructose was oxidatively degraded by $FeCl_3$ with a Pyrex-filtered light according to the Eq. 1, and more than 80 mol% of D-fructose oxidized was converted to D-erythrose, demonstrating that the oxidation process has high specificity. The reaction was shown in the preceding letter to proceed *via* formation of the Fe(III)-D-fructose complex.[14] This conclusion was deduced from the results that little difference was observed for the reactions under aerobic and anaerobic conditions and that the action spectrum of the quantum yield for the reduction of Fe(III) coincided with the absorption band of the complex. The formation of D-erythrose can best be explained by the oxidative cleavage of the bond between C-2 and C-3 of D-fructose. Therefore, it is quite probable that both or at least one of hydroxyl groups at C-2 and C-3 are involved in coordination with Fe(III). Though Charley *et al.* presented the possible structure of the Fe(III)-D-fructose complex precipitated from a weakly basic solution, no experimental evidences as to the position of iron chelation were shown,[5] and the structure of the complex in an acidic solution is not yet clear now. It is worth to note that lead tetraacetate also cleaves the bond between C-2 and C-3 of D-fructose to yield 3-*O*-glycoloyl-D-erythrose.[20] This reaction was reported to proceed from β-D-fructofuranose where hydroxyl groups at C-2 and C-3 are in *cis* configuration feasible for metal coordination. In our photoreaction, D-erythrose instead of its glycolic ester was directly formed. As formations of formaldehyde, CO, CO_2, and H_2 were observed, glycolic ester unit may be further degraded into these compounds.

The reaction was linearly dependent on the light intensity. Therefore, higher initial D-fructose concentrations increased the rate because of the increase in the concentration of the complex. However, higher initial Fe(III) concentrations decreased the rate. As the free Fe(III) ion itself has the absorption at the region where the complex shows its absorption band (300—400 nm), the result is explained by assuming that light absorption of the complex was comparatively decreased because of the light absorption by the free Fe(III) ion. To clarify more detailes of the reaction, however, the structure and other properties of the complex have still to be studied.

Photooxidation of D-glucose was also shown to proceed *via* formation of the Fe(III)-D-glucose complex, and photochemical properties of the complex were substantially similar to those of the Fe(III)-D-fructose complex. However, more than two moles of Fe(III) with respect to the D-glucose oxidized was reduced during photoirradiation, and the time course of the reaction was more complex compared to that of D-fructose (Fig. 4). Though Fe(III) decreased almost linearly, consumption of D-glucose became slower as the reaction proceeded, suggesting that the primary oxidation product was further oxidized by Fe(III). As shown in Table 3, D-arabinose was oxidized to D-erythrose in a high yield under similar conditions. Therefore, it is likely that D-glucose is oxidatively degraded to the primary product, D-arabinose, which is subsequently oxidized to D-erythrose according to the Eq. 2. This

$$\begin{aligned} \text{D-glucose} + 2\text{Fe(III)} &\xrightarrow{h\nu} \\ &\text{D-arabinose} + 2\text{Fe(II)} + 2\text{H}^+ \\ \text{D-arabinose} + 2\text{Fe(III)} &\xrightarrow{h\nu} \\ &\text{D-erythrose} + 2\text{Fe(II)} + 2\text{H}^+ \end{aligned} \qquad (2)$$

view is further supported by the following fact. The sum of the amount of D-arabinose and D-erythrose is almost the same as the amount of D-glucose decreased, and the total amount of monosaccharides oxidized by $FeCl_3$ is approximately the half of the Fe(III) reduced if we assume the Eq. 2 (Table 2). Lead tetraacetate is also known to cause the stepwise degradation of α-D-glucose into 3-*O*-formyl-D-arabinose, which is further degraded to 2,3-di-*O*-formyl-D-erythrose.[21]

The first and second steps of the reaction in the Eq. 2 are the oxidative cleavage of the bond between C-1 and C-2 of monosaccharides. Since the photooxidation of D-fructose cleaved the bond between C-2 and C-3, it seems that the photooxidation by Fe(III) causes the

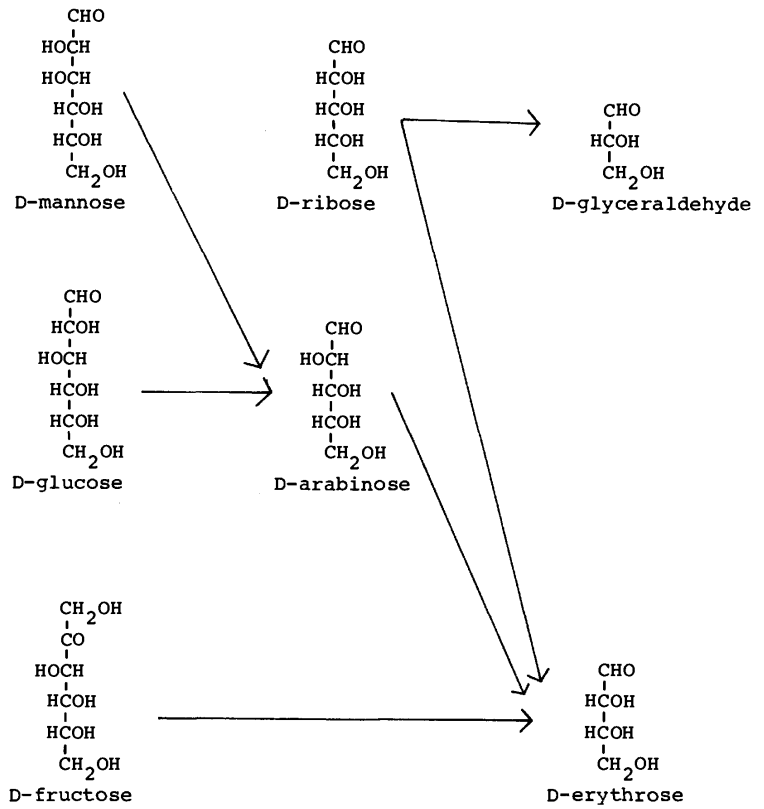

Fig. 5. Oxidative degradation of monosaccharides by $FeCl_3$ with irradiation of a Pyrex-filtered light.

cleavage of the bond between the anomeric and its adjacent carbons. In order to test whether this is the general feature of the oxidation of monosaccharides by $FeCl_3$, we studied the oxidation of D-mannose and D-ribose. Reaction of D-mannose was quite similar to that of D-glucose, suggesting that D-mannose is also oxidized stepwise *via* D-arabinose to D-erythrose. These are also the bond cleavage at the anomeric carbon. While in the case of D-ribose, approximately two moles of Fe(III) with respect to the D-ribose oxidized was reduced, suggesting that both D-erythrose and D-glyceraldehyde are directly formed from D-ribose. Though the formation of D-erythrose is due to the cleavage of the bond between C-1 and C-2, the formation of D-glyceraldehyde may be the result of the cleavage of the bond between C-2 and C-3. The latter process does not involve the anomeric carbon at C-1, and is different from other results observed here. Unlike D-arabinose, hydroxyl groups of D-ribose at C-2 and C-3 are *cis*-diol. This may enable the participation of the C-3 hydroxyl group in coordination with Fe(III), and can be the possible reason for the formation of D-glyceraldehyde. Indeed, Ca^{2+} and La^{3+} are reported to bind preferentially with α-furanose and α-pyranose forms of D-ribose which have three consecutive *cis*-hydroxyl groups from C-1 to C-3.[22]

The results presented in this paper demonstrated that many of monosaccharides are oxidatively degraded by $FeCl_3$ with irradiation of a near-UV to visible light under aerobic conditions. Except for D-ribose, the degradation processes are selective. These degradation pattern of monosaccharides are summarized in Fig. 5.

References

1) A. L. Lehninger, "Biochemistry," 2nd ed Worth Publishers, New York, N. Y. (1975), Chap. 10.
2) J. A. Rendleman, Jr., *Adv. Carbohydr. Chem.*, **21**, 209 (1966).
3) S. J. Angyal, *Pure Appl. Chem.*, **35**, 131 (1973).
4) D. H. Brown and J. MacPherson, *J. Inorg. Nucl. Chem.*, **32** 3309 (1970).
5) P. J. Charley, B. Sarkar, C. F. Stitt, and P. Saltman, *Biochim. Biophys. Acta*, **69** 313 (1963).
6) J. S. G. Cox, R. E. King, and G. F. Reynolds, *Nature*, **207**, 1202 (1965).
7) J. Briggs, P. Finch, M. C. Matulewicz, and H. Weigel, *Carbohydr. Res.*, **97**, 181 (1981).
8) S. A. Barker, P. J. Somers, and J. Stevenson, *Carbohydr. Res.*, 331 (1974).
9) G. O. Phillips, *Adv. Carbohydr. Chem.*, **18**, 9 (1963).
10) A. W. Adamson, W. L. Waltz, E. Zinato, D. W. Watts, P. D. Fleichauer, and R. D. Lindholm, *Chem. Rev.*, **68**, 541 (1968).
11) V. I. Stenberg, S. P. Singh, N. K. Narain, and S. S. Parmer, *J. Org. Chem.*, **42**, 171 (1977).
12) S. Rajan and D. Ramesh, *J. Org. Chem.*, **44**, 138 (1979).
13) A. Cox and T. J. Kemp, *J. Chem. Soc., Faraday Trans. I*, **71**, 2490 (1975).
14) K. Araki, M. Sakuma, and S. Shiraishi, *Chem. Lett.*, **1983**, 665.
15) R. Wachowiak and K. A. Connors, *Anal. Chem.*, **51**, 27 (1979).
16) S. Honda, K. Kakehi, and T. Takiura, *Anal. Chim. Acta*, **77**, 125 (1975).
17) "Kagakubinran," 2nd ed, The Chemical Society of Japan, Maruzen, Tokyo (1975), p. 1534.

18) K. Biemann, D. C. DeJongh, and H. K. Schnose, *J. Am. Chem. Soc.*, **85**, 1763 (1963).
19) D. C. DeJongh , *J. Org. Chem.*, **30**, 453 (1965).
20) A. S. Perlin and C. Brice, *Can. J. Chem.*, **34**, 541 (1956).
21) A. S. Perlin, *Can. J. Chem.*, **42**, 2365 (1964).
22) R. E. Lenkinski and J. Reuben, *J. Am. Chem. Soc.*, **98**, 3089 (1976).

Syntheses and Properties of Dinuclear Copper(II) Complexes with 2,6-Bis[bis(2-pyridylmethyl)aminomethyl]-4-methylphenol

Masatatsu SUZUKI,*,† Hajime KANATOMI, Youichi DEMURA, and Ichiro MURASE
Laboratory of Chemistry, College of General Education, Kyushu University, Ropponmatsu, Chuo-ku, Fukuoka 810
(Received October 11, 1983)

The dinucleating ligand, 2,6-bis[bis(2-pyridylmethyl)aminomethyl]-4-methylphenol](Hbpmp), formed two types of dinuclear copper(II) complexes, $[Cu_2(bpmp)X_2]^{n+}$(X=Cl^-, N_3^- py(pyridine), or Him(imidazole), and n=1 or 3), and $[Cu_2(bpmp)X]^{2+}$(X=CH_3COO^- or im^-). On the basis of the dinucleating nature of the ligand (bpmp), the elemental analyses and the conductivity measurements in acetonitrile, it is concluded that the complexes have dimeric unit of $[Cu_2(bpmp)X_2]^{n+}$ or $[Cu_2(bpmp)X]^{2+}$. In $[Cu_2(bpmp)X_2]^{n+}$ type complexes, two copper(II) ions are linked only by a single phenolate bridge. Magnetic susceptibilities of those complexes obey Curie-Weiss law in the temperature range 80—300 K with the Weiss constants ≈ -4 K, indicating that weak antiferromagnetic interactions are present in these complexes. In $[Cu_2[bpmp)X]^{2+}$ type complexes, however, two copper(II) ions are bridged by phenolate and acetate, or phenolate and imidazolate. Cryomagnetic measurements of the acetato and the imidazolato complexes showed antiferromagnetic interactions with the $-2J$ values of 82 and 66 cm^{-1}, respectively. All the complexes exhibited absorption bands at 20000—22000 cm^{-1} except for the azido complex. The origin of those bands are discussed.

Various types of quinquedentate and septidentate dinucleating ligands (L) such as Schiff-bases derived from 2,6-diformyl-4-methylphenol and various amines, 2,6-bis[bis[2-(2-pyridyl)ethyl]aminomethyl]-4-methylphenol (Hbpep), *etc.*, have been designed.[1-6] Dinuclear copper(II) complexes with those ligands are of current interest as models for the active sites of type III coppers such as hemocyanin, tyrosinase, and multicopper oxidases. General formula of those complexes is $[Cu_2(L)X]^{2+}$, in which two copper ions are linked by two bridging groups, *viz.*, phenolate or alkoxide, and additional bridging ligand (X) (X= OH^-, Cl^-, N_3^-, $C_3H_3N_2^-$ (pyrazolate), CH_3COO^-, *etc.*).

In the previous studies,[7-9] however, we found that the dinucleating ligand, 2,6-bis[bis(2-pyridylmethyl)-aminomethyl]-4-methylphenol (Hbpmp) forms new type of five-coordinate dinuclear cobalt(II) complexes, $[Co_2(bpmp)X_2]^+$ (X=Cl^-, Br^-, NCS^-, and N_3^-), in which two cobalt(II) ions are linked only by a single phenolate bridge. In those complexes, two vacant coordination sites (the sixth coordination sites) are positioned in close proximity and some of the complexes react reversibly with molecular oxygen to form μ-peroxo complexes. Such type of dinuclear copper(II) complexes bridged only by a single phenolate group is rare and attractive for studying interactions with various molecules such as hydrogen peroxide, ascorbic acid, *etc.*, with two copper(II) ions. Therefore, we have undertaken to prepare such type of dinuclear copper(II) complexes with bpmp, $[Cu_2(bpmp)X_2]^{n+}$. This paper deals with the preparations, and magnetic and electronic properties of those complexes. $[Cu_2(bpmp)X]^{2+}$ type complexes in which X acts as bridging ligand are also reported, where X represents CH_3COO^- or im^- (imidazolate).

Experimental

Preparation. The dinucleating ligand, Hbpmp, was prepared according to the literature.[7]

$[Cu_2(bpmp)(py)_2](ClO_4)_3 \cdot 2H_2O$. Pyridine (1.5 mmol) was added to a solution of $Cu(ClO_4)_2 \cdot 6H_2O$ (1 mmol) and Hbpmp (0.5 mmol) in methanol (50 cm^3) with stirring. The blue crystals deposited were filtered, washed with ethanol, and dried *in vacuo*.

$[Cu_2(bpmp)(Him)_2](ClO_4)_3 \cdot H_2O$. Imidazole (1.5 mmol) was added to a hot methanol solution (50 cm^3) of $Cu(ClO_4)_2 \cdot 6H_2O$ (1 mmol) and Hbpmp (0.5 mmol) with stirring to give blue oil. The resulting oil was dissolved in 50 cm^3 of methanol on heating to give violet solution. On cooling, the blue crystals formed were collected by filtration, washed with ethanol, and air dried *in vacuo*.

$[Cu_2(bpmp)(N_3)_2]ClO_4$. A solution of sodium azide (1.5 mmol) in water was added to a solution of $Cu(ClO_4)_2 \cdot 6H_2O$ (1 mmol) and Hbpmp (0.5 mmol) in 50 cm^3 of CH_3CN and CH_3OH mixture (1:1). The resulting brown solution was filtered and the filtrate was allowed to stand overnight to give brown crystals, which were collected by filtration, washed with ethanol and dried *in vacuo*.

$[Cu_2(bpmp)Cl_2]ClO_4 \cdot CH_3OH \cdot H_2O$. A solution of NaCl (1.5 mmol) in water was added to a solution of $Cu(ClO_4)_2 \cdot 6H_2O$ (1 mmol) and Hbpmp (0.5 mmol) in 50 cm^3 of aqueous methanol (1:1). The resulting brown solution was allowed to stand overnight to give blue grey crystals, which were collected by filtration, washed with ethanol, and dried *in vacuo*.

$[Cu_2(bpmp)(CH_3COO)](ClO_4)_2$. Sodium acetate (0.05 mmol) was added to a solution of $Cu(ClO_4)_2 \cdot 6H_2O$ (1 mmol) and Hbpmp (0.05 mmol) in methanol (30 cm^3). To the resulting brown solution was added 50 cm^3 of ethanol to give brown crystals, which were collected by filtration, washed with ethanol, and dried *in vacuo*.

$[Cu_2(bpmp)im](ClO_4)_2 \cdot 1.5CH_3CN$. A solution of CH_3ONa (1 mmol) in methanol (5 cm^3) was added to a solution of $Cu(ClO_4)_2 \cdot 6H_2O$ (1 mmol), Hbpmp (0.5 mmol), and Him (0.5 mmol) in acetonitrile (30 cm^3) to give a dark brown solution. Addition of ethanol to the brown solution gave brown crystals, which were collected by filtration, washed with ethanol, and dried *in vacuo*.

Measurements. The electronic spectra in solution and in solid were obtained with a Hitachi EPS-3T recording spectrophotometer and infrared spectra were recorded with a Hitachi 295 spectrophotometer by means of KBr disk. Magnetic susceptibilities were measured by Faraday method in the temperature range 80—300 K. Diamagnetic correction was made using Pascal's constants.[10] Molar conductivities of the complexes were determined in acetonitrile solution (10^{-3} mol dm^{-3}) at 25°C.

†Present adress: Department of Chemistry, Faculty of Science, Kanazawa University, Kanazawa 920.

Results and Discussion

$[Cu_2(bpmp)X_2]^{n+}$ Type Complexes. As was mentioned before, dinucleating ligands (L) such as bpep have been shown to form $[Cu_2(L)X]^{2+}$ type complexes. However, the addition of NaX to a mixture of Hbpmp and $Cu(ClO_4)_2 \cdot 6H_2O$ gave a new type of dinuclear complexes, $[Cu_2(bpmp)X_2]^+$ (X=Cl$^-$ and N_3^-).

The infrared spectra of $[Cu_2(bpmp)X_2]ClO_4$ complexes indicated the presence of uncoordinated perchlorate ions because no splitting of the ν(Cl-O) bands was observed definitely. The azido complex exhibited a single strong ν_{asymm} (N_3) band at 2038 cm^{-1}, suggesting that each azide ion coordinates to copper(II) ion in a similar way. In addition, the molar conductivities of those complexes indicated the presence of 1:1 electrolytes in acetonitrile (Table 1).[11] Those observations imply that the complexes have dimeric unit of $[Cu_2(bpmp)X_2]^+$ in which each X$^-$ ion coordinates to copper(II) ion and two copper(II) ions are linked only by a single phenolate bridge as was found for the corresponding dinuclear cobalt(II) complexes.[9] A possible structure of $[Cu_2(bpmp)X_2]^+$ type complexes is given in Fig. 1.

The addition of such bases as pyridine or imidazole to a mixture of Hbpmp and $Cu(ClO_4)_2 \cdot 6H_2O$ in methanol also afforded $[Cu_2(bpmp)X_2]^{3+}$ type complexes. The infrared spectra and molar conductivities also suggested that the complexes have dimeric unit of $[Cu_2(bpmp)X_2]^{3+}$ in which two copper(II) ions are bridged only by a single phenolate.

The present dinucleating ligand (bpmp) contains two tripodal parts ($N(CH_2py)_2(CH_2C_6H_5O^-)$). It is known that the tripod ligands which form three five-membered chelate rings tend to enforce trigonal bipyramidal copper(II) complexes with an additional unidentate ligand.[12] In general, trigonal bipyramidal copper(II) complexes show a band with a high energy shoulder in the d-d region.[13] However, $[Cu_2(bpmp)Cl_2]^+$ shows a band at *ca.* 14000 cm^{-1} with a low energy shoulder at $\approx$10000 cm^{-1} both in solid and acetonitrile (Fig. 2 and Table 2). This spectral pattern is indicative of a square pyramidal or a distorted square pyramidal structure about copper(II) ion.[13] An additional band is observed at 20000—22000 cm^{-1} both in solid and in acetonitrile. The complexes containing phenolate group(s) have been shown to display

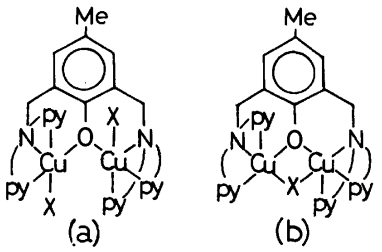

Fig. 1. Possible structures of $[Cu_2(bpmp)X_2]^{n+}$ (a) and $[Cu_2(bpmp)X]^{2+}$ (b) type complexes.

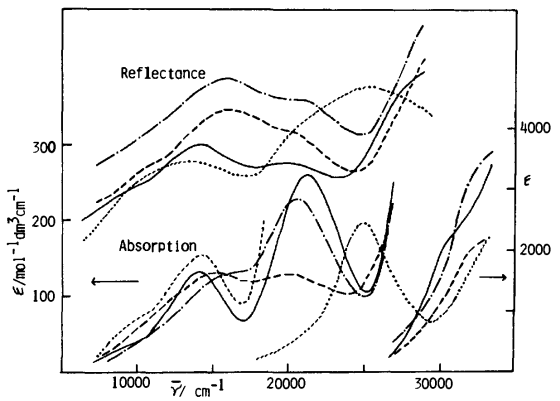

Fig. 2. Reflectance and absorption spectra of $[Cu_2(bpmp)Cl_2]ClO_4 \cdot CH_3OH \cdot H_2O$ (——), $[Cu_2(bpmp)(N_3)_2]ClO_4$ (------), $[Cu_2(bpmp)(py)_2](ClO_4)_3 \cdot 2H_2O$ (----), and $[Cu_2(bpmp)(Him)_2](ClO_4)_3 \cdot H_2O$ (—·—).

Table 1. Elemental analyses and molar conductivities of complexes

Complex	Found(Calcd) (%)			Molar conductivity
	C	H	N	Ω^{-2} cm^2 mol^{-1}
$[Cu_2(bpmp)Cl_2]ClO_4 \cdot CH_3OH \cdot H_2O$	46.62(46.56)	4.32(4.48)	9.68(9.58)	154
$[Cu_2(bpmp)(N_3)_2]ClO_4$	47.00(47.17)	4.32(3.96)	20.13(20.00)	131
$[Cu_2(bpmp)(py)_2](ClO_4)_3 \cdot 2H_2O$	45.00(44.94)	3.91(4.12)	9.62(9.75)	432
$[Cu_2(bpmp)(Him)_2](ClO_4)_3 \cdot H_2O$	42.26(42.23)	3.89(3.91)	12.62(12.63)	374
$[Cu_2(bpmp)(CH_3COO)](ClO_4)_2$	45.81(45.96)	4.09(3.97)	9.17(9.19)	272
$[Cu_2(bpmp)(im)](ClO_4)_2 \cdot 1.5CH_3CN$	47.88(47.59)	4.36(4.15)	13.46(13.52)	229

Table 2. Electronic spectral data

Complex	Reflectance spectra $\tilde{\nu}/10^3$ cm^{-1}			Absorption spectra[a] $\tilde{\nu}/10^3$ cm^{-1} (ε/mol^{-1} dm^3 cm^{-1})		
$[Cu_2(bpmp)Cl_2]ClO_4 \cdot CH_3OH \cdot H_2O$	10[s]	13.9	19.6	10[s]	14.2(131)	21.3(258)
$[Cu_2(bpmp)(N_3)_2]ClO_4$		13.2[b]	25.0	10[s]	14.3(153)	24.9(2450)
$[Cu_2(bpmp)(py)_2](ClO_4)_3 \cdot 2H_2O$	11[s]	15.9	20.0[s]		15.3(130)	20.0(129)
$[Cu_2(bpmp)(Him)_2](ClO_4)_3 \cdot H_2O$		15.7	21.3		15.4(137)[s]	20.5(230)
$[Cu_2(bpmp)(CH_3COO)](ClO_4)_2$	9.6[s]	15.3	21.7	11.6(110)	13.5(110)	22.4(319)
$[Cu_2(bpmp)(im)](ClO_4)_2 \cdot 1.5CH_3CN$	11.8		20.6	11.7(209)	14.3(180)[s]	21.5(329)

a) In acetonitrile. b) Broad band. s: Shoulder.

TABLE 3. MAGNETIC DATA OF COMPLEXES

Complex	μ_{eff}/BM		θ/K	$-2J$/cm^{-1}	g	$N\alpha/10^{-6}$ cgs mol^{-1}[a]
	80 K	297 K				
$[Cu_2(bpmp)Cl_2]ClO_4\cdot CH_3OH\cdot H_2O$	1.84	1.87	−4			
$[Cu_2(bpmp)(N_3)_2]ClO_4$	1.78	1.81	−5			
$[Cu_2(bpmp)(py)_2](ClO_4)_3\cdot 2H_2O$	1.80	1.83	−4			
$[Cu_2(bpmp)(Him)_2](ClO_4)_3\cdot H_2O$	1.79	1.83	−5			
$[Cu_2(bpmp)(CH_3COO)](ClO_4)_2$	1.32	1.75		82	2.05	80
$[Cu_2(bpmp)(im)](ClO_4)_2\cdot 1.5CH_3CN$	1.43	1.75		66	2.05	60

a) cgs mol$^{-1}\times 4\pi\times 10^{-6}\rightarrow$m^3 mol^{-1}.

phenolate (Opπ) to copper(II) ($d_{x^2-y^2}$) charge-transfer (CT) bands in the visible or the near-ultraviolet region.[5,6,14,15] It is unlikely that the band is ascribed to the d-d transitions since such a (distorted) square pyramidal complex with ClN_3O donor set would not exhibit the d-d band at such high energy. It is also unlikey that chloride (pπ) to copper CT transitions occur at such low energy; chloride to copper CT transitions would be expected to occur at about 30000 cm^{-1}.[16] Therefore, we believe that the band at 20000—22000 cm^{-1} is ascribed to phenolate to copper CT transition. A shoulder observed at 30000 cm^{-1} is assigned to chloride to copper CT transitions.

The azido complex exhibits a broad band at 13000 cm^{-1} in the reflectnace spectrum, while in the absorption spectrum, this band is resolved into a single band and a low energy shoulder. This spectral pattern is also indicative of a (distorted) square pyramidal structure. An intense band (ε=2500 mol^{-1}dm^3 cm^{-1}) is observed at 25000 cm^{-1}. This band is assigned to azide to copper CT transitions. Phenolate to copper CT transition may be hidden under this intense band.

The pyridine and the imidazole complexes exhibit the d-d band maxima at 15000—16000 cm^{-1} in the reflectance spectra, which are shifted to blue (1000—2000 cm^{-1}) compared with those of the chloro and the azido complexes. These blue shifts of the d-d band maxima of the former two complexes are attributed to the stronger ligand field strengths of pyridine and imidazole. The pyridine and the imidazole complexes show bands at 20000—21000 cm^{-1}. We tentatively assigned those bands to phenolate to copper CT transitions. If these assignments are correct, the energies of phenolate to copper CT transitions of $[Cu_2(bpmp)X_2]^{n+}$ type complexes are much lower than that of $[Cu_2(bpep)N_3]^{2+}$ (26000 cm^{-1}). This shift of the CT transition energies may be attributed to the geometries of the Cu-O-Cu moieties.[17]

Sakurai *et al.*[18] reported that $[Cu_2(tba)_2pcp]^{3+}$ (tba=tris(2-benzimidazolylmethyl)amine and pcp=4-chlorophenolate) in which two copper(II) ions are bridged only by a single phenolate group shows a reduced magnetic moment (1.7 BM[††]) at room temperature in acetone. However, magnetic property of this complex has not been fully investigated. The magnetic susceptibilities of the present complexes obey Curie-Weiss law in the temperature range 80—300 K with Weiss constants of −4— −5 K (Fig. 3 and Table 3). This implies that, although antiferromagnetic interactions are present between two copper(II) ions, they are very weak. Thus in these complexes, phenolic oxygens are not good mediator for antiferromagnetic superexchange pathway. In order to discuss their magnetisms more fully, precise structure data are necessary.

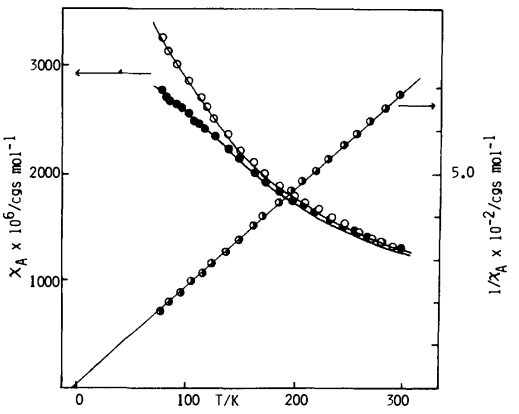

Fig. 3. Temperature dependence of inverse magnetic susceptibilities of $[Cu_2(bpmp)Cl_2]ClO_4\cdot CH_3OH\cdot H_2O$ (◑), and temperature dependence of magnetic susceptibilities of $[Cu_2(bpmp)(CH_3COO)](ClO_4)_2$ (●) and $[Cu_2(bpmp)im](ClO_4)_2\cdot 1.5CH_3CN$ (○). Solid curves for $[Cu_2(bpmp)(CH_3COO)](ClO_4)_2$ and $[Cu_2(bpmp)im](ClO_4)_2\cdot 1.5CH_3CN$ are drawn based on the Eq. 1 using the parameters listed in Table 3.

As was mentioned before, the dinucleating ligand, bpep, forms $[Cu_2(bpep)X]^{2+}$ type complexes [X=Cl$^-$ and N_3^-),[5] whereas bpmp forms $[Cu_2(bpmp)X_2]^+$ type complexes. This suggests that in the bpmp complexes, it is difficult for the binding sites available for linking two copper ions by one atom bridge such as Cl$^-$ to approach in close proximity. Thus the chelate ring size of dinucleating ligand has a significant influence on stereochemistry of dinuclear copper(II) complex. It was attempted to prepare $[Cu_2(bpmp)X]^{2+}$ type complexes containing one atom bridge (X), and $[Cu_2(bpmp)(OH)](ClO_4)_2$ was obtained (*vide infra*).

$[Cu_2(bpmp)X]^{2+}$ Type Complexes. The addition of NaOH to a mixture of Hbpmp and $Cu(ClO_4)_2\cdot 6H_2O$ in aqueous acetonitrile afforded green powder. The elemental analysis of the green powder is in agreement with $[Cu_2(bpmp)(OH)](ClO_4)_2$. Although magnetic susceptibility data over temperature range 80—300 K suggested that antiferromagnetic interaction is present in this complex, the data could not be explained on the basis of the Bleaney-Bowers equation.[19] The preparation of the complex was repeated several times

[††] 1 BM=0.9273$\times 10^{-23}$ JT^{-1}.

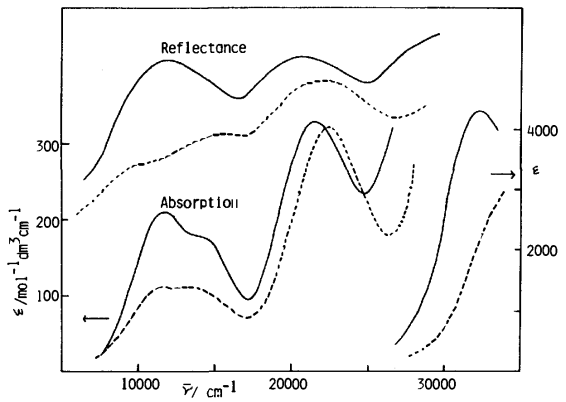

Fig. 4. Reflectance and absorption spectra of $[Cu_2(bpmp)im](ClO_4)_2 \cdot 1.5CH_3CN$ (——) and $[Cu_2(bpmp)(CH_3COO)](ClO_4)_2$ (----).

under various conditions. However, magnetic susceptibilities of those complexes were found to be highly dependent on the preparative conditions. Thus, in this experiment, magnetically pure $[Cu_2(bpmp)(OH)](ClO_4)_2$ could not be obtained.

On the other hand, the acetate-bridged complex, $[Cu_2(bpmp)(CH_3COO)](ClO_4)_2$, was easily obtained by mixing Hbpmp, $Cu(ClO_4)_2 \cdot 6H_2O$, and CH_3COONa in methanol. The infrared spectrum showed that $\Delta\tilde{\nu}(\tilde{\nu}_{asymm}(CO_2^-) - \tilde{\nu}_{symm}(CO_2^-))$ is $\approx 120\,cm^{-1}$, suggesting that the acetate ion acts as bridging ligand in syn-syn configuration.[20] The reflectance spectrum exhibits three bands at 9600, 15300, and 21700 cm^{-1} (Fig. 4). The former two bands are assigned to the d-d bands and this spectral pattern suggests a (distorted) square pyramidal coordination geometry about copper(II). The absorption spectrum is different from the reflectance spectrum, implying that the structural change occurs in acetonitrile. The band at 21700 cm^{-1} can be assigned to phenolate to copper CT transition and/or bridging acetate to copper CT transition, since dimeric copper(II) acetate monohydrate shows carboxylate to copper CT transition in this region.[21]

Such dinuclear copper(II) complexes with acetate bridge in syn-syn configuration and additional bridging ligand are rare.[3,4] Reed *et al.*[4] reported that $[Cu_2(L\text{-}Et)(CH_3COO)](ClO_4)_2$ (L-Et=1,3-bis[bis(1-ethylbenzimidazole-2-ylmethyl)amino]-2-propanolate) is essentially spin free. However, the present complex showed demagnetization by spin-pairing. Magnetic susceptibility data can be explained on the basis of the Bleaney-Bowers equation,

$$\chi_A = Ng^2\beta^2/3KT[1 + 1/3\exp(-2J/KT)]^{-1} + N\alpha, \quad (1)$$

where the symbols have their usual meanings. The $-2J$, g, and $N\alpha$ values were determined by the best fit of the χ_A values to the Bleaney-Bowers equation (1) (Fig. 3 and Table 3). The $-2J$ value thus obtained is 82 cm^{-1}, indicating that antiferromagnetic interaction is present between two copper(II) ions.

In the course of the preparation of $[Cu_2(bpmp)(Him)_2](ClO_4)_3$ (blue crystals) in acetonitrile, very small amount of brown crystals were obtained as a byproduct. The elemental analysis showed that the brown compound has a chemical composition of $[Cu_2(bpmp)(im)](ClO_4)_2 \cdot 1.5CH_3CN$. This brown compound was easily prepared by the method described in the experimental section. Since the complex contains imidazolate and phenolate anions, the imidazolate and phenolate are expected to act as bridging ligands. The conductivity measurement indicated the presence of a 2:1 electrolyte in acetonitrile. This implies that the complex has a dimeric unit, $[Cu_2(bpmp)im]^{2+}$, in acetonitrile.

The complex shows a single band at 11800 cm^{-1} in the reflectance spectrum, whereas in the absorption spectrum this band is resolved into a band and a high energy shoulder. As was mentioned before, trigonal bipyramidal complexes show a band with a high energy shoulder and the energies of the main bands are much lower than those of square pyramidal complexes with the same donor sets. Thus the electronic spectra both in solid and in acetonitrile suggest that the complex adopts a trigonl bipyramidal structure. The complex also exhibits a band at 21500 cm^{-1} both in solid and in acetonitrile. This band is assigned to imidazolate ($p\pi$) to copper(d_{z^2}) or less probably to phenolate to copper(d_{z^2}) CT transition. The magnetic susceptibilities were measured in the temperature range 80—300 K. The experimental data can be well explained on the basis of the Bleaney-Bowers equation (Fig. 3). This supports that the complex has a dinuclear unit with an imidazolate bridge. The $-2J$ value obtained is 66 cm^{-1}, indicating the presence of antiferromagnetic interaction between two copper(II) ions. Since the complex is trigonal bipyramidal, the magnetic d orbital (d_{z^2}) seems to interact mainly with the bridging imidazolate and only weakly with bridging phenolate which is in the equatorial plane. Therefore, it is probable that the bridging imidazolate provides the major superexchange pathway for the antiferromagnetic interaction between copper(II) ions. The magnitude of the antiferromagnetic interaction for the present complex is comparable to those of the imidazolate-bridged dinuclear copper(II) complexes so far reported.[22]

Our thanks are due to Prof. S. Kida, Prof. H. Okawa, Dr. Y. Nishida, and Dr. M. Mikuriya for their helpful disucssions.

References

1) H. Okawa, *Bull. Chem. Soc. Jpn.*, **43**, 3019 (1970).
2) R. Robson, *Inorg. Nucl. Chem. Lett.*, **6**, 125 (1970).
3) W. Mazurek, K. J. Berry, K. S. Murray, M. J. O'connor, M. R. Snow, and A. G. Wedd, *Inorg. Chem.*, **21**, 3071 (1982).
4) V. Mckee, J. V. Dagdigian, R. Bau, and C. A. Reed, *J. Am. Chem. Soc.*, **103**, 7000 (1981).
5) K. D. Karlin, J. C. Hayes, J. P. Hutchinson, and J. Zubieta, *J. Chem. Soc., Chem. Commun.*, **1983**, 376.
6) T. N. Sorrel, M. R. Malachowski, and D. L. Jameson, *Inorg. Chem.*, **21**, 3250 (1982).
7) M. Suzuki, H. Kanatomi, and I. Murase, *Chem. Lett.*, **1981**, 1742.
8) M. Suzuki, I. Ueda, H. Kanatomi, and I. Murase, *Chem. Lett.*, **1983**, 185.
9) M. Suzuki, H. Kanatomi, and I. Murase, *Bull. Chem. Soc. Jpn.*, **57**, 36 (1984).
10) F. E. Mabbs and D. J. Marchin, "Magnetisms and

Transition-metal Complexes," Chapman and Hall, London (1973), p. 5.
11) W. J. Geary, *Coord. Chem. Rev.*, **7**, 81 (1971).
12) K. D. Karlin, J. C. Hayes, S. Juen, J. P. Hutchinson, and J. Zubieta, *Inorg. Chem.*, **21**, 4108 (1982).
13) M. Duggan, N. Ray, B. Hathaway, G. Tomlinson, P. Brint, and K. Pelin, *J. Chem. Soc., Dalton Trans.*, **1980**, 1432.
14) A. R. Amundsen, J. Whelan, and B. Bosnich, *J. Am. Chem. Soc.*, **99**, 6730 (1977).
15) E. W. Ainscough, A. G. Bingham, A. M. Brodie, J. M. Husbands, and J. E. Plowman, *J. Chem. Soc., Dalton Trans.*, **1981**, 1701.
16) M. Suzuki, H. Kanatomi, H. Koyama, and I. Murase, *Bull. Chem. Soc. Jpn.*, **53**, 1961 (1980) and unpublished results.
17) S. Kida, Y. Nishida, and M. Sakamoto, *Bull. Chem. Soc. Jpn.*, **46**, 2428 (1973).
18) T. Sakurai, K. Narisako, and A. Nakahara, *Chem. Lett.*, **1981**, 1181.
19) B. Bleaney and K. D. Bowers, *Proc. R. Soc. London, Ser. A*, **1952**, 214.
20) G. B. Deacon and R. J. Phillips, *Coord. Chem. Rev.*, **23**, 227 (1980).
21) L. Dubicki, *Aust. J. Chem.*, **25**, 1141 (1972).
22) G. Kolks, S. J. Lippard, J. V. Waszczak, and H. R. Lilienthal, *J. Am. Chem. Soc.*, **104**, 717 (1982) and references therein.

Magnetic and Spectral Properties of 3,5-Dichloropyridine Adducts of Dimeric Copper(II) Acetate, Chloroacetate, and Dichloroacetate

Yoneichiro MUTO,* Tadashi TOKII, Kiyohiko CHIJIWA, and Michinobu KATO†
Department of Chemistry, Faculty of Science and Engineering, Saga University, Saga 840
†*Aichi Prefectural University, Mizuho-ku, Nagoya 467*
(Received October 19, 1983)

Three complexes with the empirical formula of $Cu(RCOO)_2 \cdot L$, where $R=CH_3$, CH_2Cl, or $CHCl_2$ and L=3,5-dichloropyridine, were prepared and studied. These complexes display the antiferromagnetic behavior typical of dimeric copper(II) carboxylates. The singlet-triplet splitting energy ($-2J$) is 349 cm^{-1} for the acetate, 340 cm^{-1} for the monochloroacetate and 312 cm^{-1} for the dichloroacetate. Comparison of their magnetic and electronic spectral properties with those of the corresponding pyridine adducts indicates that both the $-2J$ and $\tilde{\nu}_{max}$(absorption maximum of Band I) values of the respective 3,5-dichloropyridine adducts are higher than those of the pyridine adducts. The influence of the pyridines on both the magnetic and spectral properties was discussed.

It has already been pointed out that the antiferromagnetic interaction in dimeric copper(II) carboxylate adducts, $[Cu(RCOO)_2 \cdot L]_2$ (*cf.* Fig. 1), tends to increase as either the addend ligand L or the carboxylate substituent R becomes a stronger electron donor.[1] Therefore, the singlet-triplet separation ($-2J$, a measure of the magnitude of the magnetic interaction) is expected to increase as the pK_a of L becomes higher.[2] In the previous study of dimeric copper(II) acetate adducts with thiazoles,[3] however, we have found that, while the pK_a of thiazole (2.44)[4] is lower than that of pyridine (5.32),[5] the $-2J$ value of the thiazole adduct (344 cm^{-1}) is higher than that of the pyridine adduct (325 cm^{-1}).[6]

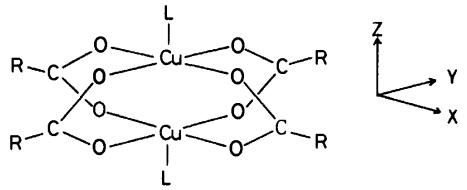

Fig. 1. Molecular structure of $[Cu(RCOO)_2 \cdot L]_2$ with reference axes marked.

In the present study, we have prepared copper(II) acetate, chloroacetate and dichloroacetate complexes with 3,5-dichloropyridine (3,5-Cl_2py) as the addend ligand which is a much weaker base (pK_a=0.67)[7] than pyridine (py). The magnetic and spectral properties of the copper(II) carboxylate complexes with 3,5-dichloropyridine and pyridine were compared with each other and the influence of the addend ligands on the magnetic interaction was discussed. The magnetic susceptibilities of dimeric copper(II) acetate complexes with 4-cyanopyridine (4-CNpy)[8] and caffeine (caf)[9] were also re-examined to contribute to the discussion.

Experimental

Syntheses. $Cu(CH_3COO)_2 \cdot L$ (L=3,5-Cl_2py and 4-CNpy): A solution of L (5 mmol) in ethanol (5 ml) was added to a solution of $Cu(CH_3COO)_2 \cdot H_2O$ (5 mmol) in ethanol (30 ml) with a few drops of glacial acetic acid. After the solution had been allowed to stand overnight at *ca.* 5 °C in a freezer, the separated green crystals were collected, washed with ethanol and dried at *ca.* 60 °C.

$Cu(CH_3COO)_2 \cdot caf$: This complex was prepared according to the method of Melnik.[9]

$Cu(ClCH_2COO)_2 \cdot L$ and $Cu(Cl_2CHCOO)_2 \cdot L$ (L=3,5-Cl_2py and py): A solution of L (5 mmol) in chloroform (20 ml) was added to one of the carboxylates (5 mmol), $Cu(ClCH_2COO)_2$ and $Cu(Cl_2CHCOO)_2$, suspended in chloroform (30 ml). After the resulting solution had been concentrated to one-third of its volume, it was allowed to stand overnight at *ca.* 5 °C in a freezer. The green crystals were collected, washed with benzene and dried at *ca.* 60 °C.

The results of the elemental analyses are given in Table 1.

TABLE 1. ANALYTICAL DATA

Complex	Found (Calcd) (%)			
	C	H	N	Cu
$Cu(CH_3COO)_2$(3,5-Cl_2py)	32.70 (32.79)	2.75 (2.75)	4.05 (4.25)	19.17 (19.28)
$Cu(CH_3COO)_2$(4-CNpy)	41.87 (42.03)	3.62 (3.53)	9.94 (9.80)	22.32 (22.24)
$Cu(CH_3COO)_2$(caf)	38.38 (38.35)	4.31 (4.29)	14.96 (14.91)	16.83 (16.91)
$Cu(ClCH_2COO)_2$(3,5-Cl_2py)	27.06 (27.13)	1.76 (1.77)	3.48 (3.51)	15.90 (15.95)
$Cu(ClCH_2COO)_2$(py)	33.00 (32.79)	2.77 (2.75)	4.13 (4.25)	19.19 (19.28)
$Cu(Cl_2CHCOO)_2$(3,5-Cl_2py)	23.07 (23.13)	1.08 (1.08)	2.93 (3.00)	13.43 (13.60)
$Cu(Cl_2CHCOO)_2$(py)	27.61 (27.13)	1.80 (1.77)	3.43 (3.51)	15.78 (15.95)

Physical Measurement. Magnetic susceptibilities in the temperature range of 80—300 K were determined by the Faraday method. The correction for diamagnetic contribution (χ_{dia}) was made by use of Pascal's constants.[10] The cryomagnetic data were fitted to the Bleaney-Bowers equation (1) allowing for the presence of paramagnetic impurity,[11]

$$\chi_A = \frac{Ng^2\beta^2}{3kT}\left[1+\frac{1}{3}\exp\left(\frac{-2J}{kT}\right)\right]^{-1}(1-P) + \frac{Ng_i^2\beta^2}{4kT}\cdot P + N\alpha, \quad (1)$$

where P is the mole fraction of the noncoupled copper(II) impurity, g_i is the average g factor for the impurity which was fixed at 2.2 throughout the present study, and the other symbols have their usual meanings. The best-fit parameters, $-2J$, g, $N\alpha$, and P, were obtained by using a nonlinear least-squares program written by T. Nakagawa (The University of Tokyo) and Y. Oyanagi (The University of Tsukuba), SALS (model D), on a FACOM M-200 computer at the Nagoya University Computation Center. As a convenient statistical indicator of the quality of the least-squares fits, the discrepancy index, σ_{dis}, was employed:

$$\sigma_{dis} = \left[\frac{\sum(\chi_{obsd}-\chi_{calcd})^2}{\sum\chi_{obsd}^2}\right]^{1/2} \quad (2)$$

The thermal magnetic data are shown in Figs. 2 and 4 as plots of χ_A *vs.* T. The values of χ_{dia}, g, $N\alpha$, P, $-2J$, and σ_{dis} are summarized in Table 2.

Reflectance spectra were recorded on a Hitachi Recording Spectrophotometer 323.

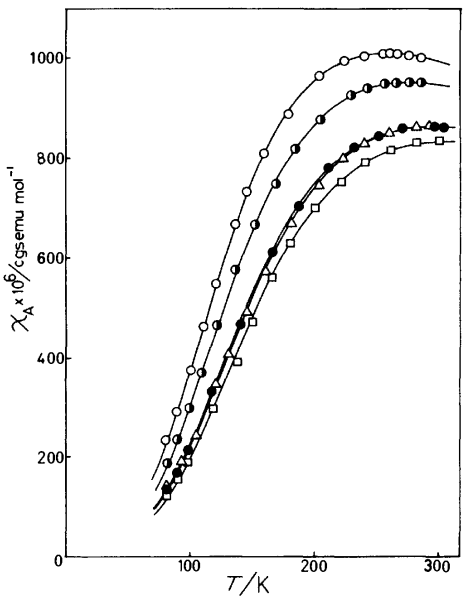

Fig. 2. Variation of magnetic susceptibilities with temperature.
(□) $Cu(CH_3COO)_2(3,5\text{-}Cl_2py)$, (△) $Cu(ClCH_2COO)_2(3,5\text{-}Cl_2py)$, (●) $Cu(ClCH_2COO)_2(py)$, (◑) $Cu(Cl_2CHCOO)_2(3,5\text{-}Cl_2py)$, (○) $Cu(Cl_2CHCOO)_2(py)$.
The solid curves were obtained as described in text.

Results and Discussion

The variable-temperature magnetic susceptibility data of the complexes prepared in the present study are well represented by Eq 1, indicating that the complexes all have a dimeric structure similar to that found for copper(II) acetate monohydrate, $[Cu(CH_3COO)_2\cdot H_2O]_2$.[12] From Table 2, we can see the following trends in the magnetic properties. First, the antiferromagnetic interactions in the respective 3,5-dichloropyridine adducts are stronger than those in the corresponding pyridine adducts. Secondly, the $-2J$ values in both the series of 3,5-dichloropyridine and pyridine adducts decrease as the parent carboxylic acids become stronger.

The reflectance spectra of the complexes resemble with each other in shape and are quite similar to those of $[Cu(CH_3COO)_2(py)]_2$ (*cf.* Fig. 3).[13] The spectra show two bands having maxima at *ca.* 26000 cm^{-1} (Band II)[14] and *ca.* 14000 cm^{-1} (Band I)[14] with a shoulder at *ca.* 8000 cm^{-1}. The wave numbers of the

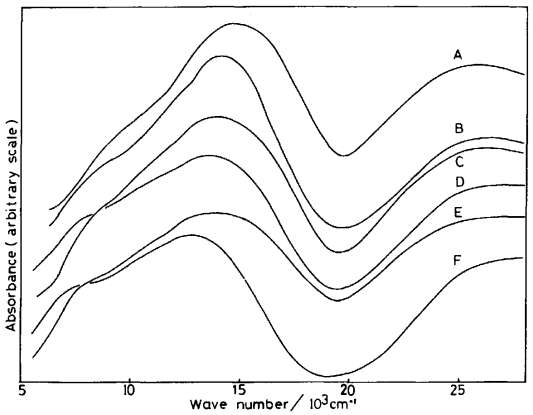

Fig. 3. Reflectance spectra of $Cu(CH_3COO)_2(3,5\text{-}Cl_2py)$ (A), $Cu(CH_3COO)_2(py)$ (B), $Cu(ClCH_2COO)_2(3,5\text{-}Cl_2py)$ (C), $Cu(ClCH_2COO)_2(py)$ (D), $Cu(Cl_2CHCOO)_2(3,5\text{-}Cl_2py)$ (E), and $Cu(Cl_2CHCOO)_2(py)$ (F).

TABLE 2. MAGNETIC DATA

Complex	$\chi_{dia}\times10^6$ / cgs emu[a]	g	$N\alpha\times10^6$ / cgs emu[a]	$P\times10^2$	$-2J$ / cm^{-1}	$\sigma_{dis}\times10^3$
$Cu(CH_3COO)_2(3,5\text{-}Cl_2py)$	−153	2.27_3	60	0.28	349	8.08
$Cu(CH_3COO)_2(py)$[b]	−121	2.18_1	60	1.10	333	2.22
$Cu(CH_3COO)_2(4\text{-}CH_3py)$[b]	−132	2.18_2	60	0	333	1.73
$Cu(CH_3COO)_2(4\text{-}CNpy)$	−127	2.24_3	60	0	345	7.45
$Cu(CH_3COO)_2(caf)$	−163	2.24_6	60	0.04	353	6.39
$Cu(ClCH_2COO)_2(3,5\text{-}Cl_2py)$	−181	2.28_7	60	0.43	340	4.41
$Cu(ClCH_2COO)_2(py)$	−147	2.26_2	60	0.18	333	4.56
$Cu(Cl_2CHCOO)_2(3,5\text{-}Cl_2py)$	−209	2.28_8	80	0.17	312	3.15
$Cu(Cl_2CHCOO)_2(py)$	−175	2.25_5	68	0.49	288	2.93

a) 1 cgs emu $mol^{-1}=4\pi\times10^{-6}$ m^3 mol^{-1}. b) Ref. 13.

Table 3. Reflectance spectral data

Complex	Band I $\tilde{\nu}_{max}/10^3$ cm^{-1}		Band II $\tilde{\nu}_{max}/10^3$ cm^{-1}
$Cu(CH_3COO)_2(3,5\text{-}Cl_2py)$	14.7	9.5[a]	25.7
$Cu(CH_3COO)_2(py)$[b]	14.1	9.1[a]	26.4
$Cu(ClCH_2COO)_2(3,5\text{-}Cl_2py)$	14.0	8.0[a]	26.2
$Cu(ClCH_2COO)_2(py)$	13.6	7.5[a]	26.5
$Cu(Cl_2CHCOO)_2(3,5\text{-}Cl_2py)$	13.6	7.7[a]	broad
$Cu(Cl_2CHCOO)_2(py)$	12.8	7.4[a]	broad

a) Shoulder. b) Ref. 13.

band maxima ($\tilde{\nu}_{max}$) are listed in Table 3 and their spectral curves are shown in Fig. 3. For comparison, the reflectance spectral curve of $[Cu(CH_3COO)_2(py)]_2$[13] is given in Fig. 3. It is now generally recognized that Bands I and II can be assigned respectively to a ligand field transition involving the positive hole promotion $d_{x^2-y^2} \rightarrow d_{xz}$, d_{yz}[15,16] (*cf.* the coordinate system given in Fig. 1) and to a charge transfer from the carboxylato-oxygen atoms to the metal ion.[17,18] Accordingly, Band I is expected to be sensitive to the nature of both the ligands $RCOO^-$ and L. As can be seen in Table 3 and Fig. 3, the $\tilde{\nu}_{max}$ values of Band I for the 3,5-dichloropyridine adducts are higher than those for the corresponding pyridine adducts. The order of the increase in the $\tilde{\nu}_{max}$ values is the same as that in the $-2J$ values, giving a linear relation between the $\tilde{\nu}_{max}$ and $-2J$ values ; *i.e.*, "higher $\tilde{\nu}_{max}$—higher $-2J$". This linear relation may be explained in terms of the electroneutrality principle[19] as follows. In dimeric copper(II) carboxylate adducts, $[Cu(RCOO)_2 \cdot L]_2$, when the L→Cu donation becomes weaker, the covalent Cu—O bonds in the CuO_4 basal plane will become stronger to maintain the electroneutrality over the whole molecule; *i.e.*, a weaker L→Cu donation will cause a stronger ligand field of the four carboxylato-oxygen atoms around the metal ion. This leads to a larger splitting of the d-d energy levels, resulting in a blue shift of Band I. This assumption is consistent with the observation by Dubicki and Martin[8] that, in a series of dimeric copper(II) acetate adducts with pyridine analogues, Band I shifts to a higher energy as the pK_a of the addend ligand decreases. For the mechanism of the magnetic interaction in dimeric copper(II) carboxylates, experimental evidence[20-23] shows that the spin-coupling between the unpaired electrons of copper(II) ions operates predominantly by superexchange interaction through the bridging carboxylato ligands rather than by direct Cu—Cu interaction. Accordingly, the magnetic interaction will become stronger as the Cu—O bonds become stronger. In the present complexes, the increase in both $-2J$ and $\tilde{\nu}_{max}$ accompanied with the replacement of pyridine with 3,5-dichloropyridine takes place in accord with the expectation based on their pK_a values (py=5.32[6] and 3,5-Cl_2py=0.67[7]) as stated above. The effect of Cu→L π-back-donation on the magnetic interaction in the present adducts may not be entirely negligible. However, the π-back-donation will make the metal more positive and thus will enhance the antiferromagnetic interaction: an effect of the same trend as caused by weak L→Cu σ donation.

From the experimental results and discussion stated above, we can conclude that, contrary to the result by Jotham, Kettle and Marks,[1] the antiferromagnetic interaction in dimeric copper(II) carboxylate adducts should become stronger as the basicity of the addend ligands becomes weaker. The values of $-2J$ for dimeric copper(II) acetate adducts with some pyridine analogues were previously reported to decrease as the pK_a values of the addend ligands decrease: 4-CH_3py (325 cm^{-1})>4-CH_3COpy (311 cm^{-1})>4-CNpy (300 cm^{-1}).[8] However, we have found the reverse order: 4-CH_3py (333 cm^{-1})<4-CNpy (345 cm^{-1}) (*cf.* Table 2 and Fig. 4). We have further found that the $-2J$ of the 4-cyanopyridine adduct of dimeric copper(II) trichloroacetate (229 cm^{-1}) is higher than that of the corresponding pyridine adduct (189 cm^{-1}).[24] The present result can explain the apparent anomalous magnetism of dioxane adducts. Dioxane has no appreciable π-acceptor ability, and it usually appears to be the weakest base (pK_a=−2.92)[25] in a series of adducts for a given copper(II) carboxylate dimer. Thus, dioxane adducts usually give the highest values in both $-2J$ and $\tilde{\nu}_{max}$ (Band I) for dimeric copper(II) carboxylate adducts.[26] For the 3,5-dichloropyridine and pyridine adducts, both $-2J$ and $\tilde{\nu}_{max}$ values decrease as the parent carboxylic acid becomes stronger (*cf.* Tables 2 and 3). This trend can be explained in terms of weakening of the ligand field strength of the four carboxylato-oxgen atoms.[8,27]

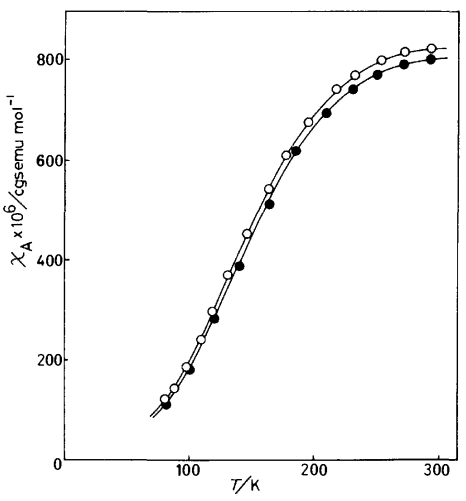

Fig. 4. Variation of magnetic susceptibilities with temperature.
(●) $Cu(CH_3COO)_2$(caf), (○) $Cu(CH_3COO)_2$(4-CNpy). The solid curves were obtained as described in text.

It must be noted here that the extremely high $-2J$ values have been reported for dimeric copper(II) acetate adducts of quinuclidine ($495 \pm 49\,cm^{-1}$)[28] and caffeine ($700\,cm^{-1}$).[9] These high $-2J$ values are unacceptable on referring to our present conclusion. The pK_a value of quinuclidine (11.49)[29] is very large. Actually, Jotham, Kettle, and Marks have re-evaluated the $-2J$ value of the quinuclidine adduct to be $318\,cm^{-1}$ by applying a least-squares fitting procedure to the reported magnetic data.[1] For the caffeine adduct, the reported magnetic susceptibilities do not agree completely with the values calculated by Eq. 1 using the reported parameter values of $-2J=700\,cm^{-1}$, $g=2.20$, $N\alpha=0$, and $P=0$. Accordingly, we repeated the magnetic measurement on the newly prepared caffeine adduct. The least-squares fitting of the cryomagnetic data gave a $-2J$ value of $353\,cm^{-1}$ (*cf.* Table 2 and Fig. 4). These renewed $-2J$ values are not abnormally high and are just comparable to those reported for well-characterized dimeric copper(II) acetate adducts.[20]

The present study was partially supported by a Grant-in-Aid for Scientific Reseach No. 58540395 from the Ministry of Education, Science and Culture.

References

1) R. W. Jotham, S. F. A. Kettle, and J. A. Marks, *J. Chem. Soc., Dalton Trans.*, **1972**, 428.
2) W. E. Marsh, G. O. Carlisle, and M. V. Hanson, *J. Mol. Struct.*, **40**, 153 (1977); *J. Inorg. Nucl. Chem.*, **39**, 1839 (1977).
3) T. Tokii and Y. Muto, *Bull. Chem. Soc. Jpn.*, **56**, 2363 (1983).
4) A. Albert, R. Goldacre, and J. Phillips, *J. Chem. Soc.*, **1948**, 2240.
5) G. J. Hawkins and D. D. Perrin, *J. Chem. Soc.*, **1962**, 1351.
6) E. Kokot and R. L. Martin, *Inorg. Chem.*, **3**, 1306 (1964).
7) A. Fischer, W. J. Galloway, and J. Vaughan, *J. Chem. Soc.*, **1964**, 3591.
8) L. Dubicki and R. L. Martin, *Inorg. Chem.*, **5**, 2203 (1966).
9) M. Melník, *J. Inorg. Nucl. Chem.*, **43**, 3035 (1981).
10) P. W. Selwood, "Magnetochemistry," Interscience Publishers, New York (1956), pp. 78 and 91.
11) A. P. Ginsberg, *Inorg. Chim. Acta Rev.*, **5**, 45 (1971).
12) J. N. van Niekerk and F. R. L. Schoening, *Acta Crystallogr.*, **6**, 227 (1953).
13) M. Kato, Y. Muto, and T. Tokii, 37th Annual Meeting of the Chemical Society of Japan, Tokyo, April 1978, Proceedings I, p. 255; ACS/CSJ Chemical Congress, April 1979, Honolulu, Hawaii, Abstracts I, Inorg. 465.
14) S. Yamada, H. Nakamura, and R. Tsuchida, *Bull. Chem. Soc. Jpn.*, **30**, 953 (1957)
15) G. F. Kokoszka, H. C. Allen Jr., and G. Gordon, *J. Chem. Phys.*, **42**, 3693 (1965).
16) C. W. Reimann, G. F. Kokoszka, and G. Gordon, *Inorg. Chem.*, **4**, 1082 (1965).
17) L. Dubicki, *Aust. J. Chem.*, **25**, 1141 (1972).
18) S. Kida, Y. Nishida, and M. Sakamoto, *Bull. Chem. Soc. Jpn.*, **46**, 2428 (1973).
19) L. Pauling, "The Nature of the Chemical Bond," 3rd ed, Cornell Univ. Press, New York (1960), p. 172.
20) R. J. Doedens, *Prog. Inorg. Chem.*, **21**, 209 (1976).
21) D. M. L. Goodgame, N. J. Hill, D. F. Marsham, A. C. Skapski, M. L. Smart, and P. G. H. Troughton, *J. Chem. Soc., Chem. Commun.*, **1969**, 629.
22) R. A. Zelonka and M. C. Baird, *Inorg. Chem.*, **11**, 134 (1972).
23) R. L. Beddoes, J. A. Connor, D. Dubowski, A. C. Jones, O. S. Mills, and R. Price, *J. Chem. Soc., Dalton Trans*, **1979**, 781.
24) H. Horie, K. Matsuyama, F. Utsunomiya, T. Tokii, Y. Muto, M. Kato, and I. Suzuki, 33rd Conference on Coordination Chemistry of the Chemical Society of Japan, Toyonaka, October 1983, Proceedings, p. 498.
25) E. M. Arnett and C. Y. Wu, *J. Am. Chem. Soc.*, **82**, 4999 (1960)
26) M. Melník, *Finn. Chem. Lett.*, **1978**, 255; *Coord. Chem. Rev.*, **36**, 1 (1981).
27) T. Tokii and Y. Muto, *Bull. Chem. Soc. Jpn.*, **49**, 1849 (1976).
28) E. D. Stevens and J. T. Yoke, *Inorg. Chim. Acta.*, **4**, 244 (1970).
29) R. G. Pearson and F. W. Williams, *J. Am. Chem. Soc.*, **76**, 258 (1954).

Reactions of *trans*-Chloro(cyanomethyl)bis(triphenylphosphine)- and Chloro-(cyanomethyl){1,2-bis(diphenylphosphino)ethane}palladium(II) Complexes with Various Thallium(I) β-Diketonates††

Noriaki ISHIO, Yukio NAKAMURA,* and Seichi OKEYA†
Faculty of Science, Osaka City University, Sumiyoshi-ku, Osaka 558
†*Faculty of Education, Wakayama University, Fukiage, Wakayama 640*
(Received October 25, 1983)

Reactions of *trans*-chloro(cyanomethyl)bis(triphenylphosphine)palladium(II), *trans*-[PdCl(CH_2CN)(PPh_3)$_2$] (**1**), with an equimolecular amount of Tl(β-dik) (β-dik=etac, acac, tfac, bzac, and dbm) in dichloromethane afforded the *O,O'*-chelated β-dik complexes [Pd(CH_2CN)(β-dik)(PPh_3)] (**3**). Hydrogen peroxide oxidation and chloride abstraction by $AgClO_4$ or $AgBF_4$ of **1** gave the neutral [PdCl(CH_2CN)PPh_3]$_n$ and the cationic [Pd(CH_2CN)(PPh_3)$_2$]$_m$$X_m$ (X=ClO_4 or BF_4), respectively, from either of which complexes **3** were also obtained by the reactions with the β-dik anions. No pure product corresponding to **3** was isolated by a similar treatment of **1** with Tl(hfac). On the other hand, chloro(cyanomethyl){1,2-bis(diphenylphosphino)ethane}palladium(II), [PdCl(CH_2CN)(dppe)] (**2**), reacted only with Tl(hfac) in refluxing acetone to give the cationic [Pd(CH_2CN)(dppe)]$_2$-(hfac)$_2$, which was also derived from **2** *via* [Pd(CH_2CN)(dppe)]$_2$$X_2$ (X=ClO_4 or BF_4).

In recent years many cyanoalkyl complexes of the type [MX(RCN)L_2] (M=Pd^{II}, Pt^{II}; X=halides or other monoanions; R=$(CH_2)_n$ (n=1,2,3), $CH_2C_6H_4$; L_2=2PPh_3, diphosphines) have been prepared[1-7] and their structures and various kinds of reactions have been studied extensively.[5-14] Among the cyanoalkyls examined, the complexes of *o*-cyanobenzyl, [MX(*o*-$CH_2C_6H_4CN$)L_2], underwent the widest range of reactions: (1) displacement of L by bidentate phosphorus ligands, (2) insertion of CO in the σ M-C bond, (3) formation of the cationic *cis*-[M($CH_2C_6H_4CN$)L_2]$_2$-(BF_4)$_2$ by abstraction of X,[6,7] and (4) nucleophilic attack by alcohols, thiols, and other nucleophiles on the coordinated CN group.[6,10-12] Moreover, the thermodynamically unstable *cis*-[PtX($CH_2C_6H_4CN$)-(PPh_3)$_2$] (X=Cl, Br) isomerized to the trans isomers, the reaction being catalyzed by free PPh_3.[6]

Although the cyanomethyl complexes of platinum-(II), [PtX(CH_2CN)L_2], have been also known to undergo the similar reactions to (1) and (3), and cis-trans isomerization,[3,5] only few studies have been performed on reactions of the palladium(II) analogue[2,14] which was found to decompose on irradiation in the solid state or in solution.[9] In this paper, we report the reactions of *trans*-[PdCl(CH_2CN)(PPh_3)$_2$] (**1**) and [PdCl(CH_2CN)-(dppe)] (**2**) with various Tl(β-dik) to know what kind of bonding mode is found for the β-dik ligands in the product complexes since β-dik anions are well-known as versatile ligands to coordinate to metal ions in various kinds of bonding modes.[15]

Results and Discussion

Thallium(I) β-diketonates employed, except 1,1,1,5,5,5-hexafluoro-2,4-pentanedionate, readily react with **1** in dichloromethane at room temperature to yield the *O,O'*-chelated β-dik complexes [Pd(CH_2CN)(β-dik)PPh_3] (**3**). Hydrogen peroxide oxidation of **1** in a dichloromethane-acetone mixture causes precipitation of the rather insoluble neutral species [PdCl(CH_2CN)PPh_3]$_n$ (**4**), from which complexes 3 are also produced by the reactions with Tl(β-dik). Abstraction of chloride from **1** by $AgClO_4$ or $AgBF_4$ in a dichloromethane-methanol mixture gives the less soluble cationic species [Pd(CH_2CN)(PPh_3)$_2$]$_m$$X_m$ (**5**) (X=ClO_4 (**5a**) or BF_4 (**5b**)), which reacts with K(β-dik) in the same solvent mixture to afford **3**. Thus, complexes **3** can be derived from **1** by the three routes.

In the case of the reaction with the hfac anion which is the least basic β-dik ligand employed, the complex of type **3** can not be obtained by any route mentioned above. This is presumably because of incapable displacement of the coordinated PPh_3 by the hfac anion (see Experimental section). Instead, the cationic *trans*-[Pd(CH_2CN)(S)(PPh_3)$_2$](hfac) (**6**) is isolated, after some make-up, from the reaction mixture of **5** and K(hfac). The complex contains an acetone molecule (S) in the coordination sphere.

In the reactions of **2**, which bears the chelating diphosphine ligand, with the more basic β-dik anions, the formation of the complexes containing the centralcarbon-bonded or *O*-unidentate β-dik ligand is expected. Nevertheless, such a product can not be isolated as a pure solid in these reactions. On the contrary, Tl(hfac) reacts with **2** in refluxing acetone to give the cationic [Pd(CH_2CN)(dppe)]$_2$(hfac)$_2$ (**7**) with the *N*-bonded CN groups. When the chloride ion is abstracted from **2** by $AgClO_4$ or $AgBF_4$ to yield [Pd(CH_2CN)(dppe)]$_2$$X_2$ (**8**) (X=ClO_4 (**8a**) or BF_4 (**8b**)) and then **8** is allowed to react with K(hfac), complex **7** is also produced by the anion exchange.

All the reactions are summarized in Scheme 1. The analytical and molecular weight data for the newly prepared complexes are listed in Table 1.

Characterization of the O,O'-Chelated β-dik Complexes 3. As is seen in Table 2, the IR spectra of complexes **3a—3e** exhibit a sharp band at the 2200—2212 cm^{-1} region, which is assigned to the ν(C≡N) vibration of the free CN group.[16] The bands of strong to medium intensities at the 1620—1500 cm^{-1} region are assigned to the ν(C···O) + ν(C···C) vibrations of the *O,O'*-chelated β-dik ligands.[17]

††In this paper β-dik represents a monoanion of ethyl 3-oxobutanoate (etacH) or that of β-diketones such as 2,4-pentanedione (acacH), 1,1,1-trifluoro-2,4-pentanedione (tfacH), 1,1,1,5,5,5-hexafluoro-2,4-pentanedione (hfacH), 1-phenyl-1,3-butanedione (bzacH), and 1,3-diphenyl-1,3-propanedione (dbmH).

Table 3 lists the ^1H NMR data for the *O,O'*-chelated β-dik complexes **3** in $CDCl_3$. The spectrum of **3b** is very simple and exhibits three singlets at 1.63, 1.98, and 5.23 ppm and a doublet at 1.35 ppm with relative intensities of 3:3:1:2 in addition to other signals assignnable to the phenyl protons. The doublet is due to the cyanomethyl protons which couples to cis ^{31}P, the coupling constant being 3.0 Hz appropriate for cis coupling.[2] The 5.23-ppm signal is due to the methine proton of the acac ligand and others due to the methyl protons, of which the higher-field signal at 1.63 ppm is assigned to the methyl cis to P and the lower one at 1.98 ppm to trans to P by reference to the data for the analogous complexes [PdCl(acac)PPh_3], [Pd(acac)(acac-

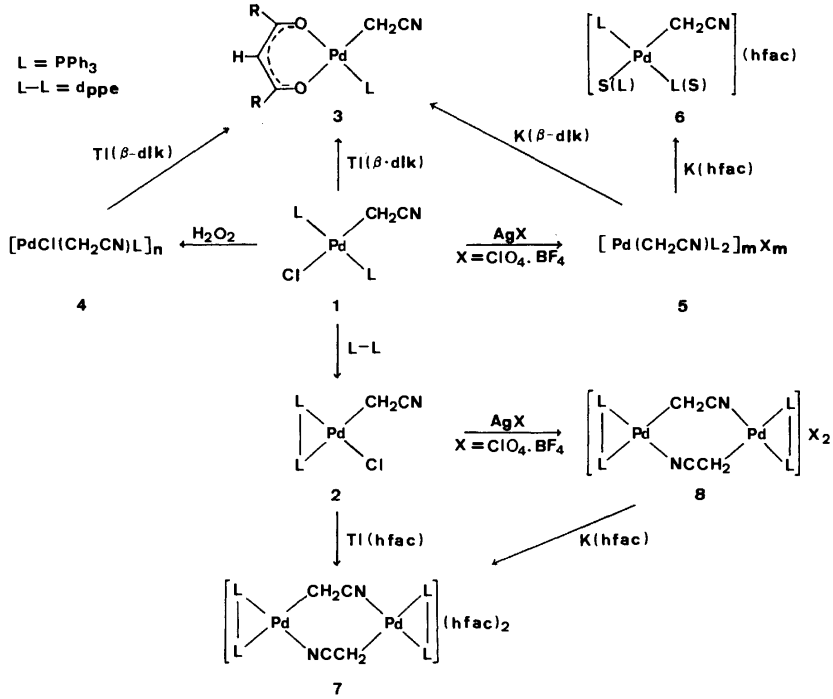

Scheme 1.

TABLE 1. ANALYTICAL DATA FOR THE NEWLY PREPARED COMPLEXES

No.	Complex	Found(Calcd)			
		C(%)	H(%)	N(%)	Mol wt[a]
3a	[Pd(CH_2CN) (etac)PPh_3]	58.43(58.06)	4.95(4.87)	2.60(2.60)	540(538)
3b	[Pd(CH_2CN) (acac)PPh_3]	59.11(59.13)	4.79(4.76)	2.80(2.76)	493(508)
3c	[Pd(CH_2CN) (tfac)PPh_3]	53.73(53.45)	3.76(3.77)	2.32(2.49)	527(562)
3d	[Pd(CH_2CN) (bzac)PPh_3]	62.93(63.22)	4.58(4.60)	2.41(2.46)	558(570)
3e	[Pd(CH_2CN) (dbm)PPh_3]	66.46(66.52)	4.45(4.47)	2.25(2.21)	646(632)
4	[PdCl(CH_2CN)PPh_3]$_n$	53.66(54.03)	3.86(3.85)	3.07(3.15)	
5a	[Pd(CH_2CN) (PPh_3)$_2$]$_m$(ClO_4)$_m$	58.13(59.24)	4.17(4.19)	1.78(1.82)	385[b] (771)[c]
5b	[Pd(CH_2CN) (PPh_3)$_2$]$_m$(BF_4)$_m$	58.67(60.23)	4.30(4.26)	1.84(1.85)	376[b] (758)[c]
6	[Pd(CH_2CN) (C_3H_6O) (PPh_3)$_2$] (hfac)	59.08(59.00)	4.24(4.20)	1.54(1.50)	
7	[Pd(CH_2CN) (dppe)]$_2$(hfac)$_2$	52.17(52.71)	3.62(3.62)	1.84(1.86)	504(1504)
8a	[Pd(CH_2CN) (dppe)]$_2$(ClO_4)$_2$	52.25(52.20)	4.15(4.08)	2.19(2.17)	452[b] (1289)
8b	[Pd(CH_2CN) (dppe)]$_2$(BF_4)$_2$	53.39(53.26)	4.20(4.15)	2.22(2.22)	424[b] (1263)

a) In CH_2Cl_2 at 28 °C unless otherwise stated. b) In CH_3CN at 39 °C. c) The formula weight was calculated as m=1.

TABLE 2. CHARACTERISTIC IR BANDS (cm^{-1}) IN NUJOL

No.	ν(C≡N)	ν(C=O)+ν(C=C)	No.	ν(C≡N)	Anion (X)
3a	2205m	1605vs, 1567w, 1509s	**5a**	2247s	1090vs, br, 925w, 620s (ClO_4)
3b	2200s	1583s, 1564s, 1510s	**5b**	2245s	1058s, br, 750m, 560s (BF_4)
3c	2212s	1618vs, 1580m, 1570sh 1518m, 1510sh	**6**	2200m 2200s, 2250w[b]	1673s, 1548s, 1520w (hfac)[c]
3d	2207s	1592s, 1585sh, 1570sh 1560s, 1510s	**7**	2234s	1670s, 1588w, 1552s (hfac)[c]
3e	2210m	1590s, 1545vs, 1515vs	**8a**	2240m	1100vs, br, 940w, 630s (ClO_4)
4	2250s, 2260sh	315w, 280w[a]	**8b**	2240s	1058s, br, 750w, 520s (BF_4)

a) ν(Pd–Cl). b) In $CHCl_3$. c) ν(C=O)+ν(C=C).

Table 3. ^{1}H NMR Data for the *O,O'*-chelated β-dik complexes **3** in $CDCl_3$[a]

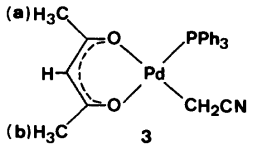

3

No.	cis / trans	Isomer[b]	β-dik CH3(a)	β-dik CH3(b)	β-dik CH	β-dik CH2CN
3a[c]	1 / 2	cis	1.62	OEt	4.73	1.49d (3.0)
		trans	OEt	1.97		
3b			1.63	1.98	5.23	1.35d (3.0)
3c	1 / —	cis	1.78		5.46	1.45d (3.0)
	2	trans		2.10		
3d	2 / 3	cis	1.80	Ph	5.96	1.44d (3.5)
		trans	Ph	2.16	5.99	1.41d (3.5)
3e			Ph	Ph	6.63	1.55d (3.0)

a) Chemical shift (δ) in ppm from internal Me_4Si at 33 °C. Figures in parentheses are $^3J(^{31}P\text{-}H)$ in Hz. d: Doublet. b) Cis and trans abbreviate cis(Me, P) and trans(Me, P), respectively. See text. c) CH_3-CH_2 signals for the ester appear at 1.28 (triplet), 4.20 (quartet) ppm (cis isomer) and at 0.77 (triplet), 3.21 (quartet) ppm (trans isomer), respectively.

C^3)PPh_3],[18] and [Pd(acac)(etac-C^3)PPh_3].[19] Complex **3e** exhibits a methine singlet at 6.63 ppm and a cyanomethyl doublet at 1.55 ppm with ^2J(P-H)=3.0 Hz.

On the other hand, the spectrum of **3a** in $CDCl_3$ is rather complex and shows two methyl signals at 1.62 and 1.97 ppm in the intensity ratio of *ca.* 1:2. Owing to the unsymmetrical nature of etac, two geometrical isomers, cis(Me,P) and trans(Me,P), coexist in the case of **3a**. By reference to the data of **3b**, these two signals at

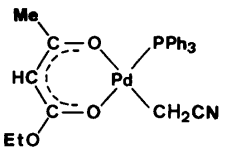

cis (Me, P)

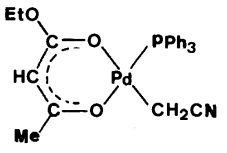

trans (Me, P)

higher and lower fields are readily attributed to the methyl protons of the cis and trans isomers, respectively. A similar situation is present in either case of **3c** and **3d**, the isomer ratios of cis to trans being *ca.* 1:2 and *ca.* 2:3, respectively. In the case of **3d**, splitting of the cyanomethyl proton signal is observed, discriminating a slightly different magnetic environment based on the different trans ligands.

Table 4. $^{31}P\{^1H\}$ NMR Data for the starting complexes and some products in $CDCl_3$[a]

No.	P (PPh_3) or P^1, P^2 (dppe)	$J(P^1\text{-}P^2)$
1	27.0	
3a-*cis*[b]	64.4	
3a-*trans*[b]	33.5	
3b	33.3	
5a[c]	25.2[d]	
2	44.1d 60.3d	23
7	50.4d, br 62.5d[e]	20
8a[c]	55.2d 65.0d	17

a) Chemical shift (δ) in ppm downfield from external H_3PO_4 and coupling constant (*J*) in Hz. d: Doublet, br: broad. b) The major component in equilibrium was assigned to trans. c) In CD_3CN. d) The half width slightly increased with increasing temperature as follows: 2 (−30 °C), 4 (−10 °C), and 10 (30 °C) Hz. e) Minor signals appear at the higher-field side (52.1 and 68.8 ppm) of each doublet. See Fig. 1.

The $^{31}P\{^1H\}$ NMR data for the starting complexes and some products in $CDCl_3$ or CD_3CN are listed in Table 4. The spectrum of **3b** in $CDCl_3$ exhibits a single signal at 33.3 ppm downfield from external H_3PO_4, while **3a** shows two signals at 33.5 and 64.4 ppm in the same solvent, disclosing the presence of cis and trans isomers in the solution. On the basis of their relative intensities, the more intense higher-field signal is assigned to the PPh_3 ligand of the trans(Me,P) isomer and the lower-field one to that of cis(Me,P) isomer.

The $^{13}C\{^1H\}$ NMR spectra of **3a**, **3b**, and *trans*-[$PdCl(CH_2CN)(PPh_3)_2$] (**1**) were measured in $CDCl_3$ using Me_4Si as internal standard at room temperature. These data are collected in Table 5. As is seen in the Table, the cyanomethyl-CH_2 signal of **1** appears at −5.0 ppm as a triplet indicating the trans configuration of two PPh_3, while that of **3b** is observed at −9.1 ppm as a doublet owing to cis coupling to one phosphorus atom. For the acac ligand in **3b**, either signal of the methyl and carbonyl carbons is splitting indicating

Table 5. $^{13}C\{^1H\}$ NMR Data for the starting complex **1** and the *O,O'*-chelated β-dik complexes **3a** and **3b** in $CDCl_3$[a]

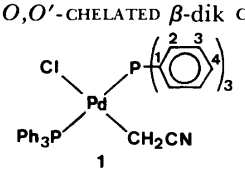

1

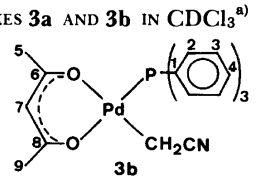

3b

No.	CH_2CN CH_2	CH_2CN CN	PPh_3 C^1	PPh_3 C^2	PPh_3 C^3	PPh_3 C^4	acac C^5, C^9	acac C^6, C^8	acac C^7
1	−5.0t (3)	124.0	129.9vt ((24))	134.7vt ((6))	128.4vt ((5))	130.5vt ((1))			
3b	−9.1d (10)	125.5	128.8d (53)	134.2d (11)	128.4d (11)	130.9d (3)	27.4 27.6d (9)	186.4 186.4d (2)	99.6

TABLE 5. (Continue)

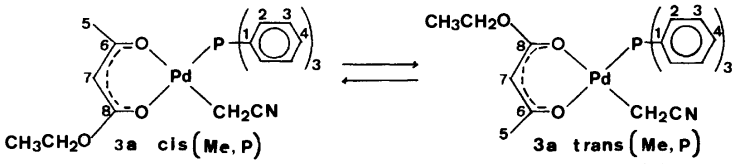

No.	CH_2CN		PPh_3				etac				
	CH_2	CN	C^1	C^2	C^3	C^4	C^5	C^6	C^7	C^8	CH_3-CH_2
3a-*cis*[b]	−9.5d (9)	125.2	128.6d (54)	134.3d (12)	128.5d (11)	131.1d[c] (3)	27.2	186.7	84.2	171.3d (2)	14.6 60.4
3a-*trans*[b]	−8.7d (9)	124.8	128.8d (52)	134.2d (12)	128.7d (11)	131.1d[c] (3)	27.3d (9)	187.2d (2)	84.3	171.0	14.2 59.5

a) Chemical shift (δ) in ppm from internal Me_4Si. Figures in parentheses and double parentheses give $J(^{31}P\text{-}C)$ and $1/2|^nJ(P\text{-}C)+^{n+2}J(P\text{-}C)|$ (n=1—4) in Hz, respectively. d: Doublet, t: triplet, vt: virtual triplet. b) Except for C^5, C^6, and C^8, the major component in equilibrium was assigned to trans. c) No splitting of signals for the cis and trans isomers was observed.

that two acetyl groups have a slightly different magnetic environment. Two singlets appearing at 27.4 and 186.4 ppm are assigned to the methyl (C^5) and carbonyl (C^6) carbons cis to P, respectively, whereas two doublets resonating at 27.6 and 186.4 ppm are attributed to those (C^9, C^8) trans to P. The $^{13}C\{^1H\}$ NMR spectrum of **3a** also discloses the presence of cis(Me,P) and trans(Me,P) isomers in solution. The ethoxycarbonyl carbon (C^8) of the cis isomer and the methyl (C^5) and acetyl carbonyl (C^6) carbons of the trans isomer couple to the trans phosphorus atom, each appearing as a doublet and hence, two sets of these signals are readily assigned as shown in Table 5. The cis and trans isomer ratio based on the ^1H NMR data is referred to assign other signals.

*Neutral Species [PdCl(CH_2CN)PPh_3]$_n$ (**4**).* The yellow precipitate obtained by hydrogen peroxide oxidation of **1** in a dichloromethane-acetone mixture gives satisfactory analysis as [PdCl(CH_2CN)PPh_3]$_n$. Four possible structures are conceivable:

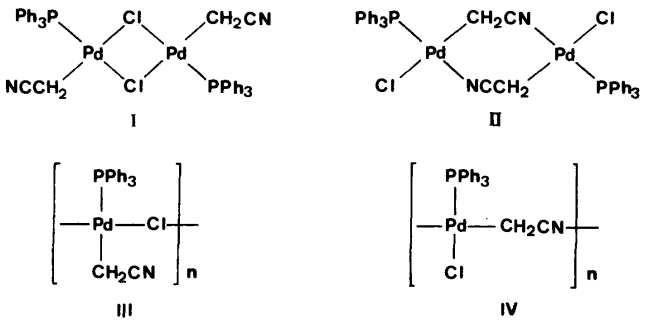

The NMR data for this species are not available because of its insolubility in any solvent appropriate to measurement. As is seen in Table 2, the IR spectrum of **4** shows two ν(Pd-Cl) bands at 315 and 280 cm^{-1}, frequencies of which are comparable to 288 cm^{-1} for **1**, indicating that the chloride-bridging structures I and III are eliminated. In contrast with **3**, species **4** exhibits two $\nu(C\equiv N)$ bands at 2250 and 2260 cm^{-1}, the former one as a strong band and the latter as a shoulder. These frequencies are 40—60 cm^{-1} higher than those for **3a—e**, revealing that the CN group coordinates to another palladium atom.[16,20] Thus, it seems likely that the *N*-bonded CN-bridging structures II and IV coexist in the solid state of **4**. This is not the case of the dimers [PdCl($CH_2C_6H_4Y$)PPh_3]$_2$ (Y=H or CN), in which the chloride-bridging structure of type I was proposed.[7]

Cationic Diphosphine Complexes. All the cationic complexes except **6** have the *N*-bonded CN-bridging structure on the basis of the $\nu(C\equiv N)$ frequencies in their IR spectra (Table 2). The cationic diphosphine complexes **8** derived from **2** are soluble only in coordinating solvents and the cations are dimeric in CH_3CN as is revealed by their molecular weight measurements (Table 1). As described earlier, this type of complex has been prepared by Ros *et al.* for the cyanomethyl complexes with platinum(II)[5] and for the *o*-cyanobenzyl complexes with platinum(II)[6] and palladium(II).[7] Addition reactions of a variety of nucleophiles to the *N*-bonded CN groups of the *o*-cyanobenzyl complexes[10-12] have been also studied. However, the present cyanomethyl complexes of palladium(II) fails to add these nucleophiles so long as we have tried briefly. The X-ray analysis for [Pt(*o*-$CH_2C_6H_4CN$)(dpe)]$_2$(BF_4)$_2$ (dpe=*cis*-1,2-bis(diphenylphosphino)ethylene) established the *N*-bonded CN-bridging structure of the dimeric cation.[21]

As is seen in Table 4, the $^{31}P\{^1H\}$ NMR spectrum of the starting PPh_3 complex **1** in $CDCl_3$ shows a singlet at 27.0 ppm, while that of the diphosphine complex **2** in the same solvent exhibits two doublets at 44.1 and 60.3 ppm with $J(P^1\text{-}P^2)$=23 Hz, reflecting a different magnetic environment of two phosphorus atoms P^1 and P^2. The higher-field signal at 44.1 ppm is assigned to P^1 trans to the CH_2CN ligand, which has the greater trans influence than chloride, while the 60.3-ppm signal is due to P^2 trans to the chloride. The spectrum of the ClO_4 salt **8a** in CD_3CN is similar to that of **2** in $CDCl_3$ and two doublets appear at 55.2 (P^1) and 65.0 (P^2) ppm with $J(P^1\text{-}P^2)$=17 Hz. The downfield shift of the P^1 and P^2 signals for **8a** compared with those of **2** can be generally understood as the coordination effect of the free CN group of **2** to another metal atom and as the replacement effect of chloride by the second CN group, although the solvent effect can not be ignored, too (see data for **7** in $CDCl_3$). The ^1H NMR spectrum of **8a** in CD_3CN shows a cyanomethyl signal at 1.34 ppm as a

Table 6. $^{13}C\{^1H\}$ NMR Data for the diphosphine complexes **2**, **7**, and **8a**[a)]

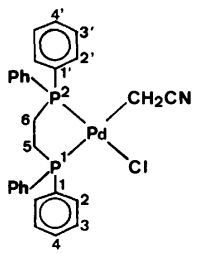

2

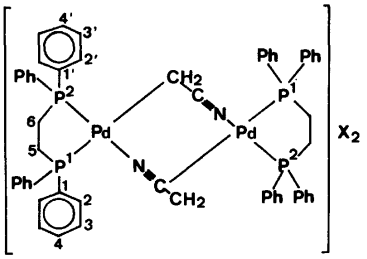

7 (X = hfac); **8a** (X = ClO_4)

No.	CH_2CN		dppe						hfac		
	CH_2	CN	C^1, $C^{1'}$	C^2, $C^{2'}$	C^3, $C^{3'}$	C^4, $C^{4'}$	C^5	C^6	CF_3	CO	CH
2[b)]	−0.7dd	125.5	129.5d	132.7d	129.0d	131.3d	24.3dd	30.9dd			
	(105)		{32}	{12}	{11}	{3}	(29)	(21)			
	((3))				129.3d	132.2d	((12))	((34))			
					{11}	{3}					
7[b)]	−2.1dd	125.7d	d)	132.9d	129.4d	131.8	24.0dd	30.7dd	118.1q	173.5q	85.2
	(92)			{12}	{10}		(31)	(18)	[291]	[31]	
	((4))	((40))		133.0d	129.7d	131.9	((9))	((36))			
				{12}	{12}						
8a[c)]	d)	126.2d	131.9d	134.1d	129.3d	133.9d	24.6dd	31.4dd			
		((43))	{41}	{12}	{13}	{3}	(33)	(18)			
				133.8d	129.2d		((9))	((37))			
				{12}	{11}						

a) Chemical shift (δ) in ppm from internal Me_4Si. Figures in parentheses, double parentheses, braces, and brackets give $J(^{31}P^1\text{-}C)$, $J(^{31}P^2\text{-}C)$, $J(^{31}P\text{-}C)$, and $J(^{19}F\text{-}C)$ in Hz, respectively. $J(^{31}P\text{-}C)$ describes $J(^{31}P^1\text{-}C^n)$ and/or $J(^{31}P^2\text{-}C^n)$. b) In $CDCl_3$. c) In CD_3CN. d) Indiscernible because of overlapping with other signals.

doublet of doublets with $^3J(P^1\text{-}H)=9.0$ and $^3J(P^2\text{-}H)=3.0$ Hz in accordance with the diphosphine-chelating structure.

Table 6 lists the $^{13}C\{^1H\}$ NMR data for the diphosphine complexes **2**, **7**, and **8a**. The starting complex **2** shows the cyanomethyl-CH_2 and -CN signals at −0.7 and 125.5 ppm, respectively. The CH_2 signal appears as a doublet of doublets by coupling to trans P^1 and cis P^2 with $^2J(P^1\text{-}C)=105$ and $^2J(P^2\text{-}C)=3$ Hz, respectively. The coupling constant of 105 Hz for $^2J(P^1\text{-}C)$ is surprisingly large, but it is not impossible because the appreciably large trans coupling constants are observed: $^2J(P\text{-}C)=75$ Hz for $[Pt(CH_3)\{P(CH_3)_2(C_6H_5)\}_3]^+$,[22] 72 Hz for $[Pt(tfac(2\text{-})\text{-}C,O)(PPh_3)_2]$,[23] and 70 Hz for $[Pd(tfac(2\text{-})\text{-}C,O)(PPh_3)_2]$[24] and *cis*-$[Pt(acac\text{-}C^1)(py)\{P(p\text{-}ClC_6H_4)_3\}_2]^+$.[25] When the cationic dimer (**8a**) with the *N*-bonded CN group is prepared, it is interesting to see that the cyanomethyl-CN signal observed at 126.2 ppm couples to a phosphorus atom, although three-bond coupling of the CN carbon in **2** to trans P^1 is not appreciated. This fact suggests that the CN carbon signal of **8a** couples to trans P^2 through C-N-Pd-P^2 bond. The large coupling constant of 43 Hz for $^3J(P^2\text{-}C)$ may be allowed when it is compared with 105 Hz for the two-bond trans coupling ($^2J(P^1\text{-}C)$) of the cyanomethyl-CH_2 signal in **2**.

In contrast to **8**, the hfac salt **7** is appreciably soluble even in noncoordinating solvents and the cation is found to be dimeric in dichloromethane by the molecular weight measurement. Figure 1 displays the temperature-dependent $^{31}P\{^1H\}$ NMR spectra of **7** in $CDCl_3$. The spectrum at 32 °C is of the basically AB quartet type, exhibiting two doublets at 50.4 (P^1) and

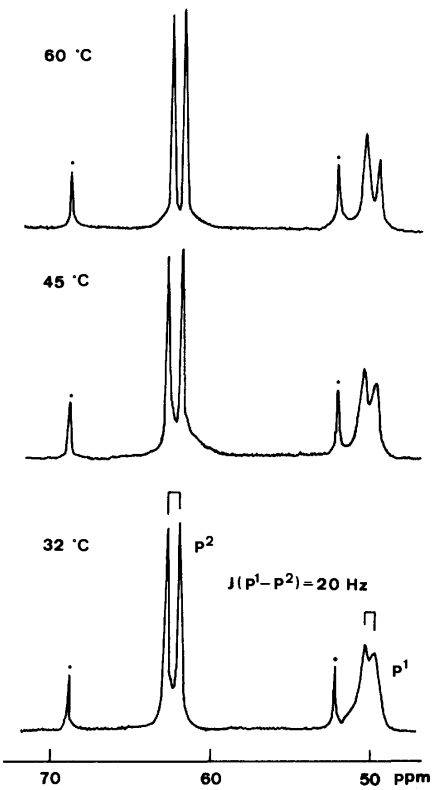

Fig. 1. Temperature-dependent $^{31}P\{^1H\}$ (24.2 MHz) NMR spectra of $[Pd(CH_2CN)(dppe)]_2(hfac)_2$ (**7**) in $CDCl_3$ with external H_3PO_4. Two minor signals denoted by asterisks are due to some decomposed species.

62.5 (P^2) ppm with J(P^1-P^2)=20 Hz, although the broadening is taking place in the higher field signal. In contrast to the ClO_4 anion, the hfac anion in **7** has the potentially coordinating power to form the five-coordinate complex. If the oxygen donor of the anion approaches from the P^1 side to the central palladium atom, the resulting complex **A** should have the trigonal-bipyramidal structure in which only the P^1 atom is appreciably sterically distorted, as exemplified below.

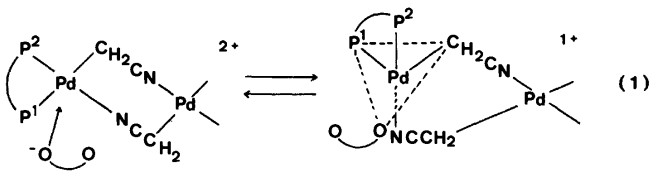

(1)

7 **A**

When the addition-elimination rate of the hfac anion in equilibrium (1) is slow on the NMR time scale, the broadening of only the P^1 signal can be observed with retention of the P^1-P^2 coupling. As the rate becomes more rapid, the normal AB quartet pattern will be restored. In fact, the broad P^1 signal sharpen gradually with increasing temperature, giving the well-resolved doublet at 60°C. Minor signals observed at each lower-field side of the two doublets increase in their intensities with time, and hence these signals can be regarded as those of some decomposed species.

In spite of the existence of equilibrium (1) in solution, the cyanomethyl-proton signal of **7** in $CDCl_3$ appears at 1.32 ppm as a doublet of doublets, the coupling constants being the same degree (^3J(P^1-H)=10.5; ^3J(P^2-H)=3.5 Hz) as those for **8a**. The methine proton of the hfac anion in **7** resonates at higher field (5.38 ppm in $CDCl_3$) than that in [Pd(hfac)$_2$] (6.42 ppm in the same solvent). Such a upfield shift is generally recognized as is due to the higher charge density on the noncoordinating anion.[26]

As is seen in Table 6, the $^{13}C\{^1H\}$ NMR spectrum of **7** in $CDCl_3$ shows three signals originated from the hfac anion in addition to the spectrum of **8a**. The CF_3-, CH-, and CO-carbon signals appear at 118.1, 85.2, and 173.5 ppm as a quartet with ^1J(C-F)=291 Hz, a singlet, and a quartet with ^2J(C-F)=31 Hz, respectively. These chemical shifts and coupling constants are very similar to those for the outer-sphere complexes [Pd(PMe$_2$Ph)$_4$](hfac)$_2$ and [Pd(dppe)$_2$](hfac)$_2$ in $CDCl_3$ and CD_3OD, respectively,[26b] indicating that the hfac ligand in **7** is present as a counter anion. The cyanomethyl-CN signal appears at 125.7 ppm as a doublet with ^3J(P^2-C)=40 Hz, also supporting the N-bonded CN-bridging structure of the cation.

Cationic Triphenylphosphine Complexes. The IR spectra of the cationic PPh_3 complexes **5** in the solid state exhibit only one sharp ν(C≡N) band at around 2250 cm^{-1} and either one of two possible structures of the cationic dimer V and polimer VI is conceivable as

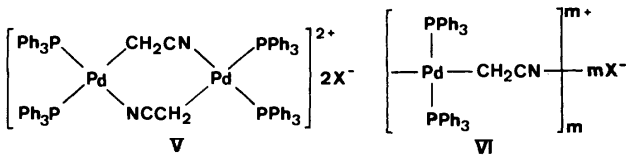

V **VI**

the solid state structure of **5**. Because of the less soluble nature in noncoordinating solvents, the molecular weight and NMR measurements of **5** were performed in CH_3CN and CD_3CN, respectively. As is seen in Table 1, each molecular weight of **5a** and **5b** has a half value of the formula weight in CH_3CN, and hence the Pd-N bonds in structure V or VI are brorken to give the following *cis*- or *trans*-PPh_3 complex in which a solvent molecule S occupies the vacant coordination site. The

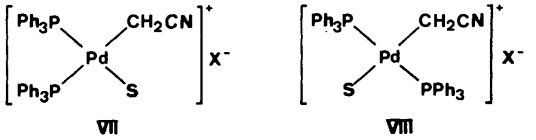

VII **VIII**

^1H NMR spectrum of **5a** at 33 °C shows a broad signal assignable to the cyanomethyl proton at 1.26 ppm from internal Me_4Si. However, when the temperature is decreased, the signal further broadens until it begin to split into three peaks at −5°C, and then gives a sharp triplet with ^3J(P-H)=6.8 Hz at −30°C. These results imply that two molecules of PPh_3 have the mutually trans configuration like structure VIII at −30°C, although the complex is stereochemically nonrigid at the higher temperature. For such a spectral change in ^1H NMR, two explanations are possible: (1) dissociation and coordination of a PPh_3 molecule in structure VIII are taking place rapidly on the NMR time scale, (2) cis-trans isomerization (Eq. 2) is taking place between structures VII and VIII *via* the cationic dimer similar to **8**, both at the higher temperatures. In

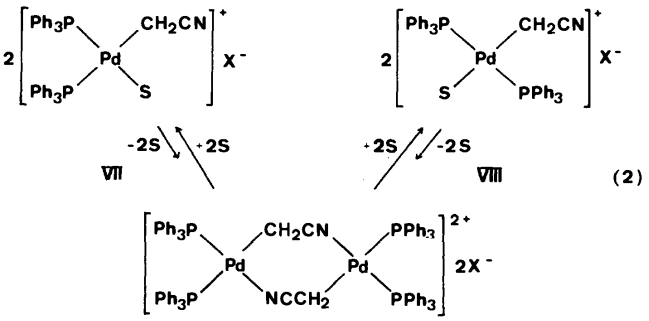

(2)

the case of (2), the isomerization can be promoted by the coordination of the free CN group in structure VII or VIII to another molecule. The choice of either one of the two mechanisms mentioned above is not possible at the present stage of investigation.

These dynamic behaviors of the species in solution are also consistent with the temperature-dependent $^{31}P\{^1H\}$ and $^{13}C\{^1H\}$ NMR data for **5a** in CD_3CN. The $^{31}P\{^1H\}$ NMR spectrum of **5a** at −30°C shows a single signal at 25.2 ppm with the half width of *ca.* 2 Hz, indicating the existence of the environmentally equivalent two phosphorus atoms at this temperature, although the half width slightly increases with increasing temperature owing to the occurrence of the stereochemical nonrigidity. In the case of the $^{13}C\{^1H\}$ NMR spectrum of **5a**, the signal intensities for the cyanomethyl-CH_2 and -CN carbons are too weak to perceive their temperature-dependent spectral changes, while the phenyl-ring carbon signals of the PPh_3 ligands are useful to examine the structural

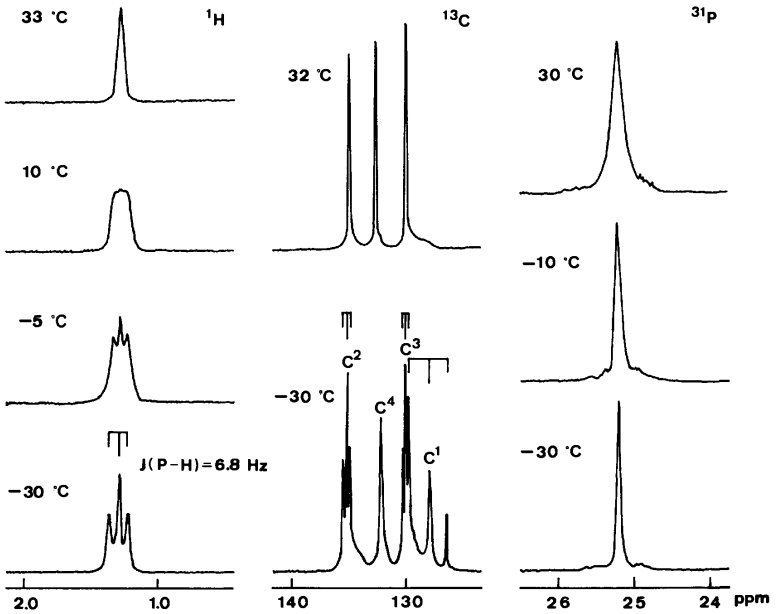

Fig. 2. Temperature-dependent ^{1}H (100 MHz), ^{13}C{^{1}H} (15.0 MHz), and ^{31}P{^{1}H} (24.2 MHz) NMR spectra of $[Pd(CH_2CN)(PPh_3)_2]_m(ClO_4)_m$ (**5a**) in CD_3CN with internal Me_4Si, external Me_4Si, and external H_3PO_4, respectively.

change of the complex in solution. At −30 °C, each signal appears at 127.8 (C^1), 134.8 (C^2), 129.8 (C^3), and 132.4 (C^4) ppm from external Me_4Si (see Table 5 for the numbering system). Except for C^4, which is most distant from P, all other carbon signals resonate as triplets by virtual coupling to the mutually trans 2P atoms, the coupling constants being 24.2 (C^1), 6.5 (C^2), and 5.1 (C^3) Hz. On the other hand, these couplings are lost at 32 °C and each signal appears as a singlet, again indicating the dynamic behavior of **5a** at this temperatures. These spectral change are summarized in Fig. 2.

Although no attempt is made to isolate the cationic species $[Pd(CH_2CN)(CH_3CN)(PPh_3)_2]X$ (X=ClO_4 or BF_4) which is thought to exist in the acetonitrile solution of **5**, a similar complex $[Pd(CH_2CN)(acetone)(PPh_3)_2](hfac)$ (**6**) can be isolated. The IR spectrum of **6** in the solid state shows a strong ν(C≡N) band at 2200 cm^{-1} and three strong to medium bands assignable to the ν(C⋯O) and ν(C⋯C) at 1673, 1548, and 1520 cm^{-1}. These frequencies are consistent with the formulation as $[Pd(CH_2CN)(acetone)(PPh_3)_2](hfac)$. When the complex is dissolved in $CHCl_3$, however, another weak band appears at the higher-frequency side of the strong ν(C≡N) band, suggesting the formation of the cationic species with the *N*-bonded CN group in the solution. The ^{1}H NMR spectrum of **6** in $CDCl_3$ at 33 °C exhibits a sharp signal at 1.43 ppm and a broad one at 5.37 ppm, which are assigned to the cyanomethyl and the hfac-CH protons, respectively. As the temperature is decreased, the CH signal moved gradually to the higher-field side and newly two signal appeared, giving three methine proton signals at 6.34, 5.72, and 4.68 ppm at −45 °C. Although such a complex behavior in the IR and ^{1}H NMR spectra of **6** predicts the formation of the *O,O'*-chelated and *O*-unidentate species of the hfac ligand in solution in addition to the existence of equilibrium (2) (X=hfac), this ambiguity is not pursued further in view of their insufficient data.

Experimental

The starting complexes *trans*-$[PdCl(CH_2CN)(PPh_3)_2]$ (**1**) and $[PdCl(CH_2CN)(dppe)]$ (**2**) were prepared according to the literature.[2]

Preparation of [Pd(CH$_2$CN)(β-dik)(PPh$_3$)] (3) by the Reactions of 1 with Tl(β-dik). General Procedure: Equimolecular amounts of an appropriate Tl(β-dik)[27] were allowed to react with **1** in dichloromethane at room temperature. Thallium(I) chloride began to precipitate immediately and the mixture was stirred for the time noted below before filtration. The filtrate was concentrated under reduced pressure and petroleum ether was added to the concentrate to obtain a crude precipitate. The color and appearance, the reaction time, the solvent of crystallization, and the yield were as follows. **3a**: White needles, 1 h, dichloromethane-petroleum ether, 62%; **3b**: yellow plates, 3 h, acetone, 89%; **3c**: yellow needles, 3 h, dichloromethane-petroleum ether, 63%; **3d**: white needles, 12 h, dichloromethane-petroleum ether, 93%; **3e**: yellow needles, 5 h, dichloromethane-petroleum ether, 98%.

In a similar reaction of **1** with Tl(hfac), only oily substance was obtained, from which a pure solid could not be isolated. The crude substance shows two ν(C≡N) bands at 2210 and 2240 cm^{-1} and their relative intensity varies with repeated preparations. The ν(C⋯O)+ν(C⋯C) bands appear at 1668s, 1638sh, and 1525s cm^{-1}, indicating that the main product contains the hfac ligand as a counter anion.[28] The signal intensity of the ^{1}H NMR spectrum reveals that the molar ratio of PPh_3 to CH_2CN in the specimen is always $1:1 \ll PPh_3:CH_2CN < 2:1$.

Preparation of the Neutral [PdCl(CH$_2$CN)(PPh$_3$)]$_n$ (4) by Hydrogen Peroxide Oxidation of 1. Acetone (20 cm^3) and a 30% aqueous solution (5 cm^3) of H_2O_2 were added successively to a dichloromethane (10 cm^3) solution of **1** (616 mg, 0.814 mmol) and the mixture was stirred for 40 h during which a small amount of white precipitate was formed. The total volume of the mixture was reduced before filtration to obtain **4** in a satisfactory yield. The yield was 326 mg (84%).

Preparation of the Cationic [Pd(CH_2CN)(PPh_3)$_2$]$_m$$X_m$ (X= ClO_4 (5a) or BF_4 (5b)) by Chloride Abstraction of 1. A methanol (10 cm^3) solution of $AgClO_4$ (260 mg, 1.25 mmol) was added to a solution of **1** (935 mg, 1.24 mmol) in dichloromethane (40 cm^3). Silver chloride began to precipitate immediately and the mixture was stirred for 24 h at room temperature before filtration. The filtrate was concentrated under reduced pressure to obtain a pale yellow powder of **5a**. The yield was 840 mg (88%). Similarly, **1** (304 mg, 0.402 mmol) in dichlomethane (20 cm^3) was allowed to react with $AgBF_4$ (78.4 mg, 0.402 mmol) in methanol (10 cm^3) for 22 h. After the same procedure as described above, addition of petroleum ether to the concentrate gave a white precipitate (214 mg) of **5b** in a 70% yield.

Reactions of 4 with Tl(acac) and Tl(tfac). A methanol (10 cm^3) solution of Tl(acac) (74 mg, 0.243 mmol) was added to a suspension of **4** (104 mg, 0.234 mmol for n=1) in acetone (20 cm^3) at room temperature. After being stirred for 10 h, the precipitated TlCl was filtered off and the filtrate was evaporated to dryness under reduced pressure. The residue was redissolved in acetone and the solution was concentrated to separate out yellow plates of **3b**. The yield was 85 mg (71%). Similarly, Tl(tfac) (127 mg, 0.356 mmol) in methanol (10 cm^3) was allowed to react with a acetone (30 cm^3) suspension of **4** (120 mg, 0.271 mmol for n=1) overnight. Filtration, concentration to dryness, and then redissolution of the residue in dichloromethane (5 cm^3) afforded a yellowish green solution, from which **3c** was deposited on addition of petroleum ether. Recrystallization from acetone-petroleum ether gave yellow crystals in a 63% yield (96%).

Reaction of 5a with K(acac). To a solution of **5a** (224 mg, 0.296 mmol for n=1) in dichloromethane (20 cm^3) was added dropwise a methanol (10 cm^3) solution of K(acac) (57 mg, 0.412 mmol). After being stirred for 2 h, the solvent was evaporated to dryness under reduced pressure. Dichloromethane (10 cm^3) was added to the residue and the undissolved $KClO_4$ was filtered off. Addition of petroleum ether to the filtrate gave a yellow plates (126 mg) of **3b** in an 84% yield.

Preparation of the Cationic [Pd(CH_2CN)(acetone)(PPh_3)$_2$](hfac) (6) by the Reaction of 5a with K(hfac). A solution of K(hfac) (70 mg, 0.282 mmol) in methanol (3 cm^3) was added slowly to a dichloromethane (20 cm^3) solution of **5a** (218 mg, 0.282 mmol for m=1). After being stirred for 10 min, the solvent was evaporated to dryness, the residue was redissolved in a small amount of acetone, and then the undissolved $KClO_4$ was filtered off. Petroleum ether was added to the filtrate and the solution was allowed to stand to separate yellow needles of **6** in a 26% yield (65 mg).

Preparation of the Cationic [Pd(CH_2CN)(dppe)]$_2$(hfac)$_2$ (7) by the Reaction of 2 with Tl(hfac). Complex **2** (232 mg, 0.400 mmol) was allowed to react with Tl(hfac) (165 mg, 0.400 mmol) in refluxing acetone over 20 h. After the solvent was evaporated to dryness, dichloromethane was added to the residue, the undissolved TlCl was filtered off, and again the solvent was evaporated to dryness. The residue was redissolved in a small amount of acetone and diethyl ether was added to precipitate acetone solvate of **7**. The product was collected, washed with diethyl ether, and then dried *in vacuo* at 50 °C for 3 h. The yield of a yellow powder of **7** was 109 mg (36%).

Preparation of the Cationic [Pd(CH_2CN)(dppe)]$_2$$X_2$ (X= ClO_4 (8a) or BF_4 (8b)) by Chloride Abstraction of 2. To a solution of **2** (160 mg, 0.275 mmol) in dichloromethane (13 cm^3) was added dropwise a solution of $AgClO_4$ (57 mg, 0.275 mmol) in methanol (15 cm^3). After being stirred for 19 h, the precipitated AgCl was filtered off and the filtrate was concentrated under reduced pressure to deposit a white powder of **8a**, which was gathered and washed with acetone and dried *in vacuo*. The yield was 136 mg (77%). In the case of the reaction of **2** with $AgBF_4$, after removal of the precipitated AgCl, the solvent was evaporated to dryness. The residue was redissolved in dichloromethane and diethyl ether was added to obtain a white precipitate of **8b**. Recrystallization twice from dichloromethane-diethyl ether gave a white powder in a 79% yield.

Reaction of 8a with K(hfac). A solution of K(hfac) (74 mg, 0.300 mmol) in methanol (10 cm^3) was added to a suspension of **8a** (120 mg, 0.132 mmol) in dichloromethane (10 cm^3). After being stirred for 2 h at room temperature, the solvent was evaporated to dryness under reduced pressure to leave **7** and $KClO_4$. The residue was redissolved in methanol and the undissolved $KClO_4$ was removed by filtration. The solvent was again evaporated to dryness and the crude product was recrystallized twice from acetone-diethyl ether to give a white powder of **7**. The yield was 119 mg (56%).

Measurements. Infrared spectra were obtained in Nujol mull or in a chloroform solution with a JASCO DS 701G (4000—200 cm^{-1}) infrared spectrophotometer. NMR spectra in $CDCl_3$ or CD_3CN were recorded on JEOL JNM MH-100 (for ^{1}H), FX-60Q (for ^{13}C and ^{31}P) instruments. Molecular weight was determined in CH_2Cl_2 (at 28 °C) or CH_3CN (at 39 °C) with a vapor pressure osmometer manufactured by Knauer, West Berlin, West Germany.

References

1) W. J. Blend, R. D. W. Kemmitt, and R. D. Moore, *J. Chem. Soc., Dalton Trans.*, **1973**, 1292.
2) K. Suzuki and H. Yamamoto, *J. Organomet. Chem.*, **54**, 385 (1973).
3) K. Suzuki, H. Yamamoto, and S. Kanie, *J. Organomet. Chem.*, **73**, 131 (1974).
4) K. Suzuki, J. Ooyama, and M. Sakurai, *Bull. Chem. Soc. Jpn.*, **49**, 464 (1976).
5) R. Ros, J. Renaud, and R. Roulet, *Helv. Chim. Acta*, **58**, 133 (1975).
6) R. Ros, J. Renaud, and R. Roulet, *J. Organomet. Chem.*, **87**, 379 (1975).
7) R. Ros, M. Lenarda, T. Boschi, R. Roulet, *Inorg. Chim. Acta*, **25**, 61 (1977).
8) A. D. Pra, G. Zanotti, G. Bombieri, and R. Ros, *Inorg. Chim. Acta*, **36**, 121 (1979).
9) R. McCrindle, G. Ferguson, A. J. McAlees, M. Parvez, and P. J. Roberts, *J. Chem. Soc., Dalton Trans.*, **1982**, 1699.
10) R. Ros, J. Renaud, and R. Roulet, *J. Organomet. Chem.*, **104**, 271 (1976).
11) R. Ros, J. Renaud, and R. Roulet, *J. Organomet. Chem.*, **104**, 393 (1976).
12) R. Ros, R. A. Michelin, T. Boschi, and R. Roulet, *Inorg. Chim. Acta*, **35**, 43 (1979).
13) K. Suzuki and M. Sakurai, *Inorg. Chim. Acta*, **20**, L13 (1976).
14) K. Suzuki and K. Hanaki, *Inorg. Chim. Acta*, **20**, L15 (1976).
15) R. C. Mehrotra, R. Bohra, and D. P. Gaur, "Metal β-Diketonates and Allied Derivatives," Academic Press, New York (1978).
16) B. N. Storhoff and H. C. Lewis, Jr., *Coord. Chem. Rev.*, **23**, 1 (1977).
17) S. Okeya, S. Ooi, K. Matsumoto, Y. Nakamura, and S. Kawaguchi, *Bull. Chem. Soc. Jpn.*, **54**, 1085 (1981).
18) S. Baba, T. Ogura, and S. Kawaguchi, *Bull. Chem. Soc. Jpn.*, **47**, 665 (1974).
19) K. Yamada, S. Baba, Y. Nakamura, and S. Kawaguchi, *Bull. Chem. Soc. Jpn.*, **56**, 1393 (1983).
20) G. Oehme, K.-C. Roeber, and H. Praceijus, *J. Organomet. Chem.*, **105**, 127 (1976).

21) D. Schwarzenbach, A. Pinkerton, G. Chapuis, J. Wenger, R. Ros, and R. Roulet, *Inorg. Chim. Acta*, **25**, 255 (1977).
22) M. H. Chisholm, H. C. Clark, L. E. Manzer, J. B. Stothers, and J. E. H. Ward, *J. Am. Chem. Soc.*, **95**, 8574 (1973).
23) S. Okeya, Y. Nakamura, S. Kawaguchi, and T. Hinomoto, *Inorg. Chem.*, **20**, 1576 (1981).
24) S. Okeya, Y. Kawakita, S. Matsumoto, Y. Nakamura, S. Kawaguchi, N. Kanehisa, K. Miki, and N. Kasai, *Bull. Chem. Soc. Jpn.*, **55**, 2134 (1982).
25) S. Okeya, Y. Nakamura, S. Kawaguchi, and T. Hinomoto, *Bull. Chem. Soc. Jpn.*, **55**, 477 (1982).
26) a) S. Okeya, H. Sazaki, M. Ogita, T. Takemoto, Y. Onuki, Y. Nakamura, B. K. Mohapatra, and S. Kawaguchi, *Bull. Chem. Soc. Jpn.*, **54**, 1978 (1981); b) S. Okeya, Y. Nakamura, and S. Kawaguchi, *ibid.*, **54**, 3396 (1981).
27) Various Tl(β-dik) complexes were prepared according to the preparative method for Tl(bzac): W. H. Nelson, W. J. Randall, and D. F. Martin, Inorg. Synth., Vol. IX, 53 (1967).
28) See text and Ref. 26.

 © 1984 The Chemical Society of Japan Bull. Chem. Soc. Jpn., 57, 1021—1025 (1984)

Kinetics and Equilibrium Studies on the Anation Reactions in Pentakis(dimethyl sulfoxide)dioxouranium(VI) and Tetrakis-(hexamethylphosphoric triamide)dioxouranium(VI) Ions in Nonaqueous Media

Hideo Doine, Yasuhisa Ikeda, Hiroshi Tomiyasu, and Hiroshi Fukutomi*

Research Laboratory for Nuclear Reactors, Tokyo Institute of Technology, O-okayama, Meguro-ku, Tokyo 152

(Received October 26, 1983)

The anation reactions in $[UO_2(dmso)_5]^{2+}$ (dmso=dimethyl sulfoxide) and $[UO_2(hmpa)_4]^{2+}$ (hmpa=hexamethylphosphoric triamide) ions by SCN^- and N_3^- have been studied by the stopped-flow method in DMSO and acetonitrile. For the anation reactions of $[UO_2(dmso)_5]^{2+}$ in DMSO as a medium, the pseudo-first order rate constant(k_{obsd}) is expressed by $k_{obsd}=\{k_{-1}+(k_1+k_{-1})\times K_{os}[X]\}/(1+K_{os}[X])$, where X=$SCN^-$ and $[UO_2(dmso)_5]^{2+}$ for the anation reactions by SCN^- and N_3^-, respectively. The values of k_1, k_{-1}, and K_{os} at 25 °C are 2.06×10^2 s^{-1}, 62 s^{-1}, 35 M^{-1} (M=mol dm^{-3}), and 7.60×10^2 s^{-1}, 0.0 s^{-1}, and 41 M^{-1} for the SCN^- and N_3^- anation reactions in $[UO_2(dmso)_5]^{2+}$, respectively. For the anation reaction in $[UO_2(hmpa)_4]^{2+}$ by SCN^-, the pseudo-first order rate constant was found to be proportional to the concentrations of $[UO_2(hmpa)_4]^{2+}$ and free HMPA: $k_{obsd}=k_f[UO_2(hmpa)_4^{2+}]+k_b[HMPA]_{free}$. The values of k_f and k_b at 25 °C are 9.70×10^3 M^{-1} s^{-1} and 9.05×10^2 M^{-1} s^{-1}, respectively. The equilibrium constants for the titled reactions were also measured at 25 °C: K=85 $M^{-1}$for the anation reaction of $[UO_2(dmso)_5]^{2+}$ by SCN^- in DMSO and K'=42.7 for the SCN^- anation reaction in $[UO_2(hmpa)_4]^{2+}$ in acetonitrile. The kinetic results suggest that the anation reactions in uranyl complexes proceed through an associative or an associative interchange mechanism.

For ligand exchange reactions in the equatorial position of uranyl complexes, it is proposed that most of the reactions proceed through the dissociation (D) or the dissociative interchange (I_d) mechanism.[1-8]

The authors have reported that the ligand substitution reactions in $[UO_2(dmf)_5]^{2+}$ (dmf=*N*,*N*-dimethylformamide) ion proceeded *via* an associative interchange (I_a) mechanism and the anation rate constant depended on the basicity of entering ligands.[9] Few other studies on the anation reactions of uranyl complexes have been reported.

A detailed kinetic and equilibrium study on the anation reactions in $[UO_2(dmso)_5]^{2+}$ and $[UO_2(hmpa)_4]^{2+}$ ions was performed for the following reactions:

$$[UO_2(dmso)_5]^{2+} + SCN^- \rightleftharpoons [UO_2(dmso)_4NCS]^+ + DMSO,$$

$$[UO_2(dmso)_5]^{2+} + N_3^- \rightleftharpoons [UO_2(dmso)_4N_3]^+ + DMSO,$$

$$[UO_2(hmpa)_4]^{2+} + SCN^- \rightleftharpoons [UO_2(hmpa)_3NCS]^+ + HMPA.$$

The reaction mechanism is discussed by comparing the results of kinetic study of these reactions with the previous results for the anation rcactions in $[UO_2(dmf)_5]^{2+}$.

Experimental

Synthesis of Complexes. The $[UO_2(dmso)_5](ClO_4)_2$ and $[UO_2(hmpa)_4](ClO_4)_2$ complexes were prepared under an atmosphere of nitrogen by refluxing hydrated uranyl perchlorate with triethyl orthoformate at 60°C for 1 h, followed by the addition of dimethyl sulfoxide and hexamethylphosphoramide at room temperature, respectively. The resulting light yellow crystals of these complexes were recrystallized from dichloromethane and washed with dried diethyl ether, and freed of the diethyl ether *in vacuo* for 2 d. Calcd for $[UO_2(dmso)_5](ClO_4)_2$: C, 13.97; H, 3.52%. Found: C, 13.45; H, 3.41%. Calcd for $[UO_2(hmpa)_4](ClO_4)_2$: C, 24.3; H, 6.12; N, 14.18%. Found: C, 24.6; H, 6.10; N, 14.50%. Elemental analysis of the complexes was carried out by using a Shimadzu CHN-1A analyzer.

Other Materials. Hexamethylphosphoric triamide (Wako Pure Chemical Ind. Ltd.) was distilled twice under reduced pressure and stored over 4A molecular sieves (Wako). Dimethyl sulfoxide (Wako) was kept in contact with barium oxide for 2 d, distilled twice under reduced pressure and stored over 4A molecular sieves. Acetonitrile (MeCN) (Wako) was dehydrated with calcium oxide and diphosphorus pentaoxide, and distilled. Triethyl orthoformate(Wako) was of guaranteed grade and used without further purification. Sodium thiocyanate (Wako) was dried at 100°C for 2 h and stored *in vacuo*. The concentration of azide ion in DMSO solution was determined by measuring sodium ion concentration with a Varian-Techtron 1100 flame-spectrophotometer. The amount of water contained in DMSO and MeCN solvents was measured by a Mitsubishi CA-02 moisture-meter and the maximum concentration was found to be less than 0.03 M. Anhydrous sodium perchlorate (Wako) was used to adjust the ionic strength of solutions to 0.2 M.

Measurement of NMR Spectra. ^1H NMR spectra were measured at 100 Hz on a JEOL JNM-FX 100 FT-NMR spectrometer equipped with a JNM-VT-3B temperature controller.

Measurement of Equilibrium Constants. The equilibrium constants between uranyl complexes and thiocyanate or azide ions were measured spectrophotometrically by using a Shimadzu UV-210A double-beam spectrophotometer with a cell compartment thermostated at 25°C. The ionic strength of sample solutions was adjusted to 0.2 M by using sodium perchlorate.

Kinetic Measurements. The anation rates were measured by using a specially designed double-beam stopped-flow apparatus with a nitrogen-pressurized flow system. The temperature of the sample solutions was adjusted by a conventional temperature controller. The memorized stopped-flow signals were introduced to a Sord microcomputer (M223 Mk III), accumulated and curve-fitted. At least ten runs were performed for cach measurement.

Results and Discussion

Equilibrium of $[UO_2(dmso)_5]^{2+}$ Ion with SCN^- and N_3^-. The ^1H NMR spectra of solutions

containing $[UO_2(dmso)_5]^{2+}$, DMSO, CD_3CN, and $(CD_3)_2CO$ were observed at −65 °C. It was shown that the structure of $[UO_2(dmso)_5]^{2+}$ was consistent with that reported by Fukutomi *et al.*, *i.e.*, a pentagonal bipyramidal structure.[2] In the case of N_3^- anation, the area of the dmso methyl proton signal varied according to the concentration of added N_3^-. It was suggested that this reaction proceeded stoichiometrically as given by Eq. 1 with a fairly large equilibrium constant. It was impossible, in fact, to determine the equilibrium constant of this reaction by measuring the spectral change. Kinetic measurements also proved that the backward reaction rate constant is zero and the equilibrium constant is fairly large.

$$[UO_2(dmso)_5]^{2+} + N_3^- \rightleftharpoons [UO_2(dmso)_4N_3]^+ + DMSO \quad (1)$$

Figure 1 shows the spectral change of $[UO_2(dmso)_5]^{2+}$ with varying the concentration of $[UO_2(dmso)_5]^{2+}$ from 0.002 to 0.006 M at a constant concentration of SCN^- (2.0×10^{-4} M). Although an isosbestic point is not observed, the most probable reaction corresponding to the spectral change seems to be

$$[UO_2(dmso)_5]^{2+} + SCN^- \overset{K}{\rightleftharpoons} [UO_2(dmso)_4NCS]^+ + DMSO. \quad (2)$$

The equilibrium constant (K) for this process was obtained from the following equation.

$$\frac{[SCN^-]}{Abs - \varepsilon_1[UO_2(dmso)_5^{2+}]} = \frac{1}{K(\varepsilon_2-\varepsilon_1)[UO_2(dmso)_5^{2+}]} + \frac{1}{\varepsilon_2-\varepsilon_1}, \quad (3)$$

where Abs is the observed absorbance, and ε_1 and ε_2 are the molar extinction coefficients of $[UO_2(dmso)_5]^{2+}$ and $[UO_2(dmso)_4NCS]^+$, respectively. The plot of

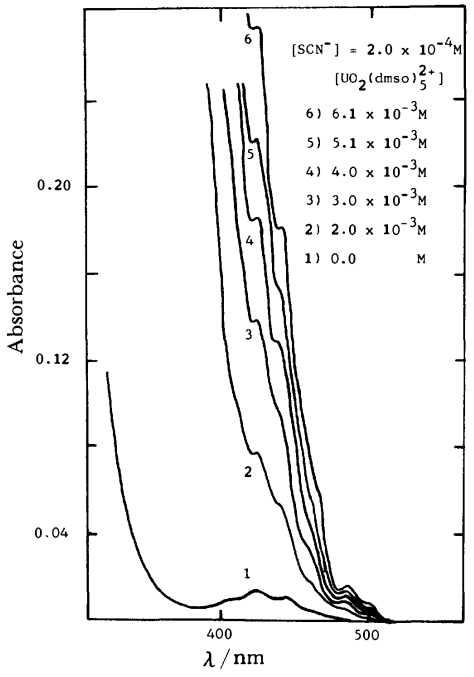

Fig. 1. The spectral change of $[UO_2(dmso)_5]^{2+}$ with varying the concentration of SCN^- in DMSO at 25 °C and ionic strength=0.2 M ($NaClO_4$).

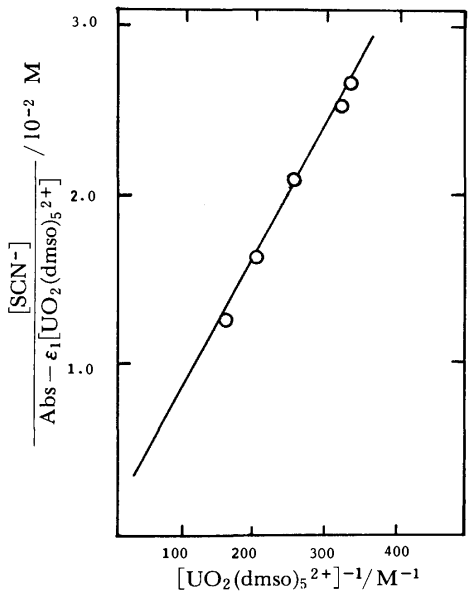

Fig. 2. The plot of $[SCN^-]/(Abs-\varepsilon_1[UO_2(dmso)_5^{2+}])$ *vs.* $1/[UO_2(dmso)_5^{2+}]$ for the anation reaction of $[UO_2(dmso)_5]^{2+}$ by SCN^- at 25 °C, 430 nm, and ionic strength=0.2 M ($NaClO_4$).

Table 1. Equlibrium constants of ligand substitution reactions in uranyl complexes at 25 °C[a]

Reaction	Solvent	K[b] / M^{-1}	K'[c]
$[UO_2(dmf)_5]^{2+}+SCN^-$	DMF	186±28	2400±210
	MeCN		2626±150
			2480±120[d]
$[UO_2(dmso)_5]^{2+}+SCN^-$	DMSO	85±9	1197±120
	MeCN		342±30
$[UO_2(hmpa)_4]^{2+}+SCN^-$	MeCN		42.7±4.0

a) The quoted errors represent the standard deviation. b) $K=[UO_2S_{n-1}L^+]/([UO_2S_n2^+][L^-]$. c) $K'=K\cdot[S]$. d) Measured in MeCN-DMF(50 vol%) mixed solvent.

$[SCN^-]/(Abs-\varepsilon_1[UO_2(dmso)_5^{2+}])$ against $1/[UO_2(dmso)_5^{2+}]$ gave a straight line as shown in Fig. 2, which supports the validity of the reaction given by Eq. 2. From the slope and intercept, the value of K was calculated and listed in Table 1.

Equilibrium of $[UO_2(hmpa)_4]^{2+}$ Ion with SCN^-. The ^1H NMR spcctra of solutions containing $[UO_2(hmpa)_4]^{2+}$, HMPA, CD_3CN, and $(CD_3)_2CO$ were observed at −65 °C. From the area ratio of the methyl proton signals of the coordinated and free HMPA, the structure of $[UO_2(hmpa)_4]^{2+}$ was proved to the same as that reported by Williams *et al.*,[10] *i.e.*, square bipyramidal. In this reaction, the equilibrium constant was measured in MeCN under the conditions of $[UO_2(hmpa)_4^{2+}]>[SCN^-]$. The value of equilibrium constant (K) was calculated by using a similar equation to Eq. 3, and is listed in Table 1.

The equilibrium constants for the reactions of $[UO_2(dmf)_5]^{2+}$ and $[UO_2(dmso)_5]^{2+}$ ions with SCN^- were also measured in MeCN under the conditions of T=25 °C and ionic strength= 0.2 M ($NaClO_4$). The

calculated values of K and K' are listed in Table 1, where K and K', denote the equilibrium constants defined as below.

$$K = \frac{[UO_2S_{n-1}NCS^+]}{[UO_2S_n^{2+}][SCN^-]}, \quad K' = K[S],$$

S = DMF, DMSO, and HMPA

As seen in Table 1, the equilibrium constants for the SCN^- anation reaction towards $[UO_2(dmf)_5]^{2+}$ ion in MeCN and DMF are consistent with each other within experimental errors. Moreover, the equilibrium constant measured in MeCN-DMF mixed solvent (50% in volume) was in good agreement with those measurcd in each solvent. The similar values of solubility parameters[11] and dielectric constants of MeCN and DMF might lead to the consistency of these results. The dielectric constant has an effect on the solvation of ions and the solubility parameter is concerned with the intermolecular forces. Thus, MeCN and DMF can be considered as almost equivalent solvents for the reactions containing relatively large ionic species. The order of K' values for the reactions of different uranyl complexes with thiocyanate ion in MeCN is consistent with the order of the donor property of the coordinated organic ligands, HMPA>TMP[12]>DMSO>DMF. Especially, the logarithmic values of the equilibrium constants showed a good linear relationship to the E_B parameter[13] of each organic ligand rather than the donor number (DN)[14] (Fig. 3).

Kinetic Study on the Reactions of $[UO_2(dmso)_5]^{2+}$ Ion with SCN^- and N_3^-. On the basis of the results of equilibrium constants measured spectrophotometrically, the pseudo-first order rate constant (k_{obsd}) for the anation reactions by SCN^- and N_3^- were measured under the conditions of $[UO_2(dmso)_5^{2+}]<[SCN^-]$ and $[UO_2(dmso)_5^{2+}]>[N_3^-]$, respectively.

Figures 4 and 5 show the plots of k_{obsd} *vs.* $[SCN^-]$ and $[UO_2(dmso)_5^{2+}]$, which do not display a simple linear relationship, and the values of k_{obsd} approach each limiting value at high concentration region of SCN^- and $[UO_2(dmso)_5]^{2+}$, respectively. Attempts were made to examine the effect of water on the anation reactions, in which the concentration of water was changed from 0.03 to 0.1 M. It was found that water made no effect on the present anation reactions in this concentration range.

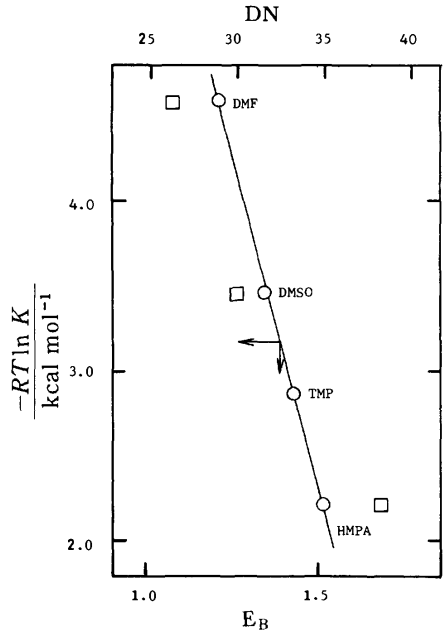

Fig. 3. The plot of $-RT\ln K$ *vs.* E_B and DN of the coordinated molecules: ○; E_B, □; DN.

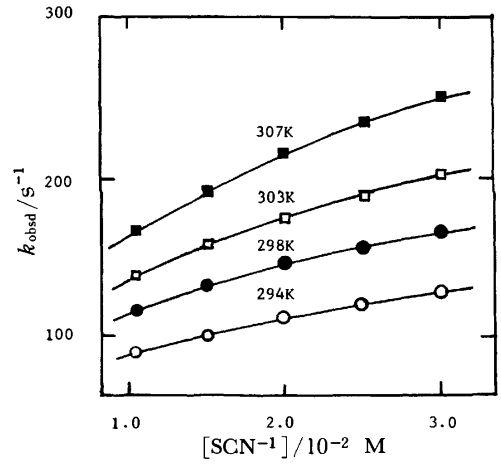

Fig. 4. Plots of k_{obs} *vs.* $[SCN^-]$ for the anation reaction of $[UO_2(dmso)_5]^{2+}$ by SCN^-. The solid lines denote the least-squares best-fit lines.

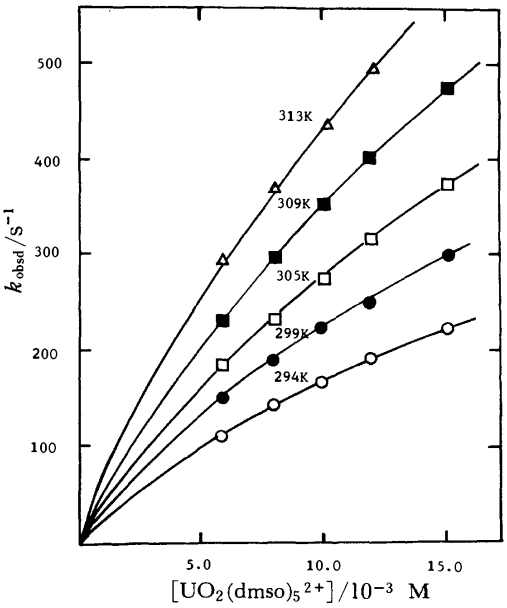

Fig. 5. Plots of k_{obsd} *vs.* $[UO_2(dmso)_5^{2+}]$ for the anation reaction by N_3^-. The solid lines denote the least-squares best-fit lines.

Taking into account the result that the anation reaction in $[UO_2(dmf)_5]^{2+}$ proceeded through the I_a mechanism,[9] the following I mechanism appears to be the most probable mehanism for the present anation reactions.

$$[UO_2(dmso)_5]^{2+} + L^- \overset{K_{os}}{\rightleftharpoons} [UO_2(dmso)_5]^{2+} \cdots L^-,$$

$$[UO_2(dmso)_5]^{2+} \cdots L^- \underset{k_{-1}}{\overset{k_1}{\rightleftharpoons}} [UO_2(dmso)_4L]^+ + DMSO,$$

were L is SCN^- or N_3^- ion, and K_{os} is the outersphere complex formation constant. According to this mechanism, the observed rate constant, k_{obsd}, is given by Eq. 4.

$$k_{obsd} = \frac{k_{-1}+(k_1+k_{-1})K_{os}[X]}{1+K_{os}[X]}, \quad (4)$$

Table 2. Kinetic parameters of ligand substitution reactions[a)]

Reaction	Temp	k_1	k_{-1}	K_{os}	k_f	k_b
	°C	s^{-1}	s^{-1}	M^{-1}	$10^4\ M^{-1}\ s^{-1}$	$10^2\ M^{-1}\ s^{-1}$
$[UO_2(dmso)_5]^{2+}+SCN^-$	21.0	160±15	41±9	41		
	25.0	206±18	62±12	35		
	30.2	281±21	73±8	29		
	34.2	404±28	85±11	35		
$[UO_2(dmso)_5]^{2+}+N_3^-$	21.0	544±35	0.0±5.0	44		
	26.3	762±20	−1.0±3.0	41		
	32.6	1035±51	3.0±5.3	35		
	36.5	1345±51	−5.1±7.2	36		
	40.0	1751±75	11.0±10.5	32		
$[UO_2(hmpa)_4]^{2+}+SCN^-$	25.0				0.97±0.03	9.05±0.50
	30.0				1.57±0.05	9.82±0.50
	34.0				2.18±0.07	11.6±0.8
	38.0				2.89±0.07	13.4±0.7

a) The quoted errors represent the standard deviation.

Table 3. Kinetic data for the ligand substitution reactions in uranyl complexes at 25 °C[a)]

Reactions	Solvents	Rate constant	ΔH^*	ΔH^*	Mechanism
		s^{-1}	kJ mol^{-1}	J $mol^{-1}\ K^{-1}$	
$[UO_2(dmso)_5]^{2+}+SCN^-$	DMSO	$k_1=2.1\times10^2$	49.6±0.8	−35.7±4.5	I_a
$[UO_2(dmso)_5]^{2+}+N_3^-$	DMSO	$k_1=7.5\times10^2$	43.3±0.9	−45.8±5.0	I_a
$[UO_2(hmpa)_4]^{2+}+SCN^-$	MeCN	$k_f=9.7\times10^3/M^{-1}$	62.6±1.5	41.1±5.3	A

a) The quoted errors respresent the standard deviation. Ionic strength=0.2 M($NaClO_4$).

where X is SCN^- and $[UO_2(dmso)_5]^{2+}$ for the anation reactions by SCN^- and N_3^-, respectively, since the measurements were carried out under the conditions of $[UO_2(dmso)_5^{2+}]<[SCN^-]$ and $[UO_2(dmso)_5^{2+}]>[N_3^-]$. When $K_{os}[X]\ll1$, Eq. 4 can be simplified to $k_{obsd}=k_{-1}+(k_1+k_{-1})K_{os}[X]$. This agrees with the dependence of k_{obs} on [X] in the low concentration region. If the values of $K_{os}[X]$ are much larger than unity, Eq. 4 becomes $k_{obsd}=k_1+k_{-1}$, which is consistent with the fact that limiting values of k_{obsd} are obtained at high [X].

The values of k_1, k_{-1}, and K_{os} were calculated by the nonlinear least-squares method and are listed in Table 2. The solid lines in Figs. 4 and 5 obtained from the calculated values agree with the experimental results. The activation parameters for k_1 obtained from the Eyring plot are shown in Table 3.

The outersphere complex formation constants for both reactions are similar as shown in Table 2. This seems to be reasonable since SCN^- and N_3^- ions have the same charge, similar size and structure. Thus the interatomic distance between $[UO_2(dmso)_5]^{2+}$ and SCN^- or N_3^- in the outersphere complexes is assumed to be the same. In this case, the Fuoss equation[15)] gives the same value for the outersphere association constant.

The interchange rate constants of the present reactions depended on the nature of the entering ligands, SCN^- and N_3^-. The difference of the reactivities, *i.e.*, $k_1^{N_3^-}/k_1^{SCN^-}\simeq3.8$ cannot be attributed to the outersphere complex formation, because the value of this ratio is larger than the corresponding value for K_{os}, $K_{os}^{N_3^-}/k_{os}^{SCN^-}\simeq1.2$ at 25 °C. Thus the different reactivity may be due to a difference in nucleophilicity of SCN^- and N_3^-.

Kinetic Study on the Reaction of $[UO_2(hmpa)_4]^{2+}$ Ion with SCN^-. On the basis of the spectrophotometric measurement of the equilibrium constant, the pseudo-first order rate constants, k_{obsd}, for the anation reaction in $[UO_2(hmpa)_4]^{2+}$ with SCN^- were measured under the conditions of $[UO_2(hmpa)_4^{2+}]>[SCN^-]$ in MeCN. The plots of k_{obsd} against the concentration of $[UO_2(hmpa)_4]^{2+}$ in Fig. 6 show a simple linear relationship. The effect of water on the present anation reaction was also examined, where the concentration of water was changed from 0.05 to 0.1 M. It was found that water made no evident effect on this reaction in this concentration range.

The simple relationship shown in Fig. 6 can be explained by an A or an I mechanism. In the A mechanism,

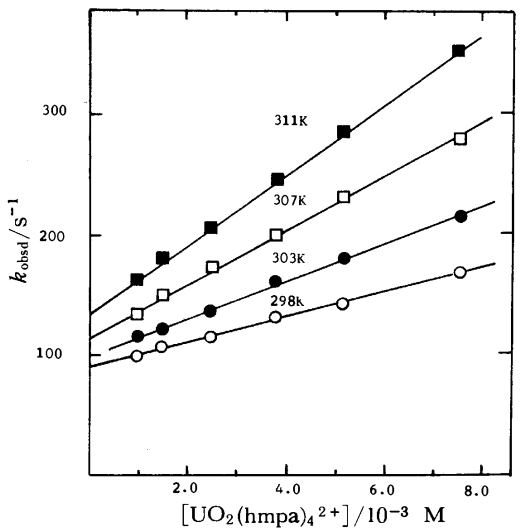

Fig. 6. Plots of k_{obsd} *vs.* $[UO_2(hmpa)_4^{2+}]$ for the anation reaction by SCN^-. The solid lines denote the least-squares best-fit lines.

$$[UO_2(hmpa)_4]^{2+} + SCN^- \underset{k_{-1}}{\overset{k_1}{\rightleftharpoons}} [UO_2(hmpa)_4NCS]^+,$$

$$[UO_2(hmpa)_4NCS]^+ \underset{k_{-2}}{\overset{k_2}{\rightleftharpoons}} [UO_2(hmpa)_3NCS]^+ + HMPA,$$

where $k_{obsd}=k_f[UO_2(hmpa)_4^{2+}]+k_b[HMPA]_{free}$ in which k_f and k_b are $k_1k_2/(k_{-1}+k_2)$ and $k_{-1}k_{-2}/(k_{-1}+k_2)$, respectively. In the I mechanism,

$$[UO_2(hmpa)_4]^{2+} + SCN^- \overset{K_{os}}{\rightleftharpoons} [UO_2(hmpa)_4]^{2+}\cdots NCS^-,$$

$$[UO_2(hmpa)_4]^{2+}\cdots NCS^- \underset{k'_{-1}}{\overset{k'_1}{\rightleftharpoons}} [UO_2(hmpa)_3NCS]^+ + HMPA,$$

where $k_{obsd}=k'_1K_{os}[UO_2(hmpa)_4^{2+}]/(1+K_{os}[UO_2(hmpa)_4^{2+}])+k'_{-1}[HMPA]_{free}$. When $K_{os}[UO_2(hmpa)_4^{2+}]$ is much smaller than unity, k_{obsd} can be simplified as follows:

$$k_{obsd} = k'_1K_{os}[UO_2(hmpa)_4^{2+}]+k'_{-1}[HMPA]_{free}.$$

Thus, both the two mechanisms can explain the experimental results shown in Fig. 6. On the other hand, as mentioned in the study on the equilibrium constant, it is shown that DMF and MeCN can be regarded as solvents having similar effect on the solvation of the species in the present study. Therefore, if the reaction proceeded through the I mechanism, the outersphere complex formation constant for this reaction is expected to be of the same order as that for the anation reaction in $[UO_2(dmf)_5]^{2+}$ with SCN^- in DMF. Since the K_{os} value for the latter reaction was $148M^{-1}$ at 25 °C[9] and the concentration range of $[UO_2(hmpa)_4]^{2+}$ is larger than 7.58×10^{-3} M, the product of K_{os} and $[UO_2(hmpa)_4^{2+}]$ has much the same value as unity. Thus it is not likely that this reaction proceeds through the I mechanism. The HMPA concentration dependence of the pseudo-first order rate constants based on the A mechanism is shown in Fig. 7 and the calculated values of k_f and k_b are listed in Table 2.

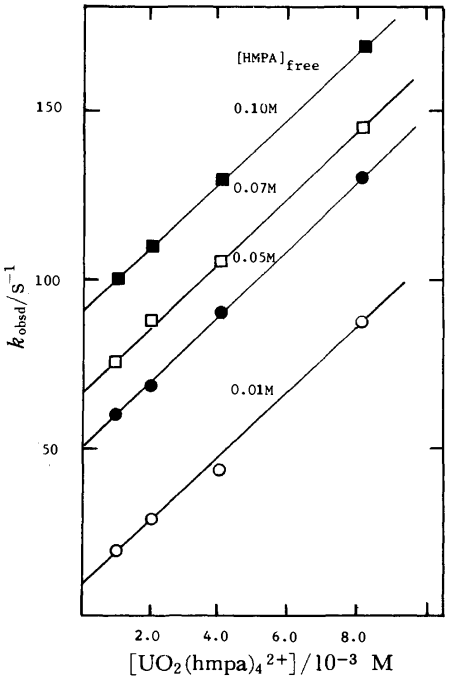

Fig. 7. Plots of k_{obsd} *vs.* $[UO_2(hmpa)_4^{2+}]$ at various concentrations of free HMPA.

It is concluded that the anation reactions in $[UO_2(dmso)_5]^{2+}$ proceeded through the Ia mechanism since the interchange rate constants depended on the nature of entering ligands, SCN^- and N_3^-. The anation reaction in $[UO_2(hmpa)_4]^{2+}$ with SCN^- ion was observed to proceed through the A mechanism, which is consistent with the results obtained by NMR[10] for the ligand exchange reaction in this complex.

It is proposed that the ligand substitution reactions in uranyl complexes with five ligands in the equatorial plane proceed through the associative interchange mechanism, while $[UO_2(hmpa)_4]^{2+}$ with less coordination number than five, reacts *via* the associative mechanism by forming a pentacoordinated intermediate.

The authors wish to express their thanks to Dr. Roderick D. Cannon of the University of East Anglia, U. K., Messrs. Takashi Kojima and Naoshi Fujiwara for their helpful discussions. This work was partly supported by the Grant-in-Aid for Developmental Scientific Research No. 584024 from the Ministry of Education, Science and Culture.

References

1) Y. Ikeda, S. Soya, H. Tomiyasu, and H. Fukutomi, *J. Inorg. Nucl. Chem.*, **41**, 1333 (1979).
2) Y. Ikeda, H. Tomiyasu, and H. Fukutomi, *Bull. Res. Lab. Nucl. Reactor*, **4**, 47 (1979).
3) R. P. Bowen, S. F. Lincoln, and E. H. Williams, *Inorg. Chem.*, **15**, 2126 (1976).
4) R. P. Bowen, G. J. Honan, S. F. Lincoln, T. M. Spotwood, and E. H. Williams, *Inorg. Chim. Acta*, **33**, 235 (1979).
5) G. J. Honan, S. F. Lincoln, and E. H. Williams, *J. Chem. Soc., Dalton Trans.*, **1979**, 1220.
6) J. Crea, R. Digiusto, S. F. Lincoln, and E. H. Williams, *Inorg. Chem.*, **16**, 2825 (1977).
7) A. M. Hounslow, S. F. Lincoln, P. A. Marshall, and E. H. Williams, *Aust. J. Chem.*, **34**, 2543 (1981).
8) C. H. Langford and H. B. Gray, "Ligand Substitution Processes," Benjamin, London (1974).
9) H. Doine, Y. Ikeda, H. Tomiyasu, and H. Fukutomi, *Bull. Chem. Soc. Jpn.*, **56**, 1989 (1983).
10) G. H. Honan, S. F. Lincoln, and E. H. Williams, *Inorg. Chem.*, **17**, 1855 (1978).
11) J. H. Hildebrand and R. L. Scott, "The Solubility of Nonelectrolytes," Reinhold, Dover (1950).
12) Unpublished data. TMP=Trimethyl phosphate.
13) a) R. S. Drago and B. B. Wayland, *J. Am. Chem. Soc.*, **87**, 3571 (1965); b) R. S. Drago, *Coord. Chem. Rev.*, **33**, 252 (1980).
14) V. Gutmann and R. Schmidt, *Coord. Chem. Rev.*, **12**, 263 (1974).
15) R. M. Fuoss, *J. Am. Chem. Soc.*, **80**, 5059 (1958).

Reaction of Organoboranes with Lead(IV) Acetate Azide. A Synthesis of Azidoalkanes from Alkenes *via* Hydroboration

Yuzuru MASUDA,* Masayuki HOSHI, and Akira ARASE
Department of Applied Chemistry, Kitami Institute of Technology, Kitami, 090
(Received March 12, 1983)

Trialkylboranes prepared from alkenes *via* hydroboration react with lead(IV) acetate azide in dichloromethane at −25 °C to form the corresponding azidoalkanes in a one-pot manner. One or two of the alkyl groups of trialkylboranes are utilized in the reaction. For example, 1-azidohexane is afforded from 1-hexene in 50% yield based on the alkene employed.

For several years, the authors have been studying the combination of alkyl groups of organoboranes[1] with ligands of metal compounds *via* the severance of carbon-boron linkage, by redox reaction of organoboranes with metal compounds.[2]

In the course of study on such oxidative transformations of trialkylboranes by metal compounds, the authors have found that lead(IV) acetate has interesting characteristics for reactions with organoboranes.

For example, it affords alkyl acetates from saturated trialkylboranes (Eq. 1),[3] 1-halo-1,2-dialkylethylenes from (1-halo-1-alkenyl)dialkylboranes (Eq. 2),[4] and (*Z*)-enol acetates from mixtures of trialkylborane and 1-alkyne (Eq. 3):[5]

$$R_3B + 2\,Pb(OCOCH_3)_4 \longrightarrow 2\,ROCOCH_3 + RB(OCOCH_3)_2 + 2\,Pb(OCOCH_3)_2 \quad (1)$$

$$R_2BCX{=}CHR' \xrightarrow{Pb(OCOCH_3)_4} RCX{=}CHR'\ (Z \text{ or } E) \quad (2)$$

$$R_3B + HC{\equiv}CR' \xrightarrow{Pb(OCOCH_3)_4} \begin{matrix} R & & OCOCH_3 \\ & C{=}C & \\ H & & R' \end{matrix} \quad (3)$$

Lead(IV) acetate azide $Pb(OAc)_{4-n}(N_3)_n$, readily prepared by reaction of lead(IV) acetate with azidotrimethylsilane at −40 to −20 °C, transfers its acetoxy and azido groups to alkenes, giving a mixture of disubstituted alkanes consisting of *vic*-diazido and *vic*-acetoxy azido compounds (Eq. 4):[6]

$$RCH{=}CH_2 \xrightarrow{Pb(OAc)_{4-n}(N_3)_n} \underset{N_3}{RCHCH_2{-}N_3} + \underset{OAc}{RCHCH_2{-}N_3} \quad (4)$$

From these results it seemed probable that azidoalkane and/or alkyl acetate would be formed in the reaction of trialkylborane with lead(IV) acetate azide (Scheme 1).

$$\left[Pb(OAc)_4 + n\,(CH_3)_3SiN_3\right] \downarrow$$

$$R_3B \xrightarrow{Pb(OAc)_{4-n}(N_3)_n} R{-}N_3 + R{-}OAc$$

$$\uparrow \quad \left[3\,R'CH{=}CH_2 + BH_3{\cdot}THF\right]$$

Scheme 1.

Results and Discussion

To a dichloromethane solution of 2 mmol of lead(IV) acetate was added 4 mmol of azidotrimethylsilane at −25 °C over 10 min. After 15 min, 2 mmol of trihexylborane was added to this solution at −25 °C and the solution was stirred at this temperature for several hours. The solution was allowed to warm up to room temperature (20 °C). GLPC analysis of the reaction mixture revealed that 1.26 mmol of 1-azidohexane was formed as the major product accompanied by 2-azidohexane and hexyl acetate as the minor products (Scheme 2).

$$Pb(OAc)_4 + 2(CH_3)_3SiN_3 \xrightarrow[-25\ ^\circ C]{CH_2Cl_2} \xrightarrow[-25\ ^\circ C]{(C_6H_{13})_3B} \xrightarrow{\text{room temp.}} n\text{-}C_6H_{13}\text{-}N_3 + \underset{N_3}{n\text{-}C_4H_9CHCH_3} + n\text{-}C_6H_{13}OAc$$

Scheme 2.

In any of blank experiments using pairs of trihexylborane and azidotrimethylsilane, hexyl acetate and azidotrimethylsilane, and hexyl acetate and lead(IV) acetate azide, no azidohexane was obtained. Accordingly, it is apparent that azidohexanes are formed by the reaction of lead(IV) acetate azide with trihexylborane.

The yield of azidoalkanes did not increase after the reaction over 6 h at −25 °C. This fact seems attributable to a decomposition of lead(IV) acetate azide during such a long reaction time.[6] The exchange reaction of the acetoxy group of lead(IV) acetate by the azido group was rapid at −40 to −20 °C,[6] and the reaction of trialkylboranes with lead(IV) acetate was very sluggish at temperatures below 0 °C.[3]

Accordingly, the following procedure, in which lead(IV) acetate azide was produced in the presence of trihexylborane in a one-pot manner, was examined to minimize the possibility of the unfavorable decomposition of lead(IV) acetate azide and to increase the yield of azidohexane. Thus, lead(IV) acetate was added to a solution of 2 mmol of trihexylborane in

$$R_3B + Pb(OAc)_4 \xrightarrow[CH_2Cl_2]{(CH_3)_3SiN_3} R{-}N_3 + R{-}OAc$$

Scheme 3.

dichloromethane, and then 2 mmol of azidotrimethylsilane was slowly added at −25 °C (Scheme 3). The results are shown in Table 1.

In this case, the reaction was fairly rapid and the maximum yield of azidohexanes was obtained after the reaction at −25 °C for 4 h. In Expt 4, a total 1.74 mmol (87%, based on R_3B) of 1-azidohexane and 2-azidohexane is formed, indicating that one of the three hexyl groups of trihexylborane is utilized for the reaction.

Table 2 shows how the yield varies with the amounts of lead(IV) acetate and azidotrimethylsilane. In the course of this experiment, it was recognized that a very slow addition of azidotrimethylsilane increased the yield of azidohexanes appreciably (for example, see the difference between Expts 9 and 10). Thus this step was carried out over a period of 1.5 or 2 h.

In the reactions with 2 mmol of the Pb(IV) compound (Expts 6 and 7), the total amounts of azidohexanes and hexyl acetate formed in each reaction were 1.96 and 1.93 mmol, respectively, suggesting that one equivalent of the Pb(IV) compound is required for the reaction of the first alkyl group in trihexylborane. The reaction of the second alkyl group in trihexylborane was rather sluggish compared with that of the first one. However, in the reaction with two or more equivalents of the lead(IV) compound to R_3B (2 mmol), the total amounts of the products formed in the reaction mixture exceeded 2 mmol and reached about 3.5 mmol in some cases, indicating that the second alkyl group in trihexylborane can also participate in the reaction, but not the third one.

The difference in the ratio of azide to acetate anions in the lead(IV) compound shows a small but evident effect on the product distribution. Thus, in Expts 7, 11, and 12, where the ratio is 2 or 4, the amounts of the azidohexanes are more than those in Expts 6, 10, 13, and 14, where the ratio is 1.

The amounts 12 and 13% of 2-azidohexane in Expts 11 and 12, respectively, indicate that most of the secondary hexyl groups in trihexylborane are converted to 2-azidohexane, whereas the amounts 105 and 104% of 1-azidohexane indicate that a considerable portion of the primary hexyl groups remains unreacted. These facts suggest that in this reaction the secondary alkyl group is more reactive than the primary one when they are on the same boron atom.[7] This characteristic of the reaction is well shown in Expt 29, where dicyclohexylhexylborane was employed (Table 3). However, the preference of the secondary alkyl group to the primary one is not so excellent compared to that observed in the reaction of trialkylboranes with lead(IV) acetate.[3]

In tetrahydrofuran, acetonitrile, benzene, diethyl ether, and hexane, a certain amount of 1-azidohexane could be formed, but the yields could not exceed those obtained in dichloromethane.

Similar reactions were carried out by using several alkenes as substrates in dichloromethane. The results are shown in Table 3.

In these reactions the formation of a small amount of alkyl acetate cannot be avoided. However, azidoalkanes can be isolated easily from the reaction mixture by applying simple column chromatography using silica

Table 1. Reaction[a] of trihexylborane with lead(IV) acetate azide in dichloromethane (1)

Expt No.	Reaction time/h	Yield of product/mmol(%)[b]		
		1-Azidohexane	2-Azidohexane	Hexyl acetate
1	0.5	1.30 (65)	0.10 (5)	0.14 (7)
2	1	1.42 (71)	0.12 (6)	0.12 (6)
3	1.5	1.52 (76)	0.18 (9)	0.10 (5)
4	4	1.60 (80)	0.14 (7)	0.08 (4)
5	6	1.58 (79)	0.16 (8)	0.10 (5)

a) The reactions were carried out in dichloromethane (8 ml) at −25 °C by using 2 mmol of trihexylborane, 2 mmol of lead(IV) acetate, and 4 mmol of azidotrimethylsilane. b) Determined by GLPC, based on trihexylborane.

Table 2. Reaction[a] of trihexylborane with lead(IV) acetate azide in dichloromethane (2)

Expt No.		$Pb(OAc)_4$	$(CH_3)_3SiN_3$	Yield of product/mmol(%)[b]		
		mmol	mmol	1-Azidohexane	2-Azidohexane	Hexyl acetate
6	(n-$C_6H_{13})_3B$	2	2	1.56 (78)	0.16 (8)	0.24 (12)
7	(2 mmol)	2	4	1.62 (81)	0.20 (10)	0.11 (6)
8		2.4	4.8	1.80 (90)	0.18 (9)	0.16 (8)
9[c]		4	4	1.96 (98)	0.18 (9)	0.32 (16)
10		4	4	2.32 (116)	0.18 (9)	0.30 (15)
11		4	8	2.10 (105)	0.24 (12)	0.22 (11)
12		4	16	2.08 (104)	0.26 (13)	0.14 (7)
13		6	6	2.84 (142)	0.20 (10)	0.40 (20)

a) Carried out in dichloromethane (Expts 6—8, 8 ml; 9—12, 10 ml; 13, 12 ml) by stirring for 4 h at −25 °C, then with a rise from −25 °C to room temperature over 2h, and finally for 4 h at room temperature. Azidotrimethylsilane was added very slowly (Expts 6—8 and 10, 1.5 h; 11—13, 2h). b) Determined by GLPC, based on R_3B. The yields are expressed so as to become 300% when all alkyl groups of R_3B have reacted completely. c) Azidotrimethylsilane was added over 10 min.

Table 3. Reaction[a] of trialkylboranes with lead(IV) acetate azide in dichloromethane (3)

Expt No.	R_3B (2 mmol) R=	$Pb(OAc)_4$ mmol	$(CH_3)_3SiN_3$ mmol	Yield of product/mmol(%)[b] RN_3 1-Azidoalkane	2-Azidoalkane	ROAc
14	Butyl	6	6	2.56 (128)	0.16 (8)	0.38 (19)
10	Hexyl	4	4	2.32 (116)	0.18 (9)	0.30 (15)
13		6	6	2.84 (142)	0.20 (10)	0.40 (10)
15[c]	(10 mmol)	30	30	13.6 (136)	1.01 (10)	—
16	Octyl	4	4	2.10 (105)	0.18 (9)	0.34 (17)
17		6	6	2.25 (113)	0.20 (10)	0.36 (18)
18[c]	(10 mmol)	30	30	10.6 (106)	0.90 (9)	—
19	Cyclopentyl	4	16	2.16 (108)		0.16 (8)
20[c]	(10 mmol)	20	80	10.4 (102)		—
21	Cyclohexyl	2	4	1.44 (72)		0.24 (12)
22		4	8	1.92 (96)		0.30 (15)
23		4	16	3.40 (170)		0.26 (13)
24[c]	(10 mmol)	20	80	16.2 (162)		—
25	Cyclooctyl	4	16	1.76 (88)		0.16 (8)
26[c]	(10 mmol)	20	80	8.50 (85)		—
27	Norbornyl	4	16	*exo*-, 2.24 (112)	*end*-, 0	0.42 (21)
28[c]	(10 mmol)	20	80	10.3 (103)		—
29	Dicyclohexylhexyl	2	4	hexyl, 0.24 (12)		hexyl, 0.08 (4)
				cyclohexyl, 1.16 (58)		cyclohexyl, 0.38 (19)

a) Carried out in dichloromethane (8—12 ml, except Expt Nos. marked with c) for 4 h at −25 °C, then with a rise from −25 °C to room temperature over 2 h, and finally 4 h at room temperature. Azidotrimethylsilane was added very slowly (over 1.5—2 h). b) Determined by GLPC (except Expt Nos. marked with c) based on R_3B used and expressed so as to become 300% when all alkyl group of R_3B have reacted completely. c) Preparative experiments. Azidoalkanes were isolated by column chromatography.

gel. Thus, the present reaction can be used as a general synthetic method for azidoalkanes.

The formation of azidoalkanes was moderately depressed when the reaction was carried out in the presence of added garvinoxyl (20 mol% to R_3B), a reagent for trapping radicals. Therefore, the reaction seems to proceed *via* a radical process.

When the reaction of trialkylborane involves a radical mechanism, the secondary alkyl group tends to react more easily than the primary one.[2,3] There is the same tendency in the present reactions as mentioned above.

From these results, the mechanism of the present reaction may be written as follows (Eq. 5):

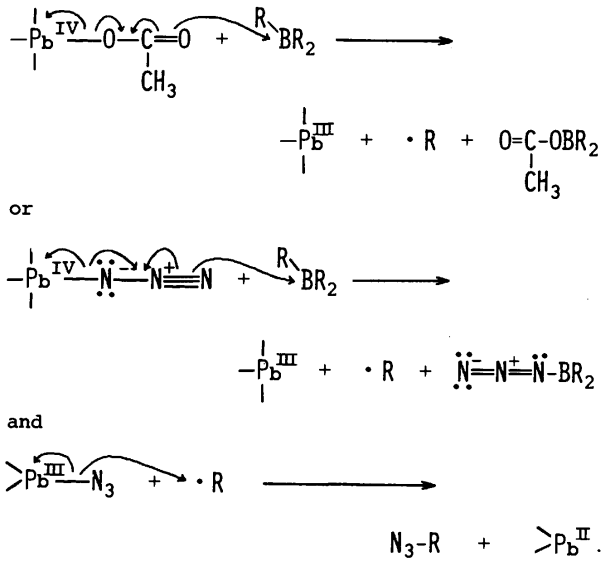

(5)

Next we offer some characteristic features of the present reaction, in comparison with reactions which have hitherto been reported.

(1) Azidoalkanes are usually prepared by reactions using haloalkanes or diazo compounds as starting materials,[8] while the present reaction makes use of alkene.

(2) Azidoalkanes have also been synthesized by reactions of alkenes with mercury(II) azide[9] where the azido group is introduced in the "Markownikoff" fashion,[10] while the present reaction is in the "anti-Markownikoff" fashion.

(3) A method for synthesis of azidoalkanes using organoboranes, iron(II) azide, and hydrogen peroxide has been reported.[11] Yields of our reaction are mostly higher than those of the above reaction.

(4) As described above (Scheme 1), diazido compounds and acetoxy azido compounds[6] are formed by the reaction of olefin with lead(IV) acetate azide,[12] while in the pesent reaction these compounds are not detected, but mainly azidoalkane is formed.

In the present reaction, contamination of 1-azidoalkane by 2-azidoalkane cannot be avoided when trialkyl-

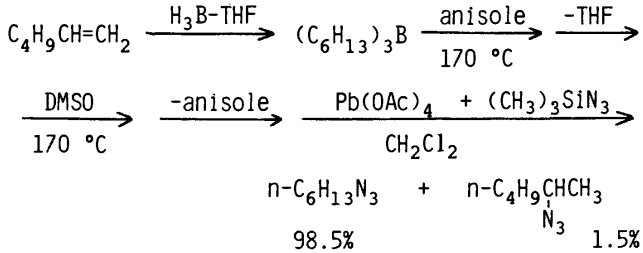

Scheme 4.

boranes from 1-alkenes are employed.[7] 2-Azidoalkane must come from the secondary alkyl groups which are originally present in trialkylboranes. Thus, to minimize the amount of 2-azidoalkane, most of the secondary alkyl groups in the trialkylborane were converted to primary alkyl groups or removed from trialkylborane by successive treatments of trialkylboranes with anisole and dimethyl sulfoxide before the reaction with lead(IV) acetate azide (Scheme 4).[13]

Although the yield was caused to be lowered a little by using this trialkylborane, the amount of 2-azidoalkane could be markedly reduced and highly isomerically pure 1-azidoalkane was obtained (97—99%).

Experimental

Instruments. GLPC was performed using a NEVA Model 1400. ^{1}H NMR spectra were obtained on a Hitachi R-20A spectrometer (60 MHz). Infrared spectra were recorded on a Hitachi 285 spectrometer. Mass spectra were obtained on a Hitachi M-52 mass spectrometer.

Materials. Commercial 1-hexene, 1-octene, cyclopentene, cyclohexene, cyclooctene, and tetrahydrofuran were dried over lithium aluminium hydride and used after distillation in an argon atmosphere. Commercial 2-norbornene and 1-butene were used without any purification. Dichloromethane was dried over phosphorus pentoxide and used after distillation in an argon atmosphere. Anisole and dimethyl sulfoxide were dried over Molecular Sieve 5A and distilled before use.

The tetrahydrofuran solution of borane,[14] lead(IV) acetate[15] (purity>98%),[16] and azidotrimethylsilane[17] (bp 93—95 °C; lit 95 °C) were prepared by the methods described in the literature.

Reaction of Trialkylboranes with Lead(IV) Acetate Azide. The following procedure is representative. A dry, 100-ml round bottomed flask, equipped with a gas inlet, a magnetic stirring bar, a septum inlet, and a dropping funnel, was flushed with argon. In this flask 3.75 ml (30 mmol) of 1-hexene was hydroborated with 10 mmol of borane in tetrahydrofuran, and then the tetrahydrofuran was removed under reduced pressure at 25 °C. In an argon atmosphere, 13.3 g (30 mmol) of lead(IV) acetate in 40 ml of dichloromethane was added to trihexylborane[14] at −25 °C and 4.20 ml (30 mmol) of azidotrimethylsilane in 10 ml of dichloromethane was added dropwise (for 2 h) through the dropping funnel. The solution was stirred at −25 °C for 4 h, then with a rise from −25 °C to room temperature over 2 h, and finally at room temperature for 4 h. The light brown color of the solution changed into white after the reaction. The reaction mixture was transferred into a separatory funnel together with 100 ml of diethyl ether and 30 ml of water. Then it was saturated with sodium chloride, and the lower aqueous layer was separated and extracted three times with diethyl ether. The combined organic layer and diethyl ether extracts were washed with a saturated aqueous sodium chloride solution, and dried over anhydrous magnesium sulfate. After evaporation of the solvent, the products were separated by column chromatography (silica gel, 150 g). On elution with pentane (200 ml) and then with a mixture of pentane (200 ml) and dichloromethane (200 ml), 1.85 g of a mixture containing 13.6 mmol of 1-azidohexane and 1.01 mmol of 2-azidohexane was obtained. The GLPC retention times, n_D values, and IR, ^{1}H NMR, and mass spectra of these products were consistent with those obtained for authentic samples.[8]

An analytical experiment was carried out by using smaller amounts of reagents, and the reaction mixture was analyzed by GLPC using the internal standard method (FFAP, supported on Diasolid M, was used as the liquid phase).

Reactions using tributylborane[14] and trioctylborane[14] were carried out under the same conditions as described above. From trioctylborane (10 mmol), on elution with hexane (200 ml) and a mixture of hexane (200 ml) and benzene (200 ml), 10.6 mmol of 1-azidooctane with 0.90 mmol of 2-azidooctane was obtained.

A reaction of tricycloalkylborane[14] was carried out under the same conditions as described above by using 10 mmol of tricycloalkylborane, 20 mmol of lead(IV) acetate, and 80 mmol of azidotrimethylsilane. From tricyclopentylborane, on elution with pentane (200 ml) and with a mixture of pentane (200 ml) and dichloromethane (200 ml), 10.4 mmol of azidocyclopentane was obtained. From tricyclohexylborane, tricyclooctylborane, and trinorbornylborane, 16.2 mmol of azidocyclohexane, 8.5 mmol of azidocyclooctane, and 10.3 mmol of *exo*-2-azidonorbornane, respectively, were obtained on elution with hexane (200 ml) and with a mixture of hexane (200 ml) and benzene (200 ml). The GLPC retention times, n_D values, and IR, ^{1}H NMR, and mass spectra of these azidocyclohexane and *exo*-2-azidonorbornane were consistent with those obtained from authentic samples.[8,10]

Reaction of Trihexylborane with Lead(IV) Acetate Azide in the Presence of Garvinoxyl. The reaction was carried out under the same conditions as described above using 2 mmol of trihexylborane, 2 mmol of lead(IV) acetate, 4 mmol of azidotrimethylsilane, and 0.20 g (20 mol%) of garvinoxyl. The total yields of 1- and 2-azidohexane in this reaction and those in the absence of garvinoxyl (in parentheses) are as follows: 30 min, 24% (56%); 45 min, 32% (61%); 2.5 h, 34% (65%); 5 h, 37% (71%).

Reaction of Trialkylborane with Lead(IV) Acetate Azide after Successive Treatments with Anisole and Dimethyl Sulfoxide. In an argon-flushed flask equipped with the same apparatus as described above and a reflux condenser, 30 mmol of 1-hexene was hydroborated with 10 mmol of borane in tetrahydrofuran. After addition of 5 ml of anisole, the tetrahydrofuran was removed under reduced pressure (20 Torr) at 25 °C. The solution was heated at 170 °C for 2 h and allowed to react with 0.5 mmol of dimethyl sulfoxide at 170 °C for 2 h. The anisole was removed under reduced pressure (3 Torr, 1 Torr≈133.322 Pa) at 50 °C. Then the reaction of trihexylborane with 30 mmol of lead(IV) acetate and 30 mmol of azidotrimethylsilane was carried out in the same manner as described above. The products were separated by column chromatography (silica gel, 150 g). On elution with pentane (200 ml) and with a mixture of pentane (200 ml) and dichloromethane (200 ml), 9.55 mmol of 1-azidohexane with 0.18 mmol of 2-azidohexane was obtained.

Similarly, 9.20 mmol of 1-azidooctane with 0.28 mmol of 2-azidooctane was obtained from 30 mmol of 1-octene.

Analytical Data of Products. *1-Azidohexane*: IR (film) ν_{N_3} 2100 cm^{-1} (v.s.); ^{1}H NMR (CCl_4, TMS) δ=0.89 (t, 3H), 1.15—1.75 (m, 8H), and 3.20 (t, 2H); n_D^{20} 1.4320 (lit[8] 1.4318). Found: C, 56.56; H, 10.29; N, 33.15%. Calcd for $C_6H_{13}N_3$: C, 56.66; H, 10.30; N, 33.04%.

1-Azidooctane: IR (film) ν_{N_3} 2100 cm^{-1} (v.s.); ^{1}H NMR (CCl_4, TMS) δ=0.87 (t, 3H), 1.15—1.70 (m, 12H), and 3.19 (t, 2H); n_D^{20} 1.4401 (lit[8] 1.4368).

Azidocyclopentane: IR (film) ν_{N_3} 2100 cm^{-1} (v.s.); ^{1}H NMR (CCl_4, TMS) δ=1.5—1.9 (m, 8H), and 3.7—4.0 (m, 1H); MS *m/z* 111 (M^+); n_D^{20} 1.4660 (lit[8] 1.4616).

Azidocyclohexane: IR (film) ν_{N_3} 2100 cm^{-1} (v.s.); ^{1}H NMR (CCl_4, TMS) δ=1.1—2.1 (m, 10H) and 3.0—3.5 (m, 1H); MS *m/z* 125 (M^+); n_D^{20} 1.4697 (lit[8] 1.4693).

Azidocyclooctane: IR (film) ν_{N_3} 2090 cm^{-1} (v.s.); ^{1}H NMR (CCl_4, TMS) δ=1.1—2.2 (m, 14H) and 3.2—3.7 (m, 1H); n_D^{20} 1.4921.

exo-*2-Azidonorbornane*: IR (film) ν_{N_3} 2100 cm^{-1} (v.s.); ^1H NMR (CCl_4, TMS) δ=0.95—1.7 (m, 8H), 2.2—2.4 (m, 2H), and 3.25—3.55 (m, 1H); MS *m/z* 137 (M^+); n_D^{20} 1.4936 (authentic sample,[10] 1.4893).

References

1) For organic syntheses using organoborane see the following reviews, for example: a) H. C. Brown, "Boranes in Organic Chemistry," Cornell Univ. Press, London (1972); b) G. M. L. Cragg, "Organoboranes in Organic Synthesis," M. Dekker, New York (1973); c) A. Pelter and K. Smith, "Comprehensive Organic Chemistry," ed by D. H. R. Barton and W. D. Ollis, Pergamon, Oxford (1979), Vol. 3, p. 689; d) A. Suzuki, *Acc. Chem. Res.*, **15**, 178 (1982).

2) A. Arase, Y. Masuda, and A. Suzuki, *Bull. Chem. Soc. Jpn.*, **47**, 2511 (1974); A. Arase and Y. Masuda, *Chem. Lett.*, **1976**, 785, 1115.

3) Y. Masuda and A. Arase, *Bull. Chem. Soc. Jpn.*, **51**, 901 (1978).

4) Y. Masuda, A. Arase, and A. Suzuki, *Chem. Lett.*, **1978**, 665; *Bull. Chem. Soc. Jpn.*, **53**, 1652 (1980).

5) Y. Masuda, M. Hoshi, and A. Arase, *Chem. Lett.*, **1980**, 413.

6) The preparation and properties of lead(IV) acetate azide are described in the following literature: E. Zbiral, *Synthesis*, **1972**, 285.

7) Trialkylboranes prepared from 1-alkenes by hydroboration are mixtures in which a primary alkyl group and/or 1-methylalkyl group are bound to a boron atom. For example, from 1-pentene, a mixture of tripentylborane (91%), dipentyl(1-methylbutyl)borane (6%), and pentylbis(1-methylbutyl)borane and tris(1-methylbutyl)borane (3%) was obtained (A. Arase, Y. Masuda, M. Itoh, M. Itoh, and A. Suzuki, *Nippon Kagaku Kaishi*, **1972**, 395). The distribution of the trialklylborane isomers derived from 1-hexene is considered to be similar to that of the trialkylborane isomers from 1-pentene described above.

8) S. R. Sandler and W. Karo, "Organic Functional Group Preparations," Academic Press, New York (1971), Vol. II, p. 268.

9) Although we tried a reaction of organoborane with mercury(II) azide, no azidoalkane was formed.

10) C. H. Heathcock, *Angew. Chem., Int. Ed. Engl.*, **8**, 134 (1969).

11) A. Suzuki, M. Ishidoya, and M. Tabata, *Synthesis*, **1976**, 687.

12) It has been reported that α-azido ketone was formed by the reaction of alkene with (diacetoxyiodo)benzene and azidotrimethylsilane: J. Ehrenfreund and E. Zbiral, *Ann. Chem.*, **1973**, 290. We tried a reaction of organoborane with (diacetoxyiodo)benzene and azidotrimethylsilane, but no azidoalkane was obtained.

13) Y. Masuda, M. Hoshi, and A. Arase, *Bull. Chem. Soc. Jpn.*, **52**, 271 (1979).

14) H. C. Brown, "Organic Syntheses *via* Boranes," Wiley, New York (1975).

15) J. C. Bailar, Jr., *Inorg. Synth.*, Vol. I, 47 (1939).

16) L. F. Fieser and M. Fieser, "Reagent for Organic Synthesis," Wiley, New York (1967), Vol. 1, p. 537.

17) L. Birkofer, A. Ritter, and P. Richter, *Chem. Ber.*, **96**, 2750 (1963); L. Birkofer and A. Ritter, *Angew. Chem.*, **77**, 414 (1965).

 © 1984 The Chemical Society of Japan Bull. Chem. Soc. Jpn., 57, 1031—1034 (1984)

Pyridoxal Methochloride Catalysis of the β-Elimination Reaction of Methyl 3-Chloroalaninate in Water

Hiroki KONDO,* Kanzi MORITA, Tatsuya KITAMIKADO, and Junzo SUNAMOTO
Department of Industrial Chemistry, Faculty of Engineering, Nagasaki University, Nagasaki 852
(Received April 11, 1983)

The β-elimination reaction of methyl 3-chloroalaninate has been investigated in the absence and presence of pyridoxal methochloride (**2**) or pyridoxal (**3**). Apparently, compound **2** was about twice as effective as **3** in the catalytic reaction that proceeds via a Schiff base of substrate and **2** or **3**. The pH-rate profiles for the catalytic reaction with **2** and **3** were analyzed in terms of ionization of the various Schiff base species present in solution. It was found that the reactivity of the Schiff base decreases as the ionization of the molecule progresses. The reaction mechanism and its relevance to the catalysis of pyridoxal phosphate-dependent enzymes are discussed.

Pyridoxal phosphate (PLP) is a coenzyme involved in the metabolism of amino acids in biological systems. These metabolic reactions include transamination, racemization and decarboxylation. They can be mimicked in model systems mostly in the presence of metal ions and at high temperature.[1] Through these biomimetic studies an insight was gained into the reaction mechanism of pyridoxal catalysis in enzymic systems. Thus, a Schiff base formed between pyridoxal and amino acid is always postulated as a key intermediate in all the reactions mentioned above. Nevertheless, much remains to be elucidated as to the catalytic mechanism of this and related vitamins, *e.g.*, the protonation state of a reactive Schiff base species. This particular problem happens because pyridoxal and the Schiff base derived therefrom can have various ionic forms in aqueous media that differ in number and/or the site of protonation.[2] We have been interested in the pyridoxal catalysis of the β-elimination reaction of amino acids in the absence of a metal ion.[3] 3-Chloroalanine is a substrate suitable for mechanistic studies, as this compound is known to undergo β-elimination spontaneously[4] and in the presence of pyridoxal.[5] In addition, an enzyme which promotes β-elimination of 3-chloro-D-alanine was recently found in *Pseudomonas putida* CR 1—1.[6] In this article, we have attempted a mechanistic study on the pyridoxal methochloride catalysis of the reaction of methyl 3-chloroalaninate (Eq. 1). This particular

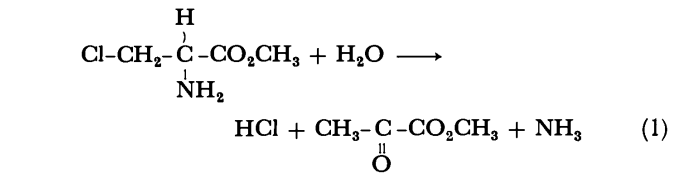

$$\mathrm{Cl\text{-}CH_2\text{-}\underset{\underset{\mathrm{NH_2}}{|}}{\overset{\overset{\mathrm{H}}{|}}{C}}\text{-}CO_2CH_3 + H_2O \longrightarrow HCl + CH_3\text{-}\overset{\overset{\mathrm{O}}{\|}}{C}\text{-}CO_2CH_3 + NH_3} \qquad (1)$$

catalyst was chosen, because there are only two ionic forms of Schiff base for this compound (Scheme 1). This should facilitate the analysis of kinetic data on the catalytic β-elimination of the substrate.

Experimental

Materials. Pyridoxal hydrochloride was obtained from Wako Pure Chemical Ind. Pyridoxal methochloride (**2**) was prepared from pyridoxal (**3**) according to the literature.[7] Methyl L-3-chloroalaninate hydrochloride (**1**) was prepared from dimethyl L-cystinate and chlorine.[8] All other chemicals were obtained from commercial sources. Glass-distilled water was used in all experiments.

Apparatus. Electronic absorption spectra were taken on a Hitachi 124 spectrophotometer. The pH values of aqueous solutions were determined with a Toa pH meter HM-5A connected with a Toa combination electrode GS 195C. Computations were carried out on a Sord microcomputer 223 Mark II with a program written in the Basic.

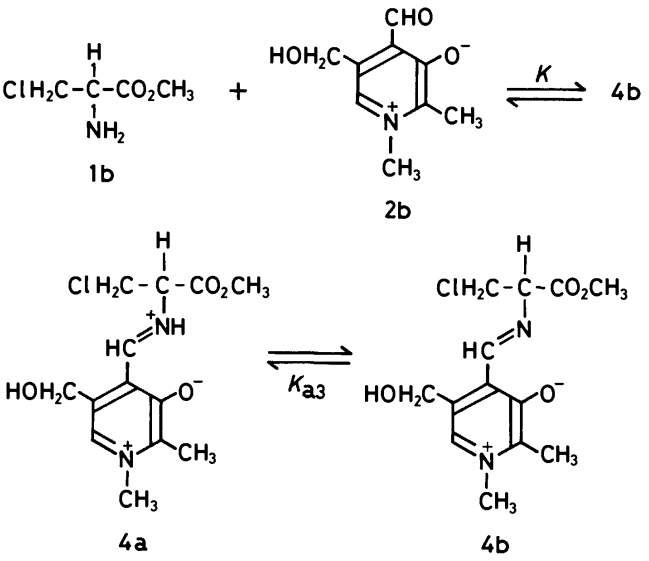

Scheme 1.

Equilibrium Measurements. Since 3-chloroalanine is labile at ambient temperatures, equilibrium studies on the formation of a Schiff base of **2** were carried out with alanine. The pertinent equilibria are depicted in Scheme 1 (but note that the amino acid illustrated is **1** but not alanine). The amino acid, **2** and the Schiff base derived thereof exist over the pH range of 5 to 11 in two ionic forms.[9] The protonated species is designated by the symbol a, while the deprotonated species by b. The acid dissociation constants of amino acid, **2** and the Schiff base are referred to as K_{a1}, K_{a2}, and K_{a3}, respectively. The pK_{a2} for **2** was determined as 4.0 by a spectrophotometric titration. The protonated form of Schiff base (HSB or **4a**) has an absorption maximum at 414 nm and the deprotonated form (SB^- or **4b**) at 374 nm. To determine both the equilibrium constant for the Schiff base formation K, defined by Eq. 2, and pK_{a3} electronic absorption spectra were

$$K = \frac{[\mathbf{4b}]}{[\mathbf{1b}]\,[\mathbf{2b}]} \qquad (2)$$

taken at pH values 6.00, 7.00, 8.00, and 9.00 by varying the concentrations of alanine (0.1, 0.2, 0.4, 0.6, 0.8, and 1.0 M) at 30.0 °C, μ=1.0 (KCl). Equilibrium was reached within a few minutes after mixing. The data were analyzed according

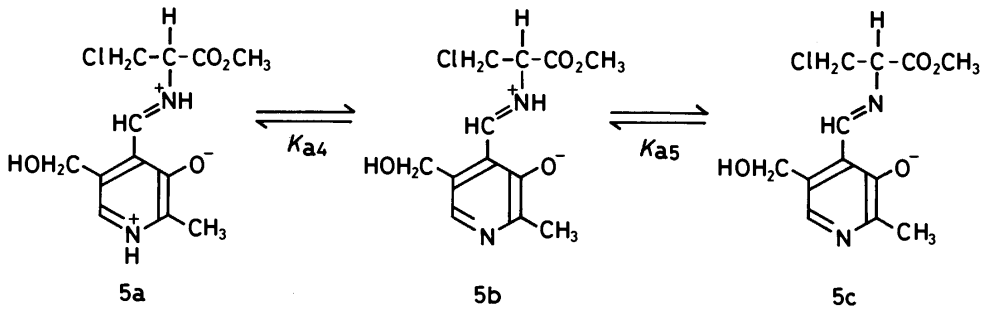

Scheme 2.

basically to the same method as that described previously.[10-12] Other pK_a values used in the calculation were 4.0 and 9.2 for **2** and alanine, respectively. The results are the following: K 5±1 M^{-1}†, pK_{a3} 8.0±0.2. The molar extinction coefficients of HSB and SB^- are 4000±1000 and 6000±1000 at 374 nm, and 8000±2000 and 1200±100 cm^{-1} M^{-1} at 414 nm, respectively. The corresponding equilibrium constant for the Schiff base of **3** and alanine was reported as 9 M^{-1}.[10]

Kinetics. All experiments were carried out at 25.0 °C, unless otherwise specified. The rate of the β-elimination reaction of **1** was determined by following the release of chloride ion by means of Volhard titration. The reaction mixture (10 ml) consisted of 0.010 M **1**, 0—0.020 M **2** or **3** in 0.10 M phosphate (pH 6—8.5) or borate buffer (pH>8.5). An aliquot (1 ml) was withdrawn from the reaction solution at appropriate time intervals, quickly transferred to a quenching solution (6 ml) containing 0.083 M silver nitrate and 1 M nitric acid and kept on ice for later titration. The excess silver ion was back-titrated with 0.1 M potassium thiocyanate in the presence of ferric ammonium sulfate as indicator. The amount of chloride ion at infinite time agreed well with the theoretical value. Data obeyed pseudo-first-order kinetics with usually a correlation coefficient 0.99 or greater.

Another reaction product, methyl pyruvate, was determined by the 2,4-dinitrophenylhydrazone method. The hydrazone was assayed spectrophotometrically at 530 nm (ε 10500),[13] after removing the insoluble hydrazone of **2** or **3** by filtration. The amount of pyruvate at infinite time agreed well with the theoretical value.

Data Processing. The catalytic rate constant k_2 of Eq. 7 was analyzed in terms of a difference in reactivity of the Schiff base species involved. As shown in Schemes 1 and 2, the Schiff bases of **2** and **3** are present in two or three ionic forms over the pH range studied.[9] Thus this idea is formulated as in Eqs. 3 and 4 for **2** and **3**, respectively. By combining Eqs. 2 and 3 one

$$k_2[\mathbf{1}][\mathbf{2}] = k_a[\mathbf{4a}] + k_b[\mathbf{4b}] \quad (3)$$

$$k_2[\mathbf{1}][\mathbf{3}] = k'_a[\mathbf{5a}] + k'_b[\mathbf{5b}] + k'_c[\mathbf{5c}] \quad (4)$$

obtains Eq. 5, where K_{pH} is the operational equilibrium constant defined by Eq. 6. Since the pK_{a2} for **2** is known, four

$$k_2 = \{k_a[H^+] + k_b K_{a3}\} \times \frac{K_{pH}}{[H^+] + K_{a3}} \quad (5)$$

$$K_{pH} = \frac{\left\{1 + \frac{[H^+]}{K_{a3}}\right\} K}{\left\{1 + \frac{[H^+]}{K_{a1}}\right\}\left\{1 + \frac{[H^+]}{K_{a2}}\right\}} \quad (6)$$

unknown parameters, K_{a1}, K_{a3}, k_a, and k_b remain to be determined. They were optimized by essentially the same procedures as those described for the analysis of spectroscopic data. It should be noted here that the Schiff base formation constants K used in the calculation were those for alanine, because we were unable to determine the corresponding values for **1** precisely. Although the equilibrium constants for alanine and **1** may not be exactly identical, it would be reasonable to assume that the relative magnitudes of the constants for **2** and **3** do not differ significantly between alanine and **1**. We have confirmed that as long as this assumption holds, the main conclusions drawn by this data processing do not change appreciably.

† 1 M=1 mol dm^{-3}.

Results

The β-elimination reaction of **1** in buffered aqueous media obeyed a pseudo-first-order rate law with respect to the substrate both in the absence and presence of catalyst **2** or **3**. It was found that the observed first-order rate constants are dependent linearly on the catalyst concentration over a 0—0.02 M range. The k_1 term of Eq. 7 represents the spontaneous reaction of the

$$k_{obsd} = k_1 + k_2[\mathbf{2} \text{ or } \mathbf{3}] \quad (7)$$

substrate. The logarithm of k_1 increases slightly with pH, but the slope of a straight line (0.12) fitted to data points is far from unity (Fig. 1), suggesting that the specific base catalysis is not working over the pH range studied. A similar insensitivity of rates to pH was reported in the β-elimination of *O*-phosphoserine over a pH range of 7 to 14.[14] It should be noted that the linear analysis of kinetic data in Fig. 1 is an approximation, as the rate increase at pH 7—8 could reflect the acid dissociation of **1a** (protonated form) to **1b**. If the data are analyzed by this scheme, **1b** is about twice as reactive as **1a**. The k_2 term refers to the catalytic reaction, proceeding via a Schiff base of the substrate

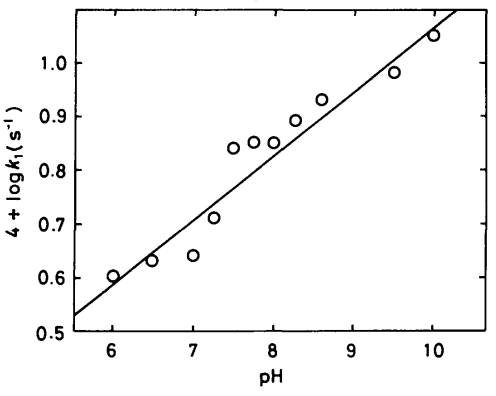

Fig. 1. pH-Dependence of the spontaneous β-elimination rate constants of **1** in water at 25.0 °C.

Table 1. Specific rate constants of individual Schiff base species in the β-elimination of **1** with **2** or **3** in water at 25.0 °C

k_a	k_b	k'_a	k'_b	k'_c
		s^{-1}		
0.11	0.017	0.070	0.010	0.004

a) For definition of the rate constants refer to Eqs. 3 and 4 and Schemes 1 and 2.

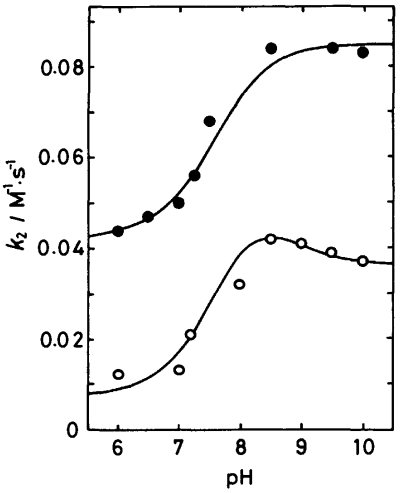

Fig. 2. pH-Rate profiles for the β-elimination of the Schiff base of **1** with **2** (●) and **3** (○) at 25.0°C. The theoretical curves were drawn based on the rate constants given in Table 1 and the following pK_a values: pK_{a1} 7.6; pK_{a2} 4.0; pK_{a3} 6.5; pK_{a4} 5.9; pK_{a5} 8.5; pK_a of **3** 4.23 and 8.70 (V. R. Williams and J. B. Nielands, *Arch. Biochem. Biophys.*,**53**, 56 (1954)).

with **2** or **3**. The treatment according to Eq. 7 is warranted, since the Schiff base formation is not extensive under the present conditions. The pH dependence of k_2 is shown in Fig. 2 for both **2** and **3**. Compound **2** is apparently twice as effective as **3** at any pH value studied.

The two pH-rate profiles for the β-elimination of the Schiff base of **1** were interpreted in terms of a difference in reactivity of the various species of Schiff base (see Experimental section). The Schiff base of **2** is present in two ionic forms, **4a** and **4b** (Scheme 1), and the experimental data are explicable by the sigmoidal curve generated with the aid of the parameters listed in Table 1. It is manifest that the protonated species (**4a**) is 6.5 times more reactive than **4b**. There are three ionic species, **5a**, **5b**, and **5c** (Scheme 2), in the Schiff base of **3** in the pH region studied, and the skewed bell-shaped curve created by the parameters listed in Table 1 fits neatly the data points. The analysis clearly reveals that the specific rate constant decreases with the degree of deprotonation on the Schiff base molecule, *i.e.*, **5a**>**5b**>**5c**.

Activation parameters for the spontaneous and **2**-catalyzed β-elimination reaction of **1** were determined at pH 10. The Schiff base of **1** and **2** exists solely in the deprotonated form (**4b**) and the parameters obtained represent those for the SB^- species (Table 2). The reaction is characterized by the large negative entropy of activation and this is compatible with the bimolecular character of β-elimination reactions.[3] The smaller enthalpy of activation for the catalytic reaction may be associated with the labilization of the substrate's α-hydrogen through formation of a Schiff base with **2**.

Discussion

The purpose of the present investigation was two-fold. A mechanistic study of PLP-dependent reactions has often been complicated, because the active Schiff base exists in a variety of ionic forms that differ in reactivity (*e.g.*, see Scheme 2). If one takes into account prototropic equilibrium between, for example, **5b** and **5d**, which could happen in a medium of low dielectric constant,[2] the number of the active Schiff bases further increases. In contrast, the number of Schiff base species derived from an *N*-substituted pyridoxal like **2** is small (Scheme 1). This should ease the analysis of kinetic data in a Schiff base reaction, as has been proven above. Moreover, the presence of a positive charge as a result of the *N*-substitution on the pyridoxal molecule should increase the electron-withdrawing ability of the catalyst, leading to labilization of the α-hydrogen of the Schiff base.[15] This idea has been supported by the finding that **2** is more effective both apparently (Fig. 2) and in terms of specific rate constants than **3** in the elimination reaction of **1** (Table 1).

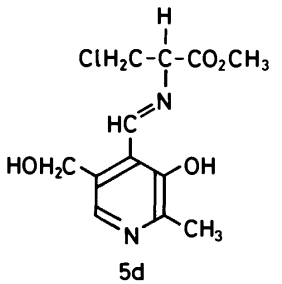

5d

The results given in Table 1 demonstrate that the Schiff bases of **2** and **3** are more reactive when they have more positive charges on them. These data agree with the above argument and may also be reasonable from a

Table 2. Activation parameters for the spontaneous and **2**-catalyzed β-elimination of **1** in water at pH 10

	Rate constant	Temperature/°C			E_a	$\Delta H^{\ddagger}$ [a]	$\Delta S^{\ddagger}$
		15	25	30	kcal mol^{-1} [b]	kcal mol^{-1} [b]	e.u.
Spontaneous	$k_1 \times 10^3/s^{-1}$	0.84	1.29	1.42	6.3	5.8	−53
Catalytic	$k_2 \times 10/s^{-1}\ M^{-1}$	0.64	0.83	1.01	5.3	4.7	−48

a) Values at 25.0 °C. b) 1 cal=4.184 J.

mechanistic point of view, as PLP serves basically as an electron sink in its catalysis.[16] It may be fair, however, to mention the kinetic equivalence of the reaction, since others dealing with similar data reached a somewhat different conclusion.[5] For example, the reaction of **4b** is equivalent kinetically to the reaction of **4a** with hydroxide ion (Eq. 8), where K_w stands for the

$$k_b[\mathbf{4b}] = k_b'' \frac{K_{a3}}{K_w} [\mathbf{4a}][OH^-] \quad (8)$$

ionization product of water. Although it is not possible to distinguish rigorously between these two mechanisms at present, we favor the k_b pathway for the following reason. It is obvious from the spectroscopic data that the Schiff base of **2** exists in two ionic forms, **4a** and **4b**. If one assumes that the k_b pathway is actually the k_b'' pathway, *i.e.*, the reaction of **4a** with OH^-, one could naturally expect a similar reaction for **4b**. Since the concentration of **4b** is over a thousand times higher than that of **4a** at pH 10, this could have brought about a pH-dependent rate increase in the alkaline region, unless **4a** is over a thousand times more reactive than **4b** in the reaction with OH^-. Hence, the lack of such a tendency at high pH values supports the contention that the k_b pathway is the more likely one.

It is noticeable that the catalytic β-elimination is not subject to the hydroxide ion catalysis. This may be understood, since the spontaneous reaction is little affected by the hydroxide ion concentration and in the catalytic reaction the electron sink labilizes the α-hydrogen so that a strong base such as hydroxide ion may not be needed for its abstraction. We suppose that water is the base responsible for the abstraction of α-hydrogen. This may raise a question about the occurrence of general base catalysis in the Schiff base reaction. An increase in phosphate buffer concentration from 0.10 to 1.0 M at pH 8 and at different catalyst concentraions gave rise to a modest increase (15% at maximum) in the observed rate, indicating that at least the buffer components used in these experiments do not affect the rates significantly. Finally, the relevance of the present data to the enzymatic catalysis is mentioned. A number of PLP-dependent enzymes including 3-chloro-D-alanine chloride-lyase show an absorption maximum at ≈420 nm.[17] Unambiguous assignment of this band is obscured, since **4a**, **5a** and **5b** provide similar spectra.[10] In light of the fact that **4a** and **5a** show the highest reactivity in the present reaction, the enzyme-bound PLP may carry a proton on the pyridine nitrogen.[15] This could explain in part a higher reactivity of the coenzyme in enzymatic systems.

The authors are grateful to Dr. J. Kikuchi for helpful discussions. This work was supported by a Grant-in-Aid for Special Project Research 56109007 from the Ministry of Education, Science and Culture.

References

1) D. E. Metzler, J. B. Longenecker, and E. E. Snell, *J. Am. Chem. Soc.*, **76**, 639 (1954).
2) D. Heinert and A. E. Martell, *J. Am. Chem. Soc.*, **85**, 183 (1963).
3) Y. Murakami and H. Kondo, *Bull. Chem. Soc. Jpn.*, **48**, 125 (1975).
4) R. I. Gregerman and H. N. Christensen, *J. Biol. Chem.*, **220**, 765 (1956).
5) K. Tatsumoto, A. E. Martell, and R. J. Motekaitis, *J. Am. Chem. Soc.*, **103**, 6197 (1981).
6) T. Nagasawa, H. Ohkishi, B. Kawakami, H. Yamano, H. Hosono, Y. Tani, and H. Yamada, *J. Biol. Chem.*, **257**, 13749 (1982).
7) D. Heyl, E. Luz, S. A. Harris, and K. Folkers, *J. Am. Chem. Soc.*, **73**, 3430 (1951).
8) L. Benoiton, *Can. J. Chem.*, **46**, 1549 (1968).
9) A Schiff base species carrying a proton on the phenolic oxygen of **4a** or **5a** may also be envisioned, but the pK_a of this group is estimated to be lower than 4. In addition, the fact that the Schiff base is unstable at such a low pH (*cf.* Eq. 6) makes this treatment warranted.
10) D. E. Metzler, *J. Am. Chem. Soc.*, **79**, 485 (1957).
11) Y. Murakami, H. Kondo, and A. E. Martell, *J. Am. Chem. Soc.*, **95**, 7138 (1973).
12) C. M. Metzler, A. Cahill, and D. E. Metzler, *J. Am. Chem. Soc.*, **102**, 6075 (1980).
13) D. E. Metzler, J. Olivard, and E. E. Snell, *J. Am. Chem. Soc.*, **76**, 644 (1954).
14) D. Samuel and B. L. Silver, *J. Chem. Soc.*, **1963**, 289.
15) J. R. Maley and T. C. Bruice, *Arch. Biochem. Biophys.*, **136**, 187 (1970).
16) D. E. Metzler, Y. Ikawa, and E. E. Snell, *J. Am. Chem. Soc.*, **76**, 648 (1954).
17) A. E. Braunstein, "The Enzymes," 3rd ed, ed by P. D. Boyer, Academic Press, New York (1973), Vol. IX, Chap. 10.

 © 1984 The Chemical Society of Japan Bull. Chem. Soc. Jpn., 57, 1035—1039 (1984)

Nonacarbonyldiiron or Pentacarbonyliron Induced Decomposition of Organic Azides and an Azirine. Novel Reduction and Carbonyl Insertion of the Complexed Nitrene Intermediate in Protic Solvents

Makoto NITTA* and Tomoshige KOBAYASHI
Department of Chemistry, School of Science and Engineering, Waseda University, Shinjuku-ku, Tokyo 160
(Received June 20, 1983)

The thermal reactions of $[Fe_2(CO)_9]$ or the photochemical reactions of $[Fe(CO)_5]$ with organic azides and an azirine in protic media have been investigated. The thermal reaction of azidobenzene (**1**) with $[Fe_2(CO)_9]$ in methanol under mild conditions gave aniline and methyl phenylcarbamate, along with *N,N'*-diphenylurea, while in the presence of water, **1** afforded aniline and *N,N'*-diphenylurea, in good combined yield. Similarly, the thermal reaction of α-azidostyrene (**4**) with $[Fe_2(CO)_9]$ in methanol gave methyl 1-phenylvinylcarbamate and acetophenone which could be derived from the corresponding enamine, while in the presence of water, **4** gave only acetophenone in good yield. The photoirradiation of $[Fe(CO)_5]$ with **1** or **4** also gave results similar to the $[Fe_2(CO)_9]$-induced reaction. However, the thermal reaction of 3-phenyl-2*H*-azirine (**5**) with $[Fe_2(CO)_9]$ in methanol gave 2,5-diphenylpyrazine in low yield, in addition to acetophenone and methyl 1-phenylvinylcarbemate, although 5 afforded only acetophenone in the presence of water. The reaction pathways for the formation of the products are discussed on the basis of the formation of a complexed nitrene intermediate, reduction of which induces amine or enamine and carbonyl insertion to yield an organic isocyanate in protic media.

Reaction of azidobenzene (**1**) with $[Fe_2(CO)_9]$ under mild conditions has been shown to give complexes such as bisnitrene complex **2** and urea-based complex **3** in benzene solution.[1,2] In the context of these reactions, the decomposition of **1** in the presence of $[Fe(CO)_5]$ and acetic acid has been studied to give *N,N'*-diphenylurea.[3] The urea-based complex **3**, which could be derived from the complexed phenylnitrene intermediate,[1,4] is proposed as the possible precursor.

In contrast to these studies, transition-metal prompted reactions of the azirine ring system, which can be considered an isomer of vinylnitrene, have been widely studied from both the synthetic and mechanistic point of view.[5,6,7-14] Among these reactions, $[Fe_2(CO)_9]$-induced reaction of 3-phenyl-2*H*-azirine (**5**) in aprotic media has been shown to give complexes such as **6**, **7**, **8**, along with pyrrole and acetophenone albeit in low combined yield.[5] However, the $[Fe_2(CO)_9]$[5] $[Fe(CO)_5]$[6] prompted reaction of α-azidostyrene (**4**) in a similar media gives the complexes **6** and **7**, along with acetophenone or 3,6-diphenylpyridazine. The complexed 1-phenylvinylnitrene is proposed as a key intermediate in the reactions of **4** and **5**. However, the best explanation for the difference of the product composition resulting from the reaction of **4** and **5** could be a further intervention of the complexed azirine in the case of **5**.[5] No reaction of **4** or **5** with $[Fe(CO)_5]$ or $[Fe_2(CO)_9]$ in protic media has been investigated.

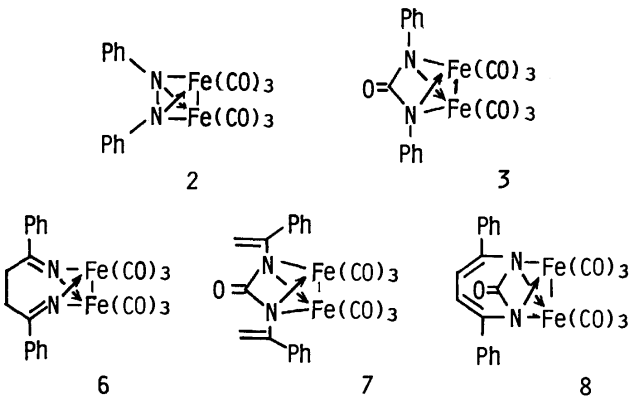

Scheme 1.

Previously the reaction of 3,5-disubstituted isoxazolines (**9**) with $[Fe(CO)_5]$ or $[Fe_2(CO)_9]$ in methanol has been shown to undergo the N-O and C_4-C_5 bond cleavage to give two fragments of aldehydes **10** and ketones **11** in good yields.[15] The complexed vinylnitrene species **12**, which could be reduced to the corresponding enamine **13** in protic media, is proposed

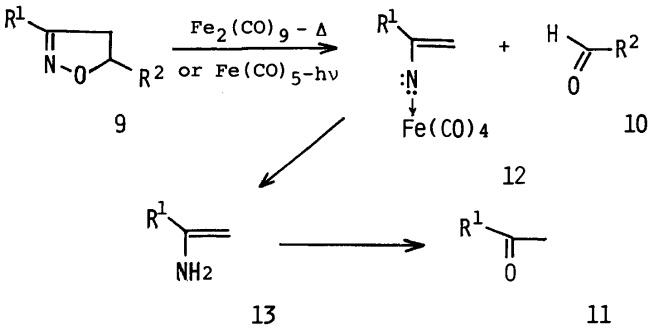

Scheme 2.

as the precursor of the ketones. In connection with the above results, it seemed conceivable that $[Fe(CO)_5]$ or $[Fe_2(CO)_9]$ induced decomposition of organic azides in protic media might provide evidence for the behavior of the complexed nitrene species. This paper describes the reduction and carbonyl insertion of the complexed nitrene species which results from the reaction of azidobenzene (**1**), α-azidostyrene (**4**), and 3-phenyl-2*H*-azirine (**5**) with $[Fe_2(CO)_9]$ or $[Fe(CO)_5]$.

Results and Discussion

Treatment of azidobenzene (**1**) with $[Fe_2(CO)_9]$ in anhydrous methanol at 50 °C afforded aniline (**14**), methyl phenylcarbamate (**15**), and *N,N'*-diphenylurea (**16**), in 21, 51, and 20% yields respectively (Table 1, entry 1). Use of acetonitrile containing water as the

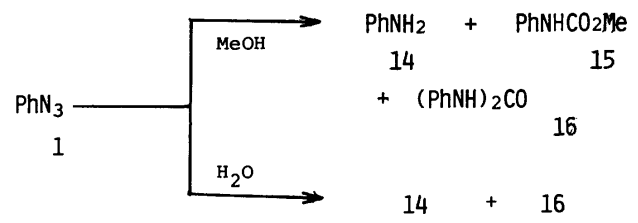

Scheme 3.

reaction solvent gave **14** and **16** in 67 and 23% yields (entry 2). The combined yield of **14**—**16** for each case is very good; the reaction conditions and the products are summarized in Table 1. The structure of the products was identified by comparison of the spectral properties with those of authentic materials. The irradiation of a solution of **1** and $[Fe(CO)_5]$ in anhydrous methanol or in acetonitrile containing water gave results similar to the $[Fe_2(CO)_9]$-induced reactions (entries 3 and 4). However, the reaction of **1** with $[Fe(CO)_5]$ in anhydrous methanol at the refluxing temperature proceeded very slowly and, gave **15** and **16** in 11 and 3% yields, with the remainder being recovered starting material (entry 5). Thus the $[Fe(CO)_5]$ could not act effectively at the low temperature and phbtochemically genarated $[Fe(CO)_4]$ species[15-17] could be very effective to induce the decomposition of **1**. At high temperature, thermal reaction of **1** with $[Fe(CO)_5]$ in acetic acid also proceeded smoothly (entries 6 and 7).

Possible pathways for the formation of the products, **14**, **15**, and **16** were shown in Scheme 4. The initial step in the present reactions is probably n-donor complexation of **1** to the thermally or photochemically generated $[Fe(CO)_4]$ species to give **17** followed by the elimination of a nitrogen molecule to give the phenylnitrene complex **18**.[1,2,5,6] In aprotic media, complexes such as **2** and **3** could be obtained from **18**.[1,2] However, the protonation and subsequent reduction of the phenylnitrene moiety of **18** by the central metal could occur in protic media such as methanol, acetonitrile containing water, or acetic acid, to give

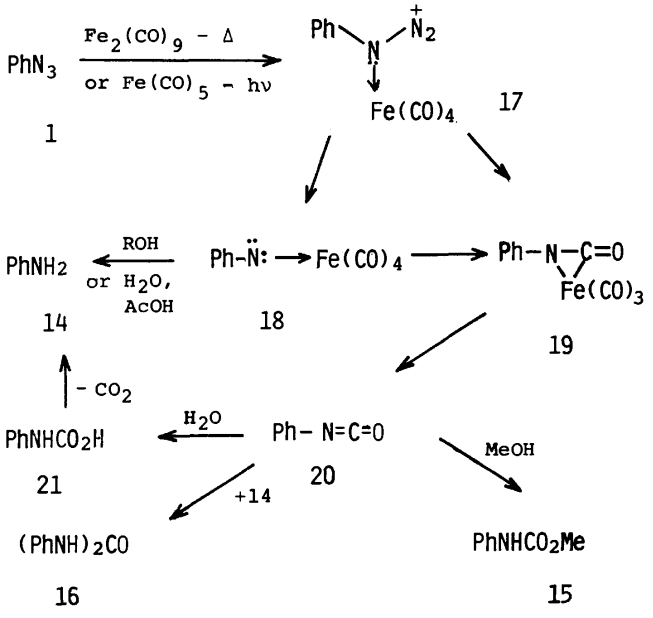

Scheme 4.

aniline **14**. The intramolecular insertion of ligand-carbonyl into metal-nitrogen bond of **18** could give the complex **19**, decomplexation of which could give phenyl isocyanate (**20**). The concerted formation of **19** from **17** may not be ruled out (*vide infra*). In contrast to the present reaction, the carbonylation of azidobenzene to give phenyl isocyanate has been shown to proceed possibly *via* free phenylnitrene under drastic conditions.[18] Phenyl isocyanate **20** is known to be trapped to give **15** in methanol, while in the presence of water, **20** would also give **14** *via* **21**. The formation of **16** can be rationalized on the basis of the reaction of **20** with **14**.[19]

Previously, thermal reaction of aromatic azides with $[Fe(CO)_5]$ in acetic acid has been shown to give *N,N'*-diphenylurea. The urea-based complex, such as **3** in Scheme 1 is proposed as the reasonable intermediate.[3] However attempted thermal reaction of **1** with $[Fe(CO)_5]$ in acetic acid at 100 °C (entry 6) gave **14** and **16** in 33 and 52% yields similarly to the case of entries 2 and 4. On the other hand, the similar reaction of **1** with $[Fe(CO)_5]$ at 100 °C in a tenfold concentrated acetic acid solution gave only **16** in 67% yield (entry 7). Thus the formation of **16** in acetic acid seems dependent on the concentration of aniline **14** which is derived from the reduction of **18** in acetic acid.[20] In a concentrated media of acetic acid, **14** is actually trapped quickly by **20** (see Experimental section), thus only **16** could be obtained in entry 7.

Similarly to the above reactions, $[Fe_2(CO)_9]$ or $[Fe(CO)_5]$ induced reactions of **4** and **5** were studied in protic solvents. The reaction conditions and the products are summarized in Table 2. Treatment of **4** with $[Fe_2(CO)_9]$ in methanol at 50 °C afforded methyl 1-phenylvinylcarbamate (**22**)[21] and acetophenone (**23**) in 44 and 18% yields (Table 2, entry 1). The carbamate **22** is labile and it is hydrolysed by TLC on silica gel to give acetophenone. Accordingly the products, **22** and **23**, in Table 2 were isolated by distillation using a Kugelrohr apparatus. A similar result was also obtained by the photoirradiation of $[Fe(CO)_5]$ and **4** (entry 3). However, the thermal reaction of **4** with $[Fe(CO)_5]$ in methanol at the refluxing temperature proceeded very slowly, and 80% of **4** was recovered (entry 4). Similar to the case of **1**, reaction of **4** with $[Fe_2(CO)_9]$ or $[Fe(CO)_5]$ in acetonitrile containing water afforded only **23** in moderated yield (entries 2 and 5).

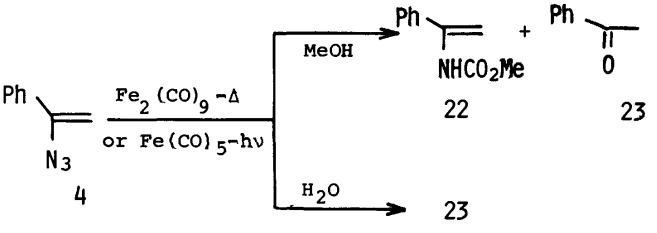

Scheme 5.

The thermal reaction of **5** with $[Fe_2(CO)_9]$ in methanol at 50 °C, on the other hand, afforded **22** and **23** in 14 and 34% yields, along with 2.2% of 2,5-diphenylpyrazine (**24**) (entry 6). It is notable that the major product from **4** in methanol is carbamate **22**, while that from **5** is acetophenone. Use of acetonitrile

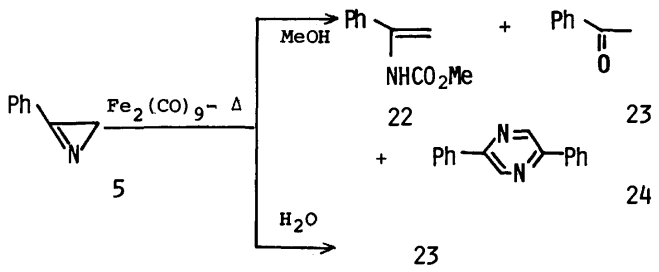

Scheme 6.

containing water as the reaction solvent **5** afforded only acetophenone **23** in 72% yield (entry 7) as in the case of entries 2 and 5 in Table 2. However, irradiation of a solution of **5** with or without [$Fe(CO)_5$] in methanol resulted in the complete disappearance of **5** and afforded **24** in 42 or 35% yield, respectively. Thus the formation of **24** might be explained by the photochemical C-C bond cleavage of the azirine ring to give nitrile ylide.[22]

The reaction pathways for **4** and **5** are very similar to the case of **1**. The carbamate **22** would arise from **4** and **5** *via* methanol-addition of 1-phenylvinyl isocyanate (**29**), which could be derived from carbonyl insertion of the complexed 1-phenylvinylnitrene **27** *via* **25** or **26**.[5,6] The protonation and the subsequent reduction of vinylnitrene moiety of **27** may occur in protic media to give enamine **31**, which may be decomposed by stray water to give **23**. This fact and the lability of **22** to hydrolysis even on TLC plates could explain the previous studies shown in Scheme 2. Another pathway for the formation of **23** would be H_2O-addition of **29** to give **30** followed by decarboxylation to give **31**. Thus in the presence of water, only **23** could be obtained. In the reaction of **4** in methanol (entries 1 and 3) **22** predominates over **23**, while in that of **5**, **23** predominates over **22** (entry 6). This fact may be explained by the direct carbonylation of **25** to give **28**. A minor amount of 2,5-diphenylpyrazine **24** may arise from addition of **27** with **26** or from dimerization of **26**,[9] in the reaction of **5**. However, C-C and/or C=N bond cleavage of the azirine ring can not be ruled out to lead to **24**.[8,9]

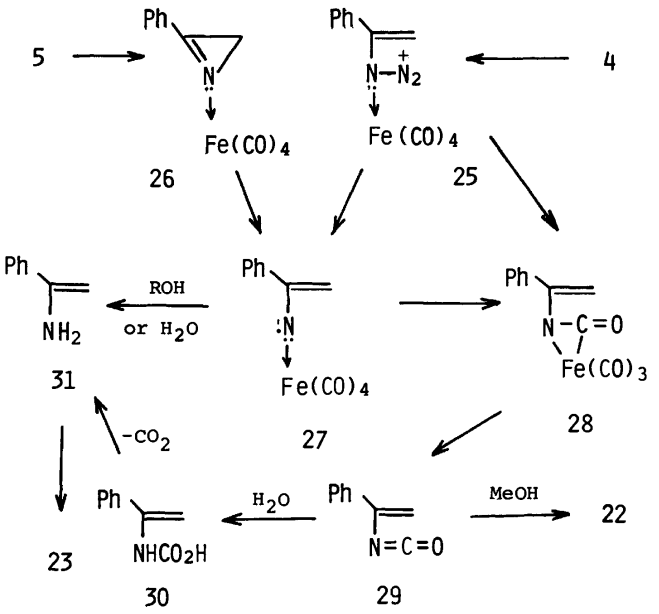

Scheme 7.

In conclusion, the decomposition of **1**, **4**, and **5** with iron carbonyl species afford complexed nitrene intermediates under mild conditions. In a protic solvent this intermediate undergoes reduction to give an amine and carbonyl insertion to give an organic isocyanate in good combined yield. No complexes, such as **2**, **3**, **6**, **7**, and **8** were obtained in protic media.

Experimental

General. Solvents were purified and dried by standard methods. All reactions were carried out under a dry nitrogen atmosphere. Photoirradiations were carried out using Rayonet photoreactor (MGR-100) fitted with RPR-350 nm lamps through a Pyrex filter. The thermal reactions were carried out under unlighted conditions. Azidobenze (**1**),[23] α-azidostyrene (**4**),[24] and 3-phenyl-2*H*-azirine (**5**)[24] were synthesized according to the literature-procedures. All of the products are known compounds and were identified by comparison of the spectral data with those of authentic samples.

Thermal Reaction of 1 with [$Fe_2(CO)_9$]. A mixture of **1** (119mg, 1mmol) and [$Fe_2(CO)_9$] (364mg, 1mmol) in 10cm^3 of anhydrous methanol or acetonitrile containing water (1 mmol) was stirred at 50 °C for a period indicated in Table 1. The solution was filtered through Celite and the filtrate was evaporated. The residue was separated by TLC on silica gel using benzene or dichloromethane as the eluent to give the products, which are summarized in Table 1.

Table 1. Reaction of azidobenzene in the presence of [$Fe_2(CO)_9$][a] or [$Fe(CO)_5$][b]

Entry	Metalcarbonyl	Solvent	Reaction conditions	Reaction time/h	Yield of product/%			
					14	**15**	**16**	**1**
1	$Fe_2(CO)_9$	MeOH	50 °C	3	21	51	20	
2	$Fe_2(CO)_9$	MeCN-H_2O[c]	50 °C	3	67	—	23	
3	$Fe(CO)_5$	MeOH	*hν*	4	10	53	20	
4	$Fe(CO)_5$	MeCN-H_2O[c]	*hν*	8	47	—	40	
5	$Fe(CO)_5$	MeOH	Reflux	8	—	11	3	>30[f]
6[d]	$Fe(CO)_5$	AcOH	100 °C	3	33	—	52	
7[e]	$Fe(CO)_5$	AcOH	100 °C	6	—	—	67	

a) An equimolar quantity of [$Fe_2(CO)_9$] was used. b) 1.2 molar equivalent amount of [$Fe(CO)_5$] was used. c) Contained an equivalent amount of water. d) 1 mol of Ph-N_3 and 2 mol of [$Fe(CO)_5$] was dissolved in 5 cm^3 of AcOH. e) 10mmol of Ph-N_3 and 20mmol of [$Fe(CO)_5$] was dissolved in 5cm^3 of AcOH. f) This compound is volatile under the workup conditions and the yield is low.

TABLE 2. REACTION OF α-AZIDOSTYRENE AND 3-PHENYL-2H-AZIRINE IN THE PRESENCE OF $[Fe(CO)_9]$[a] OR $[Fe(CO)_5]$[b]

Entry	Compound	Metalcarbonyl	Solvent	Reaction conditions	Reaction time/h	Yield of product/%		
						22	**23**	Others
1	4	$Fe_2(CO)_9$	MeOH	50 °C	3	44	18	—
2	4	$Fe_2(CO)_9$	MeCN-H_2O[c]	50 °C	3	—	71	—
3	4	$Fe(CO)_5$	MeOH	*hν*	24	53	30	—
4	4	$Fe(CO)_5$	MeOH	Reflux	8	14	5	80 (**4**)
5	4	$Fe(CO)_5$	MeCN-H_2O[c]	*hν*	24	—	67	—
6	5	$Fe_2(CO)_9$	MeOH	50 °C	7	14	34	2.2 (**24**)
7	5	$Fe_2(CO)_9$	MeCN-H_2O[c]	50 °C	24	—	72	—
8	5	None	MeOH	hν	2.5	—	—	42 (**24**)
9	5	$Fe(CO)_5$	MeOH	hν	2.5	—	—	35 (**24**)

a) An equivalent amount of $[Fe_2(CO)_9]$ was used. b) 1.2 molar equivalent amount of $[Fe(CO)_5]$ was used. c) Contained an equivalent amount of water.

Photoirradiation of **1** *with* $[Fe(CO)_5]$. A solution of **1** (119 mg, 1 mmol) and $[Fe(CO)_5]$ (232 mg, 1.2 mmol) in 20 cm^3 of anhydrous methanol or acetonitrile containing water (1 mmol) was irradiated for a period indicated in Table 1. The solution was concentrated and filtered through Celite. The filtrate was evaporated and the residue was separated by TLC on silica gel using benzene or dichloromethane as the eluent to give the products, which are summarized in Table 1.

Thermal Reaction of **1** *with* $[Fe(CO)_5]$ *in Methanol.* A solution of **1** (119 mg, 1 mmol) and $[Fe(CO)_5]$ (232 mg, 1.2 mmol) in 10 cm^3 of anhydrous methanol was refluxed for 8 h. The solution was concentrated and chromatographed on Florisil to give the products, which are listed in Table 1.

Photoirradiation of **15** *with* $[Fe(CO)_5]$. A solution of **15** (151 mg, 1 mmol) and $[Fe(CO)_5]$ (232 mg, 1.2 mmol) in 20 cm^3 of anhydrous methanol was irradiated for 5 h. The photolysate was filtered through Celite and the filtrate was evaporated. The resulting residue was recrystallized to give **15** in 100% yield.

Photoirradiation of **16** *with* $[Fe(CO)_5]$. A solution of **16** (212 mg, 1 mmol) and $[Fe(CO)_5]$ (232 mg, 1.2 mmol) in 20 cm^3 of anhydrous methanol was irradiated for 5 h. The photolysate was filtered through Celite and the filtrate evaporated. The resulting residue was recrystallized to give 100% of **16**.

Thermal Reaction of **1** *with* $[Fe(CO)_5]$ *in AcOH.* A solution of **1** (119 mg, 1 mmol) and $[Fe(CO)_5]$ (392 mg, 2 mmol) in 5 cm^3 of AcOH was heated at 100 °C for 3 h. The solution was diluted with 50 cm^3 of benzene and then neutralized with aqueous sodium hydrogencarbonate solution. The organic layer was separated and dried over sodium sulfate. After evaporation of the solvent, the residue was separated by TLC on silica gel using dichloromethane as the eluent to give **14** (31 mg, 33%) and **16** (55 mg, 52%).

Thermal Reaction of **1** *with* $[Fe(CO)_5]$ *in AcOH (Concentrated Conditions).* A solution of **1** (1.19 g, 10 mmol) and $[Fe(CO)_5]$ (392 mg, 20 mmol) in 5 cm^3 of AcOH was heated at 100 °C for 6 h. After addition of 10 cm^3 of water to this solution, the precipitated colorless crystals were collected to give **16** (782 mg, 67%). The filtrate was neutralized with aqueous sodium hydrogencarbonate solution and extracted with benzene. Evaporation of the solvent gave no other product.

Reaction of **14** *with* **20** *in AcOH.* Phenyl isocyanate **20** (101 mg, 1 mmol) was added dropwise to a stirred solution of **14** (93 mg, 1 mmol) in 5 cm^3 of AcOH. After stirring for 5 min, the solvent was evaporated and the residue was collected to give 210 mg (98%) of **16**.

Thermal Reaction of **4** *with* $[Fe_2(CO)_9]$. A solution of **4** (145 mg, 1 mmol) and $[Fe_2(CO)_9]$ (364 mg, 1 mmol) in 10 cm^3 of anhydrous methanol or acetonitrile containing water (1 mmol) was heated at 50 °C for 7 h. The solution was filtered through Celite and the filtrate was concentrated. The resulting residue was distilled *in vacuo* using a Kugelrohr apparatus to give the products, which are summarized in Table 2.

Photoirradiation of **4** *with* $[Fe(CO)_5]$. A solution of **4** (145 mg, 1 mmol) and $[Fe(CO)_5]$ (236 mg, 1.2 mmol) in 20 cm^3 of anhydrous methanol or acetonitrile containing water (1 mmol) was irradiated. The solution was concentrated and filtered through Celite. The filtrate was evaporated and the residue was distilled as described above to give the products.

Thermal Reaction of **4** *with* $[Fe(CO)_5]$. A solution of **4** (145 mg, 1 mmol) and $[Fe(CO)_5]$ (236 mg, 1.2 mmol) in 10 cm^3 of anhydrous methanol was refluxed for 7 h. The solution was concentrated and chromatographed on Florisil. The fraction eluted with hexane gave 116 mg (80%) of **4**. Then, the first fraction eluted with benzene gave 6 mg (5%) of **22**, and the second fraction gave 24 mg (13%) of **23** (Table 2, entry 4).

Thermal Reaction of **5** *with* $[Fe_2(CO)_9]$. A solution of **5** (117 mg, 1 mmol) and $[Fe_2(CO)_9]$ (364 mg, 1 mmol) in 10 cm^3 of anhydrous methanol or acetonitrile containing water (1 mmol) was heated at 50 °C for a period indicated in Table 2. The solution was filtered through Celite and the filtrate was evaporated. The residue was distilled as described above to give the products, **22** and/or **23**. After the distillation, the residual oil was purified by TLC on silica gel to give **24**: mp 196—197 °C (from EtOH).[8]

Photoirradiation of **5** *without* $[Fe(CO)_5]$. A solution of **5** (117 mg, 1 mmol) in 10 cm^3 of anhydrous methanol was irradiated for 2.5 h. The evaporation of the solvent and the following separation by TLC on silica gel gave **24** (42 mg, 41%).

Photoirradiation of **5** *with* $[Fe(CO)_5]$. A solution of **5** (117 mg, 1 mmol) and $[Fe(CO)_5]$ (232 mg, 1.2 mmol) in 10 cm^3 of anhydrous methanol was irradiated for 2.5 h. The evaporation of the solvent and the following separation by TLC on silica gel gave **24** (41 mg, 35%).

References

1) M. Decker and G. R. Knox, *Chem. Commun.*, **1967**, 1243.
2) C. D. Campbell and C. W. Rees, *Chem. Commun.*, **1969**, 537.
3) A. F. M. Iqbal, *Helv. Chim. Acta*, **56**, 655 (1976).
4) T. A. Manuel, *Inorg. Chem.*, **1**, 1703 (1964); J. A. J. Javis, B. E. Job, B. T. Kilbourn, R. H. B. Mals, P. G. Oweston, and P. F. Todd, *Chem. Commun.*, **1967**, 1149.
5) H. Alper and J. E. Prickett, *J. Chem. Soc., Chem. Commun.*, **1976**, 191; *Inorg. Chem.*, **16**, 67 (1977).
6) Y. Nakamura, K. Bachmann, H. Heimgartner, and H. Schmid, *Helv. Chim. Acta*, **61**, 589 (1978).
7) F. Bellamy, *J. C. S., Chem. Commun.*, **1978**, 998; *Tetrahedron Lett.*, **1978**, 4577.

8) H. Alper and S. Wollowitz, *J. Am. Chem. Soc.*, **97**, 3541 (1975); H. Alper, J. E. Prickett, and S. Wollowitz, *J. Am. Chem. Soc.*, **99**, 4330 (1977).
9) A. Inada, H. Heimgartner, and H. Schmid, *Tetrahedron Lett.*, **1979**, 2983; A. Inada and H. Heimgartner, *Helv. Chim. Acta*, **65**, 1489 (1982).
10) H. Alper and J. E. Prickett, *J. Chem. Soc., Chem. Commun.*, **1976**, 483; *Tetrahedron Lett.*, **1976**, 2589.
11) P. Faria des Santos Filo and U. Schuchart, *Angew. Chem., Int. Ed. Engl.*, **16**, 647 (1977).
12) K. Isomura, K. Ueno, and H. Taniguchi, *J. Chem. Soc., Chem. Commun*, **1977**, 664.
13) H. Alper and C. P. Perera, *J. Am. Chem. Soc.*, **103**, 1289 (1981).
14) T. Izumi and H. Alper, *Organometallics*, **1**, 322 (1982).
15) M. Nitta and T. Kobayashi, *Chem. Lett.*, **1983**, 51.
16) T. Kobayashi and M. Nitta, *Chem. Lett.*, **1982**, 325.
17) M. Poliakoff and J. Turner, *J. Chem. Soc., Dalton Trans.*, **1974**, 210; **1974**, 2276.
18) R. P. Bennett and W. B. Hardy, *J. Am. Chem. Soc.*, **90**, 3295 (1968).
19) S. Patai, "The Chemistry of Cyanates and Their Thio Derivatives," John Willey and Sons, Chichester, New York, Brisbane, and Toronto (1977), Part 2.
20) The reaction of phenyl isocyanate with acetic acid is known to give mixed carbamic anhydride which decomposes at room temperature to give acetic anhydride, carbon dioxide, *N*-phenylacetamide, and *N,N'*-diphenylurea; W. Dickman and F. Breest, *Chem. Ber.*, **39**, 3052 (1906). However, *N*-phenylacetamide was not detected in the present reaction.
21) T. Sakakibara and H. Alper, *J. Chem. Soc., Chem. Commun.*, **1979**, 458.
22) A. Padwa, J. Smolanoff, and A. Temper, *J. Am. Chem. Soc.*, **97**, 4682 (1975) and references cited therein.
23) *Org. Synth.*, Coll. Vol. III, p. 170.
24) G. Smolinsky, *J. Org. Chem.*, **27**, 3557 (1962).

Stereoselective Catalytic Hydrogenation of α-Hydroxy Ketoximes

Kaoru HARADA and Shozo SHIONO*
Department of Chemistry, The University of Tsukuba, Sakura-Mura, Niihari, Ibaraki 305
(Received July 11, 1983)

Two isomers(*E* and *Z*) of benzoin oxime and 2-hydroxy-1-phenyl-1-propanone oxime were catalytically hydrogenated by using palladium on charcoal and erythro amino alcohols were obtained in about 80% diastereomeric excess. The syn-anti isomerization of these oximes in the presence of palladium on charcoal was also studied in connection with the stereoselectivity of the catalytic hydrogenation of the oximes.

The stereochemistry of catalytic hydrogenation of oximes of α-keto amides[1] and Schiff bases prepared from α-keto esters with optically active amines[2] have been studied. The steric course of the catalytic hydrogenation reaction was explained by the chelation mechanism assuming that the substrate forms a five-membered chelated structure with the catalyst and subsequent hydrogenation reaction takes place from the less bulky side of the chelated substrate. This mechanism was supported by various hydrogenolytic catalytic asymmetric transamination[2-4] and also by the infrared absorption spectrum of ethyl 2-hydroxyimino-3-oxo-3-phenylpropionate on palladium metal, which was measured by using the high-sensitivity reflection method.

The substrates, which have been used in the previous studies of the chelation mechanism, contain an asymmetric center out of the chelated ring when they form a chelated structure with the catalyst. If the substrate contains an asymmetric center in the five-membered chelated ring, a relatively high asymmetric yield might be obtained by the catalytic hydrogenation. In order to examine the consideration, the catalytic hydrogenation of oximes, whose asymmetric center is in the five-membered chelated ring, was performed.

It was reported that the catalytic hydrogenation of racemic (*E*)-benzoin oxime afforded *erythro*-2-amino-1,2-diphenylethanol (*erythro*-ADE) dominantly.[6] However, the exact ratio of the diastereomer has not been clarified yet. In the present study, a cyclic reaction pathway as shown in Scheme 1 was designed and the catalytic hydrogenation of optically and racemic benzoin oxime was carried out. If the stereoselectivity of the catalytic hydrogenation is sufficiently high, optically active *erythro*-ADE could be synthesized again from optically active *erythro*-ADE used as a starting material. In addition, in order to examine the substituent effect, hydrogenation of (±)-2-hydroxy-1-phenyl-1-propanone oxime (HPPO) was also performed.

Oxime of α-keto amide has (*E*)- and (*Z*)-isomers, and only the (*E*)-isomer could form a five-membered chelated structure with the catalyst. However, the *E*—*Z* isomeric ratio of the substrate used in the catalytic hydrogenation has not been clarified yet, and the steric course of the hydrogenation of (*E*)-oximes might be different from that of (*Z*)-oximes. In order to clarify the stereochemistry of the hydrogenation of oximes, both (*E*)- and (*Z*)-isomers were isolated and each of the oximes was catalytically hydrogenated. The syn-anti isomerization of the oximes in the presence of palladium on charcoal was also studied in connection with the stereoselectivity of the catalytic hydrogenation of the oximes.

Results and Discussion

Hydrogenation of Substrates. Substrates, (*E*)- and (*Z*)-benzoin oxime and (*E*)- and (*Z*)-HPPO, were hydrogenated by using palladium on charcoal in several solvents and at various temperatures. The diastereomeric ratio of amino alcohol was determined by gas chromatographic analysis, which are summarized in Tables 1 and 2.

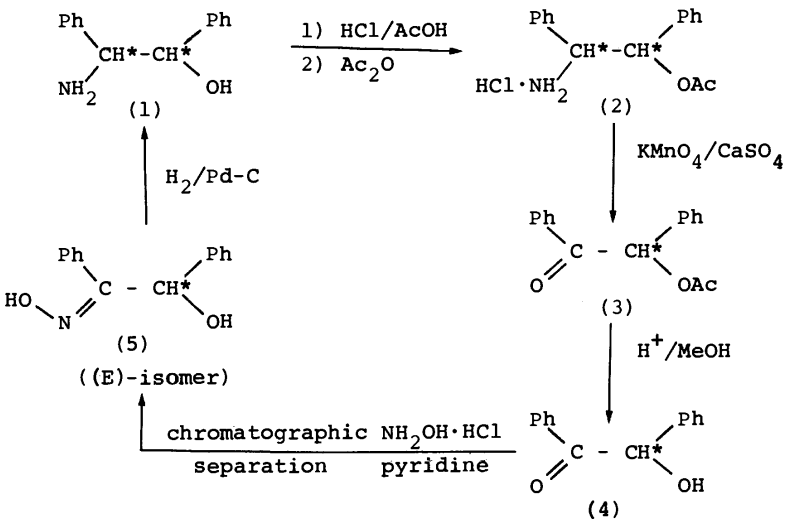

Scheme 1.

Table 1. Catalytic hydrogenation of (*E*)-oximes of *R*(—)-benzoin and racemic 2-hydroxy-1-phenyl-1-propanone

substrate	Solvent	Temp/°C	Yield/%	Erythro: Threo	O.P./%[a]	Configuration[b]
(*E*)-Benzoin oxime	MeOH	20	79	93 : 7	95	*S*
	EtOH	0	78	96 : 4		*S*
	EtOH	20	71	93 : 7		*S*
	EtOH	40	75	93 : 7		*S*
	2-PrOH	20	80	92 : 8		*S*
	DMF	20	69	94 : 6		*S*
(*E*)-2-Hydroxy-1-phenyl-1-propanone oxime	MeOH	20	89	91 : 9		—[c]
	EtOH	20	68	92 : 8		—
	EtOH	40	81	90 : 10		—
	EtOH	60	73	85 : 15		—
	AcOEt	20	69	94 : 6		—

a) Optical purity. b) Configuration of newly formed asymmetric moiety. c) Racemic oxime was used.

Table 2. Catalytic hydrogenation of (*Z*)-oximes of racemic benzoin and racemic 2-hydroxy-1-phenyl-1-propanone

Substrate	Solvent	Temp/°C	Yield[a]/%	Erythro: Threo
(*Z*)-Benzoin oxime	MeOH	20	68	88:12
	EtOH	20	71	89:11
	AcOEt	20	55	86:14
(*Z*)-2-Hydroxy-1-phenyl-1-propanone oxime	MeOH	20	59	91:9
	EtOH	20	64	93:7
	EtOH	40	75	91:9
	EtOH	60	46	85:15
	AcOEt	20	80	93:7

a) Determined by isolation.

In the hydrogenation of (*E*)-oximes of both benzoin and HPPO, erythro amino alcohols were obtained in about 80% diastereomeric excess in every solvent and at every temperature employed. Similar results were obtained in the hydrogenation of the corresponding (*Z*)-oximes.

In the case of (*E*)-benzoin oxime, the conformation of the substrate in solution could be shown in Structure 1 considering the steric repulsion between the phenyl groups of the molecule. If the hydrogenation of the (*E*)-benzoin oxime proceeds from the less bulky side of the substrate in Structure 1, *threo*-ADE would be produced, which is inconsistent with the experimental results. On the other hand, if the (*E*)-benzoin oxime forms a five-membered chelated structure with the palladium metal first as shown in structure 2, and then hydrogenation proceeds from the less bulky side of the substrate as expected by the chelation mechanism, *erythro*-ADE would be formed dominantly. In the hydrogenation of (*E*)-HPPO, the formation of erythro amino alcohol could also be explained by the chelation mechanism.

The (*E*)-oxime could also form a five-membered intramolecular hydrogen bonding between the nitrogen and the hydroxyl group at α-position. If the hydrogenation reaction proceeds from the less bulky side of the intramolecularly hydrogen bonded substrate, erythro amino alcohol could also be produced. However, examination of the molecular structure by the use of a molecular model indicates that the distance between the nitrogen and the hydroxyl group at the α-position of the (*E*)-benzoin oxime seems to be too long for the formation of rigid intramolecular hydrogen bonding. Therefore, the contribution of the hydrogen bonded steric course for the hydrogenation of (*E*)-oxime would not be so important.

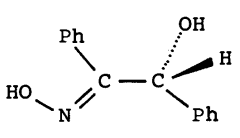

Structure 1.

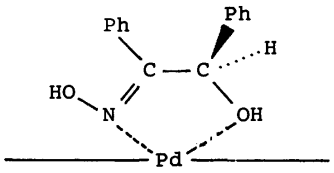

Structure 2.

According to the chelation mechanism, the stereoselectivity in the hydrogenation of (*E*)-HPPO is assumed to be smaller than that of (*E*)-benzoin oxime. However, the stereoselectivity in the hydrogenation of (*E*)-HPPO was almost the same as that in (*E*)-benzoin oxime. This might be explained by the adsorption of phenyl groups of benzoin oxime on the catalyst, and other conformation of chelated ring structure could be possible other than the prefered conformation.

On the other hand, the (*Z*)-oxime could not form the five-membered chelated structure, but could form a six-membered intramolecular hydrogen bonding. The distance between the hydroxyl group attached to nitrogen and the hydroxyl group at α-position seems to be adequate to form a rigid intramolecular hydrogen bonding by using a molecular model. If the substrate forms the six-membered intramolecular hydrogen bonding first, and then hydrogenation reaction takes place from the less bulky side of the substrate, erythro amino alcohol would be obtained. This consideration

is consistent with the experimental results. The results obtained in the hydrogenation of the (*Z*)-oxime are similar to those of the corresponding (*E*)-oxime. Considering the conformation of the substrate by using molecular model, the steric bulkiness around the diastereomeric face of the (*E*)-oxime forming the five-membered chelated structure with the catalyst is almost the same as that of the corresponding (*Z*)-oxime forming the six-membered intramolecular hydrogen bonding. This observation suggest that both (*E*)- and (*Z*)-oximes could be hydrogenated in chelated form and in intramolecular hydrogen bonded form, respectively.

Effect of Isomerization of Benzoin Oxime on the Hydrogenation. Isomerization of benzoin oxime in the presence of palladium on charcoal was observed and the time-courses of the isomerization were shown in Fig. 1. The isomerization of a few derivatives of benzoin oxime was also examined. Benzoin acetate oxime, in which the hydroxyl group of the benzoin oxime is protected by an acetyl group, isomerized in the presence of palladium on charcoal. However, *N,O*-diacetylbenzoin oxime, in which the hydroxyimino group of benzoin acetate oxime is protected by an acetyl group, did not isomerize under these conditions. These results indicate that the hydrogen atom of the hydroxyimino group of benzoin oxime might play an important role in the isomerization in the presence of palladium on charcoal. Therefore, benzoin oxime might isomerize *via* a nitroso compound and the hydrogenation of the compound to ADE might proceed as shown in Fig. 2. In order to confirm the possible

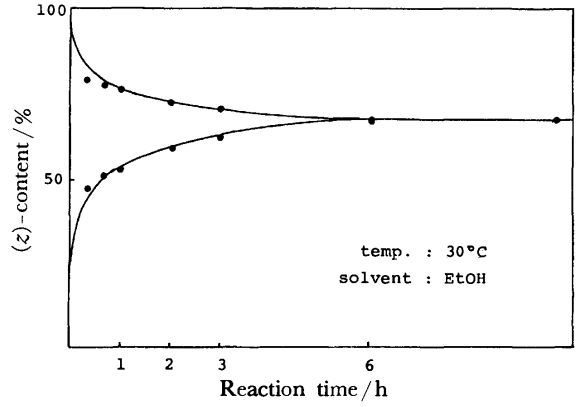

Fig. 1. Isomerization of benzoin oxime in the presence of palladium on charcoal.

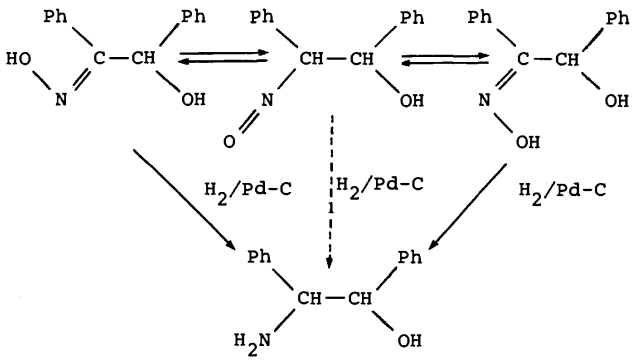

Fig. 2. Mechanism of isomerization of benzoin oxime.

hydrogenation pathway, the hydrogenation of (*E*)-benzoin oxime was carried out in CD_3OD by using palladium on charcoal. If the hydrogenation of (*E*)-benzoin oxime proceeds *via* the nitroso compound, deuterium should be combined to the asymmetric carbon attached to the amino group of ADE. ^1H NMR spectrum of ADE, which was obtained by hydrogenation of (*E*)-benzoin oxime in CD_3OD, indicates that the integrated value of proton on the asymmetric carbon attached to amino group was almost equal to that on the asymmetric carbon attached to hydroxyl group. The mass spectrum of TFA derivative of ADE obtained by hydrogenation of (*E*)-benzoin oxime in CD_3OD was almost equal to that of TFA derivatives of both *erythro*- and *threo*-ADE (Table 3). These results indicate that the hydrogenation reaction does not proceed *via* the nitroso compound but through hydrogenation of the carbon–nitrogen double bond of the substrate oxime.

TABLE 3. FRAGMENT PEAK OF MASS SPECTRA OF *N,O*-BIS (TFA)-ADE AND RELATIVE INTENSITY

N,O-Bis(TFA) derivatives	Fragment peak	Relative intensity/%
erythro-ADE	78	8.8
	107	13.1
	202[a)]	100
	203[b)]	13.3
threo-ADE	78	9.3
	107	14.1
	202[a)]	100
	203[b)]	12.4
ADE obtained by the hydrogenation of (*E*)-benzoin oxime in CD_3OD	78	8.1
	107	13.0
	202[a)]	100
	203[b)]	17.6

a) Ph-CH=NH^+-CO-CF_3. b) Ph-CH=O^+-CO-CF_3.

The influence of the syn-anti isomerization of the oximes during the hydrogenaiton was examined. In the hydrogenation of (*E*)-benzoin oxime, if it is assumed that the rate of hydrogenation reaction of the (*Z*)-oxime is much larger than that of the (*E*)-oxime, the (*E*)-oxime would isomerize to the (*Z*)-isomer first, and then the newly formed (*Z*)-isomer would be hydrogenated to form ADE. If this is the case, ADE would be obtained in rather low chemical yield in a short reaction time in the hydrogenation of (*E*)-benzoin oxime, because of the low concentration of the (*Z*)-oxime. In order to estimate the rate of hydrogenation of (*E*)- and (*Z*)-benzoin oxime, the time-courses of the chemical yield of ADE were measured. The results are shown in Fig. 3. The chemical yield of ADE obtained by hydrogenation of the (*E*)-oxime was 15% at the reaction time of 30 min, while the chemical yield of ADE obtained from the (*Z*)-oxime was 18% at the same reaction time. These results suggest that the rate of hydrogenation of the (*E*)-oxime is similar to that of the (*Z*)-oxime.

Considering the overall results, it could be concluded that (*E*)-benzoin oxime is hydrogenated mainly after forming a five-membered chelated structure with the

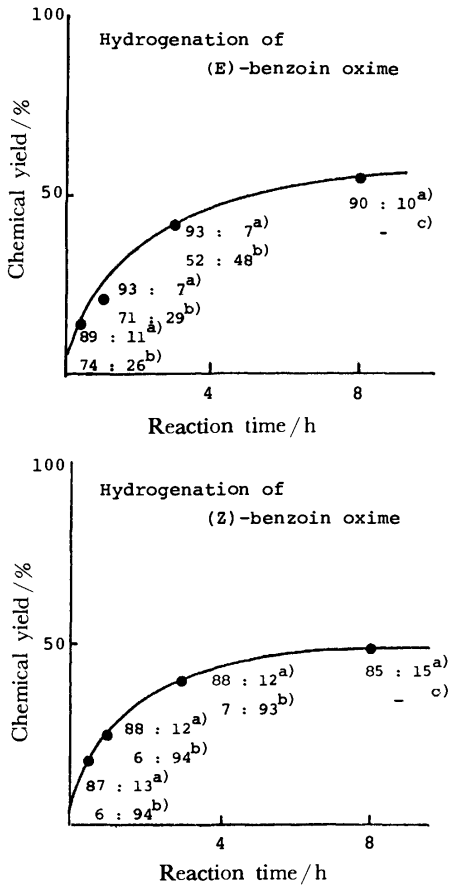

Fig. 3. Time-course of chemical yield of ADE in hydrogenation of benzoin oxime.
a) Diastereomeric ratio, erythro: threo, b) *E*-*Z* isomeric ratio, *E*:*Z*. c) *Syn-anti* isomeric ratio could not be determined.

catalyst (chelation mechanism) and (*Z*)-benzoin oxime is hydrogenated mainly after forming a intramolecular six-membered hydrogen bonding (intramolecular hydrogen bonding mechanism).

Experimental

All the melting point are uncorrected. The specific rotation were measured with a JASCO DIP-181 Digital Polarimeter. NMR spectra were obtained with a Hitachi R-24A spectrometer and the chemical shifts were given in δ values (ppm) from tetramethylsilane (TMS). Mass spectra were obtained with a Hitachi RMU-6M mass spectrometer. All the gas chromatographic analyses were carried out with a Hitachi 163 gas chromatograph. 5% Palladium on charcoal was purchased from Nippon Engelhald.

(−)-erythro-2-Amino-1,2-diphenylethyl Acetate Hydrochloride (2). (−)-*erythro*-ADE (**1**) (5.41 g, 0.025 mol) was suspended in 500 ml of AcOH. Hydrogen chloride gas was bubbled into the suspension for 9 h at 80 °C and the resulting clear solution was cooled to room temperature. Then Ac_2O was added to the mixture under stirring and the mixture was stirred for additional 5 h and concentrated *in vacuo*. The crude product obtained was recrystallized from MeOH-Ether, yield 4.74 g (64%), mp 168—169 °C, $[\alpha]_D^{11}$ −89.8° (*c* 1, MeOH), ^{1}H NMR (DMSO-d_6): δ=2.13 (s, 3H), 4.62 (d, 1H), 6.28 (d, 1H), 7.24 (m, 10H), 9.02 (s, br, 3H). Found: C, 65.92; H, 6.14; N, 4.75%. Calcd for $C_{16}H_{18}NO_2Cl$: C, 65.86; H, 6.21; N, 4.75%.

R(−)-Benzoin Acetate (3). To a suspension of $KMnO_4$ (5.02 g, 0.032 mol) and $CaSO_4 \cdot 2H_2O$ (3.75 g, 0.022 mol) in 50 ml of water and 50 ml of *t*-butyl alcohol was added (−)-*erythro*-2-amino-1,2-diphenylethyl acetate hydrochloride (**2**) (4.87 g, 0.017 mol) and the suspension was heated for 2 h at 60 °C. The reaction mixture was filtered and the residue was washed with ethyl acetate. The combined solution was washed with water and dried over magnesium sulfate and concentrated *in vacuo*. The residue was purified by column chromatography on silica gel using benzene-ethyl acetate (100:1 v/v) as an eluent. The solid obtained was recrystallized from hexane, yield 1.61 g (37.3%), mp 80.5—82 °C, $[\alpha]_D^{18}$ −214.3° (*c* 1, chloroform) (lit,[7] $[\alpha]_D^{14}$ −217.7°), ^{1}H NMR ($CDCl_3$): δ=2.15 (s, 3H), 6.81 (s, 1H), 7.66 (m, 10H). Found: C, 75.86; H, 5.64%. Calcd for $C_{16}H_{14}O_3$: C, 75.57; H, 5.54%.

R(−)-Benzoin (4). A solution of *R*(−)-benzoin acetate (**3**) (800 mg, 3.15×10^{-3} mol) in 30 ml of abs. methanol was refluxed for 2 h in the presence of a catalytic amount of concd. sulfuric acid. To the reaction mixture was added 100 ml of ethyl acetate, and organic layer was washed with saturated $NaHCO_3$ and water and dried over magnesium sulfate, and was concentrated *in vacuo*. The residue was purified by column chromatography on silica gel using benzene-ethyl acetate (20:1 v/v) as an eluent. The solid obtained was recrystallized from ethanol, yield 498 mg (75%), mp 130—131 °C (lit,[8] 132—133 °C), $[\alpha]_D^{22}$ −111.6° (*c* 1, acetone), (lit,[8] $[\alpha]_D^{25}$ −118.3°), ^{1}H NMR ($CDCl_3$): δ=4.51 (d, 1H), 5.92 (d, 1H), 7.66 (m, 10H). Found: C, 79.21; H, 5.68%. Calcd for $C_{14}H_{12}O_2$: C, 79.22; H, 5.69%.

R(−)-(E)-Benzoin Oxime (5). To a solution of *R*(−)-benzoin (**4**) (473 mg, 2.23×10^{-3} mol) in 5 ml of pyridine was added a solution of hydroxylamine hydrochloride (468 mg, 6.73×10^{-3} mol) in 5 ml of pyridine under cooling in an ice bath. The reaction mixture was stirred for 90 min at room temperature and then concentrated *in vacuo*. The residue was extracted with ethyl acetate and the extract was washed with 10% citric acid and water and dried over magnesium sulfate, and was concentrated *in vacuo*. The residue was purified by column chromatography on silica gel using benzene-ethyl acetate (5:1 v/v) as an eluent. The solid obtained was recrystallized from benzene, yield 295 mg (58%), mp 156—158 °C (lit,[7] 163—164 °C), $[\alpha]_D^{20}$ −2.9° (*c* 0.5, chloroform) (lit,[7] $[\alpha]_D^{24}$ −3.2°). Found: C, 73.97; H, 5.75; N, 6.19%. Calcd for $C_{14}H_{13}NO_2$: C, 73.99; H, 5.76; N, 6.16%.

(±)-(Z)-Benzoin Oxime. (±)-(*Z*)-Benzoin oxime was isolated by column chromatography of (±)-benzoin oxime as in the same way as *R*(−)-(*E*)-benzoin oxime. Yield from benzoin was 47%, mp 102.5—103.5 °C (lit,[9] 99 °C). Found: C, 73.88; H, 5.75; N, 6.15%. Calcd for $C_{14}H_{13}NO_2$: C, 73.99; H, 5.76; N, 6.16%.

(±)-2-Hydroxy-1-phenyl-1-propanone. To a solution of PhMgBr, prepared from bromobenzene (10.36 g, 0.066 mol) and magnesium (1.60 g, 0.066 atom), in 40 ml of ether was added a solution of lactonitrile (2.13 g, 0.03 mol) in 10 ml of ether and the mixture was refluxed for 90 min. Then 10 ml of water and 30 ml of 10% sulfuric acid was added to the mixture. The ether layer was washed with saturated $NaHCO_3$ and water and dried over magnesium sulfate, and was concentrated *in vacuo*. The residue was purified by column chromatography on silica gel using benzene-ethyl acetate (25:1 v/v) as an eluent, yield 2.35 g (57%), bp 72 °C/3 mmHg (lit,[10] 125—126 °C/14 mmHg), ^{1}H NMR ($CDCl_3$): δ=1.40 (d, 3H), 3.88 (s, 1H), 5.08 (q, 1H), 7.60 (m, 5H). Found: C, 72.62; H, 6.94%. Calcd for $C_9H_{10}O_2$: C, 71.98; H, 6.71%.

(±)-(E)-2-Hydroxy-1-phenyl-1-propanone Oxime and (±)-(Z)-2-Hydroxy-1-phenyl-1-propanone Oxime. To a solution of (±)-2-hydroxy-1-phenyl-1-propanone (1.967 g, 0.013 mol) in 20 ml of pyridine was added a solution of hydroxylamine hydrochloride (2.711 g, 0.039 mol) in 20 ml of

pyridine under cooling. The reaction mixture was stirred for an additional 2 h at room temperature and concentrated *in vacuo*. The residue was extracted with ethyl acetate and the extract was washed with 10% citric acid and water and dried over magnesium sulfate, and was concentrated *in vacuo*. The oily product obtained was purified by silica-gel column chromatography. Elution was carried out with benzene–ethyl acetate (10:1 v/v) to separate (*E*)-isomer and (*Z*)-isomer. (*E*)-Isomer was purified by thin-layer chromatography using benzene–ethyl acetate (1:1 v/v) as a developing solvent, yield 1058 mg (49.3%), oil, ^{1}H NMR (DMSO-d_6): δ=1.51 (d, 3H), 3.62 (s, 1H), 4.80 (q, 1H), 5.30 (s, 1H), 7.56 (s, 5H). Found: C, 64.60; H, 6.75; N, 8.05%. Calcd for $C_9H_{11}NO_2$: C, 65.43; H, 6.71; N, 8.47%. (*Z*)-Isomer was recrystallized from benzene, yield 441 mg (20.6%), mp 130—131 °C, ^{1}H NMR (DMSO-d_6): δ, 1.32 (d, 3H), 2.50 (s, 1H), 5.00 (s, 1H), 5.28 (q, 1H), 7.92 (m, 5H). Found: C, 65.43; H, 6.71; N, 8.44%. Calcd for $C_9H_{11}NO_2$: C, 65.43; H, 6.71; N, 8.47%.

Assignment of Structure of Two Oximes ((±)-(E)-2-Hydroxy-1-phenyl-1-propanone Oxime and (±)-(Z)-2-Hydroxy-1-phenyl-1-propanone Oxime). Of the two isomers of benzoin oxime, the (*E*)-isomer is known to be colored blue by spraying a 0.5% $CuCl_2$ solution on thin layer chromatography.[9] In the case of 2-hydroxy-1-phenyl-1-propanone oxime, one isomer was colored blue and other isomer was not colored on thin-layer chromatography, therefore the structure of the former isomer was determined as the (*E*)-isomer.

Catalytic Hydrogenation of R(−)-(E)-Benzoin Oxime (5). *R*(−)-(*E*)-Benzoin oxime 5 (20 mg, 8.8×10^{-5} mol) was hydrogenated by using 5% palladium on charcoal (10 mg) in a solvent (2 ml) (methanol, ethanol, 2-propanol and *N,N*-dimethylformamide) at a temperature (0, 20, and 40 °C) at atmospheric pressure. After hydrogenation, the solvent was removed *in vacuo*. The ratio of each diastereomers was determined by gas chromatography of the trifluoroacetyl derivative of the hydrogenated product and the chemical yield was determined by isolation.

Hydrogenations of (±)-(*Z*)-benzoin oxime, (±)-(*E*)-2-hydroxy-1-phenyl-1-propanone oxime and (±)-(*Z*)-2-hydroxy-1-phenyl-1-propanone oxime were carried out in the same way as described above. The results are summarized in Table 1 and 2.

Trifluoroacetylation of Hydrogenated Product. To a suspension of 2 mg of the hydrogenated product in 0.4 ml of ethyl acetate was added 0.2 ml of trifluoroacetic anhydride and the mixture was heated in a screw capped vial for 2 h at 80 °C. The solvent was evaporated *in vacuo* and the residue was extracted with ethyl acetate. The extract was washed with 10% citric acid, saturated $NaHCO_3$ and water and dried over magnesium sulfate, and was concentrated *in vacuo*. The residue was dissolved in ethyl acetate and the solution was injected into a gas chromatograph to determine the ratio of the diastereomers of amino alcohol. A stainless steel column (2 m×3 mm I.D.) filled with Chromosorb W AW DMCS coated with 5% SE-52 was used for determination of diastereomeric ratio of ADE obtained by the hydrogenation of (*E*)- and (*Z*)-benzoin oxime. Column temperature was raised from 100 °C to 180 °C at a rate of 1 °C per minute. The retention times of *erythro*- and *threo*-isomers were 52.6 and 56.2 min, respectively. A glass capillary column (25 m×0.3 mm I.D.) coated with a chiral stationary phase (Chirasil-Val) was used for determination of diastereomeric ratio of 1-amino-1-phenyl-2-propanol obtained by the hydrogenation of (*E*)- and (*Z*)-2-hydroxy-1-phenyl-1-propanone oxime. Column temperature was raised from 100 °C to 180 °C at a rate of 3 °C per minute. The retention times of (1*S*,2*S*)-, (1*R*,2*R*)-, (1*S*,2*R*)- and (1*R*,2*S*)-isomers were 13.12, 13.87, 14.79, and 15.28 min, respectively. The same glass capillary column was used for determination of optical purity of ADE obtained by the hydrogenation of *R*(−)-(*E*)-benzoin oxime. Column temperature was raised from 80 °C to 180 °C at a rate of 0.5 °C per minute. The retention times of (1*S*,2*R*)-, (1*R*,2*S*)-, (1*S*,2*S*)- and (1*R*,2*R*)-isomers were 65.86, 66.16, 66.86 and 67.55 minute, respectively.

Authentic threo and erythro amino alcohols (ADE and 1-amino-1-phenyl-2-propanol) were derivatized with trifluoroacetic anhydride and the products were analyzed by gas chromatography. In each analysis, only original diastereomer was detected. These results indicate that the epimerization during the derivatization would be very small or none.

Isomerization of Benzoin Oxime in the Presence of Palladium on Charcoal. To a solution of (±)-(*E*)-benzoin oxime (30 mg, 1.32×10^{-4} mol) in 3 ml of ethanol was added 5% palladium on charcoal (30 mg). After stirring for a definite time (20, 40, and 60 min and 2, 3, and 6 h) at 30 °C, 0.1 ml of the mixture was collected and filtered. The filtrate was concentrated *in vacuo* and the residue was dissolved in 0.1 ml of pyridine. To the solution was added 0.1 ml of trimethylsilylating reagent [*N,O*-bis(trimethylsilyl)-1-iminoethanol:*N*-trimethylsilylimidazole:trimethylchlorosilane 1:1:1 v/v/v] and the reaction mixture was stirred for 15 min at room temperature and was injected into a gas chromatograph with a stainless steel column (2 m×3 mm I.D.), which was filled with Chromosorb W AW DMCS coated with 5% SE-52, to determine *E–Z* isomeric ratio. Column temperature was 180 °C. The retention times of (*E*)- and (*Z*)-isomers were 14.68 and 17.94 min, respectively. Isomerization of (±)-(*Z*)-benzoin oxime was carried out in the same way as that of (±)-(*E*)-benzoin oxime.

Hydrogenation of (±)-(E)-Benzoin Oxime (Experiment of the Time-course of Reaction Yield). (±)-(*E*)-Benzoin oxime (20 mg, 8.8×10^{-5} mol) was dissolved in 2 ml of ethanol and to the solution was added 10 mg of palladium on charcoal. After stirring for a definite time (30 min, 60 min, 3 h, and 8 h) at 20 °C under hydrogen atmosphere, 0.2 ml of the mixture was collected and filtered. A solution of 1-naphthylamine (internal standard) (2 mg, 1.4×10^{-5} mol) in 0.2 ml of ethanol was added to the filtrate and concentrated *in vacuo*. The residue was trifluoroacetylated in the same way as written above. The ratio of each diastereomers and reaction yield were determined by gas chromatography of the trifluoroacetyl derivative of the hydrogenated product.

Hydrogenation of (±)-(*Z*)-benzoin oxime and analysis of the hydrogenated product were carried out in the same way as those of (±)-(*E*)-benzoin oxime.

Hydrogenation of (±)-(E)-Benzoin Oxime in CD_3OD. (±)-(*E*)-Benzoin oxime (50 mg, 2.3×10^{-4} mol) was dissolved in 5 ml of CD_3OD and the solution was stirred for 1 h at 20 °C. Then to the solution was added 25 mg of 5% palladium on charcoal and the mixture was stirred for 6 h at 20 °C under hydrogen atmosphere. Catalyst was filtered off and the filtrate was concentrated *in vacuo*.

We wish to express our sincere thanks to Dr. Shinya Nomoto for his kind advice and invaluable discussion.

References

1) K. Harada and K. Matsumoto, *J. Org. Chem.*, **32**, 1794 (1967).
2) K. Harada and T. Yoshida, *Bull. Chem. Soc. Jpn.*, **43**, 921 (1970).
3) K. Harada and Y. Kataoka, *Chem. Lett.*, **1978**, 791.
4) K. Harada and M. Tamura, *Bull. Chem. Soc. Jpn.*, **52**, 1227 (1979).
5) M. Osawa, A. Hata, K. Harada, and W. Suetaka, *Bull. Chem. Soc. Jpn.*, **49**, 1512 (1976).
6) J. Weijlard, K. Pfister, E. F. Swanezy, C. A. Robinson,

and M. Tishler, *J. Am. Chem. Soc.*, **73**, 1216 (1951).
7) H. Wren, *J. Chem. Soc.*, **1909**, 1583.
8) J. Kenyon and P. L. Patel, *J. Chem. Soc.*, **1965**, 435.
9) M. H. Jakovljevic, I. P. Tadic, and A. Stojilikovic, *J. Chromatogr.*, **12**, 70 (1963).
10) K. U. Auwers, *Ber.*, **50**, 1177 (1917).

 © 1984 The Chemical Society of Japan Bull. Chem. Soc. Jpn., 57, 1046—1051 (1984) [Vol. 57, No. 4

Effects of Surface Fluorination on Catalytic Activities and Surface Compositions of TiO_2-Al_2O_3 and TiO_2-SiO_2-Al_2O_3

Susumu Okazaki,* Akito Kurosaki, and Shinzo Suzaki
Department of Industrial Chemistry, Faculty of Engineering, Ibaraki University, Nakanarusawa, Hitachi 316
(Received July 30, 1983)

Studies showed that the ternary oxide having the atomic ratio of Ti/Si/Al=47.5/47.5/5 exhibited a high catalytic activity for cumene cracking after a surface fluorination using 1 wt% hydrofluoric acid. The catalytic activity for CH_3OH conversion into olefins was highly dependent on the preparation method. That is, the ternary mixed oxide promoted olefin formation slightly when the mixed oxide was prepared only by coprecipitation. Surface treatment, using gaseous CF_3Cl was effective in enhancing catalytic activity. Although the binary oxide, TiO_2-Al_2O_3, itself, was catalytically inactive for olefin formation, TiO_2-Al_2O_3 prepared by coprecipitation became active after the treatment using CF_3Cl. Such an enhancement was found also for the ternary oxide, TiO_2-SiO_2-Al_2O_3, and is ascribable to increased acid strength, as determined by NH_3 adsorptions at various temperatures. The XPS measurements showed that F atoms introduced into mixed metal oxides by the fluorination using CF_3Cl, selectively combined with Al atoms on the mixed oxides prepared by coprecipitation. The XPS measurements of the mixed oxides before and after fluorination using CF_3Cl showed that the coprecipitation preparation is more preferable than the impregnation method in maintaining surface composition during fluorination.

Recently TiO_2-SiO_2[1] and TiO_2-Al_2O_3[2] have been recognized as fairly strong solid acids, like SiO_2-Al_2O_3. Hence, the formation of relatively strong acid sites in the ternary oxide containing TiO_2, SiO_2, and Al_2O_3 seems promising. Furthermore, since the solid acidities of SiO_2-Al_2O_3[3,4] and TiO_2-SiO_2 are enhanced by a surface fluorination, it may be possible to obtain a stronger solid acid by surface fluorination of TiO_2-Al_2O_3 and TiO_2-SiO_2-Al_2O_3.

Since through mixing of the component oxides is very difficult, especially for the ternary oxide, the preparation method may greatly affect the solid acidity and the catalytic activity. Additionally, the method and conditions of the surface fluorination may also have a considerable effect on them.

In general, surface fluorination has been carried out by using aqueous solutions of HF,[5,6] NH_4F,[7] or NH_4HF_2.[8] Recently, gaseous fluorination using fluorohydrocarbons such as CF_3Cl and CF_2ClCF_2Cl has also been found to be effective to increase solid acidity and catalytic activities for CH_3OH conversion into olefins by Al_2O_3-Cr_2O_3,[9] and for paraffin conversion by Al_2O_3.[10]

In this work, the catalytic activities of TiO_2-Al_2O_3 and TiO_2-SiO_2-Al_2O_3 were studied with an emphasis on the effects of the preparation method and surface fluorination. The surface composition and solid acidity, which are closely related to the catalytic activities, were also examined. For comparison, the effect of surface fluorination on the catalytic activities and the surface compositions of TiO_2, Al_2O_3, SiO_2-Al_2O_3, and SiO_2-TiO_2 were investigated. Cumene cracking was selected because it is a typical reaction catalyzed by solid acids, even relatively weak ones.[11] To elucidate the nature of the strong acid sites, the CH_3OH conversion into olefins was adopted because it has been clearly established that the reaction is promoted only by fairly strong Brönsted acid sites.[12] Finally, the cyclopropane isomerization was carried out to elucidate the acid property of sites on the solid surface.

Experimental

Catalysts. Binary oxides of TiO_2 and Al_2O_3 with various atomic ratios of Ti/Al such as 9/1, 5/5, 1/9 were used as catalysts. For the TiO_2-SiO_2 catalyst, a mixed oxide of an atomic ratio of Ti/Si=1 was used as a representative species, since it has been previously determined that this ratio showed the largest acidity.[5] A typical solid acid catalyst, SiO_2-Al_2O_3 (Nikki Chemical Co. N-631L, Si/Al(atomic ratio)=85/15) was used to evaluate catalytic activities of other oxides by comparison of its catalytic activity. To determine the effect of a small Al component addition to the TiO_2-SiO_2(Ti/Si=1), the catalytic activity of the ternary oxide, TiO_2-SiO_2-Al_2O_3, with the Ti/Si/Al atomic ratio of 47.5/47.5/5 was examined.

For preparations of the single and mixed oxides, titanium tetraisopropoxide, aluminum isopropoxide or nitrate, and ethyl silicate were used as starting materials. The single oxides (TiO_2 and Al_2O_3), and TiO_2-SiO_2 were prepared by addition of aqueous solutions of the respective components to water with vigorous stirring, followed by neutralization with 28% aqueous ammonia. The TiO_2-Al_2O_3(TiO_2-Al_2O_3(Cop)) was prepared by addition of 2-propanol, containing definite amounts of alkoxides of Al and Ti, to dilute nitric acid to prevent the formation of deposits during the addition, and to ensure sufficient mixing of the components. One ternary oxide sample (TiO_2-SiO_2-Al_2O_3(Cop)) was prepared from the solution containing ethyl silicate and alkoxides of Ti and Al using the same procedure as that for the binary oxide, TiO_2-Al_2O_3(Cop).

To examine the effect of the preparation method, the mixed oxides were also prepared by impregnation. For the binary oxide, TiO_2-Al_2O_3(Imp), the impregnation was carried out by addition of TiO_2, which was prepared from alkoxide and heat-treated at 500 °C, to the aqueous solution of aluminum nitrate, followed by evaporation to dryness. For the ternary oxide, TiO_2-SiO_2-Al_2O_3(Imp), the impregnation was done in the same way by addition of TiO_2-SiO_2(Ti/Si=1), prepared by coprecipitation from titanium alkoxide and ethyl silicate, to the solution of aluminum nitrate.

All the single and mixed oxides were dried at 120 °C for 24 h and then heat-treated at 500 °C, unless otherwise noted, for 3 h before their use as a catalyst, or before surface fluorination.

Reagents. The CF_3Cl was supplied by the Mitsui Fluorochemical Co., with purity higher than 99.9%. All other reagents were commercial products of the highest grade, and were used without further purification.

Surface Treatment. The oxide surfaces were treated with hydrofluoric acid of different concentrations(0.05—10 wt%), or gaseous CF_3Cl. The treatment with the acid was

carried out by immersing the oxides (*ca.* 10 g) in a solution (*ca.* 30 ml) at room temperature for 48 h, followed by evaporation to dryness at 120 °C and heat-treatment at 500 °C for 3 h. The treatment with CF_3Cl was carried out in a reactor at 450 °C immediately before use as catalyst.

Reaction Procedure. The cyclopropane isomerization and the CH_3OH conversion into olefins (abbreviated as MTG) were carried out in a pulse reactor using He as a diluent at 150 or 250 °C, and 400 °C, respectively. The pulse size was about 1.0 μl (for CH_3OH) or 1.1 μl (for cyclopropane), and the weight of catalyst was kept constant at 30 mg (MTG) or 50 mg (cyclopropane isomerization).

The product gas of the cyclopropane isomerization was analyzed by gas chromatography using a column packed with Porapack N at 100 °C. For MTG, the pulse reactor was connected with a modified gas-chromatographic analyzer. The product gas of the MTG, including CO and CH_4, was first condensed at about −196 °C in a 3 m column packed with Tenax GC. Then the condensed products were allowed to evaporate by removal of the liquid nitrogen trap, followed by heat-treatment up to 150 °C. The evaporated gas was passed through TCD, and the composition of the product was analyzed.

The cumene cracking was carried out under ordinary pressure using a conventional flow reactor. The products were analyzed by gas chromatography using a column packed with DC 550 supported on Chromosorb (15 wt%).

Determinations of Surface Properties. Surface areas were determined by applying the BET equation for the adsorption isotherm of N_2 at −196 °C. Surface acidities were measured by the amounts of NH_3 adsorbed at different temperatures. The Brönsted and Lewis acidity was examined by observing the infrared absorption spectra of pyridine adsorbed on oxide samples which were fabricated into discs under a pressure of *ca.* 500 kg cm^{-2}.

Determinations of Surface Composition and Bonding. The compositions in the surface layer were determined by XPS, using a Shimadzu ESCA-750 analyzer. In this determination, the spectra were measured with Mg $K\alpha$ radiation; the base pressure of the spectrometer was usually below 10^{-7} Torr (1 Torr≈133.322 Pa) during the experiments. The peak positions, given by their maxima, were measured with respect to the position of C1s, for which the value of the binding energy was taken as 285 ev. The surface compositions were calculated from the area of the respective peaks (*i.e.*, the maxima in the counting rate) on the basis of photoionization cross sections at 1254 ev, in units of the C1s cross section of 22200 barns.[13] The errors inherent in such a determination are generally 10—30% of the observed value.

Results and Discussion

Catalytic Activities for Cumene Cracking before and after Fluorination Using Hydrofluoric Acid. Similar to TiO_2 and Al_2O_3, the mixed oxides with various Ti/Al atomic ratios, which were prepared from Al$(NO_3)_3$ and titanium tetraisopropoxide by coprecipitation, showed little catalytic activity before fluorination. After fluorination using 1 wt% hydrofluoric acid, only TiO_2-Al_2O_3(Ti/Al=9/1) showed a rather high catalytic activity; the concentration of hydrofluoric acid was found to be optimum at 1 wt% for enhancement of the catalytic activity. However, even the catalytic activity of the TiO_2-Al_2O_3 treated with the hydrofluoric acid at this optimum concentration (1 wt%) was less than that of the component oxide, TiO_2, fluorinated with 1 wt% hydrofluoric acid. Furthermore, the catalytic activity of the fluorinated TiO_2-Al_2O_3(Ti/Al=9/1) was far less than that of the fluorinated TiO_2-SiO_2(Ti/Si=1).[5]

Since cumene cracking can be promoted even by relatively weak Brönsted acid sites,[11] the catalytic activity for cumene cracking may be the measure of the total amount of Brönsted acid sites, including weak ones. Thus, the result indicates that the amount of total Brönsted acid sites formed on TiO_2-Al_2O_3 after fluorination may be less than that on the fluorinated TiO_2 or fluorinated TiO_2-SiO_2.

A catalyst which was more active than the fluorinated TiO_2 or fluorinated TiO_2-SiO_2 was obtained by addition of relatively small amounts of Al_2O_3 to TiO_2-SiO_2. Thus, TiO_2-SiO_2-Al_2O_3(Cop) which contained 5 atom% of Al showed higher initial catalytic activity than that of the fluorinated TiO_2 or fluorinated TiO_2-SiO_2 even before fluorination (Fig. 1). The catalytic activity of the ternary oxide was also higher than that of SiO_2-Al_2O_3 as is shown in Fig. 1. Hence, the higher catalytic activity of the ternary oxide(Cop) may be due to the coexistence of the three components(Ti, Si, and Al) itself. With surface fluorination of the ternary oxide (47.5/47.5/5)(Cop) using 1wt% hydrofluoric acid, both the initial catalytic activity and the activity maintenance were considerably increased. On the other hand, initial catalytic activity of the ternary oxide with the same atomic ratio, prepared by impregnation was noticeably lower than that of the ternary oxide(Cop). Furthermore, the activity of the fluorinated ternary oxide(Imp) decreased significantly with process time (Fig. 1); this evidence indicates the large effect of the preparation method on the catalytic activity of the mixed oxide.

Catalytic Activity for CH_3OH Conversion. Table 1 shows the catalytic activity for the MTG by various oxides, before and after fluorination. Before fluorination, ternary oxide(Cop) promoted the formation of a small amount of propene, although ternary oxide (Imp) promoted only the formation of dimethyl ether, which can be activated even by relatively weak acid

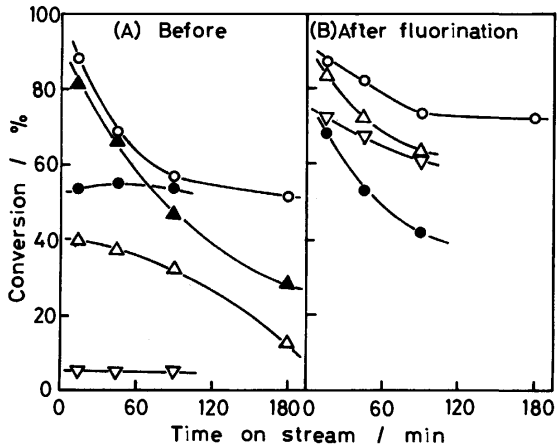

Fig. 1. Catalytic activities for cumene cracking of metal oxides before and after fluorination.
○: TiO_2-SiO_2-Al_2O_3(47.5/47.5/5)(Cop); ●: TiO_2-SiO_2-Al_2O_3(47.5/47.5/5)(Imp); △: TiO_2-SiO_2(1/1)-(Cop); ▲: SiO_2-Al_2O_3(85/15)(N-631L); ▽: TiO_2.
Reaction temperature; 350°C, W/F: 51.6 g h mol^{-1}.

Table 1. Catalytic activities of metal oxides for CH_3OH conversion

Catalyst[a]	Yield/mol%[b]					
	CO	CH_4	$CH_2=CH_2$	$CH_3CH=CH_2$	Butene	CH_3OCH_3
TiO_2-SiO_2-Al_2O_3 (Cop)						
Before fluorination	0	13.6	Trace	3.3	0	48.8
Treated with CF_3Cl	0	13.4	2.2	18.4	0.4	38.9
Treated with HF acid	0	33.6	4.3	0	0	58.8
TiO_2-SiO_2-Al_2O_3 (Imp)[c]						
treated with CF_3Cl	0	8.3	2.8	0	0.8	88.0
TiO_2-Al_2O_3 (Ti/Al=9/1)						
treated with CF_3Cl	5.2	19.0	21.4	5.2	0	42.9
SiO_2-Al_2O_3						
Before fluorination	0	0	Trace	Trace	0	76.1
Treated with CF_3Cl	0	0	5.1	11.4	0	66.8
TiO_2-SiO_2 (Ti/Si=1)						
Before fluorination	6.3	36.1	0	0	0	52.3
Treated with CF_3Cl	0	13.9	1.4	0	2.1	80.4
Al_2O_3 treated with CF_3Cl	0	0	3.6	7.9	Trace	55.4
TiO_2 treated with CF_3Cl	0	6.8	Trace	0	Trace	0

a) TiO_2 and Al_2O_3 were heat-treated at 600 °C (and the others at 500 °C) for 3 h before use as catalyst. b) These data were measured for the third pulse. c) Untreated TiO_2-SiO_2-Al_2O_3 showed little catalytic activity for CH_3OH conversion.

sites.[12] After fluorination, all oxides, except TiO_2, exhibited some degree of catalytic activity. In particular, mixed oxides containing Al and prepared by coprecipitation, such as TiO_2-Al_2O_3(Cop) and TiO_2-SiO_2-Al_2O_3(Cop), showed high activity after fluorination using CF_3Cl. The ternary oxide fluorinated with hydrofluoric acid, however, was significantly less active. Since MTG is known to be promoted only by strong acid sites,[12] these facts suggest that fluorination using CF_3Cl may be effective, but that using hydrofluoric acid is almost completely ineffective in the formation of strong acid sites.

Although TiO_2 was markedly active as a catalyst for cumene cracking after fluorination using hydrofluoric acid, it was quite inactive for the MTG after fluorination using the acid or CF_3Cl. This is plausibly ascribable to the low acid strength of the sites formed on TiO_2 by treatment with hydrofluoric acid, even though the number of these relatively weak acid sites might be fairly large.

TiO_2 fluorinated using CF_3Cl could not promote even the formation of dimethyl ether, in contrast the fluorinated Al_2O_3 appreciably increased formation of olefins besides dimethyl ether. Thus, the Al component seems important for the formation of acid sites strong enough to promote the MTG.

Acid Properties of Mixed Oxides. Infrared studies of the adsorption of pyridine were performed on TiO_2-Al_2O_3(9/1) (Cop) and TiO_2-SiO_2-Al_2O_3(47.5/47.5/5) (Cop) or (Imp) to know about the acid properties. After evacuation at 300 °C for 2 h, the sample was left in contact with 5 Torr of pyridine at room temperature for 0.5 h, and then further evacuated at 170 °C for 1 h.

TiO_2-Al_2O_3(9/1): This mixed oxide gave only bands at about 1600, 1580, 1490, and 1440 cm^{-1} which were all attributable to pyridine on Lewis acid sites.[14]

Table 2. Catalytic activities for cyclopropane isomerization

Catalyst	Reaction temperature	Conversion[a]
	°C	%
TiO_2-Al_2O_3 (Ti/Al=9/1)		
Before fluorination	150	1.0
	250	15.5
	150	19.2
Fluorinated with 1 wt% HF acid	250	93.0

a) The conversion was calculated from the result of the first pulse (for 150 °C reaction) or the third pulse (for 250 °C reaction).

Although the band at 1540 cm^{-1} due to pyridinium ion[14] was scarcely observable for the evacuated samples before and after fluorination, it became clearer after sample contact with H_2O vapor(5 Torr) for 1 min. Together with the band at about 1640 cm^{-1}, these bands indicate that Brönsted acid sites were abundantly formed on the fluorinated mixed oxide by interaction of H_2O with the surface.

The catalytic activities of mixed oxides for cyclopropane isomerization (150 and 250 °C), which is promoted not by Lewis, but by Brönsted acid sites,[15] were remarkably increased by surface fluorination, as is shown in Table 2. This fact further verified the formation of Brönsted acid sites after surface fluorination.

TiO_2-SiO_2-Al_2O_3(47.5/47.5/5): Like the spectrum for TiO_2-Al_2O_3 described above, that obtained for the ternary oxide prepared by impregnation showed the presence of only Lewis acid sites. After surface fluorination using hydrofluoric acid, a weak band specific to pyridinium ion appeared at 1540^{-1}.

On the other hand, the spectrum for the ternary oxide prepared by coprecipitation showed the bands at 1550 and 1640^{-1} due to Brönsted acid sites in addition to those due to Lewis acid sites, even before surface fluorination. The formation of the Brönsted acid sites on the unfluorinated ternary oxide may have resulted from sufficient mixing of the component metal atoms (or ions); the Brönsted acid sites may function as active sites not only for the cumene cracking but also for MTG.

NH_3 Adsorption: In order to know the strengths and numbers of acid sites, adsorption of NH_3 on various oxides, including SiO_2-Al_2O_3, was carried out at temperatures from 100 °C to 500 °C.

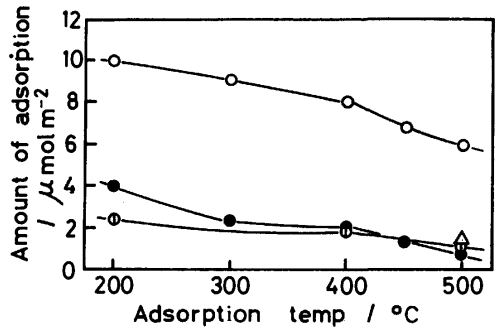

Fig. 2. NH_3 adsorptions at various temperatures.
●: TiO_2-SiO_2-Al_2O_3(47.5/47.5/5)(Cop); before treatment; ○: TiO_2-SiO_2-Al_2O_3(47.5/47.5/5)(Cop) treated with CF_3Cl; △: TiO_2-SiO_2-Al_2O_3(47.5/47.5/5)-(Cop) treated with 1 wt% hydrofluoric acid; ○: SiO_2-Al_2O_3(85/15)(N-631L).

As is shown in Fig. 2, the ternary oxide prepared by coprecipitation showed a notably high adsorptive activity for NH_3 after the surface fluorination using CF_3Cl. In particular, the amount of adsorption on the fluorinated ternary oxide at 500 °C was about 6 times that of the typical strong solid acid catalyst, SiO_2-Al_2O_3, and was higher than Al_2O_3-Cr_2O_3 fluorinated with CF_3Cl, which has been reported to be a strong acid catalyst for MTG.[9] The amount of adsorption at 500 °C on the ternary oxide(Cop), fluorinated using hydrofluoric acid, was only about the same as that on SiO_2-Al_2O_3. These facts support the suggestions that remarkably strong acid sites may be formed on the ternary oxide(Cop) treated with CF_3Cl, and that surface fluorination using CF_3Cl is far more effective in strengthening solid acidity than that using hydrofluoric acid.

Surface Compositions. Table 3 shows the surface compositions which were examined by recording the XPS spectra. As the results show, the surface composition generally differs from the designed one to a considerable extent. In particular, the Al component tends to concentrate in the surface layer, even for mixed oxides prepared by coprecipitation. Such a tendency has also been observed for the binary oxides, TiO_2-Al_2O_3, which is coprecipitated from the solution containing equimolar aluminum nitrate and

Table 3. Surface composition of various oxides

Oxide	surface composition/atom%[a]					
	O	F	Cl	Ti	Si	Al
Before fluorination						
TiO_2	74.1			25.9		
Al_2O_3	65.5					34.5
TiO_2-Al_2O_3	72.0			20.1		7.9
(9/1, Cop)				(7.2)		(2.8)
TiO_2-SiO_2	77.8			15.8	4.4	
(9/1, Cop)				(7.8)	(2.2)	
SiO_2-Al_2O_3	67.4				28.4	4.2
(8.5/1.5)					(8.7)	(1.3)
TiO_2-SiO_2-Al_2O_3	70.6			8.6	16.8	4.0
(47.5/47.5/5, Cop)				(2.9)	(5.7)	(1.4)
TiO_2-SiO_2-Al_2O_3	77.0			10.1	8.4	4.5
(47.5/47.5/5, Imp)				(4.4)	(3.6)	(2.0)
After fluorination						
TiO_2	67.5	8.4	1.4	22.7		
Al_2O_3	35.4	37.5	0			27.1
TiO_2-Al_2O_3	22.0	56.7	0	6.2		15.1
(9/1, Cop)				(2.9)		(7.1)
TiO_2-SiO_2	59.8	11.5	1.5	27.2	Trace	
(9/1, Cop)				(10.0)		
SiO_2-Al_2O_3	50.9	19.3	0		24.8	5.0
(8.5/1.5)					(8.3)	(1.7)
TiO_2-SiO_2-Al_2O_3	64.7	5.2	0	8.1	17.2	4.8
(47.5/47.5/5, Cop)				(2.7)	(5.7)	(1.6)
TiO_2-SiO_2-Al_2O_3	60.5	11.7	0	6.6	12.4	8.8
(47.5/47.5/5, Cop)				(2.3)	(4.5)	(3.2)
(HF-treated)						
TiO_2-SiO_2-Al_2O_3	61.8	20.5	0	17.7	Trace	Trace
(47.5/47.5/5, Imp)				(10.0)		

a) The numbers in parentheses indidate the atomic ratio of Ti, Si, and Al components.

ethyl silicate.[16] The higher concentration of Al component in the surface layer may possibly be due to a difference in the pH value for the precipitation as hydroxides. That is, for the precipitation of Al^{3+} as $Al(OH)_3$, the solution must be more alkaline than for Ti^{4+} and Si^{4+}; thus Al^{3+} tends to deposit as a hydroxide on the surface of the hydroxides of Ti and Si, which have already formed in the neutralization using aqueous ammonia.

Although the Al content in the surface layer of the fresh ternary oxide(Cop) is less than that in the fresh ternary oxide(Imp), the difference is relatively small. However, for the samples fluorinated with CF_3Cl, the surface composition greatly differs depending on the preparation methods. That is, during fluorination, the Al and Si components in the ternary oxide prepared by impregnation were lost largely from the surface layer, resulting in a remarkable increase of Ti content in the surface layer. On the other hand, the surface composition of the ternary oxide prepared by coprecipitation was scarcely changed by surface fluorination.

Similarly, the surface composition of SiO_2-Al_2O_3 was not appreciably changed by surface fluorination using CF_3Cl; The Si component in TiO_2-SiO_2 was lost mostly during the surface fluorination. Nevertheless, the mixed oxides were prepared by coprecipitation.

These results suggest that Al atoms may firmly combine with F atoms, especially in preference to Si atoms, and thus prevent the formation of volatile SiF_4. However, such Al atom behavior may be displayed only when the Al atoms are sufficiently close to Si atoms, so that the effect of Al component on the retention of Si component was fully exhibited in the mixed oxide prepared by coprecipitation.

Bonding in Surface Layer. Figures 3 and 4 give the detailed F1s and O1s peaks of various oxides.

F1s Peaks: The peaks due to F1s in the spectra for SiO_2-Al_2O_3, TiO_2-Al_2O_3(Cop), and the ternary oxide (Cop) were found only at 687.9, 686.9, and 687.4 eV, respectively, after fluorination using CF_3Cl. Since the peak positions are all close to that for AlF_3(687.3 eV) or Al_2O_3 fluorinated using CF_3Cl(687.4 eV), this indicates that F atoms introduced by the fluorination are selectively bound to the Al atoms in the mixed oxides.

The binding energies of the F1s peaks in the fluorinated ternary oxide(Imp) are found at 684.9 and 688.5 eV. Since the binding energy in TiO_2 fluorinated using CF_3Cl is found at 684.5 eV, the stronger peak at 684.9 eV is assignable to the F atom bound to a Ti atom in the ternary oxide(Imp), Observation of the peak due to Ti-F bonding on the surface of the ternary oxide prepared by impregnation may result from the removal of a larger amount of Al atoms as volatile aluminum chloride.

O1s Peaks: The spectrum for O1s of the fresh ternary oxide(Imp) gave two peaks, their maxima being observed at 530.3 and 532.7—533.0 eV. The former peak at 530.3 eV almost coincided with that due to TiO_2 or TiO_2-Al_2O_3, while the latter peak coincided

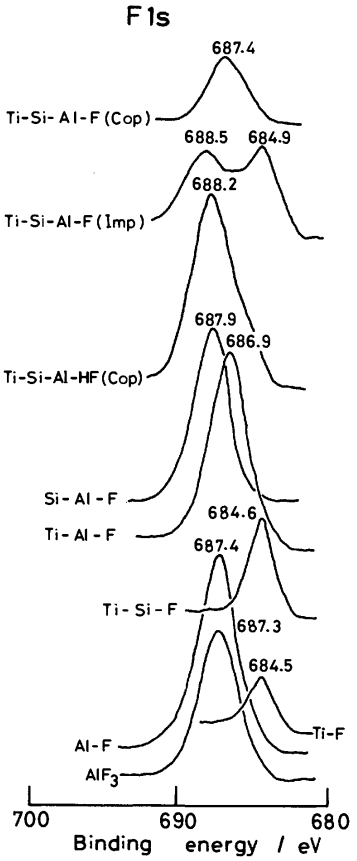

Fig. 3. XPS spectra of F1s.
Ti, Si, and Al indicate the samples of TiO_2, SiO_2 and Al_2O_3, respectively, and "-F" indicates the samples treated with CF_3Cl.

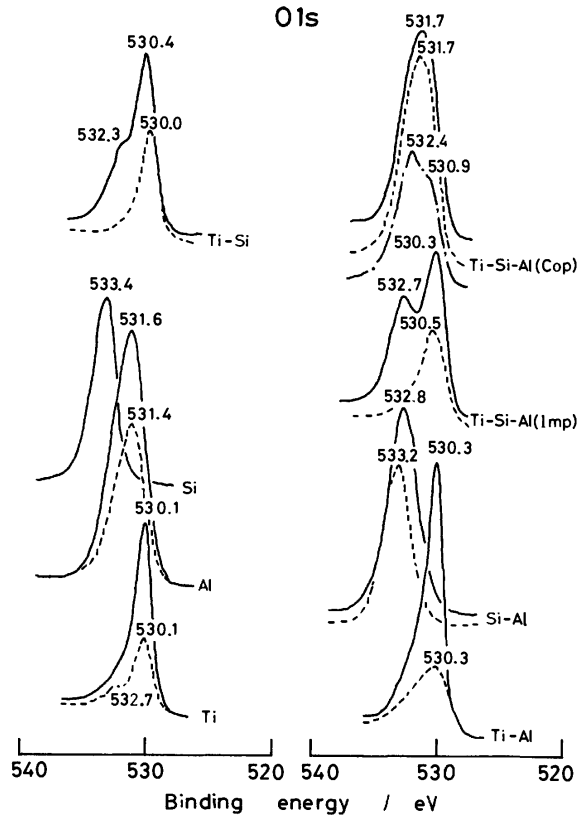

Fig. 4. XPS spectra of O1s.
Full lines and broken lines indicate the spectra for fresh oxides and treated oxides, respectively.

with that due to SiO_2 or SiO_2-Al_2O_3.

After fluorination using CF_3Cl, the ternary oxide(Imp) gave only one peak at 530.5 eV, that position almost coinciding with one obtained for fresh ternary oxide(Imp) at 530.3 eV. Furthermore, this peak position is close to that obtained for fluorinated TiO_2-(530.1 eV). Hence, the peak at 530.0 eV is assignable to the O atom bound to a Ti atom; the absence of other peaks except that 530.5 eV is compatible with the previous assumption that the surface layer of the fluorinated ternary oxide(Imp) is composed mainly of fluorinated titanium oxide.

On the other hand, for the ternary oxide(Cop), only one broad peak was given at around 531.7 eV. The peak position and shape of the peak were not changed by surface fluorination using CF_3Cl. Namely, the concentration of Ti component by the fluorination with CF_3Cl appeared improbable for the mixed oxide prepared by coprecipitation.

Thus, the preparation of the ternary oxide by coprecipitation was essential for maintaining the homogeneity in the surface compositions. The fluorination of the homogeneous surface using, not hydrofluoric acid, but gaseous CF_3Cl was remarkably effective for the formation of strong acid sites on the mixed oxide surface.

The authors wish to express their thanks to the Mitsui Fluorochemical Co., for their financial support of this study.

References

1) Y. Watanabe and N. Nojiri, *Nippon Kagaku Kaishi*, **1974**, 540.
2) R. Rodenas, T. Yamaguchi, H. Hattori, and K. Tanabe, *J. Catal.*, **69**, 434 (1981).
3) M. F. L. Johnson and J. S. Melik, *J. Phys. Chem.*, **65**, 1146 (1961).
4) C. J. Plank, D. J. Sibbett, and R. B. Smith, *Ind. Eng. Chem.*, **49**, 742 (1957).
5) S. Suzaki and S. Okazaki, *Nippon Kagaku Kaishi*, **1981**, 330; S. Okazaki, The Second Regular Meeting of Soviet-Japanese Fluorine Chemists, Moscow, June 1981, Abst., p. 109.
6) A. N. Webb, *Ind. Eng. Chem.*, **49**, 261 (1957).
7) H. J. Reitsman and C. Boelhouwer, *J. Catal.*, **33**, 39 (1974); P. O. Sochart, S. A. Selin, J. E. Damon, and P. G. Rouxhet, *J. Colloid Interface Sci.*, **70**, 209 (1979).
8) V. C. F. Holm and A. Clark, *Ind. Eng. Chem., Prod. Res. Dev.*, **2**, 38 (1963).
9) A. Kurosaki and S. Okazaki, *Bull. Chem. Soc. Jpn.*, **56**, 1279 (1983).
10) A. Kurosaki and S. Okazaki, 50th Conference for Catalysis and Catalyst, Niigata, October 1982, Abstr., $3G_205$.
11) H. A. Benesi, *J. Catal.*, **8**, 368 (1967).
12) Y. Ono, *Petrotech* **3**, 1039 (1980).
13) J. H. Scofield, *J. Electron Spectros. Relat. Phenom.*, **8**, 129 (1976).
14) E. P. Parry, *J. Catal.*, **2**, 371 (1963).
15) L. Jacob and W. K. Hall, *J. Colloid Interface Sci.*, **58**, 76 (1977).
16) N. Yamagata, I. Yoneshima, H. Hattori, and K. Tanabe, *Shokubai*, **22**, 28 (1980).

A DNMR Study of Restricted Methylene Rotation in 2-Pyridylmethyl- and 3-Methyl-2-pyridylmethyllithium

Hideki MATSUI, Akihiro YOSHINO, Tadayoshi YOSHIDA, and Kensuke TAKAHASHI*
Department of Industrial Chemistry, Nagoya Institute of Technology, Gokiso-cho, Showa-ku, Nagoya 466
(Received September 2, 1983)

Thermodynamical parameters for the restricted rotation of the title carbanions have been obtained by means of the DNMR techniques. The activation energies and entropies thus obtained are about 93 kJ mol^{-1} and 95 J K^{-1} mol^{-1} for the two carbanions studied; these values are larger than those of the similar rotations observed in arylmethanide ions. The methylene rotation is thus extremely hindered in these carbanions.

Rotational barriers about bonds with partial double-bond character have been studied extensively by means of the DNMR techniques. Especially, a lot of interesting information on rotation about the N-C bonds in amides has been obtained so far.[1] These techniques have also been applied to the hindered rotations in cations and anions with large conjugated π-systems. The barriers and the mechanism of rotation of phenyl groups in the arylmethanide-ion systems have been reported.[2-5] 2-Pyridylmethanide ions discussed in this study are one of the systems similar to the phenylmethanide ion, which is the simplest one among the arylmethanide ions. A hindered rotation about the bond between the methylene group and the pyridine ring has been previously noted.[6] The aim of this study is to obtain temperature-dependent NMR spectra of the two title carbanions (hereafter referred as **1** and **2**, as shown in Fig. 1) and to evaluate the barriers for the rotation about the bond between the pyridine ring and the α-carbon by means of the DNMR techniques.

Experimental

All reagents used were commercially available. Precursors (2-picoline and 2,3-lutidine) were dried with calcium hydride and distilled in a vacuum and then divided to a suitable amount in several Pyrex ampoules with breakable seals. Butyllithium in hexane was also ampouled with the same manner in a vacuum after filtering to remove small suspended solid particles. Precursors were reacted in vacuum with butyllithium in a small reaction vessel with a 5-mm o.d. NMR tube. About two hours after the reaction started, hexane was distilled off and *ca.* 0.35 ml of dried THF-d_8 was introduced into the system. The prepared THF-d_8 solution of the carbanion was transferred into an NMR tube, a small amount of TMS was added, and the tube was sealed off. The concentration of the sample was about 1.3 mol dm^{-3}, on the basis of the precursor used. The ^{1}H NMR spectra were recorded at a sweep time of 200 s and with a sweep width of 120 or 300 Hz, with a Hitachi R-20B spectrometer at 60 MHz equipped with a R-202VTC temperature controller. The temperature was calibrated with temperature-dependent chemical shifts of methanol (low-temperature range) or ethylene glycol (high-temperature range) using the standard equation. Theoretical DNMR spectra were calculated by a modified Quabex program[7] with a Hitachi M-170 computer and plotted with an on-line XY-plotter.

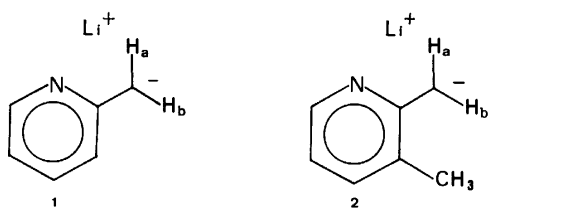

1 2-Pyridylmethyllithium 2 3-Methyl-2-Pyridylmethyllithium

Fig. 1. Numberings of the carbanions studied.

Results and Discussion

A typical ^{1}H NMR spectrum of the carbanion studied is given in Fig. 2. The first-order NMR parameters thus determined are given in Table 1. The parameters are almost consistent with those previously re-

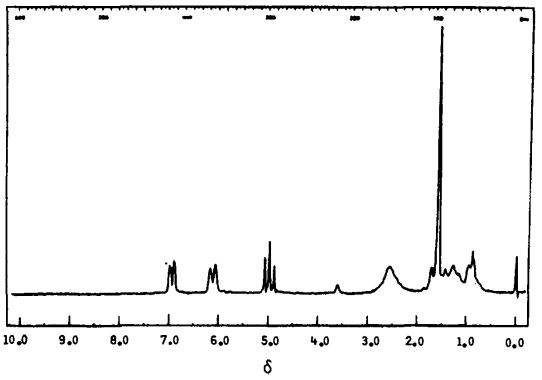

Fig. 2. ^{1}H NMR spectrum of 3-methyl-2-pyridylmethyllithium (**2**) dissolved in THF-d_8 at 60 MHz and 304.8 K. The peaks at 0.5—1.7 ppm may be due to residual butyllithium.

TABLE 1. ^{1}H NMR DATA OF 2-PYRIDYLMETHYL-(**1**) AND 3-METHYL-2-PYRIDYLMETHYLLITHIUM (**2**) IN THF-d_8 AT 304.7 K AND 60 MHz[a]

Compound	1	2
δ(2)	2.49(2.39 and 2.54 at 243.2 K)	2.59 (2.22 and 2.77 at 253.2 K)
δ(3)	5.62	1.58 (CH_3)
δ(4)	6.04	6.11
δ(5)	4.82	4.99
δ(6)	6.86	6.95
J(ab)	2.20	1.40
J(34)	9.09	—
J(35)	1.35	—
J(36)	0.96	—
J(45)	6.20	6.16
J(46)	1.97	1.60
J(56)	5.44	5.48

a) The δ values are given in ppm, referred to the internal TMS, and the J values are in Hz.

ported.[6] The DNMR analyses were carried out to the spectra of the methylene proton signals. The analyses were performed as an AB system although there is a small coupling between a methylene proton and a ring proton, as stated before.[6] The analyses need a parameter concerned with the line widths. This is determined by visual fittings of the calculated and observed spectra at both the slow- and fast-exchange limits. Two limiting T_2^* values thus determined were the same for **1** but were different for **2**. For the latter case, the T_2^* value was linearly correlated with the temperature studied. The parameters used for the DNMR analyses are given in Table 2. The chemical shift between two methylene protons of **1** was also linearly correlated with the temperature. But the value for **2** was kept constant because of the line-shape-fitting consideration. The kinetic parameters have been determined by visual fittings of the calculated lineshapes with the experimental ones. Several typical DNMR spectra are given in Fig. 3. The rate constants thus determined are given in Table 3. The thermodynamic parameters were obtained by the Eyring and Arrhenius plottings of the rate constants with inverse temperatures, one of which is shown in Fig. 4. The parameters thus determined are given in Table 4.

The hindered rotations of several substituted phenylmethanide ions have rates within the NMR-time scale and have been studied many researchers.[2,3,8-12] As compared with the values previously studied, the values obtained in this study are characteristic from

Table 2. Parameters used for the DNMR analyses of the methylene protons of 2-pyridylmethyl- (**1**) and 3-methyl-2-pyridylmethyllithium (**2**)

Compound	1	2
δ(ab)/Hz	9.50+0.040t[a]	33.2
J(ab)/Hz	2.2	1.4
T_2^*/s	0.25	0.202+0.00012t

a) The values are dependent upon the temperatures studied, which are expressed as t given in °C.

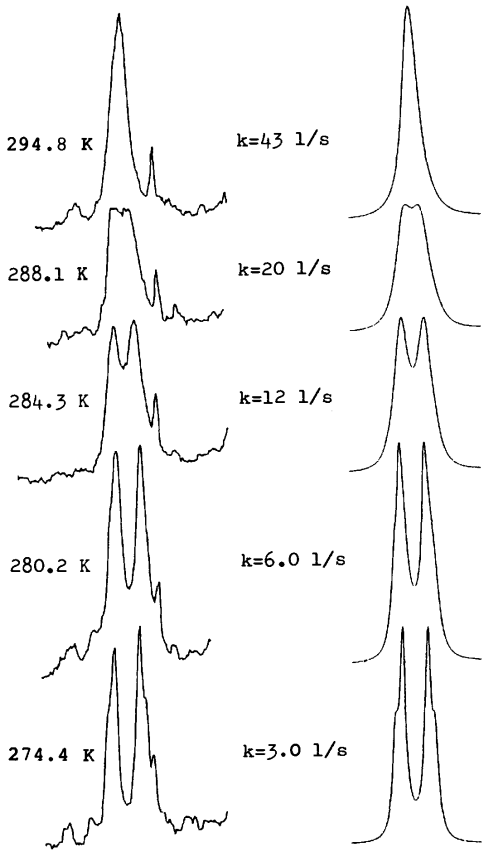

Fig. 3. Observed (left) and calculated (right) ^{1}H NMR spectra of the methylene hydrogens of 2-pyridylmethyllithium (**1**) in THF-d_8 at different temperatures and 60 MHz. An unknown peak is appeared in each oberved spectra.

Table 3. Rate constants (k) of the hindered rotation of the methylene groups in 2-pyridylmethyl- (**1**) and 3-methyl-2-pyridylmethyllithium (**2**)

1		2	
Temp/K	k/s^{-1}	Temp/K	k/s^{-1}
294.8	43±1.0	325.9	1500±100
288.1	20±1.0	314.4	470±10
284.3	12±1.0	304.8	150±10
280.2	6.0±0.1	302.8	69±1.0
274.4	3.0±0.1	298.5	37±1.0
269.4	1.1±0.1	294.8	25±1.0
263.3	0.5±0.1	288.1	12±1.0
		284.3	6.9±0.1
		274.4	1.8±0.1
		263.3	0.5±0.1

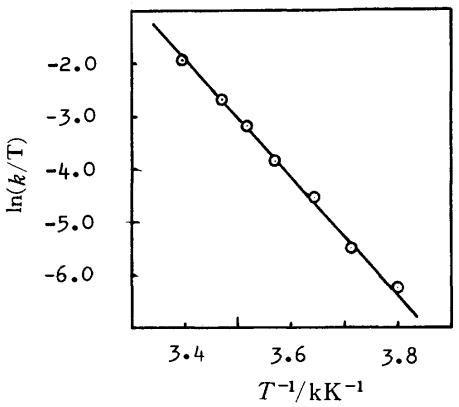

Fig. 4. An Eyring plot for the methylene rotation of 2-pyridylmethyllithium (**1**) in THF-d_8.

Table 4. Thermodynamic parameters for the hindered rotation of the methylene groups of 2-pyridylmethyl- (**1**) and 3-methyl-2-pyridylmethyllithium (**2**) in THF-d_8

Carbanion	E_a / kJ mol^{-1}	ln A	$\Delta H^{\#}$ / kJ mol^{-1}	$\Delta S^{\#}$ / J K^{-1} mol^{-1}
1	93.4±2.3	41.9±1.0	91.0±2.3	95.8±8.4
2	93.5±3.7	41.6±1.5	91.1±3.6	93.1±12.4

TABLE 5. ^{13}C NMR DATA OF 2-PYRIDYLMETHYL- (**1**) AND 3-METHYL-2-PYRIDYLMETHYLLITHIUM (**2**) IN THF-d_8 AT 298 K AND 50.3 MHz[a)]

Compound	1	2
$\delta(2)$	164.07	163.13
$\delta(3)$	115.80(157.5)[b)]	119.23
$\delta(4)$	131.27(149.5)	130.49(150)
$\delta(5)$	96.69(162)	97.22(161)
$\delta(6)$	148.55(163.5)	146.34(163.5)
$\delta(CH_2)$	57.20(150)	55.63(150)
$\delta(CH_3)$	—	20.73(124.5)

a) The δ values are given in ppm, referred to the internal TMS. b) The values in parentheses are the one-bond coupling constants between carbon and proton given in Hz.

two view points, as follows. (1) The activation energies of the 2-pyridylmethanide ions observed are larger than those observed in the similar systems. This means that the methylene rotation is extremely hindered in the carbanions studied. (2) The activation entropies are large and positive.

Generally speaking, the barrier of the hindered rotation of the aryl group in various arylmethanide ions is related to both the extent of delocalization of the electronic charge from the α-carbon to the aryl ring and the ionic nature of the carbon-metal bond.

The hindered rotations of the lithium salts have rates within the NMR-time scale for several arylmethanide ions. But for the other salts, such as the potassium and cesium ones, the barriers are too high to be studied by the DNMR techniques.[2,9,11] The reason may be the covalent nature of the carbon-metal bond. The nature of the carbon-metal bond is related to the hybridization of the α-carbon, which is reflected by the one-bond carbon-proton coupling constants. The observed ^{13}C NMR data are given in Table 5. The $^1J(CH)$ values of **1** and **2** are about 150 Hz, which are much larger than that of phenylmethyllithium (133 Hz).[13] The observed $^1J(CH)$ of the α-carbons are almost the same with those of the C_4. This shows that the α-carbons have the high sp^2-hybridized nature which is in favor with the delocalization of the extra-electronic charge from the α-carbon to the ring. And this results in a high barrier in the carbanions. This tendency is also strengthened by the nitrogen atom in the ring, whose electron-attracting nature is profitable for the charge migration from the α-carbon to the ring.

The coalescene temperatures of the two carbanions (**1** and **2**) are about 288 and 303 K. Although they are different for the two, the activation parameters are almost the same. Therefore, the introduction of the methyl group is apparently not effective for the rotation of the methylene group. This is a peculiar and unexpected result. Because some appreciable effects of the alkyl qroups were reported by Fraenkel *et al.* and Bushweller *et al.*,[2,4] it might be expected that the introduction of a methyl group at the 3-position would cause a decrease of the rotation barrier of the bond in both the electronic and steric senses. Our experimental results are thus unexpected. Therefore, it must be noted that the 3-positioned methyl group does not interfere the methylene rotation of the carbanions studied.

The observed activation entropies of the 2-pyridylmethanide ions are large and positive. This large entropy increase would be caused by the different solvations around the lithium atom accompanied with the change of the carbanions from the ground planar structure to an excited twisted one. This explanation needs more knowledge about the solvation change of the counter cation. Therefore, it is not clear at present.

References

1) "Dynamic Nuclear Magnetic Resoance Spectroscopy," ed by L. M. Jackman and F. A. Cotton, Academic Press, New York (1975).
2) G. Fraenkel, J. G. Russell, and Y.-H. Chen, *J. Am. Chem. Soc.*, **95**, 3208 (1973).
3) G. Fraenkel and M. Geckle, *J. Am. Chem. Soc.*, **102**, 2869 (1980).
4) C. H. Bushweller, J. S. Sturges, M. Cipullo, S. Hoogasian, M. W. Gabriel, and S. Bank, *Tetrahedron Lett.*, **1978**, 1359.
5) G. A. Olah and M. I. Watkins, *Proc. Natl. Acad. Sci. U.S.A.*, **77**, 703 (1980).
6) K. Takahashi, K. Konishi, M. Ushio, M. Takaki, and R. Asami, *J. Organomet. Chem.*, **50**, 1 (1973).
7) G. Binsch, *Topics in Streochem.*, **3**, 97 (1968).
8) V. R. Sandel, S. V. McKinley, and H. H. Freedman, *J. Am. Chem. Soc.*, **90**, 495 (1968).
9) S. Brownstein and D. J. Worsfold, *Can. J. Chem.*, **49**,1350 (1971).
10) F. J. Kronzer and V. R. Sandel, *J. Am. Chem. Soc.*, **94**, 5750 (1972).
11) K. Matsuzaki, Y. Shinohara, and T. Kanai, *Makromol. Chem.*, **181**, 1923 (1980); **182**, 1533 (1981).
12) T. E. Hogen-Esch and W. L. Jenkins, *J. Am. Chem. Soc.*, **103**, 3666 (1981).
13) R. Waack, M. A. Doran, E. B. Baker, and G. A. Olah, *J. Am. Chem. Soc.*, **88**, 1272 (1966).

 © 1984 The Chemical Society of Japan Bull. Chem. Soc. Jpn., 57, 1055—1057 (1984)

Thermodynamic Study on Solvent Extraction of Alkali Metal Picrates by 15-Crown-5

Yasuyuki TAKEDA,* Tsuyoshi NAMISAKI, and Shizuo FUJIWARA
Department of Chemistry, Faculty of Science, Chiba University, Yayoi-chō, Chiba 260
(Received September 22, 1983)

In order to obtain enthalpy (ΔH_1°) and entropy changes (ΔS_1°) for overall extraction reactions of 15-crown-5 (15C5) with alkali metal picrates between benzene and water, and those (ΔH_2° and ΔS_2°) for partition of 15C5 itself, overall extraction equilibrium constants of 1:1:1 complexes of 15C5 with the salts and distribution coefficients of 15C5 were determined at 20, 30, 35, and 40 °C. The ΔH_1° and ΔS_1° values of 15C5 for the alkali metals are all negative. Both the ΔH_2° and ΔS_2° values are positive. In general, the ΔH_2° and ΔS_2° values play a major role in determining the magnitude of ΔH_1° and ΔS_1° values, respectively, except the case of entropy change for the potassium system. Enthalpy (ΔH_4°) and entropy changes (ΔS_4°) for ion-pair extractions of 15C5-alkali metal ion complexes by picrate anions were calculated by using the ΔH_1° and ΔS_1° values, and the literature values for complex-formation reactions of 15C5 with alkali metal ions in water. Both ΔH_4° and ΔS_4° values vary with the alkali metal ion held in the 15C5 cavity. The ΔH_4° and ΔS_4° values for Na^+, Rb^+, and Cs^+ are all negative, whereas those for K^+ are all positive.

15-Crown-5 (15C5) constitutes a most fundamental skeleton along with 12-crown-4 and 18-crown-6 among various crown compounds. Benzo-15-crown-5 (B15C5), which is a derivative of 15C5, is used as a pendant of polymers, a moiety of bis(crown ether)s, and a colorimetric reagent. These compounds are important for analytical chemistry as versatile agents in solvent extraction. Thus, a detailed study on the extraction process of metal ions with 15C5 and B15C5 would be in order.

For the benzene/water system, extraction-selectivity tendencies of 15C5 and B15C5 for alkali metal ions are almost similar to each other, which are consistent with size relationship.[1,2] The extractability of 15C5 for the same alkali metal ion is larger than that of B15C5 except for Li^+.[1,2] For further study on the role of B15C5 in the extraction process, enthalpy and entropy changes for the overall extraction reactions of B15C5 with sodium and potassium picrates have been determined.[3] The enthalpy and entropy changes for both systems are large and negative.[3]

In the present work, enthalpy and entropy changes for the overall extraction reactions of 15C5 with alkali metal picrates, and those for partition of 15C5 itself have been determined between benzene and water. Enthalpy and entropy changes for ion-pair extractions of 15C5-alkali metal ion complexes by picrate anions were calculated by using these thermodynamic quantities and the literature values for complex-formation reactions of 15C5 with alkali metal ions in water.

Experimental

15-Crown-5 (Nisso Co., Ltd.) was used without further purification. Benzene, picric acid, NaOH, and KOH were analytical grade reagents. Rubidium and caesium hydroxides were reagent-grade. Benzene was washed three times with distilled water.

The benzene phase of 15C5 (1.3×10^{-4}—5.8×10^{-2} M; 1 M=1 mol dm^{-3}), and the aqueous phase of the alkali metal hydroxide (6.1×10^{-3}—1.2×10^{-2} M) and picric acid ((4.1—9.7)$\times10^{-3}$ M) in a stoppered glass tube (30 ml) were shaken in a thermostated water bath for 45 min and centrifuged. The initial volume of each phase was 10 ml in all the cases. Extractions were carried out at pH 10.0—11.7. The picrate in the benzene phase was back-extracted into 8 ml of 0.01 M NaOH aqueous solution, and the picrate concentration was determined spectrophotometrically (λ_{max}=356 nm, $\varepsilon=1.45\times10^4$ cm^{-1} M^{-1}). In blank experiments, there was no extraction in the absence of 15C5. Extractions were conducted at 20, 30, 35, and 40±0.3 °C.

The Distribution Coefficient of 15C5. A 13 ml benzene solution containing 15C5 (7.7×10^{-5}—6.0×10^{-4} M) and an equal volume of distilled water in a stoppered glass tube were shaken in a thermostated water bath for 40 min and centrifuged. A portion 12 ml of the benzene phase and an equal volume of aqueous solution (pH 10.5—11.0) containing NaOH (1.1×10^{-1}M) and picric acid (1.0×10^{-1} M) were placed in a stoppered glass tube and shaken. After centrifuging, the picrate in the benzene phase was back-extracted into 10 ml of 0.01 M NaOH aqueous solution, and the picrate concentration was determined spectrophotometrically (λ_{max}= 356 nm, $\varepsilon=1.45\times10^4$ cm^{-1} M^{-1}). Experiments were conducted at 20, 30, 35, and 40±0.3 °C.

Results

When an equilibrium is established between an aqueous phase of alkali metal ion (M^+) and picrate ion (A^-), and a benzene phase of crown ether (L), the equilibrium constants is defined as

$$K_{ex}=[MLA]_o/[M^+][L]_o[A^-], \quad (1)$$

$$K_{D,L}=[L]_o/[L], \quad (2)$$

$$K_{ML}=[ML^+]/[M^+][L], \quad (3)$$

$$K_{ex'}=[MLA]_o/[ML^+][A^-], \quad (4)$$

where the subscript "o" and the lack of subscript denote the organic and aqueous phases, respectively. Thus, K_{ex} can be written as

$$K_{ex}=K_{ML}K_{ex'}K_{D,L}^{-1}. \quad (5)$$

The distribution ratio of the alkali metal may be represented by

$$D=[MLA]_o/[M^+]. \quad (6)$$

The substitution of Eq. 1 into Eq. 6 gives

$$D=K_{ex}[L]_o[A^-]. \quad (7)$$

Log ($D/[A^-]$) *vs.* log $[L]_o$ plots show a straight line with a slope of 1 in every case. This indicates that the K_{ex} can be described by Eq. 1. The values of $[L]_o$ and $[A^-]$ in Eq. 7 were calculated by

Table 1. Summary of equilibrium constants

Temp/°C	$K_{D,L}$	log K_{ex}			
		Na^+	K^+	Rb^+	Cs^+
20	0.12_6	4.06	2.68	2.30	2.05
25[1]	0.15_6	3.90	2.58	2.14	1.90
30	0.16_3	3.80	2.53	2.03	1.81
35	0.20_0	3.68	2.41	1.95	1.65
40	0.22_1	3.52	2.37	1.86	1.57

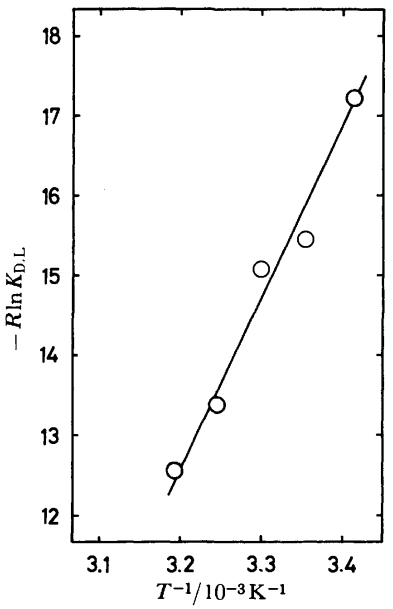

Fig. 1. $-R\ln K_{D,L}$ *vs.* T^{-1} plots for 15C5 between benzene and water.

$$[L]_o=([L]_t-[MLA]_o)/(1+K_{D,L}^{-1}), \quad (8)$$

$$[A^-]=[HA]_t-[MLA]_o, \quad (9)$$

where the subscript "t" denotes the total concentration. The equilibrium constants are listed in Table 1.

It can be seen from Figs. 1 and 2 that the $-R\ln K_{D,L}$ *vs.* T^{-1} and $R\ln K_{ex}$ *vs.* T^{-1} plots show a linear relationship. The enthalpy change (ΔH_n°) and the entropy change (ΔS_n°) for Eqs. 1 and 2 were calculated from these data by means of the following equations: $\Delta G^\circ=-RT\ln K$ and $\Delta G^\circ=\Delta H^\circ-T\Delta S^\circ$, where ΔG° and the subscript "n" designate the free energy change and the number of equation, respectively. The thermodynamic quantities are summarized in Table 2.

Discussion

As can be seen from Table 2, the $T\Delta S_2^\circ$ value is canceled by the ΔH_2° value, resulting in much greater solubility of 15C5 in water than in benzene. The ΔH_2° and $T\Delta S_2^\circ$ (at 25 °C) values of dibenzo-18-crown-6 (DB18C6) between benzene and water are 8.4 and 25 kJ mol^{-1} respectively.[5] 15-Crown-5 and DB18C6 are hydrated in an aqueous phase through hydrogen bonds between ether oxygen atoms of the crown ethers and water molecules. When the crown ethers pass over into the benzene phase from the aqueous phase, the water molecules bound to the crown ethers have to be released. The breaking of the hydrogen bonds and the release of the water molecules would lead ΔH_2° and ΔS_2° of both 15C5 and DB18C6 to positive values. The same tendency has been reported for transfer of 18-crown-6 and cryptand 222 from water to methanol (ΔH_2° and $\Delta S_2^\circ>0$).[6]

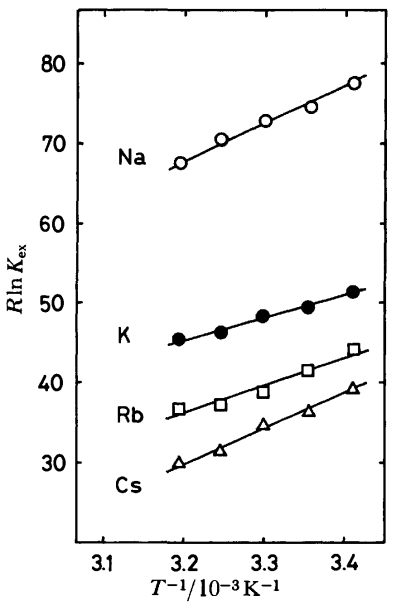

Fig. 2. $R\ln K_{ex}$ *vs.* T^{-1} plots for 15C5-alkali metal picrate systems between benzene and water.

Table 2. Thermodynamic quantities

ΔH_2°/kJ mol^{-1}=20.9		$T\Delta S_2^\circ$/kJ mol^{-1} (at 25 °C)=16.1	
	ΔH_n°/kJ mol^{-1}[a]		
	n=1	n=3[4]	n=4
Na^+	-45.3	-6.28	-18.1
K^+	-27.3	-17	10.6
Rb^+	-37.7	-7.95	-8.8
Cs^+	-42.5	-5.4	-16.2
	$T\Delta S_n^\circ$/kJ mol^{-1} (at 25 °C)[b]		
	n=1	n=3[4]	n=4
Na^+	-22.9	-2.2	-4.6
K^+	-12.5	-13.0	17
Rb^+	-25.3	-4.4	-4.8
Cs^+	-31.6	-0.6	-15

a) $\Delta H_1^\circ=-\Delta H_2^\circ+\Delta H_3^\circ+\Delta H_4^\circ$, b) $\Delta S_1^\circ=-\Delta S_2^\circ+\Delta S_3^\circ+\Delta S_4^\circ$

The ΔH_1° and ΔS_1° values of 15C5 for all the alkali metal ions are negative (Table 2). Both ΔH_1° and ΔS_1° values vary somewhat with the alkali metal ion trapped in the 15C5 cavity. Tables 1 and 2 show that the smallest $-\Delta H_1^\circ$value of K^+ is balanced by the smallest $-T\Delta S_1^\circ$ value, resulting in the second largest log K_{ex} value and the second largest $-\Delta H_1^\circ$ value of Cs^+ is canceled by the largest $-T\Delta S_1^\circ$ value, resulting in the smallest log K_{ex} value.

In general, the ΔH_2° and ΔS_2° values play a major role in determining the magnitude of ΔH_1° and ΔS_1° values, respectively, except the case of entropy change for the potassium system, whereas the ΔH_3° and ΔS_3° values play a minor role except for the potassium system.

Both ΔH_4° and ΔS_4° values vary with the alkali metal ion held in the 15C5 cavity (Table 2). This may be attributed to the fact that, since surface charge of alkali metal ions larger than the 15C5 cavity is not effectively shielded by the 15C5 ring, chemical natures of the 15C5 complexes with alkali metal ions (Na^+, K^+, Rb^+, Cs^+) are different from each other. The K_{ex} value (at 25 °C) sequences of 15C5 for the alkali mtal ions are $Na^+ \gg K^+ > Rb^+ > Cs^+$. The highest extractability for Na^+-15C5 complex is due to the largest $-\Delta H_4^\circ$ and the second smallest $-T\Delta S_4^\circ$ values. The second greatest $-\Delta H_4^\circ$ value of 15C5 complex with Cs^+ is canceled to a considerable extent by the largest $-T\Delta S_4^\circ$ value. Thus, the 15C5 complex with Cs^+ shows the lowest extractability. It is very interesting that ΔH_4° and ΔS_4° values for 15C5 complexes with Na^+, Rb^+, and Cs^+ are all negative, whereas those for 15C5 complex with K^+ are all positive. For the reaction corresponding to Eq. 4, the number of chemical species is larger for the reactant system than for the product system. This is presumably the dominant factor in determining the ΔS_4° values of 15C5 complexes with Na^+, Rb^+, and Cs^+ to be negative. The fact that, although the ΔH_4° value of the 15C5 complex with K^+ is by far the most unfavorable-or ion-pair extraction of the K^+ complex, the extraction efficiency of the K^+ complex is the second largest depends totally on much the greatest $T\Delta S_4^\circ$ value (Table 2). The reason why the ΔH_4° and ΔS_4° values of the 15C5 complex with K^+ are positive and large cannot be clearly explained at the present time. However, it is conceivable that the positive ΔS_4° value of the 15C5 complex with K^+ is due to the difference in the hydration state between the 15C5 complex with K^+ in the aqueous phase and the 15C5 complex with potassium picrate in the benzene phase.

References

1) Y. Takeda and H. Gotō, *Bull. Chem. Soc. Jpn.*, **52**, 1920 (1979).
2) Y. Takeda, Y. Wada, and S. Fujiwara, *Bull. Chem. Soc. Jpn.*, **54**, 3727 (1981).
3) Y. Takeda, *Bull. Chem. Soc. Jpn.*, **56**, 931 (1983).
4) R. M. Izatt, R. E. Terry, B. L. Haymore, L. D. Hansen, N. K. Dalley, A. G. Avondet, and J. J. Christensen, *J. Am. Chem. Soc.*, **98**, 7620 (1976).
5) A. Sadakane, T. Iwachido, and K. Tōei, *Bull. Chem. Soc. Jpn.*, **48**, 60 (1975).
6) M. H. Abraham and H. C. Ling, *Tetrahedron Lett.*, **23**, 469 (1982).

 © 1984 The Chemical Society of Japan Bull. Chem. Soc. Jpn., 57, 1058—1060 (1984) [Vol. 57, No. 4

Effects of Alkyl Chain Length on Molecular Interactions. I. Solid Complex Formation in the Pyrene-*N*-Alkyl-2,4,6-trinitroaniline Systems

Atsushi TOGASHI and Yoshio MATSUNAGA*
Department of Chemistry, Faculty of Science, Hokkaido University, Sapporo 060
(Received October 5, 1983)

Phase diagrams were prepared for the fifteen binary systems consisting of pyrene as an electron donor and *N*-alkyl-2,4,6-trinitroanilines as electron acceptors. The thermal stability of the orange 1:1 complex between pyrene and the unsubstituted 2,4,6-trinitroaniline (mp 236 °C) is drastically decreased by *N*-alkylation; *e.g.*, the *N*-pentyl-2,4,6-trinitroaniline complex melts at 97 °C. The systems with the *N*-hexyl and *N*-heptyl derivatives give two peritectics each, while most of the higher homologues produce a single peritectic or a eutectic. Unstable red solids were formed on rapid cooling of the molten pyrene-*N*-hexyl-2,4,6-trinitroaniline mixtures. This red complex becomes relatively more stable with increase of the alkyl chain length, possibly because of the enhanced tendency for chain alignment. In the systems with the *N*-pentadecyl and *N*-heptadecyl derivatives, the stable existence of the red 1:1 complex could be demonstrated.

Many organic compounds that form liquid crystals when heated have elongated molecules. Generally, these molecules have a rigid central part and one or two flexible terminal groups. The effects of the alkyl chain length in the terminal substituents on the liquid crystalline properties have been studied for a large number of homologous series. The lower homologues are commonly purely nematic, whereas the higher homologues are purely smectic. The flexible terminal groups are supposed to bring about partial breakdown of the molecular order produced by the attraction between the rigid central parts. As the nematic phase is less ordered than the smectic phase, one might assume that shorter alkyl chains tend to diminish the thermal stability of the regular molecular arrangement, while longer ones tend to restore it though the arrangement achieved is not the same as the original one. If this is so, analogous effects would be widely observable with ordinary organic solids; however, little attention has been paid to this problem.

In the present series of communications, we record studies on the effects of the alkyl chain length on intermolecular interactions such as charge transfer and proton transfer operating in solid complex formation. Systematic studies may hopefully provide a way to control such interactions. As early as 1910, Sudborough and Beard reported the preparation of 1,3,5,-trinitrobenzene complexes with aminobenzoic acids and their methyl and ethyl esters.[1] The progressive lowering of their melting points in this order appears to be consistent with the above-mentioned trends. To the authors' knowledge, no further work on such solid complexes is available.

Experimental

Materials. The yellow-colored *N*-alkyl-2,4,6-trinitroanilines were obtained by the condensation of appropriate amines with 2,4,6-trinitrochlorobenzene in boiling ethanol.[2] The alkyl groups employed and the melting points of the products were as follows: butyl, 83.5 °C; pentyl, 73.5 °C; hexyl, 70.2 °C; heptyl, 59.5 °C; octyl, 63.5 °C; nonyl, 55.6 °C; decyl, 70.2 °C; undecyl, 68.4 °C; dodecyl, 76.3 °C; tridecyl, 77.0 °C; tetradecyl, 79.0 °C; pentadecyl, 83.5 C; hexadecyl, 88.3 °C; heptadecyl, 89.0 °C; octadecyl, 91.5 °C. The pyrene, Eastman white label, was recrystallized from xylene. Binary mixtures in known proportions were melted in small test tubes, shaken well to insure homogeneity and then rapidly cooled.

Measurements. The calorimetric curves were recorded on a Rigaku Denki Thermoflex differential scanning calorimeter during the process of heating. The heating rate in this work was generally 5 °C min^{-1} but a rate as high as 20 °C min^{-1} was occasionally employed for the determination of melting points of metastable forms. The binary mixture was put into an open aluminum pan so that the color change on heating could be observed through a window. The diffuse reflectance of the solid component compounds and the molecular complexes was measured with a Beckman DK 2A spectroreflectometer. The spectrum was then plotted using the Kubelka-Munk function.

Results and Discussion

Shinomiya has prepared the phase diagram of the pyrene-2,4,6-trinitroaline system.[3] The eutectic on the donor-rich side is located at 139.5 °C and 8 mol% (hereafter, the composition is given by mol% of the acceptor) and the other one at 180.5 °C and 88 mol%. The stable 1:1 complex melts at a temperature as high as 236 °C. When the *N*-butyl and *N*-pentyl derivatives are employed as electron acceptors, the diagrams are essentially of the same type; that is, the orange 1:1 complexes melt congruently (see Fig. 1a). However, the temperatures are lowered to 104.5 and 97 °C respectively.

As is evident from Fig. 1b, the 1:1 complex becomes so unstable for the *N*-hexyl derivative that it undergoes decomposition at 85.5 °C, exhibiting a peritectic point at 55 mol%. Thus, the decrease in the thermal stability of the orange 1:1 complex by the *N*-alkylation is remarkable. In this system, another peritectic is found at 97 °C and 37 mol%, suggesting the formation of a 2:1 complex. The latter is also orange-colored. In addition, red solids crystallize when the molten mixtures around this composition are quenched. The melting point of this metastable phase (68 °C) is measurable by a rapid heating (see the shaded circles in Fig. 1b) though these red solids change monotropically to orange solids on storage at room temperature. The endothermic peak due to the melting is followed by an exothermic peak and the stable orange-colored solid is formed. The pyrene-*N*-heptyl-2,4,6-trinitroaniline system behaves similarly; however, the stabilities of the complexes are further diminished. Namely, the peri-

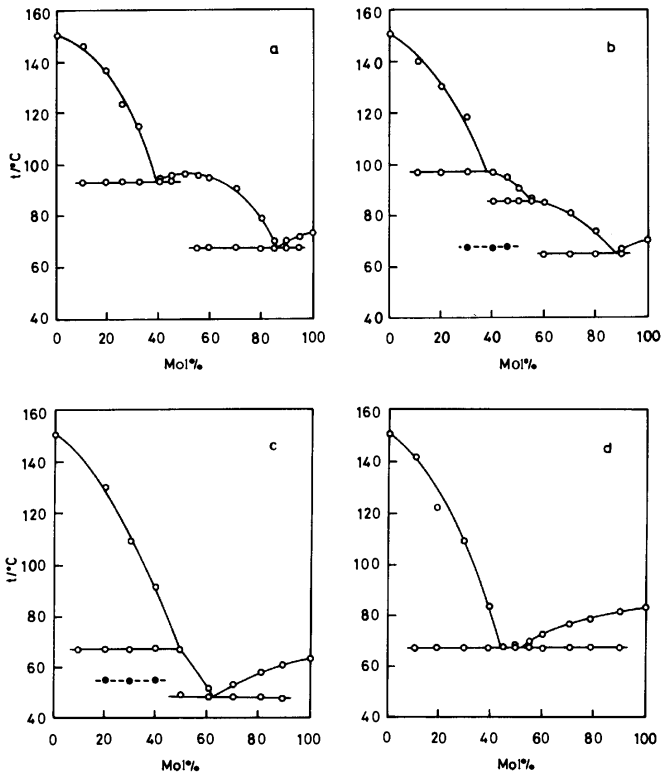

Fig. 1. Phase diagrams of the systems of pyrene with (a) *N*-pentyl-2,4,6-trinitroaniline, (b) the *N*-hexyl analogue, (c) the *N*-octyl analogue, and (d) the *N*-pentadecyl analogue. The shaded circles are the melting points of the metastable phase.

tectic due to the 1:1 complex is at 63 °C and 65 mol% and that due to the 2:1 complex at 85 °C and 38 mol%. In the composition range of the latter complex, a red complex melting at 61 °C is obtainable. The eutectic point of this system is located at 53 °C and 90 mol%.

The combination of pyrene and the *N*-octyl derivative exhibits only one peritectic at 67 °C and 48 mol%, giving no evidence for the formation of the 1:1 complex (see Fig. 1c). Metastable red solids appearing in the range from 20 to 40 mol% melt at 54.5 °C regardless of the composition. The phase diagrams of the same type were afforded by the next five higher homologues. In the case of the *N*-nonyl derivative, the system gives a peritectic at 71.5 °C and 49 mol% and a eutectic at 45.5 °C and 71 mol%. The latter temperature is the lowest among the eutectics observed in the present series. Moreover, it may be added that only in this system the red solids were so unstable that we failed to record the melting point on the calorimetric curve even with the highest rate of heating. With the *N*-decyl derivative, both the peritectic and eutectic raise appreciably; that is, the former lies at 90.5 °C and 42 mol% and the latter at 63 °C and 77 mol%. The melting point of the metastable red solid was determined as 60 °C. The peritectic and eutectic points fall again with the *N*-undecyl derivative. They are found at 76 °C and 46 mol% and at 59 °C and 73 mol%. As a result the red solids melt at 56.5 °C. The peritectic continues to fall with the *N*-dodecyl and *N*-tridecyl derivatives. They lie at 75.5 °C and 44 mol% and at 65 °C and 47 mol% respectively. On the other hand, the eutectic changes rather irregularly; that is, 64 °C and 65 mol% for the former homologue and 62.5 °C and 55 mol% for the latter. The melting point of the metastable red form shows a similar tendency to the eutectic; namely, 61.5 and 58.5 °C were recorded for these systems. Thus, the melting point of the red phase is not much affected by the alkyl chain length up to the *N*-tridecyl derivative; however, a rather large alternation in the thermal stability is demonstrated beyond this member in the series. Such an alternating effect is strongly reminiscent of the well-known alternation of the melting points of long chain compounds, which is attributed to the fact that the alkyl chains in the crystal lattice are in the form of long, straight but zig-zag chains and lie with their axes parallel.[4]

When molten mixtures of pyrene and *N*-tetradecyl-2,4,6-trinitroaniline are slowly cooled, no stable complex is found. The eutectic is located at 59 °C and 50 mol%, whereas the metastable red complex can be formed by rapid cooling in this system also. Its melting point is lower by 10 °C than the eutectic. The yellow solids exothermally produced above this melting point are mixtures of the component compounds. Therefore, the stability of the orange complex is now definitely lower than that of the red one though the latter is still metastable. The systems with the next two even-numbered homologues maintain a similar behavior. Each diagram shows only a eutectic point which is at 67.5 °C and 42 mol% and at 72 °C and 44 mol%. The red complex formed in the former system melts at 55.5 °C and that in the latter at 63.5 °C.

The systems with the *N*-pentadecyl and *N*-heptadecyl derivatives are of particular interest because in them the stable existence of the red complexes could be demonstrated. As is shown in Fig. 1d, the freezing point curve of the hydrocarbon meets a horizontal line at 68 °C and 44 mol% and that of the *N*-pentadecyl derivative at the same temperature and 53 mol%. Although the equilibrium curve involving the congruently-melting red complex is not distinguishable from the eutectic horizontal, the composition range strongly suggests that the ideal mole ratio of this phase is 1:1. In the case of the *N*-heptadecyl derivative, the binary system is somewhat complicated and has a peritectic point at 72.5 °C and 47 mol%, supporting the formation of a 1:1 complex. The eutectic point lies at 71 °C and 40 mol%. Occasionally, we obtained yellow mixtures of the solid component compounds from the melts of this system. Upon heating, this yellow mass melts but immediately solidifies into the red complex. This change is accompanied by evolution of heat.

The thermal stabilities are plotted against chain length in Fig. 2 for the above-mentioned three kinds of molecular complexes. Open circles represent the congruent or incongruent melting points of the orange 1:1 complexes. The stability diminishes rapidly with increase in the alkyl chain length and this complex can be found only in the region I which extends up to the *N*-heptyl derivative. In view of the enhanced flexing of the alkyl chains, the lowering of melting point in this region is reasonable. The metastable red complex

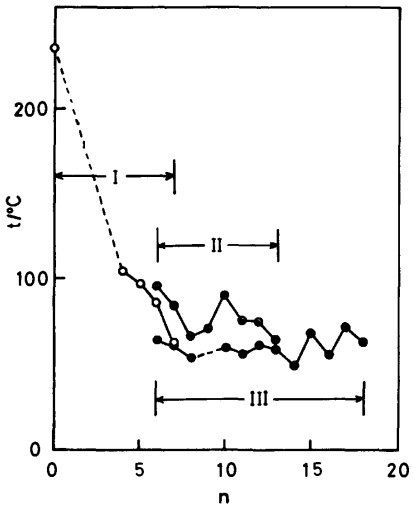

Fig. 2. Congruent or incongruent melting points of the orange-colored 1:1 complex (○), of the orange-colored 2:1 complex (⊙), and of the red-colored 1:1 complex (●) plotted against the *N*-alkyl chain length.

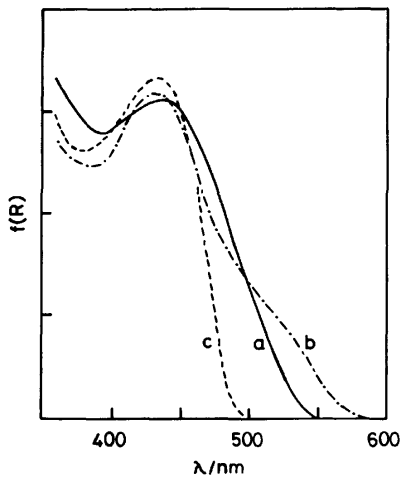

Fig. 3. Diffuse reflection spectra of (a) the orange-colored pyrene-*N*-butyl-2,4,6-trinitroaniline complex, (b) red-colored pyrene-*N*-heptadecyl-2,4,6-trinitroaniline complex, and (c) the latter acceptor compound alone.

is formed first with the *N*-hexyl derivative. The melting point fluctuates around 60°C (see shaded circles) and then tends to raise slowly with marked alternation. If one assumes that the 1:1 composition found in Fig. 1d is applicable to all the complexes in the region III, the melting point under consideration may be congruent except for the cases of the *N*-hexyl, *N*-heptyl, and *N*-octyl derivatives. When the regions I and III are overlapped with each other, the orange and red complexes may be regarded as polymorphs. The primary factor in determining the mode of molecular packing would be the charge-transfer interaction in the former complexes and the compromise between the alkyl chain alignment and the charge-transfer interaction in the latter. As is indicated by the melting point alternation, with increase in the alkyl chain length the alignment becomes relatively more important. The region II, where the orange-colored 2:1 complexes are formed, occupies about two thirds of region III. It may be noted that *N*-alkyl-2,4,6-trinitroanilines themselves also exhibit the fall of the melting point with increase of the alkyl chain length in the lower homologues and rise in the higher homologues.

The visible spectra of the orange 1:1 complex and red 1:1 complex are shown in Fig. 3. The former is represented by the *N*-butyl-2,4,6-trinitroaniline complex and the latter by the *N*-heptadecyl-2,4,6-trinitroaniline complex. For the sake of comparison, the spectrum of the acceptor is also shown. The absorption in the range from 500 to 550 nm arising from the complex formation may account for the orange color. The additional absorption appearing in the red complex is weaker but extends to about 600 nm. A shoulder may be located at about 530 nm. The shift of the absorption band to the longer wavelength-side may be interpreted by the small resonance energies in the red complex, reflecting a mode of molecular packing unfavorable to the intermolecular charge-transfer interaction. Preliminary X-ray diffraction studies on the red complexes gave patterns with a strong peak in the proximity of $2\theta = 3°$ in accordance with the parallel arrangement of the pentadecyl and heptadecyl chains.

In this connection, it may be worthwhile to mention the effects of alkyl chain length on complex formation in solution studied by Foster and Hammick.[5] They have determined the association constants for the interactions of *N*-alkylanilines with 1,3,5-trinitrobenzene and 2,4,6-trinitrotoluene in cyclohexane. According to their study, complexes of greater stability are formed with the higher homologues of both series; *e.g.*, the association constant is 8.2 l mol^{-1} for the *N*-butylaniline-1,3,5-trinitrobenzene complex and 11.6 l mol^{-1} for the corresponding *N*-dodecylaniline complex. The wavelength of the maximum absorption due to the charge-transfer interaction rises with the first few homologues of both these series, thereafter remaining sensibly constant. Because of the three dimensional order, the effects of alkyl chain length on the stability of complexes in the solid state are entirely different from those observed for the complexes in solution.

The present work was partly supported by a Grant-in-Aid for Scientific Research No. 543001 from the Ministry of Education, Science and Culture.

References

1) J. J. Sudborough and S. H. Beard, *J. Chem. Soc.*, **97**, 773 (1910).
2) P. van Romburgh and C. W. Zahn, *Recl. Trav. Chim. Pays-Bas*, **57**, 437 (1938).
3) C. Shinomiya, *Bull. Chem. Soc. Jpn.*, **15**, 259 (1940).
4) A. I. Kitaigorodskii, "Organic Chemical Crystallography," Consultant Bureau, New York (1961) p. 178.
5) R. Foster and D. L. Hammick, *J. Chem. Soc.*, **1954**, 2685.

 © 1984 The Chemical Society of Japan Bull. Chem. Soc. Jpn., 57, 1061—1066 (1984)

Kinetics of the Racemization and Dissociation of Tris(1,10-phenanthroline)-iron(II). The Aggregate Formation of the Complex Cation with 1-Alkanesulfonate Anions through Hydrophobic Interaction

Satoshi TACHIYASHIKI* and Hideo YAMATERA†

Laboratory of Chemistry, Kagawa Nutrition College, Sakado, Saitama 350-02

†*Department of Chemistry, Faculty of Science, Nagoya University, Chikusa-ku, Nagoya 464*

(Received May 28, 1983)

The kinetics of the racemization and dissociation of $[Fe(phen)_3]^{2+}$ were investigated in the presence of a series of 1-alkanesulfonate ions (n-$C_nH_{2n+1}SO_3^-$, n=2, 4, 6,...,14). The racemization rate increased, while the dissociation rate decreased, gradually as a function of the alkanesulfonate concentration at low concentrations of each alkanesulfonate. With alkanesulfonates of $n \geqq 8$, the second phase of rate changes, *i.e.*, steep increases in both rates, were observed at higher concentrations. The gradual initial changes in the rates were explained in terms of the formation of the 1:1 aggregate of the complex cation with the alkanesulfonate ion caused by hydrophobic interaction. The formation constant ($mol^{-1}\,dm^3$) increased almost exponentially from 4 (n=4) to 770 (n=14) with the increase in the alkyl-chain length, the energy of the hydrophobic interaction of the complex cation and the alkanesulfonate anion being 0.9 kJ mol^{-1} per methylene group of the latter. The second phase of the rate changes were explained in terms of the formation of the 1:m aggregate of the complex cation with the alkanesulfonate ions. The rate behavior of the hydrophobic aggregates is discussed in connection with the reaction mechanisms of the racemization and dissociation of $[Fe(phen)_3]^{2+}$.

A study of hydrophobic interaction is very important not only for understanding the nature of the interaction determining the tertiary and quarternary structures of proteins in biological systems,[1] but also for discerning the nature of the solute-solute interaction in an aqueous solution containing a hydrophobic metal complex.[2-4] However, few investigations have so far been done to clarify the nature of the interaction of a complex with a monomeric surfactant,[5] although much attention has been paid recently to the interaction of metal complexes with micelles.[6-11]

The $[Fe(phen)_3]^{2+}$ (phen=1,10-phenanthroline) ion is known to racemize by means of an intramolecular twist mechanism.[12] The nature of the twist mechanism, however, does not seem to be fully understood.[12] We previously studied the effects of inorganic anions,[13,14] inorganic cations,[15] and organic cations[15] on the rates of the racemization and dissociation of $[Fe(phen)_3]^{2+}$. The changes in the rates in the presence of inorganic anions were reasonably explained in terms of the ion-pair formation of the complex ion with the anions.[13,14] On the other hand, the effects of organic cations such as alkylammonium ions on the racemization and dissociation rates were explained by a consideration of the formation of the 1:1 aggregate of the complex and the alkylammonium cations caused by hydrophobic interaction between them.[15]

The present study is concerned with the effects of 1-alkanesulfonate ions (n-$C_nH_{2n+1}SO_3^-$, n=2, 4, 6,···, 14) on the rates of the racemization and dissociation of $[Fe(phen)_3]^{2+}$. As the hydrophobicity of alkanesulfonate anions varies with the alkyl-chain length, different effects can be expected for alkanesulfonates with different chain lengths. A comparison of the effect of each alkanesulfonate with that of the alkylammonium cation of the same alkyl-chain length will show the roles of the charge and the hydrophobic group in the interaction between the complex and organic ions, and their effects on the racemization and dissociation rates. The results will also give a basis for understanding the nature of the interaction of a metal-complex cation with ionic surfactants.

Experimental

The sodium 1-alkanesulfonates used were guaranteed-grade reagents of the Tokyo Kasei Kogyo Co., Ltd. They were recrystallized three times from an ethanol-methanol (5:1) solution and dried at 70°C *in vacuo* for 5 h. The concentrations of the solutions of these salts were determined by weighing well-dried reagents. The surface tension of the solutions of these surfactants showed no minimum around the cmc (critical micelle concentration).[16] Kinetic data were obtained at 25°C in solutions containing the perchlorate of the complex (5×10^{-5} mol dm^{-3}) and a sodium alkanesulfonate. Racemization was followed by polarimetry, and dissociation, by spectrophotometry. For measuring the dissociation rates, $NiCl_2$ (5×10^{-4} mol dm^{-3}) was added to the sample solution as a scavenger of the liberated phenanthroline. For the systems containing dodecane- and tetradecanesulfonates, the measurements were carried out at a low $NiCl_2$ concentration of 1×10^{-4} mol dm^{-3} to minimize the precipitation of nickel(II) sulfonate. The first-order rate constants for racemization and dissociation were obtained, respectively, from the $\ln [\alpha_0/\alpha_t]$ *vs.* t and $\ln[(D_0-D_t)/(D_0-D_\infty)]$ *vs.* t plots, where α and D, with the subscripts showing the time, represent the optical rotation (546 nm) and the absorbance (510 nm) of the sample solution respectively. A Union SM401 spectrometer was used for the observation of the absorption spectra. The other chemicals and procedures were the same as those described in our previous paper.[13]

Results

Profile of the Rate Changes with the Alkanesulfonate Concentrations. The kinetic results for the racemization and dissociation of $[Fe(phen)_3]^{2+}$ in the presence of various sodium alkanesulfonates (n-$C_nH_{2n+1}SO_3Na$, n=2, 4, ···, 14) are depicted in Figs. 1 ($n \leqq 6$), and 2 ($n \geqq 8$, with the abscissa on a logalithmic scale); a linear scale plot for a part of the latter is drawn in Fig. 3 for ease of comparison with Fig. 1. In solutions of the alkanesulfonates of n=2 and 4 (Fig. 1), the racemization rates increased, and the dissociation rates decreased,

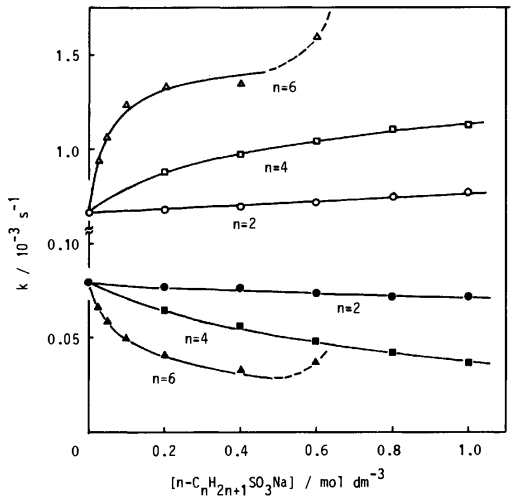

Fig. 1. The racemization (open marks) and dissociation (closed marks) rate constants of $[Fe(phen)_3]^{2+}$ in alkanesulfonate ($n \leqq 6$) solutions at 25.0°C.
○, ●: $C_2H_5SO_3Na$; □, ■: n-$C_4H_9SO_3Na$; △, ▲: n-$C_6H_{13}SO_3Na$.
The solid lines in the figure are those calculated by substituting the parameter values (Table 1) into Eq. 5.

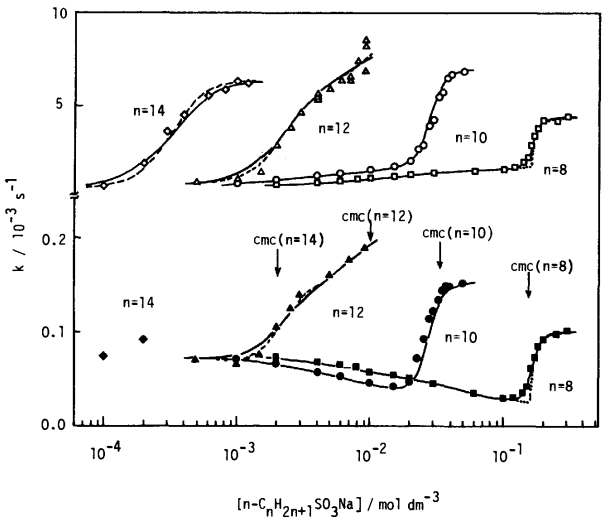

Fig. 2. The racemization (open marks) and dissociation (closed marks) rate constants of $[Fe(phen)_3]^{2+}$ in alkanesulfonate ($n \geqq 8$) solutions at 25.0°C.
○, ●: n-$C_8H_{17}SO_3Na$; □, ■: n-$C_{10}H_{21}SO_3Na$; △, ▲: n-$C_{12}H_{25}SO_3Na$; ◇, ◆: n-$C_{14}H_{29}SO_3Na$.
The solid and dotted lines in the figure are those calculated on the basis of Eqs. 10 and 15, respectyvely. For systems containing dodecane- or tetradecanesulfonate, the solid lines are those calculated by assuming the presence of 1:3 aggregates, and the broken lines, 1:4 aggregates. The parameter values given in Table 2 were used in these calculations.

monotonously with the increase in the alkanesulfonate concentration. Similar changes in the rates were also observed for sulfonates of n=6, 8, 10, 12, and 14 at concentrations lower than 0.5, 0.10, 0.015, 0.001, and 0.0001 mol dm^{-3} respectively (see Figs. 1 and 3). The changes in both the racemization and dissociation rates with the alkanesulfonate concentration were larger for the sulfonate with a longer alkyl chain. At

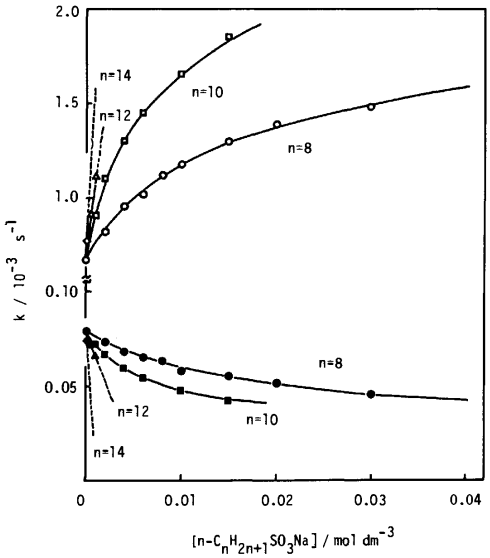

Fig. 3. The racemization (open marks) and dissociation (closed marks) rate constants of $[Fe(phen)_3]^{2+}$ in alkanesulfonate ($n \geqq 8$) solutions of low concentrations at 25.0°C.
○, ●: n-$C_8H_{17}SO_3Na$; □, ■: n-$C_{10}H_{21}SO_3Na$; △, ▲: n-$C_{12}H_{25}SO_3Na$, ◇, ◆: n-$C_{14}H_{29}SO_3Na$.

higher concentrations of the sulfonates than those mentioned above (Fig. 2), the racemization rate increased steeply with the increase in the alkanesulfonate concentration to a rate several times as large as that in water, and then it reached a plateau. The dissociation rates also increased to a rate larger than that in pure water.

Kinetics in Alkanesulfonate Solutions of the Lower Concentrations (Figs. 1 and 3): The changes in rates with the alkanesulfonate concentrations in this region are similar to those observed for $[Fe(phen)_3]^{2+}$–alkyltrimethylammonium systems. Thus, the rate changes can be thought to arise from the formation of the 1:1 aggregate[15] (or ion pair[13]) of complex ion and an alkanesulfonate ion. The following mechanism was considered:

$$[Fe(phen)_3]^{2+} + RSO_3^- \overset{K_1}{\rightleftharpoons} [Fe(phen)_3]^{2+}\cdot RSO_3^-, \quad (1)$$

$$\Delta\text{-}[Fe(phen)_3]^{2+} \xrightarrow{k_{0r}} rac\text{-}[Fe(phen)_3]^{2+}, \quad (2r)$$

$$[Fe(phen)_3]^{2+} \xrightarrow{k_{0d}} [Fe(phen)_2]^{2+} + phen \xrightarrow{fast} Fe^{2+} + 3\,phen, \quad (2d)$$

$$\Delta\text{-}[Fe(phen)_3]^{2+}\cdot RSO_3^- \xrightarrow{k_{1r}} rac\text{-}[Fe(phen)_3]^{2+}\cdot RSO_3^-, \quad (3r)$$

$$[Fe(phen)_3]^{2+}\cdot RSO_3^- \xrightarrow{k_{1d}} [Fe(phen)_2]^{2+}\cdot RSO_3^- + phen \xrightarrow{fast} Fe^{2+} + 3\,phen + RSO_3^-, \quad (3d)$$

$$K_1 = \frac{[Fe(phen)_3^{2+}\cdot RSO_3^-]}{[Fe(phen)_3^{2+}][RSO_3^-]}\frac{f_1}{f_2 f_1}, \quad (4)$$

where k_0 and k_1 are the rate constants of the complex cations not associated with and associated with the alkanesulfonate ion respectively, and where f_z represents the activity coefficient of an ion with a charge of

TABLE 1. THE FORMATION CONSTANTS OF THE 1 : 1 AGGREGATES BETWEEN $[Fe(phen)_3]^{2+}$ AND ALKANESULFONATES AND THE RATE CONSTANTS OF THE COMPLEX IN THE 1 : 1 AGGREGATES

Alkanesulfonate	Racemization		Dissociation	
	$k_{1r}/10^{-3}$ s^{-1}	K_1/mol dm^{-3}	$k_{1d}/10^{-3}$ s^{-1}	K_1/mol dm^{-3}
None	(0.67±0.03)[a]	—	(0.0795±0.0016)[b]	—
n-$C_4H_9SO_3^-$	1.24±0.06	5.5±2.0	0.0180±0.0040	3.2±0.5
n-$C_6H_{13}SO_3^-$	1.51±0.13	33±14	0.0172±0.0050	18±3
n-$C_8H_{17}SO_3^-$	2.03±0.20	85±20	0.0160±0.0030	64±8
n-$C_{10}H_{21}SO_3^-$	2.30±0.15	208±40	0.0180±0.0040	156±27
n-$C_{12}H_{25}SO_3^-$	2.5±0.6	(320±40)[c]	(0.017)[d]	320±40
n-$C_{14}H_{29}SO_3^-$	2.0±0.7	(770±120)[c]	(0.017)[d]	770±120

a) k_{0r}. b) k_{0d}. c) The values obtained from dissociation experiments. d) The value estimated from those obtained for systems containing alkanesulfonate of shorter alkyl-chain lengths.

$\pm z$ and can be calculated with the Debye-Hückel equation.[14] The rate constants for racemization and dissociation are expressed as:

$$k^{obsd} = \frac{k_0 + k_1K_1f_2[RSO_3^-]}{1 + K_1f_2[RSO_3^-]}. \quad (5)$$

Additional subscripts, r and d, may be attached to the symbols for rate constants to distinguish between racemization and dissociation. The kinetic data for $n=4$—10 (Figs. 1 and 3) were analyzed in terms of the least-squares fit to Eq. 5. The K_1 and k_1 values thus obtained are listed in Table 1.

In the cases of $n=12$ and 14 (Fig. 3), where the alkanesulfonate concentrations are very low ($[RSO_3^-] \ll 1/K_1$), Eq. 5 can be reduced to:

$$k^{obsd} = k_0 + (k_1 - k_0)K_1[RSO_3^-]. \quad (6)$$

The k_{1d} value of 0.017×10^{-3} s^{-1} was assumed for $n=12$ and 14 by extrapolation from the k_{1d} values for $n \leqq 10$, which are shown to be independent of the alkyl-chain length of the alkanesulfonate ion (Table 1). The k_{1r} values were obtained from Eq. 6 with the K_1 values obtained from dissociation experiments. The solid lines in Figs. 1 and 3 are those calculated with the parameter values listed in Table 1.

Kinetics in Solutions of Higher Alkanesulfonate Concentrations: The rate behavior of the complex ion at the sulfonate concentrations higher than 0.10, 0.015, 0.001, and 0.0001 mol dm^{-3} for n=8, 10, 12, and 14 respectively may be related to the formation of higher aggregates than 1 : 1 or to the interaction with micelles.

In order to ascertain whether or not the micelles are concerned with the observed changes in rates, the cmc values of the alkanesulfonates were determined in the presence of 5×10^{-5} mol dm^{-3} $[Fe(phen)_3]^{2+}$ by means of the surface-tension and light-scattering methods.[16] The surface tension of the solutions containing sodium alkanesulfonates decreased remarkably in the presence of 5×10^{-5} mol dm^{-3} $[Fe(phen)_3]^{2+}$, and the break-point of the surface tension *vs.* concentration curve appeared at a lower concentration. This appears to be consistent with a previous finding that the cmc value of sodium dodecyl sulfate (SDS) decreased remarkably in the presence of 1×10^{-4} mol dm^{-3} $[Co(phen)_3]^{3+}$.[17] However, light-scattering measurements, which can detect the micelle formation more directly, showed that the cmc values[18] remained almost unchanged in the presence of the complex ions, and that the pre-aggregation of the complex cation with the alkanesulfonate ions took place at a concentration below the cmc. The contradictory results of the surface-tension and light-scattering experiments may have arisen from the fact that the surface-tension measurements are an indirect method of determining the cmc value, or that they cannot distinguish between the formation of micelles and that of premicellar aggregates such as a 1 : m aggregate.

Since a steep rise in the rate was observed before the alkanesulfonate concentration reached the cmc value for the $[Fe(phen)_3]^{2+}$-containing system, the observed rate changes cannot be attributed to the interaction of the complex ion with the alkanesulfonate micelle.

Let us now consider the formation of 1 : m ($m \geqq 2$) aggregates. The following equations must be added to Eqs. 1-4:

$$[Fe(phen)_3]^{2+} + m\,RSO_3^- \overset{\beta'_m}{\rightleftharpoons} [Fe(phen)_3]^{2+} \cdot m\,RSO_3^-, \quad (7)$$

$$\Delta\text{-}[Fe(phen)_3]^{2+} \cdot m\,RSO_3^- \xrightarrow{k_{mr}} rac\text{-}[Fe(phen)_3]^{2+} \cdot m\,RSO_3^-, \quad (8r)$$

$$[Fe(phen)_3]^{2+} \cdot m\,RSO_3^- \xrightarrow{k_{md}} [Fe(phen)_2]^{2+} \cdot m\,RSO_3^- + phen \xrightarrow{fast} Fe^{2+} + 3\,phen + m\,RSO_3^-, \quad (8d)$$

$$\beta'_m = \frac{[Fe(phen)_3{}^{2+} \cdot m\,RSO_3^-]}{[Fe(phen)_3{}^{2+}][RSO_3^-]^m}. \quad (9)$$

Then, the observed reaction rate constant can be expressed as:

$$k^{obsd} = \frac{k_0 + k_1\beta'_1[RSO_3^-] + \sum_{m=2}^{\infty} k_m\beta'_m[RSO_3^-]^m}{1 + \beta'_1[RSO_3^-] + \sum_{m=2}^{\infty} \beta'_m[RSO_3^-]^m}, \quad (10)$$

where k_m represents the rate constant of the complex cation associated with m alkanesulfonate anions, and where $\beta'_1 (=K_1f_2)$ and β'_m are the concentration formation constants of the 1 : 1 and 1 : m aggregates. Because of the difficulty in estimating the activity coefficients of higher aggregates, the concentration equilibrium constants were used in the analysis. Although the ionic strength of the medium was not maintained constant, it can be expected that an analysis in such a way will at least qualitatively give a proper interpretation

TABLE 2. THE m AND $\log\beta'_m$ VALUES OBTAINED FROM THE ANALYSIS OF THE KINETIC RESULTS IN SOLUTIONS OF HIGH ALKANESULFONATE CONCENTRATIONS, AND OTHER PARAMETER VALUES ASSUMED FOR THE ANALYSIS[a)]

Alkanesulfonate	m	$\log\beta'_m$	β'_1[b)]	$k_{md}/10^{-3}$ s^{-1}	$k_{mr}/10^{-3}$ s^{-1}
n-$C_8H_{17}SO_3^-$	14±2	11.8±1.6	34	0.100	4.4
n-$C_{10}H_{21}SO_3^-$	8±1	13.1±1.2	107	0.153	7.0
n-$C_{12}H_{25}SO_3^-$[c)]	3	8.0±0.3	260	0.180±0.010	7.0±1.5
	8	18.0±1.6		0.220±0.020	9.5±2.4
	4	10.8±0.1	260	0.160±0.010	6.3±0.5
	8	19.0±1.3		0.220±0.020	9.5±1.5
n-$C_{14}H_{29}SO_3^-$[d)]	3	10.8±0.3	710	—	6.3
	4	14.4±0.4	710	—	6.3

a) Each of the figures under m and $\log\beta'_m$ is the average of the values obtained from the racemization and dissociation experiments. b) $\beta'_1=K_1f_2$. c) The m values for this system are assumed by analogy with the values for the systems containing decane- and tetradecanesulfonates. d) The value of m which best fits the experimental data is 3.4. Thus, the experimental results were analyzed by assuming an integer m value of 3 or 4.

of the experimental results for two reasons. Firstly, the high charge of the higher aggregate will be reduced by ion association with sodium ions, and therefore the activity coefficient of the higher aggregate will not so greatly depend on the ionic strength of the medium. Secondly, the rate changes at the higher alkanesulfonate concentrations are observed in a narrow range of the sulfonate concentration; accordingly, the activity coefficients of the ions involved in the reaction can be regarded as almost constant in the region where the most remarkable change in rate was observed.

In addition to the free complex ion and the 1:1 aggregate, one higher aggregate species (1:m) was considered for the systems containing octane-, decane-, and tetradecanesulfonate. Under these conditions, the transformation of Eq. 10 leads to:

$$\log\left\{\frac{(k^{obsd}-k_0)+(k^{obsd}-k_1)\beta'_1[RSO_3^-]}{(k_m-k^{obsd})}\right\} = \log\beta'_m + m\log[RSO_3^-]. \quad (11)$$

The values of m and β'_m were obtained by analyzing the kinetic data in the following way. The values of k_0, k_1, and β'_1 have been obtained above from the analysis of the rates at lower sulfonate concentrations. The rate constant of the 1:m aggregate, k_m, was regarded as equal to the rate constant at the plateau (Fig. 2, Table 2). By assuming that $[RSO_3^-]$ equals the total alkanesulfonate concentration, the plot of the left-side term of Eq. 11 *vs.* $\log[RSO_3^-]$ gave approximate values of m and $\log\beta'_m$. Then, these values of m and $\log\beta'_m$ were used to calculate the $[RSO_3^-]$ value, with which the plot as described above was repeated to give better values of m and $\log\beta'_m$. This procedure was repeated until reproducible values of m, β'_m, and $[RSO_3^-]$ were obtained. The values of m and β'_m thus obtained for the systems containing octane-, decane-, and tetradecanesulfonate are listed in Table 2, along with the value of k_m assumed for the analysis. The m and β'_m values given for the octanesulfonate system are the lower limits, since the decrease in $[RSO_3^-]$ upon micelle formation was disregarded. The solid lines in Fig. 2 show the k_r and k_d values calculated with the parameter values listed in Tables 1 and 2. In the case of tetradecanesulfonate-containing systems, the solid and broken curves correspond to the formation of the 1:3 and 1:4 aggregates respectively. The good agreement between the observed and the calculated rate constants suggests that the approximations adopted in the analysis of the experimental results are reasonably good in these cases. Aggregates other than those considered above may be present in each system, but they will not appreciably differ in the aggregation number from those considered or, if they do appreciably differ, they will not be present in appreciable concentrations. Thus, no further analysis has been carried out.

The dodecanesulfonate-containing system shows a feature different from the octanesulfonate-, decanesulfonate-, and tetradecanesulfonate-containing systems; at least two steps of changes are observed in the rate increase occurring in the region of 10^{-3}—10^{-2} mol dm^{-3} (Fig. 2). In this case, analysis was carried out by assuming the presence of the 1:3 and 1:8 aggregates or the 1:4 and 1:8 aggregates. These particular aggregates were chosen by analogy with the systems containing decane- and tetradecanesulfonate. The least-squares fit of the kinetic data to Eq. 10 with m=3 and 8 or m=4 and 8 led to the parameter values listed in Table 2. These parameter values were used to calculate the rate constants at each dodecanesulfonate concentration. The solid and broken lines in Fig. 2 were obtained by assuming the formation of the 1:3 and 1:8 aggregates and of the 1:4 and 1:8 aggregates respectively. Better fits of the calculated lines to the observed rate constants were obtained when the 1:4 aggregate was assumed to exist, although the 1:3 aggregate seems more natural from the shape of the complex.

Kinetics in Micellar Solutions: As has been described above for system containing octanesulfonate, the change in rate observed above the cmc was accounted for by considering the interaction of the complex ion with monomeric sulfonate ions. If we consider the aggregate of the complex ion with the micelle in place of the 1:m aggregate, the following reactions are substituted for Eqs. 7—10:

$$[Fe(phen)_3]^{2+} + \text{micelle} \overset{K_M}{\rightleftharpoons} [Fe(phen)_3]^{2+}\cdot\text{micelle}, \quad (12)$$

$$\Lambda\text{-}[Fe(phen)_3]^{2+}\cdot\text{micelle} \xrightarrow{k_{rM}} rac\text{-}[Fe(phen)_3]^{2+}\cdot\text{micelle}, \quad (13r)$$

$$[Fe(phen)_3]^{2+}\cdot micelle \xrightarrow{k_{dM}} [Fe(phen)_2]^{2+}\cdot micelle + phen \xrightarrow{fast} Fe^{2+} + 3\,phen + micelle, \quad (13d)$$

$$K_M = \frac{[Fe(phen)_3^{2+}\cdot micelle]}{[Fe(phen)_3^{2+}][micelle]}. \quad (14)$$

Then, the observed rate constant is expressed as:

$$k = \frac{k_0 + k_1\beta'_1[RSO_3^-] + k_M K_M[micelle]}{1 + \beta'_1[RSO_3^-] + K_M[micelle]}. \quad (15)$$

When the total concentration of the surfactant (C_S) is much larger than that of the complex, [micelle] can be expressed as:

$$[micelle] = \frac{C_S - cmc}{N}, \quad (16)$$

where N is the aggregation number of the micelle. An analysis of the kinetic data for the systems of octanesulfonate leads to $K_M=(800\pm300)N\,mol^{-1}\,dm^3$, $k_{Mr}=(4.6\pm0.3)\times10^{-3}\,s^{-1}$, and $k_{1d}=(0.105\pm0.004)\times10^{-3}\,s^{-1}$. Calculation with the parameter values gives the dotted curve shown in Fig. 2. The poor agreement between the calculated and observed rates strongly suggests the existence of at least one 1:m ($m\geqq2$) species.

Discussion

The formation of aggregates of $[Fe(phen)_3]^{2+}$ with alkansulfonate ions and the racemization and dissociation of the complex in the aggregates will now be discussed in comparison with the case of the aggregates with alkyltrimethylammonium ions.

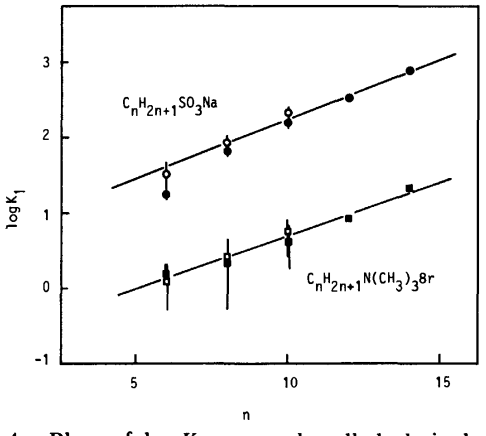

Fig. 4. Plots of $\log K_1$ versus the alkyl chain length (n) of the alkanesulfonate and alkyltrimethylammonium ions. The open marks are the results for racemization and the closed marks are those for dissociation.
○, ●: n-$C_nH_{2n+1}SO_3Na$; □, ■: n-$C_nH_{2n+1}N(CH_3)_3$-Br.

Formation of 1:1 Aggregate: Figure 4 shows the plot of the logarithm of the 1:1-aggregate formation constant ($\log K_1$) against the alkyl-chain length (n) of the sulfonate ion, together with a similar plot previously obtained for the systems containing alkyltrimethylammonium salts. A linear relationship was found between $\log K_1$ and n ($n\geqq8$), suggesting that the formation of the 1:1 aggregate is caused by hydrophobic interaction. The almost identical slopes of the two lines (Fig. 4) suggest that the interactions of the complex cation with alkanesulfonate anions and with alkyltrimethylammonium cations are of the same nature, or that hydrophobic interaction is responsible for the formation of the 1:1 aggregates. This is also supported by the result of our NMR study that the hexanesulfonate ion associates with $[Fe(phen)_3]^{2+}$ in such a way that the alkyl chain of the sulfonate ion lies on the phenanthroline ligand.[19] The energy of hydrophobic interaction between the complex and alkanesulfonate ions was estimated to be (0.9 ± 0.1) kJ mol^{-1} per methylene group from the slope of the line in Fig. 4. This is consistent with the value of (0.8 ± 0.1) kJ mol^{-1} obtained previously for the $[Fe(phen)_3]^{2+}$-alkyltrimethylammonium system.[15] The value of K_1 for each of the alkanesulfonate ions was about 40 times as large as that for the alkyltrimethylammonium ion of the same alkyl-chain length, reflecting the difference in the electrostatic energy between the cation-cation and the cation-anion interaction; this corresponds to a difference of 9.2 kJ mol^{-1} in the free-energy change in the ion-pair formation.

Formation of 1:m Aggregates: Aggregates higher than 1:1 were found to be formed for the $[Fe(phen)_3]^{2+}$-RSO_3^- system, but not for the $[Fe(phen)_3]^{2+}$-alkyltrimethylammonium system. This indicates that electrostatic attraction between the complex cation and sulfonate anions partly compensates for the repulsion between sulfonate anions, thus facilitating the formation of the 1:m aggregate. Since a remarkable increase in the rates of racemization and dissociation of $[Fe(phen)_3]^{2+}$ occurred below the cmc, premicellar aggregates must be responsible for the changes in the rates. Thus, "micellar catalysis" may, in some cases, originate from interaction with surfactant ions rather than from that with micelles.

Racemization-rate Constants of $[Fe(phen)_3]^{2+}$ in the Aggregates: The values of k_{1r} for $[Fe(phen)_3]^{2+}$ in the 1:1 aggregate were two (n=4) to three (n=10) times as large as the value of k_{0r}. This resembles our previous finding that the formation of the 1:1 aggregate with the alkyltrimethylammonium cation (n-$C_nH_{2n+1}N^+$-$(CH_3)_3$, n=6—10) increased the racemization rate of the complex ion by a factor of two to four. The similarity between these two cases shows that the difference in the charge of the organic ions has little effect on the racemization rate. This confirms the previous argument that the effect of the organic ions accelerating the racemization of $[Fe(phen)_3]^{2+}$ is caused by an interaction of the complex ion with the alkyl group of the organic ions, and not by their action as electron donors.[15]

The following mechanism is proposed for this acceleration. In a transition state of the racemization through a twist process, the metal-ligand bonds of the complex ion have to stretch to a considerable extent so as to relax the steric repulsion between the phenanthroline ligands, especially between hydrogen atoms at the 2 and 9 positions of the ligands. As a result, the hydrophobic phenanthroline ligands are exposed to the solvent more extensively in the transition state of the racemization than in the initial state; therefore, the

transition state is more hydrophobic than the initial state[20] and is more strongly stabilized by the hydrophobic interaction. Thus, the association of the complex ion with the alkylammonium or alkanesulfonate ion may lead to the acceleration of the racemization. An alternative explanation of the role of the alkyl group in accelerating the racemization may be that its aggregate formation with the complex cation removes the iceberg structure around the complex cation, thus facilitating the intramolecular twist racemization. Similar mechanisms can account for the larger values of k_{mr} for the complex in $1:m$ aggregates than the values of k_{1r} in 1:1 aggregates (Tables 1 and 2); the hydrophobic stabilization of the transition state is greater for the $1:m$ aggregate than for the 1:1 aggregate, or the iceberg structure is more efficiently removed from the complex in a $1:m$ aggregate than in a 1:1 aggregate.

Dissociation-rate Constants of $[Fe(phen)_3]^{2+}$ in the Aggregates: The values of k_{1d} for $[Fe(phen)_3]^{2+}$ in the 1:1 aggregates were one-fourth of the value of k_{0d}, and were almost independent of the value of n (n=6, 8, and 10; Table 1). The lower rate constant for the 1:1 aggregate can be related to a smaller number of water molecules in direct contact with the complex ion if the dissociation of the complex ion proceeds through a 7-coordinate transition state with a coordinated water molecule.[13] The situation is similar to the case of the hydrophobic aggregate with the alkylammonium cation.[15] However, the complex ions in the present aggregates show small but appreciable values of k_{1d}, in contrast to the very small values for the complex ion in the aggregate with alkyltrimethylammonium cations.[15] This difference indicates that the dissociation-rate constant is affected by the charge of the aggregates. The higher charge (+3) of the aggregate of the complex cation with the alkylammonium cation causes a stronger electrostriction of water around the aggregate. Therefore, the activity of the water should be lowered and the water-molecule-assisted dissociation should be retarded.

The values of k_{md} for $[Fe(phen)_3]^{2+}$ in $1:m$ aggregates were ten times as large as the value of k_{1d} (Tables 1 and 2). This may be because monomeric water molecules exist among the sulfonate ions in the $1:m$ aggregates; such water molecules should have no necessity to break hydrogen bonding with bulk water to react with the complex ion. The large k_{md} values may also result from the greater stabilization of the transition state, which should be more hydrophobic than the initial state because of the expansion of metal-ligand bonds.[20]

This research was partly supported by a Grant-in-Aid for Science Research No. 574234 from the Ministry of Education, Science and Culture. We wish to thank Professor Shoichi Ikeda and Dr. Sumio Ozeki of Nagoya University for their helpful discussions.

References

1) F. B. Armstrong and T. P. Bennett, "Biochemistry," Oxford University Press, New York (1979).
2) P. R. Michell, *J. Chem. Soc., Dalton Trans.*, **1979**, 771, and the references therein.
3) D. W. Margerum *et al.*, "Coordination Chemistry II," ACS Monograph 174, A. E. Martell, ed by American Chemical Society, Washington, D. C. (1978), pp. 140—143.
4) E. Iwamoto, Y. Tanaka, H. Kimura, and Y. Yamamoto, *J. Solution Chem.*, **9**, 841 (1980).
5) S. Tachiyashiki and H. Yamatera, *Chem. Lett.*, **1981**, 1681.
6) J. R. Cho and H. Morawetz, *J. Am. Chem. Soc.*, **94**, 375 (1972).
7) J. Holzwarth, W. Knoche, and B. H. Robinson, *Ber. Bunsenges. Phys. Chem.* **82**, 1001 (1978).
8) S. Diekmann and J. Frahm, *J. Chem. Soc., Faraday Trans. 1*, **75**, 2199 (1979).
9) V. C. Reinsborough and R. H. Robinson, *J. Chem. Soc., Faraday Trans. 1*, **75**, 2395 (1979).
10) H. Bruhn and J. Holzwarth, *Ber. Bunsenges. Phys. Chem.*, **82**, 1006 (1978).
11) K. V. Ponganis, M. A. de Araujo, and H. L. Hodges, *Inorg. Chem.*, **19**, 2704 (1980).
12) F. Basolo and R. G. Pearson, "Mechanisms of Inorganic Reactions," 2nd ed, Wiley, New York (1967), pp. 313—322.
13) S. Tachiyashiki and H. Yamatera, *Bull. Chem. Soc. Jpn.*, **55**, 1014 (1982).
14) S. Tachiyashiki and H. Yamatera, *Polyhedron*, **2**, 9 (1983).
15) S. Tachiyashiki and H. Yamatera, *Bull. Chem. Soc. Jpn.*, **55**, 759 (1982).
16) S. Ozeki, S. Tachiyashiki, S. Ikeda, and H. Yamatera, *J. Colloid Interface Sci.*, **91**, 430 (1983).
17) S. Kratohvil, K. Shinoda, and E. Matijevic, *J. Colloid Interface Sci.*, **72**, 106 (1979).
18) H. V. Tartar and A. L. M. Lelong, *J. Phys. Chem.*, **59**, 1185 (1955).
19) Y. Masuda, S. Tachiyashiki, and H. Yamatera, *Chem. Lett.*, **1982**, 1065.
20) M. J. Blandamer, J. Burgess, and S. H. Morris, *J. Chem. Soc., Dalton Trans.*, **1974**, 1717.

 © 1984 The Chemical Society of Japan Bull. Chem. Soc. Jpn., 57, 1067—1069 (1984)

Kinetics of the Racemization of Tris(1,10-phenanthroline)nickel(II). Hydrophobic Interaction of the Complex Ion with 1-Alkanesulfonate Ions

Satoshi TACHIYASHIKI* and Hideo YAMATERA†

Laboratory of Chemistry, Kagawa Nutrition College, Sakado, Saitama 350-02

†*Department of Chemistry, Faculty of Science, Nagoya University, Chikusa-ku, Nagoya 464*

(Received May 28, 1983)

The kinetics of the racemization of $[Ni(phen)_3]^{2+}$ were investigated in the presence of 1-alkanesulfonate ions (n-$C_nH_{2n+1}SO_3^-$; n=8, 10, 12, and 14). The racemization rate decreased with the increase in the alkanesulfonate concentrations in the region of low sulfonate concentrations; then, in the region of higher concentrations, it began to increase, but it never exceeded the rate in water. The rate changes at low and high alkanesulfonate concentrations were related to the formation of the 1:1 and 1:m aggregates of the complex ion with alkanesulfonate ions respectively. A comparison of the aggregate formation constants of $[Ni(phen)_3]^{2+}$ with those of $[Fe(phen)_3]^{2+}$ confirmed that hydrophobic interaction is responsible for the aggregate formation. The energy of hydrophobic interaction between $[Ni(phen)_3]^{2+}$ and an alkanesulfonate ion was estimated to be 1.0±0.1 kJ mol^{-1} per methylene group of the latter. The kinetic behavior of the racemization of $[Ni(phen)_3]^{2+}$ in the aggregates was also compared with those of the racemization and dissociation of $[Fe(phen)_3]^{2+}$, and it was discussed in relation to the racemization mechanism of $[Ni(phen)_3]^{2+}$. The reaction rates of the complexes in D_2O solutions were also reported.

Aromatic diimines, such as 1,10-phenanthroline and 2,2′-bipyridine, are among the most important ligands in coordination chemistry. Because of their hydrophobicity, metal complexes of these ligands show unique interactions with hydrophobic solutes in aqueous solutions.[1-3]

We previously measured the effects of alkylammonium cations[4] and 1-alkanesulfonate anions[5,6] on the rates of racemization and dissociation of $[Fe(phen)_3]^{2+}$. The results at low organic-ion concentrations were related satisfactorily to the formation of the 1:1 aggregates of the complex and organic ions caused by hydrophobic interactions. In solutions of higher alkanesulfonate concentrations, the rate behavior of the complex was related to the formation of the 1:m aggregates of the complex and alkanesulfonate ions.

One object of the present work is to confirm the formation of the aggregates of the tris(1,10-phenanthroline)metal ion with alkansulfonate ions and to see whether the aggregate formation occurs entirely by means of electrostatic and hydrophobic interactions or by any other interactions specific for the metal ion of the chelate. Another object is to disclose the effect of RSO_3^- on the racemization rate of $[Ni(phen)_3]^{2+}$. A comparison of the effect with those of RSO_3^- on the racemization and dissociation rates of $[Fe(phen)_3]^{2+}$ previously obtained[6] will give information regarding the racemization mechanism of $[Ni(phen)_3]^{2+}$.[7]

Experimental

The synthesis and optical resolution of $(-)_{589}$-$[Ni(phen)_3](ClO_4)_2 \cdot 3H_2O$ was carried out according to the method of Dwyer and Gyarfas;[8] $[\alpha]_{589} = -1400°$. Deutrium oxide was supplied by the Aldrich Chemical Co. (99.8 atom% D). Racemization rates were obtained at 25.0°C by following the decrease in the optical rotation (405 nm) of the solution, containing 5×10^{-5} mol dm^{-3} of the optically active complex as perchlorate and a proper concentration of 1-alkanesulfonate, on a Union PM101 automatic polarimeter. The reactions were followed for two to four half-lives. They were first order in the concentration of the metal complex in the time range studied. The racemization-rate constant was defined as $k_r = [\ln(\alpha_0/\alpha_t)]/t$, where α_0 and α_t represent the optical rotations at times zero and t respectively, and was calculated by the usual method for the first-order reactions. The racemization and dissociation rates of $[Fe(phen)_3]^{2+}$ in H_2O and D_2O were obtained at 25.0°C with 5×10^{-5} mol dm^{-3} $[Fe(phen)_3](ClO_4)_2$ in a way similar to that described in our previous paper.[6] The other chemicals and procedures were the same as those described previously.[6]

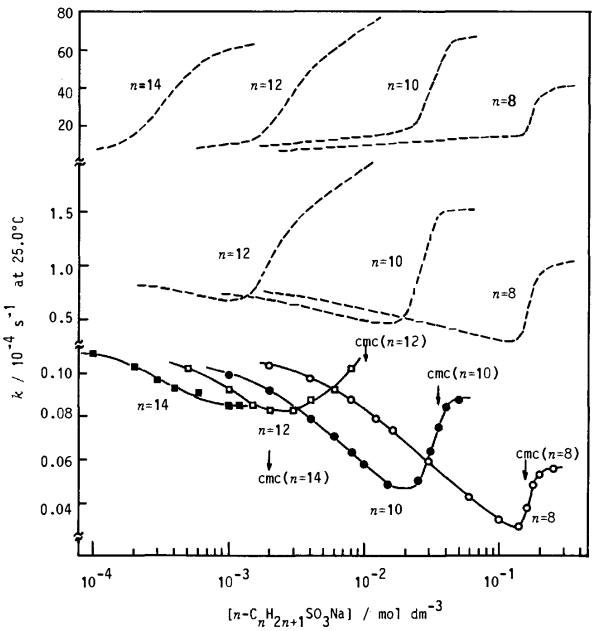

Fig. 1. The racemization rate constants of $[Ni(phen)_3]^{2+}$ (5×10^{-5} mol dm^{-3}) in the presence of sodium alkanesulfonates: ○, n-$C_8H_{17}SO_3Na$; ●, n-$C_{10}H_{21}SO_3Na$; □, n-$C_{12}H_{25}SO_3Na$; ■, n-$C_{14}H_{29}SO_3Na$. The solid curves show the values calculated on the basis of Eq. 8. The arrows indicate the cmc values for each sodium alkanesulfonate. The broken curves give the results previously obtained for the dissociation (middle) and racemization (top) of $[Fe(phen)_3]^{2+}$.

TABLE 1. THE AGGREGATION NUMBER OF ALKANESULFONATE (m) IN THE AGGREGATE WITH $[Ni(phen)_3]^{2+}$ AND THE AGGREGATE FORMATION CONSTANTS OF THE 1 : 1 (K_1) AND 1 : m (β'_m) AGGREGATE OF THE COMPLEX WITH ALKANESULFONATE AT 25.0 °C[a)]

Alkanesulfonate	K_1/mol^{-1} dm^3	m	log(β'_m/mol^{-m} dm^{3m})
n-$C_8H_{17}SO_3^-$	54±4 (70±14)	14±2 (14±2)	11.7±1.6 (11.8±1.6)
n-$C_{10}H_{21}SO_3^-$	164±14 (177±34)	8±1 (8±1)	12.8±1.6 (13.1±1.2)
n-$C_{12}H_{25}SO_3^-$[b)]	280±80 (320±40)	3 (3—4)	8.7±0.4[c)] (8.0—10.8)
		8 (8)	19.5±0.5[c)] (18.0—19.0)
n-$C_{14}H_{29}SO^{3-}$	430±390 (770±120)	3±1 (3—4)	10.5±3.5 (10.8—14.4)

a) The values in parentheses are those for the systems of $[Fe(phen)_3]^{2+}$-alkanesulfonates (from Ref. 6). b) The m values for this system are assumed to be equal to the values for the systems containing decane- and tetradecanesulfonate. c) These values were obtained by assuming k_3 and k_8 to be equal to 0.83 and 1.10 respectively.

Results

In Fig. 1, the measured rate constants of the racemization of $[Ni(phen)_3]^{2+}$ are plotted against the logarithm of the alkanesulfonate-ion concentration. The racemization and dissociation rate constants of $[Fe(phen)_3]^{2+}$ previously obtaind are also shown in the figure. A comparison of the profiles of the rate changes of the two complexes suggests that the rate behavior of $[Ni(phen)_3]^{2+}$ may be explained in a fashion similar to the case of $[Fe(phen)_3]^{2+}$;[5,6] the complex ion forms the 1:1 and 1:m ($m \geqq 2$) aggregates with alkanesulfonate ions in the regions of low and high alkanesulfonate concentrations respectively. Then, the following mechanism can be considered:

$$(-)\text{-}[Ni(phen)_3]^{2+} + RSO_3^- \overset{\beta'_1}{\rightleftharpoons} (-)\text{-}[Ni(phen)_3]^{2+}\cdot RSO_3^-, \quad (1)$$

$$(-)\text{-}[Ni(phen)_3]^{2+} + m\,RSO_3^- \overset{\beta'_m}{\rightleftharpoons} (-)\text{-}[Ni(phen)_3]^{2+}\cdot m\,RSO_3^- \quad (2)$$

$$(-)\text{-}[Ni(phen)_3]^{2+} \xrightarrow{k_0} rac\text{-}[Ni(phen)_3]^{2+}, \quad (3)$$

$$(-)\text{-}[Ni(phen)_3]^{2+}\cdot RSO_3^- \xrightarrow{k_1} rac\text{-}[Ni(phen)_3]^{2+}\cdot RSO_3^-, \quad (4)$$

$$(-)\text{-}[Ni(phen)_3]^{2+}\cdot m\,RSO_3^- \xrightarrow{k_m} rac\text{-}[Ni(phen)_3]^{2+}\cdot m\,RSO_3^- \quad (5)$$

$$\beta'_1 = \frac{[Ni(phen)_3{}^{2+}\cdot RSO_3^-]}{[Ni(phen)_3{}^{2+}][RSO_3^-]} = K_1\frac{f_2 f_1}{f_1}, \quad (6)$$

$$\beta'_m = \frac{[Ni(phen)_3{}^{2+}\cdot m\,RSO_3^-]}{[Ni(phen)_3{}^{2+}][RSO_3^-]^m}, \quad (7)$$

where k_0, k_1, and k_m represent the rate constants of the complex cation associated with zero, one, and m alkanesulfonate ions respectively, and where f_z shows the activity coefficient of an ion as a function of its charge ($\pm z$).[9] Therefore, the racemization rate constant is expressed by:

$$k = \frac{k_0 + k_1\beta'_1[RSO_3^-] + \sum_{m=2}^{\infty} k_m\beta'_m[RSO_3^-]^m}{1 + \beta'_1[RSO_3^-] + \sum_{m=2}^{\infty}\beta'_m[RSO_3^-]^m}. \quad (8)$$

The kinetic results were analyzed on the basis of Eq. 8 in a way similar to that used for the $[Fe(phen)_3]^{2+}$-RSO_3^- system.[6] The k_0, k_1, K_1 ($=\beta'_1/f_2$), m, k_m, and β'_m values thus obtained are listed in Tables 1 and 2. They were substituted into Eq. 8 to calculate the solid curves in Fig. 1.

The rate constants of the racemization of $[Ni(phen)_3]^{2+}$, as well as those of the racemization and dissociation of $[Fe(phen)_3]^{2+}$, as measured in H_2O and D_2O solutions, are listed in Table 3.

TABLE 2. RACEMIZATION RATE CONSTANTS OF $[Ni(phen)_3]^{2+}$ IN THE 1:1 AND 1:m AGGREGATES OF THE COMPLEX ION WITH ALKANESULFONATE IONS[a)]

Alkanesulfonate	k_1	k_m	m
None	(k_0=0.113±0.002)	—	—
n-$C_8H_{17}SO_3^-$	0.005±0.005	0.057	14
n-$C_{10}H_{21}SO_3^-$	0.010±0.005	0.089	8
n-$C_{12}H_{25}SO_3^-$	(≈0.010)	>0.110	8
		≈0.083	3
n-$C_{14}H_{29}SO_3^-$	(≈0.010)	0.842±0.002	3

a) $k/10^{-4}$ s^{-1} at 25.0 °C.

TABLE 3. THE REACTION RATE CONSTANTS OF $[Ni(phen)_3]^{2+}$ AND $[Fe(phen)_3]^{2+}$ IN H_2O AND D_2O SOLUTIONS AT 25.0 °C

	$k/10^{-4}$ s^{-1} in H_2O	$k/10^{-4}$ s^{-1} in D_2O	$k(D_2O)/k(H_2O)$
$[Ni(phen)_3]^{2+}$ racemization	0.113±0.002	0.090±0.002	0.80±0.03
$[Fe(phen)_3]^{2+}$ dissociation	0.795±0.016	0.587±0.006	0.74±0.03
$[Fe(phen)_3]^{2+}$ racemization	6.7±0.3	5.50±0.27	0.82±0.08

Discussion

*Formation of the 1:1 and 1:*m *Aggregates.* In octanesulfonate- and decanesulfonate-containing systems, the racemization rate of $[Ni(phen)_3]^{2+}$ changed with the alkanesulfonate concentration in a similar way to that of the dissociation rate of $[Fe(phen)_3]^{2+}$. On the other hand, in dodecanesulfonate- and tetradecanesulfonate-containing systems, the features of the rate change were somewhat different between the two complexes (Fig. 1). The results of the analysis (Table 1) showed, however, that the K_1, m, and β'_m values for the $[Ni(phen)_3]^{2+}$-RSO_3^- systems agreed with

those previously obtained for the $[Fe(phen)_3]^{2+}$-RSO_3^- systems within the limits of experimental uncertainty, even for the latter systems.[6] This confirmed that the rate changes of $[Ni(phen)_3]^{2+}$ in the dodecane- and tetradecanesulfonate solutions were also induced by the formation of the 1:1 and 1:*m* aggregates.

The essential agreements of the values for K_1, *m*, and β'_m between the two complexes (Table 1) also suggests that the formation of aggregates is not specific for the kind of metal ion in the tris(1,10-phenanthroline)metal chelate, but that hydrophobic interaction is responsible for the aggregate formation, as has been proposed previously.[6] The energy of hydrophobic interaction between $[Ni(phen)_3]^{2+}$ and RSO_3^- was estimated from the K_1 values (Table 1) to be 1.0 ± 0.1 kJ mol^{-1} per methylene group of the sulfonate ion, a value consistent with that of 0.9 ± 0.1 kJ mol^{-1} obtained for $[Fe(phen)_3]^{2+}$-RSO_3^- systems.

Rate Constants of $[Ni(phen)_3]^{2+}$ in the 1:1 and 1:m Aggregates. The Mechanism of the Racemization of the Complex: The rate *vs.* concentration curves for the racemization of $[Ni(phen)_3]^{2+}$ are analogous to those for the dissociation, rather than those for the racemization, of $[Fe(phen)_3]^{2+}$ (Fig. 1). The ratios of the rate constants, k_1/k_0 ($\approx$0.1) and k_m/k_1 ($\approx$9), for the racemization of $[Ni(phen)_3]^{2+}$ (Table 2) were of magnitudes comparable to those ($k_1/k_0\approx0.2$ and $k_m/k_1\approx10$) for the dissociation of $[Fe(phen)_3]^{2+}$. These observations may reflect the process of racemization-*via*-dissociation for $[Ni(phen)_3]^{2+}$.

While $[Fe(phen)_3]^{2+}$ was shown to dissociate by the aid of nucleophiles including water,[10] the racemization of $[Ni(phen)_3]^{2+}$ was reported to be unaffected by a strong nucleophile such as hydroxide.[11] In order to see if water is involved in the rate-determining step of the $[Ni(phen)_3]^{2+}$ racemization, studies were made for the D_2O-H_2O isotope effects of this reaction as well as the dissociation and racemization of $[Fe(phen)_3]^{2+}$. Table 3 shows that the rate in D_2O was about 80% of the rate in H_2O in each case studied. This shows that water is involved in the rate-determining step of each reaction;[12] thus, our attempt to use the H-D isotope effect for the differentiation of the reaction mechanisms failed. Considering that an intramolecular mechanism has been confirmed for the racemization of $[Fe(phen)_3]^{2+}$,[7] the participation of water molecules in the rate-determining step of the reaction may indicate that a reorganization of the hydration sphere is necessary even for the intramolecular reaction. The failure in differentiating the mechanism by means of the H-D isotope effect may also be due to the fact that the hydrogen atom of H_2O is not directly concerned with the nucleophilic attack of a water molecule, but is involved in the hydrogen bonding with other water molecules or anions.

References

1) D. W. Margerum *et al.*, "Coordination Chemistry II," ACS Monograph 174, ed by A. E. Martell, American Chemical Society, Washington, D. C. (1978), Chap. I, pp. 140—143.
2) E. Iwamoto, Y. Tanaka, H. Kimura, and Y. Yamamoto, *J. Solution Chem.*, **9**, 841 (1980).
3) P. R. Mitchell, *J. Chem. Soc., Dalton Trans.*, **1979**, 771, and the references cited therein.
4) S. Tachiyashiki and H. Yamatera, *Bull. Chem. Soc. Jpn.*, **55**, 759 (1982).
5) S. Tachiyashiki and H. Yamatera, *Chem. Lett.* **1981**, 1681.
6) S. Tachiyashiki and H. Yamatera, *Bull. Chem. Soc. Jpn.*, **57**, 1061 (1984).
7) F. Basolo and R. G. Pearson, "Mechanisms of Inorganic Reactions," 2nd ed, Wiley, New York (1967), pp. 310—313, 326—327.
8) F. P. Dwyer and E. C. Gyarfas, *J. Proc. R. Soc., N. S. Wales*, **83**, 232 (1949).
9) S. Tachiyashiki and H. Yamatera, *Polyhedron*, **2**, 9 (1983).
10) S. Tachiyashiki and H. Yamatera, *Bull. Chem. Soc. Jpn.*, **55**, 1014 (1982).
11) N. R. Davies and F. P. Dwyer, *Trans. Faraday Soc.*, **48**, 244 (1952).
12) C. J. O'Connor, E. J. Fendler, and J. H. Fendler, *J. Am. Chem. Soc.*, **96**, 370 (1974).

Kinetics of the Racemization and Dissociation of Tris(1,10-phenanthroline)-iron(II) and Tris(2,2′-bipyridine)iron(II) in Sodium Dodecyl Sulfate Solutions[1)]

Satoshi TACHIYASHIKI* and Hideo YAMATERA†
Laboratory of Chemistry, Kagawa Nutrition College, Sakado, Saitama 350-02
†*Department of Chemistry, Faculty of Science, Nagoya University, Chikusa-ku, Nagoya, 464*
(Received August 12, 1983)

The kinetics of the racemization and dissociation of $[Fe(phen)_3]^{2+}$ (phen=1,10-phenanthroline) and $[Fe(bpy)_3]^{2+}$ (bpy=2,2′-bipyridine) was investigated in aqueous sodium dodecyl sulfate (SDS) solutions. The racemization and dissociation rates of the complexes increased with the increase in the SDS concentration to reach limiting values at concentrations above the critical micelle concentration (cmc). The rate changes occurring below the cmc were explained in terms of the formation of at least three kinds of premicellar aggregates of the complex ion with dodecyl sulfate ions. In the region slightly above the cmc, where the concentration of the complex ion is larger than that of the micelle, the rates continued to increase with the increase in the micellar concentration, suggesting that the complex ions interacted with the micelles. A comparison of the kinetic behavior in aqueous micellar solutions with that in organic solvents revealed that the complexes were located inside the micelle-water interface. The mechanisms of the acceleration in the micelle were discussed.

The micellar catalysis of chemical reactions has attracted much attention recently.[2)] Most of the studies reported so far have, however, been concerned with organic reactions. Relatively few are concerned with the reactions involving metal complexes.[2)] They include studies of the Hg^{2+}-induced aquation of $[CoCl(NH_3)_5]^{2+}$,[3)] the formation of Ni^{2+} and Mn^{2+} complexes with hydrophobic ligands,[4-6)] and electron-transfer reactions of hydrophobic metal complexes[7,8)] in sodium dodecyl sulfate (SDS) solutions. In all cases, changes in rate were observed in the regions of the SDS concentration both above and below the cmc. The changes in the rate above the cmc have been discussed as an example of micellar catalysis, but less attention has been paid to the changes in rate occurring below the cmc.

We previously studied the effects of alkyltrimethylammonium bromides[9)] and sodium 1-alkanesulfonates[10,11)] on the rates of the racemization and dissociation of $[Fe(phen)_3]^{2+}$ (phen=1,10-phenanthroline). Each of the cationic and the anionic surfactants affects the rates mainly at concentrations below the cmc. The rate changes were explained by the formation of premicellar aggregates of the complex ion with the surfactant ions. Above the cmc of each system, however, we could not specify whether or not the complex ion interacted with the micelles, since the rates remained almost unchanged above the cmc.

In this paper, we will report on kinetic studies of the racemization and dissociation of $[Fe(phen)_3]^{2+}$ and $[Fe(bpy)_3]^{2+}$ (bpy=2,2′-bipyridine) in SDS solutions; investigations were made to elucidate the nature of the interaction of the complex ions with monomeric and micellar dodecyl sulfate ions below and above the cmc, and to clarify the dependence of the racemization and dissociation rates on the SDS concentration.

Experimental

The synthesis and optical resolution of $(+)_{589}$-$[Fe(phen)_3](ClO_4)_2 \cdot 2H_2O$[12)] and $(+)_{589}$-$[Fe(bpy)_3](ClO_4)_2 \cdot 2H_2O$[13)] were carried out according to the method of Dwyer and Gyarfas; $[\alpha]_{589}=1400°$ and $[\alpha]_{589}=4900°$. Sodium dodecyl sulfate from Merck (for tenside test) was recrystallized five times from ethanol and then dried under reduced pressure. Sodium chloride from Merck (Suprapur) and hydrochloric acid from Wako (Super Special Grade) were used without further purification. The kinetic measurements were carried out at 25.0 °C with the perchlorate of each complex ([complex]=5×10^{-5} mol dm^{-3}) in solutions containing SDS[14)] with and without NaCl ([NaCl]=0, 0.02, 0.15, 0.40, and 1.00 mol dm^{-3}). The dissociation rates of the complexes were observed in the presence of 5.0×10^{-4} mol dm^{-3} nickel(II) chloride, except for the systems containing HCl. (Both Ni^{2+} and H^+ are effective scavengers for the ligands released during the reactions.) The racemization rates of $[Fe(phen)_3]^{2+}$ and $[Fe(bpy)_3]^{2+}$ were observed by following the optical rotation of the solutions at 546 and 589 nm, and their dissociation rates, by following the absorbance at 510 and 520 nm, respectively. Multiple measurements under the same experimental conditions gave rate constants reproducible within ±5% and ±1% respectively for the racemization and dissociation of the complexes. The other reagents and procedures were described in our previous paper.[15)]

Results and Discussion

Interaction of $[Fe(phen)_3]^{2+}$ and $[Fe(bpy)_3]^{2+}$ with Dodecyl Sulfate Ions Below cmc. Rate Behavior of the Complexes in SDS Solutions: Figure 1 shows the observed racemization and dissociation rate constants of $[Fe(phen)_3]^{2+}$ against the SDS concentration in the absence and the presence of NaCl (0, 0.02 and 0.15 mol dm^{-3}). The dissciation rate of the complex slightly decreased, and the racemization rate slightly increased, with the increase at SDS concentrations below 0.3×10^{-3} mol dm^{-3}. In the range of $(0.3—1.0) \times 10^{-3}$ mol dm^{-3}, the rates increased steeply with the increase in the SDS concentration in the presence of NaCl, while the dodecyl sulfate of the complex was precipitated in this range of SDS concentrations in the absence of NaCl. Such a precipitation has also been reported for the $[Ru(bpy)_3]^{2+}$-SDS system[16)]. At SDS concentrations higher than 1×10^{-3} mol dm^{-3}, the increases in the rates became less steep and reached the limiting values within the range of experimental uncertainty at the SDS concentration characteristic of

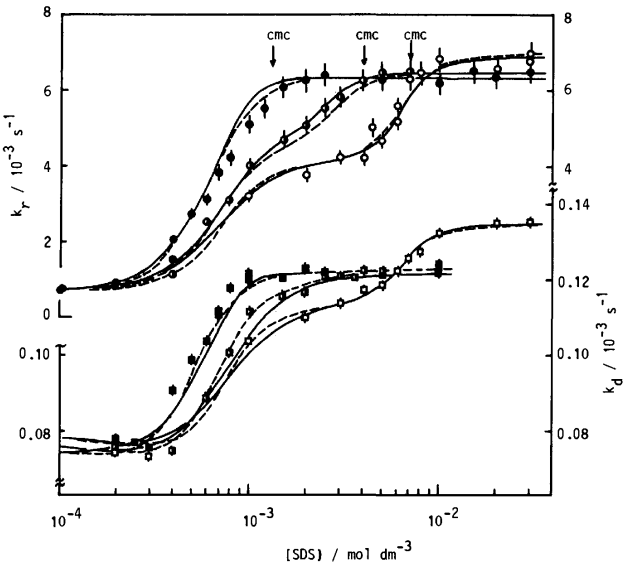

Fig. 1. Plots of the rate constants for the racemization (circles) and dissociation (squares) of $[Fe(phen)_3]^{2+}$ against the logarithm of SDS concentration. ○, □: No NaCl; ○, □: [NaCl]=0.02 mol dm^{-3}; ●, ■: [NaCl]=0.15 mol dm^{-3}. The solid (m=3) and broken (m=4) curves are those calculated by substituting the parameter values (Table 1) into Eq. 1.

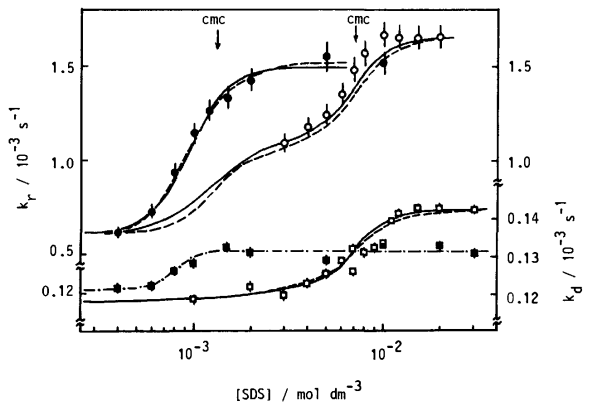

Fig. 2. Plots of the rate constants for the racemization (circle) and dissociation (square) of $[Fe(bpy)_3]^{2+}$ against the logarithm of SDS concentration. ○, □: No NaCl; ●, ■: [NaCl]=0.15 mol dm^{-3}. The solid (m=3) and broken (m=4) curves are those calculated by substituting the parameter values (Table 1) into Eq. 1.

the system. Similar features are shown by $[Fe(bpy)_3]^{2+}$, as is depicted in Fig. 2. With the rate changes of the complexes in SDS solutions, the absorption spectra of the complexes changed slightly in a fashion similar to that reported for the $[Fe(phen)_2(CN)_2]$-SDS system.[7]

Formation of the Premicellar Aggregates of the Complex Ions with Dodecyl Sulfate Ions: The cmc values of the SDS solutions containing the complex ions[17] are indicated by arrows in Figs. 1 and 2. Since the rate change in each system occurred mainly below the respective cmc, the change may be accounted for by the formation of the premicellar aggregates of the complex ions with dodecyl sulfate ions, and not by the interaction of the complex ions with micelles. The same applies to the spectral changes accompanied by the rate changes. This is in contrast to the previous reports on the $[Fe(phen)_2(CN)_2]$, $[Fe(phen)_2(CN)_2]^+$, and $[Ru(bpy)_3]^{2+}$[16] systems, in which the spectral changes of the complexes in SDS solutions were related to the incorporation of the complexes into SDS micelles.[7,8,16]

Analysis of the Kinetic Results: The racemization and dissociation rates of $[Fe(phen)_3]^{2+}$ changed with the SDS concentration in at least three steps (Fig. 1): changes in the regions of the SDS concentrations below 0.3×10^{-3} mol dm^{-3}, changes between 0.3 and 1.0×10^{-3} mol dm^{-3} and changes higher than 1×10^{-3} mol dm^{-3}. The rate changes of the three steps can be related to the formation of at least three kinds of aggregates of the complex ion with dodecyl sulfate ions.

By analogy with the previous results for the $[Fe(phen)_3]^{2+}$-1-dodecanesulfonate[11] and $[Ni(phen)_3]^{2+}$-1-dodecanesulfonate systems,[18] the first step in the rate change can be attributed to the formation of the 1:1 aggregate of the complex ion and the dodecyl sulfate ion, and the second and third steps, to the formation of 1:3 or 1:4 and 1:8 aggregates. Then, the gross rate constant, k, can be expressed as:

$$k = \frac{k_0 + k_1\beta'_1[DS^-] + k_m\beta'_m[DS^-]^m + k_8\beta'_8[DS^-]^8}{1 + \beta'_1[DS^-] + \beta'_m[DS^-]^m + \beta'_8[DS^-]^8}, \quad (1)$$

where k_0, k_1, k_m, and k_8 represent the rate constants of the complex ion aggregated with zero, one, m (m=3 or 4), and eight dodecyl sulfate ions respectively. The β'_1, β'_m, and β'_8 mean the gross concentration formation constants for the aggregates of the complex ion with one, m, and eight dodecyl sulfate ions respectively, and $[DS^-]$, the concentration of free dodecyl sulfate ions.

In the analysis of the kinetic data for the $[Fe(phen)_3]^{2+}$- SDS system, the values of β'_1, k_{1r} (k_1 for racemization), and k_{1d} (k_1 for dissociation) were assumed to be equal to the corresponding values for the $[Fe(phen)_3]^{2+}$-1-dodecanesulfonate system, *i.e.*, k_{1r}= 2.1×10^{-3} s^{-1}, $k_{1d}=0.026\times10^{-3}$ s^{-1}, and β'_1= 270, 220, and 170 $mol^{-1}dm^3$ for systems without NaCl, with [NaCl]=0.02, and 0.15 mol dm^{-3} respectively.[11] With these parameter values, the kinetic results at low SDS concentrations were analyzed graphically by disregarding the formation of the 1:8 aggregate. The transformation of Eq. 1 disregarding the $[DS^-]^8$ terms leads to this relation:

$$k = k_m - \frac{1}{\beta'_m}\frac{(k-k_0) + (k-k_1)\beta'_1[DS^-]}{[DS^-]^m}. \quad (2)$$

Plots of k *vs.* $\{(k-k_0)+(k-k_1)\beta'_1[DS^-]\}/[DS^-]^m$ should give a straight line with a slope of $-1/\beta'_m$ and an intercept of k_m for m= 3 and 4. The transformation of Eq. 1 (including the $[DS^-]^8$ terms) leads to this relation:

$$k = k_8 - \frac{1}{\beta'_8}\frac{(k-k_0) + (k-k_1)\beta'_1[DS^-] + (k-k_m)\beta'_m[DS^-]^m}{[DS^-]^8} \quad (3)$$

The k_8 and β'_8 values were obtained by plotting the rate constants at high SDS concentrations against the ratio appearing at the extreme right of Eq. 3. Then, the sets of the k_m, β'_m, k_8, and β'_8 values for m=3 and 4 were recalculated by the least-squares fit[19] of Eq. 1 to the kinetic data; they are given in Table 1. These values were

TABLE 1. FORMATION CONSTANTS OF THE 1 : m (m=3 OR 4) AND 1 : 8 AGGREGATES OF $[Fe(phen)_3]^{2+}$ OR $[Fe(bpy)_3]^{2+}$ AND DODECYL SULFATE IONS, AND THE RACEMIZATION AND DISSOCIATION RATE CONSTANTS OF THE COMPLEXES IN THE AGGREGATES IN MEDIA WITH DIFFERENT NaCl CONCENTRATIONS[a)]

Complex	[NaCl] / mol dm^{-3}	m	log β_m'[b)]	log β_8'[b)]	10^3k_{mr}/s^{-1}	10^3k_{md}/s^{-1}	10^3k_{8r}/s^{-1}	10^3k_{8d}/s^{-1}
$[Fe(phen)_3]^{2+}$	0	3	9.5±0.1	20.4±0.2	4.2±0.1	0.115±0.001	6.8±0.2	0.135±0.001
		4	12.5±0.1	21.4±0.2	4.0±0.1	0.113±0.001	6.9±0.2	0.135±0.001
	0.02	3	9.5±0.1	22.3±0.4	5.1±0.2	0.121±0.002	6.4±0.2	0.122±0.001
	0.15	4	12.7±0.1	22.9±0.4	4.4±0.3	0.119±0.002	6.5±0.3	0.123±0.003
		3	9.8±0.1	25.2±0.2	5.1±0.3	0.120±0.002	6.3±0.1	0.122±0.001
		4	13.3±0.1	25.4±0.3	4.3±0.3	0.114±0.006	6.4±0.1	0.122±0.001
$[Fe(bpy)_3]^{2+}$	0	3	8.7±0.3	19.5±0.4	1.13±0.04	0.121±0.001	1.65[c)]	0.142[c)]
		4	11.6±0.4	20.2±0.4	1.07±0.04	0.121±0.001	1.65[c)]	0.142[c)]
	0.15	3	9.2±0.1	24.0±0.1	1.19±0.09	—	1.48±0.02	—
		4	12.4±0.1	23.9±0.2	1.21±0.08	—	1.51±0.03	—

a) The parameter values of k_{0r}=0.65, k_{0d}=0.0794, 0.0757, and 0.0746, of k_{1r}=2.1, k_{1d}=0.026/10^{-3}s^{-1}and of β_1'=270, 220, and 170 for systems of [NaCl]=0, 0.02, and 0.15 mol dm^{-3} respectively, were assumed for the analysis of the results for $[Fe(phen)_3]^{2+}$-SDS systems. The values of k_{0r}=0.61 and 0.59, and of k_{0d}=0.118 and 0.122/10^{-3}s^{-1} for systems of [NaCl]=0 and 0.15 mol dm^{-3} respectively, and β_1'=0 were assumed for $[Fe(bpy)_3]^{2+}$-SDS systems. b) Average values obeained from racemization and dissociation experiments. c) Average values of the rate constants in solutions of the SDS concenration higher than 0.012 mol dm^{-3}. These values were assumed for the analysis.

used to calculate the k_r and k_d values, which are shown as the solid (for m=3) and broken (for m=4) curves in Fig. 1.

The changes in the racemization and dissociation rates of $[Fe(bpy)_3]^{2+}$ (Fig. 2) with the SDS concentration are similar to those for $[Fe(phen)_3]^{2+}$(Fig. 1). This suggests that the mechanisms of the rate changes are similar between the two complexes. Since the k_1 and β_1' values for the $[Fe(bpy)_3]^{2+}$-SDS or similar systems were not available, and since the formation of the 1:1 aggregate showed only a small effect on the measured reaction rates (as may be seen from the rate changes at low concentrations in Fig. 2), the kinetic results for the system were analyzed by disregarding the formation of the 1:1 aggregate. The disregard of the formation of the 1:1 aggregate for the $[Fe(phen)_3]^{2+}$-SDS system has little effect on the k_m, k_8, β_m', and β_8' values, although it enlarged the difference between the observed and the calculated rate constants at low SDS concentrations. For the $[Fe(bpy)_3]^{2+}$-SDS system, the calculated rate constants based on the parameter values obtained by disregarding the formation of the 1:1 aggregate agreed well with the observed values at low SDS concentrations (Fig. 2), showing that the approximation for the analysis was reasonably good. The results of the analysis for this system are listed in Table 1.

Table 1 shows that the aggregate formation constants, β_m' and β_8', are larger for systems with added NaCl than those without NaCl and larger for systems containing $[Fe(phen)_3]^{2+}$ than those containing $[Fe(bpy)_3]^{2+}$. This is natural since hydrophobic interaction is more pronounced in NaCl solutions than in solutions without NaCl, and phen is more hydrophobic than bpy.

Interaction of $[Fe(phen)_3]^{2+}$ and $[Fe(bpy)_3]^{2+}$ with SDS Micelles Above cmc. The phenomenon that the rates changed below the cmc, while they remained almost constant above the cmc, suggests that the complex ions

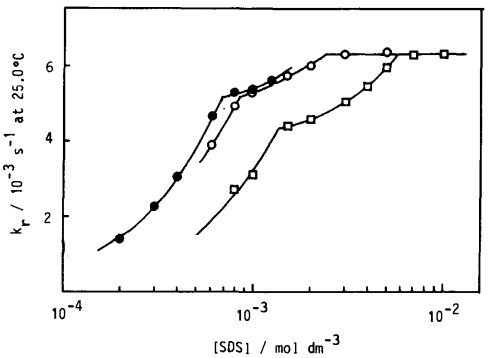

Fig. 3. Plot of the racemization rate constants of $[Fe(phen)_3]^{2+}$ against the logarithm of SDS concentration. ○, [NaCl]=0.4 mol dm^{-3}, $[Fe(phen)_3^{2+}]$=5×10^{-5} mol dm^{-3}; ●, [NaCl]=1.0 mol dm^{-3}, $[Fe(phen)_3^{2+}]$=5×10^{-5} mol dm^{-3}; □, [NaCl]=0.15 mol dm^{-3}, $[Fe(phen)_3^{2+}]$=2.5×10^{-4}mol dm^{-3}.

did not interact with micelles or that the reactivities of the complexes in the micelles were nearly the same as those in the aggregates. In order to clarify whether or not the complex ions interacted with the micelles, we measured the racemization rates of $[Fe(phen)_3]^{2+}$ in NaCl solutions ([NaCl]=0.4 and 1.0 mol dm^{-3} with [complex]=5×10^{-5} mol dm^{-3} and [NaCl]=0.15 mol dm^{-3} with [complex]=25×10^{-5} mol dm^{-3}, Fig. 3). In each case, the rate increased with an increase in the SDS concentration, steeply in the first region and then linearly and less steeply in the second region, until the rate reached a limiting value. Two break points were clearly observed. The SDS concentration at the first break point roughly corresponds to the cmc value,[20,21] suggesting that the micelles participated in the rate increase at the second step. The linear rate increase in the second region and the sharpness of the second break indicate that the association constant of the complex ions with the micelles is large and that the

TABLE 2. THE RATE CONSTANTS ($k/10^{-3}$ s^{-1}) AND THE ACTIVATION PARAMETERS OF RACEMIZATION OF $[Fe(phen)_3]^{2+}$ AND $[Fe(bpy)_3]^{2+}$ IN AQUEOUS AND MICELLAR SOLUTIONS

T/°C	$[Fe(phen)_3]^{2+}$		$[Fe(bpy)_3]^{2+}$	
	Without SDS	With SDS[a)]	Without SDS	With SDS[a)]
12.0	—	1.09(5)[b)]	—	—
15.0	—	1.73(8)	—	—
17.5	—	2.4(1)	—	—
20.0	0.30(1)	3.6(1)	0.26(1)	0.72(3)
22.5	0.42(2)	4.7(2)	0.39(2)	1.08(5)
25.0	0.65(3)	6.6(3)	0.61(3)	1.65(8)
27.5	1.00(5)	10.2(5)	0.92(4)	2.3(1)
30.0	1.53(7)	—	1.36(6)	3.3(1)
32.5	2.3(1)	—	1.98(9)	4.9(2)
35.0	3.4(1)	—	2.9(1)	6.9(3)
$\Delta H^{\ddagger}$ / kJ mol^{-1}	122.5(0.6)[b)]	98.6(1.4)	119.4(0.6)	109.9(0.7)
$\Delta S^{\ddagger}$ / J K^{-1} mol^{-1}	105(2)	43(6)	94(2)	70(2)

a) 0.02 mol dm^{-3}. b) The values in parentheses are the standard deviations.

association with the micelles was completed at the second break point. The number of $[Fe(phen)_3]^{2+}$ per micelle was calculated on the basis of the micellar concentration at the second break point and the concentration of the complex to be 6.7 and 4.3 in 0.15 and 0.4 mol dm^{-3} NaCl solutions respectively.[22] A similar number, 4.1, was reported for the $[Ru(bpy)_3]^{2+}$-SDS system.[16]

Location of the Complex Ions in a Micelle: The limiting rate of the racemization and dissociation of $[Fe(phen)_3]^{2+}$ in SDS solutions were, respectively, 10 and 1.7 times the rates in pure water, while those of $[Fe(bpy)_3]^{2+}$ were, respectively, 2.8 and 1.2 times the rates in pure water (Figs. 1 and 2). Similar increases in the reaction rates were also observed when the complex ions were dissolved in organic solvents[23-25] or were in contact with alkyl groups.[9,11] By analogy, the complex ions in the micelle are in contact with the alkyl chains of the dodecyl sulfate ions. Table 2 lists the rate constants at various temperatures for the racemization of the complexes in micellar solutions and in pure water, as well as the activation parameters. Figure 4 shows a plot of the activation enthalpy *vs.* the activation entropy for the racemization of $[Fe(phen)_3]^{2+}$ in aqueous and in alcohol-water solutions.[26] The fact that the activation parameters for the racemization of $[Fe(phen)_3]^{2+}$ in the micellar solution are close to those in pure butanols and in concentrated aqueous ethanol (0.90 mol. fraction) suggests that the complex ions were located inside the micelle-water interface or at the "Stern region"[27,28] of the micelle, and not on the interface. The activation parameters for $[Fe(bpy)_3]^{2+}$ also showed a similar, though less pronounced, tendency.

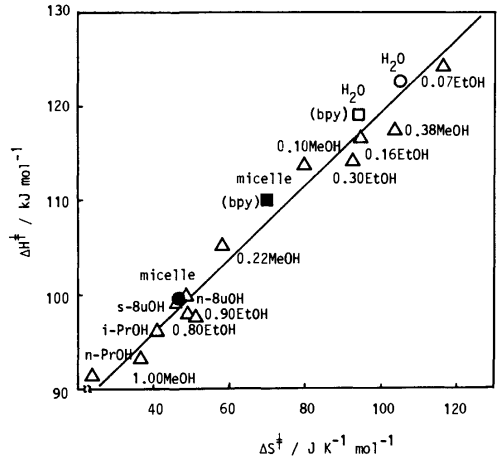

Fig. 4. Plot of activation enthalpy *vs.* activation entropy for the racemization of $[Fe(phen)_3]^{2+}$ (circle) and $[Fe(bpy)_3]^{2+}$ (square) in aqueous and micellar solutions and for the racemization of $[Fe(phen)_3]^{2+}$ in alcohol-water and alcohol solutions. ○, □: No SDS, no NaCl; ●, ■: 2×10^{-2} mol dm^{-3} SDS, no NaCl; △: alcohol-water (mole fraction of the alcohol is shown) and alcohol solutions.

Mechanism of Acceleration of the Reactions in the Micelle: The racemization of the complexes is known to proceed by means of an intramolecular twist mechanism in organic solvents.[25] The same is probably true for the complexes in the micelle. Table 2 shows that the higher rate of the racemization in micelles was brought about by the decrease in the activation enthalpy, though this decrease was partially compensated for by the decrease in the activation entropy. This can be related to the hydrophobic nature of the complex ions. In an aqueous solution, a cage-like "iceberg" structure formed around the complex ions[9] has to be broken for the complex ions to racemize, while no such iceberg structure is formed in the micelles and both $\Delta H^{\ddagger}$ and $\Delta S^{\ddagger}$ are expected to be smaller.

The dissociation rates of the complexes increased in the micelle, though the increase was much less pronounced than that of the racemization rates. The higher rate of the dissociation of $[Fe(phen)_3]^{2+}$ in the micelle is related mainly to a smaller activation enthalpy, and that of $[Fe(bpy)_3]^{2+}$, to a larger activation entropy (Table 3). This difference may be due to the difference in the mechanism of the dissociation between the two complexes; in the latter complex, dissociation

TABLE 3. THE RATE CONSTANTS ($k/10^{-3}$ s^{-1}) AND THE ACTIVATION PARAMETERS OF DISSOCIATION OF $[Fe(phen)_3]^{2+}$ AND $[Fe(bpy)_3]^{2+}$ IN AQUEOUS AND MICELLAR SOLUTIONS

T/°C	$[Fe(phen)_3]^{2+}$		$[Fe(bpy)_3]^{2+}$	
	Without SDS	With SDS[a)]	Without SDS	With SDS[a)]
15.0	0.0188(1)[b)]	0.0227(2)	0.0212(2)	0.0249(2)
20.0	0.0307(3)	0.0566(6)	0.0501(5)	0.0601(6)
25.0	0.0794(8)	0.135(1)	0.118(1)	0.143(1)
30.0	0.178(2)	0.316(3)	0.266(3)	0.329(3)
$\Delta H^{\ddagger}$ / kJ mol^{-1}	128.4(0.9)[b)]	124.6(1.3)	119.5(1.4)	122.0(1.1)
$\Delta S^{\ddagger}$ / J K^{-1} mol^{-1}	107(3)	99(5)	81(6)	91(4)

a) [SDS]=0.020 mol dm^{-3}. b) The values in parentheses are the standard deviations.

probably occurs through a five-coordinate intermediate with an open bipyridine chelate ring.

Kinetics and Mechanism of Dissociation of $[Fe(bpy)_3]^{2+}$ in Acidic Micellar Solutions: The increase in the HCl concentration increased the dissociation rate of $[Fe(bpy)_3]^{2+}$ in solutions with (1×10^{-2} mol dm^{-3}) and without SDS (Fig. 5). The rate changes with the HCl concentration can be described by the mechanism proposed by Basolo *et al.* (Fig. 6).[29] According to this mechanism, the dissociation rate constant, k', is expressed by:

$$k' = \frac{k_1'(k_2' + k_3'[H^+])}{k_{-1}' + k_2' + k_3'[H^+]}, \quad (4)$$

where k_1', k_{-1}', k_2', and k_3' are the rate constants for the reaction steps shown in Fig. 6. When $[H^+]$ is sufficiently low, the value of k' will be approximately equal to the limiting value given by:

$$k_0' = k_1'\left(\frac{k_2'}{k_{-1}' + k_2'}\right). \quad (5)$$

Then Eq. 4 is transformed to:

$$k' = k_1' - \frac{k_{-1}' + k_2'}{k_3'}\frac{k' - k_0'}{[H^+]}. \quad (6)$$

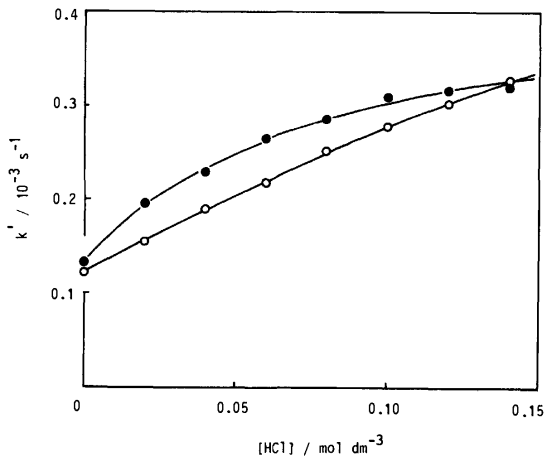

Fig. 5. Acid dependences of the dissociation rate constant of $[Fe(bpy)_3]^{2+}$ in aqueous and micellar solutions (I=0.15, NaCl): ○, No SDS; ●, 1×10^{-2} mol dm^{-3} SDS.

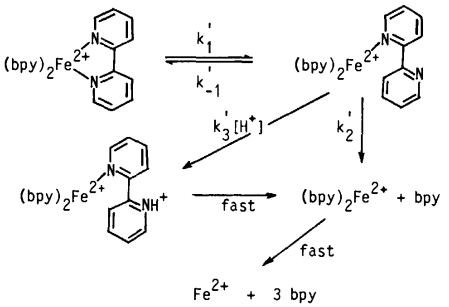

Fig. 6. Reaction scheme of the acid dependent dissociation of $[Fe(bpy)_3]^{2+}$.

TABLE 4. RESULTS OF THE ANALYSIS OF THE ACID DEPENDENCE OF THE DISSOCIATION RATE OF $[Fe(phen)_3]^{2+}$ IN AQUEOUS AND MICELLAR SOLUTIONS

	[SDS]=0	[SDS]=0.01 mol dm^{-3}
k_1' / 10^{-3} s^{-1}	1.3±0.5	0.44±0.03
k_2'/k_{-1}'	0.10±0.05	0.43±0.04
k_3'/k_{-1}' / mol^{-1} dm^3	1.8±1.1	18.1±4.3

The k' values were plotted against $(k'-k_0')/[H^+]$ to give a straight line with a slope of $-(k_{-1}'+k_2')/k_3'$ and an intercept of k_1'. These values, together with the k_0' ($=k_1'k_2'/(k_{-1}'+k_2')$) value, gave the k_2'/k_{-1}' and k_3'/k_{-1}' values listed in Table 4. The table shows that the rate constant of the formation of a five-coordinate intermediate with an open bipyridine chelate ring, k_1', is smaller in the presence of SDS than in its absence. In spite of this lower rate of intermediate formation, the dissociation rate of the complex was higher in the solution containing SDS (Fig. 5, for $[H^+]\leqq0.14$ mol dm^{-3}) because of the larger fraction of the intermediate undergoing dissociation (because of the larger $(k_2'+k_3'[H^+])/(k_{-1}'+k_2'+k_3'[H^+])$ value).

References

1) A part of this study was presented at the 28th Annual Meeting of Coordination Chemistry, Hamamatsu, Oct. 1979; Abstr. No. 3C09.

2) J. H. Fendler and E. J. Fendler, "Catalysis in Micellar and Macromolecular Systems," Academic Press, New York (1975).
3) J. R. Cho and H. Morawetz, *J. Am. Chem. Soc.*, **94**, 375 (1972).
4) J. Holzwarth, W. Knoche, and B. H. Robinson, *Ber. Bunsenges. Phys. Chem.*, **82**, 1001 (1978).
5) S. Diekmann and J. Frahm, *J. Chem. Soc., Faraday Trans. 1*, **75**, 2199 (1979).
6) V. C. Reinsborough and B. H. Robinson, *J. Chem. Soc., Faraday Trans. 1*, **75**, 2395 (1979).
7) H. Bruhn and J. Holzwarth, *Ber. Bunsenges. Phys. Chem.*, **82**, 1006 (1978).
8) K. V. Ponganis, M. A. de Araujo, and H. L. Hodges, *Inorg. Chem.*, **19**, 2704 (1980).
9) S. Tachiyashiki and H. Yamatera, *Bull. Chem. Soc. Jpn.*, **55**, 759 (1982).
10) S. Tachiyashiki and H. Yamatera, *Chem. Lett.*, **1981**, 1681.
11) S. Tachiyashiki and H. Yamatera, *Bull. Chem. Soc. Jpn.*, **57**, 1061 (1984).
12) F. P. Dwyer and E. C. Gyarfas, *J. Proc. R. Soc. N. S. Wales*, **83**, 263 (1950).
13) F. P. Dwyer and E. C. Gyarfas, *J. Proc. R. Soc. N. S. Wales*, **85**, 135 (1952).
14) Holzwarth *et al.* reported that the rate of the complex formation between 4-(2-pyridylazo)-*N*,*N*′-dimethylaniline and Ni^{2+} or Mn^{2+} in an SDS solution depended on the sample of SDS used (see Ref. 4). In our systems, however, the reaction rates did not depend on the sample of SDS used (Merck or Fluka (purmissimum grade)).
15) S. Tachiyashiki and H. Yamatera, *Bull. Chem. Soc. Jpn.*, **55**, 1014 (1982).
16) D. Meisel, M. S. Matheson, and J. Rabini, *J. Am. Chem. Soc.*, **100**, 117 (1978).
17) S. Ozeki, S. Tachiyashiki, S. Ikeda, and H. Yamatera, *J. Colloid Interface Sci.*, **91**, 430 (1983).
18) S. Tachiyashiki and H. Yamatera, *Bull. Chem. Soc. Jpn.*, **57**, 1067 (1984).
19) The least-squares fitting was carried out by using the program, "SALS" (Nakagawa and Oyanagi), in the library program of the Computer Center, Universiy of Tokyo.
20) M. L. Corrin and W. D. Harkins, *J. Am. Chem. Soc.*, **69**, 683 (1947).
21) J. N. Phillips, *Trans. Faraday Soc.*, **51**, 561 (1955).
22) The aggregation numbers of the SDS micelle were 115 and 126 in 0.15 and 0.4 mol dm^{-3} NaCl solutions respectively (Ref. 21).
23) F. M. Van Meter and H. M. Neumann, *J. Am. Chem. Soc.*, **98**, 1388 (1976).
24) S. Tachiyashiki and H. Yamatera, *Bull. Chem. Soc. Jpn.*, **54**, 3340(1981).
25) L. Seiden, F. Basolo, and H. M. Neumann, *J. Am. Chem. Soc.*, **81**, 3809 (1959).
26) S. Tachiyashiki and H. Yamatera, unpublished results.
27) F. M. Menger, *Acc. Chem. Res.*, **12**, 111 (1979).
28) Since the complex ions are about half as large as the micelle, the aggregation of the complex ions with a micelle may be regarded as the formation of a kind of mixed micelle instead of as the incorporation of the complex ions into the "Stern region" of the micelle.
29) F. Basolo, J. C. Hayes, and H. M. Neumann, *J. Am. Chem. Soc.*, **76**, 3807 (1954).

Mössbauer Spectroscopic Studies of the Effects of the $^6Li(n, \alpha)T$ Reaction in Lithium Tris(oxalato)ferrate(III)

Junko AKASHI, Yoshio UCHIDA, Tomoko KOJIMA, Motomi KATADA, and Hirotoshi SANO*
Department of Chemistry, Faculty of Science, Tokyo Metropolitan University, Fukasawa, Setagaya-ku, Tokyo 158
(Received June 4, 1983)

The chemical effects of the $^6Li(n,\alpha)T$ reaction in lithium tris(oxalato)ferrate(III) crystals were examined by means of Mössbauer spectroscopy. Neutron irradiations were carried out under different conditions in order to clarify the mechanism of the effects. The reduced iron(II) species observed in the spectrum of $Li_3[Fe(C_2O_4)_3]\cdot 4.5H_2O$, subjected to neutron irradiation (8.6×10^{15} n cm^{-2}) at 200 K, shows a larger Q.S. value than that in the spectrum of the sample neutron-irradiated at an ambient temperature (300—320 K) in a reactor, suggesting that the initially produced iron(II) species changes into another iron(II) species during the irradiation at the ambient temperature. A species identical with the initial iron(II) species produced in the neutron irradiation was found to be prepared by the pyrolysis of $Li_3[Fe(C_2O_4)_3]\cdot 4.5H_2O$. A comparison of neutron-irradiated hydrous and anhydrous $Li_3[Fe(C_2O_4)_3]$ suggests that the change in the iron(II) species is influenced by the existence of crystal water.

Mössbauer spectroscopy is one of the most useful tools in studying the chemical states nondestructively in solids. Based on the results of Mössbauer spectroscopic studies, it has been reported that iron(III) oxalate is reduced by γ-ray irradiation and that the results can be interpreted by the formation of iron(II) oxalate,[1] *i.e.*;

$$Fe_2(C_2O_4)_3 \rightarrow 2FeC_2O_4 + 2CO_2$$

Temperley suggested that the γ-ray-radiolysis of ammonium and sodium tris(oxalato)ferrate(III) could be explained by assuming this reaction;[2]

$$2M_3[Fe(C_2O_4)_3] \rightarrow 2FeC_2O_4 + 3M_2C_2O_4 \rightarrow 2CO_2,$$

while the iron(II) species observed in the Mössbauer spectrum of γ-ray-irradiated potassium tris(oxalato)-ferrate(III) was not definitely assigned to an iron(II) oxalate.[2] Bancroft *et al.* proposed this reaction;

$$2(K_3[Fe(C_2O_4)_3]\cdot 3H_2O) \rightarrow 2K_2[Fe(C_2O_4)_2(H_2O)_2] + K_2C_2O_4 + 2CO_2 + 2H_2O,$$

for the reduction induced by the γ-irradiation of the tris(oxalato)ferrate(III).[3]

Studies of the photo-irradiated potassium tris(oxalato)-ferrate(III) by using Mössbauer and infrared absorption spectroscopy have also revealed that several kinds of reduced iron species other than $FeC_2O_4\cdot 2H_2O$ were produced.[4]

Recently, we ourselves reported that a reduced iron(II) species was found in the Mössbauer spectrum taken for the $Li_3[Fe(C_2O_4)_3]\cdot 4.5H_2O$ sample subjected to the $^6Li(n,\alpha)T$ reaction,[5] although the mechanism of the formation of iron(II) species had not yet been clarified in detail.

In the present paper, the species produced by the $^6Li(n,\alpha)T$ reaction in lithium tris(oxalato)ferrate(III) were compared with those produced by thermal decomposition in order to clarify the processes caused by the $^6Li(n,\alpha)T$ reaction.

Experimental

$Li_3[Fe(C_2O_4)_3]\cdot 4.5H_2O$ was prepared by a conventional method. The particle size of the sample was adjusted to 200—350 mesh throughout this work. The difference in the effects of the particle size will be shown elsewhere. Thermogravimetry and differential scanning calorimetry were carried out for $Li_3[Fe(C_2O_4)_3]\cdot 4.5H_2O$ both in air and under nitrogen. The heating rate was kept at 5 K min^{-1}. Anhydrous $Li_3[Fe(C_2O_4)_3]$ was prepared by allowing the hydrous compound to stand for 10 min in an oven at 450 K in air. The anhydrous compound was kept in a desiccator over P_2O_5 to avoid moisture. The neutron irradiation of each 100-mg portion of the sample heat-sealed in a polyethylene envelope was carried out in a 100-kW Triga Mark II reactor at the Atomic Energy Institute of Rikkyo University. The irradiated samples were kept in liquid nitrogen until IR and Mössbauer measurements has been carried out.

In the thermal decomposition of $Li_3[Fe(C_2O_4)_3]\cdot 4.5H_2O$, a brown powder was obtained by putting the sample in an oven at 525—545 K for 5—10 min, either in air or under nitrogen, while a yellow powder was obtained when the sample was put in an oven at 500—510 K for 5—10 min under nitrogen.

The Mössbauer spectra were determined by using a constant-acceleration-type spectrometer. The isomer-shift values were reported with respect to iron foil. The infrared spctra were taken by the KBr method.

Results and Discussion

Mössbauer spectra of the neutron-irradiated (for 2 h at a fluence rate of 1.2×10^{12} n s^{-1} cm^{-2}) $Li_3[Fe(C_2O_4)_3]\cdot 4.5H_2O$ are shown in Fig. 1. The new doublet produced by the $^6Li(n,\alpha)T$ reaction shows a different Q.S. value depending on the temperature during the irradiation. The doublet A in Fig. 1(a), where the neutron irradiation was carried out at 200 K, has a larger Q.S. value (2.63 mm s^{-1}) than that (1.97 mm s^{-1}) of the doublet B shown in Fig. 1(b), where the neutron irradiation was carried out at the ambient temperature in the reactor (roughly estimated to be 300—320 K). The isomer-shift values of these doublets coincide with each other within the limits of experimental error. Figure 1(c) shows the spectrum of the same sample as that shown in Fig. 1(a) after it had been allowed to stand for 5 months at room temperature (295—298 K). The doublet A decreases in intensity, and a doublet appears at the same position as that of the doublet B. The results suggest that an unstable species which has a larger Q.S. value changes into a stable species during the irradiation at the ambient temperature or during storage for a long time at room temperature.

The results of the thermogravimetry and differential

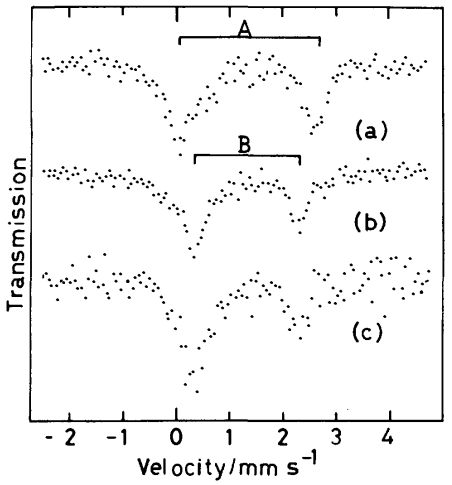

Fig. 1. Mössbauer spectra at 80 K of (a) neutron-irradiated (1.2×10^{12} n s^{-1} cm^{-2}, 2 h, at 200 K) $Li_3[Fe(C_2O_4)_3]\cdot4.5H_2O$, (b) neutron-irradiated (1.2×10^{12} n s^{-1} cm^{-2}, 2 h, at an ambient temperature) $Li_3[Fe(C_2O_4)_3]\cdot4.5H_2O$, and (c) neutron-irradiated (1.2×10^{12} n s^{-1} cm^{-2}, 2 h, at 200 K) $Li_3[Fe(C_2O_4)_3]\cdot4.5H_2O$ after storage for 5 months at room temperature.

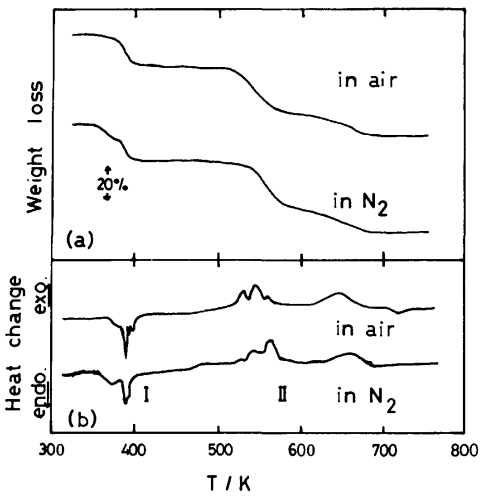

Fig. 2. (a) TG curves for $Li_3[Fe(C_2O_4)_3]\cdot4.5H_2O$ in air and under nitrogen, and (b) DSC curves for $Li_3[Fe(C_2O_4)_3]\cdot4.5H_2O$ in air and under nitrogen.

scanning calorimetry of $Li_3[Fe(C_2O_4)_3]\cdot4.5H_2O$, both in air and under nitrogen, are shown in Fig. 2. As is shown by the TG curves, the hydrous complex evolves 4.5 mol of water endothermically in stage I. The split peak in the DSC curves of dehydration indicates that the water molecules are not held uniformly in the crystal lattice. On the basis of the results, it is concluded that the dehydration ocurrs at a higher temperature in lithium tris(oxalato)ferrate(III) than the temperature reported for the corresponding potassium salt.[6-9]

For $K_3[Fe(C_2O_4)_3]\cdot3H_2O$, a decomposition reaction such as

$$K_3[Fe(C_2O_4)_3]\rightarrow K_2[Fe(C_2O_4)_2]+1/2K_2C_2O_4+CO_2$$

was proposed for the second stage under nitrogen, where one mol of CO_2 was evolved.[6-9] On the contrary, a weight change corresponding to two moles of CO_2 was observed in stage II of the thermal decomposition of $Li_3[Fe(C_2O_4)_3]\cdot4.5H_2O$, either in air or under nitrogen.

A Mössbauer spectrum of thermal-decomposition product in stage II in air is shown in Fig. 3(a). When the decomposition occurs at 525—545 K, a doublet ascribed to a high-spin iron(III) species (I.S.=0.44, Q.S.=0.95 mm s^{-1}) is observed. The same species was also found in the spectrum of the sample decomposed under nitrogen in the same temperature range. As the weight loss of the sample in stage II corresponds to two moles of CO_2, the formation of $Li[Fe(III)(C_2O_4)_2]$ may be suggested for this stage.

A Mössbauer spectrum at 80 K of the sample thermally decomposed at 500—510 K under nitrogen is shown in Fig. 3(b). The Mössbauer parameters of the iron(II) species produced thus coincide with those of

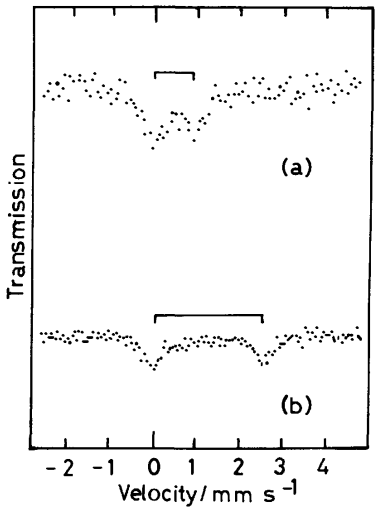

Fig. 3. Mössbauer spectra at 80 K of $Li_3[Fe(C_2O_4)_3]\cdot4.5H_2O$ (a) decomposed at 525—545 K in air, and (b) decomposed at 500—510 K under nitrogen.

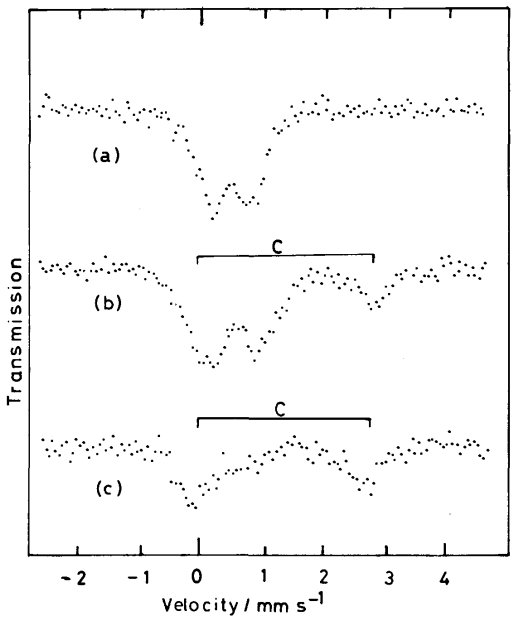

Fig. 4. Mössbauer spectra at 80 K of (a) unirradiated, (b) neutron-irradiated (5×10^{11} n s^{-1} cm^{-2}, 2 h), and (c) neutron-irradiated (1.2×10^{12} n s^{-1} cm^{-2}, 4 h) anhydrous $Li_3[Fe(C_2O_4)_3]$.

the doublet A in Fig. 1. The formation of this yellow product may correspond to a small heat change without any remarkable change in the weight at 465 K under nitrogen. The color change is accompanied by a reduction of iron(III) to iron(II), as is observed in the thermal decomposition of $K_3[Co(C_2O_4)_3]\cdot 3H_2O$ at 393 K.[6]

A Mössbauer spectrum at 80 K of anhydrous $Li_3[Fe(C_2O_4)_3]$ is shown in Fig. 4(a). The dehydration of the sample was confirmed by measuring the weight loss of the sample by heating and IR spectrum of the sample; the weight loss of the compound coincides with the theoretical value within 2%. Although the Mössbauer spectrum of $Li_3[Fe(C_2O_4)_3]\cdot 4.5H_2O$ consists of a broad single peak due to magnetic relaxation, the spectrum of the anhydrous compound consists of an asymmetric doublet with a narrower line-width. The difference between the Mössbauer spectra of the hydrous and anhydrous lithium tris(oxalato)ferrate(III) implies that the spin-spin relaxation time decreases in the anhydrous compound compared with the hydrous compound because of the decreased average Fe-Fe distance.

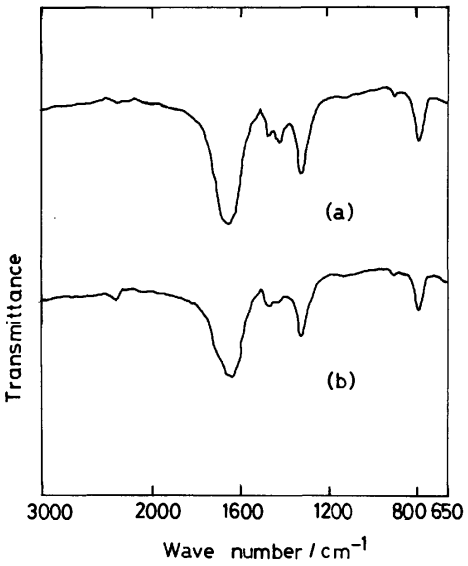

Fig. 5. IR spectra of (a) neutron-irradiated (1.2×10^{12} n s^{-1}cm^{-2}, 4 h) $Li_3[Fe(C_2O_4)_3]$, and (b) thermally decomposed (500—510 K under nitrogen) $Li_3[Fe(C_2O_4)_3]\cdot 4.5H_2O$.

Table 1. Mössbauer parameters of the species A, B, and C shown in Figs. 1 and 4, and of the thermally decomposed $Li_3[Fe(C_2O_4)_3]\cdot 4.5H_2O$

Species	I.S. / mm s^{-1}	Q.S. / mm s^{-1}
A	1.26	2.63
B	1.32	1.97
C	1.32	2.86
Product after heating at 525—545 K in air	0.44	0.95
Product after heating at 500—510 K under nitrogen	1.30	2.60

A Mössbauer spectrum of neutron-irradiated (5×10^{11} n s^{-1}cm^{-2}, 2 h, at the ambient temperature) anhydrous $Li_3[Fe(C_2O_4)_3]$ is shown in Fig. 4(b). The doublet C (I.S.=1.32, Q.S.=2.86 mm s^{-1}) is ascribed to a high-spin iron(II) species produced by neutron irradiation; it is similar in I.S. value to the doublets A and B. When the anhydrous $Li_3[Fe(C_2O_4)_3]$ is irradiated at a higher neutron fluence rate (1.2×10^{12} n s^{-1}cm^{-2}) and for a longer period (4 h) than those in Fig. 4(b), a species which has the same Mössbauer parameters as the doublet C is obtained as the main product, as is shown in Fig. 4(c). The Mössbauer parameters for the species A, B, and C, shown in Figs. 1 and 4, and the thermally decomposed products are summarized in Table 1 for the sake of comparison. As may be seen in Fig. 5, the IR spectrum of the sample shown in Fig. 4(c) is similar to that of the thermally decomposed product at 500—510 K under nitrogen. Thus, the species produced through the neutron irradiation of $Li_3[Fe(C_2O_4)_3]$ is concluded to be produced also by the thermal decomposition. Although the cause of different Q.S. values of the product in the anhydrous compound has not yet been fully elucidated, the different crystal structure of the anhydrous compound may explain the small difference in the Q.S. value of the new species produced in the original host crystal lattice.

The Fe(II) species produced in the neutron-irradiated $Li_3[Fe(C_2O_4)_3]$ and $Li_3[Fe(C_2O_4)_3]\cdot 4.5H_2O$ are ascribed to a precursor of $[Fe(C_2O_4)_2]^{2-}$ and a hydrous or anhydrous $[Fe(C_2O_4)_2]^{2-}$ species respectively. Since the weight decrease corresponding to one mol of the oxalato ligand is not observed in the neutron irradiation of the sample, decomposed fragment species, such as CO_2, produced from the oxalato ligand seem to remain in the crystal lattice of the irradiated sample.

As the spectral component C remains even after a long period of irradiation of the anhydrous compound, the change in the species A to the species B, shown in Fig. 1(a) and in Fig. 1(b) respectively, can be concluded to be related to the existence of crystal water, for instance, in such a way that the presence of water molecules is involved in stabilizing the species A to B, although further investigations are required to identify those iron(II) species.

References

1) N. Saito, H. Sano, T. Tominaga, and F. Ambe, *Bull. Chem. Soc. Jpn.*, **38**, 681 (1965).
2) A. A. Temperley, *Bull. Am. Phys. Soc.*, **12**, 924 (1967).
3) G. M. Bancroft, K. G. Dharmawardena, and A. G. Maddock, *J. Chem. Soc., A*, **1969**, 2914.
4) H. Sato and T. Tominaga, *Bull. Chem. Soc. Jpn.*, **52**, 1402 (1979).
5) J. Akashi, M. Katada, and H. Sano, *Chem. Lett.*, **1982**, 785.
6) N. Tanaka and N. Nanjo, *Bull. Chem. Soc. Jpn.*, **42**, 330 (1967).
7) N. Tanaka and K. Sato, *Bull. Chem. Soc. Jpn.*, **43**, 789 (1970).
8) K. Nagase, *Bull. Chem. Soc. Jpn.*, **45**, 2166 (1970).
9) K. Nagase, *Bull. Chem. Soc. Jpn.*, **46**, 144 (1973).

 © 1984 The Chemical Society of Japan Bull. Chem. Soc. Jpn., 57, 1079—1082 (1984)

Preparation of Aluminum Fluoride Film with Graphite Fluoride

Nobuatsu WATANABE,* Hidehiko OHARA, and Tsuyoshi NAKAJIMA
Department of Industrial Chemistry, Faculty of Engineering, Kyoto University, Sakyo-ku, Kyoto, 606
(Received July 25, 1983)

An aluminum fluoride film covered by graphite fluoride on metallic aluminum was prepared by reaction in the ternary system of aluminum, graphite and fluorine gas at 450—550 °C. The film consisted of a large amount of aluminum fluoride covered by thin graphite fluoride layers. The contact angle of a water drop on the film was around 120 °, which decreased to 85—95 ° during 45 d probably due to reaction with moisture and/or water drop. Almost no oxygen was detected in the film. The film formation would be based on the reduction of oxide layer on aluminum by carbon radical produced by thermal decomposition of graphite fluoride.

An aluminum fluoride film covered by graphite fluoride is formed by the reaction of metallic aluminum with graphite fluoride in a fluorine atmosphere at 450—600 °C.[1)]

$$Al + (CF)_n + F_2 \xrightarrow{450-600°C} \text{Aluminum fluoride film with graphite fluoride} \quad (1)$$

This film had a low surface energy with a contact angle for a water drop, *ca.* 120 ° and was an electric insulator. The value of the contact angle is the same as that on the basal plane of graphite fluoride.[2)] The fluoride film is also prepared through another route of the ternary system of aluminum, graphite and fluorine gas,[1)] in which graphite fluoride would be preferentially formed and then react with aluminum.

In this study, the preparation and structure of the aluminum fluoride film with graphite fluoride was investigated in the ternary system of aluminum, natural graphite and fluorine gas.

Experimental

An aluminum plate (18×14×0.8 mm, purity: 99.99%) was used after immersion in 10% NaOH solution for 5 min and in 3 M† HNO_3 for 10 s to remove oily material on the surface. Other starting materials were Madagascar natural graphite (40—47 μm, purity: 99.4%) and high purity fluorine gas (99.4%).

The fluoride film is prepared as follows. A nickel vessel containing the aluminum plate (2 sheets) and graphite powder (1 g) was placed in a nickel reactor, followed by pumping at room temperature. After heating to a reaction temperature, the reactor was filled with fluorine gas of 1 atm. During the reaction, the reactor was rotated at 2 min^{-1} by a motor with a mechanical seal. The fluoride film so prepared was analyzed by contact angle measurements (at 30 °C), X-ray diffractometry (by Cu$K\alpha$), X-ray microanalyzer, IR and ESCA spectroscopies.

Resuts

Contact Angle of a Water Drop on the Fluoride Film. A fluoride film having a high contact angle (Fig. 1) and smooth surface was obtained by the reaction performed at 450—500 °C. It was very difficult to prepare such a film below 400 °C, and aluminum plate was often deformed at higher temperature of 550—600 °C.

Figure 2 is the change of a contact angle on a surface film of aluminum as a function of reaction time. A

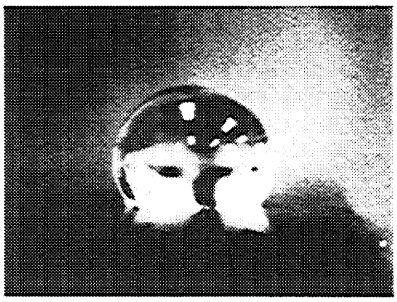

Fig. 1. Contact angle of water drop (θ) on the graphite fluoride film.
θ=125°, Preparation of the film: 500 °C, 24 h.

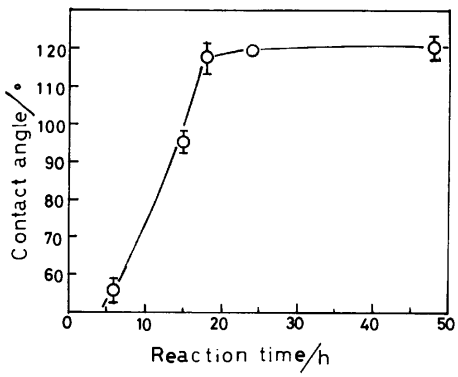

Fig. 2. Contact angle of water drop on surface film of aluminum as a function of reaction time.
Reaction temperature: 500 °C.

fluoride film with a contact angle of 120 ° was prepared by the reaction for 20 h. The change in the surface appearance with reaction time is shown in Fig. 3. At the beginning of a reaction, a white amorpous substance of 50—100 μm in thickness and with a low contact angle was formed on the surface of the aluminum (Fig. 3a). It consisted of aluminum fluoride and fluorinated aluminum carbide, as shown later from X-ray diffraction pattern and ESCA spectra. As the reaction progressed, a black part began to appear as shown in Fig. 3b, being a very thin film (<10 μm) with a higher contact angle. After 20 h, the film formation was completed. The aluminum surface was covered by a thin black film of 3—8 μm with a contact angle of 127.5 ° (Fig. 3c).

Figure 4 shows the change of the contact angles of fluoride films prepared at different temperatures with the holding time in air. The contact angle gradually decreased from 120 ° to 85—95 ° during 45 d. This might be due to reaction with moisture in air or the

†1 M=1 mol dm^{-3}

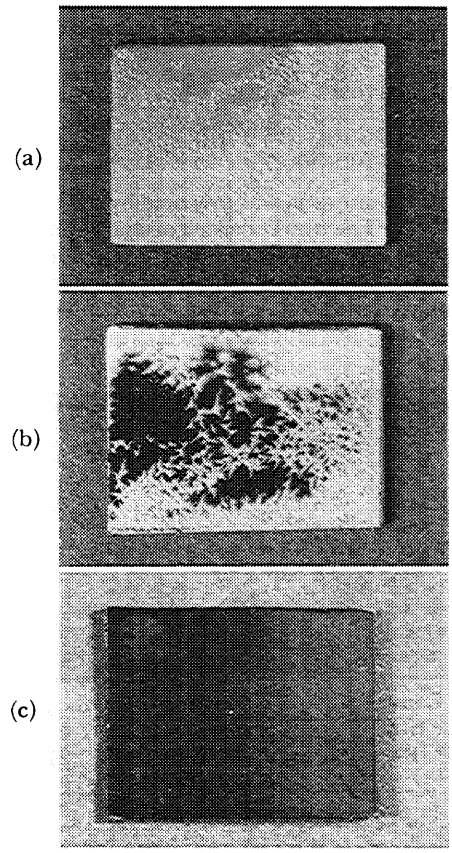

Fig. 3. Change of surface film of aluminum with reaction time.
a) Reaction: 12 h, 500 °C. Contact angle: 30.5°. Film thickness: 50—100 μm. b) Reaction: 18 h, 500 °C. Contact angle: 89° (black part), 50° (white part). c) Reaction: 24 h, 500 °C. Contact angle: 127.5°. Film thickness: 3—8 μm.

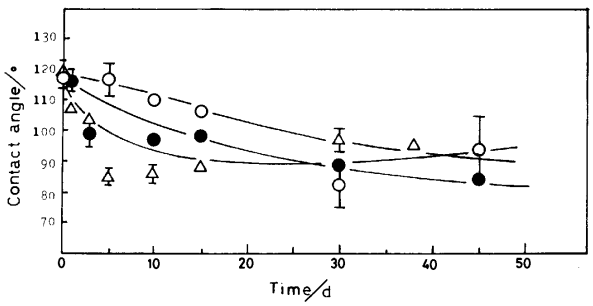

Fig. 4. Change in contact angle of water drop on surface film of aluminum as a function of time.
○: 500 °C, 18 h, ●: 500 °C, 24 h, △: 500 °C, 48 h.

water drop used in the contact angle measurement. The decrease in the contact angle was larger for a fluoride film wetted by a water drop on the contact angle measurement than for that only left in air.

IR Spectra. Figure 5 shows the IR spectra (ATR) of the fluoride films. Figure 5a was measured several days after preparation of a film having a contact angle of 92—133°. A broad absorption observed around 1220 cm^{-1} is assigned to a CF stretching vibration (1215 cm^{-1}) and CF_2 symmetric and asymmetric vibrations (1380, 1110 cm^{-1}) of graphite fluoride.[3] A strong absorption around 600 cm^{-1} indicates aluminum

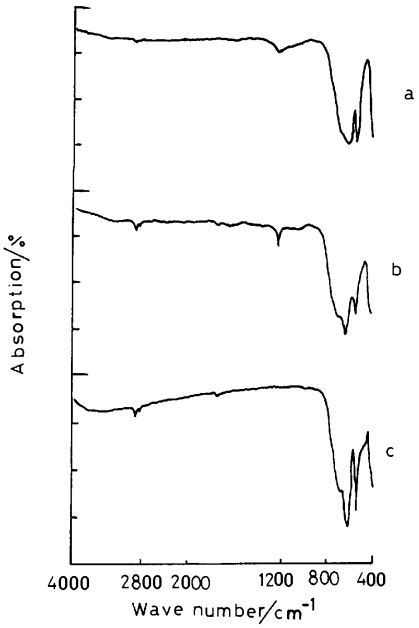

Fig. 5. IR spectra (ATR) of surface film of aluminum.
a: θ=92—133°, reaction: 500 °C, 24 h. b: θ=114→70°, reaction: 450 °C, 48 h. c: θ=Spread, reaction: 550 °C, 72 h.

fluoride. It was found from the intensity of each absorption band that the fluoride film contained a large amount of aluminum fluoride and a small amount of graphite fluoride. Figure 5b was obtained for a sample whose contact angle decreased from 114° to 70° by the reaction with moisture and water drops. In addition to a sharp absorption of the CF stretching vibration, two absorptions for carbonyl groups appeared around 1600 cm^{-1} and 2800—3000 cm^{-1}, respectively. The decrease of contact angle is probably because CF_2 group was removed by the reaction with water and the carbonyl groups were newly formed. Only carbonyl groups were found for a film on which water drop spread (Fig. 5c).

X-Ray Diffraction Pattern. An example of the X-ray diffraction pattern of a fluoride film in given in Fig. 6 where α and γ-AlF_3 and metallic aluminum were observed. No diffraction line of graphite fluoride was detected probably because of the very thin film.

X-Ray Microanalysis. Figure 7 is the elemental analysis of a cross section of a fluoride film. It was

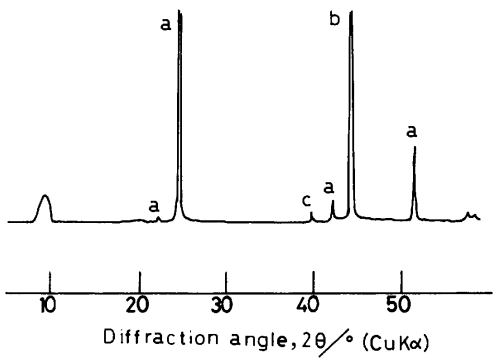

Fig. 6. X-Ray diffraction pattern of surface film of aluminum.
a: α-AlF_3, b: Al, c: γ'-AlF_3
Reaction: 500 °C, 48 h.

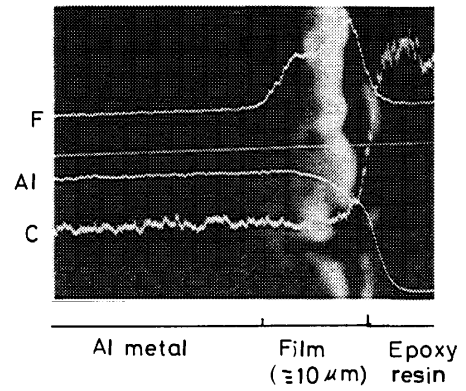

Fig. 7. Elemental analysis by X-ray microanalyser Reaction: 500 °C, 24 h.

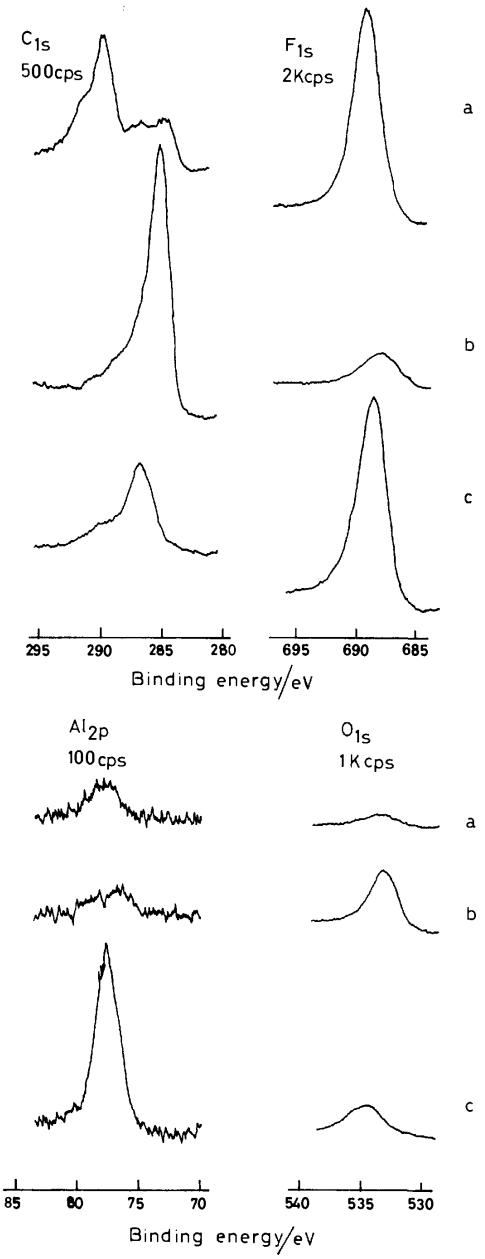

Fig. 8. ESCA spectra of surface film of aluminum. a: θ=106.3°, reaction: 450 °C, 24 h. b: θ= 121.3→83.7°, reaction: 475 °C, 48 h. c: θ=81.0°, reaction: 550 °C, 24 h.

found that the film contained large amounts of fluorine and aluminum, and a small amount of carbon. The amounts of fluorine and carbon increased toward the surface of the film while that of aluminum gradually decreased. It is surprising that no oxygen was detected in the film.

ESCA Spectra. ESCA provides the information on a chemical bond of a solid surface. Figure 8a is the spectra of a film with a high contact angle. C_{1s} spectrum had two peaks at 290.0 and 292.0 eV corresponding to CF and CF_2 groups of graphite fluoride, respectively. The position of the F_{1s} peak is the same as that of graphite fluoride. The peak for Al_{2p} was found at 77.9 eV slightly higher than that of aluminum fluoride. O_{1s} peak was observed although the peak intensity was extremely low compared with that of the F_{1s} peak. Figure 8b was obtained for a film after its contact angle decreased from 121.3° to 83.7°. The C_{1s} and F_{1s} peaks corresponding to CF and CF_2 groups were decreased remarkably by the decomposition of thin graphite fluoride layers. The C_{1s} peak, indicating hydrocarbon compounds, appeared strongly at 285.0 eV, and the F_{1s} peak was shifted to 688.0 eV near that of aluminum fluoride. On the other hand, the intensity of O_{1s} peak increased considerably probably because of the formation of carbonyl groups. Figure 8c shows the spectra of a film with a low contact angle. It seems that this sample was in the course of the formation of graphite fluoride film as shown in Fig. 3a. The C_{1s} spectrum had a strong peak at 286.7 eV which was consistent with that of aluminum carbide, Al_4C_3, fluorinated by fluorine gas at 500 °C. The peak around 290 eV indicating graphite fluoride had a low intensity. Fluorinated aluminum carbide gave an F_{1s} peak at the same position, 688.7 eV, as that of graphite fluoride. This result suggests the formation of an Al-C-F bond. The high intensity of the Al_{2p} formation of an Al-C-F bond. The high intensity of the Al_{2p} peak would be due to fluorinated carbide and aluminum fluoride since the graphite fluoride layer was not formed appreciably. The O_{1s} peak was found at a higher posi-

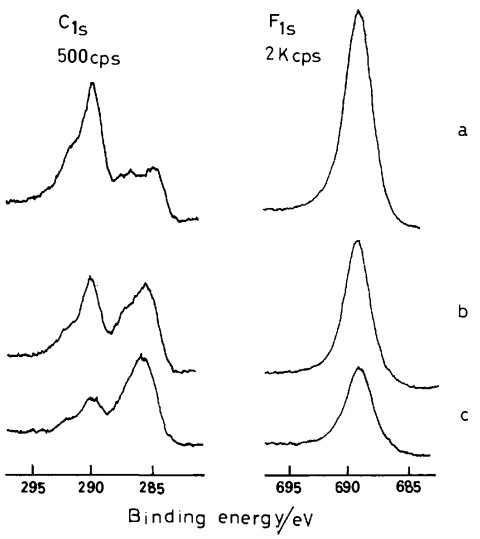

Fig. 9. ESCA spectra of surface film of aluminum. a: Film surface, b, c: polished by an emery paper.

tion than that of aluminum oxide probably because of the formation of fluoride oxide. Figure 9 is the spectra of the inside of a film obtained by polishing with an emery paper. Graphite fluoride decreased toward the inside of the film, while the peak of the fluorinated carbide at 286.7 eV increased. The latter was also decreased by further polishing and the peak for the aluminum substrate appeared.

Discussion

Structure of the Fluoride Film. From the results obtained by X-ray diffractometry, IR and ESCA spectroscopies, it was found that the fluoride film consisted of a large amount of aluminum fluoride and thin graphite fluoride layers around the film surface. The CF group comprised in graphite fluoride and fluorinated aluminum carbide rapidly decreased from the surface of the film into the inside. ESCA spectra suggested that graphite fluoride layers were chemically bonded to aluminum metal through the fluorinated aluminum carbide.

The contact angle of the water drop on the film was around 120°, which was almost equal to that for graphite fluoride prepared from flaky natural graphite.[2] The contact angle gradually decreased from *ca.* 120° to around 90°. This was explained by the IR spectra of the films. As shown by ESCA spectra, graphite fluoride on the surface of the fluoride film would have a chemical bond with the aluminum substrate through the fluorinated aluminum carbide having an ionic nature. Aluminum carbide with an ionic bond is easily decomposed by reaction with water. There would be many CF_2 groups around the edge of the graphite fluoride layer of the film as well as graphite fluoride powder. It is expected that these CF_2 groups are slightly ionic in chemical bond, being different from the CF_2 group with a covalent bond in graphite fluoride itself. For this reason, the CF_2 groups of the fluoride film would be decomposed by the reaction with moisture in air or water drop. As a result, the carbonyl groups were formed on the surface of the film.

No oxygen was detected on elemental analysis by X-ray microanalyzer. In this case, the analyzed depth is about 1 μm and the detection limit of oxygen is 0.1%. The analyzed area was a cross section of a fluoride film (≅10μm) bonded to aluminum substrate as shown in Fig. 7. In the case of ESCA, the analyzed area is the sample surface itself (2×10^{-5} m^2), and the analyzed depth is limited by the mean free path of the photoelectron in the solid; this is only several nanometers. Oxygen adsorbed on a sample surface is therefore easily detected by ESCA measurement. For example, almost the same amount of oxygen is detected for the surface of poly(tetrafluoroethylene) which does not contain oxygen in the structure. Accordingly, it can be said that the fluoride film contains almost no oxygen.

Reaction of Aluminum with Graphite Fluoride and Fluorine. The attempts to prepare a pure aluminum fluoride film on the surface of aluminum were made by electrochemical fluorination in hydrogen fluoride and by reaction with fluorine gas at a high temperature. However, they were unsuccessful because oxygen contained in the surface oxide layer of aluminum could not be removed by such fluorination reactions.[4] Since aluminum oxide is very stable, it is very difficult to reduce aluminum oxide below 600°. The reduction of an oxide film on aluminum would be attained only by chemically active species such as radicals. Graphite fluoride somewhat decomposes at 450—600°C, giving CF_2 radicals[5-7] with life time of the order of second.[8-10]

$$2(CF)_n \longrightarrow n\mathrm{C(amorphous)} + xCF_2 + yC_2F_4 \quad (2)$$

The products obtained by thermal decomposition of $(CF)_n$ are amorphous carbon, unsaturated fluorocarbons (C_2F_4, C_3F_6) and saturated fluorocarbons (CF_4, C_2F_6, C_3F_8).[5-7] It was reported that C_2F_4 does not decompose to CF_4 below 700°C.[11] The saturated fluorocarbons are therefore regarded as 2nd order products of CF_2 radicals. It is then expected that the CF_2 radical decomposes to a carbon radical and CF_4 by the disproportionation reaction.

$$2CF_2 \longrightarrow C^* + CF_4 \quad (3)$$

C*: carbon radical

This carbon radical would reduce the oxide layer of aluminum.

$$Al_2O_3 + 3C^* \longrightarrow 2Al + 3CO \quad (4)$$

$$CO + F_2 \longrightarrow COF_2 \quad (5)$$

Metallic aluminum Al* would immediately react with fluorine gas, CF_2 radical, carbon radical C* and/or graphite fluoride.

$$Al^* + 3/2F_2 \longrightarrow AlF_3 \quad (6)$$

$$Al^* + CF_2 \longrightarrow Al\text{-}CF_2 \quad (7)$$

$$Al^* + C^* \longrightarrow Al\text{-}C \quad (8)$$

$$Al^* + (CF)_n \longrightarrow Al\text{-}(CF)_n \quad (9)$$

The product of reactions (7) and (8) would further react with radical species and/or graphite fluoride to produce the fluoride film with graphite fluoride.

References

1) H. Yamada, T. Nakajima, and N. Watanabe, *Angew. Chem.*, **21**, 378 (1982); *Int. Ed.*; *Suppl.*, 939 (1982).
2) N. Watanabe, T. Nakajima, and N. Ohsawa, *Bull. Chem. Soc. Jpn.*, **55**, 2029 (1982).
3) R. J. Lagow, R. B. Badachhape, J. L. Wood, and J. L. Margrave, *J. Chem. Soc., Dalton Trans.*, **1974**, 1268.
4) H. Yamada, T. Nakajima, and N. Watanabe, *Nippon Kagaku Kaishi*, **1982**, 1305.
5) N. Watanabe, S. Koyama, and H. Imoto, *Bull. Chem. Soc. Jpn.*, **53**, 2731 (1980).
6) N. Watanabe and S. Koyama, *Bull. Chem. Soc. Jpn.*, **53**, 3093 (1980).
7) N. Watanabe, T. Kawamura, and S. Koyama, *Bull. Chem. Soc. Jpn.*, **53**, 3100 (1980).
8) P. Cadman, J. D. Scott, and J. M. Thomas, *Surf. Interface Anal.*, **1**, 115 (1979).
9) F. W. Dalby, *J. Chem. Phys.*, **41**, 2297 (1964).
10) F. X. Powell and D. R. Lide, *J. Chem. Phys.*, **45**, 1067 (1966).
11) B. Atkinson and V. A. Atkinson, *J. Chem. Soc.*, **1975**, 2086.

 © 1984 The Chemical Society of Japan Bull. Chem. Soc. Jpn., 57, 1083—1086 (1984)

Kinetic Trace Determination of Molybdenum(VI), L-Ascorbic Acid, and Thiosulfate Using Landolt Reaction by the Aid of Fluorometry

Masamitsu KATAOKA,* Hirotoshi HEMMI, and Tomihito KAMBARA†

Department of Chemistry, Faculty of Science, Hokkaido University, Kita 10, Nishi 8, Kita-ku, Sapporo 060

(Received September 19, 1983)

Trace amounts of molybdenum(VI) can be determined by the use of their catalytic effects on the peroxoborate-iodide redox reaction in acidic medium. The indicator reaction is transformed to a Landolt reaction by the addition of ascorbic acid into the reaction mixture, *i.e.*, the iodine produced by the reaction is immediately reduced by ascorbic acid. The end of the induction period of the Landolt process was fluorometrically detected by the aid of disappearence of fluorescence of Rhodamine B. Trace determination of molybdenum(VI) was carried out by employing the linear relationship between the reciprocal of induction period and catalyst concentration. The most suitable concentrations of sodium peroxoborate, potassium iodide, and hydrochloric acid in the reaction mixture were found to be 9 mM, 0.1 M, and 0.1 M, respectively. By this method, molybdenum(VI) can be determined from 80 nM to 10 mM (7.675 ng ml^{-1} to 95.95 mg ml^{-1}). The effect of foreign ions were studied and an equal amount of tungsten(VI), and 10-fold amounts of zirconium(IV), iron(II), iron(III), vanadium(IV), and copper(II) were found to show interference. Ascorbic acid and thiosulfate in micro mol l^{-1} levels were also determined by the present method employing the linear relationship between the induction period and the reductant concentration.

Kinetic methods of analysis by the aid of catalytic reactions are used in many fields of chemical analysis because of their extremely high sensitivity, and are summarized in books[1-4] and reviews[5-14]

The Landolt reaction is frequently applied to the micro-determination of various metal ions[15-23] and some reducing agents.[24] Svehla[14] reviewed the application of Landolt reaction in quantitative catalytic analysis.

The present authors had been reported kinetic micro-determinations of molybdenum(VI),[25] tungsten(VI), and vanadium(V)[26] which catalyse the redox reaction of peroxoborate-iodide system, using iodide ion-selective electrode as the tracer of reaction rate. In the present work, the indicator reaction is transformed to a Landolt reaction by the addition of L-ascorbic acid. The end of the induction period was monitored fluorophotometrically. Micro amounts of molybdenum(VI) can be determined by plotting the reciprocal of the induction period against its concentration. Also, L-ascorbic acid and thiosulfate in micro molar levels were determined by the use of the linear relationship between the induction period and their concentration.

Theory

The indicator reaction on which the present method is based proceeds as follows:

$$BO_3^- + 3\,I^- + 2\,H^+ \longrightarrow BO_2^- + I_3^- + H_2O. \quad (1)$$

In the presence of catalyst, this redox reaction proceeds with a considerable rate, but it proceeds very slowly without catalyst. In the presence of a reducing agent, *e.g.*, ascorbic acid, triiodide ions produced are immediataly reduced so that the iodide ion concentration is kept constant until all the L-ascorbic acid is oxidized.

$$C_6H_8O_6 + I_3^- \longrightarrow C_6H_6O_6 + 3\,I^- + 2\,H^+ \quad (2)$$

When ascorbic acid has been consumed completely, triiodide ions appear in the reaction mixture and the solution turns yellow. The time length necessary to elapse till the appearance of triiodide ions is called the induction period.

Concentration of hydrogen ion does not change during induction period because the oxidation of ascorbic acid releases the same number of hydrogen ions, as shown in Eq. 2. Thus, iodide and hydrogen ion concentrations remain constant so long as ascorbic acid is present. The reaction rate can be expressed as

$$-\frac{d[BO_3^-]}{dt} = (k \cdot C_k + k')[BO_3^-] \quad (3)$$

where k and k' are the products of rate constants of catalyzed and uncatalyzed reaction including the concentrations of hydrogen and iodide ion, and C_k is the catalyst concentration. Integration of Eq. 3 yields

$$\frac{1}{t} = \frac{k \cdot C_k + k'}{\ln \dfrac{[BO_3^-]_0}{[BO_3^-]_0 - [C_6H_8O_6]_0}}$$

where t is the induction period and $[BO_3^-]_0$ and $[C_6H_8O_6]_0$ are the initial concentrations of peroxoborate ion and ascorbic acid, respectively.

Hence plotting the reciprocal of induction period against catalyst concentration gives a linear calibration graph.

The end of the induction period, *i.e.*,the appearance of triiodide ion in the reaction mixture was fluorophotometrically detected by the aid of the following reaction:[27]

$$\underset{\text{(fluorescence)}}{\text{Bhodamine B}} + I_3^- \longrightarrow \underset{\text{(none-fluorescence)}}{\text{Product.}} \quad (5)$$

Here triiodide ion may act as a quenching ion.[28] Some reductants, *i.e.*, ascorbic acid and thiosulfate ion, can also be determined by utilizing the linear relationship between the induction period and their concentration.

† Present address: Hakodate Technical College, Tokura-cho, 226, Hakodate 042.

Experimental

Apparatus. All the fluorescence measurements were carried out with a Shimadzu spectrofluorophotometer, RF-510, connected with a Shimadzu recorder, U-125MU. The temperature of the fluorophotometric cell was kept constant to 25±0.5°C by the use of a Yanagimoto constant temperature bath, P8-PC. A Hitachi pH meter, F-5 was used for pH measurements.

Reagents. Molybdenum(VI) stock solution(0.01 M) was prepared by dissolving 1.7656 g of analytical reagent grade ammonium molybdate tetrahydrate obtained from Kishida Chemicals Co. into 1 dm^3 (dm^3=litre) of water. Concentration of the solution was standardized by an adding excess amount of 0.01 M Na_2H_2 edta and the solution was then back titrated with 0.01 M lead sulfate by the aid of XO metallochromic indicator at pH 5. Sodium peroxoborate solution (0.05 M) was prepared every week by dissolving 3.8465 g of sodium peroxoborate tetrahydrate obtained from Wako Pure Chemicals Co. into 0.5 dm^3 of water. It was stored in a dark bottle in a refrigerator. Potassium iodide solution (1 M) was prepared by dissolving about 166 g of reagent into 1 dm^3 of water. The stock solution was potentiometrically titrated against silver nitrate standard solution and stored in a dark bottle. Rhodamine B was obtained from Wako Pure Chemicals Co. as a chloride salt and 0.01 M stock solution was prepared by dissolving 0.4790 g of reagent into 100 ml of water. A stock solution was potentiometrically standardized with silver nitrate solution. L-Ascorbic acid was obtained from Wako Pure Chemicals Co. and a stock solution was prepared by dissolving 1.7613 g of reagent into 100 ml of water just before use. The chemicals used in this study were all of analytical reagent grade. All the water used was deionized and then twice distilled.

Procedure. The established procedure for the determination of 80 to 200 nM of molybdenum(VI) is as follows. To a 50 ml volumetric flask containing an appropriate amount of molybdenum(VI) sample solution were added 10 ml of 10 μM Rhodamine B solution and 18 ml of 50 mM sodium peroxoborate solution; the flask was filled up to the mark with water (solution A). To another 50-ml flask containing 10 ml of 1 M potassium iodide were added 3 ml of 0.1 M ascorbic acid solution and 10 ml of 1 M hydrochloric acid; this solution was diluted to the needed volume (solution B). Both solutions were thermostated at 25°C, and a 1-ml portion of solution A was transfered fluorometric cell (10×10×45 mm) in the spectrofluorophotometer. An equal amount of solution B was rapidly poured into the cell and the recorder switched on at the same time. The reaction solution in the cell was quickly mixed by using a small stirrer, and the fluorescence intensity was recorded at 555 nm of excitation and 573 nm of emission wave length. The amount of ascorbic acid added to the reaction mixture was changed according to the molybdenum(VI) ion concentration range.

Results and Discussion

Effect of pH. Effect of pH on the rate of the reaction was examined with fixed concentrations of sodium peroxoborate, potassium iodide and ascorbic acid. The pH of the reaction mixture was varied by the use of hydrochloric acid or acetate buffer. Calibration graphs for molybdenum(VI) in the concentration range from 2 to 10 μM with different pH values were obtained; the slopes of these graphs were plotted against pH. As shown in Fig. 1, the slope of the

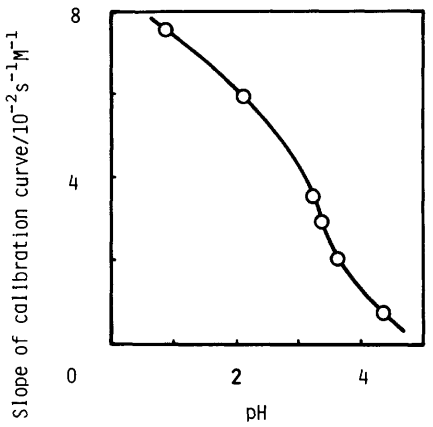

Fig. 1. Effect of pH on the slope of calibration curves. Composition of the reaction mixture: [$NaBO_3$]=2.5 mM, [KI]=1.0 mM, [Rh.B]=1.0 μM, [Asc.]=0.2 mM, temp=25±0.5°C, range of molybdenum(VI): 2 to 10 μM, pH of the reaction mixture was adjusted with HCl or acetate buffer.

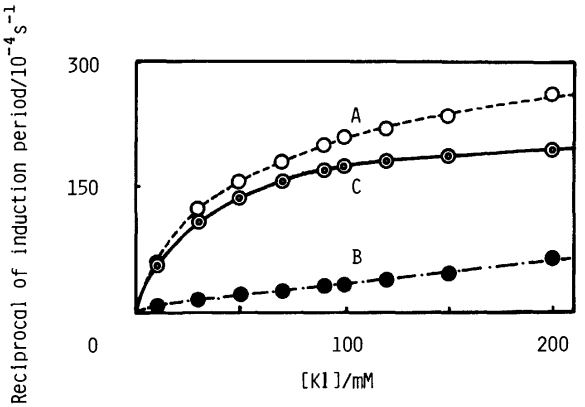

Fig. 2. Effect of potassium iodide concentration on the reciprocal of induction period.
Composition of the reaction mixture: [$NaBO_3$]=2.5 mM, [HCl]=0.1 M, [Rh.B]=1.0 μM, [Asc.]=1.0 mM, temp=25±0.5°C, A: [Mo(VI)]=6.0 μM, B: black, C: difference of reciprocal of induction period, (A—B).

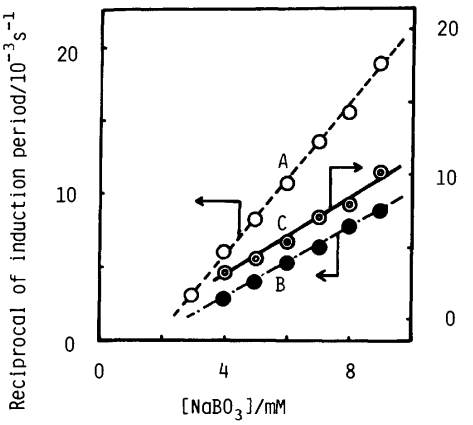

Fig. 3. Effect of potassium iodide concentration on the reciprocal of induction period.
Composition of the reaction mixture: [KI]=0.1 M, [HCl]=0.1 M, [Rh.B]=1.0 μM, [Asc.]=1.5 mM, temp=25±0.5°C, A; [Mo(VI)]=1.0 μM, B; black, C; difference of reciprocal of induction period, (A—B).

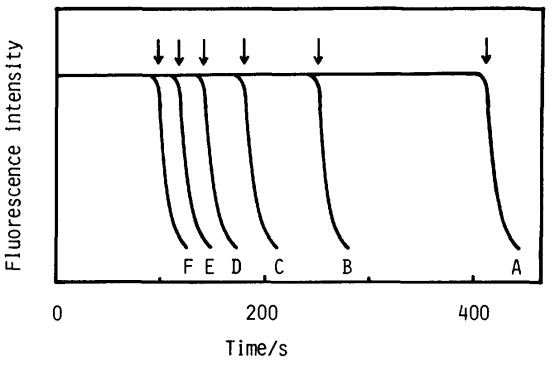

Fig. 4. Fluorescence intensity-time curve.
Composition of the reaction mixture: [KI]=0.1 M, [$NaBO_3$]=9 mM, [HCl]=0.1 M, [Rh.B]=1 μM, [Asc.]=5 mM, temp=25±0.5 °C, [Mo(VI)]: A; 0, B; 2, C; 4, D; 6, E; 8 F; 10 μM.

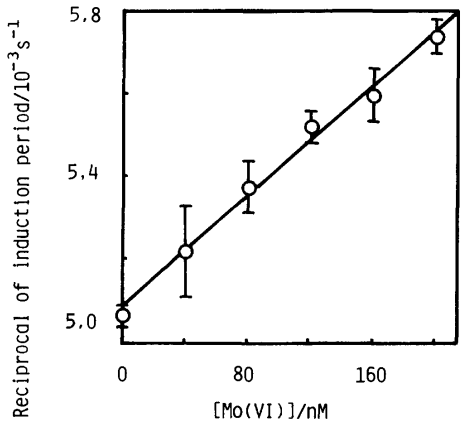

Fig. 5. Calibration curve for molybdenum(VI) (40—200 nM).
Composition of reaction mixture: [$NaBO_3$]=9.0 mM, [KI]=0.1 M, [HCl]=0.1 M, [Rh.B]=1.0 μM, [Asc.]=3 mM, temp=25±0.5 °C.

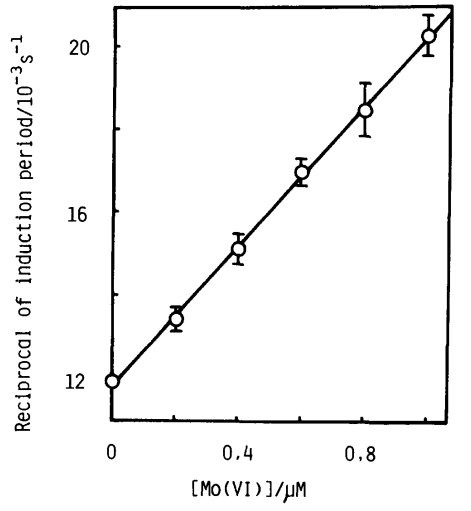

Fig. 6. Calibration curve for molybdenum(VI) (0.2—1.0 μM).
Composition of reaction mixture: [$NaBO_3$]=9 mM, [KI]=0.1 M, [HCl]=0.1 M, [Rh.B]=1.0 μM, [Asc.]=1.5 mM, temp=25±0.5 °C.

calibration curve increased with decreasing pH of the reaction mixture. The most suitable pH was found to be unity, because the rate of the blank reaction suddenly increased at pH values lower than unity.

Effect of Potassium Iodide Concentration. The dependence of iodide ion concentration on the reciprocal of induction period was investigated. The results are shown in Fig. 2. Various amounts of potassium iodide solution were added to the reaction mixture containing 6 μM of molybdenum(VI) (curve A). The blank reaction was also carried out (curve B). The differences of reciprocal of induction period are also shown in the figure (curve C). It was found that the net value (curve C) became almost constant at the iodide ion concentrations higher than 0.1 M. Thus, the concentration of potassium iodide was adjusted to 0.1 M.

Effect of Sodium Peroxoborate Concentration. The effect of peroxoborate ion concentration on the reciprocal of induction period was examined. The results are shown in Fig. 3. The net value of reciprocal of induction period increased with increasing the sodium peroxoborate concentration. However, a high peroxoborate ion concentration is not suitable because it decomposes itself by generating bubbles in the fluorometric cell. Thus, the peroxoborate ion concentration was adjusted to 9 mM.

Effect of Rhodamine B Concentration. Rhodamine B ion concentration lower than 0.1 μM is not suitable because of low fluorescence intensity. Rhodamine B ion concentration more than 0.1 mM is also not suitable because the reaction mixture becomes turbid. A concentration of 1.0 μM was adopted because the sharpness of the change in fluorescence intensity at the end of induction period is increased with decreasing its concentration.

Calibration Graph. The calibration graph for molybdenum(VI) was obtained according to the above procedure. Fluorescence intensity-time curves for various molybdenum(VI) concentrations in the range from 0 to 10 μM are shown in Fig. 4. Arrows in the figure show the end of induction period. As shown in Figs. 5 and 6, the calibration graphs of molybdenum(VI) are linear over the concentration range from 80 to 200 nM and 0.2 to 1.0 μM. The number of measurements at each molybdenum(VI) ion concentration levels are three and the graph is shown in mean and 95% confidence limit. Relative standard deviation at 8×10^{-8} and 2×10^{-7} M molybdenum(VI) concentrations are 0.47 and 0.24%, respectively.

Determination of Ascorbic Acid and Thiosulfate Ion. Since the induction period is linear to reductant concentration, micro-determination of a reducing agent such as ascorbic acid or thiosulfate is feasible. Concentration of potassium iodide, sodium peroxoborate, hydrochloric acid, Rhodamine B, and molybdenum(VI) were kept to 0.5 mM, 7.5 mM, 0.1 M, 1.0 μM, and 1.0 μM, respectively. A good calibration graph was obtained for the ascorbic acid concentration range from 1 to 10 μM. One can easily determine more concentrated ascorbic acid up to 10 mM by increasing the catalyst concentration. Thiosulfate ion in the concentration range from 2 to 10 μM was also determined by using

TABLE 1. EFFECT OF DIVERSE IONS

Diverse ion	Concentration of diverse ion			
	0.5 μM	5.0 μM	50 μM	500 μM
W^{VI}	+7.64	+49.73	—	—
Zr^{IV}	+1.48	+3.88	+113.3	—
Fe^{II}	+0.95	+4.88	+46.41	—
Fe^{III}	−0.31	+4.41	+44.63	—
Cr^{VI}	+2.44	+4.47	+13.28	—
V^{IV}	+3.18	+4.80	+11.63	+144.6
Mn^{II}	+1.27	−0.28	−3.51	−4.13
Zn^{II}	—	—	—	+0.23
Cr^{III}	—	+1.62	−8.39	−5.35
Cu^{II}	+0.58	−15.64	—	—

[$NaBO_3$]=9.0 mM, [KI]=0.1 M, [HCl]=0.1 M, [Rh.B]= 1.0 μM, [Asc.]=1.5 mM, temp=25±0.5 °C, [Mo(VI)]= 0.5 μM, Figures in the table show relative errors in percent.

the same composition of reaction solution. Relative standard deviations of 2μM ascorbic acid and 2μM thiosulfate ion concentration levels are 2.56 and 1.76%, respectively.

Interference. Interference by some diverse ions for the determination of molybdenum(VI) was evaluated; the results are shown in Table 1. The composition of the reaction solution is the same as that used for construction of the calibration graph and molybdenum(VI) concentration was kept to 0.5μM. The concentration of diverse ions were changed to 1 to 1000 times more than that of molybdenum(VI). Triplicate measurements were carried out in the presence and absence of interferent. Plus sign in the table implies acceleation of the rate of indicator reaction. Equal amounts of tungsten(VI), and tenfold amounts of zirconium(IV), iron(II), iron(III), vanadium(IV), copper(II), and chromium(VI) show interference.

References

1) K. B. Yatsimirskii, "Kinetic Methods of Analysis," Pergamon Press, Oxford (1966).
2) H. B. Mark, Jr., and G. A. Rechnitz, "Kinetics in Analytical Chemistry," Interscience Publ., New York (1968).
3) H. A. Laitinen and W. E. Harris, "Chemical Analysis," 2nd ed., McGraw-Hill, New York (1975), Chap. 21.
4) E. B. Sandell and H. Onishi, "Photometric Determination of Trace of Metals. General Aspects, in Colorimetric Determination of Trace of Metals," 4th ed, Wiley-Interscience, New York (1978), p. 200.
5) T. Fukasawa and T. Yamane, *Bunseki*, **1977**, 491.
6) S. Utsumi, *Bunseki Kagaku*, **16**, 644 (1967).
7) T. Kawashima and Y. Yonehara, *Bunseki Kagaku*, **21**, 825 (1972).
8) H. B. Mark, Jr., *Talanta*, **19**, 717 (1972).
9) A. M. Gary and J. P. Schwing, *Bull. Soc. Chim. Fr.*, **1972**, 3657.
10) R. A. Greinke and H. B. Mark, Jr., *Anal. Chem.*, **48**, 87R (1976).
11) R. A. Greinke and H. B. Mark, Jr., *Anal. Chem.*, **50**, 70R (1978).
12) H. A. Mottola and H. B. Mark, Jr., *Anal. Chem.*, **52**, 31R (1980).
13) H. Mueller and G. Werner, *Z. Chimie, Lpz.*, **16**, 304 (1976).
14) G. Svehla, *Analyst*, **94**, 513 (1969).
15) D. D. Burgness, *Mikrochim. Acta, I*, **1979**, 159.
16) H. Thompson and G. Svehla, *Z. Anal. Chem.*, **247**, 244 (1969).
17) A. M. Wilson, *Anal. Chim.*, **38**, 1784 (1966).
18) J. Bognar and O. Jellinek, *Mikrochim. Acta*, **1966**, 453.
19) J. Bognar and O. Jellinek, *Mikrochim. Acta*, **1968**, 1013.
20) J. Bognar and O. Jellinek, *Mikrochim. Acta*, **1969**, 318.
21) J. Bognar and O. Jellinek, *Mikrochim. Acta*, **1969**, 366.
22) H. Weisz and S. Pantel, *Anal. Chim. Acta*, **76**, 487 (1975).
23) H. Weisz and K. Rothmaier, *Anal. Chim. Acta*, **68**, 311 (1974).
24) J. Bognar and O. Jellinek, *Mikrochim. Acta*, **1969**, 312.
25) M. Kataoka and T. Kambara, *Denki Kagaku*, **45**, 674 (1977).
26) M. Kataoka, M. Takahashi, and T.Kambara, *Bunseki Kagaku*, **28**, 169 (1979).
27) H. Goto, *Nippon Kagaku Zasshi*, **59**, 797 (1938).
28) R. W. Stoughton and G. K. Pollefson, *J. Am. Chem. Soc.*, **61**, 2634 (1939).

 © 1984 The Chemical Society of Japan Bull. Chem. Soc. Jpn., 57, 1087—1091 (1984)

Mössbauer Study of Tin(II) Chloride Hydroxide and Tin(II) Hydroxide Oxide

Sumio ICHIBA* and Mitsuru TAKESHITA

Department of Chemistry, Faculty of Science, Hiroshima University, Higashisenda-machi, Naka-ku, Hiroshima 730

(Received September 19, 1983)

The precipitates obtained by addition of a solution of $NaHCO_3$ to a solution of $SnCl_2$ at various pH were studied by thermal analysis, Mössbauer spectroscopy, and X-ray powder diffraction. The formula of the tin(II) chloride hydroxide precipitate obtained in the range of pH 1.9—2.5 was determined as $2SnO \cdot SnCl_2 \cdot H_2O$, or $Sn_3O(OH)_2Cl_2$, and the formula of the hydroxide oxide obtained in the range of pH 7.0—7.7 was $3SnO \cdot 2H_2O$, or $Sn_3(OH)_4O$. In the intermediate pH range, the chloride ions were gradually replaced by hydroxide ions. The dehydration of hydroxide oxide to produce SnO occurred in two stages and the disproportionation reaction of SnO to SnO_2 and β-tin proceeded *via* Sn_2O_3.

When a solution of an alkali is added to a solution of a tin(II) compound, in the absence of a strong-donor anion, the precipitate is a basic chloride salt at first, but further addition of hydroxide ion results in the gradual replacement of the anion by hydroxide and finally, the precipitate turns into a hydroxide oxide. These tin(II) chloride hydroxide and hydroxide oxide have been studied by many workers and various formulas have been reported.[1-4] Among others, Donaldson *et al.* have reported that the only one preparable as a clearly defined crystalline phase of tin(II) chloride hydroxide from aqueous solution is $Sn_4(OH)_6Cl_2$[2] and that the most probable composition of the tin(II) hydroxide oxide is $5SnO \cdot H_2O$, or $Sn_5O_3(OH)_4$.[3] Howie and Moser obtained single crystals of tin(II) hydroxide oxide, they were able to establish the crystal structure by X-ray diffraction and determined the formula to be $3SnO \cdot H_2O$.[4] Furthermore, Honnick and Zuckerman synthesized tin(II) hydroxide, $Sn(OH)_2$, by an anhydrous, organometallic method.[5]

In this study, the precipitates obtained on addition of a solution of $NaHCO_3$ to a solution of $SnCl_2$ as a function of pH were examined by thermal analysis, X-ray powder diffraction, and Mössbauer spectroscopy. The thermal behavior of the tin(II) chloride hydroxide and hydroxide oxide was also examined by quenching, X-ray powder diffraction, and Mössbauer spectroscopy.

Experimental

Preparation of Tin(II) Chloride Hydroxide and Tin(II) Hydroxide Oxide. Tin(II) chloride dihydrate (2.5 g) was dissolved in 8 mol dm^{-3}-HCl (3 ml). The saturated aqueous solution of $NaHCO_3$ was added to the solution under an atmosphere of nitrogen until the pH of the solution reached the predesignated value, while the solution was stirred by means of ultrasonic waves. The white precipitates filtered off were washed throughly with de-airated water, ethanol, and diethyl ether successively under nitrogen and dried for 2 d in vacuum over potassium hydroxide pellets.

Thermal Decomposition Products of Tin(II) Chloride Hydroxide and Tin(II) Hydroxide Oxide. The samples of the thermal decomposition products for the study of the thermal behavior of the tin(II) chloride hydroxide and hydroxide oxide were prepared by heating the material in a furnace with a nitrogen gas flow up to a temperature where the reaction occurred in the DTA curve and then rapidly cooled to room temperature.

Measurements. TG and DTA heating-curves were recorded simultaneously using a Sinku-riko TGD-5000 RH instrument by heating the sample at a rate of 10 °C min^{-1} in flowing nitrogen gas. About a 10-mg sample was placed in a cell and α-alumina was used as the reference material. The Mössbauer spectra were measured using a constant acceleration type spectrometer and the accuracy was within 0.05 mm s^{-1}. The γ-ray source of calcium stannate was used at room temperature and the sample was cooled to 93 K in a liquid nitrogen cryostat. The velocity scale was calibrated against the spectra of $BaSnO_3$ and β-Sn at room temperature. All isomer shifts are reported relative to $BaSnO_3$. Mössbauer parameters were deduced from Lorentzian curves computer-fitted to the spectra by the least squares method.

Results and Discussion

TG-DTA curves of the precipitate obtained at pH 2.4 are shown in Fig. 1. The weight loss occurs in two stages; the first stage at about 170 °C is dehydration and the second stage over the range 350—550 °C is volatilization of $SnCl_2$. The TG-DTA curves of the precipitates obtained at pH 7.2 and 7.5 are shown in Figs. 2 and 3, respectively. In these cases, the dehydration occurs in two stages. It is to be noted that if the precipitates were obtained with stirring other than

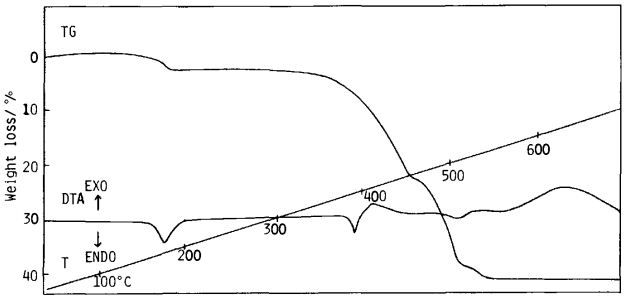

Fig. 1. The TG-DTA curves of tin(II) chloride hydroxide precipitated at pH 2.4.

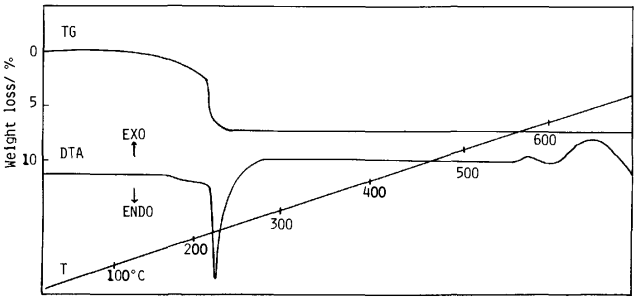

Fig. 2. The TG-DTA curves of tin(II) hydroxide oxide precipitated at pH 7.2.

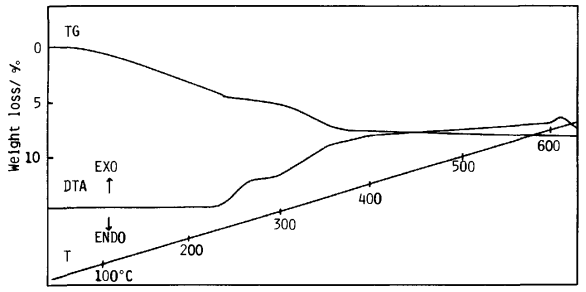

Fig. 3. The TG-DTA curves of tin(II) hydroxide oxide precipitated at pH 7.5.

Table 1. Thermal analysis data and Mössbauer parameters of the precipitates with pH

pH	Thermal analysis (wt%)			Mössbauer parameters	
	H_2O	$SnCl_2$	SnO	δ/mm s^{-1}	Δ/mm s^{-1}
1.90	4.2	39.0	56.8	3.33	1.91
2.05	4.0	39.0	57.0	3.30	1.92
2.10	4.0	37.0	59.0	3.30	1.93
2.40	4.0	39.2	56.8	3.35	1.85
2.50	4.0	32.0	64.0	3.31	1.91
2.55	6.4	12.5	81.8	2.99	2.19
2.60	7.2	20.0	72.8	3.12	2.10
2.70	8.5	17.5	74.0	3.01	2.17
2.80	5.0	12.5	82.5	2.99	2.18
3.10	4.7	13.5	81.8	2.93	2.21
3.80	5.5	10.0	84.5	2.98	2.19
4.90	5.0	4.2	90.8	2.90	2.25
5.80	5.5	2.5	93.0	2.88	2.17
6.30	6.0	0.5	94.0	2.93	2.25
6.70	7.2	0.5	92.7	2.92	2.30
6.80	7.2	0.5	92.7	2.93	2.28
6.90	8.0	0.2	91.8	2.93	2.29
7.00	7.7	0.3	92.0	2.92	2.31
7.20	8.0	0.0	92.0	2.91	2.28
7.40	8.0	0.0	92.0	2.90	2.32
7.50	7.8	0.0	92.2	2.88	2.32
7.70	7.8	0.0	92.2	2.93	2.28

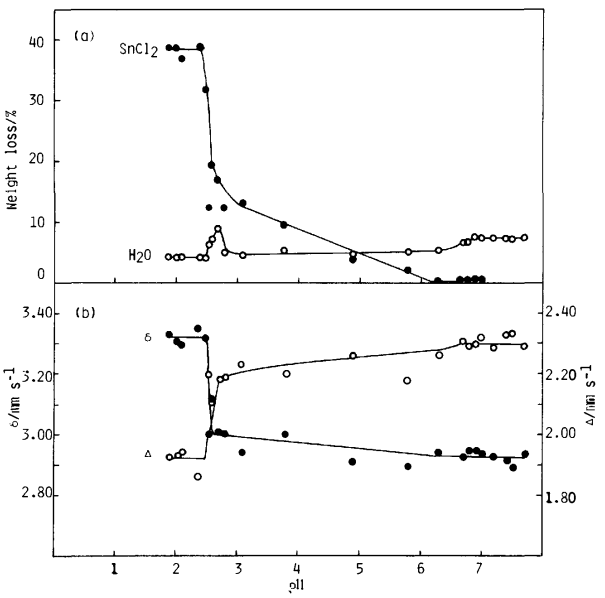

Fig. 4. The plots of the analytical data (a) and Mössbauer parameters (b) against pH.

by means of ultrasonic waves, the reliable weight loss curves could not be recorded. The analytical data, including the residual SnO from the TG curves over the pH range 1.90—7.70, are listed in Table 1, along with the Mössbauer parameters. The variations of the values against pH are schematically shown in Fig. 4.

From the analytical data in Table 1, the precipitates obtained over the pH range 1.90—2.50 are tin(II) chloride hydroxide, the formula of which is $2SnO \cdot SnCl_2 \cdot H_2O$, or $Sn_3O(OH)_2Cl_2$. The formula of the tin(II) hydroxide oxide precipitates obtained over the pH range 7.20—7.70 is $3SnO \cdot 2H_2O$, or $Sn_3(OH)_4O$. In disagreement with these formulas, Donaldson *et al.* have previously reported the formula $3SnO \cdot SnCl_2 \cdot H_2O$, or $Sn_4(OH)_6Cl_2$, for the crystalline basic chloride which was obtained by addition of ammonia solution to the solution of tin(II) chloride over the pH range1.14—4.5.[2] They have also reported the formula $5SnO \cdot 2H_2O$, or $Sn_5O_3(OH)_4$, for the tin(II) hydroxide oxide which was prepared by addition of an oxygen free solution of alkali or alkali carbonate to oxygen free solutions of tin(II) sulfate, under nitrogen, until the pH of the solution was between 10 and 12.[3] Accordingly, the Mössbauer parameters in Table 1 and the X-ray diffraction diagrams shown in Figs. 6(a), 8(a), and 10(a) are not in agreement with the data of Donaldson *et al.*[2,3,6] Another formula $3SnO \cdot H_2O$ has been reported by Howie and Moser for the single crystals of hydroxide oxide obtained from stannous perchlorate solution by prolonged passage of oxygen-free nitrogen containing a very low concentration of ammonia.[4]

Tin(II) ions complex with Cl^- in solution containing hydrochloric acid; Haight *et al.* reported the relative population of various $SnCl_n^{2-n}$ complexes at ion strength 4.0 and varying chloride ion concentration.[7] On the other hand, bivalent tin ion can hydrolyze water and Tobias found that the main product of hydrolysis is the cyclic polynuclear ion $Sn_3(OH)_4^{2+}$.[8] By neutralizing the solution of $SnCl_2$ in hydrochloric acid with $NaHCO_3$, tin(II) ions complexed with Cl^- hydrolyze water and culminate in the precipitation of the tin(II) chloride hydroxide at pH 1.9—2.5. With increasing OH^- concentration, the chloride ions are replaced by hydroxide ions, the fraction of the $Sn_3(OH)_4^{2+}$ ions increase, and finally, the single phase of $Sn_3(OH)_4O$ precipitates in the pH range above 7.0 according to the reaction:

$$Sn_3(OH)_4^{2+} + 2(OH)^- \rightarrow Sn_3(OH)_4O + H_2O.$$

The Mössbauer parameters, both the isomer shift and quadrupole splitting, of the precipitates obtained over the pH range 2.55—4.90 changed with pH from the values of the chloride hydroxide to the hydroxide oxide. Accordingly the materials are not a mixture of the chloride hydroxide and hydroxide oxide. The Cl^- ligands of Sn^{II} are gradually replaced by OH^- as the pH rises. The X-ray diagrams of those materials gave weak patterns similar to those of $Sn_3(OH)_4O$.

The Mössbauer spectra and X-ray powder diagrams of tin(II) chloride hydroxide obtained at pH 2.4 and the thermal decomposition products obtained by heating to higher temperatures are shown in Figs.5 and 6, respectively. The Mössbauer parameters deduced from the spectra and existing phases are shown in Table 2.

The dehydrated product heated up to 200 °C changes to contain two species of Sn^{II}, which are equivalent in the initial compound. The product with smaller isomer shift is coordinated with more oxygen ligands; the other product with larger shift is coordinated with more chlorine ligands. The endothermic peak at 390 °C in the DTA curve in Fig. 1 is a melting reaction because the samples heated up to 370 and 420 °C gave similar Mössbauer parameters and X-ray diagrams, as is shown

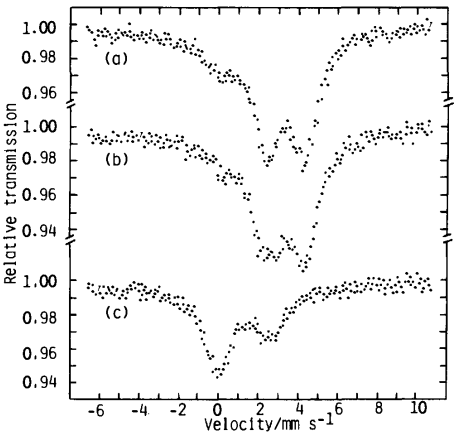

Fig. 5. Mössbauer spectra of tin(II) chloride hydroxide precipitated at pH 2.4 (a), and the thermal decomposition products by heating up to, (b) 200 °C; (c) 700 °C.

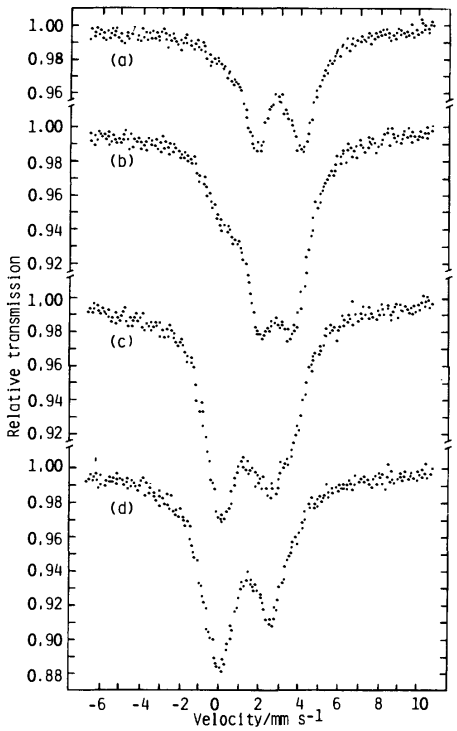

Fig. 7. Mössbauer spectra of tin(II) hydroxide oxide precipitated at pH 7.2 (a), and the thermal decomposition products by heating up to, (b) 260 °C; (c) 600 °C; (d) 700 °C.

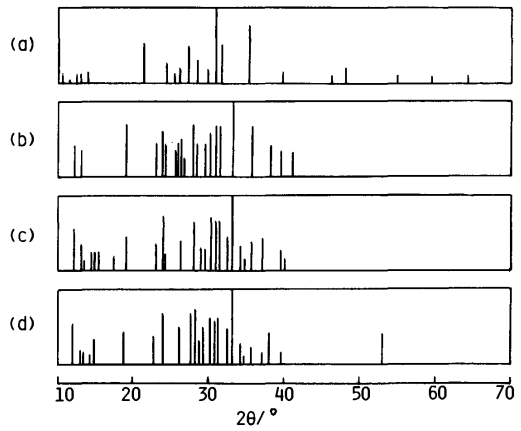

Fig. 6. X-Ray powder diagrams of tin(II) chloride hydroxide precipitated at pH 2.4 (a), and the thermal decomposition products by heating up to, (b) 200 °C; (c) 370 °C; (d) 420 °C.

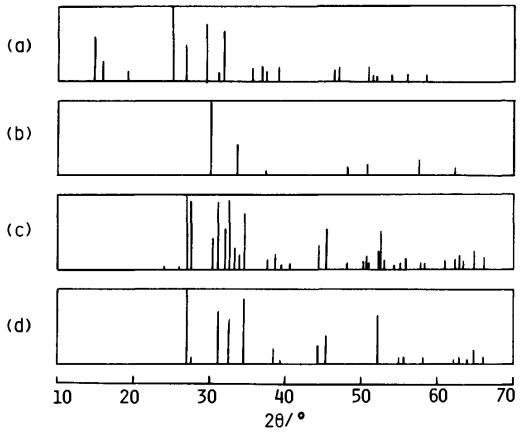

Fig. 8. X-Ray powder diagrams of tin(II) hydroxide oxide precipitated at pH 7.2 (a), and the thermal decomposition products by heating up to, (b) 260 °C; (c) 600 °C; (d) 700 °C.

TABLE 2. MÖSSBAUER PARAMETERS OF TIN(II) CHLORIDE HYDROXIDE PRECIPITATED AT pH 2.4 AND THE THERMAL DECOMPOSITION PRODUCTS BY HEATING UP TO 200, 370, 420, AND 700 °C

Temp	Sn^{II}		Sn^{IV}	Sn^{0}	Existing phase
°C	δ/mm s^{-1}	Δ/mm s^{-1}	δ/mm s^{-1}	δ/mm s^{-1}	
20	3.35	1.85			$Sn_3O(OH)_2Cl_2$
200	3.39	2.39			$Sn_3O_2Cl_2$
	3.52	1.21			
370	3.09	2.16			$Sn_3O_2Cl_2$
	3.61	1.71			
420	3.12	2.05			$Sn_3O_2Cl_2$
	3.73	1.59			
700			0.00	2.54	SnO_2, β-Sn

in Table 2 and Fig. 6, respectively. The final decomposition product heated to 700 °C is a mixture of tin(IV) oxide and β-tin as a consequence of the disproportionation reaction of SnO, which was observed in the DTA curve as the broad peak at about 600 °C.

The Mössbauer spectra and X-ray powder diagrams of tin(II) hydroxide oxide obtained at pH 7.2 and the thermal decomposition products obtained by heating to 260, 600, and 700 °C are shown in Figs. 7 and 8, respectively. The Mössbauer parameters and existing phases are shown in Table 3. The dehydration product heated to 260 °C was SnO, the product heated to 600 °C was a mixture of Sn_2O_3 and β-tin, and the final product obtained by heated to 700 °C is a mixture of SnO_2 and β-tin. Thus, in this hydroxide oxide, the disproportionation of SnO to SnO_2 and β-Sn occurs in two stages *via* Sn_2O_3 and the stages of the thermal decomposition are confirmed as :

$$2Sn_3(OH)_4O \rightarrow 6SnO \rightarrow 2Sn_2O_3 + 2\beta\text{-}Sn \rightarrow 3SnO_2 + 3\beta\text{-}Sn$$

The Mössbauer parameters and X-ray diagrams of tin(II) hydroxide oxide obtained at pH 7.5 and the thermal decomposition products by heating to 250, 420, 620, and 640 °C are shown in Figs. 9 and 10, respectively. The Mössbauer parameters and the existing phases are shown in Table 4. In the Mössbauer spectrum of Fig. 9(a), the area ratio of the tin(IV) impurity to the total was 20%. This suggests that if the

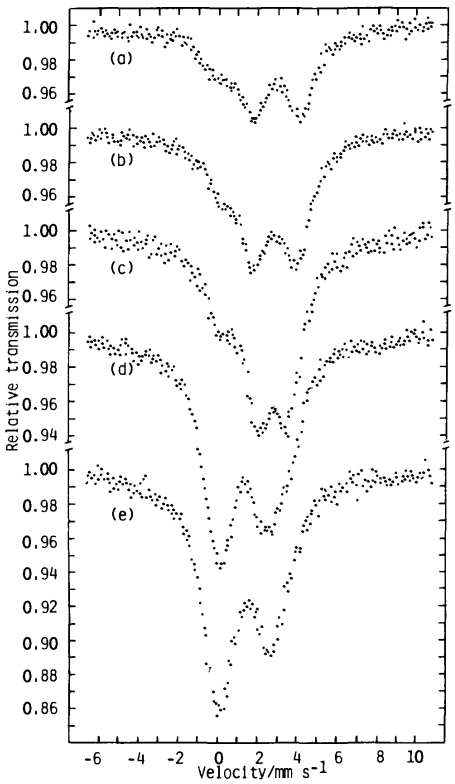

Fig. 9. Mössbauer spectra of tin(II) hydroxide oxide precipitated at pH 7.5 (a), and the thermal decomposition products by heating up to, (b) 250 °C; (c) 420 °C; (d) 620 °C; (e) 640 °C.

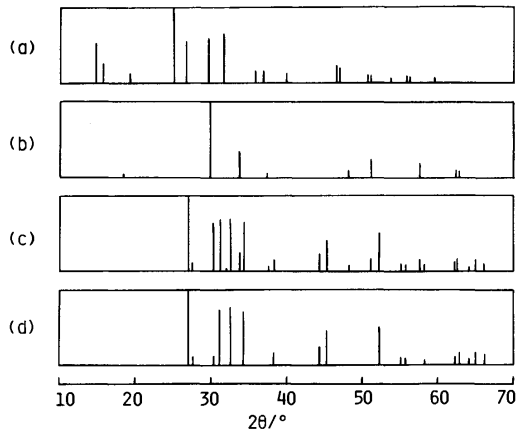

Fig. 10. X-Ray powder diagrams of tin(II) hydroxide oxide precipitated at pH 7.5 (a), and the thermal decomposition products by heating up to, (b) 370 °C; (c) 620 °C; (d) 640 °C.

Table 3. Mössbauer parameters of tin(II) hydroxide oxide precipitated at pH 7.2 and the thermal decomposition products by heating up to 260, 600, and 700 °C

Temp	Sn^{II}		Sn^{IV}	Sn^0	Existing phase
°C	δ/mm s^{-1}	Δ/mm s^{-1}	δ/mm s^{-1}	δ/mm s^{-1}	
20	2.91	2.28			$Sn_3(OH)_4O$
260	2.76	1.62			blue-black SnO
600	2.54	1.94	0.00	2.50	Sn_2O_3, β-Sn
700			0.02	2.66	SnO_2, β-Sn

Table 4. Mössbauer parameters of tin(II) hydroxide oxide precipitated at pH 7.5 and the thermal decomposition products by heating up to 250, 420, 620, and 640 °C

Temp	Sn^{II}		Sn^{IV}	Sn^0	Existing phase
°C	δ/mm s^{-1}	Δ/mm s^{-1}	δ/mm s^{-1}	δ/mm s^{-1}	
20	2.88	2.32			$Sn_3(OH)_4O$
250	2.83	2.06			amorphous
420	2.76	1.50			blue-black SnO
620	2.83	1.64	0.04	2.70	blue-black SnO, SnO_2, β-Sn
640			0.01	2.67	SnO_2, β-Sn

pH rises above 7.0, the oxidation of tin(II) to tin(IV) proceeds with the increase of pH and the stannic tin is involved in the lattice of hydroxide oxide. The product heated to 250°C, in which the first stage dehydration occurred, gave an amorphous X-ray diagram. This orange amorphous material was stable under an atmosphere of air for two weeks or more in diagreement with the previous report of Donaldson *et al.*[3] The second stage of the dehydration proceeds slowly over the temperature range 250—380°C. The disproportionation reaction of SnO, which was observed as two peaks in the DTA curve of the hydroxide oxide obtained at pH 7.2, collapsed into a small single peak and the residual SnO was still observed in the Mössbauer spectrum of the sample heated to 620°C. The final product was a mixture of SnO_2 and β-Sn and the intermediate Sn_2O_3 was not detected. These differences in the thermal behavior of the tin(II) hydroxide oxide can be ascribed to the change of tin(IV) content with pH.

References

1) J. D. Donaldson, "The Chemistry of Bivalent Tin," in "Progress in Inorganic Chemistry," ed by F. A. Cotton, John Wiley & Sons, New York (1967), Vol. 8, pp. 287—356.
2) J. D. Donaldson, W. Moser, and W. B. Simpson, *J. Chem. Soc.*, **1963**, 1727.
3) J. D. Donaldson and W. Moser, *J. Chem. Soc.*, **1961**, 835.
4) R. A. Howie and W. Moser, *Nature (London)*, **219**, 372 (1968).
5) W. D. Honnick and J. J. Zuckerman, *Inorg. Chem.*, **15**, 3034 (1976).
6) C. G. Davies and J. D. Donaldson, *J. Chem. Soc. A*, **1968**, 946.
7) G. P. Haight, J. Zoltewicz, and W. Evans, *Acta Chem. Scand.*, **16**, 311 (1962).
8) R. S. Tobias, *Acta Chem. Scand.*, **12**, 198 (1958).

Palladium(II)-Catalyzed Acetoxylation and Chlorination of 2-Alkenyl *p*-Tolyl Sulfones

Katsuyuki OGURA,* Nobuhiro SHIBUYA, Kazumasa TAKAHASHI, and Hirotada IIDA
Department of Synthetic Chemistry, Faculty of Engineering, Chiba University, Yayoicho 1-33, Chiba 260
(Received August 5, 1983)

2-Alkenyl *p*-tolyl sulfones were converted into the corresponding 3-acetoxy(or chloro)-1-alkenyl *p*-tolyl sulfones *via* π-allylpalladium complexes which reacted regiospecifically with a nucleophile such as acetate anion or chloride anion in the presence of Cu(II).

π-Allylpalladium complexes (**1**) are usually prepared by various methods starting from alkadienes, alkenes, and 2-alkenyl acetates (or chlorides), and they have often been utilized in organic synthesis.[1] Formally, these complexes

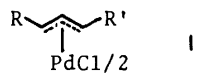

1

may be considered as allyl cation equivalents which react with various nucleophiles. In the course of our investigation to functionalize 2-alkenyl *p*-tolyl sulfones (**2**), we examined generation of di-μ-chlorobis-[1-(*p*-tolylsulfonyl)-π-allyl]dipalladium complexes (**3**) and their reactions with some nucleophiles to give substitution products such as 3-acetoxy-1-alkenyl *p*-tolyl sulfone (**4**) and 3-chloro-1-alkenyl *p*-tolyl sulfone (**5**).[2]

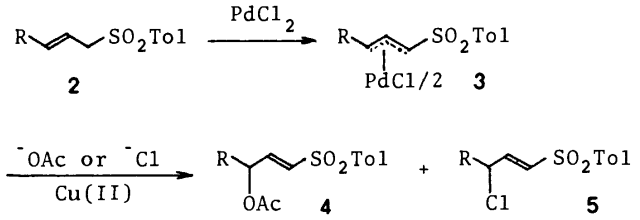

a: R = H b: R = CH_3 c: R = n-C_9H_{19} d: R = Ph

Scheme 1.

Recently, Trost and his coworkers reported on the reaction of 2-alkenyl phenyl sulfones with a Pd(O) complex, where the sulfonyl group behaves as a leaving group to form π-allylpalladium complexes.[3] This is in a sharp contrast with our findings that $PdCl_2$ reacts with **2** to give **3** without loosing the sulfonyl group. We have also found that **3** undergoes regiospecific displacement with acetate anion or chloride anion to give **4** or **5**, respectively.[4]

Results and Discussion

According to Trost's procedure for preparation of π-allylpalladium complexes from alkenes,[5] 2-propenyl *p*-tolyl sulfone (**2a**) was treated with $PdCl_2$ (1 mol equiv), $CuCl_2$ (6.1mol equiv), AcONa (13equiv), and NaCl (13 equiv) in AcOH (60°/16h). Surprisingly, the expected π-allylpalladium complex (**3a**) was not formed, but 3-chloro-1-propenyl *p*-tolyl sulfone (**5a**) and 3-acetoxy-1-propenyl *p*-tolyl sulfone (**4a**) were obtained in 60 and 29% yields, respectively. When the amount of $CuCl_2$ was decreased to 3.4 mol equiv, the acetate **3a** became the predominant product (70% yield). Furthermore, it was found that only a catalytic amount of $PdCl_2$ was needed to transform **2a** into **4a** and/or **5a**. Thus, the reaction proceeded smoothly by the use of 0.10 or 0.03 mol equiv of $PdCl_2$ as shown in Table 1 (Runs 3—5). In these cases, a large excess of $CuCl_2$ appears to oxidize Pd(0) to regenerate Pd(II). Since prolonged reaction did not cause remarkable increase of **4a** (Runs 5 and 6 of Table 1), it was concluded that **4a** is not produced from **5a**. Similar results were also obtained in the reactions of other 2-alkenyl *p*-tolyl sulfones (**2b** and **2c**). In contrast, 3-phenyl-2-propenyl *p*-tolyl sulfone (**2d**) afforded 3-acetoxy-3-phenyl-1-propenyl *p*-tolyl sulfone (**4d**) even when a large excess (6.2—6.9 mol equiv) of $CuCl_2$ was employed (Run 17—19 in Table 1).

Since the amounts of $CuCl_2$ were crucial to the ratio of **4a**:**5a**, we investigated the effect of $CuCl_2$ in more detail. As mentioned above, the acetate **4** was exclusively formed when about 6 mol equiv of $CuCl_2$ was used, whereas, when about 3 mol equiv of $CuCl_2$ was used, predominant formation of the chloride **5** was noted. Table 2 shows that the ratio of **4a**:**5a**, diminishes gradually with increase in the amount of $CuCl_2$ in the given reaction conditions. These phenomena might be attributable to a reversible reaction of $CuCl_2$ with AcONa. This may be supported by the fact that $CuCl_2$ reacted with 2 mol equiv of AcONa in AcOH to give the same mixture as that derived from $Cu(OAc)_2$ and NaCl in the molar ratio of 1:2.[6] This explanation is consistent with the observation that the absence of NaOAc increases the yield of **5a** though the reaction is somewhat slow (Runs 9 and 13 of Table 1).

Preparation of Di-μ-chlorobis[1-(p-tolylsulfonyl)-π-allyl]dipalladium (3a) and Its Reaction with Nucleophiles. As mentioned above, Trost's procedure[5] met with no success in obtaining **3a**. This may be because **3a** undergoes a smooth reaction with the coexisting AcONa in the presence of Cu(II) (*vide infra*). However, the reactions of **3b** and **3d** with nucleophiles appeared to be slow compared to that of **3a**. In fact, **3b** and **3d** were isolated by shortening the reaction time under similar conditions (see Experimental section). Later, it was found that the complex **3a** could also be obtained by treatment of **2a** with 1 mol equiv of $PdCl_2$ and 3 mol equiv of AcONa in AcOH at 60°C for 24 h. The structures of these complexes (**3a**, **3b**, and **3d**) were deduced from their IR spectra and satisfactory elemental analyses. Although **3a** was partially soluble in DMSO, rapid decomposition occurred to give the corresponding 3-hydroxy-1-propenyl *p*-tolyl sulfone. This fact made it difficult to record its NMR spectrum.

TABLE 1. DIRECT CONVERSION OF **2** TO **4** AND **5**[a]

Run	R	$PdCl_2$ (mol equiv)[b]	$CuCl_2$ (mol equiv)[b]	Temp/°C (Time/h)	Yield/%	
					4	**5**
1	H	1.0	3.4	60(75)	70	—
2		1.0	6.1	60(16)	29	60
3		0.1	2.8	60(57)	72	—
4		0.1	6.1	60(20)	12	77
5		0.03	5.9	60(18)	5	76
6		0.03	5.9	60(96)	7	84
7	CH_3	1.0	2.7	60(39)→80(98)	75	—
8		1.0	6.1	80(13)	33	63
9		1.0[c]	5.4	80(49)	9	74
10		0.1	2.7	80(52)	80	—
11		0.1	6.1	80(36)	17	80
12		0.03	2.7	80(48)	79	—
13		0.03[c]	2.7	70—80(156)	14	68
14	n-C_9H_{19}	1.0	2.7	60(140)	80	—
15		0.03	3.0	80(60)	86	—
16		0.03	6.1	80(26)	2	26
17	Ph	1.0	6.2	60(96)→80(88)	60	—
18		0.1	6.9	80(144)	53	—
19		0.03	6.9	80(144)	41	—

a) In the presence of $PdCl_2$, $CuCl_2$, AcONa (13 equiv), and NaCl (13 equiv) in AcOH. b) mol equiv to **2**. c) In the absence of AcONa.

TABLE 2. EFFECT OF THE AMOUNT OF $CuCl_2$ IN THE REACTION OF **2a**[a]

$CuCl_2$ (mol equiv)	Time	Yield/%		Ratio
	h	**4a**	**5a**	**4a**:**5a**
6.1	20	12	77	13:87
5.5	40	8(11)[b]	54(75)[b]	13:87
5.0	90	20(60)[b]	8(24)[b]	71:29
4.0	83	78(82)[b]	—	100:0
2.8	57	72	—	100:0

a) Using $PdCl_2$ (0.1 mol equiv), AcONa (13 equiv), and NaCl (13 equiv) in AcOH at 60 °C. b) The yield based on the unrecovered **2a**.

TABLE 3. REACTION OF **3a**[a]

Run	Additive (mol equiv)				Yield/%		
	$CuCl_2$	NaCl	$Cu(OAc)_2$	AcONa	**4a**	**5a**	**3a**
1	2.0	—	—	—	14	43	23
2	—	3.0	—	—	2	—	91
3	2.0	3.0	—	—	9	80	—
4	—	—	2.0	—	3	2	—[b]
5	—	—	—	3.0[c]	18	—	74
6	—	—	2.0	3.0	74	—	—
7	—	3.0	2.0	—	35	29	—

a) Stirring in AcOH at 60 °C for 48 h. b) An unidentified complex mixture which might be composed of **3a** and $Cu(OAc)_2$ was formed. c) Treatment of **3a** with 3.0 mol equiv of AcONa in AcOH at 80 °C for 48 h afforded **4a** in 88% yield.

With regard to the reactions of **3a** with acetate anion, it was observed that combined use of AcONa and $Cu(OAc)_2$ was effective to give **4a** (Table 3). Thus, **4a** was obtained in 74% yield on heating a mixture of **3a**, AcONa, and $Cu(OAc)_2$ in AcOH at 60 °C for 48 h. However, treatment of **3a** with either $Cu(OAc)_2$ or AcONa at 60 °C produced only **4a** in low yields. Analogously, stirring of **3a** with NaCl alone in AcOH did not give **5a**, and merely slow reaction of **3a** was noted when it was allowed to react with $CuCl_2$ in AcOH. However, when both $CuCl_2$ and NaCl were added to a solution of **3a** in AcOH, the reaction proceeded smoothly to afford **5a** in 80% yield together with a small amount (9%) of **4a**. In the reaction of **3a** with $Cu(OAc)_2$ and NaCl, both **4a** and **5a** were formed in 29 and 35% yields, respectively. These results indicate that a smooth conversion of **3a** to either **4a** or **5a** can be accomplished in the presence of both Cu(II) and a nucleophile (acetate anion or chloride anion, respectively). This may be interpreted in terms of the following mechanism: Cu(II) contacts the Pd(II)Cl part in **3a** to assist its departure and concurrently the nucleophile attacks the allylic carbon. At the present time, we cannot preclude the possibility that the attack of the nucleophile and the oxidation of Pd(II) of **3a** with Cu(II) occur simultaneously to give directly Pd(0) and the substitution product (**4a** or **5a**). Here it should be noted that the attack of the nucleophiles on **3a** took place at the carbon γ to the sulfonyl group to give **4** and **5**. Since the sulfonyl group is well known as a strong electron-withdrawing group,[7] the γ carbon in the allylic system of **3a** can be considered to be more positive than the α carbon. Therefore, the γ carbon appears to be the favorable site for the approach of a nucleophile.[8]

Requisite Additives for the $PdCl_2$-Catalyzed Conversion of 2 to 4 or 5. For the $PdCl_2$-catalyzed conversion of **2** to **4** or **5**, three steps must be taken into consideration: (i) transformation of **2** into the intermediary π-allylpalladium complex **3**; (ii) the reaction of **3** with a nucleophile to give Pd(0) and the substitution product (**4** or **5**); and (iii) oxidation of Pd(0) to regenerate Pd(II). The final step can be achieved by oxidation

with the coexisting Cu(II). As described previously, Cu(II) and a nucleophile appear to be neccessary to the second step. Of course, it may be also possible that the second and final steps take place simultaneously. Hitherto, Trost and his coworkers reported that three additives, $CuCl_2$, AcONa, and NaCl, were required for efficient production of π-allylpalladium complexes from acyclic and cyclic olefins and $PdCl_2$.[5] This may not be the present case because treatment of **2a** with $PdCl_2$ and AcONa gave **3a** (*vide supra*) and $PdCl_2$ (0.03 mol equiv) could catalyze the transformation of **2a** to **5a** in the presence of $CuCl_2$ (2 mol equiv) and NaCl (3 mol equiv) in AcOH (60°C/48 h: 80% yield).

For the transformation of **2a** into **4a** using 1 mol equiv of $PdCl_2$, combined use of AcONa (2 mol equiv) and $Cu(OAc)_2$ (3 mol equiv) promoted the reaction to give **4a** in 88% yield (60°C/ 48 h). However, the use of a catalytic amount of $PdCl_2$ did not result in complete transformation even in the presence of large amounts of $Cu(OAc)_2$ (4 mol equiv) and AcONa (6 mol equiv). To our surprise, however, Pd(II)-catalysis was successful if NaCl (3 mol equiv)was added. When **2a** was stirred with $PdCl_2$ (0.03 mol equiv), NaCl (3 mol equiv), $Cu(OAc)_2$ (2 mol equiv), and AcONa (6 mol equiv) in AcOH 60°C for 48 h, **4a** was obtained in 92% yield. In the $PdCl_2$-catalyzed conversion of **2a** to **5a** in the copresence of $CuCl_2$ and NaCl, NaCl not only supplies chloride anion but also is essential to the initiation of the reaction. Such a role of NaCl is intriguing, but we so far find no satisfactory interpretation. A possible explanation is that NaCl transforms $PdCl_2$ and $Pd(OAc)_2$, which is produced by oxidation of Pd(0) with $Cu(OAc)_2$, to the soluble palladates formulated as $Na_2[PdCl_n(OAc)_{4-n}]$.[9] Scheme 3 summarizes this proposed mechanism for the conversion of **2** to **4** and/or **5**.

Thus, the $PdCl_2$-catalyzed transformation of **2a** into **4a** or **5a** can be achieved by performing the reaction using $Cu(OAc)_2$-AcONa-NaCl or $CuCl_2$-NaCl, respectively. The reaction was also applied to other 2-alkenyl *p*-tolyl sulfones. The results were summarized in Table 4, showing that the present reaction conditions are general for syntheses of **4** or **5**.

Experimental

Melting points were determined on a hot-stage microscope apparatus (Yanagimoto) and are uncorrected. ^1H NMR spectra were obtained on a Hitachi R-600 spectrometer. Infrared spectra were determined with a JASCO A-200 spectrometer.

Treatment of **2a** *with* $PdCl_2$, $CuCl_2$, *AcONa, and NaCl in AcOH.* *(a) The Use* ca. *3 mol equiv of* $CuCl_2$: After a suspension containing $PdCl_2$ (468 mg: 2.64 mmol), NaCl (1.91 g: 32.7 mmol), AcONa (1.77 g: 21.6 mmol), and $CuCl_2$ (1.18 g: 8.78 mmol) in AcOH (15 ml)-Ac_2O (1.0 ml) was stirred at 90—98°C for 2 h, the suspension was cooled to 60°C. To this, a solution of **2a** (504 mg: 2.62 mmol) in AcOH (10 ml) was added and the resulting mixture was further stirred at 58—64°C for 75 h. Then, water (20 ml) was added and the mixture was extracted with four 35 ml-portions of benzene. The extracts were combined and washed successively with water, saturated aqueous $NaHCO_3$, brine, and water. After being dried over anhydrous $MgSO_4$, the extract was evaporated and separated by column chromatography on silica gel using benzene-dichloromethane (1 : 1) as an eluent to afford **4a** (454 mg: 70% yield): mp 23—24°C; IR (neat) 1745, 1384, 1318, 1303, 1280, 1230, 1148, 1095, 1038, 816, 663 cm^{-1}: ^1H NMR ($CDCl_3$) δ=2.06 (3H, s), 2.43 (3H, s), 4.78 (2H, dd, *J*=0.9 and 3.5 Hz), 6.61 (1H, td, *J*=0.9 and 15 Hz), 7.02 (1H, td, *J*=3.5 and 15 Hz), 7.32 (2H, d, *J*=9 Hz), and 7.79 (2H, d, *J*=9 Hz). Calcd for $C_{12}H_{14}O_4S + 1/20\ C_6H_6$: C, 57.22; H, 5.58%. Found: 57.31; H, 5.58%.

This compound was hydrolyzed to give 3-hydroxy-1-propenyl *p*-tolyl sulfone. A solution containing **3a** (171 mg: 0.67 mmol) and conc. hydrochloric acid (0.5 ml) in methanol (20 ml) was stirred at room temperature for 48 h. After addition of water (20 ml), the mixture was extracted with

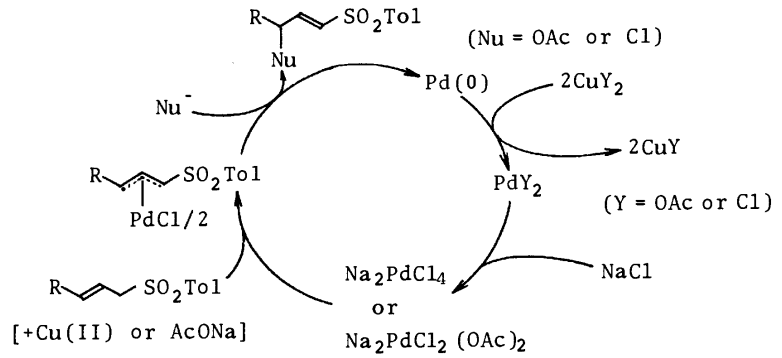

Scheme 2.

Table 4. $PdCl_2$-Catalyzed preparation of **4** or **5**

R	2→4[a]		2→5[b]	
	Conditions Temp/°C (Time/h)	Yield/%	Conditions Temp/°C (Time/h)	Yield/%
H	80(49)	92	80(30)	89
CH_3	100(30)	90	80(20)→100(56)	68
n-C_9H_{19}	100(65)	73	100(84)	57

a) Using $PdCl_2$ (3 mol%), $Cu(OAc)_2$ (2.0 mol equiv), AcONa (6.0 equiv), and NaCl (3.0 equiv) in AcOH.
b) Using $PdCl_2$ (5 mol%), $CuCl_2$ (3.0 mol equiv), and NaCl (3.0 equiv), in AcOH.

four 30 ml-portions of dichloromethane. The extracts were combined, washed with water, and evaporated under reduced pressure to give colorless crystals (131 mg: 92% yield) which were purified by recrystallization from carbon tetrachloride-dichloromethane to afford colorless needles (100 mg): mp 122—123 °C; IR (KBr) 3605, 1295, 1286, 1274, 1137, 1079, 942, 811, 665, 536, 523 cm^{-1}: ^1H NMR ($CDCl_3$) δ=2.43 (3H, s),4.34 (2H, m), 6.60 (1H, diffused d, J=15 Hz), 7.03 (1H, td, J=3 and 15 Hz), 7.33 (2H, d, J=8 Hz), 7.77 (2H, d, J=8 Hz). Calcd for $C_{10}H_{12}O_3S$: C, 56.59; H, 5.70%. Found: C, 56.61; H, 5.66%.

In the analogous manners, **4b** and **4c** were obtained. **4b**: An oil; IR (neat) 1742, 1373, 1317, 1303, 1235, 1145, 1082, 661, 568, 548, 539 cm^{-1}; ^1H NMR ($CDCl_3$) δ=1.36 (3H, d, J=6 Hz), 2.03 (3H, s), 2.41 (3H, s), 5.25—5.72 (1H, m), 6.43 (1H, dd, J=1.6 and 16 Hz), 6.90 (1H, dd, J=4 and 16 Hz), 7.31 (2H, d, J=8 Hz), and 7.73 (2H, d, J=8 Hz). Calcd for $C_{13}H_{16}O_4S$: C, 58.19; H, 6.01%. Found: C, 58.08; H, 6.15%. **4c**: An oil; IR (neat) 3030, 2860, 1748, 1375, 1320, 1301, 1235, 1150, 1087, 665 cm^{-1}; ^1H NMR ($CDCl_3$) δ=0.25—1.82 (19H, m), 2.01 (3H, s), 2.44 (3H, s), 5.13—5.56 (1H, diffused s), 6.37 (1H, d, J=15 Hz), 6.83 (1H, dd, J=4 and 15 Hz), 7.31 (2H, d, J=8 Hz), and 7.74 (2H, d, J=8 Hz). Calcd for $C_{13}H_{16}O_4S$: C, 58.19; H, 6.01%. Found: C, 58.08; H, 6.15%.

(b) The Use of ca. *6 mol equiv of* $CuCl_2$: After a suspension containing $PdCl_2$ (370 mg: 2.09 mmol), $CuCl_2$ (1.70 g: 12.7 mmol), AcONa (22.2 g: 27.1 mmol), and NaCl (1.55 g: 26.5 mmol), in AcOH (23.0 ml)-Ac_2O (1.0 ml) was stirred at 90—95 °C for 2 h, **2a** (410 mg: 2.09 mmol), was added along with AcOH (4.0 ml), and the resulting mixture was stirred at 60 °C for 16 h. After addition of water (50 ml) and extraction with four 70-ml portions of benzene-dichloromethane (3:1), the extracts were combined and washed with water, saturated aqueous $NaHCO_3$, and brine. Then, after the extract was dried over anhydrous $MgSO_4$, the solution was evaporated under reduced pressure, and the residue was subjected to column chromatography on silica gel using benzene-hexane and benzene-AcOEt as eluents to give **4a** (156 mg: 29% yield) and **5a** (291 mg: 60% yield). An analytical sample of **5a** was obtained by recrystallization from benzene-hexane: mp 58—59 °C; IR (KBr) 3046, 2921, 1302, 1276, 1141, 861, 709, 587, 530, 501 cm^{-1}: ^1H NMR ($CDCl_3$) δ=2.44 (3H, s), 4.19 (2H, dd, J=1.1 and 5.0 Hz), 6.66 (1H, dd, J=1.1 and 14.8 Hz), 6.97 (1H, dt, J=5.0 and 14.8 Hz), 7.32 (2H, d, J=8.0 Hz), and 7.77 (2H, d, J=8.0 Hz). Calcd for $C_{10}H_{11}O_2ClS$: C, 52.06; H, 4.81%. Found: C, 51.97; H, 4.80%.

Similarly, the following compounds were obtained. **5b**: Mp 37—38 °C (from hexane); IR (KBr) 1315, 1303, 1281, 1145, 1088, 963, 840, 808, 671, 578, 543 cm^{-1}; ^1H NMR ($CDCl_3$) δ=1.62 (3H, d, J=6.8 Hz), 2.44 (3H, s), 4.63 (1H, diffused quintet, J=6 Hz), 6.61 (1H, dd, J=14.8 and 0.6 Hz), 6.92 (1H, dd, J=14.8 and 5.6 Hz), 7.37 (2H, d, J=8.3 Hz), and 7.77 (2H, d, J=8.3 Hz). Calcd for $C_{11}H_{13}O_2ClS$: C, 53.99; H, 5.26%. Found: C, 54.02; H, 5.35%.

5c: Mp 30—31 °C; IR (neat) 2925, 2851, 1315, 1302, 1285, 1143, 1186, 811, 653, 588 cm^{-1}; ^1H NMR ($CDCl_3$) δ=0.67—1.90 (19H, m), 2.44 (3H, s), 4.44 (1H, dt, J=6.4 and 5.7 Hz), 6.55 (1H, d, J=14.7 Hz), 7.22 (2H, d, J=8.1 Hz), and 7.74 (2H, d, J=8.1 Hz). Calcd for $C_{19}H_{29}O_2ClS$: C, 63.93; H, 8.19%. Found: C, 63.95; H, 8.11%.

Under the similar conditions, 3-phenyl-2-propenyl *p*-tolyl sulfone (**2d**) gave **4d**: mp 108—109 °C; IR (KBr) 3080, 2925, 1739, 1314, 1301, 1236, 1139, 673, 536 cm^{-1}; ^1H NMR ($CDCl_3$) δ=2.02 (3H, s), 2.41 (3H, s), 6.18 (1H, dd, J=1.5 and 4.5 Hz), 6.25 (1H, dd, J=1.5 and 15 Hz), 6.99 (1H, dd, J=4.5 and 15 Hz), 7.16—7.61 (7H, broad), and 7.68 (2H, d, J=8 Hz). UV (EtOH) 207 (ε 11700), 239 (12000), and 277 (562) nm. Calcd for $C_{18}H_{18}O_4S$: C, 65.44; H, 5.49%. Found: C, 65.42; H, 5.43%. No **5d** was obtained in this reaction.

Acid hydrolysis of **4d** was also performed by the procedure similar to that of **3a**. 3-Hydroxy-3-phenyl-1-propenyl *p*-tolyl sulfone: mp 134—135 °C; IR (KBr) 3590, 1314, 1307, 1276, 1137, 1078, 975, 813, 756, 704, 691, and 543 cm^{-1}; ^1H NMR ($CDCl_3$) δ=2.43 (3H, s), 2.70 (1H, d, J=6 Hz, OH), 5.15—5.49 (1H, m), 6.66 (1H, d, J=16 Hz), 7.18 (1H, dd, J=3.5 and 16 Hz), 7.15—7.46 (7H, m), 7.70 (2H, d, J=8 Hz). Calcd for $C_{16}H_{16}O_3S$: C, 66.64; H, 5.59%. Found: C, 66.79; H, 5.64%.

Isolation of the π-Allylpalladium Complex (3a). A suspension involving **2a** (1.96 g: 10.0 mmol), $PdCl_2$ (1.77 g: 10.0 mmol), and AcONa (1.65 g: 20 mmol) in AcOH (100 ml)-Ac_2O (5 ml) was stirred at 60 °C for 24 h. The deposited solid was collected by filtration and transfered into a beaker. Then, the solid was triturated with benzene (10 ml) and the benzene was discarded by decantation. After this procedure was repeated five times, the solid was washed with five 10 ml-portions of water and dried over sulfuric acid under reduced pressure. An analytical sample was obtained as follows. **3a** was dissolved in DMSO-AcOH (3:2) under ice-cooling and then excess of AcOH was added to deposit **3a**. The solid (**3a**) was filtered and washed with water and dichloromethane: mp 152—164 °C (decomp); IR (KBr) 1310, 1299, 1140, 1092, 820, 802, 788, 656, 573, and 552 cm^{-1}. Calcd for $C_{10}H_{11}O_2ClPdS$: C, 35.63; H, 3.29%. Found: C, 35.23; H, 3.29%.

Isolation of the π-Allylpalladium Complexes (3b and 3d). After a suspension containing $PdCl_2$ (460 mg: 2.59 mmol), NaCl (1.94 g: 23.6 mmol), AcONa (2.77 g: 33.8 mmol), and $CuCl_2$ (943 mg: 7.01 mmol) in AcOH (14 ml)-Ac_2O (3 ml) was stirred at 95—105 °C for 2 h, a solution of **2b** (553 mg: 2.63 mmol) in AcOH (5 ml) was added and the resulting mixture was stirred at 60—65 °C for 76 h. After addition of benzene (20 ml), the mixture was extracted with four 20-ml portions of benzene. The yellow solid floating in the benzene layer was collected by filtration, washed with benzene, and dried in a desiccator to give **3b** (621 mg) as a greenish yellow solid. An analytical sample was obtained by dissolution in DMSO-AcOH (3:1) followed by reprecipitation by addition of water: mp: 168—170 °C; IR (KBr) 3060, 1595, 1308, 1301, 1150, 1079, 820, 806, 799, 654, 566 cm^{-1}. Calcd for $C_{11}H_{13}O_2ClPdS+0.9H_2O$: C, 35.96; H, 4.06%. Found: C, 35.82; H, 3.70%.

The benzene layer was washed with water and saturated aqueous $NaHCO_3$, dried over anhydrous $MgSO_4$, evaporated, and chromatographed on silica gel [elution with benzene- dichloromethane (1:2)] to give **4b** (142 mg: 20% yield).

In the similar manner, **3d** was obtained: mp 193—194 °C (decomp). Calcd for $C_{16}H_{15}O_2ClPdS+0.7H_2O$: C, 45.13; H, 3.88%. Found: C, 45.08; H, 3.69%.

Reaction of 3a with $CuCl_2$ and NaCl. A Typical Procedure: A suspension containing **3a** (506 mg: 1.50 mmol), $CuCl_2$ (404 mg: 3.00 mmol), and NaCl (263 mg: 4.50 mmol) in AcOH (19.5 ml)-Ac_2O (0.7 ml) was stirred at 60 °C for 48 h. After addition of water (40 ml), the mixture was extracted with four 50-ml portions of benzene-dichloromethane (3:1) and the organic layer was washed successively with water, saturated aqueous $NaHCO_3$, brine, and water. The organic layer was dried over anhydrous $MgSO_4$, the solvents were removed, and the resultant residue was subjected to column chromatography on silica gel using hexane-benzene (4:1) and benzene-ethyl acetate (4:1) as eluents to afford **5a** (272 mg), a mixture (6.7 mg) of **5a** and **4a** (9:1), and **4a** (35 mg). The yields of **5a** and **4a** were calculated to be 80 and 9%, respectively.

In the similar manners, **3a** was subjected to the reaction in the presence of various additives. The results were summarized in Table 3.

$PdCl_2$-Catalyzed Conversion of 2a to 4a. A Typical Procedure: A suspension involving **2a** (393 mg: 2.0 mmol), $PdCl_2$ (10.6 mg: 0.06 mmol), $Cu(OAc)_2$ (726 mg: 4.0 mmol), AcONa (985 mg: 12.0 mmol), and NaCl (351 mg: 6.0 mmol), in AcOH (26 ml)-Ac_2O (1 ml) was stirred at 60 °C for 48 h.

After addition of water (40 ml), the resulting mixture was extracted with four 60-ml portions of benzene–dichloromethane (4:1) and then the extract was washed successively with water, saturated aqueous $NaHCO_3$, brine, and water. The extract was dried over anhydrous $MgSO_4$, the solvents were removed, and the resultant residue was subjected to column chromatography on silica gel using hexane–benzene (9:11) and benzene– ethyl acetate (3:2) as eluents to give **4a** (476 mg: 92% yield).

Analogously, **2b** and **2c** were converted to **4b** (90% yield) and **4c** (73% yield), respectively, under the conditions described in Table 4.

$PdCl_2$-Catalyzed Conversion of 2a to 5a. A Typical Procedure: A suspension involving **2a** (1.00 g: 5.1 mmol), $PdCl_2$ (27.1 g: 0.153 mmol), $CuCl_2$ (2.06 g: 15.3 mmol), and NaCl (894 mg: 15.3 mmol) in AcOH (26 ml)–Ac_2O (1 ml) was stirred at 80°C for 30 h. After water (100 ml) was added, the resulting mixture was extracted with four 60-ml portions of benzene–dichloromethane (4:1). Then the organic layers was combined and washed successively with water, saturated aqueous $NaHCO_3$, brine, and water. This layer was dried over anhydrous $MgSO_4$, the solvents were removed, and the resultant residue was subjected to column chromatography on silica gel using hexane–benzene (9:11) and benzene–ethyl acetate (3:2) as eluents to give **5a** (1.09 g: 89% yield).

Similarly, **2b** and **2c** were converted **5b** (68% yield) and **5c** (57% yield), respectively, under the conditions described in Table 4.

References

1) For a review, B. M. Trost, *Tetrahedron*, **33**, 2615 (1977); J. Tuji, "Organic Synthesis with Palladium Compounds," Springer-Verlag, Heiderberg (1980); S. Murahashi and T. Hosokawa, *Yuki Gosei Kagaku Kyokai Shi*, **39**, 933 (1981); J. Tsuji, *ibid.*, **41**, 619 (1983).

2) A part of this work was reported as a preliminary communication: K. Ogura, N. Shibuya, and H. Iida, *Tetrahedron Lett.*, **22**, 1519 (1981).

3) B. M. Trost, N. R. Schmuff, and M. J. Miller, *J. Am. Chem. Soc.*, **102**, 5979 (1980).

4) During the course of our investigation, Tuji *et al.* reported γ-acetoxylation of β,γ-unsaturated ester using $Pd(OAc)_2$, AcOK, and pentyl nitrite as well as regioselective nucleophilic substitution of π-allylpalladium complexes substituted with cyano and methoxycarbonyl groups with the carbanions of dimethyl malonate and methyl acetoacetate: J. Tuji, K. Sakai, H. Nagashima, and I. Shimizu, *Tetrahedron Lett.*, **22**, 131 (1981) and J. Tuji, H. Ueno, Y. Kobayashi, and H. Okumoto, *ibid.*, **22**, 2573 (1981).

5) B. M. Trost, P. E. Strege, L. Weber, T. J. Fullerton, and T. J. Dietsche, *J. Am. Chem. Soc.*, **100**, 3407 (1978).

6) A 1:2 mixture of $CuCl_2$ and AcONa in AcOH was heated at 60°C for 48 h and then evaporated under reduced pressure, the IR spectrum of the residual solid was almost identical with that of the mixture obtained from $Cu(OAc)_2$ and NaCl (the molar ratio of 1:2) in the similar manner. The residual solid showed its IR absorption at 1620 cm^{-1} (KBr), being different from those of NaOAc [1640 (weak) and 1555 cm^{-1}] and $Cu(OAc)_2$ (1600 cm^{-1}).

7) T. Durst, "Comprehensive Organic Chemistry," ed by D. Barton and W. S. Ollis, Pergamon Press, Oxford (1979), Vol. 3, pp. 172—174.

8) The possibility that the conjugation of the sulfonyl group with the C-C double bond is a driving force for the preferable formation of **4** or **5** may be excluded because it has been the general observation that the β,γ-unsaturated sulfone is more stable than the α,β-isomer: D. E. O'Connor and W. I. Lyness, *J. Am. Chem. Soc.*, **86**, 3840 (1964); C. D. Broaddus, *ibid.*, **88**, 3865 (1966) and **90**, 5504 (1968).

9) $Na_2[PdCl_4]$ can be prepared by evaporation of a solution containing $PdCl_2$ and NaCl in the molar ratio of 1:2 in water: P. Haas, "Handbuch der Präparativen Anorganishen Chemie," ed by G. Bauer, (1954), p. 1185.

 © 1984 The Chemical Society of Japan Bull. Chem. Soc. Jpn., 57, 1097—1103 (1984)

Mass Spectra of Butyl Esters and *N*-Trifluoroacetyl Butyl Esters of Some Iminodicarboxylic Acids upon Electron Impact

Katsuhiro KAWASHIRO,* Shiro MORIMOTO, and Hideyuki YOSHIDA

Department of Chemical Engineering, Faculty of Engineering, Tokushima University, Minamijosanjima, Tokushima 770

(Received August 24, 1983)

Mass spectra (electron impact at 20 eV) of butyl esters and *N*-trifluoroacetyl (TFA) butyl esters of some iminodicarboxylic acids (IDCAs) were determined by gas chromatography-mass spectrometry. The IDCAs included iminodiacetic acid (**1**), 2-(carboxymethylamino)propionic acid (**2**), 3-(carboxymethylamino)propionic acid (**3**), 2,2′-iminodipropionic acid (**4**), 2,3′-iminodipropionic acid (**5**), 3,3′-iminodipropionic acid (**6**), *N*-methyliminodiacetic acid (**7**), and nitrilotriacetic acid (**8**). The mass spectra of the butyl ester derivatives are simple, exhibiting the corresponding molecular (M^+) ions with the exception of **5**. The α,α'-IDCAs (**1**, **2**, **4**, **7**, and **8**) are characterized by M^+, M −101 ($COOC_4H_9$) (base peak), and M −157 ($COOC_4H_9+C_4H_8$) ions. The β,β'-IDCA (**6**) is characterized by a more complex spectrum with M^+, M −73 (OC_4H_9), M −115 ($CH_2COOC_4H_9$) (base peak), M −129 ($OC_4H_9+C_4H_9$), and M −171 ($CH_2COOC_4H_9+C_4H_9$) ions. The α,β'-IDCAs (**3** and **5**) in general show spectra in which both ions characteristic of α,α'- and β,β'-IDCAs are observed. The addition of TFA to the imino nitrogens of **1**—**6** increases complexity of the resulting spectra. In these instances, although M^+ ions are usually present, neither M −101 nor M −115 ions are base peaks. The fragmentation pathways of these two volatile derivatives of the IDCAs upon electron impact are discussed.

In connection with chemical evolution, Chadha *et al.*[1] applied a discharge through a simulated Jovian atmosphere. After a reaction mixture was hydrolyzed and derivatized, they identified amino acids such as glycine and alanine, and their *N*-methyl and *N*-acetic acid derivatives (iminodicarboxylic acids, IDCAs) by gas chromatography-mass spectrometry (GC-MS). This result demonstrates that non-protein amino acids such as *N*-alkyl amino acids and IDCAs can be formed along with protein amino acids when amino acid syntheses take place prebiologically from simple molecules or gaseous mixtures *via* a Strecker mechanism. The GC-MS has been shown to be the most suitable method for unequivocal identification of amino acids and related compounds by means of retention times and mass spectral confirmation.[2-5] In these studies, an *N*-trifluoroacetylated *s*-butyl,[2-4] butyl,[1] and isopropyl[5] ester derivatives were used for GC-MS analysis.

Electron impact (EI) mass spectra of *N*-trifluoroacetyl (TFA) butyl esters of protein amino acids[6,7] and certain non protein amino acids[7,8] including β- and γ-, and *N*-alkyl amino acids, have been determined by GC-MS. Recently, Cronin *et al.*[9] have studied GC-MS of the *N*-TFA *s*-butyl esters of five carbon β-, γ-, and δ-amino acids, and presented 70 eV spectra. However, little GC-MS information is available on IDCAs at present. This prompted us to investigate GC-MS of *N*-TFA butyl esters of some IDCAs, as shown in Fig. 1, for unequivocal identification of such IDCAs present in reaction mixtures of prebiological amino acid synthesis. The reason for the *N*-TFA butyl ester derivative to be chosen in the present study, is that not only the derivatives of amino acids have widely been used for GC,[10] but also their fragmentation pathways upon electron impact have been discussed in detail.[6,7,11] Furthermore, previous authors[6,8] have suggested that various alkyl groups used in the esterification gave almost the same fragmentation pathways for amino acids.

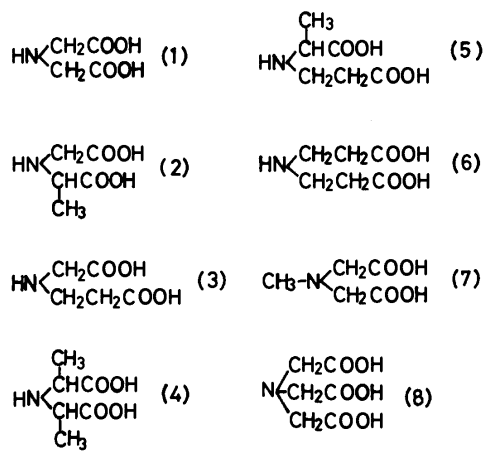

Fig. 1. Iminodicarboxylic acids.

In contrast with common amino acids, the NH of IDCAs is considered to be sterically hindered to some extent, so that trifluoroacetylation at room temperature was found to be incomplete in the case of 2,2′-iminodipropionic acid (**4**). Therefore, GC-MS of butyl ester derivatives was also studied.

The IDCAs studied in the present paper include iminodiacetic acid (**1**), 2-(carboxymethylamino)propionic acid (**2**), 3-(carboxymethylamino)propionic acid (**3**), **4**, 2,3′-iminodipropionic acid (**5**), 3,3′-iminodipropionic acid (**6**), *N*-methyliminodiacetic acid (**7**), and nitrilotriacetic acid (**8**). The structures of **1**—**8** are shown in Fig. 1. They are classified into three groups, α,α'-IDCAs (**1**, **2**, **4**, **7**, and **8**), α,β'-IDCAs (**3** and **5**), and β,β'-IDCA (**6**). Since **7** and **8** are *N*-substituted α,α'-IDCAs, only butyl ester derivatives were studied with them.

Results and Discussion

Gas Chromatography. Figure 2 shows a gas chromatographic separation of a mixture of the butyl esters of **1**—**8**. Although **1**, **2**, and **7** overlapped completely, separate experiments revealed that each IDCA except **4** gives a single GC peak. Compound **4** was found to give two GC peaks, which were evidenced by their mass spectra. This can be ascribed to the separation between diastereomers because **4** has two asymmetric carbon

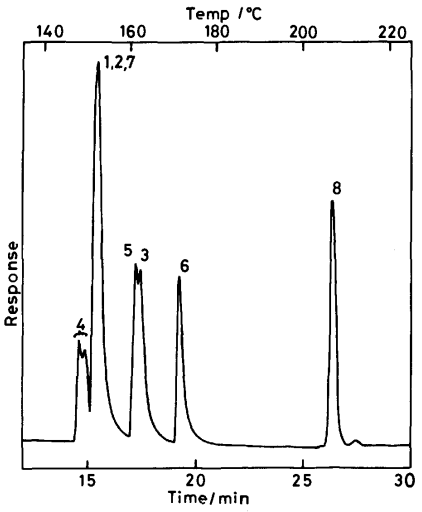

Fig. 2. Gas chromatogram of the butyl esters of **1**—**8**.
Injected: 3.12×10^{-3} μmol of each derivative.
Column: 1.5% OV-101 on Chromosorb G HP (100/120 mesh), 1 m×3 mm I.D. glass. Conditions: initial temperature, 100°C; initial hold, 5 min; program rate, 5°C/min; final temperature, 230°C. Sensitivity: 10×32.

atoms. Figure 3 shows a gas chromatographic separation of a mixture of the *N*-TFA butyl esters of **1**—**6**. Again, each derivative except **4** gave a single GC peak, while **4** gave two GC peaks due to the separation between diastereomers. As expected, the *N*-TFA butyl ester derivatives had somewhat longer retention times than the corresponding butyl ester derivatives.

Mass Spectra. *A) Butyl Ester Derivatives*: Figures 4a—c present the mass spectra of 2,2′-, 2,3′-, and 3,3′-iminodipropionic acid (**4**—**6**). Characteristic ions for **1**—**8** are listed in Table 1. The molecular ions (M^+) are present in all the spectra except **5**. The α,α′-IDCAs give very simple spectra upon electron impact. The base peaks are always M−101 ions which can originate from the following cleavage with charge retention on the nitrogen atoms:

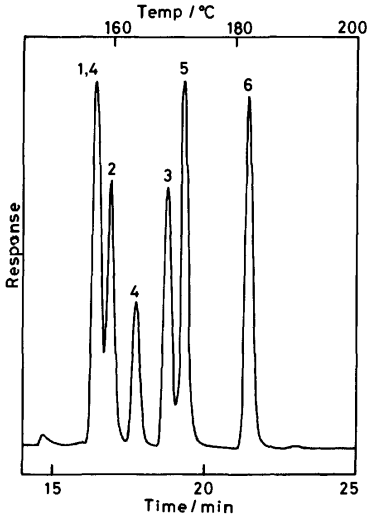

Fig. 3. Gas chromatogram of the *N*-TFA butyl esters of **1**—**6**.
Injected: 4.16×10^{-3} μmol of each derivative.
Conditions are the same as in Fig. 2. Sensitivity: 10×64.

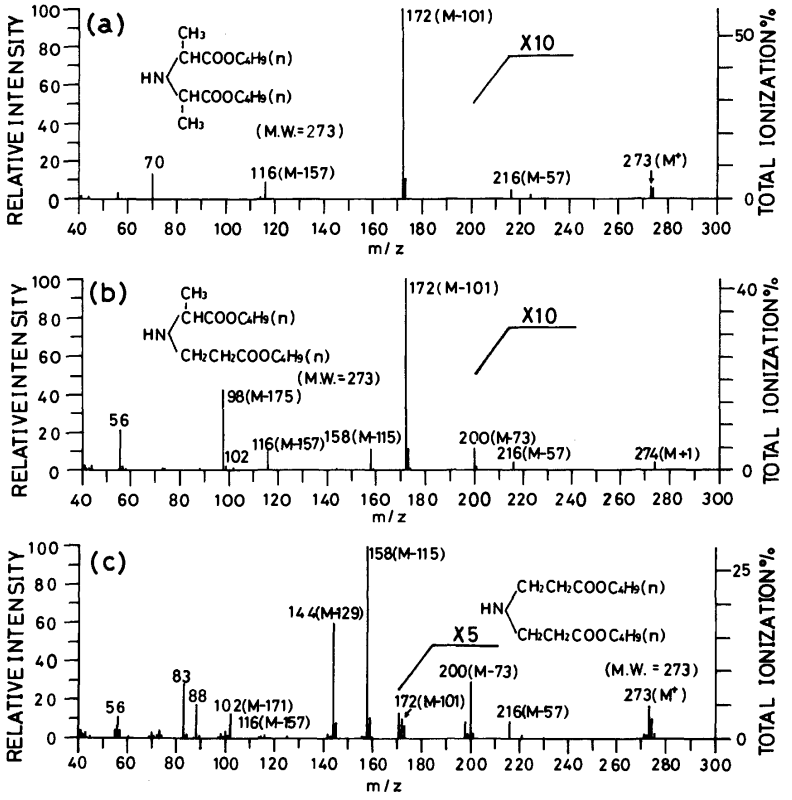

Fig. 4. Mass spectral fragmentations of the butyl esters of IDCAs. a: **4**, b: **5**, and c: **6**.

TABLE 1. SELECTED IONS FROM THE MASS SPECTRA OF THE BUTYL ESTERS OF **1**—**8**[a]

Parent IDCA	M+	M−57	M−73	M−101	M−115	M−129	M−157	M−171	Others
1	245	188	—	144	130	116	88	—	171, 56
	(10.6)	(3.9)		(100)	(0.2)	(0.2)	(31.2)		(6.3) (58.9)
2	259	202	—	158	—	130	102	—	56
	(0.3)	(0.8)		(100)		(0.6)	(43.4)		(25.8)
3	259	202	186	158	144	—	102	88	185, 84, 56
	(4.3)	(3.4)	(2.2)	(100)	(15.2)		(13.0)	(4.5)	(4.6) (38.9) (43.8)
4[b]	273	216	—	172	—	—	116	—	70
	(0.6)	(0.4)		(100)			(8.9)		(13.8)
5	—	216	200	172	158	—	116	102	98, 56
		(0.5)	(1.2)	(100)	(12.0)		(10.7)	(1.5)	(42.8) (22.0)
6	273	216	200	172	158	144	116	—	102, 88, 83
	(3.5)	(1.8)	(5.9)	(2.0)	(100)	(59.3)	(0.1)		(13.1) (17.5) (28.7)
7	259	202	—	158	—	—	102	—	—
	(6.0)	(0.8)		(100)			(13.1)		
8[c]	359	302	—	258	—	230	202	—	158
	(3.3)	(0.5)		(100)		(0.1)	(5.5)		(20.6)

a) Values in parentheses indicate relative intensity. b) The first gas chromatographic peak. c) A tributyl ester.

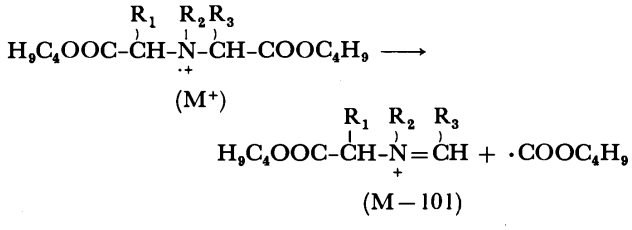

The predominance of the M−101 ($COOC_4H_9$) ion can be explained in terms of its increased stability due to resonance as described by Biemann *et al.*[12] Another prominent ion for the α,α'-IDCAs, the M−157 ion, results from the M−101 ion by the loss of 1-butene from the residual ester portion *via* a McLafferty rearrangement. Since **7** is an isomer of **2**, its spectrum is similar to that of **2**. However, some differences are noted between the two isomers. Compound **7** carrying a methyl group on the imino nitrogen is characterized not only by a more intense M^+ ion but also by a larger total ionization of the base peak (M−101) than **2**, as shown in Tables 1 and 2.

The β,β'-IDCA exhibits a more complex spectrum than the α,α'-IDCAs (Fig. 4c). The ion at m/z 158 (M−115) is a base peak, which arises from the M^+ ion by the loss of $CH_2COOC_4H_9$ due to alpha-beta bond cleavage (α-cleavage to the imino nitrogen). Because the M−115 ($CH_2COOC_4H_9$) ion resulting from the cleavage is very stable, the fragmentation losing $COOC_4H_9$ from the M^+ ion does not take place to any appreciable extent. Consequently, the M−101 ion typical of the α,α'-IDCAs is of minor importance in this case. The M−115 ion produces the M−171 ion at m/z 102 by the loss of 1-butene from the residual ester portion *via* a McLafferty rearrangement. An important M−73 ion results from the M^+ ion by the loss of OC_4H_9 from either of the two ester portions. This M−73 (OC_4H_9) ion is characteristic of the β,β'- and α,β'-IDCAs, namely those bearing a butoxycarbonyl group at the beta position to the imino nitrogen, and is not present in the spectra of the α,α'-IDCAs (Table 1). One possible explanation for the stability of the M−73 ion has been proposed by Lawless and Chadha[8] as follows:

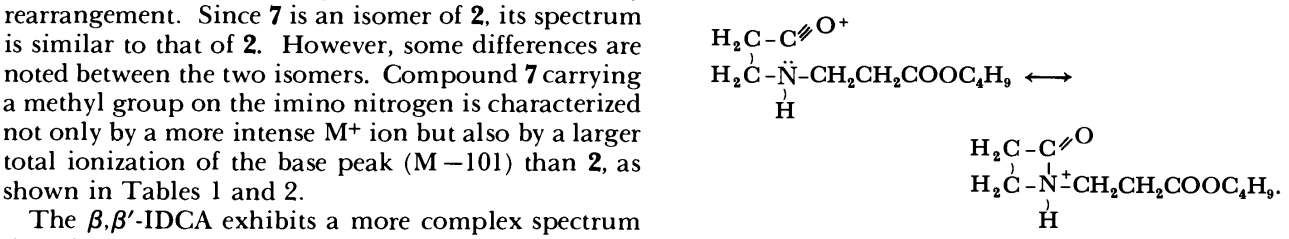

However, the M−73 peaks observed for **3**, **5**, and **6** are much smaller than those of *N*-TFA-β-amino acid butyl esters reported by Lawless and Chadha.[8] This difference may be explained in terms of the stability of such a cyclized ion as shown above. In the *N*-TFA-β-amino acid butyl esters, the *N*-TFA group is considered to stabilize the resultant cyclized ions through electron-withdrawing. The prominent M−129 ion at m/z 144 originates from the loss of 1-butene from the residual ester portion of the M−73 ion *via* a McLafferty rearrangement. This M−129 ($OC_4H_9 + C_4H_8$) ion is missing in the spectra of the α,β'-IDCAs but present with a low intensity in those of certain α,α'- IDCAs (**1**, **2**, and **8**).

As shown in Fig. 4b, α,β'-IDCAs are characterized by spectra exhibiting both ions typical of the α,α'- and β,β'-IDCAs with the exception of the M−129 ion observed for **6**. However, base peaks are always M−101 and not M−115 ions, indicating that a butoxycarbonyl group (a), defined below, is more preferentially split

TABLE 2. TOTAL IONIZATION OF BASE PEAKS OF THE BUTYL ESTERS OF **1**—**8**

Parent IDCA	Base peak/m/z	Origin	Total ionization/%
1	144	M−101	20
2	158	M−101	38
3	158	M−101	20
4	172	M−101	60
5	172	M−101	42
6	158	M−115	29
7	158	M−101	66
8	258	M−101	42

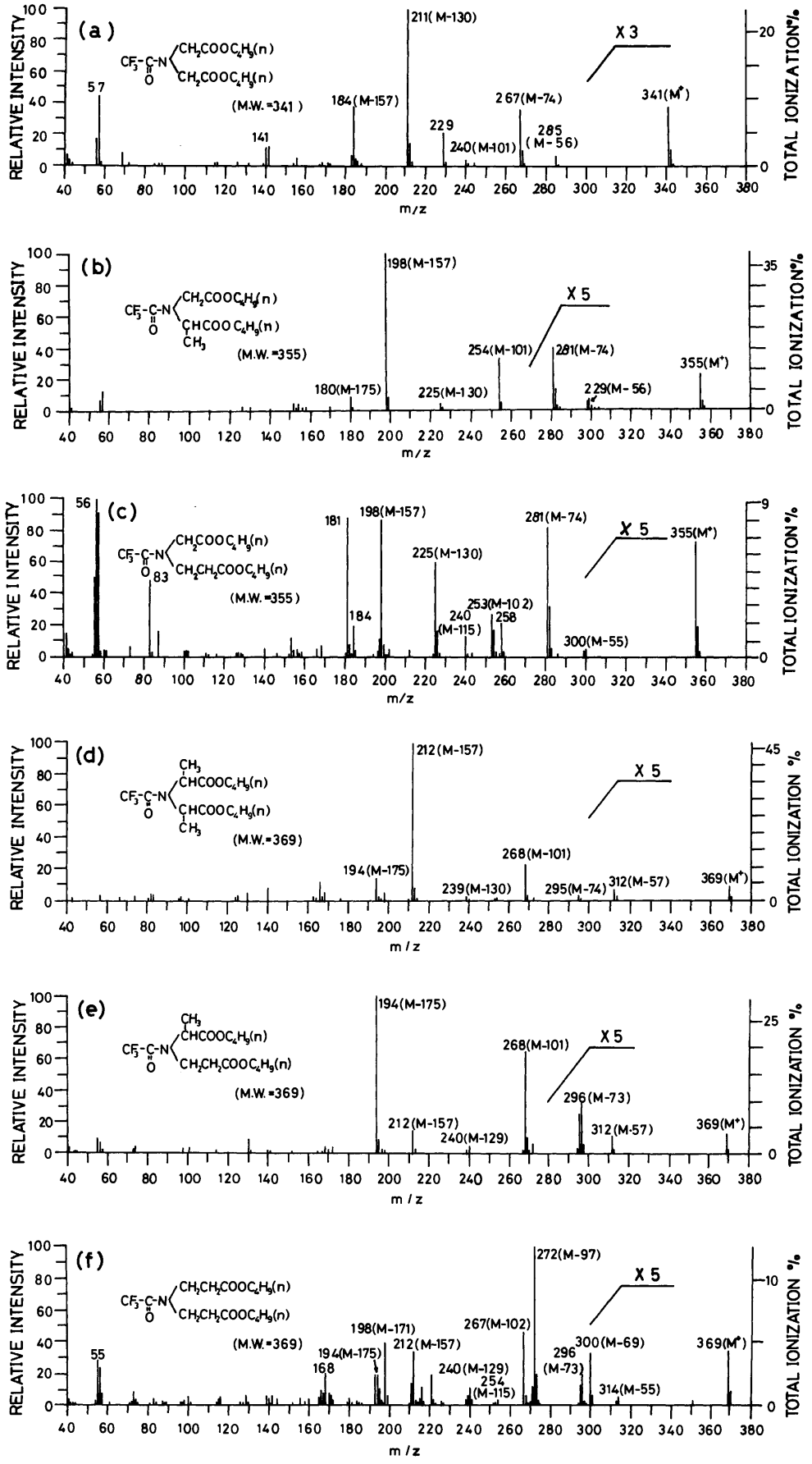

Fig. 5. Mass spectral fragmentations of the *N*-TFA butyl esters of IDCAs. a: **1**, b: **2**, c: **3**, d: **4**, e: **5**, and f: **6**.

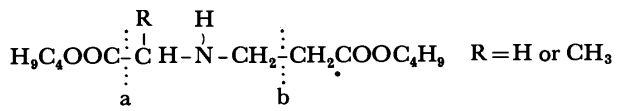

off than a butoxycarbonylmethyl one (b), also defined above, by α-fission to the imino nitrogen atom. A prominent M−175 ion is observed for **3** and **5**, which corresponds to the one resulting from the M−157 ion by the loss of H_2O,[6] or from the M−101 ion by the loss of 1-butanol.[7] Fragmentation pathways for the α,β'-IDCAs are presented in Scheme 1 as an illustrative example, which involves both the pathways characteristic of α,α'- and β,β'-IDCAs.

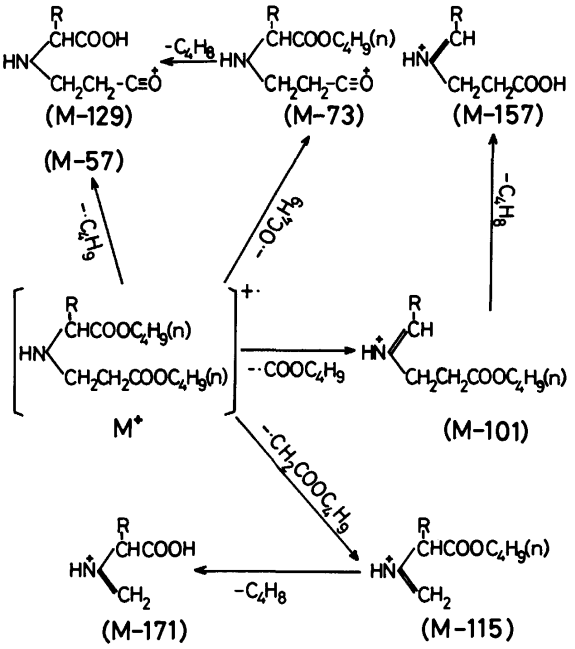

Scheme 1. Fragmentation pathways of the butyl esters of the α,β'-IDCAs.

As shown in Table 1, the M−57 ion is consistently present in all the spectra, which arises from the loss of a butyl group from the corresponding M^+ ion. The M+1 ion is also observed for **1**—**8**, and in certain instances (**2** and **5**) this ion is more intense than the corresponding M^+ ion.

As shown in Table 2, the total ionization of the base peak (M−101) generally depends on the structure of IDCA. The IDCAs carrying a methyl group on an α-carbon or an imino nitrogen atom have larger total ionization.

In conclusion, the α,α'-IDCAs are characterized by the M^+, M−101 (base peak), and M−157 ions. The β,β'-IDCA is characterized by a more complex spectrum with the M^+, M−73, M−115 (base peak), M−129, and M−171 ions. The α,β'-IDCAs generally show spectra in which both ions characteristic of α,α'- and β,β'-IDCAs are present. The M−101 and not M−115 ion is a base peak for the α,β'-IDCAs.

B) N-TFA Butyl Ester Derivatives: Figures 5a—f show the mass spectra of *N*-TFA butyl esters of **1**—**6**. In general, each spectrum is more complex than that of the corresponding butyl ester derivative. However, M^+ ions are present in all the spectra. The M−101 (loss of a butoxycarbonyl) ion which is a base peak for the butyl ester derivatives with the exception of **6**, becomes less significant in these instances. This may be due to the fact that a strong electron-attractive TFA group attached to an imino nitrogen atom will decrease the stability of the ion. It is noted that the important ions, M−73 (loss of a butoxyl group), M−74 (loss of 1-butanol), M−129 (loss of a butoxyl group and 1-butene), and M−130 are consistently present in all the spectra. The M−130 ion is observed at *m/z* 225 for **3** and its elementary composition was determined to be $C_7H_6NO_4F_3$ by a high-resolution mass measurement, which corresponds to the loss of 1-butanol and 1-butene from the M^+ ion. Accordingly, the M−130 ion is considered to result from the M−74 ion by the loss of 1-butene *via* a McLafferty rearrangement. The M−74 ion arises from the loss of 1-butanol from either of the two ester portions of the M^+ ion. Gelpi *et al.*[6] have found, for the *N*-TFA butyl esters of aspartic and glutamic acids, that the cleavage of one of the butoxyl groups to give the M−73 ion is accompanied by removal of 1-butanol to give the M−74 ion. This fragmentation is significant especially for the *N*-TFA butyl esters of IDCAs, but not for the butyl ester derivatives.

In the high mass region, two ions, M−55 and M−56, are usually present, although not as major peaks in any instances. The former ion may be explained in terms of a double hydrogen rearrangement. The latter ion results from the loss of 1-butene from the M^+ ion *via* a McLafferty rearrangement.

For the α,α'-IDCAs (**1**, **2**, and **4**), the M−74 and M−130 ions are more intense than the M−73 and M−129 ions, respectively. In the case of **1**, the M−130 ion at *m/z* 211 is a base peak. Additional characteristic ions are M−157 (loss of a butoxycarbonyl and 1-butene) and M−175 (loss of a butoxycarbonyl and 1-butanol). The former ion is a base peak for **2** and **4**.

In contrast, the β,β'-IDCA (**6**) shows a more complex spectrum (Fig. 5f) than the α,α'-IDCAs. The base peak at *m/z* 272 corresponds to a fragment, M−97 (CF_3CO), which was confirmed by a high-resolution mass measurement. Other unusual ions are M−69 (CF_3) at *m/z* 300 and M−102 ($COOC_4H_9$+H) at *m/z* 267, the elementary compositions of which were also confirmed by high-resolution mass measurements. The M−102 ion is more intense than the M−101. This fact is in good agreement with results obtained for β-amino acid derivatives,[7,8] since **6** is an *N*-substituted β-alanine. The stability of the M−102 ion for β-amino acids has been explained in terms of resonance by Lawless and Chadha.[8] Additional characteristic ions are M−115 (loss of a butoxycarbonylmethyl) at *m/z* 254 and M−171 (loss of a butoxycarbonylmethyl and 1-butene) at *m/z* 198. The characteristic ions of the α,α'-IDCAs such as the M−157 and M−175 ions are also observed. In contrast with the α,α'-IDCAs, the M−74 and M−130 ions are less intense than the M−73 and M−129 ions, respectively.

For the α,β'-IDCAs (**3** and **5**), fragmentations become more complicated. As shown in Fig. 5c, **3** exhibits a spectrum in which both ions characteristic of the α,α'- and β,β'-IDCAs are present. The elementary composition of an unusual ion at *m/z* 181 was determined to be $C_6H_6NO_2F_3$ by a high-resolution mass measurement, which corresponds to a fragment, M−174

($COOC_4H_9 + OC_4H_9$). The origin and structure of this ion are unkown. On the other hand, **5** exhibits an almost identical spectrum (Fig. 5e) with that of the corresponding α,α'-IDCA (**4**), except that the base peak is M−175 at *m/z* 194, and that the M−74 and M−130 ions are less intense than the M−73 and M−129 ions, respectively. Although the M−102 ion is present with a very low intensity, another ion typical of the β,β'-IDCA, M−115, is not observed. This fact indicates that either of the fragmentation characteristics of α,α'- or β,β'-IDCAs can take place predominantly depending on the structures of α,β'-IDCAs. Fragmentation pathways for the α,β'-IDCAs are presented in Scheme 2 as an illustrative example. The structures of the M−74 and M−130 ions are unknown.

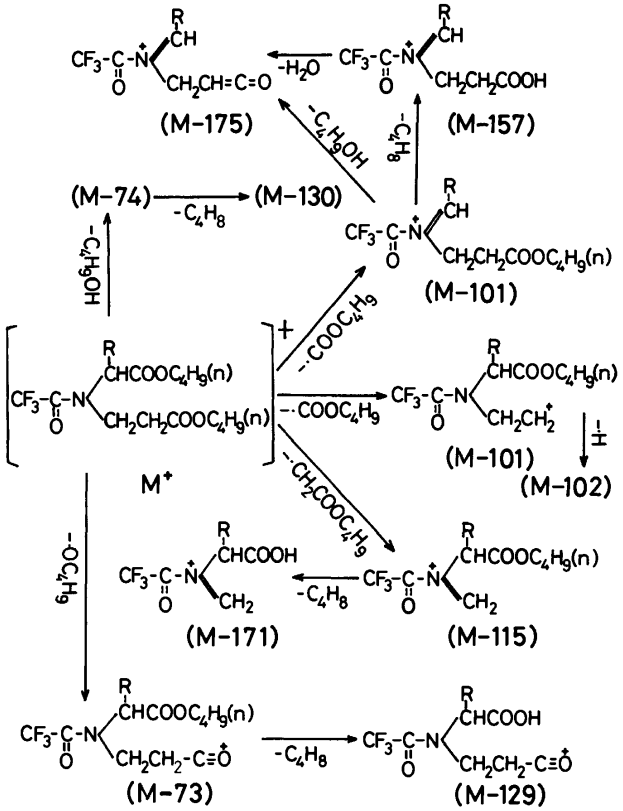

Scheme 2. Fragmentation pathways of the *N*-TFA butyl esters of the α,β'-IDCAs.

Although fragmentation pathways for the *N*-TFA butyl esters of the IDCAs are more complicated than those for the butyl ester derivatives, it seems possible to identify unknown IDCAs by noting the characteristic ions described above.

Experimental

All the melting points were determined with a Yanagimoto micro melting point apparatus and were not corrected. ^1H NMR spectra were measured with a Hitachi R-24B spectrometer using DSS as an internal standard. Thin layer chromatography was carried out on silica gel 60 F_{254} (Merck) using the following solvent system: *n*-BuOH–AcOH–H_2O (4:1:1, v/v).

Preparation of IDCAs. Compound **1** was obtained from Wako Pure Chemical Industries, Ltd. and **8** was prepared by the method reported previously.[13]

2-(Carboxymethylamino)propionic Acid (2). Compound **2**·HCl was prepared from DL-alanine (5.6 g, 63 mmol) and chloroacetic acid (5.9 g, 62 mmol) in the presence of 4 M LiOH (1 M=1 mol dm^{-3}) (46.4 ml) according to the method of Okamoto *et al.*[14] The aqueous solution of **2**·HCl was poured into an ion-exchange column (2.0ϕ×100 cm, Amberlite CG 120 (H form)) and then **2** was eluted with H_2O. The fractions containing **2** were concentrated to give crystals of free **2**: these were recrystallized from H_2O-acetone: yield 2.47 g (27%); mp (decomp) 229—232° (lit,[15] 222—223°C); R_f 0.04. Found: C, 40.55; H, 6.10; N, 9.52%. Calcd for $C_5H_9NO_4$: C, 40.82; H, 6.17; N, 9.52%.

3-(Carboxymethylamino)propionic Acid (3). A solution of *N*-(2-cyanoethyl)glycine[16] (2.56 g, 20 mmol) in 6 M HCl (50 ml) was refluxed on a sand bath for 2 d. The reaction mixture was evaporated to dryness and the residue was dissolved in a minimum amount of H_2O. The solution was treated with Amberlite CG 120 (H form) (2.0ϕ×21 cm) by the method described for **2**. The fractions containing **3** were evaporated to dryness and the residue was recrystallized from H_2O-ethanol: yield 1.29 g (44%); mp (decomp) 195—198°C; R_f 0.07; NMR (trifluoroacetic acid (TFA)) δ=7.86 (2H, br, NH_2^+), 4.22 (2H, t, J=4.7 Hz, N^+CH_2CO), 3.91—3.40 (2H, m, $N^+C\underline{H_2}CH_2$), and 3.10 (2H, t, J=5.4 Hz, $CH_2C\underline{H_2}CO$). Found: C, 40.64; H, 5.96; N, 9.32%. Calcd for $C_5H_9NO_4$: C, 40.82; H, 6.17; N, 9.52%.

2,2'-Iminodipropionic Acid (4). Compound **4**·HCl was prepared from DL-alanine (5.97 g, 67 mmol) and 2-bromopropionic acid (10.2 g, 67 mmol) in the presence of 1 M NaOH (250 ml) according to the procedure of Karrer and Appenzeller.[17] The free acid was obtained by ion-exchange chromatography and then recrystallized from H_2O-acetone: yield 5.09 g (47%); mp (decomp), 250—252°C (lit,[18] 233—235°C); R_f 0.12. Found: C, 44.72; H, 7.02; N, 8.71%. Calcd for $C_6H_{11}NO_4$: C, 44.72; H, 6.88; N, 8.69%.

2,3'-Iminodipropionic Acid (5). Compound **5** was prepared from *N*-(2-cyanoethyl)-DL-alanine[16] (2.84 g, 20 mmol) by the method described for **3**: yield 0.88 g (27%); mp (decomp) 200—203°C; R_f 0.13; NMR (TFA) δ=7.75 (2H, br, NH_2^+), 4.64—4.04 (1H, m, CH), 3.92—3.34 (2H, m, N^+CH_2), 3.09 (2H, t, J=5.8 Hz, CH_2CO), and 1.81 (3H, d, J=7.3 Hz, CH_3). Found: C, 44.84; H, 6.69; N, 8.92%. Calcd for $C_6H_{11}NO_4$: C, 44.72; H, 6.88; N, 8.69%.

N-(2-Cyanoethyl)-β-alanine. This compound was prepared by the cyanoethylation of β-alanine (44.5 g, 0.55 mol) with acrylonitrile (29.2 g, 0.50 mol) according to the procedure of McKinney *et al.*[16] and recrystallized from H_2O-acetone: yield 38.1 g (52%); mp (decomp) 144—146°C; R_f 0.19; NMR (TFA) δ=7.75 (2H, br, NH_2^+), 3.99—3.77 (4H, m, N^+CH_2), and 3.24—2.96 (4H, m, $CH_2CN + CH_2CO$). Found: C, 49.44; H, 7.38; N, 19.03%. Calcd for $C_6H_{10}N_2O_2 \cdot 1/4\ H_2O$: C, 49.14; H, 7.22; N, 19.10%.

3,3'-Iminodipropionic Acid (6). Compound **6** was prepared from *N*-(2-cyanoethyl)-β-alanine (2.84 g, 19.4 mmol) by the method described for **3**. After the hydrolyzate was poured into a column packed with Amberlite CG 120 (H form), the column was washed with H_2O to remove neutrals at first, and then the product was eluted with 2% aq pyridine: yield 1.98 g (63%); mp (decomp) 157—159°C; R_f 0.11; NMR (TFA) δ=7.56 (2H, br, NH_2^+), 3.83—3.30 (4H, m, N^+CH_2), and 3.05 (4H, t, J=7.1 Hz, CH_2CO). Found: C, 44.49; H, 6.91; N, 8.72%. Calcd for $C_6H_{11}NO_4$: C, 44.72; H, 6.88; N, 8.69%.

N-Methyliminodiacetic Acid (7). Compound **7** was prepared from sarcosine (3.0 g, 34 mmol) and chloroacetic acid (3.1 g, 33 mmol) in the presence of 4 M LiOH (16.8 ml) by the method described for **2**. After being recrystallized from H_2O-acetone and dried in a vacuum desiccator at room temperature, the product was identified as a hemihydrate: yield

Table 3. Elution times and relative color constants of some IDCAs on ion-exchange chromatography

IDCA	Elution time/min	Relative color constant[a)]
1	42	0.99
2	42	0.32
5	64	0.009
3	66	0.30
Gly	94	1.00

a) Color constant of Gly: 87.6 μmol^{-1}.

2.50 g (49%); mp (decomp) 231—234 °C (lit,[19] 226—227 °C (free acid)); R_f 0.07; NMR (TFA) δ=8.40 (1H, br, NH^+), 4.38 (4H, s, CH_2CO), and 3.31 (3H, s, N^+CH_3). Found: C, 38.18; H, 6.29; N, 8.72%. Calcd for $C_5H_9NO_4 \cdot 1/2H_2O$: C, 38.46; H, 6.46; N, 8.97%.

Ion-exchange Chromatography. Ion-exchange chromatography was carried out with a Sibata amino acid analyzer AA-600 under the following conditions: Column, 0.25ϕ×50 cm packed with Aminex A-4 (Bio-Rad); flow rate of eluent (pH 3.25 citrate buffer, 0.2 M Na^+), 6 ml/h; flow rate of ninhydrin solution, 3 ml/h; jacket temperature, 30 °C. The time of heating in the reaction bath (100 °C) was designed to be 30 min. Each of the IDCAs was chromatographed separately, and its color constant was calculated by the common $H \times W$ method. Among the IDCAs, **4** and **6** were negative to color development with ninhydrin,[20] so that their elution times could not be determined. The ion-exchange chromatographic data are listed in Table 3. It was unsuccessful to separate a mixture of the IDCAs with the amino acid analyzer.

Derivatization for Gas Chromatography. For the preparation of butyl ester derivatives, each individual IDCA (0.1 mmol) was refluxed for 30 min with 1-butanol (5 ml) which was 5.2 M in dry HCl, and then complete solubilization was achieved. Excess reagent was distilled off at 50 °C under reduced pressure. The residual ester hydrochloride was dissolved in a minimum amount of H_2O. After being made alkaline with K_2CO_3, the solution was repeatedly extracted with CH_2Cl_2 (20 ml×4). The extracted solution was dried (Na_2SO_4), filtered, and then evaporated carefully to dryness at room temperature leaving an oil. The butyl ester derivative was taken up in CH_3NO_2 (2 ml), 1 μl portions of which were usually injected into the gas chromatographic column. For the preparation of *N*-TFA butyl ester derivatives, an ester hydrochloride prepared as above was suspended in CH_2Cl_2 (1 ml), to which $(CF_3CO)_2O$ (0.5 ml) was added. After being left overnight at room temperature, the reaction mixture was carefully evaporated to dryness, and then taken up in CH_3NO_2 (2 ml) for gas chromatography. When $(CF_3CO)_2O$ was added to the ester hydrochlorides of the *N*-substituted IDCAs (**7** and **8**), the corresponding butyl ester derivatives were liberated in the free state. In the case of **4**, trifluoroacetylation with $(CF_3CO)_2O$ at room temperature was incomplete due to steric hindrance. However, it was found that trifluoroacetylation was completed in 60 min at 100 °C; in this experiment 1 ml of $(CF_3CO)_2O$ was added.

Gas Chromatography. Gas chromatography was carried out with a Hitachi gas chromatograph 163 equipped with a flame ionization detector (H_2 flow rate, 35 ml/min). A single column technique was used. The conditions for gas chromatography were as follows: column, 1 m×3 mm I. D. glass packed with 1.5% OV-101 on Chromosorb G HP (100/120 mesh) (Shimadzu); injection port, 200 °C; flow rate of N_2 (carrier gas), 30 ml/min. The column oven was operated isothermally at 100 °C for 5 min after injection and then programmed to be heated up to 230 °C at a rate of 5 °C/min.

Gas Chromatography-Mass Spectrometry. Mass spectra were measured with a JEOL JMS-D 300 mass spectrometer, which was connected through a jet separator (glass) with a JGC-20 KP gas chromatograph. Each volatile derivative was chromatographed on a glass column (1 m×2 mm I. D.) containing 3% OV-101 on Chromosorb G HP (100/120 mesh) (Shimadzu) using He as carrier gas. The GC-MS combination was operated with the following parameters: injection port, 200 °C; separator, 250 °C; ionizing voltage, 20 V; ionizing current, 300 μA; accelerating voltage, 3.0 kV; ion source, 210 °C. The spectrometer was continuously scanned every 5 s.

The authors wish to thank Miss Yasuko Yoshioka, Faculty of Pharmaceutical Sciences, Tokushima University for obtaining mass spectra by gas chromatography-mass spectrometry.

References

1) M. S. Chadha, J. G. Lawless, J. J. Flores, and C. Ponnamperuma, "Experiments in Jovian Atmosphere," in "Molecular Evolution 1," ed by R. Vuvet and C. Ponnamperuma, North-Holland Publishing Co., Amsterdam (1971), pp. 143—151.

2) K. Kvenvolden, J. Lawless, K. Pering, E. Peterson, J. Flores, C. Ponnamperuma, I. R. Kaplan, and C. Moore, *Nature*, **228**, 923 (1970).

3) K. A. Kvenvolden, J. G. Lawless, and C. Ponnamperuma, *Proc. Natl. Acad. Sci. U.S.A.*, **68**, 486 (1971).

4) D. Ring, Y. Wolman, N. Friedmann, and S. L. Miller, *Proc. Natl. Acad. Sci. U.S.A.*, **69**, 765 (1972).

5) J. P. Ferris, J. D. Wos, D. W. Nooner, and J. Oro, *J. Mol. Evol.*, **3**, 225 (1974).

6) E. Gelpi, W. A. Koenig, J. Gibert, and J. Oro, *J. Chromatogr. Sci.*, **7**, 604 (1969).

7) K. R. Leimer, R. H. Rice, and C. W. Gehrke, *J. Chromatogr.*, **141**, 121 (1977).

8) J. G. Lawless and M. S. Chadha, *Anal. Biochem.*, **44**, 473 (1971).

9) J. R. Cronin, G. U. Yuen, and S. Pizzarello, *Anal. Biochem.*, **124**, 139 (1982).

10) P. Hušek and K. Macek, *J. Chromatogr.*, **113**, 139 (1975).

11) M. Sakamoto, N. Tsuji, F. Nakayama, and K. Kajima, *J. Chromatogr.*, **235**, 75 (1982).

12) K. Biemann, J. Seibl, and F. Gapp, *J. Am. Chem. Soc.*, **83**, 3795 (1961).

13) K. Kawashiro, S. Morimoto, and H. Yoshida, *Bull. Chem. Soc. Jpn.*, **56**, 792 (1983).

14) K. Okamoto, J. Hidaka, and Y. Shimura, *Bull. Chem. Soc. Jpn.*, **44**, 1601 (1971).

15) G. Stadnikoff, *Ber.*, **40**, 4350 (1907). Compound **2** was prepared by the hydrolysis of *N*-(1-cyanoethyl)glycine ethyl ester with aq HCl.

16) L. L. McKinney, E. H. Uhing, E. A. Setzkorn, and J. C. Cowan, *J. Am. Chem. Soc.*, **72**, 2599 (1950).

17) P. Karrer and R. Appenzeller, *Helv. Chim. Acta*, **25**, 595 (1942).

18) J. V. Dubsky, *Ber.*, **49**, 1045 (1916). Compound **4** was prepared by the hydrolysis of 2,2′-iminodipropionitrile with aq HCl or aq $Ba(OH)_2$.

19) W. Eschweiler, *Justus Liebigs Ann. Chem.*, **279**, 39 (1894). Compound **7** was prepared as a free acid by the hydrolysis of *N*-methyliminodiacetonitrile with aq $Ba(OH)_2$.

20) P. Karrer, H. Koenig, and R. Legler, *Helv. Chim. Acta*, **24**, 861 (1941).

Oxidation of *S,S*-Diaryl-*N*-(*p*-tolylsulfonyl)sulfilimines and *N*-Unsubstituted *S,S*-Diaryl-sulfilimines with Potassium Hyperoxide Anion Radical ($O_2^{\cdot-}$) in the Presence of 1-Bromopropane, Benzoyl Chloride, *p*-Tolylsulfonyl Chloride, Carbon Tetrachloride, Chloroform, or Dichloromethane in Aprotic Media

Kunihiko AKUTAGAWA, Naomichi FURUKAWA,* and Shigeru OAE*,†
Department of Chemistry, University of Tsukuba, Sakura-mura, Niihari-gun Ibaraki 305
(Received September 2, 1983)

The reaction of *S,S*-diaryl-*N*-(*p*-tolylsulfonyl)sulfilimines and *N*-unsubstituted diaryl-sulfilimines with hyperoxide anion radical ($O_2^{\cdot-}$) in the presence of 18-crown-6 as a catalyst together with 1-bromopropane/benzene, benzoyl chloride/benzene, *p*-tolylsulfonyl chloride/benzene, carbon tetrachloride, chloroform, or dichloromethane, gave the corresponding sulfoximines, through nucleophilic oxidation with an intermediary dioxy species formed upon treatment of organic halides with potassium hyperoxide (KO_2).

Oxidation is considered to be one of the most important class of reactions which take place on the sulfur atom of organosulfur compounds along with substitution and reduction.[1] We have been carrying out systematic investigations on the oxidation of organosulfur compounds of various oxidation states,[2] and suggested that the oxidation which takes place on the sulfur atom is classified mainly into three different types of reactions, based on the electronic demand of the oxidant, *i.e.*, direct one electron transfer oxidation, electrophilic oxidation, and nucleophilic oxidation. The tricoordinate organosulfur species such as sulfoxides[2] and especially thiosulfinic *S*-esters[2] are believed to be good models for studying the mechanism of these oxidations and substantial amount of knowledge has been accumulated on the electrophilic and nucleophilic oxidations.[1] Although sulfilimines are relatively new commers among organosulfur compounds, the chemistry of sulfilimines, isoelectronic species of sulfoxides, has recently been extensively investigated,[3] the oxidation of sulfilimines is the most effective method to prepare sulfoximines which are widely used as important reagents for organic syntheses such as an alkylidene transfer reagent.[4] Sodium hypochlorite[5] and sodium perbenzoate[6] have been shown to be excellent oxidants to convert the sulfilimines to the corresponding sulfoximines. In many cases, however, many other oxidants, which are used in the oxidation of sulfoxide have been found to react with sulfilimines, affording various undesirable products together with the desired products, sulfoximines, as minor products and sometimes not affording the corresponding sulfoximine at all, or not reacting at all with other oxidants, recovering the original sulfilimines.[7] In general, electrophilic oxidation of sulfilimines fails to afford the corresponding sulfoximines, while nucleophilic one is expected to oxidize sulfilimines successfully to the corresponding sulfoximines.

Hyperoxide anion radical ($O_2^{\cdot-}$) is known to be an effective nucleophile in aprotic solvents.[8] Alkyl halide is known to react with hyperoxide anion radical through an S_N2 mechanistic path and yields the alkyl peroxide as an overall product *via* formation of alkylperoxyl radical and alkyldioxy anion[9] in the initial step. The *p*-tolylsulfonyl chloride-potassium hyperoxide reaction yields an intermediate *i.e.*, *p*-tolylsulfonylperoxoate anion which oxidized sulfoxides, phosphines, or electrophilic olefins to afford the corresponding sulfones, phosphine oxides or epoxides.[2] Although *S,S*-diaryl-*N*-(*p*-tolylsulfonyl)-sulfilimines have not been oxidized readily with various oxidizing systems, many of these oxidizing systems are electrophilic oxidants. According to a concept of electrophilic and nucleophilic oxidations,[10] *N*-(*p*-tolylsulfonyl)sulfilimines are liable to be attacked by nucleophilic oxidants, since the central sulfur atom is tricoordinate and hence the electron density around the central sulfinimidoyl sulfur atom is decreased. Meanwhile, since the following dioxy species, *i.e.*, alkyldioxy species (ROO^-), acyldioxy species ($AcOO^-$), or sulfonyldioxy species($TsOO^-$), generated *in situ* in the treatment of alkyl halide, acyl halide, or tosyl chloride with hyperoxide anion radical, are believed to be markedly more nucleophilic oxidizing agents than hyperoxide anion radical alone, even *S,S*-diaryl-*N*-(*p*-tolylsulfonyl)sulfilimines, which are inert to hyperoxide anion radical alone, are expected to be selectively oxidized with the reactive dioxy intermediates to afford the corresponding sulfoximines successfully, as in the nucleophilic oxidation of *S,S*-diaryl-*N*-(*p*-tolylsulfonyl)sulfilimine with such a powerful nucleophilic oxidant as hypochlorite anion.[5b]

This paper describes the successful oxidations of sulfilimines with hyperoxide anion radical in a few reaction systems.

Results and Discussion

S,S-*Diaryl*-N-*(p-tolylsulfonyl)sulfilimine.* Hyperoxide anion radical was generated *in situ* by mixing potassium hyperoxide and 18-crown-6 as a catalyst in an apropriate solvent such as benzene under argon atmosphere. At first,when *S,S*-diphenyl-*N*-(*p*-tolylsulfonyl)sulfilimine was treated with hyperoxide anion radical in the presence of 18-crown-6 as catalyst in benzene without any additive, such as an organic halide, there was no formation of any oxidized pro-

† Present adress; Okayama University of Sciences, Ridai-cho, Okayama 700.

duct, *i.e.*, the corresponding sulfoximine, and the sulfilimine was recovered quantitatively after 24 h. A few additives were examined which are capable of generating more effective dioxy species to convert *S,S*-diphenyl-*N*-(*p*-tolylsulfonyl)sulfilimine to the corresponding sulfoximine selectively. Addition to such an alkyl halide, as 1-bromopropane to the above reaction system in the presence of 18-crown-6 or "dicyclohexyl-18-crown-6" was found to give the corresponding sulfoximine in 91% or 94% yields respectively. Diphenyl sulfoxide, an isoelctromer of the sulfilimine, was also oxidized to diphenyl sulfone in this reaction system. Other additives, such as benzoyl chloride and *p*-tolylsulfonyl chloride, were also found to be effective in the oxidation of *S,S*-diphenyl-*N*-(*p*-tolylsulfonyl)sulfilimine to the sulfoximine under mild conditions. The results are summarized in the following equation 1.

$$\mathrm{Ph\text{-}\underset{\downarrow}{\underset{X}{S}}\text{-}Ph} \xrightarrow[\text{Solvent}]{\mathrm{KO_2/crown/additive}} \mathrm{Ph\text{-}\overset{O}{\overset{\uparrow}{\underset{\downarrow}{\underset{X}{S}}}}\text{-}Ph} \qquad (1)$$

X: $NSO_2C_6H_4CH_3$-*p*, O, NH.
Crown: 18-crown-6, "dicyclohexyl-18-crown-6".
Additive: 1-bromopropane, PhCOCl, TsCl, CH_2Cl_2, $CHCl_3$, CCl_4.
Solvent: benzene.

This oxidation, however, did not proceed at all without the crown ether. Thus, the sulfilimine is considered to be oxidized by the intermediary reactive dioxy anion species, incipiently formed *in situ* in the treatment of these organic halides with hyperoxide anion radical in the presence of the crown ether (Eq. 2).

$$\mathrm{PrBr} + \mathrm{O_2^-} \longrightarrow \mathrm{PrOO^-}$$
$$\mathrm{PrOO^-} + \mathrm{O_2^-} \longrightarrow \mathrm{PrOO^-} + \mathrm{O_2}$$
$$\mathrm{Ph\text{-}\underset{\downarrow}{\underset{NTs}{S}}\text{-}Ph} + \mathrm{PrOO^-} \longrightarrow \mathrm{Ph\text{-}\overset{O}{\overset{\uparrow}{\underset{\downarrow}{\underset{NTs}{S}}}}\text{-}Ph} + \mathrm{PrO^-} \qquad (2)$$

Several other sulfilimines were also converted to the corresponding sulfoximines in good yields. Halogenated solvents such as dichloromethane, chloroform, or carbon tetrachloride[11] were also found to assist the oxidation of this type. These results were summarized in Table 1. *S*-(*p*-Nitrophenyl)-*S*-phenyl-*N*-(*p*-tolylsulfonyl)sulfilimine was found to afford unidentified products. No original sulfilimine was recovered.** *S*-Methyl-*S*-phenyl-*N*-(*p*-tolylsulfonyl)-sulfilimine was not oxidized at all in this system. The original sulfilimine was recovered though the isoelectronic methyl phenyl sulfoxide was readily oxidized to the corresponding sulfone in 78% yield.

Table 1. Oxidation of *N*-tosylsulfilimines

$$\mathrm{Ph\text{-}\underset{\downarrow}{\underset{NTs}{S}}\text{-}R} + \mathrm{KO_2} \xrightarrow[\text{r.t. Solvent}]{\mathrm{R'X/18\text{-}Crown\text{-}6}} \mathrm{Ph\text{-}\overset{O}{\overset{\uparrow}{\underset{\downarrow}{\underset{NTs}{S}}}}\text{-}R}$$

R	Time/h	Solvent R'X	Yield/%[a]
Ph	3	Benzene PrBr	91
Ph	24	Benzene None	0
Ph	2	Benzene *p*-TsCl	94
Ph	3	Benzene PhCOCl	86
Ph	2	CH_2Cl_2	97
Ph	2	$CHCl_3$	92
Ph	2	CCl_4	90
p-Tol	2	CH_2Cl_2	87
p-ClC_6H_4	2	CH_2Cl_2	91
p-$NO_2C_6H_4$	10	CH_2Cl_2	0
Me	24	CH_2Cl_2	Trace

a) Isolated yield.

In this reaction, the relatively acidic α-hydrogen atom of this sulfilimine may be immediately deprotonated by hyperoxide anion radical, or peroxyl radical to stop the reaction, because of the formation of the hydroperoxy species (HOO^-) which are incapable of nucleophilic oxidation. Incidentally, acetonitrile was found to react with disulfide in the presence of hyperoxide anion radical to form bis(arylthio)acetonitrile.[2,13] Initial formation of cyanomethyl radical has been proposed for this reaction. The formation of peroxide ion (O_2^{2-}), which may exist in this reaction system by disproportionation of hyperoxide anion (O_2^{2-}) can be ruled out, since the reaction of *S,S*-diphenyl-*N*-(p-tolylsulfonyl)sulfilimine with Na_2O_2 in the presence of 18-crown-6 in benzene under argon atmosphere resulted in the partial reduction of this sulfilimine to give diphenyl sulfide in 30% yield together with the recovered sulfilimine in 70% after 24 h. Dimethyl sulfide and methyl phenyl sulfide were found not to be oxidized at all under these conditions. Thus, treatment of a mixture of *S,S*-diphenyl-*N*-(*p*-tolylsulfonyl)sulfilimine and phenyl *p*-tolyl sulfide with potassium hyperoxide in dichloromethane at 25 °C for 2 h in the presence of catalytic amount of 18-crown-6 in argon atmosphere gave *S,S*-diphenyl-*N*-(*p*-tolylsulfonyl)sulfoximine quantitatively, recovering the added phenyl *p*-tolyl sulfide quantitatively, but not phenyl *p*-tolyl sulfoxide or sulfone (Eq. 3).

$$\mathrm{Ph\text{-}\underset{\downarrow}{\underset{NTs}{S}}\text{-}Ph} + \mathrm{Ph\text{-}S\text{-}Tol}(p\text{-}) \xrightarrow[\mathrm{CH_2Cl_2}]{\mathrm{KO_2/18\text{-}crown\text{-}6}} \mathrm{Ph\text{-}\overset{O}{\overset{\uparrow}{\underset{\downarrow}{\underset{NTs}{S}}}}\text{-}Ph} + \mathrm{Ph\text{-}S\text{-}Tol}(p\text{-}) \qquad (3)$$

Phenyl *p*-tolyl sulfide was not oxidized at all even after prolonged reaction time, 24 h, with this nucleophilic oxidation system. These results strongly support that

** Upon addition of this sulfilimine into the solution of hyperoxide anion in benzene in the presence of 18-crown-6 without any additive, *e.g.*, 1-bromopropane, one finds rapid color change (from colorless heterogeneous solution into dark bluish solution) of the solution, which eventually gave unidentified products, without recovering the starting material. Perhaps, an S_{RN} type substitution reaction[12] of hyperoxide anion radical with this sulfilimine, which is activated by nitro group, would have taken place involving one electron transfer from hyperoxide anion into the sulfilimine, followed by subsequent reaction of the aromatic anion radical with oxygen or hyperoxide anion radical, or subsequent breaking down to give unidentified products.

the reactive dioxy anion species (ROO^-) was initially formed and then oxidized *S,S*-diphenyl-*N*-(*p*-tolylsulfonyl)sulfilimine, but not the sulfide. The hydroperoxide (ROOH) intermediate may not be formed during the reaction, since it would readily oxidize the sulfide but not the sulfilimine in this system. Although there is no legitimate evidence to clarify the mechanism for this oxidation by ROO^-, we propose that this oxidation may involve the initial formation of unstable sulfurane intermediate by the nucleophilic attack of dioxy anion toward the electrophilic center of sulfinimidoyl sulfur atom of the sulfilimine which readily breaks down to the corresponding sulfoximine and alkoxide anion in the subsequent step as shown in Eq. 4. This sulfurane intermediate has been proposed in the nucleophilic oxidation of sulfoxides or sulfilimines with hypochlorite anion.[2,5b] Nor was there any good correlation between the effect of substituent and the yield of the sulfoximine as depicted in Table 1, unlike those of the nucleophilic oxidation of sulfoxides by perbenzoic acid[14] or alkyldioxy anion[14] or of *N*-(arylsulfonyl)sulfilimine by hypochlorite anion[5b] in which fairly good Hammett correlations have been found to hold. A similar phenomenon was observed in the oxidation of sulfoxide with hyperoxide anion radical in the presence of di-*p*-tolyl disulfide,[2] or in the S_N2 type substitution reaction of primary or secondary alkyl halide with hyperoxide anion radical.[9,15]

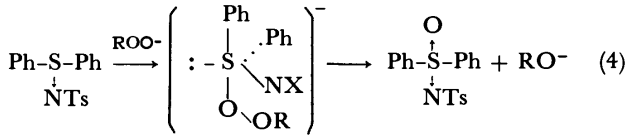

(4)

Similar dioxy anion species have been postulated in the epoxidation of electrophilic olefins or in the oxidation of sulfoxides to the corresponding sulfones.[16,17] Gibian and Ungermann found that dimethyl sulfoxide used as solvent was oxidized during the reaction of alkyl halide with hyperoxide anion radical by the intermediary active oxidizing species, an alkyldioxy anion.[15]

Thus, in the presence of organic halides and a catalytic amount of the crown ether, potassium hyperoxide was found to oxidize *S,S*-diaryl-*N*-(*p*-tolylsulfonyl)sulfilimines which have no nitro group to the corresponding sulfoximines.

N-Unsubstituted S,S-Diarylsulfilimine. *N*-Unsubstituted diarylsulfilimines were reported to be oxidized selectively to the corresponding sulfoximines by sodium hypochlorite,[5a] potassium permanganate,[7a] and sodium periodate.[16] No good result was obtained by oxidation with *m*-chloroperbenzoic acid,[7a] and hydrogen peroxide in acidic media such as acetic acid[7a] or in neutral media.

In the absence of alkyl halide, unsubstituted diphenylsulfilimine did not react with potassium hyperoxide in the presence of 18-crown-6 in benzene only to afford the recovered sulfilimine even after 24 h. However, the same oxidation in the presence of 1-bromopropane proceeded successfully giving the corresponding sulfoximine in 75% yield. The sulfilimine was also oxidized in dichloromethane which functions both as solvent and reactant, affording the corresponding sulfoximine in a good yield. These results are listed in Table 2. *S*-(*p*-Nitrophenyl)-*S*-phenylsulfilimine reacted with potassium hyperoxide in the absence of alkyl halide to afford various unidentified products, but not afford the corresponding sulfoximine. The oxidation of the unsubstituted sulfilimine is considered to proceed similarly as in the case of *S,S*-diphenyl-*N*-(*p*-tolylsulfonyl)sulfilimine, namely *via* involving sulfurane as an intermediate as shown in equation 4.

Table 2. Oxidation of *N*-unsubstituted sulfilimines

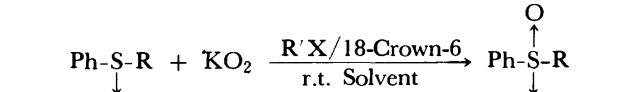

R	Time/h	Solvent R'X	Yield/%[a]
Ph	3	Benzene PrBr	75
Ph	24	Benzene None	0
Ph	1	CH_2Cl_2	84
p-Tol	1	CH_2Cl_2	89
p-$NO_2C_6H_4$	10	CH_2Cl_2	0

a) Isolated yield.

All these reactions reveal clearly that tricoordinate organosulfur compounds are oxidized to the corresponding tetracoordinate sulfur compounds much more effectively by nucleophilic oxidants as we have anticipated.

In summary, *S,S*-diaryl-*N*-(*p*-tolylsulfonyl)sulfilimines and unsubstituted diarylsulfilimines were selectively oxidized to the corresponding sulfoximines upon treatment with potassium hyperoxide in the presence of organic halides.

Experimental

General. Melting points of the products were measured by Yanaco instrument and were uncorrected. IR spectra were obtained using a Hitachi 215 spectrophotometer. ^1H NMR spectra of all the compounds were obtained with a Hitachi Perkin-Elmer R-20 spectrometer in 20% deuteriochloroform solution using tetramethylsilane as an internal standard. Liquid chromatographs were obtained by Yanaco-L-1030 instrument using methanol as an eluent. Thin layer chromatographs were carried out with Merck DC-Plastikofolien Kieselgel 60 F 254 Art 5735 with fluorescent indicator using various solvents and mixed solvents. Development was followed with UV light or by coloring with iodine. Silica gel used for column chromatography was either of Wako or Merck chromatographic grade. Elemental analyses were carried out by the Chemical Center of this University. Potassium hyperoxide was obtained from Veutron Alfa Products. 18-Crown-6 and "dicyclohexyl-18-crown" were obtained from Wako Pure Chemicals and used after drying *in vacuo* at 60—70°C. Anhydrous dichloromethane, chloroform, and carbon tetrachloride were obtained by distillation of first grade commercial products and then dried over calcium dichloride just before use. Benzene was purified by distillation similarly and dried over metal sodium under nitrogen. *p*-Tolylsulfonyl chloride from Wako Pure Chemicals were used after recrystallization from hexane.

Benzoyl chloride was purified by distillation after dehydration with calcium dichloride. Extra pure reagent 1-bromopropane from Wako Pure Chemicals was used directly without any further treatment. Other chemicals were of reagent grade.

Materials. *N*-(*p*-Toylylsulfonyl)sulfilimines *i.e.*, *S,S*-dimethyl-, *S*-methyl-*S*-phenyl-. *S,S*-diphenyl-, *S*-(*p*-tolyl)-*S*-phenyl-, *S*-(*p*-chlorophenyl)-*S*-phenyl-, *S*-(*p*-nitrophenyl)-*S*-phenyl-*N*-(*p*-tolylsulfonyl)sulfilimines were prepared by treatment of the corresponding sulfides with chloramine-T in methanol, according to the method reported earlier.[19] *N*-Unsubstituted sulfilimines *i.e.*, *S,S*-diphenyl-, *S*-phenyl- *S*-(*p*-tolyl)-, *S*-(p-nitrophenyl)-*S*-phenylsulfilimines were prepared by treatment of the corresponding *N*-(*p*-tolylsulfonyl)sulfilimines with concentrated sulfuric acid and then with aqueous sodium hydroxide solution according to a known method.[7a]

Reaction of S,S-*Diphenyl*-N-(p-*tolylsulfonyl*)*sulfilimine with Potassium Hyperoxide in Benzene in the Presence of 1-Bromopropane and Catalytic Amount of 18-Crown-6.* To a finely powdered potassium hyperoxide (252 mg, 3.5 mmol) was injected a solution of the title sulfilimine (501 mg, 1.4 mmol) and 18-crown-6 (0.08 mmol) in dry benzene and then a solution of 1-bromopropane (260 mg, 2.1 mmol) in the same solvent was added into a two-necked flask under dry argon atmosphere at room temperature. The resulting heterogeneous mixture stirred at the same temperature for 3 h. The reaction was monitored by TLC or HPLC until the substrate disappeared nearly completely. After the reaction, the reaction mixture was poured into a large excess of ice-water, extracted with chloroform, washed with water, and dried over anhydrous magnesium sulfate. The solvent was removed under reduced pressure, and the crude corresponding sulfoximine was obtained. Purification was accomplished by column chromatography through silica gel using chloroform as an eluent. The corresponding sulfoximine was obtained in 91% yield. In the reactions in which *p*-tolylsulfonyl chloride and benzoyl chloride were used as organic halides, the above mentioned procedure was also applied.

Oxidation of S,S-*Diphenyl*-N-(p-*tolylsulfonyl*)*sulfilimine with Potassium Hyperoxide in Dichloromethane in the Presence of 18-Crown-6.* A solution of the title sulfilimine (500 mg, 1.4 mmol) in dry dichloromethane was added to a finely powdered potassium hyperoxide (252 mg, 3.5 mmol) and dry 18- crown-6 (0.07 mmol) in a two-necked flask under dry argon atmosphere at room temperature. The mixture was stirred at the same temperature for 2 h, monitoring by HPLC. After the consumption of the substrate, the work-up described before was carried out. The corresponding sulfoximine was obtained in 97% yield.

Oxidation of N-*Unsubstituted Diphenylsulfilimine with Potassium Hyperoxide in Dichloromethane in the Presence of 18-Crown-6.* To a finely powdered potassium hyperoxide (440 mg, 6.2 mmol) was added a solution of the title sulfilimine (500 mg, 2.5 mmol) and dry 18-crown-6 in dry dichloromethane in a two-necked flask under dry argon atmosphere at room temperature. The heterogeneous solution was stirred at the same temperature for 1 h. After the starting sulfilimine was found to have disappeared, upon monitoring by TLC or HPLC, the reaction mixture was poured into excess water. After the usual work-up and separation by column chromatography, diphenyl sulfide (6%) and diphenylsulfoximine (84%) were obtained.

We express our thanks to Dr. Toshikazu Takata for his collaboration.

References

1) S. Oae, "Organic Chemistry of Sulfur," Kagaku Dojin, Kyoto (1982), p. 263.
2) S. Oae and T. Takata, *Tetrahedron Lett.*, **21**, 3689 (1980); S. Oae, T. Takata, and Y. H. Kim, *Bull. Chem. Soc. Jpn.*, **54**, 2712 (1981).
3) S. Oae and N. Furukawa, " Chemistry of Sulfilimines and Related Derivatives ," ACS Monograph, No. 179, 1983, p. 79.
4) C. R. Johnson, *Acc. Chem. Res.*, **6**, 341 (1973).
5) a) N. Furukawa, K. Akutagawa, T. Yoshimura, and S. Oae, *Synthesis*, **1982**, 77; b) N. Furukawa, K. Akutagawa, T. Yoshimura, and S. Oae, *Tatrahedron Lett.*, **22**, 3989 (1981).
6) S.-L. Huang and D. Swern, *J. Org. Chem.*, **44**, 2510 (1979).
7) a) T. Yoshimura, T. Omata, N. Furukawa, and S. Oae, *J. Org. Chem.*, **41**, 1728 (1976); b) S. Oae, K. Harada, K. Tsujihara, and N. Furukawa, *Int. J. Sulfur Chem., Part A*, **2**, 491 (1972).
8) D. T. Sawyer and M. J. Gibian, *Tetrahedron*, **35**, 1471 (1979); D. T. Sawyer and J. S. Balentine, *Acc. Chem. Res.*, **14**, 393 (1981).
9) M. V. Merritt and D. T. Sawyer, *J. Org. Chem.*, **35**, 2157 (1970); R. Dietz, A. E. J. Forno, B. E. Larcombe, and M. E. Peover, *J. Chem. Soc., B*, **1970**, 816; J. Jr. San Fillipo, C. I. Chern, and J. S. Valentine, *J. Org. Chem.*, **40**, 1678 (1975); R. A. Johnson and E. G. Nidy, *J. Org. Chem.*, **40**, 1680 (1975).
10) S. Oae and T. Takata, *Tetrahedron Lett.*, **21**, 3213 (1980).
11) J. L. Roberts Jr. and D. T. Sawyer, *J. Am. Chem. Soc.*, **103**, 712 (1981).
12) A. Frimer and I. Rosenthal, *Tetrahedron Lett.*, **1976**, 2809.
13) S. Oae, T. Takata, and Y. H. Kim, *Tetrahedron*, **37**, 37 (1981).
14) R. Curci, F. Difuria, and G. Modena, *J. Chem. Soc., Perkin Trans. 2*, **1979**, 603; R. Curci, A. Giovine, and G. Modena, *Tetrahedron*, **22**, 1235 (1966); R. Curci and G. Modena, *Tetrahedron*, **23**, 1227 (1966).
15) M. J. Gibian and T. Ungermann, *J. Org. Chem.*, **41**, 2500 (1976).
16) T. Nagano, K. Aragane, and M. Hirobe, 6th Symposium on Progress of Reaction and Synthesis, 1979, Abstract, p. 114.
17) M. Miura, M. Nojima, and S. Kusabayashi, *J. Chem. Soc., Chem. Commun.*, **1982**, 1352.
18) P. Stoss and G. Satzinger, *Tetrahedron Lett.*, **1974**, 1973.
19) K. Tsujihara, N. Furukawa, K. Oae, and S. Oae, *Bull. Chem. Soc. Jpn.*, **42**, 2631 (1969).

Ion Exchange Resins Anchoring 1,8-Diazabicyclo[5.4.0]undec-7-ene

Tomomichi ISHIKAWA* and Atsushi YONEYAMA
Department of Industrial Chemistry, Faculty of Technology, Tokyo Metropolitan University, Fukasawa, Setagaya-ku, Tokyo 158
(Received September 13, 1983)

The synthesis of polymeric quaternary ammonium salts linked 1,8-diazabicyclo[5.4.0]undec-7-ene(DBU) to chloromethylated polystyrenes is described. The polymers so obtained become anion exchangers with both quaternary ammonium and tertiary amino groups. The values of the total ion-exchange capacities indicated that the quaternization of the tertiary amino groups on the polymers with hydrochloric acid is difficult. The chloride forms of the resins, in spite of their bulky and steric quaternary ammonium groups containing DBU, were effective as ion exchangers for a variety of bulky anions such as sulfate, oxalate, hexacyanoferrate(II), hexacyanoferrate(III), and tris(oxalato) ferrate(III) ions. The free base forms of the resins gave low reactivity for chloride and sulfate ions. Some examples of the application of the resins is also reported.

Quaternary ammonium polymers have been used as ion exchange resins, catalysts and polyelectrolytes for a long time, and have also generated considerable interest in biological and medical fields in recent years.[1] The reaction of chloromethylated polystyrene with a variety of tertiary amines yields polymeric ammonium salts. On the other hand, "ionen polymers" can be prepared from tertiary diamino compounds with dihaloalkanes. 1,8-Diazabicyclo[5.4.0]undec-7-ene (DBU) possessing two tertiary amino groups is a potent organic base which is useful for the dehydrohalogenation of alkyl halides,[2] the *O*-alkyl cleavage of hindered methyl esters[3] and the oxidative coupling of diphenylmethanimine.[4] Because it is known that one mole of two functional compounds can be reacted with one chloromethyl group on the polymers,[5] anion exchange resins containing both strongly and weakly basic groups will be obtained by treating chloromethylated polystyrene with DBU:

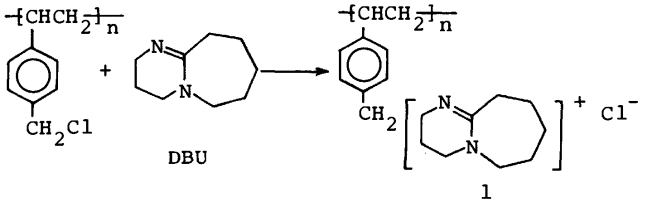

1

We have studied the reactivity of these basic groups, especially the basicity of the weakly basic groups. In this paper we describe new anion exchange resins of this type which have been prepared for the first time, and the properties of these resins have been investigated.

Experimental

Materials. Chloromethylated polystyrenes were prepared by chloromethylation of soluble polystyrene (DP 1100; Asahi Dow Chem. Co.) and 2% divinylbenzene-styrene copolymer(200—400 mesh; Eastman Kodak Co.) according to Ref.[6,7] Commercial DBU (Extra Pure; Sanyo Kasei Kogyo Co.) was purified by distillation; bp 88—89 °C (400 Pa). *N,N*-Dimethylformamide(DMF) was dried by the usual method and distilled befor use. The other materials were of reagent grade.

Preparation of Quaternary Ammonium Polymers. A 300 cm³, four necked round bottomed flask equipped with a stirrer, reflux condenser, and thermometer was charged with the desired amount of chloromethylated polystyrenes, DBU, and DMF. The reaction mixture was stirred at 40 °C for 6—7 h, and then filtered (in the case of the soluble chloromethylated polystyrene, after poured into ethyl acetate) and washed several times with methanol. The product was dried under reduced pressure.

Determination of Ion-exchange Capacities. Salt splitting capacity and total ion-exchange capacity were determined by the general method[8] for strongly and weakly basic anion exchange resins.

General Method of Ion Exchange. About 0.3 g of the chloride forms of the resins was shaken overnight with 100 cm³ of 0.1 mol cm⁻³ salts aq solution, and then recovered by filtration. The resin was washed with water, dried *in vacuo* and submitted to elemental analysis.

Adsorption Measurement. Metalic Salts: About 0.3 g of the chloride forms of the resins was shaken for 4 d with 100 cm³ of 0.1 mol cm⁻³ copper(II) or mercury(II) chloride aq solution, and then recovered by filtration. The resin was washed with water, dried *in vacuo* and submitted to elemental analysis.

Iodine: About 0.1 g of the chloride forms of the resins was shaken overnight with 30 cm³ of the desired concentration of iodine-chloroform solution or iodine-potassium iodide aq solution, and then recovered by filtration. The resin was washed with water, and dried *in vacuo*. The iodine adsorbed was determined by iodometry and elemental analysis.

Results and Discussion

Quaternary Ammonium Polymers. Polymer-supported quaternary ammonium salts were prepared from polystyrenes by a route which involves chloromethylation and subsequent amination. Styrene homopolymer and 2% divinylbenzene-styrene copolymer were used in this work, because higher crosslinking and poorer swelling chloromethylated polystyrenes seem to be insufficient for practical amination with bulky amine such as DBU. Egawa and co-worker[9] also reported that the anion exchange resins derived from the styrene copolymers containing divinylbenzene of less than 2% are useful for the absorption of the metalic ions.

The chloromethylation of styrene homopolymer and 2% divinylbenzene-styrene copolymer gave two chloromethylated polymers containing 19.3 and 21.4% of chlorine, respectively. The chloromethylated polymers were treated with the various amounts of DBU. The yields of the aminated polymers were based

TABLE 1. REACTION OF DBU WITH CHLOROMETHYLATED POLYSTYRENE[a)]

Run[b)]	Material mol ratio DBU/CSU[c)]	Product					
		Yield	Content[d)]		Relative distribution of constitutional sequence[e)]		
			DBU	Cl	*l*	*m*	*n*
		%	mequiv g^{-1}	mequiv g^{-1}			
1	1.69	72.5	1.91	1.84	0.078	0.548	0.374
2	1.80	76.6	2.31	2.13	0.078	0.418	0.504
3	1.00	87.3	2.78	2.74	0.078	0.228	0.694
4	1.20	94.4	2.89	2.81	0.078	0.137	0.785
5	1.50	97.7	3.10	2.90	0.078	0.055	0.867
6	2.06	97.5	3.05	2.88	0.078	0.082	0.840
7	1.49	91.9	3.04	2.98	0.170	0.006	0.824

a) At 40 °C for 6h in DMF. b) Runs 1—6; 2% divinylbenzene-styrene copolymer, Run 7; styrene homopolymer. c) CSU : Chloromethylstyrene unit. d) Determined by elemental analysis. e) See Fig. 1.

on the chloromethylated polystyrenes. The DBU and chlorine contents of the products were determined by elemental analysis. The results are summarized in Table 1. It is apparent that the chlorine contents are in good agreement with the DBU contents which were calculated on the basis of the nitrogen contents. These results indicate that one molecule of DBU reacted with one chloromethyl group to give the ion pairs of the chloride ion with the quaternary ammonium ion. Notwithstanding that all the chloromethyl groups had reacted, they do not convert quantitatively into quaternary ammonium groups.

The IR spectrum of the quaternary ammonium polymer shows an absorption band at 3350 cm^{-1} (OH of alcohol). On the other hand, the absorption responsible for the C-Cl bond (660 cm^{-1}) in the chloromethylated polystyrenes disappeared.

From these results, all the chloromethyl groups unreacted with DBU appeared to be changed to hydroxymethyl groups by the hydrolysis, perhaps because of the presence of a small amount of water in the reaction mixture. Therefore, the constitutional sequence of the polymers obtained in this work will be presented as Fig. 1.

The value of *l*, *m*, and *n* in the Fig. 1 were determined on the basis of the chlorine contents of the original chloromethylated polystyrenes and the nitrogen contents of the aminated polymers. The results are given in Table 1. In such Runs 1—3 which were carried out in the insufficiently dehydrated DMF, the value of *m* becomes higher than those of Runs 4—7 in the almost anhydrous DMF.

The reaction of the soluble chloromethylated polystyrene with DBU was completed under homogeneous condition in DMF. However, the aminated products, which were precipitated with ethyl acetate and then dried, were insoluble in DMF, perhaps because of the formation of crosslinks.

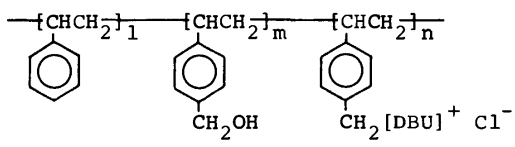

Fig. 1. Constitutional sequence.

Exchange Capacities of Basic Resins. The aminated polymers described in this paper can behave as a strongly basic anion exchanger as well as a weakly basic anion exchanger, because of the presence of both the quaternary ammonium groups and the tertiary amino groups in the polymers. The anion exchange capacities (salt splitting capacities) and total ion exchange capacities are given in Table 2. As can be seen from this table, the values of salt splitting capacity are considerably lower in comparison with the values for commercial strongly basic anion exchange resins. The salt splitting capacity was determined by titrating the sodium hydroxide which is formed according to Scheme 1.

$$\text{(P)-[DBU]}^{+}\text{Cl}^{-} \xrightarrow{\text{NaOH}} \text{(P)-[DBU]}^{+}\text{OH}^{-}$$
1 **2**

$$\xrightarrow{\text{NaCl}} \text{(P)-[DBU]}^{+}\text{Cl}^{-} + \text{NaOH}$$
3

Scheme 1.

Table 2 also gives the DBU and chlorine contents of the starting chloride form **1**, the intermediate free base form **2**, and the resulting chloride form **3** of the polymers in the Scheme 1. It was shown that **2** contained negligible chlorine, showing that all the chloride ions had been virtually displaced by hydroxide ions, while the chlorine content of **3** was extremely low in comparison with that of **1**. From these results, for this polymer the low values of salt splitting capacity seem to be ascribable to the higher selectivity of adsorption of hydroxide ion than that of chloride ion.

The total exchange capacities were calculated from the amounts of hydrochloric acid reacting with the polymer **2** according to Scheme 2.

$$\text{(P)-[DBU]}^{+}\text{OH}^{-} \xrightarrow{\text{HCl}} \text{(P)-[DBU]}_{2}^{2+}\text{H}\ 2\text{Cl}^{-}$$
2 **4**

Scheme 2.

Table 2. Ion-exchange capacity

Resin		SSC[c]	TIEC[d]	[TIEC]	Content	
					DBU	Cl
No[a]	Form[b]	mequiv g^{-1}	mequiv g^{-1}	2 [DBU]	mequiv g^{-1}	mequiv g^{-1}
2	1	0.61	2.62	0.567	2.31	2.13
2	2	—	—	—	2.65	0.16
2	3	—	—	—	2.58	0.41
2	4[e]	—	—	—	2.16	2.30
4	1	0.65	3.33	0.576	2.89	2.81
5	1	0.68	3.43	0.553	3.10	2.90
7	1	0.73	3.64	0.596	3.05	2.98

a) Run number in Table 1. b) In Scheme 1. c) Salt splitting capacity. d) Total ion-exchange capacity. e) Product obtained by treating the chloride forms of the resin with hydrochloric acid.

In the Table 2 the values of the ratio of the total exchange capacities to the number of nitrogen atoms are relatively low in comparison with the value expected from the polymer **4**. This result indicates that the reaction of the tertiary amino groups on the polymer **2** with hydrochloric acid is very difficult. This appears to be caused by an electrostatic effect owing to the close contacts[10] between the quaternary ammonium groups derived from the two tertiary amino groups on the DBU molecule.

The pK_a of DBU was 11.5, while that of the DBU bound on the polymer was 5.1, which is nearly equal to that of pyridine.

Application of Polymer Anchoring DBU. In this work, polymers anchored by bulky quaternary ammonium groups were prepared. Therefore, the ion exchange reactions with a variety of bulky anions such as sulfate, oxalate, hexacyanoferrate(II), hexacyanoferrate(III), and tris(oxalato)ferrate(III) were carried out. The chloride forms of the polymers were used in these reactions. The results are given in Table 3. In the determination of the ion exchange capacity, a difference of less than 5% was found between the values determined by elemental analysis of the Na_2SO_4-treated polymer and by titration of the sodium chloride produced in the solution after treatment. For potassium hexacyanoferrate(III), moreover, the value determined by iodometry of $K_3[Fe(CN)_6]$ remaining in the solution after the treatment was in near agreement with that by elemental analysis of the treated polymer. Therefore, in the other cases the exchange capacities were determined by elemental analysis. The results show that the polymers allow an ion exchange reaction with each bulky anion.

Table 3. Ion exchange with various salts[a]

Salt used	Ion exchange capacity[b]	Content of Cl[b]
	mequiv g^{-1}	mequiv g^{-1}
Na_2SO_4	1.22 (1.17)[c]	0.33
$Na_4[Fe(CN)_6]$	0.691	0.11
$K_3[Fe(CN)_6]$	0.852 (0.888)[c]	0.30
$(NH_4)_3[Fe(C_2O_4)_3]$	0.730	0.34
$Na_2C_2O_4$	1.43	0.21
$(NH_4)_2C_2O_4$	1.45	0.13

a) The chloride forms of the resin containing 2.89 mequiv g^{-1} of DBU was used. b) Determined by elemental analysis. c) Determined by volumetric analysis.

The absorption of metalic ions with the anion exchange resin bound tetraethylenepentamine has been investigated[9] at various pH values. It is found that the absorption increases with an increase of the pH value; at pH 4.5, it is nearly maximized in mercury(II) chloride but reaches only half a maximum value in copper(II) chloride. Table 4 gives the DBU and chlorine contents of the products obtained by treating the chloride forms

Table 4. Adsorption of $CuCl_2$ and $HgCl_2$[a]

Salt used	pH	Content	
		DBU	Cl
		mequiv g^{-1}	mequiv g^{-1}
$CuCl_2$	4.5	2.84	2.80
$HgCl_2$	4.2	1.78	2.30

a) The chloride forms of the resin containing 2.89 mequiv g^{-1} of DBU was used.

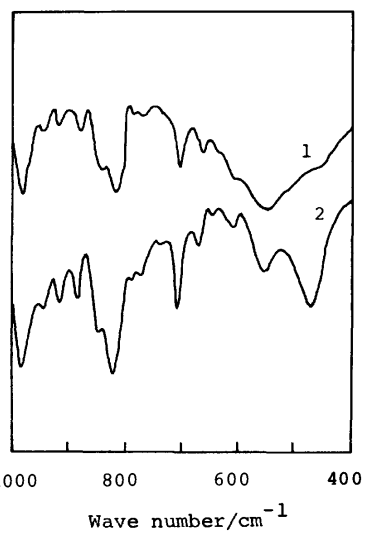

Fig. 2. IR spectra of the polymers.
1: Starting polymer. 2: Polymer treated with $HgCl_2$.

Table 5. Adsorption of iodine[a]

Meterial mole ratio I_2/DBU	Solvent	Observed ratio	
		I/DBU[b]	I/DBU[c]
0.471	$CHCl_3$	0.924	0.924
1.09	$CHCl_3$	1.69	1.67
1.42	$CHCl_3$	1.94	1.80
1.89	$CHCl_3$	1.98	1.92
1.81	KI aq	3.05	1.82

a) The chloride forms of the resin containing 2.89 mequiv g^{-1} of DBU was used. b) Determined by elemental analysis. c) Determined by iodometry.

of the aminated polymers with aqueous solutions of mercury(II) or copper(II) chloride at pH 4—5. The values were determined by elemental analysis. The product obtained by treatment with mercury(II) chloride gave a lower DBU content than for the starting polymer. The IR spectrum of this product is shown in Fig. 2; it indicates the characteristic absorption band at 460 cm^{-3}, perhaps on ν_{N-Hg}[11], which is not observed for the starting polymers. These results are probably associated with the formation of a polymer-mercury complex. The mercury content of the product determined by atomic absorption analysis was 2.13 mequiv g^{-1}, which is reasonably consistent with that calculated from the nitrogen content. On the other hand, in the case of copper(II) chloride the DBU and chlorine contents of the product are almost consistent with those of the starting polymer. Both the starting and $CuCl_2$-treated polymers gave identical IR spectra. These results indicate that this resin can be used for separation of mercury and copper ions.

The reaction of iodine with the chloride forms of the aminated polymers was carried out in chloroform or in aqueous solution of potassium iodide. The amounts of iodine adsorbed were determined by elemental analysis and iodometry. The values of the ratio of iodine atoms to one DBU-moiety in the polymers are given in Table 5. In chloroform, the values by iodometry were closely consistent with those calculated from the nitrogen content. In this case, about one molecule of iodine seems to be adsorbed with one DBU-moiety on the polymers. On the other hand, in the KI aq solution the value I/DBU by elemental analysis is about one and a half times the number of the value by iodometry. This result indicates that the chloride ions on the polymer were displaced with triiodide ions formed from iodine and potassium iodide.

References.

1) "Polymeric Amines and Ammonium Salts," ed by J. Goethals, International Symposium on Polymeric Amines and Ammonium Salts, Ghent, Belgium, September 1979, IUPAC Publication, Pergamon, London (1980).
2) H. Oediger and Fr. Moler, *Angew. Chem., Int. Ed. Engl.*, **6**, 76 (1967).
3) E. J. Parish and D. H. Miles, *J. Org. Chem.*, **38**, 1223 (1973).
4) H. Hayashi, T. Tanaka, N. Shigemoto, and T. Okazaki, *Chem. Lett.*, **1977**, 981.
5) C. C. Leznoff and J. Y. Wong, *Can. J. Chem.*, **50**, 2892 (1972).
6) G. D. Jones, *Ind. Eng. Chem.*, **44**, 2686 (1952).
7) R. S. Feimberg and R. B. Merrifield, *Tetrahedron*, **30**, 3209 (1974).
8) "Kinosei-Kobunshi," in "Kobunshi-Jikkengaku," 1st ed by S. Kambara, Kyoritsu-Shuppan, Tokyo (1974), Vol. 7, Chap. 1, p. 25.
9) H. Egawa and H. Saheki, *Kogyo Kagaku Zasshi*, **74**, 772 (1971).
10) A. Rembaum, *J. Polym. Sci.*, **B6**, 159 (1968).
11) K. Ueno and A. E. Matell, *J. Phys. Chem.*, **59**, 998 (1955); **60**, 934, 1270 (1956); S. Mizushima, I. Nakagawa, and D. M. Sweeny, *ibid.*, **25**, 1006 (1956).

Ion Radicals of Organometallic Compounds. III. Positional Effects on the Thermodynamics of Formation and the Kinetics of Decomposition of (Methyl-substituted Benzene)-tricarbonylchromium Cation Radicals

Tamio IKESHOJI† and Vernon D. PARKER*
Laboratory for Organic Chemistry, Norwegian Institute of Technology, University of Trondheim, N-7034 Trondheim-NTH, Norway
(Received September 17, 1983)

Reversible oxidation potentials, rate constants, and activation parameters are reported for the formation and decomposition reactions of all isomers of (methyl-substituted benzene)tricarbonylchromium cation radicals. The reversible potentials were observed to depend both on the number and the positions of the methyl substituents. It was found that the effects on the reversible potentials of adding single methyl substituents to similar structures were additive. The activation energies and entropies for the decomposition reactions were found to be grouped into four different categories depending upon the numbers of adjacent unsubstituted positions on the methylarene ligands. Within each group the deviations from the averages were less than experimental error. The differences in activation parameters are explained in terms of how effective bonding is between the chromium atom and the arene ligands in the cation radicals.

In previous papers of this series we have examined the thermodynamics and kinetics of the formation and decomposition reactions of (arene)tricarbonylchromium cation radicals in acetonitrile.[1,2] The arene moieties were either methylbenzene[1] or benzenes substituted with heteroatom-containing substituents.[2] The (methyl-substituted benzene)tricarbonylchromium complexes show four main oxidation peaks during linear sweep voltammetry measurements at stationary platinum electrodes.[1] The cation radicals of the complexes are generated at the first reversible oxidation wave (wave I) and decompose by a first order chemical reaction (Eq. 1) followed by electron transfer reaction (Eq. 2),

$$MCr(CO)_3^+ \xrightarrow{k} M + Cr(CO)_n^+ + (3-n)CO \quad (1)$$

$$Cr(CO)_n^+ + MCr(CO)_3^+ \rightleftharpoons Cr(CO)_m^{2+} + MCr(CO)_3 + (n-m)CO \quad (2)$$

i.e. an ECE_h mechanism. Both the activation parameters and the oxidation potentials were observed to be related to the number of methyl substituents. The more highly substituted complexes show the higher activation energies for the decomposition reactions of the cation radicals, *i.e.* form the kinetically more stable cations. For the same cation radicals the more highly substituted ones are formed at the lower potentials, *i.e.* are the more thermodynamically stable. However, a number of discrepancies were observed for the parameters obtained for the 7 complexes studied, $(CH_3)_n$-$C_6H_{6-n}Cr(CO)_3$ with $n=0$ to 6, with one isomer for each value of n. For example, the difference in oxidation potentials of 1,4-$(CH_3)_2C_6H_4Cr(CO)_3$ and 1,3,5-$(CH_3)_3$-$C_6H_3Cr(CO)_3$ was only 1 mV while the difference in activation energies for the decompositions of the corresponding cation radicals was 3.9 kcal mol^{-1}. †† On the other hand the difference in activation energies for the decomposition reactions of the cation radicals of 1,3,5-$(CH_3)_3C_6H_3Cr(CO)_3$ and 1,2,4,5-$(CH_3)_4C_6H_2Cr(CO)_3$ was observed to be only 0.3 kcal mol^{-1}. This suggests that the effects of methyl substitution on the ease of the formation and the ease of the decomposition of the cation radicals differ.

In order to obtain more insight on the effects of methyl substitution on the formations and the decompositions, oxidation potentials and kinetic parameters were obtained for all of the remaining isomers of (methyl-substituted benzene)tricarbonylchromium complexes.

Experimental

All measurements were carried out in acetonitrile with 0.1 mol dm^{-3} *n*-Bu_4NBF_4 and Ag/Ag$^+$ (0.01 mol dm^{-3} $AgNO_3$ in acetonitrile with 0.1 mol dm^{-3} *n*-Bu_4NBF_4) as reference electrode. The concentration of the substrate was 2.0 mmol dm^{-3}. The measurements of reversible oxidation potentials were performed at −10°C in order to attain reversibility over a wide range of sweep rates. The kinetic measure ments of rate constants were performed by derivative cyclic voltammetry (DCV) in the typical temperature range of −10°C to 25°C with an interval of 5°C. Activation energies (E_a) and activation entropies (ΔS^*) were obtained by Arrhenius correlations of rate constants. The details of the measurement procedure were reported in previous papers.[1,3,4]

In this paper the complexes are identified according to the number of the methyl substituents as follows:

(0)=$C_6H_6Cr(CO)_3$,
(1)=$CH_3C_6H_5Cr(CO)_3$,
(1,2), (1,3,), (1,4)=dimethyl-substituted complexes,
(1,2,3), (1,2,4), (1,3,5)=trimethyl-substituted complexes,
(1,2,3,4), (1,2,3,5), (1,2,4,5)—tetramethyl-substituted complexes,
(5)=$(CH_3)_5C_6HCr(CO)_3$,
(6)=$(CH_3)_6C_6Cr(CO)_3$.

Results

Reversible oxidation potentials of the complexes and kinetic parameters for the decomposition reactions of their cation radicals are shown in Table. 1. The reversibility was confirmed from the result that the potential differences of the oxidation and reduction peaks of cyclic voltammograms were close to *ca.*

†Present address: Government Industrial Research Institute Tohoku. 4-2-1, Nigatake, Sendai 983.

†† 1 cal=4.184 J.

TABLE 1. REVERSIBLE OXIDATION POTENTIALS OF (METHYL SUBSTITUTED BENZENE) TRICARBONYLCHROMIUM COMPLEXES AND KINETIC PARAMETERS OF THE DECOMPOSITION REACTION OF THE COMPLEXES[a)]

Complex[b)]	E_{rev}[c)]/mV	k[d)]/s^{-1}	E_a[e)]/kcal mol^{-1}	$-\Delta S^{\neq}$[f)]/cal K^{-1} mol^{-1}
(1,2)	409	892(20)[g)]	8.6(0.2)[g)]	18.3(0.6)[g)]
(1,3)	417	569(6)	8.8(0.1)	18.5(0.3)
(1,2,3)	375	567(7)	8.9(0.1)	18.2(0.3)
(1,2,4)	374	117(3)	10.3(0.2)	16.6(0.4)
(1,2,3,4)	337	106(6)	10.4(0.4)	16.3(1.4)
(1,2,3,5)	358	7.8(0.4)	14.7(0.3)	7.2(1.6)

a) In acetonitrile containing n-Bu_4NBF_4 (0.1 mol/dm^3). b) See text for the structures. c) The reversible oxidation potential at −10 °C *vs.* Ag/Ag^+ of wave I. d) The rate constant at 25 °C calculated from the Arrhenius plots. e) The activation energy. f) The activation entropy. g) All errors are 95% confidence calculated according to the theory of least squares as described in Ref. 12.

60 mV at high scan rates where the two peaks were observed to have the same height. In this case these two peaks did not shift according to the chemical reaction (Eq. 1) of the ECE_h mechanism.

Discussion

Reversible Oxidation Potentials of the Complexes. The reversible electrode potentials for the oxidation of all of the complexes in acetonitrile are plotted *vs.* the number of methyl substituents in Fig. 1. Linear regression anaiysis gives a slope of −33.6 mV/methyl group with a correlation coefficient of 0.985. There are differences in oxidation potentials within each group of isomers, *i.e.* those with 2, 3, and 4 methyl substituents. These differences affect the overall correlation. The points represented as black circles in Fig. 1 show the effect of additional methyl groups on two basic structural units, corresponding to 1,3-dimethyl- and 1,3,5-trimethylbenzene complexes.

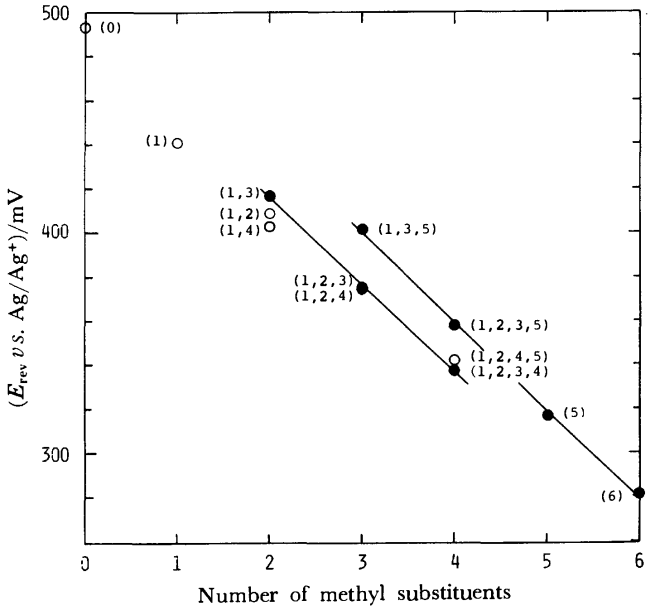

Fig. 1. Relation between reversible oxidation potentials and the structures of the complexes. See text for the structures.
(●) E_{rev} on lines.

The linear regression line for the first case has a slope of −40.0 mV/(additional methyl group) and a correlation coefficient of 0.999. In these cases the effect of additional methyl groups on the reversible oxidation potentials is additive. This suggests that the scatter observed in Fig. 1 is due to the fact that the magnitude of the effect of a methyl substituent is dependent upon the total structure and that the reversible oxidation potentials cannot be considered independent of the substitution existing before the addition of the group.

Another interesting aspect of the correlations in Fig. 1 is that the line for 1,3-substituted complexes lies only 16 mV below the other line on the potential scale. This means that an additional meta methyl substituent has much smaller effect on the reversible oxidation potentials than the addition of substituents ortho to those in the basic structural unit.

Some of the effects of methyl substitution on the reversible oxidation potentials could be due to steric interactions between the methyl groups and the carbonyl groups. In complexes (0)[5-7)] and (6)[8)] the steric configuration of H and CH_3 of the arene in relation to CO is the staggered structure **1**, and in complex (1)[9)] it is the eclipsed form **2** due to electron donation from CH_3.[10)] It is possible that ortho substitution

makes the staggered form energetically more favorable and meta substituents favor the eclipsed form. This effect could cause the difference in the potentials. With regard to conformation, it should be noted that the configuration around the chromium atom in the neutral complexes is tetrahedral, but there is a possibility that the change in oxidation state of chromium in going to the cation radical is accompanied by a change in configuration. Unfortunately the detailed structures of the cation radicals are not known, the rotational barriers in arene-$Cr(CO)_3$ are small,[10)] and thus further discussion of steric effects would be highly speculative.

TABLE 2. GROUPS DIVIDED ACCORDING TO THE ACTIVATION ENERGY AND THE STRUCTURE OF TRICARBONYLCHROMIUM COMPLEXES

Group	Designation	Structures of benzenes in complexes	E_a/kcal mol^{-1}	$-\Delta S^*$/cal K^{-1} mol^{-1}
1	3	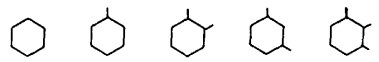	8.6 (0.3)	18.2 (0.7)
2	2	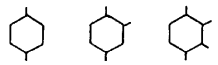	10.3 (0.1)	16.2 (0.4)
3	1	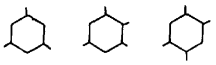	14.4 (0.3)	8.1 (1.3)
4	0	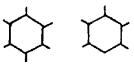	17.0 (1.4)	5

Activation Parameters for the Decomposition Reactions of the Cation Radicals. The complexes can be divided into four groups according to the magnitudes of the activation parameters as shown in Table 2 and Fig. 2. These division also correspond to the substitution pattern of the methylarene ligand. Those complexes having three or more adjacent unsubstituted positions form the first group. The activation energies (E_a) for these compounds were found to be 8.6 ± 0.3 kcal mol^{-1} and the corresponding activation entropies (ΔS^*) equal to -18.2 ± 0.7 cal K^{-1} mol^{-1}. The standard deviations are well within the experimental errors for the determination of any of the parameters. This fact implies that the parameters can be considered to be equal for all members of the group. The second group has two adjacent unsubstituted positions and in this case E_a are equal to 10.3 ± 0.1 kcal mol^{-1} and ΔS^* were estimated to be -16.2 ± 0.4 cal K^{-1} mol^{-1}. The complexes in the third group have only H substituents with adjacent methyl substituents and in all these cases there are two or three such H substituents. The activation parameters were estimated to be 14.4 ± 0.3 kcal mol^{-1} (E_a) and -8.1 cal K^{-1} mol^{-1} (ΔS^*). The final group has only two members, the complexes of haxamethyl- and pentamethylbenzene, and the activation energies averaged 17.0 ± 1.4 kcal mol^{-1} and ΔS^* was evaluated as -5 cal K^{-1} mol^{-1} in both cases.

The data in Table 2 conform well to an isokinetic relationship.[11] The data are plotted in Fig. 3. The linear regression slope is equal to 601 K, *i.e.*, the isokinetic temperature, with a correlation coefficient of 0.995. The relationship implies an inversion of relative rate constant at temperatures above and below 601 K. However, the apparent isokinetic temperature is so far removed from the range in which the parameters were determined that we place little significance on it. On the other hand the linear relationship does exist and we point this out without becoming involved in a discussion of the possible significance of the relationship, which is in itself controversial.[11]

The most stable cation radical complex, both from a thermodynamic (E_{rev}) and a kinetic (k and E_a) points of view, is that derived from hexamethylbenzene. The least stable is that from benzene. This fact suggests that steric effects have little to do with the relative stability of the cation radicals. If we assume that the

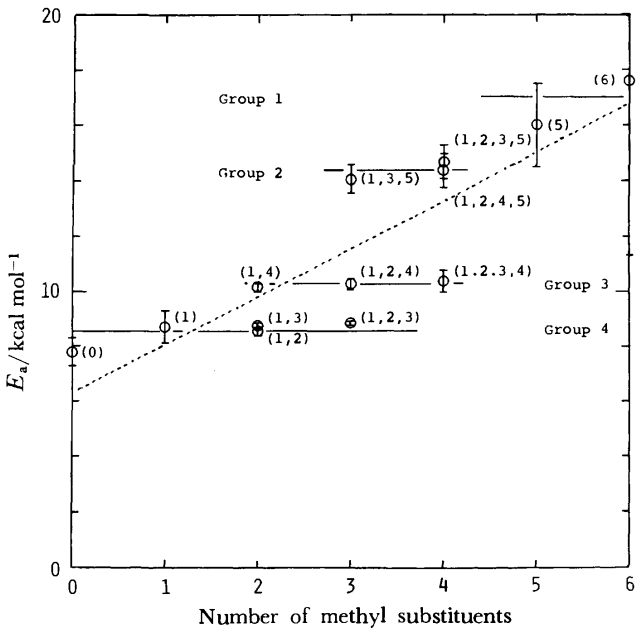

Fig. 2. Relation between activation energies of decomposition reactions of the cation radicals from the complexes and their structures. See text for the structures.
(——) Mean value of E_a in each group. (------) Linear regression line.

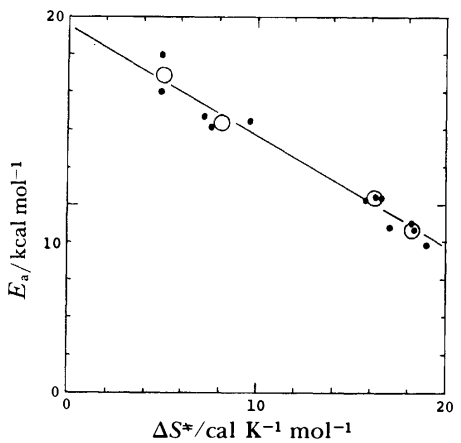

Fig. 3. Isokinetic relationship obtained from E_a and ΔS^* in Table 2.
(—○—) From Table 2. (●) Each isomer.

most important electronic effect of the methyl substituents is an inductive one, the positions where methyl is attached are the ones most affected by the substituent. All positions in the hexamethylbenzene complex cation radical are affected equally by the methyl groups. This would allow a maximum degree of transmission of the inductive effects of the methyl groups providing that Cr is located with the same relationship to all the C atoms of the benzene ring. Any unsubstituted position brings about a decrease in the donation of electrons from the methylarene ligand to the chromium atom. The complex of pentamethylbenzene forms a less stable cation radical than the corresponding hexamethylbenzene complex. The effect is amplified by having two or three unsubstituted positions as is the case for the group 3 complexes. The difference in stability becomes greater when adjacent positions are unsubstituted as in groups 2 and 1. In these cases the chromium atom could not be located equidistant from all of the ring carbon atoms except in (0) and have the maximum effect of the methyl groups at the substituted positions. There are most likely differences in the geometries of the cation radical complexes depending upon the substitution pattern.

In conclusion the linear relationship observed between the thermodydnamic and kinetic stabilities, with some scattering, can be considered to be due to different but similar aspects in three states. The thermodynamic stabilitites are related to two states of them, *i.e.* neutral complex and cation complex. On the other hand the kinetic stabilites are related to another set of two states, *i.e.* cation complex and transition state to decomposition.

We wish to thank the Royal Norwegian Council for Science and Technology for a fellowship to T.I.

References

1) T. Ikeshoji and V. D. Parker, *Acta Chem. Scand., Ser. B*, **37**, 715 (1984).
2) T. Ikeshoji and V. D. Parker, *Acta Chem. Scand.* (in Press).
3) E. Ahlberg and V. D. Parker, *Acta Chem. Scand., Ser. B*, **34**, 97 (1980).
4) E. Ahlberg and V. D. Parker, *J. Electroanal. Chem.*, **121**, 73 (1981).
5) P. Corradini and G. Allegra, *J. Am. Chem. Soc.*, **81**, 2271 (1959).
6) M. F. Bailey and L. F. Dahl, *Inorg. Chem.*, **4**, 1341 (1965).
7) R. Bernald and P. Coppens, *Acta Cryst.*, **B29**, 2515 (1973).
8) M. F. Bailey and L. F. Dahl, *Inorg. Chem.*, **4**, 1298 (1965).
9) F. Meurs and H. van Koningsveld, *J. Organomet. Chem.*, **131**, 4238 (1977).
10) T. A. Albright and B. K. Carpenter, *Inorg. Chem.*, **19**, 3092 (1980) and references therein.
11) J. F. Bunnett, "Investigation of Rates and Mechanisms of Reactions," ed by E. S. Lewis, Wiley, New York (1974), Part I, Chap. VIII.
12) O. L. Davies and P. L. Goldsmith, "Statistical methods in Research and Production," ICI (1972).

 © 1984 The Chemical Society of Japan Bull. Chem. Soc. Jpn., 57,1116—1122(1984) [Vol. 57, No. 4

Copper(II)-Catalyzed Transamination of Hydrophobic Pyridoxamine with Pyruvic Acid in Functionalized Bilayer Vesicles†

Yukito MURAKAMI,* Jun-ichi KIKUCHI, Akio NAKANO,†† Kazunari AKIYOSHI, and Toru IMORI
Department of Organic Synthesis, Faculty of Engineering, Kyushu University, Hakozaki, Higashi-ku, Fukuoka 812
(Received October 26, 1983)

The copper(II)-catalyzed transamination of 2-methyl-3-hydroxy-4-aminomethyl-5-(dodecylthiomethyl)pyridine (C_{12}SPM) with sodium pyruvate was investigated in an aqueous medium at pH 6.8, μ 0.10 (KCl), and 30.0 ±0.1 °C in the presence of molecular aggregates of *N,N*-ditetradecyl-*N*$^{\alpha}$-[6-(trimethylammonio)hexanoyl]-L-alaninamide bromide (N^+C_5Ala2C_{14}), *N,N*-ditetradecyl-*N*$^{\alpha}$-[6-(trimethylammonio)hexanoyl]-L-histidinamide bromide (N^+C_5His2C_{14}), or hexadecyltrimethylammonium bromide (CTAB). The reaction afforded the corresponding pyridoxal analogue (C_{12}SPL) and alanine as the final products upon addition of edta which liberates the copper(II) ion from the coordination sites of the aldimine Schiff-base. The coordination interaction between the copper(II) ion and C_{12}SPM, which takes place prior to the transamination, was clarified by electronic spectroscopy. The reactivity of the 2:1 (ketimine:Cu^{II}) complex was found to be much larger than that of the 1:1 complex in the molecular assemblies of N^+C_5Ala2C_{14} and CTAB, and the formation of the former species was more pronounced in the N^+C_5Ala2C_{14} vesicle. The bilayer vesicle formed with N^+C_5His2C_{14} allowed the formation of the 1:1 complex in preference to that of the 2:1 complex, and the coordination-free imidazolyl group of the amphiphile effectively catalyzed the isomerization as a general base.

Pyridoxal-5′-phosphate (PLP) is known to catalyze various transformation reactions of amino acids such as transamination, elimination, racemization, and decarboxylation as the coenzyme in biological systems.[1] Although most of the PLP-dependent enzymatic reactions can be simulated by nonenzymatic systems,[2] such nonenzymatic reactions are much less efficient than the corresponding enzymatic ones with respect to reactivity, substrate specificity, and reaction selectivity. In order to improve the catalytic efficiency of model systems for the PLP-dependent enzymes, micellar surfactants,[3] synthetic polymers,[4] and macrocyclic compounds[5] have been utilized in recent years to simulate the functions of apoenzymes. We have reported previously that a bilayer membrane composed of a synthetic peptide lipid can provide a reaction field favorable for the transamination of PLP with a hydrophobic amino acid.[6]

In the present work, we prepared hydrophobic vitamin B_6 analogues, C_{12}SPM and C_{12}SPL, and investigated the reaction of C_{12}SPM with pyruvate in single-walled vesicles of N^+C_5Ala2C_{14} and N^+C_5His2C_{14} as effected by the copper(II) ion. The kinetic behavior of the transamination reaction was analyzed in the light of metal-coordination modes observed for C_{12}SPM and its ketimine Schiff-base with the copper(II) ion. The kinetic effect of single-walled vesicles formed with N^+C_5His2C_{14} on the transamination is to be discussed in view of the base catalysis of the histidyl residue.

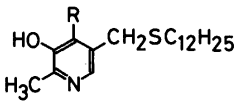

C_{12}SPM (R = CH_2NH_2)
C_{12}SPL (R = CHO)

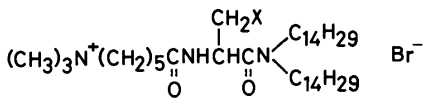

N^+C_5Ala2C_{14} (X = H)
N^+C_5His2C_{14} (X =)

Experimental

Spectroscopic data were taken on a Union Giken SM-401 UV-visible spectrophotometer and a Hitachi R-24B NMR spectrometer. pH-Measurements were carried out with a Beckman expandomatic SS-2 pH meter equipped with a Metrohm EA-125 combined electrode after calibration with a combination of appropriate standard aqueous buffers. Melting points were measured with a Yanaco MP-S1 apparatus (hot-plate type). Elemental analyses were performed at the Microanalysis Center of Kyushu University.

Hexadecyltrimethylammonium bromide (CTAB) of Nakarai Chemicals was recrystallized from ethanol, mp 237—239 °C (decomp). *N,N*-Ditetradecyl-*N*$^{\alpha}$-[6-(trimethylammonio)hexanoyl]-L-alaninamide bromide (N^+C_5Ala2C_{14}) and *N,N*-ditetradecyl-*N*$^{\alpha}$-[6-(trimethylammonio)hexanoyl]-L-histidinamide bromide (N^+C_5His2C_{14}) were prepared as described elsewhere.[6,7] 2-Methyl-3-hydroxy-4-aminomethyl-5-(dodecylthiomethyl)pyridine dihydrobromide (C_{12}SPM·2HBr) and 2-methyl-3-hydroxy-4-formyl-5-(dodecylthiomethyl)pyridine (C_{12}SPL) were prepared as described below.

2-Methyl-3-hydroxy-4-aminomethyl-5-(bromomethyl)pyridine Dihydrobromide (PMBr). Pyridoxamine dihydrochloride (1.0 g, 4.2 mmol) dissolved in 48% aqueous hydrobromic acid (25 ml) was refluxed for 2 h. After the mixture was evaporated to dryness *in vacuo*, the crude product was dissolved in methanol and purified by reprecipitation with ether; yield 1.3 g (81%), mp 265—270 °C (decomp).

2-Methyl-3-hydroxy-4-aminomethyl-5-(dodecylthiomethyl)pyridine Dihydrobromide (C_{12}SPM·2HBr). A solution of 1-dodecanethiol (530 mg, 2.6 mmol) in dry ethanol (5 ml) was added dropwise to 50 mg of sodium metal dissolved in dry ethanol (5 ml) with stirring under nitrogen atmosphere. PMBr (400 mg, 1.0 mmol) dissolved in dry ethanol (50 ml) was added dropwise to the resulting mixture with stirring under nitrogen at 0 °C. The mixture was evaporated to dryness *in*

† Contribution No. 716 from this Department.
†† Present address: Department of Food Science, Toa University, Shimonoseki, Yamaguchi 751.

vacuo, and the residue was recrystallized from methanol. The crude product dissolved in methanol was treated with 48% aqueous hydrobromic acid, evaporated to dryness, and purified by gel-filtration chromatography on columns of Toyopearl HW-40 fine and Sephadex LH-20 in this sequence with methanol as an eluant to afford a white solid: yield 0.17 g (33%), mp 193— 194 °C (decomp); ^{1}H-NMR (CD_3OD, TMS) δ=0.88 [3H, t, $S(CH_2)_{11}\underline{CH_3}$], 1.27 [20H, m, $SCH_2(\underline{CH_2})_{10}CH_3$], 2.50 [2H, t, $S\underline{CH_2}(CH_2)_{10}CH_3$], 2.67 [3H, s, 2-$\underline{CH_3}$ on pyridine ring], 3.96 [2H, s, $\underline{CH_2}S(CH_2)_{11}CH_3$], 4.39 [2H, s, $\underline{CH_2}NH_3^+$], and 8.16 [1H, s, 6-H on pyridine ring].

Found: C, 47.15; H, 7.72; N, 5.66%. Calcd for $C_{20}H_{36}N_2OS \cdot 2HBr$: C, 46.70; H, 7.45; N, 5.45%.

2-Methyl-3-hydroxy-4-formyl-5-(dodecylthiomethyl)pyridine (C_{12}SPL). A mixture of potassium hydroxide (1.37 g, 9.8 mmol), C_{12}SPM·2HBr (0.10 g, 0.19 mmol), α-oxoglutaric acid (1.46 g, 10 mmol), and zinc nitrate (0.116 g, 0.39 mmol) in methanol (200 ml) was stirred for 24 h at room temperature, and evaporated to dryness *in vacuo*. The residue was suspended in 2 mol dm^{-3} aqueous hydrochloric acid (100 ml), and extracted with chloroform (3 × 50 ml). The chloroform extract was washed with water, dried over anhydrous sodium sulfate, and evaporated to dryness *in vacuo*. The crude product was purified by gel-filtration chromatography on a column of Sephadex LH-20 with methanol as an eluant to afford a pale yellow oil: yield 29 mg (39%); ^{1}H-NMR ($CDCl_3$, TMS) δ=0.89 [3H, t, $S(CH_2)_{11}\underline{CH_3}$], 1.29 [20H, m, $SCH_2(\underline{CH_2})_{10}CH_3$], 2.35 [2H, br s, $S\underline{CH_2}(CH_2)_{10}CH_3$], 2.51 [3H, s, 2-$\underline{CH_3}$ on pyridine ring], 3.90 [2H, s, $\underline{CH_2}S(CH_2)_{11}CH_3$], 7.87 [1H, s, 6-H on pyridine ring], and 10.45 [1H, s, CHO].

Found: C, 68.06; H, 9.46; N, 4.01%. Calcd for $C_{20}H_{33}NO_2S$: C, 68.34; H, 9.46; N, 3.98%.

Kinetic Measurements. The reaction medium was prepared as follows. (i) An appropriate amount of the stock solution of one of the amphiphiles ($N^+C_5Ala2C_{14}$, $N^+C_5His2C_{14}$, and CTAB) in ethanol was placed in a glass vessel, and evaporated *in vacuo* to remove the solvent completely. An aqueous HEPES (2-[4-(2-hydroxyethyl)-1-piperazinyl]ethanesulfonic acid) buffer (2.5 mmol dm^{-3}, pH 6.8) containing 0.1 mol dm^{-3} potassium chloride was added to the residue. (ii) An aqueous dispersion of the amphiphile thus prepared was sonicated for 2 min with a probe-type sonicator at 30-W power (W-220F, Heat Systems-Ultrasonics). The resulting vesicle solution was sufficiently clear and gave good kinetic reproducibility. Each run was initiated by adding 20 µl of an aqueous solution of C_{12}SPM (5.0 × 10^{-3} mol dm^{-3}), an appropriate quantity of an aqueous solution of $Cu(ClO_4)_2$ which was standardized by conventional chelatometric titration (1.0 × 10^{-2} mol dm^{-3}), and 100 µl of a freshly prepared aqueous solution of sodium pyruvate (0.1 mol dm^{-3}) to 2.0 ml of the reaction medium which was pre-equilibrated at 30.0 ± 0.1 °C in a thermostated cell set in the spectrophotometer.

Results and Discussion

Spectral Change in the Course of Transamination. The transamination reaction of C_{12}SPM with sodium pyruvate, as effected by the presence of single-walled vesicles of $N^+C_5Ala2C_{14}$ and $N^+C_5His2C_{14}$ as well as by CTAB micelles, was followed spectrophotometrically in the aqueous HEPES buffer at pH 6.8, μ 0.10 (KCl), and 30.0 ± 0.1 °C. Figure 1 shows the spectral change observed along the progress of transamination in the presence of the $N^+C_5Ala2C_{14}$ vesicle. The absorption spectrum of C_{12}SPM in the single-walled vesicle shows a maximum at 293 nm and a shoulder at 315 nm. This indicates the presence of two species which are different in protonation site from each other (Scheme 1).[8,9] The charged form (PM_1) was primarily observed in dioxane-water (1:9 v/v), and the fraction of the neutral

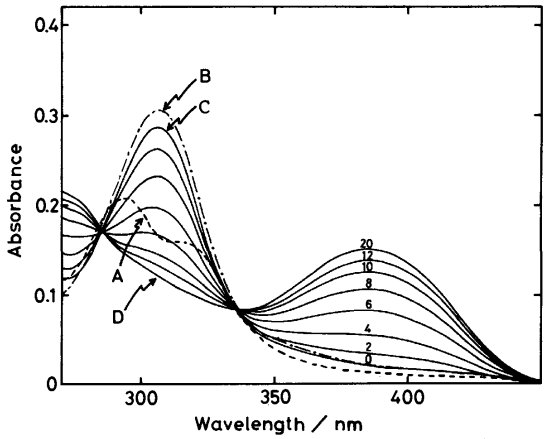

Fig. 1. Spectral change along the progress of transamination of C_{12}SPM (5.0×10^{-5} mol dm^{-3}) with sodium pyruvate (5.0×10^{-3} mol dm^{-3}) in the presence of $Cu(ClO_4)_2$ (5.0×10^{-5} mol dm^{-3}) and $N^+C_5Ala2C_{14}$ vesicle (1.0×10^{-3} mol dm^{-3}) in an aqueous HEPES buffer (2.5×10^{-3} mol dm^{-3}) at pH 6.8, μ 0.10 (KCl), and 30.0±0.1 °C: A, C_{12}SPM alone; B, Cu^{II}-C_{12}SPM species; C, Cu^{II}- ketimine species; D, Cu^{II}-aldimine species. Nunerals refer to reaction periods (in min) for the ketimine-aldimine isomerization.

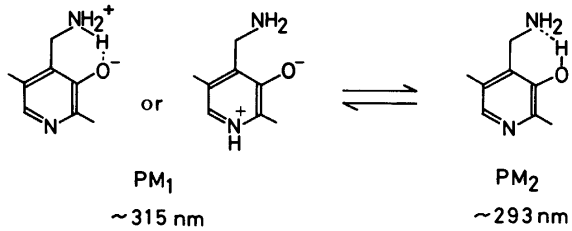

Scheme 1.

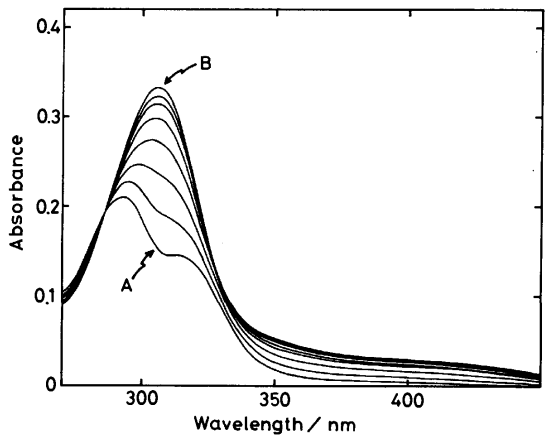

Fig. 2. Electronic absorption spectra of C_{12}SPM (5.0×10^{-5} mol dm^{-3}) in an aqueous HEPES buffer (2.5×10^{-3} mol dm^{-3}) at pH 6.8, μ 0.10 (KCl), and 30.0±0.1 °C in the presence of $N^+C_5Ala2C_{14}$ vesicle (1.0×10^{-3} mol dm^{-3}) and varying amounts of $Cu(ClO_4)_2$: 0, 5.1×10^{-6}, 1.0×10^{-5}, 1.5×10^{-5}, 2.0×10^{-5}, 2.5×10^{-5}, 3.0×10^{-5}, and 5.0×10^{-5} mol dm^{-3} (read from A to B).

form (PM_2) increased with an increase in dioxane content. The microenvironmental polarity for the pyridoxamine moiety of C_{12}SPM in the aggregates was evaluated from the relative intensities of the absorption maxima for these species. As a result, both vesicular and micellar systems provide a microenvironment equivalent to that provided by dioxane-water (1:1 v/v) (Kosower's *Z*-value, 87).[10] Addition of $Cu(ClO_4)_2$ resulted in an immediate shift of the absorption maximum to 306 nm along with an increase in intensity as shown in Fig. 2. This spectral change is analogous to that observed for the formation of the Cu^{II}-pyridoxamine complex in methanol[9] and attributed to the formation of the Cu^{II}-C_{12}SPM complex (**1** in Scheme 2). Subsequently, the ketimine Schiff-base complex (**2** in Scheme 2), having an absorption maximum at 305 nm, was formed instantaneously upon addition of sodium pyruvate to the solution. The intensity of this peak decreased with time, isosbestic points being observed at 286 and 335 nm. A new absorption band appeared at 385 nm and increased in intensity as the reaction proceeded. The absorption spectrum observed at the final stage of reaction was identical with that of the copper complex of the aldimine Schiff-base of C_{12}SPL formed with alanine (**3** in Scheme 2). When an aqueous solution of tetrasodium ethylenediaminetetraacetate (edta; 10-fold molar excess over Cu^{II} ion) was added to the final solution, the spectrum changed immediately indicating the formation of the metal-free aldimine Schiff-base of C_{12}SPL formed with alanine. This Schiff-base was hydrolyzed to C_{12}SPL and alanine completely within 1 h. The isomerization of the ketimine Schiff-base to the corresponding aldimine was not observed in the absence of $Cu(ClO_4)_2$. Similar reaction behavior was found in other amphiphile systems of the present study. Table 1 summarizes the spectral parameters for various species formed in the present amphiphile systems.

In the light of these observations, the overall reaction pathway is explicitly given in Scheme 2. Matsumoto *et al.* reported that the reaction of pyridoxamine with

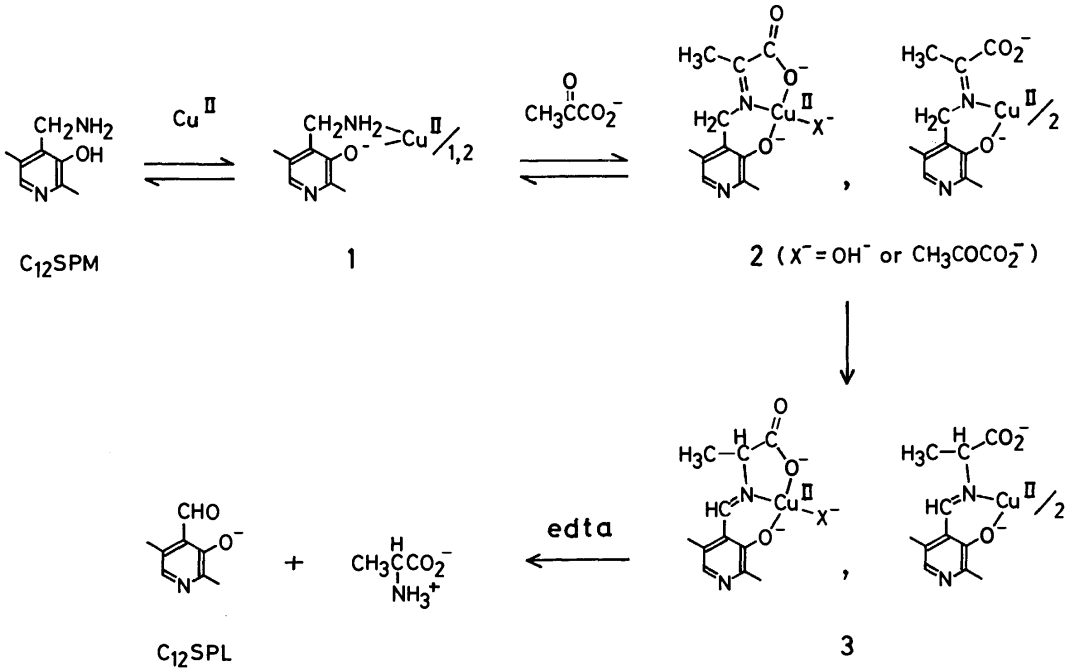

Scheme 2.

Table 1. Spectral parameters[a] for chemical species involved in the Cu^{II}-catalyzed transamination of C_{12}SPM with sodium pyruvate in various amphiphile systems at 30.0±0.1 °C[b]

Species[c]	Amphiphile		
	$N^+C_5Ala2C_{14}$	$N^+C_5His2C_{14}$	CTAB
C_{12}SPM	293 (4.2×10^3) 315sh (3.1×10^3)	294 (4.2×10^3) 315sh (3.1×10^3)	295 (3.9×10^3) 314sh (3.7×10^3)
Cu^{II}-C_{12}SPM (**1**)	306	309	305
Cu^{II}-KSB (**2**)	305	307	304
Cu^{II}-ASB (**3**)	385	392	388

a) Wavelengths (nm) at absorption maxima. Molar absorption coefficients are given in parentheses. b) Cationic amphiphile systems in an aqueous HEPES buffer (2.5×10^{-3} mol dm^{-3}) at pH 6.8 and μ 0.10 (KCl): $N^+C_5Ala2C_{14}$, 1.0×10^{-3} mol dm^{-3}; $N^+C_5His2C_{14}$, 1.0×10^{-3} mol dm^{-3}; CTAB, 3.0×10^{-3} mol dm^{-3}. Initial concentrations of reactants: C_{12}SPM, 5.0×10^{-5} mol dm^{-3}; $Cu(ClO_4)_2$, 5.0×10^{-5} mol dm^{-3}; sodium pyruvate, 5.0×10^{-3} mol dm^{-3}. c) For structures of metal complexes, see Scheme 2; KSB, ketimine Schiff-base; ASB, aldimine Schiff-base.

α-keto acids and copper(II) ion yielded the Cu^{II}-aldimine chelates in methanol, but the rate-determining step was not unambiguously defined.[11] In the present transamination reaction, however, the isomerization of the Cu^{II}-ketimine chelate to the Cu^{II}-aldimine chelate is exclusively the rate-determining step without any ambiguity, since the reaction time course was not influenced by the mixing mode of the reactants, simultaneous or sequential, and showed a monophasic kinetic feature. The absorption bands characteristic of the Cu^{II}-ketimine and -aldimine chelates were used to determine the rates of isomerization reaction.

Metal-coordination Behavior of C_{12}SPM. Prior to the transamination reaction, the copper(II) ion undergoes coordination with C_{12}SPM as shown in Scheme 2. The π-π^* transition bands appearing in the 300-nm range are due to the pyridoxamine chromophore of C_{12}SPM in the N^+C_5Ala2C_{14} vesicle, and their intensities increased upon addition of $Cu(ClO_4)_2$ (Fig. 2). The simplest coordination equilibrium would involve the formation of the 1:1 (C_{12}SPM:Cu^{II}) complex (Eq. 1).

$$C_{12}SPM + Cu^{II} \rightleftharpoons Cu^{II}(C_{12}SPM) \quad (1)$$

This is not the case, however, since the value of $[Cu^{II}(C_{12}SPM]/[C_{12}SPM][Cu^{II}]$ varied as the concentration of $Cu(ClO_4)_2$ was changed. Alternatively, the copper-coordination scheme, which involves the formation of both 2:1 and 1:1 (C_{12}SPM:Cu^{II}) complexes (Eq. 2), was utilized to analyze the equilibrium data.

$$2(C_{12}SPM) \underset{K_1}{\overset{Cu^{II}}{\rightleftharpoons}} Cu^{II}(C_{12}SPM)_2 \underset{K_2}{\overset{Cu^{II}}{\rightleftharpoons}} 2\,Cu^{II}(C_{12}SPM) \quad (2)$$

The formation of such 2:1 and 1:1 chelate species has been also reported for the coordination of Cu^{II} ion with pyridoxamine in aqueous media.[12] The observation of an isosbestic point at 286 nm (Fig. 2) assures that the present 2:1 and 1:1 chelates have an identical molar absorption coefficient as given in terms of the C_{12}SPM unit. Now, the respective stability constants (K_1 and K_2), defined by Eqs. 3 and 4, were evaluated by the least-squares analysis in a manner similar to that applied to the zinc(II)-paracyclophane system.[13]

$$K_1 = \frac{[Cu^{II}(C_{12}SPM)_2]}{[C_{12}SPM]^2[Cu^{II}]} \quad (3)$$

$$K_2 = \frac{[Cu^{II}(C_{12}SPM)]^2}{[Cu^{II}(C_{12}SPM)_2][Cu^{II}]} \quad (4)$$

The total concentration of C_{12}SPM bound to Cu^{II} at a given concentration of $Cu(ClO_4)_2$ ($c=[Cu^{II}(C_{12}SPM)]+2[Cu^{II}(C_{12}SPM)_2]$) is calculated by Eq. 5.

$$c = \frac{\Delta A}{A_c - A_f}[C_{12}SPM]_0 \quad (5)$$

Here, A_c and A_f denote the absorbance in the presence of sufficiently excess $Cu(ClO_4)_2$ and that in its absence, respectively, at a selected wavelength close to the absorption maxima of the Cu^{II}-C_{12}SPM complexes; ΔA is the absorbance change with respect to A_f at the intermediate concentration range of $Cu(ClO_4)_2$; and $[C_{12}SPM]_0$ denotes the total concentration of C_{12}SPM. Combining Eqs. 3, 4, and 5, we obtain Eq. 6.

$$(K_1K_2)^{1/2}[C_{12}SPM]([Cu^{II}]_0 - c) + K_1[C_{12}SPM]^2(2[Cu^{II}]_0 - c) = c \quad (6)$$

Here, $[Cu^{II}]_0$ is the initial concentration of $Cu(ClO_4)_2$. This equation is in the form, $aX + bY = Z$, where a and b are $(K_1K_2)^{1/2}$ and K_1, respectively, and X, Y, and Z are experimentally observable. K_1 and K_2 were determined by the least-squares analysis using all the experimental sets of (X, Y, Z) at various concentrations of $Cu(ClO_4)_2$. The results are summarized in Table 2. The observed total concentration of C_{12}SPM bound to Cu^{II} was computationally reproduced quite satisfactorily by the aid of the K_1 and K_2 values determined as above for the whole concentration range of $Cu(ClO_4)_2$ employed in the present study (Fig. 3).

Figure 4 shows the calculated molar distributions of the 2:1 and 1:1 chelate species of C_{12}SPM in the three different molecular assemblies as a function of the Cu^{II} concentration. In both N^+C_5Ala2C_{14} vesicle and CTAB micelle, the fraction of the 2:1 complex is greater than that of the 1:1 complex in a low concentration range of Cu^{II}, while the fraction of the latter exceeds that of the former at higher Cu^{II} concentrations. Meanwhile, the

Table 2. Stability constants for copper(II) complexes of C_{12}SPM in various amphiphile systems at 30.0±0.1 °C[a]

	N^+C_5Ala2C_{14}	N^+C_5His2C_{14}	CTAB
K_1/mol^{-2} dm^6	3.0×10^{10}	1.8×10^{10}	1.1×10^{11}
K_2	0.26	320	42

a) Cationic amphiphile systems in an aqueous HEPES buffer (2.5×10^{-3} mol dm^{-3}) at pH 6.8 and μ 0.10 (KCl): N^+C_5Ala2C_{14}, 1.0×10^{-3} mol dm^{-3}; N^+C_5His2C_{14}, 1.0×10^{-3} mol dm^{-3}; CTAB, 3.0×10^{-3} mol dm^{-3}.

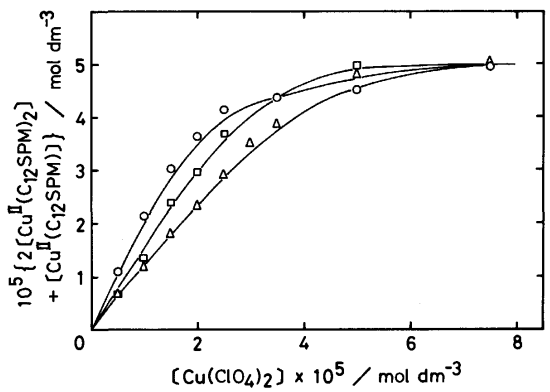

Fig. 3. Correlations between total concentrations of $Cu(ClO_4)_2$ and Cu^{II}-C_{12}SPM complexes in an aqueous HEPES buffer (2.5×10^{-3} mol dm^{-3}) at pH 6.8, μ 0.10 (KCl), and 30.0±0.1 °C in the presence of N^+C_5Ala2C_{14} (○, 1.0×10^{-3} mol dm^{-3}), N^+C_5His2C_{14} (△, 1.0×10^{-3} mol dm^{-3}), and CTAB (□, 3.0×10^{-3} mol dm^{-3}). Solid lines refer to the calculated data by the aid of evaluated stability constants (K_1 and K_2, Table 2); total concentration of C_{12}SPM, 5.0×10^{-5} mol dm^{-3}.

1:1 complex is formed predominantly over the whole concentration range of $Cu(ClO_4)_2$ in the $N^+C_5His2C_{14}$ vesicle. This result strongly indicates that the imidazolyl group of $N^+C_5His2C_{14}$ undergoes coordination with the copper(II) ion which leads to the formation of the 1:1 complex in preference to that of the 2:1 complex.[14]

Kinetic Behavior of Isomerization Reaction. The isomerization of the Cu^{II}-ketimine Schiff-base to the corresponding Cu^{II}-aldimine chelate was followed by means of electronic absorption spectroscopy at 30.0 ± 0.1 °C in the presence of cationic amphiphiles.

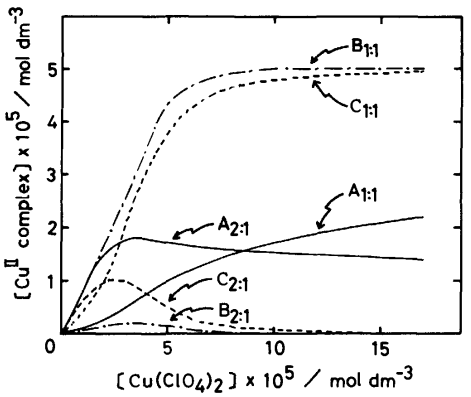

Fig. 4. Distributions of Cu^{II}-$C_{12}SPM$ complexes in an aqueous HEPES buffer (2.5×10^{-3} mol dm^{-3}) at pH 6.8, μ 0.10 (KCl), and 30.0 ± 0.1 °C in the presence of $N^+C_5Ala2C_{14}$ (A, 1.0×10^{-3} mol dm^{-3}), $N^+C_5His2C_{14}$ (B, 1.0×10^{-3} mol dm^{-3}), and CTAB (C, 3.0×10^{-3} mol dm^{-3}). Subscripts 1:1 and 2:1 denote the 1:1 and 2:1 ($C_{12}SPM$:Cu^{II}) complexes, respectively; total concentration of $C_{12}SPM$, 5.0×10^{-5} mol dm^{-3}.

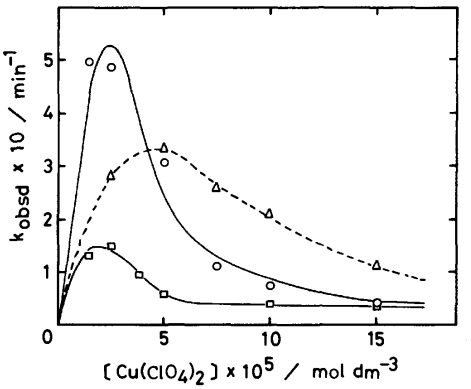

Fig. 5. Correlations between total concentration of $Cu(ClO_4)_2$ and first-order rate constant for the isomerization of Cu^{II}-ketimine to Cu^{II}-aldimine in an aqueous HEPES buffer (2.5×10^{-3} mol dm^{-3}) at pH 6.8, μ 0.10(KCl), and 30.0 ± 0.1 °C in the presence of $N^+C_5Ala2C_{14}$ (○, 1.0×10^{-3} mol dm^{-3}), $N^+C_5His2C_{14}$ (△, 1.0×10^{-3} mol dm^{-3}), and CTAB (□ 3.0×10^{-3} mol dm^{-3}) with initial concentrations: $C_{12}SPM$, 5.0×10^{-5} mol dm^{-3}; sodium pyruvate, 5.0×10^{-3} mol dm^{-3}. Solid lines refer to the calculated data on the basis of Eq. 7 and evaluated kinetic parameters (Table 3).

The absorbance increase due to the formation of the Cu^{II}-aldimine chelate was monitored at 385 nm to determine the reaction rate. The observed rate constant, k_{obsd}, was plotted against the total concentration of $Cu(ClO_4)_2$ as shown in Fig. 5.

In both $N^+C_5Ala2C_{14}$ vesicle and CTAB micelle, the rate constant reaches a maximum and then falls down sharply as the Cu^{II} concentration increases. This overall feature is completely reproducible in several sets of kinetic runs. In the light of the coordination behavior of $C_{12}SPM$ with the copper(II) ion, it can be considered that the copper-binding scheme for the formation of Cu^{II}-ketimine Schiff-base complexes involves both 2:1 and 1:1 (ketimine:Cu^{II}) chelate species as shown in Scheme 2. The observed correlations given in Fig. 5 can be reproduced by summing up the reaction rates of both 1:1 and 2:1 complexes; the former and latter complexes are designated as $Cu^{II}(KSB)$ and $Cu^{II}(KSB)_2$ with specific rate constants, k_1 and k_2 (per ketimine Schiff-base), respectively. The specific rate constant for the metal-free ketimine Schiff-base is neglected under the present conditions. The kinetic expression, on the basis of Scheme 3, is given by Eq. 7, where $[Cu^{II}\text{-KSB}]_T$ is the total concentration of the Cu^{II}-ketimine chelates as given in terms of the ketimine Schiff-base unit.

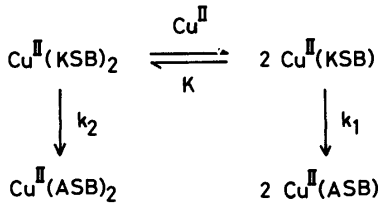

KSB : ketimine Schiff-base
ASB : aldimine Schiff-base

Scheme 3.

$$k_{obsd}[Cu^{II}\text{-KSB}]_T = k_1[Cu^{II}(KSB)] + 2k_2[Cu^{II}(KSB)_2] \quad (7)$$

The concentrations of $Cu^{II}(KSB)$ and $Cu^{II}(KSB)_2$ are interrelated by the stability constant (K) defined by Eq. 8.

$$K = \frac{[Cu^{II}(KSB)]^2}{[Cu^{II}(KSB)_2][Cu^{II}]} \quad (8)$$

The determination of K values was not made by the spectral method which was applied to the Cu^{II}-$C_{12}SPM$ system, because the coordination behavior given by Eq. 8 is accompanied with the isomerization reaction. Accordingly, the values of k_1, k_2, and K were obtained by the regression analysis which minimizes the sum of the squares of errors (U) applied to all the experimental data (Eq. 9).

$$U = \sum \{k_{obsd}[Cu^{II}\text{-KSB}]_T - k_1[Cu^{II}(KSB)] - 2k_2[Cu^{II}(KSB)_2]\}^2 \quad (9)$$

The value of $[Cu^{II}\text{-KSB}]_T$ was evaluated from the final concentration of the Cu^{II}-aldimine Schiff-base

Table 3. Specific rate constants for isomerization reaction of Cu^{II}-ketimine to Cu^{II}-aldimine and stability constants for Cu^{II}-ketimine chelates in amphiphile systems at 30.0±0.1 °C[a)]

Parameter	Amphiphile	
	$N^+C_5Ala2C_{14}$	CTAB
k_1/min^{-1}	0.041	0.036
k_2/min^{-1}	0.70	0.17
K	20	130

a) Cationic amphiphile systems in an aqueous buffer (2.5×10^{-3} mol dm^{-3}) at pH 6.8 and μ 0.10 (KCl): $N^+C_5Ala2C_{14}$, 1.0×10^{-3} mol dm^{-3}; CTAB, 3.0×10^{-3} mol dm^{-3}.

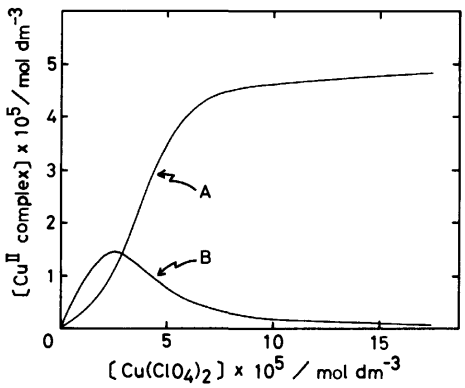

Fig. 6. Distributions of Cu^{II}-ketimine chelates in an aqueous HEPES buffer (2.5×10^{-3} mol dm^{-3}) at pH 6.8, μ 0.10 (KCl), and 30.0±0.1 °C in the presence of $N^+C_5Ala2C_{14}$ vesicle (1.0×10^{-3} mol dm^{-3}): A, 1:1 (ketimine:Cu^{II}) chelate; B, 2:1 chelate. Initial concentrations: $C_{12}SPM$, 5.0×10^{-5} mol dm^{-3}; sodium pyruvate, 5.0×10^{-3} mol dm^{-3}.

produced by the isomerization reaction,[15)] since the Cu^{II}-ketimine chelate was quantitatively converted into the corresponding Cu^{II}-aldimine chelate.

The kinetic parameters thus obtained for the isomerization carried out in the aggregates of $N^+C_5Ala2C_{14}$ and CTAB are listed in Table 3, and the calculated molar distributions of individual chelate species in the $N^+C_5Ala2C_{14}$ vesicle are shown in Fig. 6 as a function of the Cu^{II} concentration. In a manner as observed for the Cu^{II}-$C_{12}SPM$ system, the fraction of the 2:1 complex is greater than that of the 1:1 complex in a low Cu^{II} concentration range. However, the formation of the 1:1 complex is more facilitated with the terdentate ketimine Schiff-base than with the bidentate $C_{12}SPM$. It is noteworthy that the reactivity of the 2:1 complex is much larger than that of the 1:1 complex in the molecular assemblies of $N^+C_5Ala2C_{14}$ and CTAB, and that the formation of the former species is more pronounced in the $N^+C_5Ala2C_{14}$ vesicle. In order that the isomerization must take place (**2** →**3** in Scheme 2), the hydrogen atom substituted on the carbon atom, interposed between the Schiff-base nitrogen and 4-carbon atom of the pyridine ring, needs to be displaced first. The polarization of the C_4'-H bond of a given Schiff-base chelate is important in facilitating its cleavage. Thus, the effective charge on Cu^{II} must exert much effect on the reactivity. The 2:1 complex, in which the carboxylate group of the ketimine Schiff-base is free from coordination, retains positive charge on Cu^{II} more effectively than the 1:1 complex, in which three coordination sites are occupied with the anionic groups. Such a charge effect provided on Cu^{II} has been also claimed for the β-elimination reaction of *O*-phosphoserine with glyoxylate and copper(II) ions.[16)]

As shown in Fig. 5, the correlation between rate and Cu^{II} concentration observed in the $N^+C_5His2C_{14}$ vesicle is considerably different from those in the molecular aggregates of $N^+C_5Ala2C_{14}$ and CTAB. In the light of the coordination behavior of $C_{12}SPM$ with the copper(II) ion, the primary species in a concentration range of $Cu(ClO_4)_2$ higher than 5.0×10^{-5} mol dm^{-3} must be the 1:1 Cu^{II}-ketimine chelate. However, the observed rate constant reaches a maximum at the Cu^{II} concentration of 5.0×10^{-5} mol dm^{-3} and then falls down gradually as the Cu^{II} concentration increases beyond this range. This rate profile can be understood on the basis of the coordination behavior of the imidazolyl group of $N^+C_5His2C_{14}$ with the copper(II) ion. The coordination interaction of the imidazolyl group with Cu^{II} tends to stabilize the 1:1 Cu^{II}-ketimine chelate since the residual coordination site of Cu^{II} in the 1:1 chelate is occupied with the imidazolyl group and to inhibit the formation of the corresponding 2:1 chelate. In a concentration range of $Cu(ClO_4)_2$ lower than 5.0×10^{-5} mol dm^{-3} where all the copper(II) ions are exclusively coordinated to the ketimine Schiff-base, the isomerization reaction of the Cu^{II}-ketimine chelate is catalyzed by the imidazolyl group free from coordination with the copper(II) ion (Fig. 7). We have already confirmed the catalytic assistance of the imidazolyl group as a general base in the transamination reaction of PLP with *N*-dodecyl-L-alaninamide in the $N^+C_5His2C_{14}$ vesicle.[6)] At higher concentrations of $Cu(ClO_4)_2$ beyond 5.0×10^{-5} mol dm^{-3}, the excess copper(II) ion tends to form the Cu^{II}-imidazole complexes to reduce an amount of the free imidazolyl group. On this ground, the reactivity of the

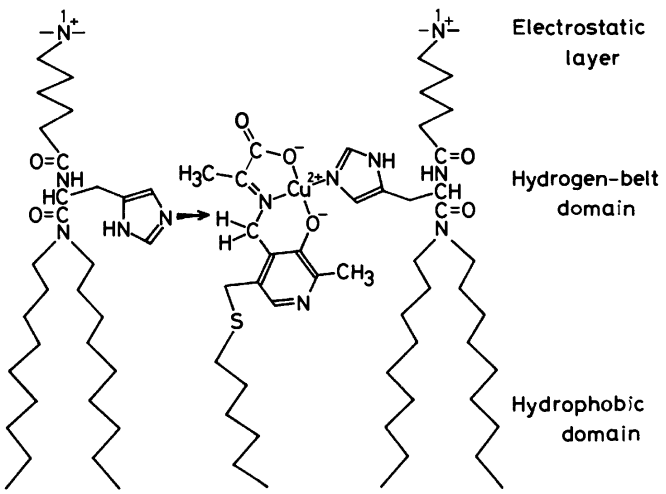

Fig. 7. Schematic representation of the isomerization mechanism for the Cu^{II}-ketimine complex in the $N^+C_5His2C_{14}$ vesicle.

1:1 complex in the $N^+C_5His2C_{14}$ vesicle must be facilitated by the general base catalysis of the metal-free imidazolyl group.

In conclusion, it became apparent that the copper(II)-catalyzed transamination of $C_{12}SPM$ with pyruvate in the cationic vesicles proceeds to give $C_{12}SPL$ and alanine as the final products. The detailed kinetic investigation of the isomerization of the Cu^{II}-ketimine to the corresponding Cu^{II}- aldimine clarified the following aspects. (i) In the bilayer vesicle formed with $N^+C_5Ala2C_{14}$, the formation of the reactive 2:1 (ketimine:Cu^{II}) complex is more favored than in the ordinary cationic micelles. (ii) The bilayer vesicle formed with the amphiphile having the histidyl residue ($N^+C_5His2C_{14}$) allows the formation of the 1:1 complex in preference to that of the 2:1 complex, and the coordination-free imidazolyl group of the amphiphile effectively catalyzes the isomerization as a general base.

The present work was supported in part by Grant-in-Aid for Scientific Research No. 58430016 from the Ministry of Education, Science and Culture.

References

1) E. E. Snell and S. J. Dimari, "The Enzymes," 3rd ed, ed by P. D. Boyer, Academic Press, New York (1970), Vol. 2, Chap. 7; A. E. Braunstein, "The Enzymes," 3rd ed, ed by P. D. Boyer, Academic Press, New York (1973), Vol. 9, Chap. 10.

2) D. E. Metzler, Y. Ikawa, and E. E. Snell, *J. Am. Chem. Soc.*, **76**, 648 (1954); T. C. Bruice and R. M. Topping, *ibid.*, **85**, 1480 (1963); A. E. Martell, "Advances in Enzymology," ed by A. Meister, John Wiley & Sons, New York (1982), Vol. 53, pp. 163—199.

3) Y. Murakami and H. Kondo, *Bull. Chem. Soc. Jpn.*, **48**, 541 (1975); H. Kondo, J. Kikuchi, and J. Sunamoto, *Tetrahedron Lett.*, **1983**, 2403.

4) Y. N. Belokon', V. I. Tararov, T. F. Savel'eva, and V. M. Belikov, *Makromol. Chem.*, **181**, 2183 (1980).

5) R. Breslow, M. Hammond, and M. Lauer, *J. Am. Chem. Soc.*, **102**, 421 (1980); H. Kuzuhara, T. Komatsu, and S. Emoto, *Tetrahedron Lett.*, **1978**, 3563.

6) Y. Murakami, A. Nakano, and K. Akiyoshi, *Bull. Chem. Soc. Jpn.*, **55**, 3004 (1982).

7) Y. Murakami, A. Nakano, A. Yoshimatsu, K. Uchitomi, and Y. Matsuda, *J. Am. Chem. Soc.*, in press.

8) D. E. Metzler and E. E. Snell, *J. Am. Chem. Soc.*, **77**, 2431 (1955).

9) Y. Matsushima and A. E. Martell, *J. Am. Chem. Soc.*, **89**, 1322 (1967).

10) J. Llor and M. Cortijo, *J. Chem. Soc., Perkin Trans. 2*, **1977**, 1111.

11) S. Matsumoto, Y. Karube, and Y. Matsushima, *Chem. Pharm. Bull.*, **23**, 1819 (1975).

12) N. Al-Awadi, M. S. El-Ezaby, and H. Abu-Soûd, *Inorg. Chim. Acta*, **67**, 131 (1982).

13) Y. Murakami, Y. Aoyama, and J. Kikuchi, *J. Chem. Soc., Perkin Trans. 1*, **1981**, 2809.

14) An absorption band appeared in the 620-nm range upon addition of $Cu(ClO_4)_2$ to the $N^+C_5His2C_{14}$ vesicle. This is attributable to the ligand-field band due to the coordinated copper(II) ion. However, quantitative evaluation of the stability constant for the Cu^{II}-$N^+C_5His2C_{14}$ complex was not possible due to insolubility of the complex in aqueous media.

15) Both 2:1 and 1:1 chelate species were assumed to have an identical molar absorption coefficient per aldimine Schiff-base unit in a similar manner as considered for the Cu^{II}-$C_{12}SPM$ complexes.

16) M. S. Mohan and E. H. Abbott, *Inorg. Chem.*, **17**, 3083 (1978).

 © 1984 The Chemical Society of Japan Bull. Chem. Soc. Jpn., 57, 1123—1127 (1984)

Bis(trimethylsilyl) Sulfate Catalysis in γ-Lactonization of Cyclopropanecarboxylates Activated by Carbonyl Substituents on α-Carbon

Yoshitomi MORIZAWA, Tamejiro HIYAMA,*,† Koichiro OSHIMA, and Hitosi NOZAKI
Department of Industrial Chemistry, Kyoto University, Yoshida, Sakyo-ku, Kyoto 606
(Received October 31, 1983)

The title reaction of 1-carbonyl substituted cyclopropanecarboxylates proceeds under C(1)-C(2) bond cleavage to produce γ-lactones. Stereochemically, the reaction takes two pathways: (1) substrates with a cationstabilizing group like vinyl on C(2) give thermodynamically favored γ-lactones having the thermodynamically more stable arrangement of substituents irrespective of the configuration of the cyclopropane substrates, (2) substrates without such a cation-stabilizing group afford γ-lactones under *ca.* 70% inversion at C(2) reaction center.

Organosilicon reagents such as iodotrimethylsilane or cyanotrimethylsilane are silicon version of hydroiodic acid or hydrocyanic acid and exhibit characteristic Lewis acidity of trimethylsilyl silicon as well as remarkably increased nucleophilicity of iodide or cyanide group.[1-4] Among the silylated inorganic acids bis(trimethylsilyl) sulfate (BTS)[5-7] is characterized by its high Lewis acidity and low nucleophilicity, although the synthetic application of this reagent has been limited so far only to silylation of active hydrogen compounds.[8-10] Previous work has been related to the protective tetrahydropyranylation of alcohols as well as the deprotection.[11] We have found that the appropriately activated cyclopropanecarboxylates are readily transformed into γ-butyrolactones in the presence of BTS.[12]

Transformation of Doubly Activated Cyclopropane into γ-Butyrolactones. Treatment of diethyl 2-vinyl-1,1-cyclopropanedicarboxylate[13] (**1**) with BTS in 1,2-dichloroethane produces the γ-butyrolactone **2** in 98% yield. The reaction of dimethyl 2-vinyl-1,1-

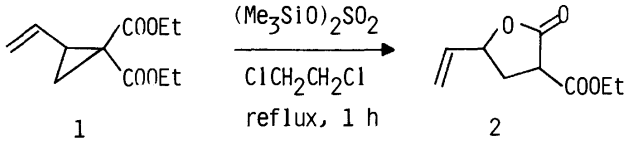

1 2

Scheme 1.

cyclopropanedicarboxylate gave the lactone in a lower yield (46%) after prolonged reaction time (10 h). Other possible product such as ethyl 3-cyclopentene-1,1-dicarboxylate or a seven-membered ring lactone was not detected at all. The BTS catalyst is markedly expedient for this transformation as other Lewis acids induced rearrangement to **3** and/or nucleophilic ring opening leading to **4** at the expence of the yields of **2** as listed in Table 1. Ethyl chrysanthemate, *trans*-2-vinyl-1-(1-oxo-3-phenylpropyl)cyclopropane, and ethyl *trans*-2-phenylcyclopropanecarboxylate did not produce the corresponding γ-lactones. Obviously the *gem*-dicarbonyl substituents on a cyclopropane carbon are required for the lactonization of this kind. Notably, the catalyzed oxavinylcyclopropane rearrangement takes place under mild conditions (40—80 °C) as compared with the purely thermal reaction proceeding at over 280 °C.[14,15]

† Present address: Sagami Chemical Research Center, 4-4-1 Nishiohnuma, Sagamihara, Kanagawa 229.

Extension of the reaction to other cyclopropanecarboxylates are summarized in Table 2. Diethyl *trans*-2-methyl-3-(*cis*-1-propenyl)-1,1-cyclopropanedicarboxylate (**5**) (Scheme 2) was converted into the lactone **6**

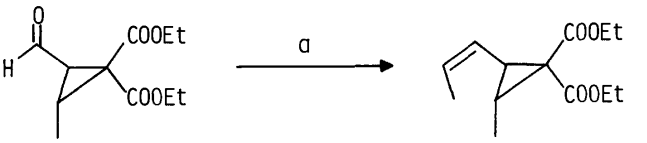

5

a: $Ph_3PCH_2CH_3Br$, n-BuLi.

Scheme 2.

of the depicted stereochemistry. Although the *trans* arrangement of the methyl and 1-propenyl appendages in **5** is retained in the product **6**, the isomerization of the *cis* C=C bond to *trans* is remarkable.[16] Retention of the stereochemistry at the cyclopropane carbon occurs also in the transformation of **7**[17] to the lactone **8**. The structure of **8** is based on ^{1}H-NMR spectral data (J_{ab}=6.7 Hz, J_{bc}=6.7 Hz, J_{bd}=3.1 Hz, J_{be}=9.3 Hz). Examination of the molecular model shows that dihedral angle of H_a-C-C-H_b is almost the same as that of H_b-C-C-H_c with respect to **8**. In contrast the *endo*-propenyl isomer of **8** is incapable of giving such a set of coupling constants. This is consistent with the *exo*-1-propenyl structure of **8**. Similar transformation of **9** gives **10** whose stereochemistry of phenyl substituent is tentatively assigned as *exo* on the basis of similar observations.

On the other hand, however, opposite stereochemistry prevails in the reaction of substrates having no cation-stabilizing substituent like 1-propenyl group. The dihydro derivative **11**[17] was transformed into an 82:18 mixture of the *endo*-propyl lactone **12a** and *exo*-isomer **12b**. The stereochemical assignment is

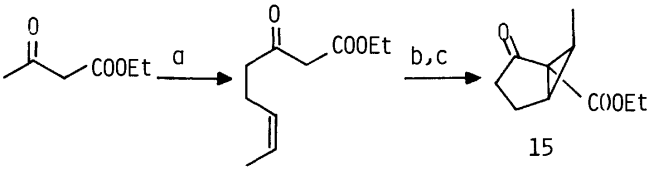

15

a: NaH, n-BuLi, Br

b: p-$CH_3C_6H_4SO_2N_3$, $(C_2H_5)_3N$, c: $Cu(acac)_2$, toluene, reflux.

Scheme 3.

Table 1. Transformation of diethyl 2-vinyl-1, 1-cyclopropanedicarboxylate (**1**) with Lewis acid catalyst

Reagent	Solvent	Temp/°C	Yield[a]/%		
			2	**3**	**4**
$(Me_3SiO)_2SO_2$	$ClCH_2CH_2Cl$	80	98	—	—
H_2SO_4	CH_2Cl_2	25	61	14	—
$Me_3SiOSO_2CF_3$	CH_2Cl_2	25	33[b]	33[b]	—
$Me_3SiOClO_3$[c]	PhH	25	39	—	47 (**4a**, X=Ph)
$Me_3SiOClO_3$	CH_2Cl_2	25	30	36	—
Me_3SiI	CH_2Cl_2	25	—	—	87 (**4b**, X=I)
$BF_3 \cdot OEt_2$	CH_2Cl_2[d]	25	0	0	0
Et_2AlCl-$AgBF_4$	CH_2Cl_2	25	—	48	31 (**4c**, X=Cl)
$TiCl_4$	CH_2Cl_2[e]	25	0	0	0

a) Isolated yield. b) Based on the consumed starting material. c) Prepared from $AgClO_4$ and Me_3SiCl. d) Complex mixture of products. e) Starting material was recovered quantitatively.

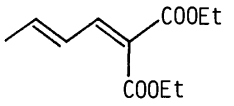

3

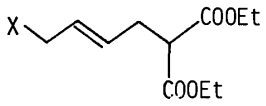

4

Table 2. Transformation of α-carbonyl substituted cyclopropanecarboxylates into γ-butyrolactone with BTS catalyst[a]

Substrate	Temp/°C	Yield/%	Product(s) (ratio)
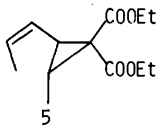 5	40[b]	60(98)[c]	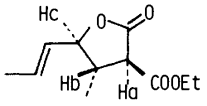 6
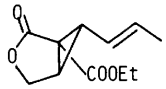 7	80	39[d]	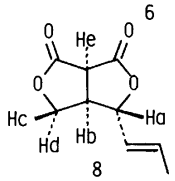 8
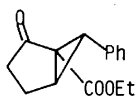 9	80	28[f]	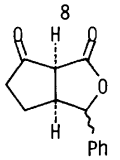 10
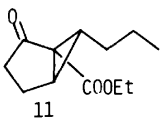 11	80	79[e]	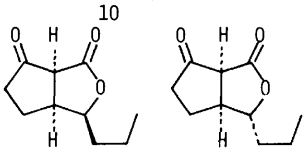 12a (82 : 18) 12b

Substrate	Temp/°C	Yield/%	Product(s) (ratio)
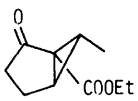 13	80	71	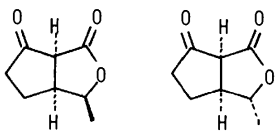 14a (65 : 35) 14b
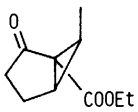 15	80	28[d]	14a (23 : 77) 14b
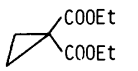 16	80	8(29)[c]	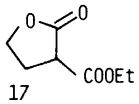 17

a) Typically 1 mol of the substrate was heated in the presence of 2 mol of BTS in 1,2-dichloroethane. b) The reaction was carried out in dichloromethane. c) Based on the consumed starting material. d) Other product was polymeric material ($R_f \simeq 0$ on TLC) only. e) BTS (1 mol) was employed. f) A by-product, ethyl 2-benzyl-5-oxo-1-cyclopentene-1-carboxylate 18 (24%), was formed.

based on the fact that the *endo* hydrogen in the bicyclic system appears at higher field than the *exo* one (see experimental part).[18] Similarly, compound **13**[17] gave a 65:35 mixture of **14a** and **14b**. The somewhat sluggish reaction of the *endo* methyl isomer **15** (Scheme 3) gave the *exo* methyl lactone **14b** predominantly. Thus, the γ-lactonization of **11**, **13**, and **15** mostly accompanies the inversion of the configuration at C(2) center. Thermal vinylcyclopropane-cyclopentene rearrangement (*ca.* 300 °C) proceeds with approximately 70% inversion at the migrating terminus.[19,20] Diethyl 1,1-cyclopropanedicarboxylate (**16**) isomerizes to γ-lactone[21] sluggishly.

Experimental

Distillation was carried out in Kugelrohr (Büchi). All mps and bps were not corrected. All ^{1}H-NMR spectra (tetramethylsilane as an internal standard) were obtained on a Varian EM 390 spectrometer, chemical shifts being given in ppm units. The IR spectra of neat liquid film samples (unless otherwise

noted) were measured on a Shimadzu IR-27G spectrometer, MS on a Hitachi RMU-6L spectrometer, and exact mass on a Hitachi M 80 spectrometer. Preparative TLC plates were prepared with Merck Kiesel-gel PF_{254}. Column chromatography was carried out with silica gel (Wakogel C-100) at atmospheric pressure.

Synthesis of Diethyl trans-*2-Methyl-3-(*cis-*1-propenyl)-1,1-cyclopropanedicarboxylate (5).* Butyllithium (1.44 M** hexane solution 3.2 ml, 4.6 mmol) was added to a THF (10 ml) solution of ethyltriphenylphosphonium bromide (1.70 g, 4.6 mmol) at 0 °C. After stirring for 15 min diethyl 2-formyl-3-methyl-1,1-cyclopropanedicarboxylate[22] (0.70 g, 3.1 mmol) in THF (4 ml) was added at 0 °C and the reaction mixture was stirred for 30 min. Workup followed by column chromatography (hexane–ethyl acetate=20:1) gave **5** (0.39 g, 53% yield): bp 70—75 °C (bath temperature)/0.03 Torr***: ^{1}H-NMR (CCl_4) δ=1.12 (*J*=7.2 Hz, 3H), 1.25 (t, *J*=6.0 Hz, 3H), 1.30 (t, *J*=6.0 Hz, 3H), 1.5—2.3 (m+dd (δ=1.77, *J*=1.5, 6.8 Hz), 4H), 2.38 (t, *J*=8.0 Hz, 1H), 3.9—4.3 (m, 4H), 4.91 (ddd, *J*=8.0, 10.5, 1.5 Hz, 1H), 5.48 (dq, *J*=10.5, 6.8 Hz, 1H); IR 2980, 1730, 1370, 1293, 1207, 1140, 1067 cm^{-1}; MS *m/z* (rel intensity) 241 (M^++1, 5), 240 (M^+, 21), 225 (11), 194 (63), 165 (51), 149 (99), 121 (38), 93 (100), 79 (61). Found: C, 65.18; H, 8.61%. Calcd for $C_{13}H_{20}O_4$: C, 64.98; H, 8.39%.

Synthesis of Ethyl endo-*6-Methyl-2-oxobicyclo[3.1.0]hexane-1-carboxylate (15).* Ethyl acetoacetate (0.52 g, 4.0 mmol) dissolved in THF (5 ml) was added to sodium hydride (60% in oil, 0.19 g, 4.8 mmol) suspended in THF (15 ml) at 0 °C. After 20 min butyllithium (1.70 M hexane solution, 2.6 ml, 4.4 mmol) was added and the reaction mixture was stirred for 20 min at 0 °C. (*Z*)-1-Bromo-2-butene (0.60 g, 4.4 mmol) dissolved in THF (3 ml) was then added and stirred for 45 min. Workup and purification by column chromatography (benzene–ethyl acetate=30:1) gave ethyl (*Z*)-3-oxo-6-octenoate (0.65 g, 89% yield): bp 73 °C (bath temperature)/0.03 Torr; ^{1}H-NMR (CCl_4) δ=1.27 (t, *J*=6.9 Hz, 3H), 1.60 (d, *J*=5.1 Hz, 3H), 2.1—2.7 (m, 4H), 3.27 (s, 2H), 4.10 (q, *J*=6.9 Hz, 2H), 5.1—5.7 (m, 2H); IR 2980, 1745, 1326, 1237, 1032 cm^{-1}; MS *m/z* (rel intensity) 184 (M^+, 17), 166 (5), 112 (47), 97 (71), 69 (79), 55 (100). Found: C, 64.97; H, 8.79%. Calcd for $C_{10}H_{16}O_3$: C, 65.19; H, 8.75%.

The β-keto ester (0.57 g, 3.1 mmol) was converted into the corresponding diazo compound with *p*-toluenesulfonyl azide (0.64 g, 3.2 mmol) and triethylamine (0.49 ml, 3.5 mmol) in acetonitrile (10 ml) (r.t., 4 h). The diazo compound was then heated in toluene (10 ml) with $Cu(acac)_2$ (0.10 g) at reflux for 8 h. Concentration and column chromatography (benzene–ethyl acetate=30:1) gave **15** (0.36 g, 63% yield): bp 105—109 °C (bath temperature)/1 Torr; ^{1}H-NMR (CCl_4) δ=1.17 (d, *J*=6.6 Hz, 3 H), 1.32 (t, *J*=6.9 Hz, 3H), 1.5—2.7 (m, 6H), 4.12 (q, *J*=6.9 Hz, 2H); IR 3000, 1755, 1730 cm^{-1}; MS *m/z* (rel intensity) 183 (M^++1, 10), 182 (M^+, 10), 154 (44), 137 (88), 136 (86), 112 (100), 80 (66), 57 (97). Found: C, 65.88; H, 7.73%. Calcd for $C_{10}H_{14}O_3$: C, 65.92; H, 7.74%.

Synthesis of Ethyl 6-Phenyl-2-oxobicyclo[3.1.0]hexane-1-carboxylate (9). This compound was prepared similarly starting from (*E*)-3-chloro-1-phenyl-1-propene in 68% overall yield: mp 86.0—86.5 °C (hexane, prism); ^{1}H-NMR ($CDCl_3$) δ=0.88 (t, *J*=7.2 Hz, 3H), 2.0—2.5 (m, 4H), 2.90 (d, *J*=5.4 Hz, 1H), 3.1—3.3 (m, 1H), 3.91 (q, *J*=7.2 Hz, 2H), 7.2—7.4 (m, 5H); IR ($CHCl_3$) 2970, 1746, 1724, 1503, 1375, 1348, 1180, 1036 cm^{-1}; MS *m/z* (rel intensity) 245 (M^++1, 7), 244 (M^+, 20), 198 (53), 170 (30), 157 (28), 129 (100), 115 (43), 91 (40). Found: C, 73.82; H, 6.44%. Calcd for $C_{15}H_{16}O_3$: C, 73.75; H, 6.60%.

Transformation of 1 into Ethyl-2-Oxo-5-vinyltetrahydrofuran-3-carboxylate (2). *A Typical Procedure for the Transformation with BTS*: Diethyl 2-vinyl-1,1-cyclopropanedicarboxylate (**1**) (82 mg, 0.4 mmol) dissloved in 1,2-dichloroethane (2 ml) was heated to reflux in the presence of BTS (0.20 g, 0.8 mmol) for 1 h. The reaction mixture was poured into brine (10 ml) and extracted with ethyl acetate (10 ml×3). Column chromatography (silica gel, benzene–ethyl acetate=30:1) gave the γ-butyrolactone (**2**) (70 mg, 98% yield): bp 125—130 °C (bath temperature)/0.06 Torr; ^{1}H-NMR (CCl_4) δ=1.34 (t, *J*=6.9 Hz, 3H), 2.0—2.9 (m, 2H), 3.48 (dd, *J*=9.6, 5.7 Hz, 1H), 4.24 (q, *J*=6.9 Hz, 2H), 4.7—5.2 (m, 1H), 5.2—5.6 (m, 2H), 5.7—6.2 (m, 1H); IR 3000, 1780, 1740, 1162 cm^{-1}; MS *m/z* (rel intensity) 184 (M^+, 3), 183 (2), 155 (18), 137 (51), 110 (100). Found: C, 58.57; H, 6.65%. Calcd for $C_9H_{12}O_4$: C, 58.69; H, 6.57%.

Reaction of Diethyl 2-Vinyl-1,1-cyclopropanedicarboxylate with Sulfuric Acid. The compound **1** (72 mg, 0.34 mmol) dissolved in 1,2-dichloroethane (2 ml) was treated with sulfuric acid (97%, 0.01 ml) at 0 °C for 5 h. Workup and preparative TLC (hexane–ethyl acetate=2:1) gave **2** (R_f 0.40—0.50, 38 mg, 61% yield) and diene **3** (9 mg, 14% yield). The diene **3** gave bp 97 °C (bath temperature)/1 Torr; ^{1}H-NMR (CCl_4) δ=1.29 (t, *J*=6.9 Hz, 3H), 1.32 (t, *J*=6.9 Hz, 3H), 1.91 (d, *J*=6.0 Hz, 3H), 4.16 (q, *J*=6.9 Hz, 2H), 4.20 (q, *J*=6.9 Hz, 2H), 6.17 (dq, *J*=6.0, 15.0 Hz, 1H), 6.50 (dd, *J*=10.5, 15.0 Hz, 1H), 7.11 (d, *J*=10.5 Hz, 1H); IR 2999, 1738, 1728, 1643, 1605, 1240, 1058, 980 cm^{-1}; MS *m/z* (rel intensity) 210 (M^+, 50), 197 (19), 171 (56), 169 (60), 138 (67), 137 (67), 121 (100), 110 (86). Found: *m/z* 212.1054. Calcd for $C_{11}H_{16}O_4$: M, 212.1048.

Reaction of Diethyl 2-Vinyl-1,1-cyclopropanedicarboxylate with Trimethylsilyl Perchlorate. Trimethylsilyl perchlorate was prepared by mixing silver perchlorate (100 mg, 0.48 mmol) and chlorotrimethylsilane (72 mg, 0.48 mmol) in benzene at room temperature for 30 min and filtration of the precipitated salt. To the benzene solution of the catalyst, diethyl 2-vinyl-1,1-cyclopropanedicarboxylate **1** (53 mg, 0.25 mmol) in benzene (2 ml) was added and the mixture was stirred at room temperature for 2 h. Preparative TLC (hexane–ethyl acetate=10:1) gave **2** (18 mg, 39% yield) and **4a** (34 mg, 47% yield). The compound **4a** gave bp 110—113 °C (bath temperature)/0.05 Torr; ^{1}H-NMR (CCl_4) δ=1.23 (t, *J*=7.2 Hz, 4H), 1.24 (t, *J*=7.2 Hz, 2H), 2.4—2.9 (m, 2H), 3.0—3.5 (m, 3H), 4.08 (q, *J*=7.2 Hz, 2.7H), 4.11 (q, *J*=7.2 Hz, 1.3H), 5.3—5.8 (m, 2H), 6.9—7.4 (m, 5H); IR 3000, 1736, 1610, 970, 746, 698 cm^{-1}; MS *m/z* (rel intensity) 291 (M^++1, 1), 290 (M^+, 2), 271 (2), 199 (11), 130 (100), 115 (26), 91 (33). Found: C, 70.59; H, 7.81%. Calcd for $C_{17}H_{22}O_4$: C, 70.32; H, 7.64%.

Reaction of 1 with Iodotrimethylsilane. To diethyl 2-vinyl-1,1-cyclopropanedicarboxylate (0.07 g, 0.33 mmol) dissolved in 1,2-dichloroethane (2 ml), iodotrimethylsilane (0.07 ml, 0.72 mmol) was added at room temperature. The reaction mixture was stirred for 18 h. Column chromatography (silica gel, hexane–ethyl acetate=5:1) gave diethyl (4-iodo-2-butenyl)propanedioate (**4b**) whose structure was assigned spectrometrically (0.10 g, 87% yield): ^{1}H-NMR (CCl_4) δ=1.30 (t, *J*=6.9 Hz, 3H), 2.58 (dd, *J*=6.9, 4.8 Hz, 2H), 3.30 (t, *J*=6.9 Hz, 1H), 3.80 (t, *J*=6.6 Hz, 2H), 4.19 (q, *J*=6.9 Hz, 2H), 5.7—5.9 (m, 2H); IR 3000, 1758, 1738, 1235, 1155, 1035 968 cm^{-1}; MS *m/z* (rel intensity) 249 (14), 213 (M^+−I, 57), 181 (15), 139 (46), 111 (55), 95 (54), 67 (100).

*Ethyl 2-Oxo-5-(*trans-*1-propenyl)tetrahydrofuran-3-carboxylate (6)*: Bp 137—138 °C (bath temperature)/0.055 Torr; ^{1}H-NMR ($CDCl_3$) δ=1.13 (d, *J*=6.0 Hz, 3H), 1.35 (t, *J*=6.9 Hz, 3H), 1.80 (d, *J*=6.3 Hz, 3H), 2.53 (ddq, *J*=6.0, 11.8, 10.4 Hz, 1H, H_b), 3.10 (d, *J*=11.8 Hz, 1H, H_a), 4.24 (q(*J*=6.9 Hz)+dd (H_c), totally 3H), 5.51 (dd, *J*=14.7, 7.2 Hz, 1H), 5.80 (dq, *J*=14.7, 6.3 Hz, 1H); The coupling constant J_{ab}=11.8, J_{bc}=10.4 Hz is consistent to the *trans*-relationship of protons on γ-butyrolactone

** 1 M=1 mol dm^{-1}.

*** 1 Torr=133.322 Pa.

ring.[20] IR 2980, 1782, 1738, 1174, 966 cm^{-1}; MS *m/z* (rel intensity) 213 ($M^+ + 1$, 2), 212 (M^+, 2), 167 (33), 139 (94), 115 (52), 98 (84), 95 (88), 86 (100). Found: C, 62.29; H, 7.72%. Calcd for $C_{11}H_{16}O_4$: C, 62.25; H. 7.60%.

*4-(1-*trans*-Propenyl)-3,7-dioxabicyclo[3.3.0]octane-2,8-dione (8)*: Bp 143—146°C (bath temperature)/0.04 Torr; ^{1}H-NMR (CCl_3) δ=1.85 (d, J=6.3 Hz, 3H), 3.2—3.6 (m, 1H, H_b), 3.73 (d, J=9.3 Hz, 1H, H_e), 4.34 (dd, J=10.3, 3.1 Hz, 1H, H_d), 4.65 (dd, J=10.3, 6.7 Hz, 1H, H_c), 4.83 (dd, J=7.4, 6.7 Hz, 1H, H_a), 5.61 (dd, J=7.4, 15.0 Hz, 1H), 6.06 (dq, J=6.3, 15.0 Hz, 1H); IR 2940, 1800, 1755, 1193, 964 cm^{-1}; MS *m/z* (rel intensity) 183 ($M^+ + 1$, 3), 182 (M^+, 14), 167 (18), 85 (100), 68 (81). Found: C, 59.18; H, 5.53%. Calcd for $C_9H_{10}O_4$: C, 59.33; H, 5.53%.

4-Propyl-3-oxabicyclo[3.3.0]octane-2,8-dione (12): Bp 128—130°C (bath temperature)/0.03 Torr; ^{1}H-NMR (CCl_4) δ=1.01 (t, J=7.6 Hz, 3H), 1.1—2.6 (m, 8H), 2.9—3.4 (m, 1H), 3.4—3.6 (m, 1H), 4.2—4.4 (m, 0.18H), 4.5—4.8 (m, 0.82H); upon irradiation at δ 1.78 the multiplet at δ 4.2—4.4 (ascribed to **12b**) turned into a doublet (J=4.2 Hz) and the one at δ 4.5—4.8 (attributed to **12a**) to a doublet of J=5.0 Hz. IR 2960, 1786, 1738, 1187, 1139 cm^{-1}; MS *m/z* (rel intensity) 183 ($M^+ + 1$, 1), 182 (M^+, 5) 139 (19), 110 (27), 68 (100). Found: C, 65.75; H, 7.90%. Calcd for $C_{10}H_{14}O_3$: C, 65.91; H, 7.74%.

4-Methyl-3-oxabicyclo[3.3.0]octane-2,8-dione (14) Obtained by the Reaction of exo*-6-Methyl-2-oxobicyclo[3.1.0]hexane-1-carboxylate (13)*: Bp 110—115°C (bath temperature)/0.03 Torr; ^{1}H-NMR ($CDCl_3$) δ=1.49 (d, J=6.9 Hz, 3H), 1.8—2.6 (m, 4H), 2.9—3.4 (m, 1H), 3.43 (d, J=7.6 Hz, 0.65H), 3.50 (dd, J=7.8, 1.6 Hz, 0.35H), 4.49 (dq, J=6.3, 4.5 Hz, 0.35H), 4.84 (dq, J=6.3, 5.1 Hz, 0.65H); upon irradiation at δ 1.49 the double of quartet at higher field turned to a doublet (J=4.5 Hz) and the one at lower field to a doublet of J=5.1 Hz. IR 2980, 1784, 1734, 1186, 1140 cm^{-1}; MS *m/z* (rel intensity) 155 ($M^+ + 1$, 12), 154 (M^+, 12), 110 (45), 82 (25), 68 (100). Found: C, 62.07; H, 6.56%. Calcd for $C_8H_{10}O_3$: C, 62.32; H, 6.54%.

4-Methyl-3-oxabicyclo[3.3.0]octane-2,8-dione from endo*-6-Methyl-2-oxobicyclo[3.1.0]hexane-1-carboxylate (15)*: ^{1}H-NMR ($CDCl_3$) δ=1.48 (d, J=6.9 Hz, 3H), 1.6—2.6 (m, 4H), 2.8—3.5 (m + d (δ 3.38, J=8.4 Hz), 1H), 4.2—4.4 (m, 0.77H), 4.4—4.8 (m, 0.23H).

4-Phenyl-3-oxabicyclo[3.3.0]octane-2,8-dione (10): Bp 148—155°C (bath temperature)/0.04 Torr; ^{1}H-NMR (CCl_4) δ=1.9—2.7 (m, 4H), 3.2—3.5 (m + d (δ 3.45, J=7.7 Hz), 2H), 5.23 (d, J=4.2 Hz, 1H), 7.1—7.6 (m, 5H); IR 3030, 2960, 1785, 1748, 1496, 1457, 1163, 699 cm^{-1}; MS *m/z* (rel intensity) 217 ($M^+ + 1$, 5), 216 (M^+, 14), 198 (24), 174 (14), 149 (36), 110 (41), 105 (56), 91 (22), 67 (100). Found: C, 72.46; H, 5.46%. Calcd for $C_{13}H_{12}O_3$: C, 72.21; H, 5.59%.

Financial support by the Nissan kagaku Kogyo Ltd. and the Ministry of Education, Science, and Culture, (Grant-in-Aid for Special Project Research No. 57118006) is acknowledged.

References

1) I. Fleming in "Comprehensive Organic Chemistry", Derek Barton and W. D. Ollis, Pergamon Press, Oxford (1979) Vol. 3, pp. 541—686.

2) E. W. Colvin, "Silicon in Organic Synthesis", Butterworths, London (1981).

3) W. P. Weber, "Silicon for Organic Synthesis", Springer-Verlag, Berlin (1983).

4) K. Utimoto, Y. Wakabayashi, T. Horiie, M. Inoue, Y. Shishiyama, M. Obayashi, and H. Nozaki, *Tetrahedron*, **39**, 967 (1983).

5) W. Patnode and F. C. Schmidt, *J. Am. Chem. Soc.*, **67**, 2272 (1945).

6) N. Duffaut, R. Calas, and J. Dunogues, *Bull. Soc. Chim. Fr.*, **1963**, 512.

7) M. Schmidt and H. Schmidbsur, *Chem. Ber.*, **94**, 2446 (1961).

8) L. H. Sommer, G. T. Kerr, and F. C. Whitmore, *J. Am. Chem. Soc.*, **70**, 445 (1948).

9) W. Kantlehner, E. Hang, and W. W. Mergen, *Synthesis*, **1980**, 460.

10) M. G. Voronkov, V. K. Roman, and E. A. Maletina, *Synthesis*, **1982**, 277.

11) Y. Morizawa, I. Mori, T. Hiyama, and H. Nozaki, *Synthesis*, **1981**, 899.

12) A part of this work was published in a communication form: Y. Morizawa, T. Hiyama, and H. Nozaki, *Tetrahedron Lett.*, **22**, 2297 (1981).

13) K. C. Murdock snd R. B. Angier, *J. Org. Chem.*, **27**, 2395 (1962).

14) D. E. McGreer and J. W. McKinley, *Can. J. Chem.*, **51**, 1487 (1973).

15) Inverse transformation, nemely cyclopropanecarboxylate from γ-butyrolactone, has been recently reported: S. Danishefsky, R. L. Funk, and J. F. Kerwin, Jr., *J. Am. Chem. Soc.*, **102**, 6889 (1980). Transformation of cyclopropanecarboxylate ester into γ-butyrolactone with iodotrimethylsilane also reported: S. P. Brown, B. S. Bal, and H. W. Pinnack, *Tetrahedron Lett.*, **22**, 4891 (1981).

16) Accordingly, we may assume an intermediate which prefers W form of an allylic cation. A recent communication refers to the stereochemistry of alumina-catalyzed oxavinylcyclopropane rearrangement proceeding with retention of the configuration at the migrating terminus. However, the conclusion should be suspended until the specificity is observed with respect to all stereoisomers of the substrate. M. E. Alonso and A. Morales, *J. Org. Chem.*, **45**, 4530 (1980).

17) T. Hiyama, Y. Morizawa, H. Yamamoto, and H. Nozaki, *Bull. Chem. Soc. Jpn.*, **54**, 2151 (1981).

18) a) F. A. Bovey, "NMR Data Table for Organic Compounds," John Wiley and Sons, New York (1967), Vol. 1, pp. 224, 399—445; b) I. Tabushi, K. Fujita, and R. Oda, *Tetrahedron Lett.*, **1967**, 3755.

19) G. D. Andrew and J. E. Baldwin, *J. Am. Chem. Soc.*, **98**, 6705 (1976).

20) Two pathways below stem from the intermediate (iv) and apparently compete each other. When R^2 is propenyl, the path A involving a zwitter ionic intermediate (v) is preferred and cyclizes to give the product (vi) exclusively. As the methyl ester corresponding to **1** reacted reluctantly, liberation of ethyl cation may be crucial at the transformation of v into vi. The substrates without 1-alkenyl group react, in turn, *via* the

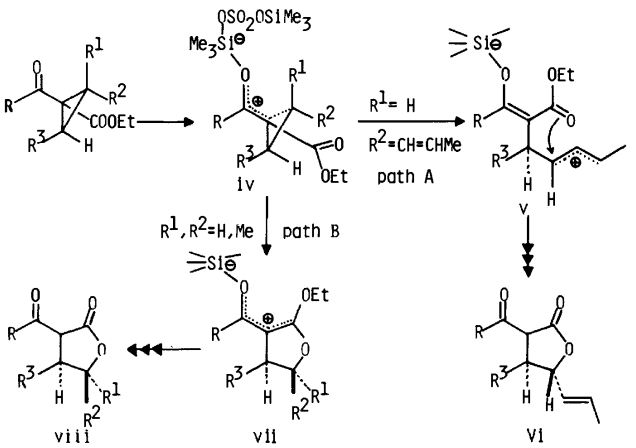

path B to give an intermediate vii which then collapse to the product viii. The intermediacy of pentacoordinate silicon species such as iv, v, and vii seems reasonable in view of such pentacoordinate silicon compounds isolated and well-documented. E. L. Klanberg and E. L. Muetterties, *Inorg. Chem.*, **7**, 155 (1968); F. P. Boer and J. W. Turley, *J. Am. Chem. Soc.*, **91**, 4134 (1969) and references cited therein. L. H. Sommer, "Stereochemistry, Mechanism and Silicon." McGraw-Hill, New York (1965); H. Kwart and K. King, "d-Orbitals in the Chemistry of Silicon, Phosphorus and Sulfur," Springer-Verlag, Heidelberg (1977), p. 149.

21) E. L. Eliel, R. M. Pietrusiewicz, and L. M. Jewell. *Tetrahedron Lett.*, **1979**, 3649.

22) G. Bonavent, M. Gausse, M. Guitard, and R. F.-Jullien, *Bull. Soc. Chim. Fr.*, **1964**, 2462.

23) W. Brugel, "Handbook of NMR Spectral Parameters," Heyden and Son Ltd., London (1979), Vol. 1, p. 245.

Rate and Equilibrium of the Hydration of 1,3-Benzodithiolylium Ion

Tadashi OKUYAMA* and Takayuki FUENO
Faculty of Engineering Science, Osaka University, Toyonaka, Osaka 560
(Received November 12, 1983)

Rates and the equilibrium constant of hydration of 1,3-benzodithiolylium ion were spectrophotometrically measured at 30 °C in aqueous acidic solutions. The hydrate was stable below pH 5 and $pK_R^+ = -0.40$. The cation does not seem to be very stable as compared with the corresponding dithiolanylium ion.

Considerable attention has recently been focused on the chemistry of 1,3-dithiolylium ions[1-3] because of their potential aromaticity and their use in the synthesis of tetrathiafulvalene derivatives. The CMR chemical shifts of the cations were considered to be evidence for the aromaticity by some authors[4,5] while the opposite conclusion was reached from similar results by others.[6] Equilibrium constants of the hydration of some 1,3-dithiolylium ions were measured in 50% ethanol: pK_R^+ of 2-(*p*-methoxyphenyl)-4-phenyl-1,3-dithiolylium ion **1** was found to be 4.11.[7] The saturated dithiolanylium ion **2** has a similar pK_R^+ value (4.1).[8] That is, the π-electonic sextet of the former cation contributes little to its equilibrium stability.

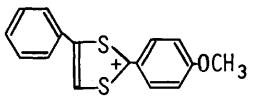

1, $pK_R^+ = 4.11$

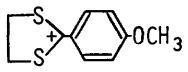

2, $pK_R^+ = 4.1$

In the present study, we have measured pK_R^+ and rates of hydration of an easily available cation, 1,3-benzodithiolylium ion **3**, in order to compare its stability with the dithiolanylium analogue.

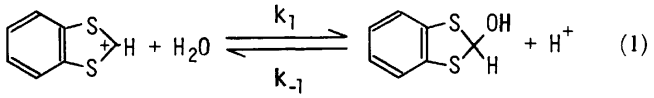

3 **4** (1)

Results

The cation **3** is stable in strong acid, having UV absorption maxima at 238 (log ε 3.65), 253.2 (3.85), 257.5 (3.81), and 308.5 (3.62) nm. On dilution of acid, the absorption at longer wavelength diminishes with formation of a strong absorption at 226.5 nm (log ε 4.49). The spectrum was stable at least for several days in acid solutions and even in unbuffered water (pH≈5). The spectrum at low acidities closely resembles that of 2-isopentyloxy-1,3-benzodithiole which has absorption maximum at 226 nm with log ε 4.42 in aqueous solution. On acidifying strongly the unbuffered solution of **3**, the absorption at 226.5 nm immediately disappears with simultaneous regeneration of the absorption due to the original cation **3**; *i.e.*, the spectrum change is rapid and reversible. The change must be due to the equilibrium between the cation **3** and its hydrate **4** (Eq. 1). The hydrate **4** must be responsible for the absorption at 226.5 nm.

Absorbance changes at 226 and 330 nm (shoulder of the spectrum of **3**) were measured at 30 °C with changing acidity in hydrochloric and perchloric acid solutions. The absorbance changes are plotted against the acidity function H_R[9,10] in Fig. 1, plots following sigmoid curves with $pK_R^+ = -0.40$.

Rates of the absorbance decrease at 226 nm were measured at 30 °C on a stopped-flow spectrophotometer by mixing a stock solution of **4** obtained by dissolving **3** in unbuffered water and an aqueous perchloric acid solution of an appropriate concentration. Results are given in Table 1. Observed pseudo-first-order rate

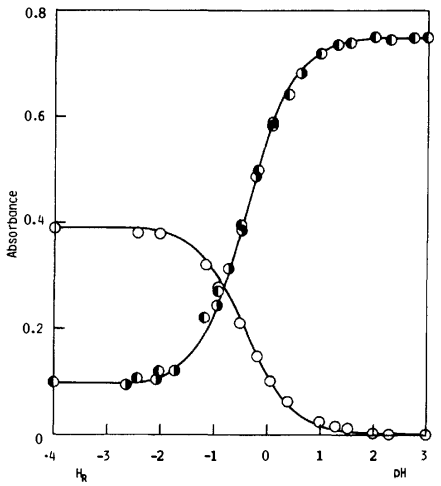

Fig. 1. Absorbance changes measured at 226 nm in HCl (◐) and $HClO_4$ (◑) with the substrate concentration of 2.46×10^{-5} mol dm^{-3} and measured at 330 nm in HCl solutions (○) with the substrate concentration of 1.33×10^{-4} mol dm^{-3}. Solid curves are sigmoid of $pK_R^+ = -0.40$.

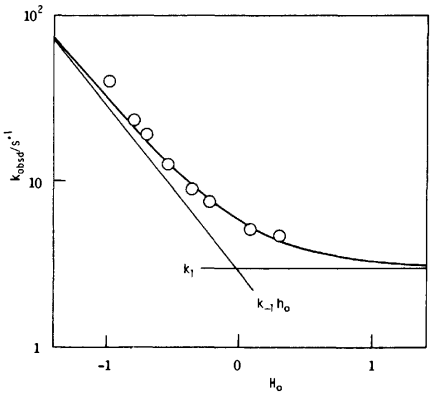

Fig. 2. Plots of log k_{obsd} against H_0. Reaction conditions are given in footnote a of Table 1. The solid curve is calculated with $k_1 = 3.0$ s^{-1} and $k_{-1} = 2.9$ dm^3 mol s^{-1}.

Table 1. Rate constants for reaction 1 at 30 °C

$[HClO_4]$/mol dm^{-3} [a]	k_{obsd}/s^{-1}	[HCl]/mol dm^{-3} [b]	k_{obsd}/s^{-1}
0.391	4.75	1.0×10^{-4}	9.13
0.587	5.20	5.0×10^{-4}	8.75
0.978	7.52	2.5×10^{-3}	9.05
1.174	8.86	5.0×10^{-3}	9.50
1.468	12.8	5.0×10^{-2}	9.18
1.761[c]	19.2	0.25	9.28
1.957[c]	23.5		
2.348[c]	40.0		
2.935[d]	101.9		

a) Rates were measured by the absorbance decrease at 226 nm in aqueous solutions containing 1 vol% of CH_3CN. The initial concentration of the substrate (**4**) was 2.46×10^{-5} mol dm^{-3}. b) Rates were measured by the absorbance decrease at 308 nm in 1 : 1 (v/v) CH_3CN-H_2O of μ=0.25. The initial concentration of the substrate (**3**) was about 1.3×10^{-4} mol dm^{-3}. c) Temperature may slightly higher than 30 °C because of heat of mixing. d) Temperature was about 33 °C owing to heat of mixing.

constants k_{obsd} are plotted logarithmically against the acidity function H_0[9,10] Fig. 2.

Disappearance of **3** was also followed at 308 nm by a stopped-flow mixing of a stock solution of **3** in dry acetonitrile and an aqueous hydrochloric acid solution of the ionic strength of 0.50 maintained with KCl, the resultant reaction solution being 1:1 (v/v) CH_3CN-H_2O of μ=0.25. The rate constant was nearly independent of acid concentration [HCl] over the range 1.0×10^{-4}—0.25 mol dm^{-3} as listed in Table 1.

In alkaline solutions, reactions seemed to be somewhat more complicated. When 30μl of the stock solution of **3** in acetonitrile (2×10^{-3} mol dm^{-3}) was added to 3 ml of a borate buffer (pH=9.1) or aqueous NaOH (0.01 mol dm^{-3}), the solution became usually turbid. However, a clear solution of the same composition was always obtained when the aqueous solution (unbuffered) of **3** containing 2 vol% CH_3CN was mixed with an appropriate alkaline solution. The latter solutions in dilute NaOH (0.01—0.1 mol dm^{-3}) showed an absorption maximum at 243 nm, which disappeared in a few hours. The clear borate buffer solution of **3** had the absorption of 226 nm which gradually changed to the absorption of $\lambda_{max}\approx240$ nm and then disappeared, the final spectrum showing no maximum absorption above 220 nm. These spectral changes did not have any clear isosbestic point.

Discussion

Reaction of the cation **3** with water was previously studied and was found to give dimeric and trimeric products as shown in Eq. 2.[11,12] The reaction was

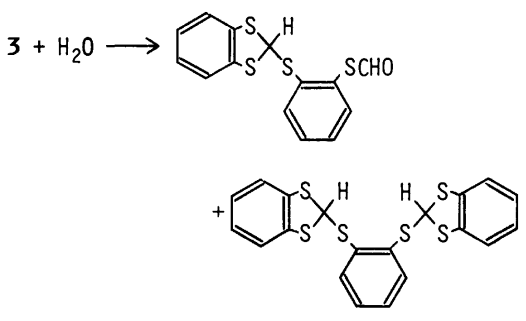

(2)

undertaken in relatively high concentration of **3** and a small amount of water, resulting in polymeric products.

The reaction carried out in very dilute solutions at acidic pH is obviously simple and UV spectral and kinetic behavior conforms with the equilibrium hydration (Eq. 1). Ring-opening reaction of the hydrate **4** must be reversible, if occur, and the equilibrium favors the cyclic structure (**4**).

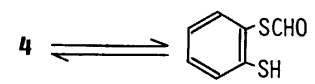

(3)

The reaction seems to proceed further in alkaline solutions, probably to give the ring-open product followed by the hydrolysis of a resultant thioformic acid *S*-ester (Eq. 4). Direct dissolution of a stock solution

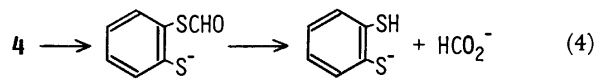

(4)

of **3** in CH_3CN into an aqueous alkaline solution, however, resulted in turbidity probably owing to the polymeric products (Eq. 2). Because of very rapid reaction, the local concentration of **3** may be high in this case. Thus, the reaction in always dilute solution which avoids bimolecular reactions between two substrate molecules is distinctly different from that in higher concentrations. Examination of the products in a preparative sense was impossible in the former mild reaction.

The pK_R+ value of **3** (−0.40) is smaller than that of 4-phenyl-1,3-dithiolylium ion (*ca.* 2)[7,13] but seems to be close to that of dithiolanylium ion.[14] The pK_R+ values of 2-(*p*-methoxyphenyl) derivatives of the unsaturated and saturated cations (**1** and **2**) are also similar to each other[7,8] as mentioned above. Equilibrium stabilities of 1,3-dithiolylium and 1,3-benzodithiolylium ions (relative to their hydrates) are not much greater than the corresponding saturated systems (dithiolanylium ions). The π-electronic sextet of the former cations does not seem to be effective in their stabilization in the above sense.

The rate of disappearance of the cation **3** (9.13 s^{-1} in 1 : 1 (v/v) CH_3CN-H_2O at 30 °C) is about 1/10 of that of 2-methyl-1,3-dithiolanylium ion (88 s^{-1}). That is, the

rate of decay of **3** is smaller but that of formation of **3** (from the hydrate) is greater than that of a similar saturated analogue (since the equilibrium constants are similar).

Kinetic measurements were also carried out in essentially aqueous solutions (containing 1 vol% of CH_3CN) at 30 °C with use of a stock solution of the hydrate **4** in water by following its disappearance to form **3** in acidic solutions. The rate constant k_{obsd} for the reversible reaction (Eq. 1) is the sum of the rate constants for the forward and reverse reactions.

$$k_{obsd} = k_1 a_w + k_{-1} h_0 , \quad (5)$$

where a_w and h_0 stand for the activity of water and the acidity function (10^{-H_0}),[9,10] respectively. The value h_0 corresponds to $[H^+]$ in dilute acid. The value a_w diminishes with acidity but it is not smaller than 0.9 in the present acidity range ($H_0 > -1$); the effect of a_w is small. Thus, rate constants k_{obsd} are logarithmically plotted against H_0[10] in Fig. 2. In the acidity scale of H_0, $H_R = -0.40$ (pK_R^+) corresponds to -0.02,[10] where $k_1 a_w = k_{-1} h_0$. The theoretical curve calculated with $k_1 = 3.0\,s^{-1}$ and $k_{-1} = 2.9\,dm^3\,mol^{-1}s^{-1}$ according to Eq. 5 is shown in Fig. 2. The range of acidity examined was necessarily narrow because of no equilibrium formation of **3** at low acidities and of heat of mixing at high acidities. Upward deviations of the observed points at high acidities may in part be due to the temperature rise on mixing.[16]

The rate of decomposition of **3** (k_1) is 1/3 of that observed in 1 : 1 CH_3CN-H_2O. The enhanced rate in the aqueous organic medium may be ascribed to instability of the cation in the less polar solvent.

Experimental

Materials. 2-Isopentyloxy-1,3-benzodithiole and 1,3-benzodithiolylium (**3**) perchlorate were prepared according to the method of Nakayama.[12] Acetonitrile was distilled from P_2O_5. Glass-distilled water was used throughout the work.

Equilibrium Measurements. Hydrochloric and perchloric acid solutions were prepared from concentrated HCl and 70% $HClO_4$, respectively, and concentrations were determined by titration. A stock solution of **3** was obtained by dissolving a weighed amount of the perchlorate in dry CH_3CN, concentration being usually 2.5×10^{-3} mol dm^{-3}. Into 3.0 ml of acid in a quartz cuvette equilibrated at 30 ± 0.1 °C was introduced 30 μl of the stock solution of **3** from a microsyringe and the absorbance was measured on a Shimadzu UV 200 spectrophotometer. Measurements were made in triplicate under the same conditions and averages are plotted in Fig. 1. Other spectral measurements were carried out in a similar way.

Kinetic Measurements. Rates were measured on a Union RS 1100 stopped-flow spectrophotometer at 30 ± 0.2 °C by mixing the acid solution with a dilute stock solution of **3** in CH_3CN or in aqueous solution (as a form of **4**). The aqueous stock solution was prepared by dissolving 1.0 ml of the stock solution of **3** in CH_3CN into water in a 50 ml volumetric flask. Good pseudo-first-order kinetics were observed over 3 halflives. Averages of 4 or 5 measurements are summarized in Table 1.

The authors thank S. Kawao for the preparation of 2-isopentyloxy-1,3-benzodithiole.

References

1) H. Prinzbach and E. Futterer, *Adv. Heterocycl. Chem.*, **7**, 39 (1966).
2) N. Lozac'h and M. Stavaux, *Adv. Heterocycl. Chem.*, **27**, 151 (1980).
3) R. D. Hamilton and E. Campaine, *Chem. Heterocycl. Compd*, **30**, 271 (1977).
4) G. A. Olah and J. L. Grant, *J. Org. Chem.*, **42**, 13 (1977).
5) K. Sakamoto, N. Nakamura, M. Oki, J. Nakayama, and M. Hoshino, *Chem. Lett.*, **1977**, 1133.
6) U. Timm, U. Plücken, H. Petersen, and H. Meier, *J. Heterocycl. Chem.*, **16**, 1303 (1979).
7) K. Hirai, *Tetrahedron*, **27**, 4003 (1971).
8) T. Okuyama, W. Fujiwara, and T. Fueno, *J. Am. Chem. Soc.*, **106**, 657 (1984).
9) C. H. Rochester, "Acidity Functions," Academic Press, London and New York (1970).
10) A. J. Kresge, H. J. Chen, G. L. Capen, and M. F. Powell, *Can. J. Chem.*, **61**, 249 (1983).
11) D. Buza and J. Szymoniak, *Rocz. Chem.*, **48**, 765 (1974).
12) J. Nakayama, K. Fujiwara, and M. Hoshino, *Bull. Chem. Soc. Jpn*, **49**, 3567 (1976).
13) A. Takamizawa and K. Hirai, *Chem. Pham. Bull.*, **18**, 865 (1970).
14) Our unpublished results show that 2-methyl-1,3-dithiolanylium ion has $pK_R^+ = 0.27$.
15) T. Okuyama, unpublished results.
16) Mixing of 6 mol dm^{-3} $HClO_4$ with water resulted in a temperature rise of 30 to 33 °C. Mixing of 4.7 mol dm^{-3} $HClO_4$ with water, which gives a resultant solution of $H_0 = -1.0$, gave rise to only about 0.5 °C temperature rise.

 © 1984 The Chemical Society of Japan Bull. Chem. Soc. Jpn., 57, 1131—1137 (1984)

Cycloaddition Reactions of Heteroaromatic Thioketones with Maleic Anhydride, Norbornene, Acrylonitrile, Styrene, and 2-Chloroacrylonitrile

Haruo OHMURA and Shinichi MOTOKI*

Department of Chemistry, Faculty of Science, Science University of Tokyo, Kagurazaka, Shinjuku-ku, Tokyo 162

(Received November 18, 1983)

Heteroaromatic thioketones react with maleic anhydride, norbornene, acrylonitrile, and styrene to form the Diels-Alder adducts, respectively. The thioketones also undergo cycloaddition with 2-chloroacrylonitrile followed by elimination of hydrogen chloride to give heteroaromatic analogues of *o*-quinodimethan derivatives. In these reactions, the thioketones act as a heterodiene on the dienophiles to give [4+2]cycloadducts regioselectively.

Recently, it has been found that α,β-unsaturated thiocarbonyl compounds, such as thiochalcone, 2-(arylmethylene)tetralin-1-thione, underwent cycloaddition reactions as reactive heterodienes with various olefins.[1]

On the other hand, the conjugated system made up of an aromatic or heteroaromatic ring and the side chain double bond can react as a diene.[2] For example, styrene has been known to react with dicyanoacetylene in this manner.[3] In 2-vinylfuran or 2-vinylthiophene, two diene systems are present in the molecule but the one involving the side chain is more reactive than heteroaromatic ring toward maleic anhydride.[4] As the heteroaromatic thioketones, aryl 2-furyl thioketones **1** and aryl 2-thienyl thioketones **3**, are relatively stable and readily available, we were interested in their properties as α,β-unsaturated thioketones. Previously, a part of the results of the study was reported.[5]

In the present paper, we wish to describe the detailed results of the cycloaddition reactions of these heteroaromatic thioketones with maleic anhydride, norbornene, acrylonitrile, styrene, and 2-chloroacrylonitrile.

Results and Discussion

1. The Reaction with Maleic Anhydride. The reaction of 2-furyl phenyl thioketone (**1a**) with maleic anhydride gave the cycloadduct **2a**. The structure of **2a** was confirmed by the IR, ^{1}H NMR, and mass spectra and elemental analysis. The IR spectrum of **2a** showed bands at 1860 and 1780 cm^{-1} due to the anhydride linkage. The mass spectrum showed a molecular ion peak at *m/z* 286 and retro Diels-Alder type fragments at *m/z* 188 (thioketone) as base ion peak and *m/z* 98 (maleic anhydride). In the ^{1}H NMR spectrum, the signal at δ 3.80 coupled with H-2, H-3, and H-4 is assigned to H-3a. The double-doublet and doublet at δ 4.05 and 4.24 are assigned to H-4 and H-5, respectively. The two double-doublet at δ 5.72 and 6.76 are assigned to olefinic protons of dihydrofuran ring (H-3 and H-2, respectively). These data and elemental analysis are consistent with the proposed structure **2a**.

2-Furyl mesityl thioketone (**1b**) gave the similar cycloadduct **2b**.

The reaction of aryl 2-thienyl thioketones (**3a**) with maleic anhydride was carried out in refluxing xylene, because the reaction needed prolonged reflux in benzene.

The reaction of phenyl 2-thienyl thioketone (**3a**) with maleic anhydride gave an aromatized cycloadduct **4a**. In the ^{1}H NMR spectrum, the singlet at δ 5.14 is assigned to benzylic proton (H-7). The mass spectrum showed no retro Diels-Alder fragment.

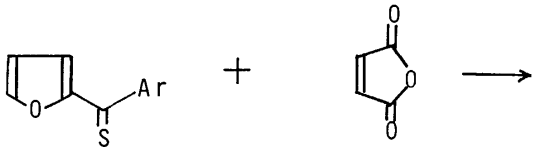

1a, Ar=Phenyl
b, Ar=Mesityl

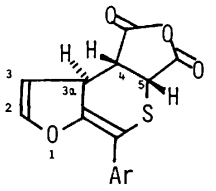

2

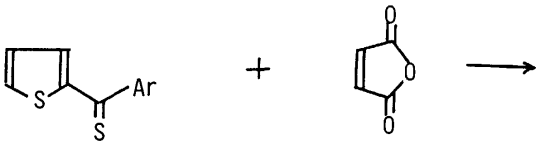

3a, Ar=Phenyl
b, Ar=Mesityl
c, Ar=p-ClC$_6$H$_4$

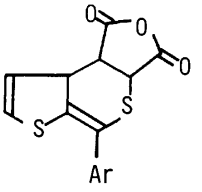

4'

1,3-Shift

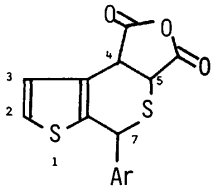

4

TABLE 1. THE REACTION WITH MALEIC ANHYDRIDE

Thioketone	Ar	Product	Reaction time	Solvent	Yield/%	Mp θ_m/°C
1a	Phenyl	**2a**	10 min	Benzene	56	124—125
1b	Mesityl	**2b**	1 h	Benzene	69	134—135
3a	Phenyl	**4a**	4 h	Xylene	12	146—147
3c	*p*-ClC_6H_4	**4c**	8 h	Xylene	18	193—194

TABLE 2. THE REACTION WITH NORBORNENE

Thioketone	Ar	Product	Reaction time	Solvent	Yield/%	Mp θ_m/°C
1a	Phenyl	**5a**	50 min	Benzene	80	122—125
1b	Mesityl	**5b**	2 h	Benzene	76	121—122
3a	Phenyl	**6a**	20 min	Xylene	60	139—142
3b	Mesityl	**6b**	4 h	Xylene	74	158—160
3c	*p*-ClC_6H_4	**6c**	30 min	Xylene	56	120—121

Probably the thioketone reacted with maleic anhydride to give the initial cycloadduct **4a'** which rearranged to aromatized adduct **4a** owing to its tendency to restore the aromatic system.

The reaction of *p*-chlorophenyl 2-thienyl thioketone (**3c**) with maleic anhydride gave a similar aromatized product **4c**. The results are presented in Table 1.

2. The Reaction with Norbornene. The reaction of 2-furyl phenyl thioketone (**1a**) with norbornene gave the cycloadduct **5a**. The IR spectrum of **5a** showed bands at 2960(C-H), 2880(C-H), and 1650(C=C) cm^{-1}. The mass spectrum showed ion peak at *m/z* 282 as parent ion peak and retro Diels-Alder fragment at *m/z* 188 (thioketone) as base ion peak. The ^1H NMR spectrum showed two multiplets at δ 1.08—1.76 and 2.00—2.36 for the signals of aliphatic protons in norbornane moiety, and a double-doublet at δ 2.78 and a double-double-doublet at δ 3.26 ($J_{9,10}$=10.0, $J_{8,9}$=2.1, and $J_{7,9}$=1.5 Hz) for H-2 and H-9, respectively. Two double-doublet at δ 5.52 and 6.64 are assigned to olefinic protons of H-8 and H-7, respectively.

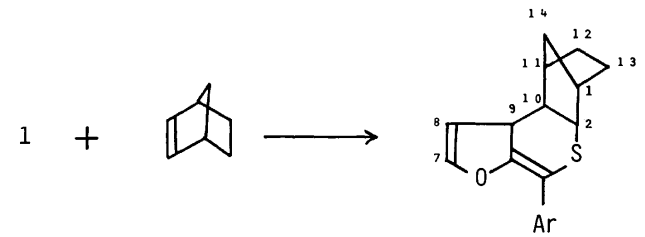

5

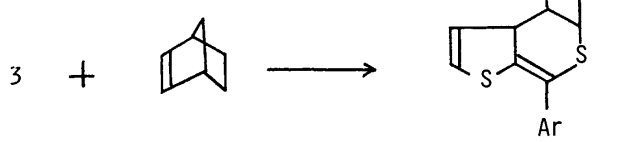

6

The reaction of 2-furyl mesityl thioketone (**1b**), aryl 2-thienyl thioketones **3a**, **3b**, and **3c** with norbornene gave similar cycloadducts **5b**, **6a**, **6b**, and **6c**, respectively. The structures were confirmed on the basis of the spectral data. The results are presented in Table 2.

3. The Reaction with Acrylonitrile and Styrene. The reaction of heteroaromatic thioketone with acrylonitrile or styrene gave the sole regioisomeric adduct.

The reaction of 2-furyl mesityl thioketone (**1b**) with acrylonitrile gave the adduct **7b**. In the ^1H NMR spectra of **7b**, the signals of H-2, H-3, and H-4,5 appeared at δ 6.54, 5.50, and 2.52—3.12 and the splitting pattern of H-3a signal ($J_{3a,4}$=10.4, $J_{3,3a}$=2.5, and $J_{2,3a}$=2.1 Hz) was similar to that of H-9 in **5**. These results are consistent with the structure **7b** rather than that of its regioisomer. Besides the adduct **7b**, the stereoisomer **7b'** with respect to H-3a and H-4 ($J_{3a,4}\approx$2 Hz) was separated by column chromatography.

The reaction of 2-furyl phenyl thioketone (**1a**) with acrylonitrile gave 1,3-rearranged product **8a**. The mass spectrum of **8a** showed an ion peak at *m/z* 241 as parent ion peak. In the ^1H NMR spectrum, the multiplet at δ 3.00—3.12 and the double-doublet at δ 4.06 are assigned to H-5 and H-4, respectively. Presence of the singlet at δ 5.00 assignable to H-7 evidently indicates that the product is not the initial adduct **7a** but its rearranged compound **8a**.

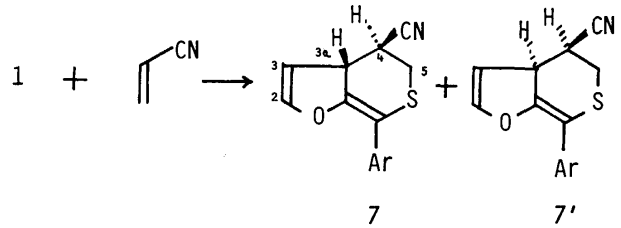

7 7'

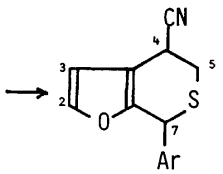

8

The reaction of mesityl 2-thienyl thioketone (**3b**) with acrylonitrile gave two stereoisomeric adducts **9b** and **9b'**.

Aromatization of the initial adduct was also observed in the reaction of phenyl 2-thienyl thioketone (**3a**) with acrylonitrile. In this case, the product **10** were separated into two stereoisomers. The ^1H NMR spectra of these

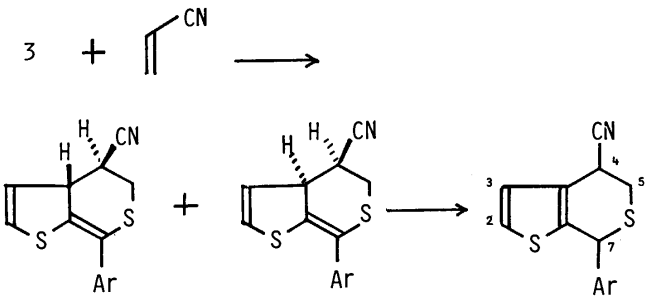

9 9′ 10

isomers showed a singlet at δ 5.20 and 5.25 for the benzylic proton (H-7), respectively. Differences in the ^{13}C NMR spectra were also observed obviously.

When the reaction of 2-furyl mesityl thioketone (**1b**) with styrene was carried out similarly, a [4+2]-cycloadduct **11b** was obtained. The reaction of aryl 2-thienyl thioketones **3a** and **3c** with styrene gave mixture of the aromatized products **12a** and **12a′**, and of **12c** and **12c′**, respectively. All attempts to isolate two isomers were unsuccessful. In the ^1H NMR spectra, two sets of signals were observed. This indicates that the product is a mixture of stereoisomers, the ratio of which was determined by intensity ratio of the two signals for benzylic proton (1 : 1).

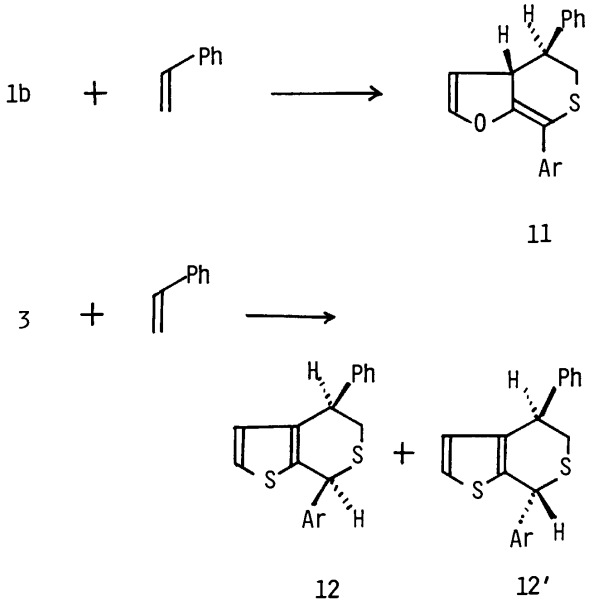

11

12 12′

4. Stereoisomer in the Products. It is possible to consider two diastereomers in the products **7**, **9**, and **11** with respect to each two asymmetric carbon atoms C-3a and C-4 [Type **A**]. The products actually obtained are classified into two groups, those having large coupling constants ($J_{3a,4}$=10.0, 10.4, and 10.4 Hz for **7b**, **9b**, and **11b**, respectively) and those having small coupling constants ($J_{3a,4}\approx$2 and 2.3 Hz for **7b′** and **9b′**, respectively) between H-3a and H-4 in the ^1H NMR spectra. The large J value indicates[6] 3a-4 trans configuration (axial-axial) as represented by the structure $\mathbf{A}_1$ (or its enantiomer) and the small J value indicates 3a—4 cis configuration (structure $\mathbf{A}_2$, axial-equatrial).[7] It can be seen from Table 3 that the cis isomers are preferentially produced in the reaction with acrylonitrile.

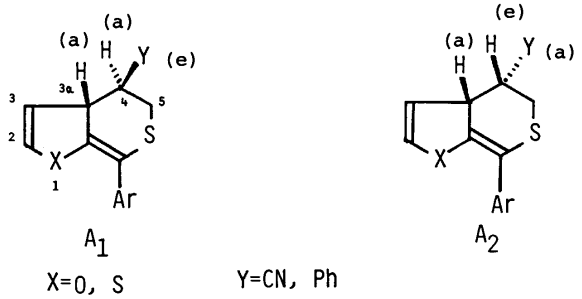

A_1 A_2

X=O, S Y=CN, Ph

The products **5** and **6** have each five asymmetric carbon atoms C-1, C-2, C-9, C-10, and C-11 [Type **B**]. However, H-2, H-10 and H-1, H-11 are undoubtedly in cis relationship to each other.[8] Therfore, only four diastereomers are possible in these adducts. All the compounds of Type **B** obtained in the present study had large coupling constant ($J_{9,10}\approx$10 Hz) between H-9 and H-10 which indicates 9-10 trans configuration (structure $\mathbf{B}_1$ or $\mathbf{B}_2$, axial-axial). Chemical shift in the ^{13}C NMR spectra of the bridged carbon (C-14) of norbornane moiety suggests that the product probably has exo configuration ($\mathbf{B}_2$) rather than endo one ($\mathbf{B}_1$).[9]

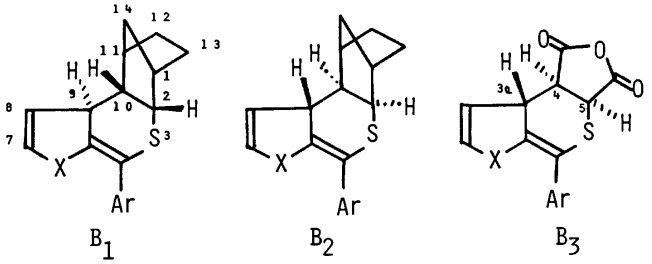

B_1 B_2 B_3

X=O, S

Table 3. The reaction with acrylonitrile

Thioketone	Ar	Product	Reaction time[a]	Yield/%	Mp θ_m/°C
1a	Phenyl	**8a**	30 min	67	133—135
1b	Mesityl	**7b**	30 min	5	158—160
		7b′		80	130—132
3a	Phenyl	**10a**[b]	3 h	36	119—122
		10a′		37	150—153
3b	Mesityl	**9b**	6 h	18	129—130
		9b′		79	194—195

a) The reactions were carried out in refluxing dry benzene. b) As a matter of convenience, the stereoisomeric adducts are represented in this way. However, it is difficult to distinguish clearly between these stereoisomers **10a** and **10a′**.

Table 4. The reaction with styrene

Thioketone	Ar	Product	Reaction time[a]/h	Yield/%	Mp θ_m/°C
1b	Mesityl	**11b**	9	40	144—146
3a	Phenyl	**12a, 12a'**	1	15	—
3c	*p*-ClC_6H_4	**12c, 12c'**	4	17	—

a) The reactions were carried out in refluxing dry benzene.

Table 5. The reaction with 2-chloroacrylonitrile

Thioketone	Product	Reaction time[a]/min	Yield/%	Mp θ_m/°C	IR ν(CN)/cm^{-1}	^{13}C NMR δ C-4
1a	**14a**	10	56	85—87	2190	76.5
1b	**14b**	20	60	135—136	2190	74.6
3a	**16a**	60	63	103—105	2190	80.2
3b	**16b**	120	76	156—158	2190	79.1
3c	**16c**	60	69	165—166	2200	80.8

a) The reactions were carried out in refluxing dry benzene.

The adduct with maleic anhydride **2** was found to have 3a-4 trans, 4-5 cis configuration (**B_3**).

5. The Reaction with 2-Chloroacrylonitrile. The cycloaddition reactions of aryl 2-furyl thioketones **1** or aryl 2-thienyl thioketones **3** with 2-chloroacrylonitrile in refluxing benzene gave an unstable adduct **13** or **15**. As these adducts readily eliminate hydrogen chloride, attempt to isolate them in a pure form was unsuccesful. However, when triethylamine was added to the reaction mixture, the color of the solution turned immediately from yellow to deep red and triethylamine hydrochloride was precipitated. Column chromatography of the mixture gave *o*-quinodimethan-type derivatives of furan and thiophene **14** or **16** as stable red crystals.

The IR spectra of **14** or **16** showed an intense absorption at 2190—2200 cm^{-1} due to the cyano group and the ^1H NMR spectra showed the singlet at δ 3.68—3.78 for methylene protons (H-5). In the ^{13}C NMR spectra, the C-4 signal is unusually upfield from the one in ordinary olefinic carbons. This suggests a considerable contribution of zwitter ionic structure such as **II** or **III** to the resonance state of **14** or **16**.

In general, *o*-quinodimethans are generated by flash-vacuum thermolysis[10] or by 1,4-elimination from the ammonium salt.[11] Furo[3,4-*c*]pyridine (**17**), 2,3-dimethylene-2,3-dihydrofuran (**18**),[12] and 2,3-dimethyleneindolin (**19**)[11] are the example of heteroaromatic *o*-quinodimethans. However, all of these compounds are unstable and are isolated only as their dimer or can be trapped by suitable capture. High stabilities of **14** and **16** are presumably ascribed to

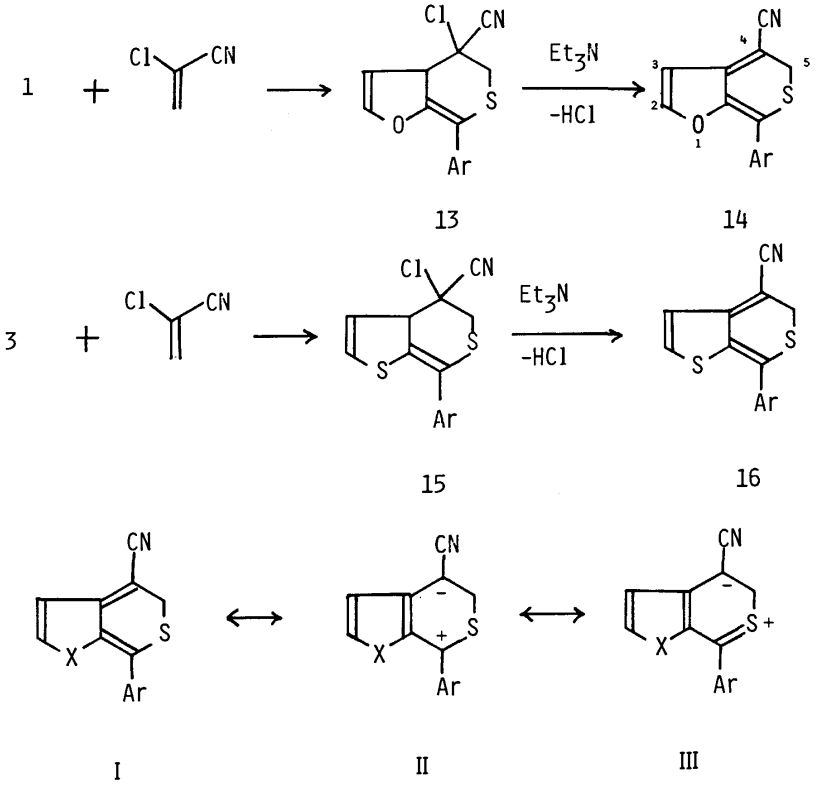

the electron-withdrawing effect of cyano group and electron-releasing effect of sulfur atom.

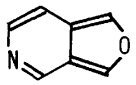
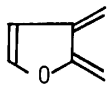
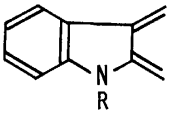

17 18 19

6. Summary. In heteroaromatic thioketones, thiocarbonyl group conjugated with ring double bond reacted preferentially as a diene. The reactivity of these thioketones was in agreement with the extent of the aromaticity of the furan and thiophene ring as expected. Regioselectivity of the reaction of heteroaromatic thioketones agreed with those of previously reported α,β-unsaturated thioketones.[1] It is found that the adduct obtained from mesityl 2-furyl or 2-thienyl thioketones do not tend to undergo 1,3-hydrogen shift.

Experimental

All the melting points are uncorrected. The IR spectra were determined on a Hitachi Model 260-10 infrared spectrometer. The ^{1}H NMR and ^{13}C NMR spectra were recorded on a JEOL JNM-FX 100 spectrometer using Me_4Si as internal standard at 100 MHz or 25 MHz, respectively. The mass spectra were recorded on a Hitachi double-focusing mass spectrometer RMU-7M operating at an ionizing potential of 70 eV. Silica gel (Wako gel C-200) was used for column chromatography.

Heteroaromatic thioketones **1** or **3** were prepared by the reaction of the corresponding ketone and Lawesson reagent [2,4-bis(4-methoxyphenyl)-1,3,2,4-dithiadiphosphetane 2,4-disulfide][13] or P_4S_{10}.[14] The thioketones were purified by column chromatography on Florisil gel (100—200 mesh) using dichloromethane-hexane (1:4) as eluent. 2-furyl phenyl thioketone (**1a**): blue liquid; 2-furyl mesityl thioketone (**1b**): blue liquid; phenyl 2-thienyl thioketone (**3a**): blue liquid (lit,[15] blue liquid); mesityl 2-thienyl thioketone (**3b**): blue liquid; *p*-chlorophenyl 2-thienyl thioketone (**3c**): deep green needles, mp 61—62 °C (lit,[15] mp 63 °C).

Cycloaddition Reaction of Heteroaromatic Thioketone with Dienophile. General Procedure: A solution of the thioketone (5 mmol) and dienophile (5 mmol or slightly excess) in dry benzene or xylene (5 cm^3) was refluxed under a nitrogen atmosphere until all the thioketone was consumed as indicated by TLC. The solvent was evaporated and the residue was recrystallized directly or chromatographed on silica gel to give the cycloadduct.

*7-Phenyl-3a,4-dihydro-5H-thiopyrano[3,4-b]furan-4,5-dicarboxylic Anhydride (**2a**)*: Colorless needles (from benzene-hexane) IR (KBr) 1860 (C=O) and 1780 (C=O) cm^{-1}; ^{1}H NMR ($CDCl_3$) δ=3.80(ddd, J=6.6, 2.2, and 2.2 Hz, 1H), 4.05(dd, J=9.6 and 6.6 Hz, 1H), 4.24 (d, J=9.6 Hz, 1H), 5.72 (dd, J=2.5 and 2.2 Hz, 1H), 6.76 (dd, J=2.5 and 2.2 Hz, 1H), 7.12—7.40 (m, 3H), and 7.60—7.76 (m, 2H); MS m/z (rel intensity) 286 (M$^+$, 8), 188 (thioketone, 100), 160(9), 155(10), and 98 (maleic anhydride, 7). Found: C, 62.92; H, 3.54; S, 11.26%. Calcd for $C_{15}H_{10}O_4S$: C, 62.93; H, 3.52; S, 11.20%.

*7-Mesityl-3a,4-dihydro-5H-thiopyrano[3,4-b]furan-4,5-dicarboxylic Anhydride (**2b**)*: Chromatographed by eluting with benzene; colorless crystals (from benzene-hexane); IR (KBr) 3120, 2980, 1880 (C=O), and 1790 (C=O) cm^{-1}; ^{1}H NMR ($CDCl_3$) δ=2.16 (s, 6H), 2.28 (s, 3H), 3.12 (dd, J=12.0 and 12.0 Hz, 1H), 3.66 (ddd, J=12.0, 3.0, and 2.5 Hz, 1H), 4.20 (d, J=12.0 Hz, 1H), 5.78 (dd, J=3.0 and 3.0 Hz, 1H), 6.68 (dd, J=3.0 and 2.5 Hz, 1H), and 6.84 (broad s, 2H); MS m/z (rel intensity) 328 (M$^+$, 21), 255 (51), 230 (thioketone, 100), 213 (58), 197 (51), and 169 (46). Found: C, 66.10; H, 4.99; S, 9.76%. Calcd for $C_{18}H_{16}O_4S$: C, 65.84; H, 4.91; S, 9.76%.

*7-Phenyl-4,5-dihydro-7H-thieno[2,3-c]thiopyran-4,5-dicarboxylic Anhydride (**4a**)*: Chromatographed by eluting with benzene-hexane (1:1); slightly yellow crystals (from ligroin); IR(KBr) 1870 (C=O) and 1790 (C=O) cm^{-1}; ^{1}H NMR($CDCl_3$) δ=4.48 (d, J=8.5 Hz, 1H), 4.62(dd, J=8.5 and 1.0 Hz, 1H), 5.14(s, 1H), 7.20(broad s, 2H), and 7.31(broad s, 5H); MS m/z (rel intensity) 302(M$^+$, 44), 229(74), 203(14), and 153(100). Found: C, 59.58; H, 3.27; S, 21.05%. Calcd for $C_{15}H_{10}O_3S_2$: C, 59.59; H, 3.33; S, 21.21%.

*7-(p-Chlorophenyl)-4,5-dihydro-7H-thieno[2,3-c]thiopyran-4,5-dicarboxylic Anhydride (**4c**)*: Chromatographed by eluting with benzene; purple crystals (from benzene-hexane); IR(KBr) 1870 (C=O) and 1790 (C=O) cm^{-1}; ^{1}H NMR($CDCl_3$) δ=4.56(d, J=1.0 Hz, 2H), 5.28(s, 1H), and 7.04—7.34(m, 6H); MS m/z (rel intensity) 338(M$^+$, 12), 336(M$^+$, 29), 308(5), 263(54), and 153(100). Found: C, 53.52; H, 2.62; S, 18.59%. Calcd for $C_{15}H_9O_3S_2Cl$: C, 53.49; H, 2.69; S, 19.04%.

*exo-4-Phenyl-6-oxa-3-thiatetracyclo[9.2.1.0^{2,10}.0^{5,9}]tetradeca-4,7-diene (**5a**)*: Chromatographed by eluting with benzene; red crystals (from ethanol); IR(KBr) 2960, 2880, and 1650 cm^{-1}; ^{1}H NMR($CDCl_3$) δ=1.08—1.76(m, 6H), 2.00—2.36(m, 3H), 2.78(dd, J=8.2 and 1.5 Hz, 1H), 3.26(ddd, J=10.0, 2.1, and 1.5 Hz, 1H), 5.52(dd, J=2.1 Hz, 1H), 6.64(dd, J=2.1 and 1.5 Hz, 1H), 7.00—7.36(m, 4H), and 7.68—7.84(m, 1H); MS m/z (rel intensity) 282(M$^+$, 28), 188(thioketone, 100), and 187(48). Found: C, 76.48; H, 6.40; S, 11.20%. Calcd for $C_{18}H_{18}OS$: C, 76.56; H, 6.42; S, 11.35%.

*exo-4-Mesityl-6-oxa-3-thiatetracyclo[9.2.1.0^{2,10}.0^{5,9}]tetradeca-4,7-diene (**5b**)*: Slightly yellow crystals (from ethanol); IR(KBr) 3120, 2950, 2870 and 1680 cm^{-1}. ^{1}H NMR($CDCl_3$) δ=1.10—1.84(m, 6H), 2.04—2.28(m, 2H), 2.20(s, 6H), 2.27(s, 3H), 2.37(broad s, 1H), 2.88(dd, J=8.2 and 1.1 Hz, 1H), 3.20(dd, J=10.0 and 2.2 Hz, 1H), 5.46(dd, J=2.2 and 2.2 Hz, 1H), 6.50(dd, J=2.2 and 1.6 Hz, 1H), and 6.80(broad s, 2H); MS m/z (rel intensity) 324(M$^+$, 55), 283(4), 230(thioketone, 100), 213(61), 202(30), 197(53), and 169(25). Found: C, 77.71; H, 7.43; S, 9.76%. Calcd for $C_{21}H_{24}OS$: C, 77.73; H, 7.46; S, 9.88%.

*exo-4-Phenyl-3,6-dithiatetracyclo[9.2.1.0^{2,10}.0^{5,9}]tetradeca-4,7-diene (**6a**)*: Chromatographed by eluting with benzene-ligroin (1:1); yellow crystals (from benzene-hexane); IR (KBr) 3060, 3010, 2960, 2880, 1640, and 1600 cm^{-1}; ^{1}H NMR($CDCl_3$) δ=1.05—1.78(m, 6H), 2.10—2.34 (m, 2H), 2.41 (broad s, 1H), 2.76(dd, J=8.2 and 1.1 Hz, 1H), 3.43(ddd, J=10.0, 2.8, and 1.8 Hz, 1H), 5.95(dd, J=9.0 and 2.8 Hz, 1H), 6.32(dd, J=9.0 and 1.8 Hz, 1H), and 7.02—7.68 (m, 5H); MS m/z (rel intensity) 298(M$^+$, 100), 265(69), and 204(92). Found: C, 72.32; H, 6.11; S, 21.63%. Calcd for $C_{18}H_{18}S_2$: C, 72.44; H, 6.08; S, 21.48%.

*exo-4-Mesityl-3,6-dithiatetracyclo[9.2.1.0^{2,10}.0^{5,9}]tetradeca-4,7-diene (**6b**)*: Chromatographed by eluting with benzene-hexane (1:2); slightly yellow needles (from benzene-hexane); IR(KBr) 3070, 2945, 2870, 1605, and 1570 cm^{-1}; ^{1}H NMR($CDCl_3$) δ=1.32—1.86(m, 6H), 2.00—2.32(2H), 2.19(s, 6H), 2.26(s, 3H), 2.44(broad s, 1H), 2.84(dd, J=8.0 and 1.4 Hz, 1H), 3.35(ddd, J=10.4, 2.2, and 2.0 Hz, 1H), 5.90 (dd, J=8.0 and 2.2 Hz, 1H), 6.26(dd, J=8.0 and 2.0 Hz, 1H), and 6.80(broad s, 2H); MS m/z (rel intensity) 340(M$^+$, 47), 246(thioketone, 100), 213(84), and 198(27). Found: C, 73.98; H, 7.22; S, 18.92%. Calcd for $C_{21}H_{24}S_2$: C, 74.07; H, 7.10; S, 18.83%.

*exo-4-(p-Chlorophenyl)-3,6-dithiatetracyclo[9.2.1.0^{2,10}.0^{5,9}]-tetradeca-4,7-diene (**6c**)*: Chromatographed by eluting with benzene; red crystals (from ethanol); IR(KBr) 3060, 2960, 2890, 1595, 1490, and 1095 cm^{-1}; ^{1}H NMR($CDCl_3$) δ=1.12—1.76(m, 6H), 2.12—2.48 (m, 3H), 2.76(dd, J=8.0 and 1.0 Hz,

1H), 3.45(ddd, J=10.0, 2.5, and 1.5 Hz, 1H), 5.96(dd, J=6.0 and 2.5 Hz, 1H), 6.32(dd, J=6.0 and 1.5 Hz, 1H), 7.16—7.30(m, 2H), and 7.48—7.64(m, 2H); MS m/z (rel intensity) 334(M^+, 12), 332(28), 240(43), 238(thioketone, 100), 205(35), and 127(21). Found: C, 64.82; H, 5.16; S, 19.43%. Calcd for $C_{18}H_{17}S_2Cl$: C, 64.94; H, 5.15; S, 19.26%.

trans-*4-Cyano-7-mesityl-3a,4-dihydro-5H-thiopyrano[3,4-b]furan (7b)*: Chromatographed by eluting with benzene-hexane (2:3); orange crystals (from ethanol); IR(KBr) 3100, 2910, 2840, 2225(CN), 1680, 1610, and 1140 cm^{-1}; ^1H NMR($CDCl_3$) δ=2.22(s, 3H), 2.25 (s, 6H), 2.52—3.12(m, 3H), 3.72(ddd, J=10.4, 2.5, and 2.1 Hz, 1H), 5.50(dd, J=2.8 and 2.5 Hz, 1H), 6.54(dd, J=2.8 and 2.1 Hz, 1H), and 6.84(broad s, 1H); MS m/z (rel intensity) 283(M^+, 64), 230(88), 213(100), 202(46), 197(97), and 169(69). Found: C, 72.36; H, 6.27; N, 4.90; S, 11.52%. Calcd for $C_{17}H_{17}NOS$: C, 72.05; H, 6.05; N, 4.94; S, 11.31%.

cis-*4-Cyano-7-mesityl-3a,4-dihydro-5H-thiopyrano[3,4-b]furan (7b')*: Slightly yellow crystals (from ethanol); IR(KBr) 3100, 2975, 2925, 2850, 2225(CN), 1700, and 1610 cm^{-1}; ^1H NMR($CDCl_3$) δ=2.27(s, 6H), 2.36(s, 3H), 2.85—3.25(m, 2H), 3.58—3.75(m, $J\approx$2 Hz, 2H), 5.30(dd, J=3.0 and 2.1 Hz, 1H), 6.60(dd, J=3.0 and 2.0 Hz, 1H), and 6.85(broad s, 1H); MS m/z (rel intensity) 283(M^+, 65), 230(thioketone, 100), 213(97), 202(42), 197(92), and 169(100). Found: C, 72.16; H, 5.88; N, 4.93; S, 11.58%. Calcd for $C_{17}H_{17}NOS$: C, 72.05; H, 6.05; N, 4.94; S, 11.31%.

4-Cyano-7-phenyl-4,5-dihydro-7H-thiopyrano[3,4-b]furan (8a): Colorless needles (from ethanol); IR(KBr) 3140(furan ring), 3060, 3025, 2950, 2250(CN), and 1600 cm^{-1}; ^1H NMR($CDCl_3$) δ=3.00—3.12(m, 2H), 4.06(dd, J=7.5 and 5.7 Hz, 1H), 5.00(s, 1H), 6.47(d, J=1.4 Hz, 1H), and 7.04—7.40(m, 6H); MS m/z (rel intensity) 241(M^+, 100), 213(7), 195(21), 188(19), 187(42), 183(M^+−CN−S, 21), and 167(183−O, 36). Found: C, 69.38; H, 4.37; N, 5.95; S, 13.26%. Calcd for $C_{14}H_{11}NOS$: C, 69.69; H, 4.60; N, 5.80; S, 13.29%.

trans-*4-Cyano-7-mesityl-3a,4-dihydro-5H-thieno[2,3-c]thiopyran (9b)*: Chromatographed by eluting with dichloromethane-hexane (2:3); orange crystals (from ethanol); IR(KBr) 3060, 2920, 2250(CN), 1610, 1535, and 860 cm^{-1}; ^1H NMR($CDCl_3$) δ=2.20(s, 3H), 2.24(s, 6H), 2.65—3.46(m, 3H), 3.95(ddd, J=10.7, 2.6, and 2.6 Hz, 1H), 5.86(dd, J=6.3 and 2.6 Hz, 1H), 6.32(dd, J=6.3 and 2.6 Hz, 1H), and 6.83(broad s, 2H); MS m/z (rel intensity) 299(M^+, 58), 264(16), 246(thioketone, 64), 213(100), and 198(23). Found: C, 68.22; H, 5.72; N, 4.73; S, 21.20%. Calcd for $C_{17}H_{17}NS_2$: C, 68.19; H, 5.72; N, 4.68; S, 21.41%.

cis-*4-Cyano-7-mesityl-3a,4-dihydro-5H-thieno[2,3-c]thiopyran (9b')*: Colorless crystals (from ethanol); IR(KBr) 3060, 2910, 2245(CN), 1605, and 850 cm^{-1}; ^1H NMR($CDCl_3$) δ=2.26(s, 6H), 2.39(s, 3H), 3.02—3.56(m, 2H), 3.64—3.82(m, 1H), 3.88—4.03(m, $J\approx$2.3 Hz, 1H), 5.63(dd, J=6.3 and 2.3 Hz, 1H), 6.40(dd, J=6.3 and 2.1 Hz, 1H), and 6.85(broad s, 2H); MS m/z (rel intensity) 299(M^+, 45), 213(100), and 198(23). Found: C, 68.66; H, 5.48; N, 4.66; S, 21.98%. Calcd for $C_{17}H_{17}NS_2$: C, 68.19; H, 5.72; N, 4.68; S, 21.41%.

4-Cyano-7-phenyl-4,5-dihydro-7H-thieno[2,3-c]thiopyran (10a): Chromatographed by eluting with dichloromethane-hexane (2:3); colorless crystals (from ethanol); IR(KBr) 3060, 3025, 2925, 2250(CN), and 1600 cm^{-1}; ^1H NMR($CDCl_3$) δ=3.05—3.25(m, 2H), 4.05—4.32(m, 1H), 5.25(s, 1H), and 6.95—7.35(m, 7H); MS m/z (rel intensity) 257(M^+, 100), 230(13), 210(58), 204(thioketone, 63), 203(77), and 180(M^+−Ph, 28). Found: C, 65.66; H, 4.12; N, 5.41; S, 24.82%. Calcd for $C_{14}H_{11}NS_2$: C, 65.34; H, 4.31; N, 5.44; S, 24.91%.

4-Cyano-7-phenyl-4,5-dihydro-7H-thieno[2,3-c]thiopyran (10a'): Orange crystals (from ethanol); IR (KBr) 3040, 2920, 2250 (CN), and 1490 cm^{-1}; ^1H NMR ($CDCl_3$) δ=3.08—3.25 (m, 2H), 4.10—4.35 (m, 1H), 5.20 (s, 1H), 7.00 (d, J=5.0 Hz, 1H), and 7.10—7.40 (m, 5H); MS m/z (rel intensity) 257(M^+, 100), 230 (13), 210 (78), 204 (thioketone, 64), 203 (74), and 180 (M^+−Ph, 27). Found: C, 65.09; H, 4.24; N, 5.30; S, 24.63%. Calcd for $C_{14}H_{11}NS_2$: C, 65.34; H, 4.31; N, 5.44; S, 24.91%.

trans-*4-Phenyl-7-mesityl-3a,4-dihydro-5H-thiopyrano[3,4-b]furan (11b)*: Chromatographed by eluting with benzene-hexane (1:2); yellow needles (from ethanol); IR (KBr) 3105, 3030, 2930, 2840, 1690, and 1610 cm^{-1}; ^1H NMR ($CDCl_3$) δ=2.27 (s, 3H), 2.31 (s, 3H), 2.34 (s, 3H), 2.60—3.25 (m, 3H), 3.78 (ddd, J=10.4, 2.1, and 2.0 Hz, 1H), 4.92 (dd, J=2.7 and 2.1 Hz, 1H), 6.40 (dd, J=2.7 and 2.0 Hz, 1H), 6.85 (broad s, 2H), and 7.08—7.45(m, 5H); MS m/z (rel intensity) 334 (M^+, 12), 230 (100), 214 (55), 202 (27), 197 (50), 187 (24), and 169 (31). Found: C, 79.08; H, 6.35; S, 9.29%. Calcd for $C_{22}H_{22}OS$: C, 79.00; H, 6.63; S, 9.59%.

4,7-Diphenyl-4,5-dihydro-7H-thieno[2,3-c]thiopyran (12a) and (12a'): Chromatographed by eluting with benzene-hexane (1:3); orange crystals (from ethanol); IR (KBr) 3100, 3060, 3030, 2910, 1600, 730, and 710 cm^{-1}; ^1H NMR ($CDCl_3$) δ=2.76—3.28 (m, 2H), 4.35—4.45 (m, 1H), 5.24 (s, 0.5H), 5.35 (s, 0.5H), 6.46 (d, J=5.0 Hz, 0.5H), 6.50 (d, J=5.0 Hz, 0.5H), 7.00 (d, J=5.0 Hz, 0.5H), 7.04 (d, J=5.0 Hz, 0.5H), and 7.05—7.40 (m, 10H); MS m/z (rel intensity) 308 (M^+, 53), 262 (49), 230 (42), 204 (thioketone, 100), 203 (97), and 184 (48). Found: C, 73.69; H, 5.11; S, 20.63%. Calcd for $C_{19}H_{16}S_2$: C, 73.98; H, 5.23; S, 20.79%.

7-(p-Chlorophenyl)-4-phenyl-4,5-dihydro-7H-thieno[2,3-c]thiopyran (12c) and (12c'): Chromatographed by eluting with benzene-hexane (2:3); yellow crystals (from ethanol); IR (KBr) 3120, 2910, 1600, and 1490 cm^{-1}; ^1H NMR ($CDCl_3$) δ=2.75—3.22 (m, 2H), 4.15—4.45 (m, 1H), 5.20 (s, 0.5H), 5.32 (s, 0.5H), 6.47 (d, J=5.7 Hz, 0.5H), 6.52 (d, J=5.7 Hz, 0.5H), 7.00 (d, J=5.7 Hz, 0.5H), 7.05 (d, J=5.7 Hz, 0.5H), and 7.00—7.40 (m, 9H); MS m/z (rel intensity) 344 (M^+, 17), 342 (38), 296 (21), 264 (37), 261 (42), 238 (54), and 203 (100). Found: C, 66.43; H, 4.32; S, 18.97%. Calcd for $C_{19}H_{15}S_2Cl$: C, 66.55; H, 4.41; S, 18.70%.

Reaction of Heteroaromatic Thioketone with 2-Chloroacrylonitrile. A mixture of heteroaromatic thioketone (5 mmol) and 2-chloroacrylonitrile (1 cm^3) was refluxed in dry benzene (5 cm^3) under a nitrogen atmosphere until all the thioketone had been consumed as evidenced by TLC analysis. The reaction mixture was cooled and triethylamine (2 cm^3) was added in the solution. The solution was refluxed for 30 min. The color of the solution turned immediately deep red. The mixture was cooled to room temperature and the precipitated triethylamine hydrochloride was filtered off. The filtrate was evaporated and the residue was purified by column chromatography. The eluate was evaporated and the residue was recrystallized from ethanol to give **14** or **16**.

4-Cyano-7-phenyl-5H-thiopyrano[3,4-b]furan (14a): Chromatographed by eluting with benzene-hexane (2:1); red needles; IR (KBr) 3150, 3100, 3060, 2190, and 1630 cm^{-1}; ^1H NMR ($CDCl_3$) δ=3.68 (s, 2H), 6.26 (d, J=2.7 Hz, 1H), 7.22 (d, J=2.7 Hz, 1H), 7.28—7.48(m, 3H), and 7.60—7.80 (m, 2H); MS m/z (rel intensity) 239 (M^+, 64), 238 (100), 213 (6), 209 (9), 121 (6), and 77 (7). Found: C, 70.33; H, 4.05; N, 6.08; S, 13.24%. Calcd for $C_{14}H_9NOS$: C, 70.27; H, 3.79; N, 5.85; S, 13.40%.

4-Cyano-7-mesityl-5H-thiopyrano[3,4-b]furan (14b): Chromatographed by eluting with benzene-hexane (1:2); red needles; IR (KBr) 3130, 2975, 2920, 2190, 1640, 1610, 1580, 1550, 1150, 860, and 790 cm^{-1}; ^1H NMR ($CDCl_3$) δ=2.20 (s, 6H), 2.29 (s, 3H), 3.74 (s, 2H), 6.20 (d, J=2.5 Hz, 1H), 6.87 (broad s, 2H), and 7.08 (d, J=2.5 Hz, 1H); MS m/z 281(M^+, 100), 266 (42), 252 (21), 248 (44), and 238 (20). Found: C, 72.34; H, 5.44; N, 4.79; S, 11.38%. Calcd for $C_{17}H_{15}NOS$: C, 72.57; H, 5.37; N, 4.98; S, 11.39%.

4-Cyano-7-phenyl-5H-thieno[2,3-c]thiopyran (16a): Chromatographed by eluting with benzene-hexane (2:3); red crystals; IR (KBr) 3120, 2190, 1580, 1520, 1490, 1095, 980, 760, and 700 cm^{-1}; ^1H NMR ($CDCl_3$) δ=3.73 (s, 2H), 6.68 (d, J=7.0 Hz, 1H), 7.10 (d, J=7.0 Hz, 1H), and 7.20—7.60 (m, 5H); MS m/z (rel intensity) 255 (M^+, 80), 254 (100), 229 (7), and 222 (7). Found: C, 65.75; H, 3.28; N, 5.57; S, 25.20%. Calcd for $C_{14}H_9NS_2$: C, 65.85; H, 3.55; N, 5.49; S, 25.11%.

4-Cyano-7-mesityl-5H-thieno[2,3-c]thiopyran (16b): Chromatographed by eluting with dichloromethane-hexane (1:3); reddish purple needles; IR (KBr) 3090, 2970, 2920, 2190, 1610, 1585, 1530, 1505, 1100, 850, and 770 cm^{-1}; ^1H NMR ($CDCl_3$) δ=2.19 (s, 6H), 2.28 (s, 3H), 3.78 (s, 2H), 6.63 (d, J=5.9 Hz, 1H), 6.85 (broad s, 2H), and 7.02 (d, J=5.9 Hz, 1H); MS m/z (rel intensity) 297 (M^+, 100), 282 (29), 264 (55), 212 (17), and 178 (M^+—mesityl, 13). Found: C, 68.84; H, 5.03; N, 4.60; S, 21.22%. Calcd for $C_{17}H_{15}NS_2$: C, 68.95; H, 5.08; N, 4.71; S, 21.56%.

7-(p-Chlorophenyl)-4-cyano-5H-thieno[2,3-c]thiopyran (16c): Chromatographed by eluting with dichloromethane-hexane (2:3); red silky needles; IR (KBr) 2975, 2200, 1580, 1490, 1195, 820, and 755 cm^{-1}; ^1H NMR ($CDCl_3$) δ=3.76 (s, 2H), 6.70 (d, J=6.3 Hz, 1H), 7.11 (d, J=6.3 Hz, 1H), and 7.20—7.84 (m, 4H); MS m/z (rel intensity) 291 (M^+, 35), 290 (56), 289 (77), 288 (100), 256 (16), 231 (16), and 178 (19). Found: C, 57.99; H, 2.79; N, 4.81; S, 22.03%. Calcd for $C_{14}H_8NS_2Cl$: C, 58.03; H, 2.78; N, 4.83; S, 22.13%.

References

1) T. Karakasa and S. Motoki, *J. Org. Chem.*, **43**, 4147 (1978); **44**, 4151 (1979); T. Karakasa, H. Yamaguchi, and S. Motoki, *ibid.*, **45**, 927(1980).

2) Th. Wagner-Jautgg, *Synthesis*, **1980**, 165.

3) E. Ciganek, *J. Org. Chem.*, **34**, 1923 (1969).

4) "Organic Reactions," John Wiley & Sons, New York (1948), Vol. 4, p. 36.

5) H. Ohmura and S. Motoki, *Chem. Lett.*, **1981**, 235.

6) P. Gosslin, S. Masson, and A. Thuillier, *Tetrahedron Lett.*, **1980**, 2421.

7) In the cis isomer, another conformation (H_{3a}-equatorial, H_4-axial) is considered. However, the condensed thiopyran ring containing a double bond in 7-position could not have equatorial conformation on H-3a.

8) J. G. Martin and R. K. Hill, *Chem. Rev.*, **61**, 537(1961).

9) G. C. Levy, R. L. Lichter, and G. L. Nelson "Carbon-13 Nuclear Magnetic Resonance Spectroscopy," 2nd ed, John Wiley & Sons, New York (1980), p. 61.

10) W. S. Trahanovsky, T. J. Cassady, and T. L. Woods, *J. Am. Chem. Soc.*, **103**, 6691 (1981).

11) E. R. Marinelli, *Tetrahedron Lett.*, **23**, 2745 (1982).

12) U. E. Wiersum, *Aldrichimica Acta*, **14**, 53 (1981).

13) B. S. Pedersen, S. Scheibye, N. H. Nilsson, and S.-O. Lawesson, *Bull. Soc. Chim. Belg.*, **87**, 223 (1978).

14) J. W. Scheeren, P. H. J. Ooms, and R. J. F. Nivard, *Synthesis*, **1973**, 149.

15) C. Andrieu, Y. Mollier, and N. Lozac'h, *Bull. Soc. Chim. Fr.*, **1965**, 2457.

Quinazoline Derivatives from 2-Phenyl-4-quinazolinylhydrazine

Hassan Ahmed EL-SHERIEF,* Abdalla Mohamed MAHMOUD, and Ahmed Ahmed ESMAIEL

Chemistry Department, Faculty of Science, Assiut University, Assiut, Egypt

(Received December 1, 1982)

Formic acid and acetyl and benzoyl chloride were treated with 2-phenyl-4-quinazolinylhydrazine (**1**) under mild conditions to afford the corresponding hydrazides which were converted into 5-phenyl[1,2,4]triazolo[1,5-*c*]quinazoline, 2-methyl-5-phenyl[1,2,4]triazolo[1,5-*c*]quinazoline, and 2,5-diphenyl[1,2,4]triazolo[1,5-*c*]quinazoline (**3a**) respectively by heating over their melting points. Reaction of **1** with aldehydes produced the corresponding hydrazones which give the corresponding [1,2,4]triazolo[1,5-*c*]quinazolines (**3a**—**i**) on pyrolysis. Carbon disulfide underwent ring closure with **1** to 5-phenyl-1,2,4-triazolo[4,3-*c*]quinazoline-3-thiol which was readily converted into the corresponding alkylthio compounds by treatment with alkyl halides. Further, 4-(4-arylmethylene-5-oxo-2-phenyl-2-imidazolinylamino)-2-phenylquinazolines were obtained *via* the condensation of 4-arylmethylene-2-phenyl-2-oxazolin-5-ones with **1**.

Literature survey has revealed that some heterocyclic compounds such as 2-hydrazinoquinoxaline which has hydrazino group ortho to ring nitrogen can be cyclized to the corresponding[1,2,4]triazolo[4,3-*a*]quinoxalines[1] *via* the reaction with organic acids, acid chlorides and/or acid anhydrides and the acylated intermediate was not obtained. In some cases, however, only the acylated intermediates were obtained, depending on the nature of heterocyclic compound.[2] The isomerization in ring-fused 1,2,4-triazoles induced by acid or heat has been reported for several of these ring systems.[3,4] A particularly facile isomerization was observed with[1,2,4]triazolo[4,3-*c*]quinazoline system to its [1,2,4]triazolo[1,5-*c*]quinazoline isomer.[5]

It was of interest to mention that the products obtained from the reaction of 2-phenyl-4-quinazolinylhydrazine (**1**) with acyl chlorides, formic acid, or aldehydes depend mainly on the reaction conditions applied.

The reaction of **1** with benzoyl chloride in chloroform containing anhydrous potassium carbonate yielded 2-benzoyl-1-(2-phenyl-4-quinazolinyl)hydrazine (**2a**), while heating a mixture of **1** and benzoyl chloride at 170—175 °C for 1 h, the isomer **2b** was obtained as a major product. Heating of **2a** in benzoyl chloride at 170 °C for 1 h gave the isomer **2b**. Further, heating of both **2a** and **2b** above their melting points for 15 min gave 2,5-diphenyl[1,2,4]triazolo[1,5-*c*]quinazoline (**3a**), which was obtained directly by refluxing a mixture of **1** and benzoyl chloride for 2 h, as shown in

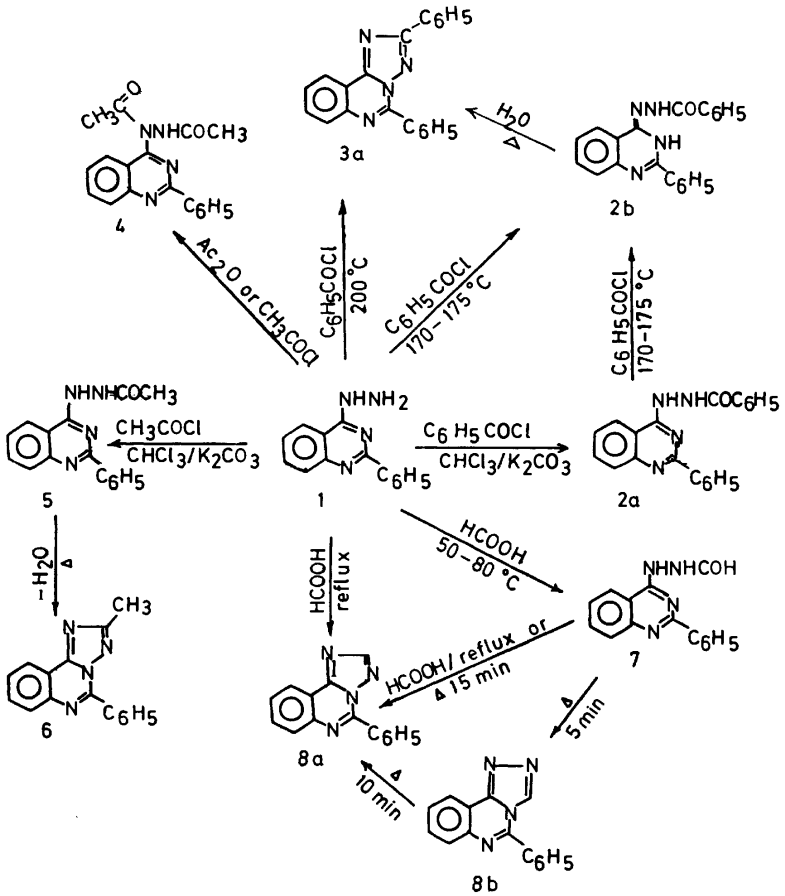

Scheme 1.

Scheme 1.

The structures of **2a**, **2b**, and **3a** were established on the basis of their IR, UV, and Mass spectral analysis. Refluxing of **1** with acetic anhydride or acetyl chloride for 2 h gives 1,2-diacetyl-1-(2-phenyl-4-quinazolinyl)hydrazine (**4**). 2-Acetyl-1-(2-phenyl-4-quinazolinyl)hydrazine (**5**) was obtained by the reaction of **1** with acetyl chloride in chloroform containing anhydrous potassium carbonate, which was cyclized to 2-methyl-5-phenyl[1,2,4]triazolo[1,5-*c*]quinazoline (**6**), by heating above its melting point for 15 min (Scheme 1).

It was reported by Potts[5] that 5-phenyl[1,2,4]-triazolo[1,5-*c*]quinazoline (**8a**) was obtained by direct cyclization of **1** with formic acid, while its [4,3-*c*]-quinazoline isomer (**8b**) was achieved by the reaction of **1** with triethyl orthoformate.

In our investigation both isomers **8a** and **8b** were obtained through the formation of *N*-formyl intermediate **7** which was obtained by conducting the reaction of **1** with formic acid at 55—80 °C for 45 min. Heating of **7** over its melting point for 5 min gave **8b**, which was readily isomerized to **8a** by further heating above its melting point for 10 min. On the other hand, **8a** was obtained directly by continuous heating of **7** for 15 min or by refluxing of **7** with formic acid for 1 h.

The UV spectra of **3a**, **6**, and **8a** were characterized by the location of the principal absorption band at shorter wavelength relative to that of **2a**, **5**, and **7** respectively. The observed blue shift (52—58 nm) may be due to the shortening of conjugation as a result of their cyclization to 1,2,4-triazolo ring system.

Reaction of **1** with the appropriate aldehydes in ethanolic solution containing piperidine yielded the corresponding hydrazones (**9a**—**i**). While carrying the same reaction in the absence of solvent at 210—220 °C for 2 h, cyclization took place and the [1,2,4]-triazolo[1,5-*c*]quinazolines (**3a**—**i**) were obtained.

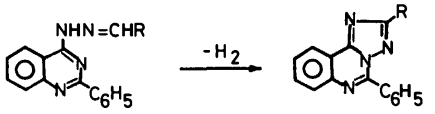

9 3

R	R
a: C_6H_5	f: $C_6H_4CH_3$-p
b: C_6H_4Br-p	g: $C_6H_4NO_2$-p
c: C_6H_4Cl-p	h: $C_6H_4NO_2$-m
d: C_6H_4Cl-m	i: 2-thienyl
e: $C_6H_4OCH_3$-p	

On the other hand, heating of **9a** above its melting point for 1 h, it was cyclized to **3a**. The IR spectra of **9a**—**i** revealed an absorption band at 3370—3350 cm^{-1} attributed to NH group, which disappeared in compounds **3a**—**i**. The UV spectra of **9** were characterized by the presence of a principal absorption band at 362—382 nm, while the UV spectra of **3** exhibited a principal absorption band at 300—310 nm. The observed blue shift (62—72 nm), probably due to the shortening of conjugation as a result of cyclization.

The NMR spectrum of **3e** (in DMSO) showed a singlet at δ=3.8 (3H, OCH_3), a multiplet at 6.8—7.8 (9H, aromatic protons) and another multiplet at 8.4—8.6 (4H, of quinazoline ring); while the NMR spectrum of **3f** showed a singlet at δ=2.6 (3H, CH_3), a multiplet at 7.2—7.8 (9H, aromatic protons) and at 8.2—8.5 (4H, of quinazoline ring).

In the mass spectra of these fused ring systems molecular ions were obtained for all compounds studied.

Further, it was reported that carbon disulfide reacted with 2-pyridylhydrazines[2,6] or 2-thiazolylhydrazines[7] to produce 1,2,4-triazolo[4,3-*a*]pyridine-3-thiols and thiazolo[2,3-*c*]-1,2,4-triazole-3-thiols respectively.

Similarly, reaction of **1** with carbon disulfide provided a convenient synthesis of 5-phenyl-1,2,4-triazolo[4,3-*c*]-quinazoline-3-thiol (**10**), which was readily converted to the corresponding 3-alkylthio compounds (**11a**—**e**) with alkyl halides in basic medium.

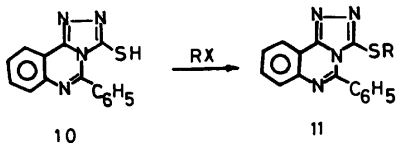

10 11

R
11 a: CH_3
b: C_2H_5
c: $CH_2(CH_2)_2CH_3$
d: $CH_2C_6H_5$
e: $CH_2COOC_2H_5$

The NMR spectrum of **11b** (in $CDCl_3$) showed a triplet at δ=1.3 (J=6 Hz, 3H, CH_3), a quartet at 3.3 (J=6 Hz, 2H, CH_2), and a multiplet at 7.5—8.3 (9H, aromatic protons), while the NMR spectrum of **11d** (in $CDCl_3$) showed signals at δ=4.7 (s, 2H, CH_2) and at 7.4—8.8 (m, 14 H, aromatic protons).

Furthermore, the hitherto unreported reaction of **1** with 4-arylmethylene-2-phenyl-2-oxazolin-5-ones (**12**)[8] in benzene or xylene afforded the corresponding 1-(2-phenyl-4-quinazolinyl)-2-(2-benzamido-3-arylacryloyl)-hydrazine (**13**). The IR spectra of **13** showed two bands characteristic of the stretching vibration of two carbonyl groups at 1680—1670 cm^{-1} and at 1650—1640 cm^{-1} in addition to the NH band appeared at 3320—3290 cm^{-1}.

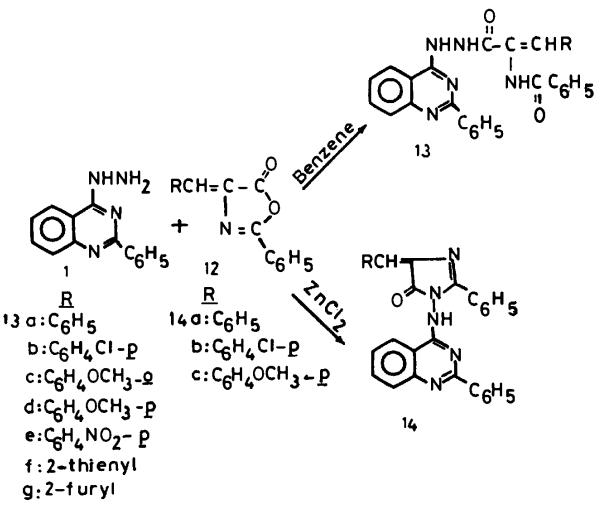

1 12 13 14

R	R
13 a: C_6H_5	14 a: C_6H_5
b: C_6H_4Cl-p	b: C_6H_4Cl-p
c: $C_6H_4OCH_3$-o	c: $C_6H_4OCH_3$-p
d: $C_6H_4OCH_3$-p	
e: $C_6H_4NO_2$-p	
f: 2-thienyl	
g: 2-furyl	

When **12** was allowed to react with **1** in the presence of anhydrous zinc chloride, the corresponding 4-(4-arylmethylene-5-oxo-2-phenyl-2-imidazolin-1-ylamino)-2-phenylquinazolines (**14a—d**) were produced directly.

On the other hand, **14a** was also obtained by heating of **13a** above its melting point for 5 min in the presence of anhydrous zinc chloride. The IR spectra of **14a—d** showed absorption bands at 1690—1680 cm^{-1} and 3280—3240 cm^{-1} which were assigned to C=O and NH stretching frequencies respectively. The mass spectrum of **14c** showed a molecular ion peak at *m/e* 497, which agreed with the molecular weight expected.

Experimental

Melting points reported are uncorrected. Elemental analysis was carried out on a CHN analyzer. IR spectra were recorded on a Perkin-Elmer infracord. NMR spectra were recorded by a Varian EM 60 MHz spectrometer. Mass spectra were taken on MAT 112 Massenspectrometer.

2-Phenyl-4-quinazolinylhydrazine (**1**) was prepared as previously described by Postovskii, mp 215 °C, lit,[9] mp 214—215 °C.

2-Benzoyl-1-(2-phenyl-4-quinazolinyl)hydrazine (**2a**). To a solution of **1** (5.9 g, 0.025 mol) in dry chloroform (100 ml) containing anhydrous potassium carbonate (0.5 g), benzoyl chloride (0.02 mol) was added slowly. After the addition was complete, the reaction mixture was stirred at room temperature for 30 min and then heated on a steam bath for 1 h. The mixture was filtered, evaporated and the crude product was collected and crystallized from ethanol as yellow needles, 7 g (82%); mp 248 °C. IR(KBr), 3360 (NH), 3220(NH), 1650 cm^{-1} (C=O); UV(ethanol), λ_{max} 248 (log ε 4.59), 320(4.0), 356 nm (3.84); MS (70 eV), M^+, *m/e* (rel intensity) 340 (100%), 221(53%), 205(38%), 103 (59%), 102(65%). Found: C, 74.11; H, 4.70; N, 16.45%. Calcd for $C_{21}H_{16}N_4O$: C, 74.10; H, 4.47; N, 16.46%.

The isomer **2b** was obtained by heating a mixture of **1** (0.02 mol) and benzoyl chloride (0.04 mol) at 170—175 °C for 1 h. The product was isolated by pouring the reaction mixture into cooled 5% sodium carbonate solution. The crude product crystallized from ethanol as colorless needles, 4.5 g (66%), mp 260 °C. IR (KBr); 3320(NH), 3210 (NH), 1660 cm^{-1} (C=O); UV (ethanol) λ_{max} 232(log ε 4.56), 256 (4.5), 308 nm(4.06); MS (70 eV), M^+, *m/e* (rel intensity) 340 (80%), 322 (100%), 219(35%). Found: C, 73.92; H, 4.83; N, 16.32%. Calcd for $C_{21}H_{16}N_4O$: C, 74.10; H, 4.74; N, 16.46%.

The same product was also obtained by heating of **2a** (1 g) in benzoyl chloride (5 ml) at 170—175 °C for 1 h.

2,5-Diphenyl[1,2,4]triazolo[1,5-c]quinazoline (**3a**). A mixture of **1** (4.69 g, 0.02 mol) and benzoyl chloride (0.04 mol) was refluxed for 2 h. The product was isolated as before and crystallized from ethanol as colorless needles, 4.6 g (72%).

The same compound was also obtained by heating of **2a** or **2b** (1 g) over their melting points for 15 min, and crystallized from ethanol, 0.5 g (63%). There is no melting point depression and the infrared spectrum was superimposable on that of **3a** prepared according to the above procedure (Table 2).

1,2-Diacetyl-1-(2-phenyl-4-quinazolinyl)hydrazine (**4**). **1** (2.3 g, 0.01 mol) was refluxed with acetic anhydride or acetyl chloride (10 ml) for 2 h. The colorless product separated was collected and crystallized from ethanol as colorless needles, 2.8 g (87%), mp 255 °C; IR (KBr); 3300 (NH), 1700, 1670 cm^{-1} (C=O), NMR, δ=2.5 (s, 3H, CH_3CO), 2.7 (s, 3H, CH_3CO), 3.0 (s, 1H, NH), 7.7—9.0 (m, 9H, aromatic protons).

Found: C, 67.36; H, 5.11; N, 17.28%. Calcd for $C_{18}H_{16}N_4O_2$: C, 67.49; H, 5.03; N, 17.49%.

2-Acetyl-1-(2-phenyl-4-quinazolinyl)hydrazine (**5**). It was prepared from **1** (9.2 g, 0.04 mol) and acetyl chloride (0.02 mol) in chloroform solution containing anhydrous potassium carbonate as previously described in **2a**. The crude product was crystallized from ethanol as pale orange prisms, 2 g (74%), mp 252—253 °C. IR (KBr) 3300, 3220 (NH), 1650 cm^{-1} (C=O).

Found: C, 69.18; H, 5.15; N, 20.46%. Calcd for $C_{16}H_{14}N_4O$: C, 69.05; H, 5.07; N, 20.13%.

Refluxing of **5** (1 g) with acetic anhydride or acetyl chloride (5 ml) for 1 h yielded **4** (0.9 g; 75%).

2-Methyl-5-phenyl[1,2,4]triazolo[1,5-c]quinazoline (**6**). **5** (1 g) was heated above its melting point for 10 min and after cooling to room temperature, crystallized from methanol as colorless needles, 0.6 g (60%), mp 128 °C; IR (KBr) 3050 (C–H), 1615 cm^{-1} (C=N); UV (ethanol) λ_{max} 259 (log ε 4.38), 264(4.25), 294 (4.3) nm; MS (70 eV), M^+, *m/e* (rel intensity) 260 (100%), 219 (36%); NMR, δ=2.7 (s, 3H, CH_3), 7.5—7.8 (m, 5H, C_6H_5), 8.5—8.8 (m, 4H, quinazoline ring).

Found: C, 73.71; H, 4.56, N, 21.31%. Calcd for $C_{16}H_{12}N_4$: C, 73.83; H, 4.65; N, 21.52%.

2-Formyl-1-(2-phenyl-4-quinazolinyl)hydrazine (**7**). A mixture of **1** (1 g) and formic acid (6 ml) was heated at 50—80 °C for 45 min and the excess acid was evaporated under reduced pressure. The crude product was collected and crystallized from ethanol as yellow crystals, 0.8 g (71%), mp 240 °C; IR (KBr) 3270, 3220(NH), 1650 cm^{-1}, (C=O); UV (ethanol), λ_{max} 275 (log ε 3.99), 288 sh (3.86), 350 nm (3.25).

5-Phenyl-1,2,4-triazolo[4,3-c]quinazoline (**8b**). **7** (1 g) was heated above its melting point for 5 min and after cooling, crystallized from ethanol as colorless needles, 0.7 g (77%); mp 207 °C, lit[5] mp 205—206 °C.

Found: C, 73.00; H, 4.38; N, 22.41%. Calcd for $C_{15}H_{10}N_4$: C, 73.16; H, 4.09; N, 22.75%.

5-Phenyl[1,2,4]triazolo[1,5-c]quinazoline (**8a**). Heating of **7** (1 g) as described above for 15 min gave colorless needles from ethanol 0.8 g (88%), mp 185 °C, lit[5] mp 184—185 °C.

The same product was also obtained by refluxing a mixture of **1** (0.5 g) and formic acid (3 ml) for 1 h as described[5] before, or by heating of **8b** (0.5 g) above its melting point for 10 min. UV (ethanol), λ_{max} 249 (log ε 4.22), 292 nm, (3.89).

Found: C, 73.18; H, 4.16; N, 22.54%. Calcd for $C_{15}H_{10}N_4$: C, 73.16; H, 4.09; N, 22.75%.

Reaction of 2-Phenyl-4-quinazolinylhydrazine (**1**) *with Aldehydes* (**9a—i**). A mixture of **1** (0.01 mol), aromatic aldehyde (0.012 mol), ethanol (30 ml), and piperidine (0.2 ml) was refluxed for 4 h. The separated hydrazone was filtered and crystallized from the same solvent as yellow to red needles. The same products were also obtained by fusion of **1** with the appropriate aldehyde for 2 min (Table 1).

2-Aryl-5-phenyl[1,2,4]triazolo[1,5-c]quinazolines (**3a—i**). A mixture of appropriate aldehyde (0.015 mol) and **1** (0.01 mol) was heated at 210—220 °C for 2 h. The pyrolysis residue in the reaction flask was cooled and triturated with cold ethanol. The crude product was dissolved in ethanol–benzene (charcoal), forming colorless needles of **3a—i** (Table 2).

3a was also obtained by heating **9a** for 1 h at 210—215

Table 1. Aromatic aldehyde (2-phenyl-4-quinazolinyl)hydrazones (**9a—i**)

Compd No.	Mp θ_m/°C	Yield %	Mol formula	Calcd (Found)(%) C	H	N	λ_{max}/nm (log ε)
9a	134	81	$C_{21}H_{16}N_4$	77.76 (77.66	4.97 4.89	17.27 17.21)	362 (3.96)
b	170	87	$C_{21}H_{15}N_4Br$	62.54 (62.58	3.75 3.64	13.89 13.68)	370 (4.10)
c	172	86	$C_{21}H_{15}N_4Cl$	70.29 (70.36	4.21 4.11	15.61 15.46)	368 (4.06)
d	162	74	$C_{21}H_{15}N_4Cl$	70.29 (70.03	4.21 4.36	15.61 15.36)	364 (4.14)
e	145	72	$C_{22}H_{18}N_4O$	74.56 (74.31	5.12 5.26	15.81 15.88)	382 (4.00)
f	138	76	$C_{22}H_{18}N_4$	78.08 (78.22	5.36 5.28	16.56 16.41)	364 (3.96)
g	238	89	$C_{21}H_{15}N_5O_2$	68.28 (68.11	4.09 4.01	18.96 18.80)	376 (3.98)
h	213	86	$C_{21}H_{15}N_5O_2$	68.28 (68.06	4.09 4.12	18.96 18.76)	370 (3.74)
i	201	70	$C_{19}H_{14}N_4S$	69.07 (69.16	4.27 4.41	16.96 16.74)	381 (3.77)

Table 2. 2-aryl-5-phenyl[1,2,4]triazolo[1,5-*c*]quinazolines (**3a—i**)

Compd No.	Mp θ_m/°C	Yield %	Mol formula	Calcd (Found)(%) C	H	N	λ_{max}/nm (log ε)
3a[a]	170	65	$C_{21}H_{14}N_4$	78.24 (78.13	4.38 4.29	17.38 17.36)	300 (3.80)
b	235	50	$C_{21}H_{13}N_4Br$	62.86 (62.60	3.27 3.21	13.96 13.74)	300 (3.51)
c	182	70	$C_{21}H_{13}N_4Cl$	70.69 (70.71	3.67 3.56	15.70 15.76)	300 (3.78)
d	165	62	$C_{21}H_{13}N_4Cl$	70.69 (70.81	3.67 3.46	15.70 15.61)	305 (3.35)
e[b]	178	72	$C_{22}H_{16}N_4O$	74.98 (74.81	4.58 4.38	15.90 15.81)	310 (3.74)
f[c]	185	84	$C_{22}H_{16}N_4$	78.47 (78.21	4.75 4.36	16.64 16.51)	303 (3.34)
g	234	45	$C_{21}H_{13}N_5O_2$	68.66 (68.86	3.57 3.46	19.06 19.15)	299 (4.17)
h	175	56	$C_{21}H_{13}N_5O_2$	68.66 (68.71	3.57 3.48	19.06 18.78)	301 (3.90)
i[d]	210	35	$C_{19}H_{12}N_4S$	69.49 (69.18	3.68 3.56	17.06 17.15)	310 (3.69)

a) MS, M^+, *m/e* (rel intensity), 322(100%), 219(30%). b) MS, M^+, *m/e* (rel intensity), 352(100%), 219(39%).
c) MS, M^+, *m/e* (rel intensity), 336(100%), 219(25%). d) MS, M^+, *m/e* (rel intensity), 328(100%), 219(24%).

Table 3. 3-Alkylthio-5-phenyl-1,2,4-triazolo[4,3-*c*]quinazolines (**11a—e**)

Compd No.	Mp θ_m/°C	Yield %	Mol formula	Calcd (Found)(%) C	H	N	S
11a	140	64	$C_{16}H_{12}N_4S$	65.73 (65.63	4.14 4.36	19.16 19.28	10.97 10.47)
b	185	68	$C_{17}H_{14}N_4S$	66.64 (66.48	4.61 4.56	18.29 18.42	10.47 10.31)
c	163	72	$C_{19}H_{18}N_4S$	68.24 (68.02	5.43 5.48	16.75 16.61	9.59 9.26)
d[a]	101	52	$C_{22}H_{16}N_4S$	71.72 (71.94	4.38 4.16	15.21 15.46	8.70 8.66)
e	186	77	$C_{19}H_{16}N_4O_2S$	62.62 (62.43	4.43 4.26	15.37 15.18	8.80 9.12)

a) Recrystallized from benzene–pet. ether (60—80 °C).

TABLE 4. 1-(2-PHENYL-4-QUINAZOLINYL)-2-(2-BENZAMIDO-3-ARYLACRYLOYL)HYDRAZINES (**13a—g**)

Compd No.	Mp θ_m/°C	Yield %	Mol formula	Calcd(Found)(%) C	H	N
13a	220	82	$C_{30}H_{23}N_5O_2$	74.21 (74.00	4.77 4.55	14.42 14.90)
b	185	86	$C_{30}H_{22}ClN_5O_2$	69.30 (69.20	4.26 4.03	13.47 13.25)
c	190	91	$C_{31}H_{25}N_5O_3$	72.22 (72.11	4.89 4.81	13.58 13.47)
d	228	76	$C_{31}H_{25}N_5O_3$	72.22 (72.20	4.89 4.79	13.58 13.50)
e	229	88	$C_{30}H_{22}N_6O_4$	67.92 (67.70	4.18 4.07	15.84 15.88)
f	227	85	$C_{28}H_{21}N_5O_2S$	68.42 (68.40	4.31 4.26	14.25 14.16)
g	199	86	$C_{28}H_{21}N_5O_3$	70.73 (70.71	4.45 4.52	14.73 14.83)

TABLE 5. 4-(4-ARYLMETHYLENE-5-OXO-2-PHENYL-2-IMIDAZOLIN-1-YLAMINO)-2-PHENYLQUINAZOLINES (**14a—d**)

Compd No.	Mp θ_m/°C	Yield %	Mol formula	Calcd (Found)(%) C	H	N
14a	248	45	$C_{30}H_{21}N_5O$	77.07 (77.18	4.53 4.50	14.98 14.88)
b	239	56	$C_{30}H_{20}ClN_5O$	71.78 (71.76	4.02 4.13	13.95 13.90)
c	264	42	$C_{31}H_{23}N_5O_2$	74.83 (74.70	4.66 4.56	14.08 14.18)
d	265	58	$C_{28}H_{19}N_5OS$	71.02 (71.31	4.04 4.22	14.79 14.81)

°C. The pyrolysis residue, treated as described above yielded **3a**, no depression of melting point occurred on admixture with the sample prepared by the reaction of **1** with benzoyl chloride.

*5-Phenyl-1,2,4-triazolo[4,3-c]quinazoline-3-thiol (**10**).* **1** (2 g), methanol (100 ml), potassium hydroxide (0.7 g), and carbon disulfide (6 ml) were refluxed for 4 h. After removal of the excess solvent, dilute potassium hydroxide was added and the alkaline solution was filtered and acidified. The crude product was collected and crystallized from ethanol-benzene mixture as colorless needles, 1.89 g (75%), mp 265—268 °C; UV (ethanol) λ_{max} 290 nm (log ε 3.97).

Found: C, 64.45; H 3.58; N 20.36; S 11.50%. Calcd for $C_{15}H_{10}N_4S$: C, 64.73; H, 3.62; N, 20.13; S, 11.52%.

*Reaction of **10** with Alkyl Halides (**11a—e**).* A solution of **10** (0.59 g, 0.002 mol) and sodium hydroxide (0.1 g) in water (10 ml) was stirred while the appropriate alkyl halide (0.004 mol) was added dropwise. The reaction mixture was stirred for 2 h, then the excess alkyl halide was evaporated and the residue crystallized from ethanol, forming colorless needles of the products **11a—e** (Table 3).

*1-(2-Phenyl-4-quinazolinyl)-2-(2-benzamido-3-arylacryloyl)hydrazines (**13a—g**).* A mixture of **1** (1 g; 0.004 mol) and 4-arylmethylene-2-phenyl-2-oxazolin-5-one (**12**) (0.005 ml) in 30 ml dry benzene or ethanol was refluxed for 1 h. The reaction mixture was cooled and the product was filtered and recrystallized from ethanol to give **13a—g** nearly in a quantitative yield (Table 4).

*4-(4-Arylmethylene-5-oxo-2-phenyl-2-imidazolin-1-ylamino)-2-phenylquinazolines (**14a—d**).* A mixture of **1** (1 g; 0.004 mol), **12** (0.005 mol), and 0.1 g of anhydrous zinc chloride was fused together for 5 min. Benzene was added to the reaction mixture and filtered. The product was recrystallized from benzene-ethanol mixture to give **14a—d** in 40—60% yield (Table 5). **14c** was also obtained by heating **13d** above its melting point for 5 min in the presence of anhydrous zinc chloride.

References

1) D. Shiho and S. Tagami, *J. Am. Chem. Soc.*, **82**, 4044 (1960).

2) K. T. Potts and H. R. Burton, *J. Org. Chem.*, **31**, 251 (1966); D. Shiho and S. Tagami, *Yakugaku Zasshi*, **76**, 804 (1965).

3) G. W. Miller and F. L. Rose, *J. Chem. Soc.*, **1965**, 3357, 3369; K. T. Potts, H. R. Burton, and S. K. Roy, *J. Org. Chem.*, **31**, 265 (1966); K. T. Potts and S. W. Schneller, *J. Heterocycl. Chem.*, **5**, 485 (1968).

4) J. A. Bee and F. L. Rose, *J. Chem. Soc., C.*, **1966**, 2031; G. W. Miller and F. L. Rose, *ibid.*, **1966**, 5642.

5) K. T. Potts and E. G. Brugel, *J. Org. Chem.*, **35**, 3448 (1970).

6) D. S. Tarbell, C. W. Todd, M. C. Paulson, E. G. Linstrom, and V. P. Wystrack, *J. Am. Chem. Soc.*, **70**, 1381 (1948).

7) K. T. Potts and S. Husain, *J. Org. Chem.*, **36**, 10 (1971).

8) M. Crawford and W. T. Little, *J. Chem. Soc.*, **1959**, 729; E. Erlenmeyer, *Justus Liebigs Ann. Chem.*, **275**, 1 (1893).

9) I. Ya. Postovskii, N. N. Vereschagina, and S. L. Mertsalov, *Khim. Geterotsikl. Soedin., Akad. Nauk Latv. SSR*, **1966**, 130.

Effect of Ethanol on the Inclusion Complex Formation between β-Cyclodextrin and Pyrene

Akira NAKAJIMA

Department of Electronic Engineering, Faculty of Engineering, Saitama Institute of Technology, Okabe, Saitama 369-02

(Received June 2, 1983)

Synopsis. The effect of the addition of ethanol on the formation of the inclusion compound between β-cyclodextrin and pyrene in aqueous solution has been studied. Based on the time dependences of the fluorescence spectra of pyrene as a probe, the rate constants estimated for the inclusion and further association in the presence of ethanol have been discussed.

It has been reported[1] that macromolecular inclusion compounds have a considerable effect on the reactivity of the substrates included. Much interest has recently been shown in the inclusion compounds of cyclodextrins,[2,3] since they exhibit appreciable enzyme-like activity, and a variety of practical applications are extending. It seems that few studies have been made on the effect of a third component, though it may occasionally have a significant influence on the enzymatic reactions.

Previously, a system of β-cyclodextrin (βCD) and pyrene in aqueous solution has been investigated utilizing the intensity enhancement phenomenon[4] and the association constant has been estimated.[5] In this work, the effect of ethanol on the rates of inclusion and further association has been studied in the same system.

Experimental

Pyrene was recrystallized and vacuum-sublimed, and βCD was purified by repeated recrystallizations from water. Ethanol was dried and fractionally distilled.

The sample solutions were carefully prepared using deionized water from an aqueous solution of pyrene which was well saturated by allowing it to stand in contact with pyrene microcrystals for more than a week. No excimer-like emission nor impurity emission was detected in these solutions. The initial concentration of pyrene, C_p, was estimated to be 2.5×10^{-7} M (1 M=1 mol dm^{-3}) by measuring the low absorbance at 334 nm. The volumetric preparation of a solution and the subsequent measurement required at least two minutes, after which the spectral changes with time were observed.

Fluorescence spectra were recorded at about 13 °C on a Shimadzu 210A spectrophotometer with some minor modifications. The excitation was made employing a combination of a high-intensity monochromator and a Xe-lamp stabilized over the wavelengths (about 15 nm width) for the second peak of the second absorption band of pyrene (319—322 nm).

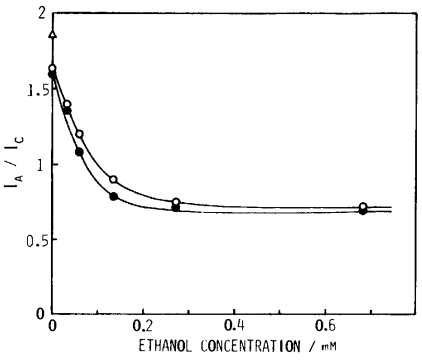

Fig. 1. Changes in I_A/I_C ratios with ethanol concentrations in aqueous solutions of βCD (8.5×10^{-4} M) and pyrene (2.5×10^{-7} M). After 30 min (○) and a week (●), and without βCD (△).

Results and Discussion

It is now well known[4,6,7] that the intensities of vibronic bands in the fluorescence spectrum of pyrene vary strikingly with the solvent polarity and the ratio of the intensity of the band A at 373 nm (I_A) to that of the band C at 384 nm (I_C) can be regarded as a measure of the polarity of medium,[6] the phenomenon being effectively employed here to probe the microenvironments. It is observed that the intensity ratio I_A/I_C is 1.87 in pure water but 0.58 in a nonpolar solvent.

The changes in the I_A/I_C ratios with varying ethanol concentrations in the solutions containing given amounts of pyrene and βCD are illustrated in Fig. 1. As can be seen, the effect of the addition of ethanol is very remarkable; the reaction is considerably speeded at concentrations more than 0.2 M. The ratios are also found to change with time.

The decrease of the I_A/I_C value from 1.87[8] implies that considerable part of pyrene dissolved is included within the βCD cavity, where the environment has a polarity corresponding to an I_A/I_C value of 0.68.[5]

The variations of the I_A/I_C ratios with time for various ethanol concentrations are shown in Fig. 2. Inspection of the behaviors of these curves reveals that they consist of two portions, associated with a fast and a slow process. The fast initial decay, which appears to be almost completed within a minute, is likely due to the inclusion of pyrene by βCD, while the subsequent slow decrease may be ascribed to a

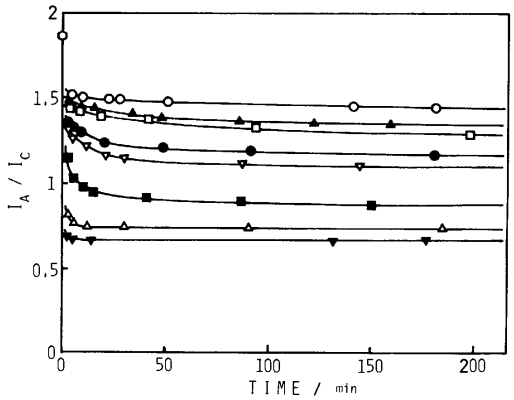

Fig. 2. Variations of I_A/I_C ratios with time in aqueous solutions of βCD (1.9×10^{-3} M) and pyrene (2.5×10^{-7} M). Concentration of ethanol (M): 0 (○), 1.4×10^{-3} (▲), 4.1×10^{-3} (□), 8.2×10^{-3} (●), 1.4×10^{-2} (▽), 4.1×10^{-2} (■), 0.14 (△), 1.7 (▼), and without βCD (0).

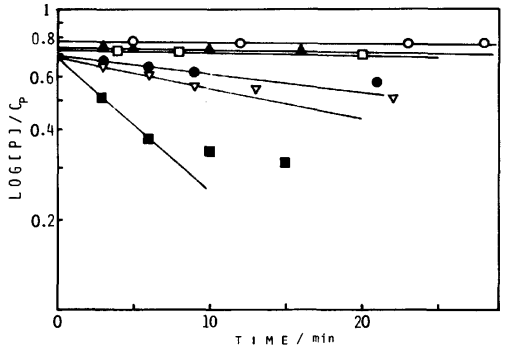

Fig. 3. Plot of log $[P]/C_P$ *vs.* t.

further association of the resulting inclusion compounds. As clearly shown in Fig. 2, the inclusion and the further association are appreciably accelerated by the addition of ethanol.

According to these observations, the reaction scheme may be expressed as follows:

$$P + D \underset{k_2}{\overset{k_1}{\rightleftharpoons}} PD,$$

$$PD + D \underset{k_4}{\overset{k_3}{\rightleftharpoons}} PD_2,$$

where P and D denote pyrene and βCD, respectively, and PD and PD_2 represent respectively the 1:1 and 1:2 complexes formed from them. Though the association may produce various complex species,[8] here PD_2 is taken as most probable. These rate constants are considered as functions of ethanol concentration, [Et].

Thus, the kinetic equations are given by

$$\frac{d[P]}{dt} = -k_1[P][D] + k_2[PD],$$

$$\frac{d[PD]}{dt} = k_1[P][D] - (k_2+k_3[D])[PD] + k_4[PD_2].$$

At relatively short times the term associated with $[PD_2]$ can be neglected and [D] is practically equal to C_D, the total βCD concentration, because of $[P] \ll C_D$.

Then, the solution has the form:

$$[P] = A\exp(-k_+t) + B\exp(-k_-t),$$

where $k_\pm = (a \pm \sqrt{a^2 - 4b})/2,$

$$a = (k_1+k_3)C_D + k_2, \quad b = k_1k_3C_D^2.$$

By using the initial conditions that $[P]=C_P$ and $[PD]=0$ at $t=0$,

$$A = (k_1C_D - k_-)C_P/(k_+ - k_-),$$

$$B = (k_+ - k_1C_D)C_P/(k_+ - k_-).$$

It can be assumed here that $k_1C_D \gg k_2 \approx k_3C_D \gg k_4$.

Accordingly, a rough approximation gives

$$k_+ \approx k_1C_D, \; k_- \approx k_3C_D,$$

$$A \approx C_P, \; B \approx k_2C_P/k_1C_D = C_P/KC_D;$$

$$[P]/C_P \approx \exp(-k_1C_Dt) + \exp(-k_3C_Dt)/KC_D.$$

Thus, the rate constant k_3 together with the equilibrium constant K can be estimated from the slowly decreasing portion of the curves. In the present experiment, however, the value of k_1 cannot be obtained owing to the considerably rapid changes.

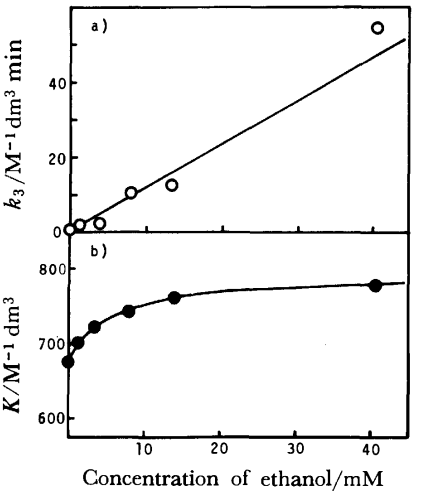

Fig. 4. Plots of k_3 (a) and K (b) against ethanol concentration.

To interpret the time-dependent behaviors on the basis of the above scheme, the concentrations of pyrene dissolved in the water phase, [P], need to be evaluated, and the following formula[5] has been employed:

$$\frac{I_A}{I_C} = \frac{k_P^A\phi_P\varepsilon_P[P] + k_{PD}^A\phi_{PD}\varepsilon_{PD}[PD]}{k_P^C\phi_P\varepsilon_P[P] + k_{PD}^C\phi_{PD}\varepsilon_{PD}[PD]},$$

Where ϕ's are the quantum yields ($\phi_{PD}/\phi_P \approx 1.5$),[5] ε's are the absorption coefficients ($\varepsilon_{PD}/\varepsilon_P \approx 1$),[6] and k^A or k^C represents the fraction of the spectral intensity for the A or C band. The assumption that $[P]+[PD] \approx C_P$ at $t \approx 0$ has been used.

Figure 3 shows plots of log $[P]/C_P$ *vs.* t, which are found to be fairly linear at small t. From the slopes and intercepts of the lines approximate values of k_3 and K are obtained. Furthermore, k_3 as well as K is plotted against the ethanol concentration in Fig. 4. As shown, k_3 appears to depend linearly on [Et], implying the possibility of the formation of a four-component complex PD_2Et.

In constrast to k_3, K does not change so much with [Et] since not only k_1 but k_2 depends on [Et]. Only an order-of-magnitude agreement is obtained between the value of K ($675\,M^{-1}dm^3$) and that ($190\,M^{-1}dm^3$) estimated previously,[5] and the discrepancy may be due largely to the times for measurement, various approximations, different pyrene and βCD concentrations, temperatures, *etc.*

References

1) J. H. Fendler and E. J. Fendler, "Catalysis in Micellar and Macromolecular Systems," Academic Press, New York (1975).

2) M. L. Bender and M. Komiyama, "Cyclodextrin Chemistry," Springer-Verlag, Berlin (1978).

3) W. Saenger, *Angew. Chem. Int. Ed. Engl.*, **19**, 344 (1980).

4) A. Nakajima, *Kagaku No Ryoiki*, **33**, 49 (1979).

5) A. Nakajima, *Spectrochim. Acta*, **39A**, 913 (1983).

6) A. Nakajima, *Bull. Chem. Soc. Jpn.*, **44**, 3272 (1971).

7) K. Kalyanasundaram and J. K. Thomas, *J. Am. Chem. Soc.* **99**, 2039 (1977).

8) H. E. Edwards and J. K. Thomas, *Carbohydr. Res.*, **65**, 173 (1978).

The Crystal Structure of the B′-Form of Heptadecanoic Acid

Midori GOTO* and Eiichi ASADA†
National Chemical Laboratory for Industry, 1-1, Higashi, Yatabe, Ibaraki 305
(Received July 8, 1983)

Synopsis. X-Ray structural determination of the B′-form of heptadecanoic acid showed that the unit cell contains two crystallographically independent molecules. All-trans zigzag chains are found in both molecules.

Odd numbered fatty acids are known to crystallize in three polymorphic forms, named A′, B′, and C′.[1] Informations relating to the properties of these are collected in Table 1. The B′-form of pentadecanoic acid has been studied by von Sydow using two-dimentional X-ray diffraction data.[2] We have now been able to obtain fairly good single crystals of the B′-form of heptadecanoic acid and investigated its crystal structure.

Experimental

The heptadecanoic acid was prepared from methyl heptadecanoate by hydrolysis. The B′-form crystals were obtained by crystallization from a 2,2,4-trimethylpentane solution. A crystal with dimensions of $0.6\times0.3\times0.05$ mm^3 was used for the structure determination. The cell dimensions and the diffraction intensities were measured on a Rigaku-Denki four circle diffractometer by using graphite monochromated Cu-$K\alpha$ radiation at room temperature. Crystal data are as follows: $C_{17}H_{34}O_2$ (B′-form); M.W=270.46; triclinic, $P\bar{1}$; a=5.561(1), b=8.018(1), c=47.90(1)Å; α=114.18(1), β=114.96(1), γ=80.22(1)°; D_x=1.017 g cm^{-3}. All independent reflections within the range of $2\theta\leqq120°$ were collected by the use of the 2θ—ω scan mode with a scanning rate 4° (2θ) min^{-1}. Correction for absorption was not applied. A total 1028 independent reflections with $|F_o|\geqq3\sigma(|F_o|)$ were obtained.

Structure Determination

The positions of the carbon atoms were obtained from three dimensional Patterson maps. The positions of the oxygen atoms were obtained by difference synthesis. The positions of the hydrogen atoms, with the exception of carboxyl hydrogen atoms, were calculated by assuming C-H distances of 1.10 Å and a tetrahedral arrangement. The structure was refined

TABLE 1. POLYMORPHISM OF SATURATED ODD-NUMBERED FATTY ACIDS

Number of carbon atoms		11	13	15	17
Crystal form and subcell	A′		t[6]	t*[10]	t*[10]
	B′		t[2,8]	t	t
	C′	m[9]	m*[10]	m*[10]	m*[10]
Crystal form	from 2,2,4-trimethyl pentane		A′	B′	B′
			(stable form at room temp)		
	from melt	C′[10]	A′	B′	B′
Transition on heating			C′	C′	C′

t; triclinic, m; monoclinic t*, m*; The crystal structure has not been determined; The crystal system was deduced from powder diffraction data.[10]

TABLE 2. FRACTIONAL ATOMIC COORDINATES (×10^4) AND THERMAL PARAMETERS FOR NON-HYDROGEN ATOMS

$$B_{eq}=\frac{4}{3}\Sigma_i\Sigma_j\beta_{ij}\boldsymbol{a}_i\cdot\boldsymbol{a}_j.$$

Atom	X	Y	Z	B_{eq}/Å^2
C17	3346(30)	6513(24)	4636(3)	10.0
C16	4627(27)	5606(20)	4379(3)	8.0
C15	3499(22)	6244(17)	4094(3)	5.7
C14	4801(22)	5256(16)	3840(3)	5.5
C13	3623(21)	5933(16)	3549(2)	4.8
C12	4992(20)	4974(15)	3305(2)	4.7
C11	3823(20)	5658(15)	3010(2)	4.5
C10	5178(20)	4698(15)	2760(2)	4.5
C9	4026(20)	5393(15)	2470(2)	4.4
C8	5346(20)	4414(15)	2218(2)	4.4
C7	4248(20)	5131(15)	1938(3)	4.6
C6	5547(19)	4152(15)	1682(2)	4.4
C5	4539(19)	4880(15)	1409(2)	4.1
C4	5854(20)	3919(15)	1154(2)	4.4
C3	4907(18)	4653(14)	877(2)	3.5
C2	6537(19)	3737(14)	661(2)	4.0
C1	5818(19)	4351(14)	372(2)	3.7
O1	4073(13)	5459(9)	315(2)	4.4
O2	7309(12)	3608(9)	201(2)	4.5
C34	-837(34)	1505(23)	4669(3)	10.5
C33	-1774(26)	511(19)	4305(3)	7.1
C32	-406(23)	1198(16)	4151(3)	5.8
C31	-1472(20)	238(16)	3771(2)	4.8
C30	-132(21)	934(15)	3619(2)	4.7
C29	-1251(20)	-30(15)	3230(2)	4.6
C28	113(20)	681(15)	3083(2)	4.4
C27	-1019(20)	-289(15)	2697(3)	4.8
C26	338(19)	431(15)	2547(2)	4.1
C25	-748(20)	-549(15)	2168(2)	4.5
C24	559(19)	165(14)	2003(2)	4.2
C23	-508(19)	-848(14)	1630(2)	4.1
C22	714(20)	-141(15)	1457(2)	4.4
C21	-476(20)	-1190(15)	1083(2)	4.3
C20	573(19)	-479(14)	897(2)	4.2
C19	-899(20)	-1521(15)	523(2)	4.4
C18	-392(20)	-790(14)	308(3)	4.4
O3	1587(13)	194(10)	416(2)	5.3
O4	-2078(14)	-1287(11)	3(2)	6.1

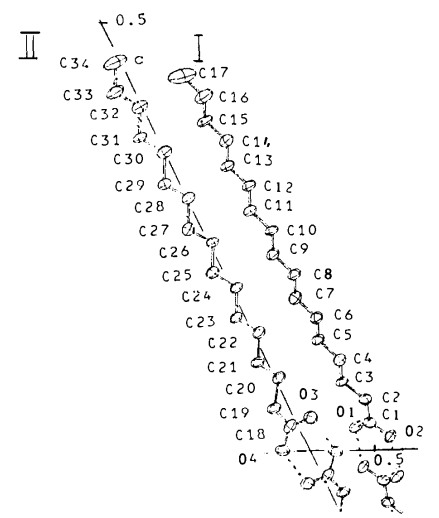

Fig. 1. ORTEP drawing along the b-direction and the numbering system of atoms.
The ellipsoids are drawn to enclose 40% probability.

†Present address: Toyohashi University of Technology 1-1, Hibarigaoka, Tenpaku-cho, Toyohashi, Aichi 440.

by the block-diagonal least-squares method using the UNICS III system.[3] The R-value was reduced to 0.077. The final atomic parameters[4] are listed in Table 2.

Results and Discussion

The B′-form of heptadecanoic acid has a characteristic layer structure, such as is usually found in fatty acids. As shown in Fig. 1, the molecules form all-trans zigzag chains, in contrast to the case of the B-form of stearic acid,[5] in which the bond between the second and third carbon atoms takes a gauche conformation. The structural parameters are shown in Table 3. The subcell, *i.e.* the cell which describes the repetition in the hydrocarbon chains,[1] was found to be orthorhombic, with the following dimensions: a_s=5.0 Å, b_s=7.4 Å, and c_s=2.54 Å, similar to that of the B-form of stearic acid.[5]

The conformations of the two molecules (I, II) in the asymmetric unit are similar to each other. These molecules are joined in pairs by hydrogen bonds between the carboxyl groups with the O···O distances of 2.64(1) Å (I-I) and 2.62(1) Å (II-II). The dihedral angles between the planes containing the carboxyl groups was 11° (I-I), and 21° (II-II), nearly the same as those in the other fatty acids.[6,7] The second closest oxygen contact distance is 3.2 Å as shown in Fig. 2.

TABLE 3. STRUCTURAL PARAMETERS

Interatomic distance (l/Å)

C34	C33	1.49(2)	C22	C21	1.52(1)	C11	C10	1.55(2)
C33	C32	1.54(2)	C21	C20	1.53(1)	C10	C9	1.56(2)
C32	C31	1.55(2)	C20	C19	1.53(2)	C9	C8	1.54(2)
C31	C30	1.53(2)	C19	C18	1.51(2)	C8	C7	1.52(2)
C30	C29	1.52(2)	C18	O3	1.26(1)	C7	C6	1.55(2)
C29	C28	1.52(2)	C18	O4	1.29(2)	C6	C5	1.50(2)
C28	C27	1.52(2)	C17	C16	1.54(2)	C5	C4	1.55(2)
C27	C26	1.54(2)	C16	C15	1.51(2)	C4	C3	1.52(2)
C26	C25	1.53(2)	C15	C14	1.55(2)	C3	C2	1.54(2)
C25	C24	1.57(2)	C14	C13	1.54(2)	C2	C1	1.53(2)
C24	C23	1.51(1)	C13	C12	1.53(2)	C1	O1	1.22(1)
C23	C22	1.57(2)	C12	C11	1.57(2)	C1	O2	1.31(1)

Bond angle (ϕ/°)

C32	C33	C34	111.9(13)	C15	C16	C17	113.1(12)
C31	C32	C33	112.2(10)	C14	C15	C16	111.7(11)
C30	C31	C32	112.1(10)	C13	C14	C15	111.1(9)
C29	C30	C31	112.0(9)	C12	C13	C14	110.5(9)
C28	C29	C30	111.2(9)	C11	C12	C13	110.9(9)
C27	C28	C29	110.5(9)	C10	C11	C12	111.1(9)
C26	C27	C28	110.7(9)	C 9	C10	C11	110.9(9)
C25	C26	C27	110.6(9)	C 8	C16	C17	111.0(9)
C24	C25	C26	112.3(9)	C 7	C15	C16	111.6(9)
C23	C24	C25	111.2(9)	C 6	C14	C15	111.2(9)
C22	C23	C24	112.3(9)	C 5	C13	C14	111.8(9)
C21	C22	C23	110.0(9)	C 4	C12	C13	112.0(9)
C20	C21	C22	112.0(9)	C 3	C11	C12	113.2(9)
C19	C20	C21	108.8(9)	C 2	C10	C11	108.5(9)
C18	C19	C20	114.1(9)	C 1	C 2	C 3	114.6(9)
C18	C19	O3	122.1(9)	C 1	C 2	O 1	112.7(10)
C18	C19	O4	115.7(10)	C 1	C 2	O 2	113.2(9)
O3	C19	O4	122.2(9)	O 2	C 1	O 1	124.1(12)

Torsion angle (ϕ/°)

C17	C16	C15	C14	-178(1)	C34	C33	C32	C31	-177.1(
C16	C15	C14	C13	-180(1)	C33	C32	C31	C30	179(1)
C15	C14	C13	C12	178(1)	C32	C31	C30	C29	-179(1)
C14	C13	C12	C11	-179(1)	C31	C30	C29	C28	-180(1)
C13	C12	C11	C10	-180(1)	C30	C29	C28	C27	180(1)
C12	C11	C10	C9	-179(1)	C29	C28	C27	C26	180(1)
C11	C10	C9	C8	-179(1)	C28	C27	C26	C25	179(1)
C10	C9	C8	C7	-180(1)	C27	C26	C25	C24	179(1)
C9	C8	C7	C6	-180(1)	C26	C25	C24	C23	179(1)
C8	C7	C6	C5	-178(1)	C25	C24	C23	C22	179(1)
C7	C6	C5	C4	179(1)	C24	C23	C22	C21	-179(1)
C6	C5	C4	C3	-179(1)	C23	C22	C21	C20	178(1)
C5	C4	C3	C2	175(1)	C22	C21	C20	C19	-176(1)
C4	C3	C2	C1	-180(1)	C21	C20	C19	C18	171(1)
C3	C2	C1	O1	-1(2)	C20	C19	C18	O3	19(1)
C3	C2	C1	O2	177(1)	C20	C19	C18	O4	-162(1)

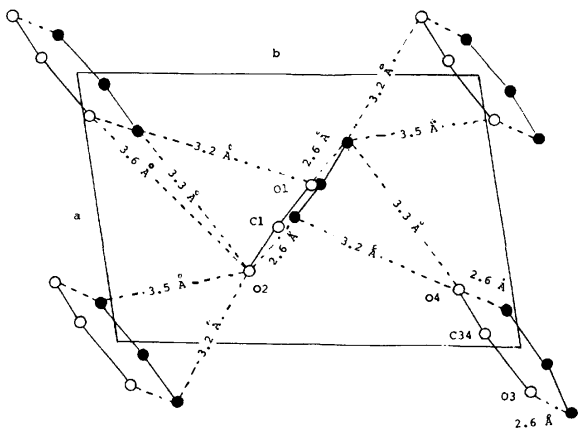

Fig. 2. Carboxyl groups projected along the c* axis.

This value agrees well with that of the B-form of stearic acid.[5] Von Sydow[2] reported that the hydrogen bond was formed between the crystallographically independent molecules (such as I-II) in the structure of the B′-form of pentadecanoic acid. We reinvestigated it and found that the hydrogen bond is formed between the two molecules related by a center of symmetry as in the B′-form of heptadecanoic acid.[8]

It is known that in the odd-numbered fatty acids a transition B′⇄C′ is reversible but in the even numbered ones a transition B⇄C is not.[1] This difference may be related to the fact that in the odd members the molecular conformation of the B′-form is similar to that of the C′-form because both of them have all-trans zigzag chains but in the even members the B-form has a bond of gauche conformation whereas the C-form does not.[5]

We are grateful to Professor Y. Iitaka of the University of Tokyo for his encouragement and helpful discussions. We are indebted to Dr. T. Sakurai and Miss K. Kobayashi of the Institute of Physical and Chemical Research for the programs UNICS III used in this work.

References

1) E. von Sydow, *Arkiv Kemi*, **39**, 231 (1956).
2) E. von Sydow, *Acta Crystallogr.*, **7**, 823 (1954).
3) T. Sakurai and K. Kobayashi. *Rikagaku Kenkyusho Hokoku*, **55**, 69 (1978).
4) The lists of structure factors, the atomic parameters for the hydrogen atoms and anisotropic thermal parameters for the non-hydrogen atoms are deposited at the Office of the Chemical Society of Japan. (Document No. 8402).
5) M. Goto and E. Asada, *Bull. Chem. Soc. Jpn.*, **51**, 2456 (1978).
6) M. Goto and E. Asada, *Bull. Chem. Soc. Jpn.*, **53**, 2111 (1980).
7) M. Goto and E. Asada, *Bull. Chem. Soc. Jpn.*, **51**, 70 (1978).
8) M. Goto, to be published.
9) E. von Sydow, *Acta Crystallogr.*, **8**, 810 (1955).
10) R. T. O'Conner, "Fatty Acids," ed by K. S. Markley, Interscience, New York (1960), Part 1, p. 285.

Solvent Effects on the Intensity of the nπ* Absorption Spectra of 1-Phenylethylenetrithiocarbonate and *p*-Benzoquinones

Yasufumi JINNOUCHI, Motohisa KOHNO, and Akira KUBOYAMA*

National Chemical Laboratory for Industry, Tsukuba Research Center, Yatabe, Ibaraki 305

(Received August 22, 1983)

Synopsis. The nπ* absorption intensities of 1-phenylethylene trithiocarbonate (**1**), *p*-benzoquinone (**2**), and 2,5-di-*t*-butyl-p-benzoquinone (**3**) in nonpolar solvents are compared with the theoretical ones calculated by the use of Abe's formula, in which the Onsager-cavity field is used. For **3**, the theoretical intensities are well correlated with the observed ones, whereas for the others there are discrepancies, especially for **1**. These discrepancies are attributed to strong dispersion-force interactions with the solvents.

Experimental data about solvent effects on the intensity of the electronic absorption spectra are still scarce. Previously, however, we found that the intensity of the nπ* absorption spectrum of *p*-benzoquinone (PBQ) in carbon disulfide is far stronger than that in heptane.[1] Recently, we also found that the intensification of the thiocarbonyl nπ* absorption spectrum of 1-phenylethylene trithiocarbonate (PTC) in carbon disulfide is greater than that of PBQ. In the studies of the solvent effects on the intensity of the nπ* absorption spectra PTC is favorable in that the nπ* absorption spectrum is at far longer wavelengths than the longest wavelength ππ* absorption spectrum and in that the steric hindrance about the thiocarbonyl group is small.

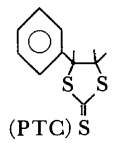

Experimental

Measurements. The absorption spectra have been obtained by means of a Cary 14 self-recording spectrophotometer. The integrated absorption intensities of the spectra were obtained by measuring the weight of the section papers, on which the areas are the same as those surrounded by the absorption curves and the baselines. In order to minimize errors which might be caused by any unevenness of the quality of the section papers used, they were calculated from the ratio of the weight of a portion of an absorption spectrum to that of a polygon[2] inscribed in it. In this method, the errors were within 0.4%.

Materials. The PTC (Toyotama Kogyo Co.) was purified by vacuum sublimation (mp 85.0—86.0°C). The PBQ (Tokyo Kasei Kogyo Co.) was purified by sublimation (mp 115.0—116.0°C). The 2,5-di-*t*-butyl-*p*-benzoquinone (2,5-PBQ) (Tokyo Kasei Kogyo Co.) was twice recrystallized from cyclohexane (mp 152.7°C). All the solvents employed, *i.e.*, cyclohexane, benzene, carbon tetrachloride, and carbon disulfide, were of a spectro-grade (all from Wako Pure Chemical Industries Co. except for the carbon disulfide of E. Merck), and were used without further purification. GR-grade 1-methylnaphthalene (Tokyo Kasei Kogyo Co.) was purified by vacuum distillation.

Results and Discussion

The long-wavelength absorption spectra of PTC in several nonpolar solvents in Fig. 1 can safely be assigned to the thiocarbonyl nπ* spectrum[1,3] from their positions and from the intensity and solvent effects on their positions; this nπ* transition has previously been thought to be essentially forbidden, like that of quinones,[1] in view of the weak intensity of these spectra. The intensity of the nπ* spectra of PTC and quinones is thought to be essentially due to the vibronic mixing of the nπ* and the closest allowed ππ* state.[4]

In Tables 1 and 2, the ratios of the *f*-values (oscillator strengths) of the nπ* spectra in various nonpolar solvents and that in cyclohexane are compared with those obtained by means of Abe's formula,[5]

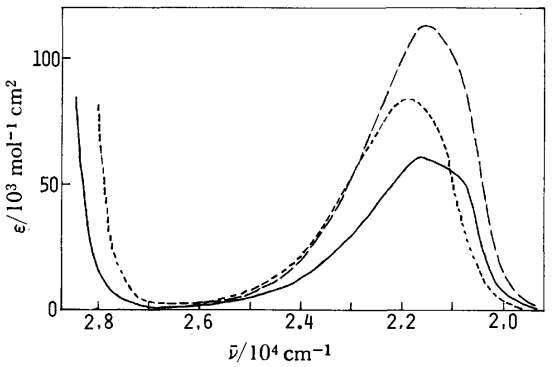

Fig. 1. The nπ* absorption spectra of 1-phenylethylene trithiocarbonate in nonpolar solvents. ——: Cyclohexane, ----: benzene, — —: carbon disulfide.

TABLE 1.[a] 1-PHENYLETHYLENE TRITHIOCARBONATE ($f_{C_6H_{12}}=3.60\times10^{-4}$)

Solvent	n_D^{20}	$\bar{\nu}_{max}$	ε_{max}	$f_X/f_{C_6H_{12}}$	
		cm⁻¹	10³ mol⁻¹ cm²	Obsd	Theoret.
Cyclohexane	1.426	21650	60.5	1.00	1.000
Carbon tetrachloride	1.460	21800	80	1.21	0.978
Benzene	1.501	21900	84	1.19	0.949
1-Methyl-naphthalene	1.617	22000	101.5	1.28	0.864
Carbon disulfide	1.628	21600	112.5	1.35	0.841

a) f_X denotes the *f*-value in the solvent X.

TABLE 2.[a] *p*-BENZOQUINONE (**1**) ($f_{C_7H_{16}}=1.73\times10^{-4}$) AND 2,5-di-*t*-BUTYL-*p*-BENZOQUINONE (**2**) ($f_{C_6H_{12}}=2.68\times10^{-4}$)

	Solvent	n_D^{20}	$\bar{\nu}_{max}$	f_X/f_{HC}[b]	
			cm^{-1}	Obsd	Theoret.
1	Heptane	1.388	21850	1.00	1.000
	Carbon tetrachloride	1.460	21850	1.02	0.943
	Carbon disulfide	1.628	21750	1.04	0.811
2	Cyclohexane	1.426	21850	1.00	1.000
	Carbon tetrachloride	1.460	21900	0.98	0.972
	Carbon disulfide	1.628	21750	0.84	0.839

a) f_X denotes the *f*-value in the solvent X. b) f_{HC} denotes $f_{C_7H_{16}}$ in **1** and $f_{C_6H_{12}}$ in **2**.

derived with the Onsager-cavity field, on the basis of the quantum-mechanical theory. In obtaining the observed *f*-values, the factor of $(1/n_D^{20})$[2] (n_D^{20}: refractive index of the D-line at 20°C) is included.[5,6] In Abe's work,[5] the formula derived with the Onsager-cavity field best reproduced the observed results among the many formulas thus far derived by many authors. In 2,5-PBQ, the observed results are close to the theoretical ones, while in PTC and PBQ the observed results are far from the theoretical ones, especially in PTC. The above results can be interpreted as follows.

In 2,5-PBQ, solvent molecules can hardly ever approach the carbonyl oxygen atoms because of the heavy steric hindrance caused by the two *t*-butyl groups. In PBQ, the hydrogen atoms attached to the α-carbon atoms cause something of a steric hindrance to the approach of solvent molecules to its carbonyl oxygen atoms. On the other hand, in PTC there is no such steric hindrance. Moreover, in PTC the bond length of the thiocarbonyl C-S bond is longer than that of the C-O bonds of PBQ, and the 3p lone-pair orbital of the sulfur atom is far more spread outward than the 2p lone-pair orbital of the oxygen atoms of PBQ. Therefore, solvent molecules can approach more easily to the thiocarbonyl sulfur atom of PTC than to the oxygen atoms of PBQ.

From the above discussion, the before-mentioned discrepancy of the observed results from the theoretical ones may be concluded to be essentially related to the approachability of solvent molecules to these heteroatoms. As the main interaction between nonpolar solvent molecules and these heteroatoms, which causes the intensification of the $n\pi^*$ spectra, any interaction but the dispersion-force interaction can hardly ever be cited. Previously Koyanagi[7] theoretically proved that the dispersion-force interaction between solvents and a solute may cause mixing between a forbidden state and the allowed states of the solute, resulting in an intensification of the forbidden spectrum, and later Koyanagi *et al.*[7,8] experimentally showed this on the $n\pi^*$ absorption spectra of carbonyl compounds. The dispersion-force interaction is very sensitive to the distance between the component molecules. Moreover, it becomes, in general, stronger with decreases in the ionization potentials of the component molecules. The ionization potential of the 3p lone-pair electron of the thiocarbonyl sulfur atom in PTC is considerably lower than that of the 2p lone-pair electrons of the carbonyl oxygen atoms in PBQ. Consequently, the dispersion-force interaction of PTC with solvents may be considerably stronger than that of PBQ. Therefore, the main cause of the before-mentioned discrepancy of the observed results may be attributed to the strong dispersion-force interaction of PTC and PBQ with the nonpolar solvents.

Generally speaking, the blue-shift of an $n\pi^*$ spectra in a solvent relative to that in saturated hydrocarbons shows that there are some specific interactions between the solvent and the solute, such as hydrogen-bond formation and charge-transfer and electrostatic interactions.[1] The $n\pi^*$ spectrum of PTC in carbon disulfide is at almost the same position as that in cyclohexane.[1] This fact may show that specific interactions between carbon disulfide and PTC are very small. Therefore, the remarkable enhancement of the $n\pi^*$ absorption intensity of PTC in carbon disulfide can hardly ever be attributed to the complex formation between carbon disulfide and PTC.

References

1) A. Kuboyama, *Bull. Chem. Soc. Jpn.*, **33**, 1027 (1960); *Tokyo Kogyo Shikensho Hokoku*, **57**, 541 (1962).
2) The area of the polygon can be easily calculated.
3) a) J. W. Sidman, *Chem. Rev.*, **58**, 689 (1958); b) S. F. Mason, *Quart. Rev.*, **15**, 287 (1961).
4) J. A. Pople and J. W. Sidman, *J. Chem. Phys.*, **27**, 1270 (1957); Ref. 3a; D. C. Moule and A. D. Walsh, *ibid.*, **75**, 67 (1975).
5) T. Abe, *Bull. Chem. Soc. Jpn.*, **43**, 625 (1970).
6) H. Baba, "Jikkenkagaku Koza," ed by The Chemical Society of Japan, Maruzen, Tokyo (1965), Ser. 11, p. 22.
7) M. Koyanagi, *J. Mol. Spectrosc.*, **25**, 273 (1968).
8) K. Nakashima, K. Uchida-Kai, M. Koyanagi, and Y. Kanda, *Bull. Chem. Soc. Jpn.*, **55**, 415 (1982); K. Nakashima and M. Koyanagi, *ibid.*, **55**, 3923 (1982).

Freezing of Water as Aggregated with Cationic Surfactants in Deuterochloroform

Junzo SUNAMOTO,* Tomiko HAMADA, and Hiroki KONDO
Department of Industrial Chemistry, Faculty of Engineering, Nagasaki University, Nagasaki 852
(Received May 25, 1983)

Synopsis. Freezing of water solubilized with the cationic CTAX(hexadecyltrimethylammonium halides) and QDX (dihexadecyldimethylammonium halides) in deuterochloroform was observed by ^{1}H-NMR method. The freezing of water was largely affected by the characteristics of the water-surfactant aggregates by the R-value(=[H_2O]/[surfactant]) and the structure of surfactant. In the 0.20 M (1 M=1 mol dm^{-3}) CTABr/0.16 M H_2O/$CDCl_3$ system, for example, the apparent freezing was observed at about −20 °C.

Various surfactants form aggregates with polar solutes, usually water molecules, in apolar media. People call the aggregates "reversed micelles" sometimes. "The aggregates" can provide specific and restricted reaction field for various chemical reactions[1] irrespectively of the concept of the cmc and aggregation number. In such a specific system equilibria, rates, and pathways of chemical reactions can be controlled by continuously and simultaneously changing the micropolarity and microviscosity of the reaction field and the activity of the cosolubilizates as a function of water content in the system.[2] Extending a series of our studies on the characterization of "the aggregates" or "reversed micelles", in this work, we would like to report an apparent freezing of water in the system. For this purpose, ^{1}H-NMR method for the water proton signal was utilized.[3,4]

Experimental

All the spectra were obtained using a JEOL 100 MHz NMR spectrometer at various probe temperatures with TMS as an internal standard. The probe temperature was calibrated carefully with methanol proton signals before and after measurements. Water content was determined on a Kyoto Electronics MFG Karl-Fischer Moisture Automatic Titrater, Model MK-AIII. Through all the runs deuterochloroform was employed as a bulk solvent to form the water-surfactant aggregates. Surfactants were the same as those used in a previous work.[3]

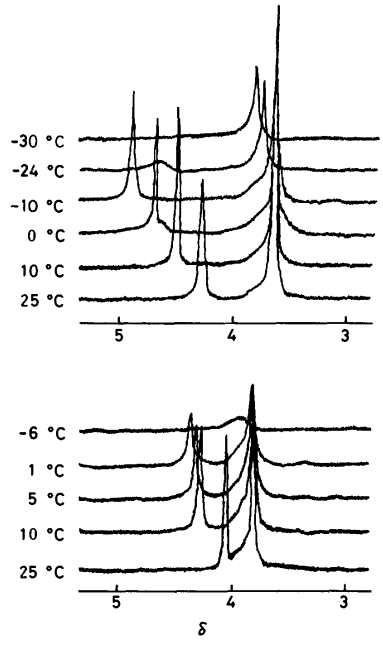

Fig. 1. NMR proton signals of water (lower field) and N-methyl group (upper field) of 0.20 M CTACl/0.444 M H_2O/$CDCl_3$ (top) and 0.10 M QDCl/0.245 M H_2O/$CDCl_3$ (bottom) at various temperatures.

Results and Discussion

Since the life time of both water protons, located in bulk phase and interacting with surfactant, is faster than the NMR time scale, only one signal of water proton was observed by NMR.[3]

First, lowering the probe temperature causes a downfield shift of the water proton signal with a concomitant line-broadening (Fig. 1). Further lowering the temperature shows a sudden and large line-broadening and a shift toward upper magnetic field of the signal. Hence, this point was defined tentatively as the apparent freezing point of water in this system. Second, the chemical shift of water proton siganl was due to both the R-value(=[H_2O]/[surfactant]) and the structure of surfactant.[3,4]

Water in deuterochloroform containing no surfactants shows a signal at 1.96 ppm (25.0 °C). In the cationic surfactant-water aggregates, water molecules interact with the strongly electronegative cation-head of surfactants by means of coordination-type.[3] This means that the water proton signal in micellar system appears downfield far from the value in chloroform: In the present cationic aggregates, the water proton

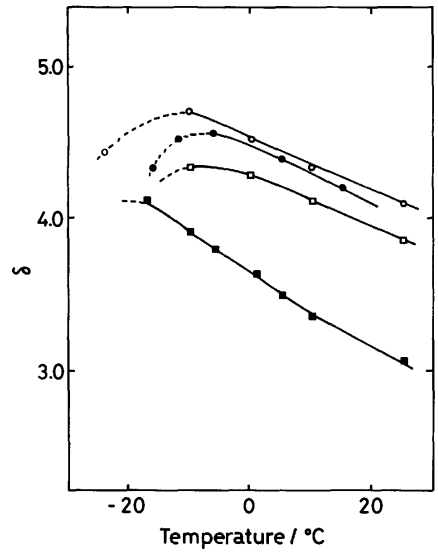

Fig. 2. Chemical shifts of water proton signal in the 0.20 M CTAX/$CDCl_3$ system as a function of the probe temperature: -○-, CTACl (R=2.22); -●-, CTABr (R=2.24); -□-, CTABr (R=2.04); -■-, CTABr (R=0.80), respectively. Drastic line-broadenings were observed over the broken line region.

signals were usually observed around 3—5 ppm (Figs. 1 and 2). Increasing the R-value produces hydrogen bonding between water molecules themselves and causes the paramagnetic shift of the proton signal as seen in Fig. 2. The chemical shift of the water proton under consideration seems to finally reach the value of pure bulk water (4.66 ppm). From the same reason, it is certain that upon lowering temperature the mobility of water molecules decreases and simultaneously both the hydrogen bonding between water molecules and the interaction between water and surfactants become stronger, resulting in further downfield shift of the signal (Fig. 2). Freezing and solubility decrease of water with lowering of temperature lead to a phase separation of the system. This was observed in a drastic change on the chemical shift and line width of the water proton signal. The apparent freezing point thus obtained was largely affected by the R-value, structure of surfactant, and bulk solvent. For example, in the case of CTABr aggregates in $CDCl_3$, the apparent freezing point was about $-20°C$ for $R=0.80$, $-10°C$ for 2.04, and $-6°C$ for 2.22, respectively. For QDBr micelles, it was about $-1°C$ for $R=0.60$ and $0°C$ for 2.45. However, in the case of anionic AOT aggregates in $CDCl_3$, no decrease in the freezing temperature was observed even when the R-value was below unity.

In any event, the nature of water bound to surfactants in apolar media is rather different from that of bulk water. In addition, the present work suggests to us that one can conduct chemical reactions in an aqueous system even below $0°C$ if an appropriate system was provided with the water-surfactant aggregates in apolar media.[5]

References

1) J. H. Fendler and E. J. Fendler, "Catalysis in Micellar and Macromolecular Systems," Academic Press, London, (1975), Chap. 10.

2) J. Sunamoto, "Control of Reactions in Extremely Restricted Environment Provided by Reversed Micelles," in "Solution Behavior of Surfactants-Theoretical and Applied Aspects," ed by K. L. Mittal and E. J. Fendler, Plenum Publishing Co. (1982), Vol. 2, p. 767.

3) J. Sunamoto, T. Hamada, T. Seto, and S. Yamamoto, *Bull. Chem. Soc. Jpn.*, **53**, 583 (1980).

4) H. Kondo, T. Hamada, S. Yamamoto, and J. Sunamoto, *Chem. Lett.*, **1980**, 809.

5) J. Sunamoto, H. Kondo, T. Hamada, S. Yamamoto, Y. Matsuda, and Y. Murakaki, *Inorg. Chem.*, **19**, 3668 (1980).

ESR Studies of Spin-Spin Dipolar Interaction in Pure and Diluted Phenoxyl Radical Solids

Kazuo MUKAI,* Kyozo UEDA, Kazuhiko ISHIZU, and Seigo YAMAUCHI†
Department of Chemistry, Faculty of Science, Ehime University, Matsuyama 790
†*Department of Chemistry, Faculty of Science, Kyoto University, Sakyo-ku, Kyoto 606*
(Received August 26, 1983)

Synopsis. ESR studies have been carried out on powder samples of pure phenoxyl (2,6-di-*t*-butyl-4-phenylphenoxyl) and 3% phenoxyl diluted in its diamagnetic corresponding phenol matrix. The dipolar splittings due to the spin pairs in closest approach have been observed for both the pure and 3% phenoxyl.

Recently, many investigations have been performed for the magnetic properties of some organic stable neutral radicals, including phenoxyl radicals. The magnetic susceptibility of these radicals deviates from the Curie-Weiss law at low temperatures and shows a broad maximum. This behavior of the paramagnet could be well described by the Heisenberg one-dimensional model or .singlet-triplet equilibrium model with isotropic antiferromagnetic exchange interaction: The value of the spin-spin exchange interaction (J) between neighboring radical molecules in these radical solids has been determined, by comparing experimental curve of susceptibility with theoretical one.[1] However, the examples that the property of the spin-spin dipolar interaction (D) in these radical solids has been clarified are very limited.[2,3] Recently, ESR studies have been carried out on powder samples of pure galvinoxyl and 1% galvinoxyl doped in its diamagnetic corresponding phenol matrix, which has the same crystal structure with that of galvinoxyl at 293 K. The existence of radical pairs in both the pure galvinoxyl and 1% galvinoxyl has been confirmed by the observation of the ESR zero-field splittings at 77 K, and, thus, by comparing the observed zero-field splittings, the mechanism of a first-order phase transition from paramagnetic to diamagnetic (or weak paramagnetic) reported previously for galvinoxyl at 85 K has been discussed.[4,5]

In the present work, in order to clarify the property of the spin-spin dipolar interaction in organic radical solids, we have measured the ESR spectra of powder samples of pure 2,6-di-*t*-butyl-4-phenylphenoxyl[6] (**1**) (abbreviated to phenoxyl hereafter) (see Fig. 1) and 3% phenoxyl diluted in its diamagnetic corresponding phenol matrix in the temperature range 293—77 K and 4.2 K.

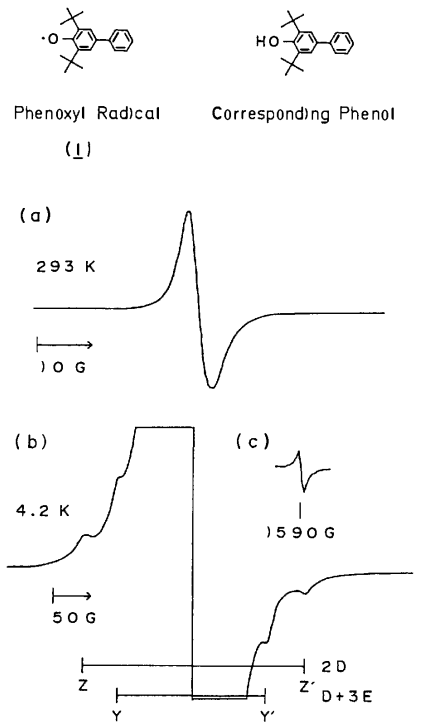

Fig. 1. ESR spectrum of a powder of phenoxyl (**1**); (a) $\Delta m_s=\pm1$ transition spectrum at 293 K, (b) $\Delta m_s=\pm1$ transition spectrum at 4.2 K, and (c) $\Delta m_s=\pm2$ transition spectrum at 4.2 K.

Experimental

Radical concentration of **1** was obtained from the results of the paramagnetic susceptibility measurements at 20°C, after correcting for the diamagnetic contribution ($\chi_{dia}=-0.204\times10^{-3}$ emu/mol) calculated by the Pascal's method. The value was 99% for **1**, assuming the Curie law. The powder sample of 3% phenoxyl diluted in its diamagnetic corresponding phenol matrix was prepared according to the procedure used for diluted galvinoxyl.[4]

Results and Discussion

The ESR spectrum of powder sample of the phenoxyl (**1**) at 293 K shows an exchange-narrowed, Lorentz-type absorption with a width of 4.5 G (1 G=10^{-4} T) located at g=2.0047, as shown in Fig. 1(a). When the temperature is lowered, the linewidth starts to increase gradually, and becomes 6.5 G at 77 K. In addition to the strong central singlet, two pairs of weak, broad side peaks were observed with the same order of intensity at 4.2 K, as shown in Fig. 1(b). The two pairs of absorption lines will be due to zero-field splittings arising from the intermolecular spin-spin dipolar interaction of two electrons in a triplet state.[7] In fact, the forbidden transition ($\Delta m_s=\pm2$) was observed at about 1590 G, as shown in Fig. 1(c). The zero-field splitting parameters and g-tensor values were evaluated as $|D|=148.2\pm0.4$ G and $|E|=17.0\pm0.4$ G and $g_{zz}=2.0027\pm0.0003$ (Z,Z') and $g_{yy}=2.0044\pm0.0003$ (Y,Y'), respectively. This phenomenon will be considered to be similar to the cases of some TCNQ salts and bisgalvinoxyl biradical, which also exhibit ESR zero-field splittings at low temperatures.[3,8] The magnetic susceptibilities of the above TCNQ salts and the bisgalvinoxyl biradical were well explained by singlet-triplet equilibrium model with lower singlet

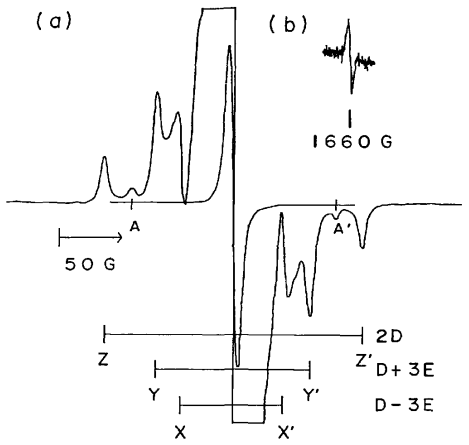

Fig. 2. ESR spectrum of a powder of 3% phenoxyl (**1**) at 293 K; (a) $\Delta m_s=\pm 1$ transition spectrum and (b) $\Delta m_s=\pm 2$ transition spectrum.

and upper triplet states. Therefore, our ESR data of the phenoxyl (**1**) indicate that this radical is a ground singlet with a thermally accessible triplet state.

The ESR spectrum of 3% phenoxyl at 293 K shows three pairs of absorption lines (Z,Z'; Y,Y'; and X,X') with the same order of intensity, as shown in Fig. 2(a). The three pairs of absorption lines apparently represent zero-field splittings arising from the intermolecular dipolar interaction of two electrons in a triplet state; thus, the zero-field splitting parameters and g-tensor values were evaluated as $|D|=101.3\pm 0.4$ G and $|E|=6.9\pm 0.4$ G and $g_{zz}=2.0043\pm 0.0003$ (Z,Z'), $g_{yy}=2.0042\pm 0.0003$ (Y,Y'), and $g_{xx}=2.0045\pm 0.0003$ (X,X'), respectively. In addition, the other weak $\Delta m_s=\pm 1$ absorptions (A,A') with a separation of about 161 G were observed in the ESR spectra, as shown in Fig. 2(a). The weak absorptions may be due to a radical triad.[9]

Careful measurements of the positions of the resonance lines show that this zero-field splitting is linearly temperature-dependent with $d|D|/dT=-(28\pm 2)\times 10^{-3}$ G K^{-1}. In the same way the $|E|$ thermal dependence is estimated to be about $d|E|/dT=-(4\pm 2)\times 10^{-3}$ G K^{-1}. This result may be interpreted as arising from the thermal expansion of the crystal lattice. The zero-field splitting parameters observed at 4.2 K are $|D|=109.3\pm 0.4$ G and $|E|=7.9\pm 0.4$ G. Here, the calculated average interelectronic distances, using a model of two point dipoles, are 6.50 Å at 293 K and 6.34 Å at 4.2 K for 3% phenoxyl. The spectrum at 4.2 K is similar to those above 77 K, and at 4.2 K, no deviation from linear temperature-dependency has been observed in D and E values.

In the present experiments, we observed the dipolar splittings due to the spin-pairs in closest approach for both the pure and 3% phenoxyl (**1**) at 4.2 K.[4] If the crystal structure of the phenol precursor of **1** is the same as that of phenoxyl (**1**), the value of the dipolar splitting observed for the diluted phenoxyl crystals will be considered to be the same as that of the neat phenoxyl crystal. However, the D and E parameters ($|D|=148.2$ G and $|E|=17.0$ G) obtained for pure phenoxyl are very different from those ($|D|=109.3$ G and $|E|=7.9$ G) obtained for 3% phenoxyl (**1**) at 4.2 K. Therefore, at first, we expected that the pure phenoxyl may show a first-order phase transition at low temperature, as observed for galvinoxyl,[5] and measured the Debye-Scherrer X-ray diffraction patterns at 293 K. However, the diffraction patterns observed for the pure phenoxyl and the corresponding phenol did not agree with each other in their diffraction angles and intensities at 293 K, contrary to our expectations. Both the phenoxyl radical (**1**) and the corresponding phenol may be considered to be biphenyl derivatives; the molecule of biphenyl is planar or nearly so in both the solid and triplet state, but twisted 30—40° around the central single bond in the vapor and in solution. Thus, the degree of twisting of biphenyl molecule is clearly due to a delicate balance of nonbonded repulsion and conjugation. In a previous paper,[10] it is reported that the phenoxyl radical (**1**) has planar character, because the inter-ring bond acquires some double-bond character in the phenoxyl radical in view of a valence-bond. On the other hand, the corresponding phenol does not acquire such double bond character, showing different crystal structure with that of the pure phenoxyl.

As described above, we observed the zero-field splittings due to the spin-pairs in closest approach for the pure phenoxyl at 4.2 K; the result indicates that this radical is a ground singlet with a thermally accessible triplet state. However, usually, the powder sample of the radical solids shows an "exchange-narrowed" single ESR absorption line, because of strong spin-spin exchange interaction operating between neighboring radical molecules. Consequently, the examples that the property of the spin-spin dipolar interaction (D) in the radical solids has been clarified are very limited.[2,3] Therefore, the observation of the dipolar splittings in phenoxyls diluted in their diamagnetic corresponding phenol matrices may be of significance.

The authors are much obliged to Professor Noboru Hirota of Kyoto University for the ESR measurements at 4.2 K.

References

1) N. Azuma, *Bull. Chem. Soc. Jpn.*, **55**, 1357 (1982), and references cited therein.
2) F. Genoud and M. Decorps, *Mol. Phys.*, **34**, 1583 (1977).
3) K. Mukai and J. Sakamoto, *J. Chem. Phys.*, **68**, 1432 (1978).
4) K. Mukai and A. Sogabe, *J. Chem. Phys.*, **72**, 598 (1980).
5) K. Mukai, K. Ueda, K. Ishizu, and Y. Deguchi, *J. Chem. Phys.*, **77**, 1606 (1982).
6) E. Müller, A. Schick, and K. Scheffler, *Chem. Ber.*, **92**, 474 (1959).
7) E. Wasserman, L. C. Snyder, and W. A. Yager, *J. Chem. Phys.*, **41**, 1763 (1964).
8) D. B. Chesnut and W. D. Phillips, *J. Chem. Phys.*, **35**, 1002 (1961).
9) N. Azuma, H. Ohya-Nishiguchi, J. Yamauchi, K. Mukai, and Y. Deguchi, *Bull. Chem. Soc. Jpn.*, **47**, 2369 (1974).
10) K. Mukai and N. Inagaki, *Bull. Chem. Soc. Jpn.*, **53**, 2695 (1980).

Paramagnetic Cobalt(III) Complexes with Organic Ligands. VIII.[1] The NMR Spectra of Paramagnetic Tetraammine(5-nitrosalicylato)cobalt(III) Chloride Nitrate Hydrate and the Related Compounds

Yoshihisa YAMAMOTO,* Shigezo SHIMOKAWA,† and Eiji YAMADA†
Faculty of Pharmaceutical Sciences, Higashi Nippon Gakuen University, Ishikari-Tobetsu, Hokkaido 061-02
†*NMR Laboratory, Faculty of Engineering, Hokkaido University, Sapporo 060*
(Received July 13, 1983)

Synopsis. The ring proton signals have been assigned for the ^{1}H NMR spectra of the green paramagnetic tetraammine(5-nitrosalicylato)cobalt(III) chloride nitrate hydrate and (quadridentate amine)(5-nitrosalicylato)cobalt(III) chloride nitrate hydrate, $[Co(5\text{-}NO_2sal)L]Cl\cdot NO_3\cdot nH_2O$ (L: $(NH_3)_4$, trien, 2,3,2-tet, and 3,2,3-tet). The ^{1}H NMR spectra indicate that the unpaired electron on the coordinated 5-nitrosalicylato ligand of the title complexes is located over the π-orbital of the chelated ligand

Previously, we have been concerned with the XPS[1,2] of the green paramagnetic tetraammine(5-nitro(or nitroso)salicylato)cobalt(III) complexes, *i.e.*, it has been established that an unpaired electron of these complexes is delocalized partly on the cobalt atom and partly on the chelated ligand (coordinated 5-nitrosalicylato ligand). In the NMR spectra of these complexes, the signals of the ammine proton have been assigned,[3] but the ring proton and carbon signals of the chelated ligand have so far remained unsolved. We have now devised appropriate conditions for the measurement of the NMR spectra of the green paramagnetic cobalt(III) complexes. The present paper deals with the measurement of the ring protons of the green paramagnetic tetraammine(5-nitrosalicylato)cobalt(III) chloride nitrate hydrate and the related compounds.

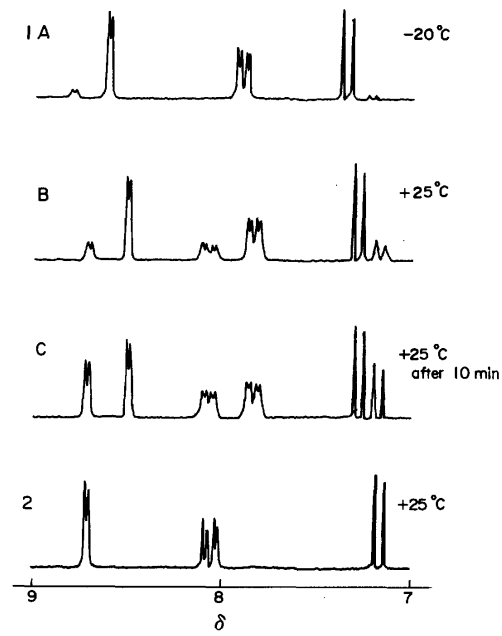

Fig. 1. The ^{1}H NMR spectra of the paramagnetic complex **1** and the diamagnetic complex **2** in 1.8 mol dm^{-3} D_2SO_4.
1A-C: $[Co(5\text{-}NO_2sal)(NH_3)_4]Cl\cdot NO_3\cdot H_2O$,
2: $[Co(5\text{-}NO_2sal)(NH_3)_4]NO_3\cdot H_2O$.

Results and Discussion

The ^{1}H NMR spectra of the chelated ligand of the green paramagnetic tetraammine(5-nitrosalicylato)-cobalt(III) chloride nitrate hydrate, $[Co(5\text{-}NO_2sal)(NH_3)_4]Cl\cdot NO_3\cdot H_2O$ (**1**), have not previously been observed, because the measurement is difficult. However, appropriate conditions for the NMR measurement of the green paramagnetic cobalt(III) complexes are now established as follows: The concentration and solvent, temperature and accumulation number are $4.6\pm0.2\times10^{-2}$ mol dm^{-3} in 1.8 mol D_2SO_4 solution, -20°C and two hundred times, respectively. On the other hand, the ^{13}C NMR spectrum of **1** did not show the expected signals, because of paramagnetism. The ^{1}H NMR spectra of **1**, as is shown in Fig. 1(A), have indicated three ring protons at δ 7.36, 7.91, and 8.61 under the same conditions. This spectrum showed six signals at 25°C as is shown in Fig. 1(B). In addition, after 10 min, as is shown in Fig. 1(C), these signals decrease with increase of the ring proton signals at δ 7.16, 8.05, and 8.71; these are chemical shifts of the ring protons of the corresponding orange diamagnetic nitrate hydrate, $[Co(5\text{-}NO_2sal)(NH_3)_4]NO_3\cdot H_2O$ (**2**). Finally, the ring proton signals of **1** are similar to those of **2**. Thus, the signals at δ 7.36 (d, H), 7.91 (dd, H),and 8.61 (d, H) of **1** have been assigned to the H_3, H_4, and H_6 ring protons, respectively. The chemical shifts and the coupling constants of the ring protons of **1** are closely similar to those of **2** as is shown in Table 1. Thus, the σ-bonds which are formed from protons and carbons (sp^2 configuration) of the chelated ligand of **1** resemble the σ-bonds of **2**, *i.e.*, the partly unpaired electron can not be delocalized over a hydrogen of the chelated ligand and a substituted methyl group[3] of the corresponding green paramagnetic tetraammine(4-methyl-5-nitrosalicylato)cobalt(III) chloride trihydrate, $[Co(4\text{-}Me\text{-}5\text{-}NO_2sal)(NH_3)_4]Cl_2\cdot 3H_2O$ (**3**), previous reported. It can be concluded that the partly unpaired electron on the chelated ligand is localized over the π-orbital of the chelated ligand. This is in agreement with the XPS results,[2] *i.e.*, the C ls binding energy and FWHM of **1** are different from those of **2**. Then, the electronic state of the π-orbital of the chelated ligand of **1** should be different from that of **2**.

The ring proton signals of the corresponding green paramagnetic (5-nitrosalicylato)cobalt(III) complexes with the quadridentate amine ligands such as trien (**4**, **5**), 2,3,2-tet (**6**), and 3,2,3-tet (**7**) were measured under the same conditions and the results are collected in Table 1. The ring proton signals of the chelated ligand

TABLE 1. ^{1}H NMR SPECTRA OF COMPLEXES **1**, **2**, AND **4**—**7**

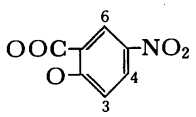

No.	Complex	H_3 δ	$^3J_{HCCH}$ Hz	H_4 δ	$^3J_{HCCH}$ Hz	$^4J_{HCCCH}$ Hz	H_6 δ	$^4J_{HCCCH}$ Hz	Temp °C
1	[Co(5-NO_2sal) (NH_3)$_4$]Cl·NO_3·H_2O	7.36 d	9.6	7.91 dd	9.6	4.0	8.61 d	4.0	−20
		7.28 d	9.6	7.85 dd	9.6	4.0	8.50 d	4.0	+25
4	[Co(5-NO_2sal)trien]Cl·NO_3·2H_2O	7.34[a]		7.92[a]			8.64[a]		+25
5	[Co(4-Me-5-NO_2sal)trien] Cl·NO_3·2H_2O	7.27 s		—			8.34 s		+25
6	[Co(5-NO_2sal) (2,3,2-tet)] Cl·NO_3·2H_2O	7.40 d	9.6	7.96 d	9.6		8.66[a]		+25
7	[Co(5-NO_2sal) (3,2,3-tet)] Cl·NO_3·2H_2O	7.22 d	9.6	7.78 dd	9.6	4.0	8.46 d	4.0	+25
2	[Co(5-NO_2sal) (NH_3)$_4$]NO_3·H_2O	7.16 d	9.3	8.05 dd	9.3	3.5	8.71 d	3.5	+25

Solvent: 1.8 mol dm^{-3} D_2SO_4; Standard: internal DSS (δ=0). a: broad signal.

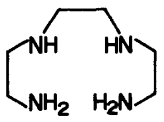

trien

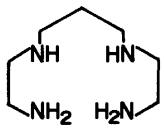

2,3,2-tet

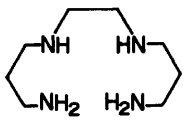

3,2,3-tet

of complex **7** are very sharp similar to those of **1**, though those of complex **4** are broad. Thus, the ring proton signals of the chelated ligand of complexes **4**—**7** are sharp with the increase of the total number of the center methylene carbons of the quadridentate amine ligands. This property is attributable to the coordinated quadridentate ligands.[4]

On the other hand, the ammine proton signals at δ 3.44 (s, 6H) and 3.94 (s, 6H) of **1** are similar to those (δ 3.44 (s, 6H) and 3.94 (s, 6H)) of **2** under the same conditions. This result agrees with that of XPS of **2**,[2] *i.e.*, the N ls binding energy of ammine ligands of **1** is similar to that of **2**.

Experimental

Measurements. The NMR spectra were recorded with Varian XL-200 NMR spectrometer.

Complexes. Green paramagnetic tetraammine- or (quadridentate amine)(5-nitrosalicylato)cobalt(III) chloride nitrate hydrate[5] (**1**, **4**—**7**) and orange diamagnetic tetraammine(5-nitrosalicylato)cobalt(III) nitrate hydrate[3] (**2**) were prepared by the methods of the previous papers.

References

1) Part VII: Y. Yamamoto, H. Kudo, M. Mori, and H. Konno, *Bull. Chem. Soc. Jpn.*, **55**, 136 (1982).
2) Y. Yamamoto, M. Mori, and H. Konno, *Bull. Chem. Soc. Jpn.*, **54**, 1995 (1981).
3) Y. Yamamoto, *Bull. Chem. Soc. Jpn.*, **51**, 2894 (1978).
4) Y. Yamamoto, H. Kudo, and E. Toyota, *Bull. Chem. Soc. Jpn.*, **56**, 1051 (1983).
5) Y. Yamamoto, K. Ito, H. Yoneda, and M. Mori, *Bull. Chem. Soc. Jpn.*, **40**, 2580 (1967); Y. Yamamoto, E. Toyota, and N. Mitsudera, *ibid.*, **53**, 3517 (1980); Y. Yamamoto and H. Kudo, *ibid.*, **57**, 287 (1984).

The Crystal Structure of Calcium Sulfite Hemihydrate

Takashi MATSUNO,* Hiroaki TAKAYANAGI,† Kimio FURUHATA,† Masumi KOISHI,†† and Haruo OGURA†

School of Medicine, Kitasato University, Kitasato, Sagamihara 228

†*School of Pharmaceutical Sciences, Kitasato University, Shirokane, Minato-ku, Tokyo 108*

††*Faculty of Pharmaceutical Sciences and Institute of Colloid and Interface Science, Science University of Tokyo, Ichigaya, Funagawaramachi, Shinjuku-ku, Tokyo 162*

(Received August 3, 1983)

Synopsis. The crystal data for calcium sulfite hemihydrate are orthorhombic, Pbcn, a=10.664(1), b=6.495(1), c=9.823(1) Å, and Z=8. The structure consists of two alternating layers. The calcium ions are coordinated by six O atoms: Five originate from the sulfite ions, and one from the water molecule.

There are only two papers relating the crystal structures of calcium sulfite: One reports the cell dimensions of calcium sulfite hemihydrate crystal[1] and the other the crystal structure of calcium sulfite tetrahydrate.[2]

This study deals with the crystal structure of calcium sulfite hemihydrate obtained as a stable phase in the temperature range from 0 to 98°C.

Experimental

Preparation. Single crystals of the hemihydrate were synthesized from calcium chloride solution(1.0 M, 1M= 1 mol dm^{-3}) and sodium sulfite solution (1.0 M) by the diffusion method (25°C, 4 weeks). Single crystals were obtained in the form of transparent plates with thicknesses of 0.1—0.4 mm. Analysis: Found: CaO, 43.3; SO_2, 49.5; H_2O, 7.1%. Calcd for $CaSO_3 \cdot 0.5H_2O$: CaO, 43.4; SO_2, 49.6; H_2O, 7.0%.

Determination of the Cell Constants and Collection of the Intensity Data. A crystal with the approximate dimension of 0.2×0.1×0.2 mm was used for the determination of cell constants and the collection of intensity data at 18°C. The cell constants were determined by the least-squares method based on the 2θ values of 21 reflections. Crystal data: $CaSO_3 \cdot 0.5H_2O$, $F.W.$=129.1, orthorhombic, space group Pbcn, a=10.664(1), b=6.495(1), c=9.823(1) Å, V=680.4(3) Å^3, Z=8, D_c=2.521, D_m= 2.51 g cm^{-3} (by flotation method). The reflection data for X-ray structural determination were collected with a Rigaku automatic four-circle diffractometer using graphite-monochromatized Cu$K\alpha$ radiation. Background was counted for 5 s at either side of each peak. The fluctuations in intensity of the three standard reflections measured every 50 reflections were about 1.1% during the data collection. Intensities of 741 independent reflections were measured up to θ=70°. Reflections having intensities stronger than four times the respective standard deviations were treated as observed. 519 non-zero reflections were obtained and corrected for Lorentz and polarization factors, but no correction was made for absorption.

Determination and Refinement of the Structure

The structure was determined by the symbolic addition method.[3] All the non-hydrogen atoms in the asymmetric unit were located from the E map. Refinement of atomic parameters was carried out by the full-matrix least-squares method, the quantity minimized being $\sum w(|F_o| - |F_c|)^2$ with w=1.0 for all the reflections. Four cycles of the least-squares refinement of the coordinates with isotropic temperature factors gave an R value of 0.082. Anisotropic temperature factors were introduced for all the atoms except hydrogen atoms, the R value being slightly reduced to 0.081. The atomic scattering factors for S and O were given by Cromer and Mann,[4] and that for Ca by International Tables for X-ray Crystallog-

TABLE 1. ATOMIC COORDINATES(×10^4), THEIR ESTIMATED STANDARD DEVIATIONS(IN PARENTHESES) AND EQUIVALENT ISOTROPIC TEMPERATURE FACTORS

Atom	X	Y	Z	B_{eq}[a]/Å^2
Ca(1)	1458(2)	5124(3)	1314(2)	1.0
S(1)	1287(2)	1690(4)	3849(3)	1.3
O(1	526(8)	3657(13	3985(8)	1.9
O(2)	2150(8)	1811(14)	5055(8)	2.4
O(3)	2089(8)	2095(13)	2606(8)	2.1
O(4)	0	7562(17)	2500	1.7

a) B_{eq} defined according to Hamilton(1959).[7]

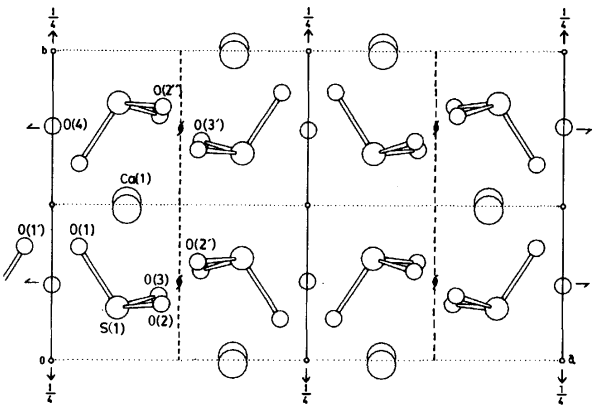

Fig. 1. Projection of the structure along the c axis and numbering of the atoms.

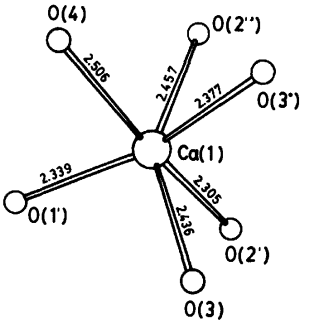

Fig. 2. Environment of the calcium ion. Interatomic distances are in Å units.

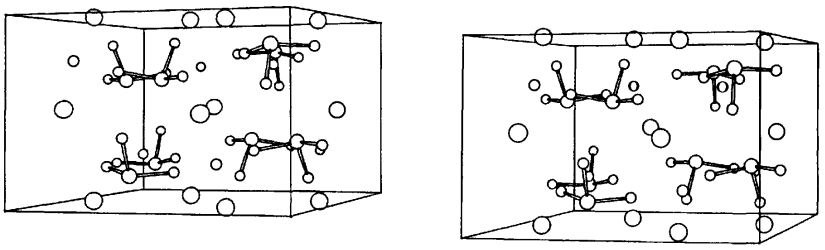

Fig. 3. Stereoscopic view of the structure.

TABLE 2. INTERATOMIC DISTANCES AND BOND ANGLES WITH THEIR ESTIMATED STANDARD DEVIATIONS IN PARENTHESES

Interatomic	Distance l/Å	Bond angle	ϕ/°
Ca(1)-O(1')	2.339(1)	O(1')-Ca(1)-O(4)	75.79(1)
Ca(1)-O(2')	2.305(1)	O(2')-Ca(1)-O(3)	70.20(1)
Ca(1)-O(2")	2.457(1)	O(2")-Ca(1)-O(3')	68.69(1)
Ca(1)-O(3)	2.436(1)	O(1')-Ca(1)-O(3)	89.22(1)
Ca(1)-O(3')	2.377(1)	O(2')-Ca(1)-O(3')	99.23(1)
Ca(1)-O(4)	2.506(1)	O(2")-Ca(1)-O(4)	84.74(1)
Sulfite ion		O(2')-Ca(1)-O(2")	88.76(1)
S(1)-O(1)	1.519(1)	O(3)-Ca(1)-O(3')	88.67(1)
S(1)-O(2)	1.502(1)	Sulfite ion	
S(1)-O(3)	1.514(1)	O(1)-S(1)-O(2)	102.4(1)
O(1)-O(2)	2.354(1)	O(1)-S(1)-O(3)	103.1(1)
O(1)-O(3)	2.375(1)	O(2)-S(1)-O(3)	106.3(1)
O(2)-O(3)	2.414(1)		

raphy.[5] The dispersion corrections for atomic scattering factors of Ca and S are 0.3 and 0.3 for $\Delta f'$ and 1.4 and 0.6 for $\Delta f''$, respectively. At the final stage of the refinement the difference Fourier map showed only featureless peaks. For these calculations, computer programs made by Stewart *et al.*[6] were used. Anisotropic temperature factors of the non-hydrogen atoms and the complete F_o-F_c data are deposited as Document No. 8406 at the Office of the Editor of the Bulletin of the Chemical Society of Japan. The final atomic coordinates, their estimated standard deviations, and equivalent isotropic temperature factors are given in Table 1.

Description and Discussion of the Structure

A projection of the structure along the c axis and the numbering of the atoms are shown in Fig. 1. The oxygen atoms O(1)-O(3) belong to the sulfite ion, and the oxygen atom O(4) belongs to the crystal water. The oxygen atoms of water molecules are situated on the twofold axes. No such sulfite ions in a disordered state as observed in the structure of calcium sulfite tetrahydrate[2] exists in that of the hemihydrate crystal. The interatomic distances and angles are given in Table 2. The S-O and O-O interatomic distances and O-S-O bond angles in the $S(1)O_3^{2-}$ ion are 1.502(1)—1.519(1) Å, 2.354(1)—2.414(1) Å, and 102.4(1)—106.3(1)°, respectively. These values are similar to those (1.52(2)—1.53(3) Å, 2.37(1)—2.39(1) Å, 102.2(3)—102.9(4)°) calculated from the atomic coordinates[2] of the sulfite ion in the ordered state in the structure of the tetrahydrate crystal. The coordination of O atoms around the Ca(1) ion is shown in Fig. 2. The calcium ions are coordinated by six O atoms. This number is the same as that of the Ca-coordinated O atoms in the tetrahydrate crystal.[2] Five of them originate from the $S(1)O_3^{2-}$ ions(O(1'), O(2'), O(2''), O(3), O(3')), and the other from the water molecule(O(4)). The Ca(1)-O(4) distance of 2.506(1) Å is longer than the other Ca(1)-O distances(2.305(1)-2.457(1) Å). For the tetrahydrate crystal, contrary to the hemihydrate crystal, the Ca-O(sulfite ion) distances(2.52(1)-2.53(7) Å) are longer than the Ca-O (water) distances (2.38(1)-2.45(1) Å).[2] The average Ca-O distance in the hemihydrate crystal (2.403 Å) is slightly shorter than 2.45 Å in the tetrahydrate crystal.

It can be presumed that the high thermostability of the hemihydrate is caused by the existence of Ca-O bondings stretched like a net all over the crystal and by the absence of the sulfite ions in a disordered state. A stereoscopic view of the crystal structure is shown in Fig. 3. The structure consists of two alternating layers similar to those in the tetrahydrate crystal: One consists of the calcium ions alone, and the other of the sulfite ions and water molecules. They are parallel to the (010) plane.

References

1) K. Setoyama, S. Takahashi, and M. Sekiya, *Gypsum Lime*, **141**, 3 (1976).

2) T. Matsuno, H. Takayanagi, K. Furuhata, M. Koishi, and H. Ogura, *Chem. Lett.*, **1983**, 459.

3) I. L. Karle and J. Karle, *Acta Crystallogr., Sect. A*, **16**, 969 (1963); **21**, 894 (1966).

4) D. Cromer and J. Mann, *Acta Crystallogr., Sect. A*, **24**, 321 (1968).

5) "International Tables for X-Ray Crystallography," Kynoch Press, Birmingham (1962), Vol. III.

6) J. M. Stewart *et al.*, Technical Report TR-192 (June, 1972), The X-Ray System of Crystallographic Programs for Any Computer, Computer Science Center, University of Maryland.

7) W. C. Hamilton, *Acta Crystallogr.*, **12**, 609 (1959).

Application of Liquid Crystals for Gas-Liquid Chromatography

Sakumitsu SAKAGAMI* and Minoru NAKAMIZO
National Industrial Research Institute of Kyushu, Tosu, Saga 841
(Received August 11, 1983)

Synopsis. A liquid crystalline homologous series of *N*-[4-(4-alkoxybenzoyloxy)benzylidene]-4-cyanoanilines was applied as a stationary liquid phase for the gas-liquid chromatographic separation of various positional isomers. It is shown that the nematic phase has higher selectivity for several positional isomers compared with the other mesomorphic phases.

Liquid crystals are anisotropic liquids and they exhibit interesting solvent properties due to the rod-like shape and the ordered arrangement of their molecules. These unique solvent properties of liquid crystals were used for the first time as the stationary phase in gas-liquid chromatography (GLC) for the separation of the positional isomers of various disubstituted benzenes.[1] Recently, the separation of various solutes such as polycyclic aromatic hydrocarbons,[2] steroid epimers,[3] and *Z*/*E* mixtures of fatty alcohols[4] has been carried out with good success using liquid crystalline stationary phases in GLC.

Most GLC studies reported so far have been made with the use of nematic liquid crystals. However, from the viewpoint of practical application there exists a disadvantage that the use of the nematic stationary phases is confined to their limited mesomorphic temperature ranges. In connection with an attempt to obtain liquid crystals with a wide mesomorphic temperature range the smectic[5,6] and re-entrant nematic phases[7] have been recently applied to the separation of the various positional isomers.

In order to develop GLC using liquid crystals as the liquid phase it seems worthwhile to study the solubility and selective affinity of the various solutes in these different liquid crystalline phases. In this report we describe a study of the separation of some positional isomers in different mesomorphic phases by use of a homologous series of *N*-[4-(4-alkoxybenzoyloxy)benzylidene]-4-cyanoanilines.

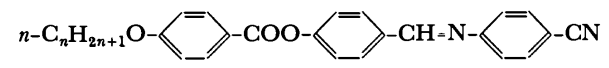

(n=7, 9, and 12)

Experimental

Materials. 4-Dodecyloxybenzoic acid was synthesized according to the known method[8] while the other lower homologues were commercially obtained. These 4-alkoxybenzoic acids were converted to acid chlorides by treatment with thionyl chloride, and then esterified by a reaction with 4-hydroxybenzaldehyde in ether solution including triethylamine. Finally, the substituted benzaldehydes formed were coupled with 4-cyanoaniline in ethanol solution. The crude liquid crystals were purified by successive recrystallization from ethanol. The solutes chosen were commercially obtained and used without further purification.

Apparatus and Procedure. The liquid crystalline texture and the transition temperatures were determined by a Nikon polarizing microscope equipped with a Mettler FP 52 microfurnace and control unit. Checks on the transition temperatures were made using a Rigaku differential scanning calorimeter.

The support material employed was 100—120 mesh Chromosorb W HP. The support was coated with the liquid crystalline compounds by using chloroform as solvent, followed by gradual elimination of the solvent by evaporation. The concentration of the liquid phase in the packing of the coated support was 2.5 wt%. The columns were conditioned at 240°C for 2 h prior to initial use.

A Hitachi 163 gas chromatograph equipped with a flame-ionization detector was used. The flow-rate of the carrier gas (nitrogen) was measured using a soap-bubble flow meter.

Results and Discussion

The transition temperatures and the liquid crystalline phases of the compounds studied are given in Table 1. The C_7 and C_9 homologues have been reported by Weissflog *et al.*[9] and the transition temperatures determined in this study are in good agreement with the published data. The C_7 member exhibits both the smectic A and nematic phases while another liquid crystalline phase, *i.e.*, re-entrant nematic phase is monotropically observed for the C_9 member. As shown in Table 1, the C_{12} homologue exhibits no nematic phase. This is not surprising because the disappearance of the nematic phase is not unusual, and has been frequently observed as the alkoxy chain length increases in other homologous series of liquid crystalline materials.[10]

To estimate the selective affinity of the different liquid crystalline phases toward the various solutes we have measured relative retention(α) of some positional isomers on the liquid crystalline stationary phases. The chosen solute isomers and their relative retention determined in this study are compiled in Table 2.

The separation of *m*- and *p*-xylenes by GLC is a classically difficult one because of their similar boiling points and polarities. However, it should be stressed that both the nematic phase of the C_7 homologue and the re-entrant nematic phase of the C_9 member can separate this isomeric pair. Separation of compounds on the basis of molecular shape is the most characteristic feature of the liquid crystalline stationary phase in GLC.[11] Roughly, the more rod-like a solute is, the

TABLE 1. TRANSITION TEMPERATURES OF LIQUID CRYSTALS STUDIED (°C)

n	Re-entrant nematic	Smectic C	Smectic A	Nematic	Isotropic
7			(72)	113	264
9	(92)		95	224	246
12		(74)	83		245

The parentheses show the monotropic transition.

TABLE 2. RELATIVE RETENTION OF THE SOLUTE ISOMERS STUDIED

Solutes	Temperature °C	C_7	C_9	C_{12}
m- and *p*- Xylenes	75	1.05(N)	1.02(Re N)	—[a] (S_A)
m- and *p*- Dibromobenzenes	130	1.14(N)	1.08(S_A)	1.09 (S_A)
m- and *p*- Chloroacetophenones	130	1.20(N)	1.14(S_A)	1.14 (S_A)
1- and 2- Chloronaphthalenes	130	1.12(N)	1.07(S_A)	1.07 (S_A)
Phenanthrene and Anthracene	210	1.14(N)	1.12(S_A)	1.12 (S_A)

The relative retention is equal to 1.00 for the *m*- and 1- isomers and phenanthrene, respectively. The parentheses indicate the liquid crystalline phases. N: nematic, S_A: smectic A, Re N: re-entrant nematic.
a) The isomers of *m*- and *p*-xylenes can not be separated at 75 °C in the smectic A phase of C_{12} homologue.

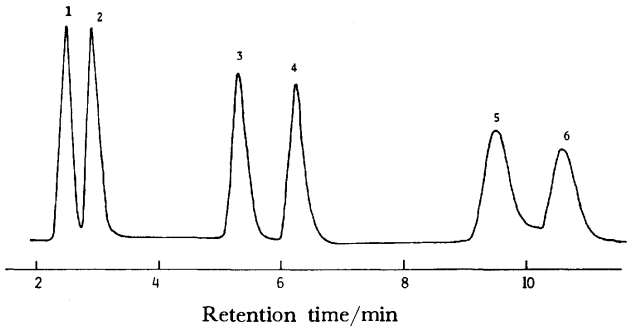

Fig. 1. Gas chromatogram of a mixture of dibromobenzenes, chloroacetophenones and chloronaphthalenes observed in the nematic phase on a C_7 column. Oven temperature, 130°C; injection temperature, 250°C; flame-ionization detector; nitrogen flow-rate, 25 ml/min. Peaks 1: *m*-dibromobenzene, 2: *p*-dibromobenzene, 3: *m*-chloroacetophenone, 4: *p*-chloroacetophenone, 5: 1-chloronaphthalene, 6: 2-chloronaphthalene.

easier it should fit into the liquid crystalline lattice and hence the greater its solubility should be. As is expected, the retention time for the isomer with the more rod-like shape (*p*-isomer) is longer than that for the *m*-isomer. It is also noteworthy to state that the relative retention of xylene isomers observed in the nematic phase is higher than that in the re-entrant nematic state. This result is likely to indicate that the nematic phase has much higher selective affinity toward the positional isomers compared with the re-entrant nematic phase.

Isomeric pairs of dibromobenzenes, chloroacetophenones and chloronaphthalenes can be separated almost completely at 130°C on all the mesomorphic stationary phases studied, as shown in Fig. 1. As mentioned previously, the length to breadth ratio of the molecules plays an important role for the separation of the solute isomers on the liquid crystalline stationary column. It is apparent in Fig. 1 that the isomer with the more rod-like shape (*p*- and 2-isomer) is retained longer than that with less rod-like shape. Similarly, a complete separation of phenanthrene and anthracene can be achieved at 210°C using a liquid crystalline column, as shown in Table 2. In addition, it should be emphasized that a value of relative retention toward all the positional isomers obtained in the nematic phase is much higher relative to the corresponding values found in the smectic A and re-entrant nematic phases.

In conclusion, we believe that the C_7 member of the homologous series studied is likely to be most useful stationary liquid phase in GLC because it exhibits a wide nematic temperature range and a unique selectivity for a mixture of various positional isomers.

References

1) H. Kelker, *Z. Anal. Chem.*, **198**, 254 (1963).
2) G. M. Janini, K. Johnston, and W. L. Zielinski, Jr., *Anal. Chem.*, **48**, 670 (1975).
3) W. L. Zielinski, Jr., K. Johnston, and G. M. Muschik, *Anal. Chem.*, **48**, 907 (1976).
4) R. Lester and D. R. Hall, *J. Chromatogr.*, **190**, 35 (1980).
5) J. E. Haky and G. M. Muschik, *J. Chromatogr.*, **214**, 161 (1981).
6) S. Sakagami and M. Nakamizo, *J. Chromatogr.*, **234**, 357 (1982).
7) S. Sakagami, *J. Chromatogr.*, **246**, 121 (1982).
8) B. Jones, *J. Chem. Soc.*, **1935**, 1874.
9) W. Weissflog, G. Pelzl, A. Wiegeleben, and D. Demus, *Mol. Cryst. Liq. Cryst.*, **56**, 295 (1980).
10) D. Demus, H. Demus, and H. Zaschke, "Fluessige Kristalle in Tabellen," Verlag, Leipzig (1974).
11) G. M. Janini, *Adv. Chromatogr.*, **17**, 231 (1979).

Binuclear Metal Complexes. LIV.[1] Strongly Spin-coupled Copper(II)-Iron(III) Complex of a Salen Homolog Containing Pendant Phenolic Group

Wakako KANDA, Hisashi ŌKAWA,* and Sigeo KIDA
Department of Chemistry, Faculty of Science, Kyushu University 33, Hakozaki, Higashiku, Fukuoka 812
(Received October 27, 1983)

Synopsis. A copper(II)-iron(III) binuclear complex of *N,N'*-disalicylidene-2-methyl-4-(2-hydroxy-5-methylphenyl)-1,2-butanediamine has been prepared and characterized. Cryomagnetic measurements revealed the presence of an antiferromagnetic spin-exchange interaction of $J=-70\,cm^{-1}$ between the metal ions.

Magnetical investigations of copper(II)-iron(III) complexes are of current interest in connection with the models for the active site of cytochrome oxidase where the iron(III) center of cytochrome a_3 and copper(II) are strongly spin-coupled.[2,3] However, only few copper(II)-iron(III) complexes are magnetically characterized.[4-6]

N,N'-Disalicylideneethylenediaminatocopper(II) and its congeners can act as bidentate chelating agents through the phenolic oxygens. Sinn and coworkers have used these complexes to synthesize a number of binuclear and trinuclear metal complexes.[7] However, no polynuclear complexes of salen analogues containing iron(III) have been obtained, mainly because of their low stability. Recently, we synthesized a new salen analogue containing a pendant phenolic group, *N,N'*-disalicylidene-2-methyl-4-(2-hydroxy-5-methylphenyl)-1,2-butanediamine (abbreviated as H_2(sal-Hpen)).[8] Its iron(III) complex Fe(sal-pen) was shown to be of five-coordination with the pendant phenolic oxygen at the apical position.[7] In this study we report the synthesis, characterization, and magnetism of the copper(II)-iron(III) complex Fe(sal-pen)$CuCl_2$.

Experimental

Preparations. H_2(sal-Hpen) and Fe(sal-pen) were prepared by the method in the preceding paper.[8]

Fe(sal-pen)$CuCl_2$. A suspention of Fe(sal-pen) (0.10 g) and anhydrous $CuCl_2$ (0.33 g) in an ethanol-dichloromethane mixture (1:1, 30 cm^3) was refluxed with stirring for 2 d. Reddish purple solution thus obtained was slowly condensed in a vacuum desiccator to give purple brown crystals.

Found: C, 49.41; H, 4.39; N, 4.43%. Calcd for Fe(sal-pen)$CuCl_2 \cdot 3/2H_2O$: C, 49.59; H, 4.47; N, 4.44%.

Magnetic Measurements. Magnetic susceptibilities were measured in the temperature range 80—300 K by the Faraday method, the apparatus being calibrated with $[Ni(en)_3]S_2O_3$.[9] Magnetic moments were calculated by the equation, $\mu_{eff}=2.828(\chi_M \times T)^{1/2}$, where χ_M is the molar susceptibility per iron and copper atoms corrected for diamagnetism by the use of Pascal's constants.

Results and Discussion

The analytical results demonstrate the stoichiometry of the complex to be Fe(sal-pen)$CuCl_2$. However, this does not rule out the possibility of coprecipitation of Fe(sal-pen) and $CuCl_2$. The complexes obtained, however, appeared uniform prismatic crystals under microscopic observation. The color of the dichloromethane solution gradually changed from purple-brown to dark brown, suggesting the decomposition of the complex. Thus, the investigations were carried out on solid samples.

The infrared spectrum of Fe(sal-pen)$CuCl_2$ showed appreciable band shifts compared with that of Fe(sal-pen); the C=N stretching and skeletal bands were shifted from 1610 and 1540 cm^{-1} to 1630 and 1550 cm^{-1}, respectively. The shift of the skeletal band to the higher frequency suggests the binuclear structure bridged by the phenolic oxygens.[10] The magnetic moment of Fe(sal-pen)$CuCl_2$ is 5.2 BM at room temperature, which is lower than that of Fe(sal-pen) (5.8 BM†). The ESR spectrum of Fe(sal-pen)$CuCl_2$ exhibited a very weak signal near $g=2$ and differs from the spectrum of Fe(sal-pen) which exhibits a strong signal near $g=3.7$. All these facts clearly demonstrate that Fe(sal-pen)$CuCl_2$ is a new heteronuclear complex, bridged by the phenolic oxygens of the salen skeleton (Fig. 1).

The magnetic moment of the complex (5.2 BM) is much lower than the spin-only value (6.2 BM) for the high-spin iron(III)-copper(II) system. Further, the moment decreased to 4.7 BM when the temperature was lowered to the liquid nitrogen temperature. These facts suggest the operation of the intramolecular spin-exchange interaction. The magnetic behavior is best understandable by assuming a high-spin iron(III) coupled with copper(II). Such a spin-coupling results in two total spin states $S_T=3$ and $S_T=2$ with an energy gap of $|6J|$ based on the Heisenberg model ($H=-2JS_1 \cdot S_2$). The molar susceptibility can be calculated using the simplified Van Vleck's equation,[11]

$$\chi_M = \frac{Nq^2\beta^2}{kT} \times \frac{5\exp(-6J/kT)+14}{5\exp(-6J/kT)+7} + N\alpha,$$

where β is the Bohr magneton, N Avogadro's constant, k the Boltzmann constant, g the Landé splitting factor,

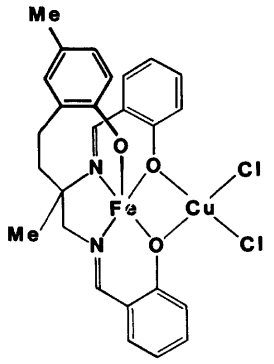

Fig. 1. Possible structure of Fe(sal-pen)$CuCl_2$.

† 1 BM=0.9273×10^{-23} J T^{-1}.

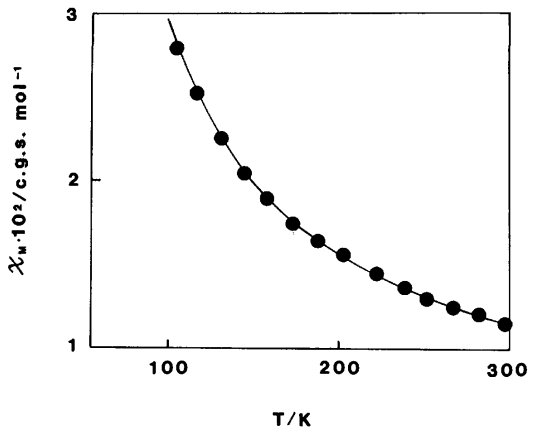

Fig. 2. Temperature-variation of magnetic susceptibility of Fe(sal-pen)$CuCl_2$. The solid curve is drawn based on the theoretical susceptibility equation for the (S=5/2)-(S=1/2) system with the parameters g=1.98, $-J$=70 cm^{-1}, and $N\alpha$=0.

J the exchange integral, and $N\alpha$ the temperature-independent paramagnetism. The experimental χ_M *vs.* T plot was best reproduced by the theoretical curve by assuming $-J$=70 cm^{-1}, g=1.98, and $N\alpha$=0. Thus, the existence of a strong antiferromagnetic spin-exchange interaction between the metal ions in Fe(sal-pen)$CuCl_2$ has been established through the present study.

References

1) Part LIII: M. Nakamura, H. Ōkawa, and S. Kida, *Inorg. Chim. Acta*, **75**, 9 (1983).
2) M. F. Tweedle, L. J. Wilson, L. Garcia-Iniguez, G. T. Babcock, and G. Palmer, *J. Biol. Chem.*, **253**, 8065 (1978).
3) T. H. Moss, E. Shapiro, T. E. King, H. Beinert, and C. Hartzell, *J. Biol. Chem.*, **253**, 8072 (1978).
4) H. Ōkawa, W. Kanda, and S. Kida, *Chem. Lett.*, **1980**, 1281.
5) J. Jaud, Y. Journaux, J. Galy, and O. Kahn, *Nouv. J. Chim.*, **4**, 629 (1980).
6) C. K. Chang, M. S. Koo, and B. Ward, *J. Chem. Soc., Chem. Commun.*, **1982**, 716.
7) E. Sinn and C. M. Harris, *Coord. Chem. Rev.*, **4**, 391 (1969).
8) W. Kanda, H. Ōkawa, and S. Kida, *Bull. Chem. Soc. Jpn.*, **56**, 3268 (1983).
9) N. F. Curtis, *J. Chem. Soc.*, **1961**, 3147.
10) B. Coles, C. M. Harris, and E. Sinn, *Inorg. Chem.*, **8**, 2607 (1969).
11) J. H. Van Vleck, "Theory of electric and Magnetic Susceptibilities," Oxford University Press, London and New York (1932), Chap. 12.

Thermal Decomposition of *t*-Butyl Heptafluoroperoxybutyrate

Hideo SAWADA,* Hidehiko HAGII, Kazuyoshi AOSHIMA, and (the late) Takeshi ARAI
Chemicals and Explosives Research Laboratory, Nippon Oil & Fats Co., Ltd., Taketoyo, Chita-gun, Aichi 470-23
(Received July 21, 1983)

Synopsis. The decomposition of *t*-butyl heptafluoroperoxybutyrate (TBH) was studied in both toluene and methanol. Kinetic and product studies from the thermolysis showed that this peroxy ester decomposes heterolytically in nonpolar solvents like toluene with homolysis, whereas in methanol this peroxy ester undergoes principally transesterification.

Although the mechanisms for the thermolysis of a series of peroxy esters have been extensively investigated,[1] studies of fluorinated peroxy esters have been few. Bartlett *et al.* reported that the *t*-butyl peroxy esters derived from strong organic acids might well undergo ionic cleavage in polar solvents[2] and *t*-butyl peroxytosylate decomposes heterolytically with Criegee rearrangement in absolute methanol to give acetone dimethyl acetal and toluenesulfonic acids.[3] Hedaya *et al.* reported that 1-methoxy-1-methylethyl *p*-nitroperbenzoate (*p*-$NO_2C_6H_4CO_2OC(CH_3)_2(OCH_3)$) decomposes heterolytically in methanol to give rise to Criegee-type products *via* 1,1-dimethoxyethylium ion intermediate.[4] These results suggest that *t*-butyl peroxy esters derived from perfluorinated organic acids ($R_fCO_2OC(CH_3)_3$, R_f=perfluorinated alkyl, aryl) would decompose similarly to give Criegee-type products. We wish to report herein on the results of the thermal decomposition of *t*-butyl heptafluoroperoxybutyrate (TBH) in both toluene and methanol.

Results and Discussion

The thermal decomposition of TBH was carried out in both toluene and methanol at 10.0—85.0 °C as shown in Table 1. For decomposition of TBH in toluene at 65.0—85.0 °C, autocatalysis was observed in the absence of pyridine and the first-order rate constants could not be obtained. However rates of decomposition following a first-order rate constant were obtained at 10.0—30.0 °C and autocatalysis was not observed. The values of the activation enthalpy and entropy for the thermal decomposition of TBH in toluene and in methanol were $\Delta H^*=89.5\pm4.2$ kJ mol^{-1}, $\Delta S^*=-74.1\pm12.1$ J K^{-1} mol^{-1}, and $\Delta H^*=44.4\pm2.1$ kJ mol^{-1}, $\Delta S^*=-167.8\pm7.1$ J K^{-1} mol^{-1}, respectively.

When TBH decomposed in toluene, 1,2-diphenylethane, which would result from radical cleavage, was obtained as shown in Table 2. Additionally the bulk polymerization of styrene initiated by TBH was studied at 50—60 °C. The thermal polymerization of styrene may be considered negligible at these temperatures. Bulk polymerization of styrene was observed and the rate constants of the polymerization were shown in Table 3. From the rate constants, the value of the activation energy of the polymerization was 94.6 ± 9.2 kJ mol^{-1}, which suggests that the polymerization of styrene initiated by TBH is not cationic but radical.[5] These results indicate that TBH would decompose homolytically in toluene.

On the other hand, the activation parameters for the thermal decomposition of TBH in toluene have small values compared with those of *t*-butyl peroxy esters which are expected to decompose homolytically; for example, *t*-butyl peroxypivalate, in chlorobenzene, $\Delta H^*=125.5$ kJ mol^{-1}, $\Delta S^*=46.4$ J K^{-1} mol^{-1}.[6] The smaller values of the enthalpy and the entropy of activation suggest that TBH would decompose in part with heterolysis. The rates of decomposition followed a first-order rate equation in the presence of pyridine, however, the first-ordsr rate constants drifted upwards remarkably after about 60% reaction at 85 °C. From this result, it can be seen that the autocatalysis was not completely suppressed even when pyridine was present. Decomposition products in toluene at 85 °C in the presence of pyridine were studied and the results were shown in Table 2. Heptafluorobutyric acid resulted from the thermolysis of TBH and reacted with pyridine to give pyridinium heptafluorobutyrate (**3**). Furthermore, 2-methoxy-1-propene (**1**), which would

Table 1. Rate constants for the thermal decomposition of 0.10 M[a] TBH in toluene and in methanol

Temp/°C	$k_d\times10^5$/s^{-1}	Solvent
65.0	1.88±0.05	Toluene[b,c]
75.0	4.66±0.15	
80.0	7.06±0.12	
85.0	12.03±0.46	
10.0	7.19±0.07	Methanol[d]
15.0	9.37±0.31	
19.6	13.04±0.26	
30.0	26.04±0.99	

a) 0.10 M=0.10 mol dm^{-3}. b) 0.10 M pyridine was added. c) Analysis by iodometry. d) Analysis by infrared spectra.

Table 2. Main products from the thermal decomposition of 0.10 M TBH and 0.10 M pyridine in toluene at 85 °C for 7 h

Product	Peroxy ester(mol/mol)
$CH_2=C(CH_3)_2$	0.02
$CH_3OC(CH_3)=CH_2$	0.08
$CF_3CF_2CF_2CO_2C(CH_3)_3$	0.07
$CF_3CF_2CF_2CO_2^{(-)}H\overset{(+)}{N}$ 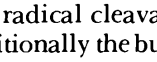	0.81[a]
$PhCH_2CH_2Ph$	0.08

a) Isolated yield.

Table 3. Rate constants for the bulk polymerization of styrene initiated by 0.03 M TBH

Temp/°C	$R_P\times10^2$/mol l^{-1}h^{-1}
50	7.77±0.64
55	12.16±0.84
60	22.43±0.64

result from ionic cleavage, was obtained as shown in Table 2. Olah *et al.* reported that the 1-methoxy-1-methylethylium ion (**2**) can also be isolated by the reaction of *t*-butyl peracetate with magic acid in SO_2ClF at −78 °C.[7] These results indicate that TBH would decompose partially with homolysis and partially with heterolysis which might contain both the autocatalysis (path A) and Criegee rearrangement (path B) according to the Scheme 1.

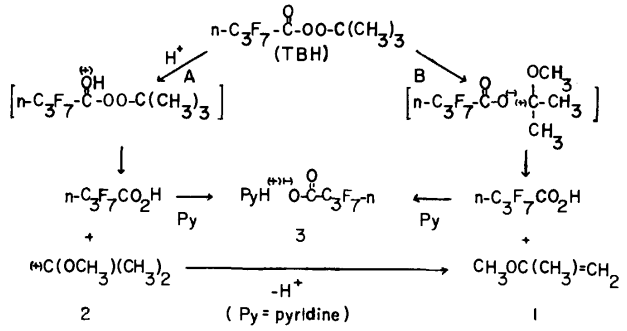

Scheme 1.

In the thermal decomposition of TBH in methanol, it is of interest that the entropy of activation for the decomposition has a large negative value compared with those of *t*-butyl peroxy esters derived from strong organic acids; TBH $\Delta S^{\ddagger} = -167.8 \pm 7.1\ J\ K^{-1}\ mol^{-1}$; *t*-butyl *p*-nitroperbenzoate, in methanol, $\Delta S^{\ddagger} = -28.0\ J\ K^{-1}\ mol^{-1}$;[8] *t*-butyl peroxytosylate, in metanol, $\Delta S^{\ddagger} = 3.8\ J\ K^{-1}\ mol^{-1}$.[3] From this large negative value of the entropy of activation and the observation of *t*-butyl hydroperoxide in decomposition products as shown in Table 4, it may be concluded that the thermal decomposition of TBH in methanol is principally dependent upon the following transesterification.

$$n\text{-}C_3F_7CO_2OC(CH_3)_3 + CH_3OH \longrightarrow n\text{-}C_3F_7CO_2CH_3 + (CH_3)_3COOH$$

On the other hand, 2,2-dimethoxypropane (**5**) in Table 4, which would result from nucleophilic attack of methanol on the 1-methoxy-1-methylethylium ion (**4**) as shown in Scheme 2, was obtained in 33% yield. The formation of 2,2-dimethoxypropane (**5**) also suggests that TBH would decompose in part with Criegee rearrangement. From the fact that methyl

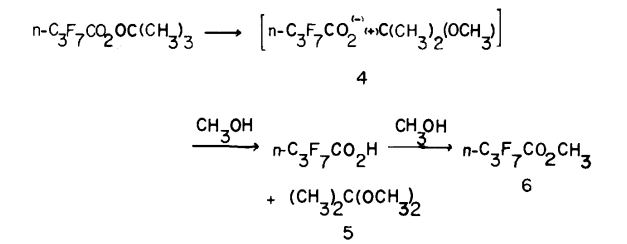

Scheme 2.

Table 4. Products from the thermal decomposition of 0.10 M TBH in methanol at 40 °C for 3 h

Product	Peroxy ester(mol/mol)
$CF_3CF_2CF_2CO_2CH_3$	0.93
$(CH_3)_3COOH$	0.65 (0.66)[a]
$(CH_3)_2C(OCH_3)_2$	0.33
$(CH_3)_2CO$	trace

a) Yield by iodometric analysis.

heptafluorobutyrate (**6**) can be quantitatively obtained by the reaction of heptafluorobutyric acid with methanol even at room temperature, **6** in Scheme 2 would result from the methyl-esterification of heptafluorobutyric acid as well as transesterification.

Experimental

TBH was prepared by the reaction of *t*-butyl hydroperoxide with heptafluorobutyryl chloride in the presence of pyridine and distilled carefully, bp 39.5—40.0 °C/17 mmHg (1 mmHg = 133.322 Pa). The infrared spectra showed the characteristic peroxy ester carbonyl band at 1815 cm^{-1}. ^{1}H-NMR($CF_2ClCFCl_2$) $\delta = 1.36$ (9H s). Mass *m/z* 286(M^+), 271, 197, 169, 150, 119, 100, 73, 69, 58, 57 (base), 55, 50, 45, 43, 42, 41, 39, 31, 29, 27, and 15; Calcd for $C_8H_9O_3F_7$: C, 33.58; H, 3.17%. Found: C, 32.50; H, 2.99%. The rates of decomposition of TBH were measured by iodometric titration or disappearance of the carbonyl stretching peak of the peroxy ester at 1815 cm^{-1}. The products of complete decomposition of TBH in both toluene and methanol were identified from the result obtained by GC/MS and the retention times of GLC compared with authentic samples.

The authors are indebted to Mr. Katsushi Katsura at the Tsukuba Central Research Laboratory of Nippon Oil & Fats Co., Ltd. for GC/Mass spectrometric measurement.

References

1) *Cf.* C. Rüchardt, *Fortschr. Chem. Forsch.*, **6**, 251 (1966).
2) P. D. Bartlett and B. T. Storey, *J. Am. Chem. Soc.*, **80**, 4954 (1958).
3) P. D. Bartlett and T. G. Traylor, *J. Am. Chem. Soc.*, **83**, 856 (1961).
4) E. Hedaya and S. Winstein, *Tetrahedron Lett.*, **1962**, 563.
5) P. J. Flory, "Principles of Polymer Chemistry," Cornell University Press, Ithaca, New York (1953).
6) P. D. Bartlett and D. M. Simons, *J. Am. Chem. Soc.*, **82**, 1753 (1960).
7) G. A. Olah, D. G. Parker, and N. Yoneda, *J. Org. Chem.*, **42**, 32 (1977).
8) E. Hedaya and S. Winstein, *J. Am. Chem. Soc.*, **89**, 1661 (1967).

Studies of Bitter Peptides from Casein Hydrolyzate. VIII.[1] Bitter Taste of Cyclic Analog of BPIa (Arg-Gly-Pro-Pro-Phe-Ile-Val)[2]

Ichizo MIYAKE, Katsushige KOUGE, Hidenori KANEHISA, and Hideo OKAI*

Department of Fermentation Technology, Faculty of Engineering, Hiroshima University, Shitami, Saijo-cho, Higashihiroshima 724

(Received September 16, 1983)

Synopsis. In order to elucidate the structure-taste relationship of bitter peptide BPIa (Arg-Gly-Pro-Pro-Phe-Ile-Val), *cyclo*-BPIa was synthesized. The result of both taste and CD examinations suggested that the bitterness of BPIa is caused by its spatial structure, which is analogous to that of *cyclo*-BPIa.

In our synthetic investigations of bitter peptide BPIa isolated from casein hydrolyzate by Minamiura *et al.*,[3] it has been confirmed that N-terminal arginine residue and C-terminal hydrophobic moiety are necessary for an intence bitterness of BPIa and that the spatial structure of whole molecule attributed to prolylproline in the center also contributes to its bitter taste. We also assume that N- and C-terminals of BPIa are situated close together by prolylproline. In order to confirm our assumption, we synthesized *cyclo*-BPIa, in which N-terminal arginine and C-terminal valine residues were combined, and compared its bitter taste with that of BPIa.

The synthetic route for *cyclo*-BPIa is shown in Fig. 1. Boc-Pro-Pro-Phe-Ile-Val-OBzl, which was an intermediate in the synthesis of BPIa,[4] was hydrogenated to yield the corresponding acid (**1**). It was condensed with H-Arg(NO_2)-Gly-OBzl·HCl (**3**) by the DCC-HOBt method and the resulting protected heptapeptide (**4**) was converted to the corresponding acid (**5**) by a saponification reaction. **5** was esterfied by the DCC-HONSu method to afford the corresponding active ester (**6**). After the amino protection of **6** was removed by the action of hydrogen chloride in 98% formic acid, the resulting heptapeptide active ester hydrochloride (**7**) was treated with pyridine under high-dilution conditions for cyclization. The reaction mixture yielded a clude N^G-nitro substituted cyclic heptapeptide (**8**), which was then purified by passing through columns of acidic and basic ion exchangers. **8** thus obtained was hydrogenated in the presence of palladium black to yield *cyclo*-BPIa (**9**). The homogeneity of the final product was confirmed by thin-layer chromatography, amino acid analysis, paper electrophoresis, and elemental analysis.

The taste of *cyclo*-BPIa was organoleptically determined by panel evaluation with four people. *cyclo*-BPIa possessed an extremely bitter taste: its threshold value was 0.02 mM (1 M=1 mol dm^{-3}). The value was of the same level as BPIa; the threshold value of BPIa was 0.05 mM. The CD curves of both *cyclo*-BPIa and BPIa measured in water are presented in Fig. 2. *cyclo*-BPIa has a curve with a negative trough at 202 nm; BPIa possesses a similarly shaped curve.

The results of both taste and CD examinations suggested that the bitter taste of BPIa is caused by its characteristic molecular shape, which is analogous to that of *cyclo*-BPIa.

Experimental

All the melting points are uncorrected. Thin-layer chromatography was carried out on Merck silica gel G with the solvent systems: R_f^1, *n*-BuOH-AcOH-pyridine-H_2O (4:1:1:2, v/v); R_f^2, $CHCl_3$-MeOH (5:1, v/v). Opical rotations were measured on a Union PM-101 polarimeter. Amino acid analysis in acid hydrolyzate with 6 M HCl at 110 °C for 72 h was performed with a Hitachi amino acid analyzer, KLA-5 type. Prior to analyses, the compounds were dried over phosphorus pentaoxide at 66 °C and 2 mmHg (1 mmHg=133.332 Pa) for 2 h.

Boc-Pro-Pro-Phe-Ile-Val-OH (1). This was prepared from Boc-Pro-Pro-Phe-Ile-Val-OBzl[4] (7.62 g, 10 mmol) in

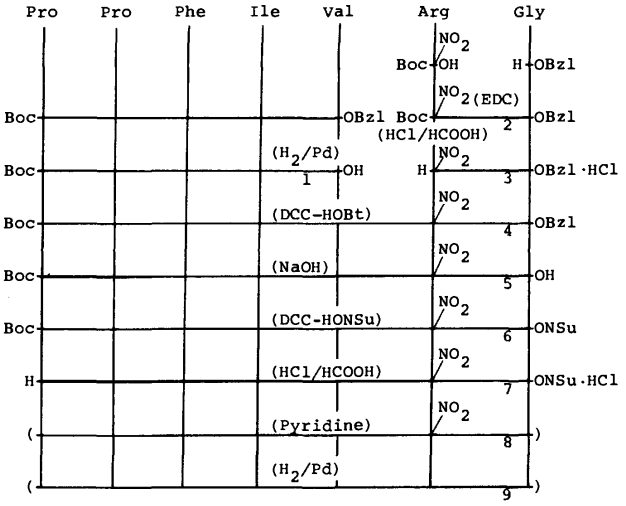

Fig. 1. Synthesis of *cyclo*-BPIa.

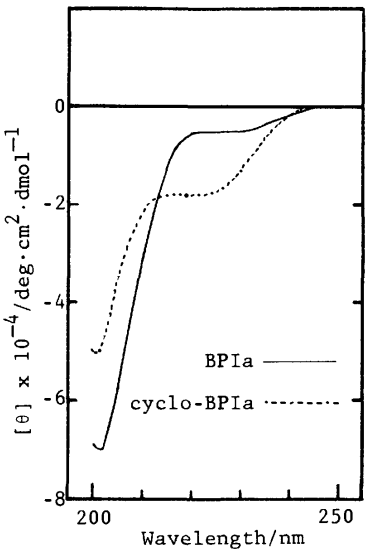

Fig. 2. CD curves of *cyclo*-BPIa and BPIa.

MeOH (30 ml) by hydrogenation in the presence of Pd black; yield 5.95 g (89%); mp 169—171 °C; $[\alpha]_D^{20}$ −96° (*c* 1, MeOH); R_f^1 0.86 and R_f^2 0.73.

Found: C, 62.34; H, 8.16; N, 10.26%. Calcd for $C_{35}H_{53}O_8N_5$: C, 62.57; H, 7.95: N, 10.43%.

Boc-Arg(NO$_2$)-Gly-OBzl (**2**). This was prepared from Boc-Arg(NO_2)-OH (9.60 g, 30 mmol) and H-Gly-OBzl·TsOH (12.12 g, 36 mmol) in acetonitrile (100 ml) by the EDC method;[5] yield 10.85 g (76%); mp 96 °C; $[\alpha]_D^{20}$ −11° (*c* 1, MeOH); R_f^1 0.91 and R_f^2 0.77

Found: C, 51.61; H, 6.31; N, 17.88%. Calcd for $C_{20}H_{30}O_7N_6$: C, 51.49; H, 6.48; N, 18.02%.

H-Arg(NO$_2$)-Gly-OBzl·HCl (**3**). This was prepared from **2** (4.66 g, 10 mmol) by the action of hydrogen chloride in 98% formic acid. The product was obtained as a hygroscopic solid; yield 4.02 g (100%); R_f^1 0.76 and R_f^2 0.31.

Boc-Pro-Pro-Phe-Ile-Val-Arg(NO$_2$)-Gly-OBzl (**4**). This was prepared from **1** (5.38 g, 8 mmol) and **3** (4.02 g, 10 mmol) in DMF (20 ml) by the DCC-HOBt method.[6] The product was recrystallized from hot MeOH; yield 5.14 g (63%); mp 231—232 °C; $[\alpha]_D^{20}$ −41.5° (*c* 1, DMF); R_f^1 0.91 and R_f^2 0.76.

Found: C, 58.59; H, 7.31; N, 15.03%. Calcd for $C_{50}H_{73}O_{12}N_{11}$: C, 58.86; H, 7.21; N. 15.10%.

Boc-Pro-Pro-Phe-Ile-Val-Arg(NO$_2$)-Gly-OH (**5**). Compound **4** (5.1 g, 5 mmol) was saponified with 1 M NaOH (7.5 ml) in MeOH (10 ml). The purification was done by the extraction with *n*-BuOH: yield 4.42 g (97%); mp 105 °C (decomp); $[\alpha]_D^{20}$ −32.3° (*c* 1, DMF); $R_f^1$0.56 and R_f^2 0.21.

Found: C, 54.11; H, 7.27; N, 16.15%. Calcd for $C_{43}H_{67}O_{12}N_{11}\cdot H_2O$: C, 54.47; H, 7.34; N, 16.25%.

Boc-Pro-Pro-Phe-Ile-Val-Arg(NO$_2$)-Gly-ONSu (**6**). To a solution of **5** (1.37 g, 1.5 mmol) and HONSu (0.35 g, 3 mmol) in DMF (5 ml), DCC (0.62 g, 3 mmol) was added with stirring at 0 °C. The reaction mixture was stirred for 3 h at 0 °C, then at room temperature overnight. DCUrea was filtered off and a large amount of ether was poured into the filtrate. The precipitate thus obtained was collected by filtration. It was recrystallized from acetonitrile; yield 1.26 g (82%); mp 193 °C; $[\alpha]_D^{20}$ −46.1° (*c* 0.5, DMF); R_f^1 0.91 and R_f^2 0.81.

Found: C, 54.58; H, 7.15; N, 15.90%. Calcd for $C_{47}H_{70}O_{14}N_{12}\cdot 1/2H_2O$: C, 54.47; H, 6.91; N, 16.22%.

cyclo(*-Arg(NO$_2$)-Gly-Pro-Pro-Phe-Ile-Val-*) (**8**). Compound **6** (0.51 g, 0.5 mmol) was dissolved in 98% formic acid and 3.5 M hydrogen chloride in dioxane (10 ml) at 0 °C. After 30 min, the solution was evaporated *in vacuo* and the oily residue was solidified with ether (yield 0.44 g). The active ester hydrochloride (**7**) thus obtained was dissolved in DMF (5 ml) and the solution was added dropwise to pyridine (250 ml) with stirring. The reaction mixture was stirred for 24 h at room temperature and evaporated *in vacuo*. The residual oil was dissolved in a mixture of dioxane (50 ml) and water (10 ml). The solution was passed successively through columns (1.2 cm×12.5 cm) of Amberlite CG-120 (H^+ form) and Amberlite CG-400 (OH^- form). The columns were washed with the same solvent and the collected effluent was evaporated *in vacuo*; then the product was collected by the aid of water (yield 51 mg). It was recrystallized from MeOH-ether; yield 41 mg (10%); mp 221 °C (decomp); $[\alpha]_D^{20}$ −56.3° (*c* 0.5, MeOH); R_f^1 0.83 and R_f^2 0.65.

Found: C, 52.51; H, 6.98; N, 17.52%. Calcd for $C_{38}H_{57}O_9N_{11}\cdot 3H_2O$: C, 52.70; H, 7.33; N, 17.79%.

cyclo(*-Arg-Gly-Pro-Pro-Phe-Ile-Val-*) (**9**). Compound **8** (40 mg, 0.005 mmol) was dissolved in MeOH (2 ml) and AcOH (2 ml) and hydrogenated in the presence of Pd black for 24 h. The filtrate from catalyst was evaporated *in vacuo* and the oily residue was crystallized by the aid of ether. It was recrystallized from water-acetone; yield 40 mg (97%); mp 198 °C (decomp); $[\alpha]_D^{20}$ −31.4° (*c* 0.5, MeOH); R_f^1 0.57 and R_f^2 0.05. Amino acid ratios in acid hydrolyzate: Arg 1.11, Gly 0.97, Pro 2.01, Phe 1.09, Ile 1.00, Val 0.95.

Found: C, 53.38; H, 7.70; N, 15.30%. Calcd for $C_{38}H_{58}O_7N_{10}\cdot CH_3COOH\cdot 4H_2O$: C, 53.44; H, 7.85; N, 15.58%.

Paper Electrophoresis. This was carried out under the conditions previously reported.[7] *cyclo*-BPIa migrated toward the cathode and revealed a single spot by spraying Sakaguchi reagent; ninhydrin gave the same result. The R_{Arg} value[8] of *cyclo*-BPIa was 0.58.

CD Measurement. This was performed with a JASCO J-20A. A cell of path length 0.2 mm was used and runs were made at ambient temperature.

Sensory Test. Taste of cyclo-BPIa was organoleptically determined in the same manner as described in the previous pepers.[1,4,7]

The authors wish to express their thanks to Associate Professor Michio Kondo of Saga University for the CD measurement. Thanks are also due to Dr. Shinji Okumura of Ajinomoto Co. Inc., for supplying some amino acids.

References

1) Part VII. T. Shigenaga, K. Otagiri, H. Kanehisa, and H. Okai, *Bull. Chem. Soc. Jpn.*, **57**, 103 (1984).

2) The abbreviations recommended by IUPAC-IUB commission of Biochemical Nomenclature (*J. Biol. Chem.*, **247**, 977 (1972)) have been used. Amino acid symbols except glycine denoted L-configuration. Additional abbreviations: DCC, dicyclohexylcarbodiimide: DCUrea, *N,N'*-dicyclohexylurea; DMF, *N,N*-dimethylformamide; EDC, 1-ethyl-3-(3-dimethylaminopropyl)carbodiimide; HOBt; 1-hydroxybenzotriazole; HONSu, *N*-hydroxysuccinimide.

3) N. Minamiura, Y. Matsumura, J. Fukumoto, and T. Yamamoto, *Agric. Biol. Chem.*, **36**, 588 (1972).

4) H. Fukui, H. Kanehisa, N. Ishibashi, I. Miyake, and H. Okai, *Bull. Chem. Soc. Jpn.*, **56**, 766 (1983).

5) J. C. Sheehan, J. Preston, and P. A. Cruickshank, *J. Am. Chem. Soc.*, **87**, 2492 (1969).

6) W. König and R. Geiger, *Chem. Ber.*. **103**, 788 (1970).

7) I. Miyake, K. Kouge, H. Kanehisa, and H. Okai, *Bull. Chem. Soc. Jpn.*, **56**, 1678 (1983).

8) The electrophoretic mobility was recorded as R_{Arg}, the ratio of the distance the compound moved to that which a standard arginine spot moved on the same electrophoreogram.

Silver Ion-induced Allylation of Furan with Cyclopropyl Halides

Nobujiro SHIMIZU,* Kenji WATANABE, and Yuho TSUNO
Department of Chemistry, Faculty of Science, Kyushu University 33, Hakozaki, Higashi-ku, Fukuoka 812
(Received, September 22, 1983)

Synopsis. Allyl species generated from 1-bromo-2-phenylcyclopropane and seven different 1,1-dihalocyclopropanes with the aid of silver perchlorate reacted with furan in a regio- and stereoselective manner to give a series of 2-allylfuran derivatives in fair to good yields.

The S_N1 like reactions of cyclopropyl halides generally proceed *via* a stereoelectronically controlled ring-opening rearrangement to allyl cation intermediates.[1,2] Although this unique behavior of cyclopropyl halides provides a useful synthetic route to cyclic alkenes which are not readily accessible by other methods,[3] only a few examples have been reported on the reactions between the allyl species formed from cyclopropyl halides and substrates other than solvent nucleophiles.[4] Trapping of such the species by furan seems to be of synthetic interest in view of the fact that direct alkylation reactions of furan including allylation often cause extensive resinification.[5,6] We here report the results of the silver ion-induced reaction of furan with various cyclopropyl halides **1a**—h.

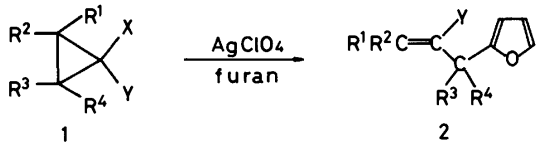

1 2

a R^1—R^4=Me, X = Y = Br
b R^1—R^3=Me, R^4=H, X=Y=Br
c R^1=R^2=Me, R^3=R^4=H, X=Y=Br
d R^1=Ph, R^2=Me, R^3=R^4=H, X=Y=Br
e R^1=Ph, R^2—R^4=H, X=Y=Br
f R^1=n-Pr, R^2—R^4=H, X=Y=Br
g R^1—R^4=Me, X=Y=Cl
h R^1=Ph, R^2—R^4=H, X=Br, Y=H

On exposure to silver perchlorate in THF/ether (1:3), 1,1-dibromo-2,2,3,3-tetramethylcyclopropane (**1a**) rapidly reacted with furan at room temperature to give 2-(2-bromo-1,1,3-trimethyl-2-butenyl)furan (**2a**) in 40% isolated yield together with 3-bromo-2,4-dimethyl-1,3-pentadiene (35%) which was shown to be the principal product in the absence of furan. Allyl species formed from cyclopropyl halides **1b**—h and silver perchlorate also reacted with furan to give the corresponding 2-allylfuran derivatives **2b**—h in moderate to good yields. The results are given in Table 1. Typical experimental procedure consists of treating a halide (**1**, 10 mmol) with silver perchlorate (2 equiv.) in THF/ether (1:3) in the presence of excess furan (*ca.* 5 equiv.) and calcium carbonate (as a buffer) at ambient temperature or under reflux.

Among 1,1-dihalocyclopropanes **1a**—g, ease of the reaction decreased in the order **1a**>**1b**≫**1c**—g and prolonged exposure to silver perchlorate was needed for the last series of halides. A marked difference in reactivity was also seen between the two stereoisomers of a cyclopropyl bromide **1h**. Thus, when a mixture of (*E*)-and (*Z*)-**1h** (1:1.47) was treated with silver perchlorate in the presence of furan in THF/ether (1:3) under reflux for 30 min, the (*E*)-isomer was completely consumed to give *trans*-**2h** in excellent yield, whereas the (*Z*)-isomer remained unchanged, in accord with the theoretical prediction.[1]

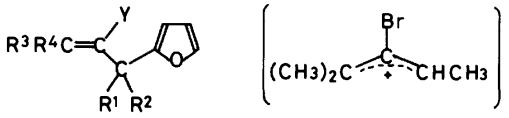

3 4

Unsymmetrical halides **1b**—f and **1h** are expected to give a regioisomeric product **3** besides **2** but actually, furan preferentially reacted with the less heavily alkylated (or arylated) carbon site of the allyl species generated from these halides yielding **2** as the exclusive product. It should be noted, however, that the silver ion-induced reaction of these halides with methanol in place of furan gave the corresponding methyl ethers of type **3** as the major product.[7] Table 2 shows the change in regioselectivity in the silver ion-induced reaction of **1b** with various substrates. In contrast to methanol, *t*-butyl alcohol preferred the secondary carbon site rather than the tertiary site of the allyl species **4** formed from **1b**. Presumably, a small nucleophile such as methanol would preferentially react with the most electron positive site but the steric effects must be the major factor to control selectivity for bulky substrates including aromatic rings.

It is also worth stating that besides the stereospecific conversion of (*E*)-**1h** to *trans*-**2h**, the formation of **2** from **1d**—f was highly stereoselective yielding a single

TABLE 1. SILVER ION-INDUCED REACTION OF FURAN WITH CYCLOPROPYL HALIDES

Halide	Conditions[a]	Yield/% of **2** (*Z*/*E*)[b]
1a	rt, 1 h	40[c]
1b	rt, 1 h	76
1c	reflux, 6 h	73
1d	reflux, 6 h	73 (8.7)
1e	reflux, 6 h	61 (*Z*)[d]
1f	reflux, 6 h	54 (*Z*)[e]
1g	reflux, 6 h	60[f]
1h[g]	reflux, 0.5 h	37, 93 (*E*)[h]

a) Reactions were carried out in THF/ether (1:3) by stirring a mixture of **1**, silver perchlorate (2—3 equiv), furan (*ca.* 5 equiv), and calcium carbonate under conditions given. b) Isolated yield. c) 3-Bromo-2,4-dimethyl-1,3-pentadiene was also formed (35%). d) A mixture of **2e** and **3e** in the ratio 8.4:1. e) A mixture of **2f** and **3f** in the ratio 24:1. f) 3-Chloro-2,4-dimethyl-1,3-pentasiene was also formed (25%). g) (*Z*)/(*E*)=1.47. h) Corrected for the recovery of (*Z*)-**1h** which remained unchanged.

Table 2. Regioselectivity in the silver ion-induced reactions of **1b**[a]

Nucleophile (S-H)	$(CH_3)_2C{=}C(Br)-CHCH_3$:	$(CH_3)_2C(Br)-C{=}CHCH_3$
	S	S
Furan	≈100:0	
Anisole[b]	≈100:0	
MeOH[c]	36:64	
i-PrOH[c]	54:46	
t-BuOH[c]	80:20	

a) Reaction were carried out in THF/ether (1 : 3) using **1b**, silver perchlorate, and a nucleophile in the molar ratio 1 : 2 : 5 (0 °C, 45 min). b) A mixture of *p*- and *o*-isomers (1.9 : 1) was obtained in 82% yield. c) The corresponding ethers were formed in high yields.

stereoisomer or near so. The (*Z*)-structure may be deduced for the abundant isomer from the reported stereochemical observation on the Ag(I)-induced solvolysis of 1,1-dihalocyclopropanes.[2] This was in fact true and the reductive dehalogenation of **2e** with LAH in boiling THF[8] gave *trans*-**2h** as the principal product. These results are explicable in terms of the stereocontrolled ring-opening formation of (*Z*)-allyl cations from **1d**—f in preference to the isomeric (*E*)-cations.[1,9]

Experimental

NMR spectra were determined in carbon tetrachloride using a Hitachi R-600 spectrometer. IR spectra were recorded on a Hitachi 260-10 spectrophotometer.

Silver Perchlorate-Induced Reaction of Furan with Cyclopropyl Halides. The following procedure for the preparation of 2-(2-bromo-1,3-dimethyl-2-butenyl)furan (**2b**) is representative.

Into a stirred mixture of silver perchlorate (4.05 g, 20 mmol), furan (3.5 g), and calcium carbonate (2 g) in THF/ether (1 : 3, 20 ml) was added a solution of 1,1-dibromo-2,2,3-trimethylcyclopropane (**1b**, 2.36 g, 9.8 mmol) in ether (2 ml) during the period of 15 min at room temperature. The mixture was stirred for additional 45 min at ambient temperature and quenched with saturated sodium chloride solution. A crude oil obtained after usual workup was distilled to give an allylfuran **2b** (1.76 g, 76%): bp 95—98 °C (14 Torr: 1=Torr 133.3 Pa); IR 3130, 1650, 1505, 1150, 1080, 1010, 910 and 740 cm^{-1}; NMR δ=1.40 (3H, d, J=7 Hz), 1.92 (6H, s), 4.17 (1H, q, J=7 Hz), 6.00 (1H, m), 6.20 (1H, m), and 7.24 (1H, m). Found: C; 52.31, H; 5.74%. Calcd for $C_{10}H_{13}BrO$: C; 52.42, H; 5.72%.

Similarly, furan derivatives **2a** and **2c**—h were obtained and characterized. They showed IR bands near 3130, 1640, 1505, 1150, 1010, 920, and 730 cm^{-1} and NMR signals of the furan ring protons near δ=6.0, 6.2, and 7.2. **2a**: NMR δ=1.20 (3H, s), 1.52 (6H, s), and 1.84 (3H, s). **2c**: bp 97—98 °C (17 Torr); NMR δ=1.90 (6H, s), 3.80 (2H, s) (Found: C; 50.22, H; 5.20%). **2d** (as a mixture of (*E*)- and (*Z*)-isomers in the ratio 1 : 8.7): bp 114—117 °C (3 Torr); NMR (signals of the less abundant isomer were shown in italics.) δ=*2.17* (s) and 2.21 (s) (together 3H), 3.66 (s) and *3.97* (s) (together 2H), and 7.22 (5H, s). **2e**+**3e** (8.4 : 1): bp 123—126 °C (2 Torr); NMR for **2e** δ=3.90 (2H, s), 6.72 (1H, s), and 7.2—7.6 (5H, m) (Found: C; 59.03, H; 4.14%), and for **3e** δ=4.99 (1H, s), 5.45 (1H, s), 5.67 (1H, s), and 7.26 (5H, s). **2f**+**3f** (24 : 1): bp 96—100 °C (14 Torr); NMR for **2f** δ=0.92 (3H, t, J=7 Hz), 1.44 (2H, m), 2.18 (2H, q, J=7 Hz), 3.70 (2H, s), and 5.19 (1H, t, J=6 Hz) (Found: C; 52.18, H; 5.74%), and for **3f** δ=0.95—2.0 (7H, m), 3.56 (1H, t, J=7 Hz), 5.45 (1H, broad s), and 5.65 (1H, broad s). **2g**: bp 85—87 °C (15 Torr); NMR δ=1.23 (3H, s), 1.52 (6H, s), and 1.86 (3H, s) (Found: C; 66.60, H; 7.68%). **2h**: NMR δ=3.51 (2H, d, J=5 Hz), 5.98 (1H, m) 6.18—6.32 (2H, m), 6.60 (1H, d, J=16 Hz), and 7.2—7.4 (6H, m).

Reduction of 2b, 2e, and 2f with LAH. A mixture of **2b** (1.28 g, 15.6 mmol) and LAH (0.5 g) in THF (10 ml) was heated under reflux for 5 h. A crude oil (801 mg) obtained after workup was distilled to give 2-(1,3-dimethyl-2-butenyl)furan (450 mg): bp 105—109 °C (92 Torr); IR 1590, 1010, and 730 cm^{-1}. NMR δ=1.27 (3H, d, J=7 Hz), 1.70 (6H, s), 3.65 (1H, m), 5.15 (1H, d, J=8 Hz), 5.85 (1H, m), 6.15, (1H, m), and 7.20 (1H, m) (Found: C; 79.82, H; 9.42%).

Similarly, **2e** and **2f** were reduced to **2h** and 2-(2-hexenyl)furan, respectively. NMR of the latter compound: δ=1.90 (3H, t, J=7 Hz), 1.42 (2H, m), 2.00 (2H, m) , 3.30 (2H, m), 5.4—5.6 (2H, m), 5.87 (1H, m), 6.16 (1H, m), and 7.20 (1H, m).

References

1) R. Hoffmann and R. B. Woodward, *Acc. Chem. Res.*, **1**, 17 (1968).
2) S. R. Sandler, *J. Org. Chem.*, **32**, 3876 (1967).
3) W. Kirmse, "Carbene Chemistry," Academic Press, New York (1971).
4) C. Müller and P. Weyerstahl, *Tetrahedron*, **31**, 1787 (1975); G. Paradisi and G. Zecchi, *Gazz. Chim. Ital.*, **104**, 881 (1974); L. Skattebøl and B. Boulette, *J. Org. Chem.*, **31**, 81 (1966).
5) R. M. Acheson, "An Introduction to the Chemistry of Heterocyclic Compounds," A Wiley-Interscience, New York (1976).
6) For direct allylation of furan, see: H. M. R. Hoffmann and N. F. Janes, *J. Chem. Soc., C*, **1969**, 1756.
7) For regiochemistry of the S_N1 solvolysis of allyl halides and esters, see: R. H. DeWolfe and W. G. Young, "The Chemistry of Alkenes," ed by S. Patai, Interscience, New York (1964).
8) S. K. Chung, *J. Org. Chem.*, **45**, 3153 (1980).
9) P. v. R. Schleyer, T. M. Su, M. Saunders, and J. C. Rosenfeld, *J. Am. Chem. Soc.*, **91** 5174 (1969); H. Mayer, W. Förner, and R. v. R. Schleyer, *ibid.*, **101**, 6032 (1979).

Reaction Efficiency of Exciplexes in Singlet Sensitized Decomposition of Dibenzoyl Peroxide

Hiroaki MISAWA, Akihide KITAMURA,† Hirochika SAKURAGI, and Katsumi TOKUMARU*
Department of Chemistry, University of Tsukuba, Sakura-mura, Ibaraki 305
(Received November 5, 1983)

Synopsis. Quantum yields were measured for aromatic hydrocarbon-sensitized decomposition of dibenzoyl peroxide in benzene. For the sensitizers employed, naphthalene, phenanthrene, triphenylene, and chrysene, the ratio of the rate constants for decay and radical formation from intermediate exciplexes was found to be similar (0.2—0.4), indicating that the reactivity of the peroxide moiety in the intermediate is independent of the structural factors of the sensitizers as far as examined.

Exciplexes have been proposed as reactive intermediates in many photochemical reactions though they are not necessarily emissive.[1-3] In some cases the exciplexes may be too reactive to be alive in sufficiently long lifetimes to exhibit emission.[3,4] However, few works have been carried out to actually examine intrinsic reactivity of the exciplexes from the viewpoint of structural factors of sensitizers.[2,5,6]

Previously, singlet excited aromatic hydrocarbons have been revealed to sensitize decomposition of dibenzoyl peroxide (BPO) in solution.[7-9] The reaction was proposed to proceed through short lived reactive exciplexes which either bring about homolytic decomposition of the peroxide moiety into free radicals or deactivate into the original components in the ground state as shown in the following scheme, where Sens and P denote a sensitizer and the peroxide, respectively, and k_q, k_r, and k_d mean the rate constants of the processes concerned.

This paper describes an attempt to determine the relative reactivity of the exciplexes in singlet sensitized decomposition of BPO in relation to structural factors of the hydrocarbon sensitizers.

$$^1\text{Sens}^* + \text{P} \xrightarrow{k_q} {}^1(\text{Sens}\cdot\text{P})^* \quad (1)$$

$$^1(\text{Sens}\cdot\text{P})^* \xrightarrow{k_r} \text{Free radicals} + \text{Sens} \quad (2)$$

$$^1(\text{Sens}\cdot\text{P})^* \xrightarrow{k_d} \text{Sens} + \text{P} \quad (3)$$

Scheme 1.

Results and Discussion

Benzene solutions of a sensitizer (3.0×10^{-3}—3.0×10^{-2} mol dm^{-3}) and varying concentrations of BPO (1.2×10^{-3}—3.1×10^{-2} mol dm^{-3}) were irradiated under argon atmosphere with 366-nm light (for chrysene as sensitizer) or 313-nm light (for triphenylene, phenanthrene, and naphthalene) isolated from a 400 W high pressure mercury lamp, and the quantum yields for decomposition of BPO were determined at low conversion of BPO (less than 20%) using potassium tris(oxalato)ferrate(III) actinometry.[10]

According to Scheme 1, the quantum yield for disappearance of BPO is expressed by Eq. 4, where τ_S^0 means the lifetime of the singlet excited sensitizer in the absence of the peroxide.

$$\Phi^{-1} = (1 + 1/k_q\tau_S^0[\text{P}])(1 + k_d/k_r) \quad (4)$$

For each sensitizer employed, the reciprocal of the quantum yield is linearly correlated with the reciprocal of the peroxide concentration, and the intercept, $(k_r+k_d)/k_r$, exceeds unity (Fig. 1). This means clearly that the reaction proceeds through formation of some reactive intermediates like exciplexes. The results analyzed according to Eq. 4 are summarized in Table 1.

In Table 1 are also listed the $k_q\tau_S^0$ values determined by fluorescence quenching in benzene using the single photon counting technique,[11] the singlet excitation energies[10] and oxidation potentials[12] of the sensitizers. The $k_q\tau_S^0$ value obtained from the quantum yield measurements for each sensitizer satisfactorily agrees well with that from the fluorescence quenching.

As Table 1 indicates, the observed ratios of the rate constants for decay and radical formation from the exciplexes, k_d/k_r, are not significantly varied (0.21—0.41) among the unsubstituted polycyclic aromatic hydrocarbons employed, naphthalene, phenanthrene, triphenylene, and chrysene. This fact indicates that the reactivity of the peroxide moiety in the intermediate does not depend upon such structural factors of the sensitizers as the singlet excitation energies of the sensitizers, E_S, and the extent of charge transfer from the excited sensitizer to BPO in the exciplex, $E_{ox}-E_S$. This observation might be accounted for by the facts that the low energy (*ca.* 31 kcal mol^{-1}, 1 cal=4.184 J)[13] is required for the cleavage of the peroxide linkage compared to the singlet excitation energies of the sensitizers (Table 1) and that the

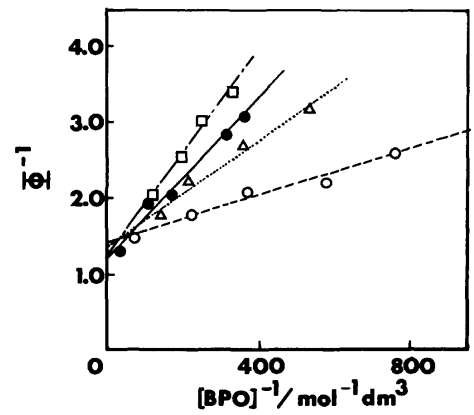

Fig. 1. Stern-Volmer plots of reciprocal quantum yields *vs.* reciprocal concentrations of BPO in aromatic hydrocarbon sensitized decomposition of BPO. Sensitizers: naphthalene (○), triphenylene (□), phenanthrene (△), and chrysene (●).

†Present address: Department of Chemistry, College of Arts and Sciences, Chiba University, Yayoi-cho, Chiba 260.

TABLE 1. RELATIVE REACTIVITY OF THE EXCIPLEXES IN SINGLET SENSITIZED DECOMPOSITION OF DIBENZOYL PEROXIDE AND STRUCTURAL FACTORS OF THE SENSITIZERS

Sensitizer	k_d/k_r	$k_q\tau_S^{0}$ a)	$k_q\tau_S^{0}$ b)	E_S c)		E_{ox} d)	$E_{ox}-E_S$
		$dm^3 mol^{-1}$		kcal mol^{-1}	eV	V	eV
Naphthalene	0.41	930	810	92	3.99	1.87	-2.12
Triphenylene	0.29	200	170	83.4	3.62	1.80	-1.82
Phenanthrene	0.38	400	310	82.8	3.59	1.71	-1.88
Chrysene	0.21	230	240	79.2	3.43	1.56	-1.87

a) From quantum yield measurements. b) From fluorescence quenching.
c) Singlet excitation energy from Ref. 10 d) Oxidation potential *vs.* SCE in CH_3CN with Et_4NClO_4.

overall process of the sensitization gives free radical products arising from benzoyloxyl and phenyl radicals, but not any ionic products at all.[7-9]

Attempts to determine the quantum yields by employing other sensitizers like anthracene, 9,10-diphenylanthracene, pyrene, and perylene were abandoned, since these sensitizers were found to be fairly consumed during the reaction in contrast to the above sensitizers which were recovered more than 80% after the reaction.

Experimental

Materials. Dibenzoyl peroxide was purified by reprecipitation from dichloromethane-methanol. Triphenylene was prepared according to literature.[14] The other aromatic hydrocarbons, naphthalene, phenanthrene, chrysene, anthracene, 9,10-diphenylanthracene, pyrene, and perylene, were commercially available. The aromatic hydrocarbons were purified by column chromatography on silica gel with petroleum ether as eluent and recrystallized from hexane. Benzene (special grade) was distilled before use.

Measurement of Quantum Yields. The quantum yields for disappearance of BPO were determined in benzene under argon atmosphere employing potassium tris(oxalato)ferrate(III) as actinometer. Irradiation was carried out with 366-nm light for chrysene, anthracene, 9,10-diphenylanthracene, pyrene, and perylene and with 313-nm light for naphthalene, phenanthrene, and triphenylene. From a 400 W high pressure mercury lamp 366-nm light was isolated through a Toshiba UV-D36B glass filter and 313-nm light through a Toshiba UV-D33S and a K_2CrO_4/Na_2CO_3 solution filter.[10] The amounts of the remaining BPO were determined by HPLC (column: Zorbax ODS, solvent: $CH_3OH-H_2O=85:15$). Although BPO was decomposed on direct irradiation with 313-nm light, its quantum yield was less than 1% compared with the sensitized decompositions and can be satisfactorily neglected in the present investigation.

References

1) P. S. Engel and B. M. Monroe, *Adv. Photochem.*, **8**, 245 (1970); M. Koizumi, S. Kato, N. Mataga, T. Matsuura, and Y. Usui, "Photosensitized Reactions," Kagaku Dojin, Kyoto (1978), p. 271; H. Sakurai and C. Pac, "Kagaku Sosetsu," ed by Chem. Soc. Jpn., Gakkai Shuppan Center, Tokyo (1982), pp. 37, 75.

2) R. A. Caldwell and D. Creed, *Acc. Chem. Res.*, **13**, 45 (1980).

3) R. S. Davidson, *Adv. Phys. Org. Chem.*, **19**, 1 (1983).

4) H. Sakuragi, K. Tokumaru, H. Itoh, K. Terakawa, K. Kikuchi, R. A. Caldwell, and C.-C. Hsu, *J. Am. Chem. Soc.*, **104**, 6796 (1982).

5) H. D. Becker, *Pure Appl. Chem.*, **54**, 1589 (1982).

6) A. M. Swinnen, M. van der Auweraer, F. C. de Schryver, C. Windels, R. Goedeweeck, A. Vannerem, and F. Meeus, *Chem. Phys. Lett.*, **95**, 467 (1983); F. C. de Schryver, N. Boens, and J. Put, *Adv. Photochem.*, **10**, 359 (1977).

7) T. Nakata, K. Tokumaru, and O. Simamura, *Tetrahedron Lett.*, **1967**, 3303; T. Nakata and K. Tokumaru, *Bull. Chem. Soc. Jpn.*, **43**, 3315 (1970).

8) K. Tokumaru, A. Ohshima, T. Nakata, H. Sakuragi, and T. Mishima, *Chem. Lett.*, **1974**, 571.

9) A. Kitamura, H. Sakuragi, M. Yoshida, and K. Tokumaru, *Bull. Chem. Soc. Jpn.*, **53**, 1393, 2413 (1980).

10) S. L. Murov, "Handbook of Photochemistry," Marcel Dekker, New York (1973).

11) A. Kitamura, Thesis, University of Tsukuba, 1980.

12) The oxidation potentials were determined *vs.* SCE in acetonitrile using Et_4NClO_4(0.1 mol dm^{-3}) as a supporting electrolyte.

13) I. Jaffe, E. J. Prosen, and M. Szwarc, *J. Chem. Phys.*, **27**, 416 (1957).

14) T. Sato, *Yuki Gosei Kagaku Kyokai Shi*, **30**, 293 (1972).

 © 1984 The Chemical Society of Japan Bull. Chem. Soc. Jpn., 57, 1169—1173 (1984)

On the Penetration Rate and the Role of Acids in the Control of Impregnation Profiles

Masaharu KOMIYAMA* and Robert P. MERRILL†
Department of Chemical Engineering, Faculty of Engineering, Tohoku University, Aramaki Aoba, Sendai 980
†*School of Chemical Engineering, Cornell University, Ithaca, New York 14853 U.S.A.*
(Recieved June 2, 1983)

Two factors which play important roles in determining the concentration profiles in the impregnation of porous catalysts, *viz.*, penetration rate of impregnating solution and the use of acids, were examined. The flow rate of impregnating solution into a spherical dry pellet consisting of polydispersed pores obeyed the equation which assumed constant pressure differential at the liquid front independent of its position in the pellet. The adsorption behavior of nickel ions onto γ-alumina strongly depended on the pH of the solution, and very weakly on the kind of acids used. By controlling the pH of the impregnating solution, it was possible to obtain a surface impregnation, a uniform impregnation and a subsurface impregnation for nickel on γ-alumina.

Many catalysts in common use are produced by impregnating a pellet of a porous support with a solution of catalyst precursors. During the impregnation and subsequent drying, small crystallites of the catalyst precursors are deposited on the internal surface of the support material. The mass transfer processes involved in the impregnation and drying steps typically do not reach equilibrium, resulting in non-uniform concentration profiles of impregnant along the radius of the support pellet. The importance of designing and/or controlling these concentration profiles, or impregnation profiles, has been recognized, because optimized impregnation profiles may bring about higher overall reaction rate,[1] better light-off performance,[2,3] longer catalyst life,[3,4] and/or conservation of expensive catalyst metals.[5,6]

In order to design and control the impregnation profiles the factors influencing the profiles must be identified by constructing appropriate impregnation models. The impregnation step involves the time-dependent flow of impregnating solution into a dry pellet and adsorption of impregnant onto the pore wall. The interior dispersal of impregnant during this step has been analyzed in detail by Vincent and Merrill,[7] for single-component impregnation using a single-pore model. Their analysis has since been expanded in two directions: models for single-component impregnation into a porous sphere[8] and the multi-component impregnation using the single-pore model[9] have been presented. This paper examines experimentally two aspects of these two developments.

The expansion of the single-pore model to a three-dimensional porous sphere is like the one-dimensional model based on the analysis of Washburn[10] who assumed a succession of Pourselle steady states. Its derivation involved an assumption, *viz.*, constant pressure differential at the liquid front independent of its position inside the pellet (*cf.* Fig. 1 (a)). Impregnation profiles calculated from this expanded model quantitatively agreed with experimental impregnation profiles,[8] although no theoretical or experimental basis for the assumption was presented. The dynamics of liquid uptake during catalyst impregnation is not well understood, and is at the stage of being closely examined.[11] In the first part of this paper we examine this process, by directly measuring the penetration rate of a liquid into a spherical pellet.

Kulkarni *et al.*[9] have expanded the single-component model to multi-component impregnation using the single-pore model of Vincent and Merrill[7] and assuming competitive adsorption among the impregnants. For the preparation of subsurface impregnation employing various acids, their model calculations were in qualitative agreement with some of the Pt/γ-alumina impregnation profiles reported by Shyr and Ernst,[12] although the sharp breakthroughs observed in Ni/γ-alumina subsurface impregnation profiles[8] (*cf.* Fig. 4) were not reproduced. This may be an indication that for this particular system the mechanism of producing subsurface impregnation by the use of acids may not by a simple competitive adsorption between the nickel ions and the acid species. The latter part of the present paper examines the mechanism of controlling impregnation profiles by the use of acids in the preparation of Ni/γ-alumina catalysts.

Experimental

Spherical γ-alumina pellets of about 4 mm-diameter supplied by Universal Oil Products were employed as the porous support. Their pretreatment and characterization are found elsewhere.[8] The poze size distribution of the alumina support is bimodal, with peak radii at around 2.5 nm (found by nitrogen adsorption) and in between 0.1 to 0.3 μm (observed by scanning electron microscopy, SEM).

The rate of 1-bromonaphthalene penetration into the alumina sphere was examined by using a light microscope with a calibrated eyepiece. 1-Bromonaphthalene was chosen as a model liquid because its refractive index of 1.66 is nearly the same with that of γ-alumina, which is 1.7. Thus alumina contacted with 1-bromonaphthalene becomes transparent, enabling one to observe through a light microscope the position of the penetrating liquid front as a function of time.

Effects of acids on nickel adsorption on γ-alumina were examined by aqueous phase adsorption measurements, which were carried out by soaking powdered (<65 mesh) alumina pellets into solutions of nickel nitrate with or without additives such as citric acid or hydrochloric acid. Adsorption experiments were performed in a constant-temperature bath at 20.0 °C with continuous stirring for 1 h. The temperature and the contact time were chosen to simulate the actual catalyst impregnation. After one hour the alumina powder

was separated from the solution by centrifuge, and the solution pH was measured. The amount of nickel ion adsorbed onto the solid surface was determined spectrophotometrically from the incremental loss of Ni(II) species in the liquid phase by adding an appropriate amount of KCN to the solution, thus converting nickel ion into a cyanide complex, and measuring its absorption at 310 nm.[13] Such a procedure was necessary in order to measure the small difference in nickel concentration caused by its adsorption on γ-alumina, because the absorption sensitivity of nickel aquo complex at around 400 nm was not sufficient to make reliable measurements.

A series of Ni/γ-alumina catalysts, designed to demonstrate the effects of pH on impregnation profiles, were prepared by impregnating alumina pellets with pH-adjusted aqueous solutions of nickel nitrate. Solution pH was adjusted by the addition of citric acid and/or ammonium hydroxide. Detailed procedures for the catalyst preparation are found elsewhere.[8] For the measurements of the impregnation profiles of the finished catalysts, a JEOL JXA 733 electron microprobe was employed. Detailes of sample preparation and procedure for this measurement are also presented elsewhere.[8]

Results and Discussion

Penetration Rate of Impregnating Solution. The three-dimensional impregnation model developed earlier,[8] which is an extension of a single-pore model proposed by Vincent and Merrill,[7] predicts the penetration rate of the liquid front into a spherical pellet by the following equation:

$$(1-\Gamma)^3 = 1-\tau^{1/2}, \qquad (1)$$

where Γ is the reduced radial position in a sphere, or one minus the fractional radius, and τ is the reduced time, or actual time divided by t_L which is the time necessary for the liquid to reach the center of the pellet. It was assumed[8] in deriving the above equation that the pressure differential is constant at the liquid front regardless of its position in the sphere. This assumption is depicted in Fig. 1 (a), where the pressure profiles along the radius of a pellet which is represented by a long single pore of the length of the pellet radius are shown for two positions of liquid front. Also note that pressure differential along the radius of the pellet at any given time is approximated by a linear function.

The validity of this assumption and its physical basis may become clearer by examining directly the actual rate of liquid penetration, or the front velocity of the penetrating liquid, and comparing it with the model prediction. Figure 2 shows measurements of the front positions of 1- bromonaphthalene penetrating into γ-alumina spheres as functions of time τ. Two sets of measurements are shown, which represent the upper and the lower bound of measurements among a number of pellets tested. The solid line in the figure was calculated by using the above Eq.(1) which is non-dimensionalized and thus is applicable to any liquid penetration. The model calculation agrees well with the measured front positions in the range of $\Gamma>0.3$. Where $\Gamma<0.3$, the actual Γ is larger than predicted. This results from very large initial front velocities followed by a period of near zero velocity.

In order to interpret these results consider first a pellet consisting of monodispersed pores, for which

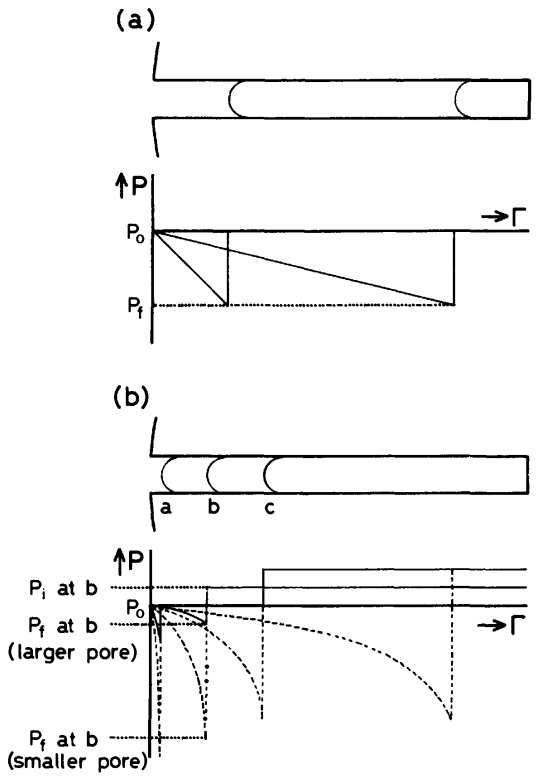

Fig. 1. Pressure profiles in the impregnating solution along the radius of a pellet.
(a) Model profile assumed in the three-dimensional impregnation model; (b) profile concieved from the results of the liquid penetration measurements. Solid lines: larger pores. Broken lines: smaller pores. P_i: Pressure inside the pellet; P_o: pressure outside the pellet; P_f: pressure at the liquid front.

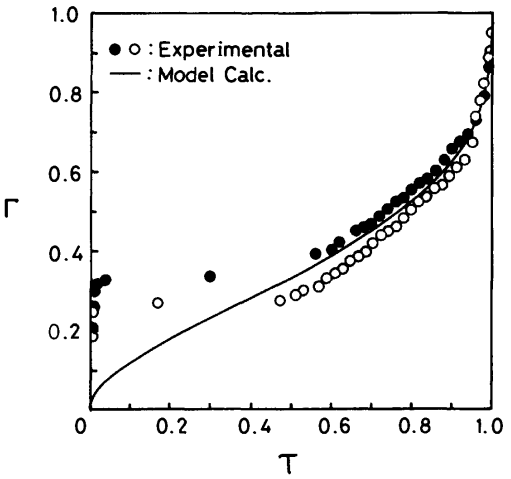

Fig. 2. Non-dimensionalizad penetration depth, $\Gamma=z/L$, of 1-bromonaphthalene into γ-alumina pellet as a function of non-dimensionalized time, $\tau=t/t_L$. Open and closed circles: experimental; solid line: model calculation using Eq. (1).

pressure profiles along the radius of the pellet at various times are represented by solid lines in Fig. 1 (b). For each profile there is a monotonic decrease in pressure up to the meniscus of the liquid front followed by a

discontinuous increase across the meniscus. At the onset of impregnation (point **a** in Fig. 1 (b)), the pressure inside the pellet, P_i, is similar to that outside the pellet, P_o, and the liquid penetrates with the capillary pressure, $(P_i-P_f)\simeq(P_o-P_f)$, as driving force. As the liquid progresses (point **b**), it compresses the air inside the pellet, raising P_i higher than P_o. Since the pressure drop at the liquid front, (P_i-P_f), is fixed for a given pore-liquid system, this higher P_i results in smaller driving force, (P_o-P_f), slowig down the rate of liquid penetration. Penetration will be stopped when P_i is balanced with the capillary pressure, *i.e.*, $P_o=P_f$ (point **c**) and the driving force for flow is zero.

In the case of a pellet consisting of polydispersed pores, such as the present one, the situation will be more complicated. At the early stage of impregnation liquid is mainly carried into the pellet through larger pores which have higher mass flow than smaller pores.[7,8] The flow through these larger pores will eventually be stopped by the process discussed above. The data in Fig. 2 indicate that this happens at $\Gamma\simeq0.3$, which gives P_i of about 3 atmosphere. This corresponds to the capillary pressure of the pores with radius of about 0.7 μm, which is in the larger end of the pore size distribution observed by SEM.

Even after liquid in the larger pores is halted, however, liquid in smaller pores, with pressure profiles represented by the broken lines in Fig. 1 (b), advance due to the higher capillary pressure. Volume occupied by this advancing liquid will be compensated by a receding meniscus in larger pores, keeping P_i constant. As a consequence liquid in larger pores is slowly pushed back, eventually making the pores empty to serve as air-escape channels. In the present system this is a long process as seen from the flat portion of the measured liquid front positions in Fig. 2, *i.e.*, the region where the observed velocity of the front is zero. Note that the wavelength of white light, which was used in the microscope, peaks above 1 μm so that neither the receding meniscus in larger pores nor the advancing meniscus in the smaller pores can be detected. The opening of the air channels is confirmed by air bubbles which are observed to form at the exterior of pellet at *ca.* $\tau=0.5$. Once the air channels are established, P_i will be kept constant at this level by advancing liquid to keep the channels open. Since the pressure drop at the liquid front is fixed for a given liquid-pore system, constant P_i means constant P_f, fulfilling the assumption described above.

It follows from the above discussion that there are two limiting cases in which the assumption of constant P_f holds. One is the early stage of impregnation (*e.g.*, point **a**), where $(P_o-P_f)\simeq(P_i-P_f)$. In this case (P_i-P_o) could be neglected compared to the driving force, (P_o-P_f), and P_f holds approximately constant. Note that this limiting case would dominate the impregnation process if a support consisting of very small pores is used. The pressure balancing in such system would not occur until very late in the impregnation process, *i.e.*, point **c** for example in Fig. 1 (b), which is displaced close to $\Gamma=1$. The other limiting case is the later stage of impregnation, where P_f is kept constant by the mechanism discussed above. Also note here that if a support consisting of relatively large pores is used, the pressure balancing would occur very early stage in the impregnation, *i.e.*, point **c** is displaced close to $\Gamma=0$, and this limiting case will dominate the impregnation. These two limiting cases are obvious in the data shown in Fig. 2, where early stage ($\tau=0$—0.03) corresponds to the former case and later stage ($\tau=0.4$—1) to the latter case. At intermediate level ($\tau=0.03$—0.4) during which either limit is appropriate, there is a transition from the larger pore-dominated region to the smaller pore region.

Effects of Acids on the Adsorption Behavior of Nickel. The effect of nitric acid addition on nickel ion adsorption on γ-alumina powder has already been reported.[8] Its results showed that the amount of nickel ion adsorbed during one hour of contact time is strongly influenced by the pH of the solution. Nickel adsorption on γ-alumina was shown to be inhibited below a pH of about 4, and the amount of nickel adsorption abruptly increased at around a pH of 5.2. The adsorption continuously increased past the pH of pure nickel salt solution to the basic side. While such adsorption behavior was presumed to be a pH effect rather than an example of competitive adsorption, and methods of preparing subsurface impregnation utilizing this pH effect has been demonstrated,[8] these results were not conclusive since it used only one acid species and there still remains the possibility that competitive adsorption of some form is still operative.[9]

In Fig. 3 adsorption as a function of pH is plotted for a number of other acids commonly used to prepare subsurface impregnation of Ni/γ-alumina. In order to simplify the presentation, data points for hydrochloric acid and glicine are replaced by lines connecting through them in the figure, since the scatter in the adsorption data was very small for those acids. Plotted in the figure is the final pH of the solution measured after alumina powder was separated by a centrifuge. It shows that regardless of the kind of acid added to the solution, nickel adsorption abruptly increases at a pH of about 5.2. These results support the previous discussion[8] that nickel adsorption on γ-alumina surface is

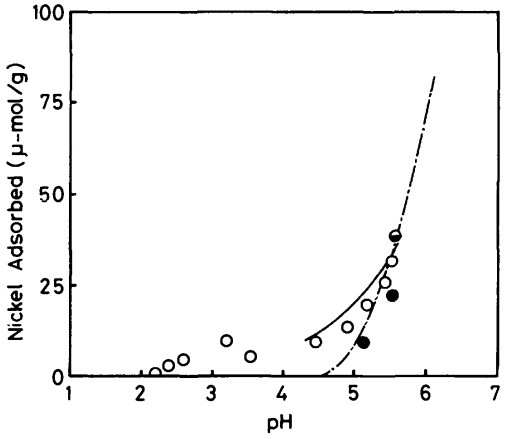

Fig. 3. The effect of pH on $Ni(NO_3)_2$ adsorption on γ-alumina. Initial concentration of $Ni(NO_3)_2$: 0.00988M. Contact time: 1h. Plotted pH are those after the contact. Additives: none (◒), citric acid (○), oxalic acid (●), hydrochloric acid (——), glycine (—·—).

controlled by the pH of the solution and not by competitive adsorption. The kind of acid species used to control pH seems to have little effect on the extent of adsorption.

A close examination of Fig. 3 shows, however, that the acids can be grouped into two types: One that inhibits nickel adsorption completely below pH of about 4, and another that allows weak adsorption even below that pH. Nitric acid,[8] oxalic acid, and glicine belong to the former while citric and hydrochloric acids belong to the latter.

This work is not intended to elucidate the physical chemistry of the pH effect. Some possible explanations have been suggested previously.[8] A detailed discussion on pH-dependent adsorption of metal cations onto oxide surfaces is given by Brunell.[14] Here we concentrate on the utilization of this pH effect for the control of impregnation profiles.

pH-Controlled Catalyst Impregnation. The strong effect of pH upon the amount adsorbed provides a degree of freedom in controlling the concentration profiles in the impregnation of porous catalysts. By exploiting these effects subsurface, uniform and/or surface impregnation can be produced.

The preparation of subsurface impregnation, through manipulating pH, has been demonstrated[8] for Ni/γ-alumina system using nitric acid as pH controller. The effects of concentrations of nitric acid and nickel salt were examined and discussed in detail.[8] When a support immersed in an impregnating solution of low pH, cation adsorption on the pore wall is inhibited at first. If the pH controlling species is adsorbed on the pore wall, then as the solution penetrates the pore its local pH gradually increases. At some point along the axis of the pore the pH may increase to the point where adsorption of the co-impregnated metal cation becomes appreciable. This should result in an outer shell of metal free adsorbate and a subsurface impregnation past the point where the critical pH is achieved, provided that molecular diffusion along the axis of the pore is small enough.

Figure 4 compares the nickel concentration profile of a sample using nitric acid (profile **a**) and citric acid (profile **b**) to suppress adsorption at the exterior of the pellet. In these plots the nickel concentration, determined by X-ray fluorescence, is presented as a function of fractional radius. A value of 1.0 in the radius represent the exterior of the pellet. In profile **b** the open circles are for pellets sectioned after drying and the solid circles are for pellets sectioned before drying. It is clear in profile **b** that the surface enhanced concentration is due to segregation during drying,[8] and therefore not pertinent to this discussion of the impregnation step.

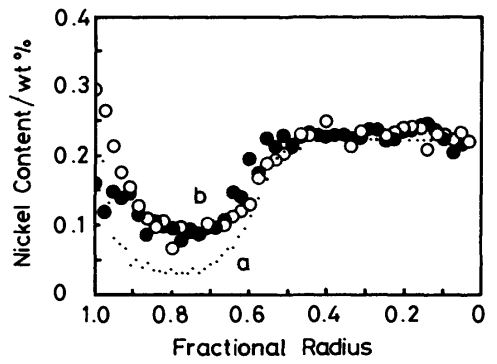

Fig. 4. Nickel subsurface impregnation produced by using nitric acid (profile **a**, dotted line) and citric acid (profile **b**, open and closed circles) as pH controller. Initial concentrations: $Ni(NO_3)_2$, 0.0247 M (1 M= 1 mol dm^{-3}); HCl, 0.000982 M; citric acid, 0.0012 M.

Profiles **a** and **b** are very similar to each other, indicating that both acids play almost identical roles, *i.e.*, pH control, in producing subsurface impregnation.

Two minor differences are noted between these two profiles. First, the acid concentration necessary to create the same thickness for the low metal loading band (fractinal radius>0.6) is higher for citric acid than for nitric acid. This is understood from the above pH-controlled impregnation mechanism, which assumes that the nickel adsorptivity is controlled by local pH. Since the dissociation constant of citric acid is much lower than that of nitric acid, a higher concentration of citric acid is necessary in order to obtain the same pH profile along the radius of the pellet and thus to create the similar nickel concentration profiles. Second, the amount of nickel deposition at the low loading region (0.9>fractional radius>0.6) is higher when citric acid was used as pH-controller than when nitric acid was used. In case of profile **a** in Fig. 4 the deposition in this region was considered to be produced by the overlap of the leading edge of the breakthrough and the tail of the surface-segregated deposition band. A higher loading in the surface region for profile **b** is attributed to the low but non-negligible adsorption below pH=4 for citric acid-controlled adsorption (*cf.* Fig. 3). In contrast to nitric acid,[8] citric acid does not completely inhibit the adsorption of nickel ions in the region where pH of the penetrating solution is still low.

It is expected from the results presented in Fig. 3 and the mechanism of pH-controlled subsurface impregnation deduced from it, that it may also be possible to produce a profile with a high concentration at the surface of the pellet if the pH of the impregnating solution is adjusted to higher side where adsorptivity enhancement is observed instead of inhibition (see Fig. 3). Presented in Fig. 5 are the nickel concentration profiles of the samples impregnated with solutions of varying initial pH. The same concentrations of nickel nitrate and citric acid were employed for all samples in Fig. 5 as well as the sample in Fig. 4, profile **b**, The initial pH was adjusted by adding an appropriate amount of ammonium hydroxide to the solution. Only the initial value of pH is presented in the figure, since it is not possible to determine experimentally the final pH of the solution in the pore at the end of the impregnation. As a control, single-component impregnation was also performed and the resulting profile is shown in Fig. 5 (sample No. F-1). Note that there is no evidence of significant surface segregation in any of these samples. There is no disparity between closed and open circles.

Nickel nitrate at this concentration produces a uniform impregnation profile as shown in Fig. 5, control sample No. F-1. When the initial pH was adjusted to

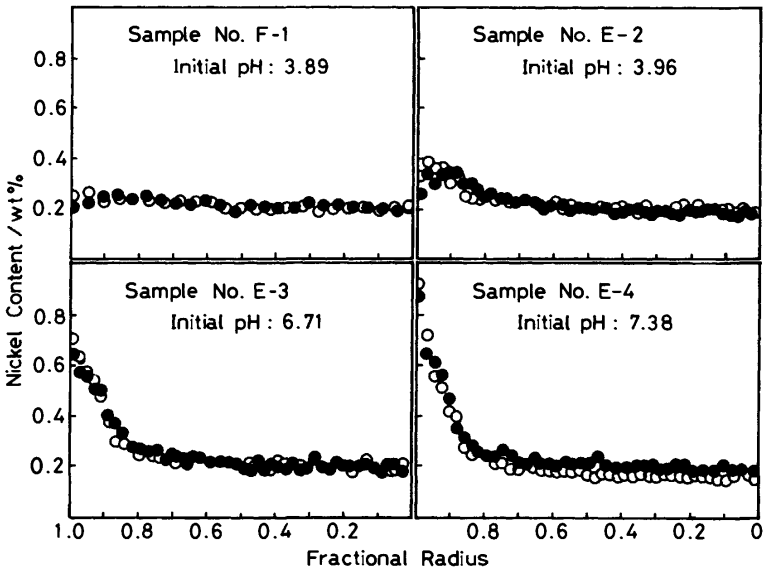

Fig. 5. Nickel concentration profiles impregnated at various initial pH.

the acidic side where adsorption inhibition occurs, subsurface impregnation was produced as discussed above (Fig. 4, profile **b**). When the starting pH was adjusted to higher side where nickel adsorption is enhanced, surface impregnation profiles resulted (Fig. 5, sample Nos. E-2 through E-4). Note that the higher the initial pH of the solution, the larger the nickel concentration near the outer surface of the pellet. The mechanism is exactly the same as that which produced subsurface impregnations except that adsorption enhancement occurs near the external surface of the pellet instead of inhibition.

While this pH effect adds another degree of freedom in engineering impregnation profiles, it also adds complication to the modeling of the impregnation process. Major parameters which play important roles in determining impregnation profiles involve characteristics of metal cation adsorptivity such as maximum amount of adsorption or an adsorption rate coefficient.[7] The consequence of the above pH effect is the dependence on local pH of these otherwise constant parameters. Models for the pH-controlled impregnation must consider these parameters as functions of local pH of the solution in the pore, which depends both on Γ and τ. It is not surprising, therefore, that models describing inhibition *via* competitive adsorption[9] do not predict the sharpness of the concentration.

For subsurface impregnation (acidic side pH control) using nitric acid, the pH effect was represented as a step function,[8] *viz.*, complete inhibition below pH=5.2 and single component behavior above that pH. Such an approach was justified because with this acid the pH dependence of nickel adsorption can be closely approximated by a step function, and also because of the resulting good agreement between the actual impregnation profiles and the ones calculated using this approximation, as reported earlier.[8] Such a treatment, however, may not be appropriate for the case of higher side pH control or acidic side control using acids like citric acid, because the nickel adsorption behavior for these cases cannot be approximated by a step function of pH. Further work is necessary in order to formulate an impregnation model incorporating such pH effects.

The work is partially supported by the Grant for Scientific Research No. 57750699 from the Japanese Ministry of Education, Science and Culture.

References

1) R. W. Maatman, *Ind. Eng. Chem.*, **51**, 913 (1959).
2) E. R. Becker, and J. Wei, *J. Catal.*, **46**, 365 (1977).
3) L. L. Hegedus, J. C. Summers, J. C. Schlatter, and K. Baron, *J. Catal.*, **56**, 321 (1979).
4) E. R. Becker, and J. Wei, *J. Catal.*, **46**, 372 (1977).
5) S. Minhas, and J. J. Carberry, *J. Catal.*, **14**, 270 (1969).
6) T. G. Smith, and J. J. Carberry, *Can. J. Chem. Eng.*, **53**, 347 (1975).
7) R. C. Vincent, and R. P. Merrill, *J. Catal.*, **35**, 206 (1974).
8) M. Komiyama, R. P. Merrill, and H. F. Harnsberger, *J. Catal.*, **63**, 35 (1980).
9) S. S. Kulkarni, G. R. Mauze, and J. A. Schwarz, *J. Catal.*, **69**, 445 (1981).
10) E. W. Washburn, *Phys. Rev.*, **17**, 273 (1921).
11) S. -Y. Lee, and A. Aris, "Preparation of Catalysts III," ed by G. Poncelet, P. Grange, and P. A. Jacobs, Elsevier, Amsterdam (1983), p. 35.
12) Y. S. Shyr, and W. R. Ernst, *J. Catal.*, **63**, 425 (1980).
13) T. M. Florence, *Anal. Chim. Acta*, **19**, 548 (1958).
14) C. P. Brunell, "Preparation of Catalysts II," ed by B. Delmon, P. Grange, P. Jacobs, and G. Poncelet, Elsevier, Amsterdam (1979), p. 51.

Regularity in Homolytic Lattice Energies of Anhydrous Formate, Acetate, Oxalate, and Glycolate of Metals**

Minoru SAKIYAMA* and Shigeo MURATA
Chemical Thermodynamics Laboratory, Faculty of Science, Osaka University, Toyonaka 560
(Received July 30, 1983)

The homolytic lattice energy ΔU_R of an ionic crystal M_xA_y was defined as the standard internal energy change at 298.15 K for the following vaporization process to yield neutral species M and A: $(1/x)M_xA_y(c)=M(g)+(y/z)A(g)$. ΔU_R and $[\Delta U_R-(y/x)\Delta H_f^\circ(A,g)]$ were calculated for formates and acetates and for oxalates and glycolates, respectively, of metals, and were analyzed empirically. ΔU_R(formate)$\simeq\Delta U_R$(acetate) holds for every metal. ΔU_R of oxalates and glycolates may be expressed as follows: ΔU_R(oxalate or glycolate)$=a\Delta U_R$(formate or acetate)$+b(y/x)$, where a is the constant close to unity, and b is the constant which is, possibly, close to zero for oxalates and about 40 kJ mol^{-1} for glycolates. The linear relations in ΔU_R were discussed in relation to crystal structure of the salts and carboxyl O-H bond dissociation energy of the corresponding carboxylic acids.

The cohesion energy of an ionic crystal of formula M_xA_y has been usually expressed as the lattice energy U_L which is defined as the standard internal energy change ΔU° for the following heterolytic (ionic) vaporization of the crystal at 298.15 K:

$$M_xA_y(c) = xM^{m+}(g) + yA^{n-}(g), \quad (1)$$

where m and n are the numbers of ionic charges in the units of e. U_L is given as follows:

$$U_L = x\Delta H_f^\circ(M^{m+}, g) + y\Delta H_f^\circ(A^{n-}, g) - \Delta H_f^\circ(M_xA_y, c) - (x+y)RT. \quad (2)$$

For most of polyatomic anions, reliable experimental data of standard enthalpy of formation in gaseous state are not availble at present. Within the extent of the present compounds, reliable data are available only for acetate anion,[1] so it is impossible to carry out a satisfactory empirical analysis in terms of U_L for the present compounds. On the other hand, reliable data are more abundant for the correseponding gaseous neutral species (free radical). A formed by loss of n electrons from a polyatomic anion A^{n-}. Within the extent of the present compounds, $\Delta H_f^\circ(A,g)$ has been determined precisely for formate and acetate free radicals.[2,3]

Here, the homolytic lattice energy ΔU_R is defined as the standard internal energy change at 298.15 K of the following homolytic (nonionic) vaporization of an ionic crystal M_xA_y (c):

$$(1/x)M_xA_y(c) = M(g) + (y/x)A(g). \quad (3)$$

ΔU_R is given as follows:

$$\Delta U_R = \Delta H_f^\circ(M, g) + (y/x)\Delta H_f^\circ(A, g) - (1/x)\Delta H_f^\circ(M_xA_y, c) - [(x+y)/x]RT. \quad (4)$$

Correspondingly, the heterolytic lattice energy ΔU_I is defined by the equation: $\Delta U_I=(1/x)U_L$. ΔU_I is related with ΔU_R according to:

$$\Delta U_I = \Delta U_R + \sum_1^m I(M, i) + C_1 + (y/x)[\sum_1^n A(A, j) + C_2], \quad (5)$$

where $I(M, i)$ is the i-th ionization energy of species M, $A(A, j)$ is the j-th electron affinity of species A, and C_1 and C_2 are $[\Delta U^\circ(298.15\ K)-\Delta U^\circ(0\ K)]$ for the processes: $M(g)=M^{m+}(g)+me$ and $A(g)+ne=A^{n-}$, respectively where e denotes electron.

** Contribution No. 58 from Chemical Thermodynamics Laboratory, Faculty of Science, Osaka University.

In this paper, ΔU_R of formates and acetates and $[\Delta U_R-(y/x)\Delta H_f^\circ(A, g)]$ of oxalates and glycolates are analyzed empirically and discussed in relation to crystal structure of the salts and O-H bond dissociation energy of the corresponding carboxylic acids.

Procedure and Results

Most of the standard enthalpies of formation used in the present analysis were taken from Ref. 4. The data from other sources are collected in Table 1. From these data, ΔU_R was calculated according to Eq. (4) and presented in Table 2 for formates and acetates. The plot of ΔU_R (acetate) against ΔU_R (formate) is shown in Fig. 1. A straight line passes close to the plots and the origin in

TABLE 1. STANDARD ENTHALPIES OF FORMATION AT 298.15 K TAKEN FROM SOURCES OTHER THAN Ref. 4

Species	$-\Delta H_f^\circ$/kJ mol^{-1}
$HOCH_2CO_2H(g)$	582.4[a)]
$HO_2CCO_2H(g)$	731.6[6)]
$(CH_3CO_2)_2Mg(c)$	1367.7[5)]
$HCO_2(g)$	151±8[2)]
$CH_3CO_2(g)$	208±4[3)]

a) Estimated value. See the text for the method of estimation.

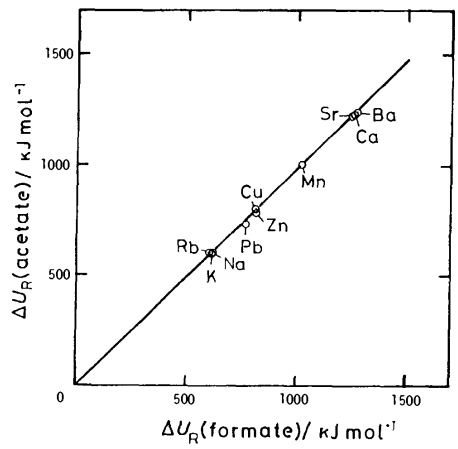

Fig. 1. ΔU_R (acetate) *vs.* ΔU_R (formate) plot. For the definition of ΔU_R, see the text. The straight line is expressed with the equation: ΔU_R (acetate)$=$ 0.9818ΔU_R (formate).

Table 2. Homolytic lattice energies ΔU_R of anhydrous formate and acetate of metals, and $[\Delta U_R-(y/x)\Delta H_f^\circ(A, g)]$ of anhydrous glycolate and oxalate of metals

	ΔU_R		$[\Delta U_R-(y/x)\Delta H_f^\circ(A, g)]$	
	kJ mol^{-1}		kJ mol^{-1}	
	Formate	Acetate	Glycolate	Oxalate
Na(I)	620	603	1003	761
Mg(II)	—	1095	1892	1410
Al(III)	—	1584	—	—
K(I)	613	599	992	758
Ca(II)	1257	1234	2027	1532
Mn(II)	1018	1006	—	1303
Co(II)	990	—	—	1269
Ni(II)	994	—	—	1280
Cu(II)	811	808	1582	—
Zn(II)	810	787	1591	—
Rb(I)	602	605	—	740
Sr(II)	1249	1228	2001	1528
Ag(I)	—	471	—	617
Cd(II)	—	—	—	1018
Cs(I)	—	607	—	—
Ba(II)	1268	1241	2034	1542
Hg(II)	—	455	—	732
Tl(I)	—	497	—	—
Pb(II)	766	736	—	1039

For symbols, see the text.

this figure. Linear regression analysis gave the following result:

$$\Delta U_R(\text{acetate})/\text{kJ mol}^{-1} = 0.9818\Delta U_R(\text{formate})/\text{kJ mol}^{-1}, \quad (6)$$

with standard deviation from the fit s_f of 9 kJ mol^{-1}.

It is not possible at present to calculate ΔU_R for oxalates and glycolates, since $\Delta H_f^\circ(g)$ is not available for oxalate and glycolate free radicals. Instead, $[\Delta U_R-(y/x)\Delta H_f^\circ(A, g)]$ calculated according to Eq. (4) was given in Table 2 and plotted against ΔU_R (formate) in Figs. 2 and 3. The upper lines express the results of the linear regression analysis of the data of bivalent metal cations. The lower lines were drawn so that they were parallel with the corresponding upper lines with intercepts 141(=282/2) and 399(=798/2), respectively, in Figs. 2 and 3. Thus, the whole data may be expressed by the following equations:

$$[\Delta U_R(\text{oxalate})-(y/x)\Delta H_f^\circ(O_2CCO_2, g)]/\text{kJ mol}^{-1} = 0.9965\Delta U_R(\text{formate})/\text{kJ mol}^{-1} + 282(y/x), \quad (7)$$

with the maximum deviation of 6 kJ mol^{-1} ands s_f of 5 kJ mol^{-1} for uni- and bivalent metal cations, respectively, and

$$[\Delta U_R(\text{glycolate})-(y/x)\Delta H_f^\circ(HOCH_2CO_2, g)]/\text{kJ mol}^{-1} = 0.9728\Delta U_R(\text{formate})/\text{kJ mol}^{-1} + 399(y/x), \quad (8)$$

with the maximum deviation of 5 kJ mol^{-1} and s_f of 6 kJ mol^{-1} for uni- and bivalent metal cations, respectively.

Similar plots, though not shown, were made for the pairs of oxalate-acetate and glycolate-acetate, with

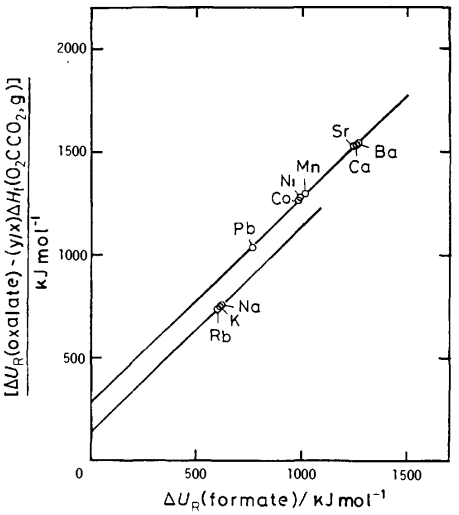

Fig. 2. $[\Delta U_R(\text{oxalate})-(y/x)\Delta H_f^\circ(O_2CCO_2, g)]$ *vs.* ΔU_R (formate) plot.
(y/x) is equal to 1/2 and 1 for mono- and divalent metals, respectively. The straight lines are expressed with the equation: $[\Delta U_R\text{ (oxalate)}-(y/x)\Delta H_f^\circ(O_2CCO_2,g)]=0.9965\Delta U_R\text{ (formate)}+282(y/x)$.

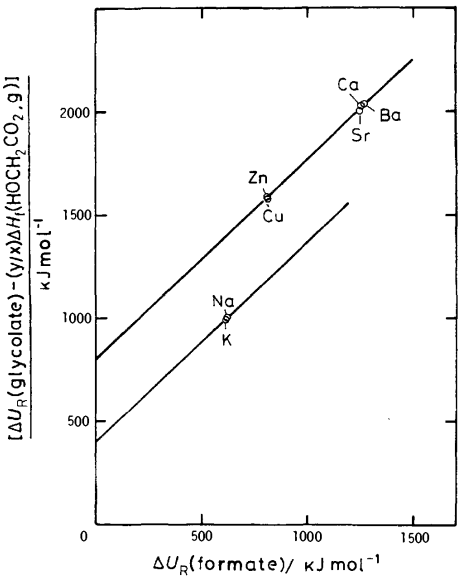

Fig. 3. $[\Delta U_R\text{ (glycolate)}-(y/x)\Delta H_f^\circ(HOCH_2CO_2, g)]$ *vs.* ΔU_R (formate) plot.
(y/x) is equal to 1 and 2 for mono- and divalent metals, respectively. The straight lines are expressed with the equation: $[\Delta U_R\text{ (glycolate)}-(y/x)\Delta H_f^\circ(HOCH_2CO_2, g)]=0.9728\Delta U_R\text{ (formate)}+399(y/x)$.

similar results. The linear relations are expressed as follows:

$$[\Delta U_R(\text{oxalate})-(y/x)\Delta H_f^\circ(O_2CCO_2, g)]/\text{kJ mol}^{-1} = 1.0239\Delta U_R(\text{acetate})/\text{kJ mol}^{-1} + 275(y/x), \quad (9)$$

with the maximum deviation of 8 kJ mol^{-1} and s_f of 8 kJ mol^{-1} for uni- and bivalent metal cations, respectively, and

$$[\Delta U_R(\text{glycolate})-(y/x)\Delta H_f^\circ(HOCH_2CO_2, g)]/\text{kJ mol}^{-1} = 0.9965\Delta U_R(\text{acetate})/\text{kJ mol}^{-1} + 397(y/x), \quad (10)$$

with the maximum deviation of 5 kJ mol^{-1} and s_f of 11 kJ mol^{-1} for uni- and bivalent metal cations, respectively.

While univalent metals are limited to alkali metals for the pairs of oxalate-formate, glycolate-formate, and glycolate-acetate, Ag(I) is also included in the plots of the pair oxalate-acetate. This shows that the linear relation for univalent metals is not specific to alkali metals.

Discussion

Prior to the discussion of each of relations in ΔU_R given in Eqs. (6)—(10), two remarks are presented here. Firstly, it is to be noted that the linear relations hold even for compounds of Mn(II), Co(II), Ni(II), and Cu(II), which are the cations with unfilled 3d orbitals. In order to study the effect of the d-orbital splitting on ΔU_R, the difference in ΔU_I between these compounds and the corresponding Ca compounds Ca_xA_y was calculated using equation (2) and the definition: $\Delta U_I = U_L/x$,

$$\Delta U_I(M_xA_y) - \Delta U_I(Ca_xA_y) = \Delta H_f^\circ(M^{2+}, g) - \Delta H_f^\circ(Ca^{2+}, g) - \Delta H_f^\circ(M_xA_y, c) + \Delta H_f^\circ(Ca_xA_y, c). \quad (11)$$

As shown in Table 3, the difference in ΔU_I changes significantly with cation species, but it barely depends on anion species. Thus, the stabilization energy due to the d-orbital splitting of each cation is nearly independent of anion species. The stabilization energy was evaluated by the crystal field theory,[7] resultant values up to 300 kJ mol^{-1}. More recently, a molecular orbital approach[8] was reported, giving the values of several hundred kJ mol^{-1} or less. Whatever the exact values may be, the conclusion derived above, together with the fact that the coefficients of the first terms on the right-hand sides of Eqs. (6)—(10) are close to unity, shows that even if the effect of the 3d-orbital splitting was corrected, the resultant values would satisfy these equations.

Secondly, the linear relations in ΔU_R given in Eqs. (6)—(10), in connection with Eq. (5), leads to the corresponding linear equations in ΔU_I, although it is unknown whether the proportionality holds for the pair of formate-acetate.

Now, the discussion on each linear relation is started. For the pair of formate-acetate, ΔU_R (formate)$\simeq\Delta U_R$ (acetate) holds. Crystal structure has been determined for formates of Na,[9] Ca,[10,11] Sr,[10] Ba,[11] and Cu(II).[12] These crystals are characterized by the coordination of the metal cations with four or more carboxyl oxygen atoms. Hence, ΔU_R may be divided into two parts: The contribution from metal-oxygen interactions and that from the other interactions, both in the crystalline states. The former is considered to be more dominant than the latter. The observed approximate equality in ΔU_R suggests that the crystal structures of formates and acetates of a metal are similar and, in view of the similarity of chemical structure of the anions, the magnitude of metal-oxygen interaction energy is also similar between formate and acetate of a metal.

Table 3. The difference between heterolytic lattice energy ΔU_I of formate, acetate, oxalate, and glycolate of Mn(II), Co(II), Ni(II), Cu(II), and Zn(II), and ΔU_I of the corresponding Ca compounds

Cation M(II)	$[\Delta U_I(M_xA_y) - \Delta U_I(Ca_xA_y)]$/kJ mol^{-1}			
	Formate	Acetate	Oxalate	Glycolate
Mn(II)	251	262	—	261
Co(II)	402	—	—	406
Ni(II)	489	—	—	500
Cu(II)	522	542	523	524
Zn(II)	457	457	468	—

For the pairs of oxalate-formate and oxalate-acetate, it is clear from Eqs. (7) and (9), that ΔU_R (oxalate) is expressed by a linear function of ΔU_R (formate) or ΔU_R (acetate), with a coefficient close to unity and a second term proportional to (y/x). Furthermore, from the similarity in chemical structure of the anions as a whole, the relation: ΔU_R(formate)$\simeq\Delta U_R$(oxalate)$\simeq\Delta U_R$ (acetate), is expected to hold for every metal. Substitution of an assumed value of ΔH_f° (O_2CCO_2, g)$=-279$ kJ mol^{-1}, into Eqs. (7) and (9), leads to the following approximate equality relations:

$$\Delta U_R(\text{oxalate})/\text{kJ mol}^{-1} = 0.9965\Delta U_R(\text{formate})/\text{kJ mol}^{-1} + 3(y/x), \quad (12)$$

and

$$\Delta U_R(\text{oxalate})/\text{kJ mol}^{-1} = 1.0239\Delta U_R(\text{acetate})/\text{kJ mol}^{-1} - 4(y/x). \quad (13)$$

The assumed value of $\Delta H_f^\circ(HOCH_2CO_2, g)$ was then used to calculate the mean O-H bond dissociation energy $\bar{D}$(O-H) of oxalic acid, which was defined as ΔU° (298.15 K) for the reaction: $(1/2)HO_2CCO_2H(g) = (1/2)O_2COO_2(g) + H(g)$. $\bar{D}$(O-H) was calculated to be 443 kJ mol^{-1}. Similarly, corresponding O-H bond dissociation energies D(O-H) of formic and acetic acids, defined as ΔU°(298.15 K) of the reactions: $RCO_2H(g) = RCO_2(g) + H(g)$, where R is H or CH_3, were calculated to be 443 and 440 kJ mol^{-1}, respectively. Agreement of the calculated value of $\bar{D}$(O-H) of oxalic acid with D(O-H) of formic and acetic acids strongly suggests that $\Delta H_f^\circ(O_2CCO_2, g)\simeq-279$ kJ mol^{-1} and the relation: ΔU_R(formate)$\simeq\Delta U_R$(oxalate)$\simeq\Delta U_R$(acetate) holds. Thus, ΔH_f°(g) of oxalate biradical, which would be determined experimentally only with difficulty, could be estimated with some grounds. In addition, the coefficients of the first terms of Eqs. (11) and (12) which are close to unity, suggest the similarity in the character of crystal structure and the magnitude of metal-oxygen interaction energy of a metal oxalate with formate and acetate of the same metal.

For the pairs of glycolate-formate and glycolate-acetate, Eqs. (8) and (10) show that ΔU_R(glycolate) is expressed by a linear functions of ΔU_R(formate) or ΔU_R(acetate), with a coefficient close to unity and a second term proportional to (y/x). The assumption that ΔU_R(formate)$\simeq\Delta U_R$(glycolate)$\simeq\Delta U_R$(acetate), or equivalently that $\Delta H_f^\circ(HOCH_2CO_2, g) = -398$ kJ mol^{-1}, leads to the result: D(O-H)$=400$ kJ mol^{-1} for carboxyl O-H of glycolic acid. ΔH_f°(g) of glycolic acid used in this calculation was obtained by estimation

using the group contribution method,[13,14] with an estimated value of $[C-(CO)(O)(H)_2]=-34.3$ kJ mol^{-1}. Hence, this value is more uncertain than the rest. Even so, the value of D(O-H) given above is significantly smaller than the corresponding values of formic and acetic acids.

Instead, it was assumed that D(O-H)=443 kJ mol^{-1} for carboxyl O-H of glycolic acid, in accordance with those of formic and acetic acids. This implies that $\Delta H_f^\circ(HOCH_2CO_2, g)=-355$ kJ mol^{-1}. Substitution of this value to Eqs. (8) and (10) leads to the following equations:

$$\Delta U_R(\text{glycolate})/\text{kJ mol}^{-1} = 0.9728\Delta U_R(\text{formate})/\text{kJ mol}^{-1} + 44(y/x), \quad (14)$$

and

$$\Delta U_R(\text{glycolate})/\text{kJ mol}^{-1} = 1.0239\Delta U_R(\text{acetate})/\text{kJ mol}^{-1} + 42(y/x), \quad (15)$$

Among the glycolates, crystal structure has been determined only for Cu(II) glycolate.[15] In this crystal, Cu(II) is coordinated with four carboxyl and two hydroxyl oxygen atoms of glycolate anions, *i.e.* glycolate anion is tridentate, whereas formate and acetate anions are bidentate. In addition, each hydroxyl oxygen atom forms a remarkably short intermolecular hydrogen bond 0.257 nm long to the carboxyl oxygen atom of a second neighbouring complex. The short O-H···O hydrogen bond corresponds to the hydrogen bond energy of about 40 kJ mol^{-1}.

For Cu(II) glycolate, the second terms of Eqs. (14) and (15) may be interpreted in terms of (1) the intermolecular hydrogen bond in the crystal, which is cleaved in the gaseous state, and (2) the change in the electronic structure and probably the molecular structure as well, of the hydroxyl moiety of glycolate anions, accompanying homolytic vaporization. Contributions from these sources to ΔU_R(glycolate) are clearly proportional to (y/x) and independent of metal species. It is to be noted that the contribution from the former source is sufficiently large to account for mostly the second terms by itself. The latter contribution is considered to be smaller than the former. The other possible extra effects arising from the fact that glycolate is a tridentate anion, may not be included in the causes of the second terms, since it seems unlikely that these extra effects are independent of metal species.

Equations (14) and (15) suggest that crystal structure of every glycolate is similar to that of Cu(II) glycolate. Intermolecular hydrogen bond would be present and metal cations would be coordinated with carboxyl and hydroxyl oxygen atoms, in the crystal of every glycolate. The total magnitude of metal-oxygen interaction energy does depend on metal species, but is independent of the kind or the combination of coordinating oxygen atoms (carboxyl and hydroxyl), as is reflected in the coefficients of the first terms which are close to unity.

Thus, it has been shown that the empirical analysis of crystal cohesion energy in terms of ΔU_R can be used to obtain various informations on crystal structure and inter-ion interactions in the crystal, at least within the extent of the present compounds.

Table 4. Estimated standard enthalpies of formation in crystalline state of metal formates, acetates, glycolates, and oxalates

Cathion	$-\Delta H_f^\circ(M_xA_y, c)$/kJ mol^{-1}			
	Formate	Acetate	Glycolate	Oxalate
Mg(II)	1276(A)	—	—	—
Al(III)	1749(A)	—	2452(A)	3428(A)
Mn(II)	—	—	1514(F)	—
Co(II)	—	970(F)	1343(F)	—
Ni(II)	—	969(F)	1342(F)	—
Cu(II)	—	—	—	963(FA)
Zn(II)	—	—	—	959(FA)
Rb(I)	—	—	916(FA)	—
Ag(I)	350(A)	—	586(A)	—
Cd(II)	634(O)	621(O)	1412(O)	—
Cs(I)	698(A)	—	930(A)	1371(A)
Hg(II)	711(A)	—	1192(A)	—
Tl(I)	481(A)	—	715(A)	933(A)
Pb(II)	—	—	1347(FA)	—

F, A, and O in the parentheses show that ΔU_R of the corresponding formate, acetate, and oxalate, was used to derive the estimated value, respectively. The values with parenthesized FA are the mean values of those obtained by correlation with ΔU_R of formate and that of acetate.

Apart from the analysis of ΔU_R described so far, the regularity in ΔU_R or $[\Delta U_R-(y/x)\Delta H_f^\circ(A,g)]$ enables us to estimate $\Delta H_f^\circ(c)$ of a compound M_xA_y, from that of another compound of the same metal, by using equations (6)—(10) and then Eq. (4). The estimated values are presented in Table 4.

References

1) W. W. Wentworth, E. Chen, and J. C. Steelhammer, *J. Phys. Chem.*, **72**, 2671 (1968).
2) S. W. Benson, "Thermochemical Kinetics", 2nd ed, John-Wiley and Sons, New York (1976), p. 299.
3) H. E. O'Neal and S. W. Benson, "Free Radicals," ed by J. K. Kochi, John-Wiley and Sons, New York (1975), p. 296.
4) D. D. Wagman, W. H. Evans, V. B. Parker, I. Halow, S. M. Bailey, R. H. Schumm, and K. L. Churney, "Selected Values of Chemical Thermodynamic Properties," NBS Technical Note 270-3 (1968), 270-4 (1969), 270-5 (1971), 270-6 (1971), 270-7 (1973), and 270-8 (1981), U.S. Government Printing Office, Washington, D. C.
5) S. Murata, M. Sakiyama, and S. Seki, *Netsu Sokutei*, **4**, 89 (1977).
6) J. B. Pedley and J. Rylance, "Sussex-N. P. L. Computer Analysed Thermochemical Data: Organic and Organometallic compounds," University of Sussex, Brighton (1977).
7) See for example, P. George and D. S. McLure, *Prog. Inorg. Chem.*, **1**, 381 (1959).
8) J. K. Burdett, *J. Chem. Soc., Dalton Trans.*, **1976**, 1725.
9) P. L. Markila, S. J. Rettig, and J. Trotter, *Acta Crystallogr., Sect. B*, **31**, 2927 (1975).
10) T. Watanabe and M. Matsui, *Acta Crystallogr., Sect. B*, **34**, 2731 (1978).
11) N. Burger, H. Fuss, and S. A. Mason, *Acta Crystallogr., Sect. B*, **33**, 1968 (1977).

12) G. A. Barclay and C. H. L. Kennard, *J. Chem. Soc.*, **1961**, 3289.
13) S. W. Benson and J. H. Buss, *J. Chem. Phys.*, **29**, 546 (1958).
14) J. D. Cox and G. Pilcher, "Thermochemistry of Organic and Organometallic Compounds," Academic Press, London (1970), Chap. 7.
15) C. K. Prout, R. A. Armstrong, J. R. Carruthers, J. G. Forrest, P. Murray-Rust, and F. J. C. Rosotti, *J. Chem. Soc., A*, **1968**, 2791.

 © 1984 The Chemical Society of Japan Bull. Chem. Soc. Jpn., 57, 1179—1183 (1984)

Photoelectrochemical Oxidation of Alcohols on Polycrystalline Zinc Oxide

Ju-seong LEE,† Tamihiko KATO, †† Akira FUJISHIMA,* and Kenichi HONDA
Department of Synthetic Chemistry, Faculty of Engineering, The University of Tokyo, Bunkyo-ku, Tokyo 113
(Received August 29, 1983)

The current doubling behavior of alcohols was studied on an n-type ZnO polycrystalline electrode. The increase in photocurrent due to alcohols on the ZnO depended on pH of the solution. The photocurrent was almost doubled in alkaline solution. It was found that the ZnO photoanode dissolved in the neutral aqueous solution but the dissolution reaction of ZnO was completely suppressed in alkaline solution at a sufficiently large pH. From the experimental results obtained by the rotating ring disk electrode and gas chromatographic and mass spectrometric analyses, a mechanism of the current-doubling reaction is proposed.

Most recent investigations of semiconductor electrodes have been concerned with the utilization of solar energy in which water is photoelectrolyzed to hydrogen and oxygen.[1-8]

Some studies of the electrochemical behavior of organic substances at semiconductor electrodes have been reported.[9-13] For example, Morrison *et al.*[14,15] reported a "current doubling effect" due to the anodic behavior of aqueous formate ion or alcohols at an illuminated zinc oxide single crystal semiconductor electrode. To account for the mechanism of current doubling they suggested that holes formed by photoirradiation of an n-type semiconductor react with the current doubling agent R to give R^{+}, which then donates an electron to the conduction band and becomes R^{2+}. However, the photodissolution reaction of zinc oxide was not mentioned.

Subsequently, similar effects were reported on other semiconductor electrodes. Gerischer *et al.*[16,17] found current doubling behavior on a cadmium sulfide single crystal electrode when alcohols or aldehydes were added to the electrolyte. Tamura *et al.*[18] observed that the photooxidation current for a titanium dioxide single crystal electrode was increased by the addition of alcohols in acidic aqueous solution.

Our earlier studies[19-22] with the zinc oxide electrode in neutral aqueous solution showed that as the photocurrent was increasd, oxygen evolution could not be observed but zinc ions were detected in the electrolyte solution after the photoelectrolysis. The amount of zinc ions dissolved was almost equivalent to the charge of holes that flowed to the zinc oxide surface. These facts indicated that the current doubling effect may not always follow Morrison's mechanism.

In this paper, we re-examine the mechanism of current doubling by using a polycrystalline zinc oxide electrode and alcohols as the current doubling agent in solutions of various pH. Experimental measurements were made by rotating ring-disk electrode (RRDE) and gas chromatographic and mass spectrometric analyses of reaction products produced from a photoelectrolysis.

Experimental

Polycrystalline n-type zinc oxide pellets were made by pressing ZnO powder of reagent grade with a pressure of 0.5 t/cm^2 and then heating the pellets for 3 h at 1300 °C in air.[21] Two kinds of semiconductor electrodes were made; one was of the conventional type and another was for a ring-disk electrode system. The pellet for photoelectrochemical measurements and macrophotoelectrolysis was 17 mm-diameter and about 2 mm-thick. The pellet for a smaller size cell, which was used for mass spectrometric analysis was 8 mm-diameter and about 2 mm-thick. After an ohmic contact was made with an In-Ga alloy, a lead wire was connected with silver paste, and then all surfaces except one side were covered with an epoxy resin.

The pellet for the ring-disk electrode was assembled with a 6 mm-diameter zinc oxide disk and an amalgamated gold ring 7 mm in inner diameter and 9 mm in outer diameter. The ring-disk electrode is schematically shown in Fig. 1 (a). The experimental setup of the RRDE followed previous paper.[23]

The faces of both zinc oxide electrodes, which were exposed to the electrolyte solution, were polished with alumina powder, etched in 1 : 1 HCl-water mixed solution for 10 s, and then washed with distilled water.

A macroelectrolysis cell consisted of two compartments separated by a cation exchange membrane (Asahi Garasu, Selemion CMV). The volumes of anolyte and catholyte chambers were 100 and 80 ml, respectively. As shown in Fig. 1 (b), the cell was equipped with the polycrystalline n-type zinc

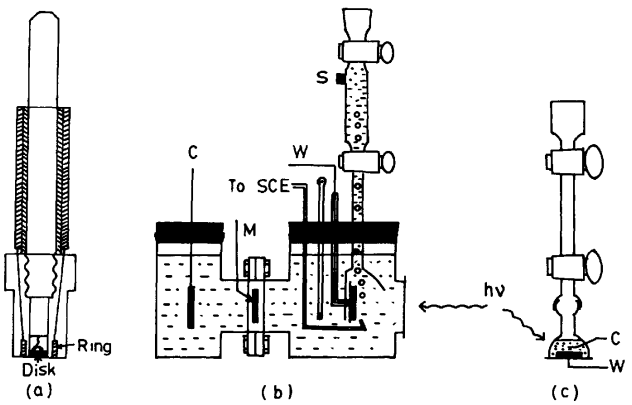

Fig. 1. Schematic diagrams of ring-disk electrode and photoelectrolysis cells.
(a) Ring-disk electrode, (b) macrophotoelectrolysis cell, (c) microphotoelectrolysis cell.
W: Working electrode, C: counter electrode, M: ion exchange membrane, S: rubber stopper.

† Department of Industrial Chemistry, College of Engineering, Hanyang University, Seoul 133, Korea.
†† Department of Industrial Chemistry, Nagoya Institute of Technology, Gokiso, Showa-ku, Nagoya 466.

oxide working electrode, a platinum wire counter electrode, and a saturated calomel electrode (SCE) as a reference electrode. A smaller size cell, which was used for mass spectrometric analysis, was equipped with two electrodes, such as ZnO photoanode and Pt cathode, and the volume of electrolyte was 1 ml, as shown in Fig. 1 (c).

The light source was a 500 W high pressure mercury arc lamp (Ushio Denki) and the wavelength of the illuminating light was fixed at 360±30 nm by means of a glass filter (Toshiba Kasei, UV-D2). Current-potential behavior of the zinc oxide electrode was measured with a potentiostat/galvanostat system (Hokuto Denko), with a saturated calomel electrode as a reference and platinum as a counter electrode. All chemicals were of reagent grade. The oxygen and organic compounds produced were analyzed by means of gas chromatography (Hitachi Model 163) and mass spectrometry (Ulvac YTP-150). In the case of the gas chromatographic analysis, all liquid compounds except formaldehyde were analyzed by using polyethylene glycol 2000, polyethylene glycol 20 M and Chromosorb 101 (FID, temp 120 °C), and formaldehyde was chromatographed with Porapax N (TCD, temp 100 °C). The electrolyte solutions after electrolysis were injected into the gas chromatograph. Oxygen evolved was analyzed with Molecular Sieve SA on 60/80 mesh. The carrier gas was helium at a flow of 40 ml/min. The zinc ions in the electrolyte solutions were analyzed spectrophotometrically by using Zincon reagent in a pH 9.0 buffer solution. Before all experiments, the solutions were purged with nitrogen gas for more than 30 min.

Results

Typical current-potential curves for the electrolyte solution at pH 6 and 13 are shown in Fig. 2. In the dark, no anodic current was observed in both the presence or the absence of a current doubling agent, such as methyl alcohol. In the solution at pH 6, the anodic photocurrent appeared at −0.45 V *vs.* SCE, and then reached saturation under anodic polarization. With the addition of methyl alcohol to the solution, the saturated photoanodic current was increased by a factor of only 1.1. On the other hand, in the solution at pH 13, the onset potential of the anodic photocurrent was more negative by 0.4 V than the potential in the neutral solution. By addition of methyl alcohol to the alkaline solution, the photocurrent was almost doubled.

The pH dependences of the photocurrent ratio (i/i_0) of ZnO for various alcohols added to solution are shown in Fig. 3, where i and i_0 are the photocurrent in the presence and in the absence of a current doubling agent, respectively. The ratio i/i_0 increased for the solution containing a primary or secondary alcohol above pH 10, whereas the increase was not observed for a tertiary alcohol solution. Thus it was found that the increase in the photocurrent of ZnO for given alcohol depended very much on the pH of the solution, an effect which is important for the discussion of the reaction mech-

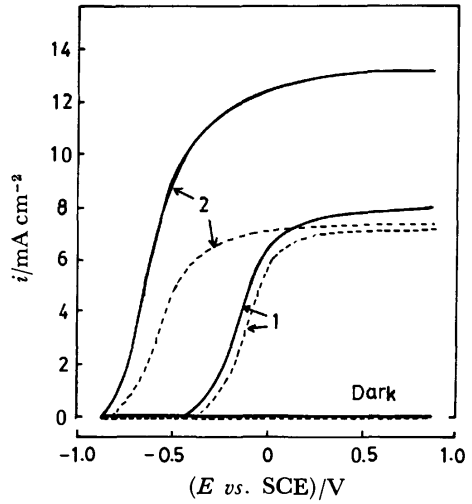

Fig. 2. Current-potential curves for polycrystalline n-type ZnO under illumination (λ=360+30 nm).
1: 0.2 M Na_2SO_4(pH 6), 2: 0.2 M Na_2SO_4+0.1 M NaOH (pH 13).
Dotted lines: [CH_3OH]=0; solid lines: [CH_3OH]= 0.5 M

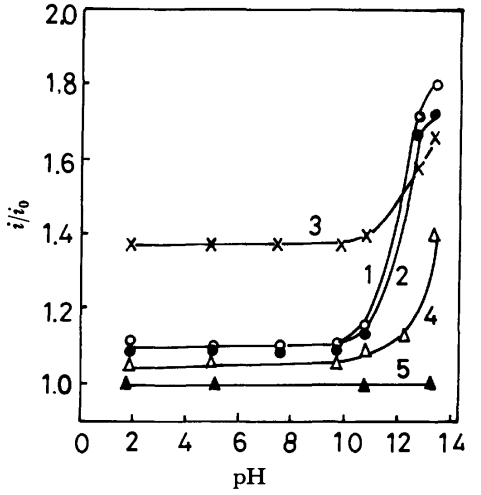

Fig. 3. pH dependence of the photocurrent ratio (i/i_0) of the ZnO electrode set at 1.0 V *vs.* SCE for various alcohols.
1: 0.5 M CH_3OH, 2: 0.5 M C_2H_5OH, 3: 0.5 M i-C_3H_7OH, 4: 0.5 M ethylene glycol, 5: 0.5 M t-C_4H_9OH

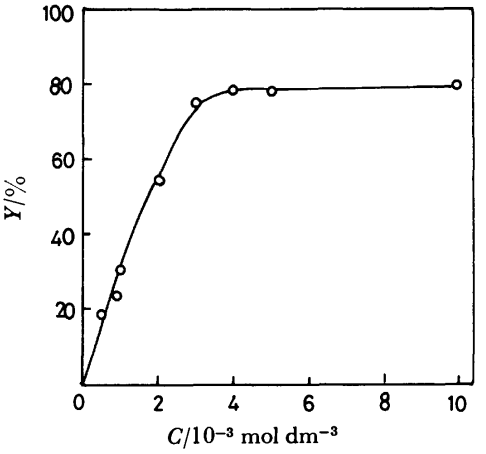

Fig. 4. Relative increase of photocurrent indicated by parameter Y on the dependence of methyl alcohol concentration in 0.2 M Na_2SO_4+0.1 M NaOH (pH 13). Disk potential was fixed at 1.0 V *vs.* SCE and rotating speed was 1000 min^{-1}.

anism. In addition to the pH effect, the α hydrogen of alcohols may be involved with the current doubling photoelectrochemical oxidation reaction.

To obtain more information on the current doubling behavior, the rotating disk electrode method was employed. For convenience, the effects of methyl alcohol concentration was evaluated by the parameter $Y=100(i-i_0)/i_0$ which references the increase in current to the photocurrent in an alkaline electrolyte. The dependence of the value of Y on the concentration of methyl alcohol in a solution containing 0.2 M Na_2SO_4+0.1 M NaOH (pH 13) (1 M=1 mol dm^{-3}) is shown in Fig. 4. The maximum Y value of 80% was obtained for CH_3OH at concentrations $\geq 4\times10^{-3}$ M. In case of methyl alcohol, the RRDE technique was applied to determine which reaction occurred on the ZnO photoanode in neutral

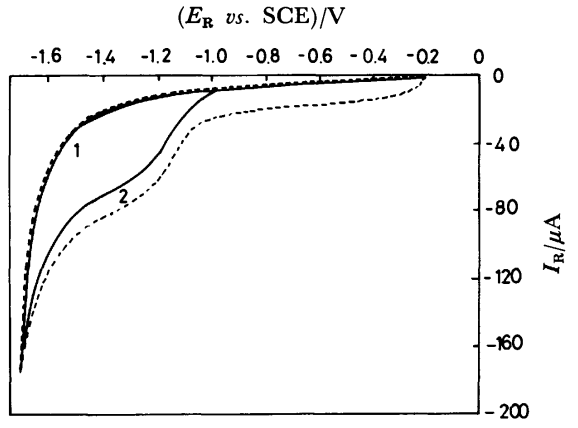

Fig. 5. Dependences of Au(Hg) ring current on the ring potential in a solution of 0.2 M Na_2SO_4(pH 6).
1: I_0: 0 μA (in dark), 2: I_0: dotted line 142 μA, solid line 182 μA (under illumination).
Dotted line is for $[CH_3OH]=0$ and solid line for $[CH_3OH]=5\times10^{-3}$ M.
The disk ZnO potential was fixed at 1.0 V *vs.* SCE. Rotating speed and scan rate were 1000 min^{-1} and 30 sV^{-1}, respectively.

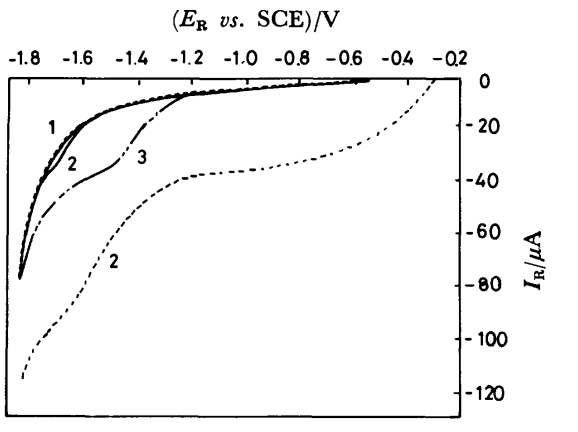

Fig. 6. Dependences of Au(Hg) ring current on the ring potential in a solution of 0.2 M Na_2SO_4+0.1 M NaOH(pH 13).
1: I_0: 0 μA (in dark), 2: I_0: dotted line 290 μA, solid line 540 μA (under illumination), 3: $[Zn^{2+}]=5\times10^{-5}$ M was added in dark.
Other conditions are the same as in Fig. 5.

and alkaline solutions. The current-potential curves at the disk and the ring electrode in solutions containing 0.2 M Na_2SO_4 are shown for pH 6 and 13 in Figs. 5 and 6, respectively. As shown in Fig. 5, for dark conditions at pH 6, the disk current was negligibly small at the fixed potential of +1.0 V *vs.* SCE, and at the ring electrode hydrogen evolution occurred at potentials more cathodic than −1.5 V *vs.* SCE. Under illumination in the absence of methyl alcohol, an anodic photocurrent flowed at the zinc oxide electrode. At the same time, a reduction current appeared at the ring electrode in the potential ranges more cathodic than −0.2 and −1.0 V, which corresponds to the reduction of oxygen and zinc ion, respectively. By addition of methyl alcohol to the solution, the magnitude of the disk photocurrent increased almost 1.1 or 1.2 times, but the ring current due to the reduction of zinc ion showed little change and the ring current for oxygen reduction disappeared from the current-potential curves.

However, in the alkaline solution (pH 13) the behaviors of the ring and the disk currents were different from those in the neutral solution. As shown in Fig. 6, under illumination on the disk electrode of the ZnO in the absence of methyl alcohol, the ring reduction current due to oxygen appeared from −0.3 V *vs.* SCE but that due to the zinc ion was not observed. The dotted curve 2 of the ring current in Fig. 6 almost coincides with the reduction of oxygen at the dropping mercury electrode reported by Kolthoff.[24] Therefore, the first cathodic wave corresponds to the reduction of dissolved oxygen to hydrogen peroxide and the second wave to the reduction of peroxide to hydroxide ion.

By addition of methyl alcohol to the solution of pH 13, the disk photocurrent increased nearly two times that of the initial photocurrent. At the same time, the reduction current which corresponds to the reduction of oxygen disappeared in the potential range between −0.3 and −1.6 V, but a new wave appeared at a potential of about −1.6 V *vs.* SCE. This new wave might correspond to a reduction current due to formaldehyde formed by photoelectrolysis of methyl alcohol. If dissolution of ZnO photoelectrode occurred in alkaline solution as well as in the neutral solution, the reduction wave of Zn^{2+} should have been observed in Fig. 6. Upon addition of zinc ion to the solution of pH 13, the ring current corresponding to the reduction of Zn^{2+} appeared at a potential of −1.25 V (curve 3 in Fig. 6).

From the experimental results shown in Figs. 5 and 6, it is concluded that the n-type ZnO photoanode dissolved in the neutral aqueous solution but not in the alkaline aqueous solution around pH 13, with or without a current doubling reagent.

In addition to the experimental results of the RRDE measuremnt, the weight changes of the ZnO anode before and after macroelectrolysis under illumination were measured. The weight loss in neutral solution was quantitatively proportional to the quantity of electricity flowed, but a weight change of ZnO could not detect in the alkaline solution at pH 13. Consequently, the ZnO photoanode does not dissolve in adequately alkaline solution during macrophotoelectrolysis, a result which confirms the RRDE measurements.

The data in Table 1 show the results obtained by

Table 1. Photoelectrochemical reaction of polycrystalline *n*-type ZnO electrode in alcoholic solution

Electrolyte	Av. photocurrent density/mA cm^{-2}	Quantity of electricity / C	Current efficiency/%		
			Zn^{2+}	O_2	Org. compd
Without alcohol					
1	6.8	50	98.2	95.5	—
2	7.0	50	0	100.2	—
With 0.5 M MeOH					Formaldehyde
1	7.8	100	99.3	0	18.5
2	13.5	100	0	0	75.0
With 0.5 M EtOH					Acetaldehyde
1	8.2	100	97.9	0	93.8
2	11.8	100	0	0	95.3
With 0.5 M *i*-PrOH					Acetone
1	11.2	100	98.8	0	81.1
2	12.5	100	0	0	90.7

Electrolyte: 1; 0.2 M Na_2SO_4 (pH 6), 2; 0.2 M Na_2SO_4+0.1 M NaOH (pH 13). Illumination wavelength; 360± 30 nm.

macrophotoelecrolysis. In neutral solution in the absence of alcohol, the current efficiencies of evolved oxygen and dissolved Zn^{2+} ion are almost 100%, respectively. On the other hand, in the alkaline solution in the absence of alcohol, the current efficiency for dissolved Zn^{2+} was zero but that of evolved oxygen was maintained at 100%. By addition of alcohols 0.5 M) to the neutral or alkaline solution, oxygen evolution was not observed. In these cases, aldehyde or ketone which corresponds to the oxidation product of a primary or secondary alcohol was observed. During photoelectrolysis the pH of the anolyte decreased gradually in the alkaline alcoholic solution but in the case of the neutral solution the pH of the anolyte was almost constant.

Photoelectrolysis resulted in formation of a small amount of formaldehyde compared with the amount of acetaldehyde or acetone produced. To examine this phenomena, the gas evolved from the electrolyte solution was analyzed by mass spectrometry after the continuous photoelectrolysis to one half the theoretical charge (quantity of electricity) in the alkaline 0.1 M CH_3OH solution (pH 13) using the small size cell. The mass spectrum showed strong signals of H_2 (*m/z* 2), unreacted methyl alcohol (*m/z* 31, 32), formaldehyde (*m/z* 18, 29, 30), CO_2 (*m/z* 44), and a very weak signal of formic acid (*m/z* 46).[25] Hydrogen probably was evolved from the Pt cathode during the electrolysis. The CO_2 is the oxidation product of methyl alcohol on ZnO where part of the formaldehyde produced is oxidized to CO_2.

Discussion

In general, when an oxide or hydrous oxide is immersed in an aqueous solution, protons and hydroxide ions become adsorbed.[26] The pH-dependence of the adsorption on the surface of the ZnO electrode could be explained by assuming reactions (1) and (2) at the electrode surface facing the electrolyte solution, that is, hydroxide ions are adsorbed on Lewis acid sites in alkaline solution and protons are adsorbed on Lewis base sites in weak acid or neutral solution.

$$ZnO + OH^- \longrightarrow ZnO\text{-}OH^- \text{ (in alkaline solution)}, \quad (1)$$

$$ZnO + H^+ \longrightarrow ZnO\text{-}H^+ \text{ (in weak acid or neutral solution)}. \quad (2)$$

The photo-produced holes coming to the ZnO surface may interact with, and oxidize, these adsorbed hydroxide ions or surfaces adsorbed protons. For example, hydroxyl radicals could be produced by reactions (3) and (4)

$$ZnO\text{-}OH^- + h^+ \longrightarrow ZnO + \cdot OH, \quad (3)$$

$$ZnO\text{-}H^+ + h^+ \longrightarrow Zn^{2+} + \cdot OH. \quad (4)$$

Thus the corrosion of the ZnO can occur readily in the neutral solution and be suppressed in alkaline solution. Then, the $\cdot CH_2OH$ radical formed by the reaction between the $\cdot OH$ radical and the α hydrogen of alcohol as in reaction (5) can result in donation of an electron to the conduction band of ZnO, as in reaction (6),

$$\cdot OH + CH_3OH \longrightarrow \cdot CH_2OH + H_2O, \quad (5)$$

$$\cdot CH_2OH + OH^- \longrightarrow HCHO + H_2O + e^-. \quad (6)$$

The net reaction occurring in alkaline solution is obtained by combining reactions (1), (3), (5), and (6)

$$CH_3OH + 2OH^- + h^+ \longrightarrow HCHO + 2H_2O + e^-. \quad (7)$$

The net reaction in weak acid or neutral solution is obtained by combining reactions (2), (4), (5), and (6).

$$ZnO + CH_3OH + h^+ \longrightarrow Zn^{2+} + HCHO + H_2O + e^- \quad (8)$$

Yamase *et al.*,[27] using an esr spin trapping method, detected simultaneously $\cdot OH$ and $\cdot CH_2OH$ radicals as intermediate of the photocatalytic reaction in an aqueous methyl alcohol solution containing polytungstate ion. Thus, reaction (5) is substantiated by their results.

The pH of the alkaline methyl alcohol solution after photoelectrolysis decreased in proportion to the quantity of electricity, but the pH of the neutral solution was much the same as that of the initial solution.

Hence, the observation of current increase (*e.g.* current doubling) makes it clear that hydroxide ion is involved in the reaction mechanism, as in Eq. (6). It is apparent that the current increasing reaction easily takes place in the alkaline solution for which $[OH^-] \geq 10^{-4}$M. In the case of the neutral solution, the small current increasing can be accounted for by the low concentration of hydroxide ions.

As a result of mass spectrometric and chemical analysis, considerable amount of carbon dioxide is detected after photoelectrolysis. This result supported the fact that formaldehyde is produced by oxidation of methyl alcohol on a ZnO photoanode and that the formaldehyde which is produced seems to be oxidized further up to carbon dioxide.

It is also concluded that the n-type ZnO photoanode dissolved in the neutral aqueous solution but not in the alkaline aqueous solution around pH 13, with or without a current doubling reagent.

References

1) A. Fujishima and K. Honda, *Nature*, **238**, 37 (1972).
2) H. Gerischer, *J. Electroanal. Chem.*, **58**, 263 (1975).
3) A. J. Nozik, *Ann. Rev. Phys. Chem.*, **29**, 189 (1978).
4) M. Tomkiewicz and H. Fay, *Appl. Phys.*, **18**, 1 (1979).
5) M. S. Wrighton, *Acc. Chem. Res.*, **12**, 303 (1979).
6) F. F. Fan, B. L. Wheeler, A. J. Bard, and R. N. Noufi, *J. Electrochem. Soc.*, **128**, 2042 (1981).
7) R. A. Simon, A. J. Ricco, and M. S. Wrighton, *J. Am. Chem, Soc.*, **104**, 2031 (1982).
8) D. G. Canfield and S. R. Morrison, *Appl. Surface Sci.*, **10**, 493 (1982).
9) T. Freund and W. P. Gomes, *Cat. Rev.*, **3**, 1 (1969).
10) S. N. Frank and A. J. Bard, *J. Am. Chem. Soc.*, **99**, 4667 (1977).
11) K. Nakatani and H. Tsubomura, *Bull. Chem. Soc. Jpn.*, **50**, 783 (1977).
12) B. Kraeutler and A. J. Bard, *J. Am. Chem. Soc.*, **99**, 7729 (1977).
13) J. Ludvik, J. Klima, J. Volke, A. Kurfurst, and J. Kuthan, *J. Electroanal. Chem.*, **138**, 131 (1982).
14) S. R. Morrison and T. Freund, *J. Chem. phys.*, **47**, 1543 (1967); *Electrochim. Acta*, **13** 1344 (1968).
15) W. P. Gomes, T. Freund, and S. R. Morrison, *J. Electrochem. Soc.*, **115**, 818 (1968); *Surface Sci.* **13**, 201 (1968).
16) H. Gerischer and H. Rösler, *Chemie-Ing.-Tech.*, **42**, 176 (1970).
17) K. Micka and H. Gerischer, *J. Electroanal. Chem.*, **38**, 397 (1972).
18) M. Miyake, H. Yoneyama, and H. Tamura, *Chem. Lett.*, **1976** 635; *Denki Kagaku*, **45**, 411 (1977).
19) A.Fujishima, Ph. D Thesis, The University of Tokyo (1971).
20) A. Fujishima and K. Honda, *Denki Kagaku*, **40**, 33 (1972).
21) A. Fujishima, T. Kato, E. Maekawa, and K. Honda, *Bull. Chem. Soc. Jpn.*, **54**, 1671 (1981).
22) Y. Maeda, A. Fujishima, and K. Honda, *J. Electrochem. Soc.*, **128**, 1731 (1981).
23) T. Inoue, T. Watanabe, A. Fujishima, K. Honda, and K. Kohayakawa, *J. Electrochem. Soc.*, **124**, 719 (1977).
24) I. M. Kolthoff and C. S. Miller, *J. Am. Chem. Soc.*, **83**, 1013 (1941).
25) J. G. Grasselli, Edited, "Atlas of Spectral Data and Physical Constants for Organic Compounds," CRC Press, Ohio (1973).
26) S. R. Morrison, "Electrochemistry at Semiconductor and Oxidized Metal Electrodes," Plenum Press, N. Y. (1980).
27) T. Yamase and N. Takabayashi, Symposium on Catalytic Chemistry to be concerned in Solar Energy Conversion, Abstract p. 46, held on June 3, 1983 at Institute of Physical and Chemical Research, Saitama, Japan.

The Complexation of Zinc Tetraphenylporphyrintrisulfonate by Viologen and Its Role in Photoredox Processes

Ichiro Okura,* Shin Kusunoki, and Shigetoshi Aono
Department of Chemical Engineering, Tokyo Institute of Technology, Meguro-ku, Tokyo 152
(Received August 31, 1983)

The formation of the cation radicals of viologen dyes was established when an aqueous solution containing zinc tetraphenylporphyrintrisulfonate (Zn-$TPPS_3$), viologen dye, and 2-mercaptoethanol was irradiated by visible light. The reduction of viologen has been studied kinetically; its reduction rate may be expressed as follows:

$$v = \frac{d[V^+]}{dt} = \left(\frac{k_3[Zn\text{-}TPPS_3]_0}{1+K_1[V^{2+}]+K_2[V^+]}\right)\left(\frac{k_4[V^{2+}]}{k_{-3}+k_4[V^{2+}]}\right)\left(\frac{k_6[RSH]}{k_5[V^+]+k_6[RSH]}\right),$$

where $[V^{2+}]$, $[V^+]$, and [RSH] are the concentrations of the oxidized form and the reduced form of viologen, and 2-mercaptoethanol respectively. On the basis of the rate expression, a reaction mechanism containing the complexation of Zn-$TPPS_3$ by viologen was proposed. On the addition of hydrogenase to the above photo-irradiation system, hydrogen evolution was observed by the irradiation of visible light.

Photochemical redox systems have been developed for the purpose of solar-energy utilization.[1] The systems, containing, as shown in the following scheme, a photosensitizer (S), an electron donor (D), and an electron carrier (C), have been used to evolve hydrogen from water when a suitable catalyst is present:

$$\underset{D_{ox}}{D} \quad \underset{S \xrightarrow{h\nu} S^*}{S^+} \quad \underset{C}{C^+} \quad \text{Catalyst} \quad \underset{1/2H_2}{H^+} \qquad (1)$$

As photosensitizers, metallo-porphyrins have been employed extensively in these studies.[2] As catalysts, hydrogenase and colloidal platinum are predominant. Methylviologen has been used almost exclusively as an electron carrier.

As both the photosensitizer and the electron carrier serve as redox catalysts in the above reaction, the overall reaction may be expressed as follows:

$$D + H^+ \xrightarrow{h\nu} D_{ox} + 1/2H_2. \qquad (2)$$

When EDTA, triethanolamine, or 2-mercaptoethanol (RSH) is used as an electron donor, the following reactions occur:

$$(HOOCCH_2)_2N(CH_2)_2N(CH_2COOH)_2 + H_2O \longrightarrow (HOOCCH_2)_2N(CH_2)_2NHCH_2COOH + CO_2 + HCHO + H_2, \qquad (3)$$

$$N(CH_2CH_2OH)_3 + H_2O \longrightarrow NH(CH_2CH_2OH)_2 + CHOCH_2OH + H_2, \qquad (4)$$

$$2RSH \longrightarrow RSSR + H_2. \qquad (5)$$

The overall reaction shown above, the light-induced oxidation of the electron donor, involves a net solar energy storage, and part of the light energy is also stored. If back reaction proceeds upon the addition of a suitable catalyst and the stored light energy is taken out as heat, the stored solar energy can be used when needed. In the cases of Reactions (3) and (4), complex products with three or four components are formed, and it may not be easy to get the starting materials by means of the back reaction. In the case of Reaction (5), however, the back reaction proceeded easily. When cystine was used as the disulfide (RSSR), the starting material, cysteine, was produced with the palladium catalyst by the hydrogenation of RSSR under mild reaction conditions (at 30 °C; hydrogen pressure: 1 atm). By the conversion of cysteine to cystine and hydrogen, about 30 kJ mol^{-1} of light energy is stored. Therefore, the hydrogen production reaction expressed by Reaction (5) seems to be suitable for a solar-energy-storage system.

The photoreduction of electron carriers should proceed nicely to get an efficient hydrogen evolution, provided the hydrogen evolution rate is determined by the photoreduction of the electron carrier as is shown in Eq. (1). For this purpose, suitable combinations of the components and the optimum reaction conditions are discussed in this study.

Experimental

Materials. All the chemicals, obtained from the Tokyo Kasei Kogyo Co., were of the highest available purity. The ethyl-, propyl-, and butylviologens were synthesized according to the literature.[3] The zinc *meso*-tetraphenylporphyrintrisulfonate (Zn-$TPPS_3$) was synthesized by refluxing $TPPS_3$ and zinc acetate (molar ratio; 1:10) in methanol for 2 h.

Desulfovibrio vulgaris cells (Miyazaki type, which has kindly been provided by Prof. T. Yagi of Shizuoka Univ.) were cultured according to the literature.[4] The hydrogenase [H_2: ferricytochrome C_3 oxidoreductase, EC 1.12.2.1] from *Desulfovibrio vulgaris* was purified according to Yagi's method.[5] The concentration of hydrogenase is not known, but it has the ability to produce 4.88 μmol of hydrogen when this reaction system is used: hydrogenase (0.5 ml)-methylviologen (4.15×10^{-6} mol)-$Na_2S_2O_4$ (2.87×10^{-5} mol) in 6.0 ml of 0.02 mol dm^{-3} of Tris-HCl buffer (pH 7.0) at 30 °C for 10 min.

Measurement Procedure. The sample solution, which consisted of the photosensitizer, the viologen dye, 2-mercaptoethanol, and hydrogenase (if included) in 0.02 mol dm^{-3} of the Tris-HCl buffer (pH 7.0; this value is suitable for hydrogenase), was deaerated by repeated freeze-pump-thaw cycles. A typical experiment was performed as follows under anaerobic conditions. To 8.33×10^{-8} mol dm^{-3} of the photosensitizer, 1.26×10^{-4} mol dm^{-3} of the viologen dye and 0.21 mol dm^{-3} of RSH as a reducing agent in water, 0.5 ml of hydrogenase (if included) was added. The volume of the mixture was then adjusted to 6.0 ml with 0.02 mol dm^{-3} of the Tris-HCl buffer (pH 7.0). In the photolysis with

continuous irradiation, the sample, in a Pyrex cell equipped with a magnetic stirrer, was irradiated with light from a 200-W tungsten lamp. Light at wavelengths less than 390 nm was cut off by a Toshiba L-39 filter. A portion of the evolved hydrogen was collected *via* a sampling valve and analyzed by means of gas chromatography.

Results and Discussion

Photoreduction of Viologen Dyes by RSH. When an aqueous solution containing Zn-TPPS$_3$, viologen dye, and RSH was irradiated, the formation of the viologen cation radical was observed. As is shown in Fig. 1, the concentration of the viologen radical increased rapidly at the beginning of the reaction, and then reached a constant value. When the light was then cut off, the concentration of the cation radical decreased gradually. The difference in the constant values may depend on the difference in the photoinduced viologen-reduction rates and the backward reaction rates in the absence of light.

As is shown in Figs. 2, 3, and 4, the initial rate of cation-radical formation (the slopes of the curves at the beginning of the reaction in Fig. 1) increases at any viologen-dye concentration, and then decreases after a maximum point. To clarify this abnormal phenomenon, the rate decrease at a higher viologen concentration, the following experiments were carried out.

Complexation of Zn-TPPS$_3$ by Viologen Dyes. When Zn-TPPS$_3$ was mixed with ethylviologen, the characteristic Soret absorption band (418 nm) decreased with the increase in the ethylviologen concentration, and a new spectrum appeared which has a characteristic absorption band at 425 nm through the isosbestic point at 422 nm (Fig. 5). Similar complex formations between metalloporphyrins and methylviologen have recently been reported.[6]

When the complex is formed by the following reaction:

$$\text{Zn-TPPS}_3 + \text{EtV}^{2+} \overset{K_1}{\rightleftharpoons} \text{complex} \qquad (6)$$

EtV^{2+}: ethyl viologen,

the equilibrium constant, K_1, is expressed by:

$$K_1 = \frac{[\text{complex}]}{[\text{Zn-TPPS}_3][\text{EtV}^{2+}]}. \qquad (7)$$

This equation can be rewritten as follows by using the initial Zn-TPPS$_3$ concentration, $[\text{Zn-TPPS}_3]_0$:

$$\frac{[\text{Zn-TPPS}_3]_0}{[\text{complex}]} = 1 + \frac{1}{K_1[\text{EtV}^{2+}]}. \qquad (8)$$

As the complex concentration is calculated from the absorbance of the complex, the relation between

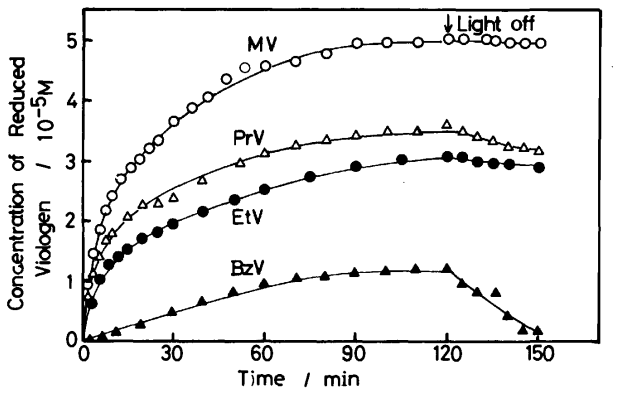

Fig. 1. Time dependence of reduced viologen concentration. (1 M=1 mol dm^{-3})
Reaction conditions; Zn-TPPS$_3$, 8.33×10^{-8} mol dm^{-3}; RSH, 0.21 mol dm^{-3}; methylviologen (MV), 1.26×10^{-4} mol dm^{-3}; ethylviologen (EtV), 1.22×10^{-4} mol dm^{-3}; propylviologen (PrV), 9.50×10^{-5} mol dm^{-3}; benzylviologen (BzV), 1.42×10^{-4} mol dm^{-3}; reaction temp, 30°C.

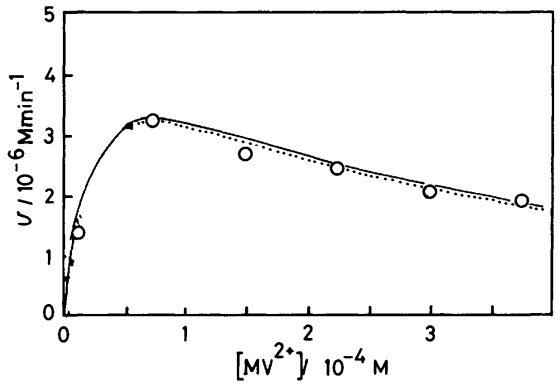

Fig. 2. Relation between photo-induced reduction rate of methylviologen and its concentration.

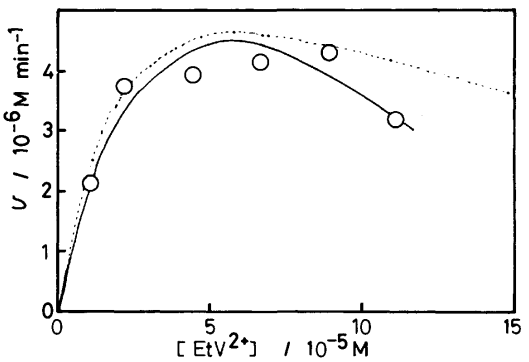

Fig. 3. Relation between photo-induced reduction rate of ethylviologen and its concentration.

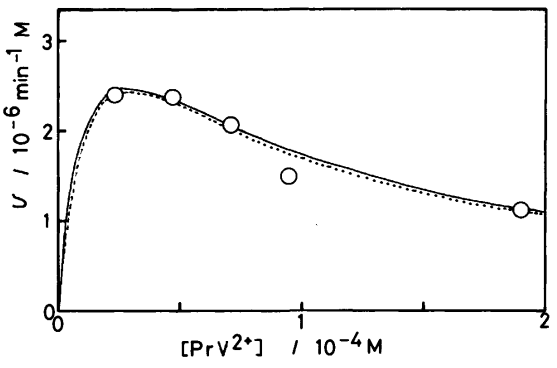

Fig. 4. Relation between photo-induced reduction rate of propylviologen and its concentration.

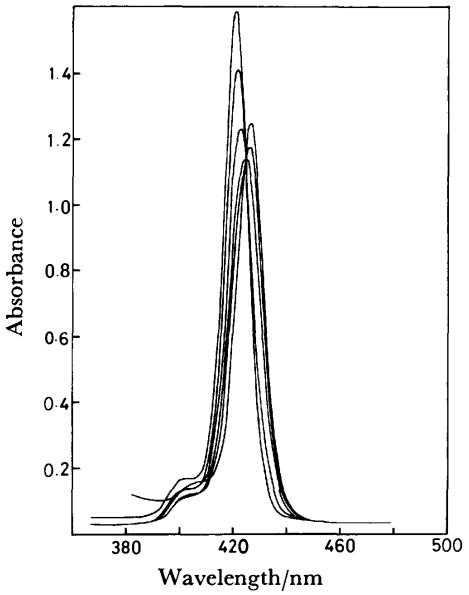

Fig. 5. Spectrum change of Zn-TPPS$_3$ by the addition of ethylviologen.

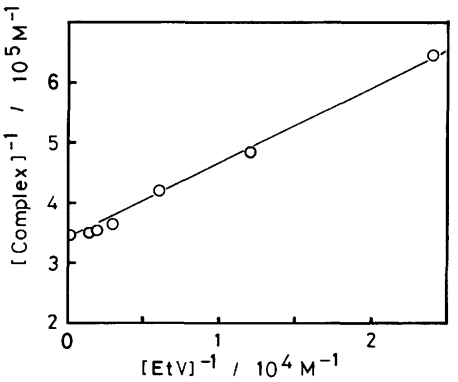

Fig. 6. Relation between [complex]$^{-1}$ and [EtV^{2+}]$^{-1}$.

[complex]$^{-1}$ and [EtV^{2+}]$^{-1}$ can be plotted to as shown in Fig. 6. The good linear relation between [complex]$^{-1}$ and [EtV^{2+}]$^{-1}$ shows the formation of a 1 : 1 complex of Zn-TPPS$_3$ and ethylviologen.

When other viologen dyes were used, the respective complex formation was observed, as is shown in Fig. 7. The equilibrium constants obtained by Eq. (8) are listed in Table 1.

The reduced form of viologen dye also produced a complex with Zn-TPPS$_3$. When the benzylviologen reduced by $Na_2S_2O_4$, for example, was added to Zn-TPPS$_3$, a new spectrum (Fig. 8 Spectrum c) was observed, which shows that Zn-TPPS$_3$ forms a complex with reduced benzylviologen.

Complex formation was also observed when metal-free porphyrin, TPPS$_3$, was used (the data is not shown); this shows that the central metal of the metalloporphyrin does not play an important role in the complex formation, but that the porphyrin ring combines with viologen dye.

Kinetics and Mechanism of Photo-induced Reduction of Viologen Dyes. As has been mentioned above, Zn-TPPS$_3$ forms complexes with both oxidized and

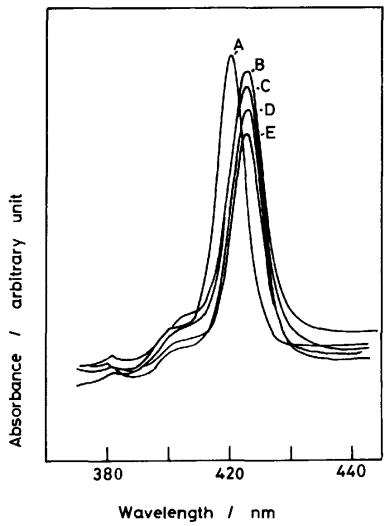

Fig. 7. Spectrum change of Zn-TPPS$_3$ by the addition of viologens.
A: Zn-TPPS$_3$, B: Zn-TPPS$_3$+methylviologen, C: Zn-TPPS$_3$+propylviologen, D: Zn-TPPS$_3$+ethylviologen, E: Zn-TPPS$_3$+butylviologen.

Table 1. List of K_1 and k_4/k_{-3} values

	K_1/dm^3 mol^{-1}	(k_4/k_{-3})/dm^3 mol^{-1}
Methylviologen	$(2.1\pm0.1)\times10^4$	$(8.2\pm0.8)\times10^3$
Ethylviologen	$(2.9\pm0.1)\times10^4$	$(1.0\pm0.1)\times10^4$
Propylviologen	$(3.0\pm0.1)\times10^4$	$(2.9\pm0.2)\times10^4$

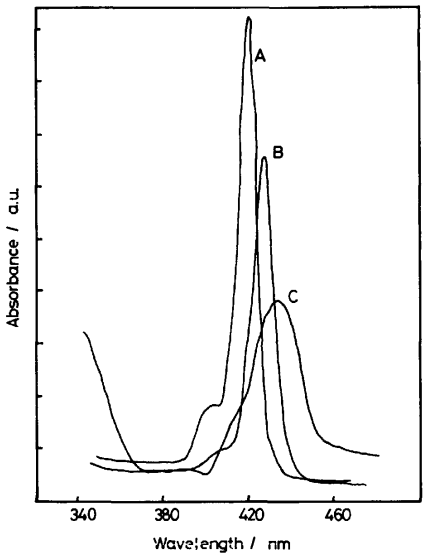

Fig. 8. Spectrum change of Zn-TPPS$_3$ by the addition of benzylviologen and reduced benzylviologen.
A: Zn-TPPS$_3$, B: Zn-TPPS$_3$+benzylviologen, C: Zn-TPPS$_3$+reduced benzylviologen.

reduced forms of viologen dyes. After comparing the reaction mechanisms reported for similar systems[7] and the above results, the following scheme containing complex-formation processes may be proposed:

$$\text{Zn-TPPS}_3 + \text{V}^{2+} \overset{K_1}{\rightleftharpoons} [\text{Zn-TPPS}_3\ \text{V}^{2+}]_{\text{complex}},$$

$$Zn\text{-}TPPS_3 + V^+ \overset{K_2}{\rightleftharpoons} [Zn\text{-}TPPS_3\ V^+]_{complex},$$

$$Zn\text{-}TPPS_3 \underset{k_{-3}}{\overset{h\nu, k_3}{\rightleftharpoons}} Zn\text{-}TPPS_3^*,$$

$$Zn\text{-}TPPS_3^* + V^{2+} \xrightarrow{k_4} Zn\text{-}TPPS_3^+ + V^+,$$

$$Zn\text{-}TPPS_3^+ + V^+ \xrightarrow{k_5} Zn\text{-}TPPS_3 + V^{2+},$$

$$Zn\text{-}TPPS_3^+ + RSH \xrightarrow{k_6} Zn\text{-}TPPS_3 + 1/2\ RSSR,$$

where V^{2+} and V^+ are oxidized and reduced forms of viologen dyes respectively. K_1 and K_2 are equilibrium constants. k_{-3}, k_4, k_5, and k_6 are rate constants, but k_3 is not, for it is a function of light flux. As the fraction of light absorption is small under these experimental conditions, *i.e.*, as the εCl value is small enough, ΦI_0 can be replaced by k_3[Zn-TPPS$_3$]$_0$.

If the complexes are not effective for viologen photoreduction, and if only free Zn-TPPS$_3$ is effective for this reaction, as Rougee *et al.* have previously established by a similar system,[6a] the following rate expression can be derived on the basis of the above reaction mechanism by the use of the steady-state approximation for [Zn-TPPS$_3$*] and [Zn-TPPS$_3^+$]:

$$v = \frac{d[V^+]}{dt} = \left(\frac{k_3[\text{Zn-TPPS}_3]_0}{1+K_1[V^{2+}]+K_2[V^+]}\right)\left(\frac{k_4[V^{2+}]}{k_{-3}+k_4[V^{2+}]}\right) \times \left(\frac{k_6[RSH]}{k_5[V^+]+k_6[RSH]}\right). \quad (9)$$

At the initial state of the reaction, V^+ grows linearly with the reaction time, for the rate of the back reaction, Zn-TPPS$_3^+$ reduction by V^+, is negligibly small at this stage. Equation (9) is rewritten as follows:

$$v = \left(\frac{k_3[\text{Zn-TPPS}_3]_0}{1+K_1[V^{2+}]}\right)\left(\frac{k_4[V^{2+}]}{k_{-3}+k_4[V^{2+}]}\right), \quad (10)$$

or

$$\frac{1}{v(1+K_1[V^{2+}])} = \left(\frac{1}{k_3[\text{Zn-TPPS}_3]_0}\right)\left(1+\frac{k_{-3}}{k_4[V^{2+}]}\right). \quad (11)$$

According to Eq. (11), $1/v(1+K_1[V^{2+}])$ should be linearly related to $1/[V^{2+}]$, and the intercept, $1/k_3$[Zn-TPPS$_3$]$_0$, should not depend on the type of viologen dye. The good linear relations and the same intercept in the cases of methylviologen and ethylviologen, as shown in Fig. 9, indicate that Eq. (9) is adequate. From the slopes and the intercept of the straight lines, the ratios of such rate constants as k_4/k_{-3} (as shown in Table 1) and k_3 were obtained. By using the values listed in Table 1 and k_3, the relations between v and $[V^{2+}]$ are obtained from Eq. (9); they are shown by the dotted lines in Figs. 2, 3, and 4. The experimental values agree well with the theoretial results except for some deviations in the case of ethylviologen. The good fittings of the curves show that the above-mentioned scheme explains the experimental results satisfactorily.

A typical time dependence of the viologen-radical concentration is shown in Fig. 10. The time course can be obtained by integrating Eq. (9). As $[V^{2+}]_0 \ll [RSH] \simeq$ constant under these experimental conditions, and if $K_1 \simeq K_2$, Eq. (9) can be rewritten as follows:

$$\left(\frac{k_4[V^{2+}]}{k_{-3}+k_4[V^{2+}]}\right)\frac{1}{v} = \left(\frac{k_3[\text{Zn-TPPS}_3]_0}{1+K_1[V^{2+}]_0}\right)^{-1}\left(1+\frac{k_5[V^+]}{k_6[RSH]}\right). \quad (12)$$

This relation is confirmed by the good linearity of the $\left(\frac{k_4[V^{2+}]}{k_{-3}+k_4[V^{2+}]}\right)\frac{1}{v}$ *vs.* $[V^+]$ plot, as is shown in Fig. 11. From the slope and the intercept of the straight line, the ratio of the rate constants, k_5/k_6, is obtained. By

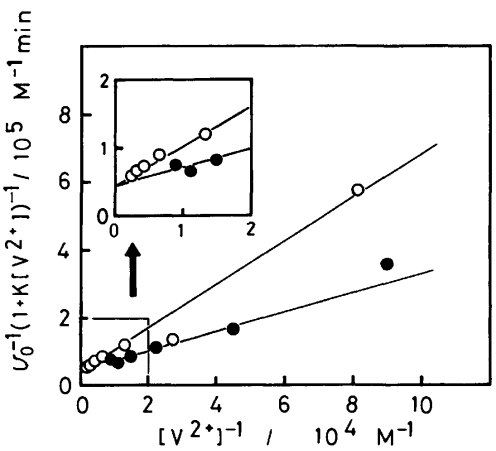

Fig. 9. Relation between $V_0^{-1}(1+K_1[V^{2+}])^{-1}$ and $[V^{2+}]^{-1}$.

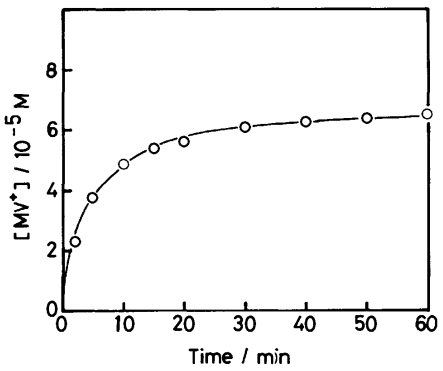

Fig. 10. Time dependence of reduced methylviologen concentration.
Reaction conditions: Zn-TPPS$_3$, 1.31×10^{-7} mol dm^{-3}; RSH, 0.85 mol dm^{-3}; methylviologen, 6.92×10^{-5} mol dm^{-3}, —: calculated; ○: observed.

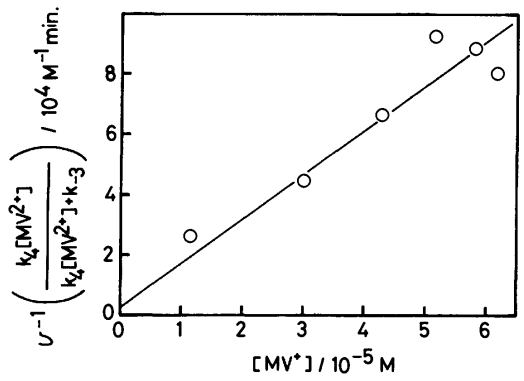

Fig. 11. Relation between $v^{-1}\left(\frac{k_4[MV^{2+}]}{k_4[MV^{2+}]+k_{-3}}\right)$ and $[MV^{2+}]$.

integrating Eq. (11), Eq. (13) can be obtained:

$$\frac{k_5[V^+]^2}{2k_6[RSH]} - \frac{k_{-3}}{k_4}[V^+]\left(1-\frac{k_5}{k_6[RSH]}\right) - \frac{k_4}{k_{-3}}\left(1+\frac{k_5}{k_6[RSH]}\right)\ln\left(\frac{[V^{2+}]_0-[V^+]}{[V^{2+}]_0}\right) = \frac{k_3[Zn\text{-}TPPS_3]_0}{1+K_1[V^{2+}]_0}t. \quad (13)$$

By using the constant values obtained from Figs. 9, 11, and Table 1, the time dependence of $[V^+]$ can be plotted on the basis of Eq. (13), as is shown by the solid line in Fig. 10. The good fit of the observed data (open circles) and the calculated data (solid line) indicates that Eq. (9) is adequate for expressing the kinetic data; it also supports the proposed reaction mechanism.

Photo-induced Hydrogen Evolution with Hydrogenase. As the reduced forms of methy-, ethyl-, propyl-, and benzylviologens have been known to produce hydrogen in the presence of a suitable catalyst, an attempt was made to produce hydrogen by the use of an electron-transfer system conbinning Zn-TPPS$_3$ and viologen dyes.[8]

By the addition of hydrogenase to the system containing RSH, Zn-TPPS$_3$, and viologen dye, photo-induced hydrogen evolution was carried out. Experiments were preformed by using higher initial concentrations of viologen dye in order to minimize the free Zn-TPPS$_3$, where more than 70% of the porphyrin is complexed, and also by using the optimum concentration, where the maximum reduction rate of viologen dye is given as is shown in Figs. 2, 3, and 4. In these experiments, an excess amount of hydrogenase was used to make the rate-determining step of the hydrogen-evolution reaction to the photoreduction of viologen dyes. As is shown in Figs. 12 and 13, a continuous hydrogen evolution was observed in both cases. The higher hydrogen evolution rate was obtained by using the optimum concentration of the viologen dyes.

We wish to express our appreciation to Professor Tominaga Keii and Professor Yoshio One for their stimulating and helpful discussions.

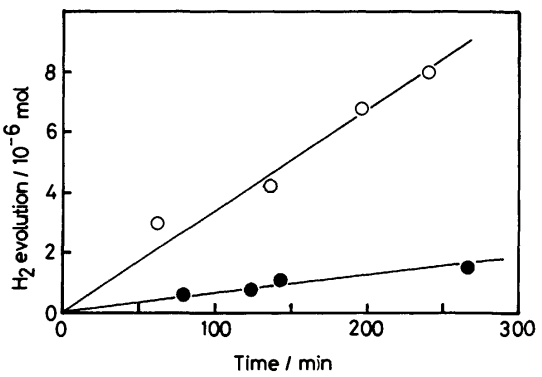

Fig. 12. Time dependence of hydrogen evolution. Reaction conditions; Zn-TPPS$_3$, 1.31×10^{-7} mol dm^{-3}; RSH, 0.21 mol dm^{-3}; ethylviologen, 5.53×10^{-4} mol dm^{-3} (●), 2.22×10^{-5} mol dm^{-3} (○); hydrogenase, 1.0 ml; reaction temp, 30°C.

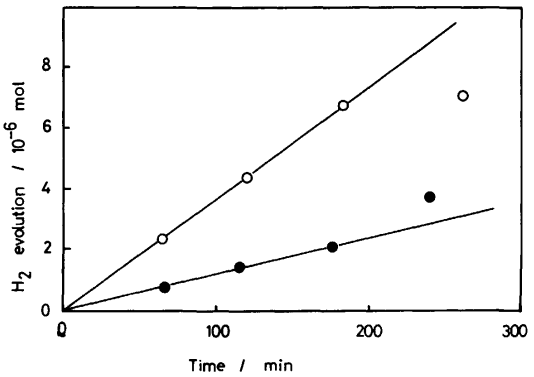

Fig. 13. Time dependence of hydrogen evolution. Reaction conditions; Zn-TPPS$_3$, 1.31×10^{-7} mol dm^{-3}; RSH, 0.21 mol dm^{-3}; methylviologen, 3.46×10^{-4} mol dm^{-3} (●), 7.40×10^{-5} mol dm^{-3} (○); hydrogenase, 1.0 ml; reaction temp, 30°C.

References

1) a) J. -M. Lehn and J. P. Sauvage, *Nouv. J. Chim.*, **1**, 499 (1977); b) M. Kirch, J. -M. Lehn, and J. P. Sauvage, *Helv. Chim. Acta*, **62**, 1345 (1979); c) K. Kalyanasundaram, J. Kiwi, and M. Gratzel, *ibid.*, **61**, 2720 (1978); d) K. Kalyanasundaram and M. Gratzel, *J. Chem. Soc., Chem. Commun.*, **1979**, 1137; e) A. Moradpour, E. Amouyal, P. Keller, and H. Kagan, *Nouv. J. Chim.*, **2**, 547 (1978); f) A. I. Krasna, *Photochem. Photobiol.*, **29**, 267 (1979); g) I. Okura and N. Kim-Thuan, *J. Mol. Catal.*, **5**, 311 (1979); h) I. Okura, S. Nakamura, N. Kim-Thuan, and K. Nakamura, *ibid.*, **6**, 261 (1979); i) I. Okura and N. Kim-Thuan, *J. Chem. Soc., Chem. Commun.*, **1980**, 84; j) I. Okura and N. Kim-Thuan, *J. Chem. Soc., Faraday Trans. 1*, **76**, 2209 (1980); k) K. Takuma, M. Kajiwara, and T. Matsuo, *Chem. Lett.*, **1977**, 1199; l) I. Okura and N. Kim-Thuan, *J. Mol. Catal.*, **6**, 227 (1979); m) I. Okura, M. Takeuchi, and N. Kim-Thuan, *Chem. Lett.*, **1980**, 765; n) K. Kalyanasundaram and M. Gratzel, *Helv. Chim. Acta*, **63**, 478 (1980); o) T. Yagi, Proc. Natl. Acad. Sci., U.S.A., **73**, 2947 (1976).

2) a) J. R. Darwent, P. Douglas, A. Harriman, G. Porter, and M. -C. Richoux, *Coord. Chem. Rev.*, **44**, 83 (1982), and the references therein; b) A. B. P. Lever, B. S. Ramaswamy, and S. Licoccia, *J. Photochem.*, **19**, 173 (1982).

3) A. G. Evans, J. P. Evans, and M. W. Baker, *J. Chem. Soc., Perkin Trans. 2*, **1977**, 1787.

4) T. Yagi, M. Honya, and N. Tamiya, *Biochim. Biophys. Acta*, **153**, 699 (1968).

5) T. Yagi, *J. Biochem.*, **68**, 694 (1970).

6) a) M. Rougee, T. Ebbesen, F. Ghetti, and R. V. Bensasson, *J. Phys. Chem.*, **86**, 4404 (1982); b) J. A. Shelnutt, *J. Am. Chem. Soc.*, **103**, 4275 (1981); c) I. Okura, S. Aono, M. Takeuchi, and S. Kusunoki, *Bull. Chem. Soc. Jpn.*, **55**, 3637 (1982).

7) a) C. R. Bock, T. J. Meyer, and D. G. Whitten, *J. Am. Chem. Soc.*, **96**, 4710 (1974); b) H. D. Gafney and A. W. Anderson, *ibid.*, **94**, 8238 (1972); c) R. C. Young, T. J. Meyer, and D. G. Whitten, *ibid.*, **97**, 4781 (1975).

8) I. Okura, S. Aono, and S. Kusunoki, *Inorg. Chim. Acta*, **71**, 77 (1983).

The Molecular Structures of (+)-6-Benzylsparteine, (Ethyl)(bromo)[(+)-6-benzylsparteine]magnesium(II),† and Dibromo[(+)-6-benzylsparteine]magnesium(II).†† Structure and Reactivity of the Grignard Reagent-(−)-Sparteine Derivative Complexes for Asymmetric Selective Polymerization of Racemic Methacrylates.

Hiroyuki KAGEYAMA, Kunio MIKI, Yasushi KAI, Nobutami KASAI,*
Yoshio OKAMOTO,** and Heimei YUKI**,†††
Department of Applied Chemistry, Faculty of Engineering, Osaka University, Yamadaoka, Suita, Osaka 565
***Department of Chemistry, Faculty of Engineering Science, Osaka University, Machikaneyama, Toyonaka, Osaka 560*
(Received October 19, 1983)

(+)-6-Benzylsparteine (**a**) crystallizes in orthorhombic systems; $P2_12_12_1$, a=10.711(1), b=25.868(4), c=6.804(1) Å, and Z=4; EtMgBr-(+)-6-benzylsparteine (**b**) also belongs to orthorhombic system; $P2_12_12_1$, a=11.020(4), b=23.660(10), c=8.666(6) Å and Z=4; and $MgBr_2$-(+)-6-benzylsparteine toluene solvate (**c**), orthorhombic system; $P2_12_12_1$, a=16.654(3), b=19.723(4), c=8.637(2) Å and Z=4. The structure of **a** was solved by the direct method and those of **b** and **c** by the heavy atom method. Refinements were carried out by the block-diagonal least-squares procedure; R values are: (**a**) 0.055. (**b**) 0.169, and (**c**) 0.118, respectively for 1342, 1445, and 1501 reflections. The **a** molecule takes a one-boat form, whereas by coordination to the Mg atom it changes into all-chair form in **b** and **c** molecules. The Mg atom has a distorted tetrahedral geometry; **b**, Mg-N=2.13(4) and 2.19(4), Mg-C 2.34(5) and Mg-Be=2.506(16) Å and N-Ng-N=83.1(14)°; **c**, Mg-N=2.08(3) and 2.17(3), Mg-Br=2.454(12) and 2.473(12) Å and N-Mg-N=85.8(10)°. The structures of these molecules are compared with those of (−)-sparteine complexes with EtMgBr, t-BuMgCl, and $MgCl_2$. On the basis of the molecular structures determined the activity of these Grignard reagent-(−)-sparteine derivatives for the enantiomer-selective polymerization of MBMA is discussed.

Asymmetric selective (enantiomer-selective) polymerization of racemic (*RS*)-α-methylbenzyl methacrylate (MBMA) has been investigated with homogeneous Grignard reagent-(−)-sparteine derivative catalysts in toluene at −78 °C.[1] Sparteines combined with the Grignard reagents were (−)-sparteine, (−)-α-isosparteine, (−)-6-ethylsparteine, (+)-6-benzylsparteine, (−)-Δ^5-dehydrosparteine, and (−)-$\Delta^{5,11}$-didehydrosparteine. Among the complexes formed between Grignard reagent and (−)-sparteine (or its derivatives), EtMgBr-(−)-sparteine has a high activity, whereas t-BuMgCl-(−)-sparteine and EtMgBr-(−)-α-isosparteine has no activity, in the asymmetric selective polymerization of racemic (*RS*)-MBMA (Table 1). EtMgBr-(+)-6-benzylsparteine was also found active for the polymerization mentioned above but it is less active than EtMgBr-(−)-sparteine.

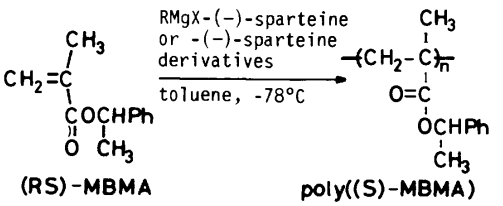

In order to obtain informations on the structural dependence of the reactivity and monomer-selectivity of these catalysts, molecular structures of EtMgBr-(−)-sparteine[2], t-BuMgCl-(−)-sparteine[3] and related complex $MgCl_2$-(−)-sparteine[3], and EtMgBr-(−)-α-

Table 1. Asymmetric selective polymerization of (*RS*)MBMA with Grignard reagent-(−)-sparteine(or sparteine derivative) complexes in toluene at −78 °C[1]

Sparteine ligand and Grignard reagent	Time h	Yield %	$[\alpha]_D^{20}$(OP) polymer °(%)	$[\alpha]_D^{20}$(OP) recovered monomer °(%)	Tacticity/% I	H	S
(−)-Sparteine							
EtMgBr	1	41.4	−102.2(82)	+30.4(57)	94	5	1
t-BuMgCl	96	0.4	0	0 (0)			
(+)-6-Benzylsparteine							
EtMgBr	99	14.1	−82.9(66)	+6.2(12)	77	14	9
(−)-α-Isosparteine							
EtMgBr	22	0					

† Abbreviated as EtMgBr-(+)-6-benzylsparteine.
†† Abbreviated as $MgBr_2$-(+)-6-benzylsparteine.
††† Present address, Tezukayama-Gakuin Women's Junior College, Tezukayama, Sumiyoshi-ku, Osaka 558.

isosparteine[4] have been determined by means of X-ray diffraction. This paper deals with the molecular structure of EtMgBr-(+)-6-benzylsparteine and related complex $MgBr_2$-(+)-benzylsparteine. Interests on the molecular conformation promoted the crystal structure analysis of (+)-6-benzylsparteine.

Experimental

(+)-6-Benzylsparteine was recrystallized from a methanol solution. EtMgBr-(+)-6-benzylsparteine was prepared by mixing the crystalline powder of (+)-6-benzylsparteine and ether solution of EtMgBr under nitrogen atmosphere, because the reaction of a toluene solution of (+)-6-benzylsparteine and ether solution of EtMgBr gave $MgBr_2$-(+)-6-benzylsparteine instead of EtMgBr-(+)-6-benzylsparteine.

Crystals of (+)-6-benzylsparteine, EtMgBr-(+)-6-benzylsparteine, and $MgBr_2$-(+)-6-benzylsparteine used had approximate dimensions of 0.38×0.25×0.23, 0.68×0.33×0.25, and 0.13×0.25×0.5 mm, respectively. Crystals of EtMgBr-(+)-6-benzylsparteine and $MgBr_2$-(+)-6-benzylsparteine are both sensitive to moisture in air, and they were sealed in glass capillary tubes under nitrogen. Each crystal was mounted on a Rigaku automated, four-circle diffractometer. Nickel-filtered Cu $K\alpha$ radiation (λ=1.5418 Å) was used for the former organic crystal, and graphite monochromatized Mo $K\alpha$ radiation (λ=0.7107 Å) for the later two Mg-complexes, respectively. Unit-cell dimensions of each crystal were determined by the least-squares fit using 2θ values of high order, strong reflections.

Crystal Data. (+)-6-Benzylsparteine (**a**), $C_{22}H_{32}N_2$, M 324.5, orthorhombic, space group $P2_12_12_1$, a=10.711(1), b=25.868(4), c=6.804(1) Å, V=1885.1(4) Å^3, D_c=1.143 g cm^{-3} for Z=4, μ(Cu $K\alpha$)=5.07 cm^{-1}; EtMgBr-(+)-6-benzylsparteine (**b**), $C_{24}H_{37}N_2MgBr$, M 457.8, orthorhombic, space group $P2_12_12_1$, a=11.020(4), b=23.660(10), c=8.666(6) Å, V=2260(2) Å^3, D_c=1.350 g cm^{-3} for Z=4, μ(Mo $K\alpha$)=19.7 cm^{-1}; $MgBr_2$-(+)-6-benzylsparteine toluene solvate(c), $C_{22}H_{32}N_2MgBr_2 \cdot C_7H_8$, $F.W.$ 600.8, orthorhombic, space group $P2_12_12_1$, a=16.654(3), b=19.723(4), c=8.637(2) Å, V=2836.8(9) Å^3, D_c=1.407 g cm^{-3} for Z=4, μ(Mo $K\alpha$)=30.7 cm^{-1}.

Reflection intensities were measured by the θ-2θ scan technique at a 2θ rate of 4° min^{-1}. The scan widths were $\Delta 2\theta$=(2.0+0.3tanθ)° for the former organic crystal and $\Delta 2\theta$=(2.4+0.7tanθ)° for the latter two Mg-complexes. Backgrounds were counted for 7.5 s at both ends of a scan. Four standard reflections were measured after every 60 reflections, which showed less than 5% fluctuations throughout the data collection. A total of 1408 reflections was measured for (+)-6-benzylsparteine, of which 1346 were non-zero reflections. The reflection profiles of EtMgBr-(+)-sparteine were not so sharp, and only 1445 reflections ($|F_o|>3\sigma(F_o)$) out of 2369 measured were used for the structure analysis. For $MgBr_2$-(+)-6-benzylsparteine 2942 reflections were measured but only 1501($|F_o|>3\sigma(F_o)$) could be used. Usual Lp corrections were applied but corrections for absorption and extinction were ignored.

Structure Solution and Refinement

(a) (+)-6-Benzylsparteine. The structure was solved by the direct method (*MULTAN* 78),[5] and all the C and N atoms could be located on the E map. The refinement of the structure was carried out by the block-diagonal least-squares procedure (*HBLS* V).[6] The function minimized was $\sum w(\Delta F)^2$. During the course of the refinement four strong reflections (200, 230, 031, and 160), which were considered largely affected by the extinction, were excluded. Hydrogen atoms were located on a difference Fourier map, which were refined isotropically while the other anisotropically. The final R index was 0.055 (R_W=0.092) for 1342 non-zero reflections. The weighting schemes used at the final stage of the refinement were $w=\{\sigma^2(F_o)+0.01024|F_o|^2\}^{-1}$ for $|F_o|>0$ and w=0.63654 for $|F_o|=0$. The final atomic parameters are listed in Table 2.††††

(b) EtMgBr-(+)-6-benzylsparteine. The Br atom

Table 2. Final atomic positional parameters, of (+)-6-benzylsparteine, with estimated standard deviaitions in parentheses

a) Anisotropic atoms.

Atom	x	y	z	B_{eq}[12]/Å^2
N(1)	0.9110(3)	0.4216(2)	0.0795(6)	3.9
N(2)	0.6163(3)	0.3744(2)	-0.1125(5)	3.0
C(2)	0.4936(4)	0.3781(2)	-0.2008(6)	3.9
C(3)	0.4005(4)	0.4050(2)	-0.0636(8)	4.8
C(4)	0.3965(4)	0.3785(2)	0.1376(7)	4.1
C(5)	0.5299(4)	0.3734(2)	0.2187(6)	3.2
C(6)	0.6218(4)	0.3464(2)	0.0767(6)	2.9
C(7)	0.7575(4)	0.3515(2)	0.1553(6)	3.0
C(8)	0.8493(4)	0.3273(2)	0.0108(6)	3.5
C(9)	0.8424(4)	0.3592(2)	-0.1764(6)	3.4
C(10)	0.7103(4)	0.3581(2)	-0.2558(6)	3.5
C(11)	0.8921(4)	0.4150(2)	-0.1343(7)	3.5
C(12)	1.0145(4)	0.4246(2)	-0.2409(8)	4.4
C(13)	1.0676(5)	0.4777(2)	-0.1915(10)	6.0
C(14)	1.0763(5)	0.4856(2)	0.0296(10)	6.0
C(15)	0.9518(5)	0.4740(2)	0.1277(9)	5.1
C(17)	0.7964(4)	0.4091(2)	0.1882(6)	3.7
C(18)	0.5837(4)	0.2878(2)	0.0541(6)	3.2
C(19)	0.5941(4)	0.2549(2)	0.2381(6)	3.0
C(20)	0.6943(4)	0.2214(2)	0.2642(7)	3.7
C(21)	0.7019(5)	0.1902(2)	0.4323(7)	4.3
C(22)	0.6103(5)	0.1923(2)	0.5734(7)	4.4
C(23)	0.5101(4)	0.2246(2)	0.5475(7)	4.1
C(24)	0.5009(4)	0.2552(2)	0.3801(7)	3.7

b) Isotropic atoms.

Atom	x	y	z	B/Å^2
H(2a)	0.464(5)	0.341(2)	-0.226(8)	3.4(11)
H(2b)	0.497(4)	0.401(2)	-0.327(7)	2.7(10)
H(3a)	0.316(5)	0.405(2)	-0.123(8)	3.0(10)
H(3b)	0.427(4)	0.442(2)	-0.047(8)	3.3(11)
H(4a)	0.353(5)	0.344(2)	0.122(8)	3.0(10)
H(4b)	0.349(5)	0.400(2)	0.234(9)	3.8(11)
H(5a)	0.527(4)	0.353(2)	0.343(7)	2.9(10)
H(5b)	0.562(5)	0.409(2)	0.249(8)	2.7(10)
H(7)	0.761(4)	0.333(2)	0.283(7)	2.0(9)
H(8a)	0.825(4)	0.290(2)	-0.017(6)	1.8(9)
H(8b)	0.938(4)	0.328(2)	0.067(7)	2.3(9)
H(9)	0.898(5)	0.345(2)	-0.282(8)	3.6(11)
H(10a)	0.706(5)	0.385(2)	-0.368(8)	3.3(11)
H(10b)	0.691(4)	0.322(2)	-0.298(7)	2.7(10)
H(11)	0.826(4)	0.441(2)	-0.178(7)	2.3(10)
H(12a)	1.002(5)	0.422(2)	-0.390(9)	3.5(11)
H(12b)	1.077(5)	0.398(2)	-0.197(8)	3.5(11)
H(13a)	1.005(5)	0.504(2)	-0.256(8)	4.7(13)
H(13b)	1.151(6)	0.482(2)	-0.264(8)	4.5(12)
H(14a)	1.103(5)	0.523(2)	0.063(8)	3.5(11)
H(14b)	1.141(5)	0.461(2)	0.087(9)	3.9(11)
H(15a)	0.887(5)	0.501(2)	0.076(8)	3.5(11)
H(15b)	0.957(6)	0.478(2)	0.281(9)	4.6(13)
H(17a)	0.722(4)	0.430(2)	0.139(8)	2.6(10)
H(17b)	0.815(5)	0.419(2)	0.332(9)	3.9(12)
H(18a)	0.637(5)	0.271(2)	-0.059(9)	3.5(11)
H(18b)	0.493(4)	0.286(2)	0.003(7)	2.4(10)
H(20)	0.763(4)	0.221(2)	0.156(7)	1.5(9)
H(21)	0.779(4)	0.166(2)	0.449(7)	3.2(11)
H(22)	0.618(4)	0.171(2)	0.698(7)	2.5(10)
H(23)	0.445(5)	0.226(2)	0.647(9)	3.2(11)
H(24)	0.420(5)	0.278(2)	0.369(8)	3.0(10)

was located by three-dimensional Patterson function. Positions of the Mg, N, and C atoms except the C(16) were determined by the subsequent Fourier synthesis. The structure was first refined isotropically by the block-diagonal least-squares procedure (*HBLS* V) with unit weight. The temperature factor of the C(1) atom fell on a negative value, and it was corrected and fixed as B=4.67 Å^2 which was derived from the Wilson statistics of structure amplitudes. The C(16) atom could be located on a difference Fourier map and fixed at the position. At the final stage of the anisotropic refinement the anomalous dispersion of all the non-hydrogen atoms was considered. However, the R index converged to a rather high value of 0.169(R_w=0.188) for 1445 reflections. The final atomic parameters are listed in Table 3.††††

(c) $MgBr_2$-(+)-6-benzylsparteine Toluene Solvate. The crystal of this complex was expected as that of EtMgBr-(+)-6-benzylsparteine, but the three-dimensional Patterson function could not be interpreted well. Three big peaks, found on the E map based on the phases using the *MULTAN* 78 program, supported to interprete the Patterson function as the complex was $MgBr_2$-(+)-6-benzylsparteine. The N and C atoms were then located on the Fourier synthesis based on the phases of the Mg and two Br atoms. The structure was refined by the *HBLS* V program with unit weight. Subsequent Fourier and difference syntheses revealed the location of seven C atoms of toluene, the solvent of crystallization. None of the hydrogen atoms could be located. The R index was 0.118 (R_w= 0.126) for 1501 reflections at the final stage of the anisotropic refinement: the anomalous dispersion of Br, Mg, N, and C atoms was considered. The final atomic parameters are given in Table 4.††††

Table 3. Final atomic positional parameters, of EtMgBr-(+)-6-benzylsparteine, with estimated standard deviations in parentheses

a) Anisotropic atoms.

Atom	x	y	z	B_{eq}[12]/Å^2
Br	0.3580(4)	0.3635(2)	-0.0705(6)	5.3
Mg	0.536(2)	0.3805(6)	0.1038(15)	4.0
N(1)	0.458(3)	0.3966(11)	0.325(4)	3.2
N(2)	0.639(3)	0.3164(11)	0.231(3)	2.8
C(2)	0.714(3)	0.2910(13)	0.102(5)	3.5
C(4)	0.549(4)	0.2211(16)	0.056(6)	5.3
C(5)	0.483(4)	0.2481(16)	0.182(5)	3.7
C(6)	0.567(4)	0.2722(16)	0.308(4)	3.6
C(7)	0.494(3)	0.2996(14)	0.442(5)	3.2
C(8)	0.579(3)	0.3263(14)	0.567(6)	4.4
C(9)	0.649(4)	0.3747(14)	0.467(6)	6.0
C(10)	0.712(3)	0.3490(13)	0.334(4)	2.1
C(11)	0.560(4)	0.4291(17)	0.420(6)	5.5
C(12)	0.509(4)	0.4547(13)	0.566(6)	4.0
C(13)	0.423(4)	0.5041(18)	0.513(5)	4.7
C(14)	0.312(4)	0.4710(16)	0.448(6)	5.5
C(15)	0.359(4)	0.4440(15)	0.287(5)	4.3
C(17)	0.397(4)	0.3451(16)	0.401(6)	5.6
C(18)	0.640(4)	0.2246(16)	0.373(5)	4.8
C(19)	0.584(3)	0.1763(14)	0.459(4)	2.6
C(20)	0.575(3)	0.1737(14)	0.621(5)	3.9
C(21)	0.532(4)	0.1274(15)	0.703(5)	4.8
C(22)	0.489(4)	0.0796(17)	0.613(6)	5.4
C(23)	0.490(4)	0.0803(16)	0.456(6)	5.0
C(24)	0.542(4)	0.1261(12)	0.373(5)	3.5

b) Isotropic atoms.

Atom	x	y	z	B/Å^2
C(3)	0.650(4)	0.2698(14)	-0.021(4)	4.0(8)
C(1)	0.674(4)	0.4436(16)	-0.007(5)	4.7(9)
C(16)	0.765	0.4218	-0.100	15(3)

†††† Tables of observed and calculated structure factors and anisotropic thermal parameters of (+)-6-benzylsparteine, EtMgBr-(+)-6-benzylsparteine, and $MgBr_2$-(+)-6-benzylsparteine toluene solvate, are kept at the Chemical Society of Japan, Document No. 8417.

Table 4. Final atomic positional parameters, of $MgBr_2$-(+)-6-benzylsparteine toluene solvate, with estimated standard deviations in parentheses

Atom	x	y	z	B_{eq}[12]/Å^2
Br(1)	0.4524(3)	0.1648(3)	-0.4109(6)	6.7
Br(2)	0.3287(3)	0.1758(3)	-0.8188(6)	7.2
Mg	0.3250(7)	0.1949(5)	-0.5359(12)	3.9
N(1)	0.235(2)	0.141(2)	-0.422(3)	3.3
N(2)	0.247(2)	0.282(2)	-0.507(3)	3.0
C(2)	0.289(2)	0.336(2)	-0.594(5)	5.0
C(3)	0.374(3)	0.351(2)	-0.526(4)	4.8
C(4)	0.372(2)	0.362(2)	-0.336(4)	3.8
C(5)	0.317(2)	0.308(2)	-0.269(4)	3.7
C(6)	0.238(2)	0.301(2)	-0.336(4)	3.8
C(7)	0.181(2)	0.245(2)	-0.263(3)	2.6
C(8)	0.099(2)	0.237(2)	-0.338(4)	3.7
C(9)	0.118(2)	0.211(2)	-0.513(4)	4.2
C(10)	0.174(2)	0.268(2)	-0.594(4)	3.8
C(11)	0.163(2)	0.139(2)	-0.512(4)	3.3
C(12)	0.093(2)	0.088(2)	-0.461(5)	5.4
C(13)	0.136(2)	0.016(2)	-0.447(4)	4.3
C(14)	0.207(2)	0.018(2)	-0.342(6)	5.9
C(15)	0.270(2)	0.071(2)	-0.389(5)	4.1
C(17)	0.226(2)	0.172(2)	-0.259(4)	4.5
C(18)	0.188(3)	0.371(2)	-0.328(5)	5.4
C(19)	0.161(2)	0.389(2)	-0.157(4)	3.1
C(20)	0.085(2)	0.382(2)	-0.117(4)	3.7
C(21)	0.055(3)	0.402(2)	0.027(5)	7.4
C(22)	0.114(3)	0.433(2)	0.132(5)	6.4
C(23)	0.189(3)	0.444(2)	0.087(5)	6.1
C(24)	0.218(3)	0.422(2)	-0.072(5)	5.8
C(25)	-0.055(4)	0.023(3)	-0.102(6)	11.6
C(26)	-0.017(4)	0.077(3)	-0.045(6)	11.5
C(27)	0.060(3)	0.069(3)	0.015(6)	9.1
C(28)	0.098(4)	0.124(3)	0.072(6)	10.9
C(29)	0.059(4)	0.198(3)	0.072(7)	12.6
C(30)	-0.006(3)	0.199(4)	0.010(5)	10.4
C(31)	-0.057(3)	0.139(2)	-0.053(5)	6.4

Atomic scattering factors[7] and coefficients of anomalous dispersion[8] used were taken from International Tables for X-Ray Crystallography, Vol. IV. All the computations were done on an ACOS 700S computer at the Crystallographic Research Center, Institute for Protein Research, Osaka University.

Results and Discussion

Molecular Structures. Perspective views(*ORTEP* II)[9] of (+)-6-benzylsparteine, EtMgBr-(+)-6-benzylsparteine, and $MgBr_2$-(+)-6-benzylsparteine molecules are depicted in Figs. 1, 2, and 3, respectively. Bond lengths and bond angles in these complexes are given in Figs. 4, 5 and 6, respectively.

(a) (+)-6-Benzylsparteine: The remarkable feature of the structure is that this molecule takes a one-boat form: six-membered ring made by the C(7), C(8), C(9), C(11), N(1), and C(17) atoms is in a boat form, whereas all of the other rings in chair forms. The C(2)-N(2)-C(6)-[115.5(3)°] and C(11)-N(1)-C(15) angles[111.7(4)°] are respectively larger than the corresponding angles in

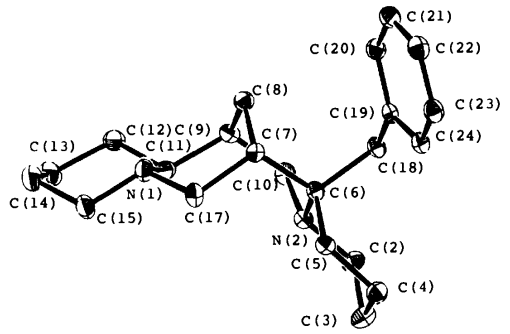

Fig. 1. A perspective view of (+)-6-benzylsparteine molecule with the numbering scheme of atoms. Non-hydrogen atoms are drawn as thermal ellipsoids with 20% probability level.[9]

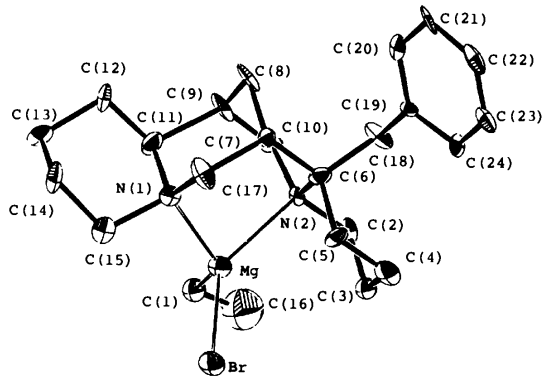

Fig. 2. A perspective view of EtMgBr-(+)-6-benzylsparteine molecule with the numbering scheme of atoms. Non-hydrogen atoms are drawn as thermal ellipsoids with 20% probability level.[9]

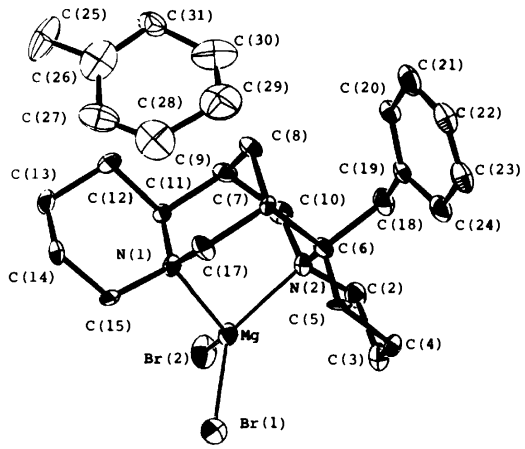

Fig. 3. A perspective view of $MgBr_2$-(+)-6-benzylsparteine and toluene, the crystalline solvent molecules with the numbering scheme of atoms. Non-hydrogen atoms are drawn as thermal ellipsoids with 20% probability level.[9]

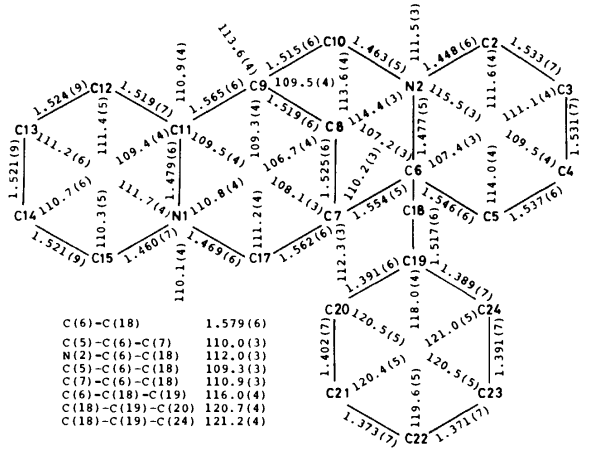

Fig. 4. Selected bond lengths [l/Å] and bond angles [ϕ/°] in (+)-6-benzylsparteine molecule.

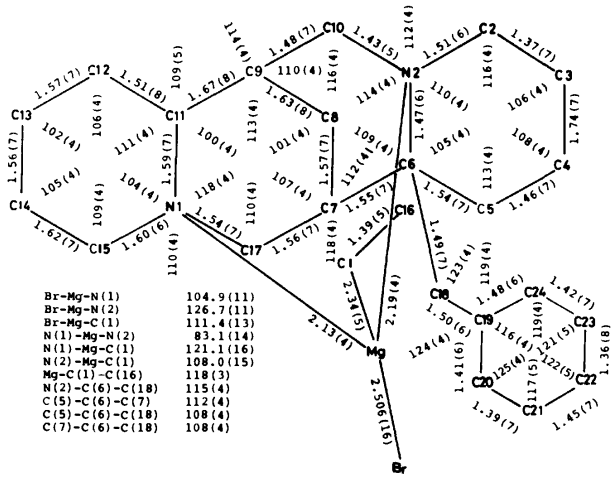

Fig. 5. Selected bond lengths [l/Å] and bond angles [ϕ/°] in EtMgBr-(+)-6-benzylsparteine molecule.

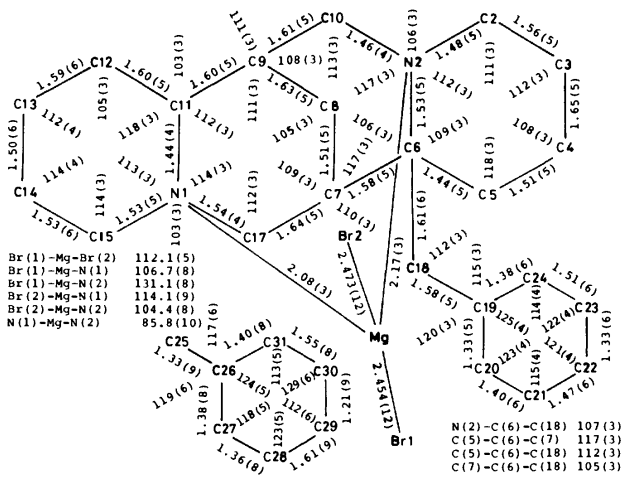

Fig. 6. Selected bond lengths [l/Å] and bond angles [ϕ/°] in $MgBr_2$-(+)-6-benzylsparteine and toluene, the crystalline solvent molecule.

sparteine skeleton in 17β-methylsparteine diperchlorate [109.6(6) and 107.9(5)°][10] and episparteine N(16)-oxide sesquiperchlorate [110.6(3) and 109.0(3)°],[11] of which the sparteine moieties have one-boat form. Whereas the C(5)-C(6)-(7) angle [110.0(3)°] is smaller than those [115.8(7) and 116.5(3)°] in the two sparteine derivatives mentioned below.

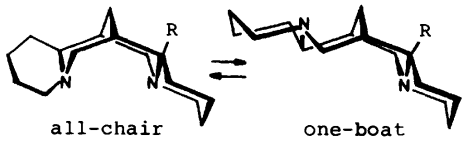

(b) EtMgBr-(+)-6-benzylsparteine: The sparteine skeleton in the (+)-6-benzylsparteine moiety has an all-chair form, and its structure is similar to those found in EtMgBr-(−)-sparteine,[2] *t*-BuMgCl-(−)-sparteine,[3] and $MgCl_2$-(−)-sparteine.[3] The spatial arrangement of the alkyl and halogen ligands the sparteine skeleton through the Mg atom is, similar to that in *t*-BuMgCl-(−)-sparteine,[3] reverse to that in EtMgBr-(−)-sparteine.[2] The coordination geometry around the Mg atom is distorted tetrahedral, which is similar to those observed in Grignard reagent-(−)-sparteine complexes.

(c) $MgBr_2$-(+)-6-benzylsparteine: The sparteine skeleton in the present complex also has an all-chair conformation. Distorted tetrahedral geometry is observed around the Mg atom.

(d) Structure of the Sparteine Skeleton in RMgX-(−)-sparteine Derivative Complexes. Through the five

Table 5. Comparison of the coordination geometry around the Mg atom with estimated standard deviations in parentheses

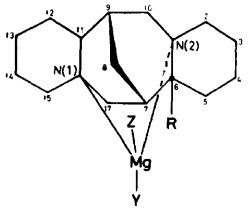

(a) Bond length[l/Å]

	Mg-N(1)	Mg-N(2)	Mg-Y			Mg-Z		
			Mg-C	Mg-Cl	Mg-Br	Mg-C	Mg-Cl	Mg-Br
EtMgBr-(−)-sparteine	2.14(2)	2.16(3)	2.24(3)					2.482(9)
t-BuMgCl-(−)-sparteine	2.171(12)	2.175(12)		2.332(7)		2.19(2)		
$MgCl_2$-(−)-sparteine	2.150(9)	2.160(9)		2.269(5)			2.279(6)	
EtMgBr-(+)-6-benzylsparteine	2.13(4)	2.19(4)			2.506(16)	2.34(5)		
$MgBr_2$-(+)-6-benzylsparteine	2.08(3)	2.17(3)			2.452(12)			2.473(12)
EtMgBr-(−)-α-isosparteine	2.165(13)	2.195(13)	2.224(15)					2.506(6)

(b) Bond angle[ϕ/°]

	N(1)-Mg-N(2)	Y-Mg-N(1)	Y-Mg-N(2)	Z-Mg-N(1)	Z-Mg-N(2)	Y-Mg-Z
EtMgBr-(−)-sparteine	84.0(8)	114.4(10)	129.6(10)	108.3(6)	103.4(7)	115.1(8)
t-BuMgCl-(−)-sparteine	83.9(5)	100.8(4)	117.4(4)	119.5(6)	116.2(6)	114.7(5)
$MgCl_2$-(−)-sparteine	85.0(4)	108.0(3)	123.3(3)	112.6(3)	105.8(3)	117.6(2)
EtMgBr-(+)-6-benzylsparteine	83.1(14)	104.9(11)	126.7(11)	121.1(16)	108.0(15)	111.4(13)
$MgBr_2$-(+)-6-benzylsparteine	85.8(10)	106.7(8)	131.1(8)	114.1(9)	104.4(8)	112.1(5)
EtMgBr-(−)-α-isosparteine	83.9(5)	106.1(6)	129.7(6)	122.9(4)	101.4(4)	112.1(5)

RMgX-(−)-sparteine derivative complexes except EtMgBr-(−)-α-isosparteine, the (−)-sparteine ligand and sparteine skeleton of (+)-6-benzylsparteine ligand take all-chair form, and all of them have the same structure: corresponding bond lengths and bond angles are respectively equal within the range of error.

The (−)-sparteine ligand (or sparteine skeleton) consists of four fused N-containing six-membered rings; the fusion of N(1)-containing ring to the central symmetrically-fused two rings is different from that of N(2)-containing ring. The approximately Λ-shaped (−)-sparteine ligand has a cavity in which a Mg atom can coordinate. The C(7)-side of the cavity is spatially less open than the C(9)-side because of the unsymmetrical structure of (−)-sparteine ligand.

The (−)-α-isosparteine ligand has a C_2 symmetry. A half of its cavity is very similar to that of the C(7)-side of (−)-sparteine. The whole cavity of this ligand is more likely Λ-shaped and spatially less open than that of (−)-sparteine.

(e) Coordination Geometry around the Mg Atom in RMgX-(-)-sparteine Derivative Complexes: The geometry around the Mg atom is summarized in Table 5. In each complex the Mg atom has a distorted tetrahedral geometry. As shown in Table 5, two Mg-N bond lengths are equal [av. 2.15 Å], and the N-Mg-N angle is sharp and solid [83.1—85.8, av. 84.3°]. Regardless the geometrical relation of the alkyl and halogen ligands to the sparteine skeleton mentioned before, the Y-Mg-N(2) angle is larger than the Y-Mg-N(1), whereas the Z-Mg-N(2) angle is smaller than the Z-Mg-N(1). The Y-Mg-Z angle is slightly larger than the tetrahedral angle. Among the Mg-Y and Mg-Z bond lengths, the Mg-Cl lengths in *t*-BuMgCl-(−)-sparteine [2.332(7) Å] is much longer than those in dichloride, $MgCl_2$-(−)-sparteine [2.269(5) Å]. Similarly, the Mg-Br bond lengths in EtMgBr-(−)-sparteine, EtMgBr-α-isosparteine and EtMgBr-(+)-6-benzylsparteine look like longer than those in dibromide, $MgBr_2$-(+)-6-benzylsparteine though it is not fully significant. The Mg-C bond lengths in four complexes are equal [2.19(2)—2.34(5), av. 2.25 Å] within the range of error.

(f) Structure-dependence of Reactivity of RMgX-(−)-sparteine Derivative Complexes for the Asymmetric Selective Polymerization of (RS)-*MBMA*: In Table 6 summarized are molecular structures of EtMgBr-(−)-sparteine,[2] *t*-BuMgCl-(−)-sparteine,[3] EtMgBr-(+)-6-benzylsparteine (present study), and EtMgBr-(−)-α-isosparteine[4] and also results of enantiomer-selective

TABLE 6. STRUCTURE AND REACTIVITY OF RMgX-(−)-SPARTEINE DERIVATIVE COMPLEXES

Complex	Molecular Structure			Reactivity for the enantiomer selective polymerization of (*RS*)-MBMA (Ref. Table 1)
	Solid ball and spoke model[13]	Space-filling model[13]	Substrate-accomodation in the neighborhood of Mg atom	
EtMgBr-(−)-sparteine	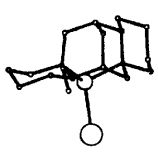	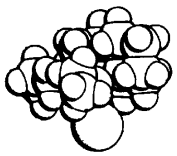	Sufficiently large	Good
t-BuMgCl-(−)-sparteine	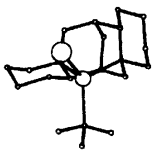	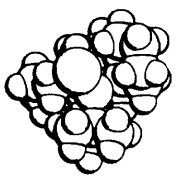	No	No
EtMgBr-(+)-6-benzylsparteine	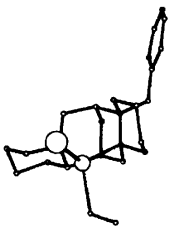	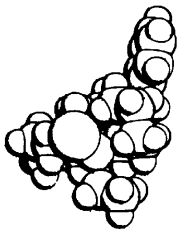	Small	Poor
EtMgBr-(−)-α-isosparteine	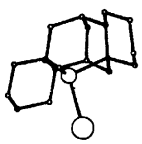	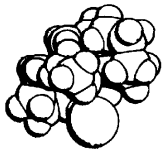	No	No

polymerization of (*RS*)-MBMA initiated by these complex catalysts.[1] Discussion will be limited on the structural feature because the activity and selectivity of these complex catalysts has already been discussed in detail.[1]

It has been reported that the polymerization of MBMA proceeds in a coordination mechanism: the structure of the active center, which presumably depend on the structure of the sparteine skeleton and the geometry around the Mg atom, is considered of most importance.

In catalytically active EtMgBr-(−)-sparteine, the Et group coordinates to the Mg atom at the spatially less opened C(7)-side of the cavity (Y=Et) whereas the bulky Br ligand at the more opened C(9)-side. The Et group is not so large. The Mg atom, therefore, has a sufficient space to accommodate the MBMA, the substrate in its neighborhood.

On the other hand, in the inactive *t*-BuMgCl-(−)-sparteine, the bulky *t*-Bu ligand covers the Mg atom at the spatially more opened C(9)-side and the Cl ligand at the C(7)-side of the cavity (Y=Cl and Z=*t*-Bu). The spatial arrangement of alkyl and halogen ligands is reverse to that of EtMgBr-(−)-sparteine. As is clearly seen from the space-filling model[13] of this molecule (Table 6), there is no room spatially to accommodate the substrate in the neighborhood of the Mg atom.

In the poorly active EtMgBr-(+)-6-benzylsparteine, the all-chair form (+)-6-benzylsparteine ligand has a structure very close to the (−)-sparteine ligand except the benzyl group. The cavity under Λ-shaped sparteine skeleton is therefore very close to that of (−)-sparteine ligand. The Et ligand in this complex coordinates to the Mg atom at the more opened C(9)-side of the cavity. The alkyl and halogen ligands spatially arranged reverse to that of EtMgBr-(−)-sparteine (Y=Br and Z=Et).

In EtMgBr-(−)-α-isosparteine, the cavity of (−)-α-isosparteine is less opened than that of (−)-sparteine. The Mg atom coordinate deep in the cavity covered with Et and Br ligands, which leads the inactivity of this complex.

Crystal Structure. The packing of molecules in crystals of (+)-6-benzylsparteine, EtMgBr-(+)-6-benzylsparteine, and $MgBr_2$-(+)-6-benzylsparteine toluene solvate are drawn in Figs. 7, 8, and 9.

(a) (+)-6-Benzylsparteine: Rather loose molecular contacts are observed between carbon atoms of the benzyl group in one molecule and those of bridge-head carbons in the other molecule: The closest intermolecular atomic contact being 3.682(6) Å [C(24) (x, y, z)···C(9) $(-0.5+x, 0.5-y, -z)$].

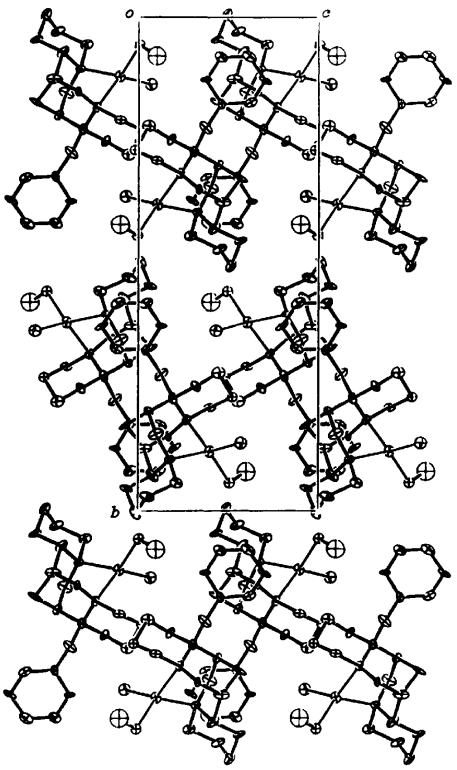

Fig. 8. The crystal structure of EtMgBr-(+)-6-benzylsparteine.[9]

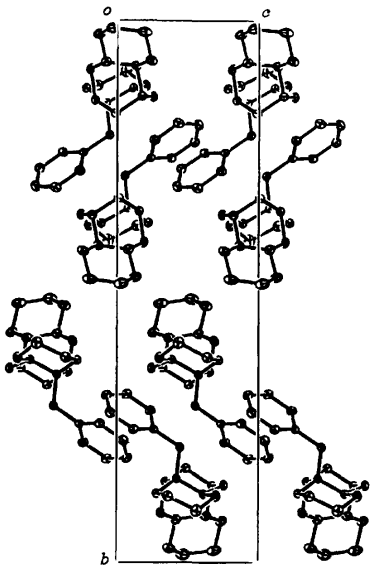

Fig. 7. The crystal structure of (+)-6-benzylsparteine.[9]

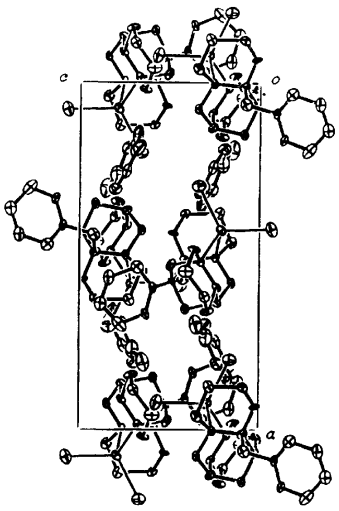

Fig. 9. The crystal structurre of $MgBr_2$-(+)-6-benzylsparteine toluene solvate.[9]

(b) EtMgBr-(+)-6-benzylsparteine: The molecular packing in the crystal is determined by the van der Waals contacts between carbon atoms of the benzyl group in one molecule to those of sparteine skeleton in the other molecule. The shortest intermolecular atomic contact is found between C(22) (x, y, z) and C(10) ($-0.5+x$, $0.5-y$, $1-z$) [3.52(7) Å].

(c) $MgBr_2$-(+)-6-benzylsparteine Toluene Solvate: The Mg complexes in the crystal are loosely bound to toluene molecules by van der Waals forces. The closest intermolecular atomic contact is 3.56(7) Å [both C(30) (x, y, z)···C(8) (x, y, z) and C(31) (x, y, z)···C(4)($-0.5+x$ $0.5-y$, $-z$)], whereas the shortest distance between Mg complexes is 3.74(4) Å [C(9) (x, y, z)···Br ($-0.5+x$, $0.5-y$, $-1-z$)].

A part of the cost of the present study is defrayed by the Grant-in-Aid for Scientific Research (No. 56470069), Ministry of Education, Science and Culture.

References

1) Y. Okamoto, K. Suzuki, T. Kitayama, H. Yuki, H. Kageyama, K. Miki, N. Tanaka, and N. Kasai, *J. Am. Chem. Soc.*, **104**, 4618 (1982).
2) H. Kageyama, K. Miki, N. Tanaka, N. Kasai, Y. Okamoto, and H. Yuki, *Bull. Chem. Soc. Jpn.*, **56**, 1319 (1983).
3) H. Kageyama, K. Miki, Y. Kai, N. Kasai, Y. Okamoto, and H. Yuki, *Bull. Chem. Soc. Jpn.*, **56**, 2411 (1983).
4) H. Kageyama, K. Miki, Y. Kai, N. Kasai, Y. Okamoto, and H. Yuki, *Acta Crystallogr., Sect. B*, **38**, 2264 (1982).
5) P. Main, S. E. Hull, L. Lessinger, G. Germain, J. P. Declercq, and M. M. Woolfson, *MULTAN-78*; "A System of Computer Programs for the Automatic Solution of Crystal Structures from X-ray Diffraction Data," University of York, England (1978).
6) T. Ashida, *HBLS V*, "The Universal Crystallographic Computing System-Osaka," The Computation Center, Osaka Univ., (1973), p. 55.
7) "International Tables for X-Ray Crystallography," The Kynoch Press, Birmingham (1974), Vol, IV, p. 71.
8) "International Tables for X-Ray Crystallography," The Kynoch Press, Birmingham (1974), Vol, IV, p. 148.
9) C. K. Johnson, *ORTEP* II, ORNL-5138, Oak Ridge National Laboratory, Tennessee (1976).
10) D. Pyzalska, M. Gawron and T. Borowiak, *Acta Crystallogr., Sect.B*, **35**, 256 (1979).
11) H. Maluszynska and Y. Okaya, *Acta Crystallogr., Sect. B*, **33**, 3049 (1977).
12) W. C. Hamilton, *Acta Crystallogr.*, **12**, 609 (1959).
13) *PLUTO* 78, "User Manual for Cambridge Crystallographic Database," Crystallographic Data Centre, University Chemical Laboratory, Cambridge (1978).

Decay Mechanism of the Aromatic Hydrocarbon Biradical, 1,1′-Biacenaphthene-2,2′-diyl. Effects of Solvent and Heavy-atom Perturbation

Harumichi KOBASHI,* Reiko KONDO,† Hiroki IKAWA,† and Toshifumi MORITA
Department of Chemistry, Faculty of Engineering, Gunma University, Kiryu, Gunma 376
(Received, November 10, 1983)

Effects of solvents and heavy-atom (H-A) containing compounds on the lifetime of the title biradical (**1**) have been examined to elucidate the decay mechanism of **1** in fluid solutions by means of nanosecond laser spectroscopy. **1** was quenched effectively by H-A compounds such as diethylmercury and iodoethane. The decay rates of **1** showed no explicit correlation with solvent polarities, while a linear correlation was found between the decay rate and the sum of squares of the spin-orbit (S-O) coupling factors of heavy atoms involved in the solvents; chlorobezene, 1,2-dichloroethane, dichloromethane, bromobenzene, and dibromomethane. It has been shown that (i) the biradical lifetime is determined by intersystem crossing (ISC) from the triplet to singlet spin state prior to chemical reactions, (ii) ISC is enhanced by H-A perturbation through the S-O interaction, and (iii) the reactivity of the singlet biradical (^{1}**1**) but not the triplet one (^{3}**1**) sways the product distribution in the triplet-sensitized photodimerization of acenaphthylene.

Since a direct detection of Norrish type II biradicals in fluid solution,[1] dynamic properties of these biradicals have been studied considerably.[2] However, our knowledges about dynamic behavior of aromatic hydrocarbon biradicals have been still scarce in comparison with those for type II biradicals.[3]

Previously we reported an observation of aromatic hydrocarbon biradical **1** as an intermediate in the triplet-sensitized photocycloreversion of trans-dimer (t-D) of acenaphthylene.[4] The biradical **1** is also supposed as an intermediate for the triplet-sensitized photodimerization of acenaphthylene (A).[5,6] This reaction is known to be a typical example of a photochemical H-A effect[7] and to undergo a significant effect of solvent polarity.[6] Therefore, examinations of solvent and H-A effects on the biradical lifetime may be favorable for elucidating the decay behavior of **1** in relation to the dimerization reaction.

This paper deals with a nanosecond laser photolysis study of the biradical **1** under the influence of H-A compounds and solvents with various polarities, in order to clarify the decay mechanism of **1** having a characteristic structure different from the type II biradicals. It was of interest whether the decay rate of a triplet biradical would be determined by a chemical reaction or by ISC prior to chemical reactions. We here make it clear that the decay of **1** proceeds *via* the latter mechanism. We also intend to relate quantitatively the decay rates of **1** to the S-O interaction factors, because the already-known results of H-A effects on biradicals are only qualitative.[1a,3a] The present results show an explicit correlation between them, indicating that the decay rate is enhanced by H-A compounds through the S-O interaction. At the same time, a complex formation between **1** and EtI is proposed and a role of the biradical in the dimerization reaction is also discussed.

Experimental

Materials. The trans-dimer of acenaphthylene (t-D) and benzophenone (BP) were the same as those reported previously.[4] Benzene, toluene, 1,4-dioxane, and acetone were all spectrograde reagents (Dotite). Dibromomethane (Wako, GR grade) was used without further purification. Dichloromethane, 1,2-dichloroethane, chlorobenzene, bromobenzene, pyridine, and acetonitrile were purified by the usual methods. Iodoethane (Wako, GR grade), diethylmercury (Wako, CP grade), and diethyl sulfide (Wako, EP grade) were distilled under vacuum just before use.

Nanosecond Laser Photolysis. The 1,1′-biacenaphthene-2,2′-diyl (**1**) was observed by a nanosecond laser photolysis method at 347 nm.[4] The solutions used contained both t-D ($\geq 2\times10^{-3}$ mol dm^{-3}) and BP ($\approx 4\times10^{-3}$ mol dm^{-3}) as a triplet sensitizer. The lifetime of **1** was measured by monitoring the time-dependent intensity of its characteristic absorption band at 380 nm. When the absorption band of **1** was overlapped by a long-lived absorption of byproduct, *e.g.*, benzophenone ketyl radical, the interference absorption at 380 nm was subtracted from the observed absorption to obtain a true decay time of **1**. The quenching experiments of **1** by Et_2Hg, EtI, and Et_2S were performed in benzene solutions. All solutions were degassed by the usual freeze-pump-thaw method. The lifetime measurements were performed at 20±1 °C.

Results and Discussion

Transient Absorption Spectra. Before examination of the external solvent effects, transient absorption spectra of **1** were observed in each solvent at room temperature. The typical spectra are illustrated in Fig. 1. Figure 1a is the previously observed spectra in benzene given for comparison.[4] Figure 1b shows time-resolved absorption spectra observed in dichloromethane. The spectral profiles resemble well those given in Fig. 1a. Namely, in the early stage of time after excitation, absorption bands due to ^{3}BP and ^{3}t-D are observed around 530 and 450 nm respectively. Both bands decay rapidly and a strong absorption band grows around 380 nm. This is the characteristic absorption band of **1** (Fig. 1b-2). This band decays with the first-order kinetics. Figure 1c pictures the transient spectra in 1,4-dioxane. The absorption of **1** is observed also around 380 nm. In this case, a distinct absorption band with maximum at 545 nm still remains after disappearance of **1**. The absorption band monitored at 545 nm

† Present address: Japan Information Processing Service Co. Ltd., Kabuto-cho, Chuo-ku, Tokyo 103.

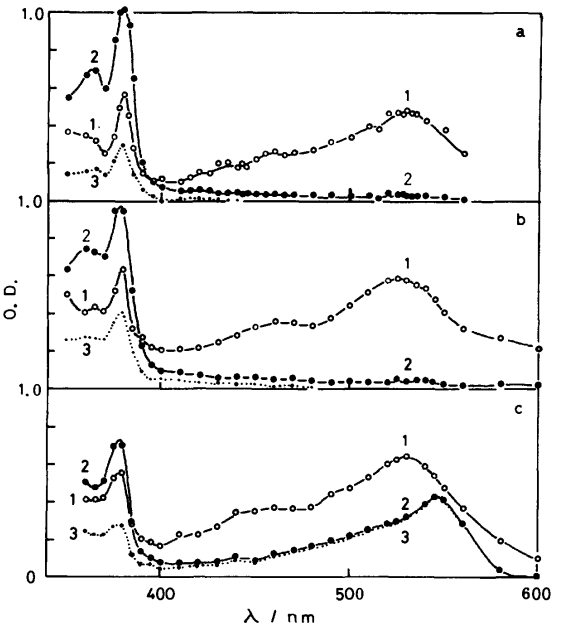

Fig. 1. Transient absorption spectra observed in the BP-t-D system. Solvent and delay time after the beginning of laser oscillation:
a) Benzene; (1) 40 ns, (2) 230 ns, (3) 730 ns, b) dichloromethane; (1) 40 ns, (2) 260 ns, (3) 660 ns, c) 1,4-dioxane; (1) 60 ns, (2) 280 ns, (3) 660 ns.

decayed slowly with the second-order kinetics. This long-lived transient can be identified to benzophenone ketyl radical (BPH·) from comparing the spectrum and decay kinetics with those of BPH· in the literatures.[8] The BPH· observed here is not a transient produced by a reaction between **1** and BP, because the absorbance of BPH· around 545 nm does not increase as the absorbance of **1** at 380 nm decreases during the time interval 280—660 ns (Fig. 1c). Furthermore, if BP in the ground state caused H-atom abstraction from ^{3}t-D, the abstraction reaction should occur in benzene or in dichloromethane as well. But no BPH· absorption is observed in these solvents (Figs. 1a and b). The BPH·, therefore, is not also a transient originated from the reaction between ^{3}t-D and BP. It is considered that BPH· forms through H-abstraction reaction by ^{3}BP from the solvent 1,4-dioxane which is a fairly good H-donor.[9] Because BPH· disappears much slower than **1**, the decay of BPH· is negligible in the time range required to analyze the biradical lifetime (τ_B). Then, the value of τ_B in 1,4-dioxane can be estimated by a simple procedure in which the absorbance of BPH· ($D_{BPH\cdot}$) is subtracted from the observed absorbance (D_{obsd}) using the following equation:

$$D_{obsd} - D_{BPH} = (D^0_{obsd} - D_{BPH\cdot})\exp(-t/\tau_B),$$

where D^0_{obsd} is the observed absorbance at the time origin arbitrarily taken in the time domain where the decay curve is exponential.

Quenching of 1 by H-A Containing Compounds. Figures 2a, 2b, and 2c present the Stern-Volmer plots of lifetimes against concentrations of the quenchers Et_2Hg, EtI, and Et_2S, respectively, in benzene. The quenching by Et_2Hg shows a good linear relation

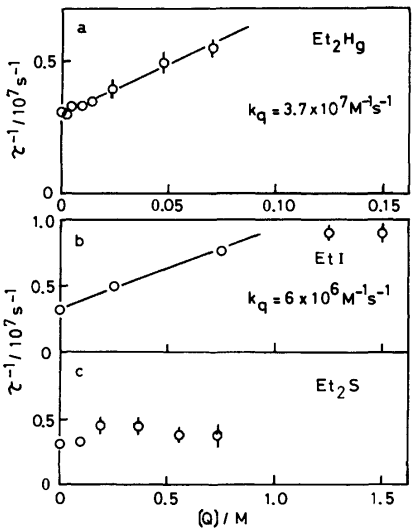

Fig. 2. Stern-Volmer plots of the inverse lifetime τ^{-1} *vs.* quencher concentration [Q]. The quencher Q: a) Et_2Hg, b) EtI, c) Et_2S. (1 M = 1 mol dm^{-3})

with the rate constant k_q: 3.7×10^7 dm^3 mol^{-1} s^{-1} (Fig. 2a). The quenching curve by EtI approaches gradually the maximum value near *ca.* 1×10^7 s^{-1} with increasing [EtI]. In the range of [EtI]<1 mol dm^{-3} the curve can be approximated by a straight line corresponding to k_q: *ca.* 6×10^6 dm^3 mol^{-1} s^{-1}. This line is added into Fig. 2b. Figure 2c indicates that Et_2S is not an effective quencher for **1**. Thus, the quenching efficiencies correspond to the order of magnitude of the atomic number of heavy atoms (Hg, I, and S) in the quenchers, suggesting that the quenching events are caused by external H-A effect.

The nonlinearity of the Stern-Volmer plots, as shown in Fig. 2b, has been frequently observed in the high concentration region of quenchers (>1 mol dm^{-3}). As for the quenching mechanism there are some interpretations in terms of the decrease of the activity coefficients of quenchers,[10] the change of radiationless transition induced by change of solvent composition,[11] and the formation of ground- or excited-state complex.[12,13] In recent studies the exciplex mechanism appears to be an appropriate one to the H-A effect of EtI on the quenching of both excited singlet and triplet states of aromatic hydrocarbons.[14,15] Since **1** is composed of aromatic hydrocarbon moieties similar to chromophores in the exciplex forming systems noted above, a weak complex formation may be expected between **1** and EtI. We attempted to analyze the quenching curve for EtI from a view point of the complex formation, although no explicitly spectral evidence indicating the complex formation was observed up to the heighest concentration (2.5 mol dm^{-3}) of EtI so far as we examined.[16] The quenching curve bending downward suggests the existence of the so-called dynamic equilibrium[17] represented as follows:

$$\mathbf{1} + \mathrm{EtI} \underset{k_b}{\overset{k_a}{\rightleftharpoons}} \mathbf{1}\cdots\mathrm{EtI}, \qquad (1)$$

with τ_B^{-1} and τ_C^{-1}

where τ_B and τ_C are the lifetimes of **1** in the absence of EtI and the complex **1**···EtI respectively, k_a and k_b are the rate constants of association and dissociation processes respectively, and the equilibrium constant K is defined by k_a/k_b. When the dynamic equilibrium condition,

$$k_a[\mathrm{EtI}],\ k_b \gg \tau_B^{-1},\ \tau_C^{-1}, \tag{2}$$

holds completely, the apparent lifetime (τ) of **1** in the presence of EtI should satisfy the following two relations expressed by Ware *et al.*[18] and Rayner and Wyatt[19] respectively:

$$(\tau^{-1}-\tau_B^{-1})^{-1} = (\tau_C^{-1}-\tau_B^{-1})^{-1}(1+K^{-1}[\mathrm{EtI}]^{-1}), \tag{3}$$

and

$$[\mathrm{EtI}]^{-1}(\tau^{-1}-\tau_B^{-1}) = K(\tau_C^{-1}-\tau^{-1}). \tag{4}$$

Although both equations are derived from the same kinetic assumption (Eq. 2), Eq. 3 is sensitive to τ values in the relatively low concentration region of the quencher and Eq. 4 reflects rather well the variation in τ in the relatively high concentration region. Figures 3a and 3b show the relations corresponding to Eqs. 3 and 4 respectively for the lifetimes (τ) measured at 8 different concentrations of EtI in the range of 0.25—2.5 mol dm^{-3}. Both equations fit well the experimental results. The values of K 0.64±0.06 dm^3 mol^{-1} and τ_C 65± 5 ns are obtained from Fig. 3a and K 0.72±0.09 dm^3 mol^{-1} and τ_C 69±13 ns are obtained from Fig. 3b. A good agreement in each K and τ_C values estimated from the two different kinetic expressions suggests strongly the existence of **1**···EtI in the equilibrium as indicated in Eq. 1. The complex formation contributes to enhancement of the biradical decay through the S-O interaction as is indicated later.

Effects of H-A Solvents and Solvent Polarities. Table 1 lists the values of biradical lifetimes (τ_B)

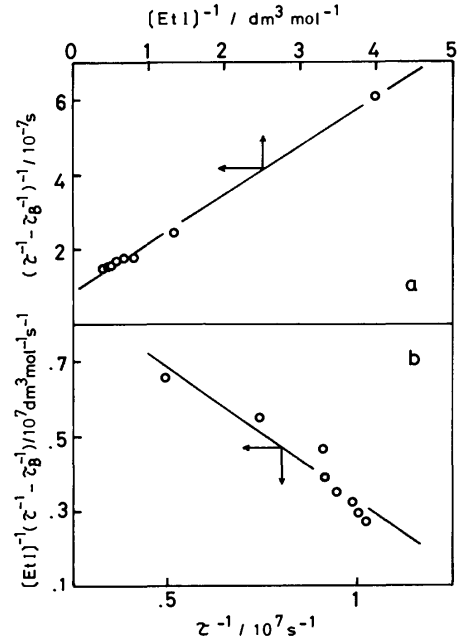

Fig. 3. Kinetic relations corresponding to (a) Eq. 3 and (b) Eq. 4.

Table 1. Decay times of **1** in various solvents at 20 °C

Solvent	ε	$\sum\zeta^2/10^6$ cm^{-2}	τ_B/ns
1,4-Dioxane	2.21		270
Benzene	2.28		300
Toluene	2.38		290
Bromobenzene	5.39	6.05	152
Chlorobenzene	5.71	0.34	289
Dibromomethane	7.04	12.1	84
Dichloromethane	8.93	0.69	295
1,2-Dichloroethane	10.66	0.69	350
Pyridine	13.23		290
Acetone + 1,2-Dichloroethane (1 : 1 in volume)	15.7[a]		380
Acetonitrile + Benzene (1 : 1 in volume)	24.6[a]		310

a) The values of mixed solvents are obtained by assuming additivity: $\varepsilon_{mix}=\sum\chi_i\varepsilon_i$, where χ_i is the molar fraction and ε_i corresponds to ε of i-th component solvent.

measured in several solvents together with those of dielectric constant (ε) of the solvents. The errors in τ_B values are *ca.* 10%. The mixed solvents were employed as highly polar solvents because of low solubility of t-D in neat acetone or acetonitrile. For H-A solvents of bromobenzene, chlorobenzene, dibromomethane, dichloromethane, and 1,2-dichloroethane the sum of squares of S-O interaction factors (ζ) of halogen atoms involved in the solvents are additionally given in Tabel 1.[20] The $\sum\zeta^2$ values are a measure of the magnitude of transition probability induced by S-O interaction; $k_{ISC}\propto\langle^1\phi|H_{SO}|^3\phi\rangle^2\propto\sum\zeta^2$, where k_{ISC} is the probability of ISC induced by heavy atoms and $\langle^1\phi|H_{SO}|^3\phi\rangle$ is the S-O coupling matrix element between singlet and triplet states.

The τ_B values in the H-A solvents decrease with the order of 1,2-dichloroethane, dichloromethane, chlorobenzene, bromobenzene, and dibromomethane. This tendency is parallel to that for the quenching rate constants in the addition effect of H-A compounds. To show this effect quantitatively, Fig. 4 illustrates a relation between τ_B^{-1} and $\sum\zeta^2$. There exists a linear relation. Therefore, it is evident that the S-O interaction is the origin of the H-A solvent effect enhancing the decay rate of **1**. Although the compounds involving Cl- or S-atom show no recognizable H-A effect, this seems due to much smaller S-O interaction factors of these atoms than those of Br- and I-atoms.

Next we notice the effect of solvent polarity on the lifetime. The τ_B values in Table 1 do not show any appreciable correlation with solvent polarities and are close to one another except for the lifetimes in bromobenzene and dibromomethane (H-A solvents). Accordingly, the biradical lifetimes can be regarded to be almost independent on solvent polarity. In contrast, it is known that a lifetime of the Norrish type II biradical **2** derived from 4-methyl-1-phenyl-1-pentanone depends strongly on the polarity and hydrogen-bonding strength of solvents.[1a,2a] Such influence of H-bonding ability is not found for the case of **1**. These different

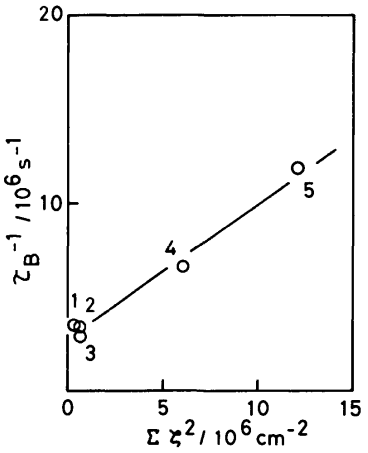

Fig. 4. The relation between the inverse lifetime of **1** (τ_B^{-1}) and the S-O interaction parameter ($\Sigma\zeta^2$); 1) chlorobenzene, 2) dichloromethane 3) 1,2-dichloroethane, 4) bromobenzene, and 5) dibromomethane.

features between **1** and **2** as to the solvent effects seem to arise from difference in their molecular structures. That is, **1** has a structure composed of two identical aromatic π-radical sites with no or weak H-bonding property but **2** consists of two different radical sites one of which has a hydroxyl group to cause readily H-bonding with basic solvents. Besides **1** would have a smaller dipole moment than **2**. Therefore, it is understood that **1** is less sensitive to the solvent polarity as well as H-bonding ability.

Decay Mechanism of 1 and Photodimerization of Acenaphthylene. A previous report[4] demonstrated that (i) **1** is a triplet-derived biradical with a fairly long life, (ii) its decay rate is approximately temperature-independent, (iii) the frequency factor of an Arrhenius plot for the decay rate constant is so small (1.9×10^6 s^{-1} in benzene) as to suggest a spin-forbidden nature of the decay process, and (iv) **1** is quenched by oxygen, a paramagnetic molecule, with a nearly diffusion-controlled rate constant 0.9×10^{10} dm^3 mol^{-1} s^{-1} in benzene at 20 °C. These properties of **1** resemble quite well those of familier triplet state type II biradicals. From these knowledges, **1** has been ascribed to be a biradical in the triplet spin state (^{3}**1**). We here discuss the decay mechanism of ^{3}**1** relating the mechanism of photodimerization of A on the basis of the previously-mentioned results together with already-known results of the photodimerization reaction.

In an examination of solvent effect on the triplet-sensitized dimerization of A, it has been reported that the logarithm of the ratio between the yields of the products t-D and c-D, log[t-D]/[c-D], correlates linearly with the Kirkwood-Onsager parameter $(\rho/M)(\varepsilon-1)/(2\varepsilon+1)$ where ρ is the solvent density and M is the molecular weight of solvent.[6,21] Nevertheless, as seen from Table 1, the decay rate of ^{3}**1** is not governed by the above relation and other solvent polarity parameters. It turns out, therefore, that ^{3}**1** does not concern directly the reaction steps determining the product distribution of c- and t-D. Since the τ_B values are approximately unaltered in the several kinds of light-atom solvents, it is supposed that ^{3}**1** does not react directly with the solvents. The validity of this supposition may be justified by the fact that the material balance of the dimerization reaction is approximately 100% in several solvents; cyclohexane, benzene, and methanol.[5] Because byproduct formation is negligible even in the H-A solvent, 1-bromopropane,[5,22] it may be also plausible that the biradical quenching by the H-A perturbers is not due to chemical reactions between ^{3}**1** and the perturbers. The spin-allowed dissociation of ^{3}**1**$\rightarrow{}^3$A*+A is thermally forbidden, so that this process is difficult to take place. ^{3}**1** is considered to exist in the potential minimum, *i.e.*, the relaxed state, since its lifetime was observably long. Then, a fairly high activation energy (at least, a few kcal mol^{-1}) would be required for the biradical decay if ^{3}**1** caused spin inversion concomitantly with bond beaking (*i.e.*, ^{3}**1**$\rightarrow$2A) in which ^{3}**1** must be activated thermally in the triplet state potential surface to take a conformation favorable for the dissociation yielding 2A. However, no activation energy was observed for the decay rate of ^{3}**1** in benzene.[4] Therefore, the spin-forbidden process of ^{3}**1**$\rightarrow$2A does not seem to participate in the radiationless decay of ^{3}**1**. Hence, the lifetime of ^{3}**1** must be determined by the rate of ISC as a physical process from the triplet to the singlet spin state (^{1}**1**) both in the presence and absence of the perturbers (X). The most reasonable decay routes of ^{3}**1** can be represented as follows:

$$^3\mathbf{1} \xrightarrow[(+X)]{\text{ISC}} {}^1\mathbf{1} \begin{cases} \nearrow \text{c-D} \\ \rightarrow \text{t-D} \\ \searrow 2\text{A} \end{cases}, \qquad (5)$$

where ^{1}**1** decays so rapid as unable to be observed by the nanosecond laser photolysis. Since ^{3}**1** involves no decay process other than ISC, the increase in the rate of ISC induced by the H-A compounds does not lead to increase in the total yield of the dimers in the triplet-sensitized dimerization reaction. This suggestion is consistent with the previous results that a kinetic analysis for the yield of the dimers can be treated without regard to the enhancement of biradical spin relaxation and hence H-A solvents may act only as solvents with certain polarities on the product distribution.[22,23]

It is known that the quantum yields for directly excited photodissociation of c- and t-D, which are assumed to dissociate via respective biradical states in the singlet multiplicity,[24,25] are different from each other.[25-27] These results imply that the reactivity of ^{1}**1** depends strongly on its conformation immediately after generation. Such importance of biradical conformation in determining product distribution has been proposed for type II biradicals.[2b,28] On the other hand, the present result regarding effect of solvent polarity suggests that the conformations of ^{3}**1** in various solvents are not so much different from one another as to vary the ISC rate depending on difference of solvent polarities, since the rate of ISC is determined normally by the magnitude of S-O interaction matrix element which is sensitive to conformation of a biradical. Such circumstance would be the case for ^{3}**1** at the moment when ISC occurs. If the conformation does not change during ISC, the conformations of ^{1}**1** immediately after generation would be nearly identical to one another in different

solvents as the case for ^{3}**1** is so. Therefore, it may be thought that the product distribution of c- and t-D is swayed by the solvent-dependent rate constants of ^{1}**1** producing c- and t-D but not by difference in the conformations of ^{1}**1** immediately after generation.[29] However, further study about dynamic nature of the short-lived singlet biradical ^{1}**1** will be needed to elucidate a detailed mechanism of the solvent effect on the product distribution.

It has been pointed out that two types of spin inversion concerning the mechanism of ISC in a triplet biradical are assumed: One is a spin inversion leading to singlet biradical prior to chemical reactions (Mechanism I) and the other is a spin inversion occuring concurrently with reactions to yield some products of the singlet state (Mechanism II).[30] In the present case, it is clear that ISC corresponds to Mechanism I, since no direct chemical reaction occurs in the triplet biradical while the singlet biradical may be an actual intermediate which plays an essential role in determining the product distribution.

The authors are grateful to Prof. Haruo Shizuka for his interest and critical manuscript reading.

References

1) a) R. D. Small, Jr. and J. C. Scaiano, *Chem. Phys. Lett.*, **50**, 431 (1977); b) J. Faure, J. -P. Fouassier, D. -J. Lougnot, and R. Salvin, *Nouv. J. Chem.*, **1**, 15 (1977).

2) a) R. D. Small, Jr. and J. C. Scaiano, *Chem. Phys. Lett.*, **59**, 246 (1978); b) J. C. Scaiano, *Tetrahedron*, **38**, 819 (1982) and references therein. c) H. Hayashi and S. Nagakura, *Bull. Chem. Soc. Jpn.*, **53**, 1519 (1980). d) H. Hayashi, and S. Nagakura, Y. Ito, Y. Umehara, and T. Matsuura, *Chem. Lett.*, **1980**, 939; e) R. A. Caldwell, T. Majima, and C. Pac, *J. Am. Chem. Soc.*, **104**, 629 (1982).

3) a) M. Gisin, E. Rommel, J. Wirz, M. N. Burnett, R. M. Pagni, *J. Am. Chem. Soc.*, **101**, 2216 (1979); b) S. Takamuku and W. Schnabel, *Chem. Phys. Lett.*, **69**, 399 (1980); c) M. Demuth, W. Amrein, C. O. Bender, S. E. Braslavsky, U. Burger, M. V. George, D. Lemmer, and K. Schaffner, *Tetrahedron*, **37**, 3245 (1981); d) T. Okada, K. Kida, and N. Mataga, *Chem. Phys. Lett.*, **88**, 157 (1982); e) D. F. Kelley and P. M. Rentzepis, *J. Am. Chem. Soc.*, **105**, 1820 (1983).

4) H. Kobashi, H. Ikawa, R. Kondo, and T. Morita, *Bull. Chem. Soc. Jpn.*, **55**, 3013 (1982).

5) D. O. Cowan and R. L. Drisko, *Tetrahedron Lett.*, **1967**, 1255.

6) H. -M. Hartmann, W. Hartmann, and G. O. Schenck, *Chem. Ber.*, **100**, 3146 (1967).

7) J. C. Koziar and D. O. Cowan, *Acc. Chem. Res.*, **11**, 334 (1978).

8) J. A. Bell and H. Linschitz, *J. Am. Chem. Soc.*, **85**, 528 (1963); F. Wilkinson and A. Garner, *Photochem. Photobiol.*, **27**, 659 (1978).

9) In fact, it is already known that ^{3}BP abstracts efficiently a hydrogen atom from 1,4-dioxane; G. Porter and M. R. Topp, *Proc. R. Soc. London, Ser. A*, **315**, 163 (1970).

10) T. Medinger and F. Wilkinson, *Trans. Faraday Soc.*, **61**, 620 (1965).

11) H. Kokubun, *Bull. Chem. Soc. Jpn.*, **42**, 919 (1969).

12) W. R. Ware and C. Lewis, *J. Chem. Phys.*, **57**, 3546 (1972).

13) S. P. McGlynn, T. Azumi, and M. Kinoshita, "Molecular Spectroscopy of the Triplet State," Printice-Hall, Englewood Cliffs, New Jersey (1969), Chap. 8.

14) Y. Shimizu and T. Azumi, *J. Phys. Chem.*, **86**, 22 (1982).

15) M. C. Tamargo and D. O. Cowan, *J. Am. Chem. Soc.*, **104**, 1107 (1982).

16) In neat dibromomethane solution the absorption peak of **1** shows a slight red-shift to 385 nm. However, it is not able to discard possibilities of other mechanisms at the present stage of investigation.

17) J. B. Birks, "Photophysics of Aromatic Molecules," Wiley-Interscience, London (1970), p. 309.

18) W. R. Ware, D. Watt, and J. D. Holmes, *J. Am. Chem. Soc.*, **96**, 7853 (1974).

19) D. M. Rayner and P. A. H. Wyatt, *J. Chem. Soc., Faraday Trans. 2*, **70**, 945 (1974).

20) D. S. McClure, *J. Chem. Phys.*, **17**, 905 (1949).

21) J. Powling and H. J. Bernstein, *J. Am. Chem. Soc.*, **73**, 1815 (1951).

22) Byproduct formation has been also neglected in a kinetic scheme for analyzing quantum yields of the dimers in cyclohexane solution containing EtI: D. O. Cowan and J. C. Koziar, *J. Am. Chem. Soc.*, **96**, 1229 (1974).

23) D. O. Cowan and J. C. Koziar, *J. Am. Chem. Soc.*, **97**, 249 (1975); D. O. Cowan and R. L. E. Drisko, *ibid.*, **92**, 6281; 6286 (1970).

24) J. Michl, *Mol. Photochem.*, **4**, 243; 257 (1972).

25) S. Yamamoto, M. Hoshino, and M. Imamura, *Chem. Phys. Lett.*, **98**, 615 (1983).

26) R. Livingstone and K. S. Wei, *J. Phys. Chem.*, **71**, 541 (1967).

27) N. Y. C. Chu and D. R. Kearns, *J. Phys. Chem.*, **74**, 1255 (1970).

28) Y. Ito and T. Matsuura, *J. Am. Chem. Soc.*, **105**, 5237 (1983).

29) Additionally speaking, the formation rates of c- and t-D may be related to the rates of ^{1}**1** deforming to the conformational isomers which are favorable to yield immediately c- and t-D respectively, because both isomers would be subject to the solvent effects related to the Kirkwood-Onsager parameter in different degrees of stabilization respectively corresponding to their dipole moments as rotational isomers of halogenoethanes are.[21]

30) a) M. S. Platz, *J. Am. Chem. Soc.*, **102**, 1192 (1980); b) S. S. Shaik, *ibid.*, **101**, 2736 (1979).

Aqueous Dispersion of Iron Oxide by Acrylic Oligomer Surfactants

Kunio ESUMI,* Kimihiko OGIHARA, and Kenjiro MEGURO
Department of Applied Chemistry and Institute of Colloid and Interface Science, Science University of Tokyo, Kagurazaka, Shinjuku-ku, Tokyo 162
(Received November 18, 1983)

The aqueous dispersion of iron oxide by acrylic oligomer surfactants was examined by particle size and zeta potential measurements. Iron oxide particles were suspended in an aqueous iron(III) chloride solution to render the surface positively charged. The iron oxide particles so prepared were then flocculated by the addition of a small amount of acrylic oligomer surfactant. The flocs of iron oxide could be redispersed by further addition of acrylic oligomer surfactant. The flocculation and the redispersion processes can be explained in terms of a "two-fold adsorption layer" mechanism of the acrylic oligomer surfactant. The concentrations of acrylic oligomer surfactants needed to achieve flocculation and redispersion decreased with an increase in acrylic content of the oligomer surfactants.

Recently, from the standpoint of environment pollution and of conservation of resources, water-base dispersion has become attractive rather than an organic-base one. Thus, it is important to prepare stable dispersions in aqueous solution. Although many kinds of surfactants have been utilized[1-3] for this purpose, they have some deficiencies such as poor film formation and sensitivity to water vapor after drying the film. Of these surfactants, oligomer surfactants[4-7] which exhibit characteristics of low molecular surfactant and of polymer surfactant have been developed and employed for dispersion of pigments due to suitable properties such as improvement of film formation and resistance to water vapor. However, there are few reports concerning dispersion of pigments by oligomer surfactants.

In this work, to elucidate an interaction of oligomer surfactant and pigment, dispersion of iron oxide by acrylic oligomer surfactants in diluted system was studied by measuring the particle size and the zeta potential.

Experimental

Materials. The oligomer surfactants used in this work were synthesized by co-oligomerization[5] of acrylic acid, acrylonitrile, and 1-dodecanethiol, followed by neutralization with potassium hydroxide. The chemical structure and analytical properties of the oligomer surfactants obtained are given in Table 1. All the chemicals were of reagent grade. The water used was purified by passing through Milli-Q Reagent Grade Water Systems until its specific conductivity fell below $10^{-7}\,\Omega^{-1}\,cm^{-1}$. As a pigment, α-Fe_2O_3 was supplied by Titan Chemicals. The specific surface area and isoelectric point of the sample were 6.4 m^2/g and 1.9, respectively.

Procedure. The suspensions of iron oxide were prepared as follows: 0.01 g of solids was added to 150 cm^3 of a desired aqueous solution and treated for 5 min in a Bransonic ultrasonic bath. The particle size distribution was determined by a centrifugal particle size analyzer CP-50 (Shimadzu Seisakusho Co., Ltd.). The zeta potential of the sample was measured with a Laser Zee 500 (Pen Kem Inc.) electrophoresis apparatus.

Results and Discussion

To elucidate the effect of oligomer surfactants on the dispersion of iron oxide, it is necessary to obtain a well dispersed system. For this purpose, iron oxide solids were suspended in aqueous iron(III) chloride solutions. From the facts[8] that the mean particle sizes show a minimum value and the zeta potential of the iron oxide reaches a maximum value at about 0.5 mmol dm^{-3} iron(III) chloride, the stock dispersion in 0.5 mmol dm^{-3} iron(III) chloride was used in further studies.

On the addition of a small amount of oligomer surfactant(I) to aqueous suspensions of iron oxide particles in 0.5 mmol dm^{-3} iron(III) chloride, the iron oxide particles flocculated, but the flocs redispersed on further addition of the same surfactant. The mean particle size of the iron oxide increased with rising concentration of oligomer surfactant(I), reached a maximum value at 0.016 mmol dm^{-3} and then decreased on further addition of oligomer surfactant(I) as shown in Fig. 1(a). The positively charged iron oxide particles in an aqueous iron(III) chloride solution were discharged in the presence of oligomer surfactant(I) and then the charge was reversed to negative on further addition of this surfactant (Fig. 1(b)). The zero point of charge of iron oxide was about 0.016 mmol dm^{-3} of oligomer surfactant(I); this value corresponds to the concentration of oligomer surfactant(I) at which the maximum mean particle size was established.

The flocs formed by the addition of this surfactant could be easily suspended in toluene by shaking, which indicates that the surface of the solids became hydrophobic by adsorption of oligomer surfactant(I). The behavior of the other oligomer surfactants(II)—(V)

TABLE 1. OLIGOMER TYPE SURFACTANTS

$$C_{12}H_{25}S\text{-}\left(CH_2CH(CN)\right)_x\text{-}\left(CH_2CH(COOK)\right)_y\text{-}\left(CH_2CH(COOH)\right)_z\text{-}H$$

Oligomer	x	y	z	MW[a]
(I)	0	9.5	3.8	1530
(II)	3.6	7.0	2.2	1325
(III)	6.8	2.8	11.4	1700
(IV)	6.5	5.7	2.0	1320
(V)	11.9	4.5	2.9	1539

a) Average molecular weight calculated from elemental analysis.

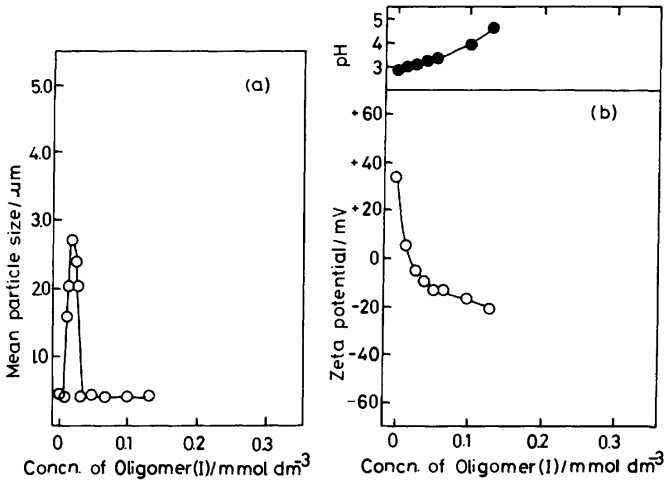

Fig. 1. The variation of the mean particle size and the zeta potential of iron oxide in the presence of 0.5 mmol dm^{-3} iron(III) chloride as a function of added oligomer surfactant(I).

was analogous to that of oligomer surfactant(I).

The redispersion of the iron oxide flocs was investigated by further addition of oligomer surfactant(I). Figure 1(a) shows that the mean particle size of iron oxide flocs decreased with the concentration of the oligomer surfactant(I). The complete redispersion occurred at about 0.029 mmol dm^{-3} of oligomer surfactant(I). In the cases of the other oligomer surfactant(II)—(V), similar results were obtained.

A model for the mechanisms of flocculation and redispersion processes can be explained in terms of the "two-fold adsorption layer" similar to that suggested earlier.[9,10] That is, the iron oxide is positively charged in an aqueous iron(III) chloride solution providing a well dispersed state characterized by a minimum in the mean particle size and a maximum in the zeta potential. On addition of a low concentration of oligomer surfactant(I), the particles are discharged and their size increases. As the hydrocarbon chains of the oligomer surfactant(I) are oriented outward, the particles become hydrophobic and flocculation takes place. On further addition of oligomer surfactant(I), the adsorption of this surfactant occurs by a hydrophobic-hydrophobic interaction resulting in a two-fold layer with the ionized groups of the second layer oriented towards the solution. Accordingly, the particles are recharged and redispersion is achieved, mainly due to the electric repulsion. For the other oligomer surfactant(II)—(V), the mechanism mentioned above can also be applied for the flocculation and the redispersion of iron oxide.

Furthermore, the flocculation and redispersion states of iron oxide by addition of oligomer surfactants were estimated by applying the D.L.V.O. theory.[11] According to the D.L.V.O. theory the total potential energy V between the two particles is obtained by a summation of the repulsive potential V_R and the attractive potential energy V_A:

$$V = V_R + V_A. \tag{1}$$

For this system, V_R for spherical particles is given:

$$V_R = \frac{\varepsilon a \psi_0^2}{2} \ln(1 + e^{-\kappa H}), \tag{2}$$

where ψ_0 is the surface potential of the particles, "a" the particle radius, ε dielectric constant of the medium, κ the reciprocal of the thickness of double layer and H the shortest distance between the two particles. Attractive potential energy V_A is given by the Hamaker equation,[12] assuming the attraction between the particles is entirely based upon the London-van der Waals forces and $H \ll a$,

$$V_A = -\frac{Aa}{12} \frac{1}{H}, \tag{3}$$

where A is the Hamaker constant. Substituting Eq. 2 and Eq. 3 into Eq. 1, we obtain:

$$V = \frac{\varepsilon a \psi_0^2}{2} \ln(1 + e^{-\kappa H}) - \frac{Aa}{12H}. \tag{4}$$

Assuming ψ_0 equals to zeta potential and using the proper value of A, the values of V for all the systems can be obtained from Eq. 4.

The values of V for iron oxide suspensions dispersed with oligomer surfactant(I) in the presence of iron(III) chloride are plotted as a function of H in Fig. 2. Here, the value of A (4.5×10^{-13} erg)[2] is used for number of 1 and 2, and A (4.7×10^{-14} erg)[13] for number of 3 and 4. The latter value was obtained from consideration of the two-fold adsorption layer. In number of 1, the repulsive force operates between the two iron oxide particles when they approach, resulting in the stable suspensions. On the other hand, V becomes negative values over all the H for the concentration of the number of 2 indicating unstable suspensions. In the numbers of 3 and 4, V becomes positive values. This suggests that the suspensions become stable. For the other oligomer surfactants, similar potential curves were obtained like that of oligomer surfactant(I). Thus, the flocculation and redispersion states of iron oxide can be explained

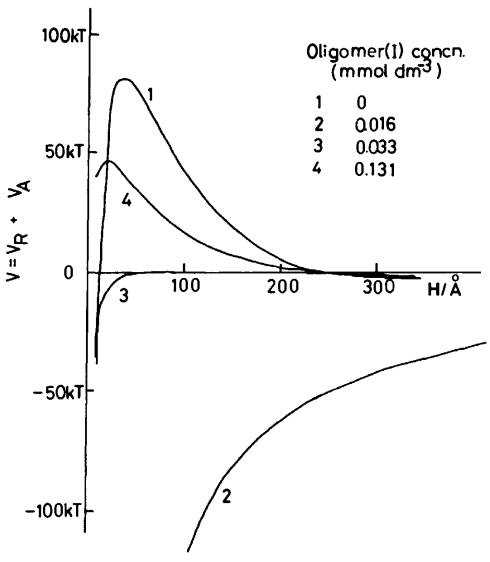

Fig. 2. The relation between V and stability for oligomer surfactant(I).

Table 2. Maximum flocculation and redispersion concentration for iron oxide dispersion

Oligomer	C_{mf}/mmol dm^{-3}	C_{rd}/mmol dm^{-3}
(I)	0.016	0.029
(II)	0.023	0.060
(III)	0.035	0.094
(IV)	0.045	0.061
(V)	0.032	0.10

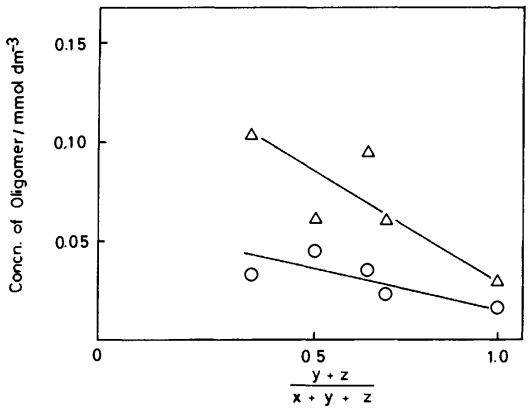

Fig. 3. The variation of the maximum flocculation and the redispersion concentration as a function of acrylic content in oligomer surfactants: (○) maximum flocculation concentration, (△) redispersion concentration.

by the D.L.V.O. theory.

To study the effect of different composition of oligomer surfactants on the dispersion of iron oxide, the maximum flocculation and redispersion concentration values are listed in Table 2 and plotted in Fig. 3. As the acrylic content in the oligomer surfactant molecule increases, the maximum flocculation concentration gradually decreases, while the redispersion concentration decreases more steeply than for the maximum flocculation concentration. The above results suggest that the oligomer surfactant with the higher acrylic content is adsorbed effectively to the positively charged iron oxide, thus resulting in lowering the maximum flocculation concentration. On the other hand, since oligomer surfactants with lower acrylic content seem to be coiled more closely in the solution, the adsorption of a second layer due to hydrophobic-hydrophobic interaction would not occur effectively. Furthermore, as oligomer surfactants with lower acrylic content contain less ionized groups, the second layer of the oligomer surfactant with the lower acrylic content would not enhance electric repulsion significantly. Therefore, to attain redispersion by adding oligomer surfactant with a lower acrylic content, more dense adsorption at the second layer is required. Thus, the redispersion concentration with oligomer surfactant with lower acrylic content becomes higher. It is found that a different composition of the oligomer surfactant molecule on the dispersion of iron oxide provides a different flocculation and a redispersion concentration.

The authors express their thanks to Miss S. Oguro and Miss A. Miyamoto for their assistance through this work.

References

1) R. J. Akers and P. W. Piley, *J. Colloid Interface Sci.*, **48**, 162 (1974).
2) N. Moriyama, *J. Colloid Interface Sci.*, **50**, 80 (1975).
3) W. Carr, *J. Oil Col. Chem. Assoc.*, **54**, 155 (1971).
4) Y. Ishigami, S. Suzuki, S. Yamazaki, and H. Suzuki, *J. Jpn. Colour Mater.*, **54**, 671 (1981).
5) K. Ogihara, H. Watanabe, K. Esumi, and K. Meguro, *Yukagaku*, **32**, 25 (1983).
6) K. Yamada and H. Mori, *Yukagaku*, **24**, 526 (1975).
7) N. Moriyama, *Colloid Polym. Sci.*, **254**, 726 (1976).
8) K. Ogihara, S. Tomioka, K. Esumi, and K. Meguro, *J. Jpn. Colour Mater.*, **55**, 546 (1982).
9) K. Meguro, *Kogyo kagaku Zasshi*, **58**, 905 (1955).
10) E. Matijević and R. H. Ottewill, *J. Colloid Sci.*, **13**, 242 (1958).
11) E. J. W. Verwey and J. Th. G. Overbeek, "Theory of the stability of Lyophobic Colloids," Elsevier, Amsterdam, New York (1948), p. 106.
12) H. C. Hamaker, *Physica*, **4**, 1058 (1937).
13) B. Vincent, *J. Colloid Interface Sci.*, **42**, 270 (1973).

Catalytic Activity of MoO_3 and V_2O_5 Highly Dispersed on TiO_2 for Oxidation Reactions

Takehiko Ono,* Yoshiro Nakagawa, Hisashi Miyata, and Yutaka Kubokawa
Department of Applied Chemistry, University of Osaka Prefecture, Sakai, Osaka 591
(Received December 3, 1983)

The structure of Mo-Ti oxide catalysts has been investigated by using IR and XRD techniques. At a low Mo content, MoO_3 is highly dispersed on TiO_2, an amorphous phase being formed. Simultaneously, a shift of the Mo=O band from 995 cm^{-1} to 950 and 905 cm^{-1} takes place. The maximum rate of the oxidation of C_2H_5OH and C_3H_6 over Mo-Ti-6(atom% of Mo) is attributable to the weakening of the Mo=O bond. The ^{18}O tracer and kinetic studies of the oxidation of C_3H_6 over Mo-Ti and V-Ti oxides suggest that a redox mechanism is applicable, the rate constants of reduction and reoxidation step being determined. The promoter action of TiO_2 support is attributed mainly to the increase in the rate of reduction step.

Previously we have reported that the promoter effect observed with V-Sn and Mo-Sn oxide catalysts in C_3H_6 oxidation arises from the formation of an amorphous material between each component in those composite catalysts.[1-3] It has been also shown that an amorphous phase formed with V-Ti oxides[4] at a low vanadium content is characterized by vanadate dispersed on TiO_2 in a monolayer, its distorted structure bringing about the weakening of V=O bond, *i.e.*, enhancement of the activity for the oxidative dehydrogenation of C_2H_5OH. As regards Mo-Ti oxide catalysts, a number of workers have studied the correlation between the surface structure and the catalytic activity by means of various techniques such as XRD,[5] IR,[5,6,7] XPS,[8] and *etc.*[7,9] Our understanding of this problem, however, is very far from complete.

In this work, the structure of Mo-Ti oxide catalysts have been investigated in a similar manner to that used in the studies of V-Ti oxides,[4] its correlation with the activity for the oxidative dehydrogenation of C_2H_5OH being examined. With V-Sn and V-Mo oxide catalysts, the nature of the oxygen species responsible for C_3H_6 oxidation has been recently discussed on the basis of the results of ^{18}O tracer and kinetic studies.[2] Similar studies have been extended to Mo-Ti as well as V-Ti oxide catalysts, since such studies are expected to provide information on the nature of the active phase of those catalysts.

Experimental

Materials. Mo-Ti oxides were prepared as follows: The slurry containing desired quantities of TiO_2 (p-25, Degussa) and ammonium heptamolybdate was evaporated with constant stirring. The dried product was calcined at 400 °C. MoC_3 was prepared by heating ammonium heptamolybdate at 450 °C. The surface area of the catalysts determined by the BET method were as follows: TiO_2, 45; Mo-Ti-3 (containing Mo in 3 atom%), 43; Mo-Ti-6, 41; Mo-Ti-24, 30; Mo-Ti-55, 15; MoO_3, 2 m^2/g. The V-Ti oxide catalysts used were the same as those in the previous paper.[4] $^{18}O_2$(99.1 atom%) was obtained from B.O.C. Limited (U. K.).

Apparutus and Procedures. The catalytic oxidation of C_3H_6 and C_2H_5OH was carried out in a closed circulation system (*ca.* 290 cm^3). The reaction products such as CH_2=CHCHO, CO, CO_2, CH_3CHO, and CH_3COCH_3, were analyzed by gas chromatography. The ^{18}O% in the reaction products were determined with a Hitachi RMU-6E mass spectrometer using the following ionization voltage: 80 eV for CO and CO_2, 15.5 eV for H_2O, and 15 eV for CH_2=CHCHO. X-Ray diffraction patterns (XRD) of the catalysts were obtained on both Rigaku Denki D-3F and RAD-rA diffractometers using Cu $K\alpha$ radiation with a Ni filter. With RAD-rA, the goniometer moter system and the signal were interfaced with a versatile data-aquisition system. The RAD-rA diffractometer can detect a small amount of crystalline MoO_3 at a lower Mo content. IR spectra of Mo-Ti oxides were recorded on a Hitachi EPI-G2 infrared spectrometer.

Results and Discussion

Structure of Mo-Ti Oxides. XRD patterns of Mo-Ti oxides showed only lines due to MoO_3 and TiO_2 phases. Figure 1 shows the XRD patterns of MoO_3 phase in Mo-Ti-3 and -6 as well as in their corresponding mechanical mixtures of pure MoO_3 and TiO_2. The intensities of the diffraction lines due to MoO_3 in the Mo-Ti catalysts are much smaller than those of the corresponding mixtures. With Mo-Ti-3, about 100% of the Mo oxide is present as an amorhous phase and

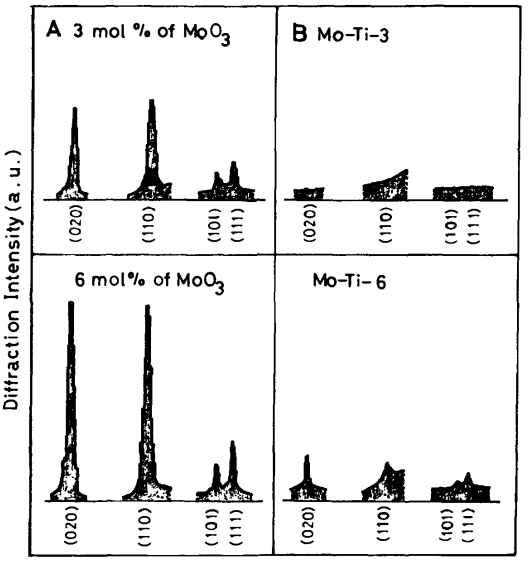

Fig. 1. X-Ray diffraction intensities of Mo-Ti oxides. (A) Mechanical mixtures of molybdenum and titanium oxides; (B) Mo-Ti oxide catalysts. (*hkl*) denote the crystal planes of MoO_3. Each diffraction line was integrated at 0.05° intervals of diffraction angle for 20 s.

with Mo-Ti-6 about 80—90%. Figure 2 shows the average intensities with Mo-Ti-24 and -55 together with the corresponding values for Mo-Ti-3 and -6. With Mo-Ti-24 and -55 catalysts MoO_3 crystals are somewhat oriented in a particular direction. As shown in Fig. 2, most of MoO_3 is amorphous at a low Mo content, its crystallinity increasing at a higher Mo content.

The IR spectra of Mo-Ti oxides containing more than 24 atom% of Mo show sharp bands at 995 and 885 cm^{-1} due to MoO_3(Fig. 3c, d). With Mo-Ti-3 and -6, these band are scarcely observed (Fig. 3 a, b). As has been done in the case of V-Ti oxides,[4], the TiO_2 disk, the weight of which corresponds to the TiO_2 content in the Mo-Ti oxides, was placed in the reference beam in order to offset the absorption due to TiO_2. As shown in Fig. 3e, f, the new bands at 950 and

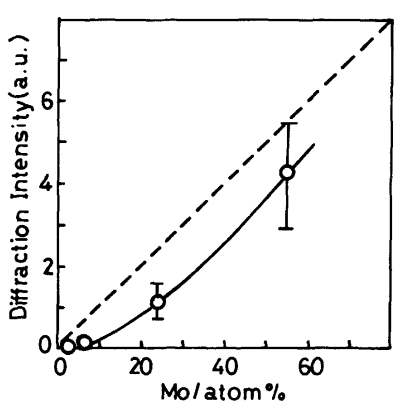

Fig. 2. X-Ray diffraction intensities of MoO_3 in the TiO_2-MoO_3 mixtures (dotted line) and in Mo-Ti catalysts (solid line) as a function of Mo content.

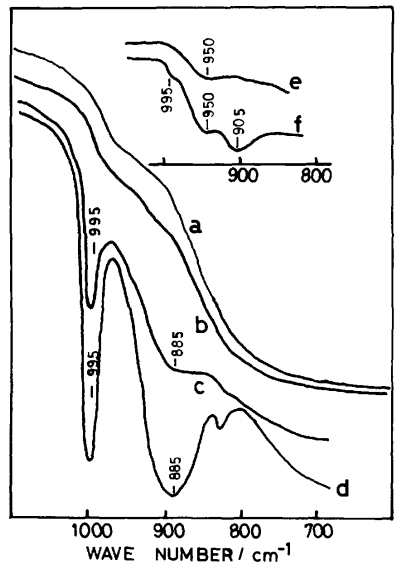

Fig. 3. IR spectra of Mo-Ti oxides. (a) Mo-Ti-3; (b) Mo-Ti-6; (c) Mo-Ti-24; (d) Mo-Ti-55; (e) and (f) the absorption due to TiO_2 were subtracted from (a) and (b) by placing the disk in the reference beam, respectively. 75 mg of KBr disk in 1 wt% of sample was used.

905 cm^{-1} appear with Mo-Ti-3 and -6 catalysts.

According to a number of workers,[10-13] the Raman spectra of various molybdenum-oxygen polyanions show two or three bands in each frequency region of about ≈200, 310—370, 500—600, 700—850, and 900—1000 cm^{-1}; the bands in the last region have been assigned to the stretching vibration of terminal Mo=O groups.[14] From these results the bands at 950—900 cm^{-1} observed with Mo-Al oxide catalysts have been attributed to the surface molybdate on alumina by Jezirowski *et al.*[14] A similar assignment has been made with the bands around 970 cm^{-1} for Mo-Si oxide catalysts.[15,16] Thus the two bands at 950 and 905 cm^{-1} seem to be assigned to terminal Mo=O stretches of the surface molybdate on TiO_2.

The bands at 995(s), 885(s), 820(w), 600(s), and 480(w) cm^{-1} are observed with IR spectra of crystalline MoO_3, while the bands at 995(m), 821(s), 668(w), and 494(vw) cm^{-1} appear in its Raman spectra.[16,17] The band at 995 cm^{-1} appears in both spectra, while the band at 885 cm^{-1} in the IR alone, suggesting that the vibrational modes attributable to both bands appear to be different from each other. Since it has been established that the band at 995 cm^{-1} is assigned to the Mo=O stretching vibration, some other assignment should be made for the band at 885 cm^{-1}.

From these facts it is concluded that with Mo-Ti oxide catalysts at a low Mo content, MoO_3 is highly dispersed on TiO_2 and present as an amorphous state which is characterized by the surface molybdate on TiO_2. Its formation results in distortion of the structure, *i.e.*, shift of the Mo=O band from 995 cm^{-1} to 950 and 905 cm^{-1}. A similar conclusion has been drawn for V-Ti oxides where formation of surface vanadate on TiO_2 brings about the shift of the V=O band from 1020 to 980 cm^{-1}.[4]

Oxydative Dehydrogenation of C_2H_5OH over Mo-Ti Catalysts. Figure 4 shows the rate of oxydative dehydrogenation of C_2H_5OH and the selectivity towards CH_3CHO formation as a function of Mo content at 180 °C. The major product is CH_3CHO, the remainder being $CH_3COOC_2H_5$ and trace of CO_2. The rate passes through a maximum around Mo-Ti-6. The maximum rate is *ca.* 4 times and 30—40 times larger than that at MoO_3 and TiO_2, respectively. There is no marked difference between the rates of oxidation in the presence and absence of oxygen (Fig. 4). Furthermore, essentially the same selectivities towards CH_3CHO formation is obtained with both oxidations. This suggests that lattice oxygen is responsible for the oxydative dehydrogenation over Mo-Ti oxide catalysts.

The rate measurements at various O_2 and C_2H_5OH pressures showed that with MoO_3 the order of the reaction is −0.5 in C_2H_5OH and zero in O_2, while with Mo-Ti-3 and Mo-Ti-6 the corresponding order is zero and 0.2—0.3, respectively. This suggests that the kinetics observed with MoO_3 is in disagreement with what is expected from a redox mechanism; the negative order in C_2H_5OH might arise from its strong adsorption.

As described above, with Mo-Ti-3 and -6 almost the whole MoO_3 is present as the amorphous surface species, while with Mo-Ti oxides containing more than

above 20 atom% of Mo, a considerable fraction MoO_3 consists of crystalline MoO_3.

Accordingly, in the region of a low Mo content, the activity of Mo-Ti oxides for the dehydrogenation of C_2H_5OH increases with increasing Mo content owing to the increase in the concentration of amorphous surface species. In the region of a high Mo content, the increase in the Mo content will cause an increase in the fraction of crystalline MoO_3 which is less active than the surface molybdate species. Thus, it is explicable that the oxidation activity passes through a maximum around 6 atom% of Mo. Such a feature is the same as that with V-Ti oxide catalysts as reported previously.[4]

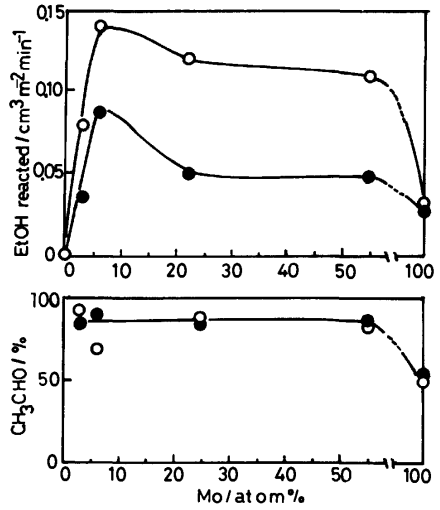

Fig. 4. Oxydative dehydrogenation of C_2H_5OH over Mo-Ti oxide catalysts at 180°C. (○) $P(C_2H_5OH)=6$ Torr and $P(O_2)=18$ Torr; (●) $P(C_2H_5OH)=6$ Torr and $P(N_2)=20$ Torr; 1 Torr=133.3 Pa.

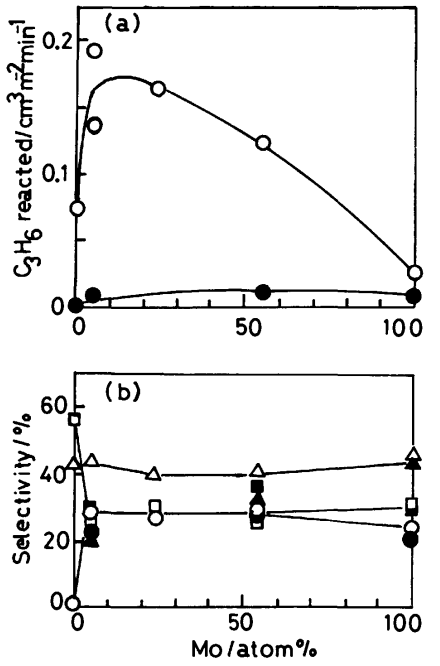

Fig. 5. Rates and product selectivities in C_3H_6 oxidation as a function of Mo content at 400°C. (a) ○ $P(C_3H_6)=23$ Torr and $P(O_2)=25$ Torr, ● $P(C_3H_6)=23$ Torr. (b) ○●, CH_2=CHCHO; □■ CO_2; △▲ CO. Solid symbols denote the results in the absence of gaseous oxygen.

C_3H_6 Oxidation over Mo-Ti and V-Ti Catalysts. Figure 5 shows the rates of C_3H_6 oxidation and the product selectivities as a function of Mo content at 400 °C. The rate of oxidation passes through a maximum around Mo-Ti-6. Almost the same distribution of the products is obtained in the whole range of the Mo content, *i.e.*, the selectivity towards CH_2=CHCHO formation is 25—30%, the remainder being CO, CO_2, and traces of CH_3COCH_3. With TiO_2, there is no formation of CH_2=CHCHO. With MoO_3 and Mo-Ti-6, essentially the same distribution of the products was obtained with both oxidations in the presence and absence of oxygen.

Similar studies have been extended to V-Ti oxide catalysts. The rate of oxidation at 320 °C also passed through a maximum around V-Ti-10 (atom% of V) catalyst. The selectivity towards CH_2=CHCHO formation decreased with decreasing vanadium content from 15—20% for V_2O_5 to 2—3% for V-Ti-10, the remainder being CO and CO_2. No formation of CH_2=CHCHO was observed with TiO_2. The rate of oxidation over V-Ti-10 is *ca.* 4 times higher than that over V_2O_5 and *ca.* 60 times than over TiO_2.

The dependence of the rate of oxidation upon O_2 and C_3H_6 pressure has been investigated with Mo-Ti as well as V-Ti oxides. As shown in Fig. 6, with increasing O_2 pressure, the rate of oxidation increases markedly for Mo-Ti-6 and V-Ti-10, while a slight increase in the rate is observed for MoO_3 and V_2O_5. There was no marked difference in the dependence of the rate of oxidation on C_3H_6 pressure over V-Ti-10 and V_2O_5. The situa-

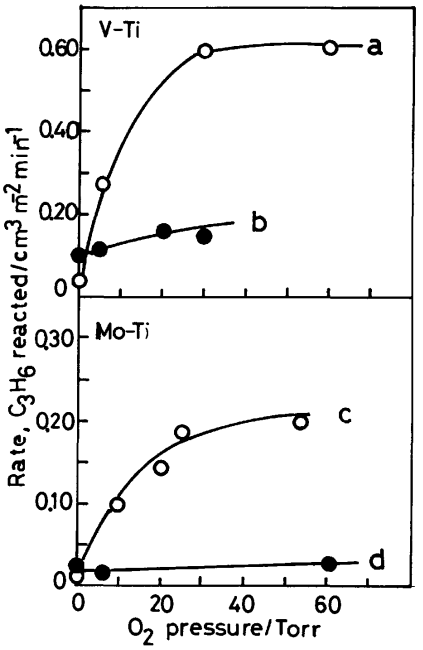

Fig. 6. Rates of C_3H_6 oxidation as a function of oxygen pressure. (a) and (b) are for V-Ti-10 and V_2O_5, respectively, at 320°C and (c) and (d) for Mo-Ti-6 and MoO_3 at 400°C. $P(C_3H_6)=23$ Torr.

tion, however, was different with Mo-Ti-6 and MoO_3, *i.e.*, the order in C_3H_6 was *ca.* 0.3 for Mo-Ti-6 but *ca.* 0.9 for MoO_3.

^{18}O Tracer and Kinetic Studies of C_3H_6 Oxidation. A large dependence of the rate of C_3H_6 oxidation on oxygen pressure observed with Mo-Ti-6 and V-Ti-10 suggests the possibility of participation of adsorbed oxygen in the oxidation. In order to obtain information on the nature of oxygen species responsible for the C_3H_6 oxidation over those catalysts, the oxidation of C_3H_6 has been investigated using $^{18}O_2$ tracer (99 atom%) with the results shown in Table 1 and Fig. 7. Little or no change in the ^{18}O content of the oxygen occurred during the reaction. According to the work of Blanchard *et al.*,[18] the exchange of oxygen through CO_2 appears to be negligible under the present experimental conditions.

In spite of the use of 99% of $^{18}O_2$, the ^{18}O content in the products at the initial stages of the reaction ranges from 20 to 30% for Mo-Ti-6 and MoO_3 and 15 to 20% for V-Ti-10 and V_2O_5. This indicates that the lattice oxygen(^{16}O) is responsible for the oxidation over both oxide catalysts. As has been done by Keulks *et al.*,[19] assuming uniform distribution of the incorporated ^{18}O among the sublayer of the oxides and the number of oxygen atoms in unit area (20 μmol/m^2), the extent of participation has been determined as follows: V_2O_5(*ca.* 10 layers)>V-Ti-10(*ca.* 5 layers)>V-Ti-2(*ca.* 1 layer) and Mo-Ti-6(*ca.* 5 layers)=MoO_3(*ca.* 5 layers).

As described previously,[2] even in the case where the surface anion vacancies are not refilled from gaseous oxygen, the following equation based on a simple redox mechanism holds, as far as the diffusion of the oxide ion is rapid as compared to the surface reduction;[2]

$$k_1P(C_3H_6)\theta = k_2P(O_2)^{0.5}(1-\theta), \quad (1)$$

where k_1 is the rate constant for reduction step and k_2 for reoxidation step. θ and $1-\theta$ refer to the surface oxide ions and anion vacancies, respectively, which corresponds to the surface Mo=O species and anion vacancies formed by oxygen removed from it, respectively, in view

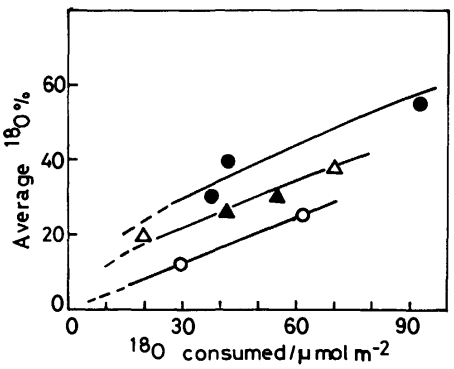

Fig. 7. Average ^{18}O%[a] in the products *vs.* amount of ^{18}O consumed[b] in C_3H_6 oxidation. V-Ti-10(●) and V_2O_5(○) at 320°C, Mo-Ti-6(▲) and MoO_3 (△) at 400°C. a),b) See Table 1.

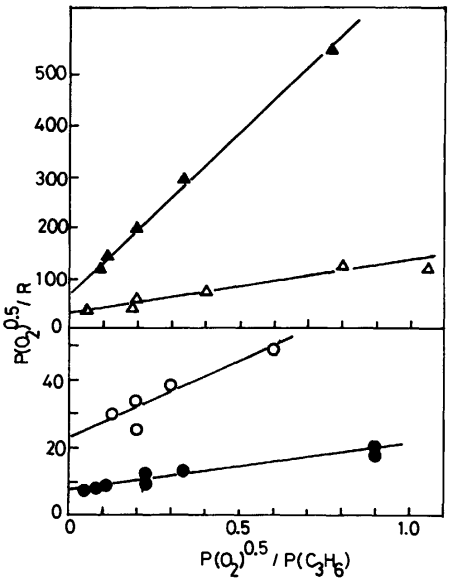

Fig. 8. Plots of $P(O_2)^{0.5}/R$ *vs.* $P(O_2)^{0.5}/P(C_3H_6)$ for MoO_3(▲), Mo-Ti-6(○), V_2O_5(△), and V-Ti-10 (●).
Experimental conditions are the same as in Fig. 5 for Mo–Ti oxides and in Fig. 6 for V-Ti oxides, respectively. R denotes the rate of C_3H_6 oxidation.

Table 1. ^{18}O contents in the products of C_3H_6 oxidation over Mo-Ti and V-Ti oxide catalysts

Catalyst	Temp °C	React. time min	Products/μ mol m^{-2} and ^{18}O content/%[a]				Total yield[c] μ mol-oxygen atoms m^{-2}	Average[d] ^{18}O %	Lattice oxygen[e] participated layers
			CO_2	CO	H_2O[b]	CH_2=CHCHO			
Mo-Ti-6	400	3	7.4(24)	7.1(34)	17(—)	3(19)	42	26	*ca.* 5
MoO_3	400	5.5	2.9(19)	4.2(21)	8(—)	0.8(33)	19	20	*ca.* 5
		15	13(34)	13(39)	28(—)	3(50)	70	37	
V-Ti-10	320	0.2	5(28)	9(33)	7(—)	—	26	30	
		0.3	4(36)	13(43)	17(—)	—	41	40	*ca.* 5
		1.0	14(54)	25(59)	38(39)	—	91	50	
V_2O_5	320	1	3.5(12)	7.5(13)	11(11)	0.45(25)	27	13	*ca.* 10
		3	7.5(25)	16(25)	24(20)	0.75(31)	55	25	

a) Values in parentheses. b) Calculated from hydrogen balance. c) These values were nearly the same as that obtained from the amount of $^{18}O_2$ consumed in the oxidation. d) (Total amount of ^{18}O/total amount of oxygen) × 100. e) See Ref. 19. $P(C_3H_6)=23$ Torr, $P(^{18}O_2)=8$ Torr.

Table 2. Values of k_1 and k_2 for Mo-Ti and V-Ti oxide catalysts

Catalyst	Temp/°C	k_1[a]	k_2[b]
MoO_3	400	0.0015	0.015
Mo-Ti-6	400	0.024	0.04
V_2O_5	320	0.01	0.04
V-Ti-10	320	0.08	0.12

a) $cm^3\ Torr^{-1}\ min^{-1}\ m^{-2}$, b) $cm^3\ Torr^{-1/2}\ min^{-1}\ m^{-2}$.

of the importance of the Mo=O species in the oxidation. The following rate equation results:

$$R = \frac{k_1 k_2 P(C_3H_6) P(O_2)^{0.5}}{k_1 P(C_3H_6) + k_2 P(O_2)^{0.5}}. \quad (2)$$

As shown in Fig. 8, the plots of $P(O_2)^{0.5}/R$ *vs.* $P(O_2)^{0.5}/P(C_3H_6)$ is approximately linear, suggeting that this equation is applicable to the results. Table 2 shows the values of k_1 and k_2 thus obtained.

Both k_1 and k_2 values increase on going from MoO_3 to Mo-Ti-6 and from V_2O_5 to V-Ti-10. The increase in the k_1 value is much larger than that for the k_2 value. Thus, the promoter action of TiO_2 in V-Ti and Mo-Ti oxides is attributed mainly to the increase in the rate of reduction step. Such a relative change of k_1 and k_2 is expected from the weakening of the Mo=O bond as described above. Thus, the rate maximum observed with both oxidation (Figs. 4 and 5) are explicable on the same basis. A large dependence of the rate of oxidation on oxygen pressure over Mo-Ti-6 and V-Ti-10 catalysts is also explicable from high values of k_1/k_2, *i.e.*, the high reducibility of surface molybdate or vanadate on TiO_2. The maximum rate of oxidation for Mo-Ti-6 and V-Ti-10 is explicable in a manner similar to that with the oxydative dehydrogenation of C_2H_5OH, *i.e.*, by the change in the concentration of the surface species with the Mo or V content.

Recently a number of workers have investigated the promoter effect observed with V-Ti oxides in the oxidation reaction, making various proposals.[20-24] The results described above indicate that similar mechanisms are involved in the promoter effects with both Mo-Ti and V-Ti oxides; The role of TiO_2 support in those oxide catalysts is to enhance the activity per one site in addition to the increase in the number of active sites. From the results in the present work together with those obtained previously,[4] it might be concluded that the promoter action due to formation of the amorphous phase (a highly dispersed oxide catalyst) is expected for other composite oxide catalysts.

Akimoto *et al.*[6] have reported that both adsorbed molecular oxygen and lattice oxygen participates in the production of maleic anhydride from 1,3-C_4H_6 over Mo-Ti catalysts. In the case of V-Sn oxide catalysts at a low V content, we have also suggested the participation of both adsorbed and lattice oxygens in the oxidation on the basis of the results of ^{18}O tracer as well as kinetic studies.[2] With Mo-Ti and V-Ti oxide catalysts, however, it seems unnecessry to take into account the possibility of adsorbed oxygen, since the dependence of the rate of oxidation on O_2 and C_3H_6 pressure is explicable by the concept that only lattice oxygen participates in the oxidation.

With the C_3H_6 oxidation over Mo-Ti oxide, there is a marked difference between the rates of oxidation in the presence and absence of oxygen. Such a feature is contrast with a slight difference between the both rates for the oxydative dehydrogenation of C_2H_5OH. It should be noted that the number of lattice oxygen atoms consumed on the oxidation of one molecule is 1—2 with C_2H_5OH but 9—10 with C_3H_6, the lattice oxygen producing CO, CO_2, H_2O, and CH_2=CHCHO for C_3H_6 oxidation. Furthermore, the reaction temperature is much higher for the C_3H_6 oxidation. Accordingly, the extent of oxygen removed from the Mo=O species during the reaction is expected to be much smaller for C_2H_5OH dehydrogenation than for the C_3H_6 oxidation. Thus, a small enhancement of the rate of C_2H_5OH dehydrogenation by the presence of oxygen is explicable.

The authors wish to thank Mr. Makoto Sakaguchi for carrying out part of the experiments.

References

1) T. Ono, Y. Nakagawa, and Y. Kubokawa, *Bull. Chem. Soc. Jpn.*, **54**, 343 (1981).
2) T. Ono and Y. Kubokawa, *Bull. Chem. Soc. Jpn.*, **55**, 1748 (1982).
3) T. Ono, T. Ikebata, and Y. Kubokawa, *Bull. Chem. Soc. Jpn.*, **56**, 1284 (1983).
4) Y. Nakagawa, T. Ono, H. Miyata, and Y. Kubokawa, *J. Chem. Soc., Faraday Trans. 1*, **79**, 2929 (1983).
5) K. Yu. Adzhamov, A. K. Senchikhina, T. G. Alkazov, and K. M. Mekhtiev, *Kinet. Catal.*, **16**, 589 (1975).
6) M. Akimoto and E. Echigoya, *J. Catal.*, **29**, 191 (1973).
7) J. Rivasseau, P. Canesson, and M. Blanchard, *J. Phys. Chem.*, **84**, 2972 (1980).
8) K. Tanaka, K. Miyahara, and Ke. Tanaka, *Bull. Chem. Soc. Jpn.*, **54**, 3106 (1981).
9) M. Ai, *Bull. Chem. Soc. Jpn.*, **49**, 1328 (1976).
10) W. P. Griffith and P. J. B. Lesniak, *J. Chem. Soc.*, A, 1066 (1969).
11) J. Fuchs and K. F. Jahr, *Z. Naturforsch.*, B, **23**, 1380 (1968); J. Fuchs and J. Brudgam, *ibid.*, **32**, 853 (1977).
12) K. H. Tytko and B. Schonfeld, *Z. Naturforsch.*, **30**, 471 (1975).
13) R. Mattes, H. Bierbusse, and J. Fuchs., *Z. Anorg. Allg. Chem.*, **385**, 230 (1971).
14) H. Jeziorowskii and H. Knözinger, *J. Phys. Chem.*, **83**, 1166 (1979).
15) S. R. Seyedmouir, S. Abdo, and R. F. Howe, *J. Phys. Chem.*, **86**, 1232 (1982).
16) H. Jeziorowskii, H. Knözinger, P. Grange, and P. Gajardo, *J. Phys. Chem.*, **84**, 1825 (1980).
17) F. R. Brown, Leo E. Makrovsky, and K. H. Rhee, *J. Catal.*, **50**, 162 (1977).
18) M. Blanchard and G. Longuet, *Kinet. Catal.*, **14**, 20 (1973).
19) G. W. Keulks and L. D. Krenzke, *Proc. 6th. Int. Congr. Catal.*, London, 1976, Vol. 2, p. 806; L. D. Krenzke and G. W. Keulks, *J. Catal.*, **61**, 316 (1980).
20) D. J. Cole, C. F. Cullis, and D. J. Hucknall, *J. Chem. Soc., Faraday Trans. 1*, **72**, 2185 (1976).
21) Y. Murakami, M. Inomata, A. Miyamoto, and K. Mori, *Proc. 7th Int. Congr. Catal.*, Tokyo, 1980, P. 1344; A. Miyamoto, Y. Yamazaki, M. Inomata, and Y. Murakami, *J. Phys. Chem.*,

85, 2366, 2372 (1981); M. Inomata, K. Mori, A. Miyamoto, T. Ui, and Y. Murakami, *ibid.*, **87**, 754 (1983).
22) G. C. Bond and K. Buckeman, *Discuss. Faraday Soc.*, **1982**, 235.
23) A. Andersson, *J. Catal.*, **76**, 144 (1982).
24) M. Akimoto, M. Usami, and E. Echigoya, *Bull. Chem. Soc. Jpn.*, **51**, 2195 (1978).

Kinetics and Equilibrium Studies of the Formation of a Cobalt(II) Complex with *N*-(8-Quinolyl)aminoacetic Acid

Yasuo HARA,† Ken-ichi OKAMOTO, Jinsai HIDAKA, and Hisahiko EINAGA*,††
Department of Chemistry, University of Tsukuba, Ibaraki 305
††*Institute of Materials Science, University of Tsukuba, Ibaraki 305*
(Received August 3, 1983)

Stopped-flow kinetic and equilibrium studies have been made of the formation of a cobalt(II) complex with *N*-(8-quinolyl)aminoacetic acid in 0.10 mol dm^{-3} aqueous sodium chloride containing 12 vol% ethanol at 25 °C. Octahedral mono- and bis-ligand complexes were formed *via* the two pathways of the reactions of deprotonated and monoprotonated ligand species with the aquacobalt(II) ion. The coordination mechanism is discussed.

It is interesting to study spectrochemically the coordination characteristics of aromatic multidentate ligands to matal ions, which take several kinds of coordination geometry depending on the ligand employed, because the ligating groups are incorporated into the rigid frame of the aromatic ligand and because the electronic absorption spectrum of the ligand reflects its coordination mode. Furthermore, the nature of the ligating groups and the steric restriction due to the planarity of the ligand qualify the coordination behavior and mechanism of the metal ion.

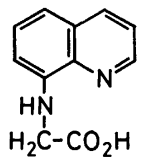

Hqaa

The present study relates to the formation of a cobalt(II) complex with *N*-(8-quinolyl)aminoacetic acid (Hqaa).[1] In order to obtain detailed information on the coordination reaction characteristics, the coordination state of cobalt(II) and the coordination behavior of the ligand were spectrochemically and kinetically investigated. There has been only one paper concerning the ligand based on potentiometry.[2]

Experimental

Reagents. The ligand, QAA,[1] was synthesized by the condensation of chloro- or bromoacetic acid with 8-aminoquinoline in an alkaline medium, with some modifications of the literature procedure.[2] It was obtained as a monohydrochloride salt and was purified by repeated crystallizations from an aqueous solution. Calcd for $C_{11}H_{10}N_2O_2 \cdot HCl$: C, 55.35; H, 4.64; N, 11.73%. Found: C, 55.63; H, 4.59; N, 12.02%.

An aqueous cobalt(II) solution was prepared from analytical grade chloride salt from the Wako Pure Chemicals Ind. Co., Ltd., Osaka, and was acidified slightly with HCl to prevent its hydrolysis. It was then standardized by titration with EDTA. All the other chemicals were of an analytical or equivalent grade and were used without further purification.

Measurements. Electronic absorption spectral measurements were made with JASCO spectrophotometers, models UVIDEC-1 and SS-25, to the latter of which were attached a stopped-flow apparatus, Model SFC-5; a data processor, Model DP-500; and a RIKADENKI X-Y recorder, Model RW-11. The protonation and stability constants were determined spectrophotometrically at 340 nm in the former and at 303.5 nm in the latter in a 0.10 mol dm^{-3} aqueous sodium-chloride solution containing 12 vol% ethanol at 25.0±0.1 °C. Nitrogen gas was passed through the solution before the absorption spectral measurements to avoid any possible oxidation of cobalt(II). Kinetic runs were made at 303.5 nm under a pseudo-first-order kinetic condition with respect to the metal-ion or ligand concentration. The rate constant, k_{obsd}, was calculated from this relation:

$$\ln \{A_{eq}/(A_{eq}-A_t)\} = k_{obsd} \cdot t,$$

where A_t and A_{eq} stand for the absorbances at 303.5 nm at time t and at equilibrium respectively. The hydrogen-ion concentration was calculated from the measured pH value, pH_{meas}, with a HORIBA pH meter, Model F7-SS, with glass and 3.33 mol dm^{-3} potassium chloride calomel electrodes, according to this relation:

$$-\log [H^+] = pH_{meas} + \log f_{H^+}.$$

The activity coefficient of the hydrogen ion, f_{H^+}, was estimated by defining a 12 vol% ethanol aqueous solution containing 0.0100 mol dm^{-3} HCl and 0.0900 mol dm^{-3} NaCl as $-\log [H^+] \equiv 2.00$. The f_{H^+} value estimated under these conditions agreed well, within the limits of experimental error, with the literature data of 0.83.[3] The hydrogen-ion concentration was adjusted mainly with an acetic acid-sodium acetate buffer solution, whose concentration was maintained as low as possible (usually less than 0.5×10^{-2} mol dm^{-3}) in order to confirm that there was no meaningful influence on the complex formation of cobalt(II) with QAA under the equilibrium and kinetic conditions adopted.

Results and Discussion

Electronic Absorption Spectra. Figures 1 and 2 show the electronic absorption spectra of QAA and its cobalt(II) complexes respectively. The qaa^- species gives two distinct absorption maxima, at 29.20×10^3 and 39.40×10^3 cm^{-1}, due to the $\pi\rightarrow\pi^*$ transitions, which shift bathochromically on protonation at the heterocyclic nitrogen atom (Fig. 1). The coordination of the terdentate ligand qaa^- to cobalt(II) brings about remarkable spectral features; several absorption maxima in the $(31.70—33.70)\times10^3$ cm^{-1} region and a maximum at 43.20×10^3 cm^{-1} are characteristic of the mono-QAA complex, and there are in addition a maximum at 39.53×10^3 cm^{-1} and a shoulder around

† Present address: Yokkaichi Works, Japan Synthetic Rubber Co., Ltd., Yokkaichi, Mie 510.

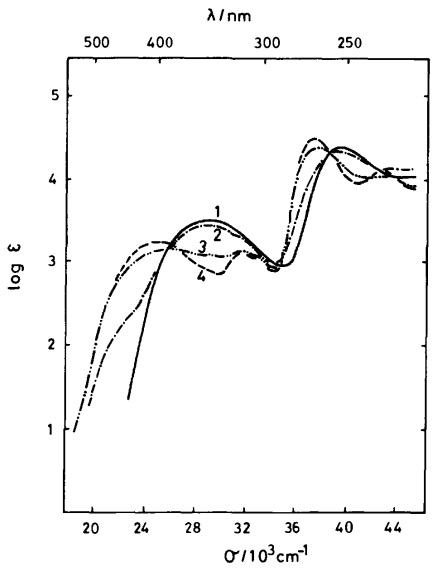

Fig. 1. Absorption spectra of QAA. 1: pH 9.70 (qaa^-); 2: pH 4.50; 3: pH 2.86; and 4: pH 0.38 ($H_3\ qaa^{2+}$).

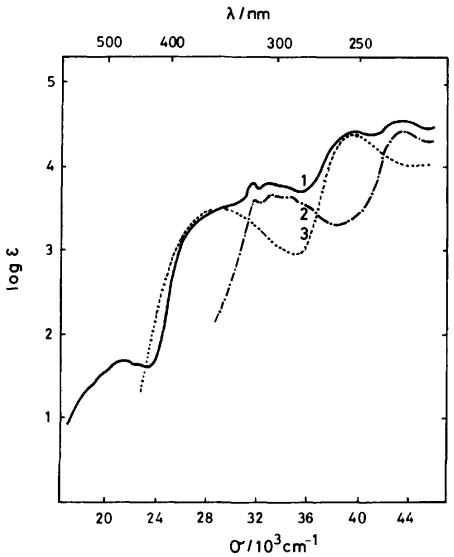

Fig. 2. Absorption spectra of the QAA complex. 1: $[Co(qaa)_2]$; 2: $[Co(qaa)(H_2O)_3]^+$; and 3: qaa^-.

$29.07\times10^3\ cm^{-1}$ of the bis-QAA complex. This shows that the transitions of π electrons related to the coordinated ligand are influenced by the numbers and arrangement of its chromophores.

The electronic absorption spectra in the d-d transition region of the bis-QAA complex and a typical cobalt(II) complex with octahedral coordination are given in Fig. 3. The absorption spectrum of the bis-QAA complex can be well correlated to that of a Schiff-base complex of the $[Co(N)_4(O)_2]$ type,[4] and the absorption maxima at 10.20×10^3 and 21.19×10^3 cm^{-1} of the bis-QAA complex can be assigned to the $^4T_{1g}(F)$-$^4T_{2g}(F)(O_h)$ and $^4T_{1g}(F)$-$^4T_{1g}(P)(O_h)$ transitions respectively.

Hence, it can be concluded that the QAA complex has an octahedral coordination and that the mono-

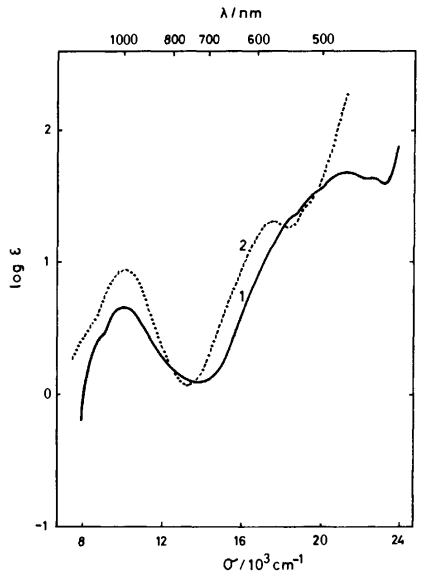

Fig. 3. Absorption spectra in the d-d transition region of $[Co(qaa)_2]$ and a Schiff base complex, $[Co(L)_2(py)_2]^+$, with octahedral coordination.[4] 1: $[Co(qaa)_2]$ and 2: $[Co(L)_2(py)_2]^+$, L: *ortho*-$OC_6H_4CHN(CH_2)_3CH_3$.

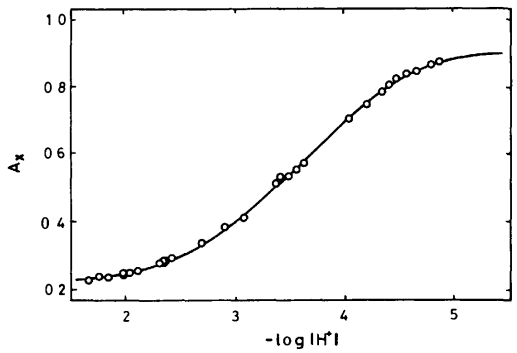

Fig. 4. Relation between A_x and $-\log[H^+]$ for QAA. Concentration of QAA, 1.41×10^{-4} mol dm^{-3}. Bald line is a theoretical curve drawn by using K_{a1} of $10^{4.04}$ and K_{a2} of $10^{2.99}$.

and bis-QAA complexes can be expressed as $[Co(qaa)(H_2O)_3]^+$ and $[Co(qaa)_2]$ respectively.

Stability. The protonation constants of QAA were determined by the use of the following relation (*cf.* Appendix I):

$$A_x = A_2 + \frac{(A_0-A_2)+(A_1-A_2)K_{a1}[H^+]}{1+K_{a1}[H^+]+K_{a1}K_{a2}[H^+]^2}. \quad (1)$$

Here, K_{a1} (=[Hqaa]/[H^+][qaa^-]) and K_{a2} (=[H_2qaa^+]/[H^+][Hqaa]) are the protonation constants related to the heterocyclic nitrogen base and the carboxylate group;[5] A_0 and A_2 are absorbances corresponding to the qaa^- and $H_2\ qaa^+$ species; A_1 is an intrinsic absorbance of the Hqaa species, and A_x is an absorbance when these ligand species coexist. Equation (1) was solved by the curve-fitting method[6] with a normalized curve of:

$$Y = \{(A_0-A_2)+bt\}/(1+at+t^2) \text{ and } X = \log t, \quad (2)$$

with $\log K_{a1}K_{a2}=2(X-\log[H^+])$, $\log K_{a1}/K_{a2}=2\log a$,

Table 1. Protonation constants of QAA

$\log (K_{a1}/\text{mol}^{-1}\,\text{dm}^3)$	$\log (K_{a2}/\text{mol}^{-1}\,\text{dm}^3)$	Condition	Reference
4.26	2.98	0.1 mol dm^{-3} aqueous sodium perchlorate, 25 °C potentiometry[a]	2
4.04±0.05	2.99±0.05	0.10 mol dm^{-3} aqueous sodium chloride containing 12 vol% ethanol, 25 °C spectrophotometry	Present work

a) The $\log K_{a3}$ value related to protonation at the imino-nitrogen atom has been estimated to be 1.9.[2]

Table 2. Stability constants and related data

$\log (\beta_{11}/\text{mol}^{-1}\,\text{dm}^3)$	$\log (\beta_{12}/\text{mol}^{-2}\,\text{dm}^6)$	$-\Delta G^\circ_{11}$/kJ mol^{-1} [a]	$-\Delta G^\circ_{12}$/kJ mol^{-1} [a]	Condition	Reference
3.7	7.5	—	—	0.1 mol dm^{-3} aqueous sodium perchlorate,25 °C potentiometry	2
4.82±0.05	9.51±0.10	27.5±0.3	54.3±0.6	0.10 mol dm^{-3} aqueous sodium chloride containing 12 vol% ethanol, 25 °C spectrophotometry	Present work

a) Calculated by this relation: $-\Delta G^\circ_{1j}=RT\ln\beta_{1j}$ without the extrapolation of β_{1j} to the zero ionic strength ($j=1$ and 2).

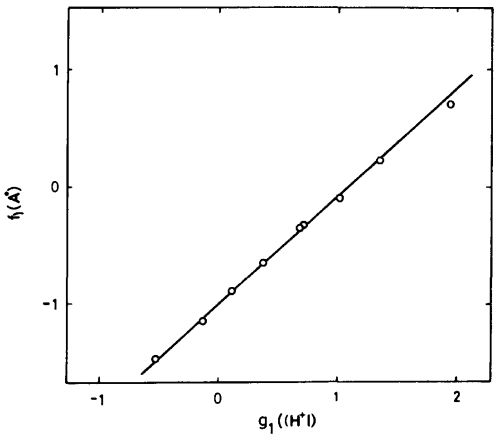

Fig. 5. Relation between $f_1(A')$ and $g_1([H^+])$. $f_1(A')\equiv \log\{(A'-A_{11g})/(A_{m.c}-A')\}$, $g_1([H^+])=-\log\{[H^+]-(K_{a2}[H^+]+1+1/K_{a1}[H^+])\}$. C_M, 1.60×10^{-2} mol dm^{-3} and C_L, 1.60×10^{-4} mol dm^{-3}.

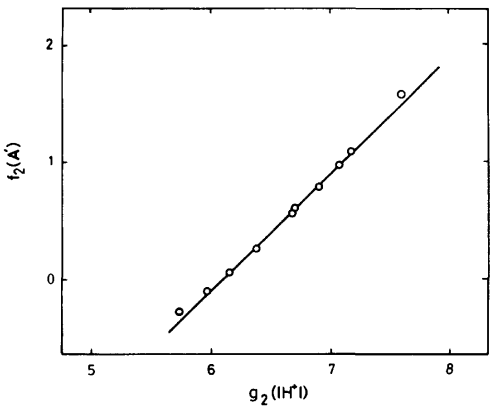

Fig. 6. Relation between $f_2(A')$ and $g_2([H^+])$. $f_2(A')\equiv \log\{(A'-A_{11g})/(A_{b.c}-A_{11g})\}-3\log\{(A_{b.c}-A')/((A_{b.c}-A_{11g})\}$, $g_2(H^+])\equiv-2\log\{[H^+](K_{a2}[H^+]+1+1/K_{a1}[H^+])\}$. C_M, 8.02×10^{-5} mol dm^{-3} and C_M, 1.60×10^{-4} mol dm^{-3}.

and $\log(A_1-A_2)=\log b+(1/2)(\log K_{a2}/K_{a1})$. Figure 4 shows the results, from which the K_{a1} and K_{a2} values were calculated; they are summarized in Table 1, together with those in the literature.[2]

The stability constants were determined by means of this relation:

$$\log\{(A'-A_{11g})/(A_{m.c}-A')\} = \log\beta_{11}C_M/K_{a1} - \log\{[H^+](K_{a2}[H^+]+1+1/K_{a1}[H^+])\}, \quad (3)$$

for the mono-QAA complex (β_{11}) under the condition of $C_M\gg C_L$, and by this relation:

$$\log\{(A'-A_{11g})/(A_{b.c}-A_{11g})\} - 3\log\{(A_{b.c}-A')/(A_{b.c}-A_{11g})\} = \log 4\beta_{12}C_M^2/K_{a1}^2 - 2\log\{[H^+](K_{a2}[H^+]+1+1/K_{a1}[H^+])\}, \quad (4)$$

for the bis-QAA complex (β_{12}) under the condition of $2C_M=C_L$ (*cf.* Appendix II). Here, C_M and C_L are the total concentrations of cobalt(II) and QAA respectively; A_{11g}, $A_{m.c}$, and $A_{b.c}$ denote absorbances corresponding to the ligand, the mono-QAA complex, and the bis-QAA complex respectively, and A' is the absorbance when the ligand and the complex coexist. Figures 5 and 6 show the findings on the relation between the absorbance term and the hydrogen-ion-concentration term in Eqs. (3) and (4), from which β_{11} and β_{12} were determined; they were summarized in Table 2, together with those in the literature.[2]

It is noteworthy that the stability constant of the mono-QAA complex is very close to the second step-by-step stability constant (β_{12}/β_{11}), as given in Table 2; this differs from general tendency for the step-by-step stability constants to decrease with increased

numbers of the coordinated ligands.[7] The molecular model reveals that there are no steric factors in QAA to bring about this particular aspect and that there are more possible geometrical isomers for the bis than for the mono-QAA complex, *i.e.*, six for the former and two for the latter. The relatively large values of the second step-by-step stability constant as compared with the first one may reflect either the bis-QAA complex being in equilibrium for some of its geometrical isomers or the mutual stabilizing interactions between the coordinated ligands in the bis-QAA complex.

Kinetics. By taking into consideration the protonation constants of QAA, the hydrolysis constant of cobalt(II) ($\log K_{OH}=-9.85$ (0 mol dm^{-3}, 25 °C) or -9.82 (1.0 mol dm^{-3}($NaClO_4$), 25 °C), $K_{OH}=[[Co(OH)(H_2O)_5]^+][H^+]/[[Co(H_2O)_6]^{2+}]$,[8] the stability constants of the mono- and bis-QAA complexes, and the rapid attainment of equilibria for the protolytic processes[9] as compared with the complex formation processes, which proceed at pH 2—5, the reaction pathways of the QAA complex can be given as follows (j=0—2);

$$[Co(H_2O)_6]^{2+} + H_jqaa^{(j-1)+} \xrightarrow{k_{0j}} [Co(qaa)(H_2O)_3]^+ + jH^+, \quad (\mathbf{I})$$

$$[Co(qaa)(H_2O)_3]^+ + H_jqaa^{(j-1)+} \xrightarrow{k_{1j}} [Co(qaa)_2] + jH^+. \quad (\mathbf{II})$$

In case the rate-determining step is in Stage **I**, Eqs. 6 and 7 can be deduced under the pseudo-first-order kinetic conditions with respect to the cobalt(II) and QAA concentrations (*cf.* Appendix III);

$$\begin{aligned} &d[[Co(qaa)(H_2O)_3]^+]/dt \\ &= k^M_{obsd}([[Co(qaa)(H_2O)_3]^+]_{eq} - [[Co(qaa)(H_2O)_3]^+]) \\ &= (k_{02}[H_2qaa^+] + k_{01}[Hqaa] + k_{00}[qaa^-])[[Co(H_2O)_6]^{2+}] \\ &\quad - (k_{-02}[H^+]^2 + k_{-01}[H^+] + k_{-00})[[Co(qaa)(H_2O)_3]^+], \end{aligned} \quad (5)$$

$$k^M_{obsd} = \{C'_M/(K_{a1}K_{a2}[H^+]^2 + K_{a1}[H^+] + 1) + 1/\beta_{11}\} \times (k_{02}K_{a1}K_{a2}[H^+]^2 + k_{01}K_{a1}[H^+] + k_{00}), \quad (6)$$

$$\begin{aligned} &d[[Co(qaa)_2]]/dt \\ &= k^L_{obsd}([[Co(qaa)_2]]_{eq} - [[Co(qaa)_2]]), \end{aligned}$$

$$k^L_{obsd} = \frac{\{C'_L/(K_{a1}K_{a2}[H^+]^2 + K_{a1}[H^+] + 1)\}^2 + 1/\beta_{12}}{C'_L/(K_{a1}K_{a2}[H^+]^2 + K_{a1}[H^+] + 1)} \times (k_{02}K_{a1}K_{a2}[H^+]^2 + k_{01}K_{a1}[H^+] + k_{00}), \quad (7)$$

where k^M_{obsd} and k^L_{obsd} are the observed rate constants under the condition of $C_M' \gg C_L'$ and $C_L' \gg C_M'$; k_{0j} is the forward rate constant for the pathway of $[Co(H_2O)_6]^{2+}$ and $H_j qaa^{(j-1)+}$; k_{-0j} is the backward rate constant for the same pathway; C_M' and C_L' are the total concentrations of cobalt II and QAA, and the suffix "eq" denotes the equilibrium state. Under the pseudo-first-order kinetic condition with respect to the ligand, Stage **II** may possibly be the rate-determining step and Eq. 8 can be deduced analogously:

$$k^L_{obsd} = \{C'_L/(K_{a1}K_{a2}[H^+]^2 + K_{a1}[H^+] + 1) + \beta_{11}/\beta_{12}\} \times (k_{12}K_{a1}K_{a2}[H^+]^2 + k_{11}K_{a1}[H^+] + k_{10}), \quad (8)$$

where k_{1j} is the forward rate constant for the pathway of $[Co(qaa)(H_2O)_3]^+$ and $H_j qaa^{(j-1)+}$. Hence, the reaction pathways can be deduced by plotting the $[H^+]$ dependence of $k^M_{obsd}{}'$ and $k^L_{obsd}{}'$, which are defined as follows;

$$k^M_{obsd}{}' \equiv k^M_{obsd}/\{C'_M/(K_{a1}K_{a2}[H^+]^2 + K_{a1}[H^+] + 1) + 1/\beta_{11}\}, \quad (6')$$

$$k^L_{obsd}{}' \equiv k^L_{obsd}\{C'_L/(K_{a1}K_{a2}[H^+]^2 + K_{a1}[H^+] + 1)\}/[\{C'_L/(K_{a1}K_{a2}[H^+]^2 + K_{a1}[H^+] + 1)\}^2 + 1/\beta_{12}], \quad (7')$$

or:

$$k^L_{obsd}{}' \equiv k^L_{obsd}/\{C'_L/(K_{a1}K_{a2}[H^+]^2 + K_{a1}[H^+] + 1) + \beta_{11}/\beta_{12}\}. \quad (8')$$

Figures 7 and 8 depict the $[H^+]$ dependences of $k^M_{obsd}{}'$ and $k^L_{obsd}{}'$ respectively, as defined by Eq. 7′. No meaningful result was obtained when $k^L_{obsd}{}'$ was defined by means of Eq. 8′. It can be concluded that the rate-determining step for both the mono- and bis-QAA complexes are in Stage **I** and that the reaction pathways of $[Co(H_2O)_6]^{2+}$ with Hqaa and with qaa^- really hold true. The rate constants and related data are summarized in Table 3.

The rate constants for the octahedral cobalt(II) complexes abstracted in Table 4 have been reported. All these ligands form cobalt(II) complexes by means of the preliminary formation of an outer-sphere complex, followed by transformation to the inner-sphere complex; then the chelate complexes are formed with a liberation of the coordinated water from the outer-sphere complex as the mechanistic rate-determining step.[10-19] The two exceptions are β-alaninate and 3-aminobutyrate, which show the chelate-ring closure as the rate-determining step.[16,17] In this reaction mechanism, the formation rate constant (k_f) can be equated with a product of the

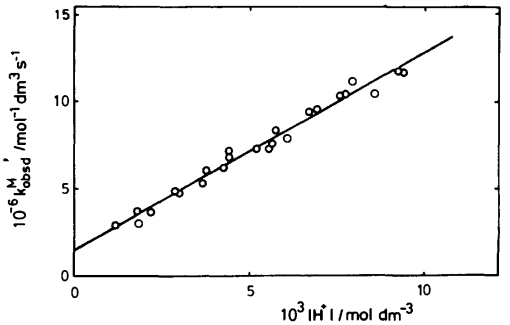

Fig. 7. Relation between $k^M_{obsd}{}'$ and $[H^+]$. C'_M, (2.01—7.99)$\times 10^{-3}$ mol dm^{-3} and C'_L, 8.02×10^{-5} mol dm^{-3}.

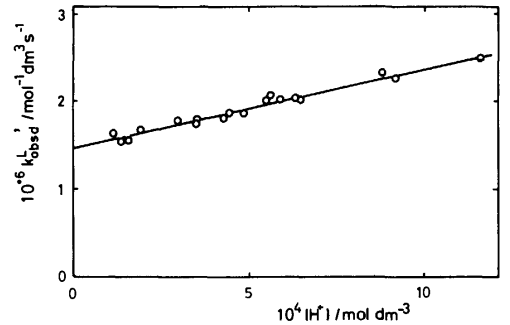

Fig. 8. Relation between $k^L_{obsd}{}'$ and $[H^+]$. C'_M, 8.02×10^{-6} mol dm^{-3} and C'_L, (2.01—4.02)$\times 10^{-4}$ mol dm^{-3}.

Table 3. Rate constants and related data

Pathway[a]	k_{0j}/mol^{-1} dm^3 s^{-1}	k_{-0j}/mol^{-j} dm^{3j} s^{-1} [b]	ΔG^{*}_{0j}/kJ mol^{-1} [c]	ΔG^{*}_{-0j}/kJ mol^{-1} [c]	Condition[d]
Co^{2+}+Hqaa	$(1.08\pm0.13)\times10^5$	—	—	—	$C_M' \gg C_L'$
(j=1)	$(0.85\pm0.08)\times10^5$	—	—	—	$C_L' \gg C_M'$
	$(1.0\pm0.1)\times10^5$	$(1.7\pm0.6)\times10^4$	44.4±0.2	48.8±1.0	Average
Co^{2+}+qaa$^-$	$(1.50\pm0.23)\times10^6$	—	—	—	$C_M' \gg C_L'$
(j=0)	$(1.47\pm0.10)\times10^6$	—	—	—	$C_L' \gg C_M'$
	$(1.5\pm0.2)\times10^6$	$(2.3\pm0.6)\times10$	37.7±0.3	65.2±0.7	Average

a) Abbreviation: Co^{2+}, $[Co(H_2O)_6]^{2+}$. b) k_{-0j} was calculated by means of this relation: $k_{-0j}=k_{0j}K_{a1}{}^j/\beta_{11}$. c) $\Delta G^{*}_{0j\,(\text{or}\,-0j)}$ was calculated by means of this relation: $\Delta G^{*}_{0j\,(\text{or}\,-0j)}=-RT(\ln k_{0j\,(\text{or}\,-0j)}-\ln kT/h)$, where R, T, k, and h have the usual meanings. d) 0.10 mol dm^{-3} aqueous sodium chloride containing 12 vol% ethanol, 25 °C.

Table 4. Formation-rate constants of cobalt(II) complexes concerned

Ligand[a]	k_f/mol^{-1} dm^3 s^{-1} [b]	Remarks[c]	Reference
Ammonia	9.5×10^4	0.1 mol dm^{-3} (NH_4NO_3), 20 °C, $k^{-H_2O}=8\times10^5$ s^{-1}	10
Imidazole	1.3×10^5	0.15 mol dm^{-3} (KNO_3), 25 °C, $k^{-H_2O}=4.4\times10^5$ s^{-1}	11
phen	3.2×10^5	No specification, 25 °C	12
5-NO_2-phen	1.6×10^5	No specification, 25 °C	12
bpy	6.3×10^4	No specification, 25 °C	12
tpy	2.5×10^4	No specification, 25 °C	13
Glycinate	1.5×10^6	0.10 mol dm^{-3} (—), 25 °C	14
Glycinate	4.6×10^5	0.15 mol dm^{-3} (KNO_3), 25 °C, $k^{-H_2O}=2.6\times10^5$ s^{-1}	11
Diglycinate	2.0×10^5	0.10 mol dm^{-3} (—), 25 °C	14
Diglycinate	4.6×10^5	0.15 mol dm^{-3} (KNO_3), 25 °C, $k^{-H_2O}=2.6\times10^5$ s^{-1}	11
Triglycinate	3.1×10^5	0.10 mol dm^{-3} (—), 25 °C	14
Tetraglycinate	2.6×10^5	0.10 mol dm^{-3} (—), 25 °C	14
pyc	1×10^7	0.10 mol dm^{-3} (—), 20 °C	15
α-Alaninate	6.0×10^5	0.10 mol dm^{-3} (KNO_3), 20 °C, $k^{-H_2O}=3\times10^5$ s^{-1}	16
β-Alaninate	7.5×10^4	0.10 mol dm^{-3} (KNO_3), 20 °C	16
2-Aminobutyrate	2.5×10^5	0.1 mol dm^{-3} (KNO_3), 20 °C	17
3-Aminobutyrate	2.0×10^4	0.1 mol dm^{-3} (KNO_3), 20 °C	17
pda	4.0×10^4	0.1 mol dm^{-3} (KNO_3), 15 °C	18
sal	1.3×10^5	0.10 mol dm^{-3} (KNO_3), 20 °C	19
5-ssal	2.7×10^5	0.10 mol dm^{-3} (KNO_3), 20 °C	19
qaa$^-$	1.5×10^6	0.10 mol dm^{-3} (NaCl), 25 °C	Present work

a) Abbreviations: phen, 1,10-phenanthroline; 5-NO_2-phen, 5-nitro-1,10-phenanthroline; bpy, 2,2′-bipyridine; tpy, 2,2′ : 6′,2″-terpyridine; pyc, 2-pyridinecarboxylate; pda, 4-(2-pyridylazo)-*N*,*N*-dimethylaniline; sal, salicylate; and 5-ssal, 5-sulfosalicylate. b) k_f is the rate constant for the formation of the mono-ligand cobalt(II) complex. c) The value of k^{-H_2O} has been reported, for example, to be 1.35×10^6 s^{-1} (0.1 mol dm^{-3} ($HClO_4$), 25 °C)[20] and $(2.15\text{—}2.35)\times10^6$ s^{-1} (0.2—0.35 mol dm^{-3} ($HClO_4$) and 2 mol dm^{-3} (NH_4NO_3),[21] 25 °C) by ^{17}O-NMR line-broadening measurements related to coordinated water, 2×10^5 s^{-1} (20 °C)[22] by ultrasonic absorption measurement and $(3.18\pm0.17)\times10^6$ s^{-1} (25 °C)[23] by ^{17}O-NMR relaxation time and line-broadening measurements.

formation constant of the outer-sphere complex (K_{os}) and the rate constant for the liberation of the coordinated water from the cobalt(II) ion (k^{-H_2O}), which then should be independent of the entering ligands. Table 4 reveals that the formation-rate constant for the complex with qaa$^-$ is in line with those for the complexes with glycinate, α-alaninate, *etc.*, even with no calculation of k^{-H_2O} from the estimated K_{os} and k_f values. Hence, it can be concluded that QAA forms a cobalt(II) complex in a "normal substitution" mode[16,17] through the preliminary formation of the outer-sphere complex, followed by the substitution of the coordinated water, with its liberation as the ultimate rate-determining step.

A comparison of k_{01} and k_{00} in Table 3 reveals that, as in the case of glycinate,[11] the carboxylato group of QAA coordinates more feasibly than does the heterocyclic nitrogen atom. The molecular model shows that the imino nitrogen atom may be less easily coordinated because its accessibility toward the metal atom is less than that of any other donor atoms in the ligand. Therefore, it can be stated that the carboxylato group of QAA coordinates first to the aquacobalt(II) ion as a unidentate ligand, followed by the donations of imino and heterocyclic nitrogen atoms to complete two five-membered chelate rings; this is followed by the coordination of the second QAA in a more rapid manner because of the labilization of the remaining coordinated water,[11] thus completing the bis-QAA complex.

Appendix

In this section, M, ML, ML_2, L, HL, and H_2L are used as simplified expressions of $[Co(H_2O)_6]^{2+}$, $[Co(qaa)(H_2O)_3]^+$, $[Co(qaa)_2]$, qaa^-, Hqaa, and H_2qaa^+; the molar absorption coefficients of the last five of those are ε_{11}, ε_{12}, ε_0, ε_1, and ε_2 respectively.

I. The following relations are given based on definitions in the text and the materials balance:

$$A_x = \varepsilon_0[L] + \varepsilon_1[HL] + \varepsilon_2[H_2L], \quad (A\text{-}1)$$

$$A_0 = \varepsilon_0[L]_m = \varepsilon_0 C_{11g}, \quad (A\text{-}2)$$

$$A_1 = \varepsilon_1[HL]_m = \varepsilon_1 C_{11g}, \quad (A\text{-}3)$$

$$A_2 = \varepsilon_2[H_2L]_m = \varepsilon_2 C_{11g}, \quad (A\text{-}4)$$

$$C_{11g} = [L] + [HL] + [H_2L] = [L]_m = [HL]_m = [H_2L]_m, \quad (A\text{-}5)$$

where C_{ug} is the total concentration of QAA. The suffix m specifies the portion of the concentration, in which only the unique ligand species is present. By taking K_{a1} and K_{a2} into consideration and by inserting Eqs. A-2—A-5 into Eq. A-1 with suitable rearrangements, Eq. 1 can be derived.

II. In an acidic solution of pH 2—5, where the complex formation proceeds, the following relations hold for the equilibrium:

$$C_M = [M] + [ML] + [ML_2], \quad (A\text{-}6)$$

$$C_L = [L] + [HL] + [H_2L] + [ML] + 2[ML_2] = [L]_i + [HL]_i + [H_2L]_i, \quad (A\text{-}7)$$

$$A' = \varepsilon_0[L] + \varepsilon_1[HL] + \varepsilon_2[H_2L] + \varepsilon_{11}[ML] + \varepsilon_{12}[ML_2], \quad (A\text{-}8)$$

$$A_{b.c} = \varepsilon_{12} C_M, \quad (A\text{-}9)$$

$$A_{11g} = \varepsilon_0[L]_i + \varepsilon_1[HL]_i + \varepsilon_2[H_2L]_i. \quad (A\text{-}10)$$

Here, the suffix i specifies the initial concentration of the ligand. Under the condition of $2C_M = C_L$, the bis-QAA complex is assumed to be dominant over the mono-QAA complex. Hence, the following relations are derived from Eqs. A-6—A-10 by taking K_{a1} and K_{a2} into consideration:

$$[L] = (C_L - 2[ML_2])/(1 + K_{a1}[H^+] + K_{a1}K_{a2}[H^+]^2), \quad (A\text{-}11)$$

$$[M] = \{(A_{b.c} - A')/(A_{b.c} - A_{11g})\} C_M, \quad (A\text{-}12)$$

$$[ML_2] = \{(A' - A_{11g})/(A_{b.c} - A_{11g})\} C_M, \quad (A\text{-}13)$$

The application of Eqs. A-11—A-13 into Eq. A-14:

$$\beta_{12} = [ML_2]/[M][L]^2, \quad (A\text{-}14)$$

and suitable rearrangements give us Eq. 4.

III. When Stage **I** is the rate-determining step, the following relations can be given under the condition of $C_M' \gg C_L'$:

$$C_M' = [M] + [ML] \approx [M] = [M]_{eq}, \quad (A\text{-}15)$$

$$C_L' = [L] + [HL] + [H_2L] + [ML] = [L]_{eq} + [HL]_{eq} + [H_2L]_{eq} + [ML]_{eq}. \quad (A\text{-}16)$$

By using Eqs. A-15 and A-16 together with Eq. A-17:

$$\beta_{11} = [ML]_{eq}/[M]_{eq}[L]_{eq}. \quad (A\text{-}17)$$

Equation 5 can be transformed into Eq. A-18:

$$\begin{aligned} d[ML]/dt &= (k_{02}K_{a1}K_{a2}[H^+]^2 + k_{01}K_{a1}[H^+] + k_{00}) \times ([M][L] - [ML]/\beta_{11}) \\ &= (k_{02}K_{a1}K_{a2}[H^+]^2 + k_{01}K_{a1}[H^+] + k_{00}) \times \{C_M'/(K_{a1}K_{a2}[H^+]^2 + K_{a1}[H^+] + 1) + 1/\beta_{11}\} \times ([ML]_{eq} - [ML]). \end{aligned} \quad (A\text{-}18)$$

A comparison of Eq. A-18 with Eq. 5 gives Eq. 6, which can be rewritten as:

$$k_{02}K_{a1}K_{a2}[H^+]^2 + k_{01}K_{a1}[H^+] + k_{00} = k^M_{obsd}', \quad (A\text{-}19)$$

by using the definition given in Eq. 6′. It was used for the data analysis.

Equations 7 and 8 can be derived from Eq. 5 in an analogous way.

References

1) Abbreviations: QAA, *N*-(8-quinolyl)aminoacetate ligand. H_3qaa^{2+}, H_2qaa^+, Hqaa, and qaa^- refer to various protonated and deprotonated species of QAA.

2) T. Tanabe, K. Kimura, and S. Takamoto, *Nippon Kagaku Zasshi*, **90**, 598 (1969).

3) J. Kielland, *J. Am. Chem. Soc.*, **59**, 1675 (1937).

4) H. Nishikawa and S. Yamada, *Bull. Chem. Soc. Jpn.*, **37**, 1154 (1964).

5) A. Albert and E. P. Serjeant, "Ionization Constants of Acids and Bases," Methuen, London (1962), Chaps. 7 and 8.

6) L. G. Sillen, *Acta Chem. Scand.*, **10**, 186 (1956).

7) For example, "Coordination Chemistry," ed by A. E. Martell, Van Nostrand-Reinhold, New York (1971), Vol.1, Chap. 8.

8) "Stability Constants of Metal-Ion Complexes," ed by L. G. Sillén and A. E. Martell, The Chemical Society, London (1971), Suppl. No. 1, Sp. Publ. No. 25, p. 23.

9) M. Eigen, *Pure Appl. Chem.*, **6**, 97 (1963).

10) D. B. Rorabacher, *Inorg. Chem.*, **5**, 1891 (1966).

11) G. G. Hammes and J. I. Steinfeld, *J. Am. Chem. Soc.*, **84**, 4639 (1962).

12) R. H. Holyer, C. D. Hubbard, S. F. A. Kettle, and R. G. Wilkins, *Inorg. Chem.*, **4**, 929 (1965).

13) R. H. Holyer, C. D. Hubbard, S. F. A. Kettle, and R. G. Wilkins, *Inorg. Chem.*, **5**, 622 (1966).

14) G. Davies, K. Kustin, and R. F. Pasternack, *Inorg. Chem.*, **8**, 1535 (1969).

15) A. Kowalak, K. Kustin, and R. F. Pasternack, *J. Phys. Chem.*, **73**, 281 (1969).

16) K. Kustin, R. F. Pasternack, and E. M. Weinstock, *J. Am. Chem. Soc.*, **88**, 4610 (1966).

17) K. Kowalak, K. Kustin, R. F. Pasternack, and S. Petrucci, *J. Am. Chem. Soc.*, **89**, 3126 (1967).

18) R. G. Wilkins, *Inorg. Chem.*, **3**, 520 (1964).

19) J. C. Williams and S. Petrucci, *J. Am. Chem. Soc.*, **95**, 7619 (1973).

20) T. J. Swift and R. E. Connick, *J. Chem. Phys.*, **37**, 307 (1962); **41**, 2553 (1964).

21) P. E. Hoggard, H. W. Dodgen, and J. P. Hunt, *Inorg. Chem.*, **10**, 959 (1971).

22) M. Eigen and K. Tamm, *Z. Elektrochem.*, **66**, 107 (1962).

23) Y. Ducommun, K. E. Newman, and A. E. Merbach, *Inorg. Chem.*, **19**, 3696 (1980).

Kinetic Studies of the Hydrolysis of Diketene Catalyzed by the Chloropalladium(II) Complex

Seichi OKEYA* and Shinichi KAWAGUCHI*,†

Faculty of Education, Wakayama University, Fukiage, Wakayama 640
†*Faculty of Science, Osaka City University, Sumiyoshi-ku, Osaka 558*

(Received September 12, 1983)

When diketene and sodium tetrachloropalladate(II) are mixed in aqueous solution, color of the solution changes promptly from dark red to yellow. During this fast primary reaction about one equivalent of diketene is consumed and acetoacetic acid (H_2A) is retained as a trihapto ligand in $[PdCl_2(HA)]^-$ (**2**). The succeeding steady hydrolysis of diketene (S) proceeds as a pseudo first-order reaction, obeying the rate law: $-d[S]/dt=k_{obsd}[S]=(k_0+k_{cat})[S]$, $k_{cat}=k_{obsd}-k_0=(k_1+k_2/[H^+])[Pd^{II}]/[Cl^-]$, where $k_1=2.0\times10^{-5}$ s^{-1} and $k_2=2.96\times10^{-6}$ mol dm^{-3} s^{-1} at 0 °C and $\mu=1.0$ mol dm^{-3} ($HClO_4$ and $NaClO_4$). A mechanism which postulates complex **2** as the effective catalyst is proposed to explain the observed two-term rate equation.

Diketene consists of a four-membered lactone ring adjacent to a vinyl function and suffers attack of various nucleophiles and electrophiles to cleave the ring.[1] Tezuka *et al.* found that sodium tetrachloropalladate catalyzes the alcoholysis of diketene to afford acetoacetic esters.[2] Ethyl acetoacetate (etacH) forms a stable dinuclear palladium(II) complex $[PdCl(etac)]_2$, in which the β-keto ester ligand was confirmed by X-ray analysis to be coordinated with palladium in the η-allylic fashion.[3] Okeya *et al.* also found that the solvolysis reactions of diketene in water and acetone are catalyzed by palladium(II) complexes.[4] Palladium(II) complexes of the reaction products, acetoacetic acid and 2,2,6-trimethyl-4*H*-1,3-dioxin-4-one, were characterized and inferred to have the η-allylic structure. In fact the crystal and molecular structure of the former complex (**1**) was determined by X-ray crystallography.[5]

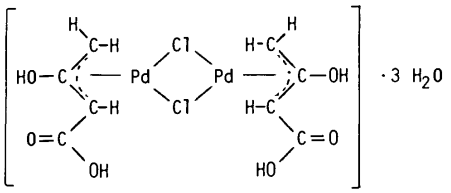

1

Palladium(II) forms a lot of organometallic compounds and is useful as catalysts for synthetic reactions.[6] As is exemplified by the famous Wacker reaction,[7] palladium participates in redox processes in most of the catalytic reactions. The spontaneous reaction of diketene with water is very slow[8] but is catalyzed by acids to produce acetone and carbon dioxide *via* acetoacetic acid.[9] The tetrachloropalladate(II) is very effective as a catalyst for this hydrolysis reaction but shows no sign of redox process involved. With the aim of elucidating the mechanism of this interesting catalysis a kinetic study was undertaken.

Experimental

Materials. A stock aqueous solution of sodium tetrachloropalladate(II) was prepared by dissolving palladium(II) chloride and sodium chloride in the mole ratio of 1 : 5. The exact concentrations of palladium and total chloride were determined by chemical analysis. Diketene (99.9% in purity) was supplied by Daicel Co., Ltd. and vacuum-distilled just before use. Other reagents such as perchloric acid, sodium perchlorate, sodium hydroxide, sodium chloride, and palladium(II) chloride as well as analytical reagents and indicators were of the AR grade and used as supplied.

Kinetic Measurement. A mixture of diketene and sodium tetrachloropalladate(II) in aqueous solution was stirred in a thermostated (±0.3 °C) reaction vessel. The solution was kept at $\mu=1.0$ mol dm^{-3} by virtue of sodium perchlorate and perchloric acid. By one minute after admixing the substrate with the catalyst color of the solution changed from dark red to yellow, indicating variation in the palladium(II) coordination sphere. Time zero for the steady reaction was set at this point and an aliquot was taken out from the reaction mixture and poured into an ethanol solution of about twice equivalents of dimethylglyoxime to quench the reaction. The mixture was titrated with a sodium hydroxide solution (0.1 mol dm^{-3}). Bromothymol Blue was used as an indicator (color changing from yellow to green) and the solution was kept throughout in ice and handled promptly. The initial concentration of diketene (S) for the steady reaction was calculated from Eq. 1,

$$[S]_0 = [S]_a - \{[NaOH]_0 - 2[Pd^{II}] - [HClO_4]\}, \quad (1)$$

where $[S]_a$ stands for the total concentration of diketene employed initially and $[NaOH]_0$ gives the concentration of alkali solution needed for neutralization of the aliquot. The amount of diketene consumed in the primary process is nearly equivalent to $[Pd^{II}]$. For each kinetic run diketene was used to make the $[S]_0$ value be in the region 0.15—0.20 mol dm^{-3}. Progress of the reaction thereafter was followed by taking aliquots at appropriate time intervals and titrating them in a similar way. The spontaneous hydrolysis of diketene in the absence of palladium(II) was also studied analogously.

Determination of the Hydrogen and Chloride Concentrations. It is usually rather difficult to determine accurately the hydrogen ion concentration in a solution with high ionic strength.[10] In this study an empirical method was used to relate an observed pH value to the hydrogen ion concentration. Solutions of hydrochloric acid at various concentrations were adjusted to $\mu=1.0$ mol dm^{-3} with sodium perchlorate and their pH values were determined. A calibration curve was thus drawn and the pH values of reaction mixtures were applied to this curve to evaluate their hydrogen ion concentrations.

As will be discussed shortly, the palladium(II) complex involved in the steady reaction is presumed to be $[PdCl_2(HA)]^-$ (H_2A=acetoacetic acid) and the concentration

of free chloride ions was calculated from the equation,

$$[Cl^-] = [Cl^-]_t - 2[Pd^{II}],$$

where $[Cl^-]_t$ represents the total concentration of chloride ions inclusive of those retained in the palladium(II) coordination sphere.

Instruments. The pH determination was performed with a Hitachi-Horiba M-5 pH meter. A reference electrode of the double junction type was used in order to prevent the perchlorate interference. Absorption spectra were measured by means of a Hitachi EPS-3T recording spectrophotometer.

Results and Discussion

Spontaneous hydrolysis of diketene in the absence of the palladium(II) catalyst proceeds as a first order reaction and $k_0=1.67\times10^{-5}$ s^{-1} at 0 °C and $\mu=1.0$ mol dm^{-3}. Addition of hydrochloric acid slightly lowers the rate, k_0 for example being 1.44×10^{-5} s^{-1} when [HCl] is 0.05 mol dm^{-3}. On the other hand the reaction is accelerated very remarkably by addition of sodium hydroxide.

The stepwise stability constants (K_n in dm^3 mol^{-1}) of the complexes $PdCl_n(H_2O)_{4-n}^{(2-n)+}$ were determined by Elding[11] at 25 °C and $\mu=1.00$ mol dm^{-3}: $K_1=(2.98\pm0.06)\times10^4$, $K_2=(1.92\pm0.13)\times10^3$, $K_3=(2.6\pm0.2)\times10^2$, and $K_4=(2.37\pm0.10)\times10$. When the chloride ion concentration lies in the 0.02—0.2 mol dm^{-3} region as is the case for the present study, the chloropalladium(II) complex seems to exist as a mixture of $[PdCl_4]^{2-}$, $[PdCl_3(H_2O)]^-$, and $[PdCl_2(H_2O)_2]$.

When an aqueous solution of diketene is added to an aqueous solution of $Na_2[PdCl_4]$, color of the solution changes in one minute from dark red to yellow. The absorption spectrum of this solution has a maximum at 360 nm (ε=*ca.* 1200), and does not change during the progress of reaction. As is seen in Fig. 1, the λ_{max} slightly shifts to longer wave length side with increasing chloride concentration. It may be presumed that the dichloropalladium(II) complex coordinated with acetoacetic acid in an η-allylic fashion, $[PdCl_2(HA)]^-$ (**2**), is produced by the following fast reactions and works as an effective catalyst for the succeeding steady reaction. Complex **2** may be contaminated with a small amount of aqua counterpart **2′** in equilibrium 3. Since the chloride ion is a weaker ligand than the aqua ligand in the spectrochemical series, shift of the equilibrium 3 to the left hand side causes red shift of the absorption maximum. Thus $[PdCl(H_2O)(en)]^+$ and $[PdCl_2(en)_2]$ absorb at 360 and 370 nm, respectively.[12]

$$\left.\begin{aligned}
[PdCl_4]^{2-} + S + H_2O &\xrightarrow{\text{fast}} [PdCl_2(HA)]^- + H^+ + 2Cl^- \\
[PdCl_3(H_2O)]^- + S &\xrightarrow{\text{fast}} [PdCl_2(HA)]^- + H^+ + Cl^- \\
[PdCl_2(H_2O)_2] + S &\xrightarrow{\text{fast}} [PdCl_2(HA)]^- + H^+ + H_2O
\end{aligned}\right\} \quad (2)$$

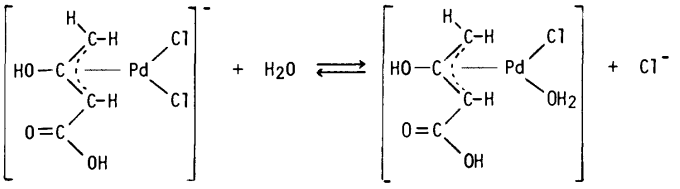

2 **2′** (3)

When diketene is used up, color of the solution returns to red gradually. On being cooled below 0 °C the yellow solution deposits complex **1** but the red solution does not. The ^{1}H NMR assay indicates that complex **1** is converted into **2** in aqueous solution containing excess chloride ions, but either of them is not thermodynamically stable under these circumstances. Even when sodium acetoacetate is added to aqueous solution of $Na_2[PdCl_4]$, no sign of reaction is observed. Thus complex **2** is not formed by the reaction of $[PdCl_4]^{2-}$ with acetoacetic acid, but seems to be involved as an intermediate in the catalytic reaction.

The succeeding rather slow hydrolysis of diketene was followed by the titration method. The hydrogen ion concentration of the reaction mixture remained almost constant during the progress of reaction, indicating that acetoacetic acid, the reaction product, hardly ionizes in the acidic solution. Contributions from added perchloric acid and produced hydrochloric acid were subtracted from the observed hydrogen ion concentration, and the remaining part was related to the ionization of the η^3-coordinated acid in complex **2**.

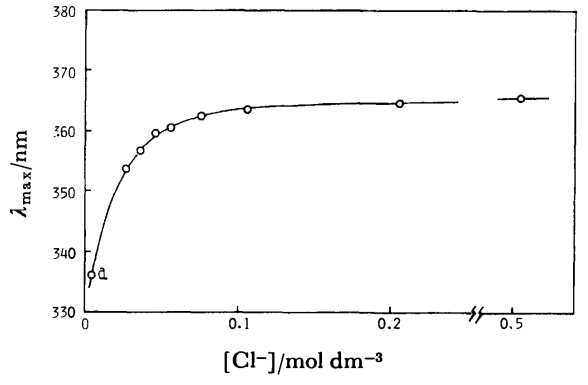

Fig. 1. Variation of λ_{max} of the reaction mixture with the concentration of chloride ions. Point a shows the λ_{max} of a solution containing complex **1** and diketene.

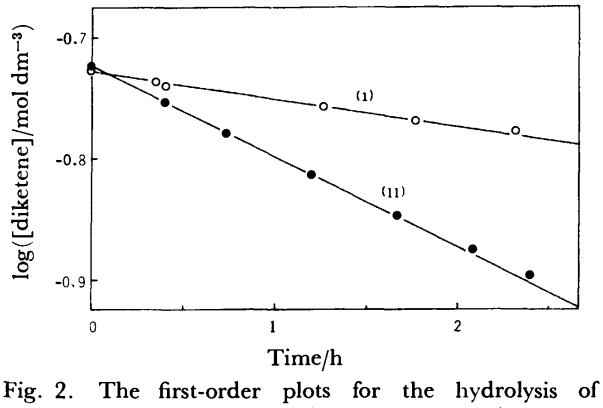

Fig. 2. The first-order plots for the hydrolysis of diketene in the absence (i) and presence (ii) of the Pd^{II} catalyst at 0 °C and $\mu=1.0$ mol dm^{-3}. $[Cl^-]=0.050$ mol dm^{-3}, $[H^+]=0.021\pm0.001$ mol dm^{-3}, and $[Pd^{II}]=0.0100$ mol dm^{-3}.

In this way the acid dissociation constant K_a (1) of **2** was estimated to be in the range 10^{-2}—10^{-3} mol dm^{-3} and is a little smaller than that of complex **1** (3.2×10^{-2} mol dm^{-3} at 18 °C).[4,5]

As is shown in Fig. 2, the reaction proceeds as a pseudo first order reaction up to 30—50% conversion. Since the spontaneous uncatalyzed hydrolysis is also a first order reaction, contribution of the catalyzed reaction is given by Eq. 4.

$$-\frac{d[S]}{dt} = k_{obsd}[S] = (k_0+k_{cat})[S],\ k_{cat} = k_{obsd} - k_0. \quad (4)$$

Both of the rate constants k_{obsd} and k_0 for the overall and uncatalyzed reactions, respectively, were measured more than four times under the same conditions and averaged.

Figures 3 and 4 show that $(k_{obsd}-k_0)$ is proportional to the palladium(II) concentration and also to reciprocal of the chloride concentration. Dependence of $(k_{obsd}-k_0)$ on the hydrogen ion concentration at constant palladium(II) and chloride concentrations is shown in Fig. 5. If the rate constants are plotted against the reciprocal of hydrogen ion concentration, a straight line is obtained (Fig. 6). Thus the pseudo first order rate constant for the catalyzed reaction is expressed by Eq. 5, and k_1= 2.0×10^{-5} s^{-1} and k_2=2.96×10^{-6} mol dm^{-3} s^{-1} at 0 °C and μ=1.0 mol dm^{-3}.

$$k_{obsd} - k_0 = \left(k_1+\frac{k_2}{[H^+]}\right)\frac{[Pd^{II}]}{[Cl^-]}. \quad (5)$$

The Eyring plots of rate data in Table 1 for the catalyzed and spontaneous reactions gave $\Delta H^{\ddagger}$=53 kJ mol^{-1} for both reactions. It should be added that the rate data reported in this paper may be accurate to ±10%.

Mechanism of Catalyzed Hydrolysis. Hydrolysis reactions of aliphatic lactones in weakly acidic solutions have been studied rather extensively.[13] For example, rates of hydrolysis of β-propiolactone and

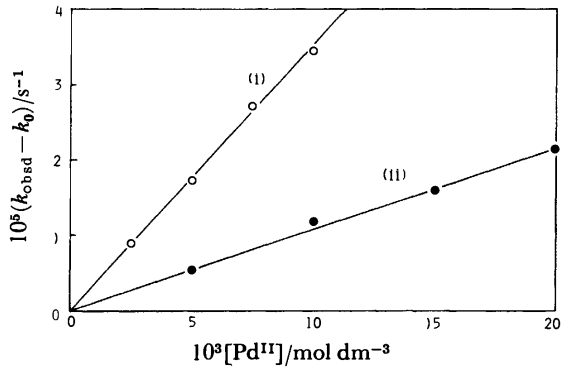

Fig. 3. Dependence of $(k_{obsd}-k_0)$ on the palladium(II) concentration at 0 °C, μ=1.0 mol dm^{-3}, and [H$^+$]=0.021±0.001 mol dm^{-3}. (i) [Cl$^-$]=0.050 mol dm^{-3}. (ii) [Cl$^-$]=0.180 mol dm^{-3}.

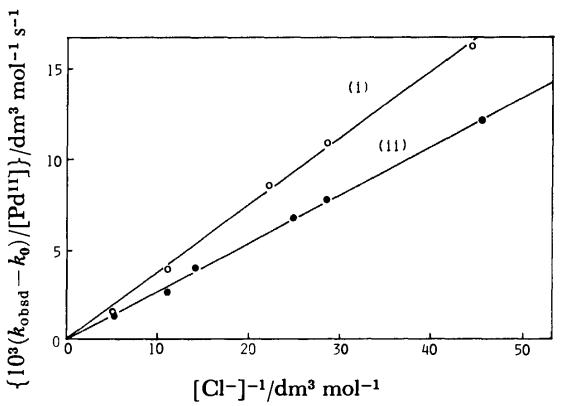

Fig. 4. Dependence of $(k_{obsd}-k_0)$ on the reciprocal of chloride concentration at 0 °C and μ=1.0 mol dm^{-3}. (i) [Pd^{II}]=0.0050 mol dm^{-3} and [H$^+$]=0.0080 ±0.0002 mol dm^{-3}. (ii) [Pd^{II}]=0.0100 mol dm^{-3} and [H$^+$]=0.0123±0.0005 mol dm^{-3}.

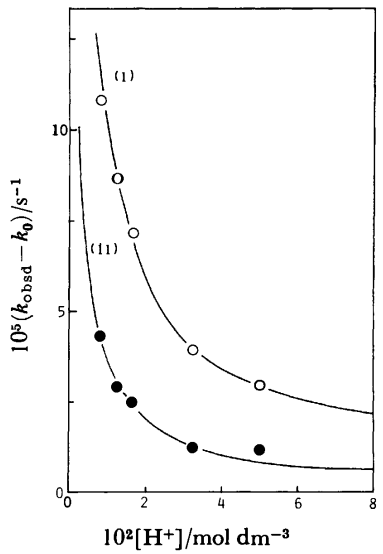

Fig. 5. Dependence of $(k_{obsd}-k_0)$ on the hydrogen ion concentration at 0 °C, μ=1.0 mol dm^{-3}, and [Pd^{II}]=0.0050 mol dm^{-3}. (i) [Cl$^-$]=0.015 mol dm^{-3}. (ii) [Cl$^-$]=0.045 mol dm^{-3}.

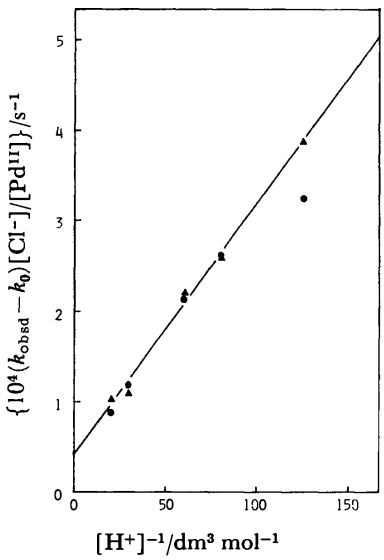

Fig. 6. Plot of $(k_{obsd}-k_0)[Cl^-]/[Pd^{II}]$ against reciprocal of the hydrogen ion concentration. Rate data are the same as those of Fig. 5, [Cl$^-$] being 0.015(●) or 0.045(▲)mol dm^{-3}.

Table 1. Rates of hydrolysis of diketene at various temperatures and $\mu=1.0$ mol dm^{-3}, $[Cl^-]=0.195$ mol dm^{-3}, $[H^+]=0.008$ mol dm^{-3}

T/K	$10^5 k_0$/s^{-1}	$10^5 k_{obsd}$/s^{-1}	$10^3(k_{obsd}-k_0)/[Pd^{II}]$[a]/dm^3 mol^{-1} s^{-1}
303	17.3	27.2	19.8
293	8.45	13.3	9.70
283	3.76	5.89	4.26
278	2.34	3.74	2.80
273	1.56	2.37	1.62

a) $[Pd^{II}]=0.0050$ mol dm^{-3}.

γ-butyrolactone were reported to be 1.88×10^{-4} and 5.00×10^{-5} s^{-1}, respectively, in neutral solutions at 37 °C.[14] The β-lactone is usually less stable and hydrolyzed more readily than the γ-lactone. In the molecule of diketene, the C=C function is attached to the β-lactone ring and the strain energy was estimated[15] as 94.1 kJ mol^{-1}. The rotational spectrum suggested that diketene is not planar.[16] Thus diketene is thermodynamically less stable and more reactive than β-propiolactone. In fact the hydrolysis rate of diketene was reported by van Duuren *et al.*[14] to be 2.0×10^{-3} s^{-1} at 25 °C and pH 7. This value is much larger than the present data in Table 1, but does not allow a direct comparison because of lacking in description of ionic strength. Higher ionic strength decreases the hydrolysis rate, k_0 at 0 °C being 3×10^{-5} s^{-1} at $\mu\approx0$ and 1.56×10^{-5} s^{-1} at $\mu=1.0$ mol dm^{-3}.

β-Propiolactone reacts with alcohol both in the absence and presence of acid catalysts to give 3-alkoxypropionic acid.[17] The alkyl-oxygen bond seems to be cleaved in this reaction (Eq. 6) as well as in hydrolysis.[18] On the other hand the reaction between diketene and alcohol results in the acetoacetic ester[1] probably by virture of the acyl-oxygen fission (Eq. 7).

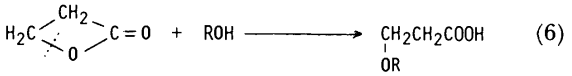

(6)

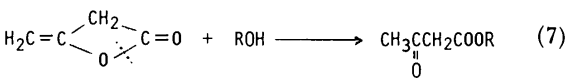

(7)

Alcoholysis of diketene catalyzed by palladium(II) seems to proceed according to the same mechanism and analogously hydrolysis of diketene both in the absence and presence of palladium(II) may involve the acyl-oxygen fission.

Since either of β-propiolactone and γ-butyrolactone shows no sign of interaction with $[PdCl_4]^{2-}$ in aqueous solution, diketene must coordinate with palladium(II) not through the oxygen atom(s) but through the C=C bond in the primary step of catalysis. Displacement of two chloride ligands and a methylene proton of diketene may give rise to a trihapto complex of the diketene anion, which in turn will be hydrolyzed rapidly to give complex **2** (Eq. 8).

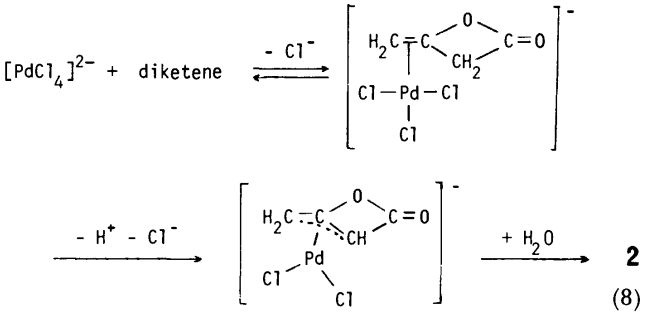

(8)

The succeeding steady reaction obeys the two term rate equation 5. The rate-determining step may be the nucleophilic attack of a water molecule (k_1) or a hydroxide anion (k_2) on the diketene ligand in the intermediate complex **3** as is shown in Eq. 9 for the k_2 path.

The enol tautomer of acetoacetic acid in the presumed complex **4** must be very unstable and rapidly displaced by a chloride anion to recover complex **2** and the product acetoacetic acid. Although the intermediate complexes postulated in this scheme have not been characterized, the rate equation 5 is readily interpreted on the assumption that complex **2** functions as the effective catalyst for hydrolysis of diketene. Pietropaolo *et al.*[19] studied kinetically the reaction between $[PdCl_4]^{2-}$ and 1,3-cyclohexadiene to form an η-allylic complex and proposed the following mechanism which involves the nucleophilic attack of methanol on the coordinated olefinic double bond as the rate-determining step in accordance with the observed rate law, rate$=k[PdCl_4^{2-}][\text{diene}]/[Cl^-]$. The mechanism is

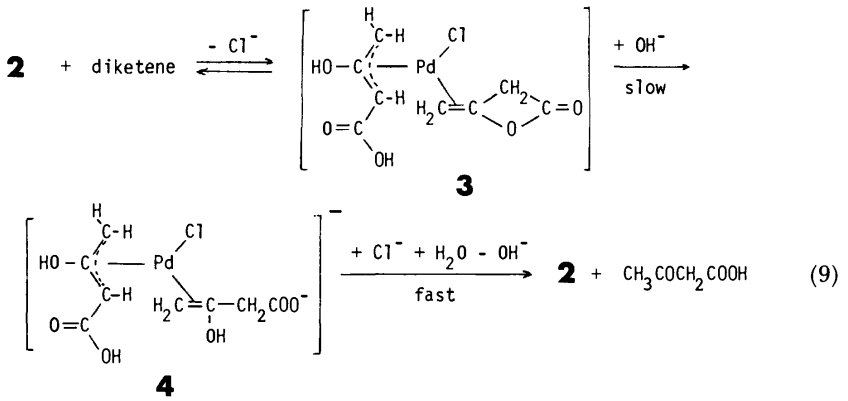

(9)

quite similar to that proposed here for the steady hydrolysis of diketene.

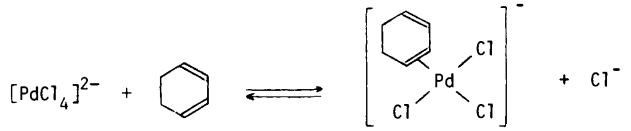

5

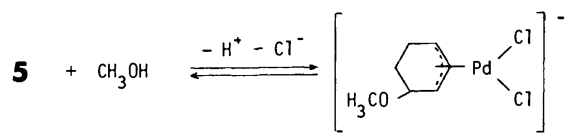

6

We thank Daicel, Ltd. for the generous gift of diketene.

References

1) R. N. Lacey, "The Chemistry of Alkenes," ed by S. Patai, Interscience Publishers, New York (1964), p. 1190; R. N. Lacey, "Advances in Organic Chemistry," ed by R. A. Raphael *et al.*, Interscience Publishers, New York (1960), Vol. II, p. 240.

2) Y. Tezuka, T. Ogura, and S. Kawaguchi, *Bull. Chem. Soc. Jpn.*, **42**, 443 (1969).

3) K. Oda, N. Yasuoka, T. Ueki, N. Kasai, and M. Kakudo, *Bull. Chem. Soc. Jpn.*, **43**, 362 (1970).

4) S. Okeya, T. Ogura, and S. Kawaguchi, *Kogyo Kagaku Zasshi*, **72**, 1656 (1969).

5) S. Okeya, T. Ogura, S. Kawaguchi, K. Oda, N. Yasuoka, N. Kasai, and M. Kakudo, *Inorg. Nucl. Chem. Lett.*, **5**, 713 (1969).

6) P. M. Maitlis, "The Organic Chemistry of Palladium," Academic Press, New York (1971), Vol. I and II.

7) G. W. Parshall, "Homogeneous Catalysis," Wiley-Interscience, New York (1980), p. 101.

8) A. B. Boese, *Ind. Eng. Chem.*, **32**, 16 (1940).

9) N. T. M. Wilsmore and F. Chick, *J. Chem. Soc.*, **93**, 946 (1908).

10) H. Kakihana, H. Ohtaki, H. Ogino, Y. Masuda, and Y. Sasaki, *Bunseki Kagaku*, **17**, 264 (1968).

11) L. I. Elding, *Inorg. Chim. Acta*, **6**, 647 (1972).

12) J. S. Coe, J. R. Lyons, and M. D. Hussain, *J. Chem. Soc., A*, **1970**, 90.

13) A. A. Frost and R. G. Pearson, "Kinetics and Mechanism," Wiley, New York (1961), p. 316.

14) B. L. van Duuren and B. M. Goldschmidt, *J. Med. Chem.*, **9**, 77 (1966).

15) M. Mansson, Y. Nakase, and S. Sunner, *Acta Chem. Scand.*, **22**, 171 (1968).

16) F. Mönnig, H. Dreizler, and H. D. Rudolph, *Z. Naturforsch., B*, **22**, 1471 (1967).

17) T. L. Gresham, J. E. Jansen, F. W. Shaver, J. T. Gregory, and W. L. Beears, *J. Am. Chem. Soc.*, **70**, 1004 (1948).

18) S. G. Waley, "Mechanism of Organic and Enzymic Reactions," Oxford University Press (1962), p. 227.

19) R. Pietropaolo, E. Rotondo, E. Faraone, and D. Pietropaolo, *J. Organomet. Chem.*, **60**, 197 (1973).

Phase Equilibria in the Ln_2O_3-V_2O_3-V_2O_5 (Ln=Dy and Ho) Systems at 1200 °C

Kenzo KITAYAMA* and Takashi KATSURA
Department of Chemistry, Faculty of Science, Tokyo Institute of Technology, Ookayama, Meguro-ku, Tokyo 152
(Received October 4, 1983)

Phase equilibria in the systems, Dy_2O_3-V_2O_3-V_2O_5 and Ho_2O_3-V_2O_3-V_2O_5, were established at 1200 °C by changing the oxygen partial pressure from 4.32 to −7.50 Pa in terms of $\log P_{O_2}$. In both systems, Ln_2O_3, $LnVO_4$, $LnVO_3$, V_nO_{2n-1}(n=2—7), VO_2, and $Ln_8V_2O_{17}$($4Ln_2O_3 \cdot V_2O_5$) are stable, and compounds with mole ratio Ln_2O_3/V_2O_5=5/1 are not stable under the present experimental conditions. On the basis of the established phase diagrams, the standard Gibbs energies of reactions, (1) $3\,Dy_2O_3+2\,DyVO_3+O_2=Dy_8V_2O_{17}$, (2) $DyVO_3+1/2\,O_2=DyVO_4$, (3) $3\,Ho_2O_3+2\,HoVO_3+O_2=Ho_8V_2O_{17}$, and (4) $HoVO_3+1/2\,O_2=HoVO_4$, were determined to be −278, −123.8, −277, and −122.4 kJ, respectively. $LnVO_4$, $Ln_8V_2O_{17}$, V_2O_3, and VO_2 have nonstoichiometric compositions. $\Delta G°$ values for reactions (2) and (4) fit well on the linear line presented by us.

The phase equilibria in the Ln_2O_3-V_2O_3-V_2O_5 systems[1-8] at 1200 °C were established by changing the oxygen partial pressures from 4.32 (air) to −7.50 or −8.00 Pa in terms of $\log P_{O_2}$. These established phase diagrams showed different patterns one another because of the differences of compounds coexisting under the experimental conditions although systems with Gd_2O_3[4] and Eu_2O_3[8] showed a similar pattern. Besides, the standard Gibbs energies of reactions found in the established diagrams and crystallographic data of the compounds presented for the systems have been obtained. It has also been established that the relationship between the ionic radius and $\Delta G°$ of reaction, $LnVO_3+1/2\,O_2=LnVO_4$, is linear provided that the lanthanoid elements can be divided into two groups.

In the present study, Dy_2O_3 and Ho_2O_3 were chosen as Ln_2O_3. In the Dy_2O_3-V_2O_5 and Ho_2O_3-V_2O_5 systems, compounds with mole ratio Ln_2O_3/V_2O_5 4/1 and 5/1 were stable[9] in the air from 600 to 1500 °C in addition to the well-known $LnVO_4$. So new types of phase equilibria will be expected.

Only one report was available about Dy_2O_3-V_2O_3 system,[10] in which one compound $DyVO_3$ with the congruent melting point at 2100 °C was found and it is nonstoichiometric toward V_2O_3 side in the temperature range from about 1800 to 2000 °C. The Ho_2O_3-V_2O_3 system has not been completely studied on account of the instability of V_2O_3 in the air, but $HoVO_3$ is well-known as a stable phase.

The crystallographic properties of $DyVO_3$, $HoVO_3$, $DyVO_4$, and $HoVO_4$ were investigated by many researchers.[11-14]

The objectives of the present study are: (1) preparation of the detailed phases diagrams of both systems at 1200 °C in order to determine the stable compounds under the present experimental conditions, (2) calculation of the standard Gibbs energies of reactions appeared in the established phase diagrams, and (3) examination of the fitness of present data on the linear relationship between the standard Gibbs energies of reactions and the ionic radius of the lanthanoid elements.

Experimental

Analytical grades of Dy_2O_3 (99.9%), Ho_2O_3 (99.9%), and V_2O_5, which was made by heating NH_4VO_3 of the guaranteed grade at 500 °C in the air for about 24 h, were used as the starting materials. Desired Dy_2O_3/V_2O_5 and Ho_2O_3/V_2O_5 mole ratios of samples were obtained by mixing appropriate quantities throughly in an agate motar under ethyl alcohol. The mixtures were treated by the procedures described in the previous paper.[1] The apparatus and procedures for controlling the oxygen partial pressures and keeping a constant temperature, the method of thermogravimetry, the criterion for an equilibrium establishment, the method of measurement of the actual oxygen partial pressure, and the method of chemical analysis are the same as those reported in the previous papers.[1,15-19]

Results and Discussion

Phase Equilibria. It was ascertained by the preliminary studies that Dy_2O_3 is stable under the present experimental ranges of the oxygen partial pressure. Seven samples with Dy_2O_3/V_2O_5 mole ratios 85/15, 8/2, 7/3, 65/35, 1, 35/65, and 15/85 were prepared to be used in the thermogravimetric experiments. The thermogravimetric results for three samples with mole ratios 85/15, 7/3, and 35/65 are shown in Fig. 1 as representative. In Fig. 1 the ordinate is the oxygen partial pressure represented in $\log P_{O_2}$ in the Pa unit and the abscissa is the composition shown by W_{O_2}/W_T, where W_{O_2} is the weight gain of the samples from the reference weight at $\log P_{O_2}$=−7.50, which is a point in the oxygen partial pressures where Dy_2O_3, $DyVO_3$, and V_2O_3 are stable, and W_T is the total weight increase of samples which might get if V_2O_3 in the samples at the reference state changed to V_2O_5 in the higher oxygen partial pressures. The W_{O_2}/W_T ratio was usually shown in the range from 0.995 to 1.00 in the air. Figure 1 shows the different patterns one another, and in the oxygen partial pressure range from $\log P_{O_2}$=−7.50 to −4.85 (Fig. 1a) the weight change was not observed. The value of $\log P_{O_2}$=−4.85 is the oxygen partial presure of the gas phase in equilibrium with the phase assemblages R+A_2+

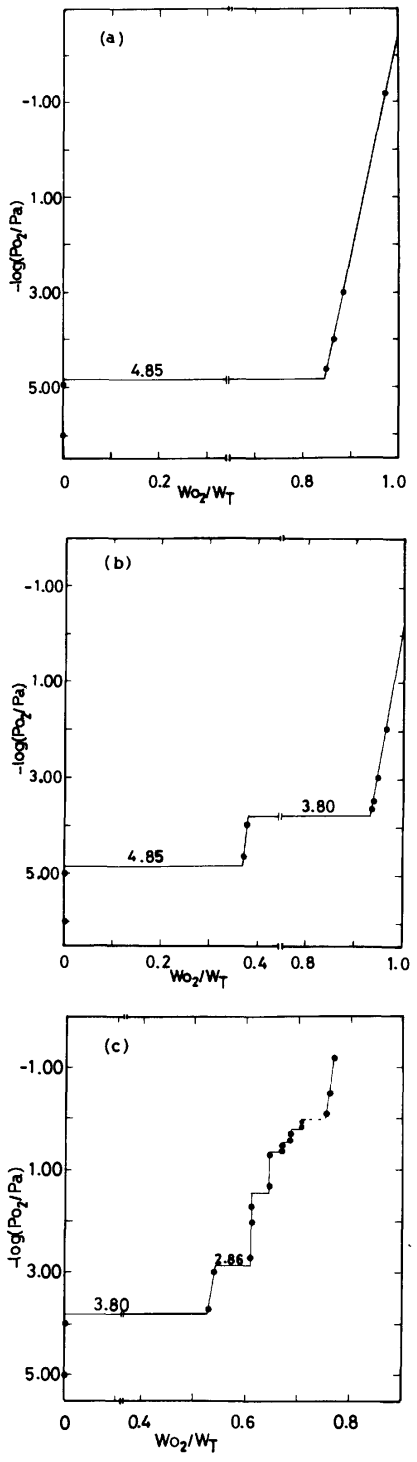

Fig. 1. The relationships between $-\log(P_{O_2}/\text{Pa})$ and the compositions, W_{O_2}/W_T, of the samples.
(a) $Dy_2O_3/V_2O_5=85/15$, (b) $Dy_2O_3/V_2O_5=7/3$, (c) $Dy_2O_3/V_2O_5=35/65$.

C which symboles will be shown in Table 2. In the range higher than $\log P_{O_2}=-4.85$, the weight changes linearly with the change in oxygen partial pressures. Figure 1b shows two oxygen partial pressures, −4.85 and −3.80 in $\log P_{O_2}$, in equilibrium. The latter corresponds to that of Reaction (2) in Table 4, and Fig. 1c have six oxygen partial pressures in equilibrium

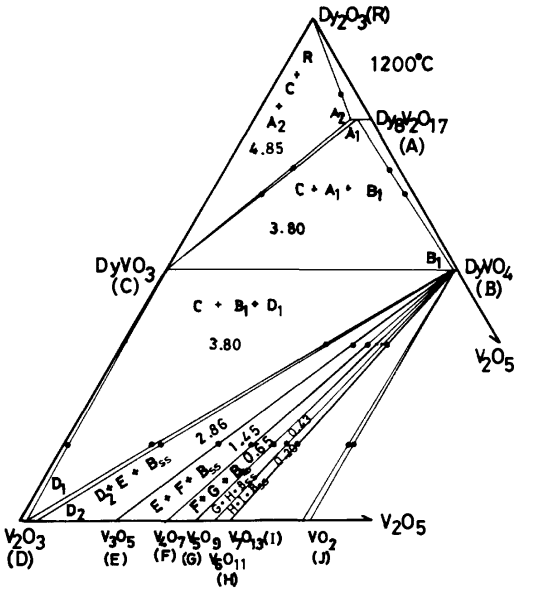

Fig. 2. Phase equilibria in the Dy_2O_3-V_2O_3-V_2O_5 system at 1200 °C. Numerical values in the three solid phases regions are the oxygen partial pressures in equilibrium in $-\log P_{O_2}$. Symbols are the same as those in Table 2.

in which five values correspond to those of the reactions in the V-O system.[1)]

In Table 1 the results of identification of phases are shown. In the first column are shown the compositions of the starting materials in mole%, in the second the experimental conditions of the oxygen partial pressure in terms of $\log P_{O_2}$ in Pa, in the third the experimental durations in hours, and in the last the phases that were found in the respective quenched samples using X-ray powder diffractometer with Cu $K\alpha$ radiation.

Based upon the above thermogravimetric results and the results of identification of phases, a phase diagram of the system can be constructed and is shown in Fig. 2. The following phases are stable; $V_nO_{2n-1}(n=2—7)$, VO_2, Dy_2O_3, $DyVO_4$, $DyVO_3$, and $Dy_8V_2O_{17}(4Dy_2O_3\cdot V_2O_5)$. The compound $5Dy_2O_3\cdot V_2O_5$ reported by Brusset *et al.*[9)] as the stable phase was not found.

The stability of Ho_2O_3 under the present experimental conditions was confirmed by preliminary experiments. Seven samples with Ho_2O_3/V_2O_5 mole ratios 85/15, 8/2, 7/3, 6/4, 1, 35/65, and 15/85 have also been used in the thermogravimetric experiments. The value of $\log P_{O_2}=-7.50$ was selected as the reference oxygen partial pressure by the similar reason as described above. In Fig. 3 the relationships between the oxygen partial pressure and the composition of samples are shown as those in Fig. 1 with the representative samples having mole ratios 85/15, 6/4, and 15/85. Figure 3 shows similar patterns to Fig. 1.

Quenched samples were used for the identification of phases and the phases were identified by X-ray powder diffractometer with Cu $K\alpha$ radiation. The results are shown in Table 1 together with those of the Dy_2O_3-V_2O_3-V_2O_5 system. Figure 4 was depicted by using

above experimental results as those in Fig. 2. Figures. 2 and 4 give similar patterns each other. In addition to the seven oxides in the V_2O_3-V_2O_5 system, Ho_2O_3, $HoVO_4$, $HoVO_3$, and $Ho_8V_2O_{17}$($4Ho_2O_3 \cdot V_2O_5$) are stable. These phase diagrams are very simple having only one compound between Ln_2O_3 and $LnVO_4$. This type of the phase diagram was found in the systems of Eu, Gd, and Er. It was very interesting that

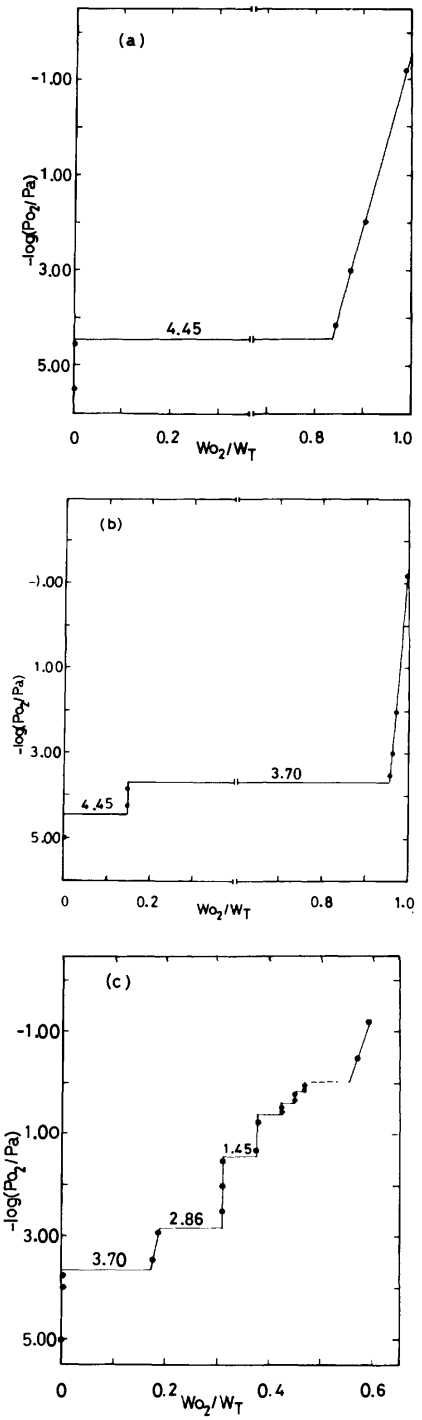

Fig. 3. The relationships between $-\log(P_{O_2}/\text{Pa})$ and the compositions, W_{O_2}/W_T of samples.
(a) Ho_2O_3/V_2O_5=85/15, (b) Ho_2O_3/V_2O_5=6/4, (c) Ho_2O_3/V_2O_5=15/85.

Table 1. Identification of phases

Starting materials mol%		$-\log(P_{O_2}/\text{Pa})$	Time h	Phases
Dy_2O_3	V_2O_5			
85	15	7.50	8	$Dy_2O_3+DyVO_3$
		5.00	27	$Dy_2O_3+DyVO_3$
		4.50	22	$Dy_2O_3+Dy_8V_2O_{17}$
		−4.32	63	$Dy_2O_3+Dy_8V_2O_{17}$
65	35	7.50	8	$Dy_2O_3+DyVO_3$
		5.00	27	$Dy_2O_3+DyVO_3$
		4.50	22	$DyVO_3+Dy_8V_2O_{17}$
		2.50	27	$DyVO_4+Dy_8V_2O_{17}$
		−4.32	63	$DyVO_4+Dy_8V_2O_{17}$
35	65	7.50	8	$DyVO_3+V_2O_3$
		4.50	22	$DyVO_3+V_2O_3$
		3.30	28	$DyVO_4+V_2O_3$
		2.00	27	$DyVO_4+V_3O_5$
		1.00	28	$DyVO_4+V_4O_7$
		0.55	39	$DyVO_4+V_5O_9$
		0.35	41	$DyVO_4+V_6O_{11}$
		0.10	56	$DyVO_4+V_7O_{13}$
		−0.55	39	$DyVO_4+VO_2$
15	85	7.50	8	$DyVO_3+V_2O_3$
		4.50	22	$DyVO_3+V_2O_3$
		3.30	28	$DyVO_4+V_2O_3$
		2.00	27	$DyVO_4+V_3O_5$
		1.00	28	$DyVO_4+V_4O_7$
		0.55	39	$DyVO_4+V_5O_9$
		0.35	41	$DyVO_4+V_6O_{11}$
		0.10	56	$DyVO_4+V_7O_{13}$
		−0.55	39	$DyVO_4+VO_2$
Ho_2O_3	V_2O_5			
85	15	6.00	24	$Ho_2O_3+HoVO_3$
		4.00	24	$Ho_2O_3+Ho_8V_2O_{17}$
		−4.32	63	$Ho_2O_3+Ho_8V_2O_{17}$
70	30	6.00	24	$Ho_2O_3+HoVO_3$
		3.90	24	$Ho_2O_3+Ho_8V_2O_{17}$
		3.00	24	$HoVO_4+Ho_8V_2O_{17}$
		−4.32	63	$HoVO_4+Ho_8V_2O_{17}$
35	65	6.00	24	$HoVO_3+V_2O_3$
		4.00	24	$HoVO_3+V_2O_3$
		3.00	26	$HoVO_4+V_2O_3$
		2.00	26	$HoVO_4+V_3O_5$
		1.00	48	$HoVO_4+V_4O_7$
		0.55	48	$HoVO_4+V_5O_9$
		0.30	47	$HoVO_4+V_6O_{11}$
		0.10	48	$HoVO_4+V_7O_{13}$
		−0.50	32	$HoVO_4+VO_2$
15	85	6.00	24	$HoVO_3+V_2O_3$
		4.00	24	$HoVO_3+V_2O_3$
		3.00	26	$HoVO_4+V_2O_3$
		2.00	26	$HoVO_4+V_3O_5$
		1.00	48	$HoVO_4+V_4O_7$
		0.55	48	$HoVO_4+V_5O_9$
		0.30	47	$HoVO_4+V_6O_{11}$
		0.10	48	$HoVO_4+V_7O_{13}$
		−0.50	32	$HoVO_4+VO_2$

these elements are located in the middle of the lanthanoid.

$DyVO_4$, $HoVO_4$, $Dy_8V_2O_{17}$, and $Ho_8V_2O_{17}$ have nonstoichiometric compositions, and the relationships between the oxygen partial pressure and the compositions were obtained as follows: $N_O/N_B=4.23\times10^{-3}\log P_{O_2}-1.38\times10^{-4}$ for $DyVO_4$, $N_O/N_L=8.80\times10^{-3}\log P_{O_2}+6.37\times10^{-3}$ for $HoVO_4$, $N_O/N_A=0.045\log P_{O_2}-0.098$ for $Dy_8V_2O_{17}$, and $N_O/N_K=0.079\log P_{O_2}-0.023$ for $Ho_8V_2O_{17}$, where N_O is the mole fraction of oxygen atom in the compounds and N_A, N_B, N_K, and N_L are the mole fractions of the $Dy_8V_2O_{17}$, $DyVO_4$, $Ho_8V_2O_{17}$, and $HoVO_4$ components in the compounds, respectively.

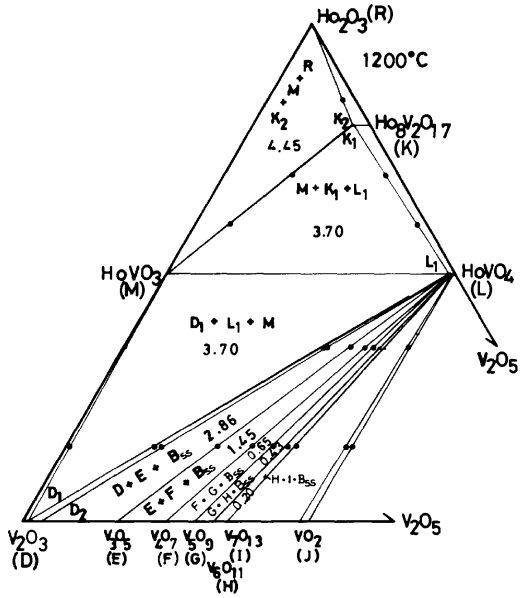

Fig. 4. Phase equilibria in the Ho_2O_3-V_2O_3-V_2O_5 system at 1200 °C. Numerical values in the three solid phases regions are the oxygen partial pressures in equilibrium in $-\log P_{O_2}$. Symbols are the same as those in Table 2.

Table 2 lists the compositions of the compounds at various oxygen partial pressures, stability ranges of the compounds in terms of $\log P_{O_2}$, the symbols of the compounds, and the activities of the components described above. The activities of the components in the solid solutions were calculated by means of the Gibbs-Duhem equation with the data of thermogravimetry, for example N_O/N_A *vs.* $\log P_{O_2}$ described above. A detailed method of the calculation has been discussed in the previous paper.[18]

Lattice constants of the compounds $DyVO_3$, $DyVO_4$, $Dy_8V_2O_{17}$, $HoVO_3$, $HoVO_4$, and $Ho_8V_2O_{17}$ are tabulated in Table 3. Present values are in good agreement

Table 2. Compositions, symbols, stability ranges in the oxygen partial pressures, and activities of component in the solid solutions

Component	Composition	Symbol	$-\log(P_{O_2}/\text{Pa})$	$-\log a_i$
$Dy_8V_2O_{17}$	$Dy_8V_2O_{17.0}$	A	-2.1[a]$-$$-4.32$	0.55
	$Dy_8V_2O_{16.73}$	A_1	3.80	0.15
	$Dy_8V_2O_{16.69}$	A_2	4.85	0
$DyVO_4$	$DyVO_{4.00}$	B	0.0[a]$-$$-4.32$	0.016
	$DyVO_{3.98}$	B_1	3.80	0
$Ho_8V_2O_{17}$	$Ho_8V_2O_{17.0}$	K	-0.3[a]$-$$-4.32$	0.45
	$Ho_8V_2O_{16.7}$	K_1	3.70	0.13
	$Ho_8V_2O_{16.6}$	K_2	4.45	0
$HoVO_4$	$HoVO_{4.00}$	L	0.7[a]$-$$-4.32$	0.020
	$HoVO_{3.97}$	L_1	3.70	0

a) These values were obtained by extrapolating the thermogravimetric results.

Table 3. Cell dimensions of compounds

Sample	$-\log(P_{O_2}/\text{Pa})$	a/Å	b/Å	c/Å	β/°	V/Å^3	Ref
$DyVO_3$	7.50	5.311±0.003	5.618±0.003	7.602±0.004		226.8±0.2	
	5.00	5.305±0.002	5.613±0.002	7.603±0.002		226.4±0.2	
		5.299	5.594	7.593		225.1	11
		5.302	5.602	7.601			12
$DyVO_4$	−4.32	7.157±0.002		6.317±0.002		323.6±0.2	
	3.50	7.157±0.002		6.315±0.002		323.5±0.2	
		7.1434		6.313			13
$Dy_8V_2O_{17}$	−4.32	10.69 ±0.05	8.81 ±0.14	15.75 ±0.12	99.1±0.5	1460±20	
	4.50	10.71 ±0.08	8.65 ±0.08	15.48 ±0.28	98.8±0.5	1420±30	
$HoVO_3$	4.00	5.283±0.002	5.609±0.002	7.580±0.002		224.6±0.2	
	6.00	5.277±0.002	5.597±0.002	7.579±0.002		223.8±0.2	
		5.276	5.592	7.576		223.5	11
$HoVO_4$	−4.32	7.129±0.002		6.293±0.002		319.8±0.2	
	3.50	7.129±0.002		6.300±0.004		320.2±0.3	
		7.1214		6.2926			14
$Ho_8V_2O_{17}$	−4.32	10.69 ±0.10	8.43 ±0.05	15.22 ±0.36	98.4±0.7	1360±35	
	4.00	10.65 ±0.08	8.61 ±0.07	15.49 ±0.28	99.0±0.5	1400±30	

TABLE 4. THE STANDARD GIBBS ENERGIES OF REACTIONS

Reaction	$-\log(P_{O_2}/Pa)$	$\frac{-\Delta G^\circ}{kJ}$
(1) $3\,Dy_2O_3+2\,DyVO_3+O_2=Dy_8V_2O_{17}$	4.85±0.05	278±1
(2) $DyVO_3+1/2\,O_2=DyVO_4$	3.80±0.03	123.8±0.5
(3) $3\,Ho_2O_3+2\,HoVO_3+O_2=Ho_8V_2O_{17}$	4.45±0.07	277±2
(4) $HoVO_3+1/2\,O_2=HoVO_4$	3.70±0.03	122.4±0.5

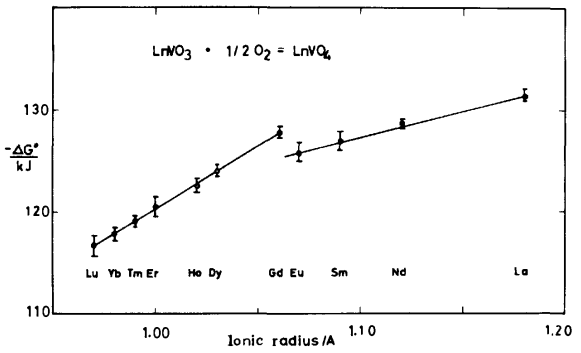

Fig. 5. The relationship between the ionic radius of lanthanoid elements with eight coordination and the ΔG° values of reaction, $LnVO_3+1/2\,O_2=LnVO_4$.

with those quoted in the Table. There are no considerable differences in values of the samples which were prepared under the different conditions of oxygen partial pressures. Lattice constants of $Dy_8V_2O_{17}$ and $Ho_8V_2O_{17}$ were determined with the data of $4\,Tm_2O_3 \cdot V_2O_5$.[20] Experimental errors are still large compared with the data of other compounds.

Calculation of the Standard Gibbs Energies of Reactions. On the basis of the present phase equilibria, the standard Gibbs energies of the reactions appeared in the systems, except for the partial system of V_2O_3-V_2O_5, can be calculated by an equation, $\Delta G^\circ=-RT\ln K$, where R is the gas constant, T, the absolute temperature, and K, the equilibrium constant of each reaction. Chemical reactions appeared in the phase diagrams, the oxygen partial pressures in equilibrium for each reaction, and ΔG° values obtained are shown in Table 4. Activities of each component in solid solutions, which are necessary for the calculation, are given in Table 2.

The Relationship between ΔG° and Ionic Radius. In the series of Ln_2O_3-V_2O_3-V_2O_5 system, the common reaction, $LnVO_3+1/2\,O_2=LnVO_4$, appeares in all the systems. It is very interesting to correlate the ΔG° values of reactions with some properties of lanthanoid elements. In a previous report,[7] we have graphically presented the linear relationship between ΔG° values and the ionic radius of lanthanoid elements with eight coordination, provided that the lanthanoid series was subdivided into two groups. The present program is to ascertain whether or not the data obtained in the present systems fit well to the previous linear relation. The values of the present systems are plotted in Fig. 5 with open circles. These circles are well fit on the line which has been drawn using the data of previous results of another systems.

References

1) K. Kitayama and T. Katsura, *Bull. Chem. Soc. Jpn.*, **50**, 889 (1977).
2) K. Kitayama and T. Katsura, *Bull. Chem. Soc. Jpn.*, **51**, 1358 (1978).
3) K. Kitayama, T. Sugihara, and T. Katsura, *Bull. Chem. Soc. Jpn.*, **52**, 458 (1979).
4) K. Kitayama and T. Katsura, *Bull. Chem. Soc. Jpn.*, **55**, 1820 (1982).
5) K. Kitayama, D. Zoshima, and T. Katsura, *Bull. Chem. Soc. Jpn.*, **56**, 689 (1983).
6) K. Kitayama, C. Mizokuchi, and T. Katsura, *Bull. Chem. Soc. Jpn.*, **56**, 695 (1983).
7) K. Kitayama and T. Katsura, *Bull. Chem. Soc, Jpn.*, **56**, 1084 (1983).
8) K. Kitayama, H. Sou, and T. Katsura, *Bull. Chem. Soc. Jpn.*, **56**, 3415 (1983).
9) H. Brusset, F. Madaule-Aubry, B. Blanck, J. P. Glaziou, and J. P. Laude, *Can. J. Chem.*, **49**, 3700 (1971).
10) A. K. Molodkin, V. N. Belan, Yu. E. Bogatov, and V. I. Moskalenko, *Zh. Neorg. Khim.*, **27**, 1033 (1982).
11) G. J. McCarthy, C. A. Sipe, and K. E. McIlvried, *Mater. Res. Bull.*, **9**, 1279 (1974).
12) B. Reuter, *Col. Int. C. N. R. S.*, 1053 (1965).
13) J. C. P. D. S. Card No. 16-870.
14) J. C. P. D. S. Card No. 15-764.
15) T. Katsura and H. Hasegawa, *Bull. Chem. Soc. Jpn.*, **40**, 561 (1967).
16) N. Kimizuka and T. Katsura, *J. Solid State Chem.*, **13**, 176 (1975).
17) T. Katsura and A. Muan, *Trans. AIME*, **230**, 77 (1964).
18) N. Kimizuka and T. Katsura, *J. Solid State Chem.*, **15**, 151 (1975).
19) N. Kimizuka and T. Katsura, *Bull. Chem. Soc. Jpn.*, **47**, 1801 (1974).
20) H. Brusset, R. Mahe, and J. P. Laude, *Bull. Soc. Chim. Fr.*, **1973**, 495.

Synthesis and Stereoselectivity of Cobalt(III) Complexes of Quadridentate Ligands Possessing SNNS Array of Donor Atoms

Kazuaki YAMANARI,* Norimatsu TAKESHITA, and Yoichi SHIMURA
Department of Chemistry, Faculty of Science, Osaka University, Toyonaka, Osaka 560
(Received November 17, 1983)

Several thiolato complexes of $[Co(SNNS)(diamine)]^+$ type were prepared (diamine stands for en=1,2-ethanediamine, *R*-pn=(*R*)-1,2-propanediamine, and *RR*-chxn=(*R*,*R*)-1,2-cyclohexanediamine) and characterized from their visible-UV absorption, circular dichroism, and ^{13}C NMR spectra, where SNNS denotes two kinds of open-chain quadridentate ligands, H_2endet=3,6-dimethyl-3,6-diazaoctane-1,8-dithiol and *R*-H_2pndet=(*R*)-3,4,6-trimethyl-3,6-diazaoctane-1,8-dithiol. Both the SNNS ligands gave the two geometrical isomers, *cis*-α(dark green) and *cis*-β(dark violet), whereas 3,7-dimethyl-3,7-diazanonane-1,9-dithiolate(2−) ligand gave no stable monomeric complex. Interestingly, stereoselective complex formation was found in *Δ*-*cis*-α-[Co(*R*-pndet)(en or *RR*-chxn)]$^+$, *Δ*(S^NR^N)-*cis*-β-[Co(endet)(*R*-pn or *RR*-chxn)]$^+$, and *Δ*(S^NR^N)-*cis*-β-[Co(*R*-pndet)(en or *RR*-chxn)]$^+$, the *Δ*-*cis*-α configuration of the former complex being the novel one having the equatorially-oriented terminal chelate rings on the tertiary nitrogen atoms.

In a previous communication, we reported the stereochemistry of cobalt(III) complexes with a quadridentate ligand having SNNS donor set. Two geometrical isomers of the $[Co(N)_4(thiolato)_2]^+$ type complex were first separated by column chromatography.[1] The earlier attempt to prepare this type of complexes using bidentate ligand was unsuccessful in spite of the chromatographic analysis.[2] These circumstances show that the quadridentate ligand possessing SNNS donor set is promising for the stereochemical investigation of cobalt(III) complexes.

In this paper, three kinds of open-chain SNNS quadridentate ligands 3,6-dimethyl-3,6-diazaoctane-1,8-dithiol(H_2endet), 3,7-dimethyl-3,7-diazanonane-1,9-dithiol(H_2tndet), and (*R*)-3,4,6-trimethyl-3,6-diazaoctane-1,8-dithiol(*R*-H_2pndet) were used to prepare several cobalt(III) complexes $[Co(SNNS)(diamine)]^+$ (diamine=en, *R*-pn, and *RR*-chxn), $[Co(SNNS)(CN)_2]^-$, and [Co(SNNS)(aet)].[3] The complexes were separated, optically resolved by the chromatographic techniques, and characterized from their visible-UV absorption, circular dichroism(CD), and ^{13}C NMR spectra. For the complex $[Co(SNNS)(diamine)]^+$, the two geometrical isomers, *cis*-α and *cis*-β, are possible as shown in Fig. 1. This type of geometrical isomers were found for the endet and *R*-pndet ligands, whereas no stable mononuclear complex was detected for the tndet ligand. Furthermore, the optically active *R*-pndet ligand showed complete stereoselectivity in *cis*-α and *cis*-β-[Co(*R*-pndet)(en or *RR*-chxn)]$^+$.

Experimental

Preparation of Ligand. *3,6-Dimethyl-3,6-diazaoctane-1,8-dithiol(H_2endet), $[HSCH_2CH_2N(CH_3)CH_2-]_2$*: The ligand was prepared from thiirane[4] and *N*,*N*′-dimethyl-1,2-ethanediamine as described by Karlin and Lippard.[5] ^{13}C NMR (benzene): δ=22.99 ($CH_2\underline{C}H_2SH$), 42.66 ($N\underline{C}H_3$), 55.72 ($N\underline{C}H_2CH_2SH$), and 61.13 ($N\underline{C}H_2CH_2N$). Found: C,48.25; H,9.53; N,13.05%. Calcd for H_2endet·1/6 C_6H_6=$C_9H_{21}N_2S_2$: C, 48.53; H,9.56; N,12.65%. A solution of H_2endet (1 mmol) in methanol (5 cm^3) was added to a warm solution of $Ni(CH_3CO_2)_2\cdot 4H_2O$ (1 mmol) in methanol (10 cm^3). The brown solid, which separated immediately, was filtered, washed with ethanol, and vacuum dried. Found: C, 36.24; H, 6.85; N, 10.56%. Calcd for [Ni(endet)]=$C_8H_{18}N_2S_2Ni$: C, 36.25; H, 6.85; N ,10.57%.

3,7-Dimethyl-3,7-diazanonane-1,9-dithiol(H_2tndet), $[HSCH_2CH_2N(CH_3)CH_2-]_2CH_2$: This ligand was obtained in the same manner as that of H_2endet, where *N*,*N*′-dimethyl-1,3-propanediamine[6] is substituted for *N*,*N*′-dimethyl-1,2-ethanediamine. ^{13}C NMR (benzene): δ=23.10 ($CH_2\underline{C}H_2SH$), 25.70 ($NCH_2\underline{C}H_2CH_2N$), 42.34 ($N\underline{C}H_3$), 55.67 ($N\underline{C}H_2CH_2SH$), and 60.87 ($N\underline{C}H_2CH_2CH_2N$). Found: C,51.01; H, 9.85; N,12.09%. Calcd for H_2tndet·1/6 C_6H_6=$C_{10}H_{23}N_2S_2$: C, 51.02; H, 9.85; N, 11.90%. A solution of H_2tndet (1 mmol) in methanol (5 cm^3) was added to a warm solution of $Ni(CH_3CO_2)_2\cdot 4H_2O$ (1 mmol) in methanol (10 cm^3). To this mixture was added 0.3 g of $NaClO_4$ dissolved in 2 cm^3 of methanol. The resulting solution was concentrated by a rotary evaporator to give dark brown crystals, which were collected by filtration and washed with ethanol. Found: C, 26.52; H, 5.06; N, 6.91%. Calcd for $[Ni\{Ni(tndet)\}_2](ClO_4)_2$=$C_{18}H_{40}N_4S_4O_8Cl_2Ni_3$: C, 26.50; H, 4.94; N, 6.87%.

(R)-*3,4,6-Trimethyl-3,6-diazaoctane-1,8-dithiol(*R*-H_2pndet), $HSCH_2CH_2N(CH_3)CH(CH_3)CH_2N(CH_3)CH_2CH_2SH$*: The ligand was prepared from thiirane and (*R*)-*N*,*N*′-dimethyl-1,2-propanediamine[7] according to the same method. The purity was relatively low compared with those of H_2endet and H_2tndet and therefore checked by the nickel(II) complex formation. The dark brown Ni(II) trimer was obtained in a similar way by the method of the above tndet complex. Found: C, 28.22; H, 5.51; N, 6.92%. Calcd for $[Ni\{Ni(R\text{-pndet})\}_2]Br_2\cdot CH_3OH$=$C_{19}H_{44}N_4S_4Br_2ONi_3$: C, 28.22; H, 5.48; N, 6.93%.

Preparation and Separation of the Cobalt(III) Complexes. cis-α- *and cis*-β-*[Co(endet)(diamine)]ClO_4 (diamine=en, R-pn, and RR-chxn)*: To a solution of 3.15 g of $[Co(en)_3]Cl_3\cdot 3H_2O$ in 20 cm^3 of water was added a mixture of 1.74 g of H_2endet and 0.6 g of NaOH in 20 cm^3 of water. The mixed solution was stirred for 2 h at room temperature. After filtration of the gummy precipitate, the resulting dark green filtrate was poured onto a column of SP-Sephadex C-25 (Na^+ form 4×50 cm), washed with water, and eluted with 0.1 mol

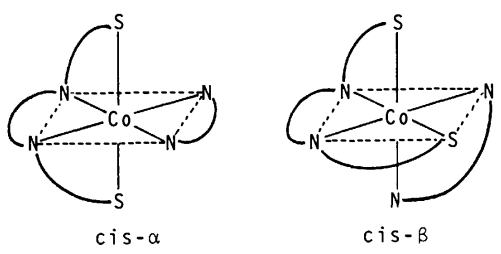

Fig. 1. Two geometrical isomers of $[Co(SNNS)(diamine)]^+$.

dm^{-3} $NaClO_4$. Two partly overlapping bands, dark green and dark violet, were eluted in this order. The total yield of the desired products was *ca.* 30% and the amount of the former isomer was somewhat higher than that of the latter one. As described later, the dark green and the dark violet isomers were assigned to *cis*-α- and *cis*-β-[Co(endet)(en)]$^+$, respectively. Each eluate was concentrated in a vacuum evaporator to give crystals of the desired perchlorate salt. Found for the dark green isomer (*cis*-α): C, 28.33; H, 6.20; N, 13.12%. Found for the dark violet isomer (*cis*-β): C, 28.17; H, 6.22; N, 13.17%. Calcd for [Co(endet)(en)]ClO_4=$C_{10}H_{26}N_4S_2O_4CoCl$: C, 28.27; H, 6.17; N, 13.19%. The perchlorate salt was converted into the corresponding chloride salt using a column of QAE-Sephadex A-25 (Cl^- form). The highly soluble chloride salt was used for ^{13}C NMR measurements.

The complexes containing *R*-pn or *RR*-chxn ligand were prepared and separated in the same manner as described above except for the use of Δ-[Co(*R*-pn)$_3$]$^{3+}$ or Δ-[Co(*RR*-chxn)$_3$]$^{3+}$, respectively, as a starting material. The two geometrical isomers, dark green and dark violet, were obtained in each case. Found for the dark green *R*-pn isomer: C, 29.59; H,6.34; N, 12.41%. Calcd for *cis*-α-[Co(endet)(*R*-pn)]$ClO_4\cdot 0.5H_2O$=$C_{11}H_{29}N_4S_2O_{4.5}CoCl$: C, 29.50; H, 6.53; N, 12.51%. Found for the dark violet *R*-pn isomer: C, 30.35; H, 6.51; N, 12.80%. Calcd for *cis*-β-[Co(endet)(*R*-pn)]ClO_4=$C_{11}H_{28}N_4S_2O_4CoCl$: C, 30.10; H, 6.43; N, 12.77%. Found for the dark green *RR*-chxn isomer(*cis*-α): C, 35.10; H, 6.75; N, 11.70%. Found for the dark violet *RR*-chxn isomer(*cis*-β): C, 35.14; H, 6.74; N, 11.60%. Calcd for [Co(endet)(*RR*-chxn)]ClO_4=$C_{14}H_{32}N_4S_2O_4CoCl$: C, 35.11; H, 6.73; N, 11.70%.

Diastereomer Separation of cis-α- *and* cis-β-*[Co(endet)(diamine)]*$^+$*(diamine=*R-*pn and* RR-*chxn)*: The general procedure in chromatography was as follows: Small amount of each isomer was dissolved in water, adsorbed onto a column of cation exchanger (Dowex 50W×2, Na^+ form; 3×15 cm) and eluted with 0.3 mol dm^{-3} Na_2SO_4. The eluate was collected into 5 cm^3 portions and the CD spectra of the fractions were measured. Two diastereomers were confirmed in each of *cis*-α-[Co(endet)(*R*-pn)]$^+$ and *cis*-α-[Co(endet)(*RR*-chxn)]$^+$, though the elution order is reversed, namely the last eluted isomer $(-)^{CD}_{570}$-*cis*-α-[Co(endet)(*R*-pn)]$^+$ corresponding to the first eluted one $(-)^{CD}_{570}$-*cis*-α-[Co(endet)(*RR*-chxn)]$^+$. On the other hand, both *cis*-β-[Co(endet)(*R*-pn)]$^+$ and *cis*-β-[Co(endet)(*RR*-chxn)]$^+$ gave the only one diastereomer, which showed the two negative CD bands in the first d-d absorption band region. In the cases of *cis*-α complexes, the oxidation products, probably sulfenato complexes, partly overlapped on the front of the first eluted band, which was collected and rechromatographed in the same manner. The diastereomer separation using SP-Sephadex C-25(Na^+ form) gave almost the same results even when the optically active reagents such as *RR*-$C_4H_4O_6^{2-}$ and [Sb_2(*RR*-$C_4H_2O_6)_2$]$^{2-}$ were used as an elution agent. These chromatographic results were supported by the ^{13}C NMR data as shown later.

cis-α *and* cis-β-*Na[Co(endet)(CN)$_2$]*: To a suspension of Na[$CoBr_2(CN)_2(NH_3)_2$](2.19 g) in 50 cm^3 of water, which was prepared by treating *cis(CN)-cis(SO$_3$)-trans(NH$_3$)*-[$Co(CN)_2(SO_3)_2(NH_3)_2$]$^{3-}$ [8] with a HBr solution, was added a solution of H_2endet (1.39 g) and NaOH (0.53 g) in 15 cm^3 of water and the mixture was stirred for 3 h. After filtration of the precipitate, the filtrate was poured onto a column of QAE-Sephadex A-25 (Cl^- form, 3×50 cm), washed with water, and eluted with 0.08 mol dm^{-3} NaCl. The two bands, red purple and light brown, were eluted in this order. Each band was concentrated, reloaded onto a column of Sephadex G-15 to remove the NaCl, and eluted with water. The eluate was evaporated to dryness because of high solubility in water or ethanol. Found for the red purple isomer: C, 26.90; H, 4.99; N, 12.50%. Calcd for *cis*-α-Na[Co(endet)$(CN)_2$]$\cdot 2H_2O\cdot 1.2$NaCl=$C_{10}H_{22}N_4S_2O_2CoNa_{2.2}Cl_{1.2}$: C, 26.90; H, 4.97; N, 12.55%. Found for the light brown isomer: C, 32.33; H, 5.84; N, 14.72%. Calcd for *cis*-β-Na[Co(endet)$(CN)_2$]$\cdot 2H_2O$=$C_{10}H_{22}N_4S_2O_2CoNa$: C, 31.91; N, 5.89; N, 14.89%.

fac(S)-*[Co(endet)(aet)]*: To a solution of $[Co(NH_3)_6]Cl_3$ (0.53 g) in 10 cm^3 of water was added a solution of H_2endet (0.46 g) and Haet (0.15 g) in 10 cm^3 of water and the mixture was stirred 2 h at room temperature. After filtration of the precipitate, the filtrate was poured onto a column of Sephadex A-25 (Cl^- form), and eluted with water. The dark green band was collected and evaporated to dryness below 20 °C. Found: C, 34.88; H, 7.06; N, 12.24%. Calcd for *fac(S)*-[Co(endet)(aet)]=$C_{10}H_{24}N_3S_3Co$: C, 35.18; H, 7.08; N, 12.31%.

Complexes Containing tndet Ligand: The same preparative method as that of [Co(endet)(en)]$^+$ was applied to this system. The solution of $[Co(en)_3]Cl_3$ became temporarily dark green by the addition of tndet ligand but then changed to dark brown to give a large amount of a gummy precipitate. The column chromatograph of the filtrate gave no desirable monomeric species in this system. The change of diamine from en to *R*-pn or *RR*-chxn led to similar results.

cis-α- *and* cis-β-*[Co(*R*-pndet)(diamine)]*$^+$*(diamine=en and* RR-*chxn)*: The complexes were prepared in the same manner as that of [Co(endet)(diamine)]$^+$ where *R*-H_2pndet was substituted for H_2endet. The column chromatography using Dowex 50W×2 (Na^+ form, 3×15 cm; 0.4 mol dm^{-3} NaCl) gave the two geometrical isomers, green and violet in this order, for both [Co(*R*-pndet)(en)]$^+$ and [Co(*R*-pndet)(*RR*-chxn)]$^+$. The earlier eluted green band was rechromatographed to remove the partly overlapping oxidation products. Each band was fractionated into 5 cm^3 portions and their CD spectra were checked. Interestingly, each band was composed of a single species, that is, complete stereoselectivity was observed in *cis*-α(green)- and *cis*-β(violet)-[Co(*R*-pndet)(diamine)]$^+$ (diamine=en and *RR*-chxn). No solid complex was isolated because of their low yield. The concentration value for the CD intensity determination was calculated from the measured absorbance using the absorption coefficient of *cis*-α- or *cis*-β-[Co(endet)(*R*-pn)]$^+$.

cis-α- *and* cis-β-*[Co(endese)(en)]*$^+$ *and* cis-α- *and* cis-β-*[Co(endesi)(en)]*$^+$ *(endese=3,6-dimethyl-3,6-diazaoctane-1,8-disulfenic acid, [HOSCH$_2$CH$_2$N(CH$_3$)CH$_2$-]$_2$ and endesi=3,6-dimethyl-3,6-diazaoctane-1,8-disulfinic acid, [HO$_2$SCH$_2$CH$_2$N(CH$_3$)CH$_2$-]$_2$)*: A stoichiometric amount of 0.6% aqueous H_2O_2 (1.76×10^{-2} mmol) was added to a solution of *cis*-α- or *cis*-β-[Co(endet)(en)]ClO_4(0.88×10^{-2} mmol) in 5 cm^3 of water, leading to an orange-red solution instantly. The oxidation was followed by the absorption spectral measurements. The absorption spectra of *cis*-α- and *cis*-β-[Co(endese)(en)]$^+$ in Table 1 were measured when the absorption intensity became maximum in the region of 380—420 nm, which is the characteristic region to the coordinated sulfenato group. The formation of the corresponding sulfinato complex was negligible because the oxidation from the coordinated sulfenato to the sulfinato group proceeds approximately 10^3 times slower than that from the coordinated thiolate to the sulfenate.[9]

The corresponding sulfinato complex *cis*-α- or *cis*-β-[Co(endesi)(en)]$^+$ was prepared in the same manner using a large excess of 30% H_2O_2 and kept to standing for 1 or 2 d to complete the reaction. In the case of *cis*-α-[Co(endesi)(en)]$^+$ the desired solid complex was obtained. Found: C, 23.73; H, 5.40; N, 10.98%. Calcd for *cis*-α-[Co(endesi)(en)]$ClO_4\cdot H_2O$ =$C_{10}H_{28}N_4S_2O_9CoCl$: C, 23.70; H, 5.57; N, 11.05%. The data of *cis*-β-[Co(endesi)(en)]$^+$ in Table 1 were calculated by assuming that the absorption coefficient at 31250 cm^{-1} is

the same as that of the *cis*-α isomer at 28380 cm^{-1}.

Measurement. The visible and ultraviolet absorption spectra were measured on a Hitachi 330 spectrophotometer and CD spectra with a JASCO MOE-1 spectropolarimeter in aqueous solutions. The ^{13}C NMR spectra were recorded with a JEOL FX-90Q NMR spectrometer.

Results and Discussion

Characterization of Geometrical Isomers. The *cis*-α and *cis*-β isomers (Fig. 1) of the $[Co(endet)(en)]^+$ complex have C_2 and C_1 symmetries, respectively, and are assignable on the basis of ^{13}C NMR spectra. The dark green isomer showed five signals (26.30, 45.21, 52.53, 62.25, and 72.71 ppm) and therefore is assigned to the *cis*-α geometry. The dark violet isomer showed ten signals (17.74, 26.60, 29.20, 42.37, 46.76, 47.11, 58.24, 63.88, 64.34, and 70.89 ppm), which is consistent with the *cis*-β geometry. The absorption spectra of

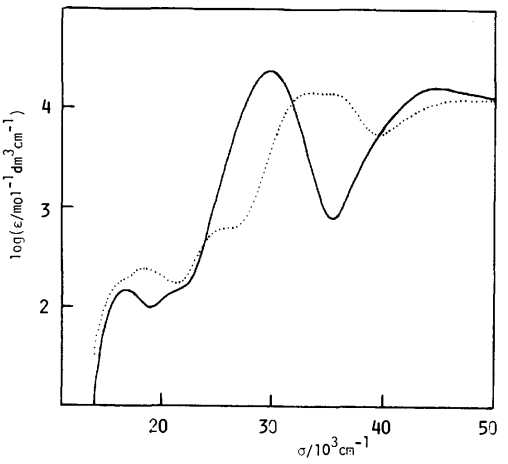

Fig. 2. Absorption spectra of $[Co(endet)(en)]ClO_4$: *cis*-α (——) and *cis*-β (----).

Table 1. Absorption data of $[Co(SNNS)X_2]^{n+}$

SNNS	X_2	Assignment	Wave number (Intensity) $\sigma_{max}/10^3$ cm^{-1}($\log(\varepsilon/mol^{-1}$ dm^3 $cm^{-1})$)		
			1st band	2nd band	CT band
endet	en	*cis*-α	16.95(2.18)		29.69(4.35)
			21.3 (2.18)[a]		44.54(4.18)
		cis-β	16.4 (2.24)	25.9(2.75)[a]	33.50(4.15)
			18.57(2.37)		35.21(4.14)
					47.2 (4.07)[a]
	R-pn	*cis*-α	16.93(2.16)		29.76(4.33)
			21.1 (2.07)[a]		44.50(4.18)
		cis-β	16.3 (2.25)[a]	25.7(2.87)[a]	33.40(4.14)
			18.65(2.41)		35.09(4.13)
					46.73(4.09)
	RR-chxn	*cis*-α	16.84(2.23)		29.66(4.31)
			21.1 (2.21)[a]		43.76(4.20)
		cis-β	16.1 (2.19)[a]	25.5(2.53)[a]	33.67(4.14)
			18.52(2.37)		34.97(4.14)
					45.56(4.13)
	2CN	*cis*-α	18.94(2.64)		32.45(4.36)
			25.3 (2.55)[a]		45.8 (4.15)[a]
					49.19(4.21)
		cis-β	17.0 (1.96)[a]	27.23(3.30)	34.57(4.10)
			21.5 (2.83)[a]		38.3 (4.00)[a]
	aet	*fac(S)*	16.20(2.60)	21.6(2.78)[a]	34.60(4.26)
				28 (3.50)[c]	36.7 (4.20)[a]
					46.8 (4.00)[a]
endese[b]	en	*cis*-α	19 (2.85)[a]		23.50(4.30)
					35.59(3.45)
					44.54(4.25)
		cis-β	19.62(3.06)		25.81(3.93)
					34.51(3.81)
					46.30(4.01)
endesi[b]	en	*cis*-α	20 (2.3)[a]		28.38(4.06)
					42.23(4.11)
		cis-β	20.6 (2.8)[a]		31.25(4.06)
					33.3 (4.04)
					44.39(4.13)

a) Shoulder. b) See Experimental section. c) This band may be due to the oxidized impurities.

$[Co(N)_4(S)_2]$ type complexes are shown in Fig. 2 and Table 1. The first d-d absorption band of each isomer is composed of two components. Since the interval between the components is larger for the dark green isomer than for the dark violet, the former isomer can be assigned to the *cis-α* structure of *trans(S)* chromophore and the latter to the *cis-β* of *cis(S)*. The complexes showed an intense band in 29000—34000 cm^{-1} region, which is assigned to the $Co(\sigma^*) \leftarrow S(\sigma)$ ligand-to-metal charge transfer (LMCT) transition.[10] The LMCT band of the *cis-α* isomer appears at 29690 cm^{-1} but that of the *cis-β* at 33500 cm^{-1} with its splitting component at 35210 cm^{-1}. Such a difference has been observed between geometrical isomers having two sulfide (thioether)[11] or sulfito[12] donor atoms: In general the charge transer (CT) band of *trans(S)* isomer locates at lower energy than that of *cis(S)* one. Thus the relative positions of CT bands confirm the above structural assignments. This criterion is also valid for the other complexes $[Co(endet)(R\text{-pn})]^+$, $[Co(endet)(RR\text{-chxn})]^+$, $[Co(R\text{-pndet})(en)]^+$, and $[Co(R\text{-pndet})(RR\text{-chxn})]^+$: the first eluted green isomer has the *cis-α* geometry and the second eluted violet one the *cis-β* geometry.

The absorption spectra of other thiolato complexes $[Co(endet)(CN)_2]^-$ and [Co(endet)(aet)] are shown in Fig. 3. In $[Co(endet)(CN)_2]^-$ three geometrical isomers, *cis-α*, *cis-β*, and *trans(CN)*, are possible. The red purple isomer exhibited the single LMCT band at 32450 cm^{-1} and therefore is assigned to the *cis-α* geometry. If the initial *cis(CN)*-configuration of the starting material $Na_3[Co(CN)_2(SO_3)_2(NH_3)_2]$ is retained after the reaction, the light brown isomer should have the *cis-β* geometry in agreement with the presence of two LMCT components at 34570 and 38300 cm^{-1}. The green isomer of [Co(endet)(aet)] showed the very similar absorption spectrum to *fac(S)*-$[Co(aet)_3]$ and *fac(S)*-$[Co(L\text{-cysteinato})_3]^{3-}$.[10] Thus this isomer can be assigned to the *fac(S)* geometry with *cis-β* configuration of the quadridentate ligand. The *mer(S)* configuration is very novel for a $[Co(N)_3(thiolato)_3]$ type complex and there has been no example except *mer(S)*-[Co(2-pyridinethiolato)$_3$].[13]

Figure 4 presents the absorption spectra of $[Co(endese)(en)]^+$ and $[Co(endesi)(en)]^+$. The usual oxidation reactions with H_2O_2 do not involve Co-S cleavage[9,10,14] and the initial geometrical structures should be retained. In fact, both the *cis-α* sulfenato and *cis-α* sulfinato complexes showed the intense CT band at lower energy side than the corresponding *cis-β* complexes, respectively (Table 1).

Synthesis and Stereochemistry of the Complexes of Sulfur-containing Quadridentate Ligand. Several cobalt(III) complexes with quadridentate ligands possessing NSSN array of donor atoms, $NH_2(CH_2)_xS(CH_2)_yS(CH_2)_zNH_2$, have been studied so far.[15] The results showed that only the *cis-α* isomer is formed in the case of $x=y=z=2$ and only the *cis-β* and *trans* isomers in the case of $x=z=2$ and $y=3$ for the mononuclear $[Co(NSSN)X_2]$ complexes. The skeleton of present thiolato ligands $HS(CH_2)_xN(CH_3)(CH_2)_yN(CH_3)(CH_2)_z$-SH is similar to the above one except for the position of sulfur atoms. However, the present SNNS ligands gave both *cis-α* and *cis-β* isomers in the case of $x=y=z=2$ (endet and *R*-pndet) and no mononuclear species in the case of $x=z=2$ and $y=3$ (tndet). Such striking difference can be attributable to the high bridging ability of thiolato groups and the special property of the tndet ligand described below.

Nickel(II) acetate reacted with H_2endet in methanol solution to give the brown complex [Ni(endet)]. However, the tndet ligand did not give the mononuclear complex but the trimeric one $[Ni\{Ni(tndet)\}_2](ClO_4)_2$. A similar Ni(II) trimer has been reported on the occasion of the detritylation of 1,9-bis(tritylthio)-3,7-diazanonane),[16] the trimer being probably in equilibrium with the monomer in methanol. This was confirmed from the synthesis of some mixed-metal trimer by allowing the Ni(II) trimer to react with Pd^{2+} or Cd^{2+}.[17] The synthesis of $[Co(tndet)(diamine)]^+$ was unsuccessful and some kind of polynuclear complex, whose composition was poorly characterized, was formed in the present case. Recently, Lippard and his co-workers prepared the iron complexes of H_2endet and H_2tndet ligands. Zubieta and his co-workers also reported the molybdenum complexes of the same ligands. In

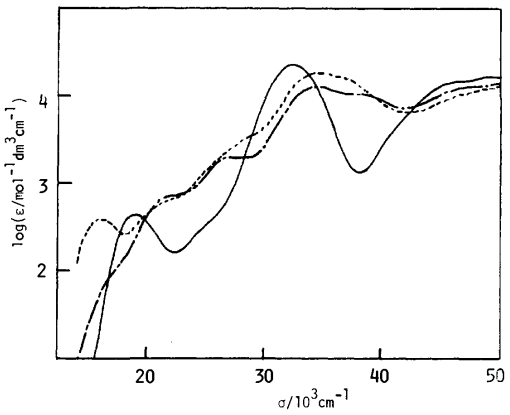

Fig. 3. Absorption spectra of *cis-α*-$[Co(endet)(CN)_2]^-$ (——), *cis-β*-$[Co(endet)(CN)_2]^-$ (– – – –), and *fac(S)*-[Co(endet)(aet)] (----).

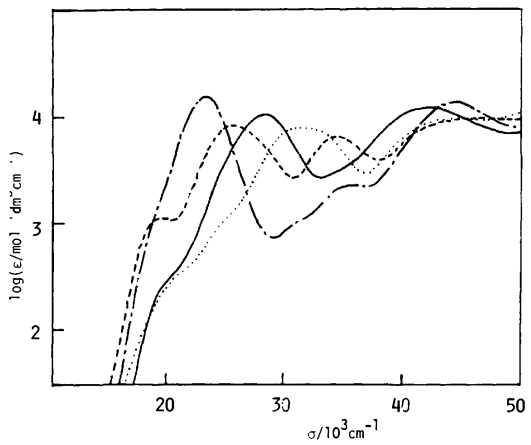

Fig. 4. Absorption spectra of *cis-α*-$[Co(endese)(en)]^+$ (– – – –), *cis-β*-$[Co(endese)(en)]^+$ (----), *cis-α*-$[Co(endesi)(en)]^+$ (——), and *cis-β*-$[Co(endesi)(en)]^+$ (……).

these investigations, some unusual structures were found for the complexes containing tndet ligand: The pseudo tetrahedral complex [Fe(Htndet)$(NO)_2$] has a 12-membered chelate ring in which the two nitrogen atoms of the quadridentate ligand are not coordinated to the iron atom.[18] A similar feature of the structure was found in [Mo_2O_4(Htndet)$_2$].[19] In these cases the tndet ligand is protonated to produce a six-membered ring $\underline{\text{N-C-C-C-N-H}}$ with a chair conformation, which is responsible for the poor complex formation in the present tndet ligand.

The synthetic efforts was also made for [Co(endet)X_2], where X_2 denotes 2(NH_3), 2(NO_2^-), $C_2O_4^{2-}$, $CH_3COCHCOCH_3^-$, CO_3^{2-}, 2(CN^-), and aet^-, all preparations except the latter two ligands producing no mononuclear cobalt(III) complex. This fact means that the stable complex is formed only when the remaining two coordination sites are occupied by such tightly bound ligands as 2(CN^-) and aet^-.

Stereoselective Formation of Diastereomers. Figure 5 shows the ^{13}C NMR spectra of *cis*-α- and *cis*-β-[Co(endet)(*RR*-chxn)]$^+$. The *cis*-α isomer exhibited twelve signals (24.73 (strong), 25.60, 27.06, 33.46, 34.54, 52.25, 52.69, 59.35, 61.52 (strong), 63.58, 72.19, and 73.38 ppm in D_2O), which imply the *cis*-α isomer having C_2 symmetry is a diastereomeric mixture of $\Delta(R^NR^N)(R^CR^C)$ and $\Lambda(S^NS^N)(R^CR^C)$. On the other hand, the *cis*-β isomer showed fourteen signals (23.79, 24.22, 25.85, 28.72, 32.24, 34.30, 45.13, 50.55, 56.84, 61.66, 62.14, 62.96, 65.83, and 69.13 ppm in DMSO-d_6), which indicate the stereoselective formation of single C_1 *cis*-β diastereomer. These results are completely in accord with those of the chromatographic separation: Two diastereomers were confirmed for *cis*-α-[Co(endet)(*R*-pn)]$^+$ and *cis*-α-[Co(endet)(*RR*-chxn)]$^+$, whereas the single diastereomer was found for *cis*-β-[Co(endet)(*R*-pn)]$^+$ and *cis*-β-[Co(endet)(*RR*-chxn)]$^+$.

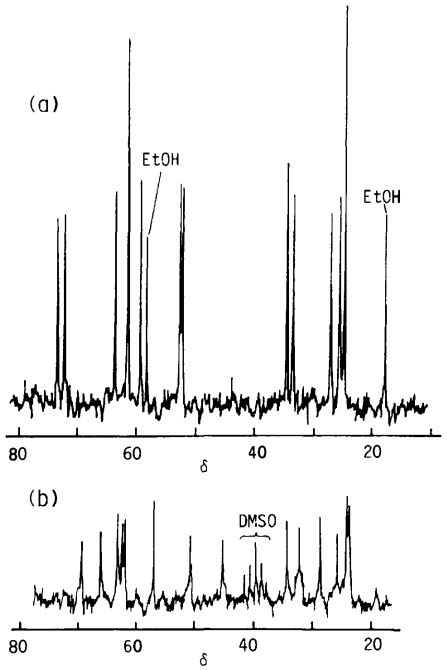

Fig. 5. ^{13}C NMR spectra of [Co(endet)(*RR*-chxn)]$^+$: (a) *cis*-α in D_2O; ethanol(δ 58.27 vs Me_4Si) was used as the internal standard. (b) *cis*-β in DMSO-d_6; DMSO (δ 39.5 vs Me_4Si) was used as the internal standard.

The CD spectra of *cis*-α diastereomers are shown in Figs. 6 and 7. The earlier eluted *R*-pn isomer *cis*-α-$(+)^{CD}_{600}$-[Co(endet)(*R*-pn)]$^+$ corresponds to the later eluted *RR*-chxn one *cis*-α-$(+)^{CD}_{600}$-[Co(endet)(*RR*-chxn)]$^+$ (Fig. 6). Both the *cis*-α-$(+)^{CD}_{600}$ isomers showed a positive dominant CD band in the first absorption band region and therefore are assigned to the $\Lambda(S^NS^N)$ absolute

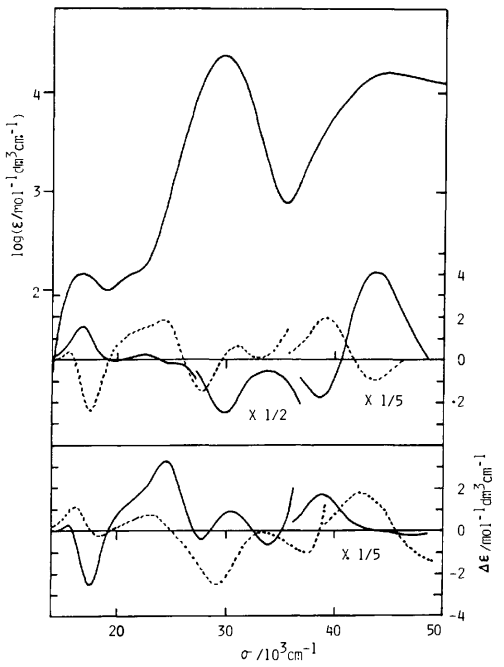

Fig. 6. Absorption and CD spectra of *cis*-α-[Co(endet)-(*R*-pn)]$^+$ (upper): 1st eluted $(+)^{CD}_{600}$-isomer (——) and 2nd eluted $(-)^{CD}_{570}$-isomer (----). CD spectra of *cis*-α-[Co(endet)(*RR*-chxn)]$^+$(lower): 1st eluted $(-)^{CD}_{570}$-isomer (——) and 2nd eluted $(+)^{CD}_{600}$-isomer (----).

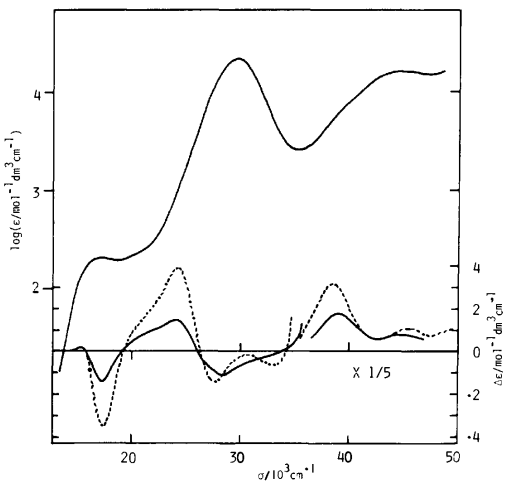

Fig. 7. Absorption and CD spectra of *cis*-α-[Co(*R*-pndet)(diamine)]$^+$: diamine=en (——) and *RR*-chxn (----).

TABLE 2. CD DATA OF [Co(SNNS)(diamine)]$^+$

SNNS	diamine	Assignment	Wave number (Intensity) $\sigma_{ext}/10^3$ cm^{-1}($\Delta\varepsilon$/mol^{-1} dm^3 cm^{-1})	
[*cis*-α complexes]				
endet	*R*-pn	$\Lambda(S^NS^N)$	16.84(+1.54)	29.87(−4.95)
			19.5 (−0.035)	38.76(−8.84)
			22.57(+0.240)	43.73(+20.4)
		$\Delta(R^NR^N)$	15.55(+0.350)	27.78(−1.48)
			17.57(−2.39)	31.2 (+0.678)
			21.5 (+1.50)[a]	39.2 (+9.77)
			24.27(+1.85)	43.67(−4.72)
	RR-chxn	$\Delta(R^NR^N)$	15.5 (+0.272)	27.28(−0.389)
			17.45(−2.42)	30.40(+0.864)
			21.5 (+1.3)[a]	33.86(−0.631)
			24.53(+3.15)	38.93(+8.16)
				47.2 (−1.1)
		$\Lambda(S^NS^N)$	16.25(+1.04)	29.41(−2.38)
			18.4 (−0.25)	37.74(−0.987)
			22.94(+0.694)	42.37(+8.51)
R-pndet	en	$\Delta\lambda(R^NR^CR^N)$	15.3 (+0.164)	28.3 (−1.12)
			17.18(−1.43)	31.5 (−0.4)[a]
			21.5 (+0.9)[a]	39.20(+8.84)
			24.00(+1.46)	44.80(+3.81)
	RR-chxn	$\Delta\lambda(R^NR^CR^N)$	15.22(+0.144)	27.62(−1.46)
			17.33(−3.52)	33.11(−0.692)
			21.2 (+1.6)[a]	38.54(+15.8)
			24.21(+3.92)	45.25(+5.04)
[*cis*-β complexes]				
endet	*R*-pn	$\Lambda(S^NR^N)$	16.47(−1.50)	32.31(+28.2)
			20.75(−1.65)	36.04(−33.3)
			24.48(+2.60)	43.29(+10.5)
	RR-chxn	$\Lambda(S^NR^N)$	16.31(−1.64)	32.27(+29.3)
			20.62(−1.85)	35.84(−31.8)
			24.39(+3.26)	43.10(+8.82)
R-pndet	en	$\Delta\lambda(S^NR^CR^N)$	16.35(−1.32)	32.21(+26.6)
			20.62(−1.87)	35.91(−34.0)
			24.69(+2.72)	42.94(+8.41)
	RR-chxn	$\Delta\lambda(S^NR^CR^N)$	16.31(−1.82)	32.27(+33.5)
			20.64(−2.43)	35.91(−36.6)
			24.39(+3.62)	42.55(+7.70)

a) Shoulder.

configuration concerning the skew pair of chelate rings and the tertiary nitrogen atoms. The remaining diastereomers *cis*-α-$(-)^{CD}_{570}$-[Co(endet)(*R*-pn)]$^+$ and *cis*-α-$(-)^{CD}_{570}$-[Co(endet)(*RR*-chxn)]$^+$ exhibited a negative main CD band in the same region, which are assigned to the $\Lambda(R^NR^N)$ absolute configuration.

Each single diastereomer was found in *cis*-α-[Co(*R*-pndet)(en)]$^+$ and *cis*-α-[Co(*R*-pndet)(*RR*-chxn)]$^+$. When the methyl group on the medial chelate ring of quadridentate ligand takes an equatorial position, the medial chelate ring is fixed to the most stable λ conformation. Therefore, two diastereomers, $\Delta\lambda(R^NR^CR^N)$ and $\Lambda\lambda(S^NR^CS^N)$, are possible for *cis*-α-[Co(*R*-pndet)(diamine)]$^+$ in Fig. 8. Each the obtained diastereomer showed three CD bands, (+), (−), and (+), from the lower energy side in the first absorption

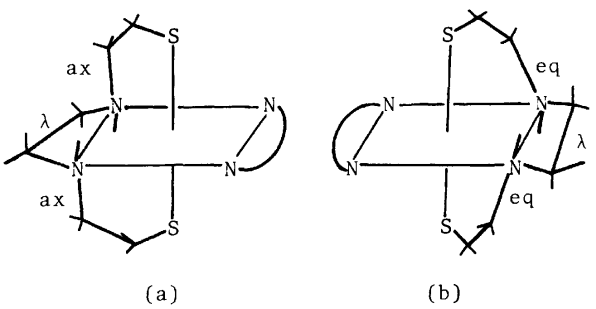

Fig. 8. Two diastereomers of *cis*-α-[Co(*R*-pndet)(diamine)]$^+$: (a) $\Lambda\lambda(S^NR^CS^N)$ and (b) $\Delta\lambda(R^NR^CR^N)$.

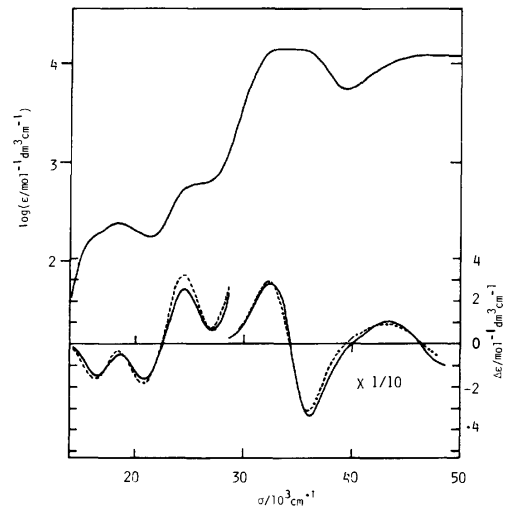

Fig. 9. Absorption and CD spectra of *cis*-β-[Co(endet)(diamine)]$^+$: diamine=*R*-pn (——) and *RR*-chxn (----).

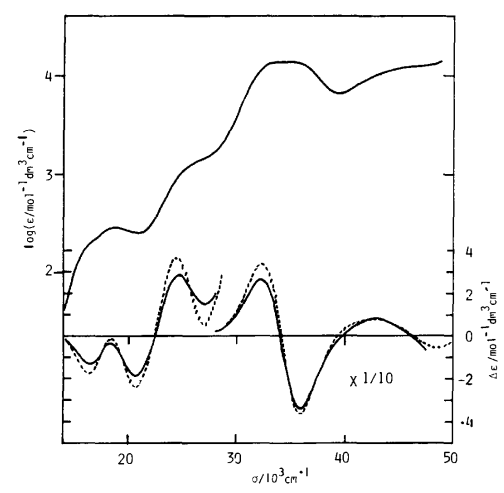

Fig. 10. Absorption and CD spectra of *cis*-β-[Co(*R*-pndet)(diamine)]$^+$: diamine=en (——) and *RR*-chxn (----).

band region (Fig. 7). Since the negative CD band becomes dominant, the complexes can be assigned to the $\Delta\lambda(R^NR^CR^N)$ absolute configuration which has the equatorially oriented terminal chelate rings on the tertiary nitrogen atoms. It has long been generally thought that the configuration $\Lambda\lambda(S^NR^CS^N)$ is more preferable in *cis*-α geometry because the configuration $\Delta\lambda(R^NR^CR^N)$ suffers the greatest ring strain in the backbone and two adjacent chelate rings. However, the latter $\Delta\lambda(R^NR^CR^N)$ or the related $\Delta\lambda(R^NR^CR^CR^N)$ configuration has been recently reported in several chromium(III) and cobalt(III) complexes containing the quadridentate ligands such as (*S*)-*N*,*N*′-bis(2-pyridylmethyl)-1,2-propanediamine, (1*S*,2*S*)-*N*,*N*′-bis(2-pyridylmethyl)-1,2-cyclohexanediamine(abbrev. *SS*-picchxn),[20] and (1*R*,2*R*)-*N*,*N*′-dimethyl-1,2-cyclohexanediamine-*N*,*N*′-diacetate (*N*,*N*′-Me$_2$-*RR*-chxnda).[21] The configurations of Λ-*cis*-α-[CrCl$_2$(*RR*-picchxn)]-

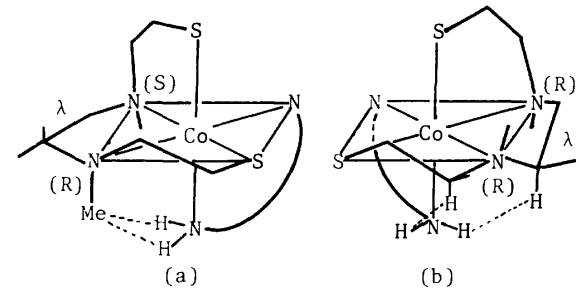

Fig. 11. Possible diastereomers of *cis*-β-[Co(*R*-pndet)(diamine)]$^+$: (a) $\Delta\lambda(S^NR^CR^N)$ and (b) $\Delta\lambda(R^NR^CR^N)$.

ClO$_4$[22] and Δ-*cis*-α-[Co(*N*,*N*′-Me$_2$-*RR*-chxnda)(en)]ClO$_4$[23] have been explicitly determined by the X-ray structure analysis. The CD spectral patterns of *cis*-α-[Co(*R*-pndet)(en)]$^+$ and *cis*-α-[Co(*R*-pndet)(*R*-chxn)]$^+$ are very similar to that of Δ-*cis*-α-[Co(*N*,*N*′-Me$_2$-*RR*-chxnda)(en)]$^+$, especially in the first absorption band region.[20] This fact supports that the present *cis*-α complexes have the rare $\Delta\lambda(R^NR^CR^N)$ configuration.

The CD spectra of the *cis*-β complexes, [Co(endet)(*R*-pn)]$^+$, [Co(endet)(*RR*-chxn)]$^+$, [Co(*R*-(pndet)(en)]$^+$, and [Co(*R*-pndet)(*RR*-chxn)]$^+$ are shown in Figs. 9 and 10. They are very resemble to one another all over the regions measured. The results indicate that each the *cis*-β diastereomer is formed stereoselectively in agreement with the ^{13}C NMR results and has the same absolute configuration. The Δ configuration is assigned to these complexes on the basis of the net negative CD sign in the first absorption band region.

In *cis*-β-[Co(*R*-pndet)(diamine)]$^+$, only two diastereomers, $\Delta\lambda(S^NR^CR^N)$ and $\Lambda\lambda(R^NR^CR^N)$, are possible owing to the λ conformation of the medial chelate ring as in Fig. 11. In the $\Lambda\lambda(R^NR^CR^N)$ structure(b), there is a steric repulsion between the two amine protons of bidentate diamine and the two methylene protons adjacent to the tertiary amine of the quadridentate. On the other hand, the steric crowding between the methyl group on the *R*-N atom and the amine protons of bidentate diamine in the $\Delta\lambda(S^NR^CR^N)$ structure(a) can be eliminated partly by the conformational change of the terminal chelate ring. Therefore the actual diastereomer is limited to the $\Delta\lambda(S^NR^CR^N)$ configuration. In conclusion, all the four *cis*-β complexes obtained stereoselectively can be assigned to $\Delta(S^NR^N)$ configuration on the basis of the analogous CD patterns.

References

1) K. Yamanari, N. Takeshita, T. Komorita, and Y. Shimura, *Chem. Lett.*, **1981**, 861.

2) C. Stein, S. Bouma, J. Carlson, C. Cornelius, J. Maeda, C.Weshler, E. Deutsch, and K. O. Hodgson, *Inorg. Chem.*, **15**, 1183 (1976).

3) Abbreviations used for ligands are as follows: en=1,2-ethanediamine, $NH_2CH_2CH_2NH_2$; *R*-pn=(*R*)-1,2-propanediamine, $NH_2CH(CH_3)CH_2NH_2$; *RR*-*chxn*=(*R*,*R*)-1,2-cyclohexanediamine, $\boxed{CH_2CH_2CH(NH_2)CH(NH_2)CH_2CH_2}$; and Haet=2-aminoethanethiol, $NH_2CH_2CH_2SH$.

4) S. Searles, E. F. Lutz, H. R. Hays, and H. E. Mortensen, *Org. Synth.*, **42**, 59 (1962).
5) K. D. Karlin and S. J. Lippard, *J. Am. Chem. Soc.*, **98**, 6951 (1976).
6) W. O. Kermack and T. W. Wight, *J. Chem. Soc.*, **1935**, 1421.
7) J. A. Tiethof and D. W. Cooke, *Inorg. Nucl. Chem. Lett.*, **8**, 1013 (1972).
8) A. V. Babaeva and I. B. Baranovskii, *Zh. Neorg. Khim.*, **7**, 783 (1962); *Chem. Abstr.*, **57**, 402g.
9) D. L. Herting, G. P. Sloan, A. W. Carbral, and J. H. Kruger, *Inorg. Chem.*, **17**, 1649 (1978).
10) M. Kita, K. Yamanari, and Y. Shimura, *Bull. Chem. Soc. Jpn.*, **55**, 2873 (1982).
11) J. Hidaka, S. Yamada, and Y. Shimura, *Chem. Lett.*, **1974**, 1487; K. Yamanari, J. Hidaka, and Y. Shimura, *Bull. Chem. Soc. Jpn.*, **50**, 2451, 2643 (1977).
12) K. Akamatsu, J. Hidaka, and Y. Shimura, *Bull. Chem. Soc. Jpn.*, **50**, 533 (1977).
13) M. Kita, K. Yamanari, and Y. Shimura, *Chem. Lett.*, **1983**, 141.
14) I. K. Adzamli, K. Libson, J. D. Lydon, R. C. Elder, and E. Deutsch, *Inorg. Chem.*, **18**, 303 (1979).
15) J. H.Worrell and D. H. Busch, *Inorg. Chem.*, **8**, 1563, 1572 (1969); B. Bosnich, W. R. Kneen, and A. T. Phillip, *ibid.*, **8**, 2567 (1969), *J. Chem. Soc., A*, **1970**, 264; J. H. Worrell, T. E. MacDermott, and D. H. Busch, *J. Am. Chem. Soc.*, **92**, 3317 (1970); R. W. Hay, P. M. Gidney, and G. A. Lawrence, *J. Chem. Soc., Dalton Trans.*, **1975**, 779.
16) R. W. Hay, A. L. Galyer, G. A. Lawrence, *J. Chem. Soc., Dalton Trans.*, **1976**, 939.
17) M. G. B. Drew, D. A. Rice, and K. M. Richards, *J. Chem. Soc., Dalton Trans.*, **1980**, 2075.
18) L. M. Baltusis, K. D. Karlin, H. N. Rabinowitz, J. C. Dowan, and S. J. Lippard, *Inorg. Chem.*, **19**, 2627 (1980).
19) P. L. Dahlstrom, J. R. Hyde, P. A. Vella, and J. Zubieta, *Inorg. Chem.*, **21**, 927 (1982).
20) Y. Yamamoto and Y. Shimura, *Bull. Chem. Soc. Jpn.* **53**, 395 (1980), **54**, 2924, 3351 (1981).
21) S. Yoshikawa, M. Asami, M. Inoue, and S. Yano, presented at the 29th Symposium on the Coordination Chemistry in Japan, Hamamatsu, 1979, Abstract, No. 1B09.
22) Y. Yamamoto, Y. Hata, and Y. Shimura, *Chem. Lett.*, **1981**, 1559.
23) T. Murata, M. Asami, M. Yashiro, S. Yano, M. Kosaka, and S. Yoshikawa, presented at the 33rd Symposium on the Coordination Chemistry in Japan, Osaka, 1983, Abstract, No. 1A16.

 © 1984 The Chemical Society of Japan Bull. Chem. Soc. Jpn., 57, 1235—1239 (1984)

Isolation and Assignment of Two Isomers of *trans*(NO_2)-Dinitrobis-[(*S*)-2-aminomethylpyrrolidine]-cobalt(III) Perchlorate

Masahiko SABURI,* Yasuhiko YOKOWO, and Sadao YOSHIKAWA*
Department of Synthetic Chemistry, Faculty of Engineering, The University of Tokyo, Hongo, Bunkyo-ku, Tokyo 113
(Received November 18, 1983)

Two possible isomers (trans,cis and trans,trans) of *trans*-(NO_2)-[($Co(NO_2)_2$(ampr)$_2$]ClO_4 (ampr= (*S*)-2-aminomethylpyrrolidine) were isolated separately by fractional recrystallization. The dinitro complexes were converted to the corresponding *trans*(Cl,NO_2)-[$CoCl(NO_2)$(ampr)$_2$]$^+$ complexes. Based on the circular dichroism and ^{13}C-NMR spectral data, it was shown that the less soluble dinitro complex gave the single isomer of the chloronitro complex, while the more soluble one yielded two diastereomeric chloronitro complexes. Thus, the former is assigned to the trans,cis configuration, and the latter to the trans,trans, taking the geometries of the complexes into consideration.

Two stereoisomers, designated as trans,trans and trans,cis,[1] are possible for the *trans*(X)-[$CoX_2(N\text{-}N')_2$]$^{n+}$ complexes, where *N*-*N*′ refers to an unsymmetrical diamine ligand (see Fig. 1). Each pair of two equivalent amino groups, *N* and *N*′, disposes in trans fashion for the trans,trans and in cis for the trans,cis isomer, respectively. 1,2-Propanediamine, one of the representative unsymmetrical diamine, has been shown to give the trans,trans isomer for its dichlorocobalt(III) complex with the optically active form.[2]

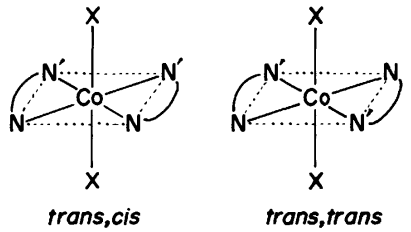

Fig. 1. Two possible isomers of *trans*(X)-[CoX_2-$(N\text{-}N')_2$]$^{n+}$ ion.

Although the formation of *trans,cis*-[$CoCl_2$((*R*)-pn)$_2$]$^+$ ion ((*R*)-pn=(*R*)-1,2-propanediamine) was claimed,[3] no detailed spectral evidence has been reported.

Most of mono-N-alkyl-substituted 1,2-diamines gave rise to the trans,trans configuration, as exemplified by *N*-methyl-1,2-ethanediamine,[1,4] (*S*)-1-methylamino-2-propanamine,[5] and (*S*)-1-ethylamino-2-propanamine.[6] It was found that (*R*)-*N*,*N*′-dimethyl-1,2-propanediamine afforded both of the trans,trans and trans,cis isomers of dinitrocobalt(III) complex.[7] This is the sole example reported so far, where the two possible isomers were isolated separatly.

In a previous paper,[8] we reported on the cobalt(III) complexes of (*S*)-2-(methylaminomethyl)pyrrolidine (=*N*-Meampr), which is a chiral unsymmetrical 1,2-diamine derived from (*S*)-proline. The [CoX_2(*N*-Meampr)$_2$]$^+$ (X=NO_2^- or Cl^-) complexes take specifically the trans,cis configuration.[8] We supposed that the unique predominance of the trans,cis isomer over the trans,trans for *N*-Meampr complexes was due, at least in part, to the presence of pyrrolidine ring in the ligand. With a view to elucidate the effect of pyrrolidinyl moiety build in a diamine molecule, the stereochemical features of cobalt(III) complexes with (*S*)-2-amino-methylpyrrolidine (=ampr) were investigated in this study. If the steric effect of pyrrolidine ring supresses any other factors controlling the geometry of complexes, the trans,cis isomer would be exclusively formed even for the ampr complexes.

Experimental

trans,cis-*Dinitrobis[(S)-2-aminomethylpyrrolidine]cobalt(III) Perchlorate,* trans,cis-*[Co(NO_2)$_2$(ampr)$_2$]ClO_4.* Sodium hexanitrocobaltate(III) (4.04 g; 0.01 mol) was added to a solution of ampr (2.00 g; 0.02 mol) in water (30 cm^3), and the resultant solution was heated at 60—65 °C for 15 min. Sodium perchlorate (4.0 g) dissolved in water (4 cm^3) was added, and the solution was cooled in a refrigerator overnight. Yellow crystals were filtered off, washed with ethanol and diethyl ether, and air-dried. Yield; 1.5—2.0 g. The filtrate (designated as F-1) was kept for obtaining the trans,trans isomer.

The crystals obtained above were recrystallized fractionally from warm water (80 °C). Less soluble yellow fine needle crystals were collected, washed with ethanol and diethyl ether, and air-dried. Yield; 0.5—0.8 g. Found: C, 26.24; H, 5.64; N, 18.82%. Calcd for $C_{10}H_{24}N_6O_8ClCo$: C, 26.65; H, 5.37; N, 18.65%.

trans,trans-*Dinitrobis[(S)-2-aminomethylpyrrolidine]cobalt(III) Perchlorate,* trans,trans-*[Co(NO_2)$_2$(ampr)$_2$]ClO_4.* The filtrate from the trans,cis isomer was gradually evaporated at room temperature to separate out brown crystals (0.5—1.0 g) after several days. The same product was also obtained from the filtrate F-1. Brown crystals were recrystallized from warm water (80 °C). Found: C, 26.92; H, 5.75; N, 18.39%. Calcd for $C_{10}H_{24}N_6O_8ClCo$: C, 26.65; H, 5.37; N, 18.65%.

trans,cis-*Chloronitrobis[(S)-2-aminomethylpyrrolidine]cobalt-(III) Perchlorate,* trans,cis-*[CoCl(NO_2)(ampr)$_2$]ClO_4 (Chloronitro-1).* *trans,cis*-[$Co(NO_2)_2$(ampr)$_2$]ClO_4 (0.65 g) was added to 1 M HCl (10 cm^3; 1 M=1 mol dm^{-3}), and heated for 5 min at 65 °C with occasional stirring. To the mixture was added $LiClO_4$ (1.0 g), and cooled in an ice bath. The crystals were filtered off, washed with ethanol and diethyl ether, and air-dried. Yield; 0.55 g. The crude product was recrystallized from hot water. Found: C, 27.07; H, 5.38; N, 16.01%. Calcd for $C_{10}H_{24}N_5O_6ClCo$: C, 27.28; H, 5.50; N, 15.91%.

trans,trans-*Chloronitrobis[(S)-2-aminomethylpyrrolidine]cobalt(III) Perchlorate,* trans,trans-*[CoCl(NO_2)(ampr)$_2$]ClO_4 (Chloronitro-2).* *trans,trans*-[$Co(NO_2)_2$(ampr)$_2$]ClO_4 (7.8 g) was

added to 8 M HCl (27 cm^3), and the mixture was heated at 70—75 °C for 5 min with occasional stirring. To the mixture was added $LiClO_4$ (4 g), and the whole was cooled in an ice bath for 3 h. Orange-red precipitate thus formed was filtered off, and washed with ethanol and diethyl ether. Yield; *ca.* 5 g. The precipitate was dissolved in warm water (80 cm^3 at 70 °C), and filtered while hot. To the filtrate was added concd. HCl (5 cm^3), and cooled in a refrigerator overnight. Orange-red crystals were collected, washed with ethanol and diethyl ether, and air-dried. Found: C, 27.22; H, 5.11; N, 15.48%. Calcd for $C_{10}H_{24}N_5O_6Cl_2Co$: C, 27.28; H, 5.50; N, 15.91%.

trans,trans-*Chloronitrobis[(S)-2-aminomethylpyrrolidine]cobalt(III) Chloride,* trans,trans-*[CoCl(NO$_2$)(ampr)$_2$]Cl (Chloronitro-3).* The filtrate after the removal of crude *trans,trans*-$[CoCl(NO_2)(ampr)_2]ClO_4$ mentioned above was poured into a mixture of ethanol (100 cm^3) and diethyl ether (500 cm^3), and the mixture was cooled in a refrigerator. Reddish pink precipitate deposited was collected and washed with diethyl ether. The crude product was recrystallized from methanol and diethyl ether. Found: C, 31.52; H, 6.16; N, 18.47%. Calcd for $C_{10}H_{24}N_5O_2Cl_2Co$: C, 31.93; H, 6.44; N, 18.62%.

trans,cis-*Dichlorobis[(S)-2-aminomethylpyrrolidine]cobalt(III) Perchlorate,* trans,cis-*[CoCl$_2$(ampr)$_2$]ClO$_4$.* *trans,cis*-$[Co(NO_2)_2(ampr)_2]ClO_4$ (1.5 g) was added to concd HCl (15 cm^3) and heated on a steam bath, until deep green crystals began to appear. The mixture was cooled in a refrigerator overnight, and the crystals were collected and washed with ethanol and diethyl ether. Yield; 0.75 g. The crude product was recrystallized from concd HCl. Found: C, 27.91; H, 5.78; N, 13.39%. Calcd for $C_{10}H_{24}N_4O_4Cl_3Co$: C, 27.94; H, 5.63; N, 13.05%.

trans,trans-*Dichlorobis[(S)-2-aminomethylpyrrolidine]cobalt(III) Perchlorate,* trans,trans-*[CoCl$_2$(ampr)$_2$]ClO$_4$.* *trans,trans*-$[Co(NO_2)_2(ampr)_2]ClO_4$ (3.3 g) was added to concd HCl (35 cm^3), and heated on a steam bath, until the solution became deep green. To the solution was added 70% $HClO_4$ (5 cm^3), and the whole was cooled in a refrigerator overnight. Green crystals were collected and washed in a usual way. Yield; 0.9 g. Found: C, 27.69; H, 5.59; N, 12.98%. Calcd for $C_{10}H_{24}N_4O_4Cl_3Co$: C, 27.94; H, 5.63; N, 13.05%.

Measurements. Visible and ultraviolet absorption spectra were obtained with a Hitachi 340 spectrophotometer. Circular dichroism spectra were recorded with a JASCO J-500 spectropolarimeter. ^{13}C-NMR spectra were obtained on a JEOL PFT-100 spectrometer (24.75 MHz), using TMS as an external reference.

Results and Discussion

It was demonstrated that $[Co(NO_2)_2(ampr)_2]ClO_4$, the dinitrocobalt(III) complex of ampr prepared by a reaction of ampr with $Na_3[Co(NO_2)_6]$ and succesive addition of $NaClO_4$, could be fractionated into two distinct crystalline products from aqueous solution; *i.e.* less soluble brownish yellow needles and more soluble brown blocks. Both forms equally showed the elemental analytical data corresponding to the formula $[Co(NO_2)_2(C_5H_{12}N_2)_2]ClO_4$, and, further, exhibited almost identical electronic absorption spectra. The spectra showed the absorption band characteristic of cobalt(III) complexes with the nitro group at 29000 cm^{-1}, so that the nitro ligands were considered to locate at the trans position to each other in the two forms.[1,5] The circular dichroism (CD) spectra of these dinitro complexes were, however, apparently different to each other as shown in Fig. 2. The numerical spectral data are summarized in Table 1. These findings unambiguously indicated that the two possible isomers of *trans*(NO_2)-$[Co(NO_2)_2(ampr)_2]ClO_4$ (illustrated as structures **a** and **b** in Fig. 3) were isolated.

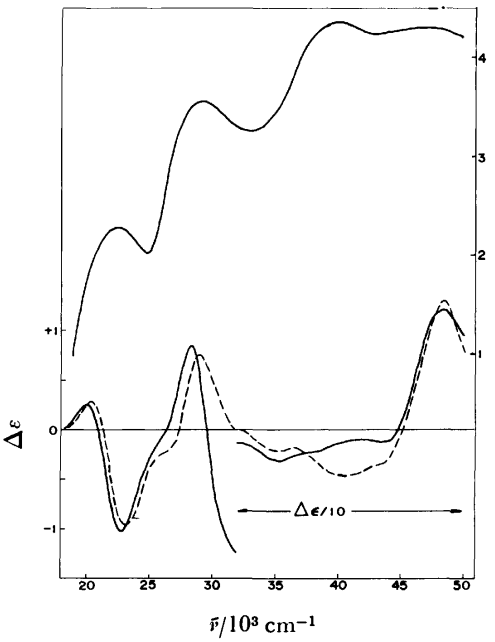

Fig. 2. Electronic absorption and CD spectra for the less soluble (trans,cis isomer; ——) and the more soluble form (trans,trans isomer; — — —) of *trans*-$(NO_2)[Co(NO_2)_2(ampr)_2]ClO_4$.

With a view to assign both the fractions of *trans*-(NO_2)-$[Co(NO_2)_2(ampr)_2]ClO_4$ to either of structure **a** (trans,cis) and **b** (trans,trans), the dinitro complexes were converted into the chloronitro complexes. Figure 3 suggests that *trans,cis*-$[Co(NO_2)_2(ampr)_2]^+$ ion gives the single species of *trans,cis*-$[CoCl(NO_2)(ampr)_2]^+$ ions (structure **c**), while *trans,trans*-$[Co(NO_2)_2(ampr)_2]^+$ ion yield, in principle, two diastereomeric *trans,trans*-$[CoCl(NO_2)(ampr)_2]^+$ ions (structure **d** and **e**). In practice, the less soluble dinitro complex gave a chloronitro complex as perchlorate (chloronitro-1) in an almost quantitative yield, and the more soluble dinitro complex also afforded another chloronitro complex as perchlorate (chloronitro-2). It was interestingly found that the third chloronitro complex could be isolated from the filtrate of chloronitro-2 as chloride salt (chloronitro-3).

It was reported that *trans*- and *cis*-$[CoCl(NO_2)(en)_2]^+$ ion (en=1,2-ethanediamine) showed the absorption bands assignable to the d-d transition at 21600 and 20100 cm^{-1}, respectively.[9] The absorption spectra of chloronitro complexes of ampr resembled to one another, and exhibited the first absorption bands at *ca.* 20900 cm^{-1} (Fig. 4 and Table 1). It is certain that the ligand field provided by ampr, an *N*-substituted 1,2-diamine, is somewhat weaker than that of en,[10] so that three chloronitro complexes could be reasonably assigned to the *trans*(Cl,NO_2) configuration.

Table 1. Absorption and CD data of $[CoXY(ampr)_2]^+$ complexes

Complex	Absorption		CD	
	$\tilde{\nu}_{max}/cm^{-1}$	($\log \varepsilon$)	$\tilde{\nu}_{ext}/cm^{-1}$	($\Delta\varepsilon$)
trans,cis-$[Co(NO_2)_2(ampr)_2]ClO_4$[a]	22,700	(2.29)	20,040	(+0.26)
			22,620	(−1.03)
	29,000	(3.54)	28,250	(+0.84)
	39,600	(4.38)	35,210	(−2.97)
			38,600	(−2.0)[d]
	47,500	(4.26)	43,860	(−1.4)
			48,250	(+12.1)
trans,trans-$[Co(NO_2)_2(ampr)_2]ClO_4$[a]	22,400	(2.28)	20,400	(+0.29)
			23,090	(−0.96)
	29,000	(3.54)	26,000	(−0.25)[d]
			28,980	(+0.75)
	39,800	(4.36)	35,210	(−2.1)
			40,500	(−4.6)
	47,300	(4.30)	43,860	(−3.0)[d]
			48,250	(+12.7)
trans,cis-$[CoCl(NO_2)(ampr)_2]ClO_4$[b] (Chloronitro-1)	20,400	(1.97)	17,330	(+0.12)
			19,650	(−0.81)
			22,320	(+0.30)
	28,900	(3.10)	27,030	(+0.34)
			32,790	(−0.88)
trans,trans-$[CoCl(NO_2)(ampr)_2]ClO_4$[b] (Chloronitro-2)	20,350	(1.96)	16,260	(−0.03)
			17,240	(+0.03)
			19,570	(−0.83)
	28,740	(3.19)	26,880	(+0.51)
			30,030	(−0.12)[d]
			33,600	(−1.1)[d]
trans,trans-$[CoCl(NO_2)(ampr)_2]Cl$[b] (Chloronitro-3)	20,420	(1.97)	19,340	(−1.03)
			22,220	(+0.42)
	28,800	(3.17)	26,880	(+0.79)
			29,500	(−0.53)[d]
trans,cis-$[CoCl_2(ampr)_2]ClO_4$[c]	16,000	(1.72)	14,750	(+0.37)
			16,470	(−0.77)
	21,410	(1.46)	20,880	(+0.63)
	25,450	(1.77)	26,740	(+0.42)
trans,trans-$[CoCl_2(ampr)_2]ClO_4$[c]	16,000	(1.71)	14,750	(+0.33)
			16,450	(−0.74)
	21,410	(1.50)	20,870	(+0.59)
	25,640	(1.81)	26,740	(+0.39)

a) In H_2O. b) In 1 M NaCl. c) In methanol. d) Shoulder.

Further, the CD spectra of chloronitro complexes were obviously different from one another, and did not change after recrystallization. This means that the three possible diastereomer of *trans*(Cl,NO_2)-$[CoCl(NO_2)(ampr)_2]^+$ ion could be isolated separately. Thus, the more soluble dinitro complex, which gave rise to two isomers of chloronitro complex, should have the trans,trans structure, and, therefore, the less soluble dinitro complex should take the trans,cis configuration.

If the above mentioned assignments are valid, chloronitro-1 must have the trans,cis configuration (structure **c**), in which the two ampr ligands are in unequal circumstances due to the C_1 symmetry of **c**. On the other hand, chloronitro-2 and -3 are considered to adopt either of the trans,trans configurations (structure **d** or **e**) with C_2 symmetry. In those structures, the two ampr molecules should be situated in the identical environment, though the environment of ampr in **d** is intrinsically different from that in **e**. In order to make sure the assignment, ^{13}C-NMR spectra of chloronitro complexes were examined.

The ^{13}C-NMR spectrum of chloronitro-3 was obtained in 1 M DCl solution, the data being given in Table 2. The spectrum showed five resonances, with the incidental overlap of two signals at 49.8 ppm. This support that chloronitro-3 certainly adopts the trans,trans configuration and consists of the single species, though the exact structure, **d** or **e**, of this isomer has not been established. The chloro-

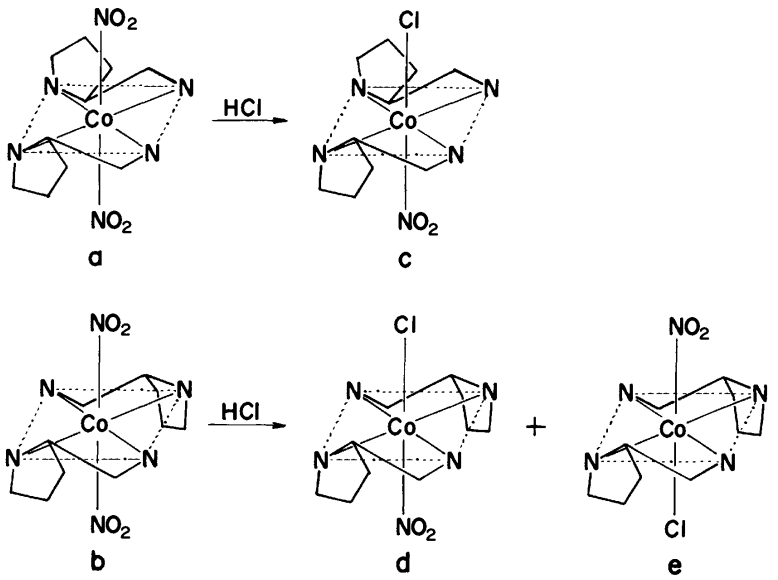

Fig. 3. Structures of *trans,cis*-$[Co(NO_2)_2(ampr)_2]^+$ ion (**a**), *trans,trans*-$[Co(NO_2)_2(ampr)_2]^+$ ion (**b**), *trans,cis*-$[CoCl(NO_2)(ampr)_2]^+$ ion (**c**), and *trans,trans*-$[CoCl(NO_2)(ampr)_2]^+$ ion (**d** and **e**).

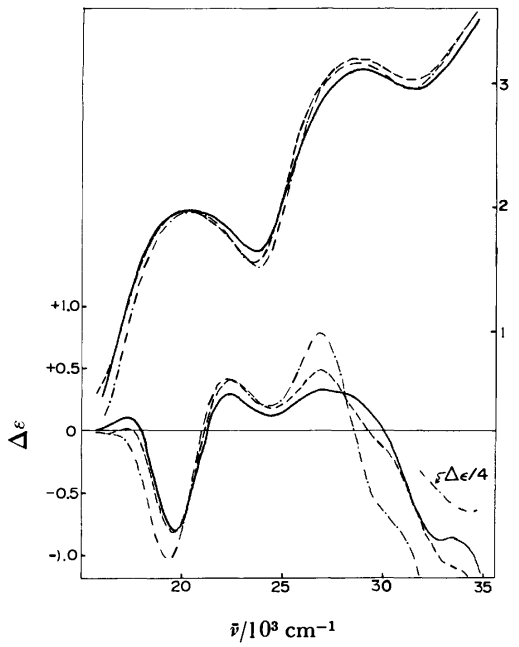

Fig. 4. Absorption and CD spectra of chloronitro-1 (——), chloronitro-2 (— — —), and chloronitro-3 (—·—·—).

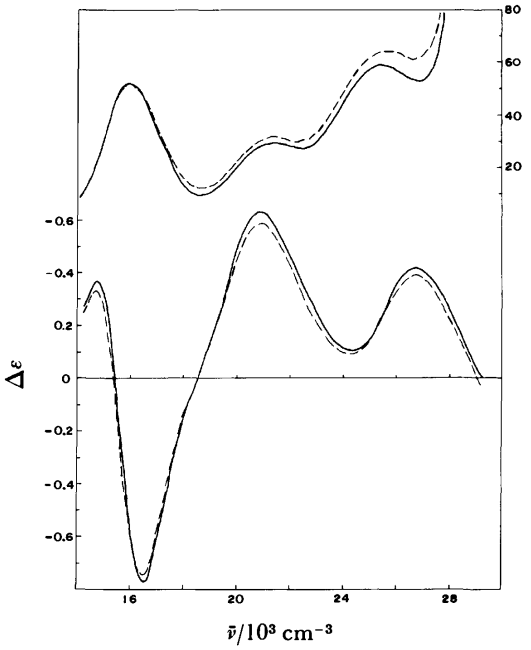

Fig. 5. Visible absorption and CD spectra of *trans,cis*-$[CoCl_2(ampr)_2]ClO_4$ (——), and *trans,trans*-$[CoCl_2(ampr)_2]ClO_4$ (— — —).

nitro-1 and -2 provided no satisfactory spectra in DCl solution because of the low solubility of the complexes and structural changes (the aquation of the chloride ligand and/or trans-cis isomerization) occured during the measurements.

The ^{13}C-NMR spectrum of chloronitro-1 could, however, be taken in a mixture of 1 M DCl and acetone. Although a few signals were occasionally overlapped, the spectrum could be analyzed to be composed of ten resonances as given in Table 2. This means that two ampr ligands are in the different circumstances, being consistent with the expected stereochemical requirements from the structure **c**. Thus, the ^{13}C-NMR features of chloronitro complexes, as well as the absorption and CD spectral data, confirmed without conflict that the less soluble dinitro complex adopted the trans,cis configuration, while the more soluble one took the trans,trans configuration.

It is clarified, therefore, that both trans,cis and trans,trans isomers exist with respect to ampr complexes. The steric effects brought about by pyrrolidine ring appeared not to be so significant in ampr complexes, compared with those found in *N*-Meampr complexes, where only the trans,cis isomer is existent. This is possibly due to the difference in the steric repulsions

Table 2. ^{13}C-NMR spectral data[a] of chloronitro complexes

trans,trans-$[CoCl(NO_2)(ampr)_2]Cl$[b] (chloronitro-3)	*trans,cis*-$[CoCl(NO_2)(ampr)_2]ClO_4$[c] (chloronitro-1)	Assignments[d]
27.01 (1)[e]	27.00 (2)	C_3, C_4
27.68 (1)	27.35 (1)	
	27.78 (1)	
49.81 (2)	49.24 (1)	C_1, C_5
	50.10 (3)	
65.41 (1)	65.04 (1)	
	65.47 (1)	C_2

a) Ppm from TMS (external). b) Measureed in 1 M DCl. c) Measured in a mixture of 1 M DCl and acetone. d) The order of carbon atoms in ampr is as follows; 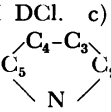 . e) The values in parentheses are approximate relative intensities of the signals.

between pyrrolidinyl moiety and *N*-methylamino (-NH(CH_3)) group in *N*-Meampr complexes, and between pyrrolidinyl and primary amino (-NH_2) group in ampr complexes, particularly in the trans,trans configuration. The steric repulsion must be considerably severer in *N*-Meampr complexes than in ampr complexes. Hence, it is shown that the steric effect of pyrrolidine ring is not so pronounced as to give solely the trans,cis isomer for complexes with any diamines having this ring.

Finally, both of the dinitro complexes were converted into the corresponding *trans*(Cl)-dichloro complexes. No configurational change was expected during this conversion, as the cases of other *N*-substituted 1,2-diamine complexes.[1,5,6] The absorption and CD spectra of two isomers resembled closely to each other, though slight differences were still acknowledged (Fig. 5). This displays a novel example of isolation of two diastereomers possible for *trans*(Cl)-$[CoCl_2(N\text{-}N')_2]^+$ ion.

References

1) D. A. Buckingham, L. G. Marzilli, and A. M. Sargeson, *Inorg. Chem.*, **7**, 915 (1968).
2) Y. Saito and H. Iwasaki, *Bull. Chem. Soc. Jpn.*, **35**, 1131 (1962).
3) C. J. Hawkins, E. Larsen, and I. Olsen, *Acta Chem. Scand.*, **19**, 1915 (1965).
4) W. T. Robinson, D. A. Buckingham, G. Chandler, L. G. Marzilli, and A. M. Sargeson, *J. Chem. Soc., D*, **1970**, 539.
5) M. Saburi, Y. Tsujito, and S. Yoshikawa, *Inorg. Chem.*, **9**, 1476 (1970).
6) T. Kitamura, M. Saburi, and S. Yoshikawa, *Inorg. Chem.*, **16**, 585 (1977).
7) J. A. Tiethof and D. W. Cooke, *Inorg. Nucl. Chem. Lett.*, **8**, 1013 (1972).
8) T. Kitamura, Y. Sato, M. Saburi, and S. Yoshikawa, *Bull. Chem. Soc. Jpn.*, **50**, 1780 (1977).
9) K. Yamasaki, J. Hidaka, and Y. Shimura, *Bull. Chem. Soc. Jpn.*, **50**, 2624 (1977).
10) For example: J. A. Tiethof and D. W. Cooke, *Inorg. Chem.*, **11**, 315 (1972).

 © 1984 The Chemical Society of Japan Bull. Chem. Soc. Jpn., 57, 1240—1254 (1984) [Vol. 57, No. 5

Synthesis and Isomerism of Mixed (Amine)(carboxylato) Complexes with the $[Pd(N)_n(O)_{4-n}]$-type (n=1—4) and Their Circular Dichroism Spectra

Kazuhiko NAKAYAMA,* Takashi KOMORITA, and Yoichi SHIMURA
Department of Chemistry, Faculty of Science, Osaka University, Toyonaka, Osaka 560
(Received December 8, 1983)

A large number of mixed-ligand $[Pd(N)_n(O)_{4-n}]$-type complexes (n=1—4) which contain at least one optically active ligand were synthesized and isolated in a systematic manner. (*S*)-Propylenediamine, (2*S*)-N^1,N^1-diethyl-1,2-propanediamine, and (*S*)-amino carboxylates were employed as one ligand, which is optically active; ammonia, diamines, amino carboxylates, acetates, and dicarboxylates as the other ligand occupying the remaining coordination sites. Isomerism could be detected in the mixed complexes of an unsymmetrical diamine and an amino carboxylate and has been discussed on the basis of ^{13}C NMR and CD spectra. Moreover, the influence of optically inactive ligands on the vicinal CD spectra has been examined, and also the additivity of vicinal CD contributions of two different optically active ligands has been demonstrated.

The electronic structure of d^8 square-planar complexes has been studied most extensively on $[MCl_4]^{2-}$ (M=Pt and Pd)[1] which are easy to deal with theoretically and experimentally. In a separate paper,[2] we reported on the electronic structures of *cis*- and *trans*-$[Pd(Cl)_2(N)_2]$-type complexes. An extension of the work to complexes containing nitrogen and oxygen atoms which are most popular as coordinating atoms is desirable to understand systematically the electronic structure of square-planar palladium(II) complexes. Although it is desired to use as simple ligands as possible in order to study the d-d absorption spectra, there have been known few examples of the isolation of mixed-ligand palladium(II) complexes comprising of such *N*- and/or *O*-ligands. This seems to be ascribed to the lability of palladium(II) complexes and to retarded development of systematized synthetic routes. Unavailability of ion exchange column chromatography, which serves as a very powerful tool for separating some chemical species in the case of cobalt(III), chromium(III), rhodium(III) complexes *etc.*, is also responsible for the situation.

In 1932, Drew *et al.*[3] isolated $[Pd(en)(NH_3)_2]Cl_2$, $[Pd(en)(py)_2]Cl_2$, and $[Pd(NH_3)_2(py)_2]Cl_2$ and observed that the former two complexes were obtained only by the action of ammonia or pyridine(py) on $[PdCl_2(en)]$, the action of ethylenediamine(en) on $[PdCl_2(NH_3)_2]$ or $[PdCl_2(py)_2]$ causing disproportionation to give $[Pd(NH_3)_4]Cl_2$ or $[Pd(py)_4]Cl_2$ as well as $[Pd(en)_2]Cl_2$, respectively. According to these investigations $[Pd(NH_3)_2(py)_2]Cl_2$ can be obtained either from $[PdCl_2(NH_3)_2]$ or from $[PdCl_2(py)_2]$, where excess pyridine is necessary in the case of the former starting material but in the latter case the calculated quantity of ammonia must be used because excess ammonia replaces the coordinated pyridine molecules. These observations suggest that the order of introduction of ligands is important in the synthesis of mixed-ligand palladium(II) complexes.

Although the kinetics of the mixed-ligand palladium(II) complexes of ethylenediamine and a variety of amino carboxylates has been systematically investigated by Lim,[4] no isolation and spectroscopic studies of the complexes have been undertaken at all. The examples of the isolation of $[Pd(N)_2(O)_2]$-type complexes with simple ligands are limited to $[Pd(ox)(NH_3)_2]$[5] and $[Pd(CH_3CO_2)_2L_2]$ (L=py, $NH(C_2H_5)_2$, $N(C_2H_5)_3$, and (bipyridine)$_{1/2}$)[6] except bis(amino carboxylato) complexes.[7,8] None of these complexes, however, are suited for investigation of d-d spectra because of low solubility, isomerization reaction, and/or the presence of the low energy intraligand transitions. As to the mixed-ligand palladium(II) complexes of an amino carboxylate and a (di)carboxylate, no reports could be found even on the preparation.

This paper deals with the synthesis and isolation of mixed-ligand $[Pd(N)_n(O)_{4-n}]$-type complexes (n=1—4) containing (di)amine(s) as an *N*-ligand, (di)carboxylate(s) as an *O*-ligand, and an amino carboxylate as an *N*,*O*-ligand. Then, the mixed-ligand complexes comprising of (*S*)-propylenediamine or (2*S*)-N^1,N^1-diethyl-1,2-propanediamine and an unsymmetrical bidentate ligand such as an amino carboxylate should exhibit isomerism; this could be actually detected in the amino carboxylato complexes, and has been discussed on the basis of ^{13}C NMR and CD spectra. Moreover, we have examined the additivity of vicinal CD contributions of two optically active ligands and the influence of optically inactive ligands on the vicinal CD spectra. The following abbreviations are used for ligands in the present paper: *S*-pn, (*S*)-propylenediamine $NH_2CH_2CH(CH_3)NH_2$; tn, trimethylenediamine $NH_2CH_2CH_2CH_2NH_2$; N^1,N^1-Et_2-(*S*)-pn, (2*S*)-N^1,N^1-diethyl-1,2-propanediamine $NH_2CH(CH_3)CH_2N(C_2H_5)_2$; *N*,*N*-$Me_2$en, *N*,*N*-dimethylethylenediamine $NH_2CH_2CH_2N(CH_3)_2$; *N*,*N*-Et_2en, *N*,*N*-diethylethylenediamine $NH_2CH_2CH_2N(C_2H_5)_2$; Hgly, glycine $NH_2CH_2CO_2H$; β-Hala, β-alanine $NH_2CH_2CH_2CO_2H$; *S*-Hala, (*S*)-alanine $NH_2CH(CH_3)CO_2H$; *S*-Hpro, (*S*)-proline $\overline{NHCH_2CH_2CH_2CHCO_2H}$; *S*-Hser, (*S*)-serine $NH_2CH(CH_2OH)CO_2H$; *S*-Hleu, (*S*)-leucine $NH_2CH\{CH_2CH(CH_3)_2\}CO_2H$; *S*-Hhpro, (*S*)-hydroxyproline $\overline{NHCH_2CH(OH)CH_2CHCO_2H}$; H(*N*,*N*-$Me_2$gly), *N*,*N*-dimethylglycine $N(CH_3)_2CH_2CO_2H$; H_2ox, oxalic acid HO_2CCO_2H; H_2mal, malonic acid $HO_2CCH_2CO_2H$; Ham,amino carboxylic acid.

Experimental

[Pd(N)$_4$]-type Complexes. *1) [Pd(S-pn)(NH$_3$)$_2$]Cl$_2$*: Concentrated aqueous ammonia (*ca.* 26.5%, 120 mg) was added to a suspension of 400 mg of [PdCl$_2$(*S*-pn)][2] in 15 cm^3 of water, with stirring at room temperature. The resulting clear solution was evaporated to 1—2 cm^3 under reduced pressure and then diluted with 5 cm^3 of methanol. After removal of a small amount of [PdCl$_2$(*S*-pn)] reproduced, the solution was mixed with one drop of concentrated aqueous ammonia and 3 cm^3 of ether, and allowed to stand at room temperature. White crystals were collected, washed with a mixture of methanol—ether, and dried in air. Yield: 310 mg. Found: C, 12.57; H, 5.65; N, 19.42%. Calcd for $C_3H_{16}N_4Cl_2Pd$: C, 12.62; H, 5.65; N, 19.62%.

2) [Pd(S-pn)(en)]Cl$_2$: An aqueous solution containing 73 mg of ethylenediamine was mixed with 300 mg of [PdCl$_2$(*S*-pn)] suspended in 10 cm^3 of water and the mixture was stirred at 40 °C. The resulting solution was filtered and concentrated to a small volume under reduced pressure. Addition of ethanol to the concentrate warmed gave white precipitate, which was collected, washed with a mixture of water-ethanol, and dried *in vacuo*. Yield: 290 mg. Found: C, 18.67; H, 5.92; N, 17.34%. Calcd for [Pd(*S*-pn)(en)]Cl$_2$·0.5H$_2$O=$C_5H_{19}N_4Cl_2O_{0.5}Pd$: C, 18.73; H, 5.97; N, 17.48%.

3) [Pd(S-pn)$_2$]Cl$_2$: This complex was obtained from [PdCl$_2$(*S*-pn)] by the same method as in *2)*, in a 72% yield. The content of water of crystallization is different from that reported for [Pd(*R*-pn)$_2$]Cl$_2$.[9] Found: C, 21.68; H, 6.20; N, 16.81%. Calcd for [Pd(*S*-pn)$_2$]Cl$_2$·0.5H$_2$O=$C_6H_{21}N_4Cl_2O_{0.5}Pd$: C, 21.54; H, 6.33; N, 16.75%.

4) [Pd(S-pn)(tn)]Cl$_2$: An aqueous solution containing this complex was prepared in the same way as in *2)*. The solution was evaporated under reduced pressure to give a sirup, which was dissolved in ethanol. After filtration the ethanol solution was mixed with ether and allowed to stand in a refrigerator. The desired product was obtained as white crystals in an 82% yield. Found: C, 21.04; H, 6.37; N, 16.35%. Calcd for [Pd(*S*-pn)(tn)]Cl$_2$·H$_2$O=$C_6H_{22}N_4Cl_2OPd$: C, 20.97; H, 6.45; N, 16.31%.

5) [Pd(N^1,N^1-Et$_2$-(S)-pn)(NH$_3$)$_2$]Cl$_2$: A suspension of 610 mg of [PdCl$_2$(*N*^{1},*N*^{1}-Et$_2$-(*S*)-pn)][10] in 10 cm^3 of water was mixed with concentrated aqueous ammonia (*ca.* 26.5%, 300 mg) and the mixture was stirred at 40 °C. An evaporation of the resulting pale yellow solution gave a sirup, which was dissolved in a mixture of ethanol-ether and stored in a freezer for 4 d. Yellow blocks deposited were mechanically separated from a small amount of white powder and identified as [PdCl(NH$_3$)(*N*^{1},*N*^{1}-Et$_2$-(*S*)-pn)]Cl by the absorption spectrum and elemental analysis (yield: 370 mg). Found: C, 25.99; H, 6.48; N, 12.97%. Calcd for [PdCl(NH$_3$)(*N*^{1},*N*^{1}-Et$_2$-(*S*)-pn)]Cl=$C_7H_{21}N_3Cl_2Pd$: C, 25.90; H, 6.52; N, 12.95%. Its electronic absorption(AB) and CD data in a 0.10 M KCl aqueous solution (1 M=1 mol dm^{-3}) were as follows in $\sigma_{max}/10^3$ cm^{-1} (ε/mol^{-1} dm^3 cm^{-1}) and $\sigma_{ext}/10^3$ cm^{-1} ($\Delta\varepsilon$/mol^{-1} dm^3 cm^{-1}), respectively; AB: 29.3 (346), 47.8 (17000) and CD: 23.6 (−0.027), 27.9 (+0.12), 32.0 (−0.73).

The monochloro complex (220 mg) was dissolved in a minimum quantity of warm water and diluted with 3 cm^3 of ethanol containing one drop of concentrated aqueous ammonia. The resulting almost colorless solution was mixed with ether to give faint yellow needles, which were washed with a mixture of 95%-ethanol-ether and dried in air. Yield: 140 mg. Found: C, 23.46; H, 7.33; N, 15.38%. Calcd for [Pd(*N*^{1},*N*^{1}-Et$_2$-(*S*)-pn)(NH$_3$)$_2$]Cl$_2$·H$_2$O=$C_7H_{26}N_4Cl_2OPd$: C, 23.38; H, 7.29; N, 15.58%. This complex is liable to decompose even in the crystalline state.

6) [Pd(N^1,N^1-Et$_2$-(S)-pn)(tn)]Cl$_2$: An aqueous solution of 130 mg of *N*^{1},*N*^{1}-Et$_2$-(*S*)-pn was added to 250 mg of [PdCl$_2$(tn)] suspended in 13 cm^3 of water, with stirring at *ca.* 55 °C. The resulting solution was evaporated to dryness and the residue was dissolved in a small amount of warm methanol. After filtration the methanol solution was mixed with acetone and allowed to stand in a refrigerator to give faint yellow crystals, which were washed with a mixture of water-acetone and dried *in vacuo*. Total yield: 300 mg. Found: C, 31.42; H, 7.38; N, 14.75%. Calcd for $C_{10}H_{28}N_4Cl_2Pd$: C, 31.47; H, 7.39; N, 14.68%.

7) [PdL(S-pn)]Cl$_2$ (L=N^1,N^1-Et$_2$-(S)-pn and N,N-*Et$_2$en)*: These complexes were prepared from [PdCl$_2$(*S*-pn)] by a method similar to that in *6)*, but crystallized from ethanol by adding acetone. Yield: 75—85%. Found: C, 28.77; H, 7.66; N, 13.46%. Calcd for [Pd(*N*^{1},*N*^{1}-Et$_2$-(*S*)-pn)(*S*-pn)]Cl$_2$·2H$_2$O=$C_{10}H_{32}N_4Cl_2O_2Pd$: C, 28.76; H, 7.72; N, 13.41%. Found: C, 27.71; H, 7.29; N, 14.29%. Calcd for [Pd(*N*,*N*-Et$_2$en)(*S*-pn)]Cl$_2$·1.25H$_2$O=$C_9H_{28.5}N_4Cl_2O_{1.25}Pd$: C, 27.71; H, 7.36; N, 14.36%.

*8) [PdL(N^1,N^1-Et$_2$-(S)-pn)]Cl$_2$ (L=*N,N-*Et$_2$en and* N,N-*Me$_2$en)*: Each of these complexes was obtained from [PdCl$_2$L][11] in a manner similar to that in *6)*, but crystallization was performed from warm ethanol or methanol by adding ether. Yield: 80—85%. Found: C, 36.87; H, 8.06; N, 13.32%. Calcd for [Pd(*N*,*N*-Et$_2$en)(*N*^{1},*N*^{1}-Et$_2$-(*S*)-pn)]Cl$_2$=$C_{13}H_{34}N_4Cl_2Pd$: C, 36.85; H, 8.09; N, 13.22%. Found: C, 33.40; H, 7.60; N, 14.29%. Calcd for [Pd(*N*,*N*-Me$_2$en)(*N*^{1},*N*^{1}-Et$_2$-(*S*)-pn)]Cl$_2$=$C_{11}H_{30}N_4Cl_2Pd$: C, 33.39; H, 7.64; N, 14.16%.

9) Other Complexes: The complex [Pd(*N*^{1},*N*^{1}-Et$_2$-(*S*)-pn)$_2$]Cl$_2$ was prepared according to the method reported,[10] but the content of water of crystallization was different. Found: C, 35.57; H, 8.47; N, 11.82%. Calcd for [Pd(*N*^{1},*N*^{1}-Et$_2$-(*S*)-pn)$_2$]Cl$_2$·2H$_2$O=$C_{14}H_{40}N_4Cl_2O_2Pd$: C, 35.49, H, 8.51; N, 11.82%. The complex [Pd(*N*^{1},*N*^{1}-Et$_2$-(*S*)-pn)(en)]Cl$_2$ was prepared in our previous work.[11]

[Pd(N)$_3$(O)]-type Complexes. *1) [Pd(gly)(S-pn)]ClO$_4$*: A suspension of 400 mg of [PdCl$_2$(*S*-pn)] in 15 cm^3 of water was mixed with an aqueous solution (5 cm^3) containing 120 mg of glycine and 65 mg of sodium hydroxide. The mixture was stirred for 30 min at 45 °C to turn into a clear lemon yellow solution, which was treated with 200 mg of sodium perchlorate and evaporated to dryness under reduced pressure. After washing with cold water, the crude product was recrystallized from warm water by adding methanol. Yield: 270 mg. Found: C, 17.03; H, 4.01; N, 11.87%. Calcd for $C_5H_{14}N_3ClO_6Pd$: C, 16.96; H, 3.99; N, 11.87%.

*2) [PdL(en)]ClO$_4$ (L=*S-*ala and* S-*ser)*: These complexes were prepared from [PdCl$_2$(en)] by the same method as in *1)*, in a 75—80% yield. Found: C, 17.05; H, 4.08; N, 11.85%. Calcd for [Pd(*S*-ala)(en)]ClO$_4$=$C_5H_{14}N_3ClO_6Pd$: C, 16.96; H, 3.99; N, 11.87%. Found: C, 16.43; H, 3.89; N, 11.35%. Calcd for [Pd(*S*-ser)(en)]ClO$_4$=$C_5H_{14}N_3ClO_7Pd$: C, 16.23; H, 3.81; N, 11.36%.

3) [Pd(S-ala)(tn)]ClO$_4$: Silver oxide (380 mg) was mixed with 400 mg of [PdCl$_2$(tn)] suspended in 12 cm^3 of water and the mixture was stirred at room temperature for 20 min in the dark. After the silver chloride had been filtered off, perchloric acid (60%, 266 mg) and (*S*)-alanine (141 mg) were successively added to the filtrate. The reaction mixture was stirred for 20 min and evaporated to dryness. A water-methanol (1:9) solution of the residue was mixed with ether and allowed to stand in a refrigerator, giving pale yellow crystals, which were washed with a mixture of methanol-ether and dried *in vacuo*. Yield: 510 mg. Found: C, 18.83; H, 4.76; N, 10.91%. Calcd for [Pd(*S*-ala)(tn)]ClO$_4$·H$_2$O=$C_6H_{18}N_3ClO_7Pd$: C, 18.67; H, 4.70; N, 10.88%.

4) [Pd(β-ala)(S-pn)]ClO$_4$: This complex was prepared by a method similar to that in *3)*, but crystallization was performed in an aqueous medium by adding ethanol carefully and

allowing to stand at room temperature for 4 d. Yield: 190 mg. Found: C, 19.33; H, 4.55; N, 11.12%. Calcd for [Pd(β-ala)(*S*-pn)]$ClO_4 \cdot 0.5H_2O$=$C_6H_{17}N_3ClO_{6.5}Pd$: C, 19.11; H, 4.54; N, 11.14%.

5) [Pd(S-leu)(en)]ClO_4: This was obtained in the same manner as in *3)*, but ethanol was used in place of ether in crystallization. Yield: 75%. Found: C, 24.34; H, 5.12; N, 10.54%. Calcd for $C_8H_{20}N_3ClO_6Pd$: C, 24.26; H, 5.09; N, 10.61%.

6) [Pd(S-ala)(S-pn)]ClO_4: Silver perchlorate (290 mg) and silver oxide (165 mg) were successively added to a suspension of 350 mg of [$PdCl_2$(*S*-pn)] in 12 cm^3 of water and the mixture was stirred at room temperature for 15 min in the dark. The silver chloride was filtered off and the filtrate was mixed with an aqueous solution (3 cm^3) containing 124 mg of (*S*)-alanine. After 20 min of stirring the mixture was evaporated under reduced pressure to give a sirup, which was dissolved in a methanol-ethanol (1:4) mixture (6 cm^3) and allowed to stand at room temperature. The desired product separated was washed with a mixture of methanol-ethanol and dried *in vacuo*. Yield: 370 mg. Found: C, 19.61; H, 4.40; N, 11.35%. Calcd for $C_6H_{16}N_3ClO_6Pd$: C, 19.58; H, 4.38; N, 11.42%.

7) [Pd(S-pro)(S-pn)]ClO_4: This complex was prepared by the same method as in *6)*, but a mixture of methanol-ethanol (1:1) was used as the solvent for crystallization. The crude product was recrystallized from warm water by adding acetone. Yield: 25%. Found: C, 24.48; H, 4.67; N, 10.65%. Calcd for $C_8H_{18}N_3ClO_6Pd$: C, 24.38; H, 4.60; N, 10.66%.

8)[PdL(en)]ClO_4 *(L=S-pro and S-hpro)*: Each of these complexes was prepared from [$PdCl_2$(en)] in the same way as in *6)*, but crystallized from hot water by adding ethanol. Yield: 85—90%. Found: C, 22.18; H, 4.28; N, 11.02%. Calcd for [Pd(*S*-pro)(en)]ClO_4=$C_7H_{16}N_3ClO_6Pd$: C, 22.12; H, 4.24; N, 11.06%. Found: C, 21.29; H, 4.13; N, 10.57%. Calcd for [Pd(*S*-hpro)(en)]ClO_4=$C_7H_{16}N_3ClO_7Pd$: C, 21.23; H, 4.07; N, 10.61%.

*9) [Pd(*N,N-*Me*$_2$*gly)(*N^1,N^1-*Et*$_2$-(S)-*pn)]*ClO_4: A suspension of 470 mg of [$PdCl_2$(N^1,N^1-Et_2-(*S*)-pn)] in 15 cm^3 of water was treated with 320 mg of $AgClO_4$ and 180 mg of Ag_2O in the same manner as in *6)*. The resulting solution was mixed with an aqueous solution of 215 mg of *N,N*-dimethylglycine hydrochloride pre-neutralized with Ag_2O. The mixture was stirred at room temperature for 1 h and evaporated to dryness. The crude product was recrystallized from hot water; yield 410 mg. Found: C, 30.34; H, 5.95; N, 9.51%. Calcd for $C_{11}H_{26}N_3ClO_6Pd$: C, 30.15; H, 5.98; N, 9.59%.

10) [Pd(β-ala)(N^1,N^1-*Et*$_2$-*(S)-pn)]*ClO_4: This complex was obtained in the same manner as in *9)*, using β-alanine in place of *N,N*-dimethylglycine hydrochloride and silver oxide, in a 65% yield. Found: C, 28.19; H, 5.79; N, 9.82%. Calcd for $C_{10}H_{24}N_3ClO_6Pd$: C, 28.32; H, 5.70; N, 9.91%.

cis-[Pd(N)$_2$*(O)*$_2$*]-type Complexes.* *1) [Pd*$_2$*(μ-OH)*$_2$*(S-pn)*$_2$*](*ClO_4*)*$_2$: This complex could be isolated as an intermediate product in the preparation of [Pd(amino carboxylato)(*S*-pn)]ClO_4.

A suspension of 300 mg of [$PdCl_2$(*S*-pn)] in 12 cm^3 of water was treated with 250 mg of $AgClO_4$ and 145 mg of Ag_2O in the same way as described for [Pd(*S*-ala)(*S*-pn)]ClO_4. The resulting solution was evaporated to dryness under reduced pressure and the residue was dissolved in a small amount of methanol. After filtration the methanol solution was mixed with ethanol and chilled in an ice-bath to give yellow precipitate, which was collected after 1.5 h, washed with ethanol and ether, and dried *in vacuo*. Yield: 230 mg. Found: C, 12.18; H, 3.82; N, 9.11%. Calcd for $C_6H_{22}N_4Cl_2O_{10}Pd_2$: C, 12.13; H, 3.73; N, 9.43%. This complex, as well as the corresponding nitrate and hydrogencarbonate salts described below, tends to decompose in an ethanol solution and is sensitive to heat.

2) [Pd$_2$*(μ-OH)*$_2$*(S-pn)*$_2$*](*NO_3*)*$_2$: This was prepared by a method similar to that in *1)* using $AgNO_3$ in place of $AgClO_4$. Crystallization was performed from water by adding acetone at room temperature. The solubility of this complex exhibits a negative temperature gradient in a solvent system of water-acetone. Yield: 35%. Found: C, 13.78; H, 4.32; N, 15.87%. Calcd for $C_6H_{22}N_6O_8Pd_2$: C, 13.88; H, 4.27; N, 16.19%. The nitrate is most unstable among the three kinds of the dimer salts.

3) [Pd$_2$*(μ-OH)*$_2$*(S-pn)*$_2$*](*HCO_3*)*$_2$: The mixture [$PdCl_2$(*S*-pn)] (250 mg) and Ag_2CO_3 (95%, 290 mg) suspended in 15 cm^3 of water was stirred for 15 min at 55—60 °C. The AgCl was filtered off in hot and the filtrate was chilled in an ice-bath. Yellow crystals were collected, washed with cold water, methanol, and ether, and dried *in vacuo*. Yield: 100 mg. Found: C, 18.34; H, 4.50; N, 10.72%. Calcd for $C_8H_{24}N_4O_8Pd_2$: C, 18.58; H, 4.68; N, 10.83%. This complex was also obtained by adding aqueous solution of $NaHCO_3$ to that containing [Pd_2(μ-OH)$_2$(*S*-pn)$_2$]$(ClO_4)_2$.

4) [Pd(CH_3CO_2*)*$_2$*(S-pn)]*: A suspension of 350 mg of [$PdCl_2$(*S*-pn)] in 10 cm^3 of water was stirred with 330 mg of Ag_2O for 15 min at room temperature. After removal of AgCl, to the solution was added 167 mg of acetic acid diluted with 2 cm^3 of water. The mixture was stirred for 15 min at *ca.* 55 °C and then evaporated to a small volume under reduced pressure and chilled in an ice-bath to give yellow crystals. The crystals were washed with cold methanol and ether, and dried *in vacuo*. Total yield: 320 mg. Found: C, 28.10; H, 5.40; N, 9.38%. Calcd for $C_7H_{16}N_2O_4Pd$: C, 28.15; H, 5.40; N, 9.38%.

5) [PdL(S-pn)] (L=ox and mal): These complexes were obtained by the same method as in *4)*, but crystallized from a more dilute solution. Yield: 75—80%. Found: C, 22.41; H, 3.75; N, 10.44%. Calcd for [Pd(ox)(*S*-pn)]=$C_5H_{10}N_2O_4Pd$: C, 22.36; H, 3.75; N, 10.43%. Found: C, 25.39; H, 4.25; N, 9.92%. Calcd for [Pd(mal)(*S*-pn)]=$C_6H_{12}N_2O_4Pd$: C, 25.50; H, 4.28; N, 9.91%. The oxalato complex was also obtained by a reaction of [$PdCl_2$(*S*-pn)] with silver oxalate.

6) [Pd(ox)(N^1,N^1-*Et*$_2$-*(S)-pn)]*: A suspension of 300 mg of [$PdCl_2$(N^1,N^1-Et_2-(*S*)-pn)] in 15 cm^3 of water was treated with 300 mg of silver oxalate. The solution filtered was evaporated to dryness under reduced pressure and the crude product was recrystallized from a minimum amount of warm water by adding acetone; yield 110 mg. Found: C, 33.24; H, 5.60; N, 8.60%. Calcd for $C_9H_{18}N_2O_4Pd$: C, 33.29; H, 5.59; N, 8.63%.

[Pd(N)(O)$_3$*]-type Complexes.* *1) K[Pd(*CH_3CO_2*)*$_2$*(S-ala)]*: An aqueous solution (18 cm^3) containing K[$PdCl_2$(*S*-ala)][8] (360 mg) and acetic acid (144 mg) was cooled in an ice-bath and then stirred with 285 mg of freshly prepared silver oxide for 8 min in the dark. After removal of AgCl the solution was evaporated to a small volume and mixed with acetone. On standing in a refrigerator overnight, the desired product was obtained as orange-brown crystals, which were washed with a mixture of water-acetone and dried *in vacuo*. Total yield: 210 mg. Found: C, 23.64; H, 3.44; N, 4.00%. Calcd for $C_7H_{12}NO_6KPd$: C, 23.91; H, 3.44; N, 3.98%. This complex is thermally labile and decomposes gradually even at room temperature in an aqueous solution.

2) K[Pd(mal)(S-ala)]: The crude poduct was obtained in the same manner as in *1)* using malonic acid in place of acetic acid, and recrystallized from water by adding acetone; yield 30%. Found: C, 21.41; H, 2.47; N, 4.13%. Calcd for $C_6H_8NO_6KPd$: C, 21.47; H, 2.40; N, 4.17%

Measurements. Electronic absorption spectra were recorded with a Hitachi 330 spectrophotometer and CD spectra with a JASCO MOE-1 spectropolarimeter. Unless otherwise noted, all the measurements were made in aqueous solutions

at room temperature. A 10-cm cell was employed for the CD measurements in the long wavelength region in order to acquire a higher precision. ^{13}C NMR spectra were taken on a JEOL FX-90Q NMR spectrometer in D_2O containing 1,4-dioxane as an internal standard (δ=67.40).

Results and Discussion

Synthesis of the Mixed-ligand Complexes. In the synthesis of palladium(II) complexes comprising of two kinds of ligands, a ligand possessing higher affinity for palladium [which we will call a higher-affinity ligand hereafter] should be introduced firstly, as the study by Drew *et al.*[3] suggests. When the order is reversed, a disproportionation reaction tends to occur, affording the complexes each having one kind of ligands. Generally, *N*-ligands coordinate to palladium more strongly than *O*-ligands; then, $[Pd(N\text{-}O)(N\text{-}N)]^+$ and $[Pd(O\text{-}O)(N\text{-}N)]$ complexes should be synthesized from $[PdCl_2(N\text{-}N)]$, and $[Pd(O\text{-}O)(N\text{-}O)]^-$ should be from $[PdCl_2(N\text{-}O)]^-$. The order of the affinity with respect to diamine ligands was obtained from the observation of the disproportionation in the course of the synthesis of $[Pd(N)_4]$-type complexes, being as follows:

en ≈ *S*-pn > tn > *N*,*N*-Me$_2$en
> N^1,N^1-Et$_2$-(*S*)-pn ≈ *N*,*N*-Et$_2$en ≫ NH_3.

The disproportionation reaction proceeded also when excess lower-affinity ligand was allowed to react with a dichloro complex of higher-affinity ligands. All the $[Pd(N)_4]$-type complexes under investigation were obtained in accord with the above order of affinity. The reaction of ammonia with $[PdCl_2(N^1,N^1\text{-Et}_2\text{-}(S)\text{-pn})]$ apparently does not proceed by one step but by two steps [Eq. (1)], that is, the intermediate product

$$[PdCl_2(N^1,N^1\text{-Et}_2\text{-}(S)\text{-pn})] \xrightarrow{NH_3} \mathbf{I} \xrightarrow{NH_3} [Pd(NH_3)_2(N^1,N^1\text{-Et}_2\text{-}(S)\text{-pn})]Cl_2 \quad (1)$$

where **I** is

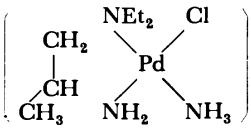

$[PdCl(NH_3)(N^1,N^1\text{-Et}_2\text{-}(S)\text{-pn})]Cl$ was isolated. The action of twice the equimolar quantity of ammonia on the dichloro complex gave only the intermediate chloroammine complex, indicating that the remaining chloro ligand is resistant to the substitution with ammonia. Judging from this observation, the intermediate is supposed to possess structure **I** because an ammine ligand is considered to be more bulky than a chloro ligand.

$[Pd(N)_3(O)]$-type complexes were synthesized by the following three methods [Eqs. (2)—(4)]. The method of Eq. (2) is useful only when a desired product crystallizes with ease and is sufficiently less soluble than sodium chloride (*e.g.* $[Pd(gly)(S\text{-pn})]ClO_4$ and $[Pd(S\text{-ala})(en)]ClO_4$). When the complexes are highly soluble, the method of Eq. (3), where both perchloric acid and amino carboxylic acid are employed in an equimolar amount with the starting dichloro complex is effective. The method of Eq. (4) is essentially the same as that of Eq.(3), but it is noticed that all the reactions proceed under nearly neutral conditions.

$$[PdCl_2(N\text{-}N)] + H(N\text{-}O) + NaOH \xrightarrow[H_2O]{NaClO_4} [Pd(N\text{-}O)(N\text{-}N)]ClO_4 + 2NaCl \quad (2)$$

$$[PdCl_2(N\text{-}N)] + Ag_2O \xrightarrow[H_2O]{} \frac{1}{2}\left[\begin{array}{c}H\\O\\ \left(N\diagdown Pd\diagup N\right)\\ \left(N\diagup O\diagdown N\right)\\H\end{array}\right](OH)_2 + 2AgCl \xrightarrow[H_2O]{H(N\text{-}O)+HClO_4} [Pd(N\text{-}O)(N\text{-}N)]ClO_4 \quad (3)$$

$$[PdCl_2(N\text{-}N)] + AgClO_4 + \frac{1}{2}Ag_2O \xrightarrow[H_2O]{} \frac{1}{2}\left[\begin{array}{c}H\\O\\ \left(N\diagdown Pd\diagup N\right)\\ \left(N\diagup O\diagdown N\right)\\H\end{array}\right](ClO_4)_2 + 2AgCl \xrightarrow[H_2O]{H(N\text{-}O)} [Pd(N\text{-}O)(N\text{-}N)]ClO_4 \quad (4)$$

The di-μ-hydroxo complex of *S*-pn, which is an intermediate in the reactions of Eqs.(3) and (4), could be isolated as nitrate and hydrogencarbonate, as well as perchlorate. The following equilibria with regard to the dimer perchlorate were confirmed by absorption and CD spectral measurements [See also Fig. 1; the shoulder at 45.5×10^3 cm^{-1} of the dimer complex is assigned to a charge transfer transition, Pd← O(μ-OH)]. The equilibrium constant of equilibrium (i) for the corresponding en complexes has been determined by Lim and Martin.[12]

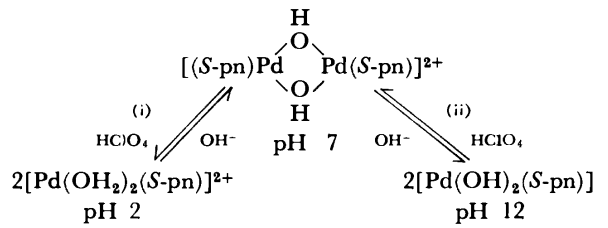

The preparation of $[Pd(S\text{-ala})(NH_3)_2]ClO_4$ was attempted according to both Eqs. (3) and (4), but the contamination with the bis(alaninato) complex prevented the isolation of the pure product. The purity was not improved by recrystallization. This seems to be primarily caused by the mechanism that the ammonia liberated during the course of recrystallization promotes a disproportionation reaction.

cis-$[Pd(N)_2(O)_2]$-type complexes could not be obtained by the method of Eq. (5). The reaction proceeded only incompletely even by the use of excess dicarboxylate, which indicates high affinity of a chloro ligand over *O*-ligands for palladium. Thus it is necessary that chloride ions are removed from the

$$[PdCl_2(S\text{-pn})] + M_2(O\text{-}O) \xrightarrow[H_2O]{} [Pd(O\text{-}O)(S\text{-pn})] + 2MCl \ (M=\text{alkali metal}) \quad (5)$$

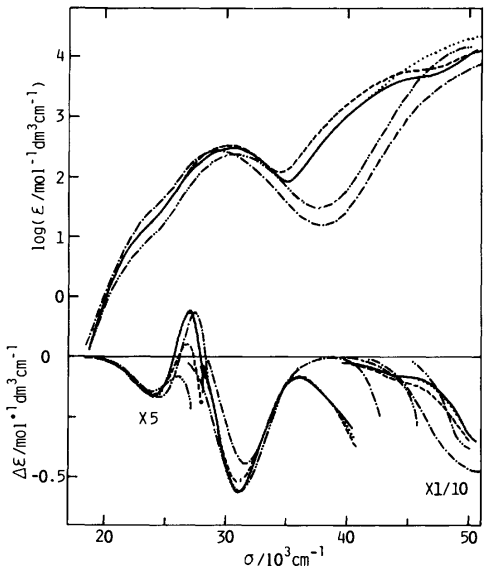

Fig. 1. Absorption and CD spectra of $[Pd_2(\mu\text{-}OH)_2(S\text{-}pn)_2]X_2$. ——: X=$ClO_4$ in H_2O, —·—: X=ClO_4 in 0.01 M $HClO_4$ (=2×[$Pd(OH_2)_2$(S-pn)]$(ClO_4)_2$), —··—: X=ClO_4 in 0.01 M NaOH (=2×[$Pd(OH)_2$(S-pn)], ----, X=HCO_3 in H_2O, and ……: X=NO_3 in H_2O.

reaction system. The method of Eq. (6) satisfies this

$$[PdCl_2(S\text{-pn})] + Ag_2O \xrightarrow[H_2O]{} \frac{1}{2}[(S\text{-pn})Pd(\mu\text{-}OH)_2Pd(S\text{-pn})](OH)_2 + 2AgCl$$

$$\xrightarrow[H_2O]{H_2(O\text{-}O)} [Pd(O\text{-}O)(S\text{-pn})] \quad (6)$$

requirement. The calculated quantity of a dicarboxylic acid is sufficient here, and a desired product can be isolated from the salt free system. The method of Eq. (7)

$$[PdCl_2(S\text{-pn})] + Ag_2(O\text{-}O) \xrightarrow[H_2O]{} [Pd(O\text{-}O)(S\text{-pn})] + 2AgCl \quad (7)$$

was also effective for the synthesis of the oxalato complex. Attempts to synthesize the carbonato complex by this method, however, were unsuccessful, and the hydrogen carbonate salt of the same di-μ-hydroxo complex as is seen in Eq. (6) was obtained instead. The same material was also obtained by metathesis of an authentic sample of the corresponding perchlorate with sodium hydrogencarbonate.

[Pd(N)(O)$_3$]-type complexes could not be obtained by reaction (8) but by (9) in analogy with the case of

$$K[PdCl_2(S\text{-ala})] + M_2(O\text{-}O) \xrightarrow[H_2O]{} K[Pd(O\text{-}O)(S\text{-ala})] + 2MCl \quad (8)$$

$$K[PdCl_2(S\text{-ala})] + Ag_2O + H_2(O\text{-}O) \xrightarrow[H_2O]{} K[Pd(O\text{-}O)(S\text{-ala})] + 2AgCl \quad (9)$$

cis-[Pd(N)$_2$(O)$_2$]-type complexes. Chloro ligands must be removed in the presence of a dicarboxylic acid because otherwise some decomposition occurs and it seems to be concerned with the instability of the di-μ-hydroxo complex [(S-ala)Pd(μ-OH)$_2$Pd(S-ala)] in a basic solution [Eq. (10)]. The malonato complex

$$K[PdCl_2(S\text{-ala})] + Ag_2O \xrightarrow[H_2O]{} \frac{1}{2}[(S\text{-ala})Pd(\mu\text{-}OH)_2Pd(S\text{-ala})] + KOH + 2AgCl \quad (10)$$

obtained according to Eq. (9) had been somewhat contaminated by the disproportionation products, but it could be purified by recrystallization. The use of oxalic acid in place of malonic acid gave only a mixture of the disproportionation products. The direct method where silver oxalate is used as in Eq. (7) also led to the same result.

Isomerism. As both S-pn and am$^-$ are unsymmetrical bidentate ligands, their mixed-ligand complexes should exhibit geometrical isomerism. We will call the configurations of two isomers *cis*(CH$_3$,O) and *trans*(CH$_3$,O) by considering the relative positions between the methyl group of S-pn and the coordinating oxygen atom of am$^-$. The ^{13}C NMR spectra of the β-ala, S-pro, and S-ala complexes varied with time, which was ascribed to the variation of distribution of such isomers: the β-ala and S-pro complexes comprise exclusively one isomer in the crystalline state and the S-ala complex also roughly so, whereas in solution each of them changes slowly into a mixture of the two isomers (approximately equimolar). The gly complex was found to be such a mixture even in the crystalline state. All the resonances were assigned on the basis of comparison with those of the related complexes[13] and by the INEPT method[14] (Table 1). The chelate ring carbons C(1) and C(2) of S-pn exhibit different

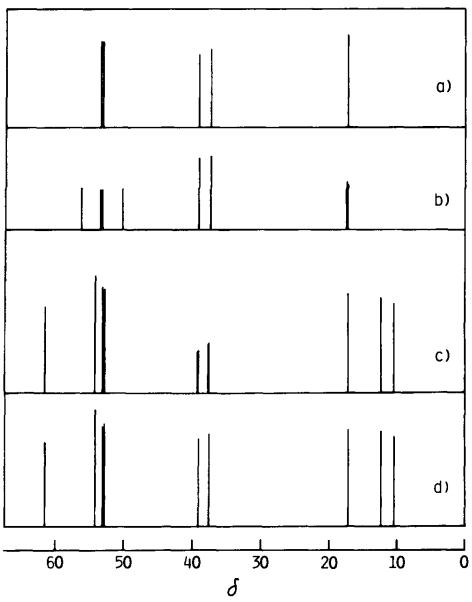

Fig. 2. Diagramatic representation of the ^{13}C NMR spectra of a) [Pd(β-ala)(S-pn)]$^+$ recorded immediately after dissolution, b) [Pd(β-ala)(S-pn)]$^+$ after 110 h, c) [Pd(β-ala)(N^1,N^1-Et_2-(S)-pn)]$^+$ recorded immediately after dissolution, and d) [Pd(β-ala)(N^1,N^1-Et_2-(S)-pn)]$^+$ after 120 h; the resonance for the carbonyl carbon being omitted.

TABLE 1. ^{13}C NMR CHEMICAL SHIFTS FOR SELECTED $[Pd(N)_4]$- AND $[Pd(N)_3(O)]$-TYPE COMPLEXES[a,j]

Complex[b] $(L_1)(L_2)$		*S*-pn			am⁻					Others	
		C(1)	C(2)	C(3)	C(α)	C(β)	C(γ)	C(δ)	C(c)		
(gly)(*S*-pn)		50.52 52.58	55.78 53.72	17.31	47.27				186.68 186.73		
(*S*-ala)(*S*-pn)	c)	50.55 52.50[e]	55.70 53.64[e]	17.39	54.67	19.67			187.57		
	d)	50.55 52.50	55.75 53.69	17.39	54.67	19.67			187.57		
(*S*-pro)(*S*-pn)	c)	52.45	53.48	17.44	64.85	30.34	25.68	52.61	f)		
	d)	50.39 52.39	55.53 53.42	17.45	64.85	30.29	25.57	52.55	188.06		
(β-ala)(*S*-pn)	c)	53.20	53.48	17.34	37.44	39.17			181.29		
	d)	50.32 53.20	56.39 53.47	17.49 17.33	37.43	39.16			181.22		
(*S*-ala)(en)					54.78	19.67			187.52	45.73[h]	47.79[h]
(*S*-leu)(en)					57.16	43.02	24.49	21.51 23.19	187.62	45.73[h]	47.73[h]
(*S*-hpro)(en)					63.39	38.58	70.71	59.16	187.62	45.62[h]	47.79[h]
(en)(*S*-pn)		51.39	54.53	17.64						46.57[h]	

	S-pn			N^1,N^1-Et_2-(*S*)-pn (or N,N-Et_2en)					Others	
	C(1)	C(2)	C(3)	C(1′)	C(2′)	C(3′)	C(4′)	C(5′)		
(N,N-Et_2en)-(*S*-pn)	51.01	54.75	17.58	57.19	43.94		55.45	11.78 12.06		
(N^1,N^1-Et_2-(*S*)-pn)-(*S*-pn)	51.28	54.59	17.69	62.66	52.42	17.55	55.86 56.35	11.43 12.79		
(N^1,N^1-Et_2-(*S*)-pn)-(N,N-Me_2en)				62.52	52.10	17.48	55.86 56.54	11.22 13.20	50.71[g] 51.85[g]	42.78[h] 66.42[i]

	am⁻			N^1,N^1-Et_2-(*S*)-pn					Others	
	C(α)	C(β)	C(c)	C(1′)	C(2′)	C(3′)	C(4′)	C(5′)		
(N,N-Me_2gly)-(N^1,N^1-Et_2-(*S*)-pn)	68.32		181.98	62.80	52.23	17.13	54.13 55.05	11.00 12.14	51.45[g] 51.61[g]	
(β-ala)-(N^1,N^1-Et_2-(*S*)-pn) c)	37.59 37.62	39.15 39.26	181.52	61.63	52.94	17.26	53.21 54.36	10.50 12.34		
d)	37.56	39.12	181.46	61.60	52.94	17.23	53.22 54.37	10.49 12.34		

a) ppm from Me_4Si. b) $(L_1)(L_2) \equiv [Pd(L_1)(L_2)]^{n+}$. c) Recorded immediately after dissolution. d) Recorded in equilibrium (See text). e) Weak. f) Not scanned. g) $(\underline{C}H_3)_2N$-. h) $H_2N\underline{C}H_2$-. i) $(CH_3)_2N\underline{C}H_2$-. j) Ligand carbons are named as follows.

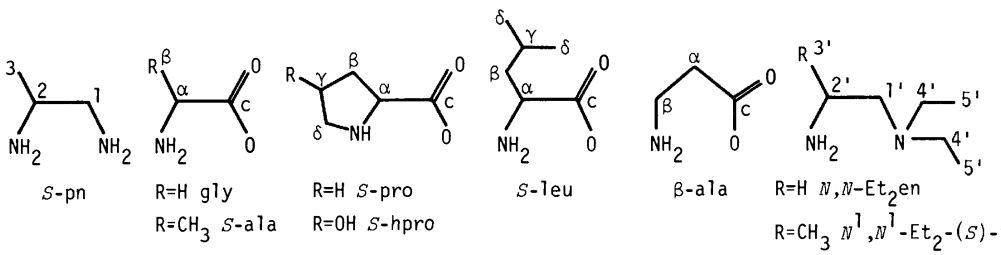

chemical shifts between a pair of isomers, and this is also the case for the carbonyl carbon C(c) of the gly complex and the methyl carbon C(3) of *S*-pn in the β-ala complex. For example, the ^{13}C NMR specirum of the β-ala complex showed six signals correspoding to six different carbons when it was recorded immediately after dissolution; whereas after equilibration (110 h) it showed three additional signals, which are assigned to C(1), C(2), and C(3) (Fig. 2 and Table 1). The variable distribution of the isomers could be also detected by CD spectra. The main negative CD band in the d-d transition region increased in intensity with time after dissolution in the β-ala and *S*-pro complexes, but decreased in the *S*-ala complex

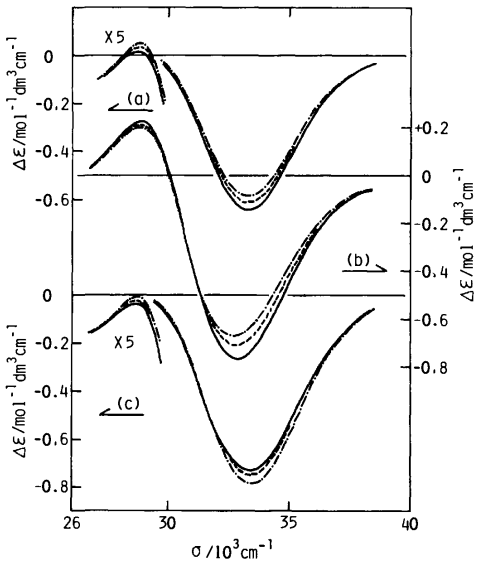

Fig. 3. CD spectral variation with time after dissolution for [PdL(*S*-pn)]ClO_4. (a) L=β-ala; —·—: 0 h, ----: 24 h, and ——: 110 h (in equilibrium). (b) L=*S*-pro; —·—: 0 h, ----: 5 h, and ——: 30 h (in equilibrium). (c) L=*S*-ala; —·—: 0 h, ----: 5 h, and ——: 12 h (in equilibrium).

(Fig. 3). This suggests that the configuration of the isomer predominant in the crystalline state of the former complexes is different from that of the latter complex, which is compatible with the deduction from the ^{13}C NMR spectra. In one isomer of every complex, the difference in chemical shifts between C(1) and C(2) is small (*ca.* 1.3, 1.0, and 1.2 ppm for the β-ala, *S*-pro, and *S*-ala complexes, respectively), and in the other isomer it is large (*ca.* 6.1, 5.1, and 5.2 ppm, respectively). The predominant isomer in the crystalline state is the former for the β-ala and *S*-pro complexes, and the latter for the *S*-ala complex (Table 1).

The configuration was determined by examination of the time-dependent ^{13}C NMR and CD spectra of [Pd(β-ala)(N^1,N^1-Et_2-(*S*)-pn)]$^+$. In the NMR spectrum recorded immediately after dissolution, each of the α- and β-carbon of β-ala showed two signals; and after 120 h (in equilibrium) one of the two signals disappeared and the remaining one increased in intensity (Fig. 2). This fact suggests that the complex comprises a mixture of a pair of isomers in the crystalline state, but in solution isomerizes slowly to the more stable isomer.[15] The steric interaction between the amino group of β-ala and the diethylamino group of N^1,N^1-Et_2-(*S*)-pn is expected to be more significant than that between the carboxyl oxygen of β-ala and the diethylamino group.[16] Therefore, structure **II** can be assigned to the more stable isomer.

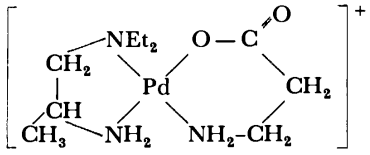

II *trans*(CH_3,*O*)

Although the CD variation with time was unexpectedly small, it was reproducible: +0.021→+0.014 (at 350 nm) and −0.919→−0.903 (at 299 nm), given as $\Delta\varepsilon$/mol^{-1} dm^3 cm^{-1} for 0 h→120 h (See also Fig. 8). Thus, the main band varies in the positive direction. This variation can be correlated to the isomerization of the *cis*(CH_3,*O*) to the *trans*(CH_3,*O*) isomer on the basis of the above structural assignment. Therefore, the predominant isomer in the crystalline state of [Pd(*S*-ala)(*S*-pn)]ClO_4, which exhibits the same CD variation as [Pd(β-ala)(N^1,N^1-Et_2-(*S*)-pn)]ClO_4, is *cis*-(CH_3,*O*); and those of [Pd(β-ala)(*S*-pn)]ClO_4 and [Pd(*S*-pro)(*S*-pn)]ClO_4, which exhibit the reverse CD variation, are *trans*(CH_3,*O*). These results are summarized in Table 2.

It is worth noting that the complexes with a six-membered amino carboxylato chelate ring isomerize evidently more slowly than those with a five-membered one, and have comparable rate of isomerization (or racemization) with the [Pd(N)$_4$]-type complexes with two five-membered chelate rings.[11] Although [Pd(N)$_4$]-type complexes such as [Pd(N^1,N^1-Et_2-(*S*)-pn)(*S*-pn)]$^{2+}$ should also exhibit similar isomerism, it could be detected by neither of ^{13}C NMR nor CD spectra.

^{13}C NMR Spectra. A convenient rule concerning ^{13}C NMR spectra is derived from the assignment of isomers given in the preceding section: A carbon atom adjacent to the coordinated *N*-atom resonates at *ca.* 1 ppm higher or lower magnetic field when an *O*-atom occupies the coordination site trans or cis to the *N*-atom, respectively, in comparison with the case that an *N*-atom occupies the same site instead of *O*-atom (Compare the data for a pair of isomers of [Pd(am)(*S*-pn)]$^+$ with those for [Pd(en)(*S*-pn)]$^{2+}$). Using this rule, two carbon signals of en in the [Pd(*S*-am)(en)]$^+$ complexes can be readily assigned on reference to that of en in [Pd(en)(*S*-pn)]$^{2+}$ (46.57

Table 2. Isomerization of [Pd(N)$_3$(O)]-type complexes[a]

Complex[b] (L_1)(L_2)	Variation of distribution of isomers[c]	Net change	Direction of CD variation[d]
(β-ala)(*S*-pn)	*trans* → [*trans*+*cis*(≈1:1)]	*trans* → *cis*	−
(*S*-pro)(*S*-pn)	*trans* → [*trans*+*cis*(≈1:1)]	*trans* → *cis*	−
(*S*-ala)(*S*-pn)	[*trans*<*cis*] → [*trans*+*cis*(≈1:1)]	*cis* → *trans*	+
(β-ala)(N^1,N^1-Et_2-(*S*)-pn)	[*trans*+*cis*(≈1:1)] → *trans*	*cis* → *trans*	+

a) *trans*≡*trans*(CH_3,*O*) and *cis*≡*cis*(CH_3,*O*). b) (L_1)(L_2)≡[Pd(L_1)(L_2)]$^+$. c) In crystal→in solution at equilibrium. d) For the main band in the d-d transition region.

ppm). Accordingly, the signals at *ca.* 45.7 and 47.8 ppm are assigned to the carbon atom adjacent to the *N*-atom trans and cis to the *O*-atom, respectively.

CD and Absorption Spectra. 1) [Pd(N)$_4$]-type Complexes: The spectra of the complexes containing *S*-pn and N^1,N^1-Et$_2$-(*S*)-pn as an optically active ligand are shown in Figs. 4 and 5, respectively; the numerical data being given in Tables 3 and 4. The absorption curves are composed of an unsymmetrical broad band and a lower-lying shoulder in the d-d transition region, the latter being a spin-forbidden d-d band. The shape of the spin-allowed d-d band can be characterized by the half-value width parameters and the unsymmetry parameter.[2] These parameters for the complexes studied in this paper are listed in Table 5.

The CD spectra in the spin-forbidden d-d region show two negative bands, more distinctly in the N^1,N^1-Et$_2$-(*S*)-pn complexes. In the spin-allowed d-d region, all complexes of the [Pd(N)$_4$]-type show only one negative band except the tn complexes, which exhibit an additional weak positive band in the lower energy side. The intensity of the main negative band is lower for the ammine complexes than for the en and tn complexes and it is almost equal for the latter two complexes, when compared within one of the series of *S*-pn or N^1,N^1-Et$_2$-(*S*)-pn complexes (Figs. 4 and 5). The main CD band lies at higher energy by (0.5—1.1) $\times 10^3$ cm^{-1} than the spin-allowed d-d absorption peak for all the complexes including the tn complexes. Thus, it is expected that the complexes other than the tn complexes also have another transition component in the lower energy side of the main band. The CD band for the lower energy component is, however, undetectable probably because of its low intensity. The minimum of $|\Delta\varepsilon|$ around 30×10^3 cm^{-1} seems to arise from such a CD band, and is included in Table 4. This and the main negative band

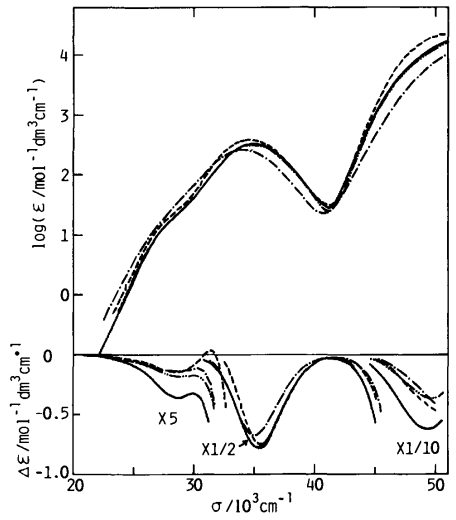

Fig. 4. Absorption and CD spectra of $[PdL(S\text{-pn})]Cl_2$. ——: L=*S*-pn, —·—: L=$(NH_3)_2$, —··—: L=en, and ----: L=tn.

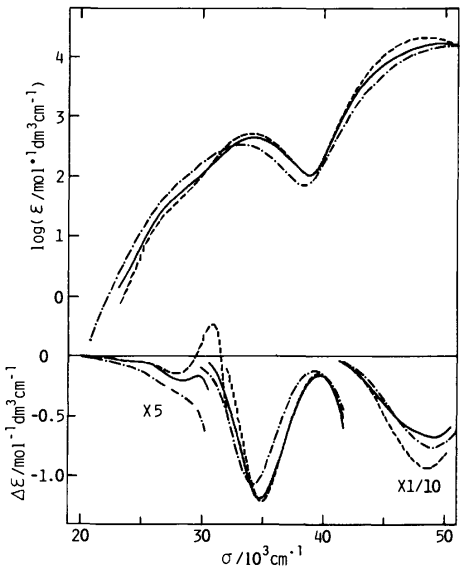

Fig. 5. Absorption and CD spectra of $[PdL(N^1,N^1\text{-Et}_2\text{-}(S)\text{-pn})]Cl_2$. ——: L=en, —·—: L=$(NH_3)_2$, and ----: L=tn.

Table 3. Absorption data[a] of $[Pd(N)_4]$-type complexes ($[Pd(L_1)(L_2)]Cl_2\cdot nH_2O$)

$(L_1)(L_2)$	n	$\sigma_{max}/10^3$ cm^{-1} (ε/mol^{-1} dm^3 cm^{-1})			
		Spin-forbidden d-d	Spin-allowed d-d	Charge transfer	
(*S*-pn)$(NH_3)_2$	0	28.4 sh (30)	34.08 (261)		
(*S*-pn)(en)	0.5	28.8 sh (23)	34.86 (310)		
(*S*-pn)$_2$	0.5	28.8 sh (24)	34.89 (328)		
(*S*-pn)(tn)	1	28.6 sh (26)	34.63 (387)		
(N^1,N^1-Et$_2$-(*S*)-pn)$(NH_3)_2$	1	27.4 sh (58)	33.12 (337)		
(N^1,N^1-Et$_2$-(*S*)-pn)(en)	1	28.2 sh (54)	34.21 (443)	49.90 (16600)	
(N^1,N^1-Et$_2$-(*S*)-pn)(*S*-pn)	2	28.2 sh (54)	34.19 (481)	49.85 (17300)	
(*N*,*N*-Et$_2$en)(*S*-pn)	1.25	28.0 sh (54)	34.15 (422)	49.70 (16800)	
(N^1,N^1-Et$_2$-(*S*)-pn)(tn)	0	28.0 sh (39)	33.97 (515)	48.43 (20500)	
(N^1,N^1-Et$_2$-(*S*)-pn)$_2$	2	27.4 sh (48)	33.57 (603)	44.48 (14600)	48.2 sh (13300)
(N^1,N^1-Et$_2$-(*S*)-pn)(*N*,*N*-Et$_2$en)	0	27.6 sh (49)	33.58 (579)	44.39 (14400)	48.4 sh (12200)
(N^1,N^1-Et$_2$-(*S*)-pn)(*N*,*N*-Me$_2$en)	0	27.8 sh (47)	33.83 (572)	46.06 (15900)	48.0 sh (15000)

a) sh: Shoulder (ε is for the value σ given).

TABLE 4. CD DATA[a] OF $[Pd(N)_4]$-TYPE COMPLEXES ($[Pd(L_1)(L_2)]Cl_2$)[b]

$(L_1)(L_2)$	$\sigma_{ext}/10^3$ cm^{-1} ($\Delta\varepsilon$/mol^{-1} dm^3 cm^{-1})		
	Spin-forbidden d-d	Spin-allowed d-d	Charge transfer
(*S*-pn)$(NH_3)_2$	28.57 (−0.027)	30.42m 35.06 (−0.68)	
(*S*-pn)(en)	28.74 (−0.038)	29.90m 35.34 (−0.79)	49.41 (−3.7)
(*S*-pn)$_2$	24 sh (−0.012) 28.78 (−0.073)	29.99m 35.36 (−1.55)	49.26 (−6.3)
(*S*-pn)(tn)	24.5 sh (−0.007) 28.53 (−0.030)	31.35 (+0.005) 35.59 (−0.75)	50.76 (−4.8)
(N^1,N^1-Et$_2$-(*S*)-pn)$(NH_3)_2$	24 sh (−0.016) 28 sh (−0.062)	34.25 (−1.07)	48.9 (−7.7)
(N^1,N^1-Et$_2$-(*S*)-pn)(en)	24.5 sh (−0.010) 28.22 (−0.042)	29.59m 34.82 (−1.19)	49.02 (−6.8)
(*N*,*N*-Et$_2$en)(*S*-pn)	27.03 (−0.024)	29.50m 34.77 (−0.85)	48.6 (−1.8)
(N^1,N^1-Et$_2$-(*S*)-pn)(*S*-pn)	24.5 sh (−0.021) 28.18 (−0.079)	29.53m 34.97 (−2.10)	47.62 (−8.9)
(N^1,N^1-Et$_2$-(*S*)-pn)(tn)	24.7 sh (−0.010) 28.00 (−0.029)	30.86 (+0.053) 35.01 (−1.21)	48.52 (−9.4)
(N^1,N^1-Et$_2$-(*S*)-pn)(*N*,*N*-Me$_2$en)	23.5 sh (−0.009) 29.0 sh (−0.10)	34.16 (−0.85)	45.3 (−6.3) 47.8 (−6.5)
(N^1,N^1-Et$_2$-(*S*)-pn)(*N*,*N*-Et$_2$en)	23.5 sh (−0.011) 27.14 (−0.032)	28.61m 34.20 (−1.16)	45.0 (−3.1) 47.8 (−3.6)
(N^1,N^1-Et$_2$-(*S*)-pn)$_2$	23.5 sh (−0.025) 26.67 (−0.045)	28.74m 34.13 (−2.85)	44 sh (−6.9) 48.5 (−9.6)

a) m: The minimum of $|\Delta\varepsilon|$ (See text); sh: shoulder ($\Delta\varepsilon$ is given for the value σ given). b) Water of crystallization is omitted (See Table 3).

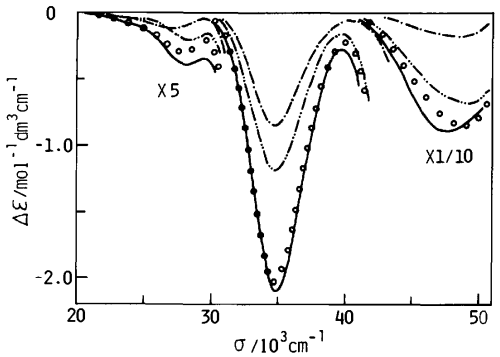

Fig. 6. CD spectra of $[Pd(N,N\text{-}Et_2en)(S\text{-}pn)]Cl_2$ (—·—), $[Pd(N,N^1\text{-}Et_2\text{-}(S)\text{-}pn)(en)]Cl_2$ (—··—), and $[Pd(N^1,N^1\text{-}Et_2\text{-}(S)\text{-}pn)(S\text{-}pn)]Cl_2$ (——); and CD curve calculated from $[\Delta\varepsilon(\text{—·—})+\Delta\varepsilon(\text{—··—})]$ (oooo).

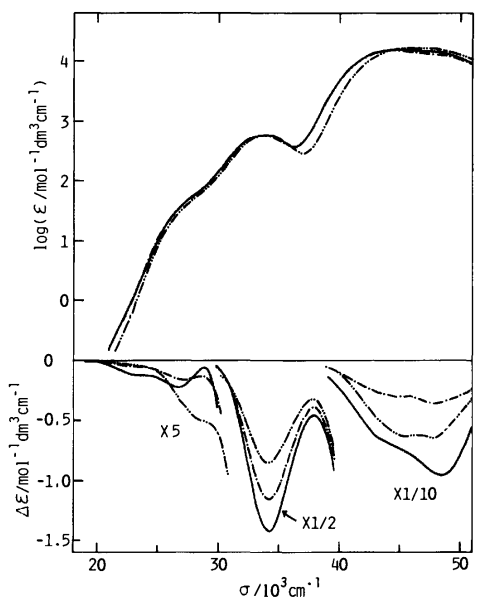

Fig. 7. Absorption and CD spectra of $[Pd(N^1,N^1\text{-}Et_2\text{-}(S)\text{-}pn)_2]Cl_2$ (——), $[Pd(N,N\text{-}Et_2en)(N^1,N^1\text{-}Et_2\text{-}(S)\text{-}pn)]Cl_2$ (—·—), and $[Pd(N,N\text{-}Me_2en)(N^1,N^1\text{-}Et_2\text{-}(S)\text{-}pn)]Cl_2$ (—··—).

are assigned to $^1A_{2g}$ and $^1E_g \leftarrow {}^1A_{1g}$ (D_{4h}), respectively, and it is expected that the $^1B_{1g} \leftarrow {}^1A_{1g}$ transition, which is magnetic dipole forbidden, occurs at higher energy than the $^1E_g \leftarrow {}^1A_{1g}$ transition as in $[PdCl_4]^{2-}$ and *cis*-$[Pd(Cl)_2(N)_2]$-type complexes.[1,2]

The CD spectrum of $[Pd(N^1,N^1\text{-}Et_2\text{-}(S)\text{-}pn)(S\text{-}pn)]^{2+}$ comprising two different optically active ligands can be reproduced well by the sum of the CD curves of $[Pd(N,N\text{-}Et_2en)(S\text{-}pn)]^{2+}$ and $[Pd(N^1,N^1\text{-}Et_2\text{-}(S)\text{-}pn)(en)]^{2+}$, which have the same structure as the first complex except for the disposition of *C*-methyl group (Fig. 6). Thus the two optically active ligands contribute independently to the optical activity of $[Pd(N^1,N^1\text{-}Et_2\text{-}(S)\text{-}pn)(S\text{-}pn)]^{2+}$. The complexes having two *N*,*N*-dialkylethylenediamine ligands exhibited a splitting with the absorption and CD bands which are assigned to Pd←N(σ) charge transfer(CT) transitions (Fig. 7). The complexes with only one *N*,*N*-dialkylethylenediamine

Table 5. Band shape parameters for the spin-allowed d-d band of $[Pd(N)_n(O)_{4-n}]$-type complexes ($n=1-4$)

Complex	$\Delta\sigma^-$ a) / 10^3 cm^{-1}	$\Delta\sigma^+$ a) / 10^3 cm^{-1}	$\Delta\sigma_{1/2}$ a) / 10^3 cm^{-1}	Unsymmetry parameter b)
$[Pd(S\text{-pn})(NH_3)_2]^{2+}$	2.75	2.83	5.58	1.4
$[Pd(S\text{-pn})(en)]^{2+}$	2.55	2.77	5.31	4.1
$[Pd(S\text{-pn})_2]^{2+}$	2.53	2.74	5.27	4.0
$[Pd(S\text{-pn})(tn)]^{2+}$	2.51	2.76	5.27	4.7
$[Pd(N^1,N^1\text{-Et}_2\text{-}(S)\text{-pn})(NH_3)_2]^{2+}$	3.20	2.91	6.11	−4.7
$[Pd(N^1,N^1\text{-Et}_2\text{-}(S)\text{-pn})(en)]^{2+}$	2.73	2.68	5.42	−0.9
$[Pd(N^1,N^1\text{-Et}_2\text{-}(S)\text{-pn})(S\text{-pn})]^{2+}$	2.67	2.70	5.37	0.6
$[Pd(N,N\text{-Et}_2\text{en})(S\text{-pn})]^{2+}$	2.85	2.70	5.55	−2.7
$[Pd(N^1,N^1\text{-Et}_2\text{-}(S)\text{-pn})(tn)]^{2+}$	2.53	2.66	5.19	2.5
$[Pd(gly)(S\text{-pn})]^+$	2.72	2.79	5.51	1.3
$[Pd(\beta\text{-ala})(S\text{-pn})]^+$	2.45	2·73	5.18	5.4
$[Pd(S\text{-ala})(en)]^+$	2.68	2.76	5.44	1.5
$[Pd(S\text{-ala})(S\text{-pn})]^+$	2.64	2.74	5.38	1.9
$[Pd(S\text{-ala})(tn)]^+$	2.53	2.83	5.37	5.6
$[Pd(S\text{-pro})(en)]^+$	2.75	2.80	5.56	0.9
$[Pd(S\text{-pro})(S\text{-pn})]^+$	2.78	2.80	5.58	0.4
$[Pd(S\text{-ser})(en)]^+$	2.70	2.78	5.47	1.5
$[Pd(S\text{-leu})(en)]^+$	2.71	2.76	5.46	0.9
$[Pd(S\text{-hpro})(en)]^+$	2.70	2.79	5.49	1.6
$[Pd(\beta\text{-ala})(N^1,N^1\text{-Et}_2\text{-}(S)\text{-pn})]^+$	2.65	2.79	5.44	2.6
$[Pd(CH_3CO_2)_2(S\text{-pn})]$ c)	2.60	3.08	5.68	8.5
$[Pd(ox)(S\text{-pn})]$	2.59	2.74	5.33	2.8
$[Pd(mal)(S\text{-pn})]$	2.88	2.83	5.70	−0.9
$[Pd_2(\mu\text{-OH})_2(S\text{-pn})_2]^{2+}$	3.02	2.75	5.77	−4.7
$[Pd(OH_2)_2(S\text{-pn})]^{2+}$ d)	2.53	3.09	5.62	10.0
$[Pd(OH)_2(S\text{-pn})]$ e)	2.94	2.97	5.91	0.5
$[Pd(ox)(N^1,N^1\text{-Et}_2\text{-}(S)\text{-pn})]$	2.96	2.63	5.59	−5.9
$[Pd(CH_3CO_2)_2(S\text{-ala})]^-$ c)	2.43	2.99	5.43	10.3
$[Pd(mal)(S\text{-ala})]^-$	2.91	2.98	5.89	1.2

a) $\varepsilon=\varepsilon_{max}/2$ for $\sigma=\sigma_{max}-\Delta\sigma^-$ and for $\sigma=\sigma_{max}+\Delta\sigma^+$; and $\Delta\sigma_{1/2}=\Delta\sigma^-+\Delta\sigma^+$. b) unsymmetry parameter$=\{(\Delta\sigma^+-\Delta\sigma^-)/\Delta\sigma_{1/2}\}\times100$. c) In 0.50 M CH_3CO_2Na. d) $[Pd_2(\mu\text{-OH})_2(S\text{-pn})_2](ClO_4)_2$ in 0.01 M $HClO_4$. e) $[Pd_2(\mu\text{-OH})_2(S\text{-pn})_2](ClO_4)_2$ in 0.01 M NaOH.

Table 6. Absorption data a) of $[Pd(N)_3(O)]$-type complexes ($[Pd(L_1)(L_2)]ClO_4$)

$(L_1)(L_2)$	$\sigma_{max}/10^3$ cm^{-1} (ε/mol^{-1} dm^3 cm^{-1})		
	Spin-forbidden d-d	Spin-allowed d-d	Charge transfer
(gly)(*S*-pn)	26.2 sh (18)	32.75 (270)	
(β-ala)(*S*-pn) b)	26.0 sh (16)	32.48 (415)	51.28 (21200)
(*S*-ala)(en)	26.4 sh (18)	32.89 (283)	
(*S*-ala)(*S*-pn)	26.4 sh (18)	32.91 (308)	
(*S*-ala)(tn) c)	26.4 sh (22)	32.55 (384)	50.45 (23200)
(*S*-pro)(en)	26.6 sh (24)	32.96 (292)	51.18 (23400)
(*S*-pro)(*S*-pn)	26.6 sh (25)	32.98 (299)	51.18 (23900)
(*S*-ser)(en)	26.4 sh (19)	32.79 (280)	
(*S*-leu)(en)	26.4 sh (19)	32.88 (289)	
(*S*-hpro)(en)	26.6 sh (23)	32.91 (291)	51.28 (22100)
(β-ala)(N^1,N^1-Et$_2$-(*S*)-pn)	26.0 sh (40)	32.05 (609)	49.14 (18000)
(N,N-Me$_2$gly)(N^1,N^1-Et$_2$-(*S*)-pn)	26.0 sh (37)	32.55 (516)	44.5 sh (14400) 48.60 (17500)

a) sh: Shoulder (ε is for the value σ given). b) Hemihydrate. c) Monohydrate.

ligand exhibited no such splitting (Fig. 5). Therefore, the splitting seems to be concerned with the structure that two dialkylamino groups occupy the trans sites. However, none of the complexes showed any splitting of the spin-allowed d-d band unlike the *trans*-$[Pd(Cl)_2(N)_2]$-type complexes.[2] The CD intensity of $[Pd(N,N\text{-}Et_2en)(N^1,N^1\text{-}Et_2\text{-}(S)\text{-pn})]^{2+}$ is smaller than a half of that of $[Pd(N^1,N^1\text{-}Et_2\text{-}(S)\text{-pn})_2]^{2+}$, additivity not holding (Fig. 7). This fact can be explained by supposing some difference between the ligand-ligand interactions of the two complexes. The explanation is also applicable to the significantly different CD curves of the *N,N*-Et_2en and the *N,N*-Me_2en complex.

2) [Pd(N)$_3$(O)]-type Complexes: The absorption and CD spectra are shown in Figs. 8—10 and the numerical data in Tables 6 and 7. It is noteworthy that the CD patterns of the complexes with *S*-pn or N^1,N^1-Et_2-(*S*)-pn are very similar to those of the corresponding [Pd(N)$_4$]-type complexes. Namely, the CD patterns of $[Pd(gly)(S\text{-pn})]^+$ and $[Pd(\beta\text{-ala})(S\text{-pn})]^+$ are similar to those of $[Pd(en)(S\text{-pn})]^{2+}$and $[Pd(tn)(S\text{-pn})]^{2+}$, respectively, and those of $[Pd(\beta\text{-ala})(N^1,N^1\text{-}Et_2\text{-}(S)\text{-pn})]^+$ and $[Pd(N,N\text{-}Me_2gly)(N^1,N^1\text{-}Et_2\text{-}(S)\text{-pn})]^+$ to those of $[Pd(tn)(N^1,N^1\text{-}Et_2\text{-}(S)\text{-pn})]^{2+}$ and $[Pd(N,N\text{-}Me_2en)(N^1,N^1\text{-}Et_2\text{-}(S)\text{-pn})]^{2+}$, respectively. The intensity of the main CD band (in the spin-allowed d-d region) for the [Pd(N)$_3$(O)]-type complexes was *ca.* 60—80% comparing with the corresponding [Pd(N)$_4$]-type complexes. Thus, two types of complexes seem to possess much the same electronic structure, but their CD intensities are influenced not only by the kind of the coordinating atoms but also by the chelate ring size and the con-

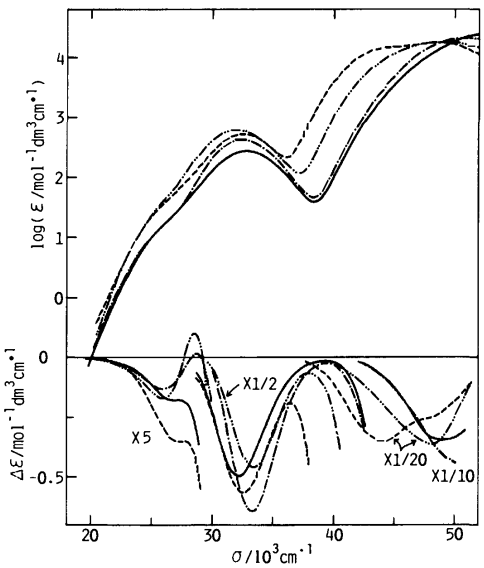

Fig. 8. Absorption and CD spectra of $[Pd(gly)(S\text{-pn})]ClO_4$ (——), $[Pd(\beta\text{-ala})(S\text{-pn})]ClO_4$ (—·—), $[Pd(\beta\text{-ala})(N^1,N^1\text{-}Et_2\text{-}(S)\text{-pn})]ClO_4$ (—··—), and $[Pd(N,N\text{-}Me_2gly)(N^1,N^1\text{-}Et_2\text{-}(S)\text{-pn})]ClO_4$ (----); the first two complexes being in the isomer equilibrium.

TABLE 7. CD DATA[a] OF [Pd(N)$_3$(O)]-TYPE COMPLEXES ($[Pd(L_1)(L_2)]ClO_4$)[b]

$(L_1)(L_2)$	$\sigma_{ext}/10^3$ cm^{-1} ($\Delta\varepsilon$/mol^{-1} dm^3 cm^{-1})		
	Spin-forbidden d-d	Spin-allowed d-d	Charge transfer
(gly)(*S*-pn)	22.5 sh (−0.006) 26.92 (−0.036)	32.20 (−0.50)	48.9 (−3.5)
(β-ala)(*S*-pn)[c]	26.03 (−0.027)	28.72 (+0.003) 33.31 (−0.64)	
(*S*-ala)(en)	21.05 (+0.0007) 25.06 (−0.0061)	30.10 (+0.077) 34.23 (−0.35)	42.44 (+0.16) 48.1 sh (−2.4)
(*S*-ala)(*S*-pn)[c]	22.5 sh (−0.005) 26.32 (−0.034)	28.63 m 33.42 (−0.73)	41.25 (+0.05) 50.51 (−8.4)
(*S*-ala)(tn)	21.74 (+0.0007) 25.92 (−0.0079)	29.57 (+0.017) 34.97 (−0.16)	43.5 (+0.3)
(*S*-pro)(en)	21.1 (−0.0006) 24.7 sh (+0.015)	29.11 (+0.28) 33.52 (−0.30)	46.36 (−2.6)
(*S*-pro)(*S*-pn)[c]	21.83 (−0.0034) 25.28 (−0.0043)	28.82 (+0.23) 32.86 (−0.77)	46.19 (−4.6)
(*S*-ser)(en)	24.34 (−0.0052)	29.69 (+0.093) 33.94 (−0.49)	46.34 (−1.6)
(*S*-leu)(en)	25.19 (−0.010)	28.67 (+0.027) 33.47 (−0.60)	44.84 (−1.2)
(*S*-hpro)(en)	20.51 (−0.0002) 24.7 sh (+0.015)	29.15 (+0.27) 34.25 (−0.20)	46.90 (−2.3)
(β-ala)(N^1,N^1-Et_2-(*S*)-pn)[d]	25.94 (−0.035)	28.56 (+0.021) 33.47 (−0.92)	48.17 (−7.3)
(N,N-Me_2gly)(N^1,N^1-Et_2-(*S*)-pn)	27.25 (−0.070)	32.57 (−0.57)	44.21 (−7.1) 48.0 sh (−5.1)

a) As in Table 4. b) Water of crystallization is omitted (See Table 6). c) In equilibrium (See Fig. 3). d) Immediately after dissolution.

formation of an optically inactive ligand.

The vicinal CD caused by an optically active amino carboxylate ligand possesses a pattern of + and − from lower energy in the spin-allowed d-d region for all the (*S*)-amino carboxylato complexes studied here, but the intensity ratio of the positive to the negative band is diverse (Figs. 9 and 10). The *S*-pro and *S*-hpro complexes exhibited a positive band with a high intensity relative to the other amino carboxylato complexes. This phenomenon is characteristic of the complexes with a coordinated asymmetric *N*-atom.[17,18] Moreover, the CD corresponding to the absorption band at *ca.* $51\times10^3\,cm^{-1}$ also showed different features from those for the other complexes in agreement with the assignment of the band to a Pd←N(σ) CT transition.

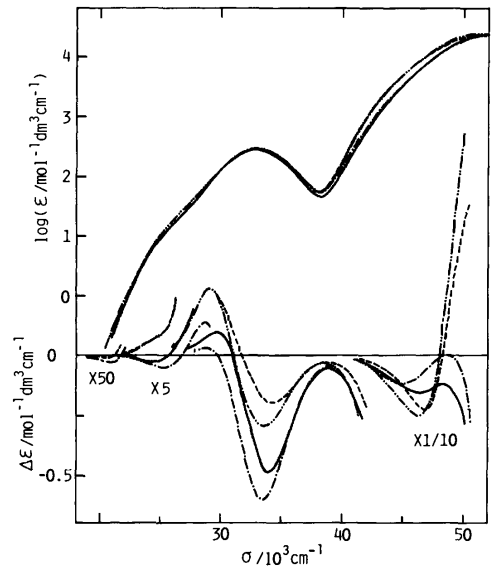

Fig. 9. Absorption and CD spectra of [PdL(en)]-ClO_4. ——: L=*S*-ser, —·—: L=*S*-leu, —··—: L=*S*-pro, and ----: L=*S*-hpro.

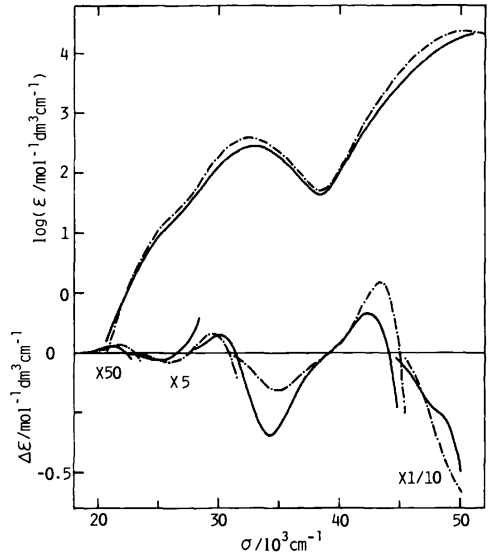

Fig. 10. Absorption and CD spectra of [Pd(*S*-ala)L]-ClO_4. ——: L=en and —·—: L=tn

The pattern of the vicinal CD of the *S*-ala complexes does not depend on the ring size of optically inactive diamine ligands, but the intensity does, particularly in the spin-allowed d-d region (Fig. 10). This situation contrasts with that in the corresponding *S*-pn complexes of $[Pd(N)_4]$-type (Fig. 4). A positive CD band occurring at the lower edge of the Pd←N(σ) CT absorption band is a general characteristic of the palladium(II) complexes containing *S*-ala. Although the corresponding absorption band was observed as a shoulder in $[Pd(S\text{-ala})_2]$,[19] it was hardly detected in the complexes containing only one *S*-ala ligand. The band is assigned to an orbitally-forbidden CT transition rather than a spin-forbidden CT one because the band differs in CD sign from the adjacent allowed CD band.

The additivity of the vicinal CD contributions of *S*-pn and *S*-am was demonstrated with regard to the *S*-ala and *S*-pro complexes (Fig. 11). The almost perfect additivity may be expected since a ligand-ligand interaction is considered to be smaller in these cases than in $[Pd(N^1,N^1\text{-Et}_2\text{-}(S)\text{-pn})(S\text{-pn})]^{2+}$, even for which such an additivity holds. However, it should be noted that the CD data of $[Pd(S\text{-am})(S\text{-pn})]^+$ used in the analysis was taken for an approximately equimolar mixture of the geometrical isomers.

As $[Pd(gly)(S\text{-pn})]^+$ and $[Pd(S\text{-ala})(en)]^+$ are considered to have almost the same electronic energy level scheme, some informations will be obtained about the vicincal effects of *S*-pn and *S*-ala by comparing the CD spectra of the two complexes. We previously de-

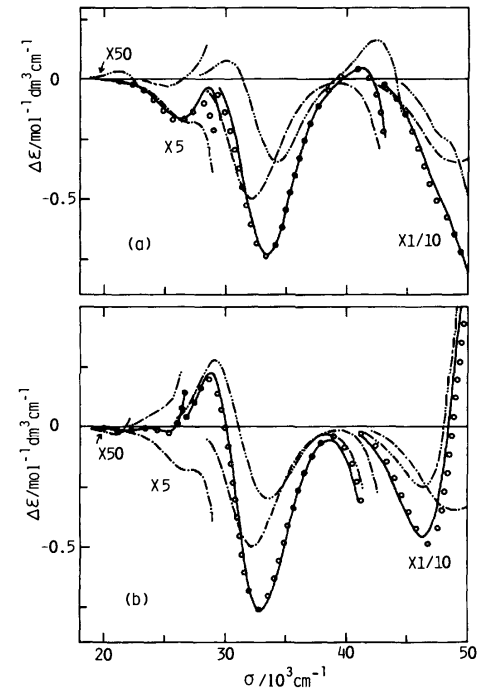

Fig. 11. CD spectra of $[Pd(gly)(S\text{-pn})]ClO_4$ (—·—), $[PdL(en)]ClO_4$ (—··—), and $[PdL(S\text{-pn})]ClO_4$ (——), all in the isomer equilibrium; and CD curves calculated from $[\Delta\varepsilon(\text{—·—})+\Delta\varepsilon(\text{—··—})]$ (oooo). (a) L=*S*-ala and (b) L=*S*-pro.

monstrated with regard to [$PdCl_2$(*S*-pn)] that the main negative CD band in the spin-allowed d-d region was primarily based on the $^1E_g \leftarrow {}^1A_{1g}$ transition, although it included a minor contribution by the $^1B_{1g} \leftarrow {}^1A_{1g}$ transition (D_{4h}).[2] This situation seems to be also the case for the *S*-pn complexes of various types, [Pd(*S*-pn)$(N)_n(O)_{2-n}$] (n=0—2), from an examination of the absorption and CD data (Figs. 4, 8, and 12). On the other hand, the main negative CD band of [Pd(*S*-ala)(en)]$^+$ shows a shift by *ca.* 2×10^3 cm^{-1} to higher energy than that of [Pd(gly)(*S*-pn)]$^+$, although the corresponding absorption band does not (Fig. 11a). Thus, it is reasonable to consider that the vicinal contribution by *S*-ala exhibits a dispersion pattern of + and − from lower energy for the $^1E_g \leftarrow {}^1A_{1g}$ transition (D_{4h}). The CD spectrum of [$Pd(CH_3CO_2)_2$(*S*-ala)]$^-$ supports this deduction (*vide infra*).

3) cis-[Pd(N)$_2$(O)$_2$]-type Complexes: The absorption and CD spectra are shown in Fig. 12 and the numerical data in Tables 8 and 9. The absorption and CD spectra of [$Pd(CH_3CO_2)_2$(*S*-pn)] measured in H_2O are different from those in the aqueous solutions containing acetate ions. It seems that the coordinated acetate ions are released by aquation in H_2O, judging from the similarity of the absorption and CD spectra to those of [$Pd(OH_2)_2$(*S*-pn)]$^{2+}$ (Fig. 1). The enhancement of absorbance around 40×10^3 cm^{-1} in H_2O is ascribable to the di-μ-hydroxo complex formed partly.

The CD pattern in the spin-allowed d-d region is various, depending upon the optically inactive ligands: + and −; − and +; and − for the CH_3CO_2, ox, and mal complexes, respectively. The complexes containing monodentate ligands exhibit a positive CD band in the lower energy side of the main negative CD band. This situation differs from that found in the [$Pd(N)_4$]- and [$Pd(N)_3(O)$]-type complexes. The ox complex exhibits a positive CD band in the higher energy side of the main negative CD one, being unique in the series of *S*-pn complexes. It is reasonable to assign the CD band to the $^1B_{1g} \leftarrow {}^1A_{1g}$ transition (D_{4h}) from its position and low intensity. If this is true, it is a very unique example that the CD band for the transition was observed definitely. Although the corresponding band did not appear in [Pd(ox)(N^1,N^1-Et_2-(*S*)-pn)], the CD features are very similar to those of [Pd(ox)(*S*-pn)] in the spin-allowed d-d region, particularly in the width of the main band. Thus it is likely that the CD band of interest is canceled out by the main band.

4) [Pd(N)(O)$_3$]-type Complexes: The absorption and CD spectra are shown in Fig. 13 and the numerical data

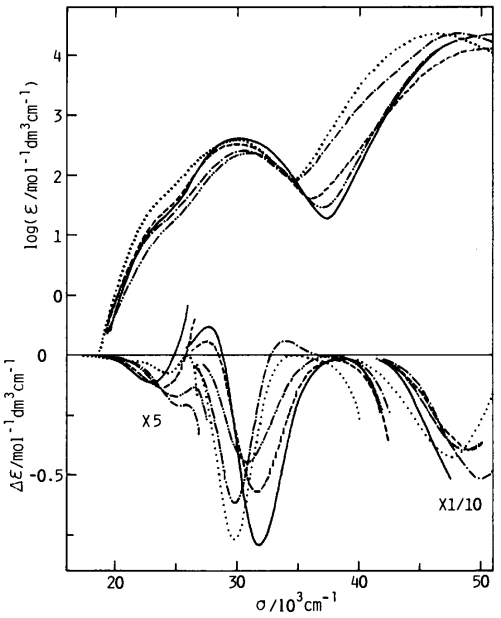

Fig. 12. Absorption and CD spectra of [PdL(*S*-pn)] and [Pd(ox)(N^1,N^1-Et_2-(*S*)-pn)] (·····). L=$(CH_3CO_2)_2$ in 0.50 M CH_3CO_2Na (—·—) and in H_2O (----); L=ox in H_2O (—·—); and L=mal in H_2O (—··—).

TABLE 8. ABSORPTION DATA[a] OF *cis*-[$Pd(N)_2(O)_2$]- AND [$Pd(N)(O)_3$]-TYPE COMPLEXES

Complex	Solvent	$\sigma_{max}/10^3$ cm^{-1} (ε/mol^{-1} dm^3 cm^{-1})		
		Spin-forbidden d-d	Spin-allowed d-d	Charge transfer
[$Pd(CH_3CO_2)_2$(*S*-pn)]	0.50 M CH_3CO_2Na	24.2 sh (23)	30.09 (417)	
[Pd(ox)(*S*-pn)]	H_2O	24.4 sh (20)	30.53 (258)	48.19 (22600)
[Pd(mal)(*S*-pn)]	H_2O	24.8 sh (18)	31.01 (234)	
[$Pd_2(\mu$-$OH)_2$(*S*-pn)$_2$]$(ClO_4)_2$[b,c]	H_2O	24.0 sh (20)	30.47 (299)	45.5 sh (4400)
	0.01 M $HClO_4$	24.4 sh (37)	29.24 (274)	
	0.01 M NaOH	24.0 sh (11)	30.80 (234)	
[$Pd_2(\mu$-$OH)_2$(*S*-pn)$_2$]$(HCO_3)_2$[b,c]	H_2O	24.0 sh (20)	30.21 (332)	45.5 sh (4800)
	0.01 M $HClO_4$	24.4 sh (37)	29.25 (273)	
	0.01 M NaOH	24.0 sh (11)	30.77 (230)	
[$Pd_2(\mu$-$OH)_2$(*S*-pn)$_2$]$(NO_3)_2$[b]	H_2O	24.0 sh (19)	30.50 (300)	51.84 (22800)
[Pd(ox)(N^1,N^1-Et_2-(*S*)-pn)]	H_2O	23.8 sh (43)	29.97 (388)	46.43 (22900)
K[$Pd(CH_3CO_2)_2$(*S*-ala)]	0.05 M CH_3CO_2Na	21.8 sh (17)	27.92 (414)	
K[Pd(mal)(*S*-ala)][d]	H_2O	22.0 sh (9)	28.86 (197)	49.63 (26100)

a) sh: Shoulder (ε is for the value σ given). b) Molar absorption coefficient is based on palladium. c) Another band was observed at *ca.* 39.5×10^3 cm^{-1} as a shoulder. d) Another band was observed at *ca.* 44×10^3 cm^{-1} as a shoulder.

TABLE 9. CD DATA[a] OF *cis*-$[Pd(N)_2(O)_2]$- AND $[Pd(N)(O)_3]$-TYPE COMPLEXES

Complex	Solvent	$\sigma_{ext}/10^3$ cm^{-1} ($\Delta\varepsilon$/mol^{-1} dm^3 cm^{-1})		
		Spin-forbidden d-d	Spin-allowed d-d	Charge transfer
$[Pd(CH_3CO_2)_2(S\text{-pn})]$	0.50 M CH_3CO_2Na	22.94 (−0.024)	27.67 (+0.12) 31.80 (−0.79)	
[Pd(ox)(*S*-pn)]	H_2O	21 sh (−0.005) 25.32 (−0.042)	25.88 m 29.83 (−0.62) 34.01 (+0.06)	50.00 (−5.2)
[Pd(mal)(*S*-pn)]	H_2O	24.93 (−0.035)	26.46 m 30.79 (−0.45)	48.83 (−4.0)
$[Pd_2(\mu\text{-}OH)_2(S\text{-pn})_2](ClO_4)_2$[b]	H_2O	23.98 (−0.032)	26.95 (+0.039) 30.96 (−0.56)	44.5 sh (−0.8)
	0.01 M $HClO_4$	24.45 (−0.033)	27.42 (+0.038) 31.58 (−0.44)	50.76 (−4.7)
	0.01 M NaOH	23.85 (−0.029)	26.11 m 31.21 (−0.56)	
$[Pd_2(\mu\text{-}OH)_2(S\text{-pn})_2](HCO_3)_2$[b]	H_2O	23.91 (−0.031)	26.80 (+0.011) 31.02 (−0.52)	45 sh (−1.1)
	0.01 M $HClO_4$	24.47 (−0.033)	27.43 (+0.032) 31.65 (−0.43)	
	0.01 M NaOH	23.95 (−0.028)	26.18 m 31.30 (−0.55)	
$[Pd_2(\mu\text{-}OH)_2(S\text{-pn})_2](NO_3)_2$[b]	H_2O	24.02 (−0.034)	26.94 (+0.037) 30.96 (−0.56)	44.5 sh (−0.8)
[Pd(ox)(N^1,N^1-Et_2-(*S*)-pn)]	H_2O	21 sh (−0.010) 24.31 (−0.031)	25.93 m 29.80 (−1.54)	47.62 (−8.5)
K[Pd(CH_3CO_2)$_2$(*S*-ala)]	0.05 M CH_3CO_2Na	17.9 (+0.001) 20.88 (−0.0044)	25.91 (+0.081) 27.2 sh (+0.078) 31.31 (−0.14)	39.5 (+0.03)
K[Pd(mal)(*S*-ala)]	H_2O	20.37 (−0.0027)	26.62 (+0.17) 30.61 (−0.27)	39.7 (+0.07) 48.83 (−5.9)

a) As in Table 4. b) $\Delta\varepsilon$ is based on palladium.

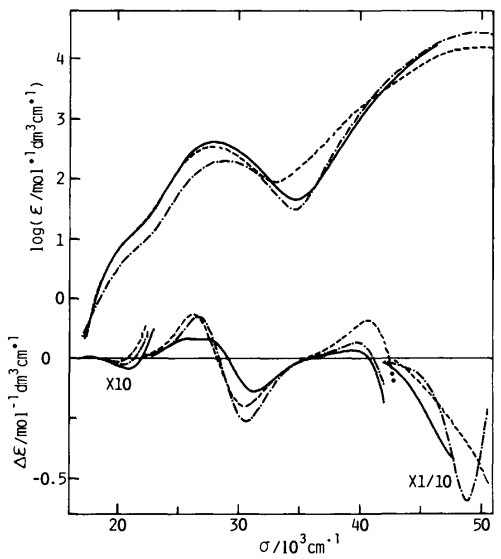

Fig. 13. Absorption and CD spectra of K[PdL(*S*-ala)]. L=$(CH_3CO_2)_2$ in 0.50 M CH_3CO_2Na (——) and in H_2O (----); and L=mal in H_2O (—·—).

in Tables 8 and 9. The K[Pd(CH_3CO_2)$_2$(*S*-ala)] complex aquates in water free from acetate ions similarly to [Pd(CH_3CO_2)$_2$(*S*-pn)]; the band ascribed to the di-μ-hydroxo complex was obviously observed as a shoulder around 40×10^3 cm^{-1}. Both the absorption and CD spectra of the acetato complex were essentially the same in 0.50 and 1.0 M CH_3CO_2Na. The CD spectrum showed a pattern of +, +, and − from lower energy in the spin-allowed d-d region; the lowest-lying positive band is assigned to the $^1A_{2g}\leftarrow{}^1A_{1g}$ transition and the following dispersion is to the $^1E_g\leftarrow{}^1A_{1g}$ one (D_{4h}). Apparently, only one positive band is observed in the other alaninato complexes including the [Pd(*S*-ala)(N)$_2$]-type ones, which is ascribed to the overlapping of the two positive bands. This explanation implies a relatively large separation between the $^1A_{2g}$ and $^1E_g\leftarrow{}^1A_{1g}$ transitions in $[Pd(CH_3CO_2)_2(S\text{-ala})]^-$, being compatible with the large value of unsymmetry parameter (Table 5). Consequently, the vicinal CD caused by *S*-ala ligand is considered to exhibit the definite pattern over the d-d and CT transition region, irrespective of the other ligand coordinated together. Similar CD spectra have been also observed in [Pd(*S*-ala)$_2$] and $[PdCl_2(S\text{-ala})]^-$.[19]

References

1) K. Nakayama, T. Komorita, and Y. Shimura, *Bull. Chem. Soc. Jpn.*, **57**, 972 (1984).
2) K. Nakayama, T. Komorita, and Y. Shimura, *Bull. Chem. Soc. Jpn.*, in press.
3) H. D. K. Drew, F. W. Pinkard, G. H. Preston, and W. Wardlaw, *J. Chem. Soc.*, **1932**, 1895.
4) M. C. Lim, *J. Chem. Soc., Dalton Trans.*, **1977**, 1398; **1978**, 726; *Inorg. Chem.*, **20**, 1377 (1981).

5) F. G. Mann, D. Crowfoot, D. C. Gattiker, and N. Wooster, *J. Chem. Soc.*, **1935**, 1642.
6) T. A. Stephenson, S. M. Morehouse, A. R. Powell, J. P. Heffer, and G. Wilkinson, *J. Chem. Soc.*, **1965**, 3632.
7) For example, F. W. Pinkard, E. Sharratt, W. Wardlaw, and E. G. Cox, *J. Chem. Soc.*, **1934**, 1012; E. W. Wilson, Jr., and R. B. Martin, *Inorg. Chem.*, **9**, 528 (1970); O. Vicol, S. Repede, and V. Lascar, *Bull. Inst. Politeh. Iasi, Sect. 2*, **25**, 17 (1980); O. Yamauchi and A. Odani, *J. Am. Chem. Soc.*, **103**, 391 (1981).
8) E. A. Sullivan, *Can. J. Chem.*, **57**, 62 (1979).
9) H. Ito, J. Fujita, and K. Saito, *Bull. Chem. Soc. Jpn.*, **40**, 2584 (1967).
10) M. Suzuki and Y. Nishida, *Inorg. Chim. Acta*, **34**, 61 (1979).
11) K. Nakayama, T. Komorita, and Y. Shimura, *Bull. Chem. Soc. Jpn.*, **54**, 1056 (1981).
12) M. C. Lim and R. B. Martin, *J. Inorg. Nucl. Chem.*, **38**, 1911 (1976).
13) L. E. Erickson, J. E. Sarneski, and C. N. Reilley, *Inorg. Chem.*, **14**, 3007 (1975); S. Yano, T. Tukuda, M. Saburi, and S. Yoshikawa, *ibid.*, **17**, 2520 (1978); T. Ama and T. Yasui, *Bull. Chem. Soc. Jpn.*, **52**, 79 (1979).
14) INEPT=Insensitive Nuclei Enhanced by Polarization Transfer; G. A. Morris and R. Freeman, *J. Am. Chem. Soc.*, **101**, 760 (1979).
15) It was confirmed by ^{13}C NMR spectra that the crystals formed in the aged solution comprised only one isomer; therefore, the distribution of the isomers in solid state seems to depend on the synthetic method adopted.
16) K. M. Wellman and B. -K. Wong, *J. Chem. Soc., Chem. Commun.*, **1969**, 1213.
17) B. Bosnich and E. A. Sullivan, *Inorg. Chem.*, **14**, 2768 (1975).
18) Y. Nakayama, S. Ooi, and H. Kuroya, *Bull. Chem. Soc. Jpn.*, **52**, 1377 (1979).
19) K. Nakayama, T. Komorita, and Y. Shimura, unpublished work.

Kinetics and Mechanism of Complex Formation of Nickel(II) with 1-(2-Pyridylazo)-2-naphthol in Acetic Acid[1)]

Akiharu HIOKI, Shigenobu FUNAHASHI, and Motoharu TANAKA*
Laboratory of Analytical Chemistry, Faculty of Science, Nagoya University, Chikusa-ku, Nagoya 464
(Received December 15, 1983)

The complex formation reactions of nickel(II) nitrate, nickel(II) acetate, and nickel(II) chloride with 1-(2-pyridylazo)-2-naphthol (PAN) in acetic acid (HOAc) to form the 1:1 nickel(II)–PAN complex have been studied kinetically by using a stopped-flow technique. The second-order rate constants and activation parameters at 25 °C are $k=(1.4\pm0.1)\times10^4$ mol^{-1} kg s^{-1}, $\Delta H^*=51.2\pm1$ kJ mol^{-1}, $\Delta S^*=6.4\pm4$ J mol^{-1} K^{-1}, and $\Delta V^*=23.4\pm2.4$ cm^3 mol^{-1} for $Ni(NO_3)_2$, $k=(1.1\pm0.1)\times10^4$ mol^{-1} kg s,$^{-1}$, $\Delta H^*=49.5\pm1$ kJ mol^{-1}, $\Delta S^*=-1.3\pm4$ J mol^{-1} K^{-1}, and $\Delta V^*=15.5\pm2.6$ cm^3 mol^{-1} for $Ni(OAc)_2$, and $k=(4.8\pm0.1)\times10^4$ mol^{-1} kg s^{-1}, $\Delta H^*=51.4\pm1$ kJ mol^{-1}, $\Delta S^*=17.0\pm4$ J mol^{-1} K^{-1}, and $\Delta V^*=35.4\pm5.5$ cm^3 mol^{-1} for $NiCl_2$. The positive value of ΔV^* strongly suggests a dissociative mode of activation.

Kinetics of the complexation of nickel(II) ion has been studied extensively in aqueous solution and it has proved that the reactions proceed *via* the Eigen mechanism.[2-4)] On the other hand, studies in nonaqueous solvents are not numerous.[5-7)] Acetic acid has been utilized as a useful solvent in the titration of weak bases since Conant and Hall,[8)] and the acid-base equilibria in this solvent have been studied first by Kolthoff and Bruckenstein,[9a)] and later by Tanaka and Nakagawa.[9b)] There are not many studies on the complex formation of metal ions in acetic acid.[10)] We have recently reported the solvent-exchange rate on copper(II) acetate[11)] and manganese(II) perchlorate[12)] in acetic acid.

In this paper we describe the rates of reactions of nickel(II) species ($Ni(NO_3)_2$, $Ni(OAc)_2$, and $NiCl_2$) with 1-(2-pyridylazo)-2-naphthol (PAN or Hpan) in acetic acid. This is the first kinetic study on complex formation of a simple metal ion with an acyclic ligand in acetic acid.[13)]

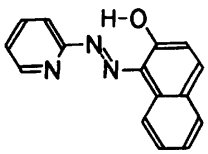

PAN or Hpan

Experimental

Reagents. In order to keep the reaction medium as dry as possible, extreme care was taken in the purification and preparation of all reagents and compounds. All reagents and solutions were stored in a glove box or a desiccator.

Acetic Acid: The purification of acetic acid was described previously.[14)] The water content of acetic acid and acetic acid solutions was confirmed to be less than 5×10^{-3} mol kg^{-1} by the Karl-Fisher titration.

PAN: PAN (Dojindo Laboratories, Kumamoto) was purified by sublimation.

Nickel(II) Salts: Hydrated nickel(II) nitrate (reagent grade) was recrystallized from distilled water. The hydrate was dissolved in acetic acid containing a small amount of nitric acid. Acetic anhydride equivalent to the water involved was added to the nickel(II) nitrate solution. Anhydrous nickel(II) nitrate precipitates. The precipitate was washed with acetic anhydride and then with acetic acid. This compound is formulated as $Ni(NO_3)_2\cdot6HOAc$.[15)] The crystals of nickel(II) acetate and nickel(II) chloride were prepared similarly and solvated salts may be formulated as $Ni(OAc)_2\cdot4HOAc$ and $NiCl_2\cdot4HOAc$. Each nickel solution was prepared by dissolving these crystals in acetic acid.

Lithium Salts: Reagent grade lithium perchlorate, lithium nitrate, and lithium chloride were recrystallized from distilled water and dried at 170, 130 and 120 °C respectively. Perchloric acid solution and lithium acetate were prepared by the methods described previously.[10)]

Measurements. A highly sensitive spectrophotometer (SM 401, Union Giken Co. Ltd., Osaka) and a Carl Zeiss spectrophotometer (Model PMQ II) were used for the measurements of absorption spectra. Reaction rates at atmospheric pressure were measured by means of a highly sensitive stopped-flow spectrophotometer.[10,16)] The temperature of the reaction cell was maintained to within ±0.1 °C. At high-pressures up to 55 MPa the reactions were followed by using a high-pressure stopped-flow apparatus.[17)] At 25 °C acetic acid freezes at 55 Mpa.

Equilibria in Acetic Acid. In acetic acid almost all substances exist as the non-dissociating form because of its low dielectric constant ($\varepsilon=6.18$ at 20 °C).[18)] Thus it is important to consider separately the ionization and dissociation. Overall dissociation of AB is expressed by Eq. 1.

$$AB \overset{K_i}{\rightleftharpoons} A^+B^- \overset{K_d}{\rightleftharpoons} A^+ + B^- \quad (1)$$

An overall dissociation constant K_D is defined by Eq. 2.

$$K_D = \frac{[A^+][B^-]}{[AB]+[A^+B^-]} = \frac{K_iK_d}{1+K_i}, \quad (2)$$

where K_i is an ionization constant and K_d is a dissociation constant.[9a)] Available values of K_D are $10^{-12.53}$ for H_2O,[19)] $10^{-10.1}$ for HNO_3,[20)] $10^{-8.55}$ for HCl,[9a)] $10^{-5.87}$ for $HClO_4$,[21)] $10^{-6.79}$ for LiOAc,[21,22)] $10^{-7.1}$ for LiCl,[21,23)] $10^{-5.80}$ for $LiClO_4$,[24)] and $10^{-7.63}$ for $Ni(OAc)_2$ ($Ni(OAc)_2\rightleftharpoons NiOAc^+ + OAc^-$).[25)] K_d can be calculated by an equation of the type derived by Fuoss and Kraus for ion-pair formation,[26)] at least to a correct order of magnitude. The K_d value is estimated to be about 10^{-6} mol dm^{-3} for all of these 1:1 electrolytes. Then values of K_i are estimated to be $10^{-6.5}$ (H_2O), $10^{-4.1}$ (HNO_3), $10^{-2.5}$ (HCl), $10^{-0.7}$ (LiOAc), $10^{-1.1}$ (LiCl), and $10^{-1.6}$ ($Ni(OAc)_2$).

From the K_i value of $Ni(OAc)_2$, it may be concluded that two OAc^- ions in $Ni(OAc)_2$ exist in the first coordination sphere of nickel(II). Since the Edwards E_n value[27)] (the electron-donating property) of chloride ion (1.24) is similar to that of

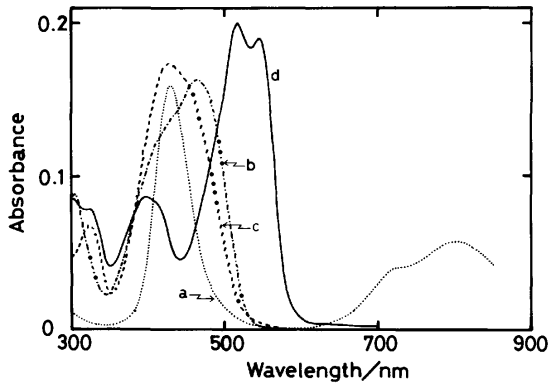

Fig. 1. Absorption spectra of nickel(II) chloride, the acid and base forms of PAN, and the nickel(II)-PAN complex in acetic acid.
a: $[NiCl_2]=1.12\times10^{-2}$ mol kg^{-1}; b: $[PAN]=9.43\times10^{-6}$ mol kg^{-1}; c: $[PAN]=9.43\times10^{-6}$ mol kg^{-1}, $[HClO_4]=5.5\times10^{-5}$ mol kg^{-1}; d: $[PAN]=9.43\times10^{-6}$ mol kg^{-1}, $[Ni(OAc)_2]=2.02\times10^{-4}$ mol kg^{-1}.

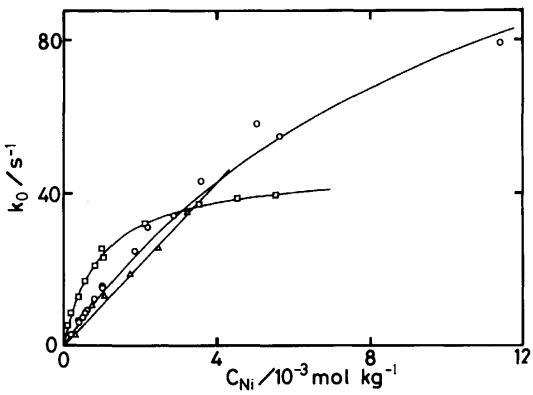

Fig. 2. Conditional first-order rate constant k_0 as a function of the nickel(II) concentration C_{Ni}.
○: $Ni(NO_3)_2$; △: $Ni(OAc)_2$; □: $NiCl_2$.
Each point is an average of several determinations. The solid curves are calculated with the constants obtained.

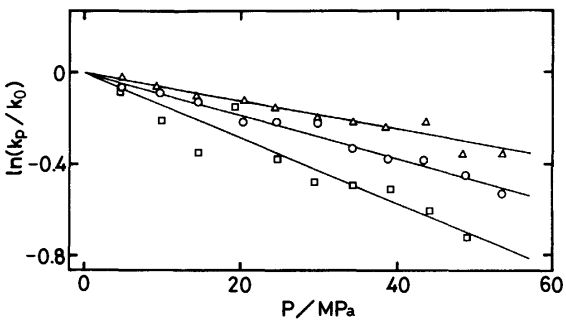

Fig. 3. Pressure dependence of ln k at 25.0 °C.
○: $Ni(NO_3)_2$; △: $Ni(OAc)_2$; □: $NiCl_2$.
Each point is an average of several determinations. The straight lines are calculated by using the ΔV^* values in Table 2.

acetate ion (0.95), two chloride ions in $NiCl_2$ are thought also to be in the first coordination sphere of nickel(II). The absorption spectra of nickel(II) nitrate, acetate, and chloride in acetic acid show their typical octahedral geometry (see Fig. 1-a for $NiCl_2$).[28] The molar absorption coefficients of nickel(II) solutions are independent of concentration of nickel(II) salts. The complexation rate of $Ni(NO_3)_2$ does not change even in the presence of HNO_3 up to 10^{-3} mol kg^{-1} (*vide infra*). These facts are consistent with solvolysis of nickel(II) salts not occurring in acetic acid.

The addition of perchloric acid (the strongest acid) to an acetic acid solution of PAN changes PAN to its acid form (see Fig. 1), protonated at nitrogen of the pyridyl group of PAN, while the addition of lithium acetate, the strongest base, causes little change in the absorption spectrum. From the change of the spectra the mole fraction of ionized PAN ([HpanH$^+$OAc$^-$]+[HpanH$^+$])/[Hpan] is estimated to be about 0.05 at most. Thus PAN exists practically as the base

$$\text{Hpan} + \text{HOAc} \rightleftharpoons \text{HpanH}^+\text{OAc}^- \rightleftharpoons \text{HpanH}^+ + \text{OAc}^- \quad (3)$$

form (Hpan) in acetic acid.

Absorption spectrum was measured for mixtures of the 2×10^{-5} mol kg^{-1} PAN solution with the 2×10^{-5} to 2×10^{-3} mol kg^{-1} nickel(II) solution. At the nickel(II) concentration higher than 2×10^{-4} mol kg^{-1}, the complexation of PAN is quantitative and the reverse reaction can be neglected. The reaction system is expressed by Eq. 4.

$$\text{Hpan} + NiX_2 \longrightarrow \text{Ni(pan)X} + \text{HX}, \quad (4)$$

where X^- is NO_3^-, OAc^-, or Cl^-. The spectrum of the 1:1 nickel(II)-PAN complex is shown in Fig. 1-d. The pan$^-$ ion is a tridentate ligand. The 1:1 nickel(II)-PAN complex tends to decompose slowly with half-life of several hours.

Results and Discussion

Kinetic measurements were carried out at 516, 544, and 554 nm for $Ni(NO_3)_2$, at 516 nm and 544 nm for $Ni(OAc)_2$, and 516 nm and 540 nm for $NiCl_2$ in large excess nickel concentration over PAN. The change in absorbance at each wavelength as a function of reaction time was satisfactorily fitted to the pseudo-first-order rate law. A conditional first-order rate constant k_0 involving the nickel(II) concentration was obtained by the relation: $\ln(A_\infty-A_t)=\ln(A_\infty-A_0)-k_0t$, where A_0, A_t, and A_∞ denote the absorbances at initial time, at time t, and at infinite time, respectively.

The rate of formation of the 1:1 nickel(II)-PAN complex is first order with respect to PAN. Conditional first-order rate constants under various conditions are summarized in Table 1. The plots of k_0 against the nickel(II) concentration are given in Fig. 2. The effect of water in acetic acid on k_0 was checked by the addition of various amounts of water up to 6×10^{-2} mol kg^{-1}. Though k_0 decreases slightly with increasing water concentration, the presence of water up to 5×10^{-3} mol kg^{-1} does not affect the rate. At lower concentrations of the nickel(II) the data show a linear relationship through the origin and then $k_0=kC_{Ni}$, where k is a second-order rate constant and C_{Ni} is a total concentration of nickel(II). At higher C_{Ni} the data deviate from the straight line. This deviation will be considered later in detail.

The activation parameters obtained from the temperature dependence of k (17.0—35.0 °C), *i.e.* the Eyring plot, are tabulated in Table 2. By the transition state

theory, the relation between k and pressure P is given as $(\partial \ln k/\partial P)_T=-\Delta V^{\neq}/RT$. As apparent from Fig. 3, the rate constant varies linearly with pressure: the activation volume, $\Delta V^{\neq}$, is independent of pressure. The values of $\Delta V^{\neq}$ are also summarized in Table 2.

Since the reactions of $Ni(NO_3)_2$ and $NiCl_2$ with PAN produce HNO_3 and HCl, respectively, the effect of these acids on the reaction rate was examined. When these acids are added to the acetic acid solution of PAN, PAN changes into an acid form. From the change of the absorption spectra, the equilibrium constants of Eq. 5, $K_{PAN\text{-}HX}$, were calculated to be 4.3×10^2 mol^{-1} kg for HNO_3 and 4.2×10^4 mol^{-1} kg for HCl.

$$Hpan + HX \overset{K_{PAN\cdot HX}}{\rightleftharpoons} HpanH^+X^- \quad (5)$$

Moreover under conditions where $[Ni(NO_3)_2]=2.04\times10^{-3}$ mol kg^{-1} and $[PAN]=1.15\times10^{-5}$ mol kg^{-1}, the presence of 100-fold excess of HNO_3 over [PAN] did not affect the reaction rate as expected from the $K_{PAN\text{-}HNO_3}$ value. Under conditions where $[NiCl_2]=2.60\times10^{-4}$ mol kg^{-1} and $[PAN]=1.15\times10^{-5}$ mol kg^{-1}, the addition of HCl twice as much as PAN decreased the reaction rate by *ca.* 6%. After all the reaction rate is not affected by HNO_3 or HCl generated by the complexation.

The addition of various amounts of lithium perchlorate and lithium acetate to a PAN solution resulted in the change in the spectra with an isosbestic point at 456 nm. The reaction corresponds to equilibrium 6.

$$Hpan + Li^+ClO_4^- + HOAc \rightleftharpoons HpanH^+ClO_4^- + LiOAc \quad (6)$$

Table 1. Conditional first-order rate constants for the reaction of nickel(II) with PAN

T / °C	[PAN]$\times10^5$ / mol kg^{-1}	$C_{Ni}\times10^4$ / mol kg^{-1}	k_0 [a] / s^{-1}		T / °C	[PAN]$\times10^5$ / mol kg^{-1}	$C_{Ni}\times10^4$ / mol kg^{-1}	k_0 [a] / s^{-1}	
		$Ni(NO_3)_2$			20.0	4.46	7.47	7.57±0.08	(4)
25.0	4.31	5.65	8.34±0.21	(5)	25.0	4.46	7.47	10.6 ±0.2	(7)
25.0	4.31	28.4	34.2 ±0.3	(9)	30.0	4.46	7.47	15.5 ±0.1	(6)
25.0	4.31	56.5	55.0 ±0.7	(8)	35.0	4.46	7.47	20.7 ±0.3	(6)
25.0	4.31	114	79.3 ±1.4	(5)			$NiCl_2$		
25.0	4.31	199	103 ±2	(5)	17.0	0.983	1.98	4.46±0.11	(3)
25.0	4.31	338	121 ±1	(10)	17.0	0.983	4.02	6.40±0.03	(3)
25.0	0.986	2.03	2.96	(1)	17.0	4.27	10.0	12.7 ±0.2	(4)
25.0	0.986	4.05	6.16±0.03	(3)	17.0	4.27	35.5	17.9 ±0.3	(4)
25.0	0.986	5.08	7.56±0.11	(4)	17.0	4.27	55.4	19.2 ±0.3	(4)
25.0	0.986	6.11	9.24±0.13	(4)	25.0	0.971	0.989	5.25±0.08	(6)
25.0	0.986	8.14	12.1 ±0.2	(5)	25.0	0.971	1.92	8.62±0.25	(7)
25.0	0.986	10.2	14.9 ±0.1	(5)	25.0	0.971	3.96	12.6 ±0.3	(6)
25.0	4.30	4.03	6.46±0.13	(5)	25.0	0.971	5.59	16.9 ±0.1	(6)
25.0	4.30	10.1	15.5 ±0.1	(9)	25.0	0.971	8.20	21.0 ±0.5	(6)
25.0	4.30	22.0	31.1 ±0.5	(8)	25.0	0.971	10.4	23.0 ±0.7	(7)
25.0	4.30	35.8	43.1 ±0.8	(5)	25.0	4.27	9.96	25.4 ±0.3	(3)
25.0	4.30	50.5	58.1 ±0.4	(4)	25.0	4.27	35.4	37.3 ±0.6	(3)
17.0	4.44	18.6	13.0 ±0.2	(7)	25.0	4.27	45.5	38.8 ±0.4	(4)
20.0	4.44	18.6	17.0 ±0.2	(8)	25.0	4.27	55.4	39.6 ±0.2	(4)
25.0	4.44	18.6	24.8 ±0.4	(5)	30.0	0.983	1.98	12.5 ±0.2	(4)
30.0	4.44	18.6	35.0 ±0.4	(7)	30.0	0.983	4.02	20.0 ±0.7	(4)
35.0	4.44	18.6	47.8 ±0.4	(6)	30.0	4.27	10.0	35.3 ±0.4	(5)
		$Ni(OAc)_2$			30.0	4.27	35.5	56.9 ±0.6	(5)
25.0	0.990	2.88	2.78±0.08	(4)	30.0	4.27	55.4	62.1 ±0.4	(5)
25.0	4.31	10.8	12.9 ±0.2	(5)	35.0	0.983	1.98	18.5 ±0.2	(3)
25.0	4.31	17.4	18.7 ±0.6	(5)	35.0	0.983	4.02	29.8 ±0.6	(2)
25.0	4.31	24.8	25.6 ±0.9	(5)	35.0	4.27	10.0	51.3 ±0.7	(4)
25.0	4.31	32.3	35.0 ±0.4	(5)	35.0	4.27	35.5	91.6 ±0.4	(4)
17.0	4.46	7.47	5.94±0.09	(6)	35.0	4.27	55.4	93.5 ±1.6	(4)

a) Figures in parentheses (the last column) indicate the number of runs, and ± indicates the standard deviation.

Table 2. Activation parameters for the complex formation of nickel(II) with PAN in acetic acid

Reaction	k(25 °C) / mol^{-1} kg s^{-1}	$\Delta H^{\neq}$ / kJ mol^{-1}	$\Delta S^{\neq}$ / J mol^{-1} K^{-1}	$\Delta V^{\neq}$ / cm^3 mol^{-1}
$Ni(NO_3)_2$+PAN	$(1.4\pm0.1)\times10^4$	51.2±1	6.4±4	23.4±2.4
$Ni(OAc)_2$+PAN	$(1.1\pm0.1)\times10^4$	49.5±1	−1.3±4	15.5±2.6
$NiCl_2$+PAN	$(4.8\pm0.1)\times10^4$	51.4±1	17.0±4	35.4±5.5

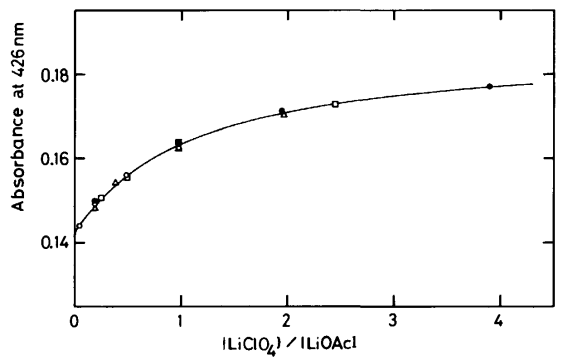

Fig. 4. Effect of lithium acetate and lithium perchlorate on spectra of PAN.
[PAN] = 1.53×10^{-5} mol kg^{-1}, [$LiClO_4$]/mol kg^{-1} = 1.59×10^{-4} (○); 3.17×10^{-4} (△); 7.90×10^{-4} (□); 3.16×10^{-3} (●).

Taking into consideration the ionization of PAN shown by Eq. 3, the equilibrium constant for Eq. 6 was determined to be [HpanH$^+$$ClO_4^-$][LiOAc][Hpan]$^{-1}$×[Li$^+$$ClO_4^-$]$^{-1}$=0.91±0.03 by analyzing the change in absorbance at 426 nm (see Fig. 4). The similar phenomena have been reported previously.[29,30]

As apparent from Fig. 2, the plots for nickel(II) nitrate and nickel(II) chloride deviate from the straight line with increasing nickel(II) concentration. The deviation is thought to be due to a fast equilibrium in which PAN interacts with nickel(II) species to form a nonreactive species. The nonreactive species of PAN seems to be a quadrupole ion-pair of the acid form of PAN, similar to the species that Bruckenstein and Kolthoff have shown for Methyl Yellow.[31] It is reasonable that the extent of the deviation, *i.e.*, the ion-pair formation, parallels the ionization constants K_{PAN-HX} for HOAc,[32] HNO_3, and HCl. The conditional first-order rate constant is given by the relation: $k_0 = kC_{Ni}/(1+KC_{Ni})$, where K is a formation constant of a nonreactive ion-pair. The value of K for $Ni(NO_3)_2$ is 92 mol^{-1} kg at 25.0 °C and those for $NiCl_2$ are 1206, 1007, 927, and 842 mol^{-1} kg at 17.0, 25.0, 30.0, and 35.0 °C, respectively.

The reactivity of nickel(II) chloride is higher than the hexasolvento nickel(II) involved in the nitrate. This is just as expected from the following equation:[33]

$$\log k_{ML}^{-S} = \log k_M^{-S} + \gamma E(L), \quad (7)$$

where k_{ML}^{-S} and k_M^{-S} denote the rate constants of solvent exchange at ML and M, respectively, E(L) the electron donating ability of L, and γ a constant characteristic of the metal ion M.

As stated earlier, the electron donating ability (E_n) of chloride (1.24) is not much different from that of acetate (0.95). Although a similar enhancement of reactivity is expected for nickel acetate, nickel acetate is the least reactive among these three nickel species. This may be due to the coordination of acetate with nickel as a hydrogen bridged dimer bidentate as follows:[34]

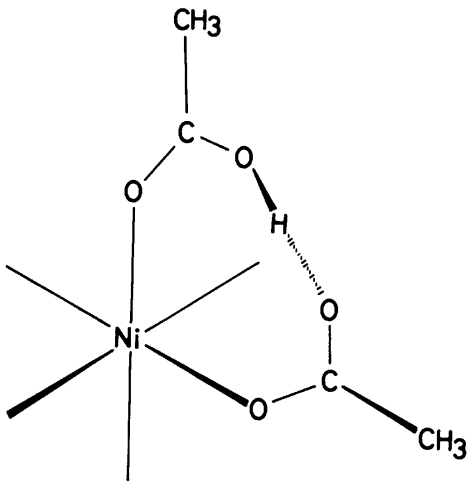

Therefore the reactivity of the acetate is anticipated to be less than expected from its E_n value: we observe hardly the bound ligand effect for the acetate in its complexation in acetic acid. The E_n value for acetate (0.95) is not for the dimeric acetate but for the simple acetate.

The values of activation enthalpy are much the same for the present three systems (see Table 2). The parallel relation between ΔV^* and ΔS^* is observed. Since the activation volumes are positive and considerably large, these reactions are concluded to proceed via a dissociative-interchange mechanism. The dissociative character increases in the order: acetate<nitrate<chloride.

References

1) Metal Complexes in Acetic Acid. 6. Part 5, see Ref. 12.
2) R. G. Wilkins, "The Study of Kinetics and Mechanism of Reactions of Transition Metal Complexes," Allyn and Bacon, Boston (1974).
3) A. E. Martell, "Coordination Chemistry," American Chemical Society, Washington, D. C. (1978), Vol. 2.
4) J. Burgess, "Metal Ions in Solution," Ellis Horwood, New York (1978).
5) P. K. Chattopadhyay and B. Kratochvil, *Can. J. Chem.*, **54**, 2540 (1976).
6) K. Ishihara, S. Funahashi, and M. Tanaka, *Inorg. Chem.*, **22**, 2564 (1983).
7) H. P. Bennetto and Z. S. Imani, *J. Chem. Soc., Faraday Trans. 1*, **71**, 1143 (1975), and references therein.
8) a) N. F, Hall and J. B. Conant, *J. Am. Chem. Soc.*, **49**, 3047 (1927); b) J. B. Conant and N. F. Hall, *ibid.*, **49**, 3062 (1927).
9) a) I. M. Kolthoff and S. Bruckenstein, *J. Am. Chem. Soc.*, **78**, 1 (1956); b) M. Tanaka and G. Nakagawa, *Anal. Chim. Acta*, **33**, 543 (1965).
10) S. Funahashi, T. Nishimoto, P. Banerjee, K. Sawada, and M. Tanaka, *Bull. Chem. Soc. Jpn.*, **53**, 1555 (1980), and references therein.
11) S. Funahashi, T. Nishimoto, A. Hioki, and M. Tanaka, *Inorg. Chem.*, **20**, 2648 (1981).
12) A. Hioki, S. Funahashi, and M. Tanaka, *Inorg. Chem.*, **22**, 749 (1983).
13) a) S. Funahashi, K. Saito, and M. Tanaka, *Bull. Chem. Soc. Jpn.*, **54**, 2695 (1981); b) A. Hioki, S. Funahashi, and M. Tanaka, *Inorg. Chim. Acta*, **76**, L151(1983).

14) K. Sawada, H. Ohtaki, and M. Tanaka, *J. Inorg. Nucl. Chem.*, **34**, 625 (1972).
15) P. W. N. M. van Leeuwen and W. L. Groeneveld, *Recl. Trav. Chim. Pays-Bas*, **87**, 86 (1968).
16) M. Tanaka, S. Funahashi, and T. Nagamura, Paper No. 63, Abstracts of 1977 Pittsburgh Conference on Analytical Chemistry and Applied Spectroscopy.
17) K. Ishihara, S. Funahashi, and M. Tanaka, *Rev. Sci. Instrum.*, **53**, 1231 (1982).
18) W. Dannhauser and R. H. Cole, *J. Am. Chem. Soc.*, **74**, 6105 (1952).
19) S. Bruckenstein and I. M. Kolthoff, *J. Am. Chem. Soc.*, **79**, 5915 (1957).
20) W. Poscham and A. Engelbrecht, *Z. Phys. Chem. (Leipzig)*, **248**, 177 (1971).
21) S. Bruckenstein and I. M. Kolthoff, *J. Am. Chem. Soc.*, **78**, 2974 (1956).
22) O. W. Kolling and H. E. Gracey, *Inorg. Chem.*, **11**, 2556 (1972).
23) T. L. Smith and J. H. Elliott, *J. Am. Chem. Soc.*, **75**, 3566 (1953).
24) S. Winstein, P. E. Klinedinst, Jr., and G. C. Robinson, *J. Am. Chem., Soc.*, **83**, 885 (1961).
25) O. W. Kolling and J. L. Lambert, *Inorg. Chem.*, **3**, 202 (1964).
26) R. M. Fuoss and C. A. Kraus, *J. Am. Chem. Soc.*, **55**, 1019 (1933).
27) J. O. Edwards, *J. Am. Chem. Soc.*, **76**, 1540 (1954).
28) A. B. P. Lever, "Inorganic Electronic Spectroscopy," Elsevier, New York (1968); pp. 333—349.
29) T. Higuchi, J. A. Feldman, and C. R. Rehm, *Anal. Chem.*, **28**, 1120 (1956).
30) I. M. Kolthoff and S. Bruckenstein, "Treatise on Analytical Chemistry," ed by I. M. Kolthoff and P. J. Elving, Interscience Encyclopedia, New York (1959), Part I, Vol. I, pp. 511—518.
31) S. Bruckenstein and I. M. Kolthoff, *J. Am. Chem. Soc.*, **78**, 10 (1956).
32) $K_{PAN\text{-}HX}$ for HOAc, the mole fraction of ionized PAN in acetic acid, is less than 0.05.
33) a) M. Tanaka, *J. Inorg. Nucl. Chem.*, **35**, 965 (1973); **36**, 151 (1974); b) M. Tanaka and S. Yamada, *J. Chem. Soc., Chem. Commun.*, **1976**, 178.
34) M. Tanaka, N, Nakasuka and S. Sasane, *J. Inorg. Nucl. Chem.*, **31**, 2591 (1969).

 © 1984 The Chemical Society of Japan Bull. Chem. Soc. Jpn., 57, 1260—1264 (1984) [Vol. 57, No. 5

Oxidation of Lipids. V. Oxidation of Methyl Linoleate in Aqueous Dispersion

Yorihiro YAMAMOTO, Shunichi HAGA, Etsuo NIKI,* and Yoshio KAMIYA
Department of Reaction Chemistry, Faculty of Engineering, The University of Tokyo, Hongo, Bunkyo-ku, Tokyo 113
(Received August 9, 1983)

The rate and products of oxidation of methyl linoleate dispersed in water by Triton X-100 were measured at 50 °C. The oxidation was initiated by water- or oil-soluble azo-initiators. The oxidation proceeded smoothly by both types of initiators without any noticeable induction period and a constant rate of oxygen uptake was observed. Conjugated diene hydroperoxides were formed almost quantitatively. The oxidizability for methyl linoleate in aqueous dispersion was obtained as $k_p/(2k_t)^{1/2}=0.032(\text{s}\cdot\text{mol/L-oil})^{-1/2}$ where k_p and k_t are the rate constants for propagation and termination reactions, respectively. This value was similar to that observed in the homogeneous oxidation in chlorobenzene. L-Ascorbic acid inhibited the oxidation initiated by water-soluble initiator but it could not inhibit the oxidation initiated by oil-soluble initiator. 2,6-Di-*t*-butyl-4-methylphenol inhibited the oxidation initiated by both initiators. On the other hand, α-tocopherol was effective for the oxidation initiated by oil-soluble initiator and it incompletely inhibited the oxidation initiated by water-soluble initiator.

The oxidation of polyunsaturated fatty acids has received renewed attention recently in connection with the deterioration of foods and oils and with the peroxidation in biological systems.[1-6] In the course of our study on the oxidation of lipids and its inhibition,[7-10] we have extended the work to the oxidation of methyl linoleate in water dispersion. Methyl linoleate was chosen as a substrate since its oxidation proceeds by a straightforward mechanism to give four isomeric hydroperoxides quantitatively at the initial stage.[7,9,11-20] The azo compounds were used as a radical initiator in order to obtain a constant rate of chain initiation.

Experimental

Material. Methyl linoleate was obtained from Sigma Chemical Co. and used as received. Prior to the oxidation, little conjugated diene hydroperoxides were observed by HPLC analysis (see later text). Ethyl palmitate was purchased from Tokyo Kasei Kogyo Co. and used as received. 2,2′-Azobis(2,4-dimethylpentanenitrile) (AMVN) and 2,2′-azobis(2-amidinopropane) hydrochloride (AAPH) used as a radical initiator were obtained from Wako Pure Chemical Industries. L-Ascorbic acid and Triton X-100 were their highest grade available. Commercial 2,6-di-*t*-butyl-4-methylphenol (BMP) was recrystallized from methanol. Natural D-α-tocopherol was kindly supplied from Eisai Co.

Procedure. Appropriate amounts of methyl linoleate, ethyl palmitate, and AMVN (and, if necessary, benzene solution of BMP and α-tocopherol) were taken into a 30 ml Pyrex glass ampoule and dissolved into benzene. The ampoule was connected to the water aspirator and benzene was removed at room temperature. The removal of benzene was checked by the weight. Five ml of 0.01 M (1 M=1 mol dm^{-3}) aqueous Triton X-100 (when necessary, L-ascorbic acid was dissolved in this solution) was added into the ampoule and shaken vigorously on Vortex mixer for two minutes. The oxidation initiated by a water-soluble initiator, AAPH, dissolved in an aqueous Triton X-100 was carried out by a similar procedure.

The ampoule was degassed and then oxygen was introduced into the vessel. The oxidation was carried out at 50 °C under atmospheric pressure of oxygen for the desired time. The rate of oxygen uptake was followed by pressure decrease using a pressure transducer connected to the vessel.

The oxidation was ceased by cooling the ampoule, then methanol was added into the ampoule in order to homogenize the aqueous dispersion. The consumption of methyl linoleate was measured by GLC. An aliquot of methanol solution was evacuated using the evaporator and the reside was dissolved in hexane. This hexane solution was analyzed by HPLC to determine the amounts of hydroperoxides formed, using a silica-gel column and hexane/isopropyl alcohol/acetic acid (1000:10:1, v/v/v) as the eluent. The extinction coefficient was taken from the literature.[12]

Results and Discussion

Oxidation of Methyl Linoleate (LH) Micelle Initiated by Oil-soluble Initiator. Table 1 shows the results of AMVN-initiated oxidation of LH in an aqueous dispersion at 50 °C. As shown in Fig. 1 (Run 2), the oxidation of LH proceeded smoothly without any noticeable induction period and a constant rate of oxygen uptake was observed.

The oxidation of LH initiated by oil-soluble initiator (IN_2I) proceeds by the mechanism[9] shown below:

$$\text{initiation} \quad (IN_2I)_{oil} \longrightarrow 2eI\cdot + N_2 + (1-e)\text{I-I}, \quad (1)$$

$$I\cdot + O_2 \xrightarrow{LH,\ O_2} IOOH + LO_2\cdot, \quad (2)$$

$$\text{propagation} \quad LO_2\cdot + LH \xrightarrow{k_p} LOOH + L\cdot, \quad (3)$$

$$L\cdot + O_2 \rightleftharpoons LO_2\cdot, \quad (4)$$

$$\text{termination} \quad LO_2\cdot + LO_2\cdot \xrightarrow{k_t} \text{nonradical products.} \quad (5)$$

The rate of oxygen uptake ($-dO_2/dt$) is given by

$$-dO_2/dt = R_i^{1/2}[LH]k_p/(2k_t)^{1/2}, \quad (6)$$

where k_p, k_t, and R_i are the rate constants for Reactions 3 and 5, and rate of initiation, respectively. The rate of initiation was measured by the Eq. 7 from the induction period (t_{inh}) observed in the presence of inhibitor (InhH). The constant n is the number of peroxyl radicals trapped by one inhibitor and it was assumed to be 2.[21]

$$R_i = n[\text{InhH}]/t_{inh}. \quad (7)$$

Table 1. Oxidation of methyl linoleate (LH) dispersed in 5 ml 0.01 M aqueous Triton X-100 at 50 °C initiated by AMVN

Run No.	1	2	3	4	5	6	7	8	9	10
LH (mmol)	0.606	0.867	1.09	1.45	1.46	1.49	1.71	1.77	2.37	2.93
[LH]/(mol/L-oil)	0.605	1.10	1.14	1.48	1.49	1.50	1.60	1.80	2.41	3.02
Ethyl palmitate (ml)	0.8	0.5	0.6	0.5	0.5	0.5	0.5	0.4	0.2	0
[AMVN]/(mol/L-oil)	0.208	0.230	0.219	0.024	0.101	0.066	0.170	0.206	0.202	0.067
$(-dO_2/dt)\times10^5$/(mol/L-oil/s)	3.43	6.14	6.77	2.60	4.74	4.21	7.04	8.30	9.14	7.82
$R_i\times10^6$/(mol/L-oil/s)	2.45	2.76	2.57	0.28	1.18	0.78	2.00	2.42	2.39	0.81
Kinetic chain length	13.5	22.2	25.8	92.4	39.6	53.4	34.7	33.8	37.8	96.2
$(k_p/(2k_t)^{1/2})\times10^3$/(s·mol/L-oil)$^{-1/2}$	36.2	33.9	37.0	33.2	29.2	31.8	31.1	29.6	24.6	28.7
cis,trans-LOOH/*trans,trans*-LOOH	0.34		0.48	0.59	0.54	0.51		0.50	0.64	0.82

Table 2. Inhibition of oxidation of methyl linoleate (LH) dispersed in 5 ml 0.01 M aqueous Triton X-100 at 50 °C initiated by AMVN[a)]

Run No.	2	11	12	13	14
LH (mmol)	0.867	0.894	0.859	0.841	0.837
[LH]/(mol/L-oil)	1.10	1.05	1.10	1.08	1.08
Ethyl palmitate (ml)	0.5	0.5	0.5	0.5	0.5
[AMVN]/(mol/L-oil)	0.230	0.233	0.235	0.233	0.237
BMP (μmol)		2.54			
α-Tocopherol (μmol)			2.30		2.30
L-Ascorbic acid (μmol)				75.1	75.1
t_{inh}/min	0	39	35	0	41
$(-dO_2/dt)\times10^5$/(mol/L-oil/s)	6.14	(1.27)5.93	(0.56)5.39	6.49	(0.86)6.52
$R_i\times10^6$/(mol/L-oil/s)	2.76	2.75	2.76	2.74	2.79
Kinetic chain length	22.2	(3.6)21.2	(1.0)19.0	23.3	(2.1)22.8
$(k_p/(2k_t)^{1/2})\times10^3$/(s·mol/L-oil)$^{-1/2}$	33.9	32.8	29.5	36.3	36.1

a) The numbers in the parentheses are the rate of oxidation and kinetic chain length during the induction period.

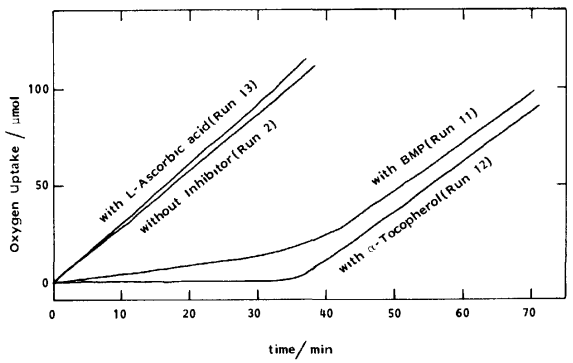

Fig. 1. Rate of oxygen uptake in the AMVN-initiated oxidation of methyl linoleate dispersed in aqueous Triton X-100 at 50 °C.

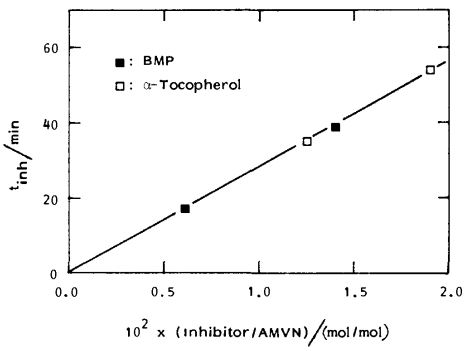

Fig. 2. Plot of induction period(t_{inh}) against the ratio of inhibitor to AMVN concentration in the AMVN-initiated oxidation of methyl linoleate in aqueous dispersion at 50 °C.

Figure 1 shows that the induction period was observed in the presence of BMP or α-tocopherol (Runs 11 and 12). The induction period is produced because BMP or α-tocopherol scavenges the chain carrying peroxyl radicals by Reactions 8 and 9, and suppresses

$$LO_2\cdot + InhH \xrightarrow{k_{inh}} LOOH + Inh\cdot, \quad (8)$$

$$LO_2\cdot + Inh\cdot \longrightarrow Inh\text{-}OOL, \quad (9)$$

the oxidation. As the inhibitor consumed, the rate of oxidation increases and when all the inhibitor is exhausted the oxidation proceeds at the same rate as that in the absence of an inhibitor; that is, the lines for Runs 11 and 12 after the induction period are parallel with the line for Run 2.

Table 2 summarizes the effect of inhibitors on the AMVN-initiated oxidation of LH in an aqueous dispersion. The rate of oxidation during the induction period was smaller when α-tocopherol was used as the inhibitor than when BMP was used. This is the reason why α-tocopherol traps the chain carrying peroxyl radicals faster than BMP.[8,21)]

Figure 2 shows the induction period changes as a

function of the ratio of inhibitor to AMVN. A good linear correlation was observed and the slope for α-tocopherol was identical with that for BMP, suggesting the same stoichiometric number n for both inhibitors.

Equation 6 suggests that the rate of oxygen uptake is the first order with respect to the concentration of the substrate. Figure 3 shows the plot of $-dO_2/dt$ as a function of [LH] $R_i^{1/2}$ and a linear correlation was obtained. This also supports that the oxidation proceeds by the Reactions 1 to 5. The slope gives the oxidizability, $k_p/(2k_t)^{1/2}$, as 0.032 $(s \cdot mol/L\text{-}oil)^{-1/2}$.

Oxidation of Methyl Linoleate(LH) Micelle Initiated by Water-soluble Initiator. A constant rate of oxygen uptake was observed in the oxidation of LH micelle initiated by AAPH as shown in Fig. 4 (Run 23), which indicates that the rate of radical formation in the oil region of micelle was constant nevertheless radicals were initially formed in the aqueous phase.[22]

Table 3 summarizes the effect of Triton X-100 on the AAPH-initiated oxidation of LH in an aqueous dispersion. When Triton X-100 was not added and LH was floating on the water-air interface, little oxygen uptake was observed (Run 15). The rate of oxygen uptake increased with an increase in the concentration of Triton X-100 (Runs 16—19). However, an appreciable rate of oxygen uptake was observed in the oxidation of 0.1 M aqueous Triton X-100 alone (Run 20), therefore the concentration of Triton X-100 was kept constant at 0.01 M.

Table 4 summarizes some representative results of the AAPH-initiated oxidation of LH dispersed in 5 ml of 0.01 M aqueous Triton X-100 at 50 °C. The rate of initiation (R_i) was calculated from the induction period (t_{inh}) produced in the presence of BMP (see later results). The oxidizability, $k_p/(2k_t)^{1/2}$, was calculated from equa-

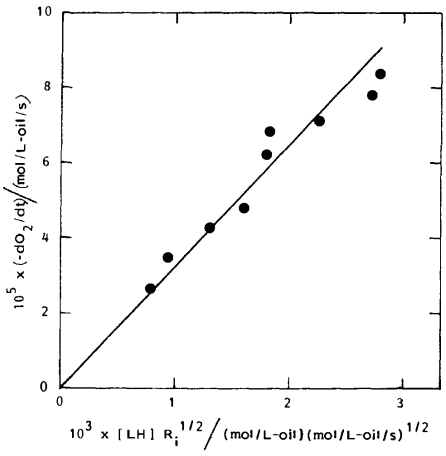

Fig. 3. Plot of the rate of AMVN-initiated oxidation of methyl linoleate (LH) in aqueous dispersion at 50 °C *vs.* [LH] $R_i^{1/2}$.

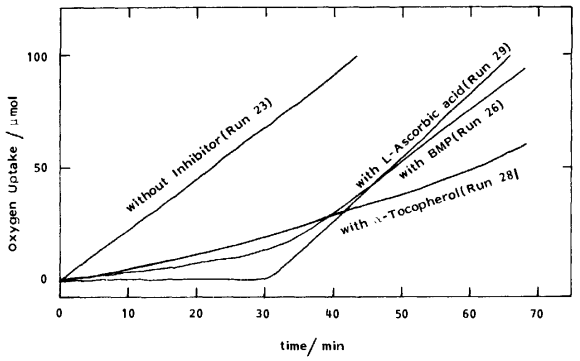

Fig. 4. Plot of oxygen uptake in the AAPH-initiated oxidation of methyl linoleate dispersed in aqueous Triton X-100 at 50 °C.

Table 3. Effect of Triton X-100 on the AAPH-initiated oxidation of methyl linoleate (LH) in 5 ml water at 50 °C

Run No.	15	16	17	18	19	20
LH (mmol)	0.873	0.971	0.903	0.858	0.893	0
[LH]/(mol/L-oil)	3.02	3.02	3.02	3.02	3.02	
AAPH (μmol)	80.8	91.5	90.8	90.5	88.9	94.5
Triton X-100 (mmol/L-soln[a])	0	1.7	10	50	100	100
$(-dO_2/dt) \times 10^6$/(mol/L-soln/s)	0	1.50	7.17	5.87	12.3	0.99

a) Concentration in total aqueous solution.

Table 4. AAPH-intiated oxidation of methyl linoleate (LH) dispersed in 5 ml 0.01 M aqueous Triton X-100 at 50 °C

Run No.	21	22	23	24	17	25
LH (mmol)	0.490	0.832	0.843	0.890	0.903	1.403
[LH]/(mol/L-oil)	3.02	3.02	3.02	3.02	3.02	3.02
AAPH (μmol)	90.4	93.0	91.9	91.9	90.8	97.0
[AAPH]/(mmol/L-soln)	17.5	17.6	17.4	17.4	17.1	17.8
$(-dO_2/dt) \times 10^4$/(mol/L-oil/s)	2.23	1.43	1.36	1.32	1.27	0.94
$R_i \times 10^6$/(mol/L-oil/s)	3.40	2.06	2.01	1.91	1.85	1.28
Kinetic chain length	65.0	68.8	67.2	68.5	68.2	72.9
$(k_p/(2k_t)^{1/2}) \times 10^3/(s \cdot mol/L\text{-}oil)^{-1/2}$	40.0	32.9	31.8	31.6	30.9	27.5

Table 5. Inhibition of AAPH-initiated oxidation of methyl linoleate (LH) dispersed in 5 ml 0.01 M aqueous Triton X-100 at 50 °C[a)]

Run No.	23	26	27	28	29	30
LH (mmol)	0.843	0.854	0.891	0.828	0.853	0.866
[LH]/(mol/L-oil)	3.02	3.02	3.02	3.02	3.02	3.02
AAPH (μmol)	91.9	96.7	91.5	91.1	92.6	95.6
[AAPH]/(mmol/L-soln)	17.4	18.3	17.3	17.3	17.5	18.1
BMP (μmol)		0.50	1.01			
α-Tocopherol (μmol)				0.50		
L-Ascorbic acid (μmol)					2.01	3.04
t_{inh}/min	0	30.5	61.5	?	30	45
$(-dO_2/dt) \times 10^4$/(mol/L-oil/s)	1.36	(0.14) 1.41	(0.17) 1.40		(0) 1.48	(0) 1.48
$R_i \times 10^6$/(mol/L-oil/s)	2.01	2.10	1.91	2.03	2.00	2.04
Kinetic chain length	67.2	(5.8) 66.6	(7.8) 72.5		(0) 73.5	(0) 72.0
$(k_p/(2k_t)^{1/2}) \times 10^3$/(s·mol/L-oil)$^{-1/2}$	31.8	32.2	33.4		34.6	34.3

a) The numbers in the parentheses are the rate of oxidation and kinetic chain length during the induction period.

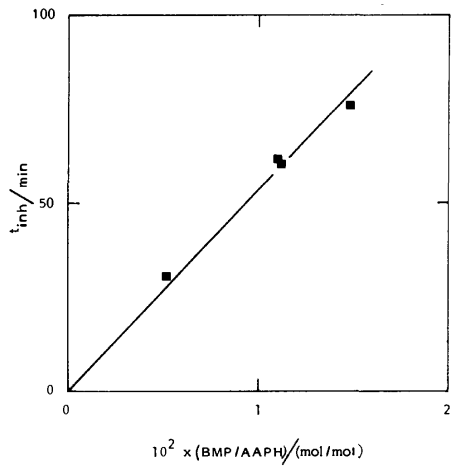

Fig. 5. Plot of induction period(t_{inh}) against the ratio of BMP to AAPH concentration in the AAPH-initiated oxidation of methyl linoleate in aqueous dispersion at 50 °C.

Table 6. Products of the oxidation of methyl linoleate (LH) dispersed in aqueous Triton X-100 at 50 °C

Run No.	4	21	17	25
LH (μmol)	1451	490	903	1403
Initiator	AMVN	AAPH	AAPH	AAPH
Time/min	40	30	50	60
ΔO_2/μmol	61	65	114	157
ΔLH/μmol		51	80	135
Hydroperoxides analyzed by HPLC (μmol)				
13-*cis,trans*-LOOH	11.8	13.4	24.6	32.6
13-*trans,trans*-LOOH	19.2	16.7	29.0	40.4
9-*trans,cis*-LOOH	10.9	11.8	21.7	30.0
9-*trans,trans*-LOOH	19.3	16.0	28.0	38.3
Total LOOH	61	58	103	141
Kinetic chain length	92.4	65.0	68.2	72.9
ΔO_2/initial LH	0.042	0.13	0.13	0.11

tion 6 as 0.032 (s·mol/L-oil)$^{-1/2}$ on the average of Runs 17, 22, 23, and 24. This value agreed well with that obtained in the AMVN-initiated oxidation of LH dispersed in an aqueous Triton X-100. These values were also in good agreement with the oxidizability obtained in the oxidation of LH in chlorobenzene at 50 °C; 0.033 (M·s)$^{-1/2}$.[23)]

The effect of inhibitors on the AAPH-initiated oxidation of LH in an aqueous dispersion is summarized in Table 5 and Fig. 4. Water-soluble inhibitor, L-ascorbic acid, suppressed the oxidation (Runs 29 and 30). BMP also inhibited the oxidation (Runs 26 and 27) and we can calculated the concentration of radical produced in the oil region of micelle in an unit time (R_i) from the induction period (T_{inh}) by Eq. 7. Figure 5 shows the plot of t_{inh} against the ratio of BMP to AAPH and a linear correlation was obtained. On the other hand, α-tocopherol inhibited the oxidation incompletely as shown in Fig. 4.

Products. Table 6 summarizes the oxygen uptake, substrate reacted, and the formation of hydroperoxides in the oxidation of methyl linoleate (LH) in an aqueous dispersion at 50 °C. As observed in the oxidation of LH in an homogeneous solution, the major products were for isomeric conjugated diene hydroperoxides: (9*Z*,11*E*)-13-hydroperoxy-, (9*E*,11*E*)-13-hydroperoxy-, (10*E*,12*Z*)-9-hydroperoxy-, and (10*E*,12*E*)-9-hydroperoxyoctadecadienoic acid methyl esters. The amounts of oxygen uptake, substrate disappearance, and the formation of hydroperoxides agreed fairy well with each other. Figure 6 shows the dependence of *cis,trans*-LOOH/*trans,trans*-LOOH ratio on the concentration of substrate in the oil phase. The intersections and the slopes were the same independent of the initiators. Furthermore, the *cis,trans* to *trans,trans* ratios were similar to those obtained in the homogeneous oxidation of LH in solution at 50 °C.[9)]

In conclusion, the oxidation of methyl linoleate dispersed in an aqueous Triton X-100 was initiated by not only oil-soluble initiator but also water-soluble initiator, and a constant rate of oxygen uptake was observed. Water-soluble inhibitor, L-ascorbic acid, inhibitd the oxidation initiated by water-soluble initiator but it could not inhibited the oxidation initiated by

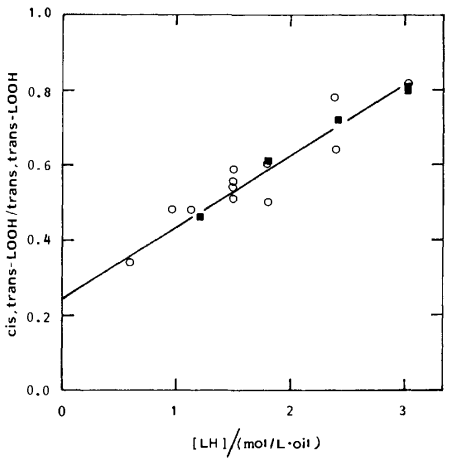

Fig. 6. Plot of *cis,trans*-LOOH/*trans,trans*-LOOH ratio against methyl linoleate (LH) concentration in the AMVN-(○) and AAPH-(■) initiated oxidation of LH in aqueous dispersion at 50 °C.

oil-soluble initiator. Oil-soluble inhibitor, BMP and α-tocopherol, inhibited the oxidation initiated by both inhibitors. The oxidizability for methyl linoleate in an aqueous dispersion was similar to that observed in the homogeneous oxidation in chlorobenzene. Furthermore, conjugated diene hydroperoxides were formed almost quantitatively and *cis,trans/trans,trans* ratios were similar to those obtained in the homogeneous oxidation. Thus, the oxidation of methyl linoleate in an aqueous dispersion proceeds in the oil region by the similar rate and mechanism as in homogeneous solution.

A gift of α-tocopherol from Eisai Co. Ltd. is gratefully acknowledged.

References

1) W. O. Lundberg, "Autoxidation and Antioxidants," Interscience, New York (1962).
2) "Free Radicals in Biology," ed by W. A. Pryor, Academic Press, New York (1976), Vol. 1, and subsequent series.
3) "Tocopherol, Oxygen and Biomembranes," ed by C. de Duve and O. Hayaishi, Elsevier/North-Holland, Amsterdam (1978).
4) "Biochemical and Clinical Aspects of Oxygen," ed by W. S. Caughey, Academic Press, New York (1979).
5) "Autoxidation in Food and Biological Systems," ed by M. G. Simic and M. Karel, Plenum, New York (1980).
6) "Oxygen and Oxy-Radicals in Chemistry and Biology," ed by M. A. J. Rodgers and E. L. Powersm, Academic Press, New York (1981).
7) Y. Yamamoto, E. Niki, and Y. Kamiya, *Bull. Chem. Soc. Jpn.*, **55**, 1548 (1982).
8) E. Niki, R. Tanimura, and Y. Kamiya, *Bull. Chem. Soc. Jpn.*, **55**, 1551 (1982).
9) Y. Yamamoto, E. Niki, and Y. Kamiya, *Lipids*, **17**, 870 (1982).
10) J. Tsuchiya, E. Niki, and Y. Kamiya, *Bull. Chem. Soc. Jpn.*, **56**, 229 (1983).
11) W. A. Pryor, J. P. Stanley, E. Blair, and G. B. Cullen, *Arch. Environ. Health*, **31**, 201 (1976).
12) H. W. S. Chan and G. Levett, *Lipids*, **12**,99 (1977).
13) E. E. Dumelin and A. L. Tappel, *Lipids*, **12**, 894 (1977).
14) E. N. Frankel, W. E. Neff, W. K. Rohwedder, B. P. S. Khambay, R. F. Garwood, and B. C. L. Weedon, *Lipids*, **12**, 901, 908, 1055 (1977).
15) H. W. S. Chan, G. Levett, and J. A. Matthew, *Chem. Phys. Lipids*, **24**, 245 (1979).
16) S. H. Fatemi and E. G. Hammond, *Lipids*, **15**, 379 (1980).
17) N. A. Porter, R. A. Wolf, and H. Weenen, *Lipids*, **15**, 163 (1980).
18) N. A. Porter, B. A. Weber, H. Weenen, and J. A. Khan, *J. Am. Chem. Soc.*, **102**, 5597 (1980).
19) N. A. Porter, L. S. Lehman, B. A. Weber, and K. J. Smith, *J. Am. Chem. Soc.*, **103**, 6447 (1981).
20) D. K. Park, J. Terao, and S. Matsushita, *Agric. Biol. Chem.*, **45**, 2071 (1981).
21) G. W. Burton and K. U. Ingold, *J. Am. Chem. Soc.*, **103**, 6472 (1981).
22) Although it is not clealy established, we believe substantially all of AAPH is distributed in an aqueous phase because AAPH is very soluble in water but insoluble in oil and because L-ascorbic acid can inhibit the AAPH-initiated oxidation whereas it can not inhibit the AMVN-initiated oxidation.
23) Y. Yamamoto, E. Niki, and Y. Kamiya, unpublished data.

The Formation of the Main Skelton of Bicyclomycin by the Cyclization of 6-Hydroxy-3-(3-hydroxypropyl)-2,5-piperazinedione Derivatives

Yoshiaki SATO, Chung-gi SHIN,* Satoshi SUMIYA, Yoshiharu NAKAJIMA, and Juji YOSHIMURA†
Laboratory of Organic Chemistry, Faculty of Technology, Kanagawa University, Rokkakubashi, Kanagawa-ku, Yokohama 221
†*Laboratory of Chemistry for Natural Products, Faculty of Science, Tokyo Institute of Technology, Nagatsuta, Midori-ku, Yokohama 227*
(Received September 17, 1983)

This paper describes the synthesis of 3-(3-*t*-butoxypropyl)-6-hydroxy-2,5-piperazinedione derivatives by the hydroxylation of the corresponding 2,5-piperazinedione with *N*-bromosuccinimide (NBS) in the presence of water and the subsequent cyclization to 2-oxa-7,9-diazabicyclo[4.2.2]decane-8,10-dione derivatives (**11**). The reversible interconversion between the spiro[oxolane-2,2′-piperazine]-3′,6′-dione prepared previously and the bicyclo compound **11** was established. The formation mechanisms and the structural confirmation of **11** and the other products are discussed.

Bicyclomycin, produced by *Streptomyces (St.) sapporonensis*[1] and *St. aizunensis*,[2] is found to have an interesting bicyclostructure and a marked bioactivity.[3-6] The very interesting and important investigation on the correlation between the structure and the bioactivity attracked and prompted us to synthesize the bicyclomycin and its analogs. Many workers have attempted the synthesis of bicyclomycin,[7-12] more recently, it has been reported that Nakatsuka *et al.* have succeeded in the total synthesis.[13] We also reported briefly the facile conversion of 1-benzyl-3-(3-hydroxypropyl)-2,5-piperazinedione (**3**) (2,5-piperazinedione=PDO) derivative to the corresponding bicyclo compound.[10]

In the present paper, we wish to report in detail the synthesis of the main framework of bicyclomycin. The structural determination and the formation mechanisms are discussed.

Results and Discussion

Synthesis of 3,6-Bridged PDO. The starting 1-benzyl-3-(3-hydroxypropylidene)-PDO (**1**), derived by the cyclization of diethyl (*Z*)-2-chloroacetylamino-2-pentendioate[14,15] with benzylamine and the reduction of the resulting 3-[2-(ethoxycarbonyl)ethylidene]-PDO derivative with $LiAlH_4$,[14] was treated with isobutene to give 1-benzyl-3-(3-*t*-butoxypropylidene)-PDO (**2**). The subsequent hydrogenation of **2** with 10% Pd/C gave 1-benzyl-3-(3-*t*-butoxypropyl)-PDO (**4**) in a good yield.

According to the method for the selective hydroxylation of 6-position of PDO derivative reported recently,[14] the compound **4** was treated with *N*-bromosuccinimide (NBS) in a mixture of chloroform and water to give reaction products as a mixture. The crude mixture thus obtained was chromatographed on a silica-gel column to give three fractions, from which the compounds **2**, **10**, and **9** were in turn obtained in 28, 21, and 29% yields respectively. The latter two were identified as 1-benzyl-3-(3-*t*-butoxypropylidene)-6-hydroxy-PDO (**10**) and 3-(3-*t*-butoxypropyl)-6-hydroxy-PDO (**9**). In addition, the compound **9** separated above and newly obtained by the catalytic hydrogenation of **10** with 10% Pd/C was found to be comprised of two stereoisomers, which could be separated purely to give **9a** and **9b** (*ca.* 1:1 ratio).

On the other hand, in order to block the 4-position,

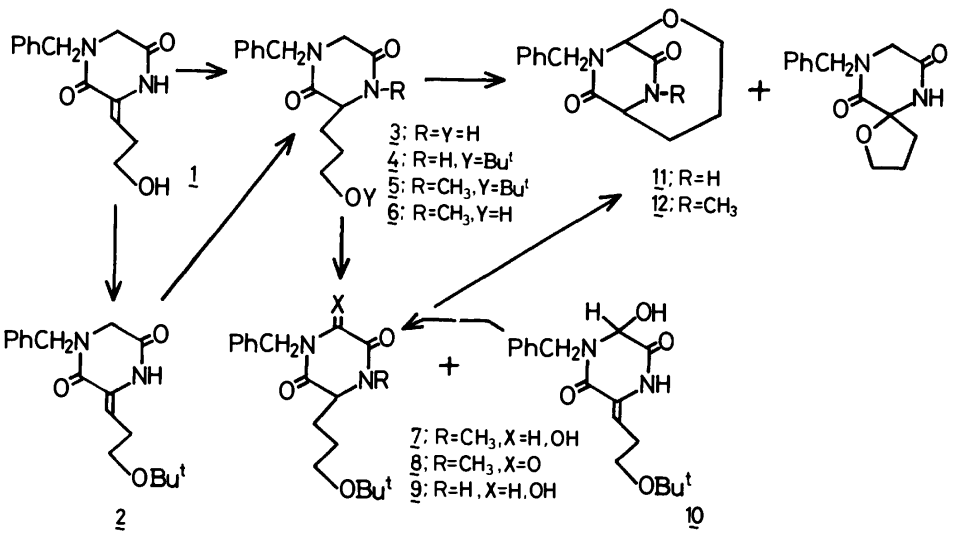

Scheme 1.

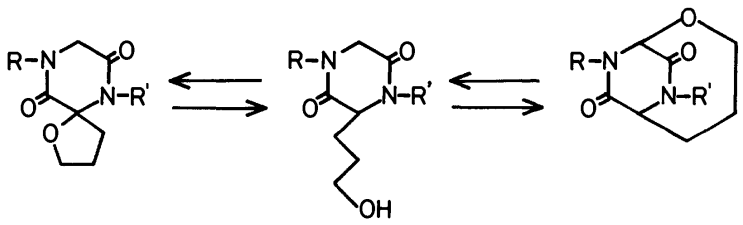

Fig. 1.

according to the method reported previously,[16] the compound **4** was subjected to the methylation with methyl iodide, followed by the reaction of the resulting 1-benzyl-3-(3-*t*-butoxypropyl)-4-methyl-PDO (**5**) with NBS in the presence of water. The reaction products thus obtained as a mixture were separated on a silica-gel column to give two kinds of colorless crystals, which were identified as 1-benzyl-5-(3-*t*-butoxypropyl)-4-methyl-2,3,6-piperazinetrione (**8**) and the corresponding 6-hydroxy-PDO (**7**) obtained in a 26% and a 40% yield respectively.

In order to examine whether or not the *N*-unmasked **3**[14] can be hydroxylated at the 6-position, the substrate **3** was also made to react with NBS in the presence of water. As a result, the expected hydroxylation of **3** took place. The resulting product, yielded as an intermediate, was cyclized to give the 3,6-bridged PDO and spiro-PDO derivatives. The two products thus obtained were readily characterized to be 9-benzyl-2-oxa-7,9-diazabicyclo[4.2.2]decane-8,10-dione (**11**) and 4'-benzylspiro[oxolane-2,2'-piperazine]-3',6'-dione[14] in a 28% and a 38% yield respectively.

On the other hand, the similar reaction of **3** with NBS in chloroform in the absence of water gave an oily product, which was assigned to be a mixture of 3-, 6-bromo, and 3,6-dibromo derivatives of **3** based on the spectroscopic analyses. However, the attempts to separate the above mixture purely have been unsuccessful so far. Consequently, the hydroxylation mechanism is supposed to be the bromination of **3** in the first step and then the substitution of bromine with hydroxyl group at 3- and 6-positions. Furthermore, from the above results and the fact that the spiro compound easily converted into **3**,[14] the reversible interconversion route between the spiro and 3,6-bridged compounds (**11**) *via* **3** was first ascertained and established here, as is illustrated in Fig. 1.

In addition, in order to obtain **11** in a higher yield, the cyclization of 1-benzyl-6-hydroxy-3-(3-hydroxypropyl)-PDO *in situ*, formed as an intermediate by the treatment of **9** with trifluoroacetic acid, was successful. **11** was obtained in a 95% yield from **9a** and in a 90% yield from **9b**. **7** was similarly worked up to give 7-methyl derivative of **11** (**12**) in a quantitative yield. Therefore, the formation mechanisms of **11** and **12** could be unambiguously concluded to be the decomposition of *t*-butoxyl group of **7** and **9** with trifluoroacetic acid to hydroxyl group, followed by the immediate cyclization by the intramolecular dehydration between 3-(3-hydroxypropyl) and 6-hydroxyl groups.

The yields, physical constants, and spectral data of **4**—**8** and **9** are summarized in Table 1.

In the NMR spectrum of **11**, the signal of the proton at the 1-position appeared in the δ 4.20 as a multiplet and the signal at δ 5.01 is attributable to 6-proton, which is splitting as a doublet (J=1.2 Hz) of the long range coupling due to the *W*-letter relationship between NH and 1-proton. In consequence, the 3,6-bridged PDO (**11** and **12**) thus obtained was found to have a boat structure, as in the corresponding spiro derivative;[14] this is illustrated in Fig. 2.

Synthesis of 3-Methoxy-3,6-bridged PDO. To

Table 1. 3-Alkyl-2,5-piperazinedione derivatives (**4**—**9**)

Compound No.	Yield %	Mp θ_m/°C	Formula	Found (Calcd) (%) C	H	N	NMR spectrum, δ in $CDCl_3$ 3-H J/Hz	6-H J/Hz	OH	NH (N-CH_3)
4	92	120—122[a]	$C_{18}H_{26}N_2O_3$	68.01 (67.90	8.45 8.23	8.86 8.80)	4.00 m	3.77 s		7.74
5	98	97—98[b]	$C_{19}H_{28}N_2O_3$	68.70 (68.64	8.74 8.49	8.48 8.43)	4.03 dd (5.0, 6.0)	3.84 q[g] (18.0)		(2.98)
6	92	73—75[c]	$C_{15}H_{20}N_2O_3$	65.23 (65.19	7.34 7.30	9.89 10.14)	4.04 t (5.0)	3.84 s	4.40 s	(2.96)
7	40	134—135[d]	$C_{19}H_{28}N_2O_4$	65.35 (65.49	8.19 8.10	8.08 8.04)	3.95 dd (5.0, 6.0)	5.03 d (5.5)	6.53 d	(2.96)
8	26	59—60[a]	$C_{19}H_{26}N_2O_4$	65.61 (65.87	7.66 7.57	7.83 8.09)	4.28 dd (4.0, 5.5)			(3.04)
9a	29	204—206[e,f]	$C_{18}H_{26}N_2O_4$	64.38 (64.65	7.88 7.84	8.31 8.38)	4.06 m	4.96 d (5.0)	5.90 d	7.64
9b		Syrup					4.16 m	4.96 bs	5.8—6.4 bs	7.96

a) Colorless needles from dibutyl ether. b) Colorless needles from hexane. c) Colorless prisms from benzene-hexane. d) Colorless needles from CCl_4. e) Decomposition. f) Colorless needles from benzene. g) AB quartet.

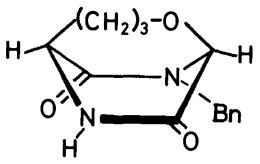

Fig. 2.

generalize the synthesis of the 3,6-bridged PDO, 3-alkoxy- and 3-hydroxy-3-(3-*t*-butoxypropyl)-PDO derivatives newly synthesized here were made to undergo the cyclization reaction. According to the method reported previously,[17] the compound **2** was treated with NBS in a mixture of dioxane and water to give colorless crystals, which were identified as 1-benzyl-3-(1-bromo-3-*t*-butoxypropyl)-3-hydroxy-PDO (**14**) in a 97% yield. In this case, the hydroxylation at the both 3- and 6-positions of **2** did not take place, but only **14** was obtained selectively. The subsequent hydrogenolysis of bromine on **14** with 10% Pd/C gave the corresponding 3-(3-*t*-butoxypropyl)-3-hydroxy-PDO derivative (**16**) in a 94% yield.

On the other hand, the methoxylation of **2** with NBS in methanol was also achieved, followed by the similar hydrogenolysis of the resulting 3-(1-bromo-3-*t*-butoxypropyl)-3-methoxy-PDO derivative (**13**) gave 1-benzyl-3-(3-*t*-butoxypropyl)-3-methoxy-PDO (**15**) in a 95% yield. For the purpose of the conversion of *t*-butoxyl group, **15** was treated with organic acid such as glacial acetic acid; the unexpected elimination of methanol readily occurred to give the starting material **2** quantitatively. Hence, to prevent the methoxyl group from being eliminated it is necessary to protect the 4-position of **15**.[14] The methylation of **15** with methyl iodide[16] gave the corresponding 4-methyl-PDO derivative of **15** (**17**) in a 71% yield.

Next, the reaction of **17** with NBS in a mixture of chloroform and water was performed to obtain a crystalline product as a mixture. Subsequently, by the usual column chromatograph method, the crude mixture was separated purely to give two fractions: The first fraction gave colorless crystals, identified as the corresponding 2,3,6-piperazinetrione derivative of **17** (**18**) in a 23% yield, while the second one gave a colorless syrup, which was also identified as the corresponding 6-hydroxy-PDO derivative of **17** (**19**) in a 40% yield. Although the compounds **17** and **19** thus obtained did not give satisfactory elemental analyses because of the difficulty of purification, their structures could be exactly confirmed by the further transformation to **18** and to the 6-acetoxy derivative of **19** (**20**) respectively.

In order to activate the 6-hydroxyl group, the compound **19** was acetylated by the usual method, followed by the treatment of **20** obtained with trifluoroacetic acid. As a result, the cyclization proceeded quickly to give the reaction products as a mixture. The subsequent separation of the mixture on a silica-gel column gave a syrup from the first fraction and colorless crystals from the second one. These compounds were characterized to be 9-benzyl-6-methoxy-7-methyl-2-oxa-7,9-diazabicyclo[4.2.2]decane-8,10-dione (**22**) in a 54% yield and the authentic 4'-benzyl-5'-hydroxy-1'-methylspiro-[oxolane-2,2'-piperazine]-3',6'-dione (**23**)[14] in a 32% yield respectively.

From the above results, interestingly, even if both 3- and 4-positions were protected with methoxyl and methyl groups respectively, it was found that the spiro formation reaction could be carried out to give **23**.

The yields, physical constants, and spectral data of **13**—**19**, and **20** are summarized in Table 2.

From the NMR spectral data of **22**, the disappearance of the signals due to *t*-butyl of 3-*t*-butoxypropyl at the 3-position and those due to methyl of acetoxyl groups at the 6-position, and the appearance of methylene protons at δ 2.95 (dd, J=5.0 Hz, J=7.5 Hz), 4-methyl protons at δ 2.95 (s), 3-methyl group at δ 3.32 (s), and 6-proton at δ 5.07 (s) indicate unambiguously the formation of the expected bicyclo compound (**23**).

Further work including the cyclization of **16** and **21** is now in progress and the results will be published later.

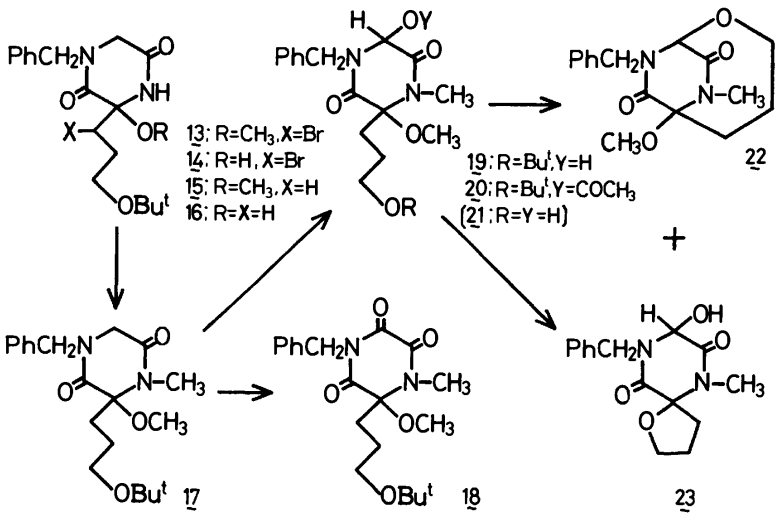

Scheme 2.

TABLE 2. 3-SUBSTITUTED 3-ALKYL-2,5-PIPERAZINEDIONE DERIVATIVES (**13**—**20**)

Compound No.	Yield %	Mp θ_m/°C	Formula	Found (Calcd) (%) C	H	N	NMR spectrum, δ in $CDCl_3$ 6-H J/Hz	OCH_3 (OH), s	NCH_3 (NH), s
13	96	138[a]	$C_{19}H_{27}N_2O_4Br$	53.47 (53.40	6.47 6.37	6.39 6.56)	3.94 d (1.5)	3.30	(8.54)
14	97	141—142[b]	$C_{18}H_{25}N_2O_4Br$	52.17 (52.31	6.17 6.10	6.64 6.78)	3.85 s	(7.20)	(8.90)[g]
15	95	Syrup	$C_{19}H_{28}N_2O_4$	65.30 (65.49	8.12 8.10	8.06 8.04)	3.88 q[f] (17.5)	3.18	(8.34)
16	94	149—150[c]	$C_{18}H_{26}N_2O_4$	64.61 (64.65	7.91 7.84	8.15 8.38)	3.86 q[f] (18.0)	(5.82)	(7.92)
17	71	Syrup					3.90 s	3.12	2.90
18	28	111—112[d]	$C_{20}H_{28}N_2O_5$	63.28 (63.81	7.51 7.50	7.23 7.44)		3.05	3.01
19	40	Syrup					5.06 s 5.12 s	2.90 2.98	3.04
20	89	102—103[e]	$C_{22}H_{32}N_2O_6$	62.57 (62.84	7.80 7.67	6.54 6.66)	6.42 s	3.04	2.88

a) Colorless needles from benzene-hexane. b) Colorless needles from CCl_4. c) Colorless needles from benzene. d) Colorless needles from dibutyl ether. e) Colorless needles from hexane. f) AB quartet. g) Measured in DMDO-d_6.

Experimental

All the boiling and melting points are uncorrected. The IR spectra were recorded with a Hitachi EPI-G3 Spectrometer. The NMR spectra were measured with a JNM-PS-100 Spectrometer (Japan Electron Optics Laboratory Co., Ltd), using tetramethylsilane as an internal standard.

Preparation of **2**. Into a solution of **1** (3.0 g, 11.54 mmol) in CH_2Cl_2 (250 ml), we stirred concentrated H_2SO_4 (1.2 ml). Isobutene gas was then introduced into the resultant solution under cooling, till the volume of the solution became about 350 ml. After the mixture was allowed to stand at room temperature overnight, an aqueous solution of $NaHCO_3$ (100 ml) was added with vigorous stirring. The organic layer was washed with water and then dried over anhydrous Na_2SO_4. Removal of CH_2Cl_2 gave crystals, which were recrystallized from dibutyl ether to give colorless prisms. Yield 88%, mp 123—125 °C. IR (KBr): 3180 (NH), 1680, 1635 (CO) cm^{-1}. NMR ($CDCl_3$): δ=1.24 (s, Bu^t), 6.28 (t, -CH=, J=8.0 Hz), 9.56 (bs, NH). Found: C, 67.82; H, 7.84; N, 8.78%. Calcd for $C_{18}H_{24}N_2O_3$: C, 68.33; H, 7.65; N, 8.85%.

Preparation of **4**. A solution of **2** (1.2 g, 3.80 mmol) in methanol (60 ml) was hydrogenated catalytically with 10% Pd/C (120 mg) at room temperature for 30 min. After filtering off Pd/C, the methanol solution was concentrated to give crude crystals, which were recrystallized from dibutyl ether to give colorless needles. IR (KBr): 3240 (NH), 1695, 1660 (CO) cm^{-1}.

Preparation of **5**. Into a solution of **4** (450 mg, 1.41 mmol) in DMF (5 ml), we stirred 55% NaH (74 mg, 1.70 mmol) at room temperature. After the evolution of hydrogen ceased, methyl iodide (240 mg, 1.69 mmol) was added to the resulting solution, with stirring for 15 min. Into the reaction solution was added ice water (20 ml) and then the resulting solution was extracted twice with benzene (30 ml). The benzene layer was washed twice with water and then dried over anhydrous Na_2SO_4. Removal of benzene gave crystals, which were recrystallized from hexane to give colorless needles. IR (KBr): 1650 (CO) cm^{-1}.

Preparation of **6**. After a solution of **5** (400 mg, 1.20 mmol) in trifluoroacetic acid (3 ml) was allowed to stand at room temperature for 2 h, the resulting solution was concentrated under reduced pressure to give a residual product. The residue thus obtained was purified on a silica-gel column using a mixture of chloroform and acetone (5:1 v/v) as the eluent. Concentration of the fraction obtained gave crude crystals, which were recrystallized from benzene-hexane to give colorless prisms. IR (KBr): 3350 (OH), 1660 (CO) cm^{-1}.

Reaction of **4** *with NBS-Water*. Into a solution of **4** (2.0 g, 6.29 mmol) in chloroform (200 ml) was added water (20 ml) and NBS (1.34 g, 7.55 mmol) at room temperature. After stirring for 2 h, the organic layer which separated was washed with water and then dried over anhydrous Na_2SO_4. After removal of chloroform, the residue was chromatographed on a silica-gel column using a mixture of chloroform and acetone (10:1 v/v) as the eluent. Four fractions thus obtained were concentrated under reduced pressure and each resulting product was purified by means of the recrystallization or on the silica-gel column to give **2**, **10**, **9a**, and **9b** respectively. **2**; Yield 28%. **9a**; IR (KBr): 3200, 1705, 1670, 1665, and 1630 cm^{-1}. **9b**; IR: 3250, 1680 cm^{-1}. **10**; Yield 21%, mp 134—136 °C (colorless prisms from benzene-hexane). IR (KBr): 3300 (OH), 3200 (NH), 1690 (CO), 1620 (C=C) cm^{-1}. NMR ($CDCl_3$): δ=1.22 (s, 9H, Bu^t), 5.06 (bs, 1H, 6-H), 5.7—6.0 (OH), 6.30 (t, -CH=, J=8.0 Hz), 9.70 (bs, NH). Found: C, 65.08; H, 7.22; N, 8.49%. Calcd for $C_{18}H_{24}N_2O_4$: C, 65.04; H, 7.28; N, 8.43%.

Hydrogenation of **10**. A solution of **10** (225 mg, 0.678 mmol) in methanol (20 ml) was catalytically hydrogenated with 10% Pd/C (30 mg) at room temperature for 30 min to give a mixture of **9a** and **9b** (*ca.* 1:1) in a 93% yield.

Reaction of **5** *with NBS-Water*. Into a solution of **5** (1.0 g, 3.01 mmol) in a mixture of chloroform (20 ml) and water (5 ml), we stirred NBS (643 mg, 3.61 mmol) at room temperature for 6 h. The resulting chloroform layer was washed with water and then dried over anhydrous Na_2SO_4. After removal of chloroform, the residue obtained was chromatographed on a silica-gel column using a mixture of

chloroform and acetone (20:1 v/v) as the eluent. The two fractions thus obtained were concentrated to give **8** and **9** respectively. **8**; IR (KBr): 1720, 1690 (CO) cm^{-1}. **9**; IR: 3170 (OH), 1675, 1650 (CO) cm^{-1}.

Reaction of 3 with NBS-Water. In a similar manner, the treatment of **3** (800 mg, 3.05 mmol) with a solution of NBS (600 mg, 3.37 mmol) in a mixture of chloroform (30 ml) and water (3 ml) was worked up for 3 h to give two kinds of products, **11** and the corresponding spiro derivative[14] in a 28 and a 38% yield respectively. **11**; Mp 200—202 °C (colorless prisms from benzene-hexane). IR (KBr): 3230 (NH), 1800 1670 (CO) cm^{-1}. NMR ($CDCl_3$): δ=1.7—2.3 (m, 4H, $-CH_2-$), 3.4—4.0 (m, 2H, $-O-CH_2-$), 4.20 (m, 1H, $-C\underline{H}-CH_2-$, 6-H), 5.01 (d, 1H, $-C\underline{H}-OCH_2-$, $J_{3\text{-H,NH}}$=1.2 Hz, 3-H), 7.68 (s, NH). Found: C, 65.01; H, 6.34; N, 10.66%. Calcd for $C_{14}H_{16}N_2O_3$: C, 64.60; H, 6.20; N, 10.76%.

Cyclization of 9a and 9b. A solution of **9** (300 mg, 0.898 mmol) in CF_3COOH (2 ml) was allowed to stand at room temperature for 2 h. After removal of CF_3COOH, the residual product was dissolved in benzene (20 ml) and the resulting solution was washed with water and then dried over anhydrous Na_2SO_4. Concentration of the solution gave **11** in a 95% yield from **9a** and in a 90% yield from **9b**.

Preparation of 12. From 6: The treatment of **6** (110 mg, 3.99 mmol) with NBS (71 mg, 3.99 mmol) in chloroform (10 ml) was carried out under reflux for 1 h to give **12** as an unstable colorless crystals. Yield 48%. IR (KBr): 1670 (CO) cm^{-1}. NMR ($CDCl_3$): δ=1.5—2.4 (m, 4H, $-CH_2-$), 2.96 (s, 3H, $N-CH_3$), 3.3—3.9 (m, 2H, $-O-CH_2-$), 4.12 (dd, 1H, $-C\underline{H}-CH_2-$, J=3.0, 4.5 6-H), 5.12 (s, 1H, $-C\underline{H}-OCH_2-$, 3-H).

From 7: Treatment of **7** (240 mg, 6.89 mmol) in CF_3COOH (2 ml) at room temperature for 2 h gave **12** in a 98% yield.

Preparation of 13. Into a mixture of **2** (900 mg, 2.85 mmol) in methanol (10 ml), we stirred NBS (507 mg, 2.85 mmol) at room temperature for 10 min. After removal of methanol, the residue was dissolved in chloroform (20 ml) and the resulting solution was washed twice with water and then dried oved anhydrous Na_2SO_4. Concentration of the solution gave crystals, which were recrystallized from benzene-hexane to give colorless needles. IR (KBr): 3160 (NH), 1680 (CO) cm^{-1}.

Preparation of 14. Similarly, the treatment of **2** (900 mg, 2.85 mmol) with NBS (507 mg, 2.85 mmol) in a mixture of dioxane (10 ml) and water (5 ml) was worked up to give **14** as colorless needles from CCl_4. IR (KBr): 3200 (NH, CO), 1660 (CO) cm^{-1}.

Preparation of 15. A solution of **13** (900 mg, 2.11 mmol) in methanol (50 ml) was catalytically hydrogenated with 10% Pd/C (100 mg) in the presence of triethylamine (220 mg, 2.18 mmol) at room temperature for 15 min. After the Pd/C was filtered off, the methanol solution was concentrated. The residue was dissolved in CH_2Cl_2 (50 ml) and the resulting solution was washed twice with water and then dried over anhydrous Na_2SO_4. After removal of CH_2Cl_2, the residual syrup thus obtained was purified on a silica-gel column using a mixture of chloroform and acetone (10:1 v/v) as the eluent. Evaporation of the solvent gave **15** as a colorless syrup. IR (KBr): 3220 (NH), 1680 (CO) cm^{-1}.

Preparation of 16. Similarly, the hydrogenation of **14** (1.1 g, 2.66 mmol) with 10% Pd/C (100 mg) in methanol (60 ml) in the presence of triethylamine (270 mg, 2.66 mmol) was performed to give **16** as colorless needles from benzene. IR (KBr): 3240 (OH, NH), 1690, 1640 (CO) cm^{-1}.

Preparaation of 17. Into a solution of **15** (1.2 g, 3.45 mmol) in THF (40 ml), we stirred 55% NaH (150 mg, 3.45 mmol) at room temperature. After the evolution of hydrogen ceased, methyl iodide (580 mg, 4.08 mmol) was added to the resulting solution with stirring. After continuing the stirring for 1 h, the reaction solution was neutralized with acetic acid. After removal of THF, the residue obtained was dissolved in ethyl acetate (30 ml) and the resulting solution was washed twice with water and then dried over anhydrous Na_2SO_4. Concentration of the solution gave the residual syrup, which was purified on a silica-gel column using a mixture of chloroform and acetone (30:1 v/v) to give **17** as a colorless syrup. IR (KBr): 1660 (CO) cm^{-1}.

Reaction of 17 with NBS-Water. Into a solution of **17** (850 mg, 2.35 mmol) in a mixture of chloroform (20 ml) and water (5 ml), we stirred NBS (460 mg, 2.58 mmol) at room temperature overnight. The resulting organic layer was washed with water and dried over anhydrous Na_2SO_4 and finally concentrated. The residue thus obtained was chromatographed on a silica-gel column using a mixture of chloroform and acetone (20:1 v/v) as the eluent. The first fraction gave trione derivative **18**, and the second one gave 6-hydroxy derivative **19**. **18**; IR (KBr): 1745, 1685 (CO) cm^{-1}. **19**; IR: 3300 (OH), 1660 (CO) cm^{-1}.

Acetylation of 19. A solution of **19** (700 mg, 1.85 mmol) in acetic anhydride (5 ml) in the presence of sodium acetate (3 mg) was heated at 100 °C for 1 h. After removal of acetic anhydride under reduced pressure, the residue was purified on a silica-gel column using a mixture of chloroform and acetone (30:1 v/v) as the eluent. The fraction was concentrated under reduced pressure to give the corresponding acetyl derivative (**20**). IR (KBr): 1760, 1690 (CO) cm^{-1}.

Cyclization of 20. A solution of **20** (650 mg, 1.55 mmol) in CF_3COOH (5 ml) was allowed to stand at room temperature for 2 h. The reaction solution was concentrated under reduced pressure and the residue was chromatographed on a silica-gel column using a mixture of chloroform and acetone (10:1 v/v) as the eluent. The first fraction gave bicyclo compound **22** and the second one gave the spiro compound **23** in a 32% yield. **22**: Yield 54%, syrup. IR (KBr): 1680 (CO) cm^{-1}. NMR ($CDCl_3$): δ=1.3—1.9 (m, 2H, $-CH_2-$), 2.16 (dd, 2H, $-CH_2-$, J=5.0, 7.5 Hz), 2.95 (s, 3H, $N-CH_3$), 3.32 (s, 3H, OCH_3), 3.3—4.0 (m, 2H, $-OCH_2-$), 5.07 (s, 1H, $-C\underline{H}-OCH_2-$, 3-H). Found: N, 9.20%. Calcd for $C_{16}H_{20}N_2O_4$: N, 8.98%.

References

1) T. Miyoshi, N, Miyairi, H, Aoki, M. Kohsaka, H. Sakai, and H. Imanaka, *J. Antibiot.*, **25**, 569 (1972).

2) S. Miyamura, N. Ogasawara, H. Otsuka, S. Niwayama, H. Tanaka, T. Take, T. Uchiyama, H. Ochiai, K. Abe, K, Koizumi, K. Asao, K. Matsuki, and T. Hoshino, *J. Antibiot.*, **25**, 610 (1972); S. Miyamura, N. Ogasawara, H. Otsuka, S. Niwayama, H. Tanaka, T. Take, T. Uchiyama, and H. Ochiai, *ibid.*, **26**, 479 (1973).

3) T. Kamiya, S. Maeno, M. Hashimoto, and Y. Mine, *J. Antibiot.*, **25**, 576 (1972).

4) Y. Tokuma, S. Koda, T. Miyoshi, and Y. Morimoto, *Bull. Chem. Soc. Jpn.*, **47**, 18 (1974).

5) H. Maag, J. F. Blount, D. L. Coffen, T. V. Steppe, and F. Wong, *J. Am. Chem. Soc.*, **100**, 6786 (1978).

6) M. Nishida, Y. Mine, T. Matsubara, S. Goto, and S. Kuwahara, *J. Antibiot.*, **25**, 582 (1972).

7) L. V. Dunkerton and R. M. Ahmed, *Tetrahedron Lett.*, **21**, 1803 (1980).

8) S. Nakatsuka, K. Yoshida, and T. Goto, *Tetrahedron Lett.*, **22**, 2009, 4973 (1981).

9) R. M. Williams, *Tetrahedron Lett.*, **22**, 2341 (1981); R. M. Williams, O. P. Anderson, R. W. Armstrong, J. Josey, H. Meyers, and C. Eriksson, *J. Am. Chem. Soc.*, **104**, 6092 (1982).

10) C. Shin, Y. Sato, and J. Yoshimura, *Tetrahedron Lett.*,

22, 2401 (1981).
11) T. Fukuyama, B. D. Robins, and R. A. Sachleben, *Tetrahedron Lett.*, **22**, 4155 (1981).
12) P. Yates and J. H. Hoare, *Can. J. Chem.*, **61**, 519 (1983).
13) S. Nakatsuka, K. Yamada, O. Asano, K. Yoshida, and T. Goto, 47th National Meeting of the Chemical Society of Japan, Kyoto, April 1983, Abstr. No. 3H-14.
14) C. Shin, Y. Sato, S. Honda, and J. Yoshimura, *Bull. Chem. Soc. Jpn.*, **56**, 2652 (1983).
15) C. Shin, K. Sato, A. Ohtsuka, K. Mikami, and J. Yoshimura, *Bull. Chem. Soc. Jpn.*, **46**, 3876 (1973).
16) C. Shin, Y. Sato, M. Hayakawa, M. Kondo, and J. Yoshimura, *Heterocycles*, **16**, 1573 (1981).
17) C. Shin, Y. Sato, H. Ohmatsu, and J. Yoshimura, *Bull. Chem. Soc. Jpn.*, **54**, 1137 (1981).

The Reaction of 5-Benzylidene-2,3,4,5-tetrahydropyridine with Some Nucleophiles

Yujiro NOMURA, Takashi BANDO, Yoshito TAKEUCHI,* and Shuji TOMODA
Department of Chemistry, College of Arts and Sciences, The University of Tokyo, Komaba, Meguro-ku, Tokyo 153
(Received September 30, 1983)

The reaction 5-benzylidene-2,3,4,5-tetrahydropyridine (**1**) with nucleophilic reagents, such as sodium tetrahydroborate, lithium tetrahydridoaluminate, organometallic reagents, pyrrole, or ethyl propiolate, has been studied. The reaction of **1** with sodium tetrahydroborate, lithium tetrahydridoaluminate, phenylmagnesium bromide, butyllithium gave exclusively respective 1,2-adducts. The reaction with pyrrole gave a tricyclic 1:1 adduct while **1** formed a 1:2 adduct with ethyl propiolate.

As an extension of our recent work directed toward the synthesis of 5-benzylidene-2,3,4,5-tetrahydropyridine (**1**)[1] which is featured with the α, β-unsaturated imine moiety fixed in *s-trans* conformation, we have investigated its reactivity toward nucleophiles. Two reaction modes are *a priori* expected: 1,2-addition of a nucleophile (Nu^-) to the C=N bond would provide a 2-substituted 3-benzylidenepiperidine (**2**), whereas conjugate addition (1,4-addition) of a nucleophile would afford 5-(α-substituted benzyl)-2,3,4,5-tetrahydropyridie (**3**) (Scheme 1). Compounds having the general structure **2** have recently attracted considerable attention in view of their potential clinical application as antihistamine and anticholine drugs.[2] On the other hand, the cyclic imine **3** may serve as a useful precursor to a variety of piperidine alkaloids and other natural alkaloids.[3] Herein we wish to report the results of such reactions of **1** with several nucleophiles which have been carried out in an attempt to synthesize these compounds (**2** and **3**).

Results and Discussion

Hydride Reduction of 1. Reduction of the C=N bond of **1** with a hydride reagent (1,2-addition) would produce 3-benzylidenepiperidine (**2a**, Nu=H), to which access has thus far been difficult using the conventional synthesis methodology.[1] On the other hand, 1,4-reduction would ultimately afford 3-benzylpiperidine (**4**) *via* partially reduced 5-benzyl-2,3,4,5-tetrahydropyridine (**3a**, Nu=H). It is generally accepted that in the reduction of α,β-unsaturated ketones 1,4-reduction tends to be more preferred with sodium tetrahydroborate than with lithium tetrahydridoaluminate.[4] In practice, however, the reduction of **1** with either reagent gave exclusively desired **2a** in 90% ($NaBH_4$, methanol, r.t.) or 85% ($LiAlH_4$, ether, 0 C). Structural identification of **2a** was based on spectral data (MS, IR, and ^1H and ^{13}C NMR). A molecular ion peak at *m/z* 173 in the mass spectrum was consistent with the molecular formula ($C_{12}H_{15}N$). ^1H NMR spectrum showed a characteristic singlet at δ 6.27 due to the benzylidene proton and one exchangeable proton at δ 2.13 (NH) in addition to eight methylene and five aromatic protons. The IR spectrum indicated a medium band at 1650 cm^{-1} due to the C=C bond conjugated with the phenyl group. In line with these data, its ^{13}C NMR spectrum exhibited ten peaks, six of which showed up in the sp^2-C region (δ 123.03—139.72), suggesting the presence of one C=C bond besides the aromatic ring.

Such a selective 1,2-hydride reduction of **1** is surprising for two reasons; (a) as described earlier, sodium

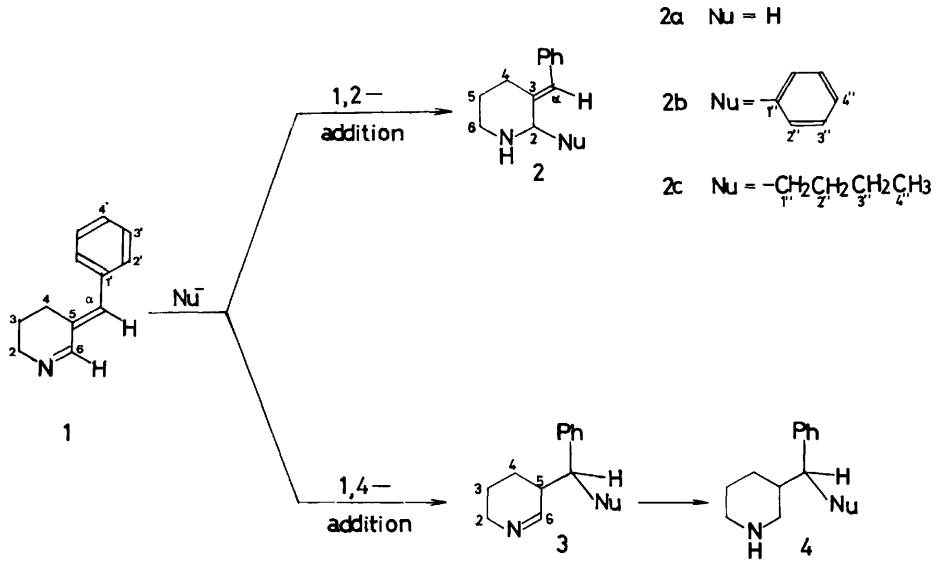

Scheme 1.

tetrahydroborate reduction of α,β-unsaturated ketones or aldehydes normally gives a mixture of 1,2- and 1,4-reduction products with the latter being predominant.[4] (b) lithium tetrahydridoaluminate reduction of 3-phenyl-2-propenal shows a discrete tendency depending on the reaction temperature; 3-phenyl-2-propen-1-ol is produced at −10 °C as a result of preferential 1,2-reduction,[5] whereas at 25 °C in diethyl ether 3-phenyl-1-propanol is obtained exclusively.[6] It should be noted here that in the case of **1** possessing an α,β-unsaturated imine structure with a phenyl group at the β-carbon, the reduction with lithium tetrahydridoaluminate at higher temperature (tetrahydrofuran, reflux, 0.5 h) resulted in the same product **2a** (79% yield); neither **3a** nor **4** was detected.

Reaction with Organometallic Compounds. The less reactive trend of the benzylidene C=C bond of **1** toward nucleophiles in comparison with α,β-unsaturate aldehyde was exposed more clearly by the reaction with organometallic compounds. Thus the reaction of **1** with excess phenylmagnesium bromide in diethyl ether at room temperature provided 3-benzylidene-2-phenylpiperidine (**2b**, Nu=Ph) exclusively in 56% yield. The structure of the product **2b** was confirmed by combustion analysis and spectral data (MS, IR, ^{1}H and ^{13}C NMR). The molecular formula ($C_{18}H_{19}N$) was established by elemental analysis (C, H, and N) and mass spectral molecular weight, *m/z* 249 (M^+). The assigned structure was compatible with the ^{1}H NMR spectrum which revealed characteristic signals at δ 1.93 (br s, 1H, NH, exchangeable with D_2O) and δ 5.90 (br s, 1 H, benzylidene proton) in addition to aromatic and alicyclic protons.

An analogous reaction mode was observed in the reaction of **1** with *n*-butyllithium at −78 °C in THF which resulted in the formation of 3-benzylidene-2-butylpiperidine (**2c**; Nu=*n*-Bu) in 95% yield. The structure of **2c** was characterized by the spectral data (MS, IR, ^{1}H and ^{13}C NMR). The ^{13}C NMR showed eight aliphatic carbons (δ 14.14—61.33) and six sp^2-carbons (δ 122.00—137.82); the peak due to the C=N bond was not detected, suggesting that the 1,2-adduct was the sole product. In agreement with this conclusion, the ^{1}H NMR indicated one benzylidene proton (δ 6.27). but no peak around δ 8 due to azomethine proton was detected.

It is noteworthy that both phenylmagnesium bromide and phenyllithium react with α,β-unsaturated imines, which can assume an *s-cis* conformation, to provide 1,4-adducts exclusively.[7] The above reaction therefore suggests an important synthetic approach for introduction of various alkyl or aryl substituent at C2 of the piperidine bearing exocyclic double bond at C3. Hence the present two-step sequence for preparation of such compounds (**2b**, **2c**) starting from 2,3,4,5-tetrahydropyridine[1,8] is much simpler and more economical than the previous methods.[9,10]

In order to prepare compounds of type **3**, we examined the reaction of organocuprates (I) (Li[R_2Cu], R=alkyl or aryl). However, desired 1,4-adducts could not be obtained under various conditions; only the starting material was recovered unchanged.

Reaction with Other Nucleophiles. The pronounced tendency of 1,2-addition of the above anionic nucleophiles could be reversed by the use of nonanionic nucleohiles, such as pyrrole. The reaction of **1** with excess pyrrole at 130 °C for 14 h gave 5-phenyl-1,3,4,4a, 5,9a-hexahydro-2*H*-pyrrolo[1',2':1,5]pyrrolo[2,3-*b*]pyridine(**6**) in 32% yield. Structural assignment was based on analytical and spectral data (MS, IR, ^{1}H and ^{13}C NMR). The presence of the fused pyrrole ring was evident by IR (1490 cm^{-1}, pyrrole ring skeletal vibration) as well as by ^{13}C NMR spectrum (four sp^2-carbons at δ 101.51(d), 111,85(d), 111.85(d)† and 142.32(s)). In its ^{1}H NMR spectrum, the three olefin protons absorbed at δ 5.83(d, *J*=3 Hz), 6.27(t, *J*=3 Hz) and 6.70(d, *J*=3 Hz) and two protons at δ 5.10(d, *J*=6 Hz) and 4.01(d, *J*=6 Hz) were assigned to the benzylic proton and the methine proton adjacent to the two nitrogen atoms, respectively. These NMR data were consistent with the tricyclic structrue **6**. This was also supported by analytical and mass spectral data.

Structure **6** suggested possible intervention of intermediate **5**, which may have been formed by 1,4-addition of pyrrole to the conjugated imine system of **1** (scheme 2). The reaction may be regarded as an electrophilic substitution of **1** with pyrrole which usually undergo such reactions preferentially at C2. This reaction therefore presents striking contrast to the previously mentioned examples of 1,2-addition of charged nucleophiles. It is very interesting that such a complex heterocyclic system can be constructed in one step by this reaction.

The other uncleophile examined was ethyl propiolate which is usually regarded as an electrophile because of its electron deficient triple bond. However, its conjugate base often functions as a nucleophile.[11]

Thus the reaction of **1** with ethyl propiolate (r.t., 13h, 73%; reflux, 0.5 h, 68%) afforded **9**. The structural elucidation of ethyl 4-[1-(2-ethoxycarbonylvinyl)-1,4,5,6-tetrahydro-3-pyridyl]-4-phenyl-2-butynoate (**9**) was based on spectroscopic data (MS, IR, ^{1}H and ^{13}C NMR). The mass spectral molecular ion peak (M^+=367) as well

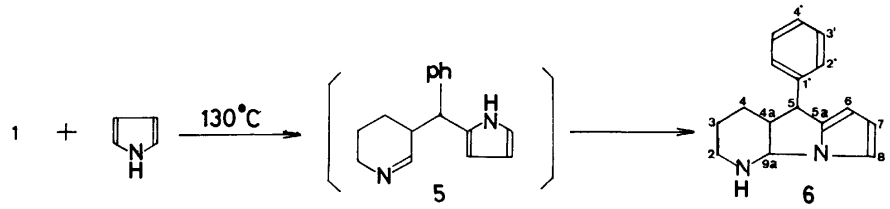

Scheme 2.

† Two signals are degenerated at the decoupling condition (see Experimental).

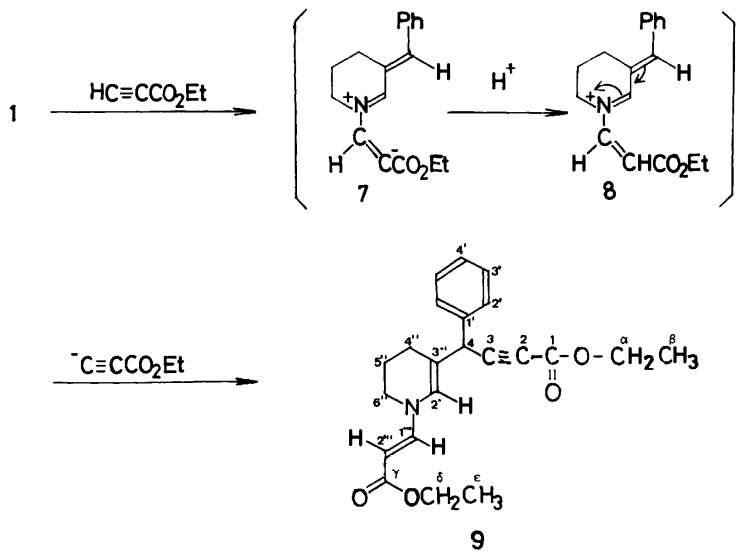

Scheme 3.

as ^{13}C NMR spectrum (a total of 20 peaks) established the molecular formula ($C_{22}H_{25}O_4N$). The presence of a *trans* C=C bond was suggested by ^{13}C NMR (δ 88.58 (d) and 150.33 (d)) and ^1H NMR (δ 4.85 (d, J=12 Hz) and 7.42 (d, J=12 Hz)).[12] The proton absorption at δ 4.85 disappeared upon addition of D_2O in agreement with the general behavior of the β-proton of an enamine system.[13] The other double bond was identified as a part of the endocyclic enamine segment on the basis of ^{13}C NMR (δ 127.42 or 127.96 (d) and 133.54 (s)) and ^1H NMR (δ 4.76(s)). The triple bond was evident by ^{13}C NMR (δ 77.47 (s) and 82.67 (s)) as well as by IR (2220 cm^{-1}).

The formation of **9** could be most simply rationalized by initial attack of one molecule of ethyl propiolate at the nitrogen of **1** to form the zwitter ion **7** and subsequent 1,6-addition of a second molecule of the acetylenic ester *via* the nitrilium ion intermediate **8**.[12] A similar reaction has previously been observed between pyridine and metyl propiolate to afford the 1,2-dihydropyridine **10**.[14]

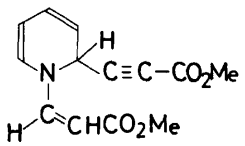

10

In summary, although our intention to synthesize both **2** and **3** could not entirely be satisfied in the present investigation, compounds **2** are potentially useful as anticholine or antihistamine drugs and the unanticipated formation of compounds **6** and **9** is intriguing not only because of the initial mechanism (1,4-addition) of their formation, but also because of their unique structural feature which is otherwise only difficultly accessible.

Experimental

All reactions were performed under dry inert conditions. Solvents used were purified by distillation over appropriate drying agent under dry nitrogen atmosphere. Mass spectra were measured on a Hitachi-Perkin Elmer RMU-6D spectrometer. Infrared spectra were recorded on a JASCO DS-403G spectrometer. ^1H NMR spectra were obtained with a JEOL MH-100 spectrometer. ^{13}C NMR spectra were recorded on a JEOL FX-90Q spectrometer operated at 22.5 MHz. Typical acquisition parameters were spectral width 5000 Hz, flip angle 30° and pulse delay 2s with 8192 data points. The ^{13}C NMR spectral data of the products (**2a**, **2b**, **2c**, **6**, and **9**) were collected in Table 1 and assignments were rationalized at the end of this section. All chemical shifts were reported in δ relative to internal tetramethylsilane.

5-Benzylidene-2,3,4,5-tetrahydropyridine (1).[1] A mixture of 2,3,4,5-tetrahydropyridine trimer (α-isomer) (32.5 g, 0.131 mol) and benzaldehyde (45.6 g, 0.430 mol) in absolute methanol (500 ml) was heated under reflux for 4 h. After removal of the solvent *in vacuo*, the residue was fractionally distilled to afford 28.0 g(42%) of 5-benzilidene-2,3,4,5-tetrahydropyridine (**1**): bp 108—110 °C (0.25 mmHg)

Reaction of 1 with Sodium Tetrahydroborate. Sodium tetrahydroborate (509 mg, 13.5 mmol) dissolved in methanol (20 ml) was added dropwise with stirring to a solution of **1** (1.085 g, 6.35 mmol) in methanol (30 ml) at ambient temperature. After additional 2 h stirring, concentrated hydrochloric acid (10 ml) was added to the reaction mixture. After removal of the solvent, water (15 ml) was added to the residue. The resultant solution, saturated with potassium carbonate, was extracted with diethyl ether. After drying the extract over anhydrous sodium sulfate and subsequent removal of ether *in vacuo*, 3-benzylidenepiperidine (**2a**) (984 mg, 90%) was obtained as colorless oil. ^1H NMR($CDCl_3$): δ 1.57(quintet, J=6 Hz, 2H), 2.13(s, 1H), 2.50(t, J=6 Hz, 2H), 2.90(t, J=6 Hz, 2H), 3.37(s, 2H), 6.27(s, 1H), and 7.00—7.40(m, 5H); IR(neat): 745 and 700 cm^{-1}; MS: M^+=173.

Reaction of 1 with Lithium Tetrahydroaluminate. A): A solution of **1** (983 mg, 5.75 mmol) in absolute ether (10 ml) was added dropwise with stirring to dry dietyl ether (15 ml) suspended with lithium tetrahydridoaluminate (500 mg, 13.2 mmol) at 0 °C. After additional 2 h stirring, ice-water was added to the reaction mixture. The organic layer was separated, dried with anhydrous sodium sulfate, and evapo-

Table 1. C-13 chemical shifts (δ) for **1**, **2a**—**2c**, **6** and **9**[a]

1		**2a**	**2b**	**2c**	**6**		**9**	
C6	163.64	C2	55.42	65.98	61.33	C9a	69.72	C2'	127.42[c]
C5	131.70	C3	139.72	142.48	142.37	C4a	50.66	C3''	133.54
C4	21.63	C4	27.85	27.41	26.11	C4	23.16	C4''	24.11
C3	25.03	C5	29.04	28.98	28.98	C3	25.35	C5''	25.02
C2	49.70	C6	47.02	45.24	43.39	C2	41.39	C6''	45.94
Cα	136.11	Cα	123.03	124.93	122.00	C5	47.00	C4	56.99
C1'	135.93	C1'	137.44	137.71	137.82	C1'	137.74	C1'	135.71
C2'	129.43[b]	C2'	128.83[b]	128.88[b]	128.94[b]	C2'	128.33[b]	C2'	128.88[b]
C3'	128.42[b]	C3'	128.07[b]	127.96[b]	128.01[b]	C3'	127.69[b]	C3'	128.34[b]
C4'	128.00	C4'	126.23	126.23	126.12	C4'	126.52	C4'	127.96[c]
		C1''		141.34	31.48	C5a	142.32	C3	82.67
		C2''		127.96[b]	29.36	C6	111.85	C2	77.47
		C3''		128.29[b]	22.81	C7	101.51	C1	153.04
		C4''		126.99	14.14	C8	111.85	Cα	62.19
								Cβ	13.98
								C1'''	150.33
								C2'''	88.58
								Cγ	169.08
								Cδ	59.21
								Cε	14.57

a) Measured in $CDCl_3$ on a JEOL FX-90Q spectrometer operated at 22.5 Hz (See Experimental section for acquisition conditions). b, c) Assignments may be reversed.

rated to afford **2a** (843 mg, 85%).

B): A solution of **1** (529 mg, 3.09 mmol) in dry tetrahydrofuran (10 ml) was added to dry tetrahydrofuran (15 ml) suspended with lithium tetrahydridoaluminate (494 mg, 13.0 mmol) under reflux. After continued reflux for 30 min, ice-water was added to the reaction mixture. The organic layer was separated, dried with anhydrous sodium sulfate, and evaporated to leave **2a** (421 mg, 79%).

Reaction of 1 with Phenylmagnesium Bromide. A solution of bromobenzene (2.5 ml, 23.9 mmol) in absolute dietyl ether (14 ml) was added under nitrogen atmosphere to magnesium powder (600 mg, 24.7 mmol) to form phenylmagnesium bromide. Subsequently, a solution of **1** (1.070 g, 6.26 mmol) dissolved in absolute ether (6 ml) was added to the Grignard reagent. The mixture was stirred for 14 h at ambient temperature and then poured into ice-cold 10% hydrochloric acid. The usual work-up followed by purification by silica-gel column chromatography using diethyl ether/dichloromethane (1 : 1) as an eluant afforded 3-benzylidene-2-phenylpiperidine (**2b**) (870 mg, 56%); mp 60.0—60.5 °C (sublimed, uncorrected); ^{1}H NMR ($CDCl_3$) δ 1.67 (quintet, J=6 Hz, 2H), 1.93 (broad s, 1H), 2.17—3.00 (m, 4H), 4.43 (broad s, 1H), 5.90 (broad s, 1H) and 7.00—7.56 (m, 10H); IR (KBr) 754, and 692 cm^{-1}; MS m/z 249 (M^+); Found: C, 86.71; H, 7.47; N, 5.85%. Calcd for $C_{18}H_{19}N$: C, 86.70; H, 7.68; N, 5.62%.

Reaction of 1 with Butyllithium. Butyllithium dissolved in hexane (1.51 mol/l, 4 ml) was added under nitrogen atmosphere to a cold (−78 °C) solution of **1** (500 mg, 2.92 mmol) in tetrahydrofuran (10 ml) and stirred for 45 min at −78 °C. The reaction was quenched with 10 ml of water and the resultant solution, saturated with potassium carbonate, was extracted with ether. The extract was dried over anhydrous sodium sulfate and the ether removed *in vacuo*. 3-Benzylidene-2-butylpiperidine (**2c**) was obtained as colorless oil. ^{1}H NMR ($CDCl_3$) δ 0.93 (t, 3H), 1.01—2.00 (m, 8H), 2.20 (broad, 1H), 2.33—3.33 (m, 4H), 3.60 (t, 1H), 6.27 (broad s, 1H) and 7.20 (m, 5H); IR (neat) 740 and 695 cm^{-1}; MS m/z 229 (M^+).

Reaction of 1 with Pyrrole. **1** (989 mg, 5.78 mmol) was dissolved in pyrrole (10 ml) and heated under reflux for 14 h. After removal of excess pyrrole *in vacuo*, the residue was purified by dry alumina column chromatography using hexane-dichloromethane-diethyl ether (1 : 1 : 1) as an eluent to afford 5-phenyl-1,3,4,4a,5,9a-hexahydro-2*H*-pyrrole[1',2' : 1,5]-pyrrolo[2,3-*b*]pyridine (**6**) (442 mg, 32%); mp 82.5—83.0 °C (sublimed, uncorrected); ^{1}H NMR ($CDCl_3$) δ 1.20—2.23 (m, 5H), 2.40—3.00 (m, 3H), 4.01 (d, J=6 Hz, 1H), 5.10 (d, J=6 Hz, 1H), 5.83 (d, J=3 Hz, 1H), 6.27 (t, J=3 Hz, 1H) 6.70 (d, J=3 Hz, 1H) and 7.00—7.57 (m, 5H); IR (KBr) 1490 (pyrrole ring), 748, 733, 720, 705 and 672 cm^{-1}; MS m/z 238 (M^+); Found (Calcd): C 80.63 (80.63), H 7.55 (7.61), N 11.91 (11.75).

Reaction of 1 with Ethyl Propiolate. A): A mixture of ethyl propiolate (9.77 mmol) and **1** (500 mg, 2.92 mmol) dissolved in benzene (20 ml) was heated under reflux for 30 min under nitrogen atmosphere. After removal of solvent *in vacuo*, the residue was purified by dry silica-gel column chromatography using hexane-dichloromethane-diethyl ether (2 : 1 : 1) as an eluant to afford ethyl 4-[1-(2-ethoxycarbonylvinyl)-1,4,5,6-tetrahydro-3-pyridyl]-4-phenyl-2-butynoate (**9**) (725 mg, 68%).

B): A mixture of ethyl propiolate (9.77 mmol) and **1** (456 mg, 2.67 mmol) dissolved in benzene (20 ml) was stirred under nitrogen atmosphere at ambient temperature for 13 h. After removal of solvent *in vacuo*, the residue was purified as described above to provide **9** (713 mg, 73%). ^{1}H NMR ($CDCl_3$) δ 1.20 (t, J=7 Hz, 3H), 1.25 (t, J=7 Hz, 3H), 1.43—2.00 (m, 2H), 2.20—2.60 (m, 1H), 2.70—3.00 (m, 1H), 3.33 (t, 2H), 4.12 (q, J=7 Hz, 2H), 4.20 (q, J=7 Hz, 2H), 4.76 (s, 1H), 4.85 (d, J=12 Hz, 1H exchangeable with D_2O), 6.50 (broad s, 1H), 7.00—7.47 (m, 5H) and 7.42 (d, J=12 Hz, 1H); IR (neat): 2220 (-C≡C-), 1710 (-C=C-CO-O-), 748, and 698 cm^{-1}; MS m/z 367(M^+).

^{13}C NMR Spectra. ^{13}C NMR chemical shift values are tabulated in Table 1. The assignment was made chiefly by the splitting pattern under off-resonance decoupling

conditions and by comparison with the compounds having similar (or partially similar) structures. The numbering of carbon atoms (see the structures in the schemes) is in some cases provided only for the sake of easy comparison.

5-Benzylidene-2,3,4,5-tetrahyropyridine (1): The low field signal of imine carbon atom was already described.[1] The assignment of C2′ and C3′ signals was based on the spin-lattice relaxation times (T_1). Thus, it is expected that C3′ relax faster than C2′. The chemical shift data for styrene[15] was also taken into consideration.

3-Benzylidenepiperidines (2a—c): Comparison with the δ values for **2a—c** with those of **1** leaves little uncertainty in the assignment except that the assignment for C2′ and C3′ may be reversed. The differentiation of signals due to two aromatic rings of **2b** was made based on the assumption that C1′—C4′ resonances are in much the same field among three compounds **2a—c**.

5-Phenyl-1,3,4,4a,5,9a-hexahydro-2H-pyrrolo[1′,2′:1,5]pyrrolo-2,3-b]pyridine (6): Of the two monoprotonated carbon resonances at δ 47.00 and δ 50.66, the latter can be assigned to C4a because of apparently shorter relaxation time due to the greater number of protons in the vicinity. Of the four sp^2-carbons of pyrrole moiety, two give a degenerate signal at δ 111.85, which should inevitably be assigned to C6 and C8 from chemical shift consideration. This assignment was confirmed by the observation that under weak decoupling condition the peak split into a pair of doublet with different splitting which reflects the distance between the carbon in question and the nitrogen atom. A high-field shift of unprotonated α-carbon resonance into protonated β-carbon region seems characteristic of α-carbons of 1,2-disubstituted pyrrole.[16]

Ethyl-[1-(2-ethoxycarbonylvinyl)-1,4,5,6-tetrahydro-3-pyridyl]-4-phenyl-2-butynoate (9): There are in **9** four sp^2-hydridized enamine carbon atoms, of which the signal due to the unprotonated C3″ is assigned based on chemical shift consideration. Peaks at δ 88.58 and 150.33, are assigned to C2‴ and C1‴, respectively, since the corresponding carbon nuclei of enamino ester resonate at δ 84.0 and 160.6, respectively.[17] Hence, the peak at δ 127.42 or 127.96 is due to C2‴, an unsaturated α-carbon of 1,2,3,4-tetrahydropyridine moiety which resonates at δ 132—133.[18]

Of the two signals at δ 77.47 and 82.67 due to two sp-hybridized carbons, the latter which shows a small coupling with H4 is assigned to C3. Of the signals due to two sets of OCH_2-CH_3 moiety, peaks at δ 13.98 and 62.19 are assigned to Cβ and Cα, respectively, based on comparison with the δ values for ethyl propiolate.[19] Similarly, C=O signal in higher field as an ester carbonyl carbon (δ 153.04) was assigned to C1.[19] This is an additional support for the presence of -C≡CCOO- moiety.

The present work was partially supported by a Grant-in-Aid for Scientific Research No. 443007 from the Ministry of Education, Science and Culture.

References

1) Y. Nomura, T. Bando, Y. Takeuchi, and S. Tomoda, *Bull. Chem. Soc. Jpn.*, **56**, 3199 (1983).
2) S. Ohki, N. Ozawa, Y. Yabe, and H. Matsuda, *Chem. Pharm. Bull.*, **24**, 1362 (1976), and references cited therein.
3) For comprehensive reviews on the piperidine alkaloids, see; "The Alkaloids," ed by M. F. Grundon, The Chemical Society, London (1976), **7**, pp. 54—64.
4) a) H. C. Brown and H. M. Hess, *J. Org. Chem.*, **34**, 2206 (1969); b) W. R. Jackson and A. Zurgiyah, *J. Chem. Soc.*, **1965**, 5280.
5) F. A. Hochstein and W. G. Brown, *J. Am. Chem. Soc.*, **70**, 3484 (1948).
6) R. F. Nystrom and W. G. Brown, *J. Am. Chem. Soc.*, **70**, 3738 (1948).
7) a) H. Gilman and G. C. Gainer, *J. Am. Chem. Soc.*, **71**, 2327 (1949); b) H. Kogen, K. Tomioka, S-I. Hashimoto, and K. Koga, *Tetrahedron Lett.*, **21**, 4005 (1980).
8) Synthesis of 2,3,4,5-tetrahydropyridine; C. Schopf, A. Komzak, F. Braun, and E. Jacobi, *Justus Liebigs Ann. Chem.*, **559**, 1 (1948).
9) Bischler-Napieralski reaction; S. Sugasawa and S. Ushioda, *Tetrahedron*, **5**, 48 (1959).
10) a) A. I. Meyers and J. J. Ritter, *J. Org. Chem.*, **23**, 1918 (1958); b) R. E. Gawley and E. J. Termine, *Tetrahedron Lett.*, **23**, 307 (1982).
11) R. M. Acheson, "Advances in Heterocyclic Chemistry," ed by A. R. Katritzky, Academic Press, New York (1963), Vol 1, pp. 125—165.
12) Although the value of the coupling constant (J=12 Hz) between the olefinic protons falls in "an ambiguous range" as an informative evidence for stereochemical assignment, α-amino-α,β-unsaturated esters, obtained by the reaction between enamines and ethyl propiolate, generally possess the C=C bond having *trans* configuration. It is therefore highly likely that the stereochemistry of the C=C in **9** is *trans*: C. B. Kanner and U. K. Pandit, *Tetrahedron*, **37**, 3513 (1981).
13) A. G. Cook, "Enamines," Marcel Dekker, New York (1969), p. 117.
14) A. Crabtree, A. W. Johnson, and J. C. Tebby, *J. Chem. Soc.*, **1961**, 3497.
15) G. K. Hamer, I. R. Peat, and W. F. Reynolds, *Can. J. Chem.*, **51**, 897 (1973).
16) E. Breitmeier and W. Voelter, "^{13}C NMR Spectroscopy," Verlag Chemie, Weinheim (1978).
17) S. Rajappa and K. Nagarajan, *J. Chem. Soc., Perkin Trans. 2*, **1978**, 921; C1=84.0, C2=160.6 for $Me_2NC^2(Me)=C^1HCOOEt$.
18) Y. Nomura, T. Bando, Y. Takeuchi and S. Tomoda, *Tetrahedron Lett.*, **1979**, 3453.
19) δ values for ethyl propiolate $HC^3\equiv C^2C^1OOC^1'H_2C^{2+}$-$H_3$; C1=152.8, C2=76.5, C3=75.1, C1′=62.4, C2′=13.9.

The Willgerodt-Kindler Reaction between Polycyclic Aromatic Amines and Benzaldehyde. Formation of 1,3-Thiazines

Yujiro NOMURA, Takashi HAYAMA, Yoshito TAKEUCHI,*
Shuji TOMODA, and Yuko KATO
Department of Chemistry, College of Arts and Sciences, The University of Tokyo, Komaba, Meguro-ku, Tokyo 153
(Received December 15, 1983)

The title reaction performed under typical conditions of the Willgerodt-Kindler reaction afforded "abnormal" product 1,3-thiazines. A mechanism involving the Diels-Alder reaction between *N*-benzylidenearylamine and thiobenzaldehyde has been suggested to explain the formation of 1,3-thiazines.

The Willgerodt-Kindler reaction,[1] in which ketones or aldehydes are allowed to react with amines in the presence of elemental sulfur under thermal conditions, is well known as an effective method for the preparation of thioamides. We now report the formation of abnormal products, 1,3-thiazines in the reaction between benzaldehyde and polycyclic aromatic amines under the typical Willgerodt-Kindler conditions[2] and present evidence for the possible intervention of thiobenzaldehyde, an elusive species which has attracted considerable attention in recent years.[3]

Results and Discussion

Typical reaction conditions are illustrated by the reaction between 1-naphthylamine (**1**) and benzaldehyde (**2a**). A mixture of **1**, **2a** and an excess powdered sulfur was heated at 140—150 °C for 48 h under a nitrogen atmosphere. Brisk evolution of hydrogen sulfide was evident by the positive test on lead tetraacetate paper during the reaction. The dark viscous reaction mixture was purified by column chromatography to give 2,4-diphenyl-4*H*-naphtho[1,2-*d*][1,3]thiazine (**3a**, 29% yield) and *N*-(1-naphthyl)thiobenzamide (48% yield)[2] in addition to two minor products, 2,4-diphenyl-1,4-dihydro-2*H*-naphtho[1,2-*d*][1,3]thiazine (**4a**, 6% yield) and an unidentifiable compound (11% yield).

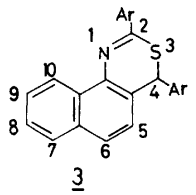

3

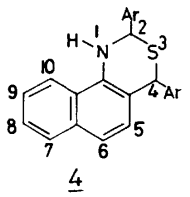

4

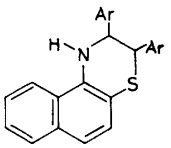

4′

The structures of the 1,3-thiazine (**3a**) and dihydrothiazine (**4a**) were assigned by spectral data (IR, ^{1}H and ^{13}C NMR, MS) and elemental analysis. With regard to the structure of dihydrothiazine (**4a**), the position of the heteroatoms in the thiazine ring system was determined by its ^{1}H NMR data. The proton of C-2 showed up as a doublet (δ 5.26, J=5.5 Hz), whereas that of C-4 appeared as a singlet (δ 5.41). This indicated that the structure of **4a** is more consistent with the 1,3-thiazine ring system represented by formula **4** (Ar=Ph) than structure **4′**. The most explicit evidence for the structure of thiazine (**3a**) was obtained by dehydrogenation of dihydrothiazine (**4a**) over elemental sulfur in refluxing pyridine: **4a** was converted into **3a** in 80% yield.

The reactions between **1** and *p*-substituted benzaldehydes (**2**) are summarized in Table 1. The yield of **3** varies from 24 to 35%. The structures of these compounds **3** were assigned on the basis of spectral (^{1}H and ^{13}C NMR, IR, MS) and analytical data. Although these reactions afforded thioamides as the major product, the formation of **3** is significant since such an easy preparation of 1,3-thiazines has not been reported to date.[4]

Table 1. Synthesis of 1,3-thiazines (**3**, **12**, **13**, and **14**) from aromatic amines (**1**, **9**, **10**, and **11**)

Amine	ArCHO(**2**)[a]	Reagent/mmol			Conditions	1,3-Thiazine	Yield/%[b]
		1	**2**	S	Temp/°C, Time/h		
1	**2a**	10	20	30	150, 48	**3a**	29
1	**2b**	10	20	22	145, 42	**3b**	35
1	**2c**	10	20	23	145, 41	**3c**	24
9	**2a**	20	40	40	140, 7	**12**	13
10	**2a**	2.6	5.3	5.3	145, 22[c]	**13**	32
11	**2a**	2.8	6.8	6.3	145, 24[c]	**14**	22

a) **2a**: Benzaldehyde, **2b**: *p*-chlorobenzaldehyde, **2c**: *p*-bromobenzaldehyde. b) Isolated, unoptimized yield. c) In 4-Methylpyridine.

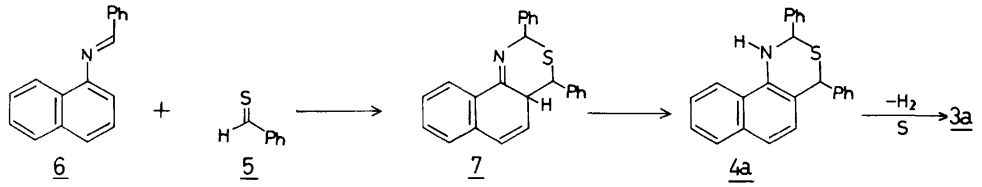

(Eq. 1)

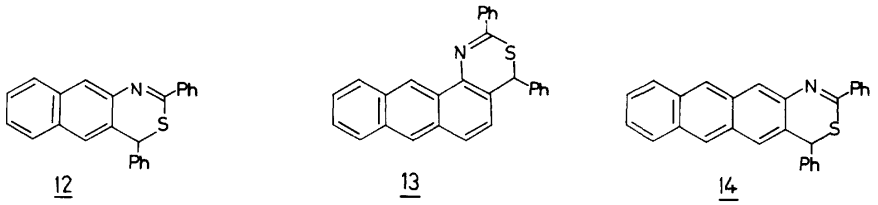

With a view to extend this reaction to other amines, we were particularly intrigued by the mechanism which might involve thiobenzaldehyde (**5**): It was anticipated that 1,3-thiazine might have arisen from the Diels-Alder reaction between **5** and *N*-benzylidene-1-naphthylamine **6**, a 2-aza-1,3-butadiene in which the C=C bond is incorporated in the naphthalene ring. It is well established that aldehydes react with hydrogen sulfide in the presence of amine to afford thioaldehydes.[5] As shown in Eq. 1, thermal cycloaddition between **5** and **6** would give rise initially to **7**, which undergoes 1,3-H shift to afford dihydrothiazine **4a** (Eq. 1).

Conversion of **4** into **3** under the reaction conditions may be readily understood since **4** was transformed to **3** upon dehydrogenation with elemental sulfur as described earlier. In order to demonstrate possible intervention of **5**, **6** was allowed to react with **5** generated *in situ* from *S*-benzyl phenylmethanethiosulfinate (**8**).[3a] Indeed, when a mixture of **6** and a large excess **8** in toluene was heated at 100 °C for 20 h in the presence of 4A Molecular Sieves, **4a** was isolated in 47% yield. Mixed melting point as well as spectral data (^{1}H NMR and IR) unequivocally established the structure of this product. The formation of the thioamide was not observed in this reaction. It should be noted here that the reaction of 2-aza-1,3-butadiene and thiocarbonyl compound has not previously been reported.[6]

Synthesis of 1,3-thiazines under Willgerodt-Kindler conditions can also be applied to other aromatic amines, such as 2-naphthylamine (**9**), 1-anthrylamine (**10**) and 2-anthrylamine (**11**) (Table 1). Structure assignments of the products (**12**, **13**, and **14**) were based on spectral data (NMR, IR and MS) and combustion analysis. In the cases of **9** and **11**, the structures of the 1,3-thiazines (**12** and **14**, respectively) were more consistent with formulas **12** and **14** rather than with **12'** and **14'**. The absence of IR band near 810 cm^{-1} precluded the possibility of 1,2,3,4-tetrasubstituted benzene ring structures.

In summary, while the yield of 1,3-thiazines is not high, the present reaction as well as the reaction between 2-aza-1,3-diene and thiocarbonyl compound may suggest a useful general entry to 1,3-thiazine system, to which access has been difficult,[4] by appropriate choice of reaction conditions.

Experimental

All reactions were performed under dry nitrogen. Mass spectra were measured with a Hitachi RMU-6MG Spectrometer. ^{1}H NMR and ^{13}C NMR spectra were measured with a Varian EM-390 spectrometer and a JEOL FX-90Q spectrometer, respectively, using $CDCl_3$ as solvent. Chemical shifts were recorded in δ scale relative to internal tetramethylsilane. IR spectra were recorded on a JASCO A-102 Spectrometer and the frequencies are given in reciprocal centimeter.

General Procedure of the Willgerodt-Kindler Reactions. The ratio of the reagents and reaction conditions are included in Table 1. Solvent was not used except for the preparation of **13** and **14**, for which 4-methylpyridine was used as the solvent. To a mixture of arylamine and benzaldehyde was added powdered sulfur and the mixture was stirred at 140—150 °C for 7—48 h in an oil bath under a nitrogen atmosphere. The resulting dark brown mixture was dissolved in dichloromethane and the unchanged sulfur was removed by filtration. The filtrate was concentrated and chromatographed on a silica-gel column (dichloromethane:hexane= 1—2:5) to give 1,3-thiazine in the yield shown in Table 1. In the case of **2a**, dihydro-1,3-thiazine **4a** was also separated.

Spectral and analytical data of 1,3-thiazine and **4a** now follow;

3a: Mp 175—176 °C; MS (70 eV) *m/z* 351 (M^+); ^{1}H NMR ($CDCl_3$) δ=5.40 (s, 1H, H-4), 7.15 (s, 5H, Ph), 7.4—7.9 (m, 10H, Ar), and 8.93—9.06 (m, 1H, Ar); ^{13}C NMR ($CDCl_3$) δ=158.4 (s), 141.8 (s), 139.5 (s), 138.5 (s), 133.8 (s), 131.5 (d), 130.5 (s), 128.7 (d), 128.5 (d), 127.8 (d), 127.7 (d), 127.6 (d), 127.4 (d), 126.5 (d), 125.6 (d), 124.1 (d), 117.3 (s), and 45.8 (d); IR (KBr) 1540, 1490, 1450, 1235, 940, and 810 cm^{-1}.

Found: C, 82.12; H, 4.89; N, 3.90; S, 9.06%. Calcd for $C_{24}H_{17}NS$: C, 82.02; H, 4.88; N, 3.99; S, 9.12%.

4a: Mp 182—183 °C; MS (70 eV) *m/z* 353 (M^+); ^{1}H NMR ($CDCl_3$) δ=4.80 (br s, 1H), 5.26 (d, *J*=5.5 Hz, 1H), 5.41 (s, 1H), and 7.20—7.96 (m, 16H); ^{13}C NMR ($CDCl_3$) δ=145.2 (s), 139.7 (s), 138.9 (s), 133.8 (s), 129.6 (d), 129.2 (d), 128.9 (d), 128.8 (d), 128.5 (d), 127.7 (d), 127.2 (s), 126.6 (d), 126.3 (d), 125.8 (d), 125.3 (d), 120.3 (d), 118.8 (d), 115.5 (s), 57.5 (d), and 48.2 (d); IR (KBr) 3400, 1565, 1510, 1460, 1400, 1110, and 800 cm^{-1}.

Found: C, 81.54; H, 5.22; N, 3.77;, S, 8.69%. Calcd for $C_{24}H_{19}NS$: C, 81.55; H, 5.42; N, 3.96; S, 9.07%.

3b: Mp 161—162 °C; MS (70 eV) *m/z* 420 (M^+); ^{1}H NMR ($CDCl_3$) δ=5.41 (s, 1H), 6.9—8.1 (m, 13H), and 8.97—9.16 (m, 1H); ^{13}C NMR ($CDCl_3$) δ=156.6 (s), 140.1 (s), 139.3 (s), 137.7 (s), 136.6 (s), 133.8 (s), 130.4 (s), 129.9 (s), 129.5 (d), 128.9 (d), 128.7 (d), 128.2 (d), 127.6 (d), 126.7 (d), 125.4 (d), 123.9 (d), 116.6 (s), and 45.0 (d); IR (KBr) 1535, 1483, 1232, 1167, 1089, 1010, and 930 cm^{-1}.

Found: C, 68.57; H, 3.45; N, 3.27; S, 7.95; Cl, 17.14%. Calcd for $C_{24}H_{15}NSCl_2$:C, 68.58; H, 3.60; N, 3.33; S, 7.63; Cl, 16.87%.

3c: Mp 140—141 °C; MS (70 eV) *m/z* 509 (M^+); ^{1}H NMR ($CDCl_3$) δ=5.35 (s, 1H), 6.85—8.10 (m, 13H), and 8.76—8.96 (m, 1H); ^{13}C NMR ($CDCl_3$) δ=140.6 (s), 137.1 (s), 133.8 (s), 131.7 (d), 130.2 (s), 129.6 (d), 129.0 (d), 128.2 (d), 127.6 (d), 126.7 (d), 126.3 (s), 125.3 (d), 124.6 (s), 123.9 (d), 121.8 (s), 116.6 (s), and 45.1 (d); IR (KBr) 1575, 1540, 1483, 1391, 1235, 1070, 1007, and 930 cm^{-1}.

Found: C, 56.64; H, 2.85; N, 2.66; S, 6.40; Br, 31.71%. Calcd for $C_{24}H_{15}NSBr_2$: C, 56.60; H, 2.97; N, 2.75; S, 6.30; Br, 31.38%.

12: Mp 201—202 °C; MS (70 eV) *m/z* 351 (M^+); ^{1}H NMR ($CDCl_3$) δ=6.10 (s, 1H), 7.00 (br s, 5H), 7.47 (m, 5H), 7.92 (m, 4H), and 8.18 (m, 2H); ^{13}C NMR ($CDCl_3$) δ=158.7, 141.9, 130.0, 133.6, 131.5, 130.3, 129.3, 129.1, 129.0, 128.8, 128.4, 128.4, 127.6, 127.1, 127.0, 126.9, 125.6, 123.2, 115.3, and 41.1; IR (KBr) 1540, 1490, 1445, 1260, 1240, 1195, 975, and 915 cm^{-1}.

Found: C, 82.15; H, 4.67; N, 3.98; S, 9.12%. Calcd for $C_{24}H_{17}NS$: C, 82.02; H, 4.88; N, 3.99; S, 9.12%.

13: Mp 185—186 °C; ^{1}H NMR ($CDCl_3$) δ=5.46 (s, 1H), 7.2 (br s, 6H), 7.41—7.62 (m, 5H), 7.85—8.43 (m, 6H), and 9.54 (s, 1H); IR (KBr) 1541, 1490, 1445, 1230, 1173, 1133, 939, and 795 cm^{-1}.

Found: C, 83.76; H, 4.50; N, 3.75; S, 8.21%. Calcd for $C_{28}H_{19}NS$: C, 83.76; H, 4.77; N, 3.49; S, 7.98%.

14: Mp 250—251 °C; ^{1}H NMR ($CDCl_3$) δ=6.26 (s, 1H), 7.2—8.2 (m, 16H), 8.49 (s, 2H); IR (KBr) 1540, 1492, 1447, 1255, 1170, and 965.

Found: C, 83.55; H, 4.48; N, 3.49; S, 8.23%. Calcd for $C_{28}H_{19}NS$: C, 83.76; H, 4.77; N, 3.49; S, 7.98%.

*Reaction of **4a** with Sulfur to Give **3a**.* To a solution of **4a** (35 mg, 0.1 mmol) in dry pyridine (10 mL) was added excess powdered sulfur and the mixture refluxed for 20 h. The resulting dark resinous material was dissolved in dichloromethane (60 mL). The solution was washed with water, 1 M hydrochloric acid (60 mL), aqueous sodium hydrogencarbonate, and water, dried over magnesium sulfate, and concentrated. The residue was chromatographed on a silica-gel column to give **3a** (28 mg, 80% yield), which was identified by comparison of spectral (IR and ^{1}H NMR) data of authentic **3a**.

*Synthesis of **4a** from **6** and **5** Generated from **8**.* A mixture of **6** (0.39 g, 1.7 mmol) and **8** (4.37 g, 17 mmol)[3a] in toluene (5 ml) was placed in a tube and 4A Molecular Sieves (4 g) was added. The tube was thoroughly purged with dry nitrogen and heated at 100 °C for 20 h. The reaction mixture was filtered to remove the molecular sieves and the filtrate concentrated in vacuo. It was then subjected to column chromatographic separation on silica gel (80 g) eluting with hexane:dichloromethane (10:3) to afford **4a** (280 mg, 47% yield). Mixed melting point, IR and ^{1}H NMR spectral comparison unambiguously established its structure.

References

1) E. V. Brown, *Synthesis*, **1975**, 358.
2) K. Kindler, *Justus Liebigs Ann. Chem.*, **431**, 187 (1923).
3) a) J. E. Baldwin and R. C. G. Ropetz, *Tetrahedron*, **39**, 1487 (1983); b) R. Okazaki, A. Ishii, N. Fukuda, H. Oyama, and. N. Inamoto, *J. Chem. Soc., Chem. Commun.*, **1982**, 1187; c) E. Vedejs and D. A. Perry, *J. Am. Chem. Soc.*, **105**, 1683 (1983); d) E. Vedejs, T. H. Eberlein, and D. L. Varie, *ibid*, **104**, 1445 (1982).
4) Review of 1,3-thiazines; G. Prota, "Organic Compounds of Sulfur, Selenium and Tellurium," The Chemical Society, London (1975).
5) R. Mayer, G. Hiller, M. Nitzschke, and J. Jentzsch, *Angew. Chem., Int. Ed. Engl.*, **2**, 370 (1963).
6) The Diels-Alder reaction of thiocarbonyl compounds itself has been reported previously.[3a,c,d]

NAD(P)$^+$-NAD(P)H Models. 49. Proximity Effect of a Phenyl Group on the Electron Transfer Process

Atsuyoshi Ohno,* Hisami Kobayashi Takehiko Goto,† and Shinzaburo Oka
Institute for Chemical Research, Kyoto University, Uji Kyoto 611
†*Department of Resource Chemistry, Faculty of Engineering University of Iwate, Morioka, Iwate 020*
(Received November 11, 1983)

1-Propyl-1,4-dihydronicotinamide (PNAH), 1-(3-phenylpropyl)-1,4-dihydronicotinamide (**1a**), 1-(2-phenylthioethyl)-1,4-dihydronicotinamide (**1b**), and 1-(4-phenylthiobutyl)-1,4-dihydronicotinamide (**1c**) and their 4-deuterated analogs are synthesized as NAD(P)H-models and subjected to the reduction of *m*-nitro-α,α,α-trifluoroacetophenone in the presence or absence of magnesium ion in acetonitrile. Kinetics at 323 K have been studied. Kinetic isotope effect is small (2.33) only when **1a** or **1b** is employed for the reduction in the presence of magnesium ion, whereas it appears large (≈3.2) under other conditions. The result has been interpreted in terms of steric interference by a proximate phenyl group on the approach of the substrate to form a binary (in the absence of magnesium ion) or ternary (in the presence of magnesium ion) complexes. Thermodynamic parameters for the formation of complexes between the models and magnesium ion have been studied. It has been elucidated that enthalpy of complexation is small for **1a** than others. However, the small enthalpy of complexation is compensated by small entropy of complexation affording almost constant free-energy of complexation throughout the models studied.

In a series of reports from our laboratory, we have emphasized that a complex of 1,4-dihydropyridine derivative and magnesium ion plays an important role in biomimetic reductions with NAD(P)H-models. The magnesium ion assists polarization of electron cloud on dihydropyridine moiety to migrate an electron onto a substrate.[1,2]

X-Ray crystallography and other evidence have revealed that zinc ion in certain liver alcohol dehydrogenases (LADH) is tetrahedrally coordinated by cysteinyl SH and/or histidinyl nitrogen.[3,4] It is commonly accepted that the zinc ion in the enzyme behaves as a Lewis acid to polarize the carbonyl group of a substrate.[5] However, it is not obvious whether tetrahedrally coordinated zinc ion in an enzyme can accommodate a carbonyl group as an extra ligand.[6] At least in the mimetic reactions, metal ions with an chelating reagent exerted no catalytic activity.[1]

In order to understand the mechanism of enzymic oxidation-reduction with NAD(P$^+$)-NAD(P)H coenzyme, not only interactions between the coenzyme and a substrate but also the effect of environment in the pocket of enzyme should be taken into account. The pocket is entirely surrounded by hydrophobic moieties.[6] Thus, we synthesized NAD(P)H-models with a phenyl or phenylthio substituent. This paper will describe the effect of magnesium ion on the kinetics of reduction with the model of this type in acetonitrile.

Results

Models employed for the study were PNAH and **1**. Although the substrate, *m*-nitro-α,α,α-trifuoroacetophenone (**2**) exerted no evidence for the formation of a complex with magnesium ion in acetonitrile, the models formed finite complexes that were detectable spectrophotometrically. The results are listed in Table 1. Kinetics were studied at 323 K in the presence or absence of magnesium perchlorate. Kinetics with 4-deuterated models were also studied and primary kinetic isotope effects were calculated according to Steffens and Chipman equation.[7] Results are summarized in Table 2.

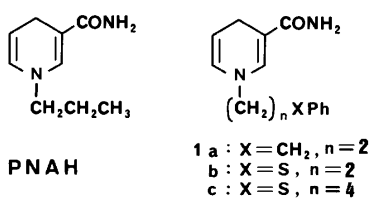

PNAH

It was already reported that water content in the solvent acetonitrile affects the rate of reduction.[8] In order to confirm the constancy of kinetic isotope effect on the variation of water content, we also studied kinetics for the reduction of **2** with PNAH and PNAH-4-*d* in acetonitriles containing 0.1 and 1.0% v/v of water, respectively. The kinetic isotope effect observed in these systems were the same as that listed in Table 2. Adduct-formation was not recognized. Thus, kinetic isotope effects listed in Table 2 can be definitely divided into two classes, small (≈2.3) and large (≈3.2).

Discussion

It is apparent from Table 2 that the phenyl group on the third atom of the substituent chain exerts small kinetic isotope effect in the coexistence of magnesium ion. The observation is in contrast with that from PNAH, where kinetic isotope effects are large both in the presence and absence of magnesium ion. Energy diagram for the reduction with PNAH has been proposed to be consisted of two energy barriers, one of which that corresponds to the initial electron transfer process is lower than the other that corresponds to the proton (or hydrogen atom) transfer process. Therefore, the rate-determining step of the reduction involves largely the movement of hydrogen nucleus exerting large kinetic isotope effect. Since magnesium ion catalyzes the process of electron transfer, the presence of magnesium ion does not affect the magnitude of kinetic isotope effect, although it accelerates the rate.

Table 1. Association constants and thermodynamic parameters for the complex between the model and magnesium ion in acetonitrile[a)]

	PNAH	**1a**	**1b**	**1c**
10^{-1} K/mol dm^{-3}				
at 283 K	1901±67	1579±46	—	1729±85
at 293 K	1532±46	1472±44	1310±46	1420±36
at 303 K	1382±64	1368±35	1128±45	1225±32
at 313 K	1132±41	1203±47	892±42	972±43
at 323 K	919±44	948±41	724±24	780±37
$\Delta H°$/kJ mol^{-1}	−13.34±0.04	−6.82±0.02	−15.22±0.04	−14.96±0.05
$\Delta S°$/J mol^{-1} deg^{-1}	34.7±0.12	56.4±0.16	26.8±0.08	28.3±0.11
$\Delta G°$/kJ mol^{-1}	−23.88±0.07	−23.92±0.07	−23.37±0.07	−23.54±0.09

a) Errors are standard deviations.

Table 2. Rate constants and kinetic isotope effects for the reduction of *m*-nitro-α,α,α-trifluoroacetophenone in acetonitrile[a)]

Model	$[Mg^{2+}]$ = 0 mol dm^{-3}		$[Mg^{2+}]$ = 1.9×10^{-2} mol dm^{-3}	
	$10\,k$[b)]	k^H/k^D	$10\,k$[b)]	k^H/k^D
PNAH[c)]	2.98 ±0.062		6.43±0.127	
PNAH-4-*d*[c)]	1.96 ±0.065	3.17	4.21±0.060	3.23
1a	2.76 ±0.056		5.27±0.052	
1a-4-*d*	1.77 ±0.027	3.61	3.77±0.043	2.33
1b	0.742±0.008[d)]		2.38±0.035	
1b-4-*d*	0.488±0.010[d)]	3.17	1.70±0.024	2.33
1c	2.16 ±0.051		5.51±0.107	
1c-4-*d*	1.38 ±0.021	3.55	3.63±0.044	3.15

a) Errors are standard deviations. Errors in kinetic isotope effects are about 10% for each. [Substrate] = 2.20×10^{-2} mol dm^{-3}. [Model] = 1.00×10^{-3} mol dm^{-3}. b) dm^3 mol^{-1} min^{-1}. c) Data from ref. 2. d) [Substrate] = 4.50×10^{-2} mol dm^{-3}. [Model] = 2.30×10^{-3} mol dm^{-3}.

The present results indicate that **1a** and **1b** behave similarly to PNAH when magnesium ion is absent, whereas, in its presence, contribution of the initial electron transfer process to the rate-determining step becomes quite important in the reductions with **1a** and **1b**. It should be noted, however, that catalytic effect of magnesium ion in the reductions with **1a** and **1b** is as large as that in the reduction with PNAH. When the chain length becomes longer as seen in **1c**, the effect of phenyl group diminishes.

CPK-models for **1** suggest that the phenyl group in **1a** or **1b** locates very closely to the dihydropyridine ring. Thus, there is no doubt that a phenyl group closely situated to the dihydropyridine ring makes, by the assistance of magnesium ion, the movement of hydrogen nucleus easier. There are three possibilities to interpret the present result based on the reaction Scheme 1.

$$MH + S \underset{k_{-1}}{\overset{k_1}{\rightleftharpoons}} MH^+S^- \xrightarrow{k_2} M\cdot HS\cdot \xrightarrow{k_3} M^+ + HS^-, \qquad (1)$$
$$\qquad\qquad\qquad

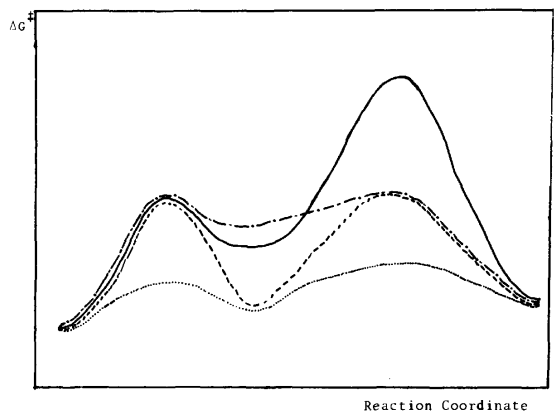

Fig. 1. Schematic energy diagram for the Reduction. The full line corresponds to the reduction without magnesium ion. Broken, dotted, and dashed lines correspond categories **1**, **2**, and **3** described in the text, respectively.

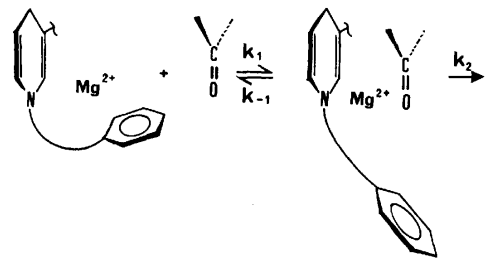

Scheme 1.

350 nm, there is no doubt that the magnesium ion primarily interacts with the dihydropyridine moiety. Nevertheless, the phenyl group in the model interrupts the approach of a substrate to form a composite ternary complex. The free-energy of transition state for the formation of initial intermediate, therefore, becomes higher than that with PNAH.

Once the intermediate is formed, on the other hand, competition takes place between the substrate and the phenyl group to ligate on the magnesium ion, and the free-energy level of the intermediate may be the same as that with PNAH (*cf.* Scheme 1). In other words, partition of the intermediate toward the reactants and products becomes less favored in the direction to the former. The energy level of the transition state for the k_2 (or k_2')-step, or migration of a hydrogen nucleus, is lowered and kinetic isotope effect becomes smaller.

Thermodynamic parameters listed in Table 1 indicate an interesting classification: although all models studied have equal free-energy of complexation, the enthalpy for **1a** is much smaller than those for others and the entropy compensates its minority. We do not have an appropriate explanation for this phenomenon. However, it seems probable that proximate phenyl group again interferes the approach of magnesium ion on complexation. The situation is improved in **1b** by the affinity of lone-pair electrons on sulfur.

Table 2 also shows that substitution of a methylene group in **1a** by a sulfur atom decreases the reactivity regardless the presence or absence of magnesium ion in the reaction system. The same trend was reported and the inhibitory effect of sulfur atom was attributed to the interference on the initial one-electron transfer process.[9] Characteristic absorption at around 350 nm from dihydropyridine moiety appears at shorter wavelength in **1b** than in other models (see Experimental), which suggests that **1b** is suffered from electronic distortion in its cyclic dienamine structure. Probably this is the reason of less ability to donate an electron to an acceptor. It is apparent, from Tables 1 and 2, that the sulfur substituent in the side-chain of model compound exerts different effects both in thermodynamics and kinetics from the corresponding methylene group. However, the proximity effect of the phenyl group is so large that present result alone is not sufficient to discuss on the effect of sulfur. Further and detailed discussion on the effect of sulfur substituent will be reserved for a forthcoming report from our laboratory.

Experimental

Melting and boiling points were not corrected.

Instruments. UV, NMR, and mass spectra were obtained on Union Giken SM-401, JEOL JNMFX-100, and Hewlett Packard 5992B GC/mass spectrometers, respectively. A Yanaco G-1800F was used for GLC analyses.

Materials. Acetonitrile was distilled over phosphorus pentaoxide five times and kept over potassium carbonate under argon atmosphere. The acetonitrile was refluxed over calcium hydride several hours, then distilled from the same pot under argon atmosphere prior to the use. Magnesium perchlorate was dried over phosphorus pentaoxide for a couple of days under reduced pressure at 400 K. The water content in a solution which was subjected to the kinetic or thermodynamic measurement was determined on GLC (30% bis(2-cyanoethyl) ether, 1 m, 313 K) prior and after the experiment and found to be less than 0.075% v/v.

1-Propyl-1,4-dihydronicotinamide (PNAH) and PNAH-4-*d* were prepared as described previously.[10] 1-(3-phenylpropyl)-1,4-dihydronicotinamide (**1a**), 1-(2-phenylthioethyl)-1,4-dihydronicotinamide (**1b**), and 1-(4-phenylthiobutyl)-1,4-dihydronicotinamide (**1c**) and their 4-deuterated analogs were prepared similarly. Deuterium contents were measured on GC/MS and NMR to be more than 99.5% for all deuterated compounds.

1a: λ_{max}=232 nm (ε=5.13×10³) and 352 nm (ε=5.36×10³) in acetonitrile at 303 K. Found: C, 74.05; H, 7.59; N, 11.42%. Calcd for $C_{15}H_{18}N_2O$: C, 74.35; H, 7.49; N, 11.56%.

1b: λ_{max}=254 nm (ε=8.48×10³) and 347 nm (ε=5.41×10³) in acetonitrile at 303 K. Found: C, 64.51; H, 6.26; N, 10.71%. Calcd for $C_{14}H_{16}N_2OS$: C, 64.59; H, 6.19; N, 10.76%.

1c: λ_{max}=256 nm (ε=1.01×10⁴) and 351 nm (ε=5.45×10³) in acetonitrile at 303 K. Found: C, 66.35; H, 7.00; N, 9.88%. Calcd for $C_{16}H_{20}N_2OS$: C, 66.63; H, 6.99; N, 9.71%.

m-Nitro-α,α,α-trifluoroacetophenone (**2**) was prepared according to a literature procedure.[11]

Kinetic Procedure. Solutions for kinetic studies were prepared under an atmosphere of argon and placed in a UV cell (0.1 dm) equipped with a silicon rubber stopper. The cell compartment of the spectrometer was also filled with dry argon and kept at 323±0.05 K. As a standard procedure, both sample and reference celles were filled with solutions of a substrate (and magnesium perchlorate, when necessary) in acetonitrile to obtain a difference spectrum. Then an acetonitrile solution of a model compound was injected into the sample cell by using a syringe to start the reaction.

The kinetics was followed by observing the decrease in the

intensity at 380 nm from a model. The spectrometer was attached by an NEC PC-8001 computor and absorptions at appropriate time intervals were monitored over 3 half-lives through the computer. One observed absorption was the avarage of 80 consecutive input. More than 50 points were monitored for a run. The data were automatically subjected to the least-squares treatment to give a pseudo-first order rate constant. Standard deviation and correlation coefficient for each run were better than ±1% (better than ±0.75% in most runs) and 0.9999, respectively. More than 5 runs were averaged to obtain rate constants listed in Table 2.

Thermodynamic Parameters. Equilibrium constants at appropriate temperatures were obtained by similar procedure as described above and according to the equation proposed by Creighton.[12]

References

1) A. Ohno, T. Kimura, H. Yamamoto, S. G. Kim, S. Oka, and Y. Ohnishi, *Bull. Chem. Soc. Jpn.*, **50**, 1535 (1977).

2) A. Ohno, H. Yamamoto, and S. Oka, *J. Am. Chem. Soc.*, **103**, 2041 (1981).

3) C.-I. Brändén, H. Jörnvall, H. Eklund, and B. Furugren, "The Enzymes," ed by P. D. Boyer, Academic Press, New York, N. Y. (1975), Vol. XI, Part A, Chap. 3, pp. 103—190.

4) M. J. Adams, J. R. Helliwell, and C. E. Bugg, *J. Mol. Biol.*, **112**, 183 (1977).

5) For Example, see D. S. Sigman, J. Hajdu, and D. J. Creighton, "Bioorganic Chemistry," ed by E. E. van Tamelen, Academic Press, New York, N. Y. (1978), Vol. 4, Chap. 14, pp. 385—407.

6) In horse liver alcohol dehydrogenase, the substrate oxygen ligates on the zinc ion as one of four ligands; a) H. Eklund, J. -P. Samama, L. Wallén, C. -I. Brändén, Å. Åkeson, and T. A. Jones, *J. Mol. Biol.*, **146**, 561 (1981); b) H. Eklund, B. V. Plapp, J. -P. Samama, and C. -I. Brändén, *J. Biol. Chem.*, **257**, 14349 (1982).

7) J. J. Steffens and D. M. Chipman, *J. Am. Chem. Soc.*, **93**, 6694 (1971).

8) A. Ohno, H. Kobayashi, K. Nakamura, and S. Oka, *Tetrahedron Lett.*, **24**, 1263 (1983).

9) A. Ohno, H. Kobayashi, S. Oka, and T. Goto, *Tetrahedron Lett.*, **24**, 5123 (1983).

10) A. Ohno, S. Yasui, K. Nakamura, and S. Oka, *Bull. Chem. Soc. Jpn.*, **51**, 290 (1978).

11) R. Stewart and R. Van der Linder, *Can. J. Chem.*, **38**, 399 (1960).

12) D. J. Creighton, Ph. D. Thesis, University of California, Los Angeles, 1972, pp. 174—175.

 © 1984 The Chemical Society of Japan Bull. Chem. Soc. Jpn., 57, 1283—1289 (1984)

Catalytic Activity of Highly Dispersed Palladium. III. The Effect of Added Zirconium Oxide upon Palladium Metal Surface Revealed by a Combined Infrared Spectroscopic and Thermal Desorption Study of Carbon Monoxide Adsorption

Bu Yong LEE, Yasunobu INOUE,*,† and Iwao YASUMORI

Department of Chemistry, Tokyo Institute of Technology, Ookayama, Meguro-ku, Tokyo 152

†*Analysis Center, Technological University of Nagaoka, Nagaoka, Niigata 949-54*

(Received August 11, 1983)

A combined infrared spectroscopic (IR) and thermal desorption (TD) study of CO adsorption was carried out to reveal the nature of Pd surface which is modified by the addition of ZrO_2. The TD spectra of CO from SiO_2- or α-Al_2O_3-supported Pd showed two broad peaks, α at 340 K and β at 530 K. The addition of ZrO_2 in a range of atomic ratios of Zr/Pd=0.5—3.0 produced a new broad peak δ at 390—420 K and the β peak shifted toward higher temperature by 16—19 K. The IR spectra of CO on Pd/SiO_2 catalysts, consisting of two broad bands: A (2030—2070 cm^{-1}) and B (1880—1920 cm^{-1}), were modified by the addition of ZrO_2 to give rise to a new sharp band, B_h (1970—1985 cm^{-1}) and to make the A band narrower. From the correspondence of the variation in intensities and position of the IR bands with those in the fraction of coverage of CO with temperature, the α peak was correlated to the A band, the δ peak to the B_h band, and the β peak to the B band. The changes in the TD peaks and the IR bands caused by added ZrO_2 were semiquantitatively compared and are discussed in terms of the electronic and geometric effects; a high electron density state of Pd surface atoms as well as the formation of adsorption sites with specific structure is proposed. A brief study was made for the role of the sites in the catalytic hydrogenation of ethylene and cyclohexene.

In this series of studies, which aims at clarifying the support effect in heterogeneous catalysis, the remarkable role of ZrO_2 in the catalytic behavior of dispersed palladium has been pointed out.[1,2] The Pd metal surfaces, in the presence of ZrO_2, exhibited an enhanced activity for the cyclohexene hydrogenation, causing a change in kinetic behavior. The XPS study showed that the Pd metal atoms were slightly negatively charged as a consequence of electron transfer from ZrO_2 to the metal and that this was mainly responsible for their prominent activities. It was also found that the ZrO_2 brought Pd metal to a highly dispersed state and increased the percentage exposed. These effects might be realted to the preferential fromation of the active sites with peculiar structures. Such ZrO_2-affected Pd metal surfaces may give rise to specific adsorptive properties as well, since the interaction with admolecules is much influenced by the changes in structure and electronic state. Therefore, a combined infrared spectroscopic (IR) and thermal desorption (TD) study of CO adsorption was undertaken to ascertain the adsorptive behavior and, further, to prove the advantage of using CO as a sensitive probe for investigating the details of characteristics of the surface.

In the present study, attention was paid to the following points. First, numerous IR measurements of adsorbed CO on metal surfaces have shown that the position of absorption band changed markedly according to the preparation methods of dispersed metals such as the procedures of metal loading, pretreatment, *etc.*[3] However, such disturbing influences can be avoided or, at least, minimized, when the samples to be measured are prepared with the same procedure. In the present study, thus, the silica- and α-alumina-supported Pd, ZrO_2-added Pd/SiO_2 and Pd/α-Al_2O_3, and the ZrO_2-supported Pd were prepared in the same way as exactly as possible. The produced catalysts were characterized by the X-ray diffraction and CO chemisorption methods.

Secondly, the IR band frequencies are also affected not only by the interaction between admolecule and surface, but also by the interactions such as dipole-dipole coupling and/or direct repulsion between admolecules[4] and, therefore, by the fraction of surface coverage. Thus, in order to reveal the contribution of the metal support interaction on adsorption, it is desirable to make the influence of the latter as low as possible; this situation will be attained in the case that the spectra obtained at similar low fractions of coverage are compared with each other for the similar adsorbed states. In this regard, the combination of IR spectroscopy with TD technique which is able to distinguish among the adsorbed states is indispensable. The catalytic activities of the prepared catalysts were briefly examined for the hydrogenation of ethylene and cyclohexene.

Experimental

The Pd/SiO_2 (2.1% in weight) and ZrO_2-added catalysts were prepared in a manner similar to those employed previously for the Pd/α-Al_2O_3 and ZrO_2-added catalysts.[1,2] The Aerosil silica 130, obtained from the Nihon Aerosil Co., was washed with 0.1 mol dm^{-3} nitric acid and then rinsed thoroughly with ion-exchanged water. The catalysts thus prepared were pretreated *in situ* in the TD or IR cell by oxidation, reduction and then evacuation at the same temperature of 723 K. This reduction temperature was higher than 523 K, *viz.*, a temperature employed in pretreatment of the catalysts for the previous kinetic studies,[1,2] since the TD experiments required Pd surfaces which are stable and resistive for heating up to 700 K. The supported catalysts were characterized by the X-ray diffraction and CO chemisorption methods.

The apparatus used for the TD and IR experiments were almost the same as those reported previously.[5] In the TD study, the catalysts were exposed to a CO atmosphere at room temperature, cooled down to 78 K, and then evacuated at the same temperature before a TD run. The temperature of the catalysts was raised at a rate of 13 K $min.^{-1}$ Under similar

Table 1. Characterization of the catalysts and ZrO_2 effects upon turn-over frequency of ethylene and cyclohexene hydrogenation

Support	Zr/Pd ratio	Amount of CO adsorbed (at 273 K) / molecule g-Pd^{-1}	$D_{CO}^{a)}$/%	$D_X^{b)}$/nm	Turn-over frequency(N_t)$^{c)}$	
					$C_2H_4+H_2$	$C_6H_{10}+H_2$
SiO_2	0	3.23×10^{20}	5.7	84	1.7	—$^{d)}$
	0.5	4.38	7.7	52	2.3	—
	1.0	5.21	9.2	20	3.3	—
	3.0	7.37	13.0	15	6.4	—
α-Al_2O_3	0	0.95×10^{20}	1.7(2.3)$^{e)}$	108	(1.4)	0.1(0.1)$^{e)}$
	0.5	1.07	1.9(3.0)	90	(6.1)	0.7(0.7)
	2.5	1.65	2.9(5.0)	55	(6.9)	0.8(0.7)
ZrO_2	—	3.5×10^{20}	6.2(10.1)	30	7.5	1.3(1.2)

The values in parentheses were for the catalysts pretreated at 523 K.
a) Percentage exposed (dispersion) evaluated by assuming one CO admolecule on each Pd atom. b) Particle size derived from X-ray line broadening. c) Partial pressure of each reactant: 40 Torr; reaction temperatures: 301 K for cyclohexene hydrogenation and 273 K for ethylene hydrogenation. d) Because of the take-up of cyclohexene by SiO_2 support, a direct comparison under the same conditions was difficult. e) See Ref. 2.

adsorption conditions, the ZrO_2 and SiO_2 supports themselves gave rise to a single peak of CO around 255 and 287 K, respectively, but no peak at all above 300 K. When the pressure of introduced CO was high, these peaks were superposed on a part of the CO peak desorbed from Pd metal. Such contribution of the interfering peak was compensated by extracting the peak-height which corresponds to that from the supports. In the IR study, CO was introduced at room temperature into the IR cell, and the spectra were recorded at the same temperature.

The catalytic hydrogenations of ethylene and cyclohexene were studied by using a closed circulation system up to 40 Torr (1 Torr=133.3 Pa) of partial pressure of each reactant and at temperatures between 273 and 301 K.

Results

Table 1 shows the observed characteristics of the supported Pd catalysts and ZrO_2-added catalysts. By the addition of ZrO_2, the particle size of Pd metals changed from 84 to 15 nm for Pd/SiO_2 and from 108 to 55 nm for Pd/α-Al_2O_3 catalysts. These changes were reflected in an increase in the percentage exposed. Table 1 also shows the turn-over frequency, N_t, of ethylene and cyclohexene hydrogenations; these values were evaluated on the assumption that the number of surface Pd atoms is equal to that of CO molecules adsorbed. With increasing Zr/Pd ratio, N_t's raised considerably for both reactions; at Zr/Pd=2.5—3, it increased by factors of 4—5 for the ethylene hydrogenation and 7—8 for the cyclohexene hydrogenation. As is shown by parentheses, the N_t's for the cyclohexene hydrogenation were the same within experimental error independent of pretreatment temperature: 523 or 723 K.

TD Spectra. Figure 1 shows the TD spectra of CO adsorbed on the Pd/SiO_2 catalysts. Two peaks were mainly observed, at 330—350 K (α peak) and at around 530 K (β peak); the latter peak had a shoulder γ around 600 K. Above 600 K, the spectra contained small peaks due to CO_2. The surface coverage, θ, was defined as the ratio of the amount of CO adsorbed to that at saturation. The β-peak was saturated at around θ=0.4, whereas the α-peak continued to increase with increasing θ. Figure 2 shows the TD spectra of CO desorbed from the ZrO_2-added Pd/SiO_2 catalysts. By the addition of ZrO_2 at a ratio of Zr/Pd=1, two main peaks were again observed but a peak appeared clearly at *ca.* 420 K (δ peak), and the β peak shifted toward high temperature by 16 K. With an increase in θ, the saturation of the β-peak occurred, followed by a considerable growth of the α, γ, and δ-peaks. Figure 3 shows the TD spectra at Zr/Pd=3. The δ-peak was more evidently observed, and the β-peak appeared at 547 K.

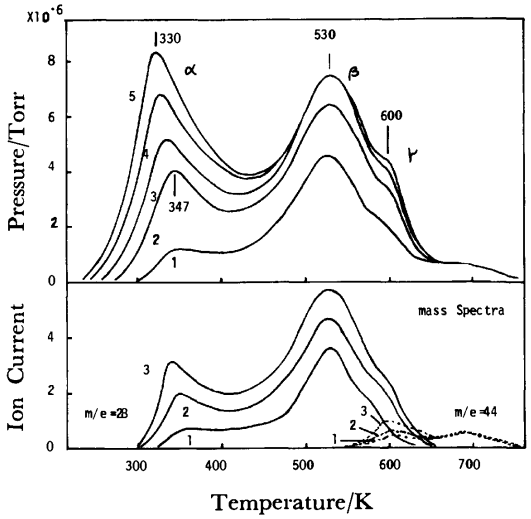

Fig. 1. Thermal desorption spectra of CO from Pd/SiO_2 catalyst.
1. θ=0.13, 2. 0.26, 3. 0.35, 4. 0.49, 5. 0.59.

In continuation of the previous studies,[1,2] the α-alumina was employed as support, and the effects of added ZrO_2 were examined. As is shown in Fig. 4, the Pd metals on α-Al_2O_3 provided almost identical TD spectra of CO with those obtained by using the silica support. When ZrO_2 was loaded at a ratio of Zr/Pd=0.5 on this surface, a broad hump emerged at around 400 K,

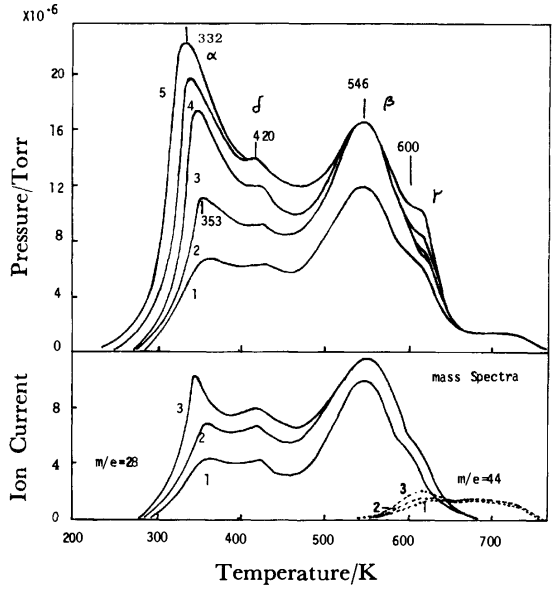

Fig. 2. TD spectra of CO from ZrO_2-added Pd/SiO_2 catalyst (Zr/Pd=1.0).
1. θ=0.15, 2. 0.20, 3. 0.34, 4. 0.47, 5. 0.58.

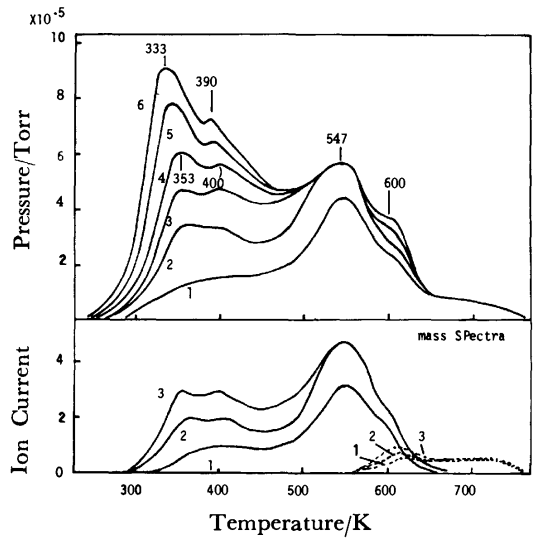

Fig. 3. TD spectra of CO from ZrO_2-added Pd/SiO_2 catalyst (Zr/Pd=3.0).
1. θ=0.07, 2. 0.21, 3. 0.31, 4. 0.47, 5. 0.54.

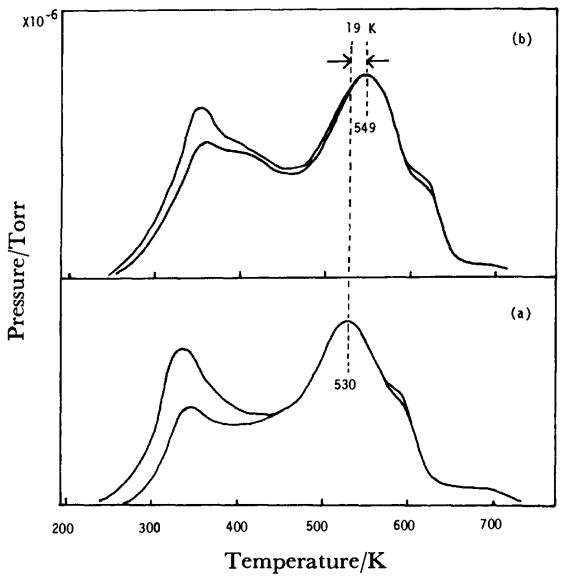

Fig. 4. Change in TD spectra of CO with ZrO_2 addition.
a) $Pd/\alpha-Al_2O_3$; 1. θ=0.50, 2. θ=0.69, b) ZrO_2-added Pd/α-Al_2O_3 (Zr/Pd=0.5); 1. θ=0.58,2. θ=0.61.

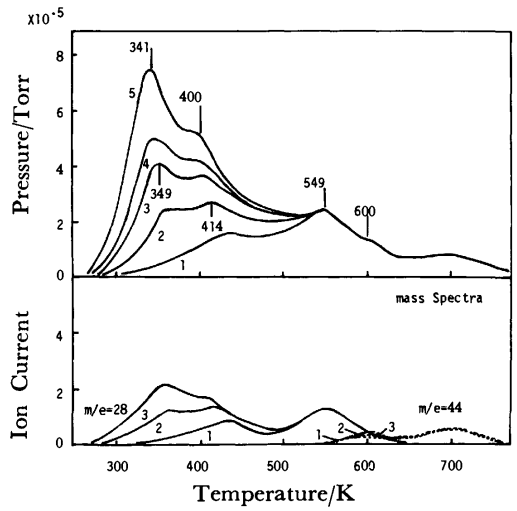

Fig. 5. TD spectra of CO from ZrO_2-supported Pd catalyst.
1. θ=0.08, 2. 0.12, 3. 0.26, 4. 0.40, 5. 0.59.

and the β-peak shifted by 19 K toward higher temperature. It is to be noted that the ZrO_2 effect was analogous on both inert supports.

The relative intensity of the δ-peak was enhanced with an increase in the Zr/Pd ratio. As the other extreme, ZrO_2 was used as support; as is shown in Fig. 5, the corresponding δ-peak was clearly observed, and the β-peak appeared at 549 K.

IR Spectra. Figure 6 shows the IR spectra of CO adsorbed at room temperature on the silica-supported Pd surface and their changes upon subsequent heat treatment. As is reported elsewhere,[3] two broad bands, A and B, appeared; with an increase in the amount of CO adsorbed, the A-band at higher frequency shifted from 2029 to 2071 cm^{-1}, and the B band at lower frequency from 1880 to 1920 cm^{-1}. When gaseous CO was evacuated at room temperature, the A-band was remarkably attenuated with a shift to 2045 cm^{-1}, whereas the B-band was weakened to a lesser extent, giving a band at 1903 cm^{-1}. Further evacuation at 453 K caused almost complete disappearance of the A-band, but the B-band remained stable up to 533 K. The variations of IR spectra upon evacuation at elevated temperature occurred in a reverse way as the increase of the CO exposure.

The IR spectra for the ZrO_2-added catalysts are shown in Fig. 7. At Zr/Pd=0.1, the spectra below 2000 cm^{-1} exhibited a sharp band, B_H, centered at 1970 cm^{-1} and a shoulder tailing toward lower frequency, whereas the A-band appeared at 2097 cm^{-1} with narrow peak width. These spectral features became more distinct with

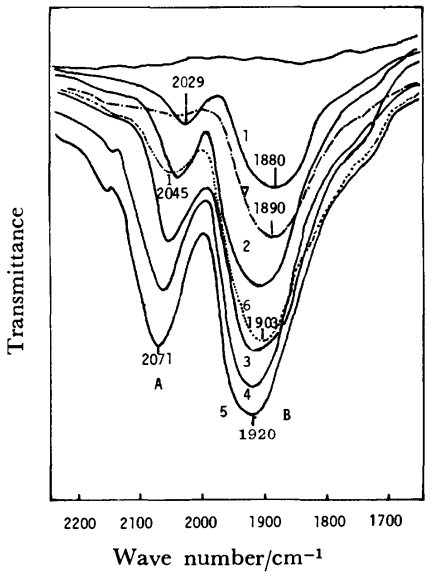

Fig. 6. IR spectra of CO adsorbed on Pd/SiO_2 catalyst and their changes upon evacuation at different temperatures.
1. $\theta=0.21$, 2. 0.35, 3. 0.47, 4. 0.59, 5. 0.67, 6. evacuated at 298 K for 20 min, 7. at 453 K for 20 min.

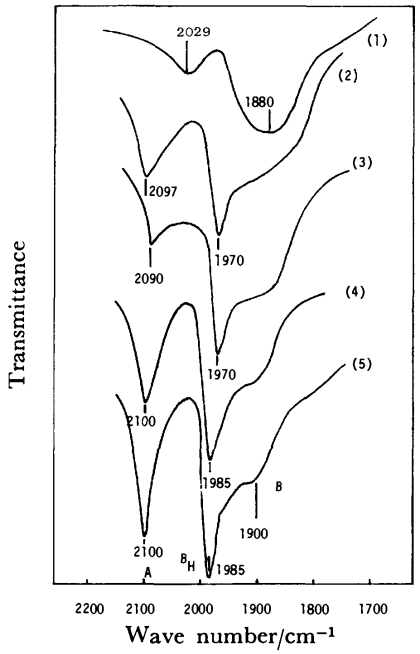

Fig. 7. Changes in IR spectra of adsorbed CO with increasing ratio of Zr/Pd ratio.
1. Zr/Pd=0 (Pd/SiO_2); $\theta=0.21$, 2. 0.1; 0.2, 3. 0.5; 0.22, 4. 1.0; 0.42, 5. 3.0; 0.68.

increasing Zr/Pd ratio; the addition of ZrO_2 at Zr/Pd=0.5—3.0 produced the B_H-band at 1970—1985 cm^{-1} and the A-band at 2090—2100 cm^{-1}. At the different exposures of CO, the spectral changes caused by added ZrO_2 were clearly observed, which indicated that the above-mentioned features are not coverage-dependent but are due to the intrinsic effect of added ZrO_2 oxide.

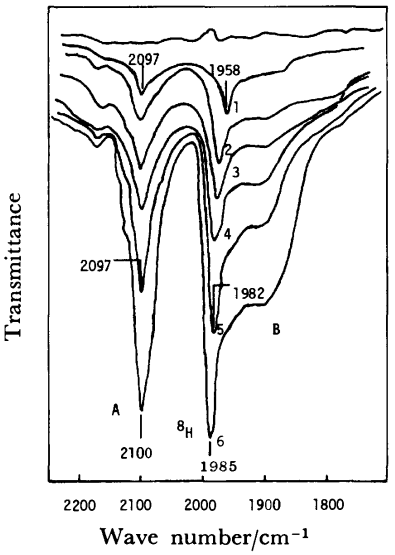

Fig. 8. IR spectra of CO on the ZrO_2-added catalyst (Zr/Pd=3.0) as a function of CO exposure.
1. $\theta=0.21$. 2. 0.34, 3. 0.48, 4. 0.54, 5. 0.68, 6. 0.80.

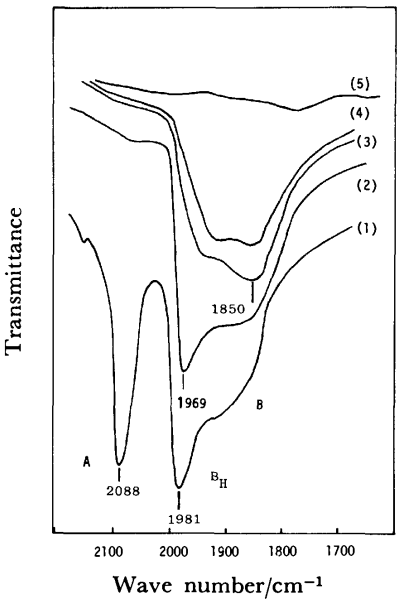

Fig. 9. Variations in IR spectra with evacuation temperature.
ZrO_2-added catalyst (Zr/Pd=0.5)
1. before evacuation ($P_{CO}=1$ Torr), 2. evacuated at 298 K for 40 min, 3. at 423 K for 20 min, 4, at 573 K for 30 min, 5. at 673 K for 20 min.

The IR spectra of the ZrO_2-added catalyst as a function of the CO exposure are shown in Fig. 8. The catalysts with the Zr/Pd ratio greater than 1.0 clearly exhibited ZrO_2-affected spectra even at low CO exposure, and, with increasing CO exposure, both A- and B_H-bands shifted to a lesser extent, in contrast to a large shift in the ZrO_2-absent catalysts. It is to be noted that the behavior of the band developments with CO exposure were different. Figure 9 shows the spectral variation upon heat treatment at different temperatures after CO adsorption at room temperature. For the catalyst with

Zr/Pd=0.5, evacuation at 298 K caused the preferential and complete removal of the A-band, and further evacuation at 423 K resulted in the almost complete disappearance of the B_H band. Thanks to this evacuation, the remaining band, B, clearly manifested itself at an absorption frequency of 1850 cm^{-1}. Evacuation at 673 K annihilated completely the IR spectra in this region but produced a band around 1500 cm^{-1}, probably ascribable to the carbon dioxide species formed by disproportionation; such a result is in agreement with the TD results.

Discussion

In the absence of ZrO_2, the IR and TD spectra each provided two broad bands and peaks; these exhibited the corresponding changes upon increasing the amount of adsorbed CO as well as upon evacuation at different temperatures. The intensity of the A band in the IR spectra continued to increase above θ=0.4 and was easily removed by evacuation at 300 K; this seems to have a common base with the TD α-peak which is present only at high surface coverage and in lower temperature. Since the B-band was produced first and resisted heating up to 550 K, it is evident that this band is associated with the TD β and γ-peaks appearing at low coverage and in higher temperature. The remarkable effects of the added ZrO_2 upon the CO adsorption on the Pd surfaces were well reflected by the generation of the sharp B_H band at 1980 cm^{-1} and the clearer appearance of the δ-peak desorbed at an intermediate temperature region.

In the Pd carbonyl complexes, a linearly-coordinated CO[6] was found to have a stretching frequency at 2050—2169 cm^{-1}, whereas the three-fold coordinated CO produced the frequency at 1800 cm^{-1} or below.[7] Furthermore, many studies of CO adsorbed on Pd metals have shown that the absorption band of CO in the 2050—2100 cm^{-1} range is the stretching vibration of a linearly-bonded CO, whereas the band of a range 2000—1800 cm^{-1} is associated with the multiply-bonded CO such as a bridged one.[8-18] This classification allows us to assign the B_H- and B-bands to the C-O stretching frequency of CO coordinated on multiple Pd atoms and the A-band to that coordinated linearly.

Kokes *et al.*[15] suggested that a stretching frequency of 1970 cm^{-1}, corresponding to the characteristic B_H band, is due to the bridge-bonded CO which shares one of two Pd atoms with a linearly bonded CO, *viz.*,

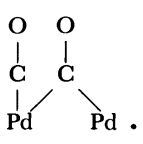

This assignment, however, does not seem to hold for in the present case, since the B_H-band still remained after the linear CO was completely removed by evacuation. Boudart *et al.*[16] obtained a band of 1980 cm^{-1} as a shoulder at CO pressure of as high as 300 Torr on the silica-supported Pd, suggesting that the band is ascribable to intermolecular interaction as a result of the compression of the admolecule and is favored for the larger Pd particles. However, the present results showed that the spectral features could be distinguished depending on the absence or presence of ZrO_2 component, irrespective of the CO coverage. Furthermore, Table 1 indicates the opposite trend as to the particle-size effect; the B_H-band became intensive with the decrease in size.

In a recent combined IR-reflection absorption and LEED study using single crystals of Pd which expose the (100), (111), or (210) surface, Bradshaw and Hoffmann[19] showed that the C-O stretching vibrational frequency in the region 1880—1970 cm^{-1} was observed for θ<0.5 and CO is adsorbed on the two-fold coordination sites, which exist as bridge-site on the (100) plane as well as the (210) surface as the stepped (100) plane, whereas the frequency in the region 1800—1880 cm^{-1} was only observed for θ<0.3 and CO is adsorbed on the three-fold coordination sites on the (111) surface. They also showed that, on the (100) surface, the band associated with a linear-bonded CO appeared at 2096 cm^{-1} even for $\theta \cong 0.5$ in the case of the CO adlayer of poor ordering. The present IR spectra show that the IR band below 2000 cm^{-1} for Pd/SiO_2 catalyst covered broadly the range of the band for the ZrO_2-added catalysts, and the B-band still existed even in the presence of ZrO_2 (as a shoulder around 1880 cm^{-1}), thereby suggesting that the ZrO_2 effect can be related to the remarkable development of the narrow B_H-band. Thus, the consolidation of the above assignment and the fact that the B_H-band grew with increasing Zr/Pd ratio for similar CO coverage, as is shown in Fig. 7, lead to the consideration that the ZrO_2-affected Pd metal surfaces possess two-fold coordination sites of high density. This might be expected in case that the (100) plane and/or high index planes such as (210) were preferentially exposed, for instance, relative to the (111) plane. However, the extraordinarily narrow B_H band seems to reflect the existence of more specific dual sites such as isolated ones. The previous study showed that Pd metal atoms are able to interact strongly with ZrO_2 through the oxygen atoms.[2] When such incorporation of the metal with the oxide is taken into account, it is not unreasonable to consider that the ZrO_2 addition promoted the formation of the sites which have arrangements distinguishable from the usual largely-extended flat planes, *e.g.*, those like facets confined partially by ZrO_2 or a pair of protruded Pd atoms.

In the TD spectra, the position of the β-CO desorption peak remained almost unchanged as the CO coverage increased. This invariance is in agreement with the view that the CO desorption obeys the first-order kinetics.[20] Therefore, the shift of CO-desorption peak to higher temperature side by the presence of ZrO_2 component is indicative of the formation of stronger bonds between Pd metal and CO, since the adsorption of CO on Pd surfaces takes place *via* a nonactivated process.[21]

The β-CO corresponds to the CO remaining after evacuation at around 423 K, and the IR spectra gave rise to the absorption band at 1890 cm^{-1} for the Pd/SiO_2 catalysts and the band at 1850 cm^{-1} for the ZrO_2-added Pd/SiO_2 (Zr/Pd=0.5—3.0) catalysts. The presence of ZrO_2 actually caused a shift of the absorption band to

lower frequency, at least by 40 cm^{-1}. The direction of respective variation in the TD and IR spectra is in line with the generally accepted view in which the weakening of bonds between C and O atoms resulted in the strenghtening of the admolecule-surface bonding, as is accounted for in terms of a back-donation of a metal electron into the $2\pi^*$ orbital of the molecule.

Since the β-state corresponds to that of CO at a small coverage, it is considered that the effects of intermolecular interaction upon the IR-band frequency and TD-peak position are safely minimized. Thus, the above-mentioned shift appears to reflect the changes in an intrinsic metal-admolecule interaction in the absence or presence of ZrO_2. Thus, the enhancement of back-donating electrons arises from a high electron density of Pd metal atoms, which is indicative of electron transfer from ZrO_2 to the metal. This finding gives support to the previous conclusion obtained by using X-ray photoelectron spectroscopy.[2]

The variation in the heat of adsorption, ΔE, usually accompanies the shift of the C-O stretching vibrational frequency of the admolecule, ΔW. The experimental data on the CO-Pd systems[19,22,23] show that the energetic ratio of $\Delta W/\Delta E$ is retained in the range 1.5×10^{-2}—15×10^{-2}. The calculation for the present ZrO_2-caused shifts of the β-peak and B band showed that this ratio was about 7×10^{-2}, which falls within the region described above. From the shifts of the δ-peak and the B_H band, relative to the β-peak and B band respectively, the ratio was roughly estimated to be 3×10^{-2}. Such agreement gives support to the assignments for the TD peaks and IR bands. As to the α-peak, we need some caution, since the α-state present at low temperature is somewhat a function of evacuation time prior to the TD run as well depending on the validity of the correction in elimiating a contribution of interfering peaks which originate from the supports.

With CO exposure, the broad A-band due to a linearly-bonded CO moved to higher frequency for the Pd/SiO_2 catalysts, in agreement with the well-established view,[3] whereas the sharp A band for the ZrO_2-added catalysts showed a little shift. This invariance and narrowing of the peak seem to be an indication of ZrO_2 effects, suggesting that the CO accepts a compensative back-donation from the ZrO_2-affected Pd metal atoms or that it is adsorbed on the confined sites which make the molecule free from the neighbouring ones.

Thus, the ZrO_2 component exerts not only electronic influence but also some geometric effects, in the sense that the surface sites with specific structures are preferentially produced on the ZrO_2-added Pd metal. The previous study found that with increasing addition of ZrO_2 to Pd/α-Al_2O_3 catalysts the change in the kinetic parameters of the cyclohexene hydrogenation became negligibly small near a ratio of Zr/Pd=0.5, whereas the turn-over frequency continued to increase. It is likely that this can be correlated with the increase in the number of the specific sites. It is of interest to see that the ZrO_2 effects appear in the hydrogenation of unsaturated hydrocarbons such as ethylene, *cis*-2-butene and cyclohexene. The relative catalytic activities of the ZrO_2-added Pd/α-Al_2O_3 catalysts with reference to Pd/α-Al_2O_3 catalysts were increased with increasing dispersion (percentage exposed) in similar way for the hydrogenation of these olefines.[24]

Finally, in a recent IR study in connection with the catalytic hydrogenation of CO, Vannice *et al.*[25] showed that Pd metals on TiO_2 behave as in the case of the metal in Pt/TiO_2 catalysts; the strong metal-support interaction (SMSI) effect was generated after heating at 773 K such that the catalytic activity as well as the adsorptive properties was drastically reduced in spite of the presence of Pd metal particles with considerable surface area. In the present system, however, we observed little SMSI effect. The N_t for the cyclohexene hydrogenation was almost the same, independent of pretreatment temperature, *i.e.*, 1.2 for the 523 K-reduced Pd/ZrO_2 and 1.3 for the 723 K-treated one. Although a detailed comparison is needed, this fact seems to reflect a moderate interaction of the Zr cation through oxygen atoms with the metal, leading to a favorable catalytic effect, compared with an overly strong interaction of the Ti cation.

This research was supported by the Grant-in-Aid for Scientific Research (No. 58104003) from the Ministry of Education, Science and Culture.

References

1) B. Y. Lee, Y. Inoue, and I. Yasumori, *Bull. Chem. Soc. Jpn.*, **54**, 13 (1981).
2) B. Y. Lee, Y. Inoue, and I. Yasumori, *Bull. Chem. Soc. Jpn.*, **54**, 3711 (1981).
3) L. H. Little, "Infrared Spectra of Adsorbed Species," Academic Press, London (1966), p. 203; R. Van Hardeveld and F. Hartog, *Adv. Catal.*, **22**, 75 (1972).
4) B. E. Nieuwenhuys, *Surface Sci.*, **105**, 505, (1981) and references herein.
5) S. Moriki, Y. Inoue, E. Miyazakia, and I. Yasumori, *J. Chem. Soc., Faraday Trans. 1*, **78**, 171 (1982).
6) E. P. Kundig, D. McIntosh, M. Moskovits, and G. A. Ozin, *J. Am Chem. Soc.*, **95**, 7234 (1973); J. H. Darling and J. S. Odgen, *Inorg. Chem.*, **11**, 666 (1972); *J. Chem. Soc., Dalton Trans.*, **1973**, 1079.
7) E. R. Corey, L. F. Dahl, and W. Beck, *J. Am. Chem. Soc.*, **85**, 1202 (1963).
8) R. P. Eischens, S. A. Francis, and W. A. Pliskin, *J. Phys. Chem.*, **60**, 194 (1956); R. P. Eischens and W. A. Pliskin, *Adv. Catal.*, **10**, 1 (1958).
9) C. W. Garland, R. C. Lord, and P. F. Toriano, *J. Phys. Chem.*, **69**, 1188 (1956).
10) J. K. A. Clarke, G. Farren, and H. E. Rubalcava, *J. Phys. Chem.*, **71**, 2376 (1976).
11) R. F. Baddour, M. Modell and U. K. Heusser, *J. Phys. Chem.*, **72**, 10 (1968).
12) R. Queau and R. Poilblanc, *J. Catal.*, **27**. 200 (1972).
13) Y. Soma-Noto and W. M. H. Sachtler, *J. Catal.*, **32**, 315 (1974).
14) R. W. Rice and G. L. Haller, *J. Catal.* **40**, 249 (1975).
15) A. Palazov, C. C. Chang, and R. J. Kokes, *J. Catal.*, **36**, 338 (1975).
16) E. L. Kugler and M. Boudart, *J. Catal.*, **59**, 201 (1979).
17) C. M. Grill and R. D. Gonzalez, *J. Phys. Chem.*, **84**, 878 (1980); C. M. Grill, M. L. Mclaughlin, J. M. Stevenson, and R. D. Gonzalez, *J. Catal.*, **69**, 454 (1981).
18) M. A. Vannice and S. Y. Wang, *J. Phys. Chem.*, **85**, 2543 (1981).

19) A. M. Bradshaw and F. M. Hoffmann, *Surface Sci.*, **72**, 513 (1978).
20) S. Ladas, H, Poppa, and M. Boudart, *Surface Sci.*, **102**, 151 (1981).
21) T. Engel and G. Ertl, *Adv. Catal.*, **28**, 1 (1979).
22) G. Ertl and J. Koch, *Z. Naturforsch., A*, **25**, 1906 (1970).
23) J. C. Tracy and P. W. Palmberg, *J. Chem. Phys.*, **51**, 4852 (1969).
24) B. Y. Lee, Y. Inoue, and I. Yasumori, to be published.
25) M. A. Vannice, S. Y. Wang and S. H. Moon, *J. Catal.*, **71**, 152 (1981); S. Y. Wang, S. H. Moon, and M. A. Vannice, *ibid.*, 167 (1981).

Physicochemical Studies of an Activated Europium Ion-exchanged Mordenite

Tsuyoshi ARAKAWA,* Midori TAKAKUWA, Gin-ya ADACHI, and Jiro SHIOKAWA

Department of Applied Chemistry, Faculty of Engineering, Osaka University, 2-1, Yamadaoka, Suita, Osaka 565

(Received September 5, 1983)

The physicochemical properties of an activated Eu(III) ion-exchanged mordenite (Eu-M) have been studied by the measurement of the fluorescence of the europium ion. When Eu-M (the exchanged level; 3.7%) was degassed only above 300 °C, a band emission which peaked at 488 nm appeared. This band emission was associated with the Eu^{2+} 5d-4f transition. The peak of the band emission shifted linearly to a shorter wavelength with the increase in the exchanged level of the Eu ions. For the Eu-M sample, which was reduced by H_2 at 500 °C, the peak position of the band emission was almost 499 nm in all cases, and the quantum yield for a reduced sample was larger than that for a dehydrated sample. The quantum yield for a reduced sample fell off extremely above the exchanged level of 6%. Moreover, the Eu^{2+}–Eu^{2+} energy transfer in the reduced samples was discussed.

Several attempts have been made to identify the structures and chemical properties of europium-exchanged zeolites. The presence of Eu^{4+} in zeolite A has been postulated by X-ray analysis.[1] Electron-paramagnetic resonance has been applied to study the ligand coordinations of europium-exchanged mordenite, zeolite Y, and zeolite A.[2,3] A Mössbauer study of europium-exchanged zeolite has been reported.[4,5] These techniques are, however, of restricted applicability. On the other hand, fluorescence spectroscopy can be helpful for rare-earth ion-exchanged zeolites, though the rare-earth mordenites have rarely been studied by the use of fluorescence techniques.[6] We ourselves have previously studied the physicochemical properties of rare-earth ion-exchanged zeolites from the measurement of the fluorescence of the rare-earth ions in an attempt to clarify the catalytic properties of these compounds.[7] Especially, it has been found that a part of the Eu^{3+} ion in zeolite Y and mordenite is reduced to the Eu^{2+} ion by dehydration in a vacuum or inert gases. That is, on Eu^{3+} ion-exchanged zeolites, the emission band for Eu^{3+} decreased and the band emission due to Eu^{2+} appeared as Eu^{3+} ion-exchanged zeolites were degassed above 300 °C. The fluorescence of Eu^{2+} has been studied, and a number of Eu^{2+}-containing phosphors emitting in the blue or ultraviolet region have been described.[8-10] In general, the Eu^{2+}-doped phosphors are made by the reduction of the Eu^{3+}-doped samples at higher temperatures (800 °C$<T$) in an hydrogen atmosphere. Therefore, it is noteworthy that the reduction of Eu^{3+} to Eu^{2+} in zeolites takes place easily upon degassing at low temperatures.

In this paper, the fluorescence properties of Eu^{2+} for an activated Eu ion-exchanged mordenite (Eu-M) will be reported in more detail.

Experimental

Materials. The Eu-M samples were prepared starting from Na-mordenite which had been supplied by the Norton Company. The parent mordenite had the following composition: $Na_8(AlO_2)_8\cdot(SiO_2)_{40}\cdot 24H_2O$. The mordenite was ion-exchanged in solutions containing $EuCl_3$, washed, dried at 100 °C, and calcined in air at 450 °C. The close correspondence between the decrease in the sodium content and the increase in the europium content indicated that a simple ion-exchanged process had occurred. The exchanged mordenites were analyzed for europium by means of X-ray fluorometry and for sodium by means of flame photometry. Thus, the exchanged levels (100x (%); $Na_{8(1-x)}\cdot Eu_{8\cdot x}(AlO_2)_8\cdot(SiO_2)_{40}\cdot 24H_2O$) of the europium ion were found to be 0.1, 0.5, 1.4, 3.7, 5.8, 6.7, and 8.0%.

Methods and Procedures. The emission and excitation spectra were measured using a Shimadzu Recording Absolute Spectrofluorophotometer (RF-502) at room temperature. The UV spectra were taken with a Shimadzu UV-180 apparatus, using MgO as the reference. The particle size of the Eu-M samples was made to fall in the range of 10^{-5}—10^{-4} m so that the light-scattering would be as uniform as possible. The UV spectra in the region from 200 to 400 nm were recorded using a glass filter (UV-D25), since the UV spectra in the region of 250—400 nm were affected by the fluorescence of the divalent europium ion as will be described below, Prior to the measurement, the samples in a quartz cell were dehydrated at the desired temperature for 4 h under a pressure of 10^{-5} Torr (1 Torr=133.322 Pa) and then cooled at room temperature. The reduced samples were obtained by treatment at 500 °C for 1 h in a hydrogen atmosphere. The quantum yield (Q_0) of fluorescence was derived from the following equation:[11]

$$Q_0 = \frac{Q_{\text{sample}}}{Q_{\text{CaWO}_4:\text{Pb}}} \times \frac{I_{\text{CaWO}_4:\text{Pb}}}{I_{\text{sample}}}, \qquad (1)$$

where Q_{sample} and $Q_{\text{CaWO}_4:\text{Pb}}$ are the photoluminescence outputs where, therefore, I_{sample} and $I_{\text{CaWO}_4:\text{Pb}}$ are the numbers of absorbed photons, as obtained from the UV spectra.

Gas-consumption Experiments. When the Eu-M sample was reduced by hydrogen, the amount of hydrogen consumption was accurately determined as a function of the time by measuring the pressure drop. Reoxidation was also investigated by measuring the oxygen-pressure drop in the same apparatus, which consisted of a closed circuit containing a circulation pump in series with a quartz tube reactor and a cold trap. The volume of the system was 180 cm^3; the rate of circulation of the gas was 1000 $cm^3\ min^{-1}$. The pressure drop was monitored on a digital manometer (Validyne CD-23). The accuracy of the gas-uptake measurements was better than ±0.002 mmol.

Lifetime Measurement. The fluorescence lifetimes were measured using a Nitrogen Laser (337 nm) with a lifetime of less than 5 ns. Also, for the measurement of the lifetimes a monochrometer was used to enable us to select the emission wavelength. The lifetimes were determined from the oscilloscope trace as the slope of log I *vs.* t.

Results and Discussion

Europium Spectra for the Dehydrated Samples. When the Eu-M sample (exchanged level: 3.7%) was degassed above 300 °C, the band-emission (Curve 1), peak at 488 nm newly appeared, as is shown in Fig. 1. The optimum excitation wavelength was 315 nm. The quantum yield was 4.3%. A new band emission in the short-wavelength UV region must be due to the $4f^65d$-$4f^7$ transition for the Eu^{2+} ion, as has been described elsewhere.[9] In the dehydrated Eu-M samples, the emission band for the Eu^{3+} ion under excitation with 300-nm radiation, which has its peaks at around 572 ($^5D_0$-$^7F_0$), 580 ($^5D_0$-$^7F_1$), and 624 nm ($^5D_0$-$^7F_2$), was observed (*cf.* Fig. 2). When Eu-M was dehydrated at 500 °C, the emission lines were observed on the foot of the band emission for the Eu^{2+} ion. No position of the emission lines changed between before and after the dehydration. However, the relative intensity of the $^5D_0$-$^7F_0$, $^5D_0$-$^7F_1$, and $^5D_0$-$^7F_2$ emissions varied with an elevation of the temperature. This fact is mainly attributable to the change in the local environment of the Eu^{3+} ion, with a loss of coordinated water molecules, as has been described elsewhere.[12] The mass-spectroscopic analysis of the noncondensable gaseous material evolved during the evacuation above 300 °C for Eu-M revealed that the gas was oxygen. The amount of oxygen evolved from Na-M was negligibly small. The evolved oxygen for Eu-M samples increased, though, with the increase in the exchange level of Eu ions. The degree of reduction for Eu^{3+} to Eu^{2+} in mordenite during the evacuation at 500 °C for 4 h was about 30%, judging from the measurement of the magnetic susceptibility, as has been described elsewhere.[12] Moreover, the total evolved oxygen amounted to one oxygen molecule desorbing per Eu^{2+} ion. Although we no clear data of the dissociation of adsorbed water,[12] it is probable that the dissociation of adsorbed water occurs as follows, in a manner similar to that occurring on the other rare-earth ion-exchanged zeolites; $Ln(OH_2)_2^{+3} \rightarrow Ln(OH)_2^+ + 2H^+$.[13] Thus, it can be considered that the reduction of Eu^{3+} in mordenite proceeds mainly according to Eq. (2):

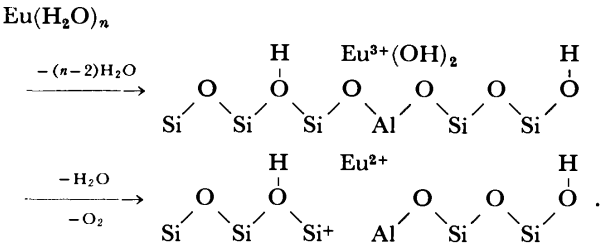

(2)

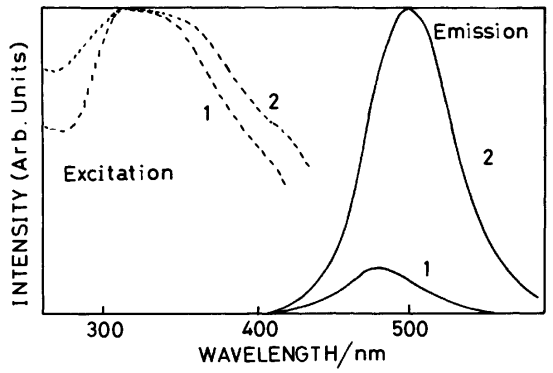

Fig. 1. Fluorescence spectra of Eu-M (3.7%) after degassing at 500 °C for 4 h (1) and reducing at 500 °C for 2 h (2).

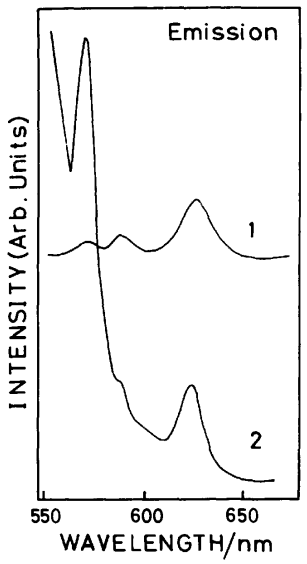

Fig. 2. Emission spectra of the Eu^{3+} ion in Eu-M (3.7 %). Excitation with 300 nm radiation. (1) After degassing at 25 °C for 2 h. (2) After degassing at 500 °C for 4 h.

The peak position of the band emission of Eu^{2+} in dehydrated samples changed with the concentration of europium ions in mordenite. However, the optimum excitation wavelength was 315 nm in all cases. Therefore, the excitation process of Eu-M may be thought to be relatively unimportant. Figure 3 gives the relationship between the wavelength of the peak position and the exchanged level of the europium ion. The peak position of the band emission shifts linearly to a shorter wavelength as the exchanged level increases. Similar behavior has been observed for the system of $SrMgP_2O_7$: Eu^{2+} or $Sr_{1-x}Ba_xAlF_5$:Eu^{2+}.[14] The wavelength for the band emission in Eu^{2+} ions is determined by two factors: on the one hand, the splitting of the 5d levels by the crystal field of the surrounding oxygen ions, and, on the other hand, the energy gap between the 4f ground state and the center of gravity of the 5d excited levels. The UV spectra of dehydrated samples with different exchanged levels are shown in Fig. 4. The peak of the absorption spectra in the UV region was about 300 nm in all cases. The split of the absorption bands attributable to the allowed electric dipole transitions between the 4f and 5d states was not clearly observed. Therefore, it

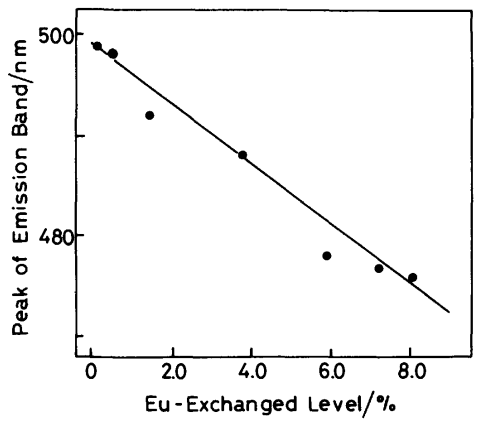

Fig. 3. The relationship between the peak position of the emission band for Eu^{2+} and the exchanged level of europium ion.

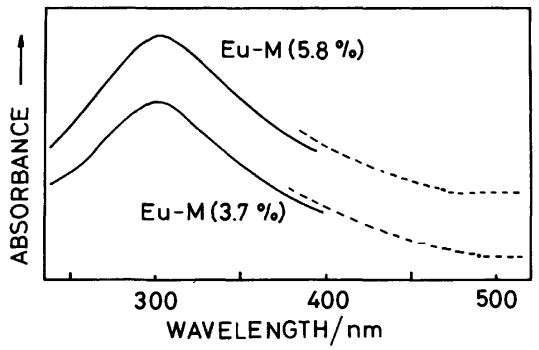

Fig. 4. The absorption spectra of the dehydrated samples. The solid lines are the spectra with a glass filter (UV-D25). The dotted lines are the spectra without the filter.

can be anticipated that the possibility of the peak shift is rarely present. The absorption edge, however, shifted to a shorter wavelength with the increase in the exchanged level of the europium ion. These results were consistent with the results for the shift of the band emission. The peak shift may be attributed to an increase in the fraction of Eu^{2+} ions which interact with each other in dipolar coupled pairs.[3] In this case, the exchanged sites will play an important part in the formation of dipolar coupled pairs.

The structure of Na mordenite has the space group Pbcn, a=17.92 (1), b=20.31 (1), and c=7.48 (7) Å.[15] Only the I′, IV, and VI sites are occupied by Na cations in a dehydrated Na mordenite. The percentages of occupancy for the sites are 43% (I′), 36% (IV), and 21% (VI). Jacobs *et al.*[16] have pointed out that, in Cu-Y, a small number of supercage oxygen ions were capable of causing a rupture or considerable weakening of the Si(Al)-O bond under evacuation at 623 K. In Na-M, the VI site faces the large channel, much like the supercage in the Y-type zeolite. Thus, it appears that the Eu^{3+} ions which occupy the VI site are easily reduced to Eu^{2+} ions during the dehydration, according to Eq. (2). The VI site is a wall site in the large channel, and the cation on the VI site sticks out of the wall somewhat. That is, the Eu^{2+} ions on the VI site are able to interact directly with each other. Also, the fraction of Eu^{3+} ions for the VI site is 21% if the Eu^{3+} ions are ion-exchanged according to the percentage of occupancy for each site. Since the degree of the reduction of the Eu^{3+} ions was about 30% under the evacuation, it is thought that the Eu^{3+} ions are slightly localized to the VI site. Therefore, the fraction of the Eu^{2+} ions which interact with each other in dipolar coupled pairs will be enhanced as the concentration of the Eu ions increases. Thus, in dehydrated Eu-M samples, a shift of the peak position would be observed as the Eu^{2+} concentration increased. Further physicochemical evidence should be collected to support the phenomena of the peak shift.

Europium Spectra for the Reduced Sample. The emission spectrum after the treatment at 500 °C in a hydrogen atmosphere is shown in Fig. 1 (Curve 2). The emission spectrum of Eu^{2+} for the reduced sample was distinct from that for the dehydrated sample. For Eu-M (3.7%), the peak position of the band emission is 499 nm under the optimum excitation of 315 nm, and the quantum yield (27.2%) is larger than that for the dehydrated sample (4.3%).

The stoichiometry of the reduction-reoxidation of dehydrated and reduced Eu-M samples at 500 °C can be derived from the data of Table 1. For Na-M, an oxygen or hydrogen pressure drop was rarely observed. After the dehydration of Eu-M, the small amount of oxygen was consumed. The amount of oxygen corresponds to 30% of the total Eu ions. The degree of reduction for Eu^{3+} to Eu^{2+} in mordenite was about 30%, as has been described elsewhere.[12] Also, we have concluded from the experiments of the thermal-programmed desorption (TPD) of oxygen that one oxygen molecule is adsorbed to an Eu^{2+} ion in mordenite.[17] Thus, the amount of oxygen estimated from the pressure drop is consitent with the amount of oxygen needed to reoxidize. On the other hand, the amount of oxygen needed to reoxidize after the reduction of hydrogen is consistent with the total number of Eu ions. The amount of hydrogen consumed, however, was 1.4 times the total amount of Eu ions in all cases. After the reduction at 500 °C, the sample was degassed and then exposed to oxygen at the same temperature. It was subsequently cooled to 25 °C under an oxygen atmosphere and then degassed for 1 h at the same temperature. After these operation, the TPD spectroscopy was done; the results

Table 1. Gas consumption (mmol g^{-1}) at 500 °C

Exchanged level (%)	Eu^{3+} ion (mmol g^{-1})	Cycle No.	H_2	O_2
5.8	0.044	1		0.013[a]
		2	0.058	0.043[b]
		3	0.060	0.044[b]
7.2	0.055	1		0.016[a]
		2	0.075	0.050[b]
		3	0.078	0.052[b]

a) Oxygen uptake at 500 °C for 2 h after dehydration. b) After the reduction of H_2, the circular system was evacuated for 1 h and then the reduced sample was reoxidized by O_2; reoxidation time: 0.5 h.

will be described elsewhere.[17] Thus, it was clear from the TPD experiment that the amount of desorbed oxygen from the reduced sample was almost consistent with that for the dehydrated sample described above. Also, the degree of reduction was about 100%, judging from the measurement of magnetic susceptibility, as has been described elsewhere.[12] Therefore, the amount of hydrogen consumed should be twice the amount of oxygen needed to reoxidize if oxygen does not desorb under the evacuation at 500 °C after oxygen exposure. As has been described above, it appears that the Eu^{3+} ions which occupy the VI site are easily reduced to Eu^{2+} ions during the dehydration, while other Eu^{3+} ions which exist on the I′ or IV site are reduced only under the reducing atmosphere. Since the I′ and IV sites are shaded by the (Si, Al)O_4 network,[15] the increase in the quantum yield for the reduced sample may be attributed to the increase in the isolated Eu^{2+} ions. That is, it is considered that, in the emission spectrum for the reduced sample, the emission band with a peak at 488 nm is concealed in the foot of the emission band with a peak at 499 nm.

Concentration Dependence. In Fig. 5, we plot the quantum yield *vs.* the exchanged-Eu-ion concentration for the reduced samples in comparison with that for the dehydrated samples. The quantum yield stays relatively constant up to almost 6%, but above that point it decreases abruptly. This phenomenon may be recorded in terms of the concentration-quenching effect. In order to discuss the concentration-quenching phenomenon in more detail, we have considered the Eu^{2+}—Eu^{2+} energy transfer in an reduced Eu-M. Since the transfer occurs mainly *via* dipole-dipole interaction,[18] the probability, $P_{Eu^{2+}-Eu^{2+}}$, of energy tranfer between Eu^{2+} ions by means of this interaction has been given as;

$$P_{Eu^{2+}-Eu^{2+}} = 6.3\times10^{27}\frac{Q_A}{R^6\tau_{Eu}}\frac{1}{E^4}\int f_{Eu}(E)F_{Eu}(E)dE, \quad (3)$$

where Q_A is the absorption cross-section of the Eu^{2+} ions (in cm^2 eV); R, the distance between the Eu^{2+} ions (Å); τ_{Eu}, the decay time of the fluorescence (in s); E the energy transferred (in ev), and $\int f_{Eu}(E)F_{Eu}(E)dE$, the overlap between emission and excitation bands. Blasse defined a critical distance, R_c, between two luminescent centers, S and A, as the distance for which the probability of transfer from S to A equals the probability of the radiative emission of S. This means that $P_{Eu^{2+}-Eu^{2+}}\cdot\tau_{Eu^{2+}}=1$ in terms of Eq. (3). Thus, R_c can be found from this equation;

$$R_c^6 = 6.3\times10^{27}\frac{Q_A}{E^4}\int f_{Eu}(E)F_{Eu}(E)dE. \quad (4)$$

Also, the critical distance R_c (in Å) can be estimated by geometrical considerations as follows:

$$R_c \simeq 2\left(\frac{3V}{4\pi x_c N}\right)^{1/3}, \quad (5)$$

where V is the volume of the unit cell (in $Å^3$); x_c the activator atom fraction (the concentration) at which the quenching starts, and N, the number of sites per unit cell at which the activator atoms enter. In this paper, we assume that, for the critical concentration, the average shortest distance between nearest activator ions is equal to the critical distance, R_c. Thus, the R_c value for the reduced sample, 22 Å, is derived from Eq. (5), as V is 2.72×10^3 $Å^3$, x_c is 0.06, and N is 8. This value is the same as that in the system of $BaBPO_5$; Eu^{2+} (22 Å).[18] 22 Å is the distance separating one Eu^{2+} ion and another Eu^{2+} ion when the quenching starts in Eu-M. If the Eu^{2+}-Eu^{2+} distance is expressed in terms of 3.4 Å×n, where 3.4 Å is the mean interatomic distance between Na nearest neighbors in Na mordenite, as has been described above and n is the number of exchanged sites, n is 6.5. $P_{Eu^{2+}-Eu^{2+}}$ is varied by the factor of $\left(\frac{R_c}{R}\right)^6\frac{1}{\tau_{Eu}}$, which is derived from Eqs. (3) and (4). Since τ_{Eu} is$\simeq10^{-6}$ s, as is shown in Table 2, in the reduced Eu-M the transfer probability for the separation of 3.4 Å is $\simeq10^{10}$ s^{-1}.

The concentration-quenching effect was also observed at a low concentration of Eu^{2+} ions in the dehydrated Eu-M, as is shown in Fig. 5. If Eu^{2+} ions disperse statistically, R_c is 46 Å, as x_c is 0.006 (the effective Eu^{2+} fraction is 0.02×0.3, since the degree of reduction is about 30%). The R_c value of 46 Å is much larger than the maximum R_c (27 Å).[10,19] Since the concentration-quenching effect is observed at a low concentration, it is probable that a Eu^{2+} ion, which is easily produced by the dehydration, is present at the specific site and in the neighborhood of another Eu^{2+} ion to be able to affect the concentration quenching as has been described above.

Since the fluorescence is a phenomenon depending on many variables, such as the concentration of the luminescent activator, its coordination, and the host lattice, the interpretation of results is not always easy. However, it is specific in the sence that it can solve certain problems which are very difficult to solve with

Table 2. Decay time of the reduced Eu-M samples at room temperature

Exchanged level (%)	Pretreatment	$\tau/10^{-6}$ s
3.7	500 °C, Reduced	3.5
5.8	500 °C, Reduced	3.5

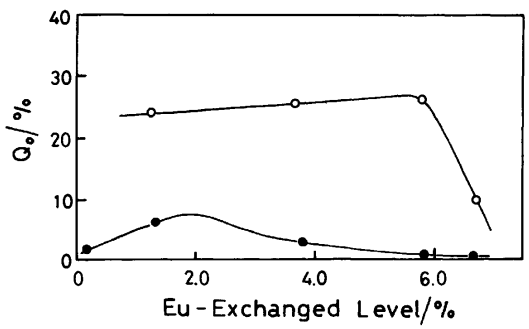

Fig. 5. Concentration quenching of the Eu^{2+} emission of the reduced samples (—○—) and the dehydrated samples (—●—).

other techniques, *e.g.*, the prediction of dipole-dipole interaction. Thus, it is considered that the results in this paper lead to a method of investigating the physicochemical properties of rare-earth ion-exchanged zeolites, although fluorescence spectroscopy is by no means a new technique. Further detailed studies to investigate these problems are now in progress.

We are grateful to Professor H. Mikawa and Dr. Y. Shirota of Osaka University for their support in the measurement of the decay time.

References

1) R. L. Firor and K. Seff. *J. Am. Chem. Soc.*, **100**, 976, 978 (1978).
2) L. E. Iton and J. Turkevich, *J. Phys. Chem.*, **81**, 435 (1977).
3) L. E. Iton, C. M. Brodbeck, S. L. Suib, and G. D. Stucky, *J. Chem. Phys.*, **79**, 1185 (1983).
4) E. A. Samuel and W. N. Delgass, *J. Chem. Phys.*, **62**, 1590 (1975).
5) S. L. Suib, R. P. Zerger, G. D. Stucky, R. M. Emberson, P. G. Derrunner, and L. E. Iton, *Inorg. Chem.*, **19**, 1858 (1980).
6) G. T. Pott and W. H. J. Stork, *J. Catal. Rev. Sci. Eng.*, **12**, 163 (1975).
7) T. Arakawa, T. Takata, G. Adachi, and J. Shiokawa, *J. Chem. Soc. Chem. Commun.*, **1979**, 453; *J. Lumin.*, **20**, 325 (1979).
8) W. C. Nieeuwpoort and G. Blasse, *Solid State Commun.*, **4**, 227 (1966).
9) G. Blasse, W. L. Wanmaker, J. W. terVrugt, and A. Brill, *Philips Res. Rep.*, **23**, 189 (1968).
10) G. Blasse and A. Brill, *Philips Tech. Rev.*, **31**, 304 (1970).
11) J. N. Denas and G. A. Crosby, *J. Phys. Chem.*, **75**, 991 (1971).
12) T. Arakawa, T. Takata, M. Takakuwa, G. Adachi, and J. Shiokawa, *Mater. Res. Bull.*, **17**, 171 (1982).
13) J. W. Ward, *J. Catal.*, **14**, 365 (1969).
14) M. V. Hoffman, *J. Electrochem. Soc.*, **115**, 560 (1968); **118**, 933 (1971).
15) J. L. Schleuker, J. J. Pluth, and J. V. Smith, *Mater. Res. Bull.*, **14**, 751 (1979).
16) P. A. Jacobs, W. de Wile, R. A. Schoonheydt, J. B. Uytterhoeven, and H. Beger, *J. Chem. Soc., Faraday Trans., 1*, **72**, 1221 (1976).
17) T. Arakawa, M. Takakuwa, T. Takata, and J. Shiokawa, *Mater. Res. Bull.*, to be published.
18) D. L. Dexter, *J. Chem. Phys.*, **21**, 836 (1953).
19) G. Blasse, *Philips Res. Rep.*, **24**, 131 (1969).
20) A. L. N. Stevels and A. D. M. Schrama-de Pauw, *J. Electrochem. Soc.*, **123**, 691 (1976).

 © 1984 The Chemical Society of Japan Bull. Chem. Soc. Jpn., 57, 1295—1298 (1984)

The Crystal Structure of *N,N,N',N'*-Tetramethylpiperazinediium Bis(2,4-dinitrophenolate) Dihydrate

Fujiko IWASAKI* and Kiyoshi MUTAI†

Department of Materials Science, The University of Electro-Communications, Chofu, Tokyo 182
†*Department of Chemistry, College of Arts and Sciences, The University of Tokyo, Meguro-ku, Tokyo 153*

(Received September 8, 1983)

The crystal structure of *N,N,N',N'*-tetramethylpiperazinediium bis(2,4-dinitrophenolate) dihydrate has been determined by the X-ray method. The crystals are triclinic, space group $P\bar{1}$, a=11.504(2), b=8.239(2), c=7.119(2) Å, α=106.22(2), β=99.67(2), γ=92.31(2)°, Z=1. The final R is 0.067 for 2743 reflections. Two dinitrophenolate anions are connected by hydrogen bonds, *via* the water molecules, forming a dimeric unit related by the center of symmetry. *N,N,N',N'*-Tetramethylpiperazinediium ion has a chair conformation.

Reaction of 2,4-dinitrofluorobenzene with 2-(dimethylamino)ethanol gave 2,4-dinitrophenyl 2-(dimethylamino)ethyl ether (**1**) as a viscous liquid. On standing long at room temperature or heating in DMF, **1** gave yellow precipitates (**2**), whose NMR spectrum showed only three broad singlets at 3.3—4.0 ppm in addition to an AMX pattern in the aromatic region. In order to elucidate the character of **2** an X-ray structure analysis was undertaken.

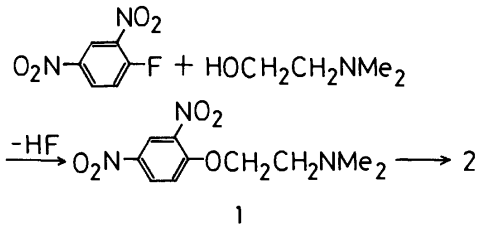

1

Experimetal

Yellow crystals were grown from an EtOH-H_2O mixed solution. Intensity data were collected on a Rigaku automatic diffractometer AFC4 using graphite-monochromated Mo $K\alpha$ radiation. A specimen with approximate dimensions 0.4×0.4×0.2 mm was used. Reflections within the range 2θ<60° were measured by the ω-2θ scan technique with a scanning speed of 4°/min in 2θ and scan widths of $\Delta\omega$=1.1°+0.5°tanθ. At both ends of the scan range 10 s background counts were taken for each reflection. 2743 reflections had $|F_o| \geq 3\sigma(F_o)$ and were considered as observed. No absorption correction was applied.

Structure Determination

Crystals belong to the triclinic system, and the centrosymmetric space group $P\bar{1}$ was assumed on the basis of the intensity statistics. Unsuccessful attempts were made to solve the structure with MULTAN78.[1] E-maps obtained from the four sets of signs showed honeycomb-like arrays of peaks from which unambiguous recognition of molecules was impossible.

The space group was assumed to be $P\bar{1}$ and attempts to solve the structure with MULTAN78 gave two fragments of 2,4-dinitrophenolate anion (2,4-DNP$^-$). Examination of the structure showed that one fragment related to the other with the center of symmetry. Reassuming the space group to be $P\bar{1}$, the parameters were refined by a block-diagonal least-squares method to R value of 0.49. A Fourier map showed two other fragments; one was assigned to the water oxygen and the other to NC_4 of the tetramethylammonium group. All non-hydrogen atoms were refined with anisotopic temperature factors. A difference synthesis was calculated from which the positions of the hydrogen atoms in 2,4-DNP$^-$, H_2O, and $(CH_2)_2N(CH_3)_2$ were found. Examination of the structure revealed that the cation was not a tetramethylammonium, but an *N,N,N',N'*-tetramethylpiperazinediium whose center of inversion was coincident with that of the crystal symmetry. All the atoms were then refined with several cycles of block-diagonal least-squares using anisotropic temperature factors for the non-hydrogen atoms and isotropic ones for the H atoms. The quantity minimized was $w(|F_o|-k^{-1}|F_c|)^2$ where w=0.8 if $|F_o|$<2.0, w=1.0 if $2.0 \leq |F_o| \leq 8.0$ and $w=(8.0/|F_o|)^2$ if $|F_o|$>8.0. The final R value was 0.067 for all observed reflections. Scattering factors were taken from "International Tables for X-Ray Crystallography".[2] All computations were performed on a HITAC M180 computer of the Data Processing Center of the University of Electro-Communications, using the programs UNICS III,[3] MULTAN78 and ORTEP.[4] The final atomic parameters are given in Table 1.[5]

Discussion

Crystal data: $(C_8H_{20}N_2)^{2+} \cdot 2(C_6H_3N_2O_5^- \cdot H_2O)$.†† Triclinic, space group $P\bar{1}$, a=11.504 (2), b=8.239 (2), c=7.119 (2) Å, α=106.22 (2), β=99.67 (2), γ=92.31 (2)°, V=636.0 (2) Å^3, D_x=1.427 g cm^{-3}, Z=1.

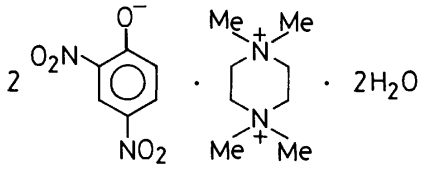

Figure 1 shows the atomic numbering of the crystal-chemical unit. Stereoscopic view of the structure and the projection along the b axis are shown in Figs. 2 and 3 respectively. The structure analysis established that the compound consists of two 2,4-dinitrophenolate

†† From the structure analysis.

Table 1. Atomic coordinates ($\times 10^4$, for H $\times 10^3$) and isotropic temperature factors

For non-H atoms $B=B_{eq}=4/3\sum_i\sum_j\beta_{ij}a_i\cdot a_j$.
The e.s.d.'s in parentheses refer to last digits.

Atom	x	y	z	B/Å^2
C(1)	2840(2)	171(3)	1493(4)	3.9
C(2)	3611(2)	-1065(3)	1924(3)	3.2
C(3)	4823(2)	-713(2)	2472(3)	3.1
C(4)	5325(2)	866(2)	2611(3)	3.1
C(5)	4627(2)	2127(3)	2207(4)	3.7
C(6)	3440(2)	1779(3)	1669(4)	4.1
N(2)	3148(2)	-2760(2)	1777(3)	4.5
N(4)	6591(2)	1206(2)	3136(3)	3.9
O(1)	1734(1)	-67(3)	996(4)	6.4
O(21)	2098(2)	-3157(3)	1416(4)	6.3
O(22)	3828(2)	-3773(3)	2026(7)	12.1
O(41)	7189(1)	147(2)	3610(3)	5.4
O(42)	7036(2)	2571(2)	3059(3)	5.7
OW	-350(1)	-1995(2)	692(3)	4.0
NP	9193(1)	6256(2)	4550(2)	2.7
CP(1)	9088(2)	5427(2)	6154(3)	2.9
CP(2)	9748(2)	5080(2)	2988(3)	2.8
CP(3)	9903(2)	7961(2)	5394(4)	3.9
CP(4)	7982(2)	6521(3)	3592(4)	4.2
H(3)	530(2)	-155(3)	267(4)	4.7(6)
H(5)	497(2)	318(3)	236(4)	4.9(6)
H(6)	297(2)	262(3)	132(4)	5.0(6)
HW(1)	-78(2)	-139(3)	28(4)	5.1(6)
HW(2)	33(2)	-162(3)	79(4)	4.9(6)
H(11)	882(2)	621(3)	717(4)	3.8(5)
H(12)	849(2)	449(3)	558(3)	2.5(4)
H(21)	987(2)	570(3)	206(4)	3.8(5)
H(22)	916(2)	414(3)	233(3)	2.7(4)
H(31)	946(2)	863(3)	632(4)	4.8(6)
H(32)	1068(3)	784(4)	617(4)	5.5(6)
H(33)	997(3)	837(4)	433(4)	5.7(7)
H(41)	806(3)	707(4)	262(4)	5.7(7)
H(42)	762(3)	719(4)	468(4)	5.5(6)
H(43)	751(2)	541(3)	306(4)	4.8(6)

anion (2,4-DNP$^-$), one *N,N,N′,N′*-tetramethylpiperazinediium (TMP^{2+}) ion and two water molecules. Thus the substance is a salt of 2DNP$^-$ and TMP^{2+}. Many picrate compounds have been known,[6] but this is the first example of the existence of 2,4-DNP$^-$ in the crystal. Two 2,4-DNP$^-$ anions are connected by the hydrogen bonds, *via* the water molecules, forming a dimeric unit related by the center of symmetry at (0,0,0) as shown in Fig. 3.

The result of the structure analysis suggests that 2,4-dinitrophenyl(dimethylamino)ethyl ether (**1**) cleaved between -O- and -CH_2- in the course of the reaction, and two -$CH_2CH_2NMe_2$ associated to form a TMP^{2+} ring. Thus the formation of **2** is nucleophilic cleavage of either C-O bond in Ar-O-CH_2 moiety intramolecularly or intermolecularly by the dimethylamino group. Primary and secondary amines usually displace the OCH_2 group through the Meisenheimer complexes, while tertiary amines can also cleave the O-CH_2 bond.[7]

Bond lengths and bond angles are listed in Table 2. The dimensions of 2,4-DNP$^-$ anion are close to those in the picrate anion. The C=O length (1.254 Å) is shorter than that of C-O (1,343 Å) in 2,4-dinitrophenol[8] and only slightly longer than the corresponding ones in the picrates. The angle at C(1) is typically low at 114.3° and the C-C bonds show characteristic variations in length. The C(1)-C(2) and C(1)-C(6) distances show some single-bonded character and the C(5)-C(6) length is shorter than the normal C-C aromatic length. The

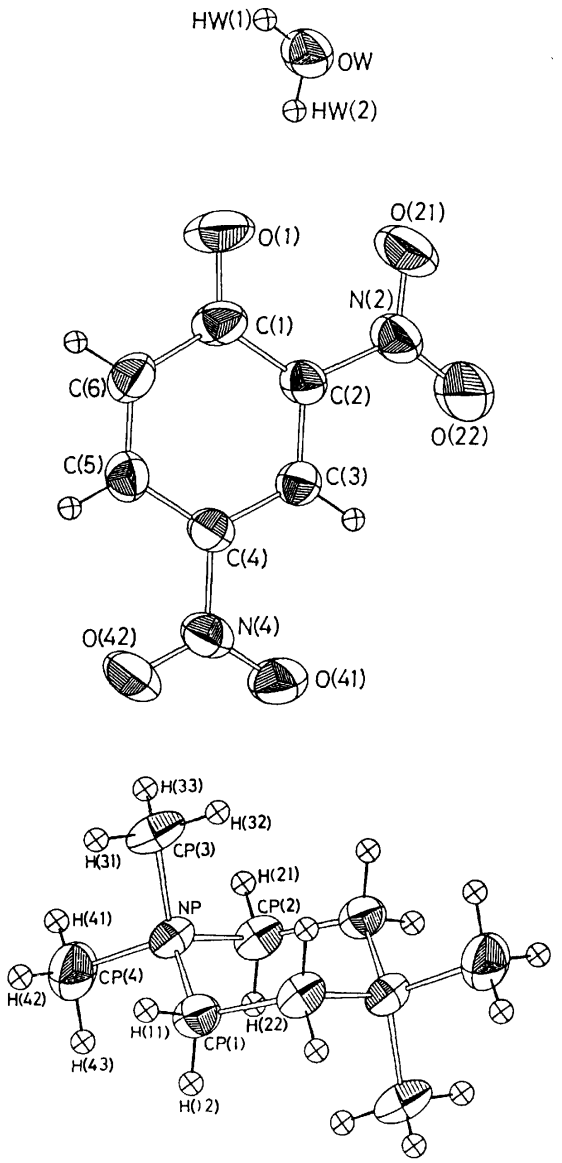

Fig. 1. Atomic numbering of the crystal chemical unit. Each non-H atom is represented as a thermal ellipsoid with a 50% probability.

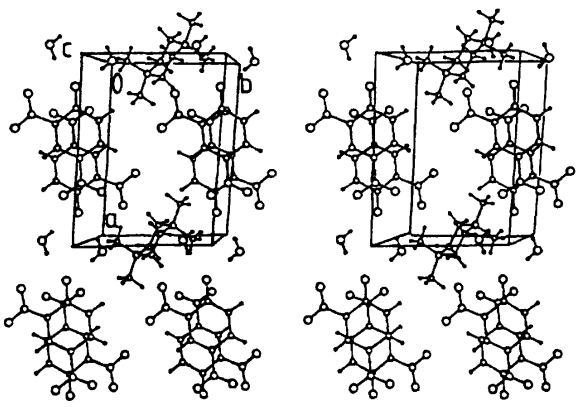

Fig. 2. Stereoscopic view of the crystal structure.

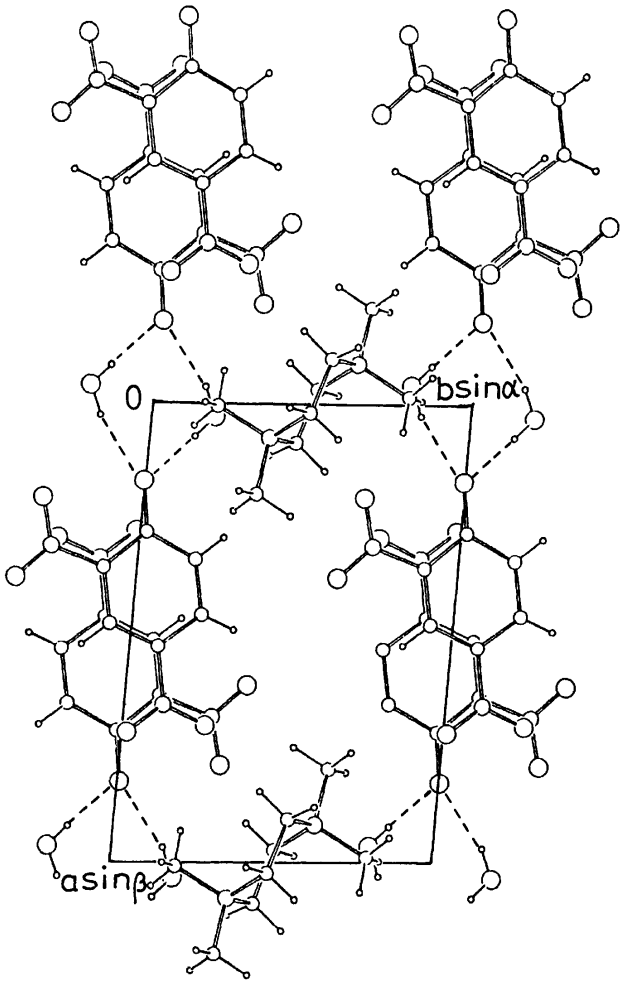

Fig. 3. Projection of the structure along the c axis.

benzene ring is planar, deviations being within 0.002 Å. Deviations of O(1), N(2), and N(4) from this plane are 0.006, 0.02, and 0.03 Å respectively. The two nitro groups are tilted only slightly from the mean plane of the benzene ring by 4.5 and 6.1° for the groups of N(2) and N(4) respectively. Some shortenings for the N-C lengths are found; N(2)-C(2) (1.444 Å) has the same value of the corresponding N-C bond in 2,4-DNP. The N(4)-C(4) length (1.436 Å) is significantly shorter than that of 2,4-DNP, but close to those in picrates. These shortenings of N-C bonds are due to the quinonoidal character of the anion.

The dimensions of O⁻···H-O hydrogen bonds between 2,4-DNP⁻ and H_2O are also listed in Table 2. The normal to the mean plane of the benzene ring of 2,4-DNP⁻ is almost parallel to the c axis and the average length between the ring planes of two 2,4-DNP⁻ related by the center of symmtry at (1/2,0,0) is 3.351 Å.

The piperazinediium ring exhibits the space-group imposed $\bar{1}$ (Ci) symmetry, and also shows the 2/m symmetry with a good approximation. The endocyclic C-N length is 1.505 Å and exocyclic C-N bonds are 1.507 and 1.498 Å. These values are longer than those usually found in C-N single bonds (1.47—1.49 Å), but similar values are reported for $C(sp_3)$-N^+(alkyl)$_3$ bonds in 1,1-dimethyl-4-phenylpiperazinium iodide,[9] (+)-*N*-2-(benzylmethylamino)propyl propionanilide hydrobromide,[10] and *trans*-2,5-dimethylpiperazine dihydrochloride.[11] The C-C length is 1.502 Å, which is significantly shorter than that in cyclohexane (1.520 Å). One of the reasons for the long C-N bond may be a nonbonding repulsion between ring hydrogens and methyl hydrogens. There are some short contacts between the axial hydrogens and the axial methyl

Table 2. Bond lengths and angles with their estimated standard deviations

Superscript (i) $-x\ -y\ -z$ (ii) $2-x\ 1-y\ 1-z$

Distance	*l*/Å	Distance	*l*/Å
C(1)-C(2)	1.440(3)	O(1)···OW^{i}	2.753(3)
C(1)-C(6)	1.432(4)	C(3)-H(3)	0.92(3)
C(1)-O(1)	1.254(4)	C(5)-H(5)	0.91(3)
C(2)-C(3)	1.379(3)	C(6)-H(6)	0.96(3)
C(2)-N(2)	1.444(3)	OW-HW(1)	0.80(3)
C(3)-C(4)	1.373(3)	OW-HW(2)	0.81(3)
C(4)-C(5)	1.402(3)	CP(1)-H(11)	0.93(3)
C(4)-N(4)	1.436(3)	CP(1)-H(12)	0.96(2)
C(5)-C(6)	1.351(4)	CP(2)-H(21)	0.97(3)
N(2)-O(21)	1.203(4)	CP(2)-H(22)	0.96(2)
N(2)-O(22)	1.196(6)	CP(3)-H(31)	0.97(3)
N(4)-O(41)	1.218(3)	CP(3)-H(32)	1.00(3)
N(4)-O(42)	1.236(3)	CP(3)-H(33)	0.93(3)
NP-CP(1)	1.504(3)	CP(4)-H(41)	0.94(3)
NP-CP(2)	1.506(3)	CP(4)-H(42)	0.99(3)
NP-CP(3)	1.507(3)	CP(4)-H(43)	0.99(3)
NP-CP(4)	1.498(3)	O(1)···HW(2)	1.98(3)
CP(1)-CP^{ii}(2)	1.502(3)	O(1)···HW^{i}(1)	1.96(3)
O(1)···OW	2.764(3)		

Angle	θ/°	Angle	θ/°
C(2)C(1)C(6)	114.3(2)	C(6)C(5)H(5)	121(2)
C(2)C(1)O(1)	125.5(3)	C(1)C(6)H(6)	117(2)
C(6)C(1)O(1)	120.2(3)	C(5)C(6)H(6)	120(2)
C(1)C(2)C(3)	122.4(2)	HW(1)OWHW(2)	108(3)
C(1)C(2)N(2)	121.2(2)	NPCP(1)H(11)	108(2)
C(3)C(2)N(2)	116.3(2)	NPCP(1)H(12)	107(1)
C(2)C(3)C(4)	119.5(2)	CP^{ii}(2)CP(1)H(11)	108(2)
C(3)C(4)C(5)	121.1(2)	CP^{ii}(2)CP(1)H(12)	113(1)
C(3)C(4)N(4)	119.0(2)	H(11)CP(1)H(12)	108(2)
C(5)C(4)N(4)	119.9(2)	NPCP(2)H(21)	106(2)
C(4)C(5)C(6)	119.3(2)	NPCP(2)H(22)	106(1)
C(1)C(6)C(5)	123.4(3)	CP^{ii}(1)CP(2)H(21)	109(1)
C(2)N(2)O(21)	121.1(2)	CP^{ii}(1)CP(2)H(22)	114(1)
C(2)N(2)O(22)	118.8(3)	H(21)CP(2)H(22)	109(2)
O(21)N(2)O(22)	120.1(3)	NPCP(3)H(31)	105(2)
C(4)N(4)O(41)	119.7(2)	NPCP(3)H(32)	110(2)
C(4)N(4)O(42)	118.1(2)	NPCP(3)H(33)	107(2)
O(41)N(4)O(42)	122.2(2)	H(31)CP(3)H(32)	108(2)
CP(1)NPCP(2)	108.5(2)	H(31)CP(3)H(33)	114(3)
CP(1)NPCP(3)	111.2(2)	H(32)CP(3)H(33)	113(3)
CP(1)NPCP(4)	109.2(2)	NPCP(4)H(41)	109(2)
CP(2)NPCP(3)	111.3(2)	NPCP(4)H(42)	106(2)
CP(2)NPCP(4)	108.3(2)	NPCP(4)H(43)	108(2)
CP(3)NPCP(4)	108.2(2)	H(41)CP(4)H(42)	114(3)
NPCP(1)CP^{ii}(2)	112.4(2)	H(41)CP(4)H(43)	114(3)
NPCP(2)CP^{ii}(1)	112.4(2)	H(42)CP(4)H(43)	106(2)
C(2)C(3)H(3)	121(2)	O(1)HW(2)OW	162(3)
C(4)C(3)H(3)	120(2)	O(1)HW^{i}(1)OW^{i}	173(3)
C(4)C(5)H(5)	120(2)	HW(2)O(1)HW^{i}(1)	92(1)

Table 3. Some intermolecular contacts with their estimated standard deviations

Superscript (none)	x	y	z	(iii)	x	$1+y$	z
(iv)	$1+x$	$1+y$	z	(v)	$1-x$	$-y$	$-z$
(vi)	$1-x$	$-y$	$1-z$				

Distance	l/Å	Distance	l/Å
O(42)···CP(1)	3.297(3)	C(1)···O^{v}(42)	3.423(3)
O(42)···CP(4)	3.287(3)	C(2)···O^{v}(42)	3.355(3)
O(21)···OW	3.020(3)	C(3)···C^{v}(5)	3.385(3)
CP(4)···O^{iii}(41)	3.156(4)	OW···CP^{v}(2)	3.292(3)
CP(2)···OW^{iv}	3.264(3)	O(21)···CP^{v}(2)	3.401(3)
CP(3)···OW^{iv}	3.321(3)	O(21)···CP^{vi}(1)	3.279(3)
CP(4)···OW^{iv}	3.464(3)	O(41)···C^{vi}(2)	3.350(3)
C(1)···N^{v}(4)	3.357(3)	N(2)···N^{vi}(4)	3.444(3)

group; H(12)···H(43) and H(22)···H(43) are 2.29 and 2.27 Å respectively. The mean endocyclic CCN angle is 112.4° and the CNC angle is 108.5°. The exocyclic CNC angles average to 109.6°. The mean value of the ring torsion angle is 55.7° (min. 55.0—max. 57.2°). For cyclohexane derivatives and heterocyclic compounds in the chair conformation a correlation exists between the average torsion angle, ϕ, and the average ring bond angle, θ: $\cos\phi=-\cos\theta/(1+\cos\theta)$.[11] In the present case $\phi_{calcd}=55.8°$ for $\theta_{obsd}=111.1°$, which is compared with the observed value of 55.7°. This value shows that the ring in TMP^{2+} is more flat than the perfect chair model of cyclohexane with tetrahedral bond angles and torsion angles of 60°.

Some of the shorter intermolecular contacts are listed in Table 3. There are distinctly short C-H···O contacts between O(42)···CP(1), O(42)···CP(4), CP(4)···O^{iii}(41), CP(2)···OW^{iv}, OW···CP^{v}(2), and O(21)···CP^{vi}(1).

References

1) P. Main, S. E. Hull, L. Lessinger, G. Germain, J. P. Declercq, and M. M. Woolfson, MULTAN78. A system of Computer Programs for the Automatic Solution of Crystal Structures from X-Ray Diffraction Data. Univs. of York, England and Louvain-la-Nerve, Belgium. (1978).

2) "International Tables for X-Ray Crystallography," Birmingham, Kynoch Press (1974), Vol. IV.

3) T. Sakurai, and K. Kobayashi. *Rikagaku Kenkyusho Hokoku,* **55**, 69 (1979).

4) C. K. Johnson, ORTEP, Report ORNL-3794, Oak Ridge National Laboratory, Tennessee (1965).

5) The tables for the anisotropic temperature factors for nonhydrogen atoms and the F_o—F_c list are deposited as Document No. 8414 at the Office of the Editor of the Bulletin of the Chemical Society of Japan.

6) C. L. Johns, G. H. Milburn, L. Sawyer, and D. L. Hughes, *Acta Crystallogr., Sect. B,* **37**, 1548 (1981).

7) M. Kohn and F. Grauer, *Monatsh. Chem.*, **34**, 1751 (1913); E. Herter and J. Luhrmann, *Z. Elektrochem.*, **45**, 405 (1939); R. S. Cahn, *J. Chem. Soc.*, **1931**, 1121.

8) F. Iwasaki and Y. Kawano, *Acta Crystallogr., Sect. B,* **33**, 2455 (1977).

9) C. Chothia and P. Pauling, *Acta Crystallogr., Sect. B,* **34** 2986 (1978).

10) P. Singh and F. R. Ahmed, *Acta Crystallogr., Sect. B,* **25**, 1901 (1969).

11) J. C. J. Bart, I. W. Bassi, and R. Scordamaglia, *Acta Crystallogr., Sect. B,* **34**, 2760 (1978).

Association between Polar Molecules. III. ^1H and ^{13}C NMR Studies on the Dipole Association of Acetonitrile Derivatives with Tetramethylurea and Dibutyl Sulfoxide in Nonpolar Solvents

Tatsuya TAKAGI,* Hideaki FUJIWARA, and Yoshio SASAKI
Faculty of Pharmaceutical Sciences, Osaka University, 1-6 Yamadaoka, Suita, Osaka 565
(Received September 24, 1983)

Dipole association between acetonitrile derivatives and polar substances such as tetramethylurea and dibutyl sulfoxide is investigated in nonpolar solvents. Association parameters and thermodynamic parameters are derived and discussed in relation to the substituent constants. ^1H and ^{13}C NMR chemical shifts show that the major structures of the associate are antiparallel. Association energies are also determined using semiempirical MNDO MO method, which supports the experimental results for energies as well as structures.

It is important to study the association between polar molecules in order to elucidate the structure of polar liquids, various solvent effects, *etc.* Hitherto, few studies have been reported[1-3] about major structures of super systems for dipolar association; Saito *et al.*[1] and Frurip *et al.*[2] indicated that a partial dipole was more important than a classical one for dipolar association, using ^{13}C NMR and *ab initio* SCF MO method respectively. However, more exhaustive studies are surely necessary to understand the factors governing the strength of association and the structre of the associate.

In previous reports,[4] we have investigated the intermolecular interactions between *p*-substituted benzonitriles or *p*-substituted nitrobenzenes and hexamethylphosphoric triamide (HMPA), dibutyl sulfone (DBSN), dibutyl sulfoxide (DBSX), and tetramethylurea (TMU) by analyzing the NMR concentration dependence. One conclusion of the study is that the association is governed mainly by electrostatic interactions. It also indicated that the association takes place around the CN group in the case of the association of *p*-substituted benzonitriles with HMPA, as evidenced by the correlation between the association parameters and the substituent constants (σ_I, σ_π)[5] or dipole moments, and by the ^{32}P chemical shift in HMPA.

In the present study, we have investigated the association of aliphatic nitriles, in which the electric charges are less delocalized than in aromatic ones and the local dipole moments are expected to play an important role in the association. ^1H and ^{13}C NMR measurements and MO calculations are utilized to obtain more detailed information about the association, especialy the equilibrium structure of such super systems.

Experimental

(Dimethylamino)acetonitrile was synthesized from dimethylamine and formaldehyde according to the literature.[6] Other nitriles were of commercial grade; they were distilled under reduced pressure and stored over Molecular Sieve 4A. Cyclohexane for solvent was washed with mixed acid, alkaline solution and water succesively; and dried over calcium chloride. It was stored over Molecular Sieve 4A after distilling three times over calcium hydride. Carbon tetrachloride was similarly washed with alkaline solution and water, distilled over calcium hydride, and finally stored over Molecular Sieve 4A. TMU and DBSX were prepared in the same way as in the previous report.[4b]

^{13}C NMR spectra were observed with a HITACHI R-900M FT NMR spectrometer operating at 22.36 MHz and at 35 °C with 16k data points, using the peak of CCl_4 as internal references. Errors in the shift measurements were less than ±0.05 ppm. ^1H NMR measurements were made as in the previous report[4b] using cyclohexane as solvent.

The sample solution for T_1 measurements was sealed under nitrogen atmosphere and the height of the solution was adjusted to 20 mm. The spin-lattice relaxation times were measured by the fast inversion-recovery method[7] which uses the (180°-τ-90°-5″-HS) pulse sequence. T_1 values were obtained from the regression coefficients for 17 data points of τ and such measurements were repeated more than twice to test the reproducibility of the experiment. Errors in the measurements of T_1 were estimated to be ±10%.

The association parameters were determined in the same way as in the previous report.[4b] Molecular orbital calculations using semiempirical CNDO/2,[8a] INDO,[8b] and MNDO[8c] MO methods were performed by the programs[8d,e] after slight modifications by the authors. The molecular geometries used for the MO calculations were experimental ones from microwave spectra and calculated ones from MNDO MO method *i.e.*, TMU.

All numerical calculations were performed on an NEAC S-900 model II computer at the Computer Center, Osaka University and HITAC M-200H computer at the Computer Center, Institute of Molecular Sciences.

Results and Discussion

Changes in ^1H and ^{13}C NMR Shift. Estimated Structure of the Associate: Variations of ^1H NMR Shifts in CH_3OCH_2CN and $(CH_3)_2NCH_2CN$ on addition of TMU or DBSX are shown in Fig. 1. In contrast to the shifts of the methylene group, those of the methyl group show only small concentration dependences. Also the change was very small for the ^1H shift of TMU when these nitriles were added to the solution. These facts suggest that the association takes place near the CN and C=O groups.

^{13}C NMR shift also changes on addition of the partner molecule (Tables 1 and 2). The changes of shifts are evident at 1-C of each nitrile (Table 1) and at the carbonyl carbon (Table 2). These facts are also consistent with the above results for the ^1H shift.[9]

^{13}C Spin-Lattice Relaxation Times: It is well known that in monosubstituted benzenes ^{13}C spin-lattice relaxation times at the ortho or the meta positions are smaller than those at the para position. Levy *et al.*[10]

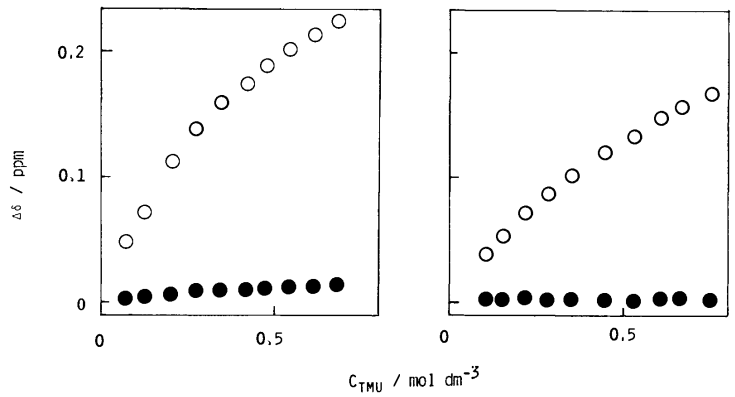

Fig. 1. Concentration dependence of ^1H NMR shifts for the CH_3OCH_2CN (left) or $(CH_3)_2NCH_2CN$ (right) plus TMU systems.
○: methylene proton, ●: methyl proton.

TABLE 1. VARIATIONS OF ^{13}C CHEMICAL SHIFTS OF R-CH_2CN ON ADDITION OF TMU(UPPER) OR DBSX(LOWER) IN CCl_4[a]

	Δδ/ppm						
	H	$(CH_3)_2N$	CH_3	C_6H_5	CH_3O	Cl	CH_3S
1-C	0.48	0.39	0.42	0.50	0.42	0.69	0.51
2-C	0.24	−0.09	0.06	−0.14	0.07	0.36	−0.18
3-C			−0.09	0.45[b]			
4-C		0.00			−0.03		−0.09
1-C	0.70	0.53	0.54	0.62	0.50	0.85	0.63
2-C	0.29	0.10	0.10	−0.08	0.13	0.48	−0.12
3-C			−0.05	0.53[b]			
4-C		0.07			0.01		−0.06

a) Equimolar (0.7 mol dm^{-3}) solutes is added. b) Ipso carbon of C_6H_5.

TABLE 2. VARIATIONS OF THE ^{13}C CHEMICAL SHIFTS OF TMU ON ADDITION OF R-CH_2CN IN CCl_4[a]

	H	$(CH_3)_2N$	CH_3	C_6H_5	CH_3O	Cl	CH_3S
C*-O	0.14	0.18	0.15	0.18	0.27	0.48	0.20
-C*H_3	−0.02	0.00	0.00	0.03	0.00	0.06	0.01

a) Equimolar (0.7 mol dm^{-3}) solutes is added.

interpreted this is due to anisotropic tumbling, *i.e.*, superior rotation around the symmetry axis. This superiority in rotation is expected to be reduced on addition of another polar molecule if they associate side by side. In the present case, the effect of the association on the relaxation time is investigated with nitrobenzene and TMU, adding 0—2.8 mol dm^{-3} of TMU to the 0.7 mol dm^{-3} solution of nitrobenzene in CCl_4. Nitrobenzene is chosen for the reason of higher solubility here. The results are given in Table 3. The higher the concentration of TMU, the more the r-value (Eq. 1)

$$r = \frac{T_1(\text{ortho}) + T_1(\text{meta})}{2T_1(\text{para})}, \quad (1)$$

approaches to 1. This is consistent with the loss of superiority in molecular rotation around the symmetry axis on addition of polar molecules indicating the increased moment of inertia around the axis.

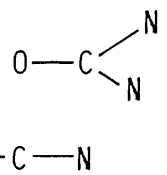

Fig. 2. Association models for the acetonitrile derivatives plus TMU systems.

All above experimental results support the idea that the polar molecules associate in the way shown in Fig. 2. For the compound treated here, electric charges are mainly distributed near the CN, C=O, and S=O groups, as calculated by CNDO/2 MO method or as reported by others.[11]

Determination of Association Parameters. The concentration dependence of the shifts at 2-C of the nitriles were measured and analyzed by nonlinear regression analsis and the equilibrium constant K and

the association shift Δ_{AB} were obtained (Table 4). 1:1 associates were assumed, similarly to the previous reports,[4] considering the results of Job plots. Plots of the association constants for the two systems containing TMU and DBSX show a linear relationship (Fig. 3), indicating similarity in the governing factor and the mode of the association in both systems. Regression analyses of the data according to the relation $y=ax$ result in

$$\ln K(\text{DBSX}) = 1.39 \ln K(\text{TMU}) \quad (2)$$
$$(n=6,\ R=0.987),^{12)}$$
$$\Delta_{AB}(\text{DBSX}) = 0.92\Delta_{AB}(\text{TMU}) \quad (3)$$
$$(n=6,\ R=0.996).$$

In *p*-substituted benzonitriles plus DBSX or TMU system, similar regression analyses result in

$$\ln K(\text{DBSX}) = 1.56 \ln K(\text{TMU}) \quad (4)$$
$$(n=6,\ R=0.943),$$
$$\Delta_{AB}(\text{DBSX}) = 0.87\Delta_{AB}(\text{TMU}) \quad (5)$$
$$(n=12,\ R=0.939).$$

As the coefficients are almost the same in both systems, the factor of association in the system containing aliphatic nitriles is similar to the one containing aromatic nitriles. Plots of $\ln K$ or Δ_{AB} against σ_i[5] show a significant correlation and the regression analyses in the system with TMU result in

$$\ln K = 4.11\sigma_i + 0.10 \quad (6)$$
$$(n=6,\ R=0.921,\ t=4.71),^{13)}$$
$$\Delta_{AB} = 11.08\sigma_i + 0.34 \quad (7)$$
$$(n=6,\ R=0.895,\ t=4.01),$$

and those in the system with DBSX result in

$$\ln K = 3.43\sigma_i + 0.72 \quad (8)$$
$$(n=6,\ R=0.958,\ t=6.68),$$
$$\Delta_{AB} = 11.11\sigma_i + 0.29 \quad (9)$$
$$(n=6,\ R=0.880,\ t=3.70).$$

Polar substituent effect for aliphatic compounds could be divided into two parts, *i.e.*, field effect and σ-inductive effect.[14] Tsuno[15] claimed that σ_i represent the former mainly. If this is also the case here, the association of the nitriles with TMU or DBSX is seen to be induced by the electric field effect.

Enthalpies ($\Delta H°$), entropies ($\Delta S°$), and Gibbs' free energies ($\Delta G°$) can be determined from van't Hoff plots after measuring the temperature dependence of the association constants (Fig. 4). These plots are obtained from the dependence of the shift on concentration as well as on temperature (Fig. 5). The results are given in Table 5. The $\Delta H°$ values derived amount to -8—-13 kJ mol^{-1}, which are about the same as those for the association of aromatic nitro or cyano compounds with HMPA and for weak hydrogen bonding. For this system, an enthalpy-entropy compensation relation, which held approximately for the aromatic nitro or cyano compounds plus HMPA systems, is not appropriate here (R=0.621). This may he due to larger steric effects for the aliphatic systems than that for the aromatic ones.

The orders of $\Delta G°$ or $\Delta H°$ are not the same as those of the dipole moments of nitriles, or more correctly, they gave a negative correlation, as was pointed out in the previous reports[4b] with aromatic systems. These facts indicate that multipole-multipole interaction, therefore, partial dipole is more important for the association of the nitriles with other polar molecules.

Calculation of Association Energy. In order to

Table 3. ^{13}C T_1 values in $C_6H_5NO_2$

TMU added / mol dm^{-3}	T_1/s			r
	ortho	meta	para	
0	11.0	12.5	5.3	2.2
0.7	11.0	11.0	6.2	1.8
1.4	10.5	10.1	6.9	1.5
2.1	9.7	8.8	6.0	1.5
2.8	9.7	8.0	6.3	1.4

Table 4. Association constants and association shifts for the R-CH_2CN plus TMU(upper) or DBSX(lower) systems

	$(CH_3)_2N$	CH_3	C_6H_5	CH_3O	Cl	CH_3S
K/mol^{-1} dm^3	1.06	1.22	1.70	1.86	5.55	2.43
Δ_{AB}/ppm	0.39	0.34	0.47	0.41	0.78	0.59
K/mol^{-1} dm^3	2.26	1.99	3.05	3.12	7.51	3.97
Δ_{AB}/ppm	0.31	0.30	0.43	0.36	0.76	0.54

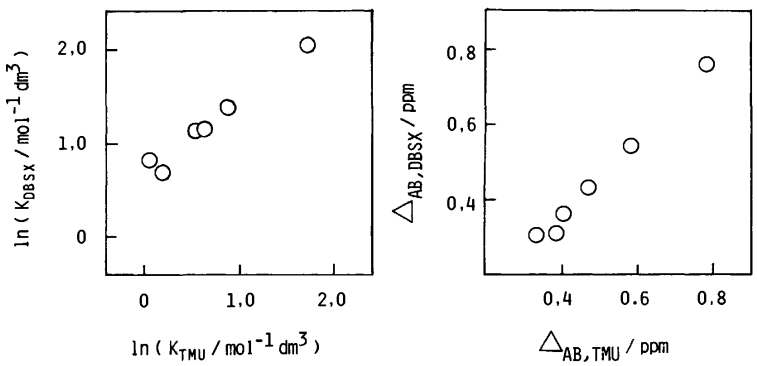

Fig. 3. Correlation of association parameters between the two systems of acetonitriles plus TMU and acetonitriles plus DBSX.

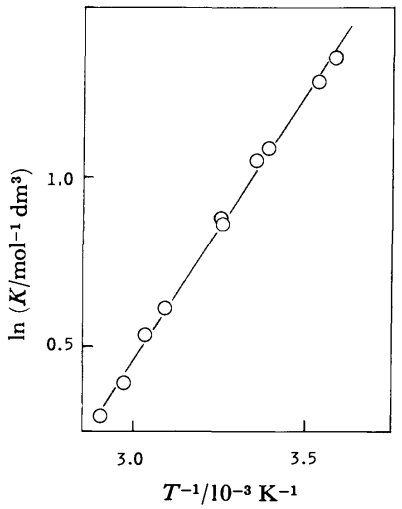

Fig. 4. van't Hoff plots for the dipole association between CH_3SCH_2CN and TMU. Similar results are reached for other systems.

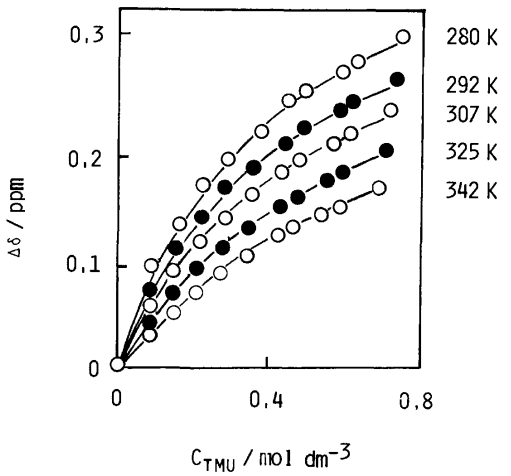

Fig. 5. Concentration and temperature dependence of the ^1H chemical shift of methylene protons in the CH_3OCH_2CN for the CH_3OCH_2CN plus TMU system in cyclohexane.

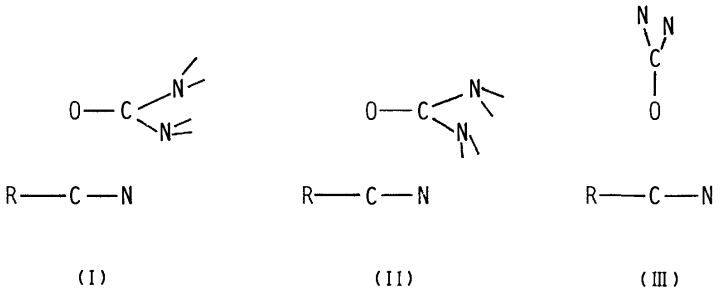

Fig. 6. Association models for the acetonitrile plus TMU systems.

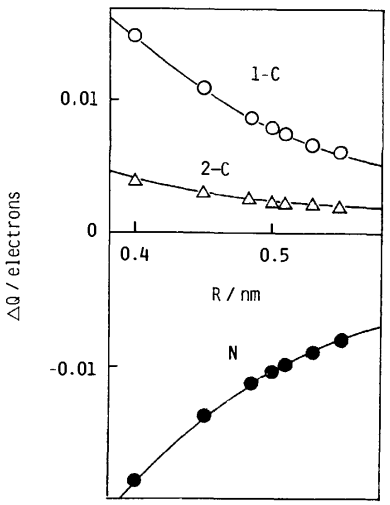

Fig. 7. Plots of association distance *vs.* change of atomic population for the acetonitrile plus TMU system calculated using MNDO MO method.

confirm the predicted structure of the associate, as mentioned before, we calculated the association energy using the super-molecule method under some molecular disposition. Three dispositions are shown in Fig. 6. Calculations by the CNDO/2 MO method gave an association distance R=0.147 nm and an association energy

TABLE 5. THERMODYNAMIC PARAMETERS FOR THE R-CH_2CN PLUS TMU SYSTEMS

	$\Delta H°$ / kJ mol^{-1}	$\Delta S°$ / J mol^{-1} K^{-1}	$\Delta G°$ / kJ mol^{-1}
$(CH_3)_2N$	−9.84	−31.0	−0.32
CH_3	−8.17	−24.8	−0.54
C_6H_5	−9.76	−25.5	−1.33
CH_3O	−10.45	−29.4	−1.42
Cl	−11.52	−22.9	−4.48
CH_3S	−13.25	−36.0	−2.19

TABLE 6. ASSOCIATION PARAMETERS FOR THE CH_3CN PLUS TMU SYSTEM CALCULATED BY MNDO MO METHOD

	ΔE / kJ mol^{-1}	R / nm
I	−2.12	0.458
II	−3.40	0.471
III	−1.43	0.433

ΔE=−241 kJ mol^{-1} on the model II. Apparently, the energy is overestimated and the distance is underestimated. Similar results are reached by the INDO MO method. This tendency is well known as typical of the

CNDO/2 or INDO MO method. On the other hand, the MNDO MO calculation gives more practical results (Table 6), which accord well with the order of the experimental values. This method also supports model II as the most stable disposition, where the changes in formal charges induced at atoms when association occurs can be calculated against the association distance under model II (Fig. 7). The changes in ^{13}C chemical shifts are in the same order with the experimental ones, when they are estimated from the changes in formal charges on the basis of ≃200 ppm/electron.

The authors thank the Institute for Molecular Science for allotment of CPU time of the HITAC M-200H computer.

References

1) H. Saito, Y. Tanaka, S. Nagata, and K. Nukada, *Can. J. Chem.*, **51**, 2188 (1973).
2) D. J. Frurip, L. A. Curtius, and M. Blender, *J. Phys. Chem.*, **82**, 2555 (1978).
3) M. R. Dagnino, G. LaManna, and L. Paoloni, *Chem. Phys. Lett.*, **39**, 552 (1976).
4) a) H. Fujiwara, T. Takaba, Y. Yamazaki, and Y. Sasaki, *J. Chem. Soc., Faraday Trans. 1*, **75**, 79 (1979); b) H. Fujiwara, T. Takagi, Y. Yamazaki, and Y. Sasaki, *J. Chem. Soc., Faraday Trans. 1*, **78**, 347 (1982).
5) Y. Yukawa and Y. Tsuno, *Nippon Kagaku Zasshi*, **86**, 873 (1965).
6) R. A. Turner, *J. Am. Chem. Soc.*, **68**, 1607 (1946).
7) G. C. Levy, *J. Magn. Reson.*, **18**, 199 (1975).
8) a) J. A. Pople and G. A. Segal, *J. Chem. Phys.*, **43**, S136 (1965); *ibid.*, **44**, 3289 (1966); b) J. A. Pople, D. L. Beveridge, and P. A. Dobosh, *ibid.*, **47**, 2026 (1967); c) M. J. S. Dewar and W. Thiel, *J. Am. Chem. Soc.*, **99**, 4899 (1977); d) J. A. Pople, D. L. Beveridge, and P. A. Dobosh, *QCPE*, **10**, 141 (1978); e) W. Thiel, *ibid.*, **11**, 353 (1978).
9) In case of benzeneacetonitrile and chloroacetonitrile exceptionally, the shift of 2-C and 3-C, respectively, changed much larger. This fact may be explained as indicating different major structure of associate for this case, but no further studies have yet been done.
10) G. C. Levy, J. D. Carginol, and F. A. L. Anet, *J. Am. Chem. Soc.*, **95**, 1527 (1973).
11) P. Mauret, J.-P. Fayet, and C. Jehl, *Bull. Chim. Soc. Fr.*, **1976**, 429.
12) R: Multiple correlation coefficient.
13) $t=r\{(n-2)/(1-r^2)\}^{1/2}$, n: number of data, r: correlation coefficient.
14) a) L. M. Stock, *J. Chem. Educ.*, **49**, 400 (1972); b) R. D. Topsom, *Prog. Org. Chem.*, **12**, 1 (1976).
15) Y. Tsuno, *Kagaku*, **36**, 412 (1981).

Conductivity and Ion Association of Some Diastereoisomeric Salts in Water. I. Δ-[Co(NO$_2$)$_2$(en)$_2$]Δ-[Co(edta)] and Λ-[Co(NO$_2$)$_2$(en)$_2$]Δ-[Co(edta)] at 15, 25, and 35 °C

Haruhiko YOKOYAMA

Department of Chemistry, Yokohama City University, 22-2 Seto, Kanazawa-ku, Yokohama 236

(Received October 4, 1983)

Electric conductivities of the diastereoisomeric salts, Δ(−)$_{589}$-[Co(NO$_2$)$_2$(en)$_2$]Δ(+)$_{546}$-[Co(edta)] and Λ-(+)$_{589}$-[Co(NO$_2$)$_2$(en)$_2$]Δ(+)$_{546}$-[Co(edta)], were measured in water at 15, 25, and 35 °C. Results were analyzed in terms of the conductivity equations of Fuoss-Hsia and Pitts. The obtained values of the ion-association constant are large and decrease with increasing temperature. The results can not be entirely explained by the electrostatic theories of ion association and suggest the formation of contact ion pairs, attributable to the existence of interactions other than simple electrostatic ones between the complex ions. No appreciable difference is found in the obtained thermodynamic parameters of ion association between the two salts. Ion-solvent interactions and effective sizes of the dissolved complex ions are also discussed in connection with the estimation of the closest distance of approach of the ions.

In recent years, many studies have been made on the stereoselectivity in ion association between optically active ions.[1-8] In particular, the association of L-tartrate ion with Δ- and Λ-[Co(en)$_3$]$^{3+}$ was widely investigated. Appearance of the stereoselectivity is attributed to the differences in structure and stability of ion pairs, and suggests the existence of ion-ion interactions other than simple electrostatic ones such as the Bjerrum-type ion association.[9,10] The hydrogen-bonding has often been presumed to be the most probable extra interaction for the association of [Co(en)$_3$]$^{3+}$ with dicarboxylate ions or other anions.[4-8,11,12] Such extra interactions are of importance for studies of ion-ion and ion-solvent interactions in the vicinity of dissolved complex ions. However, they are not necessarily investigated well.

Optically active *cis*-bis(ethylenediammine)dinitrocobalt(III) ion and (ethylenediaminetetraacetato)cobaltate(III) ion are frequently used as agents for resolution of optical isomers of complex ions.[13] The absolute configurations for (−)$_{589}$-enantiomer of *cis*-[Co(NO$_2$)$_2$(en)$_2$]$^+$ and (+)$_{546}$-enantiomer of [Co(edta)]$^-$ have been determined to be Δ-form by X-ray diffraction studies.[14,15] With respect to the solubilities of the diastereoisomeric salts, Δ-[Co(NO$_2$)$_2$(en)$_2$]Δ-[Co(edta)] and Λ-[Co(NO$_2$)$_2$(en)$_2$]Δ-[Co(edta)], the former is less soluble than the latter in water. The stereoselectivity has been observed on the rate of amino-hydrogen exchange of Δ- and Λ-[Co(NO$_2$)$_2$(en)$_2$]$^+$ in aqueous mixed electrolyte solutions containing Λ-[Co(edta)]$^-$.[16] However, no detailed information has been provided about the nature of the interactions between the complex ions. In the present study, conductivities of the above diastereoisomeric salts in water were observed at 15, 25, and 35 °C. From the analysis of conductivity data, we examined whether extra interactions are present between the complex ions or not, and whether these interactions, if present, are stereoselective or not.

The reason why such 1:1-type salts were chosen is given below. Strong 1:1 electrolytes such as sodium chloride have been usually thought to dissociate almost completely into ions in aqueous solutions.[17a] This is consistent with the prediction from the electrostatic theories of ion association.[9,10] Both ions, *cis*-[Co(NO$_2$)$_2$(en)$_2$]$^+$ and [Co(edta)]$^-$, are monovalent ones of large size. Simple electrostatic interactions may therefore be considered to be almost absent. This makes it easy to discuss the experimental results. The conductivity measurements were made with solutions of single salts alone. Consequently, the analysis of experimental data is very simple compared to the case for mixed electrolyte solutions with which most of the above studies on stereoselectivity have been carried out. The coexistence of other ions complicates not only the analysis but the explanation of results, owing to competitions or cooperative phenomena on ion association.[18]

The conductivity method is very effective to investigate ion association of 1:1 electrolytes, because it is very sensitive to a lowering of the conductivity due to the formation of noncharged ion pairs. Moreover, conductivity data obtained for 1:1 electrolytes can be precisely analyzed by using the excellent theoretical conductivity equations of Fuoss-Hsia and Pitts for a symmetrical electrolyte.[19,20] Pethybridge and Spiers have measured conductivities of the following 1:1 salts in water at 25 °C: *trans*-[Co(NO$_2$)$_2$(en)$_2$]X (X$^-$=Cl$^-$, Br$^-$, I$^-$, NO$_3^-$, ClO$_4^-$, and [Co(edta)]$^-$), *cis*-[Co(NO$_2$)$_2$(en)$_2$]X (X$^-$=I$^-$ and NO$_3^-$), and M[Co(edta)] (M$^+$=Li$^+$, Na$^+$, K$^+$, and Et$_4$N$^+$).[21,22] They analyzed their experimental data by use of the equations of Fuoss-Hsia and Pitts and found out that each electrolyte is slightly associated in water. The results obtained in the present study will be compared to theirs.

The measurements of conductivity were made by employing the linear-bridge conductometer developed by Katayama *et al.*[23] This apparatus is very favorable to examine a temperature dependence of conductivity since the temperature of the solution can be detected simultaneously with the observation of conductivity. The enthalpy and entropy of ion association will be estimated from the temperature dependence of the ion-association constant and will be used to discuss the nature of interactions between the complex ions.

Experimental

Materials. Δ- *and* Λ-*[Co(NO$_2$)$_2$(en)$_2$]X (X$^-$=Br$^-$ and*

I^-): The optically active bromide salts were prepared following the method of Dwyer and Garvan[24] from the nitrite of the racemic complex,[25] and were recrystallized from warm water (*ca.* 60 °C) by cooling in ice immediately after filtration. The recrystallization was repeated until a constant rotation result was obtained. The iodide salts were obtained by adding potassium iodide to aqueous solutions of the purified bromide salts, and recrystallized in the same manner as the bromide salts. Each salt was air-dried at room temperature. The $[\alpha]_{589}$ values of Δ- and Λ-$[Co(NO_2)_2(en)_2]Br$ were $-44°\pm1°$ and $+44°\pm1°$, respectively. Those of the iodides of Δ- and Λ-complexes were $-39°\pm1°$ and $+39°\pm1°$, respectively.

KΔ-*[Co(edta)]·2H₂O*: The optically active potassium salt was prepared following the method of Dwyer and Garvan.[26] The obtained salt was purified by fractional crystallization and air-dried at room temperature. The value of $[\alpha]_{546}$ was $+1010°\pm5°$.

Δ-*[Co(NO₂)₂(en)₂]*Δ-*[Co(edta)]·3H₂O*: This less soluble diastereoisomeric salt was prepared by adding KΔ-[Co(edta)]·$2H_2O$ to an aqueous solution of Δ-$[Co(NO_2)_2(en)_2]$-Cl, which was prepared by the double decomposition of the iodide of the complex and silver chloride in warm water (*ca.* 60°C). The obtained salt was recrystallized from warm water (*ca.* 45 °C) by the addition of ethanol. The absence of potassium and chloride ions was ascertained by adding sodium tetraphenylborate and silver nitrate, respectively, to an aqueous solution of the salt. After air-drying at room temperature, the number of molecules of the crystal water was confirmed to be three by the dehydration under vaccum by the use of a Cahn electrobalance.[27] The value of $[\alpha]_{546}$ was $+574°\pm5°$. The density of the crystal was 1.74 g cm^{-3} at 25 °C.

Λ-*[Co(NO₂)₂(en)₂]*Δ-*[Co(edta)]·H₂O*: This more soluble diastereoisomeric salt was prepared by adding ethanol to a warm aqueous solution (*ca.* 60 °C) containing equimolar proportions of the salts: Λ-$[Co(NO_2)_2(en)_2]I$ and KΔ-[Co(edta)]·$2H_2O$. The obtained salt was recrystallized twice from warm water (*ca.* 40 °C) by adding ethanol and was air-dried at room temperature. The check for potassium and iodide ions and the confirmation of the number of molecules of the crystal water were performed in the manner described above. The value of $[\alpha]_{546}$ was $+735°\pm5°$. The density of the crystal was 1.79 g cm^{-3} at 25 °C.

ORD and Electronic Absorption Spectra of the Diastereoisomeric Salts in Dilute Aqueous Solutions. The measurements of ORD and absorption spectra were carried out with a JASCO ORD/UV-5 spectropolarimeter and a Hitachi 139 spectrophotometer. The molar rotation of Δ-$[Co(NO_2)_2(en)_2]\Delta$-[Co(edta)] in water was identical with the sum of those of Δ-$[Co(NO_2)_2(en)_2]Br$ and KΔ-[Co(edta)] at any wave length from about 340 to 700 nm within the experimental error. A similar additivity was observed for Λ-$[Co(NO_2)_2(en)_2]\Delta$-[Co(edta)]. The absorption spectra of both diastereoisomeric salts in the wave length region of about 280 to 700 nm agreed with each other and with the prediction from those of *cis*-$[Co(NO_2)_2(en)_2]Br$ and K[Co(edta)] within the experimental error.

Conductivity Measurements. All solutions were made up by weight just before conductivity measurements. The conductivity of water used for the preparation was lower than 2.0×10^{-7} S cm^{-1} at 25 °C. The concentration of solutions on the molar scale at each temperature was determined by density measurements.

The conductivity measurements were made at 1000 Hz with a Fuso 360 linear-bridge conductometer according to the procedure described by Katayama *et al.*[23] The conductivity cell used was a four-necked flask with a 250 cm^3 capacity which was equipped with a thermistor, a nitrogen inlet, a magnetic stirrer, and two platinized platinum electrodes. The cell constant was 0.13702 cm^{-1}.

The conductivities of solutions were measured at 15.0, 25.0, and 35.0 °C in an atmosphere of purified nitrogen gas. Before the beginning of the measurements, dissolved carbon dioxide was removed by bubbling moistened nitrogen gas through the solution in the cell for about 50 min. During the bubbling, the solution was cooled to a temperature a little below 15 °C. The measurement was started from this temperature. The solution was warmed slowly at a speed of 0.02—0.03 °C/min to a temperature a little above 15 °C, while the change of resistance of the solution was recorded together with that of resistance of the thermistor inserted in the cell. Immediately after the recording, the solution was warmed at a high speed of 0.5—0.8 °C/min to a temperature a little below 25 °C. Subsequent procedures were made in a similar manner. A set of runs was accomplished in every case within about 2.5 h after the preparation of the solution. Throughout the measurements, the solution was protected from light.

The resistance readings of the linear bridge were calibrated by the substitution method with a precision decade resistance box (Dekabox DB62, Electro Scientific Industries; accuracy ±0.02%). The observed conductivity data were corrected for the conductivity of the solvent and for the minor conductivity change considered to be due to the aquation of *cis*-$[Co(NO_2)_2(en)_2]^+$.[28] The reproducibility of the conductivity measurements was about ±0.1%. The precision of the temperature measurements was ±0.003 °C.

Density Measurements. The density measurements were performed at (25.00±0.02) °C with all solutions used for the conductivity measurements, employing an Ostwald-type pycnometer of 10 cm^3 capacity. An approximately linear relationship was found between concentrations and densities for solutions of each diastereoisomeric salt. The density of the most concentrated solution was also measured at 15.0 and 35.0 °C to determine its molar concentration; these values were used to estimate that of the other solutions where a similar linear relationship was assumed to hold at these temperatures. The density measurements for solutions of *cis*-$[Co(NO_2)_2(en)_2]Br$ and K[Co(edta)] were carried out at 25.0 °C by using an Ostwald-type pycnometer of 50 cm^3 capacity, in order to estimate the partial molar volumes of the complex ions.

Results

Hereafter, the diastereoisomeric salts, $\Delta(-)_{589}$-$[Co(NO_2)_2(en)_2]\Delta(+)_{546}$-[Co(edta)] and $\Lambda(+)_{589}$-$[Co(NO_2)_2(en)_2]\Delta(+)_{546}$-[Co(edta)], will be often expressed by the abbreviations, Δ-Δ and Λ-Δ salts, respectively.

The observed values of molar conductivity, Λ (obsd), are summarized in Tables 1 and 2, where c is the molar concentration of a salt. In Fig. 1, the values of Λ (obsd) for each salt are plotted against those of $\sqrt{c}$. No appreciable difference in the plot is present between the Δ-Δ and Λ-Δ salts at any temperature.

The data of the density, d, obtained for aqueous solutions of the diastereoisomeric salts can be reproduced as a function of c:

$$d(\Delta\text{-}\Delta \text{ salt, } 25\,°C)/\text{g cm}^{-3} = (0.99704\pm0.00002) + (0.301\pm0.003)c$$

and

$$d(\Lambda\text{-}\Delta \text{ salt, } 25\,°C)/\text{g cm}^{-3} = (0.99705\pm0.00002) + (0.299\pm0.003)c.$$

Table 1. Molar conductivities of Λ-$[Co(NO_2)_2(en)_2]\Lambda$-[Co(edta)] in aqueous solutions at 15, 25, and 35 °C

Temp=15 °C		Temp=25 °C		Temp=35 °C	
c / 10^{-3} mol dm^{-3}	Λ(obsd) / S cm^2 mol^{-1}	c / 10^{-3} mol dm^{-3}	Λ(obsd) / S cm^2 mol^{-1}	c / 10^{-3} mol dm^{-3}	Λ(obsd) / S cm^2 mol^{-1}
1.0064	39.57	1.0043	50.31	1.0013	61.87
1.4646	39.04	1.4616	49.64	1.4572	61.01
1.9495	38.59	1.9454	49.08	1.9396	60.36
2.4314	38.15	2.4263	48.52	2.4190	59.62
3.0350	37.64	3.0287	47.91	3.0195	58.94
3.8935	37.10	3.8854	47.24	3.8737	58.13
5.0228	36.42	5.0125	46.38	4.9973	57.10
6.4907	35.71	6.4773	45.57	6.4577	56.00
8.3986	34.69	8.3813	44.29	8.3560	54.59
10.478	33.84	10.456	43.25	10.425	53.47

Table 2. Molar conductivities of Λ-$[Co(NO_2)_2(en)_2]\Lambda$-[Co(edta)] in aqueous solutions at 15, 25, and 35 °C

Temp=15 °C		Temp=25 °C		Temp=35 °C	
c / 10^{-3} mol dm^{-3}	Λ(obsd) / S cm^2 mol^{-1}	c / 10^{-3} mol dm^{-3}	Λ(obsd) / S cm^2 mol^{-1}	c / 10^{-3} mol dm^{-3}	Λ(obsd) / S cm^2 mol^{-1}
1.0417	39.61	1.0396	50.31	1.0364	61.80
1.5322	38.97	1.5291	49.55	1.5244	60.92
2.0226	38.58	2.0184	49.06	2.0123	60.34
2.5025	38.12	2.4974	48.50	2.4899	59.62
2.9623	37.79	2.9562	48.12	2.9472	59.22
4.0161	37.06	4.0078	47.21	3.9957	58.11
5.1694	36.34	5.1586	46.31	5.1430	57.02
6.5361	35.66	6.5224	45.50	6.5027	55.90
8.1154	34.85	8.0984	44.48	8.0739	54.80
10.505	33.84	10.483	43.25	10.451	53.35

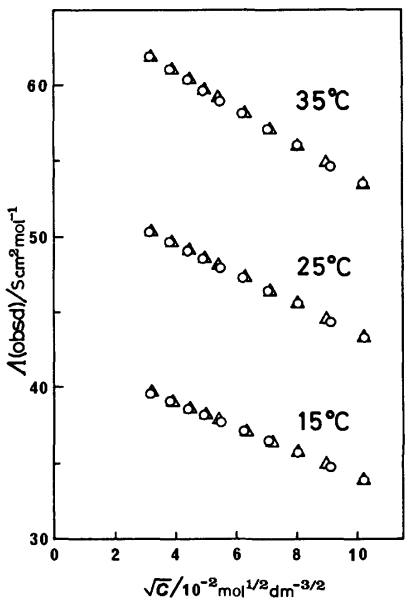

Fig. 1. Plot of Λ(obsd) against $\sqrt{c}$.
○, Λ(obsd) values for the Δ-Δ salt; △, Λ(obsd) values for the Λ-Λ salt.

From these data, the values of the partial molar volume of a salt at infinite dilution, V^∞(salt), were evaluated to be 318±4 cm^3 mol^{-1} for the Δ-Δ salt and 320±4 cm^3 mol^{-1} for the Λ-Λ salt according to the conventional manner.[29]

The values of V^∞(salt) for *cis*-$[Co(NO_2)_2(en)_2]$Br and K[Co(edta)] were estimated to be 175±2 and 181±2 cm^3 mol^{-1}, respectively, from the density data of their solutions: d(*cis*-$[Co(NO_2)_2(en)_2]$Br, 0.009972 mol dm^{-3}, 25 °C)=0.99880 g cm^{-3} and d(K[Co(edta)], 0.009161 mol dm^{-3}, 25 °C)=0.99893 g cm^{-3}. From these results, the values of the partial molar volume of an ion, V^∞(ion), can be estimated to be 145±2 and 177±2 cm^3 mol^{-1} for *cis*-$[Co(NO_2)_2(en)_2]^+$ and $[Co(edta)]^-$, respectively, using $V^\infty(Br^-, 25\ °C)$=30.1 cm^3 mol^{-1} and $V^\infty(K^+, 25\ °C)$=3.6 cm^3 mol^{-1}.[29,30] The sum of the partial molar volumes of the complex ions, 322±3 cm^3 mol^{-1}, agreeds closely with the above values of V^∞(salt) obtained for the diastereoisomeric salts.

Discussion

Analysis of Conductivity Data. The plot of Λ(obsd) against $\sqrt{c}$ gives a straight line in each case, but

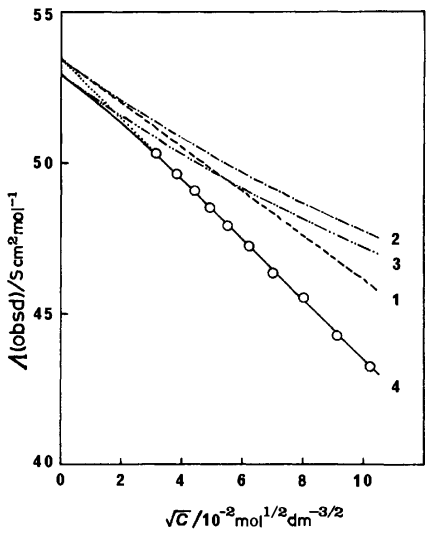

Fig. 2. Λ(obsd) values and theoretical curves for the Δ-Λ salt at 25 °C.
O, Λ(obsd) values.
Curve 1 (----) is the Onsager limiting slope drawn with a value of 53.45 S cm² mol⁻¹ for the limiting molar conductivity, Λ^∞, obtained by extrapolation of Λ(obsd) to $\sqrt{c}=0$. Curves 2 (—·—) and 3 (—··—) are Fuoss-Hsia's theoretical curves for a completely dissociated electrolyte with Λ^∞=53.45 and 52.93 S cm² mol⁻¹, respectively, on the assumption of a value of 7.0 Å for the closest distance of approach of ions. Curve 4 (——) is the theoretical curve of Fuoss-Hsia or Pitts with a set of a, K, and Λ^∞ values given in Table 3 (each set ranging a=1—9 Å gives almost the same curve).

does not obey the Onsager limiting law,[17b] as illustrated in Fig. 2. Further, the Λ (obsd) values lie considerably below the theoretical curves predicted for a completely dissociated electrolyte by the conductivity equation of Fuoss-Hsia.[19] Such negative deviations from the theoretical curves are considered to be due to the ion association. In this study, the conductivity data were analyzed by assuming the following ion association between the complex ions:

$$M^+ + A^- \rightleftharpoons M^+A^-, \quad (1)$$

where the symbol M^+ refers to the complex cation, Δ-$[Co(NO_2)_2(en)_2]^+$ or Λ-$[Co(NO_2)_2(en)_2]^+$, and the symbol A^- to the complex anion, Δ-$[Co(edta)]^-$. The analysis was made by using the Fuoss-Hsia equation[19] and the Pitts equation[20] for a symmetrical electrolyte.

The Fuoss-Hsia equation can be written symbolically as

$$\Lambda=\alpha(\Lambda^\infty-\Delta\Lambda_e)[1+(\Delta X/X)]/(1+1.5\phi), \quad (2)$$

where α is the degree of dissociation, Λ^∞ is the limiting molar conductivity, $\Delta\Lambda_e$ is the electrophoretic term, $\Delta X/X$ is the relaxation term, and 1.5ϕ corresponds to the term related to the obstruction effect.[17c] The symbol ϕ denotes the volume fraction occupied by the obstructions, approximated by $(4\pi N_A c/3000)(a/2)^3$ where N_A is the Avogadro number and a is the closest distance of approach of ions. The expressions for the electrophoretic and relaxation terms have been given by Fuoss and Hsia. The electrophoretic term is a function of αc, a, T, z, η_0, and, ε, where T is the absolute temperature, z is the absolute value of charge number of ions, and η_0 and ε are the viscosity and the dielectric constant of the solvent, respectively. The relaxation term is a function of these parameters and Λ^∞.

The Pitts equation for an incompletely dissociated electrolyte can be written symbolically as

$$\Lambda^\infty-(\Lambda/\alpha)=\Lambda^\infty P_1+P_2-P_3, \quad (3)$$

where P_1 is a function of αc, a, T, z, and ε, and where P_2 and P_3 are functions of these parameters as well as η_0. In practice, however, the following modified equation was used for the analysis instead of Eq. 3:

$$\Lambda=\alpha[\Lambda^\infty(1-P_1)-P_2+P_3]/(1+1.5\phi), \quad (4)$$

This obtained by rearranging Eq. 3 and introducing an obstruction term identical with that involved in Eq. 2.

The ion-association constant, K, was estimated for a given value of a in the following way. With an assumed value of Λ^∞, the degree of dissociation, α, was calculated by usig Eq. 2 or 4 through a successive approximation. The result was inserted in the following equation to obtain the value of K:

$$K=\frac{1-\alpha}{\alpha^2 c y_M y_A}, \quad (5)$$

where y_M and y_A are the activity coefficients of the free ions, expressed by the Debye-Hückel equation:

$$\log y_M=\log y_A=-A_{DH}\sqrt{\alpha c}/(1+B_{DH}a\sqrt{\alpha c}), \quad (6)$$

where A_{DH} and B_{DH} represent the theoretical coefficients.[17d] In these calculations, the values of η_0 and ε of water were taken from the monograph of Robinson and Stokes.[17e] The best-fit values of Λ^∞ and K for a given a value were determined by the least-squares method with the molar conductivity, Λ.

In Table 3, the results obtained on the assumption of several values for a are summarized, together with the values of the standard deviation, σ.[31] The obtained values of Λ^∞ are not much dependent on a, whereas those of K are somewhat changed by the choice of the value of a. The best values of Λ^∞ and K as well as of a are usually determined by the minimization of σ. However, this is not necessarily a good criterion for the determination of the best parameter values, because, as can be seen from Table 3, the variation of σ with a is only slight over a rather wide range of a and the value of a giving the minimum value of σ depends on the conductivity equation used for the analysis. The former reason is substantiated by the fact that the Λ(obsd) values can be theoretically reproduced well with any set of the values of Λ^∞ and K for a=1—9 Å as illustrated in Fig. 2. Further details have been described in the earlier papers.[31] We shall discuss what value of a should be taken as the best value after considering the effective sizes of the dissolved complex ions.

Ionic Radii of the Complex Ions and Ion-Solvent Interactions. From the results of the conductivity measurements, we can obtain the information concerning

Table 3. Λ^{∞} and K values at 25 °C for the Δ-Δ and Λ-Δ salts obtained with the Fuoss-Hsia equation (Eq. 2) and the Pitts equation (Eq. 4) by assuming several values for a

Salt	a/Å	With Eq. 2 (Fuoss-Hsia)			With Eq. 4 (Pitts)		
		Λ^{∞} / S cm² mol⁻¹	K / dm³ mol⁻¹	σ / S cm² mol⁻¹	Λ^{∞} / S cm² mol⁻¹	K / dm³ mol⁻¹	σ / S cm² mol⁻¹
Δ-Δ	1.0	52.90±0.07	7.9±0.7	0.0691	52.91±0.07	8.5±0.6	0.0682
	3.0	52.92±0.07	9.5±0.6	0.0673	52.93±0.07	10.0±0.6	0.0671
	5.0	52.93±0.07	10.9±0.6	0.0668	52.93±0.07	11.0±0.6	0.0670
	7.0	52.93±0.07	11.8±0.6	0.0671	52.92±0.07	11.9±0.6	0.0673
	9.0	52.90±0.07	12.2±0.7	0.0681	52.91±0.07	12.4±0.7	0.0684
	11.0	52.86±0.08	12.1±0.8	0.0730	52.88±0.07	12.7±0.7	0.0705
Λ-Δ	1.0	52.96±0.04	8.1±0.6	0.0422	52.98±0.04	8.7±0.6	0.0415
	3.0	52.99±0.04	9.7±0.5	0.0411	52.99±0.04	10.1±0.5	0.0410
	5.0	53.00±0.04	11.0±0.5	0.0410	53.00±0.04	11.2±0.5	0.0410
	7.0	52.99±0.04	12.0±0.5	0.0410	52.99±0.04	12.0±0.5	0.0411
	9.0	52.97±0.04	12.4±0.6	0.0418	52.97±0.04	12.6±0.6	0.0416
	11.0	52.93±0.05	12.3±0.6	0.0459	52.95±0.05	12.8±0.6	0.0433

the ionic radii of the complex ions in the following way. From the values of Λ^{∞}(25 °C) for a=1—9 Å, the sum of the limiting molar conductivities of *cis*-[Co(NO$_2$)$_2$(en)$_2$]$^+$ and [Co(edta)]$^-$ is considered to be 52.9 to 53.0 S cm^2 mol^{-1}. For Λ^{∞}([Co(edta)]$^-$, 25 °C), a value of 26.17±0.10 S cm^2 mol^{-1} has been reported by Pethybridge and Spiers.[22] The use of this value leads to Λ^{∞}(*cis*-[Co(NO$_2$)$_2$(en)$_2$]$^+$, 25 °C)=26.8±0.1 S cm^2 mol^{-1}.[32] By employing these Λ^{∞}(ion) values, the Stokes radii, r_s,[33] are evaluated to be 3.4$_4$ Å for *cis*-[Co(NO$_2$)$_2$(en)$_2$]$^+$ and 3.5$_2$ Å for [Co(edta)]$^-$.

The ionic radii of the complex ions can also be estimated from their partial molar volumes, V^{∞}(ion). According to Glueckauf's study,[34] V^{∞}(ion) of a univalent ion of large size is expressed by

$$V^{\infty}(\text{ion}) = 2.52(r+0.55)^3 - 33/(r+1.38), \quad (7)$$

where r corresponds to the crystallographic radius of the ion. The first term refers to the intrinsic volume of the ion and the second term to the electrostriction volume loss. Equation 7 was employed for the estimation of the ionic radii of the complex ions by regarding these ions as spherical. Substituting V^{∞}(ion)= 145±2 cm^3 mol^{-1} for *cis*-[Co(NO$_2$)$_2$(en)$_2$]$^+$ and V^{∞}(ion)=177±2 cm^3 mol^{-1} for [Co(edta)]$^-$ in Eq. 7, we obtain r=3.3$_7$ Å and 3.6$_3$ Å, respectively. The r value is in fair agreement with the r_s value for each complex ion. This suggests that both complex ions are not appreciably hydrated.

Information relating to the ion-solvent interaction can be provided from the temperature dependence of the Walden products: Λ^{∞}(salt)η_0/10^{-4} S N s mol^{-1}= 0.474 (15 °C), 0.471 (25 °C), and 0.468 (35 °C) which are calculated from the averaged values of Λ^{∞} (salt) obtained for the Δ-Δ and Λ-Δ salts. These Λ^{∞}(salt)η_0 values decrease slightly as the temperature increases. The temperature coefficient, d ln {Λ^{∞}(salt)η_0}/dT, is evaluated to be -6×10^{-4} K^{-1} close to that of Me$_4$N$^+$.[35] This implies that at least one of *cis*-[Co(NO$_2$)$_2$(en)$_2$]$^+$ and [Co(edta)]$^-$ is a structure-breaker. The latter ion may be classified as a structure-breaker from the fact that the viscosity B{[Co(edta)]$^-$} coefficient in the Jones-Dole equation increases with increasing temperature.[36] For *cis*-[Co(NO$_2$)$_2$(en)$_2$]$^+$, there is no available information about the temperature dependence of the B coefficient. However, it is interesting that the values of V^{∞}(ion) and Λ^{∞}(ion) for *cis*-[Co(NO$_2$)$_2$(en)$_2$]$^+$ are very closely similar to those for tetrakis(2-hydroxyethyl)ammonium ion, (HOCH$_2$CH$_2$)$_4$N$^+$: V^{∞}(ion)=146.8 cm^3 mol^{-1} [37] and Λ^{∞}(ion)=27.0 S cm^2 mol^{-1} at 25 °C.[38] Both the Walden product Λ^{∞}(ion)η_0 and the B(ion) coefficient for (HOCH$_2$CH$_2$)$_4$N$^+$ are known to be nearly independent of temperature.[35,38]

From the above consideration, the complex ions, *cis*-[Co(NO$_2$)$_2$(en)$_2$]$^+$ and [Co(edta)]$^-$, are presumed to have no hydration shell and to be able to come into contact to each other. Therefore, it seems reasonable that the value of a is taken to be equal to the sum of the values of r or r_s obtained for the complex ions: a=7.0$_0$ Å from the r values or a=6.9$_6$ Å from the r_s values. These values of a are considered to be moderate values because the prediction from the distance between the central cobalt(III) atoms of the two complex ions ranges from about 5 to 9 Å dependent on the direction of approach of the ions. Such a range arises from the unsymmetrical shape of the complex ions and the complexity of their surface. For these reasons, the best value of a was assumed to be equal to 7.0 Å for the diastereoisomeric salts in water.

Ion-Ion Interactions. The results obtained by assuming 7.0 Å as the best value of a are shown in Table 4. The K values for each salt are considerably larger than those predicted by the electrostatic theories of ion association.[9,10,39] According to the Bjerrum theory,[9] the values of K are expected to be equal to zero since the Bjerrum critical distance q (=3.58 Å at 25 °C for a 1:1 electrolyte)[17g] is smaller than 7.0 Å. From the theoretical equation presented by Yokoyama and Yamatera,[40] the values of K/dm^3 mol^{-1} are estimated to be 0.23 (15 °C), 0.24 (25 °C), and 0.25 (35 °C). The Fuoss theory[39] predicts 2.38 (15 °C), 2.41 (25 °C), and 2.44 (35 °C)

Table 4. Λ^{∞} and K values at 15, 25, and 35 °C for the Δ-Δ and Λ-Λ salts obtained by assuming a=7.0 Å with the Fuoss-Hsia equation (Eq. 2) and the Pitts equation (Eq. 4)

Salt	Temp °C	With Eq. 2 (Fuoss-Hsia)		With Eq. 4 (Pitts)	
		Λ^{∞} / S cm² mol⁻¹	K / dm³ mol⁻¹	Λ^{∞} / S cm² mol⁻¹	K / dm³ mol⁻¹
Δ-Δ	15	41.66±0.04	12.9±0.4	41.66±0.04	12.9±0.4
	25	52.93±0.07	11.8±0.6	52.92±0.07	11.9±0.6
	35	65.03±0.08	11.0±0.8	65.02±0.09	11.1±0.8
Λ-Λ	15	41.72±0.04	13.1±0.7	41.72±0.04	13.2±0.7
	25	52.99±0.04	12.0±0.5	52.99±0.04	12.0±0.5
	35	65.12±0.05	11.4±0.5	65.11±0.05	11.4±0.5

Table 5. Thermodynamic parameters of ion association, $\Delta G°$, $\Delta H°$, and $\Delta S°$, at 25 °C obtained by assuming a=7.0 Å

		$\Delta G°$ / kJ mol⁻¹	$\Delta H°$ / kJ mol⁻¹	$\Delta S°$ / J K⁻¹ mol⁻¹
Experimental value				
with Eq. 2(Fuoss-Hsia)	Δ-Δ	−6.12±0.13	−5.8±0.4	1.1±1.6
	Λ-Λ	−6.16±0.11	−5.3±0.7	2.9±2.8
with Eq. 4(Pitts)	Δ-Δ	−6.13±0.13	−5.7±0.3	1.4±1.4
	Λ-Λ	−6.17±0.12	−5.3±0.7	3.0±2.8
Theoretical value				
by Yokoyama-Yamatera[40]		3.55	3.54	−0.03
by Fuoss[39]		−2.18	0.93	10.4

for K/dm³ mol⁻¹.

The K value for each salt decreases as the temperature is raised, contrary to the prediction from the electrostatic theories. This tendency means that the ion association is an exothermic reaction. The standard enthalpy and entropy of ion association, $\Delta H°$ and $\Delta S°$, were estimated from the temperature dependence of the ion-association constant. The $\Delta H°$ value was derived from the slope of a linear plot of log K against T^{-1}, while the $\Delta S°$ value was calculated from the equation, $\Delta S°=(\Delta H°-\Delta S°)/T$, where $\Delta G°$ is the standard Gibbs free energy of ion association. The obtained values of $\Delta G°$, $\Delta H°$, and $\Delta S°$ are shown in Table 5 and are compared with those predicted by the electrostatic theories of ion association.[39,40]

Table 5 shows that the relation, $\Delta H°<T\Delta S°\approx 0$, is valid for the observed values of $\Delta H°$ and $\Delta S°$. This relation is distinct from $T\Delta S°>\Delta H°>0$ obtained for the ion association of 2:2 electrolytes such as $MgSO_4$.[23,41] The negative $\Delta H°$ values can not be predicted from the ion-association theories.[39,40] Such values of $\Delta H°$ will be attributed to the existence of short-range forces almost independent of the dielectric constant of the medium. The $\Delta S°$ values nearly equal to zero may suggest that the ion association occurs without the release of the hydration water molecules of the complex ions. This is consistent with the presumption that the complex ions, *cis*-$[Co(NO_2)_2(en)_2]^+$ and $[Co(edta)]^-$, are not appreciably hydrated. Consequently, the comparatively large values of K for each salt are considered to imply the formation of contact ion pairs resulting from interactions other than simple electrostatic ones between the complex ions.

It has been found that tetraalkylammonium halides, R_4NX, are slightly associated in water and the K values of the salts decrease with increasing temperature in a similar manner as observed in the present study.[42] Pethybridge and Spiers have reported the fact that the K values in water for 1:1 electrolytes including R_4NX increase with increasing the sum of the crystallographic radii, $\sum r$(cryst).[21,22,43] Such a trend is the reverse of that predicted by the ion-association theories of Bjerrum[9] and Yokoyama-Yamatera.[10] The Fuoss theory predicts that the ion-association constant increases with increasing the a value at $a>2q/3$ ($a>2.39$ Å at 25 °C).[17h] However, his theory can not also give the negative $\Delta H°$ value for any ion association in water. Therefore, the phenomenon of ion association of 1:1 electrolytes is considered to be due to existence of ion-ion interactions other than the simple electrostatic ones.

Pethybridge and Spiers have expressed graphically the relationship between K and $\sum r$ (cryst).[21,22,43] If we estimate the value of K for the diastereoisomeric salts from this relationship, a value of 4—5 dm³ mol⁻¹ can be obtained.[44] However, this value of K is much smaller than the experimental ones given in Table 4. This implies that different kinds of extra interactions exist between the complex ions. The most effective interaction among them may be the hydrogen-bonding between the hydrogen atoms of amino groups of *cis*-$[Co(NO_2)_2(en)_2]^+$ and the oxygen atoms of calboxyl

groups of $[Co(edta)]^-$. The ion-association constants of the Δ-Δ and Λ-Δ salts are somewhat larger than that of *trans*-$[Co(NO_2)_2(en)_2][Co(edta)]$: $K \approx 9\ dm^3\ mol^{-1}$.[45] This may be mainly attributed to the difference not only in the magnitude of the dipole moment of the complex cations, but in the ease of the formation of the hydrogen bonds. In the case of the *trans*-isomer, the nitro groups are considered to be more unfavorably located for the hydrogen-bonding than in the case of the *cis*-isomer.

Stereoselectivity. The ion pairs, Δ-$[Co(NO_2)_2(en)_2]^+\Delta$-$[Co(edta)]^-$ and Λ-$[Co(NO_2)_2(en)_2]^+\Delta$-$[Co(edta)]^-$, can not be stereochemically the same. However, as shown in Table 5, no appreciable difference between the two ion pairs is found in the thermodynamic properties of ion-pair formation. Although the ΔH° value of the Δ-Δ salt seems to be slightly smaller than that of the Λ-Δ salt, it is indefinite because of the experimental error. The difference in solubilities of the Δ-Δ and Λ-Δ salts would have to be interpreted from that in their crystal structures.

Yamatera and Fujita have observed the rate of amino-hydrogen exchange of Δ- and Λ-$[Co(NO_2)_2(en)_2]^+$ ($0.039\ mol\ dm^{-3}$) under the presence of Λ-$[Co(edta)]^-$ ($0.035\ mol\ dm^{-3}$) in D_2O and found out that the rate constant for the Λ-complex cation is 0.86 times that for the Δ-complex cation.[16] The hydrogen-deutrium exchange rate is thought to be slowed down by means of the ion association. If the hydrogen-deutrium exchange rate of the associated complex cations were negligibly small compared with that of the free ion, the degree of dissociation for the Λ-complex cation should be 0.86 times that for the Δ-complex cation. However, such a large difference in the degree of dissociation can not be derived from the present results. Therefore, in order to explain the difference in the observed rate constant, the associated complex cations should be supposed to contribute to the hydrogen-deutrium exchange rate. In addition, the extent of the contribution of the associated Δ-complex cation should be greater than that of the associated Λ-complex cation. The hydrogen-deutrium exchange of $[Co(en)_3]^{3+}$ has been considered to be assisted by the OD^- ion.[5] If a similar mechanism is assumed also in the case of Δ- and Λ-$[Co(NO_2)_2(en)_2]^+$, the difference in the extent of the contribution to the exchange rate between the two associated complex cations may be attributed to the difference in the ease of N-H bond breaking caused by the association with Λ-$[Co(edta)]^-$ as well as the difference in the affinity of the associated complex cations with the OD^- ion.

The author is gratefully indebted to Professor Nobuyoshi Shinohara of Yokohama City University for his helpful discussion, Dr. Masataka Ozaki for the use of a Cahn electrobalance, and Dr. Shunzo Katayama of the Institute of Physical and Chemical Research for his helpful advice and suggestions on the conductivity measurements. I would also like to thank Mr. Michio Nishimura for his asistance. The present work was partially supported by a Grant-in-Aid for Scientific Research No. 354227 from the Ministry of Education, Science and Culture.

References

1) K. Ogino and U. Saito, *Bull. Chem. Soc. Jpn.*, **40**, 826 (1967).
2) H. Yamatera and M. Fujita, *Bull. Chem. Soc. Jpn.*, **42**, 3043 (1969).
3) H. Yoneda, K. Miyoshi, S. Suzuki, and T. Taura, *Bull. Chem. Soc. Jpn.*, **47**, 1661 (1974).
4) M. Fujita and H. Yamatera, *Bull. Chem. Soc. Jpn.*, **49**, 1301 (1976).
5) M. Fujita and H. Yamatera, *Bull. Chem. Soc. Jpn.*, **50**, 2672 (1977).
6) H. Yokoyama, The Proceedings of the 27th Conference on Coordination Chemistry of the Chemical Society of Japan, Matsumoto, September 1977, p. 87.
7) T. Taura, *J. Am. Chem. Soc.*, **101**, 4221 (1979).
8) A. Tatehata, M. Iiyoshi, and K. Kotsuji, *J. Am. Chem. Soc.*, **103**, 7391 (1981).
9) N. Bjerrum, *Kgl. Danske Videnskab. Selskab.*, **7**, No. 9 (1926).
10) H. Yokoyama and H. Yamatera, *Bull. Chem. Soc. Jpn.*, **48**, 1770, 3002 (1975).
11) K. Miyoshi, C. E. Oh, and H. Yoneda, *Bull. Chem. Soc. Jpn.*, **53**, 2815 (1980).
12) S. F. Mason and B. J. Norman, *J. Chem. Soc., A*, **1966**, 307.
13) W. T. Jordan and B. J. Brennan, L. R. Froebe, and B. E. Douglas, *Inorg. Chem.*, **12**, 1827 (1973).
14) K. Matsumoto and H. Kuroya, *Bull. Chem. Soc. Jpn.*, **45**, 1755 (1972).
15) K. Okamoto, T. Tsukihara, J. Hidaka, and Y. Shimura, *Bull. Chem. Soc. Jpn.*, **51**, 3534 (1978).
16) Ref. 2. The footnote in Ref. 2 is related to $[Co(en)_3]^{3+}$, $[Co(NO_2)_2(en)_2]^+$, and tartrate ion, and in the case of *l*-$[Co(edta)]^-$ the notation *l* denotes $(-)_{546}$(private communication, 1981).
17) R. A. Robinson and R. H. Stokes, "Electrolyte Solutions," 2nd ed, Butterworths, London (1959). a) Chaps. 7, 9, and 14; b) Chap. 7, p. 142; c) Chap. 11, pp. 310—313; d) Chap. 9, p. 229; e) Appendix 1.1, p. 457; g) Chap. 14; h) Appendix 14.3, p. 551.
18) Represented by the ion association of complex cations with perchlorate ion added to solutions in order to hold a constant ionic strength. See, for example, Ref. 3; H. Yokoyama and H. Yamatera, The Proceedings of the 20th Conference on Coordination Chemistry of the Chemical Society of Japan, Tokyo, November 1970, p. 57; L. Johansson, *Coord. Chem. Rev.*, **12**, 241 (1974).
19) R. M. Fuoss and K. -L. Hsia, *Proc. Natl. Acad. Sci. U. S. A.*, **57**, 1550 (1967); **58**, 1818 (1968).
20) E. Pitts, *Proc. R. Soc. London, Ser. A*, **217**, 43 (1953); E. Pitts, B. E. Tabor, and J. Daly, *Trans. Faraday Soc.*, **65**, 849 (1969).
21) A. D. Pethybridge and D. J. Spiers, *J. Chem. Soc., Faraday Trans. 1*, **9**, 64 (1976).
22) A. D. Pethybridge and D. J. Spiers, *J. Chem. Soc., Faraday Trans. 1*, **9**, 73 (1976).
23) S. Katayama, *Bull. Chem. Soc. Jpn.*, **46**, 106 (1973); *J. Solution Chem.*, **5**, 241 (1976); *Rep. I. P. C. R.*, **53**, 212 (1977); K. Takahashi, S. Katayama, and R. Tamamushi, *ibid.*, **49**, 13 (1973).
24) F. P. Dwyer and F. L. Garvan, *Inorg. Synth.*, **6**, 195 (1960).
25) J. Springbørg and C. E. Chäffer, *Inorg. Synth.*, **14**, 63

(1973).
26) F. P. Dwyer and F. L. Garvan, *Inorg. Synth.*, **6**, 192 (1960).
27) Two water molecules of *Δ*-[$Co(NO_2)_2(en)_2$]*Δ*-[Co(edta)]·$3H_2O$ and the water molecule of *Λ*-[$Co(NO_2)_2$-$(en)_2$]*Δ*-[Co(edta)]·H_2O were dehydrated at room temperature *in vacuo*, while the third water molecule of the former salt was dehydrated by heating above *ca.* 90 °C *in vacuo*.
28) Pethybridge and Spiers have observed the increase with time in the conductivity for *trans*-[$Co(NO_2)_2(en)_2$]X (X^-= Cl^-, Br^-, I^-, NO_3^-, ClO_4^-, and $[Co(edta)]^-$) and *cis*-[Co-$(NO_2)_2(en)_2$]X (X^-=I^- and NO_3^-): about 0.01% per hour except for *trans*-[$Co(NO_2)_2(en)_2$][Co(edta)].[21] In the present study, the rate of increase in the conductivity for the diastereoisomeric salts was about 0.02% per hour at 25 °C. This value is consistent with the above value, since the increase per the molar conductivity of the complex cation can be estimated to be equal to about 0.04% per hour in both cases. For *trans*-[$Co(NO_2)_2(en)_2$][Co(edta)], the rate of increase in the conductivity has been reported to be about 0.1% per hour at 25 °C, much greater than that obtained for the other salts.[21] This abnormal value was explained by suggesting that the aquation of the complex cation is catalyzed by the hydrogen ion liberated as a result of hydrolysis of $[Co(edta)]^-$. If such a phenomenon occurred actually, the rate of increase in the conductivity would have to be accelerated with increase of concentration of the salt. However, no dependence of the rate on the concentration has been found in their study.[21]
29) F. J. Millero, *Chem. Rev.*, **71**, 147 (1971); "The Partial Molal Volumes of Electrolytes in Aqueous Solutions," in "Water and Aqueous Solutions," ed by R. A. Horne, Wiley-Intersciene, New York (1972), Chap. 13.
30) R. Zana and E. Yeager, *J. Phys. Chem.*, **71**, 521 (1967).
31) H. Yokoyama and H. Yamatera, *Bull. Chem. Soc. Jpn.*, **48**, 2708, 2719 (1975).
32) This value is slightly smaller than the value of 27.4±0.3 S cm^2 mol^{-1} reported by Pethybridge and Spiers.[21] A value of 27.7±0.4 S cm^2 mol^{-1} for Λ^∞(*trans*-[$Co(NO_2)_2$-$(en)_2]^+$) has been also given by them.[21] The sum of the values of Λ^∞(*trans*-[$Co(NO_2)_2(en)_2]^+$) and $\Lambda^\infty([Co(edta)]^-)$ becomes 53.87 S cm^2 mol^{-1}, much smaller than the value of 62.26 S cm^2 mol^{-1} obtained from the experimental data for *trans*-[$Co(NO_2)_2(en)_2$][Co(edta)].[21] Such discrepancy is not found for the Λ^∞ values of the diastereoisomeric salts in the present study.
33) Expressed by $r_s/Å=0.820/\Lambda^\infty/(\eta_0/\text{poise})$ where 1 poise=10^{-1} kg m^{-1} s^{-1}. See, for example, Ref. 17, Chap. 2, p. 44.
34) E. Glueckauf, *Trans. Faraday Soc.*, **61**, 914 (1965).
35) R. L. Kay, "Ionic Transport in Water and Mixed Aqueous Solvents," in "Water," ed by F. Franks, Plenum Press, New York (1973), Vol. 3, Chap. 4.
36) M. Yasuda, *Bull. Chem. Soc. Jpn.*, **41**, 139 (1968); K. Mizutani and M. Yasuda, The Proceedings of the 24th Conference on Coordination Chemistry of the Chemical Society of Japan, Kanazawa, October 1974, p. 373.
37) W.-Y. Wen and S. Saito, *J. Phys. Chem.*, **69**, 3569 (1965): estimated from V^∞ {$(HOCH_2CH_2)_4NBr$}=176.9 cm^3 mol^{-1} by assuming $V^\infty(Br^-)$=30.1 cm^3 mol^{-1}.[29,30]
38) D. F. Evans, G. P. Cunningham, and R. L. Kay, *J. Phys. Chem.*, **70**, 2974 (1966); G. P. Cunningham, D. F. Evans, and R. L. Kay, *ibid.*, **70**, 3998 (1966).
39) R. M. Fuoss, *J. Am. Chem. Soc.*, **80**, 5059 (1958).
40) Ref. 10. The ion-association constant is given by

$$K = \frac{8\pi N_A a^3}{1000} \sum_{n=1}^{\infty} \frac{b^{2n+2}}{(2n+2)!(2n-1)},$$

where b is the Bjerrum parameter given by $b=z^2e^2/\varepsilon kTa$.
41) H. Yokoyama and H. Yamatera, *Bull. Chem. Soc. Jpn.*, **54**, 2286 (1981).
42) R. Fernandez-Prini, *Trans. Faraday Soc.*, **64**, 2146 (1968).
43) A. D. Pethybridge and D. J. Spiers, *J. Chem. Soc., Chem. Commun.*, **1974**, 423.
44) From the K-$\sum r$ (cryst) graph given in Refs. 21, 22, and 43, a value of 2—3 dm^3 mol^{-1} for K can be read at $\sum r$ (cryst)=7.0 Å. However, this value can not be directly used for comparison with that obtained in the present study for the following reason. All the K values shown in the K-$\sum r$ (cryst) graph correspond to those obtained by the analysis with the assumption of a value of 3.58 Å for a. Further, the $\sum r$ (cryst) values for several electrolytes in this graph seem to be somewhat overestimated, as exemplified by the ionic radius of *trans*- or *cis*-[$Co(NO_2)_2(en)_2]^+$ which is assumed to be 4.3 Å, larger than 3.4 Å assumed in the present study. Considering these differences in the treatment, the value of K read at $\sum r$ (cryst)=7.0 Å is thought to have to be raised by about 2 dm^3 mol^{-1}.
45) In Ref. 21, K=8 dm^3 mol^{-1} is given for this salt. However, this value corresponds to that obtained by the analysis with the assumption of a=3.58 Å. If a=7.0 Å is assumed, a value of about 9 dm^3 mol^{-1} is obtained for K.

NMR Study of Protonated Halothiophenes. II. An *ab Initio* Self-consistent Field Calculation of the Protonation of Chlorothiophenes

Yukihide YAMASHITA, Hiroyuki KOBAYASHI, Akihiro YOSHINO,
Kensuke TAKAHASHI,* and Tyo SONE†
Department of Industrial Chemistry, Nagoya Institute of Technology, Gokiso-cho, Showa-ku, Nagoya 466
†*Department of Applied Chemistry, Faculty of Engineering, Yamagata University, Jonan, Yonezawa 992*
(Received October 17, 1983)

The STO-3G method was applied to the protonation of thiophene and chlorothiophenes. The optimized structures and charge densities thus obtained are consistent with the experimental results obtained from the ^{1}H NMR spectral data. In the neutral molecule, the β-chloro substituent lowers the total energy more than the α-one; however, the latter stabilizes the protonated state more than the former.

We have observed the halothiophenium ions produced from halothiophenes at rather low temperatures.[1-4] The NMR parameters thus obtained are useful in discussing the properties of such ions. Molecular orbital calculations are also done as supplements to the experimental results. Such calculations have previously been done by many researchers.[4-6] The system of thiophenes has the problem of whether the calculations should be carried out with or without the d-orbitals on the sulfur atom.[7]

This study has been performed by using the minimal basis set, the so-called STO-3G method.[8] The method is a very simple *ab initio* calculation and has a problem as to the quantitative determination of the properties.[9] However, the results are good enough to discuss the problems qualitatively.

Procedure

The calculation was carried out by using the HITAC M-200H computer and the Library Program (IMSPAK) installed in the Computer Center, Institute of Molecular Science, at Okazaki. The basis wave functions used were the STO-3G minimal basis set.[10] For the optimization of the structure, an initial structure was taken from that obtained by Bak *et al.*,[11] while the distance of the C-Cl bond was taken from that of Harshbarger *et al.* (1.7095 Å).[12] The structure of the thiophenium ion was assumed to be on a plane except for the atoms bonded to the protonated sp^3-carbon, which has an initial bonding angle with two out-of-plane atoms of 109.5°.

For chlorothiophenium cations, the SCF initial molecular orbitals were composed from those of the anionic ones because, when they were composed from the cationic ones, the SCF calculations did not converge with the optimized structures.

Results and Discussion

Structure of Thiophene, Chlorothiophenes, and Their Cations. The optimized structures of thiophene are given in Table 1, along with its experimental results and other calculated values. The values obtained by the STO-3G method are shorter in the double bond and longer in the single bond than those calculated by Amato *et al.*[13]

Table 1. Comparison of structure determinations of thiophene

Bond length	Bak *et al.* (1961) *l*/Å	Amato *et al.* (1982) *l*/Å	This work *l*/Å
S-C	1.7140±0.0014	1.726	1.732
C=C	1.3696±0.0017	1.348	1.335
C-C	1.4232±0.0023	1.432	1.454
C_α-H	1.0776±0.0015	1.067	1.079
C_β-H	1.0805±0.0014	1.069	1.080
Bond angle	**θ/°**	**θ/°**	**θ/°**
∠CSC	92.17±0.1	91.2	90.4
∠SCC	111.47±0.3	111.8	112.7
∠SCH	119.85±0.8	120.7	120.4
$\angle C_3C_4H_4$	124.27±0.1	123.6	123.1
∠CCC	112.45±0.2	112.6	112.1

The optimized structures of chlorothiophenes and their cations are summarized in Figs. 1 and 2. The ring-interior-angle of the substituted carbons of chlorothiophenes increases, while the bond lengths concerned with the carbons generally increase, as compared with those calculated for thiophene. Further, the bond-lengths of the C_β-H and the C_β-Cl bonds are longer than those corresponding to the C_α-H and the C_α-Cl bonds. As would be expected, the bond angles of the protonated carbons approach the tetrahedral angle. Since only one 3*H*-thiophenium ion has been calculated, the discussion of the cations will hereafter be limited to the 2*H*-thiophenium ions. In the protonated state, the bond lengths of the C_2-C_3, the C_4-C_5, and the S-C_2 bonds increase, while the reverse shortening appears in the C_3-C_4 and the S-C_5 bonds. These features are expressed schematically in Scheme 1. The C-H bond length increases in the order of the 4-, 3-, and 5-positions in the thiophene ring of the cationic state as compared with that in the neutral molecule; however, conversely, the C-Cl bond lengths decrease in the same order. On the other

Scheme 1.

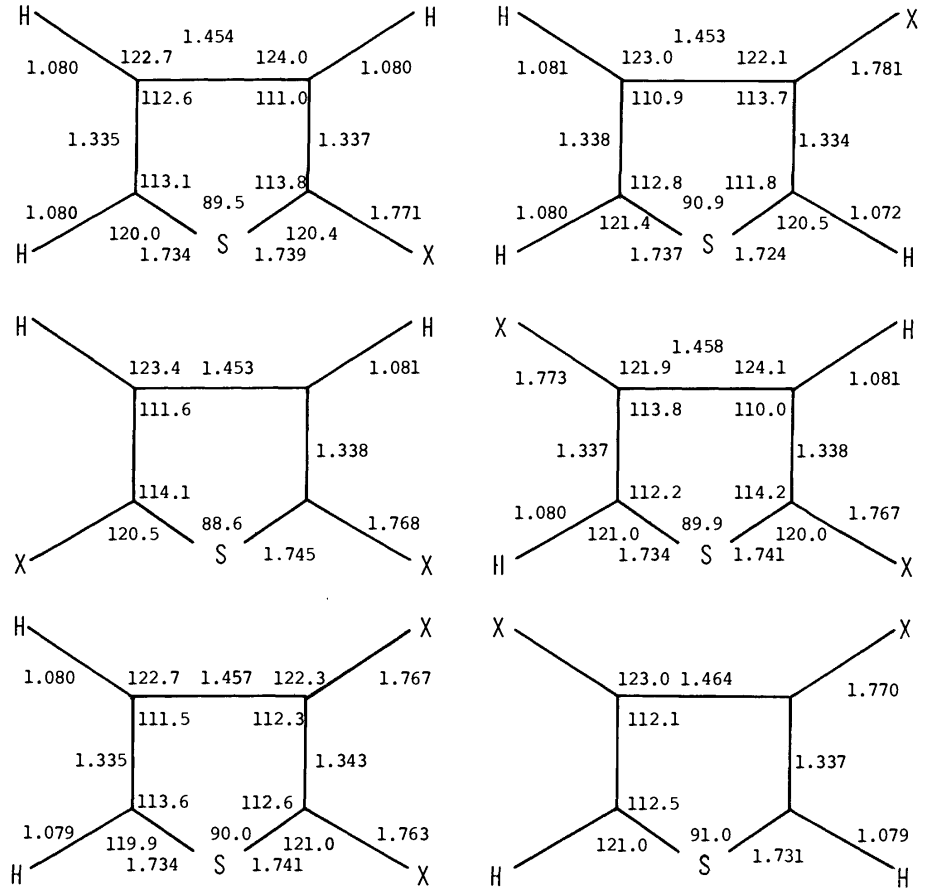

Fig. 1. Comparison of optimized geometries for chlorothiophenes.
Bond lengths in Å and angles in degrees. X denotes chlorine atom.

TABLE 2. TOTAL CHARGES OF THIOPHENE, CHLOROTHIOPHENES, AND THEIR CATIONS AS OBTAINED BY CLOSED-SHELL-SCF CALCULATIONS WITH A MINIMAL BASIS SET

	S	C_2	C_3	C_4	C_5	$X_{2(1)}$	$X_{2(2)}$	X_3	X_4	X_5
Thiophene	0.254	−0.177	−0.084	−0.084	−0.177	0.071		0.063	0.063	0.071
2-Cl	0.293	−0.074	−0.074	−0.076	−0.171	−0.136		0.084	0.074	0.081
3-Cl	0.285	−0.171	0.024	−0.075	−0.169	0.093		−0.152	0.083	0.083
2,5-Cl_2	0.328	−0.070	−0.067	−0.067	−0.070	−0.120		0.093	0.093	−0.120
2,3-Cl_2	0.317	−0.072	0.029	−0.069	−0.164	−0.103		−0.119	0.091	0.091
2,4-Cl_2	0.320	−0.068	−0.066	0.030	−0.165	−0.118		0.101	−0.135	0.101
3,4-Cl_2	0.311	−0.164	0.028	0.028	−0.164	0.101		−0.120	−0.120	0.101
2*H*	0.471	−0.205	0.060	−0.074	−0.031	0.153	0.153	0.155	0.143	0.174
2*H*,5-Cl	0.474	−0.202	0.061	−0.069	0.043	0.155	0.155	0.160	0.151	0.071
2*H*,3-Cl	0.477	−0.202	0.139	−0.070	−0.031	0.160	0.160	0.035	0.154	0.178
2*H*,3,5-Cl_2	0.480	−0.200	0.139	−0.066	0.043	0.162	0.162	0.041	0.162	0.078
2*H*,2,5-Cl_2	0.491	−0.097	0.059	−0.062	0.050	0.170	−0.027	0.169	0.158	0.089
2*H*,4,5-Cl_2	0.492	−0.197	0.060	0.018	0.043	0.160	0.160	0.170	0.001	0.094
2*H*,3,4-Cl_2	0.495	−0.199	0.138	0.016	−0.028	0.165	0.165	0.054	0.005	0.189

hand, the 3- and 5-(C-H) bonds are longer than those of the neutral molecules, although the situation is reversed with the 3- and 5-(C-Cl) bonds. This shows that the resonance effect of the chlorine atom plays a role in the cationic state. The expected structural model shown in Scheme 1 is consistent with the experimental finding that the values of J_{34} (*ca.* 5.5 Hz) are larger than those of J_{45} (*ca.* 4.0 Hz) in halogeno-substituted 2*H*-thiophenium ions.[2,3]

Charge Distributions. The total and π electronic charges of thiophene, chlorothiophenes, and their cations are tabulated in Tables 2 and 3. The protonations of these molecules occurred at the most negative carbons expected from the present calcula-

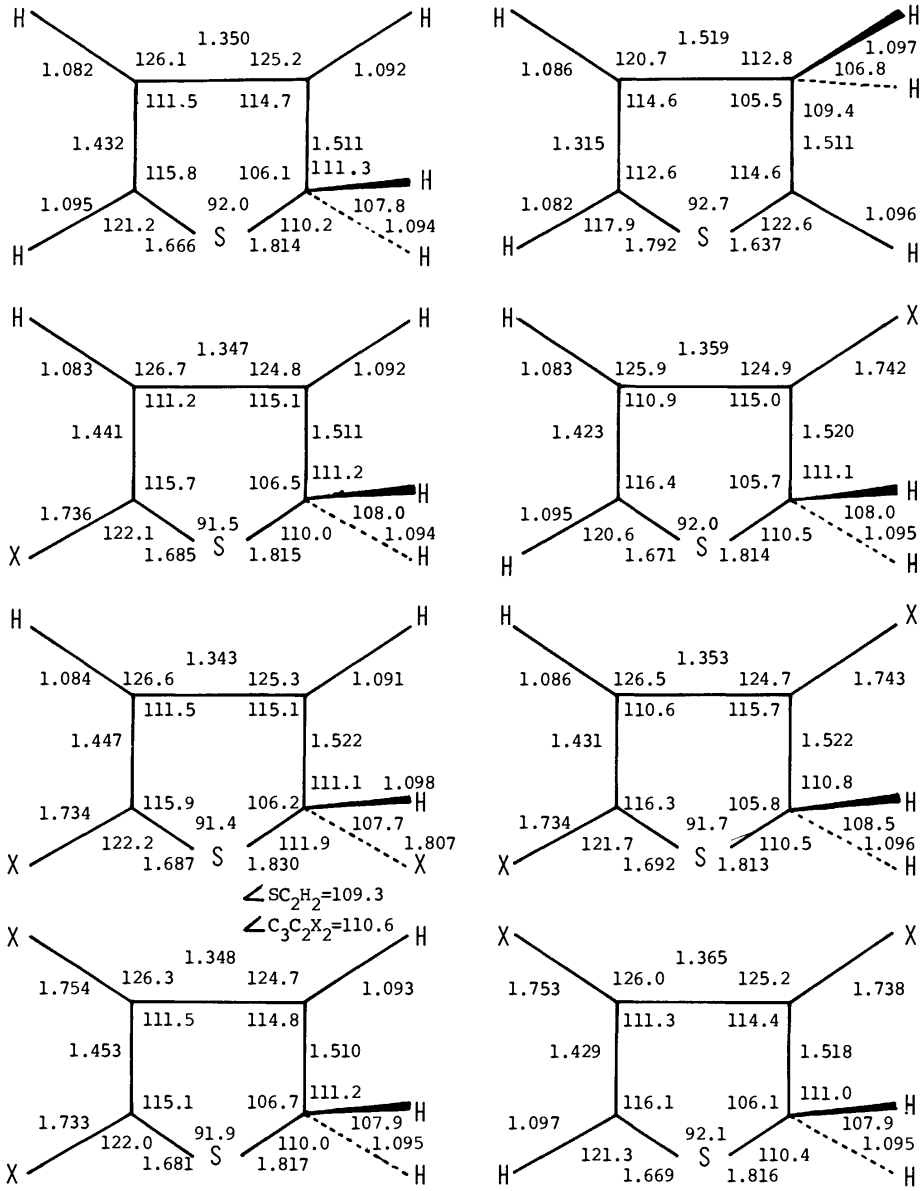

Fig. 2. Comparison of optimized geometries for thiophenium ions.
Bond lengths in Å and angles in degrees. X denotes chlorine atom.

tions. However, the ^{1}H NMR chemical shifts are not directly proportional to the calculated charge densities on the hydrogen atoms for the neutral molecules.

In the cationic states, the chlorine atoms all have a positive charge except for the atoms bonded to the sp^3-hybridized carbon. This shows that the resonance effect of the chlorine atom is important in the cationic state. Table 3 shows that the positive charges on the thiophenium ions are localized more at the 5-carbon than at the 3-carbon. Table 4 summarizes the π-charge-density differences between the neutral molecules and the corresponding cations. From the table, the excess π-charge densities can be seen to be located more at the 5-carbon than at the 3-carbon. For the thiophenium ions, the calculated electronic densities of the hydrogens bonded to the sp^2-hybridized carbons are proportional to the observed ^{1}H chemical shifts, as is shown in Fig. 3. The proportional coefficient is about 100 ppm/electron. The dotted lines in the figure show that the chlorine substituents cause a shielding effect in spite of attracting the electron from the hydrogens. The coefficients of the dotted lines are −25, −35, and −58 ppm/electron, from the bottom to the top in the figure. These values show the effects of the charge on the 4-, the 3-, and the 5-hydrogens respectively.

Energies. The total calculated energies of thiophene, chlorothiophenes, and their protonated species are given in Table 5. The total energies of the molecules are dependent upon the methods used. The values for thiophene obtained with several methods are shown in the table. The β-chloro substituent lowers the energy more than does the α-one. The α-protonation lowers the energy more than does the β-one in thiophene; the difference is about 48 kJ mol^{-1} (0.01877 a.u.). This result is consistent with the experimental result

reported in the previous study, in which only the α-protonation products have been observed, but not the β-ones.[2)]

The following schemes can be considered from the total-energy consideration of Table 5. In each case, the right system is more stable than the left system. Therefore, the protonation of thiophene is easier than that of

Table 3. π-Orbital charges of the ring atoms of thiophene, chlorothiophenes, and their cations obtained by closed-shell-SCF calculations with a minimal basis set

	S	C_2	C_3	C_4	C_5
Thiophene	0.230	−0.071	−0.046	−0.046	−0.071
2-Cl	0.226	−0.117	−0.034	−0.045	−0.066
3-Cl	0.234	−0.062	−0.095	−0.052	−0.058
2,5-Cl_2	0.221	−0.111	−0.034	−0.034	−0.111
2,3-Cl_2	0.230	−0.111	−0.085	−0.050	−0.054
2,4-Cl_2	0.230	−0.103	−0.042	−0.092	−0.059
3,4-Cl_2	0.240	−0.052	−0.100	−0.100	−0.052
2*H*	0.410	—	0.260	−0.059	0.334
2*H*,5-Cl	0.377	—	0.257	−0.064	0.272
2*H*,3-Cl	0.393	—	0.208	−0.063	0.324
2*H*,2,5-Cl_2	0.368	—	0.241	−0.054	0.292
2*H*,3,5-Cl_2	0.360	—	0.204	−0.068	0.263
2*H*,4,5-Cl_2	0.392	—	0.244	−0.104	0.266
2*H*,3,4-Cl_2	0.405	—	0.196	−0.105	0.320

Table 4. Additional π-orbital charges of the ring atoms of the thiophenium ion and chlorothiophenium ions

	S	C_2	C_3	C_4	C_5
2*H*	0.180	—	0.306	−0.013	0.405
2*H*,5-Cl	0.151	—	0.302	−0.030	0.389
2*H*,3-Cl	0.159	—	0.303	−0.011	0.382
2*H*,2,5-Cl_2	0.147	—	0.275	−0.020	0.403
2*H*,3,5-Cl_2	0.130	—	0.296	−0.026	0.366
2*H*,4,5-Cl_2	0.162	—	0.294	−0.019	0.377
2*H*,3,4-Cl_2	0.165	—	0.296	−0.005	0.372

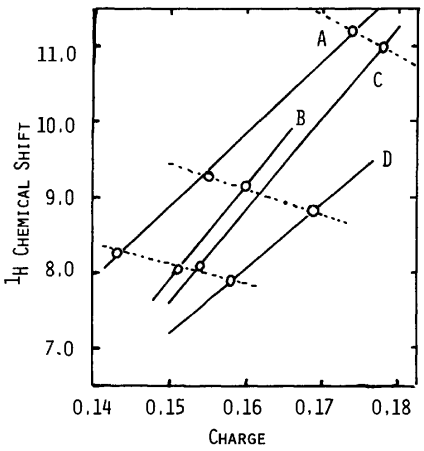

Fig. 3. Correlation of ^{1}H chemical shifts of protons attached to the sp^2-hybridized carbons with total calculated charges in thiophenium and chlorothiophenium ions; A, thiophenium ion; B, 2*H*-5-chloro-; C, 2*H*-3-chloro-; D, 2*H*-2,5-dichlorothiophenium ions.

Table 5. Calculated total energies of thiophene, chlorothiophenes, and their cations

Thiophene	−545.09237 a. u.
	−550.4174[a)]
	−550.5353[a)]
	−550.66185[b)]
2-Cl	−999.09392
3-Cl	−999.09655
2,3-Cl_2	−1453.09271
2,4-Cl_2	−1453.09521
2,5-Cl_2	−1453.09289
3,4-Cl_2	−1453.09517
2*H*	−545.50151
3*H*	−545.48274
2*H*,5-Cl	−999.48935
2*H*,3-Cl	−999.49025
2*H*,2,5-Cl_2	−1453.46314
2*H*,3,5-Cl_2	−1453.47739
2*H*,4,5-Cl_2	−1453.47021
2*H*,3,4-Cl_2	−1453.47100

a) See Ref. 7b, b) See Ref. 13.

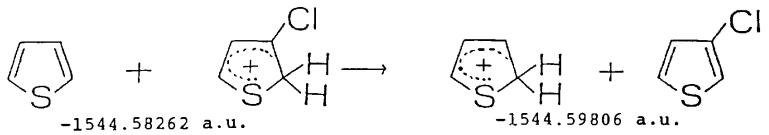

Scheme 2.

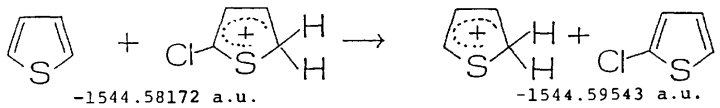

Scheme 3.

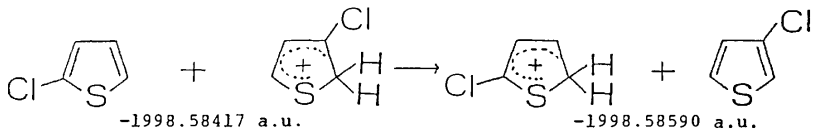

Scheme 4.

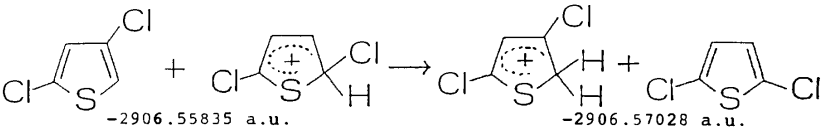

Scheme 5.

chlorothiophene. Scheme 4 is essentially interesting, for the chlorine substituent stabilizes the neutral molecule at the β-position more than at the α-position. However, Scheme 4 shows that the α-substituent is more effective than the β-one for the protonation. In other words, the resonance stabilization effect is stronger in the α-chlorine than in the β-one in the protonated state. Other interesting schemes appear below. The 2,4-dichlorothiophenium ion is more stable than the 2,5-one. However, the rearrangement has not occurred from the 2,5-dichlorothiophenium ion to the 2,4-one in the experiments,[1,2] though such a rearrangement has been observed in the dibromothiophenium ions.[3]

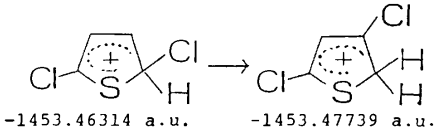

Scheme 6.

Conclusion

The STO-3G method was applied to the protonation of thiophene and chlorothiophenes. The optimized structures and charge densities thus obtained are consistent with those expected from the ^{1}H NMR spectral observations. The β-chlorine atom lowers the total energy more than the α-one in the neutral molecules; however, the latter substituent is more effective than the former in the resonance stabilization of the cationic state of the molecules.

References

1) Y. Yokoyama, Y. Yamashita, K. Takahashi, and T. Sone, *Chem. Lett.*, **1981**, 813.
2) Y. Yokoyama, Y. Yamashita, K. Takahashi, and T. Sone, *Bull. Chem. Soc. Jpn.*, **56**, 2208 (1983).
3) Y. Yamashita, A. Yoshino, K. Takahashi, and T. Sone, The 46th National Meeting of the Chemical Society of Japan, Niigata, Oct., **1982**, Abstr., 4P15.
4) W. C. Ermler and R. S. Mulliken, *J. Am. Chem. Soc.*, **100**, 1647 (1978).
5) J. L. Devlin, III, J. F. Wolf, R. W. Taft, and W. J. Hehre, *J. Am. Chem. Soc.*, **98**, 1990 (1976).
6) R. S. Greenberg, M. M. Bursey, and L. G. Pedersen, *J. Am. Chem. Soc.*, **98**, 4061 (1976).
7) a) D. T. Clark, *Tetrahedron*, **24**, 2663 (1968); b) P. McArdle and A. R. Manning, *J. Chem. Soc., Chem. Commun.*, **1970**, 319; c) M. H. Palmer, R. H. Findlay, and A. J. Gaskell, *J. Chem. Soc., Perkin Trans. 2*, **1974**, 420; d) M. H. Palmer and F. H. Findlay, *ibid.*, **1975**, 1223; e) Y. Osamura, O. Sayanagi, and K. Nishimoto, *Bull. Chem. Soc. Jpn.*, **49**, 845 (1976).
8) a) W. J. Hehre, R. Ditchfield, R. F. Stewart, and J. A. Pople, *J. Chem. Phys.*, **51**, 2657 (1969); b) W. J. Hehre, R. Ditchfield, R. F. Stewart, and J. A. Pople, *ibid.*, **52**, 2769 (1970).
9) a) R. Ditchfield, W. J. Hehre, and J. A. Pople, *J. Chem. Phys.*, **54**, 724 (1971); b) W. J. Hehre and W. A. Lathan, *ibid.*, **56**, 5255 (1972); c) W. J. Hehre, R. F. Stewart, and J. A. Pople, *ibid.*, **51**, 2657 (1969).
10) W. J. Hehre, W. A. Lanthan, R. Ditchfield, M. D. Newton, and J. A. Pople, *QCPE* No. **236**, Quantum Chemistry Program Exchange, Indiana University, Bloomington, Indiana.
11) B. Bak, D. Christensen, L. Hansen-Nygard, and J. R. Andersen, *J. Mol. Spectrosc.*, **7**, 58 (1961).
12) W. R. Harshbarger and S. H. Bauer, *Acta Crystallogr., Sect. B*, **26**, 1010 (1970).
13) J. S. Amato, S. Karady, R. A. Reamer, H. B. Schlegel, J. P. Springer and L. M. Weinstock, *J. Am. Chem. Soc.*, **104**, 1375 (1982).

 © 1984 The Chemical Society of Japan Bull. Chem. Soc. Jpn., 57, 1317—1320 (1984)

An Analysis of the $E(0_g^+)$ Ion-pair State of Bromine through Stepwise Excitation Technique

Takashi Ishiwata, Atsuto Tokunaga, Tsutomu Shinzawa, and Ikuzo Tanaka*
Department of Chemistry, Tokyo Institute of Technology, Ohokayama, Meguro-ku, Tokyo 152
(Received November 16, 1983)

The pulses of the fundamental and its frequency doubled outputs from a tunable dye laser are used to promote a stepwise exciation of the $E(0_g^+)$-$X^1\Sigma_g^+$ transition through the $B^3\Pi(0_u^+)$ state in molecular bromine. The double resonance is detected by the associated UV emission which originates from the $E(0_g^+)$ state radiating back to the $B^3\Pi(0_u^+)$ state. The $E(0_g^+)$ state is analyzed in detail on the basis of the selection rules of two transition components and the E-B fluorescence spectrum. The molecular parameters are derived as T_e= 49778.5 cm^{-1}, ω_e=150.8 cm^{-1}, $\omega_e x_e$=0.41 cm^{-1}, and r_e=3.197 Å for the $^{79}Br_2$ isotope species.

The electronic structure of diatomic halogens has been studied many times both theoretically and experimentally, and yet several important problems remain unsolved with regard to the existence and positions of certain electronic states.[1] In particular, the high-lying excited states of the ion-pair type are the subjects of recent interest and curiosity, because of their recent use in the development of the laser emissions in the ultraviolet and vacuum ultraviolet regions.[2-5] Designing a halogen laser system requires detailed spectroscopic and kinetic data on the emitting state itself as well as the surrounding electronic states.

It is well-known that the ion-pair states of Br_2 correlate with $Br^-(^1S)+Br^+(^3P, ^1D, ^1S)$ at the dissociation limit and the dominant attractive term in their potential function is simply $-e^2/r$. Therefore, all the ion-pair states are empirically taken to have relatively large internuclear distances (3.2 Å) and dissociation energies (35000 cm^{-1}) with small vibrational frequencies (150 cm^{-1}), and to group in accordance with the energies of the various Br^+ states.[6] Thus the 6 states ($0_u^+(D)$[7], $0_g^+(E)$[8], 1_u, 1_g, 2_u, and $2_g(D')$)[9] from $Br^+(^3P_2)$ would belong to the lowest group lying at around 49000 cm^{-1}, the 2 states ($0_u^+(F)$[10] and $0_g^+(f)$[11]) from $Br^+(^3P_0)$ and the 4 (0_u^-, 0_g^-, 1_u, and 1_g) from $Br^+(^3P_1)$ would locate near 53000 cm^{-1}. The 6 states (0_u^+, 0_g^+, 1_u, 1_g, 2_u, and 2_g) from $Br^+(^1D)$ would be expected at around 60000 cm^{-1}, and 2(0_u^+ and 0_g^+) from $Br^+(^1S)$, very considerably higher.

This work is part of a series[7,10,11] where the spectroscopic properties of the ion-pair states are examined for the Br_2 molecule. Since its optical pumping from the ground state requires large Franck-Condon shifts due to the large internuclear separation of the ion-pair states, our method involves a stepwise excitation through the $B^3\Pi_{0_u^+}$ state as an intermediate. The g or u ion-pair states can be proved if one or virtual two-photon transitions originate from the B state. In the experiment described here, the Br_2 molecules are pumped to the B state by the output of a tunable dye laser operated in the visible region and subsequently excited into the $E(0_g^+)$ ion-pair state by its second harmonics in the ultraviolet. It is obvious that the excitation proceeds only if the double resonance condition is satisfied for the two transition components. We can detect the resonances by the E-B emission and the stepwise processes are analyzed.

Experimental

The experimental apparatus is similar to that used in previous experiments.[11] Briefly, a nitrogen laser pumped dye laser provided 8 ns pulses with an energy of 1 mJ/pulse and 0.1 Å resolution, and a KDP crystal was installed for frequency doubling (conversion efficiency 5%). Both the fundamental laser light and its frequency doubled output passed through a UV fluorescence cell to excite the Br_2 molecules in a stepwise process. The fluorescence was dispersed by a 50 cm monochrometer in the second order and detected by a photomultiplier. The output signals were amplified ten times and averaged by a boxcar integrator.

To exclude the spectral congestion problem, monoisotopic $^{79}Br_2$ was used in the experiments. A sample pressure was 3.1 Torr (1 Torr=133.3 Pa). The emission spectra were recorded with a spectral resolution of 0.2 Å and studied as a function of excitation wavelength.

Results and Discussion

When the $^{79}Br_2$ molecules were excited both by the fundamental and its second harmonic outputs of the dye laser operated in the wavelength region between 595 and 621 nm, several series of fluorescent progressions were observed at around 310 nm. These closely resemble the $f(0_g^+)$—$B^3\Pi_{0_u^+}$ system of Br_2 (265—285 nm) which we have recently analyzed.[11] The emission bands consisted of the P and R doublets, and the vibrational spacing observed at the shortest wavelength was about 155 cm^{-1}, close to the vibrational frequency of the B state (ω_e=167.6 cm^{-1}).[12] From its position in the spectrum, the emission under study appears to be the $E(0_g^+)$—$B^3\Pi_{0_u^+}$ system observed by Tellinghuisen and co-workers[8] in conventional discharge experiments. In our case, the pumping to the E state was obviously achieved by a stepwise excitation through the B state. As a matter of fact, the emission vanished by blocking either the visible or the ultraviolet laser light with a suitable glass filter.

Table 1 summarizes the strong double resonance signals observed in the experiment. The laser frequencies noted here correspond to the positions of the rotational lines of the B-X absorption involved in the excitation process. Under our experimental conditions, the relaxations in the intermediate B state are negligible, so that the assignments of the following E-B transitions were straightforward. The rotational quantum number (J)

Table 1. Observed transitions and term values of the double resonance experiments on $^{79}Br_2$

$E(0_g^+)$ ←($h\nu_{UV}$ a)— $B(^3\Pi_{0_u^+})$ ←($h\nu_{VIS}$)— $X(^1\Sigma_g^+)$	$h\nu_{VIS}/cm^{-1}$	$T^E_{v,J}/cm^{-1}$
$v=0$, $J=33$ b) (0—11) P_{34} c) (11—4) P_{35} d)	16118.8	49900.0 e)
0 33 (0—11) P_{34} (11—4) R_{33}	16122.9	49900.9
1 57 (1—10) R_{56} (10—3) P_{57}	16249.2	50140.3
1 101 (1—9) R_{100} (9—2) R_{99}	16274.0	50431.5
1 101 (1—9) P_{102} (9—2) R_{101}	16263.2	50431.5
2 11 (2—10) P_{12} (10—3) P_{13}	16339.3	50158.1
2 37 (2—7) P_{38} (7—1) P_{39}	16532.9	50208.6
2 46 (2—7) P_{47} (7—1) R_{46}	16526.7	50242.1
3 46 (3—9) R_{45} (9—2) P_{46}	16469.1	50389.6
3 87 (3—8) P_{88} (8—1) P_{89}	16493.0	50617.0
3 95 (3—8) P_{96} (8—1) R_{95}	16483.1	50677.4
4 43 (4—11) P_{44} (11—3) P_{45}	16411.2	50526.6
4 86 (4—10) R_{85} (10—2) P_{86}	16447.5	50756.1
5 65 (5—10) R_{64} (10—2) P_{65}	16538.7	50771.0
7 58 (7—9) R_{57} (9—1) P_{58}	16753.6	51025.4
9 19 (9—11) P_{20} (11—2) R_{19}	16784.1	51189.8

a) Excitation was performed by the second harmonics of the laser light used for the B-X transition ($h\nu_{UV}=2h\nu_{VIS}$). b) Definition of the final level in the E state. c) Assignment to the E-B transition. d) Assignment to the B-X transition. e) Term values of the final (v, J) level in the E state relative to the potential minimum of the ground state.

of the ion-pair state was derived from the emission spectrum depending on whether the P or R line was in resonance with the UV laser wavelength. The absolute v' numbering was established by the characteristic intensity pattern of the fluorescent progression. The internuclear distance of the ion-pair states (typically r_e=3.2 Å) is much longer than that of the B state (r_e=2.68 Å). The low-v level of the ion-pair state will display in emission a band system whose intensity distribution is modulated according to the probability distribution of the upper wavefunction. For example, the fluorescence spectra in Fig. 1 show (a) a double and (b) a single peak in emission envelope, and can be assigned to originate from the vibrational level of (a) v'=1 and (b) v'=0, respectively. The interpretation is confirmed by the energy level analyses and Franck-Condon calculations as described below.

The term energies $T^E_{v,J}$ of the ion-pair state in Table 1 were calculated relative to the potential minimum of the ground state. They were determined by adding the fundamental ($h\nu_{VIS}$) and its second harmonic ($h\nu_{UV}$) frequencies to the vibrational and rotational terms of the ground state levels (G''_v and $F''_v(J)$) from which the stepwise transitions originate (Eq. 1).

$$T^E_{v,J} = h\nu_{VIS} + h\nu_{UV}(=2h\nu_{VIS}) + G''_v + F''_v(J) \quad (1)$$

Based on these derived term energies, we calculated the absolute wavelength positions of the expected P and R doublets in the emission spectra of the $E(0_g^+)$—$B^3\Pi_{0_u^+}$ transition using the known molecular constants of the B state.[12] The calculated values agreed with the experimentally derived ones within our experimental accuracy (±0.2 Å) and the transition from the E state terminates on the high vibrational levels of the B state as shown in Fig. 1.

The molecular constants of the $E(0_g^+)$ state were

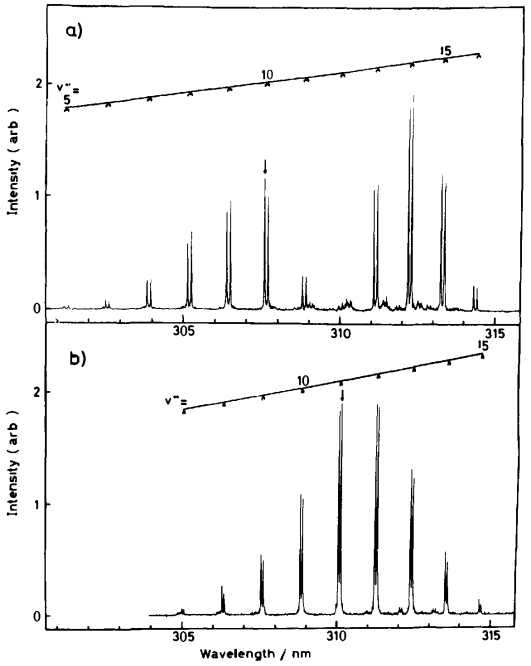

Fig. 1. Fluorescence spectrum of Br_2 corresponding to the $E(0_g^+) \rightarrow B^3\Pi_{0_u^+}$ transition.

$X^1\Sigma_g^+ \xrightarrow{h\nu_{VIS}} B^3\Pi_{0_u^+} \xrightarrow{h\nu_{UV}} E(0_g^+)$ $h\nu_{VIS}(cm^{-1})$

(a) (11-4) R_{33} (0-11) P_{34} 16122.9

(b) (10-3) P_{57} (1-10) R_{56} 16249.2

Spectral slitwidth, 0.2 Å. The UV laser wavelength is indicated by an arrow.

calculated to fit the term values to the form;

$$T^E_{v,J} = T_e + \omega_e\left(v+\frac{1}{2}\right) - \omega_e x_e\left(v+\frac{1}{2}\right)^2 + \left\{B_e - \alpha_e\left(v+\frac{1}{2}\right)\right\}J(J+1) - DJ^2(J+1)^2. \quad (2)$$

where the values of α_e and D were estimated from the following relations[13] in order to reduce the parameter of the higher order.

$$\alpha_e = 6B_e(\sqrt{\omega_e x_e \cdot B_e} - B_e)/\omega_e, \quad (3)$$

$$D = 4B_e^3/\omega_e^2. \quad (4)$$

The B_e values were calculated based on r_e values at around 3.2 Å at intervals of 0.001 Å and the equations fitted by the least squares method iteratively. Using sets of the derived constants, we have calculated the Franck-Condon factors for the E-B system.[14] The potential curve of the B state was constructed by the RKR method, while we approximated the potential curve of the E state by a Morse function using a set r_e value, and ω_e and $\omega_e x_e$ values determined from Eqs. 2, 3, and 4. Since the fluorescence intensity distribution shows a strong J dependence, the effective potential curve, $U_J(r)$, for the corresponding J level was used in the Franck-Condon calculations,

$$U_J(r) = V_0(r) + J(J+1)\hbar^2/2\mu r, \quad (5)$$

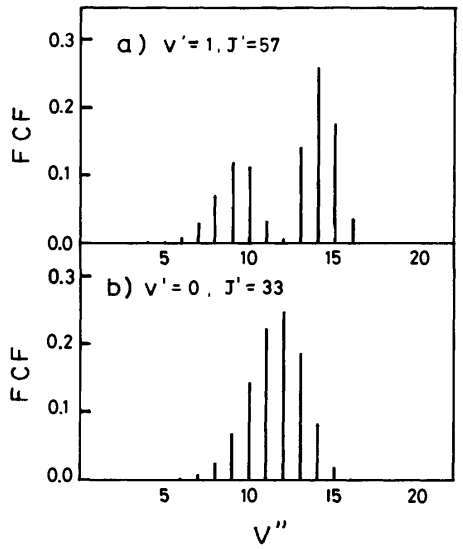

Fig. 2. Calculated Franck-Condon factors of the E $(0_g^+) \rightarrow B^3\Pi_{0_u^+}$ transition.

Table 2. Molecular parameters of the E(0_g^+) state for $^{79}Br_2$

Parameter	Value
T_e/cm^{-1}	49778.53(52)[a]
ω_e/cm^{-1}	150.78(27)
$\omega_e x_e/cm^{-1}$	0.41(3)
B_e/cm^{-1}	0.04180[c]
α_e/cm^{-1}	1.47×10^{-4}
D/cm^{-1}	1.28×10^{-7}
$r_e/Å$	3.197

a) Values in parentheses denote twice the standard deviation (2σ) and apply to the last digits of the constants. b) Calculated value corresponding to $r_e=3.197$ Å. c) From the Franck-Condon factor analysis. The accuracy is estimated to be ±0.003 Å assuming that the emission intensities fluctuate by 10%.

where $V_0(r)$ denotes the potential curve for $J=0$.

We found that the intensity distributions were fairly consistent with the results of the FCF calculations with setting $r_e=3.197$ Å. Typical examples of the agreements are shown in Fig. 2 for the fluorescence series from (a) $v'=1$, $J'=57$ and (b) $v'=0$, $J'=33$, corresponding to the results in Fig. 1 (a) and (b). Measured intensities are not corrected for instrumental sensitivity because this was essentially constant in the wavelength region under experiment. The derived spectroscopic parameters of the E(0_g^+) ion-pair state are listed in Table 2.

With the completion of this work, the E(0_g^+) ion-pair state of Br_2 correlating with $Br^-(^1S)+Br^+(^3P_2)$ has been spectroscopically characterizd in detail. The 310 nm emission system observed in the spectrum of discharge experiments can be definitely attributed to the E(0_g^+)—$B^3\Pi_{0_u^+}$ transition. This system was first studied by Venkateswarlu and Verma,[15] who deduced that the lower state was the $B^3\Pi_{0_u^+}$ state. Berwanger, Viswanathan, and Tellinghuisen[8] recently re-analyzed the spectrum based on a completely different vibrational numbering, but still using the B state as the terminating state. The set of molecular constants of the E state given here are in very good agreement with the values reported by Tellinghuisen and coworkers and obviously support their analyses.[8]

Finally, it should be pointed out that the selective excitation technique for ion-pair states of diatomic halogens is now available through stepwise processes. Efforts are being made in this laboratory to elucidate the relaxation processes involving these high-lying electronic states, especially for the inert gas-halide excimer formation mechanism in the reaction between inert gases and halogen molecules.

The authors acknowledge the assistance of Dr. J. T. Hougen of the National Bureau of Standards for supplying them with the RKR and Franck-Condon factor computer program.

References

1) See for example; K. P. Huber and G. Herzberg, "Molecular Spectra and Molecular Structure. IV. Constants of Diatomic Molecules," Van Nostrand Reinhold, New York (1978).

2) J. J. Ewing and C. A. Brau, *Appl. Phys. Lett.*, **27**, 557 (1975).

3) J. R. Murray, J. C. Swingle, and C. E. Turner, Jr., *Appl. Phys. Lett.*, **28**, 530 (1976).

4) J. K. Rice, A. K. Hays, and J. R. Woodworth, *Appl. Phys. Lett.*, **31**, 31 (1977).

5) A. K. Hays, *Opt. Commun.*, **28**, 209 (1979).

6) J. Tellinghuisen, P. Berwanger, J. G. Ashmore, and K. S. Viswanathan, *Chem. Phys. Lett.*, **84**, 528 (1981).

7) T. Ishiwata, A. Tokunaga, T. Shinzawa, and I. Tanaka, *Bull. Chem. Soc. Jpn.* in press.

8) P. Berwanger, K. S. Viswanathan, and J. Tellinghuisen, *J. Mol. Spectrosc.*, **91**, 275 (1982).

9) A. Sur and J. Tellinghuisen, *J. Mol. Spectrosc.*, **88**, 323 (1981).

10) a) T. Ishiwata, T. Shinzawa, A. Tokunaga, and I. Tanaka, *Chem. Phys. Lett.*, **101**, 350 (1983); b) T. Shinzawa, A. Tokunaga, T. Ishiwata, I. Tanaka, K. Kasatani, M. Kawasaki, and H. Sato, *J. Chem. Phys.*, in press.

11) T. Ishiwata, T. Ohtoshi, and I. Tanaka, *J. Chem. Phys.*, in press.
12) R. F. Barrow, T. C. Clark, J. A. Coxon, and K. K. Yee, *J. Mol. Spectrosc.*, **51**, 428 (1974).
13) See for example; "Molecular Spectra and Molecular Structure. I. Spectra of Diatomic Molecules," Van Nostrand Reinhold, New York (1950), pp. 106—108.
14) We have used the version from Hougen of the RKR and Franck-Condon factor program which was originally written by Zare, Schmeltekopf, Harrop, and Albritton for use in their article in *J. Mol. Spectrosc.*, **46**, 37 (1973).
15) P. Venkateswarlu and R. D. Verma, *Proc. Indian Acad. Sci.*, **46**, 416 (1957).

 © 1984 The Chemical Society of Japan Bull. Chem. Soc. Jpn., 57, 1321—1327 (1984)

The Adsorption of Dodecyldimethylammonium Bromide on Aqueous Surfaces of Sodium Bromide Solutions

Hideshi Okuda,† Sumio Ozeki, and Shoichi Ikeda*
†*Nagoya Municipal Industrial Research Institute, Atsuta, Nagoya 456*
Department of Chemistry, Faculty of Science, Nagoya University, Chikusa, Nagoya 464
(Received November 18, 1983)

The surface tension of aqueous NaBr solutions of dodecyldimethylammonium bromide has been measured by the drop weight method at different surfactant and NaBr concentrations. By applying the Gibbs adsorption isotherm, surface excess densities of surfactant cation, Na^+ and Br^- are derived as functions of surfactant concentration at different NaBr concentrations. The rational mean activity coefficients of surfactant and NaBr are both approximated by a common expression satisfying the Brønsted principle for mixed electrolytes and containing the ionic strength as a variable. Surface excess density of surfactant cation increases with increasing surfactant concentration and has a general tendency still increasing even at the critical micelle concentration. Some comparison of the behavior of surface excess densities of ions between the present bromide system and the previous chloride system is made. The Corrin-Harkins plot for the critical micelle concentration consists of two straight lines intersecting at 0.015 mol dm^{-3} NaBr.

We have recently established the thermodynamic method for estimating surface excess densities of ionic species or solute components on aqueous surfaces of electrolyte solutions from measurements of their surface tension as functions of solute concentrations.[1-3] This method is based on the Gibbs adsorption isotherm for plane surfaces of dilute solutions and has been applied for aqueous solutions of mixed electrolytes having a common counterion, such as aqueous NaCl solutions of dodecyldimethylammonium chloride (DDAC).[4,5]

In the present work we briefly review the thermodynamic method, measure the surface tension of aqueous NaBr solutions of dodecyldimethylammonium bromide (DDAB), and apply the method to the experimental data. We will be concerned with the Gibbs adsorption isotherm for aqueous NaBr solutions of DDAB, in which no micelles are yet formed. Then we can derive the surface excess densities of three ionic species. We will further examine the effects of counterion species on the adsorption isotherms of ionic species and the critical micelle concentration (cmc) and standard free energy of micellization of dodecyldimethylammonium ions, by comparing the present results with those previously obtained for aqueous NaCl solutions of DDAC.[5]

Theoretical

Let us denote a cationic surfactant and sodium halide by DX and NaX, respectively, which have a common halide anion X^-. As we have already derived the Gibbs adsorption isotherm for aqueous solutions of DDAC-NaCl system,[5] we will here present brief derivation of the Gibbs adsorption isotherm.

In terms of species present in solution, H_2O, D^+, Na^+, and X^-, we can represent the Gibbs adsorption isotherm in the form

$$-d\gamma = \Gamma_{H_2O}d\mu_{H_2O} + \Gamma_{D^+}d\mu_{D^+} + \Gamma_{Na^+}d\mu_{Na^+} + \Gamma_{X^-}d\mu_{X^-}, \quad (1)$$

where γ is the surface tension of solution, Γ_i and μ_i are the surface excess density and chemical potential of species, i, respectively. Introducing the Gibbs convention, $\Gamma_{H_2O}=0$, the surface excess densities of ions have definite values. Then, by means of the condition of electroneutrality on aqueous surfaces

$$\Gamma_{D^+} + \Gamma_{Na^+} = \Gamma_{X^-}, \quad (2)$$

we have the Gibbs adsorption isotherm in terms of components

$$-d\gamma = \Gamma_D \cdot d\mu_{DX} + \Gamma_{Na} \cdot d\mu_{NaX}. \quad (3)$$

The chemical potentials of solute components, DX and NaX, can be expressed by their molar concentrations, C and C_s, and from these expressions we obtain

$$-d\gamma = RT\left[\left\{\left(1+\frac{C}{C+C_s}\right)\Gamma_{D^+}+\frac{C}{C+C_s}\Gamma_{Na^+}\right\}d\ln C + \left\{\frac{C_s}{C+C_s}\Gamma_{D^+}+\left(1+\frac{C_s}{C+C_s}\right)\Gamma_{Na^+}\right\}d\ln C_s + \Gamma_{D^+}\,d\ln y_{\pm}^2+\Gamma_{Na^+}\,d\ln y_{s\pm}^2\right], \quad (4)$$

where R is the gas constant, T the temperature, and $y_\pm$ and $y_{s\pm}$ are the molar mean activity coefficients of DX and NaX, respectively.

The molar mean activity coefficients of DX and NaX, $y_\pm$ and $y_{s\pm}$, can be related to their rational mean activity coefficients, $f_\pm$ and $f_{s\pm}$, by[6a]

$$\frac{y_\pm}{f_\pm} = \frac{y_{s\pm}}{f_{s\pm}} = \frac{\rho_w}{\rho - \frac{M-2M_w}{1000}C - \frac{M_s-2M_w}{1000}C_s}, \quad (5)$$

where M_w, M, and M_s are the molecular weights of H_2O, DX, and NaX, respectively, and ρ_w and ρ are the densities of water and solution, respectively.

As was demonstrated previously,[5] the rational mean activity coefficients of DX and NaX can both be approximately represented as a function of ionic strength, $C+C_s$,

$$\log f_\pm = \log f_{s\pm} = -\frac{P\sqrt{C+C_s}}{1+Qa\sqrt{C+C_s}} + B_s(C+C_s), \quad (6)$$

where the constants, P and Q, of the Debye-Hückel electrostatic term are determined by the temperature

and the dielectric constant, and the ionic radius, a, serves as an adjustable parameter.[6b] The salting-out constant, B_s, is characteristic of NaX.

Then we have following identities, which are abbreviated by η and η_s, respectively:

$$\eta = \left(\frac{\partial \ln y_{\pm}^2}{\partial C}\right)_{C_s} = \left(\frac{\partial \ln y_{s\pm}^2}{\partial C}\right)_{C_s}, \quad (7)$$

$$\eta_s = \left(\frac{\partial \ln y_{\pm}^2}{\partial C_s}\right)_{C} = \left(\frac{\partial \ln y_{s\pm}^2}{\partial C_s}\right)_{C}. \quad (8)$$

The change of surface tension of solution can be formally related to the changes in concentrations of DX and NaX by

$$-\mathrm{d}\gamma = RT(\Gamma' \,\mathrm{d}\ln C + \Gamma'_s \,\mathrm{d}\ln C_s), \quad (9)$$

where Γ' and Γ'_s are given by

$$\Gamma' = \left(1+\frac{C}{C+C_s}+\eta C\right)\Gamma_{D^+} + \left(\frac{C}{C+C_s}+\eta C\right)\Gamma_{Na^+}, \quad (10)$$

$$\Gamma'_s = \left(\frac{C_s}{C+C_s}+\eta_s C_s\right)\Gamma_{D^+} + \left(1+\frac{C_s}{C+C_s}+\eta_s C_s\right)\Gamma_{Na^+}. \quad (11)$$

Solving equations 10 and 11, we obtain the surface excess densities of two cations as

$$\Gamma_{D^+} = \frac{1}{2+\eta C+\eta_s C_s}\left\{\left(1+\frac{C_s}{C+C_s}+\eta_s C_s\right)\Gamma' - \left(\frac{C}{C+C_s}+\eta C\right)\Gamma'_s\right\}, \quad (12)$$

$$\Gamma_{Na^+} = \frac{1}{2+\eta C+\eta_s C_s}\left\{-\left(\frac{C_s}{C+C_s}+\eta_s C_s\right)\Gamma' + \left(1+\frac{C}{C+C_s}+\eta C\right)\Gamma'_s\right\}, \quad (13)$$

and that of an anion as

$$\Gamma_{X^-} = \frac{1}{2+\eta C+\eta_s C_s}(\Gamma'+\Gamma'_s), \quad (14)$$

From Eqs. 5 and 6, we obtain

$$\eta = \eta_0 - \frac{2\left\{\left(\frac{\partial \rho}{\partial C}\right)_{C_s} - \frac{M-2M_w}{1000}\right\}}{\rho - \frac{M-2M_w}{1000}C - \frac{M_s-2M_w}{1000}C_s}, \quad (15)$$

$$\eta_s = \eta_0 - \frac{2\left\{\left(\frac{\partial \rho}{\partial C_s}\right)_{C} - \frac{M_s-2M_w}{1000}\right\}}{\rho - \frac{M-2M_w}{1000}C - \frac{M_s-2M_w}{1000}C_s}, \quad (16)$$

where

$$\eta_0 = \frac{2.303P}{(1+Qa\sqrt{C+C_s})^2\sqrt{C+C_s}} - 4.606B_s. \quad (17)$$

The density of aqueous NaX solution of DX is given by

$$\rho = \rho_s + (1-\bar{v}\rho_s)c, \quad (18)$$

where c (g cm^{-3})$=MC/1000$ is the weight concentration of solution, ρ_s is the density of solvent or aqueous NaX solution, and $\bar{v}$ is the partial specific volume of surfactant, DX. At surfactant concentrations lower than the critical micelle concentration

$$\left(\frac{\partial \rho}{\partial C}\right)_{C_s} = \frac{(1-\bar{v}\rho_s)M}{1000}, \quad (19)$$

$$\left(\frac{\partial \rho}{\partial C_s}\right)_{C} = \left(1-\frac{\bar{v}MC}{1000}\right)\left(\frac{\partial \rho_s}{\partial C_s}\right)_{C}. \quad (20)$$

Experimental

Materials. Dodecyldimethylammonium bromide (DDAB) was prepared from pure *N,N*-dimethyldodecylamine by passing dry HBr gas through its ethanolic solution and recrystallizing the resulting crystals from 1:1 acetone-diethyl ether mixtures three times. Commercial *N,N*-dimethyldodecylamine was purchased from Tokyo Kasei Kogyo Co., Inc., and purified by fractional distillation.

NaBr was of reagent grade from Wako Pure Chemical Industries, Inc., and was ignited on an evaporating dish and stored in a desiccator.

Methods. The surface tension of aqueous solutions was determined at 25±0.01 °C by means of the drop weight method, using a capillary tip of outer radius, r. The capillary was kept perpendicular, and its upper end was connected through rubber tubing to a burette, half-filled with water, so that the drop formed on the capillary tip could be kept at a desired size or released to fall at a desired instant by manipulating the burette. The capillary tip was kept in a glass bottle dipped in a water thermostat. Each drop was suspended on the tip for over 3 min before being allowed to fall, and five to ten drops of each solution were collected in a weighing bottle for weighing.

Surface tension, γ (mN m^{-1}), of solution was calculated from the weight, m, of a drop by the Harkins-Brown equation[7a]

$$\gamma = (mg/r)F, \quad (21)$$

where g is the gravitational acceleration (980 cm s^{-2}) and F is the correction factor, defined by V/r^3, V being the drop volume. The effective outer radius, r, of the capillary tip was determined by measuring the drop weight of distilled water, by assuming its surface tension to be 71.96 mN m^{-1},[7b] and it was found to be 0.3484 cm.

Density measurements of aqueous solutions were performed on an Anton Paar Precision Density Meter, DMA 02D. The temperature was kept at 25±0.01 °C by circulating water of constant temperature around the cell housing. The density meter was calibrated by using distilled water and air as standards, by assuming their densities to be 0.99704 g cm^{-3} and 0.00119 g cm^{-3}, respectively.

Results

Figure 1 shows the relation of surface tension, γ, with the logarithm of molar concentration of DDAB, log C, at different NaBr concentrations, C_s. Surface tension decreases with increasing surfactant concentration at concentrations up to the cmc, C_0, and also with increasing NaBr concentration. Values of Γ' can be obtained from the slope of the surface tension curves by

$$\Gamma' = -\frac{1}{RT}\left(\frac{\partial \gamma}{\partial \ln C}\right)_{C_s}. \quad (22)$$

At concentrations up to the cmc, we can apply the expression of the Gibbs adsorption isotherm developed above. At concentrations higher than the cmc, surface tension always remains constant, which is designated as γ_0, and it is clear that $\Gamma'=0$ for $C \geqq C_0$.

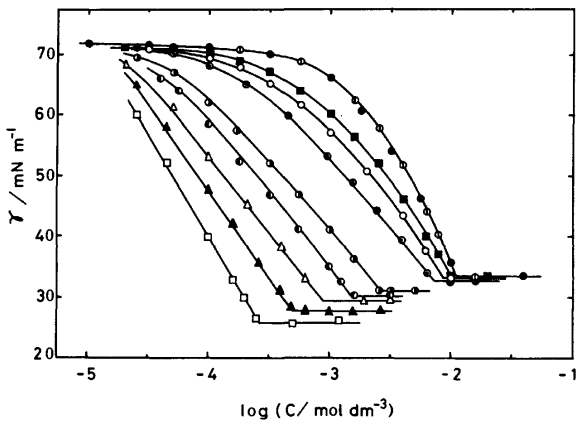

Fig. 1. Variation of surface tension with the logarithm of surfactant concentration at different NaBr concentrations.
C_s/mol dm^{-3}: ●; 0, ⦶; 1×10^{-4}, ■; 5×10^{-3}, ○; 0.01, ⊙; 0.02, ◑; 0.10, ◐; 0.20, △; 0.50, ▲; 1.00, □; 2.00.

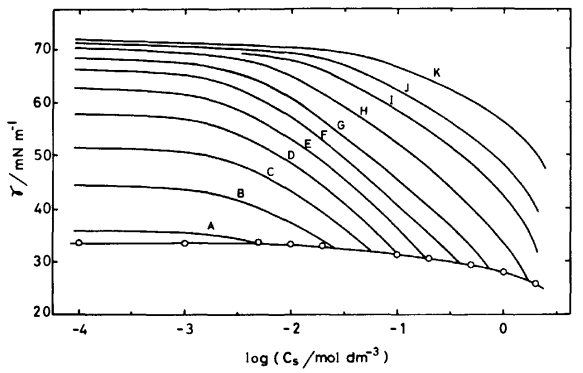

Fig. 2. Variation of surface tension with the logarithm of NaBr concentration at different surfactant concentrations. ○: Constant surface tension, γ_o, at a given NaBr concentration, obtained at surfactant concentrations higher than the critical micelle concentration.
$-\log C$/mol dm^{-3}: A; 2.0, B; 2.2, C; 2.4, D; 2.6, E; 2.8, F; 3.0, G; 3.2, H; 3.5, I; 3.8, J; 4.0, K; 4.3.

In Fig. 2 surface tension is replotted against the logarithm of molar concentration of NaBr at different surfactant concentrations. The lowest curve gives dependence of the constant surface tension on NaBr concentration, the constancy being observed at surfactant concentrations higher than the cmc. From the slope of surface tension curves we can obtain values of Γ'_s by

$$\Gamma'_s = -\frac{1}{RT}\left(\frac{\partial\gamma}{\partial \ln C_s}\right)_C. \tag{23}$$

Table 1 summarizes relevant numerical data at the cmc derived from Figs. 1 and 2. With increasing NaBr concentration, values of Γ' at the cmc decreases in the range of NaBr concentrations up to 0.10 mol dm^{-3}, and then increases at higher NaBr concentrations. On the other hand, values of Γ'_s at the cmc increases monotonously with increasing NaBr concentrations.

Figure 3 shows the density of aqueous NaBr solutions of DDAB as a function of surfactant concentration. It is

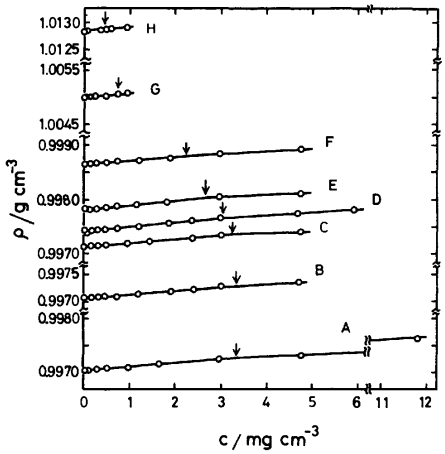

Fig. 3. Density of aqueous NaBr solutions of surfactant as a function of its concentration (g cm^{-3}). Arrows indicate the location of the critical micelle concentrations.
C_s/mol dm^{-3}: A; 0, B; 1×10^{-4}, C; 1×10^{-3}, D; 5×10^{-3}, E; 0.01, F; 0.02, G; 0.10, H; 0.20.

Table 1. Critical micelle concentration, apparent surface excess densities, and constant surface tension at the critical micelle concentration for aqueous NaBr solutions of dodecyldimethylammonium bromide at 25 °C

C_s / mol dm^{-3}	C_o / mmol dm^{-3}	Γ' at C_o / 10^{-10} mol cm^{-2}	Γ'_s at C_o / 10^{-10} mol cm^{-2}	γ_o / mN m^{-1}
0	11.1	8.96		33.6
1×10^{-4}	11.1	8.96	0.08	33.6
1×10^{-3}	10.9	8.41	0.23	33.6
5×10^{-3}	10.1	6.58	1.02	33.3
0.01	8.83	5.42	1.74	33.2
0.02	7.38	4.54	2.63	32.9
0.10	2.51	4.45	3.40	31.2
0.20	1.51	4.48	3.38	30.4
0.50	0.859	4.56	3.80	29.1
1.00	0.506	4.99	5.16	27.6
2.00	0.269	5.24	7.07	25.7

Table 2. Partial specific volume and partial molar volume of dodecyldimethylammonium bromide below and above the critical micelle concentration in aqueous NaBr solutions

C_s	c_o	$C \leqq C_o$		$C \geqq C_o$	
		$\bar{v}$	$\bar{V}$	$\bar{v}$	$\bar{V}$
mol dm^{-3}	mg cm^{-3}	cm^3 g^{-1}	cm^3 mol^{-1}	cm^3 g^{-1}	cm^3 mol^{-1}
0	3.27	0.935	275.2	0.958	282.0
1×10^{-4}	3.27	0.930	273.7		
1×10^{-3}	3.21	0.926	272.5		
5×10^{-3}	2.97	0.928	273.1	0.955	281.1
0.01	2.60	0.928	273.1		
0.02	2.17	0.933	274.6	0.950	279.6

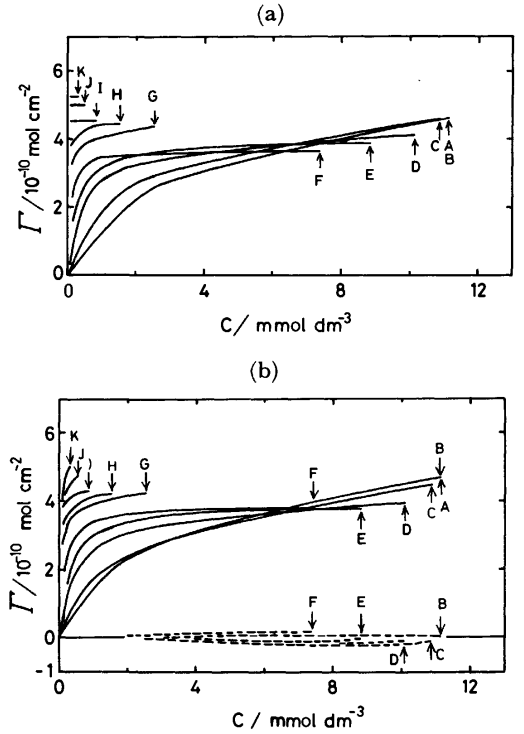

Fig. 4. Adsorption isotherms of ions on aqueous surfaces at different NaBr concentrations. (a) Γ_{D^+} *vs.* C, (b) Γ_{Na^+} (----) and Γ_{Br^+} (——) *vs.* C. Arrows indicate the location of the critical micelle concentrations.
C_s/mol dm^{-3}: A; 0, B; 1×10^{-4}, C; 1×10^{-3}, D; 5×10^{-3}, E; 0.01, F; 0.02, G; 0.10, H; 0.20, I; 0.50, J; 1.00, K; 2.00.

seen that Eq. 18 holds well for the relation between the density and surfactant concentration below the cmc, and, as shown in Table 2, the partial specific volume of DDAB is found to be 0.93 cm^3 g^{-1} at surfactant concentrations lower than the cmc, irrespective of NaBr concentration. Above the cmc, the slope of the density curves becomes less steep, indicating that the partial specific volume of DDAB abruptly increases beyond the cmc, as shown in Table 2.

In applying Eqs. 12, 13, and 14 we use the values

$$P = 0.5115, \quad Qa = 1.316, \quad B_s = 0.075, \qquad (24)$$

where the value of B_s has been determined by adapting the tabulated activity data of NaBr up to 4.0 mol dm^{-3} [6c] to Eq. 6. Then we can derive the surface excess densities of surfactant cation, Na^+ and Br^-. Figure 4 shows the surface excess densities of ions plotted against the surfactant concentration. It is seen in Fig. 4(a) that the value of Γ_{D^+} increases more rapidly and approaches the saturated value at a low surfactant concentration, as the NaBr concentration is 5×10^{-3}, 0.01, or 0.02 mol dm^{-3} or it is higher than 0.20 mol dm^{-3}. When the NaBr concentration is 0.10 mol dm^{-3} or it is lower than 1×10^{-3} mol dm^{-3}, Γ_{D^+} appears to increase without reaching their saturation even at the cmc. It is seen in Fig. 4(b) that the value of Γ_{Br^-} increases without reaching its saturated value except that the NaBr concentration is 0.01 or 0.02 mol dm^{-3}. The value of Γ_{Na^+} is very low in its absolute value and is almost zero for all NaBr concntrations.

Recently, it was found that the surface tension-concentration curves of aqueous solutions of decylammonium chloride or dodecylammonium chloride show a break point at a low surfactant concentration.[8,9] Such a break point can be more clearly observed when the mixed adsorbed film is present.[9] The presence of the break point gives the discontinuity to the surface excess density of surfactant ion, indicating the establishment of equilibrium between two kinds of "surface phases." In the present data such a break point is not detectable at all NaBr concentrations and there is no discontinuity in the surface excess density curves.

Table 3 gives the values of Γ_{D^+}, Γ_{Na^+}, and Γ_{Br^-} at the cmc for different NaBr concentrations, and Fig. 5 shows these values as functions of the square root of NaBr concentration. With increasing NaBr concentration up to 0.01 mol dm^{-3}, the value of Γ_{D^+} at the cmc decreases. After passing the minimum, it increases gradually with increasing NaBr concentration.

Discussion

Surface Excess Densities of Ions. As shown in Fig. 4(a), the surface excess density of surfactant cation, Γ_{D^+}, at several NaBr concentrations still increases without reaching its saturation even at the cmc. Such behavior was not observed in the DDAC-NaCl system.[4,5] As shown in Fig. 4(b), the surface excess density of Br^-, Γ_{Br^-}, also increases even at the cmc at several NaBr concentrations. In the DDAC-NaCl system Γ_{Cl^-} behaves in the same way only at high NaCl concentrations.

Table 3. Surface excess densities of surfactant cation, Na^+ and Br^- at the critical micelle concentration

C_s	Γ_{D^+} at C_o	Γ_{Na^+} at C_o	Γ_{Br^-} at C_o
mol dm^{-3}	10^{-10} mol cm^{-2}	10^{-10} mol cm^{-2}	10^{-10} mol cm^{-2}
0	4.68		4.68
1×10^{-4}	4.68	0.04	4.73
1×10^{-3}	4.55	−0.11	4.44
5×10^{-3}	4.22	−0.18	4.04
0.01	3.83	−0.05	3.78
0.02	3.62	0.19	3.81
0.10	4.36	−0.11	4.25
0.20	4.45	−0.22	4.23
0.50	4.55	−0.26	4.30
1.00	4.99	−0.18	4.81
2.00	5.24	−0.23	5.02

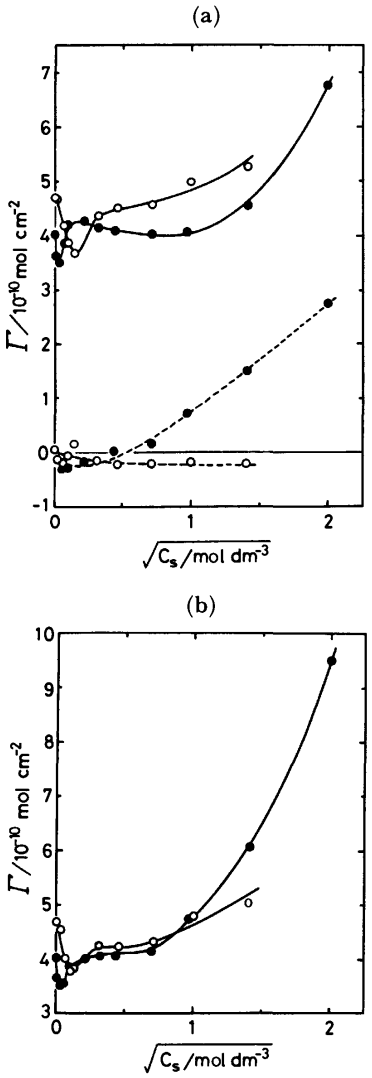

Fig. 5. The change of surface excess densities of ions at the critical micelle concentration.
(a) Γ_{D^+} (——) and Γ_{Na^+} (----) *vs.* $\sqrt{C_s}$, (b) Γ_{X^-} *vs.* $\sqrt{C_s}$. X^-: Br^- or Cl^-.
○: DDAB-NaBr, ●: DDAC-NaCl.

The values of Γ_{D^+} and Γ_{Br^-} at the cmc in the DDAB-NaBr system are essentially equal to their saturated values, respectively, at a given NaBr concentration. In Fig. 5 the values of Γ_{D^+}, Γ_{Na^+} and Γ_{Br^-} at the cmc are plotted against the square root of NaBr concentration, together with the saturated values of Γ_{D^+}, Γ_{Na^+}, and Γ_{Cl^-} in the DDAC-NaCl system.[4,5]

It is clear in Fig. 5(a) that the value of Γ_{D^+} at the cmc for the DDAB-NaBr system is higher than that for the DDAC-NaCl system at the same concentrations of sodium salts except at 0.01 and 0.02 mol dm^{-3}. This means that the effect of salting-out of Br^- is stronger than that of Cl^-, which is apparently exhibited in the values of B_s in Eq. 6, *i.e.*, 0.075 for NaBr and 0.055 for NaCl.[5,6b] It is also seen that the value of Γ_{Na^+} at the cmc for the DDAB-NaBr system is almost constant at NaBr concentrations higher than 0.20 mol dm^{-3}. For the DDAC-NaCl system the value of Γ_{Na^+} at the cmc increases rapidly and becomes positive at NaCl concentrations higher than 0.20 mol dm^{-3}. The reason for the large difference in Γ_{Na^+} at high salt concentrations is not clear, but it is certain that the difference between the two systems arises from the surface tension data themselves, since the treatment based on the ideal solution approximation also leads to such a difference in Γ_{Na^+}.

In Fig. 5(b) it is seen that the value of Γ_{Br^-} at the cmc for the DDAB-NaBr system is of the same order of magnitude as that of Γ_{Cl^-} at the cmc for the DDAC-NaCl system, as long as the concentrations of sodium salts are lower than 1.0 mol dm^{-3}. At concentrations higher than 1.0 mol dm^{-3}, the value of Γ_{Cl^-} at the cmc for the DDAC-NaCl system increases rapidly. This is because the value of Γ_{Na^+} for the DDAC-NaCl system, *i.e.*, the adsorption of NaCl, increases more rapidly.

The Corrin-Harkins Relation. Figure 6 shows the Corrin-Harkins plot for the cmc of the DDAB-NaBr system together with that of the DDAC-NaCl system. For the DDAB-NaBr system a linear relation holds at low and high counterion concentrations, respectively:

$$\log C_o = -0.452 \log (C_o + C_s) - 2.83, \quad C_s \leqq 0.015, \qquad (25)$$

$$\log C_o = -0.758 \log (C_o + C_s) - 3.33, \quad C_s \geqq 0.015. \qquad (26)$$

The threshold concentration of NaBr for the two linear plots at low and high counterion concentrations, 0.015 mol dm^{-3}, is lower than that obtained by light scattering measurement,[10] 0.095 mol dm^{-3}.

For the DDAC-NaCl system the Corrin-Harkins plot of the cmc is linear at NaCl concentrations up to 0.50 mol dm^{-3}:

$$\log C_o = -0.621 \log (C_o + C_s) - 2.98, \quad C_s \leqq 0.50, \qquad (27)$$

and at higher NaCl concentrations than 0.50 mol dm^{-3}, a linear relation no longer holds between the logarithm of the cmc and the logarithm of the concentration of Cl^-.[5]

As the cmc is a good measure of stability of the micellar state relative to the monomeric state, the lower value of the cmc for the DDAB-NaBr system than that for the DDAC-NaCl system clearly indicates the stabili-

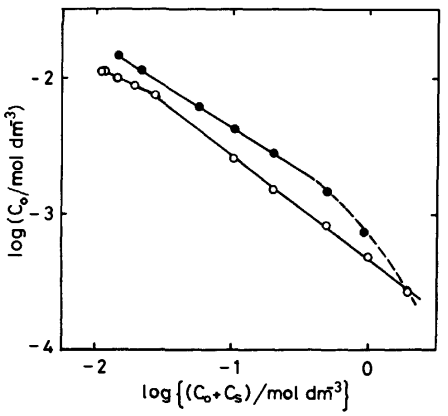

Fig. 6. Relation of the logarithm of the critical micelle concentration with the logarithm of ionic strength. ○: DDAB-NaBr, ●: DDAC-NaCl.

zation of dodecyldimethylammonium micelle by binding of Br^- stronger than binding of Cl^-. Similar relations of the lower value of the cmc of the bromide system than that of the chloride system were observed for surfactants having a dodecyl group[11,12] and surfactants having an octadecyl group.[13]

Standard Free Energy of Micellization. In terms of the pseudo-phase model for the micelle,[14] in which the solution of surfactant monomer is an ideal solution and the micelle is a separated phase, the standard free energy of micellization per mole of surfactant is given by

$$\Delta G_m^\circ = RT \ln X_o, \tag{28}$$

where X_o is the mole fraction of surfactant at the cmc. When expressed by the molar concentration of surfactant at the cmc, C_o, we have

$$\Delta G_m^\circ = RT \ln \frac{M_w C_o}{1000\rho_o - (M_s - M_w)C_s}, \tag{29}$$

where ρ_o denotes the density of solution at the cmc.

Table 4 gives the values of $-\Delta G_m^\circ$ for the DDAB-NaBr system, together with those for the DDAC-NaCl system. The micelles are both stabilized more as the ionic strength is increased. The stabilization of micelle is 0.7 kJ mol^{-1} more effective for the DDAB-NaBr system compared with that for the DDAC-NaCl system, as long as the ionic strength is lower than 0.05 mol dm^{-3}.

Surface Tension. We had originally attempted to measure the surface tension of solution by means of the Wilhelmy hanging plate method, but the downward shift of the plate was not reproducible at all. Thus we decided to employ the drop weight method for surface tension measurements.

For the surface tension measurements of aqueous solutions of a cationic surfactant, either in the presence or absence of added salt, we have found that the hanging plate method does not give any reproducible results, owing to the built-up of the cationic on the glass plate (and also possibly on the platinum plate) and the resulting change in contact angle. For the surface tension measurements of aqueous solutions by means of Wilhelmy hanging plate method, the contact angle of solution on the plate must be nearly zero. But in the case of cationic surfactants such as the derivatives of long-chain alkylammonium, this condition is never satisfied generally.

Table 4. Standard free energy of micellization of dodecyldimethylammonium bromide in aqueous NaBr solutions and dodecyldimethylammonium chloride in aqueous NaCl solutions at 25 °C

C_s / mol dm^{-3}	DDAB−NaBr $-\Delta G_m^\circ$ / kJ mol^{-1}	DDAC−NaCl $-\Delta G_m^\circ$ / kJ mol^{-1}
0	21.1	20.4
1×10^{-4}	21.1	20.4
1×10^{-3}	21.2	20.5
5×10^{-3}	21.3	20.6
0.01	21.7	21.0
0.02	22.1	
0.05		22.5
0.10	24.8	23.5
0.20	26.0	24.5
0.50	27.4	26.1
1.00	28.7	27.9[a]
2.00	30.3	30.3
4.00		34.1

a) $C_s = 0.94$ mol dm^{-3}.

The drop weight method is universally applicable for the measurements of surface tension of aqueous solutions of any surfactant. It permits to measure even the time change of surface tension, as referred to above.

The tendency of the relations between surface tension and surfactant concentration and between surface tension and the concentration of sodium salt in the present DDAB-NaBr system is analogous to those of the previous DDAC-NaCl system.[5] As it is seen in Fig. 1, the surface tension of the DDAB-NaBr system decreases with increasing the surfactant concentration up to the cmc and also with increasing the NaBr concentration, as was observed for the DDAC-NaCl system. At surfactant concentrations higher than the cmc, the surface tension remains constant in both of these systems.

Comparing the surface tension of two systems at the same concentration of the sodium salt, the surface tension of the DDAB-NaBr system is lower than that of the DDAC-NaCl system at all surfactant concentrations and also at all concentrations of sodium salt.

Partial Molar Volume. Table 2 gives the values of the cmc identified as the break point of the density curves of solution. These values are in agreement with those derived from the surface tension measurements.

The partial molar volume, $\bar{V}=M\bar{v}$, of DDAB changes abruptly at the cmc, and their values above and below the cmc are given in Table 2. The change in partial molar volume of DDAB by the micellization is 5—8 cm^3 mol^{-1}, depending on the NaBr concentration. The observed values for DDAB are comparable with that for DDAC in water, 8.4 cm^3 mol^{-1}. They are also roughly of the same order of magnitude or smaller than those for surfactants having a dodecyl group.[15,16]

One of the authors (H. O.) wishes to thank Dr. Kōichi Mase and Mr. Yoshikazu Terada for generous support and encouragement during this work.

References

1) S. Ikeda, *Bull. Chem. Soc. Jpn.*, **50**, 1403 (1977).
2) S. Ikeda and S. Ozeki, *Bull. Chem. Soc. Jpn.*, **53**, 1837 (1980).
3) S. Ikeda, *Adv. Colloid Interface Sci.*, **18**, 93 (1982).
4) S. Ozeki, M. Tsunoda, and S. Ikeda, *J. Colloid Interface Sci.*, **64**, 28 (1978).
5) S. Ozeki and S. Ikeda, *Bull. Chem. Soc. Jpn.*, **53**, 1832 (1980).
6) R. A. Robinson and R. H. Stokes, "Electrolyte Solutions," 2nd ed, Butterworths Scientific Publications, London (1959), a) p. 32; b) p. 235; c) p. 492.
7) W. D. Harkins, "Physical Methods of Organic Chemistry," ed by A. Weisberger, Part 1, Chap. IX, (a) p. 374; (b) p. 369.
8) K. Motomura, S. Iwanaga, Y. Hayami, S. Uryu, and R. Matuura, *J. Colloid Interface Sci.*, **80**, 32 (1981).
9) M. Aratono, S. Uryu, Y. Hayami, K. Motomura, and R. Matuura, *J. Colloid Interface Sci.*, **93**, 162 (1983).
10) S. Ozeki and S. Ikeda, *Colloid Polymer Sci.*, in press.
11) H. B. Klevens, *J. Am. Oil Chemists' Soc.*, **30**, 74 (1953).
12) E. W. Anacker and H. M. Ghose, *J. Phys. Chem.*, **67**, 1713 (1963).
13) P. F. Grieger and C. A. Kraus, *J. Am. Chem. Soc.*, **70**, 3803 (1948).
14) K. Shinoda and E. Hutchinson, *J. Phys. Chem.*, **66**, 577 (1962).
15) J. M. Corkill, J. F. Goodman, and T. Walker, *Trans. Faraday Soc.*, **63**, 759 (1967).
16) E. Vikingstad, A. Skauge, and H. Høiland, *J. Colloid Interface Sci.*, **72**, 59 (1979).

 © 1984 The Chemical Society of Japan Bull. Chem. Soc. Jpn., 57, 1328—1330 (1984) [Vol. 57, No. 5

The Preparation of DL-Isoleucine by Asymmetric Transformation

Chikara HONGO,* Ryuzo YOSHIOKA, Masanori TOHYAMA, Shigeki YAMADA,† and Ichiro CHIBATA††

Research Laboratory of Applied Biochemistry, Tanabe Seiyaku Co., Ltd., 16-89, Kashima-3-chome, Yodogawa-ku, Osaka 532

(Received December 2, 1983)

The chemical synthesis of isoleucine leads to a mixture of DL-isoleucine and DL-alloisoleucine. The preparation of DL-isoleucine from the mixture was studied. When the mixture was reacted with 1,5-naphthalenedisulfonic acid in water, DL-isoleucine formed the less soluble 1,5-naphthalenedisulfonate and could be separated in the form of the salt from the mixture. The soluble DL-alloisoleucine salt was easily epimerized by heating in acetic acid in the presence of salicylaldehyde and free isoleucine mixture. Asymmetric transformation between the two diastereoisomeric racemates was carried out by the simultaneous combination of the fractional crystallization of the less soluble DL-isoleucine salt and the epimerization of the soluble DL-alloisoleucine salt. DL-Isoleucine salt was obtained in a yield of up to 95% from a DL-isoleucine–DL-alloisoleucine mixture or even from DL-alloisoleucine.

L-Isoleucine (L-Ile) is an essential amino acid useful as a nutrient or a food additive. The chemical synthesis of isoleucine leads to a mixture (Ile-mixture) of DL-Ile and DL-alloisoleucine (DL-allo-Ile), since the amino acid has two asymmetric carbon atoms. In order to obtain L-Ile from the mixture by a conventional optical-resolution method, such as the asymmetric hydrolysis of *N*-acyl-DL-amino acids by aminoacylase, it is necessary to separate DL-Ile from the Ile-mixture before the optical resolution.[1,2] Several methods for the separation of DL-Ile from the Ile-mixture are known. For example, DL-Ile or the sodium salt can be separated from the mixture by fractional crystallization with an appropriate solvent in which DL-Ile or the salt is less soluble than DL-allo-Ile or its sodium salt.[3,4] Also, *N*-acetyl-DL-Ile may be obtained as the more soluble fraction in a similar way.[2,5,6] In these methods, however, the crystallization must be systematically repeated several times to isolate the pure product; this results in low yields and is time-consuming.[7] Generally, the separation of the diastereoisomers of isoleucine is so difficult and tedious that no method to meet industrial demands is found in literatures. To develop practical and convenient methods for the production of DL-Ile, we have studied the separation of DL-Ile from the Ile-mixture by fractional crystallization and the preparation of DL-Ile by asymmetric transformation, *i.e.*, by a combination of fractional crystallization and simultaneous epimerization.

It has been well known that some aromatic sulfonic acids have been used as specific precipitating reagents for the separation of amino acids.[8] We have ourselves previously developed a technique using aromatic sulfonic acids for the optical resolution of DL-amino acid by means of a preferential crystallization procedure.[9-12] Aromatic sulfonic acids were chosen because they vary greatly in properties and easily form salts with any kind of amino acid; also, their salts tend to form racemic mixtures suitable for optical resolution by means of the preferential crystallization procedure. In the present study, with a similar idea, the separation of DL-Ile from the Ile-mixture was investigated using aromatic sulfonic acids. We prepared a wide variety of aromatic sulfonates of the Ile-mixture and screened the salts suitable for the separation. As a result, the salt of DL-Ile with 1,5-naphthalenedisulfonic acid (NDS) was found to form easy handling crystals from water in a good yield and to be very suitable for the separation of the two diastereoisomeric racemates. When the Ile-mixture was reacted with NDS in water, DL-Ile selectively crystallized as the less soluble salt, which was composed of two moles of DL-Ile and one mole of NDS, while soluble DL-allo-Ile·NDS remained almost quantitatively in the mother liquor. The DL-Ile·NDS obtained by the above procedure was contaminated with approx. 7% of DL-allo-Ile·NDS, but the sulfonate once recrystallized from water had an allo-Ile content as low as 0.3%.

From an economic point of view, it is wasteful to discard the DL-allo-Ile remaining in the mother liquor because the epimerization of DL-allo-Ile leads to a mixture of DL-Ile and DL-allo-Ile, from which DL-Ile can be separated in the form of the salt with NDS, as has been described above. Therefore, we investigated the epimerization of the DL-allo-Ile·NDS remaining in the filtrate after the separation of the DL-Ile·

Table 1. Effects of salicylaldehyde and Ile-mixture on the epimerization of L-Ile·NDS[a]

Additive	Molar equiv	Epimerization degree/%
None	—	3
Salicylaldehyde	1.0	7
Ile-mixture	1.0	5
	2.0	7
Salicylaldehyde/	1.0/1.0	39
Ile-mixture	1.0/2.0	43
	1.0/5.0	45
	1.0/10.0	44

a) The reaction was carried out at 100 °C for 3 h in acetic acid containing 5% water.

† Present address: Research Planning & Investigation Division, Tanabe Seiyaku Co., Ltd., 16-89, Kashima-3-chome, Yodogawa-ku, Osaka 532.

†† Present address: Research & Development Headquarters, Tanabe Seiyaku Co., Ltd., 16-89, Kashima-3-chome, Yodogawa-ku, Osaka 532.

NDS. Our previous report[13] showed that various optically active α-amino acids were easily racemized by heating them moderately in an acetic acid solution in the presence of a catalytic amount of aldehyde. Although the NDS salt of DL-allo-Ile was epimerized only a little in the same way, the epimerization of DL-allo-Ile·NDS was found to be greatly accelerated by heating it in an acetic acid solution in the presence of large amounts (one molar equivalent or above) of salicylaldehyde and free Ile-mixture. The effects of salicylaldehyde and the free Ile-mixture on the epimerization of L-Ile·NDS are shown in Table 1.

Then, using the epimerization method described above, we studied the asymmetric transformation between two diastereoisomeric racemates by the simultaneous combination of the fractional crystallization of the less soluble DL-Ile·NDS and the epimerization of the soluble DL-allo-Ile·NDS. DL-Ile·NDS was fractionally precipitated even under the epimerizing conditions, while the precipitated crystals were nevermore epimerized. In the liquid phase, the epimerization of DL-allo-Ile·NDS proceeded simultaneously, and the equilibrium shifted in favor of DL-Ile·NDS as a whole by the continuous precipitation of DL-Ile·NDS from the epimerizing solution, so that a direct conversion of DL-allo-Ile·NDS into DL-Ile·NDS could be achieved by a so-called second-order asymmetric transformation. Starting with the Ile-mixture (Ile/allo-Ile ratio=56.4/43.6), DL-Ile·NDS (Ile/allo-Ile ratio=89.8/10.2) was obtained in a yield of 90% based on the original weight of the Ile-mixture by means of a reaction at 100 °C for 16 h. Also, starting with DL-allo-Ile, crystals of DL-Ile·NDS (Ile/allo-Ile ratio=93.1/6.9) were precipitated in a yield of up to 94.5% based on the original weight of DL-allo-Ile·NDS by means of a reaction at 100 °C for 30 h. The change in the composition of both diastereoisomeric racemates during the reaction is shown in Fig. 1. When the DL-Ile·NDS obtained above was once recrystallized from water, the ratio of Ile/allo-Ile was larger than 1000/2.

Although second-order asymmetric transformation has been reported for numerous examples of the diastereoisomeric salt of a racemic modification, including some amino acids with an optically active resolving agent,[14-16] no report has described the asymmetric transformation between two optically stable diastereoisomeric racemates in the absence of any auxiliary chiral agent. The present one-step asymmetric transformation method for the preparation of DL-Ile from a synthetic mixture of DL-Ile and DL-allo-Ile has a definite advantage and is suitable for industrial application.

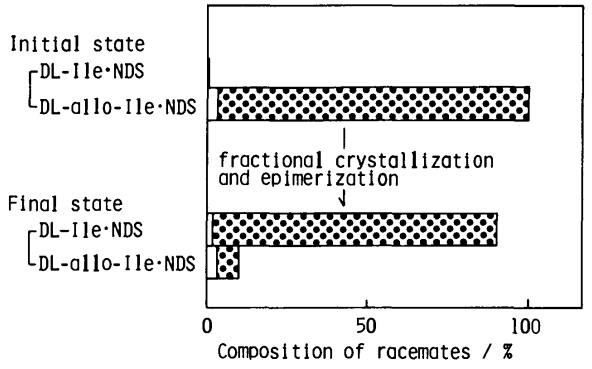

Fig. 1. The change of the composition by asymmetric transformation.

▩, crystals of NDS salt; □, NDS salt in solution.

Experimental

Materials. The diastereoisomeric mixture (Ile-mixture), consisting of 56.4% DL-Ile and 43.6% DL-allo-Ile, and L-Ile manufactured by our company, Tanabe Seiyaku Co., Ltd., were used. The DL-allo-Ile was prepared by the method of Greenstein *et al.*[2] The 1,5-naphthalenedisulfonic acid, salicylaldehyde, and other chemicals were obtained from the Tokyo Kasei Kogyo Co., Ltd.

Analyses. All samples were air-dried overnight at 50 °C. Elemental analyses were performed with a Perkin-Elmer 240 elemental analyzer. Amino acid analyses were performed by means of a Hitachi high-speed amino-acid analyzer, Model 835 [resin, Hitachi Custom Resin 2619; eluting buffer, 0.2 M sodium citrate buffer (1 M=1 mol dm^{-3}, pH 4.25); column temperature, 55 °C]. Under the conditions employed, the lower limit of the detection of allo-Ile was approximately 0.05%. The optical rotation was measured with a Perkin-Elmer 141 automatic polarimeter.

Separation of DL-Ile·NDS by Fractional Crystallization. A mixture of the Ile-mixture (10.0 g) and NDS (13.6 g; water content, 19.3%) was dissolved in water (120 ml) by heating at 80 °C and then allowed to stand in a refrigerator overnight. The crystals thus precipitated were collected by filtration, washed with a small amount of cold water, and dried to give crude DL-Ile·NDS (10.8 g); apparent yield, 91.3% (based on the DL-Ile in the starting Ile-mixture); DL-Ile/DL-allo-Ile ratio=93.5/6.5. The crude DL-Ile·NDS (10.8 g) was recrystallized twice from water (110 ml) to give pure DL-Ile·NDS (6.3 g); yield, 53.2% (based on the DL-Ile in the starting Ile-mixture); DL-allo-Ile, undetected; mp 240—241 °C (decomp). Found: C, 48.07; H, 6.27; N, 4.85; S, 11.71%. Calcd for $C_{22}H_{34}N_2O_{10}S_2$: C, 47.99; H, 6.22; N, 5.09; S, 11.64%. Solubility in water (g/100 ml): 1.84 (20 °C), 2.22 (30 °C).

Epimerization of Ile·NDS. The experiments aimed at the epimerization of Ile·NDS were carried out by using L-Ile·NDS,** since the optical rotations of L-Ile and D-allo-Ile are nearly equal in magnitude and opposite in sign. A mixture of L-Ile·NDS (0.1 g), salicylaldehyde (0.018 ml, 1.0 mol per 1.0 mol of L-Ile·NDS), an Ile-mixture (0.023—0.23 g, 1.0—10.0 mol per 1.0 mol of L-Ile·NDS), and 95% acetic acid*** (10 ml) was heated in a sealed tube at 100 °C for 3 h. The reaction mixture was diluted with 1 M-hydrochloric acid (5 ml), and the optical rotation was measured. The epimeriza-

** L-Ile·NDS was prepared as follows. A mixture of L-Ile (13.1 g) and NDS (14.5 g) was dissolved in water (50 ml) at an elevated temperature, and then the solution was allowed to stand in a refrigerator overnight. The resulting precipitates were collected, washed with cold water, and air-dried at 50 °C to give L-Ile·NDS (22.5 g); mp 253—254 °C (decomp), $[\alpha]_D^{25}$ +13.4° (c=1, water). The product was composed of 2 mol of L-Ile, 1 mol of NDS, and 1 mol of water.

*** Although the extent of epimerization decreased with the increase in the water content of acetic acid, as has been described in our previous report,[13] acetic acid containing 5% water was used in order to dissolve the L-Ile·NDS.

tion degree was calculated as follows:

$$\frac{\text{initial optical rotation} - \text{final optical rotation}}{\text{initial optical rotation}} \times 100.$$

The effects of the salicylaldehyde and the Ile-mixture on the epimerization of L-Ile·NDS are shown in Table 1.

Production of DL-*Ile·NDS by Asymmetric Transformation. From Ile-Mixture*: An Ile-mixture (13.1 g), NDS (17.9 g, water content, 19.3%; equivalent amount with Ile-mixture, 13.1 g), acetic anhydride (18.0 ml; equimolar amount with water contained in NDS, 17.9 g), and a combination of an Ile-mixture (2.2 g) and salicylaldehyde (0.22 ml) to accelerate the epimerization of DL-allo-Ile·NDS were added to glacial acetic acid (30 ml). The mixture once completely dissolved, and soon most of the Ile·NDS precipitated. The mixture was then stirred at 100 °C for 16 h. The crystals thus precipitated were quickly collected by filtration, washed with a small amount of acetic acid, and dried to give crude DL-Ile·NDS (24.8 g); yield, 90.1% (based on Ile-mixture·NDS), Ile/allo-Ile=89.8/10.2. The Ile/allo-Ile ratio of the mother liquor was 41.5/58.5. The crude DL-Ile·NDS (24.8 g) was recrystallized from water (300 ml) to give DL-Ile·NDS (17.6 g); Ile/allo-Ile ratio=1000/2.

From DL-*Allo-Ile*: DL-Allo-Ile (13.1 g, 100 mmol), NDS (14.3 g, water content 19.3%, 40 mmol), salicylaldehyde (0.26 ml, 2.5 mmol), and acetic anhydride (14.4 ml; equimolar amount with water contained in NDS, 14.3 g) were added to glacial acetic acid (60 ml). The mixture was stirred at 100 °C, seeded with finely pulverized crystals of DL-Ile·NDS (0.01 g) after 3 h, and further stirred for 30 h at the same temperature. The reaction mixture was then cooled to room temperature and stirred for 1 h. The crystals thus precipitated were collected by filtration, washed with a small amount of acetic acid, and dried to give DL-Ile·NDS (20.8 g); yield, 94.5% (based on DL-allo-Ile·NDS); Ile/allo-Ile=93.1/6.9. The Ile/allo-Ile ratio of the mother liquor was 40.7/59.3. The change in the composition of both diastereoisomeric racemates during the reaction is shown in Fig. 1.

Preparation of Pure DL-*Ile*. Recrystallized DL-Ile·NDS (16.0 g) was dissolved in water (800 ml). The solution was passed through a column of Amberlite IR-45 (70 ml, OH-form), and the column was washed with water. The effluent and washed water were concentrated, and methanol (45 ml) was added to the concentrated solution. The crystals thus precipitated were collected by filtration, washed with a small amount of cold water, and dried to give DL-Ile (7.3 g); DL-allo-Ile, undetected.

References

1) J. P. Greenstein and M. Winitz, "Chemistry of the Amino Acids," Wiley, New York, N.Y. (1961), Vol. 3, p. 2043.
2) J. P. Greenstein, L. Levintow, C. G. Baker, and J. White, *J. Biol. Chem.*, **188**, 647 (1951).
3) E. Abderhalden and W. Zeisset, *Z. Physiol. Chem.*, **195**, 121 (1931).
4) A. C. Shabica, U. S. Patent 2456742 (1948).
5) W. A. H. Huffman and A. W. Ingersoll, *J. Am. Chem. Soc.*, **73**, 3366 (1951).
6) J. P. Greenstein, S. M. Birnbaum, and L. Levintow, *Biochem. Prep.*, **3**, 84 (1953).
7) W. M. Laird, S. Matai, and R. L. M. Synge, *Biochem. J.*, **116**, 911 (1970).
8) J. P. Greenstein and M. Winitz, "Chemistry of the Amino Acids," Wiley, New York, N.Y. (1961), Vol. 1, p. 658.
9) S. Yamada, M. Yamamoto, and I. Chibata, *J. Agric. Food Chem.*, **21**, 889 (1973).
10) S. Yamada, M. Yamamoto, and I. Chibata, *J. Org. Chem.*, **38**, 4408 (1973).
11) S. Yamada, M. Yamamoto, C. Hongo, and I. Chibata, *J. Agric. Food Chem.*, **23**, 653 (1975).
12) S. Yamada, C. Hongo, and I. Chibata, *Agric. Biol. Chem.*, **42**, 1521 (1978).
13) S. Yamada, C. Hongo, R. Yoshioka, and I. Chibata, *J. Org. Chem.*, **48**, 843 (1983).
14) M. M. Harris, "Progress in Stereochemistry," ed by W. Klyne and P. B. D. Mare, Butterworths Scientific Publications, London (1958), Vol. 2, p. 157.
15) G. J. Mathews, U. S. Patent 3808254 (1974).
16) J. C. Clark, G. H. Phillipps, and M. R. Steer, *J. Chem. Soc., Perkin Trans., 1*, 475 (1976).

 © 1984 The Chemical Society of Japan Bull. Chem. Soc. Jpn., 57, 1331—1335 (1984)

Sorption of Ammonia/Ammonium Ion on Crystalline Hydrous Titanium Dioxide Fibers

Takayoshi SASAKI,* Yū KOMATSU, and Yoshinori FUJIKI
National Institute for Research in Inorganic Materials
1-1 Namiki, Sakura-mura, Niihari-gun, Ibaraki 305
(Received August 5, 1983)

The sorption of ammonia/ammonium ion has been studied on crystalline hydrous titanium dioxide fibers with a layer structure, which are prepared from potassium tetratitanate ($K_2Ti_4O_9$). From the measurement of the distribution coefficient, it was found that this material strongly preferred ammonium ion to sodium ion. The results of the pH titration curves indicated that this material showed a wide range of acidities toward ammonia/ammonium ion and had 2.63 mequiv/g of an apparent capacity which was about a half of the theoretical ion-exchange capacity. The characterizations of the ammonium adsorbed solid phase at various loading levels were carried out by measuring the X-ray powder diffractograms and the water contents. From these studies, it was concluded that the sorption-desorption reaction of ammonia/ammonium ion on this material took place almost reversibly in three stages.

Recently Fujiki *et al.* have prepared a crystalline hydrous titanium dioxide with a fibrous form from potassium tetratitanate ($K_2Ti_4O_9$).[1,2] This material, which was named "crystalline hydrous titanium dioxide fibers," has been attractive because it has a layer structure and is supposed to be highly selective for some metal ions. We have studied the sorption of the microquantities of alkali metals, alkaline earth metals and divalent transition metals and determined their order of selectivity.[3-5] Considerably large differences of the affinities were observed between these metal ions, and some mutual separations of these metals were achieved on the column of this material.[4,5] We have also proposed that this material can be used advantageously to immobilize the dangerous nuclides such as cesium and strontium in a high-level radioactive waste solution.[6,7]

On the other hand, much attention has been paid to the problem of removal of ammonia/ammonium ion from an aqueous solution during the last decade. Some kinds of ion-exchangers such as zirconium phosphate are being employed to remove ammonia/ammonium ion from human blood, *e.g.* artificial kidney machine.[8,9] The sorption of ammonia/ammonium ion on crystalline hydrous titanium dioxide fibers, however, has not been studied yet, although they are promising for such a practical use because they are suitable for column operations because of their fibrous form. The sorption on this material is expected to be different from that on zirconium phosphate because there are some differences in the layer arrangement or the characteristics of the exchangeable protons. Thus it is interesting and important, from both fundamental and practical viewpoints, to study the sorption of ammonia/ammonium ion on crystalline hydrous titanium dioxide fibers.

In this paper, the sorption of ammonia/ammonium ion on crystalline hydrous titanium dioxide fibers is studied and the mechanism and characteristics of the sorption are also discussed.

Experimental

Reagents. Titanium dioxide used was of 99.98% purity. All the other chemicals were of analytical grade. Distilled, deionized water was used throughout the experiments.

Preparation of Crystalline Hydrous Titanium Dioxide Fibers. Crystalline hydrous titanium dioxide fibers were prepared as described previously;[5] potassium tetratitanate ($K_2Ti_4O_9$) fibers were grown by slow-cooling a K_2MoO_4 flux melt containing a mixture of K_2CO_3 and TiO_2 (1:3 molar ratio). The obtained fibers were placed in a column and converted into a hydrogen form by passing through 1 mol dm^{-3} hydrochloric acid as given by Eq. 1.

$$K_2Ti_4O_9 + 2H^+ + nH_2O \longrightarrow H_2Ti_4O_9 \cdot nH_2O + 2K^+. \quad (1)$$

After the concentration of potassium ion in the effluent became negligible, the resulting product was washed with water and dried in the air to a constant weight. The chemical formula of this material can be written as $H_2Ti_4O_9 \cdot 1.3H_2O$ taking into account the fact that the weight loss at 800 °C was 11.49%. The theoretical ion-exchange capacity is calculated to be 5.53 mequiv/g.

Distribution Coefficients. Distribution coefficients of ammonium ion were obtained by shaking 0.2 g of the material with 0.02 dm^3 of 1×10^{-3} mol dm^{-3} NH_4Cl solution at 25±0.5 °C. The pH value of the solution was controlled with hydrochloric acid. After the equilibrium was attained, the supernatant solutions were analyzed for their pH values and ammonium ion contents. The ammonium ion contents were determined by means of a TOA AE-235 ammonium ion selective electrode. The distribution coefficients were calculated by using

$$K_d = \frac{\text{moles of ammonium ion per 1 g of the material}}{\text{moles of ammonium ion per 1 cm}^3 \text{ of the solution}} \ (\text{cm}^3/\text{g}).$$

The concentrations of ammonium ion in the material were calculated from the differences between initial and final concentrations of solutions.

pH Titration Curve. The titrations for ammonia/ammonium ion were carried out batchwise; in the forward titration, 0.5 g of the material was shaken with 0.05 dm^3 of 0.1 mol dm^{-3} ($NH_4Cl+NH_3H_2O$) solution at 25±0.5 °C until the equilibrium was attained. The ratio of NH_4Cl/NH_3H_2O was varied from 0.1 M/0.0 M to 0.0 M/0.1 M (1 M= 1 mol dm^{-3}). After the pH value at equilibrium was measured, the ammonium content in the solution was determined by the standard acidimetric titration in the presence of formaldehyde. The solid was filtered off, washed and dried in the air at room temperature. The ammonium content in the solid was determined by the Kjeldahl method.

In the backward titration, 0.5032 g of the end product in the forward titration was treated with 0.05 dm^3 of 0.1 mol dm^{-3} (NH_4Cl+HCl) solution. Other procedures were similar to those in the forward titration. The pH titration curve for potassium ion was obtained in a similar way by using 0.1 mol dm^{-3} (KCl+KOH) solution.

Apparatus. The pH values of the solution were measured by a TOA HM-20E digital pH meter. X-Ray powder diffractograms were obtained by a Philips X-ray diffractometer with Cu $K\alpha$ radiation.

Results and Discussion

Distribution Coefficients. In order to determine the equilibration time, 0.2 g of the material was shaken with 0.02 dm^3 of 1×10^{-3} mol dm^{-3} NH_4Cl solution (pH=2.0) at 25±0.5 °C. Figure 1 shows the percent uptake of ammonium ion as a function of time. It was confirmed that 2 d shaking was enough to attain the equilibrium. Thus all the experiments were carried out by shaking the fibers with solutions for 3 d.

Figure 2 shows the pH dependence of distribution coefficients (K_d) of ammonium ion. The dashed lines denote the data of alkali metals obtained previously under similar experimental conditions.[3] The linear relationship was observed between log K_d and pH with a slope of +1. This fact indicated that the sorption of ammonium ion took place by an ideal ion-exchange reaction as given by Eq. 2.

$$x\mathrm{NH_4^+(aq)} + \mathrm{H_2Ti_4O_9\cdot}n\mathrm{H_2O(s)} \rightleftharpoons (\mathrm{NH_4})_x\mathrm{H_{2-}}_x\mathrm{Ti_4O_9\cdot}n'\mathrm{H_2O(s)} + x\mathrm{H^+(aq)} \quad (0<x<0.04), \tag{2}$$

where the subscripts "aq" and "s" represent aqueous and solid phases, respectively.

The order of selectivity was found to be Cs>Rb>K>NH_4>Na>Li. In the case of alkali metals, this order was parallel to their ionic radii. Since the ionic size of ammonium ion is almost the same as that of potassium ion, the affinities of these two ions are expected to be almost equal with each other, which is actually true from Fig. 2.

Table 1 gives the distribution coefficients and separation factors of ammonium ion and alkali metal ions at a pH value of 2.0. A large value of separation factor was observed between ammonium ion and sodium ion. This fact will be one of advantages when this material is employed to remove ammonium ion from a solution which contains a large amount of sodium ion.

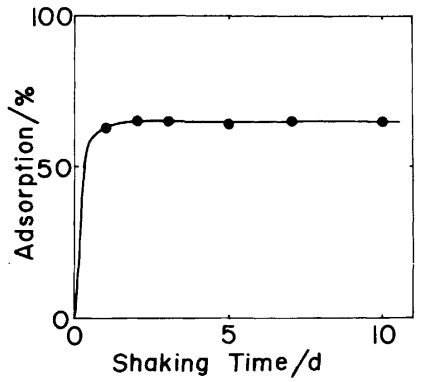

Fig. 1. Time dependence of the sorption of ammonium ion.
Exchanger: 0.2 g, solution: 0.02 dm^3 of 1×10^{-3} mol dm^{-3} NH_4Cl (pH=2.0).

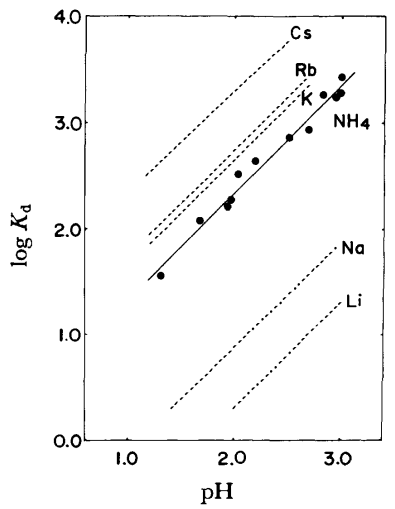

Fig. 2. pH dependence of distribution coefficients of ammonium ion.
Exchanger: 0.2 g, solution: 0.02 dm^3 of 1×10^{-3} mol dm^{-3} NH_4Cl.

Table 1. Distribution coefficients (K_d) and separation factors (α_A^B) of ammonium ion and alkali metal ions at pH=2.0

Ion	Cs	Rb	K	NH_4	Na	Li
K_d	2460	563	458	225	8.0	2.1
α_A^B	4.4	1.2	2.0	28.1	3.8	

$\alpha_A^B = K_d^B/K_d^A$ for neighboring ions. Data for alkali metal ions are from Ref. 3.

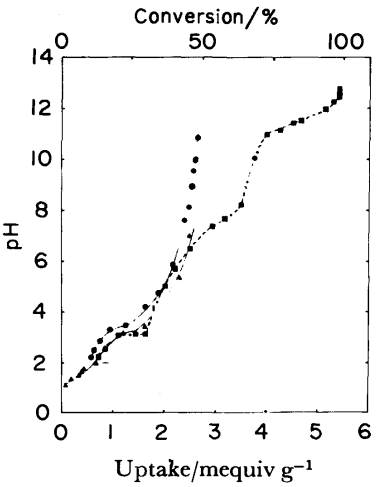

Fig. 3. pH titration curve.
—●— Ammonia/ammonium ion (forward); exchanger: 0.5 g, solution: 0.05 dm^3 of 0.1 mol dm^{-3} (NH_4Cl+NH_3H_2O), —▲— ammonia/ammonium ion (backward); exchanger (ammonium form): 0.5032 g, solution: 0.05 dm^3 of 0.1 mol dm^{-3} (NH_4Cl+HCl), —■— potassium ion (forward); exchanger: 0.2 g, solution: 0.02 dm^3 of 0.1 mol dm^{-3} (KCl+KOH).

pH Titration Curve. pH titration curves for ammonia/ammonium ion (forward and backward) are shown in Fig. 3. pH titration curve for potassium ion is also shown for comparison. The exchangeable protons in crystalline hydrous titanium dioxide fibers had a wide range of acidities toward ammonia/ammonium ion. The inflection point was observed at 25—30% conversion, which indicated that 25—30% of the exchangeable protons were more acidic than the others. The backward titration curve had a similar curvature to the forward one except for a slight difference. The apparent capacity for ammonia/ammonium ion was 2.63 mequiv/g which was about a half of the theoretical ion-exchange capacity of this material, whereas almost complete exchange was achieved with potassium ion.

Characterization of Ammonium-Adsorbed Solid Phase. Figure 4 shows the X-ray powder diffractograms of the material at various loading levels of ammonium in the forward titration. In most of the ion-exchange processes of inorganic ion-exchangers with a layer structure, two immiscible phases are observed; one is an unexchanged phase and the other is an exchanged phase with a different interlayer distance from that of the unexchanged phase.[10,11] In this work, however, X-ray diffractograms changed continuously, which indicated that ammonia/ammonium ion is taken into crystalline hydrous titanium dioxide fibers without phase transition.

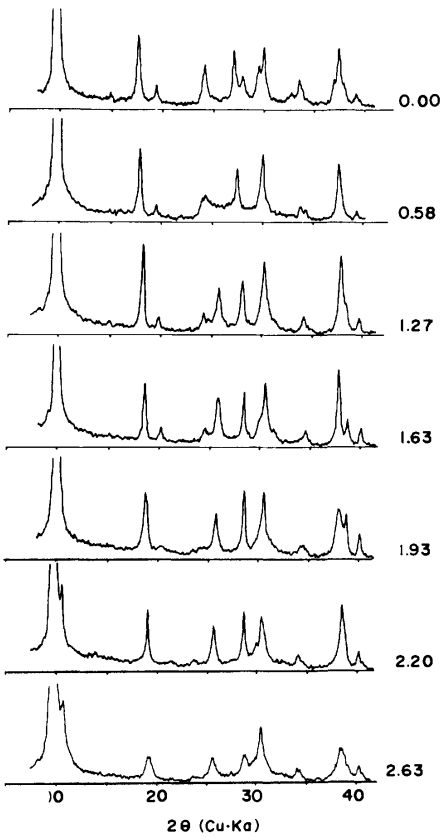

Fig. 4. Schematic diagrams of X-ray powder diffractograms of the ammonium adsorbed phase in forward titration. Numerals represent the uptake of ammonia/ammonium ion (mequiv/g).

Figure 5 shows the *d*-spacing of the strongest reflection, which appeared near the 2θ value of 10° in the X-ray diffractograms, as a function of ammonium loading. This reflection is from (200) plane and is attributable to the interlayer of the material.[12] Its spacing was determined by using potassium hexatitanate ($K_2Ti_6O_{13}$) as an internal standard.

Figure 6 shows the water content of the ammonium-adsorbed solid phase as a function of loading. The weight loss was determined by heating the ammonium-adsorbed solid phase at 800 °C for 1 h. The water content was calculated from the weight loss by assuming the decomposition given by Eq. 3.

$$(NH_4)_xH_{2-x}Ti_4O_9\cdot nH_2O(s) \longrightarrow 4TiO_2(s) + xNH_3(g) + (n+1)H_2O(g) \quad (3)$$

where subscripts "s" and "g" represent solid and gas phases, respectively.

Figure 7 shows the *d*-spacing of the (200) reflection at various loadings of ammonium in the backward titration. The *d*-spacings coincided roughly with those of

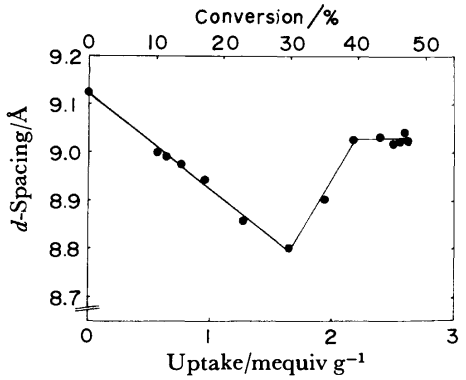

Fig. 5. *d*-Spacing of the (200) reflection as a function of loading in forward titration.

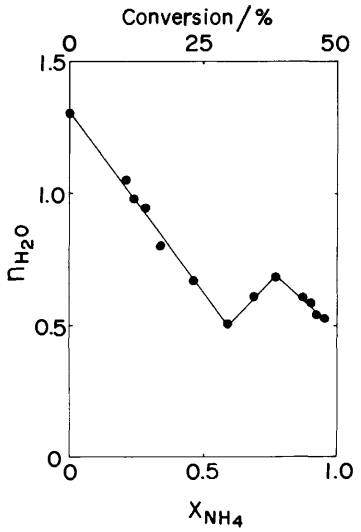

Fig. 6. Water content of the ammonium adsorbed solid phase in forward titration.
x_{NH_4} and n_{H_2O} correspond to the subscripts in the chemical formula of the ammonium adsorbed solid phase, $(NH_4)_xH_{2-x}Ti_4O_9\cdot nH_2O$.

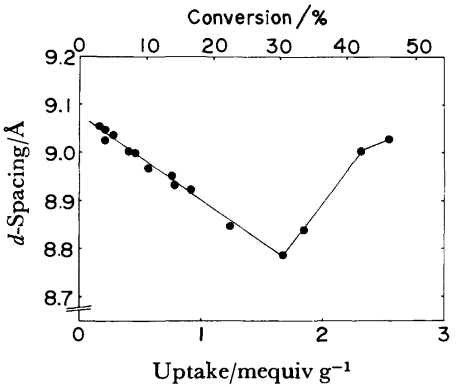

Fig. 7. *d*-Spacing of the (200) reflection as a function of loading in backward titration.

the material in the forward titration, which indicated that the sorption-desorption reaction took place almost reversibly. A slight difference between the forward and backward titration curves may be due to the loss of crystallinity of the material used in the backward titration which was the end product in the forward titration.

Mechanism of the Sorption of Ammonia/Ammonium Ion. There are two possible explanations for the sorption of ammonia/ammonium ion; one is an NH_4^+/H^+ exchange reaction and the other is a direct addition of NH_3 to the protons in the exchanger giving ammonium ion. Alberti and his co-workers have reached a conclusion after detailed investigations that the sorption on crystalline zirconium phosphate took place by the direct addition of NH_3.[12] In the case of crystalline hydrous titanium dioxide fibers, the sorption can be explained by the NH_4^+/H^+ exchange in the pH range of 1.0 to 3.0 from distribution coefficients shown in Fig. 2. However it is difficult to determine which way of the sorption process was predominant in the higher pH region from the result of pH titration curve.

As described above, about a half of the exchangable protons was replaced by ammonia/ammonium ion. The plots of the interlayer distance and the water content of the ammonium-adsorbed solid phase showed two distinct turning points at 30 and 40% conversion. These facts suggested that the ammonia/ammonium ion uptake took place in three stages; stage I [0—30% conversion], stage II [30—40% conversion] and stage III [40—48% conversion].

In stage I, ammonia/ammonium ion uptake proceeded accompanying the continuous decrease in interlayer distance and water content. This phenomenon can be explained as follows; the ammonium ion adsorbed between the layers can make a hydrogen-bond with an unexchanged hydroxyl group in an adjacent layer. As the ammonium loading increased, the number of hydrogen-bond increased, which induced the continuous decrease in interlayer distance. The water content also decreased linearly. The value of $d\,n_{H_2O}/d\,x_{NH_4}$ was 1.33 which was approximately equal to the number of water molecules per formula weight of the material. From these facts, it is suggested that the ammonia/ammonium ion was taken into the lattice by forming a hydrogen-bond and expelling the water around the sorption site.

In stage II, the ammonia/ammonium ion uptake gave rise to increase in interlayer distance and water content. In the X-ray powder diffractograms, a new tiny shoulder appeared beside the (200) reflection as seen in Fig. 4. It seems that ammonia/ammonium ion uptake beyond 30% of the conversion caused a slight distortion of the lattice of the material. If this is true, the sorption in this stage will require more energy than in stage I and the sorption will proceed in the higher pH region. This expectation is actually the case as shown in Fig. 3.

In stage III, no definite change was observed in the X-ray powder diffractograms, which suggested that the ammonium ion already adsorbed between the layers may act like a "pillar" and the material can accomodate additional ammonia/ammonium ion without an appreciable change in interlayer distance.

In conclusion, the sorption process can be summarized by the following three equation:

stage I
$$H_2Ti_4O_9\cdot 1.3H_2O + 0.6NH_3(NH_4^+) \quad [9.1\ \text{Å}]$$
$$\longrightarrow (NH_4)_{0.6}H_{1.4}Ti_4O_9\cdot 0.5H_2O + 0.8H_2O \quad [8.8\ \text{Å}] + (0.6H^+)$$

stage II
$$(NH_4)_{0.6}H_{1.4}Ti_4O_9\cdot 0.5H_2O + 0.2NH_3(NH_4^+) \quad [8.8\ \text{Å}]$$
$$+ 0.2H_2O \longrightarrow (NH_4)_{0.8}H_{1.2}Ti_4O_9\cdot 0.7H_2O \quad [9.0\ \text{Å}] + (0.2H^+)$$

stage III
$$(NH_4)_{0.8}H_{1.2}Ti_4O_9\cdot 0.7H_2O + 0.15NH_3(NH_4^+) \quad [9.0\ \text{Å}]$$
$$\longrightarrow (NH_4)_{0.95}H_{1.05}Ti_4O_9\cdot 0.5H_2O + 0.2H_2O \quad [9.0\ \text{Å}] + (0.15H^+),$$

where numerals in brackets correspond to the *d*-spacings of the (200) reflection.

Only a half of the exchangeable protons can be replaced by ammonia/ammonium ion. This phenomenon cannot be attributed to the steric effect, because almost all of the exchangeable protons were exchanged by potassium ions whose size is approximately equal to that of ammonium ion. This fact can also be explained by the hydrogen-bond formation of the ammonium ion between the layers. The stable pair of ammonium ion and an unexchanged hydroxyl group, which is hydrogen-bonded with each other, may be a good explanation for the fact that the apparent capacity was about a half of the theoretical ion-exchange capacity.

References

1) N. Ohta and Y. Fujiki, *Yogyo Kyokai Shi*, **88**, 9 (1980).
2) N. Ohta and Y. Fujiki, *Yogyo Kyokai Shi*, **89**, 134 (1981).
3) Y. Komatsu, Y. Fujiki, and T. Sasaki, *Bunseki Kagaku, Sect. E*, **31**, E225 (1982).
4) Y. Komatsu, Y. Fujiki, and T. Sasaki, *Bunseki Kagaku,*

Sect. E, **32**, E33 (1983).
5) T. Sasaki, Y. Komatsu, and Y. Fujiki, *Sep. Sci. Technol.*, **18**, 49 (1983).
6) Y. Fujiki, Y. Komatsu, T. Sasaki, and N. Ohta, *Nippon Kagaku Kaishi*, **1981**, 1656.
7) T. Sasaki, Y. Komatsu, and Y. Fujiki, *Chem. Lett.*, **1981**, 957.
8) A. Gordon, O. S. Betler, M. Greenbaum, L. Marantz, T. Gral, and H. M. Maxwell, *Trans. Am. Soc. Artif. Int. Organs*, **17**, 253 (1971).
9) N. Nakabayashi, *Jinkō Zōki*, **4**, 253 (1975).
10) J. P. Gupta, N. J. Manning, and D. V. Norwell, *J. Inorg. Nucl. Chem.*, **40**, 87 (1978).
11) G. Alberti, R. Bertrami, U. Constantino, and J. P. Gupta, *J. Inorg. Nucl. Chem.*, **39**, 1057 (1977).
12) H. Izawa, S. Kikkawa, and M. Koizumi, *J. Phys. Chem.*, **86**, 5023 (1982).

Electronic Absorption, Magnetic Circular Dichroism, and Circular Dichroism Spectra of *cis*- and *trans*-[Pd(Cl)$_2$(N)$_2$]-type Complexes and Their Electronic Structures

Kazuhiko NAKAYAMA,* Takashi KOMORITA, and Yoichi SHIMURA
Department of Chemistry, Faculty of Science, Osaka University, Toyonaka, Osaka 560
(Received September 26, 1983)

The electronic absorption and MCD spectra of [PdCl$_2$L] (L=ethylenediamine(en), 1,3-propanediamine, *N,N*-dimethylethylenediamine, *N,N'*-dimethylethylenediamine, *N,N*-diethylethylenediamine, and *N,N*-dimethyl-1,3-propanediamine) and *trans*-[PdCl$_2$(L)$_2$] (L=EtNH$_2$, Me$_2$NH, Me$_3$N, *n*-BuNH$_2$, *i*-BuNH$_2$, *s*-BuNH$_2$, *t*-BuNH$_2$, and *rac*-pea (pea=1-phenylethylamine)), and CD spectra of [PdCl$_2$L] (L=(*S*)-1,2-propanediamine-(*S*-pn) and (2*S*)-*N*^{1},*N*^{1}-diethyl-1,2-propanediamine) and *trans*-[PdCl$_2$(*S*-pea)$_2$] have been measured over the visible-near UV region, together with the corresponding spectra of [PtCl$_2$L] (L=en and *S*-pn). The examination of the three kinds of spectra as well as their Gaussian analyses indicates that the splitting pattern of metal d orbitals for the cis type complexes is similar to that for [PdCl$_4$]$^{2-}$, and that as to the trans complexes the $d_{x^2-y^2}\leftarrow d_{xz}$ and d_{yz} transitions split largely to give apparent two spin-allowed d-d bands characteristic of the trans complexes. The average energy of the $d_{x^2-z^2}\leftarrow d_{xz}$ and d_{yz} transitions for the trans complexes is approximately equal to the energy of the $d_{x^2-y^2}\leftarrow d_{xz,yz}$ (D_{4h}) ones for the cis complexes. The transition energies of $d_{x^2-z^2}\leftarrow d_{xy}$ and d_{z^2} do not differ largely between both types of complexes. The assignments of high-intensity bands have also been made tentatively.

Palladium(II) complexes generally exhibit a less informative d-d absorption spectrum than the platinum analogs because of a small splitting of the metal d orbitals. Although three spin-allowed d-d bands are expected in a D_{4h} symmetry (or four in D_{2h}), most of palladium(II) complexes exhibit only a single unsymmetrical band. This situation makes assignment difficult for the d-d spectra of palladium(II) complexes. In the case of [PdCl$_4$]$^{2-}$,[1] the difficulty could be overcome by a concurrent examination of the MCD and absorption spectra and by a comparison with the corresponding spectra of [PtCl$_4$]$^{2-}$.

There have been known a few rare examples exhibiting a distinct splitting of spin-allowed d-d bands.[2,3] The typical examples are *trans*-[Pd(Cl)$_2$(N)$_2$]-type complexes,[2] but there has been no detailed investigation of them. Although the electronic and CD spectra of some complexes of *cis*-[M(Cl)$_2$(N)$_2$]-type (M=Pt and Pd) were reported by Ito *et al.*,[4] the discussion of electronic structure was almost limited to the platinum complexes. The concurrent study of *cis*- and *trans*- [Pd(Cl)$_2$(N)$_2$]-type complexes is desirable to understand systematically the electronic structure of square-planar palladium (II) complexes.

This paper presents new spectral assignment for *cis*- and *trans*-[Pd(Cl)$_2$(N)$_2$]-type complexes on the basis of the absorption, MCD, and CD spectra and their Gaussian analysis. These spectral and analytical data have been compared with those of [PdCl$_4$]$^{2-}$ [1] and [PtCl$_2$(en)]; a similarity of spectra and electronic structure such as noted between [PtCl$_4$]$^{2-}$ and [PdCl$_4$]$^{2-}$ [1] is also found between [PtCl$_2$(en)] and [PdCl$_2$(en)]. Although every *cis*-[Pd(Cl)$_2$(N)$_2$]-type complex gives MCD with a nearly ideal A-term pattern in the spin-allowed d-d region, the MCD is based not only on a transition to a degenerate excited state but on all the spin-allowed d-d transitions. Each of four transitions of the trans complexes proves to exhibit either CD or MCD selectively. In addition, the relationship between the electronic structures of the cis and the trans complexes has been discussed in detail.

Experimental

trans-[PdCl$_2$(L)$_2$] Complexes. *1) L=MeNH$_2$*: Palladium chloride (350 mg) was mixed with an aqueous solution of methylamine (20%, 10 cm^3). The mixture was heated at *ca.* 50 °C with stirring to give an almost colorless solution. After filtration the filtrate cooled was treated with concentrated hydrochloric acid (430 mg), giving yellow needles, which were collected, washed with water, ethanol, and ether; and dried *in vacuo*. Yield: 415 mg. Found: C, 10.13; H, 4.20; N, 11.71%. Calcd for *trans*-[PdCl$_2$(MeNH$_2$)$_2$]=C$_2$H$_{10}$N$_2$Cl$_2$Pd: C, 10.03; H, 4.21; N, 11.70%.

2) L=Me$_2$NH, EtNH$_2$, and n-*PrNH$_2$, and* n-*BuNH$_2$*: Each of these complexes was obtained in good yield by a method similar to that in *1)*. Found: C, 18.05; H, 5.27; N, 10.55%. Calcd for *trans*-[PdCl$_2$(Me$_2$NH)$_2$]=C$_4$H$_{14}$N$_2$Cl$_2$Pd: C, 17.96; H, 5.28; N, 10.47%. Found: C, 17.99; H, 5.25; N, 10.52%. Calcd for *trans*-[PdCl$_2$(EtNH$_2$)$_2$]=C$_4$H$_{14}$N$_2$Cl$_2$Pd: C, 17.96; H, 5.28; N, 10.47%. Found: C, 24.51; H, 6.10; N, 9.50%. Calcd for *trans*-[PdCl$_2$(*n*-PrNH$_2$)$_2$]=C$_6$H$_{18}$N$_2$Cl$_2$Pd: C, 24.38; H, 6.14; N, 9.48%. Found: C, 29.58; H, 6.82; N, 8.64%. Calcd for *trans*-[PdCl$_2$(*n*-BuNH$_2$)$_2$]=C$_8$H$_{22}$N$_2$Cl$_2$Pd: C, 29.69; H, 6.85; N, 8.66%.

3) L=Me$_3$N: After bis(benzonitrile)dichloropalladium(II)[5] (400 mg) had been dissolved in 2 cm^3 of acetone at 50 °C, a small amount of undissolved solid was filtered off and washed with a minimum volume of acetone. An aqueous solution of trimethylamine (30%, 450 mg) was added dropwise to the combined filtrate and washings, with stirring at room temperature. Continuous stirring and cooling gave orange-brown crystals, which were collected, washed with cold acetone, and dried *in vacuo*. Yield: 150 mg. Found: C, 24.50; H, 6.10; N, 9.41%. Calcd for *trans*-[PdCl$_2$(Me$_3$N)$_2$]=C$_6$H$_{18}$N$_2$Cl$_2$Pd: C, 24.38; H, 6.14; N, 9.48%.

4) L=Et$_2$NH: Diethylamine (99%, 160 mg) diluted with acetone (1 cm^3) was added dropwise to a solution (filtered if necessary) of bis(benzonitrile)dichloropalladium(II) (400 mg) in acetone (8 cm^3), with stirring at room temperature. After 1.5 hours of stirring, the desired orange-yellow product was filtered off, washed with water, ethanol, and ether;

and dried *in vacuo*. Yield: 220 mg. Found: C, 29.99; H, 6.87; N, 8.56%. Calcd for *trans*-[PdCl$_2$(Et$_2$NH)$_2$]=C$_8$H$_{22}$N$_2$Cl$_2$Pd: C, 29.69; H, 6.85; N, 8.66%.

5) L=i-*PrNH$_2$*: This was prepared by a method similar to that in *4)*. The crude product was recrystallized from *N,N*-dimethylformamide at *ca.* 80 °C. Found: C, 24.56; H, 6.19; N, 9.51%. Calcd for *trans*-[PdCl$_2$(*i*-PrNH$_2$)$_2$]=C$_6$H$_{18}$N$_2$Cl$_2$Pd: C, 24.38; H, 6.14; N, 9.48%.

6) L=s-*BuNH$_2$*: An acetone solution (1 cm^3) of *s*-butylamine (153 mg) was added dropwise with stirring to a solution of bis(benzonitrile)dichloropalladium(II) (400 mg) in acetone (4.5 cm^3). The mixture was stirred for half an hour and then concentrated to about one-fourth of its original volume. Yellow crystals were obtained from the concentrate by addition of ether followed by stirring for 2 h in an ice-bath. Yield: 230 mg. Found: C, 29.83; H, 6.89; N, 8.67%. Calcd for *trans*-[PdCl$_2$(*s*-BuNH$_2$)$_2$]=C$_8$H$_{22}$N$_2$Cl$_2$Pd: C, 29.69; H, 6.85; N, 8.66%.

7) L=i-*BuNH$_2$ and* rac-*pea*: These were prepared in the same way as in *6)*. In the case of the *rac*-pea complex, the crude product was recrystallized from carbon tetrachloride at *ca.* 70 °C. Found: C, 29.78; H, 6.81; N, 8.71%. Calcd for *trans*-[PdCl$_2$(*i*-BuNH$_2$)$_2$]=C$_8$H$_{22}$N$_2$Cl$_2$Pd: C, 29.69; H, 6.85; N, 8.66%. Found: C, 35.65; H, 3.87; N, 4.84%. Calcd for *trans*-[PdCl$_2$(*rac*-pea)$_2$]·CCl$_4$=C$_{17}$H$_{22}$N$_2$Cl$_6$Pd: C, 35.60; H, 3.87; N, 4.88%.

8) L=t-*BuNH$_2$*: This was prepared in the same manner as in *4)*, but a twofold concentration was adopted for the reaction mixture. The crude product was recrystallized from *N,N*-dimethylformamide at 70—75 °C. Found: C, 29.86; H, 6.85; N, 8.67%. Calcd for *trans*-[PdCl$_2$(*t*-BuNH$_2$)$_2$]=C$_8$H$_{22}$N$_2$Cl$_2$Pd: C, 29.69; H, 6.85; N, 8.66%.

9) L=S-*pea*: This complex was obtained by a method similar to that of Bosnich.[2] Found: C, 40.89; H, 4.61; N, 5.77%. Calcd for *trans*-[PdCl$_2$(*S*-pea)$_2$]·0.4CCl$_4$=C$_{16.4}$H$_{22}$N$_2$Cl$_{3.6}$Pd: C, 40.93; H, 4.61; N, 5.82%.

[PdCl$_2$L] Complexes. L=en, S-*pn, tn,* N,N-*Me$_2$en,* N,N′-*Me$_2$en,* N,N-*Et$_2$en,* N^1,N^1-*Et$_2$-(S)-pn, and* N,N-*Me$_2$tn*: These complexes were prepared according to the methods described in the literature[6] or ones similar to them.

[PtCl$_2$L] Complexes. L=en and S-*pn*: These were obtained by a method similar to that reported[7] (K$_2$PtCl$_4$: ligand=1:1).

Measurements. Electronic absorption, MCD, and CD spectra were recorded with the same apparatus and in the same manner as described elsewhere.[1,6] Spectral measurements of *trans*-[Pd(Cl)$_2$(N)$_2$]-type complexes were made in DCE (1,2-dichloroethane) and in methanol, and *cis*-[Pd(Cl)$_2$(N)$_2$]- and *cis*-[Pt(Cl)$_2$(N)$_2$]-type ones in 0.20 M KCl and 0.50 M HCl aqueous solutions, respectively, all at room temperature (1 M=1 mol dm^{-3}). No spectra of *trans*-[PdCl$_2$L$_2$] (L=MeNH$_2$, Et$_2$NH, *n*-PrNH$_2$, and *i*-PrNH$_2$) could be obtained because of their virtual insolubility in both DCE and methanol, and the spectrum of *trans*-[PdCl$_2$(Me$_3$N)$_2$] in methanol could not be obtained because of its decomposition in the solvent.

Gaussian Analyses. Gaussian analyses of absorption, MCD, and CD spectra were carried out in the same way as described previously.[1] Standard deviations given in Tables 2, 6, 7, 12, and 13 are from the observed values of ε, $\Delta\varepsilon$, or $\Delta\varepsilon_M$ for the corresponding calculated values.

Results and Discussion

Ligand-field Absorption Bands. The typical electronic absorption spectra of *cis*- and *trans*-[Pd(Cl)$_2$(N)$_2$]-type complexes[8] are shown in Fig. 1. The absorption curves of the cis complexes are composed

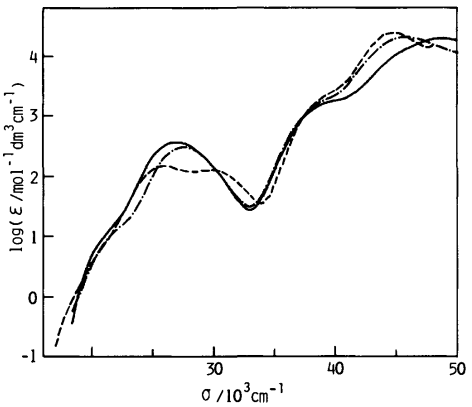

Fig. 1. A comparison of the absorption spectra of typical *cis*- and *trans*-[Pd(Cl)$_2$(N)$_2$]-type complexes. ——: [PdCl$_2$(en)] in 0.20 M KCl. —·—: [PdCl$_2$(tn)] in 0.20 M KCl. ----: *trans*-[PdCl$_2$(EtNH$_2$)$_2$] in DCE.

of an unsymmetrical main band (spin-allowed d-d band) and a lower-lying shoulder (spin-forbidden d-d band) in the ligand field transition region, being similar to that of [PdCl$_4$]$^{2-}$.[1] On the other hand, the spin-allowed d-d band of the trans complex, spreads toward both high and low energies as compared with those of the cis complexes to split into two bands (Fig. 1). Although such a distinct splitting has not been found in the ligand field absorption spectra of *trans*-[Pd(*S*-ala)$_2$][9] and *trans*-[Pd(*N*-Megly)$_2$],[10] one shoulder and one peak have been observed corresponding to the split bands. Therefore, it is reasonable to consider that the difference in ligand-field strength between two kinds of ligating atoms mainly determines the magnitude of the splitting.

For simplicity, we discuss the electronic structure of *cis*- and *trans*-[Pd(Cl)$_2$(N)$_2$]-type complexes under holohedrized symmetries.[11] Namely, the cis and trans complexes are approximately described by D_{4h} and D_{2h} symmetries, respectively. Then, the cis complexes should give rise to three spin-allowed d-d transitions ($^1A_{2g}$, $^1B_{1g}$, and $^1E_g \leftarrow {}^1A_{1g}$) similarly to [PdCl$_4$]$^{2-}$; and the trans complexes four (^1A_g, $^1B_{1g}$, $^1B_{2g}$, and $^1B_{3g} \leftarrow {}^1A_g$).

In the preceding paper,[1] we demonstrated that the absorption and MCD spectra of [PdCl$_4$]$^{2-}$ can be easily correlated with those of the platinum analog, [PtCl$_4$]$^{2-}$, by taking into account two points: firstly the energy separation of the $\Gamma_2(^1A_{2g})$ and $\Gamma_5(^1E_g)$ excited states is considerably large in the latter complex in comparison with the former; and secondly, in [PtCl$_4$]$^{2-}$ singlet-triplet transitions remarkably increase in absorption and MCD intensities and give more complicated spectra. Such a spectral resemblance between palladium and platinum complexes has been also found in [MCl$_n$(OH$_2$)$_{4-n}$]$^{2-n}$ (M=Pd and Pt; n=0—4).[12] Thus, it is helpful to examine first the spectra of [PtCl$_2$(en or *S*-pn)], which is expected to exhibit larger energy separations between d-d excited states than the palladium analog.

1) [PtCl$_2$(en or S-pn)] Complex: The absorption, MCD, and CD spectra are shown in Fig. 2 together

TABLE 1. SPECTRAL DATA OF $[PtCl_2L]$ COMPLEXES

L=en				L=*S*-pn	
Absorption		MCD		CD	
σ_{max} / 10^3 cm^{-1}	ε / mol^{-1} dm^3 cm^{-1}	σ_{ext} / 10^3 cm^{-1}	$\Delta\varepsilon_M$ / mol^{-1} dm^3 cm^{-1} T^{-1}	σ_{ext} / 10^3 cm^{-1}	$\Delta\varepsilon$ / mol^{-1} dm^3 cm^{-1}
		24.0	+0.0015		
27.8 sh[a]	35	27.2	−0.0035	26.6	−0.13
		30.6	+0.0077		
33.28	240	34.4	+0.0089	33 sh	−0.1
37.5 sh	117	38.1	−0.018	36.7	−0.46
48.76	6500	45.4	−1.1	45.2	+1.2

a) sh: shoulder (ε or $\Delta\varepsilon$ is for the value of σ given).

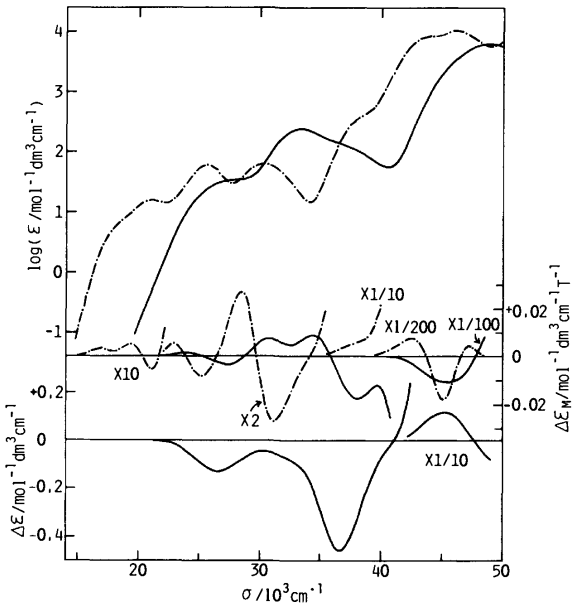

Fig. 2. Absorption and MCD spectra of $[PtCl_2(en)]$ (——) and $K_2[PtCl_4]$ (—·—); and CD spectrum of $[PtCl_2(S\text{-pn})]$ (——), all in 0.50 M HCl.

with the absorption and MCD spectra of $[PtCl_4]^{2-}$, and the numerical data in Table 1. Although the splitting of the d-d absorption band of $[PtCl_2(en)]$ is not so pronounced as observed for $[PtCl_4]^{2-}$, these two spectra can be easily correlated to each other. Such a correlation is also observed between their MCD spectra, except that the band corresponding to a negative band at 25.2×10^3 cm^{-1} of $[PtCl_4]^{2-}$ disappears in $[PtCl_2(en)]$ (Fig. 2). The dispersion of MCD at *ca.* 36×10^3 cm^{-1} is considered to be primarily composed of a negative A term, and assigned to the $\Gamma_5(^1E_g)\leftarrow\Gamma_1(^1A_{1g})$ transition. The dispersion changes sign around the middle of the whole spin-allowed d-d absorption band. From this fact and the similarities to $[PtCl_4]^{2-}$ as described above, the $\Gamma_2(^1A_{2g})$ and $\Gamma_3(^1B_{1g})\leftarrow\Gamma_1(^1A_{1g})$ transition components are reasonably considered to lie in the lower and higher energy side of the $\Gamma_5(^1E_g)\leftarrow\Gamma_1(^1A_{1g})$ transition, respectively. The results of Gaussian analysis on the basis of this deduction are tabulated in Table 2, together with

TABLE 2. GAUSSIAN-ANALYSIS DATA FOR THE ABSORPTION CURVE OF $[PtCl_2(en)]$

σ_{max} / 10^3 cm^{-1}	ε / mol^{-1} dm^3 cm^{-1}	$\Delta\sigma_{1/2}$ / 10^3 cm^{-1}	S[a]	Assignment[b] $\leftarrow\Gamma_1(^1A_{1g})$
27.3 f[c]	32 f	4.94	168	d)
30.96	12.6	3.89	52.2	$\Gamma_5(^3B_{1g})$
33.04	210	3.57	798	$\Gamma_2(^1A_{2g})$
36.10	111	3.97	471	$\Gamma_5(^1E_g)$
38.89	53.3	3.60	205	$\Gamma_3(^1B_{1g})$
	SD[e] = 0.43			

a) S(band area) = 1.0645 × (ε_{max}/mol^{-1} dm^3 cm^{-1}) × ($\Delta\sigma_{1/2}$/10^3 cm^{-1}). b) On the basis of holohedrized symmetry. c) f: fixed value. d) Spin-forbidden d-d transitions. e) Standard deviation (See Experimental).

the assignment. The three spin-allowed d-d transitions are blue-shifted by 6.8×10^3 cm^{-1} on the average from $[PtCl_4]^{2-}$.[1] The blue shift of the $\Gamma_2\leftarrow\Gamma_1$ transition is larger than the average shift by 0.6×10^3 cm^{-1}, and on the contrary that of the $\Gamma_5\leftarrow\Gamma_1$ transition is smaller by the same amount; thus the proximity of the Γ_2 and Γ_5 excited states relative to the case of $[PtCl_4]^{2-}$ makes the splitting of the spin-allowed d-d band less distinct.

The dispersion of MCD at *ca.* 36×10^3 cm^{-1} deviates from an ideal A-term pattern even by assuming such a positive B term as in $[PtCl_4]^{2-}$ for the $\Gamma_3(^1B_{1g})\leftarrow\Gamma_1(^1A_{1g})$ transition, which may be due to the reduction of symmetry from D_{4h}. The deformed dispersion pattern further suggests that the $\Gamma_5(^1E_g)\leftarrow\Gamma_1(^1A_{1g})$ transition exhibits a positive B term in addition to a negative A term because the zero point of the dispersion lies at lower energy than the corresponding absorption component obtained by Gaussian analysis. The positive band at 30.6×10^3 cm^{-1} can be assigned to a positive lobe of the negative A term based on the $\Gamma_5(^3B_{1g})\leftarrow\Gamma_1(^1A_{1g})$ transition by analogy with $[PtCl_4]^{2-}$.[1] Then a negative B term is required for the $\Gamma_2(^1A_{2g})\leftarrow\Gamma_1(^1A_{1g})$ transition in order to reproduce the observed curve because the negative lobe of the negative A term for $\Gamma_5(^3B_{1g})\leftarrow\Gamma_1(^1A_{1g})$ is expected to be overlapping the band based on $\Gamma_2(^1A_{2g})\leftarrow\Gamma_1(^1A_{1g})$.

As for the CD spectrum of $[PtCl_2(S\text{-pn})]$, the shoul-

Table 3. Absorption data of [$PdCl_2L$] complexes

L=en	*N,N*-Me$_2$en	*N,N'*-Me$_2$en	*N,N*-Et$_2$en	tn	*N,N*-Me$_2$tn
		$\sigma_{max}/10^3$ cm^{-1}	(ε/mol^{-1} dm^3 cm^{-1})		
22.0 sh[a] (17)	22.0 sh (38)	22.1 sh (36)	21.8 sh (35)	22.5 sh (15)	21.7 sh (33)
26.93 (360)	26.31 (425)	26.52 (408)	26.18 (443)	27.59 (300)	26.38 (430)
39.5 sh (1670)	38.0 sh (2030)	38.3 sh (2080)	38.1 sh (2900)	39.3 sh (1860)	36.9 sh (1650)
45.3 sh (11400)	42.6 sh (13200)				
48.97 (19400)	45.34 (20900)	45.50 (21100)	44.80 (18100)	45.81 (20200)	43.40 (20900)

a) sh: shoulder (ε is for the value of σ given).

Table 4. MCD data of [$PdCl_2L$] complexes

L=en	*N,N*-Me$_2$en	*N,N'*-Me$_2$en	*N,N*-Et$_2$en	tn	*N,N*-Me$_2$tn
		$\sigma_{ext}/10^3$ cm^{-1}	($\Delta\varepsilon_M$/mol^{-1} dm^3 cm^{-1} T^{-1})		
25.8 (+0.022)	25.3 (+0.018)	25.4 (+0.019)	25.1 (+0.016)	26.1 (+0.027)	25.1 (+0.027)
29.1 (−0.023)	28.7 (−0.020)	28.9 (−0.023)	28.3 (−0.021)	29.4 (−0.020)	28.3 (−0.020)
39.3 (+0.36)	37.8 (+0.44)	38.0 (+0.45)	37.6 (+0.45)	39 sh[a] (+0.4)	36.9 (+0.40)
				43.2 (+1.7)	40.7 (+0.88)
47.2 (−0.67)	44.5 (−0.57)	44.5 (−0.59)	44.2 (−0.55)	47.6 (−2.4)	45.0 (−1.5)

a) sh: shoulder.

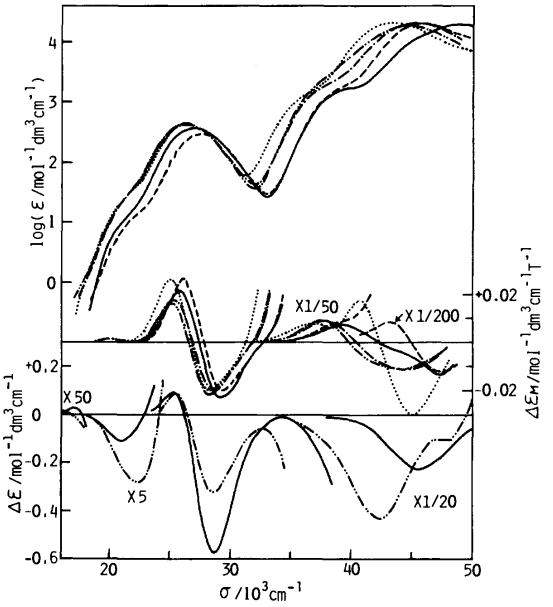

Fig. 3. Absorption, MCD, and CD spectra of [$PdCl_2L$] in 0.20 M KCl. For absorption and MCD spectra, ——: L=en, ----: L=tn, —·—: L=*N,N*-Me$_2$en, —··—: L=*N,N*-Et$_2$en, and ·····: L=*N,N*-Me$_2$tn; and for CD spectra, ——: L=*S*-pn and —··—: L=*N*^{1},*N*^{1}-Et$_2$-(*S*)-pn.

Table 5. CD data of [$PdCl_2L$] complexes

L=*S*-pn		L=*N*^{1},*N*^{1}-Et$_2$-(*S*)-pn	
σ_{ext} / 10^3 cm^{-1}	$\Delta\varepsilon$ / mol^{-1} dm^3 cm^{-1}	σ_{ext} / 10^3 cm^{-1}	$\Delta\varepsilon$ / mol^{-1} dm^3 cm^{-1}
17.2	+0.0006		
21.2	−0.022	22.4	−0.056
25.4	+0.093	25.4	+0.091
28.8	−0.58	28.6	−0.32
45.7	−4.5	42.3	−8.6
		47.6	−2.1

der around 33×10^3 cm^{-1} and the main band at 36.7×10^3 cm^{-1} were assigned to $\Gamma_2(^1A_{2g})$ and $\Gamma_5(^1E_g)\leftarrow\Gamma_1(^1A_{1g})$, respectively, by Ito *et al.*[13] However, the latter band lies in somewhat higher energy than the $\Gamma_5(^1E_g)\leftarrow\Gamma_1(^1A_{1g})$ component obtained by the Gaussian analysis of the absorption spectrum. This fact can be rationalized by considering that the $\Gamma_3(^1B_{1g})\leftarrow\Gamma_1(^1A_{1g})$ ($d_{x^2-y^2}\leftarrow d_{z^2}$) transition at 38.9×10^3 cm^{-1} is exhibiting a weak negative CD band,[14] which is due to the magnetic moment aquired through the reduction of symmetry (C_{2v} from D_{4h}). This will be demonstrated in the case of [$PdCl_2$(*S*-pn)] (*vide infra*).

2) [PdCl$_2$(en or S-pn)] Complex: The absorption, MCD, and CD data are given in Fig. 3 and Tables 3—5 together with those of the related complexes, and discussed on the basis of the results for [$PtCl_2$(en or *S*-pn)] described above. The spin-allowed d-d band exhibits a swelling in the higher energy side, which corresponds to the shoulder observed at *ca.* 37.5×10^3 cm^{-1} in [$PtCl_2$(en)]. The relative position of the zero point of the apparent A term (*ca.* 27.4×10^3 cm^{-1}) to the main CD band is also the same as that in [$PtCl_2$(en)]. On the basis of this resemblance, the Gaussian analysis of the absorption spectrum of [$PdCl_2$(en)] was carried out (Table 6). Three spin-allowed d-d components are assigned to $^1A_{2g}$, ^1E_g, and $^1B_{1g}\leftarrow{}^1A_{1g}$ from lower energy, which for convenience we denote bands I, II, and III, respectively (Table 6).

Although the MCD spectrum shows a nearly ideal A-term pattern, or dispersion, in the spin-allowed d-d region, the dispersion band is difficult to attribute only to the $^1E_g\leftarrow{}^1A_{1g}$ transition. A positive B term based on the $^1B_{1g}\leftarrow{}^1A_{1g}$ transition is expected to be included in the negative lobe of the dis-

TABLE 6. GAUSSIAN-ANALYSIS DATA FOR THE ABSORPTION CURVES OF $[PdCl_2L]$ COMPLEXES

No.[a]	σ_{max} / 10^3 cm^{-1}	ε / mol^{-1} dm^3 cm^{-1}	$\Delta\sigma_{1/2}$ / 10^3 cm^{-1}	S[b]	σ_{max} / 10^3 cm^{-1}	ε / mol^{-1} dm^3 cm^{-1}	$\Delta\sigma_{1/2}$ / 10^3 cm^{-1}	S
		L=en				L=tn		
	22.0 f[c]	14 f	3.48	51.9	22.5 f	13.5 f	3.50	50.3
I	26.16	270	3.35	963	26.71	195	3.26	676
II	28.07	179	3.07	584	28.32	156	3.02	500
III	30.08	72.8	3.13	243	30.27	69.5	3.13	232
	39.5 f	1600 f	4.70 f		39.3 f	1700 f	4.40 f	
		SD[d]=0.46				SD=0.31		
		L=*N*,*N*-Me$_2$en				L=*N*,*N*-Me$_2$tn		
	22.0 f	27.5 f	3.27	95.3	21.7 f	28.5 f	3.32	101
I	25.55	298	3.23	1023	25.51	268	3.18	908
II	27.30	215	3.10	711	27.05	228	2.99	725
III	29.32	85.4	3.16	288	28.98	98.0	3.08	321
	38.0 f	1900 f	4.30 f		36.9 f	1500 f	4.40 f	
		SD=0.65				SD=0.64		

a) Band number. b) S(band area)$=1.0645\times(\varepsilon_{max}/\text{mol}^{-1}\,\text{dm}^3\,\text{cm}^{-1})\times(\Delta\sigma_{1/2}/10^3\,\text{cm}^{-1})$. c) f: fixed value. d) Standard deviation (See Experimental).

TABLE 7. GAUSSIAN-ANALYSIS DATA FOR THE CD CURVE OF $[PdCl_2(S\text{-pn})]$

No.[b]	3 components[a]			2 components[a]		
	σ_{ext} / 10^3 cm^{-1}	$\Delta\varepsilon$ / mol^{-1} dm^3 cm^{-1}	$\Delta\sigma_{1/2}$ / 10^3 cm^{-1}	σ_{ext} / 10^3 cm^{-1}	$\Delta\varepsilon$ / mol^{-1} dm^3 cm^{-1}	$\Delta\sigma_{1/2}$ / 10^3 cm^{-1}
	21.2 f[c]	−0.023 f	2.99	21.2 f	−0.023 f	3.00 f
I	25.98	+0.153	2.72	26.05	+0.205	2.66
II	28.42	−0.488	3.17	28.72	−0.583	3.89
III	30.18	−0.183	3.29			
		SD[d]$=2.3\times10^{-3}$			SD$=4.1\times10^{-3}$	

a) See text. b) Band number. c) f: fixed value. d) Standard deviation.

persion by analogy with $[PtCl_4]^{2-}$ and $[PdCl_4]^{2-}$.[1] Moreover, a positive B term in addition to a negative A term is assigned to $^1E_g\leftarrow{}^1A_{1g}$ because the dispersion changes sign at lower energy than the corresponding absorption component (band II) obtained by Gaussian analysis; the situation resembles that in $[PtCl_2(en)]$. A negative B term is consequently predicted for band I in order to reproduce the observed MCD curve. The prediction is parallel with that made on a different basis in the case of $[PtCl_2(en)]$. As the MCD spectra of *cis*-$[M(Cl)_2(N)_2]$-type complexes (M=Pt and Pd) are of a poor precision because of low solubility of the complexes, their Gaussian analyses were not performed. However, it was found that the MCD as well as the absorption spectra of $[PtCl_2(en)]$ and $[PdCl_2(en)]$ nicely corresponded to each other.

The CD spectrum of $[PdCl_2(S\text{-pn})]$ was analyzed by assuming two or three components in the spin-allowed d-d region (Table 7.) The component corresponding to the $^1B_{1g}\leftarrow{}^1A_{1g}$ transition (which is magnetic dipole forbidden in a D_{4h} symmetry) is neglected in the former case, where the half-value width of the negative band became rather wide relative to that of the positive band. The two-component case is further inferior to the three-component one with respect to coincidence between the positions of the CD and absorption components for band II and to standard deviation. Thus, it seems reasonable to assign a weak negative CD band to the $^1B_{1g}\leftarrow{}^1A_{1g}$ transition, as expected in the case of $[PtCl_2(S\text{-pn})]$.

TABLE 8. BAND SHAPE PARAMETERS FOR THE SPIN-ALLOWED d-d BAND OF $[PdCl_2L]$ COMPLEXES

L	$\Delta\sigma^-$[a] / 10^3 cm^{-1}	$\Delta\sigma^+$[a] / 10^3 cm^{-1}	$\Delta\sigma_{1/2}$[a] / 10^3 cm^{-1}	Unsymmetry parameter[b]
en	2.14	2.61	4.75	9.9
N,*N*-Me$_2$en	2.04	2.46	4.51	9.3
N,*N*'-Me$_2$en	2.11	2.56	4.67	9.6
N,*N*-Et$_2$en	2.07	2.47	4.54	8.8
tn	2.07	2.36	4.43	6.5
N,*N*-Me$_2$tn	2.01	2.28	4.30	6.3
cf. $K_2[PdCl_4]$	1.68	2.44	4.12	18.4

a) See text; these parameters are obtained from the observed intact absorption curve, not by Gaussian analysis.[15] b) See text.

3) Other cis-*[Pd(Cl)$_2$(N)$_2$]-type Complexes*: It is concluded that these complexes possess the same elec-

tronic structure with regard to metal d orbitals as [PdCl$_2$(en)] from the similarity of their absorption, MCD, and CD spectra. The spin-allowed d-d absorption bands are similarly unsymmetrical. We characterize the band shape by half-value width parameters[15] $\Delta\sigma^-$, $\Delta\sigma^+$, and $\Delta\sigma_{1/2}$ ($\varepsilon=\varepsilon_{max}/2$ at $\sigma=\sigma_{max}-\Delta\sigma^-$ and $\sigma_{max}+\Delta\sigma^+$; and $\Delta\sigma_{1/2}=\Delta\sigma^-+\Delta\sigma^+$) and unsymmetry parameter, $(\Delta\sigma^+-\Delta\sigma^-/\Delta\sigma_{1/2})\times100$. The parameters for the *cis*-[Pd(Cl)$_2$(N)$_2$]-type complexes are given in Table 8, which leads to the following findings. (1) $\Delta\sigma^+$ is larger than $\Delta\sigma^-$ for all the complexes. The bands of the complexes with a five-membered chelate ring are (2) more highly unsymmetrical and (3) wider than those of the complexes with a six-membered chelate ring. (4) An introduction of alkyl groups on amine nitrogen atom(s) makes the band widths smaller; this is more pronounced with tertiary amine than with secondary amine. It is interesting to interprete the findings in terms of the results of Gaussian analysis for the absorption spectra. Findings (1) and (2) can be explained primarily by the relative position of band II. The band II's of the en, *N*,*N*-Me$_2$en, tn, and *N*,*N*-Me$_2$tn complexes lie at energies higher than the observed absorption peaks by 1.14, 0.99, 0.77, and 0.67×10^3 cm^{-1}, respectively. The unsymmetry parameters decrease in this order. Findings (3) and (4) are attributable to a variation in the energy difference between the three bands, particularly between bands I and II. Accordingly, the transition energy of band I ($^1A_{2g}\leftarrow{}^1A_{1g}$) is affected by the variation of ligands in a different fashion from those of the other two bands (*i.e.* ^1E_g and $^1B_{1g}\leftarrow{}^1A_{1g}$). This result is compatible with the assignment of band I to an electronic transition in the coordination plane.

The MCD spectra in the d-d transition region are similar to one another and shifted together with the absorption spectra by the variation of ligands, which suggests that all the complexes possess a common electronic structure. A detailed examination of the MCD spectra shows that the intensity ratio of the positive to the negative lobe of the dispersion gives its larger absolute value for the complexes with a six-membered chelate ring than for those with a five-membered one.

The CD pattern of [PdCl$_2$(*N*^{1},*N*^{1}-Et$_2$-(*S*)-pn)] is similar to that of [PdCl$_2$(*S*-pn)] (Fig. 3). The negative band in the spin-forbidden d-d region becomes intense as compared with [PdCl$_2$ (*S*-pn)], whereas the main negative band in the spin-allowed d-d

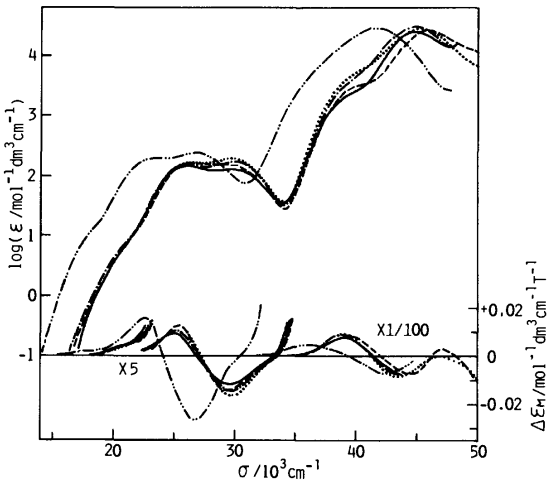

Fig. 5. Absorption and MCD spectra of *trans*-[PdCl$_2$L$_2$]. ——: L=EtNH$_2$ in DCE, ----: L=EtNH$_2$ in methanol, —·—: L=Me$_2$NH in DCE, ·····: L=Me$_2$NH in methanol, and —··—: L=Me$_3$N in DCE.

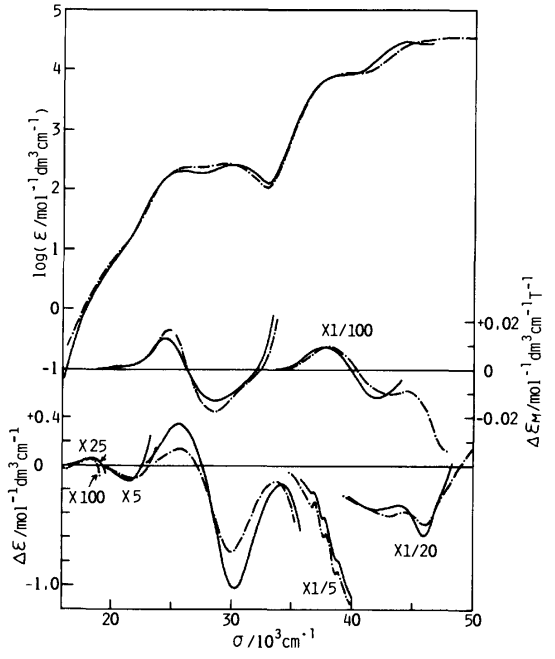

Fig. 4. Absorption and MCD spectra of *trans*-[PdCl$_2$ (*rac*-pea)$_2$], and CD spectra of *trans*-[PdCl$_2$(*S*-pea)$_2$]. ——: in DCE and —·—: in methanol.

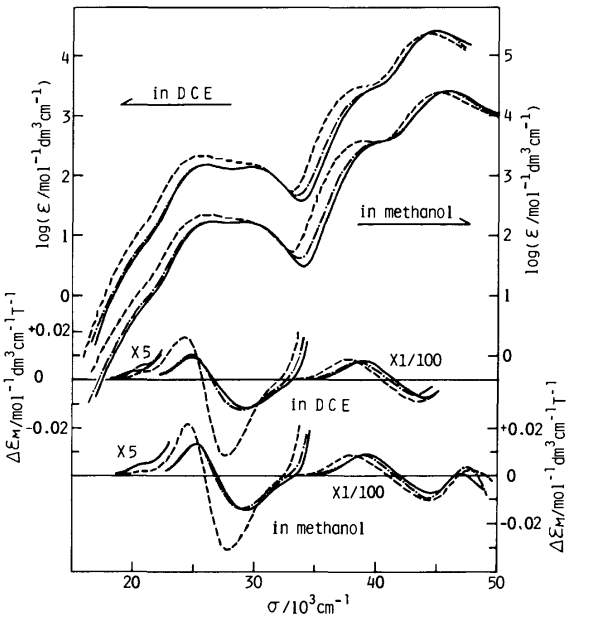

Fig. 6. Absorption and MCD spectra of *trans*-[PdCl$_2$L$_2$] in DCE and methanol. ——: L=*n*-BuNH$_2$, —·—: L=*s*-BuNH$_2$, and ----: L=*t*-BuNH$_2$.

TABLE 9. ABSORPTION, MCD, AND CD DATA OF *trans*-$[PdCl_2(pea)_2]$[a)]

Absorption		MCD		CD		Absorption		MCD		CD	
σ_{max} / 10^3 cm^{-1}	ε / mol^{-1} dm^3 cm^{-1}	σ_{ext} / 10^3 cm^{-1}	$\Delta\varepsilon_M$ / mol^{-1} dm^3 cm^{-1} T^{-1}	σ_{ext} / 10^3 cm^{-1}	$\Delta\varepsilon$ / mol^{-1} dm^3 cm^{-1}	σ_{max} / 10^3 cm^{-1}	ε / mol^{-1} dm^3 cm^{-1}	σ_{ext} / 10^3 cm^{-1}	$\Delta\varepsilon_M$ / mol^{-1} dm^3 cm^{-1} T^{-1}	σ_{ext} / 10^3 cm^{-1}	$\Delta\varepsilon$ / mol^{-1} dm^3 cm^{-1}
		in DCE						in methanol			
										16.4	−0.0004
				18.5	+0.0026					18.4	+0.0005
21.3 sh[b)]	13	21.5 sh	+0.0020	21.6	−0.025	21.2 sh	13	21 sh	+0.0017	21.9	−0.023
		24.5	+0.013					24.8	+0.017		
25.81	200			25.7	+0.34	26.53	236			25.8	+0.14
		28.6	−0.013					28.6	−0.018		
30.08	255			30.3	−1.02	29.44	264			30.1	−0.72
				36.6	−1.1					36.7	−1.7
		37.6	+1.0	37.5	−2.2			38.0	+1.0	37.7	−3.0
39 sh	8200			38.7 sh	−3.9					38.6	−4.5
				39.5 sh	−5.0	39.5	8900			39.6 sh	−5.5
		42.0	−1.2	42.0	−7.3			43.2	−1.0	43.0	−8.4
44.35	28200					45.2 sh	29000				
				45.8	−11.7					46.0	−9.9
						48.26	35700				

a) Absorption and MCD data are for *rac*-pea complex, and CD ones for *S*-pea complex. b) sh: shoulder (ε, $\Delta\varepsilon_M$, or $\Delta\varepsilon$ is for the value of σ given).

TABLE 10. ABSORPTION DATA OF *trans*-$[PdCl_2L_2]$ COMPLEXES

L=$EtNH_2$	Me_2NH	Me_3N	*n*-$BuNH_2$	*i*-$BuNH_2$	*s*-$BuNH_2$	*t*-$BuNH_2$
		σ_{max}/10^3 cm^{-1} (ε/mol^{-1} dm^3 cm^{-1})				
			in DCE			
21.5 sh[a)] (9.6)	21.4 sh (9.4)	19.0 sh (18)	21.5 sh (10)	21.5 sh (10)	21.3 sh (10)	21.1 sh (17)
25.90 (147)	26.01 (155)	23.72 (202)	25.97 (152)	25.94 (155)	25.87 (155)	25.53 (215)
29.74 (128)	29.85 (175)	26.82 (240)	29.85 (138)	29.75 (144)	29.71 (137)	29.6 sh (156)
39.8 sh (2500)	39.5 sh (3900)	36.7 sh (6300)	39.8 sh (2900)	39.8 sh (2900)	39.4 sh (2700)	38.6 sh (3000)
44.80 (24300)	44.78 (30200)	41.67 (28000)	44.86 (25800)	44.8 (25200)	44.9 (25300)	44.33 (23000)
			in methanol			
21.5 sh (9.2)	21.3 sh (9.0)		21.5 sh (9.7)	21.5 sh (9.5)	21.2 sh (9.5)	21.1 sh (16)
26.56 (163)	26.49 (171)		26.67 (173)	26.64 (171)	26.40 (174)	26.04 (225)
29.2 (158)	29.63 (196)	b)	28.99 (168)	29.04 (170)	29.03 (166)	29.4 sh (177)
40.1 sh (3200)	39.7 sh (5100)		40.1 sh (3600)	40.1 sh (3700)	39.8 sh (3700)	38.94 (3680)
45.85 (26200)	45.27 (28300)		45.79 (26400)	45.8 (26500)	45.7 (26400)	45.21 (24300)

a) sh: shoulder (ε is for the value of σ given). b) Decomposition.

Table 11. MCD data of *trans*-[$PdCl_2L_2$] complexes

L=$EtNH_2$	Me_2NH	Me_3N	*n*-$BuNH_2$	*i*-$BuNH_2$	*s*-$BuNH_2$	*t*-$BuNH_2$
		$\sigma_{ext}/10^3$ cm^{-1} ($\Delta\varepsilon_M$/mol^{-1} dm^3 cm^{-1} T^{-1})				
			in DCE			
21 sh[a] (+0.001)	21 sh (+0.001)	18 sh (+0.002)	20.5 sh (+0.0007)	21 sh (+0.0012)	21 sh (+0.0013)	21 sh (+0.0031)
25.1 (+0.0094)	25.2 (+0.011)	22.5 (+0.016)	24.9 (+0.0095)	24.8 (+0.010)	24.9 (+0.011)	24.2 (+0.018)
29.7 (−0.012)	29.7 (−0.014)	26.7 (−0.027)	29.4 (−0.012)	29.3 (−0.011)	29.0 (−0.012)	27.7 (−0.032)
39.1 (+0.8)	38.8 (+0.9)	36.0 (+0.5)	39.0 (+0.8)	38.9 (+0.8)	38.5 (+0.8)	37.7 (+0.9)
		42.3 (−0.7)	43.9 (−0.7)		43.3 (−0.6)	43.6 (−0.9)
			in methanol			
21.5 sh(+0.001)	21 sh (+0.001)		21 sh (+0.001)	21 sh (+0.0010)	21 sh (+0.0010)	21 sh (+0.0019)
25.4 (+0.013)	25.4 (+0.013)		25.3 (+0.013)	25.2 (+0.013)	25.2 (+0.013)	24.5 (+0.022)
29.4 (−0.014)	29.8 (−0.016)	b)	29.4 (−0.014)	29.1 (−0.014)	28.9 (−0.014)	27.8 (−0.031)
39.4 (+0.8)	39.0 (+1.0)		39.3 (+0.9)	39.3 (+0.9)	39.0 (+0.9)	38.0 (+0.9)
44.6 (−0.7)	43.4 (−0.9)		44.5 (−0.7)	44.1 (−0.9)	44.2 (−0.9)	44.4 (−1.0)
47.0 (+0.3)					47.4 (+0.4)	47.7 (+0.2)

a) sh: shoulder ($\Delta\varepsilon_M$ is for the value of σ given). b) Decomposition.

Table 12. Gaussian-analysis data for the spectra of *trans*-[$PdCl_2(pea)_2$]

No.[a]	Absorption			S[b]	MCD			CD		
	σ_{max} / 10^3 cm^{-1}	ε / mol^{-1} dm^3 cm^{-1}	$\Delta\sigma_{1/2}$ / 10^3 cm^{-1}		σ_{ext} / 10^3 cm^{-1}	$\Delta\varepsilon_M$ / mol^{-1} dm^3 cm^{-1} T^{-1}	$\Delta\sigma_{1/2}$ / 10^3 cm^{-1}	σ_{ext} / 10^3 cm^{-1}	$\Delta\varepsilon$ / mol^{-1} dm^3 cm^{-1}	$\Delta\sigma_{1/2}$ / 10^3 cm^{-1}
	21.3 f[c]	10 f	3.16	33.6	21.5 f	+0.0017 f	2.38	21.8 f	−0.028 f	2.80
1	24.70	101	3.08	331	24.69	+0.0145	2.89	24.74	+0.145	2.31
2	26.53	142	3.49	526	26.44	−0.0024	3.15	26.18	+0.280	2.77
3	29.21	110	3.11	363	28.56	−0.0115	3.62	29.67	−0.170	2.23
4	30.95	187	3.55	706	30.68	−0.0029	3.26	30.55	−0.896	3.53
	38.3 f	7600 f	4.00 f		37.6 f	+0.97 f	4.00 f			
		SD[d] = 0.54				SD = 0.00011			SD = 0.0036	

a—d) As in Table 6.

region weak. This observation can be explained by considering that the spin-forbidden transition takes its intensity from the spin-allowed transition through an increased spin-orbit coupling and that substancial cancellation occurs between bands I and II which have a CD sign opposite to each other.

4) trans-[Pd(Cl)$_2$(N)$_2$]-type Complexes: The absorption, MCD, and CD data are given in Figs. 4—6 and Tables 9—11. Since absorption spectra in DCE show a more distinct splitting in the d-d transition region than those in methanol, the data in DCE will be primarily used in the following discussion on the d-d transitions. At first, we will examine *trans*-[PdCl$_2$(*rac*- or *S*-pea)$_2$] complex, for which all the

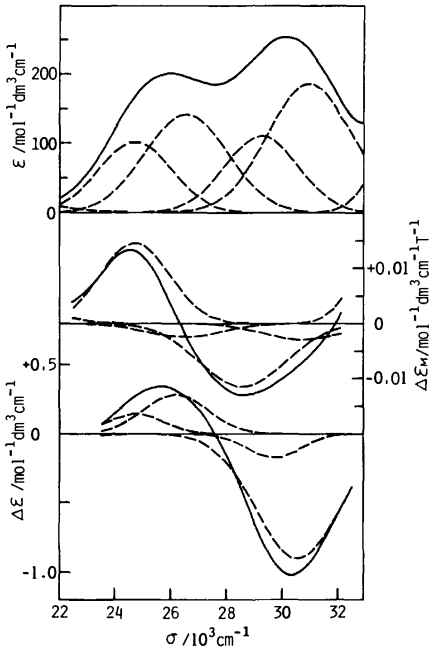

Fig. 7. Gaussian analysis curves for three spectra of *trans*-[PdCl$_2$(pea)$_2$] in DCE. ----: Gaussian components and ——: sum of them.

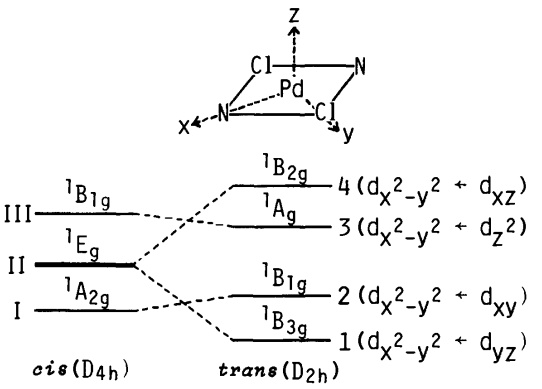

Fig. 8. The orderings of the singlet excited states arising from d-d transitions for *cis*- and *trans*-[Pd(Cl)$_2$(N)$_2$]-type complexes (on the basis of holohedrized symmetry) and the relation between them. I—III and 1—4 represent component band numbers of the cis and trans complexes, respectively (See also Tables 6, 12, and 13).

three kinds of spectra are available. The MCD and the CD spectrum each exhibit a positive and a negative band in the spin-allowed d-d region, and the positions of these four (two MCD and two CD) bands are different from one another. It is sufficient to take into account only B terms for an interpretation of the MCD because the complex has no degenerate excited state. Therefore, it is reasonable to consider that the four bands approximately correspond one by one to the four spin-allowed d-d transitions. On the basis of this consideration, the Gaussian analyses of the three spectra were carried out (Fig. 7 and Table 12). We denote the four components bands 1, 2, 3, and 4 from lower energy (Table 12). The assignment of the bands will be made in the following paragraph.

The Gaussian analyses of absorption spectra for the other trans complexes were performed by analogy with the case of the pea complex (Table 13). In assigning the spectra of the trans complexes, it is helpful to compare them with those of the cis analogs. It is *trans*-[PdCl$_2$(EtNH$_2$)$_2$] that is most suited for a comparison with [PdCl$_2$(en or tn)]. The transition energies for bands 2 and 3 of *trans*-[PdCl$_2$(EtNH$_2$)$_2$] are close to those for bands I and III of [PdCl$_2$(en or tn)], respectively, and the average energy of bands 1 and 4 of the trans complex to the energy of band II of the cis complex (Tables 6 and 13). From these facts, bands 1, 2, 3, and 4 can be assigned to $^1B_{3g}$, $^1B_{1g}$, ^1A_g, and $^1B_{2g}$←^1A_g transitions ($d_{x^2-y^2}$←d_{yz}, d_{xy}, d_{z^2}, and d_{xz}), respectively. The assignment is summarized in Fig. 8, together with that for the corresponding cis complex; the Cartesian coordinate axes are also shown. Figures 7 and 8 visuallize how the four spin-allowed d-d bands overlap to look like two bands in *trans*-[Pd(Cl)$_2$(N)$_2$]-type complexes.

The band area (or oscillator strength) of bands 3 and 4 increased with an introduction of alkyl groups on the nitrogen atoms (Fig. 5 and Table 13). The pronounced effect was found with the band 4 of *trans*-[PdCl$_2$(*rac*-pea)$_2$] complex, which exhibited a strong absorption based on pea ligands in the near-UV region (Table 12). On the other hand, the area of band 1 is hardly affected by the variation of ligands (Table 13). These results support the above assignment where bands 4 and 1 are attributed to transitions from the d_{xz} and d_{yz} orbitals, respectively, which lie in the planes containing only *N*-ligands and only chloro ligands, respectively. In the *S*-pea complex, the CD for band 4 is intense, whereas for bands 1 and 3 weak (Fig. 7). That is to say, high CD intensity is observed for the transition from the d_{xz} orbital lying in the plane containing only optically active ligands, and low for the transition from the d_{yz} orbital lying in the plane containing only optically inactive ligands (Cl) as well as for the transition magnetic dipole-forbidden. This description suggests a certain relation connecting vicinal CD and its intensity with electronic structure.

The replacement of EtNH$_2$ ligand by *n*-BuNH$_2$ caused scarcely any change in the position and intensity of every absorption component. On the other hand, the replacement by *t*-BuNH$_2$ caused shifts

to lower energies by *ca.* 1×10^3 cm^{-1} for bands 1, 2, and 4, and by *ca.* 2×10^3 cm^{-1} for band 3; in addition, the intensities of bands 3 and 4 were increased remarkably (Table 13). The anomalous behavior of band 3 was also observed in the MCD spectra (Fig. 6), and can be explained by considering that a repulsive interaction between the bulky *t*-butyl groups and the d_{z^2} electrons raised the energy of the d_{z^2} orbital. The energy shift caused by the repulsion is only 1×10^3 cm^{-1}, and the remaining shift by 1×10^3 cm^{-1} is attributed to the relative lowering of the $d_{x^2-y^2}$ orbital because this should lower all the d-d transition energies equally. The latter shift was also observed in the Me_3N complex (red shift of *ca.* 3×10^3 cm^{-1} relative to the $EtNH_2$ complex; Fig. 5 and Table 13).

It will be instructive to examine the energy separation of bands 1 and 4 in predicting the splitting for the other trans type complexes. We have empirically found that the transition energy of $^1E_g\leftarrow{}^1A_{1g}$ (D_{4h} approximation) for $[Pd(Cl)_n(N)_{4-n}]$- and $[Pd(N)_n(O)_{4-n}]$-type complexes is approximately given by $\sum_{i=1}^{4} e_i$, where e_i is an energy fraction assigned to each ligand. Because the average energy of $d_{x^2-y^2}\leftarrow d_{xz}$ and d_{yz} transitions for *trans*-$[Pd(Cl)_2(N)_2]$-type complexes is approximately equal to the transition energy of $d_{x^2-y^2}\leftarrow d_{xz,\,yz}$ for the cis analogs as described above, the empirical rule may be extended as follows: the average energy of $d_{x^2-y^2}\leftarrow d_{xz}$ and d_{yz} transitions for $[Pd(L_1)(L_2)(L_3)(L_4)]$ is approximately given by $\sum_{i=1}^{4} e_i$ ($\equiv E_{av}$). The typical values of e_i for chloro and amine ligands are 5.5 and 8.6×10^3 cm^{-1}, respectively. The former value was obtained from the transition energy of $^1E_g\leftarrow{}^1A_{1g}$ for $[PdCl_4]^{2-}$,[1] and the latter by averaging those for $[Pd(NH_3)_4]^{2+}$, $[Pd(en)_2]^{2+}$, and $[Pd(tn)_2]^{2+}$.[16] Using these values, E_{av} for $[Pd(Cl)_2(N)_2]$ can be calculated to be 28.2×10^3 cm^{-1}. The values obtained by Gaussian analyses are 28.07 and 28.32×10^3 cm^{-1} for band II's of $[PdCl_2(en)]$ and $[PdCl_2(tn)]$, respectively, and 28.10×10^3 cm^{-1} for the average energy of bands 1 and 4 of *trans*-$[PdCl_2(EtNH_2)_2]$. Thus, the empirical rule holds well for the complexes. The separation between bands 1 and 4 is about 6.2×10^3 cm^{-1} for all the *trans*-$[Pd(Cl)_2(N)_2]$-type complexes (Table 13). This value amounts to just twice as large as the difference between e_i's of chloro and amine ligands. Consequently, bands 1 and 4 possess the transition energies equal to E_{av}'s of $[Pd(Cl)_3(N)]$ and $[Pd(Cl)(N)_3]$ chromophores, respectively. The calculated values of E_{av} for the former and the latter type complexes are 25.1 and 31.3×10^3 cm^{-1}, which satisfactorily agree with the positions of the Gaussian components of the *trans*-$[Pd(Cl)_2(N)_2]$-type complexes except the Me_3N and *t*-$BuNH_2$ complexes (Table 13). The exceptions cannot be ascribed to the lowered ligand-field strength of only the amine ligands; because, if so, the splitting between bands 1 and 4 would be smaller. It must be considered that the ligand-field strength of the chloro ligand is simultaneously lowered in the two complexes.

MCD spectra in the d-d transition region are more intense in methanol than in DCE for all the trans complexes studied here (Figs. 4—6; Tables 9 and

Table 13. Gaussian-analysis data for the absorption curves of *trans*-$[PdCl_2L_2]$ complexes in DCE

No.[a]	σ_{max} / 10^3 cm^{-1}	ε / mol^{-1} dm^3 cm^{-1}	$\Delta\sigma_{1/2}$ / 10^3 cm^{-1}	S[b]	σ_{max} / 10^3 cm^{-1}	ε / mol^{-1} dm^3 cm^{-1}	$\Delta\sigma_{1/2}$ / 10^3 cm^{-1}	S	σ_{max} / 10^3 cm^{-1}	ε / mol^{-1} dm^3 cm^{-1}	$\Delta\sigma_{1/2}$ / 10^3 cm^{-1}	S
	L=$EtNH_2$				L=Me_2NH				L=Me_3N			
	21.5 f[c]	7.0 f	3.03	22.6	21.4 f	7.3 f	3.00	23.3	19.0 f	13 f	3.08	42.6
1	24.97	82.6	3.12	275	24.96	86.2	3.11	286	21.99	104	2.95	326
2	26.78	94.4	3.51	353	26.79	103	3.42	374	23.83	136	3.12	450
3	29.51	68.5	3.27	238	29.46	100	3.02	322	26.47	133	3.36	475
4	31.22	70.4	3.87	290	31.13	97.8	3.55	369	28.08	130	4.16	573
	39.8 f	2200 f	4.30 f		39.6 f	3500 f	4.00 f		36.7 f	4100 f	4.10 f	
		SD[d]=0.28				SD=0.38				SD=0.64		
		L=*n*-$BuNH_2$				L=*n*-$BuNH_2$[e]				L=*t*-$BuNH_2$		
	21.5 f	7.0 f	3.10	23.1	21.5 f	7.7 f	3.20	26.2	21.1 f	13.5 f	2.99	43.0
1	24.99	86.1	3.18	292	25.24	85.9	3.22	294	24.07	105	2.83	315
2	26.79	96.3	3.53	362	26.94	109	3.41	395	25.67	124	2.93	387
3	29.48	73.6	3.21	251	29.31	85.0	3.16	286	27.53	107	3.33	379
4	31.18	77.0	3.82	313	30.93	86.5	3.93	362	30.23	127	3.90	525
	39.8 f	2600 f	4.20 f		40.1 f	3300 f	4.10 f		38.6 f	3000 f	4.40 f	
		SD=0.29				SD=0.38				SD=0.54		

a—d) As in Table 6. e) In methanol.

11). On the contrary, the CD spectrum of the *S*-pea complex is less intense in methanol. The Gaussian-analysis result of absorption spectra for the *n*-$BuNH_2$ complex indicates that the energy separations between four d-d components are reduced in methanol in comparison with those in DCE (Table 13). Therefore, the CD spectrum in methanol is partly explained by a cancellation between the positive and the negative band; whereas the MCD spectrum by a larger mixing between the d-d vibronic excited states in which $^1B_{3g}$ and ^1A_g are involved, because the magnitude of a contribution to a B term is inversely proportional to the energy difference between the states which are mixed. The overlapping B terms may be considered to form a pseudo A term.[18] The separation of bands 1 and 4 for the *n*-$BuNH_2$ complex is smaller by 0.5×10^3 cm^{-1} in methanol than in DCE, indicating that the difference between the ligand-field strengths of chloro and amine ligands decreases in methanol. This is conceivably ascribed to the relative weakening of the ligand-field strength of the amine ligand by hydrogen bondings with methanol, which is more polar than DCE.

High-intensity Bands. The high-intensity bands observed above 35×10^3 cm^{-1} of *cis*- and *trans*-$[Pd(Cl)_2(N)_2]$-type complexes are attributable to dipole allowed charge transfer transitions from their intensities, and moreover to ones with ligand-to-metal nature (LMCT) because the bands of the trans complexes are blue-shifted with replacing DCE solvent by methanol. There are three kinds of LMCT to be considered here: Pd(σ^*)←Cl(π), Cl(σ), and N(σ).

The shoulder located in $(35—40)\times10^3$ cm^{-1} for the cis complexes is assigned to Pd(σ^*)←Cl(π) transition, to which a negative B term corresponds. In $[PdCl_2(en)]$, another shoulder is observed at *ca.* 45.3×10^3 as well as the peak at 49.0×10^3 cm^{-1} (Fig. 3). The corresponding shoulder is barely appreciable in the *N,N*-Me$_2$en complex, but undetectable in the *N,N'*-Me$_2$en and *N,N*Et$_2$en complexes owing to the overlapping of the neighboring intense band. Their MCD spectra show a broad negative band above 40×10^3 cm^{-1}, supporting the presence of more than one component. Although the CD spectrum of the *S*-pn complex exhibits only a negative CD band corresponding to the absorption shoulder, that of the N^1,N^1-Et$_2$-(*S*)-pn complex shows an additional minor negative band in the higher energy side of the main band. Figure 9 shows the absorption spectra of $[PdCl_2(N,N'$-Me$_2$en$)]$ in 0.20 M KCl and in an aqueous solution. In the latter solution, the d-d absorption band is blue-shifted and the shoulder at *ca.* 38×10^3 cm^{-1} remarkably reduced. The observations are attributed to a significant degree of aquation of the complex, being consistent with the assignment of the shoulder to Pd(σ^*)←Cl(π). Since the band centered at 45.5×10^3 cm^{-1} still retains a considerable intensity (ε_{max}=15000), it seems to contain a Pd(σ^*)←N(σ) as well as a Pd(σ^*)←Cl(σ) transition. Then, the lower and the higher absorption (or CD) component in the en (or N^1,N^1-Et$_2$-(*S*)-pn) complex are assigned to Pd(σ^*)←N(σ) and Cl(σ) transitions, respectively. This assignment is based on the expectation that the CT transition from the nitrogen atoms will exhibit more intense vicinal CD than that from the chlorine atoms since the nitrogen atoms lie more close to the asymmetric carbon atom of an N^1,N^1-Et$_2$-(*S*)-pn or *S*-pn ligand than the chlorine atoms. The assignment then suggests that the molecular orbitals comprising mainly Cl(σ) orbitals lie below those comprising mainly N(σ) ones. The situation is the reverse of that having been accepted generally. In any case no definitive experimental evidence seems available for the point.

The spectra of the complexes with a six-membered chelate ring are likewise assigned. The MCD of the tn and the *N,N*-Me$_2$tn complex show a negative A-term pattern around the absorption bands occurring at 45.8 and 43.4×10^3 cm^{-1}, respectively. The sign of the "A" terms is the same as for a Pd(σ^*)←N(σ) transition in $[Pd(N)_4]$-type complexes with one or two tn ligands[16] but the reverse of the sign of the A term for a Pd(σ^*)←Cl(σ) transition in $[PdCl_4]^{2-}$.[1] Thus, it is likely that the MCD of the tn or *N,N*-Me$_2$tn complex is contributed mainly from the former kind of transition.

The absorption bands above 35×10^3 cm^{-1} of the trans type complexes are assigned in comparison with those of the cis type complexes discussed above. The shoulder around $(39—40)\times10^3$ cm^{-1}, which shows a negative B term, is assigned to a Pd(σ^*)←Cl(π) transition; and the band centered at *ca.* 45×10^3 cm^{-1}, which shows a positive and a negative B term in methanol, is to a composite of Pd(σ^*)←Cl(σ) and N(σ).

The absorption, MCD, and CD spectra above 40×10^3 cm^{-1} in $[PtCl_2$(en or *S*-pn)$]$ are quite different from those of $[PdCl_2$(en or *S*-pn)$]$ in the corresponding region (Figs. 2 and 3). Thus, it is irrational to assign the absorption band at *ca.* 48.8×10^3 cm^{-1} to the same set of transitions as in $[PdCl_2(en)]$. As the band exhibits a positive A-term pattern in the MCD spectrum it may be attributed to a d-p transition (p_z←$d_{xz,yz}$), because the corresponding transition in $[PtCl_4]^{2-}$ gives an A term with the same sign.[1] More data need to be accumulated on complexes with different chromophores containing nitrogen and/or chlorine for a more detailed assignment of all the above high-intensity bands.

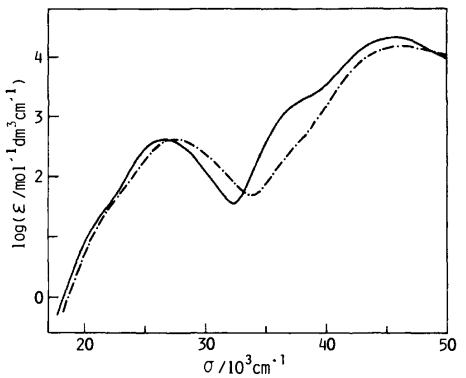

Fig. 9. Absorption spectra of $[PdCl_2(N,N'$-Me$_2$en$)]$ in 0.20 M KCl (——) and in H_2O (—·—).

References

1) K. Nakayama, T. Komorita, and Y. Shimura, *Bull. Chem. Soc. Jpn.*, **57**, 972 (1984).
2) B. Bosnich, *J. Chem. Soc., A*, **1966**, 1394.
3) T. Komorita, J. Hidaka, and Y. Shimura, *Bull. Chem. Soc. Jpn.*, **41**, 854 (1968); **44**, 3353 (1971).
4) H. Ito, J. Fujita, and K. Saito, *Bull. Chem. Soc. Jpn.*, **42**, 2863 (1969).
5) J. R. Doyle, P. E. Slade, and H. B. Jonassen, *Inorg. Synth.*, **6**, 218 (1960).
6) K. Nakayama, T. Komorita, and Y. Shimura, *Bull. Chem. Soc. Jpn.*, **54**, 1056 (1981).
7) L. F. Heneghan and J. C. Bailar, Jr., *J. Am. Chem. Soc.*, **75**, 1840 (1953).
8) In this paper, diamine chelate complexes have been investigated in place of *cis*-bis(monoamine) complexes because of fast isomerization of the latter complexes to the corresponding trans ones in solution.
9) E. A. Sullivan, *Can. J. Chem.*, **57**, 62 (1979).
10) K. Nakayama, T. Komorita, and Y. Shimura, unpublished work.
11) C. E. Schäffer and C. K. Jørgensen, *K. Dan. Vidensk., Mat. Fys. Medd.*, **34**, No. 13 (1965).
12) L. I. Elding and L. F. Olsson, *J. Phys. Chem.*, **82**, 69 (1978).
13) H. Ito, J. Fujita, and K. Saito, *Bull. Chem. Soc. Jpn.*, **40**, 2584 (1967).
14) Because the transition of interest correlates to a $\Gamma_3(^1B_{1g}) \leftarrow \Gamma_1(^1A_{1g})$ one (D_{4h}), which has no magnetic moment, the CD intensity is expected to be low.
15) C. K. Jørgensen, *Acta Chem. Scand.*, **8** 1495 (1954).
16) K. Nakayama, T. Komorita, and Y. Shimura, submitted for publication in *Bull. Chem. Soc. Jpn.*
17) P. N. Schatz and A. J. McCaffery, *Quart. Rev.*, **23**, 552 (1969).
18) S. B. Piepho, P. N. Schatz, and A. J. McCaffery, *J. Am. Chem. Soc.*, **91**, 5994 (1969).

Ion Exchange Studies of Zinc Chloride and/or Perchlorate in Ethylene Glycol

Tetsu KUMAGAI
Himeji Institute of Technology, Shosha, Himeji, Hyogo 671-22
(Received October 11, 1983)

The formation constants of zinc chloride and/or perchlorate in ethylene glycol were measured by a cation exchange method using the resin for forced-flow liquid chromatography in three systems: zinc chloride, zinc perchlorate, and zinc chloride and perchlorate together. The values obtained for the formation constants were: $\log \beta_1^{Cl}=3.03$, $\log \beta_2^{Cl}=4.80$, $\log \beta_1^{ClO_4}=2.34$, and $\log \beta_2^{ClO_4}=2.50$. The formation constant for the mixed complex of zinc, $\log k_m^{ClO_4}$, was 0.7 at the ionic strength of 0.1. The formation constants of zinc chloride in ethylene glycol containing 5 v/v% of water were 2.73 for $\log \beta_1^{Cl}$ and 4.18 for $\log \beta_2^{Cl}$, and those containing 10% of water were 2.32 for $\log \beta_1^{Cl}$ and 3.46 for $\log \beta_2^{Cl}$.

There are many methods to investigate the chemical equilibria of metal-ion complexes in aqueous solution, such as photometry, polarography, conductivity measurement, ion exchange method,[1-8] solvent extraction,[9-11] and potentiometric measurement.[12] However, the detailed studies in nonaqueous solution have been so far performed mainly by electrochemical methods. The cation exchange method using a radioactive tracer is expected to be available for studies of the chemical equilibria in nonaqueous systems. The method may be applicable to sparingly soluble compounds in nonaqueous solvents by the rise in specific activities of radio isotopes. The resins for the forced-flow liquid chromatography may withstand most of the organic solvents and attain equilibrium fairly rapidly with the ions in the solvents, compared with the ordinary ion exchangers. In the previous paper,[14] we investigated the distribution of zinc chloride and bromide complexes between the aqueous methanol solution and the cation exchange resin. The present work has extended the research to the distribution of zinc chloride and perchlorate between the cation exchange resin and ethylene glycol and has estimated the consecutive formation constants of zinc chloride and perchlorate by using a computer.

Data Treatment

The equilibria in the ethylene glycol solutions are expressed as follows:

$$Zn^{2+} + 2Cl^- = ZnCl_2 \qquad \beta_1^X,\ \beta_2^X, \qquad (1)$$

$$Zn^{2+} + 2ClO_4^- = Zn(ClO_4)_2 \qquad \beta_1^Y,\ \beta_2^Y, \qquad (2)$$

$$ZnCl^+ + ClO_4^- = ZnClClO_4 \qquad K_m^Y, \qquad (3)$$

$$ZnClO_4^+ + Cl^- = ZnClClO_4 \qquad K_m^X, \qquad (4)$$

$$Zn^{2+} + Na_2R = ZnR + 2Na^+ \qquad \beta_1^R,\ \beta_2^R, \qquad (5)$$

$$ZnCl^+ + Na_2R = ZnClNaR + Na^+ \qquad K_m^{RX}, \qquad (6)$$

$$ZnClO_4^+ + Na_2R = ZnClO_4NaR + Na^+ \qquad K_m^{RY}. \qquad (7)$$

Here the superscripts are X=Cl^- and Y=ClO_4^-. Concentrations of zinc in two phases are described as

$$\begin{aligned}(C_{Zn})_R &= C_{ZnR} + C_{ZnXNaR} + C_{ZnYNaR} \\ &= m_{ZnR} + m_{ZnXNaR} + m_{ZnYNaR}, \qquad (8)\\ (C_{Zn})_E &= C_{Zn} + C_{ZnX} + C_{ZnX_2} + C_{ZnY} \\ &\quad + C_{ZnY_2} + C_{ZnXY} \\ &= (m_{Zn} + m_{ZnX} + m_{ZnX_2} + m_{ZnY} + m_{ZnY_2} + m_{ZnXY})/\rho, \qquad (9)\end{aligned}$$

$$D = (C_{Zn})_R/(C_{Zn})_E. \qquad (10)$$

Here $(C_{Zn})_R$ is total zinc in the resin at equilibrium, $(C_{Zn})_E$ is total zinc in the solution at equilibrium, m_X is weight molarity and ρ is density. The distribution ratio, D, of zinc can be expressed as the ratio of $(C_{Zn})_R$ and $(C_{Zn})_E$. Equations 8—10 can be rewritten using equations 1—7 as follows:

$$\begin{aligned}(C_{Zn})_R = \Bigg(&\frac{\gamma_{Zn}m_{Zn}}{\gamma_{ZnR}\gamma_{Na}^2 m_{Na}^2}\cdot\beta_2^R + \frac{\gamma_{Zn}\gamma_X m_{Zn}m_X}{\gamma_{Na}\gamma_{ZnXNaR}m_{Na}}\cdot K_m^{RX}\beta_1^X \\ &+ \frac{\gamma_{Zn}\gamma_Y m_{Zn}m_Y}{\gamma_{Na}\gamma_{ZnYNaR}m_{Na}}\cdot K_m^{RY}\beta_1^Y\Bigg)\cdot\gamma_{Na_2R}m_{Na_2R}, \qquad (8')\end{aligned}$$

$$\begin{aligned}(C_{Zn})_E = \Bigg(&m_{Zn} + \frac{\gamma_{Zn}\gamma_X m_{Zn}m_X}{\gamma_{ZnX}}\cdot\beta_1^X + \frac{\gamma_{Zn}\gamma_X^2 m_{Zn}m_X^2}{\gamma_{ZnX_2}}\cdot\beta_2^X \\ &+ \frac{\gamma_{Zn}\gamma_Y m_{Zn}m_Y}{\gamma_{ZnY}}\cdot\beta_1^Y + \frac{\gamma_{Zn}\gamma_Y^2 m_{Zn}m_Y^2}{\gamma_{ZnY_2}}\cdot\beta_2^Y \\ &+ \frac{\gamma_{Zn}\gamma_X\gamma_Y m_{Zn}m_X m_Y}{\gamma_{ZnXY}}\cdot\beta_1^X K_m^Y\Bigg)\Big/\rho, \qquad (9')\end{aligned}$$

$$\begin{aligned}D = \gamma_{Zn}m_{Na_2R}\rho\cdot\Bigg\{&\frac{\beta_2^R}{\gamma_{Na}^2 m_{Na}^2} + \frac{\gamma_X m_X}{\gamma_{Na}m_{Na}}\cdot K_m^{RX}\beta_1^X \\ &+ \frac{\gamma_Y m_Y}{\gamma_{Na}m_{Na}}\cdot K_m^{RY}\beta_1^Y\Bigg\}\Bigg/ \\ &\{1 + \textstyle\sum\gamma_X^n m_X^n\beta_n^X + \sum\gamma_Y^n m_Y^n\beta_n^Y + \gamma_X\gamma_Y m_X m_Y\beta_1^X K_m^Y\}. \qquad (10')\end{aligned}$$

Here γ stands for the activity coefficient of each ion, γ_{Na_2R}, γ_{ZnR}, γ_{ZnXR}, and γ_{ZnYR} can be regarded as 1 and $\gamma_{ZnX}=\gamma_{ZnY}$, $\gamma_{ZnX_2}=\gamma_{ZnY_2}=\gamma_{ZnXY}\cdot\gamma_X$, γ_Y, γ_{Zn}, and γ_{Na} are calculated from Debye-Hückel's theory as

$$\gamma_X = \gamma_\pm^{1/2} = \left\{\frac{-A|Z^+Z^-|I^{1/2}}{1+BdI^{1/2}}\right\}^{1/2}, \qquad (11)$$

$$A = 8.1622\times\frac{\rho^{1/2}}{\varepsilon^{3/2}}\times 10^2 \quad B = 2.9127\times\left\{\frac{\rho}{\varepsilon}\right\}^{1/2}\times 10^8$$

at 25 °C. (12)

Here d denotes parameter of ionic radius, I represents ionic strength, m_{Na_2R} is expressed as g resin (Na-form)/dm^3 ethylene glycol, and ε is the dielectric constant of ethylene glycol. The constant of 5% aqueous ethylene glycol was obtained graphically by interpolation of the constants of 100, 90, and 80% ethylene glycol.[13]

In the Zn^{2+}-Cl^--ClO_4^- system, the distribution coefficient can be transformed as a function of chloride ion concentration, m_X, because m_X+m_Y=const. Sodium ions are originated from sodium chloride and sodium perchlorate, and these compounds are assumed to be completely dissociated in pure or aqueous ethylene glycol. Hence the relation that $m_{Na}=m_X+m_Y$ holds good. β_1^R is negligible, because it is expected that $\beta_2^R \gg \beta_1^R$. Equation 10 is arranged into fractional functions as follows:

1. (X=Cl or ClO_4)

$$D^* = \frac{P_{(1)}+P_{(2)}L^2}{1+P_{(3)}L+P_{(4)}L^2} \quad (13)$$

$L=\gamma_X m_X$, $D^*=D\gamma_{Na}^3 m_{Na}^3/\gamma_{Zn}$, $P_{(1)}=\beta_2^R m_{Na_2R}$,
$P_{(2)}=\beta_1^X K_m^{RX} m_{Na_2R}$, $P_{(3)}=\beta_1^Y$, and $P_{(4)}=\beta_2^R$.

2. (X=Cl and Y=ClO_4)

$$D^* = \frac{P_{(1)}+P_{(2)}m_X+P_{(3)}m_Y}{1+P_{(4)}m_X+P_{(5)}m_X^2+P_{(6)}m_Y+P_{(7)}m_Y^2+P_{(8)}m_Xm_Y} \quad (14)$$

$D^*=D\gamma_{Na}^3 m_{Na}^3/\gamma_{Zn}$, $P_{(1)}=m_{Na_2R}\beta_2^R$,
$P_{(2)}=m_{Na_2R}\beta_1^X K_m^{RX}\gamma_X\gamma_{Na}m_{Na}m_X$,
$P_{(3)}=m_{Na_2R}\beta_1^Y K_m^{RY}\gamma_{Na}\gamma_Y m_{Na}m_Y$, $P_{(4)}=\gamma_X\beta_1^X$,
$P_{(5)}=\gamma_X^2\beta_2^X$, $P_{(6)}=\gamma_Y\beta_1^Y$, $P_{(7)}=\gamma_Y^2\beta_2^Y$,
$P_{(8)}=\gamma_X\gamma_Y m_X m_Y \beta_1^X K_m^Y$.

γ_X, γ_Y, γ_{Na}, and γ_{Zn} were calculated from Eqs. 11 and 12 as a function of the ionic strength. These coefficients have constant values at constant ionic strenth. Parameters P_i were calculated by the nonliner least-squares method, a modified Gauss-Newton method, using a computer and were determined by enlisting the aid of a curve fitting method using computer graphics.

Experimental

Ethylene glycol was purified by distilling it under reduced pressure after drying over zeolite and was stored in closed bottles. Zinc-65 tracer was supplied as chloride by New England Nuclear, Boston, Mass., U.S.A. It was heated on a hot plate, adding perchloric acid to convert it into a zinc perchlorate form, and was dissolved in ethylene glycol. Sodium chloride and sodium perchlorate were dried at 110 °C and stored over phosphrous pentaoxide in a desiccator. Perchloric acid, sodium chloride, sodium perchlorate, and zinc perchlorate were guaranteed reagent grade. The cation exchange resin (mean radius, 15.5 μm), Hitachi custom ion exchange resin 2611 for the liquid chromatograph, was washed with hydrochloric acid and was transformed into the Na-form by sodium chloride solution. After washed with water to remove chloride ion, the resin was dried in vacuum and stored in a desiccator.

From 25 to 100 mg of the resin was taken in an Erlenmyer flask with a glass-stopper, and 20 ml of ethylene glycol solution containing sodium chloride and/or sodium perchlorate, zinc perchlorate, perchloric acid, and a radio-zinc tracer was added. Perchloric acid was added to minimize the loss of zinc that was caused by the adsorption on the vessel wall. The flask was set in the water bath with a thermostat at 25 °C and stirred by a teflon-coated bar. After the equilibrium was attained, both the solution and the resin were transferred to a centrifugal tube, and the two phases were separated centrifugally. Distribution coefficients were calculated from the ratio of radioactivity between the two phases. Two milliliters of solution phase were pipetted into a test tube and radioactivities were counted by a well-type scintillation counter (Metro Electronics Model PbW-6).

Results and Discussion

The attainment of the distribution equilibrium was checked by measuring the variation of the distribution coefficient of zinc *vs.* the stirring time. As shown in Fig. 1, little influence of the stirring time was observed upon the distribution of zinc between the glycol phase and the resin; the distribution attained equilibrium within 1 h at the latest and varied little within at least 48 h.

Stirring for 24 h was adopted in the experiment, because ethylene glycol has a somewhat higher viscosity than water, and then the resin was more difficult to disperse in the glycolic solution than in the aqueous one. The correct distribution coefficients can not be observed in high concentration range of zinc because of the comparatively low exchange capacity of the resin and in very low zinc concentration because of the adsorption on the resin. Figure 2 shows the influence of zinc perchlorate concentration on the distribution coefficients. The coefficients have a constant value for solutions ranging in concentration from 5×10^{-7} to 10^{-4} mol dm^{-3}. Therefore the initial zinc concentration was kept at 1×10^{-6} mol dm^{-3} throughout the experiment. It is expected from Eq. 10 that there exist a proportional relation between the distribution coeffi-

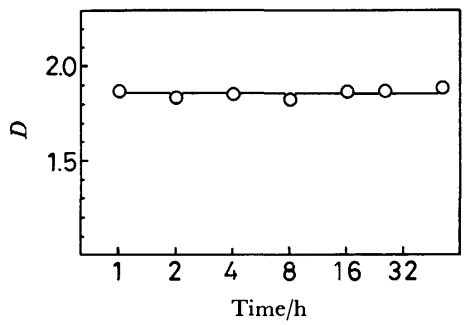

Fig. 1. Influence of stirring time.
NaCl: 0.05 mol dm^{-3}, resin: 2.5 g dm^{-3}, $Zn(ClO_4)_2$: 1×10^{-6} mol dm^{-3}.

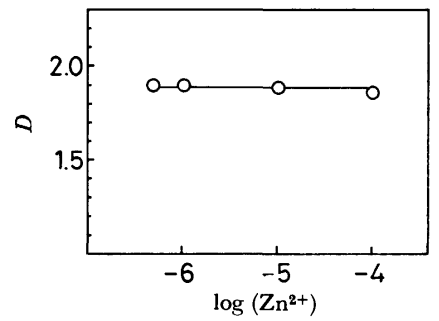

Fig. 2. Influence of initial zinc concentration.
NaCl: 0.05 mol dm^{-3}, resin: 2.5 g dm^{-3}.

cient and the resin amount. The relation is shown in Fig. 3; plots of log D^* *vs.* the resin amount give straigth lines with the slope of about 1 in the various concentrations of sodium perchlorate and chloride.

Figures 4—7 show the plot of log D^* *vs.* a_{Cl} or a_{ClO_4} on the distribution of zinc chloride and perchlorate between the glycol phase and the ion exchanger; the concentrations of chloride and perchlorate ions in the figures are converted into the activities by using Debye-Hückel's theory. The curves in these figures are depicted by means of regression analysis on Eqs. 13—

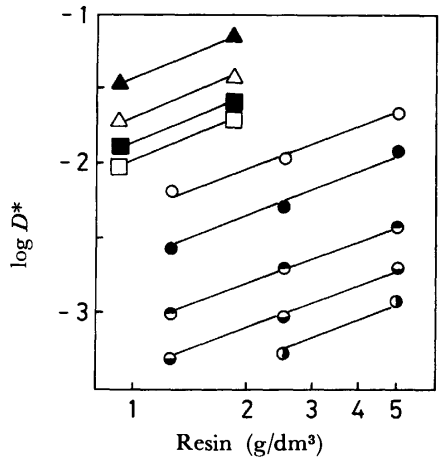

Fig. 3. Effect of resin amount in sodium chloride and sodium perchlorate system.
▲: $NaClO_4$ 0.02 mol dm^{-3}, △: $NaClO_4$ 0.04 mol dm^{-3}, ■: $NaClO_4$ 0.1 mol dm^{-3}, □: $NaClO_4$ 0.2 mol dm^{-3}, ○: NaCl 0.02 mol dm^{-3}, ●: NaCl 0.04 mol dm^{-3}, ◓: NaCl 0.07 mol dm^{-3}, ◒: NaCl 0.1 mol dm^{-3}, ◑: NaCl 0.2 mol dm^{-3}.

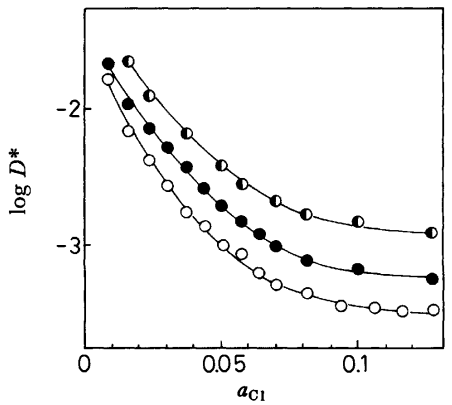

Fig. 4. Distribution coefficients of zinc chloride system.
○: Resin 1.27 g dm^{-3}, ●: resin 2.52 g dm^{-3}, ◐: resin 5.0 g dm^{-3}.

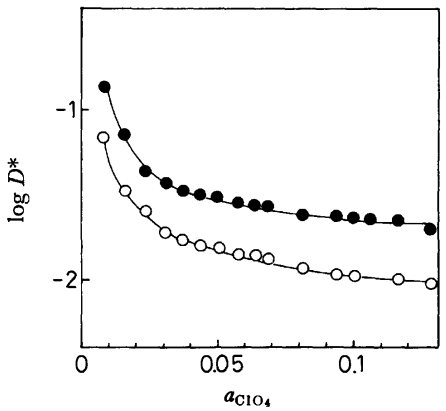

Fig. 5. Distribution coefficients of zinc perchlorate system.
○: Resin 0.909 g dm^{-3}, ●: resin 1.82 g dm^{-3}.

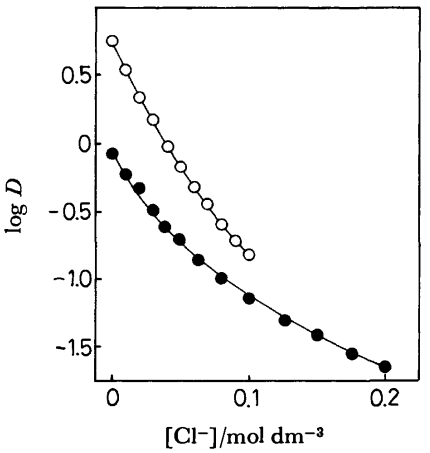

Fig. 6. Distribution coefficients of zinc at constant ionic strength (zinc-sodium chloride-sodium perchlorate system).
○: Ionic strength 0.1, ●: ionic strength 0.2, resin 2.5 g dm^{-3}

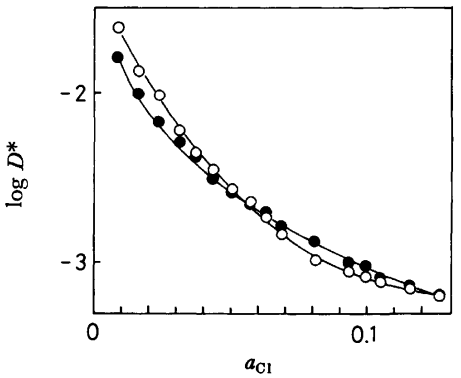

Fig. 7. Distribution coefficients of zinc chloride in the ethylene glycol solutions containing water.
○: 5% water ethylene glycol, resin 1.82 g dm^{-3}.
●: 10% water ethylene glycol, resin 1.36 g dm^{-3}.

TABLE 1. FORMATION CONSTANTS OF ZINC CHLORIDE AND ZINC PERCHLORATE

log β	β_1^X	β_2^X	K_m^X
X=Cl, pure E.G.	3.03±0.05	4.80±0.05	—
X=Cl, 5% water-E.G.	2.73±0.05	4.18±0.05	—
X=Cl, 10% water-E.G.	2.32±0.06	3.46±0.06	—
X=ClO_4	2.34±0.07	2.50±0.07	—
Ionic strength 0.1	—	—	0.7±0.1

E.G.=Ethylene glycol.

14, and these show good accordance with the experimental data. The formation constants of zinc chloride and perchlorate are listed in Table 1.

In the zinc chloride and perchlorate system, the number of parameters in Eq. 14 are too many to get exact values. Consequently, the values of β_n^X and β_n^Y in Eq. 14 were calculated by substituting β_n^X and β_n^Y obtained in the zinc chloride and zinc perchlorate system in Eq. 13. The values of the formation constant obtained by the present ion exchange method are close to those determined by the nonaqueous liquid-liquid extraction method.[10]

The ion exchange method has a bright prospect for developing research on the chemical equilibria of metals in the nonaqueous system, especially in terms of the application to the sparing by soluble salts in nonaqueous solvent.

References

1) J. R. Fryer and D. F. C. Morris, *Talanta*, **15**, 1309 (1968).
2) D. F. C. Morris and E. L. Short, *J. Chem. Soc.*, 1961, 5148.
3) E. L. Short and D. F. C. Morris, *J. Inorg. Nucl. Chem.*, **18**, 192 (1961).
4) Sture Fronaeus, *Acta. Chem. Scand.*, **5**, 859 (1951).
5) B. G. F. Carleson and H. Irving, *J. Chem. Soc.*, 1954, 1953.
6) D. F. C. Morris and E. L. Short, *J. Chem. Soc.*, 1962, 2672.
7) J. Penciner, I. Eliezer, and Y. Marcus, *J. Phys. Chem.*, **69**, 2955 (1965).
8) W. Libus, D. Puchalska, and T. Szuchnicka, *J. Phys. Chem.*, **72**, 2075 (1968).
9) M. Matsui, H. Doe, T. Hirade, and T. Shigematsu, *Anal. Lett.*, **12**(A13), 1385 (1979).
10) H. Doe, M. Matsui, and T. Shigematsu, *Bull. Inst. Chem. Res. Kyoto Univ.*, **57**, 343 (1979).
11) H. Doe, M. Matsui, and T. Shigematsu, *Bull. Inst. Chem.* Res. Kyoto Univ., **58**, 133 (1980).
12) H. Doe, M. Matsui, and T. Shigematsu, *Bull. Inst. Chem. Res. Kyoto Univ.*, **58**, 154 (1980).
13) T. F. Humbel and J. P. Scherrer, *Helv. Phys. Acta*, **26**, 17 (1953).
14) S. Iwasaki, M. Sugiyama, M. Matsui, and T. Kumagai, *Bull. Inst. Chem. Res. Kyoto Univ.*, **61**, 340 (1983).

Equilibrium Solubilities of Iodine Vapor in Water

Isao SANEMASA,* Toyohisa KOBAYASHI, Cheng Yun PIAO, and Toshio DEGUCHI
Department of Chemistry, Faculty of Science, Kumamoto University, Kurokami 2-39-1, Kumamoto 860
(Received October 5, 1983)

Equilibrium solubilities of iodine vapor in water were measured by introducing iodine vapor, in equilibrium with solid iodine, into water and by circulating it in a closed system, and Henry's law constants were determined. Equilibrium distributions of iodine vapor between a gas phase and an aqueous phase were also measured by another method, and partition coefficients were determined. The solubilities of iodine vapor in water estimated from both the Henry's law constants and the partition coefficients are compared with those of solid iodine reported in the literature. Thermodynamic parameters for the hydration of iodine vapor are evaluated experimentally.

A large number of papers have been published on solubilities of iodine in water.[1] All of them are concerned with saturated solutions prepared through direct contact of solid iodine with water. On the other hand, in the field of nuclear power plant, there are some publications on the partition study of iodine vapor between air and water.[2,3,4] The experimentally determined partition coefficients, however, differ from literature to literature. Both the solubility of solid iodine in water and the iodine vapor pressure are known at a given temperature, so the partition coefficient can be predicted provided the iodine vapor behaves ideally.[5] However, the partition coefficients reported in the literature are not consistent with the prediction.

In our previous paper we reported a method of preparing solutions saturated with solute by use of solute vapor. The method has successfully been applied to determining Henry's law constants of metallic mercury and some liquid aromatic hydrocarbons.[6,7] The present paper is concerned with an extension of the method to such solutes as iodine which exists in the solid state at ordinary temperatures. Another technique was also employed for estimation of partition coefficients of iodine vapor between the gas phase and the aqueous phase.

Experimental

Materials. The iodine used as solute was of analytical reagent grade and used without further purification. Deionized-redistilled water was used as solvent. Analytical reagent grade carbon tetrachloride was used for solvent extraction and for the preparation of iodine standard solutions.

Apparatus and Procedures. The apparatus, used to prepare aqueous solutions saturated with iodine vapor, is shown in Fig. 1. It is composed of a separatory funnel (100 cm^3), A, two condensers, B and C, a bottle (300 cm^3), D, and a Viton diaphragm pump (Iwaki Type AP-32 Z), P. Gas inlet-type adaptors are mounted in A and D. Teflon and glass pipes, both of ϕ=8 mm, are used for connection. Solid iodine is packed in the upper condenser B (ϕ 8 mm×200 mm), the top end of which is equipped with a coarse sintered glass disk and the bottom part is plugged with glass wool. We will hereinafter refer to condenser B packed with solid iodine and separatory funnel A containing *ca.* 50 cm^3 water as the "solute reservoir" and "solubility flask," respectively. Lower condenser C and bottle D serve to trap water droplets and to keep the air and the solute reservoir in thermal equilibrium. The temperature of the solubility flask is held constant by circulating water through a surrounding jacket from a thermostated bath. The temperature of the solute reservoir is also maintained constant in the same way by using another thermostated bath. These thermostats are controlled within ±0.02 °C. The assembled apparatus was placed in a chamber, the temperature of which was kept higher than that of the solute reservoir in order to prevent the iodine vapor from condensing inside the apparatus. Aqueous solutions saturated with iodine vapor were prepared as follows: after the desired temperatures for the solubility flask and solute reservoir were attained, the pump was started, and the iodine vapor, which had been generated by allowing air to flow through the solute reservoir, was introduced into the solubility flask *via* a sintered glass ball, and circulated as indicated in Fig. 1. The iodine vapor pressure inside the solubility flask can be fixed at any desired value by controlling the temperature of solute reservoir. At the beginning of this study, iodine crystals purified by sublimation were packed in the solute reservoir. However, the fine crystals tended to pack together inside the column so tightly during the course of continuous air-circulation as to make the further aeration through the column difficult. Then, we used coarse iodine crystals. The circulation rate, which could be changed by means of a Variac, was set at 0.8 $dm^3\ min^{-1}$ in most instances. After the

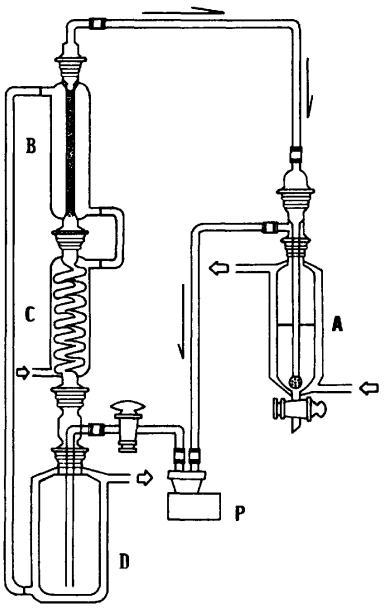

Fig. 1. Solubility apparatus.
The solid arrows indicate the direction of air-circulation.

solubility equilibrium was attained, a stopcock on the bottom of the solubility flask was opened. The first portion of *ca.* 10 cm^3 was discarded and the following 10 cm^3 portions were transferred successively into three cylindrical separatory funnels, in which 10 cm^3 CCl_4 had previously been placed. Each separatory funnel had been calibrated so that the volume of an aqueous solution poured into it might be read out. Mixtures in the separatory funnels were hand-shaken and allowed to stand for 30 min, and then, after dehydrating the CCl_4 phase with anhydrous sodium sulfate, absorbances were measured at 514 nm using a Hitachi Model 100-50 spectrophotometer against a blank extract as the reference. Standard solutions were prepared by weighing out of suitable quantities of solid iodine, followed by dilution with CCl_4 in volumetric flasks. Calibration curves were constructed by using iodine standard solutions of the order of 10^{-3} mol dm^{-3} in the same way as described in our previous paper.[7]

The apparatus, used to determine partition coefficients of iodine vapor between air and water, is shown in Fig. 2. A large separatory funnel of *ca.* 5 dm^3 capacity, to be called the "partition flask," was connected to a Viton diaphragm pump of the same type as pump P shown in Fig. 1 through Teflon tubes (ϕ=8 mm) and two glass adaptors, one of which was attached to a sintered glass ball and was long enough to reach nearly the bottom of the partition flask. The temperature inside the partition flask was kept constant by circulating water through a surrounding jacket from a thermostated bath. A particular attention was paid in assembling the apparatus so as to minimize the section exposed out of the jacket, down to a volume as small as 42.5 cm^3. Aqueous iodine solutions were prepared by using the apparatus shown in Fig. 1 with the solubility flask replaced by one of 300 cm^3 capacity. An aliquot of the iodine solution thus prepared was poured into the partition flask and another aliquot was used to determine the iodine concentration. The pump was operated at a flow rate less than 0.1 dm^3 min^{-1} and the air was circulated at least 10 min. The iodine concentration in the aqueous phase after this air-circulation was measured. The time required to attain the equilibrium partition was preliminarily investigated with a result that 10 min-circulation is sufficient. The air-circulation, however, needed to be made intermittently, lest the temperature of the aqueous phase should decrease owing to the heat of evaporation of the solvent water. From preliminary experiments the best way of the air-circulation was found to be as follows: the air was circulated for 1 min, then the solution was allowed to stand for another 1 min, and finally the operation was repeated at least 10 times.

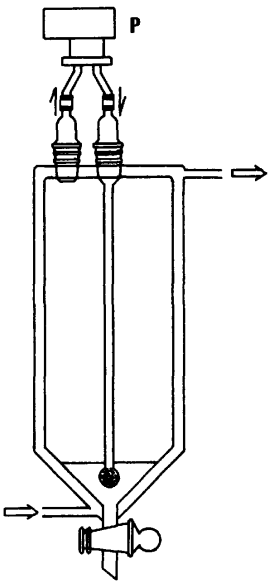

Fig. 2. Partition apparatus.
The solid arrows indicate the direction of air-circulation.

Results

The Time Required for Attaining the Solubility Equilibrium. The time required to attain the equilibrium solubility was checked by taking a small amount of aqueous solution from the bottom of the solubility flask directly into a cuvette and by measuring the absorbance at 460 nm without solvent extraction. The results are shown in Fig. 3. The absorbance readings begin to rise, reach a maximum after 30—90 min according to the rate of air-circulation, and thereafter remain constant. On the basis of this observation, subsequent experiments were carried out at a constant circulation rate of 0.8 dm^3 min^{-1} and iodine concentrations in sample solutions withdrawn after 60 min-circulation were measured.

Solubility as a Function of Iodine Vapor Pressure. It is an essential requirement, as we have emphasized in our previous paper,[7] to keep the temperature of solubility flask $\geqq$ the temperature of solute reservoir $<$ the room temperature. For this reason, the solubility runs were made by raising the temperature of solute reservoir up to that of solubility flask while the latter was maintained constant. The results are given in Table 1. The vapor pressure of iodine at a given temperature of solute reservoir was estimated from the equation $\log PT^{3/2}=16.945-3464/T$, where P is vapor pressure in Pa and T is absolute temperature. This equation was derived by reference to literature.[8,9] The equilibrium solubilities are plotted against iodine vapor pressure in Fig. 4, from which we can see that the solubility obeys Henry's law at respective temperatures of water. In Fig. 4 are also shown the results obtained under conditions such that the temperature of solute reservoir was set higher than that of solubility flask. Under such circum-

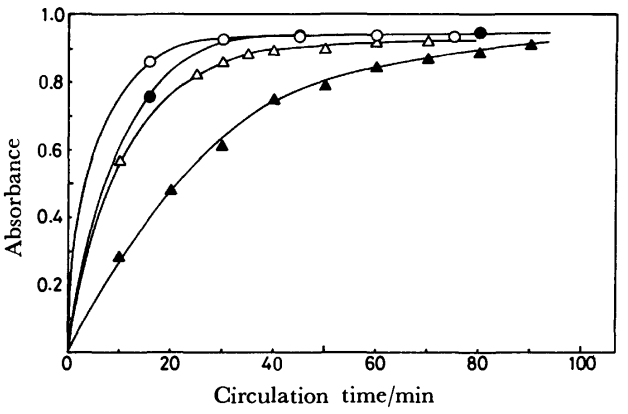

Fig. 3. Absorbance changes of iodine dissolved in water *vs.* circulation time.
Air-circulation rate: 0.8 (○), 0.5 (●), 0.3 (△), 0.2 dm^3 min^{-1} (▲).

Table 1. Solubilities of iodine as a function of its vapor pressure

Temperature of solid I_2 / °C	Vapor pressure of I_2[a] / Pa	Solubility[b] / 10^{-4} mol dm^{-3}
Temperature of water: 15.00 °C		
5.00	6.68	3.88, 3.91, 3.74
10.00	10.79	5.90, 5.81, 5.81, 5.78
15.00	17.14	9.12, 9.12, 9.09
Temperature of water: 20.00 °C		
5.00	6.68	2.51, 2.52, 2.52
10.00	10.79	4.51, 4.61, 4.50
15.00	17.14	6.90, 6.84, 6.88
20.00	26.78	10.5, 10.6, 10.7
Temperature of water: 25.00 °C		
10.00	10.79	3.33, 3.32, 3.22
15.00	17.14	5.18, 5.22, 5.21
20.00	26.78	8.11, 8.14, 8.09
25.00	41.20	12.1, 12.1, 12.1
Temperature of water: 30.00 °C		
5.00	6.68	1.53, 1.53
10.00	10.79	2.53, 2.51, 2.51
15.00	17.14	3.93, 3.94, 3.93
20.00	26.78	6.42, 6.40, 6.39
25.00	41.20	9.44, 9.59
30.00	62.48	13.8, 13.9
Temperature of water: 35.00 °C		
5.00	6.68	1.11
10.00	10.79	1.64
15.00	17.14	2.88
20.00	26.78	4.62
25.00	41.20	7.04
29.32	59.09	10.6
31.33	69.63	12.3
35.00	93.43	16.1

a) The vapor pressure of iodine, P (in Pa), was estimated by $\log PT^{3/2} = 16.945 - 3464/T$, where T is absolute temperature. b) A set of two or more solubility values indicates that experiments were carried out under the same conditions on different days.

stances, iodine vapor condenses inside the solubility flask, and the solid appears in the aqueous phase mostly in the bottom and a little on the surface. Solutions thus prepared were allowed to stand for at least 3 h without air-circulation, and aliquots were pipetted off from the middle part of the aqueous phase to measure iodine concentrations. The results varied widely and the reproducibility was poor as can be seen in Fig. 4.

Gas-Water Partition Coefficients of Iodine. The partition coefficient, K_P, is defined according to literature as follow:[3,4] K_P=(concentration of I_2 in aqueous phase in mol dm^{-3})/(concentration of I_2 in gaseous phase in mol dm^{-3}). In the present study, the concentration of iodine in the gaseous phase was not measured but estimated from the iodine concentrations in the aqueous phase before and after equilibrium, C_B and C_A (in mol dm^{-3}), respectively, by $K_P = C_A(10^3 \times V - v)/v(C_B - C_A)$, where v is the volume of aqueous phase (cm^3) and V is the volume of partition flask (V=4.9165 dm^3). The results are given in Table 2.

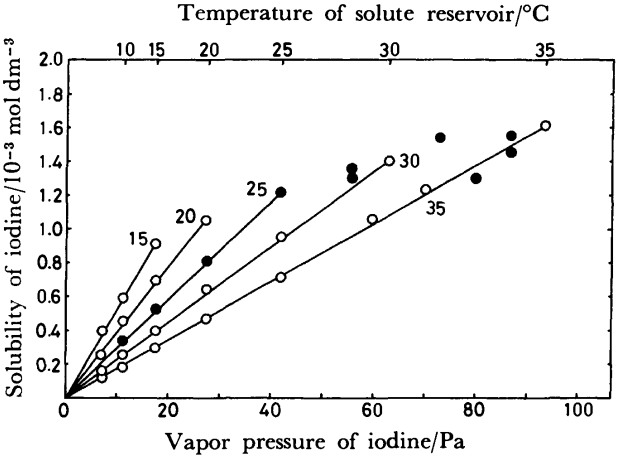

Fig. 4. Equilibrium solubility of iodine *vs.* iodine vapor pressure.
The figure near each solid line indicates the temperature of water. The solid circles are the results obtained under conditions such that the temperature of water was held constant at 25 °C while the temperature of solid iodine was raised beyond 25°C.

Discussion

Solubilities of Iodine in Aqueous Solutions. The primary purpose of the present study is to determine whether the method proposed here can be used for preparing aqueous solutions of desired iodine concentration. The most important problem is whether an aqueous solution is saturated with iodine vapor. It was experimentally confirmed that equilibrium solubilities obey Henry's law. However, this does not necessarily mean that solutions are saturated actually 100% with iodine vapor. Thus, solutions saturated, say, 90% can be expected to obey Henry's law in appearance provided the imperfect saturation is maintained constant throughout the range of iodine vapor pressure investigated. In this study, therefore, we employed the partition method, too, in which the problem of imperfect saturation need not be considered so long as the gas-water partition equiliblium is attained. The partition coefficients determined here are tabulated in Table 3, together with some available literature values. Though the data reported so far in the literature are scanty, our present results seem to be in reasonable agreement with those reported by Eguchi *et al.*[3]

The Henry's law constant, K_H, is expressed in the following well-known equation

$$K_H = P/X_2, \quad (1)$$

where P is the partial pressure of iodine vapor in Pa and X_2 is the mole fraction of dissolved iodine in water. Based on the definition of partition coefficient and on the assumption that the iodine vapor in the gaseous

phase is ideal, the partition coefficient can be written as

$$K_P = 55.51\, X_2/(PR^{-1}\, T^{-1}), \quad (2)$$

where the factor 55.51 is the mole number of 1 dm³ water and R and T have their usual significances, R being 8.3145×10^3 dm³ Pa K⁻¹ mol⁻¹. From Eqs. 1 and 2, we can derive the Henry's law constant from the partition coefficient as

$$K_H^* = 4.615 \times 10^5\, T/K_P. \quad (3)$$

We will specify as K_H^* the Henry's law constant as derived from the partition coefficient. In Table 4 are listed the values of K_H and K_H^*, the former being determined by applying the least-squares method to the data given in Table 1. The solubilities of iodine vapor in water were estimated from Eq. 1. Table 4 shows that the solubilities of iodine vapor are somewhat lower than those of solid iodine. Is there any essential difference between the solubilities of vapor and solid? They should both be equal to each other in principle if there is no possibility of any alteration, in physicochemical properties of the solid interface, to occur during the contact of the solid iodine with water, such as formation of hydrated iodine crystals (water molecule-included iodine crystals). It is supposed that an imperfect saturation with iodine vapor may give rise to the lower solubilities. However, this explanation seems to be unlikely since the values of K_H are lower than those of K_H^* over the temperature range studied. At present we cannot offer any satisfactory explanations for the difference observed between the solubilities of iodine vapor and solid iodine.

It should be mentioned that the present method for determining partition coefficients, though rapid and simple, suffers from three inherent disadvantages, and therefore the K_H^* values estimated seem to be less reliable than those of K_H. Firstly, iodine concentrations in the gaseous phase were estimated indirectly. Secondly, a part of the aqueous phase was caused to splash inside the partition flask during the course of air-bubbling. The partition equilibrium between the droplets and the gaseous phase might require much longer time, and therefore the volume of the aqueous phase initially taken, v, should be corrected for these droplets. Thirdly, in deriving Eq. 2, the iodine vapor in gase-

Table 2. Gas-water partition of iodine vapor

Temperature °C	Volume of aqueous phase cm³	Concentration of iodine in aqueous phase, 10^{-4} mol dm⁻³: Before equilibrium	Concentration of iodine in aqueous phase, 10^{-4} mol dm⁻³: After equilibrium[a]	Partition coefficient K_P[b]
15.00	50	2.29	1.27	121
	100	4.57	3.28	122
	200	1.99	1.67	123
20.00	50	0.897	0.445	95.8
	100	3.99	2.60	90.1
	200	8.24	6.56	92.1
25.00	50	9.73	4.12	71.5
	100	3.40	2.02	70.5
	100	4.35	2.57	69.5
	100	4.72	2.89	76.1
	100	5.23	3.02	65.8
	100	7.82	4.59	68.4
	100	8.86	5.24	69.7
	100	5.00	3.55[c]	118
	100	8.18	5.37[d]	92.2
	100	6.05	3.63[e]	72.0
	100	6.92	4.17[e]	72.9
	100	10.5	6.30[e]	71.8
	100	0.724	0.423[f]	67.6
	100	5.83	3.51[f]	72.7
	200	9.02	6.74	69.7
30.00	50	3.92	1.36	51.7
	100	1.78	0.931	52.8
	200	6.49	4.47	52.2
35.00	50	5.20	1.60	43.3
	100	2.88	1.37	43.7
	200	1.19	0.774	43.9
40.00	50	5.86	1.60	36.6
	100	12.1	5.24	36.8
	200	5.73	3.48	36.5
45.00	100	0.486	0.186	29.9
	100	4.16	1.55	28.6
	100	4.42	1.65	28.7
	100	5.44	2.09	30.0
	100	7.38	2.83	30.0
50.00	100	2.74	0.895	23.4
	100	3.55	1.17	23.7
	100	4.13	1.37	23.9

a) The air-circulation time was 10 min unless otherwise noted. b) Partition coefficients, K_P, were calculated by $K_P = C_A(10^3 \times V - v)/v(C_B - C_A)$, where C_B and C_A are concentrations of iodine before and after equilibrium, respectively, v is the volume of aqueous phase (cm³), and V is the volume of the partition flask (4.9165 dm³). c) The air-circulation time was 0.5 min. d) The air-circulation time was 1 min. e) The air-circulation time was 5 min. f) The air-circulation time was 30 min.

Table 3. Partition coefficients of iodine vapor, K_P

Temperature °C	This work	Literature a)	Literature b)	Literature c)
15	122			
20	92.7	122		
25	70.2±2.9[d]		70	103—114
30	52.2			
35	43.6			
40	36.6		35	32.0—37.6
45	29.4			
50	23.7			
60	15.8[e]		17	
70	10.0[e]			16.4—18.4

a) Ref. 2. b) Ref. 3. c) Ref. 4. d) In calculating the mean value, the data obtained at air-circulation times of 0.5, 1, and 5 min were omitted. e) Estimated by extrapolation of $\log K_P$ *vs.* $1/T$, where T is absolute temperature.

Table 4. Henry's law constants and solubilities of iodine

Temperature °C	Henry's law constant 10^6 Pa		Solubility of iodine vapor 10^{-4} mol dm^{-3} Estimated from		Solubility of solid iodine 10^{-4} mol dm^{-3} Literature values	
	K_H	K_H* a)	K_H	K_H* a)	b)	c)
15.0	1.03±0.04	1.09	9.23±0.36	8.73		9.717
20.0	1.39±0.06	1.46	10.7 ±0.5	10.2	10.2	11.27
25.0	1.86±0.03	1.96	12.3 ±0.2	11.7	13.2	13.11
30.0	2.44±0.06	2.68	14.2 ±0.3	12.9	15.2	15.28
35.0	3.19±0.02	3.26	16.3 ±0.1	15.9		17.87
40.0		3.95		19.4	20	20.07
45.0		4.99		22.3		24.63
50.0		6.29		25.5	28	29.03

a) Derived from the partition coefficient, K_P, by $K_H^* = 4.615 \times 10^5 T/K_P$, where T is absolute temperature. b) Taken from Ref. 1. c) Taken from Ref. 14.

Table 5. Thermodynamic parameters of iodine corresponding to solution, vaporization, and hydration processes at 25 °C

	Solution process	Vaporization process	Hydration process		
			Calcd[a]	Exptl[b]	Lit[c]
ΔG / kJ mol^{-1}	26.40	19.360	7.040	7.20 (7.32)	6.987
ΔH / kJ mol^{-1}	22.70	62.421	−39.72	−41.7 (−38.3)	−39.52
ΔS / J K^{-1} mol^{-1}	−12.41	144.428	−156.8	−164 (−153)	−156.0

a) Calculated by subtracting the value for vaporization from that for solution process. b) Estimated from the temperature dependence of Henry's law constant. The values designated in parentheses were estimated from partition coefficients. In both cases the temperature dependence of ΔH was neglected. c) Taken from Ref. 12.

ous phase was postulated to be ideal. This assumption, however, may be permissible because of its low pressure. These disadvantages might lead to relatively large deviations for the measured K_P values and, therefore, for the estimated K_H* values, as compared with the K_H values. However, it is difficult to explain why, at respective temperatures of water, the value of K_H* is lower than that of K_H, the difference amounting to as much as *ca.* 10% in the extreme case.

In the beginning of this work, we used aqueous solutions acidified with perchloric acid, 10^{-4} mol dm^{-3}, as well as pure water. However, the difference in the two results could not be regarded as significant, and according to the literature,[10] the hydrolysis constant of the reaction $I_2+H_2O \rightarrow HIO+H^+ + I^-$ has been reported to be in the order of 10^{-13} at 25 °C. These facts, therefore, suggest that the hydrolysis may be neglected over the iodine concentration range concerned in the present study. Indeed, it has been pointed out from partition experiments that the hydrolysis of iodine does occur at very low iodine concentrations less than *ca.* 4×10^{-5} mol dm^{-3}.[11] This concentration range is much lower than those of solutions saturated with iodine.

The method described in this paper is considered to be useful to prepare aqueous solutions of desired iodine concentrations below saturation. The method is suitable for studying possible interactions between iodine and hydrophobic substances in aqueous environment by measuring solubility increments.

Thermodynamic Parameters of Hydration of Iodine Vapor. While it has previously been shown that thermodynamic parameters of hydration of iodine vapor can be evaluated from solubility data of solid iodine,[12] it is considered desirable to confirm them experimentally. The temperature dependence of Henry's law constants has led to an estimation of thermodynamic parameters which correspond to the hydration of iodine vapor. The results are given in Table 5, together with literature values. The solution of solid iodine in water can be divided into two processes: vaporization and hydration. This is shown in Scheme 1.

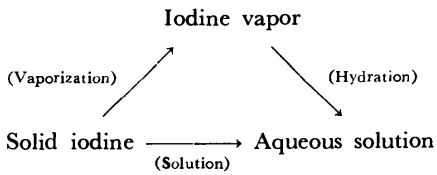

Scheme 1.

Thermodynamic parameters for each process are related to one another as follows:

$$\Delta G\,(\text{solution}) = \Delta G\,(\text{vaporization}) + \Delta G\,(\text{hydration}),$$
$$\Delta H\,(\text{solution}) = \Delta H\,(\text{vaporization}) + \Delta H\,(\text{hydration}),$$
$$\Delta S\,(\text{solution}) = \Delta S\,(\text{vaporization}) + \Delta S\,(\text{hydration}).$$

Values of ΔG, ΔH, and ΔS for the vaporization process are available from literature,[13] and those for the solution process are reported in literature.[14] Using these literature values, we have calculated the values of ΔG, ΔH, and ΔS for the hydration process. The results are given in Table 5. The agreement between the experimental and the calculated values is fairly good.

We wish to thank the Ministry of Education of people's Republic of China for the support offered to C. Y. Piao who was on leave from Yan Bian University.

References

1) The solubility data of iodine is summarized in W. L. Linke, "Solubilities of Inorganic and Metal-Organic Compounds," 4th ed, Am. Chem. Soc., Washington, D. C. (1955), Vol. I, p. 1254.
2) R. F. Taylor, *Chem. Eng. Sci.*, **10**, 68 (1959).
3) W. Eguchi, M. Adachi, and M. Yoneda, *J. Chem. Eng. Jpn.*, **6**, 389 (1973).
4) Y. Nishizawa, Y. Kigoshi, S. Oshima, and T. Maekawa, *Nihon Genshiryoku Gakkai Shi*, **11**, 205 (1969).
5) For instance, at 25 °C, the partition coefficient can be predicted to be 79.4 provided that the solubility of solid iodine in water is 13.2×10^{-4} mol dm^{-3} and that the vapor pressure of iodine is 41.20 Pa.
6) I. Sanemasa, *Bull. Chem. Soc. Jpn.*, **48**, 1795 (1975).
7) I. Sanemasa, M. Araki, T. Deguchi, and H. Nagai, *Bull. Chem. Soc. Jpn.*, **55**, 1054 (1982).
8) G. P. Baxter, C. H. Hickey, and W. C. Holmes, *J. Am. Chem. Soc.*, **29**, 127 (1907).
9) H. Chihara and N. Nakamura, *Bull. Chem. Soc. Jpn.*, **41**, 1787 (1968).
10) J. D. Burger and H. A. Liebhafsky, *Anal. Chem.*, **45**, 600 (1973).
11) C. C. Lin, *J. Inorg. Nucl. Chem.*, **43**, 3229 (1981).
12) A. B. Lindenberg, *C. R. Acad. Sci. Paris*, **273**, 1129 (1971).
13) C. D. Cox, *J. Chem. Thermodyn.*, **10**, 903 (1978).
14) R. W. Ramette and R. W. Sandford, Jr., *J. Am. Chem. Soc.*, **87**, 5001 (1965).

 © 1984 The Chemical Society of Japan Bull. Chem. Soc. Jpn., 57, 1358—1361 (1984) [Vol. 57, No. 5

Application of Gel Chromatography to Determining Formation Constants of Inclusion Compounds of Cyclodextrins

Isao SANEMASA,* Takemi MIZOGUCHI, and Toshio DEGUCHI
Department of Chemistry, Faculty of Science, Kumamoto University, Kurokami 2-39-1, Kumamoto 860
(Received October 27, 1983)

The gel filtration technique (Hummel and Dreyer method) was applied to determining formation constants of inclusion complexes of α- and β-cyclodextrins. As guest substances, *p*-nitrophenolate, *p*-nitrophenol, benzoate, and benzoic acid were used. Formation constants were determined at room temperature (25—30 °C) using Sephadex G-10 gel in aqueous buffered solutions of a constant ionic strength of 0.5 with NaCl or with phosphate buffer, and the results were compared with literature values. The method is applicable to such guest substances as exhibit strong adsorption onto the gel matrix.

It is generally accepted that cyclodextrins (CyDs) form inclusion complexes with a wide variety of inorganic and organic compounds in aqueous solutions. The CyD has a cavity, the interior side of which is considered to be hydrophobic, and some hydrophobic molecules can be accommodated in the cavity as guests. Thus, the CyD itself acts as a host. Several methods to determine formation constants of CyD inclusion complexes have been reported which utilize solubility,[1] kinetics,[2] pH potentiometry,[3] polarography,[4] calorimetry,[5,6] optical rotation,[7] NMR,[7,8] CD spectrum,[9,10] UV-visible spectrum,[2,4,5,7,11,12] positron annihilation,[13] and anion-exchange HPLC.[14]

A simple method of gel filtration chromatography has been successfully applied to studies on the association of macromolecules with low-molecular-weight ligands since it was first proposed by Hummel and Dreyer.[15] The method is based on the fact that associated complexes as well as free macromolecules are excluded from the gel phase, whereas small ligands are permeable into the gel, thus permitting the separation of the two. The method therefore makes use of a sieving effect of gel. In the gel chromatographic behavior, however, there have been observed some side-effects other than the sieving effect. Among them, adsorption of solute onto gel matrix is important, especially in such a case that the solute is a hydrophobic substance such as aromatic hydrocarbons.[16] The adsorption effect will be much more pronounced with the most tightly cross-linked Sephadex G-10. It was suggested, though not proved experimentally, that the interaction of ligands with gel matrix does not interfere with the determination of macromolecule-ligand association constants by the Hummel and Dreyer method.[17]

This paper is concerned with the application of gel chromatography to such a system that the ligand (guest) exhibits affinity to the gel matrix as well as to the macromolecule (host). We have chosen *p*-nitrophenolate, *p*-nitrophenol, benzoate, and benzoic acid as guests, because their formation constants with CyDs have abundantly been reported.

Experimental

Materials and Sample Preparations. Cyclodextrins (α- and β-CyDs from Wako) of reagent grade were recrystallized from water and dried over phosphorus pentaoxide. Benzoic acid and *p*-nitrophenol were of analytical reagent grade and used without further purification. Sephadex G-10 and Blue Dextran 2000 were obtained from Parmacia (Uppsala, Sweden). Phosphate buffer (Na_2HPO_4–NaOH for pH=11; NaH_2PO_4–H_3PO_4 for pH=3.5) and hydrochloric acid were used to adjust pH of eluents. Eluents, which contain guest molecules at various concentrations, $[guest]_0$, were prepared by dissolving *p*-nitrophenol or benzoic acid in buffered solutions and by applying a dilution with the same solutions. Ionic strength was adjusted to 0.5 with the buffer itself in the case of benzoate or with sodium chloride in the other cases. A suitable amount of the dried CyD was weighed out and dissolved in the eluent to prepare a CyD sample solution of known concentration.

Apparatus and Procedures. A 7.8 mm×19.5 cm glass-column packed with Sephadex G-10 gel was pre-equilibrated with the eluent. A 0.550 cm^3 aliquot of the CyD sample solution was applied to the pre-equilibrated column by using a sample injector (Kyowa Seimitsu Type KWM-4V-2) and then eluted with the eluent at a constant flow rate by means of a peristaltic pump (Atto Type SJ-1211). The absorbance of the eluant was monitored at the outlet of the column by a JASCO Type UVIDEC-100-III equipped with a flow-cell of 10 mm optical path length and recorded on a chart by a Hitachi Model 056. Both positive and negative peak areas were measured by cutting the chart and weighing the pieces.

Results

Experiments were carried out at room temperature (25—30 °C) under the conditions shown in Table 1. The formation constants of α- and β-CyDs inclusion complexes with *p*-nitrophenolate, *p*-nitrophenol, benzoate, or benzoic acid determined in this work are given in Table 2, together with literature values available. The data in Table 2 indicate that the present results are in reasonable agreement with the literature.

Discussion

Chromatograms were obtained by monitoring UV-visible absorbance of the guest in eluant, whose concentration, $[guest]_0$, is known. A typical chromatogram is shown in Fig. 1, which consists of a pair of positive and negative peaks. The negative peak reflects the guest lost by being incorporated into the CyD. It is desirable to assign the positive peak to a elution band of CyD, however this was not demonstrated in the present work because of the difficulty of detecting the eluted CyD.

Table 1. Experimental conditions to determine formation constants of cyclodextrin-guest inclusion complexes[a]

Guest present in eluent:	*p*-Nitrophenolate	*p*-Nitrophenol	Benzoate	Benzoic acid
$[Guest]_0/10^{-5}$ mol dm^{-3}:	1.03—0.103	10.2—1.02	5.14—1.03	2.05—0.513
$[\alpha\text{-CyD}]/10^{-3}$ mol dm^{-3}:[b]	2.55—10.5	5.12—18.1	5.18—16.0	5.04—15.6
$[\beta\text{-CyD}]/10^{-3}$ mol dm^{-3}:[b]	4.92—9.99	4.93—10.3	5.00—10.4	4.97—10.5
Ionic strength (with):	0.5(NaCl)	0.5(NaCl)	0.5(Na_2HPO_4)	0.5(NaCl)
pH of eluent:	11	3.5	11	0.05 mol dm^{-3}
Adjusted with:	Na_2HPO_4-NaOH	NaH_2PO_4-H_3PO_4	Na_2HPO_4-NaOH	HCl
Flow rate/cm^3 min^{-1}:	2.5	2.5	1.0	2.5
Wavelength monitored/nm:[c]	396	327	232	237

a) Temperatures are in the range of 25—30 °C. b) The volume of CyD sample solutions introduced to the column (Sephadex G-10) is 0.550 cm^3. c) Isosbestic points.

Table 2. Formation constants of cyclodextrin-guest inclusion complexes

Cyclo-dextrin	Formation constant/mol^{-1} dm^3 [a]	
	This work	Literature values
Guest: *p*-Nitrophenolate anion		
α-CyD	2270±230	1890(25°),[b] 3703(14°),[c] 2500(25°),[d] 1587(25°),[d] 2703(23°),[d] 2439[e]
β-CyD	818±146	769(20°),[e] 1020,[e] 476(25°)[f]
Guest: *p*-Nitrophenol		
α-CyD	210±43	341(22°),[g] 385(14°),[c] 417(10°),[h] 200(30°),[h] 126(25°)[i]
β-CyD	314±63	244,[j] 1000(25°)[i]
Guest: Benzoate anion		
α-CyD	11±2	10.5(25°),[k] 9.69(30°),[k] 12,[l] 9.8(25°)[m]
β-CyD	35±1	
Guest: Benzoic acid		
α-CyD	783±52	751(25°),[k] 1000(25°),[l] 800(25°),[m] 583(30°)[k]
β-CyD	632±59	604[j]

a) The temperatures at which formation constants have been determined are indicated in parentheses when specified in the literature. b) Ref. 5. c) Ref. 11. d) Ref. 7. e) Ref. 4. f) Ref. 12. g) Ref. 13. h) Ref. 9. i) Ref. 6. j) Ref. 10. k) Ref. 3. l) Ref. 2. m) Ref. 8.

For all the CyD-guest combinations studied here, the elution volume of the positive peak was found to be nearly equal to the void volume. Based on this observation, α- and β-CyDs, with molecular weights 973 and 1135, respectively, are supposed to be completely excluded from the gel phase. Incidentally, the approximate exclusion limit of molecular weight is said to be 700, in general, for Sephadex G-10.

The formation constant, K, was determined for the reaction

$$\text{CyD} + \text{guest} \rightleftharpoons \text{CyD}\cdot\text{guest}. \quad (1)$$

In the calculation we assumed a stoichiometry of 1 : 1 for the CyD·guest based on the following two pieces of experimental evidence. Firstly, the UV-visible spectra

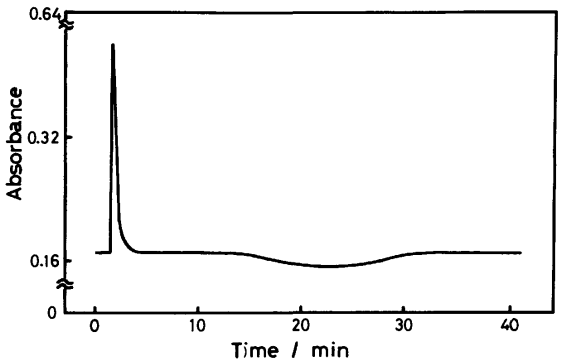

Fig. 1. Elution profile of β-cyclodextrin-*p*-nitrophenolate system.
Concentration of *p*-nitrophenolate anion in eluent: 1.03×10^{-5} mol dm^{-3}, concentration of β-CyD dissolved in eluent: 5.23×10^{-3} mol dm^{-3}, chart speed: 5 mm min^{-1}, AUFS: 0.64.

of all the CyD-guest combinations studied here were demonstrated to have isosbestic points. Secondly, ^{13}C NMR studies have revealed that benzoate anion form a 1:1 complex with α-CyD.[3] The formation constant can be expressed by using the amount of the CyD complex formed, $Q_{\text{CyD·guest}}$, the initial amount of CyD introduced to the column, $Q_{\text{CyD,o}}$, and the concentration of guest in the eluent, $[\text{guest}]_0$, as follows:[18]

$$K = Q_{\text{CyD·guest}}/[\text{guest}]_0(Q_{\text{CyD,o}} - Q_{\text{CyD·guest}}). \quad (2)$$

From the positive or negative peak area we can estimate the value of $Q_{\text{CyD·guest}}$. The negative peak area always leads to $Q_{\text{CyD·guest}}$, while this is not necessarily the case for the positive peak by the spectrophotometric measurement. Although CyDs have no absorbances in the UV-visible range investigated, the absorbance due to the guest changes with the concentration of the coexisting CyD. However, when the absorbance of the guest in the eluant is monitored at an isosbestic point, the positive and negative peak areas should be equal to each other. In Table 3 is shown such an example for *p*-nitrophenolate, from which formation constants have been determined.

The accuracy of the formation constant determined by the present method depends primarily on the con-

Table 3. Cyclodextrin-*p*-nitrophenolate anion complexes. formation constant and the amount of the complex formed

$10^5\times[\text{guest}]_0$[a] / mol dm^{-3}	$10^3\times[\text{CyD}]$[b] / mol dm^{-3}	$10^8\times Q_{\text{CyD·guest}}$[c] / mol		$10^{-1}\times K$[d] / mol^{-1} dm^3	
		e)	f)	e)	f)
Host: α-Cyclodextrin					
1.03	9.91	12.1	10.3	220	187
	4.96	5.74	5.47	209	199
	2.55	3.14	3.20	222	227
0.516	9.87	6.05	6.18	218	223
	5.26	3.15	3.73	213	253
	2.80	1.52	1.59	193	202
0.103	10.5	1.50	1.45	253	244
	5.04	0.727	0.769	255	267
	2.78	0.386	0.388	246	247
Host: β-Cyclodextrin					
1.03	9.64	4.13	3.81	76.2	70.3
	7.35	2.94	3.49	71.1	84.5
	5.23	2.27	2.15	77.2	73.1
0.516	9.99	2.32	2.15	82.2	76.1
	7.95	1.94	1.98	86.4	88.2
	5.04	1.10	1.57	77.2	110
0.103	9.99	0.508	0.539	89.8	95.3
	7.88	0.446	0.462	100	104
	4.92	0.144	0.162	51.7	58.2

a) Concentration of *p*-nitrophenolate anion in the eluent. b) Concentration of CyD dissolved in the eluent. c) Amount of the complex formed. d) Formation constant. e) Estimated from the positive peak. f) Estimated from the negative peak.

centration of the guest present in the eluent. That is, if $[\text{guest}]_0=K^{-1}$, a 50% of the total CyD molecules exists in the complexed form, and the most precise results are to be expected. The concentrations of CyD and guest have been fixed in this work so that the negative peak appearing on the chromatogram can be clearly recognized. The limit of Beer's law restricts the concentration of CyD as well as that of guest in the eluent. The positive peak is generally sharp, and the absorbance is apt to exceed the limit of Beer's law. The absorbance vs. concentration of guest was checked preliminarily by using the flow-cell. In the present work the product, $[\text{guest}]_0\cdot K$, falls in the order of 10^{-4} when the value of K is of the order of 10, for example, as with α-CyD-benzoate complex. This means that only 0.01% of the total CyD molecules is involved in association with the guest. Nevertheless, it is noticeable that the present results are in reasonable agreement with the literature.

Some of previous studies have suggested that several inorganic anions can form an adduct with CyDs, thereby affecting the formation of CyD inclusion complexes. In this work, we have studied effects of some electrolytes and their ionic strength on the formation of α-CyD complex with *p*-nitrophenolate. The results are shown in Table 4. As will be seen from Table 4, the formation constants measured decrease with increasing ionic strength and the effect is pronounced for NO_3^-. This is in accord with the literature.[6,11] The data of formation constants presented in this paper were obtained under the condition of ionic strength 0.5 adjusted with NaCl except for benzoate, in contrast to phosphate buffer in this case.

Table 4. Effects of electrolyte and ionic strength on the formation constant of α-cyclodextrin-*p*-nitrophenolate[a]

Electrolyte	Ionic strength	Formation constant / 10 mol^{-1} dm^3
KNO_3	0.5	119
	0.3	160
	0.1	195
$NaNO_3$	0.5	122
	0.1	176
KCl	0.5	217
	0.1	222
NaCl	0.5	227
	0.1	233
Na_2HPO_4	0.5	204
	0.3	189
	0.1	212
Phosphate buffer[b]		241

a) Concentration of *p*-nitrophenolate: 5.16×10^{-6} mol dm^{-3}; concentration of α-CyD: of the order of 5×10^{-3} mol dm^{-3}. b) Ionic strength was not adjusted. The ionic strength of buffer (Na_2HPO_4-NaOH) itself was less than 0.05.

Table 5. K_{av} values of guest substances in Sephadex G-10 gel column

Guest substance	Electrolyte used to adjust ionic strength[a]	K_{av}[b]
p-Nitrophenolate	$NaNO_3$	5.9
	NaCl	10.0
	Na_2HPO_4	20.3
p-Nitrophenol	NaCl	21.4
Benzoate	NaCl	1.2
	Na_2HPO_4	2.2
Benzoic acid	NaCl	11.7

a) The ionic strength was adjusted to 0.5. b) The K_{av} value is defined as $(V_e-V_o)/(V_t-V_o)$, where V_e, V_o, and V_t are the elution volume, the void volume, and the total bed volume, respectively.

Cyclodextrins are cyclic oligosaccharides made up of α-1,4-linked D-glucopyranose units. On the other hand, Sephadex G-type gel is prepared by closs-linking polysaccharide dextran with epichlorohydrin. In view of the chemical similarity between these two, similar associations with hydrophobic solutes are probable. Indeed, the affinity of the dextran gel matrix for aromatic and pseudoaromatic substances is particularly striking.[16] In Table 5 are given K_{av} values measured under the same experimental conditions that have been used for formation constants. Table 5 clearly indicates that the guest substances are strongly adsorbed on Sephadex G-10 gel. The order of K_{av} for a given guest may be explained in terms of hydration of the electrolyte, that is, the larger the hydration of electrolyte, the more pronounced the adsorption of the guest onto the gel. In the case of benzoate with the smallest K_{av} value, the ionic strength was adjusted with phosphate buffer,

and thereby the negative peak was made to be retarded. In this case, the ionic strength being adjusted with NaCl, the negative peak appeared so closely to the positive one that no plateau between the two peaks was observed.

The Hummel and Dreyer method is principally based on the sieving function of the gel column, that is, small ligands can be separated from both macromolecules and their associated complexes. In the present chromatography, the separation is due to the adsorption onto the gel phase rather than the sieving. The interaction of small ligands with the gel matrix does not interfere at all with the evaluation of their association with macromolecules so long as the adsorption equilibrium of ligands between the gel phase and the eluent is maintained during the course of chromatography, or it is established rapidly compared with the flow rate of the eluent.

The gel filtration method will serve as a useful technique to determine the formation constant of inclusion compounds of CyDs with various hydrophobic guest substances. However, it should be mentioned that the hydrophobic guests give rise to very broad negative peaks and often make it difficult to measure the peak area. The positive peak is preferable to the negative one if CyDs are pure enough to exhibit no absorbance at the monitoring wavelength.

We wish to thank Mr. Yoshiyuki Nagai for his assistance to the present experiments.

References

1) H. Schlenk and D. M. Sand, *J. Am. Chem. Soc.*, **83**, 2312 (1961).
2) R. L. VanEtten, J. F. Sebastian, G. A. Clowes, and M. L. Bender, *J. Am. Chem. Soc.*, **89**, 3242 (1967).
3) R. I. Gelb, L. M. Schwartz, R. F. Johson, and D. A. Laufer, *J. Am. Chem. Soc.*, **101**, 1869 (1979).
4) T. Osa, T. Matsue, and M. Fujihira, *Heterocycles*, **6**, 1833 (1977).
5) A. Cooper and D. D. MacNicol, *J. Chem. Soc., Perkin Trans. 2*, **1978**, 760.
6) E. A. Lewis and L. D. Hansen, *J. Chem. Soc., Perkin Trans. 2*, **1973**, 2081.
7) R. J. Bergeron, M. A. Channing, G. J. Gibeily, and D. M. Pillor, *J. Am. Chem. Soc.*, **99**, 5146 (1977).
8) R. J. Bergeron, M. A. Channing, and K. A. McGovern, *J. Am. Chem. Soc.*, **100**, 2878 (1978).
9) K. Harata, *Bull. Chem. Soc. Jpn.*, **51**, 2737 (1978).
10) H. Shimizu, A. Kaito, and M. Hatano, *Bull. Chem. Soc. Jpn.*, **52**, 2678 (1979).
11) F. Cramer, W. Saenger, and H.-Ch. Spantz, *J. Am. Chem. Soc.*, **89**, 14 (1967).
12) I. Tabushi, N. Shimizu, T. Sugimoto, M. Shiozuka, and K. Yamamura, *J. Am. Chem. Soc.*, **99**, 7100 (1977).
13) E. S. Hall and H. J. Ache, *J. Phys. Chem.*, **83**, 1805 (1979).
14) K. Uekama, F. Hirayama, S. Nasu, N. Matsuo, and T. Irie, *Chem. Pharm. Bull.*, **26**, 3477 (1978).
15) J. P. Hummel and W. J. Dreyer, *Biochim. Biophys. Acta*, **63**, 532 (1962).
16) J.-C. Janson, *J. Chromatogr.*, **28**, 12 (1967).
17) S. Kadokura, T. Miyamoto, H. Ito, and H. Inagaki, *Polym. J.*, **14**, 121 (1982).
18) N. Yoza, *J. Chem. Educ.*, **54**, 284 (1977).

 © 1984 The Chemical Society of Japan Bull. Chem. Soc. Jpn., 57, 1362—1366 (1984) [Vol. 57, No. 5

Synthesis of Sydnone Compounds Having Heterocyclic Groups at the 4-Positions from 4-(Bromoacetyl)sydnones

Toshio FUCHIGAMI,* Takushi GOTO, Mou-Yung YEH,†
Tsutomu NONAKA,* and Hsien-Ju TIEN†
Department of Electronic Chemistry, Graduate School at Nagatsuta Tokyo Institute of Technology, Nagatsuta, Midori-ku, Yokohama 227
†*Department of Chemistry, National Cheng Kung University, Tainan, Taiwan, Republic of China*
(Received November 24, 1983)

New sydnone derivatives having heterocyclic substituents such as 4-thiazolyl, 3-thienyl, 2H-1,4-benzothiazin-3-yl, 2H-1,4-benzoxazin-3-yl, and 1,2-dihydro-3-quinoxalinyl groups at the 4-positions were prepared from 4-bromoacetyl-3-arylsydnones (**1**). Sydnone compounds substituted by a 1,2,3-triazol-4-yl group were prepared *via* new type phosphonium ylids derived from **1**. Electroreduction of **1** was also attempted in order to prepare a syndnone derivatives having a furyl group.

Although sydnone compounds are interesting in their chemical, physical, and biological properties,[1] their syntheses are limited[2] because a sydnone ring is unstable to acid, alkali, and heat.

As a part of a broad program to study on the synthesis of sydnone compounds and their properties,[3] we have investigated possible synthetic methods for sydnones having heterocyclic groups at their 4-positions: In earlier works, sydnone derivatives substituted directly by 4-thiazolyl,[4,5] 4-sydnonyl,[6,7] 1,2,4-thiadiazol-5-yl,[8] 1,2,4-oxadiazol-5-yl,[9] 3,4-dihydro-1,2,4-oxadiazol-3-yl,[9] 1,2,4-oxadiazol-5-yl,[8] and 1,2,4-triazol-3-yl[8] groups were successfully synthesized. In most of the above synthesis,[8,9] derivatives of sydnone-4-carboxylic acids were used as the starting materials and they were converted into the desired sydnone compounds having heterocyclic groups *via* acyclic intermediates.

Haloacetyl groups are known as good precursors to heterocyclic groups.[10] We have found that 4-bromoacetyl-3-arylsydnones (**1**) could be easily prepared *via* 4-acetyl-3-arylsydnones from the corresponding 4-unsubstituted 3-arylsydnones.[4,11] In this paper, we wish to report the synthesis of new sydnone compounds substituted directly by heterocyclic groups at the 4-positions from **1**.

Results and Discussion

*Reaction of 4-Bromoacetyl-3-phenylsydnone (**1a**) with Thioamides (**2a,b**) and Amidine (**2c**).* Only one synthetic reaction using **1** has been reported by us: It was found that **1a** reacted with thiourea to give 4-(2-amino-4-thiazolyl)-3-phenylsydnone.[4,5] This is the first synthesis of a sydnone having a heterocyclic group at the 4-position, except for 4,4′-bisydnone.[7]

At the first stage of investigation, an analogous reaction (Scheme 1) to the above was examined by using thioamides (**2a,b**) and benzamidine (**2c**) instead of thiourea.

Thiobenzamide (**2a**) reacted readily with **1a** suspended in ethanol at room temperature to form 3-phenyl-4-(2-phenyl-4-thiazolyl)sydnone (**3a**) in a good yield. 3-Phenyl-4-thiocarbamoylsydnone (**2b**) did not react with **1a** under the same conditions. When the reaction was carried out under reflux for a short time, 2,4-bis(3-phenyl-4-sydnonyl)thiazole (**3b**) was obtained in a good yield.

4-(2-Phenyl-4-imidazolyl)-3-phenylsydnone (**3c**) was expected to be formed from **1a** and benzamidine (**2c**), since it is known that α-bromoacetophenone reacts with **2c** to give the corresponding imidazole compound.[12] However, **3c** could not be obtained in ethanol at either room temperature or higher one and decomposition of **1a** and/or **3c** seemed to occur. The reaction in DMF instead of ethanol also gave a similar result. These unsuccessful results may be due to the decomposition of sydnone rings by a strong base of **2c**.

*Reaction of 4-Bromoacetyl-3-phenylsydnone (**1a**) with N,N-Disubstituted Thioamide (**4**).* It is known that the reaction of α-bromoacetophenone with *N,N*-disubstituted thioamides gives the corresponding thiophene

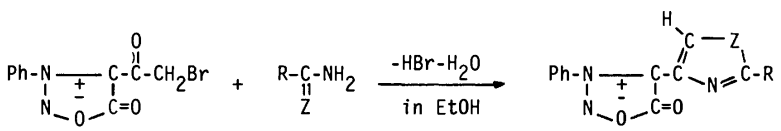

1a 2a~c 3a~c

a: R=Ph, Z=S
b: R=Ph-N(+)(-)C(=O)-O-N=C-, Z=S
c: R=Ph, Z=NH

3a: 80%
3b: 86%
3c: 0%

Scheme 1.

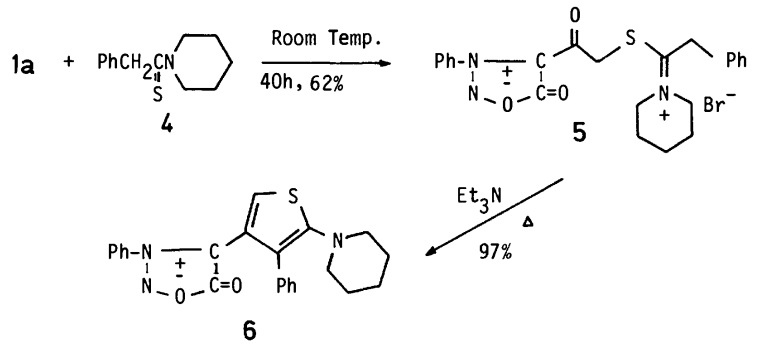

Scheme 2.

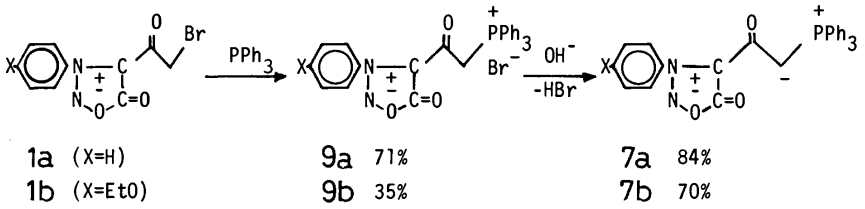

Scheme 3.

compounds.[13]

4-(Bromoacetyl)sydnone **1a** reacted with *N*-[benzyl-(thiocarbonyl)]piperidine (**4**) in dichloromethane at room temperature to form a salt (**5**) (Scheme 2). The structure of **5** was confirmed by IR and mass spectra and elemental analysis. A peak at *m/z* 403 (M^+—HBr—H_2O) was observed in the mass spectrum. The salt **5** decomposes gradually in the air.

The conversion of **5** into 3-phenyl-4-(4-phenyl-5-piperidino-3-thienyl)sydnone (**6**) was successfully carried out by heating **5** with triethylamine in ethanol. In the IR spectrum of **6**, absorption of the carbonyl group of the original **5** disappeared and the molecular ion peak at *m/z* 403 was observed in the mass spectrum.

Synthesis of Phosphonium Ylids (7) from 1 and Triphenylphosphine and their Conversion to 4-(1H-1,2,3-Triazol-4-yl)sydnones (8). It is known that phenacylidentriphenylphosphorane reacts with *p*-toluenesulfonyl azide to give 3-tosyl-4-phenyl-1,2,3-triazole.[14] Since the reaction proceeds under mild conditions, this method seems to be applicable to the synthesis of sydnone derivatives having a 1,2,3-triazol-4-yl group.

First, the synthesis of phosphonium ylid was attempted. Phosphonium bromide (**9**) was obtained by the reaction of **1** with triphenylphosphine in acetonitrile at room temperature. Treatment of **9** with aqueous sodium hydroxide provided phosphonium ylid **7** in a good yield. The structure of **7** was confirmed by comparison of IR spectra of **7** with those of **9**: The C=O stretching vibration band of **9** was at 1660—1670 cm^{-1}, while that of **7** was at 1530—1540 cm^{-1}. The shift was analogous to that of observed in the case of phenacylidenetriphenylphosphorane. The ylid **7** thus obtained melts around 200 °C and was found to be stable.

Next, the synthesis of 4-(1,2,3-triazol-4-yl)sydnone (**8**) from **7** was carried out. The reaction of **7** with

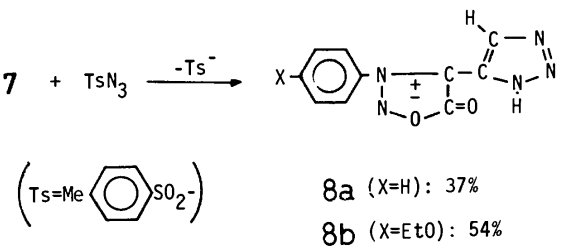

Scheme 4.

p-toluenesulfonyl azide took place in dichloromethane at room temperature, however **8** could not be obtained. The desired product **8** was obtained by the reaction in benzene under reflux for a long time. It is known that a tosyl group is easily eliminated from 4-aryl-3-tosyl-1,2,3-triazole under reflux in ethanol.[14] In a similar manner, **8** seems to be formed by hydrolysis of 3-aryl-4-[3-(*p*-tolylsulfonyl)-1*H*-1,2,3-triazol-4-yl]sydnone formed initially under the reaction conditions used.

Electroreduction of 4-Bromoacetyl-3-phenylsydnone (1a). Barba *et al.*[15] have recently reported an interesting electroreduction of α-bromoacetophenone to 2,4-diphenylfuran. Using the electrochemical method, the synthesis of a sydnone having a furyl group from 4-(bromoacetyl)sydnone (**1a**) was attempted.

The electroreduction of **1a** was carried out by means of controlled potential electrolysis at a mercury pool cathode in a DMF solution containing lithium perchlorate as a supporting electrolyte in a divided cell. One Faraday (96480 C)/mol of charge was coulometrically passed at −0.15 V *vs.* Ag/$AgNO_3$ (saturated in DMF). Products separated by a column chromatograph were not the expected furan compound but 4-acetyl-3-phenylsydnone (22% yield and 44% current efficiency) and the corresponding reduction dimer, 1,4-bis(3-phenyl-4-sydnonyl)-1,4-butanedi-

Table 1. Synthesis of sydnone derivatives (**11**—**13**)

X	Z	Solvent	Molar ratio (amine/**2**)	Reaction time (Temp)	Product (Yield/%)
H	S	EtOH	1	5 min (rt)	**11a**(85)
EtO	S	EtOH	1	1 h (rt)	**11b**(83)
H	O	DMF	1	30 h (rt)	**12** (15)
H	NH_2	EtOH	1	1 h (rt)	**13a**(0)
H	NH_2	EtOH	1	5 min (reflux)	**13a**(0)
H	NH_2	EtOH	2	5 min (reflux)	**13a**(80)
H	NH_2	DMF	1	75 min (rt)	**13a**(43)
H	NH_2	DMF	2	75 min (rt)	**13a**(82)
EtO	NH_2	EtOH	2	10 min (60 °C)	**13b**(72)

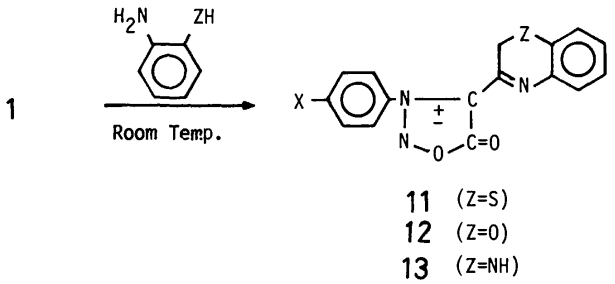

11 (Z=S)
12 (Z=O)
13 (Z=NH)

Scheme 5.

one (**10**) (7% yield and 7% current efficiency) whose structure was assigned from IR and mass spectra and analytical data.

Although a few papers deal with electrooxidation[16-18] and polarography[2b] of sydnones, no report of the electroreduction of sydnone compounds by means of preparative electrolysis has been published.[19] In this situation, it is interesting to note that the electroreduction of **1a** proceeded without any decomposition of the sydnone ring.

*Synthesis of Sydnone Compounds Having Six-membered Heterocyclic Groups (**11**, **12**, **13**).* The synthesis of sydnones substituted by six-membered heterocyclic groups at the 4-position has not been reported. In this work, the synthesis of such sydnone compounds was attempted using the reaction of **1** with *o*-aminophenol, *o*-aminobenzenethiol, and *o*-phenylenediamine.

o-Aminobenzenethiol reacted readily with **1** in ethanol at room temperature to give 4-(2*H*-1,4-benzothiazin-3-yl)sydnone (**11**) in a good yield, while *o*-aminophenol did not give the corresponding 4-(2*H*-1,4-benzoxazin-3-yl)sydnone (**12**) under the same conditions. Recently, Schrider *et al.*[20] prepared 2*H*-1,4-benzoxazines by heating α-bromoacetophenones and *o*-aminophenol in acetone in the presence of excess potassium carbonate. Using their procedure the reaction of **1a** with *o*-aminophenol was attempted. However, only decomposition took place even when the reaction was carried out at room temperature and no desired **12** was formed. After several trials, **12** could be synthesyzed by changing the solvent and base to DMF and 1 equiv. of sodium hydroxide, respectively. The compound **12** was very sensitive to base and the use of excess amount of the base caused the decomposition of **12**.

In the reaction with *o*-phenylenediamine, as shown in Table 1, the yield of 4-(3,4-dihydro-2-quinoxalinyl)-sydnone (**13**) strongly depended on the reaction conditions. When 2 equiv. of the diamine was used, the expected product **13** was obtained in satisfactory yields.

The new types of sydnone compounds thus prepared are expected to be pharmacologically active and screening tests of several biological activities of these sydnones are currently under investigation.

Experimental

^{1}H NMR spectra were recorded at 60 MHz on a Varian EM360 NMR spectrometer using DMSO-d_6 and Me_4Si as solvent and an internal standard, respectively. IR spectra were obtained on a Hitachi 295 infrared spectrometer. Electron impact mass spectra were determined at 30 eV on a JEOL JMS-D100 mass spectrometer by direct introduction *via* probe.

*4-Bromoacetyl-3-(p-ethoxyphenyl)sydnone (**1b**).* Using the procedure similar to preparation of **1a**,[4] the crude product was obtained. Recrystallization from ethanol provided pure **1b** as a yellow solid. Yield, 71%. Mp 133—134 °C. IR (KBr) 3000, 2950, 2900 (ν_{C-H}), 1770, and 1690 cm^{-1} ($\nu_{C=O}$). MS: *m/z* (rel intensity) 298 (M^++2−NO, 2), 296 (M^+−NO, 2), 270 (M^++2−NO−CO, 24), 268 (M^+−NO−CO, 24), and 148 (100). Found: C, 44.00; H, 3.20; N, 8.41; Br, 24.24%. Calcd for $C_{12}H_{11}N_2O_3Br$: C, 44.06; H, 3.39; N, 8.56; Br, 24.43%.

*3-Phenyl-4-(2-phenyl-4-thiazolyl)sydnone (**3a**).* To a stirred solution of 0.39 g (2.84 mmol) of thiobenzamide in 10 ml of ethanol was added 0.80 g (2.83 mmol) of **1a** and the mixture was stirred at room temperature for 10 min. The yellow precipitates were collected by filtration and washed with ethanol; 0.73 g, 80%. Recrystallization from ethanol provided 0.68 g (75%) of pure **2a** as pale yellow needles. Mp 183—183.5 °C. IR (KBr) 1770 cm^{-1} ($\nu_{C=O}$). ^{1}H NMR δ=7.47 (s, 5H, $C_6\underline{H}_5$), 7.80 (s, 5H, $C_6\underline{H}_5$), and 8.15 (s, 1H, thiazol C-$\underline{H}$). MS: *m/z* (rel intensity) 321 (M^+, 30) and 263 (M^+−NO−CO, 100). Found: C, 63.50; H, 3.23; N, 13.12; S, 10.26%. Calcd for $C_{17}H_{11}N_3O_2S$: C, 63.54; H, 3.45; N, 13.08; S, 9.98%.

*2,4-Bis(3-phenyl-4-sydnonyl)thiazole (**3b**).* After a mixture of 0.39 g (1.39 mmol) of **1a** and 0.30 g (1.36 mmol) of 3-phenyl-4-thiocarbamoylsydnone in 2 ml of ethanol was refluxed for 15 min, yellow precipitates appeared. After cooling, the precipitates were collected by filtration and washed with ethanol; 0.47 g, 86%. Mp 241—242.5 °C (de-

comp). Recrystallization from dichloromethane-hexane provided pure 0.37 g (66%) of **2b** as yellow needles. Mp 242—243 °C (decomp). IR (KBr) 1775 and 1765 cm^{-1} ($\nu_{C=O}$). ^1H NMR δ=7.45—7.83 (m, 10H, $C_6\underline{H}_5$), 8.21 (s, 1H, thiazol C-$\underline{H}$). MS: *m/z* (rel intensity) 405 (M^+, 5), 347 (M^+—NO—CO, 10), 289 (M^+—2NO—2CO, 5), and 147 (100). Found: C, 56.26; H, 2.63; N, 17.24; S, 8.04%. Calcd for $C_{19}H_{11}N_5O_4S$: C, 56.29; H, 2.74; N, 17.28; S, 7.91%.

1-[2-Phenyl-1-[(3-phenyl-4-sydnonyl)carbonylmethylthio]ethylidene]piperidinium Bromide (5). A mixture of 0.78 g (3.56 mmol) of *N*-[benzyl(thiocarbonyl)]piperidine (**4**)[21] and 1.00 g (3.53 mmol) of **1a** in 15 ml of dichloromethane was allowed to stand for 40 h at room temperature. The resulting precipitates were collected by filtration and pale pink prisms (0.95 g, 54%) were obtained. The filtrate was concentrated under reduced pressure and 0.14 g (8%) of a precipitating solid was obtained. Recrystallization from dichloromethane-ether provided 0.72 g (41%) of pure **5** as a pale pink solid. Mp 183—185 °C (decomp). IR (KBr) 1780 and 1720 cm^{-1} ($\nu_{C=O}$). MS: *m/z* (rel intensity) 403 (M^+—HBr—H_2O, 45) and 345 (M^+—HBr—H_2O—NO—CO, 100). Found: C, 55.20; H, 4.86; N, 8.21; S, 6.32; Br, 16.09%. Calcd for $C_{23}H_{24}N_3O_3SBr$: C, 54.98; H, 4.82; N, 8.46; S, 6.38; Br, 15.90%.

3-Phenyl-4-(4-phenyl-5-piperidino-3-thienyl)sydnone (6). A mixture of 0.60 g (1.19 mmol) of **5** and 0.13 g (1.29 mmol) of triethylamine in 20 ml of ethanol was refluxed for 30 min. After concentration, the residue was mixed with *ca.* 50 ml of water. A precipitating solid was collected by filtration, washed with water, and 0.47 g (97%) of a yellow solid was obtained. Mp 129.5—133 °C (decomp). Recrystallization from aq ethanol provided 0.29 g (59%) of pure **6** as a yellow solid. Mp 131—133 °C (decomp). IR (KBr) 1760 cm^{-1} ($\nu_{C=O}$). ^1H NMR δ=1.43 (br. S, 8H, $C\underline{H}_2$), 4.55 (s, 2H, $C\underline{H}_2$), 6.39 (s, 1H, thiophene C-$\underline{H}$), 7.23 (s, 5H, $C_6\underline{H}_5$), and 7.64 (s, 5H, $C_6\underline{H}_5$). MS: *m/z* (rel intensity) 403 (M^+, 7), 345 (M^+—NO—CO, 13), and 64 (100). Found: C, 68.51; H, 5.50; N, 10.04%. Calcd for $C_{23}H_{21}N_3O_2S$: C, 68.46; H, 5.25; N, 10.41%.

(3-Phenyl-4-sydnonylcarbonylmethyl)triphenylphosphonium Bromide (9a). To a stirred solution of 4.00 g (14.9 mmol) of triphenylphosphine in 60 ml of acetonitrile was added a solution of 4.00 g (14.1 mmol) of **1a** in 20 ml of acetonitrile and the mixture was stirred for 2 h. After concentration of the solution, ether was added and 5.45 g of insoluble material was collected by filtration. Mp 208—210 °C (decomp). Recrystallization from dichloromethane-hexane provided 2.70 g (50%) of pure **9a** as pale yellow crystals. Mp 209—211 °C (decomp). IR (KBr) 1775 and 1670 cm^{-1} ($\nu_{C=O}$). ^1H NMR δ=5.65 (s, 1H, C$\underline{H}$), 5.85 (s, 1H, C$\underline{H}$), 7.63, 7.75, and 7.88 (s, 20H, $C_6\underline{H}_5$). Found: C, 61.96; H, 4.10; N, 5.38%. Calcd for $C_{28}H_{22}N_2O_3BrP$: C, 61.67; H, 4.07; N, 5.14%.

(3-Phenyl-4-sydnonylcarbonylmethylene)triphenylphosphorane (7a). To a stirred solution of 1.96 g (9.94 mmol) of **9a** in 40 ml of dichloromethane was added 10 ml of 10% sodium hydroxide at room temperature. After the dichloromethane layer had been separated and dried over sodium sulfate, concentration of the solution provided 1.40 g (84%) of **7a**. Mp 222—224 °C (decomp). IR (KBr) 1760 and 1530 cm^{-1} ($\nu_{C=O}$). ^1H NMR δ=4.56, 4.96 (s, 1H, C$\underline{H}$), 7.60, 7.62, and 7.71 (s, 20H, C_6H_5). Found: C, 72.61; H, 4.49; N, 5.97%. Calcd for $C_{28}H_{21}N_2O_3P$: C, 72.41; H, 4.56; N, 6.03%.

[3-(p-Ethoxyphenyl)-4-sydnonylcarbonylmethylene]triphenylphosphorane (7b). Phosphonium bromide (**9b**) was prepared from **1b** and triphenylphosphine. IR (KBr) 1780 and 1660 cm^{-1} ($\nu_{C=O}$). Without purification, crude **9b** was used for the preparation of **7b**. By the procedure similar to the preparation of **7a**, crude **7b** was obtained from **9b**. Mp 196—197 °C. Recrystallization from dichloromethane-hexane provided pure **7b** as yellow crystals. Mp 196—197 °C. IR (KBr) 1750 and 1540 cm^{-1} ($\nu_{C=O}$). MS: *m/z* (rel intensity) 508 (M^+, 3) and 262 (PPh_3, 100). Found: C, 70.67; H, 4.89; N, 5.37%. Calcd for $C_{30}H_{25}N_2O_4P$: C, 70.86; H, 4.96; N, 5.51%.

3-Phenyl-4-(1H-1,2,3-triazol-4-yl)sydnone (8a). A mixture of 1.00 g (2.15 mmol) of **7a** and 0.50 g (2.54 mmol) of *p*-toluenesulfonyl azide in 80 ml of benzene was refluxed for 44 h. Black oily material was obtained after concentration of the solution. A solution of the oil in a small amount of ethyl acetate was allowed to stand for one week and crystals precipitated. Colorless needles were collected by filtration and washed with ethyl acetate, 0.18 g (37%). Mp 215—217 °C. Recrystallization from dichloromethane-hexane provided pure 0.12 g (24%) of **8a** as colorless needles. Mp 215—217 °C. IR (KBr) 3160 (ν_{NH}), 1715 ($\nu_{C=O}$), and 1605 cm^{-1} ($\nu_{C=N}$). ^1H NMR δ=7.79 (s, 5H,$C_6\underline{H}_5$), 8.13 (br. s, 1H, triazole C-$\underline{H}$), and 15.49 (br. s, 1H, N$\underline{H}$). MS: *m/z* (rel intensity) 229 (M^+, 12), 171 (M^+—NO—CO, 87), and 77 (C_6H_5, 100). Found: C, 52.20; H, 2.87; N, 30.58%. Calcd for $C_{10}H_7N_5O_2$: C, 52.40; H, 3.08; N, 30.56%.

3-(p-Ethoxyphenyl)-4-(1H-1,2,3-triazol-4-yl)sydnone (8b). In a similar manner, the reaction of **7b** with *p*-toluenesulfonyl azide was carried out. After the reaction, benzene was removed by evaporation and black oily material remained. The oil was dissolved in dichloromethane and the solution was treated with active charcoal. Concentration of the solution to dryness provided a solid. Recrystallization from dichloromethane-hexane (4:1) provided pure **8b** as colorless needles (54%). Mp 241—242 °C. IR (KBr) 3130 (ν_{NH}), 3000, 2920, 2860 (ν_{C-H}), and 1740 cm^{-1} ($\nu_{C=O}$). ^1H NMR δ=1.38 (t, 3H, C$\underline{H}_3$), 4.14 (q, 2H, C$\underline{H}_2$), 7.16 (d, 2H, *p*-EtOC$_6\underline{H}_4$), 7.70 (d, 2H, *p*-EtOC$_6\underline{H}_4$), 8.04 (s, 1H, triazole C-$\underline{H}$), 15.30 (br. s, 1H, N$\underline{H}$). MS: *m/z* (rel intensity) 273 (M^+, 18) and 215 (M^+—NO—CO, 100). Found: C, 52.70; H, 3.85; N, 25.28%. Calcd for $C_{12}H_{11}N_5O_3$: C, 52.75; H, 4.06; N, 25.63%.

Electroreduction of 4-Bromoacetyl-3-phenylsydnone (1a). An H-type cell divided with a sintered glass diaphragm was used. The cathode and anode were a mercury pool (7.07 cm^2) and a platinum plate (2.5×2.5 cm^2), respectively. 50 ml and 30 ml of 0.2 M $LiClO_4$/MeCN solution were used as catholyte and anolyte, respectively. To the catholyte was added 1.42 g (5 mmol) of **1a** and electricity was supplied. The cathode potential and temperature were maintained at −0.15 V *vs.* Ag/$AgNO_3$ (sat. in DMF) (an initial cathodic current density, 1.13 A/dm^2) and at 20 °C, respectively, during electrolysis. When 495 C (1.03F/mol) was passed, the cathodic current decreased to the background level. After electrolysis, the brown catholyte was concentrated under reduced pressure below 60 °C and 50 ml of water was added. The mixture was extracted respeatedly with dichloromethane and the extracts were washed with water, and then dried over anhydrous sodium sulfate. After the extract solution had been concentrated, the remaining reddish oily material was subjected to TLC (silica gel). Elution with dichloromethane provided 0.22 g (22%) of 4-acetyl-3-phenylsydnone (first elution component) and 0.15 g (7%) of 1,4-bis(3-phenyl-4-sydnonyl)-1,4-butandione (**10**) (second component). Product **10**: mp 237—238 °C (decomp). IR (KBr) 3080 (ν_{CH}), 2930 (ν_{CH_2}), 1780 ($\nu_{C=O}$ of sydnone ring), and 1660 cm^{-1} ($\nu_{C=O}$). *m/z* 406 (M^+). Found: C, 58.87; H, 3.20; N, 13.71%. Calcd for $C_{20}H_{14}N_4O_6$: C, 59.12; H, 3.47; N, 13.79%.

4-(2H-1,4-Benzothiazin-3-yl)-3-phenylsydnone (11a). To a stirred solution of 0.30 g (1.06 mmol) of **1a** in 2 ml of ethanol was added a solution of 0.14 g (1.08 mmol) of *o*-

aminobenzenethiol in 2 ml of ethanol at room temperature. After stirring for 5 min, *ca.* 10 ml of water was added to the reaction mixture and a resulting solid was collected by filtration. Washing with ethanol provided 0.28 g (85%) of an orange yellow solid. Mp 166—168 °C (decomp). Recrystallization from ethanol provided 0.25 g (76%) of pure **11a** as orange yellow needles. Mp 166—168 °C (decomp). IR (KBr) 3060, 2990 (ν_{C-H}), 1770 ($\nu_{C=O}$), and 1590 cm^{-1} ($\nu_{C=N}$). ^1H NMR δ=3.84 (s, 2H, $C\underline{H}_2$), 6.56—7.26 (m, 4H, aromatic C-$\underline{H}$), and 7.93 (s, 5H, $C_6\underline{H}_5$). MS: *m/z* (rel intensity) 309 (M^+, 53) and 251 (M^+—NO—CO, 100). Found: C, 62.35; H, 3.89; N, 13.49; S, 10.36%. Calcd for $C_{16}H_{11}N_3O_2S$: C, 62.12; H, 3.58; N, 13.58; S, 10.37%.

4-(2H-1,4-Benzothiazin-3-yl)-3-(p-ethoxyphenyl)sydnone (11b). By the same procedure, the pure product **11b** was directly obtained without purification. Mp 132—134 °C. IR (KBr) 3000, 2950, 2900 (ν_{C-H}), 1775 ($\nu_{C=O}$), and 1600 cm^{-1} ($\nu_{C=N}$). ^1H NMR δ=1.38 (t, 3H, $C\underline{H}_3CH_2O$), 3.80 (s, 2H, $C\underline{H}_2$), 4.17 (q, 2H, $CH_3C\underline{H}_2O$), 6.56—7.30 (m, 4H, aromatic C-$\underline{H}$), 7.12 (d, 2H, *p*-$EtOC_6\underline{H}_4$), and 7.68 (d, 2H, *p*-$EtOC_6\underline{H}_4$). MS: *m/z* (rel intensity) 353 (M^+, 11), 295 (M^+—NO—CO, 17), and 44 (100). Found: C, 61.33; H, 4.21; N, 11.80; S, 8.91%. Calcd for $C_{18}H_{15}N_3O_3S$: C, 61.15; H, 4.28; N, 11.89; S, 9.07%.

4-(2H-1,4-Benzoxazin-3-yl)-3-phenylsydnone (12). To a mixture of 0.40 g (3.67 mmol) of *o*-aminophenol, 3.9 ml of 1M† sodium hydroxide and 20 ml of DMF was added a solution of 1.00 g (3.53 mmol) of **1a** in 5 ml of DMF. The mixture was allowed to stand for 30 h. To the brown reaction mixture was added *ca.* 100 ml of water and a precipitating solid was collected, and then washed with water. The solid was chromatographed on silica gel (70—230 mesh). Elution with benzene provided 0.15 g (15%) of almost pure **12**. Mp 162.5—163.5 °C (decomp). Recrystallization from dichloromethane-hexane provided **12** as yellow needles. Mp 162.5—163.5 °C (decomp). IR (KBr) 3070 (ν_{C-H}), 1770 ($\nu_{C=O}$), and 1605 cm^{-1} ($\nu_{C=N}$). ^1H NMR δ=5.05 (s, 2H, $C\underline{H}_2$), 6.70—7.10 (m, 4H, aromatic C-$\underline{H}$), and 7.93 (s, 5H, $C_6\underline{H}_5$). MS: *m/z* (rel intensity) 293 (M^+, 57) and 235 (M^+—NO-CO, 100). Found: C, 65.60; H, 3.61; N, 14.24%. Calcd for $C_{16}H_{11}N_3O_3$: C, 65.53; H, 3.78; N, 14.33%.

4-(3,4-Dihydro-2-quinoxalinyl)-3-phenylsydnone (13a). To a hot solution of 0.16 g (1.45 mmol) of *o*-phenylenediamine in 2 ml of ethanol was added 0.20 g of **1a** and the mixture was refluxed for *ca.* 5 min. After cooling, 0.17 g (80%) of resulting reddish precipitate were collected by filtration. Recrystallization from dichloromethane-hexane provided pure **13a** as reddish crystals. Mp 143—146 °C (decomp). IR (KBr) 3430 (ν_{NH}), 1775 ($\nu_{C=O}$), and 1610 cm^{-1} ($\nu_{C=N}$). ^1H NMR δ=4.23 (d, 2H, *J*=1.8 Hz, $C\underline{H}_2$), 6.08 (d, 1H, *J*=1.8 Hz, N$\underline{H}$), 6.31—7.01 (m, 4H, aromatic C-$\underline{H}$), and 7.69 (s, 5H, $C_6\underline{H}_5$). MS: *m/z* (rel intensity) 292 (M^+, 18), 248 (M^+—CO_2, 27), 234 (M^+—NO—CO, 45), and 44 (100). Found: C, 65.62; H, 4.21; N, 19.14%. Calcd for $C_{16}H_{12}N_4O$: C, 65.75; H, 4.14; N, 19.17%.

When DMF was used as a solvent, the reaction was carried out at room temperature. After the reaction, addition of water to the reaction mixture provided the crude product of **13a**.

4-(3,4-Dihydro-2-quinoxalinyl)-3-(p-ethoxyphenyl)sydnone (13b). By the same procedure, pure **13b** was obtained without purification by the reaction of **1b** in ethanol. Mp 162.5—163 °C. IR (KBr) 3380 (ν_{NH}), 3000, 2950, 2900 (ν_{C-H}), 1780, 1760 ($\nu_{C=O}$), and 1610 cm^{-1} ($\nu_{C=N}$). ^1H NMR δ=1.40 (t, 3H, $C\underline{H}_3$), 4.00—4.36 (m, 4H, $CH_3C\underline{H}_2$, and $C\underline{H}_2NH$), 6.12 (s, 1H, N$\underline{H}$), 6.40—7.18 (m, 4H, aromatic C-$\underline{H}$), 7.22 (d, 2H, *p*-$EtOC_6\underline{H}_4$), and 7.73 (d, 2H, *p*-$EtOC_6\underline{H}_4$). MS: *m/z* (rel intensity), 336 (M^+, 26), 278 (M^+—NO—CO, 81), and 276 (100). Found: C, 64.07; H, 4.60; N, 16.54%. Calcd for $C_{18}H_{16}N_4O_3$: C, 64.28; H, 4.79; N, 16.66%.

† 1 M=1 mol dm^{-3}.

Referenes

1) a) F. H. C. Stewart, *Chem. Rev.*, **64**, 129 (1964); b) M. Ohta and H. Kato, "Non-benzenoid Aromatics," Academic Press, New York (1969), p. 117; c) C. G. Newton and C. A. Ramsden, *Tetrahedron*, **38**, 2965 (1982).

2) M.-Y. Yeh, H.-J. Tien, and T. Nonaka, *J. Org. Chem.*, **48**, 1382 (1983).

3) a) H.-J. Tien, T. Nonaka, T. Fuchigami, T. Sekine, and M. Ohta, *Nippon Kagaku Kaishi*, **1978**, 1308; b) M.-Y. Yeh, H.-J. Tien, J.-T. Chow, and T. Nonaka, *Bull. Chem. Soc. Jpn.*, **54**, 947 (1981).

4) H.-J. Tien, K. Kanda, A. Chinone, and M. Ohta, *Bull. Chem. Soc. Jpn.*, **46**, 3304 (1973).

5) Upadhya *et al.* also synthesized sydnones substituted by a 4-thiazolyl group: K. G. Upadhya, B. V. Badami, G. S. Puranik, V. N. Biradar, and S. Nanjappa, *Arch. Pharm. (Weinheim, Ger.)*, **313**, 684 (1980); *Chem. Abstr.*, **94**, 47195y (1981).

6) H.-J. Tien and M.-Y. Yeh, *J. Chinese Chem. Soc. (Taipei)*, **24**, 123 (1977).

7) Stewart also synthesized sydnones substituted by a 4-sydnonyl group: F. H. C. Stewart, *J. Chem. Soc.*, **1963**, 701.

8) T. Fuchigami M.-Y. Yeh, T. Goto, T. Nonaka, and H.-J. Tien, *Bull. Chem. Soc. Jpn.*, **57**, 116 (1984).

9) M.-Y. Yeh, T. Nonaka, T. Goto, M.-C. Hsu, T. Fuchigami, and H.-J. Tien, *Bull. Chem. Soc. Jpn.*, **56**, 3535 (1983).

10) Most recently, we have reported a novel preparation of 4-aminothiazole compounds from haloacetyl derivatives and alkoxythiocarbonylcyanamide salts: T. Fuchigami and T. Nonaka, *J. Org. Chem.*, **48**, 3340 (1983); T. Fuchigami, M.-Y. Yeh, T. Nonaka, and H.-J. Tien, *Bull. Chem. Soc. Jpn.*, **56**, 3851 (1983).

11) H.-J. Tien and M. Ohta, *Bull. Chem. Soc. Jpn.*, **45**, 2944 (1972).

12) F. Kunckell, *Chem. Ber.*, **34**, 637 (1901).

13) H. Hartmann and R. Manger, *Z. Chem.*, **6**, 28 (1966).

14) G. R. Harrey, *J. Org. Chem.*, **31** 1587 (1966).

15) F. Barba, M. D. Veasco, and A. Guirado, *Synthesis*, 625 (1981).

16) H.-J. Tien, T. Nonaka, T. Fuchigami, and T. Sekine, *J. Electrochem. Soc. Jpn.*, **47**, 449 (1979).

17) H.-J. Tien, T. Nonaka, and M.-Y. Yeh, *J. Chinese Chem. Soc. (Taipei)*, **28**, 161 (1981).

18) H.-J. Tien, T. Nonaka, and T. Sekine, *Chem. Lett.*, **1979**, 283.

19) A sydnone ring is very easily reduced at cathodes to decompose. The synthesis of 4-aminosydnones by electroreduction of 4-nitrosydnones was not successful because the reduction of the ring is easier than that of the nitro group: H.-J. Tien, T. Nonaka, and T. Fuchigami, unpublished results.

20) D. R. Scridhar, C. V. R. Sastry, O. P. Bansal, and P. P. Rao, *Synthesis*, 912 (1981).

21) E. C. Kornfeld, *J. Org. Chem.*, **16**, 131 (1951).

 © 1984 The Chemical Society of Japan Bull. Chem. Soc. Jpn., 57, 1367—1370 (1984)

Asymmetric Hydrogenation of Schiff Base Prepared from α-Keto Ester with Aliphatic Amino Acid Ester

Kaoru HARADA and Shozo SHIONO
Department of Chemistry, The University of Tsukuba, Sakura-Mura, Niihari, Ibaraki 305
(Received November 29, 1983)

Catalytic hydrogenation of Schiff bases prepared from α-keto esters with amino acid esters was carried out under various conditions. A significant substituent effect of the alkyl group of the ester moiety of amino acid on the stereoselectivity was observed in the hydrogenation of the Schiff bases prepared from methyl pyruvate with (*S*)-alanine ester. Higher asymmetric yields were obtained as the ester residue of amino acid ester became bulkier. A clear temperature effect on the asymmetric hydrogenation was also observed. These results could be explained by the chelation mechanism.

Several studies on the asymmetric hydrogenation of carbon-nitrogen double bonds have been performed.[1-3] In the previous study, hydrogenolytic asymmetric transamination of Schiff bases, prepared from α-keto ester with optically active benzylic amine and optically active aromatic amino acid ester, has been carried out.[4-7] The steric course of the catalytic hydrogenation was explained by the chelation mechanism assuming that the substrate forms a five-membered chelated intermediate with the catalyst and then hydrogenation reaction takes place from the less bulky side of the chelated substrate. The chelation mechanism was supported by the infrared absorption spectrum of ethyl 2-hydroxyimino-3-oxo-3-phenylpropionate on palladium metal which was measured by using the high-sensitivity reflection method.[8] Recently, asymmetric synthesis of amino acid by hydrogenation of the Schiff bases prepared from aliphatic amino acid *t*-butyl esters and methyl pyruvate, followed by oxidative cleavage of carbon-nitrogen single bond was reported by Yamada *et al.*[9] In the present study, the catalytic hydrogenation of Schiff bases prepared from α-keto ester with several aliphatic amino acid esters was carried out in order to examine the steric course of this kind of asymmetric hydrogenation.

Results and Discussion

Schiff bases prepared from α-keto esters with several aliphatic amino acid esters were hydrogenated with 5% palladium on charcoal in several solvents and at various temperatures. The solvents used are methanol, ethanol, 2-propanol, and ethyl acetate, and the reaction temperatures used are in a range −10—+30 °C. The diastereomeric ratio of the resulting iminodicarboxylic acid was determined by gas chromatographic analysis after derivatization of the hydrogenated product to *N*-(trifluoroacetyl)iminodicarboxylic acid diisopropyl ester.

Hydrogenation of the Schiff bases prepared from methyl pyruvate with four kinds of amino acid ester (methyl, ethyl, isopropyl, and *t*-butyl) was carried out in order to examine the substituent effect of the ester group of the chiral moieties on the asymmetric yield. The results were shown in Fig. 1 and Tables 1 and 2. When (*S*)-alanine ester was used as a chiral moiety, (2*S*,2′*S*)-2,2′-iminodipropionic acid was produced dominantly in all cases, and higher asymmetric yield was obtained as the ester group of the amino acid ester became larger as shown in Fig. 1. When (*R*)-2-aminobutyric acid ester was used as a chiral moiety, (*R*)-2-[(*R*)-1-carboxyethylamino]butyric acid was produced dominantly, and similar substituent effect in the ester group of the amino acid ester on the asymmetric yield was observed as shown in Table 2. These results indicate that the asymmetric yield of the newly formed iminodicarboxylic acid depends strongly on the bulkiness of the ester group of the chiral amino acid ester, but depends little on the bulkiness of the alkyl group of the amino acid used as the chiral moiety.

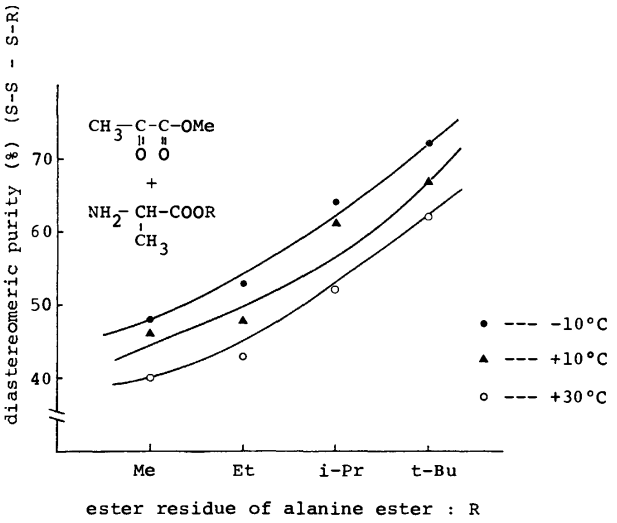

Fig. 1. Substituent effect on the asymmetric yield.

Hydrogenation of the Schiff bases prepared from methyl 2-oxobutyrate with (*S*)-alanine ester was carried out in order to examine the substituent effect of the alkyl group attached to the carbonyl group of the α-keto ester. The results were summarized in Table 3. (*S*)-2-[(*S*)-1-Carboxyethylamino]butyric acid was obtained dominantly in all cases and higher asymmetric yields were obtained as the ester residue of the amino acid ester became bulkier. An interesting result obtained is that lower asymmetric yield was obtained by using methyl 2-oxobutyrate rather than methyl pyruvate.

Hydrogenation of Schiff bases prepared from (*S*)-alanine with ethyl pyruvate instead of methyl pyruvate was carried out. The results were summarized in Table

Table 1. Hydrogenation of Schiff bases prepared from (*S*)-alanine ester and methyl pyruvate

Entry	Ester residue	Solvent	Temp/°C	d.p./%[a,b]	Yield/%[c]
1	Me	MeOH	−10	48	64
2	Me	MeOH	10	46	74
3	Me	MeOH	30	40	46
4	Me	EtOH	10	41	45
5	Me	*i*-PrOH	10	42	65
6	Me	AcOEt	−10	45	66
7	Me	AcOEt	10	38	45
8	Me	AcOEt	30	33	58
9	Et	MeOH	−10	53	59
10	Et	MeOH	10	48	69
11	Et	MeOH	30	43	55
12	Et	EtOH	10	45	45
13	Et	*i*-PrOH	10	48	63
14	Et	AcOEt	10	38	61
15	*i*-Pr	MeOH	−10	64	77
16	*i*-Pr	MeOH	10	61	57
17	*i*-Pr	MeOH	30	52	62
18	*i*-Pr	EtOH	10	58	63
19	*i*-Pr	*i*-PrOH	10	61	51
20	*i*-Pr	AcOEt	10	53	57
21	*t*-Bu	MeOH	−10	72	58
22	*t*-Bu	MeOH	10	67	65
23	*t*-Bu	MeOH	30	62	70

a) Diastereomeric purity. b) The configuration of newly formed chiral center were all S. c) Based on methyl pyruvate.

Table 2. Hydrogenation of Schiff bases prepared from (*R*)-2-aminobutyric acid ester and methyl pyruvate

Entry	Ester residue	Solvent	Temp/°C	d.p./%[a,b]	Yield/%[c]
1	Me	MeOH	−10	52	76
2	Me	MeOH	10	48	83
3	Me	MeOH	30	41	81
4	Me	EtOH	10	40	30
5	Me	*i*-PrOH	10	34	64
6	Me	AcOEt	10	26	39
7	Et	MeOH	10	45	75
8	*i*-Pr	MeOH	10	63	80
9	*t*-Bu	MeOH	10	69	68

a) Diastereomeric purity. b) The configuration of newly formed chiral center were all *R*. c) Based on methyl pyruvate.

4. The results obtained by the use of ethyl pyruvate were almost the same as that obtained by the use of methyl pyruvate.

A Schiff base has two geometric isomers, *E* and *Z*. The major isomer of the substrate Schiff base used in this asymmetric hydrogenation could be the E isomer because the alkoxycarbonyl group of the α-keto esters

Table 3. Hydrogenation of Schiff bases prepared from (*S*)-alanine ester and methyl 2-oxobutyrate

Entry	Ester residue	Solvent	Temp/°C	d.p./%[a,b]	Yield/%[c]
1	Me	MeOH	10	25	42
2	Me	*i*-PrOH	10	23	36
3	Me	AcOEt	10	20	39
4	Et	MeOH	10	32	37
5	*i*-Pr	MeOH	10	43	36

a) Diastereomeric purity. b) The configuration of newly formed chiral center were all *S*. c) Based on methyl 2-oxobutyrate.

Table 4. Hydrogenation of Schiff bases prepared from (*S*)-alanine ester and ethyl pyruvate

Entry	Ester residue	Solvent	Temp/°C	d.p./%[a,b]	Yield/%[c]
1	Me	MeOH	10	46	61
2	Et	MeOH	10	51	73
3	*i*-Pr	MeOH	10	60	53

a) Diastereomeric purity. b) The configuration of newly formed chiral center were all *S*. c) Based on ethyl pyruvate.

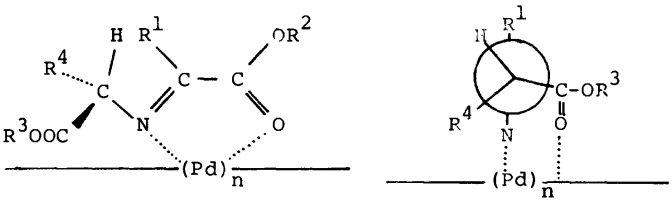

Fig. 2. Palladium-substrate complex.

are much bulkier than methyl or ethyl groups attached to the α-carbon of α-keto esters. If this is the case, the substrate-catalyst complex could be expected to form prior to catalytic hydrogenation as expected by the chelation mechanism. This five-membered chelated intermediate of the Schiff base used in the present study could be depicted as shown in Fig. 2. Considering the steric interaction between the alkyl substituent at the α-carbon of the α-keto ester and amino acid residue and the adsorption of the ester carbonyl oxygen of amino acid ester to catalyst, the conformation of the chiral moiety of the Schiff base with the catalyst could be that as shown in Fig. 2. The existence of the five-membered chelated structure could be supported by the following experimental results listed in Table 1—4 and Fig. 1. 1) The stereoselectivity in the hydrogenation of the Schiff base depends strongly on the bulkiness of the ester group of the amino acid ester. 2) Lower asymmetric yields were obtained by the use of α-keto esters with larger alkyl groups. 3) The use of ethyl pyruvate instead of methyl pyruvate gave practically no effect on the stereoselectivity in the hydrogenation of Schiff base.

Hydrogenation of Schiff base was carried out in several solvents at various temperatures. A clear temperature effect on the stereoselectivity was observed (Tables 1 and 2). Higher asymmetric yields were obtained at

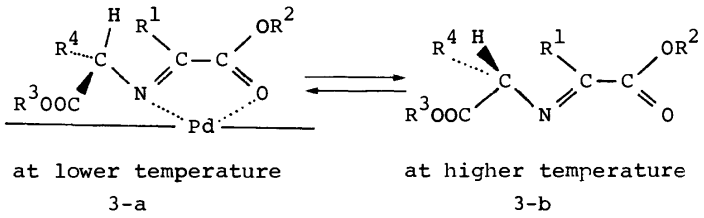

Fig. 3. Conformation of substrate at lower and at higer temperature.

lower temperature than at higher temperature. The Schiff base could form an intermediate chelated complex prior to the hydrogenation at lower temperature. On the other hand, the chelated complex might be liberated from the palladium surface to form a structure as shown in Fig. 3-b at higher temperature. Therefore, the proportion of nonchelated structure increases at higher temperature and this would result in the decrease in the stereoselectivity.

The stereoselectivity in the hydrogenation depends little on the solvent employed. In most cases, higher asymmetric yields were obtained in alcohols than in ethyl acetate. These effects might be explained by a hydrogen bonding between the solvent molecule and the ester group of the amino acid ester in the Schiff base. If the ester group of the amino acid ester in the chelated substrate forms a hydrogen bonding with alcohol, the relative steric bulkiness increases at the diastereomeric face, and this could make the stereoselectivity increase in the alcohols.

The results obtained above are summarized as follows. The stereoselectivity in the hydrogenation depends strongly on the bulkiness of the ester group of the amino acid ester and the alkyl group attached to α-carbon of α-keto ester. The use of bulkier ester group of amino acid ester afforded iminodicarboxylic acid in higher stereoselectivity. Lower asymmetric yields were obtained by the use of methyl 2-oxobutyrate than methyl pyruvate. The hydrogenation at lower temperature afforded iminodicarboxylic acid in higher stereoselectivity.

Considering the overall results, it could be concluded that the hydrogenation of the substrate used in this study proceed via the five-membered chelated intermediate.

Experimental

All the gas chromatographic analyses were carried out with a Hitachi 163 chromatograph, and the peaks on the chromatogram were integrated with a Hitachi 834-30 chromatogrocessor. 5% Palladium on charcoal was purchased from Nippon Engelhald.

General Procedure of Preparation and Hydrogenation of Schiff Base. To a suspension of methyl alaninate hydrochloride (279 mg, 2×10^{-3} mol) in 4 ml of benzene was added a solution of triethylamine (202 mg, 2×10^{-3} mol) in 1 ml of benzene and then a solution of methyl pyruvate (204 mg, 2×10^{-3} mol) in 1 ml of benzene was added to the mixture. After stirring for 1 h at 30 °C, 1 g of anhydrous magnesium sulfate was added to the mixture and the stirring was continued for 22 h at 30 °C. The mixture was filtered and the filtrate was concentrated *in vacuo*. The residue was dissolved in 6 ml of methanol and the solution was stirred with 50 mg of 5% palladium on charcoal for 9 h at 10 °C under hydrogen atmosphere. Catalyst was filtered off and the filtrate was concentrated *in vacuo*. The residue was dissolved in 20 ml of 6M-HCl[†] and the solution was refluxed for 12 h and the hydrolyzate was concentrated *in vacuo*. The residue was dissolved in a small volume of water and charged on a Dowex 50-X8 (H^+ form) column. The column was washed thoroughly with water and then eluted with 2 M-aqueous ammonia. The eluate containing iminodicarboxylic acid was concentrated *in vacuo*. One twentieth of the evaporated residue was treated with 2-propanol saturated with hydrogen chloride gas and then with trifluoroacetic anhydride in order to obtain the derivative of iminodicarboxylic acid for gas chromatographic analysis. Three quarter of the evaporated residue was dissolved in a small volume of water and charged on a column of Dowex 1-X8 (HCOOH form). The column was washed thoroughly with water and then eluted with 2 M-HCOOH. The eluate was concentrated *in vacuo* and obtained iminodicarboxylic acid, yield 178 mg (74%, based on methyl alaninate hydrochloride).

Determination of diastereomeric purity of hydrogenated product. To the residue obtained above was added 1 ml of 2-propanol saturated with hydrogen chloride gas and the mixture was heated for 1 h at 110 °C in a screw capped vial and was concentrated *in vacuo*. To the residue were added 0.5 ml of CH_2Cl_2 and 0.5 ml of trifluoroacetic anhydride and the mixture was heated for 2 h at 110 °C in a screw capped vial. The reaction mixture was concentrated *in vacuo* and the residue was extracted with ethyl acetate. The extract was washed with 10% citric acid, saturated $NaHCO_3$ and dried over magnesium sulfate, and was concentrated *in vacuo*. The residue was dissolved in ethyl acetate and the solution was injected into a gas chromatograph equipped with a glass capillary column (25 m×0.3 mm i.d.) coated with a chiral stationary phase (Chirasil-Val). The column temperature was raised from 80 °C to 180 °C at a rate of 3 °C per minute for the analysis of the diastereomeric ratio of 2,2′-iminodipropionic acid. The column temperature was raised from 80 °C to 180 °C at a rate of 0.25 °C per minute for the analysis of the diastereomeric ratio of 2-(1-carboxyethylamino)-butyric acid.

Authentic iminodicarboxylic acid, (2*S*,2′*S*)- and (2*S*,2′*R*)-2,2′-iminodipropionic acid and (*R*)-2-[(*R*)-1-carboxyethylamino]butyric acid and (*R*)-2-[(*S*)-1-carboxyethylamino]-butyric acid, were derivatized under same conditions. In each analysis of authentic derivatized samples, only a derivatized original diastereomer was detected. These results indicate that the epimerization during the derivatization would be none.

References

1) E. J. Corey, R. J. McCally, and H. S. Sachdev, *J. Am.*

† 1 M=1 mol dm^{-3}.

Chem. Soc., **92**, 2476 (1970).
2) J. P. Charles, H. Christol, and G. Solladie, *Bull. Soc. Chim. Fr.*, **1972**, 1124.
3) R. Meric and J-P. Vigneron, *Tetrahedron Lett.*, **1974**, 2059.
4) K. Harada and T. Yoshida, *Bull. Chem. Soc. Jpn.*, **43**, 921 (1970).
5) K. Harada and T. Yoshida, *J. Org. Chem.*, **37**, 4366 (1972).
6) K. Harada and Y. Kataoka, *Tetrahedron Lett.*, **1978**, 2103.
7) K. Harada and Y. Kataoka, *Chem. Lett.*, **1978**, 791.
8) M. Osawa, A. Hata, K. Harada, and W. Suetaka, *Bull. Chem. Soc. Jpn.*, **49**, 1512 (1976).
9) S. Yamada and S. Hashimoto, *Tetrahedron. Lett.*, **1976**, 997.

 © 1984 The Chemical Society of Japan Bull. Chem. Soc. Jpn., 57, 1371—1376 (1984)

Aggregate Morphology and Hydrogenation Reactivity of Functionalized Bilayer Membrane Composed of Peptide Lipid Having NADH Activity†

Yukito MURAKAMI,* Jun-ichi KIKUCHI, Koji NISHIDA, and Akio NAKANO††
Department of Organic Synthesis, Faculty of Engineering, Kyushu University, Hakozaki, Higashi-ku, Fukuoka 812
(Received December 19, 1983)

A peptide lipid bearing the 1,4-dihydronicotinamide moiety, *N,N*-dihexadecyl-N^{α}-[1-(6-trimethylammoniohexyl)-1,4-dihydro-3-pyridylcarbonyl]-L-alaninamide bromide [N^+C_6(NAH)Ala2C_{16}], and its dehydrogenated form, *N,N*-dihexadecyl-N^{α}-[1-(6-trimethylammoniohexyl)pyridinium-3-ylcarbonyl]-L-alaninamide chloride bromide [N^+C_6(NA^+)Ala2C_{16}], were prepared. Both lipids formed bilayer membranes when they were dispersed in aqueous media, and the 1,4-dihydronicotinamide and nicotinamide moieties of the respective lipid molecules were placed in the so-called hydrogen-belt domain upon membrane formation. In an aqueous dispersion of the latter dicationic lipid, relatively small multilayered vesicles were predominantly formed while the related monocationic lipids bearing the same double alkyl chain composed much larger vesicles and/or lamellae. Formation of the charge-transfer (CT) complex of the nicotinamide moiety of N^+C_6(NA^+)Ala2C_{16} with 3-indolylacetic acid was much enhanced in the membrane through tight electrostatic interaction. The bilayer membrane composed of N^+C_6(NAH)Ala2C_{16} acted as a potential reductant toward anionic substrates in aqueous media. The high reactivity is gained primarily by the effective incorporation of the substrates into the hydrogen-belt domain through electrostatic, hydrogen bonding, and CT interactions and partly by the proximity effect which becomes valid between the 1,4-dihydronicotinamide moiety and the bound substrate molecule.

Currently, there is growing attention to the physical properties and aggregation behavior of synthetic lipids in aqueous media.[1] Since synthetic bilayer membranes provide hydrophobic and organized microenvironments to various extents, it is of much interest to carry out various organic reactions in such organic media. Coenzyme NAD(P)H is one of the most frequently occurring cofactors for electron-transfer reactions in biological systems, and the activity of integral enzymes is often sensitive to the change in lipid composition of membranes where such enzymes are bound.[2] Meanwhile, synthetic membranes may simulate the functions of apoproteins by providing hydrophobic and organized microenvironments for NAD(P)H.

We have previously clarified that peptide lipids compose stable bilayer vesicles having a tripartite structure: a hydrophobic zone formed with aliphatic double chains, a hydrophilic zone with ionic head groups, and a hydrogen-belt domain with amino acid residues interposed between the former two zones.[3,4] In addition, we have found that the hydrogen-belt domain serves as effective sites for hydrolysis and transamination reactions which simulate the functions of esterase and vitamin B_6-dependent transaminase, respectively.[5] In the present work, we prepared a peptide lipid bearing the 1,4-dihydronicotinamide moiety, N^+C_6(NAH)-Ala2C_{16}. The lipid was so designed as to place the dihydronicotinamide moiety in the hydrogen-belt domain when the membrane is formed. In the light of the aggregate morphology of N^+C_6(NAH)Ala2C_{16} examined herein, we studied the reduction of various substrates with the single-compartment bilayer vesicles in aqueous media.

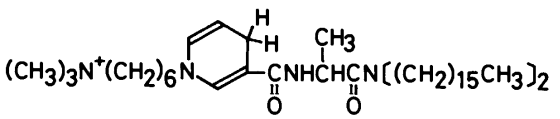

N^+C_6(NAH)Ala2C_{16}

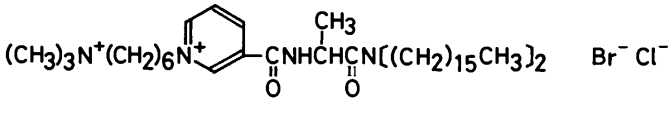

N^+C_6(NA^+)Ala2C_{16}

Experimental

General Analyses and Measurements. Elemental analyses were performed at the Microanalysis Center of Kyushu University. Melting points were measured with a Yanagimoto MP-S1 apparatus (hot-plate type). ^{1}H-NMR spectra were taken on either a Hitachi R-24B or a Hitachi Perkin-Elmer R-20 spectrometer. pH-Measurements were carried out with a Beckman expandomatic SS-2 pH meter equipped with a Metrohm EA-125 combined electrode after calibration with a combination of appropriate standard aqueous buffers. Fluorescence and electronic absorption spectra were obtained with a Hitachi 650-60 spectrofluorometer and a Union Giken SM-401 high-sensitivity spectrophotometer, repsectively. Rapid reactions between the 1,4-dihydronicotinamide moiety and substrates were monitored with a Union Giken RA-401 stopped-flow spectrophotometer. The fluorescence polarization measurements were made on a Union Giken FS-501A fluorescence polarization spectrophotometer equipped with a Sord microcomputer M200 Mark II; the emission at 449 nm was monitored upon excitation at 360 nm with a slit width of 3.5 nm for both excitation and emission sides. The fluorescence polarization (P) was calculated by Eq. 1, where I is the fluorescence intensity, and

† Contribution No. 719 from this Department.
†† Present address: Department of Food Science, Toa University, Shimonoseki, Yamaguchi 751.

the subscripts v and h refer to the orientations, vertical and horizontal, respectively, for the excitation and analyzer polarizers in this sequence; *e.g.*, I_{vh} indicates the fluorescence intensity measured with a vertical excitation polarizer and a horizontal analyzer polarizer.[6]

$$P = (I_{vv} - C_f I_{vh})/(I_{vv} + C_f I_{vh}). \quad (1)$$

C_f is the grating correction factor, given by I_{hv}/I_{hh}. A JEOL JEM-200B electron microscope, installed at the Research Laboratory for High Voltage Electron Microscopy of Kyushu University, was used for morphological measurements. The detail of sample preparation for electron microscopy has been described elsewhere.[4]

Differential Scanning Calorimetry (DSC). The phase transition temperature (T_m, temperature at a peak maximum of DSC thermogram) for an amphiphile was measured with a differential scanning calorimeter (Daini Seikosha SSC-560U): heating rate, 2 °C/min; chart speed, 0.5 cm/min; sensitivity, 0.025 mcal/s/(full scale); temperature and transition heat being calibrated with benzophenone (48 °C) and/or water (0 °C). Each 50-μl sample of an aqueous dispersion [2.0 (w/w)%] in redistilled and deionized water was weighed and sealed into a silver capsule. The enthalpy change for phase transition (ΔH) was determined by measuring the peak area of DSC thermogram.

Materials. Sodium 2,4,6-trinitrobenzenesulfonate (TNBS), 2,6-dichloroindophenol (DCIP) (both from Wako Pure Chemical Industries), and Malachite Green (Merck) were obtained from commercial sources as guaranteed reagents and used without further purification. *N*-Methylacridinium chloride[7] and trifluoroacetophenone[8] were prepared according to the procedures reported in literature, and the products were identified by various spectroscopic measurements.

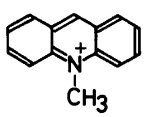

N-Methylacridinium

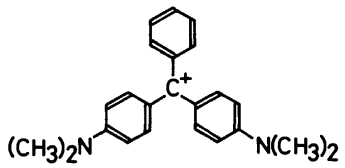

Malachite Green

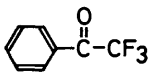

Trifluoroacetophenone

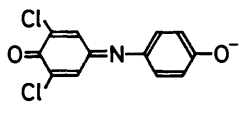

DCIP

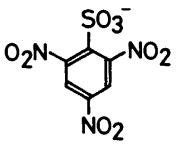

TNBS

N,N-*Dihexadecyl*-N$^{\alpha}$-*nicotinoyl*-L-*alaninamide [(NA)Ala-2C$_{16}$].* Trifluoroacetic acid (25 g, 220 mmol) was added to a dry dichloromethane solution (20 ml) of *N,N*-dihexadecyl-N$^{\alpha}$-(*t*-butoxycarbonyl)-L-alaninamide[9] (6.0 g, 9.4 mmol), and the mixture was stirred for 30 min at room temperature. Evaporation of an excess amount of trifluoroacetic acid *in vacuo* gave a pale brown oil. Elimination of the *t*-butoxycarbonyl group was confirmed by ^{1}H-NMR spectroscopy. The amine thus formed was dissolved in dry benzene (20 ml), and the solution was cooled to 0 °C. Triethylamine (6.0 g, 60 mmol) was added dropwise to the solution, and then nicotinoyl chloride (3.7 g, 26 mmol) dissolved in dry benzene (20 ml) was added dropwise to the mixture in 20 min at 0 °C with stirring. The resulting mixture was stirred for 30 min at 0 °C and then washed with saturated aqueous sodium chloride (3×50 ml). After being dried over Na_2SO_4, the solution was evaporated to dryness *in vacuo*. The residue was chromatographed on a column of silica gel (Wako gel C-100) with ethyl acetate as an eluant. Evaporation of the solvent gave a pale brown solid: yield 4.5 g (75%): ^{1}H-NMR ($CDCl_3$, TMS) δ=0.88 [6H, t, $(CH_2)_{15}C\underline{H}_3$], 1.25 [56H, m, $CH_2(C\underline{H}_2)_{14}CH_3$], ≈1.8 [3H, m, $CH(C\underline{H}_3)$], 3.32 [4H, t, NCH_2], 5.03 [1H, m, $C\underline{H}(CH_3)$], 7.30 [2H, m, CONH and pyridine-5H], 7.99 [1H, d, pyridine-4H], 8.60 [1H, d, pyridine-6H], and 9.00 [1H, s, pyridine-2H].

6-Chlorohexyltrimethylammonium Bromide. A mixture of 30% aqueous trimethylamine (5.6 g, 28 mmol), 1-bromo-6-chlorohexane[10] (5.7 g, 29 mmol), and methanol (20 ml) was stirred for 40 h at room temperature. After evaporation of the solvent *in vacuo*, the residue was dissolved in water (20 ml) and washed with ether (2×20 ml). Evaporation to dryness gave a white solid: yield 5.0 g (68%), mp 113—114 °C; ^{1}H-NMR (D_2O, DSS) δ=1.0—2.1 [8H, m, $CH_2(C\underline{H}_2)_4CH_2$], 3.07 [9H, s, $(CH_3)_3N^+$], 3.33 [2H, t, N^+CH_2], and 3.58 [2H, t, CH_2Cl].

N,N-*Dihexadecyl*-N$^{\alpha}$-*[1-(6-trimethylammoniohexyl)pyridinium-3-ylcarbonyl]*-L-*alaninamide Chloride Bromide [N$^+$C$_6$(NA$^+$)Ala2C$_{16}$].* A mixture of (NA)Ala2C$_{16}$ (4.5 g, 6.9 mmol) and 6-chlorohexyltrimethylammonium bromide (3.5 g, 14 mmol) in dry *N,N*-dimethylformamide (10 ml) was stirred for 17 h at 120 °C under nitrogen. After the mixture was cooled to room temperature, the solvent was removed *in vacuo*, and the crude product was purified by gel-filtration chromatography on columns of Sephadex LH-20 and Toyopearl HW-40 fine in this sequence with methanol as an eluant: a pale brown glassy solid, yield 3.0 g (47%); ^{1}H-NMR ($CDCl_3$, TMS) δ=0.88 [6H, t, $(CH_2)_{15}C\underline{H}_3$], 1.26 [64H, m, $CH_2(C\underline{H}_2)_{14}CH_3$ and $N^+CH_2(C\underline{H}_2)_4CH_2$], ≈1.6 [3H, m, $CH(C\underline{H}_3)$], 2.8—3.7 [6H, m, NCH_2 and $(CH_3)_3N^+C\underline{H}_2$], 3.34 [9H, s, $(CH_3)_3N^+$], 4.90 [3H, m, $N^+(CH_2)_5C\underline{H}_2$ and $C\underline{H}(CH_3)$], 8.23 [1H, t, pyridine-5H], 8.95 [1H, d, pyridine-4H], 9.50 [1H, m, CONH], 9.90 [1H, d, pyridine-6H], and 10.38 [1H, s, pyridine-2H].

Found: C, 67.00; H, 10.37; N, 6.34%. Calcd for $C_{50}H_{96}BrClN_4O_2$: C, 66.68; H, 10.72; N, 6.22%.

N,N-*Dihexadecyl*-N$^{\alpha}$-*[1-(6-trimethylammoniohexyl)-1,4-dihydro-3-pyridylcarbonyl]*-L-*alaninamide Bromide [N$^+$C$_6$(NAH)-Ala2C$_{16}$].* A solution of N$^+$C$_6$(NA$^+$)Ala2C$_{16}$ (140 mg, 0.16 mmol) and 1-benzyl-1,4-dihydronicotinamide[11] (280 mg, 1.3 mmol) in dry methanol (2 ml) was placed in an ice bath, protected from room light, and stirred for 1 h under nitrogen atmosphere. The product was purified by gel-filtration chromatography on a column of Toyopearl HW-40 superfine with dry methanol as an eluant: a yellow solid, yield 40 mg (31%); λ_{max} (methanol) 356 nm (ε 6000); ^{1}H-NMR ($CDCl_3$, TMS) δ=0.88 [3H, t, $(CH_2)_{15}C\underline{H}_3$], 1.26 [64H, m, $CH_2(C\underline{H}_2)_{14}CH_3$ and $N^+CH_2(C\underline{H}_2)_4CH_2$], ≈1.8 [3H, m, $CH(C\underline{H}_3)$], 2.8—3.7 [10H, m, NCH_2, $N^+C\underline{H}_2(CH_2)_4C\underline{H}_2$, and pyridine-4H], 3.38 [9H, s, $(CH_3)_3N^+$], 4.80 [2H, m, $C\underline{H}(CH_3)$ and pyridine-5H], 5.65 [1H, d, pyridine-6H], 6.25 [1H, d, CONH], and 6.88 [1H, s, pyridine-2H].

Found: C, 70.26; H, 11.59; N, 6.48%. Calcd for $C_{50}H_{97}BrN_4O_2$: C, 69.33; H, 11.29; N, 6.47%.

The absence of chloride ion in the purified product was

confirmed by qualitative analysis.[12] The product decomposed gradually in the air at room temperature. Therefore, freshly prepared samples were used for all the measurements. A 1,6-dihydronicotinamide isomer was obtained as a by-product in the hydrogen transfer reaction between a 1,4-dihydronicotinamide and its dehydrogenated species.[13] However, the 1,6-isomer of N^+C_6(NAH)Ala2C_{16} was not detected in the purified product by NMR analysis.

Kinetic Measurements. For the reduction of 2,6-dichloroindophenol (DCIP) and sodium 2,4,6-trinitrobenzenesulfonate (TNBS) with N^+C_6(NAH)Ala2C_{16} in aqueous media, the reaction rate was measured with the stopped-flow spectrophotometer. Single-compartment vesicles of the lipid (4.0×10^{-4} mol dm^{-3}) were prepared by injecting 50 μl of an ethanol solution of the lipid into 5 ml of an aqueous phosphate buffer (0.01 mol dm^{-3}, pH 7.1), while ethanol solutions of the substrates were mixed with the same buffer to give final substrate concentrations of 4.0×10^{-5} mol dm^{-3} with the 1 (v/v)% ethanol content. Equal volumes of both vesicle and substrate solutions were rapidly mixed to initiate the reaction. The reaction was followed by monitoring the absorbance change at 600 nm (the absorption maximum for DCIP)[14] or 462 nm (the absorption maximum for the reduced form of TNBS).[15] As for the reduction of the substrates with 1-propyl-1,4-dihydronicotinamide (PNAH)[16] in the phosphate buffer (0.01 mol dm^{-3}, pH 7.1, 50 (v/v)% ethanol), the reaction was relatively slow and the rate was measured with the ordinary spectrophotometer. The reduction of *N*-methylacridinium chloride, Malachite Green, and trifluoroacetophenone was monitored by the ordinary spectrophotometric method: the absorbance changes at 357 (the absorption maximum for *N*-methylacridinium chloride),[17] 617 (the absorption maximum for Malachite Green),[18] and 370 nm (the absorption due to the 1,4-dihydronicotinamide moiety)[19] were measured, respectively.

Results and Discussion

Morphology of Aggregates. The peptide lipid bearing the 1,4-dihydronicotinamide moiety, N^+C_6(NAH)Ala2C_{16}, forms bilayer membranes in aqueous media. The phase transition parameters evaluated by differential scanning calorimetry (DSC) for its aqueous dispersion are as follows: T_m, 19.5 °C; ΔH, 33 kJ mol^{-1} (Fig. 1a). This is consistent with the formation of multi-walled vesicles and/or lamellae. In the light of our previous study, these parameters are primarily manipulated by the size of the double alkyl-chain segment of peptide lipids. The parameters obtained for N^+C_6(NAH)Ala2C_{16} are in good agreement with those observed for peptide lipids having the same double chain segment such as N^+C_nAla2C_{16} (n=2, 5, 7, and 10).[20]

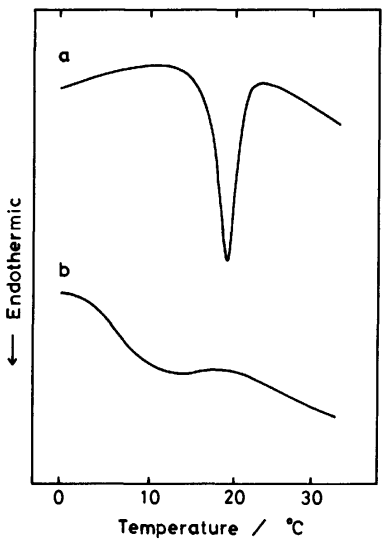

Fig. 1. DSC thermograms for aqueous dispersions of peptide lipids: a, N^+C_6(NAH)Ala2C_{16}; b, N^+C_6-(NA^+)Ala2C_{16}.

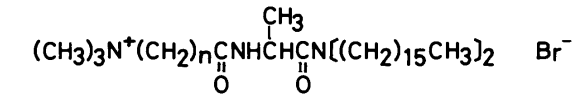

N^+C_nAla2C_{16}

In order to prepare single-walled bilayer vesicles of N^+C_6(NAH)Ala2C_{16}, the injection method which was originally employed for the formation of single-walled liposomes[21] was adopted in this work to avoid degradation of the 1,4-dihydronicotinamide group, which was detected to occur spectrophotometrically under ordinary sonication conditions. The solution thus obtained was sufficiently clear for the following various measurements in contrast to the slightly turbid dispersion of the lipid.

The electronic absorption and fluorescence maxima of N^+C_6(NAH)Ala2C_{16} in ethanol at 15 °C were observed at 353 and 448 nm, respectively, and identical with those of 1-propyl-1,4-dihydronicotinamide (PNAH). Since these spectroscopic maxima for the 1,4-dihydronicotinamide moiety are much sensitive to the microenvironmental polarity, such polarity in the so-called hydrogen-belt domain of the single-walled vesicle was evaluated by referring to the corresponding spectra of PNAH in various media. As a result, the present hydrogen-belt domain with absorption and fluorescence maxima at 359.5 and 455 nm, respectively, provides a microenvironment equivalent to that provided by ethanol-water (1:1 v/v) (solvent polarity Y-parameter, 1.665).[22] In addition, the fluorescence polarization (P=0.317) for the 1,4-dihydronicotinamide moiety of N^+C_6(NAH)Ala2C_{16} in the single-walled aggregate at 15 °C is larger than that measured in ethanol (0.114). This must be attributed to the tight side-by-side arrangement of the amphiphile molecules in the aggregated state.

An aqueous dispersion of N^+C_6(NA^+)Ala2C_{16}, the dehydrogenated counterpart of N^+C_6(NAH)Ala2C_{16}, shows a broad endothermic peak in the 5—20 °C range as shown in Fig. 1b. The morphological transformation of multi-walled bilayer aggregates, composed of natural and/or synthetic lipids, into smaller vesicles are reflected on the phase transition behavior between the gel and liquid-crystalline states; decrease in ΔH along with peak-broadening and shift of T_m to lower temperature.[20,23] The DSC thermogram for an aqueous dispersion of N^+C_6(NA^+)Ala2C_{16} is almost comparable to that for a sonicated solution of N^+C_5Ala2C_{16}. This implies that dicationic amphi-

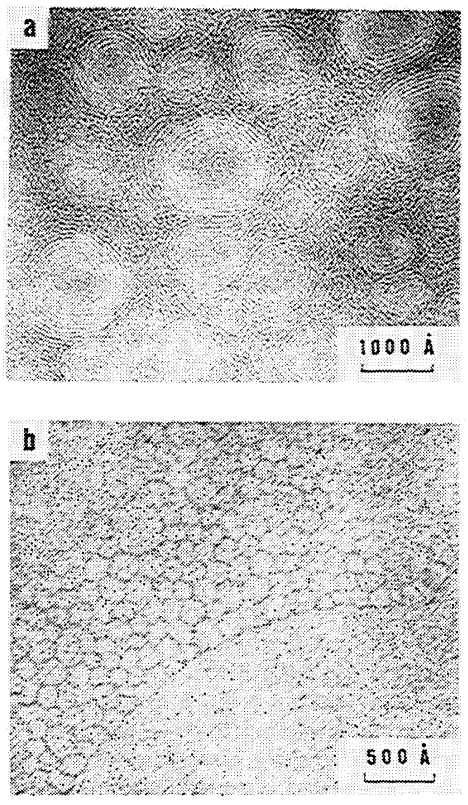

Fig. 2. Electron micrographs negatively stained with uranyl acetate: a, 10 mmol dm^{-3} aqueous dispersion of $N^+C_6(NA^+)Ala2C_{16}$; b, 10 mmol dm^{-3} aqueous solution of $N^+C_6(NA^+)Ala2C_{16}$ sonicated for 2 min at 30 W.

philes are inclined to form smaller aggregates compared with those of the corresponding monocationic ones having the same double alkyl chains when they are dispersed in water. Indeed, the electron micrograph of an aqueous dispersion of $N^+C_6(NA^+)Ala2C_{16}$ shows the presence of multi-walled vesicles with 500—1500 Å diameter (Fig. 2a) without forming straight or bent lamellae observed for aqueous dispersions of $N^+C_nAla2C_{16}$ (n=2, 5, 7, and 10).[20] The difference in aggregate morphology is apparently due to the extensive electrostatic repulsion among the $N^+C_6(NA^+)Ala2C_{16}$ molecules in the aggregated state. Sonication of an aqueous dispersion of $N^+C_6(NA^+)Ala2C_{16}$ with a probe-type sonicator for 2 min at 30 W resulted in a clear solution state which gave an electron micrograph indicating the presence of small particles in a manner as observed for sonicated solutions of $N^+C_nAla2C_{16}$[20] (Fig. 2b).

We have reported previously that an amphiphile involving the nicotinamide moiety as a polar head group, *N,N*-didodecyl-N^{α}-[6-(3-carbamoylpyridinio)-hexanoyl]-L-alaninamide bromide [$(NA^+)C_5Ala2C_{12}$], forms sngle-compartment vesicles in aqueous media upon sonication and provides molecular organization much favorable for the formation of charge-transfer (CT) complexes with electron donors such as 3-indolylacetic acid.[24] The CT interaction of $N^+C_6(NA^+)Ala2C_{16}$ (sonicated in water) with 3-indol-

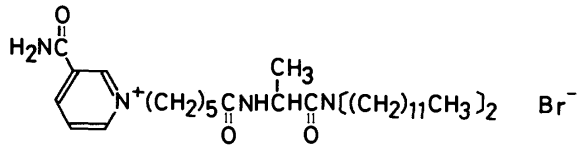

$(NA^+)C_5Ala2C_{12}$

ylacetic acid was quite effective and showed the biphasic CT complex formation in a manner as observed with the vesicular system composed of $(NA^+)C_5Ala2C_{12}$. The formation constant for the CT complex thus obtained on a 2:1 (nicotinamide *vs.* 3-indolylacetic acid) stoichiometry is 7.3×10^3 mol^{-1} dm^3 at 25 °C in water.[25] Thus, it is reasonable to consider that such CT interaction is also effective for the vesicular system composed of $N^+C_6(NAH)Ala2C_{16}$, the 1,4-dihydronicotinamide moiety being the CT donor. Hence, the highly organized molecular aggregates formed with $N^+C_6(NAH)Ala2C_{16}$ and its dehydrogenated counterpart are expected to be utilized as effective reaction sites capable of promoting redox reactions due to the so-called proximity effect when substrate species, acting as CT-acceptors or -donors, are incorporated into them.

Reactivity of $N^+C_6(NAH)Ala2C_{16}$ Membrane in the Reduction of Various Substrates. In order to evaluate the reactivity of $N^+C_6(NAH)Ala2C_{16}$ membrane prepared by the injection method, the following substrates were used: cationic, *N*-methylacridinium chloride and Malachite Green; nonionic trifluoroacetophenone; anionic, 2,6-dichloroindophenol (DCIP) and sodium 2,4,6-trinitrobenzenesulfonate (TNBS). The reactions were carried out in an aqueous phosphate buffer (0.01 mol dm^{-3}, pH 7.1) containing 1 (v/v)% ethanol. In general, the reaction rate for reduction with NAD(P)H models is much influenced by the nature of microenvironment where the reaction takes place.[17,26] Prior to the kinetic analysis of the substrate-binding process with the membrane and the subsequent reduction, a reference reaction was examined in a homogeneous solution which provides the polarity equivalent to that in the $N^+C_6(NAH)Ala2C_{16}$ membrane: the hydrogenation with PNAH was investigated in ethanol-water (1:1 v/v).

As for the reduction of the cationic and neutral substrates, each substrate underwent reaction at an identical rate regardless of the nature of media, ethanol-water or membrane. This implies that the electrostatic repulsion on the positively charged surface of the membrane toward the cationic substrates inhibits the effective incorporation of the substrates into the membrane while the hydrophobic interaction between the hydrophobic domain of the membrane and the neutral substrate disturbs to attain the effective substrate concentration in the hydrogen-belt domain.

As for the reduction of the anionic substrates, however, the marked rate acceleration was observed in the membrane system. As shown in Table 1, the reaction rates for the reduction of DCIP and TNBS in the bilayer membrane were enhanced by 72- and 1.1×10^5-fold, respectively, relative to those in ethanol-water

Table 1. Apparent first-order rate constants for the reduction of 2,6-dichloroindophenol (DCIP) and sodium 2,4,6-trinitrobenzenesulfonate (TNBS) with 1,4-dihydronicotinamide derivatives at 15.0 °C[a)]

Substrate	1,4-Dihydronicotinamide	Medium[b)]	k_{obsd}/s^{-1}
DCIP	N^+C_6(NAH)Ala2C_{16}[c)]	A	9.4×10^{-1}
DCIP	PNAH	B	1.3×10^{-2}
TNBS	N^+C_6(NAH)Ala2C_{16}[c)]	A	2.5
TNBS	PNAH	B	2.3×10^{-5}

a) Initial concentrations: 1,4-dihydronicotinamide derivatives, 2.0×10^{-4} mol dm^{-3}; substrates, 2.0×10^{-5} mol dm^{-3}. b) A, phosphate buffer (0.01 mol dm^{-3}, pH 7.1) containing 1 (v/v)% ethanol; B, phosphate buffer (0.01 mol dm^{-3}, pH 7.1) containing 50 (v/v)% ethanol. c) Single-walled vesicles.

(1:1 v/v). Although the high reactivity of both of the anionic substrates in the membrane is undoubtedly due to the favorable electrostatic interaction which takes the substrates in the membrane surface, other interaction modes, which take the substrates into the hydrogen-belt domain, must be operative. Before such effects are discussed, the kinetic analysis needs to be carried out on the basis of the pseudo-phase concept[27,28] which was originally adopted for the analysis of micellar reactions.

According to the Berezin's concept which quantitatively explain the micellar effect on a bimolecular reaction,[27] the pseudo-first-order rate constant, k_{obsd}, is given by the following equation:

$$k_{obsd} = \frac{k_m P_{TNBS} P_{NAH} C\bar{V} + k_w(1-C\bar{V})}{[1+(P_{TNBS}-1)C\bar{V}][1+(P_{NAH}-1)C\bar{V}]}[NAH]_0. \quad (2)$$

Here, k_m and k_w represent the second-order rate constants in the bilayer membrane and in water, respectively; P_{TNBS} and P_{NAH} denote the partition coefficients of TNBS and N^+C_6(NAH)Ala2C_{16}, respectively, between the membrane and water, *e.g.*, $P_{TNBS}=[TNBS]_m/[TNBS]_w$ where the subscripts, m and w, stand for the membrane and water phases, respectively; $\bar{V}$ is the partial molar volume of the lipid in the membrane; C designates the stoichiometric lipid concentration minus its critical aggregate concentration (CAC); and $[NAH]_0$ is the total lipid concentration. Under the present kinetic conditions, the following assumptions are valid: (i) the rate of reaction in water is neglected, *i.e.*, $k_m P_{TNBS} P_{NAH} C\bar{V} \gg k_w(1-C\bar{V})$; (ii) the $(1-C\bar{V})$ term approximately equals 1 because of the low lipid concentration; (iii) C is nearly equals $[NAH]_0$ and $P_{NAH}C\bar{V} \gg 1$ because of the extremely low CAC;[29] (iv) the binding constant for incorporation of TNBS into the N^+C_6(NAH)Ala2C_{16} membrane, defined by $K_{TNBS}=(P_{TNBS}-1)\bar{V}$, nearly equals $P_{TNBS}\bar{V}$ because of $P_{TNBS} \gg 1$. Thus, Eq. 2 may be simplified to Eq. 3, which is subsequently rearranged to give Eq. 4.

$$k_{obsd} = \frac{k_m K_{TNBS}[NAH]_0}{\bar{V}(1+K_{TNBS}[NAH]_0)}, \quad (3)$$

$$\frac{1}{k_{obsd}} = \frac{\bar{V}}{k_m K_{TNBS}[NAH]_0} + \frac{\bar{V}}{k_m}. \quad (4)$$

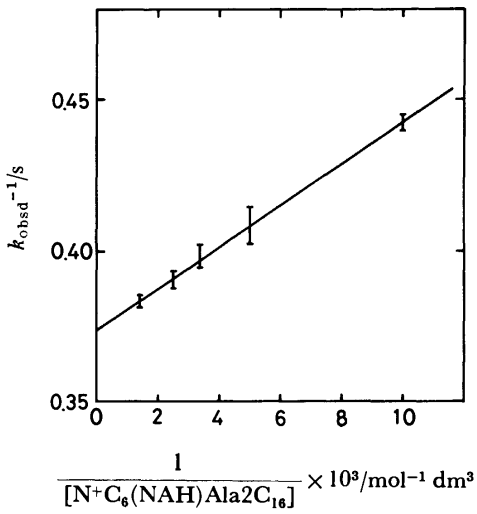

Fig. 3. Kinetic analysis on the basis of Eq. 4 for the reduction of TNBS with N^+C_6(NAH)Ala2C_{16} membrane in a phosphate buffer (0.01 mol dm^{-3}, pH 7.1) containing 1 (v/v)% ethanol at 15.0°C.

The plot of $1/k_{obsd}$ *vs.* $1/[NAH]_0$ gave a straight line correlation as illustrated in Fig. 3, and the K_{TNBS} value determined from its intercept and slope is 5.5×10^4 mol^{-1} dm^3. If one may employ 0.75 mol^{-1} dm^3 for the $\bar{V}$ value, which is calculated from the volume per lipid molecule for egg yolk phosphatidylcholine vesicles,[30] the second-order rate constant in the membrane is 2.0 mol^{-1} dm^3 s^{-1}. This assumption for $\bar{V}$ is reasonable since all the average vesicle parameters for single-walled vesicles of N^+C_5Ala2C_{16} and egg lecithin are comparable to each other as reported previously.[20] The second-order rate constant in the present membrane is 17-fold greater than the corresponding value in the homogeneous solution (0.115 mol^{-1} dm^3 s^{-1}). Consequently, the marked overall rate enhancement observed for the reduction of TNBS primarily originates in the effective substrate incorporation into the hydrogen-belt domain of the membrane. Such efficient binding behavior may come from the three interaction modes: (i) the electrostatic attraction which takes the substrate molecules in the membrane surface, (ii) the CT interaction between the 1,4-dihydronicotinamide and the substrate, and (iii) the hydrogen bonding interaction between the substrate and the hydrogen-belt domain. The latter two interactions may act to translocate the substrate molecules from the membrane surface to the hydrogen-belt domain.

In conclusion, the bilayer membrane formed with the cationic peptide lipid bearing the 1,4-dihydronicotinamide moiety, N^+C_6(NAH)Ala2C_{16}, acts as a potential reductant toward anionic substrates in aqueous media. The high reactivity primarily originates in the effective binding of such substrates to the lipid membrane, which is brought about by the three different interaction modes as stated above. The side-by-side arrangement of the 1,4-dihydronicotinamide moieties in the hydrogen-belt domain of the membrane may contribute in part to the overall

rate enhancement due to the proximity effect brought about by the CT and hydrogen-bonding interactions.

References

1) J. H. Fendler, "Membrane Mimetic Chemistry," John Wiley & Sons, New York (1982), Chap. 6.
2) R. B. Gennis and A. Jonas, *Annual Rev. Biophys. Bioeng.*, **6**, 195 (1977).
3) Y. Murakami, A. Nakano, and K. Fukuya, *J. Am. Chem. Soc.*, **102**, 4253 (1980); Y. Murakami, Y. Aoyama, A. Nakano, T. Tada, and K. Fukuya, *ibid.*, **103**, 3951 (1981).
4) Y. Murakami, A. Nakano, and H. Ikeda, *J. Org. Chem.*, **47**, 2137 (1982).
5) Y. Murakami, A. Nakano, A. Yoshimatsu, and K. Fukuya, *J. Am. Chem. Soc.*, **103**, 728 (1981); Y. Murakami, A. Nakano, and K. Akiyoshi, *Bull. Chem. Soc. Jpn.*, **55**, 3004 (1982); Y. Murakami, J. Kikuchi, A. Nakano, K. Akiyoshi, and T. Imori, *ibid.*, in press.
6) T. Azumi and S. P. McGlynn, *J. Chem. Phys.*, **37**, 2413 (1962).
7) G. Mooser, H. Schulman, and D. S. Sigman, *Biochemistry*, **11**, 1595 (1972).
8) K. T. Dishart and R. Levine, *J. Am. Chem. Soc.*, **78**, 2268 (1956).
9) This material was prepared by a procedure similar to that reported for the synthesis of *N,N*-didodecyl-N^{α}-(*t*-butoxycarbonyl)-L-alaninamide.[4]
10) S. A. Fusari, K. W. Greenlee, and J. B. Brown, *J. Am. Oil Chem. Soc.*, **28**, 416 (1951).
11) Y. Kurusu, K. Nakajima, and M. Okawara, *Kogyo Kagaku Zasshi*, **71**, 934 (1968).
12) T. Momose, Y. Ueda, and Y. Mukai, *Bunseki Kagaku*, **9**, 360 (1960).
13) H. Minato, T. Ito, and M. Kobayashi, *Chem. Lett.*, **1977**, 13.
14) K. Wallenfels and M. Gellrich, *Justus Liebigs Ann. Chem.*, **621**, 149 (1959).
15) L. C. Kurz and C. Frieden, *Biochemistry*, **16**, 5207 (1977).
16) P. Karrer and F. J. Stare, *Helv. Chim. Acta*, **20**, 418 (1937).
17) J. Hajdu and D. S. Sigman, *Biochemistry*, **16**, 2841 (1977).
18) H. Kitano, M. Katsukawa, and N. Ise, *Bioorg. Chem.*, **11**, 412 (1982).
19) J. J. Steffens and D. M. Chipman, *J. Am. Chem. Soc.*, **93**, 6694 (1971).
20) Y. Murakami, A. Nakano, A. Yoshimatsu, K. Uchitomi, and Y. Matsuda, *J. Am. Chem. Soc.*, in press.
21) S. Batzri and E. D. Korn, *Biochim. Biophys. Acta*, **298**, 1015 (1973); J. M. H. Kremer, M. W. J. v. d. Esker, C. Pathmamanoharan, and P. H. Wiersema, *Biochemistry*, **16**, 3932 (1977).
22) A. H. Fainberg and S. Winstein, *J. Am. Chem. Soc.*, **78**, 2770 (1956).
23) D. Papahadjopoulos, S. Hui, W. J. Vail, and G. Poste, *Biochim. Biophys. Acta*, **448**, 245 (1976); Y. Okahata, R. Ando, and T. Kunitake, *Ber. Bunsenges. Phys. Chem.*, **85**, 789 (1981).
24) Y. Murakami, Y. Aoyama, J. Kikuchi, K. Nishida, and A. Nakano, *J. Am. Chem. Soc.*, **104**, 2937 (1982).
25) For definition of the formation constant and the experimental method, see reference 24.
26) P. van Eikeren and D. L. Grier, *J. Am. Chem. Soc.*, **98**, 4655 (1976).
27) I. V. Berezin, K. Martinek, and A. K. Yatsimirskii, *Russ. Chem. Rev.*, **42**, 787 (1973).
28) J. H. Fendler and W. L. Hinze, *J. Am. Chem. Soc.*, **103**, 5439 (1981).
29) In general, CAC's for amphiphiles of this type are lower than 2×10^{-5} mol dm^{-3}.[3,24]
30) C. Huang and J. T. Mason, *Proc. Natl. Acad. Sci. U.S.A.*, **75**, 308 (1978).

Synthesis and Properties of the Tristyrylmethyl Anion

Koichi KOMATSU, Shuzo SHIRAI, Isao TOMIOKA, and Kunio OKAMOTO*
Department of Hydrocarbon Chemistry, Faculty of Engineering, Kyoto University, Sakyo-ku, Kyoto 606
(Received December 20, 1983)

The title anion (**3**) having a C_{3v} symmetric structure was generated from newly synthesized tristyrylmethane (**4**) and was characterized by means of ^1H and ^{13}C NMR spectroscopy. The pK_a value of **4** was determined as 20.1 in DMSO-EtOH (9:1), indicating considerable conjugative stabilization of the anion **3**. The cyclic voltammetry of **3** in acetonitrile exhibited only irreversible one-electron oxidation peak corresponding to the formation of a chemically unstable radical species. Whereas quenching the anion **3** with H_2O or Me_3SiCl quantitatively afforded the cross-conjugated triene **6** (R=H or Me_3Si), the reaction of **3** with the tropylium ion yielded 1,1'-bicycloheptatrienyl (29%), as well as the triene **6** ($R=C_7H_7$) (66%), demonstrating that **3** can also acat as a one electron reductant.

Although linearly-conjugated open-chain pentadienyl anions (**1**) have been extensively studied by means of ^1H and ^{13}C NMR spectroscopy[1] and shown to be generally predominated by the "W" conformation, the NMR study on its cross-conjugated derivative, the 3-vinylpentadienyl anion (**2**), seems to be quite limited. For example, **2** and some of its alkylated derivatives were observed by NMR[1c,2] but no NMR data was reported for a variety of cross-conjugated carbanions with aryl substituents prepared by Kuhn *et al.*[3] Here we wish to report on the properties of the newly synthesized tristyrylmethyl anion (**3**), which can also be looked upon as a tri-vinylog of the long-known triphenylmethyl (trityl) anion.

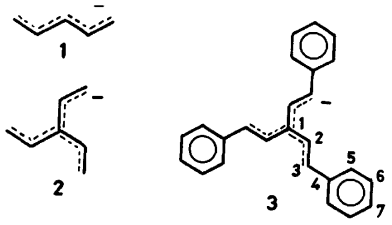

The parent hydrocarbon, tristyrylmethane (**4**), was synthesized in 53% overall yield from methyl 3-phenylpropanoate as shown in Scheme 1. Upon treatment with an equimolar amount of *n*-BuLi or *t*-BuOK in THF, the hydrocarbon **4** afforded a deep blue solution of the anion **3**, which was quite sensitive to air but could be stored unchanged for more than a year when sealed under vacuum.

The ^1H and ^{13}C NMR data for the anion **3** are shown in Table 1 together with those for the parent hydrocar-

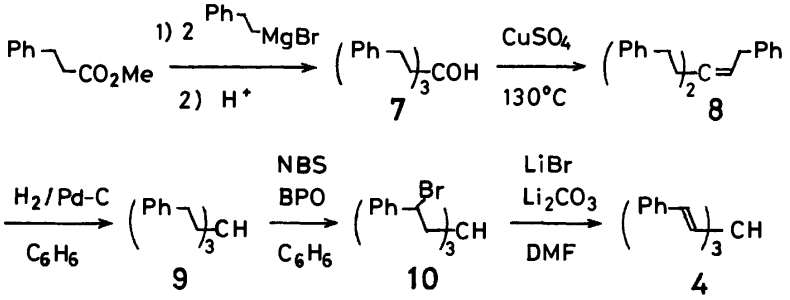

Scheme 1.

TABLE 1. ^1H AND ^{13}C NMR DATA FOR **3** AND **4**, AND EMPIRICAL AND CALCULATED π-ELECTRON DENSITIES (ρ) FOR **3**

Position	δ_{1H} (300 MHz)			δ_{13C} (25 MHz)			ρ (**3**)	
	4[a]	**3**·K^+[b]	**3**·Li^+[b]	**4**[a]	**3**·K^+[b]	**3**·Li^+[b]	Emp[c]	Calcd[d]
1	3.96[e]	—	—	48.5	100.2	101.9	1.211	1.204
2	6.34[f]	7.10[h]	7.11[h]	130.7	131.6	132.2	1.010	1.000
3	6.52[g]	5.88[h]	5.84[h]	130.5	106.1	105.5	1.173	1.163
4	—	—	—	137.2	144.3	144.9	0.929	1.000
5	7.40	7.08	7.06	126.1	123.5	123.1	1.062	1.033
6	7.31	6.94	6.93	128.4	128.9	128.8	1.028	1.000
7	7.23	6.56	6.53	127.2	120.9	120.0	1.079	1.033

a) In $CDCl_3$. b) In THF-THF-d_8 (9:1). c) Estimated from δ_{13C} of **3**·K^+ according to the ρ-δ relationship obtained for K^+ salts of open-chain carbanions: $\rho=(289.5-\delta)/156.3$ (Ref. 1e). d) Calculated by simple HMO ($\beta_{1,2}=\beta_{3,4}=0.9$). e) q ($J=6.6$ Hz). f) dd ($J=16.2$, 6.6 Hz). g) d ($J=16.2$ Hz). h) d ($J=15.0$ Hz).

bon **4**. Close similarity of the ^1H and ^{13}C chemical shifts for **3**·K^+ to those for **3**·Li^+ suggests that these salts exist as "loose" or "solvent-separated" ion pairs with little interaction between the cation and the anion. Remarkable upfield shifts noted for the ^{13}C NMR signals of C-1 and C-3 in **3**, as well as of C-5 and C-7 although in lesser amounts, indicate the presence of high electron densities on these carbons in agreement with the results of MO calculations (Table 1).

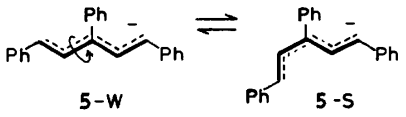

Scheme 2.

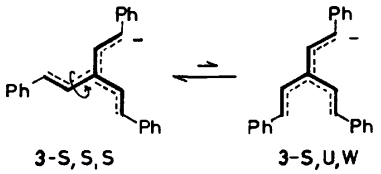

Scheme 3.

1,3,5-Triphenylpentadienyl anion **5** was reported to be in a rapid equilibrium between the "W" and "S" forms having comparable stability (Scheme 2) and to exhibit ^{13}C NMR line broadening at −5 °C.[10] For the present anion **3**, the corresponding rotation of the inner bond inevitably results in the formation of the sterically unfavorable "U" shape for one of the pentadienyl moieties (Scheme 3). Thus, the ^{13}C NMR line broadening of the C-3 and C-2 signals was observed at −45 °C for **3**·Li^+ in THF, but at lower temperatures the C-3 signal reappeared at δ 103.7 as a sharp singlet with the relative intensity comparable to the original one, while the C-1 signal remained almost unchanged. This observation may be taken as evidence that the equilibrium shown in Scheme 3 lies far to the left favoring the symmetric structure, although at the low temperatures the C-2 signal was obscured by overlapping with the more slowly broadening phenyl signals and observation of the signals for **3**-S,U,W, if any, was precluded by the low S/N ratio resulting from decreased solubility of **3**·Li^+ itself.

The electronic spectrum of the anion **3** in DMSO exhibited the longest-wavelength absorption at 585 nm (log ε 4.75) with a shoulder at 540 nm (log ε 4.72). The acidity of the hydrocarbon **4**, which measures the stability of the anion **3**, was then determined on the basis of this absorption in DMSO-EtOH (9:1) by the spectrophotometric method of Kuhn and Rewicki[3b] using the H_- function corrected with 9-phenylfluorene (pK_a 18.5)[4,5] as a standard. The pK_a of **4** was found to be 20.1±0.2, indicating that **4** is about 10^{12} times more acidic than triphenylmethane (pK_a 32.5)[5] owing to the great conjugative stabilization of the anion **3**.

In order to compare the redox behavior of the anion **3** with that of the trityl anion, which exhibits two successive oxidation steps leading to the radical and to the cation,[6] cyclic voltammetry was conducted on the anion **3** generated with *t*-BuOK in acetonitrile. The voltammogram obtained at the scan rate of 0.1 V/s exhibited an irreversible anodic peak corresponding to the oxidation of **3** to the radical at −1.33 V *vs.* Ag/Ag^+, from which was estimated the $E_{1/2}$ value[7] as −1.38 V *vs.* Ag/Ag^+ (−1.09 V *vs.* SCE),[8] 0.11 V less negative than $E_{1/2}$ for the trityl anion (−1.20 V *vs.* SCE).[6] No peak corresponding to further oxidation of the radical was observable nor did the peak at −1.33 V become reversible upon increasing the scan rate up to 1 V/s, indicating that the radical species is chemically unstable and decomposes during measurement.

Finally, quenching reactions of the anion **3** were conducted with excessive H_2O and Me_3SiCl, and were found to give the cross-conjugated triene **6** (R=H and Me_3Si) in 100 and 79% yields, respectively (Scheme 4). In contrast, the reaction of **3**·Li^+ with an equimolar amount of the tropylium ion afforded 1,1′-bicycloheptatrienyl, the one-electron reduction product of the tropylium ion,[9] in 29% yield in addition to the triene **6** (R=C_7H_7) (66%). This result clearly demonstrates that the anion **3** can act not only as a nucleophile but also as a one-electron donor towards a stable carbocation.

Experimental

General. Melting points are uncorrected. The elemental analyses were performed by the Microanalytical Center, Kyoto University, Kyoto. The IR and visible spectra were recorded on Hitachi 215 and Hitachi 200-10 spectrometers, respectively. The ^1H NMR spectra were taken with a Hitachi R-24 (60 MHz) or, when specified, with a Nicolet NP-300 NB (300 MHz) spectrometer with Me_4Si as the internal standard. The ^{13}C NMR spectra were recorded on a JEOL FX-100 (25 MHz) spectrometer operated in the Fourier transform mode.

Tris(2-phenylethyl)methanol (7). A solution of methyl 3-phenylpropanoate (16.4 g; 0.100 mol) in ether (50 ml) was added dropwise over 0.5 h to a stirred solution of 2-phenylethylmagnesium bromide, prepared from 2-phenylethyl bromide (40.7 g; 0.220 mol) and Mg (5.35 g; 0.220 mol) in ether (100 ml). After refluxing for 3 h, the reaction mixture was hydrolyzed with saturated NH_4Cl and worked up in the usual way to give **7** (32.9 g; 95.5%) as white needles: mp 68.8—70.0 °C; IR (KBr) ν 3500 cm^{-1} (OH); NMR

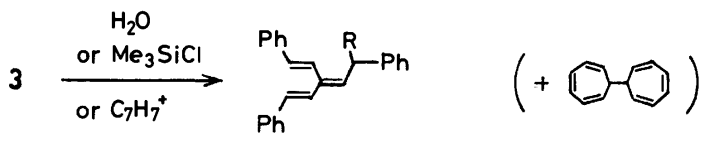

6 (R=H, $SiMe_3$, C_7H_7)

Scheme 4.

($CDCl_3$) δ=7.20 (s, 15H), 2.67 (m, 6H), 1.86 (m, 6H), and 1.33 (s, 1H). Found: C, 86.97; H, 8.10%. Calcd for $C_{25}H_{28}O$: C, 87.16; H, 8.19%.

1,5-Diphenyl-3-(2-phenylethyl)-2-pentene (8). A stirred mixture of **7** (15.3 g; 44.3 mmol) and anhydrous $CuSO_4$ (5.39 g; 33.8 mmol) was heated at 130 °C for 0.5 h and then extracted with ether to give **8** (14.6 g; 100%) as a colorless viscous oil; IR (neat) ν 1660 cm^{-1} (C=C); NMR (CCl_4) δ=7.11 (s, 15H), 5.28 (t, 1H), 3.17 (d, 2H), and 2.9—2.2 (m, 8H).

Tris(2-phenylethyl)methane (9). A solution of **8** (15.4 g; 47.2 mmol) in benzene (50 ml) was catalytically hydrogenated over 5% Pd-C (2 g) for 2 d to give **9** (16.0 g; 100%) as a colorless viscous oil; NMR (CCl_4) δ=7.01 (s, 15H), 2.45 (m, 7H), and 1.58 (m, 6H).

Tris(2-bromo-2-phenylethyl)methane (10). A mixture of **9** (11.3 g; 34.3 mmol), *N*-bromosuccinimide (17.9 g; 101 mmol), and benzoyl peroxide (1.0 g; 4.1 mmol) in CCl_4 (60 ml) was stirred at room temperature for 1 h and at 80 °C for 1 h. The cooled mixture was filtered, evaporated, and crystallized from hexane to give **10** (11.9 g; 61.4%) as yellow crystals: NMR (CCl_4) δ=7.21 (s, 15H), 4.82 (t, 3H), and 2.15 (m, 7H).

Tristyrylmethane (4). A dried mixture of Li_2CO_3 (4.12 g; 55.8 mmol) and LiBr (4.14 g; 47.7 mmol) was added portionwise over 15 min to a stirred solution of **10** (6.00 g; 10.6 mmol) in DMF (50 ml) at 10 °C. After heating the stirred mixture at 100 °C for 1.7 h, the mixture was treated with water and worked up to give **4** (3.10 g; 90.6%) as pale brown powder. Recrystallization from hexane-benzene (1:1) afforded 2.70 g of off-white prisms: mp 110.0—111.0 °C; IR (KBr) ν 1650 cm^{-1} (C=C). Found: C, 93.00; H, 6.80%. Calcd for $C_{25}H_{22}$: C, 93.12; H, 6.88%.

The Tristyrylmethyl Anion (3). Method A (Preparation under Vacuum): The NMR Spectra; Under a stream of argon, the hydrocarbon **4** was added to an equimolar amount of *t*-BuOK or neat *n*-BuLi (obtained by evaporation of the hexane solution) in an NMR tube connected to a vacuum line. An appropriate amount of dry THF-THF-d_8 (9:1) was vacuum distilled into this mixture to give a 0.1 M solution. The tube was then sealed under vacuum and subjected to NMR measurements.

The Electronic Spectrum; A diluted solution (2.79×10^{-5} M[1]) of **4** in DMSO (5.00 ml) was placed in a 1-cm cell connected to a vacuum line. The cell was equipped with a mixing compartment containing *t*-BuOK (1 mg; 0.009 mmol). After the DMSO solution was degassed by three freeze-pump-thaw cycles, the whole assembly was sealed under vacuum, and the solution mixed with *t*-BuOK and subjected to the measurement.

Quenching with H_2O; Water (1 ml) was vacuum distilled into a solution of **3**·K^+, prepared as described above from **4** (0.0405 g; 0.126 mmol) and *t*-BuOK (0.020 g; 0.18 mmol) in THF (3 ml). The resultant pale yellow solution was worked up and purified by PTLC over SiO_2 developed with hexane-benzene (2:1) to give **6** (R=H) (0.0400 g; 100%) as a colorless viscous oil; NMR (300 MHz) ($CDCl_3$) δ=7.44—7.14 (m, 15H), 7.10 (d, J=16.4 Hz, 1H), 6.95 (d, J=15.9 Hz, 1H), 6.73 (d, J=16.4 Hz, 1H), 6.69 (d, J=15.9 Hz, 1H), 5.97 (t, J=7.8 Hz, 1H), and 3.69 (d, J=7.8 Hz, 2H).

Method B (Preparation under Nitrogen): Quenching with Me_3SiCl; *n*-BuLi (1.4 M in hexane) (5.0 ml; 7.0 mmol) was added to a stirred and deaerated solution of **4** (0.471 g; 1.46 mmol) in dry THF (10 ml) under dry nitrogen. To the resultant deep blue solution was immediately added Me_3SiCl (2.6 g; 24 mmol) to give a pale yellow suspension, which was evaporated, hydrolyzed, and extracted with ether. The crude product was purified by PTLC over SiO_2 developed with hexane-benzene (2:1), affording **6** (R=Me_3Si) (0.449 g; 79.0%) as a pale yellow viscous oil: NMR (300 MHz) ($CDCl_3$) δ=7.40—7.05 (m, 15H), 6.94 (d, J=16.2 Hz, 1H), 6.90 (d, J=16.2 Hz, 1H), 6.52 (d, J=16.2 Hz, 1H), 6.31 (d, J=16.2 Hz, 1H), 6.21 (d, J=12.0 Hz, 1H), 3.52 (d, J=12.0 Hz, 1H), and −0.06 (s, 9H).

The pK_a Measurements. The pK_a value was determined by the method of Kuhn and Rewicki,[3b] using the H_ function reported by Bowden and Stewart and corrected with the known pK_a of 9-phenylfluorene (18.59).[4] The visible spectra were measured under vacuum as described above in 5.00 ml of DMSO-EtOH (90:10 by mol, also used were mixtures of 85:15 and 80:20 by mol) using NaOEt (0.05 mmol, obtained by evaporation of 0.500 ml of a 0.1 M ethanolic solution) as a base.

Cyclic Voltammetry. The measurements were performed by the method and apparatus previously reported,[10] on a sample solution freshly prepared by adding *t*-BuOK (0.0202 g; 0.180 mmol) to a stirred solution of **4** (0.0502 g; 0.156 mmol) and dried Bu_4NClO_4 (0.513 g; 1.50 mmol) in dry acetonitrile (15 ml) under an atmosphere of nitrogen.

Reaction of 3·Li^+ with Tropylium Tetrafluoroborate. A solution of 3·Li^+ was prepared as described above by vacuum distillation of dry THF (100 ml) into a 200 ml flask containing a stirring bar, **4** (2.90 g; 9.00 mmol), and *n*-BuLi (9.18 mmol, obtained by evaporation of 6.7 ml of 1.37 M solution in hexane). The flask was equipped with a side-arm containing tropylium tetrafluoroborate (1.60 g; 9.00 mmol). After sealing the whole equipment under vacuum, the tropylium salt was added from the side-arm into the stirred solution of 3·Li^+. The mixture was stirred for 16 h, hydrolyzed, and worked up to give the crude product, which was then separated by PTLC over SiO_2 developed with hexane-benzene (3:1). From the fraction with R_f 0.75 was obtained 1,1′-bicycloheptatrienyl (0.233 g; 28.5%) identified by spectral comparison with an authentic sample, while the fraction with R_f 0.52 afforded **6** (R=C_7H_7) (2.43 g; 65.6%) as a colorless viscous oil; ^1H NMR (300 MHz) ($CDCl_3$) δ=7.44—7.12 (m, 15), 7.06 (d, J=16.2 Hz, 1H, H-8), 6.87 (d, J=15.9 Hz, 1H, H-8′), 6.67 (d, J=16.2 Hz, 1H, H-7), 6.63 (d, J=15.9 Hz, 1H, H-7′), 6.62 (t, J=4.8 Hz, 2H, H-6,6′), 6.19 (dd, J=9.3, 4.8 Hz, 1H, H-5), 6.04 (dd, J=9.3, 4.8 Hz, 1H, H-5′), 5.89 (d, J=10.2 Hz, 1H, H-1), 5.30 (dd, J=9.3, 5.7 Hz, 1H, H-4), 5.07 (dd, J=9.3, 5.7 Hz, 1H, H-4′), 4.12 (dd, J=10.7, 10.2 Hz, 1H, H-2), and 2.08 (dt, J=10.7, 5.7 Hz, 1H, H-3); ^{13}C NMR

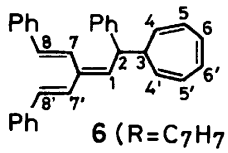

6 (R=C_7H_7)

($CDCl_3$) δ=142.9—124.2 (24 peaks), 46.7 (d, C-2), and 44.7 (d, C-3). From the fraction with R_f 0.29 was obtained a pale yellow viscous oil (0.856 g), which is supposed to be a polymeric material having structural units derived from the tristyrylmethyl radical based on its ^1H NMR exhibiting very broad signals corresponding to phenyl and olefinic protons in a ratio of about 15:5.

[1] 1 M=1 mol dm^{-3}.

References

1) a) R. B. Bates, D. W. Gosselink, and J. A. Kaczynsky, *Tetrahedron Lett.*, **1967**, 205; b) S. Brenner and J. Klein, *Isr. J. Chem.*, **7**, 735 (1969); c) R. B. Bates, S. Brenner, C. M. Cole, E. W. Davidson, G. D. Forsythe, D. A. McCombs, and A. S. Roth, *J. Am. Chem. Soc.*, **95**, 926 (1973); d) W. T. Ford and M. Newcomb, *ibid.*, **96**, 309 (1974); e) D. H. O'Brien, A. J. Hart,

and C. R. Russell, *ibid.*, **97**, 4410 (1975); f) D. H. Hunter, R. E. Klinck, R. P. Steiner, and J. B. Stothers, *Can. J. Chem.*, **54**, 1464 (1976).

2) R. B. Bates, S. Brenner, and C. M. Cole, *J. Am. Chem. Soc.*, **94**, 2130 (1972).

3) a) R. Kuhn and D. Rewicki, *Angew. Chem.*, **79**, 648 (1967); b) R. Kuhn and D. Rewicki, *Justus Liebigs Ann. Chem.*, **704**, 9, 250 (1967), and earlier publications cited therein.

4) K. Bowden and R. Stewart, *Tetrahedron*, **21**, 261 (1965).

5) D. J. Cram, "Fundamentals of Carbanion Chemistry," Academic Press, New York (1965). For the review on more recently determined values, see R. F. Cookson, *Chem. Rev.*, **74**, 5 (1974).

6) S. Bank, C. L. Ehrlich, and J. A. Zubieta, *J. Org. Chem.*, **44**, 1454 (1979).

7) For the irreversible CV peak, $E_{1/2}$ can be theoretically correlated with the value at 85% of the peak height: R. Breslow and W. Chu, *J. Am. Chem. Soc.*, **95**, 411 (1973); R. N. Adams, "Electrochemistry at Solid Electrodes," Marcel Decker, New York (1969).

8) The Ag/0.01 M $AgNO_3$ employed in this work has +0.291 V *vs.* SCE: C. K. Mann, "Electroanalytical Chemistry," ed by A. J. Bard, Marcel Decker, New York (1969), Vol. 3.

9) W. von E. Doering and L. H. Knox, *J. Am. Chem. Soc.*, **79**, 352 (1957).

10) K. Komatsu, K. Masumoto, Y. Waki, and K. Okamoto, *Bull. Chem. Soc. Jpn.*, **55**, 2470 (1982).

Chemical Synthesis of Fully Active and Heat-stable Fragments of Heat-stable Enterotoxin of Enterotoxigenic *Escherichia coli* Strain 18D

Shoko YOSHIMURA, Toshifumi TAKAO, Haruo IKEMURA, Saburo AIMOTO, Yasutsugu SHIMONISHI,* Saburo HARA,† Tae TAKEDA,†† Yoshifumi TAKEDA,†† and Toshio MIWATANI††

Institute for Protein Research, Osaka University, Yamada-oka 3-2, Suita, Osaka 565
†*Department of Chemistry, College of Science, Osaka University, Toyonaka, Osaka 560*
††*Research Institute for Microbial Diseases, Osaka University, Yamada-oka 3-1, Suita, Osaka 565*

(Received December 20, 1983)

Two shorter peptides of a heat-stable enterotoxin (ST_p), which is produced by enterotoxigenic *Escherichia coli* strain 18D, were prepared by two different procedures; i) chemical synthesis and ii) Edman-degradation of ST_p. These peptides (designated as $ST_p(4—18)$ and $ST_p(5—18)$) corresponded to 15 and 14 amino acid residues in the sequence of ST_p without three and four residues, respectively, of the N-terminus. Peptides $ST_p(4—18)$ and $ST_p(5—18)$ prepared by chemical synthesis had the same biological and physicochemical properties as the peptides obtained by the Edman method. Furthermore, they showed almost the same toxicity as native and synthetic ST_p, and their toxicity was neutralized by anti-native ST_p antisera. Synthetic $ST_p(4—18)$ had similar heat-stability to ST_p, but synthetic $ST_p(5—18)$ was much more heat-stable. These findings suggest that the sequence from the Cys residue near the N-terminus to the C-terminal residue is extremely important for the unique characters of toxicity and heat-stability of the toxin.

Various strains of enterotoxigenic *Escherichia coli* (ETEC) from animal hosts produce heterologous low-molecular-weight, heat-stable enterotoxins (ST's), which are responsible for acute diarrhea in man and various domestic animals. Burgess *et al.*[1] reported two distinct ST's, one (ST_a) being methanol-soluble and active in neonatal piglets and infant mice but inactive in weaned pigs, and the other (ST_b) being methanol-insoluble and active in weaned pigs but inactive in infant mice. Recently, we[2-4] isolated two kinds of ST_a (designated as ST_h and ST_p) in pure form from human strains SK-1 and 18D of ETEC, respectively. These ST_a's, which were active in suckling mouse assay, were found to have the amino acid sequences shown in Fig. 1. Slightly before our description,[4] Chan and Giannella[5] reported the amino acid sequence of an ST from ETEC strain 18D to be as shown in Fig. 1. The amino acid sequence of ST_p determined by us was very similar to that of ST proposed by Chan and Giannella,[5] but differed in two residues at positions 11 and 18 from the N-terminus, although we[4] isolated and purified ST_p from the same strain, ETEC 18D, that Chan and Giannella[5] used. To elucidate these discrepancy, we[6] synthesized ST_p and ST with the amino acid sequences proposed by us[4] and Chan and Giannella,[5] respectively, and confirmed that the former had the same biological and physicochemical properties as native ST_p isolated from ETEC strain 18D. Lallier *et al.*[7,8] and Ronnberg *et al.*[9] also purified ST produced by a porcine strain F11 (P155) and human strain C57/26C2 of ETEC, respectively, and reported their amino acid sequences to be as illustrated in Fig. 1. Their amino acid sequences were identical with that of ST_p from ETEC strain 18D determined by us.[4]

These toxins have great structural similarity, although the sequences of their N-terminal regions differ. The sequences from the Tyr residue near the N-terminus to the Tyr residue at the C-terminus are identical, except at the 4th residue from the C-terminus, although the sequence of toxin proposed by Chan and Giannella[5] also differs at the 11th and 18th residues. Six half-cystine residues are conserved in the same positions and intramolecularly linked by disulfide bonds, suggesting that these toxins have similar molecular conformations, although the

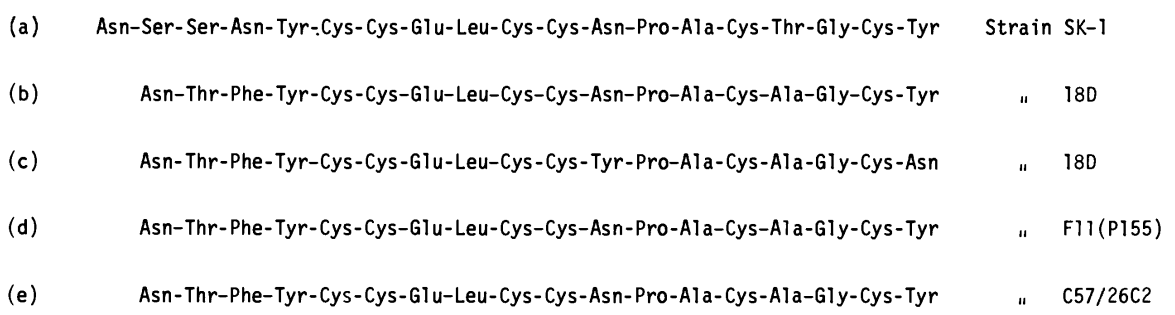

Fig. 1. Comparison of amino acid sequences of ST: (a) ST_h isolated from ETEC strain SK-1, reported in Ref. 3); (b) ST_p isolated from ETEC strain 18D by us;[4] (c) an ST isolated from ETEC strain 18D by Chan and Giannella;[5] (d) an ST isolated from a porcine strain (F11(P155)) of ETEC, reported in Ref. 8); (e) an ST isolated from ETEC strain C57/26C2, reported in Ref. 9).

positions of the disulfide linkages have not yet been determined. Moreover, ST_h and ST_p have the same activities in suckling mouse assay[3,4] and their activity is neutralized by homologous and heterologous *anti*-ST_p and *anti*-ST_h antisera.[10] These findings imply that the common region of the primary structures of these toxin molecules is important for their biological activity and heat-stability.

This paper reports the chemical syntheses of shorter peptides of ST_p, which constitute the common primary sequence of these toxins, but without N-terminal 3 and 4 amino acid residues, respectively, of the N-terminal sequence of ST_p. The preparation of shorter peptides of ST_p by stepwise Edman-degradation of ST_p is also described. Synthetic shorter peptides of ST_p (ST_p (4—18) and ST_p (5—18)) were confirmed to have the same properties as the peptides derived from ST_p by Edman-degradation and to have almost the same biological activities as native and synthetic ST_p. Interestingly, synthetic ST_p (5—18) was more heat-stable than native ST_p.

Experimental

The general experimental and analytical methods used were described in the preceding paper.[6] The abbreviations used in this paper are those recommended by the IUPAC-IUB: *J. Biol. Chem.*, **247**, 977 (1972). Additional abbreviations are: MBzl, *p*-methylbenzyl; TFA, trifluoroacetic acid; DMF, *N,N*-dimethylformamide; TEA, triethylamine.

Boc-Tyr-Cys(MBzl)-Cys(MBzl)-OMe (1). Boc-Cys(MBzl)-Cys(MBzl)-OMe[11] (21.9 g, 40 mmol) was dissolved in TFA (40 ml), stirred at room temperature for 30 min and concentrated to a syrup under reduced pressure. The syrup was mixed with dioxane containing 1 equiv of HCl and concentrated under reduced pressure to a syrup, which was dissolved in DMF (80 ml). Meanwhile, Boc-Tyr-N_2H_3 (13.0 g, 44 mmol) was dissolved in DMF (80 ml), cooled below −20 °C and mixed with 4.39 M HCl (1M=1 mol dm^{-3}) in dioxane (9.1 ml). The solution was stirred with isopentyl nitrite (6.5 ml, 50 mmol) at the same temperature for 35 min and then mixed with the above DMF solution and TEA (20.1 ml). The mixture was stirred at 0 °C for 2 d in a refrigerator. The resulting precipitate was filtered off and the filtrate was concentrated to an oil under reduced pressure. The oil was dissolved in AcOEt and washed successively with 0.1 M HCl, 5% aq $NaHCO_3$ and water. The washed solution was dried over anhydrous Na_2SO_4 and concentrated to a solid under reduced pressure. The solid was crystallized from a mixture of AcOEt, MeOH and hexane; wt 26.0 g (91.6%), mp 160—161 °C, $[\alpha]_D^{23}$ −39.2° (*c* 1.0, DMF).

Found: C, 62.45; H, 6.59; N, 5.72; S, 9.05%. Calcd for $C_{37}H_{47}O_7N_3S_2$: C, 62.61; H, 6.68; N, 5.92; S, 9.02%.

Boc-Tyr-Cys(MBzl)-Cys(MBzl)-N_2H_3 (2). Compound **1** (17.8 g, 25 mmol) was dissolved in a mixture of DMF (50 ml) and MeOH (300 ml). The solution was cooled in an ice-bath, mixed with 100% hydrazine hydrate (50 ml), and then stirred at room temperature for 2 h. The solution was concentrated under reduced pressure and the residue was mixed with water. The solid formed was collected and recrystallized from MeOH and ether; wt 17.0 g (95.5%), mp 194—195 °C, $[\alpha]_D^{23}$ −16.2° (*c* 1.0, DMF).

Found: C, 60.68; H, 6.53; N, 9.76; S, 8.95%. Calcd for $C_{36}H_{47}O_6N_5S_2$: C, 60.91; H, 6.68; N, 9.87; S, 9.02%.

Boc-Tyr-Cys(MBzl)-Cys(MBzl)-Glu(OBu^t)-Leu-OEt (3). Compound **2** (14.2 g, 20 mmol) was dissolved in DMF (100 ml), cooled to −20 °C, and mixed with 4.39 M HCl in dioxane (2.95 ml). The solution was stirred with isopentyl nitrite (2.86 ml, 22 mmol) at the same temperature for 20 min and then mixed with H-Glu(OBu^t)-Leu-OEt·HCl[11] (8.4 g, 22 mmol) and TEA (21.2 ml). The mixture was stirred at 0 °C for 4 d in a refrigerator. The precipitate formed was filtered off and the filtrate was concentrated to an oil under reduced pressure. The oil was dissolved in AcOEt and washed successively with 0.1 M HCl, 5% aq $NaHCO_3$ and water. The washed solution was dried over anhydrous Na_2SO_4 and concentrated under reduced pressure. The residue was crystallized from AcOEt and hexane; wt 19.0 g (93.1%), mp 153 °C (sintered) and 173 °C (melted), $[\alpha]_D^{23}$ −21.2° (*c* 0.5, DMF).

Found: C, 62.27; H, 7.49; N, 6.83; S, 6.20%. Calcd for $C_{53}H_{75}O_{11}N_5S_2$: C, 62.27; H, 7.40; N, 6.85; S, 6.26%.

Boc-Tyr-Cys(MBzl)-Cys(MBzl)-Glu(OBu^t)-Leu-N_2H_3 (4). Compound **3** (18.4 g, 18 mmol) was dissolved in EtOH (200 ml) and mixed with 100% hydrazine hydrate (40 ml) in an ice-bath. The mixture was stirred at room temperature for 4.5 h. The solution was concentrated under reduced pressure to a solid, which was collected with water. The crude material was crystallized from DMF and ether; wt 15.3 g (83.1%), mp 223 °C (decomp), $[\alpha]_D^{23}$ −11.6° (*c* 0.5, DMF).

Found: C, 59.38; H, 6.89; N, 9.46; S, 6.37%. Calcd for $C_{51}H_{73}O_{10}N_7S_2 \cdot H_2O$: C, 59.69; H, 7.37; N, 9.56; S, 6.24%.

Boc-Tyr-Cys(MBzl)-Cys(MBzl)-Glu(OBu^t)-Leu-Cys(MBzl)-Cys(MBzl)-Asn-Pro-Ala-Cys(MBzl)-Ala-Gly-Cys(MBzl)-Tyr-OBzl (5). Boc-Cys(MBzl)-Cys(MBzl)-Asn-Pro-Ala-Cys(MBzl)-Ala-Gly-Cys(MBzl)-Tyr-OBzl[6] (3.22 g, 2.0 mmol) was dissolved in TFA (40 ml), stirred at room temperature for 50 min, and then concentrated under reduced pressure. Meanwhile, compound **4** (2.42 g, 2.4 mmol) was dissolved in DMF 14 ml, cooled below −20 °C, and mixed with 4.39 M HCl in dioxane (4.2 ml). The mixture was stirred with isopentyl nitrite (0.35 ml, 2.7 mmol) at the same temperature for 20 min and then mixed with the above residue and TEA (2.87 ml). The mixture was stirred at 0 °C for 2 d in a refrigerator. The precipitate formed was filtered off and the filtrate was concentrated to a solid under reduced pressure. The solid was washed with 0.1 M HCl and water and crystallized first from DMF and ether and then from DMF and EtOH; wt 4.40 g (88.5%), mp 231 °C (decomp), $[\alpha]_D^{23}$ −37.5° (*c* 0.32, DMF). Amino acid ratio in the acid hydrolysate: Asp, 1.05 (1); Glu, 1.05 (1); Pro, 1.00 (1); Gly, 0.98 (1); Ala, 2.00 (2); Leu, 1.02 (1); Tyr, 2.18 (2).

Found: C, 61.54; H, 6.85; N, 9.10; S, 7.60%. Calcd for $C_{128}H_{164}O_{23}N_{16}S_6$: C, 61.82; H, 6.65; N, 9.01; S, 7.72%.

Boc-Cys(MBzl)-Cys(MBzl)-Glu(OBu^t)-Leu-Cys(MBzl)-Cys-MBzl)-Asn-Pro-Ala-Cys(MBzl)-Ala-Gly-Cys(MBzl)-Tyr-OBzl (6). This compound was synthesized as described previously.[6] Amino acid ratio in the acid hydrolysate: Asp, 1.06 (1); Glu, 1.00 (1); Pro, 1.07 (1); Gly, 1.00 (1); Ala, 2.02 (2); Leu, 1.01 (1); Tyr, 0.97 (1).

Removal of Protecting Groups and Air-oxidation: Protecting groups of compounds **5** and **6** were removed by treatment with anhydrous liquid hydrogen fluoride[12] and the deprotected peptides in dilute solution (5×10^{-5} M) were air-oxidized at pH 8.0, as described previously.[6]

Edman-degradation: Synthetic ST_p (1-18)[6] (1.4 mg, 0.7 μmol) was dissolved in 50% aq pyridine (300 μl). The solution was adjusted to pH 9.5 by the addition of *N*-methylmorpholine and mixed with phenyl isothiocyanate (30 μl). The mixture was kept at 40 °C for 1 h under a stream of nitrogen. The excess reagent used was removed by three washings with benzene (1 ml) and the aqueous layer was lyophilized. The residue was treated with a few drops of TFA at 40 °C for 20 min. TFA was removed under a stream of nitrogen and the residue was dissolved in water

(200 μl) and washed three times with AcOEt (0.5 ml). The aqueous layer was lyophilized. The lyophilized material was purified by HPLC, as described below, and the purified material was degraded by the Edman method under similar conditions to those described above.

Ion-exchange Chromatography: Ion-exchange chromatography of synthetic peptides was performed on a column (2×33 cm or 1.6×25 cm) of DEAE-Sephadex A-25 (acetate form). The material adsorbed on the ion-exchanger was eluted with a linear-gradient of 0 to 0.5 M acetic acid.

High-performance Liquid Chromatography (HPLC): HPLC was performed on a hand-made column (8×300 mm) packed with LiChrosorb RP-8 (Merck, 5 μm particle size) and on a YMC packed column ODS AM-312 (6×150 mm) (Yamamura Chemical Laboratory Co. Ltd., Kyoto, 5 μm particle size) for semipreparative separation and for analysis, respectively. LiChrosorb RP-8 was equilibrated with 0.01 M ammonium acetate (pH 5.7) containing 10% acetonitrile as an organic modifier. YMC packed column was equilibrated with 0.05% TFA (pH 2.2) containing 10% acetonitrile. Both columns were developed at a flow rate of 1 ml/min with a linear-gradient of 10% to 30% acetonitrile.

Biological Assay: ST activity was assayed in suckling mice of 2—4 d old, as described previously.[2] The minimum toxic activity, designated as 1 mouse unit, was the amount of peptide causing sufficient fluid accumulation in the intestine of the test animal to give a weight ratio of the entire intestine to that of the rest of the body of over 0.09.

Heat-stability: Synthetic peptides were tested for heat-stability with analysis by HPLC as described previously.[6]

Results and Discussion

Syntheses of ST_p (4–18) and ST_p (5–18). Two kinds of heat-stable enterotoxins (ST_h and ST_p) active in suckling mouse were isolated from various strains of ETEC and their amino acid sequences were determined by us[2-4] and others.[5,7-9] These toxins have the same sequence from the Tyr residue near the N-terminus to the C-terminal Tyr residue, except for the 4th residue from the C-terminus, as illustrated in Fig. 1, suggesting that this common sequence is important for their biological activity. On the other hand, we[6] recently obtained ST_p from a chemically synthesized linear peptide with the whole amino acid sequence proposed by us.[4] Since this synthetic ST_p had the same biological and physicochemical properties as native ST_p, it seemed to have the same structure, including disulfide linkages, as native ST_p, although the positions of the three disulfide linkages in ST_p have not yet been determined. Because of the structural similarities of ST_h and ST_p, we attempted to synthesize shorter peptides of ST_p covering the common sequence of the toxin, by the same procedure as that used for synthesis of ST_p. Protected pentadeca- and tetradecapeptides (**5** and **6**) were synthesized by similar procedures to those described previously[6] and then treated with anhydrous liquid hydrogen fluoride[12] to remove all the protecting groups. Then dilute solutions (5×10^{-5} M) of the linear peptides with free thiol groups were air-oxidized at pH 8.0 under similar conditions to those described previously.[6] Toxic peptides were isolated from the air-oxidized solution by successive ion-exchange chromatography (Figs. 2 and 3) and HPLC (Figs. 4 and 5). The purified peptides, ST_p (4—18) and ST_p (5—18), were ob-

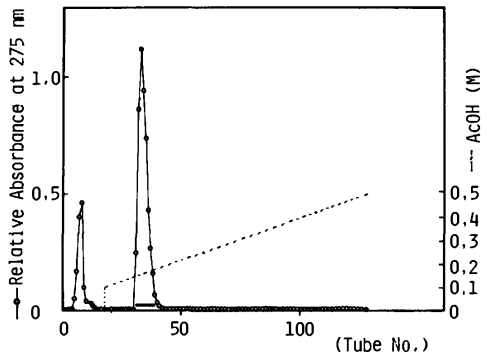

Fig. 2. Chromatography on DEAE-Sephadex A-25 of deprotected and air-oxidized material from compound **5**. Fractions indicated by a horizontal bar showed toxicity and were collected. Column size: 1.3×16.5 cm; fractionation size: 4.5 ml/tube; flow rate: 45 ml/h.

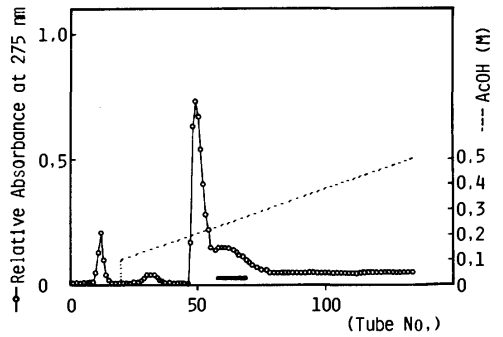

Fig. 3. Chromatography on DEAE-Sephadex A-25 of deprotected and air-oxidized material from compound **6**. The toxic fractions shown by a horizontal bar were collected. Column size: 1.6×25 cm; fractionation size: 4.5 ml/tube; flow rate: 20 ml/h.

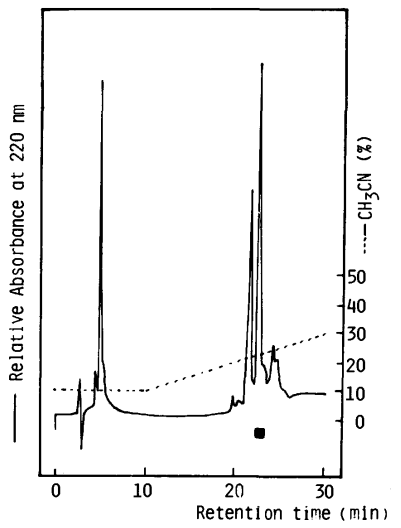

Fig. 4. Semipreparative HPLC of the toxic fraction shown by a horizontal bar in Fig. 2 on a LiChrosorb RP-8 column (5 μm, 8×300 mm). The toxicity was observed in the peak fraction shown by a horizontal bar.

tained in about 6.0% and 10.9% yield from the protected peptides **5** and **6**, respectively.

Preparation of Shorter Peptides of ST_p by Stepwise Edman-degradation. To examine whether synthetic shorter peptides of ST_p (ST_p(4—18) and ST_p(5—18)) were intramolecularly linked by the disulfide bonds in the same way as in native ST_p, we degraded synthetic ST_p (1—18),[6] which has the same biological and physicochemical properties as native ST_p and therefore seems to have the same disulfide linkages as the latter, by the Edman method. Peptides lacking one to four amino acid residues from the N-terminus of ST_p-(1—18) were purified on a semipreparative column of HPLC. The purities of the isolated peptides was confirmed by analytical HPLC, as illustrated in Figs. 6b—e. Removal of N-terminal hydrophilic amino acid residues Asn and Thr from the 1st and 2nd positions of ST_p increased the retention times of the degraded peptides ST_p (2—18) and ST_p (3—18) on HPLC. Further removal of the hydrophobic amino acid residues Phe and Tyr from the 3rd and 4th positions of ST_p gave shorter peptides, ST_p (4—18) and ST_p (5—18), which were eluted earlier than ST_p (1—18). ST_p (1—18) and the degraded peptides were eluted separately from a YMC ODS-column, as shown in Fig. 6f. The recoveries of the degraded peptides in Edman-degradation were 52—56%.

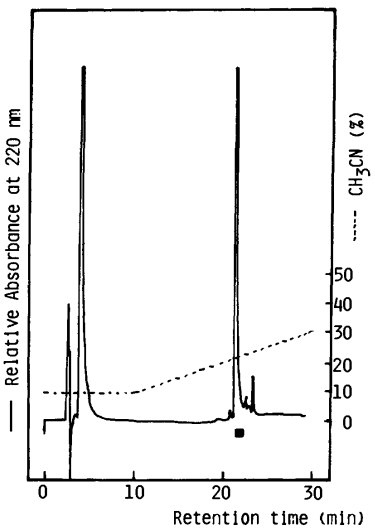

Fig. 5. Semipreparative HPLC on a LiChrosorb RP-8 (5 μm, 8×300 mm) of the fraction shown by a horizontal bar in Fig. 3.

Identification of Synthetic and Edman-degraded Peptides. *i) Amino Acid Analyses*: The amino acid compositions of synthetic peptides (ST_p (4—18) and ST_p (5—18)) and the Edman-degraded peptides (ST_p-(2—18) to ST_p (5—18)) are summarized in Table 1. The results indicate that the N-terminal amino acid residues of ST_p (1—18) were removed stepwise by Edman-degradation.

ii) Mass Spectra: Synthetic and Edman-degraded peptides were subjected to FAB mass spectrometry. As shown in Fig. 7, synthetic ST_p (4—18) and ST_p (5—18), like the Edman-degraded peptides (ST_p(4—18) and ST_p-(5—18)), gave intense signals at m/z=1609 and 1446. The results indicated that the molecular weights of synthetic ST_p (4—18) and ST_p (5—18) were 1608 and 1445, respectively, and hence that these synthetic peptides were intramolecularly linked by three disulfide bonds.

iii) HPLC: The synthetic peptides (ST_p (4—18) and ST_p (5—18)) were coeluted with the respective peptides prepared by the Edman method from LiChrosorb RP-8,

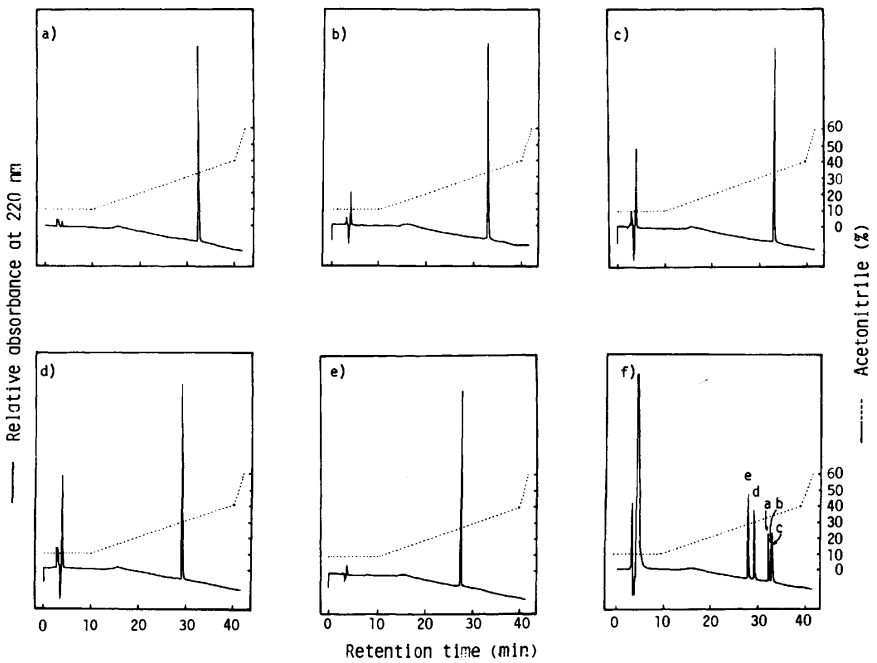

Fig. 6. HPLC profiles on a YMC ODS-column (6×150 mm) of shorter peptides of ST_p prepared by Edman-degradation: a) The starting peptide ST_p (1-18), b) ST_p(2-18), c) ST_p(3-18), d) ST_p(4-18), e) ST_p(5-18), and f) a mixture of a), b), c), d), and e).

Table 1. Amino acid compositions of synthetic peptides and Edman-degraded peptides of ST_p

	Synthetic peptides			Edman-degraded peptides			
	ST_p	ST_p[4-18]	ST_p[5-18]	ST_p[2-18]	ST_p[3-18]	ST_p[4-18]	ST_p[5-18]
Asp	2.00(2)	1.08(1)	1.08(1)	1.03(1)	1.02(1)	1.03(1)	1.04(1)
Thr	1.00(1)			0.95(1)			
Glu	1.11(1)	1.03(1)	1.05(1)	1.01(1)	1.01(1)	1.02(1)	1.06(1)
Pro	1.07(1)	1.22(1)	1.25(1)	0.93(1)	1.09(1)	1.06(1)	0.97(1)
Gly	0.99(1)	1.02(1)	1.02(1)	1.02(1)	0.99(1)	1.04(1)	1.03(1)
Ala	2.00(2)	2.00(2)	2.00(2)	2.00(2)	2.00(2)	2.00(2)	2.00(2)
1/2 Cys	5.25(6)	5.44(6)	5.05(6)	5.16(6)	5.16(6)	5.26(6)	5.18(6)
Leu	0.96(1)	1.09(1)	1.00(1)	1.02(1)	1.01(1)	1.03(1)	1.07(1)
Tyr	1.86(2)	2.05(2)	0.91(1)	1.95(2)	1.95(2)	1.95(2)	0.98(1)
Phe	0.98(1)			0.97(1)	0.94(1)		

Values were calculated as mol/mol of Ala; numbers in parentheses indicate theoretical values.

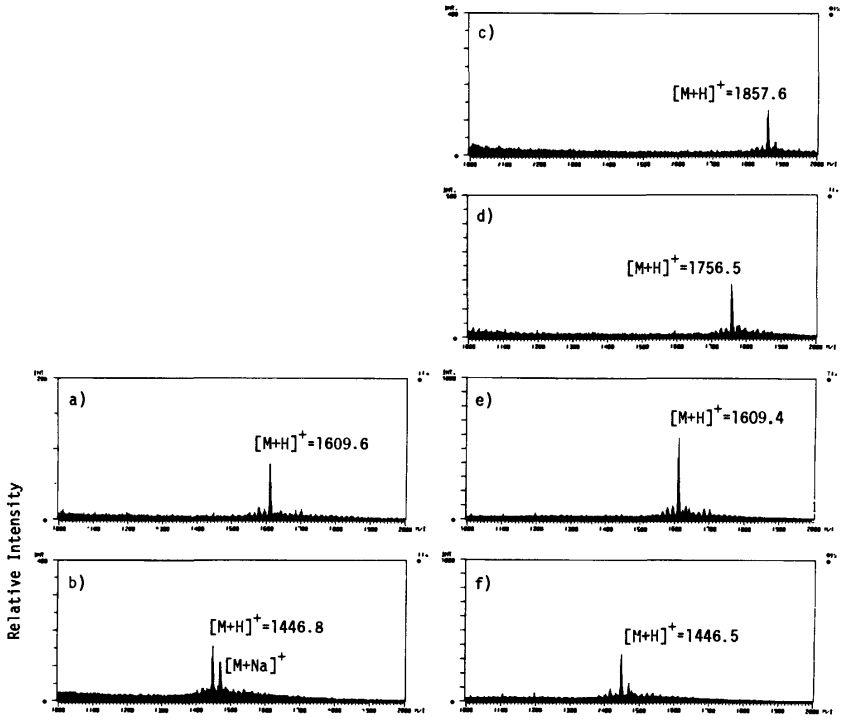

Fig. 7. Positive FAB mass spectra: (first column) synthetic peptides a) ST_p(4–18), b) ST_p(5–18); (second column) Edman degraded peptides c) ST_p(2–18), d) ST_p(3–18), e) ST_p(4–18), and f) ST_p(5–18).

as shown in Fig. 8. These results indicated that the synthetic ST_p (4—18) and ST_p (5—18) were intramolecularly linked by three disulfide bonds in the same positions as in native ST_p.

Biological Activities of Synthetic and Edman-degraded Peptides. The synthetic peptides (ST_p (4—18) and ST_p (5—18)) and Edman-degraded peptides (ST_p (2—18), ST_p (3—18), ST_p (4—18), and ST_p (5—18)) were assayed by the fluid accumulation test using suckling mice.[2] As seen in Table 2, these shorter peptides of ST_p all showed toxicity at a dose of about 1.5—2 ng, which was almost the same value as that of native and synthetic ST_p. Thus the sequence from the Tyr residue near the N-terminus to the C-terminal Tyr residue, which is the same in ST_h and ST_p, except for the 4th residue from the C-terminus, had the same biological

Table 2. Some biological properties of ST_p related peptides

	Minimum effective dose/ng	Neutralization by anti-native ST_p antiserum
Synthetic peptides		
ST_p[1-18]	1	+
ST_p[4-18]	0.8—1	+
ST_p[5-18]	0.8—1	+
Edman-degraded peptides		
ST_p[2-18]	0.5—2	+
ST_p[3-18]	1.5—2	+
ST_p[4-18]	1—2	+
ST_p[5-18]	1	+

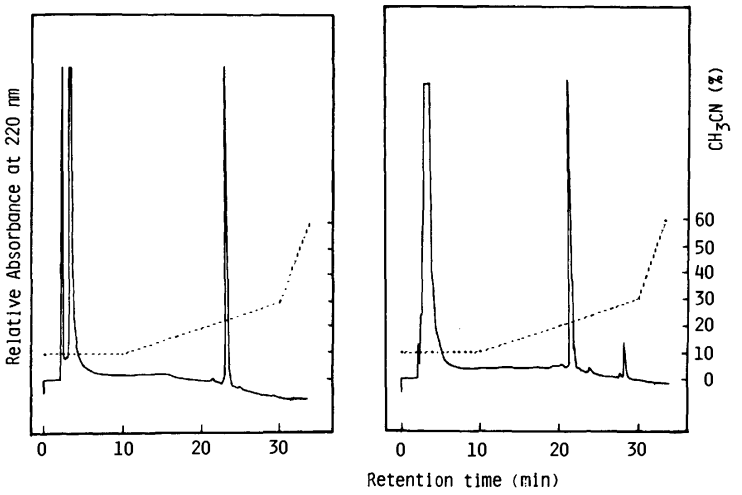

Fig. 8. HPLC profiles on a column (4×250 mm) of LiChrosorb RP-8 of mixtures of a) synthetic ST_p-(4–18) and the Edman-degraded peptide ST_p(4–18) and b) synthetic ST_p(5–18) and the Edman-degraded peptide ST_p(5–18).

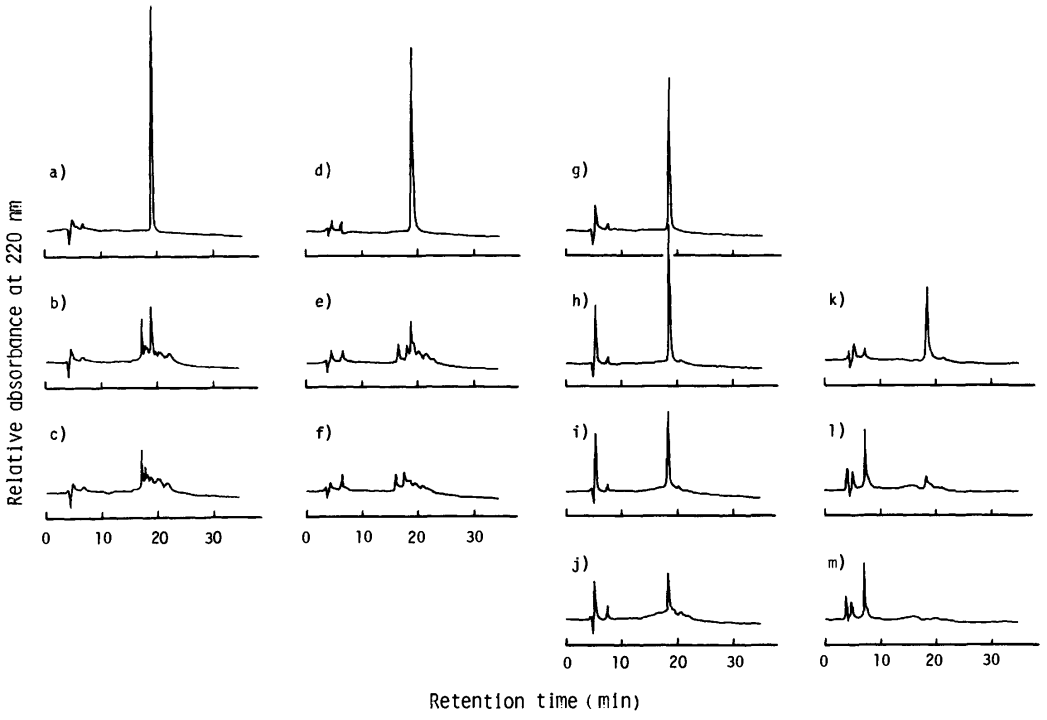

Fig. 9. Comparison of heat-stabilities of synthetic ST_p(1-18) and its shorter peptides: (first column) synthetic peptide ST_p(1-18) a) untreated, b) after 10 min at 100 °C, c) after 30 min at 100 °C; (second column) synthetic ST_p(4–18) d) untreated, e) after 10 min at 100 °C, f) after 30 min at 100 °C; (third and fourth columns) synthetic ST_p(5–18) g) untreated, h) after 10 min at 100 °C, i) after 30 min at 100 °C, j) after 60 min at 100 °C, k) after 10 min at 120 °C, l) after 30 min at 120 °C, and m) after 60 min at 120°C.

activity as that of the whole sequence in ST_p. The results also show that the Tyr residue at the 4th position of ST_p was not necessary for expression of toxicity.

Furthermore, the toxicity of the synthetic and Edman-degraded peptides was found to be neutralized by anti-native ST_p antisera,[10] as shown in Table 2. These results suggest that the three dimensional structure from the Cys residue near the N-terminus to the C-terminal Tyr residue, including the three disulfide linkages, is extremely important for the expression of the toxicity of ST_p, because the reductive cleavage of disulfide linkages destroys the toxicity of the toxin. If the receptor for ST_p is on the epithelial cell membrane in the intestine, the site for binding of ST_p to the receptor may be located in this three dimensional structure. Studies on this possibility are now in progress.

Heat-stabilities of Synthetic Peptides ST_p (4—18) and ST_p (5—18). The name "heat-stable" is based on

the observation[14,15] that the toxicity of this toxin is not lost on heating the toxin for 30 min in boiling water. Recently we[6,13] found that the heat-stability of the toxin can be examined by HPLC. By this HPLC procedure, we compared the heat-stabilities of synthetic ST_p-(4—18) and ST_p (5—18) with that of synthetic ST_p (1—18). ST_p (4—18) showed similar stability to ST_p (1—18) under the conditions examined, as illustrated in Figs. 9a—f. On the other hand, ST_p (5—18) was found to be more stable than ST_p (4—18) and ST_p (1—18) and after heating in boiling water for 60 min, about half its peak height was retained, as shown in Figs. 9g—j, whereas on similar treatment synthetic ST_p (1—18) and ST_p-(4—18) were almost completely destroyed. The HPLC profiles of ST_p (5—18) treated at 120 °C (Figs. 9k—m) were similar to those of ST_p (1—18) and ST_p (4—18) boiled at 100 °C. ST_p (5—18) was completely destroyed by treatment for 60 min at 120 °C. Thus, removal of the four N-terminal amino acid residues, especially the 4th Tyr residue, increased the heat-stability of the toxin. The enhanced structural stability of ST_p (5—18) may be due to decreased perturbation of the molecule on heating as a result of the absence of the N-terminal sequence.

This work was partly supported by a Grant-in-Aid for Scientific Research No. 58122002 from the Ministry of Education, Science and Culture.

References

1) M. N. Burgess, R. J. Bywater, C. M. Cowley, N. A. Mullan, and P. M. Newsome, *Infect. Immun.*, **21**, 526 (1978).
2) Y. Takeda, T. Takeda, T. Yano, K. Yamamoto, and T. Miwatani, *Infect. Immun.*, **25**, 978 (1979).
3) S. Aimoto, T. Takao, Y. Shimonishi, S. Hara, T. Takeda, Y. Takeda, and T. Miwatani, *Eur. J. Biochem.*, **129**, 257 (1982).
4) T. Takao, T. Hitouji, S. Aimoto, Y. Shimonishi, S. Hara, T. Takeda, Y. Takeda, and T. Miwatani, *FEBS Lett.*, **152**, 1 (1983).
5) S. -K. Chan and R. A. Giannella, *J. Biol. Chem.*, **256**, 7744 (1981).
6) S. Yoshimura, M. Miki, H. Ikemura, S. Aimoto, Y. Shimonishi, T. Takeda, Y. Takeda, and T. Miwatani, This *Bull. Chem. Soc. Jpn.*, **57**, 125 (1984).
7) R. Lallier, F. Bernard, M. Gendreau, C. Lazure, N. G. Seidah, M. Chretien, and S. St-Pierre, *Anal. Biochem.*, **127**, 267 (1982).
8) C. Lazure, N. G. Seidah, M. Chretien, R. Lallier, and S. St-Pierre, *Can. J. Biochem. Cell Biol.*, **61**, 287 (1983).
9) B. Ronnberg, T. Wadstrom, and H. Jornvall, *FEBS Lett.*, **155**, 183 (1983).
10) T. Takeda, Y. Takeda, S. Aimoto, T. Takao, H. Ikemura, Y. Shimonishi, and T. Miwatani, *FEMS Microbiol. Lett.*, **20**, 357 (1983).
11) H. Ikemura, unpublished.
12) S. Sakakibara, Y. Shimonishi, Y. Kishida, M. Okada, and H. Sugihara, *Bull. Chem. Soc. Jpn.*, **40**, 2164 (1967).
13) S. Aimoto, H. Watanabe, H. Ikemura, Y. Shimonishi, T. Takeda, Y. Takeda, and T. Miwatani, *Biochem. Biophys. Res. Commun.*, **112**, 320 (1983).
14) H. W. Smith and C. L. Gyles, *J. Med. Microbiol.*, **3**, 387 (1970).
15) D. G. Evans, D. J. Evans, Jr., and N. F. Pierce, *Infect. Immun.*, **7**, 873 (1973).

Manufacture of Pure Titanium(IV) Oxide by the Chloride Process. III. Precipitation of Hydrous Titanium(IV) Oxide in Hydrochloric Acid Solution at Elevated Temperatures

Eiichi NARITA,* Hitoshi TAKEUCHI, Naoto HORIGUCHI, and Taijiro OKABE
Department of Applied Chemistry, Faculty of Engineering, Tohoku University, Aramaki, Sendai 980
(Received June 10, 1983)

Thermal hydrolysis of titanium(IV) in hydrochloric acid solutions (0.2 mol dm^{-3} in Ti(IV); 2 mol dm^{-3} in HCl) was carried out at temperatures up to 110 °C to investigate the effects of heating rate, heating temperature, aging time, and coexisting ions on the particle shape, size, crystal form, crystalline size, and content of water of the hydrous titanium(IV) oxide precipitated. The resulting polycrystalline particles having rutile structure were all distorted ellipsoids at the beginning of the hydrolysis, and gradually changed to spheres with rising temperature or with the duration of time. However, no effects of heating rate on the particle shape and size distribution were observed at the beginning of the hydrolysis. On the other hand, the precipitation rate of titanium(IV) measured at a constant temperature remarkably depended on the temperature; marked changes in the particle size distribution and mean particle size were observed during the reaction. The precipitation rate was well expressed by the rate equation based on the rate-determining step of the surface chemical reaction. The apparent activation energy was 111 kJ mol^{-1}. Although no effects of coexisting cations such as iron(III) and aluminium(III) were recognized, the presence of sulfate and fluoride ions significantly affected the particle shape and size of such precipitates. Anatase-type hydrous titanium(IV) oxide consisting of spherical particles of narrow size distribution was also obtained in the presence of fluoride ion.

As a new manufacturing process of titanium(IV) oxide, the authors previously proposed the Chloride Process,[1,2] in which both production of titanium(IV) oxide and recovery of iron compounds in higher state of purity were expected. This process is based on the leaching of ilmenite ore in concentrated hydrochloric acid solutions and on the selective recovery of titanium(IV) and iron(III) from the resulting leach liquor by solvent extraction with tributyl phosphate (TBP). In this process, ilmenite ore, which occurs abundantly in nature, can be used. The other important feature is that using hydrochloric acid as the leachant allows easier recovery of useful free acid from its waste solution than using sulfuric acid does.[3-5] The kinetics of leaching of ilmenite ore[1] and the solvent extraction of titanium(IV) and iron(III) using TBP[2] have been already studied. As the third unit process for producing hydrous titanium(IV) oxide from the back-extracted solution containing titanium(IV), the thermal decomposition[5,6] or the thermal hydrolysis[7,8] can be useful. In the conventional manufacturing process, *i.e.*, the sulfate process, thermal hydrolysis is extensively used.[9]

It is generally known that the rutile-type hydrous titanium(IV) oxide is produced in hydrochloric acid solutions by the thermal hydrolysis.[10] Recently Matijević *et al.*[11,12] also studied the thermal hydrolysis of titanium(IV) in hydrochloric acid solutions to clarify the optimum conditions for the preparation of titanium(IV) oxide hydrosol of narrow size distribution. On the other hand, the effect of various additives such as NO_3^-, Cl^-, SO_4^{2-}, and F^- ions on the crystal structure of the resulting hydrous titanium(IV) oxide was also investigated in the hydrolysis of titanium(IV) chloride,[7,10] in the aerial oxidation of titanium(III) chloride,[13] and in the hydrothermal treatment of amorphous titanic acid.[14] In addition, from the viewpoint of the kinetics of the hydrolysis[8] and of the mechanism of the particle growth,[15] the thermal hydrolysis of titanium(IV) chloride has been investigated. However, in the course of our development of the Chloride Process, further information about the factors influencing the particle properties of the hydrous titanium(IV) oxide precipitated by the thermal hydrolysis of titanium(IV) in hydrochloric acid solutions was necessary. This study will deal with the effect of process variables such as heating rate, heating temperature, aging time, and coexisting ions on the particle shape, size, crystal form, crystalline size, and content of water of the precipitates. The relation between the particle growth behavior and the precipitation rate of titanium(IV) was also investigated.

Experimental

Reagents. Commercial extra-pure titanium(IV) chloride (Wako Pure Chem. Ind., Ltd.) was purified by distillation at 61 °C and 64 mmHg (1 mmHg≈133.322 Pa) before being used. The titanium(IV) chloride stock solution was prepared by dissolving a 25 cm^3 portion of the distillate in 200 cm^3 analytical grade concentrated hydrochloric acid (Wako Pure Chem. Ind., Ltd.) and then by filtrating through a 0.66 μm teflon millipore filter to remove insoluble materials as impurities. The reaction solution used in the experiment was prepared by diluting the stock solution with hydrochloric acid solution. Additive ions were previously added as sodium salts in the case of anion and as chloride in the case of cation to the hydrochloric acid solution. All other reagents were of the highest purity grade available.

Procedure. Hydrochloric acid solution containing titanium(IV) (0.2 mol dm^{-3} in Ti(IV); 2 mol dm^{-3} in HCl) was transferred in a Vitro Dynamics rectangular parallelepiped microslide (inner size: 0.3 mm×3.0 mm×50 mm) and then both ends of the slide were sealed using epoxy resin adhesive. After this procedure, the slide was heated in the small-sized silicone oil bath equipped with a Sinku Riko HPC-5000 thermal program controller for the hydrolysis of titanium(IV). The oil bath was designed to allow us to observe the precipitation behavior of titanium(IV) in the

slide. After the lapse of a fixed time, the slide was taken out and rapidly quenched to room temperature. Subsequently, the slide was destroyed and the precipitate which had formed on the inner side of the slide was washed with 2 mol dm^{-3} hydrochloric acid and distilled water, and then dried over diphosphorus pentaoxide under reduced pressure. As an experiment to measure the precipitation rate of titanium(IV), the thermal hydrolysis was similarly carried out using a cylindrical glass sealed tube (36 cm^3 in volume). The resulting suspension was first quenched and then centrifuged. The supernatant solution was withdrawn to analyze for titanium ion. The percentage precipitation of titanium(IV) was calculated from the titanium ion concentrations in solution before and after the hydrolysis. The precipitate was washed and dried by the procedures described above.

Analysis. The observation of the particle shape and the measurement of the particle size distribution of the precipitate were performed using a Hitachi-Akashi MSM 4C-102 Scanning Electron Microscope. The X-ray diffraction patterns were obtained using a Rigaku Denki Geigerflex 2013 with Ni filtered Cu $K\alpha$ radiation, with 30 kV and 10 mA. The crystalline size of the precipitate was obtained by the line-broadening method,[16] based on the half-value width of X-ray diffraction peaks of 2θ=27.42° (110) for the rutile and of 2θ=25.28° (101) for the anatase, respectively. DTA and TG were obtained using a Rigaku Denki Thermoflex over the range from room temperature to 1200 °C. The rate of temperature rise was 10 °C min^{-1}. The concentrations of titanium ion and hydrochloric acid were analyzed by colorimetric method[17] and neutralization, respectively.

Results and Discussion

Effect of Heating Rate. Hydrochloric acid solution containing titanium(IV) was heated from room temperature with the heating rates of 0.2, 1.0, and 2.0 °C min^{-1}. The turbidity point is defined here as the temperature at which turbidity was observed in the solution by the hydrolysis of titanium(IV). The turbidity points observed were 77, 87, and 97 °C, respectively. Scanning electron micrographs of the precipitated particles obtained at the turbidity point or above under the heating rate of 1.0 °C min^{-1} are shown in Fig. 1. The particle shape of the precipitate obtained at the turbidity point was that of a distorted ellipsoid, an aggregate of two or three small particles. As the temperature was raised further, the shape changed to sphericity with an increase in the particle size. A similar result was obtained under the heating rate of 0.2 °C min^{-1}. X-Ray diffraction revealed that all these precipitates were rutile-type hydrous titanium(IV) oxide.

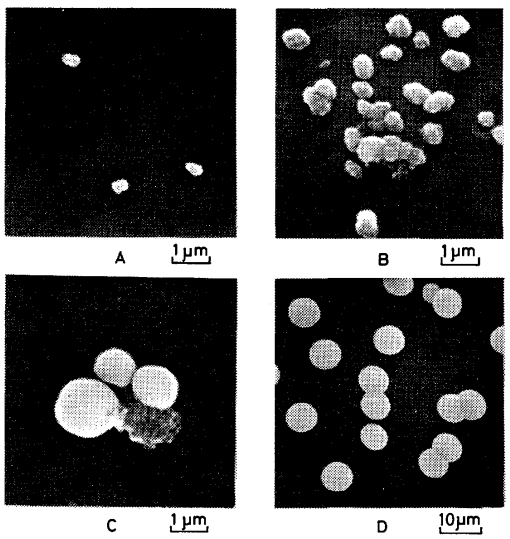

Fig. 1. Scanning electron micrographs of the precipitated particles obtained at different temperatures.
HCl: 2.10 mol dm^{-3}, Ti(IV): 0.230 mol dm^{-3}, heating rate (°C min^{-1})—1.0(A: 87 °C (turbidity point), B: 95 °C, C: 105 °C), 0.2(D: 105°C).

Figure 2 shows the effect of the heating rate on the particle size distribution of the precipitates obtained at the turbidity points. No marked differences can be detected in the distribution histogram and mean particle size, δ. Therefore, it was concluded that the particle shape and size of the hydrous titanium(IV) oxide were not affected by the heating rate. In the experiments conducted in 4 mol dm^{-3} hydrochloric acid, the same results were obtained, except for a rise in the turbidity point of about 10 °C.

Effect of Aging Time. Hydrochloric acid solution containing titanium(IV) was heated at a rate of 1.0 °C min^{-1}, and then maintained at the desired temperatures in all subsequent experiments. Figure 3 shows the effect of the aging time on the particle size distribution at 95 °C. The mean particle size increased with the duration of the aging. The other impressive feature was that the tailing phenomenon was recognized in the distribution histograms after the lapse of 1—3 h and then disappeared after the lapse of 6 h. These precipitates were all spherical in shape, having the rutile structure. The results obtained in the experiments conducted at 88 °C were approximately the same as those described above.

The precipitation rate of titanium(IV) measured at 88, 91, and 95 °C are shown in Fig. 4. A rapid precipitation step was found at 2—4 h for 88 °C, and also at 1—3 h for 95 °C. It is noticeable here that these rapid precipitation steps correspond to the time at which the tailing phenomenon shown in Fig. 3 appeared. The disappearance of the tailing phenomenon at 6 h also seemed

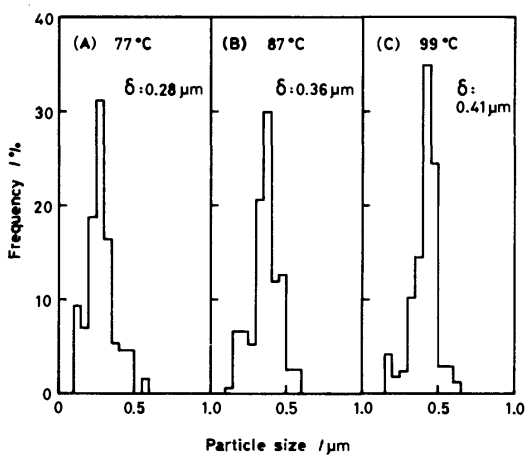

Fig. 2. Effect of heating rate on the particle size distribution of the precipitates obtained at the turbidity point.
HCl: 2.10 mol dm^{-3}, Ti(IV): 0.230 mol dm^{-3}, heating rate (°C min^{-1})—A: 0.2, B: 1.0, C: 2.0.

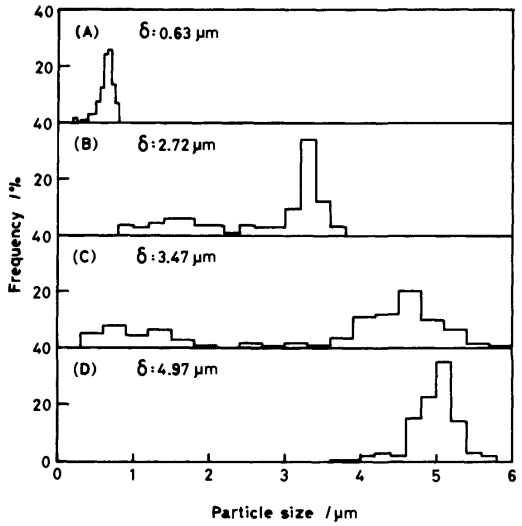

Fig. 3. Effect of aging time on the particle size distribution of the precipitates.
HCl: 2.13 mol dm^{-3}, Ti(IV): 0.220 mol dm^{-3}, temperature: 95 °C, aging time (h)—A: 0, B: 1, C: 3, D: 6.

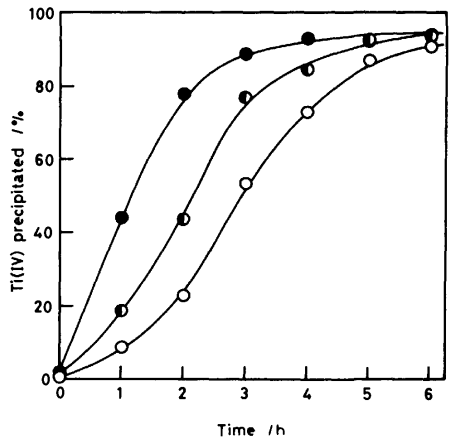

Fig. 4. Effect of temperature on the precipitation rate of Ti(IV) in HCl solution.
HCl: 2.16 mol dm^{-3}, Ti(IV): 0.219 mol dm^{-3}, temperature (°C)—○: 88, ◐: 91, ●: 95.

to be due to the growth of the particles by the dissolution-reprecipitation or by the annexation of small particles on the bigger ones.

Analysis of Particle Growth Rate. The analysis of the particle growth was carried out using the crystal growth theory. This analysis is based on the assumption that nucleation is finished at once in the beginning step of the crystal growth. In the case that the particle growth is limited by the surface chemical reaction, the precipitation rate is written as follows:[18]

$$\frac{dX}{dt} = \alpha X^{2/3}(1-X). \quad (1)$$

Here

$$\alpha = \{36\pi V^2(C_o - C_e)^2 N\}^{1/3} G, \quad (2)$$

where X is the molar fraction of precipitation (−), t the time (h), V the volume per unit molar of precipitate (m^3 kg mol^{-1}), Co the initial solute concentration in bulk solution (kg mol m^{-3}), C_e the solubility of the precipitate (kg mol m^{-3}), N the particle number per unit volume (m^{-3}), and G the transfer coefficient (m h^{-1}). By integration of Eq. 1, Eq. 3 was obtained:

$$\alpha t = \int_0^{X^{1/3}} \frac{3}{1-y^3} dy = I. \quad (3)$$

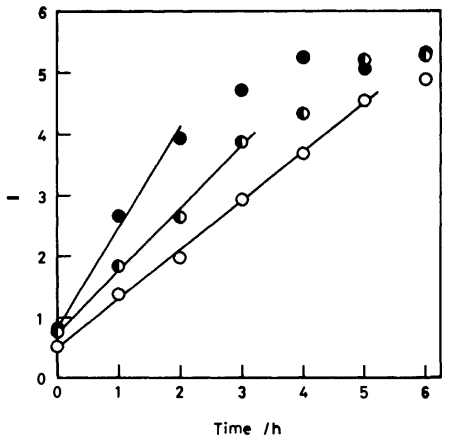

Fig. 5. Effect of temperature on the precipitation rate of Ti(IV) in HCl solution—I *versus* t.
HCl: 2.16 mol dm^{-3}, Ti(IV): 0.219 mol dm^{-3}, temperature (°C)—○: 88, ◐: 91, ●: 95.

Figure 5 shows the relationship between I and t. At 88 °C a good linear dependence of I on t was observed. This means that the precipitation rate of titanium(IV) is well expressed by Eq. 1. The linear dependence was also observed at early steps at 91 and 95 °C. However, there was not a linear relationship between I and t in the precipitation curves after 3 h at 91 °C or after 2 h at 95 °C. This deviation from the rate equation was thought to be dependent on the change in the rate-determining step from the surface chemical reaction process to the diffusion process of titanium(IV). The apparent activation energy calculated from the Arrhenius plots of α, which was given from the slope of the straight lines in Fig. 5, was 111 kJ mol^{-1}. This value indicates the reasonability of the assumption used in this analysis that the particle growth is limited by the surface chemical reaction.

Effect of Coexisting Ions. The effect of sulfate and fluoride ions, both which have stronger complexing ability for titanium(IV) than chloride ion does, on the particle shape, size, crystal form, crystalline size, and content of water of the precipitate was investigated in detail. Scanning electron micrographs of the precipitated particles obtained in the presence of these anions at 95 °C after 6 h are shown in Fig. 6, together with that obtained in the absence of these anions. The precipitated particles were perfectly spherical in shape; X-ray diffraction revealed that crystal form corresponded to rutile-type hydrous titanium(IV) oxide. On the other hand, the particle shape of the precipitate was irregular plate-like in the presence of sulfate ion and slightly distorted spherical in the presence of fluoride ion. The reason for this difference is as yet unclear. The other important feature was that both precipitates were ana-

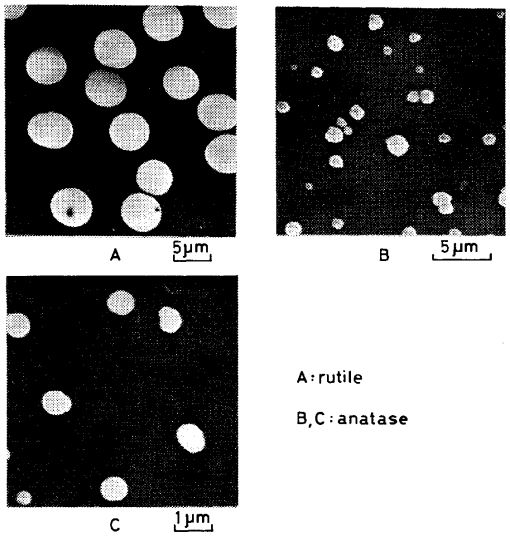

Fig. 6. Scanning electron micrographs of the precipitated particles obtained in the presence of sulfate and fluoride ions.

HCl: 2.13 mol dm^{-3}, Ti(IV): 0.220 mol dm^{-3}, temperature: 95°C, anion added—A: none, B: 0.480 mol dm^{-3} Na_2SO_4, C: 0.112 mol dm^{-3} NaF.

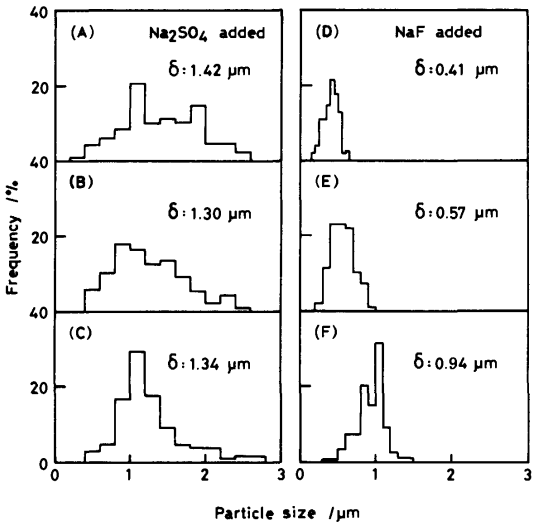

Fig. 7. Effect of coexisting anions on the particle size distribution of the precipitates.
HCl: 2.13 mol dm^{-3}, Ti(IV): 0.220 mol dm^{-3}, temperature: 95 °C, anion added—A—C: 0.480 mol dm^{-3} Na_2SO_4, D—F: 0.112 mol dm^{-3} NaF, Aging time (h)—A,D: 1, B,E: 3, C,F: 6.

tase-type hydrous titanium(IV) oxide; this result agrees with those reported by earlier workers.[7,10,13,14]

The effect of both anions on the particle size distribution is shown in Fig. 7. In the presence of sulfate ion, the distribution was broadened, although the mean particle size became smaller. However, in the presence of fluoride ion, the range of the distribution was extremely narrow, so that the particles can be regarded as monodispersed, whereas the mean particle size became even smaller. Although Matijević *et al.*[11,12] had reported the preparation method of rutile-type titanium(IV) oxide consisting of spherical particles of narrow size distribution, it was found here that a similar result on the formation of anatase-type titanium(IV) oxide could be obtained by the addition of fluoride ion.

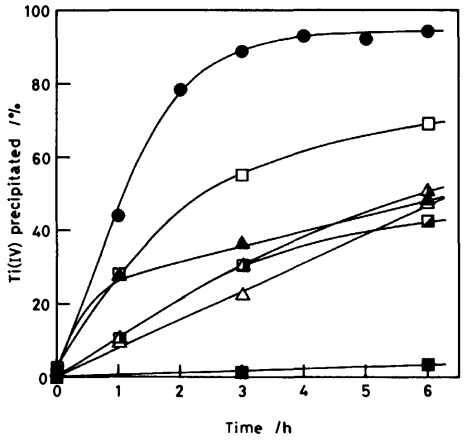

Fig. 8. Effect of coexisting anions on the precipitation rate of Ti(IV) in HCl solution.
HCl: 2.12 mol dm^{-3}, Ti(IV): 0.219 mol dm^{-3}, temperature: 95°C, anion added—None: ● Na_2SO_4 (mol dm^{-3}): △ 0.10, ▲ 0.20, ▲ 0.46, NaF (mol dm^{-3}): □ 0.10, ◪ 0.20, ■ 0.44.

Figure 8 also shows the effect of both anions on the precipitation rate of titanium(IV). In general, the precipitation rate decreased in the presence of these anions. The degree of the decrease in the precipitation rate was correlative with the stability constant of each titanium(IV) complex, as shown below (25 °C):

$$\frac{[TiOCl^+]}{[TiO^{2+}][Cl^-]} = 3.55,^{19} \quad (4)$$

$$\frac{[TiOSO_4]}{[TiO^{2+}][SO_4^{2-}]} = 1.69\times10^2,^{20} \quad (5)$$

$$\frac{[TiOF^+]}{[TiO^{2+}][F^-]} = 2.75\times10^6.^{21} \quad (6)$$

The precipitation rate decreased with increasing the concentration of fluoride ion. The initial precipitation rate oppositely increased with increasing the concentration of sulfate ion. This conflicting result can be explained by the phenomenon that sulfate ion exists mostly as HSO_4^- under the conditions of 90 °C and 2 mol dm^{-3} hydrochloric acid, as can be estimated from the following equation:

$$\frac{[SO_4^{2-}]}{[HSO_4^-]} = 3.97\times10^{-4}.^{23} \quad (7)$$

Namely, the increase in the initial precipitation rate seemed to be due to the actual decrease in acid concentration.

The time changes in the mean particle size of the precipitate obtained at different temperatures in the presence or absence of these anions are shown in Fig. 9. In general, the mean particle sizes increase with the duration of the aging, except in the case of the presence of sulfate ion, and decreased with an increase in the complexing ability of these anions for titanium(IV). It

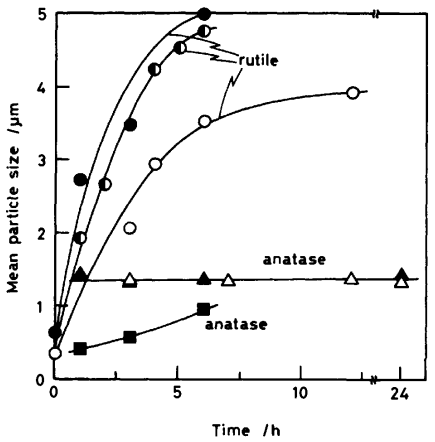

Fig. 9. Effects of temperature and coexisting anions on the mean particle size of the precipitates.
HCl: 2.13 mol dm^{-3}, Ti(IV): 0.220 mol dm^{-3},

	○ ◐ ●	△ ▲	■
Temperature/°C	78 88 95	78 95	95
Anion added	None	0.480 mol dm^{-3} Na_2SO_4	0.112 mol dm^{-3} NaF

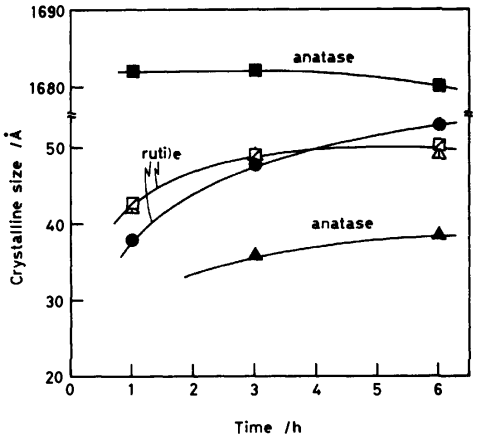

Fig. 10. Effect of coexisting ions on the crystalline size of the precipitates.
HCl: 2.2 mol dm^{-3}, Ti(IV): 0.22 mol dm^{-3}, temperature: 95 °C, ion added—●: none, ▲: 0.20 mol dm^{-3} Na_2SO_4, ■: 0.20 mol dm^{-3} NaF, ⊠: 0.02 mol dm^{-3} $FeCl_3$, ⚠: 0.01 mol dm^{-3} $AlCl_3$.

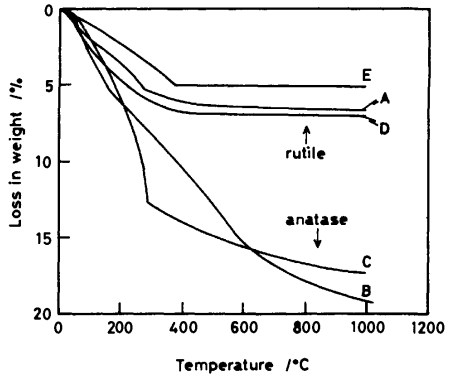

Fig. 11. TG curves of the precipitated particles obtained in the presence of various ions.
HCl: 2.2 mol dm^{-3}, Ti(IV): 0.22 mol dm^{-3}, temperature: 95 °C, ion added—A: none, B: 0.20 mol dm^{-3} Na_2SO_4, C: 0.20 mol dm^{-3} NaF, D: 0.01 mol dm^{-3} $FeCl_3$, E: 0.01 mol dm^{-3} $AlCl_3$.

was also found that the mean particle size increased with an increase in the heating temperature, as shown in Fig. 3, whereas no changes was observed in the case of the presence of sulfate ion.

The effect of coexisting cations such as iron(III) and aluminium(III), which would be contained in the hydrochloric acid leach liquor of ilmenite ore, was also investigated here. With regard to the coprecipitation behavior, about 5% of the initial concentration of iron(III) was incorporated in the hydrous titanium(IV) oxide precipitate, whereas no aluminium(III) was incorporated. Therefore, it is necessary to remove iron(III) from the leach liquor containing titanium(IV) by solvent extraction using TBP before the thermal hydrolysis.[2)]

Figure 10 shows the effect of the coexisting ions on the crystalline size of the precipitates. No changes in the crystalline size were observed in the presence of these cations, although it varied drastically in the presence of anions. Especially in the presence of fluoride ion, the crystalline size became extremely large, and increased with increasing the concentration of fluoride ion. The enlargement in the crystalline size was observed in the fluoride ion concentration of 0.05 mol dm^{-3} or above, whereas time dependences were generally not recognized. On the contrary, the crystalline size became slightly smaller in the presence of sulfate ion.

TG curves of the precipitated particles obtained in the presence or absence of various additional ions are shown in Fig. 11. The rutile-type hydrous titanium(IV) oxides obtained in pure hydrochloric acid solution or in the presence of such cations were found to contain 5—7% of water. The anatase-type hydrous titanium(IV) oxides obtained in the presence of sulfate and fluoride ions indicated that a large weight loss occurred in the heating process. Since the sulfate ion decomposes at temperature higher than 700 °C, most of this weight loss (16—17%) of Sample B can be regarded as the release of water. However, the rapid weight loss of Sample C at about 285 °C corresponded with the close-neighboring peaks of sharp exothermic peak (293 °C) and endothermic peak (300 °C) on the DTA curve. Therefore, this rapid weight loss seemed to be dependent on the formation and sublimation of TiF_4. From these results, the content of F^- ion in the precipitate was calculated as 0.82%. It can be said that the anatase-type hydrous titanium(IV) oxide contains a larger amount of water than the rutile-type one.

The results show that the particle shape, size, crystal form, crystalline size, and content of water of the hydrous titanium(IV) oxide precipitated in hydrochloric acid solution can be controlled in the limited range by varying the heating temperature, aging time, and addition of such anions.

References

1) H. Tsuchida, E. Narita, H. Takeuchi, M. Adachi, and T. Okabe, *Bull. Chem. Soc. Jpn.*, **55**, 1934 (1982).
2) E. Narita, H. Takeuchi, H. Ichikawa, T. Odagawa, and T. Okabe, *Bull. Chem. Soc. Jpn.*, **56**, 1832 (1983).
3) A. Conners, *CIM Bulletin*, **68**, 75 (1975).
4) J. W. Burtch, *CIM Bulletin*, **68**, 96 (1975).
5) G. H. Rupy and C. J. Jewell, *CIM Bulletin*, **68**, 89 (1975).
6) N. R. Iammartino, *Chem. Eng.*, **83**, 100 (1976).
7) K. Funaki and Y. Saeki, *Kogyo Kagaku Zasshi*, **59**, 1291 (1956).
8) J. Shiokawa, A. Matsumoto, and H. Kawakami, *Rep. Asahi Glass Found. Ind. Tech.*, **16**, 431 (1970).
9) N. Ohta, *Kagaku Keizai*, **28**, 49 (1981).
10) H. B. Weiser and W. O. Milligan, *J. Phys. Chem.*, **38**, 513 (1934).
11) E. Matijević, M. Budnik, and L. Meites, *J. Colloid Interface Sci.*, **61**, 302 (1977).
12) M. Visca and E. Matijević, *J. Colloid Interface Sci.*, **68**, 308 (1979).
13) M. Kiyama, T. Akita, Y. Tsutsumi, and T. Takada, *Chem. Lett.*, **1972**, 21.
14) F. Izumi, *Bull. Chem. Soc. Jpn.*, **51**, 1771 (1978).
15) T. Iida, K. Yamaoka, N. Nojiri, and H. Nozaki, *Kogyo Kagaku Zasshi*, **69**, 2088 (1966).
16) K. Kubo, E. Suito, Y. Nakagawa, and S. Hayakawa, "Funtai," Maruzen, Tokyo (1962), p. 186.
17) E. B. Sandell, "Colorimetric Determination of Traces of Metals," 3rd ed, Interscience Publishers Inc., New York (1959), pp. 524, 870.
18) K. Hayashi and Y. Nurishi, *Kagaku No Ryoiki*, **18**, 26 (1964).
19) B. I. Nabivanets and L. N. Kudritskaya, *Russ. J. Inorg. Chem.*, **12**, 789 (1967).
20) A. K. Babko, E. A. Mazurenko, and B. I. Nabivanets, *Russ. J. Inorg. Chem.*, **14**, 1091 (1969).
21) V. Caglioti, L. Ciavatta, and A. Liberti, *J. Inorg. Nucl. Chem.*, **15**, 115 (1960).
22) M. Pourbaix, "Atlas of Electrochemical Equilibria in Aqueous Solution," Pergamon Press, Oxford *etc.* (1966), p. 545.

Kinetics and Mechanism of Bromine Addition to Derivatives of Unsaturated Aliphatic Carboxylic Acids in Aqueous Solution

Syed Ahamed Mohamed Farook,† Seshaiyer Viswanathan, and (the late) Ramachandran Ganesan

Department of Physical Chemistry, University of Madras, Madras-600 025, India

(Received December 23, 1982)

This paper deals with the kinetics of bromine addition to unsaturated compounds in presence of added bromide ions at 22, 30, 38, 46, and 54 °C. The substrates used were acrylamide (AAm), methyl acrylate (MA), ethyl acrylate (EA), butyl acrylate (BA), *t*-butyl acrylate (*t*BA), methacrylamide (MAAm), methyl methacrylate (MMA), ethyl methacrylate (EMA), methyl crotonate (MC), and ethyl crotonate (EC). The kinetics was followed potentiometrically. The activation parameters ($\Delta H^{\neq}$, $\Delta S^{\neq}$, and $\Delta G^{\neq}$) were calculated and compared. Estimation of product ratio of bromohydrin to dibromide showed the absence of any correlation of the product formation with reactivity of the substrates. The observed parameters are discussed in relation to the proposed reaction mechanisms.

Although a number of mechanisms have been proposed for the bromination in presence of bromide ions,[1-3] controversy still persists regarding the electrophilic activity of the tribromide species.[2-8] We reinvestigated these mechanisms with the help of kinetic experiments, product analysis and salt effects.

Experimental

Materials. Acrylamide,[9] methacrylamide,[10] and esters[11] were purified. Crotonates were prepared according to the reported procedures.[12] Sodium bromide was recrystallised three times from distilled water, and dehydrated at 120 °C for 5 d and kept in a vacuum desiccator over sodium hydroxide. All other inorganic chemicals used were of guaranteed reagents.

Kinetic Procedures. All the kinetic experiments were carried out by potentiometric method using Pt, Br_2/Br^-, and glass electrodes fitted into a specially fabricated reaction vessel.[13,14]

Analysis of Products. To study the regioselectivity factor mainly by ^1H NMR technique for the substrates, MMA and EMA a slight excess of bromine at various bromide concentrations was employed. After completion of the reaction potassium iodide and then sodium thiosulfate were added to remove unreacted bromine. After saturation with NaCl the products were ether extracted, dried over anhydrous sodium sulfate and then distilled off ether. The remaining liquid was used for analysis by TLC, GC, IR, and ^1H NMR studies, as the case may be.

Authentic bromohydrins were prepared[15] and separated by column chromatography. The ^1H NMR spectrum of methyl 2-bromo-3-hydroxy-2-methylpropionate (CCl_4/TMS) showed a singlet (3H, H_a) at δ 1.90, a singlet (1H, H_b) at δ 3.31,

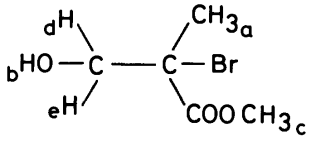

(exchangeable with D_2O), a singlet (3H, H_c) at δ 3.85, and a pair of doublets (2H, $H_{d,e}$) one pair at δ 3.72 and another pair at δ 4.90 resulting from the diastereotropic and hence anisochronous hydrogens on the carbon bearing the hydroxyl group (J_{gem}, 11 Hz). Similarly, the ^1H NMR spectrum of methyl 3-bromo-2-hydroxy-2-methylpropionate (CCl_4/TMS) showed a characteristic singlet at δ 1.49 for 2-methyl group.

† Present address: Department of Cemistry, A. G. C. W., Karaikal, Pondicherry State 609 602, India.

The ^1H NMR spectrum of methyl 2,3-dibromo-2-methylpropionate (CCl_4/TMS) showed a singlet (3H, H_a) at δ 2.0, a singlet (3H, H_b) at δ 3.8 and a pair of doublets (2H, $H_{c,d}$) situated at δ 3.66 and δ 4.19 resulting from the diastereotropic and hence anisochronous hydrogens on the carbon bearing the bromine (J_{gem}, 10 Hz).

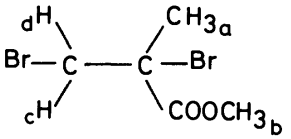

Results and Discussion

In each reaction, the emf falls linearly with time (Fig. 1) showing first-order in bromine. The pseudo-first-order rate constants (k_1) were obtained from the slope of the plots.[16] The second-order rate constant, k_2(obsd),

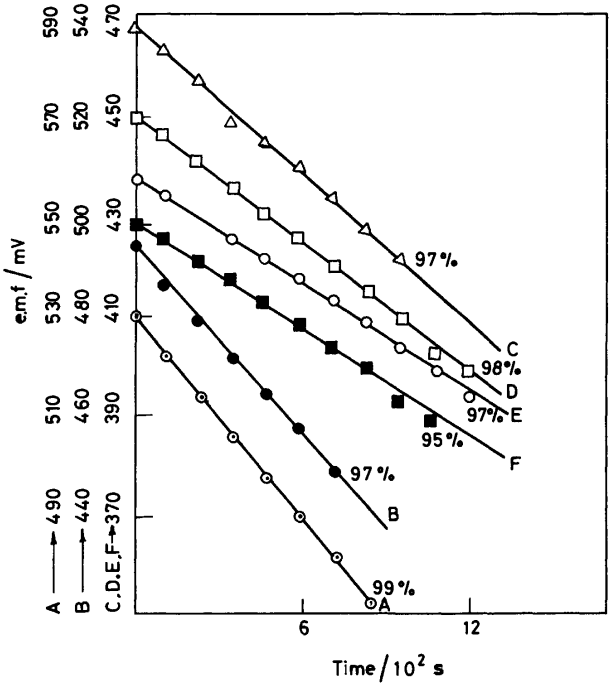

Fig. 1. Pseudo first-order plots for AAm-Br_2 reaction in water at 22 °C. The various $[Br^-]$'s/mol dm^{-3} used are A: 0.01, B: 0.05, C: 0.10, D: 0.20, E: 0.3, F: 0.40. $[AAm]=8.0\times10^{-3}$ mol dm^{-3}, $[Br_2]=6.0\times10^{-5}$ mol dm^{-3}, $[HClO_4]=1.0\times10^{-2}$ mol dm^{-3}.

can be obtained by dividing k_1 by the substrate concentration (S). The constancy in k_2(obsd) values for AAm and MAAm for a variation of the substrate concentration by a factor of 6 indicates the first-order in substrate.

The acids like $HClO_4$, HNO_3, and H_2SO_4 had no effect on the rate constant even for a 100 times variation in concentration thus excluding the contribution of hypobromous acid to reaction. Further, the possibility of the reaction by bromine cation can be neglected in presence of such a high concentration of bromide used. It is therefore reasonable to assume that the reaction may proceed mainly by Br_2 and Br_3^- species. Hence, k_2(obsd), a composite parameter, is given by the equation:[2]

$$k_2(\text{obsd}) = (k_{Br_2} + k_{Br_3^-} K[Br^-])/(1 + K[Br^-]), \quad (1)$$

where k_{Br_2} is the rate constant for the attack by Br_2 species and $k_{Br_2^-}$ for the Br_3^- species; and K, the tribromide formation constant for $Br_2 + Br^- \rightleftharpoons Br_3^-$. Employing least square method for the K values of Scaife and Tyrrell,[17] the values at other required temperatures have been evaluated. Values of k_{Br_2} and $k_{Br_3^-}$ were calculated from the plots of k_2(obsd) $(1 + K[Br^-])$ *vs.* $[Br^-]$ (Fig. 2). Activation parameters were calculated by employing k_{Br_2} and $k_{Br_3^-}$ (Table 1). The values of ΔH^*, ΔS^*, and ΔG^* (at 303 K) are given in Tables 2 and 3.

It is clear from the Table 2 that the ΔH^* values for the methyl-substituted alkenic compounds are lower than that of the corresponding unsubstituted ones. It is evident that the introduction of a methyl group, which causes electron accession to the alkenic linkage by both inductive (+I) and hyperconjugative effects, brings down the activation enthalpy and correspondingly the reaction rate of the methyl-substituted compound increases.

The methacrylic esters react faster than their isomeric crotonates (Table 2). In MMA and EMA, resonance structure-**2** facilitates the retention of the negative charge on the alkenic carbon atom whereas in alkyl crotonates, where the methyl group is present on β-carbon, resonance structure-**1** reduces the electron density on the alkenic carbon atom,

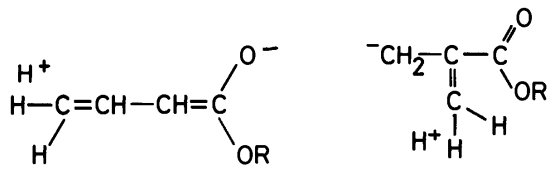

1 2

where R = $-CH_3$ or $-C_2H_5$

When ΔH^* values of all these substrates were compared, it was observed that the activation enthalpy remains almost constant in each of the following sets of

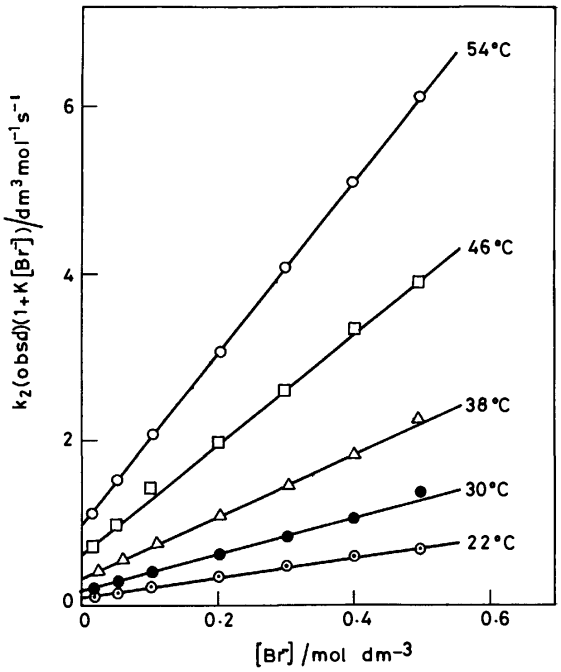

Fig. 2. Determination of k_{Br_2} and $k_{Br_3^-}$ at different temperatures for EA-Br_2 reaction in water.

TABLE 1. RATE CONSTANTS (k_{Br_2} and $k_{Br_3^-}$) AT DIFFERENT TEMPERATURES

Compound	22 °C		30 °C		38 °C		46 °C		54 °C		Average value of
	k_{Br_2}	$k_{Br_3^-}$	k_{Br_2}	$k_{Br_3^-}$	k_{Br_2}	$k_{Br_3^-}$	k_{Br_2}	$k_{Br_3^-}$	k_{Br_2}	$k_{Br_3^-}$	$k_{Br_2}/k_{Br_3^-}$
AAm	0.82	0.30	1.67	0.58	3.10	1.03	5.35	1.97	9.20	3.36	2.82
AAM	1.25	0.24	2.54	0.45	4.15	0.88	8.05	1.61	13.80	2.69	5.14
at μ=0.5 mol dm^{-3}											
MA	0.06	0.04	0.12	0.09	0.23	0.18	0.40	0.32	0.68	0.49	1.35
MA	0.08	0.04	0.17	0.08	0.36	0.16	0.71	0.28	0.95	0.44	2.21
at μ=0.5 mol dm^{-3}											
EA	0.10	0.07	0.17	0.13	0.33	0.25	0.66	0.46	1.00	0.77	1.36
BA	0.09	0.07	0.21	0.14	0.38	0.23	0.65	0.46	1.01	0.77	1.43
tBA	0.34	0.21	0.67	0.49	1.19	0.70	2.40	1.43	3.60	2.78	1.53
MAAm	24.50	7.85	47.00	13.55	81.50	24.50	139.00	39.26	215.00	70.32	3.30
MMA	3.10	1.44	5.80	2.67	10.60	4.62	16.80	8.16	28.00	13.60	2.15
MMA	4.75	1.24	8.75	2.30	13.40	4.24	26.80	7.04	39.00	11.84	3.56
at μ=0.5 mol dm^{-3}											
EMA	5.90	2.59	9.30	4.30	18.40	8.10	27.60	13.57	50.00	25.18	2.15
MC	1.38	0.55	2.83	1.06	5.15	1.96	8.95	3.26	13.70	5.24	2.63
EC	2.35	0.82	4.68	1.65	8.30	2.95	14.00	5.12	22.80	7.87	2.83

Units for k_{Br_2} and $k_{Br_3^-}$ are in dm^3 mol^{-1} s^{-1}.

Table 2. Activation parameters for the addition of Br_2 species

Compound	ΔH^*	ΔS^*	ΔG^*
	kJ mol^{-1}	J K^{-1} mol^{-1}	kJ mol^{-1}
AAm	55.3	−59.0	73.3
AAm[a)]	54.9	−56.1	72.0
MA	57.0	−75.3	79.6
MA[a)]	57.8	−68.7	78.7
EA	55.3	−77.0	78.7
BA	55.7	−75.3	78.3
*t*BA	55.3	−66.1	75.3
MAAm	49.4	−49.8	64.5
MMA	49.8	−66.1	69.9
MMA[a)]	48.6	−67.0	69.1
EMA	48.6	−65.7	68.7
MC	52.8	−62.8	71.6
EC	51.5	−62.4	70.3

a) At μ=0.5 mol dm^{-3}.

Table 3. Activation parameters for the addition of Br_3^- species

Compound	ΔH^*	ΔS^*	ΔG^*
	kJ mol^{-1}	J K^{-1} mol^{-1}	kJ mol^{-1}
AAm	56.1	−64.9	75.8
AAm[a)]	56.1	−66.1	76.2
MA	57.0	−77.4	80.0
MA[a)]	56.1	−80.8	80.4
EA	57.0	−74.1	79.5
BA	55.6	−78.3	79.5
tBA	57.4	−62.8	76.2
MAAm	49.8	−59.4	67.4
MMA	51.5	−67.0	72.0
MMA[a)]	51.5	−68.2	72.0
EMA	51.9	−61.1	70.3
MC	51.5	−74.9	74.1
EC	51.9	−70.3	72.8

a) At μ=0.5 mol dm^{-3}.

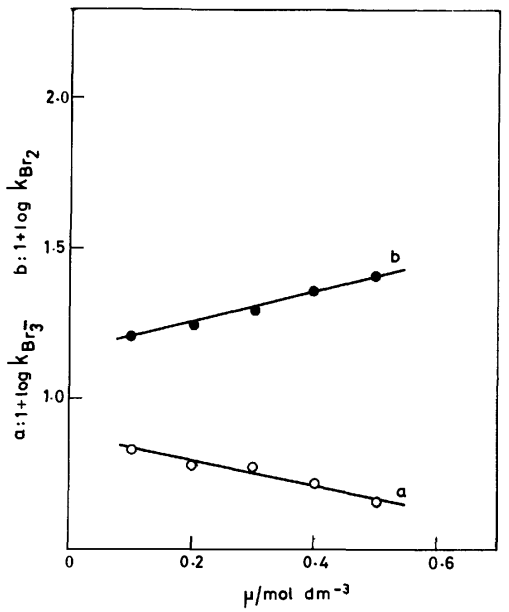

Fig. 3. Effect of ionic strength on k_{Br_2} and $k_{Br_3^-}$ for AAm-Br_2 reaction in water at 30°C.

compounds:
(i) CH_2=CHCOR$_1$; R$_1$=-NH_2, -OBu^t, -OBu, -OEt, -OMe, (ii) CH_2=C(Me)COR$_2$; R$_2$=-NH_2, -OEt, -OMe, and (iii) CHMe=CHCOR$_3$; R$_3$=-OEt, -OMe. In spite of constancy in ΔH^*, the variations in the rate constant for the compounds in each set are reflected in their ΔS^* values (Table 2). That the values of ΔG^* remain more or less constant indicates a similar reaction mechanism operating in these cases.

It was observed that the value of k_{Br_2} increases in much the same manner as does k_2(obsd) with increasing ionic strength (Fig. 3). The observed increase in rate is in accord with Hughes-Ingold theory of solvent action for a reaction in which the transition state is stabilised more than the initial state.[18] While k_{Br_2} increased with increasing ionic strength $k_{Br_3^-}$ decreased (Fig. 3). This trend was observed at all the experimental temperatures in the bromination of substrates such as AAm, MA, and MMA. However, the added $NaNO_3$ does not affect the activation enthalpy of the reaction (Table 2).

It was observed that the ratio (Q) of k_{Br_2} to $k_{Br_3^-}$ is greater for the extra methyl-substituted compounds. For each substrate, Q remains constant at all the experimental temperatures. In the present investigation, a comparison was, therefore, made between the reactivity of the substrate and the mean value of the ratio of k_{Br_2} to $k_{Br_3^-}$ obtained at all temperatures. It was observed that Q varied regularly in a set of compounds. For example, in compounds having the common structure CH_2=CHCOR (R= -OMe, -OEt, -OBu, -OBu^t, -NH_2), CH_2=C(Me)COR R=-OMe, -OEt, -NH_2) and CHMe=CHCOR R= -OMe, -OEt), Q increased with the increasing order of the reactivity of the substrate in each set.

Both by potentiometry and by titrimetry, the stoichiometry of alkene-bromine reactions was found to be 1:1. The values of product ratio, (P_r= [Bromohydrin]/[Dibromide]) were determined in order to find out the relation, if any, between the two reaction paths namely the attack by Br_2 and Br_3^- species, on the one hand, and the different products (bromohydrin and dibromide), on the other. When 1 mol of bromohydrin was formed by the attack of water, 1 mol of HBr will be liberated. The estimation of the liberated acid gave directly the amount of bromohydrin formed. The difference between the amount of bromine initially taken and the bromohydrin formed gave the amount of dibromide formed during the reaction. The product ratio of bromohydrin to dibromide did not agree with that calculated on the basis of Kanyaev's view[1] (Table 4).

When the observed product ratio values of all the substrates studied were compared at any particular bromide concentration, it did not fall under any correlation. The values of P_r neither follow the reactivities of the substrates[1] nor the relative reactivity ratio of Br_2 and Br_3^-.[2] Instead of comparing different substrates for the correlation of reaction rate and the product composition, an attempt was made in the present investigation to study such effect on a single substrate itself. According to Kanyaev[1] and Atkinson[2]

TABLE 4. PRODUCT RATIO THE VALUES OF [BROMOHYDRIN]/[DIBROMIDE] AT VARIOUS [Br^-]'S AT 30 °C

[Br^-]	AAm		MA		EA		BA		tBA		MAAm	
mol dm^{-3}	Obsd	Calcd[a)]	Obsd	Calcd[a)]	Obsd	Calcd[a)]	Obsd	Calcd[a)]	Obsd	Calcd[a)]	Obsd	Calcd[a)]
0.01	—	—	18.18	8.45	48.08	8.06	9.02	9.54	7.54	8.54	131.37	21.83
0.05	—	—	—	—	4.82	1.61	2.14	1.91	2.72	1.71	9.61	4.37
0.10	4.20	1.80	2.59	0.84	1.88	0.81	1.16	0.95	1.63	0.85	3.88	2.18
0.15	—	—	—	—	—	—	0.72	0.64	1.17	0.57	2.54	1.46
0.20	1.74	0.90	1.04	0.42	1.10	0.40	0.59	0.48	0.92	0.43	2.07	1.09
0.25	—	—	—	—	—	—	0.48	0.38	0.75	0.34	1.75	0.87
0.30	1.25	0.60	0.83	0.28	0.72	0.27	0.41	0.32	0.67	0.28	—	—
0.40	1.03	0.45	0.74	0.21	0.50	0.20	—	—	—	—	—	—
0.50	0.85	0.37	0.58	0.17	0.37	0.16	—	—	—	—	—	—

a) The calculated values of [bromohydrin]/[dibromide] based on Kanyaev's view.[1)]

the ratio of bromohydrin to dibromide should increase with k_{Br_2}. To examine this fact P_r was determined by carrying out the acrylamide-bromine reaction at various concentrations of added salts like $NaNO_3$ and Na_2SO_4. Though the ratio $k_{Br_2}/k_{Br_3^-}$ increases with the increase of ionic strength by adding $NaNO_3$, P_r decreased; and the product analysis in presence of nitrate revealed that this is due to the incorporation of NO_3^- in the product. In presence of added Na_2SO_4 P_r remained almost constant (Table 5). The present investigation reveals therefore, the following facts: i) the effect of ionic strength on the ratio in presence of non-participating radicals like SO_4^{2-} clearly indicates that there exists no relation between reaction rates and product distribution; ii) P_r was unaffected much by temperature and iii) the increase of acid concentration even by 100 fold did not alter P_r.

TABLE 5. EFFECT OF [$NaNO_3$], [Na_2SO_4], AND TEMPERATURE ON THE PRODUCT RATIO, P_r=[BROMOHYDRIN]/[DIBROMIDE] AT [Br^-]=0.1 mol dm^{-3} FOR AAm-BROMINE REACTION

Effect of $NaNO_3$		Effect of Na_2SO_4		Effect of temperature	
[$NaNO_3$]		[Na_2SO_4]		Temp	
mol dm^{-3}	P_r	mol dm^{-3}	P_r	°C	P_r
0.0	4.18	0.0	4.10	22	4.02
0.1	3.94	0.1	4.07		
0.2	3.69	0.2	3.80	30	4.10
0.3	3.29	0.3	4.07		
0.4	3.29	0.4	4.07	38	4.18
0.5	3.24	0.5	3.80		
0.6	2.65	0.6	3.80	46	4.18
1.0	2.53	—	—		

Contrary to the earlier observations[7,15)] the present investigation shows the formation of a small amount of bromohydrin (2.3%) even at [Br^-]=2 mol dm^{-3} and an appreciable amount of bromohydrin at [Br^-]=0.5 mol dm^{-3} (Tables 4 and 6). The products are, therefore, formed by the competitive attack by bromide, water, *etc.*

The aspect of regioselectivity was considered for the bromination of MMA and EMA. The product analysis by GC has shown the formation of three products and they were identified as a dibromide and two isomeric bromohydrins by comparing the retention time with those of authentic samples. Further, NMR spectrum showed three singlets at δ 2.00, δ 1.90, and δ 1.49 for C-2 methyl protons of 2,3-dibromo-, 2-bromo-3-hydroxy-, and 3-bromo-2-hydroxy- compounds as identified by the spectra of authentic samples. The nucleophilic attack by Br^-, Br_3^-, solvent molecule, *etc.*, may be on either of the two carbon atoms of the alkenic linkage giving rise to a dibromide and isomeric bromohydrins. The results also show that the bromonium ion formed in these cases did not favour any unsymmetrical bromonium structure. The regioselectivity value[19)] is fluctuating around 0.5. In spite of unsymmetrical nature of the substrate, the intermediate behaves almost like a symmetrical one. This may probably be due to the fact that in methyl acrylates a Me(+I) group on C-2 partially compensates for the influence of ester group

TABLE 6. THE PERCENT OF VARIOUS PRODUCTS (BY NMR SPECTRAL ANALYSIS) AT DIFFERENT [Br_r^-]'S FOR MMA, EMA-BRONINE REACTION IN AQUEOUS MEDIUM

[Br_r^-]	MMA				EMA			
mol dm^{-3}	A(%)	B(%)	C(%)	R(B)	A(%)	B(%)	C(%)	R(B)
0.01	25.48	34.08	40.44	0.46	17.86	39.29	42.85	0.48
0.05	26.09	35.87	38.04	0.49	42.17	16.87	40.96	0.29
0.10	45.71	30.00	24.29	0.55	70.37	14.81	14.81	0.50
0.20	63.58	18.17	17.10	0.50	—	—	—	—
0.30	75.83	12.92	11.25	0.54	—	—	—	—
0.40	—	—	—	—	73.21	7.15	19.65	0.27
0.50	78.22	14.22	7.56	0.65	—	—	—	—
2.00	97.72	0.91	1.37	0.40	—	—	—	—

A: 2,3-dibromo-, B: 2-bromo-3-hydroxy-, C: 3-bromo-2-hydroxy-compounds.

R: Regioselectivity factor, $R(B)=\frac{B}{B+C}$.

(—I) on the same C-2 position. Thus the occurrence of isomeric compounds almost in equal proportion gives evidence for non-regiospecificity or non-regioselectivity in its product formation.

In order to find out the possibility of any cis-addition (*via* the addition of Br_3^- whose structure is slightly bent in the solid state[20] which may be favourable for a cis-addition) the study of stereochemistry was extended to methyl crotonate-bromine reaction in water in presence of bromide ions. The reaction mixture was fractionated by silica-gel column chromatography and a number of small fractions were collected and ^1H NMR spectra were taken for the first, the middle and the last fractions. The ^1H NMR spectrum of the dibromo compound namely the methyl 2,3-dibromobutanoate (CCl_4/TMS) showed a doublet at δ 1.92 (3H, $J=6$ Hz, H_a) a singlet at

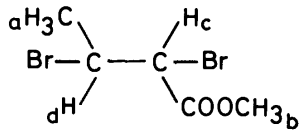

δ 3.82 (3H, H_b) and a multiplet centered at δ 4.42 (2H, $H_{c,d}$); the methyl-decoupled spectrum showed a doublet at δ 4.36 ($J=5.2$ Hz) instead of a complex multiplet present in the original spectrum. This is compared with similarly methyl-decoupled spectrum of an authentic sample of erythro-dibromo product of methyl crotonate prepared, where bromination occurs only by trans addition.[21] Comparison shows that the dibromo compound obtained in the bromination in aqueous medium in the present case is also an erythro isomer (trans addition). Spectra for other fractions of dibromo compounds were also found to be similar for protons at C-2 and C-3 positions ($J=5.2$ Hz).[22] Absence of threo isomer completely rules out a cis-addition. The attempts to detect the presence of π-complex, if any, in water by UV spectrophotometric method were not successful. However, interactions between alkene and bromine leading to a π-complex cannot be ruled out and π-complex may be small to be detected spectrophotometrically. From a kinetic point of view, however, such a small concentration is quite sufficient, as the π-complex is formed in a fast equilibrium step. The absence of spectrophotometric evidence for alkene-bromine π-complex could not be considered as a total negative evidence for its formation. Dewar *et al.*[23] have also stressed this point.

Reaction Mechanism. The experimental results show that the contribution to the reaction by Br_2 and Br_3^-, species is quite appreciable. The fact that the experimental values of k_2(obsd) $(1+K[Br^-])$ and the calculated values, $(k_{Br_2}+k_{Br_3^-}K[Br^-])$ are in total agreement with each other indicates that bromination, under the experimental conditions, occurs mainly by Br_2 and Br_3^- species. As a representative example, the observed and calculated values of k_2(obsd) $(1+K[Br^-])$ for the bromination of AAm in water at 22 °C are provided in Table 7. In the following two sections are discussed two mechanisms one for the reaction between alkene and Br_2 species and the other for alkene and Br_3^- species.

Mechanism of the Bromination of Alkenes by Br_2 Species. Based on the effect of ionic strength on

Table 7. The observed and calculated values of k_2(obsd) $(1+K[Br^-])$ for the bromination of AAm in water at 22 °C

$[Br^-]$/mol dm^{-3}	0.01	0.05	0.10	0.20	0.30	0.40	0.50
Obsd	1.73	2.15	2.64	3.30	4.44	5.15	6.15
Calcd	1.76	2.13	2.59	3.52	4.43	5.37	6.06

k_{Br_2} and on the formation of exclusive stereospecific but non-regiospecific, anti-addition products and in the light of the points discussed, the kinetic scheme for the bromination of alkene by Br_2 species in aqueous medium may be represented as follows:

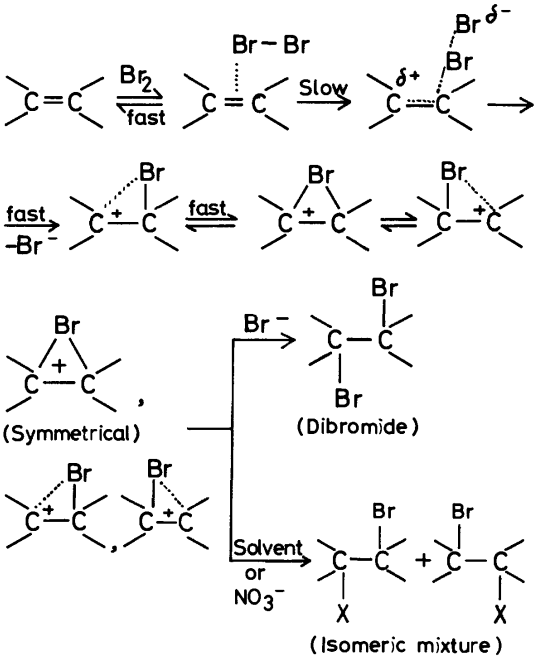

Thus it may be formulated that molecular bromine first attaches to double bond of alkenic compounds in a fast equilibrium step to form an intermediate complex, which then decomposes to give a carbonium ion. The carbonium ion rearranges to a bromonium ion which by subsequent fast steps readily forms dibromide, bromohydrin or bromo nitrates by the reaction with bromide, water molecule or with nitrate ions, respectively.

Mechanism of the Bromination of Alkenes by Br_3^-, Species. A number of mechanisms for the bromination of alkenes by Br_3^- species have been proposed by earlier workers.[2-8] The data collected on the rate constants correspond well with the following rate expression: rate $=k_{Br_3}[S][Br_3^-]$. Alternatively, the rate expression can also be represented as, rate $=k_{Br^-}[S][Br_2][Br^-]$. These two rate expressions cannot be distinguished kinetically. While the former represents the addition of Br_3^- by a bimolecular mechanism, the latter represents Br^- catalysed termolecular mechanism.

A possible mechanism for Br_3^- addition is envisaged in the present investigation for the first time on the basis of experimental kinetic parameters and the product analysis. Irrespective of whether the bromination is between alkene and Br_2 or between alkene and Br_3^-, the value of ΔH^* is observed to be the

same in either case for a given substrate. There is thus every reason to believe that the approach of Br_2 or Br_3^- towards alkene should be quite similar. Since the structure of Br_3^- species even in solid state was predicted to be linear[20] and unsymmetrical[24] and carrying a single negative charge and since the Br_3^- structure in solution is even more uncertain, the approach to alkene by both Br_2 and Br_3^- species (in keeping with more or less same ΔH^* obtained in either case) can be unequivocally depicted as

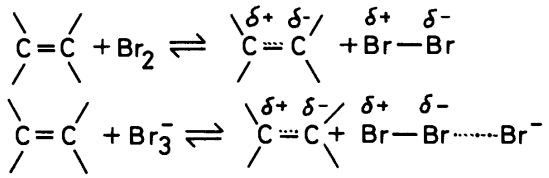

It should be stressed at this point that the ionic strength effect is to increase the rate (k_{Br_2}) of alkene-Br_2 species reaction while decreasing that of alkene-Br_3^- species. As already stated the rate enhancement in the former case is due to the formation of polar or ionic intermediate from neutral molecules and can be represented in all probability as

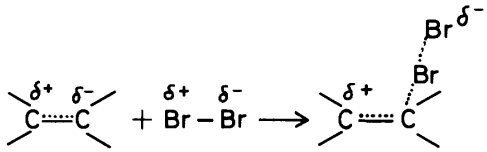

On the other hand, the decrease in rate ($k_{Br_3^-}$) with μ found in the reaction between alkene and Br_3^- species may be attributed to the less polar character of the transition state as compared to the reactants, a neutral molecule and an ionic species, and may be represented as follows:

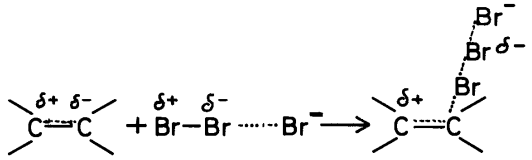

3

Similarly, a less-charged activated complex can be equivally possible in Br^--catalysed mechanism too, as shown below

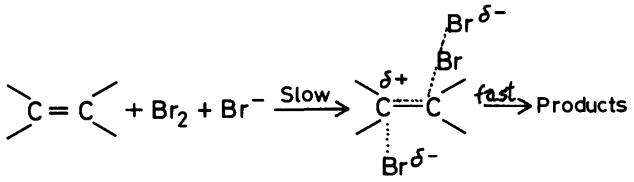

Further, the Br^--catalysed reaction is stereospecific whereas structure **3** formed by Br_3^- can still lead to non-stereospecific products. However, in the present study, the product analysis made on the reaction between methyl crotonate and bromine showed a nil contribution of threo product. To account for this stereospecificity it is necessary to propose bromonium ion structure in Br_3^--addition also. Hence the activated complex (Structure **3**) giving rise to a bromonium ion should involve breakage of two Br-Br bonds in contrast to the addition by Br_2 species where only one bond needs to be broken. Thus the breakage of two Br-Br bonds may take place one at a time as in

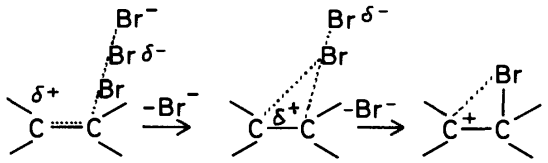

or the two Br-Br bonds may break simultaneously as in

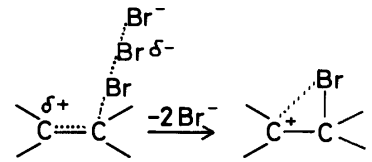

Futhermore, this bromonium ion must be either symmetrical or equilibrium mixture of two unsymmetrical forms in accordance with regioselectivity factor around 0.5. Otherwise, a single unsymmetrical structure formed by Br_3^- alone (and not by Br_2) might result in a regioselective products. The participation by Br_3^- as an electrophile is proved further in the present study as follows.

Substitution of a methyl group at the alkenic carbon increases both k_{Br_2} and $k_{Br_3^-}$. The methyl substitution accordingly, decreases activation enthalpy in either case. If we assume that $k_{Br_3^-}$ is especially due to Br^--catalysed reaction, then the product formed by this step should be only dibromide. And the solvent incorporated and salt (NO_3^-) incorporated products should then result from bromonium ion formed due to addition of Br_2 species. It is evident that if Kanyaev's view[1] namely bromohydrines are exclusively formed by the addition to alkene by Br_2 species and dibromide by Br_3^- species, is correct, then one can expect that both the observed and calculated product ratios, [bromohydrin]/[dibromide], should agree with each other. As already pointed out, the bromonium ion formation during the course of the reaction seems inevitable to explain the observed 'stereospecific *cum* non-regioselective' products. Also the dibromide formation in this situation is warranted. If this were so, the amount of bromohydrin formed should be actually lower than that predicted by calculation. This means that the observed ratio of bromohydrin to dibromide should be less than the calculated value. This expectation arises from the assumption that $k_{Br_3^-}$ is due to Br^- catalysis. However, the experimental P_r has been found to be greater than the calculated one (Table 4). It is quite clear that the formation of more of bromohydrin than the expected amount should have resulted only from Br_3^--addition. So the observation that bromohydrin is formed in rather large quantity than dibromide, cannot be explained by Br^--catalysed mechanism alone. All the foregoing arguments strongly suggest that Br_3^- species acts as an electrophile. Otherwise either nucleophilic attack by Br_3^- or bromide-catalysed reaction should have resulted only in a dibromide compound, which is not found to be the case.

In conclusion, the addition of bromine to alkenes in aqueous medium in presence of bromide in the present investigation is stereospecific and non-regioselective antiaddition. Though $k_{Br_3^-}$ is a composite term, in the

present set of substrates, electrophilic-bimolecular addition by Br_3^- species is more favourable. The activated complex formed by Br_3^- species is less polar than the one formed from the alkene-Br_2 species. The formation of activated complex is the slow step of the bromination. Besides dibromide, other products such as bromohydrins and bromonitrates too are formed due to incorporation of solvent and added salts like nitrates.

We thank the University Grants Commission of India for a teacher fellowship to one of us (S.M.F.).

References

1) N. P. Kanyaev, *J. Can. Chem. U.S.S.R.*, **29**, 825 (1959); **26**, 3037 (1956).
2) J. R. Atkinson and R. P. Bell, *J. Chem. Soc.*, **1963**, 3260.
3) R. P. Bell and M. Pring, *J. Chem. Soc. B*, **1966**, 1119.
4) P. B. D. de la Mare, *Quart. Rev. London*, **3**, 126 (1949).
5) P. B. D. de la Mare, "Electrophilic Additions to Unsaturated Systems," Elsevier, New York (1966).
6) K. Nozaki and R. A. Ogg, *J. Am. Chem. Soc.*, **64**, 697, 704, 709 (1942).
7) J. H. Rolston and K. Yates, *J. Am. Chem. Soc.*, **91**, 1469, 1477, 1483 (1969).
8) J. E. Dubois and E. Bienvenue-Goetz, *Bull. Soc. Chim. Fr.*, **1968**, 2086.
9) F. S. Dainton and M. Tordoff, *Trans. Faraday Soc.*, **53**, 499 (1957).
10) F. S. Dainton and W. D. Sisley, *Trans. Faraday Soc.*, **59**, 1369 (1963).
11) Rohm and Haas, "Technical Bulletin for Monomeric Acrylic-esters," 3rd ed (1951), p. 8.
12) A. I. Vogel, "A Textbook of Practical Organic Chemistry," 3rd ed, Longmans, Green and Co., London (1956), p. 927.
13) R. P. Bell and R. R. Robinson, *Proc. R. Soc. London, Ser. A*, **270**, 411 (1962).
14) S. Mohamed Farook, Ph. D. Thesis, University of Medras, February, 1980.
15) D. R. Dalton, V. P. Dutta, and D. C. Jones, *J. Am. Chem. Soc.*, **90**, 5498 (1968).
16) R. P. Bell and E. N. Ramsden, *J. Chem. Soc.*, **1958**, 161.
17) D. B. Scaife and H. J. V. Tyrrell, *J. Chem. Soc.*, **1958**, 386.
18) E. D. Hughes, *Trans. Farady Soc.*, **37**, 763 (1941).
19) J. E. Dubois and J. R. Chretien, *J. Am. Chem. Soc.*, **100**, 3507 (1978).
20) R. B. Heslop and K. Jones, "Inorganic Chemistry, A Guide to Advanced Study," Elsevier Scientific Publishing Co. (1976).
21) F. Velichko, V. I. Dostovalova, L. V. Vinogradova, and R. Kh. Freidlina, *Izv. Akad. Nauk., U.S.S.R. Ser. Khim.*, **1978**, 734; *Chem. Abstr.* **89**, 42223t (1978).
22) R. C. Fahey, *J. Am. Chem. Soc.*, **88**, 4681 (1966).
23) M. J. S. Dewar and C. C. Thomson, *Tetrahedron*, **7**, 97 (1966).
240 A. G. Maki and R. Forneris, *Spectrochim. Acta, Part A*, **23**, 867 (1967).

A New Version of Inclusion of Overlap Charges in ω-Technique. π-Bond Energies, Heats of Formation, and Resonance Energies of Conjugated Hydrocarbons

Vindhya Prasad TEWARI, Krishna Behari LAL, and Arun Kumar SRIVASTAVA*
Department of Chemistry, University of Allahabad, Allahabad 211002, India
(Received March 31, 1983)

With systematic approximations to Roothaan equation it has been possible to deduce the IOC-ω-technique (inclusion of overlap charges in ω-technique) which apparently approximates the SCF-equations by bringing in an approximate correction for the two center-two electron repulsion integrals and represents a better version of PPP (Pariser-Parr-Pople) method by involving the hybrid integrals which have been completely neglected in PPP-approximations. In the present communication a new version of IOC-ω-Technique has been used for evaluating the π-bond energies, heats of formation and resonance energies of some conjugated hydrocarbons. The calculated values are found to be in excellent agreement with the experimental data and with some previously calculated values.

In the framework of LCAO-MO approximations Roothaan[1] has given $F_{\mu\nu}$ as,

$$F_{\mu\nu} = H^C_{\mu\nu} + \sum_{\lambda}\sum_{\sigma} P_{\lambda\sigma}\{(\mu\nu, \lambda\sigma) - 1/2(\mu\lambda, \nu\sigma)\}, \quad (1)$$

where $H^C_{\mu\nu}$ is the matrix element involving core Hamiltonian such that,

$$H^C_{\mu\nu} = \int \phi_\mu \left(-\frac{h^2}{8\pi^2 m}\right)\nabla^2 - \sum_{\sigma} V_\sigma \phi_\nu \mathrm{d}\tau, \quad (2)$$

and $(\mu\nu, \lambda\sigma)$ the electron repulsion integral represented as,

$$(\mu\nu, \lambda\sigma) = \iint \phi_\mu(1)\,\phi_\nu(1)\frac{e^2}{r_{12}}\phi_\lambda(2)\,\phi_\sigma(2)\,\mathrm{d}\tau_1\,\mathrm{d}\tau_2. \quad (3)$$

It has been shown[2] that if all electron repulsion integrals are neglected except for one centre integrals $(\mu\mu, \mu\mu)$, two centre integrals $(\mu\mu, \sigma\sigma)$ and the hybrid integrals $(\mu\mu, \mu\sigma)$, since the other integrals are of very small magnitude, then the diagonal matrix elements of Eq. 1 reduces to,

$$\begin{aligned} F_{\mu\mu} &= H^C_{\mu\mu} + 1/2\,p_{\mu\mu}(\mu\mu, \mu\mu) + 1/2\sum_{\sigma\neq\mu} p_{\mu\sigma}(\mu\mu, \mu\sigma) \\ &\quad + \sum_{\mu\neq\sigma} q_\sigma\,(\mu\mu, \sigma\sigma) \\ &= H^C_{\mu\mu} + 1/2\sum p_{\mu\sigma}(\mu\mu, \mu\sigma) + \sum_{\mu\neq\sigma} q_\sigma(\mu\mu, \sigma\sigma). \end{aligned} \quad (4)$$

However, the coulomb integral, $H^C_{\mu\mu}$, neglecting the penetration integral, is approximated as,[3]

$$H^C_{\mu\mu} = I_\mu - \sum_{\mu\neq\sigma}(\mu\mu, \sigma\sigma)$$

where I_μ is the valence state ionization potential of an electron associated with atom μ. Equation 4 therefore leads to,

$$F_{\mu\mu} = I_\mu + 1/2\sum_{\sigma} p_{\mu\sigma}(\mu\mu, \mu\sigma) + \sum_{\sigma\neq\mu}(q_\sigma - 1)(\mu\mu, \sigma\sigma). \quad (5)$$

Since the integral $(\mu\mu, \mu\sigma)$ obviously depends upon the charge distribution $\phi_\mu\,\phi_\sigma$ so that it can be made proportional to the overlap integral $S_{\mu\sigma}$,

$$(\mu\mu, \mu\sigma) = 2\omega_\mu\, s_{\mu\sigma} \quad (6)$$

where ω_μ is a proportionality constant which may be written as,

$$\omega_\mu = 1/2(\mu\mu, \mu\mu), \quad (7)$$

in case of $\mu = \sigma$.

However, ω_μ is treated as an empirical parameter in order to cover up the deficiencies in the method due to several approximations involved. Inserting Eq. 6 in Eq. 5,

$$F_{\mu\mu} = I_\mu + \omega_\mu \sum p_{\mu\sigma}\, s_{\mu\sigma} + \sum_{\sigma\neq\mu}(q_\sigma - 1)\,(\mu\mu, \sigma\sigma). \quad (8)$$

At this stage a new parameter α_μ has been defined as,

$$\alpha_\mu = I_\mu + \omega_\mu.$$

In terms of this parameter Eq. 8 will assume the following form,

$$\begin{aligned} F_{\mu\mu} &= \alpha_\mu + \omega_\mu\left(\sum_{\sigma} p_{\mu\sigma}\, s_{\mu\sigma} - 1\right) \\ &\quad + \sum_{\sigma\neq\mu}(q_\sigma - 1)\,(\mu\mu, \sigma\sigma). \end{aligned} \quad (9)$$

For most of the molecules last term of Eq. 9 would be very small and in fact will be equal to zero for alternant hydrocarbons. Therefore, this last term may be neglected and consequently Eq. 9 will assume the following form,

$$\begin{aligned} F_{\mu\mu} &= \alpha_\mu + \omega_\mu\left(\sum_{\sigma} p_{\mu\sigma}\, s_{\mu\sigma} - 1\right) \\ &= \alpha_\mu + \omega_\mu\{1/2\sum_{\sigma}(p_{\mu\sigma}\, s_{\mu\sigma} + p_{\sigma\mu}\, s_{\sigma\mu}) - 1\}. \end{aligned} \quad (10)$$

The last line of Eq. 10 follows from the fact that in the expansion of Eq. 1 both $(\mu\mu, \mu\sigma)$ and $(\mu\mu, \sigma\mu)$ type integrals will occur but since there is no difference between them the factor 1/2 has been included to avoid the counting of them twice. If ω_μ is treated as a negative parameter Eq. 10 will become,

$$F_{\mu\mu} = \alpha_\mu + \omega_\mu\{1 - 1/2\sum_{\sigma}(p_{\mu\sigma}\, s_{\mu\sigma} + p_{\sigma\mu}\, s_{\sigma\mu})\}, \quad (11)$$

which has been used in our calculation as diagonal matrix element. $F_{\mu\mu}$ as derived in Eq. 1 approximates the SCF equations by bringing in an approximate correction for the two centre-two electron repulsion integral and represents a better version of PPP-method since it involves hybrid integrals which have been completely neglected in PPP-metod and which are in no way negligible as they can be as large as 3.5 eV.[4] The success of the technique can also be attributed to the fact that the inclusion of overlap charges permits the ω-technique to make use of orthogonal atomic orbitals (OAO's) rather than usual nonorthogonal slater type

atomic orbitals (STAO's). The ω-technique, which has been put to successful use by Aihara,[5] can be said to be a simplified version of PPP-method (for example see Doggett[6]) which is based on zero differential overlap (ZDO) approximations of Pariser, Parr and Pople[3,7] and since these approximations are valid only over OAO's and not over usual non-orthogonal STAO's, the use of OAO's is essentially warranted in it. It has been shown by Gupta[8] that this necessity in ω-technique is fulfilled by inclusion of overlap charges. This is arrived at by deducing the IOC-ω-technique (inclusion of overlap charges in ω-technique) in the framework of Lowdin's OAO's. In the present communication the following form of the off diagonal matrix element has been used for the first time in the framework of IOC-ω-technique,

$$F_{\mu\nu} = K S_{\mu\nu} (F_{\mu\mu} \cdot F_{\nu\nu})^{1/2}, \tag{12}$$

where K is a dimensionless constant and $S_{\mu\nu}$ are the overlap integrals. Since $F_{\mu\nu}$ represents the energy of interaction between atomic orbitals μ and ν, the simple arithmatic mean, an approximation used by Wolfsberg and Helmholtz,[9] evidently takes into account only an average interaction between atomic orbitals whereas a use of geometric mean[10] will incorporate all the possible interactions between different atomic orbitals.

In most of the semiempirical π-electron calculations, using variant of the Pariser-Parr-Pople[3,7] (PPP-method), the choice of parameters required to give optimum agreement with experiment is specific for a particular property, or is valid for a specific class of compounds, and cannot therefore, generally be extended to other molecular properties or to different class of molecules. In the present work a set of parameters has been developed which when applied to a given molecular property, *e.g.* ionization potential produces good results and also give satisfactory results when used to calculate other properties, *e.g.* electron affinity, π-bond energies, heats of formation and resonance energies of different class of compounds.

π-Bond Energy. In molecular orbital theory the π-electronic energy of a molecule is given by,

$$E_\pi = \text{Total molecular orbital energy} = \sum_\mu \sum_\nu p_{\mu\nu} F_{\mu\nu}. \tag{13}$$

Substituting the values of $F_{\mu\mu}$ and $F_{\mu\nu}$ from Eqs. 11 and 12 into Eq. 13, we shall get the following expression for the total π-elecronic energy,

$$E_\pi = \sum_\mu q_\mu \alpha + \omega \sum_\mu q_\mu (1-q_\mu) - \omega S \sum_\mu \sum_{\sigma \neq \mu} q_\mu p_{\mu\sigma} + KS \sum_\mu \sum_\nu p_{\mu\nu} \{(\alpha + \omega(1-q_\mu) - \omega S \sum_\sigma p_{\mu\sigma})(\alpha + \omega(1-q_\nu) - \omega S \sum_\sigma p_{\nu\sigma})\}^{1/2}. \tag{14}$$

Now, consider the energy liberated when n carbon atoms with p-electrons combine to form π-bonds, *i.e.* energy ($E_{\pi b}$). The total π-electronic energy of a molecule is given by the algebraic sum of the energy of electrons in p-orbital of widely separated carbon atoms and the π-bond energy ($E_{\pi b}$). The former may be equated to $\sum q_\mu \alpha$. Hence, the remaining terms of Eq. 14 give π-bond energy. For alternant hydrocarbons with $q_\mu = 1$, we have,

$$E_{\pi b} = -\omega S \sum_\mu \sum_{\sigma \neq \mu} q_\mu p_{\mu\sigma} + 2KS \sum_{\mu<\nu} \sum p_{\mu\nu} \{(\alpha - \omega S \sum p_{\mu\sigma})(\alpha - \omega S \sum p_{\nu\sigma})\}^{1/2}. \tag{15}$$

Heat of Formation. The heat of formation of a molecule in its equilibrium configuration is the additive sum of the bond energies. The total bond energy of a molecule is given by the sum of the total σ-bond energy, $E_{\sigma b}$ and total π-bond energy, $E_{\pi b}$. The following expression provides a simple route to calculate heats of formation of hydrocarbons.

$$\Delta H_f = E_{\sigma b} + E_{\pi b} = N_C E_{CC} + N_H E_{CH} + E_{\pi b}, \tag{16}$$

where E_{CC} and E_{CH} are the bond energies of C-C and C-H bonds respectively and N_C and N_H are the number of C-C and C-H bonds respectively.

Resonance Energy. If a compound possesses more than one structure, the resonance energy is regarded as a physical measure of the most stable structure relative to other possible structure. Among the various possible definitions of the term resonance energy, the most important is one due to Mulliken and Parr[11] (empirical resonance energy), which is taken as the differences between the bond energies of structure I and II,

$$E_R = E_{b(I)} - E_{b(II)}, \tag{17}$$

where I represents an aromatic structure with all bonds equal to 1.40Å and II represents a structure with alternating C-C bond length and C=C bond length. The bond energies may be calculated with the help of the following equations,

$$E_{b(I)} = NE_C + N_H E_H + E_{\pi b(I)}, \tag{18}$$

and

$$E_{b(II)} = N_1 E_1 + N_2 E_2 + N_H F_H. \tag{19}$$

In which $E_{\pi b(I)}$ is the π-bonding energy of structure I and $N = N_1 + N_2$. E_1 and E_2 are the energies of a C-C bond of length 1.48 Å and C=C bond of length 1.34 Å respectively. N_1, N_2, N_H, and E_H represent the number of single and double bonds and number of C-H bonds and energy of carbon-hydrogen bonds respectively.

Now, since the values of E_1 and E_2 are very uncertain, we shall use the following scheme instead of using them directly,

$$E_R = NA_0 + (N_1 - N_2) A_1 + E_{\pi b(I)} \tag{20}$$

where,

$$A_0 = E_C - \frac{E_1 + E_2}{2}, \tag{21}$$

$$A_1 = \frac{E_2 - E_1}{2}. \tag{22}$$

However, A_0 and A_1 are to be treated as empirical parameters.

Values of Parameters. In the present communication, it has been assumed that the overlap integral $S_{\mu\nu}$ vanishes for non-neighbouring μ, ν and it

TABLE 1. π-BOND ENERGIES AND HEATS OF FORMATION OF ALTERNANT HYDROCARBONS

Compound	$E_{\pi b}$/eV	Present work	Ref. 16	Ref. 17	Experimetal Ref. 18
Benzene	7.91	57.29	57.52	57.16	57.16
Naphthalene	13.43	90.67	90.516	90.61	90.61
Anthracene	18.95	124.05	123.655	123.89	123.93
Naphthacene	24.44	157.40	156.096	157.11	157.56
Biphenyl	16.10	109.80	—	109.75	109.76
Styrene	10.28	76.12	—	75.91	75.83
Stilbene	18.57	128.73	—	128.54	128.48
Pyrene	22.03	138.73	138.956	138.62	138.88
Perylene	27.64	172.00	169.599	172.15	172.04
Phenanthrene	19.07	124.17	123.460	124.22	124.20
Triphenylene	25.03	157.99	156.624	157.94	157.76
Benzo [*c*] phenanthrene	24.68	157.64	156.067	157.77	157.56
Benz [*a*] anthracene	24.60	157.56	—	157.58	157.49
Chrysene	24.68	157.64	156.157	157.77	157.73
Av. dev.		0.12	0.765	0.11	

TABLE 2. EMPIRICAL RESONANCE ENERGIES OF ALTERNANT HYDROCARBONS

Compound	Present work	Ref. 19			Ref. 20	Experimental Ref. 21
		Huckel	Pople	SPO		
Benzene	1.55	1.318	1.318	1.318	1.560	1.553
Naphthalene	2.61	2.312	2.429	2.258	1.645	2.631
Anthracene	3.67	3.365	3.382	3.039	4.147	3.601
Naphthacene	4.70	4.206	4.278	3.750	5.126	4.744
Biphenyl	3.16	—	—	—	—	—
Styrene	1.80	1.80	—	—	—	—
Stilbene	3.51	—	—	—	—	—
Pyrene	4.41	—	—	—	—	4.696[a)]
Perylene	5.56	4.998	5.713	4.961	4.779	5.447[a)]
Phenanthrene	3.79	3.372	3.750	3.386	4.020	3.937
Triphenylene	5.29	4.479	5.236	4.643	4.416	5.076
Benzo [*c*] phenanthrene	4.94	—	—	—	4.822	4.727
Benz [*a*] anthracene	4.86	—	—	—	—	4.813
Chrysene	4.94	—	—	—	4.918	5.024
Av. dev.	0.09		0.246		0.286	

a) Ref. 22.

has a constant value S for μ, and ν directly bonded. S has been assigned a value of 0.25. ω has been taken to 1.4. Both the values have been extensively used by several workers.[12,13] K has been assigned a value of 1.634, which is very close to its value quoted in literature.[14] E_{CC} and E_{CH} are taken as 3.80 and 4.43 respectively, as proposed by Dewar and Gleicher.[15] A_0 and A_1 have been assigned values as −1.06 and 0.84 respectively. α has been taken to be 7.00.

Results and Discussion

In Table 1, we have listed the values of heat of formation obtained with Eqs. 15 and 16 along with some previously calculated values[16,17] and with available experimental values.[18] A close study of Table 1, shows that our calculated values are generally in excellent agreement with the experimental values. The values calculated by the present method (av.dev. = 0.12) are also in good agreement with Dellano[17] (av.dev. = 0.11) and are better than those calculated by Srivastava[16] (av.dev. = 0.765). Table 2, enlists the empirical resonance energy calculated by the present method along with some previously calculated values[19,20] and the relevant experimental data.[21,22] From Table 2, it is amply clear that the values obtained by the present method are in excellent agreement with the observed experimental values. The values calculated by the present technique (av. dev. = 0.09) are better than those calculated by Srivastava[20] (av. dev. = 0.286) and Dewar[19] (av. dev. = 0.246) PPP-method.

It is worth mentioning that the same set of parameters have been used for the calculation of different ground state properties of various class of compounds. Thus the values obtained are in good agreement with experimental values.

References

1) C. C. J. Roothaan, *Rev. Mod. Phys.*, **23**, 69 (1951).
2) S. P. Gupta and B. Krishna, *J. Phys. B*, **5**, 1101 (1972).
3) J. A. Pople, *Trans. Faraday Soc.*, **49**, 1375 (1953).
4) R. McWeeny, Quarterly Progress Report of Solid State and Molecular Group MIT (1954).
5) J. Aihara, *Bull.Chem. Soc. Jpn.*, **53**, 2689 (1980).
6) G. Doggett, *Mol. Phys.* **16**, 225 (1966).

7) R. Pariser and R. G. Parr, *J. Chem. Phys.*,**21**, 466, 767 (1953).
8) S. P. Gupta, *Indian J. Chem.*, **13**, 717 (1975).
9) M. Wolfsberg and C. Helmholtz, *J. Chem. Phys.*, **20**, 837 (1952).
10) C. J. Ballhausen and H. B. Gray, *Inorg. Chem.*, **1**, 111 (1962).
11) R. S. Mulliken and R. G. Parr, *J. Chem. Phys.*, **19**, 1271 (1951).
12) N. Muller and R. S. Mulliken, *J. Am. Chem. Soc.*, **80**, 3489 (1958).
13) A. Streitwieser, Jr., and P. M. Nair, *Tetrahedron*, **5**, 149 (1959).
14) J. S. Yadava, P. C. Misra, and D. K. Rai, *Indian J. Pure Appl. Phys.*, **11**, 163 (1973).
15) M. J. S. Dewar and G. J. Gleicher, *J. Chem. Phys.*, **44**, 759 (1966).
16) A. K. Srivastava and B. Krishna, *Indian J. Pure Appl. Phys.*, **10**, 627 (1972).
17) G. R. Dellano, Ph. D. Thesis, University of Texas, Texas, U.S.A. (1968).
18) M. J. S. Dewar, "The Molecular Orbital Theory of Organic Chemistry," Mc-Graw Hills, New York (1969), pp. 170, 171.
19) M. J. S. Dewar and A. L. H. Chung, *J. Chem. Phys.*, **42**, 756 (1965).
20) A. K. Srivastava and B. Krishna, *Indian J. Pure Appl. Phys.*, **11**, 56 (1973).
21) G. W. Wheland, "Resonance in Organic Chemistry," John Wiley & Sons, New York (1955), p. 98.
22) F. Klages, *Ber.*, **82**, 358 (1949).

A Novel Synthesis of Azophenines

J. R. MERCHANT,* Gail MARTYRES, and N. M. SHINDE
Organic Chemistry Department Institute of Sience, Bombay-400 032 India
[1]*D. G. Reparel College, Bombay-400016,India*
(Received March 7, 1983)

Aarylamines react with polyhaloalkanes in the presence of copper bronze to yield azophenines.

In the course of our work on the reactions of arylamines with polyhaloalkanes we investigated the reaction of aniline and some substituted anilines with 1,1,2,2-tetrachloroethane and hexachloroethane in the presence of copper bronze. Heating the arylamines with the alkyl halide in the presence of a catalytic quantity of copper bronze for 2—4 h afforded bright red compounds, isolated as single substances (TLC, chloroform-methanol) in 25—35% yield. The latter dissolved in concentrated sulfuric acid, giving a deep violet solution, which on dilution gave back the red colour. The sulfuric acid solution on heating at about 300 °C turned blue and when alkali was added to it a red coloration was observed. This property as well as the spectral and analytical data indicated that these compounds were probably *N,N'*-diphenyl-2,5-dianilino-*p*-benzoquinone diimines or azophenines.[1] This assumption was confirmed since azophenine (**1a**)[1] on heating with zinc and hydrochloric acid gave back aniline and *p*-phenylenediamine. The known azophenines were synthesized by previously reported methods and were found to be identical with our compounds. The literature methods reported so far are tedious, involve separation of mixtures and afford extremely low yields of the azophenines. These include the condensation of quinone with *N*-ethylideneaniline or *N*-benzylideneaniline in dry toluene[2] under anhydrous conditions to yield azophenine along with a dark red amorphous residue which does not melt up to 360 °C. Azophenines have also been obtained (in about 1% yield) by the peroxidase oxidation of a mixture of amines[3] as well as by the periodic acid oxidation of aniline.[4] γ-Irradiation of a mixture of aniline and bromobenzene afforded azophenine in a mixture of other products.[5] Benzofurazan-1-oxide, not an easily accessible starting material, on heating with aniline hydrochloride in aniline is reported to furnish azophenine.[6]

Azophenine (**1a**) has been prepared[3] by oxidizing *N,N'*-diphenyl-*p*-phenylenediamine with mercury(II) oxide to *p*-benzoquinone dianil and heating the latter with aniline.

Most of the above methods cannot be used to prepare substituted azophenines. The method described by us constitutes a simple and novel synthesis of azophenines (especially the *p*-substituted compounds) which are reported to be important intermediates in the synthesis of dyes,[7] such as Induline 3B and 6B and Nigrosine CF New. Indulines are blue basic dyes which could be prepared by heating azophenines with the arylamine concerned.

Mechanistically, it is indicated that polyhaloalkanes and copper bronze react to generate a sufficient amount of copper(II) chloride *in situ* which acts as an oxidising agent in the presence of the amine to yield an *N*-phenyl-*p*-benzoquinone diimine as an intermediate. The latter reacts with an excess of the amine to give the azophenine. The intermediacy of *N*-phenyl-*p*-benzoquinone diimine was established by preparing it as described by Goldschmidt[8] by oxidation of an ethereal solution of aniline with lead oxide. In the case of *p*-alkoxy substituted anilines the corresponding diimines were obtained by the method of Willstätter and Kubli[9] involving the silver oxide oxidation of *N*-phenyl-*p*-alkoxy-*p*-phenylenediamines. The diimines so obtained were allowed to react with excess of the corresponding amines to afford the expected azophenines. To confirm our assumptions, *p*-phenetidine (6.85 g) was heated with dry copper(II) chloride (0.135 g) on a steam bath for 4 h when the corresponding azophenine (**1c**) was isolated in about 1.8 g yield.

It is pertinent to mention here that the oxidation of *p*-anisidine with peroxidase in presence of acetic acid has been reported[10] to yield the corresponding azophenine in about 5% yield. The mechanism for the formation of azophenines in our reaction can be depicted as follows.

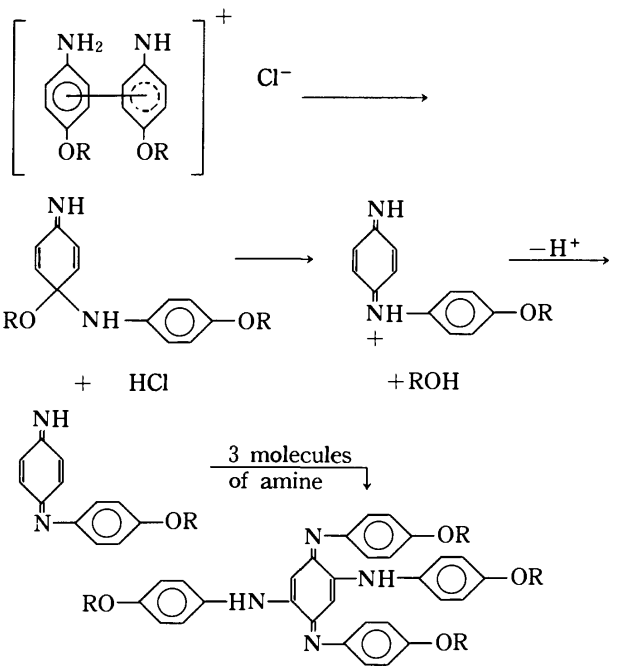

The formation of free radicals during the reaction could be ruled out since no 4-alkoxyazobenzene could be isolated during the reaction. Also *p*-benzoquinone, a known product of the oxidation of amines, is not an intermediate since its reaction with amines under mild conditions affords only 2,5-dianilino-*p*-benzoquinones.[11] Further, it is well known that quinones do not

TABLE 1. AZOPHENINES

Compound	Formula	Mp θ_m/°C	Found (Calcd) (%)		
			C	H	N
1a	$C_{30}H_{24}N_4$	242—244	82.0 (81.8	5.6 5.4	12.5 12.7)
1b	$C_{34}H_{32}N_4O_4$	230—232	72.6 (72.8	5.4 5.7	10.4 10.2)
1c	$C_{38}H_{40}N_4O_4$	237—239	74.3 (74.0	6.8 6.5	9.2 9.0)
1d	$C_{46}H_{56}N_4O_4$	220—222	75.0 (75.1	7.4 7.3	8.3 8.3)
1e	$C_{50}H_{64}N_4O_4$	155—157	75.8 (75.6	7.6 7.5	7.6 7.7)

easily form anils with amines.

Amines with strongly electron-donating groups like the alkoxyl in the *p*-position were found to take part in the reaction while amines with electron-withdrawing groups like a nitro group or a halogen atom in this position failed to yield the azophenine. The above reaction with *N,N*-dimethyl-*p*-phenylenediamine was also unsuccessful. When amines substituted at the *o*- or *m*-positions were employed, the reaction failed to occur probably due to steric hindrance.

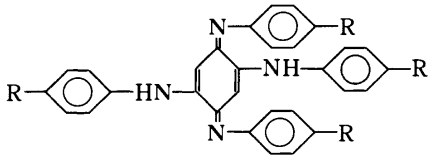

1: **a**, R=H; **b**, R=$-OCH_3$; **c**, R=$-OC_2H_5$; **d**, R=$-OC_3H_7$; **e**, R=$-OC_4H_9$

Experimental

General Procedure. For Azophenine (1a), Tetra-p-methoxyazophenine (1b),[10] *and Tetra-p-ethoxyazophenine (1c)*: The amine (10 g), (aniline, *p*-anisidine or *p*-phenetidine) hexachloroethane or 1,1,2,2-tetrachloroethane (6 g) and copper bronze (40 mg) were heated on a boiling water bath for 2 h to give a black mass which was decomposed and washed with dilute hydrochloric acid and the residue refluxed with ethanol and filtered to afford a reddish brown solid. The latter was crystallized from pyridine and then from dioxane in dark red needles.

The spectral data of **1b** are as follows: UV $\lambda_{max}^{dioxane}$: nm (log ε): 305 (4.37), 420 (4.25); IR (KBr): 3350 (N-H), 1600, 1580, 1540, 1490, and 1450 (aromatic), 1050 (C-O-C) cm^{-1}; MS: *m/z* 560 (M^+). The NMR spectrum of **1b** could not be taken due to its insolubility in the usual solvents.

The IR and mass spectral data of **1c** are as follows: IR (KBr): 3360 (N-H), 1600, 1580, 1540, 1490, 1450 (aromatic), 1040 (C-O-C) cm^{-1}; MS: *m/z* 616 (M^+).

Tetra-p-propoxyazophenine (1d): The reaction was carried out as above with *p*-propoxyaniline. The black mass obtained was repeatedly recrystallized from ethanol to afford a reddish-violet solid. IR (KBr): 3360 (N-H), 1600, 1580, 1540, 1480, 1450 (aromatic), 1050 (C-O-C) cm^{-1}.

Tetra-p-butoxyazophenine (1e): The procedure used was similar to the general procedure. The black mass obtained was chromatographed over a silica-gel column. Elution with hexane-acetone (70:30) afforded a deep reddish-violet solid which was crystallized from ethanol. The NMR spectrum of compound **1e** is as follows: NMR ($CDCl_3$) δ=0.8—1.2 (12H, m, four $-CH_3$), 1.26—2.0 (16H, m, eight $-CH_2$), 3.76—4.19 (8H, q, four $-OCH_2$), 5.63 (2H, s, two =CH-), 6.66—7.76 (16H, m, aromatic protons).

We are grateful to the Ciba-Geigy Research Centre, Bombay, for the spectra recorded and the UGC for the award of a fellowship to GM.

References

1) O. N. Witt and E. Thomas, *Ber.*, **16**, 1102 (1883).
2) M. Lora Tamayo and F. Fontan Yanes, *Anales Real Soc., Espan. Fis. y Quim Ser. B*, **44**, 583 (1948); *Chem. Abstr.*, **42**, 8176a (1948).
3) G. M. K. Hughes and B. C. Saunders, *J. Chem. Soc.*, **1956**, 3814.
4) Hiroya Tanabe, *Yakugaku Zasshi*, **77**, 867 (1958); *Chem. Abstr.*, **52**, 1093 (1958).
5) G. A. Swan and P. S. Timmons, *J. Chem, Soc.*, **1958**, 4669.
6) P. Ruggli and F. Buchmeier, *Helv. Chim. Acta*, **28**, 850 (1945).
7) E. H. Rodd, "Chemistry of Carbon Compounds," Elsevier, Amsterdam, **1954**, Vol. 3, p. 724.
8) S. Goldschmidt, *Ber.*, **53**, 35 (1920).
9) R. Willstatter and H. Kubli, *Ber.*, **42**, 4135 (1909).
10) G. H. Daniels and B. C. Saunders, *J. Chem. Soc.*, **1951**, 2112.
11) I. L. Finar, "Organic Chemistry," Longman, London (1973), Vol. 1, p. 725.

Vibrational Energy Levels and Infrared Absorption Intensities of Carbon Monoxide

Tomoo MIYAZAKI,* Azuma MATSUURA, and Hisao TAKEUCHI

Department of Applied Chemistry, Faculty of Science and Engineering, Waseda University, Ohkubo, Shinjuku-ku, Tokyo 160

(Received July 14, 1983)

Synopsis. The vibrational energy levels and infrared absorption intensities of carbon monoxide have been calculated with due consideration for the mechanical and electrical anharmonicities of vibration by the use of ab initio molecular orbital calculation in which the C-I treatment and polarization functions were introduced.

The dipole moment of carbon monoxide, as a function of the interatomic distance, is a problem of absorbing interest not only in itself but in relation to the infrared absorption intensity. In this paper, the potential energy of the CO vibration and the dipole moment function have been studied by comparison between theoretical values and observations about the wave number and intensity in the infrared absorption spectrum of carbon monoxide. One of the remarkable features of this work is that the infrared absorption intensities are calculated by the use of a dipole moment function involving the higher order terms and by vibrational wave functions obtained from the variation method in which the potential energy function involving the higher order terms are adopted. Another feature is that the atomic polarizations of the C and O atoms which bring about the unexpected dipole moment of the CO molecule are determined. The calculations have been performed by employing the GAUSSIAN 76 and 80 programs provided by the QCPE and HITAC M-280H/M-200H system of the Computer Center in The University of Tokyo.

In the first step of this work, the results of several ab initio calculations on the dipole moment (μ), gross atomic population (P_{AA}), force constant (K), and total energy (E) at the theoretical equilibrium distance (R_{eq}) of the CO molecule were compared with observations.

TABLE 1. COMPARISON OF RESULTS FROM SEVERAL AB INITIO CALCULATIONS OF CO

Method[a,b,c]	R_{eq} / Å	μ[d] / D[e]	P_{OO}	P_{CC}	K / mdyn Å^{-1} [e]	E / a.u.[e]
STO-6G	1.1458	−0.0578	8.2148	5.7852	24.283	−112.30421
STO-6G-CI	1.1802	−0.2442	8.1614	5.8386	19.580	−112.43701
631G	1.1307	+0.5728	8.3492	5.6508	21.078	−112.66722
631G-CI	1.1942	+0.5402	8.3536	5.6464	21.044	−112.77613
631G*	1.1136	+0.2625	8.2777	5.7223	24.231	−112.73734
631G*-CI	1.1396	+0.1648	8.2620	5.7380	20.231	−112.85647
6311G	1.1237	+0.4677	8.3276	5.6724	20.968	−112.69949
6311G-CI	1.1439	+0.4909	8.3237	5.6763	18.265	−112.90340
6311G*	1.1047	+0.1532	8.1863	5.8137	24.076	−112.76948
6311G*-CI	1.1216	+0.1679	8.1801	5.8199	21.558	−113.05573
Obsd	1.1283	−0.112			19.02	−113.377

a) The Gaussian 76 was employed on all cases except for 6311G and 6311G* methods with or without CI treatment. b) The CI calculation for the STO-6G method was performed by considering all possible singly and doubly excited configurations. The CI calculations were performed by considering single and double excitations within the limits of orbital number 3 to 14 and 3 to 15 for the 631G and 631G* methods respectively. c) The CI calculation with Gaussian 80 was performed by considering all double excitations under condition of a frozen core. d) The Cartesian axis used in this calculation is as follows:

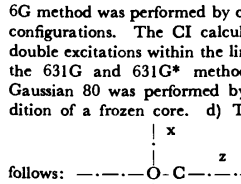

e) 1 D = 10^{-18} g$^{1/2}$ cm$^{5/2}$ s^{-1}, 1 mdyn Å^{-1} = 10^5 g s^{-2}, 1 a.u. = 4.35981×10^{-11} g cm^2 s^{-2}.

These values are listed in Table 1. Generally, the application of CI treatment leads to a slight increase of the theoretical bond distance and to a slight decrease of the theoretical force constant. On the basis of these results, we chose the STO-6G-CI and 6311G*-CI meth-

TABLE 2. COEFFICIENTS OF POTENTIAL ENERGY, V, AND DIPOLE MOMENT, μ, FUNCTIONS

$V(Q)$[a] $= (1/2)\lambda Q^2 + gQ^3 + hQ^4 + iQ^5 + jQ^6$

$\mu(Q)$[a] $= \mu_0 + M_1Q + M_2Q^2 + M_3Q^3 + M_4Q^4$

	Coefficients of $V(Q)$			Coefficients of $\mu(Q)$[d]	
	STO-6G-CI[b]	6311G*-CI[c]		STO-6G-CI[b]	6311G*-CI[c]
λ	0.82872×10^{29}	0.82784×10^{29}	μ_0	-0.2442×10^{-18}	0.1679×10^{-18}
g	-0.51761×10^{49}	-0.51565×10^{49}	M_1	4.90130×10	13.00971×10
h	0.21014×10^{69}	0.20980×10^{69}	M_2	0.50706×10^{21}	1.07712×10^{21}
i	-0.06554×10^{89}	-0.06898×10^{89}	M_3	-0.58929×10^{41}	-0.71974×10^{41}
j	0.01889×10^{109}	0.01920×10^{109}	M_4	-0.11907×10^{61}	-0.03150×10^{61}

Unit: $Q = g^{1/2}$ cm, $V = g\ cm^2\ s^{-2}$, $\mu = \mu_0 = g^{1/2}\ cm^{5/2} s^{-1}$.

a) $L/g^{-1/2} = 2.962707\times10^{19}$ (The unit of internal coordinate, R, in $V(R)$ is Å.). b) $\alpha = 0.989$. c) $\alpha = 0.935$. d) $\mu(Q) = -0.1120\times10^{-18} + 9.2130\times10Q - 0.1317\times10^{21}Q^2 - 0.6148\times10^{41}Q^3$ (from Young and Eachus, Ref. 3), $\mu(Q) = -0.1140\times10^{-18} + 9.3362\times10Q - 0.2196\times10^{21}Q^2 - 0.6184\times10^{41}Q^3$ (from Weisbach and Chackerian, Ref. 4), $\mu(Q) = -0.2600\times10^{-18} + 9.6666\times10Q - 0.0031\times10^{21}Q^2 - 0.8924\times10^{41}Q^3$ (from Kirby-Docken and Liu, Ref. 5).

TABLE 3. ENERGY LEVELS AND WAVE FUNCTIONS OF THE CO VIBRATION[a] (ε_v AND $\psi_v = \sum C_{vi}\phi_i^\circ$)

v	0	1	2	3	4	5
ε[b] $\times10^{13}$	2.14112	6.39337	10.60736	14.78342	18.92199	23.02403
C_{v0}	**0.99848**	−0.05312	0.00156	−0.01344	0.00559	−0.00148
C_{v1}	0.05308	**0.98686**	−0.14888	0.01308	−0.02629	0.01498
C_{v2}	0.00251	0.14861	**0.94987**	−0.26687	0.04033	−0.04163
C_{v3}	0.01454	0.01552	0.26588	**0.87239**	−0.39122	0.08764
C_{v4}	0.00169	0.03006	0.04422	0.38887	**0.74353**	−0.50298
C_{v5}	0.00012	0.00725	0.05060	0.09173	0.49871	**0.55994**
C_{v6}	0.00047	0.00110	0.01868	0.07805	0.15723	0.57409
C_{v7}	0.00008	0.00136	0.00426	0.03793	0.11397	0.23428
C_{v8}	0.00001	0.00042	0.00317	0.01160	0.06659	0.15830
C_{v9}	0.00002	0.00008	0.00134	0.00680	0.02562	0.10519
C_{v10}	0.00000	0.00008	0.00036	0.00339	0.01367	0.04853
C_{v11}	0.00000	0.00003	0.00022	0.00118	0.00739	0.02533
C_{v12}	0.00000	0.00001	0.00010	0.00060	0.00307	0.01439
C_{v13}	0.00000	0.00000	0.00003	0.00028	0.00130	0.00591

a) The values were obtained from the 6311G*-CI method. b) $\varepsilon = g\ cm^2\ s^{-2}$.

TABLE 4. WAVENUMBERS, $\tilde{\nu}$, AND ABSORPTION INTENSITIES, $A_{v'\leftarrow v}$, OF THE VIBRATIONAL SPECTRUM OF CO ($\tilde{\nu}$ = cm^{-1}, A = cm^2 s^{-1} molecule^{-1}, T = 300 K)

v→v'	STO-6G-CI		6311G*-CI		Ref.	
	$\tilde{\nu}$	$A\times10^{10}$	$\tilde{\nu}$	$A\times10^{10}$	$\tilde{\nu}$[a]	$A\times10^{10}$
0→1	2141.78	833.559	2140.79	5894.890	2143.27	2923.2[b]
1→2	2122.46	0.057272	2121.52	0.408735	2116.79	4043.2[c]
2→3	2103.41	0.000003	2102.42	0.000023	2090.38	7300.7[d]
3→4	2084.72	0.000000	2083.55	0.000000	2064.03	
0→2	4264.24	2.09954	4262.31	16.63066	4260.06	21.056[b]
1→3	4225.87	0.000233	4223.95	0.001777	4207.17	26.210[c]
2→4	4188.13	0.000000	4185.98	0.000000	4154.41	
0→3	6367.65	0.004708	6364.73	0.018628	6350.44	0.11984[b]
1→4	6310.59	0.000001	6307.50	0.000003	6271.20	0.34720[c]
2→5	6254.78	0.000000	6251.14	0.000000	6192.16	
0→4	8452.37	0.000556	8448.28	0.000113	8414.47	
1→5	8377.24	0.000000	8372.66	0.000000	8308.95	

Rotational constants (cm^{-1}): $B_e = 1.9531$, $\alpha_e = 1.4390\times10^{-2}$, $\gamma_e = 2.760\times10^{-5}$, $\delta_e = 2.027\times10^{-7}$.

a) Values calculated using vibrational constants from Mantz *et al.* (Ref. 6). b) Experimental values from Young and Eachus (Ref. 3). c) Values calculated by Billingsley and Krauss (Ref. 7). d) Value calculated by Rogers and Hillman (Ref. 8).

Table 5. Dipole moments, μ, atomic polarizations, μ_{AP}, and gross atomic populations, P_{AA}, at several CO distances (ΔR=Å, μ=Debye (10^{-18} $g^{1/2}$ $cm^{5/2}$ s^{-1}))

ΔR	STO-6G-CI					6311G*-CI				
	μ	μ^{o}_{AP}	μ^{c}_{AP}	P_{oo}	P_{cc}	μ	μ^{o}_{AP}	μ^{c}_{AP}	P_{oo}	P_{cc}
−0.08	−0.3731	+1.5450	−2.9951	8.1828	5.8172	−0.1972	+1.3769	−3.0997	8.1377	5.8623
−0.04	−0.3100	+1.5457	−2.8714	8.1710	5.8290	−0.0176	+1.3868	−3.0054	8.1572	5.8428
R_{eq}	−0.2442	+1.5328	−2.7502	8.1614	5.8386	+0.1679	+1.3816	−2.9211	8.1801	5.8199
+0.08	−0.1079	+1.4781	−2.5135	8.1473	5.8527	+0.5508	+1.3388	−2.7614	8.2320	5.7680
+0.16	+0.0277	+1.3987	−2.2812	8.1370	5.8630	+0.9418	+1.2722	−2.6074	8.2861	5.7139

ods which differ from each other in adoption of the basis set. In the next step, the detailed calculation have been performed using these two methods. According to the method of least squares, the potential energy and dipole moment functions were obtained carefully from sufficient data for distorted molecules as the higher order equations with respect to the internal coordinate (R_{CO}). These equations have been transformed to the functions with the normal coordinate (Q) by the use of the L term which relates the internal coordinate to the normal coordinate. In order to obtain the appropriate final results, these functions have been rewritten by multiplying the coordinate term by an adjusting constant (α) determined in comparison with the observed frequency of fundamental band. Table 2 records the coefficients of these potential energy and dipole moment functions. The variation method has been used to calculate the energy levels of vibration in view of the mechanical anharmonicity and the wave function (ψ) of the molecular vibration has been described by the linear combination of harmonic oscillator wave functions(ϕ°). Further details of the treatment were reported in previous papers.[1,2] The calculated energy levles and wave functions are listed in Table 3. By the use of these anharmonic wave functions and dipole moment function indicated in Table 2, the absolute infrared absorption intensities of fundamental and overtone bands have been calculated in view of the mechanical and electrical anharmonicities.[1,2] The results are summarized in Table 4 in which reference data are also included. Since the potential energy function is modified by the use of the adjusting constant (α), the calculated wave number of the fundamental band agrees well with the observed value. The calculated wave numbers of overtone bands, too, almost coincide with the observed values. From these results, we may reasonably conclude that the potential energy function obtained in this work is adequate. Furthermore, according to the perturbation treatment,[9] the rotational constants α_e, γ_e, and δ_e have been determined by the use of anharmonic wave functions as indicated in Table 3. The calculated constants are listed in the footnote of Table 4.

When the higher approximate treatment of molecular orbital calculation was adopted, the appropriate value of the dipole moment could not always be obtained. However from Table 4, in which theoretical values of infrared absorption intensities are compared with experimental values, it has been definitely recognized that the values of M_1, M_2, and M_3 in dipole moment function are improved by employing the higher approximate 6311G* calculation than STO-6G, while Amore-Bonapasta[10] reported as follows: the agreement between experimental result and theoretical function from the STO-6G method is satisfactory and better than that between experimental and 631G functions.

The last point to which special attention should be paid is the change of the direction of the dipole moment in the vicinity of the equilibrium CO distance. The values of the atomic polarization resulting from the mixing of the S and P type orbitals or the P and D type orbitals are indicated in Table 5 in which gross atomic populations are also indicated. It is notable that the absolute value of the atomic polarization, μ^{c}_{AP}, of carbon is about double that, μ^{o}_{AP}, of oxygen. The sign of μ^{c}_{AP} is negative and that of μ^{o}_{AP} is positive when the CO molecule is fixed in the coordinate indicated in the footnote of Table 1. From these results, it is evident that the unexpected sign of the CO dipole moment is caused by atomic polarizations. In the results from different methods, there are opposite tendencies as to the increase in gross atomic population with the variation of CO distance. The same tendencies are seen in the value of the dipole moment with the exception of the atomic polarization term. In view of the above facts, it is found that the theoretical result for the electronic property of carbon monoxide is highly sensitive to the difference of approximation in the method of calculation.

References

1) T. Miyazaki and H. Yamamoto, *Bull. Chem. Soc. Jpn.*, **45**, 1669 (1972).
2) T. Miyazaki, M. Ikeda, and M. Shibata, *Bull. Chem. Soc. Jpn.*, **48**, 1138 (1975).
3) L. A. Young and W. J. Eachus, *J. Chem. Phys.*, **44**, 4195 (1966).
4) M. F. Weisbach and C. Chackerian, *J. Chem. Phys.*, **59**, 4272 (1973).
5) K. Kirby-Docken and B. Liu, *J. Chem. Phys.*, **66**, 4309 (1977).
6) A. W. Mantz, J. P. Maillard, W. B. Roh, and K. N. Rao, *J. Mol. Spectrosc.*, **57**, 155 (1975).
7) F. P. Billingsley and M. Krauss, *J. Chem. Phys.*, **60**, 4130 (1974).
8) J. D. Rogers and J. J. Hillman, *J. Chem. Phys.*, **77**, 3615 (1982).
9) H. Eyring, J. Walter, and G. E. Kimball, "Quantum Chemistry," John Wiley & Sons, New York (1944), p. 269.
10) A. Amore-Bonapasta, *Indian J. Chem., Sect. A*, **21**, 91 (1982).

The Number of Water Molecules Bound to Insulin

Nobuya NAGASHIMA,* Ei-ichiro SUZUKI, and Masamichi TSUBOI†
Central Research Laboratories, Ajinomoto Co., Inc., 1-1 Suzuki-cho, Kawasaki-ku, Kawasaki 210
†*Faculty of Pharmaceutical Sciences, The University of Tokyo, Hongo, Bunkyo-ku, Tokyo 113*
(Received September 10, 1983)

Synopsis. On cooling an aqueous solution of zinc pig-insulin to −40 °C, 108 water molecules per insulin molecule have been found (by NMR) unfrozen. This number is nearly equal to what was found crystallographically of the water molecules located within 4.7 Å of the protein molecule.

It is now well known that every globular protein is biologically active only when it is hydrated. Thus, the water molecules bound to a protein molecule are considered to play an essential role in its biological function. Their molecular structures as found in the crystal also involve a great amount of water, and these structures has been supposed to be kept on going from crystals to aqueous solutions. As a powerful tool for characterizing such protein-bound water, we have recently developed[1] a full computerized apparatus, whose main part is a broad-line pulsed NMR spectrometer with a Lamor frequency of 20 MHz, for the observation of a proton (Bruker, minispec p20). In this apparatus, the in-put is an aqueous solution of the sample protein now in question, while the out-put is the unfrozen-water content *versus* the temperature curve, where unfrozen water is defined as water molecules with protons of $T_2 > 70\ \mu s$ (here, T_2 is the spin-spin relaxation time). At any temperature below 0 °C, the usual solvent water is frozen, and the T_2 values for such water molecules are much shorter than 10 μs. Only some H_2O molecules in a special environment, such as hydrating water of a protein molecule, may be kept unfrozen, may keep a long T_2, and may be detected (as unfrozen water) by the present apparatus. The purpose of this paper is to compare what is found with this apparatus and what is found by an X-ray crystallographic study with regard to the hydration of insulin.

The sample of Zn pig-insulin powder was kindly provided by Dr. Noriyoshi Sakabe, Nagoya University; it is the same as what was subjected to his and his collaborators' crystallographic study.[2-4] Elementary analyses for this powder gave: C, 47.24; H, 6.80; N, 13.93%. This is consistent with the chemical formula of $C_{256}H_{383}N_{66}O_{76}S_6 \cdot (1/3)Zn \cdot 28H_2O$, so the water content of this powder was estimated to be 8.0 ±1.0%. This means that dry matter (DM) content=92.0 ±1.0%. The water content was also determined by measuring the weight decrease on keeping the powder sample at 115 °C for 8 h. This gave a value of H_2O content=9.4±1.0% (dry matter content=90.6 ±1.0%). A 29.2-mg portion of this powder (which should involve 26.9 mg of dry matter) was dissolved into 0.22 ml of distilled water, and this solution was then placed at the proper position in our apparatus. The out-put is illustrated in Figs. 1 and 2. As may be seen in Fig. 1, the unfrozen-water content drops suddenly at −1.5 °C (after some supercooling) in the process of cooling; this corresponds to the freezing of the solvent water. On further cooling, the unfrozen-water content is gradually lowered from 1.3 to 0.4 gH_2O/gDM. After it reaches 0.33_8 gH_2O/gDM at −25 °C, it remains nearly constant until −50 °C. In the course of warming, this unfrozen-water content is kept till the temperature becomes −10 °C, whereupon it suddenly increases. Thus, the unfrozen-water content 0.33_8 gH_2O/gDM at −40 °C seems to have some special significance; this unfrozen-water content corresponds to 108 H_2O molecules/insulin molecule, and to 216 H_2O molecules/two insulin molecules (see Table 1).

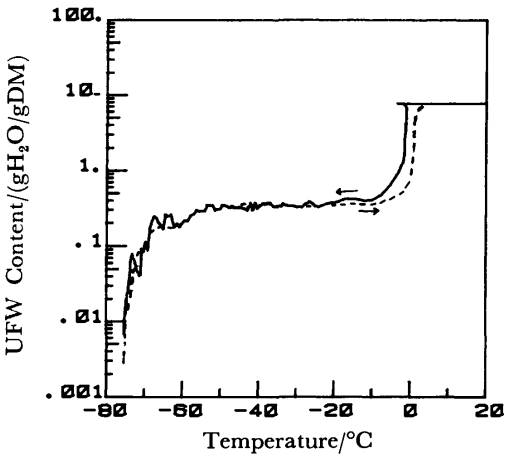

Fig. 1. Unfrozen water content *versus* temperature curves for zinc pig-insulin solution. The unfrozen water (UFW) content is given by g H_2O per g DM (dry matter). Solid line was obtained in the process of cooling (freezing curve), and dashed line was obtained in the process of warming (thawing curve).

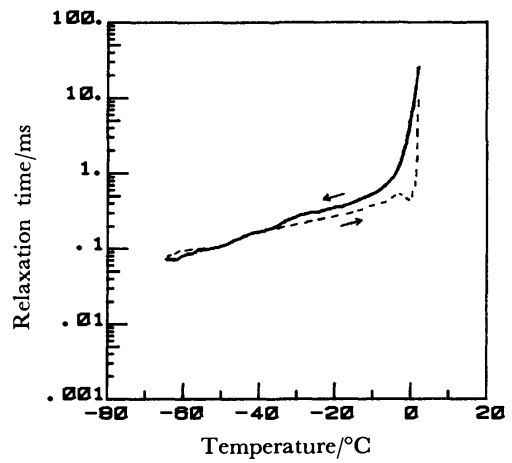

Fig. 2. T_2 (spin-spin relaxation time) *versus* temperature curves for zinc pig-insulin solution. Solid line was obtained in the process of cooling, and dashed line was obtained in the process of warming.

Table 1. Number of water molecules bound to the pig insulin molecule

X-Ray crystallography[a]					NMR (Present work)		
Nearest atom in insulin	Distance Å	Number per asymmetric unit		Temperature range in which the water is kept unfrozen °C	T_2 ms	UFW content gH_2O/gDM	Number per two insulin molecules
N or O	2.7—3.3	117	124				
C	3.2	7					
				214	−50——25	0.1--0.3	0.33_8	216
N or O	3.3—4.7	43	90				
C	3.3—4.7	47					
N or O	4.7—5.0	5	11				
C	4.7—5.0	6					
				66	−25——8	0.3—0.5	0.10_0	64
Not found			55[b]				

a) Refs. 2—4. b) This may be greater than 55, because the total number of water molecules in the crystal was determined by chemical analysis, while the located molecules may have occupancy factors with values slightly less than 1.0 (private communication from Dr. N. Sakabe).

For the rhombohedral two-zinc porcine insulin crystal, a high-resolution (1.2 Å) X-ray diffraction analysis has been made.[2-4] A chemical analysis indicated that its asymmetric unit involves 2/3 Zn+2 insulin molecules+280 H_2O. Of these 280 H_2O, 225 were crystallographically determined. Among them, 214 H_2O molecules were found within the distance of 4.7 Å from the nearest atoms of insulin, and 11 H_2O molecules at distances of 4.7—5.0 Å from the nearest atoms. The remaining 55 H_2O molecules were not found because of their disorder and the larger temperature factors (see Table 1). Therefore, the water molecules remaining unfrozen in the −50——25 °C range (or in the −50——10 °C range in the thawing curve; see Fig. 1) may be correlated with the water of hydration located within 4.7 Å of the protein molecule. This may be called "tightly bound" water. The remaining 66 H_2O molecules were found in the crystallographic work to be less strongly bound to the insulin molecules. This number corresponds to the amount of water kept unfrozen in the temperature range of −8——25 °C on the freezing curve (or −15——3 °C on the thawing curve) in our NMR study. This may be called "weakly bound" water. In view of the errors (about ±5%) in our unfrozen-water content estimation, it is also possible that all the crystallographically located (at 4 °C) H_2O molecules (225 in number) correspond to unfrozen water at −40 °C ("tightly bound" water). If so, all the 55 water molecules that do not appear clearly in the crystal correspond to the "weakly bound" water.

The above-mentioned apparatus can also provide an average T_2 value of the unfrozen water at every temperature.[1] As is shown in Fig. 2, the "tightly bound" water was found to have a T_2 value of 0.1—0.3 ms, and the "weakly bound" water, one of 0.3—0.5 ms. It should also be pointed out here that a hysteresis loop in the freezing-thawing curves is found not only for the unfrozen water content (see Fig. 1), but also for the unfrozen water mobility (Fig. 2). By thermal analysis with a differential scanning calorimeter (Daini Seikosha, SSC 560U), an inflection was observed in the thawing process at −32.8 °C; this means an increase in the specific heat.

In conclusion, it may be suggested that the tightly-bound water molecules (and possibly the weakly-bound water molecules also) are nearly intrinsic on the surface of the insulin molecule, and that even in its aqueous solution their sites and orientations are similar to those in the crystal. This suggestion is based merely upon a coincidence in the numbers. If it is valid, however, it may be generalized to globular proteins other than insulin.

We wish to express our thanks to Dr. Noriyoshi Sakabe, Nagoya University, for his kindness in providing the sample and for his valuable advice.

References

1) E. Suzuki and N. Nagashima, *Bull. Chem. Soc. Jpn.*, **55**, 2730 (1982).

2) N. Sakabe, K. Sakabe, and K. Sasaki, "Proc. Symp. on Proinsulin, Insulin, and C-Peptide," (Tokushima, 12—14 July 1978), ed by S. Baba, T. Kaneko, and N. Yanaihara, Excerpta Medica, Amsterdam (1978), p. 73.

3) K. Sakabe, N. Sakabe, and K. Sasaki, "Water and Metal Cations in Biological Systems," ed by B. Pullman and K. Yagi, Japan Scientific Societies Press, Tokyo (1980), p.117.

4) N. Sakabe, K. Sakabe, and K. Sasaki, "Structure Studies on Molecules of Biological Interest," ed by G. Dodson, J. P. Glusker, and D. Sayre, Clarendon Press, Oxford (1981), p.509.

Liquid Crystal Formation in Binary Systems. IX.[1] Effects of Branching of Ester Alkyl Group on the Induction of Liquid Crystals in the Alkyl 4-[4-(Dimethylamino)benzylideneamino]benzoate-4,4'-Dinitroazoxybenzene Systems

Yoshio MATSUNAGA* and Izumi SUZUKI
Department of Chemistry, Faculty of Science, Hokkaido University, Sapporo 060
(Received October 5, 1983)

Synopsis. Smectic A liquid crystals are formed not only in systems with normal alkyl esters but also with esters of branched alkyl groups such as *t*-butyl, 1,2-dimethylpropyl, and 1-ethylpropyl.

Branching of a terminal alkyl group has been shown to decrease nematic and smectic thermal stabilities relative to those of the unbranched chain compounds by Gray and Harrison.[2,3] However, the effects of branching on the liquid crystals induced in electron-donor-acceptor systems may not be the same as those found with single mesogenic compounds. Consequently, we decided to examine the effects employing binary systems consisting of nonmesogenic alkyl 4-[4-dimethylamino)benzylideneamino] benzoates as electron donors and nonmesogenic 4,4'-dinitroazoxybenzene as an electron acceptor.

The donor compounds were obtained by fusing equimolar mixtures of *p*-(dimethylamino)benzaldehyde and an appropriate alkyl *p*-aminobenzoate and purifying by repeated recrystallization from ethanol. The methyl, ethyl, two isomeric propyl, four isomeric butyl, five isomeric pentyl, and hexyl esters were prepared for this work. The acceptor compound, hereafter abbreviated as DNAO, is known to be able to produce liquid crystals when it is mixed with *N*-[4-(dimethylamino)benzylidene]-4-ethoxyaniline and related compounds.[4] The measurements were carried out as described in our earlier papers.[1,4]

A 2:1 solid molecular complex melting congruently at 179 °C is formed in the methyl ester–DNAO system. The smectic A phase induced in the composition range from 10 to 40 mol% of DNAO is metastable. The isotropic-smectic A (I-S_A) transition point at the former composition is 138 °C and that at the latter is 156 °C. The broad maximum lies at 173 °C and around 25 mol%.

As is shown in Fig. 1a, a phase diagram of the eutectic type is produced when the ethyl ester is mixed with DNAO. The I-S_A transition point curve is markedly convex upwards and appears near the eutectic point at 114 °C and 10 mol% and terminates at the intersection with the freezing point curve of DNAO at 147 °C and about 55 mol%. The effects of branching of this alkyl group are demonstrated by the phase diagrams of the isopropyl ester- and the *t*-butyl ester–DNAO systems (see Figs. 1b and 1c). The induced smectic A phases in these two systems are metastable and the maximum temperatures are 132 and 131 °C respectively. A decrease in the transition temperature by the introduction of the first methyl group to the ester ethyl group meets our expectation but, to our surprise, the effect of the second methyl group is essentially nil.

In the propyl ester–DNAO system, a smectic A phase is observable from 15 to 50 mol% (see Fig. 2a). The I-S_A transition point curve is less convex than that in the ethyl ester–DNAO system, and the maximum is found at 129 °C and around 34 mol%. By 1-methylation, the smectic A phase remains stable only in a small area. The I-S_A transition point curve reaches its maximum at 111 °C and 29 mol% (see Fig. 2b). The methylation on the penultimate carbon further reduces the thermal stability of the induced mesophase. As is shown in Fig. 2c, the smectic A phase is metastable in this binary system and a nematic phase is also induced on the acceptor-rich side. The maximum temperature of the smectic phase is 103 °C. These observations are in contrast to those made by Gray and Harrison for several series of mesogenic compounds: that is, 1-methylation generally produces the largest decrease in the thermal stability of the smectic A phase, and as the methyl group is moved to the end of the chain, the effect becomes less marked. The anomalous results described

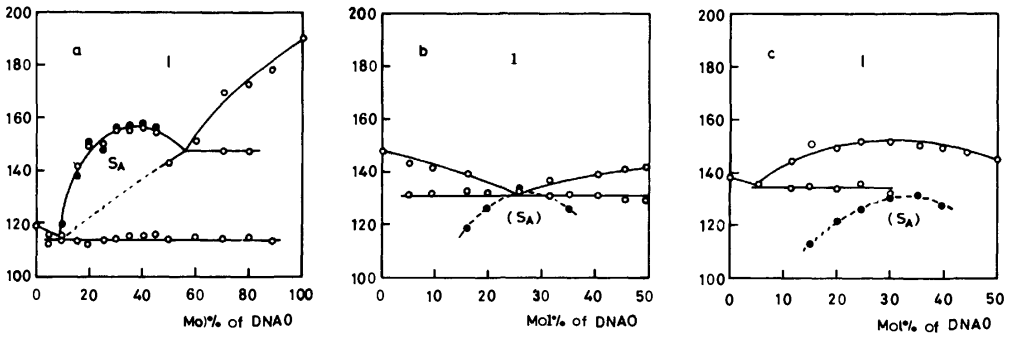

Fig. 1. Phase diagrams of the systems of DNAO with (a) the ethyl ester, (b) the isopropyl ester, and (c) the *t*-butyl ester. The open and shaded circles are transitions observed in the processes of heating and cooling respectively.

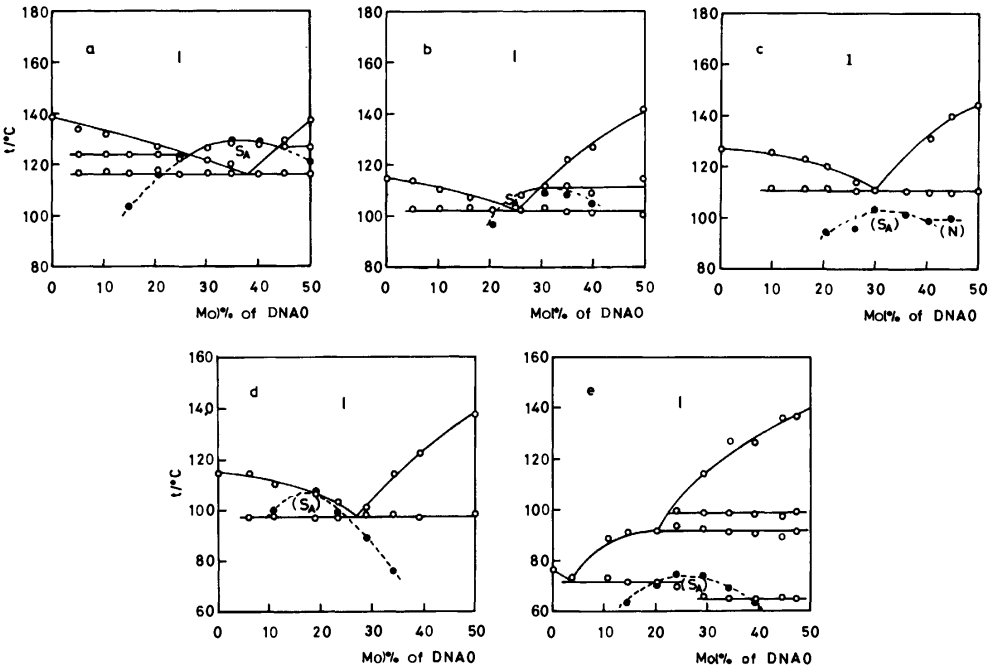

Fig. 2. Phase diagrams of the systems of DNAO with (a) the propyl ester, (b) the 1-methylpropyl ester, (c) the 2-methylpropyl ester, (d) the 1,2-dimethylpropyl ester, and (e) the 1-ethylpropyl ester. As to the open and shaded circles, see the caption of Fig. 1.

above appear to be characteristic of the present binary systems, and are in accord with the effects of the methyl substitution at both the 1 and 2 positions of the ester propyl group (see Fig. 2d). If one considers a 1-methyl group to be added to the isobutyl ester, the substitution raises the maximum I-S_A transition temperature by 3 °C, whereas if the 2-methyl group is regarded as an extra substituent, the temperature is lowered by 5 °C. Moreover, no mesophase could be observed in the neopentyl ester-DNAO system. Figure 2e presents the phase diagram of the 1-ethylpropyl ester-DNAO system. The transition temperature change by 1-ethylation to 74 °C is double that by 1-methylation.

Contrary to the above cases, the effects of methylation on the induced smectic A phase in the butyl ester-DNAO system is normal. The butyl ester and its 2-methyl and 3-methyl derivatives all produce stable smectic A phases when they are mixed with DNAO. The maximum I-S_A transition temperatures are 120, 90, and 111 °C respectively. Finally, it must be noted that the longer the unbranched alkyl group, the maximum I-S_A transition temperature becomes lower: namely, 110 °C with the pentyl ester and 108 °C with the hexyl ester. In the former case, the induced mesophase is metastable in the whole composition range. Thus, even numbers of carbon atoms in the ester alkyl group in the present binary systems tend to produce larger regions of stable existence of induced smectic A phase. This behavior may be, at least partly, ascribed to the marked odd-even alternation of the melting point of the ester as the mesophase is induced in the donor-rich composition range (compare Figs. 1a and 2a).

Although the mechanism of the transition temperature change by chain branching is not well understood even in single mesogenic compounds, branching certainly disturbs smectic order because of a steric interference with neighboring molecules. The anomalous effects observed with the ethyl and propyl esters may be tentatively explained by the difference in molecular length between the donor and acceptor. As the donor and acceptor molecules are arranged side by side in the mesophase, the 1-methyl group may be accommodated, partially at least, within room produced by the acceptor molecule which is shorter than the ester molecules. If the ester molecules are still longer and/or the point of branching is near the end of the chain, the flexible alkyl group is surrounded increasingly by like molecules and may behave as if it is in a single mesogenic compound.

The present work was partly supported by a Grant-in-Aid for Scientific Research No. 543001 from the Ministry of Education, Science and Culture.

References

1) Part VIII, E. Chino and Y. Matsunaga, *Bull. Chem. Soc. Jpn.*, **56**, 3230 (1983).
2) G. W. Gray and K. J. Harrison, *Symp. Faraday Soc.*, No. 5, 54 (1971).
3) G. W. Gray and K. J. Harrison, *Mol. Cryst. Liq. Cryst.*, **13**, 37 (1971).
4) K. Araya and Y. Matsunaga, *Bull. Chem. Soc. Jpn.*, **55**, 1710 (1982).

Emergence of Nematic Phase in Purely Smectogenic Alkyl 4-(4-Substituted Benzylideneamino)benzoates by Chain Branching of the Ester Alkyl Group

Yoshio MATSUNAGA* and Nobuhiko MIYAJIMA
Department of Chemistry, Faculty of Science, Hokkaido University, Sapporo 060
(Received November 4, 1983)

Synopsis. 2-Methylation of the ester butyl and pentyl groups in the phenyl-substituted compounds and also of the ester propyl, butyl, and pentyl groups in a number of the alkoxy-substituted compounds resulted in the production of nematic liquid crystals.

Gray and Harrison systematically studied the effects of branching of alkyl chain on the liquid crystalline behavior of 4-(4-substituted benzylideneamino)-cinnamates.[1,2] Methylation at any carbon of the ester alkyl chain was found to decrease liquid crystal stability. They noted that branching has a greater effect on nematic than on smectic thermal stability. However, there may be cases where nematic liquid crystals arise by partial destruction of smectic ordered arrangement due to methylation of the alkyl chain as subtle changes in molecular structure can strongly influence the liquid crystalline behavior. Thus, we began a study of the effects of chain branching specifically paying attention to such a possibility. In this note, we wish to report the formation of nematic liquid crystals by 2-methylation of alkyl chains (R′) in fourteen purely smectogenic compounds of the following type.

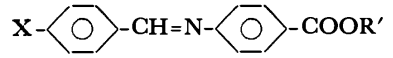

The mesogenic compounds first studied by us were alkyl 4-(4-phenylbenzylideneamino)benzoates (X=Ph) which are closely related in molecular structure to the compounds studied by Gray and Harrison. The ethyl and isopropyl esters are purely smectic in behavior. Stable nematic and smectic A phases are given by the propyl ester. As the butyl and pentyl esters exhibit only smectic properties, search for nematic phases was undertaken with all the possible methylbutyl and methylpentyl esters. The emergence is limited to the 2-methyl derivatives. The transition temperatures determined by differential scanning calorimetry are presented in Table 1 together with those of the unbranched alkyl esters. The mesophases were identified by examination of their textures with the aid of a polarizing microscope in conjunction with a heated stage.

Further examples were provided by some alkyl 4-(4-alkoxybenzylideneamino)benzoate (X=RO) series. The alkoxyl group includes all the members from methoxyl to decyloxyl. Among the propyl esters, the first two members are nematogenic, whereas the higher members are purely smectogenic (see Table 2).

We have found that five members from the propoxy to heptyloxy derivatives in the isobutyl esters exhibit nematic behavior. As in shown in Table 2, the nematic phase in the propoxy derivative is monotropic. Nevertheless, the temperature range of existence is as wide as 12 °C in this compound, and progressively decreases with lengthening of the alkoxyl group. Above octyloxy derivative a smectic A phase becomes the only observable mesophase. Thus, none of the isobutyl esters gives smectic B phase found with most of the propyl esters.

The butyl 4-(4-alkoxybenzylideneamino)benzoate series has been examined by Fishel and Patel.[3] The methoxy derivative gives no mesophase but a metastable smectic A phase is observable with the ethoxy derivative. All the higher members were reported to be purely smectic in behavior. The methoxy and ethoxy derivatives of the racemic 2-methylbutyl esters examined by us form nematic liquid crystals (see Table 3); however, the higher members give only smectic A

Table 1. Transition temperatures (°C) for alkyl 4-(4-phenylbenzylideneamino)benzoates

Ester alkyl group	Transition temperatures[a]
Butyl	C $\xrightarrow{91}$ S_B $\xleftrightarrow{98}$ S_A $\xleftrightarrow{121}$ I
2-Methylbutyl	C $\xrightarrow{77.5}$ S_B $\xleftrightarrow{88}$ S_A $\xleftrightarrow{110}$ N $\xleftrightarrow{112}$ I
Pentyl	C $\xrightarrow{84.5}$ S_B $\xleftrightarrow{94.5}$ S_A $\xleftrightarrow{123}$ I
2-Methylpentyl	C $\xrightarrow{75}$ S_B $\xleftrightarrow{80.5}$ S_A $\xleftrightarrow{106}$ N $\xleftrightarrow{113}$ I

a) C, S_B, S_A, N, and I stand for crystalline, smectic B, smectic A, nematic, and isotropic phases respectively.

Table 2. Transition temperatures (°C) for propyl and isobutyl 4-(4-substituted benzylideneamino)-benzoates

Substituent	Propyl esters	Isobutyl esters
Propoxyl	C $\xrightarrow{58}$ S_A $\xleftrightarrow{70.5}$ I	C $\xrightarrow{74.5}$ I; S_A $\xleftrightarrow{56.5}$ N $\xrightarrow{68.5}$ I
Butoxyl	C $\xrightarrow{55}$ S_B $\xrightarrow{47.5}$ S_A $\xleftrightarrow{90}$ I	C $\xrightarrow{74}$ S_A $\xleftrightarrow{74.5}$ N $\xleftrightarrow{80}$ I
Pentyloxyl	C $\xrightarrow{56.5}$ S_B $\xrightarrow{36.5}$ S_A $\xleftrightarrow{85}$ I	C $\xrightarrow{66}$ S_A $\xleftrightarrow{71}$ N $\xleftrightarrow{75}$ I
Hexyloxyl	C $\xrightarrow{61}$ S_B $\xrightarrow{38}$ S_A $\xleftrightarrow{91}$ I	C $\xrightarrow{59.5}$ S_A $\xleftrightarrow{77}$ N $\xleftrightarrow{79.5}$ I
Heptyloxyl	C $\xrightarrow{62.5}$ S_B $\xrightarrow{35.5}$ S_A $\xleftrightarrow{90.5}$ I	C $\xrightarrow{52}$ S_A $\xleftrightarrow{81}$ N $\xleftrightarrow{82}$ I

Table 3. Transition temperatures (°C) for butyl and 2-methylbutyl 4-(4-substituted benzylideneamino)-benzoates

Substituent	Butyl esters	2-Methylbutyl esters
Methoxyl	C 57.5 I	C 34.5 I; 3.5 N
Ethoxyl	C 98 I; C 63.5 S_A	C 35 S_A 47.5 N 53 I

Table 4. Transition temperatures (°C) for pentyl and 2-methylpentyl 4-(4-substituted benzylideneamino)benzoates

Substituent	Pentyl esters	2-Methylpentyl esters
Propoxyl	C 45 S_A 58 I	C 41.5 I; S_A 31.5 N 37
Butoxyl	C 29 S_A 77.5 I	C 49.5 N 53 I; S_A 49
Pentyloxyl	C 47.5 S_A 74.5 I	C 38 S_A 43.5 N 47.5 I
Hexyloxyl	C 60 S_A 79 I	C 34 S_A 54 N 57 I
Heptyloxyl	C 57 S_A 79 I	C 57 I; S_A 55.5 N 56.5

phase. These results contrast greatly with those described for the isobutyl ester series and also the findings with the 2-methylpentyl esters to be presented in next paragraph.

In the series of pentyl esters, the methoxy and ethoxy derivatives were found to be nonmesogenic and nematogenic respectively. All the other members give smectic A phase. Upon 2-methylation, the members from the propoxy to heptyloxy derivatives exhibit nematic properties (see Table 4). In this series too, the metastable phase in the propoxy derivative appears over the widest temperature range. The phase is enantiotropic in the next three members but monotropic again in the heptyloxy derivative and the range is as narrow as 1 °C in the last. Finally we add that neither the 3-methylpentyl nor 4-methylpentyl ester exhibits nematic behavior except for the methoxy derivative in the latter series. A monotropic isotropic-nematic transition occurs at 16 °C for this compound.

In conclusion, we wish to emphasize that methylation of the ester alkyl chain not only diminishes the thermal stability of smectic A mesophase, as confirmed by the ample examples presented in the four tables, but also gives rise to the appearance of nematic phase in a number of smectogens by partial destruction of the molecular order, the magnitude of which seems to be just right, in general, when the methyl group is located at the 2 position.

The present work was partially supported by a Grant-in-Aid for Scientific Research No. 58118003 from the Ministry of Education, Science and Culture.

References

1) G. W. Gray and K. J. Harrison, *Mol. Cryst. Liq. Cryst.*, **13**, 37 (1971).
2) G. W. Gray and K. J. Harrison, *Symp. Faraday Soc.*, No. 5, 54 (1971).
3) D. L. Fishel and P. R. Patel, *Mol. Cryst. Liq. Cryst.*, **17**, 139 (1972).

Determination of the Vapor Pressures of Lithium Chloride and Sodium Bromide by a Molecular Effusion-Surface Ionization Method

Hiroyuki KAWANO,* and Tsutomu KENPŌ
Department of Chemistry, Faculty of Science, Ehime University, 2-5, Bunkyō-chō, Matsuyama 790
(Received December 7, 1983)

Synopsis. By means of molecular effusion from a Knudsen cell and of thermal positive ionization on a glowing polycrystalline rhenium filament, the vapor pressure P (in atm) of LiCl or NaBr was measured as a function of cell temperature T (in K). The following equations were established empirically.

$$\log_{10} P(\mathrm{LiCl}) = (7.948\pm0.102) - (10954\pm76)/T \quad \text{for 662—848 K,}$$

$$\log_{10} P(\mathrm{NaBr}) = (7.716\pm0.072) - (11138\pm55)/T \quad \text{for 669—882 K.}$$

In order to study the chemical reactions in the gas phase or on solid surfaces, many workers have recently employed a molecular beam technique, where the beam intensity of molecules (MX) effusing from a Knudsen cell is usually evaluated thermodynamically from published data on the vapor pressure (P(MX)) of MX. Literature values of P(MX), however, scatter widely in general, thereby suggesting that reliable data on P(MX) should be obtained by precise measurements of both effusion rate and cell temperature.

From the above point of view, the present authors already tried a precise determination of the vapor pressures of CsF and CsCl, and obtained fruitful results in a previous work.[1] Therefore, the same method of thermal positive ionization was employed in this work, too, in order to detect a molecular beam of LiCl or NaBr.

In this paper the experimental data on the vapor pressure and on the entropy and enthalpy changes due to sublimation are summarized briefly and also compared with data published to date.

Experimental

Experimental apparatus and method employed in this work were the same as in the previous work.[1] A molecular beam of MX (LiCl or NaBr) effusing from a Knudsen cell heated to a temperature (T) was directed onto a polycrystalline rhenium filament (F) kept at a high temperature (T_F), and the total ion current ($I^+(M^+)$) of M^+ (Li^+ or Na^+) emitted from F was measured as a function of T or T_F. The samples (LiCl and NaBr) of optical grade were obtained from Wako Pure Chem. Ind., Ltd.

Results and Discussion

At first, the Knudsen cell was kept at a constant temperature higher than 800 K, and $I^+(M^+)$ was measured as a function of T_F in order to find a filament temperature suitable for detecting a beam of MX. In consequence, $I^+(Li^+)$ and $I^+(Na^+)$ corresponding to the cell temperatures T=840 and 885 K, for example, were constant at 38.4±1.8 and 35.6±0.6 nA in the ranges $T_F\simeq$1430—1520 and 1100—1500 K, respectively, indicating that the ionization efficiencies of LiCl and NaBr incident upon F were essentially unity in the respective ranges.

Next, $I^+(M^+)$ was measured as a function of T at T_F=constant in either of the above ranges.

Finally, the vapor pressure was evaluated from

$$P(\mathrm{MX}) = 1.27[M(\mathrm{MX})\cdot T]^{1/2}\, I^+(M^+), \qquad (1)$$

where P(MX) and $I^+(M^+)$ are expressed in atm and ampere, respectively, and M(MX) is the molecular weight of MX. This equation is the same as Eq. 3 in the previous paper.[1]

Temperature dependence of P(MX) determined by the present and other workers is illustrated in Figs. 1 and 2, which indicate that the following equation holds in general.

$$\log_{10} P(\mathrm{MX}) = A - B/T. \qquad (2)$$

The values of A and B determined empirically and of P(MX) evaluated from Eq. 2 for three selected temperatures are shown together with literature values in Table 1. The entropy and enthalpy changes ($\Delta S(\bar{T})$ and $\Delta H(\bar{T})$) due to sublimation at the mean temperature ($\bar{T}$) in the range (T_R) covered in each measurement were calculated from Eqs. 3 and 4, respectively.

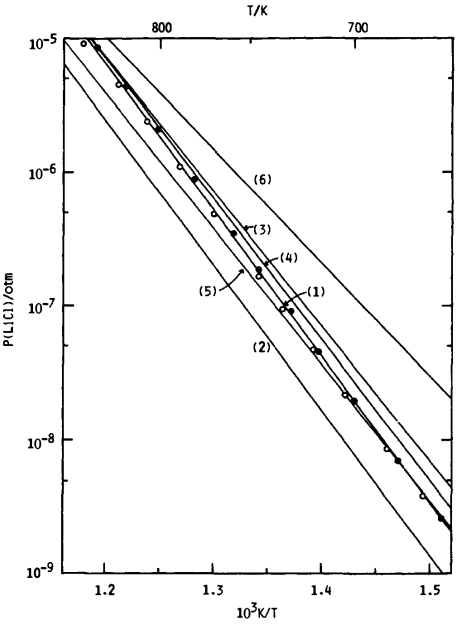

Fig. 1. Temperature dependence of the vapor pressure of LiCl.
(1): This work at T_F=1480 K (open circle) or 1510 K (solid circle), (2): Ref. 2, (3): Ref. 3, (4): Ref. 4, (5): Ref. 5, and (6): Ref. 6.

Table 1. Experimental data obtained with LiCl and NaBr by the present and other workers

Sample	T_R / K	$\overline{T}$ / K	A	B / K	P(MX)/μatm 700 K	800 K	900 K	$\Delta S(\overline{T})$ / cal† mol^{-1} K^{-1}	$\Delta H(\overline{T})$ / kcal mol^{-1}	$\Delta H(300)$ / kcal mol^{-1}	Ref.
LiCl	500—800	650	7.356±0.051	10816±32	0.0080	0.69	21.8	33.7±0.2	49.5±0.1	51.1±0.1	2
	798—877	838	6.872±0.099	10020±83	0.0361	2.22	54.8	31.4±0.5	45.8±0.4	48.2±0.4	3
	644—855	750	7.419±0.173	10483±126	0.0278	2.07	59.1	33.9±0.8	48.0±0.6	50.0±0.6	4
	783—823	803	6.829±0.124	10199±103	0.0182	1.20	31.4	31.2±0.6	46.7±0.5	49.0±0.5	5
	783-1382	1083	5.116	8430	0.118	3.79	56.2	23.4	38.6	42.1	6
	670—848	759	7.790±0.060	10858±45	0.0190	1.65	53.2	35.7±0.3	49.7±0.2	51.8±0.2	This work (a)
	662—838	750	8.148±0.042	11081±31	0.0208	1.98	68.5	37.3±0.2	50.7±0.1	52.7±0.1	This work (b)
	662—848	755	7.948±0.102	10954±76	0.0199	1.80	59.8	36.4±0.5	50.1±0.3	52.2±0.3	This work (A)
NaBr	600—900	750	7.267±0.132	11001±98	0.00356	0.328	11.1	33.3±0.6	50.3±0.4	52.2±0.4	2
	687—991	839	6.942±0.081	10748±65	0.00387	0.321	10.0	31.8±0.4	49.2±0.3	51.5±0.3	4
	833—933	883	7.275±0.054	10748±48	0.00833	0.692	21.5	33.3±0.2	49.2±0.2	51.7±0.2	5
	806-1392	1099	5.332	8842	0.0502	1.90	32.2	24.4	40.5	43.9	6
	758—911	835	7.570±0.100	11093±80	0.00528	0.506	17.6	34.6±0.5	50.8±0.4	53.1±0.4	7
	673—875	774	7.825±0.083	11206±63	0.00655	0.657	23.7	35.8±0.4	51.3±0.3	53.3±0.3	This work (c)
	669—882	776	7.625±0.066	11082±51	0.00622	0.592	20.5	34.9±0.3	50.7±0.2	52.7±0.2	This work (d)
	669—882	776	7.716±0.072	11138±55	0.00638	0.622	21.9	35.3±0.3	51.0±0.3	53.0±0.3	This work (B)

† 1 cal=4.184 J.

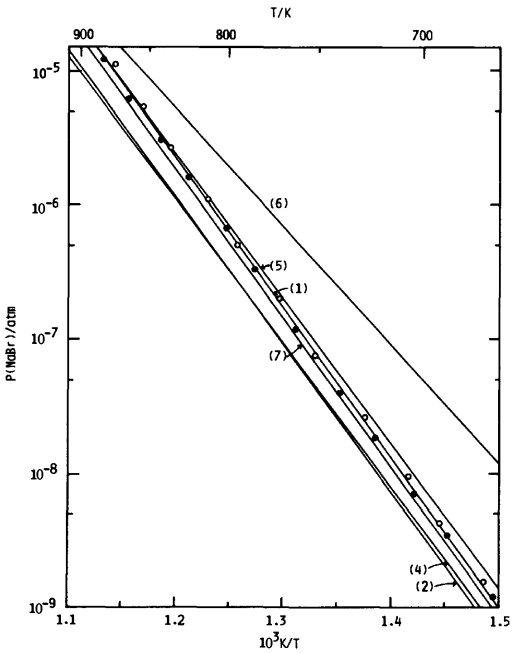

Fig. 2. Temperature depenednce of the vapor pressure of NaBr.
(1): This work at T_F=1360 K (open circle) or 1400 K (solid circle), (2): Ref. 2, (4): Ref. 4, (5): Ref. 5, (6): Ref. 6, and (7): Ref. 7.

$$\Delta S(\overline{T}) = (\ln 10)RA \equiv 4.575\,A \text{ cal mol}^{-1}\text{ K}^{-1}, \quad (3)$$

$$\Delta H(\overline{T}) = (\ln 10)RB \equiv 4.575\times10^{-3}\,B \text{ kcal mol}^{-1}, \quad (4)$$

where 1 cal is equal to 4.184 J. In a similar way as in the previous work,[1] the heat of sublimation at 300 K was calculated from

$$\Delta H(300) \simeq \Delta H(\overline{T}) + aR(\overline{T}-300). \quad (5)$$

According to the data on specific heats of MX,[2] the values of a in the range 300—800 K were taken as 2.27 and 2.16 for LiCl and NaBr, respectively, in this work.

The values of T_F in the present works (a)—(d) given in the last column in Table 1 were 1480, 1510, 1360, and 1400 K, respectively. The present works (A) and (B) indicate the average values of those (a) and (b) and those (c) and (d), respectively. As may be seen in Fig. 1 and Table 1, the values of P(LiCl) cited from Refs. 3, 4, and 5 and from Refs. 2 and 6 are close to and apart from those determined in this work, respectively. Figure 2 and Table 1 indicate that the data on P(NaBr) obtained in this work lie in the region between those quoted from Ref. 5 and those from Ref. 7, and also that the data in Ref. 6 have the largest deviation from the other data cited therein.

The above results may lead to the conclusions that the data on LiCl in Refs. 3, 4, and 5 are more reliable than those in Refs. 2 and 6, and that the data on NaBr in Refs. 5 and 7 are more accurate than those in Refs. 2, 4, and 6, and also that the data in Ref. 6 are not available for a precise evaluation of P(LiCl) or P(NaBr) in the temperature range lower than the melting point (887 K for LiCl or 1028 K for NaBr).

References

1) H. Kawano, T. Kenpō, and Y. Hidaka, *Bull. Chem. Soc. Jpn.*, **57**, 581 (1984).
2) D. R. Stull and H. Prophet, "JANAF Thermochemical Tables," 2nd ed, Natl. Bur. Stand., Washington (1971).
3) D. L. Hildenbrand, W. F. Hall, F. Ju, and N. D. Potter, *J. Chem. Phys.*, **40**, 2882 (1964).
4) M. S. Chandrasekharaiah, "Volatilities of Refractory Inorganic Compounds" in "The Characterization of High-Temperature Vapors," ed by J. L. Margrave, John Wiley & Sons, London (1967), Appendix B, pp. 495—507.
5) K. Niwa, *J. Fac. Sci. Hokkaido Imp. Univ., Ser. III*, **2**, 201 (1938).
6) G. G. Schlessinger, "Vapor Pressures, Critical Temperatures and Critical Pressures of Inorganic Compounds," in "Handbook of Chemistry and Physics," 52nd ed, ed by R. C. Weast, The Chemical Rubber Co., Cleveland, pp. D-171—D-180.
7) G. E. Cogin and G. E. Kimball, *J. Chem. Phys.*, **16**, 1035 (1948).

Crystal Structure of Dimethyltin Molybdenum Tetraoxide, $(CH_3)_2SnMoO_4$

Yukiyoshi SASAKI,* Hideo IMOTO, and Osamu NAGANO†

Department of Chemstry, Faculty of Science, The University of Tokyo, Hongo, Bunkyo-ku, Tokyo 113

(Received October 25, 1983)

Synopsis. Single-crystal X-ray analysis has shown that the title compound is tetragonal, $P4_2/mbc$, with a= 13.705(2), c=7.271(1) Å. The structure is made of octahedra of *trans*-$Sn(CH_3)_2O_4$ and tetrahedra of MoO_4. These polyhedra share apices to form a three-dimensional structure.

In 1953, Rochow *et al.* reported the synthesis of dimethyltin molybdenum tetraoxide. They treated dimethyltin dichloride with sodium molybdate in aqueous solution, and obtained the compound as a flocculent precipitate.[1] Later, ^{119}Sn Mössbauer spectroscopy of the compound showed that the asymmetry parameter of the tin atom was nearly zero, which indicated the trans-octahedral coordination.[2] Recently we have succeeded in preparing large single crystals of the compound by using isopolymolybdate as the molybdate source, and determined the structure by the single-crystal X-ray analysis.

Experimental

Dimethyltin dichloride (1 g) was added to the aqueous solution of ammonium heptamolybdate $(NH_4)_6Mo_7O_{24}\cdot 4H_2O$ (6 g in 60 cm^3 water). Immediately after the addition, pH of the solution decreased to *ca.* 2. After several hours, colorless rectangular crystals of dimethyltin molybdenum tetraoxide $(CH_3)_2SnMoO_4$ were obtained (Found: C, 7.86; H, 2.01%). The largest crystals were *ca.* 10 mm long.

Weissenberg photographs showed that the space group of the crystal was $P4_2/mbc$ (centrosymmetric) or $P4_2bc$ (noncentrosymmetric). The cell parameters were determined by least-squares refinements from 21 reflections ($45°<2\theta<60°$). X-Ray reflection data were collected with a Rigaku automated four-circle diffractometer (crystal, cubic in shape and *ca.* 0.2 mm long; radiation, Mo $K\alpha$ monochromatized by a graphite plate; scan method, ω-2θ, $2\theta\leq 60°$).[3] Intensities of three standard reflections were monitored for every 50 reflections and found to be constant. The structure was solved by the heavy atom method with the space group $P4_2/mbc$, and refined both in $P4_2/mbc$ and $P4_2bc$ by the block-diagonal least-squares method, where 879 independent reflections were used. The function minimized was $\sum w(|F_o|-|F_c|)^2$ where w=0.2 for $|F_o|<10$ and w=1 otherwise. Atomic scattering factors were taken from "International Tables for X-Ray Crystallography" (1974). The refinement in the space group $P4_2bc$ included the anomalous dispersions for heavy atoms. Computations were performed with a local version of *UNICS* at the Computer Center of the University of Tokyo.

The comparision of the results of the refinements in the space group $P4_2/mbc$ and $P4_2bc$ were summarized as follows:

(a) The final R-values were almost equal (0.031 for $P4_2/mbc$ and 0.030 for $P4_2bc$), though the number of parameters in $P4_2/mbc$ is much smaller than in $P4_2bc$ (46 for $P4_2/mbc$ and 73 for $P4_2bc$).

(b) Both refinements yielded substantially the same x and y values. Their standard deviations in $P4_2bc$ were 1—2 times larger than the corresponding values in $P4_2/mbc$.

(c) The standard deviations of the z values were very large in $P4_2bc$ (0.0006 for heavy atoms and 0.0011—0.0082 for light atoms), while in $P4_2/mbc$ they were small or zero due to the crystallographic symmetry. The z values of heavy atoms were significantly different in the two refinements, because the differences were 10 times of their standard deviations. However, for light atoms the differences of the z values were not very significant (1—3 times of their standard deviations). From these results we concluded that the space group $P4_2bc$ was very improbable.

Results and Discussion

The cell, positional, and thermal parameters are listed in Table 1, and bond lengths and angles are shown in Fig. 1.

The tin atom has the *trans*-octahedral coordination, *trans*-$Sn(CH_3)_2O_4$. This is consistent with the result of previous Mössbauer studies.[2] The molybdenum atom is tetrahedrally coordinated by four oxygen atoms. All oxygen atoms are bridging tin and molybdenum atoms (Fig. 1).

The structure extends three-dimensionally. It has zig-zag chains of $(-Sn-O-Mo-O-)_\infty$ along the a axis exactly on the plane at z=0, and identical chains along the b axis at z=1/2. These chains are not connected with other chains on the same plane, but with those on the neighboring planes through O(3) atoms (Fig. 2). The location of the tin atoms can be approximately described as a body-centered cubic arrangement as shown in Fig. 3. A unit cell contains four body-centered cells of the tin atoms. The body-centered cells are elongated 6% along the c axis, and the tin atoms are shifted on the xy plane 0.21 Å from the ideal positions. The molybdenum atoms are in the tetrahedral holes of this body-centered packing of the tin atoms, and oxygen atoms are placed between the metal atoms.

The structure of $(CH_3)_2SnMoO_4$ consists of octahedra and tetrahedra in the ratio of 1:1, and

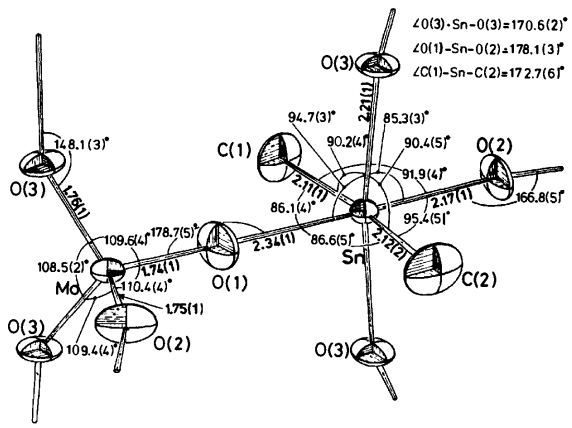

Fig. 1. ORTEP drawing of $(CH_3)_2SnMoO_4$ with bond lengths (in Å) and angles. The estimated standard deviations are in parentheses. The atoms, Sn, Mo, O(1), and O(2), are on a crystallographic mirror plane.

† Present address: Asahi Chemical Industry Co. Ltd., Yakou, Kawasaki-ku, Kawasaki 210.

Table 1. Cell,[a] positional, and thermal[b] parameters of $(CH_3)_2SnMoO_4$

	x	y	z	U_{11}	U_{22}	U_{33}	U_{12}	U_{13}	U_{23}
Sn	−0.01480(5)	0.24614(6)	0	17.1(3)	16.7(3)	10.7(2)	1.2(3)	0	0
Mo	0.24549(7)	0.10137(6)	0	15.4(3)	20.4(4)	11.8(3)	−4.0(3)	0	0
O(1)	0.1352 (7)	0.1646 (8)	0	23 (4)	53(6)	47(5)	13(4)	0	0
O(2)	0.3438 (7)	0.1831 (7)	0	30 (4)	56(6)	36(5)	−30(5)	0	0
O(3)	0.2522 (5)	0.0266 (4)	0.1965(6)	43 (3)	35(3)	9(2)	−4(3)	−2(3)	2(2)
C(1)	−0.0789(11)	0.1066 (9)	0	50 (8)	17(5)	51(8)	−13(5)	0	0
C(2)	0.0671(14)	0.3775(11)	0	75(11)	31(7)	56(9)	−28(8)	0	0

a) Space group: tetragonal $P4_2/mbc$. $a=13.705(2)$, $c=7.271(1)$ Å. b) In 10^{-3} Å^2.

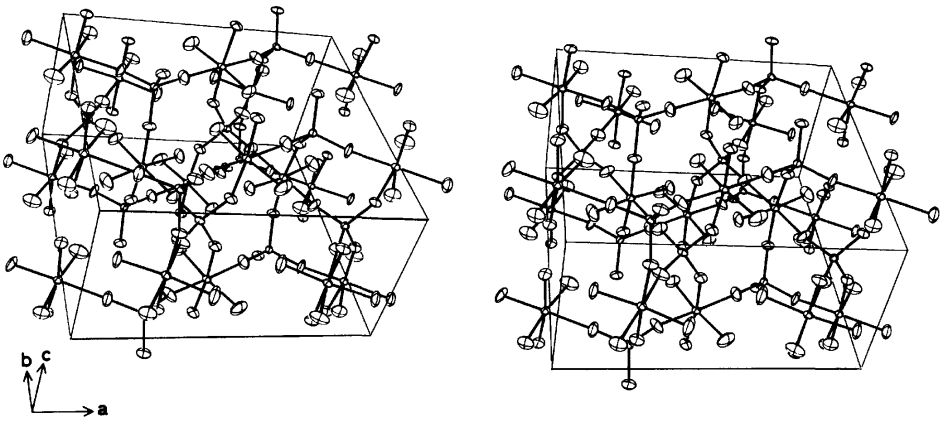

Fig. 2. Stereoscopic view of a unit cell of $(CH_3)_2SnMoO_4$ drawn by ORTEP.

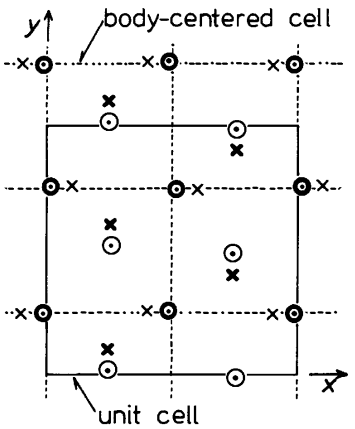

Fig. 3. Projection of metal atoms of $(CH_3)_2SnMoO_4$ along the c axis. Tin atoms are shown by open circles, and molybdenum atoms by crosses. The atoms drawn by thick lines are at $z=0$, and others at $z=1/2$.

these polyhedra share only apices. Compounds with these structural features are rare, and we have found only two examples. Neither of them is isostructural with $(CH_3)_2SnMoO_4$. The first example is a series of compounds $A(H_2O)_2BO_4$ (A=Al, In, Tl, or Fe; B= P or As).[4] These compounds have a cis coordination of aqua ligands around the A atoms in contrast with a trans coordination of methyl groups in $(CH_3)_2SnMoO_4$. The second example is the clathrate compound $Cd(NH_3)_2Hg(CN)_4\cdot 2C_6H_6$ which has octahedra of *trans*-$Cd(NH_3)_2(NC)_4$ and tetrahedra of $Hg(CN)_4$.[5] The metal atoms of this clathrate compound are arranged in the same way as the platinum and sulfur atoms in the PtS structure. This compound and $(CH_3)_2SnMoO_4$ are structurally very similar because both have approximately body-centered arrangement of the metal atoms with the *trans*-octahedral coordination. Furthermore, in the three-dimensional networks of both structures, the smallest rings are 8-membered when the CN ligand is regarded as one unit. However, the two structures are definitely different. In $(CH_3)_2SnMoO_4$ three atoms, Sn, O(2), and Mo, are shared by neighboring 8-memberd rings, while in the clathrate compound only one atom, Cd or Hg, is shared.

The authors wish to express their thanks to Akiko Kobayashi, the University of Tokyo, for X-ray data collection and for helping with the structural determination.

References

1) E. G. Rochow, D. Seyferth, and A. C. Smith, Jr., *J. Am. Chem. Soc.*, **75**, 3099 (1953).

2) N. E. Erickson, *J. Chem. Soc., Chem. Commun.*, **1970**, 1349.

3) The $|F_o|-|F_o|$ table is kept at the Office of the Editor of Bull. Chem. Soc. Jpn., as Document No. 8413.

4) K. Kitahama, R. Kiriyama, and Y. Baba, *Acta Crystallogr., Sect. B*, **31**, 322 (1975); R. Kniep, D. Mootz, and A. Vegas, *ibid.*, **33**, 263 (1977); and the references cited therein.

5) R. Kuroda, *Inorg. Nucl. Chem. Lett.*, **9**, 13 (1973).

Preparation and Characterization of the Diastereoisomers of the (*S*)- or (*R*)-1,2-Propanediaminebis(1,10-phenanthroline)cobalt(III) Ion

Akira TATEHATA* and Shigeru NATSUME
Department of Chemistry, Faculty of Science, Shizuoka University, Oya, Shizuoka 422
(Received November 19, 1983)

Synopsis. Four diastereoisomers of the type $[Co(S- or R-pn)(phen)_2]^{3+}$ (pn=1,2-propanediamine; phen=1,10-phenanthroline) were prepared and characterized by absorption, circular dichroism (CD), and ^1H NMR spectra. High stereoselectivity in the formation of the diastereoisomers was observed and the Λ-isomer of $[Co(S-pn)(phen)_2]^{3+}$ was formed in preference to the Δ-isomer.

Although some complexes of the type $[Co(aa)(phen)_2]^{n+}$ (aa=chiral α-hydroxy carboxylate ion[1] and α-amino acidate ion[2]) have been prepared and studied on the absorption and circular dichroism (CD) spectra, there is no report for this type of complex containing a chiral diamine. This Note describes the preparation and the spectroscopic properties of the optically active complexes $[Co(S- or R-pn)(phen)_2]^{3+}$ and compares the formation ratio between the diastereoisomers with that of the corresponding ethylenediamine complexes $[Co(S- or R-pn)(en)_2]^{3+}$. It is shown on the basis of ^1H NMR spectra that interligand interactions between 1,2-propanediamine and bis(1,10-phenanthroline) moiety lead to high stereoselectivity in this systems.

Experimental

1,2-propanediamine was resolved as described in the literature,[3] $[\alpha]_D^{25}$ +10.2° for *S*-(+)-pn and $[\alpha]_D^{25}$ −10.6° for *R*-(−)-pn (free diamine, 3—5% aqueous solution).

Preparation and Separation of Isomers. To a suspension of *cis*-$[CoCl_2(phen)_2]Cl\cdot 3H_2O$[4] (1 g, 1.7 mmol) in 50 cm³ of methanol, 1.5 cm³ of methanol solution of (*S*)- or (*R*)-1,2-propanediamine (10% v/v) was added with stirring. The solution was kept in a water bath (40 °C) for 3 h. The resulting yellow-orange solution was diluted with water and poured on a column of SP-Sephadex C-25 (φ2.7×50 cm) in the sodium form. Three bands were developed on the column during the elution with a 0.3 mol dm⁻³ NaCl solution. Their bands, identified as the $[Co(phen)_3]^{3+}$, $[Co(pn)(phen)_2]^{3+}$, and $[Co(pn)_2(phen)]^{3+}$, were eluted in this order from bottom of the column. The second band containing the desired complex was transfered to another SP-Sephadex column (φ2.7×90 cm) and was eluted with a 0.15 mol dm⁻³ $Na_2[Sb_2(d\text{-tart})_2]$ to separate into the diastereoisomers. The formation ratio between the diastereoisomers was calculated from the areas of the elution curve. In both cases of the *S*- and the *R*-pn complexes, Λ-isomer was always eluted earlier than Δ-isomer. The fractions for each band were combined and passed through an SP-Sephadex column (φ2.0×3 cm) after dilution with water and the adsorbed complex was eluted with a 0.5 mol dm⁻³ $NaClO_4$ solution. The solution was concentrated with a rotary evaporator under reduced pressure and was kept in a refrigerator. The specific rotations and analytical results are given in Table 1.

Measurements. Absorption and CD spectra were obtained on a Shimadzu MPS-50L recording spectrophotometer and a JASCO J-40 spectropolarimeter, respectively. ^1H NMR spectra (90 MHz) were measured on a Varian EM-390 spectrometer in D_2O solution using sodium 2,2-dimethyl-2-silapentane-5-sulfonate (DSS) as an internal standard reference. For the measurement of ^1H NMR spectra, the perchlorate salts were converted into the chloride salts with an anion exchange resin (Dowex 1-X8, Cl^- form).

Results and Discussion

The absorption and the CD spectra of $[Co(S-pn)(phen)_2]^{3+}$ are shown in Fig. 1, and their numerical data are given in Table 2. The absolute configurations of the isomers were assigned on the basis of the sign of dominant CD peak in the T_{1g} region and the CD spectra in the region of the phen ligand π-π^* transition. The configurational and vicinal effect curves under the T_{1g} band evaluated from the CD spectra of the diastereomeric pair of *R*-pn complexes are shown in Fig. 2. The configurational effect curve for Λ-$[Co(R-pn)(phen)_2]^{3+}$ is quite similar to the CD[5] for Λ-$[Co(en)(phen)_2]^{3+}$, where there is no vicinal effect. The contribution from vicinal effect exhibits a −, + CD sign pattern similar in shape to that reported for *R*-pn in Co (III) complexes containing *R*-pn and en,[6] but the relative intensities differ considerably. It is well known that the coordinated *R*-pn exists predominantly in the more stable conformation (λ gauche form) with an equatorial methyl group.[7] The above finding for the vicinal effect of the Λ-$[Co(R-pn)(phen)_2]^{3+}$ may indicate that although the coordinated *R*-pn ligand keeps the λ gauche form with an equatorial methyl group, it is subjected to different degrees of distortion because of the significant difference of the interligand interactions between the pn-en systems and the pn-phen systems. This may be also reflected on the formation ratios (Λ/Δ) of the diastereoisomers in both systems. The diastereoisomeric Λ/Δ ratio was 4.8±0.2 for the $[Co(S-pn)(phen)_2]^{3+}$, indicating that this stereoselectivity occurred in the phenanthroline complex is very higher than that for the corresponding ethylenedi-

Table 1. Elemental analyses and specific rotations of the isomers

No.	Complex	Found(Calcd) (%)			$[\alpha]_{546}$
		C	H	N	
(I)	Λ-$[Co(S-pn)(phen)_2](ClO_4)_3\cdot 2H_2O$	38.68(39.17)	3.27(3.66)	10.81(10.15)	+880°
(II)	Δ-$[Co(S-pn)(phen)_2](ClO_4)_3\cdot 3H_2O$	38.72(38.34)	3.34(3.82)	10.03(9.94)	−681°
(III)	Λ-$[Co(R-pn)(phen)_2](ClO_4)_3\cdot 3H_2O$	38.95(38.34)	3.30(3.82)	10.06(9.94)	+689°
(IV)	Δ-$[Co(R-pn)(phen)_2](ClO_4)_3\cdot 2H_2O$	38.80(39.17)	3.25(3.66)	10.11(10.15)	−889°

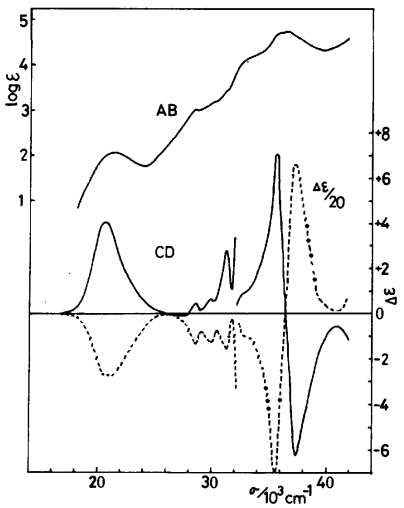

Fig. 1. Absorption and CD spectra of Λ-(+)$_{546}$-(——) and Δ-(−)$_{546}$-[Co(*S*-pn)(phen)$_2$]$^{3+}$(----).

Table 2. Absorption and CD spectral data

Complex No.[a]	Absorption $\sigma/10^3$ cm^{-1} (ε/mol^{-1} dm^3 cm^{-1})	CD $\sigma_{ext}/10^3$ cm^{-1} ($\Delta\varepsilon$/mol^{-1} dm^3 cm^{-1})
(I)	21.41 (112)	20.66(+4.08)
	35.59 sh (46500)	35.59(+141.3)
	36.50 (51500)	37.31(−125.4)
(II)	21.41 (99)	21.05(−2.78)
	35.59 sh (46900)	35.59(−140.7)
	36.50 (51700)	37.31(+132.5)

a) Complex No. is the same as those in Table 1.

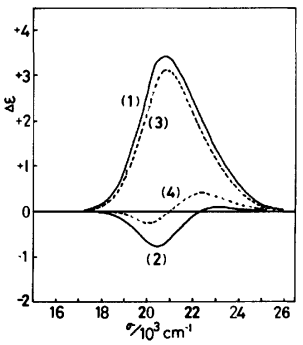

Fig. 2. Configurational effect (1) and vicinal effect curves (2) for Λ-[Co(*R*-pn)(phen)$_2$]$^{3+}$. CD spectrum (3) reported for Λ-[Co(en)(phen)$_2$]$^{3+}$ and vicinal effect curve (4) of *R*-pn reported for cobalt(III) complexes containing *R*-pn and en.

amine complex [Co(*S*-pn)(en)$_2$]$^{3+}$, for which the value of Λ/Δ=2.1 had been reported.[8] This remarkable stereoselectivity in the pn-phen systems may be attributed to intramolecular ligand-ligand interactions between the aromatic ring of the phenanthroline ligands and the *S*-pn ligand. Molecular model reveals that the methyl group of *S*-pn in the Λ-isomer is located above the aromatic ring of one phenanthroline and thus lies under the influence of the ring current (Fig. 3). Such a hydrophobic interaction (CH$\cdots\pi$ interaction) is known to function as a stabilization effect of the complexes.[9] On the other hand, the methyl group of *S*-pn in the Δ-isomer takes a position by the side of the phenanthroline plane, and therefore may cause some repulsive interactions with α-proton of the phenanthroline (Fig. 3), resulting in the less favored Δ-isomer. These situations were confirmed by the ^{1}H NMR spectra of the diastereoisomers (Fig. 4). The methyl protons in the Λ-*S* isomer (1.49 ppm) resonate at higher field than in the Δ-*S* isomer (1.62 ppm), as has been observed for the methyl protons in [Co(*S*-ala)(phen)$_2$]$^{2+}$ complexes.[2] These chemical shifts observed imply that the methyl protons in the Λ-*S* isomer are shielded by one phenanthroline ring to resonate at a high field and those in the Δ-*S* isomer are in a deshielding region near the phenanthroline plane, being in agreement with considerations from the molecular model.

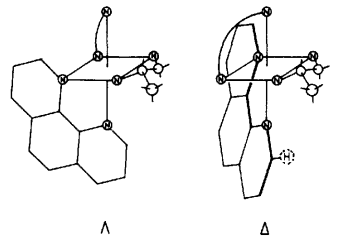

Λ Δ

Fig. 3. Structures of Λ- and Δ-[Co(*S*-pn)(phen)$_2$]$^{3+}$.

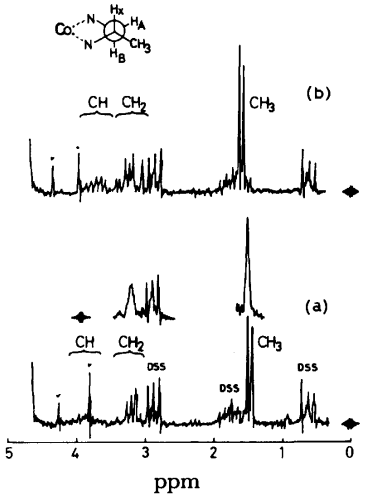

Fig. 4. ^{1}H NMR spectra of (a) Λ- and (b) Δ-[Co(*S*-pn)(phen)$_2$]$^{3+}$ in D_2O solutions.

References

1) A. Tatehata, *Inorg. Chem.*, **15**, 2086 (1976); ibid., **17**, 725 (1978).
2) A. Tatehata, *Inorg. Chem.*, **21**, 2496 (1982).
3) "Shin Jikken Kagaku Kōza," ed by the Chemical Society of Japan, Maruzen, Tokyo (1977), Vol. 8, p. 1429.
4) A. V. Ablov, Russ. *J. Inorg. Chem.*, **6**, 157 (1961).
5) L. S. Dollimore and R. D. Gillard, *J. Chem. Soc., Dalton Trans*, **1975**, 369.
6) B. E. Douglas, *Inorg. Chem.*, **4**, 1813 (1965).
7) S. Yano, H. Ito, Y. Koike, J. Fujita, and K. Saito, *Bull. Chem. Soc. Jpn.*, **42**, 3184 (1969).
8) F. P. Dwyer, T. E. MacDemott, and A. M. Sargeson, *J. Am. Chem. Soc.*, **85**, 2913 (1963).
9) H. Okawa, K. Ueda, and S. Kida, *Inorg. Chem.*, **21**, 1594 (1982), and references cited therein.

Reactions of Arenesulfonyl Chlorides with *cis*- or *trans*-β-Methylstyrene Catalyzed by Ruthenium(II) Complex

Nobumasa KAMIGATA,* Tomoo NARUSHIMA, Hideo SAWADA, and Michio KOBAYASHI
Department of Chemistry, Faculty of Science, Tokyo Metropolitan University, Fukazawa, Setagaya-ku, Tokyo 158
(Received June 16, 1983)

Synopsis. The reactions of arenesulfonyl chlorides with *cis*- or *trans*-β-methylstyrene catalyzed by dichlorotris(triphenylphosphine)ruthenium(II) in the presence of triethylamine proceeded smoothly to give only (*E*)-2-arylsulfonyl-1-phenylpropene. The recovered *cis*-β-methylstyrene was isomerized to trans form, while *trans*-β-methylstyrene did not isomerize to the cis one.

Recently, much attention has been paid to the radical reactions formed from halides treated with transition metal complexes.[1] We have reported the reactions of arenesulfonyl chlorides with vinylarenes catalyzed by dichlorotris(triphenylphosphine)ruthenium(II) (**1**) in the presence of triethylamine to give α,β-unsaturated sulfones.[2] We report here the reactions of arenesulfonyl chlorides with *cis*- or *trans*-β-methylstyrene catalyzed by ruthenium(II) complex.

The reaction of *p*-toluenesulfonyl chloride with *trans*-β-methylstyrene was carried out in benzene, using ruthenium(II) complex **1** as catalyst in the presence of a molar equivalent of triethylamine at 60 °C for 72 h in a degassed sealed tube. The reaction mixture was chromatographed on Florisil column using benzene as an eluent to give (*E*)-1-phenyl-2-(*p*-tolylsulfonyl)propene (**2a**) as colorless crystals, mp 122.5—123.0 °C (from ethanol). The stereochemistry of **2a** was confirmed by its spectral data (see Experimental section). Its stereoisomer, (*Z*)-1-phenyl-2-(*p*-tolylsulfonyl)propene (**3a**), mp 54—55 °C, prepared by oxidation of 1-phenyl-1-phenylseleno-2-(*p*-tolylsulfonyl)propane exhibited different spectral properties.

The reaction of *p*-toluenesulfonyl chloride with *cis*-β-methylstyrene was carried out under similar conditions to give also **2a**; none of its (*Z*)-isomer **3a** was detected. Similarly, reactions of several arenesulfonyl chlorides with *cis*- and *trans*-β-methylstyrene catalyzed by **1** were studied and only (*E*)-2-arylsulfonyl-1-phenylpropene (**2**) were obtained in all the cases. The results are summarized in Table 1.

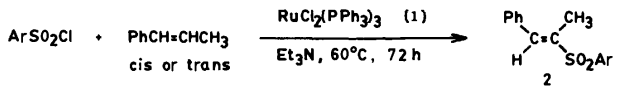

No isomerization of (*Z*)-1-phenyl-2-(*p*-tolylsulfonyl)-propene (**3a**) to its (*E*)-isomer **2a** was observed when **3a** was treated with ruthenium(II) catalyst **1** in benzene at 60 °C. This excluded the possibility that **3a** is first formed in the reaction of *p*-toluenesulfonyl chloride with *cis*- or *trans*-β-methylstyrene and then isomerized to **2a** during the reaction period. The formation of **2** may be explained by the base-catalyzed elimination of hydrogen chloride from the adduct 2-arylsulfonyl-1-chloro-1-phenylpropane (**5**) shown in Scheme 1 as one plausible mechanism. Accordingly, even though the adduct **5** formed is a mixture of threo and erythro isomers, the formation of **2** as a sole product may be accounted for by assuming that the elimination proceeded by E2 mechanism, the formation of *Z*-isomer **3** is very slow, and also the Eqs. 1—3 are equilibrium ones.

The stereochemistry of the β-methylstyrene which was recovered was examined by HPLC. No isomerization of *trans*-β-methylstyrene to *cis*-isomer was ob-

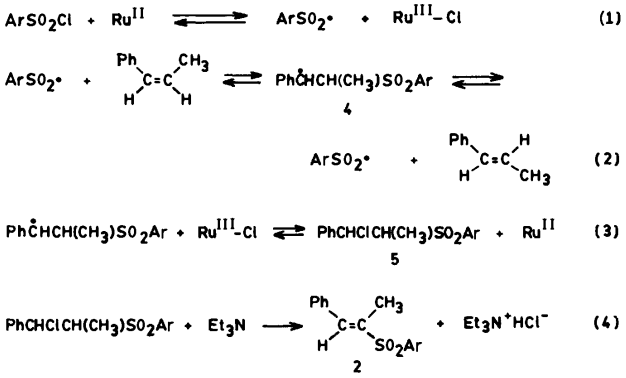

Scheme 1.

TABLE 1. REACTIONS OF ARENESULFONYL CHLORIDES WITH *cis*- OR *trans*-β-METHYLSTYRENE CATALYZED BY **1**

Sulfonyl chloride	β-Methylstyrene	Conversion of β-methylstyrene %	Product	Yield[a] %	Cis/trans ratio of recovered β-methylstyrene
p-$CH_3C_6H_4SO_2Cl$	trans	39	**2a**	67	0/100
p-$CH_3OC_6H_4SO_2Cl$	trans	43	**2b**	82	0/100
$C_6H_5SO_2Cl$	trans	35	**2c**	55	0/100
p-$ClC_6H_4SO_2Cl$	trans	40	**2d**	85	0/100
p-$CH_3C_6H_4SO_2Cl$	cis	42	**2a**	74	9/91
p-$CH_3OC_6H_4SO_2Cl$	cis	46	**2b**	70	4/96
$C_6H_5SO_2Cl$	cis	26	**2c**	73	42/58
p-$ClC_6H_4SO_2Cl$	cis	32	**2d**	69	37/63

a) The yields are based on the β-methylstyrene (cis or trans) consumed.

served, while a large part of *cis*-β-methylstyrene was found to be converted to trans form (see Table 1). The isomerization of *cis*-β-methylstyrene was not observed when a mixture of *cis*-β-methylstyrene, ruthenium(II) catalyst **1**, and triethylamine in benzene was heated at 60 °C for 72 h. This means that *cis*-β-methylstyrene does not isomerize to trans in the absence of arenesulfonyl chloride. The fact that *cis*-β-methylstyrene isomerized to trans only when a solution of *cis*-β-methylstyrene, ruthenium(II) catalyst, and arenesulfonyl chloride in benzene was heated in the presence or absence of triethylamine means that Eq. 2 in Scheme 1 is reversible and that thermodynamically stable *trans*-β-methylstyrene is preferably formed from the radical **4**.

Experimental

Measurement. Melting points and boiling points are uncorrected. The infrared absorption spectra were determined on a Hitachi Model EPI-G2 spectrophotometer using samples as KBr disks. The proton magnetic resonance spectra were recorded at 60 MHz using a Hitachi R-20B spectrometer with Me_4Si as an internal standard in $CDCl_3$. Mass spectra were determined with a JEOL JMS-07 mass spectrometer at an ionizing voltage of 30—75 eV. Elemental analyses were operated with a Perkin-Elmer 240 elemental analyzer. HPLC was carried out on a Water's ALC-204 HPLC using a silica-gel column using benzene as an eluent.

Materials. Dichlorotris(triphenylphosphine)ruthenium(II) (**1**) was prepared by the methods described in the literature.[3] *p*-Toluenesulfonyl chloride and *p*-chlorobenzenesulfonyl chloride of Tokyo Kasei Chemicals were recrystallized prior to use. Benzenesulfonyl chloride of Wako Chemicals, *cis*-β-methylstyrene of ICN Pharmaceuticals, and *trans*-β-methylstyrene of Tokyo Kasei Chemicals were purified by distillation under nitrogen prior to use. *p*-Methoxybenzenesulfonyl chloride was prepared by the methods described in the literature.[4]

General Procedures in the Reaction of Arenesulfonyl Chloride with cis- *or* trans-*β-Methylstyrene Catalyzed by 1.* A solution containing 2.0 mmol of arenesulfonyl chloride, 2.0 mmol of *cis*- or *trans*-β-methylstyrene, 2.0 mmol of triethylamine, and 0.16 mmol of **1** in 3.0 cm^3 of benzene was heated at 60 °C in a degassed sealed tube for 72 h. The remaining β-methylstyrene (cis and trans) was quantitatively analyzed by HPLC using an internal standard. The reaction mixture was chromatographed on Florisil using benzene as an eluent to give (*E*)-arylsulfonyl-1-phenylpropene **2** which were characterized by IR, ^1H NMR, and mass spectra, and elemental analyses.

*(E)-1-Phenyl-2-(p-tolylsulfonyl)propene (**2a**)*: Mp 122.5—123.0 °C. IR (KBr): 1150 and 1310 cm^{-1}. ^1H NMR ($CDCl_3$): δ=2.10 (3H, d, *J*=1.8 Hz), 2.44 (3H, s), 7.34 (2H, d, *J*=8.4 Hz), 7.38 (5H, s), 7.80 (1H, q, *J*=1.8 Hz), and 7.82 (2H, d, *J*=8.4 Hz). Mass: *m/z* 272 (M^+). Found: C, 70.26; H, 6.01%. Calcd for $C_{16}H_{16}O_2S$: C, 70.56, H, 5.92%.

*2-(p-Methoxyphenylsulfonyl)-1-phenylpropene (**2b**)*: Mp 82—83 °C. IR (KBr): 1147 and 1300 cm^{-1}. ^1H NMR ($CDCl_3$): δ=2.10 (3H, d, *J*=1.8 Hz), 3.87 (3H, s), 7.02 (2H, d, *J*=8.4 Hz), 7.39 (5H, s), 7.81 (1H, q, *J*=1.8 Hz), and 7.89 (2H, d, *J*=8.4 Hz). Mass: *m/z* 288 (M^+). Found: C, 66.70; H, 5.58%. Calcd for $C_{16}H_{16}O_3S$: C, 66.64; H, 5.59%.

*1-Phenyl-2-(phenylsulfonyl)propene (**2c**)*: Mp 88.5—89.0 °C. IR (KBr): 1152 and 1305 cm^{-1}. ^1H NMR ($CDCl_3$): δ= 2.10 (3H, d, *J*=1.8 Hz), 7.42 (5H, s), 7.86 (1H, q, *J*= 1.8 Hz), and 7.5—8.1 (5H, m). Mass: *m/z* 258 (M^+). Found: C, 69.80; H, 5.48%. Calcd for $C_{15}H_{14}O_2S$: C, 69.74; H, 5.46%.

*2-(p-Chlorophenylsulfonyl)-1-phenylpropene (**2d**)*: Mp 104—105 °C. IR (KBr): 1158 and 1310 cm^{-1}. ^1H NMR ($CDCl_3$): δ=2.13 (3H, d, *J*=1.8 Hz), 7.50 (5H, s), 7.62 (2H, d, *J*=8.4 Hz), 7.95 (1H, q, *J*=1.8 Hz), and 8.01 (2H, d, *J*=8.4 Hz). Mass: *m/z* 294 and 292 (M^+). Found: C, 61.51; H, 4.51%. Calcd for $C_{15}H_{13}ClO_2S$: C, 61.53; H, 4.48%.

*Preparation of (Z)-1-Phenyl-2-(p-tolylsulfonyl)propene (**3a**).* A solution containing 3.2 g (10.3 mmol) of *Se*-phenyl *p*-tolueneselenosulfonate and 1.46 g (12.3 mmol) of *trans*-β-methylstyrene in 11 cm^3 of benzene was heated at 80 °C in a degassed sealed tube for 20 h. Removal of the solvent left a light yellow solid, which when recrystallized from ethanol afforded 2.4 g (54%) of a colorless crystalline solid, whose structure was assigned as 1-phenylseleno-1-phenyl-2-(*p*-tolylsulfonyl)propane on the basis of its physical and spectral properties: Mp 118—119 °C. IR (KBr): 1190, 1295, and 1305 cm^{-1}. Found: C, 61.56; H, 5.19%. Calcd for $C_{22}H_{22}O_2SSe$: C, 61.53; H, 5.16%. To a solution containing of 1-phenylseleno-1-phenyl-2-(*p*-tolylsulfonyl)propane 1.0 g (2.3 mmol) in 10 cm^3 of THF, 2.0 cm^3 of 30% hydrogen peroxide was added slowly at room temperature and the mixture was stirred for an additional hour. The organic layer was extracted with ether, and the extract was dried over with anhydrous magnesium sulfate. After evaporation of the solvent, the residual oil was subjected to preparative thick-layer chromatography. The component isolated from the plate contained 0.35 g (55%) of a white solid, mp 54—55 °C (from ethanol), whose structure was assigned as (*Z*)-1-phenyl-2-(*p*-tolylsulfonyl)propene (**3a**) on the basis of its physical and spectroscopic data: Mp 54—55 °C. IR (KBr): 1150 and 1315 cm^{-1}. ^1H NMR ($CDCl_3$): δ=2.16 (3H, d, *J*=1.2 Hz), 2.33 (3H, s), 7.03 (1H, q, *J*= 1.2 Hz), 7.14 (2H, d, *J*=8.4 Hz), 7.27 (5H, s), and 7.53 (2H, d, *J*=8.4 Hz). Mass: *m/z* 272 (M^+). Found: C 70.62; H, 6.00%. Calcd for $C_{16}H_{16}O_2S$: C, 70.56; H, 5.92%.

*Attempt at the Isomerization of **3a** to **2a**.* A solution containing 102 mg (0.38 mmol) of **3a** and 84 mg (0.03 mmol) of **1** in 1.5 cm^3 of benzene was heated at 60 °C in a degassed sealed tube for 72 h. The reaction mixture was subjected to preparative thick-layer chromatography. The only one component isolated from the plate (98 mg) consisted of 100% of recovered **3a** and no **2a** was detected by its mp, IR, and ^1H NMR spectra.

Attempt at the Isomerization of cis- *or* trans-*β-Methylstyrene in the Absence of Arenesulfonyl Chloride.* A solution containing 236 mg (2.0 mmol) of *cis*- or *trans*-β-methylstyrene and 153 mg (0.16 mmol) of **1** in 3.0 cm^3 of benzene in the presence or absence of 202 mg (2.0 mmol) of triethylamine was heated at 60 °C in a degassed sealed tube for 72 h. After removal of the solvent, the residue was subjected to the elution chromatography on a short column of silica gel, using hexane as the eluent to remove the catalyst. The component concentrated by evaporation of the solvent was subjected to the HPLC. In every case, neither *cis*- to *trans*- nor *trans*- to *cis*-isomerization of β-methylstyrene was observed under these conditions.

References

1) Y. Mori and J. Tsuji, *Kagaku No Ryoiki*, **27**, 197 (1973); *Chem. Abstr.*, **78**, 146879a (1973); H. Matsumoto and Y. Nagai, *Kagaku No Ryoiki*, **30**, 50 (1976); *Chem. Abstr.*, **84**, 1589835s (1976).

2) N. Kamigata, H. Sawada, and M. Kobayashi, *J. Org. Chem.*, **48**, 3793 (1983).

3) T. A. Stephenson and G. Wilkinson, *J. Inorg. Nucl. Chem.*, **28**, 945 (1966); P. S. Hallam, T. A. Stephenson, and G. Wilkinson, *Inorg. Synth.*, **12**, 238 (1972); T. A. Stephenson, and G. Wilkinson, *J. Chem. Soc., A*, **1970**, 2497.

4) R. Adams and C. S. Marvel, *Org. Synth.*, Coll. Vol. 1, 84 (1967).

The Formation of 1,2-Bis(alkylthio)-1,2-diphenylethanes by the Lithium Diisopropylamide-induced Fragmentation of Dibenzyl Disulfide Followed by the Trapping with Some Alkyl Halides

Hideyuki IKEHIRA* and Shigeo TANIMOTO*

Institute for Chemical Research, Kyoto University, Uji, Kyoto 611

(Received October 14, 1983)

Synopsis. It was found that dibenzyl disulfide undergoes lithium diisopropylamide-induced fragmentation to afford several intermediate species which, on trapping with alkyl halides, lead to the formation of 1,2-bis(alkylthio)-1,2-diphenylethanes and α-alkylbenzyl alkyl sulfides.

The use of carbanions stabilized by the presence of one or more adjacent thioether groups has become an established technique in organic synthesis.[1-12] In some related works, we were interested in utilizing a carbanion that could be easily generated by the action of a strong base on disulfide possessing α-hydrogens. We chose dibenzyl disulfide (**1**) as a starting substrate in this research since it is easily available and relatively nontoxic. Since most of the reaction products from it are nonvolatile, it thus has advantages for small scale work. The removal of the α-hydrogens of **1** could be achieved by the addition of an easily available metalating agent such as lithium diisopropylamide (LDA). Presumably, the initially formed anionic species undergoes fragmentation followed by further conversion to the other intermediate species. These species were trapped by the addition of some alkyl halides to the reaction mixture. In this way a series of 1,2-bis(alkylthio)-1,2-diphenylethanes (**9**) were produced in fairly good yields, along with α-alkylbenzyl alkyl sulfides (**10**) (see Table 1). The structures of **9** and **10** were established from satisfactory analytical and spectral data. Table 2 shows the physical properties and analytical data of the isolated products.

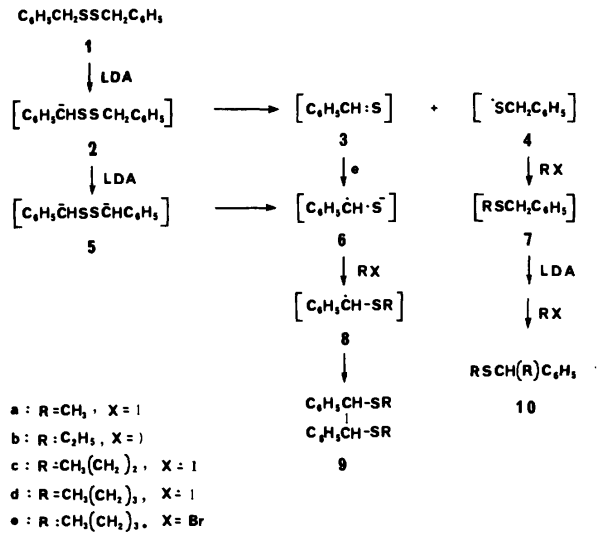

Possible routes for the formation of **9** and **10** are shown by the accompanying equations. Presumably, the initially formed anion (**2**) undergoes fragmentation to afford thiobenzaldehyde (**3**) and α-toluenethiolate anion (**4**). This type of fragmentation may be certain from the fact that, in a preliminary experiment in which **1** was treated with equimolar amounts of LDA in tetrahydrofuran at −78 °C followed by addition of ethyl iodide, the formation of benzyl ethyl sulfide was observed (76% yield) together with small amounts of **9b**, **10b**, and tarry substance. Thus, the anion (**4**) which would be formed similarly in the present reaction undergoes trapping by alkyl halides and subsequent deprotonation-alkylation sequence to afford **10**. Although the deprotonation of **4** by butyllithium leading to a dianion such as $^{-}\overline{S}CHC_6H_5$ has already been recognized by Seebach and Geiss,[14] the possibility that **4** is further deprotonated by LDA to give the same dianionic species seems to be less reasonable, since LDA is less basic than butyllithium and also, in all runs, the formation of alkyl benzyl sulfides was observed, albeit in very low yields. Hiskey and Dennis[15] have previously proposed a mechanism for the alkoxide cleavage of bis(2-oxo-2-phenylethyl) disulfide. If such a mechanism also prevails in the LDA cleavage of **1**, **3** would be attacked by **4** to afford an anion of the hemidithioacetal which undergoes deprotonation with LDA and the subsequent intramolecular rearrangement leading to dianion of 1,2-diphenyl-1,2-ethanedithiol. However, this mechanism is incompatible with the fact that, in all runs of Table 1, the sum of the yield of **9** and that of **10** is beyond 100%. Thus, it seems reasonable that there is no occurrence of any recombination of **4** with **3**. On the basis of these considerations, the source of **9** could hardly be anything else than **3**. Concerning the trapping of thioaldehydes such as thiobenzaldehyde, one or two papers[16,17] have appeared in the literature. However, the isolation of **3** by the application of a similar method failed, presumably because it is immediately converted to the radical anion (**6**) by one-electron transfer from LDA. Such one-electron transfer has already been observed[12,18,19] in the reaction of several thioketones. The formation of **6** was also evident from the appearance of its characteristic color (blue-black). Thus, **6** undergoes charge neutralization by the applied alkyl halide to

Table 1. Lithium diisopropylamide-induced fragmentation of dibenzyl disulfide(**1**), followed by trapping with some alkyl halides

Run	RX	Product (Yield/%[a])
1	CH_3I	**9a** (72), **10a** —[b]
2	C_2H_5I	**9b** (60), **10b** —[b]
3	$CH_3(CH_2)_2I$	**9c** (68), **10c** (39)
4	$CH_3(CH_2)_3I$	**9d** (77), **10d** (38)
5	$CH_3(CH_2)_3Br$	**9e**[c] (76), **10e**[c] (39)

a) Yield was calculated assuming that 1 mol of **1** produces 1 mol of product. b) Not isolated. c) The compounds **9e** and **10e** are identical to **9d** and **10d**, respectively.

Table 2. Physical properties and analytical data of the isolated products

Product[a]	Mp θ_m/°C or [Bp θ_b/°C(Torr)]	^{1}H-NMR[b] (δ, $CDCl_3$ or CCl_4)	^{13}C-NMR (δ, $CDCl_3$)	Found(Calcd)(%) C	H
9a	102—103 (lit,[13] 99.3—101 °C)	1.81(s, 6H), 4.11(s, 2H), 7.01(s, 10H)	15.15(q), 57.63(d), 127.07(d), 127.95(d), 128.59(d), 139.76(s)	69.79 (70.02)	6.52 (6.61)
9b	[163(3.5)]	1.10(t, 6H, J=7 Hz), 2.19 (q, 4H, J=7 Hz), 4.20(s, 2H), 6.9—7.3(m, 10H)	14.10(q), 25.74(t), 55.70(d), 126.95(d), 127.83(d), 128.59(d), 140.11(s)	71.28 (71.47)	7.32 (7.33)
9c	[159(2.5)]	0.83(t, 6H, J=6 Hz), 1.1—1.8 (m, 4H), 2.13(t, 4H, J=6 Hz), 4.13(s, 2H), 6.8—7.1(m, 10H)	13.51(q), 22.41(t), 33.87(t), 56.10(d), 126.95(d), 127.83(d), 128.71(d), 140.29(s)	72.74 (72.67)	7.80 (7.93)
9d	[150(2)]	0.6—1.0(m, 6H), 1.0—1.6(m, 8H), 2.0—2.4(m, 4H), 4.17(s, 2H), 6.9—7.2(m, 10H)	13.57(d), 21.94(t), 31.12(t), 31.53(t), 56.16(d), 126.95(d), 127.83(d), 128.71(d), 140.29(s)	73.69 (73.68)	8.46 (8.43)
10c	[87(1.5—2.0)]	0.7—1.0(m, 6H), 1.0—1.8(m, 4H), 2.0—2.7(m, 4H), 3.55(t, 1H, J=7 Hz), 7.0—7.4(m, 5H)	—[c]	74.80 (74.93)	9.51 (9.68)
10d	[111(2.5)]	0.7—1.2(m, 6H), 1.2—2.0(m, 8H), 2.0—2.7(m, 4H), 3.67(t, 1H, J=7 Hz), 7.0—7.4(m, 5H)	—[c]	76.07 (76.20)	9.93 (10.23)

a) The research for stereochemical assignment of the structures of **9a–d** has not been done. b) The measurement of ^{1}H-NMR was carried out with **9a–d** in $CDCl_3$ and with **10c**, **10d** in CCl_4. c) Not measured.

generate the radical species (**8**), which on subsequent dimerization of itself leads to **9**. This explanation would mean that only half of the dibenzyl disulfide molecule is utilized in the formation of **9**. However, it is not tenable since it does not accommodate the experimental fact that the yields of **9**, which are calculated provided that 1 mol of **1** produce 1 mol of **9**, are beyond 50%. This problem could be solved by postulating that another process involving a further deprotonation of **2** followed by the S-S bond fission of the resulting dianion (**5**) to afford **6** is competitively operative. Such an assumption is also compatible with the facts that, in all runs of Table 1, **9** has been produced in more excess than **10** and that the employment of a fourfold excess or more of LDA under otherwise identical conditions results in increased yields of **9** and slightly decreased yields of **10**. For example, with propyl iodide as the trapping agent, the yield of **9c** was 75% and that of **10c** was 34%. However, there has not been any direct evidence for the occurrence of the conversion of **5** to **6**.

Experimental

Lithium Diisopropylamide(LDA)-induced Fragmentation of Dibenzyl Disulfide (1) Followed by the Trapping with Some Alkyl Halides. General Procedure: To LDA, prepared from diisopropylamine (0.36 g, 3.6 mmol) in tetrahydrofuran (7 ml) and 1.56 molar solution (2.18 ml, 3.4 mmol) of butyllithium in hexane, was added at −78 °C 0.27 g (1.1 mmol) of **1** in tetrahydrofuran (4 ml). The reaction mixture was allowed to warm to −15 °C and the stirring was continued for 1 h at that temperature. The mixture was cooled again to −78 °C, and an appropriate alkyl halide (3.3 mmol) was added with stirring. The stirring was continued for 1 h at −10—−5 °C and then for 24 h at room temperature. The mixture was quenched with water (100 ml) and a saturated aqueous solution (20 ml) of ammonium chloride, and then extracted with ether (3×60 ml). The combined ethereal extract was dried over magnesium sulfate and concentrated under reduced pressure to give a residue, which was sujected to preparative TLC on silica gel using ethyl acetate-hexane as the eluent. In Runs 1 and 2, however, the R_f values of **9a** and **9b** were almost same with those of **10a** and **10b**, respectively. Thus, the obtained mixture, which is composed of **9a** and **10a**, was distilled under vacuum to remove **10a** from the mixture, and the residue was again subjected to preparative TLC on silica gel using the same eluent. In the similar manner, only **9b** was isolated in Run 2.

References

1) S. Oae, W. Tagaki, and A. Ohno, *Tetrahedron*, **20**, 417, 427, 437, 443 (1964).
2) A. I. Shatenshtein and H. A. Gvozdeva, *Tetrahedron*, **25**, 2749 (1969).
3) K. C. Bank and D. L. Coffen, *J. Chem. Soc., D*, **1969**, 8.
4) S. Wolfe, A. Rauk, L. M. Tel, and I. G. Csizmadia, *J. Chem. Soc., D*, **1970**, 96.
5) D. J. Peterson, *J. Org. Chem.*, **32**, 1717 (1967).
6) E. J. Corey and D. Seebach, *J. Org. Chem.*, **31**, 4097 (1966).
7) E. J. Corey and M. Jautelat, *Tetrahedron Lett.*, **1968**, 5787.
8) S. R. Wilson. G. M. Georgiadis, H. N. Khatri, and J. E. Bartmess, *J. Am. Chem. Soc.*, **102**, 3577 (1980).
9) S. R. Wilson and P. Caldera, *J. Org. Chem.*, **47**, 3319 (1982).
10) D. Seebach and E. J. Corey, *J. Org. Chem.*, **40**, 231 (1975).
11) B. Harirchian and P. Magnus, *J. Chem. Soc., Chem. Commun.*, **1977**, 522.
12) H. Ikehira, S. Tanimoto, T. Oida, and M. Okano, *J. Org. Chem.*, **48**, 1120 (1983).
13) K.-H. Geiss, D. Seebach, and B. Seuring, *Chem. Ber.*, **110**, 1833 (1977).
14) D. Seebach and K.-H. Geiss, *Angew. Chem.*, **86**, 202 (1974).
15) R. G. Hiskey and A. J. Dennis, *J. Org. Chem.*, **33**, 563 (1968).
16) J. E. Baldwin and R. C. G. Lopez, *J. Chem. Soc., Chem. Commun.*, **1982**, 1029 and references cited therein.
17) E. Vedejs, T. H. Eberlein, and D. L. Varie, *J. Am. Chem. Soc.*, **104**, 1445 (1982) and references cited therein.
18) H. Ikehira, S. Tanimoto, and T. Oida, *Bull. Chem. Soc. Jpn.*, **56**, 2537 (1983).
19) A. Ohno, K. Nakamura, M. Uohama, S. Oka, T. Yamabe, and S. Nagata, *Bull. Chem. Soc. Jpn.*, **48**, 3718 (1975).

Cyclosadol, Isocyclosadol, and Other Related Triterpene Alcohols Obtained from 24-Methylenecycloartanol by Acid-catalyzed Isomerization

Naoto SHIMIZU, Toshihiro ITOH, Yoshiyuki ICHINOHE, and Taro MATSUMOTO*
College of Science and Technology, Nihon University, 1-8, Kanda Surugadai, Chiyoda-ku, Tokyo 101
(Received October 18, 1983)

Synopsis. The acid-catalyzed isomerization of 24-methylenecycloartanol with sulfuric acid afforded cyclosadol (23*E*-Δ^{23}), isocyclosadol (23*Z*-Δ^{23}), and other isomers, including lanostane- and cucurbitane-type isomers with (23*E*)- and (23*Z*)-Δ^{23}- and Δ^{24}-unsaturated side chains. The phytochemical significance of the isomers is discussed.

Our recent study of the acid-catalyzed isomerization of cycloartane (9β,19-cyclolanostane) triterpene alcohols has shown that this isomerization is quite useful in obtaining several lanostane- and cucurbitane [19(10→9β)*abeo*-lanostane]-type isomers.[1] In this study we undertook the isomerization of 24-methylenecycloartanol (24-methylene-9β,19-cyclo-5α-lanostan-3β-ol, **1a**), a cycloartane triterpene alcohol widely distributed in plants,[2,3] in order to prepare several isomers of **1a**. Since **1a** is considered to be the key intermediate of sterol biosynthesis in some plants,[2] the isomerization products which have a structural similarity to **1a** are also considered to be especially worthwhile from the points of view of phytochemistry and sterol biogenesis.

The isomerization of **1a** with sulfuric acid was performed in isopropyl alcohol at 80 °C for 12 h.[1] The compositions of the isomerized products were, after acetylation, carefully determined by GLC to be as follows: Cyclosadol[4-6] [(23*E*)-24-methyl-9β,19-cyclo-5α-lanost-23-en-3β-ol, **1b**, 24%], isocyclosadol [(23*Z*)-24-methyl-9β,19-cyclo-5α-lanost-23-en-3β-ol, **1c**, 7%], cyclobranol[7] (24-methyl-9β,19-cyclo-5α-lanost-24-en-3β-ol, **1d**, 30%), (23*E*)- (**2b**, 2%) and (23*Z*)-24-methyl-5α-lanosta-8,23-dien-3β-ol (**2c**, 1%), 24-methyl-5α-lanosta-8,24-dien-3β-ol (**2d**, 3%), (23*E*)- (**3b**, 12%) and (23*Z*)-24-methyl-5α-lanosta-9(11),23-dien-3β-ol (**3c**, 3%), 24-methyl-5α-lanosta-9(11),24-dien-3β-ol (**3d**, 14%), (23*E*)-24-methyl-10α-cucurbita-5,23-dien-3β-ol (**4b**, 0.5%), 24-methyl-10α-cucurbita-5,24-dien-3β-ol (**4d**, 0.5%), (23*E*)-24-methylcucurbita-5(10),23-dien-3β-ol (**5b**, 2%), and 24-methylcucurbita-5(10),24-dien-3β-ol (**5d**, 1%).

The carbon skeletons of **1**—**5** were established by comparing their ^{1}H NMR spectra with those of **1a** and the relevant compounds described previously.[1] The double bond of the side chains **b** and **c** was found to be located at C-23 by the observation of a mass-fragmentation ion at *m/z* 325 ($M^+-C_7H_{13}-HOAc$) for the acetyl derivatives.[5,6] The configurations of 23*E* (**b**) and 23*Z* (**c**) were established on the basis of the ^{1}H NMR spectra as compared with those of two model olefins, (2*E*)- (**6**) and (2*Z*)-3,4-dimethyl-2-pentene (**7**).[5] The acetyl derivatives with the side chain **d** were established to have a C-24(25) double bond by the ^{1}H NMR, which showed three overlapping olefinic methyl singlets due to the 26-H$_3$, 27-H$_3$, and 28-H$_3$ protons.[7]

Thirteen isomers were obtained by the acid-catalyzed isomerization of **1a**. Among them, two cycloartane isomers, a (23*E*)-Δ^{23}-isomer (**1b**) in *Zea mays*[4-6] and Δ^{24}-isomer (**1d**), have been detected as natural products in several seed-bearing plants,[3] and their possible intermediacy in sterol biosynthesis has been suggested.[2,6] Although the occurrence of the other eleven isomers has not yet been reported, these isomers are also considered to be of significance from the phytochemical and sterol biogenetic points of view. In particular, taking into account the fact that the (23*E*)- and (23*Z*)-isomers of 24-ethylcholesta-5,23-dien-3β-ol both occur as natural products,[8] the occurrence of (23*Z*)-Δ^{23}-compounds such as **1c** can be expected in seed-bearing plants, especially in *Z. mays*. On the other hand, since some 24-methylenated lanostenes, such as **2a** and **3a**, have been detected in some plants,[3] the natural occurrence of several of the lanostane-type isomers prepared in this study can be expected. Some Cucurbitaceae plants have recently been shown to contain 10α-cucurbita-5,24-dien-3β-ol;[9] hence, the occurrence of its higher homologs, such as **4b** and **4d**, is highly probable in these plants.

Experimental

The melting points are uncorrected. The argentic TLC (silica gel-$AgNO_3$, 4:1) was developed 4 times with

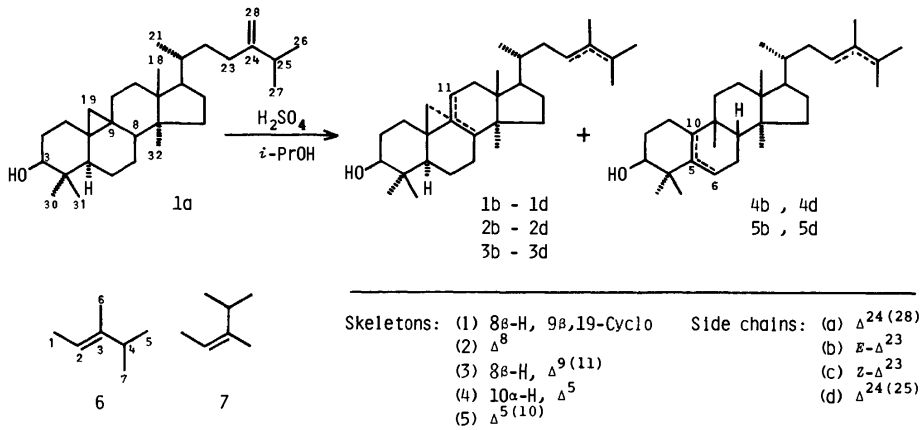

Table 1. Melting points, chromatographic data, and relative intensities (in percent) of selected mass-spectral fragments of the acetates of some new triterpene alcohols

Acetate	Mp θ_m/°C	R_c TLC	RRT HPLC	RRT GLC	m/z 482	467	439	422	407	398	379	355	353	339	325	300	297	295	288	273
1c	131—133	0.85	0.95	2.04	23	17	—	100	70	—	40	4	23	—	55	34	13	8	—	—
2b	112—114	0.86	0.82	1.77	36	100	—	2	73	—	7	7	—	—	10	—	5	5	—	—
2c	—	0.86	0.80	1.72	25	100	—	5	67	—	4	5	—	—	10	—	4	5	—	—
2d	153—155	1.01	0.89	2.12	46	100	—	4	77	4	2	2	—	2	—	—	2	2	—	—
3b	149—151	0.40	0.85	2.02	15	44	27	5	39	—	5	100	—	—	29	—	12	22	—	—
3c	—	0.40	0.83	1.95	17	59	21	2	64	—	6	100	—	—	34	—	8	19	—	—
3d	170—172	0.42	0.92	2.43	33	76	6	12	100	63	6	55	—	8	—	—	10	16	—	—
4b	128—130	0.58	0.63	1.59	7	9	—	31	22	—	—	—	—	—	14	—	9	5	100	64
4d	179—181	0.78	0.68	1.94	3	3	—	15	12	8	—	—	—	3	—	—	3	2	100	56
5b	163—165	0.82	0.62	1.40	12	33	—	100	83	—	8	—	—	—	42	8	8	2	—	—
5d	200—202	1.02	0.67	1.74	15	34	—	100	83	—	10	—	—	15	—	5	10	5	—	—

Table 2. ^{1}H NMR data[a] of the acetates of some new triterpene alcohols

Acetate	18-H_3[b]	19-H_3[b,c]	30-H_3[b]	31-H_3[b]	32-H_3[b]	21-H_3[d,e]	26-H_3/27-H_3[d]	28-H[b]	23-H[f]	25-H[g]	Others
1c	0.96	0.34(*d*, 4.4) 0.57(*d*, 3.9)	0.85	0.89	0.89	0.85(5.1)	0.95(6.8)	1.61	5.04(6.8)	2.80(6.8)	—
2b	0.69	1.00	0.88	0.88	0.88	0.84(5.6)	0.99(6.8)	1.55	5.16(6.0)	2.18(6.8)	—
2c	0.69	0.99	0.88	0.88	0.88	0.84(5.1)	0.95(6.8)	1.61	5.03(6.8)	2.80(7.1)	—
2d	0.69	1.00	0.88	0.88	0.88	0.92(4.4)	1.63(*s*)	1.63	—	—	—
3b	0.65	1.07	0.87	0.89	0.74	0.84(5.6)	0.99(6.8)	1.55	5.16(6.0)	2.17(6.8)	5.20(*m*, 11-H)
3c	0.65	1.06	0.87	0.89	0.74	0.84(5.1)	0.95(6.8)	1.60	5.03(6.8)	2.80(7.1)	5.20(*m*, 11-H)
3d	0.65	1.07	0.87	0.89	0.74	0.92(5.8)	1.63(*s*)	1.63	—	—	5.20(*m*, 11-H)
4b	0.81	0.91	1.04	1.04	0.85	0.84(5.6)	0.98(6.8)	1.56	5.16(6.0)	2.19(6.8)	5.50(*d*, 5.5, 6-H)
4d	0.81	0.91	1.04	1.04	0.85	0.92(4.4)	1.62(*s*)	1.62	—	—	5.50(*d*, 5.5, 6-H)
5b	0.79	1.00	0.96[h]	0.93[h]	0.84	0.82(4.9)	0.98(6.3)	1.55	5.14(6.8)	2.17(6.4)	—
5d	0.79	1.00	0.96[i]	0.93[i]	0.84	0.92(4.4)	1.62(*s*)	1.62	—	—	—

a) Given as δ values. Figures in parentheses denote J values in Hz. b) Singlet unless otherwise specified. c) Cyclopropyl methylene signal as for **1c**. d) Doublet if not otherwise specified. e) Assigned with the aid of the lanthanoid-induced-shift techniques.[11] f) Triplet. g) Septet. h) and i) The assignment in each row may be inverted, although that given here is preferred.

CCl_4-CH_2Cl_2 (5:1). The HPLC was carried out on a Partisil 5 ODS-2 column (25 cm×10 mm i.d.) using an UV detector and monitoring at 212 nm (mobile phase, MeOH-H_2O, 98:2). The GLC was performed with a 30 m×0.3 mm i.d. SCOT OV-17 glass capillary column at 260 °C. The R_c-values (relative mobilities) in the argentic TLC and the RRTs (relative retention times) in the HPLC and GLC were expressed relative to cholesteryl acetate (1.00). The MS spectra (70 ev) were taken by means of a probe injection. The ^{1}H NMR spectra (100 MHz) were obtained in a $CDCl_3$ solution, with Me_4Si as the internal standard. The 24-methylenecycloartanol (**1a**)[10] was kindly donated by the Riken Vitamin Co. (Tokyo). The isomerization of **1a** (500 mg) was carried out with conc H_2SO_4 (4 cm^3) in isopropyl alcohol (40 cm^3) while the mixture was being stirred at 80 °C for 12 h. The separation of the isomerization products was performed by the same way as has been described in the previous paper,[1] but the eventual isolation of each product was achieved by HPLC in this study. All of the other techniques used in this study[1] and the full ^{1}H NMR data[5] of **6** (4-H, *septet*, δ= 2.22, J=6.9 Hz; 6-H_3, *s*, δ=1.56) and **7** (4-H, *septet*, δ=2.83, J=6.9 Hz; 6-H_3, *s*, δ=1.59) have been described previously.

The High-resolution MS Data of New Triterpene Alcohols. The molecular ions (M^+) observed in the high-resolution MS for the acetates of the eleven new triterpene alcohols may be described as follows: The acetates of **1c** (m/z 482.4104; the molecular formulas of this and the subsequent compounds are $C_{33}H_{54}O_2$, calcd 482.4121), **2b** (m/z 482.4085), **2c** (m/z 482.4109), **2d** (m/z 482.4087), **3b** (m/z 482.4096), **3c** (m/z 482.4102), **3d** (m/z 482.4084), **4b** (m/z 482.4146), **4d** (m/z 482.4112), **5b** (m/z 482.4146), and **5d** (m/z 482.4160). The molecular formulas for the fragment ions described in Table 1 were taken from the MS data of the relevant compounds and may be summarized as follows; m/z 467 ($C_{32}H_{51}O_2$), 439 ($C_{30}H_{47}O_2$), 422 ($C_{31}H_{50}$), 407 ($C_{30}H_{47}$), 398 ($C_{27}H_{42}O_2$), 379 ($C_{28}H_{43}$), 355 ($C_{24}H_{35}O_2$), 353 ($C_{26}H_{41}$), 339 ($C_{25}H_{39}$), 325 ($C_{24}H_{37}$), 300 ($C_{22}H_{36}$), 297 ($C_{22}H_{33}$), 295 ($C_{22}H_{31}$), 288 ($C_{21}H_{36}$), and 273 ($C_{20}H_{33}$).

References

1) N. Shimizu, T. Itoh, M. Saito, and T. Matsumoto, *J. Org. Chem.*, **49**, 709 (1984).

2) W. R. Nes and M. L. McKean, "Biochemistry of Steroids and Other Isopentenoids," University Park Press, Baltimore, Md. (1977).

3) T. Itoh and T. Matsumoto, *Yukagaku*, **28**, 231 (1979).

4) H. Pinhas, *Bull. Soc. Chim. Fr.*, **1969**, 3027.

5) T. Itoh, N. Shimizu, T. Tamura, and T. Matsumoto, *Phytochemistry*, **20**, 1353 (1981).

6) F. Scheid and P. Benveniste, *Phytochemistry*, **18**, 1207 (1979); F. Scheid, M. Rohmer, and P. Benveniste, *ibid.*, **21**, 1959 (1982).

7) T. Endo, O. Misu, and Y. Inaba, *Yukagaku*, **18**, 255 (1969).

8) T. Itoh, D. Sica, and C. Djerassi, *J. Org. Chem.*, **48**, 890 (1983).

9) T. Itoh, T. Tamura, T. M. Jeong, T. Tamura, and T. Matsumoto, *Lipids*, **15**, 122 (1980).

10) T. Itoh, T. Tamura, and T. Matsumoto, *Lipids*, **10**, 454 (1975).

11) N. Shimizu, T. Itoh, and T. Matsumoto, unpublished results.

Asymmetric Synthesis of Alanine by Catalytic Hydrogenation of Chiral N^{α}-Acetyldehydroalaninamides

Kaoru HARADA* and Michiaki TAKASAKI
Department of Chemistry, University of Tsukuba, Niihari, Ibaraki 305
(Received December 12, 1983)

Synopsis. Asymmetric hydrogenation of chiral N^{α}-acetyldehydroalaninamides was studied. The asymmetric yield of the resulting alanine was in the range 0—24%. The effects of reaction temperature, solvent polarity and asymmetric moieties on the asymmetric yields were examined.

Several studies[1-7] have been performed on asymmetric reduction of α,β-dehydroamino acid derivatives yielding amino acids. Among these studies, heterogeneous hydrogenations of optically active linear derivatives of dehydroamino acids were reported,[1,2] and the steric course of the asymmetric hydrogenation was explained by the application of the Prelog rule.[8] However, no detailed studies on the effects of temperature and solvent polarity on asymmetric hydrogenation have been reported. In the present study, asymmetric catalytic hydrogenation of chiral N^{α}-acetyldehydroalaninamides was carried out and the temperature dependence on the asymmetric hydrogenation was studied using various solvents.

The chiral N^{α}-acetyldehydroalaninamides used were N^{α}-acetyl-*N*-[(*S*)-methylbenzyl]dehydroalaninamide (**3-a**), *N*-[(*R*)-α-ethylbenzyl]amide (**3-b**), and *N*-[(*R*)-1-(1-naphthyl)ethyl]amide (**3-c**). The compounds **3-a**, **b**, and **c** were prepared by the coupling of *N*-acetyldehydroalanine (**1**) and the corresponding chiral amines (**2-a**, **b**, and **c**) with dicyclohexylcarbodiimide in the presence

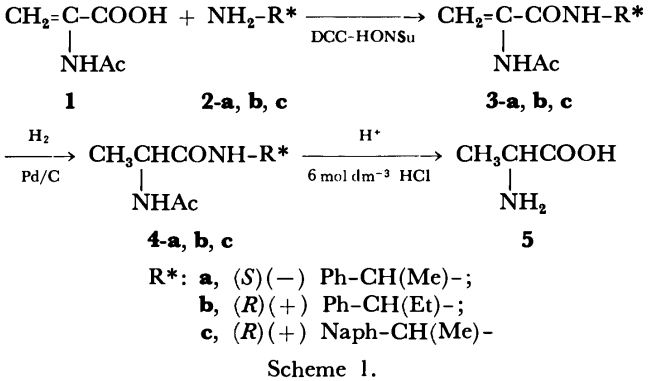

Scheme 1.

of *N*-hydroxysuccinimide. The hydrogenation reactions were carried out at 1 atm of hydrogen by using palladium on charcoal suspended in several solvents (methanol, ethanol, 2-propanol, and ethyl acetate). The reaction temperature was in the range of −50 °C to 50 °C. After the hydrogenation, the resulting N^{α}-acetylalaninamides (**4-a**, **b**, and **c**) were hydrolyzed to form alanine. The chemical yield of alanine was in the range of 78—98% as determined by an amino acid analyzer. The asymmetric yield of alanine was determined by gas chromatographic analysis employing a chiral stationary phase (Chirasil-Val[9]).

The results are summarized in Figs. 1, 2, and 3. In the reaction of compound **3-a**, a clear temperature effect on the asymmetric yield was observed. With the decrease in solvent polarity, the asymmetric yield of (*R*)-alanine increased at lower temperature. The effect observed could not be explained by the application of the Prelog rule,[8] which was employed in the previous reports.[1,2] Since a similar temperature effect was observed in the reaction of compound **3-b**, the same reaction mechanism would prevail in the hydrogenation of these two compounds.

In the reaction of compound **3-c**, the temperature effect was not so large. With the decrease in solvent polarity, the asymmetric yield of (*R*)-alanine increased except in the reaction using ethyl acetate as the solvent. This result was definitely different from the results

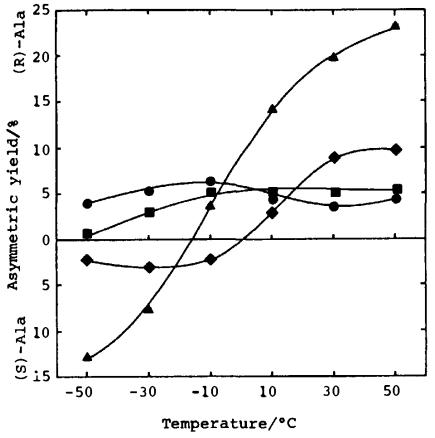

Fig. 1. Temperature effect in asymmetric hydrogenation of compound **3-a**. ●: In methanol, ■: in ethanol, ◆: in 2-propanol, ▲: in ethyl acetate.

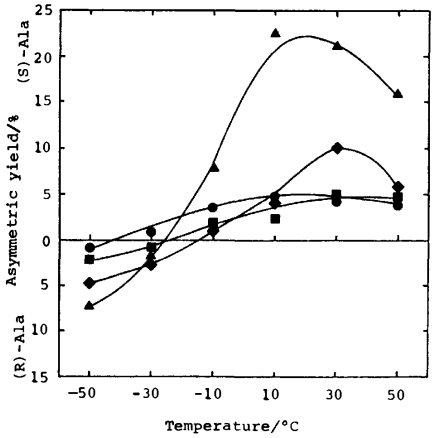

Fig. 2. Temperature effect in asymmetric hydrogenation of compound **3-b**. ●: In methanol, ■: in ethanol, ◆: in 2-propanol, ▲: in ethyl acetate.

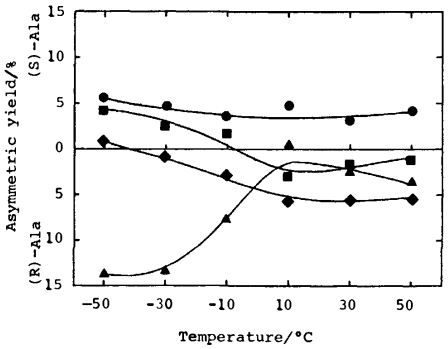

Fig. 3. Temperature effect in asymmetric hydrogenation of compound **3-c**. ●: In methanol, ■: in ethanol, ◆: in 2-propanol, ▲: in ethyl acetate.

obtained in the reactions of compounds **3-a** and **b**. Therefore, mechanisms prevailed in the reaction of compound **3-c** could be distinct from those of compounds **3-a** and **b**.

The results obtained could indicate the participation of several reaction mechanisms in the asymmetric synthesis. The mechanisms in these reactions could be changed by the reaction temperature, solvent polarity and asymmetric moieties.

Experimental

All the melting points were uncorrected. Optical rotations were measured with a JASCO DIP-181 Digital Polarimeter. The gas chromatographic analysis were carried out with a Hitachi 163 gas chromatograph and the peaks on the chromatogram were integrated with a Hitachi 834-30 chromatoprocessor. Amino acid analysis were carried out with a Yanagimoto LC-5S instrument.

N$^{\alpha}$-Acetyl-N-[(S)-methylbenzyl]dehydroalaninamide (3-a). *N*-Acetyldehydroalanine[10] (**1**) (3.25 g, 25 mmol) was dissolved in ethyl acetate (60 ml) together with (*S*)-methylbenzylamine (**2-a**) (3.00 g, 25 mmol), *N*-hydroxysuccinimide (2.9 g, 25 mmol) and dicyclohexylcarbodiimide (6.18 g, 25 mmol) at −15 °C. Stirring was continued at −15 °C for 1 h and at room temperatue for 10 h. The solution was filtered and the filtrate was washed with 10% aqueous citric acid, saturated aqueous sodium hydrogencarbonate and brine and dried over magnesium sulfate, and was concentrated *in vacuo*. The resulting crude product was purified by column chromatography (silica-gel column, 4 mm i.d.×350 mm). From the eluate with benzene–ethyl acetate (3:1), white solid was obtained, yield, 1.48 g (26.3%). It was recrystallyzed from methanol for elemental analysis, mp 119—121 °C, $[\alpha]_D^{15}$ −21.2° (*c* 0.523, methanol), Found: C, 67.19; H, 7.05; N, 11.97%. Calcd for $C_{13}H_{16}N_2O_2$: C, 67.22; H, 6.79; N, 12.06%.

Other *N$^{\alpha}$*-acetyldehydroalaninamides (**3-b** and **c**) were prepared in a similar way. The physical properties were as follows: **3-b**; mp 135—137 °C, $[\alpha]_D^{15}$ +20.2 (*c* 0.523, methanol), Found: C, 68.02; H, 7.57; N, 11.18%. Calcd for $C_{14}H_{18}N_2O_2$; C, 68.27; H, 7.37; N, 11.37%. **3-c**; mp 111—113 °C, $[\alpha]_D^{15}$ −61.8 (*c* 0.964, methanol), Found: C, 72.30; H, 6.59; N, 9.82%. Calcd for $C_{17}H_{18}N_2O_2$: C, 72.32; H, 6.43; N, 9.92%.

Alanine (5). The compound **3-a** (23 mg, 0.1 mmol) was dissolved in 5 ml of methanol and hydrogenated with 5% palladium on charcoal (100 mg) for 24 h at 30 °C under hydrogen (1 atm). After the reaction was over, the catalyst was removed by filtration, and the filtrate was evaporated to dryness. The resulting *N$^{\alpha}$*-acetylalaninamide (**4-a**) was hydrolyzed with 6 mol dm^{-3} HCl at 110 °C in a sealed tube with refluxing in a toluene bath for 10 h. A part of the solution was diluted appropriately and analyzed with an amino acid analyzer to determine the chemical yield of alanine (96.3%). A part of the resulting alanine was converted to *N*-(trifluoroacetyl)alanine isopropyl ester in the usual mammer and then subjected to gas chromatographic analysis employing a chiral stationary phase (Chirasil-Val[9]). The peaks due to (*R*)- and (*S*)-alanine on the chromatogram were in baseline separation.

References

1) J. S. Sheehan and R. E. Chandler, *J. Am. Chem. Soc.*, **83**, 4795 (1961).
2) M. Nakayama, G. Maeda, T. Kaneko, and H. Katsura, *Bull. Chem. Soc. Jpn.*, **44**, 1150 (1971).
3) N. Izumiya, S. Lee, T. Kanmera, and H. Aoyagi, *J. Am. Chem. Soc.*, **99**, 8346 (1977).
4) T. Kanmera, S. Lee, H. Aoyagi, and N. Izumiya, *Tetrahedron Lett.*, **1979**, 4483.
5) I. Ojima and T. Suzuki, *Tetrahedron Lett.*, **21**, 1239 (1980).
6) D. Meyer, J.-C. Poulin, H. B. Kagan, H. L.-Pinto, J.-L. Morget, and P. Fromageot, *J. Org. Chem.*, **45**, 4680 (1980).
7) K. Omura, T. Ito, and A. Nakamura, *Chem. Lett.*, **1980**, 481.
8) V. Prelog, *Helv. Chim. Acta*, **36**, 308 (1953).
9) H. Frank, G. J. Nicolson, and E. Bayer, *J. Chromatogr.*, **146**, 197 (1978).
10) T. Wieland, G. Ohnacker, and W. Ziegler, *Chem. Ber.*, **90**, 194 (1957).

The Reaction of Fluorenethione *S*-Tosylimide with Grignard Reagents

Takao SAITO, Michio NAKANE, and Shinichi MOTOKI*

Department of Chemistry, Faculty of Science, Science University of Tokyo, Kagurazaka 1-3, Shinjuku-ku, Tokyo 162

(Received December 26, 1983)

Synopsis. Fluorenethione *S*-tosylimide reacted with Grignard reagents to afford both the thiophilic and carbophilic products depending on the solvent used.

Thione *S*-imides have three potential reactive sites (carbon, sulfur, nitrogen atoms) on the cumulated system, and hence reactions with nucleophiles, *e.g.* Grignard reagents include interesting possible modes of the site selectivity, *viz.* carbophilic, thiophilic, and azophilic reactions.

Only one example has been reported first by Senning *et al.*[1] on the reaction of thione *S*-imide (*S,S'*-diphenyl trithiocarbonate *S,S*-dioxide *S''*-*t*-butylimide) with organometallic reagents (phenyllithium) giving carbophilic adduct.[2]

In this paper we will describe the reaction of fluorenethione *S*-tosylimide (**1**) with some Grignard reagents.

Results

The reactions were carried out by adding a twofold excess of a Grignard reagent to thione *S*-imide (**1**) at low temperature in diethyl ether or THF (method A), or *vice versa* (method B).[3]

The reactions in diethyl ether (0.06 mol/l of **1**) afforded products **2—7** (Scheme 1, Table 1). It is unambiguous that sulfenamide **2** was produced by the attack of the nucleophile R of the Grignard reagent to the 9-carbon of the fluorenylidene ring in **1**. *N*-Substituted tosylamide (**3**) would be formed by the sulfur extrusion from **2**, which was observed independently, and/or by the reaction of **6** with a Grignard reagent.

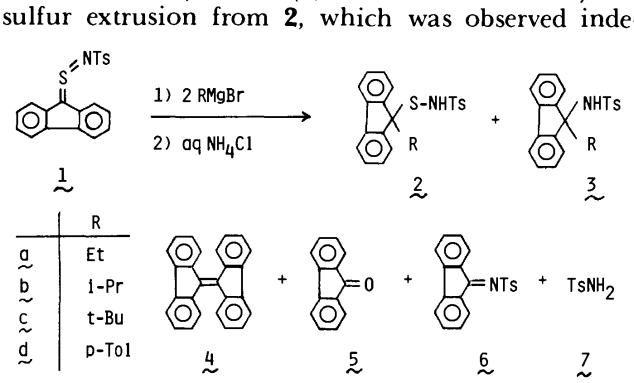

Scheme 1.

TABLE 1. REACTION OF FLUORENETHIONE *S*-TOSYLIMIDE (**1**) WITH GRIGNARD REAGENTS

R	Solvent (Method)	Reaction time/h	Yield/% Carbophilic adducts 2	3	Thiophilic adduct 4	By-products 5	6	7
a	E (A)	2.5	17	a)	29	12	2	48
b	E (A)	3.5	23	a)	18	28	15	32
c	E (A)	2.5	24	a)	2	18	10	62
d	E (B)	1.0	6	16	2	54	0	35
a	THF (A)	1.0	0	0	99	a)	a)	99
d	THF (B)	1.0	0	0	87	6	5	64

a) Trace amount, checked by TLC.

In contrast, the reactions in THF gave 9,9'-bifluorenylidene (**4**) as a major product, and the formation of **2** and **3** was not detected (Table 1).

Discussion

Probable mechanisms of the reaction are shown in Scheme 2 on the basis of polar and single electron transfer (SET) mechanisms in general Grignard reactions.[4] The negatively charged nitrogen of **1** coordinates the positive magnesium of the reagent (**8**), followed by the slow SET giving **9** and **10**.[5] The intermediary **8** (**9**) and **10** are key species giving thiophilic and carbophilic adducts, respectively. The carbophilic attack of R· to the 9-carbon of the fluorenylidene ring in **10** gives **2** *via* **15**. The new Grignard reagent (**11**) formed by the thiophilic attack of R in **8** (**9**) further reacts with another molecule of **1** on the sulfur atom to afford **4** *via* **12—14**.

Similar reaction mechanisms have been reported in the reaction of fluorenethione *S*-oxide (sulfine) with organolithium reagents,[6] where no carbophilic reaction product was obtained.[7] On the contrary, sulfilimine **16** which corresponds to sulfoxide formed by the thiophilic reaction of the sulfine was not detected. The sulfilimine **16** or **11** might produce **5** and **7** by hydrolysis.

In the reactions in diethyl ether, the yields of the carbophilic adducts (**2**, **3**) are in the order of **c**(R=*t*-Bu) ≥**b**(R=*i*-Pr)>**a**(R=Et), and the yields of the thiophilic adducts (**4**) are in the order of **a**(R=Et)>**b**(R=*i*-Pr)> **c**(R=*t*-Bu). This result is consistent with the view that the more radical property of tertiary alkyl (*t*-Bu) stabilized preferentially attacks the carbon atom in **10** whereas the less radical property of primary alkyl (Et) instantly forms the thiophilic adduct **11**.[8] On the other hand, the reaction in THF implies that the solvent effect (higher solubility for **1**: concentration dependence, polarity) of THF makes the route to thiophilic adduct **4** favorable.

Experimental

All the melting points are uncorrected. IR spectra were measured on a Hitachi Model 260-10 spectrometer. Mass spectra were recorded on a Hitachi double-focusing mass spectrometer RMU-7M operating at an ioninzing potential of 70 eV. ^{1}H- and ^{13}C-NMR spectra were measured on a JEOL-FX 100 spectrometer in $CDCl_3$ using TMS as an internal standard.

Fluorenethione *S*-tosylimide (**1**) was prepared by the method reported previously.[9]

Reaction of 1 with Grignard Reagents. General Procedure: 1) A diethyl ether solution (7 cm^3) of a Grignard reagent (7.0 mmol) was added with stirring to a suspension of **1** (1.21 g, 3.32 mmol) in 48 cm^3 of diethyl ether at −15 °C (0 °C in THF) under nitrogen atmosphere (method A). 2) A suspension of **1** (1.47 g, 4.02 mmol) in

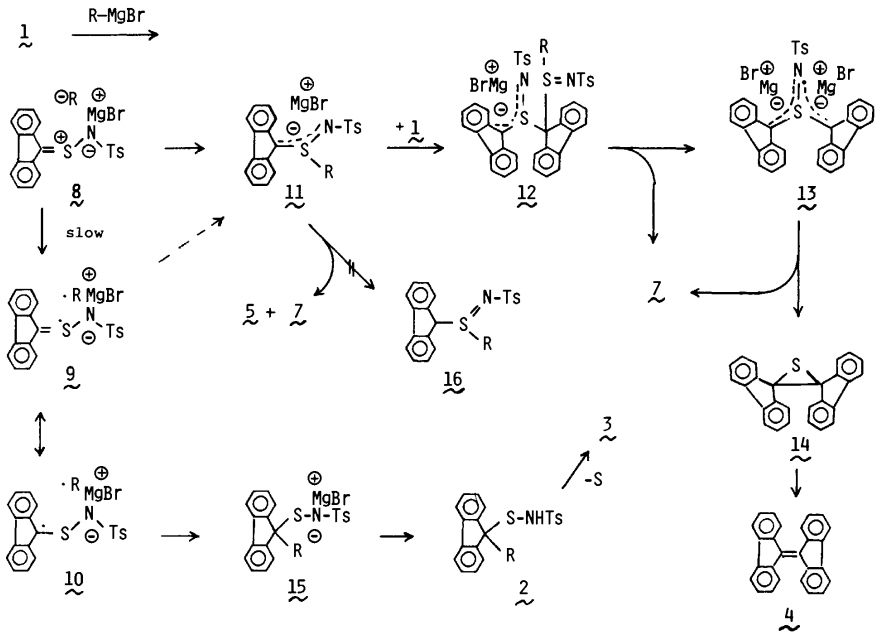

Scheme 2.

ether (30 cm³) was added to *p*-tolylmagnesium bromide ethereal solution (37 cm³) under the same conditions as described for method A (method B). After being stirred for 1—3.5 h at −15 °C (0 °C in THF), the reaction mixture was rinsed with aq NH_4Cl and water, dried over Na_2SO_4, and concentrated *in vacuo*. The residue was column-chromatographed on silica gel (Wako C-200) using hexane, benzene, dichloromethane, and methanol as eluents to give the products **2—7**. The products **4—7** were identified by comparison of the spectral data with those of authentic samples.

2a: Mp 150—151 °C; IR (Nujol) 3320 cm^{-1} (NH), 1160, 1100 (SO_2); MS *m/z* 395 (3%, M^+), 193 (100, M^+—SNHTs); ^{1}H-NMR ($CDCl_3$) δ 0.44 (t, *J*=8 Hz, 3H, CH_3), 2.34 (s, 3H, CH_3(Ts)), 2.60 (q, *J*=8 Hz, 2H, CH_2), 5.70 (s, 1H, NH), 7.13—7.70 (m, 12H, Ar-H); ^{13}C-NMR ($CDCl_3$) δ 65.0 (9-C), 28.7 (CH_2), 21.5 (CH_3(Ts)), 8.8 (CH_3). Found: C, 66.88; H, 5.37; N, 3.33; S, 16.13%. Calcd for $C_{22}H_{21}NS_2O_2$: C, 66.81; H, 5.35; N, 3.53; S, 16.22%.

2b: Mp 138—139 °C; IR (Nujol) 3210 cm^{-1} (NH), 1165, 1100 (SO_2); MS *m/z* 409 (1, M^+), 207 (100, M^+—SNHTs); ^{1}H-NMR ($CDCl_3$) δ 0.94 (d, *J*=7 Hz, 6H, CH_3), 2.37 (s, 3H, CH_3(Ts)), 2.86 (sept, *J*=7 Hz, 1H, CH), 5.59 (s, 1H, NH), 7.12—7.68 (m, 12H, Ar-H); ^{13}C-NMR ($CDCl_3$) δ 68.9 (9-C), 32.7 (CH), 21.5 (CH_3(Ts)), 8.8 (CH_3). Found: C, 67.51; H, 5.68; N, 3.26; S, 15.63%. Calcd for $C_{23}H_{23}NS_2O_2$: C, 67.45; H, 5.66; N, 3.42; S, 15.66%.

2c: Mp 161—163 °C; IR (Nujol) 3250 cm^{-1} (NH), 1165, 1100 (SO_2); MS *m/z* 423 (1, M^+), 221 (100, M^+—SNHTs); ^{1}H-NMR ($CDCl_3$) δ 0.98 (s, 9H, CH_3), 2.34 (s, 3H, CH_3(Ts)), 5.16 (s, 1H, NH), 6.90—7.62 (m, 12H, Ar-H); ^{13}C-NMR ($CDCl_3$) δ 73.3 (9-C), 38.5 (C(CH_3)$_3$), 21.5 (CH_3(Ts)), 27.0 (CH_3). Found: C, 68.10; H, 5.94; N, 3.20; S, 15.06%. Calcd for $C_{24}H_{25}NS_2O_2$: C, 68.50; H, 5.95; N, 3.31; S, 15.14%.

2d: Mp 131—135 °C; IR (Nujol) 3325 cm^{-1} (NH), 1170, 1100 (SO_2); MS *m/z* 365 (1, M^+—Tol), 287 (21, M^+—NHTs), 196 (81, Fl=S^+), 91 (100, Tol^+); ^{1}H-NMR ($CDCl_3$) δ 2.25 (s, 3H, CH_3(Tol)), 2.30 (s, 3H, CH_3(Ts)), 5.88 (s, 1H, NH), 6.84—7.48 (m, 16H, Ar-H). Found: C, 70.89; H, 5.10; N, 3.08; S, 14.00%. Calcd for $C_{27}H_{23}NS_2O_2$: C, 70.87; H, 5.07; N, 3.06; S, 14.01%.

3d: Mp 182.5—184 °C; IR (Nujol) 3250 cm^{-1} (NH), 1165, 1100 (SO_2); MS *m/z* 425 (27, M^+), 270 (37, M^+—Ts), 255 (100, M^+—NHTs), 91 (23, Tol^+); ^{1}H-NMR ($CDCl_3$) δ 2.16 (s, 3H, CH_3), 2.22 (s, 3H, CH_3(Ts)), 6.33 (s, 1H, NH), 6.72—7.44 (m, 16H, Ar-H). Found: C, 76.11; H, 5.44; N, 3.30; S, 7.55%. Calcd for $C_{27}H_{23}NSO_2$: C, 76.21; H, 5.45; N, 3.29; S, 7.53%.

References

1) S. Holm, J. A. Boerma, N. H. Nilsson, and A. Senning, *Chem. Ber.*, **109**, 1069 (1976).

2) Tamagaki and Oae *et al.* reported some reactions of 4,5-benzo-1,2-dithiole-3-thione *S*-arenesulfonimides with nucleophiles, *viz.* amines, thiols, halides, and phosphines, including the initial thiophilic attack. S. Tamagaki, K. Sakaki, and S. Oae, *Bull. Chem. Soc. Jpn.*, **47**, 3084 (1974); **48**, 2983, 2985, 2987 (1975); *Heterocycles*, **2**, 631 (1974).

3) Changes of the reaction products by the methods were not observed except for the case of *p*-tolylmagnesium bromide (**d**). A Grignard reagent **d** mainly gave decomposed products of **1** by the method A.

4) M. Ōkubo and K. Maruyama, *Kagaku*, **35**, 338, 467 (1980).

5) In canonical resonance structures I—III of α-thio radical, the contributor III is usually considered to be the major one. E. Block, "Sulfur-Containing Radicals," in "Reactions of Organosulfur Compounds," ed by A. T. Blomquist and H. H. Wasserman, Academic Press, New York (1978), Chap. 5, p. 190.

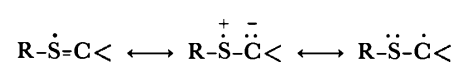

I (**9**) II III (**10**)

6) A. G. Schultz and R. H. Schlessinger, *J. Chem. Soc., Chem. Commun.*, **1970**, 747, 748.

7) See an excellent review quoting many references on reactions of varied sulfines with organometallic reagents. B. Zwanenburg, *Recl. Trav. Chim. Pays-Bas*, **101**, 1 (1982).

8) A. Ohno, M. Uohama, K. Nakamura, and S. Oka, *J. Org. Chem.*, **44**, 2244 (1979); A. Ohno, M. Uohama, and S. Oka, *Bull. Chem. Soc. Jpn.*, **54**, 3231 (1981).

9) T. Saito and S. Motoki, *J. Org. Chem.*, **42**, 3922 (1977).

An Easy Preparation of Triphenylmethyl Carboxylates

Shun-ichi HASHIMOTO, Masahiko HAYASHI, and Ryoji NOYORI*
Department of Chemistry, Nagoya University, Chikusa, Nagoya 464
(Received December 27, 1983)

Synopsis. A new recipe for triphenylmethylation of carboxylic acids and phenol is disclosed.

Triphenylmethylation of carboxylic acids has been conventionally achieved by heating triphenylmethyl bromide and metal carboxylates in nonpolar solvents.[1] Sensitive, polymerizable acrylic acids, however, can be esterified only using the expensive silver salts.[2] We found that condensation of economically accessible trimethylsilyl carboxylates (**1**) and triphenylmethyl fluoride (**2**) proceeds smoothly at room temperature in acetonitrile containing a catalytic amount of tetrafluorosilane (**3**). This facile procedure allows the easy synthesis of triphenylmethyl methacrylate (**4a**),[3] an important material for the preparation of the chiral liquid chromatographic stationary phases.[4,5]

$$\underset{\mathbf{1}}{RCOOSi(CH_3)_3} + \underset{\mathbf{2}}{(C_6H_5)_3CF} \xrightarrow{SiF_4} \underset{\mathbf{4}}{RCOOC(C_6H_5)_3} + (CH_3)_3SiF$$

a: R=CH_2=C(CH_3), **b**: R=*n*-C_9H_{19}, **c**: R=C_6H_5

In a like manner, the tetrafluorosilane-catalyzed reaction of phenyl trimethylsilyl ether and the fluoride **2** gave phenyl triphenylmethyl ether in a high yield.

Experimental

All melting points were uncorrected. IR spectra were recorded on a JASCO IRA-1 spectrometer. ^{1}H NMR spectra were measured with a JEOL JNM FX-90Q (90 MHz) spectrometer using tetramethylsilane as an internal standard. Mass spectra were determined with a Hitachi RMU-6C mass spectrometer, operating with an ionization energy of 70 eV. Tetrafluorosilane (**3**) was purchased form Matheson Co. Triphenylmethyl fluoride (**2**) was prepared by the reported method.[6] Acetonitrile was distilled from CaH_2 before use. All products are known compounds and gave consistent spectral data.

*Triphenylmethyl Methacrylate(**4a**).* To a solution of **1a** (1.25 g, 7.91 mmol) and **2** (2.07 g, 7.91 mmol) in dry acetonitrile (2 cm^3) was added a 0.08 mol dm^{-3} solution of **3** in acetonitrile (4.9 cm^3, 0.396 mmol) at 14 °C under argon atmosphere. After 6-h stirring at this temperature, the resulting yellow mixture was poured into a vigorously stirred, pH 7.4 phosphate buffer (80 cm^3) containing KF (8.0 g) which was kept at 0 °C. The whole mixture was extracted with a 2:1 mixture of ether and hexane (50 cm^3×2), and the combined organic layers were washed with aq $NaHCO_3$ and brine, dried over anhydrous Na_2SO_4, and evaporated *in vacuo*. The residual solid was recrystallized from hexane to give **4a** (2.42 g, 94% yield) as colorless prisms: Mp 98—99 °C (lit,[7] 101—102 °C); IR (CCl_4) 1725, 1490, 1140 cm^{-1}; ^{1}H NMR ($CDCl_3$) δ=1.99 (3H, dd, J=1.0, 1.4 Hz), 5.60 (1H, m), 6.23 (1H, m), 7.2—7.5 (15H, m); MS *m/z* 328 (M$^+$), 260, 259, 243, 183, 165, 105, 85, 83, 77.

The above reaction was carried out in acetonitrile-d_3 for 6 h, and the reaction mixture was subjected to ^{1}H NMR analysis, which indicated the production of the theoretical amount of trimethylfluorosilane[8] (δ=0.21, d, $J_{CH_3,F}$=7.5 Hz) in addition to **4a**.[9]

*Triphenylmethyl Decanoate (**4b**).* A mixture of **1b** (232 mg, 0.95 mmol), **2** (249 mg, 0.95 mmol), and **3** (0.08 mol dm^{-3} in acetonitrile, 0.62 cm^3, 0.05 mmol) in acetonitrile (2.5 cm^3) was stirred at 16 °C for 6 h. The reaction mixture was worked up as described above, and the oily residue was chromatographed on silica gel, which had been treated with triethylamine (2%), using a 5:1 mixture of hexane and ether as an eluent. Pure **4b** was obtained as a colorless oil (361 mg, 88%): IR (CCl_4) 1760, 1500, 1150 cm^{-1}; ^{1}H NMR ($CDCl_3$) δ=0.87 (3H, br t, J=6.0 Hz), 1.07—1.73 (14H, m) 2.43 (2H, t, J=6.8 Hz) 7.1—7.4 (15H, m); MS *m/z* 414 (M$^+$), 260, 259, 244, 243, 165, 78, 77.

*Triphenylmethyl Benzoate (**4c**).* A mixture of **1c** (372 mg, 1.92 mmol), **2** (503 mg, 1.92 mmol), and **3** (0.08 mol dm^{-3} in acetonitrile, 1.2 cm^3, 0.1 mmol) in acetonitrile (4 cm^3) was stirred at 16 °C for 4 h. Workup followed by recrystallization from a 10:1 mixture of hexane and benzene afforded **4c** (671 mg, 96%) as colorless plates: Mp 170—171 °C (lit,[1] 168—170 °C); IR (CCl_4) 1740, 1600, 1500, 1270 cm^{-1}; ^{1}H NMR ($CDCl_3$) δ=7.1—7.6 (18H, m), 8.13 (2H, J=1.5, 7.8 Hz); MS *m/z* 364 (M$^+$), 260, 259, 244, 243, 85, 83.

Phenyl Triphenylmethyl Ether. A mixture of phenyl trimethylsilyl ether (166 mg, 1.0 mmol), **2** (262 mg, 1.0 mmol), and **3** (0.08 mol dm^{-3} in acetonitrile, 0.63 cm^3, 0.05 mmol) in acetonitrile (2 cm^3) was stirred at 15 °C for 24 h. Aqueous workup followed by column chromatography on 2% triethylamine-treated silica gel using a 30:1 mixture of hexane and ether as an eluent, afforded the product (286 mg, 85%) as a colorless oil. This oil crystallized as colorless prisms from ethanol solution: Mp 103—104 °C (lit,[10] 103 °C); IR (CCl_4) 1600, 1500, 1450, 1220 cm^{-1}; ^{1}H NMR ($CDCl_3$) δ=6.6—7.1 (5H, m) 7.1—7.5 (15H, m); MS *m/z* 244, 243, 165, 94.

References

1) K. D. Berlin, L. H. Gower, J. W. White, D. E. Gibbs, and G. P. Sturm, *J. Org. Chem.*, **27**, 3595 (1962).

2) H. Yuki, K. Hatada, Y. Kikuchi, and T. Niinomi, *J. Polym. Sci. Part B*, **6**, 753 (1968).

3) For the preparation of **4a** from **1a** and triphenylmethyl trimethylsilyl ether, see: S. Murata and R. Noyori, *Tetrahedron Lett.*, **22**, 2107 (1981).

4) Y. Okamoto, K. Suzuki, K. Ohta, K. Hatada, and H. Yuki, *J. Am. Chem. Soc.*, **101**, 4763 (1979); H. Yuki, Y. Okamoto, and I, Okamoto, *ibid.*, **102**, 6356 (1980); Y. Okamoto, I. Okamoto, and H. Yuki, *Chem. Lett.*, **1981**, 835; Y. Okamoto, I. Okamoto, and H. Yuki, *J. Polym. Sci. Polym. Lett. Ed.*, **19**, 451 (1981); Y. Okamoto, S. Honda, I. Okamoto, H. Yuki, S. Murata, R. Noyori, and H. Takaya, *J. Am. Chem. Soc.*, **103**, 6971 (1981); R. Noyori, N. Sano, S. Murata, Y. Okamoto, H. Yuki, and T. Ito, *Tetrahedron Lett.*, **23**, 2969 (1982); Y. Kawada, H. Iwamura, Y. Okamoto, and H. Yuki, *ibid.*, **24**, 791 (1983).

5) A column of (+)-poly(triphenylmethyl methacrylate) coated on macroporous silica gel (Chiralpak OT) is available from Japan Spectroscopic Co. Ltd., Ishikawa-cho, Hachioji,

Tokyo.
6) G. A. Olah, J. T. Welch, Y. D. Vankar, M. Nojima, I. Kerekes, and J. A. Olah, *J. Org. Chem.*, **44**, 3872 (1979).
7) N. A. Adrova and L. K. Prokhorova, *Vysokomol. Soedin.*, **3**, 1509 (1961); *Chem. Abstr.*, **56**, 10384 (1962).
8) A. E. Newkirk, *J. Am. Chem. Soc.*, **68**, 2736 (1946).
9) Other Lewis acids such as BF_3, $AlCl_3$ (in CH_3CN), and $TiCl_4$ (in CH_2Cl_2) also acted as catalyst of this reaction.
10) A. Baeyer, *Ber.*, **42**, 2625 (1909).

Prenylation of Aromatic Amines and Nitrogen-containing Aromatic Heterocycles by Prenyl Diisopropyl Phosphate

Shuki ARAKI, Shin-ichi MANABE, and Yasuo BUTSUGAN*
Department of Synthetic Chemistry, Nagoya Institute of Technology, Gokiso-cho, Showa-ku, Nagoya 466
(Received January 5, 1984)

Synopsis. Lewis-acid catalyzed prenylation of aromatic amines with prenyl diisopropyl phosphate gave *N*-prenylated amines, whereas nitrogen-containing aromatic heretocycles gave nucleus prenylated products.

N-Alkylation of amines by trialkyl phosphates is well documented. For example, Billman *et al.* reported that trimethyl and triethyl phosphates readily alkylate various anilines to *N,N*-dialkylanilines in good yields.[1] Recently, Kinoshita and his coworkers described the methylation and ethylation of nucleic acid-bases by means of trimethyl and triethyl phosphates.[2] Moreover, they succeeded the allylation of nucleic acid-bases by triallyl phosphate.[3] *N*-Prenylation of amines by prenyl phosphates is a biogenetically important process, because naturally occurring amines such as cytkinin[4] and acrophylline,[5] which bear a prenyl group on the nitrogen atom, are proposed to be biosynthesized *via* *N*-prenylation with prenyl pyrophosphate. However, there have been no studies describing the prenylation of amines by the use of prenyl phosphate. Here we wish to report the reaction of prenyl diisopropyl phosphate (PDIPP) with aromatic amines and nitrogen-containing aromatic heterocycles in an attempt to have insight into the nature of the prenylation of amines by prenyl phosphate.

When a mixture of aniline and PDIPP was treated with boron trifluoride etherate in dimethyl sulfoxide (DMSO) at room temperature, the reaction proceeded and *N*-prenylaniline (**1**) and *N,N*-diprenylaniline (**2**) were obtained in 12 and 10% yields, respectively, after column chromatography on silica gel. As minor products, trace amounts of 2-prenylaniline (**3**) and 2-(1,1-dimethyl-2-propenyl)aniline (**4**) were also isolated from the reaction mixture. The formation of **3** and **4** may be rationalized in terms of the Lewis acid-catalyzed amino-Claisen rearrangement[6] of the initially formed *N*-prenylaniline (**1**). In the absence of the Lewis acid, the reaction did not occur. The use of polar aprotic solvents such as DMSO and *N,N*-dimethylformamide (DMF) was essential for the present reaction. In other solvent such as ether, dichloromethane, and benzene, no characterized products were obtained. Under the similar conditions, *N*-methylaniline gave 56% yield of *N*-methyl-*N*-prenylaniline (**5**) accompanied by a small amount (1.2% yield) of *N*-methyl-*N*,4-diprenylaniline (**6**). For the latter, the position of the prenyl group on the benzene ring was determined by the ^{13}C NMR spectral analysis. The prenylation of diphenylamine gave *N,N*-diphenylprenylamine (**7**) (24% yield) as the main product. Nucleus-prenylated products, 4-(or 2-)prenyldiphenylamine (**8**) (7%) and *N*-phenyl-*N*,4-(or 2)diprenylaniline (**9**) (3%) were also formed, but the prenylated position remained uncertain. Aliphatic amines such as diisopropylamine and pyrrolidine could not be prenylated by the present method.

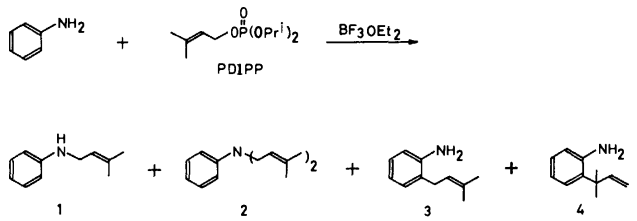

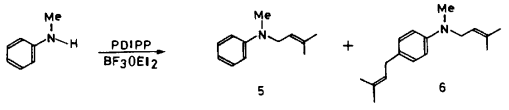

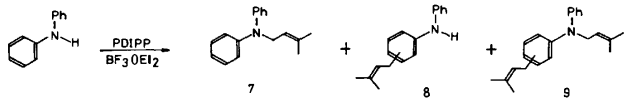

Nitrogen-containing aromatic heterocycles, pyrrole and indole, are also susceptible to prenylation by PDIPP. Pyrrole gave a mixture of 2-prenylpyrrole (**10**) (34% yield), 2-(1,1-dimethyl-2-propenyl)pyrrole (**11**) (10%), and 3-prenylpyrrole (**12**) (6%), and indole gave 3-prenylindole (**13**) (21% yield) and 3-(1,1-dimethyl-2-propenyl)indole (**14**) (5%). Unlike the cases of aromatic amines described above, *N*-prenylated products could not be found in the reaction mixtures. This result contrasts to the fact that the methylation of indole with trimethyl phosphate gives only 1-methylindole.[7]

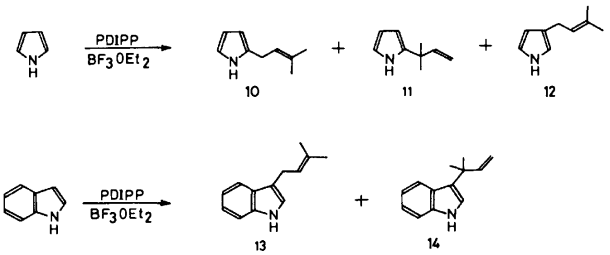

Experimental

General. Infrared spectra were recorded on a JASCO IRA-1 spectrometer. ^1H NMR spectra were determined with a Hitachi R-24A spectrometer (60 MHz). Chemical shifts (δ) are recorded in ppm downfield from Me_4Si. Mass spectra were measured on a Hitachi M-52 mass spectrometer, operating with an ionization energy of 20 eV. GLPC analyses and preparative GLPC were performed on a Yanaco G1800 gas chromatograph. Elemental analyses were performed at the Elemental Analysis Center of Kyoto University.

Reaction of Aniline with Prenyl Diisopropyl Phosphate. To a solution of aniline (470 mg, 5 mmol) and prenyl diisopropyl phosphate (1.27 g, 5.1 mmol) in DMSO (10 ml) was added boron trifluoride etherate (1.99 g, 14 mmol) at

room temperature and the mixture was stirred for 16 h. Saturated aqueous sodium hydrogencarbonate was added and the products were extracted with light petroleum. The extracts were washed with water and brine, dried over anhydrous magnesium sulfate, and concentrated. The residue was column chromatographed on silica gel with benzene as an eluent to give *N*-prenylaniline (**1**)[6] (92 mg, 12% yield), *N,N*-diprenylaniline (**2**)[6] (118 mg, 10%), and trace amounts of 2-prenylaniline (**3**)[6] (5 mg) and 2-(1,1-dimethyl-2-propenyl)aniline (**4**) (1 mg).

4: ^{1}H NMR (CCl_4) δ=6.40—7.00 (m, 5H, ring), 5.00—5.90 (m, 3H, olefin), 3.20 (br s, 2H, NH_2), 1.35 (s, 6H, CH_3).

Reaction of N-*Methylaniline with Prenyl Diisopropyl Phosphate.* To a solution of *N*-methylaniline (550 mg, 5.1 mmol) and prenyl diisopropyl phosphate (2.02 g, 8.1 mmol) in DMF (10 ml) was added boron trifluoride etherate (1.26 ml, 10 mmol) under nitrogen at room temperature and the mixture was stirred for 15 h. The reaction mixture was treated as above. Silica-gel column chromatography (benzene as an eluent) gave *N*-methyl-*N*-prenylaniline (**5**) (499 mg, 56%) and *N*-methyl-*N*,4-diprenylaniline (**6**) (15 mg, 1.2%).

5:[8] IR (neat) 2970, 2910, 1670, 1600, 1510, 1450, 1310, 1250, and 695 cm^{-1}; ^{1}H NMR (CCl_4) δ=6.40—7.30 (m, 5H, ring), 5.15 (t, J=6 Hz, 1H, olefin), 3.80 (d, J=6 Hz, 2H, CH_2), 2.80 (s, 3H, CH_3), 1.69 (s, 6H, CH_3).

6: IR (neat) 2960, 2920, 1670, 1590, 1510, 1440, 1245, and 693 cm^{-1}; ^{1}H NMR (CCl_4) δ=6.40—7.30 (m, 4H, ring), 5.10 (br t, 2H, olefin), 3.80 (d, J=6 Hz, 2H, CH_2), 3.35 (d, J=6 Hz, 2H, CH_2), 2.80 (s, 3H, CH_3), 1.65 (br s, 12H, CH_3); ^{13}C NMR ($CDCl_3$) 151.2 (s), 136.8 (s), 132.5 (s), 121.3 (s), 129.8 (d), 126.3 (d), 123.5 (d), 120.3 (d), 55.2 (t, N-CH_2), 41.5 (t, Ph$\underline{C}H_2$), 29.2 (q, N-CH_3), 25.9 (q), 25.8 (q), 18.0 (q), 17.9 (q); MS *m/z* (rel intensity) 243 (M^+; 13) and 174 (100); Found: C, 84.17; H, 10.60%. Calcd for $C_{17}H_{25}N$: C, 83.89; H, 10.35%.

Reaction of Diphenylamine with Prenyl Diisopropyl Phosphate. To a solution of diphenylamine (852 mg, 5.0 mmol) and prenyl diisopropyl phosphate (2.00 g, 8.0 mmol) in DMF (10 ml) was added boron trifluoride etherate (1.26 ml, 10 mmol) under nitrogen at room temperature and the mixture was stirred for 15 h. Work-up and column chromatography on silica gel with benzene-light petroleum (1:3) gave *N,N*-diphenylprenylamine (**7**)[9] (280 mg, 24%), 4(or 2-)prenyldiphenylamine (**8**) (85 mg, 7%), and *N*-phenyl-*N*,4(or 2)-diprenylaniline (**9**) (40 mg, 3%).

8: IR(neat) 3400, 2980, 2930, 1595, 1500, 1450, 1310, 750, and 695 cm^{-1}; ^{1}H NMR (CCl_4) δ=6.40—7.50 (m, 9H, ring), 5.15 (t, J=6 Hz, 1H, olefin), 5.05 (br s, 1H, NH), 3.24 (d, J=6 Hz, 2H, CH_2), 1.73 (s, 6H, CH_3); MS *m/z* (rel intensity) 237 (M^+; 100); Found: C, 86.09; H, 8.15%. Calcd for $C_{17}H_{19}N$: C, 86.03; H, 8.07%.

9: IR (neat) 2980, 2930, 1595, 1500, 1450, 1355, 1260, 750, and 695 cm^{-1}; ^{1}H NMR (CCl_4) δ=6.20—7.20 (m, 9H, ring), 5.20 (m, 2H, olefin), 4.03 (d, J=6 Hz, 2H, N-CH_2), 3.10 (d, J=6 Hz, 2H, CH_2), 1.62 (s, 6H, CH_3), 1.50 (s, 6H, CH_3); MS *m/z* (rel intensity) 305 (M^+; 35) and 236 (100); Found; C, 86.53; H, 9.21%. Calcd for $C_{22}H_{27}N$: C, 86.51; H, 8.91%.

Reaction of Pyrrole with Prenyl Diisopropyl Phosphate. To a solution of pyrrole (680 mg, 10.1 mmol) and prenyl diisopropyl phosphate (4.01 g, 16 mmol) in DMF (20 ml) was added boron trifluoride etherate (2.52 ml, 20 mmol) under nitrogen at room temperature and the mixture was stirred for 15 h. Work-up and column chromatography on silica gel (benzene-light petroleum=1:1) gave a mixture (679 mg, 50% yield) of 2-prenylpyrrole (**10**), 2-(1,1-dimethyl-2-propenyl)pyrrole (**11**), and 3-prenylpyrrole (**12**). GLPC analysis (Apiezon Grease L on Uniport B (15%), 1 m×3 mm, temp 130 °C, He 90 ml/min) revealed that the ratio of **10**:**11**:**12** was 68:20:12. They were separated by preparative GLPC.

10: IR (neat) 3400, 2970, 1678, 1568, 1440, 1378, 1022, 768, and 710 cm^{-1}; ^{1}H NMR ($CDCl_3$) δ=6.60 (m, 1H, pyrrole H^5), 5.75—6.20 (m, 2H, pyrrole H^3 and H^4), 5.30 (t, J=7 Hz, 1H, olefin), 3.30 (d, J=7 Hz, 2H, CH_2), 1.70 (s, 6H, CH_3); MS *m/z* (rel intensity) 135 (M^+; 100). Found: C, 80.16; H, 9.79%. Calcd for $C_9H_{13}N$: C, 79.95; H, 9.69%.

11: IR (neat) 3400, 2980, 1700, 1455, 1378, 1020, and 764 cm^{-1}; ^{1}H NMR ($CDCl_3$) δ=6.65 (m, 1H, pyrrole H^5), 5.75—6.25 (m, 3H, olefin and pyrrole H^3 and H^4), 4.85—5.20 (m, 2H, olefin), 1.35 (s, 6H, CH_3); MS *m/z* (rel intensity) 135 (M^+; 100); Found: C, 80.24; H, 9.89%. Calcd for $C_9H_{13}N$: C, 79.95; H, 9.69%.

12: IR (neat) 3400, 2910, 1680, 1550, 1436, 1372, 1052, 760 and 705 cm^{-1}; ^{1}H NMR ($CDCl_3$) δ=6.45—6.80 (m, 2H, pyrrole H^2 and H^5), 6.10 (m, 1H, pyrrole H^4), 5.35 (t, J=7 Hz, 1H, olefin), 3.20 (d, J=7 Hz, 2H, CH_2), 1.69 (s, 6H, CH_3); MS *m/z* (rel intensity) 135 (M^+; 100); Found: C, 79.97; H, 9.98%. Calcd for $C_9H_{13}N$: C, 79.95; H, 9.69%.

Reaction of Indole with Prenyl Diisopropyl Phosphate. To a solution of indole (586 mg, 5.0 mmol) and prenyl diisopropyl phosphate (2.00 g, 8.0 mmol) in DMF (10 ml) was added boron trifluoride etherate (1.26 ml, 10 mmol) under nitrogen at room temperature. The reaction mixture was stirred for 13 h and treated as above. Column chromatography on silica gel (benzene-light petroleum=1:1) gave a mixture (242 mg, 26% yield) of 3-prenylindole (**13**) and 3-(1,1-dimethyl-2-propenyl)indole (**14**) as a yellow oil. GLPC (Apiezon Grease L on Uniport B (15%), 1 m×3 mm, temp 200 °C, He 90 ml/min) of the oil showed two peaks of **13** and **14** in the ratio of 82:18. They were separated by preparative GLPC.

13:[10] IR (neat) 3420, 2960, 1640, 1450, 1360, and 740 cm^{-1}; ^{1}H NMR (CCl_4) δ=6.90—7.70 (m, 5H, benzene ring and NH), 6.70 (br s, 1H, H^2), 5.40 (t, J=7 Hz, 1H, olefin), 3.40 (d, J=7 Hz, 2H, CH_2), 1.73 (s, 6H, CH_3); MS *m/z* (rel intensity) 185 (M^+; 100).

14: IR (neat) 3420, 2960, 1640, 1450, 1360, and 740 cm^{-1}, ^{1}H NMR (CCl_4) δ=6.70—8.00 (m, 6H, benzene ring and NH), 4.75—6.50 (m, 3H, olefin), 1.49 (s, 6H, CH_3); MS *m/z* (rel intensity) 185 (M^+; 51) and 170 (100).

References

1) J. H. Billman, A. Radike, and B. W. Mundy, *J. Am. Chem. Soc.*, **64**, 2977 (1942); D. G. Thomas, J. H. Billman, and C. E. Davis, *ibid.*, **68**, 895 (1946).

2) K. Yamauchi, T. Tanabe, and M. Kinoshita, *J. Org. Chem.*, **41**, 3691 (1976); T. Tanabe, K. Yamauchi, and M. Kinoshita, *Bull. Chem. Soc. Jpn.*, **50**, 3021 (1977).

3) T. Tanabe, K. Yamauchi, and M. Kinoshita, *Bull. Chem. Soc. Jpn.*, **52**, 259 (1979).

4) L. K. Kline, F. Fittler, and R. Hall, *Biochemistry*, **8**, 4361 (1969).

5) F. N. Lahey and M. McCamish, *Tetrahedron Lett.*, **1968**, 1525.

6) N. Takamatsu, S. Inoue, and Y. Kishi, *Tetrahedron Lett.*, **1971**, 4661; *Yakugaku Zasshi*, **97**, 553, 558 (1977); J. Tanaka, K. Takabe, K. Taniguchi, and T. Katagiri, *Nippon Kagaku Kaishi*, **1981**, 1043.

7) K. Yamauchi and M. Kinoshita, *J. Chem. Soc., Perkin Trans. 1*, **1973**, 2506.

8) H. H. Kachani, J. J. Perie, and A. Lattes, *Chem. Lett.*, **1976**, 405.

9) W. E. Parham and J. R. Potoski, *J. Org. Chem.*, **32**, 278 (1967).

10) G. Casnati, M. Francioni, A. Guareschi, and A. Pochini, *Tetrahedron Lett.*, **1969**, 2485.

Oxidation of Alcohols *via* Alkoxymagnesium Halides by an NAD$^+$ Model Compound[1)]

Seiji SHINKAI,* Hiroyuki ERA, Takaharu TSUNO, and Osamu MANABE
Department of Industrial Chemistry, Faculty of Engineering, Nagasaki University, Nagasaki 852
(Received January 25, 1984)

Synopsis. Alkoxymagnesium bromides prepared from phenylmagnesium bromide and alcohols are capable of reducing an NAD$^+$ model compound to the 1,4-dihydronicotinamide in good yields. The carbonyl products were detected in quantitative yields from diphenylmethanol and 1-phenylethanol but in low yields from benzyl alcohol and aliphatic alcohols. This is a new route to 1,4-dihydronicotinamides with alcohols although it remains uncertainty whether or not the route has relevance as a model process for NAD$^+$ oxidaiton of alcohols.

In alcohol dehydrogenases, the interconversion of aldehydes (or ketones) and alcohols occurs in conjunction with that of NADH and NAD$^+$ coenzymes. In contrast to a number of investigations on the NADH model reduction of carbonyl substrates, there are only a few examples for the NAD$^+$ model oxidation of alcoholic substrates.[2-5)] The contrast suggests the difficulty to mimick the NAD$^+$-dependent oxidations in model systems. Interestingly, it is well established that 5-deazaflavin and its analogs which have the isoelectronic structure to NAD$^+$ can oxidize alcohols,[6-8)] but the mechanistic difference between 5-deazaflavin and NAD$^+$ is not well understood. One important information to exploit NAD$^+$ model oxidation would be the fact that protic or acidic media are very favorable to reduction of carbonyls by NADH,[9,10)] whereas oxidation of alcohols by 5-deazaflavin proceeds favorably in basic media.[11)] The findings are quite understandable from a viewpoint of the principle of the microscopic reversibility. Meanwhile, some metal ions such as Mg^{2+} and Zn^{2+} play a crucial role not only in the dehydrogenase reduction but also in the NADH model reduction.[12)] The principle suggests, therefore, that alcohols would be oxidized by an NAD$^+$ model compound through the metal (Mg^{2+} or Zn^{2+}) alkoxide intermediates. We here report that alkoxymagnesium halides prepared from a Grignard reagent and alcohols are capable of reducing an NAD$^+$ model compound to the 1,4-dihydronicotinamide in good yields, although the yields of the carbonyl products are in some cases unstatisfactory.

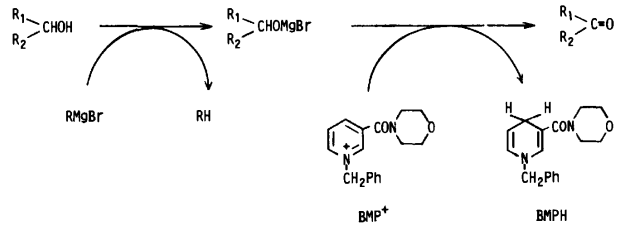

We used 1-benzyl-3-morpholinocarbonylpyridinium bromie (BMP$^+$) as an NAD$^+$ model compound. BMP$^+$ was prepared by the reaction of 3-morpholinocarbonylpyridine[2)] and benzyl bromide in benzene at reflux temperature for 4 h; mp 117—120 °C, yield 80.8%. Found: C, 55.63; H, 5.33; N, 7.49%. Calcd for $C_{17}H_{19}N_2O_2Br$: C, 56.21; H, 5.27; N, 7.71%.

1-Benzyl-3-morpholinocarbonyl-1,4-dihydropyridine (BMPH) was prepared from BMP$^+$ and $Na_2S_2O_4$ according to the method of Kim and Chaykin[13)]; oil, one spot on TLC, yield 64%. NMR (Me_2SO-d_6): 4-CH_2, δ= 3.00, 2H; morpholine protons, 3.35 (4H) an 3.52 (4H); 5- and 6-H, 4.2—4.4, 2H; N-CH_2, 5.97, 2H; 2-H and benzene protons, 7.3—7.4, 6H. The mixture of BMPH and 1-benzyl-3-morpholinocarbonyl-1,6-dihydropyridine was prepared by the reduction of BMP$^+$ by $NaBH_4$ in methanol. The ratio of 1,4- *vs.* 1,6-isomer determined on the basis of NMR[14)] was 57/43.

A typical experimental procedure is as follows: phenylmagnesium bromide (3.5 mmol) was prepared in 10 ml of anhydrous tetrahydrofuran (THF). Alcohol (3.5 mmol) was added and the reaction mixture was stirred for 3 h at room temperature under a nitrogen stream. Then, BMP$^+$ (2.8 mmol) in a mixed solvent of 20 ml THF and 20 ml *N*,*N*-dimethylformamide was added. The progress of the reaction (25 °C) was monitored analyzing the aliquot withdrawn from the reaction mixture. The yield of the dihydronicotinamide was directly determined by HPLC analysis: Shimadzu LC-3, Lichroprep RP-18, acetonitrile: water=8:2 v/v. To determine the yields of the oxidized carbonyl products the sample was once mixed with aqueous solution (pH 4) and extracted with chloroform. The chloroform solution was analyzed on GLC. Both methods had been certified by making the calibration curves using the authentic samples.

In the HPLC analysis we could detect BMPH, but

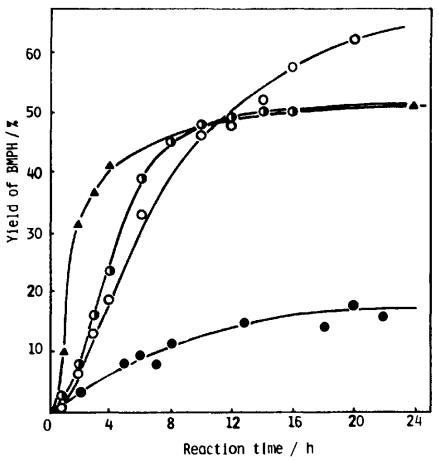

Fig. 1. Time-dependence of the yield of BMPH (1,4-isomer). ▲: Diphenylmethanol, ●: benzyl alcohol, ◑: 1-octanol, ○: cyclohexanol. The plot for 1-phenylethanol is essentially identical to that for diphenylmethanol.

Table 1. Product analysis for the reaction of BMP^+ and alkoxymagnesium bromides

Alcohol	Reaction time / h	Yield/%[a] BMPH	Yield/%[a] Carbonyl compound
Diphenylmethanol	24	51.2	100
1-Phenylethanol	24	52.0	100
Benzyl alcohol	5	8.8	0.2
	22	15.8	0.2
1-Octanol	4	24.1	0.9
	16	50.8	0.8
Cyclohexanol	8	40.3	trace ($\approx$0.1)
	20	61.9	trace ($\approx$0.1)

a) Yield based on BMP^+.

neither the 1,6-isomer nor the 4,4'-dimer[15] was detected. Speculating from the accuracy of the HPLC analysis, the yield of the 1,6-isomer (even if it was produced) would be less than 3%. The time-dependence of the BMPH yield is illustrated in Fig. 1 and the typical results are summarized in Table 1.

The oxidation of alcohols by 5-deazaflavin and its analogs affords the oxidized carbonyl products in good yields and in some cases the yields under aerobic conditions exceed 100% because of the autorecycling nature.[6-8] In the previous experiments of NAD^+ model oxidation, however, the analysis of the oxidized products was rather incomplete or unsuccessful: For example, the analysis of acetaldehyde was not carried out in the reaction with lithium ethoxide[3] and the oxidized product could not be detected in spite of the authors' best efforts in the reaction with glyceraldehyde.[4] We found that the reaction with diphenylmethanol and 1-phenyethanol affords the corresponding ketones in quantitative yields, whereas benzaldehyde expected for the oxidation of benzyl alcohol could be detected only in 0.2% yield. We first considered that the difference might be attributed to the steric difference between primary and secondary alcohols, because the unfavorable adduct formation between alkoxides and BMP^+ would be relatively suppressed in sterically crowded secondary alcohols. In fact, it was suggested in the oxidation by 5-deazaflavin analogs that to suppress the adduct formation leads to the efficient oxidation of alcohols.[8] This may be true for aromatic alcohols but is not the case for aliphatic alcohols, because the oxidation of cyclohexanol, as well as that of 1-octanol, gave only a trace amount of cyclohexanone. Two possibilities come to mind as a general scheme to explain the reaction. First, these reaction products may undergo further reaction in the strongly basic reaction solution. In relation to this, we observed that the yields increase up to 3—4% in the initial stage and then decrease. The second possibility is associated with the adduct formation proposed by Ohno *et al.*[4] In the HPLC analysis we sometimes detected a few unknown peaks (absorbing at around 350 nm) other than the 4,4'-dimer, but these peaks were not found for the oxidation of diphenylmethanol and 1-phenylethanol. Hence, the whole story of this reaction may be more complex than described by a single scheme. Further extensive studies are thus necessitated to answer this question.

It is known that 1,4-dihydronicotinamides result selectively from the oxidation of lithium ethoxide or glyceraldehyde.[3,4] Also in our reaction with alkoxymagnesium bromides, the 1,4-isomer of BMPH was produced selectively. As seen in Fig. 1, the reactions with diphenylmethanol and 1-phenylethanol ($t_{1/2}$ 1,4-2 h) was much faster than those with benzyl alcohol (6 h), 1-octanol (4 h), and cycloloxanol (7 h). It may be of some significance that the reactions yielding the corresponding carbonyl products are faster than others.

In the previous examples the yields of 1,4-dihydronicotinamides obtained from the 1:1 molar ratio reaction are not high (21—28%).[2,3] On the other hands, the yields of BMPH in the present system are much higher (50.8—61.9%) except benzyl alcohol. In particular, one can expect not only the high yield of BMPH but also the quantitative production of the ketones for the oxidation of diphenylmethanol and 1-phenethyl alcohol. We believe, therefore, that although it is still equivocal mechanistically whether or not the present reaction has direct relevance to NAD^+-dependent oxidations, the method is undoubtedly useful as a convenient route to 1,4-dihydronicotinamides with "alcohols."

References

1) Coenzyme Models 38. Part 37: S. Shinkai, Y. Ishikawa, H. Shinkai, T. Tsuno, H. Makishima, K. Ueda, and O. Manabe, *J. Am. Chem. Soc.*, **106**, 1801 (1984).

2) A. Shirra and C. J. Suckling, *J. Chem. Soc., Perkin Trans. 2*, **1977**, 759.

3) Y. Ohnishi and M. Kitami, *Tetrahedron Lett.*, **1978**, 4035.

4) A. Ohno, S. Ushida, and S. Oka, *Tetrahedron Lett.*, **23**, 2487 (1982); *Bull. Chem. Soc. Jpn.*, **56**, 1822 (1983).

5) K. Wallenfels and W. Hanstein, *Angew. Chem., Int. Ed. Engl.*, **4**, 869 (1965).

6) F. Yoneda, Y. Sakuma, and P. Hemmerich, *J. Chem. Soc., Chem. Commun.*, **1977**, 825.

7) F. Yoneda, R. Hirayama, and M. Yamashita, *Chem. Lett.*, **1980**, 1157.

8) S. Shinkai, H. Hamada, H. Kuroda, and O. Manabe, *Chem. Lett.*, **1980**, 1235; *J. Org. Chem.*, **46**, 2333 (1981).

9) P. van Eikeren and D. L. Grier, *J. Am. Chem. Soc.*, **98**, 4655 (1976).

10) S. Shinkai and T. Kunitake, *Chem. Lett.*, **1977**, 297; S. Shinkai, H. Hamada, T. Ide, and O. Manabe, *ibid.*, **1978**, 685.

11) S. Shinkai, H. Kuroda, and O. Manabe, *Tetrahedron Lett.*, **1982**, 1357.

12) For example, D. S. Sigman, J. Hadju and D. J. Creighton, "Bioorganic Chemistry," ed by E. E. van Tamelen, Academic Press, New York, (1978), Vol. 4, Chapt. 14; A. Ohno, *Kagaku Sohsetsu*, **35**, 141 (1982).

13) C. S. Y. Kim and S. Chaykin, *Biochemistry*, **7**, 2339 (1968).

14) Y. Ohnishi and S. Tanimoto, *Tetrahedron Lett.*, **1977**, 1909.

15) The 4,4'-dimer was prepared according to the method of Ohnishi and Kitami[16] and used for the HPLC analysis without further purification.

16) Y. Ohnishi and M. Kitami, *Bull. Chem. Soc. Jpn.*, **52**, 2674 (1979).

Resistance to Alkali of the Nascent Fibril Produced by *Acetobacter xylinum*

Akira KAI* and Tomoki KOSEKI
Department of Industrial Chemistry, Faculty of Technology, Tokyo Metropolitan University, Fukazawa, Setagaya-ku, Tokyo 158
(Receivd October 31, 1983)

Synopsis. The resistance of the nascent fibril produced by *Acetobacter xylinum* to alkali is lower than that of the crystalline cellulose I and higher than that of the amorphous cellulose. In the nascent fibril the cellulose chains are thougth to be in the form of cellulose sheets corresponding to the (1$\bar{1}$0) plane of cellulose I.

Investigation of the structure of the nascent fibril produced by *Acetobacter xylinum (A. xylinum)* is very important for the clarification of the biogenesis and the structure of bacterial cellulose. We have studied the structure of cellulose fibril after production by *A. xylinum*, in particular its staining behavior toward heavy metal salts[1] and its resistance to alkali.[2,3] However, the structure of nascent fibril is not yet clear enough. In this paper, therefore, the structure of nascent fibril produced by *A. xylinum* was examined from the aspects of the resistance to alkali of the never-air-dried fibrils. These were formed by glucose incubation for 3 h at 28 °C; they did not contain any crystalline microscopic fibril but were composed of 15 wt% of the amorphous fibril and 85 wt% of the fibril having the uneven staining behavior.[2]

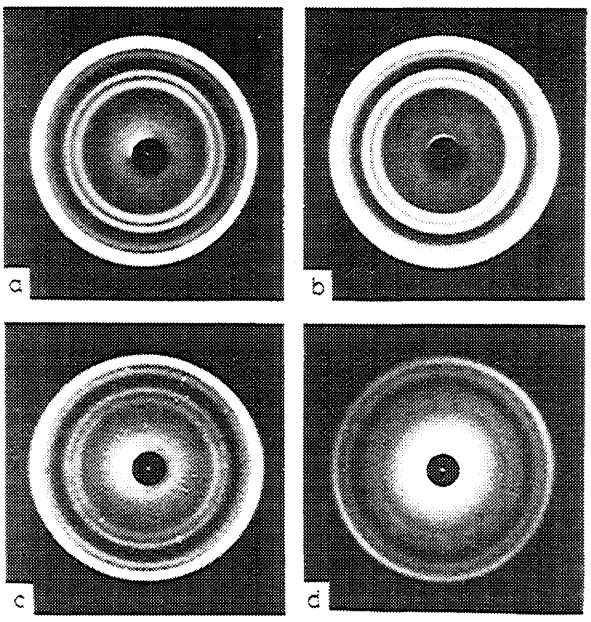

Fig. 1. X-Ray photographs of alkali-treated samples. a: Purified and dried sapmle obtained from the complex incubation for 2d at 28 °C, b: 10.8 wt% alkali-treated sample made from purified and dried sample a, c: 9.0 wt% alkali-treated never-air-dried cellulose obtained from the glucose incubation for 3 h at 28 °C, d: 10.8 wt% alkali-treated never air-dried cellulose obtained from the incubation of the same conditions as sample c.

The never-air-dried cellulose samples from the 3 h incubation were treated with 9.0 or 10.8 wt% aqueous NaOH solution. The X-ray diffraction diagram of 9.0 wt% alkali-treated sample showed only the diffraction of cellulose I, but not that of cellulose II (Fig. 1c). On the other hand, very little diffraction of the (1$\bar{1}$0) plane of cellulose II was found in the X-ray diffraction diagram of 10.8 wt% alkali-treated sample (Fig. 1d). In the diffraction diagram of the 10.8 wt% alkali-treated purified and dried sample, of course, the diffraction of cellulose II does not occur (Fig. 1b).

As described in the previous paper,[2] from the relationship between the change in the morphology of an amorphous fibril after production and the increase in the yield of cellulose with the incubation time, it is presumed that in the never-air-dried cellulose from the 3 h incubation some amorphous fibrils (about 15 wt%) are contained. However, it is considered that such amorphous fibril (15 wt%) will not shown up on the X-ray diffraction diagram of the 10.8 wt% alkali-treated sample. If the cellulose chains are arranged at random in the cross-section of an amorphous fibril, some cellulose chains in the low order region may be dissolved by alkali-treatment with 9.0—10.8 wt% aqueous NaOH solution. But, as shown in Table 1, the values for each weight of alkali-treated samples coincides with the values of each untreated sample, within the experimental errors. This result shows that the cellulose chains are not rejected by alkali-treatment. Accordingly, the X-ray test shows that the resistance of an amorphous fibril to alkali is close to that of the crystalline cellulose I.

The results shown above suggest that in the cross-section of amorphous fibril, as one of the authors described previously,[3] the cellulose chains are in the form of monomolecular layers corresponding to the (1$\bar{1}$0) plane of cellulose I. The amorphous fibril may include staining agent, water and culture substrates between (1$\bar{1}$0) planes.[3] This idea is supported by the studies on the alkali-treatment of cotton,[4,5] which conclude that the structure of a cellulose sheet formed by hydrophobic bond does not easily change by alkali-treatment.

TABLE 1. COMPARISON OF WEIGHTS OF ALKALI-TREATED AND UNTREATED NEVER-AIR-DRIED CELLULOSE FROM THE 3 h GLUCOSE INCUBATION

Concn of NaOH/wt%	Untreated	9.0	Untreated	10.8
Weight (mg/720 ml)	0.18	0.19	0.15	0.17

a) 720 ml is the volume of the culture medium.

Experimental

The culture of *A. xylinum* and the alkali-treatment of the never-air-dried cellulose were as described previously.[2,3] 40 ml of 3 wt% glucose medium (pH 6.8) was added to 200 ml of cellulose-free cell suspension and the mixture was then incubated at 28 °C for 3 h. To the incubated medium was gradually added dropwise an equal volume of aqueous NaOH, two times as dense as the given concentration. After gently making a homogeneous alkali solution, we kept the solution at 20 °C for 1 h and then added 30 vol% aqueous acetic acid solution to neutralize it. The solution was dialyzed through Cellulose Dialyzer Tubing (Nakarai Chemical Ltd, through M. W. cut-off: 8000, diameter: 90 mm, thickness: 0.09 mm) until it became sodium acetate free. The requisite quantity of cellulose for the X-ray photographing was obtained from preparing many times over (1 cycle/week). The dialyzed solution from many times preparations was boiled to collect cellulose. This collected cellulose was boiled in 1 wt% aqueous NaOH solution for 10 h under a nitrogen atmosphere, then neutralized with 1 vol% aqueous acetic acid solution and washed with distilled water until sodium acetate free. The wet cellulose was formed into a disk with the diameter of 1.5 mm and the thickness of about 1 mm for the X-ray photographing. The X-ray diffraction diagram of cellulose was taken with a flat-film camera with Ni filtered Cu $K\alpha$ radiation (35 kV, 15 mA, time of exposure: about 35 min) at specimen film distance of 50 mm.

References

1) A. Kai, J. Kogusuri, and Y. Kobayashi, *Nippon Kagaku Kaishi*, **1982**, 148.
2) A. Kai, T. Koseki, and Y. Kobayashi, *Nippon Kagaku Kaishi*, **1983**, 719.
3) A. Kai, *Bull. Chem. Soc. Jpn.*, **57**, 836 (1984).
4) J. O. Warwicker and A. C. Wright, *J. Appl. Polym. Sci.*, **11**, 659 (1967).
5) R. Jeffries and J. O. Warwicker, *Text. Res. J.*, **39**, 548 (1969).

Kinetics and Mechanism of Oxidation of Pyridoxine by Sodium *N*-Chlorobenzenesulfonamidate

Beby JAYARAM and Sarabaghatta Mayanna MAYANNA*

Department of Chemistry, Central College, Bangalore University, Bangalore-560 001, India

(Received May 16, 1983)

Synopsis. Oxidation of pyridoxine (PRX) by chloramine-B (CAB) in HCl medium at 313 K shows first order dependence each on oxidant, substrate and Cl^- ion concentrations, but is independent of $[H^+]$. A first-order retardation of rate is observed by the addition of reaction product, benzenesulfonamide. Suitable mechanism is proposed.

Aromatic *N*-halosulfonamides are compounds containing positive halogen and they act as both chlorinating and oxidising agents. The important members of this class of compounds are chloramine-T (CAT) and chloramine-B (sodium *N*-chlorobenzenesulfonamidate, CAB). Although sufficient reports are available about the mechanism of oxidation of substrates by CAT[1], information about CAB is scanty. Pyridoxine (PRX) find extensive application in pharmaceutical industries but mechanistic studies of its oxidation are meagre. It has been oxidised to pyridoxal by MnO_2[2] and $KMnO_4$[3] in acidic and alkaline media respectively. We report here the kinetics and mechanism of pyridoxine by CAB in HCl medium at 313 K.

Experimental

Chloramine-B was prepared and purified by standard procedures.[4] Pyridoxine (Fluka) was used without further purification. Aqueous solutions of the compounds were prepared in double distilled water. Heavy water (99.8%) was obtained from BARC, Bombay, India. All other reagents used were of AR grade. The reactions were followed under pseudo-first order conditions by estimating the unreacted CAB iodometrically. Experimental details are described elsewhere.[1]

Stoichiometry. Varying proportions of CAB and pyridoxine solutions in presence of HCl (0.04—0.14 M, 1M = 1 mol dm^{-3}) were mixed and the unreacted CAB was estimated. Values of $\Delta[CAB]/\Delta[PRX]$ and $\Delta[\text{pyridoxal}]/\Delta[CAB]$ in Table 1 suggest the overall reaction:

$$C_8H_{11}NO_3 + RNClNa \longrightarrow C_8H_9NO_3 + RNH_2 + NaCl.$$
$$(R = C_6H_5SO_2)$$

Benzenesulfonamide among the reaction product was detected by TLC technique.[5] Pyridoxal was identified and estimated as semicarbazone[6] (mp 509 K).

Table 1. Stoichiometry of oxidation of pyridoxine by CAB at 313 K

[HCl]/M	Δ[CAB]/Δ[PRX]	Δ[Pyridoxal]/Δ[CAB]
0.02	0.89	0.86
0.04	0.92	0.90
0.06	0.94	0.93
0.08	0.99	1.01
0.10	1.01	1.01
0.12	1.02	0.99
0.14	0.99	1.00

Results and Discussion

Oxidation of PRX by CAB was carried out at 313 K in the presence of various concentrations of HCl, H_2SO_4, and $HClO_4$ (0.04—0.14 M) but the reaction was found to be facile only in the presence of chloride ion in the solution. Hence, a detailed study was made on the kinetics of oxidation of PRX by CAB in HCl medium.

At constant [HCl] and [PRX], plots of log $(a-x)$ *vs.* time were linear indicating a first-order dependence of rate on [CAB]. The value of first-order rate constant k was independent of [CAB] (Table 2). Values of k increase with increase in [PRX] (Table 2) and a plot of log k *vs.* log [PRX], gives a straight line of slope unity, indicating first order dependence of rate on [PRX].

The rate also increases with increase in [HCl]. A plot of log k *vs.* log [HCl], shows a first-order dependent of rate on [HCl]. At constant $[H^+]$, addition of NaCl increased the rate. Plot of log k *vs.* log $[Cl^-]$ was linear with unit slope, showing first-order dependence of rate on $[Cl^-]$. The effect of $[H^+]$ at constant $[Cl^-]$ was studied. It was observed that the rate is independent of $[H^+]$ (Table 3).

Table 2. Effect of concentration of reactants on the rate

10^4[CAB]/M	10^3[PRX]/M	$10^4k/s^{-1}$
3.0	5.0	4.69±0.10
4.0	5.0	4.71±0.09
5.0	5.0	4.64±0.09
6.0	5.0	4.59±0.08
7.0	5.0	4.62±0.11
5.0	2.0	1.99±0.04
5.0	4.0	3.71±0.10
5.0	6.0	5.84±0.11
5.0	8.0	7.31±0.18
5.0	10.0	9.59±0.21
5.0	5.0	4.35±0.08[a]
5.0	5.0	4.21±0.11[b]

[HCl]=0.1 M; temp: 313 K; a) : with 0.5 M $NaClO_4$; b) : In D_2O medium.

Table 3. Dependence of reaction rate on $[H^+]$ and $[Cl^-]$ at 313 K

[HCl]/M	[NaCl]/M	$10^4k/s^{-1}$
0.06	0.08	7.53±0.15
0.08	0.06	7.59±0.15
0.10	0.04	7.55±0.18
0.12	0.02	7.60±0.16
0.14	—	7.57±0.19
0.08	—	3.98±0.11
0.08	0.02	5.10±0.14
0.08	0.04	5.96±0.10
0.08	0.06	7.20±0.16
0.08	0.08	7.71±0.16

[CAB]=5×10^{-4} M; [PRX]=5×10^{-3} M.

The effect of temperature on the rate of oxidation of PRX by CAB in HCl medium was studied. The values of k at various temperatures (K) -303, 308, 313, 318, 323 are 1.77 ± 0.03, 3.11 ± 0.08, 4.64 ± 0.09, 7.90 ± 0.15, and 13.51 ± 0.24, ($\times10^4\,s^{-1}$) respectively. From the Arrhenius plot of log k *vs.* $1/T$ ($r=-0.9984$) values of E_a (82.6 kJ mol^{-1}), ΔS^* (-45.5 J K^{-1}), ΔG^* (94.0 kJ mol^{-1}), ΔH^* (80.0 kJ mol^{-1}), and A ($2.8\times10^{10}\,s^{-1}$) were computed.

The effect of the dielectric constant of the medium was studied by adding methanol to the reaction system. A plot of log k *vs.* $1/D$, where D is dielectric constant of the medium, gives a straight line with a positive slope of value 0.8642 ($r=0.9976$).

Change in the ionic strength of the medium (0.1—0.5 M) (with $NaClO_4$) had no effect on the rate of reaction (Table 2). The effect of reaction product was studied by adding benzenesulfonamide (BSA). The rate of reaction decreased with increase in BSA, showing a first-order retardation of rate by [BSA] (Fig. 1). The reaction was also studied in D_2O medium. The solvent isotope effect was found to be 0.907.

Eqilibria present in acidified CAT solution has been clearly established.[7] No detailed information is available about the oxidative species present in acidic solution of CAB. Zilberg[8] has shown that acidification of CAB gives dichloramine-T ($RNCl_2$) and RNH_2. Mogilevski *et al.*[9] have reported the presence of HOCl in acidic CAB solution. It is likely that equilibria similar to those of CAT exist in acidified CAB solution.

Hence the probable oxidizing species are RNHCl, $RNCl_2$ and HOCl. A strict first-order dependence of rate on [CAB] (Table 2) rules out $RNCl_2$ as the oxidizing species. In acidic chloride solution, HOCl forms Cl_2 while RNHCl can be further protonated to give RN^+H_2Cl.[10] Kinetic data obtained with Cl_2 water were found to be identical with those of CAB under comparable experimental conditions. First order retardation of rate by the addition of BSA further supports the involvement of Cl_2 in the reaction sequence. Hence free chlorine can be assumed to be the reactive species, which oxidizes PRX present in the protonated form, SH^+ in acid solution.[11] Based on

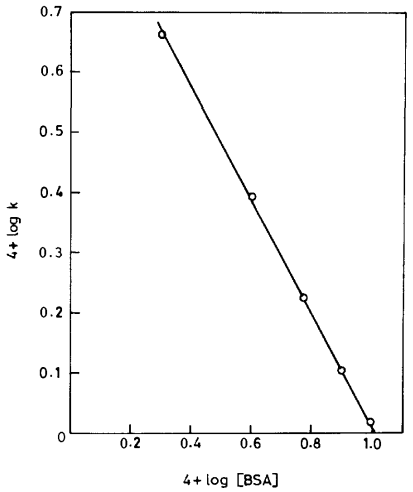

Fig. 1. Plots of log k *vs.* log [BSA].
[PRX]$=5\times10^{-3}$ M; [CAB]$=5\times10^{-4}$ M; [HCl]$=$ 0.1 M; temp$=$313 K.

these facts, the following reaction scheme may be proposed:

$$RN^+H_2Cl + Cl^- \overset{K}{\rightleftharpoons} RNH_2 + Cl_2, \quad (1)$$

$$Cl_2 + SH^+ \xrightarrow{k} \text{products}. \quad (2)$$

Scheme

From Eqs. 1 and 2, the rate law becomes,

$$\text{Rate} = \frac{kK[SH^+][CAB][Cl^-]}{[RNH_2]}. \quad (3)$$

The mechanism of oxidation of primary alcohol usually involves the hydride transfer which accounts for the high solvent isotope effect[12] ($k_{D_2O}/k_{H_2O}\approx4$ to 7). In the present system hydride transfer is unlikely in view of the observed low solvent isotope effect (0.907). Therefore a mechanism involving the formation of hypochlorite is suggested. The electron flow during oxidation is depicted as follows:

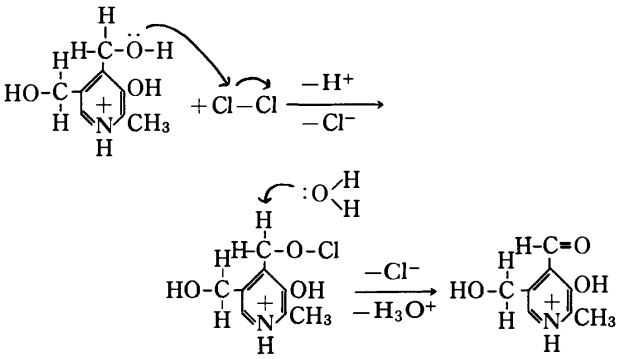

The negative entropy of activation indicates the formation of the compact hypochlorite species at the determining step. The observed neutral salt effect and slight positive dielectric constant effect on the rate support the proposed mechanism.

References

1) M. M. Campbell and Johnson, *Chem. Rev.*, **78**, 65 (1978).
2) F. Yasuo, Japan Patent 7039260 (Cl. C. 07d, A 61k) (1970); *Chem. Abstr.*, **74**, 125457p (1971).
3) S. A. Harris, D. Heyl, and K. Folkers, *J. Am. Chem. Soc.*, **66**, 2088 (1944).
4) A. Chrzaszezewska, *Bull. Soc. Sci., Lett.*, Lo'd'z, Classe III, **3**, 16 (1952); *Chem. Abstr.*, **49**, 212 (1955).
5) H. S. Yathirajan, D. S. Mahadevappa, and Rangaswamy, *Talanta*, **27**, 52 (1980).
6) "Dictionary of Organic Compounds," ed by J. R. A. Pollock and R. Stevens, Eyre and Spottilwoode Publishers Ltd., London (1965), Vol. 5, p. 2820.
7) E. Bishop and V. J. Jennings, *Talanta*, **1**, 197 (1958).
8) I. G. Zilberg, *Chem. Abstr.*, **42**, 144 (1948).
9) M. S. Mogilevskii, V. I. Malchevskaya, and E. P. Voinarovskaya, *Gig. Sanit.*, **24**, 77 (1958); *Chem. Abstr.*, **53**, 22749e (1959).
10) V. Balasubramanyan and V. Thiagarajan, *Int. J. Chem. Kinet.*, **7**, 605 (1975).
11) R. C. Harruff and W. T. Jenkis, *Org. Magn. Res.*, **8**, 548 (1976).
12) K. K. Banerji, *Indian J. Chem.*, **16A**, 595 (1978).

 © 1984 The Chemical Society of Japan Bull. Chem. Soc. Jpn., 57, 1441—1445 (1984)

Ferromagnetic Interactions in Formazanyl-Copper Complexes

Yoshiko KAWAMURA, Hiroaki OHYA-NISHIGUCHI,† Jun YAMAUCHI, and Yasuo DEGUCHI*

Department of Chemistry, College of Liberal Arts and Sciences, Kyoto University, Sakyo-ku, Kyoto 606

†*Department of Chemistry, Faculty of Sciences, Kyoto University, Sakyo-ku, Kyoto 606*

(Received April 26, 1983)

The magnetic susceptibility of four formazanyl-copper complexes have been measured by the use of a torsion balance in the range from 2 K to room temperature. Their ESR parameters have been measured on powdered samples at room temperature and the temperature of liquid nitrogen, and in solution at room temperature in order to elucidate the electronic structures of the complexes. The complexes which have shown the exchange-narrowed pattern in the spectra of powdered samples have been paramagnetic as low as 2 K. Nitro and carboxy derivatives characterized by a single, broad ESR absoption line have positive Weiss constants, indicating ferromagnetic interaction. Especially, the magnetic behavior of the carboxy derivative has been well interpreted in terms of a ground triplet-excited singlet model with the exchange parameter of 24 K. The nitro derivative showed an abnormally low magnetic moment. It has been concluded that the magnetic properties of formazanyl-copper complexes are very sensitive to substitution at the phenyl rings.

Formazans are compounds which contain a characteristic chain of atoms: -N=N-C=N-NH- and which yield tetrazolium salts upon oxidation. Since Kuhn and Jerchel drew attention to their valuable applications to biological research in 1941,[1] formazans and their tetrazolium salts have been studied extensively from various points of views.[2] In addition, it has been learned that formazans react with compounds of Cu^{2+}, Co^{2+}, and Ni^{2+} to give complexes which have two or four nitrogen atoms as ligands.[3,4] The magnetic susceptibilities of several complexes have been measured at room temperature or at three points between the temperature of liquid nitrogen and room temperature in order to ascertain the effective magnetic moments.[5,6] However, although quite a few papers have referred to the magnetic interaction among copper ions, only a few have made mention of the structures.[7] The fact that 1-(*o*-hydroxyphenyl)-3,5-diphenylformazanyl copper showed an abnormally low magnetic susceptibility was attributed to its having a binuclear form, not to its mixing of Cu^{+} and Cu^{2+}.[8] 1-(*o*-carboxyphenyl)-3,5-diphenylformazanyl copper has also been presumed to be a dimer, but it showed normal magnetic susceptibility down to the temperature of liquid nitrogen.[5,8] Therefore, the dimer structure has been proposed on the basis only of the elemental analyses and the hypothetical molecular arrangement. Though it is clear from the elemental analyses that 1-(*o*-carboxyphenyl)-3,5-diphenylformazan reacts with a divalent transition-metal ion with 1:1 stoichiometry,[3,4] the structure of the complex has been an open question for a long time.

In order to clarify the problems mentioned above, four formazanyl-copper complexes have been prepared, and ESR and magnetic-susceptibility measurements have been carried out. In this paper we will report first the results of the ESR and magnetic susceptibility measurements. Second, the magnetic properties will be discussed; they will be classified into two groups, the paramagnetic species and the ferromagnetic species. Especially, the latter will be discussed theoretically based on a ferromagnetic dimer model.

Experimental

The formazans were prepared by a method described elsewhere.[1] Bis(1,3,5-triphenylformazanyl)copper as (**1**) was prepared following the method by Hunter *et al.*, but using a different solvent. Bis[1-(*p*-chlorophenyl)-3,5-diphenylformazanyl]copper (**2**), 1-(*o*-carboxyphenyl)-3,5-diphenylformazanyl copper (**3**), and the copper complex of 1-(*p*-nitrophenyl)-3,5-diphenylformazan (**4**), were prepared by a similar method. **1**, **2**, and **4** all consisted of a fine, almost black powder, while **3** was a fine, purple powder. The elemental analyses of **1** and **2** agreed well with the calculated values; those of **4** also agreed well with the calculated values assuming the 2:1 stoichiometry of formazan and copper. The hypothetical molecular structure of **4** is shown as **4'** in Fig. 1. An amount of **3** large enough for the measurements was too difficult to obtain. The **3'** used for the measurements was a sample containing some solvent molecules. In Table 1, the

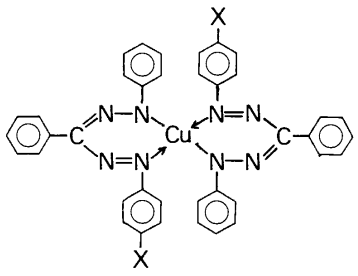

1, X=H 2, X=Cl 4', X=NO_2

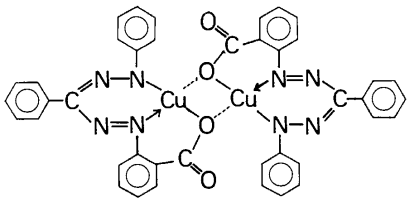

3

Fig. 1. **1**; Bis(1,3,5-triphenylformazanyl)copper, **2**; Bis[1-(*p*-chlorophenyl)-3,5-diphenylformazanyl]copper, **3**; 1-(*o*-carboxyphenyl)-3,5-diphenylformazanyl copper, **4'**; Copper complex of 1-(*p*-nitrophenyl)-3,5-diphenylformazan.

TABLE 1. ANALYTICAL DATA OF COMPLEXES

Complex	Found (%)					Calcd (%)					
	C	H	N	Cl	Cu	C	H	N	Cl	Cu	
1 $(C_{19}H_{15}N_4)_2Cu$	68.8	4.6	16.6		9.9	68.9	4.5	16.4		9.6	
2 $(C_{19}H_{14}N_4Cl)_2Cu$	61.7	3.9	14.7	9.9	9.0	62.4	3.9	15.3	9.7	8.7	
3 $(C_{20}H_{14}N_4O_2)_2Cu_2$	59.0	3.6	13.5			59.3	3.5	13.8		15.2	(1:1)
$(C_{20}H_{14}N_4O_2)_2Cu$						64.2	3.7	15.0		8.5	(1:2)
3' $(C_{20}H_{14}N_4O_2)_2Cu_2\cdot(C_5H_5N)$	62.1	3.6	12.5		14.2	61.4	3.8	14.3		13.3	
4 $(C_{19}H_{14}N_5O_2)_2Cu$	60.5	3.7	18.6		8.6	60.7	3.7	18.6		8.4	

values calculated based on the 1:1 and 1:2 stoichiometries of copper and 1-(*o*-carboxyphenyl)-3,5-diphenylformazan are also listed for comparison. It was found that **3'** has basically the 1:1 stoichiometry.

The ESR spectra were observed at room temperature and at the temperature of liquid nitrogen by using an X-band ESR spectrometer(JEOL ME-3X) equipped with 100 kHz field modulation. The molar magnetic susceptibility χ_M was measured with powdered samples of about 50—70 mg in the temperature range from 2 K to room temperature by using a magnetic torsion balance described elsewhere.[10] All the data were corrected for the diamagnetic contribution calculated by the Pascal method: -341.2×10^{-6}, -331.3×10^{-6}, -288.7×10^{-6}, and -331.6×10^{-6} emu/mol for Compounds **1**, **2**, **3'**, and **4** respectively.**

Results

ESR in Solution. In order to obtain information about the isolated paramagnetic species, the ESR spectra in benzene solutions were measured at room temperature. The isotropic hyperfine structures due to the copper nuclear spin with $I=3/2$ have been observed in **1**, **2**, and **4**. Their hyperfine coupling constants are listed in Table 2. Their spectra showed a linewidth-variation effect; the linewidth in the higher field was sharper than that in the lower field. In the case of **4**, the superhyperfine splittings due to the four ligand-nitrogen nuclei(a_N) could be further observed in the absorption line of Cu^{2+} at the highest field, as is shown in Fig. 2, and a_N was equal to 5.4 G.*** On the contrary, in the benzene solution of **3**, only a single broad line with a linewidth of about 120 G was observed at room temperature, without any hyperfine splitting due to the copper nucleus. At the temperature of liquid nitrogen the ESR spectrum of **3** showed a tendency to split further into seven components. These results can be reasonably interpreted by assuming that the two copper nuclei are coupled with each other, with a strong exchange interaction. It should be noted in Table 2 that the Cu-hyperfine coupling constants (a_{Cu}) of about 41 G are abnormally small compared with those in the Cu-complexes with a planar structure. The a_N in **4**, is also much smaller than those of the usual planar complexes. These are the characteristic features of formazanyl copper complexes.

Magnetic Properties of 1 and 2. The ESR spectra of powdered samples of four compounds are shown in Fig. 3, while their *g*-values are listed in Table 2. The hyperfine splitting of copper in **1** could not be observed.

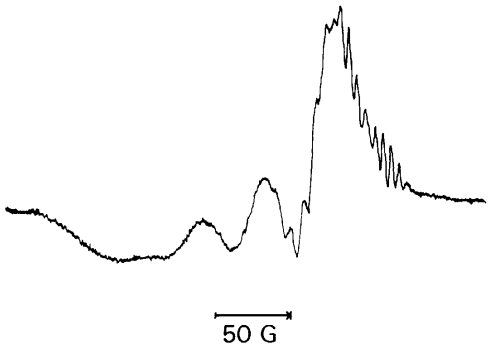

Fig. 2. ESR spectrum of **4** in benzene solution at room temperature. Note that the group at the highest field shows additional superhyperfine structure.

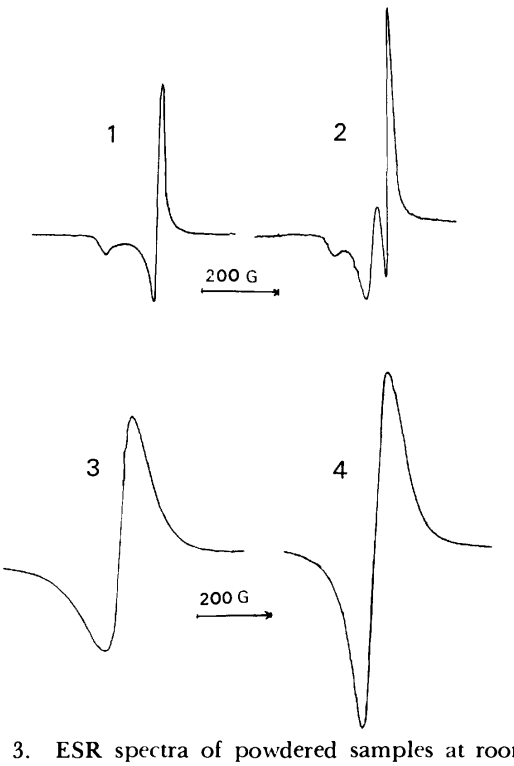

Fig. 3. ESR spectra of powdered samples at room temperature.

** The diamagnetic contribution was calculated for **4'**.
*** $1\,G=10^{-4}\,T$.

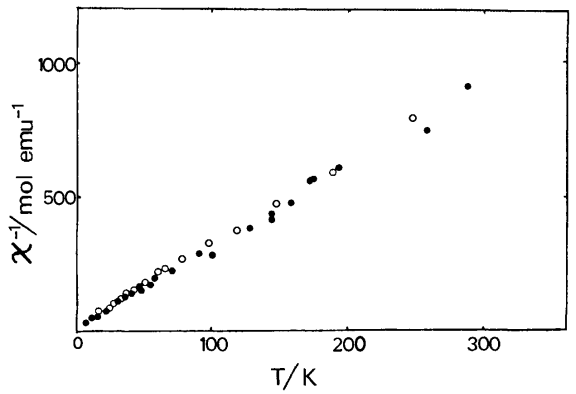

Fig. 4. The reciprocals of molar magnetic susceptibility of **1** (full circle) and **2** (open circle).

The linewidth between the halves of the absorption intensity of the parallel component, $\Delta H_{//}$, and the peak-to- peak width of that of the perpendicular component, $\Delta H_{\perp}$, were 26 and 15 G respectively. The results clearly show an exchange-narrowing effect. In Compound **2**, three components of the g-value, g_1, g_2, and g_3, were obtained. The difference in the g_{ave}-values between that at room temperature and that at the temperature of liquid nitrogen was quite small in **1** and **2**.

The reciprocal plots of χ_M of Compounds **1** and **2** *versus* the temperature are shown in Fig. 4. The most remarkable feature of these compounds is that both χ_M values follow the Curie-Weiss law described by Eq.(1):

$$\chi_M = C/(T-\theta), \quad C = Ng^2\beta^2 S(S+1)/3k, \tag{1}$$

$$\mu_{eff}/\beta = g\sqrt{S(S+1)}, \tag{2}$$

with the negative Weiss constant of -4 K. Here, the other notations have the usual meanings. This negative θ value indicates the existence of weak antiferromagnetic interaction among the magnetic species under consideration. The effective magnetic moment, μ_{eff} of **1** and **2** was estimated as 1.9β from the slopes of the $1/\chi_M - T$ (temperature) curves. This agrees well with the μ_{eff} value (1.78β) calculated with $g=2.06$ and $S=1/2$ in Eq. (2). This can be attributed to the fact that each molecule in the system possesses an isolated magnetic moment with $S=1/2$.

Magnetic Properties of **3**. The average g-value was 2.09. The ESR spectra of powdered samples of **3** and **3'** consisted of almost symmetrical broad lines without any hyperfine structure. The line shape and the g-value were almost temperature-independent.

The full circles in Fig. 5 show the experimental results of **3'**. The $1/\chi_M$ value obeys the Curie-Weiss law in the higher-temperature region (I) above 30 K. The Weiss constant in (I) was $+12$ K, indicating ferromagnetic interaction. On the other hand, the $1/\chi_M$ value in the lower-temperature region (II) deviates from the Curie-Weiss law in (I) at around 30 degrees and follows the Curie-Weiss law with a different θ value. The θ value estimated in the (II) region was almost zero. This behavior can be well interpreted in terms of the ground triplet-excited singlet model (referred to as the T-S mode),[13] as will be described later.

Magnetic Properties of **4**. The ESR spectrum observed in the powdered sample of **4** is also a single

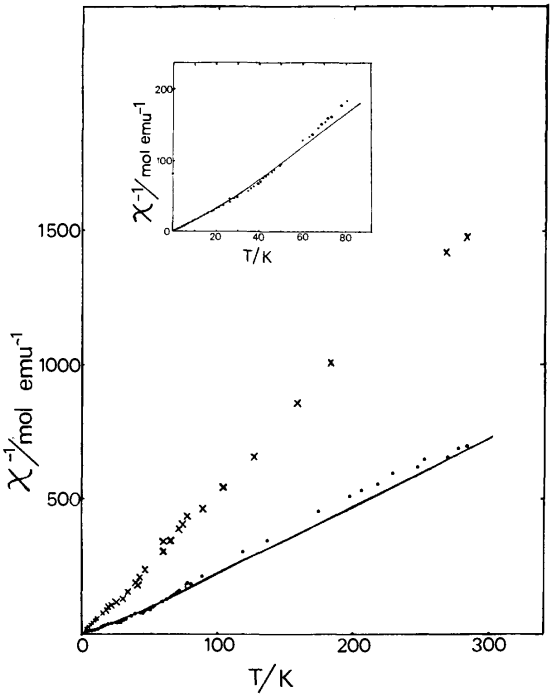

Fig. 5. The reciprocals of molar magnetic susceptibility of **3'** (full circle) and **4** (cross).
The inset shows the susceptibility of **3'** in the lower temperature region; the experimental results (full circle) and theoretical curve (solid line) based on the T-S model (see text).

broad line which is almost symmetrical and which gives an average g-value of 2.06. This is not so much different from that of **3**. However, the stoichiometry of formazan and copper of **4** was 2:1, in contrast with that of **3**, 1:1, as is seen in the elemental analyses.

The ESR in solution and stoichiometry indicate that **4** is of a monomer type, similar to **1** and **2**. On the contrary, the ESR of the powdered sample suggests a strong interaction among the copper ions, because neither the g anisotropy nor the hyperfine splitting could be observed.

A plot of the $1/\chi_M$ of **4** *versus* the T is also shown in Fig. 5. The Weiss constant extrapolated in the higher-temperature region(I) was $+11$ K, indicating that the exchange interaction in **4** is also ferromagnetic. The $1/\chi_M$ value in the lower-temperature region(II) obeys a Curie-Weiss law, with $\theta=0$ K.

Discussion

The $g_{//}$ and $g_{\perp}$ values of **1** were similar to those of Cu-tetraphenylporphyrine ($g_{//}=2.12$, $g_{\perp}=2.07$).[11] This fact indicates that the environment of the nitrogen-bonded copper ion in the present compound is square-planar. On the other hand, the three components of the g-value in **2** demonstrate that the planarity around the copper ion is no longer kept. However, the average g-value of **2**, $g_{ave}=(g_1+g_2+g_3)/3$, is not so much different from that of **1**. The slight deviation from the square-planar configulation is probably caused by the introduction of chlorine into the phenyl rings. In spite of this difference, both Compound **1** and Compound **2** showed an exchange-

Table 2. Results of ESR and magnetic susceptibility measurements

Compound	Magnetism	Weiss constant θ/K	μeff BM	g-value Room temp.	g-value Liq. nitrogen	a_{Cu}(iso) G
1	Curie-Weiss	−4	1.9	g=2.120 g=2.031 g_{ave}=2.061	g=2.121 g=2.031 g_{ave}=2.061	41.3
2	Curie-Weiss	−4	1.9	g_1=2.032 g_2=2.061 g_3=2.123 g_{ave}=2.072	g_1=2.033 g_2=2.065 g_3=2.125 g_{ave}=2.074	41.0
3′	Ferromagnetic (T-S model)	+12	1.8	g_{ave}=2.094	g_{ave}=2.100	
4	Ferromagnetic	+11	1.0 (I) 1.3 (II)	g_{ave}=2.056	g_{ave}=2.059	41.4

(I) and (II) mean the higher- and the lower-temperature regions respectively.

narrowed pattern in ESR and obeyed the Curie-Weiss law. These results indicate that these compounds are typical paramagnetic species with small exchange interactions among the mononuclear units. On the other hand,the g_{ave} of **3**, 2.09, is the largest among the four compounds; the others have almost identical g_{ave} value, about 2.06.

The g-anisotropy of the copper ion in the powdered sample of **4** could not be seen because of the single broad line, but the copper hyperfine coupling constant of **4** in solution was almost the same as those of **1** and **2**, about 41 G, and the stoichiometry was also the same. The most remarkable difference between Compound **4** and Compounds **1** and **2** was that the χ_M of **4** at 288 K, 670×10^{-6} emu/mol, is abnormally small compared with the values of the others, 1200×10^{-6} emu/mol. The χ_M value of the isolated spin system with $S=1/2$ is calculated as 1300×10^{-6} emu/mol at 288 K on a spin-only basis. Therefore, the experimental value of χ_M of **4** at 288 K is about one half of the calculated value. In order to interpret these results quantitatively, we need the crystal structure of **4**. Further experiments such as ESR measurements below the temperature of liquid nitrogen and X-ray analysis are now in progress.

In conclusion, it is characteristic in formazanyl copper complexes that a subtle perturbation such as the introduction of a substituent into the phenyl rings far from the central copper ion results in changes in the symmetry of the ligand field and the magnetic properties.

Ground Triplet-excited Singlet Model. Recently, the ferromagnetic behavior in several copper complexes has been reported and discussed in relation to their molecular structures.[12] In the present case, the ferromagnetic behavior of **3′** can be well explained on the basis of the T-S model.[13] The molar magnetic susceptibility of this model is expressed by the Bleaney-Bowers equation (3):[14]

$$\chi_M = \frac{Ng^2\beta^2}{kT}\frac{1}{3+\exp(-2J/kT)}, \quad (3)$$

where $2J$ is the energy separation between the ground triplet and the excited singlet states, and where N is the number of monomer complexes. Equation (3) indicates that the $1/\chi_M$ ratio approaches linearly to zero with a lowing of the temperature. In the higher-temperature region, χ_M can be approximated by Eq. (1), with $\theta=J/2k$. Therefore, the theoretical ratio of the slope of the $1/\chi_M$-T curve in the lower-temperature region to that in the higher-temperature region, R, can be calculated; it is equal to 0.75. The R of **3′** was found to be 0.7 ± 0.05. The θ in the higher-temperature region clearly indicates the ferromagnetic-exchange interaction. These results indicate that the ferromagnetically coupled dimeric model is adequate for **3′**. The exchange energy, J, could be estimated from the relation: $J/k=2\theta$, based on the high-temperature approximation of Eq. (3). J was equal to 24 k erg**** in this case. In conformance with the above mentioned T-S model and the estimated J value, the theoretical curve of the temperature dependence of the magnetic-susceptibility behavior was drawn with the solid line in Fig. 5; it agreed with the experimental results within the limits of experimental error. Thus, the T-S model accounts well for the susceptibility behavior of **3′**. We have carried out the magnetic-susceptibility calculations based on Cubane-type models.[15,16] The experimental data fit well at the limit of the interdimer-interaction, $J'=0$. This establishes the appropriateness of the T-S model.

It is well known that the coupling of the copper ions can be ferromagnetic when the bonding angle of Cu-O-Cu is about 90°.[17] The construction of the molecular model of **3** shows that the angle of Cu-O-Cu can be about 90°. The results of the magnetic measurement give circumstantial evidence for the molecular structure of **3** shown in Fig. 1, which had been proposed only on the basis of the elemental analyses.[5]

Thus, it can be concluded that the most possible structure of **3** is the magnetic dimer, in which the triplet state is the ground state, the energy separation $2J/k$ being 48 K. Finally, it is of interest to point out that the copper complexes having such large ligands as formazan derivatives show comparatively large ferromagnetic interactions, as is visualized in **3′** and **4**. The central chain structure of formazan has a high flexibility on complexation with metal ions. This results in a variety of magnetic properties in these

**** 1 erg = 10^{-7} J.

complexes. We are now planning to investigate such features in the other formazanyl-transition metal complexes.

The authors would like to acknowledge the helpful advice of Professor Yutaka Takaki of Osaka Kyoiku University in the preparation of formazans. They are also much obliged to Professor Mamoru Mekata for the susceptibility measurements and his helpful discussion.

References

1) R. Kuhn and D. Jerchel,*Ber.*, **74**, 941, 949 (1941).
2) A. W. Nineham, *Chem. Rev.*, **55**, 355 (1954).
3) L. Hunter and C. B. Roberts, *J. Chem. Soc.*, **1941**, 823.
4) R. Wizinger and V. Biro, *Helv. Chim. Acta*, **32**, 901 (1949).
5) E. Kishita, Y. Muto, and M. Kubo, *Aust. J. Chem.*, **11**, 309 (1958).
6) M. I. Ermakova, E. I. Krylov, and I. Ya. Postarsky, *Zh. Obshch. Khim.*, **1960**, 30.
7) A. R. Siedel and L. H. Pignolet, *Inorg. Chem.*, **19**, 2052 (1980).
8) P. Price, *J. Chem. Soc., A*, **1971**, 3371.
9) J. N. Ashley, B. M. Davis, A. W. Nineham, and R. Slack, *J. Chem. Soc.*, **1953**, 3881.
10) M. Mekata, *J. Phys. Soc. Jpn.*, **17**, 796 (1962).
11) B. A. Goodman and J. B. Raynor, *Adv. Inorg. Radiochem.*, **13**, 135 (1970), Other references are cited herein, for example: J. M. Assour, *J. Chem. Phys.*, **42**, 2477 (1965); M. C. R. Symons, *J. Chem. Soc., A*, **1969**, 2219.
12) For example: a) J. A. Santen, A. J. Duynereldt, and R. L. Carlin, *Inorg. Chem.*, **19**, 2152 (1980); b) T. Asaji, H. Sakai, and D. Nakamura, *ibid.*, **22**, 202 (1983).
13) J. J. Mooiji, A. A. K. Klassen, and E. de Boer, *Mol. Phys.*, **32**, 879 (1976).
14) B. Bleaney and K. D. Bowers, *Proc. R. Soc. London, Ser. A*, **214**, 451 (1952).
15) W. E. Hatfield and G. W. Inman, Jr., *Inorg. Chem.*, **8**, 1376 (1969).
16) L. Merz and W. Haase, *J. Chem. Soc., Dalton Trans.*, **1980**, 875.
17) P. W. Anderson,"Magnetism," ed by G. T. Rado and H. Suhl, Academic Press, New York and London (1963), Vol. 1, pp. 64—75.

Optically Active and Racemic Glycerides. I. The Thermodynamic and Structural Relationship between Optically Active and the Corresponding Racemic α-Monostearins in Their Crystalline, Molten, and Dissolved States

Makio IWAHASHI,* Yasutoshi WATANABE,† Toshihiko WATANABE,†† and Mitsuo MURAMATSU†††
Department of Chemistry, Faculty of Science, Tokyo Metropolitan University, Setagaya-ku, Tokyo 158
(Received June 8, 1983)

The thermodynamic and spectrographic properties, such as the melting temperature, the latent heat of fusion, the solubility, the heat of solution, and the infrared and NMR spectra, were studied for the stable β-forms of the optically active (*S*)- and the corresponding racemic (*RS*)-α-monostearin crystals. The phase diagram for the binary mixture and the IR spectra of (*S*)- and (*RS*)-crystals indicate that the (*RS*)- form is a racemic molecular compound consisting of (*R*)- and (*S*)-α-monostearin molecules. The latent heats of fusion for the (*S*)- and (*RS*)-α-monostearin crystals were 82.4 kJ mol^{-1} and 75.4 kJ mol^{-1} respectively. The heats of solution in benzene for the (*S*)- and the (*RS*)-crystals were 86.3 and 99.9 kJ mol^{-1} respectively. The difference in the heat of solution between the (*S*)- and the (*RS*)-crystals, $\Delta(\Delta H_S)$, was 13.6 kJ mol^{-1}, which may be attributable to the difference in the extent of hydrogen bonding. These results suggest that (*R*)- and (*S*)-molecules in the (*RS*)-form strongly interact to form a racemic pair not only in the crystalline state, but also in the molten state. Such a racemic pair dissociates into the free molecules when it is dissolved in a nonpolar solvent. The conclusion is supported by the IR and NMR spectra for both the glycerides in dissolved states.

The properties of α-monoglycerides, harmless detergents, have been studied by many investigators.[1-6] Little has yet been reported on the thermodynamic difference between optically active and (*RS*)-forms, however. The (*RS*)-form can, in general, be classified, in terms of the interaction of (*R*)- and (*S*)-molecules in the crystal, into three types of modification:[7,8] a racemic compound, a solid solution, or a mixture of (*R*)- and (*S*)-crystals. (*RS*)-α-Monoglycerides containing even carbon-chain lengths from C-12 to C-18 seem to be racemic compounds, as they appear at higher melting points than do their optically active (*S*)-forms.[9] The crystalline properties of the racemic compounds can be expected to differ from those of the optically active species. A comparative study has thus been made of the properties of these crystals: the thermodynamic and structural properties of the crystals of (*RS*)-α-monostearin were compared with those of (*S*)-α-monostearin in an effort to obtain knowledge of the interaction between (*R*)- and (*S*)-molecules in the racemic α-monostearin crystal.

Experimental

Materials. Pure (≫99%) samples of optically active (*S*)- and racemic (*RS*)-α-monostearins obtained from Fluka AG (Switzerland) were further purified by repeated recrystallizations from hexane. The melting points of these samples were 349.3 and 355.6 K respectively, in good agreement with the previously reported values[9] (349.2 K for (*S*)- and 355.2 K for (*RS*)-) for the β-form crystals. The polymorphic forms of the (*S*)- and (*RS*)-α-monostearins are the β, β′, α, and sub-α forms. The first one obtainable by slow crystallization from a solvent is the most stable[2,4,10] under ordinary conditions.

Apparatus and Procedures. The latent heat of fusion and the melting point were determined by the use of a differential scanning calorimeter (Shimadzu Model DSC-30) in the temperature range of 300—373 K at a constant rate of 5 K min^{-1} to rise the temperature. In order to obtain melting temperature-composition diagrams for mixtures of (*S*)- and (*RS*)-α-monostearins, they were mixed in benzene and allowed to stand overnight *in vacuo* to evaporate the solvent.** A standard sample of KNO_3[11] was used for calibration to obtain the latent heat of fusion. The solubility in benzene was determined at a constant temperature (±0.02 K) in the range of 281—298 K by the method of an asymptotic approach to the concentration-time curves for under- and super-saturated solutions.[12,13] About 10 h after the addition of a monostearin to the solvent, a 2.00 ml portion of a saturated solution was pipeted out through a glass tip covered with a piece of filter paper (Toyoroshi No. 5) which had been soaked in the solvent for 24 h prior to pipeting.[13] The pipeted solution was then evaporated to dryness *in vacuo* for weighing. The infrared spectra of the monostearins in crystalline state (in the KBr disks) and in the molten state (on the NaCl plate) were obtained with a Hitachi Model 260-10 spectrometer (resolving power of 0.5 cm^{-1}); those in CCl_4 solutions were obtained with a JASCO IR-A3 spectrometer (Japan Spectroscopic Co., Ltd.; resolving power of 0.7 cm^{-1}). The NMR spectra for those monostearins in benzene-d_6 (C_6D_6) were obtained with a JEOL-FX 60 NMR spectrometer.

Results and Discussion

The values of the melting point, the latent heat, ΔH_f, and the entropy, ΔS_f, of the fusion of (*S*)- and (*RS*)-α-monostearin crystals are listed on the second to fourth lines respectively in Table 1. The value of ΔH_f (75.4 kJ mol^{-1}) for the (*RS*)-form is in good agreement with that (75.4 kJ mol^{-1}) reported by T. Maruyama *et al.*[3]

Figure 1 shows the temperature dependences of the solubilities for the (*S*)- and (*RS*)-compounds in

† Present address: Tokyo Branch, Yoshitomi Pharmaceutical Co.

†† Present address: Kaken Seiyaku Co., Ltd., Tokyo.

††† Present address: Dept. of Chem., Faculty of Hygienic Sci., Kitasato Univ., Sagamihara, 228.

** Simple mixing of the two in a mortar always resulted in the appearance of two peaks on the DSC chart, the two giving a molar ratio exactly the same as that of the initial mixture. The peak positions also corresponded to the melting points for the mixture components.

benzene. The following van't Hoff equation was used to calculate the heat of solution, ΔH_s;

$$\ln C = \Delta H_s/RT + K, \quad (1)$$

where C is a solubility; R, the gas constant; T, the absolute temperature, and K, an integration constant. The activity coefficient was always assumed to be unity because of the low solubilities. The ΔH_s values are tabulated on the last line of Table 1.

In Fig. 2 the melting point is plotted against the mole fraction of (*RS*)-α-monostearin in the mixture of (*S*)- and (*RS*)-α-monostearins. The figure indicates that the (*RS*)-form is a typical racemic compound, giving an eutectic mixture at a molar ratio of 3:7. If there were a crystal of (*R*)-α-monostearin, it would have been of the same melting point as that for the crystal of the (*S*)-α-monostearin because enantiomers in general possess the same physical and chemical properties except in optical rotations and biological actions. The mp for the (*RS*)-form should thus give a maximum at an equilmolar mixture of the (*R*)- and (*S*)-compounds, implying that a racemic pair exists in the (*RS*)-crystal, as has been suggested by Larsson.[5,6] Such an implication leads to a more ordered arrangement of the molecules in the (*RS*)-crystal compared to the (*S*)-crystal, reflecting a kind of contradiction of the results on the third and fourth lines of Table 1: if we assume enthalpic and entropic identities between the liquid form (*S*)-crystal and (*RS*)-crystal, the former crystal should be in a more ordered state, with a lower enthalpy, than the latter. On the other hand, the ΔH_s values in Table 1 reveal a lower enthalpy for the (*RS*)-crystal, than that for the (*S*)-crystal, if we assume an identical state for a benzene solution of α-monostearin, whether it is (*S*) or (*RS*). In fact, the NMR pattern for a solution of the (*S*)-glyceride in benzene-d_6 (C_6D_6) was exactly the same as that of the (*RS*)-compound. The contradiction between the heat of fusion and that of solution can be clarified by assuming that the molten states of the (*S*)-form and the (*RS*)-form are different from each other. McGinn[14] has reported that "a liquid" of (*RS*)-octanol differs considerably from that of the (*R*)- or (*S*)-compound in its physical properties, such as density, boiling point, and refractive index.

The difference in the heat of solution between (*S*)- and (*RS*)-α-monostearin crystals, $\Delta(\Delta H_s)$, was 13.6 kJ mol^{-1}, which may be attributable to the difference mainly in the extent of hydrogen bonding. In fact, the OH-stretching vibration in the former crystal was different from that for the latter crystal, as shown in Fig. 3.

From the identity between (*S*)- and (*RS*)-compounds in the dissolved state and the assumption that their

TABLE 1. THERMODYNAMIC PROPERTIES OF α-MONOSTEARINS

	(*S*)-Form crystal	(*RS*)-Form crystal
Mp θ_m/K	349.3 349.2[10]	355.6 355.2[10]
Latent heat of fusion ΔH_f/kJ mol^{-1}	82.4	75.4 75.4[3]
Entropy of fusion ΔS_f/J K^{-1} mol^{-1}	235.9	212.0 213.4[3]
Heat of solution ΔH_s/kJ mol^{-1}	86.3	99.9

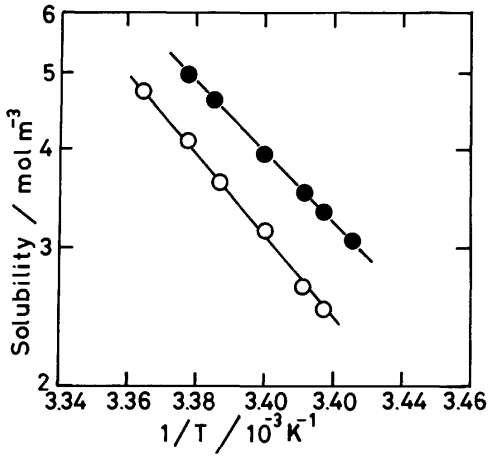

Fig. 1. Relationship between the solubilities and (1/*T*) for (*S*)- (filled symbols) and (*RS*)-α-monostearin (open) crystals.

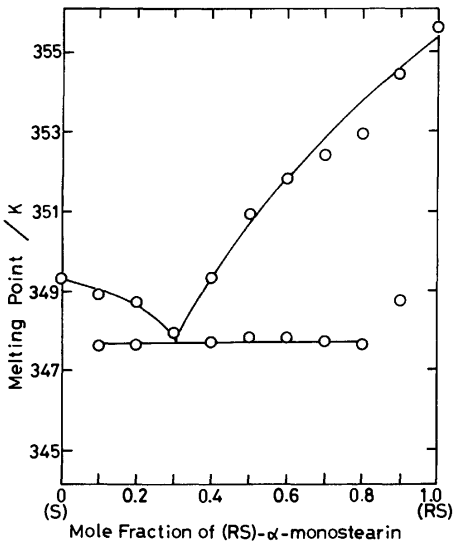

Fig. 2. Melting point of the mixture of (*S*)- and (*RS*)-α-monostearins as a function of the mole fraction of the (*RS*)-species.

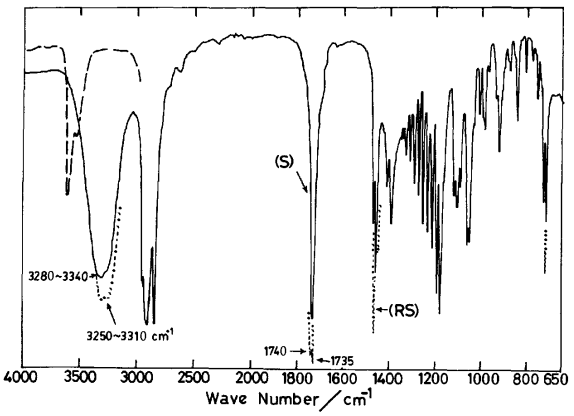

Fig. 3. Infrared spectra of α-monostearins:
Solid line expresses (*S*)-crystal in KBr disk, dotted one (*RS*)-, and dashed one (*S*)- or (*RS*)-forms in CCl_4.

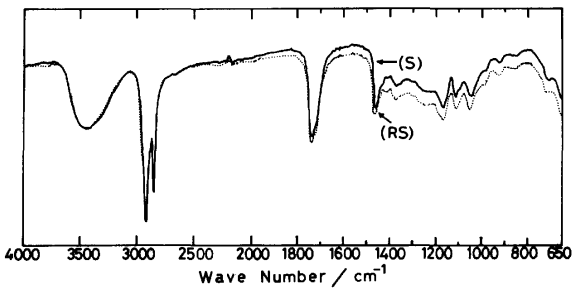

Fig. 4. Infrared spectra of α-monostearins in molten state at 358 K:
Solid line expresses (*S*)-form and dotted one (*RS*)-form on NaCl plate, respectively.

liquid states for (*S*)- and (*RS*)-crystals differ from each other, 20.6 [=(99.9−75.4)−(86.3−82.4)] kJ mol^{-1} can be calculated for the enthalpic difference between the molten (*S*)- and (*RS*)-forms, if we ignore the temperature difference between the solubility and the melting data. The enthalpic difference probably due to the difference in the intensities of the hydrogen bonding forces, the cohesive forces, and so on, between (*S*)- and (*S*)-molecules, and (*R*)- and (*S*)-molecules in their molten states. However, the IR spectra for their molten samples at 358 K did not show a remarkable difference between them, as shown in Fig. 4. The reason for that is uncertain at present.

Larsson[6] described that a unit cell of the (*S*)-α-monostearin contains eight molecules and is orthorhombic, with these dimensions; a=4.94 Å, b=8.97 Å, and c=100.4 Å, while in the (*RS*)-form, its unit cell contains also eight molecules, but gives monoclinic system with these dimensions; a=9.20 Å, b=100.5 Å, c=5.04 Å, and β=100.2°, giving a denser packing for the former as a whole. The racemic pair in the latter crystal should thus be arranged so as to give a lower density. Such a difference in the packing mode may contribute to the entropy difference $\Delta(\Delta S_f)$ between (*S*)-crystal→(*S*)-liquid (235.9 J K^{-1} mol^{-1}) and (*RS*)-crystal →(*RS*)-liquid (212.0 J K^{-1} mol^{-1}). Whatever the case, it must be stated that the $\Delta(\Delta H_f)$ difference is overwhelmed by the $\Delta(\Delta H_s)$ difference, so that the thermodynamic difference between (*S*)-crystal→(*S*)-liquid and (*RS*)-crystal→(*RS*)-liquid is much less than the thermodynamic difference between (*S*)-crystal→solution and (*RS*)-crystal→solution. This, in turn, implies that (*S*)-liquid is more different from (*RS*)-liquid than (*S*)-crystal is different from (*RS*)-crystal.

References

1) D. Chapman, *Chem. Rev.*, **62**, 433 (1962).
2) T. Maruyama, I. Niiya, M. Imamura, M. Okada, and T. Matsumoto, *Yukagaku*, **22**, 85 (1973).
3) T. Maruyama, I. Niiya, M. Imamura, and T. Matsumoto, *Yukagaku*, **26**, 104 (1977).
4) E. S. Lutton, *J. Am. Oil Chem. Soc.*, **48**, 778 (1971).
5) K. Larsson, *Ark. Kemi.*, **23**, 29 (1965).
6) K. Larsson, *Ark. Kemi.*, **23**, 35 (1965).
7) E. L. Eliel, "Stereochemistry of Carbon Compounds," McGraw-Hill Kogakusha, Tokyo (1962), p. 44.
8) T. Tachibana, T. Yoshizumi, and K. Hori, *Bull. Chem. Soc. Jpn.*, **52**, 34 (1979).
9) "Dictionary of Organic Compounds," ed by J. R. A. Polleck and R. Stevens, Eyre & Spottishwoode Publishers, London (1965), Vol. 4, p. 2350.
10) T. Malkin and M. R. E. Shurbagy, *J. Chem. Soc.*, **1936**, 1628; E. Bear and H. O. L. Fisher, *J. Am. Chem. Soc.*, **67**, 2031 (1945).
11) "Kagaku Binran," ed by the Chemical Society of Japan, Maruzen, Tokyo (1977), p. 912.
12) F. P. Krause and W. Lange, *J. Phys. Chem.*, **69**, 3171 (1965).
13) M. Muramatsu, M. Iwahashi, and K. Masumoto, *J. Chem. Eng. Data*, **20**, 6 (1975).
14) C. J. McGinn, *J. Phys. Chem.*, **65**, 1896 (1961).

 © 1984 The Chemical Society of Japan Bull. Chem. Soc. Jpn., 57, 1449—1453 (1984)

Catalytic Activities of 12-Molybdophosphoric Acid and Its Salts Supported on Silicon Dioxide for the Reduction of Nitrogen Monoxide

Isao MOCHIDA,* Toshihiro NAKASHIMA,† and Hiroshi FUJITSU

Research Institute of Industrial Science,

†*Department of Molecular Technology, Graduate School of Industrial Sciences, Kyushu University, Kasuga 816*

(Received July 25, 1983)

12-Molybdophosphoric acid and its metal salts, supported on SiO_2 (H_3PA and MPA/SiO_2), were found to exhibit significant activities for the catalytic reduction of nitrogen monoxide with hydrogen or ammonia, the latter reductant being more reactive. The activity orders of the catalysts were as follows, depending on the reductant: $Cu^{2+}>Ag^+>Ni^{2+}>Cs^+\simeq Co^{2+}\simeq H^+$ (hydrogen), $Cu^{2+}>Co^{2+}>H^+>Ag^+>Ni^{2+}>Cs^+$ (ammonia). It is of value to mention also that H_3PA/SiO_2 exhibited ten times many activity when ammonia was applied. The extent of the cation exchange (X) of $Cu_XH_{3-2X}PA/SiO_2$ influenced the catalytic activity differently, depending again on the reductant, although the maximum activity was obtained with both reductants when X was 1.1. Nitrogen monoxide was decomposed by a stoichiometric reaction with the reduced site on $Cu_{1.1}H_{0.8}PA/SiO_2$, especially when the catalyst was reduced with hydrogen, although no oxygen was detected in the product, the initial rate being comparable to that of the reduction with hydrogen. The following rate-equations were obtained with the respective reductants on $Cu_{1.1}H_{0.8}PA/SiO_2$ at 300 °C over the partial pressure range of NO (3.0—10.1 kPa) and reductants (3.0—35.5 kPa): $V=k_{H_2}P_{NO}^{0.8}P_{H_2}^{0.04}$, $V=k_{NH_3}P_{NO}^{0.6}P_{NH_3}^{0.4-0.7}$. The wide range in the magnitude of powers with respect to the ammonia partial pressure in the latter equation implies the strong adsorption of ammonia on the catalyst. These results suggest that the redox and Langmuir mechanisms are plausible for the reactions with hydrogen and ammonia respectively. An ESR study of the copper and molybdenum ions of the catalyst supports the above mechanisms.

The practical removal or reduction of NO_x in the flue gas has been widely carried out in various industries.[1] Nevertheless, techniques with higher efficiency are still extensively explored for using various catalytic reactions. The recent increase in coal firing, which tends to exhaust highly contaminated flue gas,[2] may also force the acceleration of technical development.

In the present study, the catalytic activities of heteropolyphosphoric acid and its metal salts were examined for the reactions of NO-H_2 and NO-NH_3. Since they are well known catalysts for acid-catalyzed and oxidation reactions,[3] the simultaneons activation of ammonia and nitrogen monoxide can be expected to provide an excellent activity. They are soluble in water or methanol, and can easily be recovered and regenerated when the catalyst is poisoned by fly ashes exhausted from coal. The salt forms may be durable against the alkali metal compounds which are known to poison some metal oxide catalysts severely.[4]

Experimental

Catalysts. The 12-molybdophosphoric acid ($H_3PMo_{12}O_{40}$) was purchased from the Nippon Inorganic Colour and Chemical Co. The metal salts were prepared using their corresponding metal carbonates according to the method described in the literature.[5] The salts or the acid were supported on silica gel (Merck, Kiesel gel 60HR, 350 m^2/g) from their methanol solution. The loading level of the salts or the acid was 33.3 wt%. Granules of 28—40 mesh, prepared by molding and crushing, were used for the catalytic reaction.

Reaction Procedure. The reduction of nitrogen monoxide was carried out in a fixed-bed flow reactor (8 mmϕ, Pyrex glass tube) and in a closed-circuration reactor (vol. 800 ml). The reactant gas contained 5 vol% (5.07 kPa) of nitrogen monoxide (Seitetsu Kagaku Co.), plus 10 vol% (10.1 kPa) of ammonia or hydrogen as the reductant. The catalyst weight and the total flow rate in a typical case of the flow reactor were 500 mg and 100 $cm^3\,min^{-1}$ (SV: 9200/h) respectively. The same reactant gas was supplied to the circulation reactor, where the circulation rate was 500 ml min^{-1} at a total pressure of 15.2 kPa. The rate dependence on their partial pressures was measured under partial pressures of nitrogen monoxide and reductants varying from 3.0 to 10.1 kPa (3 to 10 vol%) and from 3.0 to 35.5 kPa (3 to 35 vol%) respectively by means of a flow reactor under differential reactor conditions (conversions less than 10%). The gas composition was analyzed before and after the reaction by means of a gas chromatograph with columns packed with Porapak Q (1 m) and Molecular Sieve 13X (2 m).

Adsorption Measurements. The adsorption of NO and NH_3 was measured volumetrically with a fixed volume apparatus.

ESR Measurements. The ESR measurements were carried out at room temperature with a JEOL JES-FEIX spectrometer at a modulation frequency of 100 kHz. Mn^{2+} doped in MgO was used as the external standard to determine the g values of the paramagnetic species.

Results

Catalytic Activity for NO Reduction with Hydrogen and Ammonia. The catalytic activities of 12-molybdophosphoric acid and its stoichiometric metal salts supported on silica gel are summarized in Table 1; the reduction of NO was examined with hydrogen as a reductant. All the catalysts showed activity stable enough for more than 12 h and commonly produced nitrogen and dinitrogen monoxide, without any ammonia. The activity and selectivity varied considerably, depending on the kind of metal cation; the following activity order was deduced:

$$Cu^{2+}>Ag^+>Ni^{2+}>Cs^+\simeq Co^{2+}\simeq H^+.$$

The three active catalysts produced considerable amounts of dinitrogen monoxide; its selectivity on the nickel salt was as high as 60%, whereas no dinitrogen monoxide was found over the catalysts of much less

Table 1. Catalytic activities for $NO-H_2$ reaction over 12-molybdophosphoric acid and its metal salts supported on SiO_2

Catalyst	NO conversion/%	Selectivity (%)		Rate (mol NO/g min)
		N_2	N_2O	
H_3PA	2.0	100.0	0.0	8.9×10^{-6}
$Cu_{1.5}PA$	13.0	72.0	28.0	5.8×10^{-5}
$Ni_{1.5}PA$	4.0	40.0	60.0	1.8×10^{-5}
$Co_{1.5}PA$	1.5	0.0	100.0	6.7×10^{-6}
Ag_3PA	9.3	53.1	46.9	4.2×10^{-5}
Cs_3PA	2.4	100.0	0.0	1.1×10^{-5}

Reaction temperature: 300°C, pretreatment: 300°C-3 h (in He), catalyst weight: 0.5 g, NO: 5.0%, H_2: 10.0%, He: Carrier: 100 $cm^3 min^{-1}$.

Table 2. Catalytic activities for $NO-NH_3$ reaction over 12-molybdophosphoric acid and its metal salts supported on SiO_2

Catalyst	NO conversion/%	Selectivity (%)	
		N_2	N_2O
H_3PA	21.4	87.4	12.6
$Cu_{1.5}PA$	27.4	77.8	22.2
$Co_{1.5}PA$	24.3	88.7	11.3
$Ni_{1.5}PA$	5.3	65.8	34.2
Ag_3PA	11.2	74.2	25.8
Cs_3PA	6.0	67.9	32.1

Reaction temp: 300°C, pretreatment: 300°C-3 h (in He), catalyst weight: 0.5 g, NO: 5.0%, NH_3: 10.0%, He: Carrier: 100 $cm^3 min^{-1}$.

activity except for the cobalt salt.

The catalytic activities using NH_3 as a reductant are shown in Table 2, where the conversion and selectivity were observed 3 h after the reaction had started. Although all the catalysts showed activities higher than those with hydrogen, their activities decreased to *ca.* 80% of the initial value within 3 h and then further gradually to give *ca.* 50% after 20 h. The selectivities, however, stayed constant. The catalytic activities depended considerably on the exchanged cations, although N_2 was always the principal product over all the catalysts, regardless of the cation. The activity order was deduced to be as follows:

$$Cu^{2+}>Co^{2+}>H^{+}>Ag^{+}>Ni^{2+}\simeq Cs^{+}.$$

It must be noted that H^+ and Co^{2+} catalysts showed activities over ten times larger than those observed in the reaction with hydrogen.

The Effects of the Extents of Cation Exchange on the Catalytic Activity. The catalytic activities of the acid exchanged with Cu^{2+} at variable levels (defined as $M_XH_{3-2X}PA$, where the exchange levels of X were 0.5, 1.1, and 1.5), with hydrogen and ammonia as the reductants, are shown in Fig. 1. When hydrogen was used, the conversion of NO increased proportionally with the increase in X until X was 1.1. The acid and $Cu_{0.5}H_2PA$ produced nitrogen almost exclusively, whereas the more copper(II)-ion-exchanged one produced dinitrogen monoxide with about a 30% selectivity, in addition to the principal product of nitrogen.

The activity in the reduction with NH_3 depended more markedly on the exchange level, showing a bell-shaped correlation against X where $Cu_{1.1}H_{0.8}PA$ showed the highest activity, whereas the selectivity

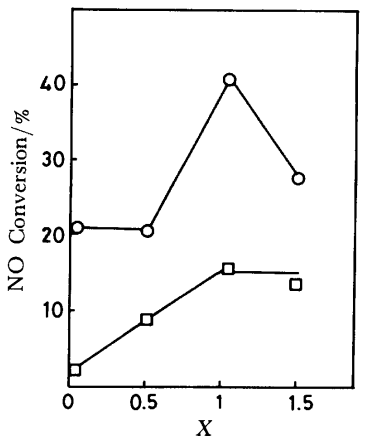

Fig. 1. The effects of the extent of cation exchange (X) on the catalytic activity of $Cu_XH_{3-2X}PA/SiO_2$. Catalyst: 0.5 g, NO and reductant: 5% and 10% in He, total flow rate: 100 $cm^3 min^{-1}$, reaction temp: 300°C, □: $NO-H_2$, ○: $NO-NH_3$.

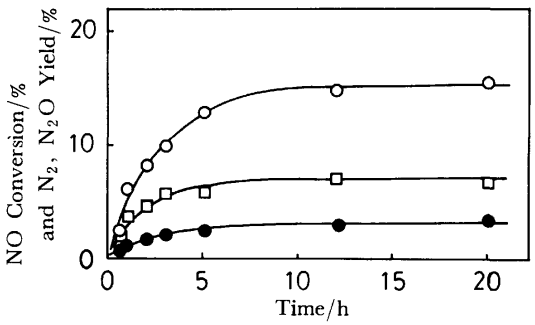

Fig. 2. Decomposition reaction of NO over $Cu_{1.1}H_{0.8}PA/SiO_2$ using a closed circulation reactor. Catalyst: 1.0 g, P_{NO}=40.3 kPa, reaction temp: 300°C. ○: NO conversion, ●: N_2 yield, □: N_2O yield.

was almost constant at all exchange levels.

Decomposition Reaction of NO over $Cu_{1.1}H_{0.8}PA/SiO_2$. The decomposition of NO was found to proceed over $Cu_{1.1}H_{0.8}PA/SiO_2$ at 300°C. Its reaction profile, as observed in a closed circulation reactor (P_{NO} = 40.3 kPa, catalyst = 1 g), is shown in Fig. 2. The reaction proceeded slowly but steadily to produce nitrogen and dinitrogen monoxide, and terminated at 10 h after the reaction started. At the end of the reaction, the reacted NO amounted to one molecule per Keggin unit of the catalyst. It must be noted that no oxygen was detected in the gas phase throughout the reaction.

The activity of reduced $Cu_{1.1}H_{0.8}PA/SiO_2$ (under a hydrogen flow at 300 °C for 20 h) observed with a flow reactor is shown in Fig. 3, where the reaction temperature, the amounts of catalyst, the partial pressure of NO, and the total flow rate were 300 °C, 0.5 g, 1.057% (1.1 kPa) in helium, and 50 $cm^3 min^{-1}$ (SV 4600/h) respectively. Although the conversion was very high at the early stage of the reaction (70% at 30 min), it decreased sharply to *ca.* 2% after 5 h and terminated after 10 h. The total amounts of decomposed NO reached 12 molecules per Keggin unit. Nitrogen was the principal product at the early stage of the reaction; however, the amount of dinitrogen monoxide increased, reaching *ca.* 40% at 1 h and then gradually decreasing with the reaction time. The reaction in the later stage was very similar to that over the unreduced catalyst.

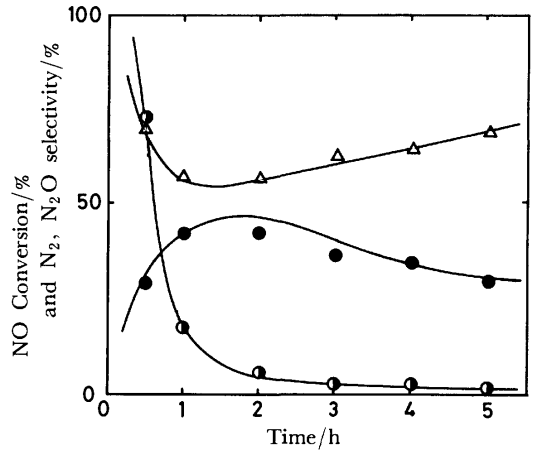

Fig. 3. Time on stream of NO decomposition over $Cu_{1.1}H_{0.8}PA/SiO_2$ reduced with hydrogen.
Catalyst: 0.5 g (reduction conditions: 300 °C, 20 h in H_2), NO: 1.06% in He, total flow rate: 50 $cm^3 min^{-1}$, reaction temp: 300 °C, ◑: NO conversion, △: N_2 yield, ●: N_2O yield.

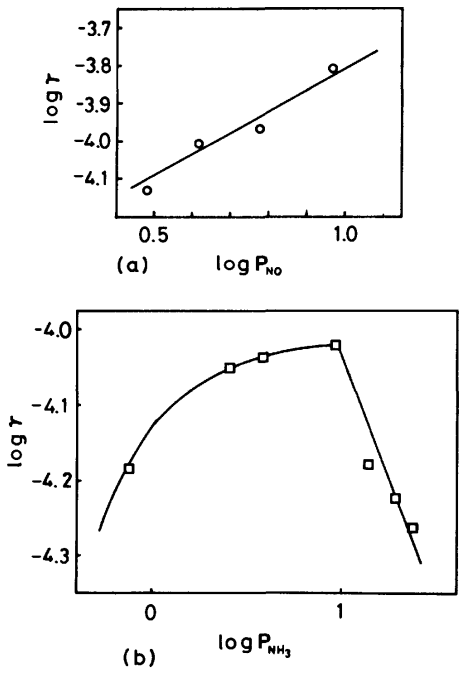

Fig. 4. The partial pressure dependence of $NO-NH_3$ reaction over $Cu_{1.1}H_{0.8}PA/SiO_2$.
a) Dependence on the partial pressure of NO, b) dependence on the partial pressure of NH_3.

Kinetic Measurements. Some kinetic studies were carried out for the reaction over $Cu_{1.1}H_{0.8}PA/SiO_2$. The logarithmic rates of the $NO-H_2$ reaction varied linearly with the partial pressures (Fig. 4), providing the following rate equation (Eq. 1):

$$r = k_{H_2} P_{NO}^{0.8} P_{H_2}^{0.04}. \quad (1)$$

For the $NO-NH_3$ reaction, a good linear correlation was obtained with NO, providing the order of 0.6 (Fig. 4a). On the other hand, a complex dependence on NH_3 was observed (Fig. 4b). The rate increased rather sharply first while the pressure was below 1.3 kPa, leveling off at *ca.* 5.3 kPa, the order being 0.4 at first and decreasing to zero. Above 10.1 kPa of NH_3 the rate decreased very sharply, providing the order of −0.7. Thus, the rate equation is described by Eq. 2 with a variable order of ammonia:

$$r = k_{NH_3} P_{NO}^{0.6} P_{NH_3}^{0.4 \sim -0.7}. \quad (2)$$

The activation energy for NO disappearance in the $NO-NH_3$ reaction was calculated to be 91.6 kJ mol^{-1}. The selectivity for N_2 was slightly decreased (85% at 300 °C to 80% at 350 °C); instead, that of N_2O increased.

The adsorption of NO and NH_3 on the H_3PA, $Cu_{0.5}H_2PA$, $Cu_{1.1}H_{0.8}PA$, and $Cu_{1.5}PA$ after pretreatment at 300 °C in He was observed at room temperature and 300 °C respectively. H_3PA adsorbed 0.5 molecule of NO per Keggin unit, whereas the cupric ion exchanged PA adsorbed one molecule per Keggin unit. *Ca.* six molecules of NH_3 were adsorbed at 300 °C on both the acid and the salts, a half of those adsorbed being subsequently desorbed by evacuation at the same temperature.

ESR Spectra of $Cu_xH_{3-2x}PA/SiO_2$. The ESR spectra of the orignal $Cu_{1.1}H_{0.8}PA/SiO_2$ and that after the heat-treatment at 300 °C *in vacuo* are illustrated in Fig. 5. The original salt exhibited only an anisotropic signal due to the cupric ion ($g_\perp = 2.222$, $g = 2.071$); however, the heat-treatment decreased its intensity very much, to one-eighth of the original value, because of the formation of Cu^+, and provided an intense signal of Mo^{5+} ($g_\perp = 1.945$, $g = 1.894$). These facts suggest that a considerable reduction takes place during the heat-treatment. The extent of reduction for $Cu_xH_{3-2x}PA/SiO_2$, based on the decrease of Cu^{2+} and the appearance of Mo^{5+}, were estimated thus: $Cu_{1.1}H_{0.8}PA$ (1.8 electron/Keggin unit) > $Cu_{0.5}H_2PA$ (1.4 electron/Keggin unit) ≃ $Cu_{1.5}PA$ (1.3 electron/Keggin unit) > H_3PA (0.7 electron/Keggin unit).

A similar spectrum was observed in the $Cu_{1.1}H_{0.8}PA$ after the reaction of $NO-H_2$. The extent of reduction did not change after the NH_3 treatment at 300 °C; however it decreased samewhat after the reaction of $NO-NH_3$, Mo^{5+} decreasing by *ca.* 10% with the increase in Cu^{2+} (twice the intensity) compared to their respective intensities after the heat-treatment.

Mechanistic Consideration. The heteropoly acid and its transition-metal salts have been well documented to exhibit significant activities in the acid-catalyzed and oxidation reactions.[3] The reduction of

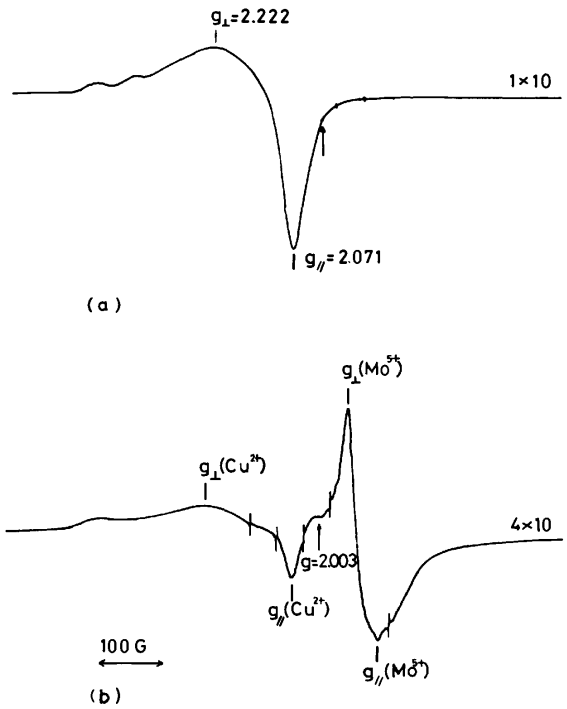

Fig. 5. ESR specra of $Cu_{1.1}H_{0.8}PA/SiO_2$.
a) Original, b) after evacuation at 300°C.

NO can be listed for one of them, although its activity is not remarkably high. Copper(II) salt supported on silica gel showed the highest activities for the reactions of both NO-H_2 and NO-NH_3: however, some different features of the catalytic reactions suggest different mechanisms.

As is shown in Fig. 6, the redox-cycle mechanism, which is similar to that for the oxidation of methacrolein,[6] is assumed in the NO-H_2 reaction over $Cu_{1.1}H_{0.8}PA/SiO_2$, where the reduction of NO by copper(I) or molybdenum(V) ions of the reduced catalyst is rate-determining, judging from the kinetic equation. The rate of NO decomposition over the catalyst reduced by hydrogen at 300°C is similar to that of NO reduction with hydrogen on the same catalyst when the rates are compared at similar reduction extents of the catalyst (as estimated by ESR measurements after the reaction). The catalytic activity is, thus, influenced by the number of reduced sites[7] and by the activation degree of NO, both of which are themseleves influenced by the cations, the transition metal ions probably being favorable for both factors since they can activate NO as well as hydrogen, the latter of which reduces the catalyst. It may be of value to mention that the most active $Cu_{1.1}H_{0.8}PA$ was revealed by ESR to be the most easily reduced by the heat-treatment. Eguchi *et al.* have also reported that the reduction of the heteropoly acid occurred upon evacuation at 300°C[8].

$$r = kP_{NO}^{0.8} P_{H_2}^{0.04}$$

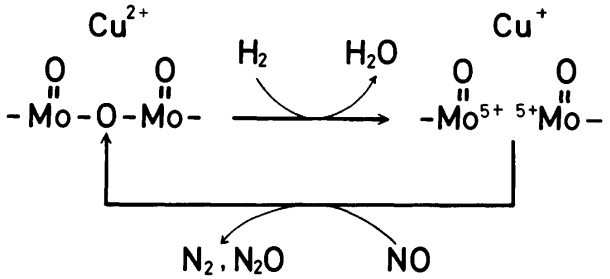

Fig. 6. Mechanism of NO-H_2 reaction over $Cu_{1.1}H_{0.8}PA/SiO_2$.

$$r = kP_{NO}^{0.6} P_{NH_3}^{0.4 \sim -0.7}$$

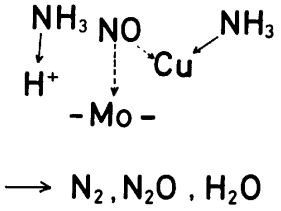

$\longrightarrow N_2, N_2O, H_2O$

Fig. 7. Mechanism of NO-NH_3 reaction over $Cu_{1.1}H_{0.8}PA/SiO_2$.

The ESR measurements suggest that the decomposition reaction of NO on the $Cu_{1.1}H_{0.8}PA/SiO_2$ may proceed by means of the stoichiometric oxidation of the reduced sites which may be produced during the heat-treatment (*ca.* 1 sites/Keggin unit). The reduction of the catalyst by hydrogen before the reaction enhances the activity; however, the reaction also terminates when the reduced sites are consumed. In the latter case, the possibility that the adsorbed hydrogen atoms[9] contribute the high activity at the early stage of the reaction cannot be excluded. No generation of a reduced site takes place during the reaction under the present conditions.

The NO-NH_3 reaction provides some contrasting mechanistic features to the NO-H_2 reaction. A plausible mechanism is illustrated in Fig. 7. The acid itself showed a significant activity, but $Cu_{1.5}PA$ was much inferior to $Cu_{1.1}H_{0.8}PA$. The ammonia treatment of $Cu_{1.1}H_{0.8}PA$ after the evacuation at 300°C causes no change in the ESR spectrum, suggesting that ammonia did not produce the reduced sites. Such results as well as the kinetic equation suggest the participation of NH_3 activation. Thus, the surface reaction between the NO adsorbed on the metal-ion sites and the NH_3 on the acidic sites seems to be rate-determining. $Cu_{1.1}H_{0.8}PA$, which contains proton as well as copper sites suitable for activating both reactants, naturally exhibits the highest activity. In contrast, the lack of any proton site on $Cu_{1.5}PA$ may lose the advantages of NH_3 activation. Excess NH_3 decreases the rate, covering the active sites for NO.

In conclusion, the heteropoly acid and its transition-metal salts were found to exhibit significant activities for the reduction of nitrogen monoxide with hydrogen and ammonia, according to their redox and acidic properties. Although the activities were not markedly high, such origins of activity may be suggestive for the catalyst design.

References

1) S. Okazaki, *Hyomen*, **20**, 504 (1982).
2) S. Gotoh, *J. Fuel Soc. Jpn.*, **62**, 378 (1983).

3) Y. Izumi and M. Otake, "Catalyst Design" in "Kagaku Sosetsu" ed by the Chemical Society of Japan, Japan Scientific Societies Press, Tokyo (1982), No. 11, p. 116, and the references listed therein.
4) H. Inaba, *J. Fuel. Soc. Jpn.*, **57**, 826 (1978); T. Nakagawa, M. Okabe, H. Miyagawa, and T. Jinbo, Steel Industry Foundation Technical Report 2-22, Steel Industry Foundation for the Advancement of Environmental Protection Technology (1980).
5) G. A. Tsigdinos, *Ind. Eng. Chem., Prod. Res. Dev.*, **13**, 267 (1974).
6) Y. Konishi, K. Sakata, M. Misono, and Y. Yoneda, *J. Catal.*, **77**, 169 (1982).
7) H. Niiyama, H. Tsuneki, and E. Echigoya, *Nippon Kagaku Kaishi*, **1979**, 996; S. Yoshida, Y. Miyata, H. Niiyama, and E. Echigoya, *Catalyst*, **22**, 220 (1980); **23**, 284 (1981).
8) K. Eguchi, N. Yamazoe, and T. Seiyama, *Chem. Lett.*, **1982**, 13.
9) T. Baba, W. Watanabe, and Y. Ono, *J. Phys. Chem.*, **87**, 2406 (1983).

 © 1984 The Chemical Society of Japan Bull. Chem. Soc. Jpn., 57, 1454—1458 (1984) [Vol. 57, No. 6

Single-crystal ESR and X-Ray Crystallographical Studies of a Binuclear Copper(II) Complex with a Coaxially Stacked Square-pyramidal Geometry

Yuji KAJIKAWA, Tosio SAKURAI,[I] Nagao AZUMA,[II] Shizue KOHNO, Sei TSUBOYAMA,[I] Kimiko KOBAYASHI,[I] Kazuo MUKAI, and Kazuhiko ISHIZU*

Department of Chemistry, Faculty of Science, Ehime University, Matsuyama 790

[I]*The Institute of Physical and Chemical Research, Wako 351*

[II]*Laboratory of Chemistry, Faculty of General Education, Ehime University, Matsuyama 790*

(Received October 3, 1983)

A binuclear complex of bis(μ-*N*,*N*′-dipicolinoyl-1,3-propanediamine)-bis(sulfato)dicopper(II) has been isolated as a blue single crystal tridecahydrate, $[\{Cu(SO_4)(ppda)\}_2]\cdot 13H_2O$, from an aqueous solution. The crystals are orthorhombic, $C222_1$, with $a=15.42(1)$, $b=24.92(2)$, $c=25.73(2)$ Å, and $Z=8$. Each copper(II) ion is in a square-pyramidal coordination with two pyridine nitrogen atoms, two carbonyl oxygen atoms, and a sulfate oxygen atom at the apex. The two equivalent copper(II) ions, about 3.9 Å apart from each other, are aligned coaxially. The eight Cu-Cu vectors are approximately parallel to one another along the c axis. The most important feature of the crystal structure is the presence of the bulky ligands and of many water molecules, which magnetically isolate the Cu-Cu coupled pair from one another. This facilitates the ESR study of the molecular anisotropies by using the single crystal, even at room temperature. The ESR parameters determined are as follows: $g_{//}=2.280(2)$, $g_{\perp}=2.067(1)$, $|D|=422.4(8)$, $|A_{//}|=170(2)$, and $|A_{\perp}|=14(1)$ in 10^{-4} cm^{-1}. Bleaney and Bowers treatments of the exchange coupling contribution in the *D* parameter indicated a ground singlet state about 7 cm^{-1} below a triplet state for the coupled copper(II) ions. A comparison of the ESR parameters measured for the single crystal with those in the aqueous solution enabled us to conclude that the molecular structure in the solution was very similar to that in the crystalline phase, apart from the coordination of sulfate ions.

The imidazole ring, as a histidine moiety, derives a function as a ligand towards transition-metal ions in a variety of biologically important metalloprotein and peptides.[1] As one simple model ligand, *N*,*N*′-dipicolinoyl-1,3-propanediamine (abbreviated as ppda, Fig. 1), which is a dipeptide with pyridyl groups in place of the imidazolyl groups, was employed to mimic the structure of the metal-active site involving the histidine ligand of related metalloproteins. In an aqueous solution, the coordination chemistry of ppda containing a copper(II) ion has been much altered as the solution is varied from an alkaline one to an acidic one.[2,3] The complex prepared in the alkaline solution has been isolated in the form of trihydrate, and it has been characterized by Ojima[2] by means of visible and IR spectroscopies. This complex is electrically neutral and is composed of mononuclear copper(II) ion. Its coordination geometry is to be ascribed to deprotonation from the amide groups. The acidified solution of this complex showed a sharp red-shift, implying protonation to the anionic nitrogen atoms.[2] ESR measurements in solution have given critical knowledge about the molecular structures: we ourselves have previously reported that the copper(II) complex

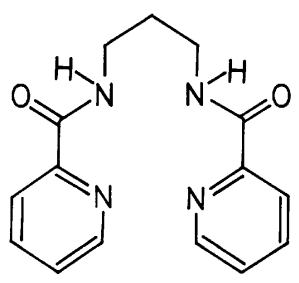

Fig. 1. The chemical structure of *N*,*N*′-dipicolinoyl-1,3-propanediamine (ppda) ligand.

stable in an alkaline solution takes a square-planar ligand geometry, while the one stable in an acidic solution behaves as an axially symmetric binuclear copper(II) complex ion.[3]

The ESR studies of the binuclear complex ion in an aqueous solution have suggested that the square-planar chromophores bearing the two equivalent copper(II) ions stack so as to possess a common *Z* axis; thus, the respective unique axes of the *g* and *D* tensors of axial symmetry coincide with the molecular unique axis.[3] This structure is quite exceptional as compared with the structures reported for a great many of copper(II) binuclear complexes.[4] In many cases, the unique axes of the two square basal planes are inclined to each other, and the observed ESR parameters are usually described in terms of a spin Hamiltonian, with a rhombic symmetry. In order to reveal the absolute molecular geometry of the ppda-copper(II) binuclear complex ion, X-ray crystallographic studies have been undertaken of those of its crystals which contain sulfate or chloride ions. The former, bis(μ-*N*,*N*′-dipicolinoyl-1,3-propanediamine)-bis(sulfato)dicopper(II) tridecahydrate, $[\{Cu(SO_4)(ppda)\}_2]\cdot 13H_2O$, has been successfully obtained as a blue single crystal in a concentrated aqueous solution. However, the crystal is easily cracked as soon as it is taken from the solution or as soon as the solution is warmed beyond room temperature. Since the crystals show such disorder, the model structure has not been refined beyond an *R* factor of 17%. In so far as we have examined, the latter crystal, $[\{CuCl_x(H_2O)_y(ppda)\}_2]\text{-}Cl_{4-2x}\cdot(2-2y)H_2O$, gave no Bragg reflection.

Although the ppda-copper(II) binuclear complex has been of interest to us as a model for active sites in metalloproteins[5] and as a bimetallic catalyst,[6] the ESR feature in the aqueous solution and the crystal and molecular structure of this complex have caused us to pay much attention to its magnetic properties. The

structure around the copper(II) ions revealed by the X-ray analysis is consistent with the structure indicated by the ESR study in the aqueous solution; this is an example of an investigation in which the crystallographic study assisted by ESR study plays a decisive role in establishing the molecular structure in solution. The prominency of this example is due to the question of whether the ESR parameters for the single molecule in the crystal are the same as those for one in the solution. Even at room temperature, the ESR spectrum of the crystal has exhibited a resolved hyperfine structure as well as a fine structure similar to that in a glassy aqueous solution, which is a very rare case. In order to compare the single-crystal ESR parameters with those obtained from the solution spectrum, therefore, the results of the single-crystal ESR and crystallographic studies of $[\{Cu(SO_4)(ppda)\}_2]\cdot 13H_2O$ are reported in the present paper.

Experimental

Materials. The ppda ligand was prepared from methyl picolinate and 1,3-propanediamine by the method of Ojima.[2] The complex was isolated by the slow evaporation of an aqueous solution containing an equimolar mixture of ppda and $CuSO_4$. Recrystallization from the aqueous solution gave deep blue rhombic-plate crystals with the plate normally along the c axis and diagonals along the a and b axes. The analogous procedure gave a solid containing chloride ions.

Exactly 200 mg of the chloride, dried in the air at room temperature, was reduced to 191.86 mg by further drying in a vacuum for 12 h at 110 °C; this indicated a formula of $[\{CuCl_x(H_2O)_y(ppda)\}_2]Cl_{4-2x}\cdot(2-2y)H_2O$. Anal. calcd for this formula: C, 39.61; H, 4.33; N, 12.32%. Found: C, 39.55; H, 4.32; N, 12.31%. $\lambda_{max}(H_2O)=680$ nm with $\varepsilon=60$. Based on this ε value, $[\{Cu(SO_4)(ppda)\}_2]\cdot 13H_2O$ was assumed for the present compound. Anal. calcd for this formula: C, 32.11; H, 5.21; N, 9.99%. Found: C, 31.97; H, 5.49; N, 10.19%.

ESR Measurements. The ESR spectra from the single crystal were observed at room temperature through the rotation of the three crystallographic axes. The spectrum from the aqueous solution was recorded at 77 K by the use of a glassy solvent containing 30% ethylene glycol. All the measurements were carried out on a JES-ME-3X X-band spectrometer equipped with a 100 kHz field modulation for the first derivative. The magnetic field was calibrated by the splitting of Mn^{II} in MgO, which had previously been corrected by the splitting of Fremy's salt ($a_N=1.300$ mT and $g=2.0054$[7]). The microwave frequency was measured with a Takeda-Riken frequency counter. The resonant-field intensities were estimated based on the spacings between the respective spectral lines and the line from Li-TCNQ taken as a secondary standard.

X-Ray Analysis. Some of the crystals recrystallized a few times were coated with a manicure while the others were sealed in glass capillaries. They were all then tested on a Rigaku automated diffractometer AFC or on a Weissenberg camera. The preliminary measurements showed that the crystals belonged to the orthorhombic system, but some of them lost their orthorhombic symmetry.

After many trials, the diffraction data were obtained for the best crystal examined. Crystal data: $C_{30}H_{58}N_8O_{25}S_2Cu_2$, F.W.=1194.1, orthorhombic, space group=$C222_1$, $a=15.42(1)$, $b=24.92(2)$, $c=25.73(2)$ Å, $V=9885(13)$ Å^3, $D_x=1.51(Z=8)$, $D_m=1.52$ g cm^{-3}. The intensity data were collected on the same diffractometer up to $2\theta=40°$. The observed data numbered 910, about 40% of the possible reflections. The intensity data were corrected for the Lorentz and polarization factors.

The intensity distribution showed some special features:

(a) only $k+l=4n$ are observed for $0kl$, with a few exceptions,

(b) only $h+k=4n$ are observed for $hk0$ at lower angles, while only $h+k=4n+2$ are observed for $hk0$ at higher angles, and

(c) 008 is extraordinary strong.

Based on these feature, the reasonable positions of the heavy atoms were obtained after several attempts.

Successive Fourier syntheses revealed the planar atomic groups around the Cu atoms, and also SO_4 groups above and below the planes. R index was reduced to about 23% by the block-diagonal least-squares method. Although the R index could be further reduced by additional cycles, the molecular shape became poor. Therefore, a constrained refinement was applied in order to keep a reasonable molecular shape. The bases for the constraint were the picolinoyl and SO_4 groups. Many residual peaks corresponding to the crystalline water molecules were added from the difference Fourier syntheses. Without the constraint, the R index could be reduced to 17%, but it was about 21% with the constraint. The atomic scattering factors were taken from the "International Tables for X-Ray Crystallography."[8]

Results and Discussion

Crystal Structure. In the asymmetric unit there are two crystallographically independent molecules, each with a two-fold axis through the central methylene carbon atoms in the bridging propane groups. One of them has two pairs of pyridyl rings, upper and lower, which overlap each other almost completely, while the other has two pairs in which the overlapping is partial. The other differences between the two geometries are not very great, so the sketch of only the latter molecule is shown in Fig. 2.

The copper(II) ion is ligated by two pyridine nitrogen atoms and by two carbonyl oxygen atoms to give a square-planar coordination geometry, and that ion is about 0.3 Å above the basal plane. The apical ligand is the oxygen atom of the sulfate ion as a proximal group (Cu-O≃2.3 Å) and the copper ion in the alternative moiety as a distal one (Cu···Cu≃3.9 Å). The two major planes of the pairs of the picolinamido

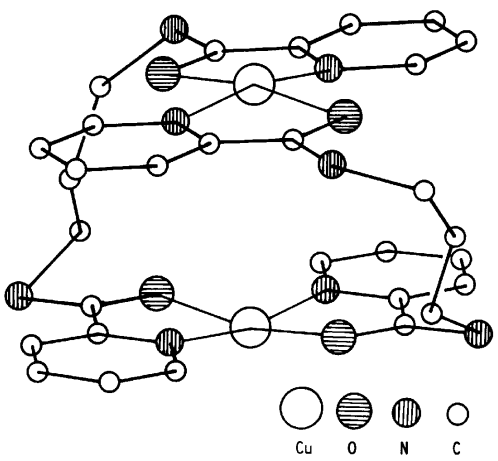

Fig. 2. The sketch of the molecular structure of $[\{Cu(ppda)\}_2]^{4+}$ moiety.

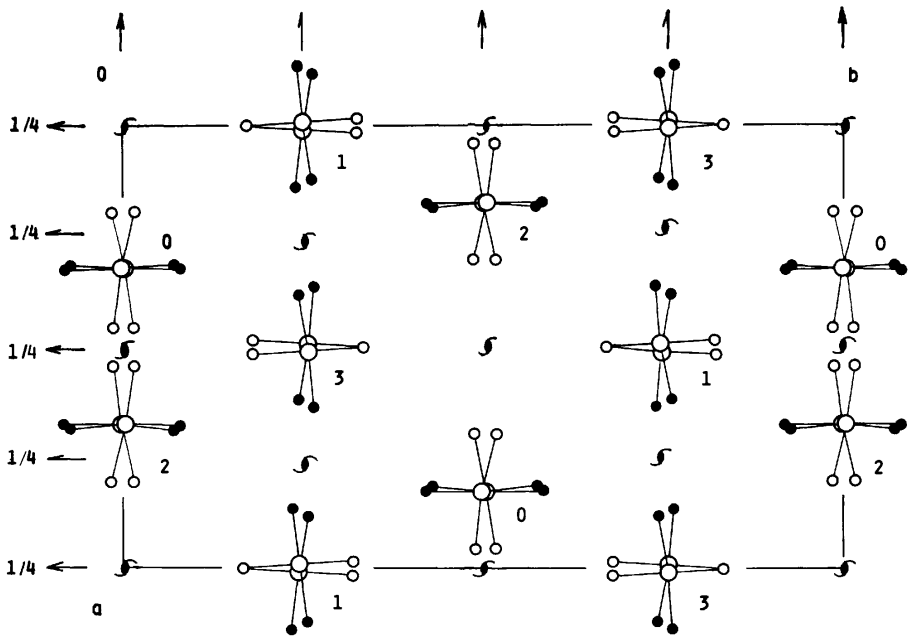

Fig. 3. The arrangement of the [{Cu(N_2O_2)}2] chromophore in the unit cell viewed along the c axis.
The large open circle stands for copper atom, the small open circle oxygen atom, and the solid circle nitrogen atom. The n figure shows the z-component of $z=n/4$ for the center of indicated Cu-Cu pair.

groups are approximately perpendicular to the Cu-Cu distance vector. The two square-planar chromophores bearing two equivalent Cu(II) ions are stacked together so that their local axes approximately coincide to form two sets of x, y, and z axes; this can be seen better in Fig. 3 than for Fig. 2.

Figure 3 shows how the pairs of the copper ions and the metal-binding sites of ppda ligands are packed in the unit cell. The crystal structure consists of a parallel array of the biplanar molecules. The directions of the two-fold axes are parallel to the a and b axes respectively. Therefore, the orientations of the molecules in the c-axis projection are perpendicular to each other. This arrangement is consistent with the extra extinction (b) mentioned in the last section.

The temperature factors of some atoms, especially those at the end of the pyridine rings, are unreasonably high. Therefore, it can not be completely denied that the result might be biased by the proposed model or by the shape of the constrained base. However, the general agreement of the F_o's with the F_c's is good, and the results are at least generally satisfactory within the limits of the quality of the diffraction data.

Magnetic Aspect of the Structure. One can concisely discuss the magnetic aspect of this crystal structure by taking each copper(II) ion to be in an identical coordination geometry of an ideal square pyramid and by taking all the *intramolecular* Cu-Cu distance vectors to be parallel to the c axis.

Then, any single copper ion shows a magnetic anisotropy of a nearly axial symmetry, and the unique axis of the anisotropy is parallel to the c axis. Because the difference between the two kinds of intramolecular Cu-Cu distances can be neglected, the binuclear paramagnetic clusters occupy identical sites of the axial symmetry. On the other hand, the small overlapping between the ligands of the molecules packed discretely indicates a very weak *intermolecular* spin-spin exchange interaction. Moreover, the shortest intermolecular Cu-Cu distance is about 8.3 Å, which is sufficiently large to take the magnitude of the *intermolecular*

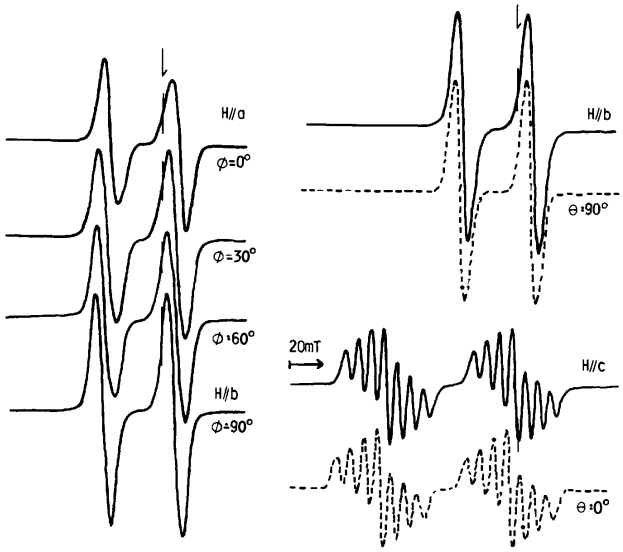

Fig 4. The ESR spectra observed (solid line) and simulated (broken line).
The spectra at left side were obtained when the applied field, $\boldsymbol{H}$, was rotated around the c axis, from $\boldsymbol{H}$//a (uppermost) to $\boldsymbol{H}$//b (lowest) at intervals of 30°. The spectra upper and below at alternative side were recorded when $\boldsymbol{H}$//b and $\boldsymbol{H}$//c, respectively. The arrow shows the resonant field of Li-TCNQ. The simulation was carried out approximating the transition probability to be $g_\perp^2(1+g_{/\!/}^2/g^2)$, where $g^2=g_{/\!/}^2\cos^2\theta+g_\perp^2\sin^2\theta$, and the line-shape function to be Gaussian, with $\sigma_{/\!/}=\sigma_\perp=4.0$ mT ($\boldsymbol{H}$//b) and $\sigma_{/\!/}=\sigma_\perp=3.2$ mT ($\boldsymbol{H}$//c).

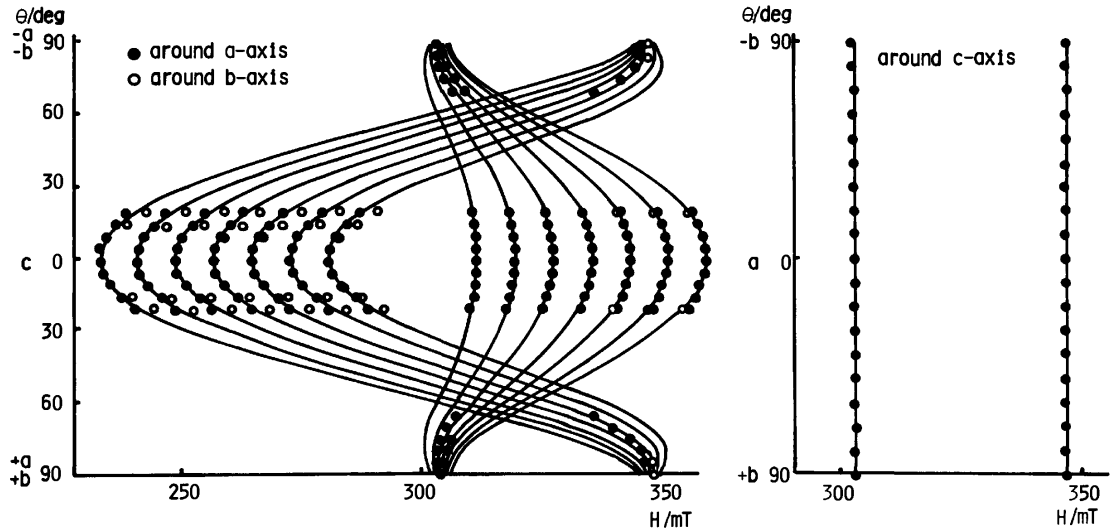

Fig. 5. The angular variation of the resonant fields observed (circles) and calculated (solid lines) when the applied field was rotated around the a and b axes (left side) and the c axis (right side).

magnetic dipolar interaction down one place from that of the *intramolecular* one. Therefore, we can take the crystal anisotropy to be the molecular anisotropy within the limits of the present approximation.

Magnetic Anisotropy. Within the limits of the approximation mentioned above, the axial symmetry of the coordination geometry places restrictions on the principal direction of the molecular coordinate system; therefore, an *a priori* deduction of the magnetic axes can be made. This contrasts with the case of the low symmetric copper binuclear complexes, for example, the $[Cu_2Cl_8]^{4-}$ anion,[9] the low symmetry of which precluded any *a priori* determination of the magnetic principal axes. Figure 4 shows the ESR spectra of the present copper binuclear complex, obtained by applying the external field parallel to the respective principal axes, which coincide with the crystallographic axes. The spectra show a fine structure from the system of $S=1$ and a hyperfine structure due to the exchange-coupled copper atoms. Some investigators have observed fine structures from authentic single crystals of copper binuclear complexes at room temperature.[10] However, they could not record any hyperfine structure from those crystals.

The angular variations of the fine and hyperfine structures are shown in Fig. 5. The error in the setting of the a, b, and c axes is believed to be less than 3°. Figure 5 indicates that the anisotropies in the g factor, the spin-spin dipolar interaction, and the hyperfine interaction are all of an axial symmetry and that the paramagnetic clusters are in equivalent sites. These results are consistent to the approximation made in this text.

In order to obtain the g tensor components ($g_{/\!/}$, $g_{\perp}$), the zero-field splitting parameter (D), and the components of the hyperfine coupling tensor ($A_{/\!/}$, $A_{\perp}$), the following spin Hamiltonian is employed:

$$\begin{aligned}\mathcal{H} &= \beta[g_{/\!/}H_zS_z+g_{\perp}(H_xS_x+H_yS_y)] \\ &+D[S_z^2-S(S+1)/3]+2J\boldsymbol{S}_1\cdot\boldsymbol{S}_2 \\ &+A_{/\!/}S_zI_z+A_{\perp}(S_xI_x+S_yI_y),\end{aligned} \tag{1}$$

where $S=S_1+S_2$, $I=I_1+I_2$, while the other symbols have their usual meanings. The simulation of the ESR spectrum from the glassy solution suggested that the exchange-coupling energy, $|J|$, is much greater than the micro-wave quantum, $W=h\nu=g\beta H_0\cong 0.3\,\mathrm{cm}^{-1}$. Under such conditions, Lund and Hatfield[11] calculated the allowed transitions:

$$\begin{aligned}&H_{1,2}/H_0 \\ &=1-[\pm 3D_1+K(m_1+m_2)/2]/W \\ &-[D_3^2/2+D_4^2/2+R^2(m_1+m_2)^2/8\pm 3D_4R(m_1+m_2)/2]/W^2 \\ &-(B_1\mp B_2)/W^2,\end{aligned} \tag{2}$$

where the meanings of the symbols are as given in their paper. Using this equation, the spin Hamiltonian parameters were determined by the nonlinear least-squares method for the data shown in Fig. 5. The starting parameters were obtained by the conventional method. The hamiltonian parameters thus obtained are as follows: $g_{/\!/}=2.280(2)$, $g_{\perp}=2.067(1)$, $|D|=422.4(8)$, $|A_{/\!/}|=170(2)$, and $|A_{\perp}|=14(1)$, in $10^{-4}\,\mathrm{cm}^{-1}$. The unique principal axis, Z, of the axial symmetry is parallel to the c axis. Based on these parameters, the angular variations of the fine and hyperfine structures are calculated to be as shown by the solid lines in Fig. 5. The spectra simulated for the $\boldsymbol{H}$//a and $\boldsymbol{H}$//c cases are presented in Fig. 4 by broken lines. The agreement of the simulated spectra with those observed is good in view of the approximation employed. The observed zero-field splitting parameter, D, is the sum of the magnetic dipolar and exchange coupling contributions:

$$D=D_{ex}-(g_{/\!/}^2+g_{\perp}^2/2)\beta^2/r^3. \tag{3}$$

Here, the second term results from the dipolar interaction and is appropriate in this particular form only if both ions occupy identical sites of axial symmetry.[12,14] The observed g components and r(Cu-Cu)=3.86 Å indicate the approximate value of $-55\times 10^{-3}\,\mathrm{cm}^{-1}$ for the dipolar contribution. On the other hand, D_{ex} depends on the sign of D. When D is negative, $D_{ex}=13\times 10^{-3}\,\mathrm{cm}^{-1}$ is obtained; hence, the

dipolar coupling rules over the zero-field splitting. If D is regarded as positive, $D_{ex}=97\times10^{-3}\,cm^{-1}$ is derived. The negative D value can be inferred in view of the long distance between the two copper ions in the binuclear complex. When one uses the simplest expression for D_{ex} given by Bleaney and Bowers:[13]

$$D_{ex}=-2J[(g_{//}-2)^2-4(g_{\perp}-2)^2]/32, \quad (4)$$

the exchange-coupling parameter, J, or a half of the energy separation between the singlet and triplet levels can be estimated to be about $-3.5\,cm^{-1}$, based on the negative D value. If D is positive, the calculated J is $-26\,cm^{-1}$. The negative J values indicate antiferromagnetic exchange-coupling between the two copper ions. In order to determine which of the J's is adequate, we measured the magnetic susceptibility of this complex by using liquid nitrogen as a coolant; we thus obtained the Weiss constant of $\theta=-4$ K. Since the binuclear complex molecules are isolated from one another in the present crystal, the J parameter obtained from the susceptibility data can be attributed to the exchange-coupled pair of the copper ions in the binuclear complex. The Weiss constant corresponds to $J=2k\theta\simeq-5.5\,cm^{-1}$, which is much closer to the value of $-3.5\,cm^{-1}$ based on the negative D value than to that of $-26\,cm^{-1}$ estimated from the positive D value. Thus, the separation between the ground-singlet and excited-triplet energy levels is estimated from the ESR parameters to be about $-7\,cm^{-1}$. The copper hypefine interaction causes a slight breakdown of the pure singlet and triplet character.[14]

In order to know how the coordination geometry is perturbed by the dissolution of the crystal in a water medium, the ESR parameters obtained for the aqueous solution are compared with those for the single crystal. The observed spectrum, shown with a solid line in Fig. 6, has been simulated with a broken line in the same figure by means of the following parameters: $g_{//}=2.280$, $g_{\perp}=2.072$, $|D|=453$, $|A_{//}|=168$, and $|A_{\perp}|=14$, in $10^{-4}\,cm^{-1}$. The values other than D are in good agreement with those for the crystal. The disagreement between the two D parameters corresponds to the shortening of the Cu-Cu distance by 2.5%, within the limits of the point-dipole approximation.[15] Therefore, one can take it for granted that the molecular structure of the present binuclear complex is retained throughout both the crystalline and solution states, apart from the coordination of the sulfate ions. We suppose that the water molecules play an important role in bringing the molecular structure in the solution into the crystalline phase as it stands, as well as in stabilizing the binuclear complex, since the ppda and the copper(II) ion in common organic solvents do not form any binuclear complex.

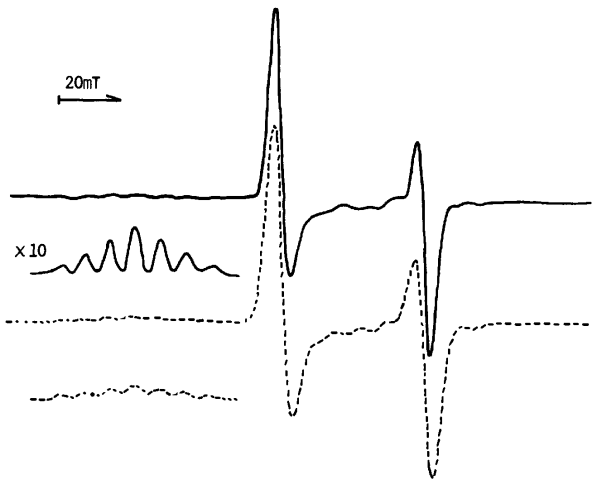

Fig. 6. The ESR spectrum of $[\{Cu(SO_4)(ppda)\}_2]\cdot13H_2O$ dissolved in 30% ethylene glycol aqueous solution at 77 K (solid line) and its simulated spectrum (broken line). The following parameters were employed in the simulation: $g_{//}=2.280$, $g_{\perp}=2.072$, $|D|=0.0453$, $|A_{//}|=0.0168$, $|A_{\perp}|=0.0014\,cm^{-1}$, and $\sigma_{//}=\sigma_{\perp}=2.5$ mT. The transition probability and the line-shape function were the same as those applied in the simulation in Fig. 4.

The authors are grateful to Professor Heijiro Ojima of Aichi Kyoiku University for his encouragement throughout this work. The crystallographic calculations were performed on a FACOM M-200 computer at this Institute using the UNICS III program system.[16] The magnetic data were processed at the Computer Center of this University.

References

1) R. J. Sundberg and R. Brucemartin, *Chem. Rev.*, **74**, 471 (1974).
2) H. Ojima, *Nippon Kagaku Zasshi*, **88**, 333 (1967).
3) Y. Kajikawa, K. Mukai, K. Ishizu, and H. Ojima, *Chem. Lett.*, **1981**, 801.
4) T. D. Smith and J. R. Pilbrow, *Coord. Chem. Rev.*, 13, 173 (1974).
5) J. A. Ibers and R. H. Holm, *Science*, **209**, 223 (1980).
6) For example, see: J. P. Collman, C. M. Elliot, T. R. Halbert, and B. S. Tovrod, *Proc. Natl. Acad. Sci. U.S.A.*, **74**, 18 (1977).
7) G. E. Pake, J. Townsend, and S. I. Weissman, *Phys. Rev.*, **85**, 682 (1952).
8) "International Tables for X-Ray Crystallography," The Kynoch Press, Birmingham (1974), Vol. IV.
9) K. T. McGregor and W. E. Hatfield, *J. Chem. Phys.*, **65**, 4155 (1976).
10) For example, see: G. F. Kokoszka and H. C. Allen, Jr., and G. Gordon, *J. Chem. Phys.*, **46**, 3013 (1967); C. Chow and R. D. Willett, *ibid.*, **59**, 5903 (1973).
11) T. Lund and W. E. Hatfield, *J. Chem. Phys.*, **59**, 885 (1973).
12) T. D. Smith, T. Lund, and J. R. Pilbrow, *J. Chem. Soc., A*, **1971**, 2786; R. H. Dunhil, J. R. Pilbrow, and T. D. Smith, *J. Chem. Phys.*, **45**, 1474 (1966); J. H. Price, J. R. Pilbrow, K. S. Murray, and T. D. Smith, *J. Chem. Soc., A*, **1970**, 968; P. D. W. Boyd and T. D. Smith, *J. Chem. Soc., Dalton Trans.*, **1972**, 839.
13) B. Bleaney and K. D. Bowers, *Proc. Roy. Soc. London, Ser. A*, **214**, 451 (1952).
14) T. D. Smith and A. E. Martell, *J. Am. Chem. Soc.*, **94**, 3029 (1972).
15) H. Yokoi and T. Isobe, *Bull. Chem. Soc. Jpn.*, **45**, 3006 (1972).
16) T. Sakurai and K. Kobayashi, *Rikagaku Kenkyusho Hokoku*, **55**, 69 (1979).

 © 1984 The Chemical Society of Japan Bull. Chem. Soc. Jpn., 57, 1459—1468 (1984)

X-Ray Structural Elucidation of a Novel Steric Effect of *o*-Methoxyl Substituents in 2,6-Dimethoxyphenylnickel(II) Complexes Mediated by *m*-Bromo Substitution

Duanjun Xu,[†] Yasushi Kai, Kunio Miki, Nobutami Kasai,* Koichi Nishiwaki, and Masanori Wada
Department of Applied Chemistry, Faculty of Engineering, Osaka University, Suita, Osaka 565
(Received October 19, 1983)

Molecular structures of novel *trans*-[NiR_2L_2] complexes, *trans*-[$Ni\{C_6H_3(OMe)_2$-2,6$\}_2(PR_3)_2$] [PR_3=PMe_3 (**1a**), PMe_2Ph (**1b**)], and their *m*-brominated derivatives, *trans*-[$Ni\{C_6H(OMe)_2$-2,6-Br_2-3,5$\}_2(PR_3)_2$] [PR_3=PMe_3 (**2a**), PMe_2Ph (**2b**)], were determined by X-ray crystal structure analysis. A remarkable effect of *m*-substitution on the conformation of the *o*-methoxyl groups was found. This correlated well with the reactivity difference toward carbon monoxide. Crystal data: **1a**: monoclinic, space group $P2_1/c$, a=8.737(2), b=18.282(3), c=16.319(4) Å, β=105.06(2)°, Z=4, R=0.062; **1b**: triclinic, space group $P\bar{1}$, a=16.993(5), b=10.180(3), c=17.177(5) Å, α=112.44(2), β=117.59(2), γ=66.25(2)°, Z=3, R=0.060; **2a**: monoclinic, space group $P2_1/c$, a=9.294(2), b=14.091(3), c=10.770(2) Å, β=92.06(3)°, Z=2, R=0.067; **2b**: triclinic, space group $P\bar{1}$, a=9.370(1), b=11.387(2), c=9.013(1) Å, α=94.52(2), β=107.24(2), γ=77.35(2)°, Z=1, R=0.058.

Several 2,6-dimethoxyphenyl derivatives of transition metals are known. There seem to be at least three characteristic features caused by the *o*-methoxyl substituents. First, the steric effect allows the facile preparation of derivatives for Ni^{II},[1] Cu^{I},[2] Ag^{I},[3] and Au^{I},[4] which display greatly increased thermal and/or chemical stabilities, making their manipulation more facile than that of common phenyl derivatives. Secondly, the coordination properties through the oxygen lone-pair electrons have been demonstrated by the X-ray molecular structures of V_2R_4·2THF[5] and Cr_2R_4,[6] [R = $C_6H_3(OMe)_2$-2,6]. This functionality also explains the facile lithiation of the phosphine methyl groups in *trans*-[$NiR_2(PR'_3)_2$] [R = $C_6H_3(OMe)_2$-2,6; PR'_3 = PMe_3 (**1a**), PMe_2Ph (**1b**)].[1] Thirdly, the mesomeric effect caused by the methoxyl oxygen atom affects the facile and stereospecific bromination (electrophilic substitution) on the 2,6-dimethoxyphenyl group, as observed for **1a** and **1b**.[1] Interestingly, some of the resulting bromophenyl complexes *trans*-[$Ni\{C_6H(OMe)_2$-2,6-Br_2-3,5$\}_2(PR'_3)_2$] [PR'_3=PMe_3 (**2a**), PMe_2Ph (**2b**)] remarkably differed from the parent complexes **1a** and **1b** in the reactivity toward carbon monoxide, which catalyzes the intermolecular exchange of the PR'_3 ligands between **1a** and **1b** but not between **2a** and **2b**.[1] In order to obtain more structural information to aid in understanding the difference, the detailed molecular structures of these complexes have now been determined by the X-ray crystal structure analysis.[7] The results revealed the additional feature caused by the *o*-methoxyl substituents: their steric effect is highly influenced by the *m*-substituents and is associated with the rotational flexibility of the methoxyl group around the C(phenyl)-O bond.

Experimental

Crystallographic Data. Complexes **1a**, **1b**, **2a**, and **2b** were prepared by the procedures previously described.[1] Single crystals were obtained by recrystallization from ethanol (**1a**, **1b**), ethyl methyl ketone (**2a**), or acetone (**2b**). Crystals of **1a**, **1b**, **2a**, and **2b** are all pale yellow in color with regular prismatic shapes. Preliminary oscillation and Weissenberg photographs taken with Cu$K\alpha$ radiation showed that crystals of **1a** and **2a** are monoclinic, whereas those of **1b** and **2b** are triclinic. Accurate unit-cell parameters were determined at room temperature by the least-squares fit of 2θ values of 30, 25, 24, and 25 strong, higher angle reflections for **1a**, **1b**, **2a**, and **2b**, respectively. The density of each crystal was measured at room temperature by a flotation method in an aqueous solution of zinc bromide. Crystal data are summarized in Table 1.

Collection and Reduction of Intensity Data. Integrated intensities were measured on an Rigaku four-circle diffractometer by the θ-2θ scan technique at a 2θ scan rate of 4° min^{-1} and a scan width of $\Delta 2\theta=(2.0+0.70\tan\theta)°$. The background intensities were measured for 7.5 s at both ends of a scan. Four standard reflections were measured after every 60 reflections in order to monitor the radiation damage and the change of the crystal orientations. No significant intensity decay of the standard reflections was observed for any of the crystals. The reflection intensities collected up to 2θ=54° ($\sin\theta/\lambda$=0.639 $Å^{-1}$) were 5492, 3885, and 3904 for **1a**, **2a**, and **2b**, among which the observed reflections ($|F_o|>3\sigma(F_o)$) were 4138, 2284, and 3206, respectively. A total of 3394 (2397 non-zero) intensities for **1b** was first measured by adopting the small unit cell, which was later found to be a subcell of the true one. Reflections for **1b** based on the true unit cell were later collected up to 2θ=50°, and among the reflections measured 6006 were classed as observed ($|F_o|>3\sigma(F_o)$). The usual Lorentz and polarization effects were corrected for the intensity data, but no absorption correction was applied.

Determination and Refinement of the Structure. The crystal data of **2a** (space group $P2_1/c$ and Z=2) and **2b** (space group $P\bar{1}$ and Z=1) show that the **2a** and **2b** molecules must lie on a crystallographic center of symmetry. The crystal structures of **1a** and **2a** were solved by the heavy atom method. The heavy atoms located from the three-dimensional Patterson maps are: a nickel atom on a general position for **1a**, two bromine atoms on general positions in addition to a nickel atom on (0,0,0) for **2a**, respectively. The crystal structure of **2b** was solved by a combined use of the Patterson function and the direct method (*MULTAN*-78),[8] and two bromine atoms were located on general positions in addition to a nickel atom on (0,0,0).

Non-hydrogen atoms for **1a**, **2a**, and **2b** were located on the subsequent Fourier maps based on the positions of the heavy atoms. These crystal structures were refined by the block-diagonal least-squares procedure (*HBLS*-V),[9] the function minimized being $\sum w(|F_o|-|F_c|)^2$. All the hydrogen atoms

[†] On leave from Department of Chemistry, Zhejian University, Hangzhou, China. 1981 Scholarship Fellow, Ministry of Education, Science and Culture, Japan.

Table 1. Crystal data of *trans*-[NiR_2L_2] complexes

	1a	**1b**	**2a**	**2b**
R	$C_6H_3(OMe)_2$-2,6	$C_6H_3(OMe)_2$-2,6	$C_6H(OMe)_2$-2,6-Br_2-3,5	$C_6H(OMe)_2$-2,6-Br_2-3,5
L	PMe_3	PMe_2Ph	PMe_3	PMe_2Ph
Formula	$C_{22}H_{36}O_4P_2Ni$	$C_{32}H_{40}O_4P_2Ni$	$C_{22}H_{32}Br_4O_4P_2Ni$	$C_{32}H_{36}Br_4O_4P_2Ni$
M	485.2	609.3	800.8	924.9
Crystal Size/mm^3	0.20×0.25×0.30	0.15×0.25×0.25	0.20×0.27×0.27	0.20×0.22×0.22
System	Monoclinic	Triclinic	Monoclinic	Triclinic
Absence of reflections	h01: l≠2n 0k0: k≠2n	None	h01: l≠2n 0k0: k≠2n	None
Space Group	$P2_1/c$	$P\bar{1}$	$P2_1/c$	$P\bar{1}$
a/Å	8.737(2)	16.993(5)	9.294(2)	9.370(1)
b/Å	18.282(3)	10.180(3)	14.091(3)	11.387(2)
c/Å	16.319(4)	17.177(5)	10.770(2)	9.013(1)
α/°		112.44(2)		94.52(2)
β/°	105.06(2)	117.59(2)	92.06(3)	107.24(2)
γ/°		66.25(2)		77.35(2)
U/Å^3	2517.1(9)	2339.8(13)	1409.6(5)	896.0(2)
Z	4	3	2	1
D_c/g cm^{-3}	1.280	1.297	1.886	1.714
D_m/g cm^{-3}	1.284	1.299	1.884	1.727
$F(000)$	1032	966	788	458
μ(Mo$K\alpha$)/cm^{-1}	7.2	5.8	36.2	31.4

Table 2. Details of the refinement

	1a	**1b**	**2a**	**2b**
No. of reflections used[a]	4138	6006	2284	3206
No. of parameters refined	407	773	219	272
Weighting parameters[b]				
a[c]	0.070	0.0365	0.1023	0.0201
b[c]	0.0	0.0003	0.0003	0.0016
GOF[d]	1.096	1.240	1.149	1.271
Final R value[e]	0.062	0.060	0.067	0.058
Final Weighted R value (R_w)[f]	0.068	0.063	0.077	0.073

a) $|F_o|>3\sigma(|F_o|)$. b) Weighting scheme used: $w=(\sigma^2_{cs}+a|F_o|+b|F_o|^2)^{-1}$, where σ_{cs} is the standard deviation obtained from counting statistics. c) Used in the final refinement. d) Goodness of fit, $\Sigma w(|F_o|-|F_c|)^2/(n-m)$, where n and m are the number of reflections used and number of parameters refined, respectively. e) $R=\Sigma||F_o|-|F_c||/\Sigma|F_o|$. f) $R_w=\{\Sigma w(|F_o|-|F_c|)^2/\Sigma w|F_o|^2\}^{1/2}$

could be located on the difference Fourier maps, which were included in the successive refinement with isotropic temperature factors. At this stage of the refinement, the weighting schemes of the form $w=(\sigma^2_{cs}+a|F_o|+b|F_o|^2)^{-1}$ for $|F_o|>3\sigma(F_o)$ were applied. σ_{cs} is the standard deviation obtained from the counting statistics. The final weighted R values are (**1a**): 0.068; (**2a**): 0.077; (**2b**): 0.073. The values of a and b used in the final refinement are given in Table 2.

The structure analysis of **1b** was first carried out in a similar way to that for **1a**, **2a**, and **2b**, by adopting the subcell. Through the process of conventional refinement, a rather curious disordered structure was found: one of the methoxyl oxygen atoms takes two positions more than 1 Å apart from each other with half occupancy probability. After the anisotropic refinement of non-hydrogen atoms (R=0.103), hydrogen atoms were included in the refinement, but the convergence was not satisfactory. At this stage, a well-exposed Weissenberg photograph was taken around the b axis; additional reflections were thus found. This fact strongly indicated the possibility of a larger unit-cell for this crystal. The unit cell dimensions were redetermined, and reflection intensities were remeasured based on the true cell. Two interesting crystallographic features were found: (i) 2/3 of the total reflections measured based on the true cell are systematically weaker than the remaining 1/3 of the reflections, (ii) the subcell had been determined by using the stronger 1/3 reflections only. These two unit cells are related by these equations:

$$a=a_S-c_S,$$
$$b=b_S,$$
$$c=a_S+2c_S,$$

where the subscript shows the cell parameters of the subcell.

The crystal structure obtained by adopting the subcell, therefore, gives only the average structure. The true cell contains three molecules, and the space group is $P\bar{1}$. Therefore, one centrosymmetric molecule [**1b-1**] must lie on (0,0,0) and the other two molecules [**1b-2**] must lie on general positions. These two molecules [**1b-1** and **1b-2**] are crystallographically equivalent in the subcell. For the redetermination of the structure, the initial position of the **1b-2** could be easily deduced from the relationship between the true cell and the subcell. The coordinates of the nickel atom on the general position were refined by introducing an artificial bias of ±0.01 (in fraction) to the y parameter. The isotropic temperature factor of 3.0 Å^2 was applied for the nickel atom as the starting parameter. After two cycles of refinement, the temperature factors of the nickel atoms with the initial positions of (0,0,0) and (2/3, +0.01, 1/3) changed to large values of 10.1 and 3.2 Å^2 respectively and those with initial positions of (0,0,0) and (2/3, −0.01, 1/3) to 2.5 and 3.5 Å^2; the resulting atomic coordinates were (0.6657, 0.0209, 0.3258) from (2/3, +0.01, 1/3) and (0.6672, −0.0268, 0.3426)

TABLE 3. FINAL ATOMIC PARAMETERS, TOGETHER WITH THEIR ESTIMATED STANDARD DEVIATIONS IN PARENTHESES[a)]

Atom	x	y	z	B_{eq}
(a) *trans*-[Ni{$C_6H_3(OMe)_2$-2,6}$_2$(PMe_3)$_2$] (**1a**)				
Ni	0.29991(7)	0.10607(3)	0.22247(4)	2.75
P(1)	0.5314(2)	0.07764(7)	0.30317(9)	3.62
P(2)	0.0638(2)	0.14287(7)	0.15554(8)	3.43
C(11)	0.6497(8)	0.1541(4)	0.3561(4)	5.8
C(12)	0.6600(8)	0.0329(4)	0.2479(5)	6.1
C(13)	0.5466(8)	0.0162(4)	0.3929(4)	6.2
C(21)	-0.0739(7)	0.0731(4)	0.0999(4)	4.6
C(22)	-0.0433(7)	0.1852(4)	0.2257(4)	4.9
C(23)	0.0399(7)	0.2135(4)	0.0746(4)	5.4
C(31)	0.1999(6)	0.0374(3)	0.2823(3)	3.3
C(32)	0.1687(6)	0.0577(3)	0.3595(3)	3.6
C(33)	0.0961(7)	0.0118(4)	0.4056(4)	4.5
C(34)	0.0570(7)	-0.0578(4)	0.3765(4)	5.0
C(35)	0.0897(7)	-0.0826(3)	0.3031(4)	4.7
C(36)	0.1604(6)	-0.0344(3)	0.2576(3)	3.7
C(37)	0.1836(8)	0.1562(4)	0.4586(4)	5.9
C(38)	0.1535(9)	-0.1251(4)	0.1504(4)	6.1
C(41)	0.4035(6)	0.1768(3)	0.1648(3)	3.6
C(42)	0.4702(6)	0.1676(3)	0.0961(4)	4.2
C(43)	0.5487(7)	0.2247(4)	0.0666(4)	5.3
C(44)	0.5598(7)	0.2916(4)	0.1038(4)	5.9
C(45)	0.4932(7)	0.3049(3)	0.1692(4)	5.4
C(46)	0.4159(6)	0.2476(3)	0.1979(4)	4.2
C(47)	0.3484(9)	0.0534(4)	0.0458(5)	6.7
C(48)	0.354(1)	0.3237(4)	0.3069(6)	7.7
O(32)	0.2200(5)	0.1277(2)	0.3854(3)	4.5
O(36)	0.1991(5)	-0.0550(2)	0.1833(3)	4.9
O(42)	0.4750(5)	0.1018(3)	0.0559(3)	5.5
O(46)	0.3435(5)	0.2563(2)	0.2637(3)	5.5
(b) *trans*-[Ni{$C_6H_3(OMe)_2$-2,6}$_2$(PMe_2Ph)$_2$] (**1b**)				
1b-1				
Ni	0	0	0	2.84
P(1)	0.08351(9)	-0.1875(2)	-0.06879(9)	3.53
C(111)	0.0237(4)	-0.2795(5)	-0.1845(4)	3.6
C(112)	-0.0114(4)	-0.3943(6)	-0.2024(4)	4.6
C(113)	-0.0583(4)	-0.4623(6)	-0.2904(5)	5.5
C(114)	-0.0700(4)	-0.4162(7)	-0.3614(4)	5.5
C(115)	-0.0362(5)	-0.3036(7)	-0.3448(4)	5.8
C(116)	0.0099(4)	-0.2350(6)	-0.2574(4)	4.6
C(12)	0.1462(4)	-0.3352(7)	-0.0094(4)	5.7
C(13)	0.1772(4)	-0.1638(7)	-0.0817(4)	5.3
C(31)	0.0828(4)	0.1156(5)	0.0360(3)	3.4
C(32)	0.0720(4)	0.2014(6)	-0.0168(4)	4.6
C(33)	0.1323(5)	0.2834(7)	0.0091(5)	6.4
C(34)	0.2043(5)	0.2808(7)	0.0876(5)	7.0
C(35)	0.2221(4)	0.1954(7)	0.1437(5)	6.0
C(36)	0.1605(4)	0.1122(6)	0.1156(4)	4.1
C(37)	-0.0301(7)	0.2862(9)	-0.1537(6)	9.2
C(38)	0.2325(5)	0.0358(8)	0.2539(5)	7.6
O(32)	-0.0041(3)	0.1917(5)	-0.0992(3)	6.5
O(36)	0.1711(3)	0.0201(5)	0.1632(3)	5.5
1b-2				
Ni	0.66785(4)	-0.02674(6)	0.34608(4)	2.75
P(1)	0.75716(9)	-0.2171(2)	0.2853(1)	3.80
P(2)	0.57664(9)	0.1721(2)	0.40187(9)	3.30
C(111)	0.6985(4)	-0.3047(5)	0.1682(4)	3.8
C(112)	0.6627(4)	-0.4194(6)	0.1472(4)	4.7
C(113)	0.6160(5)	-0.4825(6)	0.0593(4)	5.8
C(114)	0.6042(5)	-0.4334(7)	-0.0098(4)	6.6
C(115)	0.6375(5)	-0.3173(8)	0.0087(5)	6.6
C(116)	0.6853(4)	-0.2533(7)	0.0978(4)	5.4
C(12)	0.8160(4)	-0.3693(7)	0.3417(5)	6.1
C(13)	0.8547(4)	-0.1947(7)	0.2779(5)	6.4
C(211)	0.6328(4)	0.2912(5)	0.5083(4)	3.4
C(212)	0.6632(4)	0.3985(6)	0.5079(4)	4.4
C(213)	0.7106(4)	0.4839(6)	0.5882(5)	5.5
C(214)	0.7295(4)	0.4613(7)	0.6697(4)	6.0
C(215)	0.6999(5)	0.3559(7)	0.6710(4)	5.8
C(216)	0.6515(4)	0.2705(6)	0.5907(4)	4.6
C(22)	0.5070(4)	0.2949(6)	0.3257(4)	5.0
C(23)	0.4877(4)	0.1530(6)	0.4254(4)	4.9
C(31)	0.7444(3)	0.0922(5)	0.3696(3)	3.2
C(32)	0.7281(4)	0.1631(6)	0.3065(4)	3.8
C(33)	0.7805(5)	0.2524(7)	0.3219(4)	5.2
C(34)	0.8530(4)	0.2693(7)	0.4025(5)	5.5
C(35)	0.8748(4)	0.1981(6)	0.4674(4)	4.7
C(36)	0.8199(4)	0.1121(5)	0.4497(4)	3.6
C(37)	0.6263(5)	0.2129(9)	0.1605(5)	7.6
C(38)	0.9008(5)	0.0708(7)	0.5997(4)	5.8
C(41)	0.5883(4)	-0.1480(5)	0.3146(4)	3.5
C(42)	0.5954(4)	-0.2432(6)	0.3593(4)	4.1
C(43)	0.5323(5)	-0.3254(6)	0.3251(4)	5.5
C(44)	0.4613(5)	-0.3153(7)	0.2453(4)	6.1
C(45)	0.4488(4)	-0.2221(7)	0.1972(4)	4.9
C(46)	0.5118(4)	-0.1408(5)	0.2329(4)	3.7
C(47)	0.7050(5)	-0.1587(7)	0.5040(4)	5.7
C(48)	0.4462(5)	-0.0564(7)	0.0967(4)	6.2
O(32)	0.6560(3)	0.1344(4)	0.2258(3)	5.0
O(36)	0.8366(3)	0.0367(4)	0.5101(3)	4.4
O(42)	0.6668(3)	-0.2713(4)	0.4405(3)	5.9
O(46)	0.5051(3)	-0.0455(4)	0.1892(3)	4.8
(c) *trans*-[Ni{$C_6H(OMe)_2$-2,6-Br_2-3,5}$_2$(PMe_3)$_2$] (**2a**)				
Ni	0	0	0	2.22
Br(1)	0.43254(10)	-0.26991(8)	0.19628(13)	6.05
Br(2)	0.29983(12)	0.0598(1)	0.46699(10)	6.27
P(1)	-0.1878(3)	-0.0781(2)	0.07037(18)	2.84
C(11)	-0.2848(12)	-0.1530(8)	-0.0443(9)	5.2
C(12)	-0.3341(10)	-0.0047(7)	0.1260(10)	4.9
C(13)	-0.1594(10)	-0.1613(7)	0.1996(8)	4.1
C(31)	0.1313(8)	-0.0518(6)	0.1296(7)	2.8
C(32)	0.2177(9)	-0.1346(6)	0.1205(8)	3.4
C(33)	0.3180(9)	-0.1573(6)	0.2149(9)	3.8
C(34)	0.3408(9)	-0.1034(7)	0.3182(8)	4.3
C(35)	0.2571(9)	-0.0235(7)	0.3293(8)	3.8
C(36)	0.1535(8)	0.0007(6)	0.2394(7)	3.1
C(37)	0.1063(12)	-0.2080(8)	-0.0586(10)	5.5
C(38)	-0.0330(12)	0.0819(8)	0.3438(10)	5.5
O(32)	0.2188(8)	-0.1926(6)	0.0176(8)	6.7
O(36)	0.0745(7)	0.0832(5)	0.2509(6)	4.1
(d) *trans*-[Ni{$C_6H(OMe)_2$-2,6-Br_2-3,5}$_2$(PMe_2Ph)$_2$] (**2b**)				
Ni	0	0	0	2.19
Br(1)	0.54337(8)	-0.36534(7)	0.23880(8)	5.04
Br(2)	0.31851(8)	-0.28545(8)	-0.40566(8)	4.99
P(1)	0.1012(2)	0.1481(2)	-0.0450(2)	2.78
O(32)	0.2887(5)	-0.1445(4)	0.2457(5)	3.6
O(36)	0.0974(5)	-0.0827(4)	-0.3055(5)	3.8
C(111)	0.1096(6)	0.2727(5)	0.0976(7)	3.0
C(112)	-0.0225(7)	0.3554(5)	0.1014(8)	4.0
C(113)	-0.0224(8)	0.4439(6)	0.2146(10)	5.1
C(114)	0.1121(9)	0.4538(7)	0.3257(9)	5.7
C(115)	0.2455(9)	0.3734(8)	0.3244(9)	5.6
C(116)	0.2449(7)	0.2817(6)	0.2111(8)	4.1
C(12)	0.0018(8)	0.2239(6)	-0.2290(7)	4.2
C(13)	0.2950(7)	0.1088(6)	-0.0627(9)	4.2
C(31)	0.1756(6)	-0.1169(5)	-0.0286(6)	2.6
C(32)	0.2912(6)	-0.1763(5)	0.0949(6)	2.7
C(33)	0.4026(6)	-0.2734(5)	0.0695(6)	3.0
C(34)	0.4104(7)	-0.3079(5)	-0.0787(7)	3.3
C(35)	0.3045(6)	-0.2433(5)	-0.2005(6)	3.0
C(36)	0.1900(6)	-0.1495(5)	-0.1773(6)	2.9
C(37)	0.4007(9)	-0.0772(7)	0.3287(8)	4.9
C(38)	-0.0503(8)	-0.1012(7)	-0.3682(8)	4.7

a) Positional parameters are in fraction of cell edges and B_{eq} is the equivalent isotropic temperature factor calculated from the corresponding anisotropic factors.[11)]

from (2/3, −0.01, 1/3), respectively. The Fourier map based on phases of the former set of nickel positions includes many unreasonable supurious peaks especially around the methoxyl group, whereas the Fourier map calculated from the latter set of nickel positions could easily locate all the non-hydrogen atoms except two. The latter structure was then refined isotropically, and the next Fourier synthesis revealed the remaining two atoms. Refinement was then carried out in the same manner as those of **1a**, **2a**, and **2b**; it converged to a reasonable R value.

The details of the refinements for all the crystals are summarized in Table 2. The atomic scattering factors were taken from the International Tables for X-Ray Crystallography.[10)] Final atomic coordinates of four crystals, together with equivalent isotropic temperature factors B_{eq}[11)] for non-hydrogen atoms are listed in Table 3.[‖]

Computation. All the calculations were carried

[‖] Tables of anisotropic temperature factors for non-hydrogen atoms, the atomic coordinates and isotropic temperature factors for hydrogen atoms, and the observed and the calculated structure factors are deposited as Document No. 8415 at the Office of the Editor of the Bulletin of the Chemical Society of Japan.

out on an ACOS S900 computer at the Crystallographic Research Center, Institute for Protein Research, Osaka University.

Results and Discussion

Molecular Structure. The molecular structures of **1a**, **1b-1**, **1b-2**, **2a**, and **2b** are shown in Fig. 1 by the *ORTEP* drawings,[12] together with the atomic numberings. The crystallographic molecular symmetries of **1b-1**, **2a**, and **2b** are C_i. The **1a** and **1b-2** molecules have no crystallographic symmetry, but the local center of symmetry is found in these structures when the conformations of methoxyl groups are ignored. The interatomic bond distances and angles observed in these complexes are summarized in Table 4.

Coordination Geometry of Nickel Atom: The important structural parameters needed to describe the coordination geometry of nickel atom are summarized in Table 5. The first structural feature commonly observed in these complexes is that the nickel atom takes a square-planar coordination with two phenyl and two phosphine ligands on *trans*-positions. As the **1b-1**, **2a**, and **2b** molecules occur on the center of symmetry, the five atoms defining the coordination plane of nickel atom are exactly coplanar. The least-squares planes of the coordination planes in **1a** and **1b-2** are listed in Table 6. The coplanality of the five atoms in **1a** is slightly lower than that of those in **1b-2**. However, the deformation geometry of the coordination planes is the same in both structures; that is, all the four atoms bonding to the nickel atom deviate toward the same direction from nickel atom, bending away from the C(47) atom, which is the only methoxyl methyl group approaching near to nickel atom in these complexes. It is noteworthy that the P(1)-Ni-P(2) bond angle [172.5(1)°] in **1a** shows an angular deviation of

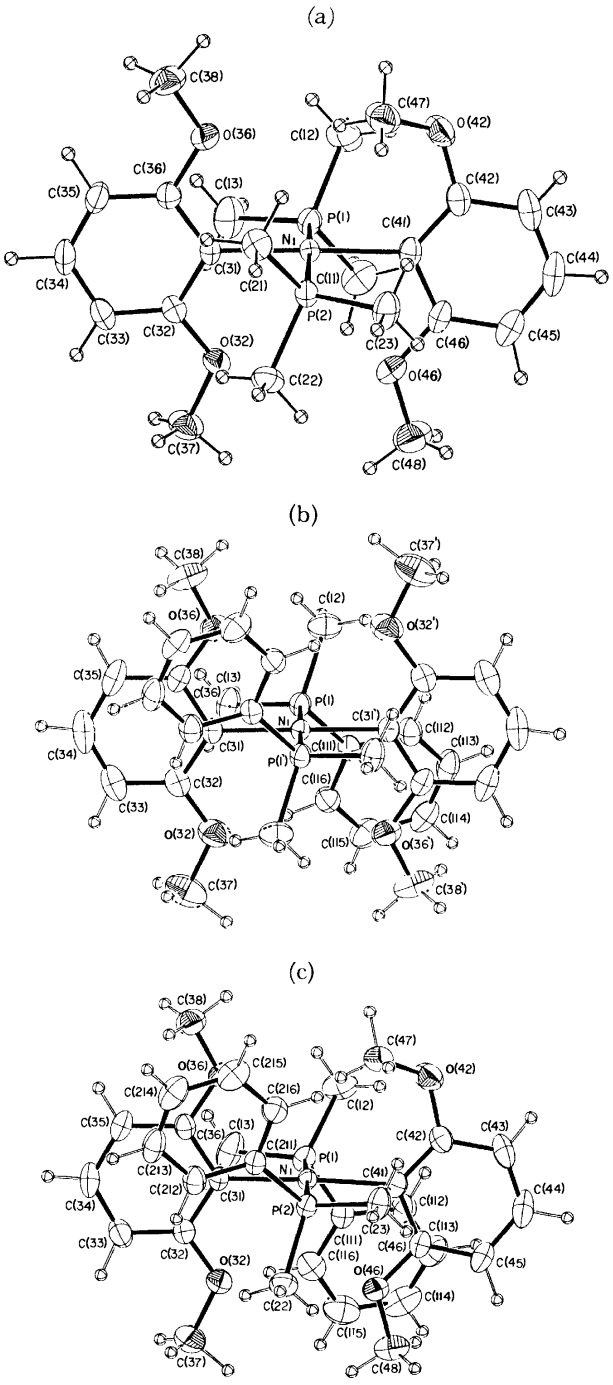

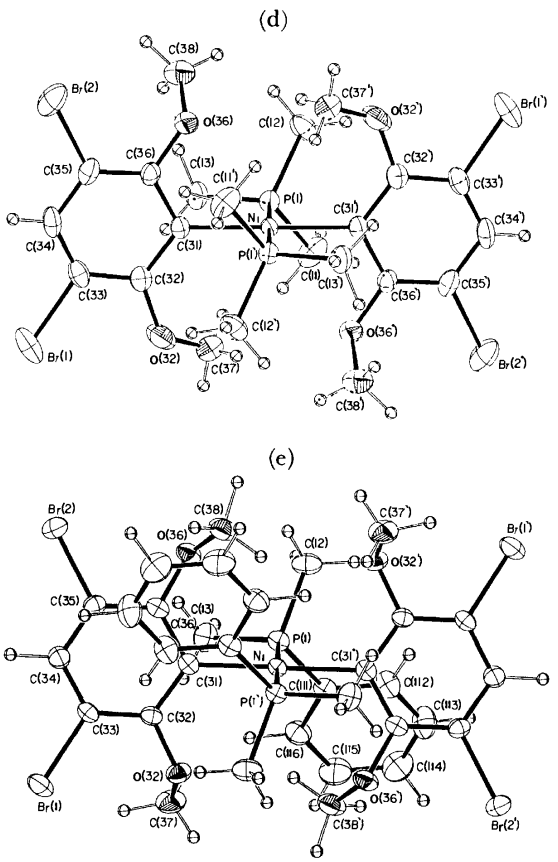

Fig. 1. Molecular structures of *trans*-[NiR_2L_2] complexes drawn by *ORTEP*-II,[12] together with the atomic numberings. Thermal ellipsoids for non-hydrogen atoms are drawn at the 30% probability level. The hydrogen atoms are shown as spheres with arbitrary temperature factor of 1.0 Å^2. a) **1a**; R=$C_6H_3(OMe)_2$-2,6, L=PMe_3, b) **1b-1**; R=$C_6H_3(OMe)_2$-2,6, L=PMe_2Ph, c) **1b-2**; R and L are same as those in **1b-1**, d) **2a**; R=$C_6H(OMe)_2$-2,6-Br_2-3,5, L=PMe_3, e) **2b**; R=$C_6H(OMe)_2$-2,6-Br_2-3,5, L=PMe_2Ph.

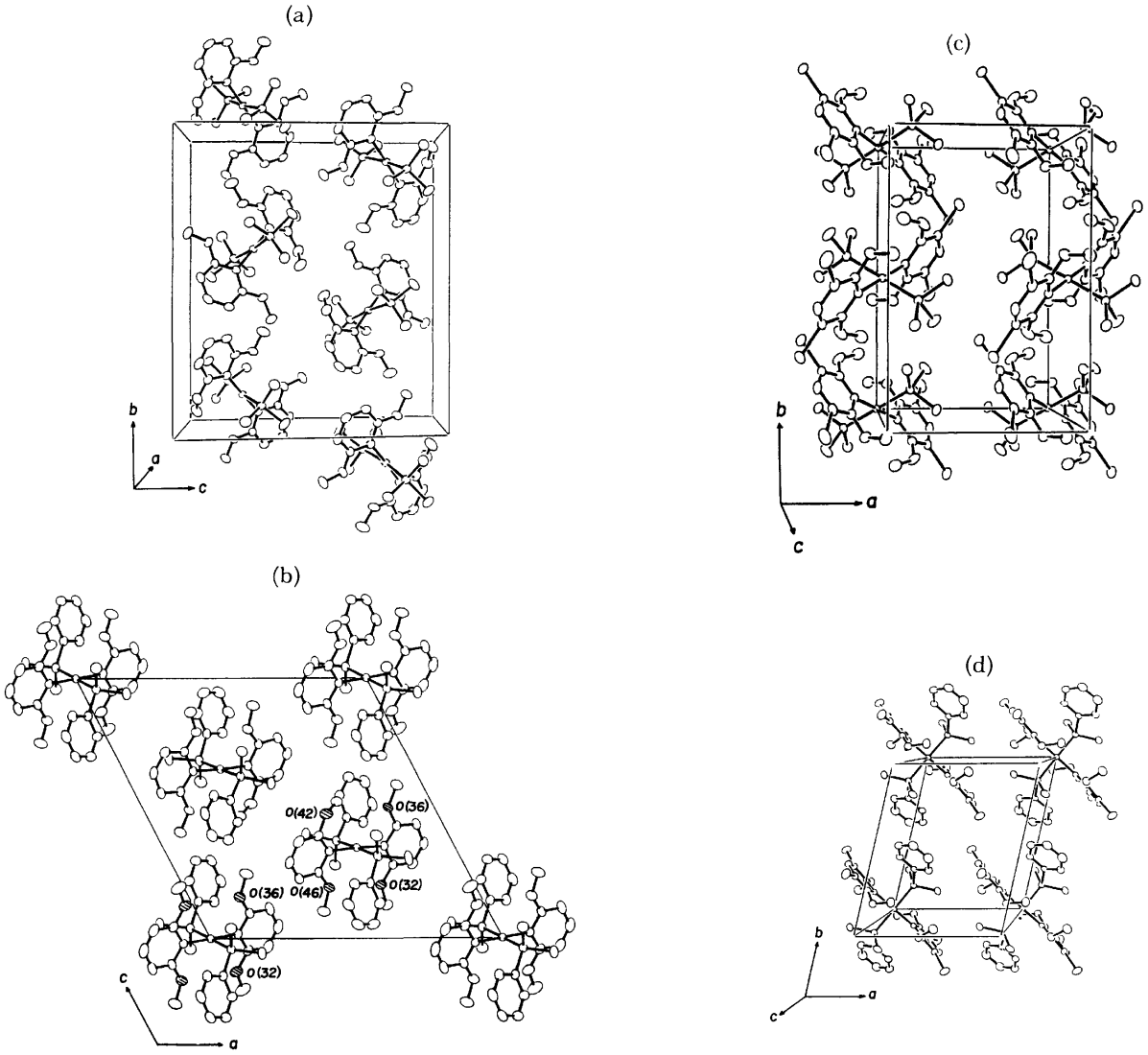

Fig. 2. Crystal structures of *trans*-[NiR_2L_2] complexes.
a) **1a**, b) **1b**, c) **2a**, and d) **2b**.

TABLE 4. INTERATOMIC BOND DISTANCES AND ANGLES, TOGETHER WITH THEIR ESTIMATED STANDARD DEVIATIONS IN PARENTHESES*

Bond distance	*l*/Å				
	1a	**1b-1**	**1b-2**	**2a**	**2b**
Br(1) -C(33)				1.925(9)	1.902(5)
Br(2) -C(35)				1.922(9)	1.909(6)
P(1) -C(11)	1.818(6)			1.836(10)	
P(1) -C(12)	1.809(7)	1.819(7)	1.827(7)	1.828(10)	1.822(7)
P(1) -C(13)	1.822(7)	1.822(7)	1.828(8)	1.831(9)	1.824(8)
P(2) -C(21)	1.825(6)				
P(2) -C(22)	1.828(6)		1.815(6)		
P(2) -C(23)	1.820(6)		1.830(7)		
P(1) -C(111)		1.826(6)	1.824(6)		1.836(6)
P(2) -C(211)			1.829(6)		
C(111)-C(112)		1.390(8)	1.383(8)		1.389(9)
C(111)-C(116)		1.380(8)	1.387(9)		1.392(9)
C(112)-C(113)		1.389(9)	1.372(9)		1.376(11)
C(113)-C(114)		1.373(9)	1.362(10)		1.379(12)

*Important parameters are selected and summarized in Tables 5 and 7.

Table 4. (Continued)

Bond distance	l/Å				
	1a	**1b-1**	**1b-2**	**2a**	**2b**
C(114)-C(115)		1.361(10)	1.379(10)		1.380(12)
C(115)-C(116)		1.380(9)	1.394(10)		1.402(11)
C(211)-C(212)			1.387(9)		
C(211)-C(216)			1.380(8)		
C(212)-C(213)			1.389(9)		
C(213)-C(214)			1.373(10)		
C(214)-C(215)			1.368(10)		
C(215)-C(216)			1.394(9)		
C(31) -C(32)	1.405(7)	1.393(8)	1.389(8)	1.423(11)	1.397(7)
C(31) -C(36)	1.391(7)	1.393(8)	1.394(8)	1.404(11)	1.399(7)
C(32) -C(33)	1.385(7)	1.388(10)	1.393(9)	1.392(12)	1.400(7)
C(33) -C(34)	1.370(8)	1.338(11)	1.369(10)	1.358(13)	1.381(8)
C(34) -C(35)	1.380(8)	1.390(11)	1.385(9)	1.375(13)	1.376(8)
C(35) -C(36)	1.396(8)	1.408(9)	1.387(8)	1.384(12)	1.390(8)
C(41) -C(42)	1.402(7)		1.389(8)		
C(41) -C(46)	1.396(7)		1.405(7)		
C(42) -C(43)	1.403(8)		1.399(10)		
C(43) -C(44)	1.356(9)		1.349(10)		
C(44) -C(45)	1.364(9)		1.379(10)		
C(45) -C(46)	1.391(8)		1.387(8)		
C(32) -O(32)	1.385(6)	1.410(8)	1.383(7)	1.377(11)	1.385(7)
C(37) -O(32)	1.413(8)	1.400(11)	1.411(10)	1.324(13)	1.430(9)
C(36) -O(36)	1.392(6)	1.377(7)	1.379(7)	1.383(10)	1.386(7)
C(38) -O(36)	1.406(8)	1.407(9)	1.422(8)	1.440(12)	1.388(9)
C(42) -O(42)	1.376(7)		1.398(8)		
C(47) -O(42)	1.392(8)		1.384(9)		
C(46) -O(46)	1.390(7)		1.381(7)		
C(48) -O(46)	1.411(9)		1.421(8)		

Bond angle	φ/°				
	1a	**1b-1**	**1b-2**	**2a**	**2b**
Ni -P(1) -C(11)	115.4(2)			115.4(3)	
Ni -P(1) -C(12)	114.1(2)	112.0(3)	115.1(3)	115.8(3)	114.5(2)
Ni -P(1) -C(13)	119.8(2)	119.4(3)	119.3(3)	118.9(3)	117.6(2)
C(11) -P(1) -C(12)	103.6(3)			101.1(5)	
C(11) -P(1) -C(13)	100.3(3)			101.4(4)	
C(12) -P(1) -C(13)	101.3(3)	100.7(4)	100.5(4)	101.6(4)	100.0(3)
Ni -P(1) -C(111)		117.4(2)	114.4(2)		116.0(2)
C(111)-P(1) -C(12)		104.0(3)	103.6(3)		103.2(3)
C(111)-P(1) -C(13)		101.0(3)	101.6(4)		103.2(3)
Ni -P(2) -C(21)	116.8(2)				
Ni -P(2) -C(22)	112.9(2)		112.3(3)		
Ni -P(2) -C(23)	119.9(2)				
C(21) -P(2) -C(22)	103.2(3)				
C(21) -P(2) -C(23)	101.4(3)				
C(22) -P(2) -C(23)	100.0(3)		101.0(3)		
Ni -P(2) -C(211)			116.4(2)		
C(211)-P(2) -C(22)			103.7(3)		
C(211)-P(2) -C(23)			102.1(3)		
C(32) -C(31) -C(36)	114.8(4)	115.7(6)	115.2(5)	115.1(7)	116.0(5)

TABLE 4. (Continued)

Bond angle	φ/°				
	1a	**1b-1**	**1b-2**	**2a**	**2b**
C(31) -C(32) -C(33)	123.3(5)	122.8(7)	123.4(6)	120.2(7)	121.4(5)
C(31) -C(32) -O(32)	113.3(4)	112.8(6)	113.8(5)	124.3(7)	119.2(5)
C(33) -C(32) -O(32)	123.4(5)	124.4(7)	122.9(6)	115.3(7)	119.1(5)
C(32) -C(33) -C(34)	118.9(5)	119.5(8)	118.6(7)	123.4(8)	121.2(5)
C(33) -C(34) -C(35)	121.1(6)	121.9(8)	121.0(7)	117.2(9)	117.5(5)
C(34) -C(35) -C(36)	118.3(5)	117.5(7)	118.4(6)	121.5(8)	121.8(5)
C(31) -C(36) -C(35)	123.5(5)	122.6(6)	123.3(6)	122.5(7)	121.6(5)
C(31) -C(36) -O(36)	114.2(4)	113.8(5)	114.2(5)	117.1(7)	120.7(5)
C(35) -C(36) -O(36)	122.2(5)	123.7(6)	122.4(5)	120.2(7)	117.5(5)
C(32) -C(33) -Br(1)				118.1(6)	120.7(4)
C(34) -C(33) -Br(1)				118.5(7)	118.1(4)
C(34) -C(35) -Br(2)				117.7(7)	118.1(4)
C(36) -C(35) -Br(2)				120.6(6)	120.1(4)
C(32) -O(32) -C(37)	118.3(4)	118.8(7)	118.9(6)	124.6(8)	114.7(5)
C(36) -O(36) -C(38)	118.0(5)	118.1(6)	118.3(5)	115.8(7)	117.9(5)
C(42) -C(41) -C(46)	114.5(5)		114.0(5)		
C(41) -C(42) -C(43)	121.9(5)		122.6(6)		
C(41) -C(42) -O(42)	123.9(5)		124.3(6)		
C(43) -C(42) -O(42)	114.1(5)		113.0(6)		
C(42) -C(43) -C(44)	120.0(6)		120.3(7)		
C(43) -C(44) -C(45)	121.1(6)		120.6(7)		
C(44) -C(45) -C(46)	118.2(6)		118.0(6)		
C(41) -C(46) -C(45)	124.3(5)		124.4(6)		
C(41) -C(46) -O(46)	113.5(5)		113.6(5)		
C(45) -C(46) -O(46)	122.2(5)		121.9(5)		
C(42) -O(42) -C(47)	119.4(5)		119.2(6)		
C(46) -O(46) -C(48)	120.2(5)		118.6(5)		
P(1) -C(111)-C(112)		121.4(5)	121.2(5)		120.3(5)
P(1) -C(111)-C(116)		121.0(5)	120.5(5)		121.2(5)
C(112)-C(111)-C(116)		117.6(6)	118.3(6)		118.3(6)
C(111)-C(112)-C(113)		121.3(6)			121.8(7)
C(112)-C(113)-C(114)		119.6(7)	120.3(7)		119.8(8)
C(113)-C(114)-C(115)		119.7(7)	119.9(7)		119.7(8)
C(114)-C(115)-C(116)		120.9(7)	120.0(7)		120.5(7)
C(111)-C(116)-C(115)		121.0(6)	120.1(7)		119.8(6)
P(2) -C(211)-C(212)			120.4(5)		
P(2) -C(211)-C(216)			121.2(5)		
C(212)-C(211)-C(216)			118.3(6)		
C(211)-C(212)-C(213)			121.0(6)		
C(212)-C(213)-C(214)			120.1(7)		
C(213)-C(214)-C(215)			119.5(7)		
C(214)-C(215)-C(216)			120.8(7)		
C(211)-C(216)-C(215)			120.4(6)		

7.5° from the exact *trans* coordination, while the other P-Ni-C and P-Ni-P bond angles in Table 5 take the value near to 90° and 180°, respectively. The second structural feature to note is that the ring planes of phenyl ligands are nearly perpendicular to the coordination plane of nickel atom. The dihedral angles between these planes in Table 5 show that almost all the phenyl ligands are normal to the coordination plane within several degrees, with one exception having the relatively large deviation of 13.9° from the right angle in the **2b** molecule. The third interesting feature is that the phosphine ligands take a very characteristic conformation, with one methyl group located roughly on the coordination plane of nickel atom regardless of the types of phosphine ligands, PMe_3 or PMe_2Ph. The torsional angles ϕ_1 and ϕ_2 in Table 5 are the measure to

TABLE 5. COORDINATION GEOMETRIES OF NICKEL ATOMS IN **1a**, **1b**, **2a**, AND **2b**

	1a	**1b-1**	**1b-2**	**2a**	**2b**
P(1) -Ni-C(31)	90.6(1)°	89.4(2)°	89.2(2)°	92.8(2)°	89.8(2)°
P(1) -Ni-C(41)	88.6(2)		89.5(2)		
P(2) -Ni-C(31)	87.7(1)		88.9(2)		
P(2) -Ni-C(41)	92.9(2)		92.3(2)		
P(1) -Ni-P(2)	172.5(1)		176.6(1)		
C(31)-Ni-C(41)	178.5(2)		176.6(3)		
ϕ_1[a]	−6.0°	−8.5°	−1.4°	−4.6°	−7.2°
ϕ_2[a]	3.2		14.4		
θ_1[b]	92.3	89.2	90.6	91.0	103.9
θ_2[b]	84.1		96.8		

a) Torsional angles around Ni-P bonds: $\phi_1=\phi_{C(31)\text{-}Ni\text{-}P(1)\text{-}C(13)}$, $\phi_2=\phi_{C(41)\text{-}Ni\text{-}P(2)\text{-}C(23)}$. b) Dihedral angles between Ni-coordination plane and phenyl ring planes: θ_1 and θ_2 correspond with the phenyl rings defined by C(31) to C(36) and by C(41) to C(46), respectively.

TABLE 6. COORDINATION PLANES OF NICKEL ATOMS IN **1a** AND **1b-2** MOLECULES

Least-squares plane through Ni, P(1), P(2), C(31), and C(41) atoms in the form of $AX+BY+CZ+D=0.0$, where X, Y, Z are the coordinates in the orthogonal unit cell in Å.

1a $0.2192X-0.6949Y-0.6849Z+3.4467=0.0$

1b-2 $-0.0545X+0.4415Y-0.8956Z+5.6687=0.0$

Atomic deviations from the least-squares plane in Å.

	Ni	P(1)	P(2)	C(31)	C(41)
1a	0.066	−0.076	−0.070	0.044	0.040
1b-2	−0.043	0.010	0.011	0.011	0.012

TABLE 7. CONFORMATIONS OF METHOXYL GROUPS AND RELATED STRUCTURAL PARAMETERS IN **1a**, **1b**, **2a**, AND **2b**

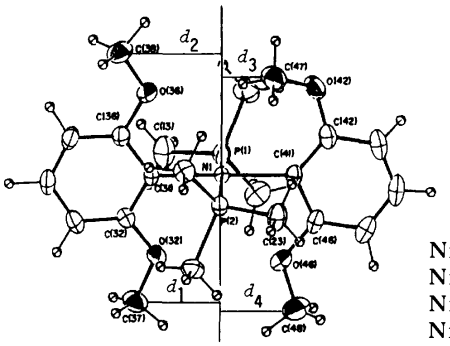

1a

	1a	**1b-1**	**1b-2**	**2a**	**2b**
ϕ_1[a]	175.0°	172.0°	173.0°	−31.8°	−106.7°
ϕ_2[a]	−175.7	−164.4	−168.6	111.7	−79.3
ϕ_3[a]	36.0		34.3		
ϕ_4[a]	176.4		164.1		
d_1[b]	2.365Å	2.516Å	2.403Å	1.339Å	2.286Å
d_2[b]	2.801	2.467	2.706	2.249	1.312
d_3[b]	1.425	2.516[c]	1.447	1.339[c]	2.286[c]
d_4[b]	2.069	2.467[c]	2.009	2.249[c]	1.312[c]
$(d_1+d_4)/2$	2.217	2.492	2.206	1.794	1.799
$(d_2+d_3)/2$	2.113	2.492[c]	2.077	1.794[c]	1.799[c]
Ni-C(31)-C(32)	120.0(3)°	123.0(5)°	121.8(4)°	126.5(6)°	122.9(4)°
Ni-C(31)-C(36)	125.2(4)	121.3(5)	122.9(4)	118.2(6)	121.1(4)
Ni-C(41)-C(42)	130.2(4)		130.5(5)		
Ni-C(41)-C(46)	115.3(4)		115.5(4)		
Ni-P(1)	2.170(2)Å	2.168(1)Å	2.168(2)Å	2.220(2)Å	2.224(1)Å
Ni-P(2)	2.175(1)		2.188(2)		
Ni-C(31)	1.933(5)	1.928(5)	1.931(5)	1.962(8)	1.945(5)
Ni-C(41)	1.954(5)		1.951(5)		

a) Torsional angles around C(phenyl)-O(methoxyl) bonds: $\phi_1=\phi_{C(31)\text{-}C(32)\text{-}O(32)\text{-}C(37)}$, $\phi_2=\phi_{C(31)\text{-}C(36)\text{-}O(36)\text{-}C(38)}$, $\phi_3=\phi_{C(41)\text{-}C(42)\text{-}O(42)\text{-}C(47)}$, and $\phi_4=\phi_{C(41)\text{-}C(46)\text{-}O(46)\text{-}C(48)}$. b) Distances from methoxyl methyl carbons to the normal of the coordination plane through Ni atom: d_1, d_2, d_3, and d_4 correspond with the C(37), C(38), C(47), and C(48) atoms, respectively. c) These parameters are not crystallographically unique but are listed for the sake of better understanding.

estimate the angular deviation of the unique methyl group of each phosphine ligand from the coordination plane; the maximum angular deviation observed is 14.4° of ϕ_2 in **1b-2** molecule.

Conformation of Methoxyl Group: The selected structural parameters for the conformations of methoxyl groups are listed in Table 7. The most interesting and important difference in the molecular structures of this series of complexes is the difference in the conformations of methoxyl groups, which are influenced very sensitively by the steric and/or electrostatic effect in the different types of phosphine ligands and/or the different substituents on *m*-positions.

The torsional angles around the O(methoxyl)-C(phenyl) bond (ϕ's in Table 7) were calculated as the measure to describe the conformation of methoxyl groups. When the methoxyl methyl groups are near the nickel atom, the ϕ angles become smaller, and when the methoxyl

methyl groups are far from the nickel atom and near the substituents on *m*-positions, the ϕ angles become larger. Five independent molecules in Table 7 are divided into three conformers according to the conformations of methoxyl groups. The **1b-1** molecule gives one extreme case (Conformer A), in which all of the four methoxyl groups (only two are crystallographically independent) take the ϕ values near to 180°, indicating that all the methoxyl groups are located far from the nickel atom and near the *m*-substituents (H atoms). The molecules **1a** and **1b-2** have similar structures (Conformer B): one of the four methoxyl groups has the angle of 36.0° in **1a** and 34.3° in **1b-2** respectively, and the remaining three methoxyl groups have ϕ angles between 164.1° and 176.4°; this shows that only one methoxyl methyl is located near the nickel atom. The *m*-brominated derivatives, **2a** and **2b**, give the third conformer (Conformer C), in which all the ϕ angles are much smaller than 180°, the maximum value being 111.7° in the **2a** molecule.

The distances from the methoxyl carbons to the normal of the coordination plane passing through the nickel atom are calculated (*d*'s in Table 7) to estimate the free space of the 5th and/or 6th coordination sites of nickel atom. The average values of these distances on each coordination site of nickel atom are devided clearly into three types corresponding to the three types of conformers found in these complexes. The Conformer A [**1b-1**] gives the longest *d* distance of 2.492 Å on both sites of the coordination plane of nickel atom. Conformer B [**1a** and **1b-2**] takes a little shorter *d* distances, between 2.077 and 2.217 Å, than the Conformer A. On the other hand, Conformer C [the *m*-substituted derivatives **2a** and **2b**] takes the shortest *d* distances of 1.794 and 1.799 Å.

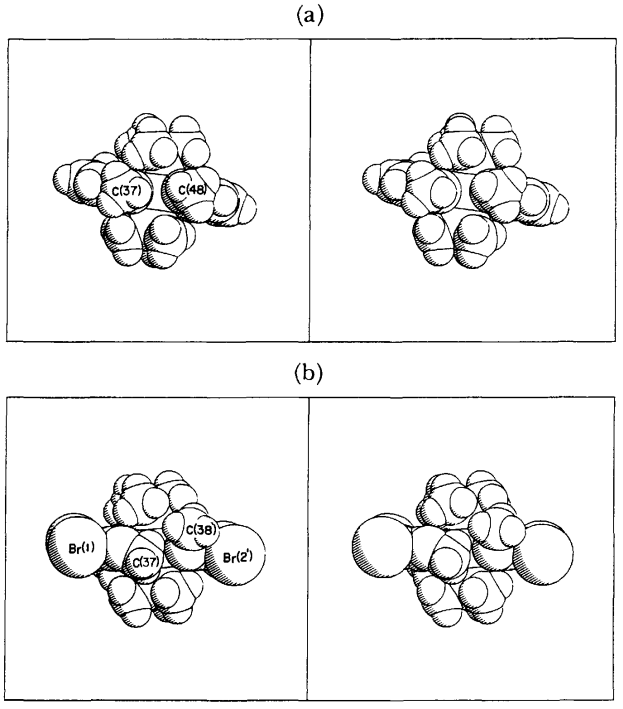

Fig. 3. Stereoscopic views of the molecular structures of **1a** and **2a** complexes shown by the space filling models drawn by *PLUTO*-78.[13] a) **1a**, b) **2a**.

The bond distances and angles included in the coordination plane of nickel atom show some interesting deformations which are correlated to the conformational differences of *o*-methoxyl groups and *m*-substituents. The Ni-C(phenyl) distances are divided into two types. The shorter ones are the Ni-C(31) bonds in *m*-unsubstituted molecules with two methoxyl groups near to the *m*-substituents: from 1.928(5) to 1.933(5) Å. The longer ones are the the Ni-C(phenyl) bonds in *m*-unsubstituted molecules with one methoxyl group near to the nickel atom, and those in *m*-brominated molecules with two methoxyl groups near to the nickel atom: from 1.945(5) to 1.962(8) Å. Similar structural deformations are also found in Ni-P distances. The Ni-P distances in *m*-brominated molecules [**2a** and **2b**: 2.220(2) and 2.224(1) Å] are significantly longer than those in *m*-unsubstituted ones [**1a**, **1b-1**, and **1b-2**: from 2.168(2) to 2.188(2) Å]. The Ni-C(phenyl)-C(phenyl) angles also reflect the steric effect of methoxyl groups. The corresponding angles associated with the phenyl ligand with different conformations of methoxyl groups, one near to the *m*-substituent and another near to the nickel atom, show a remarkable difference: Ni-C(41)-C(42) angles [130.2(4) and 130.5(5)°] are much larger than the Ni-C(41)-C(46) ones [115.3(4) and 115.5(4)°] in **1a** and **1b-2**. These structural deformations are the causes of the slightly shorter *d* distances [$(d_1+d_4)/2$] in **1a** and **1b-2** molecules (2.217 Å in **1a** and 2.206 Å in **2b**) compared to that in **1b-1** (2.492 Å); this occurs in spite of the similar conformations of the methoxyl groups on the corresponding sites of the coordination plane. The structural deformations found in these molecules show that the Ni-C(phenyl), Ni-P distances and Ni-C(phenyl)-C(phenyl) angles are very flexible and sensitive to the steric effect of the methoxyl groups onto the nickel atom and its ligand molecules.

Crystal Structures. The crystal structures of **1a**, **1b**, **2a**, and **2b** complexes are shown in Fig. 2. No intermolecular distance shorter than the normal van der Waals contact is found in these structures. The molecular packing in **1b** crystal is projected the b* axis [Fig. 2(b)], which shows surprisingly identical molecular arrangement of crystallographically independent two molecules [**1b-1** and **1b-2**] in the unit cell. The only difference in these molecules is found in the conformation of the methoxyl group [O(42)-C(47)]. This specific packing structure in **1b** resulted in the systematically weak diffraction intensities of 2/3 of the total reflections observed from this crystal.

Concluding Remarks. The intermolecular exchange of the *t*-phosphine ligands are catalyzed by carbon monoxide between **1a** and **1b** but not between **2a** and **2b**.[1] The X-ray structure determinations of these complexes seem now to have revealed the structural evidence needed to understand the reactivity differences. We observed the largest structural difference between these complexes in spatial locations of methoxyl methyl group on *o*-positions, as shown by the space filling models of **1a** and **2a** complexes in Fig. 3.[13] Probably due to the relative lack of spatial restriction, the methoxyl methyl groups in **1a** and **1b** can adopt a variety of directions around the

C(phenyl)-O bond, both in the solid state as observed and in solution, too. It then can yield spatial free coordination sites on nickel atom both above and below the four-coordination plane by taking the conformations of methoxyl groups directed toward the *m*-substituents. Both such 5th and 6th coordination sites of nickel atom in *m*-brominated complexes **2a** and **2b** are completely confined by the four methoxyl methyl groups, at least in the solid state. Due to the spatial restriction caused by the large *m*-substituents, the rotational flexibility of the methoxyl groups must be highly restricted even in solution to the direction apart from the *m*-position, toward the phosphine ligands and closer to the nickel atom. The nickel atom there must be well protected from the attack of carbon monoxide.

Another structural feature related to the reactivity difference seems to exist in the flexibilities of C-Ni-C and P-Ni-P bond angles. The observed coplanality of these five atoms in **1a** and **1b** is poorer in the crystals than that in **2a** and **2b**, which suggests the flexibility of these bond angles in **1a** and **1b** in solution. If so, this flexibility enables the coordination of the fifth ligand such as carbon monoxide on the nickel to be more facile by bending one of these bonds (C-Ni-C and P-Ni-P) toward the opposite side of the fifth ligand. The observed coplanality for **2a** and **2b** are higher in the crystals. The deviational motions of these bonds in solution must be restricted by the steric interaction between the methoxyl methyl groups locating over and below the coordination plane.

An analogous effect may be expected from the observed deviations of Ni-C-C bond angles from 120° in **1a** and **1b**.

References

1) M. Wada, K. Nishiwaki, and Y. Kawasaki, *J. Chem. Soc., Dalton Trans.*, **1982**, 1443.
2) G. van Koten, A. J. Leusink, and J. G. Noltes, *J. Organomet. Chem.*, **85**, 105 (1975).
3) A. J. Leusink, G. van Koten, and J. G. Noltes, *J. Organomet. Chem.*, **56**, 379 (1973).
4) G. van Koten, C. A. Schaap, J. T. B. H. Jastrzebski, and J. G. Noltes, *J. Organomet. Chem.*, **186**, 427 (1980).
5) F. A. Cotton and M. Miller, *J. Am. Chem. Soc.*, **99**, 7886 (1977).
6) F. A. Cotton, S. A. Koch, and M. Miller, *Inorg. Chem.*, **17**, 2087 (1978)
7) D. Xu Y. Kai, K. Miki, N. Kasai, K. Nishiwaki, and M. Wada, *Chem. Lett.*, **1983**, 591.
8) P. Main, S. E. Hull, L. Lessinger, G. Germain, J. P. Declercq, M. M. Woolfson (1978). *MULTAN*·78, A System of Computer Programs for the Automatic Solution of Crystal Structures from X-ray Diffraction Data. Univs. of York, England, and Louvain, Bergium.
9) T. Ashida (1979). *HBLS*-V, The Universal Crystallographic Computing System-Osaka, The Computation Center, Osaka Univ.
10) "International Tables for X-Ray Crystallography," Kynoch Press, Birmingham (1974), Vol. IV, p. 71.
11) W. C. Hamilton, *Acta Crystallogr.*, **12**, 609 (1959).
12) C. K. Johnson, *ORTEP*-II, Report ORNL-5138, Oak Ridge National Laboratory, Tennessee (1974).
13) *PLUTO*·78, "User Manual for Cambridge Crystallographic Database," Crystallographic Data Center, University Chemical Labolatory, Cambridge (1978).

 © 1984 The Chemical Society of Japan Bull. Chem. Soc. Jpn., 57, 1469—1472 (1984)

An Optical-optical Double Resonance Excitation of Bromine to a New D(0_u^+) Ion-pair State

Takashi Ishiwata,* Atsuto Tokunaga, Tsutomu Shinzawa, and Ikuzo Tanaka
Department of Chemistry, Tokyo Institute of Technology, Ohokayama, Meguro-ku, Tokyo 152
(Received January 5, 1984)

An optical-optical double resonance (OODR) technique utilizing a sequential three-photon absorption has been applied to study the electronic structure of Br_2. Two pulsed dye lasers were used to excite the molecules to appropriate rovibronic levels of the $B^3\Pi(0_u^+)$ state and subsequently into an ion-pair state by simultaneous two-photon transition. The OODR excitation spectra showed a number of transitions consisting of closely-spaced O, Q, and S branches which combine the $B^3\Pi(0_u^+)$ state with a new ion-pair state designated D(0_u^+). The following spectroscopic constants of the D(0_u^+) state were determined for the $^{79}Br_2$ isotope species: T_e=49925.4(6), ω_e=135.7(3), $\omega_e x_e$=0.27(3), B_e=0.04190(14), and α_e=5.9(23)×10^{-5} cm^{-1}.

It has been demonstrated that an optical-optical double resonance (OODR) method is very promising to study the spectroscopic details of high-lying electronic states in atoms and molecules.[1] In particular, this technique is attractive in the spectroscopy of diatomic halogens to explore their excited states of the ion-pair type whose precious information is normally inaccessible by the conventional single-photon spectroscopy.[2] Recently we have reported a series of ion-pair states observed in the two or three photon transitions through the $B^3\Pi_{0_u^+}$ state.[3-5] In this report, we present the analysis of a new D(0_u^+) state of Br_2 which might belong to the lowest group of ion-pair states correlating with $Br^-(^1S)+Br^+(^3P_2)$.

In our experiments the output pulses from two synchronously pumped dye lasers are focused inside a fluorescence cell containing $^{79}Br_2$ vapor from opposite directions and are aligned to overlap with each other at the focusing point. One laser, refered as the pump laser, is operated at a fixed wavelength to pump the molecules to appropriate rovibronic levels of the $B^3\Pi_{0_u^+}$ state through a visible B-X transition at around 583 nm. The setting was performed by monitoring the near-infrared B-X fluorescence. The second dye laser, the probe laser, is scanned in the wavelength region of 600—660 nm to promote two-photon transitions from the pumped levels of the B state to an ion-pair state. The OODR signals are detected by the UV emission between 240 and 290 nm.

The outputs of the dye lasers are horizontally polarized in the normal experiments. Polarization studies to examine anisotropic characters of the two-photon transitions from the B state are carried out for several of the strong transitions by changing the polarization angles of the probe laser light.

Results and Discussion

Figure 1 presents a part of a typical OODR excitation spectrum observed in the experiments on the $^{79}Br_2$ molecule. The pump laser (ν_1) was adjusted to a photon energy of 17155.9 cm^{-1} which is in resonance with the three rotational lines of the $B^3\Pi_{0_u^+}$ -$X^1\Sigma_g^+$ transition within our laser bandwidth; (9-0) P_{25} and R_{29}, and (10-0) P_{71}. The spectrum was recorded by scanning the probe laser (ν_2) using a sample pressure of 1.1 Torr (1 Torr≈133.322 Pa). There is no time delay between the pump and probe laser pulses. Under the conditions, the relaxations in the intermediate B levels are negligible, so that the OODR spectrum is very simple and the assignment is straightforward.

First of all, we found that the probe laser induced three types of transitions to form an ion-pair state by overall three-photon processes.

Type (I)	$\nu_1+(2\nu_2)$
Type (II)	$\nu_1+(\nu_1+\nu_2)$
Type (III)	$\nu_2+(2\nu_2)$

The type (I) transition denotes the (1+2) process, which corresponds to the excitation of the Br_2 molecules to the specific rovibronic levels of the B state by pump frequency (ν_1) and thence to an ion-pair state in the virtual two-photon transition by probe frequency ($2\nu_2$). On the other hand, the two-photon process in the type (II) transition proceeds by a combination of pump and probe lasers ($\nu_1+\nu_2$). The type (II) transitions appear because of temporal overlap of pump and probe laser pulses. They can be distinguished from the type (I) transitions by the dependence of the line intensities on the time delay of the two laser pulses and more easily by the polarization effects on their transition strengths. For example, when the polarization of the probe laser light is changed from horizontal to vertical, the anisotropic change of line intensities is predicted in the type (II) transitions. Because randomly oriented molecules cannot distinguish the vertically polarized photons from the horizontally polarized ones in the type (I) transitions. In the spectrum, typical results of the polarization effects for the type (II) transitions are shown in Fig. 1. These bands disappeared under the conditions of a 15 ns time delay between laser pulses, as being expected. The type (III) transitions produced by the probe laser alone appear only if the double resonance condition of two transition components is satisfied at a given frequency. They are obviously not suitable for a systematic analysis of an ion-pair state.

Secondly, the type (I) and (II) transitions clearly show the closely-spaced rotational lines, which should correspond to the O, Q, and S branches in the 0_u^+-0_u^+ transition from the following considerations. Molecular bromine belongs to the symmetry of $D_{\infty h}$ and its ion-pair states are known to be described in Hund's case c due to large multiplet splittings. From the dipole matrix elements of two-photon absorption, the symmetry species of the upper state which combine with the $B^3\Pi_{0_u^+}$ state by identical photons in the type (I)

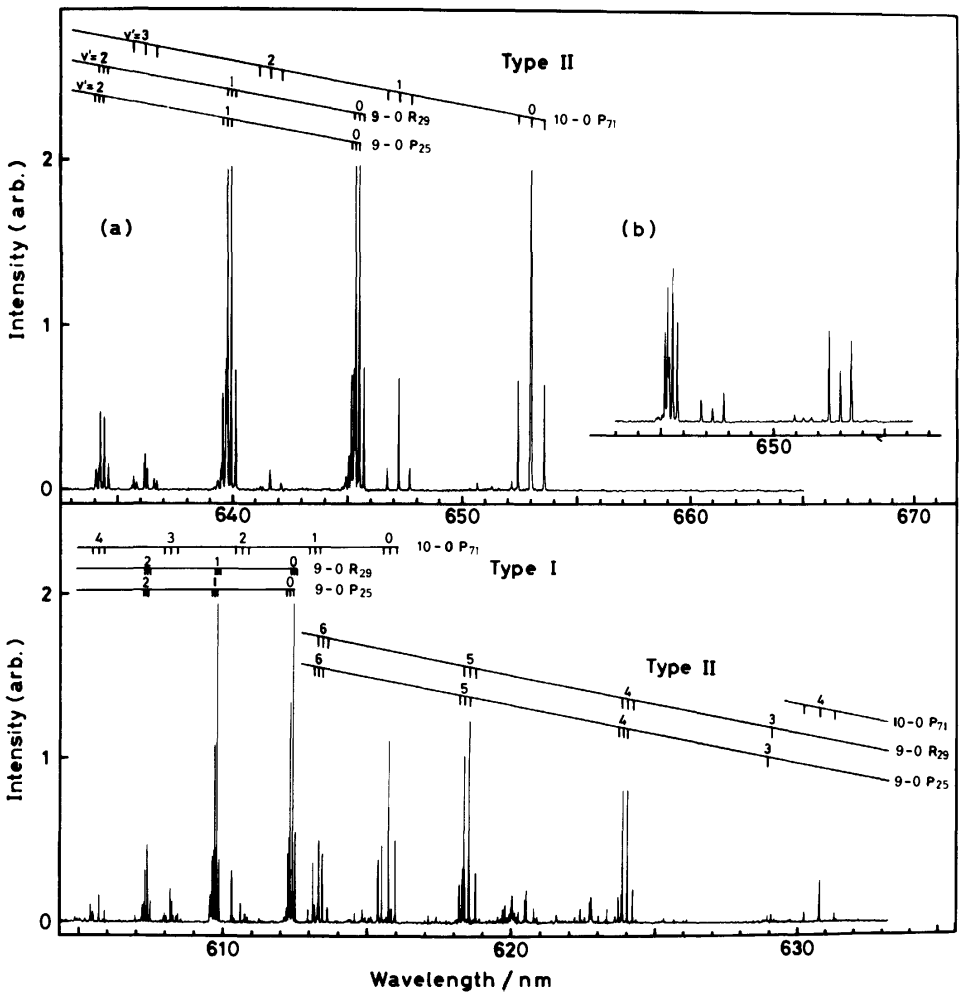

Fig. 1. A portion of the OODR excitation spectrum of $^{79}Br_2$. The pump frequency (ν_1) is in resonance with (9-0) P_{25} and R_{29}, and (10-0)P_{71} of the B-X transition within laser bandwidth. The probe laser (ν_2) was scanned in the wavelength region of 605—655 nm using dyes, Rh-610 and Rh-640. Two-photon transition from the B state proceeds according to the selection rule of $\Delta J=0, \pm2$ by the probe laser alone (type I, $2\nu_2$) and by the probe and pump lasers (type II, $\nu_1+\nu_2$). The pump laser is polarized horizontally, while the probe laser is polarized (a) horizontally and (b) vertically. No correction is made for signal intensities with the variation of laser power.

transition are 0_u^+, 1_u, and 2_u. According to the treatment of McClain and Harris,[6] their rotational selection rules are

$$\Delta J=0, \pm2 \quad \text{for the } 0^+\text{-}0^+ \text{ transition,} \tag{I}$$

$$\Delta J=0, \pm1, \pm2 \quad \text{for the } 1\text{-}0^+ \text{ and } 2\text{-}0^+ \text{ transitions,} \tag{II}$$

and also the large anisotropic behavior of the Q branch as shown in Fig. 1(b) is only expected for that of the 0^+-0^+ transition as discussed in the previous publication.[3b] The progression in the spectrum can be assigned from the splittings of the O and S branches ($\Delta\nu_{OS}$).

$$\Delta\nu_{OS}=(8J+4)B_v' \quad \text{for type (II).} \tag{III}$$

B_v' denotes the rotational constant of a v' ion-pair state (typically $B_v' \simeq 0.04\,cm^{-1}$ for lower v' levels) and J is the rotational quantum number of the $B^3\Pi_{0_u^+}$ state from which the two-photon transition originates. The type (II) transitions show a series of the progressions with intervals of around $135\,cm^{-1}$. The rotational splittings and vibrational intervals in the type (I) transitions are equal to half of the corresponding values in the type (II) transitions.

Thirdly, the intensity distribution of each progression in Fig. 1(a) shows the characteristic profiles inherent to the pumped vibrational levels of the B state. The progressions increase their intensities at the longer wavelength ends and suddenly break off. As discussed later on the basis of their Franck-Condon factors, the first levels observed at the lowest energies are assigned to the transition terminating on a $v'=0$ level of the ion-pair state.

Finally, it should be pointed out that the strong perturbation was observed in the ion-pair state. For example, the O, Q, and S branches in the $v'=3$ levels in Fig. 1 (see (10-0) P_{71}) split into two with comparable intensities. They are excluded in the following analysis of the energy level. A high resolution study utilizing etalon tuning dye lasers is in progress from which the detailed information about the perturbation by the

surrounding electronic states will be obtained.

The term energies of the ion-pair state, $T(v', J')$, relative to the potential minimum of the ground state are obtained by

$$T(v', J') = \nu_1 + 2\nu_2 + G_v'' + F_v''(J) \quad \text{for type (I),} \quad \text{(IV)}$$
$$= 2\nu_1 + \nu_2 + G_v'' + F_v''(J) \quad \text{for type (II),} \quad \text{(V)}$$

where G_v'' and $F_v''(J)$ are the vibrational and rotational energies of the $X^1\Sigma_g^+$ level, respectively. The G_v'' and $F_v''(J)$ values were determined from the constants of the Barrow, Clark, Coxon, and Yee.[7] The pump frequency (ν_1) corresponded to the position of either a P(J) or R(J) line in the B-X system. The probe frequency (ν_2) had three values in accord with the $\Delta J = 0, \pm 2$ transitions from a pumped level.

We have measured 117 rovibronic levels of a 0_u^+ ion-pair state corresponding to $0 \leqq v' \leqq 8$ and $6 \leqq J' \leqq 78$ pumped through the B-X transitions of (9-0) P_{25}, R_{29}; (10-0) P_{71}, R_{75}; (12-1) P_{51}, R_{55}; (14-2) R_5; (15-2) P_{51}. They were fitted by a least-squares method to the limited expansions;

$$T(v', J') = T_e + \omega_e\left(v' + \frac{1}{2}\right) - \omega_e x_e\left(v' + \frac{1}{2}\right)^2 + \left\{B_e - \alpha_e\left(v' + \frac{1}{2}\right)\right\} J'(J' + 1). \quad \text{(VI)}$$

The derived molecular constants are summarized in Table I.

Table 1. Molecular parameters of the D(0_u^+) state for $^{79}Br_2$

Parameter	Value
T_e/cm^{-1}	49925.4(6)[a]
ω_e/cm^{-1}	135.7(3)
$\omega_e x_e/cm^{-1}$	0.27(3)
B_e/cm^{-1}	0.04190(14)
α_e/cm^{-1}	$5.9(23)\times10^{-5}$

a) Values in parentheses denote twice the standard deviation (2σ) and apply to the last digits of the constants.

In order to confirm the absolute v' numbering of the ion-pair state, we have compared the intensity distribution of the OODR spectra with the calculated Franck-Condon factors. In the FCF calculations we used the version from Hougen of the RKR and FCF programs which were originally written by Zare, Schmeltekopf, Harrop, and Albritton for use.[8] The potential curve of the B state was constructed by using the constants of Barrow *et al.*,[7] while that of the ion-pair state was approximated by a Morse function defined by three parameters (ω_e, $\omega_e x_e$, and B_e) in Table 1. The patterns of observed vibrational progressions are reproduced in the FCF calculations as shown in Fig. 2. The calculated intensities using the different v' numbering have never fitted the observed intensities, since our spectrum includes the transition to a $v' = 0$ level of the ion-pair state. For example, the calculations by shifting the v' numbering upward have always predicted significantly strong bands at longer wavelengths which were not observed.

According to our preliminary results, the UV

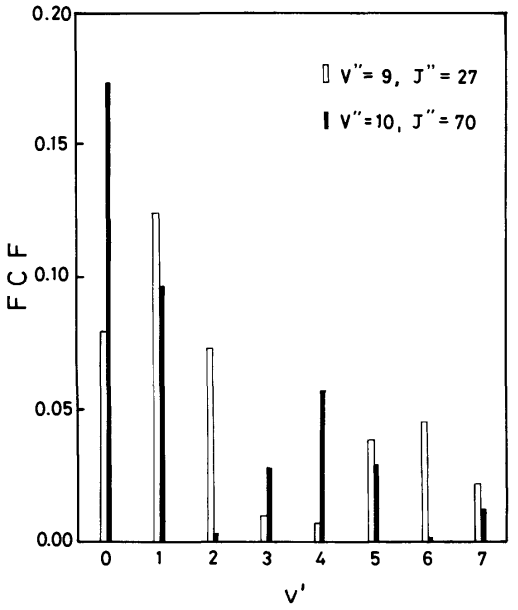

Fig. 2. Calculated Franck-Condon factors for the transitions shown in Fig. 1.

fluorescence spectrum of Br_2 observed in the experiment closely resembles that of the F(0_u^+)-$X^1\Sigma_g^+$ system analyzed recently.[5] The strong parallel bands were observed at around 269 nm. The emission system showed the vibrational structure which we could assign to a transition originating from a $v' = 0$ level of the ion-pair state and terminating on the $X^1\Sigma_g^+$ ground state at the high vibrational levels around $v'' = 48$. Other fluorescence terminating on the low valence states was present at the longer wavelengths (≈310 nm) in the spectra.

To summarize the results, a new 0_u^+ ion-pair state of Br_2 has been observed by the OODR excitation technique utilizing a sequential three-photon absorption through the B state. The new state is the third ion-pair state spectroscopically characterized in any detail among the 6 states (0_u^+, 0_g^+(E), 1_u, 1_g, 2_u, 2_g (D')) arising from $Br^-(^1S) + Br^+(^3P_2)$, and could be labelled as D(0_u^+) in the analogy of I_2. The D state lies about 1000 and 150 cm^{-1} higher than the D' and E states, respectively, with a similar equilibrium internuclear distance of 3.19 Å but with a smaller vibrational frequency of 135.7 cm^{-1}; $T_e = 48930 \pm 100\ cm^{-1}$ [12]. $\omega_e = 150.86\ cm^{-1}$, and $r_e = 3.170$ Å for D' (2_g),[9] and $T_e = 49777.96\ cm^{-1}$, $\omega_e = 150.83\ cm^{-1}$, and $r_e = 3.194$ Å for E(0_g^+).[11]

We plan further investigations on the D(0_u^+) ion-pair state of Br_2. Macdonald, Donovan, and Gower[13] have recently studied the fluorescence spectrum of Br_2 directly excited at 158 nm (F_2 laser) and reported three bound-free transitions originating from the D(0_u^+) state in the region of 210—440 nm. It is obvious that they excite the molecules to the high vibrational levels of ion-pair state more than $v' = 100$. By extending the probe frequency to analyze these high levels, we can provide the accurate potential curve of the D state which might not only answer the correct numbering of D levels in the VUV absorption but also explain the spectrum observed by Macdonald *et al.*[13]

Experimental

Experimental details were described previously.[3b] Briefly, a nitrogen laser pumped dye lasers (Molectron UV-24 and DL-14) provided 10 ns pulses with an energy of around 0.5 mJ/pulse and 0.4 cm^{-1} linewidth. The experiments were performed at 10 Hz. The signals from a solar blind photomultiplier (Hamamatsu TV R-166) were processed by a boxcar integrator (PAR 162/164) through a preamplifier (PAR 115).

The authors are grateful to Dr. J. T. Hougen of the National Bureau of Standards for supplying them the RKR and Franck-Condon factor program.

References

1) See, for example; J. I. Steinfeld and P. L. Houston, "Laser and Coherence Spectroscopy," ed by J. I. Steinfeld, Plenum, New York (1978), p. 1.

2) See, for example; K. P. Huber and G. Herzberg, "Molecular Spectra and Molecular Structure. IV. Constants of Diatomic Molecules," Van Nostrand, Reinhold, New York (1978).

3) a) T. Ishiwata, I. Fujiwara, and I. Tanaka, *Chem. Phys. Lett.*, **89**, 527 (1982); b) T. Ishiwata, I. Fujiwara, T. Shinzawa, and I. Tanaka, *J. Chem. Phys.*, **79**, 4779 (1983).

4) T. Ishiwata, H. Ohtoshi, M. Sakaki, and I. Tanaka, *J. Chem. Phys.*, **80**, 1411 (1984).

5) T. Ishiwata, T. Shinzawa, A. Tokunaga, and I. Tanaka, *Chem. Phys. Lett.*, **101**, 350 (1983).

6) W. M. McClain and R. A. Harris, "Excited States," ed by E. C. Lim, Academic Press, New York (1977), Vol. 3, p. 1.

7) R. F. Barrow, T. C. Clark, J. A. Coxon, and K. K. Yee, *J. Mol. Spectrosc.*, **51**, 428 (1974).

8) R. N. Zare, A. L. Schmeltekopf, W. J. Harrop, and D. L. Albritton, *J. Mol. Spectrosc.*, **46**, 37 (1973).

9) A. Sur and J. Tellinghuisen, *J. Mol. Spectrosc.*, **88**, 323 (1981).

10) P. Berwanger, K. S. Viswanathan, and J. Tellinghuisen, *J. Mol. Spectrosc.*, **91**, 275 (1982).

11) J. C. D. Br and, V. D. Deshpande, A. R. Hoy, and S. M. Jaywant, *J. Mol. Spectrosc.*, **100**, 143 (1983).

12) The spectroscopic parameters for the $D'(2_g)$ state were obtained in great detail by the analyses of the $D'(2_g)$-$A'(2_u{}^3\Pi)$ emission bands (280—295 nm). The relative position of $D'(2_g)$ to $A'(2_u{}^3\Pi)$ was derived as ΔT_e=35705.97(78) cm^{-1}. The error in T_e of $D'(2_g)$ is due to the uncertainty in the absolute position of the $A'(2_u{}^3\Pi)$ state as noted in Ref. 9.

13) M. Macdonald, R. J. Donovan, and M. C. Gower, *Chem. Phys. Lett.* **97**, 72 (1983).

 © 1984 The Chemical Society of Japan Bull. Chem. Soc. Jpn., 57, 1473—1477 (1984)

Effects of $Hg(ClO_4)_2$, $HgCl_2$, and $AgClO_4$ on the Conformations of Poly(*S*-carboxymethyl-L-cysteine) and Poly[*S*-(2-carboxyethyl)-L-cysteine] in Solution

Kazuki Oka, Hiroshi Maeda,* and Shoichi Ikeda*

Department of Chemistry, Faculty of Science, Nagoya University, Chikusa-ku, Nagoya 464

(Received January 5, 1984)

The effects of $Hg(ClO_4)_2$, $HgCl_2$, and $AgClO_4$ on the conformations of fully neutralized poly(*S*-carboxymethyl-L-cysteine) and poly[*S*-(2-carboxyethyl)-L-cysteine] in the absence of supporting electrolytes were examined by circular dichroism (CD) spectra. The induction of the β-form was suggested by the addition of $Hg(ClO_4)_2$ and $AgClO_4$, while it could not be concluded in the case of $HgCl_2$. Spectroscopic evidence for the coordination of metals with the two polypeptides was provided in the case of $Hg(ClO_4)_2$ and $HgCl_2$ by the appearance of a new CD band around 250—260 nm as well as the distortion of the polymer CD spectra in the region of 200—230 nm, while it was not obtained in the case of $AgClO_4$. The decrease of pH observed on addition of the three metal compounds also suggested the conformational change. Extraordinary lowering of pH and enhanced solubility were observed on addition of $HgCl_2$.

Recently, the effects of various bivalent metal ions on the conformations of poly(*S*-carboxymethyl-L-cysteine) (poly[Cys(CH_2COOH)])[1] and poly[*S*-(2-carboxyethyl)-L-cysteine](poly[Cys(CH_2CH_2COOH)])[2] were studied. Transition metal ions, such as Cu^{2+}, Cd^{2+}, Zn^{2+}, and Ni^{2+} ions, effectively induced the β-form of these two polypeptides, while alkaline earth ions such as Mg^{2+}, Ca^{2+}, and Ba^{2+} ions were not effective inducers. Based on these results, it is likely that the β-form of these polypeptides is induced *in solution* only when their negative charges are annihilated by a kind of complex formation with counterions. In other words, shielding of the charged sites on the polypeptides by condensed counterions is not effective at all, even in the case of bivalent counterions, in the induction of the β-form of these two polypeptides. The complex formation with counterions is shown by ultraviolet absorption spectra and circular dichroism (CD) in the interactions of Cu^{2+} ions with these two polypeptides.[3] These two polypeptides have carboxyl and thioether groups in the side chains, which readily react with mercury and silver. According to the suggested mechanism of the β-form induction, these two metal species are expected to induce the β-form of the two polypeptides in solution.

In the present study, the effects of $Hg(ClO_4)_2$, $HgCl_2$, and $AgClO_4$ on the conformations of the two polypeptides are examined in their fully neutralized states mainly by CD.

Experimental

Poly[Cys(CH_2COOH)] (Lot No. KO125W; M_w=12000, DP=75) and poly[Cys(CH_2CH_2COOH)] (Lot No. H920WR; M_w=16000, DP=92) are the same samples as used in the previous studies.[1-3] Here M_w and DP denote, respectively, the weight average molecular weight and degree of polymerization. Reagent grade $HgCl_2$ and $AgClO_4 \cdot H_2O$ and $Hg(ClO_4)_2$ (99%) were purchased from Nakarai Chemicals Ltd. and were used without further purification. Doubly distilled water was used to prepare the solutions.

Circular dichroism (CD) spectra were taken on a Jasco J-40 A circular dichrograph using cells of 1 and 5 mm light paths. Measurements of pH were carried out on a Hitachi-Horiba F-7 ss pH meter. These measurements were carried out at 25±2 °C.

The polymer concentration C_p is expressed in residue molarity, mol dm^{-3} (M) and is kept constant at 1×10^{-3} M in the present study. Metal concentrations C_M are expressed in molarity, mol dm^{-3} (M). The CD data are expressed in terms of the residue ellipticity $[\theta]$ based on the polymer concentration. To ascertain the time independent results, the solutions were kept at ambient temperature (25±2 °C) at least 20 h before the measurements were made.

In the present study, the two polymers were examined invariably in their fully neutralized states. Hence, they are abbreviated as poly[Cys(CH_2COONa)] and poly[Cys(CH_2CH_2-COONa)], except for the case that these abbreviations are confusing.

Results

1. $Hg(ClO_4)_2$ and $HgCl_2$. The CD spectra of poly[Cys(CH_2COONa)] in the presence of different amounts of $Hg(ClO_4)_2$ and $HgCl_2$ are shown in Figs. 1(a) and (b), respectively. In the absence of the mercury compounds, the CD spectrum of random coils at low ionic strengths is seen (curves A).[5] The CD spectra at large values of the mixing ratio C_M/C_p are different from those found on the mixtures of the β-form and random coils in the respect that a small positive CD band appears around 255 nm. This CD band is observed for both $Hg(ClO_4)_2$ and $HgCl_2$, and hence probably originates as a result of the coordination of Hg atoms to the side chains of the polypeptides. It is likely that the CD spectra in the wavelength region shorter than 230 nm are also modified. Nevertheless, the change of CD spectra by the addition of $Hg(ClO_4)_2$ can be ascribed mostly, if not all, to the induction of the β-form. The spectra of the β-forms of the two polypeptides are characterized by a negative band around 224 nm ($[\theta]\simeq-10^4$) and a positive band around 200 nm ($[\theta]\simeq3.5\times10^4$ for poly[Cys(CH_2COOH)][4] and $\simeq2\times10^4$ for poly[Cys(CH_2CH_2COOH)][5]). In the case of $HgCl_2$, definite conclusions cannot be obtained.

Residue ellipticities at 205 nm and 255 nm, $[\theta]_{205}$ and $[\theta]_{255}$, are plotted against the mixing ratio C_M/C_p in Fig. 2. The value of $[\theta]_{205}$ is tentatively chosen as a measure of the extent of the β-form induction, since the measurements at 200 nm was not always reliable due to the absorption of $HgCl_2$. The values of $[\theta]_{255}$ were mostly obtained using a cell of 5 mm light path. The

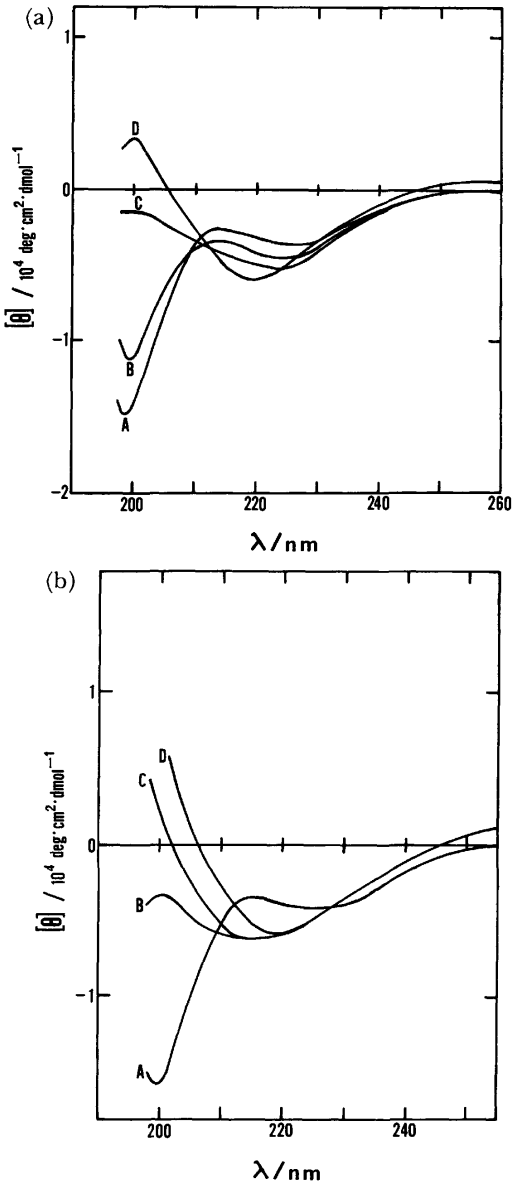

Fig. 1. CD spectra of poly[Cys(CH_2COONa)] in the presence of (a) $Hg(ClO_4)_2$ and (b) $HgCl_2$. Polymer concentration (C_P) is 1×10^{-3} M. Mixing ratios (C_M/C_P). (a); 0(A), 0.052(B), 0.156(C), and 0.259(D). (b); 0(A), 0.201(B), 0.402(C), and 1.005(D).

induction of the β-form is suggested for $Hg(ClO_4)_2$ also from the comparison with the previous results on $CuCl_2$,[1] which is given by a dashed curve in Fig. 2.

In Figs. 3(a) and (b), the CD spectra of poly[Cys(CH_2CH_2COONa)] in the presence of different amounts of $Hg(ClO_4)_2$ and $HgCl_2$ are shown, respectively. In the case of $Hg(ClO_4)_2$, the spectrum at $C_M/C_P=0.415$ resembles, in shape, that of the β-form except for the wavelength region larger than 240 nm. In the intermediate region of the mixing ratio, $0.15<C_M/C_P<0.26$, a characteristic CD pattern appears (curves C and D), which is different from the spectrum found on the mixtures of the β-form and random coils. The CD pattern found in the presence of $HgCl_2$ differs considerably from the spectrum characterizing the β-form of poly[Cys(CH_2CH_2COOH)] induced either by protonation or by the addition of bivalent metal

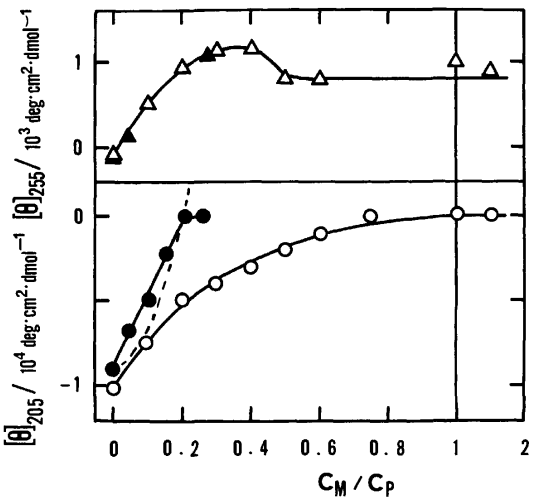

Fig. 2. Dependences of the residue ellipticities of poly[Cys(CH_2COONa)] at 205 nm ($[\theta]_{205}$) and 255 nm ($[\theta]_{255}$) on the mixing ratio (C_M/C_P). Open symbols (○, △) refer to $HgCl_2$ and filled symbols (●, ▲) refer to $Hg(ClO_4)_2$. A dashed curve represents the result on $CuCl_2$.

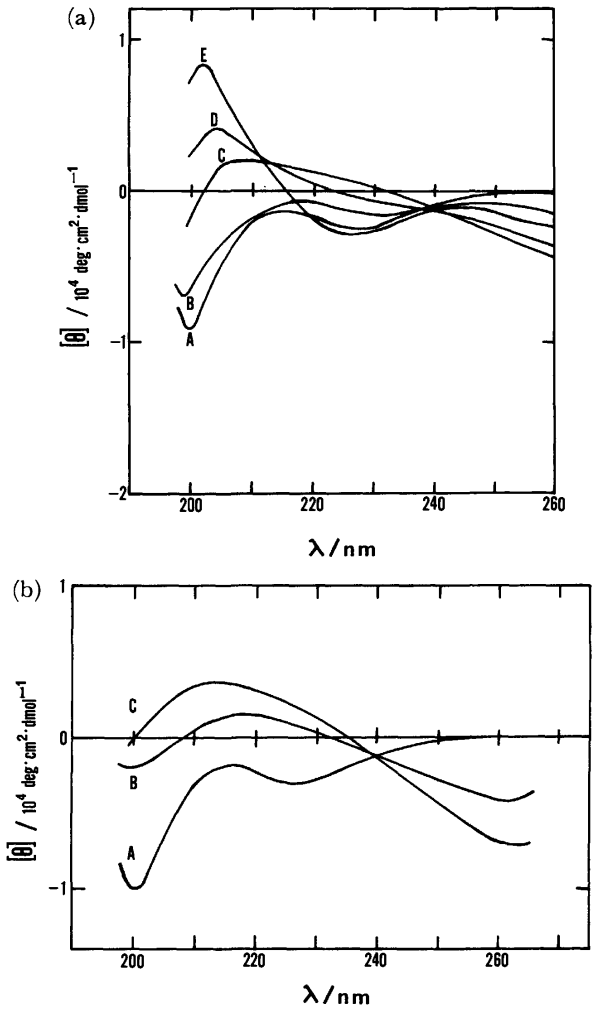

Fig. 3. CD spectra of poly[Cys(CH_2CH_2COONa)] in the presence of (a) $Hg(ClO_4)_2$ and (b) $HgCl_2$. Polymer concentration (C_P) is 1×10^{-3} M. Mixing ratios (C_M/C_P). (a); 0(A), 0.052(B), 0.156(C), 0.259(D), and 0.415(E). (b); 0(A), 0.100(B), and 0.200(C).

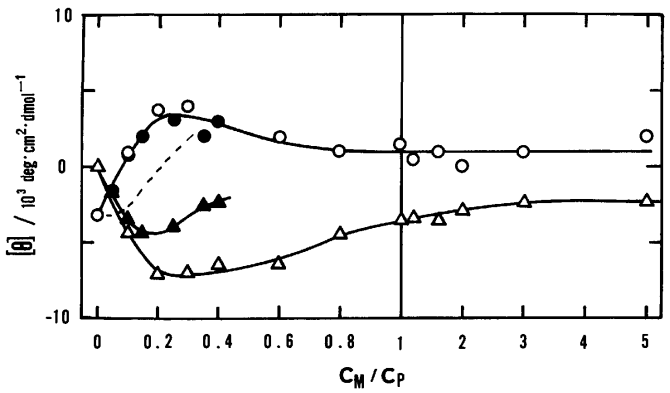

Fig. 4. Dependences of the residue ellipticities of poly[Cys(CH_2CH_2COONa)] on the mixing ratio (C_M/C_P).
210 nm (○, ●) and 260 nm (△, ▲). Open and filled symbols refer to $HgCl_2$ and $Hg(ClO_4)_2$, respectively. A dashed curve represents $[\theta]_{210}$ obtained on $CdCl_2$.

cations.[2] The CD spectra at the mixing ratios larger than about 0.2 fall between curves B and C. It is difficult to infer the induction of the β-form in the case of $HgCl_2$.

A large negative CD band appears around 260 nm for both $Hg(ClO_4)_2$ and $HgCl_2$, which becomes negligible at the wavelengths larger than 320nm. The residue ellipticities at 210 nm and 260 nm, $[\theta]_{210}$ and $[\theta]_{260}$, obtained at different mixing ratios are shown in Fig. 4 together with the previous results on $CdCl_2$[2] for 210 nm. The wavelength 210 nm is chosen partly because the characteristic CD pattern in the case of $HgCl_2$ shows the maximum around 210 nm and partly because reliable measurements of CD were hampered at 205 nm by strong absorption of $HgCl_2$. At 205 nm, CD spectra were obtained up to $C_M/C_P=0.2$ in the case of $HgCl_2$. The values of $[\theta]_{205}$ were very similar for both $Hg(ClO_4)_2$ and $HgCl_2$. Comparison of the present results with the results on $CdCl_2$ suggests the distortion of the polymer CD spectra as well as the induction of the β-form. It is likely that the β-form of poly[Cys(CH_2CH_2COOH)] is induced by the coordination of Hg atoms, at least, in the case of $Hg(ClO_4)_2$. The dependences of $[\theta]_{210}$ and $[\theta]_{260}$ on C_M/C_P are well correlated to each other, especially in the case of $HgCl_2$. This correlation also suggests that the induction of the β-form parallels the coordination of Hg atoms.

When the effects of $Hg(ClO_4)_2$ and $HgCl_2$ are compared between the two polypeptides, the characteristic CD patterns inherent to the coordination of Hg atoms are more evident in poly[Cys(CH_2CH_2COONa)] than in poly[Cys(CH_2COONa)]; a new CD band around 260 nm is more intense and the distortion of the CD spectra in the range 200—230 nm is more significant in poly[Cys(CH_2CH_2COONa)].

In Fig. 5, the dependences of pH on $Hg(ClO_4)_2$ and $HgCl_2$ concentrations (C_M) are shown in logarithmic scale for the two polypeptides. There is no appreciable difference between the effects of $Hg(ClO_4)_2$ (filled circles) and $HgCl_2$ (open circles). The profiles of pH change are very similar for the two polypeptides. The change of pH on log C_M is almost identical between the two polypeptides, when the pH values are corrected

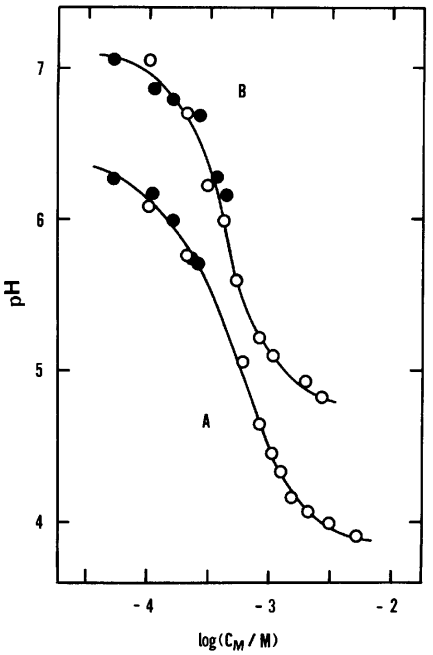

Fig. 5. Dependence of pH on the logarithm of the salt concentration (C_M).
Polymer concentration (C_P) is 1×10^{-3} M. (A) poly[Cys(CH_2COONa)] and (B) poly[Cys(CH_2CH_2COONa)]. Open and filled circles refer to $HgCl_2$ and $Hg(ClO_4)_2$, respectively.

for the difference in the intrinsic dissociation constants K_0; $pK_0=3.2$ for poly[Cys(CH_2COOH)][6] and 4.0 for poly[Cys(CH_2CH_2COOH)].[7] The correction is made in such a way that one of the two curves, either A or B, is shifted vertically by about 0.8 pH unit, which corresponds to the difference between the two values of pK_0. After the correction, these two curves are nearly identical to each other in the whole range of C_M examined. This profile of the pH change is, however, different from that expected for the effect of added salt on random coil polyelectrolytes.[8] The pH change thus suggests the conformational change. In the previous studies, pH decreased to about 4.5 on addition of the most effective species (Cu^{2+} ions) to poly[Cys(CH_2COONa)][1] while pH decreased to about 6.0 in the case of poly[Cys(CH_2CH_2COONa)][2]. In the present study, the extents of pH decrease by the addition of $HgCl_2$ are much larger than those found in previous studies, while the effects of $Hg(ClO_4)_2$ are consistent with previous data. The extraordinary lowering of pH on addition of $HgCl_2$ may suggest the coordination of $HgCl_2$ to peptide nitrogens, which releases hydrogen ions and converts the partially formed β-form to random coils.

A marked difference between $Hg(ClO_4)_2$ and $HgCl_2$ is found in Figs. 2, 4, and 5 concerning the solubilities of the two polypeptides. Precipitation of the two polypeptides did not occur at the mixing ratio of 5 in the case of $HgCl_2$. Precipitation occurred at the mixing ratios of about 0.3 for poly[Cys(CH_2COONa)] and about 0.4 for poly[Cys(CH_2CH_2COONa)] in the case of $Hg(ClO_4)_2$. The solubilities found in the case of $Hg(ClO_4)_2$ are consistent with the previous results on other bivalent metal cations, although they are the least or nearly the least among the solubilities in the

presence of bivalent cations.[1,2] It is interesting to note that the solubility in the presence of $Hg(ClO_4)_2$ is larger for poly[Cys(CH_2CH_2COONa)] than for poly[Cys(CH_2COONa)].

In conclusion, the induction of the β-form occurs on addition of $Hg(ClO_4)_2$ to the solutions of poly[Cys(CH_2COONa)] or poly[Cys(CH_2CH_2COONa)] due to the formation of a complex between them, as suggested by the appearance of a new CD band around 250—260 nm. In the case of $HgCl_2$, on the other hand, the induction of the β-form cannot be concluded, although evidence for the complex formation is obtained.

II. $AgClO_4$. In Figs. 6(a) and (b), the CD spectra of poly[Cys(CH_2COONa)] and poly[Cys(CH_2CH_2COONa)] are shown respectively in the presence of different amounts of $AgClO_4$. The change of CD spectra indicates the formation of the β-form by the addition of $AgClO_4$. This result is the first example of the β-form of these two polypeptides induced *in solution* by a univalent metal cation. Based on the mechanism suggested for the induction of the β-form of these two polypeptides deduced from previous studies, silver ions are supposed to be covalently bound to the side chains of the polypeptides. However, there is no new CD band in the whole wavelength region examined nor anomalous pattern around 200—230 nm, contrary to the case found on the addition of the mercury compounds.

In Fig. 7, the residue ellipticities at 200 nm, $[\theta]_{200}$, are shown as functions of the mixing ratio. The results on

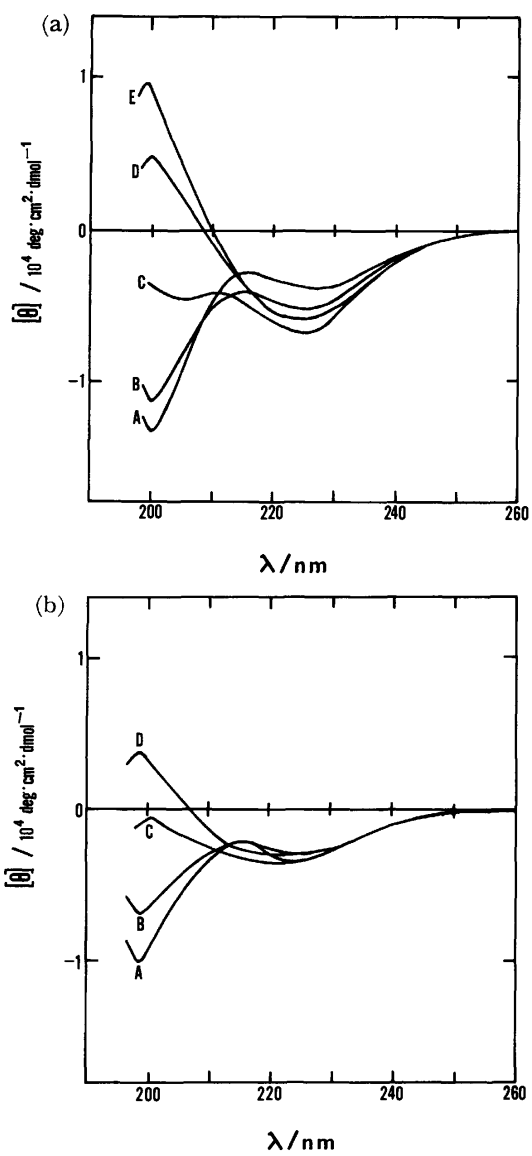

Fig. 6. CD spectra of (a) poly[Cys(CH_2COONa)] and (b) poly[Cys(CH_2CH_2COONa)] in the presence of $AgClO_4$.
Mixing ratios (C_M/C_P). (a); 0(A), 0.101(B), 0.402(C), 0.503(D), and 0.754(E). (b); 0(A), 0.102(B), 0.409(C), and 0.512(D).

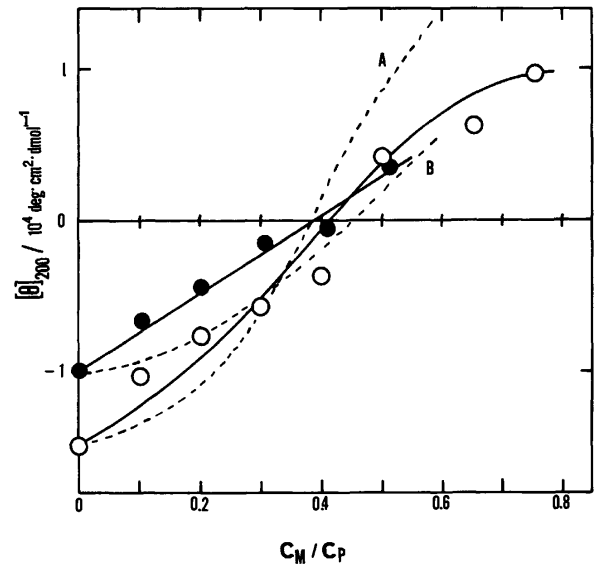

Fig. 7. Dependence of the residue ellipticity at 200 nm, $[\theta]_{200}$, on the mixing ratio (C_M/C_P).
(○) Poly[Cys(CH_2COONa)] and (●) Poly[Cys(CH_2CH_2COONa)].
Polymer concentration (C_P) is 1×10^{-3}M. Dashed curves represent the results on (A) $CuCl_2$-poly[Cys(CH_2COONa)] and (B) $CdCl_2$-poly[Cys(CH_2CH_2COONa)]. The scale of abscissa is doubly enlarged for these dashed curves.

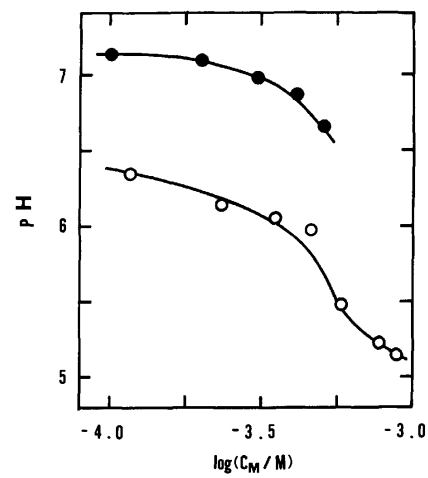

Fig. 8. Dependence of pH on the logarithm of $AgClO_4$ concentration (C_M).
(○) Poly[Cys(CH_2COONa)] and (●) poly[Cys(CH_2CH_2COONa)]. Polymer concentration (C_P) is 1×10^{-3}M.

$CuCl_2$ for poly[Cys(CH_2COONa)] (curve A)[1] and on $CdCl_2$ for poly[Cys(CH_2CH_2COONa)] (curve B)[2] are also shown. These are the most effective inducers of the β-forms of respective polypeptides in the previous studies. To facilitate the comparison, the scale of the abscissa for these bivalent cations is doubly enlarged. The induction of the β-form by $AgClO_4$ is comparable with $CdCl_2$ in the case of poly[Cys(CH_2CH_2COONa)], while it is less effective than $CuCl_2$ in the case of poly[Cys(CH_2COONa)].

In Fig. 8, values of pH of the solutions of the two polypeptides are given as functions of $AgClO_4$ concentration (C_M) in the logarithmic scale. As in the case of the mercury compounds shown in Fig. 5, the changes are nearly identical for the two polypeptides, when either of the two curves is shifted vertically by about 0.8 pH unit, the correction for the difference in the intrinsic dissociation constants. The decrease of pH is much larger than that expected for the effect of added salt on random coil polyions and hence confirms the coordination of Ag^+ ions, probably, to the side chains.

Precipitation occurred at the mixing ratios of about 0.8 for poly[Cys(CH_2COONa)] and 0.5 for poly[Cys(CH_2CH_2COONa)], which correspond to 0.4 and 0.25 in the case of bivalent ions, respectively. They are comparable with those found on $Hg(ClO_4)_2$, 0.3 and 0.4 given above. The solubility of poly[Cys(CH_2CH_2COONa)] in the presence of $AgClO_4$ is lower than that of poly[Cys(CH_2COONa)], which is consistent with the general trend found for the β-forms of these two polypeptides induced by bivalent metal cations and hydrogen ions.[1,2]

Discussion

In the present study, new CD band appears in the region of 240—260 nm and distortion of the CD spectra occurs in the region of 200—220 nm on addition of $Hg(ClO_4)_2$ or $HgCl_2$ to the solutions of poly[Cys(CH_2COONa)] and poly[Cys(CH_2CH_2COONa)]. These changes can be ascribed to the electronic transition involving Hg atoms. The absorption of $HgCl_2$ is more intense than that of $Hg(ClO_4)_2$ in the region of 200—260 nm; the molar absorption coefficients differ by about one order around 230 nm.[9] The absorption maxima are about 205 nm for $HgCl_2$ and below 190 nm for $Hg(ClO_4)_2$.[9] This can explain why the anomaly was observed more clearly for $HgCl_2$ than for $Hg(ClO_4)_2$. In the case of $AgClO_4$, which has absorption bands around 225, 210, and 194 nm,[10] neither distortion of the CD spectra occurs nor new CD band appears appreciably, although the β-form is induced.

The different solubilities of the two polypeptides are seen from Figs. 2, 4, and 5 between the solutions containing $Hg(ClO_4)_2$ or $HgCl_2$. The difference may be related to the different extents of the covalent nature of these two compounds. While $Hg(ClO_4)_2$ readily dissociates, $HgCl_2$ remains mostly undissociated in aqueous solutions. The induction of the β-form, the low solubility, and the characteristic decrease of pH are reasonably understood in the case of $Hg(ClO_4)_2$ in terms of the interactions of ionic species Hg^{2+} with the polypeptides. Contrary to the expected behavior for neutral species, the complex formation is indicated from the CD spectra in the case of $HgCl_2$. [Figs. 1(b) and 3(b)]. It is difficult, however, to infer the induction of the β-form from the CD spectra.

All the obtained data (CD spectra, pH change, and solubility) in the case of $HgCl_2$ cannot be consistently explained by assuming for the bound species either neutral species or bivalent ionic species. Explanations in terms of various possible bound species could be developed. However, it is not pertinent to present highly speculative discussions here.

References

1) H. Maeda, J. Nakajima, K. Oka, K. Ooi, and S. Ikeda, *Int. J. Biol. Macromol.*, **4**, 352 (1982).
2) K. Oka, H. Maeda, and S. Ikeda, *Int. J. Biol. Macromol.*, **5**, 342 (1983).
3) H. Maeda, K. Oka, and S. Ikeda, *Biopolymers*, submitted.
4) H. Maeda, Y. Gatto, and S. Ikeda, *Macromolecules*, in press (1984).
5) S. Ikeda, A. Fukutome, T. Imae, and T. Yoshida, *Biopolymers*, **18**, 335 (1979).
6) H. Maeda and S. Ikeda, *Biopolymers*, **14**, 1623 (1975).
7) H. Maeda and S. Ikeda, *Biopolymers*, **10**, 2525 (1971).
8) F. Oosawa, *Biopolymers*, **6**, 135 (1968).
9) H. Fromherz and K.-H. Lih, *Z. Physik. Chem.*, **A167**, 103 (1933).
10) F. Volbert, *Z. Physik. Chem.*, **A149**, 382 (1930).

The Formation of Metastable Potassium Trivanadate from Melts

Yoshiya KERA
Department of Applied Chemistry, Faculty of Science and Engineering, Kinki University, Higashi-Osaka 577
(Received May 16, 1983)

Potassium vanadates, which were prepared from melts by rapid quenching and slow cooling over the composition range of K_2O-contents of $C=(K)/(V)=0$—0.50, were examined by means of IR spectrometry and X-ray powder diffraction. In the composition range of $C\leq 0.17$, mixtures of V_2O_5, $K_2V_{18}O_{45}$, and $K_2V_8O_{21}$ were produced by the slow cooling. At the composition of $C=0.33$, however, an unknown compound and $K_2V_8O_{21}$ were the main products upon rapid quenching from melts, while at $C=0.50$ the main products were $K_3V_5O_{14}$ and an additional unknown compound. The unknown compound was confirmed to be metastable and was formed as a single compound only by a rapid quenching from melts of K_2O and V_2O_5 especially at $C=0.37$. The X-ray diffractions for the compound were characterized as $d=8.2$ (very strong), 4.05, and 3.27 Å, and the V=O stretching frequencies, as 995, 968, and 955 cm^{-1}. By comparing these characteristic data with those of lithium trivanadate and sodium trivanadate (γ-phase), it was suggested that the unknown compound was isomorphous with trivanadate ($M_{1+x}V_3O_8$).

In the previous paper, it was examined how alkali tri- and/or hexavanadates could be produced or not by the procedures of the rapid quenching and slow cooling of the melts which had been prepared from mixtures of M_2CO_3 and NH_4VO_3 or V_2O_5 as the starting materials with the composition of $C=(M)/(V)=0.33$.[1] Only in the case of K_2O-containing samples, however, was neither the trivanadate nor the hexavanadate formed by those procedures,while the mixtures of $K_2V_8O_{21}$, an unknown compound, and $K_3V_5O_{14}$ were formed. The reasons why the tri- or hexavanadate could not be formed only in the K_2O-V_2O_5 binary system, and also what the unknown compound was, have remained to be investigated. With a potassium oxide-vanadium oxide binary system, five stable compound have been reported by Holtzberg *et al.*,[2] corresponding to these five formulas: $K_2V_8O_{21}$, KVO_3, $K_{32}V_{18}O_{61}$, $K_4V_2O_7$, and K_3VO_4. Kelmers[3] also found $K_3V_5O_{14}$ as a high-temperature phase; he further suggested the existence of $K_2V_{12}O_{30}$ and metastable $K_2V_{18}O_{45}$. However, no such compounds, the composition of which is near 0.33 ($C=0.33$), have yet been reported to be formed from high-temperature melts.

On the other hand, potassium hexavanadate ($K_2V_6O_{16}$) has been prepared by Kelmers[4] from V_2O_5 solution with alkali dissolved in it. Evans and Block called the potassium vanadate prepared by this procedure potassium trivanadate(KV_3O_8) based on an exact X-ray analysis.[5] The potassium trivanadate is monoclinic; its X-ray powder data has also been shown on an ASTM-card.[6] However, any diffraction peaks are inconsistent with the unknown compound formed from high-temperature melts in a previous experiment.[1]

In the present experiment IR spectrometry and X-ray powder diffraction were used for analysing in detail the potassium vanadates formed by slow cooling and/or rapid quenching from the melts of K_2O and V_2O_5 over the composition range of $C=0$—0.50. Especially, in order to characterize the unknown compound, many samples formed in the region near $C=0.33$ were investigated.

Experimental

1) Materials and Preparations. Potassium vanadates in the composition range of $C=(K)/(V)=0$—0.17 (in atomic ratio) were prepared from K_2CO_3 (Wako Pure Chem. Co., Ltd.; guaranteed grade) and NH_4VO_3,which had been purified cautiously,[7] by the following procedures. The NH_4VO_3 was immersed into a K_2CO_3 aq soln, dried at 120 °C, and calcined in a quartz tube with opening to the air at 600 °C for 20 h. After the heating, they were cooled slowly in the furnace. The samples will be called K-1—6. Sample K-7, with the composition of $C=0.33$, was prepared by the same procedures except for the final cooling procedures; it was rapidly quenched in ice-water. For preparing Sample K-8, K_2CO_3 and V_2O_5 (both Kanto Chem. Co., Ltd.; guaranteed grade) were well mixed in the composition of $C=0.33$ in an agate mortar and then heated in a quartz tube (outer diameter, $d_o=10$ mm) with an opening to the air at 530 °C for 14 h.

TABLE 1. K-CONTENTS OF POTASSIUM VANADATES PREPARED BY MELTS AND THEIR V=O STRETCHING FREQUENCIES, AS ESTIMATED FROM Figs. 1 AND 2

Sample	C/[M]/[V]	V=O Stretching ν/cm^{-1}					
K-1	0.020(s)[a]	1022	—	—	960	—	940
K-2	0.040(s)	1022	—	—	970	—	942
K-3	0.063(s)	1020	1005	—	—	—	942
K-4	0.087(s)	1023	1000	—	972	—	941
K-5	0.119(s)	1020	1000	—	972	—	942
K-6	0.171(s)	1021	1001	—	972	—	942
K-7	0.33 (r)	—	995	985	967	955	940
K-8	0.33 (s)	—	995	—	970	955	937
K-9	0.33 (r)	—	995	985	967	955	938
K-10	0.50 (r)	—	995	980	—	955	935

a) The letters of s and r in parentheses denote the procedures of the slow cooling and the rapid quenching respectively.

Table 2. The K_2O-contents of samples V-1—7

Sample	C/(K)/(V)
V-1	0.261
V-2	0.285
V-3	0.310
V-4	0.334
V-5	0.350
V-6	0.374
V-7	0.399

After further heat-treatment at 590 °C for 8 h, it was cooled slowly in the furnace. For preparing Samples K-9 and 10, the compositions of which were $C=0.33$ and 0.50 respectively, given amounts of K_2CO_3 and NH_4VO_3 were well mixed in an agate mortar and then heated in a quartz tube ($d_o=10$ mm) with an opening to the air at 620 °C for 72 h. Finally they were quenched rapidly in ice-water. The compositions of the samples thus prepared are summarized in Table 1. In order to investigate the unknown compound in detail, K_2CO_3 and V_2O_5 were mixed well in the composition of $C=0.26$—0.40 and then heated in a quartz tube ($d_o=6$ mm) with an opening to the air at 750 °C for 22 h. After the heat-treatment they were quenched in ice-water. The compositions of the samples, V-1—7, are summarized in Table 2.

2) IR and X-Ray Measurements. The IR spectra of Samples K-1—10 were measured in the frequency range from 650 to 1200 cm^{-1} by using the normal KBr-disk method. The IR spectrometer used was JASCO, model DS-402 G. The IR spectrum for Sample V-6 was measured in the range of 400—1100 cm^{-1} by the use of a JASCO model A-202 spectrometer. The X-ray powder diffraction was carried out on all the samples in the range of $2\theta=4$—60 °. The X-ray diffractometer used was a Rigaku-Denki model; GF-Rad-γA; Cu $K\alpha$-radiation (at 40 kV, 120 mA) and a Ni-filter were used.

Results

The IR spectra of Samples K-1—7 are shown in Fig. 1, in which the spectrum of pure-V_2O_5 is also given for the sake of comparison. The 1022 cm^{-1} band appearing in pure-V_2O_5 has already been assigned to the V=O stretching vibration.[8,9] It may be seen that sharp bands appear at 1000, 972, and 942 cm^{-1} in Samples K-1—7 and that the intensities of those bands increase with an increase in the K_2O-content. In the IR spectra of Samples K-7—9, which differ in their starting materials and with the procedures used to prepare them but whose are the same in the K_2O-content ($C=0.33$), the band peaks were seen at 995, 985, 955, and 940—937 cm^{-1}, a little different from those of Samples K-1—6. In Sample K-10 ($C=0.50$), the characteristic broad and sharp bands appeared at about 980 and 935 cm^{-1} respectively, while a shoulder band seemed to appear at 995 cm^{-1}. In Samples K-8 and 10, a very weak band was seen in the region of 905—908 cm^{-1}. The frequencies for the V=O stretching bands of Samples K-1—10 are summarized in the third colum of Table 1. The 967 cm^{-1} band seems to be more intensive than the 995 cm^{-1} band in Sample K-9, while the two intensities are similar in extent in Sample K-7. The broad 980 cm^{-1} and the sharp 935 cm^{-1} bands became relatively intensive in Sample K-10. With respect to Samples K-1—6, the peak intensities for the sharp band in the region of 930—1000 cm^{-1} were estimated by drawing a base line smoothly under the bands of the spectra according to the previous papers;[1,10] their relative intensities are given in Table 3. As the band separations were not good enough for us to estimate the intensities of each peak in the K-7 —10 samples, these values were excluded from the table.

Table 3. The relative intensities of the V=O stretching bands for samples K-1—6

Sample	C/[M]/[V]	Band Intensities			
		1022	1000	972	942 cm^{-1}
K-1	0.020	0.92	0.047	0.017	0.018
K-2	0.040	0.87	0.077	0.037	0.019
K-3	0.063	0.784	0.134	0.041	0.041
K-4	0.087	0.76	0.160	0.040	0.037
K-5	0.119	0.61	0.246	0.065	0.079
K-6	0.171	0.48	0.30	0.13	0.09

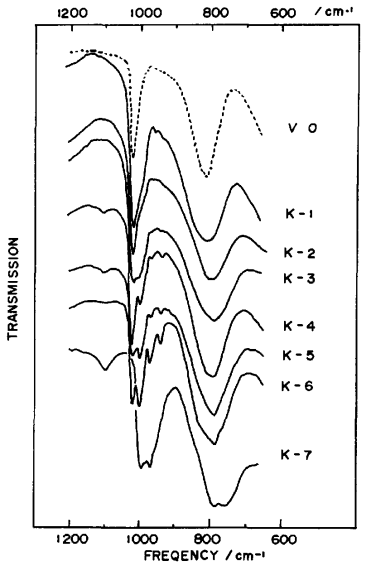

Fig. 1. IR-spectra of Samples K-1—7 recorded in the frequency range of 650—1200 cm^{-1}. The spectrum for V_2O_5 was added for comparison.

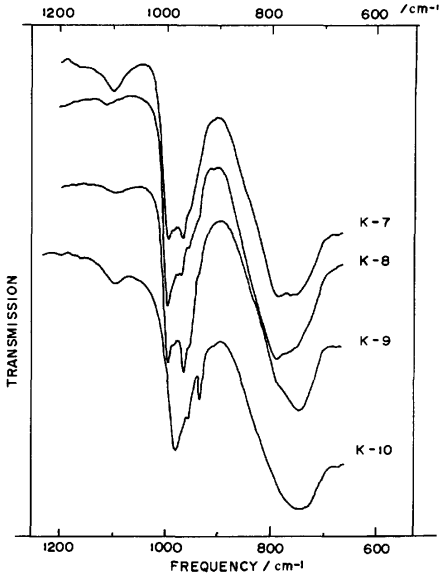

Fig. 2. IR-spectra of Samples K-7—10.

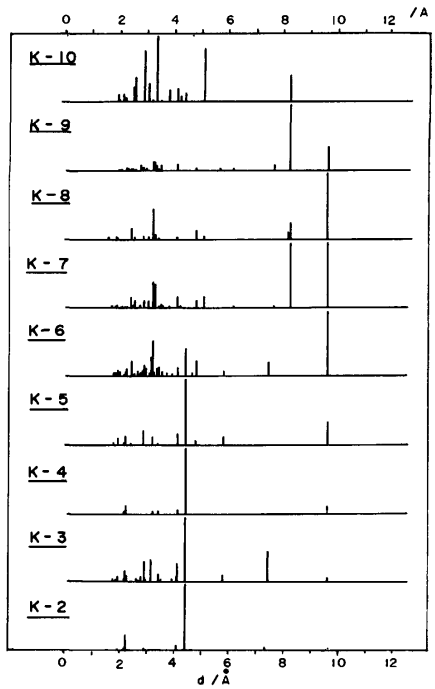

Fig. 3. The X-ray powder diffraction patterns for Samples K-2—10, recorded in the angles of 2θ =4—60° (d=22—1.54 Å).

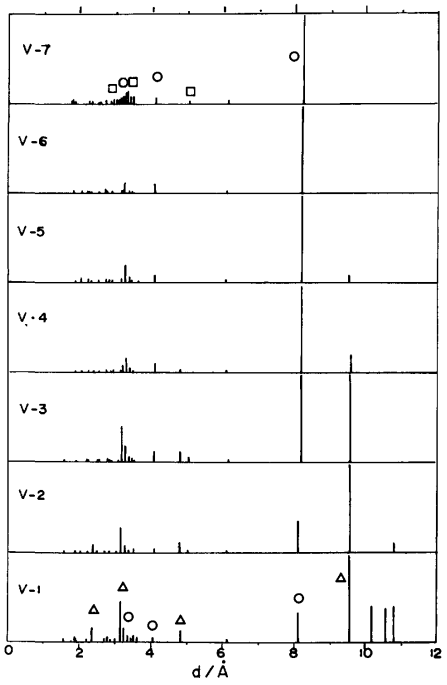

Fig. 4. The X-ray powder diffraction patterns for Samples V-1—7 recorded in the angles of 2θ=4—60° (d=22—1.54 Å). The signs, △, ○, and □, denote the lines for $K_2V_8O_{21}$,[12] the unknown compound, and $K_3V_5O_{14}$,[13] respectively. See also text.

The X-ray diffraction patterns of Samples K-2—10 are shown in Fig. 3. The diffraction peak corresponding to the interplanar spacing of d=4.38 Å, which has been characterized as V_2O_5,[11] was the highest in Samples K-2—5 (C=0.040— 0.12), but it completely disappeared in Samples K-7—10 (C=0.33—0.50). On the other hand, the peak for d= 9.60 A, characteristic of $K_2V_8O_{21}$,[12] appeared at first in the K-2 sample (C= 0.04), became intensive with an increase in the K_2O-content, and reached its highest point in the K-6—8 samples (C=0.17—0.33). In the K-10 sample (C= 0.50), the peak at d=3.28 Å, characteristic of the $K_3V_5O_{14}$ phase[13] became the highest.

At a rather low content, especially in the K-3 sample, the intensive diffraction peak appeared at d=7.4 Å, which was characteristic of the $K_2V_{18}O_{45}$ phase.[12] With respect to the highest peak at d=8.2 Å in the K-9 sample, the corresponding compound was not found out in any ASTM-cards for potassium vanadates; thus, it has been called an unknown compound. From the comparisons of the diffraction intensities at d=9.6, 8.2, and 3.28 Å, which are the highest of the compounds of $K_2V_8O_{21}$, the unknown compound, and $K_3V_5O_{14}$, respectively, $K_2V_8O_{21}$ seems to be a major component in the K-8 sample and the unknown compound seems to be the major in the K-9 sample. Similarly $K_3V_5O_{14}$ seems to be a major component in the K-10 sample.

The X-ray diffraction patterns of Samples V-1—7 are shown in Fig. 4. In the V-1 sample the most intensive peak is seen at 9.5 Å, and the second most intensive at 3.16 Å: they are characteristic of $K_2V_8O_{21}$.[12] With an increase in the potassium content (C=0.26→0.37), it may be seen in the figure that the peak at 8.2 Å, becomes intensive, while, on the contrary, that at 9.5 Å, decreases. Similarly, the intensities of the peaks at 4.05 and 3.27 Å, (marked with ○) increase relative to the peaks at 4.85, 3.15, and 2.12 Å (marked with △). Finally in the V-6 sample (C=0.374), those peaks assigned to $K_2V_8O_{21}$ disappear completely, while the very strong peak at d=8.2 Å and weak peaks at 4.05 and 3.27 Å which have been ascribed to the unknown compound remain. In Sample V-7 (C=0.399), the other peaks assigned to $K_3V_5O_{14}$[13] appear at d=5.01, 3.29, and 3.02 Å (marked with □). Therefore, it is clearly suggested that the unknown compound is formed as a single compound only by the rapid quenching from the melt at C=0.37. Furthermore, the characteristic X-ray peaks of the unknown compound may be regarded as corresponding to the interplanar distances of 8.2 (very strong), 4.05 and 3.27 Å. The IR spectrum of the

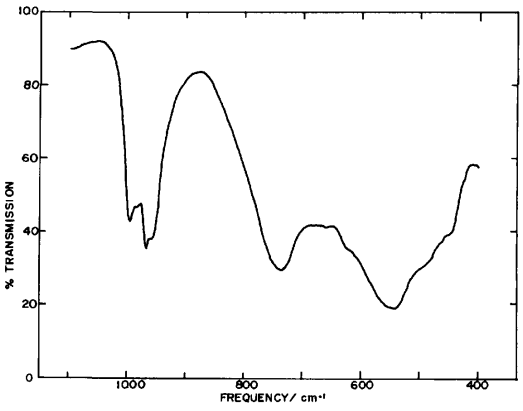

Fig. 5. IR-spectrum of Sample V-6, in which the unknown compound was regarded to be purely contained, recorded in the frequency range of 400—1100 cm^{-1}. See also text.

V-6 sample is shown in Fig. 5. The V=O stretching frequencies characteristic of this compound were determined exactly to be 995, 968, and 955 cm^{-1}.

Discussion

1) The V=O Stretching Frequencies of the Potassium Vanadates Formed from the Melts of K_2O-V_2O_5 in the Range of C=0—0.50. V_2O_5, $K_2V_{18}O_{45}$, and $K_2V_8O_{21}$ were the main components in the samples of $C=0.04$—0.17, as has been pointed out above. Furthermore, the content of the $K_2V_8O_{21}$ phase has been seen to increase with C, and simulteneously the 1000, 972, and 942 cm^{-1} bands have been seem to become intensive, while the 1022 cm^{-1} band weakens, as is shown in Fig. 1 and Table 3. The band intensities are plotted against C in Fig. 6, in which the plot for the 1022 cm^{-1} band can be linearly extrapolated toward the point at $C=0.33$ on the abscissa. As has already been noted above,the V_2O_5 phase is not contained in the samples of $C\geq0.33$. In fact, the X-ray diffraction peak for d=4.38 Å ascribed to V_2O_5 was not detected completely in Samples K-7—10. The intensities of the 1000, 972, and 942 cm^{-1} bands increase linearly with C, keeping approximntely a constant relation with one another, although the content ratio of $K_2V_8O_{21}$ and $K_2V_{18}O_{45}$ differs considerably among Samples K-2—6. Therefore, it can be suggested that the V=O stretching frequencies in $K_2V_8O_{21}$ are nearly the same as those in $K_2V_{18}O_{45}$.

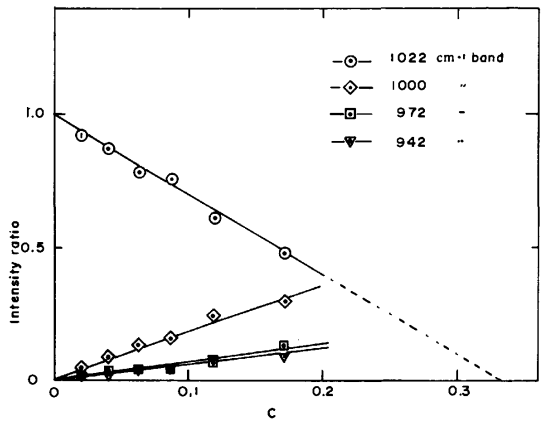

Fig. 6. Changes in the relative intensities of the V=O stretching bands (Intensity ratio) with increasing the K_2O-contents (C) for Samples K-1—6. The 1022 cm^{-1} band is ascribed to pure-V_2O_5 and the 1000, 972, and 942 cm^{-1} for $K_2V_8O_{21}$ (or $K_2V_{18}O_{45}$).

From comparisons of the IR spectra and X-ray diffraction lines between the K-8 and 9 samples, the 967 cm^{-1} band could be assigned to the unknown compound because the band in Sample K-9 was more intensive than that in Sample K-8, while, simultaneously, the existing ratio of the unknown compound to $K_2V_8O_{21}$ in K-9 was higher than that in K-8. It has been reported by Zurkova *et al.*[13] that the characteristic bands of $K_3V_5O_{14}$ were found at 985 and 940 cm^{-1}. The broad band at 980 cm^{-1} and the sharp band at 935 cm^{-1} in the K-10 sample seemed to correspond to these bands, although the frequencies deviated a little bit because of the overlapped spectrum with those of the unknown compound. Therefore, the bands at 995 and 955 cm^{-1} remaining in the spectrum of the K-10 sample could be regarded as having been caused by the unknown compound. Thus, the V=O stretching bands of the unknown compound were established as appearing at 995, 967, and 955 cm^{-1}. These values are in good agreement with those determined from the spectrum for the V-6 sample, $C=$ 0.37 (995, 968, and 955 cm^{-1} respectively).

2) Chemical Formula and Structural Features of the Unknown Compound. With the increase in C, the diffraction peaks at $d=8.2$, 4.05, and 3.27 Å, became intensive relative to those at $d=9.5$, 4.85, 3.15, and 2.12 Å, which are ascribed to the diffraction of $K_2V_8O_{21}$ ($C=0.25$)[12] untile finally, at $C=0.37$, only those lines remained, as is shown in Fig. 4. Therefore, those at $d=$ 8.2, 4.05, and 3.27 Å should be ascribed to the unknown compound. Thus, the unknown compound might be expressed by this formula: $K_{1+x}V_3O_8$ ($x=0.11$). If this $K_{1+x}V_3O_8$ is assumed to be isomorphous with lithium and sodium trivanadates ($K_{1+x}V_3O_8$, γ-phase), both the X-ray diffraction lines and the V=O stretching bands should correspond to one another. Furthermore, those values should be expected to vary more or less among themselves depending upon the alkali-metal-ion size. The strongest peak at $d=$ 8.2 Å for the $K_{1+x}V_3O_8$ compound seems to correspond to that at 6.4 Å, which has been assigned to the interplanar spacing of the (100) plane with $Li_{1+x}V_3O_{7.9}$ ($x=0.12$)[14] and that at $d=7.0$ Å with NaV_3O_8,[15] although it has not been assigned.

In order to compare the d-values of not only 8.2 Å but also 4.05 and 3.27 Å for $K_{1+x}V_3O_8$ with the the

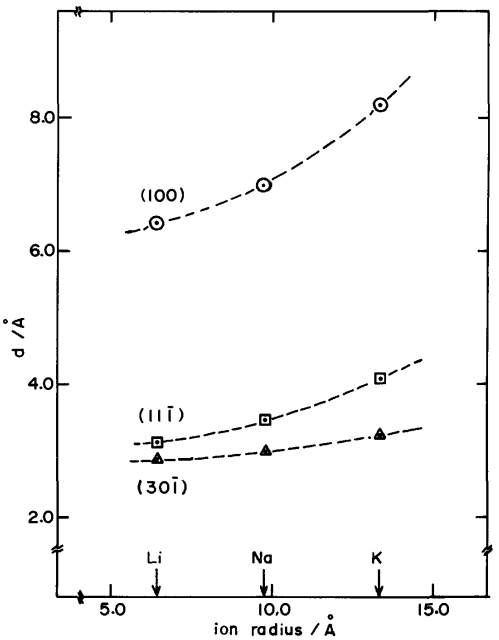

Fig. 7. Comparisons of the X-ray diffraction lines characterized to the compound $K_{1+x}V_3O_8$ (just assigned) with those referred to Li and Na-trivanadates (γ-phase) by use of the alkali metal ion radii as an parameter. The d-values for $Li_{1+x}V_8O_{7.9}$($x\leq0.12$)[14] 6.36, 3.15, and 2.216 Å has been assigned to the (100), (11$\bar{1}$), and (30$\bar{1}$), as were shown in the figure.

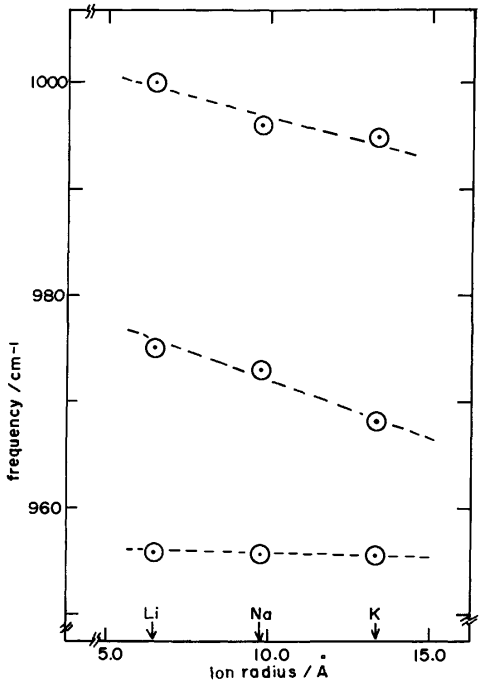

Fig. 8. Comparisons of the V=O stretching frequencies characterized to the compound $K_{1+x}V_3O_8$ (just assigned) with those reported previously for Li and Na-trivanadates[1] by use of the alkali metal ion radii as an parameter.

corresponding *d*-values for $Li_{1+x}V_3O_{7.9}$ and NaV_3O_8 respectively, the *d*- values were plotted against alkali ion radii;[16] they are shown in Fig. 7. Those values are known to correlate well with the alkali-metal-ion radii in the figure. Especially, such a large change in the *d*-value with the (100) can be understood reasonably because alkali-metal-ions are placed into the interplanar spacing along the a-axes in the monoclinic lattice. Thus, from the good coorelations, these three compounds might be concluded to be isomrphous with each other.

Such correlation is consistent with those found in the hexavanadates of potassium, ammonium, rubidium, and cesium, being isomorphous with each other, reported by Kelmers.[4] The V=O stretching bands, 995, 968, and 955 cm^{-1} for the $K_{1+x}V_3O_8$, seem to correspond to those of 1000, 975, and 957 cm^{-1} for LiV_3O_8 and those of 996 , 973, and 957 cm^{-1} for NaV_3O_8, respectively.[1] In fact, the V=O stretching frequencies also gave a good correlation to the alkali-metal-ion radii, as is shown in Fig. 8.

Therefore, throughout any discussions it should be emphasized that the metastable potassium trivanadate (KV_3O_8), being isomorphous with lithium and sodium trivanadates (γ-phase), was favorably formed, especially upon rapid quenching from high-temperature melts (≃750 °C). Furthermore, it should be noted that the present potassium trivanadate differs completely in its X-ray diffraction patterns from the potassium hexavanadate($K_2V_6O_{16}$) reported by Kelmers[4] and from the potassium trivanadates (KV_3O_8) reported by Evans and Block,[5] prepared from aq soln and regarded as isomorphous with $(NH_4)_2V_2O_{16}$, $Rb_2V_2O_{16}$ and $Cs_2V_2O_{16}$.

3) The V=O Bond Lengths of The Potassium Vanadates, $K_2V_8O_{21}$, $K_{1+x}V_3O_8$, and $K_3V_5O_{14}$. From the 1000, 972, and 942 cm^{-1} bands ascribed to the V=O stretching bands for $K_2V_8O_{21}$, the corresponding bond lengths were evaluated as 1.599, 1.618, and 1.630 Å respectively, according to the same procedure as was used in previous papers.[1,10] Similarly, the V=O bond lengths corresponding to the 995, 968, and 955 cm^{-1} bands of $K_{1+x}V_3O_8$ were evaluated as 1.603, 1.622, and 1.630 Å respectively, and those corresponding to the 980 and 935 cm^{-1} bands of $K_3V_5O_{14}$ as 1.613 and 1.645 Å respectively.

The author wishes to express his appreciation to Mr. Tetuo Yamamoto for his measurements of the IR spectra.

References

1) Y. Kera, *J. Solid State Chem.*, **51**, 205 (1984).
2) F. Holtzberg, A. Reisman, M. Berry, and M. Berkenblit, *J. Am. Chem. Soc.*, **78**, 1536 (1956).
3) A. D. Kelmers, *J. Inorg. Nucl. Chem.*, **23**, 279 (1961).
4) A. D. Kelmers, *J. Inorg. Nucl. Chem.*, **21**, 45 (1961).
5) H. T. Evans and S. Block, *Inorg. Chem.*, **5**, 1808 (1966).
6) ASTM-card No. 22-1247; *cf) National Bureau of Standards (U.S.), Mono.* **25**, Sec. 8, 56 (1970).
7) Y. Kera and K. Kuwata, *Bull.Chem. Soc. Jpn.*, **52**, 1268 (1979).
8) L. D. Fredericson, Jr., and D. M. Hansen, *Anal. Chem.*, **35**, 818 (1963).
9) Y. Kera and K. Hirota, *J. Phys. Chem.*, **73**, 3973 (1969).
10) Y. Kera, *Bull. Chem. Soc. Jpn.*, **54**, 1693 (1981).
11) H. G. Backman, F. R. Ahmed, and W. H. Barnes, *Z. Krystallogr.*, **115**, 110 (1961).
12) A. Kato, I. Mochida, and T. Seiyama, *Anal. Chim. Acta*, **54**, 168 (1971).
13) L. Zurkova, V. Sucha, C. Vargova, and J. Corba, *Coll. Czech. Chem. Commun.*, **39**, 387 (1974).
14) D. G. Wickham, *J. Inorg. Nucl. Chem.*, **27**, 1939 (1965); A. D. Wadasley, *Acta Crystallogr.*, **10**, 261 (1957).
15) G. A. Kolta, I. F. Hewaidy, N. S. Felix, and N. N. Girgis, *Thermochem. Acta*, **6**, 165 (1973).
16) L. Pauling, " The Nature of the Chemical Bond," 3rd ed, Cornell Univ. Press, New York, Ithaca (1960), p. 526.

 © 1984 The Chemical Society of Japan Bull. Chem. Soc. Jpn., 57, 1483—1486 (1984)

The Circular Dichroism Spectra of *cis*-$[Co(CN)_2(CO_3)_2]^{3-}$, *cis*-$[Co(NO_2)_2(CO_3)_2]^{3-}$, and Related Bis(dicarboxylato) Complexes

Shuhei Fujinami,* Akihide Shimoda, Toshihito Furukawa, and Muraji Shibata
Department of Chemistry, Faculty of Science, Kanazawa University, Kanazawa 920
(Received September 5, 1983)

Five kinds of *cis*-$[Co(CN)_2(OO)_2]^{3-}$ and *cis*-$[Co(NO_2)_2(OO)_2]^{3-}$ complexes ($OO=CO_3^{2-}$, ox^{2-}, mal^{2-}) have been optically resolved. As to the dicarbonato complexes, one enantiomer has been obtained in a yield far exceeding 50% because of the rapid racemization. When the carbonato ligand is replaced with an oxalato or malonato ligand, the complex becomes inert for racemization and a new Cotton peak with an opposite sign appears at the lower frequency in the first-absorption-band region. The CD spectral change is different from the change observed in *cis*-$[Co(a)_2(OO)_2]^-$ complexes ($a=NH_3$, py, en/2), suggesting the intimate participation of the unidentate ligands in determining the signs of the Cotton peaks.

It is known that the variation in the size of a dicarboxylato chelate ring causes a marked change in the CD spectra.[1-6] For example, a $[Co(CO_3)_2(en)]^-$ complex exhibits a single Cotton peak in the first-absorption-band region, while $[Co(ox)_2(en)]^-$ and $[Co(mal)_2(en)]^-$ complexes exhibit two and three Cotton peaks respectively. Such a spectral change has been utilized to assign a single Cotton peak observed in the *cis*-$[Co(a)_2(CO_3)_2]^-$ complex ($a=NH_3$, py, or en/2).[6] When the carbonato ligand is replaced with an oxalato or malonato ligand, a new Cotton peak with an opposite sign appears at a higher frequency in the first-absorption-band region. Therefore, the single Cotton peaks in the dicarbonato complexes have been assigned to the $A_{1g}\rightarrow E_g$ transition component in a holohedrized[7] D_{4h} symmetry, since this component lies at a lower frequency in the *cis*-$[Co(N)_2(O)_4]$-type complexes.

This paper deals with the optical resolutions of *cis*-$[Co(CN)_2(OO)_2]^{3-}$ and *cis*-$[Co(NO_2)_2(OO)_2]^{3-}$ complexes ($OO=CO_3^{2-}$, ox^{2-}, and mal^{2-}). These dicyano and dinitro complexes have previously been synthesized, and only *cis*-$[Co(CN)_2(CO_3)(ox)]^{3-}$ and *cis*-$[Co(CN)_2(ox)_2]^{3-}$ complexes have been optically resolved.[8,9] The CD spectral changes in the *cis*-$[Co(CN)_2(OO)_2]^{3-}$ and *cis*-$[Co(NO_2)_2(OO)_2]^{3-}$ complexes will be investigated and compared with those in the *cis*-$[Co(a)_2(OO)_2]^-$ complexes ($a=NH_3$, py, and en/2).

Experimental

1) Optical Resolution of cis-*[Co(CN)$_2$(CO$_3$)$_2$]$^{3-}$.* This complex was prepared and crystallized by adding $(+)_{589}$-$[Co(en)_3]Br_3$ and an appropriate amount of ethanol according to the method in the literature.[8] Since the dicyano complex racemized rapidly in an aqueous solution, the CD spectrum was measured by the following procedure. The brown-violet crystals[8] were quickly dissolved into a cold 0.5 mol dm^{-3} $NaHCO_3$ solution. The solution was poured onto a column of Dowex 50W-X8 (ϕ 1 cm × 1 cm, in Na^+ form) and then discharged rapidly by air-pressing the top of the column. The effluent was submitted to the measurement of the CD spectrum within the range of 50—100 nm at 5 °C. The procedure should be done as fast as possible and repeated several times to cover the region of the d-d transition bands. Each time needed to separate the complex cation was recorded in order to correct the spectrum. The separation of the cation was carried out at *ca.* 10 s, and the spectrum was recorded at a speed of 100 nm min^{-1}. Since no change in the absorption spectrum was observed after the measurement of the CD spectrum, the metal concentration was evaluated from the absorption spectral data. The height of the Cotton peak at 459 nm decreased to half after *ca.* 27 s at 5 °C in a 0.5 mol dm^{-3} $NaHCO_3$ solution. The deposited brown-violet crystals contained the $(+)^{CD}_{589}$-dicyano isomer.

2) Preparation and Optical Resolution of cis-*[Co(CN)$_2$(mal)$_2$]$^{3-}$.* This complex was prepared by a literature method with only a slight modification.[8] Malonic acid (25 g, 0.35 mol) and potassium hydrogencarbonate (25 g, 0.25 mol) were dissolved in 30 cm^3 of warm water, and the solution was stirred vigorously until the evolution of CO_2 gas ceased. The resultant solution was added to a deep red solution of *cis*-$[Co(CN)_2(CO_3)_2]^{3-}$[8] which had been prepared by using a green solution of tricarbonatocobaltate(III) (0.05 mol scale).[10] The mixed solution was adjusted to pH 5 by acetic acid and stirred at room temperature for 3 h.

After filtration, the filtrate was poured onto a column of QAE Sephadex A-25 in the Cl^- form (ϕ3 cm × 15 cm). By elution with 0.6 mol dm^{-3} KCl, red and orange bands were discharged from the column, in that order. The effluent of the orange band was concentrated to a small volume (*ca.* 10 cm^3) with the simultaneous removal of the precipitated KCl. An appropriate amount of an acetone solution of $(+)_{589}$-$[Co(en)_3](ClO_4)_3$ was added to the concentrate. After the removal of the deposited $KClO_4$, small amount of ethanol was added to the filtrate. The precipitated resolving agent was repeatedly removed, and a red diastereoisomeric salt containing the $(+)^{CD}_{546}$-dicyano complex was finally obtained. The yield was very poor. The salt was dissolved in water, and the solution was passed through a short column of Dowex 50W-X8 (ϕ 1 cm × 2 cm, in Na^+ form). The absorption spectral data of the effluent were identical with those of the literature.[8] The CD spectrum was measured by using the effluent, and the metal concentration was estimated from the absorption spectral data. The enantiomer was enough inert for racemization for the CD spectrum to be measured.

3) Optical Resolution of cis-*[Co(NO$_2$)$_2$(CO$_3$)$_2$]$^{3-}$.* This complex was prepared according to the method in the literature.[9] Into a cold solution of $K_3[Co(NO_2)_2(CO_3)_2]\cdot H_2O$ (2 g, 5 mmol, in 200 cm^3 H_2O) we stirred, in turn, a solution of $(-)_{589}[Co(gly)(en)_2]Cl_2$[11] (1.6 g, 5 mmol, in 50 cm^3 H_2O) and acetone (20 cm^3) under iced conditions. The *cis*-$[Co(NO_2)_2(CO_3)_2]^{3-}$ complex was deposited as a less-soluble pink diastereoisomeric salt. Found: C, 18.17; H, 5.26; N, 18.63%. Calcd for $[Co(gly)(en)_2]_3\cdot[Co(NO_2)_2(CO_3)_2]_2\cdot 7.5H_2O$: 18.39; H, 5.26; N, 18.52%.

The dinitro complexes was also racemized rapidly in an aqueous solution, and the CD spectrum was measured by a method similar to that used for *cis*-$[Co(CN)_2(CO_3)_2]^{3-}$. The Cotton peak at 521 nm decreased in intensity to half after *ca.* 80 s at 5 °C in a 0.5 mol dm^{-3} $NaHCO_3$ solution. No change

in the absorption spectrum was observed after the measurement of the CD spectrum. The diastereoisomeric salt contained the $(-)^{CD}_{589}$-dinitro isomer.

4) Optical Resolution of cis-*[Co(NO$_2$)$_2$(CO$_3$)(ox)]$^{3-}$.* Into a solution of *cis*-$K_3[Co(NO_2)_2(CO_3)(ox)]$[9] (4 g, 0.01 mol, in 300 cm^3 H_2O) we stirred a solution of $(+)_{589}[Co(en)_3]Cl_3$ (2 g, 5 mmol, in 50 cm^3 H_2O) at room temperature. Red diastereoisomeric salt was soon deposited. The salt was sparingly soluble in water, but it could not be recrystallized. Purification was carried out by the following method. The salt and the ion-exchange resin (Dowex 50W-X8, Na^+ form) were mixed in water, and the mixture was stirred for 20 min. The resin was filtered out, and the filtrate containing the $(-)^{CD}_{589}$-isomer of the dinitro complex was mixed with a solution containing an equimolar amount of $(+)_{589}[Co(en)_3]Cl_3$. The red salt was soon obtained. This procedure was repeated until the $\Delta\varepsilon$ value at 490 nm became constant. The CD spectrum was measured by using the solution from which the resin had been removed by filtration; the metal concentration was evaluated from the absorption spectral data. The rate of the racemization of the enantiomer was very slow compared with that of *cis*-$[Co(NO_2)_2(CO_3)_2]^{3-}$.

5) Derivation of Optically Active cis-*[Co(NO$_2$)$_2$(ox)$_2$]$^{3-}$.* Into a solution of an optically active $[Co(NO_2)_2(CO_3)(ox)]^{3-}$ isomer (5 mmol in 100 cm^3 H_2O) we successively stirred potassium oxalate (35 g, 0.21 mol) and oxalic acid (1 g, 0.01 mol) under iced conditions; the pH of the solution thereupon became *ca.* 4. After stirring for 3 h, the solution was filtered and the filtrate was poured onto a column of QAE Sephadex A-25 (ϕ2.5 cm × 15 cm, in Cl^- form). The band containing a univalent species was discharged by elution with 0.6 mol dm^{-3} KCl, and then the desired tervalent complex species was eluted with 1 mol dm^{-3} KCl. The absorption spectrum of the eluate was identical with that in the literature.[9] The eluate was also subjected to the measurement of its CD spectrum, while the metal concentration was evaluated from the absorption spectral data. The enantiomer was enough inert for racemization for the CD spectrum to be measured. The $(-)^{CD}_{589}[Co(NO_2)_2(ox)_2]^{3-}$ isomer was derived from the $(-)^{CD}_{589}[Co(NO_2)_2(CO_3)(ox)]^{3-}$ isomer.

Measurement. The absorption and CD spectra were measured with a Hitachi 323 recording spectrophotometer and a JASCO J40-C automatic recording spectropolarimeter respectively.

The CD spectrum of $(-)^{CD}_{589}[Co(CN)_2(ox)(H_2O)_2]^-$ was measured by acidifying a solution of $(-)^{CD}_{589}[Co(CN)_2(CO_3)(ox)]^{3-}$ [8] to pH 2 with perchloric acid. The spectrum was reformed to that of the parent complex on the addition of $KHCO_3$.

Results and Discussion

Optical Resolution of the Labile Complex. A series of *cis*-$[Co(CN)_2(OO)_2]^{3-}$ complexes (OO = CO_3^{2-}, ox^{2-}, mal^{2-}) has been prepared, and the optical resolutions have been successfully done for the *cis*-$[Co(CN)_2(CO_3)(ox)]^{3-}$ and *cis*-$[Co(CN)_2(ox)_2]^{3-}$ complexes by using $(+)_{589}[Co(en)_3]Br_3$ as a resolving agent.[8] The attempt to measure the CD spectrum of *cis*-$[Co(CN)_2(CO_3)_2]^{3-}$ has resulted in failure, although the anion was easily crystallized with a $(+)_{589}[Co(en)_3]^{3+}$ cation. This failure is attributable to a rapid racemization of *cis*-$[Co(CN)_2(CO_3)_2]^{3-}$ in an aqueous solution. In this study, the separation of the complex cation from the solution of the diastereoisomeric salt was done as fast as possible. A CD spectral measurement was carried out within a narrow range of wavelengths and was repeated several times under the same conditions to cover the first-absorption-band region. Since the half-life of the optical activity (*ca.* 27 s at 5 °C) is shorter than the time needed to record a CD spectrum, the recorded curve does not afford a correct CD spectrum. The curves were corrected by extrapolating the ellipticity recorded at each wavelength to that at the time when the diastereoisomeric salt had been dissolved. The corrected spectrum was reproducible with a deviation of *ca.* 4%. A dominant positive extremum appeared at 21800 cm^{-1} and a weak positive plateau, at 17500 cm^{-1}, in the first-absorption-band region.

The *cis*-$[Co(NO_2)_2(OO)_2]^{3-}$ complexes (OO = CO_3^{2-}, ox^{2-}) have been prepared, but their optical resolutions have not been reported.[9] The *cis*-$[Co(NO_2)_2(CO_3)(ox)]^{3-}$ complex was optically resolved with $(+)_{589}[Co(en)_3]Br_3$, while the *cis*-$[Co(NO_2)_2(ox)_2]^{3-}$ complex was not resolved by using resolving agents. The optically active bis(oxalato) isomer was derived from the optically resolved $[Co(NO_2)_2(CO_3)(ox)]^{3-}$. The rates of the racemization of the two dinitro complexes were very slow, so the recorded CD spectra did not need to be corrected. The $[Co(NO_2)_2(CO_3)_2]^{3-}$ complex was rapidly racemized in an aqueous solution. The half-life of the optical activity was *ca.* 80 s at 5 °C. The recorded CD spectral curves were also corrected by the method described in the case of *cis*-$[Co(CN)_2(CO_3)_2]^{3-}$. The corrected spectrum exhibits two extrema, with opposite signs, at 16400 and 19200 cm^{-1}, the extremum at the lower frequency being extremely weak.

It is characteristic that almost the whole of the dicarbonato complex in a solution could be deposited as a less-soluble diastereoisomeric salt by adding excess amounts of a resolving agent and an organic solvent; the crop of the crystals and the rate of crystallization were controlled by the amount of organic solvent added, but the optical purity was independent of the conditions. Moreover, the $\Delta\varepsilon$ value of the dominant peak in each dicarbonato complex is comparable with that in the corresponding carbonatooxalato complex, as is shown in Table 1. The high-yield resolution of the dicarbonato complexes can be explained by a so-called second-order asymmetric process.[12,13]

As to the *cis*-$[Co(NH_3)_2(CO_3)_2]^-$ complex, $Li(-)_{589}$-$[Co(NH_3)_2(CO_3)_2]$ has been deposited in the presence of $(-)_{589}[Co(ox)(en)_2]^+$, with the yield far exceeding 50%.[14] However, the $[Co(CN)_2(CO_3)_2]^{3-}$ and $[Co(NO_2)_2(CO_3)_2]^{3-}$ complexes crystallized as diastereoisomeric salts. The present dicarbonato complexes racemize more rapidly than the $[Co(NH_3)_2(CO_3)_2]^-$ complex.

CD Spectra of Bis(dicarboxylato) Complexes. The CD spectral data for the enantiomers obtained from the less-soluble diastereoisomeric salts are listed in Table 1. The CD spectral changes in a series of *cis*-$[Co(CN)_2(OO)_2]^{3-}$ complexes are illustrated in Fig. 1. Except for the dicarbonato complex, the dicyano complexes exhibit two Cotton peaks, with opposite signs, in the first-absorption-band region. It is found that the peak observed on a lower-frequency side apparently increases in intensity as the member of the

TABLE 1. ABSORPTION AND CD SPECTRAL DATA

Complex	Absorption[a]		CD	
	$\tilde{\nu}/10^3cm^{-1}$(log ε)		$\tilde{\nu}/10^3cm^{-1}$($\Delta\varepsilon$)	
$(+)^{CD}_{589}[Co(CN)_2(CO_3)_2]^{3-}$	18.3	(1.96)	17.5	(+0.18)
	22.5	(2.03)	21.8	(+1.47)
$(-)^{CD}_{589}[Co(CN)_2(CO_3)(ox)]^{3-}$	18.7	(1.90)	19.3	(−0.66)[a]
	23.0	(2.07)	22.9	(+2.17)
$(-)^{CD}_{589}[Co(CN)_2(ox)_2]^{3-}$	18.8	(1.84)	19.1	(−1.74)[a]
	23.4	(2.14)	23.5	(+3.03)
$(+)^{CD}_{589}[Co(CN)_2(mal)_2]^{3-}$	18.7	(1.60)	18.2	(+0.40)
	23.3	(2.08)	23.4	(−0.24)
$(-)^{CD}_{589}[Co(CN)_2(ox)(H_2O)_2]^{-}$	18.5	(1.70)	18.0	(−0.71)
	23.8	(2.08)	23.5	(+0.52)
$(-)^{CD}_{589}[Co(NO_2)_2(CO_3)_2]^{3-}$	18.3	(2.24)	16.4	(+0.04)
			19.2	(−3.00)
$(-)^{CD}_{589}[Co(NO_2)_2(CO_3)(ox)]^{3-}$	18.7	(2.26)	17.2	(−0.45)
			20.4	(+2.93)
$(-)^{CD}_{589}[Co(NO_2)_2(ox)_2]^{3-}$	19.1	(2.13)	18.0	(−0.39)
			20.9	(+0.87)

a) Cited from Refs. 9 and 10.

chelate ring increases.

It is troublesome to decide whether the Cotton peaks of a complex with C_2 symmetry indicate three transition components or two transition components. Both interpretations have been applied to the *cis*-$[Co(a)_2(mal)_2]^-$ (a = NH_3, en/2, and tn/2) complexes which exhibit three Cotton peaks with alternating signs.[1,6] However, Gaussian analyses of both situations have given splittings of the transition components incompatible with the predictions from an angular overlap model.[15] Since the *cis*-$[Co(CN)_2(mal)_2]^{3-}$ complex, in which the transition components are considered to be well separated from one another, exhibits two extrema, we will analyze the CD spectra of the dicarboxylato complexes with two transition components.

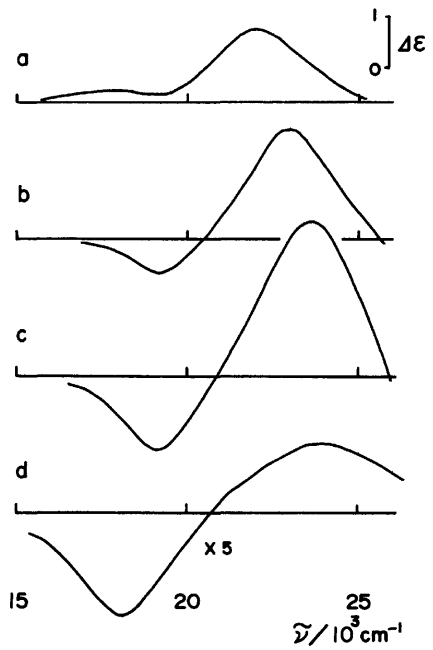

Fig. 1. CD Spectra of; a) $(+)^{CD}_{589}[Co(CN)_2(CO_3)_2]^{3-}$, b) $(-)^{CD}_{589}[Co(CN)_2(CO_3)(ox)]^{3-}$, c) $(-)^{CD}_{589}[Co(CN)_2(ox)_2]^{3-}$, d) $(-)^{CD}_{589}[Co(CN)_2(mal)_2]^{3-}$.

The angular overlap model also predicts that two of the three transition components in an octahedral parentage band will almost entirely degenerate in these dicarboxylato complexes with a holohedrized D_{4h} symmetry,[7] while the remaining one will separate well from the two components. In this situation, the Cotton peak, which increases in intensity on a lower-frequency side with the replacement of the OO chelate from CO_3^{2-} to ox^{2-} or mal^{2-}, can be assigned to the $A_{1g} \rightarrow E_g(D_{4h})$ component, while the dominant Cotton peak in *cis*-$[Co(CN)_2(CO_3)_2]^{3-}$ is attributed to $A_{1g} \rightarrow A_{2g}(D_{4h})$. Similar CD spectral changes were observed in the *cis*-$[Co(NO_2)_2(OO)_2]^{3-}$ complexes, as is shown in Fig. 2. The negative Cotton peak at a lower frequency also increases in intensity with the change from CO_3^{2-} to ox^{2-}.

These spectral changes are different from those in the *cis*-$[Co(a)_2(OO)_2]^-$ complexes (a = NH_3, py, and en/2), in which a new component has been observed on a

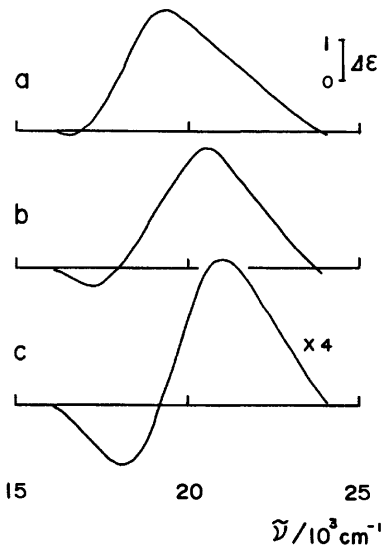

Fig. 2. CD spectra of; a) $(+)^{CD}_{589}[Co(NO_2)_2(CO_3)_2]^{3-}$, b) $(-)^{CD}_{589}[Co(NO_2)_2(CO_3)(ox)]^{3-}$, c) $(-)^{CD}_{589}[Co(NO_2)_2(ox)_2]^{3-}$.

higher-frequency side with the replacement from CO_3^{2-} to ox^{2-} or mal^{2-} and in which a single Cotton peak in each dicarbonato complex has been assigned to $A_{1g} \rightarrow E_g(D_{4h})$.[6] This difference is considered to be caused by the difference between the charges of the unidentate ligands. The unidentate a is neutral, while the cyano and nitro ligands are anionic.

Similar CD spectral changes with the ligand replacement from CO_3^{2-} to $2H_2O$ have been reported in *cis*-$[Co(N)_2(O)_4]$-[6] and *cis*-$[Co(N)_4(O)_2]$-type complexes.[16] The $(+)_{589}[Co(CO_3)(mal)(NH_3)_2]^-$ and $(-)_{589}[Co(CO_3)(NH_3)_2(py)_2]^+$ complexes exhibit (−) and (+) Cotton peaks from a lower frequency in the first-absorption-band region. When the $(-)_{589}$-$[Co(mal)(NH_3)_2(H_2O)_2]^+$ and $(-)_{589}[Co(NH_3)_2(py)_2$-$(H_2O)_2]^{3+}$ complexes are derived from these optically active carbonato complexes, two Cotton peaks, with (+) and (−) signs, from a lower frequency are observed. This phenomenon has been explained in terms of a crystal-field model of the rotatory strength in transition-metal complexes: the spectral change is ascribed to a change in the effective charge on donor atoms according to aquation.[17] Therefore, the CD spectral changes in the dicyano and dinitro complexes are regarded as the second piece of evidence indicating an intimate relation between the effective charge of donor atoms and the Cotton signs.

When a $(-)^{CD}_{589}[Co(CN)_2(ox)(H_2O)_2]^-$ complex was derived from the $(-)^{CD}_{589}[Co(CN)_2(CO_3)(ox)]^{3-}$ complex, no drastic change in the CD spectrum was observed. However, a decrease in the negative Cotton peak at a lower frequency, compared with that of the parent carbonato complex, was detected.

References

1) B. E. Douglas, R. A. Haines, and J. G. Brushmiller, *Inorg. Chem.*, **2**, 1194 (1963).
2) W. T. Jordan, B. J. Brennan, L. R. Froebe, and B. E. Douglas, *Inorg. Chem.*, **12**, 1827 (1973).
3) B. J. Brennan, K. Igi, and B. E. Douglas, *J. Coord. Chem.*,**4**, 19 (1974).
4) C. W. Van Saun and B. E. Douglas, *Inorg. Chem.*, **8**, 115 (1969).
5) W. T. Jordan and J. I. Legg, *Inorg. Chem.*, **13**, 957 (1974).
6) S. Muramoto, K. Kawase, and M. Shibata, *Bull. Chem. Soc. Jpn.*, **51**, 3505 (1978).
7) C. K. Jørgensen, "Modern Aspects of Ligand Field Theory," North-Holland Pub. Co., Amsterdam (1971).
8) S. Fujinami and M. Shibata, *Bull. Chem. Soc. Jpn.*, **46**, 3443 (1973).
9) H. Ichikawa and M. Shibata, *Bull. Chem. Soc. Jpn.*, **42**, 2873 (1969).
10) M. Shibata, *Proc. Jpn. Acad.*, **50**, 779 (1974).
11) C. T. Liu and B. E. Douglas, *Inorg. Chem.*, **3**, 1356 (1964).
12) F. P. Dwyer and E. C. Gyarfas, *J. Proc. R. Soc. N. S. W.*, **83**, 263 (1949).
13) D. H. Busch, *J. Am. Chem. Soc.*, **77**, 2747 (1955).
14) S. Muramoto and M. Shibata, *Chem. Lett.*, **1977**, 1499.
15) H. Yamatera, *Bull. Chem. Soc. Jpn.*, **31**, 95 (1958): C. E. Schäffer, *Struct. Bonding*, **5**, 68 (1968).
16) K. Tsuji, S. Fujinami, and M. Shibata, *Bull. Chem. Soc. Jpn.*, **54**, 1531 (1981).
17) S. Fujinami, K. Tsuji, and M. Shibata, *Bull. Chem. Soc. Jpn.*, **55**, 2383 (1982).

 © 1984 The Chemical Society of Japan Bull. Chem. Soc. Jpn., 57, 1487—1490 (1984)

The Influence of Anions on the Distribution Coefficients of Hard Acid-Metals for Anion-exchange Resin in $HF-H_3BO_3$ Media

Takeo ADACHI,* Hideyo YOSHIDA, Kimie IZAWA, and Sorin KIHARA†
Analytical Chemistry Laboratory, Japan Atomic Energy Research Institute, Tokai, Ibaraki 319-11
(Received October 17, 1983)

The distribution coefficients, K_d, of eighteen hard acid-metal ions for a strongly basic anion-exchange resin were determined in $HF-H_3BO_3$ media in the presence of Cl^- or NO_3^-, SO_4^{2-}, and ClO_4^-, and the relation between the adsorbabilities of the coexisting anions and the K_d values of the metal ions was discussed. The fluoride-ion concentration is quite low in $HF-H_3BO_3$ media because of the complex formation of the fluoride ion with boric acid, and most of the hard acid-metal ions have lower K_d values in $HF-H_3BO_3$ media than those in a hydrofluoric acid solution. By varying the kinds of coexisting anions and their concentrations in $HF-H_3BO_3$ media containing less than 0.02 M (1 M = 1 mol dm^{-3}) of fluoroborate ions, the K_d values of metal ions can be controlled to allow the anion-exchange separations. As fluoroborate ions, *e.g.*, BF_4^- or BF_3OH^-, are strongly adsorbed on the resin, metal ions which are strongly held on the resin can be eluted by media including fluoroborate ions in higher concentrations. By using $HF-H_3BO_3$ media and selecting the coexisting anions, an effective mutual separation of titanium-zirconium, titanium-uranium, tin-niobium, and molybdenum-tungsten can be attined.

The highly fluorinated metal complexes in a hydrofluoric acid solution change their forms to poorly fluorinated complexes when boric acid is added to the solution, because the free fluoride-ion concentration is considerably reduced by the formation of such fluoroborate ions as BF_4^- or BF_3OH^-. The free fluoride-ion concentration in $HF-H_3BO_3$ mixed media is kept constant by the buffer action due to the dissociation of fluoroborate ions, even if the free fluoride ions are consumed by the complex formation with coexisting metal ions. As the fluoroborate ions in the mixed media are strongly adsorbed on the anion-exchange resin, metal-anion comlexes held on the resin can be eluted by the aid of fluoroborate ions in a increased concentration.

In the previous paper,[1] the usefulness of $HF-H_3BO_3$ media in the anion-exchange separation of hard acid-metals was reported and it was also pointed out that a more effective mutual separation of metals can be attained if nitrate ions coexist in the mixed media.

In the present paper, for the extensive application of the mixed media in the ion-exchange separation, the distribution coefficients of metal ions on the anion-exchange resin are determined in mixed media containing various anions, and the relation between the distribution coefficients and the adsorbabilities of anions on the resin is discussed.

Experimental

Chemicals and Apparatus. The standard solutions of the metal ions were prepared by the procedures described in previous papers.[1,2] The other chemicals and apparatus were the same as those used before.

Ion-exchange Resin. A strongly basic anion-exchange resin, Diaion SA#100, a product of Mitsubishi Chemical Ind. Ltd. (8% DVB, 75—150 μm, Cl^--form), was used. After washing the resin in a column with five times as much as the column volume of 3 M HCl or HNO_3, H_2SO_4, and $HClO_4$ and with a sufficient volume of distilled water, the resin was dried to a constant weight at 70 °C and stored in a vacuum desiccator.

† Present address: Institute for Chemical Research, Kyoto University, Uji, Kyoto 611

Determination of Distribution Coefficient. Fifty ml of a definite concentration of a hydrofluoric-hydrochloric acid solution or a hydrofluoric-boric-hydrochloric acid solution containing 2×10^{-4} M of a metal ion was added to a 150-ml polyethylene bottle containing 0.5 g of the dried resin in the Cl^--form. The bottle was then shaken gently for 24 h at room temperature. After the filtration of the resin, the metal-ion concentration in the solution was determined by a suitable method, as has been described previously.[2]

The distribution coefficient, K_d, was determined by the following equation:

K_d = (Amount of metal ion in resin / Amount of metal ion in solution) × (ml of solution / g of resin).

The K_d was also determined in the media containing sulfuric, nitric, or perchloric acid instead of hydrochloric acid by the manner described above.

Column Operation. About 4 g of the dried resin, which had been swelled well with distilled water, was packed in a polyethylene column (8 mmϕ × 180 mm), and was conditioned with about 50 ml of 0.2 M HF. After the addition of a test solution containing 1—250 mg of a metal ion in 0.2 M HF, an eluent of a definite composition was passed through the column. The effluent was then collected with a fraction collector, and the concentration of the metal ion in each fraction was determined by a method described previously.[2] In the mutual-separation experiments, two kinds of metal ions were added together to the column.

Results and Discussion

In the present experiments, the coexisting anions are added as their acid forms in order to prevent the hydrolysis of the hard acid-metals.

In the following discussion, as a criterion for ion-exchange separation, we adopt Ringbom's suggestion for the column-filtration method (*i.e.*, the K_d of an adsorbed ion is larger than 10^2—$10^{2.5}$, method (*i.e.*, the K_d of an adsorbed ion is larger than 10^2—$10^{2.5}$, while that of the emerging ion is less than $10^{0.5}$—10^1).[3]

Distribution Coefficients. The distribution coefficients of the metal ion, K_d, on strongly basic anion-exchange resin were determined in hydrofluoric-boric acid media containing Cl^-, SO_4^{2-}, NO_3^-, or ClO_4^-; they are summarized in Tables 1—4. In the third column of these tables, the K_d values in the absence of boric acid are also tabulated.

Table 1. Anion-exchange distribution coefficients of metal ions in $HF-H_3BO_3-HCL$ media

Metal ion	HCl(M)	HF(M)			0.1 M HF-H_3BO_3(M)		HF(M)-0.5 M H_3BO_3		
		0.01	0.1	0.5	0.01	0.1	0.01	0.1	0.5
Ta(V)	0.1	4.8×10^3	1.1×10^4	8.9×10^3	2.9×10^3	1.8×10^3	2.9×10^3	2.2×10^3	300
	1	887	911	949	618	352	622	412	235
Nb(V)	0.1	404	577	1.1×10^3	310	97	161	87	7
	1	31	38	29	35	17	149	22	7
Sn(IV)	0.1	501	2.2×10^3	4.2×10^3	1.1×10^3	25	19	15	3
	1	460	433	45	157	800	176	1.7×10^3	577
W(VI)	0.1	83	535	1.1×10^3	83	93	325	170	3
	1	8	22	28	121	243	501	207	20
Mo(VI)	0.1	64	214	376	144	32	151	60	18
	1	36	30	33	45	14	16	19	18
Zr(IV)	0.1	698	2.2×10^3	2.2×10^3	3.5×10^3	76	160	27	3
	1	3	5	12	9	3	9	6	3
Hf(IV)	0.1	1.0×10^3	2.5×10^3	2.4×10^3	3.1×10^3	86	243	33	3
	1	3	9	18	9	3	9	5	3
Ti(IV)	0.1	939	2.2×10^3	2.6×10^3	1.5×10^3	38	10	9	3
	1	15	22	24	16	3	3	3	3
U(VI)	0.1	5	3	10	4	3	3	3	3
	1	6	5	5	3	3	3	3	3

V(V) is slightly adsorbed in HF-HCl. Al(III), V(IV), and Fe(III) are not adsorbed in either HF-HCl or $HF-H_3BO_3-HCl$.

Table 2. Anion-exchange distribution coefficients of metal ions in $HF-H_3BO_3-H_2SO_4$ media

Metal ion	H_2SO_4(M)	HF(M)			0.1 M HF-H_3BO_3(M)		HF(M)-0.5 M H_3BO_3		
		0.01	0.1	0.5	0.01	0.1	0.01	0.1	0.5
Ta(V)	0.05	6.5×10^3	2.0×10^4	1.7×10^3	1.2×10^3	1.0×10^3	1.2×10^3	1.0×10^3	272
	0.5	1.0×10^3	3.7×10^3	4.2×10^3	519	562	867	645	215
Nb(V)	0.05	410	1.1×10^3	754	249	78	306	88	8
	0.5	51	46	41	41	40	109	63	5
Sn(IV)	0.05	451	2.1×10^3	1.7×10^3	788	22	21	13	3
	0.5	8	27	52	53	73	11	30	3
W(VI)	0.05	78	810	946	155	71	889	157	7
	0.5	31	32	46	35	109	445	70	16
Mo(VI)	0.05	315	515	473	142	175	848	280	39
	0.5	46	43	45	15	3	20	6	3
Zr(IV)	0.05	772	1.7×10^3	1.1×10^3	1.0×10^3	82	320	52	3
	0.5	29	51	78	30	18	17	9	3
Hf(IV)	0.05	1.1×10^3	1.5×10^3	1.1×10^3	673	69	152	38	3
	0.5	28	68	85	27	7	14	7	3
Ti(IV)	0.05	833	1.6×10^3	1.3×10^3	867	53	20	13	3
	0.5	30	60	71	58	6	3	3	3
U(VI)	0.05	1.1×10^3	286	205	135	126	2.3×10^3	167	3
	0.5	29	14	11	10	10	44	13	3

V(V) is slightly adsorbed in HF-0.05 M H_2SO_4. Al(III), V(IV), and Fe(III) are not adsorbed in either $HF-H_2SO_4$ or $HF-H_3BO_3-H_2SO_4$.

The concentration of fluoride ions and fluoroborate ions in $HF-H_3BO_3$ media in the presence of 0.1 or 1 M of nitric acid was calculated using the dissociation constants given by Sillen *et al.*[4] and Mesmer *et al.*;[5] they are shown in Fig. 1 as a function of the hydrofluoric acid concentration, C_{HF}.

Qualitatively speaking, the K_d values of metals in $HF-H_3BO_3$ media are smaller than those in the absence of boric acid, and decrease with the increase in C_{HF}, though the K_d values in HF solutions increase or stay constant. The variation in K_d values may be explained as follows: (1) As the addition of boric acid to the hydrofluoric acid solution reduces the free fluoride-ion concentration, C_{F^-} to about one hundredth (Curves b and c in Fig. 1), the fraction of metal-anion complexes to be adsorbed onto the anion-exchange resin in $HF-H_3BO_3$ media becomes smaller than that in the absence of boric acid. (2) In a hydrofluoric acid solution, with the increase in C_{HF}, C_{F^-} and also the fraction of metal-fluoride complexes to be adsorbed onto the resin are increased. On the other hand, in $HF-H_3BO_3$ media, C_{F^-} does not increase when C_{HF} is larger than 0.1 M. (3) The concentration of fluoroborate ions in the mixed media increases with the increase in C_{HF}, and the increased fluoroborate ions which are strongly adsorbed on the resin lower the K_d values of the metals.

The influence of coexisting anions on the K_d can be interpreted by considering their adsorbabilities on the anion-exchange resin. The following selectivity

Table 3. Anion-exchange distribution coefficients of metal ions in HF-H_3BO_3-HNO_3 media

Metal ion	HNO_3 (M)	HF(M)			0.1 M HF-H_3BO_3(M)		HF(M)-0.5 M H_3BO_3		
		0.01	0.1	0.5	0.01	0.1	0.01	0.1	0.5
Ta(V)	0.1	638	1.2×10^3	3.4×10^3	963	1.5×10^3	1.5×10^3	1.7×10^3	386
	1	202	178	198	296	252	302	235	172
Nb(V)	0.1	110	130	190	68	18	71	58	3
	1	12	3	3	3	3	29	14	11
Sn(IV)	0.1	350	420	450	322	15	3	3	3
	1	3	3	3	3	3	3	3	3
W(VI)	0.1	140	185	220	28	14	112	56	5
	1	30	3	3	3	3	29	19	3
Mo(VI)	0.1	6	38	57	25	4	33	15	6
	1	5	3	5	3	3	10	8	3
Zr(IV)	0.1	82	283	418	282	6	8	3	3
	1	3	3	3	3	3	3	3	3
Hf(IV)	0.1	90	320	430	245	7	10	3	3
	1	3	3	3	3	3	3	3	3
Ti(IV)	0.1	241	344	411	302	18	3	3	3
	1	4	5	3	3	3	3	3	3

U(VI), Al(III), V(IV), V(V), and Fe(III) are not adsorbed.

Table 4. Anion-exchange distribution coefficients of metal ions in HF-H_3BO_3-$HClO_4$ media

Metal ion	$HClO_4$ (M)	HF(M)			0.1 M HF-H_3BO_3(M)		HF(M)-0.5 M H_3BO_3		
		0.01	0.1	0.5	0.01	0.1	0.01	0.1	0.5
Ta(V)	0.1	112	165	252	74	128	182	200	42
	1	38	81	73	26	46	15	18	15
Sn(IV)	0.1	5	3	3	13	12	17	15	10
	1	3	3	3	3	3	3	3	3
W(VI)	0.1	7	3	3	29	21	47	10	20
	1	3	3	3	14	10	23	8	18
Mo(VI)	0.1	3	3	38	25	4	33	15	6
	1	3	3	3	3	3	5	8	10

Nb(V), Zr(IV), Hf(IV), Ti(IV), U(VI), Al(III), V(IV), V(V), and Fe(III) are not adsorbed.

Table 5. Anion-exchange distribution coefficients of tantalum in HF-H_3BO_3-HNO_3 media

HF(M)	H_3BO_3(M)	HNO_3(M)	K_d of Ta(V)
2	1	1	25
3	1	1	19
4	2	1	7
6	2	1	3

coefficients of anions for the anion-exchange resin, referred to the Cl^- ion, K_{Cl}^A, were calculated from the data presented in a previous paper[1] according to the method of Wheaton *et al.*:[6] $K_{Cl}^{BF_4}$ 30, $K_{Cl}^{ClO_4}$ 30, $K_{Cl}^{NO_3}$ 3.3, $K_{Cl}^{(SO_4)_{1/2}}$ 1.4, and K_{Cl}^F 0.04. As ClO_4^- and BF_4^- are strongly adsorbed on the resin, in a solution containing more than 0.1 M of $HClO_4$ or 0.5 M HF-0.5 M H_3BO_3, which contains 0.1 M of BF_4^- and 0.05 M of BF_3OH^-, the K_d values of metal ions are extremely small and none of the metal ions presented in Tables 1-4 are adsorbed on the resin except Ta(V). With more concentrated HF-H_3BO_3 media, as is indicated in Table 5, Ta(V) comes not to be absorbed on the resin.

In the media where the concentration of $C_{BF_4^-}$ or $C_{BF_3OH^-}$ is less than 0.02 M, the effect of coexisting anions becomes significant. In 0.1 M HF-0.5 M H_3BO_3 media, which contain 0.01 M of BF_4^- and 0.02 M of BF_3OH^-, only Ta(V) is retained on the resin in the presence of 0.1 M $HClO_4$, but in the presence of 0.1 M HNO_3 or 0.1 M HCl instead of $HClO_4$, Nb(V) and W(VI) or Nb(V), W(VI), and Mo(VI) are retained in addition to Ta(V). In the media where $C_{BF_4^-}$ or $C_{BF_3OH^-}$ is further reduced, the adsorbed elements increase in

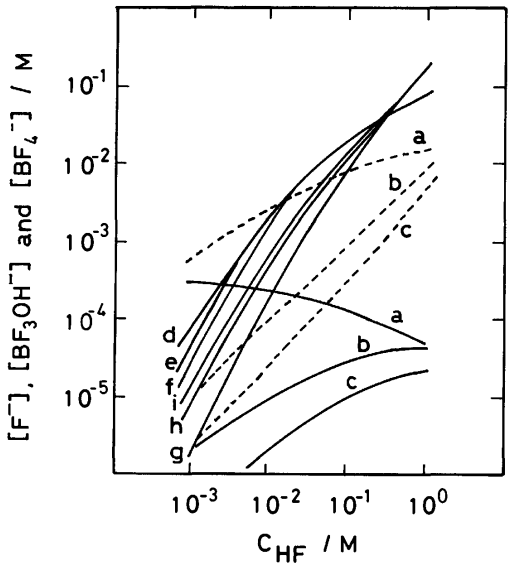

Fig. 1. Concentration of F^-, BF_3OH^-, and BF_4^- in HF and HF-H_3BO_3 media containing HNO_3.
——: HF-0.5 M H_3BO_3, ----: HF. a, b, and c [F^-]; d, e, and f: [BF_3OH^-]; g, h, and i: [BF_4^-] (a, d, and g: without HNO_3; b, e, and h: with 0.1 M HNO_3; c, f, and i: with 1 M HNO_3).

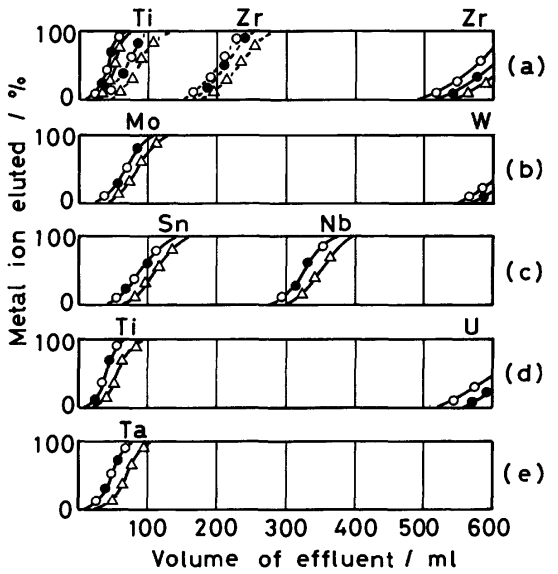

Fig. 2. Column elution behavior of metal ions in HF-H_3BO_3 containing various anions.
Column: Diaion SA#100, 4g, 8mmϕ×180mm. Flow rate: 1.0ml min^{-1}. (a) ——: 0.01 M HF-0.5 M H_3BO_3-0.1 M HCl, ----: 0.1 M HF-0.5 M H_3BO_3-0.05 M H_2SO_4, (b) 0.1 M HF-0.5 M H_3BO_3-1 M HCl, (c) 0.1 M HF-0.5 M H_3BO_3-0.1 M HCl, (d) 0.1 M HF-0.5 M H_3BO_3-0.05 M H_2SO_4, (e) 4 M HF-2 M H_3BO_3-1 M HNO_3. Amount of metal ion; ○: 1 mg, ●: 100 mg, △: 250 mg.

number; *i.e.*, Zr(IV) and Hf(IV), besides Ta(V), Nb(V), W(VI), and Mo(VI), become adsorbed on the resin in 0.01 M HF-0.1 M H_3BO_3-0.1 M HCl media.

Though the discussion above has been carried out from the viewpoint of the adsorbability of a coexisting anion, there are some exceptions which cannot be explained from this point of view. It is thought that the exceptions are due to the complex formation of metal ions with anions other than the fluoride ion and to the adsorption of non-fluorinated metal-oxoacid anions, such as MoO_4^{2-} or WO_4^{2-}, on the resin.

Mutual Separation of Hard Acid-Metals by the Column Method. Referring to the K_d values in Tables 1—4, the mutual separation of hard acid-metals that had been considered to be difficult was attempted by the column method according to the procedure described in the Experimental section. It is clear from Fig. 2 that the several mutual separations described below are possible. The elution curves of metal ions in Fig. 2 are shown in integrated forms.

(a) Ti-Zr: Only one pice of literature concerning the ion-exchange separation of Ti(IV) and Zr(IV) in a solution containing hydrofluoric acid was reported by one (T.A.) of the present authors, who used an anion-exchange resin in HF-H_3BO_3-HNO_3 media.[1] As is shown in Fig. 2 (a), an effective separation can also be attained by using HCl or H_2SO_4 instead of HNO_3.

(b) Mo-W: The anion-exchange separation of Mo(VI) and W(VI) in 3 M HF-10 M HCl[7] has been the most recommended method for these ions. The difficulty with this method is that acids of a high concentration are inevitable. In HF-H_3BO_3 media, it is possible to separate Mo(VI) from W(VI) in acid mixtures of a lower concentration, *i.e.*, 0.1 M HF-0.5 M H_3BO_3-1 M HCl, as is shown in Fig. 2 (b).

(c) Sn-Nb; Adopting the HF-H_3BO_3-HCl media, an effective separation can be attained in a less concentrated acid mixture, as is shown in Fig. 2 (c). The difference *in* K_d between Sn(IV) and Nb(V) is larger than that in the HF-HCl[8] or HF-HNO_3[9] media.

(d) Ti-U: In the general method for the anion-exchange separation of Ti(IV) and U(VI), Ti(IV) was adsorbed on the resin, whereas U(VI) was eluted. On the contrary, in the HF-H_3BO_3-H_2SO_4 media, U(VI) was adsorbed and Ti(IV) was eluted, as is shown in Fig. 2. Therefore, the media are useful for the separation of Ti(IV) in samples of a uranium matrix.

The media usually used for the elution of Ta(V) from the anion-exchange resin are composed of highly concentrated salts or acids, *e.g.*, 1 M NH_4F-4 M NH_4Cl[7] or 5 M HF-12 M HNO_3.[10] Using 4M HF-2M H_3BO_3-1 M HNO_3, as is shown in Fig. 2 (e), Ta(V) can be eluted from the column.

It is obvious from the above examples that the HF-H_3BO_3 media are useful for the effective mutual separation of hard acid-metal ions. In the practical mutual separation of two components, in order to reduce the volume of the effluents it is recommended that, after one metal ion is completely eluted from the column, the other ion should be then eluted by the use of a different composition of the eluent in which the other ion has a low K_d value. Zirconium(IV), W(VI), and U(VI) are quantitatively eluted by 100 ml of 0.1 M HF-0.5 M H_3BO_3-1 M HCl, 150 ml of 0.5 M HF-0.5 M H_3BO_3-1 M HCl, and 120 ml of 0.1 M HF-0.5 M H_3BO_3-0.5 M H_2SO_4 respectively.

In addition, the fluoroboric acids in the effluent can easily be evaporated prior to the subsequent determination. The elution behavior of metal ions are not affected by the amount of metal ions, as is demonstrated in Fig. 2, because the HF-H_3BO_3 media have a buffer action relating to C_{F^-}, as has already been mentioned.[1]

Because hydrofluoric acid is indispensable in the dissolution of most hard acid-metals, it should be stressed that the HF-H_3BO_3 media will be useful for the consecutive separation of metals in a matrix of hard acid-metals.

References

1) T. Adachi, *Bull. Chem. Soc. Jpn.*, **55**, 1824 (1982).
2) T. Adachi, *Bull. Chem. Soc. Jpn.*, **55**, 802 (1982).
3) A. Ringbom, "Complexation in Analytical Chemistry" Wiley-Intersience, New York (1963), p. 229.
4) L. G. Sillen and A. E. Martell, "Stability Constants of Metal-Ion Complexes," Special Publications Nos. 17 and 25, The Chemical Society, London (1964 and 1971).
5) R. E. Mesmer, K. M. Palen, and C. F. Baes, Jr., *Inorg. Chem.*, **12**, 89 (1973).
6) R. M. Wheaton and W. C. Bauman, *Ind. Eng. Chem.*, **43**, 1088 (1951).
7) E. J. Dixon and J. B. Headridge, *Analyst (London)*, **89**, 185 (1964).
8) J. P. Faris, U. S. DOE Report, ANL-78-78 (1978).
9) L. Danielsson, *Acta Chem. Scand.*, **19**, 1859 (1965).
10) A. I. Williams, *Analyst (London)*, **92**, 43 (1967).

 © 1984 The Chemical Society of Japan Bull. Chem. Soc. Jpn., 57, 1491—1493 (1984)

Alkali-free Magnesium Phosphate Glasses as Nitrate-ion-selective Materials for Solid-state Electrochemical Sensors

Tsuyoshi NOMURA* and Genkichi NAKAGAWA

Laboratory of Analytical Chemistry, Nagoya Institute of Technology, Gokiso-cho, Showa-ku, Nagoya 466

(Received November 2, 1983)

Ion-selective electrochemical sensors which respond to nitrate-ion activities have been developed. The sensor material consists of alkali-free magnesium phosphate glasses containing CuO, Al_2O_3, and SiO_2. The response characteristics have been observed strongly on the glass composition. Studies of the selectivity coefficient and the electrode function of nitrate-ion activities have shown that the most suitable glass composition is $10CuO:55P_2O_5:15MgO:10Al_2O_3:10SiO_2$. The potential response is linear over the nitrate-ion activities of (10^{-1}—10^{-5}) mol/dm^3, and it has a sub-Nernstian response of about 54 mV/decade change at 20 °C. The order of the selectivity is $NO_3^->ClO_4^->I^->NO_2^->Cl^->SO_3^{2-}\gg SO_4^{2-}$. Therefore, its use to determine the nitrate-ion activities in a solution containing perchlorate ions is suggested. The physical and chemical properties, such as the glass transition temperature, the softening temperature, the thermal expansion, the membrane resistance, and the chemical durability, were measured and compared with those of other glasses.

Solid electrodes for the determination and monitoring of nitrate ion have not been commercially available. Liquid ion-exchanger electrodes have been made, and used for the determination of nitrate-ion activities in various sample solutions.[1,2] However, common anions such as iodide and perchlorate interfere seriously, and the loss of the liquid ion-exchanger in the liquid electrodes can be expected. Some investigations of selective nitrate-ion solid-type sensors have been made. One of the solid-type sensors was made of PVC film, which included the optimum proportion of the nitrate-selective liquid-ion-exchanger in the PVC matrix,[3] and another was made by the film of the nitron-nitrate precipitate in the araldite matrix.[4]

There have been relatively few studies of the ion-selective electrode behavior of phosphate glasses.[5,6] Phosphate glasses containing iron oxide[5] have been investigated as materials of the cation selective membrane electrode for alkaline-earth cations. On the other hand, it has been suggested that the replacement of aluminium in the sodium alumino silicate glass by phosphorus can be expected to lead to anion-exchanger properties.[7]

We have already investigated some phosphate glass membranes as materials of ammonia-selective electrodes[8] and that of the hydrogen-ion-selective electrode in the hydrofluoric acid solution.[9] However, it is an important fact that some anion-responsive glass electrodes have apparently not been reported on to date.

In this investigation, the physical and chemical properties of alkali-free magnesium phosphate glasses containing various metal oxides, such as CuO, Ag_2O, Al_2O_3, and SiO_2, were measured, and a systematic check of the response behavior of those glass electrode was made. After several modifications of the glass compositions, some promising results were obtained for the solid-state nitrate-ion-selective sensors.

Experimental

Preparation of the Glass Membrane. The materials used were the following reagents. Orthophosphoric acid (85%) and tetramagnesium tris(carbonate)dihydroxide were used in all the systems. Dicopper(II) carbonate dihydroxide, silver carbonate, aluminium hydroxide, and silicon dioxide were used in the composition of each glass. The sample were prepared by melting it in a platinum crucible at 1200 °C for an hour; after melting, the glasses were annealed at a temperature 20 °C higher than the respective glass transition temperature for 20 min and then cooled.

The preparation of the phosphate glasses and the glass membranes has been described previously.[8]

The chemical compositions of some of the tested glasses are listed in Table 1.

Measurements of Physical and Chemical Properties. The glass-transition temperature (T_g, °C), the softening temperature (T_s, °C), and the thermal expansion (α, cm °C^{-1}) were measured with a Shimadzu TM-30-type dilatometer. The chemical durability of glass against water and the membrane resistance were measured by the method previously described in the literature.[9] The physical and chemical properties of some of the magnesium phosphate glasses containing CuO, Ag_2O, Al_2O_3, and SiO_2 are summarized in Table 2.

Reagents and Solutions. All the reagents were of an analytical grade unless otherwise specified. Sodium, potassium, and ammonium nitrate were used as nitrate standard solutions. Chloride, iodide, perchlorate, sulfate, nitrite, and sulfite salts of sodium were used as the sources of interfering anions. The water was twice-distilled. The activities of various anions were calculated from the concentration by means of the activity coefficients tabulated by Kielland.[10]

Measurements of the Membrane Potentials. The sensor element is sealed in the end of a cylindrical plastic tube, with one surface of the disk exposed to the test solution and the other to the internal-reference solution (0.1 mol/dm^3 $NaNO_3$). A double-junction-type saturated calomel reference electrode makes contact with the internal-reference solution (0.1 mol/dm^3 $NaNO_3$). The responses of each sensor are investigated by measuring the potential *vs.* SCE with a DKK IOC-10 ion-meter connected with a Sekonic model SS-250F recorder.

The electrode potential is strongly affected by prior conditioning in regard to its electrical resistance and the response

Table 1. Composition of the glasses

Glass No.	CuO	Ag_2O	P_2O_5	MgO	Al_2O_3	SiO_2
1	10	—	55	35	—	—
2	10	—	55	25	10	—
3	—	—	55	25	10	10
4	5	—	55	20	10	10
5	10	—	55	15	10	10
6	20	—	55	5	10	10
7	5	—	47	28	10	10
8	—	5	55	20	10	10

time. Thus, each sensor disc was polished on both sides with silicon carbide paper and then preconditioned in twice-distilled water for one day before use.

The membrane potentials for nitrate-ion and other anions are measured in a solution containing a 10^{-4} mol/dm^3 sulfuric acid solution at 20°C. The steady state of the membrane electrode is defined as a potential stable to a drift of less than 1 mV in 2 min in the stirred solution (600 min^{-1}). With stirring, the electrode potentials are read the same within 2 mV. As a result of determining the effect of the potential response on the membrane thickness, it can be said that the response rate and the reproducibility of the electrode potential are absolutely not affected within a thickness of 1 mm.

Results and Discussion

Physical and Chemical Properties of Glasses. As shown in Table 2, with the addition of the Al_2O_3 and SiO_2, the values of T_g and T_s of the tested glasses are increased. On the contrary, the values of the thermal expansion decrease with an increase in their metal oxides in the glass compositions. On the other hand, it was observed that the chemical durability of the glass with a lower P_2O_5 content (No. 7 glass) was rather worse than that of the other ultra-phosphate glasses. This fact suggest that the ultraphosphate glass corresponding to the network-forming structure seems to stabilize structurally more than the metaphosphate glass corresponding to the straight-chain structure.[11] Moreover, the addition of silicon dioxide may also be conducive to the advancement of the chemical durability because of its tendency forms network-forming.

Potential Response of the Magnesium Phosphate Glass Membrane. The potential response curves of some of the alkali-free magnesium phosphate glass membranes for the nitrate ion activities are shown in Fig. 1. The response characteristics of a magnesium phosphate glass membrane depend strongly upon its glass composition. In particular, glasses not containing Ag_2O or CuO show a small electrode function of the nitrate-ion activities, and the electrode potentials show an unstable behavior.

As shown in Fig. 1, when we compare the electrode function of the metaphosphate glass membrane (No. 7 glass) and the other ultraphosphate glass membrane containing copper(II) oxide, the latter is better than the former. Threfore, the suitable quantity of the P_2O_5 contents in the glass membrane, determined by means of an analysis of the nitrate-ion activities, was fixed at 55 mol%, with varied quantities of the other metal oxides.

Among the glasses examined, the $10CuO:55P_2O_5:15MgO:10Al_2O_3:10SiO_2$ glass membrane is the best in terms of stability, reproducibility, rapidity of response, and magnitude of the electrode function with nitrate-ion activities.

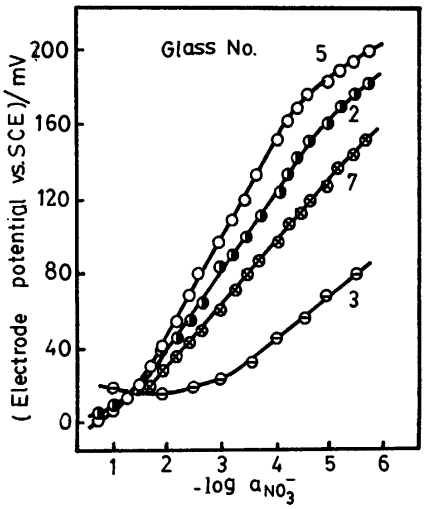

Fig. 1. Electrode response of some glasses as a function of the nitrate ion activities.
Glass compositions used in this figure were described in Table 1.

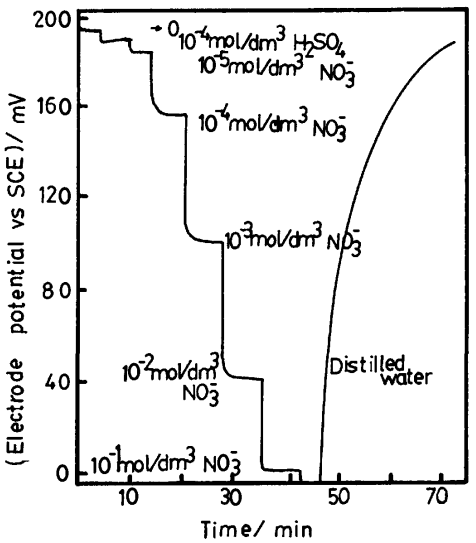

Fig. 2. Response characteristics of the No. 5 glass electrode with the nitrate ion concentration.

Table 2. Physical and Chemical Properties of the Glasses

Glass No.	Transition temperature T_g/°C	Softening temperature T_s/°C	Thermal expansion $\alpha\times10^7$/cm°C^{-1}	Chemical durability mg mm^{-2}	Memberane resistance MΩ cm^{-1}
1	508	552	125.7	2.04×10^{-2}	4.53
2	546	621	100.6	2.43×10^{-3}	6.31
3	637	717	91.2	8.87×10^{-3}	3.71
4	—	—	—	1.53×10^{-2}	6.68
5	589	678	99.7	8.51×10^{-3}	5.27
6	563	632	102.4	7.32×10^{-3}	3.79
7	568	628	91.7	4.73×10^{-2}	7.77
8	574	646	120.5	3.82×10^{-3}	8.93

The potential response of nitrate-ion activities for this glass membrane was linear over the range of (10^{-1}—$10^{-4.5}$) mol/dm^3, and the slope of the potential-concentration relationship shows a sub-Nernstian response of about 54 mV/decade change at 20 °C. However, when the range of the nitrate-ion activities is below $10^{-4.5}$ mol/dm^3 or above 10^{-1} mol/dm^3, the slope becomes small.

Figure 2 shows the response characteristics of the No. 5 glass electrode operated in the following manner. The electrode was first placed directly in twice-distilled water, to which a solution of 10^{-4} mol/dm^3 sulfuric acid was added, then the electrode was exposed to increasing concentrations of nitrate ions in the order of 10^{-5}, 10^{-4}, 10^{-3}, 10^{-2}, and 10^{-1} mol/dm^3 with the addition of the value-calculated sodium-nitrate solution. After recording the potential of the nitrate-ion activities to 10^{-1} mol/dm^3, the electrode was carefully washed with distilled water and then immersed in the twice-distilled water. The response rate with an increase in the concentration of nitrate-ion activities was observed to be somewhat faster than that with a decrease in the concentration of nitrate ions.

In solutions containing 10^{-1} and 10^{-4} mol/dm^3 of nitrate ions, equilibrium was reached within about 1 and 3 min respectively. However, after the electrode has been exposed to a nitrate concentration of 10^{-1} mol/dm^3, and then to concentrations decreasing to 10^{-5} mol/dm^3, the dynamic response time needed for reaching the equilibrium potential was more than 5 min. It is clear that 95% of the response times are about one minute expect in the case of nitrate-ion concentrations of less than 10^{-4} mol/dm^3.

Interferences of Diverse Anions and the Selectivity Coefficient of Nitrate Ion for the Other Anions. There were essentially no effects of the cations on the determination of nitrate ions when the magnesium phosphate glass electrode was used.

The effect of common anions on the determination of nitrate-ion activities was determined by means of the potential-concentration curve, and the order of magnitude of the selectivity, as regards all of the glass electrodes examined, was defined as: $NO_3^- > ClO_4^- > I^- > NO_2^- > Cl^- > SO_3^{2-} \gg SO_4^{2-}$. Therefore, sodium sulfate or sulfuric acid is used to adjust the ionic strength. The electrode function of the nitrate-ion activities and the selectivity coefficients of some of the coexisting anions for the magnesium phosphate glass electrodes are listed in Table 3. The selectivity coefficients were deternined by the mixed solution method.[12] The values of the selectivity coefficients are calculated by means of the electrode potential, with fixed quantities of the interfering ion (0.1 mol/dm^3) and a varied activity of the nitrate ions.

The selectivity coefficients of ClO_4^- and NO_2^- with the No. 5 glass electrode are smaller than that of the liquid ion-exchanger nitrate-ion selective electrode,

Table 3. Electrode function of nitrate-ion activities and selectivity coefficients of various anions

Glass No.	Electrode function mV/pa$_{NO_3^-}$	Selectivity coefficient×10^2				
		Cl^-	ClO_4^-	SO_4^{2-}	NO_2^-	SO_3^{2-}
1	31.1	—	—	—	—	—
2	42.0	3.98	15.8	0.63	1.26	2.09
3	21.3	—	—	—	—	—
4	41.6	4.57	11.7	0.59	11.2	8.73
5	54.2	3.36	7.52	0.67	3.98	1.84
6	38.5	6.31	3.16	1.58	9.32	5.25
7	35.3	16.5	21.9	5.25	10.7	7.41
8	42.6	12.6	63.1	5.01	25.1	14.5

and the electrode potentials of mixed nitrate-perchlorate solutions indicate that the effect of the perchlorate ion on a concentration of about 0.01 mol/dm^3 can be neglected for the determination of nitrate ions at concentrations above 7.5×10^{-4} mol/dm^3.

As is obvious from the results shown in Table 3, Nos. 1, 3, and 7 glasses can not be used as ion-selective electrodes because of their poor chemical durability and small electrode function. Moreover, No. 8 glass is also observed to have a poor selectivity for the other anions.

The selectivity coefficient and the electrode function show that the No. 5 glass is better for use as an ion-selective glass sensor for nitrate-ion activities than the other glasses.

We wish to thank Professor Yoshihiro Abe for his valuable advice.

References

1) P. J. Milham, A. S. Awad, R. E. Paull, and J. H. Bull, *Analyst*, **95**, 751 (1970).
2) C. J. Coetzee and H. Freiser, *Anal. Chem.*, **40**, 2071 (1968).
3) J. E. W. Davies, G. J. Moody, and J. D. R. Thomas, *Analyst*, **97**, 87 (1972).
4) U. S. Lal, M. C. Chattopadhyaya, and A. K. Dey, *Mikrochim. Acta (Wien)*, **1980**, 417.
5) A. H. Truesdell and A. M. Pommer, *Science*, **142**, 1292 (1963).
6) V. S. Bobrov, I. P. Kalmkova, and M. M. Shul'ts, *Zh. Prikl. Khim.*, **40**, 1628 (1967).
7) G. Eisenman, *Biophs. J., Part 2 Suppl.*, **1962**, 259.
8) T. Nomura and G. Nakagawa, *Bull. Chem. Soc. Jpn.*, **56**, 943 (1983).
9) T. Nomura and G. Nakagawa, *Bull. Chem. Soc. Jpn.*, **56**, 3632 (1983).
10) J. Kielland, *J. Am. Chem. Soc.*, **59**, 1675 (1937).
11) Y. Abe, *Zairyo Kagaku*, **11**, 311 (1974).
12) G. E. Baiulescu and V. V. Cosofret, "Applications of Ion-Selective Membrane Electrodes in Organic Analysis," John Wiley & Sons, New York (1977), p. 17.

Characterization of Cobalt(III) Complex with 2-Aminoethaneseleninate. Spontaneous Resolution and Crystal Structure of $(-)^{CD}_{500}$-(2-Aminoethaneseleninato)bis(ethylenediamine)cobalt(III) Nitrate

Ken-ichi Okamoto,* Takumi Konno, Masayo Nomoto, Hisahiko Einaga,† and Jinsai Hidaka

Department of Chemistry, University of Tsukuba, Sakura, Ibaraki 305

†*Institute of Materials Science, University of Tsukuba, Sakura, Ibaraki 305*

(Received December 3, 1983)

The crystal structure and the absolute configuration of the spontaneously resolved title complex cation, $(-)^{CD}_{500}$-$[Co(aesei)(en)_2]^{2+}$, has been determined by X-ray diffraction. The red crystalline needle was monoclinic, space group $P2_1$, $a=9.572(4)$, $b=10.410(3)$, $c=8.838(5)$ Å, $\beta=115.35(3)°$, $Z=2$, and the final R value was 0.035 for 2358 independent reflections with $|F_o|>3\sigma(|F_o|)$. The crystal used showed a negative CD value at 500 nm and had Δ configuration. The 2-aminoethaneseleninate is bound to the cobalt atom by the nitrogen and oxygen atoms, and the asymmetric selenium atom takes an S configuration. The value of the protonation constant (pKa) was determined to be 1.91 ± 0.05, on the basis of the major absorption spectral change at 304 nm of the title complex by spectrophotometric titration ($\mu=1.0$ mol dm^{-3} ($NaClO_4$) and 25 °C). The electronic absorption and CD spectral behavior were compared with those of the related sulfinato complexes, in which the *S*-bonded sulfinato complex, $(+)^{CD}_{500}$-$[Co(S(O)_2CH_2CH_2NH_2)(en)_2]^{2+}$, was resolved in this work.

The structure and bonding for the cobalt(III) complexes with selenium- or sulfur-containing bidentate ligands have been studied in some detail.[1-12] These complexes have only Co-Se or Co-S bonding, except for the (2-aminoethanesulfinato-N,O)bis(ethylenediamine)cobalt(III), $[Co(aesi\text{-}N,O)(en)_2]^{2+}$, obtained by photochemical preparation.[6,7] The (2-aminoethaneseleninato)bis(ethylenediamine)-cobalt(III), $[Co(aesei)(en)_2]^{2+}$, was obtained by treatment of the (2-aminoethaneselenolato)bis(ethylenediamine)cobalt(III), $[Co(aes)(en)_2]^{2+}$, with excess hydrogen peroxide. The aesei acts as a bidentate ligand and takes either of the two coordination modes, aesei-N,Se or aesei-N,O. The *S*-bonded sulfinato complex, which is obtained by a similar procedure to the aesei complex, takes up the nitrogen and sulfur coordinations, and the primary coordination sphere of the cobalt atom remains intact throughout the oxidation process.[2,10] Therefore, there has been no real evidence for the coordination mode of the seleninato complex except for the anticipation on the basis of the electronic absorption spectra of the related sulfinato complexes.[2,6,7]

The present paper deals with the preparation and spontaneous resolution of $[Co(aesei)(en)_2](NO_3)_2$. The crystal structure and absolute configuration of the $(-)^{CD}_{500}$ aesei isomer are established by X-ray diffraction studies and an investigation based on the CD spectra. The electronic absorption and CD spectra in solution of the aesei complex are discussed in comparison with the related sulfinato complexes, in which the $[Co(aesi\text{-}N,S)(en)_2]^{2+}$ isomer was resolved in this work. A preliminary report has been presented.[12]

Experimental

1) Preparation and Resolution of the Complexes. a) Spontaneous Resolution of $[Co(aesei)(en)_2](NO_3)_2$: An excess amount of 5% aqueous H_2O_2 (5 cm^3) was added to a solution containing 0.4 g of $[Co(aes)(en)_2](NO_3)_2$[9] in 7 cm^3 of water, followed by addition of 2 cm^3 of 15% HNO_3. The solution was stirred for 20 min and stood in a refrigerator for a day. The solution was adjusted to pH 7 by the addition of an queous solution of NaOH and concentrated with a rotary evaporator. The resultant seleninato complex was collected by filtration. The spontaneous resolution of the nitrate salt was observed for the needle crystals as follows; the racemic nitrate was dissolved in a small amount of water at room temperature and when the solution was kept in a refrigerator overnight, the spontaneously resolved red complex was obtained as fairly large needle crystals. A piece of one of these crystals was used for the X-ray diffraction study.

b) $(+)^{CD}_{500}$-$[Co(aesei)(en)_2](ClO_4)_2$: The $(+)^{CD}_{500}$ aesei isomer was obtained by the same procedure as that used in a), using the $(+)^{CD}_{500}$-$[Co(aes)(en)_2](ClO_4)_2$ isomer[11] instead of the racemic nitrate. This isomer shows the identical electronic absorption and CD spectra as the spontaneously resolved $(+)^{CD}_{500}$ isomer. Found: C, 13.21; H, 4.27; N, 12.94%. Calcd for $[Co(aesei)(en)_2](ClO_4)_2\cdot0.5H_2O=CoC_6H_{22}N_5O_{10}SeCl_2\cdot0.5H_2O$: C, 13.29; H, 4.28; N, 12.92%.

c) $(+)^{CD}_{500}$-$[Co(asei\text{-}N,S)(en)_2](ClO_4)_2$: This $(+)^{CD}_{500}$ aesi isomer was obtained by the same procedure as that used in b), using the $(+)^{CD}_{500}$-$[Co(SCH_2CH_2NH_2)(en)_2](ClO_4)_2$ isomer[9] instead of the $(+)^{CD}_{500}$-$[Co(aes)(en)_2](ClO_4)_2$ one. The analytical result was obtained from the racemic nitrate salt. Found: C, 16.71; H, 5.62; N, 22.91%. Calcd for $[Co(aesi\text{-}N,S)(en)_2](NO_3)_2\cdot H_2O=CoC_6H_{22}N_7O_8S\cdot H_2O$: C, 16.79; H, 5.63; N, 22.84%.

2) General Data. The electronic absorption spectra were recorded with a JASCO UVIDEC-1 spectrophotometer, and the CD spectra, with a JASCO J-20 spectropolarimeter. All measurements were carried out in aqueous solution at room temperature. The calculations were carried out on a FACOM M-200 computer at the University of Tsukuba. The protonation constant was determined by measuring the adsorbance at 304 nm in aqueous media at 25 °C and $\mu=1.0$ mol dm^{-3} ($NaClO_4$). The hydrogen ion concentration was measured with a HORIBA pH meter (F7-SS).

3) X-Ray Characterization. The unit cell parameters and intensity data were measured on a Rigaku-denki automated four-circle diffractometer (AFC-5) with a graphitemonochromatized Mo $K\alpha$ radiation ($\lambda=0.710690$ Å). A spontaneously resolved needle crystal with approximate dimensions of $0.03\times0.07\times0.7$ mm^3 was used for the intensity measurements. The unit cell parameters were determined by least-squares refinement based on 20 reflections. The systematic absence led to the space group $P2_1$. Crystal data: $CoC_6H_{22}N_7O_8Se$, $M.W.=458.2$, monoclinic, space group $P2_1$, $a=9.572(4)$, $b=10.410(3)$, $c=8.838(5)$ Å, $\beta=115.35(3)°$, $V=795.9(6)$ Å^3, $D_m=1.90$ g cm^{-3} (by the flotation), $D_x=1.91$ g cm^{-3}, and $Z=2$.

The intensity data were collected by the ω-2θ scan technique with a scan rate of 3 ° min^{-1}. During the course

of the data collection, three reflections were monitored every 40 reflections. The intensity data were converted to the Fo data in the usual manner. Absorption corrections were not applied. A total of 2603 reflections up to $2\theta=60°$ was collected, of which 2358 independent reflections with $|F_o|>3\sigma(|F_o|)$ were considered as 'observed' and used for the structure analysis.

Determination of the Crystal Structure

1) Solution and Refinement of Structure. The positions of the cobalt and selenium atoms were obtained from the three dimensional Patterson function. The difference-Fourier maps based on the cobalt and selenium positions revealed all non-hydrogen atoms. The structure was refined by a full-matrix least-squares refinement of the positional and anisotropic thermal parameters of all the non-hydrogen atoms (program RFINE by L. W. Finger, as modified by H. Horiuchi, was used). The neutral atomic scattering factors for all the non-hydrogen atoms were taken from the literature.[13] The final residual values were $R=0.036$ and $R_w=0.049$, respectively.

2) Determination of the Absolute Configuration. The absolute configuration was determined by the anomalous scattering technique. The anomalous dispersion corrections, $\Delta f'$ and $\Delta f''$, for all the non-hydrogen atoms were taken from the literature.[13] When the refinements were carried out by the use of a set of the atomic parameters containing the Δ configuration of the complex cation, the residual values converged to $R=0.035$ and $R_w=0.046$, respectively. On the contrary, the refinements in the enantiomeric atomic parameters (the Λ configuration) resulted in the residual values of $R=0.041$ and $R_w=0.055$, respectively. These facts indicate that the former is probably the correct choice, namely, the complex cation has the Δ configuration. A similar relationship between the residual values and the absolute configuration was observed for the determination of the crystal structure of cobalt(III) complexes with the *S*-(2-aminoethyl)-L-homocysteinate.[14,15] The crystal, which was used for this X-ray intensity measurement, showed the enantiomeric CD curve for that of the $(+)^{CD}_{500}$-[Co(aesei)$(en)_2]^{2+}$ isomer derived from the $(+)^{CD}_{500}$-[Co(aes)$(en)_2]^{2+}$ one. This is in line with the result that the $(+)^{CD}_{500}$ aesei isomer has been assigned to the Δ configuration from the comparison with the CD spectrum of the Δ-[Co(mea)$(en)_2]^{3+}$ isomer mea; 2-(methylthio)ethylamine).[9,11]

The final atomic parameters with their estimated standard deviations are given in Table 1. A list of structure factors and anisotropic thermal parameters of the non-hydrogen atoms is kept at the Chemical Society of Japan as Document No. 8416.

TABLE 1. POSITIONAL AND THERMAL PARAMETERS

Atom	x	y	z	B_{eq}/Å$^{2a)}$
Co	0.25167(6)	0.0	0.11276(7)	1.81
Se	-0.06427(5)	0.04554(8)	0.15590(6)	2.39
O1	0.0520(4)	-0.0458(4)	0.0985(4)	2.29
O2	-0.0878(5)	0.1826(4)	0.0473(5)	3.04
N1	0.1851(5)	0.1665(4)	-0.0006(5)	2.54
N2	0.1715(5)	-0.0733(4)	-0.1139(5)	2.47
N3	0.3147(5)	-0.1705(5)	0.2097(5)	2.60
N4	0.3256(5)	0.0842(5)	0.3356(5)	2.92
N5	0.4619(5)	0.0146(5)	0.1258(6)	3.03
C1	0.0851(7)	0.1023(7)	0.3766(6)	2.99
C2	0.2217(7)	0.1724(6)	0.3701(7)	3.15
C3	0.1390(8)	0.1502(6)	-0.1835(7)	3.47
C4	0.0607(7)	0.0220(6)	-0.2290(6)	3.23
C5	0.4603(7)	-0.2055(7)	0.1979(9)	3.63
C6	0.5582(7)	-0.0888(8)	0.2409(9)	3.99
N11	0.4785(7)	-0.5686(6)	0.2448(8)	3.84
N21	0.7421(6)	-0.7714(6)	0.4177(7)	3.42
O11	0.5894(6)	-0.5020(6)	0.2682(7)	4.72
O12	0.4169(8)	-0.6259(9)	0.1023(8)	7.22
O13	0.4301(13)	-0.5822(13)	0.3464(12)	11.39
O21	0.7180(6)	-0.8041(7)	0.2720(7)	5.14
O22	0.6499(9)	-0.8119(11)	0.4731(8)	9.27
O23	0.8529(6)	-0.7038(6)	0.5012(7)	5.33

a) B_{eq} is the equivalent isotropic temperature factor defined by Hamilton.[24]

Results and Discussion

Description of the Structure. Perspective drawing of the complex cation obtained is given in Fig. 1 and its packing mode is illustrated in Fig. 2. The bond lengths and angles with their estimated standard deviations in the complex are summerized in Table 2. The coordination geometry around the cobalt atom is approximately octahedral. The 2-aminoethaneseleninate coordinates to cobalt atom with the nitrogen and oxygen atoms instead of the nitrogen and selenium ones in the starting complex, $[Co(SeCH_2CH_2NH_2)(en)_2]^{2+}$ [3] in contrast to the case of the related sulfinato complex whose coordinated atoms remain intact during the oxidation process.[2] This suggests that the treatment of the selenolato complex with excess hydrogen peroxide is accompanied by linkage isomerization and the *O*-bonded seleninato complex is obtained. The asymmetric selenium atom in the Δ-$(-)^{CD}_{500}$-[Co(aesei-N,O)$(en)_2]^{2+}$ takes the *S* configuration as shown in Fig. 1.

The bond lengths and angles are similar to those for the [Co$(en)_2$(L)] type complexes, where L denotes the selenium- or sulfur-containing bidentate ligands.[1-5,8,14,15] The selenium-oxygen bond lengths,

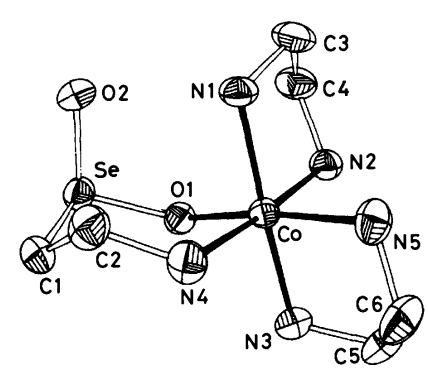

Fig. 1. A perspective drawing of Δ-$(-)^{CD}_{500}$-[Co(aesei-N,O)$(en)_2]^{2+}$ with the numbering scheme of atoms.

Se-O1 and Se-O2, are 1.698(4) and 1.680(4) Å, respectively. They are longer than those of the sulfur-oxygen ones (1.456 and 1.476 Å) in the [Co(aesi-N,S)-(en)$_2$](ClO$_4$)·(NO$_3$).[2] The bond angle of O1-Co-N4 for the six-membered chelate ring is 95.6(2)°, which is consistent with that of the cobalt(III) complexes containing amino carboxylate.[16,17] The bond angles around the selenium atom are about 100°, and this value seems tobe reasonable for the selenium atom whose tetragonal positions are occupied by the three bonding pairs and a lone pair.[18]

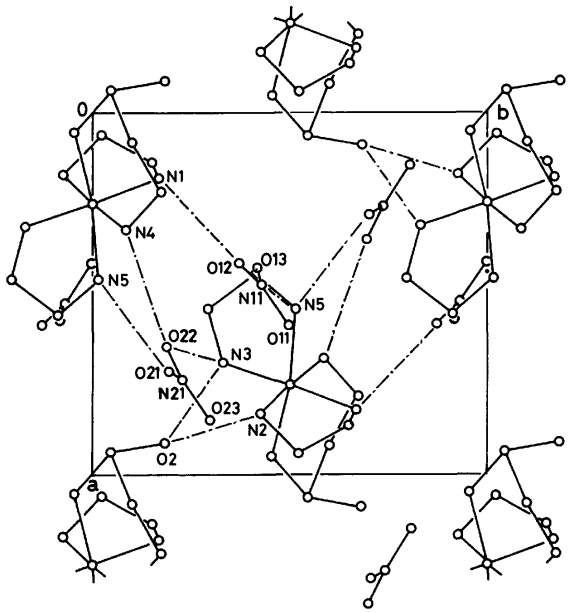

Fig. 2. A projection of the crystal packing viewed along the c axis. The hydrogen bonds are represented by the lines (-·-·-); O2-N2′, 2.802(7); O2-N3′, 2.827(6); O12-N1, 2.948(10); O12-N5′, 3.091(11); O21-N5, 2.920(8); O22-N4, 3.009(10); and O22-N3′, 3.054(10) Å.

Table 2. Intermolecular distances and bond angles (with e.s.d. 's)

Bond distance	l/Å	Bond distance	l/Å
Co-O1	1.922(4)	Co-N1	1.966(4)
Co-N2	1.967(5)	Co-N3	1.950(5)
Co-N4	1.988(5)	Co-N5	1.972(5)
Se-O1	1.698(4)	Se-O2	1.680(4)
N1-C3	1.491(8)	N2-C4	1.490(7)
N3-C5	1.487(9)	N4-C2	1.479(9)
N5-C6	1.497(8)	C1-Se	1.952(5)
C1-C2	1.520(10)	C3-C4	1.500(9)
C5-C6	1.481(10)	N11-O11	1.209(8)
N11-O12	1.286(9)	N11-O13	1.183(16)
N21-O21	1.255(9)	N21-O22	1.251(12)
N21-O23	1.223(7)		
Bond angle	**ϕ/°**	**Bond angle**	**ϕ/°**
O1-Co-N1	95.1(2)	O1-Co-N2	83.9(2)
O1-Co-N3	85.1(2)	O1-Co-N4	95.6(2)
O1-Co-N5	170.0(2)	N1-Co-N2	85.6(2)
N1-Co-N3	175.9(2)	N1-Co-N4	90.9(2)
N1-Co-N5	93.5(2)	N2-Co-N3	90.4(2)
N2-Co-N4	176.4(2)	N2-Co-N5	91.9(2)
N3-Co-N4	93.1(2)	N3-Co-N5	85.9(2)
N4-Co-N5	89.2(2)	O1-Se-O2	104.5(2)
O1-Se-C1	100.1(2)	O2-Se-C1	100.1(2)
Co-O1-Se	127.0(2)	Co-N1-C3	109.5(4)
Co-N2-C4	106.9(3)	Co-N3-C5	108.4(4)
Co-N4-C2	119.5(3)	Co-N5-C6	107.5(4)
Se-C1-C2	112.4(4)	N4-C2-C1	112.0(5)
N1-C3-C4	105.9(5)	N2-C4-C3	106.4(4)
N3-C5-C6	106.8(6)	N5-C6-C5	106.1(4)
O11-N11-O12	115.8(8)	O11-N11-O13	122.6(8)
O12-N11-O13	121.6(8)	O21-N21-O22	117.4(6)
O21-N21-O23	120.4(7)	O22-N21-O23	122.2(7)

In the present complex cation, the two gauche conformations, δ and λ, are possible for each of the two ethylenediamine chelate rings.[1-5,8,17] As shown in Fig. 1 and Table 3, both of the ethylenediamine chelate rings in the Δ-$(-)^{CD}_{500}$-[Co(aesei-N,O)(en)$_2$]$^{2+}$ isomer take up the reasonable λ gauche conformation. The six-membered chelate ring (O1-Se-C1-C2-N4) of the coordinated aesei ligand takes up a chair conformation (Table 3) and dihedral angle for the two-planes, O1-Co-N4 and Se-C1-C2, is 24.5°. This suggests that the six-membered chelate ring is distorted from the normal chair conformation, because the bond lengths and angles around the selenium atom are larger than those around the carbon atom (Table 2).

The crystal structure consists of the complex cations and nitrate anions, and the distance between the two nitrate anions is 3.140(8) Å. The O2-N2 and O2-N3 distances between adjacent complex cations are

Table 3. Displacements of atoms from the least-squares plane (d/Å)

Diamine chelate ring				
Plane 1; $0.9929X+0.1190Y-0.0007Z-1.9677=0$				
Co	0.0000	N1 0.0000	N2 0.0000	C3 −0.2292
C4	0.5024			
Plane 2; $0.0791X-0.3897Y-0.9175Z+0.6695=0$				
Co	0.0000	N3 0.0000	N5 0.0000	C5 0.3421
C6	−0.3855			
Six-membered chelate ring				
Plane 3; $0.1970X-0.8736Y+0.4451Z-0.7914=0$				
Co	0.0000	O1 0.0000	N4 0.0000	Se 0.8888
C1	0.5029	C2 0.9017		

The X, Y, and Z coordinates in Å are referred to the crystallographic axes.

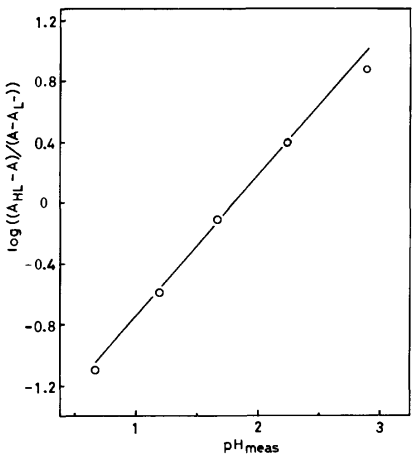

Fig. 3. Relation between pH_{meas} and $\log\{(A_{HL}-A)/(A-A_L)\}$. μ=1.0 mol dm^{-3} ($NaClO_4$), 25°C, and absorbance at 304 nm.

TABLE 4. ABSORPTION AND CD SPECTRAL DATA

Complex ion	Absorption maxima $\sigma/10^3\,cm^{-1}$ ($\log\varepsilon/mol^{-1}\,dm^3\,cm^{-1}$)	CD extrema $\sigma/10^3\,cm^{-1}$ ($\Delta\varepsilon/mol^{-1}\,dm^3\,cm^{-1}$)
$(+)^{CD}_{500}$-[Co(aesei-N, O)$(en)_2]^{2+}$	19.23(2.02)	17.15(+ 1.90)
	33.00(3.61)	27.17(− 0.52)
	47.17(4.19)	32.26(− 1.25)
		45.5 (−21.8)
$(+)^{CD}_{500}$-[Co(aesi-N, S)$(en)_2]^{2+}$	23.07(2.37)	21.05(+ 1.46)
	34.48(4.16)	24.21(− 0.48)
	47.06(4.18)	28.65(+ 0.39)
		34.97(− 4.18)
		47.2 (−22.0)
[Co(aesi-N, O)$(en)_2]^{2+}$ [a]	19.53(2.13)	
	30.67(3.61)	

a) Ref. 6).

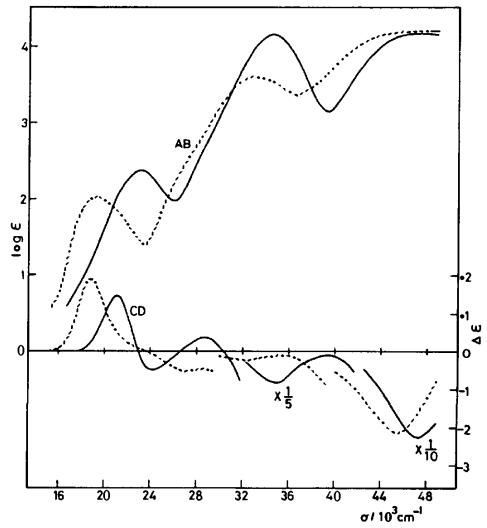

Fig. 4. Absorption and CD spectra of $(+)^{CD}_{500}$-[Co(aesei-N,S)$(en)_2]^{2+}$ (------) and $(+)^{CD}_{500}$-[Co(aesi-N,S)$(en)_2]^{2+}$ (——).

2.802(7) and 2.827(6) Å, respectively. In addition, the distances between the nitrogen atoms of the complex cation and the oxygen atoms of the nitrate anions are from 2.948 Å to 3.091 Å, as shown in Fig. 2. These distances suggest that they are hydrogen bonds.

Protonation Constant. The absorption spectral changes were reversible and an acid-base equilibrium is indicated. The value of the protonation constant (pK_a) is calculated from the following equation.

$$pK_a = -\log\gamma_H + pH_{meas} - \log\{(A_{HL}-A)/(A-A_{L^-})\},$$

where A_{HL} and A_{L^-} are the absorbances of acid and base, respectively, and A is the absorbance containing both of them. The γ_H is the activity coefficient of hydrogen ion and the value, $-\log\gamma_H = 0.13$, is calculated by the Debye-Hückel equation.[19] The value of pH_{meas} at $-\log\{(A_{HL}-A)/(A-A_{L^-})\}=0$ is determined to 1.78 ± 0.05 by least-squares treatment from Fig. 3. As a result, the value of pK_a can be determined to be 1.91 ± 0.05. The corresponding sulfinato complex, [Co(aesi-N,O)$(en)_2]^{2+}$, gave a pK_a of -0.7 (8 mol dm^{-3} ($NaClO_4$) uncorrected for H^+ activity coefficient changes).[6] This is consistent with the conclusion that the selenium atom is more "basic or soft" than the sulfur atom.[20]

Electronic Absorption and CD Spectra. The electronic absorption and CD spectra of the *A*-$(+)^{CD}_{500}$-[Co(aesei-N,O)$(en)_2]^{2+}$ isomer are shown in Fig. 4 and their data are summarized in Table 4, together with the related sulfinato complex, $(+)^{CD}_{500}$-[Co(aesi-N,S)$(en)_2]^{2+}$. This aesei isomer, which belongs to the [Co(O)$(N)_5$] type, exhibits a broad band with a vague shoulder on the higher energy side in the first absorption band region. This absorption behavior agrees well with those for the [Co(amino-carboxylato)$(en)_2$] type complexes.[21-23] The intense absorption band at *ca.* $33\times10^3\,cm^{-1}$ is weaker than that of the *Se*-bonded or *S*-bonded cobalt(III) complexes (Fig. 3 and Table 4) [2,3,5-11] Since the seleninate moiety can still interact with a cobalt center (Fig. 1), this absorption band seems to be a new charge transfer band from the seleninato chromophore to the cobalt atom. A similar absorption spectral trend was also observed for the photoproduct of the [Co(aesi-N,S)-$(en)_2]^{2+}$ complex.[6,7]

The CD spectrum shows a positive band in the first absorption band region (Fig. 4). This CD spectral behavior is consistent with those of the *A*-[Co(amino-carboxylato)$(en)_2$] type complexes.[21-23] These facts suggest that the asymmetric selenium atom contributes little to the CD band in this region. The $(+)^{CD}_{500}$-[Co(aesi-N,S)$(en)_2]^{2+}$ isomer exhibits a similar CD spectrum to that of *A*-$(+)^{CD}_{500}$-[Co(aesei-N,O)$(en)_2]^{2+}$ over the whole region, although the absorption and CD spectra of the latter shift to lower energy than those of the former. This seems to suggest that the $(+)^{CD}_{500}$ aesi isomer is also in the *A* configuration.

References

1) R. C. Elder, L. R. Florian, R. E. Lake, and A. M. Yacynych., *Inorg. Chem.*, **12**, 2690 (1973).
2) B. A. Lange, L. Libson, E. Deutsch, and R. C. Elder, *Inorg. Chem.*, **12**, 2985 (1973).
3) C. A. Stein, P. E. Ellis, Jr., R. C. Elder, and E. Deutsch, *Inorg. Chem.*, **15**, 1618 (1976).
4) W. A. Jackson, A. M. Sargeson, and P. O. Whimp, *J. Chem. Soc. Chem., Commun.*, **1976**, 934.

5) R. C. Elder, G. J. Kennard, M. D. Payne, and E. Deutsch, *Inorg. Chem.*, **17**, 1296 (1978).
6) H. Mäcke, V. H. Houlding, and A. W. Adamson, *J. Am. Chem. Soc.*, **102**, 6889 (1980).
7) V. H. Houlding, H. Mäcke, and A. W. Adamson, *Inorg. Chem.*, **20**, 4279 (1981).
8) L. Roecker, M. H. Dickman, D. L. Nosco, R. J. Doedens, and E. Deutsch, *Inorg. Chem.*, **22**, 2022 (1983).
9) K. Yamanari, J. Hidaka, and Y. Shimura, *Bull. Chem. Soc. Jpn.*, **50**, 2299 (1977).
10) M. Kita, K. Yamanari, and Y. Shimura, *Chem. Lett.*, **1980**, 275.
11) T. Konno, K. Okamoto, and J. Hidaka, *Chem. Lett.*, **1982**, 535.
12) K. Okamoto, T. Konno, M. Nomoto, H. Einaga, and J. Hidaka, *Chem. Lett.*, **1982**, 1941.
13) "International Tables for X-Ray Crystallography," The Kynoch Press, Birmingham (1974), Vol. IV.
14) K. Okamoto, M. Suzuki, and J. Hidaka, *Chem. Lett.*, **1983**, 401.
15) K. Okamoto, M. Suzuki, H. Einaga, and J. Hidaka, *Bull. Chem. Soc. Jpn.*, **56**, 3513 (1983).
16) K. Okamoto, T. Tsukihara, J. Hidaka, and Y. Shimura, *Bull. Chem. Soc. Jpn.*, **51**, 3534 (1978).
17) C. J. Hawkins, "Absolute Configuration of Metal Complexes," John-Wiley & Sons, New York (1971).
18) B. E. Douglas, D. H. McDaniel, and J. J. Alexander, "Concepts and Models of Inorganic Chemistry," 2nd ed, John-Wiley & Sons, New York (1983).
19) H. L. Schläfer, "Komplexbildung in Lösung," Springer-Verlag, Berlin (1961).
20) F. Basolo and R. G. Pearson, "Mechanisms of Inorganic Reaction," 2nd ed., John-Wiley & Sons, New York (1967).
21) C. T. Liu and B. E. Douglas, *Inorg. Chem.*, **3**, 1356 (1964).
22) D. A. Buckingham, S. F. Mason, A. M. Sargeson, and K. R. Turnbull, *Inorg. Chem.*, **5**, 1649 (1966).
23) M. Saburi, M. Homma, and S. Yoshikawa, *Inorg. Chem.*, **8**, 367 (1969).
24) W. C. Hamilton, *Acta Crystallogr.*, **12**, 609 (1959).

 © 1984 The Chemical Society of Japan Bull. Chem. Soc. Jpn., 57, 1499—1504 (1984)

Pyrolytic Sulfurization Gas Chromatography. XVI. Pyrolytic Sulfurization Reaction at Atmospheric Pressure and Its Application to the Identification of Carbon, Hydrogen, Oxygen, and Nitrogen in Organic Components

Tadashi HARA* and Fujio OKUI

Department of Chemical Engineering, Faculty of Engineering, Doshisha University, Karasuma Imadegawa, Kamigyo-ku, Kyoto 602

(Received December 5, 1983)

A new method by which the component elements: C, H, O, and N, in an organic compound can be simply, rapidly, and economically identified was established on the basis of the reaction of an organic compound with sulfur at atmospheric pressure. The apparatus for this method consists of two gas chromatographs and an original reactor for reacting an organic compound with sulfur vapor. One component separated from a given mixture by the use of one gas chromatograph was made to react with sulfur vapor in the original reactor and then the reaction products were analyzed by the use of the other gas chromatograph. The reaction products were restricted to seven kinds of compounds irrespective of the chemical structure of the target component. According to this method, the component elements: C, H, O, and N, in an organic compound could be easily identified by the reaction products within 20 min with a detection limit of a few pmol.

It is well known that gas chromatography-mass spectrometry(GC-MS) and atomic emission spectrometry(AES) using inductively coupled plasma (ICP) or microwave induced plasma(MIP) excitation are useful tools for identifying or determining component elements in a sample. However, the component elements in a sample cannot be easily identified or determined by means of GC-MS, though GC-MS can in principle clarify the chemical structure of a compound which can vaporize at relatively low temperature by its fragmentation. But complicated data analysis is required to clarify the chemical structure of the compound. On the other hand, though the component elements in a sample are easily identified by means of ICP- or MIP-AES, the applicable elements are restricted to heavy elements, such as metal elements. Few reports concerning the identification of light elements such as C, H, O, and N are available.[1-3] Moreover, both mass spectrometry and AES have the following disadvantages: 1) The apparatus is very expensive, 2) the system is very complicated, and 3) data analysis is very troublesome. Accordingly, it is now difficult to identify simply or to determine the component elements in an organic compound by means of instrumental analysis. Therefore, a new method by which the light elements such as C, H, O, and N in an organic compound can be simply, rapidly, and economically identified was investigated and successfully established. This method is based on the reaction of an organic compound with sulfur vapor at atmospheric pressure in the flow of sulfur vapor: A target component separated from a given mixture by gas chromatography is introduced to the reactor and is made to react with sulfur vapor, and then the resulting products are analyzed by gas chromatography. The apparatus used for this method consists of two gas chromatographs and an original reactor, in which a target component reacts with sulfur. The apparatus is set up by linking one gas chromatograph, the pyrolytic sulfurization reactor, and the other gas chromatograph in series in that order. This method will therefore be called "gas chromatograph-pyrolytic sulfurization reactor-gas chromatography (GC-PSR-GC)". By using GC-PSR-GC under the optimum conditions, carbon in an organic compound is mainly converted to carbon disulfide (CS_2) and/or carbonyl sulfide (COS), hydrogen to hydrogen sulfide (H_2S), oxygen to COS, and nitrogen to hydrogen cyanide (HCN). Therefore, the component elements, C, H, O, and N, in a target component can be successfully identified by observing four kinds of reaction products: CS_2, COS, H_2S, and HCN. The time necessary for an analysis by GC-PSR-GC is about 20 min.

Experimental

Reagents. The sulfur used as a reaction agant with a sample was obtained by purifying[4] commercially available sulfur (chemical pure). The organic compounds used as standard samples were of reagent grade; their purities were confirmed by gas chromatography. Helium as a carrier gas was purified in the present apparatus by passing through a stainless steel column(3 cm i.d. and 18 cm long) packed

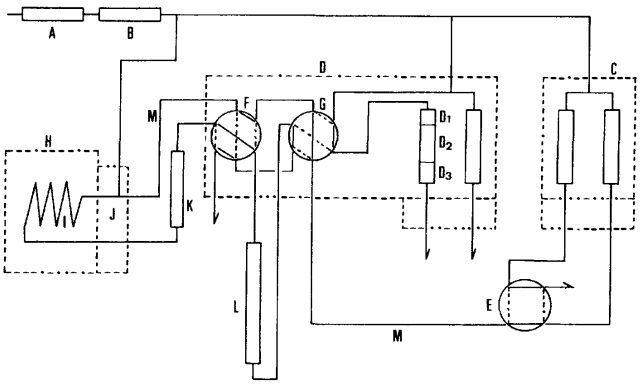

Fig. 1. Schematic flow diagram of the system.
A: Molecular sieve 5A column, B: copper column, C: gas chromatograph-I, D: gas chromatograph-II, D_1: Chromosorb 104 column, D_2: Porapak QS column, D_2: Deactigel column, E: four-way cock, F and G: six-way cocks, H: electric furnace, I: reaction tube, J: quartz-made apparatus, K: sulfur trap, L: trap column, and M: stainless steel tube.

with Molecular Sieve 5A (60—80 mesh) and a copper column (8 mm i.d. and 35 cm long) packed with sponge granular copper(12—25 mesh) heated at 380 °C.

Apparatus. The apparatus constructed for this study is schematically illustrated in Fig. 1. This apparatus consists of the following four sections: 1) Introduction section of a target component, 2) generation and condensation section of sulfur vapor as a reaction agent, 3) reaction section of the component with sulfur vapor, and 4) analysis section of the reaction products. The sections are constructed in the following detailed manners:

Section 1: A gas chromatograph(Shimadzu GC-4CPT)-I (GC-I) (C) mounted with a four-way cock(E) held at 180 °C was used for the introduction of a target component to the pyrolytic sulfurization. GC-I was operated under the optimum conditions for a sample, except that the flow rate of He as a carrier gas was set at 11 cm^3/min. All the stainless steel tubing (1.5 mm o.d. and 1.0 mm i.d.) (M) used to introduce a target component to the reactor were held at 180 °C, so as to prevent the condensation of the component in the tube.

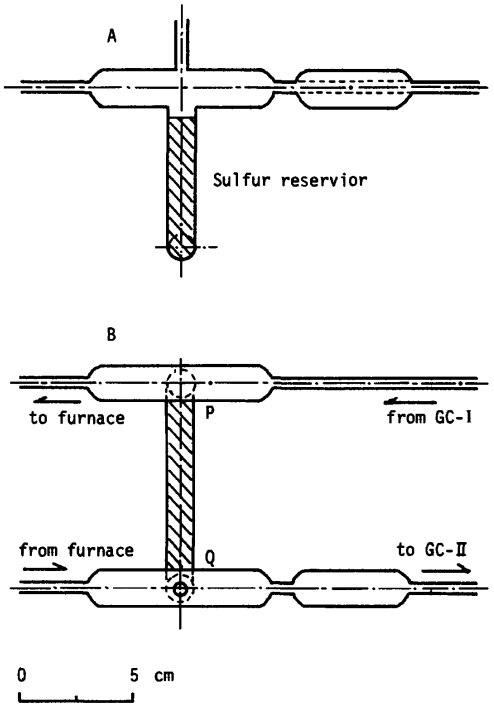

Fig. 2. The apparatus for supplying and recovering sulfur vapor.
A: Front view and B: plain.

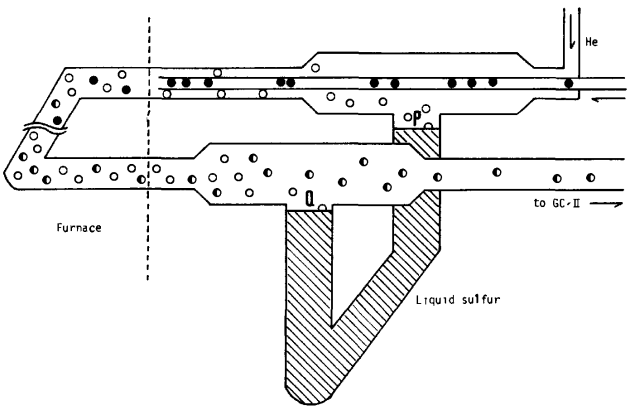

Fig. 3. The system of the pyrolytic sulfurization reaction.
○: Sulfur, ●: sample, and ◐: products.

Section 2: The quartz-made apparatus (J) by which sulfur vapor could be supplied and recovered was designed and constructed; this is shown in Fig. 2. Sulfur vapor was generated from the position P in Fig. 2 by heating it at 350 °C and was carried into the reaction section by He at a flow rate of 4 cm^3/min; then the sulfur vapor was condensed at the position Q held at 150 °C. Sulfur trap column (4 mm i.d., 6 mm o.d., and 10 cm long) (K) packed with quartz wool was connected with this apparatus for completely eliminating sulfur mist.

Section 3: A spiral quartz tube(2.5 mm i.d., 4 mm o.d., and 5 m long) (I) was used as a reaction tube by placing it in a electric furnace (Seiwa Riko Co. Ltd., FDH-15) heated at 900 °C.

Section 4: A gas chromatograph (Shimadzu GC-4CPT)-II (GC-II) (D) mounted with two six-way cocks (F and G) and a stainless steel column (3 mm i.d., 4 mm o.d., and 50 cm long) (L) for trapping the reaction products was used for analyzing the reaction products; the trap column was packed with Silica gel (60—80 mesh). The reaction products could be trapped in this column at room temperature and released from this column by heating it to 250 °C. GC-II was operated under the following conditions: A 0.25 m stainless steel column D_1 was packed with Chromosorb 104 (80—100 mesh), a 1.75 m stainless steel column D_2 with Porapak QS (80—100 mesh), and a 0.2 m stainless steel column D_3 with Deactigel (60—80 mesh) were used by linking them in series in that order. The column temperature was programmed between 80 and 185 °C at the rate of 20 °C/min. The flow rate of He carrier gas was 30 cm^3/min at room temperature.

The system for the pyrolytic sulfurization reaction between a target component and sulfur vapor by the use of the present apparatus is illustrated in Fig. 3. The component gas and sulfur vapor were mixed just before the entrance of the furnace and then the mixture components were made to react in the furnace. The reaction products thus obtained and the excessive sulfur over the pyrolytic sulfurization reaction were separated at the position of the condenser (Fig. 3, Q) by condensing the excessive sulfur vapor to liquid sulfur, and only the reaction products were introduced to the analysis system by GC-II. Therefore, this system for supplying and recovering sulfur makes it possible to minimize the sulfur consumption necessary for the analysis and allows the excessive sulfur to be reused for the next analyses.

Procedure. Several decimilligrams of a sample, either a single compound or a mixture, was injected into GC-I by the use of a microsyringe and the elution behavior of the sample was monitored by the thermal conductivity detector installed in GC-I. The target peak of the sample to be analyzed was introduced to the reactor of pyrolytic sulfurization by operating the four-way cock E, and other compounds, if present, were sent from the exit at the same time. The target component was mixed with sulfur vapor generated from a sulfur generator just before the furnace. Then their mixture were subjected to react for about 1 min during the passage through the reaction tube heated at 900 °C by the electric furnace. The products thus obtained were separated from the excessive sulfur and only the products were trapped by the trap column L at room temperature for 2.5 min after the elution from GC-I. The reaction products trapped were released from the trap column and introduced to GC-II by operating two six-way cocks (F and G) and by heating the trap column rapidly to 250 °C, followed by analysis by the use of GC-II. The peak areas of the products on the gas chromatogram of GC-II were read out by the use of

the integrator (Shimadzu digital integrator E1A). By the use of the chromatogram thus obtained, the component elements C, H, O, and N, in the target component were qualitatively identified.

Results and Discussion

Optimization of the Reaction Conditions between a Sample and Sulfur. Flow rate of carrier gas, He, for supplying a target component to the reactor was set at 11 cm^3/min, and that for supplying sulfur vapor was set at 4 cm^3/min, based on the design of the apparatus. In these experimental conditions, vaporizing temperature for supplying the sufficient sulfur necessary for the pyrolytic sulfurization of the component was examined by the use of 1 μl of toluene, which did not seem to be so reactive with sulfur (Fig. 4). Figure 4 indicates that vaporizing temperature of sulfur has to be held over about 350 °C. Therefore, the vaporizing temperature of sulfur was chosen at 350 °C as its optimum condition.

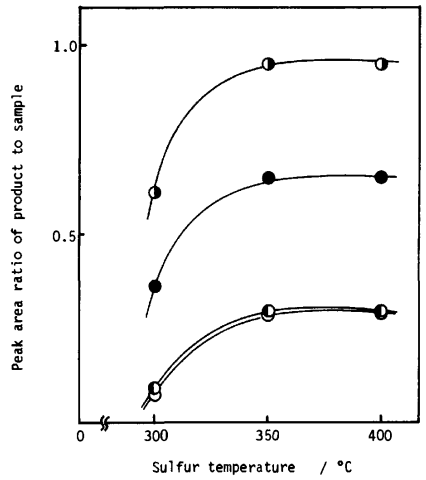

Fig. 4. Effect of the sulfur temperature on the amount of products.
○: H_2S(2.5 min-trap), ●: CS_2(2.5 min-trap), ◐: H_2S(5 min-trap), and ◑: CS_2(5 min-trap).
Conditions: Furnace temperature 900 °C.

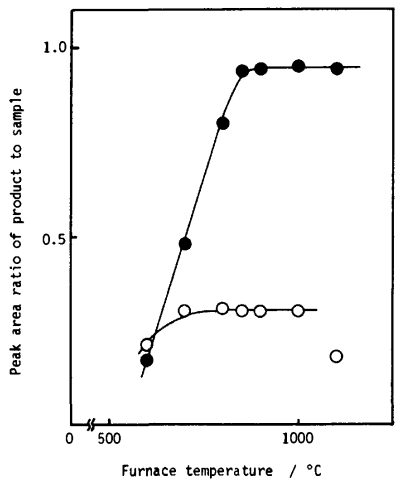

Fig. 5. Effect of furnace temperature on the amount of products.
○: H_2S and ●: CS_2. Conditions: Trap time 5 min.

The reaction temperature of the component with sulfur vapor in the electric furnace was also examined by the use of 1 μl of toluene as a standard sample; the effects of the furnace temperature on the amount of products are shown in Fig. 5. The reaction temperature has to be held over about 850 °C. Moreover, COS as a blank was produced at a temperature of over 1100 °C; this may be attributed to the fact that carbon in the component reacted with the internal surface of the reaction tube.[5] Therefore, the reaction temperature was chosen at 900 °C as its optimum condition.

Trap Time of the Reaction Products. The products from the reaction between a target component and sulfur were trapped by the stainless steel column packed with silica gel. The time necessary for trapping the products was examined; the effects of trap time on the amount of the products are shown in Fig. 6. Figure 6 indicates that a trap time over 15 min is required to trap quantitatively all the products from a target component. In the present conditions, a small

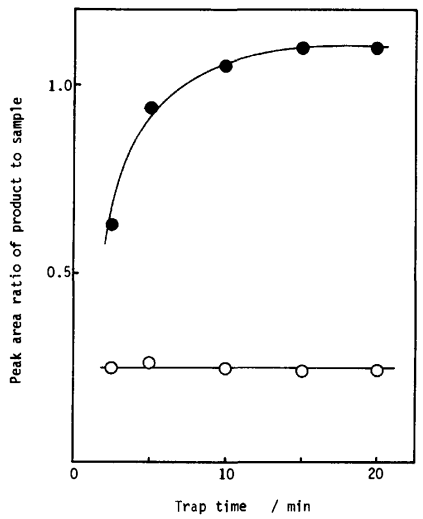

Fig. 6. Effect of trap time on the amount of products.
○: HS and ●: CS_2.

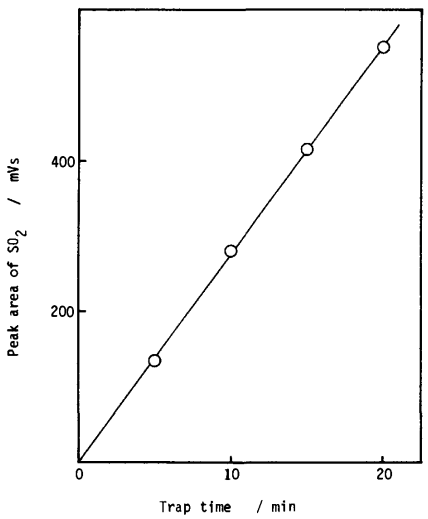

Fig. 7. Relationship between trap time and peak area of SO_2.

amount of sulfur dioxide (SO_2) was constantly produced from sulfur as its impurity, so the amount of SO_2 was measured in the range of 5—20 min of trap time by the use of the present system (Fig. 7). The amount of SO_2 is proportional to the trap time. It is generally better to minimize the analysis time and to simplify the data analysis in all qualitative identification. Therefore, the trap time for qualitative identification was chosen to 2.5 min after the elution of a target component from GC-I as its optimum condition by considering both the analysis time and the blank value of SO_2.

Reaction Products by Pyrolytic Sulfurization. The reaction products obtained by the pyrolytic sulfurization reaction under the above-mentioned conditions were investigated by subjecting several kinds of organic compounds to the GC-PSR-GC system. The reaction products were restricted to carbon dioxide (CO_2), COS, CS_2, H_2S, water (H_2O), SO_2, and HCN. Here each product was identified gas-chromatographically by analyzing a authentic sample. The results showed that carbon in an organic compound is converted to CO_2, COS, CS_2, and HCN, hydrogen to H_2S, H_2O, and HCN, oxygen to CO_2, COS, SO_2, and H_2O, and nitrogen to HCN, respectively, by the pyrolytic sulfurization reaction under the present conditions. In order to separate and determine the seven kinds of the products by gas chromatography, their optimum conditions were searched and obtained, as described in experimental term. A typical chromatogram of the products is shown in Fig. 8. This was obtained by analyzing nitromethane as a target component, from which seven kinds of products were produced by the use of GC-PSR-GC. As can be seen from Fig. 8, seven kinds of products

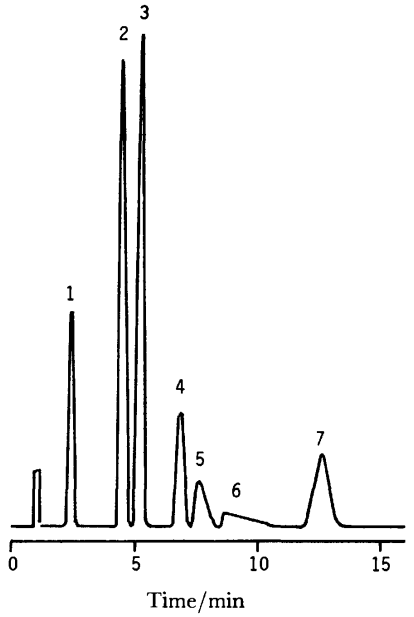

Fig. 8. Typical chromatogram of nitromethane.
1: CO_2, 2: H_2S, 3: COS, 4: SO_2, 5: HCN, 6: H_2O, and 7: CS_2.

TABLE 1. ANALYTICAL RESULTS OF VARIOUS ORGANIC COMPOUNDS

Sample	Products[a]							Components	
	CO_2	H_2S	COS	SO_2	HCN	H_2O	CS_2	Theor.	Found
Toluene	−	+	−	−	−	−	+	CH	CH
Benzene	−	+	−	−	−	−	+	CH	CH
Hexane	−	+	−	−	−	−	+	CH	CH
Cyclohexene	−	+	−	−	−	−	+	CH	CH
Triethylamine	−	+	−	−	+	−	+	CHN	CHN
Ethylenediamine	−	+	−	−	+	−	+	CHN	CHN
Pyridine	−	+	−	−	+	−	+	CHN	CHN
Acrylonitrile	−	+	−	−	+	−	+	CHN	CHN
Methyl alcohol	+	+	+	−	−	−	+	CHO	CHO
Ethyl alcohol	−	+	+	−	−	−	+	CHO	CHO
Propyl alcohol	−	+	+	−	−	−	+	CHO	CHO
Butyl alcohol	−	+	+	−	−	−	+	CHO	CHO
Acetone	−	+	+	−	−	−	+	CHO	CHO
Ethyl methyl ketone	−	+	+	−	−	−	+	CHO	CHO
Isobutyl methyl ketone	−	+	+	−	−	−	+	CHO	CHO
Acetylacetone	−	+	+	−	−	−	+	CHO	CHO
Ethylene glycol monomethyl ether	−	+	+	−	−	−	+	CHO	CHO
Dibutyl ether	−	+	+	−	−	−	+	CHO	CHO
Methyl acetoacetate	+	+	+	−	−	−	+	CHO	CHO
Methyl acrylate	+	+	+	−	−	−	+	CHO	CHO
Acetic acid	+	+	+	−	−	−	+	CHO	CHO
Propionic acid	+	+	+	−	−	−	+	CHO	CHO
Nitromethane	+	+	+	+	+	+	+	CHON	CHON
Nitroethane	+	+	+	+	+	−	+	CHON	CHON
N, N-Dimethylformamide	−	+	+	−	+	−	+	CHON	CHON
Morpholine	−	+	+	−	+	−	+	CHON	CHON

a) +, −: Shows the production or non-production of the product.

can be successfully separated one from another and can be eluted within 15 min.

Qualitative Indentification of C, H, O, and N in a Standard Sample. Many kinds of organic compounds were analyzed by GC-PSR-GC by the use of 0.4 μl of sample; the products from the sample are shown in Table 1. With regard to all samples, carbon in a sample was mainly converted to CS_2 and COS, where CS_2 became a main product in a carbon-rich compound and COS did in an oxygen-rich compound, hydrogen to H_2S, oxygen to COS, and nitrogen to HCN. Therefore, the component elements: C, H, O, and N in an organic compound could be easily identified by observing four kinds of products: CS_2, COS, H_2S, and HCN; all the samples are shown in Table 1. The component elements in the sample can be qualitatively identified without any exceptions.

Detection Limit of GC-PSR-GC. The detection limit of GC-PSR-GC was examined under the present conditions by the use of ethanol and acrylonitrile as standard samples. No products except SO_2 were observed by the blank test under the present conditions, and a small amount of COS produced by the reaction between carbon in a target component and SO_2 as an impurity of sulfur was observed when the component containing no oxygen was analyzed. Therefore, the detection limit of the present method for the products except COS was defined as the signal to noise ratio equal to two on a gas chromatogram, while that for COS was also defined as the signal to blank ratio equal to two. As a result of the investigation on the basis of above definition, the detection limit of GC-PSR-GC was a few pmol.

Identification of C, H, O, and N in a Component Separated from a Mixed Sample by Gas Chromatography. The mixed sample was artificially prepared by mixing four kinds of compounds: cyclohexene consisting of C and H, methanol consisting of C, H, and O, pyridine consisting of C, H, and N, and morpholine consisting of C, H, O, and N. This sample was subjected to GC-PSR-GC in the following manner. One μl of the sample was injected to GC-I(chromatogram of this sample is shown in Fig. 9) and the target peak of a sample was introduced to the pyrolytic sulfurization reactor by operating the four-way cock mounted with GC-I, followed by analysis by the present procedure. By repeating the above-mentioned procedure, four kinds of compounds in the mixed sample were analyzed. Each chromatogram is shown in Fig. 10. The component elements in each compound could be successfully and easily identified by the use of each chromatogram of the compound. These results indicate that all organic compounds which can be separated by gas chromatography can be subjected to GC-PSR-GC and can be qualitatively identified according to their component elements: C, H, O, and N. In other words, the present system can be expected to become a useful tool as a secondary

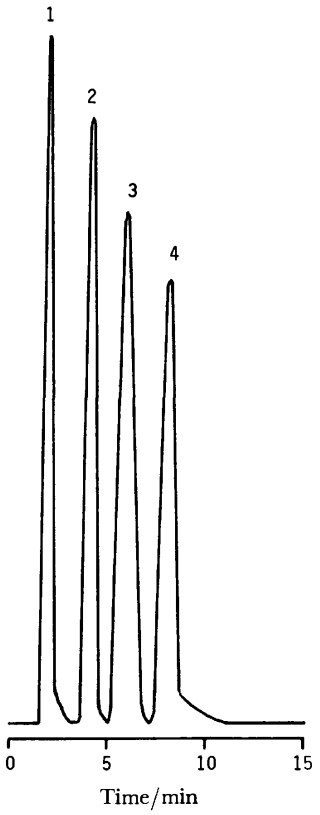

Fig. 9. Chromatogram of mixed sample by GC-I.
1: Methyl alcohol, 2: cyclohexene, 3: pyridine, and 4: morpholine.
GC conditions: Column stainless steel (3 mm i.d., 4 mm o.d., and 1 m long), column packings 5%-Silicone GE SE-30 on Chromosorb W (60—80 mesh), column temperature 60°C, flow rate 11 cm^3/min, and carrier gas He.

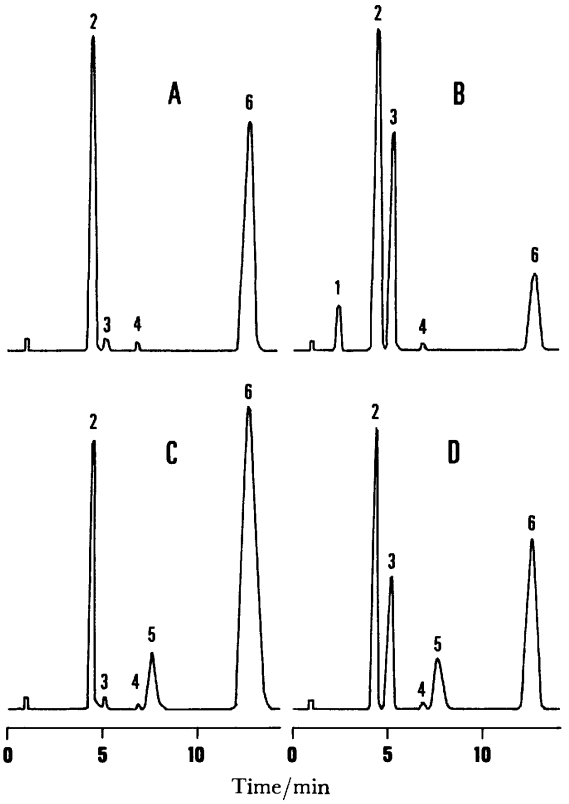

Fig. 10. Chromatograms of samples by GC-PSR-GC (A: cyclohexene, B: methyl alcohol, C: pyridine, and D: morpholine).
1: CO_2, 2: H_2S, 3: COS, 4: SO_2, 5: HCN, and 6: CS_2.

detector for gas chromatography.

Pyrolytic Sulfurization Reaction under the Present Conditions. Pyrolytic sulfurization reaction under the present conditions is discussed here on the basis of the results obtained in this study. Figure 4 indicates that the amount of CS_2 produced is influenced by the trap time, though that of H_2S is not, for each sulfur temperature. Figure 6 also indicates that the amount of CS_2 becomes constant by trapping it for over 15 min, while that of H_2S becomes constant within 2.5 min. These results can be explained by presuming the mechanism of pyrolytic sulfurization under the present conditions as follows: A target component is immediately decomposed in the furnace to gaseous compounds and carbon deposit. Then the gaseous compounds react with sulfur vapor during the passage through the reaction tube and the carbon deposit reacts with sulfur vapor at the position of the thermal decomposition until it is completely converted to CS_2. Therefore, the times necessary for the production of H_2S and CS_2 may be different. This was also experimentally proved by the use of other kinds of compounds.

Comparison of GC-PSR-GC with PSGC with Regard to Pyrolytic Sulfurization. Pyrolytic sulfurization gas chromatography(PSGC)[6-19] has been previously investigated and successfully established by the authors as a new elemental analysis method by which the atomic ratio between C, H, O, and N in an organic compound can be simultaneously determined. This method has been successfully applied to various organic compounds, such as an usual organic compound, a metal organic chelate, a polymer, and an organic halogen compound. In PSGC, a sample is made to react with sulfur in a sealed quartz tube for 1 min at 1500 °C or for 30 min at 950 °C. Therefore, a pyrolytic sulfurization reaction occurs at high pressure. On the contrary, pyrolytic sulfurization reaction by GC-PSR-GC occurs at atmospheric pressure, as described in this study. The reaction products obtained by GC-PSR-GC are the same as those obtained by PSGC, except for HCN. Nitrogen in a sample is converted to molecular nitrogen in PSGC. This suggests that the reaction conditions of PSGC are severer than those of GC-PSR-GC. The fact that pyrolytic sulfurization reaction by GC-PSR-GC is completed by reacting a sample with sulfur for 15 min at 900 °C, though the reaction by PSGC is done for 30 min at 950 °C may be explained as follows: Pyrolytic sulfurization reaction by PSGC may take a longer time to convert carbon in a sample to CS_2 at the end of the reaction. This suggests that a trace amount of carbon must react with a trace amount of sulfur at the end of the reaction since a stoichiometric amount of sulfur is present in the sealed tube, unlike the case of GC-PSR-GC.

On the basis of the above-mentioned investigation, a method for the qualitative identification of the component elements, C, H, O, and N, in an organic compound was newly established. This method, called GC-PSR-GC, is characterized by the following: 1) The component elements: C, H, O, and N, in an organic compound can be qualitatively identified, 2) data analysis is very simple, 3) this method is more simple and economical than earlier ones, and 4) this method is also useful as a secondary detector of gas chromatography. This method will contribute to progress in organic chemistry.

References

1) W. R. Mclean, D. L. Stanton, and G. E. Penketh, *Analyst*, **98**, 432 (1973).
2) S. K. Hughes, R. M. Brown, and R. C. Fry, *Appl. Spectrose.*, **35**, 400 (1981).
3) D. L. Windsor and M. B. Denton, *Anal. Chem.*, **51**, 1116 (1979).
4) T. Hara, K. Fujinaga, K. Tsuji, and F. Okui, *Bull. Chem. Soc. Jpn.*, **51**, 3079 (1978).
5) K. Imaeda, "Yūki Biryō Teiryō Bunseki," ed by Yūki Biryō Bunseki Kenkyū Kondan Kai, Nankō-dō, Tokyo (1972), p. 366.
6) K. Tsuji, K. Fujinaga, and T. Hara, *Bull. Chem. Soc. Jpn.*, **50**, 2292 (1977).
7) T. Hara, K. Fujinaga, and K. Tsuji, *Bull. Chem. Soc. Jpn.*, **51**, 1110(1978).
8) T. Hara, K. Fujinaga, and K. Tsuji, *Bull. Chem. Soc. Jpn.*, **51**, 2951 (1978).
9) T. Hara, K. Fujinaga, F. Okui, and K. Negayama, *Sci. Eng. Rev. Doshisha Univ.*, **21**, 241 (1981).
10) T. Hara, K. Fujinaga, and F. Okui, *Bull. Chem. Soc. Jpn.*, **53**, 951 (1980).
11) T. Hara, K. Fujinaga, and F. Okui, *Bull. Chem. Soc. Jpn.*, **53**, 1308 (1980).
12) T. Hara, K. Fujinaga, and F. Okui, 3rd World Chromatography Conference, Zürich, July 1980, Abstr. p. 7.
13) T. Hara, K. Fujinaga, and F. Okui, *Bull. Chem. Soc. Jpn.*, **54**, 2956 (1981).
14) T. Hara and F. Okui, *Bull. Chem. Soc. Jpn.*, **55**,329 (1982).
15) T. Hara and F. Okui, *Bull. Chem. Soc. Jpn.*, **55**, 2127 (1982).
16) T. Hara and F. Okui, *Bull. Chem. Soc. Jpn.*, **55**, 3450 (1982).
17) T. Hara, K. Fujinaga, and F. Okui, *Bull. Chem. Soc. Jpn.*, **55**, 3800 (1982).
18) T. Hara and F. Okui, *Bull. Chem. Soc. Jpn.*, **56**, 1378 (1983).
19) T. Hara, K. Fujinaga, F. Okui, and A. Arai, *Bull. Chem. Soc. Jpn.*, **56**, 3615 (1983).

 © 1984 The Chemical Society of Japan Bull. Chem. Soc. Jpn., 57, 1505—1509 (1984)

1,3-Dipolar Cycloaddition Reactions of 6-Methylenetricyclo-[3.2.1.$0^{2,7}$]oct-3-en-8-one and Its Related Compounds

Makoto NITTA,* Akihiko OMATA, and Shuji OKADA

Department of Chemistry, School of Science and Engineering, Waseda University, Shinjuku-ku, Tokyo 160

(Received August 18, 1983)

The cycloaddition reactions of 1,5-dimethyl-6-methylenetricyclo[3.2.1.$0^{2,7}$]oct-3-en-8-one (**1a**), its corresponding -8-*endo*-ol (**1b**), 1,5,8-trimethyltricyclo[3.2.1.$0^{2,7}$]oct-3-en-8-*endo*-ol (**1c**), and 5,8-dimethyl-9-methylenetricyclo[3.3.1.$0^{2,8}$]non-3-en-7-one (**2**) were investigated in order to study the origin of its stereoselectivity or site selectivity. The reaction of 2,4,6-trimethylbenzonitrile oxide (mesitonitrile oxide, MNO) with **1a, b** occurs on the *exo*-mthylene group from the *exo*-side, but on the endocyclic double bond in the case of **1c**. The compound **2** undergoes the addition of MNO on both the exocyclic and endocyclic double bonds to give a corresponding bis-adduct. On the other hand, the reaction of phenyl azide (PA) with **1a—c** occurs on the endocyclic double bond from the endo-side to give a single adduct. The reaction of 6-*exo*-methoxy-1,5,6-trimethyltricyclo[3.2.1.$0^{2,7}$]oct-3-en-8-one with MNO or PA was also studied to prove the regioselectivity of the cycloadditions of constrained vinylcyclopropane moiety.

Recently the stereoselectivities and/or site selectivities of electrophilic reactions or cycloadditions of molecules containing proximal π-bonds, such as alkylidenenorbornene and alkylidenebenzonorbornadiene have been investigated.[1-5]

In previous papers, we reported that electrophilic reactions such as solvomercuration, bromination and its related reactions on the exocyclic double bond of 1,5-dimethyl-6-methylenetricyclo[3.2.1.$O^{2,7}$]oct-3-en-8-one (**1a**) and its related compounds of general structure (**A**) exhibit a remarkable stereoselectivity to give

n = 0 or 1 X = O or H, OH Z = Br or HgOAc

(**B**).[6,7] The stereoselectivity was explained by the steric and/or electronic factor of mercurinium or bromonium ion formation and the stereoelectronic control of the endocyclic double bond for the incorporating nucleophiles. In continuation of this study, the 1,3-dipolar cycloadditions of 2,4,6-trimethylbenzonitrile oxide or phenyl azide with **1a**, its corresponding-8-*endo*-ol (**1b**), 1,5,8-trimethyl-6-methylenetricyclo[3.2.1.$0^{2,7}$]oct-3-en-8-*endo*-ol (**1c**), 5,8-dimethyl-9-methylenetricyclo[3.3.1.$0^{2,8}$]non-3-en-7-one (**2**), and 6-*exo*-methoxy-1,5,6-trimethyltricyclo[3.2.1.$0^{2,7}$]-oct-3-en-8-one (**11**) were studied to probe the origin of stereoselectivity or site selectivity. The results are described in this paper.

Results and Discussion

The reaction of 2,4,6-trimethylbenzonitrile oxide (mesitonitrile oxide, MNO) with **1a**[8] and **1b**[9] under reflux in benzene for 5 h gave 1 : 1 adducts **3a** and **3b** in 83 and 82% yields, respectively. The structural proof was based on the elemental analyses and spectroscopic data. The stereochemical arrangement of the MNO moiety of **3a** was deduced from the pseudo-contact NMR spectra obtained by using Eu(fod)$_3$. The relative down field shifts of δ's are given in parentheses in the structural formula.[10] The large values of 2.01 and 2.34 for the methyl groups as compared to the value of 1.27 for the methylene protons of the isoxazoline ring suggest the coordination of Eu(fod)$_3$ occurs on the carbonyl-oxygen and the MNO moiety is *exo* to the carbonyl group. On oxidation with pyridinium chlorochromate, **3b** was converted to **3a** in an 80%

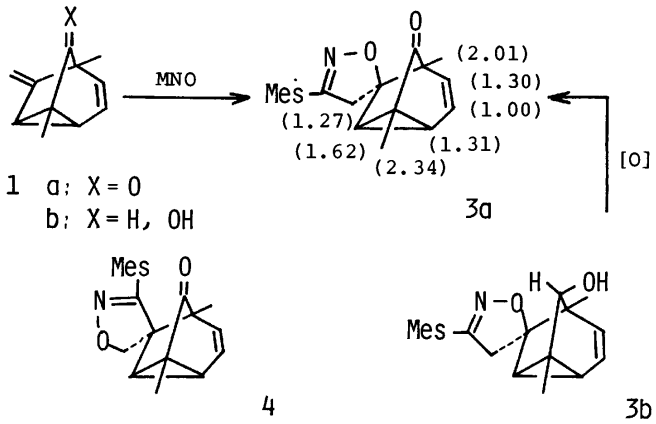

yield, therefore the stereochemistry of **3a** and **3b** were assessed. Regarding the frontier orbital theory, the regioselectivity of the present cycloadditions is explained by LUMO (MNO)-HOMO (**1a, b**) interaction, since the unsubstituted terminus of the exomethylene group (possible large HOMO coefficient) was bound to the carbon terminus of MNO (large LUMO coefficient).[11,12] The regiochemistry of **3a, b** is also favorable for a steric reason. The van der Waals nonbonded interaction energies should be very large in such material as **4** as compared to the adduct **3a, b** (*vide infra*).

In order to probe the *exo*-selectivity of the present cycloadditions, the reaction of **1c**, which has a bulky methyl group at 8-position, was studied. The reaction of **1c**[13] with MNO under reflux in benzene for 7 h gave 1 : 1 adduct **5** in a 26% yield, the remainder being recovered starting material **1c** in a 53% yield. The structural proof including the regiochemistry and the stereochemistry of the MNO moiety was assessed on the basis of the spectral data and the pseudo-contact NMR spectra.[10] The relatively large values of 2.48 and 1.70 for the methine protons of the isoxazoline ring clearly indicate the *endo*-orientation of the MNO moiety of **5**. In the adduct **5**, the terminus of the

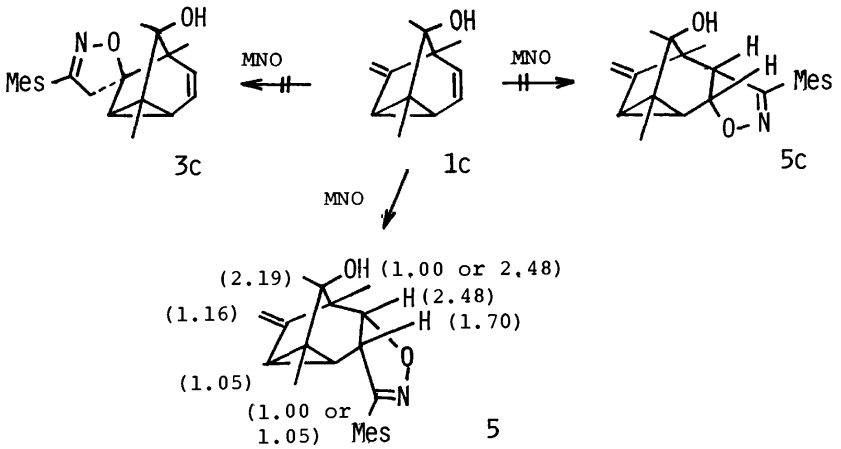

divinylcyclopropane moiety (possible large LUMO coefficient) was bound to the oxygen of MNO (large HOMO coefficient).[11,12] The bulky methyl group at 8-position of **1c** seems to prevent the *exo*-attack to give **3c**, which is expected from LUMO (MNO)-HOMO (**1c**) interaction as in the case of **1a**, **b**. The *endo*-arrangement of the MNO moiety of **5** is suggestive of the steric effect between the bulky mesityl group and two methyl groups at 1-and 5-positions. The blocked LUMO (MNO)-HOMO (**1c**) interaction to give **5c** stands in contrast to the cycloaddition of MNO with the vinylcyclopropane moiety of **11** (*vide infra*). The *endo*-attack of MNO on the *exo*-methylene group of **1c**, as well as **1a**, **b**, was prevented completely. This feature suggests a stereoelectronic effect of the endocyclic double bond[6] rather than a steric effect.

In order to probe this point, the reaction of **2**,[14] in which the *exo*-methylene group is located symmetrically with respect to the carbon skeleton, was investigated. The reaction of MNO with **2** under reflux in benzene for 20 h gave the bis-adduct **7** in a 48% yield, leaving 27% of **2**. Unfortunately the mono-adduct **6** was not isolated even in the presence of an excess amount of **2**. The structural proof and the stereochemical arrangement of the isoxazoline moiety were deduced from the spectral data.[10] The reaction of MNO with the *exo*-methylene gorup of **1a** or **1b** seemed to be faster than that with the endocyclic double bond of **1c** (*vide supra*), therefore it is suggested that the mono-adduct **6** might be the primary cycloadduct leading to **7**. An electrophilic reaction of sulfenyl chloride with **1a** could give a 1:1 adduct on the *exo*-methylene group, while that of **2** could give a 1:1 adduct on the *exo*-methylene group and a bis-adduct which can be derived from the former mono-adduct. Thus the endocyclic double bond of **2** seems to be more reactive than that of **1a**.[15] This fact may also suggest the intermediacy of **6** in the present cycloaddition. Regarding the steric hindrance of the hydrogen at the α-position of the carbonyl group, the *exo*-attack of MNO on the *exo*-methylene group of **2** seems unfavorable as compared to the endo-attack. However, MNO appeared to attack the *exo*-methylene group of **2** from the *exo*-side. Thus the *endo*-attack of **1a—c** or **2** may be prevented by the repulsive orbital interaction, which would be experienced with the endocyclic double bond.

The cycloaddition of phenyl azide (PA) to the compounds **1a—c** was carried out under reflux in cyclohexane for 1 week to give 1:1 adducts **8a—c**. No adduct on the *exo*-methylene group was obtained. The structural proof including the stereochemistry and regiochemistry was based on the spectral data.[10] Photoirradiation of **8a** could undergo a clean elimination of a nitrogen molecule to give aziridine **9**, the structure of which including stereochemistry was also confirmed by the spectral data. Since the terminus of the divinylcyclopropane moiety (possibly with a large HOMO coefficient) was bound to the nitrogen bearing no phenyl group (large LUMO coefficient),[12] the regiochemistry of the adducts **8a—c** appears to be controlled by the LUMO (PA)-HOMO (**1a**, **b**, **c**) inter-

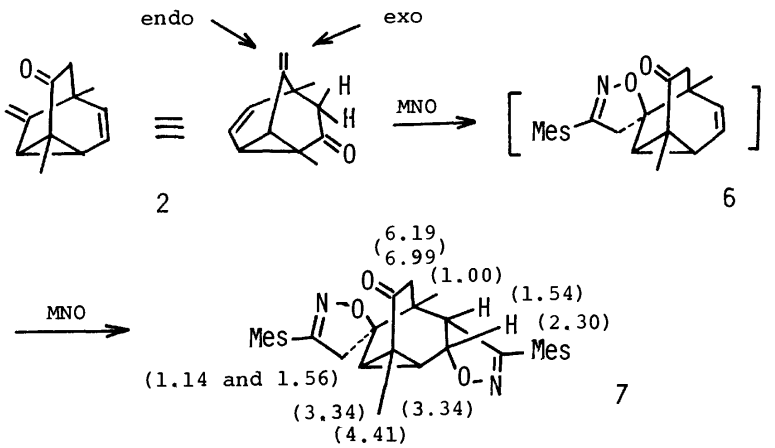

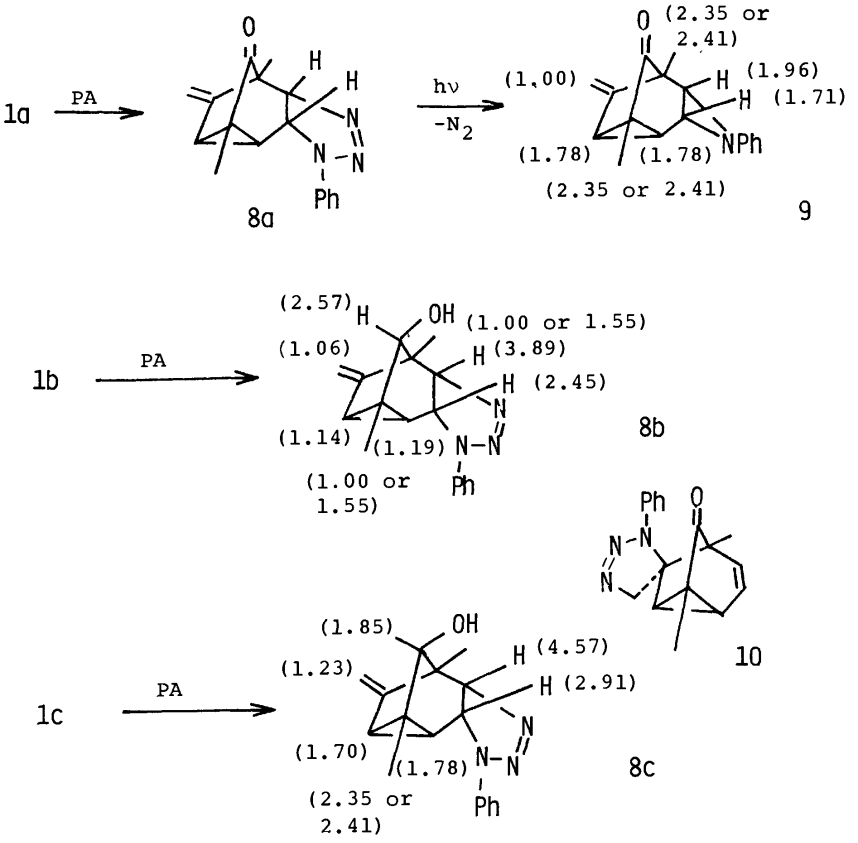

actions. The attack of PA on another terminus of the divinylcyclopropane moiety (*exo*-methylene group) to give **10** would be impossible because of the large steric hindrance. The attack of PA on the *exo*-methylene group from the *endo*-side would also be prevented because of the large steric effect and the stereoelectronic effect (*vide supra*).

The HOMO of MNO[16] and PA[12] are −8.3 and −9.5 eV, and LUMO have been estimated at +0.11 and −0.22 eV. Thus the low lying LUMO (PA), as compared to the high lying LUMO (MNO), appeared to control the regioselectivity of **8a—c**. On the other hand, the regiochemistry of **3c** or the second isoxazoline moiety of **7** seemed to be controled by HOMO

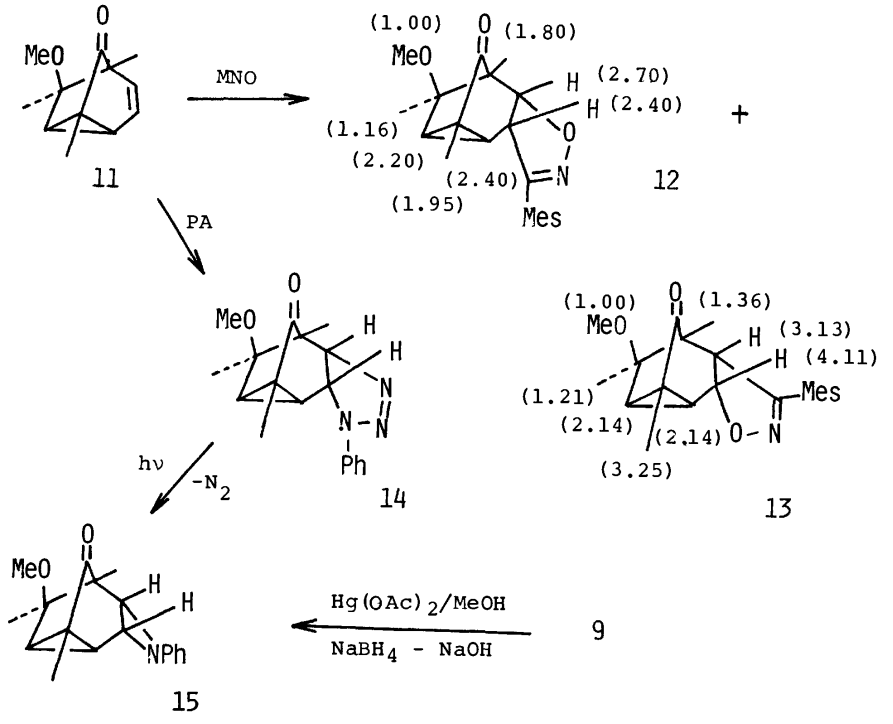

(MNO)-LUMO (**1c**) or LUMO (MNO)-HOMO (**6**) interactions, respectively.

Furthermore the cycloaddition of MNO or PA with constrained vinylcyclopropane was studied. The reaction of **11** with MNO under similar conditions gave the 1:1 adducts **12** and **13** in 13 and 10% yields, along with unreacted **11** in 70% yield. The structural proof is based on the spectroscopic data. On the other hand, the reaction of **11** with PA in cyclohexane under similar conditions described above gave single adduct **14** in 40% yield along with the unreacted **11** in 23% yield. The photoirradiation of **14** afforded 89% of aziridine **15**, which was also obtained by the methoxymercuration-demercuration of **9**. Thus the structure of **14** was established. Therefore both the high lying LUMO and HOMO of MNO, as compared to that of PA, can intervene in the cycloaddition of a constraiened vinylcyclopropane system such as **11**, while only low lying LUMO in the case of PA. In the adduct **12**, **13**, and **14**, 1,3-dipoles were incorporated from the *endo*-side to the carbonyl group. Regarding the steric effect of methyl groups at 1-and 5-positions, *endo*-orientation seems to be favorable.

In conclusion, the selective *exo*-attack on the *exo*-methylene group of **1a**, **b** and **2** giving **3a**, **b** and **6**, respectively, seems to be controlled by the stereoelectronic effect, which would prevent the *endo*-attack. The site selectivity giving **5** or **8a—c** would be caused by the sterically hindered *exo*-attack of 1,3-dipoles on the *exo*-methylene group and the stereoelectronically hindered *endo*-attack on the *exo*-methylene group. The stereochemistry and the regiochemistry of 1,3-dipolar cycloaddition of endocyclic double bond of **1a—c**, **6**, and **11** seemed to be controlled by the steric effect of the methyl groups at the ring junction and frontier orbital interaction, respectively.

Experimental

IR spectra were recorded on a Shimadzu IR-400 spectrometer. The mass spectral studies were conducted using a Hitachi RMU-60 spectrometer. All NMR spectra were recorded on a JEOL PS-100 high resolution spectrometer using tetramethylsilane as the internal standard. The shift data were obtained by adding small increments of Eu(fod)$_3$ to the sample and noting the extent to which each peak was shifted. The relative shift-slopes were obtained by dividing each of the slopes by the slope of the least shifted signal. The analyses were performed by the Science and Engineering Research Laboratory, Waseda University.

*Cycloaddition of **1a** with 2,4,6-Trimethylbenzonitrile Oxide (Mesitonitrile Oxide, MNO).* A solution of **1a** (160 mg, 1 mmol) and MNO (161 mg, 1 mmol) in 3 cm^3 of anhydrous benzene was refluxed for 5 h. After the solvent removal *in vacuo*, the residue was separated by TLC on silica gel using dichloromethane as the eluent. The first band from the TLC plates contained 20 mg (13%) of **1a**. The second band from the TLC plates gave 267 mg (83%) of the adduct **3a**: mp 150—151 °C (from hexane); IR ($CHCl_3$), 1607, 1336 cm^{-1}; NMR ($CDCl_3$), δ=1.21 (3H, s), 1.38 (3H, s), 2.12—2.33 (1H, m), 2.32 (6H, s), 2.35 (3H, s), 2.43 (1H, d, J=8.1 Hz), 3.02 (1H, d, J=18.6 Hz), 5.68 (1H, d×d, J=8.4, 3.0 Hz), 6.27 (1H, d×d, J=8.4, 5.1 Hz), 7.05—7.16 (2H, broad s); MS, m/z (rel intensity), 321 (M$^+$, 50), 159 (100). Found: C, 78.75; H, 7.21; N, 4.22%. Calcd for $C_{21}H_{23}O_2N$: C, 78.47; H, 7.21; N, 4.36%.

*Cycloaddition of **1b** with MNO.* A solution of **1b** (162 mg, 1 mmol) and MNO (161 mg, 1 mmol) in 3 cm^3 of anhydrous benzene was refluxed for 5 h. After the solvent removal *in vacuo*, the residue was separated by TLC on silica gel using dichloromethane as the eluent. The first band from the TLC plates contained 13 mg (8%) of **1b**. The second band from the TLC plates gave 265 mg (82%) of the adduct **3b**: mp 97—98 °C (from hexane); IR (CCl_4), 3561—3251, 1610, 1053 cm^{-1}; NMR (CCl_4), δ=1.41 (3H, s), 1.56—1.72 (2H, m), 2.22 (6H, s), 2.30 (3H, s), 2.57 (1H, d, J=18.6 Hz), 2.91 (1H, d, J=18.6 Hz), 3.79—3.93 (1H, broad s), 5.37 (1H, d×d, J=8.4, 1.2 Hz), 6.41 (1H, d×d, J=8.4, 5.4 Hz), 6.93—7.02 (2H, broad s). Found: C, 77.70; H, 7.47; N, 4.11%. Calcd for $C_{21}H_{25}O_2N$: C, 77.98; H, 7.79; N, 4.35%.

*Oxidation of **3b**.* To a stirred suspension of pyridinium chlorochromate (100 mg, 0.46 mmol) and anhydrous sodium acetate (20 mg, 0.24 mmol) in 0.5 cm^3 of dichloromethane, was added **3b** (100 mg, 0.31 mmol) in 0.5 cm^3 of dichloromethane under a nitrogen stream. After the reaction mixture was stirred for 5 h, it was chromatographed on Florisil using dichloromethane as the eluent to give 78 mg (80%) of the ketone **3a**, which was identified by mixed mp.

*Cycloaddition of **1c** with MNO.* A solution of **1c** (176 mg, 1 mmol) and MNO (161 mg, 1 mmol) in 3 cm^3 of benzene was refluxed for 7 h. After the solvent removal *in vacuo*, the residue was separated by TLC on silica gel using dichloromethane as the eluent. The first band from the TLC plates contained 93 mg (53%) of **1c**. The second band from the TLC plates gave 88 mg (26%) of the adduct **5**: mp 203—204 °C (from EtOH); IR ($CHCl_3$), 3694, 1608, 1070 cm^{-1}; NMR ($CDCl_3$), δ=1.08 (3H, s), 1.12 (6H, s), 1.55—1.80 (1H, m), 1.64 (1H, d, J=6.0 Hz), 2.24 (9H, s), 4.13 (1H, d×d, J=11.4, 2.4 Hz), 4.72 (1H, d, J=11.4 Hz), 4.77 (1H, s), 4.89 (1H, s), 6.81 (2H, broad s); MS, m/z (rel intensity), 337 (M$^+$, 100), 338 (100). Found: C, 77.95; H, 8.34; N, 3.92%. Calcd for $C_{22}H_{27}O_2N$: C, 78.30; H, 8.07; N, 4.15%.

*Cycloaddition of **2** with MNO.* A solution of **2** (140 mg, 0.8 mmol) and MNO (161 mg, 1 mmol) in 1.5 cm^3 of benzene was refluxed for 20 h. After the solvent removal *in vacuo*, the residue was separated by TLC on silica gel using benzene-ether (1/1) as the eluent. The first band from the TLC plates afforded 38 mg (27%) of **2**. The second band from the TLC plates contained 193 mg (48%) of the adduct **7**; mp above 250 °C (from EtOH); IR ($CHCl_3$), 2941, 1684, 1456, 1381, 1325, 891 cm^{-1}; NMR ($CDCl_3$), δ=1.22 (3H, s), 1.37 (3H, s), 1.40 (1H, d, J=7.5 Hz), 2.01 (1H, d, J=7.5 Hz), 2.23 (1H, d, J=18.3 Hz), 2.81 (18H, s), 2.84 (1H, d, J=18.3 Hz), 3.11 (1H, d, J=18.2 Hz), 3.83 (1H, d, J=10.2 Hz), 3.99 (1H, d, J=18.2 Hz), 4.54 (1H, d, J=10.2 Hz), 6.92 (4H, s); MS, m/z (rel intensity), 497 (M+1, 41), 496 (M$^+$, 100). Found: C, 77.45; H, 7.47; N, 5.33%. Calcd for $C_{32}H_{36}O_3N_2$: C, 77.39; H, 7.31; N, 5.64%.

*Cycloaddition of **1a** with Phenyl Azide (PA).* A solution of **1a** (100 mg, 0.63 mmol) and PA (150 mg, 1.27 mml) in 5 cm^3 of cyclohexane was refluxed for 7 d. After the removal of the solvent, the residue was recrystallized from carbon tetrachloride to give 104 mg (60%) of the adduct **8a**. The filtrate contained 8 mg (8 %) of **1a**. For **8a**: mp 143—145 °C (dec); IR ($CHCl_3$), 1738, 1667, 1600, 1493, 1108, 1091, 1067, 965 cm^{-1}; NMR (CCl_4), δ=1.10 (3H, s), 1.44 (3H, s), 2.45 (1H, d×d, J=7.5, 1.9 Hz), 2.67 (1H, d, J=7.5 Hz), 4.46 (1H, d×d, J=11.7, 1.9 Hz), 4.62 (1H, d, J=11.7 Hz), 4.87 (1H, s) 4.97 (1H, s), 6.86—7.47 (5H, m), MS, m/z (rel intensity), 279 (M$^+$, absent), 251 (25), 118 (100). Found: C, 72.54; H, 6.09; N, 14.15%. Calcd for $C_{17}H_{17}ON_3$: C, 73.19; H, 6.31; N, 14.04%.

*Photoirradiation of the Adduct **8a**.* A solution of **8a** (100 mg, 0.36 mmol) in 10 cm^3 of acetonitrile was irradiated with a high pressure mercury lamp (400 W) through a Pyrex filter for 24 h under a nitrogen atmosphere. After the removal

of the solvent, the residue was chromatographed on Florisil using dichloromethane as the eluent to give 80 mg (85%) of **9**: mp 128—129 °C (from hexane-benzene, 1/1); IR (CCl_4), 1751, 1664, 1601, 1492, 1407 cm^{-1}; NMR ($CDCl_3$), δ=1.29 (3H, s), 1.34 (3H, s), 2.28 (1H, d, J= 6.0 Hz), 2.36—2.55 (2H, m), 2.68 (1H, d×d, J=6.0, 3.0 Hz), 4.72 (1H, s), 4.83 (1H, s), 6.66—7.17 (5H, m). Found: C, 81.28; H, 6.66; N, 5.86%. Calcd for $C_{17}H_{17}ON$: C, 81.24; H, 6.82; N, 5.57%.

Cycloaddition of ***1b*** *with PA.* A solution of **1b** (100 mg, 0.62 mmol) and PA (147 mg, 1.24 mmol) in 5 cm^3 of cyclohexane was refluxed for 7 d. The reaction mixture was then recrystallized from hexane-CCl_4 to give 48 mg (28%) of the adduct **8b**. The filtrate contained 44 mg (44%) of **1b**. For **8b**: mp 172—174 °C (dec): IR ($CHCl_3$), 3625, 1601, 1491, 1113, 1096, 1065 cm^{-1}; NMR ($CDCl_3$), δ=1.32 (3H, s), 1.43 (3H, s), 1.58—1.79 (2H, m), 2.32—2.45 (1H, broad s), 3.76 (1H, broad s), 4.46 (1H, d×d, J=12.0, 2.4 Hz), 4.57 (1H, d, J=12.0 Hz), 4.57 (1H, s), 4.77 (1H, s). 6.86—7.40 (5H, m), MS, m/z (rel intensity), 281 (M^+, absent), 253 (28), 119 (100). Found: C, 72.99; H, 6.82; N, 14.68%. Calcd for $C_{17}H_{19}ON_3$. C, 72.57; H, 6.81; N, 14.94%.

Cycloaddition of ***1c*** *with PA.* A solution of **1c** (100 mg, 0.57 mmol) and PA (136 mg, 1.14 mmol) in 5 cm^3 of cyclohexane was refluxed for 7 d. After the removal of the solvent, the residue was recrystallized from hexane-benzene to give 50 mg (30%) of the adduct **8c**. The filtrate contained the recovered **1c** (30 mg, 30%). For **8c**: mp 145—146 °C (dec): IR ($CHCl_3$), 3549, 1600, 1494, 1110 cm^{-1}; NMR ($CDCl_3$), δ=1.20 (3H, s), 1.24 (3H, s), 1.33 (3H, s), 1.57—1.81 (2H, m), 4.51 (1H, d×d, J=12.0, 3.0 Hz), 4.55 (1H, s), 4.63 (1H, d, J=12.0 Hz), 4.73 (1H, s), 6.83—7.40 (5H, m); MS, m/z (rel intensity), 295 (M^+, absent), 267 (100). Found: C, 73.42; H, 7.17; N, 14.23%. Calcd for $C_{18}H_{21}ON_3$: C, 73.19; H, 7.17; N, 14.23%.

Cycloaddition of ***11*** *with MNO.* A solution of **11** (200 mg, 1.04 mmol) and MNO (168 mg, 1.04 mmol) in 8 cm^3 of benzene was refluxed for 6 h. After the removal of the solvent, the residue was separated by TLC on silica gel using benzene-ethyl acetate (4/1) as the eluent to give **11** (139 mg, 70%), the adduct **12** (47 mg, 13%), and the adduct **13** (36 mg, 10%). For **12**: mp 170—171 °C (from hexane-benzene); IR ($CHCl_3$), 2949, 1732, 869 cm^{-1}; NMR ($CDCl_3$), δ= 1.16 (3H, s), 1.22 (3H, s), 1.30 (3H, s), 1.53—1.68 (1H, m), 2.18—2.48 (1H, m), 2.28 (9H, s), 3.19 (3H, s), 4.04 (1H, d×d, J= 10.5, 3.0 Hz), 4.64 (1H, d, J=10.5 Hz), 6.84 (2H, broad s); MS, m/z (rel intensity), 353 (M^+, 82), 338 (32), 43 (100). Found: C, 74.76; H, 7.79; N, 3.87%. Calcd for $C_{22}H_{27}O_3N$: C, 74.75; H, 7.70; N, 3.96%. For **13**: mp 195—196 °C (from benzene); IR ($CHCl_3$), 2930, 1729, 875 cm^{-1}; NMR ($CDCl_3$), δ=0.50 (3H, s), 1.26 (3H, s), 1.35 (3H, s), 2.15 (3H, s), 2.19 (3H, s), 2.28 (3H, s), 2.28—2.38 (2H, m), 3.26 (3H, s), 3.84 (1H, d, J=10.2 Hz), 5.09 (1H, d×d, J=10.2, 3.0 Hz), 6.71 (1H, broad s), 6.84 (1H, broad s). MS, m/z (rel intensity), 353 (M^+, 68), 43 (100). Found: C, 74.68; H, 7.69; N, 3.40%. Calcd for $C_{22}H_{27}O_3N$: C, 74.75; H, 7.70; N, 3.96%.

Cycloaddition of ***11*** *with PA.* A solution of **11** (100 mg, 0.52 mmol) and PA (124 mg, 1.04 mmol) in 5 cm^3 of cyclohexane was refluxed for 7 d. After the removal of the solvent, the residue was recrystallized from hexane-benzene to give 65 mg (40%) of the adduct **14**. The filtrate contained 23 mg (23%) of **11**. For **14**: 178—179 °C (decomp); IR ($CHCl_3$), 1735, 1601, 1487, 1108, 1095 cm^{-1}; NMR (acetone-d_6), δ=1.00 (3H, s), 1.25 (3H, s), 1.44 (3H, s), 2.37—2.70 (2H, m), 3.26 (3H, s), 4.77 (2H, s), 6.87—7.50 (5H, m); MS, m/z (rel intensity), 311 (M^+, absent), 285 (85), 267 (100). Found: C, 69.07; H, 6.85; N, 13.77%. Calcd for $C_{18}H_{21}O_2N_3$: C, 69.43; H, 6.80; N, 13.50%.

Photoirradiation of ***14****.* A solution of **14** (100 mg, 0.32 mmol) in 10 cm^3 of acetonitrile was irradiated with a Rayonet Photoreactor (MGR-100) fitted with RPR-350 nm lamps through a Pyrex filter for 2 h under a nitrogen atmosphere. After the removal of the solvent, the residue was chromatographed on Florisil using dichloromethane as the eluent to give 81 mg (89%) of 15: mp 129—132 °C; IR ($CHCl_3$), 1733, 1592, 1482, 1448, 1111, 1047 cm^{-1}; NMR ($CDCl_3$), δ= 1.21 (3H, s), 1.27 (3H, s), 1.64 (3H, s), 2.03—2.57 (3H, m), 2.71 (1H, d×d, J=5.8, 3.6 Hz), 3.17 (3H, s), 6.58—7.27 (5H, m); MS, m/z (rel intensity), 283 (M^+, 12), 118 (100). Found: C, 75.43; H, 7.33; N, 5.23%. Calcd for $C_{18}H_{21}O_2N$: C, 76.29; H, 7.47; N, 4.94%.

Methoxymercuration of ***9****.* A suspension of **9** (502 mg, 2 mmol), mercury(II) acetate (638 mg, 2 mmol) in methanol (8 cm^3) was stirred for 30 min. To this reaction mixture, 8 cm^3 of 3 mol dm^{-3} sodium hydroxide solution was added and followed by reduction with 38 mg (1 mmol) of sodium borohydride in 2 cm^3 of 3 mol dm^{-3} aqueous sodium hydroxide. To this mixture, 10 cm^3 of brine and 10 cm^3 of benzene was added and then filtered. The filtrate was extracted with benzene, and the benzene extract was dried over sodium sulfate. After the removal of the solvent *in vacuo*, 439 mg (78%) of **15** was obtained.

References

1) K. Okada and T. Mukai, *J. Am. Chem. Soc.*, **100**, 6509 (1978).

2) L. A. Paquette, L. W. Hartel, R. Gleiter, and M. C. Bohm, *J. Am. Chem. Soc.*, **100**, 6510 (1978).

3) L. A. Paquette and L. W. Hartel, *J. Am. Chem. Soc.*, **101**, 7620 (1979).

4) L. A. Paquette, L. W. Hartel, R. Gleiter, M. C. Bohm, M. A. Beno, and G. G. Christoph, *J. Am. Chem. Soc.*, **101**, 7106 (1981).

5) T. Sasaki, K. Hayakawa, and S. Nishida, *J. Am. Chem. Soc.*, **103**, 565 (1981).

6) M. Nitta, A. Omata, and H. Sugiyama, *Bull. Chem. Soc. Jpn.*, **55**, 569 (1982); *Chem. Lett.*, **1980**, 1615.

7) M. Nitta, A. Omata, and H. Nakatani, *Bull. Chem. Soc. Jpn.*, **56**, 2009 (1983).

8) J. Zsindely and H. Schmid, *Helv. Chim. Acta*, **51**, 1501 (1968).

9) J. P-Katalinic, J. Zsindely, and H. Schmid, *Helv. Chim. Acta*, **57**, 223 (1974).

10) The numerical values presented in parentheses in the structural formulae in this paper are the relative down-field shifts of δ's obtained by using Eu(fod)$_3$.

11) K. N. Houk, *Acc. Chem. Res.*, **8**, 261 (1975).

12) I. Fleming, "Frontier Orbital and Organic Chemical Reactions," John Wiley and Sons, London, New York, Sydney, and Toronto, (1976).

13) G. Muhejee-Muller, P. Gilgen, J. Zsindely, and H. Schmid, *Helv. Chim. Acta*, **60**, 1758 (1977).

14) M. Nitta, A. Omata, and H. Sugiyama, *Bull. Sci. Eng. Res. Lab., Waseda Univ.*, **94**, 55 (1981).

15) M. Nitta and A. Omata, unpublished results.

16) P. Caramella, G. Cellerino, K. N. Houk, F. M. Albini, and C. Santiago, *J. Org. Chem.*, **43**, 3006 (1978); P. Caramella, G. Cellerino, P. Grunanger, F. Marinone Albini, and M. R. Re Cellerino, *Tetrahedron*, **34**, 3545 (1978); and references cited therein.

Bromination of 2,6-Dimethyl-4-methoxybenzyl Alcohol Derivatives

Munehiro NAKATANI,* Kimi TAKAHASHI, Sumie WATANABE, Atsuko SHINTOKU, and Tsunao HASE
Department of Chemistry, Faculty of Science, Kagoshima University, Koorimoto 1-Chome, Kagoshima 890
(Received August 26, 1983)

The reaction of 2,6-dimethyl-4-methoxybenzyl alcohols, ethyl ethers, and acetates, possessing electron-donating and -withdrawing groups at the benzylic position, with bromine water was studied at different temperatures. The reaction was strongly affected by the electronegativity of a benzyl substituent to afford bromination products of aromatic nuclei and 2,4-dibromo-3,5-dimethylmethoxybenzene along with 2,4,6-tribromo derivatives formed by the cleavage of C-C bond.

Bromination of bis[1-(2,6-dimethyl-4-methoxyphenyl)ethyl] ether (**1**) with bromine water in acetic acid has been reported to give acetaldehyde and 2,4-dibromo-3,5-dimethylmethoxybenzene (**4**) at 60 °C *via* bis[1-(3-bromo-2,6-dimethyl-4-methoxyphenyl)ethyl] ether (**2**).[1] A reaction mechanism involving the electrophilic displacement to **2** by bromine to give the oxonium intermediate **3**, which undergoes the cleavage of C-C bond to give the dibromide **4**, was proposed (Scheme 1). When the methoxyl group of **1** was displaced by

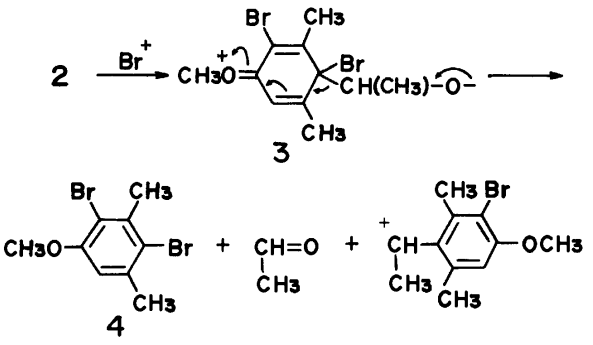

Scheme 1.

methyl group or hydrogen, the cleavage of C-C bond was not observed under the same conditions, whereas at room temperature, but not at 60 °C, 1-(2,6-dimethyl-4-methoxyphenyl)ethanol (**6a**) and 1-(2,4,6-trimethylphenyl)ethanol afforded **4** and 2,4-dibromo-1,3,5-trimethylbenzene along with acetaldehyde, respectively. These results supported that the cleavage reaction was influenced by the resonance effects of the methoxyl and methyl groups, and suggested that it should be further affected by the ease of formation of an aldehyde **5**. Similar cleavage of C-C bond have been observed in the bromination of some bromosalicylic acid and methylphenol derivatives.[2,3] We have devoted conciderable attention to the electrophilic reaction of bromine to 2,6-dimethyl-4-methoxybenzyl alcohols (**6**), ethyl ethers (**7**) and acetates (**8**), especially to the effects of R^1 and R^2 substituents (Fig. 1) on the cleavage of C-C bond. To compare the effect of substituent, a series of 2,6-dimethyl-4-methoxybenzyl alcohol derivatives, **6**, **7**, and **8**, possessing various electron-donating and -withdrawing substituents, CN, CO_2CH_3, $CONH_2$, CH_3, and H, at the benzylic position were synthesized from 3,5-xylenol *via* 2,6-dimethyl-4-methoxybenzaldehyde[4] and reaction with saturated bromine in water was studied in acetic acid at 10, 20, 30, 60 and 90 °C.

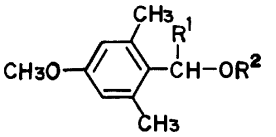

6a: R^1 = Me, R^2 = H
6b: R^1 = R^2 = H
6c: R^1 = $CONH_2$, R^2 = H
6d: R^1 = CO_2Me, R^2 = H
6e: R^1 = CN, R^2 = H

7a: R^1 = Me, R^2 = Et
7b: R^1 = H, R^2 = Et
7c: R^1 = $CONH_2$, R^2 = Et
7d: R^1 = CO_2Me, R^2 = Et
7e: R^1 = CN, R^2 = Et

8a: R^1 = Me, R^2 = Ac
8b: R^1 = H, R^2 = Ac
8c: R^1 = $CONH_2$, R^2 = Ac
8d: R^1 = CO_2Me, R^2 = Ac
8e: R^1 = CN, R^2 = Ac

Fig. 1.

Results and Discussion

The results of the reaction with bromine water at 10, 20, 30, and 60 °C are summerized in Table 1. The alcohols, **6a—e**, mainly afforded the dibromide **4** at 20 °C derived from the cleavage of C-C bond, while at the same temperature, main products from the acetates, **8a—e**, possessing the electronegative acetyl group were 3-bromo derivatives, **11a—e**. On the other hand, in the reaction of the ethyl ethers at 20 °C, **7a** (R^1= Me) and **7b** (R^1=H) afforded **4**, but **7c** (R^1=$CONH_2$), **7d** (R^1=CO_2Me) and **7e** (R^1=CN) gave 3-bromo derivatives, **10c**, **10d**, and **10e**, as main products, respec-

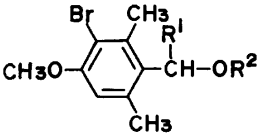

9c: R^1 = $CONH_2$, R^2 = H
9d: R^1 = CO_2Me, R^2 = H
9e: R^1 = CN, R^2 = H

10c: R^1 = $CONH_2$, R^2 = Et
10d: R^1 = CO_2Me, R^2 = Et
10e: R^1 = CN, R^2 = Et

11a: R^1 = Me, R^2 = Ac
11b: R^1 = H, R^2 = Ac
11c: R^1 = $CONH_2$, R^2 = Ac
11d: R^1 = CO_2Me, R^2 = Ac
11e: R^1 = CN, R^2 = Ac

TABLE 1. BROMINATION OF ALCOHOLS **6**, ETHYL ETHERS **7**, AND ACETATES **8** AT 10, 20, 30, AND 60 °C

Compound			Products (yield/%)			
	R^1	R^2	at 10 °C	at 20 °C	at 30 °C	at 60 °C
6a	Me	H	**11a**(43) **4**(45)	**11a**(81) **4**(14)	**11a**(3) **4**(95)	**4**(87) **14**(7) **15**(4)
6b	H	H	**4**(94)	**4**(96)	**4**(95)	—
6c	$CONH_2$	H	**9c**(43) **4**(39)	**4**(95)	**4**(92)	—
6d	CO_2Me	H	**9d**(49) **4**(44)	**4**(95)	**4**(98)	—
6e	CN	H	**9e**(85) **4**(10)	**9e**(18) **4**(74)	**4**(96)	**4**(81) **14**(6) **15**(4)
7a	Me	Et	**4**(93)	**4**(95)	**4**(96)	—
7b	H	Et	**4**(94)	**4**(97)	**4**(97)	—
7c	$CONH_2$	Et	**10c**(92)	**10c**(90) **4**(5)	**10c**(48) **4**(29) **12c**(20)	**12c**(23) **4**(67) **14**(7) **15**(3)
7d	CO_2Me	Et	**10d**(95)	**10d**(95)	**10d**(75) **4**(7) **12d**(15)	**12d**(43) **4**(39) **14**(6) **15**(4)
7e	CN	Et	**10e**(99)	**10e**(98)	**10e**(98)	**10e**(99)
8a	Me	Ac	**11a**(90) **4**(4)	**11a**(88) **4**(12)	**11a**(40) **4**(54)	**4**(87) **14**(6) **15**(2)
8b	H	Ac	**11b**(91)	**11b**(91) **4**(4)	**11b**(84) **4**(10)	**11b**(15) **4**(66) **14**(7) **15**(3)
8c	$CONH_2$	Ac	**11c**(92)	**11c**(90)	**11c**(94)	**11c**(73) **13c**(13) **4**(5)
8d	CO_2Me	Ac	**11d**(98)	**11d**(97)	**11d**(98)	**11d**(75) **13d**(13) **4**(5)
8e	CN	Ac	**11e**(45) **8e**(44)	**11e**(55) **8e**(37)	**11e**(60) **8e**(32)	**11e**(93) **4**(4)

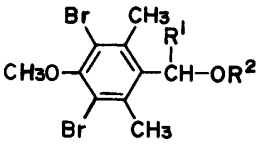

12c: $R^1 = CONH_2$, R^2 = Et **13c**: $R^1 = CONH_2$, R^2 = Ac
12d: $R^1 = CO_2Me$, R^2 = Et **13d**: $R^1 = CO_2Me$, R^2 = Ac
12e: R^1 = CN, R^2 = Et **13e**: R^1 = CN, R^2 = Ac

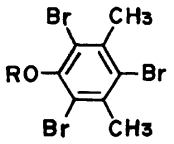

14: R = Me
15: R = H

tively. These results indicate that the C-C bond cleavage is strongly affected by the R^1 and R^2 substituents, as clarified below. Although **6a** and **6b** yielded **4** even at low temperature (10 °C), **6c**, **6d** and **6e** afforded 3-bromo derivatives, **9c**, **9d**, and **9e**, in yields of 43, 49, and 85%, respectively, along with **4**. The reaction of **6a** alone afforded a bromo acetate **11a** at low temperature and all of the alcohols, **6a—e**, gave mixtures of **4**, 2,4,6-tribromo-3,5-dimethylmethoxybenzene (**14**) and the corresponding phenol **15** at 60 and 90 °C. The resulting aldehydes from the C-C bond cleavage afforded their 2,4-dinitrophenylhydrazones, but the corresponding benzyl bromides presumed from bromination with generating hydrobromic acid in the reaction systems could not be isolated. The reaction of the ethyl ethers, **7a—e**, at 10 °C showed a similar result to that of **6a—e**, that is, **7a** and **7b** afforded **4** and **7c—e** yielded monobromides, **10c—e**. The ethers **7c—e**, however, afforded 3,5-dibromo derivatives, **12c** and **12d**, at 30 °C and **12e** at 90 °C by the second bromination on the benzene nucleus, while the first formation of **4** was recognized at 20, 30, and 90 °C, respectively. Apparently, the bromo substituent suppresses the bond cleavage reaction so that **7c** afforded 20% of **12c** at high temperature (90 °C). Both compounds having $CONH_2$ and CO_2Me groups afforded similar reaction products, but the proportions of products from **6c** and **6d** at 10 °C, and from **7c** and **7d** at 20, 30, and 60 °C revealed that the methoxycarbonyl group suppressed the C-C bond cleavage more than the carbamoyl group. Although the acetates, **8a** and **8b**, afforded the monobromides, **11a** and **11b**, at low temperature, they showed no formation of the corresponding dibromides at higher temperature. On the other hand, **8c—e** first showed the formation of dibromides, **13c**, **13d** and **13e**, at 60, 60, and 90 °C in 13, 13, and 7% yields along with **11c** (73%), **11d** (75%), and **11e** (49%), respectively. These acetates, **8c—e**, yielded **4** in 4—5% yields at 60 °C from hydrolysis of the acetate group.

Some potent points derived from our studies on the substituent effects are listed as follows: (i) The electrophilic substitution on the benzene nucleus of the alcohols **6** by bromonium ion, being accompanied by C-C bond cleavage, proceeds according to the mechanism proposed previously and the bond cleavage reaction is largely governed by the R^1 substituent. But in the reaction of the ethyl ethers, **7c—e**, and the acetates, **8c—e**, possessing electronegative carbamoyl, methoxycarbonyl and cyano groups, the bond cleavage reaction is in competition with the second bromination on benzene nucleus to give the dibromides, **12c—e** and **13c—e**. (ii) The cleavage reaction is also largely regulated by the R^2 substituent and occurred most readily in the reaction of the alcohols **6** by the easy formation of aldehydes. (iii) In each R^1 series, this reaction becomes difficult in the order of R^1=CN, CO_2Me, $CONH_2$, H, CH_3.

Experimental

All of the melting and the boiling points are uncorrected. The IR spectra were recorded with a Shimadzu IR-27C spectrophotometer. The ^1H NMR spectra were measured with JEOL JNM 60 and JNM 100 apparatus. The HPLC separation was done with Waters M45 system and Whatman

Partisil M9 Semi-prep column.

*Preparation of **6a**, **7a**, and **8a**.* To an ether soln of MeMgI prepared from MeI (8.0 g) and Mg (1.5 g), a soln of 2,6-dimethyl-4-methoxybenzaldehyde (5.0 g) was added with stirring. After refluxing for a 1/2 h, the resulting complex was decomposed with aq NH_4Cl and the ether layer was washed with aq $Na_2S_2O_3$, aq $NaHCO_3$, and water. The crude product was chromatographed over silica gel to give **6a** (4.7 g; 85%), $C_{11}H_{16}O_2$, mp 51—52 °C; IR ($CHCl_3$) 3240, 1605, 853, 830 cm^{-1}; ^1H NMR ($CDCl_3$) δ=1.45 (3H, d, J=7.2), 1.84 (1H, s), 2.37 (6H, s), 3.71 (3H, s), 5.30 (1H, q, J=7.2), 6.52 (2H, s). Found: C, 73.56; H, 9.12%. Calcd for $C_{11}H_{16}O_2$: C, 73.30; H, 8.95%. The alcohol **6a** was refluxed with a catalytic amount of TsOH in abs EtOH for 12 h and after removal of EtOH, the crude product was purified by column chromatography to give the ethyl ether **7a** (95%), $C_{13}H_{20}O_2$, bp 92—93 °C/7 mmHg (1 mmHg≈133.322 Pa); IR ($CHCl_3$) 1605, 850, 835 cm^{-1}; ^1H NMR ($CDCl_3$) δ=1.16 (3H, t, J=7.0), 1.44 (3H, d, J=7.0), 2.38 (6H, s), 3.28 (2H, q, J=7.0), 3.74 (3H, s), 4.88 (1H, q, J=7.0), 6.56 (2H, s). Found: C, 74.90; H, 9.58%. Calcd for $C_{13}H_{20}O_2$: C, 74.96; H, 9.68%. The alcohol **6a** was acetylated with Ac_2O in pyridine followed by treatment in the usual way to give the acetate **8a** (97%), $C_{13}H_{18}O_3$, bp 134—137 °C/10 mmHg; IR (liq film) 1750, 848, 827 cm^{-1}. ^1H NMR ($CDCl_3$) δ=1.51 (3H, d, J=7.0), 2.01 (3H, s), 2.41 (6H, s), 3.71 (3H, s), 6.25 (1H, q, J=7.0), 6.56 (2H, s). Found: C, 70.11; H, 8.09%. Calcd for $C_{13}H_{18}O_3$: C, 70.24; H, 8.16%.

*Preparation of **6b**, **7b**, and **8b**.* The reduction of 2,6-dimethyl-4-methoxybenzaldehyde with $LiAlH_4$ followed by the treatment with aq NaOH gave **6b** (92%), $C_{10}H_{14}O_2$, mp 70—71 °C; IR (Nujol) 3350, 1603, 853, 830 cm^{-1}; ^1H NMR ($CDCl_3$) δ=1.61 (1H, s), 2.37 (6H, s), 3.73 (3H, s), 4.60 (2H, s), 6.55 (2H, s). Found: C, 72.30; H, 8.50%. Calcd for $C_{10}H_{14}O_2$: C, 72.26; H, 8.49%. The treatment of **6b** with a catalytic amount of TsOH in abs EtOH under reflux afforded **7b** (93%), $C_{12}H_{18}O_2$, bp 117—119 °C/7 mmHg; IR ($CHCl_3$) 1605, 850, 830 cm^{-1}; ^1H NMR ($CDCl_3$) δ=1.23 (3H, t, J=6.8), 2.36 (6H, s), 3.54 (2H, q, J=6.8), 3.76 (3H, s), 4.45 (2H, s), 6.56 (2H, s). Found: C, 74.30; H, 9.29%. Calcd for $C_{12}H_{18}O_2$: C, 74.19; H, 9.34%. The acetylation of **6b** with Ac_2O in pyridine afforded **8b** (92%), $C_{12}H_{16}O_3$, mp 59—60 °C; IR ($CHCl_3$) 1745, 1603, 877, 835 cm^{-1}; ^1H NMR ($CDCl_3$) δ= 2.00 (3H, s), 2.34 (6H, s), 3.73 (3H, s), 5.15 (2H, s), 6.55 (2H, s). Found: C, 69.20; H, 7.71%. Calcd for $C_{12}H_{16}O_3$: C, 69.21; H, 7.74%.

*Preparation of **6e**, **7e**, and **8e**.* A mixture of 2,6-dimethyl-4-methoxybenzaldehyde (2 g) and anhydrous HCN (2 ml) was kept with CaO (400 mg) in a sealed tube at 50 °C for 2 h. The reaction mixture was acidified with dil H_2SO_4 followed by extraction with ether to give the cyanohydrin **6e**[5] (1.8 g; 77%), $C_{11}H_{13}NO_2$, mp 122—123 °C; IR ($CHCl_3$) 3470, 2280, 1610, 850, 834 cm^{-1}; ^1H NMR ($CDCl_3$) δ=2.47 (6H, s), 3.04 (1H, d, J=4.0), 3.77 (3H, s), 5.83 (1H, d, J= 4.0), 6.60 (2H, s). Found: C, 69.23; H, 6.91; N, 7.30%. Calcd for $C_{11}H_{13}NO_2$: C, 69.09; H, 6.85; N, 7.33%. The treatment of **6e** with a catalytic amount of TsOH in abs EtOH under reflux afforded **7e** (90%), $C_{13}H_{17}NO_2$, mp 49—59 °C; IR ($CHCl_3$) 1608, 850, 830 cm^{-1}; ^1H NMR($CDCl_3$) δ=1.41 (3H, t, J=7.0), 2.45 (6H, s), 3.67 (2H, m), 3.74 (3H, s), 5.46 (1H, s), 6.60 (2H, s). Found: C, 71.04; H, 7.90; N, 6.39%. Calcd for $C_{13}H_{17}NO_2$: C, 71.20, H, 7.82; N, 6.39%. The acetylation of **6e** with Ac_2O in pyridine afforded **8e** (98%), $C_{13}H_{15}NO_3$, mp 54—55 °C; IR (Nujol) 1770, 1610, 860, 840 cm^{-1}; ^1H NMR ($CDCl_3$) δ=2.08 (3H, s), 2.48 (6H, s), 3.73 (3H, s), 6.60 (2H, s), 6.80 (1H, s). Found: C, 66.91; H, 6.45; N, 6.11%. Calcd for $C_{13}H_{15}NO_3$: C, 66.93; H, 6.84; N, 6.01%.

*Preparation of **6c**, **7c**, and **8c**.* Into a soln of the cyanohydrin **6e** in abs EtOH, dry HCl gas was passed at 50 °C for 3 h. After removal of the solvent, the crude product was purified by column chromatography to give the glycolamide **6c** (76%), $C_{11}H_{15}NO_3$, mp 145.5—146 °C; IR (Nujol) 3500, 3350, 1670, 1585, 853, 830 cm^{-1}; ^1H NMR ($CDCl_3$) δ=2.33 (6H, s), 3.56 (1H, d, J=2.0), 3.74 (3H, s), 5.45 (1H, br), 5.75 (2H, br), 6.60 (2H, s). Found: C, 63.03; H, 7.03; N, 6.82%. Calcd for $C_{11}H_{15}NO_3$: C, 63.14; H, 7.23; N, 6.69%. The treatment of **6c** with a catalytic amount of TsOH in abs EtOH under reflux afforded **7c** (87%), $C_{13}H_{19}NO_3$, mp 121—122 °C; IR (Nujol) 3500, 3150, 1700, 1605, 875, 846, 820 cm^{-1}; ^1H NMR ($CDCl_3$) δ=1.18 (3H, t, J=6.8), 2.37 (6H, s), 3.40 (2H, q, 6.8), 3.77 (3H, s), 5.25 (1H, s), 6.20 (1H, br), 6.68 (2H, s), 6.93 (1H, br). Found: C, 65.93; H, 8.09; N, 5.89%. Calcd for $C_{13}H_{19}NO_3$: C, 65.80; H, 8.07; N, 5.90%. The acetylation of **6c** with Ac_2O in pyridine at room temperature afforded **8c** (78%), $C_{13}H_{17}NO_4$, mp 145 °C; IR (Nujol) 3490, 3200, 1755, 1700, 860, 845 cm^{-1}: ^1H NMR ($CDCl_3$) δ=2.17 (3H, s), 2.47 (6H, s), 3.80 (3H, s), 6.50—5.60 (2H), 6.60 (2H+1H, s). Found: C, 62.32; H, 6.97; N, 5.52%. Calcd for $C_{13}H_{17}NO_4$: C, 62.14; H, 6.82; N, 5.57%.

*Preparation of **6d**, **7d**, and **8d**.* The amide **6c** was hydrolyzed with 30% aq KOH and methylated with diazomethane to give the methyl glycolate **6d** (82%), $C_{12}H_{16}O_4$, mp 149—150 °C; IR (Nujol) 3480, 1750, 1605, 855, 835 cm^{-1}; ^1H NMR ($CDCl_3$) δ=2.34 (6H, s), 3.27 (1H, br s), 3.71 (6H, s), 5.46 (1H, br s), 6.56 (2H, s). Found: C, 64.26; H, 7.16%. Calcd for $C_{12}H_{16}O_4$: C, 64.27; H, 7.19%. The treatment of **6d** with a catalytic amount of TsOH in abs EtOH under reflux afforded **7d** (92%), $C_{14}H_{20}O_4$, bp 109—111 °C/7 mmHg; IR ($CHCl_3$) 1765, 1610, 845, 830 cm^{-1}; ^1H NMR ($CDCl_3$) δ=1.21 (3H, t, J=6.8), 2.41 (6H, s), 3.48 (2H, d quint, J=2.0, 6.8),[6] 3.65 (3H, s), 3.72 (3H, s), 5.29 (1H, s), 6.55 (2H, s). Found: C, 66.38; H, 8.14%. Calcd for $C_{14}H_{20}O_4$: C, 66.64; H, 7.99%. The acetylation of **7d** with Ac_2O in pyridine afforded **8d** (95%), $C_{14}H_{18}O_5$, mp 66—66.5 °C; IR (Nujol) 1750, 1735, 865, 835 cm^{-1}; ^1H NMR ($CDCl_3$) δ=2.12 (3H, s), 2.35 (6H, s), 3.66 (3H, s), 3.72 (3H, s), 6.61 (2H+1H, s). Found: C, 63.09; H, 6.77%. Calcd for $C_{14}H_{18}O_5$: C, 63.14; H, 6.81%.

*Reaction of the Alcohols **6**, the Ethyl Ethers **7**, and the Acetates **8** with Bromine Water.* To a soln of a material (100 mg) in acetic acid (15 ml), saturated bromine in water (10 ml) containing KBr (0.8 g) was added with stirring until a red colour persisted and the soln was stirred for 1 h, in which to keep the red colour, additional bromine water was sometimes added. After addition of aq $Na_2S_2O_3$, the reaction products at 10, 20, and 30 °C from **7** and **8** except for **7c** and **8c** were directly extracted with hexane from the resulting mixture, and the others were extracted with ether after neutralization with aq $NaHCO_3$. The crude product was chromatographed over silica gel and difficult congeners (**10** and **12**, and **11** and **13**) were separated by a use of HPLC with 1—2% MeOH in CH_2Cl_2.

*2,4-Dinitrophenylhydrazones of Aldehydes from **6a** and **6b**.* The reactions of **6a** and **6b** with bromine water were carried out under a N_2 stream at 90 °C and the each resulting vapour was bubbled through a soln of 2,4-dinitrophenylhydrazine in aq HCl. The precipitate was collected by filtration and recrystallized from EtOH. 2,4-Dinitrophenylhydrazone of acetaldehyde; mp 146—147 °C. 2,4-Dinitrophenylhydrazone of formaldehyde; mp 165—166 °C. They were identified by direct comparison with authentic samples.

*2,4-Dinitrophenylhydrazones of Aldehydes from **6c**, **6d** and **6e**.* Into reaction mixtures of **6c**, **6d**, and **6e** with bromine water at 60 °C, a soln of 2,4-dinitrophenylhydrazine was added and the solutions were left overnight. Each ether extract was purified by chromatography and recrystallization. 2,4-Dinitrophenylhydrazone of glyoxylamide; $C_9H_8O_6N_4$, mp 241.5—243.5 °C (decomp); IR (Nujol) 3400, 3250, 3150, 3070, 1675, 1615, 1590 cm^{-1}; MS, m/z (rel intensity) 253 (M^+, 65), 181 (28), 152 (29), 74 (100). 2,4-Dinitrophenylhydrazone of

methyl glyoxylate; $C_9H_8O_6N_4$, mp 200—202.5 °C (decomp); IR (Nujol) 3300, 3090, 1730, 1620, 1590 cm^{-1}; MS, *m/z* (rel intensity) 268 (M^+, 100), 237 (12), 180 (44), 181 (12), 152 (13). 2,4-Dinitrophenylhydrazone from **6e**; mp 126—127 °C; IR (Nujol) 3300, 1620, 1570 cm^{-1}; MS, *m/z* (rel intensity) 238 (M^+, 100), 181 (24), 152 (21).

Reaction products at 10, 20, 30, and 60 °C. **4**,[1] $C_9H_{10}OBr_2$, mp 107—110 °C; ^{1}H NMR ($CDCl_3$) δ=2.36 (3H, s), 2.58 (3H, s), 3.82 (3H, s), 6.61 (1H, s). **9c**, $C_{11}H_{14}NO_3Br$, mp 144—145 °C; IR (Nujol) 3470, 3230, 1690, 1640, 825 cm^{-1}; ^{1}H NMR (acetone-d_6) δ=2.37 (3H, s), 2.43 (3H, s), 3.82 (3H, s), 4.93 (1H, d, *J*=3.8), 5.48 (1H, d, *J*=3.8), 6.45—7.04 (2H), 6.77 (1H, s). Found: C,45.51; H, 4.99; N, 4.77%. Calcd for $C_{11}H_{14}NO_3Br$: C, 45.85; H, 4.90; N, 4.86%. **9d**, $C_{12}H_{15}O_4Br$, mp 119—120 °C; IR (Nujol) 3450, 1734, 1723, 1580, 836 cm^{-1}; ^{1}H NMR ($CDCl_3$) δ=2.37 (3H, s), 2.45 (3H, s), 3.19 (1H, d, *J*=3.0), 3.76 (3H, s), 3.86 (3H, s), 5.42 (1H, d, *J*=3.0), 6.58 (1H, s). Found: C, 47.76; H, 4.90%. Calcd for $C_{12}H_{15}O_4Br$: C, 47.54; H, 4.99%. **9e**, $C_{11}H_{12}NO_2Br$, mp 122—123 °C; IR (Nujol) 3600, 828 cm^{-1}; ^{1}H NMR ($CDCl_3$) δ=2.41 (3H, s), 2.58 (3H, s), 3.55 (1H, br), 3.83 (3H, s), 5.85 (1H, s), 6.58 (1H, s). Found: C, 48.65; H, 4.52; N, 5.01%. Calcd for $C_{11}H_{12}NO_2Br$: C, 48.91; H, 4.48; N, 5.18%. **10c**, $C_{13}H_{18}NO_3Br$, mp 140—141.5 °C; IR (Nujol) 3540, 3160, 1700, 1590, 833 cm^{-1}. ^{1}H NMR ($CDCl_3$) δ=1.17 (3H, t, *J*=7.0), 2.36 (3H, s), 2.45 (3H, s), 3.37 (2H, q, *J*=7.0), 3.82 (3H, s), 5.19 (1H, s), 6.58 (1H, s), 6.77 (2H, br). Found: C, 49.50; H, 5.51; N, 4.40%. Calcd for $C_{13}H_{18}NO_3Br$: C, 49.38; H, 5.74; N, 4.43%. **10d**, $C_{14}H_{19}O_4Br$, mp 88.5—89.5 °C; IR ($CHCl_3$) 1765, 1595, 828 cm^{-1}; ^{1}H NMR ($CDCl_3$) δ=1.19 (3H, t, *J*=7.0), 2.36 (3H, s), 2.46 (3H, s), 3.47 (2H, br quint, *J*=7.0), 3.65 (3H, s), 3.81 (3H, s), 5.26 (1H, s), 6.59 (1H, s). Found: C, 50.69; H, 5.82%. Calcd for $C_{14}H_{19}O_4Br$: C, 50.77; H, 5.78%. **10e**, $C_{13}H_{16}NO_2Br$, mp 65—65.5 °C; IR ($CHCl_3$) 2300, 1585, 840 cm^{-1}; ^{1}H NMR ($CDCl_3$) δ=1.26 (3H, t, *J*=7.2), 2.44 (3H, s), 2.60 (3H, s), 3.68 (2H, m), 3.85 (3H, s), 5.48 (1H, s), 6.60 (1H, s). Found: C, 52.35; H, 5.40; N, 4.61%. Calcd for $C_{13}H_{16}NO_2Br$: C, 52.36; H, 5.41; N, 4.70%. **11a**, $C_{13}H_{17}O_3Br$, mp 94—95 °C; IR ($CHCl_3$) 1745, 1585, 825 cm^{-1}; ^{1}H NMR ($CDCl_3$) δ=1.54 (3H, d, *J*=6.8), 2.04 (3H, s), 2.42 (3H, s), 2.57 (3H, s), 3.85 (3H, s), 6.27 (1H, q, *J*=6.8), 6.56 (1H, s). Found: C, 52.11, H, 5.48%. Calcd for $C_{13}H_{17}O_3Br$: C, 51.84; H, 5.69%. **11b**, $C_{12}H_{15}O_3Br$, mp 67—68 °C; IR ($CHCl_3$) 1740, 1593, 832 cm^{-1}; ^{1}H NMR ($CDCl_3$) δ=2.04 (3H, s), 2.37 (3H, s), 2.48 (3H, s), 3.86 (3H, s), 5.17 (2H, s), 6.62 (1H, s). Found: C, 50.20; H, 5.22%. Calcd for $C_{12}H_{15}O_3Br$: C, 50.19; H, 5.27%. **11c**, $C_{13}H_{16}NO_4Br$, mp 170—172 °C; IR (Nujol) 3450, 3120, 1690, 1585, 835 cm^{-1}; ^{1}H NMR ($CDCl_3$) δ=2.13 (3H, s), 2.46 (3H, s), 2.51 (3H, s), 3.70 (3H, s), 5.83 (2H, br), 6.59 (1H, s), 6.63 (1H, s). Found: C, 47.13; H, 4.95; N, 4.40%. Calcd for $C_{13}H_{16}NO_4Br$: C, 47.29; H, 4.89; N, 4.24%. **11d**, $C_{14}H_{17}O_5Br$, mp 77.5—79 °C; IR (Nujol) 1760, 1735, 1580, 833 cm^{-1}; ^{1}H NMR ($CDCl_3$) δ=2.08 (3H, s), 2.36 (3H, s), 2.43 (3H, s), 3.66 (3H, s), 3.80 (3H, s), 6.60 (1H, s), 6.65 (1H, s). Found: C, 48.83; H, 4.92%. Calcd for $C_{14}H_{17}O_5Br$: C, 48.71; H, 4.97%. **11e**, $C_{13}H_{14}NO_3Br$, mp 87 °C; IR (liq film) 1775, 1590, 840 cm^{-1}; ^{1}H NMR ($CDCl_3$) δ=2.10 (3H, s), 2.49 (3H, s), 2.63 (3H, s), 3.85 (3H, s), 6.59 (1H, s), 6.87 (1H, s). Found: C, 50.07; H, 4.53; N, 4.44%. Calcd for $C_{13}H_{14}NO_3Br$: C, 50.02; H, 4.52; N, 4.48%. **12c**, $C_{13}H_{17}NO_3Br_2$; IR (Nujol) 3470—3150, 1680 cm^{-1}; ^{1}H NMR ($CDCl_3$) δ=1.16 (3H, t, *J*=6.9), 2.49 (6H, s), 3.37 (2H, q, *J*=6.9), 3.83 (3H, s), 5.33 (1H, s), 5.82 (1H, br), 6.85 (1H, br). Found: C, 39.34; H, 4.60; N, 3.32%. Calcd for $C_{13}H_{17}NO_3Br_2$: C, 39.52; H, 4.34; N, 3.54%. **12d**, $C_{14}H_{18}O_4Br_2$; IR (Nujol) 1765, 1550 cm^{-1}; ^{1}H NMR ($CDCl_3$) δ=1.21 (3H, t, *J*=6.8), 2.47 (6H, s), 3.52 (2H, quint, *J*=6.8), 3.67 (3H, s), 3.82 (3H, s), 5.37 (1H, s). Found: C, 40.75; H, 4.27%. Calcd for $C_{14}H_{18}O_4Br_2$: C, 41.00; H, 4.42%. **13c**, $C_{13}H_{15}NO_4Br_2$, mp 178.5—179.5 °C; IR (Nujol) 3450—3100, 1740, 1690, 1660 cm^{-1}; ^{1}H NMR ($CDCl_3$) δ=2.12 (3H, s), 2.54 (6H, s), 3.82 (3H, s), 5.60—5.85 (2H), 6.70 (1H, s). Found: C, 38.32; H, 3.77; N, 3.35%. Calcd for $C_{13}H_{15}NO_4Br_2$: C, 38.17; H, 3.70; N, 3.42%. **13d**, $C_{14}H_{16}O_5Br_2$, mp 81.5—82.5 °C; IR (Nujol) 1730 cm^{-1}: ^{1}H NMR ($CDCl_3$) δ=2.15 (3H, s), 2.50 (6H, s), 3.71 (3H, s), 3.85 (3H, s), 6.78 (1H, s). Found: C, 39.70; H, 3.79%. Calcd for $C_{14}H_{16}O_5Br_2$: C, 39.65; H, 3.80%. **14**, $C_9H_9OBr_3$, mp 116.5 °C; ^{1}H NMR ($CDCl_3$) δ=2.59 (6H, s), 3.82 (3H, s). **15**, $C_8H_7OBr_3$, mp 165—167 °C; IR (Nujol) 3450 cm^{-1}; ^{1}H NMR ($CDCl_3$) δ=2.57 (6H, s), 6.00 (1H, br). Found: C, 26.75; H, 1.97%. Calcd for $C_8H_7OBr_3$: C, 26.77; H, 1.97%.

Reaction of 6a with Bromine Water at 90 °C. The alcohol **6a** (100 mg) was stirred with saturated bromine water in acetic acid (15 ml) at 90 °C for 1 h. The crude product was isolated in the usual way to give **4** (87 mg; 66%), **14** (31 mg; 15%), and **15** (24 mg; 12%).

Reaction of 7c with Bromine Water at 90 °C. The ethyl ether **7c** (100 mg) was treated in a manner similar to the one descrived for **6a** at 90 °C and the crude product afforded **4** (46 mg; 37%), **12c** (33 mg; 20%), **14** (34 mg; 22%) and **15** (25 mg; 17%).

Reaction of 7e with Bromine Water at 90 °C. The ethyl ether **7e** (100 mg) was treated in a similar manner as above at 90 °C and the crude product afforded **4** (5 mg; 4%), **10e** (19 mg; 14%), **12e** (110 mg; 64%), **14** (3 mg; 2%) and **15** (2 mg; 2%). **12e**, $C_{13}H_{15}NO_2Br_2$, mp 101—102 °C; ^{1}H NMR ($CDCl_3$) δ=1.26 (3H, t, *J*=6.8). 2.55 (6H, s), 3.72 (2H, m), 3.83 (3H, s), 5.83 (1H, s). Found: C, 41.38; H, 4.06; N, 3.66%. Calcd for $C_{13}H_{15}NO_2Br_2$: C, 41.41; H, 4.01; N, 3.71%.

Reaction of 8e with Bromine Water at 90 °C. The acetate **8e** (100 mg) was worked up in a similar manner as above at 90 °C to give **4** (34 mg; 27%), **11e** (66 mg; 49%), **13e** (12 mg; 7%), **14** (11 mg; 7%) and **15** (9 mg; 6%). **13e**, $C_{13}H_{13}NO_3Br_2$, mp 137.5 °C; IR ($CHCl_3$) 1765 cm^{-1}; ^{1}H NMR ($CDCl_3$) δ= 2.14 (3H, s), 2.63 (6H, s), 3.87 (3H, s), 7.03 (1H,s). Found: C, 40.06; H, 3.45; N, 3.51%. Calcd for $C_{13}H_{13}NO_3Br_2$: C, 39.92; H, 3.35; N, 3.58%.

2,4-Dinitrophenylhydrazones of Aldehydes from 8d. Into a reaction mixture of **8d** (100 mg) with bromine water at 90 °C, a soln of 2,4-dinitrophenylhydrazine was added and the reaction vessel was left overnight at room temperature. Ether extract of the reaction mixture was purified by chromatography and recrystallization to give 2,4-dinitrophenylhydrazones of methyl glyoxylate and glyoxylic acid; 18 mg and 23 mg. 2,4-Dinitrophenylhydrazone of glyoxylic acid, mp 185—188 °C; IR (Nujol) 3500—2500, 3280, 1705, 1618, 1577 cm^{-1}, afforded a methyl ester by methylation with diazomethane, which was identical with the 2,4-dinitrophenylhydrazone of methyl glyoxylate.

We wish to express our sincere gratitude to Dr. Shibata of Osaka City University for the elemental analysis.

References

1) T. Kamikawa, M. Nakatani, and T. Kubota, *Tetrahedron*, **24**, 2091 (1968).

2) E. Grovenstein, Jr. and U. V. Henderson, Jr., *J. Am. Chem. Soc.*, **78**, 569 (1956); E. Grovenstein, Jr., and G. A. Ropp, *ibid.*, **78**, 2560 (1956); I. P. Beletskaya, Kh. Vill, and D. A. Reutov, *Zh. Org. Khim.*, **3**, 615 (1967).

3) A. P. Krysin and V. A. Koptyug, *Izv. Otd. Akad. Nauk SSSR, Ser. Khim. Nauk*, **1975**, 73.

4) C. T. Davis and T. A. Geissmann, *J. Am. Chem. Soc.*, **76**, 3507 (1954).

5) M. Nakatani and T. Hase, *Bull. Chem. Soc. Jpn.*, **52**, 462 (1979).

6) Similar observation that methylene protons of alkoxyl group attached to an asymmetric carbon display one AB-type signal in ^1H NMR spectrum, has been reported. G. M. Whitesides, D. Holtz, and J. D. Roberts, *J. Am. Chem. Soc.*, **86**, 2628 (1964). As noted in the experimental section, the methylene protons of ethoxyl group of the following compounds were observed as a quartet in the case of R=H, CH_3 and $CONH_2$, but they displayed double quintet-type or multiplet spectra in the case of R=CO_2Me or CN, respectively.

 © 1984 The Chemical Society of Japan Bull. Chem. Soc. Jpn., 57, 1515—1517 (1984)

Organic Photochemical Reactions. XXX. Photoreactions of *N,N*-Dimethylpyruvamide in Methanol and Ethanol[1,2]

Kensuke SHIMA,* Kimiko TANABE, Shinpei FURUKAWA, Jouji SAITO, and Kazuhiro SHIRAHASHI
Department of Industrial Chemistry, Faculty of Engineering, Miyazaki University, Kirishima, Miyazaki 880
(Received August 29, 1983)

The photoreactions of *N,N*-dimethylpyruvamide (DMPA) in methanol and ethanol were investigated. Irradiation of DMPA in methanol gave three products (3,5-dimethyl-4-oxazolidinone, 2-hydroxy-*N*-methyl-*N*-(methoxymethyl)propanamide, and 2,3-dihydroxy-2,3-dimethyl-*N,N,N'*-trimethyl-*N'*-(methoxymethyl)-butanediamide) in good yields. The product distribution was dependent on the concentration of DMPA and methanol. Similarly, irradiation of DMPA in ethanol gave three products (3,5-dimethyl-4-oxazolidinone, 2-hydroxy-*N*-methyl-*N*-(ethoxymethyl)propanamide, and 2,3-dihydroxy-2,3-dimethyl-*N,N,N'*-trimethyl-*N'*-(ethoxymethyl)butanediamide). The mechanism for the formation of these products is discussed.

Extensive photochemical studies of α-oxo amides have recently been performed by Aoyama's group;[3-6] they considered both synthetic and mechanistic points. They reported that irradiation of *N,N*-dialkylpyruvamides in methanol gave 4-oxazolidinones as a sole product in quantitative yields.[3] In our recent study of the photoadditions of pyruvamides to alkenes,[7] we found that irradiation of *N,N*-dimethylpyruvamide (DMPA) in methanol gave not only 3,5-dimethyl-4-oxazolidinone (**1**), but also the adducts of DMPA with methanol (**2a** and **3a**) in good yields. In this paper we wish to report on the photochemical reactions of DMPA with methanol and ethanol, and to discuss the mechanism for the formation of the photoproducts.

Results and Discussion

Irradiation of DMPA in methanol resulted in the formation of three products (**1**, **2a**, and **3a**) in good yields. These products were separated by preparative GC or column chromatography on silica gel. Their structures were determined by IR, ^{1}H- and ^{13}C-NMR, mass spectra, and elemental analyses, as detailed in the experimental section. Product **1** was assigned as a derivative of 4-oxazolidinones.[3] Product **2a** was the 1:1 adduct of DMPA and methanol, whereas product **3a** was found to be 2:1 adduct of DMPA and methanol on the basis of the elemental analyses and mass spectra. **2a** was characterized as 2-hydroxy-*N*-methyl-*N*-(methoxymethyl)propanamide by IR, ^{1}H- and ^{13}C-NMR spectra.[2] **3a** was found to be the stereoisomeric mixtures of 2,3-dihydroxy-2,3-dimethyl-*N,N,N'*-trimethyl-*N'*-(methoxymethyl)butanediamide from the ^{1}H- and ^{13}C-NMR spectra. Similarly, irradiation of DMPA in ethanol gave three products (**1**, **2b**, and **3b**).

The produced amounts of **1**, **2a**, and **3a** in the irradiation of DMPA in methanol increased linearly with the irradiation time (see Fig. 1). Therefore, these products can be considered to be the primary products from DMPA. Furthermore, it was confirmed that each product remains unchanged under the irradiation in methanol. The product distribution in the photoreaction of DMPA in methanol was found to depend on the concentration of DMPA; as the concentration of DMPA increases, **3a** increases and **1** decreases (see Table 1). The effects of methanol concentration on product yields are shown in Fig. 2. In the irradiation of benzene solutions containing 0.1 mol dm^{-3} DMPA and 0—22 mol dm^{-3} methanol, the yield of **1** remains almost constant, and the yield of **2a** gradually increases

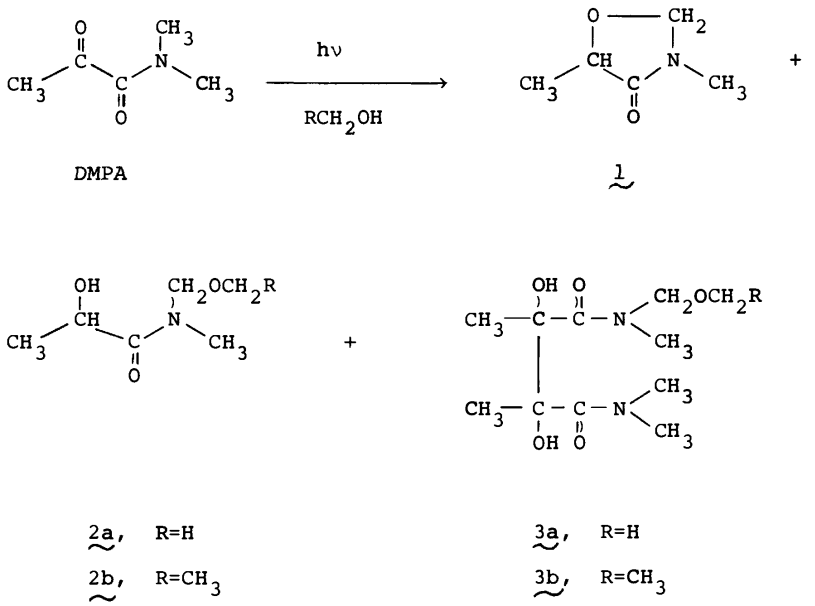

Scheme 1.

as the concentration of methanol increases. The yield of **3a** is highest at *ca.* 1.5 mol dm^{-3} of methanol and decreases at higher methanol concentration. Thus, at very high concentration of methanol, **2a** becomes the major product. The quantum yields for the formation of **1**, **2a**, and **3a** in methanol solution of 0.2 mol dm^{-3} DMPA were as follows: ϕ_1=0.098; ϕ_{2a}=0.34; ϕ_{3a}=0.065.

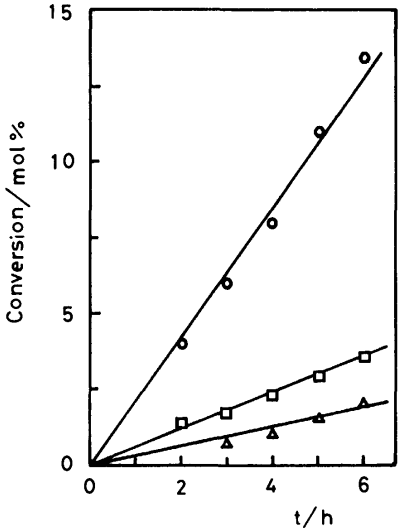

Fig. 1. Effects of irradiation time on product yields. □: **1**, ○: **2a**, △: **3a**. [DMPA]=0.2 mol dm^{-3} in methanol.

The formation of these products is most reasonably explained by a mechanism which involves a zwitterionic intermediate (**5**).[6] The formation of the oxazolidinone (**1**) and the methanol adducts (**2a** and **3a**) from the zwitterion (**5**) can be explained as shown in Scheme 2. Aoyama *et al.*[6] have proposed the mechanism in which the oxazolidinone and the methanol adduct are formed from the imminium ion (**6**), produced by the addition of proton to the zwitterion (**5**). However, it seems to be difficult to explain the formation of **3a** by the mechanism suggested by them.

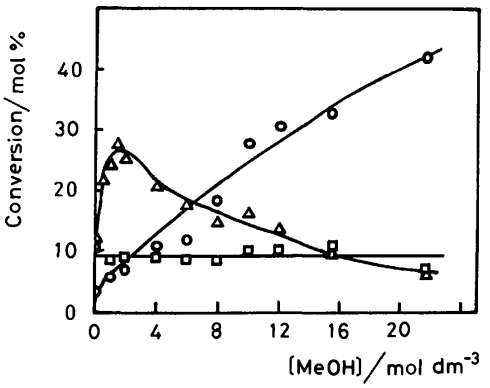

Fig. 2. Effects of methanol concentration on product yields. □: **1**, ○: **2a**, △: **3a**. [DMPA]=0.1 mol dm^{-3}.

Table 1. Concentration effects on products distribution in the photoreactions of DMPA in methanol

DMPA/g	MeOH/cm^3	Irradiation time/h	Products distribution/%		
			1	**2a**	**3a**
8.3	200	72	37	54	9
8.2	140	30	24	55	21
5.5	45	140	12	53	35

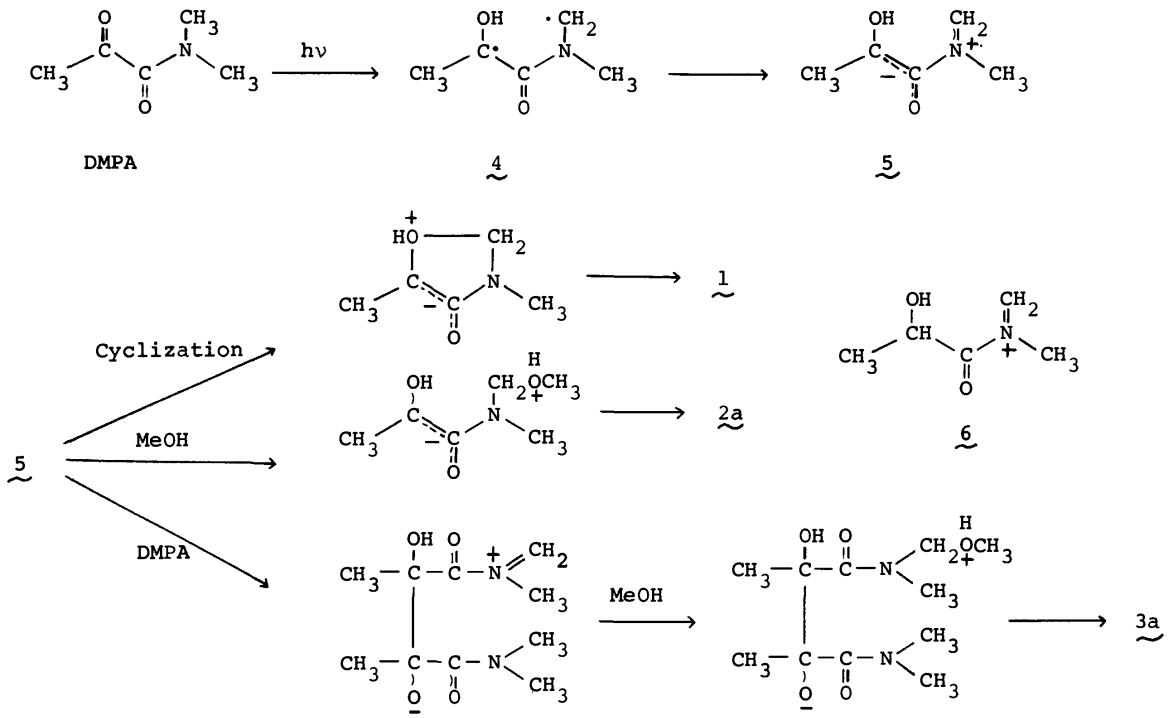

Scheme 2.

Experimental

General. ^{1}H-NMR spectra were recorded on a JEOL JNM-MH 100 machine, ^{13}C-NMR spectra on a JEOL FX 60 machine, IR spectra on a Hitachi IR 260-50 and a JASCO IRA-1 spectrometer, and mass spectra on a JEOL D-300 machine. GC were performed on a Shimadzu GC-6AM and a Hitachi 163 apparatus using a column of Si DC 550 or DEGS at 170 °C. *N,N*-Dimethylpyruvamide (bp 103—105 °C/25 mmHg[†]; lit, bp 53.8 °C/4.5 mmHg[8]) was prepared by the permanganate oxidation[9] of *N,N*-dimethyllactamide (bp 113—116 °C/14 mmHg), which in turn was prepared from the reaction of methyl lactate and anhydrous dimethylamine.[10]

Irradiation of DMPA in Methanol. A solution of DMPA (8.2 g) in 140 cm^3 of methanol was irradiated in a Pyrex doughnut-type vessel under nitrogen with a 300 W high pressure mercury lamp for 30 h. After removal of the solvent, the residue was distilled under reduced pressure to give a liquid (bp 63—130 °C/3 mmHg, 8.3 g) and a viscous oily residue (2.2 g). GC analysis of the distillate showed that it was composed of three products (**1**, **2a**, and **3a**) with the area ratio of 24:55:21. Products **1** and **2a** were isolated by preparative GC on Si DC 550 or DEGS column at 150 °C, and **3a** was isolated by column chromatography on silica gel.

3,5-Dimethyl-4-oxazolidinone (1): IR ($CHCl_3$) 1705, 1100, 1025 cm^{-1}; ^{1}H-NMR (CCl_4) δ=1.31 (3H, d, J=7 Hz, $C\underline{H}_3CH$), 2.83 (3H, s, NCH_3), 4.18 (1H, q, J=7 Hz, $CH_3C\underline{H}$), 4.92 (2H, s, OCH_2N); ^{13}C-NMR (C_6D_6) δ=17.4 (q, $\underline{C}H_3CH$), 26.5 (q, NCH_3), 74.5 (d, $CH_3\underline{C}H$), 81.5 (t, OCH_2N), 172.7 (s, C=O); MS m/z 115 (M^+). Found: C, 51.90; H, 7.97; N, 11.95%. Calcd for $C_5H_9NO_2$: C, 52.16; H, 7.88; N, 12.17%.

*2-Hydroxy-*N*-methyl-*N*-(methoxymethyl)propanamide (2a)*: IR ($CHCl_3$) 3420, 1650, 1100 cm^{-1}; ^{1}H-NMR (CCl_4) δ=1.28 (3H, d, J=7 Hz, $C\underline{H}_3CH$), 2.91 and 2.96 (3H, s, NCH_3), 3.17 and 3.26 (3H, s, OCH_3), 3.94 (1H, br. s, OH), 4.28—4.60 (1H, m, $CH_3C\underline{H}$), 4.64 —4.90 (2H, m, NCH_2O); ^{13}C-NMR (C_6D_6) δ=20.9 and 21.8 (q, $\underline{C}H_3CH$), 33.4 and 33.7 (q, NCH_3), 55.6 (q, OCH_3), 65.2 (d, $CH_3\underline{C}H$), 78.6 and 80.8 (t, NCH_2O), 174.7 (s, C=O); MS m/z 147 (M^+). Found: C, 48.74; H, 9.16; N, 9.47%. Calcd for $C_6H_{13}NO_3$: C, 48.97; H, 8.90; N, 9.52%.

*2,3-Dihydroxy-2,3-dimethyl-*N,N,N′*-trimethyl-*N′*-(methoxymethyl)butanediamide (3a)*: Bp 121—123 °C/2 mmHg; IR ($CHCl_3$) 3340, 1600, 1100 cm^{-1}; ^{1}H-NMR ($CDCl_3$) δ=1.46 (6H, br. s, CH_3C), 2.91, 2.94, 3.30, 3.38, and 3.41 (s, 12H, NCH_3 and OCH_3), 4.69, 4.87, 5.14, and 5.30 (2H, d, J=10 Hz, NCH_2O), 5.89, 6.08, and 6.23 (2H, br. s, OH); ^{13}C-NMR (CCl_4) δ=18.2 and 19.1 (q, $\underline{C}H_3C$), 32.7, 34.0, 36.9, and 37.8 (q, NCH_3), 54.3 and 55.1 (q, OCH_3), 78.3 and 79.5 (t, NCH_2O), 79.5 (s, $CH_3\underline{C}OH$), 177.8 and 186.6 (s, C=O); MS m/z 263 (M^++1, by CI). Found: C, 50.48; H, 8.50; N, 10.65%. Calcd for $C_{11}H_{22}N_2O_5$: C, 50.37; H, 8.45; N, 10.68%.

Irradiation of DMPA in Ethanol. A solution of DMPA (5.9 g) in 140 cm^3 of ethanol was irradiated in a Pyrex vessel for 40 h. After removal of the solvent, the residue was distilled under reduced pressure to give a liquid (bp 45—105 °C/0.5 mmHg, 6.1 g) and a viscous oily residue (1.3 g). GC analysis of the distillate showed that three products (**1**, **2b**, and **3b**) with the area ratio of 57:18:25 were present. Products **1** and **2b** were isolated by preparative GC, and **3b** was isolated by column chromatography on silica gel.

*2-Hydroxy-*N*-methyl-*N*-(ethoxymethyl)propanamide (2b)*: IR ($CHCl_3$) 3420, 1650, 1080 cm^{-1}; ^{1}H-NMR (CCl_4) δ=1.12—1.38 (3H, m, $OCH_2C\underline{H}_3$), 1.27 (3H, d, J=7 Hz, $C\underline{H}_3CH$), 2.97 (3H, s, NCH_3), 3.41 (2H, q, J=7 Hz, $OC\underline{H}_2CH_3$), 3.60 (1H, br. s, OH), 4.24—4.56 (1H, m, $CH_3C\underline{H}$), 4.62—4.93 (2H, m, NCH_2O); ^{13}C-NMR ($CDCl_3$) δ= 15.1 (q, $OCH_2\underline{C}H_3$) 20.9 and 21.9 (q, $\underline{C}H_3CH$), 32.7 and 33.9 (q, NCH_3), 63.8 (t, $O\underline{C}H_2CH_3$), 64.6 (d, $CH_3\underline{C}H$), 76.8 and 78.7 (t, NCH_2O), 176.5 (s, C=O); MS m/z 161 (M^+). Found: C, 52.33; H, 9.15; N, 8.72%. Calcd for $C_7H_{15}NO_3$: C, 52.15; H, 9.38; N, 8.69%.

*2,3-Dihydroxy-2,3-dimethyl-*N,N,N′*-trimethyl-*N′*-(ethoxymethyl)butanediamide (3b)*: Bp 101—102 °C/0.5 mmHg; IR ($CHCl_3$) 3320, 1600, 1100 cm^{-1}; ^{1}H-NMR ($CDCl_3$) δ=1.10—1.42 (3H, m, $OCH_2C\underline{H}_3$), 1.48 (6H, br. s, CH_3C), 2.91, 2.96, 3.38, and 3.42 (9H, s, NCH_3), 3.30—3.64 (2H, m, $OC\underline{H}_2CH_3$), 4.68, 4.87, 5.14, and 5.30 (2H, d, J=10 Hz, NCH_2O), 5.90, 6.07, and 6.23 (2H, br. s, OH); ^{13}C-NMR (C_6D_6) δ=16.0 (q, $OCH_2\underline{C}H_3$), 19.2 and 20.3 (q, $\underline{C}H_3C$), 34.3, 35.3, 37.9, and 38.8 (q, NCH_3), 63.9 (t, $O\underline{C}H_2CH_3$), 78.3 and 79.8 (t, NCH_2O), 81.2 (s, $CH_3\underline{C}OH$), 179.1 and 180.9 (s, C=O); MS m/z 277 (M^++1, by CI). Found: C, 51.91; H, 8.96; N, 10.05%. Calcd for $C_{12}H_{24}N_2O_5$: C, 52.16; H, 8.75; N, 10.14%.

The Ratio of 1: *2a*: *3a under Various Conditions.* In the experiments on the effects of irradiation time, solutions (4 cm^3) of DMPA (0.2 mol dm^{-3}) in methanol were placed in 10 mm Pyrex tubes. The samples were degassed by four freeze-pump-thaw cycles at $\approx 10^{-5}$ mmHg and sealed. The tubes were irradiated for 1—6 h with a merry-go-round apparatus using a Halos PIH 300 mercury lamp in a water bath. After the irradiation, an internal standard (vanilin) was added to each tube, and product yields were determined by GC analysis. The calibration factors were 0.69 for **1**, 3.22 for **2a**, and 2.06 for **3a**. In the experiments of the effects of methanol concentration, degassed benzene solutions (4 cm^3) containing 0.1 mol dm^{-3} of DMPA and 0—22 mol dm^{-3} of methanol were irradiated for 1 h. Light Intensities in quantum yield measurements were determined by tris(oxalato)ferrate(III) actinometry.[11]

The authors are grateful to the Research Center for Material Analysis in Miyazaki University for the use of NMR and MS spectrometers. The present work was partially supported by a Grant-in-Aid for Scientific Research No. 154163 from the Ministry of Education, Science and Culture.

[†] 1 mmHg ≈ 133.322 Pa.

References

1) Part XXIX: K. Shima, Y. Nakatake, and K. Tanabe, *Nippon Kagaku Kaishi*, **1984**, 132.
2) Reported at the 40th Annual Meeting of the Chemical Society of Japan, Fukuoka, October, 1979.
3) H. Aoyama, T. Hasegawa, M. Watanabe, H. Shiraishi, and Y. Omote, *J. Org. Chem.*, **43**, 419 (1978).
4) H. Aoyama, T. Hasegawa, and Y. Omote, *J. Am. Chem. Soc.*, **101**, 5343 (1979).
5) H. Aoyama, M. Sakamoto, and Y. Omote, *J. Chem. Soc., Perkin Trans. 1*, **1981**, 1537.
6) H. Aoyama, M. Sakamoto, K. Kuwabara, K. Yoshida, and Y. Omote, *J. Am. Chem. Soc.*, **105**, 1958 (1983).
7) K. Shima, O. Hosoyama, and K. Tanabe, *Nippon Kagaku Kaishi*, **1981**, 1326.
8) W. F. Gresham, US Patent 2429877 (to E. I. du Pont de Nemours & Co.); *Chem. Abstr.*, **1948**, 924.
9) J. W. Cornforth, *Org. Synth.* Coll. Vol. IV, 467 (1963).
10) W. P. Ratchford and C. H. Fisher, *J. Am. Chem. Soc.*, **69**, 1911 (1947).
11) C. G. Hatchard and C. A. Parker, *Proc. R. Soc. London, Ser. A*, **235**, 518 (1956).

 © 1984 The Chemical Society of Japan Bull. Chem. Soc. Jpn., 57, 1518—1521 (1984) [Vol. 57, No. 6

The Enantioface-differentiating Hydrogenation of the C=O Double Bond with Asymmetrically Modified Raney Nickel. XXXVIII. The Hydrogenation of Methyl Ketones to Optically Active Secondary Alcohols

Tsutomu OSAWA* and Tadao HARADA
Institute for Protein Research, Osaka University, Yamada-oka, Suita, Osaka 565
(Received September 22, 1983)

The enantioface-differentiating (asymmetric) hydrogenation of various methyl ketones ($R-COCH_3$) was carried out over the Raney nickel catalyst modified with (*R*,*R*)-tartaric acid and sodium bromide. The presence of an appreciable amount of carboxylic acid in the reaction system was indispensable for a high optical yield. The highest optical yield (74%) was obtained in the hydrogenation of 3,3-dimethyl-2-butanone in the presence of pivalic acid.

The development of a facile method for the preparation of optically active compounds is one of the important tasks in synthetic organic chemistry. Enantioface-differentiating (asymmetric) catalysts could be useful for a large-scale production of optically active compounds, because the reaction produces a large amount of optically active compounds from a catalytic amount of the optically active substance employed for the preparation of the catalyst.

Many attempts have been carried out to prepare optically active secondary alcohols *via* the hydrogenation of prochiral ketones over enantioface-differentiating catalysts. Several catalysts have been reported to give good optical yields in the enantioface-differentiating hydrogenation of ketones carrying polar groups or unsaturated groups.[1-4] However, no efficient catalysts have been reported for the enantioface-differentiating hydrogenation of alkyl ketones. As far as we know, the highest optical yield (43%) was attained in the hydrogenation of 3,3-dimethyl-2-butanone using an optically active phosphine-rhodium complex catalyst.[5]

As has been reported preliminarily, the Raney nickel modified with tartaric acid (TA) and sodium bromide (TA-NaBr-MRNi) is an excellent catalyst for the enantioface-differentiating hydrogenation of 2-octanone.[6] This paper will describe a successful attempt to obtain a high optical yield in the hydrogenation of 2-octanone and the application of MRNi to the hydrogenation of various methyl ketones.

Results and Discussion

It was well documented that the enantioface-differentiating hydrogenation of β-keto esters over TA-NaBr-MRNi proceeded to give an optical yield of more than 80%.[7] When the optimum conditions for the hydrogenation of β-keto esters were applied to the hydrogenation of 2-hexanone, about 30% of the optical yield was obtained.[8] This result strongly suggested that MRNi was a promising enantioface-differentiating catalyst for the hydrogenation of alklyl ketones as well as β-keto esters. However, under the same conditions as above, the hydrogenation of 2-octanone gave only a poor optical yield. Since the structural difference between 2-hexanone and 2-octanone is not significant, it was expected that the change in the reaction conditions would improve the optical yield of the hydrogenation of 2-octanone. The optical yield of the

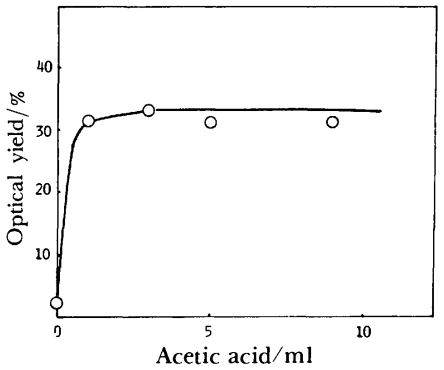

Fig. 1. The relation between the optical yield and the amount of acetic acid in the reaction system. Catalyst; RNi modified with TA (2 g) and NaBr (4 g).

hydrogenation of methyl acetoacetate (MAA) was known to be affected by the presence of carboxylic acid in the reaction system as an additive.[9,10] Thus, the effects of additives on the hydrogenation of 2-octanone were first examined. As is shown in Fig. 1, the addition of a small amount of acetic acid to the reaction system steeply increased the optical yield. Around 30% of the optical yield was obtained by the addition of 1 ml (0.02 mol) of acetic acid to 10 ml (0.064 mol) of the substrate. However, no further increase in the optical yield was observed when more than 1 ml of acetic acid was added. In order to find a more efficient substance than acetic acid, the reaction was carried out in the presence of various additives. The results are listed in Table 1. Among the compounds examined, α-branched carboxylic acids gave the best results. The best result was obtained by the use of pivalic acid. No other classes of compounds, such as hydroxy acid, alcohol, amine, and sulfonic acid, functioned as effective additives. Figure 2 shows the relationship between the amount of pivalic acid in the reaction system and the optical yield. The optical yield increased with the increase in the amount of pivalic acid until it reached a constant value. The maximum optical yield was obtained when more than 12 ml (0.11 mol) of pivalic acid was added to 10 ml (0.064 mol) of 2-octanone. The results showed that the use of a proper amount of α-branched carboxylic acid was important in obtaining a high optical yield.

In the second step, the effects of the modification variables of the nickel catalysts on the optical yields were examined, because the optical yield was also known to be affected significantly by the modification

Table 1. Effects of the additives on the optical yield

Additives	Amount	$[\alpha]_D^{20}$/°	Optical yield/%
None	—	+0.22	2
Acetic acid	3 ml	+3.2	33
Propionic acid	12 ml	+4.2	43
Hexanoic acid	13 ml	+4.2	43
Lauric acid	21 g	+3.9	40
Stearic acid	9 g	+2.9	29
Isobutyric acid	15 ml	+5.6	57
Pivalic acid	18 ml	+6.2	63
2, 2-Dimethylhexanoic acid	23 g	+5.7	58
Diphenylacetic acid	10 g	+4.1	42
Tartaric acid	10 mg	+0.11	1
3-Hydroxybutyric acid	0.01 g	+0.28	3
	11 g	—[1]	—[1]
2, 2-Dimethyl-1-propanol	9 g	+0.26	3
Triethylamine	15 ml	+0.88	9
p-Toluenesulfonic acid	7 g	—[1]	—[1]

Modifying solution: (*R*, *R*)-TA (2 g) and NaBr (4 g) in 200 ml of H_2O. 1) No hydrogen uptake.

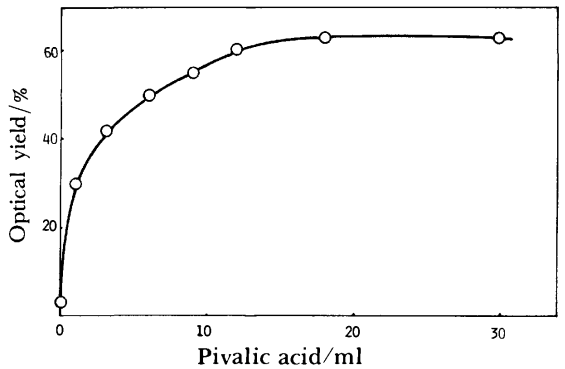

Fig. 2. The relation between the optical yield and the amount of pivalic acid in the reaction system. Catalyst; RNi modified with TA (2 g) and NaBr (4 g).

variables. Figure 3 shows the relationship between the amount of NaBr used for the preparation of MRNi and the optical yield. The optical yield increased with the increase in the amount of NaBr to reach a plateau. The constant value was obtained by the addition to TA of more than twice as much NaBr by weight.

Besides NaBr, various inorganic salts were used for the preparation of MRNi. None of the inorganic salts was found to be more effective than NaBr, as is shown in Table 2.

The modifying pH and the temperature were found to be important factors governing the optical yield of the reaction, like the hydrogenation of MAA.[7] The dependences of the optical yields on the modifying pH and the temperature are listed in Table 3. So far as we

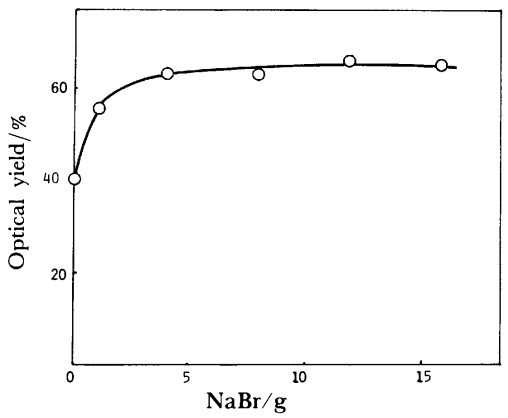

Fi. 3. The relation between the optical yield and the amount of NaBr in modifying solution. Additive; Pivalic acid (18 ml).

Table 2. Hydrogenation of 2-octanone over TA-inorganic salt-MRNi

Inorganic salt in the modifying solution(g)	Reaction		Optical yield/%
	Time	Conversion/%	
None	20 h	83	29
NaBr(14)	20 h	100	51
NaCl(16)	20 h	100	47
NaF(1.5)	20 h	100	29
NaI(0.002)	3 d	70	27
NaH_2PO_4(2)	5 d	100	4
Na_2SO_4(16)	20 h	100	31
$NaNO_3$(0.2)	3 d	100	32
LiBr(4)[1]	3 d	90	14
KBr(4)[2]	4 d	87	7
NH_4Br(4)[3]	7 d	84	6

Modifying solution: (*R*, *R*)-TA (2 g) and an appropriate amount of inorganic salt in 200 ml of H_2O. Additive; Hexanoic acid (13 ml). 1) Modifing pH was adjusted with 1 mol dm^{-3} LiOH. 2) Modifying pH was adjusted with 1 mol dm^{-3} KOH. 3) Modifying pH was adjusted with 14 mol dm^{-3} NH_4OH.

Table 3. Dependence of optical yield on the modifying temperature and modifying pH

Modifying temperature/°C	Modifying pH	Optical Yield/%
100	2.5	37
100	3.2	63
100	5	46
0	3.2	16
50	3.2	28

Modifying solution: TA (2g) and NaBr (8g) in 200ml of H_2O. Additive: Pivalic acid (18ml).

Table 4. Hydrogenation of methyl ketones ($R-CO-CH_3$) over (R, R)-TA-NaBr-MRNi

R-	$[\alpha]_D^{20}$/°	Optical yield/%	Configuration of the product
CH_3CH_2-	+6.8	49	*S*
$CH_3(CH_2)_2-$	+8.7	63	*S*
$CH_3(CH_2)_3-$	+7.6	66	*S*
$CH_3(CH_2)_4-$	+6.8	66	*S*
$CH_3(CH_2)_5-$	+6.4	66	*S*
$CH_3(CH_2)_7-$	+5.1	58	*S*
$CH_3(CH_2)_{10}-$	+4.7	65	*S*
$(CH_3)_2CH-$[1]	+3.0	63	*S*
$(CH_3)_3C-$[1]	+5.7	74	*S*
$C_6H_5(CH_2)_2-$	+8.2	58	*S*

Modifying solution: (*R*, *R*)-TA (2g) and NaBr (12g) in 200ml of H_2O. Additive: Pivalic acid (18ml). 1) MRNi was prepared from 19g of the RNi alloy.

examined, the modification at pH 3.2, and 100 °C gave the best result.

The enantioface-differentiating hydrogenations of various kinds of methyl ketones were carried out under the optimum reaction conditions for the hydrogenation of 2-octanone. The results are shown in Table 4. Unbranched methyl ketones, except for 2-butanone and 4-phenyl-2- butanone, were hydrogenated in an optical yield of around 65%. 2-Butanone and 4-phenyl-2-butanone were hydrogenated in rather low optical yields. From the comparison of the optical yields of the hydrogenation of 2-butanone, 3-methyl-2-butanone, and 3,3-dimethyl-2-butanone, it appears that there is a tendency for methyl ketones with α-alkyl substituents to be hydrogenated in higher optical yields than unbranched ones. The highest optical yield (74%) was obtained in the hydrogenation of 3,3-dimethyl-2-butanone.

Experimental

The analytical and preparative GLC of the products were carried out with a Shimadzu GC-6A gas chromatograph. The optical rotations were measured with a Perkin Elmer 241 polarimeter. The ^{1}H-NMR and IR spectra were taken with a JEOL-FX200 instrument and a Shimadzu IR 27G spectrometer respectively.

Materials. All the chemicals except for those described below were obtained from commercial sources and were used without further purification.

Tetrahydrofuran. Commercial tetrahydrofuran was dried over NaH overnight and then distilled.

Racemic 3-Hydroxybutyric Acid. This was prepared by the alkali hydrolysis of methyl 3-hydroxybutyrate which had been obtained by the hydrogenation of MAA.

2,2-Dimethylhexanoic Acid. This compound was prepared by the procedure of Pfeffer *et al.*[11]

Catalyst. Unless otherwise stated in the text, the catalyst was prepared in the following manner: a 3.8-g portion of the Raney nickel alloy (Ni:Al=42:58)was added, portion by portion,to 40 ml of a 20% aqueous NaOH solution, and then the mixture was allowed to stand at 100 °C for 1 h. After the subsequent removal of the alkaline solution by decantation, the catalyst was washed 30 times with a 30-ml portion of deionized water. The resulting catalyst was modified for 1 h at 100 °C with 200ml of an 1.0% aqueous solution of (*R*,*R*)-TA containing the stated amount of inorganic salt, the pH of which had been adjusted to 3.2 with 1 mol dm^{-3} NaOH. After the removal of the modifying solution, the catalyst was washed successively with a 20-ml portion of water, two 100-ml portions of methanol, and two 30-ml portions of anhydrous tetrahydrofuran.

Hydrogenation of Methyl Ketones. A mixture of methyl ketone (10ml) dissolved in anhydrous tetrahydrofuran (20 ml) and a stated amount of an additive was subjected to hydrogenation under an initial hydrogen pressure of 90 kg/cm^2. Hydrogenation was carried out in a 100ml autoclave at 100 °C. After the removal of the catalyst by decantation and the evaporation of the solvent, the product was dissolved in 100ml of ether and washed with a saturated aqueous solution of K_2CO_3 to remove the carboxylic acid. The ether solution was then dried over anhydrous Na_2SO_4 and concentrated *in vacuo*. As for 2-hexanol, 2-heptanol, 2-octanol, 2-decanol, 2-tridecanol, and 4-phenyl-2-butanol, simple distillations gave hydrogenated products with chemical purities of more than 98% (GLC analyses: at 130 °C, 5% Tween 80 on Shimalite W; at 100—220 °C, 2% OV-17 on Chromosorb W). In the cases of 2-butanol, 2-pentanol, 3-methyl-2-butanol, and 3,3-dimethyl-2-butanol, the products were contaminated by the solvent (tetrahydrofuran) through the simple distillation. Some of the products were further purified by preparative GLC (at 100 °C for 2-butanol, 130 °C for 2-pentanol and 3,3-dimethyl-2-butanol, 20% PEG-20M Chromosorb W; at 125 °C, 15% UCON 50HB-2000 on Chromosorb W for 3-methyl-2-butanol) and subjected to analyses of the chemical and optical purities. These products showed chemical purities of more than 98% in the GLC analyses (at 130 °C, 5% Tween 80 on Shimalite W; at 100—220 °C, 2% OV-17 on Chromosorb W). The ^{1}H-NMR spectra of the products were consistent with their structures; IR (neat) 3350—3400 cm^{-1} (OH).

Determination of Optical Yield. The optical yields of the hydrogenation of methyl ketones were estimated from the specific rotations of the pure enantiomers: (*S*)-2-butanol, $[\alpha]_D^{20}$+13.87 ° (neat);[12] (*S*)-2-pentanol, $[\alpha]_D^{20}$+13.70 ° (neat);[12] (*S*)-2-hexanol, $[\alpha]_D^{20}$+11.57 ° (neat);[12] (*S*)-2-heptanol, $[\alpha]_D^{20}$ +10.32 ° (neat);[12] (*S*)-2-octanol, $[\alpha]_D^{20}$+9.76 ° (neat):[12] (*S*)-2-decanol, $[\alpha]_D^{20}$+8.68 ° (neat);[12] (*S*)-2-tridecanol, $[\alpha]_D^{20}$+7.22 ° (neat);[12] (*S*)-3-methyl-2-butanol, $[\alpha]_D^{20}$+4.85 ° (neat);[13] (*S*)-3,3-dimethyl-2-butanol, $[\alpha]_D^{20}$+7.71 ° (neat);[14] (*S*)-4-phenyl-2-butanol, $[\alpha]_D^{20}$+14.23 ° (neat).[14]

The authors would like to thank Professor Yoshiharu Izumi, Dr. Akira Tai, and Dr. Hiroshi Ozaki, Osaka University, for their many helpful suggestions. The authors also wish to express their thanks to the Ajinomoto Co., Inc., for its financial support and to the Kawaken Fine Chemicals Co., Ltd., for providing the RNi alloy.

References

1) T. Hayashi and M. Kumada, *Acc. Chem. Res.*, **15**, 395 (1982).
2) K. Ito, T. Harada, and A. Tai, *Bull. Chem. Soc.Jpn.*, **53**, 3367 (1980); A. Tai, K. Ito, and T. Harada, *ibid.*, **54**, 223 (1981).
3) S. Murakami, T. Harada, and A. Tai, *Bull. Chem. Soc. Jpn.*, **53**, 1356 (1980).
4) Y. Hiraki, K. Ito, T. Harada, and A. Tai, *Chem. Lett.*, **1981**, 131.
5) T. Hayashi, T. Mise, and M. Kumada, *Tetrahedron Lett.*, **1976**, 4351.
6) T. Osawa and T. Harada, *Chem. Lett.*, **1982**, 315.
7) T. Harada, M. Yamamoto, S. Onaka, M. Imaida, H. Ozaki, A. Tai, and Y. Izumi, *Bull. Chem. Soc. Jpn.*, **54**, 2323 (1981); M. Nakahata, M. Imaida, H. Ozaki, T. Harada, and A. Tai, *ibid.*, **55**, 2186 (1982); A. Tai, T. Harada, Y. Hiraki, and S. Murakami, *ibid.*, **56**, 1414 (1983).
8) A. Tai, T. Harada, Y. Hiraki, and S. Murakami,*Bull. Chem. Soc. Jpn.*, **56**, 1414 (1983).
9) Y. Izumi, *Angew. Chem., Int. Ed. Engl.*, **10**, 871 (1971).
10) Y. Orito, S. Niwa, and S. Imai, *Yuki Gosei Kagaku Kyokai Shi*, **35**, 672, 753 (1977).
11) P. E. Pfeffer, L. S. Silbert, and J. M. Chirinko, Jr., *J. Org. Chem.*, **37**, 451 (1972).
12) R. H. Pickard and J. Kenyon, *J. Chem. Soc.*, **99**, 45 (1911).
13) R. H. Pickard and J. Kenyon, *J. Chem. Soc.*, **101**, 621 (1912).
14) R. H. Pickard and J. Kenyon, *J. Chem. Soc.*,**105**, 1115 (1914).

Studies of Liquid Water by Computer Simulations. III. Dynamical Properties of a 2-D Model

Yosuke KATAOKA
Department of Chemistry, Faculty of Science, Kyoto University, Sakyo-ku, Kyoto 606
(Received December 2, 1983)

Molecular dynamics simulations of a water-like system are performed at many temperatures and densities. A 2-dimensional model of water is used for the system with 144 molecules in a square cell. The calculated self-diffusion coeffcient and the dipole direction relaxation time are in good agreement with the observed values in a wide temperature-pressure plane. Cross correlation function of displacement and local orientational order parameter are computed by the time-averaged configurations, where the average of period is several times longer than the velocity correlation time. The cross correlation is observed even in the third neighbor pairs, which proves the existence of hydrogen-bonded local structure. The lifetime of this local structure is about 2×10 ps at low temperatures and low density, where density maximum is known. The lifetime of the unstable species with a rather high energy is found to be about 0.5—2 ps at low temperatures and low density.

In the first paper of this series,[1] it was shown that a simple 2-D model of water can reproduce main features of the thermodynamical behavior observed in real water over a wide region of the liquid state. In the present article, we shall study dynamical properties of 2-D water by molecular dynamics (MD) simulations.

By MD method, Rahman and Stillinger and others[2] studied static and dynamic properties of liquid water. However, a systematic study is not yet performed on the density dependence of the dynamical properties of liquid water. For this reason, we are going to perform MD simulations at many temperatures and densities. The dipole direction relaxation time and the self-diffusion coefficient will be calculated as a function of temperature and density. The effects of compression on these quantities which are in good agreement with experimental data[3,4] will be discussed. The present paper also deals with the lifetime of the local structure in liquid water which is not examined so far. Because water molecules perform oscillatory motion within the framework of hydrogen-bonded local structure, the configuration is averaged over a period longer than the correlation time of velocity. The lifetime of the local structure will be calculated by two methods, the cross correlation function of displacement and the local orientational order parameter. The dynamics of the unstable molecule which is not well bound in the hydrogen-bonded cluster will be also studied. The concentration of the unstable species will be obtained as a function of temperature and pressure and will be compared with the results of the two-state model analysis of real water.[5]

Molecular Dynamics Method

Classical mechanics describes the time evolution of our 2-D water system. The Hamiltonian H for N rigid rotor molecules consists of kinetic energy for translational and rotational motions, plus interaction potential energy.

$$H = \frac{1}{2}\sum_{i=1}^{N}(m\boldsymbol{v}_i^2 + I\dot{\varphi}^2) + \sum_{(ij)} U(\boldsymbol{R}_{ij}, \varphi_i, \varphi_j). \quad (1)$$

The linear and angular velocities are denoted by $\boldsymbol{v}$ and $\dot{\varphi}$.

The pair potential U consists of a Lennard-Jones potential and an anisotropic potential U_{anis} multiplied by a switching function S:

$$U(\boldsymbol{R}_{12}, \varphi_1, \varphi_2) = 4\varepsilon\left[\left(\frac{\sigma}{R_{12}}\right)^{12} - \left(\frac{\sigma}{R_{12}}\right)^{6}\right] + S(R_{12}; R_1, R_2, R_3)\, U_{\text{anis}}(\boldsymbol{R}_{12}, \varphi_1, \varphi_2), \quad (2)$$

where R_{12} denotes the distance between two molecules 1 and 2 and φ_1 and φ_2 the orientations of the respective molecules. The switching function S cuts down the anisotropic potential for $R_{12}<R_1$ and for $R_{12}>R_3$. The details are shown in Ref. 1.

The mass of the molecule m is 18 in units of atomic weight and the moment of inertia I is 3.34×10^{-46} g m^2. For simplicity, the center of mass is assumed to be the center of the molecule (see Fig. 2 of Ref. 1).

We shall use the following reduced units.[1] The energy E is measured in units of ε_0=24.68 kJ/mol, ($-\varepsilon_0$ is the absolute minimum of the pair potential energy, *i.e.* ε_0 is the hydrogen bond energy), the length in units of R_0=27.6 nm and area per molecule A in units of R_0^2. Pressure P is measured in units of ε_0/R_0^2. (If we replace R_0^2 by R_0^3, new reduced units can be applied to the three-dimensional real water. Such reductions of units are of course only a convention, and therefore one should be satisfied with semiquantitative comparisons between the 2 D model and real water). Temperature T is measured in units of ε_0/R, where R is the gas constant which is not shown explicitly hereafter. As for the time units we use three kinds of units:

1) Time unit for rotation
$$t_0^{\text{ROT}} = (I/\varepsilon_0)^{1/2} = 2.86 \times 10^{-14}\,\text{s},$$
2) Time unit for translation (3)
$$t_0^{\text{TR}} = (mR_0^2/\varepsilon_0)^{1/2} = 2.37 \times 10^{-13}\,\text{s},$$
3) and real time scale s.

Our system consists of 144 molecules in a square unit cell with periodic boundary condition. The coupled dynamical equations are numerically integrated[6] with time increment

$$\Delta t = 0.870 \times 10^{-15}\,\text{s} = 0.304\, t_0^{\text{ROT}}. \quad (4)$$

The total energy is conserved within 0.01% after 24000 steps, or 21 ps. At low temperatures and low density, a long run (30000 steps or 78 ps) with time increment

2.6×10^{-15} s is performed to obtain the long (20 ps) lifetime of the local structure.

At a given density the 144 molecules are placed initially within the periodic cell at random positions, with random orientations, and with no translational or rotational velocities. After some steps, the kinetic energies are reduced to decrease the temperature. This reduction was repeatedly performed to obtain several low temperature samples. In our standard run, 3000 steps are spent for the aging of the system. After this interval, the subsequent period of 30000 steps, or 26 ps is the period over which the molecular dynamics' statistical averages are calculated. Simulations are performed at about 90 state points. The static properties (energy, pressure, radial distribution function and others) thus calculated are in good agreement with the results of our Monte Carlo simulations.[1]

Kinetic Properties

A couple of dynamical quantities are calculated in a way similar to Rahman and Stillinger's method.[2] As these results are only the 2-D version of their results, in the first place only a part of these will be shown briefly in the low density region (area per molecule $A=0.957\ R_0^2$), where thermodynamic quantities of 2-D water show interesting aspects like real liquid water under normal pressure. After that, the dipole direction relaxation time and the self-diffusion coefficient will be discussed.

The velocity autocorrelation function at temperature $T=0.18\ \varepsilon_0$, area per molecule $A=0.957\ R_0^2$ crosses the horizontal axis at 0.05 ps and shows several oscillations. The Fourier spectrum has a peak at $3\times10^{13}\ s^{-1}$ with half-full-width $6\times10^{13}\ s^{-1}$. The angular velocity correlation function crosses the horizontal axis at 0.02 ps. The Fourier spectrum has a peak at $9\times10^{13}\ s^{-1}$, with half-full-width $6\times10^{13}\ s^{-1}$. These frequencies correspond to the observed ν_L and ν_T.[7] These functions show clearly that there exists an oscillatory motion of water molecules at low temperatures.

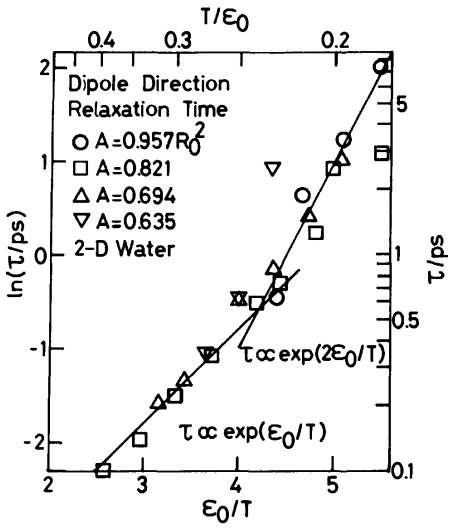

Fig. 1. The dipole direction relaxation time τ is plotted against the inverse of temperature $1/T$ at four densities.

The molecular dipole direction relaxation time τ is shown in Fig. 1 at four densities. This time constant at low densities and low temperatures has the comparable value to the measured dielectric relaxation time.[3,7] The relaxation time in the case where $A=0.821\ R_0^2$ is shorter than that in the case of low density ($A=0.957\ R_0^2$) at low temperatures $T\leq0.24\ \varepsilon_0$. This effect of compression is compared with the experiments on the dielectric relaxation under high pressure,[3] qualitatively. Figure 1 also shows that the temperature dependence of the dipole direction relaxation time τ is roughly written as $\tau\propto\exp(2\ \varepsilon_0/T)$ at low temperatures ($T\lesssim0.24\ \varepsilon_0$) and as $\tau\propto\exp(\varepsilon_0/T)$ at high temperatures ($T\gtrsim0.24\ \varepsilon_0$), where ε_0 is the hydrogen bond energy. The temperature dependence at low temperatures seems too steep, compared with the observed results on real water.[7]

The self-diffusion coefficient D is calculated from the mean-square displacement. In Fig. 2, D is shown as a function of T and P. The region between two dashed lines corresponds to liquid state. At low temperature ($T=0.18\varepsilon_0$), D is almost constant in spite of compression, thus D shows anomalous behavior similar to the observed one.[4] Figure 3 shows that the temperature dependence of D at constant density is well approximated to be $D\propto\exp(-\varepsilon_0/T)$. This depend-

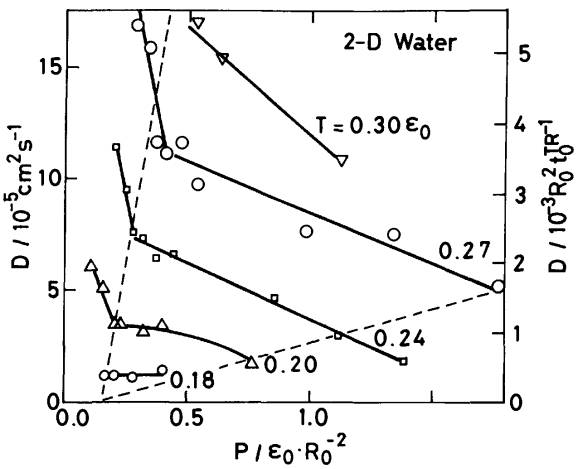

Fig 2. The self-diffusion coefficient D *vs.* pressure P plots are shown. Values of the temperature are indicated next to each curve. The region between two dashed lines corresponds to the liquid state.

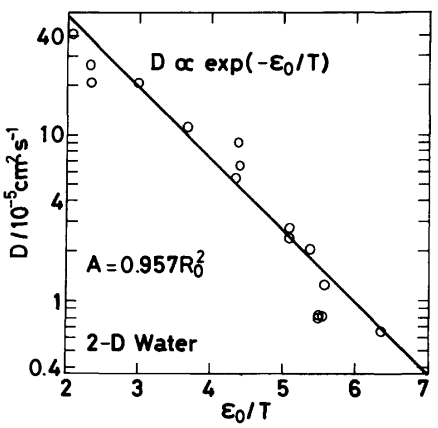

Fig. 3. Plot of D *vs.* $1/T$ at $A=0.957\ R_0^2$.

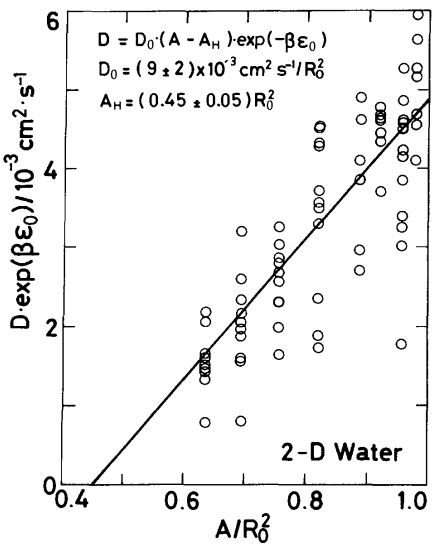

Fig. 4. Plot of $D\exp(\varepsilon_0/T)$ *vs.* area per molecule A.

ence is comparable with experimental results on real water.[7] The density dependence is shown in Fig. 4. From Figs. 3 and 4 the temperature-density dependence of D is summarized as follows;

$$\begin{aligned} D &= D_0\,(A-A_H)\exp\,(-\varepsilon_0/T), \\ D_0 &= (9\pm2)\times10^{-3}\,\mathrm{cm^2\,s^{-1}}\,R_0^{-2}, \\ A_H &= (0.45\pm0.05)\,R_0^2, \end{aligned} \tag{5}$$

although there are some deviations especially at low temperatures. It is worthwhile to notice that the value of constant A_H is close to the area of the high density ice ($0.50\ R_0^2$) and A-A_H means the area of hole in liquid water.

Thus it has been shown that the MD simulation of 2-D model can reproduce the main anomalous dynamical behavior of liquid water. On the basis of these results, the lifetime of the hydrogen-bonded cluster will be obtained in the next section.

Lifetime of Hydrogen-bonded Local Structure

Time Averaged Configuration. An oscillatory motion of water molecule is seen at low temperatures and densities as shown in the preceding section. Therefore, we use the time averaged configuration in this section in order to obtain the lifetime of hydrogen bonded local structure. The configuration is averaged over a period of 0.13 ps. This means that we study the vibrationally averaged structure (V-structure) of liquid water as discussed by Eisenberg and Kauzmann.[7,8]

Cross Correlation of Displacement. In the V-structure it is expected that the molecules in the same hydrogen-bonded cluster move to nearly the same direction on average. On the basis of this idea, we are going to calculate the cross correlation of displacement.

The position r_i of molecule i at time $t=0$ is denoted as r_i^0, and the displacement of molecule i is $r_i-r_i^0$. Figure 5 shows the cross correlation of displacement of molecule i and j $<(r_i-r_i^0)\cdot(r_j-r_j^0)>$ at low temperatures and low density with the following condition at $t=0$. As the low density ice type network of hydrogen bond is the square lattice in our model,[1] the molecular distance R_{ij} at $t=0$ is classified as follows;

$$\begin{aligned} &0.85\,R_0 < R_{ij} < 1.23\,R_0 \quad (i.e.\ R_{ij} \simeq R_0), \\ &1.23\,R_0 < R_{ij} < 1.71\,R_0 \quad (i.e.\ R_{ij} \simeq 2^{1/2}R_0), \\ &1.71\,R_0 < R_{ij} < 2.41\,R_0 \quad (i.e.\ R_{ij} \simeq 2R_0), \\ \text{or } &2.41\,R_0 < R_{ij} < 2.91\,R_0 \quad (i.e.\ R_{ij} \simeq 2^{3/2}R_0). \end{aligned} \tag{6}$$

It should be noticed that the linear part of cross correlation function ($R_{ij}-R_0$ at $t=0$) extends up to 2×10 ps. The value of tangent of this linear part is as large as about 30% of that in the

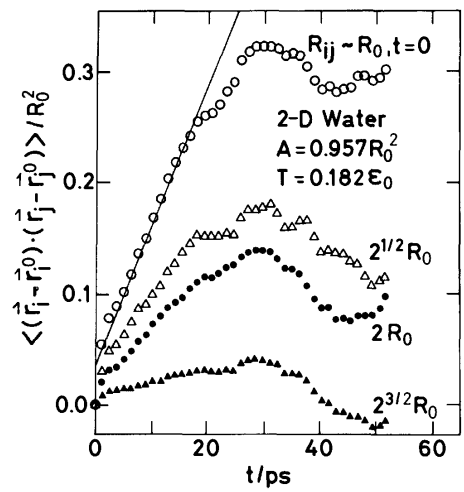

Fig. 5. The cross correlation functions $<(r_i-r_i^0)\cdot(r_j-r_j^0)>$. The initial conditions in the statistics are indicated in the figure.

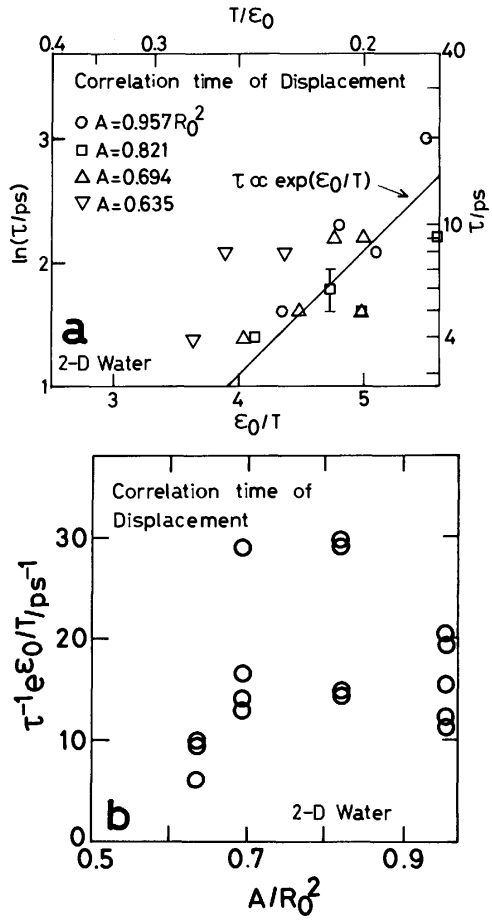

Fig. 6. a) The cross correlation time τ of displacement *vs.* the inverse of temperature $1/T$. b) Plot of $\tau^{-1}\exp(\varepsilon_0/T)$ *vs.* area per molecule A.

case of $i=j$. Thus this figure shows that molecules i and j with $R_{ij}-R_0$ at $t=0$ move collectively in a period of about 2×10 ps to nearly the same direction.

One can see cross correlation of the displacement in the cases of $R_{ij}-2^{1/2}R_0$ and $2R_0$ which is negligible in the case of more distant pair $R_{ij}-2^{3/2}R_0$. In other words cross correlation of displacement is seen even in the third neighbor pair. Figure 6 shows the temperature and density dependence of the cross correlation time τ of displacement. In Fig. 6(a), we see that the cross correlation time τ depends on temperature T as $\tau\propto\exp(\varepsilon_0/T)$ on average, where ε_0 is the energy of hydrogen bond. This temperature dependence seems reasonable (*cf.* Fig. 3). For this reason, a quantity $\tau^{-1}\exp(\varepsilon_0/T)$ is plotted against the area per molecule A in Fig. 6(b) in order to obtain the density dependence of τ. This figure shows that the cross correlation time τ at first becomes shorter due to compression from the normal density, then it becomes longer if 2-D water is compressed to the density close to that of high density ice.[1]

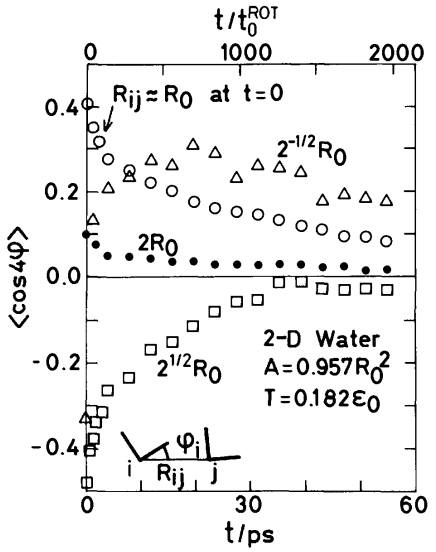

Fig. 7. Plot of $<\cos4\varphi>$ *vs.* time t. The initial conditions in the statistics are indicated in the figure.

Local Orientational Order Parameter. We performed many calculations to confirm the above lifetime by other methods. One of them will be shown in this section. The rotational motion, too, will be studied here.

At low temperatures water molecule has local orientational order due to the hydrogen bond. The angle φ_i is the orientation of the molecule i measured from the vector $\boldsymbol{R}_{ij}$ (see Fig. 2 in Ref. 1). The average $<\cos4\varphi>$ is used to examine the local orientational order, as shown in Fig. 7. In the case of low density ice at OK (Fig. 5 in Ref. 1), this order parameter has the following values:

$$<\cos4\varphi> = 1, \qquad R_{ij} = R_0, 2R_0,$$
$$<\cos4\varphi> = -1, \qquad R_{ij} = 2^{1/2}R_0. \tag{7}$$

One can see the local orientational order in the first neighbor ($R_{ij}-R_0$) and the second neighbor pair ($R_{ij}-2^{1/2}R_0$). The half-life period of $<\cos4\varphi>$ (orientational relaxation time) is 15 ps in the case of $R_{ij}-R_0$. This value is in good agreement with that of the cross correlation time of displacement.

The density dependence of orientational relaxation time is shown in Fig. 8. Figure 8(a) shows that the temperature dependence of the orientational relaxation time τ is written as $\tau\propto\exp(2\varepsilon_0/T)$ at low temperatures ($T\lesssim0.24\varepsilon_0$) (*cf.* Fig. 1). As for the density dependence, the cross correlation time of displacement and the relaxation time of $<\cos4\varphi>$ has a

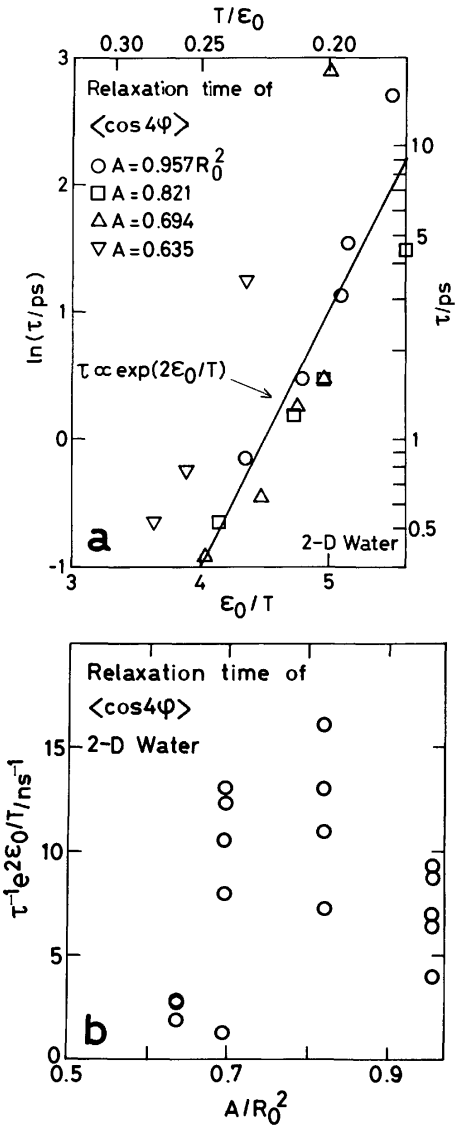

Fig. 8. a) The orientational relaxation time τ of $<\cos4\varphi>$ *vs.* the inverse of temperature $1/T$. b) Plot of $\tau^{-1}\exp(2\varepsilon_0/T)$ *vs.* area per molecule A.

similar behavior as that shown in Figs. 6(b) and 8(b). Figures 1, 6, and 8 indicate that the initial effect of pressure increase (at low temperatures and low pressure) leads to increased fluidity, known to be true in the case of real water.[3,4]

Dynamics of Unstable Species

In the preceding section it was described that molecules with the oscillatory motion are stable and are located in the hydrogen-bonded cluster. This section is devoted to the dynamics of the unstable species. On the contrary to the preceding section, the time averaged configuration is not used here.

The binding energy (BE) is defined as follows:

$$\mathrm{BE}_i = \frac{1}{2}\sum_j U_{ij} \tag{8}$$

In liquid water the distribution of BE is as wide as shown in Fig. 9 in Ref. 1.[9] The BE of the molecule with one hydrogen bond is about 0.5 ε_0. The molecule with more than one hydrogen bond may be called stable species. Thus, we call this molecule unstable species if the following condition is fulfilled:

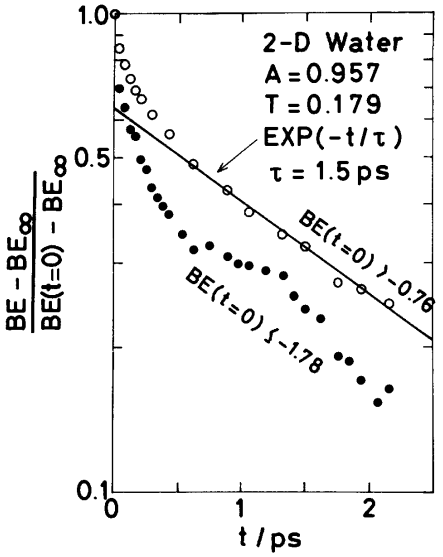

Fig. 9. The relaxation of the binding energy.

$$BE > -0.76\,\varepsilon_0. \tag{9}$$

The relaxation of BE for unstable species is shown in Fig. 9. Here, the molecules are classified according to Eq. (9), where BE is taken to be the value at $t=0$. The deviation of BE from its equilibrium value relaxes to 0.5 times the deviation at initial condition at about $t=0.5$ ps (short term) and then decays as a function $\exp(-t/\tau)$, $\tau=1.5$ ps (long term) ($A=0.957\,R_0^2$, $T=0.179\,\varepsilon_0$). The long term of relaxation time of BE is shown as a function of temperature and density in Fig. 10. It can be seen that this relaxation time τ does not depend strongly on density and that its temperature dependence is written as $\tau \propto \exp(\varepsilon_0/T)$.

The velocity autocorrelation functions

$$f^{TR}(t) = \frac{\langle \boldsymbol{v}(t)\cdot\boldsymbol{v}(0)\rangle}{\langle \boldsymbol{v}(0)\cdot\boldsymbol{v}(0)\rangle}, \tag{10}$$

of both species are shown in Fig. 11. Dynamical properties are different in two species. The behavior of $f^{TR}(t)$ for the unstable species is very similar to that of liquid Ar.[10] The unstable species has a larger self-diffusion coefficient than the stable one.

The concentration x of the unstable species is shown as a function of T and P in Fig.12. This figure is similar to the results of the mixture model by Konda and Yamamoto.[5]

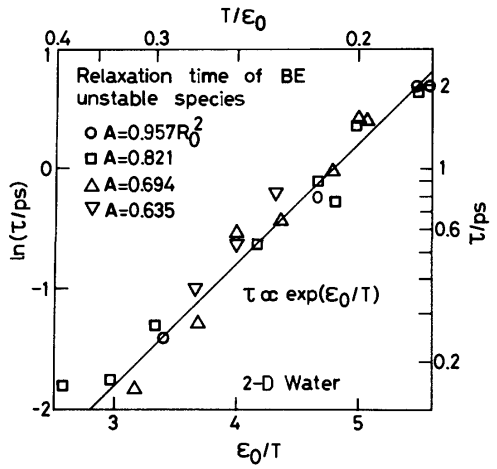

Fig. 10. The long term of the relaxation time τ of BE *vs.* the inverse of temperature $1/T$.

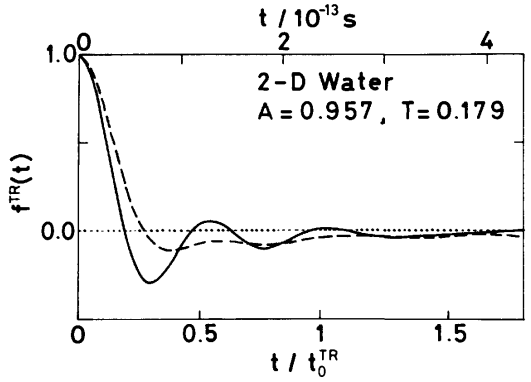

Fig. 11. The velocity autocorrelation functions. The dashed curve corresponds to the unstable species and the solid one corresponds to the stable species.

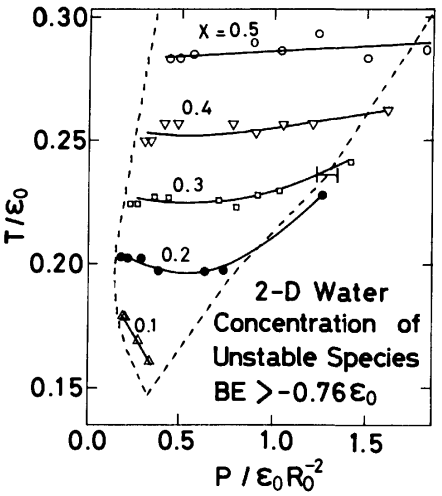

Fig. 12. The concentration of the unstable species is shown in P-T plane.

In this section, the relaxation of BE is calculated and it turned out that the short term of relaxation is about 0.5 ps and the long term one, about 1.5 ps. Therefore, classification like Eq. (9) is meaningfull in observations where the time scale in not longer than several ps. Such classification may be usefull in understanding of the anomalous behavior of liquid water, like the simple two-state model.

Concluding Remarks

The vibrationally-averaged structure (V-structure) of liquid water was discussed by Eisenberg and Kauzmann.[7,8] In the present article the size and lifetime of the vibrationally-averaged local structure in 2-D water are obtained to be about 13 molecules (as far as third neighbors) and about 2×10 ps by observing time scale of 0.13 ps at low temperatures and low density, where the density maximum is known.

The oscillatory motion of water molecule has a time constant of about 0.02—0.05 ps. The relaxation time of dipolemoment of the water molecule is about 5 ps. The binding energy relaxes with decay constants of about 0.5—1.5 ps.

The author would like to thank Professor Tsunenobu Yamamoto, Dr. Keiji Okazaki, Dr. Shuichi

Nosé, Dr. Kenkichi Okada and Dr. Kazuo Maki for kind discussions. A part of the computation was done at the Computer Center of the Institute for Molecular Science and at the Kyoto University Data Processing Center.

References

1) K. Okazaki, S.Nosé, Y. Kataoka, and T. Yamamoto, *J. Chem. Phys.*, **75**, 5864 (1981).

2) A. Rahman and F. H. Stillinger, *J. Chem. Phys.*, **55**, 3336 (1971); F. H. Stillinger and A. Rahman, *ibid.*, **57**, 1281 (1972); A. Rahman and F. H. Stillinger, *J. Am. Chem. Soc.*, **95**, 7943 (1973); F. H. Stillinger and A. Rahman, *J. Chem. Phys.*, **60**, 1545 (1974); **61**, 4973 (1974); A. Rahman, F. H. Stillinger, and H. L. Lemberg, *ibid.*, **63**, 5223 (1975); W. F. Van Gunsteren, H. J. C. Berendsen, and J. A. C. Rullmann, *Faraday Discuss. Chem. Soc.*, **66**, 58 (1978); F. H. Stillinger and A. Rahman, *J. Chem. Phys.*, **68**, 666 (1978); I. R. McDonald and M. L. Klein, *ibid.*, **68**, 4875 (1978); A. Geiger, F. H. Stillinger, and A. Rahman, *ibid.*, **70**, 4185 (1979); D. C. Rapaport and H. A. Scheraga, *Chem. Phys. Lett.*, **78**, 491 (1981); R. W. Impey, M. L. Klein, and I. R. McDonald, *J. Chem. Phys.*, **74**, 647 (1981); R. W. Impey, P. A. Madden, and I. R. McDonald, *Mol. Phys.*, **46**, 513 (1982).

3) R. Pottel and E. Asselborn, *Ber. Bunsenges. Phys. Chem.*, **83**, 29 (1979). See also Y. Lee and J. Jonas, *J. Chem. Phys.*, **57**, 4233 (1972); J. Jonas, T. DeFries, and D. J. Wilbur, *ibid.*, **65**, 582 (1976); E. Lang and H.-D. Ludemann, *ibid.*, **67**, 718 (1977); *Ber. Bunsenges. Phys. Chem.*, **84**, 462 (1980); . **85**, 603 (1981).

4) L. A. Woolf, *J. Chem. Soc., Faraday Trans. 1*, **71**, 784 (1975); **72**, 1267 (1976); D. J. Wilbur, T. DeFries, and J. Jonas, *J. Chem. Phys.*, **65**, 1783 (1976); K. Krynicki, C. D. Green, and D. W. Sawyer, *Faraday Discuss. Chem. Soc.*, **66**, 199 (1978); K. R. Harris and L. A. Woolf, *J. Chem. Soc., Faraday Trans. 1*, **76**, 377 (1980).

5) C. Konda and T. Yamamoto, *Chem. Phys. Lett.*, **50**, 324 (1977).

6) See, *e.g.* L. Verlet, *Phys. Rev.*, **159**, 98 (1967); S. Toxvaerd, *Mol. Phys.*, **29**, 373 (1975).

7) D. Eisenberg and W. Kauzmann, "The Structure and Properties of Water" Oxford U.P., New York (1969).

8) See also F. Hirata and P. J. Rossky, *J. Chem. Phys.*, **74**, 6867 (1981).

9) See also Y. Kataoka, H. Hamada, S. Nosé, and T. Yamamoto, *J. Chem. Phys.*, **77**, 5699 (1982).

10) A. Rahman, *Phys. Rev.*, **136**, A405 (1964).

Yields of Electron Transfer Reactions in the Quenching of the Phosphorescent States (^{2}E) of Tris(2,2′-bipyridine)chromium(III) and Tris(4,7-diphenyl-1,10-phenanthroline)chromium(III) Compounds

Takeshi OHNO* and Shunji KATO
Chemistry Department, College of General Education, Osaka University, Toyonaka, Osaka 560
(Received December 21, 1983)

Molar absorption coefficients of the phosphorescent states (^{2}E) of $[Cr(2,2'\text{-bipyridine})_3]^{3+}$ and $[Cr(4,7\text{-diphenyl-1,10-phenanthroline})_3]^{3+}$ were determined. The ^{2}E state of $[Cr(2,2'\text{-bipyridine})_3]^{3+}$ was reduced to $[Cr(2,2'\text{-bipyridine})_3]^{2+}$ with the yield of less than 0.2 in the quenching by iron(II) compounds. The reduction yields of $[Cr(2,2'\text{-bipyridine})_3]^{3+}$ and $[Cr(4,7\text{-diphenyl-1,10-phenanthroline})_3]^{3+}$ in the quenching of ^{2}E by aromatic amines increase with the Gibbs energy change ($-\Delta G$) in the reverse electron-transfer process. The weak dependence of the yields on ΔG can not be interpreted in terms of adiabatic reverse electron transfer in the geminate pair, which is formed in the quenching process. The electron transfer from the chromium(II) compounds of triplet spin-multiplicity to the amine radical of doublet spin-multiplicity suffers from spin-restriction.

The bimolecular electron transfer reactions of photoexcited compounds are followed by two kinds of the reverse process. The one takes place in the lifetime of the geminate radical pair formed in the electron transfer quenching. The other can be observed to occur as the second order process with respect to the free radical formed in the bulk. Hoselton *et al.*[1] proposed that the small yield of the electron transfer products in the bulk was ascribed to the fast reverse electron transfer in the geminate pair. Ohno and Lichtin also found that the yield of free radical was reduced by the reverse electron transfer competing with the dissociation of the triplet geminate pair, though every bimolecular quenching of the phosphorescent state of a dye molecule, Methylene Blue, yielded the geminate radical pair.[2-4] Moreover, they found that the rates of the reverse electron transfer are slower than those estimated from the free energy changes and the rearrangement energies involved in the process. The slower rates of the reverse electron transfers were ascribed to the spin-restriction of the process.[4,5] In this work, the product yields in the electron transfer quenching of the phosphorescent states of $[Cr(2,2'\text{-bipyridine}^*)_3]^{3+}$ and $[Cr(4,7\text{-diphenyl-1,10-phenanthroline}^*)_3]^{3+}$ are investigated by means of laser photolysis kinetic spectroscopy. Nonadiabaticity due to spin-restriction on the electron transfer reactions will be discussed.

Experimental

Apparatus. An NEC SLG-2018 Q-switched ruby laser was used in most of the experiments. The second harmonics (347 nm) of the power less than 0.1 J was generated by using temperature matching nonlinear crystal of RDA supplied by Quantum Tecknology. The laser beam (ϕ=10 mm) is vertically converged and holizontally expanded to 3 mm ×12 mm on the sample cell (10 mm×10 mm) by using two cylindrical lenses. The monitoring beam from a 150 W xenon arc lamp was set in right angles to the laser beam. Increases in light intensity of 50—100 times can be obtained by the use of a transistor-switched discharging circuit. The converged monitoring beam passes through a small aperture on the sample cell, which is located at the depth of 1—2 mm from the cell window exposed to the laser. The laser intensity at 347 nm was attenuated by insertion of a filter solution of chromium alum. The details of the laser and the monitoring apparatuses have been described elsewhere.[4] The absoption change was recorded in a transient recorder, Kawasaki Electronica M-500T or a storagescope, Iwasaki-Tsushinki TS-8123, followed by computer analysis using a laboratory-constructed mini-computer.[6] A 5 cm long cell was used for an excitation by means of xenon flash apparatus. A Hitachi 323 Spectrophotometer was used for the measurement of absorption spectra and a Hitachi MPF-2A Spectrofluorophotometer was used for the measurement of phosphorescence.

Materials. $[Cr(bpy)_3](ClO_4)_3\cdot 1/2H_2O$ was prepared by a similar method as that reported by Baker and Mehta.[7] The crude sample of $[Cr(bpy)_3](ClO_4)_3$ was purified by repeated recrystalizations from the aqueous solution and the methanol solution. $[Cr(dp\text{-}phen)_3](ClO_4)_3\cdot H_2O$ was prepared by a method of Kane-Maguire *et al.*[8] All the aromatic amines- diphenylamine(DPA), triphenylamine (TPA), 3,3′-dimethylbenzidine(DMB), 1,2-phenylenediamine (1,2-DP), 1,4-phenylenediamine (1,4-DP), *N,N,N′,N′*-tetramethylbenzidine(TMB), *N,N,N′,N′*-tetramethyl-1,4-phenylenediamine(TMPD), supplied by Tokyo Kasei or Aldrich, were purified by vacuum sublimation. Ferrocene was recrystallized from the benzene solution and ferrocenecarboxylic acid was recrystallized from the ethanol solution. $Fe(NH_4)_2(SO_4)_2\cdot 6H_2O$ and acetonitrile (AN) of Wako Pure Chemical Co. were used as supplied. Water was purified by the passage through a Millipore deionizer and filter.

Procedure. All the sample solutions were deaerated by purging with nitrogen of 99.99% purity for 15 min. All the measurements were done at 15±2 °C.

Molar Absorption Coefficients. The molar absorption coefficients of ^{2}E states were obtained on the assumption that all the $[Cr(bpy)_3]^{3+}$ or $[Cr(dp\text{-}phen)_3]^{3+}$ of 40—50 μM[1] were excited to the ^{2}E state by the laser light of 347 nm. The complete excitation of the compound to ^{2}E state was ascertained by a constant production of the transient absorbance due to ^{2}E with an attenuation of the laser intensity.

Quenching Rate Constants. Decays of the excited state absorptions of the chromium compounds were spectroscopically monitored with or without a quencher. In order not to excite the quenchers of TMPD and TMB which are photoionized on the exposure to 347 nm light, a xenon flash for the photolysis was used with a 375 nm cut-off-filter. The quenching rate constants of the excited state by TMPD

* The following abbreviations will be used hereafter, 2,2′-bipyridine: bpy, and 4,7-diphenyl-1,10-phenanthroline: dp-phen.

[1] 1 M=1 mol dm^{-3}.

and TMB (k_q) were obtained from Stern-Volmer plots of the phosphorescence intensity of the chromium(III) chelate compounds ($[Cr(NN)_3]^{3+}$).

Fractions of Electron-transfer-product Formation in the Quenching. The production of $[Cr(N-N)_3]^{2+}$ ($[Cr(N-N)_3^{2+}]_0$) or the radical cation of amine in the quenching was calculated from the absorption change by using the molar absorption coefficients of $[Cr(bpy)_3]^{2+}$ ($4860\,M^{-1}cm^{-1}$ at 560 nm[9]), $[Cr(dp\text{-}phen)_3]^{2+}$($5500\,M^{-1}cm^{-1}$ at 460 nm[10]), $TPA^{\dagger}$ ($30500\,M^{-1}cm^{-1}$ at 660 nm in dichloromethane[11]), $TMB^{\dagger}$ ($41000\,M^{-1}\,cm^{-1}$ at 474 nm in AN[12]), and $TMPD^{\dagger}$ ($12000\,M^{-1}cm^{-1}$ in H_2O[13]). The production of $[Cr(N-N)_3]^{2+}$, which decayed in several hundred microseconds, was measured after the fast disappearance of ^2E in a few microseconds. The production of ^2E state ($[^2Cr(N-N)_3^{3+}]_0$) in the presence of the quencher was monitored to be constant. The fractions of $[Cr(N-N)_3]^{2+}$ production in the quenching, denoted by F_i, were calculated as a ratio of the reaction rate constant of $[Cr(N-N)_3]^{2+}$ production (k_{et}) to the quenching rate constant (k_q) or a ratio of $[Cr(N-N)_3^{2+}]_0$ to $[^2Cr(N-N)_3^{3+}]_0$ with the complete quenching. The rate constants of $[Cr(N-N)_3]^{2+}$ production (k_{et}) were determined by using a following equation,

$$\frac{[Cr(N-N)_3^{2+}]_0}{[^2Cr(N-N)_3^{3+}]_0} = k_{et}\frac{[Q]}{k_d}, \qquad (1)$$

where [Q] is the quencher concentration and k_d is the observed decay rate constant of $^2[Cr(N-N)_3]^{3+}$ in the presence of the quencher.

Results

Absorption Spectrum of Excited State of $[Cr(N-N)_3]^{3+}$. A transient species observed after laser excitation of $[Cr(N-N)_3]^{3+}$ exhibits an absorption spectrum as in Figs. 1 and 2. The lifetimes of the excited state were 60 μs for $[Cr(bpy)_3]^{3+}$ and 200 μs for $[Cr(dp\text{-}phen)_3]^{3+}$. The transient absorbances of $^2[Cr(bpy)_3]^{3+}$ at 390 nm and of $^2[Cr(dp\text{-}phen)_3]^{3+}$ at 520 nm were measured with attenuation of the laser intensity (see Fig. 3).

Electron Transfer Quenching of ^2E by Iron(II) Compounds. Ferrocene and ferrocenecarboxylic acid of less than 0.5 mM quenched the ^2E state of $[Cr(bpy)_3]^{3+}$ in a 70% AN aqueous solution. Iron(II) ions in a 1 M HCl or a 1 M $HClO_4$ aqueous solution also quenched the ^2E. The quenching were more effective in 1 M HCl than in 1 M $HClO_4$. The quenching rate constants are shown in Table 1. As the ^2E state decayed in the presence of ferrocene, another transient species was produced, whose absorption spectrum consists of bands at 480 and 560 nm as is shown in Fig. 4. This transient spectrum is almost identical to that of $[Cr(bpy)_3]^{2+}$ reported by König and Herzog,[9] and by Serpone *et al.*[10] The iron(III) compound formed, ferro-

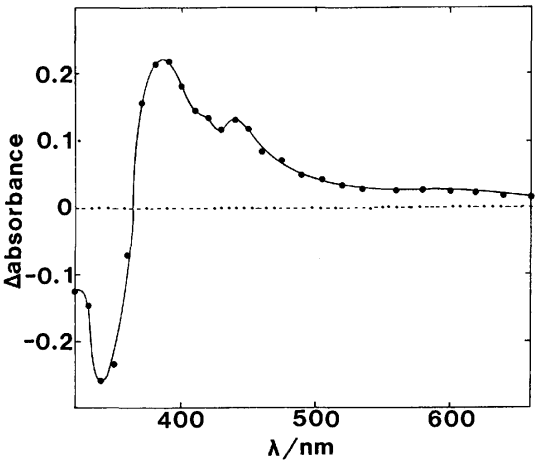

Fig. 1. Difference absorption spectrum of the photolyzed solution of $[Cr(bpy)_3]^{3+}$ (100 μM) in AN-water (1:1 by volume) just after laser excitation.

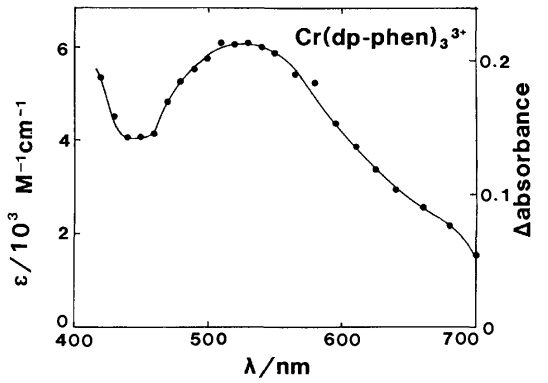

Fig. 2. Difference absorption spectrum of the photolyzed solution of $[Cr(dp\text{-}phen)_3]^{3+}$ (40 μM) in AN-water (1:1 by volume) just after laser excitation.

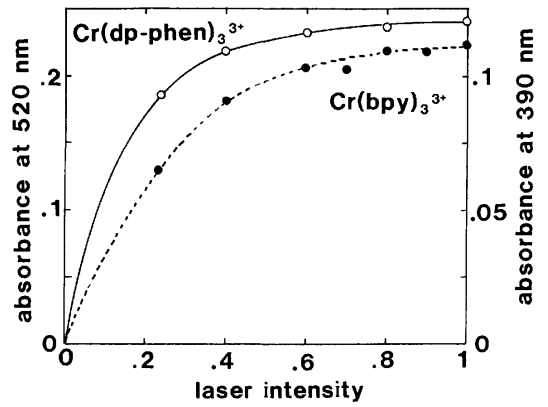

Fig. 3. Transient absorbance with attenuation of laser intensity. The closed circle: at 390 nm for $[Cr(bpy)_3]^{3+}$ of 50 μM, and the open circle: at 520 nm for $[Cr(dp\text{-}phen)_3]^{3+}$ of 40 μM.

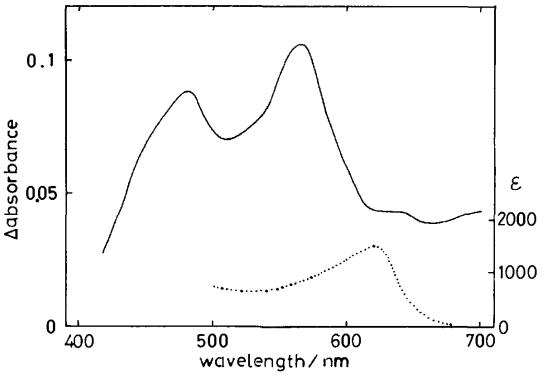

Fig. 4. Absorption spectra of the reaction intermediates. Solid line; the photolyzed solution of $[Cr(bpy)_3]^{3+}$ with ferrocene of 1.1×10^{-4} M in AN-water (7:3 by volume), dotted line; ferrocenium oxidized by $Fe(ClO_4)_3$ in 1 M $HClO_4$.

Table 1. Rate constants of quenching, electron transfer, and reverse electron transfer and redox potentials.

Compound	E°	k_q	k_{et}	k_{ret}	F_1
	V	10^9 M^{-1} s^{-1}	10^9 M^{-1} s^{-1}	10^9 M^{-1} s^{-1}	
Fe^{2+}	0.77[a]	0.007	1.2×10^{-3}	1.0	0.17
$Fe^{2+}Cl_x$		0.04	3.2×10^{-3}	1.4	0.081
Ferrocene	0.54[b]	6.2	1.1	—	0.18
Ferrocene-COOH	0.79[b]	7.3	0.50	—	0.069

a) W. M. Latimer, "Oxidation Potentials", 2nd ed, Prentice- Hall N. Y. (1952). b) H. Hemming and O. Grurtler, *J. Organomet. Chem.*, **11**, 307(1968).

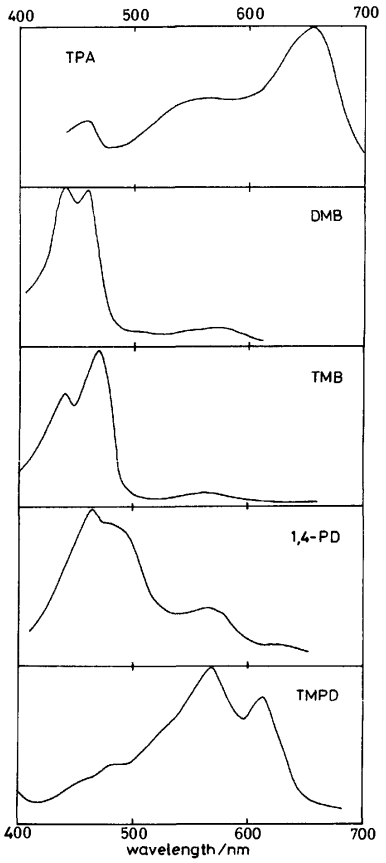

Fig. 5. Difference absorption spectra of the photolyzed solution of $[Cr(bpy)_3]^{3+}$ and the amine after the decay of ^2E. The intensity is arbitary.
a) triphenylamine, b) 3,3′-dimethylbenzidine, c) *N,N,N′,N′*-tetramethylbenzidine, d) 1,4-phenylenediamine, e) *N,N,N′,N′*-tetramethyl-1,4-phenylenediamine.

cenium ion, has a minor contribution to the transient spectrum, because ferrocenium ion which was obtained by the oxidation of ferrocene in a 1 M $HClO_4$ 70% AN aqueous solution with iron(III) ion, has a broad and weak absorption (the molar absorption coefficient is 800 $M^{-1}cm^{-1}$ at 560 nm).

The fraction of $[Cr(bpy)_3]^{2+}$ production in the quenching by the iron(II) compounds examined are less than 0.18 of the ^2E production. The values of k_{et} and F_1 are shown in Table 1.

Electron Transfer Quenching of ^2E by Aromatic Amines. Aromatic amines of DPA, TPA, DMB, 1,2-PD, 1,4-PD, TMB, and TMPD, quenched the ^2E of $[Cr(N\text{-}N)_3]^{3+}$ with the rate contants close to the diffusion-controlled

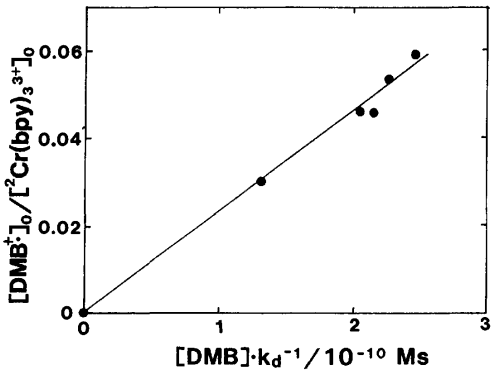

Fig. 6. Determination of k_{et} in the quenching of $^2[Cr(bpy)_3]^{3+}$ by DMB. $[DMB^+]_0$ is the production of one-electron oxidized 3,3-dimethylbenzidine in the quenching.

one (see Table 2). The quenching processes resulted in the production of the second transient species of $[Cr(N\text{-}N)_3]^{2+}$ and the radical cation of the amine. As Fig. 5 shows, transient absorption spectra were observed after the disappearance of ^2E except for the quenching by DPA. They are composed of the bands at 560 nm due to $[Cr(N\text{-}N)_3]^{2+}$ and the more intense band(s) which can be ascribed to the radical cation of the quencher, because these intense bands are in agreement with those of the radical cation reported[11-13]; the band at 660 nm is ascribed to TPA^+, the bands at 440 and 460 nm to DMB^+, the band at 465 nm to 1,4-PD^+, the band at 470 nm to TMB^+, and the bands at 580 and 615 nm to $TMPD^+$. The rate constants of the electron transfer reactions (k_{et}) are obtained by plotting Eq. 1 as is shown in Fig. 6. Most of the fractions of $[Cr(N\text{-}N)_3]^{2+}$ production measured in the quenching of $^2[Cr(bpy)_3]^{3+}$ were obtained as the ratio of k_{et} to k_q. As for $^2[Cr(dp\text{-}phen)_3]^{3+}$, all the fractions were obtained as the ratio of $[Cr(dp\text{-}phen)_3]^{2+}$ production to $^2[Cr(dp\text{-}phen)_3]^{3+}$ production with complete quenching of $^2[Cr(dp\text{-}phen)_3]^{3+}$. They are tabulated in Table 2. All the radical and $[Cr(bpy)_3]^{2+}$ formed in the quenching reactions were returned to the parent compounds via the second-order reaction, *e.g.* the reverse electron transfer.

Discussion

^2E States of $[Cr(N\text{-}N)_3]^{3+}$. The difference absorption spectra of photolyzed solution of $[Cr(N\text{-}N)_3]^{2+}$ are ascribed to the production of the excited state of $[Cr(N\text{-}N)_3]^{3+}$, ^2E which are identical to those reported by Maestri *et al.*[14] and by Serpone *et al.*[10]

TABLE 2. REDOX POTENTIALS OF AROMATIC AMINES AND RATE CONSTANTS OF ^2E WITH AROMATIC AMINES

Compound	$E°$/V	$Cr(bpy)_3^{3+}$ k_q / $10^9 M^{-1}s^{-1}$	F_1	$Cr(dp\text{-}phen)_3^{3+}$ k_q / $10^9 M^{-1}s^{-1}$	F_1
TPA	1.10[a]	2.4	0.006	9.2	0.019
DPA	1.06[a]	3.8	0	—	—
DMB	0.69[a]	3.2	0.068	6.6	0.11
1, 2-PD	(0.67)[b]	3.6	0.05	15	0.14
TMB	0.56[a]	3.5	0.115	6.7	0.21
1, 4-PD	0.41[a]	4.6	0.22	6.6	0.50
TMPD	0.25[a]	5.6	0.29	2.0	0.73

a) C. K. Mann and K. K. Barnes, "Electrochemical Reactions In Nonaqueous Systems," Marcel Deckker, N. Y. (1970). b) The value is estimated from the redox potential of 1, 4-PD assuming the difference in the redox potential between 1, 2-PD and 1, 4-PD to be equal to the difference in the redox potential between *N, N, N', N'*,-tetramethyl-1, 2-phenylenediamine and *N, N, N', N'*,-tetramethyl-1, 4-phenylenediamine.[c] c) A. Zweig, J. E. Lancaster, N. T. Neghia, and W. H. Jura, *J. Am. Chem. Soc.*, **86**, 4130(1964).

The complete conversion of $Cr(N\text{-}N)_3^{3+}$ to the ^2E state (see Fig. 3) allowed us to calculate the molar absorption coefficients of the excited states to be 3.1×10^3 M^{-1} cm^{-1} at 390 nm and to be 200 $M^{-1}cm^{-1}$ at 600 nm for $^2[Cr(bpy)_3]^{3+}$ and to be 6.0×10^3 $M^{-1}cm^{-1}$ at 520 nm for $^2[Cr(dp\text{-}phen)_3]^{3+}$ after the correction due to the depression of absorbance of the ground state. They agree in the order with the molar absorption coefficients of $^2[Cr(bpy)_3]^{3+}$ calcuated from the light absorption, which was roughly estimated from the absorbance of the sample solution in the wide wavelength region and the light intensity of non-monochromatic pumping xenon flash.[14] Since the absorption bands of ^2E except for the broad band of $^2[Cr(bpy)_3]^{3+}$ at 600 nm are too strong to be assigned as a d-d band,[15] they can be assigned to the transitions from ^2E at 13700 cm^{-1} to the doublet CT state. This assignment is in agreement with that proposed by Serpone *et al.*,[10] who studied the band shift in the absorption spectra of excited chromium(III) compounds of substituted 2,2′-bipyridine or 1,10-phenanthroline. Since strong CT transitions of ^2E states were also observed in the visible region for chromium(III) compounds, such as $[Cr(NCS)_6]^{3-}$, $[Cr(NCS)_4(NH_3)_2]^-$, Cr(acetylacetonato)$_3$, and so on,[16] an appearance of strong CT band in the visible region can be expected for the excited states of most chromium(III) compounds. Meanwhile, the weak and broad band in the visible region can be assigned to a d-d transition ($^2E\rightarrow{}^2A_2$).

The strong absorption bands of ^2E are useful to estimate the production of ^2E and to calculate the fractions (F_1) of $[Cr(N\text{-}N)_3]^{2+}$ production in the quenching process. It is parenthetically noted that a larger molar absorption coefficient of $^2[Cr(bpy)_3]^{3+}$ (7000 $M^{-1}cm^{-1}$) has been reported by Lilie and Waltz.[17] They obtained the value on an assumption made by Ferraudi *et al.*[18] that the production of $[Cr(bpy)_3]^{2+}$ in the complete quenching by Fe^{2+}_{aq} in 0.1 M $HClO_4$ might be equal to the production of $^2[Cr(bpy)_3]^{3+}$. However, since the efficiency of $[Cr(bpy)_3]^{2+}$ production in the quenching may not be unity (0.18 in 1 M $HClO_4$), this value of the molar absorption coefficient is assumed to be the possible maximum.

Electron Transfer Reaction of ^2E with Amines. The productions of $[Cr(bpy)_3]^{2+}$ and the radical cation of the aromatic amine indicate the quenching of ^2E *via* electron transfer mechanism by the amine, as has been reported by Ballardini *et al.*[19] The efficiencies (F_1) of $[Cr(N\text{-}N)_3]^{2+}$ production in the quenching reaction can be expressed as $F_1=k_{et}/k_q$ using the rate constants of electron transfer reaction (k_{et}) and quenching reaction (k_q). As Table 2 shows, the values of the F_1 increase with the decrease of the redox potential of the amine; F_1 is the largest with TMPD (0.25 V) and the smallest with DPA (1.08 V) or TPA (1.1 V). This trend in the change of F_1 can be understood by assuming the following reaction mechanism, in which a reaction intermediate, a geminate pair or a cage complex, is postulated.

$$^2[Cr(N\text{-}N)_3]^{3+}+D \longrightarrow {}^2({}^3[Cr(N\text{-}N)_3]^{2+}\text{—}{}^2D^+), \quad k_f \quad (2)$$

$$^2({}^3[Cr(N\text{-}N)_3]^{2+}\text{—}{}^2D^+) \longrightarrow {}^3[Cr(N\text{-}N)_3]^{2+}+{}^2D^+, \quad k_{dis} \quad (3)$$

$$^2({}^3[Cr(N\text{-}N)_3]^{2+}\text{—}{}^2D^+) \longrightarrow {}^4[Cr(N\text{-}N)_3]^{3+}+D. \quad k_r \quad (4)$$

The fraction of $[Cr(N\text{-}N)_3]^{2+}$ production in the quenching can be rewritten as,

$$F_1 = k_{dis}/(k_{dis}+k_r), \quad (5)$$

using the rate constants of elementary processes of the geminate pair. The dependence of k_r on the free energy change (ΔG) involved in the process is apparently reflected on the ratio of k_r to k_{dis}, which is expressed as the observable quantity, $1/F_1-1$, because the rate of electron transfer can be written as follows, provided that the electron transfer process is adiabatic,

$$k_r = (k_1k_2f_{12})^{1/2}\exp(-\Delta G/2RT), \quad (6)$$

where k_1 and k_2 are the rate constants of the self exchange electron transfer of reactants 1 and 2, respectively, and f_{12} is nearly constant.[20] Then, the final expression is as follows,

$$\ln(k_r/k_{dis}) = \ln(1/F_1-1) = -\Delta G/2RT + A', \quad (7)$$

for the adiabatic process on assuming the free energy change for the dissociation of the geminate pair to be constant. As shown in Figs. 7 and 8, the values of ln $(1/F_1-1)$ nearly fit the expected relation of Eq. 7, provided that the difference in the solvation energy and the electrostatic energy between the initial and the final states is neglected and ΔG is expressed as $E°(Cr^{III}/Cr^{II})-E°(D^+/D)$, where $E°(Cr^{III}/Cr^{II})$ and $E°(D^+/D)$ are the redox potentials of $[Cr(N\text{-}N)_3]^{3+}$

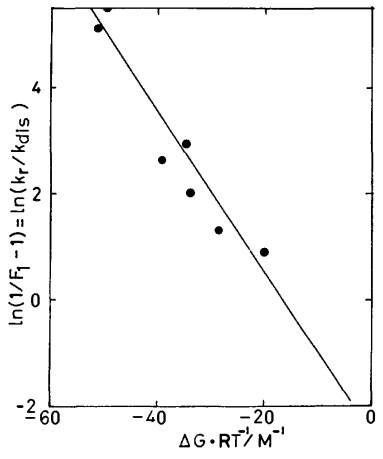

Fig. 7. The dependence of the fraction of $[Cr(bpy)_3]^{2+}$ production in the quenching reaction on the free energy change involved in the reverse electron transfer.

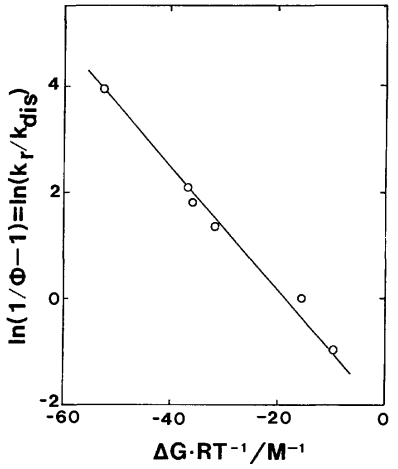

Fig. 8. The dependence of the fraction of $[Cr(dp\text{-}phen)_3]^{2+}$ production in the quenching on the free energy change involved in the reverse electron transfer.

(-0.26 V[10,21]) and the amine, respectively. However, the values (-0.14 for $[Cr(bpy)_3]^{3+}$ and -0.12 for $[Cr(dp\text{-}phen)_3]^{3+}$) of $\partial(\ln(k_r/k_{dis}))/\partial(\Delta G/RT)$ obtained from Figs. 7 and 8 are less negative compared to the ideal value (-0.5) estimated for an adiabatic electron transfer process. Since the reverse electron transfer is accompanied by spin conversion (doublet→quartet) as shown in Eq. 4, the nonadiabaticity in the process may retards the reaction rate. Actually, a less negative value(-0.07) of $\partial(\ln(k_r/k_{dis}))/\partial(\Delta G/RT)$ was obtained for the spin-inverted electron transfer between doublet organic radicals containing no heavy atom.[3,5] The larger dependence of k_r on ΔG was reported for the spin-inverted electron transfer reactions between doublet iron(III) compounds and the doublet radical of Methylene Blue,[3] and between the triplet excited state of $[Ru(bpy)_3]^{2+}$ and doublet $Cu^{+2}{}_{aq}$.[1]

An alternative explanation is that a part of the geminate pair may be converted to an exciplex in which the spin conversion more likely occurs and the reverse electron transfer occurs as a radiationless transition of the exciplex. Since the dependence of radiationless transition rate in the exciplex on ΔG is positive according to Mataga *et al.*,[22] $\partial(\ln k_r/k_{dis})/\partial(\Delta G/RT)$ is expected to be positive. This kind of switchover mechanism has been proposed to explain the radical yield in the bimolecular quenching of singlet excited state.[23]

Electron Transfer Reaction of ^2E with Iron(II) Compounds. Efficiencies of $[Cr(bpy)_3]^{2+}$ formation in the quenching by the iron(II) compounds are calculated to be 0.069—0.18 as shown in Table 1. The smaller values of the efficiencies with iron(II) ion in the 1 M hydrochloric acid than in the 1 M perchloric acid are essentially ascribed to the faster reverse electron transfer in the geminate pair because the reverse electron transfer from the bulk in the hydrochloric acid ($1.4\times10^9\,M^{-1}s^{-1}$) is faster than that in the perchloric acid ($1.0\times10^9\,M^{-1}s^{-1}$). However, since the efficiencies of net electron transfer in the quenching are much smaller than the fraction of collision complex undergoing no electron transfer in the bulk reverse process (0.53—0.67), which can be obtained from the rate constants of the reverse electron transfer (k_{ret}) and the collision complex formation (k_e) as $(k_e-k_{ret})/k_e$, other types of quenching, paramagnetic ion-induced intersystem crossing and energy transfer must be accompanied with electron transfer. It is probable that the iron(II) quenching of ^2E takes place *via* quintet iron-induced intersystem crossing,[15b] which was proposed in the iron(II) quenching of triplet excited molecule.[24] Meanwhile, the ΔG-dependence of k_q in the iron(II) quenching of ^2E led to conclusion that the principal process was not energy transfer but electron transfer.[25]

The larger rate of reverse electron transfer in the 1 M hydrochloric acid indicates the formation of $Fe^{III}Cl_{6-n}(H_2O)_n^{(3-n)+}(n=1—6)$. The larger quenching rate constant in 1 M HCl than in 1 M $HClO_4$ may sugggest the formation of the chloride complex of iron(II), which is responsible for the faster rate of reverse electron transfer in the geminate pair.

F_1 in the quenching by ferrocenecarboxylic acid is less than a half of the value by ferrocene. This reduction is ascribed to the fast reverse electron transfer in the geminate pair compared to ferrocene because $-\Delta G$ of the reverse process with ferrocenecarboxylic acid (1.06 ev) is larger than that (0.81 ev) with ferrocene.

References

1) M. A. Hoselton, C. T. Lin, H. A. Schwarz, and N. Sutin, *J. Am. Chem. Soc.*, **100**, 2283 (1978).
2) T. Ohno and N. N. Lichtin, *J. Am. Chem. Soc.*, **102**, 4636 (1980).
3) T. Ohno and N. N. Lichtin, *J. Phys. Chem.*, **86**, 354 (1982).
4) T. Ohno, S. Kato, and N. N. Lichtin, *Bull. Chem. Soc. Jpn.*, **55**, 2753 (1982).
5) T. Ohno, S. Kato, A. Yamada, and T. Tanno, *J. Phys. Chem.*, **87**, 775 (1983).
6) N. Tatebe, Ph. D. Thesis, Osaka University at Toyonaka, Japan, 1976.
7) B. R. Baker and B. D. Mehta, *Inorg. Chem.*, **4**, 848 (1965).
8) N. A. P. Kane-Maguire, J. Conway, and C. H. Langford, *J. Chem. Soc., Chem. Commun.*, **1974**, 801.

9) E. König and S. Herzog, *J. Inorg. Nucl. Chem.*, **32**, 585 (1972).
10) N. Serpone, M. A. Jamieson, M. S. Henry, M. Z. Hoffman, F. Bolletta, and M. Maestri, *J. Am. Chem. Soc.*, **101**, 2907 (1979).
11) H. D. Burrows, D. Greatorex, and J. J. Kemp, *J. Phys. Chem.*, **76**, 20 (1972).
12) S. A. Akaitis and M. Grätzel, *J. Am. Chem. Soc.*, **98**, 3549 (1976).
13) P. S. Rao and E. Hayon, *J. Phys. Chem.*, **79**, 1063 (1975).
14) M. Maestri, F. Bolletta, I. Moggi, V. Balzani, M. S. Henry, and M. Z. Hoffman, *J. Am. Chem. Soc.*, **100**, 2694 (1978).
15) a) Though an absorption band of $[Cr(bpy)_3]^{3+}$ with intensity of 400—900 $M^{-1}cm^{-1}$ between 400 and 450 nm, has been ascribed to d-d transition,[9,10] it is assigned to the singlet-triplet transition of the ligand excitation by means of low temperature spectroscopy;[15b] b) T. Ohno, S. Kato, S. Kaizaki, and I. Hanazaki, *Chem. Phys. Lett.*, **102**, 471 (1983).
16) T. Ohno, and S. Kato, *Bull. Chem. Soc. Jpn.*, **43**, 8 (1970).
17) J. Lilie and W. L. Waltz, *Inorg. Chem.*, **22**, 1473 (1983).
18) G. J. Ferrraudi and J. F. Endicott, *Inorg. Chim. Acta*, **37**, 219 (1979).
19) R. Ballardini, G. Varani, M. T. Indelli, F. Scondola, and V. Balzani, *J. Am. Chem. Soc.*, **100**, 7219 (1978).
20) R. A. Marcus, *J. Chem. Phys.*, **43**, 679 (1964); **67**, 853 (1963).
21) T. Saji and S.Aoyagi, *J. Electroanal. Chem. Interfacial Elctrochem.*, **60**, 1 (1975).
22) J. Hinatu, F. Yoshida, H. Masuhara, and N. Mataga, *Chem. Phys. Lett.*, **59**, 80 (1978).
23) P. Iwa, U. E. Steiner, E. Vogelman, and H. E. A. Kramer, *J. Phys. Chem.*, **86**, 1277 (1982).
24) P. V. Kamat and N. N. Lichtin, *J. Phys. Chem.*, **86**, 351 (1982).
25) C-T. Lin, W. Bottcher, M. Chou, C. Creutz, and N. Sutin, *J. Am. Chem. Soc.*, **98**, 6536 (1976).

Studies of the Hydrous Tin(IV) Oxide Ion-exchanger. II. Some Properties as a Cation-exchanger

Yasushi INOUE* and Hiromichi YAMAZAKI
Department of Nuclear Engineering, Faculty of Engineering, Tohoku University, Aramaki, Sendai 980
(Received September 5, 1983)

In order to elucidate the fundamental properties of hydrous tin(IV) oxide as a cation-exchanger, the stoichiometry of cation exchange and its acid-base property were studied by means of the uptake curves for alkali-metal ions. The results are summarized as follows: 1) The equivalent exchange between the hydrogen ion and either alkali-metal or alkaline-earth-metal ions holds, irrespective of the ionic strength of the solution and the extent of exchange. 2) The water content in the exchanger depends on the ionic composition. 3) This material is an amphoteric ion-exchanger, with at least two kinds of weakly dissociable ion-exchange sites, and the conditional dissociation constant depends on the ionic composition of the exchanger. The stability to various reagents was also examined.

Several studies have been carried out on the ion-exchange property of hydrous tin(IV) oxide,[1-8] but different compositions and ion-exchange properties have been reported by different investigators. This may be due to the irreproducibility of the synthesis; hence, a detailed examination of the synthetic procedure is indispensable to undertaking any further study of this material. With this point in mind, the relation between the yield of hydrous tin(IV) oxide and the conditions of precipitation for various synthetic systems, and the ion-exchange properties relevant to the synthesis were investigated in a previous paper.[9] There is little choice between the $Na_2[Sn(OH)_6]$-H_2SO_4 and $SnCl_4$-NH_3 aq systems with respect to yield or physical and ion-exchange properties, but the former system is inferior to the latter in its very lengthy washing. The exchanger is semitransparent and consists of nearly amorphous particles which are hard to be ground into particles suitable for column operation, and can be converted to the pure hydrogen form by conditioning with 0.1 mol dm^{-3} HCl. The exchanger of the H^+ form prepared from the $SnCl_4$-NH_3 aq system has a composition of $SnO_2 \cdot 2.18H_2O$ and an ion-exchange capacity of 1.18 mmol Na^+ g^{-1} (at pH 11.3). This is stable for longer than 15 months after preparation when it is stored over a saturated NH_4Cl solution.

Of the many properties which have not been investigated in detail, the acid-base property and the mechanism of adsorption are very important in understanding the material as an ion-exchanger. This induced us to examine the validity of the equivalence of cation-exchange reactions on the exchanger prepared from the recommended $SnCl_4$-NH_3 aq system and the uptake curves for various alkali-metal ions, which are useful for understanding the acid-base property of the exchanger.

Experimental

Reagents and Apparatus. The hydroxide solutions of the alkali-metal and alkaline-earth-metal ions except those of the lithium and sodium ions were prepared by passing corresponding chloride solutions through a column packed with Dowex 1-x8 anion-exchange resin in the OH^- form. All the other chemicals used were of the highest-purity grade obtained from Wako Pure Chemical Industries, Ltd. All the apparatuses were the same as described previously.[9]

Preparation of the Ion-exchanger. The synthetic system No.5 described in the preceeding paper was chosen for the preparation of the ion-exchanger.[9] Into 0.5 dm^3 of a 1 mol dm^{-3} $SnCl_4$ solution prepared by diluting liquid $SnCl_4$ with water, 1.5 dm^3 of 2% NH_3 aq was added, drop by drop, at an average rate of 20—30 cm^3 min^{-1}. The precipitate thus formed was separated from the mother liquor by a combination of decantation and filtration through Toyo No.1 filter paper under suction, uniformly dispersed into distilled water, and filtered again after being completely sedimentated. This procedure was repeated until no chloride ion was detected in the filtrate. Then the precipitate was filtered and sufficiently air-dried at room temperature. The resulting product was then immersed in distilled water to break it down into fine particles. The grains were dried again at room temperature. Particles larger than desired, if any, were ground in a porcelain mortar and sieved to obtain the required particle sizes. The exchanger of a desired particle size (100—200 mesh) was converted to the H^+ form by treating it with a 0.1 mol dm^{-3} HCl solution by the procedure described previously.[9] Finally, the exchanger was air-dried and stored in a desiccator containing a saturated NH_4Cl solution(relative humidity: 79% at 25 °C).

Conversion to Na^+ Form. The exchanger in the H^+ form was immersed in an alkaline solution, prepared by the combination of 0.1 mol dm^{-3} NaCl and 0.1 mol dm^{-3} NaOH(ionic strength=0.10, pH=11.0). Then the slurry was poured into a glass column, through which the same solution was subsequently passed until the pH of the effluent approached that of the influent. The column was then washed with distilled water, followed by acetone. Then the exchanger was taken out of the column, air-dried for 30 min, and stored in a desiccator containing saturated NH_4Cl and 5 mol dm^{-3} NaOH solutions.

Analytical Methods. The Cl^- ions were determined by the Fajans method after the solution had been neutralized. The alkali-metal ions were converted to the corresponding pure chlorides and indirectly determined by titrating the Cl^- ions. The Sr^{2+} and Ba^{2+} ions were assayed by a complexometric titration: the Zn-EDTA displacement method, using eriochrome black T as an indicator. The OH^- and CO_3^{2-} ions were determined by differential titration. The water content in the exchanger was calculated from the weight loss when it was heated in air at 850 °C to a constant weight.

Chemical Stability. In 30 cm^3 of a suitable solution, 0.25 g of the exchanger in the H^+ form was immersed for 4 d at room temperature. The tin dissolved in the supernatant solution was determined spectrophotometrically.[10]

Ion-exchange Stoichiometry. The exchanger in the H^+ form was immersed in an alkaline solution of metal ions, of suitable concentrations(ionic strength=0.0024—0.022), in a nitrogen atmosphere for longer than 2 d at room temperature,

with intermittent shaking. This was followed by chemical analysis, and the ratio of the amount of metal ions taken up in the exchanger to that of the hydrogen ions released from the exchanger was evaluated from the difference between the initial and final concentrations of the respective ions present in the solution.

The other experimental procedures were the same as those previously described.[9]

Results and Discussion

Chemical Stability. To examine the chemical stability of the exchanger, the amount of tin dissolved in various reagents was measured. The results, shown in Table 1, indicate that, in neutral or alkaline solutions, the exchanger was unstable to NaOH and K_2CO_3, whereas it was fairly stable to NaCl, Na_2CO_3, and aqueous NH_3. In acid solutions, it was very stable to HNO_3 and H_2SO_4, but dissolved appreciably into HCl, $HClO_4$, and $H_2C_2O_4$, even at concentrations as low as 1 equivalent dm^{-3}. These results show that this exchanger is easily attacked by the acids having a strong tendency to complex tin(IV) and the bases which form soluble hexahydroxostannates. As it is known that α-stannic acid dissolves easily in K_2CO_3 and that β-stannic acid is stable to HNO_3 and H_2SO_4, the charscteristics of this exchanger are intermediate between those of α- and β-stannic acids. Because β-stannic acid is the dehydration product of α-stannic acid, this exchanger is considered to be more dehydrated and more condensed than α-stannic acid.

Table 1. Chemical stability[a]

Reagent	Solution Concentration	Amount of Sn dissolved
	mol dm^{-3}	wt%
NaOH	0.10	10
	0.94	19
NH_3 aq	0.10	0.14
	1.1	0.95
K_2CO_3	0.050	14
Na_2CO_3	0.050	<0.05[b]
NaCl	0.10	<0.05[b]
HNO_3	1.1	<0.05[b]
	2.8	0.38
H_2SO_4	0.61	<0.05[b]
	1.6	0.36
HCl	0.10	<0.05[b]
	0.54	0.43
	1.2	1.7
	2.9	100
$HClO_4$	0.98	0.20
	3.1	100
Oxalic acid	0.50	7.0
Tartaric acid	0.50	<0.05[b]
Citric acid	0.50	1.4

a) Exchanger; 100—200 mesh, H^+ form. Conditions; exchanger: 0.25 g, solution: 30 cm^3, contact time: 4d at room temperature. b) Limit of detection.

Dependence of Exchange Capacity on Particle Size. The ion-exchange capacity for the Na^+ ion was measured as a function of the particle size, as is shown in Table 2. This table shows that the capacity was independent of the particle size. Hence, it can be concluded that the exchange sites are distributed uniformly in the particle.

Stoichiometry and Reversibility of Exchange Reaction. Table 3 presents the results concerning the stoichiometry of the exchange reaction between hydrogen ions on the exchanger and alkali-metal or alkaline-earth-metal ions in the solution. When the concentration of carbonate ions in a solution was decreased during contact, the amount of hydrogen ions released was determined from the difference in the sum of the carbonate and hydroxide ions before and after the equilibrium. As is shown in the last column of Table 3, the equivalent ratio of hydrogen ions released to metal ions absorbed became unity within the limits of experimental error. Therefore, the equivalent ion exchange holds irrespective of the ionic strength of the solutions, the extent of the exchange, and the kind of metal ion. From the stoichiometry of ion exchange and the dependence of the exchange capacity on the particle size, this material acts as an ideal cation-

Table 2. Dependence of cation-exchange capacity on particle size[a]

Mesh size	Cation-exchange capacity for Na^+	
	A[b]	B[c]
	pH (mmol g^{-1})	pH (mmol g^{-1})
16—28	7.52 0.61±0.02	11.39 1.22±0.02
28—42	7.49 0.61±0.02	11.38 1.24±0.02
42—70	7.49 0.61±0.02	11.36 1.22±0.03
70—100	7.48 0.60±0.02	11.35 1.22±0.02
100—200	7.52 0.63±0.02	11.40 1.19±0.02
200—350	7.53 0.62±0.03	11.38 1.21±0.02

a) Conditions; exchanger: 0.25 g, solution: 30 cm^3, at room temperature. b) A: 28.4 cm^3; 0.10 mol dm^{-3} NaCl+1.6 cm^3; 10.10 mol dm^{-3}; NaOH. c) B: 26.0 cm^3; 0.10 mol dm^{-3}; NaCl+4.0 cm^3; 0.10 mol dm^{-3}; NaOH.

Table 3. The verification of the equivalence of the exchange

System	Ionic strength	Duration of immersion	(I) Metal ions uptaken	(II) H^+ released	Stoichiometry (I)/(II)
	mol dm^{-3}	d	mequiv. g^{-1}	mequiv. g^{-1}	
Li^+/H^+	0.022	4	1.46±0.02	1.49±0.04	0.98±0.04
	(OH^-/Cl^-=1.0)[a]	4	1.47±0.02	1.51±0.04	0.97±0.04
Na^+/H^+	0.020	4	1.14±0.02	1.12±0.04	1.02±0.05
	(OH^-/Cl^-=0.86)[a]	4	1.13±0.02	1.11±0.04	1.02±0.05
Sr^{2+}/H^+	0.0024	2	0.90±0.03	0.87±0.03	1.03±0.06
		4	1.22±0.03	1.17±0.02	1.04±0.05
Ba^{2+}/H^+	0.0024	3	1.06±0.05	1.06±0.03	1.00±0.07

a) : Molar ratio.

exchanger, possessing exchange sites distributed uniformly in the particle.

Figure 1 shows the forward and backward uptake curves for sodium ions. Since these curves agree with each other, the exchange reaction can be said to proceed reversibly, and it seems that no structural change would occur upon ion-exchange.

Change in Water Content of the Exchanger. The change in the water content of the exchanger with the amount of alkali-metal ions uptaken is shown in Table 4, where the amount of water and of metal ions uptaken is normalized to the value per mole of tin in the exchanger. If we compare this value with the water content in the H^+-form exchanger, 2.16 ± 0.01 mol H_2O (mol Sn)$^{-1}$, it is clear from Table 4 that the decrease in the water content is brought about by the uptake of alkali-metal ions. As part of water is removed from the exchanger by the release of H^+ ions from the OH group by ion-exchange, the water content, as estimated from the weight loss, should be corrected by adding half the amount of metal ions uptaken if the water content in the H^+ form is compared with that in the metal form. The corrected values are shown in the last column of Table 4, which shows that the water content decreased at first to a minimum and then increased gradually with the amount of alkali-metal ions in the exchanger. Furthermore, the water content is greater for larger hydrated cations, suggesting that these cations are uptaken as hydrated ions. As will be reported in a following paper, the order of selectivity for alkali-metal ions $Li^+ \gg Na^+ > K^+ > Rb^+ \approx Cs^+$, leads to the assumption that alkali-metal ions are present in the anhydrous state. This contradicts the foregoing suggestion. These results can be understood by considering that, at the early stage of exchange, the interstitial water is excluded by ingoing anhydrous cations, which have a larger volume than the proton. When the amount of cations uptaken exceeds a certain limit, the exchanger swells to relax the distortion produced in the structure of the matrix, so it can accommodate a larger ammount of water.

Acid-Base Properties. In order to study the acid-base property of the exchanger, the uptake curves for sodium and chloride ions were measured as a function of the pH, as is shown in Fig. 2. This figure reveals that this material is an amphoteric ion-exchanger

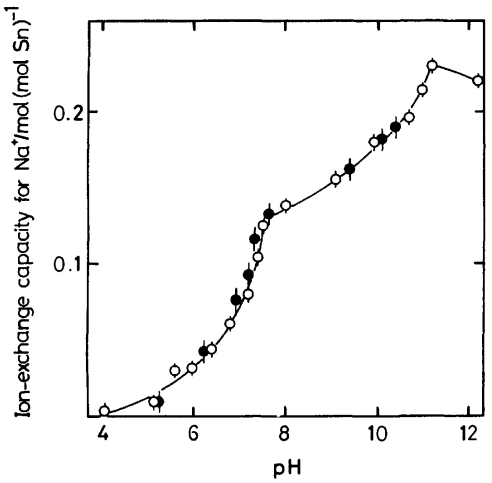

Fig. 1. Reversibility of exchange reaction between Na^+ and Cl^- ions.
○: Forward reaction, ●: Reverse reaction. Conditions; exchanger: 0.25 g, solution: 20 cm^3, temperature: R.T..

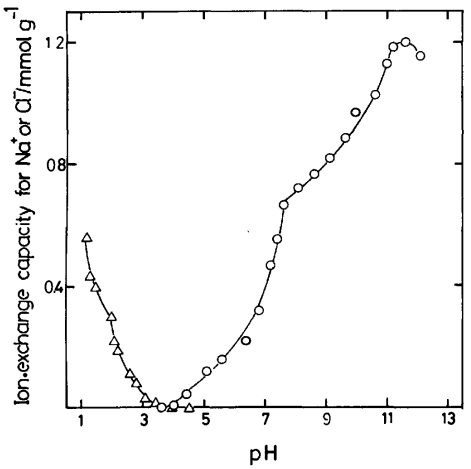

Fig. 2. Uptake curves for Na^+ and Cl^- ions.
Ions; ○: Na^+, △: Cl^-. Conditions; exchanger: 0.25 g, solution: 30 cm^3, ionic strength: 0.10, temperature: R.T..

TABLE 4. CHANGE IN WATER CONTENT OF THE EXCHANGER BY CATION EXCHANGE

System	Amount of M^+ uptaken	Weight loss[1]		M^+ content	Water content	
	mmol M^+ / g M^+ form	wt%	mmol H_2O / g M^+ form	mol M^+ / mol Sn	mol H_2O(I) / mol Sn	mol H_2O(II)[a] / mol Sn
Li^+/H^+	0.19±0.02	19.9±0.2	11.0±0.1	0.036±0.003	2.08±0.03	2.10±0.03
	0.83±0.02	18.9±0.2	10.5±0.1	0.156±0.003	1.98±0.03	2.06±0.03
	1.42±0.02	18.5±0.2	10.3±0.1	0.271±0.003	1.95±0.03	2.09±0.03
	1.74±0.02	18.5±0.2	10.4±0.1	0.332±0.004	1.96±0.03	2.13±0.03
Na^+/H^+	0.16±0.02	19.2±0.2	10.7±0.1	0.030±0.002	2.00±0.03	2.02±0.03
	0.32±0.02	17.8±0.2	9.9±0.1	0.060±0.002	1.85±0.03	1.88±0.03
	0.54±0.02	17.4±0.2	9.7±0.1	0.101±0.003	1.80±0.03	1.85±0.03
	0.81±0.02	17.2±0.2	9.5±0.1	0.152±0.004	1.79±0.03	1.87±0.03
	1.22±0.02	16.8±0.2	9.3±0.1	0.231±0.004	1.77±0.03	1.91±0.03
Cs^+/H^+	0.19±0.02	18.7±0.2	10.4±0.1	0.036±0.004	1.99±0.03	2.01±0.03
	0.28±0.02	18.0±0.2	10.0±0.1	0.054±0.004	1.93±0.03	1.96±0.03

1) : Calcinated at 850°C. a) : Water content(II)=Water content(I)+1/2 (M^+ content). Exchanger: H^+ form, 100—200 mesh, $SnO_2 \cdot (2.16\pm0.01)H_2O$.

possessing a larger ion-exchage capacity for cations than for anions and having an isoelectric point close to pH 4. The inflection points at pH 7.6 and pH 2.0 for cation and anion exchanges respectively suggest that the exchanger has at least two kinds of dissociable ion-exchange sites.

The ion-exchange reaction and its equilibrium constant can be written:

$$\overline{H} + Na = \overline{Na} + H,$$

and:

$$K = K' \cdot \frac{\bar{f}_{Na}}{\bar{f}_H} = \frac{[\overline{Na}]\bar{f}_{Na}a_H}{[\overline{H}]\bar{f}_H a_{Na}},$$

where a superscript bar indicates the exchanger phase; [ ], the concentration; a, the activity of ions in the solutions; $\bar{f}$, the activity coefficient of ions in the exchanger, and K' ($\equiv[\overline{Na}]\cdot a_H/[\overline{H}]\cdot a_{Na}$), the conditional selectivity coefficient. By introducing the total specific ion-exchange capacity, $[\bar{S}]=[\overline{Na}]+[\overline{H}]$, we get:

$$\frac{1}{[\overline{Na}]} = \frac{1}{[\bar{S}]} + \frac{a_H}{K[\bar{S}]}\cdot\frac{\bar{f}_{Na}}{\bar{f}_H}\cdot\frac{1}{a_{Na}} = \frac{1}{[\bar{S}]} + \frac{a_H}{K'[\bar{S}]}\cdot\frac{1}{a_{Na}}.$$

If K' is assumed to be constant, the $1/[\overline{Na}]$ *vs.* $1/a_{Na}$ plot will show a linear relation, because $[\bar{S}]$ and a_H are constant in the present experiment. Table 5 shows the ion-exchange capacities of the exchanger for sodium ions, measured at a constant pH (11.00±0.03) as a function of the sodium-ion concentration in the solution. The plot of $1/[\overline{Na}]$ *vs.* $1/a_{Na}$, however, was not linear, as is shown in Fig. 3. In the calculation of a_{Na} for making this plot, the values of γ_{Na} given by Kielland[11] were used except in the case of the ionic strength, 0.5, where γ_{Na} was estimated by means of this relationship: $\gamma_{Na}=\gamma_{\pm NaCl}/\gamma_{\pm KCl}$. The non-linearity does not support the assumption that K' is constant, even in the pH region, where the same kind of acidic site takes part in the exchange reaction. Hence, either the $\bar{f}_{Na}/\bar{f}_H$ ratio or K changes as the exchange reaction proceeds. The change in the $\bar{f}_{Na}/\bar{f}_H$ ratio may be brought about by the variation in the electric field in the exchanger, which would be strongly affected by the ratio of dissociated to undissociated OH groups. The dissociation of an OH group may affect the electric distribution of other OH groups. This will result in a successive change in the dissociation constant with the change in the ionic composition of the exchanger, even in the same kind of exchange site. We can not decide which is more important, the ratio of the activity coefficients in the exchanger or the dissociation constant of the exchange site, as a reason for the non-constancy of K'. In any event, this material is an amphoteric ion-exchanger possessing at least two kinds of weakly dissociable ion-exchange sites. Furthermore, for the same functional group, the degree of dissociation depends on its ionic composition.

Table 5. Effect of Na^+ concentration on the ion-exchange capacity

Concentration of Na^+ $[Na^+]$ / mol dm^{-3}	Activity of Na^+ $\gamma^*_{Na}[Na^+]$	Ion-exchange capacity[a] $[Na]$ / mmol g^{-1}
1.0×10^{-2}	9.3×10^{-3}	0.974±0.006
5.0×10^{-2}	4.3×10^{-2}	1.094±0.006
1.0×10^{-2}	8.2×10^{-2}	1.160±0.006
5.0×10^{-1}	3.6×10^{-1}	1.29 ±0.01

a) : Column exchange capacity at pH 11.0. *: Activity coefficient of Na^+ ion; J. Kielland, *J. Am. Chem. Soc.*, **59**, 1675 (1937).

In order to compare the ion-exchange behavior for the Na^+ ion with that for other cations, uptake curves were obtained for other alkali-metal ions, as is shown in Fig. 4. The curve of the Li^+ ions was similar to that of the Na^+ ions, but the specific ion-exchange capacity was greater for Li^+ than for Na^+, by 0.2 and 0.3 mmol g^{-1} respectively, at the first and second stages. Because the hydrous tin(IV) oxide possesses a micropore structure and because its mean pore radius is as small as 0.5 nm, as was reported by Selim and Zeidan,[12] the difference between the ion-exchange capacity of

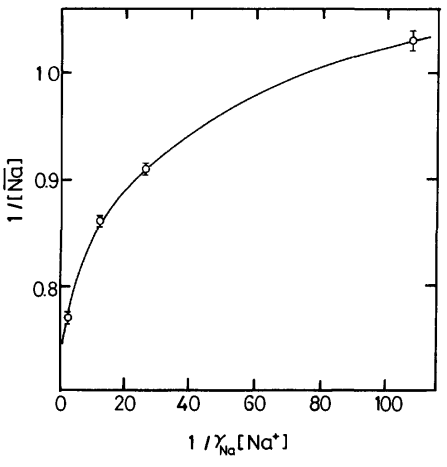

Fig. 3. $1/[\overline{Na}]$ *vs.* $1/\gamma_{Na}[Na^+]$ plot.
$[\overline{Na}]$: Column exchange capacity for Na^+ ion at pH 11.0 (mmol g^{-1}). $\gamma_{Na}[Na^+]$: Activity of Na^+ ion in the equilibrium solution.

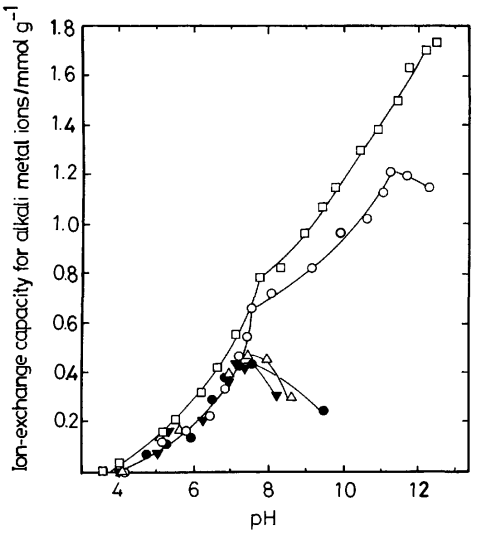

Fig. 4. Uptake curves for various alkali metal ions.
Ions; □: Li^+, ○: Na^+, ▼: K^+, ●: Rb^+, ○: Cs^+.
Conditions; exchanger: 0.25 g, solution: 30 cm^3, contact time: 4 d at room temperature.

these two ions may be attributable to an ion-sieving effect of this material. On the other hand, the uptake curves for the K^+, Rb^+, and Cs^+ ions agreed with that for the Na^+ ion in the lower pH region until the ion-exchange capacity reached around 0.45 mmol g^{-1}, whereupon it began to decrease steeply. This phenomenon can be ascribed to the dissolution of a part of the exchanger, which was verified by analyzing the amount of tin dissolved in the supernatant solution; the exchanger began to dissolve into the solution of K^+, Rb^+, and Cs^+ ions at a pH of around 7, in spite of the fact that no dissolution was observed in the solution of Na^+ and Li^+ ions. The unstability of the exchanger in alkaline solutions of heavy alkali-metal ions reflects the characteristics of α-stannic acid, which has a high solubility in K_2CO_3 and KOH. For α-stannic acid prepared by a similar method, the ion-exchange capacity for the K^+ ion was reported by Abe and Ito and by Sautereau *et al.* to be 0.54 and 0.75 mequiv. g^{-1} respectively at pH 10.[3,8] The reason for this contradiction may be the difference in the duration of immersion when the specific ion-exchange capacity was measured.

References

1) K. A. Kraus, H. O. Philips, T. A. Carlson, and J. S. Johnson, *Prog. Int. Conf. on Peaceful Use of Atomic Energy*, **28**, 3 (1958).
2) E. Merz, *Z. Electrochem.*, **63**, 288 (1959).
3) M. Abe and T. Ito, Nippon Kagaku Zasshi, **86**, 1259 (1965).
4) J. D. Donaldson and M. J. Fuller, *J. Inorg. Nucl. Chem.*, **30**, 1083, 2841 (1968); **32**, 1703 (1970).
5) P. C. Ho, F. Nelson, and K. A. Kraus, *J. Chromatogr.*, **147**, 263 (1978).
6) N. Jaffrezic-Renault, N. Karisa, H. Andrade-Martins, and N. Deschamps, *Radiochem. Radioanal. Lett.*, **37**, 257 (1979).
7) T. N. Perekohozheva, L. M. Sharygin, T. G. Malykh, and V. F. Gonchar, *Kinet. Katal.*, **15** (No. 1), 145 (1974); *Radiokhimiya*, **20**, 414, 420 (1978); **21**, 47 (1979).
8) J. Sautereau, M. Baverez, and J. M. Bloch, *Bull. Chem. Soc. Fr.*, **1977**, 207.
9) Y. Inoue and H. Yamazaki, *Bull. Chem. Soc. Jpn.*, **55**, 3782 (1982).
10) M. Ishibashi, T. Shigematsu, Y. Yamamoto, and Y. Inoue, *Bunseki Kagaku*, **7**, 473 (1958).
11) J. Kielland, *J. Am. Chem. Soc.*, **59**, 1675 (1937).
12) S. A. Selim and F. I. Zeidan, *J. Appl. Chem. Biotechnol.*, **26**, 23 (1976).

 © 1984 The Chemical Society of Japan Bull. Chem. Soc. Jpn., 57, 1539—1544 (1984)

The Effects of Salts on the Solubilities of Benzene, Toluene, Ethylbenzene, and Propylbenzene in Water

Isao SANEMASA,* Seiji ARAKAWA, Masatake ARAKI, and Toshio DEGUCHI
Department of Chemistry, Faculty of Science, Kumamoto University, Kurokami 2-39-1, Kumamoto 860
(Received October 1, 1983)

Salt effects on the solubilities of benzene, toluene, ethylbenzene, and propylbenzene were studied by making use of the solute vapor. The salting coefficients were determined at 25 °C, and the results were compared with the literature values and with those estimated by means of theoretical equations. The McDevit-Long equation did not give satisfactory predictions until the equation was multiplied by a factor of 0.4. The scaled particle theory gave a favorable agreement with the observations in most cases if suitable pair-potential parameters of solutes were used in the calculations.

The solubility of a nonelectrolyte (solute) in aqueous electrolyte solution has been found to depend on the concentration and on the type of electrolyte present in the solution. In a sufficiently dilute nonelectrolyte solution, the activity coefficient, f, in the salt solution of a given molar concentration, C, is given by:

$$\log f=\log (S_0/S)=k_s C, \quad (1)$$

where S and S_0 denote the solubility of the nonelectrolyte in salt and salt-free solutions respectively, k_s being the salting coefficient.

In a previous paper, we reported a method of preparing aqueous solutions saturated with a solute such as benzene and the alkylbenzenes by means of a technique that made use of the solute vapor.[1] By means of this technique, the solubility equilibrium can be attained within quite a short time; moreover, we can determine the equilibrium solubility as a function of the vapor pressure of the solute. The present paper is an extension of the method to determining the salting coefficients of benzene, toluene, ethylbenzene, and propylbenzene. Many data on salt effects have been reported in the literature concerning benzene and, to less extent, toluene, but little is known about the alkylbenzenes of larger molecules. Almost all of the literature data have been obtained by putting "liquid" solute in direct contact with aqueous electrolyte solutions. Here we report salting coefficients determined by solubility measurements of the solute "vapor" in the presence of some typical electrolytes. The results obtained are compared below with the literature data and with those predicted by both the McDevit-Long equation and the scaled-particle theory.

Experimental

All the electrolytes and the nonelectrolytes used were of an analytical reagent grade. Deionized-redistilled water was used as a solvent. The concentrations of the electrolyte (stock) solutions were determined by either the argentometric or the gravimetric method.

The apparatus used and the procedures of the solubility measurements were the same as those described in the previous paper.[1] The apparatus was composed of two main parts: one was a separatory funnel (300 cm^3) in which an aqueous solution of from 100 to 200 cm^3 was placed, and the other was a pear-shaped flask (50 cm^3) in which a liquid solute of from 10 to 20 cm^3 was placed. We will call the former "solubility flask," and the latter, "solute reservoir." The solubility flask and the solute reservoir were connected to each other with Teflon and glass tubes. A Viton diaphragm pump was incorporated into the assembly. By means of the pump, the solute vapor was generated by bubbling air through the solute reservoir *via* a sintered glass ball and was then introduced into the solubility flask *via* another sintered ball. The solute vapor was thus circulated in a closed system. The total pressure inside the closed system was kept under atmospheric pressure. After the solubility equilibrium had been attained, an aliquot of the aqueous solution was taken out of the bottom of the solubility flask to determine the solute concentration by means of solvent extraction-spectrophotometry.

Results

The Time Required for Attaining the Solubility Equilibrium. An aqueous solution in the presence of an electrolyte has reached equilibrium with the solute vapor within 5 min at a circulation rate of 2 $dm^3 min^{-1}$. Some examples are shown in Fig. 1.

Solubility as a Function of the Solute-vapor Pressure. The aqueous phase in the solubility flask has come to be in equilibrium with the solute vapor, while in the solute reservoir the liquid solute has attained equilibrium with the vapor of water. From this point of view, the solute phase is no longer "pure"; hence, the vapor pressure of the solute inside the solubility flask differes from that of the pure solute. However, the solubilities of water in the liquid hy-

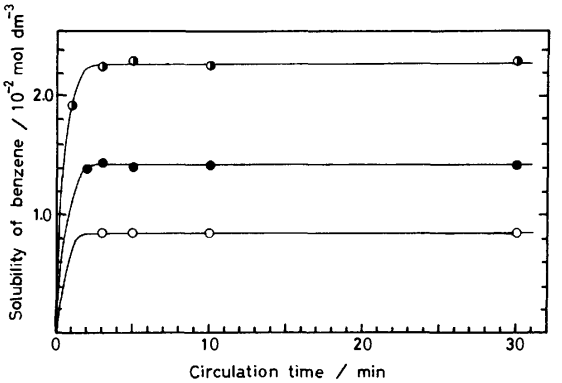

Fig. 1. Equilibrium solubility of benzene *vs.* circulation time.
Circulation rate: 2.0 dm^3/min. Pure water (○), 0.408 mol dm^{-3} $(C_2H_5)_4NBr$ (●), 0.991 mol dm^{-3} $(CH_3)_4NBr$ (◑). Temperature of aqueous solution: 35.0 (○), 25.0 °C (●, ◑). Temperature of solute reservoir: 15.0 (○), 11.8 (●), 19.0 °C (◑).

drocarbons employed here are as small as 3×10^{-3} in the mole fraction.[2] Suppose that Raoult's law is valid; then, the difference in vapor pressure between the pure and actual solutes is only 0.3% or so. We have thus considered it permissible to employ the vapor pressure of the pure solute for the present purpose, the vapor-pressure data of benzene and the alkylbenzenes being taken from previously published tabulations.[3]

In order to check whether or not the solubilities are linearly dependent on the solute-vapor pressure, preliminary experiments were made on the following solute-electrolyte combinations: benzene-tetraalkylammonium bromides, toluene-(NaCl, KCl, $BaCl_2$, and NaSCN). The solubility runs were carried out under conditions such that, at a constant temperature of the aqueous electrolyte solution, the temperature of the solute reservoir was raised nearly up to that of the aqueous solution. Some typical results are shown in Figs. 2 and 3 for a given electrolyte concentration and in Fig. 4 for a constant temperature of the aqueous electrolyte solution, 25 °C. Strictly speaking, the solute-vapor pressure inside the solubility flask may differ from that inside the solute reservoir because of such factors as solute-water and solute-electrolyte interactions in the aqueous phase and the difference in temperature between the solute reservoir and the solubility flask. However, as can be seen from Figs. 2, 3, and 4, a plot of the solubility *vs.* the vapor pressure of the pure solute appears as a straight line for each solute-electrolyte combination investigated, regardless of the salting-in or -out nature of the electrolyte.

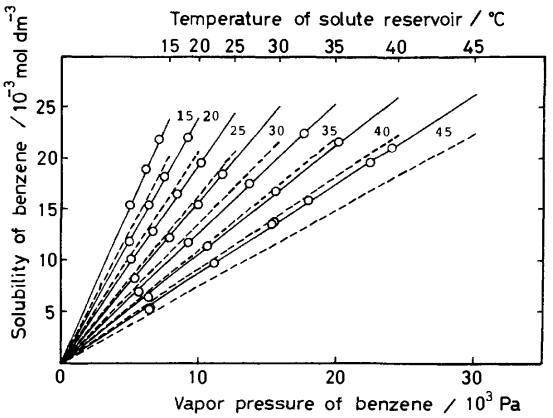

Fig. 2. Equilibrium solubility of benzene in $(CH_3)_4NBr$ aqueous solutions *vs.* vapor pressure.
Pure water (dotted line), 0.496 mol dm^{-3} $(CH_3)_4NBr$ solution (solid line). The figure near each line indicates the temperature of aqueous solution.

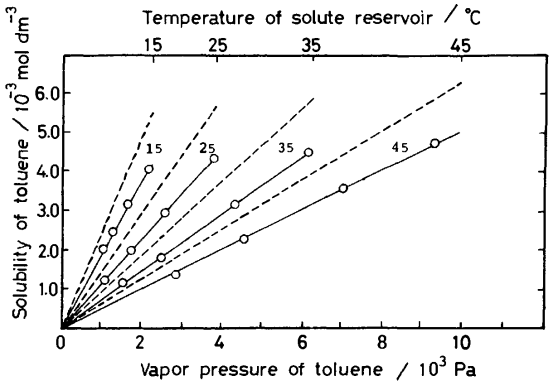

Fig. 3. Equilibrium solubility of toluene in NaCl aqueous solutions *vs.* vapor pressure.
Pure water (dotted line), 0.508 mol dm^{-3} NaCl solution (solid line). The figure near each line indicates the temperature of aqueous solution.

Experimental Salting Coefficients. The salting coefficients were all determined at 25 °C. In the beginning of this study, the solubilities were measured under conditions where the temperatures of both the solubility flask and the solute reservoir were the same. However, somewhat poor reproducibilities were then oberved. This is probably due to the fact that, because it is difficult to keep both temperatures exactly the same, the solute vapor condenses temporarily inside the solubility flask. Therefore, the solubility in each electrolyte solution, S, was estimated as follows: the equilibrium solubility was first measured keeping the solute reservoir at a temperature just below 25 °C, while the temperature of the solubility flask was maintained at 25 °C, and then the equilibrium solubility was extrapolated to find S on the assumption that the solubility obeys Henry's law. The solubility in pure water, S_0, was also estimated in the same way. The values thus determined are, at 25 °C: $10^3 \cdot S_0$ (in mol dm^{-3})=20.7 (benzene), 5.65 (toluene), 1.62 (ethylbenzene), 0.376 (propylbenzene). These values are in good agreement with those previously reported except for that of propylbenzene, which differs by *ca.* 10%.[1] In the present study, we will use as S_0 the values determined here. The salting coefficients, k_s, were determined by the least-squares method according to Eq. 1. The log (S_0/S) *vs.* C plots were almost proportional to the electrolyte concentrations up to 1 mol dm^{-3} for 1:1 electrolytes and 0.5 mol dm^{-3} for $BaCl_2$ and Na_2SO_4. The use of NaI as an electrolyte gave scattered plots and a poor reproducibility except in the case of benzene;

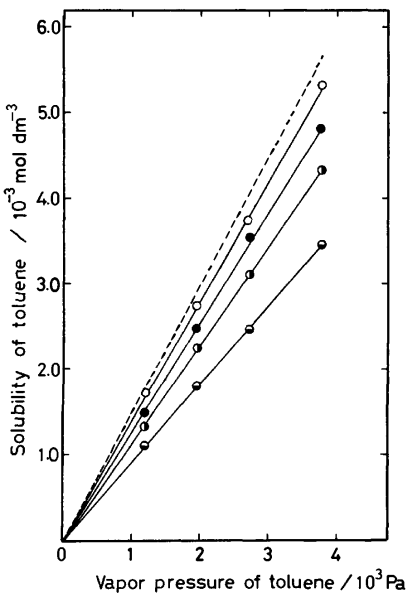

Fig. 4. Equilibrium solubility of toluene in KCl aqueous solutions *vs.* vapor pressure.
Pure water (dotted line), concentration of KCl: 0.101 (○), 0.253 (●), 0.505 (◑), 1.01 mol dm^{-3} (◒). The temperature of aqueous solution: 25.0 °C.

Table 1. Salting coefficients of benzene, toluene, ethylbenzene, and propylbenzene[a]

Electrolyte	Observed		Calculated	
	This work	Literature	M-L[b]	SPT[c]
		Benzene		
NaCl	0.188	0.195[d]	0.436(0.174)	0.199
$NaNO_3$	0.113	0.119[d]	0.314(0.126)	0.207
NaBr	0.156	0.155[d]	0.367(0.147)	0.170
NaSCN	0.048		0.168(0.067)	0.150
NaF	0.249	0.254[d]	0.681(0.272)	0.197
$NaClO_4$	0.115	0.109[d]	0.262(0.105)	0.244
KCl	0.157	0.166[d]	0.349(0.140)	0.176
NaI	0.099	0.095[d]	0.279(0.112)	0.166
$BaCl_2$	0.310	0.334[d]	1.030(0.412)	0.266
Na_2SO_4	0.514	0.548[d]	1.365(0.546)	0.512
$(CH_3)_4NBr$	−0.15	−0.15[e]	−0.54(−0.22)	1.700
$(C_2H_5)_4NBr$	−0.29	−0.25[e]	−0.80(−0.32)	2.189
		Toluene		
NaCl	0.242	0.267[f]	0.518(0.207)	0.248
$NaNO_3$	0.154		0.373(0.149)	0.258
NaBr	0.190		0.435(0.174)	0.218
NaSCN	0.066		0.199(0.080)	0.200
NaF	0.336		0.807(0.323)	0.244
$NaClO_4$	0.139		0.311(0.124)	0.299
KCl	0.214	0.205[f]	0.414(0.166)	0.222
$BaCl_2$	0.414		1.221(0.489)	0.392
Na_2SO_4	0.684	0.651[f]	1.619(0.648)	0.636
		Ethylbenzene		
NaCl	0.280		0.601(0.240)	0.286
$NaNO_3$	0.165		0.432(0.173)	0.300
NaBr	0.232		0.504(0.202)	0.256
NaSCN	0.079		0.231(0.092)	0.238
NaF	0.438		0.937(0.375)	0.281
$NaClO_4$	0.142		0.360(0.144)	0.345
KCl	0.250		0.480(0.192)	0.259
$BaCl_2$	0.457		1.417(0.567)	0.491
Na_2SO_4	0.693		1.878(0.751)	0.737
		Propylbenzene		
NaCl	0.281		0.708(0.283)	0.323
$NaNO_3$	0.153		0.510(0.204)	0.339
NaBr	0.233		0.595(0.238)	0.292
NaSCN	0.069		0.272(0.109)	0.275
NaF	0.373		1.104(0.442)	0.315
$NaClO_4$	0.131		0.425(0.170)	0.389
KCl	0.256		0.566(0.227)	0.294
$BaCl_2$	0.467		1.671(0.668)	0.582
Na_2SO_4	0.748		2.214(0.886)	0.834

a) Observed and calculated at 25 °C. b) McDevit-Long equation (multiplied by a factor of 0.4). c) Scaled-particle theory. d) Ref. 4. e) Ref. 7. f) Z. Sir, L. Strnadova, and V. Rad, *Collect. Czech. Chem. Commun.*, **45**, 679(1980).

therefore, the results for the other solutes were omitted. The observed k_s values are listed in Table 1, together with the literature values. The present results are in good agreement with the literature. Comparisons for ethylbenzene and propylbenzene cannot be made, since no data are available for these solutes in the literature at the present time.

Salting Coefficients Calculated by Means of the McDevit-Long Equation. Based on the internal pressure theory (IPT), McDevit and Long have derived this equation[4]:

$$k_s=\overline{V}_i^\circ(V_s-\overline{V}_s^\circ)/2.3\,\beta_0 RT, \qquad (2)$$

where $\overline{V}_i^\circ$ is the partial molar volume of the solute at an infinite dilution, V_s is the molar volume of the pure electrolyte, $\overline{V}_s^\circ$ is the partial molar volume of the electrolyte at an infinite dilution, and β_0 is the compressibility of pure water. At 25 °C, $\overline{V}_i^\circ$ (in $cm^3\,mol^{-1}$)=89.4 (benzene), 106 (toluene), 123 (ethylbenzene), and 145 (propylbenzene).[5] All the other parameters were taken from the literature.[4,6-8] The values of k_s calculated by means of Eq. 2 are given in Table 1.

Salting Coefficients Calculated by Means of the Scaled-particle Theory. In order to predict the salting coefficients, equations have been derived based on the scaled-particle theory (SPT) by Masterton and Lee[9] and, more recently, by Miyajima *et al.*[10] We have calculated the salting coefficients according to the latter authors, since their equations are more definite and are

more widely applicable. In the present calculations, however, we neglected the self-interaction coefficient, k_2, in the equation given by Miyajima *et al.* since, in the present case, plots of $\log(S_0/S)$ *vs.* the electrolyte concentrations are almost linear through the zero intercept. Equations leading to k_0 are expressed as functions of the hard-sphere diameter, σ; the energy parameter, ε/κ; the polarizability, α; and the apparent molar volume of salt at an infinite dilution, ϕ_0. We adopted the same values of σ and ε/κ for water as those used in Ref. 10, and the same values of σ, α, and ϕ_0 for electrolytes as those used in Ref. 1, the parameter for I^- being taken from Ref. 9. The values of ε/κ for the electrolytes have been evaluated by means of Mavroyannis-Stephen equation:

$$\varepsilon/\kappa = 2.28\times10^{-8}\alpha^{3/2}Z^{1/2}\sigma^{-6}, \quad (3)$$

where Z is the total number of electrons of species. The necessary information on the parameters used for solutes is tabulated in Table 2.

Table 2. Parameters used for solutes in calculating salting coefficients by scaled-particle theory

Solute	$10^{24}\times\alpha$ [a]	$10^{8}\times\sigma$ [b]	ε/κ [c]
	$cm^3 mol^{-1}$	cm	K
Benzene	10.43	5.46	188
Toluene	12.26	5.93	159
Ethylbenzene	14.09	6.31	145
Propylbenzene	16.03	6.67	135

a) Estimated from molar refractivity. b) Evaluated by Eq. 4 in the text. c) Evaluated by Eq. 3 in the text.

Discussion

Table 1 shows that the absolute values of the salting coefficient as calculated by means of the McDevit-Long equation are generally larger than those observed and that, if the equation is multiplied by a factor of 0.4, the calculations give the closest prediction. The various k_s values observed for a number of hydrocarbons available in the literature enable us to compare the data with those estimated by the use of Eq. 2. The results are summarized in Table 3, from which it is noticable that most ratios, k_s(obsd)/k_s(calcd), are in the range of from 0.3 to 0.4. The McDevit-Long equation implies that the k_s is linearly dependent on the molar volume of the solute at a given electrolyte. Such plots are shown in Fig. 5 using the data obtained in the present study. The k_s appears for each electrolyte to be approximately proportional up to the molar volume corresponding to

Table 3. Comparison of salting coefficients reported in the literature with those calculated by McDevit-Long equation

Solute	Molar volume	Electrolyte	k_s		Ratio [a]
			obsd	calcd	
	$cm^3 mol^{-1}$				
Benzene	89	NaCl	0.175 [b]	0.434	0.4
Chlorobenzene	101.8	NaCl	0.2090 [c]	0.497	0.42
		NaBr	0.1292 [c]	0.418	0.31
		Na_2SO_4	0.5808 [c]	1.56	0.37
Pentane	115.2	NaCl	0.221 [c]	0.562	0.39
p-Dichlorobenzene	117.8	NaCl	0.2448 [c]	0.575	0.43
		NaBr	0.1744 [c]	0.483	0.36
		Na_2SO_4	0.2925 [c]	1.799	0.16
Naphthalene	125	NaCl	0.213 [b]	0.610	0.35
		NaCl	0.260 [c]	0.610	0.43
		NaBr	0.169 [c]	0.513	0.33
		Na_2SO_4	0.716 [c]	1.909	0.38
Hexane	130.6	NaCl	0.276 [c]	0.638	0.43
		NaBr	0.161 [c]	0.536	0.30
		KCl	0.244 [c]	0.510	0.48
		Na_2SO_4	0.788 [c]	1.99	0.40
Biphenyl	149	NaCl	0.276 [c]	0.727	0.38
		NaBr	0.209 [c]	0.611	0.34
		KCl	0.255 [c]	0.582	0.44
		Na_2SO_4	0.846 [c]	2.28	0.37
Fluorene	153	NaCl	0.267 [b]	0.747	0.36
Anthracene	160	NaCl	0.238 [b]	0.781	0.30
Phenanthrene	160	NaCl	0.275 [b]	0.781	0.35
		NaCl	0.287 [c]	0.781	0.37
		NaBr	0.211 [c]	0.656	0.32
		KCl	0.279 [c]	0.625	0.45
		Na_2SO_4	0.784 [c]	2.44	0.32
Pyrene	172	NaCl	0.286 [b]	0.839	0.34
Fluoranthene	175	NaCl	0.339 [b]	0.854	0.40
Chrysene	194	NaCl	0.336 [b]	0.947	0.35
Benz[*a*]anthracene	194	NaCl	0.354 [b]	0.947	0.37

a) k_s(obsd)/k_s(calcd). b) Taken from W. E. May, S. P. Wasik, and D. H. Freeman, *Anal. Chem.*, **50**, 997 (1978). c) Taken from M. Aquan-Yuen, D. Mackay, and W. Y. Shiu, *J. Chem. Eng. Data*, **24**, 30 (1979).

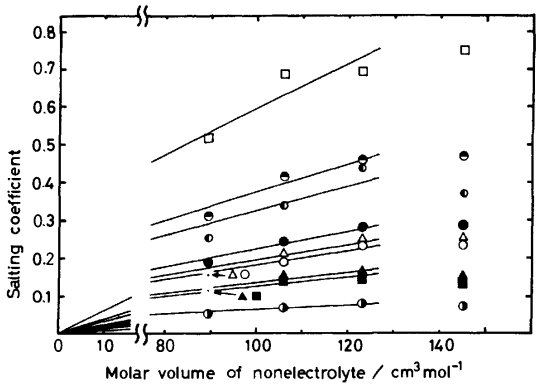

Fig. 5. Salting coefficient *vs.* molar volume of solute.
Electrolyte: Na_2SO_4 (□), $BaCl_2$ (◓), NaF (◐), NaCl (●), KCl (△), NaBr (○), $NaNO_3$ (▲) $NaClO_4$ (■), NaSCN (◑).

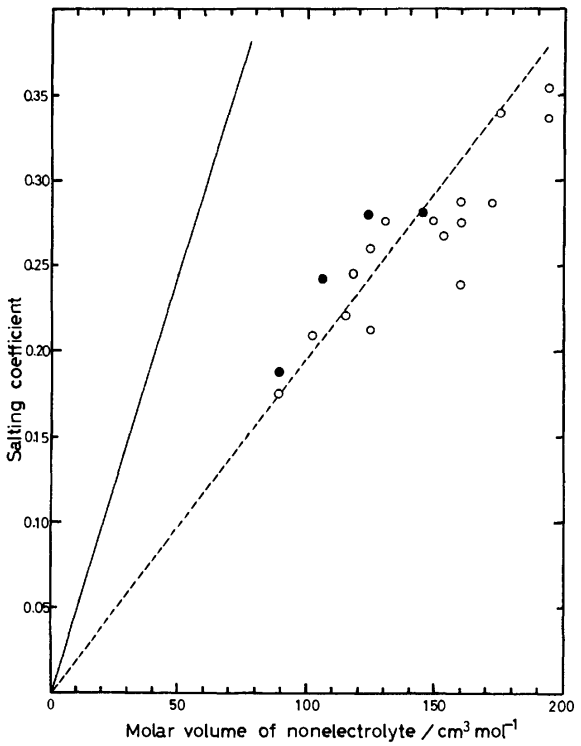

Fig. 6. Salting coefficient for NaCl *vs.* molar volume of solute.
This work (●), literature values (○).

ethylbenzene, but exhibits a poor proportionality in the vicinity of propylbenzene. According to the data shown in Table 3, the values of k_s observed for NaCl are plotted against the molar volume of each solute. The results are shown in Fig. 6, where the solid line and the dotted line indicate, respectively, the molar volume dependence of k_s expected from Eq. 2 and that of k_s multiplied the equation by a factor of 0.4. The plots in Fig. 6, though they seem to scatter around the dotted line, when inspected in more detail display a gently downward curve with an increase in the molar volume rather than a straight line.

The McDevit-Long equation gives satisfactory predictions of k_s for such solutes as H_2, N_2, O_2, CH_4, C_2H_4, and rare gases.[9,11] On the other hand, as was originally pointed out by McDevit and Long, the equation gives a k_s value for benzene consistently too high by a factor of from 2 to 3.[4] Deno and Spink also suggested that the equation must be multiplied by a factor of 0.3 to improve the agreement with the observed and the calculated k_s values of benzene.[7] It is noteworthy that the McDevit-Long equation predicts a high k_s not only for benzene, but also for such hydrocarbons as are shown in Table 3. The IPT explains the salt effect in terms of the electrostriction, $V_s - \overline{V}_s^o$ of the solvent caused by salt, and it does not take into account any interactions which may be possible between solute and solvent and between solute and electrolyte. The solute-solvent interaction should be an important factor, especially in the case of aromatic hydrocarbon solutes. Masterton *et al.* have emphasized that the solute-electrolyte interaction, especially with anions, plays a major role in the salting-in of some aromatic hydrocarbons.[12] We can see from Table 3 that the k_s(obsd)/k_s(calcd) ratio is definitely smaller for Br^- than for Cl^-. However, the solute-electrolyte interaction seems to be less important than the solute-solvent interaction, since the k_s(obsd)/k_s(calcd) ratios for various hydrocarbons are almost consistently in the range from 0.3 to 0.4. An empirical factor of from 0.3 to 0.4 cannot be explained quantitatively at present.

The SPT involves two steps: (1) the creation of a cavity in the solvent of a suitable size to accommodate a solute molecule, and (2) the interaction of a solute molecule with the solvent and electrolyte species. The theory would, therefore, reflect the characteristic interactions between solute and solvent and between solute and electrolyte. It is important in calculating k_s by means of SPT to select the most suitable values of σ and ε/κ for the solute in question. Lennard-Jones 6—12 pair potential parameters have been reported except for propylbenzene, but they differ from report to report.[13] At first we adopted the pair-potential parameters evaluated by the use of the following equations:

$$\sigma=(2.3454+0.2972\ \omega)\ (T_c/P_c)^{1/3}, \quad (4)$$

$$\varepsilon/\kappa=(0.8082-0.4504\ \omega)\ T_c, \quad (5)$$

where $\omega=-1+3\theta/7(1-\theta)\times\log P_c$, $\theta=T_b/T_c$ and where T_c, T_b, and P_c are the critical temperature, the boiling temperature, and the critical pressure of the solute respectively. These equations have been explained as being successful for nonpolar molecules.[14] We have taken the alkylbenzenes used in this study to be nearly nonpolar, with quite small dipole moments. The values of ε/κ estimated from Eq. 5 are: ε/κ (in K)=398 (benzene), 406 (toluene), 412 (ethylbenzene), and 415 (propylbenzene). The calculated k_s values, however, led to consistently lower results compared with the observations. Masterton and Lee found that Eq. 3 gave an appropriate ε/κ value in predicting the k_s of benzene.[9] Wilcox and Schrier also recommended the use of the ε/κ estimated from Eq. 3 in calculating the k_s values of polar solutes such as alcohols.[15] For the solutes considered in this work, the values of ε/κ have been determined by Eq. 3 using the corresponding σ values estimated from Eq. 4. These parameters are shown in Table 2. The calculated k_s values

are in reasonable agreements with the observations, as will be seen from Table 1, except for $NaNO_3$, NaSCN, $NaClO_4$ and tetraalkylammonium salts. The considerable discrepancies relating to NO_3^-, SCN^-, and ClO_4^- may be attributable to the uncertainty as to the true σ values for these polyatomic anions. In the case of tetraalkylammonium salts, however, the failure of SPT is inherent.

The present method to determine k_s, which makes use of solute vapor, has a potential usefulness when an anionic or cationic electrolyte is subject to being extracted into the liquid solute phase accompanying a counter ion; hence, it is difficult to determine k_s in the presence of a liquid solute.

References

1) I. Sanemasa, M. Araki, T. Deguchi, and H. Nagai, *Bull. Chem. Soc. Jpn.*, **55**, 1054 (1982).
2) J. Polak and B. C.-Y. Lu, *Can. J. Chem.*, **51**, 4018 (1973).
3) For benzene, the vapor pressure was taken from "International Critical Tables," McGraw-Hill, New York (1928), Vol. III, pp. 208, 221. For the alkylbenzenes, the vapor pressure were taken from "Kagaku Binran, Kiso-Hen II," ed by The Chemical Society of Japan, Maruzen, Tokyo (1975), pp. 710—731.
4) W. F. McDevit and F. A. Long, *J. Am. Chem. Soc.*, **74**, 1773 (1952).
5) H. B. Klevens, *J. Phys. Colloid Chem.*, **54**, 283 (1950).
6) B. Lunden, *Z. Phys. Chem.*, **192**, 345 (1943).
7) N. C. Deno and C. H. Spink, *J. Phys. Chem.*, **67**, 1347 (1963).
8) F. J. Millero, *Chem. Rev.*, **71**, 147 (1971).
9) W. L. Masterton and T. P. Lee, *J. Phys. Chem.*, **74**, 1776 (1970).
10) K. Miyajima, H. Yoshida, and M. Nakagaki, Nippon Kagaku Kaishi, **1980**, 1.
11) F. A. Long and W. F. McDevit, *Chem. Rev.*, **51**, 119 (1952).
12) W. L. Masterton, T. P. Lee, and R. L. Boyington, *J. Phys. Chem.*, **73**, 2761 (1969).
13) Pair-potential parameters have been reported in the following reports: S. Goldman, *J. Phys. Chem.*, **80**, 1697 (1976), E. Willhelm and R. Battino, *J. Chem. Phys.*, **55**, 4012 (1971), B. K. Kaul, M.D. Donohue, and J. M. Prausnitz, *Fluid Phase Equilibria*, **4**, 171(1980), and Ref. 14.
14) F. M. Mourits and H. A. Rummens, *Can. J. Chem.*, **55**, 3007 (1977).
15) F. L. Wilcox and E. E. Schrier, *J. Phys. Chem.*, **75**, 3757 (1971).

 © 1984 The Chemical Society of Japan Bull. Chem. Soc. Jpn., 57, 1545—1550 (1984)

Physicochemical Speciation of Trace Elements in River Water by Size Fractionation

Yoshiyuki TANIZAKI,* Masao YAMAZAKI, and Sumiko NAGATSUKA
Tokyo Metropolitan Isotope Research Center, Fukazawa, Setagaya-ku, Tokyo 158
(Received November 11, 1983)

Eight kinds of Millipore filters with different pore sizes (8—0.025 μm) were used for the filtration of two water samples taken from the Tama River. The filtrates were analyzed for 31 elements using a neutron activation analysis. Most alkali and alkaline earth elements were distributed in the smallest size fraction (<0.025 μm). The same fractionation pattern was also recognized for As, Se, Mo, Sb, and W, which tend to form oxoanions. But the major transition elements were concentrated in the larger size fractions (>0.45 μm). For the river water sample with higher concentration of total organic carbon, however, most of such elements were found in the smallest size fraction. The solubilities of rare earth elements bacame higher with increasing their ionic potentials.

The analysis of chemical species for various elements in natural water is of great importance not only to substantiate their geochemical behavior such as dissolution, fluidity, adsorption, and precipitation, but also to estimate the toxicity of the elements towards aquatic organisms.[1,2] For trace elements, however, it is very difficult to determine directly their chemical species hecause of their low concentrations and the complexity of their physical or chemical forms in natural water. Consequently, a physicochemical fractionation technique has been developed for an indirect speciation of the trace elements. Stumm and Bilinski first proposed that trace metal species could usefully be classified according to their size distribution.[3] Subsequently, a few workers studied the effect of filter pore size exerted on the analytical concentrations of some trace elements in filtrates of natural water.[4,5] Laxen and Harrison applied the fractionation technique to speciation of several trace elements in lake water,[6] and to effluents from sewage treatment plants and industrial processes and the river water which receives these effluents.[7,8] This fractionation technique was summarized together with other physicochemical speciation techniques such as centrifugation, ultrafiltration, dialysis and gel filtration chromatography, by Mora and Harrison.[9] But no one has applied the size fractionation technique to a systematic analysis of multielements. In this paper, therefore, we tried to clarify the size distribution of 31 elements found in river water, and to discuss their chemical species, by utilizing this technique and neutron activation analysis (NAA).

Experimental

Water Samples. The river water samples were taken from two points of the Tama River, which runs through the Metropolis of Tokyo, in November 1982 and February 1983. The two sampling points are shown in Fig. 1. They are located up-stream of the Hamura intake dam (A point) and near the Tamagawara bridge (B point). The water qualities are listed in Table 1 for the two points. The river water of B point (sample B) is more enriched in chlorine and total organic carbon (TOC) than those of the river water of A point (sample A) by a factor of 10 or above. This indicates that sample B is largely influenced by anthropogeneous pollutions. Chemical constituents in sample A, on the other hand, are mainly derived from rocks and their efflorescences in the drainage basin or by rainfall, as reported in a previous paper.[10]

Filtration. All-glass Millipore apparatus and eight kinds of Type HA millipore filters (mixed esters of cellulose) with diameter 142 mm, of average pore sizes 8, 3, 1.2, 0.45, 0.22, 0.1, 0.05, and 0.025 μm, were used for all filtrations. Decontamination of each filter was achieved by passing through 30 ml of dilute nitric acid (1:3), followed by 2-l of redistilled water under reduced pressure. The filtration of each water sample was performed in the following way. Forty liters of the water sample was pre-filtrated using the filter with pore size 8 μm, in order to remove large size particles. The filtrate was divided into eight 5-l portions. The seven portions of filtrate were filtrated once again using the other seven kinds of filters, one by one. The eight filtrates were transferred to clean 5-l polyethylene bottles, and then acidified immediately with 30 ml of nitric acid (Super Special Grade) in order to avoid any adsorption of trace elements on

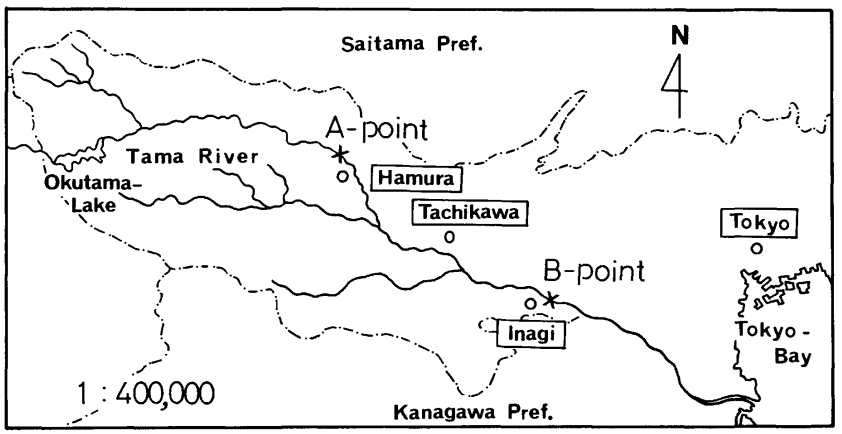

Fig. 1. Sampling locality.

Table 1. Water quality of the Tama River at the time of sampling

Parameter	River water sample	
	A	B
Sampling point	Hamura	Inagi
Date	1/11/82	16/2/83
Water temp/°C	14.7	9.8
pH	8.2	6.9
Conductivity/μS cm^{-1}	80	310
4.3 Bx/mequiv l^{-1}	0.71	1.77
ER[a]/ppm	101	402
TOC[b]/ppm	0.5	6.9
SO_4^{2-}/ppm	13	49
SiO_2/ppm	18	31
Cl^-/ppm	1.6	51.5

a) Amount of evaporated residue. b) Total organic carbon.

the wall of the bottle.

Five-liter of the water sample was taken as the original material in another polyethylene bottle without filtration and was then acidified with 30 ml of the nitric scid.

Preparation of Irradiation Samples. For the NAA in this work, two kinds of irradiation samples, an evaporated residue sample and iron(III) hydroxide coprecipitated one, were prepared from each filtrate and the original (unfiltrated) water sample. The procedures were reported in detail in our previous papers.[10-12]

Irradiation and Gamma-ray Counting. The irradiation was performed by the TRIGA-Mark II Reactor of Rikkyo University, with a thermal neutron flux of 1.5×10^{12} n/cm^{2}s. The gamma ray spectrometer consists of a high pure germanium detector with 15% efficiency and 2.0 keV resolution, and a 2048 and 4096 channel pulse height analyzer.

The evaporated residue sample was first irradiated for 1 min to determine the elements that result the short life nuclides such as Al (^{28}Al), Ca (^{49}Ca), K (^{42}K), Mg (^{27}Mg), Mn (^{56}Mn), Na (^{24}Na), and V (^{52}V); these radioactivities were measured for 100 s by the spectrometer. One month later, the same sample was irradiated once more for 12 h to determine the elements that result the long life nuclides such as Ag (^{110m}Ag), Ba (^{131}Ba), Ce (^{141}Ce), Co (^{60}Co), Cr (^{51}Cr), Cs (^{134}Cs), Fe (^{59}Fe), Ni (^{58}Co), Rb (^{86}Rb), Sb (^{124}Sb), Sc (^{46}Sc), Se (^{75}Se), Sr (^{85}Sr), Tb (^{160}Tb), and Th (^{233}Pa). The measurement of these long life activities were carried out for 50000 s after a cooling time of 2—4 weeks to reduce the short or medium life nuclides.

The iron(III) hydroxide coprecipitated sample, on the other hand, was also irradiated for 12 h to determine the elements that result the medium life nuclides such as As (^{76}As), Eu (^{152m}Eu), La (^{140}La), Lu (^{177}Lu), Mo (^{99}Mo), Sm (^{153}Sm), U (^{239}Np), W (^{187}W), and Yb (^{175}Yb), and after the cooling time of 1 d, these activities were measured for 2000 s.

Results and Discussion

The concentrations of 31 elements were determined for the eight filtrates and the original water sample by NAA. The statistical errors based on the gamma ray counting were 5—30% for Ag, Ba, Ce, Cr, Eu, Fe, La, Mg, Mn, Mo, Ni, Se, Tb, Th, and U, and less than 5% for the other 16 elements.

The, size distribution of each element is calculated in the following way. When the analytical concentration of an element in the original water sample and the filtrates resulted from the filters with pore size of 8, 3, ···, 0.05, and 0.025 μm are represented by C_T and C_8, C_3, ···, $C_{0.05}$, and $C_{0.025}$, the size distribution (S) of the elements is given by

$$
\begin{aligned}
S(>8\,\mu m) &= C_T - C_8 && F(>8\,\mu m)\\
S(8-3\,\mu m) &= C_8 - C_3 \\
S(3-1.2\,\mu m) &= C_3 - C_{1.2} && F(8-0.45\,\mu m)\\
S(1.2-0.45\,\mu m) &= C_{1.2} - C_{0.45} \\
S(0.45-0.22\,\mu m) &= C_{0.45} - C_{0.22} \\
S(0.22-0.1\,\mu m) &= C_{0.22} - C_{0.1} && F(0.45-0.025\,\mu m)\\
S(0.1-0.05\,\mu m) &= C_{0.1} - C_{0.05} \\
S(0.05-0.025\,\mu m) &= C_{0.05} - C_{0.025} \\
S(<0.025\,\mu m) &= C_{0.025} && F(<0.025\,\mu m)
\end{aligned}
$$

The results are classified into four size fractions: F (>8 μm), F (8—0.45 μm), F (0.45—0.025 μm), and F (<0.025 μm); these results are shown in Tables 2—6.

In general, chemical constituents passing through the filter with pore size 0.45 μm are defined as "dissolved", and those retained on the filter are classified as "particulate".[13] However, the "dissolved" constituents need not be in true solution but can include "colloidals".[3,9] The boundary in size between "colloidals" and "true solution" probably lies in the range of 0.01—0.001 μm.[9,14] Consequently, it is difficult to fractionate perfectly chemical constituents in the river water samples between "colloidals" and "true solution" because the smallest pore size of the Millipore filter is 0.025 μm. For convenience, it is assumed in this paper that the constituents passing through the 0.025 μm filter (F (<0.025 μm)) are mostly "true solution", and the materials with size ranging from 0.45 μm to 0.025 μm (F (0.45—0.025 μm)) are "colloidals". The materials with size larger than 0.45 μm (F (>8 μm) and F (8—0.45 μm)) are classified as "particulate".

In order to discuss systematically the fractionation results, the 31 elements are divided into 5 groups in the following manner, as shown in Tables 2—6.

Alkali and Alkaline Earth Elements (Na, K, Rb, Cs, Mg, Ca, Sr, and Ba). The total concentrations are given in the concentrations for the original (unfiltrated) water sample. For alkali and alkaline earth elements in sample A, these concentrations were considerably lower than those in sample B, although the concentration of Cs in sample A was exceptionally high, as can be seen in Table 2. The very high enrichments in Na, K and Mg concentrations for sample B indicate that the B point of the Tama River is largely influenced by anthropogeneous pollutions.

Na, K, Mg, Ca, and Sr were found only in the smallest size fraction (< 0.025 μm) for both samples A and B. It is well known that these elements are dissolved in natural water as uni- or bivalent cations. Rb and Cs in sample A were divided mainly between the particulate (>8 μm and 8—0.45 μm) and the smallest size fractions, with few colloidals (0.45—0.025 μm), although in sample B all those elements were also found in the smallest size fraction. 47% of Ba were associated with the particulate, and the remaining 53% were distributed in the smallest size fraction for sample A. For sample B, on the other hand, 15 and 85% of Ba were found in the particulate and the smallest size fractions, respectively. It is supposed that considerable parts of Rb, Cs, and Ba

TABLE 2. FRACTIONATION RESULTS OF ALKALI AND ALKALINE EARTH ELEMENTS IN THE RIVER WATER

Element	Sampling point	Size fraction(μm)				Sum total
		>8	8—0.45	0.45—0.025	<0.025	
Na	A	0(0)[a)]	0(0)	0(0)	3.39(100)	3.39 ppm
	B	0(0)	0(0)	0(0)	45.3(100)	45.3 ppm
K	A	0(0)	0(0)	0(0)	0.98(100)	0.98 ppm
	B	0(0)	0(0)	0(0)	5.9(100)	5.9 ppm
Rb	A	0.63(38.9)	0.12(7.3)	0.14(8.6)	0.73(45.1)	1.62 ppb
	B	0(0)	0(0)	0(0)	5.0(100)	5.0 ppb
Cs	A	0.071(73.2)	0.010(10.3)	0.004(4.1)	0.012(12.4)	0.097 ppb
	B	0(0)	0(0)	0(0)	0.083(100)	0.083 ppb
Mg	A	0(0)	0(0)	0(0)	1.04(100)	1.04 ppm
	B	0(0)	0(0)	0(0)	6.99(100)	6.99 ppm
Ca	A	0(0)	0(0)	0(0)	14.9(100)	14.9 ppm
	B	0(0)	0(0)	0(0)	29.0(100)	29.0 ppm
Sr	A	0(0)	0(0)	0(0)	58.2(100)	58.2 ppb
	B	0(0)	0(0)	0(0)	169(100)	169 ppb
Ba	A	2.7(33.3)	1.1(13.6)	0(0)	4.3(53.1)	8.1 ppb
	B	0.9(7.1)	1.0(7.9)	0(0)	10.8(85.0)	12.7 ppb

a) The parenthesized values are percentages of each fraction.

TABLE 3. FRACTIONATION RESULTS OF TRANSITION ELEMENTS IN THE RIVER WATER

Element	Sampling point	Size fraction(μm)				Sum total (ppb)
		>8	8—0.45	0.45—0.025	<0.025	
Sc	A	0.0855(90.5)	0.0064(6.7)	0.0011(1.2)	0.0015(1.6)	0.0945
	B	0.0414(75.4)	0.0016(2.9)	0.0010(1.8)	0.0109(19.9)	0.0549
V	A	0.46(37.7)	0.09(7.4)	0(0)	0.67(54.9)	1.22
	B	0.76(27.9)	0(0)	0(0)	1.96(72.1)	2.72
Cr	A	0.21(56.8)	0.03(8.1)	0(0)	0.13(35.1)	0.37
	B	0.28(29.0)	0.18(18.6)	0.05(5.1)	0.46(47.4)	0.97
Mn	A	8.5(88.5)	0(0)	0(0)	1.1(11.5)	9.6
	B	6.5(9.4)	2.4(3.5)	0(0)	60.3(87.1)	69.2
Fe	A	308(88.5)	35.8(10.3)	1.4(0.4)	3.0(0.9)	349
	B	151(72.2)	18.3(8.8)	24.8(11.9)	14.9(7.1)	209
Co	A	0.087(68.5)	0.019(15.0)	0(0)	0.021(16.4)	0.127
	B	0.047(12.6)	0(0)	0.012(3.2)	0.313(84.1)	0.372
Ni	A	0(0)	0(0)	0(0)	0.85(100)	0.85
	B	0.1(1.3)	0(0)	0.5(6.3)	7.3(92.4)	7.9

in sample A are held on ion exchange sites of inorganic suspended materials[15] such as clay minerals or iron(III) hydroxide, which will be explained in later discussion, by the fact that the contents of particulate Al and Fe for sample A are high.

Transition Elements (Sc, V, Cr, Mn, Fe, Co, and Ni). Sample A was more enriched in the total concentrations of Sc and Fe, and deficient in V, Cr, Mn, Co, and Ni in comparison with the concentrations in sample B, as can be seen in Table 3. This indicates that Sc and Fe in the Tama River water are mainly derived from rocks or their efflorescences, while the other five heavy metals are chiefly supplied by anthropogeneous sources.

The major parts (80% or more) of Sc, Mn, Fe, and Co in sample A were distributed in the particulate size fraction. In particular, Sc and Fe were mostly particulate (>97%), and only a few percent of those elements could be fractionated as dissolved species (<0.45 μm). It is known that Fe is the main component of suspended materials in most river water along with Al and SiO_2,[16,17] and it usually forms iron(III) hydroxide.[4,18] The concentration of Sc is very low for ordinary natural water.[10,12] It is supposed that the behavior of Sc in river water with poor TOC concentration is governed by coprecipitation with iron(III) hydroxide. For sample B, on the other hand, although approx. 80% of Sc and Fe were also associated in the particulate size fraction, the remaining 20% were fractionated as the dissolved species. For Mn and Co, 80—90% of them in sample A were found in the particulate size fraction. On the contrary, 80—90% of these elements in sample B were distributed in the smallest size fraction. In general, transition elements are known to have a strong complexing ability for organic substances such as humus.[19-21] Sample B has a

TABLE 4. FRACTIONATION RESULTS OF ARSENIC, SELENIUM, MOLYBDENUM, ANTIMONY, AND TUNGSTEN IN THE RIVER WATER

Element	Sampling point	Size fraction(μm)				Sum total (ppb)
		>8	8-0.45	0.45-0.025	<0.025	
As	A	0(0)	0(0)	0(0)	0.61(100)	0.61
	B	0(0)	0(0)	0(0)	0.79(100)	0.79
Se	A	0(0)	0(0)	0(0)	0.086(100)	0.086
	B	0(0)	0(0)	0(0)	0.13(100)	0.13
Mo	A	0(0)	0(0)	0(0)	0.24(100)	0.24
	B	0(0)	0(0)	0(0)	0.48(100)	0.48
Sb	A	0(0)	0(0)	0(0)	0.176(100)	0.176
	B	0(0)	0(0)	0(0)	0.376(100)	0.376
W	A	0(0)	0(0)	0(0)	0.072(100)	0.072
	B	0(0)	0(0)	0(0)	0.123(100)	0.123

TABLE 5. FRACTIONATION RESULTS OF RARE EARTH ELEMENTS IN THE RIVER WATER

Element	Sampling point	Size fraction(μm)				Sum total (ppt)
		>8	8—0.45	0.45—0.025	<0.025	
La	A	163(84.6)	16(8.3)	1.8(0.9)	11.9(6.2)	193
	B	245(88.1)	13(4.6)	8(3.0)	12(4.4)	278
Ce	A	493(85.7)	48(8.3)	5(0.9)	29(5.0)	575
	B	347(79.7)	51(11.6)	8(1.8)	29(6.8)	435
Sm	A	30.5(84.1)	3.4(9.4)	1.3(3.6)	1.0(2.9)	36.2
	B	15.6(77.8)	1.7(8.6)	1.4(6.9)	1.3(6.7)	20.0
Eu	A	7.97(83.5)	1.18(12.4)	0(0)	0.40(4.1)	9.55
	B	5.04(69.1)	0.52(7.1)	0.73(10.0)	1.00(13.7)	7.29
Tb	A	—	—	—	—	ND
	B	1.81(58.0)	0.26(8.3)	0.26(8.3)	0.76(24.4)	3.12
Yb	A	>9.0(85.7)		<1.3(12.5)	< 0.2(1.8)	10.5
	B	6.5(15.2)	2.2(5.1)	5.7(13.3)	28.5(66.4)	42.9
Lu	A	—	—	—	—	ND
	B	1.54(18.8)	0(0)	1.74(21.3)	4.89(59.9)	8.17

much higher TOC concentration than that of sample A, by a factor of ahout 14, as listed in Table 1. In sample B, therefore, the transition elements should be mostly present as soluble organic complexes, so that they are distributed in the smallest size fraction. However, it is very difficult to draw any quantitative conclusion about the extent of complexing of the transition elements by organic substances because we have no information on their chemical forms. This remains to be studied.

Even in sample A with poor TOC concentration, V and Cr were found in the smallest size fraction in substantial quantity (55 and 35%, respectively). This can be explained by assuming the existences of their soluble quinque- or sexivalent species such as $V_{10}O_{28}^{6-}$,[22,23] CrO_4^{2-}.[24]

Almost all Ni, which is distinct from the other six transition elements, was found in the smallest size fraction for both samples A and B. This indicates that Ni easily dissolves in natural water as a bivalent species, Ni^{2+}.[25]

The Elements Forming Oxoanions (As, Se, Mo, Sb, and W). The total concentrations of As, Se, Mo, Sb, and W in sample B were higher than those in sample A by a factor of about 2. However, the same fractionation result was observed for all of them, that they were detectable only in the smallest size fraction (<0.025 μm), as can be seen in Table 4. This result is consistent with the view that these elements tend to form soluble oxoanions such as AsO_4^{3-}, SeO_3^{2-}, MoO_4^{2-}, SbO_4^{3-}, WO_4^{2-}[12,26-31] in ordinary natural water.

Rare Earth Elements (REEs: La, Ce, Sm, Eu, Tb, Yb, and Lu). Major parts (86—94%) of La, Ce, and Sm were associated with the particulate size fraction (>8 μm and 8—0.45 μm) for both samples A and B, and those elements distributed in the colloidal (0.45—0.025 μm) and the smallest size fractions (<0.025 μm) were only several percent, as can be seen in Table 5. Europium in sample A was also found mainly in the particulate size fraction, whereas in sample B 10 and 14% of Eu were distributed in the colloidal and the smallest size fractions,respectively. Although Yb in sample A was also mostly the particulate, 33% of Tb and approx. 80% of Yb and Lu in sample B were fractionated as the dissolved species (0.45—0.025 μm and <0.025 μm). These findings suggest that the higher TOC concentration in sample B is largely contributed to the dissolution of the heavier REEs such as Tb, Yb, Lu. This conclusion is substantiated by the analytical data that the total concentrations of the heavier REEs for sample B are higher than those for sample A, even though for the light REEs, except La,

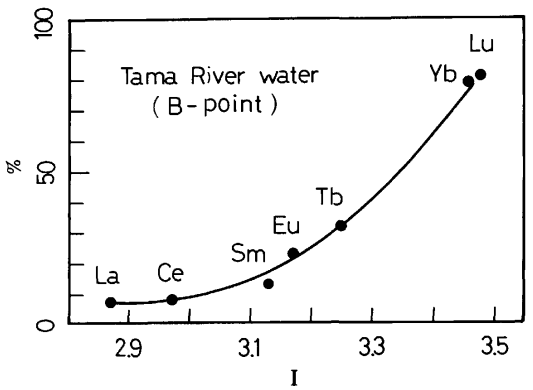

Fig. 2. Plot showing the relation between the solubilities (%) of REEs and their ionic potentials (*I*).

the higher total concentrations were found in sample A, as shown in Table 5.

The relation between the solubilities of the REEs in sample B and their ionic potentials is demonstrated by Fig.2, which is a plot of the proportions(%) of REEs fractionated as the dissolved species to their total concentrations *versus* ratios of the chemical valency to their ionic radii.[32] The diagram shows that the solubilities of the REEs increase with increasing ionic potentials. In other words, the heavier REEs with high ionic potentials tend to form the organic complexes in the river water with high TOC concentration. The monotonous increasing fashion of the solubilities for the heavier REEs illustrated in the diagram agrees with that reported by Goldberg *et al.*,[33] who have studied the behavior of REEs in marine environment.

For the light REEs, on the other hand, it is supposed that most of those elements may be coprecipitated with iron(III) hydroxide. This is explained by the following considerations. The total concentration ratios of La, Ce, and Sm to Fe in samples A and B are $(0.55—1.3)\times10^{-3}$, $(1.7—2.1)\times10^{-3}$, and $(0.96—1.0)\times10^{-4}$, and those in particulate matters in the Thames River water reported by Habib *et al.*[17] are 0.46×10^{-3}, 1.9×10^{-3}, and 0.86×10^{-4}, respectively. These values are close to the same ratios for the earth's crust presented by Taylor[34] and Wedepohl[35] $(0.53—1.2)\times10^{-3}$, $(1.2—2.1)\times10^{-3}$, and $(1.1—1.9)\times10^{-4}$. Therefore, it could be said that the behavior of light REEs in the river water is similer to that of Fe, on the process of dissolution or precipitation. Iron tends to form insoluble iron(III) hydroxide in ordinary natural water, as mentioned above, so that the light REEs also precipitate as the hydroxides.

Others (Al, Ag, Th, and U). Sample A was more enriched in the total concentrations of Al and U by a factor of about 2 in the comparison with those in sample B, as can be seen in Table 6. Silver in sample A and Th in sample B were less than the detection limits. Thorium in sample A could not be determined since no standard reference sample was prepared, so that the gamma ray counting ratio was utilized for the discussion. The higher total concentrations of Al, Th, and U in sample A indicate that those elements are mainly derived from the rocks or their efflorescences in the drainage basin, while the higher total concentration of Ag in sample B means that Ag is largely influenced by artificial pollution.

Table 6 notes that 87% of Al in sample A was associated with the particulate, and 11% was found in the smallest size fraction. For sample B, on the other hand, Al amounts distributed in the particulate and the smallest size fractions were 65 and 34%, respectively. The colloidal Al was only a few percent for both samples. Aluminium is one of the main components of suspended materials in most river water as well as Fe and SiO_2, as stated above. However, the proportion of Al fractionated as the dissolved species (0.45—0.025 μm and<0.025 μm) to the total concentration are 13 and 35% for samples A and B, and these values are much higher than those of Fe, 1.3 and 19% respectively. This can be explained in the following way. It is well known that Al in natural water not only precipitates as the hydroxide, but also forms clay minerals in the process of the rock weathering.[36] In general, clay minerals have a small size distribution (<5 μm), and a certain type of them has been found with size smaller than 0.45 μm.[37] Such materials pass through the filter with the corresponding pore size. In addition, Hem and Roberson showed that some finegrained Al compounds suspended in water may be passed through a 0.45 μm membrane filter.[38] Thus, a considerable part of Al can be fractionated as the dissolved species.

Eighty five percent of Ag was found in the particulate size fraction with 14% of the colloidal for sample B. Silver seems to be easily halogenated in the polluted river water, and is predominantly held on clay minerals or iron(III) hydroxide.

Thorium in sample A was also chiefly associated with the particulate size fraction; on the contrary, almost all U was distributed in the smallest size fraction, although approx. 20% of the particulate U was

Table 6. Fractionation results of aluminium, silver, thorium, and uranium in the river water

Element	Sampling point	Size fraction(μm)				Sum total (ppb)
		>8	8—0.45	0.45—0.025	<0.025	
Al	A	487(80.8)	37(6.1)	13(2.2)	66(10.9)	603
	B	191(58.6)	20(6.1)	5(1.5)	110(33.7)	326
Ag	A	—	—	—	—	ND
	B	1.14(74.3)	0.17(11.0)	0.21(13.7)	0.015(1.0)	1.53
Th	A	—(89.2)	—(7.6)	—(1.3)	—(1.9)	—
	B	—	—	—	—	ND
U	A	0.012(20.7)	0(0)	0.005(8.6)	0.041(70.7)	0.058
	B	0(0)	0(0)	0(0)	0.027(100)	0.027

found for sample A. The difference of the fractionation patterns between Th and U seems to arise from the differences of their chemical forms in the river water. It is well known that U tends to form the soluble sexivalent species UO_2^{2+} in most natural water.[39-41] But for Th, a quadrivalent species is the only stable form, which is probably coprecipitated with the hydroxides of Fe and Al in water.[42]

Conclusion

Using the size fractionation technique and NAA method, it was possible to obtain some knowledge about the chemical species of the trace elements existing in the Tama River water. One of the factors that governed the size distribution patterns of the trace elements was the TOC concentration in the river water. The high TOC concentration largely contributed to the dissolution of Rb, Cs, Ba, Al, U, the transition elements, and the heavier REEs. Fe, Sc, Th, and the light REEs, which tend to precipitate as the hydroxides, however, were predominantly distributed in the particulate size fraction. Na, K, Mg, Ca, Sr, Ni, As, Se, Mo, Sb, and W, which easily form the various soluble inorganic ions, on the other hand, were found only in the smallest size fraction, regardless of the TOC concentration in the river water.

Several tedious problems, however, still remain to be examined concerning the size fractionation technique. It must be kept in mind that adsorptive losses of trace elements onto the filter[43] and contamination from the filter materials[44] may occur during the filtration, which may lead to erroneous analytical results. Equilibrium conditions on chemical species of trace elements kept in the river water may be upset at the time of filtration, so that rapid treatments of the samples are required. Filters are not 100% efficient with respect to their size selectivety characteristics,[9] and the effective pore size decreases during the filtration because of filter clogging. Such problems are more insidious and require consideration in greater detail to minimize analytical errors. In order to determine exactly the chemical species of trace elements in river water, further studies will be necessary.

References

1) C. Chakoumakos, R. C. Russo, and R. V. Thurston, *Environ. Sci. Technol.*, **13**, 213 (1979).
2) H. E. Allen, R. H. Hall, and T. D. Bribin, *Environ. Sci. Technol.*, **14**, 441 (1980).
3) W. Stumm and H. I. Billinski, "Advances in Water Pollution Research," Pergamon Press, Oxford (1973), p. 39.
4) V. C. Kennedy and G. W. Zellweger, *Water Resour. Res.*, **10**, 785 (1974).
5) R. Wagemann and G. J. Brunskill, *Int. J. Environ. Anal. Chem.*, **4**, 75, (1975).
6) D. P. H. Laxen and I. M. Chandler, *Anal. Chem.*, **54**, 1350 (1982).
7) D. P. H. Laxen and R. M. Harrison, *Water Res.*, **15**, 1053 (1981).
8) D. P. H. Laxen and R. M. Harrison, *Water Res.*, **17**, 71 (1983).
9) S. J. Dē Mora and R. M. Harrison, *Water Res.*, **17**, 723 (1983).
10) Y. Tanizaki and S. Nagatsuka, *Nippon Kagaku Kaishi*, **1974**, 2094.
11) S. Nagatsuka and Y. Tanizaki, *Radioisotopes*, **23**, 693 (1974).
12) Y. Tanizaki and S. Nagatsuka, *Bull. Chem. Soc. Jpn.*, **56**, 619 (1983).
13) E. D. Goldberg, M. Baker, and D. L. Fox, *J. Mar. Res.*, **11**, 197 (1952).
14) B. Mason, "Principles of Geochemistry," Third ed, John Wiley and Sons, New York (1966), Chap. 6.
15) J. D. Hem, *Geochim Cosmochim Acta*, **40**, 599 (1976).
16) H. Teraoka and J. Kobayashi, *Geochemical J.*, **14**, 203 (1980).
17) S. Habib and M. J. Minski, *J. Radioanal. Chem.*, **63**, 379 (1981).
18) J. D. Hem and W. H. Cropper, *U. S. Geol. Surv. Water-Supply Pap.*, **No. 1459-A**, 31 (1959).
19) P. Benes, E. T. Gjessing, and E. Steinnes, *Water Res.*, **10**, 711 (1976).
20) C. Steelink, *J. Chem. Educ.*, **54**, 599 (1977).
21) E. R. Sholkovitz and D. Copland, *Geochim. Comochim. Acta*, **45**, 181 (1981).
22) R. M. Garrels and C. L. Christ, "Solutions, Minerals, and Equilibria," Harper and Row, New York (1965), Chap.4.
23) R. U. Byerrum *et al.*, "Medical and Biologic Effects of Environmental Pollutant, Vanadium," National Academy of Sciences, Washington D. C. (1974), Chap. 4.
24) A. M. Beatjer *et al.*, "Medical and Biologic Effects of Environmental Pollutant, Chromium," National Academy of Sciences, Washington D. C. (1974), Chap. 2.
25) Y. Sugimura, *Bunseki*, **1981**, 148.
26) R. M. Garrels and C. L. Christ, "Solutions, Minerals, and Equilibria," Harper and Row, New York (1965), pp.421 and 426.
27) S. Gohda, *Bull. Chem Soc. Jpn.*, **48**, 1213 (1975).
28) S. A. Gunn *et al.*, "Medical and Biologic Effects of Environmental Pollutant, Selenium," National Academy of Sciences, Washington D. C. (1976), Chap. 2.
29) M. O. Andreae, *Anal. Chem.*, **49**, 820 (1977).
30) R. Massee, H. A. van der Sloot, and H. A. Das, *J. Radioanal. Chem.*, **35**, 157 (1977).
31) M. Ishibashi and T. Fujinaga, *Nippon Kagaku Zasshi*, **88**, 76 (1967).
32) R. D. Shannon and C. T. Prewitt, *Acta Crystallogr., Sect. B*, **25**, 925 (1969).
33) E. D. Goldberg, M. Koide, R. A. Schmitt, and R. H. Smith, *J. Geophys. Res.*, **68**, 4209 (1963).
34) S. R. Taylor, *Geochim. Cosmochim. Acta*, **28**, 1273 (1964).
35) K. H. Wedepohl, "Geochemistry," Holt, Rinehart and Winston, New York (1971), p. 65.
36) F. J. Pettijohn, "Sedimentary Rocks," 2nd ed, Harper and Row, New York (1957), p. 101.
37) R. E. Grim, "Clay Mineralogy," McGraw-Hill, New York (1968), pp. 168—183 and 544—548.
38) J. D. Hem and C. E. Roberson, *U. S. Geol. Surv. Water-Supply Pap.*, **1827-A**, A24 (1968).
39) J. A. S. Adams, J. K. Osmond, and J. J. W. Rodgers, "Physics and Chemistry of the Earth, BIII," Pergamon Press, New York (1959) p. 298.
40) Y. Miyake, Y. Sugiura, and H. Tsubota, "The Natural Radiation Environment, ed by J. A. S. Adams and W. M. Lowder," The University of Chicago Press' Chicago (1964), p. 219.
41) K. Megumi and T. Mamuro, *Hoken Butsuri*, **12**, 181 (1977).
42) V. M. Goldshmidt, "Geochemistry," Clarendon Press, Oxford (1954), p. 431.
43) R. E. Truitt and J. H. Weber, *Anal. Chem.*, **51**, 2057 (1979).
44) G. E. Batley and D. Gardner, *Water Res.*, **11**, 745 (1977).

 © 1984 The Chemical Society of Japan Bull. Chem. Soc. Jpn., 57, 1551—1555 (1984)

Determination of a Small Amount of Biological Constituent by Use of Chemiluminescence. III. The Flow-injection Analysis of Protein by Direct Injection

Tadashi HARA,* Motohiro TORIYAMA, and Kazuhiko TSUKAGOSHI
Department of Chemical Engineering, Faculty of Engineering, Doshisha University, Karasuma Imadegawa, Kamigyo-ku, Kyoto 602
(Received November 29, 1983)

A flow-injection analysis method of protein by direct injection has been established by use of the luminol-hydrogen peroxide luminescence system. The determination of protein is based on the measurement of the decreasing catalytic activity of copper(II) for the chemiluminescent reaction between luminol and hydrogen peroxide. The present flow-injection analysis in which a protein solution is directly injected is quite different from the previous one in which a protein solution is injected after having been previously allowed to react with copper(II) outside the flow-through system. The optimum conditions for the determination of protein were determined with regard to reagent concentration, flow rate, reaction time, and reaction temperature. The present method is simple, rapid, and applicable to the determination of 2×10^{-4}—1×10^{-1} g dm^{-3} of protein with 40 ng of detection limit at a rate of about 30 samples per hour. The present method was also applied to the determination of the ratio of albumin to globulin in a sample. The present flow-injection system is expected to be a sensitive detector for the determination of small amounts of protein.

A new method for the determination of protein, in which use was made of the decreasing catalytic activity for the chemiluminescence (CL) reaction between 5-amino-2, 3-dihydro-1, 4-phthalazinedione(luminol) and hydrogen peroxide(H_2O_2) when copper(II) (Cu(II)) interacted with polypeptide linkage, was reported by the authors in the previous paper[1]. The method was more sensitive and applicable to a wider range of protein concentration than is available with the conventional methods. However the protein in a sample solution had to be made to react with Cu(II) at 30 °C for 50 min before its injection into a flow-injection system.

Here the flow-injection system in the previous paper has been modified to enable a protein solution to inject directly into the flow-injection system. In the previous paper,[2] protein was also determined by use of a cobalt(III) complex. However Cu(II) is used in the present work as a catalyst for the CL reaction because Cu(II) shows faster reaction with protein and smaller difference between CL responses of individual protein compared with those of cobalt(III). In the present method, the protein solution is directly injected into the flow-injection system without any pretreatment and the analytical results are obtained simply and rapidly because the reaction between Cu(II) and protein proceeds in the flow-path.

Experimental

Reagents. By diluting with the buffer solution (pH 10.15) consisting of boric acid and potassium hydroxide presented in the previous paper,[1] a 5.0×10^{-4} mol dm^{-3} luminol solution and a 2.0×10^{-6} mol dm^{-3} Cu(II) catalyst solution from a 2.0×10^{-2} mol dm^{-3} Cu(II) stock solution[1] were prepared. A 5.0×10^{-4} mol dm^{-3} H_2O_2 solution was prepared by diluting a 0.3 wt% H_2O_2 solution with water. The reagents used were of commercially available special grade.

Human serum albumin(HSA) and bovine serum α-globulin from ICN Pharmaceuticals, Inc., and human serum γ-globulin, bovine serum albumin(BSA), and bovine serum γ-globulin from Sigma Chemical Co., and control serum(Q-PAK-Chemistry Control Serum I) from HYLAND were used. All these proteins were dissolved in the buffer solution and diluted with it.

Ion exchange water was distilled for use.

Apparatus and Procedure. The schematic diagram of the apparatus used for the present flow-injection analysis is shown in Fig. 1. All the tubes and connectors used were made of Teflon. Each solution of luminol(a), H_2O_2(b), Cu(II) (c), and a buffer(d) was fed by means of 2.3×10^5 Pa gauge pressure of nitrogen gas; the flow rate was adjusted to 10 cm^3 min^{-1} by a needle valve. A 0.4 cm^3 of protein sample solution was injected into the buffer solution line through the sampling loop(k) and the six-way cook(j). The protein sample solution was first mixed with a Cu(II) catalyst solution and passed through 1.6 m of tube held at 0 °C in the cooling bath (n) *via* a 1.0 m of tube held at 95 °C in the heating bath(m). Then the solution was mixed with a H_2O_2 solution and a luminol solution in that order, and passed through the flow cell(o). The distances between T and S or U were 35 and 10 cm, respectively. The same flow cell as in the previous paper was used. The CL intensity of the solution passing through the cell was measured by a photomultiplier (p) (Hamamatsu TV Co. Ltd., R928), amplified with a amplifier(g) (Horiba Ltd., OPE-402), and recorded on a recorder(r) (Yokogawa Electric Works, Ltd., 3046). The CL intensity of the solution containing no sample was recorded

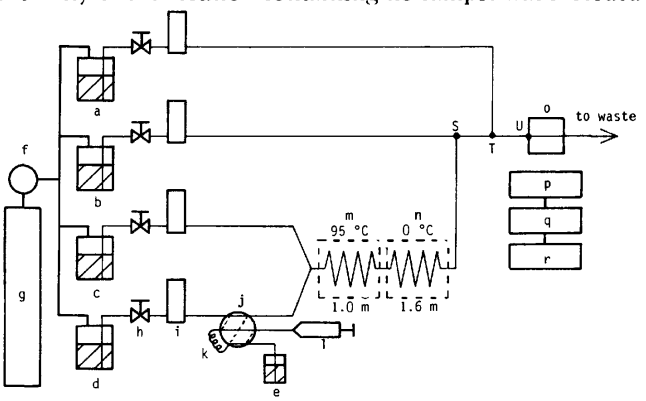

Fig. 1. Schematic diagram of the flow-injection system.
a: Luminol solution, b: H_2O_2 solution, c: Cu(II) catalyst solution, d: buffer solution, e: sample solution, f: regulator, g: N_2 bomb, h: needle valve, i: flow meter, j: six-way cock, k: sampling loop, l: cylinge, m: heating bath, n: cooling bath, o: flow cell, p: photomultiplier, g: amplifier, and r: recorder.

as a base line while the CL intensity of the solution containing protein was recorded as a negative peak because the catalytic activity of Cu(II) decreased because of the complex formation between Cu(II) and protein. The amount of protein was estimated from the peak area.

Results and Discussion

Determination of Analysis Conditions. Bovine serum albumin was used as a model protein.

The CL intensity was measured by using 0.5, 1.0, 2.0, and 3.0 m of tube held at 95 °C in the heating bath, but no difference between CL intensities was observed in all the tubes except the first one. Then a 1.0 m of tube was used for the heating bath in the following experiment.

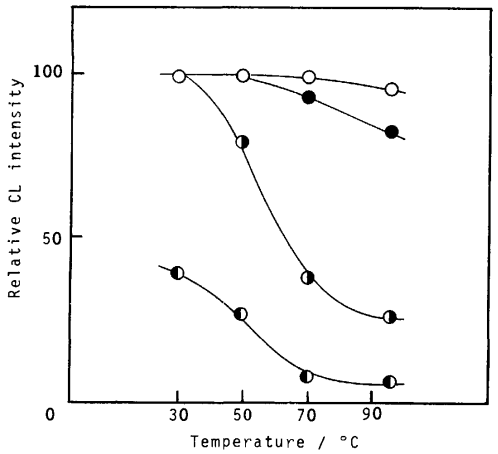

Fig. 2. Effect of heating bath temperature on relative CL intensity.[a)]
○: 2.0×10^{-4} g dm^{-3}-, ●: 1.0×10^{-3} g dm^{-3}-, ◑: 1.0×10^{-2} g dm^{-3}-, and ◐: 1.0×10^{-1} g dm^{-3}-BSA.
Conditions: 5.0×10^{-4} mol dm^{-3} luminol, 5.0×10^{-4} mol dm^{-3} H_2O_2, and 2.0×10^{-6} mol dm^{-3} Cu(II).
a) The CL intensity of the solution containing protein to the CL intensity of the solution containing no protein.

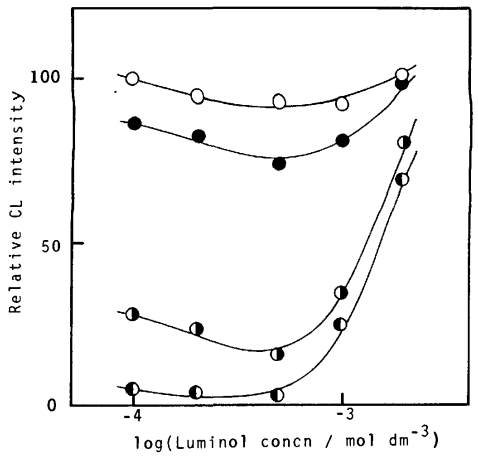

Fig. 3. Effect of luminol concn on relative CL intensity.[a)]
○: 2.0×10^{-4} g dm^{-3}-, ●: 1.0×10^{-3} g dm^{-3}-, ◑: 1.0×10^{-2} g dm^{-3}-, and ◐: 1.0×10^{-1} g dm^{-3}-BSA.
Conditions: 5.0×10^{-4} mol dm^{-3} H_2O_2 and 2.0×10^{-6} mol dm^{-3} Cu(II).
a) The CL intensity of the solution containing protein to the CL intensity of the solution containing no protein.

The effect of the temperature of the heating bath on the CL intensity is shown in Fig. 2. Each plot represents the CL intensity in the presence of BSA against the CL intensity 100 of a base line. Then the temperature of the heating bath was set at 95 °C because the CL intensity decreased with a rise of temperature.

The tube held at 0 °C in the cooling bath played two important roles: cooling the hot effluent so as not to affect the CL intensity and charging the back pressure so as not to produce a foam inside the tube in the heating bath. 1.6 m tube length was chosen to make the diffusion of the samples as small as possible.

The effect of the concentration of luminol, H_2O_2, and Cu(II) solutions on the CL intensity are shown in Figs. 3, 4, and 5. From these results, the optimum

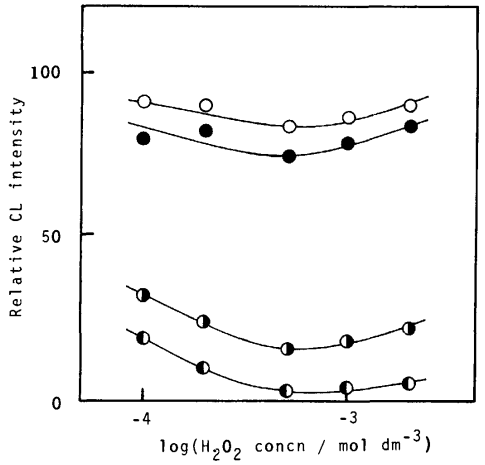

Fig. 4. Effect of H_2O_2 concn on relative CL intensity.[a)]
○: 5.0×10^{-4} g dm^{-3}-, ●: 1.0×10^{-3} g dm^{-3}-, ◑: 1.0×10^{-2} g dm^{-3}-, and ◐: 1.0×10^{-1} g dm^{-3}-BSA.
Conditions: 5.0×10^{-4} mol dm^{-3} luminol and 2.0×10^{-6} mol dm^{-3} Cu(II).
a) The CL intensity of the solution containing protein to the CL intensity of the solution containing no protein.

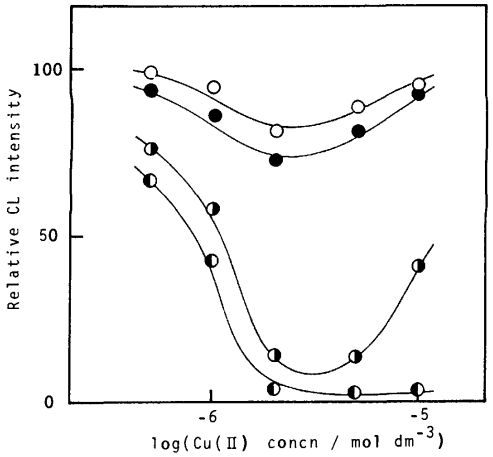

Fig. 5. Effect of Cu(II) concn on relative CL intensity.[a)]
○: 5.0×10^{-4} g dm^{-3}-, ●: 1.0×10^{-3} g dm^{-3}-, ◑: 1.0×10^{-2} g dm^{-3}-, and ◐: 1.0×10^{-1} g dm^{-3}-BSA.
Conditions: 5.0×10^{-4} mol dm^{-3} luminol and 5.0×10^{-4} mol dm^{-3} H_2O_2.
a) The CL intensity of the solution containing protein to the CL intensity of the solution containing no protein.

concentrations corresponding to maximum decreases in the CL intensity were as follows: luminol solution 5.0×10^{-4} mol dm^{-3}; H_2O_2 solution 5.0×10^{-4} mol dm^{-3}; and Cu(II) catalyst solution 2.0×10^{-6} mol dm^{-3}.

Determination of Protein. The calibration curve of BSA obtained under the above-mentioned conditions is shown in Fig. 6. As can be seen from it, 1×10^{-4}—1×10^{-1} g dm^{-3} protein gave the CL response which corresponded to the peak area of the negative peak recorded in the addition of BSA solution. The decrease of the CL intensity in the presence of protein is attributed to the lowering of the catalytic activity of Cu(II) based on the formation of a Cu(II)-polypeptide complex. The fact that the ratio of the change of peak area to the change of protein concentration is rather small seemed to be based on the diffusion of a sample and the dilution of a sample solution by additions of reagent solutions. The flow chart obtained by injecting each 1.0×10^{-4}, 5.0×10^{-3}, and 5.0×10^{-2} g dm^{-3} BSA and that obtained at a blank experiment are shown in Fig. 7.

The CL responses of HSA, human serum γ-globulin, bovine serum α-globulin, and bovine serum γ-globulin by the present method were examined in the manner used in the preparation of the calibration curve of BSA (Fig. 8). Approximately similar responses were obtained for them. This suggests that the present flow-injection system will serve as a promising detector for the determination of protein.

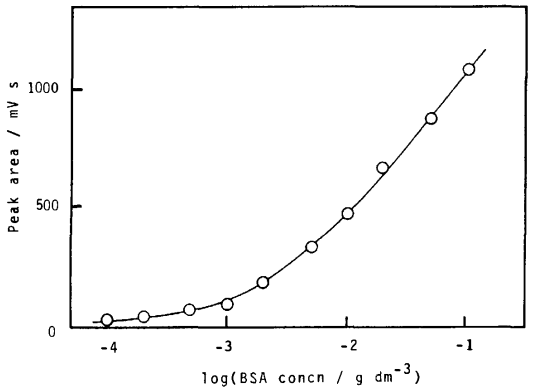

Fig. 6. Calibration curve of BSA by the present method.
Conditions: 5.0×10^{-4} mol dm^{-3} luminol, 5.0×10^{-4} mol dm^{-3} H_2O_2, and 2.0×10^{-6} mol dm^{-3} Cu(II).

Precision was not so good in the previous paper because each solution was delivered by means of a peristaltic pump, accompanied by fluctuating flow, while precision in the present work was drastically improved by means of the utilization of a gas pressure without any fluctuations in flow. Therefore the present method makes it possible to estimate a small amount of protein with the concentration range of 2×10^{-4}—1×10^{-1} g dm^{-3} and the detection limit of about 40 ng. The coefficients of variation of the present method for 10 analyses of 5.0×10^{-3} and 5.0×10^{-2} g dm^{-3} protein solutions were both 4.1%.

Estimation of the Ratio of Albumin to Globulin. The ratio of albumin to globulin(A/G) has been looked upon as an important parameter for diagnosis of the abnormal metabolism of protein in human body. Here the A/G ratio was estimated to examine whether or not the present method could be applied to a mixed protein sample.

To examine the effect of the coexisting constituents in a control serum on the CL intensity when a control serum was diluted to 2000 times of volume with a buffer solution and measured, the analytical values against HSA or a definite amount of control serum (containing 2.3×10^{-2} g dm^{-3} of protein) plus HSA were obtained by use of the calibration curve shown in Fig. 8. All the analytical values of the ordinate in Fig. 9 were represented as the amount of HSA. The difference between straight lines I and II in the analytical value was approximately equal to the protein amount of the added control serum. This means that the constituents other than protein in the serum do not significantly affect the CL intensity when a sample solution is diluted to 2000 times of volume with a buffer solution and measured. Then the present method was applied to the estimation of the A/G ratio.

Various A/G ratio of mixtures of HSA and human serum γ-globulin were subjected to the fractionation

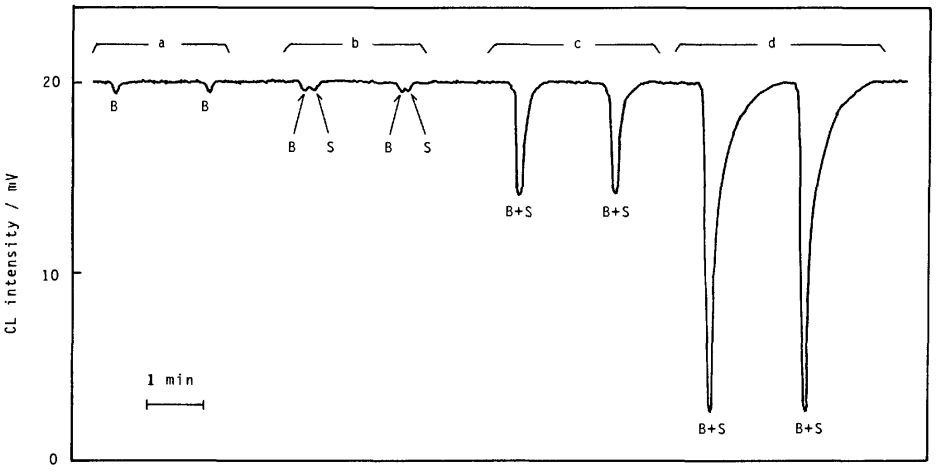

Fig. 7. Flow chart in duplicate measurements.
a: Blank value, b: 1.0×10^{-4} g dm^{-3}-, c: 5.0×10^{-3} g dm^{-3}-, d: 5.0×10^{-2} g dm^{-3}-BSA, B: blank (shock peak by the change of the flow path), and S: sample peak.
Conditions: 5.0×10^{-4} mol dm^{-3} luminol, 5.0×10^{-4} mol dm^{-3} H_2O_2, 2.0×10^{-6} mol dm^{-3} Cu(II), and 1.5 cm min^{-1} chart speed.

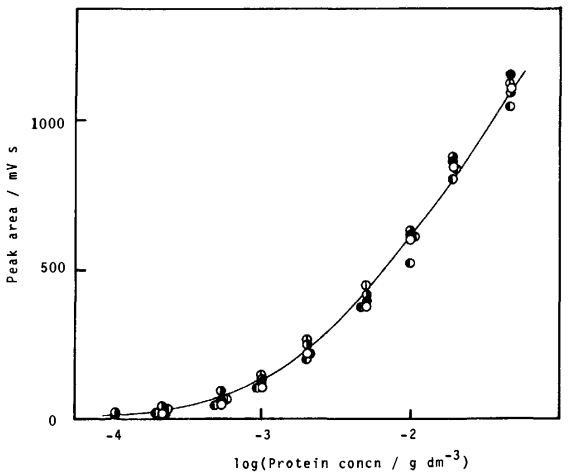

Fig. 8. Response pattern of flow-injection method for various proteins.
○: HSA, ●: human serum γ-globulin, ◑: BSA, ◐: bovine serum α-globulin, and ⊕: bovine serum γ-globulin.
Conditions: 5.0×10^{-4} mol dm^{-3} luminol, 5.0×10^{-4} mol dm^{-3} H_2O_2, and 2.0×10^{-6} mol dm^{-3} Cu(II).

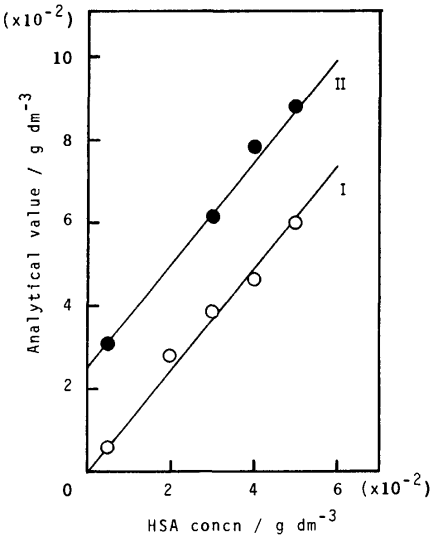

Fig. 9. Relationship between HSA concn and analytical value.
○: HSA and ●: HSA+control serum.
Conditions: 5.0×10^{-4} mol dm^{-3} luminol, 5.0×10^{-4} mol dm^{-3} H_2O_2 and 2.0×10^{-6} mol dm^{-3} Cu(II).

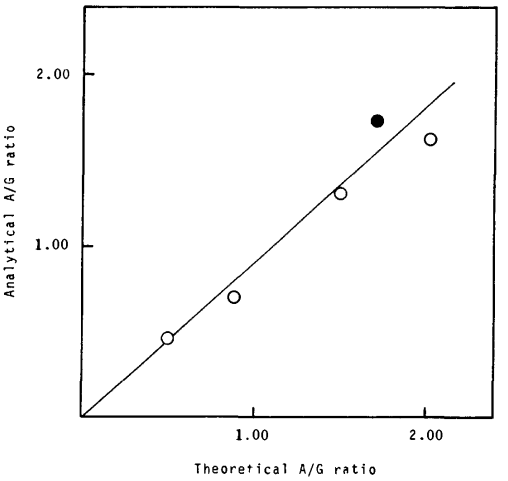

Fig. 10. Relationship between theoretical A/G ratio and analytical A/G ratio.
○: Mixture of HSA and human serum γ-globulin and ●: control serum.
Conditions: 5.0×10^{-4} mol dm^{-3} luminol, 5.0×10^{-4} mol dm^{-3} H_2O_2, and 2.0×10^{-6} mol dm^{-3} Cu(II).

using sodium sulfate as a salting-out agent, and the A/G ratio were determined on the basis of the albumin amount from the albumin fraction and of the globulin amount obtained by subtracting the albumin amount from the total amount obtained for the mixture. Neither sodium sulfite and ammonium sulfate were suitable as a salting-out agent, because the sulfite worked as a reducing agent and the ammonium salts produced a ammine complex in an alkaline solution. To 0.5 cm^3 of protein solution, the concentration of which is the same as that of protein in control serum, 0.5 cm^3 of water and 0.18 g sodium salfate were added and dissolved by shaking in a centrifugal tube. The contents was centrifuged at 10000 min^{-1} for 10 min. An aliquot volume of supernatant liquid was diluted to 1000 times of volume with the buffer solution, and the albumin amount in it and the A/G ratio were determined by the above-mentioned procedure. The relationship between theoretical and analytical values of A/G ratio is shown in Fig. 10. Though the present fractionation did not seem to give complete separation of albumin from globulin, there was a linear correlation,as shown in Fig. 10. The analytical value of the A/G ratio in a control serum was also determined similarly and is plotted in Fig. 10 against the A/G ratio of 1.71, which stood for the mean value of 1.47—2.00 estimated by different methods in eight laboratories as the A/G ratio for the same control serum. The result was almost satisfactory, but a better result would be obtained by the complete separation of albumin from globulin. The possibility of estimating the A/G ratio in human serum by the present method suggests that the combination of the present method with a continuous separation procedure for a mixed protein sample enables the system used in the present method to be a promising detector for the sensitive determination of protein.

On the basis of the results obtained, the flow-injection analysis method of protein by direct injection has been established by use of the luminol-H_2O_2 luminescence system. According to the present method, the previous reaction between Cu(II) and protein as in the previous paper is unnecessary and a protein sample solution can be directly injected into the flow system, followed by the reaction between Cu(II) and protein in the flow-path and the determination of protein. The measurement can be done at the rate of about 30 samples per hour with the concentration range of 2×10^{-4}—1×10^{-1} g dm^{-3} protein and the detection limit of about 40 ng. The present method is expected to serve as a promising detector in the near future because the method is simple, rapid, and applicable to the sensitive determination of a wide range of protein concentration.

The authors wish to thank Mr. Masakatsu Imaki (Horiba Ltd.,) for providing the apparatus necessary for the present study.

References

1) T. Hara, M. Toriyama, and K. Tsukagoshi, *Bull. Chem. Soc. Jpn.*, **56**, 1382 (1983).
2) T. Hara, M. Toriyama, and K. Tsukagoshi, *Bull. Chem. Soc. Jpn.*, **57**, 289 (1984).

 © 1984 The Chemical Society of Japan Bull. Chem. Soc. Jpn., 57, 1556—1561 (1984) [Vol. 57, No. 6

Correlation between Axial and In-Plane Coordination Bond Lengths in Tetragonal Six-coordinate Complexes of the *trans*-MX_2N_4 Type ($M=Co^{3+}$, Ni^{2+}, and Zn^{2+}). X-Ray Structural and *ab initio* Molecular Orbital Studies

Tasuku Ito,* Masako Kato, and Haruko Ito

Department of Applied Molecular Science, Institute for Molecular Science, Okazaki National Research Institutes, Okazaki 444

(Received December 16, 1983)

X-Ray data of 16 structures having coordination geometry of the *trans*-MX_2N_4 type show that (i) an out-of-plane coordination bond length decreases as an in-plane distance increases, (ii) the degree of the correlation is metal ion dependent and varies in the order, $Zn^{2+}>Ni^{2+}>Co^{3+}$. In the Ni(II) systems, complexes having stronger ligands ($X=NCS^-$) at axial positions show the weaker correlation as compared with complexes with weaker axial ligands (Cl^-). Electronic origin that causes such negative correlations has been investigated in terms of the potential energy surfaces obtained from *ab initio* MO calculations for model compounds, *trans*-$[MCl_2(NH_3)_4]$. A section of the potential surface along the M-Cl and M-N bond axes is an ellipse and the ellipse has a tilt with respect to the metal-ligand bond axes. The dependence of the M-Cl distances on the M-N distances becomes stronger, as the tilt of the ellipse increases, and/or as the ratio of the length of long to short axes of the ellipse is increased. The degree of correlation expected from the potential energy surfaces are consistent, in all respect, with experimentally observed results. The interrelationships, found both experimentally and theoretically, are associated with softness of metal ions. Among the metal ions studied, Co(III) is the hardest, Zn(II) is the softest, and Ni(II) is intermediate.

Earlier studies of tetragonally distorted octahedral metal complexes suggest that, in complexes of this type, there exists an interaction between in-plane and out-of-plane ligands through a metal ion.[1] Hathaway[2] and Gažo[1] demonstrated, on the basis of available X-ray data of metal ion salts and simple coordination compounds, correlations between in-plane and out-of-plane coordination bond lengths for some Cu(II) and Ni(II) complexes of this type. Generally, an in-plane bond distance increases as an out-of-plane distance decreases. In our recent structural study of a series of Ni(II) complexes, a similar negative correlation of the coordination bond lengths was observed.[3] It has been also noted, in solution chemistry of some Co(III) complexes of this type, that equatorial ligands affect rates of hydrolyses of the axial ligands.[4] In an NMR spectral study of five-coordinate Cd(II) porphyrin complexes with substituted pyridines at the axial position, coupling constant between ^{111}Cd and porphyrin nitrogen(^{15}N) has been found to decrease with an increase in basicity of substituted pyridine.[5] Busch and coworkers observed a similar phenomenon in ligand field electronic spectra.[6] They showed that, in Ni(II) complexes of *trans*-NiX_2N_4 type, ligand field strength of an axial ligand (Dq^z) decreases as an in-plane ligand field (Dq^{xy}) increases, and they termed it the "electronic cis effect".[6] They also reported that a series of Co(III) complexes of the same type do not show a correlation between Dq^z and Dq^{xy}.[7]

These seem to arise from the same electronic origin. The occurrence of such an interaction between in-plane and out-of-plane ligands through a metal ion, as well as the degree of the interaction, should be metal ion dependent. The present series of the studies were undertaken in order to investigate the electronic effect in more systematic and quantitative way to elucidate the role and function of the metal ion in the observed phenomenon. We have carried out X-ray analyses and *ab initio* MO calculations for a series of complexes which have the same or very similar coordination environments. As metal ions, we chose Co(III), Ni(II), and Zn(II) because of the following reasons: (i) these metal ions form tetragonal octahedral complexes of this type; (ii) routine application of an *ab initio* MO method is in hand in this laboratory for complexes of first row transition metal ions. In the experimental approach, we have determined the structures of a series of complexes of *trans*-MX_2N_4 type, where X is halide or pseudo-halide ion. Tetraazacycloalkanes with different ring sizes, 1,4,8,11-tetraazacyclotetradecane ([14]aneN$_4$), 1,4,8,12-tetraazacyclopentadecane ([15]aneN$_4$), and 1,5,9,13-tetraazacyclohexadecane ([16]aneN$_4$), were used as in-plane ligands so as to vary the M-N distance systematically.

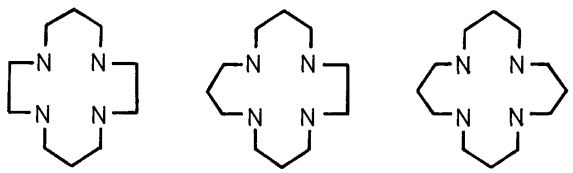

As axial ligands (X), we chose Cl^- and NCS^-, which have relatively weak and strong ligand field strengths, respectively, so that it is possible to investigate the effect of ligand field strength on the correlation between M-X and M-N distances. In the present paper, we summarize and discuss the experimental data on the coordination bond distances found in the series of studies. Structural details of Ni(II)[8] and Zn(II)[9] complexes have been described elsewhere. In the theoretical approach, we have carried out *ab initio* MO calculations on model systems, *trans*-$MCl_2(NH_3)_4$ ($M=Co^{3+}$, Fe^{2+}, Ni^{2+}, and Zn^{2+}).[10] We discuss electronic factors, or metal ion characteristics, which bring about the experimentally observed correlation of intramolecular coordination bond lengths in terms of potential en-

ergy surfaces along M-N and M-Cl bond axes.

We also showed, for the Ni(II) complexes, that the electronic cis effect is manifested in far infrared spectra due to coordination bond stretching vibrations.[8]

Results and Discussion

Correlation between Axial and In-plane Coordination Bond Lengths in trans-MX_2N_4 *Type Complexes.* Table 1 collates the average in-plane (M-N) and axial (M-X) coordination bond lengths of the complexes studied. As expected, with an increase in the number of ring members in macrocyclic ligands, the in-plane M-N distance increases. This increase amounts to 0.04—0.06 Å for each ring member added. They are not as large as expected from calculations of strain energy minimizations for free ligand molecules (0.10—0.15 Å).[11] Data reported previously for the same type of complexes with other similar tetraazamacrocyclic or diamine ligands are also included in Table 1. The correlations are shown in Fig. 1, in which the M-X distances are plotted on the vertical axis and the M-N distances horizontally. As is seen in Fig. 1, there exists a negative correlation between M-X and M-N distances for complexes of each metal ion with given axial ligands: axial coordination bond length decreases as in-plane distance increases, generally. Although there exist steric effects in the molecular and crystal structures of the compounds, that cause the large standard deviations in the average coordination bond lengths,[8,9] they are characteristic of each system and should not give rise to the correlation shown in Fig. 1. Thus, the nature of the phenomenon depicted in Fig. 1 must be electronic in origin.

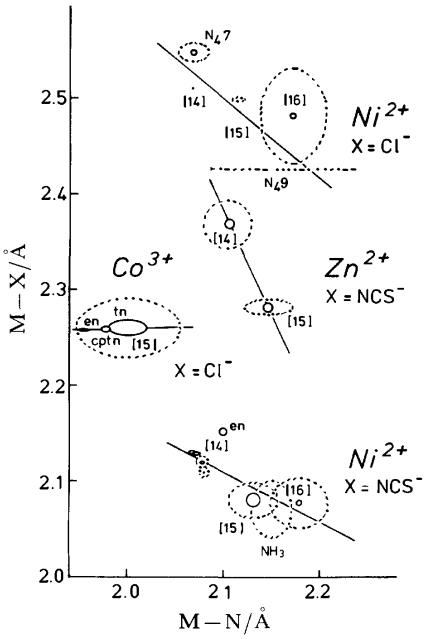

Fig. 1. Correlation between axial and in-plane coordination bond lengths in complexes of the *trans*-MX_2N_4 type. Size of a dashed ellipse or line illustrate an esd obtained upon averaging chemically or crystallographically inequivalent distances, while that of a full-line figure within the dashed one shows an arithmetic mean of esd's for individual metal-ligand distances (see footnote a) in Table 1). Ligand abbreviations: [14]=[14]aneN$_4$, [15]=[15]aneN$_4$, [16]=[16]aneN$_4$. See footnotes of Table 1 for others. For the en complex, no esd values were reported.

Table 1. Average in-plane and axial coordination bond lengths in complexes of *trans*-MX_2N_4 type[a]

Compound	M-X/Å	M-N/Å	Ref. No.
[$NiCl_2$([14]aneN$_4$)]	2.5101(4)	2.067(1)	8, 12
[$NiCl_2$([15]aneN$_4$)]	2.497(1)	2.114(10)	8
[$NiCl_2$([16]aneN$_4$)]	2.482(54)	2.171(34)	8
[$NiCl_2$(N_47)][b]	2.548(8)	2.068(16)	3
[$NiCl_2$(N_49)][c]	2.426(1)	2.161(75)	3
[$Ni(NCS)_2$([14]aneN$_4$)][d]	2.130(2)	2.067(3)	8
	2.128(2)	2.071(5)	8
	2.108(2)	2.081(5)	8
	2.119(6)	2.078(6)	8
[$Ni(NCS)_2$([15]aneN$_4$)]	2.079(20)	2.131(25)	8
[$Ni(NCS)_2$([16]aneN$_4$)]	2.077(26)	2.179(32)	8
[$Ni(NCS)_2(NH_3)_4$]	2.07(3)	2.15(2)	13
[$Ni(NCS)_2$(en)$_2$]	2.15	2.10	14
[$Zn(NCS)_2$([14]aneN$_4$)]	2.367(25)[h]	2.104(25)	9
[$Zn(NCS)_2$([15]aneN$_4$)]	2.282(8)[h]	2.146(28)	9
[$CoCl_2$([15]aneN$_4$)][e]	2.259(31)	2.001(56)	15
[$CoCl_2$(en)$_2$]$^+$	2.257(1)	1.955(4)	16
[$CoCl_2$(tn)$_2$]$^+$[f]	2.26	2.00	17
[$CoCl_2$(cptn)$_2$]$^+$[g]	2.258(3)	1.978(5)	18

a) A number in parentheses is an esd for a mean value of more than two chemically or crystallographically inequivalent bond lengths and is equal to $[\Sigma\Delta_i^2/(n-1)]^{1/2}$, where Δ_i is the deviation of i-th value in a set of n such values from arithmetic mean of the n values. In case of n=2, it is taken to be the largest of three values: the esd for one parameter (q_1), the esd for the other (q_2), or $|q_1-q_2|/2$. b) N_47=1,4,7,10-tetraazacyclotetradecane. c) N_49=1,4,7,10-tetraazacyclohexadecane. d) There are four crystallographically independent complexes in the unit cell.[8] e) Green form isomer. f) tn=1,3-Propanediamine. g) cptn=1,2-cyclopentanediamine. h) An average value of C_t-NCS distances, where C_t denotes a center of the cavity formed with four in-plane nitrogens(see Ref. 9).

In the crystal structure of *trans*-[Ni(NCS)$_2$([14]aneN$_4$)], there are four crystallographically nonequivalent molecules.[8] Interestingly, data for these four molecules show clearly a trend for the negative correlation within the very limited range of metal-ligand distances (see Fig. 1).

Among the present three metal ions, the Zn^{2+} system shows the strongest correlation, the Co^{3+} system almost no correlation, and the Ni^{2+} system is intermediate.

When the $NiCl_2N_4$ and $Ni(NCS)_2N_4$ systems are compared, the slope for the chloro complexes is steeper than that for the isothiocyanato complexes. This indicates that the weaker the axial ligand field is, the stronger is the correlation (*vide infra*). It should be noted that the Zn system has a steep slope in spite of the fact that the data have been obtained with complexes with strong axial ligands NCS^-.[19]

For the Ni(II) system, it is possible to observe changes in the M-N distances of complexes having the same in-plane ligand by altering the axial ligand. Although the number of data for such comparisons are very limited and the changes in the M-N distances are very small, it is likely that there exist negative correlations between M-X and M-N distances in each of [NiX$_2$([14]aneN$_4$)], [NiX$_2$([15]aneN$_4$)], and [NiX$_2$([16]aneN$_4$)].

Coordination geometries found for Ni(II) complexes with the N$_4$7 ligand may provide further evidence for the occurrence of such an electronic cis effect. The structures of [NiCl$_2$(N$_4$7)][3] and [Ni(NCS)$_2$(N$_4$7)][20] have been found to be of trans and cis types, respectively. It is most reasonable to consider the observed cis and trans stereochemistries to be a result of the electronically controlled cis effect in view of the relative size between the cavity of the N$_4$7 ligand and a high spin octahedral Ni^{2+}, and the relative ligand field strength between Cl^- and NCS^- ligands.[8,20]

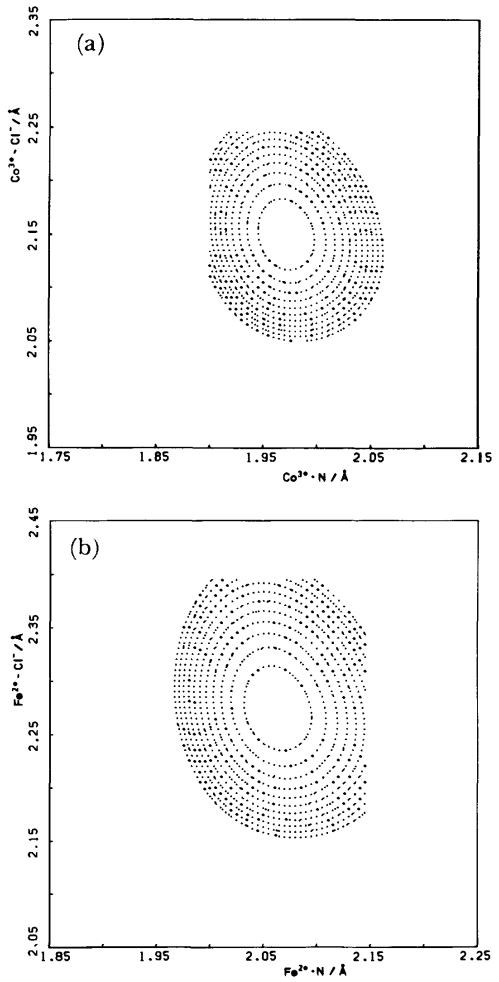

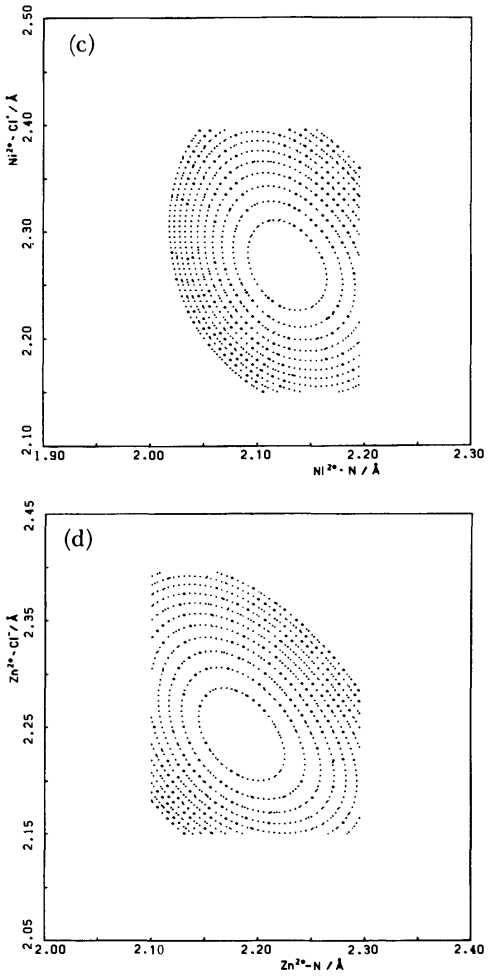

Fig. 2. Potential energy surfaces of *trans*-[MCl$_2$(NH$_3$)$_4$] along the M-Cl (vertical axis) and M-N (horizontal axis) coordination bonds: (a) *trans*-[CoCl$_2$(NH$_3$)$_4$]$^+$; (b) *trans*-[FeCl$_2$(NH$_3$)$_4$]; (c) *trans*-[NiCl$_2$(NH$_3$)$_4$]; (d) *trans*-[ZnCl$_2$(NH$_3$)$_4$]. Contours are at intervals of 0.5 kcal mol^{-1}.

Potential Energy Surfaces of trans-*[MCl$_2$(NH$_3$)$_4$] (M= Co^{3+}, Fe^{2+}, Ni^{2+}, and Zn^{2+}) along Coordination Bond Axes.* Figure 2 shows the calculated potential energy surfaces for the Co^{3+}, Fe^{2+}, Ni^{2+}, and Zn^{2+} complexes, M-Cl distances being plotted on the vertical axis and M-N distances horizontally. The MO calculations for a hypothetical low spin Fe(II) complex, *trans*-[FeCl$_2$(NH$_3$)$_4$], have been carried out in order to investigate the effect of electric charge, since experimental data have been obtained with complexes of divalent metal ions except for the Co(III) system. The Fe(II) complex is isoelectronic with the Co(III) complex and its ground state was assumed to be closed-shell singlet.[21]

The calculated maps of the potential surfaces have the following common features: (i) each contour is an

ellipse elongated in the M-Cl direction; (ii) each ellipse has an anticlockwise tilt. When the maps shown in Fig. 2 are compared, the ellipse for Co^{3+} is the closest to a circle, the axis ratio of the Zn^{2+} ellipse is the largest, and the Ni^{2+} system is intermediate. The tilt of the ellipse is the smallest for Co^{3+}, intermediate for Ni^{2+}, and the largest for Zn^{2+}. Contour lines are the most congested for Co^{3+}, while they are the farthest apart for Zn^{2+}. These features are very important in the interpretation of the experimentally observed correlation between the axial and in-plane coordination bond distances.

On the basis of the section map, we will discuss the case where the M-N distance is varied, as was done experimentally by use of the macrocyclic ligands with different ring sizes.

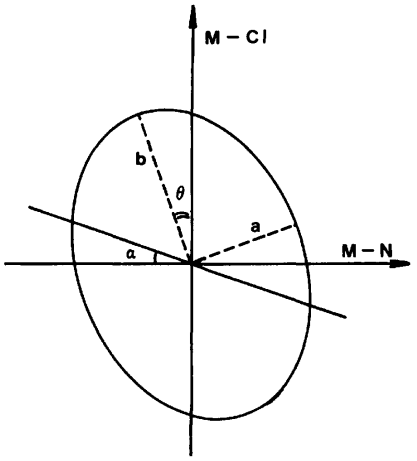

When energy minimum points at various M-N distances are connected, a line with a slope (α) is obtained. This line shows the interrelationship between the M-Cl and M-N distances under the electronically most stable circumstances. Thus, the larger the slope (α) is, the stronger is the correlation. Assuming that each contour is a perfect ellipse, α is given by the following equation,

$$\tan^{-1}\alpha=[\{1-(a/b)^2\}\sin\theta\cos\theta]/[\sin^2\theta+(a/b)^2\cos^2\theta], \quad (1)$$

where θ denotes a tilt of the ellipse and a/b represents an axis ratio of the ellipse ($b>a$). As is clear from Eq. 1, if the contour is not an ellipse but a circle ($a=b$), or if the longer axis of the ellipse is parallel to the vertical axis ($\theta=0$), α equals zero. Under such circumstances, the M-Cl distance does not change at all, even though the M-N distance is varied. The larger α value would be expected when the ellipse has a larger tilt[23] and the axis ratio of the ellipse is smaller.[24]

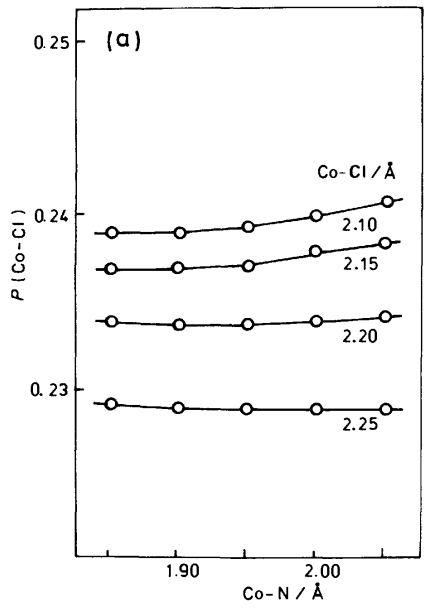

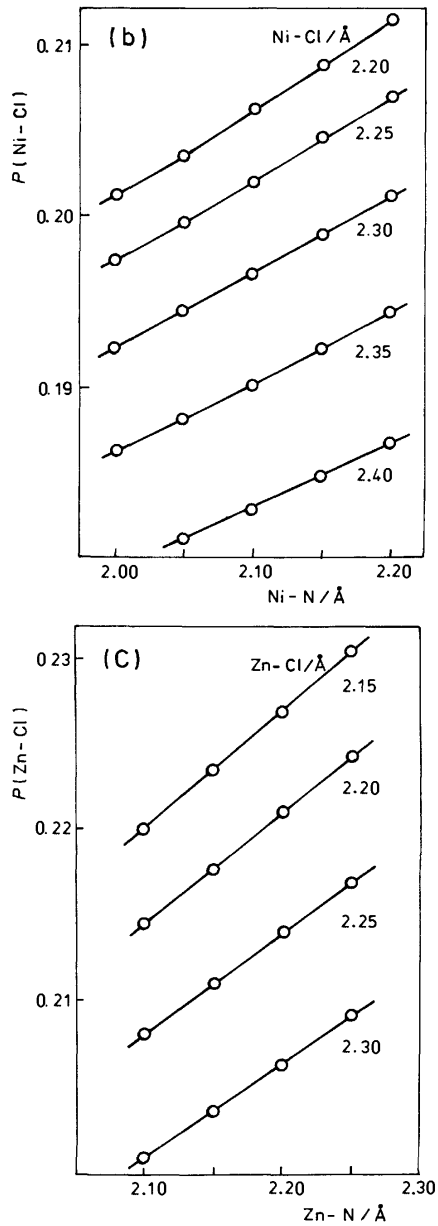

Fig. 3. M-Cl overlap population (P) as a function of M-N distances: (a) *trans*-$[CoCl_2(NH_3)_4]^+$; (b) *trans*-$[NiCl_2(NH_3)_4]$; (c) *trans*-$[ZnCl_2(NH_3)_4]$.

As the difference in the ligand field strengths between axial and in-plane ligands becomes larger, the ellipticity (a/b) decreases to give larger α. This is exemplified by the difference in the slopes for the chloro and isothiocyanato Ni(II) complexes, shown in Fig. 1 (*vide supra*). In the present systems, the ellipse becomes more nearly circular with an increase in the axial ligand field strength. The closer the ellipse is to a circle, the weaker is the correlation. The Co(III) system demonstrates such a situation (see Figs. 1 and 2(a)).

The tilt of the ellipse in Fig. 2 is 14° for Co(III), 18° for Fe(II), 31° for Ni(II), and 41° for Zn(II). The tilt reflects ease with which electrons move when the coordination bond lengths are forced to be varied. Thus, it seems that the tilt is associated with polarizability of the complex. Figure 3 shows overlap population on an M-Cl bond as a function of M-N distances. Generally, the M-Cl overlap population increases as the M-N distance increases. This arises from the fact that each metal atom tends to keep the electric charge neutral. In fact, within the computed range of M-N and M-Cl distances (the optimized distance $\pm$ *ca.* 0.25 Å, see Computational Procedures), total electron population on the metal atoms (Mulliken population) was constant within 2% for each metal atom. The values were 26.4 for Co(III), 25.5 for Fe(II), 27.5 for Ni(II), and 29.4 for Zn(II). The interrelationships depicted in Fig. 3, which are strongly metal ion dependent, are deeply related to the tilts of the ellipses of Fig. 2.

The congestion of the contour lines, *i.e.*, the slope of the potential surface, is also an important factor. If contour lines were less congested, the electronic cis effect would occur more easily. On the other hand, coordination bond lengths would not vary widely, if the slope of the potential surface were steep. It is manifested in the Co(III) system (see Figs. 1 and 2(a)). The most apparent difference in the feature of the potential surfaces between the Co(III) and Fe(II) complexes is the slopes. There is no doubt that the Co(III) surface becomes steeper by the effect of the electric charge. Higher electric charge on the metal brings about more congested contour lines.

The conclusions obtained from the features of the potential surfaces, such as the axis ratio, the tilt of the ellipse and the degree of the congestion of the contour lines, agree very well with the experimentally observed results shown in Fig. 1.

Pearson made the following statement in his paper describing the concept of Hard and Soft Acids and Bases: Softness in both the acid and base means that the repulsive part of the potential energy curve rises less sharply than for hard acids and bases.[25] According to this, it follows that the degree of the congestion of the contour lines in Fig. 2 shows hardness of the metal ions. Furthermore, softness (or hardness) is known to be directly associated with the polarizability,[25] which is correlated with the tilt of the ellipse in Fig. 2. In view of these, it is clear from Figs. 1 and 2 that, among the metal ions studied, Co(III) is the hardest, Zn(II) is the softest, and Ni(II) is intermediate. Although Pearson classifies both of Ni^{2+} and Zn^{2+} into borderline Lewis acids,[25] there is a clear difference in softness between them.

In the present MO calculations, we used a double ζ quality basis set for metal 3d orbitals and minimal basis sets for the others. The approximation might not be sufficient to describe detailed electronic structures and molecular dimensions. For example, M-Cl bond distances in the optimized structures (see below (Table 2)) are evidently shorter than the normal values.[26] However, we believe that the present calculations give sufficiently reliable results concerning the relative differences of the potential surfaces.

Both theoretically and experimentally, it has been found that the degree of correlation increases in the order, $Co^{3+}<Ni^{2+}<Zn^{2+}$. It should be pointed out that the number of d-electrons in e_g orbital in O_h symmetry increases in the same order: 0 for Co^{3+}, 2 for Ni^{2+}, and 4 for Zn^{2+}.

Computational Procedures

Geometries and Basis Set. Each ammonia ligand was assumed to have the N-H bond length of 1.00 Å and tetrahedral bond angles with its C_3 axis lying on the M-N bond. The ammonia molecules were arranged in such a manner that the entire molecule of *trans*-$[MCl_2(NH_3)_4]$ has D_{2d} symmetry.

The basis sets used were the STO-3G set for ligand atoms and the [4s3p2d] contracted set for central metal atoms, respectively.[27] For M=Co^{3+}, Fe^{2+}, and Zn^{2+}, the ground states are assumed to be closed-shell singlet, whereas, for M=Ni^{2+}, it is assumed to be triplet, and the restricted Hartree-Fock method was used in the SCF-MO calculations.

Section Maps of the Potential Surfaces along M-Cl and M-N Bond axes. In order to draw section maps of the potential energy surfaces along the coordination bond axes, we have calculated SCF MO's on 20—30 geometries for each model compound, M-N and M-Cl distances being varied by 0.05 Å near the minimized structures. Contours were drawn by means of two-dimensional spline fitting program at intervals of 0.5 kcal mol^{-1}. Coordinates for the optimum structure of each compound were obtained by smooth interpolation from the section map (Table 2).

Table 2. Optimized coordination geometries for *trans*-$[MCl_2(NH_3)_4]$.

M	M-N/Å	M-Cl/Å
Co^{3+},[a]	1.97	2.15
Fe^{2+}	2.06	2.27
Ni^{2+}	2.13	2.27
Zn^{2+}	2.18	2.25

a) For Co(III) complexes of *trans*-$CoCl_2N_4$ type, Co-N and Co-Cl distances have been found to be $\approx$1.98 Å and $\approx$2.26 Å, respectively.[18]

All the calculations were carried out by using the IMSPACK program system[28] on a HITAC M-200H computer at the Computer Center of IMS.

References

1) J. Gážo, R. Bőca, E. Jóna, M. Kabešová, Ľ. Macášková, and J. Šima, *J. Coord. Chem. Rev.*, **43**, 87 (1982), and references cited therein.

2) B. J. Hathaway and A. A. G. Tomlinson, *Coord. Chem. Rev.*, **5**, 1 (1970).

3) M. Sugimoto, J. Fujita, H. Ito, K. Toriumi, and T. Ito, *Inorg. Chem.*, **22**, 955 (1983).

4) J. F. Endicott and B. Durham, "Coordination Chemistry of Macrocyclic Compounds," ed by G. A. Melson, Plenum Press, New York, N. Y. (1979), Chap. 6.

5) D. D. Domoinguez, M. M. King, and H. J. Yeh, *J. Magn. Reson.*, **32**, 161 (1978).

6) L. Y. Martin, C. R. Sperati, and D. H. Busch, *J. Am. Chem. Soc.*, **99**, 2968 (1977).

7) Y. Hung, L. Y. Martin, S. C. Jackels, A. M. Tait, and D. H. Busch, *J. Am. Chem. Soc.*, **99**, 4029 (1977).
8) T. Ito, M. Kato, and H. Ito, *Bull. Chem. Soc. Jpn.*, in press and presented at XXII International Conference on Coordination Chemistry, Budapest, Hungary, August 1982, Abstract P. TuB14.
9) T. Ito, M. Kato, and H. Ito, *Bull. Chem. Soc. Jpn.*, in press.
10) Except for Co(III), such complexes are hypothetical.
11) L. Y. Martin, J. L. DeHayes, L. J. Zompa, and D. H. Busch, *J. Am. Chem. Soc.*, **96**, 4046 (1974).
12) B. Bosnich, R. Mason, P. T. Pauling, G. B. Robertson, and M. L. Tobe, *J. Chem. Soc., Chem. Commun.*, **1965**, 97.
13) E. K. Yukhno and M. A. Poraj-Košic, *Kristallografiya*, **2**, 239 (1957); Struc. Rep. **22**, 407.
14) B. W. Brown, and E. L. Lingafelter, *Acta Crystallogr.*, **16**, 753 (1963).
15) H. Ito, M. Kato, and T. Ito, unpublished result.
16) A. Nakahara, Y. Saito, and H. Kuroya, *Bull. Chem. Soc. Jpn.*, **25**, 331 (1952).
17) K. Matsumoto, S. Ooi, and H. Kuroya, *Bull. Chem. Soc. Jpn.*, **43**, 1903 (1970).
18) M. Goto, K. Ohta, K. Toriumi, and T. Ito, *Acta Crystallogr., Sect. B*, **37**, 1189 (1981).
19) So far we have not succeeded in the sysnthesis of *trans*-$[Zn(NCS)_2([16]aneN_4)]$. The $[14]aneN_4$, $[15]aneN_4$, and $[16]aneN_4$ ligands did not afford single crystals of six-coordinate Zn(II) complexes with Cl^- ligands at the axial positions.
20) M. Sugimoto, H. Ito, K. Toriumi, T. Ito, *Acta Crystallogr., Sect. B*, **38**, 2453 (1982).
21) It has been shown that $[Fe^{II}Cl_2([14]aneN_4)]$ is a high-spin complex.[22]
22) D. D. Watkins, Jr., D. P. Reiley, J. A. Stone, and D. H. Busch, *Inorg. Chem.*, **15**, 387 (1976).
23) This holds mathematically until θ reaches $\tan^{-1}(a/b)$, where α adopts the maximum value. When θ exceeds $\tan^{-1}(a/b)$, α gets smaller with an increase in θ.
24) This holds always irrespective of the value of θ.
25) R. G. Pearson, *J. Chem. Educ.*, **45**, 581, 643 (1968).
26) This arises from the use of STO-3G basis set for the chlorine atom, contribution of 3d orbitals being not taken into account at all.
27) The basis sets used in this study for metal atoms were similar to those used in an *ab initio* MO study on simple nickel-phosphine complexes by Morokuma *et al.*[29] The [4s3p2d] set was contracted from the (11s7p5d) primitive Gaussian set, which was modified from (12s6p4d)[30] by deleting the two most diffuse an s-type, a p-type, and a d-type functions and adding an s-type, a p-type, and a d-type functions with the exponents 0.2, 0.25, and 0.2, respectively. The 3s-type functions arising from the totally symmetric linear combination of d-type functions were removed from the basis set.
28) K. Morokuma, S. Kato, K. Kitaura, I. Ohmine, S. Sakai, and S. Obara, IMS Computer Center Library, Institute for Molecular Science, No. 0372 (1980).
29) K. Kitaura, S. Sakaki, and K. Morokuma, *Inorg. Chem.* **20**, 2292 (1981).
30) B. Roos, A. Veillard, and G. Vinot, *Theor. Chim. Acta*, **20**, 1 (1971).

A Kinetic Study on Oxidation of a Pair of Associating Thiols Having Substituted Phenyl Groups with Oxygen

Tadashi Endo,* Masao Hashimoto, Toyohiko Orii, and Masato M. Ito
Department of Chemistry, College of Science and Engineering, Aoyama Gakuin University, Chitosedai, Setagaya-ku, Tokyo 157
(Received May 31, 1983)

The rates of oxidation of 1:1 mixtures of associating thiols, each having the binding site (-CNHCNH-) and the recognition site [p-$(CH_3)_2NC_6H_4$ or R], with O_2 were measured in 80% (v/v) acetonitrile-20% water in the range of 20 to 50 °C. Oxidation of the thiol having the p-$(CH_3)_2NC_6H_4$ group proceeds about 100 times faster than that of the thiols with R. It has been found that oxidation of 1:1 mixtures of the thiols is first-order with respect to thiols and 0.7 th-order with respect to triethylamine by means of the method of initial rates. The $k_{1.7}$ values for R=C_6H_5, p-$CH_3C_6H_4$, and p-$C_2H_5C_6H_4$ were similar to one another; this makes a sharp contrast with our previous work that the selectivity (the logarithmeric ratio of the yield of the unsymmetrical disulfide to twice that of the symmetrical disulfide) changes greatly with the structures of R and temperature. It is concluded that the product ratio does not depend upon the $k_{1.7}$. The large negative activation entropies (−51 to −45 cal K^{-1} mol^{-1})† suggest that the oxidation would proceed through a highly ordered transition state.

The recognition of the methyl groups on nucleotide bases plays a significant role in living cells, whether prokaryotes or eukaryotes.[1] It is striking that highly complicated *in vivo* reactions are controlled by a rather simple modification, methylation, of the aromatic rings. Therefore, an approach to the problem of methylation from a chemical point of view would serve to elucidate the factors governing chemical reactions including those in biological systems.

As a continuing study on molecular recognition,[1-6] we examined the effect of methylation of the benzene ring on chemical selectivity.[1] A pair of thiols (**1** and **2**) were used as model compounds. Thiols **1** and **2** each

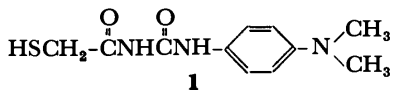

1

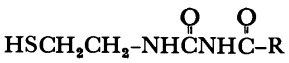

2a R =

2b R = 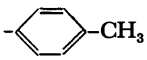

2c R = 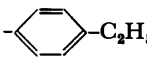

2d R = $(CH_2)_2CH(CH_3)_2$

have the binding site (-CNHCNH-) participating in intermolecular hydrogen bonding and the recognition site (p-$Me_2NC_6H_4$ or R) participating in the specific discrimination. As a model reaction, we used oxidation of a 1:1 mixture of **1** and **2** with oxygen in the presence of a catalytic amount of triethylamine (Et_3N) (Eq. 1):

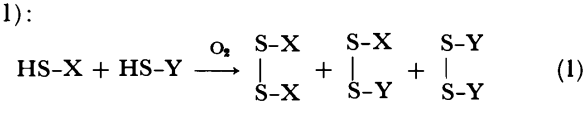

(1)

1 **2** **3** **4** **5**

The temperature dependence of the selectivity in the above oxidation has previously been reported as a function of the structures of R in 80% (v/v) acetonitrile-20% water (Fig. 1);[1,2] the selectivity (r) is represented here by the logarithmeric ratio of the yield of the unsymmetrical disulfide (**4**) to twice that of the symmetrical disulfide (**3**) {r=ln([**4**]/(2 [**3**]))}. The selectivity for R=p-MeC_6H_4 displayed a minimum (r= −0.86) at 35 °C, whereas for R=C_6H_5 the selectivity passed through a maximum (r=1.6) at 35 °C; for R=p-$C_2H_5C_6H_4$ a plot of the selectivity against temperature showed a sigmoid-like curve.

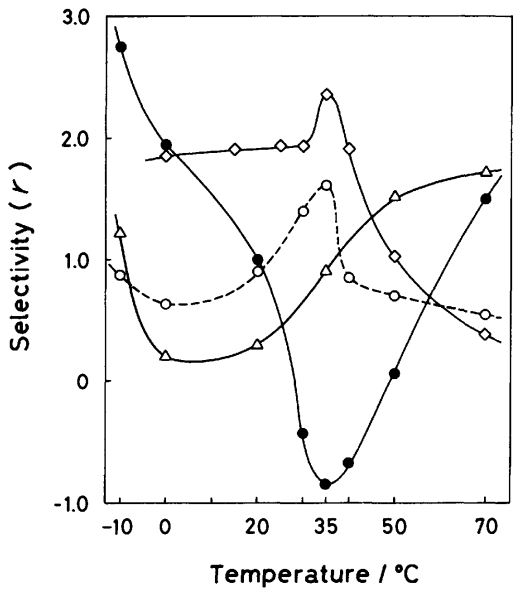

Fig. 1. Temperature dependence of the selectivity (r) in oxidation of 1:1 mixtures of **1** and **2** with O_2 in 80% (v/v) acetonitrile-20% water. ○, **1** and **2a**; ●, **1** and **2b**; △, **1** and **2c**; ◇, **1** and **2d**. We have previously represented the selectivity as the ratio of the yield of unsymmetrical disulfide **4** to that of symmetrical disulfide **3**.[1,2]

In order to elucidate the mechanism of the oxidation described above, we made a kinetic study on the oxidation under conditions similar to those where the selectivity was investigated. Measurements were performed on overall rates for 1:1 mixtures of thiols **1** and **2a**—**c** as well as on rates for the individual thiols,

† 1 cal=4.184 J.

by titration of remaining thiols with iodine. For comparison, the rates were also determined for **2d**—the thiol with an isopentyl group as the recognition site—and a 1:1 mixture of **1** and **2d**; for oxidation of the 1:1 mixture of **1** and **2d**, a plot of the selectivity against temperature showed a sharp peak of maximum selectivity (r=2.4) at 35 °C[2] under the same conditions as with oxidation of **1** and **2a—c** (Fig. 1).

Results

Kinetic Behavior of Catalytic Oxidation of Thiols. Oxidation of each thiol (**1** or **2**) was carried out in oxygen-saturated 80% (v/v) acetonitrile-20% water in the presence of Et_3N as a catalyst. Figure 2 summarizes the time course of thiol consumption where $[RSH]_0$ represents the initial concentration of thiols. Downward curvature was observed for **1** in a plot of log ($[RSH]/[RSH]_0$) against time in the presence of 0.1 equivalent of Et_3N. The use of 2.0 equivalents of Et_3N led to the pseudo first-order reaction, as might be expected from the results by Wallace *et al.*[7] that oxidation of thiols follows pseudo first-order kinetics in the presence of 2.0 equivalents of a base.

For oxidation of 1:1 mixtures of **1** and **2**, total concentration of thiols was measured. Remarkable downward curvatures were observed (Fig. 2) in the presence of 0.1 equivalent of Et_3N, the same concentration of Et_3N as in the oxidation whose selectivity is given in Fig. 1. However, on addition of 20 equivalents[8] of Et_3N, the oxidation has proved to follow

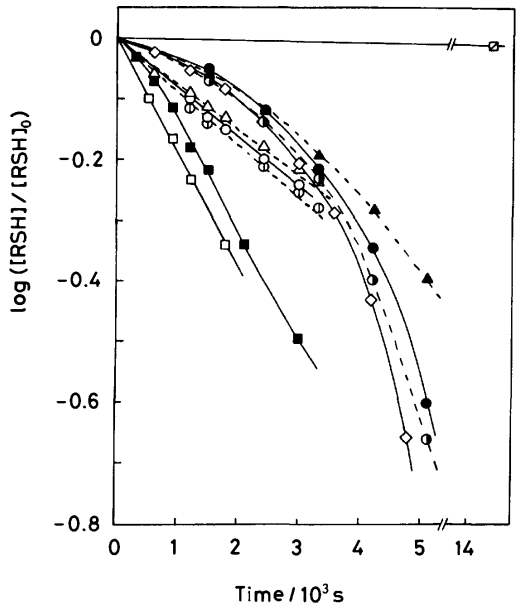

Fig. 2. Dependence of log ($[RSH]/[RSH]_0$) on time for oxidation of **1**, **2**, and their 1:1 mixtures at $[RSH]_0$=0.020 M in 80% (v/v) acetonitrile-20% water at 35.0 °C. The concentration of Et_3N as a catalyst was 0.0020 M, unless otherwise mentioned. ■, **1**; □, **1** ($[Et_3N]$=0.040 M); ⊠, **2b**; ◑, 1:1 mixture of **1** and **2a**; ●, 1:1 mixture of **1** and **2b**; ▲, 1:1 mixture of **1** and **2c**; ◇, 1:1 mixture of **1** and **2d**; ⊕, 1:1 mixture of **1** and **2a** ($[Et_3N]$=0.40 M); ○, 1:1 mixture of **1** and **2b** ($[Et_3N]$=0.40 M); △, 1:1 mixture of **1** and **2c** ($[Et_3N]$=0.40 M).

Table 1. Initial rates for oxidation of individual thiols (**1** and **2**) and overall initial rates for their 1:1 mixtures

Compd	$[Et_3N]\times10^3$/M	$v_0\times10^8$ [a]/mol l^{-1}s^{-1}
1	2.0	440
2a	2.0	3.3
2b	2.0	3.1
2c	2.0	3.3
2d	2.0	2.9
1+**2a**	2.0	200
1+**2b**	2.0	180
1+**2c**	2.0	180
1+**2d**	2.0	210
1+**2a**	400	610
1+**2b**	400	480
1+**2c**	400	450

a) Average rates until 10% consumption of thiols ($[RSH]_0$=0.020 M) (1 M=1 mol dm^{-3}) at 35.0 °C in oxygen saturated 80% (v/v) acetonitrile-20% water.

pseudo first-order kinetics.

Initial rates (v_0)—average rates until 10% consumption of thiols—for the oxidation are listed in Table 1. The thiol with the isopentyl group (**2d**) was similar to the thiols with the aromatic groups (**2a—c**) both in kinetic behavior (Fig. 2) and in the initial rates (Table 1).

Rate Equation for Oxidation of 1:1 Mixtures of Thiols. The observed downward curvatures for oxidation of 1:1 mixtures at $[Et_3N]=2.0\times10^{-3}$ M (1M=1 mol dm^{-3}) showed that rate equations were impossible to derive directly from the plots in Fig. 2. Thus we used the method of initial rates in order to determine the rate equation for the Et_3N-catalyzed oxidation. Since the concentration of oxygen is considered to be constant for low levels of conversion,[9] the rate equation becomes Eq. 2

$$v = k_n[RSH]^{n-m}[Et_3N]^m \quad (2)$$

where n represents the overall reaction order and k_n the n-th order overall rate constant for the oxidation. Putting Eq. 2 into logarithmeric form yields Eq. 3.

$$\log v = \log k_n + (n-m)\log[RSH] + m\log[Et_3N] \quad (3)$$

The v_0 values were measured at various $[RSH]_0$, with the molar ratio of **1**, **2b**, and Et_3N being fixed (1:1:0.2). Since $[Et_3N]$=0.1 $[RSH]_0$, Eq. 3 can be rewritten as Eq. 4.

$$\log v_0 = \log k_n + n\log[RSH]_0 - m \quad (4)$$

Figure 3 plots the logarithm of v_0 against log $[RSH]_0$. Linear relationship was found to exist between them. The slope of a log $[RSH]_0$—logv_0 plot for a 1:1 mixture of **1** and **2b** gave the n value of 1.7 for the oxidation.[10]

The initial rates were then measured at different Et_3N concentrations with $[RSH]_0$ fixed. In this case the first two terms on the right-hand side of Eq. 3 can be regarded as constant. Since a linear relationship exists between log v_0 and log $[Et_3N]$ (Fig. 4), the slope of the straight line gives m value in Eq. 3. The m value turned out to be 0.7, indicating that the reaction is first-order with respect to thiols.[11] Thus the rate follows the equation:

$$v = k_{1.7}[RSH][Et_3N]^{0.7} \quad (5)$$

The 1.7th-order rate constants for oxidation of 1:1 mixtures ($k_{1.7}$) were obtained at 20.0, 35.0, and 50.0 °C using Eq.5. The results are listed in Table 2. In all cases, the linear relationship existed between ln $k_{1.7}$ and $1/T$, demonstrating that Eq. 5 holds true for the temperature range described above. Activation parameters for the oxidation are also given in Table 2.

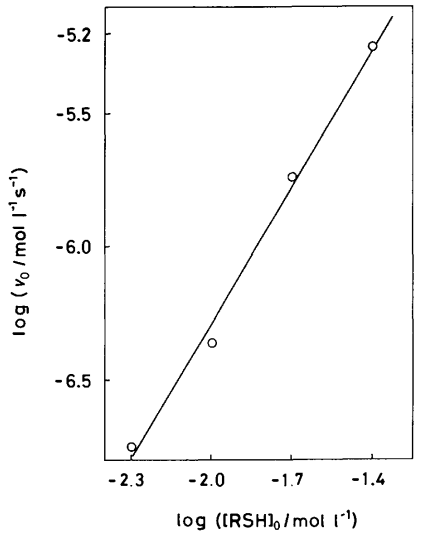

Fig. 3. Dependence of initial rates (v_0) on initial concentration of a 1:1 mixture of **1** and **2b** at [Et$_3$N]=0.1 [RSH]$_0$. The other conditions are as in Fig. 2.

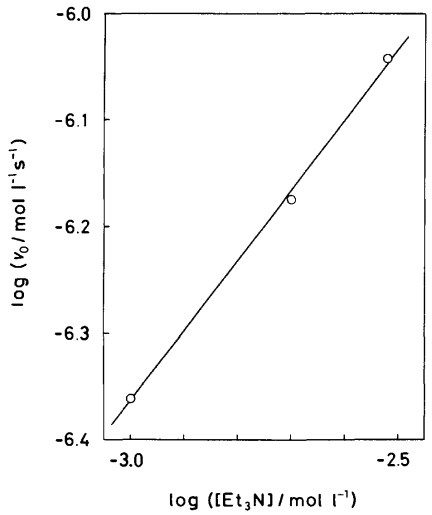

Fig. 4. Dependence of initial rates (v_0) on initial concentration of Et$_3$N at [RSH]$_0$=0.010 M. The other conditions are as in Fig. 2.

Discussion

Mechanism of the Oxidation. Base-catalyzed oxidation of thiols is known to proceed through the following reaction paths (Eqs. 6—10).[12-15]

$$RSH + Et_3N \underset{}{\overset{K_6}{\rightleftharpoons}} RS^- + Et_3NH^+ \quad k_{+6}, k_{-6} \qquad (6)$$

$$RS^- + O_2 \longrightarrow RS\cdot + O_2^{\cdot-} \quad k_7 \qquad (7)$$

$$RSH + O_2^{\cdot-} \longrightarrow RS\cdot + OOH^- \qquad (8)$$

$$OOH^- \longrightarrow OH^- + \frac{1}{2}O_2 \qquad (9)$$

$$2\,RS\cdot \longrightarrow RS\text{-}SR \qquad (10)$$

The equilibrium shown in Eq. 11 would contribute to the recovery of Et$_3$N.[13] These yield Eq. 12 as the overall stoichiometry of the oxidation.

$$Et_3N + H_2O \underset{}{\overset{K_{11}}{\rightleftharpoons}} Et_3NH^+ + OH^- \qquad (11)$$

$$2\,RSH + \frac{1}{2}O_2 \longrightarrow RS\text{-}SR + H_2O \qquad (12)$$

The rate-determining step of base-catalyzed oxidation of thiols is shown to be either the formation of thiolate anions (Eq. 6) or its oxidation to the corresponding thiyl radicals (Eq. 7).[12,13] This view appears to hold true for the oxidation presented here, considering that the oxidation is first-order with respect to thiols.[16] Uncertainty still remains about what causes the downward curvatures in kinetic profiles (Fig. 2).

An intriguing aspect of the kinetic results is the large negative activation entropies (Table 2). The activation entropies of −51 to −45 cal K^{-1} mol^{-1} for the present oxidation are more negative than those of about −20 to −10 cal K^{-1} mol^{-1} for ordinary bimolecular reactions[17]. Bimolecular reactions with highly ordered transition states generally have $\Delta S^{\neq}$ values of similar magnitude: −49 to −22 cal K^{-1} mol^{-1} for Diels-Alder reactions,[18] −43 to −22 cal K^{-1} mol^{-1} for 1,3-dipolar cycloadditions,[19] and −42 to −19 cal K^{-1} mol^{-1} for Menschutkin reactions between tertiary amines and alkyl iodides.[20] These observations suggest that the

Table 2. Temperature dependence of 1.7th order rate constants for oxidation of 1:1 mixtures of thiols (**1** and **2**) and activation parameters

Compd	T / K	$v_0\times10^{7}$ a) / mol l^{-1} s^{-1}	$k_{1.7}\times10^{3}$ / l$^{0.7}$ mol$^{-0.7}$ s^{-1}	$\Delta E^{\neq}$ / kcal mol^{-1}	$\Delta H^{\neq}$ / kcal mol^{-1}	$\Delta S^{\neq}$ / cal K^{-1} mol^{-1}
1+**2a**	293	7.9	3.1			
1+**2a**	308	20	7.7	11.2±1.9	10.5±1.9	−45±6
1+**2a**	323	36	13.9			
1+**2b**	293	8.8	3.4			
1+**2b**	308	18	7.0	9.5±0.5	8.8±0.5	−51±2
1+**2b**	323	31	12.2			
1+**2c**	293	6.7	2.6			
1+**2c**	308	18	7.0	10.7±3.0	10.1±4.0	−47±13
1+**2c**	323	28	10.8			

a) The values at [Et$_3$N]=2.0×10^{-3} mol l^{-1} in oxygen saturated 80% (v/v) MeCN-20% H$_2$O.

oxidation presented in this paper would have a highly ordered transition state.

Factors Governing the Selectivity. Oxidation of thiol **1** proceeds more than 100 times faster than that of **2** (Table 1). The initial rates for oxidation of 1:1 mixtures of **1** and **2** decreased to about half (v_0= (1.8—2.1)×10^{-6} mol l^{-1} s^{-1}) of that for oxidation of **1** (v_0=4.4×10^{-6} mol l^{-1} s^{-1}), $[\mathbf{1}]_0$ for oxidation of 1:1 mixtures being half that for oxidation of **1** (Table 1). These results indicate that the thiolate anion which is formed predominantly from the 1:1 mixtures is that derived from **1**. Thus, the selective formation of symmetrical disulfide **3** might be expected at an early stage, though the oxidation gives the high selectivity (r) in most cases (Fig. 1). However, this is not the case, because the product ratio in this type of oxidation is kinetically controlled so that the selectivity does not vary with the reaction time.[2] This fact suggests the presence of fast exchange reaction between an anion and a thiol (Eq. 13) or between a radical and a thiol (Eq. 14).

$$\underset{\mathbf{2}}{XS^-} + \underset{\mathbf{1}}{YSH} \rightleftharpoons \underset{\mathbf{2}}{XSH} + \underset{\mathbf{1}}{YS^-} \quad (13)$$

$$\underset{\mathbf{2}}{XS\cdot} + \underset{\mathbf{1}}{YSH} \rightleftharpoons \underset{\mathbf{2}}{XSH} + \underset{\mathbf{1}}{YS\cdot} \quad (14)$$

The initial rates for oxidation of 1:1 mixtures of **1** and **2a—c** are expressed by a single rate equation (Eq. 5). Further, the rate constants for the oxidation do not change appreciably with the structures of R (Table 2); this makes a sharp contrast with our previous work[1] that the selectivity alters markedly with the structures of R (Fig. 1). Accordingly, the product ratio would not be controlled in the rate-determining step.[21]

We have reported that thiols **1** and **2** associate strongly in benzene *via* two NH···O intermolecular hydrogen bonds between the inner -NHC(=O)- units in the -CNHCNH- group to form tetramers (**9—13**, reaction intermediates) as well as dimers (**6—8**) (Fig. 5).[1,22,23] The S-S bonds would be formed between the two proximate HS groups in tetramers **9—13**.[22] Each of the tetramers gives the corresponding disulfide(s) selectively when treated with oxygen.[4] The relative concentration of the tetramers would vary with the structures of R and temperature,[4] thereby leading to the selectivity alterations (Fig. 1). These selectivity data appear to reflect weak interactions[5] specific for the shape of the recognition sites of **1** and **2**.

Conclusion

Triethylamine-catalyzed oxidation of 1:1 mixtures of **1** and **2a—c** in 80% (v/v) acetonitrile-20% water follows the rate equation $v=k_{1.7}$ [RSH][Et_3N]$^{0.7}$, although a detailed mechanism of the oxidation still remains to be elucidated. The $k_{1.7}$ values for the 1:1 mixtures are similar to one another, in sharp contrast to our previous work that the selectivity varies markedly with the structures of R and temperature. This indicates that the product ratio does not depend upon the $k_{1.7}$. The present results including the large negative activation entropies are consistent with our view that the formation of disulfides **3—5** occurs *via* tetrameric intermediates **9—13**.

Experimental

Materials. All the thiols **1** and **2** were prepared as described previously.[1,24] Acetonitrile was dried and purified by distillation from calcium hydride and phosphorus pentaoxide, and stored over molecular sieves. The reaction solvent was prepared by mixing 62.58 g of dry acetonitrile with 19.96 g of water [4:1 (v/v) at 20 °C], and allowed to stand overnight under an oxygen atmosphere. Triethylamine was distilled over potassium hydroxide through a fractionating column. The iodine solution (0.001 M) containing potassium iodide (0.005 M) was titrated with 1.00×10^{-3} M aqueous sodium arsenite standard solution before use.

Determination of Rates of the Oxidation. Samples of thiols were accurately weighed into a two-necked flask and dissolved in 10.00 ml of the reaction solvent. The solution was placed in a well-stirred water bath thermostated to

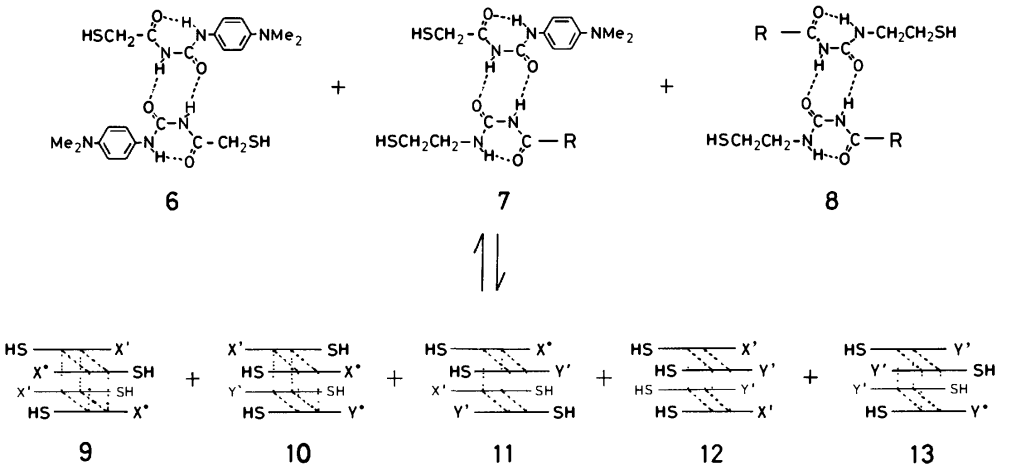

Fig. 5. Association patterns of three dimers **6—8** and association schemes of tetramers **9—13** formed by dimerization of the dimers. The hydrogen bonds (----) in the dimers and the noncovalent weak interactions (·····) responsible for the stabilization of the tetramers are shown. The symbols X′ and Y′ represent *p*-$Me_2NC_6H_4$ and R, respectively.

±0.1 °C for 5 h with stirring under an oxygen atmosphere. Oxidation of thiols was negligible in the absence of Et_3N. At time zero, an appropriate amount of Et_3N was added into the solution with a microsyringe, and time measurement was begun. At appropriate time intervals, a 0.50 ml portion of the reaction mixture was pipetted out and quenched in 5 ml of a 1:9 mixture of 3 M hydrochloric acid with acetonitrile. The amount of remaining thiols in the quenched solution was then determined by titration with the 0.001 M iodine solution.

Rate constants were determined by the method of initial rates.[17] Plots of concentration of thiols against time were constructed, and initial rates for 10% conversion were calculated. Initial rates presented in Tables 1 and 2 are average values of at least three, generally five, or more determinations. The reaction order and rate constants were evaluated from the initial rates measured at different initial concentrations of thiols and Et_3N (Figs. 3 and 4), through least square optimization.

Calculations of Activation Parameters. Activation energies were determined from the slopes of Arrhenius plots (ln k *vs.* $1/T$). Activation enthalpies and entropies were obtained from the plots of ln (k/T) against $1/T$ based on Eyring equation.[17]

We thank Mr. Kazuo Guro and Mr. Hideki Ueda for valuable assistance. We are also grateful to the referees for helpful suggestions.

References

1) T. Endo, A. Okubo, Y. Kaneko, M. Uehara, H. Tasai, A. Sato, K. Nikki, N. Nakagawa, and S. Kamei, *Bull. Chem. Soc. Jpn.*, **55**, 2224 (1982) and the references cited therein.

2) T. Endo, A. Kuwahara, H. Tasai, T. Murata, M. Hashimoto, and T. Ishigami, *Nature*, **268**, 74 (1977).

3) T. Endo, Y. Takeda, H. Kamada, S. Kayama, and H. Tasai, *Chem. Lett.*, **1980**, 417.

4) T. Endo, Y. Takeda, T. Orii, T. Murata, M. Sakai, N. Nakagawa, and K. Nikki, *Chem. Lett.*, **1980**, 1291.

5) T. Endo, K. Miyazawa, M. Endo, A. Uchida, Y. Ohashi, and Y. Sasada, *Chem. Lett.*, **1982**, 1989.

6) T. Endo, H. Tasai, K. Miyazawa, M. Endo, K. Kato, A. Uchida, Y. Ohashi, and Y. Sasada, *J. Chem. Soc., Chem. Commun.*, **1983**, 636.

7) T. J. Wallace, A. Schriesheim, and W. Bartok, *J. Org. Chem.*, **26**, 1311 (1963).

8) In the presence of 2.0 equivalents of Et_3N, downward curvature was still observed.

9) No appreciable changes took place in kinetic profiles for the oxidation with O_2 whose pressure was slightly larger than 1 atm.

10) For a 1:1 mixture of **1** and **2d**, the overall order of the oxidation became 2.2 in the thiol concentration range similar to that for **1** and **2a—c**.

11) The fact that the oxidation is first-order with respect to thiols agrees with the results by Wallace *et al.* for base-catalyzed oxidation of simple aliphatic and aromatic thiols.[7]

12) G. Capozzi and G. Modena, "Oxidation of Thiols," in "The Chemistry of the Thiol Group," ed by S. Patai, Wiley, London (1974), Part 2, Chap. 17.

13) A. A. Oswald and T. J. Wallace, "Anionic Oxidation of Thiols and Co-oxidation of Thiols with Olefins," in "Organic Sulfur Compounds," ed by N. Kharash, Pergamon Press, New York (1965), Vol. 2, Chap. 8.

14) The initial rate for oxidation of a 1:1 mixture of **1** and **2b** decreased by 33% on addition of hydroquinone (0.020 M). This suggests the participation of free radicals in the oxidation [W. A. Pryor, "Free Radicals," Mcgraw-Hill, New York (1966), Chap. 21].

15) Though O_2^- oxidizes thiols very readily [S. Oae, T. Takata, and Y. H. Kim, *Bull. Chem. Soc. Jpn.*, **54**, 2712 (1981)], it is uncertain whether or not the step in Eq. 8 contributes to the rate for the present oxidation, since O_2^- is known to be labile in aqueous media [J. Rabani and S. O. Nielsen, *J. Phys. Chem.*, **73**, 3736 (1969)].

16) If the formation of thiolate anions (Eq. 6) is rate-determining, the rate may be expressed as

$$v = 2\,k_{+6}[\mathrm{RSH}][\mathrm{Et_3N}]$$

Thus the oxidation will be first-order with respect to both thiols and Et_3N. In contrast, if the oxidation of RS^- (Eq. 7) is rate-determining, the rate may follow the expression

$$v = k_7' K_6[\mathrm{RSH}]\left(\frac{[\mathrm{Et_3N}]}{K_{11}+K_6[\mathrm{RSH}]}\right)^{0.5} \quad (k_7' = 2\,k_7[\mathrm{O_2}])$$

Provided that $K_{11} \gg K_6[\mathrm{RSH}]$, the oxidation will be first-order with respect to thiols and 0.5th-order with respect to Et_3N. Neither of the above equations completely agrees with the experimental results at an initial stage (0.7th-order with respect to Et_3N), suggesting the complex nature of the oxidation.

17) J. F. Bunnett, "From Kinetic Data to Reaction Mechanism," in "Investigation of Rates and Mechanisms of Reactions," 3rd ed, ed by E. S. Lewis, Wiley, London (1974), Part I.

18) J. Sauer and R. Sustmann, *Angew. Chem., Int. Ed. Engl.*, **19**, 779 (1980) and the references cited therein.

19) R. Huisgen, *Angew. Chem., Int. Ed. Engl.*, **2**, 633 (1963) and the references cited therein; R. Huisgen, G. Szeimies, and L. Möbius, *Chem. Ber.*, **100**, 2494 (1967) and the references cited therein.

20) A. P. Harris and K. E. Weale, *J. Chem. Soc.*, **1961**, 146.

21) Some examples have been reported in which chemical selectivity is controlled prior to the rate-determining step: see, for example, H. Ozaki, A. Tai, and Y. Izumi, *Chem. Lett.*, **1974**, 935.

22) T. Endo, Y. Takeda, T. Orii, Y. Kaneko, and M. Kondo, *Chem. Lett.*, **1979**, 1455.

23) Thiolate anions would be formed from dimers (**6—8**) and tetramers (**9—13**) as well as monomers (Fig. 5). It is uncertain whether or not the dissociation constants for the thiols alter when the thiols associate. The rate equation shown in Ref. 16 is based on the assumption that $[RS^-]$ is practically unaffected by the association.

24) T. Endo, K. Oda, and T. Mukaiyama, *Chem. Lett.*, **1974**, 443.

 © 1984 The Chemical Society of Japan Bull. Chem. Soc. Jpn., 57, 1567—1569 (1984)

Reactions of Sodium Salts of Tosylhydrazone Compounds with Silver Chromate. Formation of Indazole, Pyrazole, and Benzonitrile Derivatives

Katsuhiro SAITO,*,† Takashi TODA, and Toshio MUKAI

†*Department of Chemistry, Nagoya Institute of Technology, Gokiso-cho, Showa-ku, Nagoya 466*

Department of Chemistry, Faculty of Science, Tohoku University, Aoba, Aramaki, Sendai 980

(Received July 19, 1983)

Tropone tosylhydrazone sodium salt was allowed to react with silver chromate to give 2-tosyl-2*H*-indazole. The reaction is thought to proceed through the cyclization of the hydrazyl radical intermediate. Under the same conditions, sodium salts of *m*-nitrobenzaldehyde tosylhydrazone (**5**), benzylideneacetone tosylhydrazone derivatives (**7a** and **7b**), and β-ionone tosylhydrazone (**9**) reacted to yield *m*-nitrobenzonitrile from **5** and pyrazole derivatives from **7a**, **b**, and **9**, respectively. *m*-Nitrobenzonitrile is formed by homolytic fission of nitrogen-nitrogen bond of **5**. Formation of the pyrazole derivatives can be explained by intramolecular 1,3-dipolar additions of the corresponding diazo intermediates.

Considerable attention has been paid to the synthesis and chemistry of the heterocyclic compounds having two nitrogen atoms in the ring, *i.e.*, diaziridines, pyrazoles, and diazepines, from the viewpoint of electronic structures and the chemical reactivities of these compounds.[1]

Tosylhydrazone derivatives are readily available compounds which contain two nitrogen atoms in a molecule. It is known that one electron oxidation of amine derivatives affords amino radicals.[2] This fact suggested to us that one electron oxidation of tosylhydrazone derivatives may afford some of the above-mentioned heterocyclic compounds besides the products derived from 1,3-dipolar addition or carbenic reactions.[3] Actually, 2-phenyl-2*H*-indazole was obtained by lead tetraacetate oxidation of tropone phenyhydrazone although the yield was poor.[4]

We investigated an oxidation reaction of tropone tosylhydrazone sodium salt (**1**) with silver chromate as an oxidizing agent. The same type of reaction was carried out with sodium salts of tosylhydrazone derivatives **5**, **7**, and **9**. We wish to report the results of these investigations.

Results and Discussion

Tropone tosylhydrazone sodium salt (**1**) was allowed to react with silver chromate in anhydrous diglyme under a nitrogen stream at 125 °C for 10 min. Alumina chromatographic purification of the reaction mixture afforded 2-tosyl-2*H*-indazole (*2*) in 28% yield. The structure of **2** was deduced on the basis of the spectral properties and finally confirmed by the following experiments. Hydrolysis of **2** in basic aqueous media gave indazole (**3**) in 74% yield, implying that 2 was an indazole derivative. 1-Tosyl-1*H*-indazole (**4**) was synthesized from **3** and tosyl chloride which was isomeric to **2**.[5]

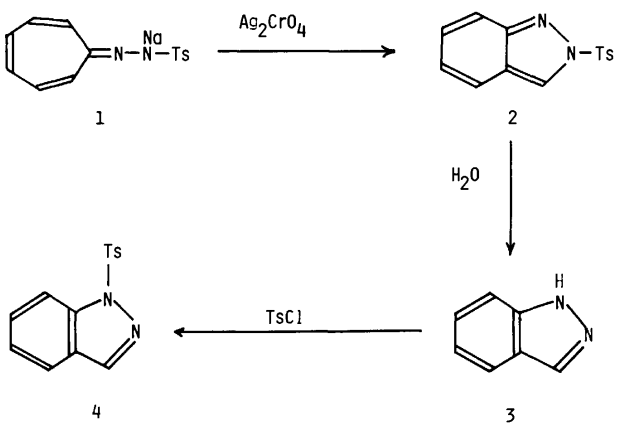

1 2 3 4

Fig. 1.

m-Nitrobenzaldehyde tosylhydrazone sodium salt (**5**) was allowed to react with silver chromate at 100 °C for 5 min to yield *m*-nitrobenzonitrile (**6**)[6] in 6% yield. Sodium salts of benzylideneacetone tosylhydrzaone derivatives (**7a** and **7b**) were also reacted under the analogous conditions to afford pyrazole derivatives (**8a** and **8b**) in yields of 70 and 44%, respectively. Similarly, β-ionone tosylhydrazone sodium salt (**9**) gave a pyrazole derivative (**10**) in 82% yield by the same reaction. The structures of **8a**, **8b**, and **10** were deduced from their spectral properties as follows. The electronic spectra are similar to those of the (aryl or arylalkyl) pyrazole derivatives.[7] Also, the chemical shift values of the pyrazole ring protons at δ 6.20 of **8a**, 6.23 of **8b**, and 5.73 of **10** correspond with those of the reported pyrazole derivatives.[8]

The mechanism for the formation of **2** is considered to be as follows. The hydrazyl radical (**11**) generated by oxidation of **1** by silver chromate cyclizes to form the 8,9-diazabicyclo[5.2.0]nonatriene intermediate (**12**). 2-Tosyl-2*H*-indazole (**2**) is formed by the loss of a hydrogen radical from the intermediate norcaradiene isomer (**13**). Bicyclo[5.2.0]nonatriene and 8,9-diazabicyclo-[5.2.0]nonatriene systems are known to rearrange to bicyclo[4.3.0]nonatriene systems *via* intermediate norcaradienes.[4,9]

The reaction of **5** was performed with the intention of synthesizing the 1-tosyl-1*H*-indazole derivative (**14**). However, a homolytic fission of the nitrogen-nitrogen bond occurred to form *m*-nitrobenzonitrile (**6**) *via* radical intermediates (**15** and **16**). This result corresponds with Binkley's finding that the benzylaminyl radical leads to benzonitrile.[10] 1,2-Benzodiazepine derivatives or pyrazole derivatives were expected to be formed in the reaction of **7**. The expected radical reaction *via* the hydrazyl radical (**19**) leading to **17**, however, did not occur, but the pyrazole derivatives (**8**) were obtained. The nitro group on the phenyl ring in **7b**, which is

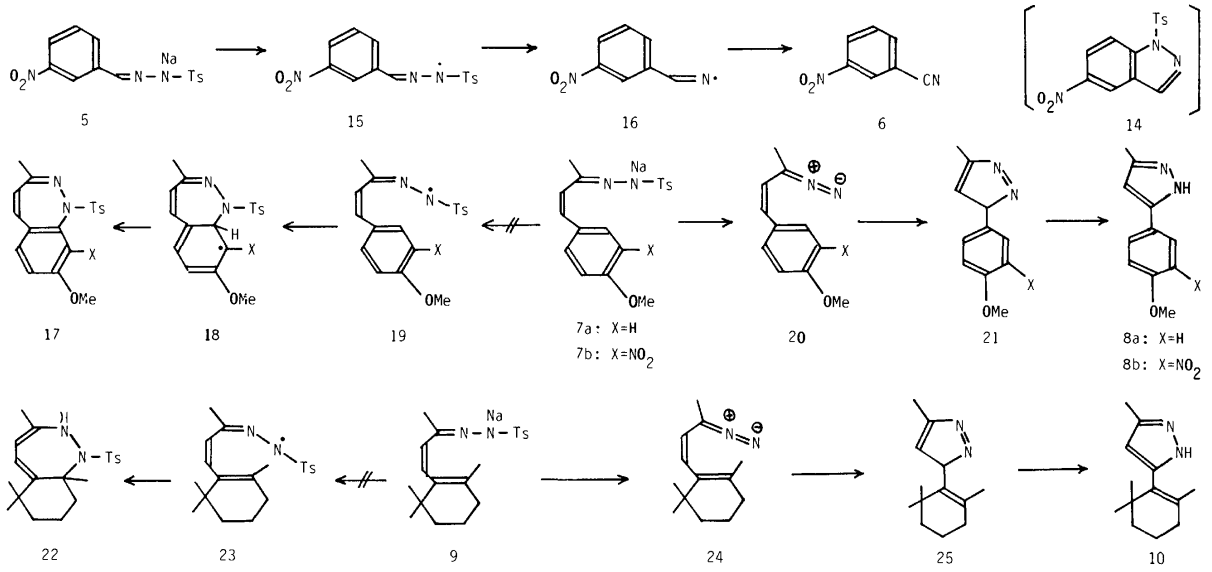

Fig. 2.

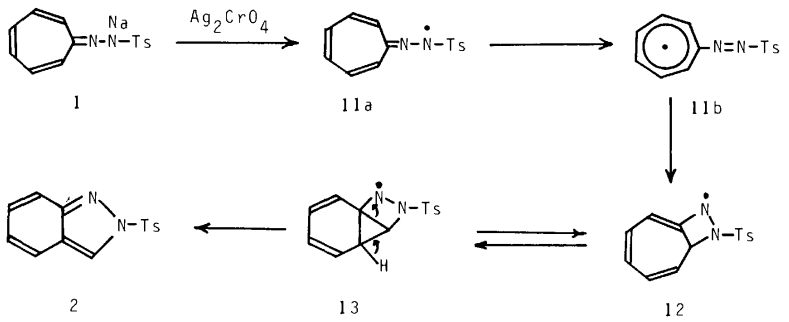

Fig. 3.

expected to stabilize the radical intermediate (**18**), did not promote the radical reaction. The reaction of **9** was performed to compare the reactivity of aliphatic double bond with that of aromatic skeleton. The cyclization reaction to form a seven-membered ring compound did not occur, but the experiment resulted in the formation of the pyrazole derivative (**10**).

The reactions of **7** and **9** are considered to proceed *via* diazo compounds **20** and **24**, respectively, because the pyrazole derivatives (**8** and **10**) did not contain any tosyl groups. The formation of pyrazoles from vinyldiazomethane derivatives is a well-documented reaction.[11]

The formation of the condensed ring indazole from **1** and the failure of phenyl substituted tosylhydrazones to form the condensed ring compounds may be explained as follows. Cycloheptatrienyl radical is readily formed from cycloheptatriene, so the hydrazyl radical (**11**) can be considered to be stabilized by the canonical formula **11b**.[12] No such stabilization effect is expected for the hydrazyl radicals **19** and **23**.

Experimental

All the melting and boiling points were uncorrected. NMR spectra were measured with a Varian HA-100 or a Hitachi R-20B spectrometer with deuteriochloroform as a solvent and tetramethylsilane as an internal standard. Benzylideneacetone derivatives were prepared according to a modification of the method of Drake and Allen.[13] All tosylhydrazones were prepared by ordinary methods from the corresponding ketones and tosylhydrazine.

Reaction of 1 with Silver Chromate. A mixtur of **1** (2.0 g, 6.8 mmol) and silver chromate (4.4 g, 13.3 mmol) in anhydrous diglyme (10 ml) was heated at 125 °C for 10 min under a nitrogen stream. After separation of the solid by filtration, the filtrate was extracted with ethyl acetate, washed with water and brine, and dried over anhydrous sodium sulfate. After filtration, the solvent was removed on a rotary evaporator to yield a tarry material, which was chromatographed on alumina using benzene as an eluent to give colorless crystals of **2** (562 mg). Recrystallization from ethyl acetate afforded pure crystals of **2** (510 mg, 28%); mp 139—140 °C; UV_{max} (MeOH) 244 nm (log ε 4.40), 276 (3.60), 288 (3.73), and 296 (3.68); IR (KBr) 3060, 1630, and 1596 cm^{-1}; NMR ($CDCl_3$) δ=2.33 (3H, s), 6.95—7.35 (4H, m), 7.5—7.7 (2H, m), 7.98 (2H, d), and 8.60 (1H, d); MS *m/z* (rel intensity) 272 (M^+, 34), 208 (29), 155 (26), and 91 (100). Found: C, 61.95; H, 4.36; N, 10.16%. Calcd for $C_{14}H_{12}O_2N_2S$: C, 61.76; H, 4.44; N, 10.29%.

Hydrolysis of 2. A solution of **2** (190 mg, 0.7 mmol) and 3 M† aqueous sodium hydroxide (10 ml) in methanol (5 ml) was heated at 90 °C for 2 h. After evaporation of methanol, the mixture was extracted with benzene, washed with water and brine, and dried over anhydrous sodium sulfate. After filtration, the solvent was removed on a rotary evaporator to yield colorless crystals of **3** (70 mg). Recrys-

† 1 M=1 mol dm^{-3}.

tallization from ethyl acetate gave pure crystals of **3** (60 mg, 74%); mp 145—146 °C (lit,[14] 146 °C).

Synthesis of 4. A solution of **3** (70 mg, 0.6 mmol) and tosyl chloride (230 mg, 1.2 mmol) in pyridine (5 ml) was heated at 110 °C for 2 h. The solution was poured into benzene (50 ml), washed with water, and dried over anhydrous sodium sulfate. After filtration the solvent was evaporated on a rotary evaporator to yield colorless crystals of **4** (160 mg). Recrystallization from ethanol gave pure crystals of **4** (140 mg, 79%); mp 111—112 °C; UV_{max} (MeOH) 237 nm (log ε 4.28) 241 (4.27), 269 (3.92), 277 (4.01), and 287 (4.00); IR (KBr) 3050, 1610, 1598, and 1360 cm^{-1}; NMR ($CDCl_3$) δ=2.33 (3H, s), 7.13—7.93 (8H, m), and 8.17 (1H, s); MS *m/z* (rel intensity) 272 (M^+, 36), 208 (34), 155 (15), 118 (100), and 91 (83). Found: C, 61.80; H, 4.20; N, 10.36%. Calcd for $C_{14}H_{12}O_2N_2S$: C, 61.76; H, 4.44; N, 10.29%.

Reaction of 5 with Silver Chromate. Sodium hydride (55%, 540 mg, 12.4 mmol) was added to a solution of *m*-nitrobenzaldehyde tosylhydrazone (3.2 g, 10.0 mmol) in anhydrous diglyme (30 ml). After evolution of hydrogen gas had ceased, silver chromate (5.2 g, 15.7 mmol) was added and the resulting mixture was heated at 100 °C for 5 min. The usual workup afforded a black tarry material, which was chromatographed on alumina using benzene as an eluent to give crystals of **6** (100 mg). Recrystallization from ethyl acetate gave pure crystals of **6** (85 mg, 6%); mp 117—118 °C (lit,[6] 117—118 °C).

Reaction of 7a with Silver Chromate. In the same way as above, a mixture of *p*-methoxybenzylideneacetone tosylhydrazone (1.7 g, 5.0 mmol), sodium hydride (55%, 300 mg, 6.9 mmol), and silver chromate (2.5 g, 7.5 mmol) in anhydrous diglyme (30 ml) was heated at 140 °C for 5 min. After the usual workup, the tarry material was chromatographed on alumina using benzene–ether (1:1) as an eluent to yield pale yellow crystals of **8a** (697 mg). Recrystallization from benzene gave pur crystals of **8a** (650 mg, 70%); mp 116—117 °C; UV_{max} (MeOH) 205 nm (log ε4.09) and 258 (4.16); IR (KBr) 3150, 2920, 1613, and 1570 cm^{-1}; NMR ($CDCl_3$) δ= 2.20 (3H, s), 3.73 (3H, s), 6.20 (1H, s), 6.76 (2H, d), 7.55 (2H, d), and 10.6 (1H, bs); MS *m/z* (rel intensity) 188 (M^+, 100), 173 (44), and 145 (13) Found: C, 70.12; H, 6.49; N, 14.73%. Calcd for $C_{11}H_{12}ON_2$: C, 70.18; H, 6.43 N, 14.88%.

Reaction of 7b with Silver Chromate. A mixture of 3-nitro-4-methoxybenzylideneacetone tosylhydrazone (2.0 g, 5.2 mmol), sodium hydride (55%, 300 mg, 6.9 mmol), and silver chromate (2.5 g, 7.5 mmol) in anhydrous diglyme (30 ml) was heated at 140 °C for 5 min. After the usual workup, the tarry material was chromatographed on alumina using benzene–ethyl acetate (1:1) as an eluent to give pale yellow crystals of **8b** (560 mg). Recrystallization from ethyl acetate gave pure crystals of **8b** (520 mg, 44%); mp 108—109 °C; UV_{max} (MeOH) 208 nm (log ε 4.10) and 252 (4.20); IR (KBr) 3150, 2950, and 1540 cm^{-1}; NMR ($CDCl_3$) δ=2.25 (3H, s), 3.90 (3H, s), 6.23 (1H, s), 7.0 (1H, d), 7.75 (1H, d), 8.05 (1H, d), and 10.6 (1H, bs); MS *m/z* (rel intensity) 233 (M^+, 100), 173 (7), 157 (19), and 130 (9). Found: C, 56.80; H, 4.77; N, 17.80%. Calcd for $C_{11}H_{11}O_3N_3$: C, 56.65; H, 4.75; N, 18.02%.

Reaction of 9 with Silver Chromate. A mixture of β-ionone tosylhydrazone (1.8 g, 5.2 mmol), sodium hydride (55%, 300 mg, 6.9 mmol), and silver chromate (2.5 g, 7.5 mmol) in anhydrous diglume (30 ml) was heated at 140 °C for 5 min. After the usual workup the oily material was chromatographed on alumina using benzene–ether (1:1) as an eluent to give a colorless oil of **10** (890 mg). Distillation under reduced pressure gave a pure oil of **10** (810 mg, 82%); bp 140 °C (bath temperature)/0.6 Torr (1 Torr ≈ 133.322 Pa); UV_{max} (MeOH) 205 nm (log ε 3.85) and 213 (sh, 3.83); IR (neat) 3100, 2960, and 1575 cm^{-1}; NMR ($CDCl_3$) δ=0.93 (6H, s), 1.40 (3H, s), 1.5—2.1 (6H, m), 2.23 (3H, s), 5.73 (1H, s), and 11.5 (1H, bs); MS *m/z* (rel intensity) 204 (M^+, 74), 189 (100), 147 (12), and 117 (21). Found: C, 76.29; H, 10.03; N, 13.68%. Calcd for $C_{13}H_{20}N_2$: C, 76.42; H, 9.87; N, 13.71%.

References

1) K. Saito, T. Toda, and T. Mukai, *Heterocycles*, **3**, 445 (1975); T. Tsuchiya, M. Enkaku, and H. Sawanishi, *J. Chem. Soc., Chem. Commun.*, **1978**, 568; H. U. Reissig and R. Huisgen, *J. Am. Chem. Soc.*, **101**, 3648 (1979); M. L. Graziano, M. R. Iesce, and R. Scarpati, *J. Chem. Soc., Chem. Commun.*, **1979**, 7; K. Saito and K. Takahashi, *Heterocycles*, **12**, 263 (1979); P. Geshe, F. Klinger, J. Streith, and H. Strub *Tetrahedron Lett.*, **21**, 4507 (1980); K. Saito, S. Iida, an T. Mukai, *Heterocycles*, **19**, 1197 (1982); D. P. Munro and J. T. Sharp, *Tetrahedron Lett.*, **23**, 345 (1982).

2) L. Horner and J. Dehnert, *Chem. Ber.*, **96**, 786 (1963).

3) R. M. Wilson and J. W. Rekers, *J. Am. Chem. Soc.*, **101**, 4005 (1979); A, Padwa and Hao Ku, *Tetrahedron Lett.*, **1979**, 4425 and **21**, 1009 (1980).

4) T. Tezuka, A. Yanagi, and T. Mukai, *Tetrahedron Lett.*, **1970**, 637.

5) K. V. Awres, *Chem. Ber.*, **58**, 2081 (1925).

6) F. Beilstein and A. Kuhlberg, *Ann.*, **146**, 317 (1868).

7) A. R. Katritzky, F. W. Maine, and S. Golding, *Tetrahedron*, **21**, 1693 (1965).

8) L. G. Tensmeyer and C. Ainsworth, *J. Org. Chem.*, **31**, 1878 (1966).

9) T. Mukai, T. Nakazawa, and K. Isobe, *Tetrahedron Lett.*, **1968**, 565; W. M. Jones and C. L. Ennis, *J. Am. Chem. Soc.*, **91**, 6391 (1969); K. Saito, T. Toda, and T. Mukai, *Bull. Chem. Soc. Jpn.*, **47**, 331 (1974).

10) R. W. Binkley, *J. Org. Chem.*, **35**, 2796 (1970).

11) C. D. Hurd and S. C. Lui, *J. Am. Chem. Soc.*, **57**, 2656 (1935); G. L. Closs, L. E. Closs, and W. A. Boll, *ibid.*, **85**, 3796 (1963); A. Ledwith and D. Parry, *J. Chem. Soc., B*, **1967**, 41; H. Hart and J. L. Brewbaker, *J. Am. Chem. Soc.*, **91**, 706 (1969); J. L. Brewbaker and H. Hart, *ibid.*, **91**, 711 (1969).

12) G. Vincow, H. J. Dauben, Jr., F. R. Hunter, and W. V. Volland, *J. Am. Chem. Soc.*, **91**, 2823 (1969), F. A. Bell, A. Ledwith, and D. C. Sherrington, *J. Chem. Soc., C*, **1969**, 2719; K. Okamoto, K. Komatsu, O. Murai, O. Sakaguchi, and Y. Matsui, *Bull. Chem. Soc. Jpn.*, **46**, 1785 (1973); M. Pomerantz, G. L. Combs, Jr., and R. Fink, *J. Org. Chem.*, **45**, 143 (1980).

13) N. L. Drake and P. Allen, *Org. Synth.*, Coll. Vol., I, p. 77 (1956).

14) E. Fischer and H. Kuzel, *Ann.*, **221**, 280 (1889).

A Basic Study of the Amino Acid Residue in Protein. The Role of Hydrocarbon Groups in Enantiomer-differentiating Acylation

Yuji HIRAKI and Akira TAI*
Institute for Protein Research, Osaka University, Yamada-oka, Suita, Osaka, 565
(Received July 30, 1983)

The enantiomer-differentiating acylation (kinetic resolution) of 1-phenylalkylamines and their derivatives was carried out with (*S*)-2-phenylbutyric anhydride and its derivatives in aqueous and nonaqueous media. On the basis of the distributions of the two diastereomeric products, the molecular interactions between hydrocarbon residues responsible for the structural recognition of the reacting molecules were studied. In nonpolar media, the (*R*,*S*)-isomer was predominantly formed over the (*S*,*S*)-isomer. Moreover, the differentiation was mainly controlled by the size of the alkyl substituents of the substrates. In aqueous media, though, the (*S*,*S*)-isomer was predominantly formed. By a comparative study of the cyclohexyl analogs of the substrates and the reagents, it was shown that alkyl-phenyl and/or phenyl-phenyl interactions were important in the recognition process. A partitioning process of the substrate into the reagent phase was not effective in the differentiation of the enantiomer by the reaction in suspensions of optically active reagents in highly aqueous media.

Noncovalent molecular interactions as well as covalent interactions[1] play an important role in molecular recognition processes. However, only limited information is available for understanding the contributions of noncovalent interactions between small hydrocarbon residues of proteinous amino acids to a molecular recognition process.[2]

In previous reports[3,4] we have described the characterization of the function of small hydrocarbon residues in molecular recognition by analyzing the product distributions of the competitive acylation of two primary amines. Here, we wish to report the results of the enantiomer-differentiating acylation (kinetic resolution; Eq.1) of racemic primary amines with optically active acid anhydride in aqueous and nonaqueous media; we will also discuss the role of the hydrocarbon residues constituting a chiral center of substrates in the differentiation process. From the logarithmic molar ratio of the two diastereomeric products (ln r value: Eq.2), the differentiation efficiency of the reaction was evaluated. Since the nucleophilicities of amino groups in (*R*)-and (*S*)-substrates are identical with each other, the ln r value can be effected to reflect the interactions between hydrocarbon residues.

$$\left.\begin{matrix}(R)\text{-R-NH}_2\\(S)\text{-R-NH}_2\end{matrix}\right\} + (S)\text{-}(R^0\text{-CO})_2\text{O} \longrightarrow \left\{\begin{matrix}(R,S)\text{-R-NHCO-R}^0\\(S,S)\text{-R-NHCO-R}^0,\end{matrix}\right. \quad (1)$$

$$\ln r = \ln\left([(S,S)\text{-R-NHCO-R}^0]/[(R,S)\text{-R-NHCO-R}^0]\right). \quad (2)$$

Results and Discussion

The Reaction System. The enantiomer-differentiating acylation of primary amine with acid anhydride (Eq. 1) is one of the simplest systems for the study of a differentiation process, for it readily proceeds without any side reactions. Acid anhydrides react quantitatively with amines not only under homogeneously-dissolved conditions in the solvent (Phase I), but also in a suspension of acid anhydride in an aqueous solvent (Phase II); however, the modes of differentiation in these solvents are completely different from each other. By the estimation of the solubility of acid anhydride under the present reaction conditions (see Experimental), it was shown that (*S*)-2-phenylbutyric anhydride was homogeneously dissolved in a water-dioxane mixture with $\chi_{H_2O}<0.77$ (Phase I). In a water-dioxane mixture with $\chi_{H_2O}>0.77$, a large fraction of the reagent was insoluble, resulting in a heterogeneous solution containing oily droplets of the reagent (Phase II).[3]

For the evaluation of the differentiation efficiency by means of the ln r value, the reaction should be carried out in the presence of so large an excess of the substrates to the reagent as to eliminate the effects of the concentration changes in the substrates during the reaction. To establish the appropriate reaction conditions, the ln r values were determined in water-dioxane ($\chi_{H_2O}=0.76$) or dioxane under a variety of relative molar ratios of the substrates to a reagent ([(*R*)-R-NH_2+(*S*)-R-NH_2]/[((*S*)-R^0-CO)$_2$O]). The ln r value became constant when the relative molar ratio of the substrates to a reagent was over four. The four molar equivalents of the substrates were treated with one molar equivalent of a reagent in the following experiments. Using this ratio of substrates to a reagent, it was also confirmed that the same ln r value was obtained in the presence and in the absence of triethylamine, an acid quencher. The ln r value was not affected by the (*S*)-2-phenylbutyric acid liberated during the reaction.

Effects of Reaction Media on the Enantiomer-differentiation of 1-Phenylalkylamines. Four 1-phenylalkylamines, *i.e.* 1-phenylethylamine, 1-phenylpropylamine, 1-phenylbutylamine, and 1-phenyl-2-methylpropylamine, were treated with (*S*)-2-phenylbutyric anhydride in dioxane, benzene, or a water-dioxane mixture ($\chi_{H_2O}=0.76$). The resulting ln r values are listed in Table 1, together with the ν_x values of the alkyl group of the substrates.[5] In dioxane the ln r values were almost zero in the reaction of 1-phenylethylamine, which meant that no appreciable recognition of the substrate structure took place. The reaction of the other three amines resulted in negative ln r values, which meant that the (*S*)-reagent favored the reaction with (*R*)-substrates. The ln r value became negative with the increase in the size of the alkyl group (ν_x): The differentia-

TABLE 1. THE ln r VALUES OBTAINED IN THE ENANTIOMER-DIFFERENTIATING ACYLATION OF 1-PHENYLALKYLAMINES WITH (*S*)-2-PHENYLBUTYRIC ANHYDRIDE IN SEVERAL SOLVENTS

Substrate (R'-CH(C_6H_5)-NH_2)	Size of R'	ln r values		
	ν_x[5] for R'	In dioxane	In benzene	In water-dioxane[a]
R'=CH_3-	0.52	0.027	0.009	0.332
R'=CH_3CH_2-	0.56	−0.066	−0.222	0.289
R'=$CH_3CH_2CH_2$-	0.68	−0.104	−0.286	0.229
R'=$(CH_3)_2CH$-	0.76	−0.356	−0.560	0.200

a) The mole fraction of water in the water-dioxane mixture (χ_{H_2O}) used in the experiments was 0.76.

tion efficiency was highest in the reaction of the substrate carrying the largest alkyl group. A similar effect of alkyl goups on the ln r value was also found in the reaction in benzene. These results suggest that enantiomer-differentiation in these solvents is mainly controlled by the size of the substituents. Since nonpolar media reduce polar interactions between reactants, the contribution of polar interactions to a differentiation process will be less in benzene than that in dioxane. Therefore, the low polarity of benzene explains why the effect of the size of the alkyl group on the ln r value was more pronounced in benzene than in dioxane.

In Phase I of a water-dioxane mixture (χ_{H_2O}=0.76), the ln r value was positive in every case. The ln r decreased in the order of the increase in the size of the alkyl group (R'-). However, the effect of the size on ln r was not so remarkable as that in benzene or dioxane. These results suggest that the effect of the size on the differentiation was overlaid with some intermolecular interaction between reagents to make the reagent select the other enantiomer in aqueous media. Thus, the modes of enantiomer-differentiation are quite different in the reactions in aqueous media and in nonaqueous media.

In order to obtain further information about the effects of the water in reaction media on enantiomer-differentiation, the enantiomer-differentiating acylation of racemic 1-phenylpropylamine with (*S*)-phenylbutyric anhydride was carried out in a water-dioxane mixture with various compositions of water. The ln r values are plotted against χ_{H_2O} in the plot (○) in Fig. 1. In Phase I, where the reaction proceeds in a homogeneous solution, ln r linearly increased with the increase in χ_{H_2O} in changing its sign from negative to positive and it reached its maximum at χ_{H_2O}=0.76. In Phase II, ln r sharply decreased with increase in χ_{H_2O}. Thus, no efficient enantiomer-differentiation is attainable by a phase-transfer process of substrates from the aqueous phase to the optically active organic phase. The reaction in Phase I will be discussed here, because we are chiefly concerned with differentiation and molecular interactions between a reagent and a substrate under homogeneous conditions.

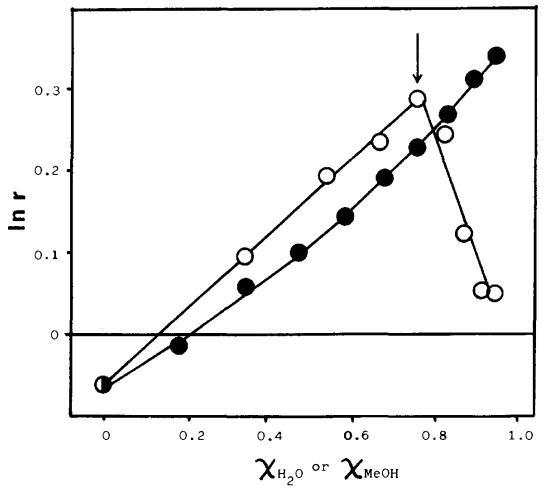

Fig. 1. The relationship between ln r value of the enantiomer-differentiating acylation with (*S*)-2-phenylbutyric anhydride and the mole fraction of water (χ_{H_2O}) or methanol (χ_{MeOH}). The ln r values were determined in the acylation of 1-phenylpropylamine in water-dioxane (○) or methanol-dioxane (●) mixed solvent.

As is shown by the (●) plot in Fig. 1, methanol had a similar effect on ln r to that of water in Phase I: ln r increased with the increase in χ_{MeOH} in changing its sign from negative to positive. Thus, the reaction in protic solvents, such as methanol and water, resulted in large positive ln r values.

The ln r values determined in various organic media are listed in Table 2, together with the solvent polarity parameters. The ln r value was very positive in polar media and almost zero or negative in nonpolar media. The dielectric constant or its related solvent parameters did not explain the increasing order of ln r values: the dielectric constants of DMF and acetonitrile are larger than that of methanol. However, it was in accordance with the increasing order of empirical solvent parameters, $E_T(30)$,[5] including the ln r values in water-dioxane (χ_{H_2O}=0.76, $E_T(30)$=52.4[7]) listed in Table 1. Thus, the remarkable changes in ln r must be a consequence of the elevation in polarity expressed by $E_T(30)$. These results suggest that the quite different molecular interactions from those caused by the bulkiness of hydrocarbon groups became important in the differentiaing process in highly polar reaction media, because bulkiness will not be affected so much by solvent polarity. In addition, water and methanol act as hydrogen-bond donors in the differentiation, since rather higher $E_T(30)$ values are assigned to hydrogen-bonded solvents than to those with high dielectric constants.[6]

Figure 2 shows the ln r *vs.* χ_{H_2O} plots in the enantiomer-differentiating acylation of 1-phenylethylamine in such aqueous media as water-dioxane, water-acetone, water-DMF and water-acetonitrile mixtures. In all cases, the ln r value increased linearly with an increase in χ_{H_2O} in Phase I, while it decreased in Phase II. The

TABLE 2. THE ln r VALUES IN ENANTIOMER-DIFFERENTIATING ACYLATION WITH (*S*)-2-PHENYLBUTYRIC ANHYDRIDE IN VARIOUS ORGANIC SOLVENTS

Solvent	Solvent Polarity[a]	ln r values	
	$E_T(30)$	Substrate structure	
	kcal mol^{-1} [c]	$CH_3CH(C_6H_5)$-NH_2	$CH_3CH_2CH(C_6H_5)$-NH_2
Methanol	55.5	0.37	0.38
Acetonitrile	46.0	0.29	0.24
DMF[b]	43.8	0.16	—
Acetone	42.2	0.15	—
Ethyl acetate	38.1	—	−0.07
Dioxane	36.0	0.03	−0.07
Benzene	34.5	0.01	−0.22

a) The empirical solvent polarity parameter $E_T(30)$-values are cited from "Solvent Effects in Organic Chemistry," by Christian Reichardt, Verlarg Chemie, New York (1979), pp. 270—272. b) *N*, *N* -Dimethylformamide is abbreviated as DMF. c) 1 cal=4.184 J.

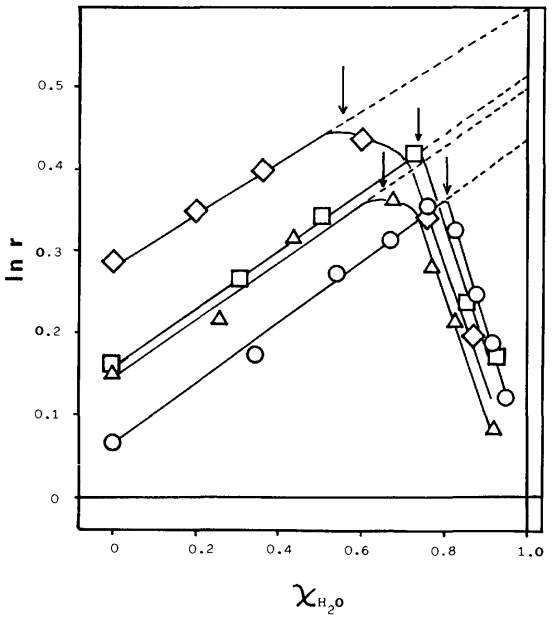

Fig. 2. The relationship between ln r value in enantiomer-differentiating acylation and the mole fraction of water (χ_{H_2O}) in several mixed solvents. (*S*)-2-Phenylbutyric anhydride and 1-phenylethylamine were employed as a reagent and a substrate respectively. The reaction was carried out in water-dioxane (○), water-acetone (△), water-DMF (□), or water-acetonitrile (◇) mixed solvent.

slopes in Phase I were similar with one another. In the water-acetonitrile mixture, the ln r value became as large as 0.44 at a maximum. The estimated ln r values in water obtained by extrapolation were not converged, as may be found in the figure. Without taking into account the solvophobic effect, the large ln r values in protic solvents cannot be explained.

The Role of Hydrocarbon Groups in Enantiomer-differentiating Acylation in Aqueous Media. As has been shown above (Table 1, Figs. 1 and 2), in the acylation of 1-phenylalkylamine derivatives with (*S*)-2-phenylbutyric anhydride the ln r value commonly exhibited a large change with an increase in the water content of the reaction media in Phase I. To ascertain the role of phenyl groups in the differentiation process, the reactions between reactants carrying no phenyl group were compared with those between reactants carrying a phenyl group.

Figure 3 shows the results of the enantiomer-differentiation of 1-phenylethylamine. In the reaction with (*S*)-2-phenylbutyric anhydride (plot (○)), no significant differentiation took place in dioxane (χ_{H_2O}=0), and the ln r value increased linearly with an increase in χ_{H_2O} in Phase I. In Phase II, the ln r value decreased to substantially zero in the very-high-water region. In the case of (*S*)-2-cyclohexylbutyric anhydride (plot (△)), the profile of the plot was the same as that of the (○) plot, though its gradient in Phase I was smaller than that of the (○) plot. In the case of (*S*)-2-ethylhexanoic anhydride (plot (□)), no appreciable differentiation took place in either Phase I or Phase II, even if a slight increase in the ln r value was detectable in Phase I.

Figure 4 shows the results of the enantiomer-differentiation of 1-cyclohexylethylamine and 1-methylbutyl-

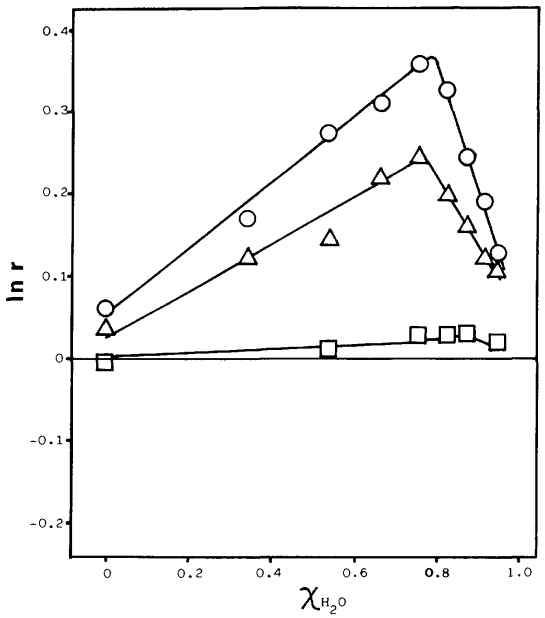

Fig. 3. The relationship between the ln r value in the acylation of racemic 1-phenylethylamine and χ_{H_2O} in water-dioxane mixed solvents. As a reagent, (*S*)-2-phenylbutyric anhydride (○), (*S*)-2-cyclohexylbutyric anhydride (△), and (*S*)-2-ethylhexanoic anhydride (□) were employed.

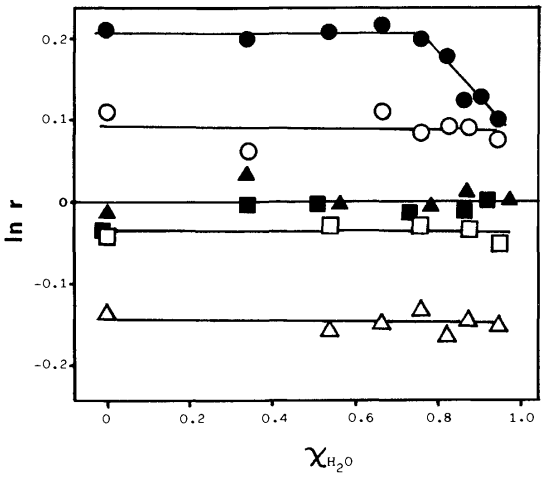

Fig. 4. The relationship between ln r value and χ_{H_2O} in water-dioxane mixed solvent. In the acylation of racemic 1-cyclohexylethylamine, (S)-2-phenylbutyric anhydride (●), (S)-2-cyclohexylbutyric anhydride (▲), and (S)-2-ethylhexanoic anhydride (■) were employes as a reagent. In the acylation of racemic 1-methylbutylamine, (S)-2-phenylbutyric anhydride (○), (S)-2-cyclohexylbutyric anhydride (△), and (S)-2-ethylhexanoic anhydride (□) were employed as a reagent.

amine. In no case, did any efficient differentiation take place, and the ln r value stayed constant in Phase I.

Thus, the large increase in the ln r value in Phase I was specific for the reaction where both reagent and substrate carry a phenyl group (Table 1, Figs. 1 and 3 plot (○)). In the reaction between a reagent and a substrate carrying only saturated hydrocarbon residues (plots (△), (□), (▲), and (■) in Fig. 4), the ln r value did not change at all in either Phase I or Phase II. These facts indicate that the existence of an alkyl-phenyl group in a reagent and the substrate is responsible for the interaction being evident in polar aqueous media. The plot (▲) in Fig. 4 suggests that the geometrical feature of a phenyl group are unimportant for the occurrence of this interaction.

The effect of a phenyl group in reactant molecules on enantiomer-differentiation in Phase I qualitatively parallels that found in the competitive acylation of two amines previously reported.[3] In that earlier report, we showed that the distinction of a phenyl group from alkyl groups easily took place due to the attractive alkyl-phenyl or phenyl-phenyl interaction, but that the distinction of alkyl groups with different chain lengths did not take place in polar aqueous media. The present results can be explained in terms of these attractive interactions. That is, enantiomer-differentiation results from a distinction between alkyl and phenyl groups in substrate molecules by means of alkyl and/or phenyl groups in a reagent molecule on the basis of alkyl-alkyl and alkyl-phenyl interactions and/or alkyl-phenyl and phenyl-phenyl interactions. On the other hand, in reaction between a reagent and a substrate carrying only saturated hydrocarbon groups, the enantiomer-differentiation does not take place, since neither alkyl-phenyl nor phenyl-phenyl interaction can be expected.

In the reaction where a phenyl group and a cyclohexyl group participated (the plot (△) in Fig. 3), the ln r value increased in Phase I, though the gradient of the plot was not large. This must be correlated with the fact that a phenyl group could slightly distinguish a branched alkyl group from an unbranched one.[8]

The results of the present study show that a phenyl group significantly influences the recognition of hydrocarbon groups by means of attractive alkyl-phenyl and/or phenyl-phenyl interactions[3] in aqueous media as well as by means of interaction based on its molecular size.

The attractive alkyl-phenyl and phenyl-phenyl interactions seem unlikely to be hydrophobic interactions between hydrocarbon groups, since no attractive interaction was found between alkyl groups (an alkyl-alkyl interaction). These attractive interactions might be a complex expression of noncovalent interactions induced in polar aqueous media. At this stage, weak solvophobic interaction and electron donor-acceptor interaction including CH···π[9] are probable candidates of the physicochemical entity of these attractive interactions.

In a biochemical field, a special aromatic character was postulated by Némethy[10] to characterize amino acid side chains. It was shown by the study of the structure-activity relationship that the aromatic character and the charge-transfer interactions were remarkably important in the expression of the biological activity of oligopeptides.[11] By the analysis of evolutionary changes in proteins, the relative mutabilities of Tyr or Phe can be said to be rather lower than those of Leu, Ile, and Val.[12] The probability of intermutation between Tyr and Phe was rather high, but probability of the mutation of Tyr or Phe to Leu, Ile, or Val was low.[12] These findings must be explained by the unique character of the phenyl groups that participate in the molecular recognition process through alkyl-phenyl or phenyl-phenyl interaction.

Experimental

Instruments. The ^{1}H-NMR and IR spectra were taken with a JEOL FX-100 spectrometer and a Shimadzu IR 27 G spectrometer respectively. The optical rotation was measured with a Perkin Elmer 241 polarimeter. The analytical GLC was carried out with a Shimadzu GC 6A gas chromatograph equipped with a Shimadzu Chromatopac C-R 1A apparatus, using a 3 m×5 mm o. d. glass column packed with 2% Silicone OV-17 on a Chromosorb W (OV-17) or Silicone OV-101 capillary column, 30 m×0.25 mm or 50 m×0.25 mm, at the stated temperature. The preparative GLC was carried out with a Shimadzu 3A instrument using a 3 m×6 mm o.d. stainless column packed with OV-17.

Materials. All the chemicals except those noted below were obtained from commercial sources and were used without further purification. The pure acetanilide used as an internal standard for the GLC analysis was obtained from Kishida Chemical, Inc., Osaka. Methyl stearate of a GLC analysis grade was obtained from Applied Science Laboratories, Inc., USA. (S)-2-Phenylbutyric acid was obtained by the preferential recrystallization of (R)-1-phenylethylamine salt from water; $[\alpha]_D^{20}$ +96.3° (*c* 10, benzene).[13] (S)-2-Phenylbutyric anhydride was prepared by the published method,[13] $[\alpha]_D^{20}$ +145° (*c* 5, benzene). (S)-2-Cyclohexylbutyric acid was prepared from optically pure (S)-2-phenylbutyric acid by hydrogenation with platinum oxide at a hydrogen pressure of 8.2 kg/cm^2 at 65 °C, $[\alpha]_D^{20}$ −1.32° (*c* 10, MeOH).[14] (S)-2-Cyclohexylbutyric anhydride was

Table 3. The retention times and analytical conditions in GLC analyses of the reaction products

Compound(R_A-CONH-R_B)[a] R_A-	R_B-	Retention time/min	GLC condition[b]
(*S*)-$CH_3CH_2CH(C_6H_5)$-	(*S*)-$CH_3CH(C_6H_5)$-	16.90	A
	(*R*)-$CH_3CH(C_6H_5)$-	17.70	A
	(*S*)-$CH_3CH_2CH(C_6H_5)$-	18.23	A
	(*R*)-$CH_3CH_2CH(C_6H_5)$-	19.26	A
	(*S*)-$CH_3(CH_2)_2CH(C_6H_5)$-	20.15	A
	(*R*)-$CH_3(CH_2)_2CH(C_6H_5)$-	21.09	A
	(*S*)-$(CH_3)_2CH(C_6H_5)$-	18.60	A
	(*R*)-$(CH_3)_2CH(C_6H_5)$-	19.90	A
	(*S*)-$cC_6H_{11}CH(CH_3)$-	19.5	B
	(*R*)-$cC_6H_{11}CH(CH_3)$-	20.4	B
	(*S*)-$CH_3(CH_2)_2CH(CH_3)$-	17.1	C
	(*R*)-$CH_3(CH_2)_2CH(CH_3)$-	17.9	C
(*S*)-$CH_3CH_2CH(cC_6H_{11})$-	(*S*)-$CH_3CH(C_6H_5)$-	16.6	D
	(*R*)-$CH_3CH(C_6H_5)$-	17.5	D
	(*S*)-$cC_6H_{11}CH(CH_3)$-	19.3	B
	(*R*)-$cC_6H_{11}CH(CH_3)$-	20.5	B
	(*S*)-$CH_3(CH_2)_2CH(CH_3)$-	22.1	C
	(*R*)-$CH_3(CH_2)_2CH(CH_3)$-	22.8	C
(*S*)-$CH_3(CH_2)_3CH(C_2H_5)$-	(*S*)-$CH_3CH(C_6H_5)$-	24.9	E
	(*R*)-$CH_3CH(C_6H_5)$-	25.9	E
	(*S*)-$cC_6H_{11}CH(CH_3)$-	31.7	E
	(*R*)-$cC_6H_{11}CH(CH_3)$-	32.3	E
	(*S*)-$CH_3(CH_2)_2CH(CH_3)$-	23.5	F
	(*R*)-$CH_3(CH_2)_2CH(CH_3)$-	24.0	F

a) Cyclohexyl and phenyl groups are denoted by cC_6H_{11} and C_6H_5 respectively. b) GLC analytical conditions are indicated by A, B, C, *etc.* A: A 3-m Silicone OV-17 column was used. The column temperature was elevated from 150°C to 250°C by 10°C/min. Methyl stearate was used as the internal standard. B: A Silicone OV-101 capillary column, 30 m×0.25 mm, was used. The column temperature was 240°C. Acetanilide was used as the internal standard. C: A Silicone OV-101 capillary column, 30 m×0.25 mm, was used. The column temperature was 170°C. Acetanilide was used as the internal standard. D: A Silicone OV-101 capillary column, 30 m×0.25 mm, was used. The column temperature was 220°C. Acetanilide was used as the internal standard. E: A Silicone OV-101 capillary column, 50 m×0.25 mm, was used. The column temperature was 175°C. Acetanilide was used as the internal standard. F: A Silicone OV-101 capillary column, 50 m×0.25 mm, was used. The column temperature was 170°C. Acetanilide was used as the internal standard.

prepared by the published method.[13] (*S*)-2-Ethylhexanoic acid was obtained by the recrystallization of (*R*)-1-phenylethylamine salt from acetonitrile, $[\alpha]_D^{20}$ +8.20° (neat).[15] (*S*)-2-Ethylhexanoic anhydride was prepared by the published method.[13] 1-Phenylpropylamine, 1-phenylbutylamine, and 1-phenyl-2-methylpropylamine were prepared from the appropriate oximes, which had themselves been prepared from propiophenone, butyrophenone, and isobutyrophenone respectively by hydrogenation with a Raney nickel catalyst in acetic anhydride at a hydrogen pressure of 90 kg cm^{-2} at 60°C and by succesive hydrolysis with 6 M HCl (1 M=1 mol dm^{-3}). The NMR and IR spectra were consistent with the desired structure; their boiling points were 98°C/20 mmHg (1 mmHg≈133.322 pa) (lit, 99—100°C/16 mmHg), 101—102°C/10 mmHg (lit, 107—109°C/16 mmHg), and 103—107°C/21 mmHg (lit, 214°C/760 mmHg) respectively. 1-Cyclohexylethylamine was prepared from *N*-acetyl-1-phenylethylamine by hydrogenation with platinum oxide in acetic acid at a hydrogen pressure of 8.2 kg cm^{-2} at 60°C and by successive hydrolysis with 6 M HCl. (*R*)-1-Cyclohexylethylamine was prepared from commercially available (*R*)-1-phenylethylamine; $[\alpha]_D^{20}$ +2.88° (*c* 5, MeOH).[16] (*R*)-1-Methylbutylamine was obtained by the preferential recrystallization of (+)-camphor-10-sulfonic acid salt from water; $[\alpha]_D^{20}$ −7.95° (*c* 5, MeOH).[17] The NMR spectra are consistent with the desired structures. The authentic samples of various amides for GLC analysis were prepared from an appropriate acid chloride and amine by a conventional method; they were then purified by preparative GLC. The NMR, IR spectra, and results of elemental analysis of each sample were consistent with the desired structures.

Reaction Procedure of Enantiomer-differentiating Acylation. In a flask, a 100-μl portion of a racemic mixture of a chiral amine (2 M dioxane solution) was dissolved in 3.8 ml of a reaction medium. To the resulting amine solution, a 100-μl portion of an optically active acid anhydride solution (0.5 M dioxane solution) was added all at once under vigorous stirring at room temperature; the mixture was then allowed to stand for 1 h. After a 100-μl portion of the internal standard (0.25 M dioxane solution), which will be specified in the following section, had been added for GLC analysis, the volume of the reaction mixture was made up to 5 ml with dioxane. GLC was used for the quantitative analysis of the products of the sample solution.

Assignment of Diastereomeric Reaction Products in GLC Analysis. The reaction shown in Eq. 1 affords two diastereomeric amides, *i.e.* the (*S,S*)-isomer and the (*R,S*)-isomer. These reaction products can be detected as two distinct peaks on a gas chromatogram. The amount of the products were determined by quantitative GLC using an internal-standard method. The analytical conditions and the retention times of the reaction products are listed in Table 3.

As far as the substrates and reagents employed in this study were concerned, the GLC peak with a shorter reten-

tion time was assigned to the (*S,S*)-isomer, while the peak with a longer retention time was assigned to the (*R,S*)-isomer, in the following manner.

In the acylation of racemic 1-phenylethylamine with (*S*)-2-phenylbutyric anhydride, the reaction product with a shorter retention time was identified with the authentic *N*-[(*S*)-1-phenylethyl]-(*S*)-2-phenylbutyramide, which had been prepared from (*S*)-2-phenylbutyric anhydride and (*S*)-1-phenylethylamine by GLC. Therefore, the reaction product with a longer retention time was identified as the (*R,S*)-isomer.

In the acylation of racemic 1-phenylpropylamine with (*S*)-2-phenylbutyric anhydride, the product with a longer retention time was identified as the (*R,S*)-isomer by a kinetic resolution of the amine. When an excess of racemic 1-phenylpropylamine was treated with (*S*)-2-phenylbutyric anhydride in benzene, the reaction product with a longer retention time was produced in excess. Moreover, the unreacted amine recovered showed a levorotatory power. Since (*S*)-1-phenylpropylamine is levorotatory,[17] the reaction product with a longer retention time was identified as the (*R,S*)-isomer.

The configurations of 1-phenylbutylamine and 1-phenyl-2-methylpropylamine have not yet been determined. Therefore, it is not possible to assign the configuration of the reaction products on the GLC. However, the results of the kinetic resolutions of both amines were the same as in the case of 1-phenylpropylamine. That is, the isomeric product with a longer retention time was obtained in excess, while levorotatory unreacted amine was recovered in either case. Since the levorotatory amine has the *S* configuration in other homologues, *i.e.*, 1-phenylethylamine and 1-phenylpropylamine, the configuration of (−)-1-phenylbutylamine and (−)-1-phenyl-2-methylpropoylamine was assumed to be also *S*. Thus, the product amide isomer with a shorter retention time in the GLC was identified as the (*S, S*)-isomer, and the other, is the (*R, S*)-isomer.

In all other cases, authentic (*R, S*)-isomers were prepared from the corresponding amine and acid anhydride. The diastereomeric products with longer retention times were identified with the authentic (*R, S*)-isomer.

Solubility of Acid Anhydride in Aqueous Media. The fraction of the acylating reagent dissolved in the water-dioxane mixture was determined by quenching it with a large excess of butylamine as follows: A 100-μl portion of (*S*)-2-phenylbutyric anhydride (0.5 M dioxane solution) was added to the solvent (0.9 ml), and the mixture was stirred vigorously. The resulting mixture was centrifuged at 2000 min^{-1} for 20 min to separate the undissolved portion of the anhydride from the solvent phase. A 50-μl portion of butylamine (2 M dioxane solution) was added to the 100-μl portion of the supernatant obtained under a vigorous stirring, after which the mixture was allowed to stand for 1 h to complete the reaction. By the quantitative GLC analysis of *N*-butylamide, the solubility of 2-phenylbutyric anhydride in aqueous media was estimated.

We wish to thank Professor Yoshiharu Izumi, Dr. Hiroshi Ozaki, and Dr. Tadao Harada of Osaka University for their helpful suggestions. Our thanks are also due to Mr. Motomasa Imaida, Mrs. Mihoko Yamamoto, and Miss Masako Yamashita for their technical assistance in preparing optically active compounds and in the GLC analyses.

References

1) Z. Simon, *Angew. Chem., Int. Ed. Engl.*, **13**, 719 (1974).
2) J. B. Jones, "Application of Biochemical Systems in Organic Chemistry," ed by J. B. Jones, C.J. Sih, and D. Perlman, John Wiley & Sons, New York (1976), Part I, pp. 15—28; W.P. Jenkes, "Catalysis in Chemistry and Enzymology," McGraw-Hill, New York (1969), Chap. 8; P. D. Ross and S. Subramanian, *Biochemistry*, **20**, 3096 (1981); P. Manavalan and P. K. Ponnuswamy, *Nature*, **275**, 673 (1978).
3) Y. Hiraki, T. Oda, and A. Tai, *Bull. Chem. Soc. Jpn.*, **56**, 2330 (1983).
4) Y. Hiraki and A. Tai, *Chem. Lett.*, **1982**, 341.
5) M. Charton, *J. Am. Chem. Soc.*, **97**, 1552 (1975).
6) C. Reichardt, "Solvent Effects in Organic Chemistry," Verlag Chemie, Weinheim (1979), p. 237.
7) E. M. Kosower, H. Dodiuk, K. Tanizawa, M. Ottolenglhi, and N. Orbach, *J. Am. Chem. Soc.*, **97**, 2167 (1975).
8) F. Kubota, Y. Hiraki, H. Ozaki, and A. Tai, 47th National Meeting of the Chemical Sciety of Japan, Kyoto, April 1983, Abstr. No. 3K30,.
9) M. Hirata, K. Abe, H. Tashiro, and M. Nishio, *Chem. Lett.*, **1982**, 777.
10) G. Némethy, *Angew. Chem., Int. Ed. Engl.*, **6**, 195 (1967).
11) P. H. A. Sneath, *J. Theor. Biol.*, **12**, 157 (1966); Simon, *Rev. Roum. Biochim.*,**5**, 319 (1968); Z. Szabadai and Z. Simon, *ibid.*, **9**, 327 (1972).
12) M. O. Dayhoff, R.M. Schwartz, and B. C. Orcutt, "Atlas of Protein Sequences and Structure, 5" National Biochemical Research Foundation, Silver Spring, Maryland (1978), (Supplement 3), Chap. 22.
13) A. Horeau, "Stereochemistry Fundamentals and Methods," ed by H. B. Kagan, Georg Thieme Publishers, Stuttgart (1977), Vol. 3, pp. 52—93.
14) P. A. Levene, R. E. Marker, and A. Roten, *J. Biol. Chem.*, **100**, 589 (1933).
15) P. A. Levene, *J. Biol. Chem.*, **91**, 687 (1931).
16) H. Herlinger, H. Kleimann, and I. Ugi, *Justus Liebigs Ann. Chem.*, **706**, 37 (1967).
17) P. A. Levene,.*J. Biol. Chem.*, **120**, 759 (1937).

Kinetics of the Ligand Exchange Reaction between Tetrakis(acetylacetonato)-thorium(IV) and Free Acetylacetone in CD_3CN and $CDCl_3$

Naoshi FUJIWARA, Hiroshi TOMIYASU, and Hiroshi FUKUTOMI*

Research Laboratory for Nuclear Reactors, Tokyo Institute of Technology, O-kayama, Meguro-ku, Tokyo 152

(Received November 14, 1983)

Kinetics of the ligand exchange reaction between tetrakis(acetylacetonato)thorium(IV) and free acetylacetone in CD_3CN and $CDCl_3$ was studied by ^1H NMR. The rate law was written as rate=k[Th(acac)$_4$][Hacac]$_{enol}$, where k=(1.0±0.1)×10^2 s^{-1} mol^{-1} kg at 0 °C in CD_3CN and (1.7±0.1)×10^2 s^{-1} mol^{-1} kg at −16 °C in $CDCl_3$. The rates were retarded by addition of bases and the retardation effect well correlated with the donor number of the bases. Under the conditions studied, the activation entropies gave large negative values. A ligand exchange mechanism passing through a nine-coordinate intermediate is proposed to interpret the kinetic law.

Thorium(IV) is one of the largest metal ions in size and gives complexes with high coordination numbers. Eight-coordination is usually common and even the existence of nine- and ten-coordinate complexes were reported.[1-6] Tetrakis(2,4-pentanedionato)thorium(IV), where hereafter the common name of the ligand, *i.e.* acetylacetonate (acac) will be used, has been known as one of the typical eight-coordinate complexes having a square antiprismatic structure. The same structure is established in such acac complexes as Zr(acac)$_4$, Hf(acac)$_4$, and U(acac)$_4$.[1]

Little has been known with respect to the kinetics of the ligand substitution in eight-coordinate complexes. Adams and Larsen[7] studied the ligand exchange in Zr(acac)$_4$ and Hf(acac)$_4$ and proposed the mechanism passing through a seven-coordinate intermediate which was formed by the partial breaking of one of the chelate rings. They also studied the ligand exchange in Th(acac)$_4$ but reported that the rate was too fast to be measured by ^1H NMR. On the other hand, the mechanism involving a nine-coordinate intermediate was proposed by Folcher *et al.*[8] in the ligand exchange of U(fod)$_4$ (fod=6,6,7,7,8,8,8-heptafluoro-2,2-dimethyl-3,5-octanedionate).

In an earlier study,[9] it was found that the rate of the ligand exchange between Th(acac)$_4$ and Hacac was measurable in chloroform by ^1H NMR. In this paper, we report in detail the kinetic results of the acac exchange in Th(acac)$_4$ and propose a possible mechanism proceeding *via* a nine-coordinate intermediate.

Experimental

Materials. Th(acac)$_4$ was synthesized by the following procedure. The solution containing 0.01 mol of thorium nitrate was stirred with 5 g of acetylacetone; then aqueous ammonia was added slowly until the pH of the solution became 5. White precipitate obtained was dried *in vacuo* for 1 d. Recrystallization of the precipitate was carried out twice first from benzene and then Hacac. Found: C, 38.0; H, 4.3%, Calcd for $C_{20}H_{28}O_8Th$: C, 38.2; H, 4.5%.

Acetylacetone was dried over anhydrous calcium sulfate and distilled twice. Acetonitrile, dichloromethane, tetrahydrofuran (THF) and chloroform-*d* ($CDCl_3$) were distilled, and dimethyl sulfoxide (DMSO), *N,N*-dimethylformamide (DMF) and hexamethylphosphoric triamide (HMPT) were distilled under reduced pressure before use. Acetonitrile-d_3 (CD_3CN) was dried over Molecular Sieve 4A.

Water contents in CD_3CN and $CDCl_3$ were determined by the Karl-Fischer method.

Measurements of UV and ^1H NMR Spectra. The UV spectra of Th(acac)$_4$, Hacac and their mixture were measured by using a Shimadzu 210A spectrophotometer with a 0.1 mm quartz cell. A JEOL JNM-FX100 FT-NMR spectrometer equipped with a JNM-VT-3B temperature controller was used for ^1H NMR measurements. The preparation of NMR samples was carried out by dissolving a small amount of sample materials, which were weighed in 5 mmϕ NMR tubes with a microbalance, in appropriate solvents.

Determination of the Fraction of Keto- and Enol-forms in Hacac. Two forms, keto and enol, of Hacac are in tautomeric equilibrium and the concentration ratio, [enol]/[keto], was determined by area measurements of methyl proton signals for keto- and enol-isomers. In order to obtain the temperature dependence of the ratio, the area measurements were performed in the temperature range from −20 to 36 °C.

Rate Analysis. The first-order rate constants of the acac exchange in Th(acac)$_4$, k_{obsd}, were determined from the line shape analysis of the NMR signals by using the two site model.[10]

Results

The absorption spectrum of Th(acac)$_4$ shows a peak at 283 nm with molar extinction coefficients, ε, of 4.9×10^4 M^{-1} cm^{-1} (1 M=1 mol dm^{-3}) in acetonitrile and 4.8×10^4 M^{-1} cm^{-1} in dichloromethane. The spectra of the mixture containing Th(acac)$_4$ and Hacac coincided with the sum of those of each component in acetonitrile and dichloromethane, and remained unchanged for several hours.

The ^1H NMR spectra of the reaction mixture in CD_3CN are shown in Fig. 1. Three methyl proton

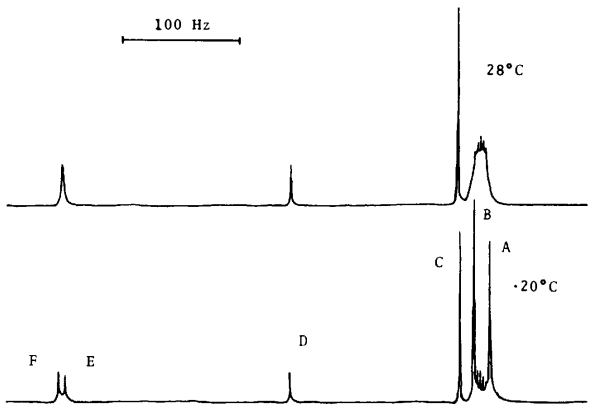

Fig. 1. ^1H NMR spectra of the reaction mixture in CD_3CN at −20 °C and 28 °C. [Th(acac)$_4$]=0.0707 mol kg^{-1} and [Hacac]$_{total}$=0.444 mol kg^{-1}.

signals and two methine proton signals were clearly observed at −20 °C. Two methyl proton signals of $Th(acac)_4$ (A) and Hacac in the enol-form (B) coalesced as the temperature was raised. Similar behavior was observed in methine proton signals of $Th(acac)_4$ (E) and Hacac in the enol-form (F). No line broadening was observed for the methyl proton signal (C) and methylene proton signal (D) of Hacac in the keto-form. Since signals A and B overlapped with the methyl proton signals of the solvent used, the rate analyses were carried out by using signals E and F.

The change of ^1H NMR signals in CD_3CN at various temperatures was very similar to that in $CDCl_3$ in the earlier work.[9] The ligand exchange reaction between $Th(acac)_4$ and Hacac in the enol-form can be described as follows.

$$Th(acac)_4 + Hacac^*_{enol} \rightleftharpoons Th(acac)_3(acac^*) + Hacac_{enol}, \quad (1)$$

where the asterisk denotes the exchanging species.

The life time of acac in the coordination site, τ_c, correlates directly with the first-order rate constant by the following equation.

$$k_{obsd} = 4\tau_c^{-1} \quad (2)$$

Plots of k_{obsd} *vs.* the concentration of $Th(acac)_4$ indicate that the values of k_{obsd} are independent of $[Th(acac)_4]$ (Fig. 2). On the other hand, plots of k_{obsd} *vs.* the concentration of Hacac in the enol-form, $[Hacac]_{enol}$, in CD_3CN and $CDCl_3$ show that the plots are linear passing through the origin (Figs. 3 and 4). These results lead to the following rate equation.

$$Rate = k_{obsd}[Th(acac)_4] = k[Th(acac)_4][Hacac]_{enol}, \quad (3)$$

where k is the second-order rate constant. The values of k and activation parameters are listed in Tables 1 and 2. These results indicate that the exchange rate is influenced by solvents, *i.e.* the rate in $CDCl_3$ is faster than that in CD_3CN. This is mainly due to the difference in activation entropy, ΔS^*, rather than the difference in activation enthalpy, ΔH^*.

Influence of the Addition of Bases. The kinetic parameters of the acac exchange in $Th(acac)_4$ were obtained also in the presence of various bases. The results are listed in Table 3. The addition of the bases retarded the exchange rate and this effect is remarkable in the case of strong bases. The order of the retardation effect is found to be as follows;

$$\underset{(38.8)}{HMPT} > \underset{(29.8)}{DMSO} > \underset{(26.6)}{DMF} > \underset{(20.0)}{THF}, \quad \underset{(18.0)}{H_2O}.$$

It is to be noted that this is the order of Gutmann's

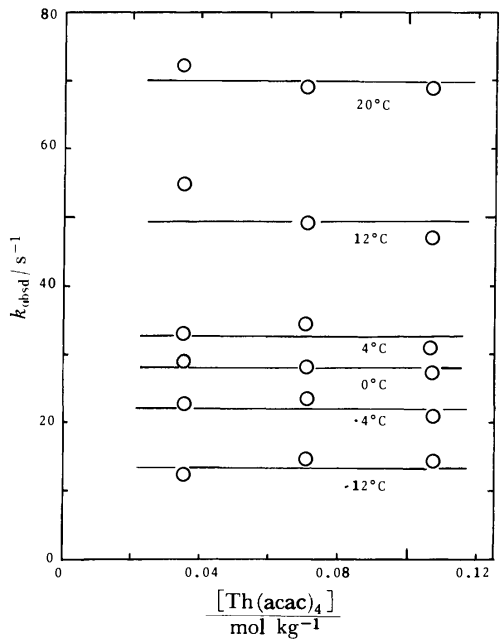

Fig. 2. Dependence of k_{obsd} on $[Th(acac)_4]$ in CD_3CN at various temperatures.

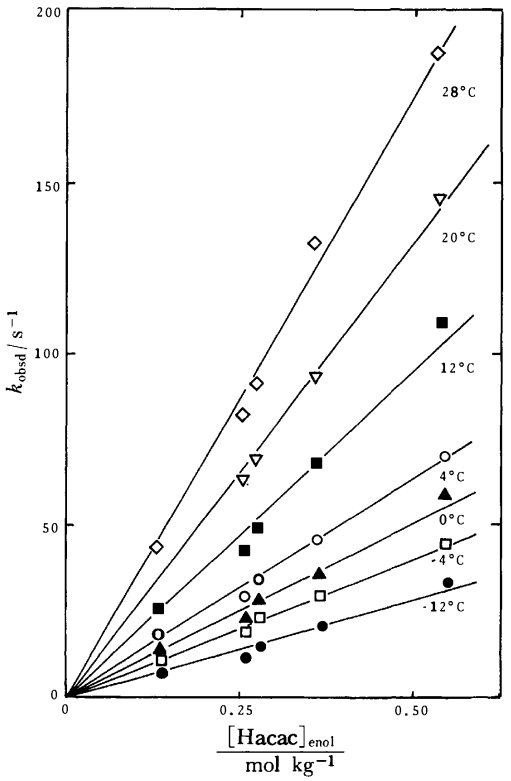

Fig. 3. Plots of k_{obsd} *vs.* $[Hacac]_{enol}$ in CD_3CN at various temperatures.

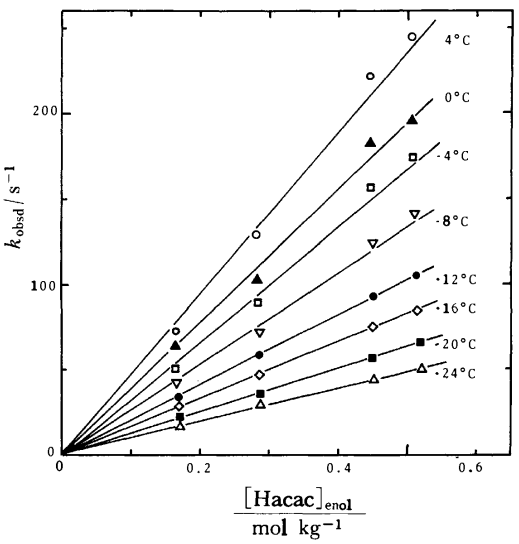

Fig. 4. Plots of k_{obsd} *vs.* $[Hacac]_{enol}$ in $CDCl_3$ at various temperatures.

donor number (DN)[11] which is given in parentheses.

The values of k_{obsd} obtained at various H_2O concentrations in CD_3CN and at various DMSO concentrations in $CDCl_3$ are listed in Tables 4 and 5, respectively. The reciprocal plots of k_{obsd} *vs.* [H_2O] or [DMSO] are shown in Figs. 5 and 6, respectively. From these results,

Table 1. Second-order rate constants and the kinetic parameters for acac exchange in CD_3CN

[Th(acac)$_4$]	[Hacac]$_{enol}$(0°C)	k(0°C)	ΔH^*	ΔS^*
mol kg^{-1}	mol kg^{-1}	s^{-1} mol^{-1} kg	kJ mol^{-1}	J mol^{-1} K^{-1}
0.0394	0.279	100	33.0±1.5	−84.9±5.2
0.0704	0.189	97.0	28.8±1.7	−100.8±6.2
0.0706	0.261	88.4	31.2±0.8	−92.9±2.7
0.0707	0.279	101	31.9±0.7	−102.9±2.4
0.0705	0.365	102	29.1±0.6	−99.2±2.1
0.0707	0.546	110	27.8±1.1	−103.3±3.8
0.107	0.280	96.3	29.8±0.5	−97.1±1.9

The water content in the solvent (CD_3CN) is 0.04 mol kg^{-1}.

Table 2. Second-order rate constants and the kinetic parameters for acac exchange in $CDCl_3$

[Th(acac)$_4$]	[Hacac]$_{enol}$(−16°C)	k(−16°C)	ΔH^*	ΔS^*
mol kg^{-1}	mol kg^{-1}	s^{-1} mol^{-1} kg	kJ mol^{-1}	J mol^{-1} K^{-1}
0.0822	0.170	164	27.9±0.6	−91.2±2.2
0.0817	0.276	166	29.4±0.5	−87.0±1.8
0.0800	0.457	165	32.9±0.7	−73.0±2.7
0.0808	0.517	159	32.8±0.9	−74.1±3.3

The water content in the solvent ($CDCl_3$) is 0.008 mol kg^{-1}.

Table 3. Kinetic parameters of the ligand exchange in the presence of bases

Solvent	Base	k(0°C)	ΔH^*	ΔS^*
		s^{-1} mol^{-1} kg	kJ mol^{-1}	J mol^{-1} K^{-1}
CD_3CN	H_2O	82.3	28.7±0.3	−102±1
	THF	81.1	29.1±1.5	−101±5
	DMF	54.8	30.1±0.6	−101±2
	DMSO	32.4	32.0±0.7	−98±2
	HMPT	9.1	39.7±1.6	−80±5
$CDCl_3$	THF	321	27.7±1.1	−95±4
	DMF	120	37.4±1.8	−68±6
	DMSO	54.3	33.5±2.3	−88±7
	HMPT	16.7	29.8±4.1	−112±13

Conditions: [Th(acac)$_4$]=0.070—0.072 mol kg^{-1}, [Hacac]$_{enol}$=0.27—0.29 mol kg^{-1}, [Base]=0.24—0.25 mol kg^{-1} in CD_3CN; [Th(acac)$_4$]=0.080—0.082 mol kg^{-1}, [Hacac]$_{enol}$=0.27—0.29 mol kg^{-1}, [Base]=0.24—0.25 mol kg^{-1} in $CDCl_3$.

Table 4. Dependence of the first-order rate constants on [H_2O] in CD_3CN

[Th(acac)$_4$]	[Hacac]$_{enol}$		[H_2O]	k_{obsd}	
mol kg^{-1}	mol kg^{-1}		mol^{-1} kg	s^{-1}	
	(0°C)	(20°C)		(0°C)	(20°C)
0.0706	0.278	—	0.074	31.5	—
0.0706	0.278	0.273	0.246	22.6	55.5
0.0701	0.276	0.271	0.477	19.0	49.4
0.0699	0.275	0.270	0.816	16.2	45.4
0.0706	0.278	0.273	1.01	12.4	40.4

Table 5. Dependence of the first-order rate constants on [D_MSO] in $CDCl_3$

[Th(acac)$_4$]	[Hacac]$_{enol}$		[DMSO]	k_{obsd}	
mol kg^{-1}	mol kg^{-1}		mol^{-1} kg	s^{-1}	
	(24°C)	(32°C)		(24°C)	(32°C)
0.0810	0.273	0.270	0.068	128	184
0.0812	0.274	0.271	0.135	83.6	127
0.0812	0.271	0.268	0.249	49.9	76.6
0.0811	0.270	0.267	0.401	31.6	50.0
0.0812	0.275	0.272	0.672	21.2	31.8

The water content in the solvent ($CDCl_3$) is 0.008 mol kg^{-1}.

k^{-1}_{obsd} can be expressed by the following equation.

$$k^{-1}_{obsd} = a + b[H_2O \text{ or DMSO}], \quad (4)$$

where a and b are constants. The intercepts of these plots agree well with the values of k^{-1}_{obsd} in the absence of bases.

Discussion

It is generally considered that the ligand exchange processes in (acetylacetonato)metal complexes consist of several steps. Two types of initiation mechanism are presented for the acac exchange reactions: 1) bond breaking of one end of the chelate bond; 2) bond formation with free Hacac at the additional coordination site without a ring opening of the chelate.

Type (1) has been proposed for the acac exchanges in $Al(acac)_3$,[12] $Co(acac)_3$,[13] and type (2) has been proposed for those in $Cr(acac)_3$, $Rh(acac)_3$, $V(acac)_3$ and $Fe(acac)_3$.[13] In the case of the acac exchange in $Al(acac)_3$, a complete dissociation of one of the coordinated acac occurs prior to an attack of entering Hacac to the complex. For most of the other acac exchange reactions which belong to type (1) or type (2), a proton transfer from incoming Hacac to coordinated acac is involved in the acac exchange processes.

The ionic radius of Th^{4+} is large enough to make nine- or ten-coordinate complexes, *e.g.* $Th(tta)_4topo$ and $Th(tta)_4tbp$, where tta, topo and tbp are 2-thenoyltrifluoroacetonate, trioctylphosphine oxide and tributyl phosphate, respectively.[3] This fact suggests that type (2) seems to be probable for the acac exchange in $Th(acac)_4$.

As shown in Fig. 7, $Th(acac)_4$ (I) forms a nine-coordinate intermediate, $Th(acac)_4Hacac^*$ (II), by the attack of free acetylacetone, and the proton of entering Hacac* is transferred to one of the coordinated acac, followed by the Th-O bond breaking of the chelate ring. Then the protonated ligand (Hacac) leaves rapidly from the coordination sphere.

Since the rate of ligand exchange of unidentate ligands is generally much faster than that of bidentate ligands in the complexes of the same metal ion [10,14] it can be assumed that complexes (I) and (II) are in fast

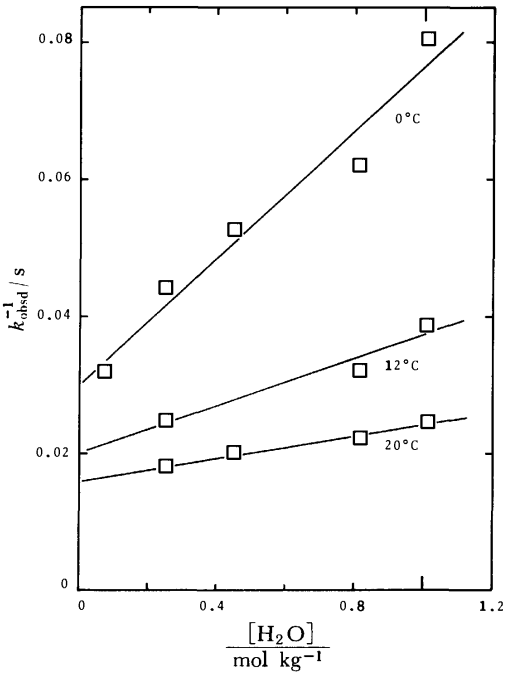

Fig. 5. Plots of k^{-1}_{obsd} against $[H_2O]$ in CD_3CN at various temperatures.

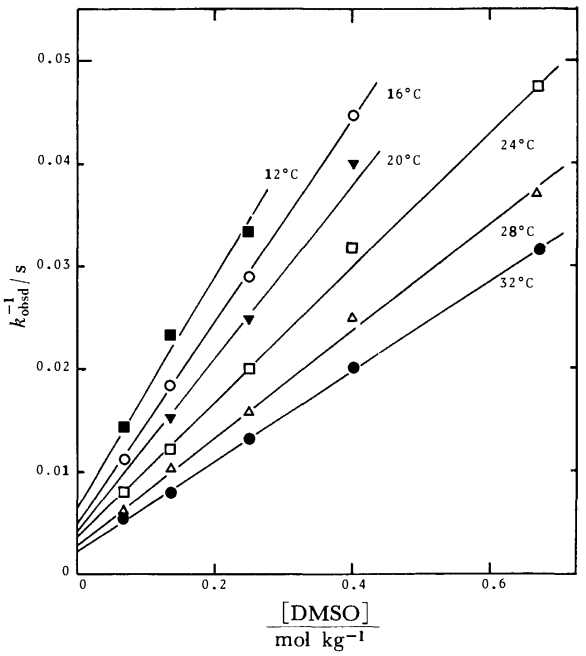

Fig. 6. Plots of k^{-1}_{obsd} against [DMSO] in $CDCl_3$ at various temperatures.

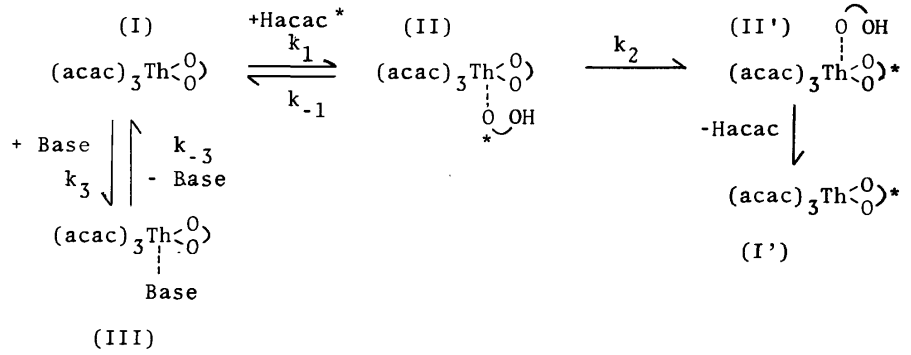

Fig. 7. Possible mechanism of the ligand exchange in $Th(acac)_4$. HOO represents Hacac in the enol-form.

equilibrium. Based on this assumption, the rate of exchange is expressed by Eq. (5).

$$\text{Rate} = \frac{k_1 k_2}{k_{-1}}[\text{I}][\text{Hacac}]_{\text{enol}} \quad (5)$$

If $[\text{I}] \gg [\text{II}]$ or $K_1[\text{Hacac}]_{\text{enol}} \ll 1$, where $K_1 = k_1/k_{-1}$, the first-order rate constant for the exchange of acac, k_{ex}, can be written by Eq. (6).

$$k_{\text{ex}} = k_2 K_1 [\text{Hacac}]_{\text{enol}} \quad (6)$$

Equation (6) is basically the same as Eq. (3), where k corresponds to k_2K_1 in the absence of water. The k_2 pathway involves two processes, *i.e.* the proton transfer from entering Hacac* to coordinated acac and the Th-O bond breaking in the chelate ring. It appears difficult to determine which process is the rate determining step from the above results.

In the case of tris(acetylacetonato) complexes,[12,13] it was often observed that the ligand exchange was accelerated in the presence of water. However, the retardation by the addition of bases including water was observed for the acac exchange in $Th(acac)_4$ as described above. A good correlation between $\ln k$ and DN as shown in Fig. 8 suggests that the donicity of bases might be important for the retardation effect. Strong donor bases may bind to $Th(acac)_4$ tightly forming adduct complex (III) and hence hinder the formation of (II).

On the assumption that complex (III) is in fast equilibrium with (I) and that the concentration of (II) is much low compared with that of (I) or (III), k_{ex} in the presence of bases is written by Eq. (7).

$$k_{\text{ex}} = \frac{k_2 K_1 [\text{Hacac}]_{\text{enol}}}{1 + K_3[\text{Base}]}, \quad (7)$$

or by Eq. (8).

$$k_{\text{ex}}^{-1} = \frac{1}{k_2 K_1 [\text{Hacac}]_{\text{enol}}} + \frac{K_3[\text{Base}]}{k_2 K_1 [\text{Hacac}]_{\text{enol}}}, \quad (8)$$

where $K_3 = k_3/k_{-3}$. Hence, when the concentration of Hacac is kept constant, the plots of k_{ex}^{-1} *vs.* [Base] should give a straight line. This relationship is the same as Eq. 4 which was determined experimentally.

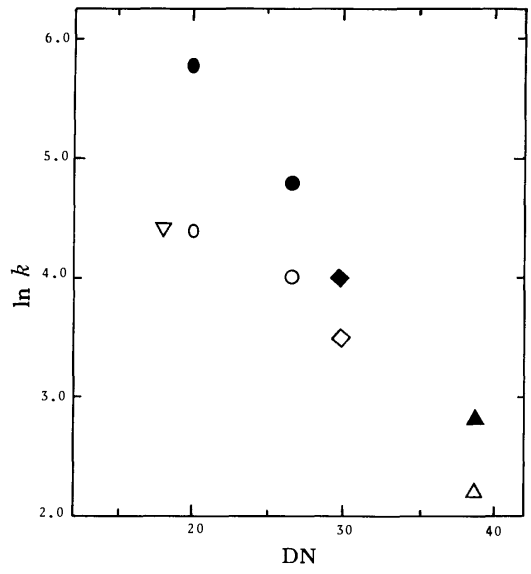

Fig. 8. Relationship between $\ln k$ and the donor number (DN) at 0°C. ▽: H_2O, ○: THF, ○: DMF, ◇: DMSO, △: HMPT in CD_3CN, and ●: THF, ●: DMF, ◆: DMSO, ▲: HMPT in $CDCl_3$.

Thus, the proposed mechanism can explain well the experimental results. The large negative values of activation entropies shown in Table 3 might support the formation of nine-coordinate intermediate.

Nishizawa and Saito[14] studied the kinetics of acac exchange in $VO(acac)_2$ and found that the reaction was retarded by the addition of DMSO. They proposed that the retardation effect was attributed to the formation of an outer-sphere intermediate with DMSO, which prohibits an associative attack by free Hacac. Unlike their interpretation in $VO(acac)_2$, the retardation by bases in the present study arises from the competition between bases and Hacac in the enol-form at the ninth coordination site. From the slopes and intercept in Figs. 5 and 6, the formation constant of the nine-coordinate adduct complex (III) was determined to be *ca.* 0.9 $\text{mol}^{-1}\,\text{kg}$ at 12°C for $Th(acac)_4H_2O$ in CD_3CN, and *ca.* 20 $\text{mol}^{-1}\,\text{kg}$ at 32°C for $Th(acac)_4$dmso in $CDCl_3$. These values indicate that the presence of such strong bases as DMSO and HMPT in solution leads to the adduct formation with bases.

In this study, it was found that $Th(acac)_4$ was the most labile of acetylacetonato complexes of quadrivalent metal ions. The order of the lability for the ligand exchange reaction is as follows:[7,15,16]

$$\text{Th(acac)}_4 \geq \text{U(acac)}_4 > \text{Zr(acac)}_4 \simeq \text{Hf(acac)}_4 > \text{Ti(acac)}_3^{+}.$$

As the ionic size of Th^{4+} is much larger than the ionic radii of Zr^{4+} and Hf^{4+}, and the electronic configuration of Th^{4+} is $5f^0$ and $6d^0$, the electric repulsion between electrons of donor molecule and Th^{4+} might be weak. These facts also support the proposed mechanism in which the reaction proceeds through the nine-coordinate intermediate for the ligand exchange reaction between $Th(acac)_4$ and Hacac.

The present work was partially supported by a Grant-in-Aid for Scientific Research No. 57470035 from the Ministry of Education, Science and Culture.

References

1) S. J. Lippard, "Eight-Coordination Chemistry," in "Progress in Inorganic Chemistry," ed by F. A. Cotton, Wiley-Interscience, New York (1967), Vol. 8, pp. 108—193.
2) M. Lenner and O. Lindgvist, *Acta Crystallogr., Sect. B*, **35**, 600 (1979).
3) L. D. C. Bok, G. F. S. Wessels, and J. G. Leipordt, *Z. Anorg. Allg. Chem.*, **404**, 76 (1974).
4) J. G. Leipordt, G. F. S. Wessels, and L. D. C. Bok, *J. Inorg. Nucl. Chem.*, **37**, 2487 (1975).
5) R. J. Hill and C. E. F. Rickard, *J. Inorg. Nucl. Chem.*, **37**, 2481 (1975).
6) M. M. Akhtar and A. J. Smith, *Acta Crystallogr., Sect. B*, **31**, 1361 (1975).
7) A. C. Adams and E. M. Larsen, *Inorg. Chem.*, **5**, 814 (1966).
8) G. Folcher, N. Keller, C. Kiener, and J. Paris, *Can. J. Chem.*, **55**, 3559 (1977).
9) N. Fujiwara, H. Tomiyasu, and H. Fukutomi, *Chem. Lett.*, **1983**, 377.
10) Y. Ikeda, H. Tomiyasu, and H. Fukutomi, *Bull. Chem.*

Soc. Jpn., **56**, 1060 (1983).
11) V. Gutmann, "Coordination Chemistry in Non-aqueous Solution," Springer-Verlag, Wien (1968).
12) K. Saito, *Pure Appl. Chem.*, **38**, 325 (1974).
13) a) H. Kido, *Bull. Chem. Soc. Jpn.*, **53**, 82 (1980); b) H. Kido and K. Saito, *ibid.*, **53**, 428 (1980); c) A. Watanabe, H. Kido, and K. Saito, *Inorg. Chem.*, **20**, 1107 (1981).
14) M. Nishizawa and K. Saito, *Bull. Chem. Soc. Jpn.*, **51**, 483 (1978).
15) G. M. Khvostik, V. N. Sokolov, G. K. Grebenshchikov, S. A. Toropov, and G. P. Kondratenkov, *Koordinatsionnaya Khimiya*, **5**, 680 (1979).
16) M. Nishizawa, H. Kido, I. Kinoshita, Y. Soma, and K. Saito, *Bull. Chem. Soc. Jpn.*, **49**, 819 (1976).

Formation Process of Niobium Nitride by the Reaction of Niobium Pentachloride with Ammonia in the Vapor Phase and Properties of the Niobium Nitride Formed

Akimasa YAJIMA, Takashi ARAI, Ryoko MATSUZAKI, and Yuzo SAEKI*
Research Laboratory of Resources Utilization, Tokyo Institute of Technology, 4259, Nagatsuta-cho, Midori-ku, Yokohama 227
(Received January 25, 1984)

The reaction products of gaseous $NbCl_5$ with ammonia were $NbCl_5 \cdot 5NH_3$ at 200 °C, $NbCl_5 \cdot 5NH_3$, Nb_4N_5, and NH_4Cl at 250—500 °C, Nb_4N_5 and NH_4Cl at 550—950 °C, δ-NbN and NH_4Cl at 1000 °C, δ-NbN, Nb_2N, NH_4Cl, and HCl at 1100 °C, and δ-NbN, Nb_2N, Nb_4N_3, δ′-NbN, ε-NbN, NH_4Cl, and HCl at 1200—1300 °C. In the vapor-phase reaction of gaseous $NbCl_5$ with ammonia, the reaction of gaseous $NbCl_5$ with ammonia to form $NbCl_5 \cdot 5NH_3$ occurs first. Above *ca.* 235 °C, the $NbCl_5 \cdot 5NH_3$ reacts with ammonia to form Nb_4N_5. Above *ca.* 1000 °C, the Nb_4N_5 decomposes to δ-NbN. Above about 1100 °C, in addition to these reactions, the nitriding of niobium, formed by the reduction of gaseous $NbCl_5$ with the hydrogen resulting from the thermal dissociation of ammonia, also occurs to form Nb_2N at 1100 °C and Nb_2N, Nb_4N_3, δ′-NbN, and ε-NbN at 1200—1300 °C. When the Nb_4N_5, formed by the vapor-phase reaction, is heated in an argon atmosphere, it changes to δ-NbN at *ca.* 1000 °C, to δ-NbN and ε-NbN at 1100—1200 °C, and then to Nb_4N_3 and δ-NbN at 1300 °C. The niobium nitrides formed above 1200 °C are uniform, ultrafine powders with particle diameters of the order of 1/100 μm.

The vapor-phase reaction of transition-metal chlorides with ammonia has recently become important for the preparation of fine powders or thin films of transition-metal nitrides, which are aquiring importance as new industrial materials. However, no information has been available on the reaction process of transition-metal chloride with ammonia in the vapor phase. The present authors have previously reported the formation processes of some nitrides of transition metals of Groups IV and V by the reaction of the chloride with ammonia.[1,2]

Concerning the vapor-phase reaction of niobium pentachloride ($NbCl_5$) with ammonia, little information has been available apart from the work of Gavrilko and Kornilov.[3] They reported the preparation of fine niobium nitride powders by a vapor-phase reaction of the $NbCl_5$-NH_3-N_2 system at 5300—9200 K, with emphasis on the effect of the reaction temperature on the specific surface area and the particle size.

In this paper, the reaction products of gaseous $NbCl_5$ with ammonia at 200—1300 °C were examined in detail. The possible reactions which were considered to occur during the reaction process on the basis of the above experiments were examined. Further, the thermal stability of the niobium nitride formed was examined. The niobium nitride formed was also examined by electron microscopy.

Experimental

Materials. The $NbCl_5$ used was prepared by the reaction of niobium powder (Nb 99.8%, Hermann C. Starck Berlin) with chlorine at 300 °C.[4] Found: Nb, 34.3; Cl, 65.6%. Calcd for $NbCl_5$: Nb, 34.39; Cl, 65.61%. Ammonia was dried by passing it over sodium hydroxide granules and barium oxide powders.

Experimental Procedures. A transparent quartz or alumina reaction tube (1000 mm length) was used for examining the reaction products of gaseous $NbCl_5$ with ammonia. Gaseous $NbCl_5$ was formed by heating solid $NbCl_5$ (12 g) at 190 °C and was carried by a stream of argon (50 cm^3/min) into the reaction zone (28 mm i.d., 250 mm length), held at a specified temperature. The $NbCl_5$ inlet tube consisted of two concentric tubes. Gaseous $NbCl_5$ carried by argon was introduced through the inner tube, and the outer tube was utilized for introducing argon (50 cm^3/min) as a sheath gas to prevent the formation of product deposits in the chloride inlet tube. Ammonia was simultaneously introduced at a flow-rate of 100 cm^3/min into the reaction zone through a separate tube. The mean flow-rate of gaseous $NbCl_5$ was 6.0 cm^3/min. A quartz or alumina tube was inserted into the reaction tube to make the removal of the reaction product easier. The reaction was allowed to proceed for 2 h.

The by-product, ammonium chloride (NH_4Cl), which was deposited outside the reaction zone, together with the niobium nitride formed, was separated by heating the mixture in an argon stream at 400 °C for 10—15 h.

Analytical. The chemical analysis of the reaction product was performed as follows. The niobium content of the $NbCl_5$-NH_3 adduct was gravimetrically determined as Nb_2O_5 after hydrolyzing the sample in 3 M†-nitric acid. The chlorine and ammonia contents were determined by the gravimetric method as AgCl and by the Kjeldahl method, respectively, from the filtrate. In the case of a mixture of the adduct and niobium nitride, the niobium and chlorine contents were gravimetrically determined after the fusion of the sample with sodium carbonate. The NH_3 content was determined by the Kjeldahl method from the filtrate after hydrolyzing the sample in 3 M-nitric acid.

The X-ray analysis of the solid product was performed with an X-ray powder diffractometer equipped with a proportional counter and using Ni filtered Cu radiation. The sample chamber of the diffractometer was maintained under a dry nitrogen atmosphere, if necessary, to prevent any contamination of the sample by atmospheric moisture during the irradiation.

The sensitivity of the quartz helix used for thermogravimetry (TG) was approximately 113 mm/g. The sample (0.2 g) was heated at a rate of 2.5 °C/min, and the flow-rate of ammonia was maintained at 50 cm^3/min.

Throughout this work, the $NbCl_5$ and the reaction products were handled in an argon atmosphere to prevent any contamination by atmospheric moisture.

Results and Discussion

Reaction Products of Gaseous Niobium Pentachloride with Ammonia. The products formed by heating

† 1 M=1 mol dm^{-3}.

gaseous $NbCl_5$ in an ammonia stream at various temperatures were examined by both X-ray analysis[5-11] and chemical analysis. Reaction temperatures above 200 °C were employed, because gaseous $NbCl_5$ was generated at 190 °C.

The product formed at 200 °C showed no clear X-ray diffraction pattern. Found: Nb, 26.1; Cl, 49.8; NH_3, 24.0%. The ratio of Nb:Cl:NH_3 was calculated to be 1:5.00:5.02. This was considered to indicate that the product formed at 200 °C had a composition of $NbCl_5 \cdot 5NH_3$ (calcd for $NbCl_5 \cdot 5NH_3$:Nb, 26.15; Cl, 49.89; NH_3, 23.96%). The reaction products at various temperatures above 200 °C are shown in Table 1. Unreacted $NbCl_5$ was not observed throughout the temperature range of this work.

At 550—1000 °C, all the products were obtained outside the reaction zone. Above 1100 °C, in addition to the δ-NbN formed outside the reaction zone, Nb_2N was formed inside the reaction zone at 1100 °C, while Nb_2N, Nb_4N_3, δ'-NbN, ε-NbN, were formed both inside and outside the reaction zone at 1200—1300 °C. The products formed below 1000 °C and the products formed outside the reaction zone above 1100 °C were in the form of powder, while the products formed inside the reaction zone at 1100—1300 °C were in the form of film. The mole percentage of $NbCl_5$ converted to the nitrides formed inside the reaction zone was 16% at 1100 °C, 21% at 1200 °C, and 44% at 1300 °C. Also, it was observed that HCl was formed in addition to NH_4Cl above 1100 °C.

The presence of the following niobium nitrides has been reported: Nb_2N (hexagonal, a_0=3.055 Å, c_0=4.994 Å;[6] N/Nb 0.40—0.50[12]), Nb_4N_3 (tetragonal, a_0=4.382 Å, c_0=4.316 Å;[7] N/Nb 0.75—0.79[12]), δ-NbN (cubic, a_0=4.376—4.392 Å; N/Nb 0.86—1.06[10]), δ'-NbN (hexagonal, a_0=2.967 Å, c_0=5.538 Å;[5] metastable phase[13]), ε-NbN (hexagonal, a_0=2.960 Å, c_0=11.270 Å;[8] N/Nb 1.000—1.018[12]), Nb_4N_5 (tetragonal, a_0=6.873 Å, c_0=4.298 Å),[5] and Nb_5N_6 (hexagonal, a_0=5.193 Å, c_0=10.380 Å).[5] It was found that all the above nitrides except Nb_5N_6 were formed by the reaction of gaseous $NbCl_5$ with ammonia.

Table 1. Reaction products of gaseous $NbCl_5$ with ammonia at various temperatures

Temp/°C	Products
200	$NbCl_5 \cdot 5NH_3$
250—300	$NbCl_5 \cdot 5NH_3 \gg Nb_4N_5$; NH_4Cl
400—450	$NbCl_5 \cdot 5NH_3$, Nb_4N_5; NH_4Cl
500	$Nb_4N_5 \gg NbCl_5 \cdot 5NH_3$; NH_4Cl
550—950	Nb_4N_5; NH_4Cl
1000	δ-NbN; NH_4Cl
1100	δ-NbN>Nb_2N; NH_4Cl, HCl
1200	δ-NbN>Nb_2N>Nb_4N_3, δ'-NbN, ε-NbN; NH_4Cl, HCl
1300	Nb_4N_3>Nb_2N, ε-NbN>δ-NbN, δ'-NbN; NH_4Cl, HCl

Reaction Process of Gaseous Niobium Pentachloride with Ammonia. To elucidate the reaction process of gaseous $NbCl_5$ with ammonia, the behavior of the $NbCl_5 \cdot 5NH_3$ and the Nb_4N_5, which had been formed during the reaction process, on heating in an ammonia stream were examined.

Behavior of $NbCl_5 \cdot 5NH_3$ on Heating in an Ammonia Stream: The TG curve of $NbCl_5 \cdot 5NH_3$ in an ammonia stream showed that the sample weight decreased continuously above about 235 °C and reached a constant value at about 460 °C. The sample after the heating to 500 °C was found by X-ray analysis to be Nb_4N_5.

In order to obtain more detailed information on the behavior of $NbCl_5 \cdot 5NH_3$ on heating in an ammonia stream, $NbCl_5 \cdot 5NH_3$ (1.0 g) in a quartz boat (70 mm length, 15 mm width, 7 mm depth) was placed in a straight reaction tube (28 mm i.d., 1000 mm length). Ammonia was introduced into the reaction tube at a flow-rate of 100 cm^3/min. The sample part was then placed in the centre of an electric furnace (300 mm heating length) maintained at a specified temperature for 1 h. The products obtained both inside and outside the boat were examined by X-ray analysis and chemical analysis. The results are shown in Table 2.

The results showed that $NbCl_5 \cdot 5NH_3$ reacted with ammonia to form Nb_4N_5 and NH_4Cl above about 235 °C and that a small part of the $NbCl_5 \cdot 5NH_3$ vaporized above about 350 °C. The formation of a small amount of Nb_4N_5 above 400 °C outside the boat was considered to indicate that the reaction of gaseous $NbCl_5 \cdot 5NH_3$ with ammonia to form Nb_4N_5 also occurred above about 400 °C.

Behavior of Nb_4N_5 on Heating in an Ammonia Stream: The samples obtained by heating Nb_4N_5 (0.1 g) in an ammonia stream (100 cm^3/min) at various temperatures of 900—1300 °C for 2 h were examined by X-ray analysis.[5,8,9] The Nb_4N_5 used was prepared by the reaction of gaseous $NbCl_5$ with ammonia at 900 °C, based on the experimental results shown in Table 1. The results are shown in Table 3. The results indicated that, on heating Nb_4N_5 in an ammonia stream above 1000 °C, Nb_4N_5 changed according to the following path: $Nb_4N_5 \rightarrow$ δ-NbN $\rightarrow$ ε-NbN $\rightarrow$ δ'-NbN.

Based on the above experimental results, the reac-

Table 2. Experimental results for $NbCl_5 \cdot 5NH_3$ on heating in an ammonia stream

Heating temp/°C	Products		Unreacted $NbCl_5 \cdot 5NH_3$/%
	In the boat	Outside the boat	
250	Nb_4N_5(11)	NH_4Cl	89
300	Nb_4N_5(46)	NH_4Cl	54
350	Nb_4N_5(75)	$NbCl_5 \cdot 5NH_3$(1), NH_4Cl	24
400	Nb_4N_5(88)	$NbCl_5 \cdot 5NH_3$(3), Nb_4N_5(<1), NH_4Cl	8
450	Nb_4N_5(91)	$NbCl_5 \cdot 5NH_3$(4), Nb_4N_5(2), NH_4Cl	3
500	Nb_4N_5(95)	$NbCl_5 \cdot 5NH_3$(4), Nb_4N_5(<1), NH_4Cl	—

The values in parentheses are the mole percentages of $NbCl_5 \cdot 5NH_3$ converted to the product.

TABLE 3. PRODUCTS OBTAINED BY HEATING Nb_4N_5 AT VARIOUS TEMPERATURES IN AN AMMONIA STREAM

Temp/°C	Products
900	Nb_4N_5
1000	δ-NbN > ε-NbN
1100	ε-NbN > δ-NbN > δ′-NbN
1200	ε-NbN > δ-NbN > δ′-NbN
1300	ε-NbN > δ-NbN > δ′-NbN

TABLE 4. PRODUCTS OBTAINED BY HEATING NIOBIUM AT VARIOUS TEMPERATURES IN A NITROGEN STREAM

Temp/°C	Products
900	Nb > Nb_2N
1000	Nb > Nb_2N > δ′-NbN, ε-NbN > Nb_4N_3
1100	Nb_2N, ε-NbN > Nb, Nb_4N_3 > δ′-NbN
1200	Nb_4N_3 > Nb_2N, ε-NbN > δ′-NbN
1300	Nb_4N_3, ε-NbN

tion process of gaseous $NbCl_5$ with ammonia can be discussed. As shown in Table 1, $NbCl_5 \cdot 5NH_3$ alone was formed at 200 °C. This fact indicates that the reaction of $NbCl_5$ with ammonia to form $NbCl_5 \cdot 5NH_3$ occurs first. The Nb_4N_5 formed at 250—950 °C is considered to be due to the reaction of $NbCl_5 \cdot 5NH_3$ with ammonia, because the $NbCl_5 \cdot 5NH_3$ reacts with ammonia above about 235 °C to form Nb_4N_5, as described above. The δ-NbN formed above 1000 °C is considered to be due to the decomposition of the Nb_4N_5, because Nb_4N_5 decomposes above about 1000 °C to form δ-NbN, as described above.

As mentioned before, Nb_2N was formed in addition to δ-NbN at 1100 °C. At 1200—1300 °C, Nb_4N_3, δ′-NbN, and ε-NbN were formed in addition to δ-NbN and Nb_2N. Above 1100 °C, HCl was formed in addition to NH_4Cl. The percentage of HCl formed to the total amount of chlorine introduced as $NbCl_5$ was 18% at 1100 °C, 51% at 1200 °C, and 92% at 1300 °C. This amount of HCl formed is considerably higher than that of HCl formed by the thermal decomposition of NH_4Cl at each temperature under the experimental conditions in this work.[1] Also, it has been reported that the thermal dissociation of ammonia under the experimental conditions in this work proceeds markedly above about 1100 °C to form hydrogen and nitrogen[1] and that the reduction of gaseous $NbCl_5$ with hydrogen proceeds markedly above about 900 °C to form niobium.[14] Considering these facts, it was considered that the reduction of gaseous $NbCl_5$ with the hydrogen resulting from the thermal dissociation of ammonia also occurred to form niobium and HCl and that the niobium formed reacted with nitrogen or ammonia to form niobium nitrides.

Then, the products obtained by heating niobium (1.0 g) in a nitrogen stream and in an ammonia stream (100 cm^3/min) at various temperatures of 900—1300 °C for 2 h were examined by X-ray analysis.[5-8,15] The experimental results in a nitrogen stream are shown in Table 4. The results in an ammonia stream were similar to those in a nitrogen stream.

Based on the above experimental results, the formation processes of the Nb_2N, Nb_4N_3, δ′-NbN, and ε-NbN, which were formed above 1100 °C by the reaction of gaseous $NbCl_5$ with ammonia, can be discussed. As seen from the results shown in Tables 3 and 4, Nb_2N and Nb_4N_3 were not formed by the heating of Nb_4N_5 in an ammonia stream, but they were formed by the nitriding of niobium. This fact was considered to indicate that the formation of Nb_2N and Nb_4N_3 was due to the nitriding of the niobium resulting from the hydrogen reduction of $NbCl_5$. δ′-NbN and ε-NbN were considered to be formed by the heating of Nb_4N_5 in an ammonia stream or by the nitriding of niobium (Tables 3 and 4). However, as shown in Table 1, δ′-NbN and ε-NbN were always obtained, together with Nb_2N and Nb_4N_3, which were formed only by the nitriding of niobium. This fact was considered to indicate that δ′-NbN and ε-NbN were formed also by the nitriding of niobium.

From the above mentioned results, the formation process of niobium nitride by the vapor-phase reaction of $NbCl_5$ with ammonia can be represented as follows. The reaction of gaseous $NbCl_5$ with ammonia occurs first to form $NbCl_5 \cdot 5NH_3$. Above about 235 °C, the $NbCl_5 \cdot 5NH_3$ reacts with ammonia to form Nb_4N_5. Above about 1000 °C, the Nb_4N_5 decomposes to δ-NbN. Above about 1100 °C, in addition to these reactions, the nitriding of niobium, formed by the reduction of gaseous $NbCl_5$ with the hydrogen resulting from the thermal dissociation of ammonia, also occurs to form Nb_2N at 1100 °C and Nb_2N, Nb_4N_3, δ′-NbN, and ε-NbN at 1200—1300 °C.

Properties of the Niobium Nitride Formed. To obtain knowledge on the thermal stability of the niobium nitride formed by the reaction of gaseous $NbCl_5$ with ammonia, the Nb_4N_5 (0.1 g), formed at 900 °C, was heated in a argon atmosphere at various temperatures for 2 h. X-ray analysis of the samples obtained after the heating showed them to be unchanged Nb_4N_5 at 900 °C, δ-NbN at 1000 °C, δ-NbN ≫ ε-NbN at 1100—1200 °C, and Nb_4N_3 > δ-NbN at 1300 °C.

A comparison of the above results with the results on heating Nb_4N_5 in an ammonia stream (Table 3) showed that δ′-NbN was not formed by the heating of Nb_4N_5 in an argon atmosphere, and that in an argon atmosphere Nb_4N_5 decomposed to Nb_4N_3, while in an ammonia stream Nb_4N_5 did not give the nitride with a N/Nb atomic ratio of less than 1, Nb_4N_3.

Finally, the niobium nitrides obtained outside the reaction zone by the reaction of gaseous $NbCl_5$ with ammonia at various temperatures were examined by electron microscopy. Some typical micrographs of the niobium nitride are shown in Fig. 1.

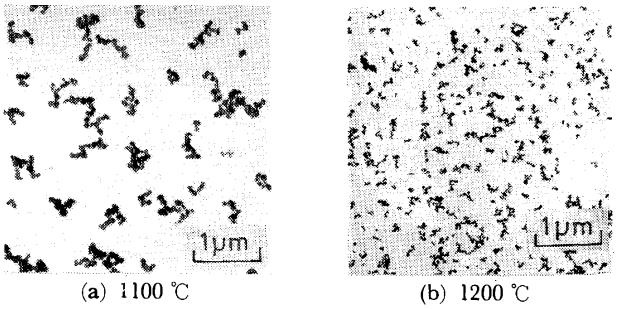

(a) 1100 ℃ (b) 1200 ℃

Fig. 1. Electron micrographs of the niobium nitrides formed at various temperatures.

As seen from Fig. 1, the niobium nitrides formed above 1200 °C under the experimental conditions in this work were uniform, ultrafine powders with particle diameters of the order of 1/100 μm.

References

1) Y. Saeki, R. Matsuzaki, A. Yajima, and M. Akiyama, *Bull. Chem. Soc. Jpn.*, **55**, 3193 (1982).
2) A. Yajima, R. Matsuzaki, and Y. Saeki, *Denki Kagaku*, **51**, 676 (1983).
3) V. P. Gavrilko and A. A. Kornilov, *Izv. Vyssh. Uchebn Zaved., Khim. Khim. Tekhnol.*, **22**, 639 (1979).
4) Y. Saeki and M. Yanai, *Denki Kagaku*, **39**, 878 (1971).
5) N. Terao, *J. Less-Common Met.*, **23**, 159 (1971).
6) JCPDS, Powder Diffraction File 20-802.
7) JCPDS, Powder Diffraction File 20-803.
8) JCPDS, Powder Diffraction File 20-801.
9) J. Pelissier, *J. Less-Common Met.*, **35**, 193 (1974).
10) G. Brauer and H. Kirner, *Z. Anorg. Allg . Chem.*, **328**, 34 (1964).
11) ASTM, Powder Diffraction File 7-7.
12) G. Brauer and R. Esselborn, *Z. Anorg. Allg. Chem.*, **309**, 151 (1961).
13) R. W. Guard, J. W. Savage, and D. G. Swarthout, *Trans. Metall. Soc. AIME*, **239**, 643 (1967).
14) Y. Saeki and T. Suzuki, *J. Electrochem. Soc. Jpn.*, **33**, 220 (1965).
15) JCPDS, Powder Diffraction File 16-1.

Condensations of 1,4-Cyclohexanediones and Secondary Aromatic Amines. The Formation of Alkyldiarylamines and Triarylamines

Kazuo HAGA,* Masayuki OOHASHI, and Ryohei KANEKO
Department of Industrial Chemistry, Faculty of Engineering, Utsunomiya Universty, Ishii-machi, Utsunomiya 321
(Received September 26, 1983)

Condensation of 1,4-cyclohexanedione with *N*-alkylarylamines gives *N*-alkyl-*N*-arylanilines, and that with diarylamines gives triarylamines. A mechanism involving dehydration of monoenamines of the 1,4-dione is proposed for the reaction. Relative rates of substituted *N*-ethylanilines on competitive reactions plotted *vs.* Hammet's σ values gave -2.0 as the ρ value. In separate reactions, however, a different tendency is noted for the yield, that is, the ease of reactions with *p*-chloro and *p*-nitro derivatives. This discrepancy is explained in terms of acidities of the conjugate acids of the amines used as the actual catalysts.

The condensations between ketones and secondary amines are known to produce enamines. Leonard and Sauers[1] reported that the condensation of 1,4-cyclohexanedione (**1**) with cycloalkylamines gave dienediamines, which converted by air oxidation to substituted *p*-phenylenediamines.

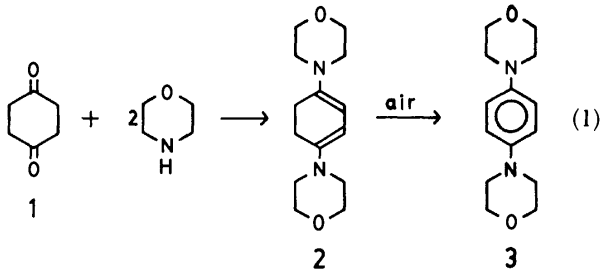

(1)

On the condensation of **1** with some secondary aromatic amines, we now have found that almost no dienediamines or phenylenediamines are obtained, but that tertiary monoamines are produced instead. In the present study, a mechanism for the reaction will be proposed and substituent effects will be discussed. This reaction is useful as a new procedure for the synthesis of tertiary aromatic amines. Preparation of 2,6-dimethyl-1,4-cyclohexanedione is also reported.

Results and Discussion

Preparation of 2,6-Dimethyl-1,4-cyclohexanedione. 2,6-Dimethyl-1,4-cyclohexanedione (**8**), one of the starting materials for the condensation reaction, was prepared as shown in Scheme 1. Ethyl 5,5-ethylenedioxy-3-methyl-2-oxocyclohexanecarboxylate (**5**) was obtained by isomerization of ethyl 5,5-ethylenedioxy-1-methyl-2-oxocyclohexanecarboxylate (**4**), and was methylated *in situ* in considerable yield. The alkaline hydrolysis of the product **6** yielded the monoacetal **7**, which on removal of the ethylenedioxy group gave 2,6-dimethyl-1,4-cyclohexanedione (**8**). This procedure was modified from the method of Mori and Matsui[2] for the methylation of ethyl 1-methyl-2-oxocyclohexanecarboxylate to afford ethyl 1,3-dimethyl-2-oxocyclohexanecarboxylate. This method for α,α'-dialkylation of cyclic ketones, exploiting the reversible cleavage of β-keto ester, was also useful for the formation of the 1,4-dione derivative.

Condensation Reaction. When the condensation of **1** and *N*-methylaniline (**9**) was carried out in

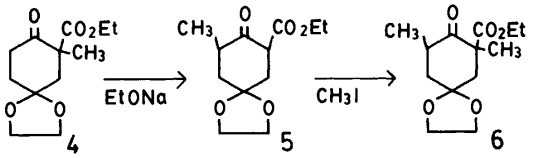

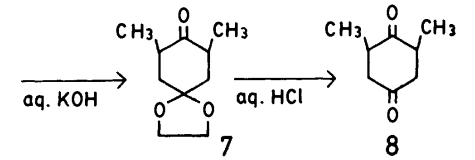

Scheme 1.

the presence of *p*-toluenesulfonic acid, *N*-methyl-*N*-phenylaniline (**10**) was obtained unexpectedly in 77% yield. The condensation of **1** with *N*-methyl-*m*-toluidine (**11**) in similar conditions gave *N*-methyl-*N*-phenyl-*m*-toluidine (**12**) which was produced also from 2-methyl-1,4-cyclohexanedione (**13**) on the reaction with *N*-methylaniline (**9**). Even diphenylamine (**14**) which is a very weak base ($pK_a=0.79$) reacted with **1** giving triphenylamine (**15**) in 72% yield, and with 2,6-dimethyl-1,4-cyclohexanedione (**8**) giving 3,5-dimethyltriphenylamine (**16**).

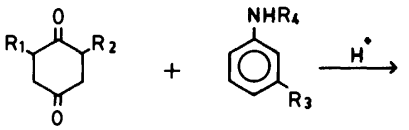

1: $R_1=R_2=H$ **9**: $R_3=H$, $R_4=CH_3$
13: $R_1=H$, $R_2=CH_3$ **11**: $R_3=R_4=CH_3$
8: $R_1=R_2=CH_3$ **14**: $R_3=H$, $R_4=C_6H_5$

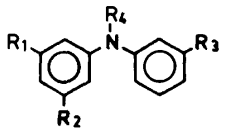

(2)

10: $R_1=R_2=R_3=H$, $R_4=CH_3$
12: $R_1=R_2=H$, $R_3=R_4=CH_3$
15: $R_1=R_2=R_3=H$, $R_4=C_6H_5$
16: $R_1=R_2=CH_3$, $R_3=H$, $R_4=C_6H_5$

These reactions (Eq. 2) show that the 1,4-diones are converted into aniline derivatives, not the product in Eq. 1, and that the amines combine selectively to the carbonyl having no substituent at α-position.

Thus, the effect of the substituent on the starting aniline was examined in order to obtain insight into

TABLE 1. CONDENSATIONS OF 1,4-CYCLOHEXANEDIONE AND *N*-ETHYLANILINES

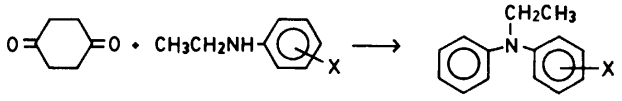

X	Reaction time/h	Product			
		Yield/%	Appearance	NMR(δ, CCl_4)	MS (rel intensity/%)
p-CH_3O	12	50.6	Cryst mp 58—59°C	1.17(3H, t), *ca.* 3.66(2H, q), 3.77(3H, s), 6.50—7.40(9H, m)	227(75)M^+, 212(100)
p-CH_3	12	42.9	Light yellow liquid	1.18(3H, s), 2.29(3H, s), 3.69(2H, q), 6.45—7.25(9H, m)	211(100)M^+, 197(62), 196(70)
m-CH_3	12	38.4	Light yellow liquid	1.20(3H, t), 2.27(3H, s), 3.71(2H, q), 6.45—7.20(9H, m)	211(100)M^+, 196(81)
o-CH_3	12	23.9	Light yellow liquid	1.20(3H, t), 2.10(3H, s), 3.61(2H, q), 6.18—7.20(9H, m)	211(58)M^+ 196(100)
H	12	58.6	Colorless liquid	1.14(3H, t), 3.67(2H, q), 6.65—7.50(10H, m)	197(62)M^+, 182(100)
p-Cl	12	75.7	Colorless liquid	1.18(3H, t), 3.68(2H, q), 6.58—7.30(9H, m)	233(18), 231(56), 216(100)
	35	85.1			
p-NO_2	12	73.1	Red cryst mp 72—73°C	1.25(3H, t), 3.80(2H, q), 6.35—6.70(2H, m), 6.75—7.68(5H, m), 7.80—8.13(2H, m)	242(59)M^+, 227(100)
	35	83.0			

the reaction mechanism. Table 1 shows the results of the condensation of **1** with some substituted *N*-ethylanilines. No definite relationship can be found between the yields of the tertiary amines and the basicity of the starting amines. However, it is worth noting that *p*-nitro and *p*-chloro substitutions lead to good yield. Therefore, **1** was treated in a solution containing *N*-ethylaniline and another aniline, and the products were analyzed by means of gas chromatography. The relative rates on the competing reactions plotted *vs.* Hammet's σ values gave −2.0 as the ρ value, as shown in Fig. 1. The reactivities, hence, decrease with the decrease of the basic strengths of the amines. In addition to Fig. 1, *N*-ethyl-*p*-nitroaniline was found to react very slowly in the competitive reaction with *N*-ethylaniline.

The aromatization of cyclohexane ring was also found on condensation of 4,4-(ethylenedioxy)cyclohexanone (**17**) with secondary aromatic amines. The reaction of **17** with *N*-methylaniline produced *N*-methyl-*N*-phenylaniline and the diacetal **18** of the 1,4-dione.

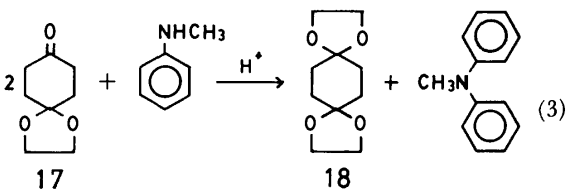

(3)

The formation of **18** shows that an acetal exchange reaction occurred in these conditions. This may produce the 1,4-dione also, which could follow the reaction in Eq. 2, because no monoenamine was obtained even if the amine was used in large excess. On the other hand, the reaction of pyrrolidine with **17** has been reported[3] to produce the corresponding enamine **19**. In an effort to determine the effect of the catalyst, this reaction was further studied, but the same results were obtained regardless of the presence of the acid.

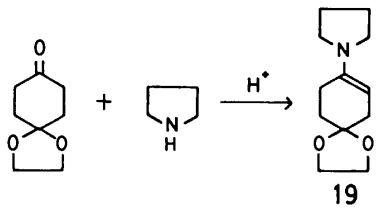

(4)

These results show that the conjugate acid of the aromatic amine is an active catalyst for the acetal-exchange reaction in these conditions but that the conjugate acid of the aliphatic amine has no or very little effect.

In spite of above results, an aromatic amine also produced a phenylenediamine derivative, as suggested in Eq. 1, if the reaction was carried out in the presence of $TiCl_4$. Under these conditions *N*-methylaniline gave *N,N'*-dimethyl-*N,N'*-diphenyl-*p*-phenylenediamine (**20**).

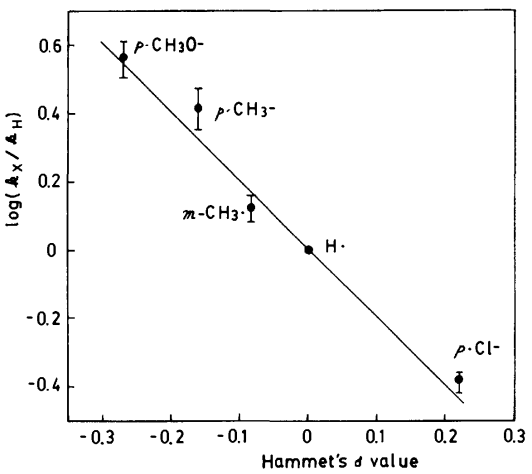

Fig. 1. Relative rates of substituted *N*-ethylanilines on the competitive reactions.

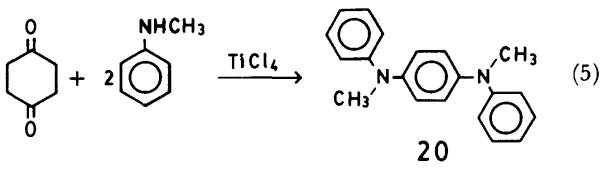

(5)

20

NMR Spectra of the Reaction Mixtures. In order to understand the differences between aromatic amine- and aliphatic amine-condensation processes, the reactions of **1** with some aliphatic or aromatic amine were followed by ^{1}H-NMR spectra of the reaction mixtures in sealed tubes under nitrogen. The spectra of the mixture of **1** and morpholine showed signals at δ 5.01 and at δ 2.13 due to the vinyl protons of the dienediamine **2** and its methylene protons and the vinyl proton of monoenamine **21** at δ 4.21. The signals due to **2** became progressively stronger as the reaction time, while those due to **21** disappeared after 4 h at 120 °C. When the sample was permitted to stand for 1 h in contact with air after the reaction, the signals due to **2** disappeared too and those due to aromatic protons of **3** appeared. ^{1}H-NMR spectra of the mixture of **1** with *N*-methylcyclohexylamime showed also signals due to the vinyl proton of monoenamine **22** at δ 4.22 along with those due to the corresponding dienediamine at δ 5.08.

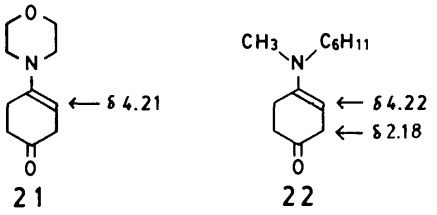

21 22

These facts show that the aliphatic amines reacted stepwise to the carbonyl groups of the 1,4-dione and that the intermediate monoenamines were produced in measurable amounts. On the contrary, ^{1}H-NMR spectra of the reaction mixture of *N*-methylaniline and **1** show the signals due to starting materials and those due to *N*-methyl-*N*-phenylaniline, but no signal ascribable to any intermediate.

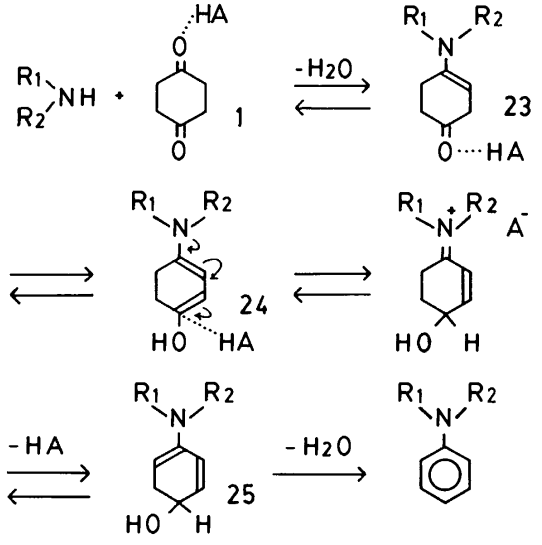

Scheme 2.

Reaction Mechanism. On the basis of the above results, the mechanism shown in Scheme 2 is proposed for the reaction of aromatic amines with the 1,4-dione catalyzed by *p*-toluenesulfonic acid. The key steps in Scheme 2 are the enolization of monoenamine **23** and the protonation to γ-position of 24. These processes and the dehydration of **25** may be fast, because no intermediate was observed by ^{1}H-NMR spectroscopy. An alternate path which involves elimination of an amine from the dienediamine can also be considered (Eq. 6):

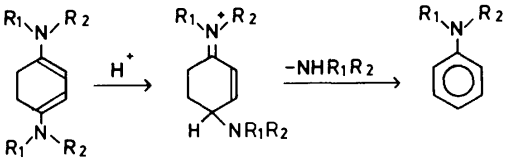

(6)

If the reaction proceeds *via* the dienediamine, the signals of the monoenamine should be observed at least in an early period of the reaction; this is because the reactivity of the residual carbonyl of the monoenamine **23** to the secondary aromatic amine should not be much greater than that of the starting ketone (**1**). Moreover, 2,6-dimethyl-1,4-cyclohexanedione (**8**) is very unlikely to produce any dienediamine because of its steric hindrance: therefore, the formation of **16** in Eq. 2 supports also Scheme 2. The discrepancy between the results of Fig. 1 and Table 1 is discussed below on the basis of the proposed mechanism.

Although there have been a number of examples of enamine formation, the mechanistic studies have been limited to the enamines derived from aliphatic amines. The addition step of aminoalcohol formation has been generally shown[3] to be noncatalytic. However, the addition reaction of weak bases such as semicarbazides or primary aromatic amines to carbonyl compounds is catalyzed by general acid catalysis. Since the addition step of the enamine formation is the same as that of the formation of the carbon nitrogen double bond, the addition of aromatic amines to **1** must occur by the general acid-catalysis. Consequently, essentially every step of the reaction in Scheme 2 is acid-catalyzed. Therefore, it is necessary to take into account not only the nucleophilicity of the amine, but also the acidity of the catalyst for discussion of the reactivity. In practice, the reactions with aromatic amines did not proceed without the acid catalyst. *p*-Toluenesulfonic acid was employed as the catalyst for the all experiments. HA in Scheme 2, then, is the conjugate acid of the amine in the mixture, and its acidity can be assumed to have a reverse tendency to the nucleophilicity of the amine. Therefore the ease of the reaction of the *N*-ethylaniline substituted with an electron-withdrawing group can be interpreted in terms of the increased acidity of its conjugate acid. The facility of the triphenylamine formation in Eq. 2 is also explained by the same reason. As seen in Fig. 1, two competitive reactions in a mixture were catalyzed by the same system, where the main acid was the conjugate acid of the more basic amine. Therefore, only nucleophilicity of the amine contributed to the relative reactivity on competitive reactions.

The fact that the condensation of **1** with aliphatic amines produced dienediamines but no tertiary monoamines is also explained by the same factor. The conjugate acids of aliphatic amines are so weak that the enolization of **23** and the protonation to 4-position of **24** are difficult. On the contrary, the formation of **23** and further addition of the aliphatic amine to the residual carbony of **23** must proceed smoothly, because the aliphatic amines react even without the acid catalyst.

On the other hand, the formation of the dienediamine derived from *N*-methylaniline in Eq. 5 may be due to the fast addition of the amine to the carbonyl activated by $TiCl_4$.

Finally we add a few comments on the present reactions from the viewpoint of organic synthesis. The formation of tertiary amines from secondary aromatic amines with halobenzene requires drastic conditions. Therefore, *N*-phenylation by use of 1,4-cyclohexanedione is worthwhile because of its mild conditions. The conditions in Table 1 are not always the most suitable. For example, increase of the catalyst concentration or of the reaction period lead to good yield of the products. As the solvent, aromatic hydrocarbonds are more favorable than polar ones such as dioxane. The reaction became slower in polar solvents.

Experimental

General. Melting points were uncorrected. ^{1}H-NMR spectra were recorded on a JNM-C-60HL spectrometer with $(CH_3)_4Si$ as an internal standard. IR spectra were taken on a JASCO Model IR-G spectrophotometer. Mass spectra were measured on a Hitachi M-80 mass spectrometer. GLPC analyses were carried out by a Hitachi 163 gas chromatograph using 1-decene or phenanthrene as an internal standard.

Materials. *N*-Ethyl-*p*-chloroaniline was prepared following a method given in "Organic Sytheses"[4]: Yield 60%; bp 89—90 °C / 2 Torr (1 Torr = 133.322 Pa). *N*-Ethyl-*p*-nitroaniline was obtained from *p*-nitroaniline in a similar manner: Yield 48%; mp 96—97 °C. *N*-Ethyl-*p*-anisidine was prepared in three steps involving acetylation of *p*-anisidine, alkylation by use of methyl iodide in the presence of sodium ethoxide, and successive hydration in basic coditions. The total yield was 28%. Found: C, 71.87; H, 8.96; N, 9.05%. Calcd for $C_9H_{13}NO$: C, 71.49; H, 8.67; N, 9.26%. The derivatives of 1,4-cyclohexanedione were all prepared from diethyl 4,4-(ethylenedioxy)pimelate (**26**). The compound **26** was obtained from furfural and malonic acid in three steps according to reported pocedures[5]: Bp 134—136 °C / 0.5 Torr (lit, 134 °C / 0.3 Torr). Ethyl 5,5-ethylenedioxy-2-oxocyclohexanecarboxylate (**27**) was prepared from **26** according to the direction of Gardner[5]: Bp 120 °C / 1 Torr (lit, 114 °C / 0.5 Torr). 4,4-(Ethylenedioxy)cyclohexanone (**17**) was obtained from **27** by hydration in 5% aq KOH for 6 h at room temperature: Yield 80%; mp 70—72 °C (lit,[6] 68—70 °C). Found: C, 61.77; H, 8.01%. Calcd for $C_8H_{12}O_3$: C, 61.52; H, 7.74%. Ethyl 5,5-ethylenedioxy-1-methyl-2-oxocyclohexanecarboxylate (**4**) and 2-methyl-1,4-cyclohexanedione (**13**) were prepared by the method of Narang.[7] Compound **4** was obtained from **26** in 59% yield: mp 71—72 °C (lit, 72 °C). Compound **13** was obtained from **4** in two steps: Yield 60%; mp 47—48 °C (lit, 47 °C). All other reagents were commercially available and were used after purification, if necessary.

2,6-Dimethyl-1,4-cyclohexanedione (8). A mixture of **4** (10 g, 4.13×10^{-2} mol) and sodium ethoxide prepared from 0.95 g (4.13×10^{-2} mol) of sodium was refluxed in ethanol (20 cm^3) for 10 h. Toluene (20 cm^3) was added to the reaction mixture, and then ethanol was gradually distilled off. An additional 20 cm^3 of toluene was added into the residue and the mixture was refluxed for 5 h. Methyl iodide (5.9 g, 4.15×10^{-2} mol) was then added at 0 °C and the mixture was allowed to stand overnight at room temperature. The mixture was refluxed for 2 h, and decomposed with 5% sodium carbonate solution (16 cm^3) and extracted with benzene. The extract was evaporated and the residue was distilled *in vacuo* to afford 6.3 g (60%) of ethyl 1,3-dimethyl-5,5-ethylenedioxy-2-oxocyclohexanecarboxylate (**6**): Bp 125 °C/1 Torr. The product (6.1 g, 2.4×10^{-2} mol) was refluxed with a mixture of 10% aqueous potassium hydroxide (30 cm^3) and ethanol (10 cm^3) for 10 h. The mixture was extracted with ether and evaporated *in vacuo*, giving 3.6 g (82%) of 2,6-dimethyl-4,4-(ethylenedioxy)cyclohexanone (**7**). The crude product (3.5 g, 1.9×10^{-2} mol) was warmed in 3 mol dm^{-3} hydrochloric acid (18 cm^3) at 80 °C for 1 h. Upon cooling to room temperature, a part of the product crystallized out of the solution, and was filtered. The filtrate was extracted with benzene and the extract was evaporated. The residue was combined with the above crystals and was recrystallized from hexane, affording 2.4 g (90%) of 2,6-dimethyl-1,4-cyclohexanedione: Total yield based on **4** is 44%; mp 84—86 °C; IR (KBr) 1707, 1142 and 2800—3000 cm^{-1}; NMR (CCl_4) δ=1.00—1.30 (6H, dd) and 1.80—3.00 (6H, m). Found: C, 68.75; H, 8.95%. Calcd for $C_8H_{12}O_2$: C, 68.55; H, 8.63%.

Condensation of 1,4-Cyclohexanediones and Secondary Aromatic Amines. The general procedure consists of a heating of 1,4-cyclohexanedione (0.5 g, 4.46×10^{-3} mol) with an equivalent of the amine and *p*-toluenesulfonic acid (20 mg) using toluene (30 cm^3) as the solvent in nitrogen atmosphere. The mixture was refluxed for 12 h under a Soxhlet extractor packed with $CaCl_2$ as desiccant, and the solution freed of the solvent *in vacuo*. The product was isolated by column chromatography on sillica gel eluted with hexane. The *N*-ethyl-*N*-phenylanilines obtained are summarized in Table 1. Some other tertiary amines obtained and their properties are presented below.

N-Methyl-*N*-phenylaniline (**10**) was obtained as a light yellow liquid from **1** and *N*-methylaniline in 77.2% yield: NMR (CCl_4) δ=3.25 (3H, s) and 6.63—7.28 (10H, m); MS, *m*/*z* 183 (M$^+$).

N-Methyl-*N*-phenyl-*m*-toluidine (**12**) was obtained as a light yellow liquid in 62.3% yield from **1** and *N*-methyl-*m*-toluidine, or in 61.6% yield from 2-methyl-1,4-cyclohexanedione and *N*-methylaniline: NMR (CCl_4) δ=2.28 (3H, s), 3.28 (3H, s) and 6.53—7.30 (9H, m); IR (neat) 1590, 1490, 750 and 690 cm^{-1}; MS, *m*/*z* 197 (M$^+$).

Triphenylamine (**15**) was obtained as crystals in 88.2% yield from **1** and diphenylamine: Mp 125—126 °C (from hexane).

3,5-Dimethyltriphenylamine (**16**) was obtained as crystals from 2,6-dimethyl-1,4-cyclohexanedione and diphenylamine in 28.9% yield: Mp 130—132 °C (from hexane); NMR (CCl_4) δ=2.20 (6H, s) and 6.45—7.35 (13H, m); IR (KBr disk) 1585, 1490, 755 and 690 cm^{-1}; MS, *m*/*z* 273 (M$^+$).

Competitive Reaction. A mixture of *N*-ethylaniline and another appropriate amine was used in the place of the amine component of the condensation described above. The competitive reaction was followed by gas chromatography every half hour until one of the amines gave 10% conversion. The relative rate (k_x/k_y) in Fig. 1 was determined from the ratios of the two products.

The Condensation of 4,4-(Ethylenedioxy)cyclohexanone (17) with N-Methylaniline. The method used here was virtually identical with that for 1,4-cyclohexanedione, but

the latter was replaced with **17**. *N*-Methylaniline (0.35 g, 3.3×10^{-3} mol) and 0.5 g (3.2×10^{-3} mol) of **17** were refluxed in toluene (30 cm^3) in presence of *p*-toluenesulfonic acid (20 mg). After 30 h, GLPC analysis showed that *N*-methyl-*N*-phenylaniline and diacetal **19** were produced in an approximately equal yield (9%).

Condensation of 17 and Pyrrolidine. The procedure was similar to that of Stork[3] except that 2×10^{-2} equivalent *p*-toluenesulfonic acid to pyrrolidine was added. The pyrrolidine enamine of **17** was produced in 82% yield: Bp 135—137 °C/3 Torr (lit, 110—120 °C/0.1—0.15 Torr); IR 1640, 1115, 1055, and 850 cm^{-1}.

Condensation of 1 and N-Methylaniline in Presence of $TiCl_4$. To a mixture of *N*-methylaniline (5.8 g, 5.42×10^{-3} mol) and **1** (1.0 g, 8.9×10^{-3} mol) in benzene (44 cm^3) a benzene solution (9 cm^3) containing $TiCl_4$ (1.88 g) was added during 20 min at below 10 °C in nitrogen atmosphere with stirring. Then the mixture was stirred for 12 h at room temperature, the precipitate was filtered, and the filtrate was evaporated. The residue was crystallized from ethanol, affording *N,N'*-dimethyl-*N,N'*-diphenyl-*p*-phenylenediamine (0.7 g, 27%) as crystals: Mp 149—150 °C; IR 1590, 1500, 860, and 840 cm^{-1}. Found: *m/z* 288.1614. Calcd for $C_{20}H_{20}N_2$: M, 288.1625.

The authors wish to thank Mr. Katsumasa Iwaya for obtaining some of the NMR spectra and Miss Machiko Nozawa for the preparation of the derivatives of 1,4-cyclohexanedione.

References

1) N. J. Leonard and R. R. Sauers, *J. Org. Chem*, **21**, 1187 (1956).
2) K. Mori and M. Matsui, *Tetrahedron*, **22**, 879 (1966).
3) G. Stork, A. Brizzolara, H. Landesman, J. Szmuszkovicz, and R. Terrell, *J. Am. Chem. Soc.*, **85**, 207 (1963).
4) R. M. Robert and P. J. Vogt, *Org. Synth.*, Coll. Vol. IV, 420 (1963).
5) P. D. Gardner, L. Rand, and G. R. Haynes, *J. Am. Chem. Soc.*, **78**, 3425 (1956).
6) M. Suzuki, *Nippon Kagaku Zasshi*, **82**, 730 (1961).
7) S. A. Narang and P. C. Dutta, *J. Chem. Soc.*, **1960**, 2843.

 © 1984 The Chemical Society of Japan Bull. Chem. Soc. Jpn., 57, 1591—1595 (1984)

Kinetic Study on Hydrolysis of Silicon Phosphate in Aqueous Alkaline Solutions[1)]

Tomoji SAEKI, Eiichi NARITA,* and Hiroyuki NAITO†

Department of Applied Chemistry, Faculty of Engineering, Tohoku University, Aramaki, Sendai 980

†*Mizusawa Factory, Mizusawa Industrial Chemicals, Ltd., Nishime, Tsuruoka 999-75*

(Received October 25, 1983)

Kinetic study of the hydrolysis of silicon phosphate, $Si_3(PO_4)_4$ (hexagonal), was carried out in borax buffer solutions (pH 5—12, temperature 20—50 °C) to investigate how it acts as a hardener for alkali silicate adhesive. The silicon phosphate was found to be hydrolyzed with a resulting release of orthophosphate ion, soluble silicate ions, and colloidal silica under mild conditions; the decomposition rate increased with decreasing the particle size of the phosphate and with increasing the pH and temperature of the buffer solution. From the analysis of the decomposition rate on the basis of the shrinking core model, it was found that the decomposition rate could be adequately expressed by the rate equation based on the mixed control of diffusion through a residual layer and surface chemical reaction. This indicates that a part of the colloidal silica which resulted from the hydrolysis remains on the surface of the silicon phosphate particle and then partially limits the overall rate of the hydrolysis. The dependence of both rate-determining steps for the decomposition rate was quantitatively indicated according to the reaction conditions.

Because of the advantages of being heat-stable, incombustible, and solvent-resistant, inorganic adhesives are increasingly being used in many fields. A silicate adhesive using alkali silicate solution (generally referred to as "water glass") as a binder is most widely utilized.[2,3)] However, it still has some weak points; for instance, the hardened silicate materials at room temperature show water sensitivity. Since the adhesive properties of the hardened silicate materials are known to be predominantly dependent on the kind of hardeners used, a number of substances such as metal powders, oxides, hydroxides, mineral acids, borates, and phosphates are now being employed.[4,5)] However, no hardener having excellent properties, especially sufficient water resistance, has yet been obtained.

The present authors[1)] have prepared silicon phosphates such as $Si_3(PO_4)_4$ and SiP_2O_7 by calcination of silica gel impregnated with a small amount of phosphoric acid at temperatures up to 1000 °C and have shown that they can be used as a satisfactory hardener for silicate adhesives. The most important feature was that these phosphates with silicate adhesives showed excellent water resistance even without heat-treatment. Although the synthesis of silicon phosphates in a large excess of phosphoric acid has been done by earlier workers,[6,7)] no information is at present available on these chemical properties. Therefore, to investigate the mechanism of the enhancement in the water insensitivity by using silicon phosphates, an understanding of the hydrolysis behavior of silicon phosphates is desirable.

In this study, the kinetics of the hydrolysis of pure silicon phosphate ($Si_3(PO_4)_4$) in aqueous alkaline solutions was investigated in detail. As a model solution, borax buffer solution having the desired pH value was used here.

Experimental

Materials. In the preparation of $Si_3(PO_4)_4$, analytical reagent grade orthophosphoric acid (P_2O_5: 63%) and commercial silica gel for chromatography (200—300 mesh) were used. A buffer solution was prepared using analytical reagent grade sodium tetraborate decahydrate and sodium hydroxide. The pH of the buffer solution was adjusted to the desired value by mixing 0.2 mol dm^{-3} $Na_2B_4O_7$ with 1.0 mol dm^{-3} NaOH.

Preparation of $Si_3(PO_4)_4$.[6)] First, 17.5 g of orthophosphoric acid was transferred to a 30 cm^3 platinum crucible and heated for 30 min at 150 °C. Subsequently, 1.0 g of dried silica gel (P_2O_5/SiO_2 molar ratio: 5.0) was added to the crucible, which was then heated again for 5 h at 220—230 °C. After cooling, the suspension was centrifuged, and the resulting white powder was washed repeatedly with ethanol to remove adsorbed acid and then dried over P_2O_5 under reduced pressure. Since $Si_3(PO_4)_4$ is hygroscopic, it was well-dried before being used for the hydrolysis experiment. Although the spontaneous particle size of $Si_3(PO_4)_4$ was different in all runs, uniform-sized particles were obtained for each run. In this investigation, four different-sized $Si_3(PO_4)_4$ (hexagonal)[8)] were used without further pulverization. As

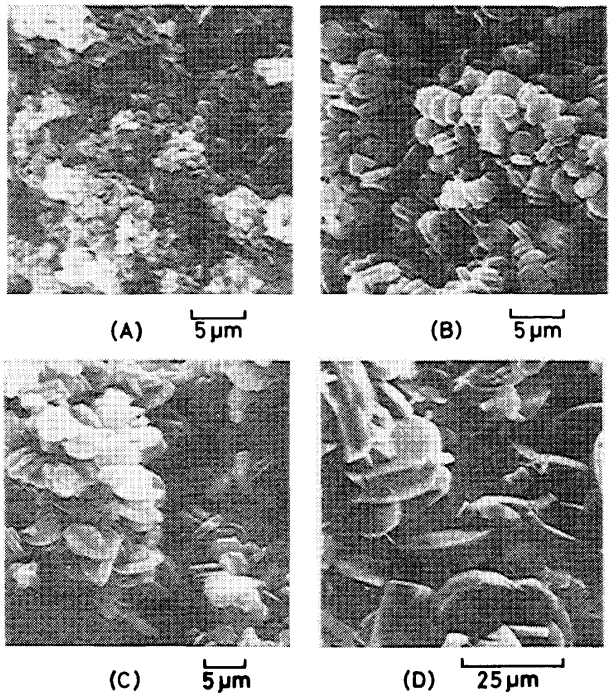

Fig. 1. Scanning electron micrographs of silicon phosphate ($Si_3(PO_4)_4$) used in this experiment.
Mean particle diameter (μm) —— A: 1.0, B: 2.2, C: 3.7, D: 22.6.

can be seen in Fig. 1, these phosphate particles were all disk-shaped. No differences in their crystal forms and chemical compositions were observed. The particle size was measured using a scanning electron microscope (Hitachi-Akashi MSM 4C-102) and the cylindrical shape equivalent diameter[9] was used as the mean particle size. The chemical composition was: Found: SiO_2, 36.6±3.2, P_2O_5, 59.5±1.9; Calcd for $Si_3(PO_4)_4$: SiO_2, 38.8, P_2O_5, 61.2%.

Measurement of Hydrolysis Rate. As the first step, 200 cm^3 of the buffer solution was transferred to a 300 cm^3 three-necked flask equipped with a mechanical stirrer (crescent shaped impeller, 60 mm×20 mm), a reflux condenser, and a thermometer and maintained at 20—50 °C. Then, a weighed amount of $Si_3(PO_4)_4$ was suspended in the buffer solution with vigorous agitation. The decomposition rate of $Si_3(PO_4)_4$ was determined by pipetting about 3 cm^3 of the suspension from the flask as regular time intervals, filtering out the insoluble residues, and chemically analyzing the supernatant solution for orthophosphate ion by colorimetric method.[10] In all experiments, no changes in the pH of the buffer solution were observed from before to after the hydrolysis.

Results and Discussion

Effect of Amount of $Si_3(PO_4)_4$ Added. Figure 2 shows the effect of changes in the amount of $Si_3(PO_4)_4$ on the decomposition rate of $Si_3(PO_4)_4$ conducted in the buffer solution of pH 11.0 at 30 °C with a stirring speed of 300 min^{-1}. The particle size of $Si_3(PO_4)_4$ used was 2.2 μm. Since the maximum difference in the percentage decomposition was only 4%, it cannot be said that there is any effect of amount of $Si_3(PO_4)_4$ under the conditions tested.

Effect of Stirring Speed. Figure 3 shows the effect of stirring speed on the decomposition rate of $Si_3(PO_4)_4$ under the same conditions as those conducted above. 0.2 g of $Si_3(PO_4)_4$ was used here. The decomposition rate was maximum at 300 min^{-1} and slightly decreased at 200 and 400 min^{-1}. When different-sized $Si_3(PO_4)_4$ were tested, the effect of stirring speed was also hardly observed under stirring speeds of 200—300 min^{-1}.

Effect of Particle Size. The decomposition rate was determined using 0.4 g of four different-sized $Si_3(PO_4)_4$, shown in Fig. 1, under the same conditions as those employed above. The result is given in Fig. 4. The decomposition rate obviously increased with de-

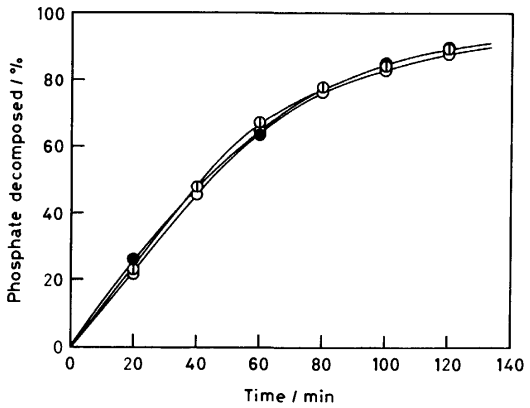

Fig. 2. Effect of amount of silicon phosphate on the decomposition rate of silicon phosphate in aqueous alkaline solution.
Particle diameter: 2.2 μm, pH: 11.0, temperature: 30 °C, stirring speed: 300 min^{-1}, amount of silicon phosphate added (g)—— ●: 0.1, ○: 0.2, ⊕: 0.4.

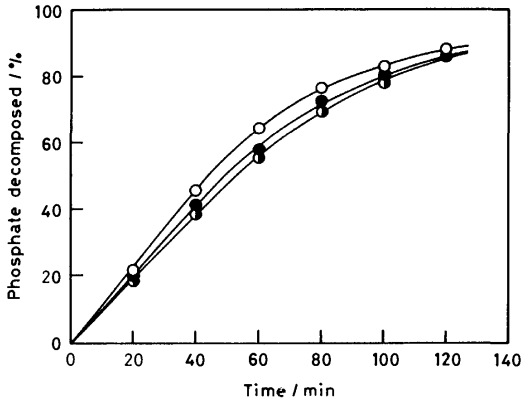

Fig. 3. Effect of stirring speed on the decomposition rate of silicon phosphate in aqueous alkaline solution.
Amount of silicon phosphate added: 0.2 g, particle diameter: 2.2 μm, pH: 11.0, temperature: 30 °C, stirring speed (min^{-1}) —— ●: 200, ○: 300, ◑: 400.

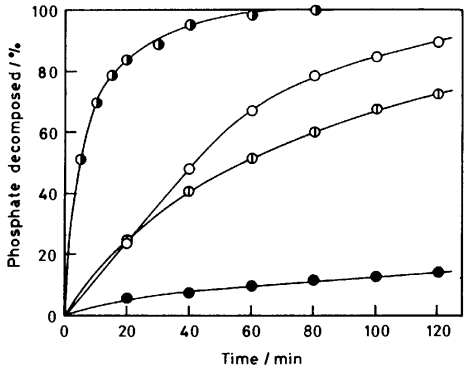

Fig. 4. Effect of phosphate particle diameter on the decomposition rate of silicon phosphate in aqueous alkaline solution.
Amount of silicon phosphate added: 0.4 g, pH: 11.0, temperature: 30 °C, stirring speed: 300 min^{-1}, particle diameter (μm) —— ◑: 1.0, ○: 2.2, ⊕: 3.7, ●: 22.6.

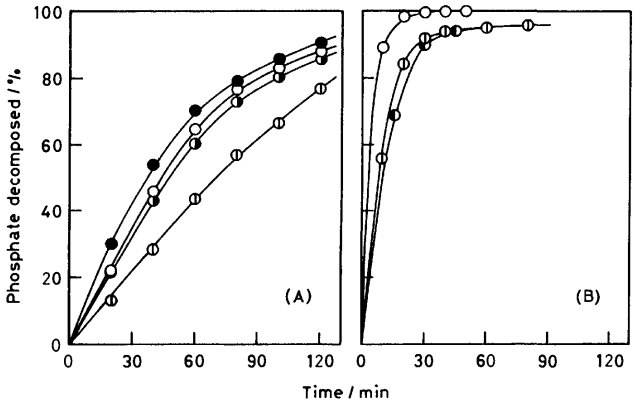

Fig. 5. Effect of pH on the decomposition rate of silicon phosphate in aqueous alkaline solution.
Amount of silicon phosphate added: 0.2 g, particle diameter: 2.2 μm, temperature: (A) 30 °C (B) 50 °C, stirring speed: 300 min^{-1}, pH —— ◐: 5.0, ⊕: 8.0, ◑: 9.5, ○: 11.0, ●: 12.0.

creasing particle size. The relationship between particle size and decomposition rate will be quantitatively discussed later.

On the basis of the data, subsequent experiments were carried out under the following conditions; particle diameter of $Si_3(PO_4)_4$, 2.2 μm; amount of $Si_3(PO_4)_4$, 0.2 g; stirring speed, 300 min^{-1}.

Effect of pH. Figure 5 shows the effect of pH on the decomposition rate of $Si_3(PO_4)_4$ at 30 °C (A) and 50 °C (B). At both temperatures, the decomposition rate increased with increasing the pH, although its effect was not so appreciable. In the experiments at 50 °C, more than 90% of the total quantity of $Si_3(PO_4)_4$ was hydrolyzed at all pH values tested.

Effect of Temperature. Fiure 6 shows the effect of temperature on the decomposition rate of $Si_3(PO_4)_4$ at pH 8.0 (A) and 11.0 (B). At both pH values, the temperature affected predominantly the decomposition rate, which increased significantly with increasing temperature.

Analysis of Hydrolysis Rate. The electron micrographs of the insoluble residues obtained from the suspensions after the decomposition of 30% and 70% of $Si_3(PO_4)_4$ are shown in Fig. 7. It was observed that the particles shrunk with progress of the hydrolysis. The profile of the residue was quite similar: the same percentage decomposition and independence of

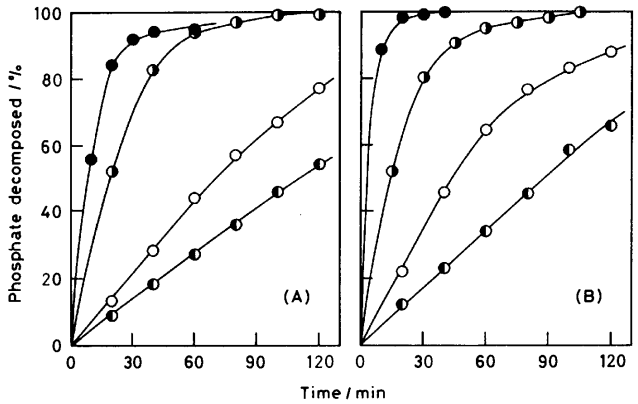

Fig. 6. Effect of temperature on the decomposition rate of silicon phosphate in aqueous alkaline solution.
Amount of silicon phosphate added: 0.2 g, particle diameter: 2.2 μm, pH: (A) 8.0, (B) 11.0, stirring speed: 300 min^{-1}, temperature (°C) —— ◐: 20, ○: 30, ◑: 40, ●: 50.

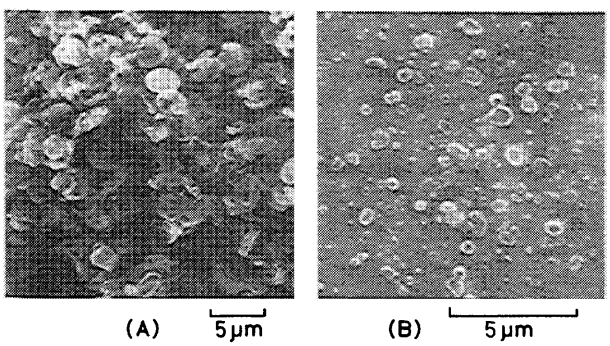

Fig. 7. Scanning electron micrographs of the decomposition residues.
Percentage decomposition (%) —— A; 30, B; 70.

the reaction conditions were found. The colloidal silica was gradually suspended in the buffer solution during the hydrolysis. According to Alexander *et al.*,[11] the solubility of the different forms of amorphous silica in water is 0.011—0.015 wt% at pH 6—9 and 25 °C, and increases to 0.2—0.4 wt% at pH 11. It also increases with a rise in temperature, but its effect is not appreciable compared to that of pH. Since the buffer solution used here contains a large amount of borate, the resulting silicate species should be present mainly as colloidal silica in it. Although the colorimetric determination of soluble silicate ion using ammonium molybdate was not so exact because of the coexistence of phosphate ion, the formation of the soluble silicate ion was identified in the buffer solution. From the results reported by Busey *et al.*,[12] the soluble silicate ions were thought to be $SiO(OH)_3^-$ and $Si(OH)_4$. Paper chromatography[13] also revealed that the phosphate ions in the buffer solution which originated from $Si_3(PO_4)_4$ were all orthophosphate ions, PO_4^{3-}. Thus $Si_3(PO_4)_4$ reacts with H_2O or OH^-, and decomposes in aqueous alkaline solution, which leads to the release of orthophosphate ion, soluble silicate ions, and colloidal silica.

Therefore, the hydrolysis reaction of $Si_3(PO_4)_4$ in aqueous alkaline solution is written as:

$$Si_3(PO_4)_4 + 6H_2O = 3SiO_2(\text{soluble and colloidal}) + 4PO_4^{3-} + 12H^+. \quad (1)$$

The decomposition rates of $Si_3(PO_4)_4$ were analyzed on the basis of the shrinking core model under the assumption that the phosphate particles form a homogeneous spherical solid phase.

The reaction in Eq. 1 can be represented simply as Eq. 2:

$$A(l) + \sigma S(s) \longrightarrow P(l). \quad (2)$$

When the reaction percentage of component P was represented as x and the steady state of the reaction was assumed, the following Eq. 3 was obtained as the rate equation:

$$\frac{dx}{dt} = \frac{3C_A V}{r_0} = \frac{1}{\frac{1}{k_L} + \frac{\sigma r_0}{D_e}\{(1-x)^{-1/3} - 1\} + \frac{1}{k_C}(1-x)^{-2/3}}. \quad (3)$$

Three rate-determining steps were studied: The diffusion in liquid film, the diffusion in residual layer, and the surface chemical reaction.[14] However, the diffusion in liquid film should not be the rate-determining step because the decomposition rate of $Si_3(PO_4)_4$ was not affected by the stirring speed but was significantly influenced by temperature, as described previously. Therefore, the following two equations were obtained for each rate-determining step by integration of Eq. 3:

i) For diffusion in residual layer (k_L, $k_C \gg D_e/r_o$)

$$1 - \frac{2}{3}x - (1-x)^{2/3} = \frac{2C_A D_e V}{\sigma r_0^2} t, \quad (4)$$

ii) For surface chemical reaction (k_L, $D_e/r_o \gg k_C$)

$$1 - (1-x)^{1/3} = \frac{C_A k_C V}{r_0} t, \quad (5)$$

In the first place, the results for the hydrolysis of $Si_3(PO_4)_4$ shown in Figs. 4 and 5 were replotted according to the rate equations shown in Eqs. 4 and 5. However, it was found that neither rate equation could express the decomposition rates satisfactorily. In general, the rate of heterogeneous reaction of a solid-liquid system is often dependent on both the rate of diffusion through residual layer and the surface chemical reaction. According to Habashi[15] and Sohn *et al.*,[16] a mixed control rate equation can be derived by combining the diffusion and chemically controlled expressions as shown in Eq. 6:

iii) For mixed control ($k_L \gg D_e/r_o$, k_C)

$$[1 - \frac{2}{3}x - (1-x)^{2/3}] + \beta[1-(1-x)^{1/3}] = kt, \quad (6)$$

where

$$\beta = \frac{2D_e}{k_C \sigma r_0},$$

$$k = \frac{2C_A D_e V}{\sigma r_0^2}.$$

The results for the hydrolysis of $Si_3(PO_4)_4$ shown in Figs. 4 and 5 are replotted according to Eq. 6 as Fig. 8. A good linear dependence of $[1-2/3x-(1-x)^{2/3}]+\beta[1-(1-x)^{1/3}]$ on time was obtained. The values of β and k used for replotting Fig. 8 were conveniently given by the slope and intercept of the straight line drawn between $[1-2/3x-(1-x)^{2/3}/t]$ and $[1-(1-x)^{1/3}/t]$ at constant temperature.[17] The values for the constants β and k for the four different-sized particles used are given in Table 1. If Eq. 6 describes the reaction conversion adequately, then the ratio of the values of k for two essentially monosized fractions should be equal to the square of the ratio of the radii. The comparison is shown as Table 2. Agreement between the expected results and those actually obtained is observed, and hence the suggestion that the hydrolysis of $Si_3(PO_4)_4$ is under mixed diffusion through residual layer and chemical reaction control is reasonable. A part of the resulting colloidal silica remains on the surface of $Si_3(PO_4)_4$ and the diffusion of the reactant through the silica layer partially controls the overall rate of the hydrolysis.

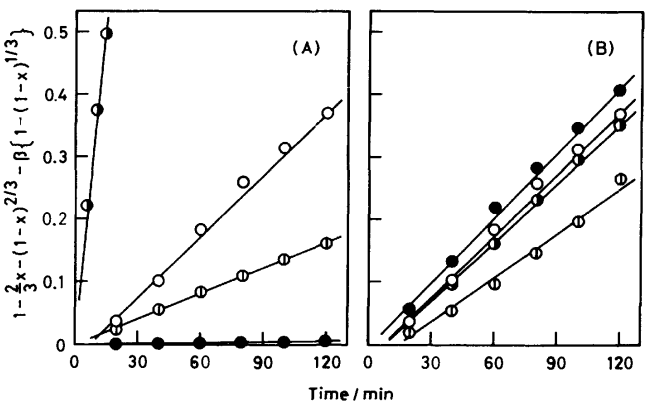

Fig. 8. Plots of decomposition data according to shrinking core model with mixed surface chemical and diffusional kinetics.
(A) Effect of phosphate particle diameter (Fig. 4), (B) Effect of pH (Fig. 5-A) (Symbols are the same as those in each Fig.).

The values for the constants β and k for various pH values and temperatures are summarized in Table 3. The value of k increased with increasing pH. On the other hand, at constant pH the value of β decreased

Table 1. Values of constants in Eq 6 for the decomposition of silicon phosphate in aqueous alkaline solution

Mean particle diameter[a] / μm	β	k / min^{-1}
1.0	0.9	1.6×10^{-2}
2.2	0.4	3.4×10^{-3}
3.7	0.2	1.4×10^{-3}
22.6	0.04	3.2×10^{-5}

a) Since the phosphate particle was disk-shaped, its diameter, d, could be calculated as follows: $d=(f\cdot h)^{1/3}$, where $f=\pi d'^2$.[9]

Table 2. Testing of Eq 6 using data from Table 1

Particle diameters used / μm		Ratio	Ratio
d_i	d_j	k_i/k_j	$(d_j/d_i)^2$
1.0	2.2	4.7	4.8
1.0	3.7	11.4	13.7
1.0	22.6	500	511
2.2	3.7	2.4	2.8
2.2	22.6	106	106
3.7	22.6	43.8	37.3

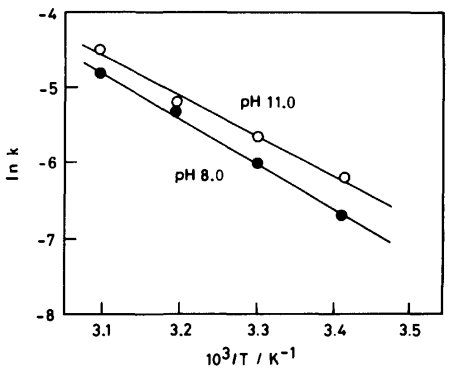

Fig. 9. Arrhenius plots for the decomposition rate of silicon phosphate in aqueous alkaline solution.
pH —— ●: 8.0, ○: 11.0.

Table 3. Values of constants in Eq. 6 and Arrhenius activation energy

pH	Temperature / °C								E_a / kJ mol^{-1}
	20		30		40		50		
	β	k / min^{-1}	β	k / min^{-1}	β	k / min^{-1}	β	k / min^{-1}	
8.0	0.5	5.7×10^{-4}	0.4	2.5×10^{-3}	0.05	4.9×10^{-3}	0.01	7.9×10^{-3}	48.8
9.5	—	—	0.4	3.2×10^{-3}	—	—	0.01	7.9×10^{-3}	—
11.0	0.5	2.0×10^{-3}	0.4	3.4×10^{-3}	0.05	5.5×10^{-3}	0.01	1.1×10^{-2}	42.7
12.0	—	—	0.4	3.5×10^{-3}	—	—	—	—	—

with increasing temperature, whereas the value of k increased. The decrease in the value of β means that the contribution of the surface chemical reaction to the overall rate of the decomposition becomes smaller. The unusual behavior, that the value of β decreased with increasing temperature in spite of the increase in silica solubility, can be explained by the relative increase of the rate of the chemical reaction.

The Arrhenius plots for the data of pH 8.0 and 11.0 are given in Fig. 9. The dependence of ln k on temperature was approximately the same at both pHs. The apparent activation energies calculated from the Arrhenius plots were 48.8 and 42.7 kJ mol^{-1} at ph 8.0 and 11.0, respectively; these are reasonable values for the mixed control reaction.

The authors wish to thank Prof. Taijiro Okabe and Dr. Tsugio Sato of the Department of Applied Chemistry, Tohoku University, for their helpful discussions and Mr. Kazuhiro Sango of Mizusawa Industrial Chemicals, Ltd. for his experimental assistance.

Nomenclature

C_A=Bulk reactant concentration (mol cm^{-3}).
D_e=Effective diffusivity of reactant through the product layer (cm^2 min^{-1}).
d=Mean particle diameter (μm).
d'=Diameter of disk-shaped particle (μm).
h=Height of disk-shaped particle (μm).
k=Overall reaction rate constant (min^{-1}).
k_C=Surface chemical reaction rate constant (cm min^{-1}).
k_L=Mass transfer coefficient (cm min^{-1}).
r_o=Initial particle radius (cm).
t=Reaction time (min).
V=Molar volume of solid reactant (cm^3 mol^{-1}).
x=Fractional conversion (−).
β=Coefficient indicating surface chemical contribution to overall rate (−).
σ=Stoichiometry factor (−).

References

1) Studies on the Preparation and Utilization of Silicon Phosphates, Part II. Part I: K. Sango, S. Sato, H. Naito, T. Saeki, T. Matsushita, and E. Narita, *Ind. Eng. Chem. Prod. Res. Dev.*, in press.
2) J. G. Vail, "Soluble Silicates, Their Properties and Uses," Reinhold Publishing Corp., New York (1952).
3) "Soluble Silicates," ed by J. S. Falcone, Jr., ACS Symposium Series 194, Am. Chem. Soc., Washington, D.C. (1982).
4) K. Kimura and A. Motegi, *Nippon Setchaku Kyokaishi*, **12**, 394 (1976).
5) K. Kimura and A. Motegi, *Nippon Setchaku Kyokaishi*, **18**, 116 (1982).
6) H. Makart, *Helv. Chim. Acta*, **50**, 399 (1967).
7) F. Liebau, G. Bissert, and N. Köppen, *Z. Anong. Allg. Chem.*, **359**, 113 (1968).
8) X-Ray powder data file (ASTM card 22-1380).
9) K. Kubo, E. Suito, Y. Nakagawa, and S. Hayakawa, "Funtai," Maruzen, Tokyo (1962), p. 75.
10) C. J. Barton, *Anal. Chem.*, **20**, 1068 (1948).
11) G. B. Alexander, W. M. Heston, and R. K. Iler, *J. Phys. Chem.*, **58**, 453 (1954).
12) R. H. Busey and R. E. Mesmer, *Inorg. Chem.*, **16**, 2444 (1977).
13) E. Karl-Kroupa, *Anal. Chem.*, **28**, 1091 (1956).
14) S. Yagi and D. Kunii, *Kagaku Kikai*, **16**, 283 (1952); *Kogyo Kagaku Zasshi*, **56**, 131 (1953).
15) F. Habashi, "Principles of Extractive Metallurgy," Gordon and Breach, New York (1969), p. 153.
16) H. Y. Sohn and M. E. Wadsworth, "Rate Processes of Extractive Metallurgy," Plenum Press, New York (1979), p. 182.
17) S. L. Pohlman and F. A. Olson, "Solution Mining Symposium," AIME Soc. Min. Eng. (1974), p. 446.

Stereoselective Formation of Rotaxanes Composed of Polymethylene-bridged Dinuclear Cobalt(III) Complexes and α-Cyclodextrin. II[1]

Kazuaki YAMANARI* and Yoichi SHIMURA
Department of Chemistry, Faculty of Science, Osaka University, Toyonaka, Osaka 560
(Received December 5, 1983)

[2]-[[(en)$_2$Co{XCH$_2$S(CH$_2$)$_n$SCH$_2$Y}Co(en)$_2$]Cl$_m$]-[α-CDX]-rotaxanes (n=8, 10, and 12 for X=Y=CO$_2^-$ (m=4); n=10 for X=CO$_2^-$ and Y=CH$_2$NH$_2$(m=5); α-CDX=α-cyclodextrin) were prepared with partial stereoselectivity and characterized from their visible-UV absorption, circular dichroism(CD), and ^{13}C NMR spectra, and elemental analysis. The rotaxane formation could be identified by the down field shift of the chemical shift due to α-CDX in the ^{13}C NMR spectra and the increase of the CD intensity in the ligand-to-metal charge transfer band region in the CD spectra. The rotaxanes always showed apparently *ΔΔ*-rich CD spectra, the highest selectivity(10% *ΔΔ*-rich) being found in the case of n=10.

α-Cyclodextrin (CDX) has the hydrophobic cavity and is an excellent host molecule for a great variety of guest molecules.[2] Using this inclusion property of CDX, Ogino first prepared the novel cobalt(III) rotaxane complexes.[3] We recently prepared similar rotaxanes consisting of a dinuclear cobalt(III) complex [(en)$_2$Co{NH$_2$(CH$_2$)$_2$S(CH$_2$)$_n$S(CH$_2$)$_2$NH$_2$}Co(en)$_2$]$^{6+}$ (n=8, 10, and 12) and α- or β-CDX starting from a mononuclear thiolato complex [Co(aet)(en)$_2$]$^{2+}$ (Haet =2-aminoethanethiol, NH$_2$CH$_2$CH$_2$SH).[1] Interestingly, the rotaxanes showed the partial stereoselectivity, which led to the relatively higher yield of *ΔΔ*-rotaxanes as compared with that of *ΛΛ*-rotaxanes.

In this paper, another thiolato complex [Co(maa)-(en)$_2$]$^+$ (H$_2$maa=mercaptoacetic acid, HSCH$_2$CO$_2$H) was used as a starting material for the synthesis of [2]-[[(en)$_2$Co{XCH$_2$S(CH$_2$)$_n$SCH$_2$Y}Co(en)$_2$]Cl$_m$]-[α-CDX].[4] As shown in Fig. 1, the preparation was carried out for the two kinds of rotaxanes: X=Y=CO$_2^-$ (m=4), and X=CO$_2^-$ and Y=CH$_2$NH$_2$(m=5). The bridging quadridentate ligands are abbreviated to dtda for n=8 (X=Y=CO$_2^-$): 3,12-dithiatetradecanedioic acid; dhda for n=10 (X=Y=CO$_2^-$): 3,14-dithiahexadecanedioic acid; doda for n=12 (X=Y=CO$_2^-$): 3,16-dithiaoctadecanedioic acid; and adha for n=10 (X=CO$_2^-$ and Y=CH$_2$NH$_2$): 16-amino-3,14-dithiahexadecanoic acid. The cobalt(III) rotaxanes and the bridged complexes (=dinuclear complexes without α-CDX) were characterized from the elemental analysis, absorption, circular dichroism(CD) and ^{13}C NMR spectra. The optically active *ΔΔ*- and *ΛΛ*-rotaxanes were also prepared starting from the resolved mononuclear complexes.

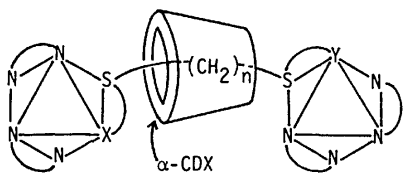

[2]-[[(en)$_2$Co{XCH$_2$S(CH$_2$)$_n$SCH$_2$Y}-Co(en)$_2$]Cl$_m$]-[α-CDX]-rotaxane

abbr.	n	X	Y	m
dtda	8	CO$_2^-$	CO$_2^-$	4
dhda	10	CO$_2^-$	CO$_2^-$	4
doda	12	CO$_2^-$	CO$_2^-$	4
adha	10	CO$_2^-$	CH$_2$NH$_2$	5

Fig. 1. The rotaxanes prepared and abbreviations of the bridging quadridentate ligands.

Experimental

Preparation and Separation of Complexes. rac-, Δ'-, *and* Λ'-*[Co(aet)(en)$_2$]ClO$_4$*:[5] This complex was prepared and optically resolved according to the published procedure.[6]

rac-, Δ- *and* Λ-*[Co(maa)(en)$_2$]ClO$_4$*: The racemate was prepared according to the literature[6] and used as a starting material. The perchlorate salt was converted into the chloride by the use of QAE-Sephadex A-25 (Cl$^-$ form).

Optical resolution of this complex was attempted using resolving agents such as K$_2$[Sb$_2$(*d*-tart)$_2$]·3H$_2$O, Ag(*d*-H$_3$tart), NH$_4$(*d*-BCS), K[Co(edta)]·2H$_2$O, and Na(*d*-HDBT) (abbrev: *d*-H$_3$tart$^-$=hydrogen (*R*,*R*)-tartrate(1−), *d*-BCS$^-$=(1*R*,3*S*,-4*S*,7*R*)-3-bromocamphor-9-sulfonate, edta^{4-}=ethylenediaminetetraacetate (4−), and *d*-HDBT$^-$=hydrogen (*R*,*R*)-di-*O*-benzoyltartrate(1−)), only the last resolving agent leading to the successful result. The racemic complex [Co(maa)(en)$_2$]Cl (10.6 g, 35 mmol) was dissolved in 150 cm^3 of water. To this solution was added dropwise a solution of Na(*d*-HDBT) (19 mmol), which was previously prepared from 7.2 g of *d*-H$_2$DBT and 0.7 g of NaOH in 200 cm^3 of water at 50 °C. The mixture was allowed to stand at room temperature for overnight with stirring. The less soluble diastereomer $(-)^{CD}_{543}$-[Co(maa)(en)$_2$](*d*-HDBT) was filtered off and washed with water and then ethanol. The filtrate was later used for gaining $(+)^{CD}_{543}$-antipode. The excess of QAE-Sephadex A-25 (Cl$^-$ form) resin was added to a suspension of the diastereomer, and the mixture was stirred for 1 h. The resultant dark violet solution was collected by filtration and 6 g of NaClO$_4$ was added to it to yield the crystals of $(-)^{CD}_{543}$-[Co(maa)(en)$_2$]ClO$_4$. This was recrystallized by dissolving in a minimum amount of water, adding NaClO$_4$, and filtering. The yield was 3 g. $\Delta\varepsilon^{CD}_{543}$=−2.32. Found: C, 19.49; H, 4.93; N, 15.29%. Calcd for *Δ*-[Co(maa)(en)$_2$]ClO$_4$=C$_6$H$_{18}$N$_4$SO$_6$ClCo: C, 19.55; H, 4.92; N, 15.20%. The initial filtrate was condensed to *ca.* 130 cm^3 by rotaevaporation at 30 °C and 2 g of NaClO$_4$ was added to it. The first crystals deposited (2.5 g) were almost racemate and removed by filtration. Further addition of NaClO$_4$ (*ca.* 4 g) gave the desired $(+)^{CD}_{543}$-[Co(maa)(en)$_2$]ClO$_4$. The yield was 3.5 g. $\Delta\varepsilon^{CD}_{543}$=+2.32. Found: C, 19.55; H, 4.89; N, 15.19%. Calcd for *Δ*-[Co(maa)(en)$_2$]ClO$_4$=C$_6$H$_{18}$N$_4$SO$_6$ClCo: C, 19.55; H,4.92; N, 15.20%.

Δ- *and* Λ-*[Co{O$_2$CCH$_2$S(CH$_2$)$_{10}$Br}(en)$_2$]ClO$_4$)Br.* To 12 cm^3 of DMSO (dimethyl sulfoxide) solution containing *Δ*- or *Λ*-[Co(maa)(en)$_2$]ClO$_4$(2 g) was added 3.25 g of 1,10-dibromodecane, and then the mixture was kept at 30 °C for 2 d. The unreactive 1,10-dibromodecane was removed by extraction with diethyl ether for several times. To the resultant dark

red oil was added *ca.* 20 cm^3 of water. The precipitate of the desired product appeared immediately and then was filtered off and washed with water, ethanol, and diethyl ether. This complex was sparingly soluble in water but very soluble in DMSO, and used as a starting material for the preparation of adha rotaxanes described later. Found for the *Δ*-complex: C, 28.99; H, 5.85; N, 8.05%. Found for *Λ*-complex: C, 28.80; H, 5.85; N, 8.05%. Calcd for $[Co\{O_2CCH_2S(CH_2)_{10}Br\}(en)_2](ClO_4)Br=C_{16}H_{38}N_4SO_6ClBrCo$: C, 28.74; H, 5.73; N, 8.38%.

*[2]-[[(en)₂Co(dtda)Co(en)₂]Cl₄]-[α-CDX]-rotaxane (**R1**) and [(en)₂Co(dtda)Co(en)₂]Cl₄ (**B1**).* The starting materials of *rac*-$[Co(maa)(en)_2]ClO_4$ (1.4 mmol) and 1,8-dibromooctane (0.84 mmol, 20% excess) were dissolved in 4 cm^3 of DMSO containing 1.25 g of *α*-CDX. The mixture was kept at 30 °C for 7 d, leading to the red solution. The unreactive dibromooctane was extracted into diethyl ether. The resultant red oil was dissolved in water, adsorbed onto a cation exchange column (SP-Sephadex C-25, Na^+ form) and eluted with 0.3 mol dm^{-3} NaCl. Six colored bands, f1—f6, were eluted in this order. The species f2(dark violet), f4(red), f5(red), and f6(red) were assigned to $[Co(maa)(en)_2]^+$, $[Co\{O_2CCH_2S(CH_2)_8Br\}(en)_2]^{2+}$, [2]-$[(en)_2Co(dtda)Co(en)_2]^{4+}$-[*α*-CDX]-rotaxane, and $[(en)_2Co(dtda)Co(en)_2]^{4+}$, respectively. The other red bands f1 and f3 were remained unknown. The eluate from the red band f6 was evaporated to a small volume. After repeated removal of NaCl deposited out, a large amount of ethanol was added to it. The resultant solution was refrigerated for 2—3 d at −15 °C. The supernatant solution was discarded, and then the precipitate was washed with ethanol several times and filtered off. Found for **B1**; C, 29.41; H, 7.09; N, 12.39%. Calcd for $[(en)_2Co(dtda)Co(en)_2]Cl_4\cdot C_2H_5OH\cdot 3.5H_2O=C_{22}H_{65}N_8S_2O_{8.5}Cl_4Co_2$: C, 29.31; H, 7.27; N, 12.43%. The rotaxane **R1** was not isolated as a solid but the yield was 3.3±0.5% (the mean for 2 preparations). The band of the rotaxane showed apparently *ΔΔ*-rich CD spectra (*ca.* 2% rich).[6]

*[2]-[ΔΔ-[(en)₂Co(dtda)Co(en)₂]Cl₄]-[α-CDX]-rotaxane (**R2**) and ΔΔ-[(en)₂Co(dtda)Co(en)₂]Cl₄ (**B2**):* These complexes were prepared and chromatographed by the same procedure as **R1** and **B1** except for the use of *Δ*-$[Co(maa)(en)_2]ClO_4$ instead of the racemate. The yield was 2.5±0.5% for **R2** and 60±5% for **B2**. Found for **R2**; C, 34.07; H, 6.73; N, 5.76%. Calcd for [2]-[*ΔΔ*-$[(en)_2Co(dtda)Co(en)_2]Cl_4$]-[*α*-CDX]-rotaxane·$11H_2O=C_{56}H_{134}N_8S_2O_{45}Cl_4Co_2$: C, 34.26; H, 6.88; N, 5.71%. Found for **B2**; C, 26.90; H, 7.01; N, 12.32%. Calcd for *ΔΔ*-$[(en)_2Co(dtda)Co(en)_2]Cl_4\cdot 0.2C_2H_5OH\cdot 6H_2O=C_{20.4}H_{65.2}N_8S_2O_{10.2}Cl_4Co_2$: C, 26.93; H, 7.22; N, 12.32%.

[2]-[[(en)₂Co(dhda)Co(en)₂]Cl₄]-[α-CDX]-rotaxane (***R3***) *and [(en)₂Co(dhda)Co(en)₂]Cl₄ (**B3**):* These complexes were prepared and chromatographed in the same manner as **R1** and **B1** except for the use of 1,10-dibromodecane instead of 1,8-dibromooctane. In the separation seven bands f1′—f7′ were eluted in this order. The species f3′(dark violet), f5′(red), f6′(red), and f7′(red) were assigned to $[Co(maa)(en)_2]^+$, [2]-$[(en)_2Co(dhda)Co(en)_2]^{4+}$-[*α*-CDX]-rotaxane, $[Co\{O_2CCH_2S(CH_2)_{10}Br\}(en)_2]^{2+}$, and $[(en)_2Co(dhda)Co(en)_2]^{4+}$, respectively. Three species f1′(pink), f2′(red), and f4′(pink) were unassignable as yet. When the eluate f2′ was allowed to stand for several days at room temperature, white precipitate of *α*-CDX was deposited. Therefore, this species is inferred as an inclusion compound of $[Co\{O_2CCH_2S(CH_2)_{10}Br\}(en)_2]^{2+}$ and *α*-CDX from the analogy of $[Co(en)_2\{NH_2(CH_2)_2S(CH_2)_{10}Br\}]Cl_3\cdot 2$(*α*-CDX) reported previously.[1] The yield was 9.6±2% for **R3** and 47±4% for **B3** (3 preparations). In this system, pronounced selectivity was observed[7]: The band f5′ showed apparently *ΔΔ*-rich (*ca.* 10%) CD spectra and f7′ *ΛΛ*-rich (*ca.* 3%). Found for **R3**; C, 34.98; H, 6.80; N, 5.55%. Calcd for [2]-[$[(en)_2Co(dhda)Co(en)_2]Cl_4$]-[*α*-CDX]-rotaxane·$0.2C_2H_5OH\cdot 11H_2O=C_{58.4}H_{139.2}N_8S_2O_{45.2}Cl_4Co_2$: C, 35.06; H, 7.01; N, 5.60%. Found for **B3**; C, 29.83; H, 7.07; N, 12.36%. Calcd for $[(en)_2Co(dhda)Co(en)_2]Cl_4\cdot 0.2C_2H_5OH\cdot 4H_2O=C_{22.4}H_{65.2}N_8S_2O_{8.2}Cl_4Co_2$: C, 29.83; H, 7.29; N, 12.43%.

*[2]-[ΔΔ-[(en)₂Co(dhda)Co(en)₂]Cl₄]-[α-CDX]-rotaxane (**R4**), ΔΔ-[(en)₂Co(dhda)Co(en)₂]Cl₄ (**B4**), [2]-[ΛΛ-[(en)₂Co(dhda)Co(en)₂]Cl₄]-[α-CDX]-rotaxane (**R5**), and ΛΛ-[(en)₂Co(dhda)Co(en)₂]Cl₄ (**B5**):* These complexes were prepared and chromatographed in the same manner as **R3** and **B3** except for the use of *Δ*- or *Λ*-$[Co(maa)(en)_2]ClO_4$ instead of the racemate. The yield was 12% for **R4** and 52% for **B4** in the *Δ*-system (1 preparation), and 7% for **R5** and 49% for **B5** in the *Λ*-system (1 preparation). Found for **R4**; C, 36.14; H, 6.98; N, 5.38%. Calcd for [2]-[*ΔΔ*-$[(en)_2Co(dhda)Co(en)_2]Cl_4$]-[*α*-CDX]-rotaxane·$2C_2H_5OH\cdot 9.5H_2O=C_{62}H_{147}N_8S_2O_{45.5}Cl_4Co_2$: C, 36.21; H, 7.20; N, 5.45%. Found for **R5**; C, 32.55 H, 6.35; N, 5.01%. Calcd for [2]-[*ΔΔ*-$[(en)_2Co(dhda)Co(en)_2]Cl_4$]-[*α*-CDX]-rotaxane·$4NaCl\cdot 1.3C_2H_5OH\cdot 8H_2O=C_{60.6}H_{139.8}N_8S_2O_{43.3}Cl_8Na_4Co_2$: C, 32.62; H, 6.32; N, 5.02%. In the case of **B4** or **B5**, the addition of ethanol to the concentrated eluate yielded the gelatinous precipitate, which contained a large amount of NaCl. Therefore, no satisfactory analytical data were obtained for **B4** and **B5**. The concentrations of their CD spectra were calculated by reference to the molar absorption coefficient of the corresponding racemate **B3**.

*[2]-[ΔΛ-[(en)₂Co(dhda)Co(en)₂]Cl₄]-[α-CDX]-rotaxane (**R6**) and ΔΛ-[(en)₂Co(dhda)Co(en)₂]Cl₄ (**B6**):* These complexes were prepared from *Δ*-$[Co\{O_2CCH_2S(CH_2)_{10}Br\}(en)_2](ClO_4)Br$ (1.3 mmol), *Λ*-$[Co(maa)(en)_2]ClO_4$ (1.4 mmol), and *α*-CDX (2.5 g) in DMSO (8 cm^3). The reaction and separation conditions were the same as those for **R3** and **B3**. The yield was 8.8% for **R6** and 46% for **B6** (1 preparation). Found for **R6**; C, 35.13; H, 6.93; N, 5.43%. Calcd for [2]-[*ΔΛ*-$[(en)_2Co(dhda)Co(en)_2]Cl_4$]-[*α*-CDX]-rotaxane·$C_2H_5OH\cdot 12H_2O=C_{60}H_{146}N_8S_2O_{47}Cl_4Co_2$: C, 35.06; H, 7.16; N, 5.45%. Found for **B6**; C, 29.45; H, 6.92; N, 12.07%. Calcd for *ΔΛ*-$[(en)_2Co(dhda)Co(en)_2]Cl_4\cdot 0.1C_2H_5OH\cdot 5H_2O=C_{22.2}H_{66.6}N_8S_2O_{9.1}Cl_4Co_2$: C, 29.13; H, 7.34; N, 12.24%.

*[2]-[[(en)₂Co(doda)Co(en)₂]Cl₄]-[α-CDX]-rotaxane (**R7**) and [(en)₂Co(doda)Co(en)₂]Cl₄ (**B7**):* The complexes were prepared and chromatographed in the same manner as **R3** and **B3** except for the use of 1,12-dibromododecane instead of 1,10-dibromodecane. The yield was 21±2% for **R7** and 44±3% for **B7** (2 preparations). The apparent selectivity was *ca.* 8% for **R7** and *ca.* 3% for **B7**.[7] Found for **R7**; C, 36.57; H, 7.09; N, 5.36%. Calcd for [2]-[$[(en)_2Co(doda)Co(en)_2]Cl_4$]-[*α*-CDX]-rotaxane·$1.8C_2H_5OH\cdot 10H_2O=C_{63.6}H_{150.8}N_8S_2O_{45.8}Cl_4Co_2$: C, 36.65; H, 7.29; N, 5.38%. Found for **B7**; C, 32.52; H, 7.33; N, 12.19%. Calcd for $[(en)_2Co(doda)Co(en)_2]Cl_4\cdot 0.4C_2H_5OH\cdot 2.5H_2O=C_{24.8}H_{67.4}N_8S_2O_{6.9}Cl_4Co_2$: C, 32.66; H, 7.45; N, 12.29%.

*[2]-[ΔΔ-[(en)₂Co(doda)Co(en)₂]Cl₄]-[α-CDX]-rotaxane (**R8**), ΔΔ-[(en)₂Co(doda)Co(en)₂]Cl₄ (**B8**), [2]-[ΛΛ-[(en)₂Co(doda)Co(en)₂]Cl₄]-[α-CDX]-rotaxane (**R9**), and ΛΛ-[(en)₂Co(doda)Co(en)₂]Cl₄ (**B9**):* The complexes were prepared and chromatographed in the same manner as **R7** and **B7** except for the use of *Δ*- or *Λ*-$[Co(maa)(en)_2]ClO_4$ instead of the racemate. The yield was 24±1% for **R8** and 39±2% for **B8** in the *Δ*-system (2 preparations), and 17±1% for **R9** and 43±2% for **B9** in the *Λ*-system (2 preparations). Found for **R8**; C, 36.89; H, 7.17; N, 5.29%. Calcd for [2]-[*ΔΔ*-$[(en)_2Co(doda)Co(en)_2]Cl_4$]-[*α*-CDX]-rotaxane·$2.5C_2H_5OH\cdot 10H_2O=C_{65}H_{155}N_8S_2O_{46.5}Cl_4Co_2$: C, 36.88; H, 7.38; N, 5.29%. Found for **B8**; C, 33.01; H, 7.29; N, 11.63%. Calcd for *ΔΔ*-$[(en)_2Co(doda)Co(en)_2]Cl_4\cdot 1.2C_2H_5OH\cdot 0.6NaCl\cdot H_2O=C_{26.4}H_{69.2}N_8S_2O_{6.2}Cl_{4.6}Na_{0.6}Co_2$: C, 33.14; H, 7.29; N, 11.71%. Found for **R9**: C, 35.83; H, 6.75; N, 5.47%. Calcd for [2]-[*ΛΛ*-$[(en)_2Co(doda)Co(en)_2]Cl_4$]-[*α*-CDX]-rotaxane·$0.5C_2H_5OH\cdot NaCl\cdot 8H_2O=C_{61}H_{139}N_8S_2O_{42.5}Cl_5NaCo_2$: C, 35.79; H, 6.84; N, 5.47%. Found for **B9**; C, 30.79; H, 7.33; N, 11.74%. Calcd for *ΛΛ*-$[(en)_2Co(doda)Co(en)_2]Cl_4\cdot 0.2C_2H_5OH\cdot$

$5H_2O$=$C_{24.4}H_{71.2}N_8S_2O_{9.2}Cl_4Co_2$: C, 30.92; H, 7.57; N, 11.82%.

[2]-[ΔΔ'-[(en)$_2$Co(adha)Co(en)$_2$]Cl$_5$]-[α-CDX]-rotaxane (**R10**), *ΔΔ'-[(en)$_2$Co(adha)Co(en)$_2$]Cl$_5$* (**B10**), *[2]-[ΛΛ'-[(en)$_2$Co(adha)-Co(en)$_2$]Cl$_5$]-[α-CDX]-rotaxane* (**R11**), *and ΛΛ'-[(en)$_2$Co(adha)-(en)$_2$]Cl$_5$* (**B11**):[9] To 8 cm^3 of DMSO solution containing α-CDX (2.5 g) was added the complexes of *Δ*(or *Λ*)-[Co{O_2CCH_2S-$(CH_2)_{10}Br$}(en)$_2$](ClO_4)Br and *Δ'*(or *Λ'*)-[Co(aet)(en)$_2$](ClO_4)$_2$, and the mixture was kept at 30 °C for 10 d. The resulting reaction mixture was diluted with 20 cm^3 of water, poured onto a column of SP-Sephadex C-25 (Na^+ form), and eluted with 0.65 mol dm^{-3} NaCl. Seven bands, f1″(pink), f2″(pink), f3″(brown), f4″(pink), f5″(orange red), f6″(red), and f7″(orange red), were eluted in this order. The two orange red bands f5″ and f7″ were the desired bands and isolated as the chloride salt in the same manner as above. The other four bands except for [Co(aet)(en)$_2$]$^{2+}$ (f3″) were low in yield and unassignable as yet. The yield was 12% for **R10** and 54% for **B10** in the *ΔΔ'*-system (1 preparation), and 6.4% for **R11** and 58% for **B11** in the *ΔΔ'*-system (1 preparation). Found for **R10**; C, 36.38; H, 7.20; N, 6.15%. Calcd for [2]-[*ΔΔ'*-[(en)$_2$Co(adha)-Co(en)$_2$]Cl$_5$]-[α-CDX]-rotaxane·$2C_2H_5OH$·$8H_2O$=$C_{62}H_{148}N_9S_2O_{42}Cl_5Co_2$: C, 36.31; H, 7.27; N, 6.15%. Found for **B10**; C, 29.84; H, 7.66; N, 12.83%. Calcd for *ΔΔ'*-[(en)$_2$Co(adha)Co-(en)$_2$]Cl$_5$·C_2H_5OH·$4.5H_2O$=$C_{24}H_{75}N_9S_2O_{7.5}Cl_5Co_2$: C, 29.74; H, 7.80; N, 13.01%. Found for **R11**; C, 34.85; H, 7.06; N, 6.05%. Calcd for [2]-[*ΔΔ'*-[(en)$_2$Co(adha)Co(en)$_2$]Cl$_5$]-[α-CDX]-rotaxane·C_2H_5OH·$0.5NaCl$·$10H_2O$=$C_{60}H_{146}N_9S_2O_{43}Cl_{5.5}Na_{0.5}Co_2$: C, 34.81; H, 7.11; N, 6.09%. Found for **B11**; C, 30.03; H, 7.68; N, 12.97%. Calcd for *ΔΔ'*-[(en)$_2$Co(adha)Co(en)$_2$]Cl$_5$·$1.1C_2H_5OH$·$4H_2O$=$C_{24.2}H_{74.6}N_9S_2O_{7.1}Cl_5Co_2$: C, 30.12; H, 7.79; N, 13.06%.

Measurement. The visible and ultraviolet absorption spectra were measured on a Hitachi 330 spectrophotometer and CD spectra with a JASCO MOE-1 spectropolarimeter in aqueous solutions. The ^{13}C NMR spectra were recorded with a JEOL FX-90Q NMR spectrometer in D_2O containing dioxane as an internal standard.

Results and Discussion

Absorption and CD Spectra. The analytical data show explicitly the formation of the rotaxanes and the

TABLE 1. ABSORPTION AND CD DATA OF THE ROTAXANE AND BRIDGED COMPLEXES

Complex	Bridging ligand	Co(III) components	Absorption[a]	σ_{max}(log ε)		CD[a] σ_{ext}(Δε)	
R2	dtda	*ΔΔ*	20.15(2.511)	27.8(2.81)[b]	18.90(−1.62)	21.25(−2.30)	27.47(+0.824)
			35.8(4.14)[b]	43.40(4.492)	38.76(−11.8)	43.1(+26.4)	
B1	dtda	*rac*	19.95(2.513)	27.8(2.71)[b]			
			35.50(4.186)	43.30(4.486)			
B2	dtda	*ΔΔ*	20.00(2.513)	27.8(2.71)[b]	18.90(−2.42)	21.16(−3.07)	27.47(+1.06)
			35.40(4.184)	43.40(4.495)	37.17(−9.29)	42.9(+35.5)	
R3	dhda	*rac*	20.04(2.514)	27.8(2.74)[b]			
			35.60(4.173)	43.50(4.483)			
R4	dhda	*ΔΔ*	20.02(2.505)	27.8(2.75)[b]	18.90(−2.32)	21.25(−2.91)	27.46(+1.02)
			35.60(4.170)	43.48(4.480)	37.33(−10.2)	42.9(+27.9)	
R5	dhda	*ΛΛ*	19.97(2.500)	27.8(2.76)[b]	18.98(+2.08)	21.28(+2.59)	27.46(−0.902)
			35.50(4.144)	43.45(4.459)	37.33(+8.42)	42.9(−29.9)	
R6	dhda	*ΔΔ*	19.97(2.518)	27.8(2.75)[b]			
			35.58(4.183)	43.26(4.496)			
B3	dhda	*rac*	19.95(2.511)	27.8(2.70)[b]			
			35.30(4.189)	43.40(4.478)			
B4	dhda	*ΔΔ*			18.92(−2.79)	21.14(−3.41)	27.46(+1.19)
					37.17(−10.7)	42.9(+40.2)	
B6	dhda	*ΔΔ*	19.98(2.497)	27.8(2.70)[b]			
			35.38(4.152)	43.30(4.458)			
R7	doda	*rac*	19.98(2.540)	27.8(2.75)[b]			
			35.50(4.175)	43.24(4.475)			
R8	doda	*ΔΔ*	19.95(2.530)	27.8(2.75)[b]	18.90(−1.53)	21.28(−1.89)	27.47(+0.632)
			35.55(4.161)	43.30(4.460)	37.31(−8.06)	43.1(+22.0)	
R9	doda	*ΛΛ*	19.90(2.534)	27.8(2.75)[b]	18.96(+1.44)	21.23(+1.71)	27.43(−0.641)
			35.60(4.162)	43.40(4.474)	37.04(+5.81)	43.1(−20.2)	
B7	doda	*rac*	19.98(2.538)	27.8(2.73)[b]			
			35.35(4.172)	43.24(4.453)			
B9	doda	*ΛΛ*	19.97(2.549)	27.8(2.75)[b]	18.98(+1.45)	21.19(+1.82)	27.47(−0.636)
			35.40(4.209)	43.40(4.500)	37.31(+6.03)	42.9(−21.2)	
R10[c]	adha	*ΔΔ'*	20.25(2.536)	28.2(2.77)[b]	20.04(−3.13)	27.40(+0.353)	
			35.28(4.221)	44.72(4.481)	35.34(−11.6)	44.4(+30.3)	
R11[c]	adha	*ΛΛ'*	20.28(2.556)	28.2(2.77)[b]	20.04(+3.27)	27.46(−0.342)	
			35.34(4.232)	44.62(4.490)	35.46(+9.87)	44.4(−31.3)	
B10[c]	adha	*ΔΔ'*	20.26(2.560)	28.1(2.73)[b]	20.12(−4.03)	27.46(+0.560)	
			35.20(4.250)	44.52(2.514)	35.34(−11.5)	44.3(+39.2)	
[Co(maa)(en)$_2$]ClO_4		*Δ*	16.2(1.50)[b]	19.33(2.180)	18.40(−2.32)	26.32(+0.714)	
			27.0(2.49)[b]	35.45(4.073)	34.84(+4.81)	44.6(+19.4)	
			45.20(4.180)				
[Co(aet)(en)$_2$]-$(ClO_4)_2$[c]		*Λ'*	16.7(1.66)[b]	20.72(2.158)	16.8(+0.844)[b]	19.12(+1.34)	21.88(−0.278)
			27.3(2.49)[b]	35.45(4.118)	26.32(+0.677)	35.09(−4.68)	45.7(−11.3)
			49.90(4.221)				

a) Wave numbers are given in 10^3 cm^{-1} unit and log ε or Δε values (in parentheses) in mol^{-1} dm^3 cm^{-1}. b) Shoulder. c) Ref. 7.

corresponding bridged complexes. The ratios C/N in these complexes are somewhat higher than the ideal values because a large amount of ethanol was used for the isolation of them. It seems that the high ability of adduct formation with organic solvent is common in the present complexes with the hydrophobic polymethylene bridging atoms.

Table 1 collects the absorption and CD data of the present complexes. The representative absorption and CD spectra of the rotaxanes and the bridged complexes are shown in Figs. 2 and 3, respectively, together with those of dhdd complexes (n=10, X=Y=CH_2NH_2) for comparison. The starting thiolato complex [Co(maa)-

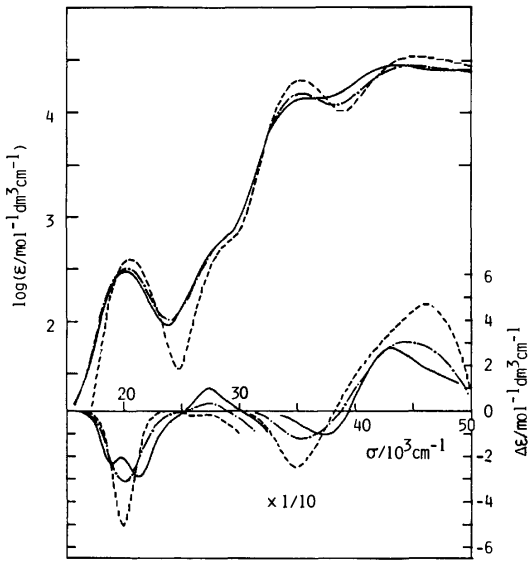

Fig. 2. Absorption and CD spectra of the rotaxanes with the bridging methylene chain length n=10: **R4** (dhda, X=Y=CO_2^-) ——; **R10** (adha, X=CO_2^- and Y=CH_2NH_2) -·-·-·; dhdd rotaxane (X=Y=CH_2NH_2)[1] ------.

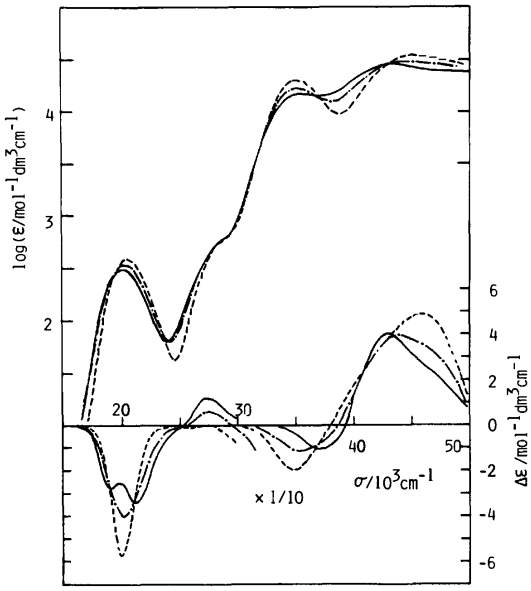

Fig. 3. Absorption and CD spectra of the bridged complexes with n=10: **B4** (dhda, X=Y=CO_2^-) ——; **B10** (adha, X=CO_2^- and Y=CH_2NH_2) -·-·-·; dhdd complex (X=Y=CH_2NH_2)[1] ------.

(en)$_2$]ClO_4 exhibits a characteristic absorption at *ca.* 610 nm (16000—17000 cm^{-1}). It is well known that this band disappears by alkylation of the thiolato groups.[6,8] Since all present complexes lack this ab-

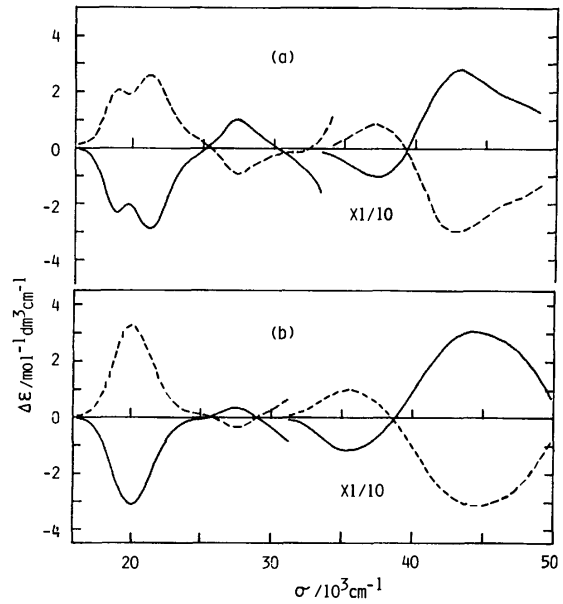

Fig. 4. CD spectra of the dhda and adha rotaxanes: (a) **R4** ($\Delta\Delta$) —— and **R5** ($\Lambda\Lambda$) ------; (b) **R10** ($\Delta\Delta$) —— and **R11** ($\Lambda\Lambda$) ------.

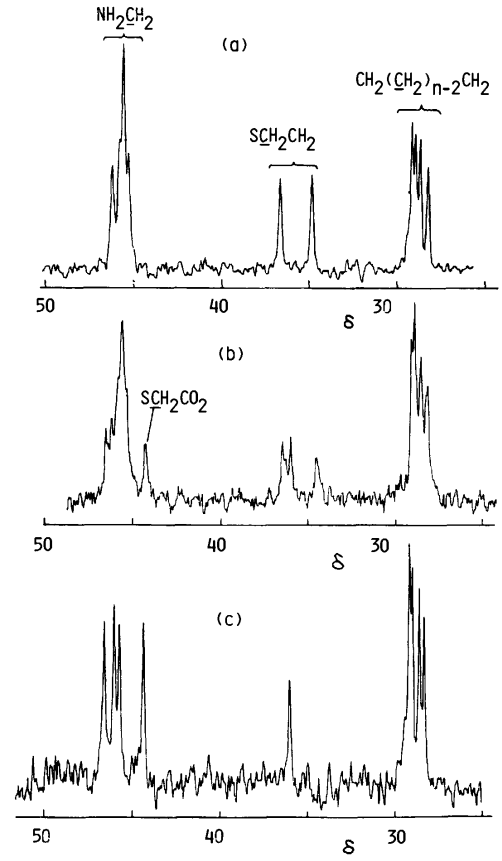

Fig. 5. ^{13}C NMR spectra of the bridged complexes: (a) dhdd complex (X=Y=CH_2NH_2),[1] (b) **B10** (X=CO_2^- and Y=CH_2NH_2), and (c) **B4** (X=Y=CO_2^-). 1,4-Dioxane (δ=67.40 *vs.* Me_4Si) was used as the internal reference. The spectral region due to the carboxyl group was omitted in (b) and (c).

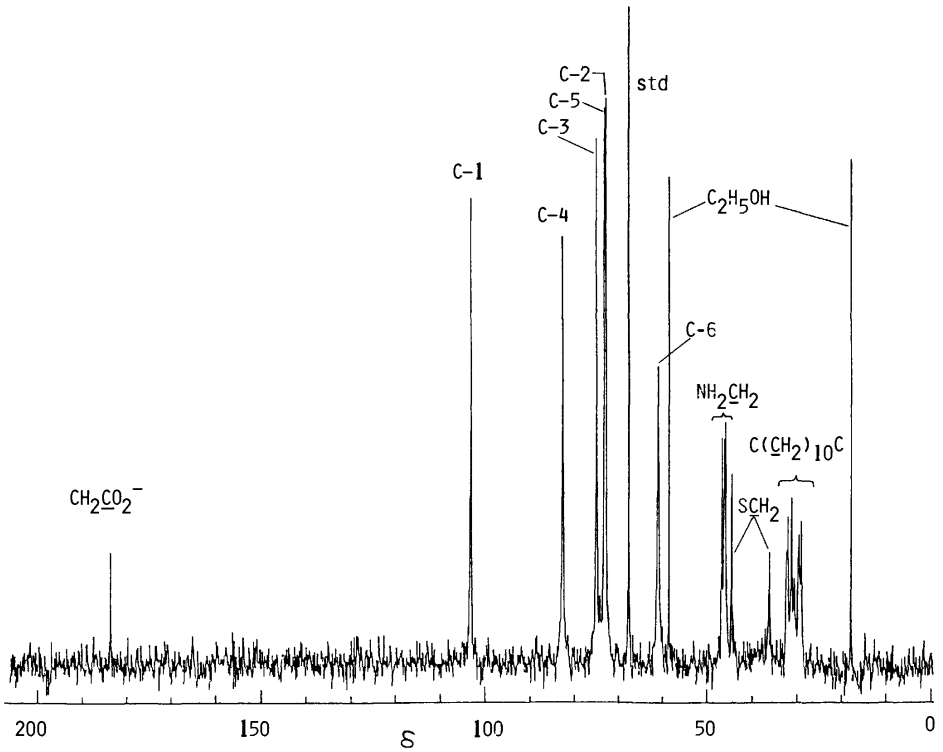

Fig. 6. ^{13}C NMR spectra of the rotaxane **R8**.

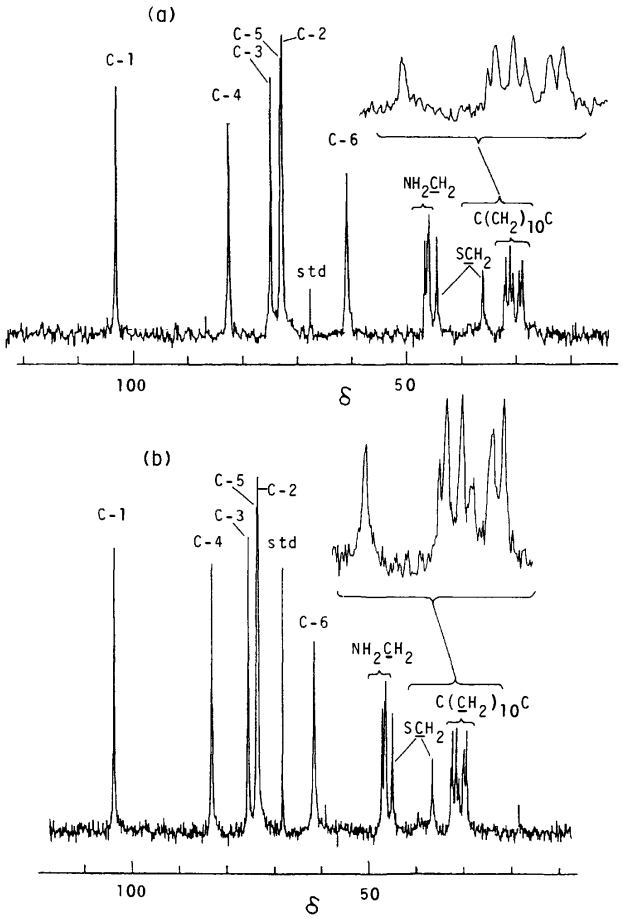

Fig. 7. ^{13}C NMR spectra of the rotaxanes **R9** (a) and **R7** (b). The spectral region due to the carboxyl group was omitted in both.

sorption, they contain only thioether donor atoms as sulfur atom. The first spin-allowed d-d absorption bands of the rotaxanes with the bridging methylene chain length $n=10$ gradually red-shift with the increase of oxygen atom, locating at 20440 cm^{-1} for the dhdd rotaxane with $2[Co(N)_5(S)]$ chromophore, at 20250 cm^{-1} for the adha one with $[Co(N)_5(S)]$ and $[Co(N)_4(S)(O)]$, and 20020 cm^{-1} for the dhda one with $2[Co(N)_4(S)(O)]$ (Fig. 2). The intense bands at *ca.* 35000 cm^{-1}, which can be assigned to the $Co(\sigma^*)\leftarrow S(\sigma)$ ligand-to-metal charge transfer (LMCT) band,[9] show apparently no such shift. The LMCT band intensity of the adha rotaxane is intermediate between those of the dhdd and dhda rotaxanes. Such a mean behavior of the adha rotaxane is also realized in the CD spectra. The absolute configurations of the present complexes can be assigned on the basis of the net CD sign in the first spin-allowed d-d absorption band region, that is, *Δ*-configuration for negative and *Λ*-one for positive.[1,6] The bridged complexes (Fig. 3) show the analogous absorption and CD spectral changes as the corresponding rotaxanes.

The rotaxanes prepared from *rac*-$[Co(maa)(en)_2]^+$ are each the mixture of four diastereomers, *ΔΔ*-, *ΛΛ*-, and two *ΔΛ*-forms (pseudo-*meso*) with respect to the bridged cobalt(III) moieties(neglecting the *R* and *S* chiralities of the donor sulfur atoms).[1] The optically active *ΔΔ* (or *ΛΛ*) rotaxane could be obtained in a pure form from the resolved starting material *Δ*(or *Λ*)-$[Co(maa)(en)_2]ClO_4$. The CD spectra of the dhda and adha rotaxanes are shown in Figs. 4(a) and 4(b), respectively. The CD spectra of the *ΔΔ*- and *ΛΛ*-rotaxanes are not completely enantiomeric to each other in each pair of diastereomers. The deviation is eminent by comparing the diastereomers in the CD intensity ratio,

$\Delta\varepsilon_{LMCT}/\Delta\varepsilon_{I}$, where $\Delta\varepsilon_{I}$ and $\Delta\varepsilon_{LMCT}$ denote the CD peak intensities in the first d-d absorption and LMCT band (*ca.* 35000 cm^{-1}) regions, respectively: The ratio is 3.25 for *ΛΛ*-dhda (**R5**) and 3.49 for *ΔΔ*-dhda (**R4**) rotaxanes, and 3.02 for *ΛΛ*-adha (**R11**) and 3.70 for *ΔΔ*-adha (**R10**) rotaxanes. It is noteworthy that all the ratios in the rotaxanes are higher than those of the corresponding bridged complexes, namely, 3.14 for dhda bridged complex (**B4**) and 2.85 for adha bridged one (**B10**). This is correlated with the sterically crowded structure of the rotaxane containing α-CDX as compared with the corresponding bridged complexes. The ratio becomes a measure to distinguish between the rotaxane and the bridged complex by the CD spectra.

^{13}C NMR Spectra. Figure 5 shows the ^{13}C NMR spectra of the bridged complexes with $n=10$. The dhdd and dhda complexes with C_2 symmetry clearly shows four resonances in the $-C(CH_2)_8C-$ region. The adha complex with C_1 symmetry exhibited the intermediate pattern. The ^{13}C NMR spectra of rotaxanes are quite different from the bridged complexes, giving the direct evidence of the rotaxane formation with α-CDX (Figs. 6—10). The rotaxane **R8** exhibited strong six signals in a low magnetic field (δ=60—105), which were assigned to α-CDX moiety[1] (Fig. 6). The other signals were assigned to $CH_2\underline{C}O_2^-$ (δ=*ca.* 182.7) and methylene carbons (δ=25—50) of $NH_2\underline{C}H_2-$, $-S\underline{C}H_2-$, and $-C(\underline{C}H_2)_{n-2}C-$ from the lower megnetic field side. The rotaxanes **R8** (Fig. 6) and **R9** (Fig. 7(a)) are composed of a single diastereomer, which has a C_1 symmetry because of the inequality of both openings of α-CDX. In the $-C(CH_2)_{10}C-$ region, they showed four strong (δ=31.75, 30.94, 29.32, and 28.72 for **R9**) and two weak (δ=32.13 and 30.45 for **R9**) resonances. Since it is reasonable to consider that each of the strong signals corresponds to two methylene carbons, the total number of the methylene resonances becomes ten in both the rotaxanes as expected. The results are consistent

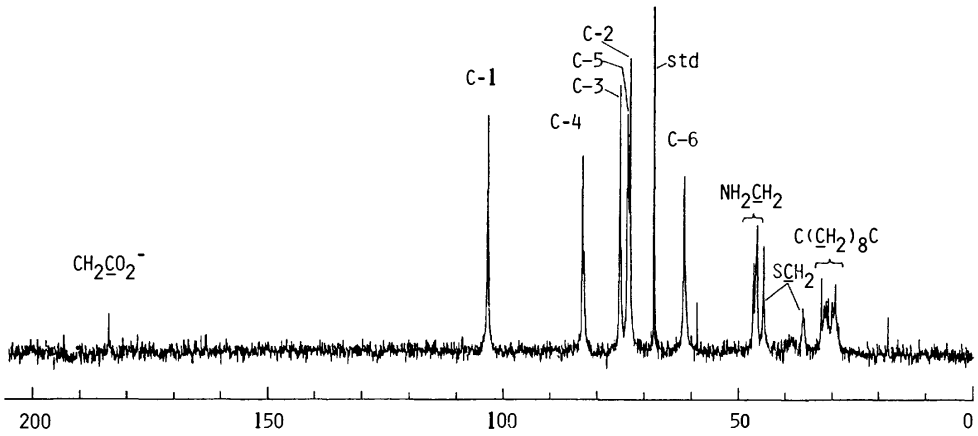

Fig. 8. ^{13}C NMR spectra of the rotaxane **R4**.

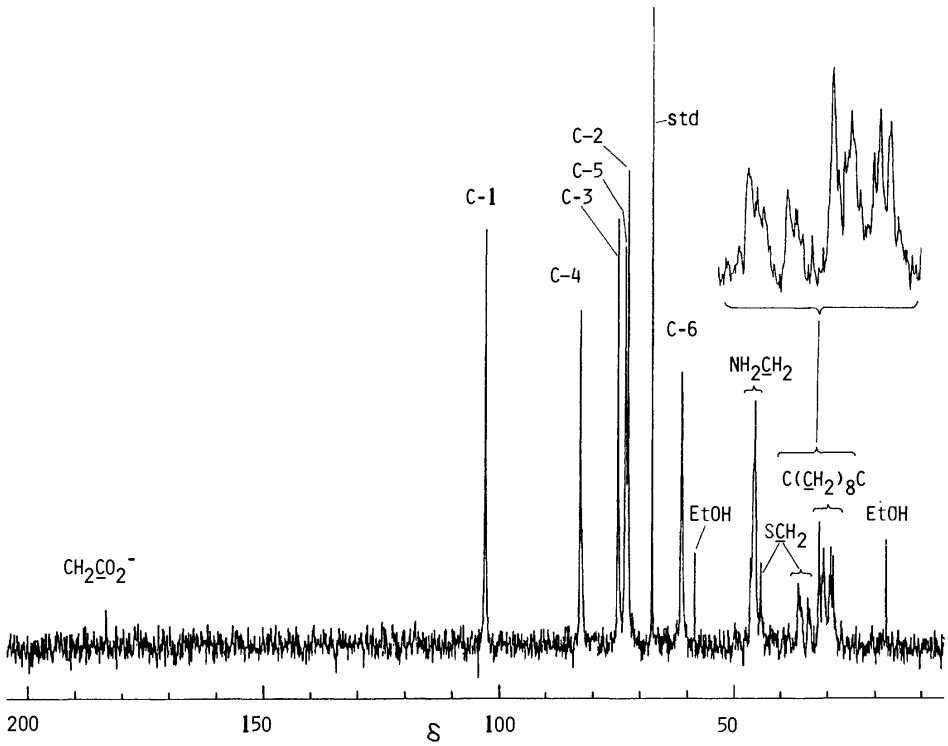

Fig. 9. ^{13}C NMR spectra of the rotaxane **R10**.

with the formation of the rotaxane with C_1 symmetry.

The characteristic features of ^{13}C NMR spectra are the same in the rotaxanes with $n=10$ (**R4** in Fig. 8 and **R10** in Fig. 9) and $n=8$ (**R2** in Fig. 10). However, a significant spectral change was observed in **R2**; two signals for each of C4, C5, and C6 in α-CDX appeared during the first several hours (Fig. 10(a)) and the higher field component in each pair became dominant with time (Fig. 10(b)). None of the final resonances corresponded to the chemical shifts of the free α-CDX. The absorption and CD spectra of the same sample after the ^{13}C NMR measurement were checked to elucidate the origin of such a change. The absorption spectrum was the same as the initial one except for the *ca.* 11% intensity decrease in the LMCT region. The pattern of the CD spectrum was the same but the CD intensity reduced to one-half its initial value. The results indicate that the decomposition reaction releasing free α-CDX does not occur and that the species with the uncoordinated thioether atoms, which will be formed by the Co-S cleavage, is also very low in concentration, if any, as judged by the absorption intensity in LMCT region. The most plausible explanation may be that the species with the uncoordinated carboxyl group in $-SCH_2CO_2$ moiety is partly produced owing to the steric crowding imposed by α-CDX. In fact, the ^{13}C-NMR change with time is most eminent only in **R2** with rather short chain length $n=8$. Such a splitting is observed only for C4 carbon in **R4** and **R10** with $n=10$ and the rotaxanes with $n=12$ had no splitting tendency.

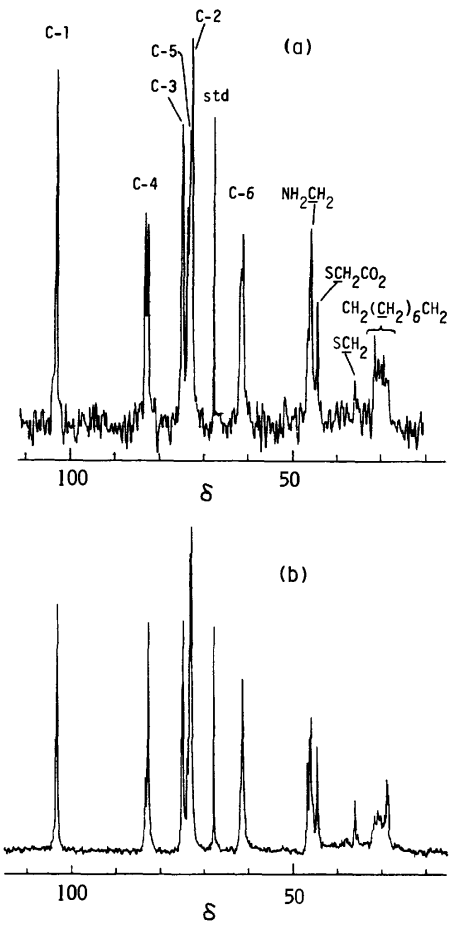

Fig. 10. ^{13}C NMR spectra of the rotaxane **R2**: (a) accumulated for *ca.* 6h after dissolution in D_2O; (b) accumulated for *ca.* 20h after dissolution in D_2O.

The chemical shifts due to α-CDX in the rotaxanes are summarized in Table 2. The assignment is after Colson *et al.*[10] and our results.[1] The chemical shifts of free α-CDX were significantly altered by the rotaxane formation, especially those of C1, C3, and C5 shifting to the down field. One of the substituent groups on each of the carbons undergoing such a large shift is directed toward the center part of the cavity of α-CDX and sterically interacted with the included polymethylene chain. This situation is responsible for the above shift. The values of the rotaxanes **R3**, **R4**, **R5**, and **R6** are very similar to one another irrespective of the absolute configurations of the cobalt(III) moieties, which is in good agreement with the earlier results.[1] The change of the bridging methylene length, however, affects the chemical shift. The resonances of C4, C5, and C6 were shifted regularly to the down field with the decrease of the methylene chain length from $n=ca.$ 17 to $n=7$,[11] whereas the chemical shifts of C1, C2, and C3 were hardly affected. The latter is relevant to the rigid hydrogen bonding network at the side of secondary hydroxyl groups on C2 and C3,[12] which makes the chemical shifts of C1, C2, and C3 insensitive to the

Table 2. ^{13}C NMR resonances due to α-CDX in the rotaxane (δ from Me_4Si)

Rotaxane	Chain length	C1	Chemical shift C4	C3	C5	C2	C6	Ref.
U1(*ΔΔ*)	7	102.50	82.95	74.55	73.47	72.36	61.63	11
R2(*ΔΔ*, dtda)	8	102.61	82.89	74.71	73.41	72.55	61.44	
7(*ΔΔ*, dtdd)	8	102.64	83.06	74.71	73.47	72.44	61.66	1
R3(*rac*, dhda)	10	102.72	82.46	74.61	72.98	72.49	61.01	
R4(*ΔΔ*, dhda)	10	102.72	82.51	74.66	73.03	72.49	61.06	
R5(*ΔΔ*, dhda)	10	102.78	82.46	74.66	72.98	72.49	61.01	
R6(*ΔΔ*, dhda)	10	102.75	82.49	74.66	73.01	72.47	61.03	
R10(*ΔΔ'*, adha)	10	102.72	82.54	74.66	73.06	72.47	61.09	
2(*rac*, dhdd)	10	102.78	82.68	74.72	73.15	72.50	61.23	1
R7(*rac*, doda)	12	102.83	82.27	74.63	72.84	72.57	60.79	
R8(*ΔΔ*, doda)	12	102.83	82.30	74.66	72.87	72.55	60.79	
R9(*ΛΛ*, doda)	12	102.78	82.24	74.61	72.82	72.49	60.74	
1(*rac*, dodd)	12	102.78	82.24	74.60	72.81	72.54	60.79	1
U2(*rac*)	*ca.* 17	102.78	81.92	74.71	72.71	72.49	60.52	11
free α-CDX		102.18	82.03	74.06	72.82	72.44	61.17	

TABLE 3. PERCENTAGE YIELD OF [2]-[[(en)$_2$Co{XCH$_2$S(CH$_2$)$_n$SCH$_2$Y}Co(en)$_2$]Cl$_m$]-[α-CDX]-rotaxane

n	Co(III) components	X=CO$_2^-$ Y=CO$_2^-$	X=CO$_2^-$ Y=CH$_2$NH$_2$	X=CH$_2$NH$_2$ Y=CH$_2$NH$_2$
n=8	*rac*	2.5(Δ−2)[b]		~0
	$\Delta\Delta$	2.5		3.5
n=10	*rac*	10(Δ−10)[b]		6(Δ−16)[b]
	$\Delta\Delta$	12	12[c]	21
	$\Lambda\Lambda$	7	6.4[c]	<7
	$\Delta\Lambda$	8.8[c]		
n=12	*rac*	21(Δ−8)[b]		16(Δ−5)[b]
	$\Delta\Delta$	24		28
	$\Lambda\Lambda$	17		14

a) The data from Ref. 1. b) Apparent optical purity[7] is indicated in parentheses with the configuration of the rich species. c) The preparative procedures are different from those of other rotaxanes. See Experimental section.

change of the bridging length. On the other hand, the hydroxyl group at C6 can rotate freely and is sensitive to the steric change. Such a steric change at C6 also influences the chemical shifts of C4 and C5. Thus, the rotaxan formation is explicitly identified by the ^{13}C NMR spectra.

Synthesis and Stereoselectivity. The yields of rotaxanes are summarized in Table 3, together with the earlier results for comparison. The yield is the highest in the doda rotaxanes with n=12 and decreases with the decrease of the chain length, namely, in the order 12>10>8. The $\Delta\Delta$-rotaxane was prepared in the highest yield among the rotaxanes with the identical chain length. This is attributable to the stereoselective inclusion by α-CDX.[13] The results are very similar to those for the earlier system (X=Y=CH$_2$NH$_2$) except for that the yields starting from the racemate are somewhat higher in the present system (X=Y=CO$_2^-$).

The highest selectivity was *ca.* 10% in the dhda rotaxane **R3**. The partial selectivity was also observed in the other rotaxanes **R1** and **R7**. It should be noted that the selectivity decreases in the order 10>12>8. This means that there is the optimum methylene length for the chiral discrimination. The rotaxanes of the present system (X=Y=CO$_2^-$, and X=CO$_2^-$ and Y=CH$_2$NH$_2$) are relatively unstable compared with those in the earlier system (X=Y=CH$_2$NH$_2$), because it was observed that the former underwent the partial racemization in the prolonged column chromatography. In conclusion, the yield and the selectivity of rotaxane are mainly dependent on the length of the bridging methylene chain and the absolute configuration of the starting cobalt(III) complex. The difference between the bidentate thiolate ligands aet and maa has a small influence on the yield and the selectivity of rotaxane.

References

1) Part I: K. Yamanari and Y. Shimura, *Bull. Chem. Soc. Jpn.*, **56**, 2283 (1983).

2) J. Szejtli, "Cyclodextrins and Their Inclusion Complexes", Akadémiai Kiadó, Budapest (1982); M. L. Bender and M. Komiyama, "Cyclodextrin Chemistry", Springer Verlag, Berlin (1978).

3) H. Ogino, *J. Am. Chem. Soc.*, **103**, 1303 (1981).

4) The nomenclature for rotaxanes is based on Schill's: G. Schill, "Catenanes, Rotaxanes, and Knots," Academic Press, New York (1971).

5) Greek letters Δ(or Λ) and Δ'(or Λ') represent the absolute configurations of [Co(maa)(en)$_2$]$^+$ and [Co(aet)-(en)$_2$]$^{2+}$, respectively.

6) K. Yamanari, J. Hidaka, and Y. Shimura, *Bull. Chem. Soc. Jpn.*, **50**, 2299 (1977).

7) The apparent optical purity of the rotaxane was calculated from the CD and absorption values in the first d-d transition region, $\Delta\varepsilon=\pm1.4$ and ε=160 per one cobalt(III) ion for the system of X=Y=CO$_2^-$.

8) K. Yamanari and Y. Shimura, *Bull. Chem. Soc. Jpn.*, **53**, 3605 (1980).

9) M. Kita, K. Yamanari, and Y. Shimura, *Bull. Chem. Soc. Jpn.*,**55**, 2873 (1982).

10) P. Colson, H. J. Jennings, and Ian C. P. Smith, *J. Am. Chem. Soc.*, **96**, 8181 (1974).

11) K. Yamanari and Y. Shimura, to be published. The rotaxanes **U1** and **U2** denote [2]-[$\Delta\Delta$-[(en)$_2$Co{NH$_2$(CH$_2$)$_2$S-(CH$_2$)$_7$S(CH$_2$)$_2$NH$_2$}Co(en)$_2$]Cl$_6$]-[α-CDX]-rotaxane and [2]-[[(en)$_2$Co{NH$_2$(CH$_2$)$_2$S(CH$_2$)$_6$O- -O(CH$_2$)$_6$S(CH$_2$)$_2$NH$_2$}-Co(en)$_2$]Cl$_6$]-[α-CDX]-rotaxane, respectively.

12) B. Casu, M. Reggiani, G. G. Gallo, and A. Vigevani, *Tetrahedron*, **22**, 3061 (1966); W. Saenger, M. Noltemeyer, P. C. Manor, B. Hingerty, and B. Klar, *Bioorg. Chem.*, **5**, 187 (1976).

13) K. Yamanari and Y. Shimura, *Chem. Lett.*, **1982**, 1957.

Photochemical Reaction of Phenyl-substituted 1,3-Diketones

Michikazu YOSHIOKA,* Tsuneji SUZUKI, and Masashi OKA
Department of Chemistry, Faculty of Science, Saitama University, Shimo-okubo, Urawa, Saitama 338
(Received October 4, 1983)

Irradiation of 2,2-dimethyl-1-phenyl-1,3-diketones with 3-ethyl or 3-isopropyl substituents gave type II cyclization product, 3-hydroxy-2,2,4-trimethyl-3-phenylcyclobutanone or 3-hydroxy-2,2,4,4-tetramethyl-3-phenylcyclobutanone, along with type I cleavage products. The type II cyclization/type I cleavage ratio is greater with a 3-isopropyl group than with a 3-ethyl group. A similar irradiation of 2,2-dimethyl-1-phenyl-1,3-butanedione gave type I cleavage products and no type II cyclization product. Irradiation of 2,4-dimethyl-1-phenyl-1,3-pentanedione gave 3-hydroxy-2,2,4-trimethyl-3-phenylcyclobutanone and propiophenone. The geometry of 3-hydroxy-2,2,4-trimethyl-3-phenylcyclobutanone which arose from 2,2-dimethyl-1-phenyl-1,3-pentanedione was cis with respect to phenyl and 4-methyl groups and that which arose from 2,4-dimethyl-1-phenyl-1,3-pentanedione was trans.

Two major photochemical processes, Norrish type I and Norrish type II, have been widely studied.[1] The type II process is the most common photoreaction of monoketones with γ-hydrogens in the alkyl chain. However, in the case of 1,3-diketones, no example of type II photoreaction where an α-hydrogen to one carbonyl group undergoes 1,5-shift to another carbonyl oxygen has been found. Non- or difficultly-enolizable aliphatic 1,3-diketones have been found to undergo type I cleavage.[2] The photochemistry of aromatic 1,3-diketones has been studied for 3-aroylchromones[3] and 2-diaza-1-aryl-1,3-diketone compounds.[4] Little attention has been given to aromatic 1,3-diketones with an sp^3 carbon α to both carbonyl groups.[5] Since, for the same electronic and spin configuration, aryl alkyl ketones undergo type I cleavage more slowly than the analogous dialkyl ketones,[6] 1-aryl-3-alkyl-1,3-diketone compounds may undergo type II photoreaction where the aromatic carbonyl oxygen abstracts a hydrogen from the α-carbon on the 3-alkyl substituent, in competition with type I cleavage. In this paper, we report the photochemistry of 1-phenyl-3-alkyl-1,3-diketone compounds.

Results and Discussion

An acetonitrile solution of 2,2,4-trimethyl-1-phenyl-1,3-pentanedione (**1a**) was irradiated under nitrogen with a Pyrex filter. After removal of the solvent, 3-hydroxy-2,2,4,4-tetramethyl-3-phenylcyclobutanone (**2a**), isobutyrophenone (**3**), enol ester (**4a**), and 1,4-diketone (**5a**) were isolated by silica gel chromatography. A similar reaction was found to occur with 2,2-dimethyl-1-phenyl-1,3-pentanedione (**1b**). As shown in Table 1, the yield of **2** was higher with **1a** than with **1b**, and the yields of **4** and **5** were lower with **1a** than with **1b**. Irradiation of 2,2-dimethyl-1-phenyl-1,3-butanedione (**1c**) gave isobutyrophenone (**3**), enol ester (**4c**), and 1,4-diketone (**5c**), along with benzaldehyde and benzoic acid. In this case, no hydroxycyclobutanone was detected. Similar irradiation of 2,4-dimethyl-1-phenyl-1,3-pentanedione (**1d**) gave propiophenone (**3d**) and 3-hydroxy-2,2,4-trimethyl-3-phenylcyclobutanone (**2d**) which was a geometrical isomer of **2b**, along with several

Table 1. Photoreaction of **1** in acetonitrile[a]

1	Irradiation time / h	Conversion / %	Yield/% 2[b]	3[c]	4[c]	5[c]
1a	3.5	78	47	2	6	8
1b	4	68	11	3	9	14
1c	11	45	—	11	7	27
1d	26	88	16	12	—	—

a) Irradiation of 20 mmol of **1** in 400 cm^3 of acetonitrile with a 450 W high-pressure mercury lamp through a Pyrex filter. b) Isolated yield. c) Determined by GLC.

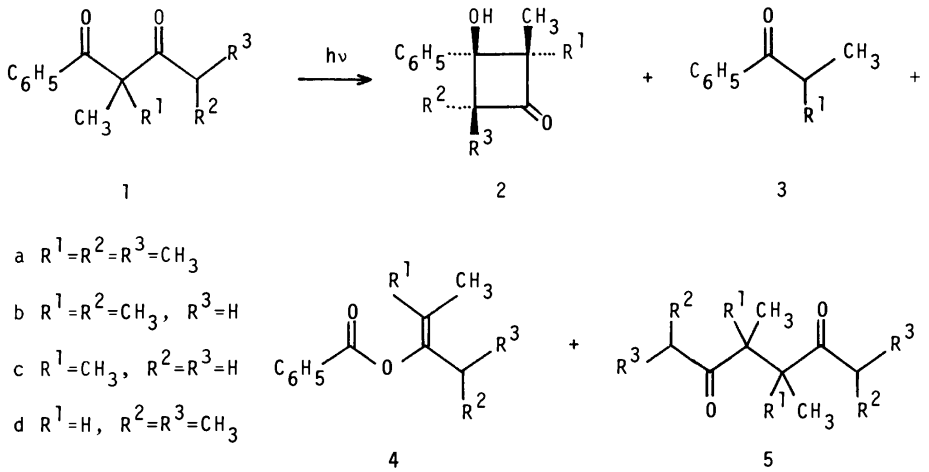

Scheme 1.

unidentified products. The structures of **2a**, **2b**, and **2d** were based on their spectroscopic and analytical properties and further supported by chemical evidence. The IR spectra showed a four-membered carbonyl band at 1770—1775 cm^{-1} and a hydroxyl band at 3600 cm^{-1}. The ^1H NMR spectrum of **2a** showed singlets at δ 1.38 and 1.40 due to four methyl groups, a singlet at δ 1.91 due to a hydroxyl group, and a singlet at δ 7.32 due to aromatic protons. This simple pattern is caused by the symmetry of the molecule. Compound **2a** underwent cycloreversion reaction to **1a** on heating at 150 °C or by treatment with aqueous sodium hydroxide. This chemical behavior strongly supports the proposed structure for **2a**. The ^1H NMR spectra of **2b** and **2d** resemble each other in their splitting patterns except for the aromatic protons, suggesting that they are geometrical isomers with respect to the phenyl and 4-methyl groups. In the spectrum of **2b**, the signal due to the aromatic protons appeared as a multiplet between δ 7.1—7.4, being consistent with the proposed structure in which the phenyl group was restricted to rotate by virtue of its cis-relationship to two methyl groups on C_2 and C_4. Whereas, in the spectrum of **2d**, the aromatic protons appeared as a singlet at δ 7.36. Compound **2b** underwent cycloreversion reaction to **1b** and **1d** in a ratio of 1:2 by heating at 150 °C, but **2d** converted mostly to **1d** under the same reaction conditions. The IR spectra of **4a—c** showed a strong band at 1730—1735 cm^{-1} due to ester carbonyl. The ^1H NMR spectra of **4a** and **4b** showed two singlets at the region between δ 1.5—1.8 due to two methyl groups attached to olefinic carbon atoms. The ^1H NMR spectrum of **4c** showed three singlets at δ 1.55, 1.75, and 1.95 due to three methyl groups attached to olefinic carbon atoms. These spectroscopic properties are consistent with the proposed structures for **4a—c**. The structures of **5a—c** were unambiguously assigned by their IR and NMR spectra.

The formation of **2** can best be explained by type II cyclization which involves 1,5-hydrogen shift from C_4 to the carbonyl oxygen on C_1. The product **3** may be formed by a type II elimination process or by a type I cleavage of the C_2-C_3 bond. It is known that α-diketones[7] and β,γ-unsaturated ketones[8] with γC-H bonds undergo type II cyclization and no type II elimination. The lack of elimination has been attributed to the perpendicular orientation of the p orbital on one radical site relative to the C_2-C_3 σ bond in the 1,4-biradical intermediate. In the 1,4-biradical formed from 1,3-diketone **1**, the C_4 radical site is allylic such that its π-system is completely perpendicular to the C_2-C_3 bond. This suggests that the 1,4-biradical will result in the formation of the cyclization product.

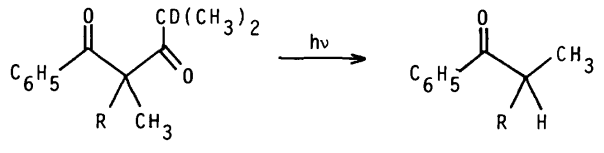

1d-d_1 R=H 3d R=H

1d-d_2 R=D 3d-d_1 R=D

Scheme 2.

Thus, **3** probably arises from a type I cleavage. In order to provide experimental information for the formation of **3**, photolysis of 2,4-dimethyl-1-phenyl-1,3-pentanedione-4-d_1 (**1d**-d_1) and 2,4-dimethyl-1-phenyl-1,3-pentanedione-2,4-d_2 (**1d**-d_2) was investigated. Photolysis of **1d**-d_1 in benzene gave propiophenone (**3d**) and not its deuterio derivative. Similar irradiation of **1d**-d_2 gave propiophenone-α-d_1 (**3d**-d_1) and no α,α-dideuterio derivative. These results suggest that **3** may arise from a type I cleavage.

It is noteworthy that **2b** and **2d** are geometrical isomers with respect to the phenyl and the 4-methyl groups. The ^1H NMR spectra of the irradiation mixtures showed no evidence for the formation of **2d** from **1b** and **2b** from **1d**. Lewis and Hilliard studied[9] the photochemistry of methyl-substituted 1-phenyl-1-butanones. They reported that both 2-methyl-1-phenyl-1-butanone and 1-phenyl-1-pentanone form 2-methyl-1-phenylcyclobutanol; however, only the trans isomer with respect to the phenyl and methyl groups is observed for 2-methyl-1-phenyl-1-butanone, whereas a 3.1:1 trans: cis ratio is observed for 1-phenyl-1-pentanone. They explained the specificity of 2-methyl-1-phenyl-1-butanone by a repulsive interaction of the phenyl and α-methyl groups in the 1,4-biradical. The interaction between the phenyl and γ-methyl groups in the 1,4-biradical was regarded as being small until the 1,4-bond is almost completely formed. The formation of *r*-3-hydroxy-2,2,*c*-4-trimethyl-3-phenylcyclobutanone **2d** from **1d** is consistent with their results. However, the preferential formation of *r*-3-hydroxy-2,2,*t*-4-trimethyl-3-phenylcyclobutanone **2b** rather than the corresponding 2,2,*c*-4-trimethyl isomer **2d** from **1b** is not expected. In the 1,4-biradical from **1b**, the methyl group on the C_4 radical site is probably trans to the C_2-C_3 bond owing to the steric effect,and the rotation of the C_1-C_2 bond is probably hindered by the interactions between the phenyl and α,α-dimethyl groups. Therefore, the transition state for cyclization of the 1,4-biradical from **1b** is pertinently depicted as **6** and results in the formation of **2b**.

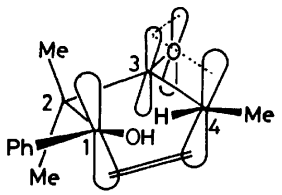

6

Scheme 3.

The formation of **4** and **5** is explained by combination of radicals resulting from type I cleavage. Diketones **1a**, **1b**, and **1c** vary only at C_4. The photochemical results of **1a—c** indicate that as the C_4-H bond strength increases the type II cyclization decreases with increasing type I cleavage. Thus, as expected, appropriate 1-phenyl-1,3-diketones with 3-alkyl substituent undergo type II cyclization *via* 1,5-hydrogen shift from carbon atom α to aliphatic carbonyl group to the aromatic carbonyl oxygen, in competition with type I cleavage. Finally, both cyclization and α-

cleavage were completely quenched by 1,3-pentadiene suggesting a triplet state reaction.

Experimental

All melting points were uncorrected. ^{1}H NMR spectra were recorded on a Varian A-60D or a JEOL FX-90Q spectrometer with tetramethylsilane as an internal standard. ^{13}C NMR spectra were recorded on a JEOL FX-90Q spectrometer. IR spectra were recorded on a JASCO IRA-2 spectrometer. GLC analyses and preparative purification were performed on a Hitachi K-53 instrument using Silicone SE-30 as the stationary phase. Irradiations were carried out with an Ushio UM-452 high-pressure mercury lamp (450 W) or a Rikoh Kagaku UVL-100 high-pressure mercury lamp (100 W) with a water-cooled Pyrex jacket. For column chromatography, Wakogel C-300 or Merck Silica Gel 60 Art. 7734 was used.

Materials. Phenyl 1,3-diketones **1a—c** were prepared by condensation of isobutyrophenone with the corresponding aliphatic aldehydes using methylanilinomagnesium bromide as the condensing agent,[10] followed by chromium(VI) oxide oxidation. Similarly, **1d** was prepared from propiophenone and isobutyraldehyde. Compound **1a** was also prepared by a similar procedures from 2,4-dimethyl-3-pentanone and benzaldehyde. The deuterio derivatives (**1d**-d_1 and **1d**-d_2) of **1d** were prepared as follows. A mixture of 400 mg of **1d**, 100 mg of TsOH, 4 cm^3 of D_2O, and 4 cm^3 of dioxane was heated under reflux for 70 h. The solvent was evaporated, and the residue was extracted with ether. A usual work-up and purification by GLC gave 2,4-dimethyl-1-phenyl-1,3-pentanedione-2,4-d_2 (**1d**-d_2). A mixture of 100 mg of **1d**-d_2, a trace amount of TsOH, 2 cm^3 of H_2O, and 2 cm^3 of dioxane was heated at 80 °C for 40 h. The same procedures as described above gave 2,4-dimethyl-1-phenyl-1,3-pentanedione-4-d_1 (**1d**-d_1).

Photolysis of 1. A typical procedure is described. A solution of 20 mmol of **1** in 400 cm^3 of acetonitrile was irradiated. The progress of the reaction was monitored by TLC and GLC. After removal of the solvent, the residue was chromatographed on silica gel eluted with a hexane–ethyl acetate mixture as eluent to give **2—5**. Compounds **2a**, **2b**, and **2d** were recrystallized from a mixture of hexane and a small amount of benzene. Compounds **3—5** were purified by preparative GLC. Yields are given in Table 1 on the basis of **1** consumed. Physical properties of the isolated products are shown bellow.

*3-Hydroxy-2,2,4,4-tetramethyl-3-phenylcyclobutanone (**2a**).* Mp 135 °C. IR ($CHCl_3$) 1775 (C=O), 3600 (OH) cm^{-1}. ^{1}H NMR ($CDCl_3$) δ=1.38 (s, 6H, Me), 1.40 (s, 6H, Me), 1 91 (s, 1H, OH), and 7.32 (s, 5H, Ph). ^{13}C NMR ($CDCl_3$) δ=18.643 (2q), 24.452 (2q), 63.538 (2s), 79.808 (s), 127.591 (d), 128.045 (2d), 128.374 (2d), 141.362 (s), and 221.386 (s). MS *m/z* (rel intensity) 218 (M$^+$, 3), 148 (M$^+$—Me_2C=C=O, 55), 105 (PhCO, 100), 77 (Ph, 96). Found: C, 77.07; H, 8.34%. Calcd for $C_{14}H_{18}O_2$: C, 77.03; H, 8.31%.

r-*3-Hydroxy-2,2,*t-*4-trimethyl-3-phenylcyclobutanone (**2b**).* Mp 126—127 °C. IR ($CHCl_3$) 1770 (C=O), 3600 (OH) cm^{-1}. ^{1}H NMR ($CDCl_3$) δ=0.80 (s, 3H, Me), 1.04 (d, *J*=7.2 Hz, 3H, Me), 1.48 (s, 3H, Me), 2.46 (s, 1H, OH), 3.96 (q, *J*=7.2 Hz, 1H, CH), and 7.1—7.4 (m, 5H, Ph). ^{13}C NMR ($CDCl_3$) δ=8.200 (q), 18.667 (q), 22.243 (q), 63.018 (d), 64.839 (s), 76.739 (s), 126.553 (2d),126.943 (d), 127.854 (2d), 140.275 (s), and 215.191 (s). MS *m/z* (rel intensity) 204 (M$^+$, 10), 148 (M$^+$—MeCH=C=O, 32), 134 (M$^+$—Me_2C=C=O, 99), 105 (PhCO, 100), 77 (Ph, 39). Found: C, 76.42; H, 7.85%. Calcd for $C_{13}H_{16}O_2$: C, 76.43; H, 7.89%.

r-*3-Hydroxy-2,2,*c-*4-trimethyl-3-phenylcyclobutanone (**2d**).* Mp 106—107 °C. IR ($CHCl_3$) 1775 (C=O), 3600 (OH) cm^{-1}. ^{1}H NMR ($CDCl_3$) δ=0.92 (s, 3H, Me), 1.22 (d, *J*=7.2 Hz, 3H, Me), 1.26 (s, 3H, Me), 1.94 (s, 1H, OH), 4.10 (q, *J*=7.2 Hz, 1H, CH), and 7.36 (s, 5H, Ph). MS *m/z* (rel intensity) 204 (M$^+$, 16), 148 (M$^+$—MeCH=C=O, 46), 134 (M$^+$—Me_2C=C=O, 67), 105 (PhCO, 100), 77 (Ph, 100). Found: C, 76.32; H, 7.89%. Calcd for $C_{13}H_{16}O_2$: C, 76.43; H, 7.89%.

*1-Isopropyl-2-methyl-1-propenyl Benzoate (**4a**).* IR (CCl_4) 1735 (C=O) cm^{-1}. ^{1}H NMR ($CDCl_3$) δ=1.08 (d, *J*=7.0 Hz, 6H, Me), 1.56 (s, 3H, Me), 1.81 (s, 3H, Me), 3.03 (hep, *J*=7.0 Hz, 1H, CH), 7.3—7.7 (m, 3H, aromatic), and 8.1—8.3 (m, 2H, aromatic). Found: C, 77.12; H, 8.33%. Calcd for $C_{14}H_{18}O_2$: C, 77.03; H, 8.31%.

*1-Ethyl-2-methyl-1-propenyl Benzoate (**4b**).* IR (CCl_4) 1730 (C=O) cm^{-1}. ^{1}H NMR ($CDCl_3$) δ=1.02 (t, *J*=7.0 Hz, 3H, Me), 1.56 (s, 3H, Me), 1.74 (s, 3H, Me), 2.36 (q, *J*=7.0 Hz, 2H, CH_2), 7.3—7.7 (m, 3H, aromatic), and 8.0—8.2 (m, 2H, aromatic). ^{13}C NMR ($CDCl_3$) δ=11.581 (q), 17.626 (q), 18.406 (q), 23.350 (t), 117.969 (s), 128.374 (2d), 129.870 (2d), 130.455 (s), 132.926 (d), 144.372 (s), and 164.791 (s). Found: C, 76.34; H, 8.01%. Calcd for $C_{13}H_{16}O_2$: C, 76.43; H, 7.89%.

*1,2-Dimethyl-1-propenyl benzoate (**4c**).*[11] IR (CCl_4) 1730 (C=O) cm^{-1}. ^{1}H NMR (CCl_4) δ=1.55 (s, 3H, Me), 1.75 (s, 3H, Me), 1.95 (s, 3H, Me), 7.2—7.6 (m, 3H, aromatic), and 8.0—8.2 (m, 2H, aromatic). Found: C, 75.55; H, 7.40%. Calcd for $C_{12}H_{14}O_2$: C, 75.76; H, 7.42%.

*2,4,4,5,5,7-Hexamethyl-3,6-octanedione (**5a**).*[12] IR (CCl_4) 1700 (C=O) cm^{-1}. ^{1}H NMR (CCl_4) δ=1.01 (d, *J*=7.0 Hz, 12H, Me), 1.21 (s, 12H, Me), and 3.03 (hep, *J*=7.0 Hz, 2H, CH). Found: C, 73.98; H. 11.59%. Calcd for $C_{14}H_{26}O_2$: C, 74.28, H, 11.57%.

*4,4,5,5-Tetramethyl-3,6-octanedione (**5b**).* IR (CCl_4) 1700 (C=O) cm^{-1}. ^{1}H NMR ($CDCl_3$) δ=1.00 (t, *J*=7.0 Hz, 6H, Me), 1.16 (s, 12H, Me), and 2.50 (q, *J*=7.0 Hz, 4H, CH_2). ^{13}C NMR ($CDCl_3$) δ=8.135 (2q), 22.438 (4q), 32.165 (2t), 52.679 (2s), and 215.841 (2s).

*3,3,4,4-Tetramethyl-2,5-hexanedione (**5c**).*[12] IR (CCl_4) 1700 (C=O) cm^{-1}. ^{1}H NMR (CCl_4) δ=1.14 (s, 12H, Me) and 2.05 (s, 6H, Me).

Pyrolysis of 2. Pyrolysis was done at 150 °C in a sealed Pyrex tube for 3 h. The ^{1}H NMR analysis revealed that **2a** was quantitatively converted to **1a**, **2b** was converted to a 1:2 mixture of **1b** and **1d**, while **2d** was converted to **1d** along with a trace of **1b**.

*Treatment of **2a** with Aqueous Sodium Hydroxide.* To a solution of 50 mg of **2a** in 6 cm^3 of acetone was added one drop of 2 M (1 M=1 mol dm^{-3}) sodium hydroxide. The mixture was stirred at room temperature for 4 h, acidified with 3 M hydrochloric acid, and extracted with ether. A usual work-up gave **1a** in quantitative yield.

*Irradiation of **1d**-d_1 and **1d**-d_2.* A solution of 40 mg of **1d**-d_1 in 4 cm^3 of benzene was placed in a Pyrex tube, and irradiated with a 100 W high-pressure mercury lamp for 5 h. From the irradiation mixture, unlabelled propiophenone was isolated by preparative GLC. A similar irradiation of **1d**-d_2 gave propiophenone-α-d_1.

*Irradiation of **1a,d** in the Presence of 1,3-Pentadiene.* a): A solution of 10 mg of **1a,d** in 1 cm^3 of acetonitrile was placed in a Pyrex tube. b): A solution of 10 mg of **1a,d** in 1 cm^3 of a 1:1 mixture of acetonitrile and 1,3-pentadiene was placed in a Pyrex tube. Both solutions were irradiated under the same conditions with a 100 W high-pressure mercury lamp for 5 h. The ^{1}H NMR analysis showed that no reaction occurred in the case of *b*), while complete disappearance of **1a,d** was observed in the case of *a*).

References

1) N. J. Turro, J. C. Dalton, K. Dawes, G. Farrington, R. Hautala, D. Morton, M. Niemczyk, N. Schore, *Acc. Chem.*

Res., **5**, 92 (1972); P. J. Wagner, *Top. Curr. Chem.*, **66**, 1 (1976).
2) H. Nozaki, Z. Yamaguti, T. Okada, R. Noyori, and M. Kawanisi, *Tetrahedron*, **23**, 3993 (1967); H. Kato, N. Miyamoto, M. Kawanisi, and H. Nozaki, *ibid.*, **26**, 2975 (1970).
3) P. G. Sammes and T. W. Wallace, *J. Chem. Soc., Perkin Trans. 1*, **1975**, 1845.
4) H. Tomioka, N. Hayashi, T. Asano, and Y. Izawa, *Bull. Chem. Soc. Jpn.*, **56**, 758 (1983).
5) M. Feldkimel-Gorodetsky and Y. Mazur, *Tetrahedron Lett.*, **1963**, 369.
6) N. J. Turro, "Modern Molecular Photochemistry" The Benjamin/Cummings Publishing Co., (1978).
7) W. H. Urry and D. J. Trecker, *J. Am. Cem. Soc.*, **84**, 118 (1962).
8) N. C. Yang and D. M. Thap, *Tetrahedron Lett.*, **1966**, 3671.
9) F. D. Lewis and T. A. Hilliard, *J. Am. Chem. Soc.*, **92**, 6672 (1970).
10) A. T. Nielsen, C. Gibbons, and C. A. Zimmerman, *J. Am. Chem. Soc.*, **73**, 4696 (1951).
11) W. M. Muir, P. D. Pitchie, and D. J. Lyman, *J. Org. Chem.*, **31**, 3790 (1966).
12) M. F. Ansell, W. J. Hickinbottom, and P. G. Holton, *J. Chem. Soc.*, **1955**, 349.

Thermal Behavior of Head-to-head Coumarin Dimers and Their Lactone-opened Derivatives

Noriyuki YONEZAWA, Yutaka IKEBE, Tsuyoshi YOSHIDA, Teruhisa HIRAI, Kazuhiko SAIGO, and Masaki HASEGAWA*

Department of Synthetic Chemistry, Faculty of Engineering, The University of Tokyo, Hongo, Bunkyo-ku, Tokyo 113

(Received October 11, 1983)

The thermal behavior of head-to-head coumarin dimers and twelve lactone-opened derivatives was investigated. Though the lactone rings in coumarin dimers are very susceptible to nucleophilic ring-opening, heating these derivatives reformed six-membered lactone rings except for certain imide and diamide derivatives. The large neiboring group effect allowed the relactonization by the attack of hydroxyphenyl group to carbonyl carbon in preference to the scission of cyclobutane ring.

Our recent studies on coumarin dimers revealed that the lactone-openig reaction of coumarin dimers[1] and the photoreaction of their lactone-opened derivatives[2,3] are as attractive as their photochemical formation which have been extensively investigated.[4-16] The large strain of the six-four-six fused ring system in coumarin dimers markedly facilitates their lactone-opening reactions by nucleophiles, permitting the smooth reaction with diamines to give high-molecular-weight polyamides. The resulting polyamides show a characteristic photochemical behavior of the transformation of the main chain *via* the asymmetric scission of the cyclobutane rings.[17-19] On the other hand, the thermal degradation of these polyamides was proposed to proceed in quite a different manner to form five-membered imide ring or six-membered lactone ring by the scission of the main chain.[19]

In the previous communication,[20] we briefly reported the thermal behavior of some lactone-opened derivatives of *syn* head-to-head coumarin dimer. In this paper, we wish to present the anomalous thermal reaction of the lactone-opened derivatives of *syn* and *anti* head-to-head coumarin dimers in detail and to discuss these reaction behaviors mainly from the point of neighboring group effect.

Experimental

Materials. *Syn* and *anti* head-to-head coumarin dimers (*syn* dimer (**1**) and *anti* dimer (**2**)) were prepared by the methods of Krauch *et al.*[9] The lactone-opened derivatives were synthesized according to the methods described in the previous paper:[1] *N,N'*-Dibutyl-*c*-3,*c*-4-bis(2-hydroxyphenyl)-*r*-1,*c*-2-cyclobutanedicarboxamide (*syn* dibutyldiamide (**3**)), *N*-butyl-*c*-3,*c*-4-bis(2-hydroxyphenyl)-*r*-1,*c*-2-cyclobutanedicarboximide (*syn* butylimide (**4**)), *N*-phenyl-*c*-3,*c*-4-bis(2-hydroxyphenyl)-*r*-1,*c*-2-cyclobutanedicarboximide (*syn* phenylimide (**5**)), and *N,N,N',N'*-tetrabutyl-*c*-3,*c*-4-bis(2-hydroxyphenyl)-*r*-1,*c*-2-cyclobutanedicarboxamide (*neo* tetrabutyldiamide (**6**)) were prepared from *syn* dimer (**1**). *Anti* dimer (**2**) was converted to 2-ethoxycarbonyl-1-(2-hydroxyphenyl)-1α,2α,2aβ,8bβ-tetrahydro-3*H*-cyclobuta[*c*]chromen-3-one (*anti* monoethyl ester (**7**)), 1-(2-hydroxyphenyl)-2-phenylcarbamoyl-1α,2α,2aβ,8bβ-tetrahydro-3*H*-cyclobuta[*c*]chromen-3-one (*anti* monoanilide (**8**)), 2-butylcarbamoyl-1-(2-hydroxyphenyl)-1α,2α,2aβ,8bβ-tetrahydro-3*H*-cyclobuta[*c*]chromen-3-one (*anti* monobutylamide (**9**)), *t*-3,*c*-4-bis(2-hydroxyphenyl)-*r*-1,*t*-2-cyclobutanedicarboxylic acid (*anti* dicarboxylic acid (**10**)), diethyl *t*-3,*c*-4-bis(2-hydroxyphenyl)-*r*-1,*t*-2-cyclobutanedicarboxylate (*anti* diethyl ester (**11**)), *t*-3,*c*-4-bis(2-hydroxyphenyl)-*r*-1,*t*-2-cyclobutanedianilide (*anti* dianilide (**12**)), *N,N,N',N'*-tetrabutyl-*t*-3,*c*-4-bis(2-hydroxyphenyl)-*r*-1,*t*-2-cyclobutanedicarboxamide (*anti* tetrabutyldiamide (**13**)), and *N,N'*-dibutyl-*t*-3,*c*-4-bis(2-hydroxyphenyl)-*r*-1,*t*-2-cyclobutanedicarboxamide (*anti* dibutyldiamide (**14**)). 2,2'-Dihydroxystilbene was synthesized by the method reported in the literature.[3]

Measurements. TG-DSC curves were recorded on a Rigaku Denki THERMOFLEX TG-DSC with the heating rate of 5 °C/min in a nitrogen stream. IR spectra were recorded on a JASCO IRA-1 spectrophotometer. ^{1}H-NMR spectra were recorded on a HITACHI R-40 spectrophotometer. High performance liquid chromatography (HPLC) was carried out by detecting UV absorbance (at 280 nm) using a Merck LiChrosorb SI60 column (4ϕ×250 mm) with benzene-ethyl acetate (50:50 or 80:20 v/v%) as an eluent. Thin layer chromatography (TLC) was performed on Merck TLC plates Silica gel 60 F_{254} using the same eluents with HPLC.

Pyrolysis. *A) Pyrolysis in a TG-DSC Pan.* Sample (5—9 mg) was placed in an aluminium pan and heated in the furnace of the TG-DSC instrument under a nitrogen atmosphere. The pyrolyzed products were analyzed by ^{1}H-NMR and IR spectroscopy without purification.

B) Pyrolysis in a Sealed Tube. Sample (*ca.* 10 mg) was placed in a sealed tube under an argon atmosphere and heated in a salt bath. The pyrolyzed product was analyzed by HPLC.

C) Pyrolysis in a Sublimation Tube. Sample (*ca.* 0.2 g) was placed in a sublimation tube and heated in an oil bath under reduced pressure (0.5—1.0 Torr, 1 Torr=133.322 Pa). The product was analyzed by HPLC and IR spectroscopy without purification.

The identification of the pyrolyzed products were accomplished by the comparison of their spectroscopic and HPLC data with those of authentic samples.

Results and Discussion

Thermal Reaction of syn *Head-to-head Coumarin Dimer Derivatives.* The thermal reaction of *syn* dimer (**1**) and its derivatives was investigated on the

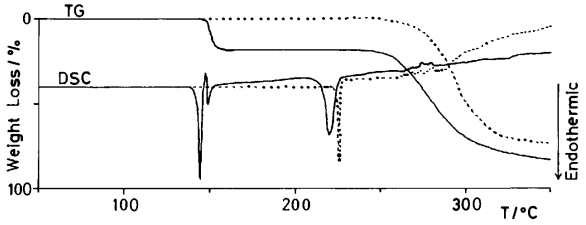

Fig. 1. TG-DSC curves of *syn* dibutyldiamide (**3**) [——] and *syn* butylimide (**4**) [----].

basis of their TG-DSC curves and the data of ^{1}H-NMR, IR, and HPLC analyses of the pyrolyzed products. Figure. 1 shows the TG-DSC curves of *syn* dibutyldiamide (**3**) and *syn* butylimide (**4**). In the TG-DSC curves of *syn* dibutyldiamide (**3**) there were sharp endo- and exothermic peaks at 144 and 147 °C, accompanying with the 16.4% weight loss. These two peaks and weight loss were attributed to melting and decomposition of *syn* dibutyldiamide (**3**) and crystallization of *syn* butylimide (**4**), formed from *syn* dibutyldiamide (**3**) with the elimination of one mole of butylamine (the calculated weight loss is 16.7%). The almost quantitative imide formation was confirmed by comparison of ^{1}H-NMR and IR spectra of the product, obtained by heating *syn* dibutyldiamide (**3**) at 200 °C in a TG-DSC pan, with those of *syn* butylimide (**4**). The thermal reaction in a solution was also carried out and monitored by ^{1}H-NMR spectroscopy. In a DMSO-d_6 solution, *syn* dibutyldiamide (**3**) remained unchanged on standing at 80 °C for 1 h. But the peaks of the cyclobutane ring protons changed completely into those of *syn* butylimide (**4**) on heating at 100 °C for 6.5 h. Moreover, HPLC analysis showed that heating *syn* butylimide (**4**) at 188 to 220 °C under reduced pressure resulted in the complete sublimation of *syn* butylimide (**4**) accompanying with the formation of a small amount of 2,2′-dihydroxystilbene. But, in the products obtained by heating at 270 °C for 3 min in a sealed tube, small amounts of coumarin and *syn* dimer (**1**) were detected along with 2,2′-dihydroxystilbene by HPLC analysis. These results indicate that under rather drastic conditions the symmetric cleavage of the cyclobutane ring *via* an anomalous relactonization occurred certainly in competition with the asymmetric scission of the cyclobutane ring, which would be the single pathway for the degradation at 220 °C.

On the other hand, a complete thermal conversion of *syn* phenylimide (**5**) into *syn* dimer (**1**) was achieved. In the TG-DSC curves of *syn* phenylimide (**5**), a broad endothermic peak in the temperature range of 181—223 °C with the weight loss of 21.4% and a sharp exothermic peak at 190 °C were observed, which correspond to the decomposition of *syn* phenylimide (**5**) with the vaporization of aniline eliminated (the calculated weight loss of aniline is 24.2%) and the crystallization of *syn* dimer (**1**)(Fig.2). Furtheremore, the decomposition mode of *syn* phenylimide (**5**) above 223 °C in TG-DSC curves was essentially the same as that of *syn* dimer (**1**). The product obtained by heating *syn* phenylimide (**5**) at 240 °C in a TG-DSC pan was identified as *syn* dimer (**1**) by ^{1}H-NMR and IR spectroscopy. This relactonization was also observed when a DMSO-d_6 solution of *syn* phenylimide (**4**) was heated at 185 °C for 1 h, giving a mixture of *syn* phenylimide (**4**) and *syn* dimer (**1**) (41:59, based on the peak areas of the cyclobutane ring protons in ^{1}H-NMR spectrum), and the finally decomposed product of *syn* dimer (**1**) was ascertained as coumarin on the basis of spectroscopic data. These thermal behaviors of the lactone-opened derivatives of *syn* dimer (**1**) are summarized in Scheme 1.

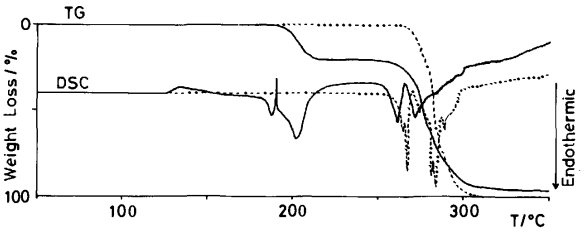

Fig. 2. TG-DSC curves of *syn* dimer (**1**) [----] and *syn* phenylimide (**5**) [——].

The difference in the thermal behaviors of *syn* butylimide (**4**) and *syn* phenylimide (**5**) is interpreted in terms of the electronic nature of their imide linkage. The less electron-donating character of the phenyl group than butyl group lowers the electron density of the imide carbonyl effectively enough to facilitate the nucleophilic attack of 2-hydroxyphenyl group in *syn* phenylimide (**5**).

In spite of the high reactivity of the lactone rings in *syn* dimer (**1**) to nucleophiles, the lactone of a phenolic acid reformed through the elimination of anilino group by the attack of *cis*-positioned 2-hydroxyphenyl group to regenerate *syn* dimer (**1**). It means that anomalously large neighboring group effect plays an important role in these thermal reactions, although phenoxyl group is a very effective leaving group in the lactone-opening reaction of *syn* dimer (**1**) as well as in general substitution reactions.

Thermal Reaction of anti *Head-to-head Coumarin Dimer Derivatives.* The thermal reaction of *anti* dimer (**2**) and its lactone-opened derivatives was investigated by analogous methods.

The thermal reaction of monolactone derivatives of *anti* dimer (**2**) such as *anti* monoethyl ester (**7**), *anti* monoanilide (**8**), and *anti* monobutylamide (**9**) was not clearly distinguished from the TG-DSC curves (Figs. 3—5), but the product sublimed on heating at 300 °C was

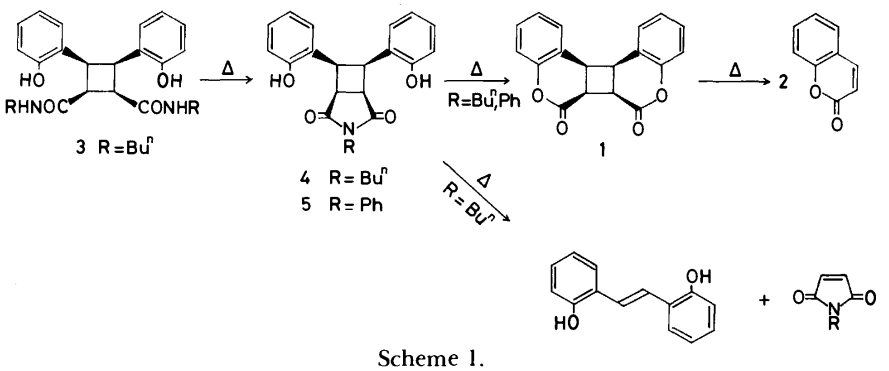

Scheme 1.

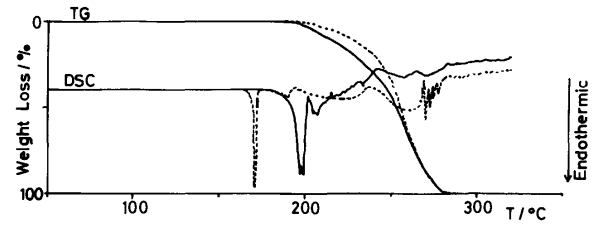

Fig. 3. TG-DSC curves of *anti* monoetyl ester (**7**) [----] and *anti* dietyl diester (**11**) [——].

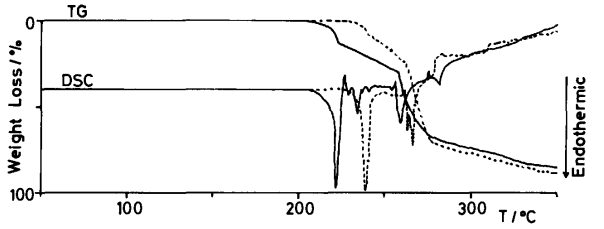

Fig. 4. TG-DSC curves of *anti* monoanilide (**8**) [----] and *anti* dianilide (**12**) [——].

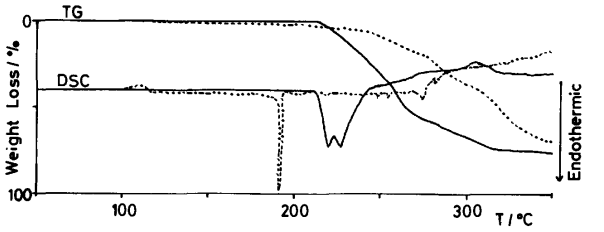

Fig. 5. TG-DSC curves of *anti* monobutylamide (**9**) [----] and *anti* dibutyldimide (**14**) [——].

solely coumarin. To clarify the reaction pathway from monolactone derivatives **7**, **8**, and **9** to coumarin, the heating in a TG-DSC pan was stopped when the weight loss corresponded to the release of one mole of alcohol or amine. The product was proved to be a mixture of the starting material and *anti* dimer (**2**) on the basis of IR and ^{1}H-NMR spectrometric data, indicating that coumarin was produced *via* anomalously relactonized *anti* dimer (**2**). The smooth relactonization was also supported by the following observation: In a DMSO-d_6 solution, *anti* monobutylamide (**9**) turned to a mixture of the starting compound **9**, *anti* dibutyldiamide (**14**), and *anti* dimer (**2**) (70:15:15, based on the peak areas of the cyclobutane ring protons in ^{1}H-NMR spectrum) on heating at 185 °C for 1 h, meaning that *anti* monobutylamide (**9**) slowly decomposed to *anti* dimer (**2**) with the elimination of butylamine, which attacked the residual lactone ring of *anti* monobutylamide (**9**) to give *anti* dibutyldiamide (**14**) (Scheme 2).

In the next stage, the thermal reactions of both lactone-opened derivatives of *anti* dimer (**2**) such as *anti* dicarboxylic acid (**10**), *anti* diethyl diester (**11**), *anti*

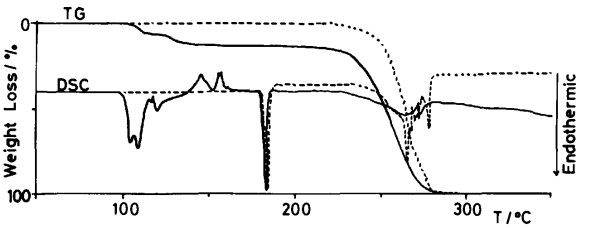

Fig. 6. TG-DSC curves of *anti* dimer (**2**) [----] and *anti* dicarboxylic acid (**10**) [——].

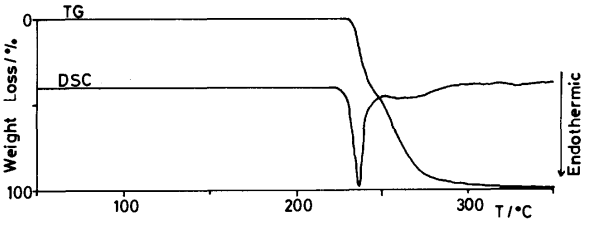

Fig. 7. TG-DSC curves of *anti* tetrabutyldiamide (**13**).

dianilide (**12**), *anti* tetrabutyldiamide (**13**), and *anti* dibutyldiamide (**14**) were carried out. The reactions except for *anti* dibutyldiamide (**14**) were made clear by comparison of their TG-DSC curves with those of the corresponding monolactone compounds **7**—**9** and *anti* dimer (**2**), suggesting that the reaction proceed *via* the monolactone compounds (Figs. 3, 4, 6, and 7). The product, obtained by heating in a TG-DSC pan up to the temperature at which the weight loss corresponded to the release of one mole of water, ethanol, aniline, or dibutylamine, was proved to be a mixture of starting material, the corresponding monolactone derivative, and *anti* dimer (**2**), and further heating was ascertained to give coumarin by TLC analysis and IR and ^{1}H-NMR spectroscopy. But, when *anti* dibutyldiamide (**14**) was heated at 216—217 °C for 30 min (corresponding to the weight loss of one mole of butylamine), the product showed IR absorptions at 1765, 1690, and 1650 cm^{-1} indicating the formation of five-membered imide. However, the thermal reaction of *anti* dibutyldiamide (**14**) in a sublimation tube *in vacuo* at 224—230 °C was found to give only *anti* monobutylamide (**9**) with starting compound **14** by TLC analysis. It is concluded that the both lactone-opened derivative of *anti* dimer (**2**) degradates successively into the corresponding monolactone derivative, *anti* dimer (**2**), and coumarin.

The thermal reactions of *anti* dimer derivatives are summarized in Scheme 3.

Thermal Reaction of neo *Tetrabutyldiamide.* The TG-DSC curves of *neo* tetrabutyldiamide (**6**) in Fig. 8 show gradual weight loss (20.3%) at 170 to 220 °C with an endothermic peak at 170 °C, which corresponds to the loss of one mole of dibutylamine (the calculated weight loss is 23.5%). Then, weight loss restarted at 239 °C and complete weight loss was achieved till

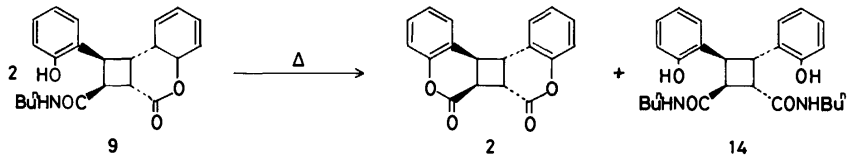

9 2 14

Scheme 2.

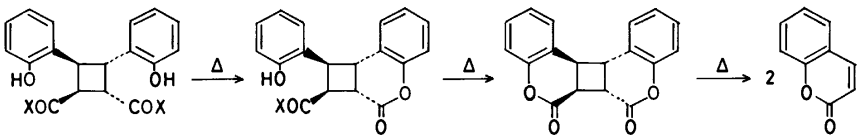

10 X=OH
11 X=OEt
12 X=NHPh
13 X=NBu^n_2
14 X=$NHBu^n$

7 X=OEt
8 X=NHPh
9 X=$NHBu^n$

2

Scheme 3.

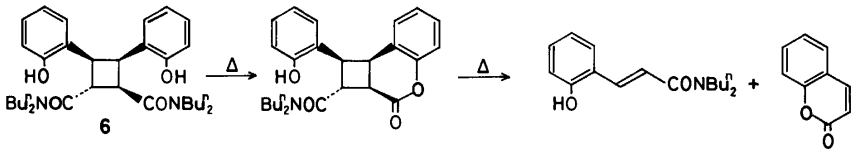

Scheme 4.

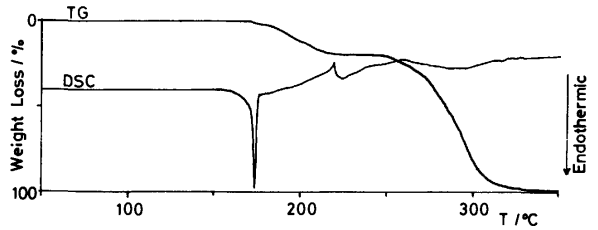

Fig. 8. TG-DSC curves of *neo* tetrabutyldiamide (**6**).

350°C. At the first stage of this reaction, *cis*-positioned carbonyl and 2-hydroxyphenyl groups were presumed to form six-membered lactone ring with the elimination of one mole of dibutylamine. But further heating did not cause the lactone formation between the *trans*-positioned residual carbonyl and 2-hydroxyphenyl groups but resulted in the scission of the cyclobutane ring (Scheme 4).

In conclusion, the imide formation is prior to other reactions when two carbonyl groups are situated in *cis* position. But, in the case of the imide formation being impossible, the relactonization between the *cis*-positioned 2-hydroxyphenyl and carbonyl groups occurs smoothly, and when both the reactions are impossible, the thermal treatment results in the scission of the cyclobutane ring.

In spite of being effective leaving groups in the nucleophilic lactone-opening reactions, 2-hydroxyphenyl groups attack carbonyl carbons of carboxyl, ester, and even amide to reproduce six-membered lactone rings as a common thermal reaction of these derivatives. This anomalous behavior clearly manifested the contribution of the large neighboring group effect in these reactions. In this point of view, the thermal behavior of coumarin dimer derivaitves is substantially influenced by the configuration of substituents on the cyclobutane ring in the similar manner with the observation in their photocleavage reaction.[3)]

References

1) N. Yonezawa and M. Hasegawa, *Bull. Chem. Soc. Jpn.*, **56**, 367 (1983).
2) M. Hasegawa, Y. Suzuki, and N. Kita, *Chem. Lett.*, **1972**, 317.
3) N. Yonezawa, T. Yoshida, and M. Hasegawa, *J. Chem. Soc., Perkin Trans. 1*, **1983**, 1083.
4) G. Ciamician and P. Silber, *Ber.*, **35**, 4128 (1902).
5) G. Ciamician and P. Silber, *Ber.*, **47**, 640 (1914).
6) R. Anet, *Can. J. Chem.*, **40**, 1249 (1962).
7) K. T. Ström, *Ber.*, **37**, 1383 (1904).
8) G. O. Schenck, I. von Wilucki, and C. H. Krauch, *Chem. Ber.*, **95**, 1409 (1962).
9) C. H. Krauch, S. Farid, and G. O. Schenck, *Chem. Ber.*, **99**, 625 (1966).
10) G. S. Hammond, C. A. Stout, and A. A. Lamola, *J. Am. Chem. Soc.*, **86**, 3103 (1964).
11) H. Morrison, H. Curtis, and T. McDowell, *J. Am. Chem. Soc.*,**88**, 5415 (1966).
12) R. Hoffman, P. Wells, and H. Morrison, *J. Org. Chem.*, **36**, 102 (1971).
13) K. Muthuramu and V. Ramamurthy, *J. Org.Chem.*, **47**, 3976 (1982).
14) J. Bregman, K. Osaki, G. M. Schmidt, and F. I. Sonntag, *J. Chem. Soc.*, **1964**, 2021.
15) N. Ramasubbu, T. N. Guru Row, K. Venkatesan, V. Ramamurthy, and C. N. Ramachandra Rao, *J. Chem. Soc., Chem. Commun.*, **1982**, 178.
16) F. D. Lewis, D. K. Howard, and J. D. Oxman *J. Am. Chem. Soc.*, **105**, 3344 (1983).
17) Y. Suzuki, M. Hasegawa, and N. Nishikawa, *J. Polym. Sci.,Polym. Lett. Ed.*, **11**, 173 (1973).
18) M. Hasegawa, N. Yonezawa, T. Kanoe, and Y. Ikebe, *J. Polym. Sci., Polym. Lett. Ed.*, **20**, 309 (1982).
19) M. Hasegawa, K. Saigo, H. Katsuki, N. Yonezawa, and T. Kanoe, *J. Polym. Sci., Polym. Chem. Ed.*, **21**, 2345 (1983).
20) M. Hasegawa, H. Katsuki, N. Yonezawa, T. Yoshida, and Y. Ikebe, *Chem. Lett.*, **1982**, 1325.

Hydrophilicity and Complexing Ability of Alkyl Lariat Ethers

Isao IKEDA, Hiroshi EMURA, and Mitsuo OKAHARA*

Department of Applied Chemistry, Faculty of Engineering, Osaka University, Yamadaoka 2-1, Suita, Osaka 565

(Received October 17, 1983)

A series of long chain alkyl lariat ethers were synthesized and their aqueous properties in the absence and presence of alkali metal cations were investigated by measuring their cloud points and complex stability constants. In spite of the presence of ether oxygen(s) in the side chain, complexing abilities toward sodium and potassium cations did not significantly differ from those of the corresponding alkyl crown ethers. As the number of ether oxygens in the side chain of lariat ethers was increased, the water solubilities were much improved and showed high cloud points. However, the degree of salting-in effect decreased and the increment of cloud point caused by addition of salts decreased, probably due to the increase of acyclicity of the polyether molecule.

Since the crown ethers have strong interactions with metal cations and ammonium ions and show characteristic behaviors, many studies about their complexing ability, phase transfer catalysis, metal cation transport, and metal cation analysis have been reported. Various kinds of substituents have been introduced onto the crown ring to improve these functions.

As the crown ring acts as a hydrophile, some crown compounds having a suitable lipophilic substituent have been synthesized and declared to have interesting properties as nonionic surface active agents. LeMoigne,[1,2] Moroi,[3] and Kuwamura[4-7] reported the surface properties of some of these crown compounds. We also have synthesized long chain alkyl crown ethers (**1**)[8-11] and *N*-(long chain alkyl) monoaza crown ethers (**2**),[9,12] and investigated their surface properties[13,14] and clarified their behaviors toward metal cations in the aqueous solution.[8,15-17] Thus, alkyl crown ethers (**1**), unlike the usual acyclic poly(oxyethylene) type nonionic surfactants, show a salting-in effect in the presence of alkali metal cations based on the formation of metal-crown ring complex.[8,16]

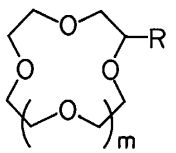

(1)

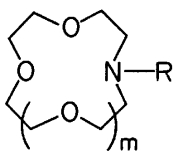

(2)

However, as the crown ring consists of a limited number of oxyethylene units and has no hydroxyl group, the hydrophilicity of this kind of surfactant is low compared with that of the usual nonionic surfactants.[15] Improvement of the hydrophilicity by enlarging the crown ring may affect the complexing ability with metal cations.

Recently, Gokel and his coworkers[18-23] and we[12,24] reported the synthesis and complexing ability of so-called "lariat ethers" (**3**, **4**) which have oxyethylene chain in the side arm. In the case of monoaza lariat ethers (**4**), not only the hydrophilicity but also the complexing ability of the molecule increased by the introduction of oligo-(oxyethylene) group.[12]

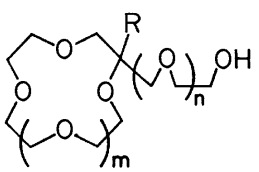

(3) R=H,CH3.

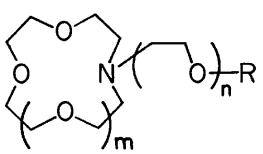

(4) R=H,alkyl.

In this paper, we report the syntheses of long alkyl chain lariat ethers (**5**) having one to three ether oxygens in the side chain and their properties affected by the side oxyethylene chain, especially the increase of hydrophilicity and the variation of salt effect by measuring the cloud point of aqueous solution in the presence of sodium or potassium chloride. The contribution of ether oxygens in the side chain to the complexation toward sodium and potassium cations was directly examined from the measurement of complex stability constants.

Experimental

Materials. The NaCl and KCl were commercial guaranteed-grade reagents, and were dried at 80 °C at reduced pressure [1 Torr(1 Torr=133.322 Pa), 6 h]. The water was deionized by passing through an ion-exchange resin column. Lariat ethers having one oxygen in the side chain (**5a—d**) were synthesized from alkyl glycidyl ethers and oligoethylene glycol according to the reported method (Scheme 1).[10] Lariat ethers having two or three oxygens in the side chain (**5e—l**) were synthesized by Williamson ether synthesis from hydroxymethyl crown ether (**7**)[10] and **8** which was prepared by chlorination of oligoethylene glycol monoalkyl ethers according to Scheme 2. As a typical procedure, preparation of 2-(dodecyloxy)ethoxymethyl-15-crown-5 (**5f**) is described. To 10 ml of *t*-butyl alcohol including 5 g (0.02 mol) of **7** (m=2), 0.35 g (0.015 mol) of sodium was dissolved and 7.5 g (0.03 mol) of 2-chloroethyl dodecyl ether (**8**, n=1) was added dropwise. After heating to reflux for 6 h, the *t*-butyl alcohol was evaporated off at reduced pressure. The residue was extracted with dichloromethane. After removal of the solvent, the oily

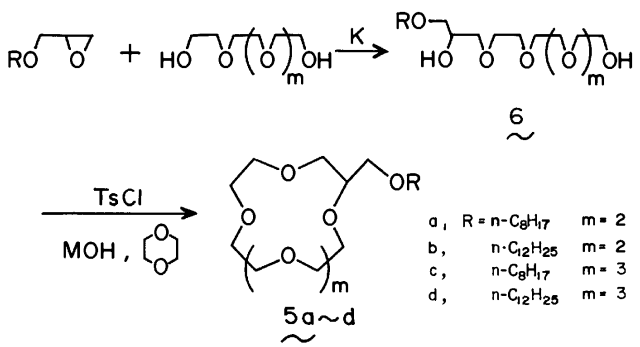

Scheme 1. Preparation of crown ethers having one oxygen atom in the side chain.

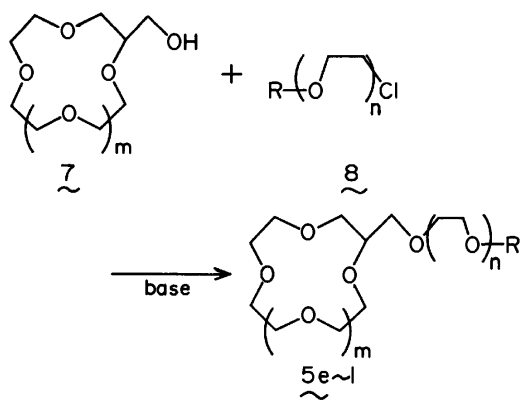

Scheme 2. Preparation of crown ethers having two to three oxygen atoms in the side chain.

material which remained was distilled by Kugelrohr apparatus to give a colorless oil (**5f**) 6.2 g (yield 67%). In Table 1 are listed the boiling points (Kugelrohr distillation) and the yields of **5**. All the ethers (**5**) showed the almost the same IR and NMR spectra. IR (cm^{-1}); 2940(s), 2860(s), 1470(m), 1350(m), 1290(w), 1250(w), 1120(s), and 940(w). NMR; δ=0.89 (t, 3H), 1.28 (12 or 20H), 3.3—3.9 (m, [4*m*+4*n*+15]H). Elemental analyses showed the good agreement within 0.4% of deviation.

Measurement of Cloud Point. The cloud point (T_{cp}) of each aqueous solution of crown compound was determined by observation with naked eyes, using a solution of 10 mg of crown ether in 1 ml of water or the salt solution of specific concentration in a test tube of 10 mm of inner diameter under heating with a rate of *ca.* 0.5 °C/min.

Measurement of Stability Constant of Complexes. Stability constants were measured by Frensdroff's method.[25]

Results and Discussion

Lariat ethers having a long alkyl group were synthesized by two procedures: those having one oxygen in the side chain (**5a—d**) were synthesized by the cyclization of alkoxymethyl oligoethylene glycol (**6**) (Scheme 1),[10,11] and those having two or three ether oxygens in the side chain (**5e—l**) were synthesized from hydroxymethyl crown ethers (**7**)[10] and α-alkyl-ω-chlorooligo (oxyethylene) (**8**) by Williamson ether synthesis (Scheme 2) since the oligoethylene glycols having an excessively long side chain were not desirable as a precursor for cyclization, from the point of difficulty in purification due to their high boiling points.

Cloud points of twelve kinds of long chain alkyl lariat ethers are listed in Table 2, together with those of alkyl crown ethers (**1**) for comparison.

When the size of crown ring and the length of alkyl chain were the same, cloud points of the crown compounds rose almost linearly with increasing the number of ether oxygen atoms in the side chain. The slopes of four straight lines were almost equal. The degree of rise in cloud point with increase of the number of ether oxygen atom in the side chain was

Table 1. Synthetic and spectral data of crown ethers

	Crown ether		MOH	Bp[a]	MS	Yield[b]
	m	*n*		θ_b/°C (Torr)	(M^+)	%
5a	2	0	NaOH	130(0.03)	362	59
5b	2	0	NaOH	150(0.05)	418	56
5c	3	0	KOH	150(0.01)	406	55
5d	3	0	KOH	180(0.01)	462	51
5e	2	1	NaOH	150(0.01)	406	65
5f	2	1	NaOH	180(0.05)	406	67
5g	2	2	NaOH	180(0.01)	462	71
5h	2	2	NaOH	200(0.01)	506	66
5i	3	1	KOH	180(0.05)	450	71
5j	3	1	KOH	200(0.03)	494	66
5k	3	2	KOH	200(0.01)	506	67
5l	3	2	KOH	220(0.01)	550	64

a) Kugelrohr distillation. b) **5a—d**: Yields of cyclization, **5e—l**: yields of side chain introduction.

Table 2. Cloud points of aqueous solution of crown ethers

	Crown ether		Cloud point		Crown ether		Clound point
	m	*n*	°C		*m*	*n*	°C
1[a]	2	—	14.0	**1**[a]	3	—	31.0
5a	2	0	25.0	**5c**	3	0	43.0
5e	2	1	39.0	**5g**	3	1	52.5
5i	2	2	50.0	**5k**	3	2	60.0
1[b]	2	—	<0	**1**[b]	3	—	18.5
5b	2	0	6.0	**5d**	3	0	28.5
5f	2	1	22.0	**5h**	3	1	41.0
5j	2	2	28.5	**5l**	3	2	51.0

a) R=C_8H_{17}. b) R=$C_{12}H_{25}$.

about 50 to 70% of that with increase of the oxygen number in the crown ring.

Many studies about the effect of added inorganic electrolytes on the cloud points of open chain poly(oxyethylene) type nonionics have been reported.[26-29] In the presence of metal salts except for the salts having a counter anion of water-destructuring type, such as SCN^-, NO_3^-, and so on, the cloud points of these open chain poly(oxyethylene) type nonionics usually fall down, due to the salting-out effect. In the case of crown ethers, however, a salting-in effect based on the complexation of crown ring with metal cations causes the rise of cloud point compared with the cases in the absence of metal salts.[8,16,17] Figures 1 and 2 show the

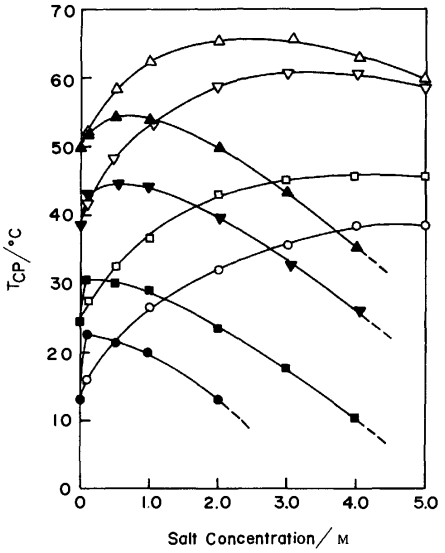

Fig. 1. Cloud points of aqueous solution of alkyl lariat ethers. —Octyl 15-crown-5 ethers—

Crown Ether	m	n	NaCl	KCl
1	2	-	○	●
5a	2	0	□	■
5e	2	1	▽	▼
5i	2	2	△	▲

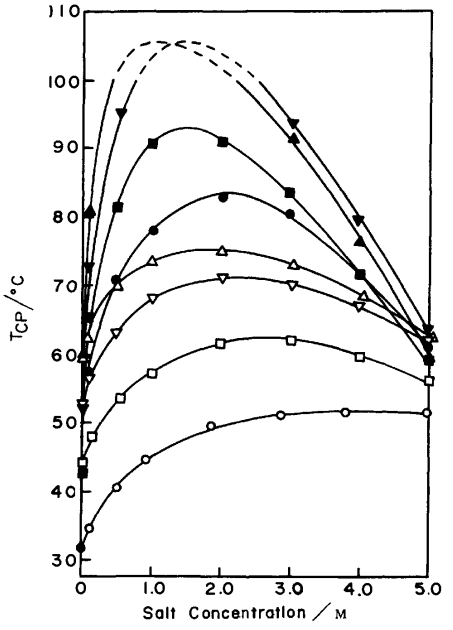

Fig. 2. Cloud points of aqueous solution of alkyl lariat ethers. —Octyl 18-Crown-6 ethers—

Crown Ether	m	n	NaCl	KCl
1	3	-	○	●
5c	3	0	□	■
5g	3	1	▽	▼
5k	3	2	△	▲

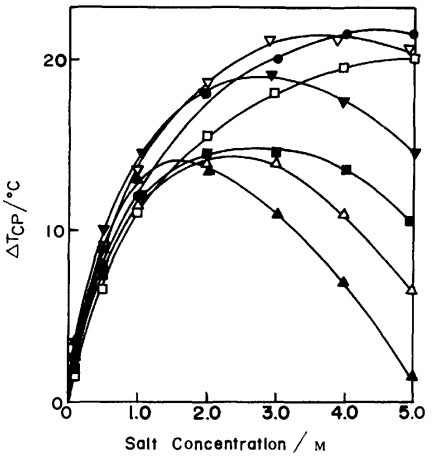

Fig. 3. Differences of cloud points (ΔT_{cp}) in the absence and presence of sodium chloride. —Dodecyl derivatives—

Crown Ether	m	n	Crown Ether	m	n
			1	3	- ●
5b	2	0 □	5d	3	0 ■
5f	2	1 ▽	5h	3	1 ▼
5j	2	2 △	5l	3	2 ▲

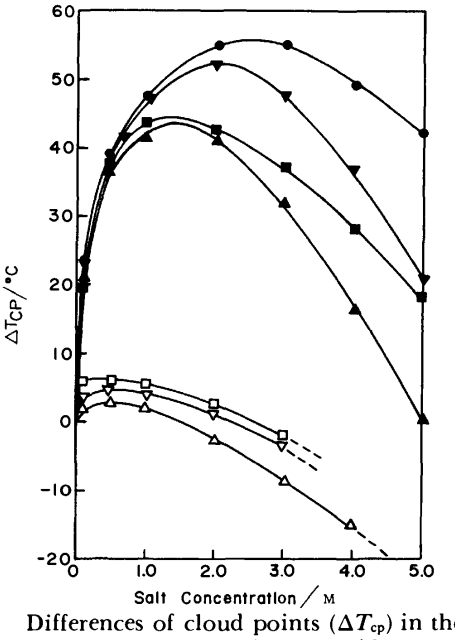

Fig. 4. Differences of cloud points (ΔT_{cp}) in the absence and presence of potassium chloride. —Dodecyl derivatives—

Crown Ether	m	n	Crown Ether	m	n
			1	3	- ●
5b	2	0 □	5d	3	0 ■
5f	2	1 ▽	5h	3	1 ▼
5j	2	2 △	5l	3	2 ▲

correlations between the cloud points of aqueous solutions of octyl derivative series of lariat ethers and the concentrations of sodium and potassium chlorides as examples. In Figs. 3 and 4 are shown the correlations of the concentration of salt and the difference of cloud point (ΔT_{CP}) between the values in the absence and presence of sodium or potassium chloride, using dodecyl derivatives as examples.

15-Crown-5-NaCl System (Figs. 1 and 3). When the salts were added to the aqueous solutions of these crown ethers, the cloud points rose, since the salting-in effect is superior to the salting-out effect. However, as the salting-out effect works concurrently, the cloud points began to fall above a certain salt concentration.[16] In the case of octyl-15-crown-5, the ΔT_{cp} was the maximum at around the concentration of 4.5 m of NaCl. And the higher the number of ether oxygen atoms in the side chain, the lower the concentration of salts at which the ΔT_{cp} was maximum, though the cloud points themselves were higher (Fig. 1). As the cloud point of dodecyl-15-crown-5 in the absence of salts was below 0 °C, the maximum values of ΔT_{cp} could not be calculated, but the homologues having one and more than one ether oxygens in the side chain, showed the same tendency as the octyl derivatives showed. This can be explained by the following reasons: as the number of oxygen atoms in the side chain increased, the water-solubility of the whole molecule was enhanced, but it became easier to salt out the molecule, probably because the acyclicity of the molecule increased. Acyclicity causes the salting-out effect, and lariat ethers are apt to be salted-out even at a lower salt concentration. The higher the number of ether oxygens in the side chain, the larger the degree of fall of cloud point by the salting-out effect.

18-Crown-6-NaCl System (Figs. 2 and 3). In this system the salting-in effect works strongly in general and the T_{cp}s rise markedly. Upon the increase of number of oxygen in the side chain, the salting-out effect became also larger and the salt concentration showing the maximum ΔT_{cp} shifted to the lower region.

18-Crown-6-KCl System (Figs. 2 and 4). It is well known that the complexes of this combination are the most stable of all the crown ether-alkali metal cation systems. They showed the largest ΔT_{cp} values, 40—50 °C, showing that they are affected by the strong salting-in effect due to the strong complexation.

15-Crown-5-KCl System (Figs. 1 and 4). In this system, different from others, the complexing ability is small and the salting-in effect is so weak that ΔT_{cp} did not exceed 10 °C. The salting-out effect begins to overcome the salting-in effect even at as low as 2 m of salt concentration.

In all the systems, the changes of ΔT_{cp} caused by the difference of alkyl chain length were almost the same in both the octyl and dodecyl series and it is obvious that the additional methylene units in the side chain bring about only the increase of lipophilicity of the molecule. Considering from the changes of cloud point of a series of the lariat ethers which have the same alkyl chain and the same crown ring, it can be concluded that ether groups in the side chain are related to hydration, namely aqueous solubility, rather than the complexation with metal cations. To confirm directly the participation of ether oxygens in the side chain to the complexation, the stability constants of complexes with sodium and potassium cations in methanol were measured and are shown in Table 3. ΔT_{cp} of lariat ethers, especially in the low salt-concentration region where the neat effect of salting-in phenomenon was revealed, showed a good correlation with their complex stability constants, as was reported in the case of alkyl crown ethers[8,15,16] and alkyl aza crown ethers.[17]

Little differences of the stability constant were found within a series of the lariat ethers which had the same crown ring.

We already reported that, for the lariat ethers **3** (R=CH_3) and **4**, the higher the number of ether oxygen atoms in the side chain, the larger the stability constants. This fact was explained as due to the participation of the ether oxygens in the side chain. In the case of **3**, the geminal methyl group forces sterically oligo(oxyethylene) chain to take an advantageous position to complexation.[24,30] And in the case of **4**, the oligo-

Table 3. Stability constants of crown ethers with sodium and potassium cations

	Crown ether		Na^+		K^+	
			log K_1		log K_1 (+log K_2)	
	m	n	MeOH[a,c]	MeOH-H_2O[b,c]	MeOH[a,c]	MeOH-H_2O[b,c]
	15-Crown-5		3.31[e]	—	3.35(+2.62)[d]	—
1[f]	2	—	3.18±0.03	2.73±0.03	3.05(+2.32)[d]	2.52±0.06
5a	2	0	3.18±0.04	2.72±0.02	3.22(+2.41)[d]	2.56±0.05
5e	2	1	3.22±0.04	2.72±0.03	3.14(+2.30)[d]	2.57±0.05
5i	2	2	3.23±0.04	2.75±0.02	3.28(+2.20)[d]	2.71±0.07
	18-Crown-6		4.30[e]	—	6.10[e]	—
1[f]	3	—	3.91±0.03	3.17±0.05	5.39±0.01	4.7[g]
5c	3	0	3.97±0.05	3.27±0.03	5.64±0.05	4.8[g]
5g	3	1	4.00±0.06	3.24±0.06	5.49±0.00	4.8[g]
5k	3	2	3.97±0.08	3.26±0.06	5.50±0.01	4.8[g]

a) in methanol. b) In water/methanol=10/90 (v/v). c) At 25 °C, values in 95% of confidence interval. d) Calculated by Frensdorff's equation. e) Values reported in Ref. 24. f) R=n-C_8H_{17}. g) Since values are dependent on the ratio of ligand and cation in the range of measured conditions, values at specific conditions (KCl=2.5 mmol·l^{-1}, 50 ml; ligand=12 mmol·l^{-1}, 20 ml) are shown.

(oxyethylene) chain can easily participate in the complexation because the junction (the nitrogen atom) of the crown ring and the side chain is flexible.[17] In the case of **5**, to the contrary, contribution of the side oligo(oxyethylene) chain to the complexation is found to be quite small. It is natural to consider that the oxygens in the side chain are apt to be located too far from the crown plane to induce-fit effectively the metal cation which complexes with the crown ring.

To determine the complexation of lariat ethers in the aqueous solution, the stability constants in methanol containing 10% of water were measured. Gokel measured the stability constants of complexes of 15-crown-5 and 18-crown-6 with sodium cation in the mixture of methanol and water and reported that the stability constants enhanced proportionally to the ratio of methanol in the mixture, and that no confusion in the order of stability constants was found between any two crown ethers.[31]

The results are shown in Table 3. The values were smaller than those in methanol, but the tendency was quite the same with that in methanol, showing that the ether oxygens in the side chain did not contribute to complexation in water either.

As a result, it can be concluded that the lariat ethers having desirable HLB and with complexing ability and selectivity of the parent alkyl crown ethers toward alkali metal cations could be designed by combining an alkyl group and a crown ring with a suitable length of oxyethylene chain.

References

1) J. LeMoigne, Ph. Gramain, and J. Simon, *J. Colloid Interface Sci.*, **60**, 565 (1977).
2) J. LeMoigne and J. Simon, *J. Phys. Chem.*, **84**, 170 (1980).
3) Y. Moroi, E. Pramauro, M. Grätzel, E. Pelizzetti, and P. Tundo, *J. Colloid Interface Sci.*, **69**, 341 (1979).
4) T. Kuwamura and T. Kawachi, *Yukagaku*, **28**, 195 (1979).
5) T. Kuwamura and S. Yoshida, *Nippon Kagaku Kaishi*, **1980**, 427.
6) S. Inokuma, N. Aoki, E. Kameyama, and T. Kuwamura, *Yukagaku*, **29**, 767 (1980).
7) S. Inokuma, T. Negishi, E. Kameyama, and T. Kuwamura, *Nippon Kagaku Kaishi*, **1982**, 479.
8) M. Okahara, P. -L. Kuo, S. Yamamura, and I. Ikeda, *J. Chem. Soc., Chem. Commun.*, **1980**, 586.
9) P. -L. Kuo, M. Miki, I. Ikeda, and M. Okahara, *J. Am. Oil Chemists'. Soc.*, **57**, 227 (1980).
10) I. Ikeda, S. Yamamura, Y. Nakatsuji, and M. Okahara, *J. Org. Chem.*, **45**, 5355 (1980).
11) I. Ikeda, H. Emura, S. Yamamura, and M. Okahara, *J. Org. Chem.*, **47**, 5150 (1982).
12) A. Masuyama, Y. Nakatsuji, I. Ikeda, and M. Okahara, *Tetrahedron Lett.*, **22**, 4665 (1981).
13) P. -L. Kuo, I. Ikeda, and M. Okahara, *Tenside Detergents* **19**, 4 (1982).
14) P. -L. Kuo, I. Ikeda, and M. Okahara, *Tenside Detergents*, **19**, 204 (1982).
15) P. -L. Kuo, I. Ikeda, and M. Okahara, *Bull. Chem. Soc. Jpn.*, **55**, 3356 (1982).
16) P. -L. Kuo. K. Tsuchiya, I. Ikeda, and M. Okahara, *J. Colloid Interface Sci.* **92**, 463 (1983).
17) A. Masuyama, P. -L. Kuo, I. Ikeda, and M. Okahara, *Nippon Kagaku Kaishi*, **1983**, 249.
18) G. W. Gokel, D. M. Dishong, and C. J. Diamond, *J. Chem. Soc., Chem. Commun.*, **1980**, 1053.
19) D. M. Dishong, C. J. Diamond, and G. W. Gokel, *Tetrahedron Lett.*, **22**, 1663 (1981).
20) R. A. Schultz, D. M. Dishong, and G. W. Gokel, *Tetrahedron Lett.*, **22**, 2623 (1981).
21) R. A. Schultz, D. M. Dishong, and G. W. Gokel, *J. Am. Chem. Soc.*, **104**, 625 (1982).
22) R. A. Schultz, E. Schlegel, D. M. Dishong, and G. W. Gokel, *J. Chem. Soc., Chem. Commun.*, **1982**, 242.
23) D. M. Dishong, C. J. Diamond, M. I. Cinoman, and G. W. Gokel, *J. Am. Chem. Soc.*, **105**, 586 (1983).
24) Y. Nakatsuji, T. Nakamura, M. Okahara, D. M. Dishong, and G. W. Gokel, *Tetrahedron Lett.*, **23**, 1351 (1982).
25) H. F. Frensdorff, *J. Am. Chem. Soc.*, **93**, 600 (1971).
26) M. J. Schick, *J. Colloid Interface Sci.*, **17**, 801 (1962).
27) H. Schott, *J. Colloid Interface Sci.*, **43**, 150 (1973).
28) H. Schott and S. -K. Han, *J. Pharm. Sci.*, **64**, 658 (1975).
29) F. Tokiwa and T. Matsumoto, *Bull. Chem. Soc. Jpn.*, **48**, 1645 (1975).
30) Y. Nakatsuji, T. Nakamura, M. Okahara, D. M. Dishong, and G. W. Gokel, *J. Org. Chem.*, **48**, 1237 (1983).
31) D. M. Dishong and G. M. Gokel, *J. Org. Chem.*, **47**, 147 (1982).

 © 1984 The Chemical Society of Japan Bull. Chem. Soc. Jpn., 57, 1617—1625 (1984)

The Thermal Isomerization of Azobenzenes. III.[1] Substituent, Solvent, and Pressure Effects on the Thermal Isomerization of Push-pull Azobenzenes

Norio NISHIMURA,* Shinya KOSAKO, and Yoshimi SUEISHI
Department of Chemistry, School of Science, Okayama University, Okayama 700
(Received July 18, 1983)

The substituent, solvent, and pressure effects on the rate of the thermal *cis*-to-*trans* isomerization of 4-dimethylamino-4′-nitroazobenzene(NDAAB) derivatives have been studied. 2-Methyl- and 2′-chloro-NDAAB isomerize faster than NDAAB, and 2′-methyl- and 2-chloro-NDAAB isomerize slower than NDAAB. For 2,2′-dimethyl- and 2,2′-dichloro-NDAAB, the rates are between those of the monosubstituted ones. These findings are very similar to those for 4-(dimethylamino)azobenzene (DAAB) derivatives, and no fundamental difference in the kinetic-substituent effects was observed between NDAAB and DAAB. The volume of activation, which is of a negative value, varies remarkably from solvent to solvent and from substituent to substituent; its magnitude increases generally with an increase in the solvent polarity. Even for DAAB and 4,4′-bis(diethylamino)azobenzene (BDEAAB), the rate is appreciably accelerated by external pressures in polar solvents. It is concluded that the observed results are more consistent with the inversion mechanism than with the rotational mechanism.

The mechanism of the thermal *cis*-to-*trans* isomerization of azobenzenes has attracted much attention for many years. Two mechanisms have been proposed. One involves rotation around the N=N double bond and includes the π-bond rupture. The other involves inversion on either or both of the azo-nitrogen atoms, the π-bond remaining intact.

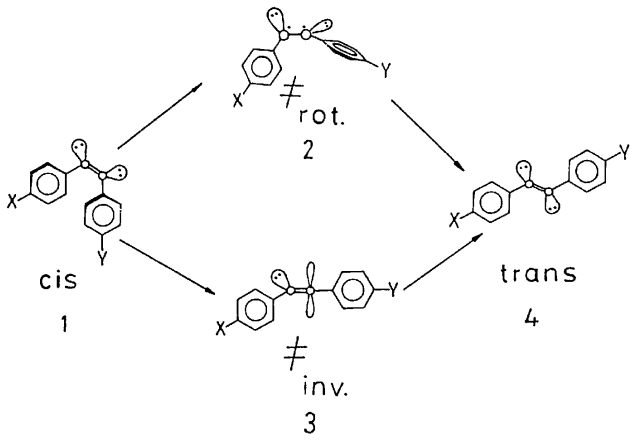

Theoretical[2,3] and experimental[4-7] approaches favor the inversion mechanism for most cases. However, the rotational mechanism has been revived recently.[8-13] Nerbonne and Weiss[10] studied the isomerization of azobenzene in the cholesteric and isotropic phases and, observing that the Arrhenius plot in a liquid crystal did not yield a single straight-line slope, suggested the rotational mechanism. Whitten *et al.*[8,9] found a large solvent effect for push-pull-substituted azobenzenes and suggested a dipolar rotational transition state **5**.

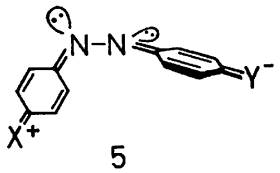

5

Asano *et al.*[11-13] reported that the isomerization rate of 4-dimethylamino-4′-nitroazobenzene (NDAAB) is considerably accelerated by external pressures in benzene and in polar solvents, but is little affected in hexane. According to them, this can be regarded as evidence for a change in the mechanism with the solvents for such push-pull azobenzenes, *i.e.*, from inversion in hexane to rotation in benzene. Indeed, such large pressure and solvent effects are consistent with the change in mechanism from solvent to solvent. However, it would be unnatural to expect such a drastic change in mechanism in nonpolar solvents. Therefore, it seems necessary to examine whether or not the proposed mechanism also accommodates other factors influencing the isomerization rate.

Several years ago, we reported on the kinetic data for the thermal isomerization of 36 kinds of azobenzene derivatives.[1,14] We found that the introduction of substituents almost invariably accelerates the rate, irrespective of the nature of the substituents. The substituent effect is of an additive nature, and the following Hammett-type equation holds approximately:

$$\log k/k_0 = \sum\sigma_{c-t}, \quad (1)$$

where k_0 and k refer to the rate constant of a standard azobenzene derivative properly chosen and that of substituted derivatives with respect to the standard one respectively, and where σ_{c-t} denotes a substituent constant characteristic of the kind and the position of the substituent in question. We also found that the wavelength at the maximum absorption of the conjugation band of a *trans*-isomer is closely related to the rate constant. Another finding is that 2-methyl-4-(dimethylamino)azobenzene isomerizes about three times faster than 4-(dimethylamino)azobenzene (DAAB), whereas the 2′-methyl group rather retards the rate. We have interpreted these facts in terms of the resonance stabilization in the inversion-transition state. However, since the rotational mechanism has been newly proposed for NDAAB, we wish to examine which of the proposed mechanisms is more compatible with the experimental observations. Our views concerning the mechanistic implications will be described in some detail.

Experimental

Materials. The NDAAB derivatives were prepared by diazo coupling from the corresponding *N,N*-di-

methylanilines and *p*-nitroanilines. The crude products were purified by column chromatography on silica gel and recrystallized from ethanol. The melting points, IR, NMR, and UV spectra were utilized for identification. For 2-methyl-NDAAB: mp 183—184 °C (lit, [15] 179—180.5 °C). For 2'-methyl-NDAAB: mp 159.5—160.5 °C (lit, [16] 161—163 °C). For 2,6-dimethyl-NDAAB: mp 169—170 °C. Found: C, 64.34; H, 6.21; N, 18.95%. Calcd for $C_{16}H_{18}N_4O_2$: C, 64.41; H, 6.08; N, 18.78%. For 2,2',6-trimethyl-NDAAB: mp 198—199 °C. Found: C, 65.45; H, 6.34; N, 17.86%. Calcd for $C_{17}H_{20}N_4O_2$: C, 65.37; H, 6.45; N, 17.94%. For 2-chloro-NDAAB: sublimed *ca.* 209 °C. Found: C, 55.35; H, 4.57; N, 18.55%. Calcd for $C_{14}H_{13}ClN_4O_2$: C, 55.18; H, 4.30; N, 18.39%. For 2'-chloro-NDAAB: mp 198—199 °C (lit, [17] 198—199 °C). For 2,2'-dichloro-NDAAB: mp 226—227 °C. Found: C, 49.36; H, 3.65; 16.41%. Calcd for $C_{14}H_{12}Cl_2N_4O_2$: C, 49.58; H, 3.57; N, 16.52%. The preparation of the other materials has been described elsewhere.[1] The solvents were purified and distilled in the usual manner.

Measurements. The pressure vessel,[18] with four optical windows, was made of SNCM-8 stainless steel and equipped with a water-circulating jacket. In this work, we used only two of the windows. High pressures were generated by means of a plunger pump and measured by means of a Heise Bourdon gauge. A turn mirror was installed between the pressure vessel and a monochrometor in order to switch the excitation light and the monitoring light. A 650-watt projector lamp was used for excitation. The light was passed through a 20-mm water layer and introduced into an inner cell. The cell was made of Teflon and consists of two compartments connected by a capillary tube (ϕ=1 mm). This made the uniform irradiation of the solution in the upper compartment possible, avoiding the mixing of the irradiated and unirradiated solutions. In order to avoid the adventitious contamination of acid which may affect the isomerization rate, small amounts of piperidine (0.3%) were added to the reaction solution. The solution was charged in the inner cell, and a desired pressure was applied to the solution through a liquid-separation piston. After a constant temperature and pressure had been attained, the solution was irradiated for *ca.* 1 min. Then the mirror was turned by 45 °, the absorption maximum of the *trans*-isomers was monitored by means of a Hitachi 139 spectrophotometer, and the absorbance was recorded. Satisfactory and reproducible first-order plots were obtained. The values of the rate constants listed in the tables are the average of several runs, the errors being within 2% in most cases. For 2,6-dimethyl- and 3-methyl-NDAAB in hexane, 2,6-dimethyl-NDAAB in CCl_4, 2,2',6-trimethyl-NDAAB and 2'-chloro-NDAAB in toluene, and NDAAB in chloroform, the errors were within 5%.

Results

The wavelengths λ_{max} (nm) at the maximum absorption of the conjugation band of *trans*-NDAAB and other substances in various solvents are given in Table 1. It is noted that λ_{max} is quite sensitive to such solvent-polarity parameters as the E_T-values; *i.e.*, the band generally exhibits a bathochromic shift with an increase in the solvent polarity, with the exception of methanol, for which a specific solvent-solute interaction takes place, probably *via* hydrogen bonding. In Tables 2—4, the first-order rate constants in several

TABLE 1. ABSORPTION MAXIMA, λ_{max}(nm) OF THE CONJUGATION BAND OF *trans*-4-DIMETHYLAMINO-4'-NITROAZOBENZENE AND OTHERS IN SOLVENTS OF DIFFERENT POLARITIES

	Hexane	CCl_4	Toluene	Benzene	$CHCl_3$	Methanol
E_T/kcal†	30.9	32.5	33.9	34.5	39.1	55.5
Compound						
NDAAB[a]	440	453	466	467	479	474
2-Me-NDAAB	450	462	477	476	490	488
2'-Me-NDAAB	440	451	462	463	470	469
2,2'-Me_2-NDAAB	449	460	471	471	480	481
2,6-Me_2-NDAAB	438	447	455	453	460	457
2,2',6-Me_3-NDAAB	442	453	462	461	467	466
2-Cl-NDAAB	439	449	458	458	468	465
2'-Cl-NDAAB	459	474	488	488	500	493
2,2'-Cl_2-NDAAB	455	465	478	478	488	487
3-Me-NDAAB	407	420	427	427	433	420
DAAB[b]	400[d]		409		409	406
2-Me-DAAB	405[d]		415		415	412
BDEAAB[c]	431[d]		448		463	470

a) 4-Dimethylamino-4'-nitroazobenzene. b) 4-(Dimethylamino)azobenzene. c) 4,4'-Bis(diethylamino)azobenzene. d) In cyclohexane. † 1 kcal=4.184 kJ.

TABLE 2. FIRST-ORDER RATE CONSTANTS ($10^3k/s^{-1}$) FOR THE THERMAL *cis*-to-*trans* ISOMERIZATION OF NDAAB AND ITS DERIVATIVES IN HEXANE

Compound	25 °C	30 °C	35 °C	40 °C	45 °C
NDAAB	2.75	4.40	6.62	10.3	
2-Me-	4.38	6.87	11.5	18.3	
2'-Me-	2.05	3.50	5.65	8.65	
2,2'-Me_2-	3.95	6.28	9.77	15.3	
2,6-Me_2-	2.38	3.75	6.00	7.63	
2,2',6-Me_3-	3.45	5.45	9.30	13.6	
2-Cl-		1.59	2.68	3.60	5.56
2'-Cl-	21.5	32.2	55.8	86.3	
2,2'-Cl_2-	5.97	7.85	12.9	23.2	33.8

solvents are listed. The activation parameters were estimated by using the least-squares method; their representative sets are given in Table 5. The isomerization rate was also followed under various pressures up to 1200 bar (1 bar=10^5 Pa) in various solvents; the rate constants for representative species in representative solvents are given in Tables 6—8. Plots of $\ln k_p/k_1$ against the external pressure p for NDAAB in various solvents are shown in Fig. 1, where k_p and k_1 are the rate constants under the external pressure of p and 1 bar respectively. The solid lines in the figure represent the following quadratic regression equation:

Table 3. First-order rate constants ($10^3k/s^{-1}$) for the thermal isomerization of NDAAB derivatives in CCl_4

Compound	20°C	25°C	30°C	35°C	40°C
NDAAB	1.65	2.70	4.37	8.35	14.4
2-Me-	4.02	6.67	11.4	19.8	
2′-Me-	1.52	2.55	4.50	8.28	
2,2′-Me_2-	3.85	6.50	11.1	17.8	
2,6-Me_2-	2.47	4.35	7.10	13.9	
2,2′,6-Me_3-	4.92	7.73	11.8	22.0	
2-Cl-	0.475	0.678	1.16	2.07	3.42
2′-Cl-		38.5	62.2	95.3	160
2,2′-Cl_2-		7.82	13.4	23.0	37.8

Table 4. First-order rate constants ($10^3k/s^{-1}$) for the thermal isomerization of NDAAB derivatives in toluene

Compound	15°C	20°C	25°C	30°C	35°C	40°C
NDAAB	4.08	6.68	11.1	17.0	28.3	
2-Me-	24.5	40.0	61.8	84.0	137	
2′-Me-	3.35	5.73	9.72	14.0	25.0	
2,2′-Me_2-	18.0	31.7	49.3	63.8	107	
2,6-Me_2-	17.8	28.3	41.3	58.5	90.3	
2,2′,6-Me_3-	33.8	44.5	70.8	104	151	
2-Cl-			2.13	3.53	5.92	10.2
2′-Cl-	119	178	267	388		
2,2′-Cl_2-		32.3	56.2	84.0	119	

Table 5. Activation parameters for the thermal isomerization of NDAAB and its derivatives in various solvents

Compound	Solvent	ΔH^*	ΔS^*	$r^{a)}$
		kcal mol^{-1}	cal K^{-1} mol^{-1}	
NDAAB	Hexane	15.7±0.2	−17.7±0.6	0.9997
	CCl_4	19.3±0.6	−5.5±1.8	0.9975
	Toluene	16.4±0.2	−12.5±0.6	0.9997
	$CHCl_3$	11.3±0.5	−24.3±1.8	0.9956
2-Me-NDAAB	Hexane	17.2±0.3	−11.6±0.9	0.9995
	CCl_4	18.5±0.3	−6.4±1.2	0.9993
	Toluene	14.2±0.4	−16.6±1.3	0.9978
2′-Me-NDAAB	Hexane	17.2±0.3	−13.0±1.0	0.9993
	CCl_4	19.7±0.5	−4.2±1.7	0.9987
	Toluene	16.8±0.4	−11.7±1.4	0.9981
	$CHCl_3$	10.3±0.5	−28.0±1.5	0.9960
2-Cl-NDAAB	Hexane	15.0±0.7	−22.0±2.3	0.9954
	CCl_4	17.9±0.7	−13.0±2.2	0.9958
	Toluene	18.6±0.2	−8.3±0.7	0.9997
	$CHCl_3$	13.0±0.1	−22.8±0.3	0.9999
2′-Cl-NDAAB	Hexane	16.8±0.5	−9.9±1.5	0.9983
	CCl_4	16.9±0.4	−8.5±1.2	0.9990
	Toluene	13.2±0.04	−17.2±0.1	0.9999
2,2′-Me_2-NDAAB	Hexane	16.2±0.1	−15.4±0.3	0.9999
	CCl_4	17.9±0.3	−8.7±0.5	0.9999
	Toluene	14.5±0.6	−16.2±2.0	0.9964
2,2′-Cl_2-NDAAB	Hexane	18.4±0.7	−7.3±2.0	0.9975
	CCl_4	19.0±0.1	−4.5±0.3	0.9999
	Toluene	14.9±0.7	−14.3±2.2	0.9957
3-Me-NDAAB	Toluene	19.6±0.6	−6.8±2.0	0.9979
	$CHCl_3$	12.6±0.3	−25.3±1.0	0.9985

a) Correlation coefficient for the plot of ln k *versus* $1/T$.

Table 6. First-order rate constants ($10^2k/s^{-1}$) at various pressures for the isomerization of azobenzene derivatives in hexane

Compound	Temp/°C	P/bar				
		1	300	600	900	1200
NDAAB	50	2.33	2.57	2.73	2.97	3.17
2-Me-NDAAB	40	1.55	1.78	2.00	2.22	2.38
2′-Me-NDAAB	50	2.40	2.55	2.65	2.77	3.03
2,2′-Me_2-NDAAB	40	1.55	1.75	1.92	2.08	2.18
2-Cl-NDAAB	50	0.753	0.805	0.835	0.878	0.882
2′-Cl-NDAAB	25	2.07	2.32	2.51	2.77	3.00
2,2′-Cl_2-NDAAB	35	1.30	1.46	1.65	1.77	1.92

Table 7. First-order rate constants ($10^2k/s^{-1}$) at various pressures for the isomerization of azobenzene in CCl_4

Compound	Temp/°C	P/bar				
		1	300	600	900	1200
NDAAB	40	1.22	1.36	1.52	1.59	1.73
2-Me-NDAAB	40	2.93	3.35	3.83	4.50	5.05
2′-Me-NDAAB	40	1.32	1.41	1.53	1.65	1.75
2,2′-Me_2-NDAAB	40	2.81	3.12	3.47	3.82	4.25
2,6-Me_2-NDAAB	40	1.82	2.42	2.90	3.47	3.95
2,2′,6-Me_3-NDAAB	25	0.775	0.928	1.13	1.32	1.48
2-Cl-NDAAB	50	0.962	1.05	1.15	1.23	1.32
2′-Cl-NDAAB	25	3.75	4.20	4.70	5.25	5.82
2,2′-Cl_2-NDAAB	40	3.93	4.47	5.08	5.51	6.05

Table 8. First-order rate constants ($10^2k/s^{-1}$) at various pressures for the isomerization of azobenzene derivatives in toluene

Compound	Temp/°C	P/bar				
		1	300	600	900	1200
NDAAB	25	1.11	1.45	1.78	2.12	2.48
2-Me-NDAAB	16	2.52	3.40	4.47	5.78	
2′-Me-NDAAB	25	0.952	1.09	1.26	1.47	1.64
2,2′-Me_2-NDAAB	25	4.35	5.75	7.33	9.00	10.7
2-Cl-NDAAB	50	2.55	2.90	3.38	3.85	4.47
2′-Cl-NDAAB	15	11.4	14.2	17.8	22.5	28.2
2,2′-Cl_2-NDAAB	25	5.25	6.75	8.61	10.4	12.6
NAAB	70	0.585	0.592	0.585	0.590	0.595
2-Me-DAAB	70	1.45	1.51	1.56	1.60	1.63
BDEAAB	50	3.00	3.18	3.35	3.47	3.58

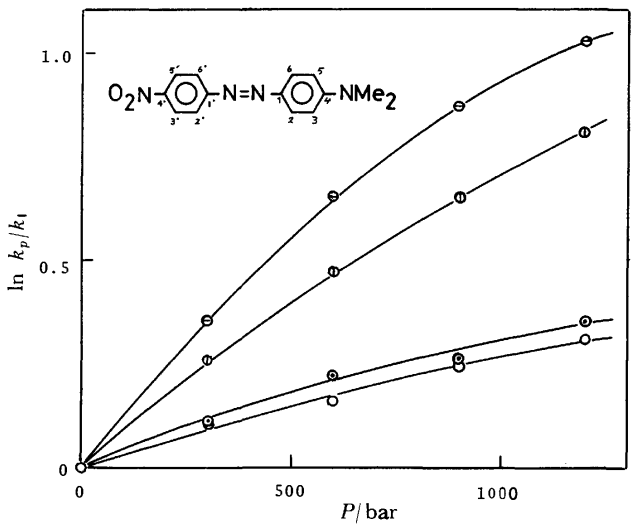

Fig. 1. Pressure effects on the first-order rate constants for the thermal *cis*-to-*trans* isomerization of 4-dimethylamino-4′-nitroazobenzene (NDAAB): (○) hexane; (⊙) CCl_4; (◑) toluene; (⊖) chloroform.

$$\ln k_p/k_1 = a + bp + cp^2. \quad (2)$$

The activation volumes at 1 bar were estimated according to Eq. 3; the values are given in Table 9:

$$\Delta V^* \approx -bRT. \quad (3)$$

Discussion

General Survey of Rate-controlling Factors. Large differences in the activation energy between azobenzenes and the corresponding iso-π-electronic stilbenes have been considered as indirect evidence of the inversion mechanism for azobenzenes.[5] Enthalpy considerations[19,20] and theoretical approaches[2,3] are compatible with this view. However, for 4-amino-4′-nitrostilbene, both the activation energy and the frequency factor drop a great deal compared with those of unsubstituted stilbene. According to Calvin and Alter,[21] the *cis*-isomer of this substance is thermally isomerized *via* a triplet state, as characterized by the very low frequency factor ($A \approx 10^5\ s^{-1}$). Hence, our data

Table 9. Activation volumes (ΔV^{*}/cm^{3}mol^{-1}) for the thermal *cis*-to-*trans* isomerization of azobenzene derivatives in various solvents (temp/°C)

Compound	Hexane	CCl_4	Toluene	$CHCl_3$	MeOH
NDAAB	−7.7(50)	−10.3(40)	−22.0(25)	−30.4(15)	
2-Me-NDAAB	−13.0(40)	−12.1(40)	−24.0(16)		
2′-Me-NDAAB	−3.2(50)	−7.1(40)	−12.0(25)	−22.1(16)	
2,2′-Me_2-NDAAB	−11.2(40)	−8.8(40)	−24.3(25)		
2,6-Me_2-NDAAB	−16.9(50)	−17.8(40)	−23.6(15)		
2,2′,6-Me_3-NDAAB	−13.7(40)	−17.6(25)	−21.9(15)		
2-Cl-NDAAB	−6.4(50)	−8.2(50)	−12.0(50)		
2′-Cl-NDAAB	−8.8(25)	−9.6(25)	−17.6(15)		
2,2′-Cl_2-NDAAB	−11.3(35)	−12.0(40)	−21.9(25)		
3-Me-NDAAB	−8.6(50)		−11.8(50)	−30.8(25)	
DAAB			−0.1(70)	−1.9(57)	−3.6(50)
2-Me-DAAB			−4.2(70)	−3.7(70)[a]	
BDEAAB	−2.9(50)		−5.7(50)	−6.8(40)	−5.0(15)

a) In chlorobenzene.

(Table 5) must preclude the intervention of the triplet state involving the rupture of the N=N π-bond.

Previously, we pointed out that the stabilization by means of the delocalization of the π-electrons in the transition state is an important rate-controlling factor. This inference has arisen from the following reasoning: if the conformation of the transition state of the species in question is similar to that of the *trans*-isomer in the sense that the phenyl rings are coplanar, the solvent and substituent effects on the isomerization rate would reflect the nature of the *trans*-isomer. As may be seen in Table 1, the conjugation band shifts to a longer wavelength almost invariably upon the introduction of the substituent, irrespective of their nature, and as the solvent polarity increases. It follows from an inspection of Tables 1—4 that, as the conjugation band of the *trans*-isomers of NDAAB derivatives shifts to a longer wavelength, the rate as a whole increases. This correlation has already been observed for DAAB derivatives.[1,14] The introduction of strong push-pull groups remarkably affects the rate and the position of the conjugation band. Because of the additive nature of the substituent effects on the rate, greatly accelerated rates are observed for NDAAB derivatives.

Very recently, Whitten and his co-workers[9,22] showed that the ΔG^{*} value for the isomerization of NDAAB is linearly related to Kosower's *Z*-values or other solvent polarity parameters, and suggested that **5** is responsible for the transition state. This conformation has also been supported by Asano *et al.* on the basis of the kinetic pressure effects.[11-13] However, we have a different idea of the conformation and the electronic structure of the activated complex, as will be discussed below.

Solvent Effects. The thermal isomerization of most azobenzenes exhibits few solvent effects. For push-pull azobenzenes such as NDAAB, however, a significant solvent effect has been observed. According to Whitten *et al*, [8,9] this favors a dipolar transition state **5**. Asano *et al.* also consider that **2** and **3** greatly differ in their polarities, and that in **2** (=**5**), the original π-electrons are transferred toward the pulling group and the newly formed positive charge center is stabilized by the pushing group. It should be noted that, in **5**, the N=N π-bond is completely ruptured. If such a charge-separated species is stabilized by solvation at the expense of the N=N π-bond rupture, the same logic must be admitted for the *cis*- and *trans*-isomers, too. Then the *trans*-isomer may have an electronic structure of the following type:

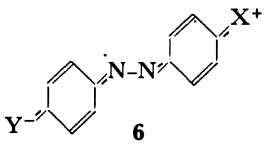

6

where the original N=N π-bond is completely broken and where charges are localized on the push and pull groups. If this were true, the dipole moment of the *trans*-isomer must be as large as 50 Debye, but this is not the case (see below). We admit that **6** is one of the canonical resonance forms, but it is not an *entity* (*cf.* **7**, **10**, and **11**).

The free energy of activation for the isomerization in the gas phase may be compensated for by solvation in a condensed medium. Laidler and Landskroener[23] gave expressions for the rate constant for reactions involving ions and dipoles. These are based on the treatment of Kirkwood, who gave general expressions for the free-energy change when a sphere with a radius *r* containing a distribution of charges is transferred from a medium of the unit dielectric constant to one of the dielectric constant ε. If azobenzenes are regarded as dipoles with no net charges, the rate constant for the thermal isomerization may be given by:

$$\ln k = \ln k_0 + \frac{3}{8kT}\left(\frac{\mu_{*}^2}{r_{*}^3} - \frac{\mu^2}{r^3}\right)\left(\frac{\varepsilon-1}{\varepsilon+1}\right), \qquad (4)$$

where k_0 is the hypothetical rate constant in a condensed medium of $\varepsilon=1$, and where μ and μ_{*} denote the dipole moments in the *cis* and transition states. We may expect that the plot of ln *k versus* $(\varepsilon-1)/(\varepsilon+1)$ makes a straight line.

In order to examine Eq. 4, the isomerization rate was followed for three representative azobenzenes in various solvents; the results are listed in Table 10. In Fig. 2, ln *k* is plotted against $(\varepsilon-1)/(\varepsilon+1)$. From the slope and assuming that $r \approx r_{*}=0.5$ nm, $T=300$ K, and $\mu=3$ D (1 Debye=3.3×10^{-30} m C), we tentatively estimated $\mu_{*} \approx 12$

Table 10. Rate constants for the thermal *cis*-to-*trans* isomerization of DAAB, NDAAB, and BDEAAB in various solvents at 25 °C

Solvent	ε	ln k/s^{-1}		
		DAAB	NDAAB	BDEAAB
Hexane	1.90	−10.3	−5.90	−7.47
Dioxane	2.21		−4.16	
CCl_4	2.23		−5.91	
Benzene	2.27	−10.16	−4.47	
Toluene	2.38		−4.50	
$CHCl_3$	4.70		−4.02	−4.71
Chlorobenzene	5.61	−9.54	−1.73	−5.40
1,2-Dichloroethane	10.37			−4.92
Acetone	20.5	−9.88	0.92[a]	−5.13
Methanol	32.6			−3.17
DMF	36.7		3.91[a]	
DMSO	48.9		4.79[a]	

a) Cited from Ref. 1.

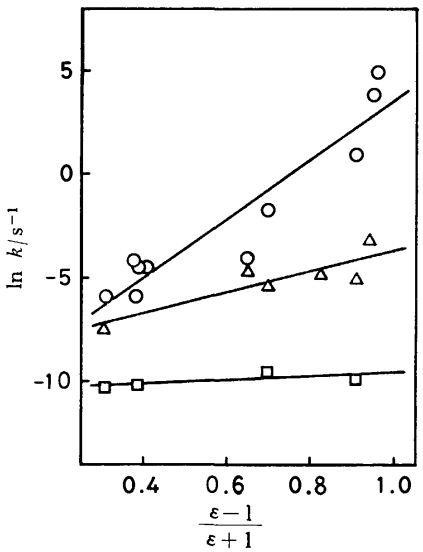

Fig. 2. Plots of ln k against $(\varepsilon-1)/(\varepsilon+1)$, according to Eq. 4: (○) NDAAB; (△) BDEAAB; (□) DAAB.

Debye for NDAAB. This may be an acceptable order of magnitude, since μ=7.91 D for *trans*-NDAAB.[24] There are very few solvent effects on DAAB, but it is notable that BDEAAB exhibits considerably greater solvent effects than DAAB, indicating a substantial polarity change upon activation. Therefore, we admit a polar *inversion* transition state for this kind of species, too (see **8** and **9** below), since a rotational dipolar structure such as **5** is quite unlikely. (Relevant discussion will be undertaken in the section on pressure effects.) The considerable scatter of the plots in Fig. 2 may indicate very complicated solvent effects on the rate, which has been often observed in Menschutkin reactions. The magnitude of the slope could then be regarded as a measure of the change in charge distribution upon activation.

Substituent Effects. As Talaty and Fargo[5] first pointed out, the introduction of substituents almost invariably accelerates the rate, regardless of the nature of the substituents. Therefore, the Hammett plot becomes V-shaped, with a mimimum near σ=0. Hall *et al.*,[25] and Herkstroeter[26] also reported similar observations for the isomerization of *N*-(hexafluoroisopropylidene)anilines and pyrazolone azomethines. They explained these observations in terms of a change in the mechanism. However, we question this and made a brief comment on it previously.[1] It has been found that the introduction of bulky substituents into *ortho* positions with respect to azomethine nitrogen always accelerates the rate. According to Kessler and his coworkers, the steric hindrance of bulky *ortho* substituents becomes less severe in the inversion-transition state than in the ground state, thus accounting for the acceleration in terms of the inversion mechanism.[27-30]

In this respect, we considered that, if we introduce substituents on *ortho* positions with respect to the azo group, and then examine the kinetic effects, it would shed light on the mechanism. Two sorts of substituents were chosen: Cl- and Me-groups. Let us regard NDAAB as the standard of the push-pull azobenzenes, since interest is focused on this species. When we examine the data in Tables 2—4, we notice some interesting points: (1) 2-Me- accelerates the rate, while 2′-Me- slightly retards it. (2) This effect tends to become more remarkable as the polarity of the solvent increases. (3) On the other hand, 2-Cl- retards the rate, while 2′-Cl- accelerates it. These kinetic substituent and solvent effects are more remarkable than those of the Me-group. (4) For 2,2′-disubstituted NDAAB, the rates fall between those of the 2- and 2′-groups. (5) The kinetic effect of 6-Me- is notable: 2-Me-$>$2,6-dimethyl, and 2,2′-dimethyl$<$2,2′,6-trimethyl in most solvents.

We previously reported that Eq. 1 approximately holds for DAAB derivatives for a specified solvent. The above findings indicate that Eq. 1 is valid for NDAAB derivatives and in other solvents, too. However, the rule is not valid for the 6-Me-group. A plausible reason for this may be the additional steric hindrance: 2-Me-$<$2,6-dimethyl in the transition state and 2,2′-dimethyl$<$2,2′,6-trimethyl in the *cis* ground state.

As is shown in Table 1, λ_{max} is sensitive to substituents: 2-Me- and 2′-Cl- shift the conjugation band to a longer wavelength, while 2′-Me- and 2-Cl- shift it to a shorter one. Fig. 3 shows the relationship between the ln k/k_0 and $\bar{\nu}_{max}$ values of the *trans*-isomers. In benzene as well as in hexane, good parallelograms can be observed. These observations suggest that the delo-

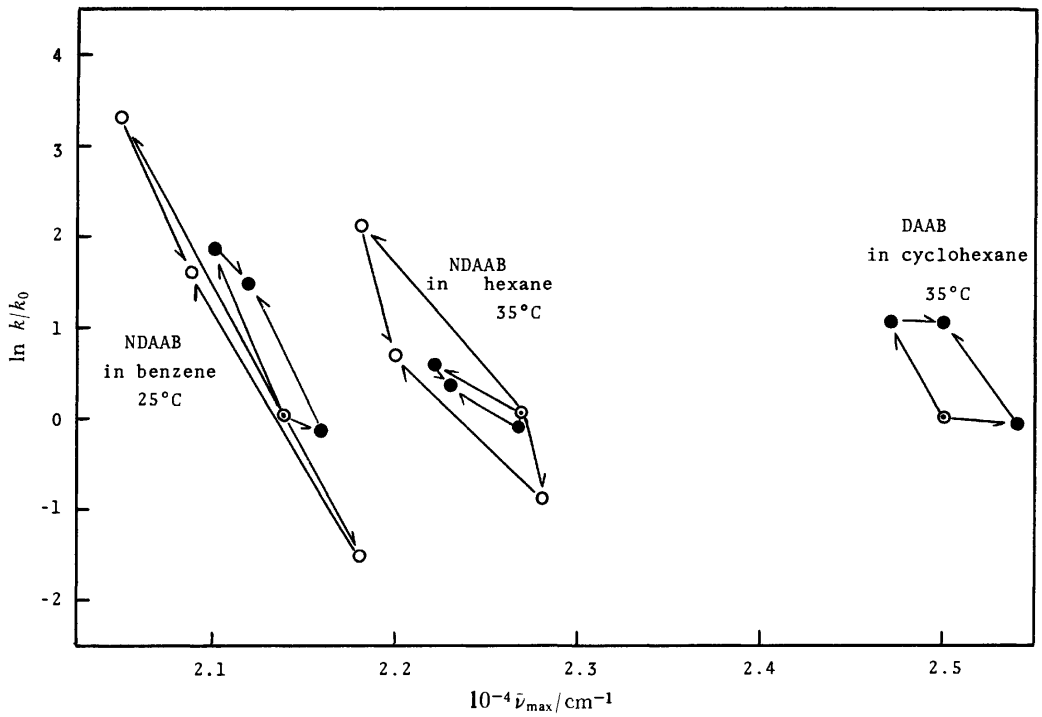

Fig. 3. Correlation between ln k/k_0 and $\bar{\nu}_{max}$ for Me-substituted (●), and Cl-substituted (○) azobenzene derivatives. Data for DAAB are cited from Ref 1.

calization of the π-electrons, and hence the mesomeric effect, are important rate-controlling factors. Therefore, the two phenyl rings must be coplanar; this supports the inversion mechanism. If **5** is assumed, the correlation shown in Fig. 3 could not be expected, since the benzene rings are twisted in relation to each other.

From the above observations, one could say that there is no indication of the mechanism change for any kind of azobenzene in any solvent. The idea that NDAAB and its homologues isomerize *via* a route to rotation in solvents other than hexane, while other azobenzenes do so *via* a route to inversion or inversion-rotation competition paths, is thus questionable.

The substantial contribution of the canonical resonance form **7**:

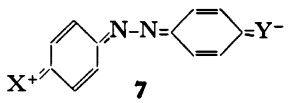

7

which is possible for push-pull azobenzenes alone, may be responsible for the enhanced rate, especially in polar solvents. This resonance contribution must be strongly forbidden in the *cis*-isomer, for which two phenyl rings are twisted by 56° out of the C-N-N-C plane,[31] as well as in the rotational transition state (compare **7** with **5**). Therefore, we can reasoably assume that, for push-pull azobenzenes, a remarkable polarity change occurs on going from the *cis* to the inversion transition state, a change which accommodates the substantial substituent and solvent effects. From the theoretical approaches,[2,3] it is known that the energy required for the hybrid change from sp^2 to sp is much less than the energy needed for the π-bond rupture. Even if the latter energy were compensated for partially by solvation in the rotational dipolar transition state, it is unlikely that *cis* push-pull azobenzene prefers a route *via* rotation to a route *via* inversion in benzene, and *vice versa* in hexane.

Linear Free-energy Relationship. According to Leffler and others,[32-36] a linear enthalpy-entropy relationship should hold for the simple interaction mechanism. If the ΔH^* *versus* ΔS^* plot is scattered, more than two interactions must be involved. Shinkai and his co-workers[7,12] have shown that the ΔH^* *versus* ΔS^* plots for various kinds of azobenzenes, but not NDAAB, constitute a straight line, while the same plots for NDAAB in various solvents, including hexane, give other straight line shifted downward, thus accounting for the change in the mechanism. Nevertheless, they opined that the mechanism change for NDAAB depends on the solvents, on the basis of the kinetic pressure effect; this is inconsistent.

If the data in Table 5 are inspected, it may be seen that ΔH^* tends to increase with the increase in ΔS^*. It may also be noted that the sets of ΔH^* and ΔS^* in hexane for NDAAB derivatives fall in the region in which other sets are involved, and we cannot see any indication of special behavior in hexane. We consider that the downward shift is not due to the mechanism change, but to the remarkable free-energy depression attributable to the extra mesomeric contribution **7** and the accompanying solvation.

Pressure Effects. We now wish to examine the pressure effects on the isomerization of various kinds of azobenzenes in various solvents with different polarities. From an inspection of Tables 6—9, we see some interesting points: (1) First of all, an appreciable acceleration in the rate by external pressures for NDAAB and its homologues can be observed, even in hexane. The values of ΔV^* are similar to those reported

by Asano *et al.*, except for that of NDAAB in hexane. (2) The pressure effect and, hence the activation volume $|\Delta V^{*}|$, tend to increase as the solvent polarity increases, but there is a distinction between CCl_4 and toluene. (3) When ln k_p is plotted against p for substituted NDAAB, we can see that the patterns of the kinetic pressure effect for 2-Me- and 2′-Cl- , 2′-Me- and 2-Cl-, and 2,2′-dimethyl and 2,2′-dichloro-NDAAB are very similar to each other. We have already pointed out that these sets of substituents exert similar effects on the rate as well as the position of $\bar{\nu}_{max}$. (4) Astonishingly, BDEAAB and DAAB also exhibit appreciable pressure effects in toluene, chloroform, and methanol (Table 9).

The above findings indicate very complex kenetic pressure effects, and it is very difficult to give a clear-cut explanation of them. It is well known, though, that if a reaction starts from a nonpolar ground state and proceeds *via* a polar transition state, a more negative activation volume is to be expected for a less polar solvent, as observed in Menschutkin reactions.[37-40] The above findings are just the reverse; therefore, they could be explained in terms of two competing reaction paths for push-pull azobenzenes for which $|\Delta V^{*}|$(inversion)≈0, and $|\Delta V^{*}|$(rotation)=20—30 cm^3 mol^{-1}.[13] However, the (4) observation excludes this, since a dipolar structure for the rotational transition state is least likely for a bis-substituted azobenzene such as BDEAAB. At the same time, it is possible to write the dipolar inversion transition state for push-push azobenzenes as follows:

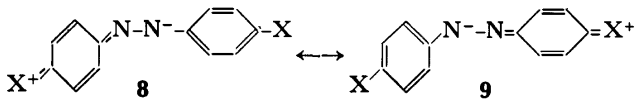

The partial charge on the molecule would cause the polarization of the surrounding solvent molecules, thus accounting for the substantial pressure and solvent effects for these kinds of azobenzenes. The red shift of the conjugation band of *trans*-BDEAAB, which is nominally a nonpolar molecule, could thus be explained (Table 1). For push-pull azobenzenes, there must be a substantial contribution of the following dipolar canonical resonance forms to the stabilization of the inversion transition state:

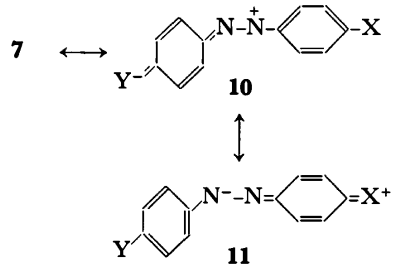

The solvent dependencies of ΔV^{*} for reactions in which a polarity change between a reactant and the activated complex takes place have hitherto been interpreted as follows: if Eq. 4 is differentiated with respect to the pressure, it follows that:

$$\left(\frac{\partial \ln k}{\partial p}\right)_T = -\frac{\Delta V^{*}}{RT} = \frac{3}{4kT}\left(\frac{\mu_{*}^2}{r_{*}^3} - \frac{\mu^2}{r^3}\right)\frac{(\partial\varepsilon/\partial p)_T}{(\varepsilon+1)^2}. \quad (5)$$

The $(\partial\varepsilon/\partial p)_T/(\varepsilon+1)^2$ term generally decreases as the polarity of a solvent increases, in agreement with the trend observed in Menschutkin reactions. However, this is nothing but a qualitative explanation. For example, ΔV^{*}(benzene)/ΔV^{*}(nitrobenzene)≈1.6(obsd) and 10(calcd) for a reaction between pyridine and methyl iodide. This large discrepancy, together with the considerable scatter in Fig. 2, may be ascribed to the neglect of specific solute-solvent interactions in the Kirkwood model. Such interactions will give rise to a polarization enhanced by polar solvents. In our case, the dipole moment in the transition state may be more susceptible to the solvent polarity, compared with the case of the Menschutkin reactions, since the transition state of substituted azobenzenes are *soft* in the sense that the π-electrons are labile(see **7**—**11**). Thus, if the effect of solvent polarity on the μ-term overwhelms the effect on the ε-term in Eq. 5, ΔV^{*} will increase with the increase in solvent polarity, and *vice versa*, the preference depending on the type of reactions. It seems that the investigation and the interpretation along these lines have not yet been well-established, and so we must suspend a straightforward conclusion.

The above assumption requires that the plot of Fig. 2 be curved concavely upward. Probably, a quadratic regression equation for NDAAB will support it, but the plots are too scattered, and therefore more sophisticated investigations are necessary. Further, the freedom to rotate around the C-N bond in the *cis* and transition states may be deeply related to the nature of the solvents as well as to the bulkiness and positions of substituents. The above findings (1)—(4), together with the solvent and substituent effects, show very complicated aspects of the isomerization of azobenzenes.

Conclusion

We have compared the kinetic substituent, solvent, and pressure effects for the thermal *cis*-to-*trans* isomerization of push-pull azobenzenes with those for other kinds of azobenzenes for which the inversion mechanism has been accepted, and have seen that there are no essential differences in kinetic behavior between them. Rather, we have observed very similar *ortho* effects between NDAAB and DAAB derivatives. Further, we have found substantial kinetic-pressure and solvent effects for symmetrically substituted azobenzene. The above findings argue in favor of the inversion mechanism and against the rotational one.

We wish to express our gratitude to Emeritus Professor Jiro Osugi and Dr. Kimihiko Hara of Kyoto University for their technical advice on the high-pressure experiments and also for their encouragement.

This work was financially supported by the Japan Society for the Promotion of Science.

References

1) Part II: N. Nishimura, T. Sueyoshi, H. Yamanaka, E. Imai, S. Yamamoto, and S. Hasegawa, *Bull. Chem. Soc. Jpn.*, **49**, 1381 (1976).

2) S. Ljunggren and G. Wettermark, *Acta Chem. Scand.*, **25**, 1599 (1971).

3) E. V. Brown and G. R. Granneman, *J. Am. Chem. Soc.*, **97**, 621 (1975).

4) P. Haberfield, P. M. Block, and M. S. Lux, *J. Am. Chem. Soc.*, **97**, 5804 (1975).
5) E. R. Talaty and J. C. Fargo, *Chem. Commun.*, **2**, 65 (1967).
6) E. Wolf and H. K. Cammenga, *Z. Phys. Chem., Neue Folge*, **107**, 21 (1977).
7) S. Shinkai, Y. Kusano, K. Shigematsu, and O. Manabe, *Chem. Lett.*, **1980**, 1303.
8) P. D. Wildes, J. G. Pacifici, G. Irick, and D. G. Whitten, *J. Am. Chem. Soc.*, **93**, 2004 (1971).
9) K. S. Schanze, T. P. Mattox, and D. G. Whitten, *J. Am. Chem. Soc.*, **104**, 1733 (1982).
10) J. M. Nerbonne and R. G. Weiss, *J. Am. Chem. Soc.*, **100**, 5953 (1978).
11) T. Asano, *J. Am. Chem. Soc.*, **102**, 1205 (1980).
12) T. Asano, T. Okada, S. Shinkai, K. Shigematsu, Y. Kusano, and O. Manabe, *J. Am. Chem. Soc.*, **103**, 5161 (1981).
13) T. Asano, T. Yano, and T. Okada, *J. Am. Chem. Soc.*, **104**, 4900 (1982).
14) T. Sueyoshi, N. Nishimura, S. Yamamoto, and S. Hasegawa, *Chem. Lett.*, **1974**, 1131.
15) K. V. Auwers and Ph. Bullmann, *Ber.*, **59**, 2719 (1926).
16) I. N. Zhmurova, *Zh. Obshch. Khim.*, **27**, 2704 (1957).
17) V. V. Kormachev, E. A. Chalykh, V. A. Kukhtin, and E. A. Chalyeh, *Zh. Obshch. Khim.*, **47**, 2621 (1977).
18) Y. Sueishi and N. Nishimura, *Bull. Chem. Soc. Jpn.*, **56**, 2598 (1983).
19) G. B. Kistiakovsky and W. R. Smith, *J. Am. Chem. Soc.*, **56**, 638 (1934).
20) J. Bineboym, A. Burcat, A. Lifshitz, and J. Shamir, *J. Am. Chem. Soc.*, **88**, 5039 (1966).
21) M. Calvin and H. W. Alter, *J. Chem. Phys.* **19**, 765 (1951).
22) K. S. Schanze, T. F. Mattox, and D. G. Whitten, *J. Org. Chem.* **48**, 2808 (1983).
23) K. J. Laidler and P. A. Landskroener, *Trans. Faraday Soc.*, **52**, 200 (1956).
24) S. Yamamoto, N. Nishimura, and S. Hasegawa, *Bull. Chem. Soc. Jpn.*, **44**, 2018 (1971).
25) G. E. Hall, W. J. Middleton, and J. D. Roberts, *J. Am. Chem. Soc.*, **93**, 4778 (1971).
26) W. G. Herkstroeter, *J. Am. Chem. Soc.*, **95**, 8686 (1973).
27) H. Kessler and D. Leibfritz, *Tetrahedron*, **25**, 5127 (1969).
28) H. Kessler, P. Bley, and D. Leibfritz, *Tetrahedron*, **27**, 1687 (1971).
29) H. Kessler, *Angew. Chem.*, **82**, 237 (1970).
30) D. Wurmb-Gerlich, F. Vogtle, A. Mannschreck, and H. A. Staab, *Justus Liebigs Ann. Chem.*, **708**, 36 (1967).
31) G. C. Hampson and J. M. Robertson, *J. Chem Soc.*, **1941**, 409.
32) J. E. Leffler and E. Grunwald, "Rates and Equilibria of Organic Reactions," Wiley, New York (1963).
33) J. E. Leffler, *J. Org. Chem.*, **20**, 1202 (1955).
34) E. V. Brown and G. R. Granneman, *J. Am. Chem. Soc.*, **97**, 621 (1975).
35) S. Hasegawa, N. Nishimura, and K. Miura, *Bull. Chem. Soc. Jpn.*, **33**, 1323 (1960).
36) J. E. Leffler, *J. Org. Chem.*, **31**, 533 (1966).
37) Y. Kondo, M. Uchida, and N. Tokura, *Bull. Chem. Soc. Jpn.*, **41**, 992 (1968).
38) H. Hartmann, H. Kelm, and G. Rinck, *Z. Phys. Chem. Neue Folge*, **44**, 335 (1965).
39) H. Hartmann, H. D. Bauer, and G. Rinck, *Z. Phys. Chem. Neue Folge*, **61**, 47 (1968).
40) T. Asano and W. J. le Noble, *Chem. Rev.*, **78**, 407 (1978).

Extrinsic Carrier-photogeneration in Poly(*N*-vinylcarbazole)

Ken-ichi OKAMOTO* and Akira ITAYA

Department of Chemical Engineering, Faculty of Engineering, Yamaguchi University, Ube, Yamaguchi 755

(Received September 5, 1983)

The carrier-photogeneration efficiency of holes in poly(*N*-vinylcarbazole) (PVCz) films was investigated by means of the time-of-flight method as a function of applied electric field, temperature, and excitation band. The extrinsic effects on the efficiency were examined; these included photooxidation of film surface and doping with a weak electron-acceptor, dimethyl terephthalate (DMTP). The experimental results were analyzed according to the Onsager theory of geminate recombination of a bound electron-hole pair with an interionic separation of r_0. The primary yield of the electron-hole pair, ϕ_0, increased from 0.02 to 0.059 with decreasing excitation wavelength. By photooxidation, it increased up to 0.09 for all the excitation bands. The r_0 was independent of the excitation band, and was identical between fresh and photooxidized films. In DMTP(1.8 mol%)-doped films, both ϕ_0 and r_0 were independent of the excitation band, although their values were different from those of undoped films. These results indicate that the extrinsic carrier-photogeneration *via* nonrelaxed exciplexes formed between singlet excitons and acceptor-like impurities or photooxidation products is predominant in PVCz films for all the excitation bands.

A number of papers have appeared in the literature concerned with the carrier-photogeneration process in poly(*N*-vinylcarbazole) (PVCz), one of the typical photoconducting polymers.[1-10] Taking account of the ionization potential (6.1 eV)[11] and the electron affinity (1.5 eV)[12] of PVCz in a solid film, the intrinsic carrier-photogeneration due to the autoionization mechanism, which has been observed for anthracene single crystals,[13] is considered only for the π-π^* excitation higher than 4.6 eV (^1B_b and ^1B_a transitions). For the lower π-π^* excitation (^1L_b and ^1L_a transitions), the extrinsic carrier-photogeneration expressed by Scheme 1 is the most probable mechanism at the present stage.[10] Photooxidation products of PVCz produced within the surface layer of a film seem to be the most probable as the acceptor-like impurity A in Scheme 1.[9]

$$^1D^* + A \longrightarrow \underset{\text{encounter complex}}{(^1D^* \cdots A)} \longrightarrow \underset{\text{nonrelaxed exciplex}}{^1(D^+A^-)^{**}} \xrightarrow{\text{thermalization}}$$

$$\underset{\text{bound electron-hole pair}}{^1(D^+ \overset{r_0}{\cdots} A^-)} \xrightarrow[P(E)]{\text{field-assisted dissociation}} \underset{\text{carriers}}{D^+ + A^-}$$

$$\downarrow \text{ geminate recombination } 1-P(E)$$

$$\underset{\text{relaxed exciplex}}{^1(D^+A^-)^*}$$

Scheme 1.

The overall carrier-photogeneration efficiency, ϕ, is given as the product of the primary quantum yield, ϕ_0, of a bound electron-hole pair with an interionic separation of r_0 and the dissociation probability, $P(E)$:

$$\phi = \phi_0 P(E). \quad (1)$$

The ϕ_0 is considered to be independent of the electric field, E. The field-dependent probability of $P(E)$, which is given by the Onsager theory,[14] is a function of r_0.

The field dependence of the photogeneration efficiency in PVCz films has been analyzed according to the Onsager theory by two groups of investigators.[4,8] They have reported that ϕ_0 is independent of the excitation wavelength and that r_0 increases in steps with decreasing excitation wavelength. However, there has been no explanation of their results. These results are quite opposite to the predictions based on the extrinsic carrier-photogeneration process expressed by Scheme 1.

The above results were obtained by means of the xerographic discharge technique. Although it is convenient and practical, especially for high fields, this technique seems inferior to the time-of-flight method because it is difficult to avoid two effects: trapped space charge due to preexposures and photodegradation of film surface caused by exposing it to corona-charge. Unfortunately, to our knowledge, there have been few reports in which the field dependence of the photogeneration efficiency has been measured in detail by means of the time-of-flight method, taking cautions to prevent any photooxidation of the films, and has been analyzed according to the Onsager theory.

In the present paper, in order to make clearer the carrier-photogeneration process, we investigate effects of the excitation wavelength and temperature on the photogeneration efficiency in PVCz over a wide range of fields by means of time-of-flight method. We also investigated the photogeneration efficiency in PVCz films which were slightly-photooxidized or doped with dimethyl terephthalate (DMTP), a weak electron acceptor, by comparing the results with that obtained for the fresh films.

Experimentals

The PVCz was prepared by free-radical polymerization (initiator: AIBN) of the highly-purified monomer and was purified by reprecipitation from a benzene solution with methanol several times. The polymer sample was stored in tubes with an argon atmosphere in the dark. Gel permeation chromatography analysis showed $M_n = 1.95 \times 10^5$ and $M_w/M_n = 2.3$. Films were cast on NESA-coated quartz plates from a benzene solution and were dried *in vacuo*. Photooxidized films were prepared by irradiating the free surface of fresh films in air for 1—18 min through a water filter (10 cm) with the full spectrum of a 500 W high pressure mercury lamp at a distance of 40 cm from the lamp. A semitransparent gold electrode with a typical area of 1 cm^2 was evaporated on a film to prepare a sandwich-type cell. Caution

was taken in all procedures of the experiment to keep the sample from being exposed to the room light. Film thickness was determined from the weight and density (1.188 g/cm^3) of a film with a known area (*ca.* 1.5 cm^2) and/or by a capacitive method.

A 3 μs light pulse from an air-gap flash was irradiated on a cell set in a cryostat with a high vacuum, better than 1.3 mPa, through appropriate narrow band pass filters. An induced transient photocurrent was observed through a series load resistor in the current or differential mode by means of a storage oscilloscope. In order to avoid the space charge effect due to previous exposures and to get reproducible results, the cell was irradiated by visible light (λ>450 nm) while short-circuited for several minutes prior to each measurement. The intensity of each light pulse was monitored by a Si photodiode equipped with a peak-hold circuit, the output of which was calibrated by means of a potassium ferrioxalate actinometer.

The dielectric constant ε of films was determined from capacitance measurements. The value of 3.38, which was determined at the frequency of 1 kHz at 23 °C, was used in the calculation of $P(E)$, neglecting the temperature dependence of ε.

The $P(E)$ was calculated according to the method developed by Geacintov and Pope.[15]

Results and Discussion

Effects of Excitation Band and Temperature on ϕ_0 and r_0 in Fresh Films. As shown in Fig. 1, three kinds of band bass filters were used in order to excite the ^1L_b, ^1L_a, and ^1B_a absorption bands. 90% of the incident light of 340, 280, and 240 nm was absorbed within layers of less than 0.51, 0.23, and 0.065 μm in depth, respectively. A typical set of transient photocurrent signals for positive gold-electrode illumination is shown in Fig. 2. The observed photocurrent signal generally had an initial spike-like signal superimposed on a longer-duration signal. This spike-like signal cannot be attributed to loss of holes by bimolecular volume-recombination in the excitation layer, as for the case of anthracene,[17] but to fast hole transport in a short duration immediately after carrier generation.[18] The number of collected carriers (holes) per unit area, N_p, was obtained from the integral of the photocurrent over the entire drift times using a set of transient signals such as shown in Fig. 2. The N_p was proportional to the light intensity, ranging from 1×10^{12} to 1×10^{14} photons/cm^2 pulse, and was independent of the film thickness, which ranged from 3 to 12 μm. These results indicate that the observed values of N_p are not affected by space-charge effects, bulk recombination, or range limitation of hole carriers. The ϕ was obtained by dividing N_p by the light intensity.

Figure 3 shows the field dependence of ϕ in fresh films for the different excitation bands. The measurements were done at 65 °C in order to avoid the complicating effects due to bulk carrier trapping in the low-field region.[2] The ϕ increased in the order of the

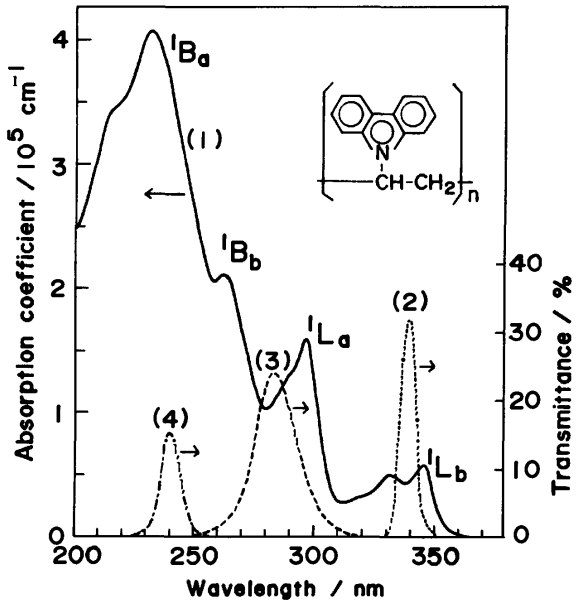

Fig. 1. Absorption spectrum of a PVCz film (1) and transmittance of band pass filters ((2)—(4)).

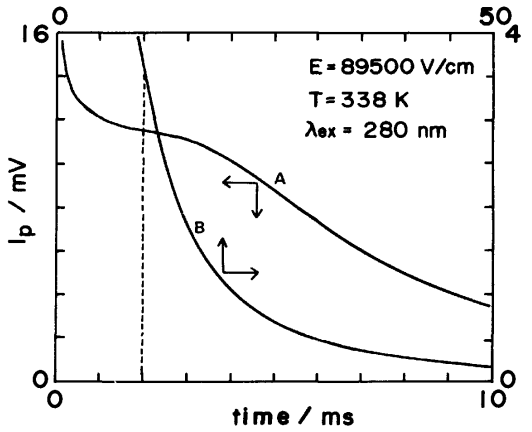

Fig. 2. A set of typical transient photocurrent signals.
(A) The early part of a signal, (B) the late part of a signal.

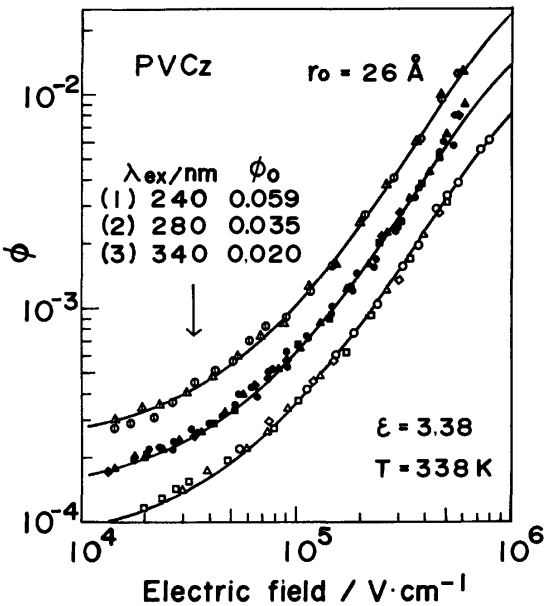

Fig. 3. Field dependence of ϕ in fresh films for different excitation bands. The solid lines were calculated from Eq. 1 with r_0 and ϕ_0 values presented in the figure.

^1L_b, ^1L_a, and ^1B_a bands. The solid lines were calculated from Eq. 1, with r_0 of 26 Å and with ϕ_0 of 0.020, 0.035, and 0.059 for the ^1L_b, ^1L_a, and ^1B_a bands, respectively. They are in good agreement with the experimental data. The results indicate that the increase in ϕ with decreasing excitation wavelength is due only to a change in ϕ_0. Although being quite opposite to the results reported in the literature,[4,8] these results are explained by the extrinsic carrier-photogeneration process (Scheme 1) mentioned below.

The singlet excitons, which migrate in a film to encounter molecules A, are the lowest excited singlet state, irrespective of the excitation wavelength, because the internal conversion from any higher excited singlet state to the lowest excited one precedes excitation energy migration. Therefore, r_0 is independent of the excitation wavelength. Taking account of the singlet exciton migration efficiency,[16] ϕ_0 is considered to increase with increasing concentration of A in the concentration range less than the order of 10^{-3} mol/mol-basic-unit (expressed by mol% hereafter). As the photooxidation proceeds preferentially near the surface of a film, the concentration of photooxidation products acting as A in Scheme 1 becomes higher on going from the bulk to the surface. Because of this concentration profile, ϕ_0 has a tendency to be higher for the excitation wavelength having higher absorption coefficient; that is, ϕ_0 increases in the order of the ^1L_b, ^1L_a, ^1B_b, and ^1B_a transitions.

Figure 4 shows the temperature dependence of ϕ in fresh films for the 340 nm excitation. The solid lines were calculated from Eq. 1 with r_0=26 Å and ϕ_0=0.020, assuming that both r_0 and ϕ_0 were independent of temperature. They are in fairly good agreement with the experimental data, indicating that both r_0 and ϕ_0 do not depend on temperature in the relatively narrow range. The result for ϕ_0 seems to be due to the fact that the singlet exciton migration length is insensitive to temperature in this range.[16]

Effects of DMTP-doping on ϕ_0 and r_0. Figure 5 shows the field dependence of ϕ in films doped with DMTP (1.8 mol%). The ϕ in these films is much larger

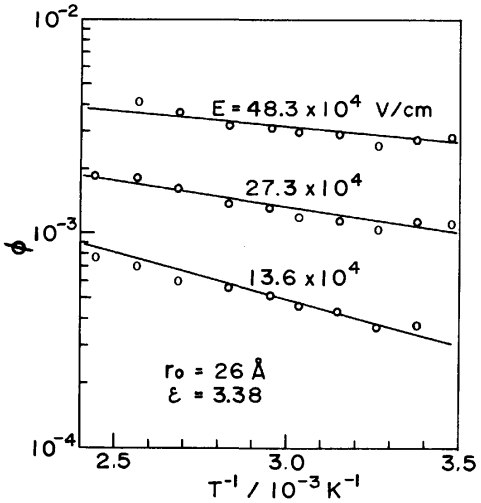

Fig. 4. Temperature dependence of ϕ in fresh films for the 340 nm excitation. The solid lines were calculated from Eq. 1 with r_0=26 Å and ϕ_0=0.020.

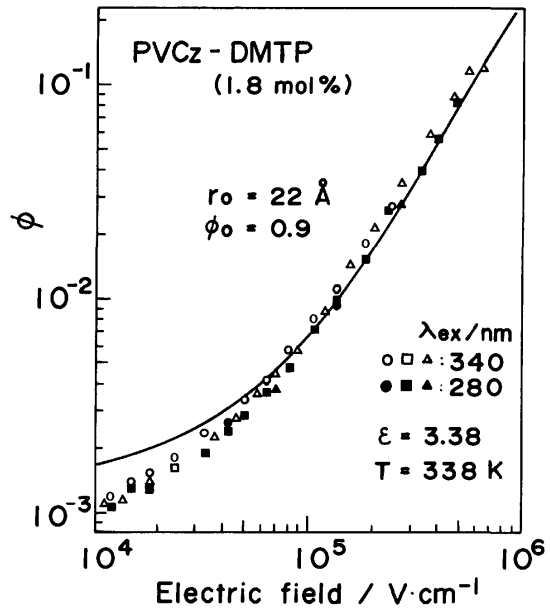

Fig. 5. Field dependence of ϕ in films doped with DMTP (1.8 mol%). The solid line was calculated from Eq. 1 with r_0=22 Å and ϕ_0=0.9.

than that in undoped films and is independent of the excitation bands. The data are in fairly good agreement with the solid line calculated from Eq. 1 with r_0= 22 Å and ϕ_0=0.9. In the DMTP-doped films, the host excimer fluorescence was almost completely replaced by the exciplex fluorescence,[16] indicating that most of the singlet excitons encounter DMTP molecules to form encounter complexes. Furthermore, the probability of triplet exciton formation from a singlet exciton by intersystem crossing is in the order of 10^{-2}.[19] It is, therefore, reasonable that the DMTP-doped films

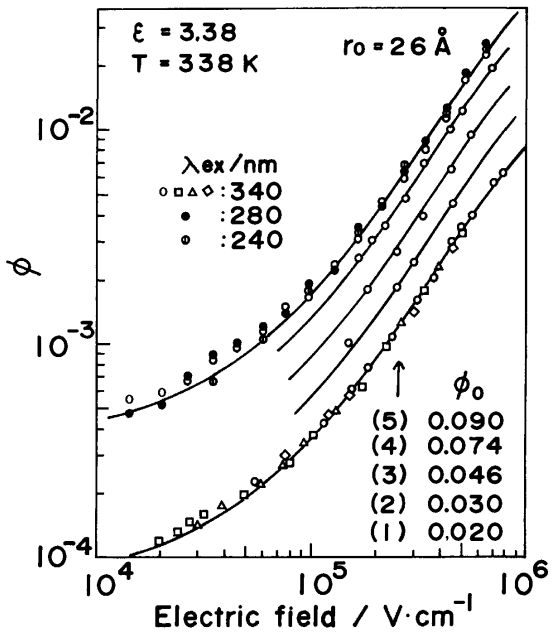

Fig. 6. Field dependence of ϕ in photooxidized films for different irradiation times. The solid lines were calculated from Eq. 1 with r_0 and ϕ_0 values presented in the figure. The irradiation time: (1) 0, (2) 0.9, (3) 3.3, (4) 9, and (5) 18 min. See the text concerning the irradiation conditions.

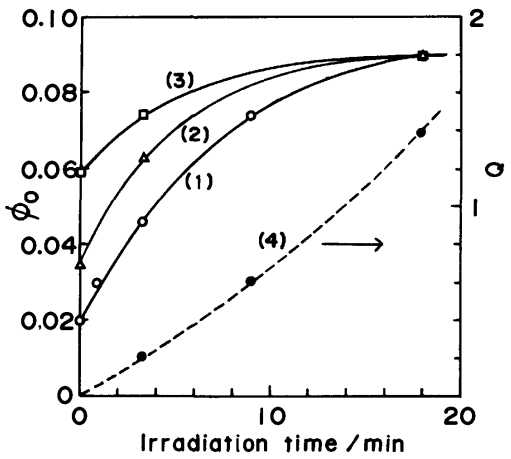

Fig. 7. Irradiation-time dependence of ϕ_0 and the quenching factor, Q, of the excimer fluorescence. ϕ_0: (1) 340 nm, (2) 280 nm, and (3) 240 nm excitation. Q: (4) 340 nm excitation.

have the ϕ_0 value of 0.9 for all the excitation bands. This high value of ϕ_0 is comparable to the value of 0.8 for PVCz films doped with 1,2,4,5-tetracyanobenzene (2 mol%) on excitation of the charge transfer band,[20] and is much larger than the value of 0.23 for films doped with 2,4,7-trinitro-9-fluorenone (6 mol%).[21] The r_0 value of 22 Å is the same as that observed from the quenching experiment of the exciplex fluorescence by electric field.[10]

Effects of Photooxidation on ϕ_0 and r_0. Figure 6 shows the field dependence of ϕ in photooxidized films for different irradiation times. The data are in good agreement with the solid lines calculated from Eq. 1 with r_0=26 Å, the same value as in fresh films, irrespective of both the excitation bands and the irradiation time. The ϕ_0 values thus determined are shown in Fig.7 as a function of irradiation time. The ϕ_0 increased rapidly with increasing irradiation time and soon leveled off to a value of 0.09 for all the excitation bands. The increase in ϕ with increasing irradiation time within the present level of photooxidation is thus explained by the increase in ϕ_0 only, which was caused by an increase in the concentration of acceptor-like photooxidation products acting as molecule A in Scheme 1.

The films irradiated in air showed remarkable changes in the fluorescence spectra, while such changes were not observed for the films irradiated in a high vacuum of 1.3×10^{-3} Pa. With irradiation time, the excimer fluorescence of PVCz films decreased and a new fluorescence band, which has been attributed to the exciplex formed between an excited carbazole chromophore and an acceptor-like photooxidation product,[9] appeared around 515 nm. The decrease in the excimer fluorescence in films is shown in Fig. 7, using a quenching factor Q. In each film, the value of Q for the 280 nm excitation was roughly twice as large as that for the 340 nm excitation. According to the random hopping model of singlet exciton migration, Q is expressed by Eq. 2:

$$Q=([A])+[T_s])/[E], \quad (2)$$

where [A] is the concentration of acceptor-like photooxidation products acting as molecule A in Scheme 1; $[T_s]$ is the concentration of non-acceptor-like photooxidation products acting as singlet exciton traps; and [E] is the concentration of the excimer-forming sites. According to Scheme 1, ϕ_0 is expressed by Eq. 3:

$$\phi_0=\phi_s^*[A]/([E]+[A]+[T_s]), \quad (3)$$

where ϕ_s^* is the quantum yield of the singlet exciton formation. The $[T_s]$ and [A] were evaluated from the Q and ϕ_0 values, taking [E] and ϕ_s^* as 0.27 mol%[16] and 0.9,[19] respectively, irrespective of the irradiation time. The $[T_s]$ and [A] thus obtained are listed in Table 1. They are the effective concentrations in the surface layer through *ca.* 0.5, 0.2, and 0.07 μm in depth for the 340, 280, and 240 nm excitations, respectively. Both $[T_s]$ and [A] were higher for the shorter-wavelength excitation, because the photooxidation proceeds preferentially near the surface of a film. With increasing irradiation time, both [A] and $[T_s]$ increased, but their ratio, $[A]/[T_s]$, decreased. This is reasonable, judging from the facts that the acceptor-like photooxidation products are intermediates and undergo further photooxidation and that the exciplex fluorescence around 515 nm was observed most strongly for the films with the Q value of 1—3.[9] The small value (0.09) of ϕ_0 observed for all the excitation bands is thus explained by a small value of the ratio, $[A]/([E]+[A]+[T_s])$, and is independent of the excitation layer.

The ϕ_0 values of 0.11[8] and 0.14[4] determined by the xerographic discharge technique are comparable to the value of 0.09 in the photooxidized films and are much larger than the value of 0.02 for the 340 nm excitation in fresh films. This suggests that the surface of films exposed to xerographic photo-discharge even in a nitrogen atmosphere is subjected to the photooxidation at a fairly high level.

The r_0 is considered to depend on the properties of acceptor-like molecules,[10] while both the fresh and photooxidized films had the identical value (26 Å) of r_0. This suggests that the main acceptor-like molecules are identical for these films. The r_0 is considered to depend on the excess energy to be dissipated. It was,

Table 1. Effect of irradiation time on [A] and $[T_s]$[a]

Irradiation time	[A]/mol%			$[T_s]$/mol%	
min	340 nm	280 nm	240 nm	340 nm	280 nm
0	0.006	0.011	0.018	≈0	≈0
3.3	0.016	0.028	—	0.019	0.077
9	0.036	—	—	0.124	—
18	0.065	0.10	—	0.315	0.67

a) 340, 280, and 240 nm are the excitation wavelengths. See the text.

nevertheless, independent of the excitation bands, as mentioned above. This indicates that the direct carrier-photogeneration from the higher excited singlet states is negligible for films investigated in this paper.

Based on the energetical considerations,[10,11] intrinsic carrier-photogeneration due to the autoionization mechanism is expected to be possible for the ^1B_b and ^1B_a excitations. Yokoyama *et al.* have proposed this mechanism for the photocurrent in copolymers of *N*-vinylcarbazole with 1-vinylnaphthalene.[22] However, the comparison of r_o and ϕ_o between the 240 nm excitation and the 280 or 340 nm excitation clearly indicates that the extrinsic carrier-photogeneration in Scheme 1 rather than the intrinsic autoionization mechanism is predominant even for the 240 nm excitation. This is reasonable, judging from both the relatively high concentration of acceptor-like impurities ([A]=0.018 mol%) in the surface layer through 0.07μm in depth of fresh PVCz films and the relatively low value of the primary quantum yield ($\phi_o<10^{-2}$) for the autoionization process in anthracene single crystals.[23] The intrinsic autoionization mechanism is considered to become important when the higher singlet excited states are formed in a bulk sample which has a low concentration of acceptor-like impurities, as is the case of the triplet-triplet annihilation in the copolymers.[22]

Conclusion. As mentioned above, the excitation wavelength dependences of r_o and ϕ_o in fresh, photooxidized and DMTP-doped films lead to the conclusion that the extrinsic carrier-photogeneration process expressed by Scheme 1 and Eq.1 is predominant in every film for all the excitation bands.

This work was supported by the Grant-in-Aid for the Scientific Research No 56550630 from the Ministry of Education, Science and Culture.

Refereces

1) P. J. Regensburger, *Photochem. Photobiol.*, **8**, 429 (1968).
2) D. M. Pai, *J. Chem. Phys.*, **52**, 2285 (1970).
3) K. Okamoto, S. Kusabayashi, and H. Mikawa, *Bull. Chem. Soc. Jpn.*, **46**, 2324, 2613 (1973).
4) G. Pfister and D. J. Williams, *J. Chem. Phys.*, **61**, 2416 (1974).
5) P. J. Reucroft and K. Takahashi, *J. Non-Cryst. Solids*, **17**, 71 (1975).
6) K. Okamoto, M. Oda, A. Itaya, and S. Kusabayashi, *Chem. Phys. Lett.*, **35**, 483 (1975).
7) M. Yokoyama, Y. Endo, and H. Mikawa, *Bull. Chem. Soc. Jpn.*, **49**, 1538 (1976).
8) P. M. Borsenberger and A. I. Ateya, *J. Appl. Phys.*, **49**, 4035 (1978).
9) A. Itaya, K. Okamoto, and S. Kusabayashi, *Bull. Chem. Soc. Jpn.*, **52**, 2218 (1979).
10) M. Yokoyama, Y. Endo, A. Matsubara, and H. Mikawa, *J. Chem.Phys.*, **75**, 3006 (1981).
11) J. Mort and A. I. Lakatos, *J. Non-Cryst. Solids*, **4**, 117 (1970).
12) W. Klöpfer, *Z. Naturforsch., A*, **24**, 1923 (1969).
13) R. R. Chance and C. L. Braun, *J. Chem. Phys.*, **64**, 3573 (1976); L. E. Lyons and K. A. Milne , *ibid.*, **65**, 1474 (1976).
14) L. Onsager, *J. Chem. Phys.*, **2**, 599 (1934); *Phys. Rev.*, **54**, 554 (1938).
15) N. E. Geacintov and M. Pope, Proceedings of the Third International Conference on Photoconductivity," ed by E. M. Pell, Pergamon, Oxford (1971), p. 289.
16) A. Itaya, K. Okamoto, and S. Kusabayashi, *Bull. Chem. Soc. Jpn.*, **50**, 22 (1977).
17) N. Karl and G. Sommer, *Phys. Status Solidi A*, **6**, 231 (1971).
18) B. Reimer and H. Baessler, *Phys. Status Solidi A*, **51**, 445 (1979); M. Fujino, H. Mikawa, and M. Yokoyama, *Photog. Sci. Eng.*, **26**, 84 (1982).
19) W. Klöpffer, *Chem. Phys.*, **57**, 75 (1981).
20) M. Yokoyama and H. Mikawa, *Photog. Sci. Eng.*, **26**, 143 (1982).
21) P. J. Melz, *J. Chem. Phys.*, **57**, 1694 (1972).
22) M. Yokoyama, M. Hanabata, T. Tamamura, T. Nakano, and H. Mikawa, *J. Chem. Phys.*, **67**, 1742 (1977).
23) R. G. Kepler, *Appl. Opt. Suppl.*, **3**, 25 (1969).

 © 1984 The Chemical Society of Japan Bull. Chem. Soc. Jpn., 57, 1631—1636 (1984)

Electrophilic Substitution Reactions on Methine Carbon of the Unsymmetrical Tetradentate Schiff Base and its Complexes with Nickel(II) and Copper(II)

Kuninobu KASUGA,* Takeo NAGAHARA, Teruaki MASUDA, Shunji KIYOTA, and Yasuo YAMAMOTO
Department of Chemistry, Faculty of Science, Shimane University, Matsue 690
(Received July 1, 1983)

A number of unsymmetrical tetradentate Schiff base complexes of nickel(II) and copper(II) having only one methine carbon in the ligand were synthesized and characterized by means of UV and ^{1}H NMR spectra. The kinetic studies of the electrophilic substitution reactions on the methine carbon with *N*-halogenosuccinimide gave no support to an aromatic character of the chelate ring, being consistent with the results of ^{1}H NMR studies for the nickel(II) complexes.

Nature of the bonding in β-diketone metal complexes has been the subject of considerable controversy. A π-bonding between ligands and metal ion in the complexes was once proposed.[1-3] However, an aromaticity of the chelate ring has been suspected on the basis of electronic spectral and ^{1}H NMR data.[4] Collman and his coworkers subsequently reported various replacements of methine protons of these complexes by electrophiles such as bromine, iodine, *N*-halogenosuccinimide, nitro derivatives, acyl derivatives, and sulfur, suggesting the aromatic character of the chelate ring.[5] Furthermore electrophilic substitution reactions on the chelate ring have been reported for mixed ligand β-diketone complexes of cobalt(III),[6] and tetradentate Schiff base complexes of nickel(II) and copper(II).[7-9] Further replacement of the halogen-substituted methine carbon of the β-diketone and tetradentate Schiff base complexes were also carried out using benzenethiol and its derivatives as a nucleophile.[8,10,11]

Although the reactions of coordinated ligands were considerably studied from the synthetic aspects, only a few studies have been reported on the reaction mechanism.[6,9,12] One of the reasons is the presence of two or more methine carbons in the chelate rings, which makes it difficult to study the reaction kinetics. In the present paper, a series of nickel(II) and copper(II) complexes with only one methine carbon in their chelate ring was prepared and the aromaticity of the chelate ring was studied by means of the ^{1}H NMR spectra and reaction kinetics of the electrophilic substitution on the methine carbon. The complexes used in the present study are shown in Fig. 1.

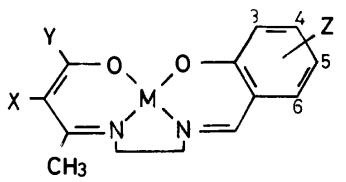

X = H , Cl , Br

Y = Me , Ph

Z = H , 3-OCH3 , 5-Br , 5-Cl

M = Ni(II) , Cu(II)

M(L-X,Y,Z)

Fig. 1. Abbreviation of the Schiff base complexes; Me and Ph denote methyl and phenyl groups, respectively.

Experimental

Complexes. [*N*-(1-Methyl-3-oxobutylidene)-*N'*-salicylideneethylenediaminato]copper(II), Cu(L-H, Me, H), was prepared by the method described before.[13] Other derivatives of copper(II) were prepared according to the similar procedure to that for Cu(L-H, Me, H). However, the method was inapplicable to the preparation of the nickel(II) complex because of a great difficulty in separating the product from the by-products such as [*N*,*N'*-bis(1-methyl-3-oxobutylidene)ethylenediaminato]nickel(II) and (*N*,*N'*-disalicylideneethylenediaminato)nickel(II). Therefore, the nickel(II) complex, Ni(L-H, Me, H), was prepared by the reaction of nickel(II) acetate and a free ligand which was previously liberated from the copper(II) complex, Cu(L-H, Me, H). Hydrogen sulfide was bubbled through a chloroform solution(50 ml) of 1.0 g (3.2 mmol) Cu(L-H, Me, H) at room temperature for 20 min. After filtering off copper(II) sulfide, active charcoal was added to the filtrate, and the mixture was stirred for several min. After filtering off charcoal, tarry crude precipitates of the free ligand were obtained by concentrating the filtrate under a reduced pressure. The pale yellowish white crystals of the free ligand were subsequently recrystallized from cyclohexane. The nickel(II) complex was precipitated after standing a methanol solution(30 ml) of 0.74 g (3.0 mmol) free ligand and 0.75 g (3.0 mmol) nickel(II) acetate tetrahydrate at room temperature for 30 min. Then, the bright brown crystals of the nickel(II) complex were recrystallized from dichloromethane added with a small amount of methanol. The other nickel(II) complexes were prepared by the reactions of nickel(II) acetate tetrahydrate and the free ligands which were liberated from the corresponding copper(II) complexes.

Halogen Derivatives. *N*-Chlorosuccinimide (CSI) (0.44 g, 3.3 mmol) was added to 30 ml of the dichloromethane solution of 0.91 g (3.0 mmol) Ni(L-H, Me, H), which was stirred at room temperature for 20 min. After concentrating the solution under a reduced pressure, [*N*-(2-chloro-1-methyl-3-oxobutylidene)-*N'*-salicylideneethylenediaminato]nickel(II), Ni (L-Cl, Me, H), was precipitated by the addition of an adequate amount of methanol. The brown crystals were subsequently recrystallized from acetone. The other chloro derivatives were also prepared according to the similar method described above. Bromo derivatives of the nickel(II) complexes were prepared using *N*-bromosuccinimide (BSI) instead of CSI (the reaction temperature was maintained below −5 °C). The halogen derivatives of the copper(II) complexes were prepared

using a similar method to the nickel(II) complexes. The chlorination of the free ligand was performed by adding 0.88 g (6.6 mmol) CSI to the 50 ml dichloromethane solution of 1.5 g (6.0 mmol) (L-H, Me, H), and was left at room temperature for 20 min. After evaporation of the solvent, the precipitates remained were dissolved in 30 ml methanol, and an adequate amount of water was added to the solution. Then, the pale yellowish white precipitates were obtained, and subsequently recrystallized from cyclohexane.

Kinetic Measurements. *N*-Chlorosuccinimide and *N*-bromosuccinimide were recrystallized from ethanol, and dried under a reduced pressure. The solvents used for kinetic measurements were dehydrated on anhydrous calcium chloride and distilled under a reduced pressure. The reaction rate was measured by the absorbance change with time on a Hitachi 215 spectrophotometer. The temperature was kept at 20.0±0.1 °C.

Other Measurements. The ^{1}H NMR spectra were recorded with a JEOL-MH 100 spectrophotometer at a frequency of 100 MHz. The chemical shifts were determined in ppm, using TMS as the internal standard. The electronic spectra in solution were measured on a Hitachi 215 spectrophotometer.

Results and Discussion

Electronic and ^{1}H NMR Spectra of the Complexes. The results of elemental analyses and yields of the complexes are listed in Table 1.

In Table 2, the electronic spectral data in benzene solutions are given. Nickel(II) complexes (**1**—**20**) show the d-d absorption bands at 550—570 nm which are characteristic of a square planar nickel(II) complex. The Ni(L-X, Ph, Z) complexes (**5**—**8** and **13**—**16**) show the d-d bands at longer wavelengths than Ni(L-X, Me, Z) (**1**—**4** and **9**—**12**). This lower-energy shift may be attributed to an electron-withdrawing effect of a phenyl group which weakens the in-plane crystal field. The 5-chloro and 5-bromo derivatives show little shift of the d-d bands, whereas the 3-methoxy derivatives (**4**, **8**, **12**, and **20**) shift the bands somewhat to longer wavelengths compared with the unsubstituted complexes (**1**, **5**, **9**, **13**, and **17**). The lower-energy shift in the methoxy derivatives may also be attributed to the electron-withdrawing effect of the methoxyl group. On the other hand, the d-d bands (560 nm) of the copper(II) complexes (**21**—**26**) show little shift. The π-π^* absorption bands in 310 to 350 nm have the following characteristic points; 1) the X substituents such as chlorine and bromine of the nickel(II) complexes (**9** and **17**) shift the bands to shorter wavelengths than Ni(L-H, Me, H) (**1**), whereas the Z substituents (**2**—**4**) to longer wavelengths. 2) In the copper(II) complexes, on the contrary, the X substituents (**24** and **25**) shift the bands to longer wavelengths, and the Z substituents scarcely shift the bands (**22** and **23**) compared with Cu(L-H, Me, H) (**21**). That is, the effect of copper(II) on the π-system of the chelate ring is different from that of nickel(II). Further studies will be performed on the effect of other metal ions on the π-π^* absorption bands.

The ^{1}H NMR data are listed in Table 3. The ^{1}H NMR signals arising from the methine proton disappear in the halogen derivatives, indicating the replacement of the methine proton with the substituents. The ^{1}H

Table 1. Elemental analyses and yields of the complexes

No.	Complex	Found/(%)			Calcd/(%)			Yield[a]
		C	H	N	C	H	N	%
1	Ni(L-H, Me, H)	55.52	5.26	9.32	55.49	5.33	9.25	68
2	Ni(L-H, Me, Cl)	49.86	4.53	8.49	49.82	4.49	8.30	62
3	Ni(L-H, Me, Br)	43.65	3.75	7.31	44.02	3.97	7.34	58
4	Ni(L-H, Me, OCH_3)	54.09	5.44	8.42	54.09	5.46	8.41	61
5	Ni(L-H, Ph, H)	62.64	4.95	7.69	62.50	4.98	7.67	30
6	Ni(L-H, Ph, Cl)	56.64	4.40	6.69	57.11	4.30	7.01	15
7	Ni(L-H, Ph, Br)	51.41	3.90	6.13	51.39	3.87	6.31	45
8	Ni(L-H, Ph, OCH_3)	60.40	5.07	6.81	60.79	5.11	7.09	53
9	Ni(L-Cl, Me, H)	49.76	4.37	8.26	49.83	4.49	8.30	42
10	Ni(L-Cl, Me, Cl)	44.92	3.52	7.43	45.21	3.80	7.53	44
11	Ni(L-Cl, Me, Br)	40.18	3.30	6.69	40.38	3.40	6.73	58
12	Ni(L-Cl, Me, OCH_3)	48.78	4.92	7.33	49.02	4.67	7.62	70
13	Ni(L-Cl, Ph, H)	56.89	4.20	6.94	57.11	4.30	7.01	62
14	Ni(L-Cl, Ph, Cl)	52.55	3.71	6.40	52.58	3.72	6.46	63
15	Ni(L-Cl, Ph, Br)	47.59	3.36	5.43	47.69	3.38	5.86	67
16	Ni(L-Cl, Ph, OCH_3)	55.78	4.49	6.37	55.92	4.47	6.52	83
17	Ni(L-Br, Me, H)	44.04	3.72	7.41	44.02	3.97	7.34	30
18	Ni(L-Br, Me, Cl)	39.92	3.13	6.32	40.38	3.40	6.73	44
19	Ni(L-Br, Me, Br)	36.29	3.11	6.32	36.49	3.07	6.08	35
20	Ni(L-Br, Me, OCH_3)	43.65	3.94	6.63	43.73	4.17	6.80	55
21	Cu(L-H, Me, H)	54.95	5.15	9.23	54.62	5.25	9.10	63
22	Cu(L-H, Me, Br)	43.41	3.55	6.89	43.47	3.93	7.24	52
23	Cu(L-H, Me, OCH_3)	53.10	5.45	8.03	53.32	5.38	8.29	60
24	Cu(L-Cl, Me, H)	49.17	4.25	8.21	49.12	4.43	8.19	56
25	Cu(L-Br, Me, H)	42.98	3.85	7.08	43.47	3.93	7.24	28
26	Cu(L-Cl, Me, Br)	39.41	3.11	6.24	39.92	3.36	6.65	34
27	(L-H, Me, H)	68.03	7.45	11.14	68.26	7.38	11.37	76
28	(L-Cl, Me, H)	59.65	6.02	9.71	59.89	6.12	9.97	26

a) Yields are in molar percentages.

NMR signals of the methyl groups are largely shifted to lower magnetic fields in the order of X=H, Cl, and Br derivatives of nickel(II). This tendency is attributable to the magnetic anisotropic effect of halogen rather than to its inductive effect.

Aromaticity of the Chelate Rings. Nature of the chelate-ring bonding of β-diketone complexes has called considerable attention for a long time. In 1945, Calvin *et al.* proposed the conjugated system of type II for the chelate-ring bonding of the complexes.[1)]

Table 2. Electronic spectra of the complexes in benzene

No.	M(L-X, Y, Z)	λ max/nm(log ε)				
1	Ni(L-H, Me, H)	340(3.87)	370^{sh}(3.62)	417(3.40)	452^{sh}(3.27)	555(2.01)
2	Ni(L-H, Me, Cl)	351(3.93)	375^{sh}(3.69)	432(3.40)	462^{sh}(3.34)	555^{sh}(2.19)
3	Ni(L-H, Me, Br)	352(4.00)	390(3.68)	419(3.58)	460^{sh}(3.38)	560(2.73)
4	Ni(L-H, Me, OCH_3)	352(3.95)	375(3.70)	427(3.43)	465^{sh}(3.30)	562(2.21)
5	Ni(L-H, Ph, H)	311(4.20)		414(3.83)	455^{sh}(3.54)	562(2.21)
6	Ni(L-H, Ph, Cl)	308(4.17)		408(3.81)	480^{sh}(3.26)	557^{sh}(2.26)
7	Ni(L-H, Ph, Br)	307(4.13)		407(3.98)	473^{sh}(3.30)	560^{sh}(2.29)
8	Ni(L-H, Ph, OCH_3)	315(4.10)		417(3.77)	456^{sh}(3.48)	564(2.18)
9	Ni(L-Cl, Me, H)	333(3.85)	393(3.69)	422(3.66)	458^{sh}(3.37)	564(2.18)
10	Ni(L-Cl, Me, Cl)	342(3.87)	387(3.65)	427(3.46)	465^{sh}(3.36)	565(2.20)
11	Ni(L-Cl, Me, Br)	342(3.82)	387(3.72)	426(3.51)	470^{sh}(3.32)	565(2.73)
12	Ni(L-Cl, Me, OCH_3)	337(3.87)	390(3.64)	420(3.49)	464^{sh}(3.26)	574(2.15)
13	Ni(L-Cl, Ph, H)	315(4.09)		413(3.77)	455^{sh}(3.46)	569(2.20)
14	Ni(L-Cl, Ph, Cl)	312(4.05)		406(3.76)	472^{sh}(3.29)	566(2.32)
15	Ni(L-Cl, Ph, Br)	312(4.12)		406(3.73)	475^{sh}(3.25)	566(2.25)
16	Ni(L-Cl, Ph, OCH_3)	318(4.09)		415(3.71)	455^{sh}(3.41)	576(2.16)
17	Ni(L-Br, Me, H)	332(3.81)	391(3.62)	422(3.57)	460^{sh}(3.35)	560(2.15)
18	Ni(L-Br, Me, Cl)	342(3.76)	387(3.61)	427(3.42)	466^{sh}(3.30)	557^{sh}(2.16)
19	Ni(L-Br, Me, Br)	342(3.82)	387(3.67)	427(3.49)	466^{sh}(3.25)	560(2.18)
20	Ni(L-Br, Me, OCH_3)	338(3.76)	391(3.63)	422(3.48)	466^{sh}(3.25)	570(2.18)
21	Cu(L-H, Me, H)	332(4.17)	393(3.69)			560(2.48)
22	Cu(L-H, Me, Br)	333(4.23)	401(3.67)			562(2.63)
23	Cu(L-H, Me, OCH_3)	333(4.23)	401(3.68)			560(2.63)
24	Cu(L-Cl, Me, H)	345(4.13)	393(3.66)			560(2.48)
25	Cu(L-Br, Me, H)	345(4.11)	393(3.63)			560(2.49)
26	Cu(L-Cl, Me, Br)	347(4.04)	403(3.61)			560(2.48)
27	(L-H, Me, H)	311(4.27)				
28	(L-Cl, Me, H)	330(4.22)				

Sh=Shoulder.

Table 3. ^1H NMR spectra of the nickel(II) complexes in chloroform-*d* (PPM)

No.	Complex	δ CH_3	δ CH_2	δ OCH_3	δ CH	δ (aromatic and azomethine protons)
1	Ni(L-H, Me, H)	2.15(6H, d)	3.33—3.53(2H, m) 3.66—3.83(2H, m)		5.51(H, s)	7.29—8.32(5H, m)
2	Ni(L-H, Me, Cl)	2.13(6H, d)	3.33—3.83(2H, m) 3.65—3.80(2H, m)		5.51(H, s)	7.59—8.25(4H, m)
3	Ni(L-H, Me, Br)	2.13(6H, d)	3.14—3.50(2H, m) 3.66—3.83(2H, m)		5.50(H, s)	7.32—8.25(4H, m)
4	Ni(L-H, Me, OCH_3)	2.15(6H, d)	3.33—3.50(2H, m) 3.66—3.86(2H, m)	4.16(3H, s)	5.51(H, s)	7.33—7.49(3H, m) 8.28(H, s)
5	Ni(L-H, Ph, H)	2.13(3H, s)	3.40—3.60(2H, t) 3.70—3.93(2H, t)		6.22(H, s)	7.19—7.76(4H, m) 8.12—8.61(6H, m)
6	Ni(L-H, Ph, Cl)	2.11(3H, s)	3.40—3.63(2H, m) 3.76—3.96(2H, m)		6.24(H, s)	7.56—8.03(3H, m) 8.12—8.58(6H, m)
7	Ni(L-H, Ph, Br)	2.10(3H, s)	3.40—3.63(2H, m) 3.76—3.96(2H, m)		6.23(H, s)	7.49—7.99(3H, m) 8.09—8.58(6H, m)
8	Ni(L-H, Ph, OCH_3)	2.15(3H, s)	3.43—3.66(2H, m) 3.73—3.96(2H, m)	4.26(3H, s)	6.24(H, s)	6.99—7.66(3H, m) 8.12—8.61(6H, m)
9	Ni(L-Cl, Me, H)	2.44(6H, s)	3.47—3.86(4H, m)			7.79—8.35(5H, m)
10	Ni(L-Cl, Me, Cl)	2.40(6H, d)	3.47—3.83(4H, m)			7.59—7.99(3H, m) 8.16(H, s)
11	Ni(L-Cl, Me, Br)	2.40(6H, d)	3.53—3.82(4H, m)			7.49—8.03(3H, m) 8.23(H, s)
12	Ni(L-Cl, Me, OCH_3)	2.43(6H, d)	3.53—3.83(4H, m)	4.19(3H, s)		7.16—7.56(3H, m) 8.25(H, s)
13	Ni(L-Cl, Ph, H)[a)]	2.46(3H, s)	3.50—3.90(4H, m)			7.16—7.66(3H, m) 8.23—8.42(6H, m)

TABLE 3. (Continue)

No.	Complex	δ CH_3	δ CH_2	δ OCH_3	δ CH	δ (aromatic and azomethine protons)
16	Ni(L-Cl, Ph, OCH_3)[a]	2.51(3H, s)	3.53—3.80(4H, m)	3.80(3H, s)		7.16—7.66(3H, m) 8.33(6H, brs)
17	Ni(L-Br, Me, H)	2.51(6H, d)	3.53—3.83(4H, m)			7.72—8.16(4H, m) 8.25(H, s)
18	Ni(L-Br, Me, Cl)	2.50(6H, s)	3.50—3.96(4H, m)			7.66—7.99(3H, m) 8.24(H, s)
19	Ni(L-Br, Me, Br)	2.53(6H, s)	3.50—3.90(4H, m)			7.99—8.33(4H, m)
20	Ni(L-Br, Me, OCH_3)	2.53(6H, s)	3.50—3.83(4H, m)	4.23(3H, s)		7.16—7.66(3H, m) 8.46(H, s)
27	(L-H, Me, H)	2.05(6H, d)	3.76—4.13(4H, m)		5.31(H, s)	7.26—7.92(4H, m) 9.08(H, s)
28	(L-Cl, Me, H)	2.34(6H, d)	3.89—4.09(4H, m)			7.33—7.99(4H, m) 9.08(H, s)

Confidence limits are ±0.02 ppm. a) in 1, 1, 2, 2-tetrachloroethane-d_2. s=singlet, d=doublet, t=triplet, m =multiplet, and br=broad. The ^1H NMR spectra of Ni(L-Cl, Ph, Cl) and Ni(L-Cl, Ph, Br) were not obtained because of their poor solubilities.

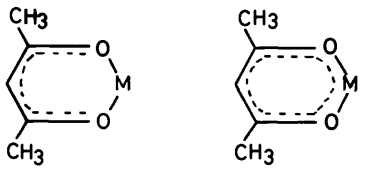

Barnum also suggested the significant π-bonding between the ligands and the metal ion on the basis of electronic spectra.[2] Further, Nakamoto suggested from the results of IR spectra that acetylacetone complexes of nickel(II), copper(II), and palladium(II) have the structure of type (II), although those of zinc(II) and cobalt(II) have that of type (I).[3] However, Cotton *et al.* pointed out that the aromaticity was unreasonable on the basis of the symmetry and energy of the metal orbitals available for the π-bonding.[4] On the other hand, Collman and his coworkers have studied the numerous electrophilic substitution reactions on the chelate rings, which support the conjugate system of type (II).[5] They also reported the quasiaromatic character of the chelate ring from the ^1H NMR spectra of diamagnetic cobalt(III) and rhodium(III) complexes with the mixed ligands of acethylacetone and its derivatives.[14]

To examine the quasiaromatic character of the chelate ring of Ni(L-H, Y, Z), we investigated the effect of the Z groups on the ^1H NMR signals of the methine proton (Table 3). If the chelate ring had the quasiaromaticity, the electron density of the methine proton is expected to change with the Z groups. In a series of the complexes with the methyl substituents at position Y, Ni(L-H, Me, Z), the methine signals are observed at 5.51 (Z=H), 5.51 (Cl), 5.50 (Br), and 5.51 ppm (OCH_3), respectively. For Ni(L-H, Ph, Z), the signals appear at 6.22 (Z=H), 6.24 (Cl), 6.23 (Br), and 6.24 ppm (OCH_3). These facts show that the effect of the Z substituents is little on the ^1H NMR signals of the methine proton, and this agrees with the ^1H NMR data investigated for a broad range of diamagnetic metal complexes of acetylacetone; the metal ions do not significantly affect the shift of the methine-proton signals.[4] Therefore, the ^1H NMR data seem to give no support for an aromaticity of the nickel(II) chelate-ring of the Schiff base complexes such as shown in aromatic compounds.

Kinetics of Electrophilic Ring-substitution Reactions. By the addition of *N*-chlorosuccinimide, the spectrum

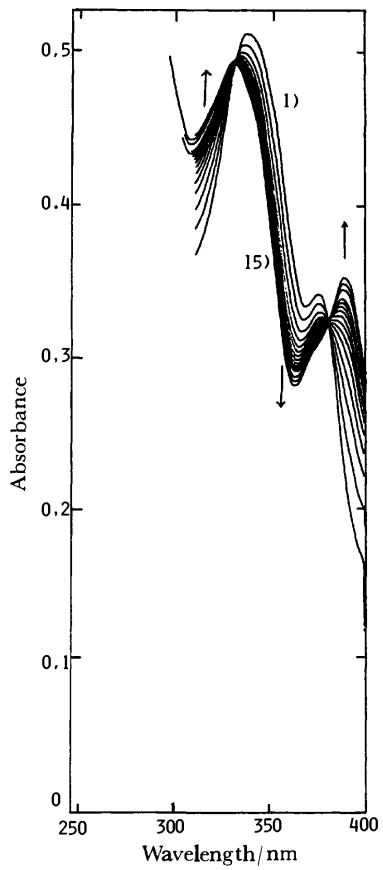

Fig. 2. Spectra changes during the reaction of Ni(L-H, Me, H) with CSI in the benzene solution at 20°C; $[Ni(L\text{-}H, Me, H)]_0=7.48\times10^{-5}$ mol dm^{-3}, $[CSI]_0=1.05\times10^{-4}$ mol dm^{-3}: 1) 40 s, 2) 1 min 40 s, 3) 2 min 40 s, 7) 6 min 40 s, 11) 10 min 40 s, 13) 15 min 40 s, 14) 20 min 40 s, and 15) 30 min 40 s, after the reaction.

TABLE 4. THE RATE CONSTANTS OF THE REACTIONS OF THE COMPLEXES WITH CSI IN A BENZENE SOLUTION

Run	$k/10^2$ mol^{-1} dm^3 s^{-1}	Conditions
1	0.53±0.03	Ni(L-H, Me, H) + CSI
2	0.51±0.04	same reactants with a few mg of the scavenger
3	0.30±0.02	Ni(L-H, Ph, H) + CSI
4	0.21±0.05	Ni(L-H, Me, Cl) + CSI
5	0.25±0.03	Ni(L-H, Me, Br) + CSI
6	0.55±0.04	Ni(L-H, Me, OCH_3) + CSI
7	8.0 ±1.2	Cu(L-H, Me, H) + CSI
8	1.1 ±0.2	(L-H, Me, H) + CSI

Isosbestic points for the reactions of the copper(II) complex and the free ligand with CSI are at 337 and 324 nm, respectively. [complex]$_0$=4.4×10^{-5}—7.5×10^{-5} mol dm^{-3}; [CSI]$_0$=1.05×10^{-4} mol dm^{-3}; temp= 20.0±0.1 °C.

of Ni(L-H, Me, H) in the benzene solution changed to that of Ni(L-Cl, Me, H) with isosbestic points at 334 and 380 nm (Fig. 2). The existence of the isosbestic points clearly indicates that only the following reaction occurs:

Ni(L-H, Me, H)+CSI→Ni(L-Cl, Me, H)+succinimide. (1)

Thus, the rate of reaction (1) is determined by an absorbance change at 393 nm. The second-order plot of $(a-b)^{-1}\ln[b(A_t-A_\infty)/\{b(A_0-A_\infty)-a(A_0-A_t)\}]$ *versus* time is linear for at least 90% completion, a and b being intial concentrations of Ni(L-H, Me, H) and CSI. A_0, A_t, and A_∞ represent the absorbances at the beginning, time t, and infinity, respectively. From the slope, the rate constant was estimated to be (5.3±0.3)×10/mol^{-1} dm^3 s^{-1}. The rate was also measured at 340 nm. The rate constant, (5.1±0.4)×10/mol^{-1} dm^3 s^{-1}, agreed with that obtained at 393 nm within an error, showing no wavelength dependence of the rate. The other rate constants were also obtained in a similar manner to that described above.

Further experiments were performed to elucidate the reaction mechanism (Table 4, Figs. 3 and 4), and the results are as follows: 1) A few mg of 2,6-di-*t*-butylphenol were added into the CSI solution and the solution was subsequently mixed with the Ni(L-H, Me, H) solution. The rate constant of the reaction (Run 2) was the same as that without scavenger (Run 1), which excludes a radical mechanism consistent with the result of the chlorination of [*N*,*N*′-bis(4,4,4-trifluoro-1-methyl-3-oxobutylidene)ethylenediaminato]nickel(II), Ni(tfac$_2$en), with CSI.[9] As shown in Fig. 3, the rate constant increased with the amount of dichloromethane added to the benzene solution. It is known that the reaction of CSI involves the radical mechanism in crystals or in solvents such as carbon tetrachloride and cyclohexane, but involves an ionic mechanism in solvents such as 1,1,2,2-tetrachloroethane and acetonitrile.[15,16] Thus, the above solvent effect observed supports the ionic mechanism. On the other hand, the rate constant decreased slightly by the addition of acetone and remarkably by ethyl ether. It has been reported that acetone and ethyl ether react with BSI to exchange α-hydrogen with bromine.[16] Thus, the addition of the solvents must decrease the concentration of CSI, resulting in the decrease of the rate constant; 2) The rate constant of the chlorination of Ni(L-H, Me, H) (Run 1) was almost the same as those of Ni(L-H, Me, Cl), and Ni(L-H, Me, Br) (Runs 3—5); 3) The rate constant of bromination with *N*-bromosuccinimide was larger than that of chlorination (the rate of bromination was so fast that the rate constant could not be determined). The smaller electron negativity of bromine may produce the cationic bromine more easily from BSI than the cationic chlorine from CSI; 4) The addition of triethylamine (3.0×10^{-5}/mol dm^{-3}) inhibited extreamly the reaction presumably because of the reaction with CSI;[16] 5) As is shown in Fig. 4, the addition of alcohols remarkably increased the

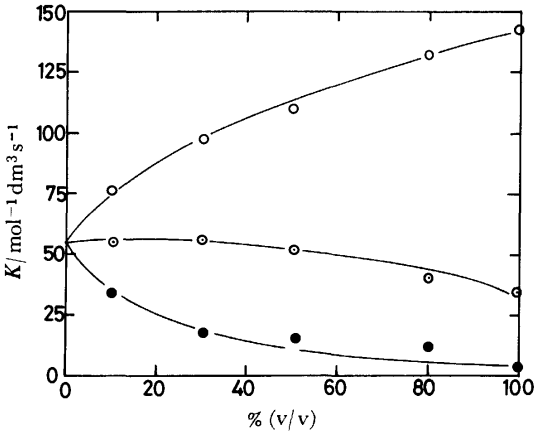

Fig. 3. The effect of solvents on the rate constant of the chlorination reaction: O, dichloromethane; ⊙, acetone; ●, diethyl ether.

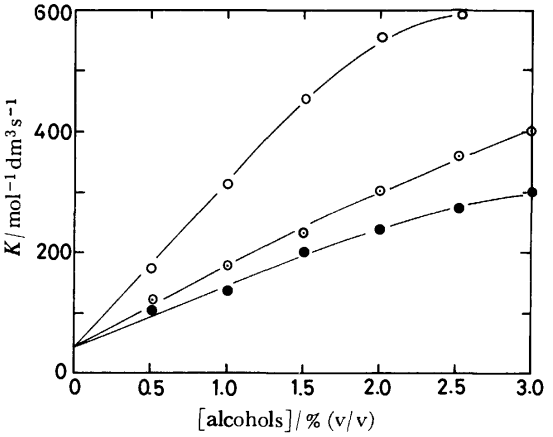

Fig. 4. The effect of alcohols on the rate constant of the chlorination: O, methyl alcohol; ⊙, ethyl alcohol; ●, butyl alcohol.

rate constant. It is reported that molecular chlorine is liberated from CSI by the addition of alcohols.[17] Thus, chlorine liberated by alcohols may accelerate the reaction rate; 6) The rate constants of the chlorination of Cu(L-H, Me, H) and (L-H, Me, H) are $(8.0\pm 1.2)\times10^2$ and $(1.1\pm0.2)\times10^2$ / mol^{-1} dm^3 s^{-1}, respectively (Runs 7 and 8).

On the basis of the above results and discussion, the chlorination of M(L-H, Y, Z) can be assumed to proceed *via* an intermediate (A)[9] or (B) in which a π-system is extended through the central metal ion. However, for the free ligand, in which an extended π-system like (B) is impossible, also proceeds the chlorination, and the order of the rate constant is Ni(II)-complex< free ligand<Cu(II)-complex. Therefore, these results indicate that the chlorination of M(L-H, Y, Z) proceeds *via* the intermediate (A) which is consistent with the result for Ni($tfac_2en$).[9]

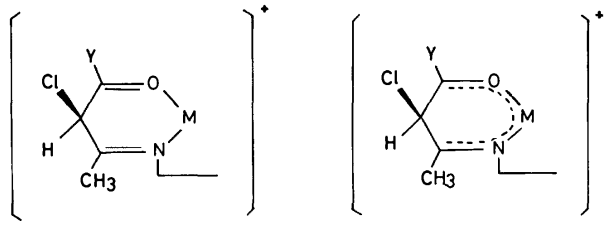

(A) (B)

That is, the electrophilic ring-substitution reaction on the chelate ring of metal complexes does not necessarily support the existence of the benzenoid resonance as shown for the β-diketone metal complexes by Collman *et al.*[5] The results agree with those obtained by the ^1H NMR studies.

The copper(II) complex shows an extremely large rate constant as compared with the nickel(II) complex and the free ligand. At present, there is no satisfactory explanation for the behavior of the copper(II) complex. The copper(II) complex may catalyze the reaction presumably *via* the formation of a CSI adduct. Further studies on the effect of the central metal ions will be performed.

References

1) M. Calvin and K. W. Wilson, *J. Am. Chem. Soc.* **67**, 2003 (1945).
2) D. W. Barnum, *J. Inorg. Nucl. Chem.*, **21**, 221 (1961).
3) K. Nakamoto, "Kinzoku Kireto II," ed by T. Sakaguchi and K. Ueno, Nankodo, Tokyo (1966), pp. 20—85.
4) R. H. Holm and F. A. Cotton, *J. Am. Chem. Soc.*, **80**, 5658 (1958).
5) J. P. Collman, *Adv. Chem. Ser.*, **37**, 78 (1963); *Angew. Chem.*, **77**, 154 (1965); K. C. Joshi and V. N. Pathak, *Coord. Chem. Rev.*, **22**, 37 (1977), and the articles cited therein.
6) K. Kuroda, K. Yoshitani, K. Kunigita, Y. Kamiida, and K. Watanabe, *Bull. Chem. Soc. Jpn.*, **49**, 2445 (1976); K. Kuroda, K. Yamaguchi, and N. Yamaoka, *ibid*, **50**, 535 (1977).
7) T. Nagahara, K. Kasuga, and Y. Yamamoto, *Inorg. Nucl. Chem. Lett.*, **17**, 235 (1981).
8) T. Nagahara, K. Kasuga, and Y. Yamamoto, *Inorg. Chim. Acta*, **47**, 37 (1981).
9) Y. Fujii, M. Ito, and K. Akiyama, *Bull. Chem. Soc. Jpn.*, **54**, 2527 (1981).
10) Z. Yoshida, H. Ogoshi, and Y. Shimizu, *Kogyo Kagaku Zasshi*, **72**, 1648 (1969).
11) Y. Yamamoto, K. Kasuga, and A. Sumita, *Bull. Chem. Soc. Jpn.*, **49**, 2021 (1976); K. Kasuga, M. Anami, and Y. Yamamoto, *ibid*, **51**, 476 (1978); K. Kasuga, T. Nagahara, and Y. Yamamoto, *J. Coord. Chem.*,**10**, 217 (1980).
12) R. W. Kluiber, *J. Am. Chem. Soc.*, **82**, 4839 (1960).
13) H. A. Kusuka, M. F. Farona, P. Paparo, and S. Potterson, *J. Coord. Chem.*, **1**, 259 (1971).
14) J. P. Collman, R. L. Marshall, and W. L. Young, *Chem. Ind. (London)*, **1962**, 1380.
15) S. D. Loss, M. Finkelstein, and R. C. Petersen, *J. Am. Chem. Soc.*, **80**, 4327 (1958); F. Dewhurst and P. K. J. Shah, *J. Chem. Soc., C*, **1970**, 1737.
16) L. Horner and E. H. Winkelmann, "*N*-Bromosuccinimide, its Properties and Reactions," in "Newer Methods of Preparative Organic Chemistry," ed by W. Forest, Academic Press, New York (1964), Vol. 3, pp. 151—198.
17) L. Zechmeister and L. Walleave, *J. Am. Chem. Soc.*, **75**, 4493 (1953); F. J. Petracek and L. Zechmeister, *ibid*, **78**, 1437 (1956).

 © 1984 The Chemical Society of Japan Bull. Chem. Soc. Jpn., 57, 1637—1642 (1984)

A Versatile Synthesis of Four-, Five-, and Six-membered Cyclic Ketones Using Methyl Methylthiomethyl Sulfoxide

Katsuyuki OGURA,*,† Mitsuo YAMASHITA, Michiyo SUZUKI, Shigeko FURUKAWA, and Gen-ichi TSUCHIHASHI*,††

Sagami Chemical Research Center, Nishi-Ohnuma 4-4-1, Sagamihara, Kanagawa 229

†*Department of Synthetic Chemistry, Faculty of Engineering, Chiba University, Yayoicho 1-33, Chiba 260*

††*Department of Chemistry, Faculty of Science and Technology, Keio University, 3-14-1 Hiyoshi, Kohokuku, Yokohama 223*

(Received October 14, 1983)

Cyclization of 1,*n*-dihalo[or bis(tosyloxy)]alkanes with methyl methylthiomethyl sulfoxide in the presence of a base (*n*-BuLi or KH) gave three-, four-, five-, and six-membered 1-methylsulfinyl-1-methylthiocycloalkanes. These cyclization products were easily converted to the corresponding ketones by acid hydrolysis except 1-methylsulfinyl-1-methylthiocyclopropane which afforded a complicated mixture. The combination of the cyclization with the acid hydrolysis thus provides a new method for synthesizing four-, five-, and six-membered cycloalkanones. Several representative preparations, such as those of substituted cyclobutanones, 3-cyclopentenone, and tetrahydro-4-pyrone, are described.

Cyclic ketones, especially five- and six-membered cycloalkanones, are widely spreaded skeletons in naturally occurring organic compounds, and development of a new methodology for constructing these skeletons is one of the most important problems in organic synthesis. Further, exploitation of various methods for ring expansion of cyclobutanones to cyclopentanones[1] is looking forward to an efficient way to make four-membered cyclic ketones. In this paper, we report a novel synthetic method of cyclobutanones, cyclopentanones, and cyclohexanones using methyl methylthiomethyl sulfoxide (**1**).[2] A previous paper[3] revealed that **1** undergoes monoalkylation on treatment with an alkyl halide (RX) in the presence of NaH and the acid hydrolysis of the resultant alkylated product gives an aldehyde (RCHO).[4] The present method for synthesis of cycloalkanones (**4**) comprizes the reaction of 1,*n*-dihalo[or bis(tosyloxy)]alkanes (**2**) with **1** to give 1-methylsulfinyl-1-methylthiocycloalkanes (**3**) and the subsequent acid-hydrolysis of **3** leading to **4**, as shown in Scheme 1.[11] The characteristic features of this cycloalkanone synthesis are as follows: i) one-step cyclization of **1** with **2** is achieved; ii) ring-strained cyclobutanone is conveniently made in a high yield, and (iii) cycloalkanones having many kinds of substituents can be easily synthesized.

Results and Discussion

For the reaction of 1,*n*-dihalo[or bis(tosyloxy)]-alkanes (**2**) with methyl methylthiomethyl sulfoxide (**1**), two types of procedures were employed: (a) with 2.2—2.8 equiv of KH in tetrahydrofuran (THF) (−10 °C—room temperature; "Method A") and (b) with 2.0—2.5 equiv of the lithio derivative (**1'**; M=Li) of **1** in THF (−70 °C—room temperature; "Method B"). The results are summarized in Table 1, showing that both Method A and Method B gave the dithioacetal *S*-oxides (**3**; *n*=3, 4, 5) of cyclobutanone, cyclopentanone, and cyclohexanone in fair to good yields starting from either the corresponding 1,*n*-dibromoalkanes (**2**; X=Br) or 1,*n*-bis(tosyloxy)alkanes (**2**; X=TolSO$_3$). However, 1-methylsulfinyl-1-methylthiocyclopropane (**3**; *n*=2) could be produced in 78% yield only by applying Method B to 1,2-bis(tosyloxy)ethane (**2**; *n*=2, X=TolSO$_3$). For the reaction of **1** with **2**, NaH could be employed as a base in place of KH, but heating the reaction mixture at 50 °C was required and the yields of **3** were relatively low [*n*=5 42%; *n*=4 46%]. The reaction of **1** with 1,3-dibromopropane (**2**; *n*=3, X=Br) in the presence of NaH in THF (50 °C/6 h) was

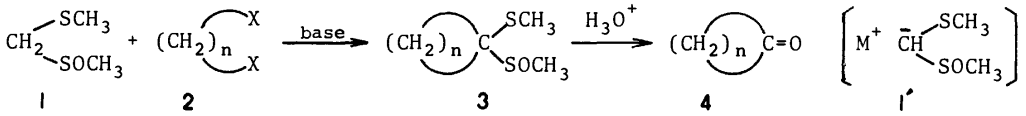

1 2 3 4 1'

Scheme 1

TABLE 1. REACTION CONDITIONS AND YIELDS IN THE CONVERSION OF **1** TO **3**

2	X=Br		X=TolSO$_3$	
	Method A[a]	Method B[b]	Method B[b]	
n=2	−15 °C/4 h→rt/48 h 4%	−15 °C/1 h→rt/48 h 33%	−15 °C/4 h→rt/19 h	78%
n=3	0 °C/1 h→rt/17 h 78%	0 °C/0.5 h→rt/ 2 h 70%	rt/18 h	91%
n=4	0 °C/1 h→rt/19 h 80%	−60 °C/1 h→rt/16 h 80%	rt/18 h	84%[c]
n=5	0 °C/1 h→rt/19 h 82%	−60 °C/2 h→rt/16 h 74%	rt/17 h	80%
n=6	0 °C—rt/20 h None[d]	−15 °C/3 h→rt/18 h None[e]	−15 °C/3 h→rt/19 h	None[f]

a) With 2.2—2.8 equiv of KH in THF. b) With 2.0—2.5 equiv of the lithio derivative (**1'**, M=Li) in THF. c) When Method A was employed, the yield of **3** (*n*=4) was 31%. d) 1,8-Bis(methylsulfinyl)-1,8-bis(methylthio) octane (**19**) and 1-methylsulfinyl-1-methylthio-7-bromoheptane (**20**) were obtained in 24 and 11% yields, respectively. e) The yields of **19** and **20** were 20 and 22%, respectively. f) The yield of **19** was 23%.

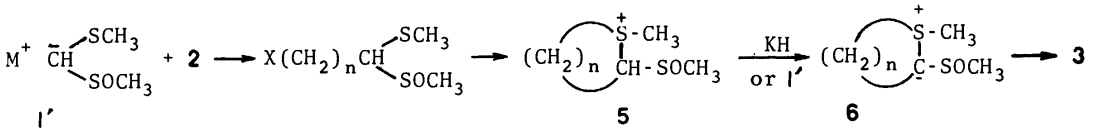

Scheme 2

accompanied with dehydrobromination to give 4-methylsulfinyl-4-methylthio-1-butene in 38% yield (82% yield based on the unrecovered **1**).

It should be noted that 1,6-dibromo [or bis(tosyloxy)]-hexane (**2**; n=6, X=Br or $TolSO_3$) did not produce the corresponding **3** (n=6) by ether Method A or Method B, in a contrast to the base-assisted cyclization of diethyl malonate with 1,n-dihaloalkanes, where a seven-membered cycloalkane derivative is favorably produced.[12] Furthermore, in the present cyclization reaction, **2** afforded the cyclic compounds (**3**) in high yields by the reaction with 2 equiv of the lithio derivative (**1′**; M=Li), indicating the involvement of a more acidic intermediate than **1**. The ring-strained **3** (n=3) is produced at a comparable rate to that of **3** (n=4 or 5). These facts seem to be in accord with the hypothesis that the cyclization may pass through an intermediary sulfonium salt (**5**), followed by the Stevens-type rearrangement to form **3**.

When **3** (n=4 or 5) was treated with a small amount of 4.5 M† sulfuric acid in diethyl ether or ethanol, an acid hydrolysis took place smoothly at room temperature to give cyclopentanone (92%) or cyclohexanone (88%), respectively. These yields were obtained by their derivation into the corresponding 2,4-dinitrophenylhydrazones. When the acid-catalyzed hydrolysis of **3** (n=5) was performed in the presence of trietyl orthoformate in ethanol, the corresponding diethyl acetal of **4** (n=5) was obtained in 83% yield. In the case of 1-methylsulfinyl-1-methylthiocyclobutane (**3**; n=3), an elevated temperature (45 °C) was required for completing the conversion to cyclobutanone. 1-Methylsulfinyl-1-methylthiocyclopropane (**3**; n=2) resisted the acid hydrolysis. Prolonged heating **3** (n=2) with sulfuric acid in ethanol resulted in complicated decomposition. Thus, the present method was shown to be suitable to the synthesis of four-, five-, and six-membered cycloalkanones. Versatility of this method is demonstrated by making certain cycloalkanone derivatives described in the following sections.

Synthesis of Tetrahydro-4-pyrone (8). The reaction of **1** with bis(2-chloroethyl) ether in the presence of KH (2.4 equiv) in THF at 0 °C—room temperature [Method A] afforded the dithioacetal *S*-oxide (**7**) which was subjected to the acid hydrolysis with 4.5 M sulfuric acid in diethyl ether (room temperature/2 h) to give **8** in an overall yield of 66%.

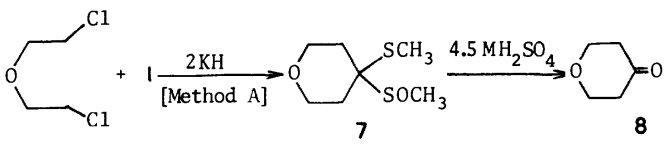

Scheme 3

†1 M=1 mol dm^{-3}.

Synthesis of 3-Cyclopentenone (10). When *cis*-1,4-dichloro-2-butene was allowed to react with 2.5 equiv of **1′** (M=Li) in THF at −78 °C—room temperature, 4-methylsulfinyl-4-methylthio-1-cyclopentene (**9**) was obtained in 78% yield. On the other hand, *trans*-1,4-dichloro-2-butene gave 1-methylsulfinyl-1-methylthio-2-vinylcyclopropane (**11**) in 76% yield under the similar reaction conditions.[13] On treatment of **9** with 4.5 M sulfuric acid in acetone-water (9:1) at room temperature, the expected 3-cyclopentenone was formed in 60% yield along with 2-cyclopentenone (6%) (by a GLC analysis). The ratio of 3-cyclopentenone/2-cyclopentenone decreased with the increase of the reaction time and reached to 2.5 after 24 h.

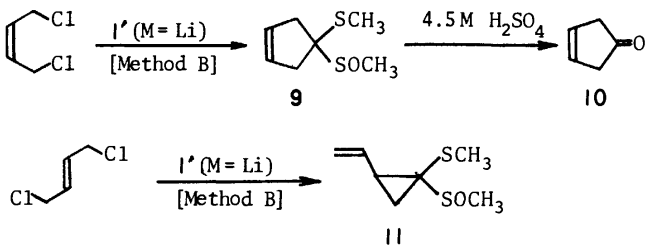

Scheme 4

Synthesis of 2- or 3-Substituted Cyclobutanones. Seebach and Corey reported an elegant synthesis of cyclobutanone by the reaction of 1,3-dithiane with 1,3-dihalopropane.[14] To practice this synthesis, a somewhat complicated procedure is necessitated to avoid the formation of the undesirable disubstituted product: After 2-(3-chloro-1-propyl)-1,3-dithiane is once produced by the reaction of the lithiated 1,3-dithiane with 1-bromo-3-chloropropane, 1-chloro-3-iodopropane, or 1,3-dichloropropane (an excessive amount), this product is again treated with n-BuLi. The use of 1,3-dibromopropane appeared to be impractical because of the formation of a cyclic sulfonium salt (**12**), which gave 1,3-bis(vinylthio)propane (**13**) on treatment with a base.[14]

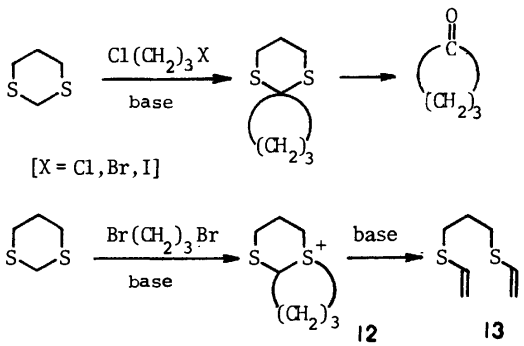

Scheme 5

In contrast, 1,3-dibromo[or bis(tosyloxy)]propane can be preferably employed for conversion of **1** to 1-methylsulfinyl-1-methylthiocyclobutane (**3**; $n=3$), a synthetic precursor of cyclobutanone as above mentioned. Furthermore, the reaction of 1,3-dibromobutane with 2.4 equiv of **1'** (M=Li) at room temperature for 46.5 h in THF furnished 1-methylsulfinyl-1-methylthio-2-methylcyclobutane (**14**) (80% yield), which consisted mainly of two diastereomer in the ratio of 1:2.[15] The acid hydrolysis of cyclization product (**14**) afforded 2-methylcyclobutanone (**15**) which was isolated as its 2,4-dinitrophenylhydrazone (77% yield).

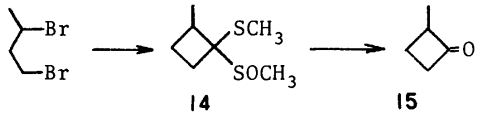

14 15

Scheme 6

By the present method, 3-substituted cyclobutanones (**18**) are simply and conveniently synthesized. Treatment of 2-benzyl-1,3-dibromopropane (**16a**) with 2.3 equiv of **1'** (M=Li) in THF [Method B] resulted in the formation of 3-benzyl-1-methylsulfinyl-1-methylthiocyclobutane (**17a**) (77% yield) as a 2:1 mixture of two diastereomers.[15] The acid hydrolysis of **17a** was effected with 4.5 M sulfuric acid in refluxing diethyl ether to yield 3-benzylcyclobutanone (**18a**) in 78% yield.

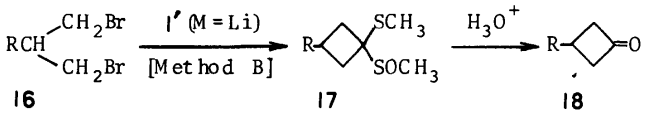

16 17 18

[a: R = $PhCH_2$ b: R = $PhCH_2O$]

Scheme 7

When 2-benzyloxy-1,3-dibromopropane (**16b**) was allowed to react with **1** according to Method B, a cyclization product (**17b**) was formed in 77% yield as a mixture of two diastereomers (1.1:1). The product (**17b**) gave 3-benzyloxycyclobutannone (**18b**) (60% yield) on treatment with perchloric acid in diethyl ether at room temperature for 24 h.

In conclusion, methyl methylthiomethyl sulfoxide (**1**) is a novel reagent for the synthesis of four-, five-, and six-membered cycloalkanones. By the use of **1**, many kinds of their derivatives can be simply and conveniently prepared.

Experimental

Melting points were determined on a hot-stage microscope apparatus (Yanagimoto) and were uncorrected. ^1H NMR spectra were obtained on Varian HA-100 and Varian EM-390 spectrometers. IR spectra were measured with a Hitachi EPI-G3 infrared spectrometer.

Reaction of 1,3-Dibromopropane with 1. A Typical Procedure: *(a) Method A;* To a suspension containing KH (1.01 g: 25.3 mmol) in THF (15 ml), was added to **1** (1.04 g: 8.39 mmol) under an argon atmosphere and the resulting mixture was stirred for 1 h under ice-cooling. After dropwise addition of 1,3-dibromopropane (2.07 g: 10.3 mmol) over 10 min, the mixture was further stirred for 1 h under ice-cooling and then at room temperatre for 17 h. CH_2Cl_2 (100 ml) was added and the deposited insoluble matter was filtered off. The filtrate was concentrated *in vacuo* and the residue was subjected to column chromatography on silica gel using CH_2Cl_2 and Et_2O as eluents to give **3** ($n=3$) as a pale yellow oil (1.08 g: 78%) along with **1** (199 mg). **3** ($n=3$): IR (neat) 1052 cm^{-1}; ^1H NMR ($CDCl_3$) $\delta=1.5$—3.1 (6H, m), 2.13 (3H, s), and 2.47 (3H, s).

This compound was transformed into the corresponding disulfone: To a solution of **3** ($n=3$) (261 mg: 1.59 mmol) in MeOH (5 ml), were added Na_2WO_4-$2H_2O$ (10 mg) and 30% aq solution (1 ml) of H_2O_2 and the resulting mixture was stirred at room temperature for 2 d. Addition of water (10 ml) deposited the disulfone as colorless crystals: mp 141.5—142 °C (from CH_2Cl_2-CCl_4); IR (KBr) 1295, 1140, 1110, 945, 771, and 505 cm^{-1}; ^1H NMR ($CDCl_3$) $\delta=2.0$—2.6 (2H, m), 2.7—3.1 (4H, m), and 3.15 (6H, s). Calcd for $C_6H_{12}O_4S_2$: C, 33.94; H, 5.70; S, 30.21%. Found: C, 33.99; H, 5.66; S, 30.27%.

(b) Method B; To a solution containing **1** (657 mg: 5.30 mmol) in THF (10 ml), was added a 1.44 mol/l hexane solution (4.0 ml) of *n*-BuLi (5.8 mmol) at −10 °C, and the mixture was stirred for 2 h. After addition of 1,3-dibromopropane (530 mg: 2.63 mmol) together with THF (3 ml), the resulting mixture was stirred under ice-cooling for 0.5 h and then at room temperature for 2 h. CH_2Cl_2 (100 ml) was added and the mixture was washed with water (30 ml). The aqueous layer was extracted with four 50-ml portions of CH_2Cl_2. The organic layer and the extracts were combined and dried (Na_2SO_4). The solvents were evaporated, and the residue was column-chromatographed on silica gel [elution with CH_2Cl_2 and CH_2Cl_2-Et_2O (4:1)] to give **3** ($n=3$) as a pale yellow oil (300 mg: 70% yield based on 1,3-dibromopropane). Employment of 1,3-bis(tosyloxy)propane in place of 1,3-dibromopropane gave **3** ($n=3$) in 91% yield as shown in Table 1.

Similarly, the following compounds were prepared. **3** ($n=2$): an oil; IR (neat) 1055 cm^{-1}; ^1H NMR ($CDCl_3$) $\delta=0.89$—1.60 (4H, m), 2.23 (3H, s), and 2.56 (3H, s). The disulfone of **3**($n=2$): mp 140—140.5 °C (from methanol); IR (KBr) 1332, 1318, 1300, and 1125 cm^{-1}; ^1H NMR ($CDCl_3$) $\delta=1.83$ (4H, s) and 3.27 (6H, s). Calcd for $C_5H_{10}O_4S_2$: C, 30.29; H, 5.08; S, 32.35%. Found: C, 30.13; H, 5.04; S, 32.34%.

3 ($n=4$): an oil; IR (neat) 1045 cm^{-1}; ^1H NMR ($CDCl_3$) $\delta=1.6$—2.3 (8H, m), 2.18 (3H, s), and 2.64 (3H, s). The disulfone of **3** ($n=4$): mp 173—173.5 °C (from CH_2Cl_2-CCl_4-hexane); IR (KBr) 1315, 1305, 1288, and 1132 cm^{-1}; ^1H NMR ($CDCl_3$) $\delta=1.7$—2.2 (4H, m), 2.2—2.7 (4H, m), and 3.17 (6H, s). Calcd for $C_7H_{14}O_4S_2$: C, 37.15; H, 6.24; S, 28.34%. Found: C, 37.29; H, 6.22; S, 28.31%. **3** ($n=5$): mp 57.5—58.5 °C (from benzene-hexane); IR (KBr) 1045 cm^{-1}; ^1H NMR ($CDCl_3$) $\delta=1.5$—2.1 (10H, m), 2.08 (3H, s), and 2.60 (3H, s). Calcd for $C_8H_{16}OS_2$: C, 49.95; H, 8.39; S, 33.34%. Found: C, 50.18; H, 8.22; S, 33.26%.

Reaction of 1,6-Dibromohexane with 1. A Typical Procedure: To a solution containing **1** (1.32 g: 10.6 mmol) in THF (10 ml), was added to 1.30 mol/l hexane solution (8.2 ml) of *n*-BuLi (10.7 mmol) and the reaction mixture was stirred at −15 °C for 2 h. After addition of 1,6-dibromohexane (1.01 g: 4.14 mmol), the resulting mixture was further stirred at −15 °C for 3 h and then at room temperature for 18 h. CH_2Cl_2 (15 ml) was added and the deposited solid was filtered off. The filtrate was concentrated, and the residue was subjected to column chromatography on Florisil using CH_2Cl_2 and AcOEt as eluents to give 1,8-bis(methylsulfinyl)-1,8-bis(methylthio)octane (**19**) as a pale brown oil (273 mg: 20% yield) and 1-methylsulfinyl-1-methylthio-7-bromoheptane (**20**) as a pale brown oil (256

mg: 22% yield). The compound **19** was identified by its derivation to 1,1,8,8-tetrakis(methylsulfonyl)octane: mp 163.5—165.5 °C; IR (KBr) 1310, 1150, and 1120 cm^{-1}; ^1H NMR (DMSO-d_6) δ=1.39 (4H, broad s), 1.59 (4H, broad s) 2.07 (4H, broad s), 3.19 (12H, s), and 5.08 (t, 2H, J=5.8 Hz). Calcd for $C_{12}H_{26}O_8S_4$: C, 33.78; H, 6.14; S, 30.07%. Found: C, 33.69; H, 6.11; S, 30.31%. The compound **20** was also converted to its disulfone derivative: mp 56—58 °C; IR (KBr) 1335, 1315, 1310, 1140, 1125, 1120, and 755 cm^{-1}; ^1H NMR ($CDCl_3$) δ=1.3—1.6 (4H, m), 1.6—2.0 (4H, m), 2.0—2.3 (2H, m), 3.15 (6H, s), and 3.93 (1H, t, J=5.5 Hz). Calcd for $C_9H_{19}O_4S_2Br$: C, 32.24; H, 5.71; S. 19.13%. Found: C, 32.64; H, 5.73; S, 19.13%.

Acid-catalyzed Hydrolysis of **3** *(n=3).* To a solution of **3** (n=3) (432 mg: 2.63 mmol) in EtOH (3 ml), was added 8 drops of 4.5 M sulfuric acid, and the resulting solution was stirred at room temperature for 18 h and then at 45 °C for 5 h. This solution was shown not to contain **3** (n=3) by a TLC analysis. A 2,4-dinitrophenylhydrazine solution (25 ml) [3.0 g/sulfuric acid (30 ml)+H_2O (20 ml)+EtOH (70 ml)] was added and the mixture was allowed to stand overnight at room temperature. Addition of water (20 ml) deposited cyclobutanone 2,4-dinitrophenylhydrazone (518 mg: 79%) as orange crystals: mp 146.5—148 °C (from EtOH and CCl_4-hexane) (lit,[16] mp 146 °C); IR (KBr) 3280, 3080, 1615, 1587, 1510, 1338, 1310, and 1270 cm^{-1}; ^1H NMR ($CDCl_3$) δ=1.9—2.5 (2H, m), 2.8—3.4 (4H, m), 7.87 (1H, d, J=10 Hz), 8.27 (1H, dd, J=2.5 and 10 Hz), 9.12 (1H, d, J=2.5 Hz), and 10.73 (1H, broad, NH). Calcd for $C_{10}H_{10}N_4O_4$: C,48.00; H, 4.02; N, 22.39%. Found: C, 47.97; H, 4.02; N, 22.17%.

Acid Hydrolysis of **3** *(n=4).* To a solution of **3** (n=4) (211 mg: 1.19 mmol) in EtOH (5 ml), was added 5 drops of 4.5 M sulfuric acid and the resulting solution was stirred at room temperature for 15 h. By the above-mentioned procedure, the resulting ketone was converted to the corresponding 2,4-dinitrophenylhydrazone (290 mg: 92%) which was identified as cyclopentanone 2,4-dinitrophenylhydrazone by comparison of its IR spectrum with that of the authentic sample.

Acid Hydrolysis of **3** *(n=5).* *a)*: To a solution of **3** (n=5) (293 mg: 1.53 mmol) in EtOH (3 ml), was added 3 drops of 4.5 M sulfuric acid and the resulting solution was stirred at room temperature for 4 h. The above-mentioned work-up gave yellow crystals (375 mg: 88%) which were identified as cyclohexanone 2,4-dinitrophenylhydrazone by comparison of their IR spectrum with that of the authentic sample.

b): To a mixture containing **3** (n=5) (10.79 g: 56.2 mmol) in Et_2O (50 ml), was added 4.5 M sulfuric acid (0.5 ml), and the resulting mixture was stirred at room temperature. Then $NaHCO_3$ (800 mg) and Na_2SO_4 were added. After the insoluble solid was filtered off, the filtrate was evaporated under atmospheric pressure. The residue was subjected to fractional distillation to afford three fractions: (i) bp 56—75 °C/80 Torr (1 Torr=133.322 pa) which was shown by an NMR analysis to consist of dimethyl disulfide (765 mg) and cyclohexanone (655 mg); (ii) bp 75—84 °C/80 Torr which consisted of dimethyl disulfide (258 mg) and cyclohexanone (1.64 g); and (iii) 50—56 °C/20—14 Torr which consisted of dimethyl disulfide (50 mg) and cyclohexanone (2.03 g). The last fraction showed the same IR spectrum to that of cyclohexanone. The yield of cyclohexanone was calculated to be 79%.

c): A mixture containing **3** (n=5) (9.18 g: 47.8 mmol), EtOH (14 ml), triethyl orthoformate (12 ml), and sulfuric acid (0.2 ml) was stirred at room temperature for 14 h. K_2CO_3 (1.5 g) was added and the mixture was further stirred for 30 min. After addition of 0.5 M aq solution (50 ml) of K_2CO_3 and extraction with three 70-ml portions of Et_2O, the extracts were combined and dried (K_2CO_3). The solvents were evaporated, and the residue was subjected to fractional distillation to give cyclohexanone diethyl acetal (6.84 g: 83% yield) as a colorless liquid having bp 100—105 °C/57 Torr (lit,[17] bp 78—85 °C/18 Torr): IR (near) 2890—2830 and 1090—1045 cm^{-1}; ^1H NMR ($CDCl_3$) δ=1.16 (6H, t, J=7 Hz), 1.2—1.8 (10H, broad), and 3.45 (4H, q, J=7 Hz). Calcd for $C_{10}H_{20}O_2$: C, 69,72; H, 11.70%. Found: C, 69.62; H, 11.43%.

Synthesis of Tetrahydro-4-pyrone (8). To a suspension containing KH (3.81 g: 95.3 mmol) in THF (30 ml), was dropwise added to **1** (4.98 g: 40.2 mmol) under ice-cooling over 30 min. After the resulting mixture was stirred for 45 min at the same temperature, bis(2-chloroethyl) ether (5.82 g: 40.7 mmol) was dropwise added over 30 min and the reaction mixture was further stirred under ice-cooling for 1 h and then at room temperature for 4 h. CH_2Cl_2 (100 ml) was added and the deposited solid was filtered off. The filtrate was evaporated and the residue was subjected to column chromatography on silica gel using Et_2O as an eluent to give 4-methylsulfinyl-4-methylthiotetrahydro-4-pyrane (**7**) contaminated with a small amount of **1** as a pale yellow oil (6.17 g).

This oil was dissolved in Et_2O (100 ml) and 4.5 M sulfuric acid (1 ml) was added. After the reaction mixture was stirred at room temperature for 2 h, $NaHCO_3$ (1.5 g) was added to neutralize the acid and then anhydrous Na_2SO_4 was added. After the mixture was allowed to stand overnight, the insoluble solid was filtered off and the filtrate was concentrated *in vacuo*. Distillation of the residue gave two fractions, a colorless liquid (384 mg) having bp 86—88 °C/59 Torr and a colorless oil (2.40 g) having bp 88—91 °C/59 Torr. The former was shown by an NMR analysis to consist of dimethyl dislfide (92 mg) and 8 (292 mg) and latter was pure **8**: IR (neat) 1720, 1217, 1088, and 990 cm^{-1}; ^1H NMR ($CDCl_3$) δ=2.50 (4H, t, J=6 Hz) and 3.98 (4H, t, J=6 Hz). Its 2,4-dinitrophenylhydrazone: mp 191.5—192.5 °C (from water-EtOH) (lit,[18] mp 186.5—187 °C). Calcd for $C_{11}H_{12}N_4O_5$: C, 47.14; H, 4.32; N, 19.99%. Found: C, 47.24; H, 4.36; N, 19.74%.

Reaction of cis-1,4-Dichloro-2-butene with **1**. To a solution of lithio derivative **1'** (M=Li) in THF (150 ml) which was prepared from 1 (24.9 g: 0.200 mol) and n-BuLi (0.200 mol), was added *cis*-1,4-dichloro-2-butene (10.0 g: 0.08 mol). The mixture was further stirred at −70 °C for 3.5 h and then at room temperature for 16.5 h, and then CH_2Cl_2 (400 ml) was added. The mixture was washed with water (100 ml) and the aqueous layer was extracted with five 100 ml-portions of CH_2Cl_2. The organic layers were combined and dried ($MgSO_4$). The solvents were evaporated, and the residue was subjected to column chromatography on Florisil using AcOEt as an eluent to give 4-methylsulfinyl-4-methylthio-1-cyclopentene (**9**) as a pale yellow oil (11.1 g: 78% yield): IR (neat) 1617 and 1050 cm^{-1}; ^1H NMR ($CDCl_3$) δ=2.24 (3H, s), 2.60 (3H, s), 2.35—3.4 (4H, m), and 5.68 (2H, s). The *S,S,S',S'*-tetraoxide derivative: mp 168—169 °C (from CCl_4); IR (KBr) 1630, 1320—1305, 1295, and 1140 cm^{-1}; ^1H NMR ($CDCl_3$) δ=3.20 (6H, s), 3.23 (4H, s), and 5.69 (2H, s). Calcd for $C_7H_{12}O_4S_2$: C, 37.48; H, 5.39; S, 28.59%. Found: C, 37.48; H, 5.38; S, 28.58%.

Acid Hydrolysis of **9** *Leading to 3-Cyclopentenone (10).* The authentic sample of **10** was synthesized by pyrolysis of tricyclo[5.2.1.$0^{2,6}$]deca-3,8-dien-5-ol according to a literature.[19] To a solution of **9** (105 mg: 0.597 mmol) in 10 ml of acetone-water (8:1) was added 2 drops of 4.5 M sulfuric acid, and the mixture was stirred at room temperature for 5 h. By a GLC analysis (20% XF1150 column, 1 m, 130 °C; nitrogen, 1 kg/cm^2; internal standard, cyclopentanone), the yields of 3-cyclopentenone and 2-cyclopentenone were shown to be 60% and 6%, espectively.

Reaction of trans-*1,4-Dichloro-2-butene with 1.* To a solution of **1'** (M=Li) in THF (30 ml) which was prepared from **1** (2.91 g: 23.5 mmol) and *n*-BuLi (23.0 mmol), was added to *trans*-1,4-dichloro-2-butene (1.32 g: 10.6 mmol) at −70 °C, and then the reaction mixture was stirred at room temperature for 2.5 h. Water (30 ml) was added and the mixture was extracted with four 50 ml-portions of CH_2Cl_2. The extracts were combined and dried (Na_2SO_4). The solvents were evaporated, and the residue was subjected to column chromatography on silica gel using CH_2Cl_2-Et_2O (4:1) as an eluent to afford 1-methylsulfinyl-1-methylthio-2-vinylcyclopropane (**11**) as a pale yellow oil (1.41 g: 76% yield):[13] IR (neat) 1632 and 1060 cm^{-1}. The corresponding *S,S,S',S'*-tetraoxide: mp 102—102.5 °C (from CCl_4 and MeOH-water); IR (KBr) 1640, 1625, 1335, 1325, 1305, 1290, of CH_2Cl_2. The extracts were combined and dried (Na_2SO_4). The solvents were evaporated, and the residue was subjected to column chromatography on silica gel using CH_2Cl_2-Et_2O (4:1) as an eluent to afford 1-methylsulfinyl-1-methylthio-2-vinylcyclopropane (**11**) as a pale yellow oil (1.41 g: 76% yield):[13] IR (neat) 1632 and 1060 cm^{-1}. The corresponding *S,S,S',S'*-tetraoxide: mp 102—102.5 °C (from CCl_4 and MeOH-water); IR (KBr) 1640, 1625, 1335, 1325, 1305, 1290, 1160, and 1130 cm^{-1}; ^1H NMR ($CDCl_3$) δ=1.80 (1H, dd, J=6.5 and 10 Hz), 2.18 (1H, dd, J=6.5 and 8 Hz), 2.96—3.22 (1H, m), 3.14 (3H, s), 3.20 (3H, s), 5.22—6.02 (3H, m). Calcd for $C_7H_{12}O_4S_2$: C, 37.48; H, 5.39; S, 28.59%. Found: C, 37.22; H, 5.23; S, 28.37%.

Synthesis of 2-Methylcyclobutanone (14) Using 1. To a solution of **1'** (M=Li) in THF (15 ml) which was prepared from **1** (1.57 g: 12.6 mmol) and *n*-BuLi (12.6 mmol), was added to 1,3-dibromobutane (1.13 g: 5.2 mmol) at −70 °C, and the reaction mixture was stirred at room temperature for 46.5 h. Water (20 ml) was added and the mixture was extracted with one 100 ml-portion and four 20 ml-portions of CH_2Cl_2. The extracts were combined, washed with brine (20 ml), and dried ($MgSO_4$). The solvents were evaporated, and the residue was subjected to colum chromatography on Florisil using CH_2Cl_2 as an eluent to afford 1-methylsulfinyl-1-methylthio-2-methylcyclobutane as a pale yellow oil (746 mg: 80% yield), which consisted mainly of two diastereomers in the ratio of 1:2; IR (neat) 1050 cm^{-1}; ^1H NMR of the major isomer ($CDCl_3$): δ=1.18 (3H, d, J=7 Hz), 1.6—4.0 (5H, m), 2.33 (3H, s), and 2.67 (3H, s); ^1H NMR of the minor isomer ($CDCl_3$): δ=1.39 (3H, d, J=7 Hz), 1.6—4.0 (5H, m), 2.18 (3H, s), and 2.47 (3H, s).

This *S*-oxide (212 mg) was dissolved in EtOH (3 ml) and 8 drops of 4.5 M sulfuric acid were added. The resulting mixture was stirred at room temperature for 15 h and then at 43—47 °C for 24 h. The thus-formed 2-methylcyclobutanone was trapped as its 2,4-dinitrophenylhydrazone (241 mg: 77%): orange crystals; mp 119.5—122 °C (from CCl_4-Et_2O); IR (KBr) 3260, 3075 2935, 2895, 1667, 1615, 1588, 1515, 1500, 1420, 1335, 1310, and 1268 cm^{-1}; ^1H NMR ($CDCl_3$) δ=1.33 (3H, d, J=7 Hz), 1.72 (1H, m), 2.33 (1H, m), 2.97 (2H, m), 3.40 (1H, m), 7.81 (1H, d, J=10 Hz), 8.22 (1H, dd, J=2.6 and 10 Hz), 9.04 (1H, d, J=2.6 Hz), and 10.67 (1H, broad, NH). Calcd for $C_{11}H_{12}N_4O_4$: C, 50.00; H, 4.58; N, 21.20%. Found: C, 50.07; H, 4.49; N, 20.99%.

Synthesis of 3-Benzylcyclobutanone (18a). The starting material 2-benzyl-1,3-dibromopropane (**16a**) was synthesized by reduction of diethyl benzylmalonate with $LiAlH_4$ in Et_2O leading to 2-benzyl-1,3-propanediol and the subsequent treatment of this diol with CBr_4 and PPh_3 in CH_3CN.[20] To a solution of 1' (M=Li) in THF (15 ml) which was prepared from **1** (1.01 g: 8.15 mmol) and *n*-BuLi (8.64 mmol), was added **16a** (1.03 g: 3.53 mmol) at −10 °C and the mixture was further stirred at −10 °C for 100 min and then at room temperature for 3 h. CH_2Cl_2 (100 ml) was added and washed with water (30 ml). The aqueous layer was extracted with two 50 ml-portions of CH_2Cl_2. The organic layers were combined, washed with brine (20 ml), and dried (Na_2SO_4). The solvenrs were evaporated, and the residue was subjected to column chromatography on silica gel using CH_2Cl_2-AcOEt (9:1) as an eluent to give 1-methylsulfinyl-1-methylthio-3-benzylcyclobutane (**17a**) as a pale yellow oil (686 mg: 77% yield): IR (neat) 1055 and 1035 (sh) cm^{-1}. ^1H-NMR ($CDCl_3$) showed that this oil consisted of two diastereomers (2:1). The methyl signals of the major isomer appeared at δ=2.12 and 2.49, while the minor isomer exhibited the methyl signals at δ=2.08 and 2.42.

The *S*-oxide (2.70 g: 10.6 mmol) was dissolved in Et_2O (140 ml), and 4.5 M sulfuric acid (2.8 ml) was added. The resulting mixture was stirred at room temperature for 2 d and then heated under a reflux for 2 d. After addition of $NaHCO_3$ and $MgSO_4$, the mixture was further stirred for a while and the insoluble solid was filterd off. The filtrate was concentrated, and the residue was subjected to column chromatography on silica gel using CH_2Cl_2 and hexane as eluents to give 3-benzylcyclobutanone (**18a**) as a colorless oil (1.13 g: 66% yield) IR (neat) 1785 cm^{-1}; ^1H NMR ($CDCl_3$) δ=2.43—3.49 (7H, m) and 7.21 (5H, s). Its 2,4-dinitrophenylhydrazone derivative: mp 138—139.5 °C (from CCl_4-hexane). Calcd for $C_{17}H_{16}N_4O_4$: C, 59.99; H, 4.74; N, 16.46%. Found: C, 60.02; H, 4.70; N, 16.46%.

The *S*-oxide (398 mg) was dissolved in Et_2O (20 ml). Then 4.5 M sulfuric acid (0.4 ml) was added and the resulting mixture was stirred at room temperature for 1 d and then heated under a reflux for 7 h. After addition of $NaHCO_3$ and $MgSO_4$, the mixture was stirred for a while and the insoluble solid was filterd off. The filtrate was subjected to the reaction with 2,4-dinitrophenylhydrazine to give the 2,4-dinitrophenylhydrazone of **18a** (417 mg: 78% yield).

Synthesis of 3-Benzyloxycyclobutanone (18b) Using 1. To a solution of **1'** (M=Li) in THF (40 ml) which was preparted from **1** (4.81 g: 38.7 mmol) and *n*-BuLi (38.5 mmol), was dropwise added to 2-benzyloxy-1,3-dibromopropane[21] (4.95 g: 16.1 mmol) at −70 °C over 15 min, and the reaction mixture was stirred at −70 °C for 2 h and then at room temperature for 15.5 h. After addition of CH_2Cl_2 (200 ml), the mixture was washed with water (30 ml). The washings were extracted with four 50 ml-portions of CH_2Cl_2. The organic layers were combined, washed with brine (30 ml), and dried ($MgSO_4$). The solvents were evaporated, and the residue was subjected to column chromatography on Florisil using AcOEt to afford 1-methylsulfinyl-1-methylthio-3-benzyloxycyclobutane (**17b**) as a pale yellow oil (3.35 g: 77% yield), which was shown by its ^1H NMR spectrum to consist of two diastereomers (1.1: 1). In the ^1H NMR spectrum, the sulfinylmethyl protons appeared at δ 2.38 (s) and 2.48 (s) in the relative intensity of 1.1:1.

After this *S*-oxide (593 mg) was dissolved in Et_2O (10 ml), 35% perchloric acid (0.45 ml) was added. The resulting mixture was stirred at room temperature for 25 h. After addition of $NaHCO_3$ and $MgSO_4$, the mixture was stirred for a while and the insoluble solid was filterred off. The filtrate was concetrated and the residue was subjected to column chromatography on silica gel using $CHCl_3$ as an eluent to give **18b** (233 mg: 60% yield) as a colorless oil; IR (neat) 1795 (sh) and 1787 cm^{-1}; ^1H NMR ($CDCl_3$) 3.10 (4H, d, J=6 Hz), 4.28 (1H, quintet, J=6 Hz), 4.45 (2H, s), and 7.28 (5H, s). Its semicarbazone: mp 164—166.5 °C (from acetone-water); IR (KBr) 3445, 3260, 3145, 2895, 2850, 1667, 1593, 1485, and 1088 cm^{-1}; ^1H NMR ($CDCl_3$) δ=3.00 (4H, m), 4.16 (1H, m), 4.42 (2H, S), 5.50 (2H, broad s), 7.29 (5H, s), and 8.70 (1H, broad s). Calcd for $C_{12}H_{15}N_3O_2$: C, 61.79; H, 6.48; N, 18.01%. Found: C, 61.80; H, 6.45; N, 17.89%.

References

1) K. Ogura, M. Yamashita, M. Suzuki, and G. Tsuchihashi, *Chem. Lett.*, **1982**, 93 and the references cited therein; R. C. Gadwood, *J. Org. Chem.*, **48**, 2098 (1983) and the references cited therein.

2) This was preliminarily reported: K. Ogura, M. Yamashita, M. Suzuki, G. Tsuchihashi, *Tetrahedron Lett.*, **1974**, 3653; K. Ogura, M. Yamashita, S. Furukawa, M. Suzuki, and G. Tsuchihashi, *ibid.*, **1975**, 2767.

3) K. Ogura and G. Tsuchihashi, *Tetrahedron Lett.*, **1971**, 3151; G. R. Newkome, J. M. Robinson, and J. D. Sauer, *J. Chem. Soc., Chem. Commun.*, **1974**, 410.

4) Methyl methylthiomethyl sulfoxide (**1**) is also utilized as a synthetic reagent for making α-hydroxy aldehydes,[5] α-amino acids,[6] α-keto acides,[7] arylacetic esters,[8] α-bromo-α-arylacetic acids,[9] and α-arylpropionic acids.[10]

5) K. Ogura and G. Tsuchihashi, *Tetrahedron Lett.*, **1972**, 2681; K. Ogura, S. Furukawa, and G. Tsuchihashi, *Chem. Lett.*, **1974**, 659.

6) K. Ogura and G. Tsuchihashi, *J. Am. Chem. Soc.*, **96**. 1960 (1974); K. Ogura, I. Yoshimura, and G. Tsuchihashi, *Chem. Lett.*, **1975**, 803.

7) K. Ogura, N. Katoh, I. Yoshimura, and G. Tsuchihashi, *Tetrahedron Lett.*, **1978**, 375.

8) K. Ogura and G. Tsuchihashi, *Tetrahedron Lett.*, **1972**, 1383; K. Ogura, Y. Itoh, and G. Tsuchihashi, *Bull. Chem. Soc. Jpn.*, **52**, 2013 (1979); K. Ogura, Y. Itoh, and G. Tsuchihashi, *Synthesis*, **1980**, 736.

9) K. Ogura, S. Furukawa, and G. Tsuchihashi, *Bull. Chem. Soc. Jpn.*, **48**, 2219 (1975).

10) K. Ogura, S. Mitamura, K. Kishi, and G. Tsuchihashi, *Synthesis*, **1979**, 880.

11) Acylic ketones can be synthesized by dialkylation of **1**, followed by an acid hydrolysis: G. Schill and P. R Jones, *Synthesis*, **1974**, 117.

12) H. O. House, "Modern Synthetic Reactions," Benjamin, California (1972), pp. 541—543.

13) Although four diastereomers are possible for **11**, one diastereomer showing two methyl signals at δ 2.35 and 2.72 along with the olefinic protons at δ 4.9—6.3 in the ^{1}H NMR spectrum was predominantly produced.

14) E. J. Corey and D. Seebach, *Angew. Chem., Int. Ed. Engl.*, **4**, 1075 and 1077 (1965); D. Seebach, N. R. Jones, and E. J. Corey, *J. Org. Chem.*, **33**, 300 (1968); D. Seebach and A. K. Beck *Org. Syn.*, **51**, 76 (1971).

15) At the present time, the stereochemical structures for these isomers are not determined.

16) N. J. Demjanow and M. Dojarenko, *Chem. Ber.*, **55**, 2737 (1922).

17) J. Boeseken and F. Tellegen, *Recl. Trav. Chim Pays-Bas*, **57**, 133 (1938).

18) M. I. Farberov, E. P. Tepenitsyna, and N. K. Shemyakina, *Dokl. Akad. Nauk SSSR*, **99**, 793 (1954); *C. A.*, **49**, 8315b (1955).

19) H. M. Hess and H. C. Brown, *J. Org. Chem.*, **32**, 4138 (1967).

20) E. H. Axelrod, G. M. Milne, and E. E. van Tamelen, *J. Am. Chem. Soc.*, **92**, 2139 (1970).

21) M. Avram, C. D. Nenitzescu, and M. Mexim, *Chem. Ber.*, **90**, 1424 (1957).

 © 1984 The Chemical Society of Japan Bull. Chem. Soc. Jpn., 57, 1643—1649 (1984)

An Account of the Site- and Regio-selectivity in the Reaction of Nitrile Oxides with Substituted *p*-Benzoquinones by Frontier Molecular Orbital Theory

Tohru HAYAKAWA, Koji ARAKI, and Shinsaku SHIRAISHI*
Institute of Industrial Science, The University of Tokyo, Roppongi, Minato-ku, Tokyo 106
(Received October 27, 1983)

The 1,3-dipolar cycloaddition reactions of nitrile oxides with substituted *p*-benzoquinones are discussed in terms of Frontier Molecular Orbital (FMO) theory. The calculation is carried out by *ab initio* Self Consistent Field (SCF) method with STO-3G basis set. The site- and regio-selectivities in the reactions are correlated with two types of FMO interactions. Some predictions have been confirmed by experimental results.

Frontier Molecular Orbital (FMO) theory is widely used to explain or predict the reactivities and the selectivities in the organic reactions. In the field of cycloaddition reactions, such as Diels-Alder and 1,3-dipolar cycloaddition reactions, it is a powerful tool to study and account for the reactions.[1-6] By applying FMO theory to cycloaddition reactions, Sustmann has classified them into three groups.[7]

We reported before[8-11] the 1,3-dipolar cycloaddition reactions of nitrile oxides with various *p*-benzoquinones, which have two kinds of potentially reactive sites, one is the carbon-oxygen double bond and the other the carbon-carbon double bond. Depending on the number, pattern, combination and kind of the substituents of the quinones, two different types of the adducts were obtained in the reactions. One is the C=O addition product, *i.e.* spiro[1, 4, 2]dioxazole derivative and the other is the C=C addition product, *i.e.* isoxazoline derivative. We tried to account for the site-selectivity and reactivity of the quinones, and also the regio-selectivity in the C=C addition reactions in terms of FMO theory. This paper describes the calculation of the energy levels of FMO's and the coefficients of FMO's on the atoms of nitrile oxides and substituted *p*-benzoquinones, and correlates the experimental results with the calculation.

Results and Discussion

The following were studied: nitrile oxides: 2,4,6-trimethylbenzonitrile oxide (**1a**) and 2,6-dichlorobenzonitrile oxide (**1b**); quinones: 2,3-dichloro-5,6-dicyano-*p*-benzoquinone (**2a**), tetrafluoro-*p*-benzoquinone (**2b**), tetrachloro-*p*-benzoquinone (**2c**), tetramethyl-*p*-benzoquinone (**2d**), tetramethoxy-*p*-benzoquinone (**2e**), 2,6-dichloro-*p*-benzoquinone (**2f**), 2-methyl-*p*-benzoquinone (**2g**), 2,5-dimethyl-*p*-benzoquinone (**2h**), and 2,6-dimethyl-*p*-benzoquinone (**2i**), 2,5,6-trimethyl-*p*-benzoquinone (**2j**). The structures are shown in Fig. 1. The reactions of **1a** with **2a**—f has been known to give 1,4,2-dioxazole derivatives through C=O addition and those with **2g**—**i** isoxazoline derivatives through C=C addition. The reactions of **1b** gave similar results, except with **2d**—f as will be discussed later. This kind of site-selectivity and the orientation of the addition (regio-selectivity in C=C addition) are to be accounted for and predicted.

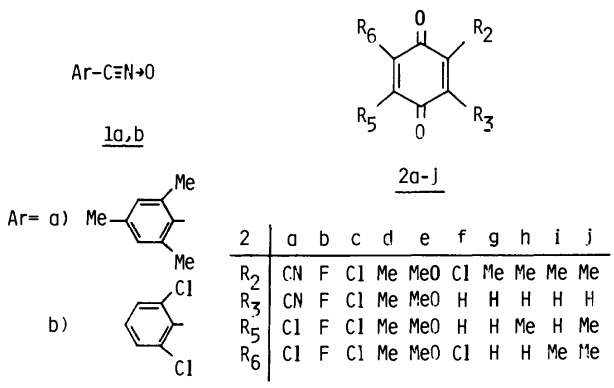

2	a	b	c	d	e	f	g	h	i	j
R_2	CN	F	Cl	Me	MeO	Cl	Me	Me	Me	Me
R_3	CN	F	Cl	Me	MeO	H	H	H	H	H
R_5	Cl	F	Cl	Me	MeO	H	H	Me	H	Me
R_6	Cl	F	Cl	Me	MeO	Cl	H	H	Me	Me

Fig. 1.

Ab Initio *SCF Calculation.* The FMO calculations on nitrile oxides, not only fulminic acid but also aromatic nitrile oxides, by semiempirical methods have been reported.[1,5] The calculation by nonempirical method has been reported only for fulminic acid[12] and no calculations for aromatic nitrile oxides have been reported as far as we know.

On the other hand, the calculations for several *p*-benzoquinones by *ab initio* method have been reported by Rozemboom *et al.*,[13] though only the one for 2-methyl-*p*-benzoquinone is available for our study. We calculated the FMO's of nitrile oxides and substituted *p*-benzoquinones by *ab initio* SCF method with STO-3G basis set.[14]

The calculation for nitrile oxides were carried out using the bond lengths (in nm) 0.1436 for C-C, 0.1147 for C-N, and 0.1243 for N-O, which are the averaged values of the X-ray results for 4-methoxy-2,6-dimethyl- and 4-bromo-2,6-dimethylbenzonitrile oxides.[15] Other geometries used are standard ones given by Pople and Gordon.[16] The methyl substituents of **1a** can have various conformations. We computed the energies for several representative conformations of the methyl groups and selected and used the most stable one for the FMO calculation. When one hydrogen of the methyl group is placed in the same plane as the aromatic nucleus of the nitrile oxides, the energy of FMO's does not exceed that of the most stable conformation by more than 0.1 eV.

The energy values and coefficient magnitudes of FMO's of nitrile oxides are given in Table 1, together with the negative values of the ionization potential (experimentally estimated HOMO energies).[12,17,18] The orderings of the calculated HOMO energy and the experimentally estimated ones are the same. Our calculation on fulminic acid gave nearly the same energy values as the one (HOMO −7.69 eV) reported by *ab initio* method. From fulminic acid to **1b**, the

Table 1. Energy levels and coefficients of FMO of nitrile oxides

Nitrile oxide	FMO	ε/eV		Cα[b]	C	N	O
		Calcd	Exptl[a]				
HCNO	LUMO	8.66		—	0.82	−0.80	0.43
	HOMO	−7.61	−10.83	—	0.54	0.14	−0.84
phCNO	LUMO	5.33		0.53	0.27	−0.42	0.29
	HOMO	−6.42	−8.96	−0.26	0.44	0.20	−0.72
1a	LUMO	5.58		0.50	0.27	−0.42	0.28
	HOMO	−6.12	−8.35	−0.32	0.41	0.21	−0.69
1b	LUMO	4.43		0.55	0.22	−0.40	0.29
	HOMO	−6.89	—	−0.24	0.46	0.18	−0.73

a) These are the negative values of the ionization potentials. b) This carbon connects with the dipole moiety.

calculated values well reflect the substituent effect. The phenyl group of benzonitrile oxide, which is a conjugative group, raises HOMO energy and lowers LUMO energy. Substitution on benzonitrile oxide with methyl groups, which are electron-releasing groups, raise both HOMO and LUMO energies; the increase in HOMO is larger than that of LUMO (**1a**). Chlorine atoms lower both HOMO and LUMO energies. The decrease in LUMO is larger than that of HOMO as a result of mixing of electron-withdrawing and -releasing natures (**1b**). Furthermore, inspection of Table 1 reveals that the nodal positions and the ordering of the magnitudes of the atomic orbital coefficients are preserved in all four calculated nitrile oxides.

The results of the calculations of the substituted *p*-benzoquinones are listed in Table 2. The geometries of quinones, *p*-benzoquinone, **2a**, **2b**, **2c**, and **2f** are those of X-ray results.[19] In the cases of methyl- and methoxy-substituted quinones, such as **2d**, **2e**, **2g**, **2h**, **2i**, and **2j**, the methyl group can take various conformations. The conformation of methyl group of **2g** used for the calculation is the same one as reported by Rozemboom *et al.*[13] and those for **2d**, **2e**, **2h**, **2i**, and **2j** are the most stable ones estimated by computation in the same way as in the case of **1a**. The geometries of quinone moieties of **2g**, **2h**, **2i**, and **2j** are derived from that of *p*-benzoquinone,[19] and those of **2d** and **2e** are X-ray results.[20] The electron affinities of these quinones[21] are also listed in Table 2. The tendency is in good accordance with that of the calculated values. The substituent effects to FMO's energies are also reasonable.

Our calculation values and those reported by Rozemboom *et al.*[13] for *p*-benzoquinone and 2-methyl-

Table 2. Energy levels and coefficients of FMO of substituted *p*-benzoquinones

Quinone	FMO	ε/eV		C_1	C_2	C_3	C_4	C_5	C_6	O_1	O_4
		Calcd	Exptl[a]								
p-Benzo-	LUMO	3.74	−1.91	−0.30	−0.34	0.34	0.30	0.34	−0.34	0.49	−0.49
quinone	HOMO	−8.23		0.20	−0.34	−0.34	0.20	−0.34	−0.34	0.44	0.44
2a	LUMO	1.61	−3.07	−0.24	−0.25	0.25	0.24	0.43	−0.43	0.44	−0.44
	HOMO	−9.34		0.10	−0.45	−0.45	0.10	−0.12	−0.12	0.30	0.30
2b	LUMO	3.02	−2.45[b]	−0.32	−0.31	0.31	0.32	0.31	−0.31	0.50	−0.50
	HOMO	−8.30		0.13	−0.33	−0.33	0.13	−0.33	−0.33	0.39	0.39
2c	LUMO	2.21	−2.49	−0.28	−0.35	0.35	0.28	0.35	−0.35	0.48	−0.48
	HOMO	−9.40		0.12	−0.32	−0.32	0.12	−0.32	−0.32	0.34	0.34
2d	LUMO	4.20	−1.66	−0.32	−0.33	0.33	0.32	0.33	−0.33	0.48	−0.48
	HOMO	−7.44		0.16	−0.35	−0.35	0.16	−0.35	−0.35	0.42	0.42
2e	LUMO	4.24		−0.36	−0.30	0.28	0.36	0.30	−0.28	0.48	−0.48
	HOMO	−6.08		0.05	−0.30	−0.32	0.05	−0.30	−0.32	0.32	0.32
2f	LUMO	2.78	−2.77	−0.30	−0.34	0.34	0.28	0.34	−0.34	0.49	−0.48
	HOMO	−8.83		0.13	−0.31	−0.33	0.18	−0.33	−0.31	0.35	0.42
2g	LUMO	3.85	−1.83	−0.32	−0.33	0.32	0.30	0.35	−0.34	0.50	−0.48
	HOMO	−8.03		0.17	−0.38	−0.41	0.20	−0.28	−0.28	0.42	0.45
2h	LUMO	3.97	−1.78	−0.31	−0.34	0.32	0.31	0.34	0.32	0.49	−0.49
	HOMO	−7.89		0.18	−0.33	−0.36	0.18	−0.33	−0.36	0.43	0.43
2i	LUMO	3.96	−1.66	−0.33	−0.33	0.33	0.29	0.33	−0.33	0.50	−0.48
	HOMO	−7.88		0.16	−0.34	−0.35	0.20	−0.35	−0.34	0.41	0.45
2j	LUMO	4.06	−1.74[b]	−0.31	−0.33	0.34	0.32	0.31	−0.32	0.48	−0.49
	HOMO	−7.70		0.17	−0.28	−0.26	0.15	−0.41	−0.41	0.43	0.41

a) The values are the negatives of the average of the EA's determined from reduction potentials and charge-transfer spectra except **2b** and **2j**. b) The values are the negatives of EA's determined from reduction potentials. c) The numbering of the atoms is the following:

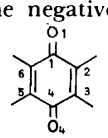

p-benzoquinone are nearly the same, the difference is due to the difference in the geometry of the quinone moiety which was employed.

C=O Addition. Figure 2 shows the FMO energy levels of the nitrile oxides and the quinones. The quinones **2a—f**, which have been found to undergo C=O addition with **1a**, have very low LUMO energy values, except for **2d** and **2e**. The energy difference between the HOMO of **1a** and the LUMO of the quinones is smaller than that between the LUMO of **1a** and the HOMO of the quinones by more than about 5 eV, except in the cases of **2d** and **2e**. This energetical analysis clearly suggests that the HOMO (nitrile oxide)-LUMO (quinone) interaction is the governing factor of C=O addition. This suggests that the reactions of **1b** with **2a—c** give C=O adducts; this is indeed the case. The reactions of **1b** with **2d—f** will be discussed later.

The kinetic data of these reactions also supports this suggestion. Reaction rate constants measured by a UV method at 20 °C[10] (Table 3) show that quinone **2a**, which has the lowest LUMO energy value, reacts most rapidly, and also that the rate in the reactions of **1b** with **2a—c** is always slower than that of **1a** with the corresponding quinones. This is reflecting the fact that **1b** has a lower HOMO energy value than **1a** by 0.65 eV.

C=C Addition. The quinones **2g—j** have been known to undergo C=C addition with **1a**, and their FMO energy levels are higher than those of quinones **2a—f**, except **2d** and **2e**, as shown in Fig 1. In addition, *p*-benzoquinone, which has been reported to undergo C=C addition with benzonitrile oxide,[22] has nearly the same FMO levels as the quinones **2g—j** and was confirmed to undergo C=C addition with **1a** and **1b** as described in the Experimental section. The energy differences between the two possible interactions are far smaller than those in the cases mentioned in the preceding section and are less than 3.9 eV with **1a** and less than 2.0 eV with **1b**. The participation of LUMO(nitrile oxide)-HOMO(quinone) interaction is considered to become important to some extent in these reactions.

The reaction rate constants were also measured as shown in Table 3. Contrary to the C=O addition, the reaction rate of the C=C addition of **1b** with **2h—j** is shown to be always faster than the corresponding one of **1a**. This indicates that the orbital interactions exerted different effects from those in C=O addition. We should take note of not only the decrease of the HOMO level of **1b** but also that of the LUMO level. As mentioned above, the decrease of the HOMO level of **1b** is only 0.65 eV, but that of the LUMO level is 1.09 eV. Because of this large decrease in LUMO of **1b**, the ener-

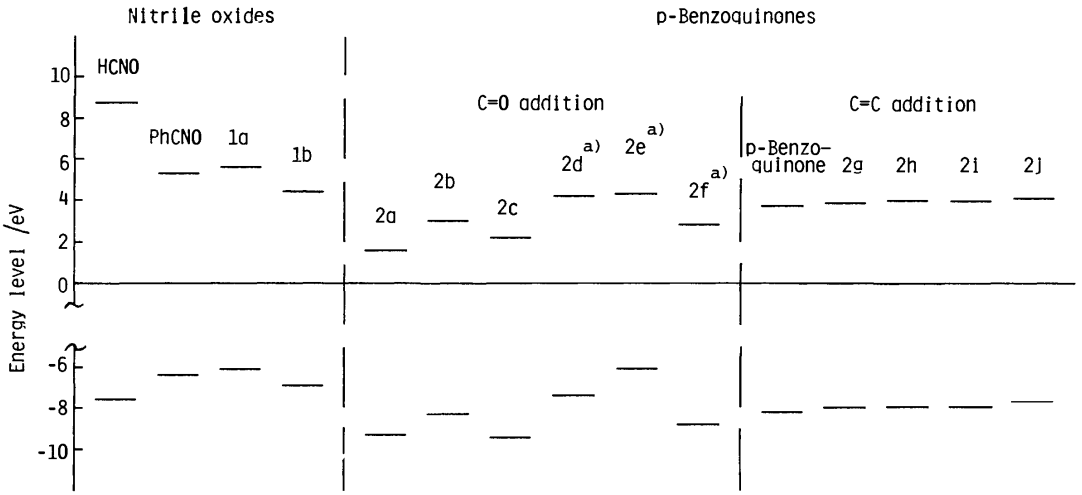

Fig. 2. Energy levles of HOMO and LUMO of nitrile oxides and substituted *p*-benzoquinones calculated by *ab initio* SCF method with STO-3G basis set.
a) The reaction with Ia gives C=O adduct.

TABLE 3. RATE CONSTANTS FOR THE REACTIONS OF NITRILE OXIDES WITH QUINONES

Quinone	Solvent	k/l mol^{-1} s^{-1} With **1a**[a]	With **1b**	Mode
2a	$CHCl_3$	3.52	5.98×10^{-2}	C=O
	C_6H_6	5.60×10^{-1}	3.60×10^{-3}	
2b	$CHCl_3$	5.18×10^{-2}	1.15×10^{-3}	C=O
2c	$CHCl_3$	1.59×10^{-2}	7.09×10^{-4}	C=O
2h	$CHCl_3$	4.77×10^{-4}	2.36×10^{-3}	C=C
	C_6H_6	9.30×10^{-4}	4.94×10^{-3}	
2i	$CHCl_3$	1.33×10^{-3}	4.50×10^{-3}	C=C
	C_6H_6	1.50×10^{-3}	5.26×10^{-3}	
2j	C_6H_6	4.35×10^{-4}	2.60×10^{-3}	C=C

a) The values for **2a—c** measured in $CHCl_3$ are reported ones.[10]

Table 4. The energy difference between LUMO(nitrile oxides)-HOMO(quinones) and HOMO(nitrile oxides)-LUMO(quinones) interaction

	2a	2b	2c	2d	2e	2f	*p*-Benzoquinone	2g	2h	2i	2j
1a	7.19	4.74	6.65	2.70	1.30	5.51	3.90	3.64	3.38	3.38	3.10
1b	5.27	2.82	4.73	0.78	−0.62	3.59	2.03	1.72	1.46	1.46	1.18

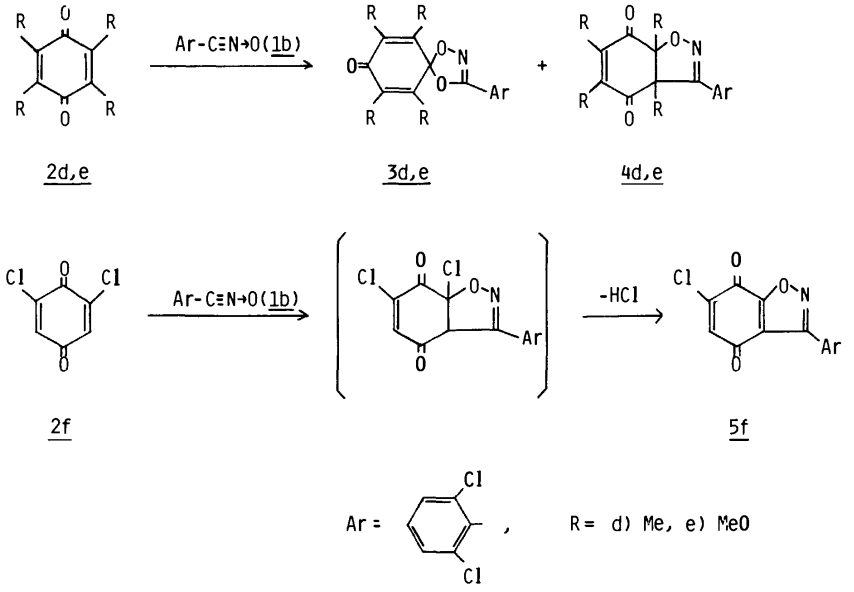

Scheme 1.

gy gain by LUMO (**1b**)-HOMO (quinone) interaction overcomes the energy loss by the HOMO (**1b**)-LUMO (quinone) interaction. This result suggests that in the reactions giving C=C adducts LUMO (nitrile oxide)-HOMO (quinone) interaction is more significant than the opposite interaction. Usually *p*-benzoquinones are thought to be electron acceptor and known to form CT complexes with many electron donors. The reactivity and selectivity of the reactions involving *p*-benzoquinones are known to be dominated by the interaction of LUMO of quinones and HOMO of nucleophiles or dienes. But in the reactions discussed here, HOMO of quinones participates in the reactions to some extent, and quinones appear to behave as if electron donors.

We show in Table 4 the energy difference between LUMO (nitrile oxide)-HOMO (quinone) and HOMO (nitrile oxide)-LUMO (quinone) interaction. The results with **1a** shows that, if the energy difference is larger than 5 eV, C=O addition will occur, and if the energy difference is less than 4 eV, C=C addition will occur, except for the cases of **2d** and **2e**. This energetical analysis predicts that the reaction of **1b** with **2f** will give C=C adduct because the energy difference is less than 4 eV. Moreover it is expected that the reaction pattern of **1b** with **2d** and **2e** will be different from that of **1a**.

In fact, **1b** underwent C=C addition with **2f** and not C=O addition. As shown in Scheme 1, isoxazoloquinone **5f** was formed in the reaction *via* C=C addition and subsequent dehydrochlorination. The structure of the product **5f** was determined by spectral data; the characterization is described in the Experimental section.

The reactions of **1b** with **2d** and **2e** were also found to proceed in a different mode from those of **1a**. Compound **1b** underwent both C=C and C=O additions with **2d** and **2e**. The results are shown in Scheme 2. The characterization of the adducts is also described in the Experimental section. Though the yields were low, the reactions were clean and no other products were detected. This is the first case of the isolation of C=C adducts in the reactions of nitrile oxides with tetrasubstituted *p*-benzoquinones and of the competitive reactions of C=C and C=O additions. Compound **2d** has FMO levels very close to those of the quinones **2g—j**, while **2e** has very close LUMO to those of **2g—j**, but a much higher HOMO level. The energy difference between the two possible interactions of **1b** with **2d** is less than 1 eV. For tetrasubstituted *p*-benzoquinones, the steric hindrance cannot be neglected. Actually, tetrafluoro-*p*-benzoquinone (**2b**) underwent only C=O addition with **1b** despite the energy difference being smaller than 4 eV. The reaction of tetramethoxy-*p*-benzoquinone (**2e**) is not clearly understood by considering the steric effect only. The higher orbital interactions involving methoxy groups may have to be considered in the interpretation of the experimental result, for which further study is needed.

Accounts for the Selectivity. In the 1,3-dipolar cycloaddition reactions, the square of the products of the coefficients of the interacting atoms and resonance integral ($C_aC_b\beta_{ab}$) should be taken into consideration, as discussed by Houk.[1] But such an approach to rationalize the site-selectivity may be applicable only for the specific addition to a bond among the same kinds of unsaturated bonds, and not among the dif-

ferent kinds of unsaturated bonds. Furthermore there are many factors which cannot be neglected: for example, Coulombic repulsion, and we cannot exactly estimate the extent of the importance of the factors.

In the reactions giving C=O adducts, which is considered to be chiefly governed by the HOMO (nitrile oxide)-LUMO (quinone) interaction, Coulombic repulsion is thought to play a significant role. The regio-selectivity of the C=O addition is clearly influenced by Coulombic repulsion but not by the overlap of the orbitals.

2,6-Dichloro-*p*-benzoquinone (**2f**) has two different C=O sites and undergoes C=O addition onto the carbonyl group of chlorine-substituted side exclusively.[9] This site-selectivity among the two C=O addition sites has been interpreted in terms of LFER theory.[10] This can also be treated by considering the primary interactions in FMO theory, *i.e.* comparison in the sum of the square of the product of the coefficients of interacting atoms and resonance integral ($Cc Co\beta co$)[1] for two possible interaction shows that the value for the addition to the substituted side (2.41) is larger than that to the unsubstituted side (2.20).

The reactions giving C=C adducts are thought to be governed chiefly by the LUMO(nitrile oxide)-HOMO (quinone) interaction. Considering this interaction, one notes that the coefficients on the carbon atom are nearly equal in **1a** or less in **1b** than those on the terminal oxygen atom. But by taking into consideration the secondary orbital interaction with the α-carbon connecting with the nitrile oxide moiety,[5,23] regio-selectivity can be explained.

For the purpose of the study of the selectivities of the reactions, we tried the reactions of nitrile oxides with 2-methyl-*p*-benzoquinone (**2g**), which has two types of carbon-carbon double bond. The C=C adduct added on the methyl-substituted side was isolated in the reactions and the formation of the adduct added on the other side was only suggested.[11] Here we could confirm the formation of the two C=C adducts by derivating the latter to the corresponding isoxazoloquinone (**8g** or **11g**) by oxidation, as shown in Scheme 2. The characterization of the adducts will be described in the Experimental section.

The quinone **2g** has a larger coefficient magnitude on the carbon atoms of the methyl-substituted C=C

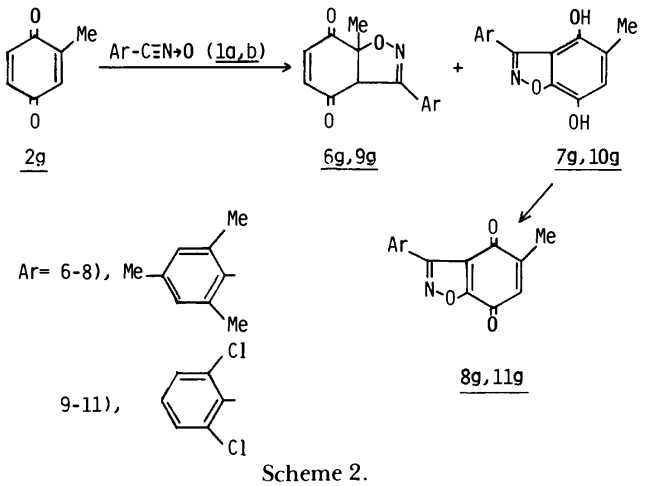

Scheme 2.

bond. The most efficient overlap of the orbitals of interacting atoms leads to the products **6g** or **9g**. The interaction leading to products **7g** or **10g** has not so efficient an overlap, and the yields of **6g** and **9g** are thought to become much larger than those of **7g** and **10g**. In fact, the yield of **6g** or **9g** is larger but not so much, which is thought to be due to the steric effect of the methyl group. In the reactions with 2,5,6-trimethyl-*p*-benzoquinone (**2j**), the cycloaddition occurred onto only the less hindered side,[11] though the coefficients of HOMOs' of the carbon atoms at the hindered side are larger than those at the less hindered side.

The orientation of the C=C addition with quinones **2f—j**[11] is in accordance with the theory that the most efficient overlap of the interacting orbitals includes secondary orbital interaction of LUMO of nitrile oxides with HOMO of quinones, as mentioned before.

In conclusion we can classify the substituted *p*-benzoquinones into two groups: One is a group giving C=O adducts, the reaction of which is chiefly governed by HOMO (nitrile oxide)-LUMO (quinone) interaction, and the other is that giving C=C adducts, the reaction of which is chiefly governed by LUMO (nitrile oxide)-HOMO (quinone) interaction. The borderline-energy-difference between two interactions may be about 4 eV, having some exceptions. Some quinones such as **2d** and **2e** gave both C=C and C=O adducts competitively in the reactions with **1b**.

Experimental

Melting points were measured using a micro-melting-point-measuring apparatus (Yazawa Co., Ltd.) and are uncorrected. Column chromatography was conducted on silica gel (Wako gel C-200) with benzene as an eluent. IR spectra were recorded with a JASCO IRA-1 spectrophotometer. UV spectra were recorded with a JASCO UVIDEC-505 spectrophotometer. ^{1}H NMR spectra were measured in $CDCl_3$ with a JEOL JMN-MH 100 spectrometer, and chemical shifts are reported in ppm from internal tetramethylsilane. Mass spectra were recorded with a Hitachi RMU-7L high resolution mass spectrometer.

Materials. 2,4,6-Trimethylbenzonitrile oxide (**1a**) and 2,6-dichlorobenzonitrile oxide (**1b**) were prepared by the method of Grundmann.[24] *p*-Benzoquinone, 2,3-dichloro-5,6-dicyano-*p*-benzoquinone (**2a**), tetrafluoro-*p*-benzoquinone (**2b**), tetrachloro-*p*-benzoquinone (**2c**), tetramethyl-*p*-benzoquinone (**2d**), and 2-methyl-*p*-benzoquinone (**2g**) were commercially obtained and were used after recrystallization. Tetramethoxy-*p*-benzoquinone (**2e**) was prepared by the method of Robinson and Vasey.[25] 2,5-Dimethyl-*p*-benzoquinone (**2h**), 2,6-dimethyl-*p*-benzoquinone (**2i**), and 2,5,6-trimethyl-*p*-benzoquinone (**2j**) were prepared by the method described in the previous paper.[11]

*Reactions of 2,4,6-Trimethylbenzonitrile Oxide (**1a**) and 2,6-Dichlorobenzonitrile Oxide (**1b**) with* p*-Benzoquinone.* A solution of 0.806 g (5 mmol) of **1a** and 1.081 g (10 mmol) of *p*-benzoquinone in 100 ml benzene was stirred for 3 d at room temperature. Solvent was then evaporated under reduced pressure, and the residue was subjected to column chromatography. 3-(2,4,6-Trimethylphenyl)-1,2-benzisoxazole-4,7-dione (0.853 g 64%) was obtained and the recrystallization was carried out from benzene-hexane. Mp 130—132 °C. IR (KBr) 1670 and 1680 cm^{-1} ($\nu_{C=O}$). ^{1}H NMR ($CDCl_3$) δ=2.07 (s, 6H, mesityl *o*-methyl), 2.35 (s, 3H, mesityl *p*-methyl), 6.74 (d, 1H, olefinic), 6.89 (d, 1H, olefinic), and 6.96 (s, 2H, aromatic).

Found: C, 71.79; H, 4.80; N, 5.49%. Calcd for $C_{16}H_{13}N_1O_3$: C, 71.65; H, 4.89; N, 5.22%.

The reaction of 2,6-dichlorobenzonitrile oxide (**1b**) with *p*-benzoquinone was conducted and worked up in a similar manner. 3-(2,6-dichlorophenyl)-1,2-benzisoxazole-4,7-dione (73%). Mp 178—180 °C. IR (KBr) 1670 and 1680 cm^{-1} ($\nu_{C=O}$) ^1H NMR ($CDCl_3$) δ=6.78 (d, 1H, olefinic), 6.87 (d, 1H, olefinic), and 7.42 (s, 3H, aromatic).

Found: C, 52.89; H, 1.53; N, 4.70%. Calcd for $C_{13}H_5N_1O_3Cl_2$: C, 53.09; H, 1.71; N, 4.76%.

*Reaction of 2,6-Dichlorobenzonitrile Oxide (1b) with Tetramethyl-*p*-benzoquinone (2d).* A solution of 0.503 g (3 mmol) of **1b** and 0.574 g (3 mmol) of **2d** in 60 ml of benzene was stirred for about one month at room temperature. The solvent was evaporated under reduced pressure, and the residue was worked up with column chromatography. The first fraction gave a mixture of starting materials and **3d**. The residue was recrystallized from benzene-hexane to give 3-(2,6-dichlorophenyl)-6,7,9,10-tetramethyl-2-aza-1,4-dioxaspiro[4.5]-deca-2,6,9-trien-8-one (**3d**), (0.14 g 13%). Mp 204—205 °C. IR (KBr) 1665 cm^{-1} ($\nu_{C=O}$) ^1H NMR ($CDCl_3$) δ=1.97 (s, 6H, methyl), 2.24 (s, 6H, methyl), and 7.47 (s, 3H, aromatic). M^+ (351.0361) was observed as a very weak signal, and fragment ion peaks at *m/z* 186.9574 and 164.0841 arising from the starting component (*i. e.* the nitrile oxide and the quinone) were very intensive in the mass spectrum. The fragmentation pattern is characteristic of C=O adducts.

Found: C, 58.03; H, 4.31; N, 3.92%; M^+, 351.0361. Calcd for $C_{17}H_{15}N_1O_3Cl_2$: C, 57.97; H, 4.29; N, 3.98%; M^+, 351.0431.

The second fraction gave yellow needles of 3-(2,6-dichlorophenyl)-3a,5,6,7a-tetramethyl-3a,7a-dihydro-1,2-benzisoxazole-4,7-dione (**4d**), (0.14 g 13%), which was recrystallized from benzene-hexane. Mp 135—136 °C. IR (KBr) 1670 and 1710 cm^{-1} ($\nu_{C=O}$) ^1H NMR ($CDCl_3$) δ=1.53 (s, 3H, methyl), 1.59 (s, 3H, methyl), 1.97 (s, 3H, methyl), 2.07 (s, 3H, methyl), and 7.31 (s, 3H, aromatic). M^+ was not observed but characteristic fragmentation of the C=C adducts, which was the elimination of angular methyl and CO, was observed in the mass spectrum.

Found: C, 57.84; H, 4.38; N, 3.91%. Calcd for $C_{17}H_{15}N_1O_3Cl_2$: C, 57.97; H, 4.29; N, 3.98%.

*Reaction of 2,6-Dichlorobenzonitrile Oxide (1b) with Tetramethoxy-*p*-benzoquinone (2e).* The reaction was conducted and worked up in the same manner as the above. The second fraction gave 3-(2,6-dichlorophenyl)-3a,5,6,7a-tetramethoxy-3a,7a-dihydro-1,2-benzisoxazole-4,7-dione (**4e**), (27%). Mp 174—176 °C. IR (KBr) 1685 and 1700 cm^{-1} ($\nu_{C=O}$) ^1H NMR ($CDCl_3$) δ=3.27 (s, 3H, methoxyl methyl), 3.84 (s, 3H, methoxyl methyl), 4.04 (s, 3H, methoxyl methyl), 4.06 (s, 3H, methoxyl methyl), and 7.31 (s, 3H, aromatic).

Found: C, 48.85; H, 3.65; N, 3.34%; M^+, 415.0302. Calcd for $C_{17}H_{15}N_1O_7Cl_2$: C, 49.06; H, 3.63; N, 3.37%; M^+, 415.0227.

The third fraction gave 3-(2,6-dichlorophenyl)-6,7,9,10-tetramethoxy-2-aza-1,4-dioxaspiro[4.5]deca-2,6,9-trien-8-one (**3e**), (13%). Mp 163—164 °C. IR (KBr) 1650 cm^{-1} ($\nu_{C=O}$) ^1H NMR ($CDCl_3$) δ=3.70 (s, 6H, methoxyl methyl), 4.12 (s, 6H, methoxyl methyl), and 7.38 (s, 3H, aromatic). M^+ was not observed, but fragment ion peaks at *m/z* 186.9576 and 288.0625 arising from the starting component (*i.e.* the nitrile oxide and the quinone) were very intense in the mass spectrum.

Found: C, 49.12; H, 3.62; N, 3.42%. Calcd for $C_{17}H_{15}N_1O_7Cl_2$: C, 49.06; H, 3.63; N, 3.37%.

*Reaction of 2,6-Dichlorobenzonitrile Oxide (1b) with 2,6-Dichloro-*p*-benzoquinone (2f).* A solution of 0.94 g (5 mmol) of **1b** and 0.885 g (5 mmol) of **2f** in 100 ml benzene was stirred for 3d at room temperature. Then the solvent was evaporated under reduced pressure. The residue was worked up with column chromatography. The first fraction gave 3-(2,3-dichlorophenyl)-6-chloro-1,2-benzisoxazole-4,7-dione (**5f**), (1.14 g 63%), which was recrystallized from hexane. Mp 142—145 °C. IR (KBr) 1680 and 1700 cm^{-1} ($\nu_{C=O}$) ^1H NMR ($CDCl_3$) δ=7.05 (s,1H, olefinic), and 7.46 (s, 3H, aromatic). The mass spectrum shows the elimination of CO from the parent ion, which is a characteristic pattern of C=C adduct.

Found: C, 47.48; H, 1.19; N, 4.53%. Calcd for $C_{13}H_4N_1O_3Cl_3$: C, 47.53; H, 1.22; N, 4.26%.

*Reaction of 2,4,6-Trimethylbenzonitrile Oxide (1a) with 2-Methyl-*p*-benzoquinone (2g).* A solution of **1a** 0.805 g (5 mmol) and **2g** 0.61 g (5 mmol) in 100 ml of benzene was stirred for about one week at room temperature. The solvent was evaporated under reduced pressure, and the residue was subjected to column chromatography. The first fraction gave the mixture of **1a** and **2g**. The second fraction gave the yellow crystals of 3-mesityl-7a-methyl-3a,7a-dihydro-1,2-benzisoxazole-4,7-dione (**6g**), (0.48 g 34%), which was recrystallized from benzene-hexane. Mp 137—139 °C. IR (KBr) 1680 and 1700 cm^{-1} ($\nu_{C=O}$) ^1H NMR ($CDCl_3$) δ=1.62 (s, 3H, angular methyl), 2.16—2.43 (m, 9H, mesityl methyl), 4.30 (s, 1H, angular methine), 6.72 (d, 1H, olefinic), 6.94 (d, 1H, olefinic), and 6.84 (s, 2H, aromatic).

Found: C, 72.02; H, 6.15; N, 5.17%. Calcd for $C_{17}H_{17}N_1O_3$: C, 72.07; H, 6.04; N, 4.94%.

The third fraction gave a glassy mass which was assumed to be 3-mesityl-5-methyl-1,2-benzoisoxazole-4,7-diol (**7g**), which can not be isolated as a pure state, from its IR spectrum (ν_{OH} at about 3200 cm^{-1}). Oxidation of **7g** was conducted with sodium dichromate in the presence of sulfuric acid in benzene-water mixture with vigorous stirring. The reaction mixture was extracted from benzene. The extract was dried over anhydrous sodium sulfate. Evaporation of the solvent gave 3-mesityl-5-methyl-1,2-benzisoxazole-4,7-dione (**8g**), (0.28 g 20%). The recrystallization was carried out from benzene-hexane. Mp 139—141 °C. IR (KBr) 1670 and 1680 cm^{-1} ($\nu_{C=O}$) ^1H NMR ($CDCl_3$) δ=2.12 (s, 6H, mesityl *o*-methyl), 2.24 (s, 3H, methyl), 2.37 (s, 3H, mesityl *p*-methyl), 6.65 (s, 1H, olefinic), and 7.00 (s, 2H, aromatic).

Found: C, 72.96; H, 5.55; N, 4.55%. M^+, 281.1084. Calcd for $C_{17}H_{15}N_1O_3$: C, 72.58; H, 5.37; N, 4.98%. M^+, 281.1053.

*The Reaction of 2,6-Dichlorobenzonitrile Oxide (1b) with 2-Methyl-*p*-benzoquinone (2g).* The reaction was conducted and worked up in the same manner as the above.

3-(2,6-Dichlorophenyl)-7a-methyl-3a,7a-dihydro-1,2-benzisoxazole-4,7-dione (**9g**), (47%). Mp 175—177 °C. IR (KBr) 1680 and 1700 cm^{-1} ($\nu_{C=O}$) ^1H NMR ($CDCl_3$) δ=1.77 (s, 3H, angular methyl), 4.51 (s, 1H, angular methine), 6.89 (d, 1H, olefinic), 7.06 (d, 1H, olefinic), and 7.42 (s, 3H, aromatic).

Fonud: C, 54.41; H, 2.87; N, 4.90%. Calcd for $C_{14}H_9N_1O_3Cl_2$: C, 54.22; H, 2.92; N, 4.52%.

3-(2,6-dichlorophenyl)-5-methyl-1,2-benzisoxazole-4,7-dione (**11g**), (31%). Mp 215—217 °C. IR (KBr) 1680 and 1685 cm^{-3} ($\nu_{C=O}$). ^1H NMR ($CDCl_3$) δ=2.14 (s, 3H, methyl), 6.71 (s, 1H, olefinic), and 7.43 (s, 3H, aromatic).

Found: C, 54.98; H, 2.13; N, 4.63%; M^+, 306.9720. Calcd for $C_{14}H_7N_1O_3Cl_2$: C, 54.54; H, 2.29; N, 4.55%; M^+, 306.9804.

The Reactions of 1b with 2a—c: The reaction was carried out using 2.5 mmol of each reactant in chloroform at room temperature for 1 d and worked up in the same manner as the above. The product of each reaction follows. The reaction gave exclusively spiro[1,4,2]dioxazole derivatives.

6,7-Dichloro-9,10-dicyano-3-(2,6-dichlorophenyl)-2-aza-1,4-dioxaspiro[4.5]deca-2,6,9-trien-8-one. Yield 77%. Mp 172—174 °C. IR (KBr) 1700 cm^{-1} ($\nu_{C=O}$). Found: C, 43.61; H, 0.79; N, 9.86%. Calcd for $C_{15}H_3N_3O_3Cl_4$: C, 43.41; H, 0.73; N, 10.12%.

6,7,9,10-Tetrafluoro-3-(2,6-dichlorophenyl)-2-aza-1,4-dioxaspiro[4.5]deca-2,6,9-trien-8-one. Yield 92%. Mp 148—150 °C. IR (KBr) 1700 cm^{-1} ($\nu_{C=O}$). Found: C, 42.70; H, 0.71; N, 3.96%. Calcd for $C_{13}H_3N_1O_3Cl_2F_4$: C, 42.42; H, 0.82; N, 3.81%.

6,7,9,10-Tetrachloro-3-(2,6-dichlorophenyl)-2-aza-1,4-dioxaspiro-[4.5]deca-2,6,9-trien-8-one. Yield 88%. Mp 165—167 °C. IR (KBr) 1695 cm^{-1} ($\nu_{C=O}$). Found: C, 36.34; H, 0.57; N, 3.34%. Cacld for $C_{13}H_3N_1O_3Cl_6$: C, 35.99; H, 0.70; N, 3.23%.

Kinetic Study. The reaction rate constants were measured by UV method at 20 °C.[10] As the solvent, benzene and chloroform were used. Equimolar portions of the solutions of a nitrile oxide and a quinone were placed in a quartz cell for UV measurement and the progress of the reaction was followed by the spectral change at the absorption maximum of the quinone or of the adduct formed. The concentration of the reactants was about $(2—4)\times10^{-3}$ mol l^{-1} in C=O addition reactions and about $(1—3)\times10^{-2}$ mol l^{-1} in C=C addition reactions.

The authors indebted to Dr. Kosugi, Department of Chemistry, Faculty of Science, University of Tokyo, for helpful advice in the *ab initio* calculation.

References

1) K. N. Houk, J. Sims, R. E. Dure, Jr., R. W. Strozier, and J. K. George, *J. Am. Chem. Soc.*, **95**, 7287 (1973); K. N. Houk, J. Sims, C. R. Watts, and L. J. Luskus, *ibid.*, **95**, 7301 (1973).
2) K. N. Houk, *Acc. Chem. Res.*, **8**, 361 (1975).
3) P. Caramella, E. Albini, T. Bandiera, A. C. Coda, P. Grunanger, and F. M. Albini, *Tetrahedron*, **39**, 689 (1983).
4) J. M. Lluch and J. Bertran, *Tetrahedron*, **38**, 1847 (1982).
5) A. Bened, R. Durand, D. Pioch, P. Geneste, J. P. Declercq, G. Germain, J. Rambaud, R. Roques, C. Guimon, and G. P. Guillouzo, *J. Org. Chem.*, **47**, 2461 (1982).
6) I. Fleming, "Frontier Orbitals and Organic Chemical Reactions," Wiley-Interscience, New York (1976).
7) R. Susimann, *Tetrahedron Lett.*, **1971**, 2717.
8) S. Shiraishi, S. Ikeuchi, M. Seno, and T. Asahara, *Bull. Chem. Soc. Jpn.*, **50**, 910 (1977).
9) S. Shiraishi, S. Ikeuchi, M. Seno, and T. Asahara, *Bull. Chem. Soc. Jpn.*, **51**, 921 (1978).
10) S. Shiraishi, S. Ikeuchi, and M. Seno, *Nippon Kagaku Kaishi.*, **1978**, 1127.
11) S. Shiraishi, B. S. Holla, and K. Imamura, *Bull. Chem. Soc. Jpn.*, **56**, 3457 (1983).
12) J. Bastide and J. P. Maier, *Chem. Phys.*, **12**, 177 (1976).
13) M. D. Rozeboom, I. M. T. Larsson, and K. N. Houk, *J. Org. Chem.*, **46**, 2338 (1981).
14) N. Kosugi and H. Kuroda, *Chem. Phys. Lett.*, **74**, 490 (1980); N. Kosugi, Program GSCF2, Program Library, The Computer Center, The University of Tokyo (1981).
15) M. Shiro, M. Yamakawa, and T. Kubota, *Acta Crystallogr., Sect. B*, **35**, 712 (1979).
16) J. A. Pople and M. Gordon, *J. Am.Chem. Soc.*, **89**, 4253 (1967).
17) J. Bastide, J. P. Maier, and T. Kubota, *J. Electron. Spectrosc. Rel. Phenom.*, **9**, 307 (1976).
18) K. N. Houk, P. Caramella, L. L. Munchausen, Y. M. Chang, A. Battaglia, J. Sims, and D. C. Kaufman, *J. Electron. Spectrosc. Rel. Phenom.*, **10**, 441 (1977).
19) For 2,3-dichloro-5,6-dicyano-*p*-benzoquinone: G. Zanotti, R. Bardi, and A. D. Pra, *Acta Crystallogr., Sect. B*, **36**, 168 (1980). For tetrafluoro-*p*-benzoquinone: P. A. Meresse and C. C. N. Chanh, *ibid.*, **30**, 524 (1974). For *p*-benzoquinone, 2,6-dichloro-*p*-benzoquinone and tetrachloro-*p*-benzoquinone: P. B. Rees, *ibid.*, **26**, 1311 (1970).
20) For tetramethyl-*p*-benzoquinone: D. Rabinovich, G. M. J. Schmidt, and E. Ubell, *J. Chem. Soc., B.* **1967**, 131. The geometry of the quinone moiety of tetramethoxy-*p*-benzoquinone is postulated to reflect half of the substituted side of 2,6-dimethoxy-*p*-benzoquinone. [H. Schmalle, O. Jarchow, and B. M. Hausen, *Naturwissenschaften*, **64**, 534 (1977)]. The geometry of the methoxyl substituents was such as gave the most stable conformation suggested by calculations referring to the X-ray data of 2-methyl-4,5-dimethoxy-*p*-benzoquinone. [J. Silverman, I. Stam-Thole, and C. H. Stam, *Acta Crystallogr., Sect. B*, **27**, 1846, (1971)].
21) E. C. M. Chen and W. E. Wentworth, *J. Chem. Phys.*, **63**, 3183 (1975).
22) T. Sasaki and T. Yoshioka, *Bull. Chem. Soc. Jpn.*, **41**, 2206 (1968).
23) M. D. Gordon, P. V. Alston, and A. R. Rossi, *J. Am. Chem. Soc.*, **100**, 5701 (1978).
24) C. Grundmann and R. Richter, *J. Org. Chem.*, **33**, 476 (1968); C. Grundmann and J. M. Dean, *ibid.*, **30**, 2809 (1965).
25) S. R. Robinson and C. Vasey, *J. Chem. Soc.*, **1941**, 660.

Synthesis of Several New Pyrazolo[5,1-*c*][1,2,4]triazoles, Imidazo[1,2-*b*]-pyrazoles, and Pyrazolo[3,4-*b*]pyrazines. Reaction of Nitrilimines with Amino- and Oxo-substituted Azoles. II

Galal Eldin Hamza ELGEMEIE, Hassan Attia ELFAHHAM, Said Ahmed Soliman GHOZLAN,† and Mohamed Hilmy ELNAGDI*,†

Department of Chemistry, Faculty of Science, Minia University, Minia, A. R. Egypt
†*Department of Chemistry, Faculty of Science, Cairo University, Giza, A. R. Egypt*

(Received July 4, 1983)

The reactivity of amino and hydroxy azoles toward nitrilimines and hydrazonoyl halides was investigated. Several novel rotes for synthesis of derivatives of known heterocyclic systems are reported.

Nitrilimines, usually synthesised *in situ* by base-catalysed elimination of halogeno acid from hydrazonoyl halides, are reactive intermediates that have found extensive use in heterocyclic syntheses.[1] Recently we reported that these reactive intermediates react readily with amino and oxo diazoles, thus, enabling preparation of a variety of new, otherwise difficult to obtain, fused azole derivatives.[2,3] We have been interested to see if reactions of this type can be utilized to constitute a general route to fused azoles. In the present paper we reported the results of our investigation on the reactivity of *N*-phenylbenzohydrazonoyl chloride (**1a**) and *N*-phenylpyruvohydrazonoyl chloride (**1b**) toward a variety of amino and oxo azoles in order to define the exact behaviour of **1a,b** toward this class of compounds.

Thus, it has been found that **1a** reacts with the aminopyrazole derivatives **2a—c** in the presence of triethylamine to yield the pyrazolo[5,1-*c*][1,2,4]triazole derivatives **3a—c**. The formation of **3a—c** is assumed to proceed *via* 2+3 dipolar cycloaddition mechanism. Similar mechanism was suggested to account for the formation of pyrazolo[5,1-*c*][1,2,4]triazole derivative from the reaction of **1a** with **2d**.[3] The 3-amino-2-pyrazolin-5-one (**4**) reacted with **1a** to yield a product with the molecular formula $C_{29}H_{22}N_6O$ (M^+=470). Two theoretically possible isomeric structure **5** and **6** were considered for the product. Structure **6** was readily ruled out based on IR and ^{1}H-NMR spectrum of the product as well as its chemical behaviour. The IR spectrum revealed absorption at 1690 cm^{-1} for ring CO group. Whereas the ^{1}H-NMR spectrum showed no pyrazole C(4)-H signal at δ_H *ca.* 6.0. Furthermore the reaction product proved to be stable under conditions reported to effect decomposition of *N*-substituted pyrazoles of structure similar to that of **6**.[3] The formation of **5** is assumed to proceed *via* reaction of **4** with two molecules of **1a** and elimination of ammonia.

In contrast to the behaviour of **2a—c**, reaction of aminopyrazole derivative **2e** with **1a** afforded *N*-alkylated product (M^+=378) which may be formulated as **7** or **8**. The isomeric structure **7** was established for the reaction product showed a signal for NH_2 at δ 5.9. Attempts to effect cyclization of this product were unsuccessful. The formation of **7** in this case is assumed to proceed *via* alkylation sequence. Alkylation of aminoazoles with hydrazonoyl halides has been previously observed.[3]

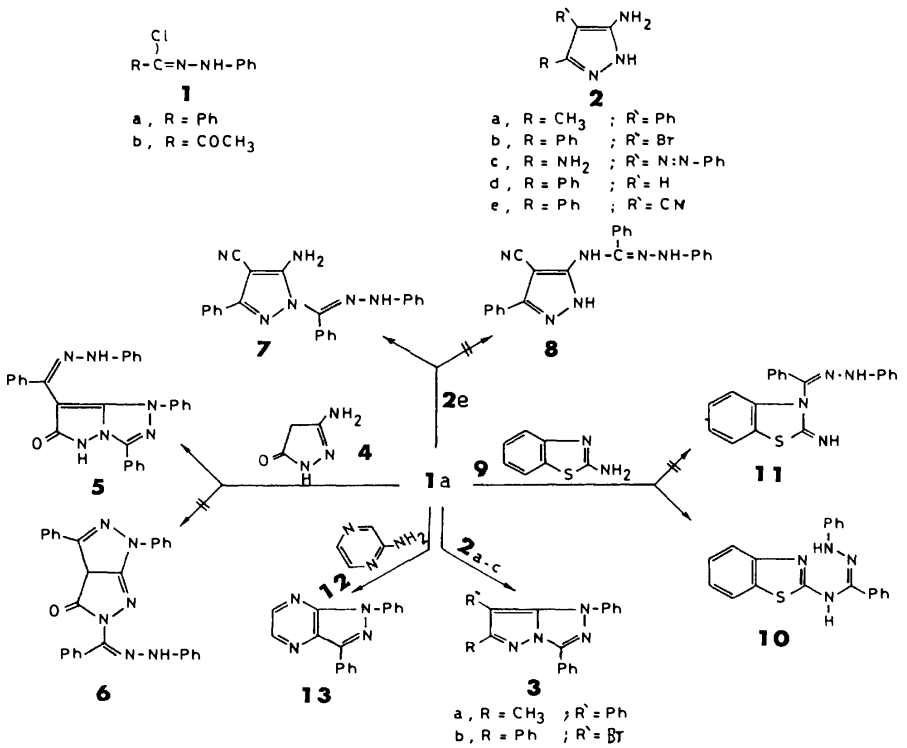

Similar to the behaviour of **2e**, 2-aminobenzthiazole (**9**) reacted with compound **1a** under the same experimental condition to yield an alkylated product, although structures **10** and **11** seemed possible, structure **11** was readily ruled out based on IR spectrum which revealed the absence of absorption at 1670—1630 cm^{-1} for exocyclic C=N.

2-Aminopyrazine (**12**) reacted with **1a** to yield the pyrazolo[3,4-*b*]pyrazine derivative **13**. The structure of **13** was established based on analytical and spectral data. The formation of **13** in this reaction represents the first observed 2+3 cycloaddition of nitrilimine to diazine derivative.

Whereas compound **1b** reacted with **2a** to yield the imidazo[1,2-*b*]pyrazole derivative **14** ($M^+=315$), it reacted with compounds **2b, c, e** to yield only the acyclic *N*-alkylated products **15a—c**. The formation of **14** may be assumed to proceed either *via* the stepwise sequence

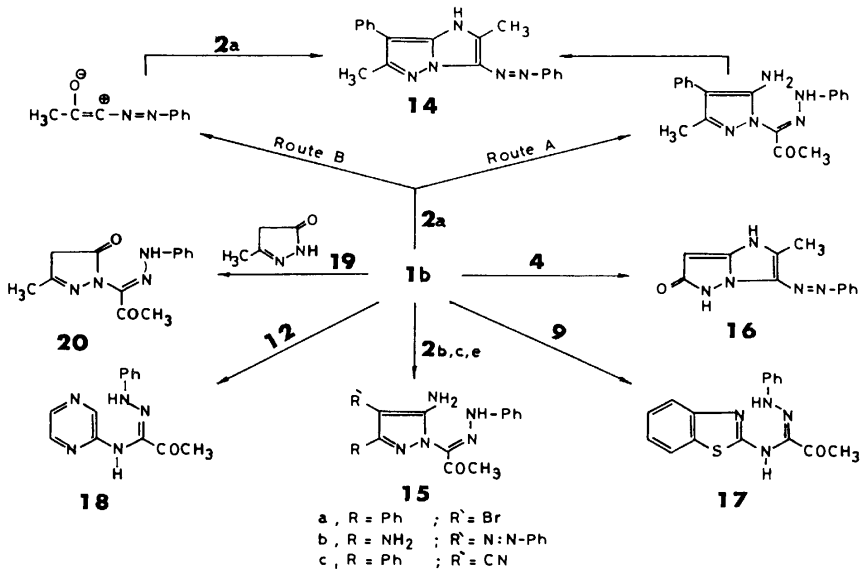

TABLE 1. LIST OF PRODUCTS OF REACTION OF THE HYDRAZONOYL CHLORIDES **1a, b** WITH AMINO- AND OXO-SUBSTITUTED AZOLES

Compound (Colour)	Crystallization solvent	Mp θ_m/°C	Yield %	Mol formula (Mol weight)	Found Calcd (%) C	H	N
3 (Yellow)	EtOH	208	74	$C_{23}H_{18}N_4$ (350)	79.2 (78.9	5.2 5.1	16.2 16.0)
3 (Yellow)	EtOH	214—216	28	$C_{22}H_{15}N_4Br$ (415)	63.3 (63.6	3.6 3.6	13.3 13.5)
3 (Yellow)	MeCOMe	236—238	85	$C_{22}H_{17}N_7$ (379)	69.8 (69.7	4.4 4.5	25.7 25.9)
5 (Buff)	MeCONMe2	246—248	24	$C_{29}H_{22}N_6O$ (470)	73.6 (74.0	4.8 4.7	17.7 17.9)
7 (Yellow)	EtOH	188	80	$C_{23}H_{18}N_6$ (378)	73.1 (73.0	4.6 4.8	22.4 22.2)
10 (Colourless)	MeCOMe	170	88	$C_{20}H_{16}N_4S$ (344)	69.6 (69.8	4.9 4.7	16.1 16.3)
13 (Colourless)	EtOH	250—252	35	$C_{17}H_{12}N_4$ (272)	75.0 (75.0	4.8 4.4	20.5 20.6)
14 (Orange)	MeCOMe	176—178	90	$C_{19}H_{17}N_5$ (315)	72.1 (72.4	5.2 5.4	22.4 22.2)
15 (Yellow)	MeCOMe	>300	90	$C_{18}H_{16}N_5OBr$ (398)	54.2 (54.3	4.4 4.0	17.8 17.6)
15 (Yellow)	MeCOMe	228—229	92	$C_{18}H_{18}N_8O$ (362)	59.8 (59.7	5.1 5.0	30.6 30.9)
15 (Yellow)	MeCOMe	242—244	88	$C_{19}H_{16}N_6O$ (344)	66.0 (66.3	5.0 4.7	24.6 24.4)
16 (Violet)	MeCONMe2	>300	82	$C_{12}H_{11}N_5O$ (241)	59.5 (59.8	4.6 4.6	29.2 29.0)
17 (Yellow)	MeCOMe	238—239	60	$C_{16}H_{14}N_4OS$ (310)	61.7 (61.9	4.7 4.5	18.2 18.1)
18 (Yellow)	MeCOMe	158—159	40	$C_{13}H_{13}N_5O$ (255)	61.0 (61.2	5.2 5.1	27.2 27.5)
20 (Brown)	MeCOMe	159	52	$C_{13}H_{14}N_4O_2$ (258)	60.5 (60.5	5.2 5.4	21.5 21.7)

TABLE 2. SPECTROSCOPIC DATA OF PRODUCTS LISTED IN Table 1

Compound	IR $\tilde{\nu}$/cm^{-1} (selected bands)	^{1}H-NMR δ
3	1640 (C=N)	2.2(3H, s, CH_3); 6.8—8.3 (15H, m, 3 phenyl protons)
3	1610 (C=N)	7.2—8.6(15H, m, 3 phenyl protons)
3	3400, 3200 (NH_2); 1625 (δNH_2); 1610 (C=N)	7.2—8.5(15H, m, 3 phenyl protons); 8.8 (2h, s, NH_2)
5	3250 (NH); 1690 (CO); 1630 (C=N)	7.2—7.8 (20H, m, 4 phenyl protons); 8.2 (1H, s, NH); 11.2 (1H, s, NH)
7	3500, 3300, 3200 (NH and NH_2); 2220 (CN); 1620 (C=N)	6.0 (2H, s, NH_2); 6.8—7.4 (15H, m, 3 phenyl protons); 10.2 (1H, s, NH)
10	3500—3300 (NH); 1610 (C=N)	7.1—7.7 (14H, m, 2 phenyl protons and C_6H_4); 8.2 (1H, s, NH); 8.4 (1H, s, NH)
13	1620 (C=N)	7.2—7.7 (10H, m, 2 phenyl protons); 8.0—8.3 (2H, m, pyrazine H-3 and H-4)
14	3500—3350 (NH); 1620 (C=N)	2.5 (3H, s, CH_3); 2.7 (3H, s, CH_3), 6.8—7.4 (10H, m, 2 phenyl protons); 12.1 (1H, br, s, NH)
15	3450, 3300, 3200 (NH and NH_2);	2.5 (3H, s, CH_3); 5.6 (2H, s, NH_2), 7.0—7.8 (10H, m, 2 phenyl protons); 10.7 (1H, br, s, NH)
15	3450—3300 (NH and NH_2); 1660 (CO); 1620 (C=N)	2.45 (3H, s, CH_3); 5.8 (2H, br, s, NH_2); 6.8—7.5 (12H, m, 2 phenyl protons and NH_2), 10.7 (1H, s, NH)
15	3500—3150 (NH and NH_2); 2220 (CN); 1660 (CO); 1620 (C=N)	2.5 (3H, s, CH_3); 6.8 (2H, s, NH_2); 7.0—7.8 (10H, m, 2 phenyl protons); 10.7 (1H, s, NH)
16	3500 (NH); 3100—2500 (chelated NH); 1700 (CO); 1610 (C=N)	Insoluble in commonly used NMR solvents
17	3500, 3200 (NH); 1705, 1680 (CO); 1620 (C=N)	
18	3500—3200 (NH); 1690 (CO);1610(C=N)	
20	3500—2500 (chelated NH); 1680—1650 (acetyl and ring CO); 1610 (C=N)	

(route A) or dipolar addition mechanism (route B). We believed that **14** is formed mainly *via* a cycloaddition mechanism as acyclic intermediate for the reaction of **1b** and **2a** could not be traced. Moreover compounds **15a—c** were found resistant to cyclization under the reaction conditions or even more drastic conditions.

Reactivity of **1b** toward **4**, **9** and **12** was also investigated. Only in the case of **4** the cyclic product **16** was obtained (M^+=241). With other aminoazoles only the alkylated products **17** and **18** were obtained. Similarly **1b** reacted with 3-methyl-2-pyrazolin-5-one (**19**) to yield the acyclic *N*-alkylated product **20**.

It may thus concluded that nitrilimines would react with aminoazoles either *via* a 2+3 dipolar cycloaddition or by alkylation sequence. The exact course of the reaction seems to depend on the nature of the aminoazole and the nitrilimine. Fused azoles can only be readily obtained from a cycloadditions, trials to cyclise products of alkylation has failed in our hands.

Experimental

All melting points are uncorrected. IR spectra were recorded (KBr) on a Pye Unicam SP-1000 spectrophotometer. ^{1}H-NMR spectra were obtained in an EM-390 spectrometer at 90 MHz with DMSO-d_6 as solvent and TMS as internal reference. Analytical data were obtained from the Analytical Data Unit at Cairo University.

Reaction of the Hydrazonoyl Chlorides 1a, b with Amino and/or Oxo-substituted Azoles. General Procedure: A suspension of compound **1a** or **1b** (20 mmol) and the appropriate amino or oxo-substituted azoles (20 mmol) in ethanol (30 ml) was refluxed with triethylamine (20 mmol) for 3 h and then evaporated to dryness under reduced pressure. The residue was washed with petroleum ether, triturated with ethanol, and the resulting solid product was filtered off and crystallized from the appropriate solvent (Table 1). Analytical and spectroscopic data are given in Table 1 and 2.

References

1) S. Y. Hong and J. E. Balwin, *Tetrahedron*, **24**, 3787 (1968).
2) H. A. Elfahham, K. U. Sadek, G. E. H. Elgemeie, and M. H. Elnagdi, *Chem. Lett.*, **1982**, 119.
3) H. A. Elfahham, K. U. Sadek, G. E. H. Elgemeie, and M. H. Elnagdi, *J. Chem. Soc., Perkin Trans. 1*, **1982**, 2663.

Synthesis and Reactions of Quinoxaline Derivatives

Mahmoud Zarif Amin BADR,* Galal Moustafa EL-NAGGAR,
Hassan Ahmad Hassan EL-SHERIEF, and Safar Ahmed MAHGOUB
Chemistry Department, Faculty of Science, Assiut University, Assiut, Egypt

(Received April 6, 1983)

Reaction of 3-methyl-2(1*H*)quinoxalinone (**1**) with alkyl, benzyl, and arenesulfonyl halides in the presence of K_2CO_3 in dry acetone gave 1-substituted 3-methyl-2(1*H*)-quinoxalinones (**2a—g**). However **1** reacts with benzoyl chloride under the same conditions to give 3-methyl-2-quinoxalinyl benzoate, while it reacts with P_2S_5 in dry pyridine to give 3-methyl-2(1*H*)quinoxalinethione (**4**). Treatment of **4** with methy iodide in the presence of K_2CO_3 in dry acetone gave 2-methyl-3-(methylthio)quinoxaline but not 1,3-dimethyl-2(1*H*)-quinoxalinethione which has been obtained from **2a** and P_2S_5 in dry pyridine. Treatment of **4** with benzyl bromide and/or *p*-nitrobenzyl bromide in the presence of K_2CO_3 in dry acetone gave 2-benzylthio and 2-(*p*-nitrobenzylthio)-3-methylquinoxalines. Syntheses of 1-methyl-3-(substituted styryl)-2(1*H*)-quinoxalinone (**8a—m**) were achieved by condensation of **2a** with aromatic aldehydes. Addition of thiophenols and mercaptoacetic acid to **8** gives 1-methyl-3-[2-(substituted phenylthio)ethyl]-2(1*H*)-quinoxalinones and 1-methyl-3-[2-(substituted phenyl)-2-(carboxymethylthio)ethyl]-2(1*H*)-quinoxalinones respectively. 1,3-Dimethyl-2(1*H*)-quinoxalinone (**2a**) condensed with ketones in the presence of $ZnCl_2$ to give 1-methyl-3-[2-(substituted phenyl)-1-alkenyl]-2(1*H*)-quinoxalinones. 1-Methyl-3-(substituted styryl)-2(1*H*)-quinoxalinethiones were produced by refluxing a mixture of **8** with P_2S_5 in dry pyridine.

Quinoxaline derivatives are important as insecticides,[1] fungicides,[2,3] antibacterials,[4] and they show important biological effects.[5,6] In continuation of our earlier work[7] on quinoxaline derivatives, the present investigation deals with the synthesis of a series of new quinoxaline and quinoxalone compounds applying new procedures which are easier and afford better yields.

It has been observed in the present study that 3-methyl-2(1*H*)-quinoxalinone[8] (**1**) reacts with alkyl, benzyl, and arenesulfonyl halides in the presence of K_2CO_3 in dry acetone to give the corresponding 1-substituted 3-methyl-2(1*H*)-quinoxalinone (**2a—g**). These compounds showed IR absorption bands between 1665—1710 cm^{-1} for C=O group and between 1600—1610 cm^{-1} for C=N group but they did not show absorption band at 3350 cm^{-1} for NH group. The UV spectra of **2b,c** in ethanol were similar to that of **1** and showed three characteristic absorption bands as shown in Table 1.

The ^{1}H-NMR spectra of compounds **2a—f** in $CDCl_3$ as a solvent were in agreement with the suggested structures and showed the signals given in Table 2.

However, when **1** was allowed to react with benzoyl chloride in the presence of anhydrous K_2CO_3 in dry acetone, the *O*-benzoylation was observed to give 3-methyl-2-quinoxalinyl benzoate (**3**).

The IR spectrum of **3** showed absorption band at 1740 cm^{-1} for C=O of the ester group. The NMR spectrum determined in $CDCl_3$ showed a singlet at δ 2.71 (3H, $-CH_3$), a symmetrical multiplet centered at δ 7.65 (5H, $-C_6H_5$) and a symmetrical multiplet centered at δ 8.2 (4H, aromatic protons of quinoxalinone nucleus).

Reaction of **1** with P_2S_5 in dry pyridine gave 3-methyl-2(1*H*)-quinoxalinethione (**4**), whose structure was confirmed by its IR spectrum which showed bands at 3350 cm^{-1} (NH) and at 1550 cm^{-1} (C=S).

Treatment of 3-methyl-2(1*H*)quinoxalinethione (**4**) with methyl iodide in the presence of K_2CO_3 in dry acetone gave 2-methyl-3-(methylthio) quinoxaline[9] (**5**). However, 1,3-dimethyl-2(1*H*)-quinoxalinethione (**6**) was not detected among the products. Compound **6** was prepared by reaction of 1,3-dimethyl-2(1*H*)-quinoxalinone (**2a**) with P_2S_5 in pyridine. However this observation does not exclude the possibility that 3-methyl-2(1*H*)-quinoxalinethione (**4**) exists in solution as 2-mercaptoquinoxaline rather than as cyclic thioamide tautomer. This was further confirmed by the similarity of the UV spectra of **6** together with that of compound **4** and their subsequent difference from that corresponding to 2-methyl-3-(methylthio)quinoxaline (**5**) (Table 3). The structures of **5** and **6** were further confirmed by NMR spectra in $CDCl_3$. Compound **5** showed a singlet at δ 2.68 (6H, $-S-CH_3$ and $-C-CH_3$) and a symmetrical multiplet centered at δ 7.8 (4H, aromatic protons), where compound **6** showed a singlet at δ 2.82 (3H, $-C-CH_3$), a singlet at δ 4.2 (3H, $N-CH_3$) and a multiplet at δ 7.4—7.9 (4H, aromatic protons).

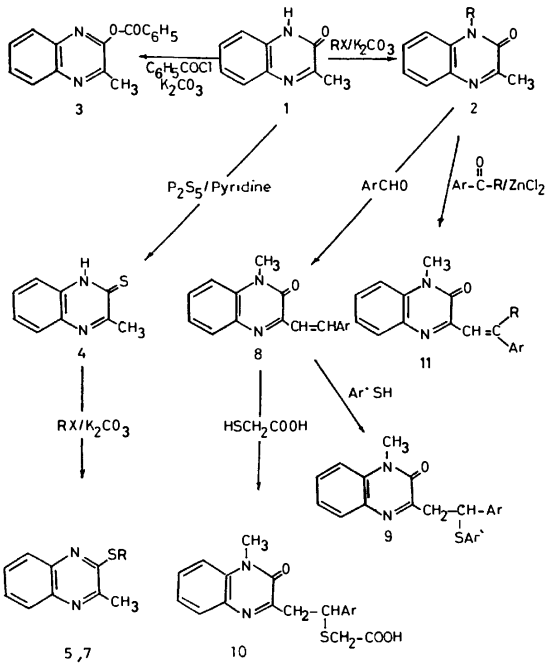

Scheme 1.

Treatment of 3-methyl-2(1*H*)-quinoxalinethione (**4**)

Table 1. UV spectral data of some 1-substituted 3-methyl-2(1*H*)-quinoxalinones

No.	R	Band I		Band II		Band III	
		λ_{max} nm	ε $dm^3\ mol^{-1}\ cm^{-1}$	λ_{max} nm	ε $dm^3\ mol^{-1}\ cm^{-1}$	λ_{max} nm	ε $dm^3\ mol^{-1}\ cm^{-1}$
1	H	278	2000	328	2300	338	1750
2b	$-CH_2C_6H_5$	282	2700	330	2900	338	2500
2c	$-CH_2C_6H_4CH_3(p)$	282	2900	330	3100	338	2500

Table 2. ^{1}H-NMR spectral data for 1-substituted 3-methyl-2(1*H*)-quinoxalinones (**2a—f**)

No.	R	N=C-CH_3	N-CH_2-Ar	Aromatic protons	N-Ar-$CH_3(p)$
2a	$-CH_3$	2.60	3.7(CH_3)	7.15—7.9 (4H)	—
2b	$-CH_2C_6H_5$	2.65	5.50	7.15—7.9 (9H)	—
2c	$-CH_2C_6H_4CH_3(p)$	2.65	5.45	7.05—7.9 (8H)	2.25
2e	$-SO_2C_6H_5$	2.75	—	7.60—8.35 (9H)	—
2f	$-SO_2C_6H_4CH_3(p)$	2.75	—	7.30—8.25 (8H)	2.50

In the above reactions substitution occurred favorably at the NH group.

Table 3. UV spectral data of substituted 2(1*H*)-quinoxalinethiones (**4**, **6**) and 2-(benzylthio)quinoxalines (**5**, **7**)

No.	Band I		Band II		Band III		Band IV	
	λ_{max} nm	ε $dm^3\ mol^{-1}\ cm^{-1}$	λ_{max} nm	ε $dm^3\ mol^{-1}\ cm^{-1}$	λ_{max} nm	ε $dm^3\ mol^{-1}\ cm^{-1}$	λ_{max} nm	ε $dm^3\ mol^{-1}\ cm^{-1}$
4	216	17100	278	9400	396	5400	—	—
5	235	10600	262	10600	345	6900	354	6800
6	217	22500	274	15800	390	8600	—	—
7a	238	7700	266	7150	347	4300	356	4150
7b	240	8700	266	10900	343	4250	355	4100

with benzyl bromide and/or *p*-nitrobenzyl bromide in the presence of K_2CO_3 in dry acetone gave 2-benzylthio and 2-(*p*-nitrobenzylthio)-3-methylquinoxalines (**7a**,**b**) respectively. Their electronic absorption spectra were similar with that of **5** (Table 3).

The ^{1}H-NMR spectrum of **7b** in CF_3 COOH showed a singlet at δ 2.55 (3H, -C-CH_3), a singlet at δ 4.35 (2H, -S-CH_2-) and a multiplet at δ 7.2—7.8 (8H, aromatic protons).

The reactivity of the 3-methyl group towards condensation reaction into the corresponding styryl compounds **8** was demonstrated either by: (A) Fusion of 1,3-dimethyl-2(1*H*)-quinoxalinone (**2a**) with the corresponding aldehyde in the presence of few drops of piperidine or (B) refluxing **2a** with the corresponding aldehyde in dry pyridine using few drops of piperidine and (C) refluxing **2a** with the corresponding aldehyde in acetic anhydride. The IR spectra of compounds **8a—m** showed bands at 1665—1650 cm^{-1} for C=O group, at 1630—1610 cm^{-1} for C=C group and at 1580 cm^{-1} C=N. It is suggested that compounds **8** are of trans configuration since a strong absorption band appeared in the region 990—980 cm^{-1} characteristic of trans olefinic configuration. The coupling constants of the styryl protons in the NMR spectra are 15—16 Hz, confirming its trans configuration.

The UV spectra of the styryl compounds (**8a**,**b**,**d**,**e**) showed a bathochromic shift of the K-band as compared with that of the parent compound (**2a**). This shift has been attributed to the difference in auxochromic character of the styryl residue at position-3 of the quinoxalinone ring in conjugation with -C=N- group. *o*-Nitrostyryl derivative (**8j**) showed less bathochromic shift than its *p*-isomer (**8i**) due to the steric hindrance at ortho-position distorting the coplanarity and conjugation (Table 4).

Table 4. UV spectral data of 1-methyl-3-styryl-2(1*H*)-quinoxalinones (**8**)

No.	Ar	λ_{max}/nm	ε/$dm^3\ mol^{-1}\ cm^{-1}$
8a	$-C_6H_5$	384	7350
8b	$-C_6H_4OCH_3(p)$	404	8800
8d	$-C_6H_4N(CH_3)_2(p)$	452	9400
8e	$-C_6H_4OH(p)$	402	6950
8i	$-C_6H_4NO_2(p)$	402	9250
8j	$-C_6H_4NO_2(o)$	394	6000

Thiophenols were added to 1-methyl-3-(substituted styryl)-2(1*H*)-quinoxalinones (**8**) to produce 1-methyl-3-[2-(substituted phenyl)-2-(substituted phenylthio)-ethyl]-2(1*H*)-qunoxalinones (**9a—e**) whose IR spectra showed band at 1670 cm^{-1} for C=O group and revealed the disappearance of C=C band at 1620—1610 cm^{-1}. The UV spectrum of **9b** in ethanol showed absorption band at λ_{max} 340 nm (ε 1800) which is close to that of **2a** λ_{max} 340 nm (ε 5500) confirming the saturation of the styryl side chain. The ^{1}H-NMR spectrum of **9b** in

Table 5. 1-Substituted 3-methyl-2-(1*H*)-quinoxalinones (**2**)

No.	1-Substituent	Mp θ_m/°C	Crystal. solvent	Yield %	Mol formula	Found (%)			Calcd (%)		
						C	H	N	C	H	N
2a	CH_3	84— 85[a)]	Pet. ether (60—80 °C)	65	$C_{10}H_{10}N_2O$	68.83	5.80	16.13	68.95	5.79	16.08
2b	$C_6H_5CH_2$-	87— 88	Pet. ether (40—60 °C)	90	$C_{16}H_{14}N_2O$	76.95	5.25	11.19	76.78	5.64	11.19
2c	*p*-$CH_3C_6H_4CH_2$-	174—175	Pet. ether (60—80 °C)	85	$C_{17}H_{16}N_2O$	77.19	6.09	10.59	77.25	6.10	10.60
2d	*p*-$NO_2C_6H_4CH_2$-	212—213	Acetone	65	$C_{16}H_{13}N_3O_3$	65.12	4.51	14.32	65.08	4.44	14.23
2e	$C_6H_5SO_2$-	126—127	Pet. ether (60—80 °C)	90	$C_{15}H_{12}N_2O_3S$	60.10	4.33	9.26	60.00	4.03	9.33
2f	*p*-$CH_3C_6H_4SO_2$-	109—110	Ethanol	89	$C_{16}H_{14}N_2O_3S$	61.15	4.50	8.81	61.14	4.49	8.91
2g	2-$C_{10}H_7SO_2$-	126—127	Acetone	90	$C_{19}H_{14}N_2O_3S$	65.37	4.21	8.09	65.14	4.03	8.00

Compounds are colorless crystals except **2e—g** are brownish crystals. a) Not changed by admixture with the reference sample.[10)]

$CDCl_3$ showed a singlet at δ 3.38 (3H, *N*-CH_3), a doublet at δ 3.58 (2H, -CH_2-side chain), a singlet at δ 3.7 (3H, -OCH_3), a triplet at δ 4.35 (1H, -CH-side chain). J_{vic} 6—7 Hz and a multiplet at δ 6.7—7.85 (13H, aromatic protons). Mercaptoacetic acid underwent addition to 1-methyl-3-styryl-2(1*H*)-quinoxalinones (**8a—c, i**) giving the products, 1-methyl-3-[2-(carboxymethylthio)-2-(substituted phenyl)ethyl]-2(1*H*)-quinoxalinones (**10a—d**). The IR spectra of **10a,c** showed bands at 1650 cm^{-1} (C=O) of quinoxalinone nucleus, at 1720 cm^{-1} (C=O) of carboxylic acid and a broad band at 2700—2500 cm^{-1} (assoc. OH). The UV spectrum of **10a** in ethanol showed a band at λ_{max} 343 nm (ε 2000) which is close to λ_{max} 340 nm (ε 5500) of the compound **2a**. The NMR spectrum of **10a** in $CDCl_3$ showed a singlet at δ 3.15 (2H, -CH_2-carboxyl); a doublet at δ 3.6 (2H-CH_2- to quinoxalinone nucleus), a singlet at δ 3.85 (3H, *N*-CH_3), a triplet at δ 4.80 (1H, -CH-side-chain), J_{vic} 6—7 Hz and a multiplet at δ 7.2—8 (9H, aromatic protons).

1,3-Dimethyl-2(1*H*)-quinoxalinone (**2a**) condensed with ketones, such as, acetophenone, *p*-bromo-, *p*-methyl-, *p*-methoxy acetophenones, and benzophenone, in the presence of zinc chloride gave 1-methyl-3-[2-(substituted phenyl)-1-alkenyl]-2(1*H*)-quinoxalinones (**11a—e**). The NMR spectrum of compound **11e** in $CDCl_3$ showed a singlet at δ 3.7 (3H, *N*-CH_3), a singlet at δ 6.85 (1H, -CH=) and a multiplet at δ 7.35—7.65 (14H, aromatic protons).

Syntheses of 1-methyl-3-(substituted styryl)-2(1*H*)-quinoxalinethiones (**12a—e**) were achieved by refluxing a mixture of **8** with P_2S_5 in dry pyridine for 5 h. In the IR spectrum of compound **12d** C=O Stretching disappeared, while two new bands at 1515, 1240 cm^{-1} for C=S group and also a band at 1610 cm^{-1} for C=C group was observed. The UV spectrum of compound **12d** in $CHCl_3$ showed a bathochromic shift for the K-band at λ_{max} 442 nm (ε 135×10^2) in comparison with its precursor 1,3-dimethyl-2(1*H*)-quinoxalinethione (**6**), λ_{max} 390 nm (ε 86×10^2), which proves the extended conjugation between the styryl residue and -C=N- group of 2(1*H*)-quinoxalinethione nucleus.

Experimental

Melting points reported are uncorrected. IR spectra were recorded on a Beckman 20 infrared spectrophotometer using KBr Wafer technique. UV spectra in ethanol on a Pye-Unicam SP 8000 Spectrophotometer and NMR spectra were recorded on a 90 MHz Bruker spectrospin and a Varian EM-390 spectrometer.

*3-Methyl-2(1H)-quinoxalinone (**1**).*[8)] Colorless crystals from ethanol, mp 245 °C (sublim). NMR exhibit a singlet at δ 2.9 (3H, -CH_3), a multiplet at δ 7.4—8.15 (4H, aromatic protons), while the NH proton at δ 7.1 disappeared by adding D_2O.

*Reactions of 3-Methyl-2(1H)-quinoxalinone (**1**) with Alkyl, Benzyl, and Arenesulfonyl Halides. General Procedure*: A mixture of 3-methyl-2(1*H*)-quinoxalinone (**1**) (0.01 mol), alkyl, benzyl, or arenesulfonyl halides (0.012 mol), and anhydrous K_2CO_3 were refluxed together for several hours in dry acetone (30 ml). The resultant *N*-substituted derivatives (**2a—g**) were crystallized from the proper solvent (Table 5).

*Synthesis of 3-Methyl-2-quinoxalinyl Benzoate (**3**).* A mixture of 3-methyl-2(1*H*)-quinoxalinone (**1**) (0.01 mol) in dry acetone, anhydrous K_2CO_3 (0.012 mol), and benzoyl chloride (0.012 mol) was heated for several hours. Acetone solution was filtered and evaporated. The product was crystallized from petroleum ether (60—80 °C) to give **3** as yellowish crystals, mp 110—111 °C, yield 2.3 g (90%). Found: C, 72.69; H, 4.68; N, 10.49%. Calcd for $C_{16}H_{12}N_2O_2$ C, 72.71; H, 4.58; N, 10.60%.

*Synthesis of 3-Methyl-2(1H)-quinoxalinethione (**4**).* A mixture of 3-methyl-2(1*H*)-quinoxalinone (**1**) (0.01 mol) and P_2S_5 (0.01 mol) was refluxed in dry pyridine (20 ml) for 5 h. The solvent was evaporated and the residue was treated with dil acetic acid. The solid product was filtered and crystallized from absolute ethanol to give **4** as orange-brown crystals, mp 250—251 °C (sublim), yield 1.4 g (85%). Found: C, 61.56; H, 4.59; N, 15.95%. Calcd for $C_9H_8N_2S$: C, 61.36; H, 4.58; N, 15.90%.

*Reaction of 3-Methyl-2(1H)-quinoxalinethione (**4**) with Alkyl and Benzyl Halides. General Procedure*: A mixture of 3-methyl-2(1*H*)-quinoxalinethione (**4**) (0.01 mol) in dry acetone, anhydrous K_2CO_3 (0.012 mol) and the corresponding alkyl or benzyl halide was heated on a steam bath for 4 h. Acetone solution was filtered and evaporated and the product was crystallized from suitable solvent.

*2-Methyl-3-(methylthio)quinoxaline (**5**)*: Colorless crystals from pet. ether (40—60 °C), mp 55—56 °C, yield 1.8 g

Table 6. 1-Methyl-3-(substituted styryl)-2(1*H*)-quinoxalinones (**8**)

No.	3-Substituent	Mp θ_m/°C	Yield %	Procedure	Mol formula	Found (%)			Calcd (%)		
						C	H	N	C	H	N
8a	$C_6H_5CH=CH-$	164—165	85	A	$C_{17}H_{14}N_2O$	78.05	5.54	10.63	77.84	5.38	10.67
8b	p-$CH_3OC_6H_4CH=CH-$	134—135	65	B, C	$C_{18}H_{16}N_2O_2$	73.86	5.62	9.30	73.95	5.53	9.58
8c	p-$CH_3C_6H_4CH=CH-$	149—150	75	A	$C_{18}H_{16}N_2O$	78.47	5.89	10.05	78.23	5.84	10.14
8d	p-$(CH_3)_2NC_6H_4CH=CH-$	197—198	83	A	$C_{19}H_{19}N_3O$	74.74	6.29	13.75	74.73	6.27	13.76
8e	p-$HOC_6H_4CH=CH-$	272—273	65	A	$C_{17}H_{14}N_2O$	73.35	5.11	10.01	73.36	5.07	10.07
8f	o-$HOC_6H_4CH=CH-$	249—250	65	A	$C_{17}H_{14}N_2O_2$	73.22	5.13	9.97	73.36	5.07	10.07
8g	p-$ClC_6H_4CH=CH-$	169—170	85	A	$C_{17}H_{13}N_2OCl$	68.75	4.50	—	68.80	4.42	—
8h	p-$BrC_6H_4CH=CH-$	183—184	90	A	$C_{17}H_{13}N_2OBr$	59.79	4.05	—	59.84	3.84	—
8i	p-$NO_2C_6H_4CH=CH-$	235—236	85	A, C	$C_{17}H_{13}N_3O_3$	66.29	4.19	13.48	66.04	4.26	13.68
8j	o-$NO_2C_6H_4CH=CH-$	155—156	80	A	$C_{17}H_{13}N_3O_3$	66.32	4.30	13.70	66.04	4.26	13.68
8k	m-$NO_2C_6H_4CH=CH-$	184—185	65	A	$C_{17}H_{13}N_3O_3$	66.31	4.40	13.57	66.04	4.26	13.68
8l	1-$C_{10}H_7CH=CH-$	168—169	75	A	$C_{21}H_{16}N_2O$	80.69	5.30	8.89	80.75	5.16	8.97
8m	2-$C_{10}H_7CH=CH-$	221—222	65	A	$C_{21}H_{16}N_2O$	80.67	5.30	9.01	80.75	5.16	8.97

All compounds crystallized from ethanol solvent, except **8f** from acetic acid. All compounds are yellow crystals, except **8d** bright deep red, **8e** bright brown, and **8h** orange crystals.

Table 7. 1-Methyl-3-[2-(carboxymethylthio)-2-(substituted phenyl)ethyl]-2(1*H*)-quinoxalinone (**10**)

No.	2-Substituent on ethyl	Mp θ_m/°C	Yield %	Mol formula	Found (%)			Calcd (%)		
					C	H	N	C	H	N
10a	C_6H_5-	169—170	80	$C_{19}H_{18}N_2O_3S$	64.52	5.20	7.82	64.40	5.12	7.91
10b	p-$CH_3C_6H_4-$	171—172	75	$C_{20}H_{20}N_2O_3S$	65.35	5.58	7.50	65.21	5.47	7.61
10c	p-$CH_3OC_6H_4-$	105—106	75	$C_{20}H_{20}N_2O_4S$	62.70	5.23	8.60	62.49	5.24	8.32
10d	p-$NO_2C_6H_4-$	118—119	85	$C_{19}H_{17}N_3O_5S$	57.35	4.33	10.48	57.14	4.29	10.52

All compounds are yellowish crystals from pet. ether (40—60 °C).

(95%). Found: C, 63.19; H, 5.35; N, 14.90%. Calcd for $C_{10}H_{10}N_2S$: C, 63.15; H, 5.30; N, 14.74%.

*2-Benzylthio-3-methylquinoxaline (**7a**)*: Colorless crystals from acetone, mp 84—85 °C, yield 2.4 g (90%). Found: C, 72.25;H, 5.34; N, 10.56; S, 12.00%. Calcd for $C_{16}H_{14}N_2S$: C, 72.16; H, 5.30; N, 10.52; S, 12.02%.

*Synthesis of 1,3-Dimethyl-2(1H)-quinoxalinone (**6**)*: From 1,3-dimethyl-2(1*H*)-quinoxalinone (**2a**) and P_2S_5 following the same procedure for the synthesis of **4**. Brown crystals from ethanol, mp 146—147 °C, yield 85%. Found: C, 63.20; H, 5.40; S, 16.90%. Calcd for $C_{10}H_{10}N_2S$: C, 63.15; H, 5.30; S, 16.82%.

*Synthesis of 1-Methyl-3-substituted Styryl-2(1H)-quinoxalinone (**8**). Procedure (A)*: In the presence of piperidine; 1,3-Dimethyl-2(1*H*)-quinoxalinone (**2a**) (0.01 mol) was fused with the corresponding aromatic aldehyde (0.012 mol) for 10 min in the presence of few drops of piperidine. The product was isolated from the reaction mixture by adding ethanol, filtered and crystallized from the proper solvent (Table 6).

Procedure (B): In the presence of pyridine solvent and piperidine; 1,3-Dimethyl-2(1*H*)-quinoxalinone (**2a**) (0.01 mol) and the appropriate aromatic aldehyde (0.012 mol) were refluxed together in dry pyridine as solvent in the presence of few drops of piperidine for 3 h after which the excess solvent was removed and the product was crystallied from suitable solvent.

Procedure (C): In acetic anhydride solvent; 1,3-Dimethyl-2(1*H*)-quinoxalinone (**2a**) (0.01 mol) and the appropriate aromatic aldehyde (0.012 mol) were refluxed together in acetic anhydride as solvent for 20 h after which the excess solvent was removed and the reaction mixture was treated as usual.

*Addition of Substituted Thiophenol to 1-Methyl-3-(substituted styryl)-2(1H)-quinoxalinone (**8**). General Procedure*: A mixture of 1-methyl-3-(substituted styryl)-2(1*H*)-quinoxalinone (**8**) (0.002 mol) and substituted thiophenol (0.004 mol) was heated at 100 °C for 2 h. The yellow-brown oil formed was triturated with pet. ether (40—60 °C) and the products obtained were crystallized from the proper solvent.

*1-Methyl-3-[2-phenyl-2-(phenylthio)ethyl]-2(1H)-quinoxalinone (**9a**)*: Colorless crystals from pet. ether (60—80 °C), mp 129—130 °C, yield 0.5 g (65%). Found: C, 74.09; H, 5.50; N, 7.45%. Calcd for $C_{23}H_{20}N_2S$: C, 74.17; H, 5.41; N, 7.52%.

*1-Methyl-3-[2-(p-methoxyphenyl)-2-(phenylthio)ethyl]-2(1H)-quinoxalinone (**9b**)*: Yellow crystals from pet. ether (40—60 °C), mp 154—155 °C, yield 0.6 g (70%). Found: C, 71.64; H, 5.60; N, 6.97%. Calcd for $C_{24}H_{22}N_2O_2S$: C, 71.62; H, 5.51; N, 6.96%.

*1-Methyl-3-[2-(p-nitrophenyl)-2-(phenylthio)ethyl]-2(1H)-quinoxalinone (**9c**)*: Yellowish crystals from pet. ether (40—60 °C), mp 141—142 °C, yield 0.45 g (55%). Found: C, 66.09; H, 4.57; N, 10.03%. Calcd for $C_{23}H_{19}N_3O_3S$: C, 66.18; H, 4.59; N, 10.07%.

*1-Methyl-3-[2-(p-methoxypenyl)-2-(p-methylphenylthio)ethyl-2(1H)-quinoxalinone (**9d**)*: Yellowish crystals from benzene and pet. ether (40—60 °C) mixture, mp 162—164 °C, yield 0.6 g (75%). Found: C, 72.13; H, 5.82; N, 6.69; S, 7.46%. Calcd for $C_{25}H_{24}N_2O_2S$: C, 72.10; H, 5.81; N, 6.73; S, 7.68%.

*1-Methyl-3-[2-(p-methoxyphenyl)-2-(o-aminophenylthio)ethyl-2(1H)-quinoxalinone (**9e**)*: Yellowish crystals from benzene and pet. ether (60—80 °C) mixture, mp 109—110 °C, yield

Table 8. 1-Methyl-3-[2-(substituted phenyl)-1-alkenyl]-2(1*H*)-quinoxalinones (**11**)

No.	2-Substituent on ethyl	Mp θ_m/°C	Yield %	Mol formula	Found (%)			Calcd (%)		
					C	H	N	C	H	N
11a	CH_3, C_6H_5-	182—183	65	$C_{18}H_{16}N_2O$	78.50	6.07	10.01	78.23	5.84	10.14
11b	CH_3, *p*-BrC_6H_4-	112—113	55	$C_{18}H_{15}N_2OBr$	60.85	4.40	8.02	60.79	4.22	7.88
11c	CH_3, *p*-$CH_3C_6H_4$	213—214	65	$C_{19}H_{18}N_2O$	78.72	6.50	9.44	78.59	6.25	9.65
11d	CH_3, *p*-$CH_3OC_6H_4$-	229—232	70	$C_{19}H_{18}N_2O$	74.59	5.97	9.07	74.49	5.92	9.15
11e	C_6H_5, C_6H_5-	189—190	85	$C_{23}H_{18}N_2O$	81.75	5.50	8.09	81.63	5.36	8.28

a) Crystallized from acetone.

Table 9. 1-Methyl-3-(substituted styryl)-2-(1*H*)-quinoxalinethiones (**12**)

No.	3-Substituent	Mp θ_m/°C	Yield %	Mol formula	Found (%)			Calcd (%)		
					C	H	S	C	H	S
12a	C_6H_5CH=CH-	170 (decomp)	50	$C_{17}H_{14}N_2S$	73.30	5.20	11.50	73.36	5.07	11.50
12b	*p*-$CH_3C_6H_4CH$=CH-	209—210	83	$C_{18}H_{16}N_2S$	73.85	5.53	10.91	73.95	5.52	10.95
12c	*p*-BrC_6H_4CH=CH-	240—241	50	$C_{17}H_{13}N_2SBr$	57.20	3.69	8.97	57.14	3.64	8.96
12d	*p*-$(CH_3)_2NC_6H_4CH$=CH-	273—274	85	$C_{19}H_{19}N_3S$	71.04	5.98	9.97	71.01	5.96	9.96
12e	*p*-$CH_3OC_6H_4CH$=CH-	194—195	75	$C_{18}H_{16}N_2OS$	70.20	5.24	10.40	70.11	5.23	10.38

All compounds crystallized from ethanol, except **12c** and **12d** from benzene. Compounds **12a, b** are black fluorescence, **12d, e** are brown fluorescence, and **12c** is dark green crystals.

0.75 g (75%). Found: C, 69.69; H, 5.60; N, 9.68%. Calcd for $C_{24}H_{23}N_3O_2S$: C, 69.91; H, 5.40; N, 9.79%.

Addition of Mercaptoacetic Acid to 1-Methyl-3-(substituted styryl)-2(1H)-quinoxalinone (8). *General Procedure*: A mixture of 1-methyl-3-(substituted styryl)-2(1*H*)-quinoxalinone (**8**) (0.002 mol) and mercaptoacetic acid (0.002 mol) was heated at 100 °C for 2 h. The yellow oil formed was triturated with pet. ether (40—60 °C) and the products obtained were crystallized from the suitable solvent (Table 7).

Condensation of 1,3-Dimethyl-2(1H)-quinoxalinone (2a) with Alkyl Aryl Ketones and Biaryl Ketones. *General Procedure*: A mixture of 1,3-dimethyl-2(1*H*)-quinoxalinone (**2a**) (0.01 mol) and the appropriate ketone (0.01 mol) was heated under reflux in the presence of anhydrous $ZnCl_2$ (0.5 g) at 180—200 °C for 3 h, the reaction mixture was cooled, extracted with ethanol, filtered and concentrated whereby the corresponding product was obtained as brown crystals by crystallization from ethanol (Table 8).

Synthesis of 1-Methyl-3-(substituted styryl)-2(1H)-quinoxalinethiones (12a—e). *General Procedure*: A mixture of **8** (0.002 mol) and P_2S_5 (0.003 mol) was refluxed in dry pyridine (30 ml) for 5 h. The solvent was evaporated and the residue was treated with dilute acetic acid. The product was filtered and crystallized from the suitable solvent (Table 9).

The author (M. Z. Badr) is indebted to Dr. R. O. Loutfy of Xerox Research Centre of Canada for running of some NMR. spectra.

References

1) R. Pavel, B. Emanuel, S. Juraj, M. Vladimir, and P. Jaromir, Czech. 146,816 (Cl. A Oln), 15 Jan. 1973, Appl. 6157—6170, 09 Sep. 1970.

2) K. Sasse, R. Wegler, H. Schempflug, and H. Jung, Ger. 1, 194, 631 (Cl. A Oln), June 10, 1965, Appl. Nov. 9, 1963.

3) C. W. Hofmann, J. J. Krajeurski, Ph. J. Kotz, J. T. Traxler, and S. S. Ristich, *J. Agric. Food Chem.*, **1**(2), 298 (1971).

4) K. Asano and S. Asai, *Yakugaku Zasshi*, **79**, 567 (1959); *Chem. Abstr.*, **53**, 21979 (1959).

5) D. Bucchini, M. Fiszman, and M. Girard, *Intervirology*, **3**, 281 (1974).

6) I. R. Mandel, U. S. 3, 749, 781 (Cl. 224—251; 261 K), 31 Jul. 1973, Appl. 80,176, 12 Oct. 1970.

7) M. Z. A. Badr, G. M. El-Naggar, H. A. H. El-Sherief, A.E. Abdel-Rahman, and M.F. Aly, *Bull. Chem. Soc. Jpn.*, **56**, 326 (1983).

8) D. C. Morrison, *J. Am. Chem. Soc.* **76**, 4483 (1954).

9) D. C. Morrison and A. Furst, *J. Org. Chem.*, **21**, 470 (1956).

10) G. W. H. Cheeseman, *J. Chem. Soc*, **1955**, 1804.

Asymmetric Reduction of Schiff's Bases with Lithium Aluminium Hydride–Monosaccharide Complexes to Give Optically Active Secondary Amines

Stephen R. Landor, Olatunji O. Sonola,*,† and Austin R. Tatchell
University of West Indies, Kingston, Jamaica
University of California, Berkeley, California, 94720 U.S.A.
Thames Polytechnic, London S.E. 18, U.K.

(Received May 10, 1983)

The asymmetric reduction of selected Schiff's bases (ketimines) with the lithium aluminium hydride–monosaccharide complexes derived from 3-*O*-benzyl-1,2-*O*-cyclohexylidene-α-D-glucofuranose gives optically active secondary amines. The absolute configuration of *N*-(1-phenylethyl)aniline was assigned as *S* by *N*-phenylation of *S*-(−)-1-phenylethylamine and hence all the levo-rotatory secondary amines obtained by this asymmetric reduction are assigned the *S*-configuration.

The asymmetric reduction of ketoximes and their *O*-substituted ether derivatives with the lithium aluminium hydride–monosaccharide complexes has been reported by us to give optically active primary amines.[1] We have now extended these investigations to the reduction of structurally related Schiff's bases (ketimines) to give optically active secondary amines. Prior to this investigation, an asymmetric reduction of ketimines was briefly reported by Cervinka and Suchan[2] who obtained "partially optically active primary amine". The primary amines so obtained were of low optical yields and have known configurations. More recently, Solladie and his coworker[3] described the introduction of a new chiral site on an *N*-chirally substituted imine by stereoselective reduction followed by subsequent hydrogenolysis of the chiral substituent on the nitrogen to give an optically active primary amine.

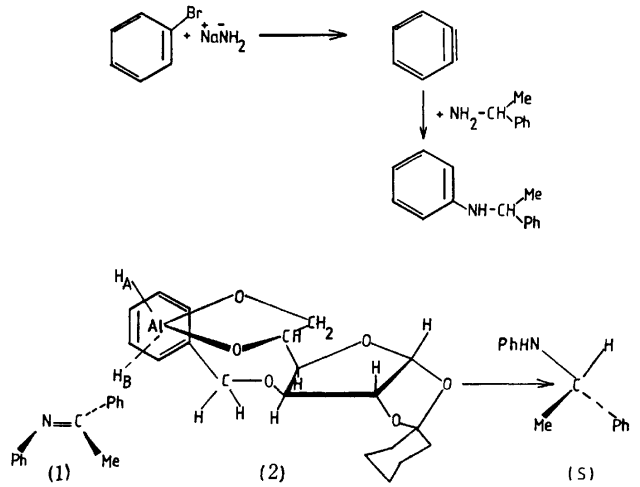

(1) (2) (S)

The reduction of ketimines with lithium aluminium hydride–3-*O*-benzyl-1,2-*O*-cyclohexylidene-α-D-glucofuranose complex (**2**) follows the same pattern as that of the oxime and oxime ethers.[1] A similar mechanism is therefore postulated for the reduction of ketimines and this is shown in **1** and **2**. A preferential hydride transfer of the less shielded H_B to the carbon of the imino group with the phenyl pointing away from the shielding 3-*O*-benzyl group of the monosaccharide derivative is predicted to give optically active secondary amines of the *S*-configuration. The *N*-phenyl group is as remote from the carbohydrate moiety as the tetrahydropyranyloxy group is in the reduction of ketone oxime ethers and, therefore, not likely to play any part in the stereoselective process. The stereoselectivity of the reduction process would thus be determined by the steric and electronic interactions between the *C*-phenyl and alkyl substituents on the ketimines and the 3-*O*-benzyl group of the carbohydrate residue.

Four examples of a homologous series of ketimines were reduced with the lithium aluminium hydride complex **2** (Table 1) and gave optically active secondary amines, all levo-rotatory, which were characterised by IR, NMR, and elemental analysis (Table 2).

The absolute configuration of *N*-(1-phenylethyl)aniline was previously reported by Wittig and Thiele.[4] A confirmation of this configuration was obtained for *N*-(1-phenylethyl)aniline by phenylation *via* the benzyne of (+)- and (−)-1-phenylethylamine and comparison of the products with that obtained from the reduction of the amine. Benzyne, generated by the action of sodamide on bromobenzene in liquid ammonia,[5] reacted with *S*-(−)-1-phenylethylamine[6,7] to give (−)-*N*-(1-phenylethyl)aniline which therefore has the *S*-configuration. This method should give minimum racemisation of the optically active amine and the optical purity of the *N*-(1-phenylethyl)aniline is estimated to be >95%. This value is much greater than the 40% ee reported by Kagan *et al.*[8] The maximum specific rotation obtained was −6.2° which was used to calculate the stereoselectivity of the asymmetric reduction and gave a maximum of excess enantiomer of 23.6% (Table 3).

The three other amines for which the configuration has not been determined previously are now assigned the *S*-configuration on the basis that in our laboratory, the asymmetric reduction with this reagent of 40 compounds comprising ketones, oximes, oxime ethers, and now ketimines has without exception given products with the *S*-configuration.[1,9]

Several methods for the synthesis of ketimines have been reported in the literature.[10] Recently, the condensation of a ketone with a primary aromatic amine in the presence of hydrogen cyanide was briefly reported to give α-amino nitriles in good yields, and these were coverted into the ketimines with methanolic potassium

† Permanent address: Ogun State Polytechnic, P.M.B. 2210, Abeokuta, Nigeria.

Table 1. Reduction of ketimines with the aluminium hydride complex of 3-*O*-benzyl-1,2-*O*-cyclohexylidene-α-D-glucofuranose

Ketimine PhRC=NPh	*N*-(1-Phenylethylidene)-aniline (R=CH_3)			*N*-(1-Phenylpropylidene)-aniline (R=CH_2CH_3)			*N*-(1-Phenylbutylidene)-aniline (R=$CH_3CH_2CH_2$)			*N*-(1-Phenyl-2-methylpropylidene)aniline (R=$(CH_3)_2CH$)		
Secondary amine	*N*-(1-Phenylethyl)aniline[a]			*N*-(1-Phenylpropyl)-aniline[b]			*N*-(1-Phenylbutyl)aniline[c]*			*N*-(1-Phenyl-2-methylpropyl)aniline[d]*		
$LiAlH_4$ (mol)	α_D^{20} / °	% e.e.†		α_D^{20} / °	% e.e.†		α_D^{20} / °	% e.e.		α_D^{20} / °	% e,e.	
0.012	−0.71	11.5	*S*	−1.08	—	*S*††	−1.40	—	*S*††	−1.26	—	*S*††
0.018	−0.98	15.8	*S*	−1.13	—	*S*	−1.54	—	*S*	−1.45	—	*S*
0.025	−1.46	23.6	*S*	−1.54	—	*S*	−1.65	—	*S*	−1.53	—	*S*
0.032	−0.94	15.2	*S*	−1.30	—	*S*	−1.66	—	*S*	−1.54	—	*S*
0.039	−0.66	10.7	*S*	−0.90	—	*S*	−1.30	—	*S*	−1.44	—	*S*
0.045	−0.58	9.4	*S*	−0.76	—	*S*	−1.08	—	*S*	−1.38	—	*S*

a) Bp 142 °C/1.5 mmHg(1 mm Hg≈133.322 Pa); b) Bp 150 °C/1.5 mmHg; c) Mp 51—52 °C; d) Mp 54—55 °C.
*: Rotations determined for chloroform solutions (*ca.* 50%). †: Maximum specific rotation obtained from this work $[\alpha]_D^{20}$ −6.20°; % excess enantiomers. ††: Configurational assignment on the basis of present work.

hydroxide at room temperature.[11]

$$R'COR + PhNH_2 + KCN \xrightarrow{HOAC} RR'C(CN)NHPh \xrightarrow{KOH\text{-}MeOH} RR'C{=}NPh$$

In our laboratory, the elimination of hydrogen cyanide from the α-amino nitrile did not proceed in reasonable yield at room temperature, but excellent yields were obtained when the reaction was carried out under reflux for 1 h. The four examples of homologous series of ketimines used for these asymmetric reductions were synthesized by this method, and their structures confirmed by IR, UV, and NMR spectroscopy and their elemental analyses.

Experimental

Thin layer chromatography of carbohydrate derivates was performed on silica gel with benzene-methanol (98:2) as solvent system and a 1,3-naphthalenediol-phosphoric acid spray for detection. The ester used in the reductions was repeatedly dried over sodium. The purity of the amines was established by GLC on a 5 ft glass column of Carbowax 20 M on Chromosorb W (for the liquid amines), and by several recrystallizations with constant melting points were obtained (in the case of the solid amines). Optical rotations (0.01°) were determined for neat samples unless otherwise stated, with a Stanley photoelectric polarimeter and/or with a Perkin-Elmer 141 polarimeter at 20 °C. NMR spectra were obtained for solutions in deuteriochloroform with Varian A60 and T60 spectrometers, tetramethylsilane being used as internal reference.

Preparation of α-Amino Nitrile. The ketone (0.66 mol) and aniline (6.12 g, 0.06 mol) were dissolved in glacial acetic acid (25 ml). The mixture was gently stirred at 0 °C while portions of solid potassium cyanide (4.3 g, 0.66 mol) were cautiously added. Stirring was continued until a solid crystallized (*ca.* 1 h). The mixture was then cooled and filtered; the solid residue was washed with water (4×100 ml) and light petroleum (bp 40—60 °C; 4×50 ml) and then crystallized from methanol, yields 80—90% ν_{max} 2230 (CN) and 3400 cm^{-1} (NH).

Preparation of Ketimines. The α-amino nitrile (0.03 mol) was dissolved in hot methanol (40 ml). To this a solution of potassium hydroxide (6.7 g, 0.12 mol) in methanol (50 ml) was carefully added and the reaction mixture heated under reflux for 1 h. Water (100 ml) was added to the cooled mixture and the organic material removed by extraction with light petroleum (bp 40—60 °C; 4×50 ml). The combined light petroleum extracts were washed with water (2×100 ml), dried ($MgSO_4$) and the solvent evaporated to give a light yellow oil which was refrigerated. The crude solid material was recrystallized from light petroleum (bp 40—60 °C) to give the pure ketimine; ν_{max} 1640—1650 cm^{-1} (C=N).

Reduction of Ketimines with the Lithium Aluminium Hydride-3-O-benzyl-1,2-O-cyclohexylidene-α-D-glucofuranose Complex. A solution of the glucofuranose (8.8 g, 0.025 mol) in dty ether (50 ml) was added to a measured volume of a standardized ethereal solution of lithium aluminium hydride (*ca.* 18—20 g l^{-1}). The mixture was heated under reflux for 90 min, after which a solution of the ketimine (0.025 mol) in dry ether (20 ml) was added. Heating under reflux was continued for 2.5 h, after which the mixture was cooled, the complex decomposed with water (15 ml) and the precipitated hydroxide filtered off and washed with ether (2×30 ml). The combined filtrate and washings were extracted with dilute hydrochloric acid (3×20 ml) to separate all basic components. The aqueous acid layer was strongly basified (6 M† NaOH) and extracted with ether (3×50 ml) and the extract washed with water (2×30 ml) and dried ($MgSO_4$). Evaporation gave an oily porduct. The optically active secondary amine was isolated by fractional distillation under reduced pressure and characterized by IR, NMR spectroscopy, and elemental analysis; its purity was checked by GLC or by recrystallization in the case of a solid product (Table 2).

Determination of the Absolute Configuration of N-*(1-phenylethyl)-aniline.* Metallic sodium (0.58 g, 0.025 mol) and an excess of liquid ammonia (20 ml) were stirred for 1 h, after which bromobenzene (4 g, 0.025 mol) was added. The resultant dark violet product was further stirred for 1 h, after which 1-phenylethylamine (3.0 g, 0.025 mol) was added dropwise with stirring. Stirring was continued for another 3 h, the reaction mixture was neutralized with dilute hydrochloric acid (3×10 ml) and the aqueous layer strongly basified (6 M NaOH). Work-up gave an oily product which was distilled under reduced pressure and then characterized by IR and NMR spectroscopy; the optical rotation

† 1 M=1 mol dm^{-3}.

Table 2. Physical and analytical data ketimines and *N*-(1-phenylalkyl)anilines

	C_6H_5-C(R)=N-C_6H_5 Chemical shifts (in τ values)		C_6H_5-CH(R)-NH-C_6H_5 Chemical shifts (in τ values)				Bp θ_b / Mp θ_m /°C at 1.5 mmHg	Yield/%	Analyses (%) Found			Calcd		
R	$2\times C_6H_5$	R	$2\times C_6H_5$	H	R	NH			C	H	N	C	H	N
Me	2.0—3.5 (10H, m)	7.38(3H, s, CH_3)	2.63—3.70 (10H, m)	5.60 (1H, dd-CH)	8.60 (3H, d, CH_3)	6.20	142	76	85.25	7.45	7.15	85.30	7.60	7.10
Et	2.0—3.4 (10H, m)	9.0(3H, t, CH_3) 7.45(2H, dd, CH_2)	2.70—3.70 (10H, m)	5.70 (1H, t, -CH)	8.40(2H, dp-CH_2) 9.20(3H, t, CH_3)	6.30	150	80	85.21	7.91	6.45	85.31	8.09	6.60
Pr	2.4—3.6 (10H, m)	9.08(3H, t, CH_3) 8.55(2H, m, CH_2) 8.00(2H, t, CH_2)	2.70—3.70 (10H, m)	5.70 (1H, t, -CH)	8.40(2H, M, CH_2) 8.82(2H, m, CH_2) 9.25(3H, t, CH_3)	6.35	51—52 mp	75	85.12	8.71	6.38	85.35	8.44	6.22
Pr^i	2.6—3.6 (10H, m)	8.80(3H, d, CH_3) 8.60(3H, d, CH_3) 7.05(1H, dd, CH)	2.75—2.60 (10H, m)	5.90 (1H, d, CH)	8.65(1H, m, CH) 9.30(3H, d, CH_3) 9.35(3H, d, CH_3)		54—55 mp	78	85.07	8.75	6.34	85.34	8.44	6.22

Table 3. 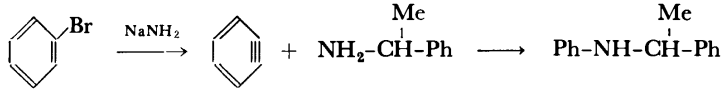

Liq NH_3 (ml)	Na (g)	C_6H_5Br (g)	1-Phenylethylamine : g rotation	*N*-(1-Phenylethyl)aniline	Yield g	Yield %	$[\alpha]_D^{20}$ °	Solvent	Concn %
20	0.58	4.0	3.0 (±)	(±) 140 °C/1.3 mmHg	3.2	64	—	—	—
20	0.58	4.0	3.0 (−) $[\alpha]_D^{20}$ −38.5°*	(−) 142 °C/1.5 mmHg	3.7	74	−6.2	$CHCl_3$	50
20	0.58	4.0	3.0 (+) $[\alpha]_D^{20}$ +38.5*	(+) 142° C/1.5 mmHg	3.4	68	+6.0	$CHCl_3$	50

*: Supplied by E. Merck, Darmstadt.

was determined.

References

1) S. R. Landor, O. O. Sonola, and A. R. Tatchell, *J. Chem. Soc., Perkin Trans. 1*, **1974**, 1902.
2) O. Cervinka, V. Suchan, O. Kotynek, and V. Dudek, *Collect. Czech. Chem. Commun.*, **30**, 2484 (1965).
3) G. Solladie and G. Demailly, *Tetrahedron Lett.*, **1975**, 2471.
4) G. Wittig and U. Thiele, *Justus Liebigs Ann. Chem.*, **726**, 1 (1969).
5) I. Tabushi, K. Okazaki, and R. Oda, *Tetrahedron Lett.*, **1967**, 3827.
6) A. W. Ingeroll, *Org. Synth*, Coll. Voll. II, 503 (1943).
7) W. Leither, *Ber.*, **64**, 2827 (1931).
8) H. B. Kagan, N. Langlois, and T. P. Dang, *J. Organomet. Chem.*, **90**, 353 (1975).
9) S. R. Landor, B. J. Miller, and A. R. Tatchell, *J. Chem. Soc., C*, **1966**, 1822; **1966**, 2280; **1967**, 197.
10) R. W. Layer, *Chem. Rev.* **63**, 498 (1963).
11) J. S. Walia, L. Heindl, H. Lader, and P. S. Walia, *Chem. Ind.*, **1968**, 155.
12) H. Felkin, *Bull. Soc. Chim. Fr.*, **1951**, 347.

Cyclic Carbonates Obtained by Reactions of Alkali Metal Carbonates with Epihalohydrins

Gabriel Rokicki* and Witold Kuran

Faculty of Chemistry, Technical University (Politechnika), Koszykowa 75, 00-662 Warsaw, Poland

(Received July 11, 1983)

A study has been carried out on the reaction of alkali metal carbonates with epihalohydrins in the presence of cation complexing agents *e.g.* crown ethers. 3-Glycidyloxypropylene carbonate was found to be formed as the main product of the reaction of epichlorohydrin with potassium carbonate promoted by 18-crown-6. The effect of various epihalohydrins and alkali metal carbonates on the reaction course was examined. It was found that the reaction of potassium hydrogencarbonate with epichlorohydrin gives 4-hydroxymethyl-1,3-dioxolan-2-one. When the reaction of epihalohydrins with potassium carbonates was carried out in the atmosphere of carbon dioxide the products contained linear carbonate linkage apart from cyclic one. From these results, a plausible mechanism was proposed for the reaction of alkali metal carbonates with epihalohydrins in the presence of crown ethers.

The polycondensation reaction of alkali metal carbonates with α,ω-dihalo compounds in the presence of crown ethers, leading to polycarbonates,[1] prompted to develop studies on the application of alkali metal carbonates for the synthesis of high polymers.

Recently we have shown the possibility of using alkali metal carbonates as substrates for the synthesis of dialkyl carbonates, which when having been subjected to transesterification yielded high-molecular-weight polycarbonates.[2]

From the literature data[3] it results that alkali metal carbonates promoted by crown ethers initiate an anionic polymerization of oxiranes. The presence of carbon dioxide in the polymerization system with propylene oxide was found to stop the polymerization. In this system cyclic propylene carbonate was formed,[3] but in rather low yield.[4]

Recently, we have shown that cyclic carbonates could be obtained in nearly quantitative yield in the reaction of carbon dioxide with oxiranes in the presence of alkali metal halides, *e.g.* potassium iodide and anion-activating agents. Potassium carbonate, however, appeared also to be an efficient catalyst for the above reaction in the case of (halomethyl) oxiranes.[4] On the other hand, the reaction of potassium carbonate with α,ω-dibromo derivatives was reported to produce cyclic carbonates.[5]

In the course of investigations on the polymerization of epihalohydrins by the potassium carbonate–crown ether system, instead of a polymeric product, we found the formation of products containing a 1,3-dioxolan-2-one ring. Thus, in this paper we decided to study the synthesis of cyclic carbonates by the reaction of alkali metal carbonates with epihalohydrins in the presence of cation complexing agents.

Cyclic carbonates were found recently[6] as rather useful monomers for a number of new polymer syntheses.

Results and Discussion

It was found that the reaction of potassium carbonate (**1a**) with epihalohydrin (1-chloro-2,3-epoxypropane (**2a**)) carried out in the presence of 18-crown-6 or benzyltriethylammonium chloride (TEBA) yielded 3-glycidyloxypropylene carbonate [4-(oxiranylmethoxymethyl)-1,3-dioxolan-2-one (**3a**)]. The IR spectrum of the post-reaction mixture did not exhibit any absorption bands characteristic for a linear carbonate linkage.

The reactions of sodium and lithium carbonates in the presence of 15-crown-5 were found also to give **3a** but in lower yield than when **1a** was used (Table 1).

Considering the structure of cyclic carbonate **3a** the following scheme of the reaction of **1a** with **2a** can be proposed.

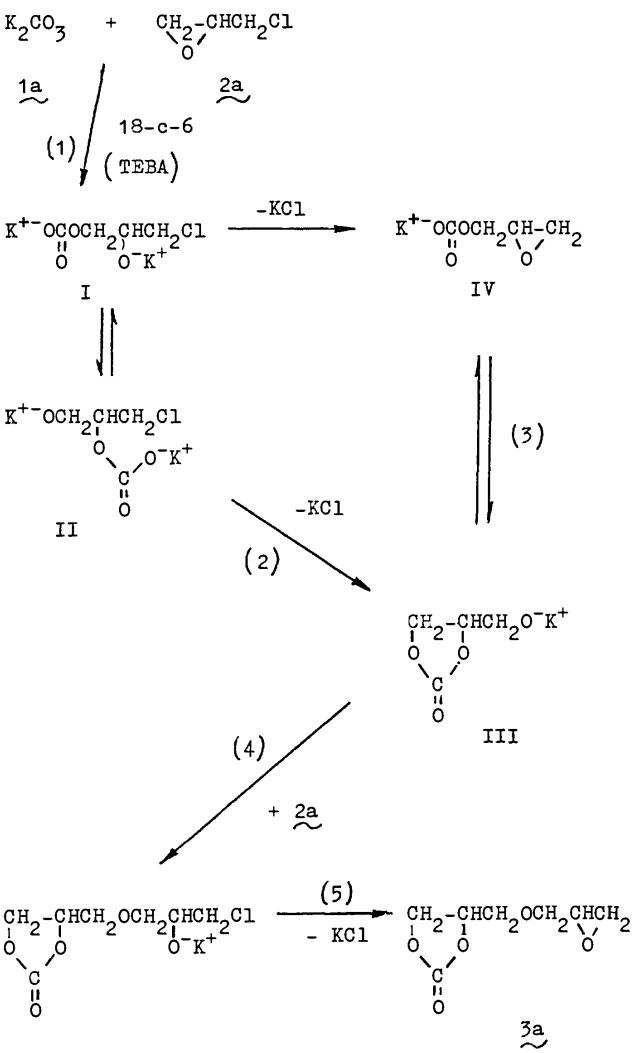

Table 1. The yield of **3a** in reaction of **2a** with alkali metal carbonates[a)]

Alkali metal carbonate	Anion activating agent	Reaction conditions: Molar ratio Carbonate/**2a**	Temp °C	Time h	Yield of **3a** %
K_2CO_3	18-c-6	1 : 4	85	24	53
		1 : 6	85	24	60
		1 : 10	90	24	65
	TEBA	1 : 6	80	20	43
Na_2CO_3	15-c-5	1 : 10	90	22	42
Li_2CO_3		1 : 10	85	24	10
$CaCO_3$	18-c-6	1 : 10	90	24	—

a) See Exptl part.

The carbonate ion, as an active nucleophilic agent when **1a** is complexed by a crown ether, can attack the C_α atom of the oxirane ring according to Eq. 1. The resulting **I** should undergo an intramolecular ester-exchange reaction leading to **II**, which can be followed by a cyclization reaction (Eq. 2) yielding **III**. The intermediate **III** can be also formed according to Eq. 3 involving an intramolecular nucleophilic attack of the carbonate ion on the oxirane ring in **IV**. The alcoholate ion in **III** can undergo reaction with **2a**, being in excess with respect to **1a** in the reaction system, and **3a** is formed as the final product (Eqs. 4 and 5).

When 1-chloro-2-methyl-2,3-epoxypropane (**2b**) was used instead of **2a** to the reaction with **1a**, a cyclic carbonate **3b** of a structure analogous to **3a** was formed (Eq. 6). This indicates that the reactions of substituted epihalohydrins with **1a** give also derivatives with oxirane and 1,3-dioxolan-2-one rings as the main reaction products.

However, in the case of the reaction of **1a** with 1-bromo-2,3-epoxypropane (**2c**) it appeared that this reaction leads to products with linear carbonate linkages besides those with 1,3-dioxolan-2-one ring as it is indicated by the appearance of an infrared absorption band at 1750 cm^{-1} (C=O in a linear carbonate linkage). This absorption band was twice less intense than that at 1803 cm^{-1}, characteristic for carbonyl of 1,3-dioxolan-2-one ring. Taking into account our previous results[7)] of studies on the reaction of **2c** with phenolates, one may consider that in the system studied a nucleophilic attack of a carbonate ion on the carbon atom bonded to a bromine atom is plausible and a linear carbonate linkage can be formed (Eq. 7).

In the course of our studies on the reaction of 4-bromomethyl-1,3-dioxolan-2-one with **1a** also a nucleophilic attack of the carbonate ion on the carbon atom bonded to bromine was shown to occur. As a result the product containing both cyclic and linear carbonate linkages was formed (Eq. 8).

When the reaction of **2a** with **1a**, promoted by a crown ether, was carried out in the presence of small amount of water, the post-reaction mixture was found to contain 4-hydroxymethyl-1,3-dioxolan-2-one (**4a**). The formation of **4a** probably results from the presence of potassium hydrogencarbonate (**1b**) in the above water-containing reaction mixture. **1b** should be formed by basic hydrolysis of carbonate groups (Eqs. 9 and 10).

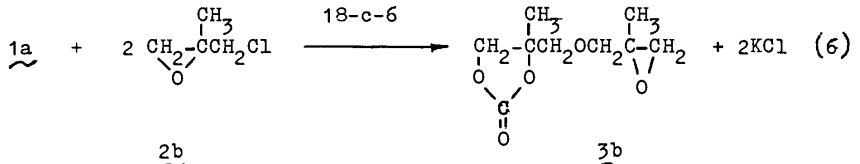

(6)

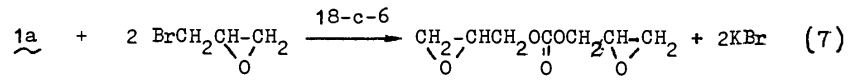

(7)

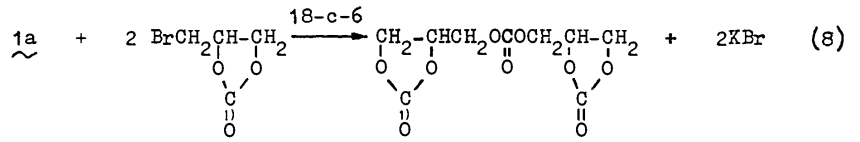

(8)

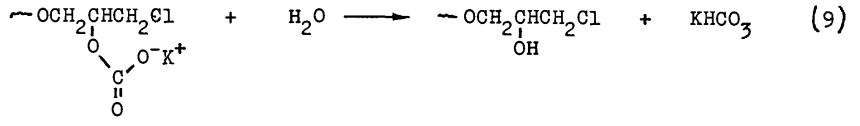

(9)

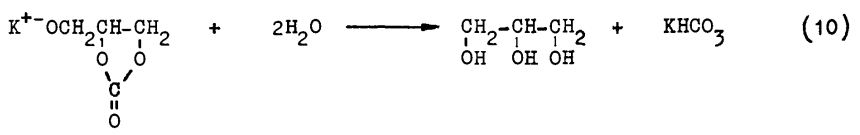

(10)

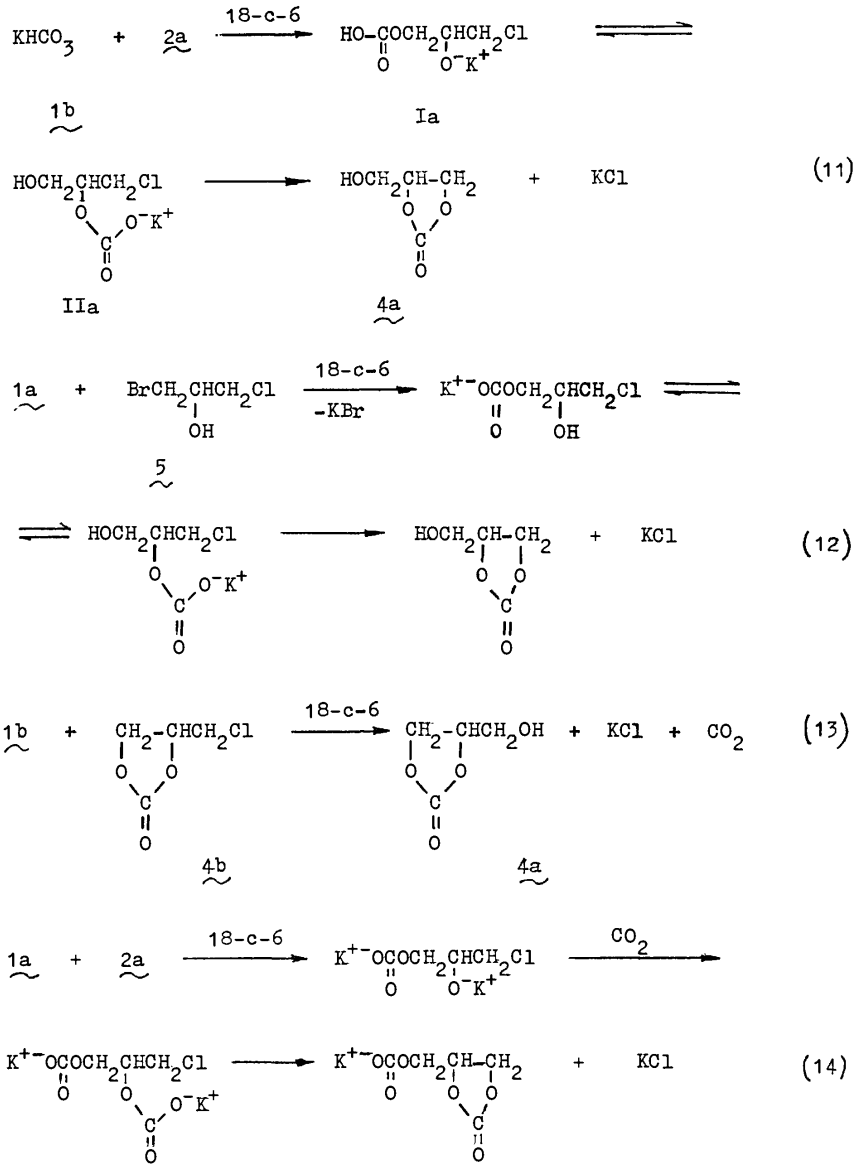

In order to confirm the above suggestion, the reaction of **1b** with **2a** in the presence of a crown ether was studied and it appeared to produce **4a** as the main product. The course of this reaction may be represented by Eq. 11.

Also in this case a nucleophilic attack of the hydrogencarbonate ion on the C_α atom of the oxirane ring of **2a** takes place, analogously as in the reaction of **1a** with **2a**. The resulting **Ia** exists in an equilibrium with the corresponding product of the intramolecular ester exchange **IIa**, which undergoes cyclization to **4a**.

Another reaction between **1a** and 1-bromo-3-chloro-2-propanol with 18-crown-6 was carried out to confirm the proposed pathway of **4a** formation (Eq. 12). Also in this case the product formed appeared to be **4a** but not 5-hydroxy-1,3-dioxan-2-one.

4a was shown to be formed also by heating of **1b** with 4-chloromethyl-1,3-dioxolan-2-one (**4b**) in the presence of a crown ether. Carbon dioxide was found to evolve during this reaction (Eq. 13).

The above data obtained are consistent with the proposed mechanism of the **4a** formation involving **1b** in the system containing **2a**, **1a**, crown ether and slight amount of water (Eqs. 9 and 10).

The reaction of **1a** with **2a** in the presence of a crown ether carried out under carbon dioxide atmosphere was found to yield products containing linear carbonate linkages (IR absorption band 1740 cm^{-1}) apart from the cyclic ones (IR absorption band 1805 cm^{-1}). Thus, this reaction occurs most probably involving the carbon dioxide addition to the secondary alcoholate ion and relatively stable carbonate ion formation followed by the cyclization to the 1,3-dioxolan-2-one ring (Eq. 14).

Such a reaction mechanism could be supported by the course of the reaction of potassium alkyl carbonate **6** with **2a** under the carbon dioxide atmosphere (Eq. 15).

The reactions run according to Eqs. 14 and 15 were accompanied by the addition of carbon dioxide to **2a** yielding **4b**. The mechanism of this addition is discussed elsewhere.[4]

3a, which is the main product of the **1a** with **2a** reaction, was subjected to the reaction with carbon

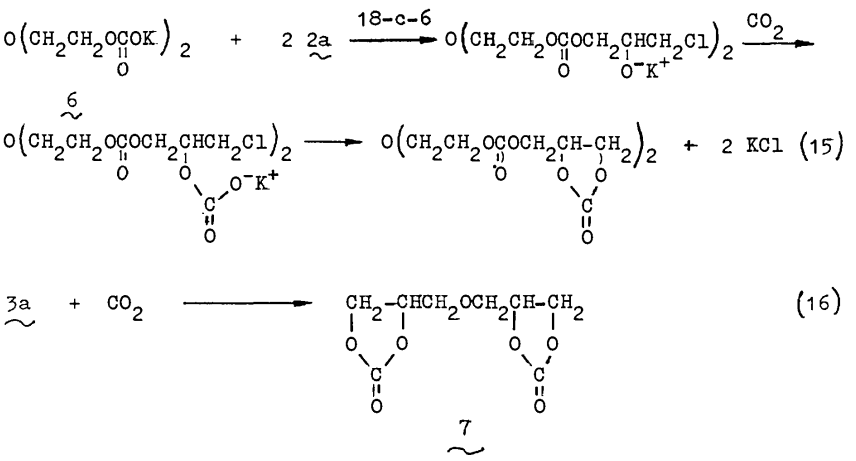

dioxide using the potassium iodide–crown ether catalyst. The product appeared to be bis(2,3-dihydroxypropyl) ether dicarbonate (**7**) (Eq. 16). **7** was obtained also in the reaction of diglycidyl ether with carbon dioxide under analogous reaction conditions.

It seems noteworthy to mention that **3a** appeared to be very well soluble in water in contrast to **7** and **4a**.

Preliminary studies on the reactions of bis(cyclic carbonate) monomers, such as **7**, showed them to be useful for the synthesis of high-molecular-weight polymers like poly(hydroxy ether)s and poly(hydroxy urethane)s.[6]

Experimental

IR spectra were recorded on a Perkin-Elmer 521 spectrometer. The ^{1}H-NMR spectra were recorded with a 100 MHz JEOL NMR spectrometer using TMS as a standard. Elemental analyses of the products were carried out with a Perkin-Elmer model 240 microanalyzer.

The content of epoxy groups in products was determined by titration with a HCl solution in dioxane.

*Reaction of Potassium Carbonate (**1a**) with 1-Chloro-2,3-epoxy propane (**2a**).* A mixture of 13.8 g (0.1 mol) of **1a**, 0.2 g (0.76 mmol) of 18-crown-6 and 55.2 g (0.6 mol) of **2a** was heated at 85 °C within 24 h. After cooling the post-reaction mixture to room temperature KCl precipitate containing unreacted **1a** was filtered off. The filtrate was distilled to give **3a**. Bp 160—166 °C/0.4 mmHg (1 mmHg≈133.322 pa). Yield 10.6 g (60%). $d^{20}=1.2793$ g/cm^3; $n^{20}=1.4605$. Found: C, 48.02; H, 5.73%. Calcd for $C_7H_{10}O_5$: C, 48.27; H, 5.80%. IR: 1805 (C=O of 1,3-dioxolan-2-one ring), 1120 (H_2C-O-CH_2), 910 cm^{-1} (HC—CH_2). Epoxide content—0.57. Molecular weight of **3a** found from epoxide content was 176 (Calcd 174.1).

*Reaction of Potassium Carbonate (**1a**) with 1-Chloro-2-methyl-2,3-epoxypropane (**2b**).* A mixture of 13.8 g (0.1 mol) of **1a**, 0.2 g (0.76 mmol) of 18-crown-6 and 63.6 g (0.6 mol) of **2b** was heated at 90 °C within 24 h. The resultant mixture was cooled and potassium salt precipitate was filtered off. 3-(β-Methylglycidyloxy)-2-methylpropylene carbonate (**3b**) was distilled at 170—174 °C/0.8 mmHg. Yield 10.5 g (52%). Found: C, 52.85; H, 6.78%. Calcd for $C_9H_{14}O_5$: C, 53.45; H, 6.99%. IR: 1800 (C=O of 1,3-dioxolan-2-one ring), 1120 (H_2C-O-CH_2), 955 cm^{-1} (C—CH_2). ^{1}H-NMR: $\delta=1.42$ (3H, CH_3C—C), 1.56 (3H, CH_3C-C-OC-O), 4.28 and 4.68 (2H, CH_2-C-OC-O).

*Reaction of Potassium Carbonate (**1a**) with 1-Bromo-2,3-epoxypropane (**2c**).* A mixture of 7.9 g (0.05 mol) of **1a**, 0.1 g (0.38 mmol) of 18-crown-6 and 34.2 g (0.25 mol) of **2c** was heated at 70 °C within 15 h. After filtration of precipitate the filtrate contained products with linear carbonate linkages beside cyclic carbonate ones. IR: 1803 (C=O of 1,3-dioxolan-2-one ring) and 1750 cm^{-1} (C=O of linear carbonate linkages). Yield 2.8 g (32%) of **3a**.

*Reaction of Potassium Hydrogencarbonate (**1b**) with 1-Chloro-2,3-epoxypropane (**2a**).* A mixture of 10.0 g (0.1 mol) of **1b**, 0.2 g (0.76 mmol) of 18-crown-6 and 27.6 g (0.3 mol) of **1a** was heated at 80 °C under stirring within 36 h. After cooling and filtration of the potassium salt an organic layer was washed with water and **4a** was distilled at 152—160 °C/0.6—0.8 mmHg. Yield 4.83 g (41%). Found: C, 40.57; H, 5.21%. Calcd for $C_4H_6O_4$: C, 40.68; H, 5.03%. IR: 1800 (C=O of 1,3-dioxolan-2-one ring), 3500 cm^{-1} (OH).

*Reaction of Potassium Carbonate (**1a**) with 1-Bromo-3-chloro-2-propanol (**5**).* A mixture of 13.8 g (0.1 mol) of **1a**, 0.2 g (0.76 mmol) of 18-crown-6 and 51.9 g (0.3 mol) of **5** was heated at 80 °C within 24 h. After cooling and filtration of potassium salt precipitate, an organic layer was washed with water and **4a** was distilled at 150—160 °C/0.8 mmHg. Yield 8.8 g (75%). Found: C, 40.52; H, 5.23%. Calcd for $C_4H_6O_4$: C, 40.68; H, 5.13%.

*Reaction of **6** with 1-Chloro-2,3-epoxypropane (**2a**) in the Carbon Dioxide Atmosphere.* In a 50 cm^3 pressure autoclave 1.3 g (7.0 mmol) of the dipotassium salt of diethylene glycol, 10 cm^3 of dioxane, 0.3 g (1.14 mmol) of 18-crown-6 were added under nitrogen. Gaseous carbon dioxide was than introduced to the system under a pressure of 30 atm during 20 min. The carbon dioxide was released and 1.65 g (17.5 mmol) of **2a** was added to the autoclave containing resulting **6** and carbon dioxide introduction under pressure was repeated. The autoclave was then heated at 80 °C within 26 h. After cooling, carbon dioxide was released and the post-reaction mixture was extracted with benzene to remove **4b**. The residue contained a product with linear and cyclic carbonate linkages. IR: 1805 (C=O of 1,3-dioxolan-2-one ring), 1740 cm^{-1} (C=O of linear carbonate linkage).

*Reaction of 3-Glycidyloxypropylene Carbonate (**3a**) with Carbon Dioxide.* In a autoclave 17.4 g (0.1 mol) of **3a**, 0.2 g (1.2 mmol) of KI and 0.1 g (0.38 mmol) of 18-crown-6 were

placed. Carbon dioxide was then introduced to the system under a pressure of 30 atm. The autoclave was heated at 120 °C within 12 h. The post-reaction mixture was washed with water. 20.2 g (93% yield) of **7** was obtained. Mp 62—64 °C. Found: C, 44.84; H, 4.74%. Calcd for $C_8H_{10}O_7$: C, 44.04; H, 4.63%.

Addition Reaction of Carbon Dioxide to Diglycidyl Ether (8) In a autoclave 13.0 g (0.1 mol) of **8**, 0.2 g (1.2 mmol) of KI and 0.1 g (0.38 mmol) of 18-crown-6 were placed.Carbon dioxide was then introduced to the system under a pressure of 30 atm and the autoclave was heated at 120 °C within 14 h. After cooling, carbon dioxide was released and the reaction product was washed with water. 21.1 g (97% yield) of **7** was obtained. Mp 62—63 °C. Found: C, 43.97; H, 4.71%. Calcd for $C_8H_{10}O_7$: C, 44.04; H, 4.63%.

The authors wish to thank the Polish Academy of Sciences for financial support within the programme MR-I-31.

References

1) K. Soga, Y. Toshida, S. Hosoda, and S. Ikeda, *Makromol. Chem.*, **178**, 2747 (1977).
2) G. Rokicki, J. Pawlicki, and W. Kuran, *Polym. J.*, **14**, 847 (1982).
3) H. Koinuma, K. Naito, and H. Hirai, *Makromol. Chem. Rapid Commun.*, **1**, 493 (1980).
4) G. Rokicki, W. Kuran, and B. Pogorzelska-Marciniak, *Mh. Chem.*, **115**, 205 (1984).
5) K. Soga, S. Hosoda, and S. Ikeda, *J. Polym. Sci., Polym. Chem. Ed.*, **17**, 517 (1979).
6) G. Rokicki, in preparation.
7) G. Rokicki, W. Kuran, and A. Nowiński, *Makromol. Chem.*, **179**, 1661 (1978).

Reactions of 2-Diazo-1,2-Diphenylethanone and Diphenyldiazomethane with Ketohydrazones

Girija Shankar Singh, Surendra Bahadur Singh, and Kailash Nath Mehrotra*

Department of Chemistry, Banaras Hindu University, Varanasi-221 005, India

(Received August 30, 1983)

The reactions of 2-diazo-1,2-diphenylethanone (**1**) with ketohydrazones (**3a—c**) in equimolecular ratio yield (diphenylacetyl)hydrazones (**4a—c**) of the corresponding benzophenones which on further treatment with **1** in equimolecular ratio leads to 1-diphenylacetylazo-1,1,3,3-tetraaryl-2-propanones (**5a—c**). The product **5a** is also obtained in the reaction of **1** with benzophenone hydrazone (**3a**) in 2 : 1 molecular ratio. The bis(acetylacetonato)copper(II)-catalyzed reaction of **1** and also of diphenyldiazomethane (**2**) with ketohydrazones (**3**) affords ketazines (**6**). The mechanistic route for the formation of products is discussed.

The thermal decomposition of 2-diazo-1,2-diphenylethanone (**1**) in the presence of amines has been observed to yield diphenylacetamides.[1] Using bis(acetylacetonato)copper(II) as a catalyst in the above reaction the products formed are benzilmonoimines.[1] Copper powder,[2] salts,[3] and complexes[4] have been employed earlier as these are known to prevent Wolff rearrangement of carbenes to ketenes in the decomposition of α-diazo ketones. Bis(acetylacetonato)copper(II)-catalyzed decomposition of diphenyldiazomethane (**2**) in the presence of primary amines gives benzophenone (*N*-substituted imines).[5] The reaction of **1** with *N*-substituted imines has been reported to yield 2-azetidinones[6] which are also formed in the reaction of diphenylketene with fluorenone acetyl (or benzoyl) hydrazones.[7] The thermal decomposition of **1** in the presence of monoanils of benzil has been observed to yield spiro-2-azetidinones.[8] The reaction of **1** with 1,1-diphenylmethanimine has been reported to form a 2-azetidinone derivative.[9] We now report the thermal decomposition of 2-diazo-1,2-diphenylethanone (**1**) in the presence of ketohydrazones (**3a—c**) to give (diphenylacetyl) hydrazones (**4a—c**) of the corresponding benzophenones, these on further reaction with **1** yield 1-diphenylacetylazo-1,1,3,3-tetraaryl-2-propanones (**5a—c**). In each step the reacting species is diphenylketene. The reaction between **1** and **3a** in 2 : 1 molecular ratio also gives the product **5a**. The bis(acetylacetonato)copper(II)-catalyzed decomposition of **1** and also of diphenyldiazomethane (**2**) in the presence of ketohydrazones **3** form ketazines **6a—g** in which benzoylphenylcarbene and diphenylcarbene, respectively, are the reacting species.

Results and Discussion

An equimolecular mixture of 2-diazo-1,2-diphenylethanone (**1**) and benzophenone hydrazone (**3a**) was heated to reflux in dry benzene for 8 h under a stream of nitrogen. The reaction product was separated by fractional crystallization from ethanol; it consisted of benzophenone(diphenylacetyl)hydrazone (**4a**). The structural assignment of **4a** was made on the basis of its analytical and spectral data.

Similar treatment of hydrazones **3b** and **3c** gave (diphenylacetyl)hydrazones **4b** and **4c**, respectively, (identified on the basis of their analytical and spectral data).

Treatment of compounds **4a—c** with **1** in equimolecular ratio gave 1-diphenylacetylazo-1,1,3,3-tetraaryl-2-propanones (**5a—c**) characterized on the basis of their analytical and spectral data. The product 1-diphenylacetylazo-1,1,3,3-tetraphenyl-2-propanone(**5a**) was also obtained in the reaction of **1** with **3a** in 2 : 1 molecular ratio. In the above reaction, benzophenone (diphenylacetyl)hydrazone (**4a**) seems to be an intermediate as shown in Scheme 1.

The product mixture, obtained from the bis(acetylacetonato)copper(II)-catalyzed reaction of **1** with **3a** in dry benzene, was separated by elution chromatography and crystallized from ethanol; it gave 2-diphenylmethylenehydrazono-1,2-diphenylethanone (**6a**). The structure of **6a** was assigned on the basis of analytical and spectral data.

Similar treatment of **1** with hydrazones **3b—f** gave 2-diarylmethylenehydrazono-1,2-diphenylethanones(**6b—f**) identified on the basis of their analytical and spectral data. Authentic samples of the products **6a—f** were prepared following the reported method[10] for comparison (analytical and spectral data).

When diphenyldiazomethane (**2**) was allowed to react with benzophenone hydrazone (**3a**), in an analogous manner, a yellow solid was obtained which was identified as benzophenone azine (**6g**) on the basis of its analytical and spectral data and also comparison (IR, NMR, and mp) with an authentic sample, prepared according to the method reported.[11]

Similar treatment of **2** with benzil monohydrazone (**3d**) afforded yellow crystalline product, characterized as ketazine **6a** on the basis of its analytical and spectral data.

Thermal decomposition of **1** may lead to benzoylphenylcarbene which has been known to undergo Wolff rearrangement to give diphenylketene[12] (Scheme 1). The products **4a—c** arise through a proton transfer from the zwitterionic intermediate **A**, formed by the addition of diphenylketene to hydrazones **3a—c**. A similar zwitterionic intermediate has been proposed earlier in the reaction of diphenylketene with *N*-benzylideneaniline to give *N*-phenylimidate.[13] Addition of a second molecule of diphenylketene to compounds **4a—c** gives rise to products **5a—c** through a proton transfer from an intermediate **B**. A similar intermediate has been proposed earlier in the reaction of benzenediazonium ion with aldehyde arylhydrazones to give bis(arylazo)methanes.[14]

The proton shift in **B** appears to be more feasible than the cyclization to β-lactams due to steric factors (pre-

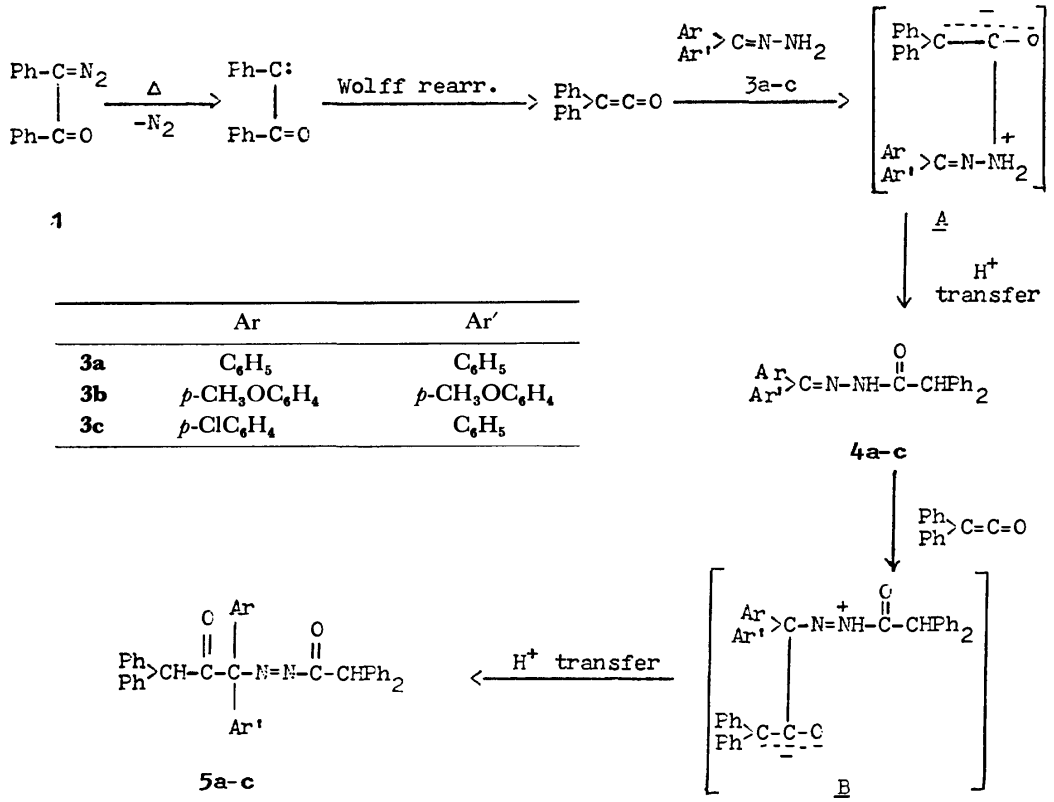

	Ar	Ar′
3a	C_6H_5	C_6H_5
3b	p-$CH_3OC_6H_4$	p-$CH_3OC_6H_4$
3c	p-ClC_6H_4	C_6H_5

Scheme 1.

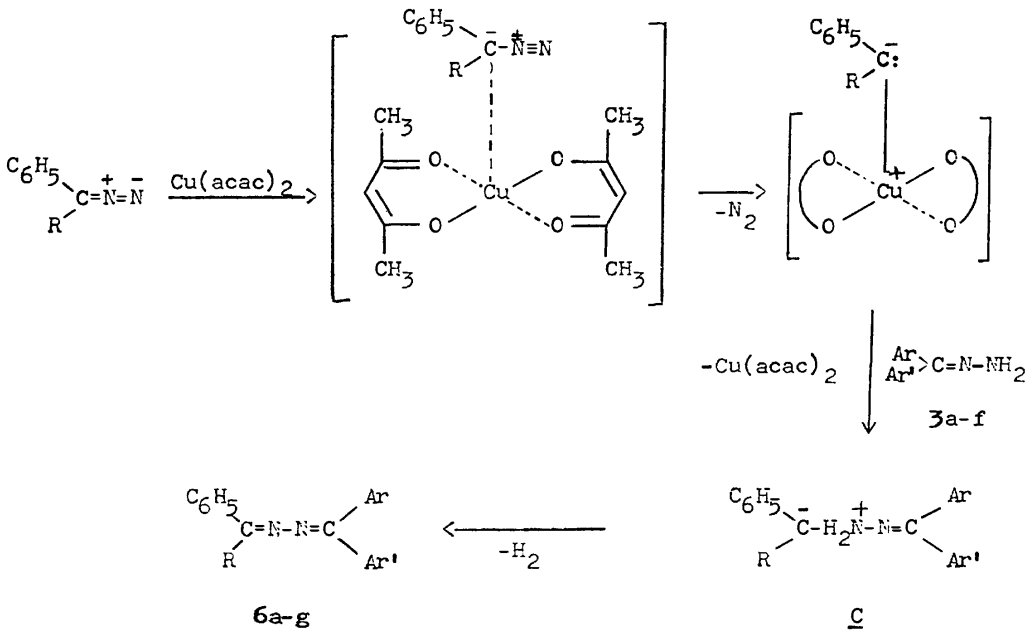

Scheme 2.

	R	Ar	Ar′	Yield/%
6a	COC_6H_5	C_6H_5	C_6H_5	88
6b	COC_6H_5	p-$CH_3OC_6H_4$	p-$CH_3OC_6H_4$	52
6c	COC_6H_5	p-ClC_6H_4	C_6H_5	55
6d	COC_6H_5	C_6H_5	COC_6H_5	92
6e	COC_6H_5	p-$CH_3OC_6H_4$	$COC_6H_4OCH_3(p$-)	71
6f	COC_6H_5	p-$CH_3C_6H_4$	$COC_6H_4CH_3(p$-)	85
6g	C_6H_5	C_6H_5	C_6H_5	60

sence of four bulky aryl groups on the terminal carbon atoms in **B**). However, in the presence of bis(acetylacetonato)copper(II), the Wolff rearrangement of the carbene is prevented[4] (Scheme 2) and in this case a carbene-copper complex is formed.[15] The respective carbenes from the complexes react with ketohydrazones to give ketazines **6a—g** through an intermediate **C**, formed by the interaction of carbenes with N–H bond of hydrazones.

Experimental

Melting points have been determined on a Büchi apparatus (capillary method) and are uncorrected. The ultraviolet spectra were obtained in 95% ethanol on a Carry-14 spectrophotometer. The infrared spectra were recorded in nujol mull on a Perkin-Elmer 720 spectrophotometer. The PMR spectral data were obtained on a Varian A-60D spectrometer in $CDCl_3$ using TMS as internal standard.

Materials. Benzil, 4,4-dimethoxybenzil, 4,4'-dimethylbenzil, and bis(acetylacetonato)copper(II) were obtained from EGA chemicals, West Germany; benzophenones and hydrazine hydrate from BDH, India; 2-diazo-1,2-diphenylethanone,[16] diphenyldiazomethane,[17] benzophenone hydrazones,[18] and benzil monohydrazones[19] were prepared according to reported methods and characterised on the basis of their analyses and spectral data.

*Preparation of Benzophenone (Diphenylacetyl)hydrazones **4a—c**. General Procedure*: A mixture containing 2-diazo-1,2-diphenylethanone (**1**) (0.01 mol) and hydrazones **3a—c** (0.01 mol) in 80 ml of dry benzene (thiophene free) in a 250 ml three necked round bottomed flask equipped with a condenser and a mercury trap was heated to reflux for 8 h under a stream of nitrogen and kept overnight at room temperature. The solvent was removed on a rotatory evaporator and residual material was triturated with ethanol. The solid obtained was recrystallized from ethanol to afford the products.

*Benzophenone (Diphenylacetyl)hydrazone (**4a**).* A yield of 80% was obtained, mp 149 °C. UV (EtOH): 290 nm; IR (Nujol): 3325 (N–H); 1690 (C=O) and 1605 cm^{-1} (C=N); NMR ($CDCl_3$) δ=8.85 (s, 1H, NH, D_2O exchangeable), 7.33 (m, 20H, aromatic protons) and 6.17 (s, 1H, CH). Found: C, 82.82; H, 5.84; N, 6.85%. Calcd for $C_{27}H_{22}N_2O$: C, 83.08; H, 5.64; N, 7.18%.

*4,4'-Dimethoxybenzophenone (Diphenylacetyl)hydrazone (**4b**).* A yield of 53% was obtained, mp 119 °C. UV (EtOH): 298 nm; IR (Nujol): 3280 (N–H); 1660 (C=O) and 1605 cm^{-1} (C=N); NMR ($CDCl_3$) δ=9.38 (s, 1H, NH, D_2O exchangeable), 7.33 (m, 18H, aromatic protons), 6.25 (s, 1H, CH) and 3.83 and 3.78 (a pair of singlet, 6H, two OCH_3 protons). Found: C, 77.27; H, 5.91; N, 6.36%. Calcd for $C_{29}H_{26}N_2O_3$: C, 77.31; H, 5.77; N, 6.22%.

*4-Chlorobenzophenone (Diphenylacetyl)hydrazone (**4c**).* A yield of 52% was obtained, mp 99 °C. UV (EtOH): 290 nm; IR (Nujol): 3280 (N–H): 1660 (C=O) and 1600 cm^{-1} (C=N); NMR ($CDCl_3$) δ=8.08 (s, 1H, NH, D_2O exchangeable), 7.20 (m, 19H, aromatic protons) and 6.00 (s, 1H, CH). Found: C, 76.10; H, 5.07; N, 6.66%. Calcd for $C_{27}H_{21}N_2OCl$: C, 76.32; H, 4.94; N, 6.59%.

*Preparation of 1-Diphenylacetylazo-1,1-diaryl-3,3-diphenylpropanones **5a—c**. General Procedure*: A similar procedure was used as described above for the preparation of **4a—c** taking 0.01 mol of **1** and 0.01 mol of **4a—c**.

*1-Diphenylacetylazo-1,1,3,3-teraphenyl-2-propanone (**5a**).* A yield of 71% was obtained, mp 177 °C. UV (EtOH): 250 nm; IR (Nujol): 1670 (C=O) and 1600 cm^{-1} (N=N); NMR ($CDCl_3$) δ=7.40 (m, 30H, aromatic protons), 5.83 (s, 1H, -CHCON=N) and 5.12 (s, 1H, CHCOC). Found: C, 83.87; H, 5.31; N, 5.02%. Calcd for $C_{41}H_{32}N_2O_2$: C, 84.25; H, 5.48; N, 4.79%.

*1-Diphenylacetylazo-1,1-bis(4-methoxyphenyl)-3,3-diphenyl-2-propanone (**5b**).* A yield of 50% was obtained, mp 140 °C. UV (EtOH): 238 nm; IR (Nujol): 1665 (C=O) and 1600 cm^{-1} (N=N); NMR ($CDCl_3$) δ=6.70 (m, 28H, aromatic protons), 5.53 (s, 1H, CHCON=N-), 4.83 (s, 1H, CHCOC) and 3.66 (s, 6H, two OCH_3 protons). Found: C, 80.45; H, 5.90; N, 4.29%. Calcd for $C_{43}H_{36}N_2O_4$: C, 80.12; H, 5.59; N, 4.34%.

*1-Diphenylacetylazo-1-(4-chlorophenyl)-1,3,3-triphenyl-2-propanone (**5c**).* A yield of 51% was obtained, mp 148 °C. UV (EtOH); 248 nm; IR (Nujol): 1670 (C=O) and 1600 cm^{-1} (N=N); NMR ($CDCl_3$) δ=7.20 (m, 29H, aromatic protons), 5.76 (s, 1H, $CHCON_2$) and 5.01 (s, 1H, CHCOC). Found: C, 79.58; H, 5.04; N, 4.26%. Calcd for $C_{41}H_{31}N_2O_2Cl$: C, 79.54; H, 5.01; N, 4.52%.

*Preparation of 1-Diphenylacetylazo-1,1,3,3-tetraphenyl-2-propanone (**5a**) from **1** and **3a**.* A yield of 52% was obtained by using a similar procedure as described above by taking **1** and **3a** in 2:1 molecular ratio.

*Preparation of Ketazines **6a—g**. General Procedure*: To a suspension containing 1 m mol of bis(acetylacetonato) copper(II) in 30 ml of dry benzene(thiophene free), heated under reflux with stirring in a 250 ml three necked round bottom flask equipped with a condenser and a mercury trap, a solution containing 0.01 mol of **1** and 0.01 mol of the hydrazones **3a—f** in 80 ml of dry benzene (thiophene free) was slowly added over a period of 3 h from a pressure equalizing funnel under a stream of nitrogen. The contents were heated to reflux for additional 4—6 h and kept overnight at room temperature. The reaction mixture was passed through a neutral alumina (10g, 1.2 cm × 10 cm^2) column and the products were eluted with benzene leaving the copper salt in column. The solvent was evaporated under reduced pressure and the residual material was triturated with ethanol to afford the products.

Similar procedure was adopted for the preparation of ketazines **6g** and **6a** by the reaction of diphenyldiazomethane (**2**) with keto hydrazones **3a** and **3d** respectively.

*2-Diphenylmethylene hydrazono-1,2-diphenylethanone (**6a**).* A yield of 88% was obtained, mp 129 °C. UV (EtOH) : 255, 315 nm; IR (Nujol): 1670 (C=O) and 1600 cm^{-1} (C=N-N=C); NMR ($CDCl_3$) δ=8.00 (m, H, aromatic protons) and 7.38 (m, H, aromatic protons). Found: C, 83.62; H, 4.92; N, 7.39%. Calcd for $C_{27}H_{20}N_2O$: C, 83.48; H, 5.19; N, 7.21%.

*2-[Bis(4-methoxyphenyl)methylenehydrazono]-1,2-diphenylethanone (**6b**).* A yield of 52% was obtained, mp 95 °C. UV (EtOH): 252, 295 nm; IR (Nujol): 1670 (C=O) and 1600 cm^{-1} (C=N-N=C); NMR ($CDCl_3$) δ=8.10 (m, 2H, aromatic protons), 7.30 (m, 16H, aromatic protons) and 3.96 and 3.81 (two s, 6H, two OCH_3 protons). Found: C, 77.60; H, 4.97; N, 6.14%. Calcd for $C_{29}H_{24}N_2O_3$: C, 77.67; H, 5.34; N, 6.25%.

*2-(4-Chloro-α-phenylbenzylidenehydrazono)-1,2-diphenylethanone (**6c**).* A yield of 55% was obtained, mp 114 °C. UV (EtOH): 255, 315 nm; IR (Nujol): 1670 (C=O) and 1600 cm^{-1} (C=N-N=C); NMR ($CDCl_3$) δ=7.66 (m, H, aromatic protons) and 7.13 (m, H, aromatic protons). Found: C, 76.80; H, 4.75; N, 6.79%. Calcd for $C_{27}H_{19}N_2OCl$: C, 76.68; H, 4.49; N, 6.62%.

*2-(α-Benzoylbenzylidenehydrazono)-1,2-diphenylethanone (**6d**).* A yield of 92% was obtained, mp 201 °C. UV (EtOH): 255, 315 nm; IR (Nujol): 1680 (C=O) and 1601 cm^{-1} (C=

N-N=C); NMR ($CDCl_3$) δ=7.99 (m, H, aromatic protons) and 7.45 (m, H, aromatic protons). Found: C, 80.76; H, 4.86; N, 6.79%. Calcd for $C_{28}H_{20}N_2O_2$: C, 80.76; H, 4.80; N, 6.73%.

*2-[4-Methoxy-α-(4-methoxybenzoyl)benzylidene hydrazono]-1,2-diphenyl-ethanone (**6e**).* A yield of 71% was obtained, mp 131 °C. UV (EtOH): 255, 320 nm; IR (Nujol): 1660 (C=O) and 1601 cm^{-1} (C=N-N=C); NMR ($CDCl_3$) δ=7.92 (m, 4H, aromatic protons), 7.13 (m, 14H, aromatic protons) and 3.83 and 3.72 (two s, 6H, two OCH_3 protons) Found: C, 75.54; H, 5.10; N, 6.03%. Calcd for $C_{30}H_{24}N_2O_4$: C, 75.62; H, 5.08; N, 5.88%.

*2-[4-Methyl-α-(4-methylbenzoyl)benzylidenehydrazone]-1,2-diphenylethanone (**6f**).* A yield of 85% was obtained, mp 151 °C. UV (EtOH): 255, 320 nm; IR (Nujol): 1670 (C=O) and 1601 cm^{-1} (C=N-N=C): NMR ($CDCl_3$) δ=7.90 (m, 4H, aromatic protons), 7.25 (m, 14H, aromatic protons), and 2.33 and 2.20 (two s, 6H, two CH_3 protons). Found: C, 81.10; H, 5.46; N, 6.22%. Calcd for $C_{30}H_{24}N_2O_2$: C, 81.06; H, 5.44; N, 6.30%.

*Benzophenone azine (**6g**).* A yield of 60% was obtained, mp 161 °C. UV (EtOH): 275, 310 nm; IR (Nujol): 1600 cm^{-1} (C=N-N=C); NMR ($CDCl_3$) δ=7.33 (m, H, aromatic protons). Found: C, 86.58; H, 5.49; N, 7.75%. Calcd for $C_{26}H_{20}N_2$: C, 86.66; H, 5.56; N, 7.78%.

*2-Diphenylmethylene hydrazono-1,2-diphenylethanone (**6a**).* A yield of 75% was obtained in the reaction of **2** with ketohydrazone **3d**, mp 129 °C, mmp 129 °C. The IR spectrum was superimposable to that of the product described above.

We are thankful to Professor B. M. Shukla for providing the facilities and to C. S. I. R., New Delhi, for grant of a fellowship to G. S. S.

References

1) S. B. Singh and K. N. Mehrotra, *Can. J. Chem.*, **59**, 2475 (1981).
2) P. Yates, *J. Am. Chem. Soc.*, **74**, 5376 (1952).
3) J. L. E. Erickson, J. M. Dechary, and M. R. Kesling, *J. Am. Chem. Soc.*, **73**, 5301 (1951).
4) M. Takebayashi, T. Ibata, H. Kohara, and B. H. Kim, *Bull. Chem. Soc. Jpn.*, **40**, 2392 (1967).
5) K. N. Mehrotra and G. S. Singh, *Indian J. Chem., Sect.B*, **21**, 672 (1982).
6) S. B. Singh and K. N. Mehrotra, *Bull. Chem. Soc. Jpn.*, **54**, 1838 (1981).
7) E. Fahr, K. Doppert, and Konigsdorfer, *Tetrahedron*, **23**, 1379 (1967).
8) S. B. Singh and K. N. Mehrotra, *Can. J. Chem.*, **60**, 1901 (1982).
9) K. N. Mehrotra, S. B. Singh, and K. N. Singh, *Indian J. Chem., Sect.B*, **21**, 146 (1982).
10) O. Gerhardt and H. Bodenkueture, *Monatsh*, **41**, 199 (1920); *Chem. Abstr.* **14**, 3409 f (1920).
11) D. B. Mobbs and H. Suschetzky, *J. Chem. Soc., C.* **1971**, 175.
12) V. Frangen, *Ann.*, **614**, 31 (1958).
13) W. Jugelt and D. Schmidt, *Tetrahedron*, **25**, 969 (1969).
14) A. F. Hegarty, "*The Chemistry of Hydrazo, Azo and Azoxy Groups*", ed by S. Patai, Interscience, New York (1975), Vol. II, p. 669.
15) H. Nozaki, H. Takaya, S. Moriuti, and R. Noyori, *Tetrahedron*, **24**, 3655 (1968).
16) C. D. Nenitzescu and E. Solomonica, *Org. Synth.*, Coll. Vol. II, 496 (1950).
17) M. Fieser and E. Fieser, "*Reagent for Organic Synthesis*," John Willey, & Sons New York (1966), Vol. I, p. 338.
18) R. Baltzly, R. B. Mehta, P. B. Russel, R.E. Brooks, E. M. Grivsky, and A. M. Steinberg, *J. Org. Chem.*, **26**, 3669 (1961).
19) L. I. Smith and H. H. Hoehn, *Org. Synth.*, Coll. Vol. III, 356 (1955).

Equilibria in the Aqueous Ternary System Containing Na^+, $CH_3CO_2^-$, and $P_2O_7^{4-}$ between 38 and 85°C

Takahiro WADA,* Fumiko YOKOTANI, and Yoshihiro MATSUO
Central Research Laboratory, Matsushita Electric Industrial Co. Ltd., 1006 Kadoma, Osaka, 571
(Received August 29, 1983)

Synopsis. The ternary system CH_3CO_2Na-$Na_4P_2O_7$-H_2O was investigated between 38 and 85 °C. No double salt occurs in this temperature range. The saturated CH_3CO_2Na solutions can contain only small amount of $Na_4P_2O_7$. The CH_3CO_2Na solutions have a very strong dehydrating influence on $Na_4P_2O_7 \cdot 10H_2O$. So, the lowest formation temperature of anhydrous $Na_4P_2O_7$ is about 47 °C.

In an earlier paper,[1] we have reported that the addition of a small amount of sodium pyrophosphate decahydrate to sodium acetate solutions is very effective for the crystal nucleation of sodium acetate trihydrate from the solutions. Subsequently, we studied the influence of preheating on crystallization of sodium acetate trihydrate from the aqueous solution with addition of a small amount of sodium pyrophosphate decahydrate and proposed an adsorption model to account for the crystal nucleation catalytic effect.[2] To complete the investigation, knowledge is required of the ternary system sodium acetate-sodium pyrophosphate-water.

The phase diagrams of the binary systems sodium acetate-water and sodium pyrophosphate-water, based on the data from Seidell's compilation[3] are shown in Fig. 1. In this figure, W_a and W_b are the mass fraction of sodium acetate and sodium pyrophosphate respectively.

This paper reports the results from the investigation of sodium pyrophosphate together with sodium acetate aqueous solution.

Experimental

Sodium acetate trihydrate, anhydrous sodium acetate, and sodium pyrophosphate decahydrate were guaranteed grade reagents. Weighed quantities of reagents and water were placed in a glass vessel equipped with a stirrer bar. The glass vessel was sealed and immersed in a water bath, whose temperature was controlled within ±0.5 °C. After the sample was stirred at a determined temperature for 6 h, the supernatant solution was pipetted off through the filter.

The pyrophosphate ion concentration was measured colorimetrically. Concentrated nitric acid was added in the dilute supernatant solution, and heated at 80 °C for about 1 h in order to decompose a pyrophosphate ion into two orthophosphate ions. Dilute sulfuric acid was further added. When ammonium molybdate aqueous solution was introduced into the solution, a yellow ammonium molybdophosphate precipitate was deposited. The precipitate was extracted with isobutyl methyl ketone. The extract was dried over anhydrous sodium sulfate. The absorbance of the extract was measured at 400 nm.

The supernatant solution was also dried at 120 °C in an oven and the total salt concentration was determined. The sodium acetate concentration was caluculated from the difference in concentration between the total salts and sodium pyrophosphate. The residual solid, which was in equilibrium with the saturated solution was separated and identified by X-ray diffraction. The solution in equilibrium with two solid phases was confirmed by analyzing the solution added by these solids.

Results

In the ternary system sodium acetate-sodium pyrophosphate-water, five isotherms between 38 and 85 °C are shown in Table 1. The solubilities of the binary systems, sodium acetate-water and sodium pyrophosphate-water, which are determined in the present ex-

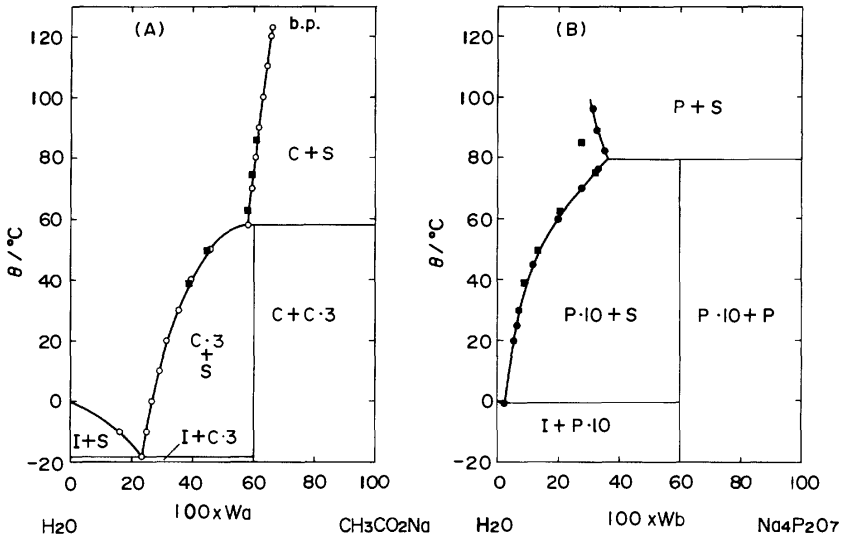

Fig. 1. Phase diagram of the binary systems, CH_3CO_2Na-H_2O (A) and $Na_4P_2O_7$-H_2O (B). Symbols: I=ICE, C=CH_3CO_2Na, C·3=$CH_3CO_2Na \cdot 3H_2O$, P=$Na_4P_2O_7$, P·10=$Na_4P_2O_7 \cdot 10H_2O$, S=Solution.
○: The data obtained by Green,[4] ●: the data obtained by Menzel and Gabler,[5] and Menzel and Sieg,[6] ■: the data obtained by the present experiment.

TABLE 1. ISOTHERMS OF THE TERNARY SYSTEM CH_3CO_2Na–$Na_4P_2O_7$–H_2O AT 38, 50, 62, 75, AND 85 °C

θ/°C	Solution 100×W_a[a]	Solution 100×W_b[b]	Solid[c] phase
38	0	8.5	P·10
	5.5	3.1	P·10
	11.1	1.1	P·10
	16.3	0.54	P·10
	21.0	0.28	P·10
	25.6	0.18	P·10
	29.9	0.14	P·10
	34.0	0.11	P·10
	37.9	0.10	P·10
	37.9	0.08	P·10+C·3
	38.5	0	C·3
50	0	12.9	P·10
	6.5	4.9	P·10
	13.4	1.6	P·10
	19.2	0.73	P·10
	25.0	0.47	P·10
	29.7	0.31	P·10
	34.0	0.24	P·10
	37.3	0.22	P·10+P
	41.6	0.10	P
	45.5	0.06	P+C·3
	45.4	0	C·3
62	0	20.4	P·10
	9.7	6.3	P·10
	19.5	2.1	P·10
	21.4	1.3	P·10+P
	24.7	1.1	P
	29.3	0.73	P
	35.5	0.24	P
62	39.9	0.10	P
	46.4	0.04	P
	51.3	0.03	P
	58.0	0.02	P+C
	58.2	0	C
75	0	31.7	P·10
	2.5	26.0	P·10
	4.8	20.6	P·10+P
	9.4	11.1	P
	20.2	2.4	P
	29.3	0.55	P
	36.9	0.13	P
	44.0	0.05	P
	50.1	0.03	P
	55.9	0.03	P
	59.2	0.02	P+C
	59.6	0	C
85	0	27.4	P
	9.3	9.3	P
	18.9	1.9	P
	27.2	0.49	P
	34.2	0.18	P
	40.9	0.09	P
	46.4	0.05	P
	51.9	0.02	P
	56.6	0.02	P
	60.8	0.02	P+C
	60.8	0	C

a) W_a is the mass fraction of CH_3CO_2Na in the system. b) W_b is the mass fraction of $Na_4P_2O_7$ in the system. c) Symbols: C=CH_3CO_2Na, C·3=$CH_3CO_2Na·3H_2O$, P=$Na_4P_2O_7$, P·10=$Na_4P_2O_7·10H_2O$.

periments are plotted in Fig. 1. From these figures, it is clear that the solubilities determined here are in good agreement with the reported data.

The solids which exist in equilibrium with the solution of the system include no double salt in the temperature range investigated. The principal interest is therefore connected with the changes in the isothermally invariant equilibria and the lowest formation temperature of the anhydrous sodium pyrophosphate. The saturated sodium acetate solutions contain only a small amount of sodium pyrophosphate and they have a very strong dehydrating influence on the sodium pyrophosphate decahydrate. Accordingly anhydrous sodium pyrophosphate must be formed at temperatures which are low compared with the corresponding one in the pure aqueous system (79.5 °C). A synopsis of the isothermally invariant equilibria below 85 °C is given in Fig. 2. There it is presumed that the solubility of sodium pyrophosphate in the sodium acetate solutions is insignificant below 0 °C. This figure gives a survey of the formation of the solid.

Isothermally invariant points were plotted, with temperature as ordinate and sodium pyrophosphate concentration as abscissa. The lowest formation temperature of anhydrous sodium pyrophosphate is determined from the point of intersection of the curves on which the solution is equilibrium with two solid phases and it is about 47 °C.

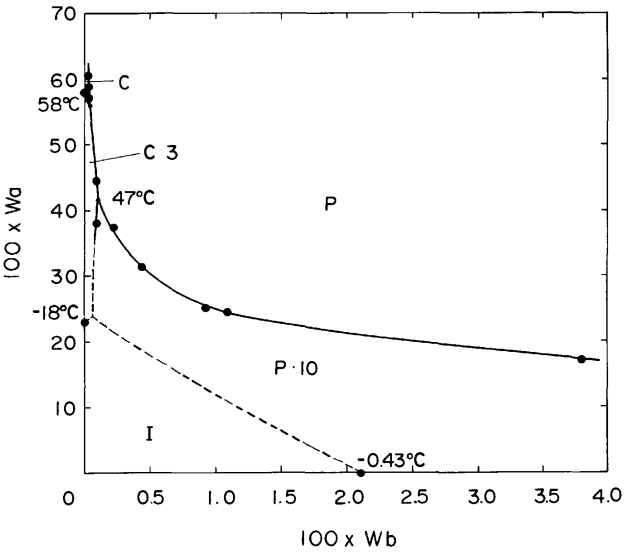

Fig. 2. Synopsis of the composition of the solutions at the invariant and univariant equlibria of the ternary system CH_3CO_2Na–$Na_4P_2O_7$–H_2O. The symbols in this figure indicate the same phases as those in Fig. 1.

The authors wish to express their thanks to Dr. Ryoichi Kiriyama for his useful discussions and to Drs. Tsuneharu Nitta, Eiichi Hirota, and Masanari Mikoda for their continuous encouragements. The authors are grateful to Miss Akiko Ueno for the colorimetric analyses. They are also grateful to Dr. Ryoichi Yamamoto for his discussions throughout this work.

References

1) T. Wada and R. Yamamoto, *Bull. Chem. Soc. Jpn.*, **55**, 3603 (1982).

2) T. Wada, K. Matsunaga, and Y. Matsuo, *Bull. Chem. Soc. Jpn.*, **57**, 557 (1984).

3) A. Seidell, "Solubility of Inorganic and Metal-Organic Compounds," 4th ed, ACS, Washington, D. C. (1965), Vol. II, pp. 854 and 1106.

4) W. F. Green, *J. Phys. Chem.*, **12**, 655 (1908).

5) H. Menzel and C. Gabler, *Z. Anorg. Allg. Chem.*, **177**, 187 (1929).

6) H. Menzel and L. Sieg, *Z. Elektrochem.*, **38**, 287 (1932).

A Direct Evidence for the Overestimation of Acidity Incidental to the Benesi Method

Shozi MISHIMA* and Tsuyoshi NAKAJIMA
Department of Synthetic Chemistry, Faculty of Engineering, Shinshu University, Wakasato, Nagano 380
(Received September 16, 1983)

Synopsis. Acid strength distributions of silica-alumina, silica-magnesia, and their mixtures were measured by the Benesi method. Overestimation of acidity has been demonstrated by the measurement that the acidity in the range $H_0 \leqq -3.0$ for the mixtures is larger than the value expected from additivity.

The amine titration method (the Johnson[1] and the Benesi[2] method), consisting essentially of titration of a solid acid by using butylamine and a series of Hammett indicators, has widely been employed[3] for determining the acid strength distribution of solid acids, which is in close connection with their catalytic activity.

The reliability of this method has not sufficiently been discussed. Matsuzaki *et al.*[4] initially pointed out that overestimation of acidity is to be involved in the Johnson method due to slow migration of the butylamine once adsorbed on weak acid sites to strong acid sites. Take *et al.*[5] experienced a difficulty in establishing adsorption equilibrium between butylamine and a thin wafer of silica-alumina even at 100 °C. From this phenomenon, they suggested the possibility that overestimation of acidity would be involved in the Benesi method for strong acid sites. The same suggestion was presented by Deeba and Hall[6] from their result obtained by column chromatography. However, such overestimation has not yet been given any experimental proof, especially for the Benesi method.

In this study, aiming at a direct demonstration of occurrence of the overestimation, mixtures of silica-alumina and silica-magnesia which possess strong and medium acid sites, respectively, were titrated by the Benesi method; the acidity for strong sites in the range $H_0 \leqq -3.0$ for the mixed samples has been found larger than that expected from additivity.

Experimental

Silica-alumina (Nikki Chem. Co., N631-L) was powdered to below 250 mesh and activated at 450 °C for 3 h in an electric furnace. Silica-magnesia was coprecipitated from an aqueous solution of sodium silicate and magnesium chloride by a similar way as reported by Ikebe;[7] the recipitate was dried at 105—110 °C and powdered to below 250 mesh, and the powder was calcined at 500 °C for 3 h befor use. Silica-alumina and silica-magnesia will be abbreviated as SA and SM, respectively. Mixtures of SA and SM were prepared simply by mixing the component powders. Benzene dried with silica gel was used as solvent. 4-Phenylazo-1-naphthylamine ($pK_a=+4.0$), *p*-dimethylaminoazobenzene ($pK_a=+3.3$), 4-(phenylazo)diphenylamine ($pK_a=+1.5$), dicinnamylideneacetone ($pK_a=-3.0$), benzylideneacetophenone ($pK_a=-5.6$), and anthraquinone ($pK_a=-8.2$) were used as indicators in the form of 4×10^{-3} mol dm^{-3} benzene solution. Butylamine solution in benzene of 0.1 mol dm^{-3} was used as titrant.

SA, SM, and their mixtures (1:1 and 1:2 in weight) were titrated by the Benesi method in the following procedure: A mixture of 0.4 g powder and 5 ml solvent was taken in each of several 50 ml Erlenmeyer's flasks and known amounts of amine were added to each flask. In this way, a series of samples was prepared in which each sample had a different amount of base added. The samples were tightly stoppered and shaken at 30 °C for 1—2 d, and then a portion of each slurry (*ca.* 1 ml) was transferred into each of several test tubes. A small amount of indicator (20—50 μl) was added to each sample and the color was observed. The acid strength distribution was determined from the amount of amine required to discolor the acid color of each indicator substantially. The transfer of slurry and addition of indicators were repeated after 1 d shaking to confirm the duplication of the preceding measurement. All the above procedure was performed in dry air to avoid moisture contamination.

Results and Discussion

The acid strength distributions obtained for SA and SM are shown in Fig. 1. SA has a 0.2 mmol g^{-1} acidity in the range $H_0 \leqq -3.0$ for strong acid sites and a 0.075 mmol g^{-1} acidity in $-3.0 < H_0 \leqq +4.0$ for medium ones. SM has a 0.35 mmol g^{-1} acidity in $-3.0 < H_0 \leqq +4.0$ but none in $H_0 \leqq -3.0$. These results are in qualitative agreement with the results obtained by Benesi.[1]

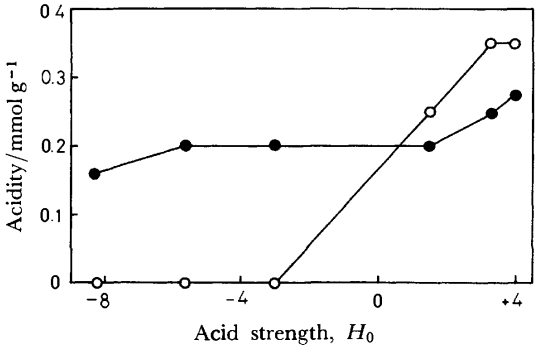

Fig. 1. Acid strength distributions of silica-alumina and silica-magnesia.
●: silica-alumina, ○: silica-magnesia.

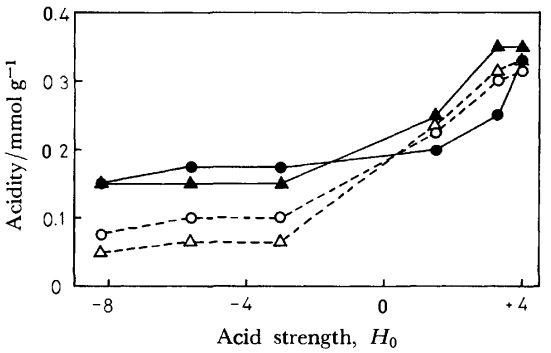

Fig. 2. Acid strength distribution of the mixtures.
● and ▲: Experimentally obtained, ○ and △: calculated from distribution of each solid for SA: SM=1:1 and 1:2, respectively.

Figure 2 shows the acid strength distributions for the mixtures of SA and SM (solid lines) in weight ratios 1:1 and 1:2. The distributions expected on the basis of additivity from the distributions of each solid are also shown in Fig. 2 (broken lines). If there is no overestimation in operation, the solid and the broken line should coincide with each other and the acidities in $H_0 \leqq -3.0$ for the 1:1 and 1:2 mixtures should be 1/2 and 1/3, respectively, of the acidity for SA given in Fig. 1. The observed acidity in $H_0 \leqq -3.0$ is, however, about two or three times larger than that expected from the distributions of each solid on the basis of the mixing ratios. Thus, these results have demonstrated the occurrence of overestimation. The degree of overestimation corresponds to 86% of the medium acid sites in SM for both the cases. Matsuzaki *et al.*,[4] Take *et al.*,[5] and Deeba and Hall[6] pointed out that butylamine adsorbs on acid sites substantially irreversibly. With the irreversibility taken into account, the observed overestimation is attributable to the irreversible adsorption of amine not only on strong sites but also on relatively weak sites. Thus, when the acid color of dicinnamylideneacetone has disappeared, the whole acid sites in $H_0 \leqq -3.0$ and the greater part of the acid sites in $-3.0 < H_0 \leqq +4.0$ will be taking part in the adsorption of amine.

For the range $-3.0 < H_0 \leqq +4.0$, the acidities of the mixtures are in agreement with those expected from the acidities of each solid within experimental errors. However, this agreement does not necessarily conclude the absence of overestimation in the medium and weak ranges $-3.0 < H_0$ since if overestimation should be operative in these ranges, weak acid sites in $+4.0 < H_0$ would be included in the estimate for the range $-3.0 < H_0 \leqq +4.0$ and since the present study made no measurement on the presence of any acid sites in the range $+4.0 < H_0$; thus, it is left to future experimental check whether or not these medium and weak ranges are free from overestimation.

Recently, it has been observed that some portions of butylamine or Hammett indicators adsorbed on strong acid sites of silica-alumina can migrate,[8] and that no overestimation occurs when a mixture of silica-alumina and nickel sulfate containing medium acid sites ($-3.0 < H_0 \leqq +1.5$) is subjected to a measurement by the Benesi method.[9] These results are different from the present findings. The difference cannot be explained reasonably at this stage for lack of detailed knowledge about the behavior of amine and indicators adsorbed on the surface of solid acid.

References

1) O. Johnson, *J. Phys. Chem.*, **59**, 827 (1955).
2) H. A. Benesi, *J. Phys. Chem.*, **61**, 970 (1957).
3) T. Yashima and N. Takahashi, *Yuki Gosei Kagaku Kyokai Shi*, **36**, 501 (1978).
4) I. Matsuzaki, Y. Fukuda, T. Kobayashi, K. Kubo, and K. Tanabe, *Shokubai*, **11**, 210 (1969).
5) J. Take, Y. Nomizo, and Y. Yoneda, *Bull. Chem. Soc. Jpn.*, **46**, 3568 (1973).
6) M. Deeba and W. K. Hall, *J. Catal.*, **60**, 417 (1979).
7) K. Ikebe, *Kogyo Kagaku Zasshi*, **61**, 437 (1958).
8) I. Matsuzaki and S. Mishima, *Shokubai*, **21**, 211 (1979).
9) I. Matsuzaki and S. Mishima, *Shokubai*, **22**, 238 (1980).

Optical Resolution of DL-Alanine by Formation of Ternary Copper(II) Complexes with L-Isoleucine

Tadashi SHIRAIWA,* Hirofumi FUKUOKA, Masahiro YOSHIDA, and Hidemoto KUROKAWA
Faculty of Engineering, Kansai University, Yamate-cho, Suita, Osaka 564
(Received October 11, 1983)

Synopsis. A ternary complex, (D-alaninato)(L-isoleucinato)copper(II) (abbreviated as [Cu(D-ala)(L-ile)]), was crystallized selectively at 0 °C from an aqueous solution containing DL-alanine (DL-Ala), L-isoleucine (L-Ile), and copper(II) acetate monohydrate ($Cu(OAc)_2 \cdot H_2O$) in the molar ratio of 1:1:1.

Many studies have been reported on optical resolution of DL-amino acids through formation of ternary copper(II) complexes.[1-4] Most of such optical resolutions have taken advantage of electrostatic ligand-ligand interaction or stereoselective ligand exchange, and little work has been reported on resolution of DL-amino acids having an aliphatic side chain through formation of ternary complexes composed of two kinds of such amino acids. This note describes the possibility of optical resolution of DL-Ala by formation of ternary copper(II) complexes with L-Ile. [Cu(D-ala)(L-ile)] was crystallized selectively at 0 °C from an aqueous solution containing DL-Ala, L-Ile, and $Cu(OAc)_2 \cdot H_2O$ in the molar ratio of 1:1:1. This was confirmed by preparation of [Cu(D-ala)(L-ile)] and [Cu(L-ala)(L-ile)]. The cis-trans isomers for the two nitrogen or two oxygen donor atoms exist in these complexes. Such geometrical isomerism was also investigated from infrared spectra.

Experimental

Amino Acids. DL-Ala and L-Ile ($[\alpha]_{436}^{20}$+78.8° (*c* 1.00, 1 mol dm^{-3} HCl)) were purchased from Wako Pure Chemical Ind., Ltd., L-Ala ($[\alpha]_{436}^{20}$+34.6° (*c* 1.00, 1 mol dm^{-3} HCl)) from Kanto Chemical Co., Ltd., and D-Ala ($[\alpha]_{436}^{20}$−34.6° (*c* 1.00, 1 mol dm^{-3} HCl)) from Sigma Chemical Co. These amino acids were recrystallized from water–ethanol.[5]

Optical Resolution. DL-Ala (0.01 mol) and L-Ile (0.01 mol) were dissolved in 70 cm^3 of water and the solution was kept at 0 °C. To the solution was added a solution containing 0.01 mol of $Cu(OAc)_2 \cdot H_2O$ in 30 cm^3 of water at 0 °C. A ternary complex [Cu(D-ala)(L-ile)] was crystallized on standing at 0 °C overnight or by adding ethanol (100, 200, 300, or 400 cm^3) to the reaction mixture. The ternary complex was filtered and dissolved in 300 cm^3 of water by being heated at a temperature below 50 °C. An acetone solution of 8-quinolinol was added to precipitate the copper(II) in the aqueous solution as bis(8-quinolinolato)-copper (II). After filtration, a mixture of Ala and L-Ile was obtained by evaporating the filtrate to dryness under reduced pressure, and thoroughly washed with acetone. On the other hand, the filtrate from the reaction mixture was treated with 8-quinolinol in a similar manner. The amounts[6] and optical purities[7] of Ala in these mixtures were determined on the basis of specific rotation and ^{1}H NMR data.

Preparation of Ternary Complexes. Ternary complexes were prepared in a similar manner to the procedure for optical resolution. An aqueous solution containing D- or L-Ala, L-Ile, and $Cu(OAc)_2 \cdot H_2O$ in the molar ratio of 1:1:1 gave crystalline ternary copper(II) complexes at 0 °C. The complexes were recrystallized from water. Elemental analysis and specific rotation of [Cu(D-ala)(L-ile)]: C, 38.28; H, 6.43; N, 10.08%; ($[\alpha]_{436}^{20}$+24.3° (*c* 0.50, 1 mol dm^{-3} HCl). [Cu(L-ala)(L-ile)]: C, 38.52; H, 6.57; N, 10.09%; ($[\alpha]_{436}^{20}$+48.3° (*c* 0.50, 1 mol dm^{-3} HCl). Calcd for $C_9H_{18}N_2O_4Cu$: C, 38.36; H, 6.44; N, 9.94%.

Measurements. Specific rotations were measured with a Union Giken high sensitivity PM-101 digital polarimeter in 1 mol dm^{-3} hydrochloric acid using a 0.5 dm path length quartz cell. ^{1}H NMR spectra were recorded on a JEOL JNM-PMX 60 NMR spectrometer in deuterium oxide. Infrared spectra were obtained in the range 4000—400 cm^{-1} with a JASCO A-102 infrared spectrophotometer by the KBr disk method.

Results and Discussion

Results of Optical Resolution. The bluish violet complex, crystallized at 20 °C from an aqueous solution containing DL-Ala, L-Ile, and $Cu(OAc)_2 \cdot H_2O$ in the molar raio of 1:1:1, was bis(L-isoleucinato)copper(II) monohydrate with a specific rotation of +62°.[8] The precipitation of this binary complex could be avoided by keeping the reacting solution at 0 °C and the ternary complex [Cu(D-ala)(L-ile)] was crysallized. The ternary complex had an optical purity of 93.4%. The specific rotation of the complex increased with an increase in the amount of added ethanol, since more soluble [Cu(L-ala)(L-ile)] was also precipitated by adding ethanol. [Cu(D-ala)(L-ile)] was almost completely precipitated by adding 400 cm^3 of ethanol, and [Cu(L-ala)(L-ile)] with an optical purity of 96.1% was obtained from the filtrate. The copper(II) within these complexes was removed with 8-quinolinol. ^{1}H NMR spectra of the mixtures obtained showed that the mixtures were composed of equimolar amounts of Ala and L-Ile. Ala in the mixture obtained from the precipitate had an abundance of D-isomer, whereas Ala from the filtrate an abundance of L-isomer. The results of optical resolution are summarized in Table 1.

These results indicate that DL-Ala was resolved into optical isomers with high optical purity by formation of the ternary copper(II) complexes with L-Ile, though the mixtures were not separated into D- or L-Ala and L-Ile.

Infrared Spectra. The geometrical isomerism existing in [Cu(D-ala)(L-ile)] and [Cu(L-ala)(L-ile)] was investigated on the basis of infrared spectra. Subtle spectral differences in 4000—1000 cm^{-1} are observed between these ternary complexes. In the range 1000—400 cm^{-1}, however, the spectral patterns are considerably different from each other as shown in Fig. 1. The differences may come from the presence of cis-trans isomers for the two nitrogen or two oxygen atoms.[9,10] The geometrical isomerism will give rise to differences in the absorption wave number of infrared active copper-ligand bands; the cis isomer should exhibit two ν_{Cu-N} and two ν_{Cu-O}, whereas the trans

Table 1. Results of optical resolutions

Amount of added ethanol	[Cu(D-ala)(L-ile)]		Ala in mixture			
	Yield	Optical purity[a]	Configuration[b]	Yield	Optical purity	Degree of resolution[c]
cm^3	g	%		g	%	%
0	0.336	93.4	D	0.10	98.5	22
			L	0.76	15.2	26
100	1.311	72.3	D	0.40	69.2	62
			L	0.44	62.2	61
200	1.547	58.4	D	0.46	62.3	64
			L	0.40	77.5	70
300	1.590	49.6	D	0.52	49.0	57
			L	0.33	81.7	61
400	1.922	39.5	D	0.58	41.8	54
			L	0.28	93.4	59

a) The optical purities were determined on the basis of the specific rotation of an equivalent mixture of [Cu(D-ala)(L-ile)] and [Cu(L-ala)(L-ile)] ($[\alpha]_{436}^{20}$ +38.0° (1 mol dm^{-3} HCl)). b) D-Isomer was obtained from the precipitate and L-isomer from the filtrate. c) Degree of resolution (%)=[Yield of Ala (g)×Optical purity (%)]/0.445 (g).

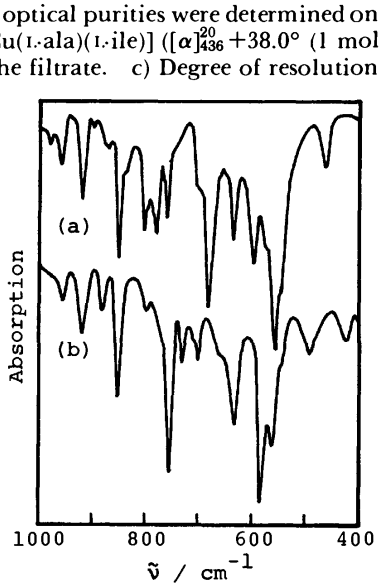

Fig. 1. Infrared spectra of the ternary copper(II) complexes.
(a): Cu[(L-ala)(L-ile)], (b): Cu[(D-ala)(L-ile)].

isomer only one for each of these modes.[10,11] In the range 500—400 cm^{-1}, [Cu(D-ala)(L-ile)] exhibits two bands at 494 and 422 cm^{-1} and [Cu(L-ala)(L-ile)] only one band at 466 cm^{-1}. These bands can be assigned to the ν_{Cu-N}, since in copper(II) complexes of amino acids, ν_{Cu-N} appears in 500—400 cm^{-1} and ν_{Cu-O} in the range below 350 cm^{-1}.[10,11] These results suggeste that [Cu(D-ala)(L-ile)] has a cis structure and that [Cu(L-ala)(L-ile)] has a trans one.

References

1) K. Harada and T. Iwasaki, *Chem. Lett.*, **1972**, 1057.
2) K. Harada and W. Tso, *Bull. Chem. Soc. Jpn.*, **45**, 2859 (1972).
3) T. Sakurai, O. Yamauchi, and A. Nakahara, *J. Chem. Soc., Chem. Commun.*, **1976**, 553.
4) O. Yamauchi, T. Sakurai, and A. Nakahara, *Bull. Chem. Soc. Jpn.*, **50**, 1776 (1977).
5) S. Akabori, T. Kaneko, and K. Narita, "Tanpaku-shitsu Kagaku, 1," Kyoritsu Shuppan, Tokyo (1954), p. 104.
6) The molar ratio and amounts of Ala and L-Ile in their mixture can be obtained from integrated data of the methyl (Ala), *s*-butyl (L-Ile), and their α-CH proton signals in ^1H NMR spectra.
7) Since the optical rotation of L-Ile in the mixture could be obtained from the amount and specific rotation of L-Ile, the optical rotation of Ala in the mixture was calculated on the basis of the corresponding difference between the mixture and L-Ile.
8) The complex bis(L-isoleucinato)copper(II) monohydrate was prepared from an aqueous solution containing $Cu(OAc)_2 \cdot H_2O$ and L-Ile in the molar ratio of 1:2. Found: C, 42.45; H, 7.72; N, 8.28%. Calcd for $C_{12}H_{26}N_2O_5Cu$: C, 42.16; H, 7.67; N, 8.19%. $[\alpha]_{436}^{20}$ +62.2° (*c* 0.50, 1 mol dm^{-3} HCl).
9) T. Sakurai, O. Yamauchi, and A. Nakahara, *Bull. Chem. Soc. Jpn.*, **49**, 169 (1976).
10) K. Nakamoto, "Infrared and Raman Spectra of Inorganic and Coordination Compound," John Wiley and Sons (1978), p. 305.
11) A. W. Herlinger, S. L. Wenhold, and I. V. Long, *J. Am. Chem. Soc.*, **92**, 6474 (1970).

The Structure of Aquatris(*m*-hydroxybenzoato)cerium(III), $[Ce(HOC_6H_4CO_2)_3(H_2O)]_n$

Yukio KOIZUMI,† Hiroshi SAWASE,† Yasuo SUZUKI,† Mamoru SHIMOI, and Akira OUCHI*
Department of Chemistry, College of Arts and Sciences, The University of Tokyo, Komaba 3-8-1, Meguro-ku, Tokyo 153
†*Department of Industrial Chemistry, Faculty of Engineering, Meiji University, Higashi-Mita, Tama-ku, Kawasaki-shi, Kanagawa 214.*
(Received December 23, 1983)

Synopsis. The crystal and molecular structure of the title complex has been determined by the use of the single-crystal X-ray diffraction method. The crystal of $CeC_{21}H_{17}O_{10}$, F. W. 569.48, was monoclinic; space group $P2_1/c$, a=13.401(2), b=19.173(5), c=8.079(1) Å, β=98.94(1)°, U=2050.6(8) Å^3, Z=4, D_m=1.84(3), D_x=1.84 Mg m^{-3}, and μ(Mo $K\alpha$)=2.31 mm^{-1}. Each cerium(III) atom is ennea-coordinated and is in a tri-capped trigonal-prism geometry. They are in a linear polymer, and each cerium(III) atom is bridged to the next metal atom by three carboxylate ligands.

The structures of lanthanoid(III) carboxylates, are actively being investigated.[1-5] The present authors showed in previous paper the structure of the lanthanoid(III) complexes of *m*-hydroxybenzoic acid with the formula of $[LnL_3(H_2O)_2]\cdot HL\cdot 2H_2O$, where Ln= La, Ce, Pr, and Nd, and HL=*m*-hydroxybenzoic acid.[6] Although the type of the complex of cerium(III) was obtained from aqueous solution containing an excess of the free acid, the titled complex was crystallized from the aqueous solution containing cerium(III) and the carboxylate ions in a stoichiometric ratio (pH≈5). Therefore, its crystal and molecular structure was determined by the single-crystal X-ray-diffraction method.

Experimental

*Synthesis of [Aquatris(*m*-hydroxybenzoato)cerium(III)] Polymer.* The cerium(III) hydroxide obtained by mixing aqueous solutions of about 1.5 g (4 mmol) of cerium(III) chloride heptahydrate and an excess of sodium hydroxide was dissolved into a hot aqueous solution of *m*-hydroxybenzoic acid (1.7 g (12 mmol) in 20 cm^3 of water). The insoluble matter was filtered off, and the filtrate was kept in a silica-gel desiccator several days, until the volume of the solution was reduced to about 10 cm^3. The precipitated crystals were filtered off and washed with water and acetone, in that order. The yield was about 1.1 g (48%).

Single-crystal X-Ray Analysis. A crystal with dimensions of 0.4×0.4×0.2 mm^3 was used for the measurement. All its edges were ground off. The reflections within the range of 3°<2θ<46° were collected on a Rigaku AFC-6A four-circle automated X-ray diffractometer with Mo $K\alpha$ radiation, where the ω-scan (3—30°) or θ-2θ-scan (30—46°) technique was employed. From the 2978 independent reflections observed, 2479|F_o|>3σ(|F_o|) were selected and used for the refinement. The intensities were corrected for the Lorentz and polarization factors, but no correction was made for the absorption or extinction.

All the calculations were carried out on a HITAC M-200H computer at the Computer Center of the University of Tokyo, using the local version of the UNICS.[7] The scattering factors were taken from the tables.[8]

Structure Determination. The structure was solved by the heavy-atom method and refined by the block-diagonal least-squares method. All non-hydrogen atoms were found, and the final R value was 0.032, with anisotropic temperature factors for all atoms.[9]

Results and Discussion

The selected final atomic coordinates and equivalent isotropic temperature factors are shown in Table 1, while the bond lengths and bond angles, in Table 2.[10] A perspective drawing of the complex, with the numbering scheme, is shown in Fig. 1; its crystal packing diagram, in Fig. 2, and a schematic presentation of the bonding modes of the ligands, in Fig. 3.

As is shown in the figures, this complex has a structure different from those of the tetracarboxylates $[ML_3(H_2O)_2]\cdot HL\cdot 2H_2O$ (M=La—Nd) or of the tricarboxylates $[ML_3(H_2O)_3]_2\cdot 2H_2O$ (M=Sm—Yb) (HL= *m*-hydroxybenzoic acid), where the complex molecules are lined parallel to the c-axis.[6] In this complex, the central cerium(III) atom is ennea-coordinated and is in a deformed tri-capped trigonal-prism geometry. One of the oxygen atoms of each ligand, O(11), O(21), and O(31), takes each cap position, while O(22) or O(32)

TABLE 1 FINAL ATOMIC COORDINATES (×10^4) AND EQUIVALENT ISOTROPIC TEMPERATURE FACTORS, WITH ESTIMATED STANDARD DEVIATIONS IN PARENTHESES

Atom	x	y	z	B_{eq}/Å$^{2a)}$
Ce	2617.0(3)	2207.0(2)	328.3(4)	1.37
O(11)	4164(3)	2661(2)	1816(5)	2.55
O(12)	4016(3)	3310(2)	4034(5)	2.14
O(21)	3071(4)	1035(2)	1469(5)	2.83
O(22)	2951(3)	1769(2)	3526(5)	2.04
O(31)	1110(3)	3020(2)	−219(5)	2.37
O(32)	1879(3)	3097(2)	2375(5)	1.90
C(11)	4542(5)	3012(3)	3062(7)	1.85
C(12)	5670(5)	3085(3)	3388(7)	1.93
C(21)	3143(4)	1164(3)	3019(7)	1.71
C(22)	3414(4)	585(3)	4230(7)	1.66
C(31)	1189(4)	3291(3)	1202(7)	1.78
C(32)	477(4)	3856(3)	1487(7)	1.98
O(W)	1004(3)	1642(3)	1248(6)	3.21

a) The equivalent isotropic temperature factors were computed using the following expression: $B_{eq}=4/3(B_{11}a^2+B_{22}b^2+B_{33}c^2+B_{13}ac\cos\beta)$. The B_{ij}'s are defined by: $\exp[-(h^2B_{11}+k^2B_{22}+l^2B_{33}+2klB_{23}+2hlB_{13}+2hkB_{12})]$.

TABLE 2. BOND LENGTHS AND BOND ANGLES, WITH ESTIMATED STANDARD DEVIATIONS IN PARENTHESES

Bond length	l/Å	Bond length	l/Å
Ce-O(11)	2.392(4)	Ce-O(21)	2.468(5)
Ce-O(22)	2.687(4)	Ce-O(31)	2.535(4)
Ce-O(32)	2.671(4)	Ce-O(W)	2.628(5)
Ce-O(12^{ii})	2.489(4)	Ce-O(22^{ii})	2.526(4)
Ce-O(32^{ii})	2.506(4)	O(11)-C(11)	1.251(7)
O(12)-C(11)	1.270(8)	O(13)-C(16)	1.376(8)
O(21)-C(21)	1.265(7)	O(22)-C(21)	1.269(7)
O(31)-C(31)	1.249(7)	O(32)-C(31)	1.273(7)
Bond angle	**Φ/°**	**Bond angle**	**Φ/°**
O(11)-Ce-O(21)	90.00(14)	O(11)-Ce-O(31)	117.93(14)
O(11)-Ce-O(22)	68.23(13)	O(11)-Ce-O(32)	80.33(13)
O(11)-Ce-O(W)	134.03(14)	O(21)-Ce-O(31)	140.15(14)
O(22)-Ce-O(32)	68.09(12)	O(11)-Ce-O(32^{ii})	138.28(13)
O(22)-Ce-O(12^{ii})	104.80(13)	O(11)-Ce-O(12^{ii})	72.91(14)
O(11)-Ce-O(22^{ii})	77.85(13)		
O(12^{ii})-Ce-O(22^{ii})	81.69(13)		

Key to symmetry operations: i. x, 0.5−y, 0.5+z; ii. x, 0.5−y, −0.5+z.

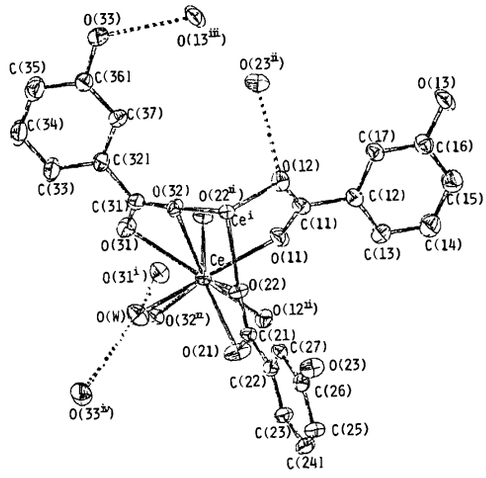

Fig. 1. The perspective drawing of the complex and the numbering scheme.

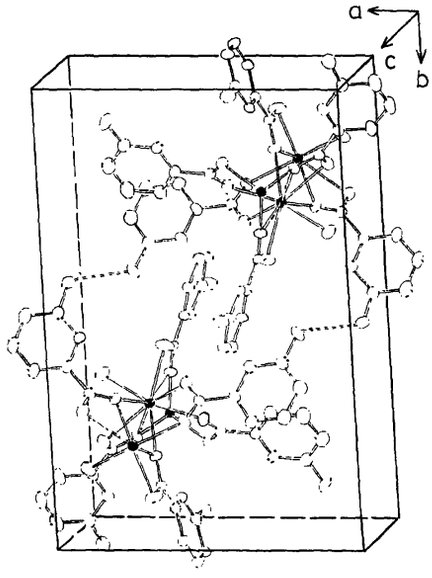

Fig. 2. The crystal packing diagram of the title complex.

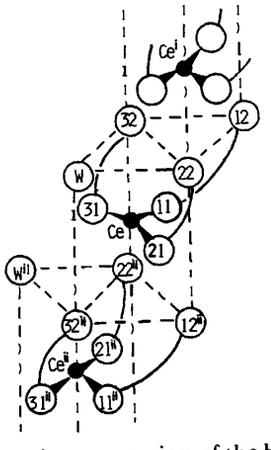

Fig. 3. Schematic presentation of the bonding modes of ligands.
(●: cerium(III), O: oxygen atoms)

take the tips of the upper triangle of the prism. The water oxygen atom, O(W), occupies the other tip of the triangle. All of the three ligands form bridges to the next cerium(III) atom, Ce^{i},[11] and O(12), O(22), and O(32) atoms are at the three tips of the bottom triangle of the prism around the Ce^{i} atom. Thus, the O(22)–O(32) edge is common to both of the triangles, as is shown in Fig. 3. The three oxygen atoms at the bottom triangle of the prism around the Ce atom are $O(12^{ii})$, $O(22^{ii})$, and $O(32^{ii})$,[11] which are parts of the bridging ligands between Ce and Ce^{ii} atoms.[11] Thus, Ce and Ce^{i}, as well as Ce and Ce^{ii}, are each bridged with three carboxylate ligands. One of the three ligands bond to each cerium(III) atom with one each oxygen atom of its carboxyl group. Each one of the other two ligands bridges two metal atoms by one carboxyl oxygen atom, and, at the same time, the other carboxyl oxygen atom of the ligand is coordinated to one of the bridged metal atoms. One of the Ce–O bondings of each latter type of ligand, Ce–O(22) or Ce–O(32), is a little longer than the other Ce–O bondings, as is shown in Table 2. The bond length of Ce–O(W) is also a little longer than the others. The difference in the C–O bond lengths of each carboxyl group of the ligands is not large: 0.019, 0.004, and 0.024 Å respectively, and the oxygen atom of the shorter C–O bond occupies the cap position.

It is found that some O···O interatomic distances are shorter than about 2.9 Å, and hydrogen bondings between the phenol oxygen atoms and the oxygen atoms of the other ligands are expected to exist; the $O(33)\cdots O(13^{iii})$, $O(12)\cdots O(23^{ii})$, $O(W)\cdots O(33^{iv})$, and $O(W)\cdots O(31^{i})$, shown in Fig. 2, are examples (2.723(7), 2.820(7), and 2.910(6) Å respectively).[11] Thus, the linear complex chains weakly bond with other chains.

The authors are greatly obliged to the Shin-Etsu Chemical Co., Ltd., for aiding the study by presenting the highly pure lanthanoid(III) oxides. The present work was partly supported by a Grant-in-Aid for Scientific Research (No. 57430011) from the Ministry of Education, Science and Culture.

References

1) G. G. Sadikov, G. A. Kukina, and M. A. Porai-Koshits, *Zh. Strukt. Khim.*, **8**, 551 (1968).
2) G. G. Sadikov and G. A. Kukina, *Zh. Strukt. Khim.*, **9**, 145 (1968).
3) G. G. Sadikov, G. A. Kukina, and M. A. Porai-Koshits, *Zh. Strukt. Khim.*, **12**, 859 (1971).
4) M. C. Favas, D. L. Kepert, B. W. Skelton, and A. H. White, *J. Chem. Soc., Dalton Trans.*, **1980**, 454.
5) M. S. Khiyalov, I. R. Amiraslanov, Kh. S. Mamedov, and E. M. Movsumov, *Koord. Khim.*, **7**, 445 (1981).
6) Y. Koizumi, H. Sawase, Y. Suzuki, T. Takeuchi, M. Shimoi, and A. Ouchi, *Bull. Chem. Soc. Jpn.*, in print.
7) "The Universal Crystallographic Computation Program System (UNICS)," ed by T. Sakurai, Crystallographic Society of Japan, Tokyo (1967).
8) "International Tables for Crystallography," Kynoch Press, Birmingham (1974), Vol. IV.
9) $R=\sum||F_o|-|F_c||/\sum|F_o|$
10) The final atomic parameters, the final F_o-F_c values, and some additional data about bond lengths and bond angles are deposited as Document No. 8418 at the Office of the Editor of Bull. Chem. Soc. Jpn.
11) Key to symmetric operations: i. x, $0.5-y$, $0.5+z$; ii. x, $0.5-y$, $-0.5+z$; iii. $1.0-x$, $1.0-y$, $1.0-z$; iv. $-x$, $-0.5+y$, $0.5-z$.

Syntheses and Circular Dichroism Studies of Oligopeptides Having Tri- or Tetra-L-prolyl Sequences

Kazuki SATO,* Masato TANAKA, and Tetsuo HAYASE†
Mitsubishi-Kasei Institute of Life Sciences, 11 Minamiooya, Machida, Tokyo 194
†*Research Center, Mitsubishi Chemical Industries Ltd., Kamoshida, Midori-ku, Yokohama 227*
(Received May 23, 1983)

Synopsis. CD spectra of many oligopeptides having tri- or tetra-L-prolyl sequences showed that a penta- or hexapeptide having a tetra-L-prolyl sequence took poly(L-proline) II helix irrespective of amino acid residues at N- or C-terminal of a L-prolyl cluster and that as to a size of the cluster, tri-L-prolyl sequence was enough to form the helix, when glycine was used as substituent.

It has been reported that oligo(L-proline)s begin to form poly(L-proline) II (PPII) helix at the tetramer, and that the pentamer or the greater has higher population of the helix.[1-4] However, there has been no report in detail on the PPII helix of oligopeptides containing a variety of amino acids other than L-proline. This paper describes syntheses and CD measurements of many oligopeptides having tri- or tetra-L-prolyl sequences (**1b—19b**, **12c**, and **14c**; see Table 1) to study effects of amino acid residues bound to the L-prolyl cluster on the formation of PPII helix.[5]

First, we synthesized sequential peptides **1b—6b**. Compound **1b** showed a negative CD band at 201 nm. Both **3b** and **5b** showed larger CD bands at longer wavelength of 203 nm (Table 1). Marked difference was not observed between **3b** and **5b**. Okabayashi *et al.* reported that Aoc-oligo(L-proline)s having some populations of PPII helix showed a CD minimum at longer wavelength than 203 nm.[2] So, the CD spectra suggests that both **3b** and **5b** have ordered conformation such as PPII helix and that **1b** has unordered one. All of Boc-[(Pro)$_4$-Gly]$_m$-OH showed large negative CD bands at 203.5 nm suggesting that all these peptides took also PPII helix. Therefore, prolyl peptides with more than five amino acid residues and at least one tri-L-prolyl sequence seem to take PPII helix. CD spectra of **7b** and **8b** support this consideration; **8b** showed a negative CD band at 203 nm similar to those of **3b** and **5b**, whereas **7b** showed a weak CD band at shorter wavelength of 200.5 nm.

TABLE 1. CD SPECTRAL DATA OF SYNTHETIC PEPTIDES[a]

Peptides	$[\theta]^{min}_{\sim 200nm}$	$[\theta]^{max}_{\sim 225nm}$
	10^3 degree cm^2 dmol^{-1}	
Boc-(Pro)$_3$-Gly-OH (**1b**)	−23.3 (201.0)	0.9 (223.0)
Boc-(Pro)$_4$-Gly-OH (**2b**)	−26.2 (203.5)	1.3 (226.5)
Boc-[(Pro)$_3$-Gly]$_2$-OH (**3b**)	−28.9 (203.0)	0.9 (227.0)
Boc-[(Pro)$_4$-Gly]$_2$-OH (**4b**)	−31.8 (203.5)	0.9 (227.5)
Boc-[(Pro)$_3$-Gly]$_3$-OH (**5b**)	−31.1 (203.0)	0.6 (227.0)
Boc-[(Pro)$_4$-Gly]$_3$-OH (**6b**)	−32.8 (203.5)	0.7 (229.0)
Boc-Gly-(Pro)$_2$-Gly-OH (**7b**)	−17.0 (200.5)	not observed
Boc-Gly-(Pry)$_3$-Gly-OH (**8b**)	−23.1 (203.0)	0.6 (228.0)
Boc-Gly-(Pro)$_4$-OH (**9b**)	−27.6 (203.5)	2.0 (229.0)
Boc-Ala-(Pro)$_4$-OH (**10b**)	−25.9 (203.5)	1.6 (225.0)
Boc-Val-(Pro)$_4$-OH (**11b**)	−25.8 (204.0)	0.8 (229.0)
Boc-Ser-(Pro)$_4$-OH (**12b**)	−23.7 (204.0)	0.8 (230.0)
Boc-Thr-(Pro)$_4$-OH (**13b**)	−21.4 (206.5)	0.4 (230.0)
Boc-Tyr-(Pro)$_4$-OH (**14b**)	−20.8 (206.5)	4.3 (228.5)
Boc-Hyp-(Pro)$_4$-OH (**15b**)	−28.8 (203.5)	2.6 (226.0)
Boc-Ala-Ser-(Pro)$_4$-OH (**16b**)	−25.0 (203.0)	0.4 (235.0)
Boc-(Pro)$_4$-Ser-OH (**17b**)	−25.2 (203.0)	1.1 (226.0)
Boc-(Pro)$_4$-Val-OH (**18b**)	−29.8 (203.5)	0.4 (227.0)
Boc-Ser-(Pro)$_4$-Gly-OH (**19b**)	−25.7 (203.0)	1.1 (227.5)
Boc-Ser-(Pro)$_4$-NH$_2$ (**12c**)	−25.9 (204.0)	1.0 (227.0)
Boc-Tyr-(Pro)$_4$-NH$_2$ (**14c**)	−22.7 (206.0)	4.2 (228.0)

a) Figures in parentheses are wavelength at $[\theta]^{extrema}$

To study the relation between amino acid sequences and CD spectra, many peptides having a variety of amino acids at either or both of N- and C-termini of tetra-L-prolyl sequence (**9b—19b**, **12c**, and **14c**) were synthesized. N-terminal substitution caused various patterns of CD spectra (**9b—15b**), however, all these peptides showed CD bands at longer wavelength than 203 nm suggesting that they took PPII helix. A tendency was observed; the longer wavelength a CD band shifted the weaker its intensity decreased. Close similarity of CD spectra between Boc-Gly-(Pro)$_4$-OH (**9b**) and Boc-(Pro)$_5$-OH (which showed a CD minimum of -31.0×10^3 degree cm^{2}dmol^{-1} at 203.5 nm)[6] suggested that Gly residue was suitable for PPII helix. As to a C-terminal substitution, clear-cut tendency was not observed in the range of this experiment (**2b**, **17b**, and **18b**). Compounds **12b**, **16b**, and **19b**, which had the same Ser-(Pro)$_4$ sequence, showed similar CD spectra to each other suggesting that chain elongation from pentapeptide (**12b**) to hexapeptides (**16b** and **19b**) did not affect significantly to PPII helix. Amide derivatives (**12c** and **14c**) showed a little larger CD bands than the corresponding peptides with free carboxyl groups (**12b** and **14b**). It seems that charged group near L-prolyl cluster is not suitable for the helix.

From CD spectra of various prolyl peptides mentioned above, we concluded that a penta- or hexapeptide having a tetra-L-prolyl sequence took PPII helix irrespective of the amino acid residues at N- or C-terminal of a L-prolyl cluster, and that as to a size of the cluster tri-L-prolyl sequence was enough to form PPII helix, when glycine is used as substituent.

Experimental

Melting points were uncorrected. Optical rotations were measured on an Union automatic polarimeter PM-201. Yields and analytical data of synthetic peptides except for some oily products are summarized in Table 2; compounds **1a—19a** with benzyl ester group at C-termini are precursors of **1b—19b**.

Boc-(Pro)$_3$-Gly-OBzl (1a). To a chilled solution of Boc-Pro-OH (4.30 g, 20 mmol), H-(Pro)$_2$-Gly-OBzl·HCl (7.92 g, 20 mmol), and TEA (2.8 ml, 20 mmol) in $CHCl_3$ (80 ml) was added EDC·HCl (3.83 g, 20 mmol), and the reaction mixture was stirred for 1 h at 0 °C and overnight at room temperature and evaporated. The residue was dissolved in EtOAc (120 ml), and the solution was washed successively with 10% citric acid, 4% $NaHCO_3$, and water, and then evaporated to a small volume after being dried over anhydrous Na_2SO_4. Addition of petroleum ether to the solution gave amorphous solid which was reprecipitated from EtOAc-petroleum ether; yield, 8.46 g (76%).

Compounds **2a—19a** were prepared as described for **1a**; in such cases that a product was soluble in water, column chromatographies with silica gel or Sephadex LH-20 were used instead of acid and alkali washings.

TABLE 2. YIELDS AND ANALYTICAL DATA OF SYNTHETIC PEPTIDES

Compound	Yield	Mp θ_m	$[\alpha]_D^{22}$ [a]	Found (%)			Calcd (%)		
	%	°C	°	C	H	N	C	H	N
1a	76	72—73	−171.2	61.54	7.42	9.87	61.57	7.31	9.90[b]
2a	68	73—75	−215.4	62.23	6.95	10.71	62.46	7.25	10.70
3a	60	125—128	−243.6	59.52	7.33	11.70	59.28	7.25	12.02[c]
4a	54	155—157	−284.6	59.27	7.50	12.31	59.25	7.28	12.34[d]
5a	34	162—165	−273.6	57.52	6.98	12.91	57.87	7.24	12.86[e]
6a	34	191—193	−314.8	59.63	7.12	13.31	59.95	7.16	13.44[f]
10a	69	212—213	−264.6	63.18	7.38	10.54	62,95	7.40	10.49
11a	73	198—200	−259.6	63.99	7.54	9.99	63.86	7.68	10.06
12a	75	192—193	−249.6	61.36	7.05	10.12	61.48	7.22	10.24
13a	71	93— 95	−233.4	60.19	7.27	9.71	60.40	7.46	9.78[f]
14a	68	120—123	−196.2	63.52	6.92	9.24	63.30	7.13	9.00[f]
15a	57	118—124	−250.6	61.00	7.06	9.53	61.06	7.34	9.62[f]
16a	66	102—104	−232.4	58.46	7.05	10.86	58.37	7.35	10.75[c]
17a	69	105—108	−213.8	59.46	6.98	9.96	59.14	7.37	9.85[c]
19a	53	105—108	−221.6	56.89	6.91	10.95	57.20	7.27	10.82[d]
1b	93	115—117	−184.4	55.91	7.40	12.13	56.10	7.38	11.90[g]
2b	75	175—177	−208.4	59.06	7.60	11.37	55.75	7.45	12.04[f]
3b	87	178—180	−254.0	55.65	7.19	13.31	55.64	7.30	13.31[c]
4b	90	203—205	−303.0	56.57	7.29	13.34	56.31	7.33	13.40[d]
5b	84	208—210	−278.0	55.74	7.16	13.85	55.66	7.26	13.91[h]
6b	88	223—225	−312.2	56.25	7.21	13.78	56.52	7.28	13.93[e]
7b	80	90— 93	−142.0	51.12	6.97	12.45	51.34	7.26	12.60[f]
8b	61	123—128	−206.4	52.54	6.92	12.72	52.35	7.32	12.72[c]
9b	67	155—157	−224.2	53.96	6.82	11.52	54.08	7.56	11.68[d]
10b	58	157—161	−242.2	53.89	7.60	11.21	54.01	7.77	11.25[h]
11b	85	143—146	−248.8	56.67	7.53	10.66	56.95	7.97	11.07[c]
12b	67	173—175	−235.6	53.42	7.35	11.09	53.41	7.52	11.12[d]
13b	72	165—168	−230.0	52.97	7.49	10.67	52.64	7.77	10.58[e]
14b	69	186—191	−186.0	56.67	7.10	9.73	56.42	7.38	9.68[e]
15b	74	174—181	−251.8	54.86	7.43	10.53	54.94	7.53	10.68[d]
16b	80	156—159	−232.6	52.56	6.88	11.87	52.46	7.53	11.84[h]
17b	72	164—166	−216.0	53.18	7.25	11.04	53.41	7.52	11.12[d]
18b	85	143—146	−223.6	56.09	7.86	10.77	56.15	8.02	10.91[d]
19b	56	172—175	−244.6	52.66	6.93	12.20	52.47	7.34	12.24[d]
12c	77	147—151	−240.0	53.70	7.44	13.43	53.49	7.69	13.37[d]
14c	70	163—166	−193.4	57.27	7.42	11.71	57.21	7.48	11.77[c]

a) *c* 1, MeOH. b) $0.5H_2O$. c) $1.5H_2O$. d) $2H_2O$. e) $3H_2O$. f) H_2O. g) $0.25H_2O$. h) $2.5H_2O$.

Boc-(Pro)$_3$-Gly-OH (1b). Compound **1a** (5.57 g, 10 mmol) dissolved in MeOH (20 ml) was hydrogenated in the presence of 5% paradium carbon (*ca.* 2 g) for 4 h at room temperature. The product was recrystallized from EtOAc-petroleum ether; yield, 4.33 g (93%).

Compounds **2b—19b** were prepared as describe for **1b**.

H-(Pro)$_3$-Gly-OBzl·HCl. Compound **1a** (2.78 g, 5 mmol) dissolved in 0.1 mol dm^{-3} hydrogen chloride in formic acid (60 ml) was allowed to stand for 30 min at room temperature and evaporated. Addition of ether to the residue gave highly hygroscopic crystals, which were used for the next reaction without further treatment.

Boc groups in other peptides (**2a—4a**, and **12a**) were removed as described above.

Boc-Ser-(Pro)$_4$-NH$_2$ (12c). Compound **12a** (137 mg, 0.2 mmol) dissolved in MeOH (3 ml) saturated with NH_3 was allowed to stand at room temperature for 3 d. After the evaporation of solvent, the residue was purified by silica gel ($CHCl_3$-MeOH; 10:1, v/v) and Sephadex LH-20 (MeOH) column chromatographies; yield, 91 mg (77%).

Compound **14c** was prepared as described for **12c**.

CD Measurements. CD spectra were measured on a JASCO J-40A spectropolarimeter at 23 °C in H_2O solution with quartz cells of 1-mm path length. The ellipticity was expressed as mean residual molar ellipticity [θ] in degree cm^2 dmol^{-1}.

We thank Drs. Tsuneko Uchida and Ukon Nagai of this institute for helpful discussion, and the members of Analysis Center, Mitsubishi Chemical Industries Ltd. for elemental analysis.

References

1) T. Isemura, H. Okabayashi, and S. Sakakibara, *Biopolymers*, **6**, 307 (1968).

2) H. Okabayashi, T. Isemura, and S. Sakakibara, *Biopolymers*, **6**, 323 (1968).

3) H. Okabayashi and T. Isemura, *Bull. Chem. Soc. Jpn.*, **43**, 20 (1970).

4) H. Okabayashi and T. Isemura, *Bull. Chem. Soc. Jpn.*, **43**, 359 (1970).

5) The abbreviations used in this paper are those recommended by IUPAC-IUB: *J. Biol. Chem.*, **247**, 977 (1972). Additional abbreviations: Boc, *t*-butoxycarbonyl; OBzl, benzyl ester; Aoc, *t*-pentyloxycarbonyl; EDC, 1-ethyl-3-(3-dimethylaminopropyl)carbodiimide; TEA, triethylamine. Symbols of amino acids denote the L-configuration.

6) M. Tanaka, K. Sato, and T. Uchida, *J. Biol. Chem.*, **256**, 11397 (1981).

Chromatographic Resolution of Racemic Compounds Containing Phosphorus or Sulfur Atom as Chiral Center

Yoshio Okamoto,* Shiro Honda, Koichi Hatada, Ichiro Okamoto,†
Yuzo Toga,† and Shiro Kobayashi*,†

Department of Chemistry, Faculty of Engineering Science, Osaka University, Toyonaka, Osaka 560
†*Research Center, Daicel Chemical Industries, Ltd., Aboshi-ku, Himeji, Hyogo 671-12*
††*Department of Synthetic Chemistry, Faculty of Engineering, Kyoto University, Kyoto 606*

(Received December 15, 1983)

Synopsis. Racemic compounds containing a phosphorus or a sulfur atom as a chiral center were resolved by high-performance liquid chromatography on optically active (+)-poly(triphenylmethyl methacrylate). The resolved compounds include insecticides such as *O*-ethyl *O*-(4-nitrophenyl) phenylphosphonothionate (EPN), *O*-(4-cyanophenyl)-*O*-ethyl phenylphosphonothionate (cyanofenfos), and 2-methoxy-4*H*-1,3,2-benzo-dioxaphosphorin 2-sulfide (salithion).

Optically active poly(triphenylmethyl methacrylate) (PTrMA)[1] has been used as an effective chiral packing material for liquid chromatographic resolution of various racemic compounds,[2-9] most of which possess an asymmetric carbon. Here, we wish to report the resolution of racemic compounds containing a phosphorus or a sulfur atom as the asymmetric center using high-performance liquid chromatography (HPLC) with a (+)-PTrMA column.

Recently, Pirkle and coworkers successfully resolved racemic sulfoxides on their chiral HPLC column.[10] However, liquid chromatographic resolution of racemic phosphoric compounds has not so far been reported.

Experimental

The synthesis of compounds **1**—**5** in Table 1 has been carried out in the following manner. **1**: Preparation procedures were similar to those in a literature.[11] Methyl methyl(phenyl)phosphinate was reacted with benzylmagnesium chloride in diethyl ether to give a crude product which was purified by chromatography (silica gel) to give white solid **1**; ^{31}P NMR ($CDCl_3$ with external standard of 85% H_3PO_4) δ= 35.2 (single peak). ^{1}H NMR ($CDCl_3$) δ=1.60 (d, J=12 Hz, 3H), 3.20 (d, J=15 Hz, 2H), 6.83—7.75 (m, 10H). IR (Nujol) 1297, 1175, 1115, 920, 897, 770, 740 cm^{-1}. TLC (acetone) R_f= 0.5. **2**: Similarly, methyl methyl(phenyl)phosphinate was allowed to react with 1-naphthylmagnesium bromide, giving rise to a solid product **2** after purification by chromatography. **3**: The hydrolysis of a spirophosphonane, 5-phenyl-1,4,6-trioxa-5-phosphaspiro[4.4]nonan-7-one, gave 2-hydroxyethyl (2-carboxyethyl)phenylphosphinate (mp 75—76 °C) whose esterification with diazomethane produced **3**. **4**: Phenylphosphonic dichloride was treated with an equimolar amount of ethanol in the presence of triethylamine in benzene followed by a further reaction with an equimolar amount of methanol in the presence of triethylamine in benzene to give **4**, bp 69—72 °C/0.2 mmHg**. **5**: Phenylphosphonic dichloride was subjected to reaction with an equimolar amount of cyclohexanol and then with methanol (equimol.) in the presence of pyridine in benzene to give **5**, bp, 105—110 °C/0.2 mmHg. ^{31}P NMR ($CDCl_3$) δ=19.1 (single peak). ^{1}H NMR ($CDCl_3$) δ=1.00—2.05 (m, 10H), 3.60(d, J=11 Hz, 3H), 4.33 (br, 1H), 7.28—7.95 (m, 5H). IR (neat) 2930, 2850, 1440, 1245, 1130, 1050, 990, 800, 557 cm^{-1}. TLC (diethyl ether) R_f=0.6.

Compounds **6**—**9** were commercially obtained.

The preparations of (+)-PTrMA[12] and the packing material[4] for HPLC were described previously. The resolution was accomplished with a JASCO TRIROTOR II chromatograph equipped with a UV detector at 15 °C, methanol (0.5 ml/min) being used as eluent.

Results and Discussion

Figure 1 shows the chromatograms of the resolution of 2-hydroxyethyl [2-(methoxycarbonyl)ethyl] phenylphosphinate (**3**), *O*-ethyl *O*-(4-nitrophenyl) phenylphosphonothionate (EPN, **6**), and 2-methoxy-4*H*-1,3,2-benzo-dioxaphosphorin 2-sulfide (salithion, **8**) on (+)-PTrMA columns; the results are summarized in Table 1 together with the data for the resolution of other racemic compounds. Most compounds in Table 1 were resolved on (+)-PTrMA. The separation factor α was increased by the addition of water to the eluent, suggesting that the chiral recognition ability of (+)-PTrMA is enhanced in a polar medium, probably due to the stronger hydrophobic interaction between the polymer and enantiomers. Phosphinate **3** was resolved most effectively. Insecticides, **6**, *O*-(4-cyanophenyl) *O*-ethyl phenylphosphonothionate (cyanofenfos, **7**), and **8** were also resolved. Although optically active isomers of **6** and **7** have already been prepared and the difference of the biological activities between the optical an-

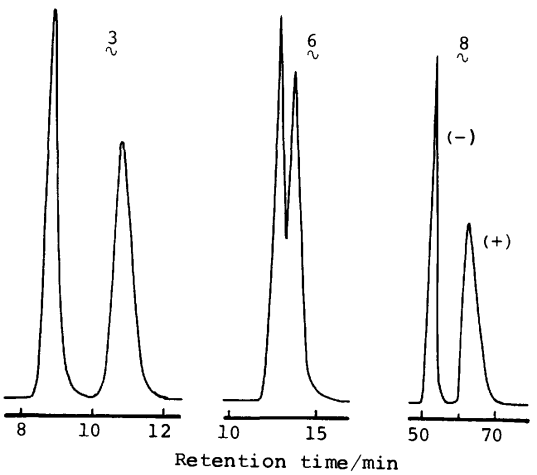

Fig. 1. Chromatograms of the resolution of **3**, **6**, and **8** on (+)-PTrMA columns. (Column: 25 cm×0.46 (id) cm for **3** and **6**; 50 cm×0.72 (id) cm for **8**, dead times of two columns were 6.4 and 30 min, respectively).

** 1 mmHg≈133.322 Pa.

*** **Note added in proof.** After submission of this Note, the optical isomers of **8** and their insecticidal activity were reported. A. Hirashima and M. Eto, *Agric. Biol. Chem.*, **47**, 2831 (1983).

Table 1. Resolution of racemic compounds on (+)-PTrMA columns[a]

Entry	Compound	k_1[b]	α[c]	R_s[d]
1	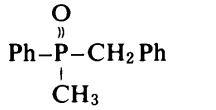	0.62 1.68[e](+) 10[f]	≈1 1.09[e] 1.14[f]	≈0.4[e] 0.84[f]
2	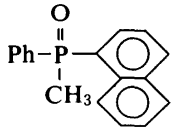	0.78(−)	1.14	≈0.5
3	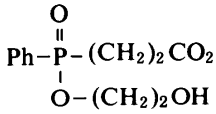	0.41(−)[g]	1.79	2.33
4	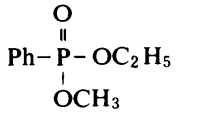	0.43	≈1	
5	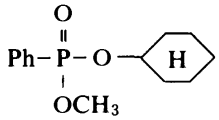	1.85	1.11	0.80
6	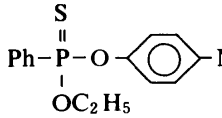	1.03(+)	1.14	0.77
7	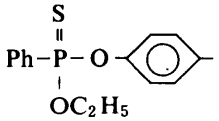	1.09(+) 17[e]	1.10 1.13[e]	≈0.3 0.67[e]
8	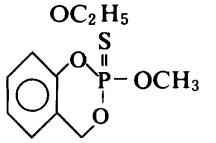	0.35[h](−)	1.45[h]	1.95[h]
9	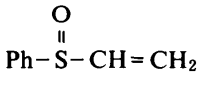	0.20(−) 0.74[e](−)	≈1 1.19[e]	0.87[e]

a) Column: 25 cm×0.46(id)cm. b) k' (capacity factor to less retained enantiomer)=(retention time of less retained enantiomer−dead time)/dead time; the sign in parenthesis is that of the optical rotation at 365 nm. c) α (separation factor)=(capacity factor to more retained enantiomer)/k_1'. d) Resolution factor=2×(difference of retention times of more and less retained enantiomers)/(sum of the band width of the two enantiomer peaks). e) Eluent: CH_3OH-H_2O(80:20). f) Eluent: CH_3OH-H_2O(60:40). g) Elipticity of the CD spectrum at 263 nm. h) Column (50 cm× 0.72(id)cm).

tipodes has been studied,[13,14] optical isomers of **8** and their activity have not yet been reported.*** These isomers are expected to show different biological activity.

Phenyl vinyl sulfoxide (**9**) was not separated with methanol as eluent but was resolved with methanol-water (80:20).

These results suggest that the (+)-PTrMA column is useful for the resolution of racemic compounds having heteroatoms.

The authors thank to Dr. Yukitoshi Narukawa for the help in preparation of the phosphorus compounds. A part of this work was supported by a Grant-in-Aid for Developmental Scientific Research No.58850188 from the Ministry of Education, Science and Culture.

References

1) Y. Okamoto, K. Suzuki, K. Ohta, K. Hatada, and H. Yuki, *J. Am. Chem. Soc.*, **101**, 4763 (1979).
2) H. Yuki, Y. Okamoto, and I. Okamoto, *J. Am. Chem. Soc.*, **102**, 6356 (1980).
3) Y. Okamoto, I. Okamoto, and H. Yuki, *Chem. Lett.*, **1981**, 835.
4) Y. Okamoto, S. Honda, I. Okamoto, H. Yuki, S. Murata, R. Noyori, and H. Takaya, *J. Am. Chem. Soc.*, **103**, 6971 (1981).
5) M. Nakazaki, K. Yamamoto, and M. Maeda, *Chem. Lett.*, **1980**, 1553; *J. Org. Chem.*, **46**, 1985 (1981).
6) R. Noyori, N. Sano, S. Murata, Y. Okamoto, H. Yuki, and I. Ito, *Tetrahedron Lett.*, **23**, 2969 (1982).
7) Y. Kawada, H. Iwamura, Y. Okamoto, and H. Yuki, *Tetrahedron Lett.*, **24**, 791 (1983).
8) M. Nakazaki, K. Yamamoto, T. Ikeda, T. Kitsuki, and Y. Okamoto, *J. Chem. Soc., Chem. Commun.*, **1983**, 787.
9) Y. Okamoto, S. Honda, E. Yashima, and H. Yuki, *Chem. Lett.*, **1983**, 1221.
10) W. H. Pirkle, J. M. Finn, B. C. Hamper, J. Schreiner, and J. R. Pribish, ACS Symp. Ser., No. 185, 245 (1982).
11) O. Korpium, R. A. Lewis, J. Chickos, and K. Mislow, *J. Am. Chem. Soc.*, **90**, 4842 (1968).
12) Y. Okamoto, H. Shohi, and H. Yuki, *J. Polym. Sci. Polym. Lett. Ed.*, **21**, 601 (1983).
13) H. Ohkawa, N. Mikami, and J. Miyamoto, *Agric. Biol. Chem.*, **41**, 369 (1977).
14) H. Ohkawa, N. Mikami, Y. Okuno, and J. Miyamoto, *Bull. Environ. Contaminat. Toxicol.*, **18**, 534 (1977).

The Study of Metal Colloids Produced by Means of Gas Evaporation Technique. II. Reaction of Metal Sols in Organic Solvents

Keisaku KIMURA

Instrument Center, Institute for Molecular Science, Myodaiji, Okazaki 444

(Received September 19, 1983)

Synopsis. The reaction of copper colloid in ethanol was studied. In the beginning of the reaction, very small particles reacted with ethanol producing ethoxide. With the proceeding of the reaction, the 577-nm characteristic copper band showed a red shift together with the broadening of the line width. This was explaind by the size dependence of the particles on the spectrum. Lead colloid was also examined.

We have recently proposed a new technique to prepare metal colloids in organic solvents.[1] It was found that the colloid stability was dependent on the kinds of metal; In, Al, Ag, and Au were stable and Pb, Sn, Ca, and Cu were unstable. In the latter case, the color of the metal colloid solution changed with time. An absorption peak was found at 213 nm, irrespective of the metal species which suggested a formation of alkoxide anion.[2] The color change was particularly prominent in copper colloid, the color of which changed from wine red to yellow within 30 min under aerobic conditions while within one day under anaerobic conditions. In the present paper, we have studied this reaction in order to clarify the cause of the time dependence of the spectrum and the origin of the 213-nm peak.

Experimental

The metal colloids were prepared by the method described in the previous report.[1] Ethanol (99.5%) was used without further purification. Hexane was distilled *in vacuo* from CaH_2 to completely exclude traces of oxygen and water. An authentic sample of ethoxide was prepared by dissolving a small grain of sodium metal in ethanol.

The time development of the spectra (room temperature) was recorded by a Hitachi 556 spectrophotometer just after the preparation of the sol in an Ar atmosphere.

Results and Discussion

Figure 1 shows the time course of the spectra of copper-ethanol colloid. The existence of an isosbestic point at 296 nm shows that the reacting system contains two components. In this system, the metal fine particles change to a single unknown product, because the 577-nm peak, which is characteristic in fine copper particles,[3] gradually decreased as time passed. The increase of the peak height of the 213-nm absorption band is suggestive of the formation of the ethoxide ion.

In the previous paper, we postulated a formation of metal ethoxide. In order to confirm this conjecture, we measured the optical absorption spectrum of the colloid in hexane solution in which no alkoxide can form. Although the fine metal particles have a tendency to coagulate in alkanes, it is possible to measure the absorption spectrum if it is immediately after the preparation of the sample. In Fig.2 is shown the absorption spectra of copper colloid in ethanol (a), and in hexane (b) together with that of ethoxide ion (c). It is clear that there is no 213-nm peak in hexane. Therefore, the 213-nm peak in ethanol is concluded as coming from ethoxide ion.

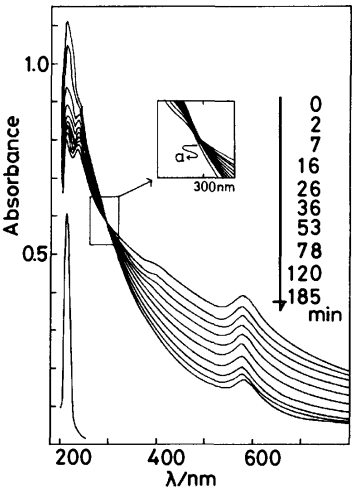

Fig. 1. Optical absorption spectra of copper colloid as a function of time. The number in the figure are the time after the preparation of the sample. The spectrum of sodium ethoxide in ethanol is also shown in the same figure. The insertion is the expansion of the region of isosbestic point. The deviation from the isosbestic point at 10 h after the preparation is shown by a.

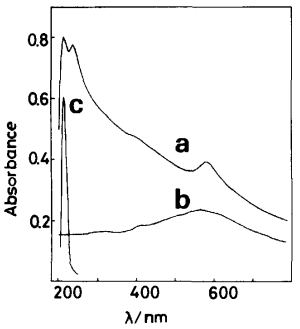

Fig. 2. Absorption spectra of copper colloid in ethanol (a) and in hexane (b). The spectrum of sodium ethoxide in ethanol is shown in c.

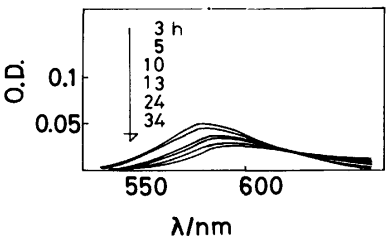

Fig. 3. Optical absorption spectra of copper colloid in the visible region as a function of time later than 3 h. Spectra are drawn after subtraction of the background slope.

Returning now to Fig.1, we notice that the 577-nm peak shifts to longer wavelength at 185 min and that the spectrum does not pass through the isosbestic point at 185 min and at 10 h after the preparation of the sample (see the expanded spectra in the insert). This peak shift is more noticeable after longer periods of time as seen in Fig. 3. After such a long reaction time, all spectra did not pass through the isosbestic point at 296 nm. These findings show that a new reaction phase has progressed. In this stage, the color of the solution gradually changed to yellow from wine red. It should also be noted in the same figure that the band width is broadened with the peak shift. The time dependences of the peak shift, of the band width at the half maxima, and of the absorption intensity are shown in Fig. 4 after correction for background absorption.

As mentioned before, the position of the absorption band of the copper colloid does not vary for the first couple of hours. When it is over 180 min, the peak gradually shifts to longer wavelength. Initially the band width decreases with time, but then it increases later than 180 min with the concurrent shifting of the peak as seen in Fig. 4. As for the intensity, it monotonously decreases with time, corresponding to the decrease of particle size. These findings show that the

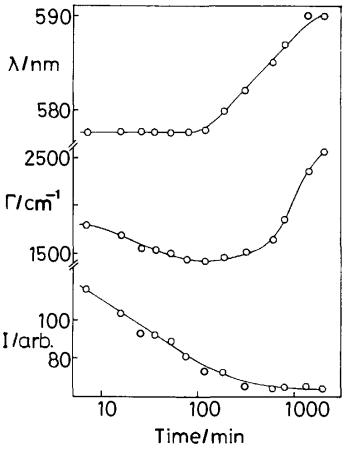

Fig. 4. The absorption peak, the band width and the absorption intensity as a function of time. These were calculated from the spectra in Fig. 3. Solid lines are for eye guide.

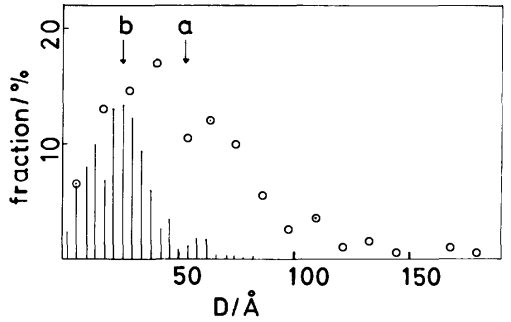

Fig. 5. The distribution of the particle size of colloids. The diameter distribution of the sample, 7 min after the preparation, is shown by circles. The average diameter is indicated by the arrow a. The histogram shows the distribution of the sample at 3 hr after the preparation. The average diameter of this sample is shown by b.

colloid system changes in the size distribution and in the average diameter and that this change becomes prominent at 180 min. The electron micrographs of the colloids were taken at 7 min and at 180 min after the preparation. The size distributions of the colloids at the different time are shown in Fig.5. Just after the preparation, the average diameter of the colloids was 53 Å and the width at the half maxima of the distribution was 60 Å. These values changed to 26 Å and 30 Å respectively at 180 min after. This finding shows that the size distribution becomes narrower and the average diameter also decreases after longer periods.

Based on these observations, we can explain the time dependence of the band width and the position of the absorption peak shown in Fig.4. In the first stage, ultrafine particles diminish rapidly because very small particles easily react with ethanol forming ethoxide. Therefore, the distribution of particle size becomes narrower, resulting in the decrement of the band width, because the absorption band is a superposition of many bands of the particles with different sizes. In the second stage, many particles reduce their radii, resulting in the reduction of the average particle size which may cause the change in the peak position and the band width.

It is well known that the spectrum of fine particles depends on the particle size. Quantum mechanical calculation shows that the band width of the surface plasmon is broadened and the peak shifts to higher energy with a decrease in the radius.[4,5] These results conflict with the present observations, if we explain the peak shift and broadening as a size dependence of a plasmon band. On the other hand, Abe *et al.* reported that the 577-nm band should not be regarded to a pure plasmon band but to interband transitions mixed with plasmon band.[3] Kreibig reported the size dependence of the interband transition edge in gold particles in which the band edge shifts toward lower energy with a decrease in size.[6] If this tendency also holds for the peak position, the peak shift is explaind by the size dependence of the interband transition of copper colloid. The 214-nm peak found in the lead-ethanol system also disappeared in the lead-hexane system. This finding is also consistent with the results of copper described above.

The author wishes to express his thanks to Messrs. S. Bandow and M. Yamakawa in technical assistance. His thanks are due to Prof. S. Sako of Mie University in obtaining the size distribution of the colloids.

References

1) K. Kimura and S. Bandow, *Bull. Chem. Soc. Jpn.*,**56**, 3578 (1983).
2) E. F. Caldin and G. Lang, *J. Chem. Soc.*, **1954**, 3737.
3) H. Abe, K. P. Charle, B. Tesche, and W. Schulze, *Chem. Phys.*, **68**, 137 (1982).
4) A. Kawabata and R. Kubo, *J. Phys. Soc. Jpn.*, **21**, 1765 (1966).
5) L. Genzel, T. P. Martin, and U. Kreibig, *Z. Phys.*, **21**, 339 (1975).
6) U. Kreibig, *J. Phys. (Paris), Colloq.*, C2, 97 (1977).

The Solubilization Site of Methylferrocene in Cationic Micelles

Katsuyoshi HOSHINO, Tetsuo SAJI, Yasuhiko OHSAWA, and Shigeru AOYAGUI*
Department of Chemical Engineering, Tokyo Institute of Technology, Ohokayama, Meguro-ku, Tokyo 152
(Received November 7, 1983)

Synopsis. The voltammetry of methylferrocene (MeFC) in a dodecyltrimethylammonium bromide micellar solution leads to the conclusion that most MeFC molecules reside in the micelle phase. They are located within the hydrophobic core where water cannot reach, judging from our finding that oxygen decomposes MeFC in the presence of water, but otherwise does not.

The most important function of aqueous micelles is to solubilize water-insoluble substances. A number of investigations have been devoted to determining the partition of such substances between the water phase and the micelle phase. Further interest has been taken in the problem of the location of the solubilizate in the micelle, *i.e.*, either the hydrophobic site in the micelle core or the hydrophilic site near the head group.[1]

This paper will deal with the solubilization site of methylferrocene (MeFC) in cationic micelles of dodecyltrimethylammonium bromide (DTMAB). In an earlier paper dealing with the cyclic voltammetry and potentiometry of ferrocene (FC) in nonionic micellar solutions, Yeh and Kuwana suggested that the environment of FC in the micelles was quite similar to that in the hydrophobic liquid membrane, but they gave no direct evidence for it.[2] Unfortunately, the generally applicable method of site determination, which is based on the different absorption maximum frequencies (λ_{max}) of the solubilizate in polar and nonpolar media, cannot be used in our case, because the λ_{max} values of MeFC in both media are very close to each other and MeFC is only poorly soluble in water. Instead, we make use of our finding that oxygen decomposes MeFC in the presence of water, but does not do so in its absence. Though this is a kind of the probe technique which has been extensively used for studying the microenvironment of the micelle, the chemical reactions of the guest substances have rarely been used for this purpose, except for quenching reactions[1] and chemical equilibria.[3-6] The redox potential of the $MeFC^{+/0}$ couple in DTMAB micellar solution is also measured to determine the partition of MeFC between the micelle phase and the water phase.

TABLE 1. SOLUBILITY AND PARTITION PARAMETER (K_R) OF FERROCENE (FC), METHYLFERROCENE (MeFC) AND BUTHYLFERROCENE (n-BuFC) IN 0.2 M Li_2SO_4 WITH AND WITHOUT 0.1 M DODECYLTRIMETHYLAMMONIUM BROMIDE AT 25 °C

Complex	$[C_W]_{sat}$[a]/mM	$[C]_{sat}$[b]/mM	10^2K_R[c]
FC[d]	0.035	1.35	2.7
MeFC	0.15	11.1	1.4
n-BuFC	0.14	8.32	1.7

a, b) Solubility of complex (C) in a) water and b) a micellar solution respectively. c) Ratio of the concentration of the complex in the water phase to that in the micelle phase. d) Data in Ref. 8.

Experimental

MeFC was prepared by the literature method.[7] The molar absorptivity values of MeFC at 250 nm, $1.8\times10^3\ M^{-1}\ cm^{-1}$ ($1\ M=1\ mol\ dm^{-3}$) in the water phase and $4.0\times10^3\ M^{-1}\ cm^{-1}$ in the micelle phase, were determined by the method described in a previous paper.[8] The other experimental procedures used in this work were also described in that paper.

Results and Discussion

According to our previous paper,[8] we can determine the partition parameter, K_R *i.e.*, the ratio of the concentration in moles of MeFC in water to that in micelles, per liter of the micellar solution, under the specific conditions of $MeFC^+$ residing only in the water phase. To see if these conditions are fulfilled, the obserbed value for the reversible half-wave potential of the $MeFC^{+/0}$ in the micellar solution ($E^r_{1/2}$) was compared with the value calculated by using the following equation:[8]

$$E^r_{1/2}=E^0_W+(RT/F)\ln(1+K_R)/K_R-(RT/F)\ln(D_0/D_R)^{1/2}, \quad (1)$$

with:

$$D_R=(D_{RM}+K_RD_{RW})/(1+K_R) \quad (2)$$

and:

$$K_R=[MeFC_W]/[MeFC_M]=[MeFC_W]_{sat}/([MeFC]_{sat}-[MeFC_W]_{sat}). \quad (3)$$

The abbreviations used are the same as have been described in a previous paper.[8]

Tables 1 and 2 summarize, respectively, the results of the spectroscopic determination of the solubility and

TABLE 2. VOLTAMMETRIC DATA OF METHYLFERROCENE (MeFC) AND METHYLFERROCENIUM ($MeFC^+$) IN 0.2 M Li_2SO_4 WITH AND WITHOUT 0.1 M DODECYLTRIMETHYLAMMONIUM BROMIDE (DTMAB) AT 25 °C[a]

Complex	DTMAB/M	D_R[b]/$cm^2\ s^{-1}$	D_0[c]/$cm^2\ s^{-1}$	$E^r_{1/2}$[d]/V	$E^r_{1/2W}$[e]/V
MeFC	0.1	0.82×10^{-6}	—	0.185	—
$MeFC^+$	0.1	—	7.1×10^{-6}	0.185	—
MeFC	0	—	—	—	0.114

a) All the voltammograms are diffusion-controlled, as is indicated by the linear plot of the peak current *vs.* the square root of the potential-scan rate. b, c) Apparent diffusion coefficients of b) $MeFC^+$ in a micellar solution respectively. d, e) Reversible halfwave potentials of the $MeFC^{+/0}$ redox system in d) a micellar solution and e) water respectively. The latter value was estimated from the peak potential in the reduction of $MeFC^+$ plus 0.029 V.

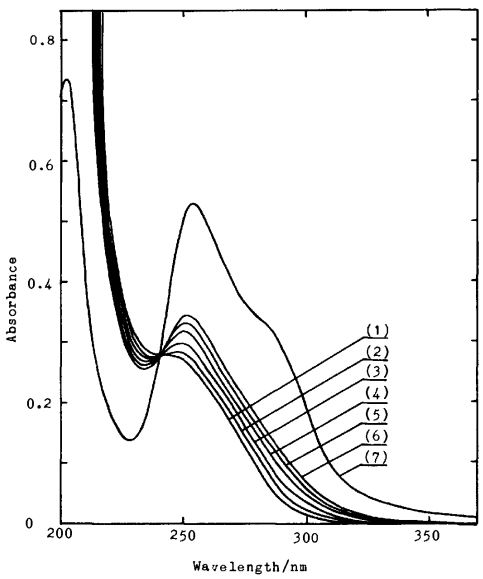

Fig. 1. UV absorption spectra of methylferrocene saturated in aqueous 0.2 M Li_2SO_4 at 25°C recorded at time t after oxygen introduction into the solution: t=(1) 0, (2) 40, (3) 87, (4) 150, (5) 203, (6) 258 min, and (7) 7 d.

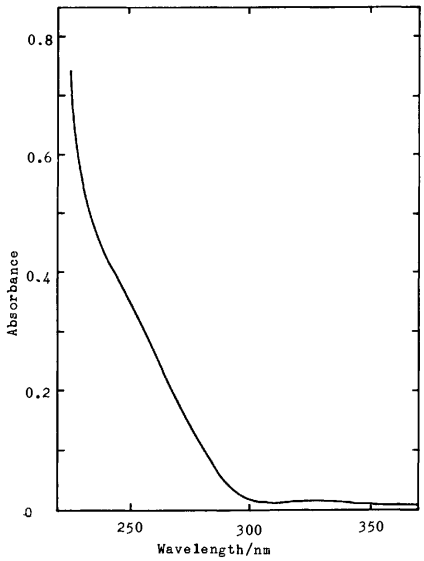

Fig. 2. UV absorption spectrum of 0.088 mM methylferrocene in an aqueous solution of 0.2 M Li_2SO_4 and 0.1 M dodecyltrimethylammonium bromide.

the voltammetric determination of the diffusion coefficient and the reversible half-wave potential. Table 1 also lists the data for FC and butylferrocene (*n*-BuFC). The ($E^r_{1/2W}$), value for the redox couple $MeFC^{+/0}$ calculated from Eqs. 1 and 3 with these data was 0.186 V *vs.* SCE. It is in excellent agreement with the experimental value of 0.185 V. Consequently, Eq. 1 applies to this redox system; hence, it can be concluded that the $MeFC^+$ ions are located only in the water phase and that most of the MeFC molecules reside in the micelle phase, as is indicated by the small K_R value of 1.4×10^{-2}.

Figure 1 shows the absorption spectra of a saturated solution of MeFC (0.15 mM) in 0.2 M Li_2SO_4, which were recorded (1) before and (2—7) after the introduction of oxygen gas into the solution. In the absence of oxygen, the 1 spectrum was kept unchanged for more than a day, but in its presence a new peak appeared at about 250 nm and grew linearly in height with the time, while the peak at 200 nm got lower. The isosbestic point at 240 nm indicates that this reaction gives only one product. The reaction scheme of the oxidation of MeFC will be discussed in a separate paper. Contrary to aqueous solutions, the spectra of MeFC in nonaqueous solvents, such as hexane, ethanol, and acetonitrile, were kept unchanged for more than 100 d in the presence of oxygen. These findings show that MeFC reacts with oxygen only in the coexistence of water.

Figure 2 shows an absorption spectrum of MeFC in a micellar solution. According to the above voltammetric results, the spectroactive species is the MeFC located in and/or on the micelle. The fact that the shape of this spectrum did not change for more than 4 h after introducing oxygen gas into the solution strongly suggests that the microenvironment of the solubilized MeFC molecules is highly hydrophobic for the following reasons: the decomposition of MeFC requires both water and oxygen; the solubilities of ferrocene and oxygen are higher in aliphatic solvents than in water; we have evidence for oxygen residing in micelles.[9] Considering the NMR experimental finding of Menger *et al.* that water molecules can penetrate into the micelle core as far as seven carbon atoms away from the head group,[10] we can conclude that the MeFC molecules reside deep in the interior of the micelle core where water molecules cannot reach. However, another finding of the same authors, that the CH≡ group substituted for the terminal methyl protons of $DTMA^+$ is located in a wet environment[11], seems incompatible with our findings, if no specific conformation of this surfactant molecule is assumed.

The authors wish to thank Dr. Masamichi Fujihira for his helpful suggestions.

References

1) J. H. Fendler and E. J. Fendler, "Catalysis in Micellar and Macromolecular Systems," Academic Press, New York (1975).
2) P. Yeh and T. Kuwana, *J. Electrochem. Soc.*, **123**, 1334 (1976).
3) N. Shoji, M. Ueno, and K. Meguro, *J. Am. Oil Chem. Soc.*, **53**, 165 (1976).
4) N. Shoji, M. Ueno, and K. Meguro, *J. Am. Oil Chem. Soc.*, **55**, 297 (1978).
5) F. M. Menger and B. J. Boyer, *J. Am. Chem. Soc.*, **102**, 5936 (1980).
6) F. M. Menger, H. Yoshinaga, K. S. Venkatasubban, and A. R. Das, *J. Org. Chem.*, **46**, 415 (1981).
7) A. N. Nesmeyanov, E. G. Paravalova, L. S. Shilovtseva, and Z. A. Beĭnoravichute, *Dokl. Akad. Nauk SSSR*, **121**, 117 (1958).
8) Y. Ohsawa and S. Aoyagui, *J. Electroanal. Chem.*, **136**, 353 (1982).
9) F. M. Menger, *Acc. Chem. Res.*, **12**, 111 (1979).
10) F. M. Menger, J. M. Jerkunica, and J. C. Johnston, *J. Am. Chem. Soc.*, **100**, 4676 (1978).
11) F. M. Henger and J. F. Chow, *J. Am. Chem. Soc.*, **105**, 5501 (1983).

Translational Energy Distribution of the Excited Hydrogen Atom (n=4) Produced in Electron-Benzene Collisions

Hirofumi KAWAZUMI, Junichi KURAWAKI, and Teiichiro OGAWA*
Department of Molecular Science and Technology, Kyushu University, Kasuga, Fukuoka 816
(Received December 26, 1983)

Synopsis. Line shapes of the Balmer-β line of H* produced in dissociative excitation of C_6H_6 were precisely measured. The translational energy distributions of H* (n=4) have two peaks at about 1 and 4 eV, and their relative intensity depends on incident electron energy.

Benzene is a basic organic molecule with a high symmetry. All six hydrogen atoms are equivalent. The dissociation mechanism of benzene for the formation of the excited hydrogen atoms should be a key process for dissociation dynamics of the organic molecule.

Benzene gives photoemissions of both its own excited states and fragment species such as H* and CH* upon collision with electrons.[1-4] Balmer series are intense, and the analysis of the Doppler line shape can give the translational energy distribution of the excited hydrogen atom.[5] The translational energy distribution is useful not only for an elucidation of dissociation mechanism of highly excited molecule but also for a correction of optical signal losses due to the high velocity of the fragments in the determination of the absolute emission cross section.

This note presents the translational energy distributions of H* (n=4) and D* (n=4) produced by controlled electron impact on C_6H_6 and C_6D_6 and their incident electron energy dependence.

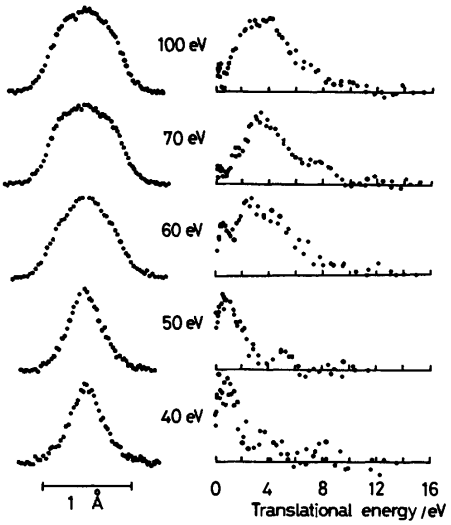

Fig. 1. High resolution spectra and translational energy distribution of H*(n=4) produced in e-C_6H_6 collisions. Electron energy: 40—100 eV, optical resolution: 0.0031—0.0042 nm.

Experimental

The apparatus has been described in detail previously.[6] The Balmer lines were measured at optical resolution of 0.0031—0.0042 nm with a Fabry-Perot interferometer; this resolution is sufficient for the analysis of the Doppler profile. Excitation function was measured with an interference filter (band width 2 nm). Benzene (research grade) was deaerated before use.

Results and Discussion

The line shapes of the Balmer-β emissions produced in e-C_6H_6 collisions were measured precisely at 90° with respect to the electron beam and the results taken at various incident electron energies are shown in the left of Fig. 1. The translational energy distributions calculated from them are shown in the right of Fig. 1.

The line shapes of H* (n=4) from C_6H_6 taken a 90° and at 55° (magic angle) and D* (n=4) from C_6D_6 taken at 90° were also recorded for comparison at an electron energy of 100 eV, as shown in Fig. 2; their translational energy distributions have been obtained. The line shapes and the translational energy distributions at 90° and at 55° agreed with each other within the experimental uncertainty; thus, effect of anisotropy seems to be small.

The translational energy distribution has a peak at 1 eV when excited at electron energies of 40—50 eV. With increasing the incident electron energy, a new peak appears at about 4 eV; the distribution shifts toward higher energy. There seems to be an additional shoulder at 6—8 eV at an electron energy of 100 eV. The translational energy distribution of H* (n=4) measured at 100 eV looks similar to those from CH_4[7]

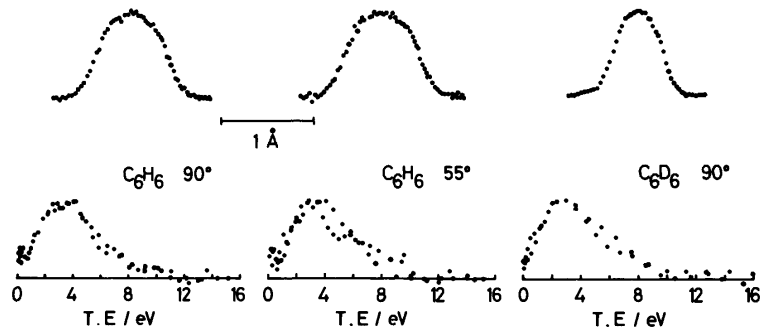

Fig. 2. High resolution spectra and translational energy distribution of H*(D*) produced in e-C_6H_6(C_6D_6) collisions at 100 eV.

and $CHCl_3$.[8] These results indicate that a few electronic excited states and a few dissociation processes take part in the production of the excited hydrogen atoms. The dissociation process, which has the peak of the translational energy distribution at 4 eV, is the major process at higher excitation energy and should proceed through repulsive potential surfaces. This process should also be symmetry forbidden, since the slope of the Fano plot for the Balmer-β emission is zero.[4]

The excited hydrogen atom with 4 eV of the translational energy has a velocity of 28000 $m \cdot s^{-1}$ and about 3 mm in 119 ns (average lifetime of H* (n=4)). A correction for the loss of the excited species is necessary for the determination of the absolute emission cross section and this correction should be estimated from the translational energy distribution. Furthermore, the fly-out rate of H* from the collision volume and the correction for the absolute emission cross section depend on the incident electron energy.

The dissociation processes are expected to be identical for isotope molecules such as H_2 and D_2,[9] and H_2O and D_2O,[10] however, the relative importance of coexisting processes are often different. In the case of benzene there is no clear quantitative difference in the translational energy distributions of H* and D* (Fig. 2).

The measured excitation function for the Balmer-β emission (0—100 eV) is similar to that reported by Beenakker and de Heer.[4] The threshold energy are 19.6±0.6 eV for C_6H_6, which agrees well with previous papers,[4,11] and 19.5±1.3 eV for C_6D_6; no obvious onset was observed except the first threshold.

The observed translational energy distributions and threshold energy indicate that a major route for the formation of the excited hydrogen atoms as lower incident electron energies is as follows:

$$C_6H_6(19.6\,eV) \rightarrow C_6H_5(\tilde{X}\,^2A_1) + H^*(n=4) + E_{excess}(2.0\,eV)$$
$$E_{excess}(2.0\,eV) = E_{trans}(\approx 1\,eV) + E_{int}(\approx 1\,eV),$$

where (19.6 eV) represents the excitation energy, E_{excess} the energy equal to the difference between the excitation energy and the calculated dissociation limit, E_{trans} the translational energy of H* and E_{int} the internal energy.

At higher incident electron energies, an enormous number of direct and multistep fragmentation paths can be estimated from thermochemical data. Doubly excited Rydberg states converging to excited ion states or doubly ionized states, which are optically forbidden and generally repulsive, should play important roles.

References

1) T. Ogawa, M. Tsuji, M. Toyoda, and N. Ishibashi, *Bull. Chem. Soc. Jpn.*, **46**, 2637 (1973).
2) K. C. Smyth, J. A. Schiavone, and R. S. Freund, *J. Chem. Phys.*, **61**, 4747 (1974).
3) T. Ogawa, N. Yamami, M. Tsuji, and Y. Nishimura, *Bull. Chem. Soc. Jpn.*, **54**, 1203 (1981).
4) C. I. M. Beenakker and F. J. de Heer, *Chem. Phys. Lett.*, **29**, 89 (1974).
5) T. Ogawa and M. Higo, *Chem. Phys. Lett.*, **65**, 610 (1979).
6) M. Higo and T. Ogawa, *Chem. Phys.*, **44**, 279 (1979).
7) T. Ogawa, J. Kurawaki, and M. Higo, *Chem. Phys.*, **61**, 181 (1981).
8) T. Ogawa, F. Miyoshi, and M. Higo, *Bull. Chem. Soc. Jpn.*, **55**, 1790 (1982).
9) M. Higo, S. Kamata, and T. Ogawa, *Chem. Phys.*, **66**, 243 (1982).
10) J. Kurawaki, K. Ueki, M. Higo, and T. Ogawa, *J. Chem. Phys.*, **78**, 3071 (1983).
11) I. Tokue and M. Ikarashi, *Bull. Chem. Soc. Jpn.*, **54**, 2565 (1981).

Determination of Solubility Products of Rare Earth Fluorides by Fluoride Ion-selective Electrode

Hisako ITOH, Hiromitsu HACHIYA, Masashi TSUCHIYA, Yasuo SUZUKI,* and Yasukazu ASANO†

Department of Industrial Chemistry, Faculty of Engineering, Meiji University, Higashimita, Tama-ku, Kawasaki 214

†*Denki Kagaku Keiki Co., Ltd. Kichijoji-kitamachi, Musashino, Tokyo 180*

(Received August 26, 1983)

Synopsis. Solubility product values of the rare earth fluorides were determined potentiometrically by using fluoride ion-selective electrodes at 25.0 °C. The pK_{sp} values of the lanthanoid fluorides decreased gradually from 20.0 to 16.9, while the value for yttrium fluoride was locate in between those of terbium and dysprosium fluorides. The value for scandium fluoride was appreciably smaller than any of the lanthanoid fluorides, as expected from the cationic radii. The solubility product value of lanthanum fluoride single crystal could not be determined, since the saturated solution was not obtained through measurements of over three months.

Generally, the solubilities of lanthanoid salts increase with increasing atomic number when the anion of the salt arises from a strong acid and decreases with increasing atomic number when the anion originates from a weak acid. For example, solubility of the sulfates increases with increasing atomic number, while that of the hydroxides or dimethylphosphates decreases with increasing atomic number.[1)]

The solubility product values of lighter and heavier rare earth fluorides were determined titrimetrically by Nikolaev *et al.*[2)] and Ikurami *et al*,.[3)] respectively. Fraustro da Silva and Queimado[4)] also determined the solubility product values of the fluorides throughout the rare earth elements in mixed solutions of sodium fluoride and rare earth nitrates by using a fluoride ion-selective electrode. They showed that the solubility of the lanthanoid fluorides increased with increasing atomic number. In this study, the solubility product values of the rare earth fluorides, including yttrium and scandium fluorides, were determined in solution containing the respective fluorides only by using a fluoride ion-selective electrode.

Experimental

Reagents. Fifteen rare earth fluorides of 99.99% purity were obtained from Shin-etsu Chem. Ind. Co., Ltd. Single crystals of lanthanum fluoride prepared for the fluoride ion-selective electrode membrane were supplied from Denki Kagaku Keiki Co., Ltd. One of the single crystals was an europium-doped lanthanum fluoride. All the other chemicals were of reagent grade.

Apparatus and Procedure. Denki Kagaku Keiki model 7200 fluoride ion-selective electrode and model 4083 double junction Ag-AgCl reference electrode were used with Denki Kagaku Keiki model IOC-10 pH/mV meter.

A portion of a fluoride powder was taken into a covered polyethylene beaker together with water, and stirred continuously at 25.0 °C until a constant millivolt reading was obtained with the fluoride ion-selective electrode. After keeping the mixture for another day without stirring at 25.0 °C, an aliquot portion of the supernatant was brought to a pH of 5 with a portion of the Denki Kagaku Keiki pH5-AB buffer solution. To prevent the formation of hydrogen fluoride in acidic solutions, the sample solution has to be kept at pH 5 by using the buffer solution, as described above.

Calculations. In a solution, a rare earth fluoride should be dissociated as described in Eq. 1:

$$LnF_3 \longrightarrow Ln^{3+} + 3F^-, \quad (1)$$

where Ln means a rare earth element. The solubility product values can be calculated by Eq. 2, if no common ions are originally present in the solution:

$$K_{sp} = [Ln^{3+}][F^-]^3 = \frac{[F^-]^4}{3}. \quad (2)$$

Since the activity coefficient of fluoride ion may be considered unity in solution of such a low concentration, the activity of fluoride ion would be equal to the concentration.

Results and Discussion

The solubility product values obtained for the powder of the rare earth fluorides are shown in Table 1. The pK_{sp} values apparently decrease with increasing atomic number of lanthanoids. This tendency agrees with the assumption that the solubility of the slightly soluble salts of lanthanoids derived from the anions of strong acids increases with increasing atomic number. On the other hand, one would expect that solubility decreases with increasing atomic number, since the size of the lanthanoid ion decreases and the lattice energy is inversely proportional to the sum of the anion and the cation radii. Fraustro da Silva and Queimado[4)] showed that the solubility product values would be affected by the lattice and hydration energies, and thus the order of the pK_{sp} values was correct.

The comparison of the solubility product values of this study with the values of Fraustro da Silva and

TABLE 1. SOLUBILITY PRODUCT VALUES OF RARE EARTH FLUORIDES

Fluoride	K_{sp}	pK_{sp}
LaF_3	3.26×10^{-21}	20.5
CeF_3	1.69×10^{-20}	19.8
PrF_3	1.54×10^{-19}	18.8
NdF_3	5.31×10^{-20}	19.3
SmF_3	1.05×10^{-19}	19.0
EuF_3	1.37×10^{-19}	18.9
GdF_3	2.36×10^{-19}	18.6
TbF_3	2.85×10^{-19}	18.5
DyF_3	8.23×10^{-19}	18.1
HoF_3	1.12×10^{-18}	18.0
ErF_3	1.52×10^{-18}	17.8
TmF_3	2.55×10^{-18}	17.6
YbF_3	6.43×10^{-18}	17.2
LuF_3	1.26×10^{-17}	16.9
YF_3	4.41×10^{-19}	18.4
ScF_3	2.98×10^{-12}	11.5

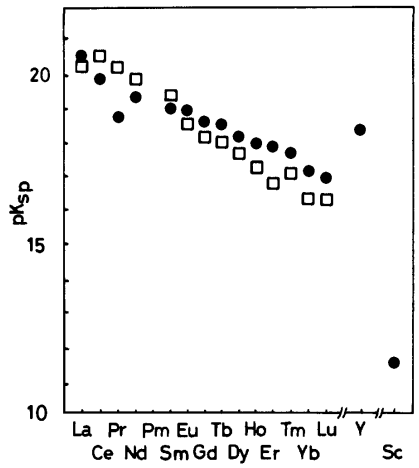

Fig. 1. A comparison of the pK_{sp} values of the rare earth fluorides at 25.0°C.
●: This work, □: Fraustro da Silva and Queimado.[4]

Queimado is given in Fig. 1. Their report were made in mixed solutions of sodium fluoride and rare earth nitrate; thus the fluoride solutions contained nitrate, sodium, and rare earth ions. In this study, the solubility product values were determined by using the rare earth fluoride powder, and the sample solutions contained only rare earth and fluoride ions. As shown in Fig. 1, the present values are in fairly good agreement with those of Fraustro da Silva and Queimado, though the present pK_{sp} slope is apparently smaller than theirs. The rather unusual pK_{sp} location of praseodymium fluoride was not corrected even after the repeated measurements. The difference of the pK_{sp} values would be attributed to the origin of the rare earth fluorides present in the solutions.

The solubility product value of lanthanum fluoride single crystal was determined by the same experimental procedures as used for the powder fluorides; however, no saturated solutions of fluoride ion were obtained even after more than three months of continuous stirring. The previously reported solubility product values[5-8] of lanthanum fluoride single crystal were widely scattered and remarkably smaller than those of the powder fluorides, possibly because of the difference in crystal size or surface. Single crystals could be dissolved at considerably slower rates than the powder fluorides. This means that lanthanum fluoride single crystal is preferable to the fluoride powder as the fluoride ion-selective electrode membranes.

References

1) C. S. G. Phillips and R. J. P. Williams, "Inorganic Chemistry," Clarendon Press, Oxford (1966), Vol. 2, p. 112.
2) N. S. Nikolaev, Sh. A. Abdurakhmanov, and Kh. Sh. Dzhuraev, *Russ. J. Inorg. Chem.*, **19**, 618 (1974).
3) D. D. Ikurami, Kh. Sh. Dzhuraev, and N. S. Nikolaev, *Dokl. Akad. Nauk Tadzh. SSR*, **9**, 35 (1970).
4) J. R. Fraustro da Silva and M. M. Queimado, *Rev. Port. Quim.*, **15**, 29 (1973).
5) G. D. Moody and J. D. R. Thomas, "Selective Ion Sensitive Electrodes," Merrow, Watford (1971).
6) M. S. Frant and J. W. Ross, *Science*, **154**, 1553 (1966).
7) J. Buffle, N. Parthasarathy, and W. Haerdy, *Anal. Chim. Acta*, **68**, 253 (1974).
8) J. Vasely and K. Stulik, *Anal. Chim. Acta*, **73**, 157 (1974).

A Short Synthesis of Dihydrojasmone, *cis*- and *trans*-Jasmones

Fumio OGURA,* Tetsuo OTSUBO, Tetsuo SAKAMOTO, and Hachiro YAMAGUCHI†
Department of Applied Chemistry, Faculty of Engineering, Hiroshima University, Shitami, Saijo, Higashi-Hiroshima 724
†*Faculty of Pharmaceutical Sciences, Fukuyama University, Fukuyama 729-02*
(Received October 7, 1983)

Synopsis. The titled jasmones were synthesized from *N,N'*-dimethyl-2-oxo-1,3-propanedisulfonanilide, a new three carbon building block for organic preparation.

2-Oxo-1,3-propanedisulfonic acid (**1**), which is easily accessible from acetone, has three kinds of reactive groups (sulfonic acid, carbonyl, and methylene groups) and seems to be a promissing intermediate for routine synthesis. But little is known about its synthetic utilization. Recently we have reported an application of the dialkyl sulfonates as practical alkylating reagents.[1] To show the utility of **1**, we now report a new synthesis of dihydrojasmone, *cis*- and *trans*-jasmones from *N,N'*-dimethyl-2-oxo-1,3-propanedisulfonanilide (**3**) through undecane- and 8-undecene-2,5-diones. The sulfonanilide can be prepared easily from the corresponding sulfonyl chloride (**2**)[1] and *N*-methylaniline and it behaves as an acetone with highly activated methylenes.

$O{=}C(CH_2X)_2$ **1**, X=SO_3H; **2**, X=SO_2Cl; **3**, X=$SO_2N(CH_3)Ph$

The process of synthesis was outlined in Scheme 1. In the case of dihydrojasmone, introduction of two necessary carbon fragments, pentyl and acetonyl groups, into **3** was conducted in one pot reaction with a high yield. Thus, the dianion generated from **3** with two equivalents of sodium hydride was allowed to react first with 3-bromo-2-methoxypropene[2] and the resulting reaction mixture was treated with one more equivalent of NaH. The unsymmetrical dianion formed was then alkylated with 1-iodopentane. The product enol ether (**4a**) was easily hydrolysed with HCl in acetic acid to the diketone (**5a**), which was desulfonated with aluminum amalgum in THF to afford 2,5-undecanedione (**6a**). The aldol cyclization of **6a** with NaOH in aq ethanol yielded dihydrojasmone (**7a**).[3] By the essentially same procedure, using *cis*- and *trans*-1-bromo-2-pentenes in place of 1-iodopentane, *cis*- and *trans*-jasmone were synthesized, respectively.

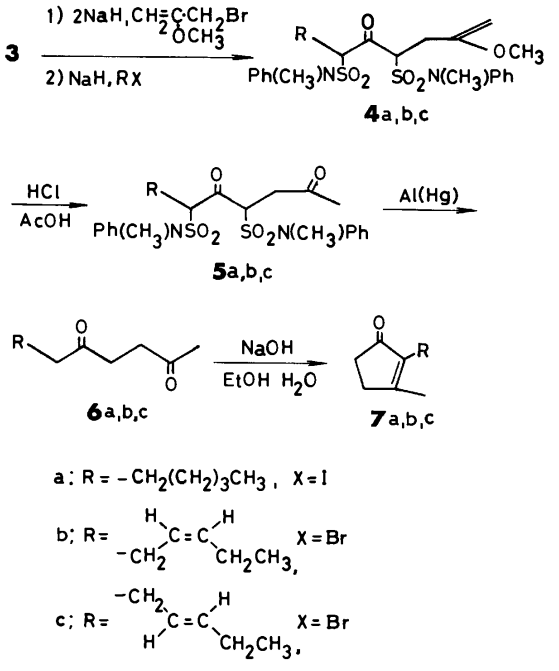

Scheme 1.

As illustrated above, the sulfonanilide (**3**) seems to be a good synthetic part for nucleophilic introduction of acetone unit. Particularly it is noteworthy that the smooth introduction of two electrophiles into the both methylene carbons of **3** is possible in one pot reaction, involving the successive generation of dianions.[4]

Experimental

The melting points were not corrected. The solvents were of a reagent grade. All the known compounds were confirmed by a comparison of the melting points and spectroscopic data with those of the authentic samples or the reported data. The reaction products were fractionated with a JAI LC-08 gel permeation liquid chromatograph (GPLC) using chloroform as eluent. The ^1H NMR spectra were recorded on a JEOL PMX-60 spectrometer in $CDCl_3$ and the shifts were given in δ unit from internal TMS. The IR spectra were measured on a Hitachi 260-30 spectrometer. The boiling points shown were bath temp.

N,N'-Dimethyl-2-oxo-1,3-propanedisulfonanilide (3). *N*-Methylaniline (149.7 g, 1.397 mol) was added dropwise to a benzene (60 cm^3) suspension of 2-oxo-1,3-propanedisulfonyl chloride (**2**, 118.9 g, 0.466 mol)[1] at 13—15 °C with stirring. After stirring was continued for 4 h at the same temperature, benzene was removed under reduced pressure and the residue was poured into aq MeOH (500 cm^3, 1:1 v/v). The mixture was made acidic with HCl and the precipitated crystals were collected by suction filtration, washed with water, and dried. Recrystallization from methanol yielded colorless crystals (122.6 g, 71%, mp 77—78 °C).[5] IR: 1725 ($\nu_{C=O}$) cm^{-1}. ^1H NMR: 3.30 (s, 6H, CH_3), 4.27 (s, 4H, CH_2), 7.35 (s, 10H, Ph). Found: C, 51.76; H, 4.96; N, 7.04%. Calcd for $C_{17}H_{20}N_2O_5S_2$: C, 51.50; H, 5.08; N, 7.07%.

N,N'-Dimethyl-2,5-dioxo-4,6-undecanedisulfonanilide (5a). Sodium hydride (60% in mineral oil, 1.20 g, net 30.0 mmol) was washed twice with hexane and suspended in DMSO 30 cm^3) under N_2. The sulfonanilide (**3**) was added to the mixture with stirring at the room temp and stirring was continued for 1 h. 3-Bromo-2-methoxypropene[2] (3.0 g, 45 mmol) was added dropwise with stirring and the mixture was stirred for 3 h at the ambient temp. Sodium hydride (60% in mineral oil, 0.60 g, net 15 mmol) was added and the mixture was stirred for 0.5 h. 1-Iodopentane (2.37 g, 12.0 mmol) was added to the mixture and stirring was continued for further 3 h at the room temp. The reaction mixture was decomposed with water (10 cm^3) and made acidic with HCl. The mixture was extracted with $CHCl_3$ and the combined extracts were washed with water and dried ($MgSO_4$). The crude product obtained on concentration under reduced pressure was subjected to GLPC fractionation. The enol ether (**5a**) was effectively separated by means of the recycle tech-

nique and hydrolyzed with AcOH (20 cm³) containing 1 M† HCl (10 cm³). The diketone (**5a**) was extracted with ether and the combined extracts were washed with 5% aq $NaHCO_3$ and water, successively, and dried (Na_2SO_4). On the vacuum concentration, **5a** was obtained as a colorless viscous oil (4.47 g, 85.5%). IR (neat): 1726 (sh, $\nu_{C=O}$), 1720 ($\nu_{C=O}$) cm^{-1}. ^1H NMR: 0.55—1.57 (m, 11H, pentyl), 2.0 (s, 3H, CH_3 of acetyl), 2.87 (d, J=6 Hz, 2H, CH_2 of acetonyl), 3.27 (s, 6H, CH_3-N), 4.76 (dd, J=10 and 4 Hz, 1H, pentyl side methine), 5.8 (t, J=6 Hz, 1H, acetonyl side methine), 7.32 (s, 10H, Ph). Found: C, 57.62; H, 6.62; N, 4.58%. Calcd for $C_{25}H_{24}N_2O_6S_2$: C, 57.45; H, 6.56; N, 4.36%.

*2, 5-Undecanedione (**6a**).* The sulfonanilide (**5a**, 2.66 g, 5.09 mmol) was dissolved in the mixture of THF (170 cm³) and water (10 cm³). Aluminum amalgum prepared from Al foil (4.12 g, 0.15 mol) was added to the solution and heated to reflux[6] for 3 h. After cooling down, the reaction mixture was digested with cold dil HCl and THF was removed under reduced pressure. The residue was extracted with ether and the combined extracts were washed with brine, dried (Na_2SO_4), and concentrated under reduced pressure. The crude diketone was purified by GPLC and bulb to bulb distillatin (bp 99—101 °C/1 Torr, 1 Torr=133.322 Pa) to yield a faintly yellow oil (0.45 g, 47.9%). IR (neat): 1703 ($\nu_{C=O}$) cm^{-1}. ^1H NMR: 0.87 (deformed t, J=5 Hz, 3H, CH_3 of hexyl), 1.07—1.85 (m, 8H, internal tetramethylenes of hexyl), 2.17 (s, 3H, CH_3 of acetyl), 2.27 (t, J=7 Hz, 2H, terminal methylene of hexyl), 2.67 (s, 4H, methylenes between carbonyls). Found: C, 70.70 H, 10.94%. Calcd for $C_{12}H_{20}O_2$: C, 70.90; H, 10.77%. Desulfonation could also be done by 6% Na(Hg) in MeOH containing Na_2HPO_4 (21% yield).

*3-Methyl-2-pentyl-2-cyclopentenone (Dihydrojasmone, **7a**).* The diketone (**6a**, 0.560 g, 3.04 mmol) was submitted to the aldol cyclization according to the reported method[3] to yield dihydrojasmone as a colorless oil (bp 110—112 °C/10 Torr, 0.39 g, 77.3%). IR (neat): 1700 ($\nu_{C=O}$), 1645 ($\nu_{C=C}$) cm^{-1}. ^1H NMR: 0.55—1.85 (m, 9H, methyl and internal trimethylenes of pentyl), 1.95—2.90 (m including s at 2.07 for CH_3 at C_3, 9H, CH_3, ring methylenes, and the terminal methylene of pentyl). Found: C, 79.53; H, 10.69%. Calcd for $C_{11}H_{18}O$: C, 79.46; H, 10.91%. 2,4-Dinitrophenylhydrazone melted at 120—121 °C.[7] Found: C, 58.92; H, 6.17; N, 16.12%. Calcd for $C_{17}H_{22}O_4N_4$: C, 58.95; H, 6.40; N, 16.17%.

*cis- and trans-N,N'-Dimethyl-2,5-dioxo-8-undecene-4,6-disulfonanilides (**5b and 5c**).* By the essentially same procedure, **3** was allowed to react first with 3-bromo-2-methoxypropene[2] and then with *cis-* or *trans-*1-bromo-2-pentene[8] in place of 1-iodopentane. Working up in the same way as in the case of **5a** yielded **5b** or **5c** as a faintly yellow viscous oil (both 86%).

*cis- and trans-8-Undecene-2,5-diones (**6b and 6c**).* The dioxodisulfonanilide (**5b**, 2.42 g, 4.65 mmol or **5c**, 1.99 g, 3.82 mmol) was refluxed in the mixture of THF and water (200 cm³, 9:1 v/v for **5b** or 130 cm³, 15:1 v/v for **5c**) with aluminum amalgum, prepared from Al foil (6.27 g, 0.23 mol for **5b** or 3.24 g, 0.12 mol for **5c**) for 3 h under stirring. Working up the reaction mixture in the same way as in the case of **6a** afforded **6b** or **6c** as a colorless oil (**6b**: bp 140 °C/2 Torr, 0.40 g, 47.3%; **6c**: bp 137 °C/4 Torr, 0.11 g, 15.8%). IR: **6b** (neat), 1710 ($\nu_{C=O}$); **6c** (neat), 1712 ($\nu_{C=O}$) cm^{-1}. ^1H NMR: **6b**, 0.95 (t, J=7 Hz, 3H, CH_3 of heptenoyl), 1.27—*ca.* 2.5 (m, 4H, allylic methylenes), 2.18 (s, 3H, CH_3 of acetyl), 2.43 (t, J=4 Hz, 2H, heptenoyl methylene neighboring to the carbonyl), 2.7 (s, 4H, methylenes between carbonyls), 5.2—5.6 (m, 2H, olefinic); **6c**, 0.95 (t, J=7 Hz, 3H, CH_3 of heptenoyl), 1.1—2.6 (m, 6H, methylenes of heptenoyl), 2.18 (s, 3H, CH_3 of acetyl), 2.68 (s, 4H, methylenes between carbonyls), 5.3—5.6 (m, 2H, olefinic). Found: **6b**, C, 71.98; H, 9.58%; **6c**, C, 72.75; 9.94%. Calcd for $C_{11}H_{18}O_2$: C, 72.49; H, 9.95%.

*2-(cis-2-Pentenyl)-3-methyl-2-cyclopentenone (cis-Jasmone, **7b**).* The diketone (**6b**, 0.303 g, 1.66 mmol) was refluxed in 0.5 M aq NaOH (5 cm³) containing ethanol (2 cm³) for 5 h. The reaction mixture was extracted with ether. The combined extracts were washed with brine, dried (Na_2SO_4), and concentrated under reduced pressure. The crude product was purified by GPLC and vacuum distillation to yield a colorless oil (bp 82—85 °C/1 Torr, 0.13 g, 50%). IR (neat): 1700 ($\nu_{C=O}$), 1650 ($\nu_{C=C}$) cm^{-1}. ^1H NMR: 0.98 (t, J=7 Hz, 3H, CH_3 of pentenyl), 1.7—2.7 (m, 6H, methylenes), 2.07 (s, 3H, CH_3 at C_3), 2.94 (d, J=5 Hz, 2H, CH_2 between double bonds), 5.1—5.7 (m, 2H, olefinic). Found: C, 79.91; H, 9.71%. Calcd for $C_{11}H_{16}O$: C, 80.44; H, 9.82%. 2,4-Dinitrophenylhydrazone melted at 115—116 °C.[9] Found: 59.05; H, 5.96; N, 15.91%. Cacld for $C_{17}H_{20}O_4N_4$: C, 59.29; H, 5.85; N, 16.27%.

*2-(trans-2-Pentenyl)-3-methyl-2-cyclopentenone (trans-Jasmone, **7c**).* The diketone (**6c**, 0.240 g, 1.32 mmol) was heated to reflux for 6 h in the mixture of ethanol (2 cm³) and 0.5 M aq NaOH (3 cm³). The reaction mixture was worked up and purified in the same way as in the case of **7b** to obtain **7c** as a colorless oil (bp 87—90 °C/1 Torr, 0.136 g, 63%). IR (neat): 1700 ($\nu_{C=O}$), 1650 ($\nu_{C=C}$) cm^{-1}. ^1H NMR: 0.94 (t, J=7 Hz, 3H, CH_3 of pentenyl), 1.6—2.7 (m, 6H, methylenes), 2.07 (s, 3H, CH_3 at C_3), 2.88 (d, J=4 Hz, 2H, CH_2 between double bonds), 5.3—5.6 (m, 2H, olefinic). Found: C, 79.88; H 9.72%. Calcd for $C_{11}H_{16}O$: C, 80.44; H, 9.82%. 2,4-Dinitrophenylhydrazone melted at 127—128 °C.[9] Found: C 59.15; H, 5 62; N, 16.16%. Calcd for $C_{17}H_{20}O_4N_4$: C, 59.29; H, 5.85; N, 16 27%.

The authors wish to express their thanks to the Asahi Glass Foundation for Industrial Technology for the generous financial aid.

References

1) F. Ogura, H. Yamaguchi, T. Otsubo, T. Nakano and T. Saito, *Bull. Chem. Soc. Jpn.*, **56**, 1257 (1983).

2) R. M. Jacobson, R. A. Raths, and J. H. McDonald III, *J. Org. Chem.*, **42**, 2545 (1977).

3) C. S. Subramaniam, P. J. Thomas, V. R. Mamdapur, and M. S. Chadha, *J. Chem. Soc., Perkin Trans. 1*, **1979**, 2346.

4) We have found that reaction of the monoanion of **3** with equimolar CH_3I afforded the mixture of a monomethylated and two dimethylated derivatives. On the other hand, selective monomethylation occurred in a nearly quantitative yield when the dianion was submitted to the same reaction.

5) H. Yamaguchi and K. Monden, *Bulletin of the Faculty of Engineering, Hiroshima University*, **24**, 13 (1975).

6) E. J. Corey and M. Chaykovsky, *J. Am. Chem. Soc.*, **87**, 1345 (1965).

7) M. Miyakawa and J. Araki, *Kogyo Kagaku Zasshi* **68**, 2236 (1965).

8) T. Kajiwara, T. Harada, and A. Hatanaka, *Agric. Biol. Chem.*, **39**, 243 (1955); L. Jaenicke and K. Saferiadis, *Chem. Ber.*, **108**, 225 (1975); M. S. Smagula, Chi-Tang Ho, and S. S. Chang, *J. Am. Oil Chem. Soc.*, **56**, 516 (1979).

9) L. Crombie and S. H. Harper, *J. Am. Chem. Soc.*, **74**, 867 (1952).

† 1 M=1 mol dm^{-3}.

Selective Mono- and Dibromination of Thymol by Electrolysis in Acetonitrile and Methanol

Isao TANIGUCHI,* Kouzou TAKADA, Hiroko YAMAGUCHI, and Kazuo YASUKOUCHI
Department of Industrial Chemistry, Faculty of Engineering, Kumamoto University, Kurokami, Kumamoto 860
(Received November 21, 1983)

Synopsis. For anodic bromination of thymol, MeCN and MeOH were suitable solvents for mono- and dibromination respectively. In MeCN, no dibrominated product was observed even when four Faradays per mole of thymol were passed.

Regioselective halogenation is one of the attractive subjects in electroorganic synthesis. Electrochemical chlorination of benzene derivatives in aqueous solutions was developed by Osa *et al.*[1] by using an α-cyclodextrin immobilized electrode. Gileadi *et al.*[2] have shown that the product ratio of bromophenols for anodic bromination of phenol depended on the charge consumed in aqueous solutions. In nonaqueous solvents, regioselective halogenation takes place at ordinary anodes. Matsuda *et al.*[3] have recently reported that para-preferential chlorination of alkoxybenzenes proceeded at a Pt electrode in *N,N*-dimethylacetamide and *N,N*-dimethylformamide, whereas in methanol, 2,4-dichlorophenetole was the product.[4] We have also reported[5] that anisole was easily brominated in high para-selectivity in acetonitrile. Recentrly, Becker[6] and Torii[7] reviewed studies of anodic halogenation. However, information on selective halogenation in nonaqueous solvents is still limited.[8]

Hence we have examined anodic bromination of thymol (*p*-cymene-3-ol) in acetonitrile (MeCN) and methanol (MeOH), because thymol derivatives are useful for medicinal materials.

Experimental

Controlled-potential electrolysis (CPE) was carried out at 25 °C by using a two-compartment cell. The amount of charge consumed was measured by a Hokuto Denko HF-201 coulometer. The working (5×8 cm^2) and the counter electrodes were Pt plates. The anolyte was 50 cm^3 in volume.

An Ag/0.01 M $AgClO_4$ in MeCN or MeOH was used as a reference electrode. Anode potentials for CPE were determined from the cyclic voltammograms of the test solutions. The products were analyzed gas chromatographically. The column used was 2 m×3 mmφ SUS packed with 5% polyethylene glycol 20 M on Uniport HP. Authentic samples of bromothymols donated from Kohjin Co., were identified by mass spectrometry. No significant difference in product distribution was observed when CPE was undertaken at temperatures between 0 and 40 °C. Throughout this paper 1 M=1 mol dm^{-3}.

Results and Discussion

Figure 1 shows the change in the yield of product as a function of the amount of charge passed for anodic bromination of thymol. In MeCN, thymol was brominated to 6-bromothymol at a current efficiency of more than 90% when up to one equivalent charge (two Faradays per mole of thymol) was passed. Further electrolysis caused a slight decrease in the amount

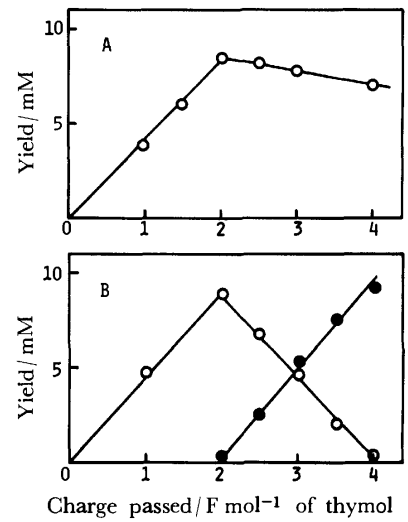

Fig. 1. Change in the yields of products as a function of the amount of charge passed for anodic bromination of thymol in MeCN (A) and MeOH (B). ○; 6-bromothymol and ●; 2,6-dibromothymol. Electrolyses were carried out in solutions consisted of 10 mM thymol, 20 mM bromide and 0.1 M perchlorate.

of 6-bromothymol, but no dibrominated product was obtained. On the other hand, in MeOH, the initial product was 6-bromothymol, as in MeCN, and was further brominated to 2,6-dibromothymol with high selectivity in a yield of *ca.* 90% at two equivalent charges. Typical results of CPE are summarized in Table 1. In MeCN, neither the anode potential nor the concentration ratio of thymol to bromide ion affected the selective monobromination (runs 1—10).

In MeOH, the total yield and the selectivity of brominated products decreased at potentials more positive than 0.55 V (*vs.* Ag/Ag^+ in MeOH). This is because oxidation of thymol itself and of the solvent both occurred (runs 11—18). No significant influence of the counter ion of the bromide ion source on the bromination behavior was observed (runs 11, 12, and 19—24). Thus, clearly, selective mono- and dibromination of thymol can be performed in MeCN and MeOH, respectively; an excess amount of bromide with respect to thymol is preferable for effective bromination in high selectivity (runs 7—10, 13, and 14).

A possible explanation for the difference in regioselectivity in MeCN and MeOH can be given as follows: (i) Since MeOH is a strong electron-acceptor (acceptor number, AN=41.3[9]), anodically generated bromine would be more polarized, $Br\overset{\delta+}{-}Br\overset{\delta-}{-}S$ where S is the solvent, in MeOH than in MeCN (AN=19.3[9]), and bromine molecules in MeOH become much more active than in MeCN. (ii) In MeCN, Br_3^- which is not active for bromination[5,10] is stable and the equilibrium of $Br_2+Br^-=Br_3^-$ lies to the right (pK=−7[11]), while unstability of Br_3^- in an amphiprotic solvent such as

Table 1. Anodic bromination of thymol

Run	Anolyte[a]	Anode potential[b]	Charge passed/ equivalent[c]	Yield of product[d]/% (Selectivity/%) 6-Bromothymol	2,6-Dibromothymol
1	MeCN-	0.85	1	85.9(100.0)	0(0)
2	Et_4NBr		2	71.6(100.0)	0(0)
3		1.0	1	89.9(100.0)	0(0)
4[e]			2	65.9(100.0)	0(0)
5		1.2	1	79.0(100.0)	0(0)
6[e]			2	64.5(100.0)	0(0)
7[f]		0.85	1	98.1(100.0)	0(0)
8[f]			2	96.4(100.0)	0(0)
9[g]		0.85	1	94.2(100.0)	0(0)
10[g]			2	97.5(100.0)	0(0)
11	MeOH-	0.35	1	88.5(98.4)	1.4(1.6)
12	NaBr		2	3.7(4.0)	87.9(96.9)
13[f]		0.35	1	93.1(98.7)	1.2(1.3)
14[f]			2	0(0)	93.8(100.0)
15		0.55	1	70.0(92.8)	5.4(7.2)
16[h]			2	8.7(10.1)	77.7(89.9)
17		0.75	1	68.4(93.4)	4.8(6.6)
18[h]			2	10.1(14.7)	58.6(85.3)
19	MeOH-	0.35	1	85.2(95.6)	3.9(4.4)
20	LiBr		2	8.8(9.0)	89.3(91.0)
21	MeOH-	0.35	1	80.0(96.3)	3.1(3.7)
22	NH_4Br		2	0.1(0.1)	88.3(99.9)
23	MeOH-	0.35	1	85.5(97.9)	1.8(2.1)
24	Et_4NBr		2	7.4(8.1)	83.5(91.9)

a) 50 cm^3 of solution consisted of 10 mM thymol, 20 mM bromide and 0.1 M perchlorate as a supporting electrolyte, except runs 7—10, 13, and 14. b) V *vs.* Ag/0.01 M $AgClO_4$ in MeCN or in MeOH. Potentials for CPE were chosen at which bromine was produced. c) One equivalent charge is 96.5 C (=2 F/mol of thymol). d) Based on 10 mM thymol. The yields were calculated from gas chromatographic data. The values also indicate the current efficiencies for the bromination. e) Oxidation of 6-bromothymol also occurred. f) 10 mM thymol and 50 mM bromide. g) 10 mM thymol and 100 mM bromide. h) Oxidation products of thymol itself were also detected.

MeOH shifts the equilibrium far to the left ($pK = -2.2$[11]). Thus, the actual concentration of Br_2 during electrolysis is larger in MeOH than in MeCN. (iii) Moreover, bulky bromine molecules may be solvated in MeCN through the dispersion force between solvent and bromine molecules, but the solvation would be unlikely in MeOH because of low acceptability of hydrogen-bond of Br_2; thus the active bromine would be larger in size in MeCN than in MeOH. Accordingly, these kinetic and steric factors make dibromination (the second bromination at 2-position) of thymol favorable in MeOH, but not in MeCN.

The following results also support the difference in regio-selectivity in MeCN and MeOH. Chlorination of anisole in MeCN gave monochlorinated products,[8] whereas in MeOH, 2,4-dichloroanisole was obtained as well, as reported by Matsuda *et al.*[4] For bromination of phenol, di- and tribromophenols were obtained in MeOH, but only in small amounts in MeCN.

On the other hand, exceptions were also observed. Bromination and iodination of anisole gave *p*-halogenoanisole in high para-selectivity and no dihalogenation took place at all, even in MeOH. This can be explained in terms of the steric hindrance at the ortho position by the methoxyl group for larger halogen molecules.

Finally, MeCN and MeOH are, rather generally, promising solvents for mono- and di- (and/or multi) halogenation of aromatic compounds, respectively.

The authors acknowledge partial financial support of this work by a Grant-in-Aid for Developmental Scientific Research from the Ministry of Education (No. 57850269).

References

1) T. Matsue, M. Fujihira, and T. Osa, *J. Electrochem. Soc.*, **126**, 500 (1979); *Bull. Chem. Soc. Jpn.*, **52**, 3692(1979).
2) T. Bejerano and E. Gileadi, *Electrochim. Acta*, **21**, 231 (1976).
3) Y. Matsuda and H. Hayashi, *Chem. Lett.*, **1981**, 661.
4) Y. Matsuda, A. Terashima, N. Sakota, and K. Nakagawa, *Denki Kagaku*, **49**, 669 (1981).
5) I. Taniguchi, M. Yano, H. Yamaguchi, and K. Yasukouchi, *J. Electroanal. Chem. Interfacial Electrochem.*, **132**, 233 (1982).
6) J. Y. Becker, "The Chemistry of Functional Groups, Suppl. D," ed by S. Patai and Z. Rappoport, John Wiley & Sons, New York (1983), Chap. 6.
7) S. Torii, "Yuuki Denkai Gousei," Koudansha, Tokyo (1981), Chap. 9.
8) I. Taniguchi, A. Tomoeda, I. Iwatani, H. Yamaguchi, and K. Yasukouchi, *Denki Kagaku*, **51**, 82 (1984).
9) V. Gutmann, *Electrochim. Acta*, **21**, 661 (1976).
10) G. Casalbore, M. Mastragostino, and S. Valcher, *J. Electroanal. Chem. Interfacial Electrochem.*, **77**, 373 (1977); **87**, 411 (1978).
11) R. Alexander, E. C. F. Ko, Y. C. Mac, and A. J. Parker, *J. Am. Chem. Soc.*, **89**, 3703 (1967).

Conformations of 3-Alkoxycarbonyl-1-tetralols and 2-Ethoxycarbonyl-4-chromanols

Kaoru HANAYA,* Takashi MURAMATSU, Shinji ONODERA,† Yusaku IKEGAMI,† and Minoru HIROTA††

Research Institute for Science Education, Miyagi University of Education, Aramaki Aoba, Sendai 980

†*Chemical Research Institute of Non-Aqueous Solutions, Tohoku University, Katahira, Sendai 980*

††*Department of Applied Chemistry, Faculty of Engineering, Yokohama National University, Hodogaya-ku, Yokohama 240*

(Received December 20, 1983)

Synopsis. The 1- or 4-hydroxyl group in cis isomers of 3-alkoxycarbonyl-1-tetralols and 2-ethoxycarbonyl-4-thiochromanols are predominantly quasi-equatorial and those of the trans isomers quasi-axial. *cis*-2-Ethoxycarbonyl-4-chromanol prefers the quasi-axial OH conformation.

Intramolecular OH···π interaction has been used as a means of configurational and conformational studies on unsaturated alcohols.[1,2] This paper deals with the conformations of the alcohols having an alkoxycarbonyl group γ to the OH group.

The ν_{OH} absorption maxima of the alcohols examined are summarized in Table 1. Basing upon that the tetralin, chroman, and thiochroman skeletons exist preferentially as a half-chair from,[2-6] the previous studies elucidated that 1-tetralol and 4-chromanol epimers with quasi-axial OH group show each only a band around 3618 cm^{-1} and the quasi-equatorial one a doublet at 3622 and 3600 cm^{-1}, as represented by **4a**—**6a** and **4b**—**6b**, respectively, in Table 1. It is therefore readily assigned that the OH groups in **1a** and **3a** prefer the quasi-equatorial orientation and those of **1b** and **3b** the quasi-axial one. In contrast with these, **2a** showed two ν_{OH} bands at 3610 and 3596 cm^{-1}, the former band being stronger. Referring to the previous results,[3] an appearance of the two bands is ascribed to the coexistence of two conformers with quasi-axial and -equatorial OH groups, the former being predominant. This means that the conformation A with both axial OH and ester groups is more predominant than the conformation B.

TABLE 1. THE OH-STRETCHING FREQUENCIES (ν_{OH}), HALF BAND-WIDTHS ($\Delta\nu_{1/2}$), AND MOLAR ABSORPTION COEFFICIENTS (ε) FOR 1-TETRALOLS, 4-CHROMANOLS, AND 4-THIOCHROMANOLS

Compound	ν_{OH}/cm^{-1}	$\Delta\nu_{1/2}$/cm^{-1}	ε
1a	3621	21	21
	3599	16	52
1b	3618	17	63
2a	3610	18	42
	3596	15	31
3a	3619	12	24
	3592	13	49
3b	3617	17	47
	3600 sh	—	—
4a[a]	3622	23	37
	3600	10	66
4b[a]	3617	12	88
5a[a]	3622	23	34
	3596	14	75
5b[a]	3616	16	89
6a[b]	3625	18	32
	3594	12	52
6b[b]	3613	18	91

a) Ref. 3a. b) Ref. 3b.

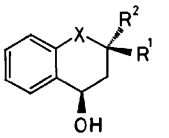

1a X=CH_2, R^1=$COOC_2H_5$, R^2=H
1b X=CH_2, R^1=H, R^2=$COOC_3H_7$
2a X=O, R^1=$COOC_2H_5$, R^2=H
3a X=S, R^1=$COOC_2H_5$, R^2=H
3b X=S, R^1=H, R^2=$COOC_2H_5$
4a X=CH_2, R^1=C_6H_5, R^2=H
4b X=CH_2, R^1=H, R^2=C_6H_5
5a X=O, R^1=C_6H_5, R^2=H
5b X=O, R^1=H, R^2=C_6H_5
6a X=S, R^1=CH_3, R^2=H
6b X=S, R^1=H, R^2=CH_3

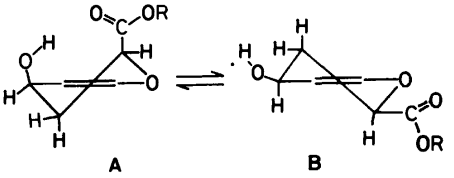

A B

To clarify the conformational equilibrium, temperature dependence of the OH absorption was examined for **2a** and **3a** in the range 10—50 °C. The result indicated that the intensity of the lower frequency band increased with a rise in temperature for both **2a** and **3a**: the intensity ratio A_{3592}/A_{3619} of the two ν_{OH} bands at 3592 and 3619 cm^{-1} for **3a** changed from 1.3 at 10 °C to 2.2 at 50 °C. Accordingly, the quasi-axial OH conformer is more stable than the quasi-equatorial one in the equilibrium. Generally speaking, 3-hydroxycyclohexanecarboxylic acid ester do not form an intramolecular hydrogen bond.[7] If the two substituents in the cis isomer are fixed in a diaxial conformation, however, both carbonyl and alkoxyl oxygen-bonded OH species should be observed.[8] Although authors can not give a decisive explanation, the band at 3610 cm^{-1} of **2a** presumably arose from the diaxial conformation which is possible to form a hydrogen bond. Examination of the $\nu_{C=O}$ bands for **1a**, **2a**, and **3a**, however, afforded no clear sign of hydrogen-bond formation.

The above interpretation is supported by the ^{1}H-NMR measurements for **1**—**6** (Table 2). The coupling constants in Table 2 can be used to deduce the relative configurations and substituent conformations by making use of the Karplus relationship between vicinal HC-CH coupling constants and dihedral angles. A simplified method[5,6,9] can be adapted to the present cases. If the 2-substituent is in the equatorial position on half-chair dihydropyran ring and all the vicinal J's have the same sign, the value of $J_{3a\text{-}4}+J_{3e\text{-}4}$ would be significantly smaller for 2,4-*trans* than for 2,4-*cis* isomers.

TABLE 2. NMR PROTON COUPLING CONSTANTS FOR 1-TETRALOLS, 4-CHROMANOLS, AND 4-THIOCHROMANOLS

Compound	HC-CH coupling in $CDCl_3$ $J_{3a,4}+J_{3e,4}$/Hz		HC-OH coupling in DMSO J_{HC-OH}/Hz	
	cis	trans	Quasi-equatorial OH	Quasi-axial OH
1a	15.4(d.d)		6.3	
1b		6.8(t)[a]		5.0
2a	10.0(t)			5.0
3a	12.5(d.d)[a]		5.8	
3b		7.2(d.d)		4.9
4a	17.0(d.d)[b]		7.1	
4b		6.0(t)[b]		5.3
5a	15.5—16.0(d.d)[c]		6.7	
5b		6.0—6.5(t)[c]		5.0
6a	15.3(d.d)[d]		6.3	
6b		5.9(t)[d]		5.4

a) Coupling constant of the acetate. b) Ref. 4. c) Refs. 5 and 6. d) Ref. 3b.

This explanation is assured with the data for **4—6** in Table 2. It is thus considered that the OH groups in **1a** and **3a** prefer the quasi-equatorial orientation and those of **1b** and **3b** the quasi-axial one. The value of $J_{3a,4}+J_{3e,4}$ (10.0 Hz) observed for **2a** is smaller than those of **1a** and **3a**, supporting the existence of the conformational equilibrium of **2a** in solution. The equilibrium is also supported by the hydroxyl ^{1}H-NMR measurements for **1—6** in dimethyl sulfoxide (DMSO) (Table 2).[10] The J_{HC-OH} of **2a** is significantly smaller than those of **1a** and **3a** and similar to those of the compounds with a quasi-axial OH group (**4b**, **5b**, and **6b**), rather than a quasi-equatorial OH group (**4a**, **5a**, and **6a**).

Experimental

3-Alkoxycarbonyl-1-tetralol (**1**),[11] 2-ethoxycarbonyl-4-chromanol (**2**),[12] and 2-ethoxycarbonyl-4-thiochromanol (**3**)[12] were prepared by reducing the corresponding ketones as reported. Since the pure *cis*-2-ethoxycarbonyl-4-thiochromanol (**3a**) was not readily isolated due to its instability, the mixture (1:1) of **3a** and **3b** was used for measurements. Then the infrared and NMR spectra of **3a** were obtained by subtracting the spectra of pure **3b** from those of the mixture.

Infrared spectra were measured using a KCl cell of 30 mm in optical length; the concentration of the CCl_4 solution was ca. 4×10^{-3} mol/dm^3. NMR spectra were measured at a probe temperature of 30 °C, using TMS as the internal standard.

References

1) H. S. Aaron, "Topics in Stereochemistry," ed by N. L. Allinger and E. L. Eliel, Interscience, New York (1979), Vol. 11, p. 11; M. Oki, H. Iwamura, T. Onoda, and M. Iwamura, *Tetrahedron*, **24**, 1905 (1968); L. Ananthasubramanian and S. C. Bhattacharyya, *J. Chem. Soc., Perkin Trans. 2*, **1977**, 1821.

2) N. Mori, S. Kasuya, H. Miyagaki, and T. Takezawa, *Bull. Chem. Soc. Jpn.*, **52**, 1423 (1979).

3) a) H. Iwamura and K. Hanaya, *Bull. Chem. Soc. Jpn.*, **43**, 3901 (1970); b) K. Hanaya, S. Onodera, S. Awano, and H. Kudo, *ibid.*, **47**, 509 (1974); c) K. Hanaya, S. Onodera, and H. Kudo, *ibid.*, **47**, 2607 (1974); d) K. Hanaya, S. Onodera, Y. Ikegami, H. Kudo, and K. Shimaya, *J. Chem. Soc., Perkin Trans. 2*, **1981**, 944.

4) S. Mitsui, A. Kasahara, and K. Hanaya, *Bull . Chem. Soc. Jpn.*, **41**, 2526 (1968).

5) B. J. Bolger, A. Hirwe, K. G. Marathe, E. M. Phiblin, M. A. Vickers, and C. P. Lillya, *Tetrahedron*, **22**, 621 (1966).

6) G. F. Katekar and A. G. Moritz, *Aust. J. Chem.*, **22**, 2337 (1969); **20**, 2235 (1967).

7) N. Mori, S. Omura, N. Kobayashi, and Y. Tsuzuki, *Bull. Chem. Soc. Jpn.*, **38**, 2149 (1965).

8) W. S. Bennet, G. Eglinton, J. W. B. Fulke, R. McCrindle, K. Hirano, A. Tahara, and W. Simon, *J. Chem. Soc., B*, **1967**, 211.

9) C. P. Lillya, S. E. Drewes, and D. S. Roux, *Chem. Ind.*, **1963**, 783.

10) K. Hanaya, H. Kudo, K. Gohke, and S. Imaizumi, *Bull. Chem. Soc. Jpn.*, **52**, 2163 (1979).

11) K. Hanaya, *Nippon Kagaku Zasshi*, **90**, 314 (1969).

12) K. Hanaya, Y. Koga, A. Yamaguchi, H. Kudo, and Y. L. Chow, *Nouveau J. Chim.*, **6**, 149 (1982).

π-Electron Distribution in Benz[*a*]indeno[1,2,3-*cd*]azulene and the Corresponding Azepinium Ion

Shigeru MURATA and Hiizu IWAMURA*
Institute for Molecular Science, Myodaiji, Okazaki 444
(Received December 21, 1983)

Synopsis. The π-electron density distribution in benz[*a*]indeno[1,2,3-*cd*]azulene and the corresponding azepinium ion has been calculated by the PPP MO method. The effects of the hetero atom and the benzo annellation on the π-electron density and bond order of the cyclopent[*cd*]azulene are discussed.

Since Hafner *et al.* synthesized the dimetyl derivatives of cyclopent[*cd*]azulene (**1**) and cyclohept[*cd*]azulene (**2**) (Hafner's hydrocarbon),[1] their electronic structures have attracted the interest of many organic and theoretical chemists.[2,3] Parent molecules **1** and **2** were treated by the self-consistent field molecular orbital theory on π-conjugated systems developed by Pariser, Parr, and Pople.[4] The essence of these theoretical calculations[5] is summarized as follows. Thermodynamically, **1** is more stable than **2** as shown by their Dewar's resonance energy of 0.018 and 0.016$|\beta|$, respectively. However there is higher olefinic character in the 5-membered rings of **1**, and therefore **1** should be kinetically less stable of the two.

Some more derivatives of **1** and **2** were synthesized, and in 1969 and 1970 crystallographic studies on 5,7-dimethyl-2-phenylcyclopentazulene[6] and 3,5,8,10-tetramethylcycloheptazulene[7] showed almost planar structure of these molecules. More recently we found a facile access to the dibenzo derivative (**1b**) of **1** *via* the photorearrangement of 1-alkoxytriptycenes.[8] The corresponding azepinium salt (**3b**) was also obtained by the hydride abstraction reaction of the similar photoproduct of 1-azatriptycene.[9]

Since the benzoannellation is so located as to block the reactive olefinic bonds in **1**, **1b** proved to be a very stable compound. These experimental work encouraged us to study the electronic structure of **1b** and **3b**.

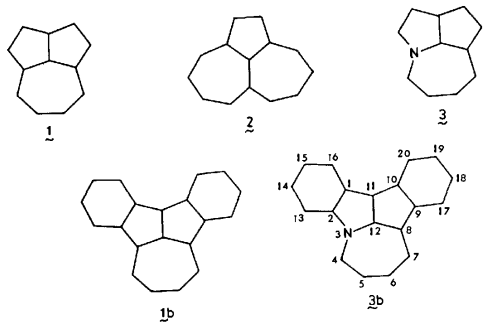

Method and Parameters

The self-consistent-field method used here is the Pariser-Parr-Pople method within the zero-differential-overlap approximation. The matrix elements of the closed shell Hartree-Fock operator are written as follows,

$$F_{rr} = -I_r + \frac{1}{2}q_r\gamma_{rr} + \sum_{s\neq r}(q_s-1)\gamma_{rs},$$

$$F_{rs} = \beta_{rs} - \frac{1}{2}p_{rs}\gamma_{rs},$$

where q_r and p_{rs} are π-electron density and bond order, respectively, and I_r is the ionization potential of atom r in its valence state, and γ_{rr} is one-center repulsion integral which is estimated as the difference between valence state ionization energy and electron affinity.

As the resonance integral, β_{rs}, a constant value was used for neighboring atoms, and for non-neighboring atoms β_{rs} was assumed to be zero. The two-center repulsion integral, γ_{rs}, was calculated by the Mataga-Nishimoto formula[10] using the standard geometries.

The parameters used in this calculation are shown in Table 1, with the Hückel parameters h and k in $\alpha_N = \alpha_C + h\beta_{CC}$, and $\beta_{CN} = k\beta_{CC}$ for initial guess.[11] These vaules were determined in reference to the DasGupta's work on nonbenzenoid hydrocarbons[5] and the study of methyleneammonium ion by Brown.[12]

The molecules discussed here are all assumed to have planar geometries, with all the carbon-carbon and carbon-nitrogen bonds being 1.39 Å and 1.36 Å, respectively. The bond angles of the cyclopent[*cd*]azulene moiety are close to those of the crystal structure[6] of related compounds and collected in Table 2. The bond angles of the annulated benzene rings are assumed to be equal to 120°.

Calculations were carried out on a Hitachi M-200H computer, using "SCF-CI-PI-MO Program with PPP Approximation" programmed by Mueller-Westrhoff and filed in the program library of the Computer Center of Institute for Molecular Science.

TABLE 1. PARAMETERS USED IN THE CALCULATIONS

I_C=11.16 ev	I_N=14.16 ev
γ_{CC}=11.134 ev	γ_{NN}=12.82 ev
β_{CC}=−1.7901 ev	β_{CN}=−2.57 ev
h=2.0	k=1.0

TABLE 2. BOND ANGLES IN MOLECULES **1**, **1b**, **3**, AND **3b** EMPLOYED FOR THE PPP CALCULATIONS[a]

Bond angle	φ/°	Bond angle	φ/°
1 and **1b**		C_{12}–C_{11}–C_1	106.0
C_1–C_2–C_3	109.6	C_{11}–C_1–C_2	108.2
C_2–C_3–C_{12}	105.2	C_{11}–C_{12}–C_8	111.0
C_3–C_{12}–C_{11}	111.0	C_{12}–C_8–C_9	105.2
C_{12}–C_{11}–C_1	106.0	C_8–C_9–C_{10}	109.6
C_{11}–C_1–C_2	108.2	C_9–C_{10}–C_{11}	108.2
C_3–C_4–C_5	125.8	C_{10}–C_{11}–C_{12}	106.0
C_4–C_5–C_6	131.2	N_3–C_4–C_5	132.6
C_7–C_8–C_{12}	124.0	C_4–C_5–C_6	126.9
3 and **3b**		C_5–C_6–C_7	131.2
C_1–C_2–C_3	108.0	C_6–C_7–C_8	125.8
C_2–N_3–C_{12}	108.5	C_7–C_8–C_{12}	124.0
N_3–C_{12}–C_{11}	109.3	C_{12}–N_3–C_4	119.8

a) Numbering scheme is given for **3b**.

Results and Discussion

In Table 3 are given the calculated π-electron densities and π-bond orders of cyclopent[*cd*]azulene (**1**) and its dibenzo derivative (**1b**) together with their azepinium derivatives (**3** and **3b**). The present results for cyclopent[*cd*]azulene agree with those of the previous calculations,[2,3,5,6] confirming the validity of our parametrization. Although the π-electron density is somewhat sensitive to choice of parameters,[5] the data in Table 3 indicate some trends which do not depend on the parameters. Firstly, we note that the charge density at the positive nitrogen center (position 3) is more effectively neutralized in **3b** than in **3**. As a result, π-electron densities are slightly reduced not only at the neighboring carbons (position 2, 4, 12) but also the remote carbon atoms (position 6, 8, 10). Secondly, the π-electron density on the benzene rings is little influenced by the change of atoms at position 3. For a third, when the dibenzo derivatives are compared with the parent compounds, it is noted that the extent of the separation of charge densities is smaller in the dibenzo derivatives. Thus **1b** and **3b** are expected to be less polar and therefore less reactive than the corresponding parent compounds.

An operational test for the validity of the calculated charge distributions is provided by the ^{1}H NMR data for **1b** and **3b**. Plots of the chemical shifts of the nonbenzenoid hydrogens 4—7 *vs.* the calculated π-electron densities gave a line as shown in Fig. 1. The slope is close to the well-known 10 ppm/π-electron. The reason why the proton at position 5 of **3** deviated from the line is not clear for the moment.

Turning now to π-bond orders (Table 3), we note that the bond alternation in the 7-membered ring is more evident in the dibenzo derivatives than in their parent compounds in which the bond orders in the 7-membered rings are more uniform and suggest the reasonably high aromatic character. Whereas the 3-12 and 8-12 bonds, which are shared by two rings of different type, have a single bond character with bond order 0.38—0.44, the 11-12 bond between the same ring types has an aromatic character with bond order 0.68—0.69 in the dibenzo derivatives. Bonds 1-2 and 9—10 on the 5-membered rings of **1** and **3** have very high bond order 0.73—0.77 which is supported by the short bond length (1.359 and 1.386 Å) found in the crystal structure of the related compounds.[6] The benzo annellation reduced the latter bond orders to 0.55—0.57 by sharing the bonds as a part of the benzene ring. Whereas the double bond character of these bonds is reduced, the bond alternation in the rest of the molecules is found to be enhanced by the benzo annellation in these systems. The trend is interpreted in terms of an increased contribution of canonical structure A over B and B′ which require the quinonoid structure of one of the benzene rings. In the aza-analogs, the extent of the bond alternation is somewhat enlarged as compared to the hydrocarbons.

Table 3. π-Electron densities and bond orders of cyclopentazulenes

Carbon atom	π-Electron densities				π-Bond orders				
	1	1b	3	3b	Bond	1	1b	3	3b
1	0.937	0.971	0.949	0.977	1-2	0.771	0.568	0.733	0.550
2	1.110	1.057	1.066	1.018	1-11	0.474	0.413	0.490	0.424
3	0.922	0.933	1.142	1.151	2-3	0.488	0.406	0.528	0.453
4	0.944	0.956	0.840	0.840	3-12	0.423	0.408	0.452	0.441
5	0.965	0.968	0.987	0.991	3-4	0.621	0.686	0.617	0.675
6	0.965	0.968	0.931	0.930	4-5	0.658	0.591	0.618	0.546
7	0.944	0.956	0.956	0.969	5-6	0.646	0.704	0.670	0.729
8	0.922	0.933	0.889	0.898	6-7	0.658	0.591	0.637	0.568
9	1.110	1.057	1.120	1.063	7-8	0.621	0.686	0.641	0.705
10	0.937	0.971	0.909	0.958	8-9	0.488	0.406	0.479	0.401
11	1.124	1.118	1.129	1.120	8-12	0.423	0.408	0.389	0.376
12	1.119	1.069	1.082	1.032	9-10	0.771	0.568	0.774	0.565
13		0.993		0.998	10-11	0.474	0.413	0.458	0.403
14		1.025		1.026	11-12	0.637	0.687	0.636	0.684
15		0.993		1.000	2-13		0.594		0.570
16		1.013		1.015	13-14		0.701		0.709
17		0.993		0.998	14-15		0.624		0.618
18		1.025		1.026	15-16		0.702		0.704
19		0.993		0.986	1-16		0.595		0.593
20		1.013		1.013	9-17		0.594		0.599
					17-18		0.701		0.696
					18-19		0.624		0.628
					19-20		0.702		0.696
					10-20		0.595		0.601

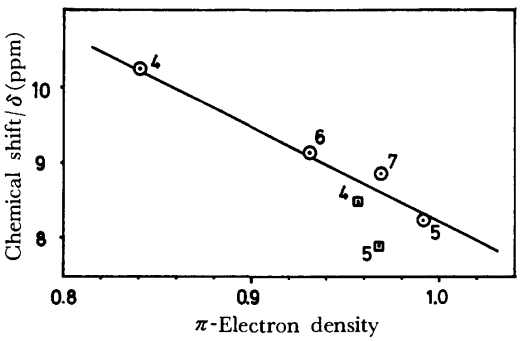

Fig. 1. Plots of chemical shifts of the non-benzenoid hydrogens *vs.* the calculated π-electron densities. □: Hydrocarbon **1b**, ⊙: azepinium salt **3b**.

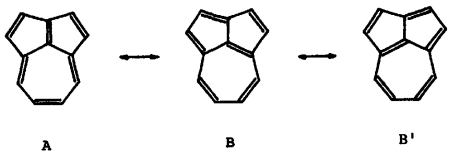

References

1) K. Hafner and J. Schneider, *Justus Liebigs Ann. Chem.*, **624**, 37 (1959).
2) A. Rosowsky, H. Fleischer, S. T. Young, R. Partch, W. H. Saunders, Jr., and V. Boekelheide, *Tetrahedron*, **11**, 121 (1960).
3) H. Chatterjee and M. A. Ali, *Tetrahedron*, **20**, 2829 (1964).
4) R. Pariser and R. G. Parr, *J. Chem. Phys.*, **21**, 466, 767 (1953); J. A. Pople, *Trans. Faraday Soc.*, **49**, 1357 (1953).
5) F. W. Birss and N. K. DasGupta, *Can. J. Chem.*, **49**, 2840 (1971). A. DasGupta and N. K. DasGupta, *Can. J. Chem.*, **52**, 135 (1974).
6) H. J. Lindner, *J. Chem. Soc., B*, **1970**, 907.
7) R. Qasba, F. Bandl, W. Hoppe, and R. Huber, *Acta Crystallogr., Sect B*, **25**, 1198 (1969).
8) Y. Kawada, H. Tukada and H. Iwamura, *Tetrahedron Lett.*, **21**, 181 (1980).
9) T. Sugawara and H. Iwamura, *J. Am. Chem. Soc.*, **102**, 7134 (1980).
10) N. Mataga and K. Nishimoto, *Z. Phys. Chem.*, **13**, 140 (1957).
11) A. Streitweiser, "Molecular Orbital Theory for Organic Chemists," Wiley, New York (1961).
12) R. D. Brown and A. Penfold, *Trans. Faraday Soc.*, **53**, 397 (1957).

Induced Circular Dichroism in the Complexes of Histidine Polypeptides with Methyl Orange. Effect of Distance between Histidine Residues

Hiroyuki YAMAMOTO,* Ayako NAKAZAWA, Tadao HAYAKAWA, Norio NISHI,† and Takumi NARUSE†
Institute of High Polymer Research, Faculty of Textile Science and Technology, Shinshu University, Ueda 386
†*Department of Polymer Science, Faculty of Science, Hokkaido University, Sapporo 060*
(Received December 22, 1983)

Synopsis. The induced circular dichroism (CD) spectra of the sequential histidine polypeptide-azo dye complexes were measured. The induced CD arose from the dye bound to the polypeptide in the random coil conformation. The intensity of the induced CD decreased with increasing distance between the intramolecular histidine residues.

The induced optical activities of complexes of anionic poly(L-glutamic acid) (PLG) with cationic dyes were first reported by Stryer and Blout.[1,2] Induced optical activities have been reported mostly for the PLG complexes. Lately, however, the complexes of cationic poly(L-lysine)-,[3,4] poly(alkyl-L-lysine)s-,[5,6] and poly(L-arginine)-azo dyes[7,8] have been reported to exhibit optical activity. In the course of our study of the induced CD of biopolymers,[4-8] we wish to report here on the induced CD due to the interaction between the cationic poly(L-histidine) (PLH) and an azo dye.

Experimental

The four histidine polypeptides, PLH (I, $[\eta]^{25}_{DCA}$=0.18), poly(His-Gly) (II, $[\eta]^{25}_{DCA}$=0.19), poly(His-βAla-Gly) (III, $[\eta]^{25}_{DCA}$=0.20), and poly(His-Gly$_3$) (IV, $[\eta]^{25}_{DCA}$=0.17) were synthesized according to the racemization-free diphenyl phosphoryl azide method (dichloroacetic acid was abbreviated as DCA).[9,10] 4-(4-dimethylaminophenylazo)benzenesulfonic acid sodium salt (Methyl Orange, MO) was guaranteed reagents (Wako). The mixtures were prepared by adding the dye solution to the polypeptide solutions; the pH values of the solutions were then brought up to the desired pH by the addition of NaOH or HCl. The final concentrations of histidine residue in polypeptides and MO were 10^{-4} mol residue dm^{-3} and 2×10^{-5} mol dm^{-3}, respectively. The absorption and CD spectra were measured with JASCO UVIDEC-1 and CD J-40A spectrometers, respectively. The molar ellipticity [θ] (degree cm^2 dmol^{-1}) and molar extinction coefficient ε (dm^3 mol^{-1} cm^{-1}) were expressed on the basis of the dye concentration.

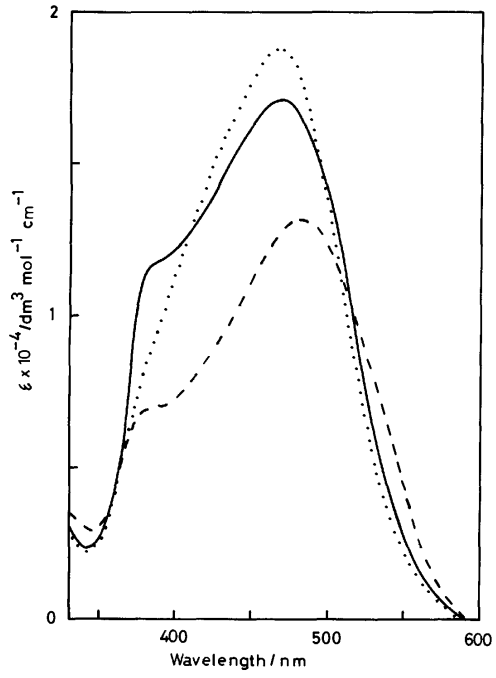

Fig. 1. Absorption spectra of the PLH (I)-MO complex in water at R/D=5: (·····) at pH 4.4, (——) at pH 4.1, and (------) at pH 3.7.

Results and Discussion

Since PLH is not soluble in water above pH 6,[11-13] the absorption and CD spectra of MO with and without polypeptides were measured over the pH range 3 to 6. Upon adding PLH (I), the position of the peak and the band shape of MO in the visible absorption spectrum were changed and the PLH (I)-dye complex exhibited the induced CD. Figure 1 shows the absorption spectra of the PLH (I)-MO complex in water as a function of pH at residue/dye (R/D)=5. At pH 4.6, the visible absorption spectrum showed a peak at 467 nm. As the pH of the solution was lowered from 4.6 to 3.1, the peak at 467 nm shifted to 506 nm. Between pH 4.3 and 3.2 an additional shoulder was observed at around 370 nm. The blue-shifted shoulder (or peak) suggests a nearly parallel orientation of the MO molecules.[3,14] At low PLH (I) concentration, R/D<2, the shoulder at 370 nm was not clear. Figure 2 shows the induced CD spectra of the PLH (I)-MO complex in

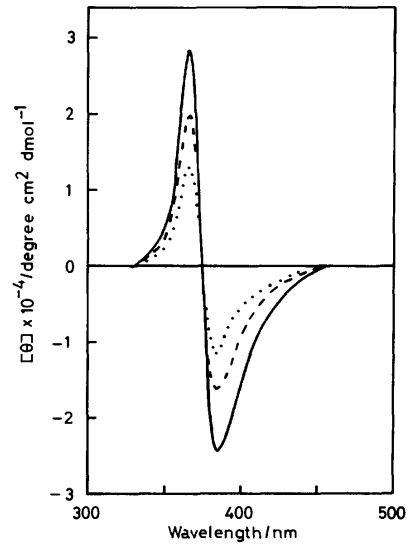

Fig. 2. Induced CD spectra of the PLH (I)-MO complex in water at R/D=5: (·····) at pH 4.4, (——) at pH 4.1, and (------) at pH 3.7.

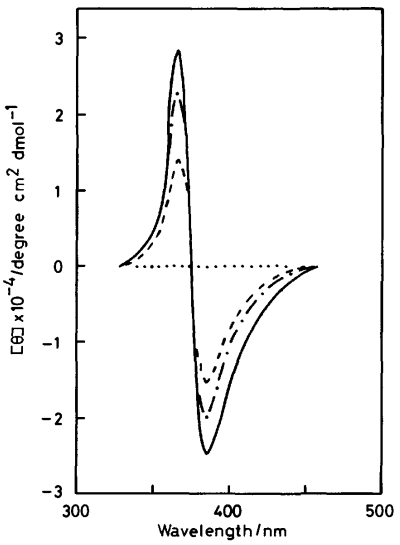

Fig. 3. Induced CD spectra of the PLH (I)-MO complex at various NaCl concentrations (at pH 4.1 and R/D=5): (——) 0 mM, (-·-·-) 0.5 mM, (------) 2 mM, and (·····) 5 mM.

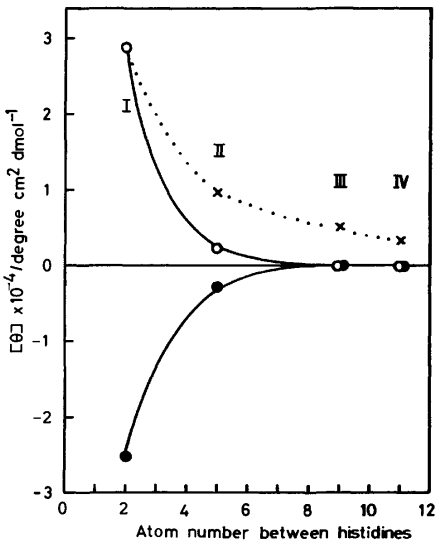

Fig. 4. Induced CD values at the extrema of the sequential polypeptide MO-complexes as a function of distance between histidine residues in water at pH 4.1 and R/D=5: ○ at 366 nm and ● at 385 nm. Samples I—IV, see text. The estimated induced CD values (× and dotted line) were calculated from the CPK model examinations, assuming the stretched backbone conformation and the nearest distances between histidine residues.

water as a function of pH at R/D=5. pH 4.1 was optimal for the induced CD of the PLH (I)-MO system, and the spectra at pH 3.7 and 4.4 showed smaller CD values. Two induced CD extrema were observed at 385 nm with $[\theta]=-25200$ and at 366 nm with $[\theta]=28800$ at pH 4.1. The PLH (I)-MO complex at pH 4.1 showed the characteristic CD bands at 222 nm with $[\theta]=2000$ and at 203 nm with $[\theta]=-4200$ (based on the histidine residue). These ellipticity values suggest that the degree of ionization of the imidazole side chains is about 50% and the conformation of the complex is a random coil.[13]

Figure 3 shows the change in the induced CD spectra of the PLH (I)-MO complex in an aqueous solution with various sodium chloride concentrations at pH 4.1 and R/D=5. With increasing concentration of sodium chloride from 0 to 0.005 mol dm^{-3}, the intensity of the induced CD became weaker. No induced CD was observed in 0.005 mol dm^{-3} sodium chloride.

The main features of the optical activities arise from the dipole-dipole couplings of the chromophores with each another. The intensity of the split Cotton effect is inversely proportional to the square of the interchromophoric distance and is changed by the dihedral angle between the transition moments.[15] In an electrostatic interaction systems, the dihedral angle between the transition moments is difficult to examine but the interchromophoric distance can be changed by sequential polypeptides. Figure 4 shows the induced CD values at the extrema of four sequential polypeptide-MO complexes as a function of distance between C_α of the histidine residues. Since the random coil conformations of the four sequential polypeptide-MO complexes do not allow the exact estimation of the distance between chromophores, we tentatively used the numbers of backbone atoms between histidine residues as abscissa. Clearly, an increased distance decreased the intensity of the induced CD. Beyond the bold approximation of the distances between the nearest intramolecular histidine residues by the CPK model examinations, the observed values of the induced CD of sequential polypeptides decreased sharply.

These results are the first observed induced CD of PLH-MO complexes and demonstrate that the intensity of the induced CD of the polypeptide-dye complex is dependent on the distance between the intramolecularly interacting chromophores.

References

1) E. R. Blout and L. Stryer, *Proc. Natl. Acad. Sci. U. S. A.*, **45**, 1591 (1959).
2) L. Stryer and E. R. Blout, *J. Am. Chem. Soc.*, **83**, 1411 (1961).
3) M. Hatano, M. Yoneyama, Y. Sato, and Y. Kawamura, *Biopolymers*, **12**, 2423 (1973).
4) H. Yamamoto, A. Nakazawa, and T. Hayakawa *J. Polym. Sci., Polym. Lett. Ed.*, **21**, 131 (1983).
5) H. Yamamoto and A. Nakazawa, *Chem. Lett.*, **1983**, 47.
6) H. Yamamoto, *Makromol. Chem.*, **184**, 1479 (1983).
7) H. Yamamoto and A. Nakazawa, *Bull. Chem. Soc. Jpn.*, **56**, 2535 (1983).
8) H. Yamamoto and A. Nakazawa, *Biopolymers*, in press.
9) T. Shioiri, K. Ninomiya, and S. Yamada, *J. Am. Chem. Soc.*, **94**, 6203 (1972).
10) N. Nishi, B. Nakajima, N. Hasebe, and J. Noguchi, *Int. J. Biol. Macromol.*, **2**, 53 (1980).
11) K. S. Norland, G. D. Fasman, E. Katchalski, and E. R. Blout, *Biopolymers*, **1**, 277 (1963).
12) S. Beychok, M. Pflumm, and J. E. Lehmann, *J. Am. Chem. Soc.*, **87**, 3990 (1965).
13) E. Peggion, A. Cosani, M. Terbojevich, an E. Scoffone, *Macromolecules*, **4**, 725 (1971).
14) M. Kasha, H. R. Rawls, and M. El-Bayoumi, *Pure Appl. Chem.*, **11**, 371 (1965).
15) N. Harada, S. L. Chen, and K. Nakanishi, *J. Am. Chem. Soc.*, **97**, 5345 (1975).

Preparation and Properties of a Mercury Selective Ion Exchanger Cerium(IV) Selenite

Jagdish Prasad RAWAT*,†, Masood Akhtar KHAN, and Pritam Singh THIND††
† *Department of Chemistry, Aligarh Muslim University, Aligarh-202001, India*
†† *Department of Chemistry, Guru Nanek Dev University, Amritsar-Punjab, India*
(Received May 8, 1982)

Synopsis. A new inorganic ion exchanger, cerium(IV) selenite has been synthesized with a cation exchange capacity of 0.98 mequiv g^{-1}. It is fairly stable in water and in dilute solutions of acids, bases and salts. The K_d values for number of metal ions were determined in different solvent systems. The exchanger possesses a high affinity for Hg(II) and hence its separation from certain metal ions have been made.

Selenites of tin,[1] titanium,[2] and tantalum[3] have been synthesized and used for various separations. However, no such studies have so far been reported on cerium(IV) selenite. Our studies on this material reveal that it is highly selective for Hg(II). As mercury is a toxic substance, its determination and separation should be of great importance. In the present report the synthesis and the ion exchange properties of cerium (IV) selenite are described as well as its possible application to separation of Hg(II) from other metal ions.

Experimental

Synthesis. Cerium(IV) selenite was prepared by mixing solutions of sodium selenite (Riedel, Germany) and ammonium cerium(IV) sulfate (British Drug House,England). The solution of 0.05 mol dm^{-3} sodium selenite was added to a solution of 0.05 mol dm^{-3} ammonium cerium(IV) sulfate in the volume ratio of 1:1 at pH 1. The pH was adjusted by adding either nitric acid or aqueous ammonia. The precipitate so obtained was kept standing for 24 h to ensure complete precipitation. It was then filtered, washed with deionized water and dried at 40 °C. The dried product was then converted to H^+ form by treatment with 1 mol dm^{-3} HNO_3.

The ion exchange capacity, which in fact is the capacity to decompose neutral salts, was determined by column operation. A solution of 1.0 mol dm^{-3} of Na^+, K^+, Mg^{2+}, Ca^{2+}, Sr^{2+}, and Ba^{2+} was passed through a column containing 1 g of exchanger. The eluted hydrogen ion concentration was then determined titrimetrically.

To determine the chemical stability, 0.5 g cerium(IV) selenite was shaken with an appropriate solution for six hours in a conical flask. The cerium[4] and selenium[5] released into the supernatant solution were determined by standard methods.

The pH titrations of cerium(IV) selenite were performed with LiOH, NaOH, KOH and aqueous ammonia in the presence of Li^+, Na^+, K^+ and NH_4^+ chlorides, respectively, by the method of Topp and Pepper.[6]

For equilibrium studies 0.5 g of exchanger in H^+ form was shaken with 50 cm^3 solution of 1.0 mol dm^{-3} sodium nitrate. The amount of released H^+ ions in the supernatant solution was determined after appropriate intervals.

The distribution coefficient (K_d values) were determined by shaking 50 cm^3 of 0.001 mol dm^{-3} solution of different metal ions with 0.5 g of the exchanger for six hours at room temperature.[3]

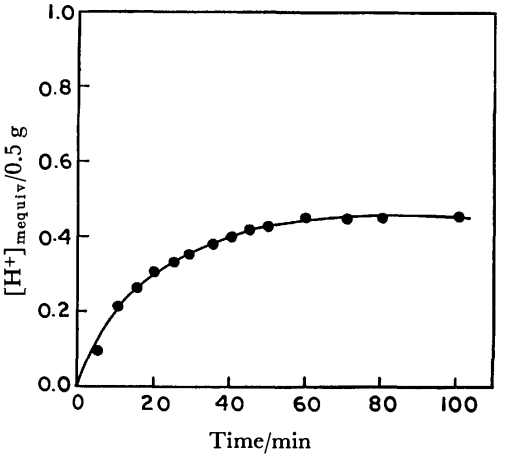

Fig. 1. Attainment of equilibrium of Na^+-H^+ exchange on cerium(IV) selenite.

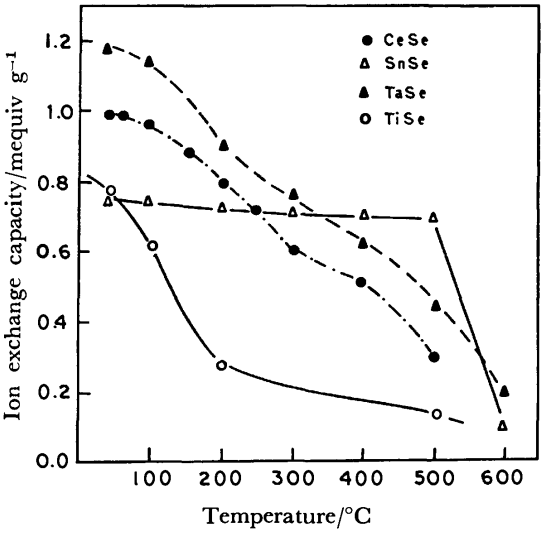

Fig. 2. Ion exchange capacity of various selenites as a function of drying temperature.

Results and Discussion

The hydrogen ion liberation capacity of cerium(IV) selenite for some uni and bivalent metal ions such as Na^+, K^+, Mg^{2+}, Ca^{2+}, Sr^{2+}, and Ba^{2+} were found to be 0.98, 0.86, 0.90, 0.80, 0.82, and 0.85 mequiv g^{-1} respectively.

The equilibrium studies (Fig. 1) show that the equilibrium is attained in 60 min. The effect of drying temperatures of cerium(IV) selenite on the ion exchange capacity (Fig. 2) indicates that the selenite also shows deterioration after 100 °C as in the case of tantalum selenite. The reason for the decrease in capacity with the increase in drying temperature upto 500 °C may be attributed to the loss of structural

Table 1. Some separations on cerium(IV) selenite columns

Separation	Eluent	Elution volume/ml	Amount of cation	
			Loaded mg	Recovered mg
Cd(II)-Hg(II)	Cd(II)-0.01 mol dm^{-3} HNO_3	0.0—80	0.74	0.74
	Hg(II)-0.1 mol dm^{-3} (HNO_3+NaNO_3)	90—160	1.6	1.6
Ni(II)-Hg(II)	Ni (II)-0.1 mol dm^{-3} HNO_3	0.0—70	0.48	0.49
	Hg(II)-0.1 mol dm^{-3} (HNO_3+NaNO_3)	80—160	1.6	1.6
Pb(II)-Hg(II)	Pb (II)-0.01 mol dm^{-3} HNO_3	0.0—90	1.6	1.6
	Hg(II)-0.1 mol dm^{-3} (HNO_3+NaNO_3)	100—170	1.6	1.5

water, selenium and attached replaceable hydrogen ion.

The results of chemical stability test of cerium(IV) selenite revealed that the material is fairly stable (less than 1.2 mg of Se and 0.28 mg of Ce were lost) in demineralized water, 2.0 mol dm^{-3} solution of each of $NaNO_3$, NH_4NO_3, HNO_3, CH_3COOH, HCOOH, and CH_3OH but less stable (3.24 mg of Se and 2.8 mg of Ce were lost) in sulphuric acid of over 2.0 mol dm^{-3}. The pH titration curves (Fig. 3) of the exchanger in H^+ form show bifunctional behaviour.

The chemical analysis revealed that Ce : Se ratio as 1 : 1.1. TGA curve showed the loss of water molecules, 11% at 200 °C. Therefore, the material possibly possesses the empirical formula $CeO_2 \cdot Se(OH)_2O \cdot nH_2O$ with a formula weight of 301 for the anhydride. The value of '*n*' the external water molecule per mole of oxide was 2.07.

The analytical importance of cerium(IV) selenite can be deduced from the K_d values of various metal ions in water, 0.1 mol dm^{-3} $NaNO_3$ and in different concentrations of HNO_3. The ion exchanger showed a selective trend in various solution as may be predicted by the K_d values, which are in parentheses *e.g.* in water: Hg^{2+} (total adsorption), Al^{3+} (1160), Pr^{3+} (700), Ho^{3+} (585), Zr^{4+} (470), Y^{3+} (440), Th^{4+} (340), La^{3+} (390), Sm^{3+} (240), Fe^{3+} (240), Ca^{2+} (200), Ba^{2+} (200), Cu^{2+} (170), Mn^{2+} (160), Sr^{2+} (110), Mg^{2+} (100), Zn^{2+} (100), Ni^{2+} (80), Cd^{2+} (68), and Pb^{2+} (55) and in 0.01 mol dm^{-3} HNO_3: Hg^{2+} (2020), Al^{3+} (640), Pr^{3+} (580), Ho^{3+} (400), Y^{3+} (340), Th^{4+} (170), La^{3+} (140), Sm^{3+} (120), Fe^{3+} (180), Ca^{2+} (70), Ba^{2+} (60), Cu^{2+} (120), Mn^{2+} (90), Sr^{2+} (40), Mg^{2+} (50), Zn^{2+} (60), Ni^{2+} (40), Cd^{2+} (20), and Pb^{2+} (10). These indicate that the exchanger shows greatest preference for Hg(II) in solvent media like H_2O and 0.01 mol dm^{-3} HNO_3, where total absorption of Hg(II) was observed. Its elution was possible only when a mixture of 0.1 mol dm^{-3} solution each of HNO_3 and $NaNO_3$ was used. The high affinity of cerium(IV) selenite for Hg(II) paved the way for its separation from most of the metal ions. For separations a glass column of 30 cm in height and of internal diameter 0.69 cm was loaded with 2 g of the exchanger. A solution was then poured into the column. The flow rate was kept 0.5 ml/min. After repeated recyclization the metal ions were eluted with an appropriate solution in which the K_d value was lowest. The separation was practically complete and the order of elution of different metals are shown in Table 1. The separations were quantitative and the errors were within admissible range.

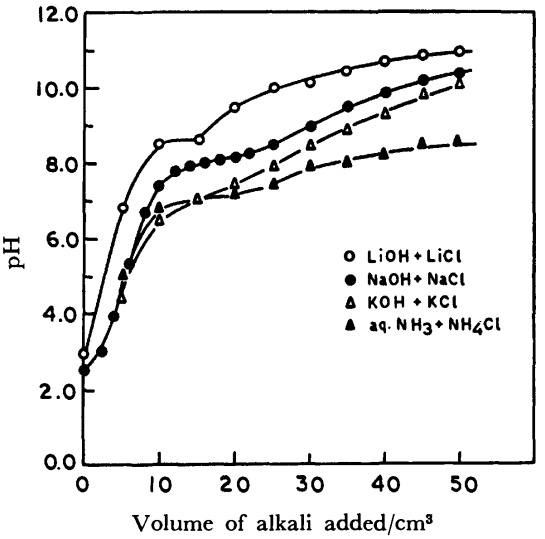

Fig. 3. pH titration curves of cerium(IV) selenite (H^+ form).

The financial support from the CSIR (India) to one of us (M. A. Khan) is gratefully acknowledged.

References

1) M. Qureshi and S. A. Nabi, *Talanta*, **19**, 1033 (1972).
2) M. Qureshi, R. Kumar, and H. S. Rathore, *Anal. Chem.*, **44**, 1081 (1972).
3) J. P. Rawat and K. P. S. Muktawat, *J. Liq. Chromatogr.*, **4**, 85 (1981).
4) H. L. Greenhanus, A. M. Feibush, and L. Gordon, *Anal. Chem.*, **29**, 1531 (1957).
5) N. H. Furman, "Standard Method of Chemical Analysis," 6th ed, Van Nostrand, Princeton (1962), Vol. 1, p. 930.
6) N. E. Topp and K. V. Pepper, *J. Chem. Soc.*, **1949**, 3299.

Amperometric Determination of Silver(I) with Hydrazine Sulfide and Its Estimation in Presence of Lead(II)

Govind S. Deshmukh, Arun G. Kulkarni,* and Shashikant N. Joshi†
Department of Chemistry, Ramnarain Ruia College Matunga, Bombay 400 019, India

(Received May 30, 1983)

Synopsis. Silver(I) has been estimated by an amperometric method using hydrazine sulfide as titrant. The titration is carried out in ammonium tartrate–ammonia supporting electrolyte (pH≈9). Further, this method is extended to determine silver(I) in presence of lead(II). Under these conditions lead(II) reacts only after all silver(I) has been precipitated. The accuracy of the procedure is comparable with that obtained in classical method.

One of the oldest procedure for the determination of silver was carried out by Lamber and Walker[1] using dead stop end point method. Potassium hexacyanoferrate(II)[2] has been used for the determination of silver at an applied potential of +0.4 V. Songina[3] titrated silver with potassium iodide at rotating platinum electrode. Thiourea[4,5] has been successfully used for estimation of silver. Deshmukh and Garde[6] determined silver using potassium thiocarbonate. Ethyl xanthate[7] was used to determine silver alone and in presence of lead. Many complexing agents like diphosphorus pentasulfide,[8] thiosemicarbazide,[9] and 8 quinolinethiol[10] have been successfully used to determine silver. Recently ethyltrithiocarbonate[11] has been reported as titrant for silver.

In the present investigation a new amperometric method for determination of silver(I) has been developed using hydrazine sulfide as titrant. The procedure is further applied for quantitative estimation of silver(I) in presence of lead(II). Preliminary studies of the polarogram characteristics of hydrazine sulfide at dropping mercury electrode revealed a well developed anodic wave in pH range 8 to 9.5 in ammonium tartrate–ammonia buffer. It was considered useful for titration of metals giving precipitates. Furthermore the anodic current of hydrazine sulfide and cathodic current of metal ions can be employed for simultaneous determination of binary mixture of silver and lead.

Experimental and Results

Solutions. Stock solutions of silver(I) and lead (II) were prepared from AnalaR grade samples. These stock solutions were standardized by classical methods.[12] The lower concentrations were then obtained by successive dilution of these stock solutions. The standard solution of hydrazine sulfide was prepared by dissolving an accurately weighed quantity of pure recrystallised sulfur in hydrazine hydrate and was protected from atmospheric contact with a layer of petroleum ether. The solution was found to be quite stable under these conditions.[13]

Ammonium tartrate solution (0.1 M (1 M=1 mol dm^{-3})) was prepared from pure sample and its pH was adjusted to 9 by concentrated ammonia.

† Present address: Forchungsinstitut, Meinsberg, 7305 Waldheim DDR.

Table 1. Amperometric determination of Ag^I with hydrazine sulfide

Supporting electrolyte: 0.1 M ammonium tartrate+ ammonia (pH≈9).
Potential applied: +0.2 V *versus* SCE.

Observation No.	Amount of Ag^I (mg)		Error
	Taken	Found	%
1	0.539	0.535	−0.74
2	0.8071	0.8011	−0.98
3	1.0788	1.0785	−0.04
4	1.3485	1.3478	−0.34
5	1.618	1.618	—
6	2.157	2.165	+0.37

A simple form of an amperometric titration unit with rotating platinum micro electrode described by Kolthoff[14] was used.

Determination of Silver(I). Preliminary experiments were carried out to study appropriate conditions for quantitative precipitation of silver in base solution of ammonium tartrate–ammonia in pH range 8 to 9.5 and following procedure was followed.

An aliquots of silver(I) solution was placed in Pyrex beaker containing 25 ml of ammonium tartrate–ammonia buffer (pH≈9). The titration was carried out at an applied potential of +0.2 V *versus* SCE. The calibrated 2 ml microburette was used for delivery of titrant. The galvanometer reading was noted initially and after each addition of titrant. The diffusion current remained constant till the whole of silver was precipitated. After the end point hydrazine sulfide gave the diffusion current of its own, resulting the regular rise in the current. The plot of volume of hydrazine sulfide added against galvanometer reading gave reverse 'L' shaped curve. The results are given in Table 1.

Determination of Silver(I) and Lead(II). Earlier results from this laboratory reported determination of lead with hydrazine sulfide.[13] Since the half wave potential of lead(II) (−0.54 V) is more negative than that of silver(I) (>O) at pH 9, the latter can be determined cathodically while lead(II) end point can be determined anodically. An attempt was, therefore, made to estimate silver(I) and lead(II) in mixed solution. The applied potential, which was chosen, was such that lead(II) was not reduced at this potential but reagent has anodic diffusion current.

Aliquots of silver(I) and lead(II) were taken in 100 ml Pyrex beaker containing 25 ml ammonium tartrate – ammonia buffer (pH≈9). The titration was performed with hydrazine sulfide. The current was noted at −0.2 V *versus* SCE. With the addition of hydrazine sulfide to mixture, diffusion current of silver (I) reduced gradually and became steady. When all

Table 2. Determination of Ag^{I} and Pb^{II} with hydrazine sulfide

Supporting electrolyte: 0.1 M ammonium tartrate+ ammonia (pH≈9).

Potential applied: −0.2 V *versus* SCE.

Observation	Amount taken (mg)		Amount found (mg)		Error/%	
	Ag^{I}	Pb^{II}	Ag^{I}	Pb^{II}	Ag^{I}	Pb^{II}
1	0.539	1.036	0.535	1.038	−0.74	+0.19
2	0.8091	2.590	0.8084	2.586	−0.08	−0.15
3	1.6182	4.144	1.5982	4.140	−0.61	−0.096
4	2.1576	1.036	2.1497	1.038	−0.36	+0.19
5	2.1576	3.108	2.165	3.105	+0.37	−0.09
6	1.0788	3.108	1.0788	3.084	—	−0.77

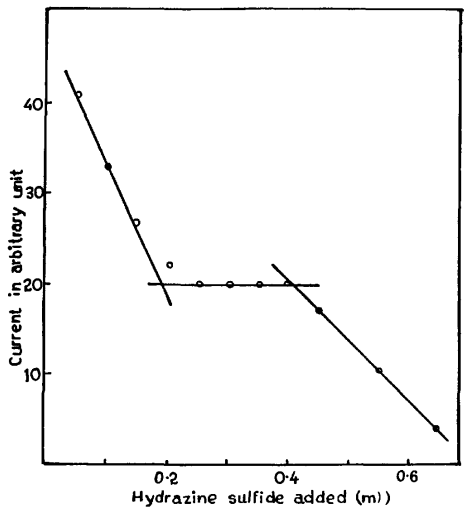

Fig. 1. A typical amperometric titration curve for mixture of Ag^{+} and Pb^{II} in tartrate buffer at −0.2 V *versus* SCE.

silver was precipitated with further addition of titrant, lead started getting precipitated. After all lead(II) was precipitated excess of reagent gave anodic diffusion current of its own. A typical titration curve is shown in Fig. 1. The first intersection gives the amount of silver(I) while second intersection gives the amount of lead(II). The results are returned in Table 2.

Besides simplicity, accuracy and time economy a significant advantage offered by the present method is the use of pure elemental sulfur directly as primary standard for preparing the solution of the titrant.

References

1) R. H. Lamber and R. D. Walker, *Ind. Eng. Chem., Anal. Ed.*, **13**, 1846 (1941).
2) R. Kalvoda and J. Zyka, *Collect. Czech. Chem. Commun.*, **15**, 630 (1950).
3) O. A. Songina., *Tr. Kom. Anal. Khim., Akad. Nauk SSSR, Otdel. Khim-Nauk*, **4**, 116 (1952).
4) A. I. Mischenko and O. A. Songina., *Zavod. Lab.*, **29**, 162 (1963).
5) N. H. Zumina and O. A. Songina., *Zh. Anal. Khim.*, **18**, 323 (1963).
6) G. S. Deshmukh and P. Garde., *Bull. Chem. Soc. Jpn.*, **40**, 1543 (1967).
7) G. S. Deshmukh and K. Saraswathi., *Bull. Chem. Soc. Jpn.*, **40**, 1545 (1967).
8) H. Chaudhari, S. S. Chaterjee, and H. S. Mahanti., *J. Indian. Chem. Soc.*, **37**, 836 (1974).
9) G. M. Norenko and A. I. Filenko., *Zh. Anal. Khim.*, **27**, 775 (1972).
10) V. I. Suprunovich, V. V. Velichko, and Y. I. Shevchenko., *Zavod. Lab.*, **44**, 525 (1978).
11) A. L. J. Rao, B. B. Brar, and B. Veerraju., *J. Electrochem. Soc. (India)*, **27**, 225 (1978).
12) A. I. Vogel, "Quantitative Inorganic Chemistry" 3rd ed, Longmans Green & Co., London (1975).
13) G. S. Deshmukh, A. G. Kulkarni, and S. N. Joshi., *Indian J. Chem., Sect.A*, **21**, 755 (1982).
14) I. M. Kolthoff and W. Stricks., *Analyst*, **78**, 405 (1953).

Preparation and Characterization of Dinitrosylmolybdenum Chelate Complexes

K. S. NAGARAJA and M. R. UDUPA*

Department of Chemistry, Indian Institute of Technology, Madras-600 036, India

(Received August 11, 1983)

Synopsis. Nitrosyl complexes of molybdenum with the composition $Mo(NO)_2L_2$ (HL=8-quinolinol, 2-mercaptobenzothiazole, 2-pyridinethiol, or ethylmercaptoacetate) have been prepared. The infrared spectral absorptions at 1740 and 1625 cm^{-1} indicate that the nitrogen monoxide groups are coordinated as NO^+ and are cis to each other. The ^1H-NMR spectral studies are also presented. The analytical, magnetic and spectral data suggest that molybdenum is in formal zero oxidation state with octahedral coordination completed by univalent bidentate ligands.

Nitrogen monoxide is a potent inhibitor for *nitrogenase*[1], a molybdoenzyme, and further nitrosyl complexes of molybdenum have been found by Zeuch[2,3] to be active disproportionatoin catalysts. With this view, the preparation and characterization of nitrosyl complexes of molybdenum with 8-quinolinol (Hoxine), 2-mercaptobenzothiazole (Hmbt), 2-pyridinethiol (Hmp), and ethylmercaptoacetate (Hetg) have been reported in the present note.

Experimental

The chemicals employed such as ammonium heptamolybdate, hydroxylammonium chloride, and ligands are pure and of Laboratory grade.

Preparation of Dinitrosylbis(8-quinolinato)molybdenum, Mo(NO)$_2$(oxine)$_2$. The interaction of ammonium heptamolybdate (0.5 g) with hydroxylammonium chloride (2.0 g) in *N,N*-dimethylformamide (20 ml) yielded green solution. 8-quinolinol (2.0 g) in ethanol (60 ml) was added to the above solution and refluxed for 1 h. The fine precipitate separated out was filtered, washed with ethanol and dried. Yield: 60%

The other complexes were also prepared by following the similar procedure as described above. The complexes are red in colour and the analytical data are listed in Table 1. The infrared, far infrared, UV-visible and ^1H-NMR spectra were recorded on Perkin-Elmer 257, Polytech IR 12, Carl Zeiss DMR 21 and Varian XL-100 spectrometers, respectively.

Results and Discussion

The complexes are found to be diamagnetic from the magnetic susceptibility measurements. The electronic transitions at 470 nm (Table 2) is attributed to charge transer transition involving $t_{2g}\rightarrow\pi^*$ (NO) or may be represented as $e(\pi^b)[d_{xz},d_{yz}]\rightarrow e(\pi^*)$ charge transfer, which has been identified[4] in a number of metal nitrosyl complexes. The other higher energy and intense absorptions are assigned[5] to internal ligand transitions. The strong absorptions observed at 1730 and 1625 cm^{-1} in the IR spectra (Fig.1) of the complexes are assigned to sym and asym stretching of NO groups. The bands suggest[6] that the NO groups are coordinated as NO^+ and further two NO groups are cis to each other. For trans configuration there will be only one mode of vibration. The strong absorption

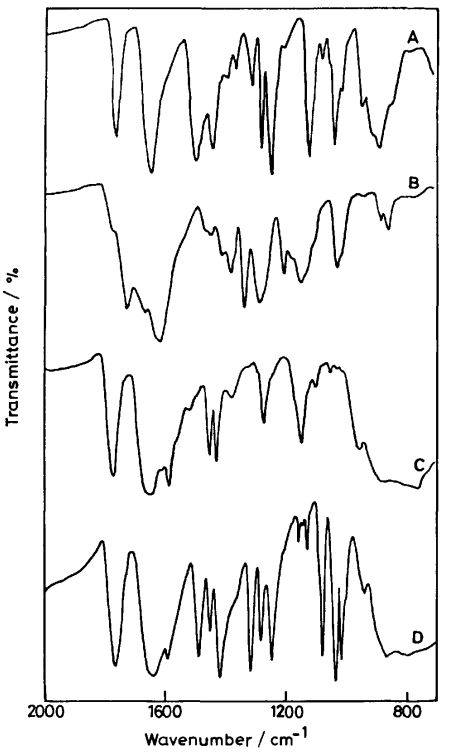

Fig. 1. Infrared spectra of (A) $Mo(NO)_2(oxine)_2$, (B) $Mo(NO)_2(etg)_2$, (C) $Mo(NO)_2(mp)_2$, and (D) $Mo(NO)_2(mbt)_2$.

in the IR spectrum of $Mo(NO)_2(oxine)_2$ at 1120 cm^{-1} (C–O) is the characteristic of the coordinated 8-quinolinol.[7] The bands at 540 and 315 cm^{-1} are due to Mo–O and Mo–N. The IR spectra of $Mo(NO)_2(mbt)_2$ and $Mo(NO)_2(mp)_2$ showed absorption at 1595 cm^{-1} (C=N) of heterocyclic ring. The absorptions in the far IR spectra at 390 and 235 cm^{-1} are due to Mo–S and Mo–N. $Mo(NO)_2(etg)_2$ has a shoulder peak at 1650 cm^{-1} (C=O). The lower value when compared with aliphatic ester (1730 cm^{-1}) indicates that the carbonyl oxygen is involved in coordination. Mo–O and Mo–S absorptions are found at 500 and 375 cm^{-1}. The absence of peak due to S–H in the last three complexes indicate deprotonation of the mercapto group. The IR spectral studies suggest that NO is coordinated as NO^+ and the complexes are of cis configuration. The univalent and bidentate nature of the ligands are also suggested by IR spectral studies.

^1H-NMR spectra of $Mo(NO)_2(mbt)_2$, $Mo(NO)_2(mp)_2$ and $Mo(NO)_2(etg)_2$ were recorded (Table 3) in $CDCl_3$ using TMS as reference. The spectrum of $Mo(NO)_2(oxine)_2$ is not recorded due to poor solubility. The NMR spectrum of $Mo(NO)_2(mbt)_2$ has a doublet of multiplet in the range δ 7.4—7.8 which is attributed to aromatic protons. The signals of the aromatic

Table 1. Analytical data of the compounds

Compound	Found (Calcd) (%)				
	H	C	N	S	Mo
$Mo(NO)_2(oxine)_2$	2.69(2.72)	48.68(48.66)	12.59(12.61)	—	21.5(21.6)
$Mo(NO)_2(mbt)_2$	1.67(1.65)	34.39(34.42)	11.45(11.46)	26.21(26.25)	19.6(19.6)
$Mo(NO)_2(mp)_2$	1.99(2.01)	36.06(36.01)	13.97(13.99)	16.00(16.02)	23.9(24.0)
$Mo(NO)_2(etg)_2$	4.32(4.30)	28.37(28.43)	6.64 (6.63)	15.16(15.18)	22.4(22.7)

Table 2. UV-visible[a] and IR[b] spectral data

Compound	λ_{max}^{c}/min (ε/dm^3 mol^{-1} cm^{-1})		$\nu_{(N-O)}$/ cm^{-1}
	$t_{2g}\rightarrow\pi^*$(NO)	Internal ligand transitions	
$Mo(NO)_2(oxine)_2$	460(200)	310(19980), 250(23450)	1700 s, 1640 s
$Mo(NO)_2(mbt)_2$	450(98)	340(15000), 285(19900)	1740 s, 1620 s
$Mo(NO)_2(mp)_2$	465(120)	275(14800), 240(20100)	1755 s, 1620 s
$Mo(NO)_2(etg)_2$	425(106)	305(12100), 250(17750)	1715 s, 1620 s

a) In methanol, b) KBr pellet.

Table 3. ^{1}H NMR spectral data

Compound	δ	Assignment
$Mo(NO)_2(mbt)_2$	7.40, 7.50, 7.54, 7.68, 7.80, 7.82, 7.84, 7.86	Aryl protons
$Mo(NO)_2(mp)_2$	7.78, 7.80, 7.82, 7.84, 7.88	Aryl protons
$Mo(NO)_2(etg)_2$	4.10, 4.14, 4.20, 4.22, 4.26	$-SCH_2-$ and $-OCH_2$
	1.14, 1.24, 1.28, 1.30, 1.32	$-COCH_2$ and $-CH_3$

protons in the spectrum of $Mo(NO)_2(mp)_2$ are observed at δ 7.82 as complex multiplet. $Mo(NO)_2(etg)_2$ has two sets of multiplet resonances in the range δ 4.2—4.8 (4H) and δ 1.40—1.80 (5H). The integrated ratio and the δ values suggest that the first set of peaks are due to $-SCH_2-$ and $-OCH_2-$ and second are due to $-COCH_2-$ and $-CH_3$ protons. In fact even the simple compound $Mo(NO)_2(Me_2dtc)_2$, which was prepared similarly, exhibited complex multiplet resonances in its ^{1}H and ^{13}C-NMR spectra, indicating cis configuration of the complex.[8]

The nitrosyls formulated as NO^+, the complexes contain $4d^6$ configuration with molybdenum in formal zero oxidation state. The presumed octahedral structure is consistent with low-spin molybdenum complex thus explaining diamagnetic behaviour.

The authors thank Council of Scientific and Industrial Research, India for the financial assistance.

References

1) E. I. Stiefel, *Prog. Inorg. Chem.*, **22**, 1 (1977).
2) E. A. Zeuch, *Chem. Commun.*, **1968**, 1182.
3) E. A. Zeuch, W. B. Hughes, D. H. Kubicek, and E. T. Kittleman, *J. Am. Chem. Soc.*, **92**, 528 (1970).
4) H. B. Gray, I. Bernal, and E. Billig, *J. Am. Chem. Soc.*, **84**, 3404 (1962).
5) C. N. R. Rao, "Ultra-violet and Visible Spectroscopy," Butterworth, London (1975).
6) B. F. G. Johnson and J. A. McCleverty, *Prog. Inorg. Chem.*, **7**, 277 (1966).
7) W. Andruchow and R. D. Archer, *J. Inorg. Nucl. Chem.*, **34**, 3185 (1972).
8) K. S. Nagaraja, Ph. D. Thesis, Indian Institute of Technology, Madras, India, 1982.

 © 1984 The Chemical Society of Japan Bull. Chem. Soc. Jpn., 57, 1707—1712 (1984)

A Model for Interactions of Amino Acid Side Chains with Watson-Crick Base Pair of Guanine and Cytosine. Crystal Structures of 9-(2-Carboxyethyl)guanine and Its Crystalline Complex with 1-Methylcytosine

Sigeo FUJITA, Akio TAKENAKA, and Yoshio SASADA*
Laboratory of Chemistry for Natural Products, Tokyo Institute of Technology, Nagatsuta, Midori-ku, Yokokama 227
(Received September 12, 1983)

A new compound, 9-(2-carboxyethyl)guanine, was successfully synthesized and its crystalline complex with 1-methylcytosine was prepared, in order to investigate the protein-nucleic acid interactions involving guanine base. The crystal structures of 9-(2-carboxyethyl)guanine (cx^{9}G) and of the complex of cx^{9}G with 1-methylcytosine (cx^{9}G:m^{1}C) were determined by the X-ray analysis. Crystal data: cx^{9}G, $P2_1/c$, a=12.221(3), b=11.022(2), c=6.961(2) Å, β=100.22(2)°; cx^{9}G:m^{1}C, $P\bar{1}$, a=8.932(1), b=12.370(1), c=7.139(1) Å, α=85.01(1), β=99.21(1), γ=86.64(1)°. In cx^{9}G, the carboxyl group is doubly hydrogen-bonded with N(2) and N(3) of the guanine moiety of the adjacent molecule, N(2)-H···O distance being 2.939(5) Å and N(3)···H-O 2.660(5) Å for N···O. In cx^{9}G:m^{1}C, the guanine moiety and 1-methylcytosine form a Watson-Crick base pair. The carboxyl group takes an O=C-OH antiperiplanar conformation and is hydrogen-bonded with N(7) of guanine in the adjacent base pair. This hydrogen bond distance is very short, 2.634(2) Å, though the unfavorable conformation of the carboxyl group. This may suggest the marked preference of the carboxyl group for N(7) of guanine in the Watson-Crick base pair. On the basis of the geometrical data found in the present crystals, some possible models of interactions were constructed and examined, for example, aspartic or glutamic acid residue in the major groove of double stranded DNA.

In order to understand the mechanism of the specific interactions between nucleic acid and protein, we have been engaged in studying on the elementary binding patterns between their components by X-ray analyses of the model crystals.[1-9] But most of them are concerned with binary systems.[1-7] As the structural basis of the interactions between protein and double stranded region of nucleic acid, the systems containing amino acid side chains and Watson-Crick base pairs are important. Two model crystals for the ternary systems of adenine-thymine-carbamoyl group[8] and of adenine-uracil-carboxyl group[9] have been reported, but no Watson-Crick base pair has been obtained.

On the other hand, model systems containing guanine base have been little studied because guanine derivatives are poorly soluble for any organic solvent and in addition appropriate guanine derivatives with amino acid side chains are not known. We have succeeded in synthesizing a new compound, 9-(2-carboxyethyl)guanine (cx^{9}G), which is a starting material to prepare model crystals covalently linked with amino acid and enables us to examine the interactions involving guanine base.

This paper describes the interaction modes between the Watson-Crick base pair of guanine-cytosine and amino acid side chains of glutamic acid and aspartic acid.

Experimental and Structure Determination

Materials. The reaction of 2-*N*-acetylguanine with β-propiolactone in the presence of 4-dimethylaminopyridine resulted in 2-carboxyethylation of the former. After purification on a silica gel column, the product was deacetylated with 6.0 equivalent of NaOH to give 9-(2-carboxyethyl)guanine (cx^{9}G). Colorless needle-like crystals of cx^{9}G were obtained from a water-acetic acid (1:1) solution. Complex of cx^{9}G and 1-methylcytosine was prepared in the dimethyl sulfoxide solution containing equimolar amounts of both components. Colorless plate-like crystals were deposited from the solution by the vapor diffusion method with ethyl acetate.

pKa Measurement. A mixture solution of 20.0 cm^3 of cx^{9}G (0.0050 mol dm^{-3}) and 2.0 cm^3 of NaOH (0.10 mol dm^{-3}) was titrated with HCl (0.10 mol dm^{-3}) and at each step the value of pH was recorded using Toshiba-Beckman pH meter. The pKa values were evaluated to be 4.1 for the carboxyl group and 2.5 for the guanine moiety from least-squares fitting.

X-Ray Work. Oscillation and Weissenberg photographs showed that the cx^{9}G crystals were twin in which the c axes of the twin components coincided but their b axes were antiparallel to each other and almost equal quantities of the components were included. Densities of the crystals were measure by the flotation method in a hexane and tetrachloromethane solution. Crystal data are listed in Table 1.

Data collection was carried out for both crystals on a Rigaku four-circle diffractometer with graphite-monochromated Cu $K\alpha$ radiation (λ=1.54184 Å). Five reference reflections monitored showed no significant intensity deterioration during the data collection. For the crystal of cx^{9}G, intensities of only one of the twin components were carefully measured; reflections with abnormally high background or unresolved reflections were excluded. Corrections were made for the Lorentz and polarization factors, but not for absorption effects. The standard deviations were estimated by the equation of $\sigma^2(F_o)=\sigma_p^2(F_o)+qF_o^2$, where q was derived from the variation of the monitored reflections and $\sigma_p(F_o)$ was due to counting statistics.[10] The experimental conditions are summarized in Table 1.

Structure Determination. The structures were solved by the direct method with the program of MULTAN 78[11] and the atomic parameters were refined by the full-matrix least-squares method. The quantity minimized in the refinement was $\sum\omega(|F_o|-|F_c|)^2$ with $\omega=1/\sigma^2(F_o)$. In the refinement, the zero-reflections with $|F_c|>F_{lim}$ were included by assuming $F_o=F_{lim}$ and $\omega=\omega(F_{lim})$, F_{lim} being the observed threshold value (Table 1). All the hydrogen atoms found on difference maps were included in the refinement. Since the $hk0$ reflections of

the crystal of cx^{9}G consist of the contributions from the both twin components, the layer scale of $hk0$ reflections was also refined. Initial value of $1/\sqrt{2}$ was evaluated by assuming 1 : 1 twin and it converged to be 0.6062 in the last some cycles of the refinement.

The space group of the complex was assumed to be $P\bar{1}$, as the normalized structure factor indicated the centrosymmetric distribution. The R value and the maximum shift of the parameters are given in Table 1. The final atomic parameters are given in Tables 2 and 3.[12] The atomic scattering factors were taken from Ref. 13.

Results and Discussion

Molecular and Crystal Structure of 9-(2-Carboxyethyl)-guanine. The bond distances and angles are shown in Fig. 1. The guanine moiety is not protonated by the carboxyl group, as expected from the lower dissociation constant of guanine moiety (pKa= 2.5). The dimensions of the carboxyl group are typical of the non-dissociated form, and the hydrogen atom of the carboxyl group appears on a difference map. The guanine moiety is planar within 0.020 Å, and its bond distances and angles are similar to those of the guanine derivatives such as 9-ethylguanine[14] and

TABLE 1. CRYSTAL DATA AND DETAILS OF EXPERIMENT AND ANALYSIS

Compound	$C_8H_9N_5O_3$[a]	$C_8H_9N_5O_3$-$C_5H_7N_3O$[b]
Formula weight	223.19	348.32
Crystal system	monoclinic	triclinic
Space group	$P2_1/c$	$P\bar{1}$
a/Å	12.221(3)	8.932(1)
b/Å	11.022(2)	12.370(1)
c/Å	6.961(2)	7.139(1)
α/°		85.01(1)
β/°	100.22(2)	99.21(1)
γ/°		84.64(1)
Cell volume/Å^3	922.8(4)	770.9(1)
Z	4	2
D_x/g cm^{-3}	1.606	1.500
D_m/g cm^{-3}	1.56	1.49
Radiation	Cu $K\alpha$	Cu $K\alpha$
μ(calcd)/cm^{-1}	11.0	9.92
Crystal size/mm^3	0.3×0.1×0.05	0.4×0.2×0.1
Scan mode	ω	$\omega/2\theta$
Scan width /°(in ω)	1.6+0.14 tanθ	1.4+0.14 tanθ
Scan speed /°(in ω) min^{-1}	2	2
2θ range/°	3—125	3—127
No. of unique reflections	1409	2202
No. of zero-reflections	247	419
q	2.31×10^{-5}	5.38×10^{-3}
F_{11m}	2.312	0.968
R	0.074	0.044
No. of reflection for R	1126	1979
Maximum shift	0.8σ	0.2σ

a) 9-(2-carboxyethyl)guanine, b) 9-(2-carboxyethyl)-guanine : 1-methylcytosine complex.

TABLE 2. FRACTIONAL COORDINATES AND ISOTROPIC TEMPERATURE FACTORS OF 9-(2-CARBOXYETHYL)GUANINE

The B values accompanied by 〈 〉 are the equivalent isotropic temperature factors calculated from anisotropic thermal parameters using the equation, $B=8\pi^2(U_1+U_2+U_3)/3$, where U_1, U_2, and U_3 are principal components of mean square displacement matrix U. Values in 〈 〉 are anisotropicity defined by $(\sum(B-8\pi^2U_i)^2/3)^{1/2}$ and those in ( ) are e.s.d.'s; they refer to last decimal places.

Atom	x	y	z	B/Å^2
N(1)	0.9363(2)	0.2522(3)	0.6940(5)	2.0<12>
C(2)	0.8321(3)	0.2237(3)	0.5951(6)	2.2<7>
N(2)	0.8054(3)	0.1057(2)	0.5719(5)	2.5<11>
N(3)	0.7563(2)	0.3070(3)	0.5235(5)	2.3<8>
C(4)	0.7966(3)	0.4222(3)	0.5518(7)	2.2<9>
C(5)	0.8993(3)	0.4578(3)	0.6507(7)	2.1<8>
C(6)	0.9773(3)	0.3690(3)	0.7305(7)	2.5<6>
O(6)	1.0718(2)	0.3848(2)	0.8249(4)	2.9<17>
N(7)	0.9081(2)	0.5822(3)	0.6503(6)	2.7<11>
C(8)	0.8116(3)	0.6220(3)	0.5571(7)	2.6<9>
N(9)	0.7400(2)	0.5271(3)	0.4898(5)	2.3<10>
C(10)	0.6234(3)	0.5362(3)	0.3912(8)	3.2<22>
C(11)	0.6042(3)	0.6359(4)	0.2432(7)	3.0<16>
C(12)	0.4828(3)	0.6463(3)	0.1552(7)	2.7<11>
O(13)	0.4582(2)	0.7516(3)	0.0716(5)	3.7<26>
O(14)	0.4163(2)	0.5660(2)	0.1616(5)	3.3<21>
H(1)	0.987(3)	0.182(3)	0.743(6)	1.5(10)
H(2A)	0.857(3)	0.045(3)	0.601(6)	1.3(10)
H(2B)	0.746(3)	0.069(3)	0.511(7)	3.1(12)
H(8)	0.792(3)	0.716(3)	0.522(6)	1.1(10)
H(10A)	0.595(3)	0.456(3)	0.312(7)	2.6(11)
H(10B)	0.572(3)	0.552(3)	0.506(7)	4.3(13)
H(11A)	0.646(3)	0.627(3)	0.144(6)	1.4(10)
H(11B)	0.635(3)	0.710(3)	0.293(6)	2.0(11)
H(13)	0.386(3)	0.758(4)	0.045(7)	5.1(13)

TABLE 3. FRACTIONAL COORDINATES AND ISOTROPIC TEMPERATURE FACTORS OF 9-(2-CARBOXYETHYL)GUANINE: 1-METHYLCYTOSINE COMPLEX

The B values accompanied by 〈 〉 are the equivalent isotropic temperature factors. Details are given in Table 2.

Atom	x	y	z	B/Å^2
C(1')	1.0048(5)	0.8948(3)	0.2296(5)	4.9<8>
N(1')	0.9994(2)	0.8192(2)	0.3984(3)	3.7<8>
C(2')	0.9113(3)	0.7329(2)	0.3757(4)	3.6<9>
O(2')	0.8399(2)	0.7251(2)	0.2156(3)	4.7<23>
N(3')	0.9059(3)	0.6611(2)	0.5284(3)	3.7<12>
C(4')	0.9862(3)	0.6738(2)	0.6980(4)	4.1<13>
N(4')	0.9770(4)	0.6016(3)	0.8447(4)	5.8<30>
C(5')	1.0781(4)	0.7604(3)	0.7250(4)	4.7<18>
C(6')	1.0820(4)	0.8304(3)	0.5726(4)	4.5<15>
N(1)	0.7208(2)	0.4788(2)	0.4697(3)	3.1<10>
C(2)	0.6357(3)	0.4783(2)	0.2906(3)	2.9<8>
N(2)	0.6497(3)	0.5590(2)	0.1607(3)	3.8<21>
N(3)	0.5436(2)	0.4032(2)	0.2449(2)	2.83<90>
C(4)	0.5480(3)	0.3255(2)	0.3922(3)	2.8<5>
C(5)	0.6313(3)	0.3177(2)	0.5740(3)	2.9<9>
C(6)	0.7258(3)	0.3997(2)	0.6232(3)	3.1<11>
O(6)	0.8085(2)	0.4077(2)	0.7773(2)	4.3<21>
N(7)	0.6068(3)	0.2222(2)	0.6764(3)	3.5<12>
C(8)	0.5109(3)	0.1761(2)	0.5584(3)	3.7<12>
N(9)	0.4704(2)	0.2354(2)	0.3838(3)	3.0<9>
C(10)	0.3749(3)	0.2005(2)	0.2177(4)	3.4<7>
C(11)	0.4639(3)	0.1796(2)	0.0594(3)	2.9<7>
C(12)	0.5972(3)	0.0936(2)	0.1129(3)	2.8<10>
O(13)	0.6197(2)	0.0310(1)	0.2572(2)	3.82<147>
O(14)	0.6940(2)	0.0888(2)	-0.0086(3)	3.9<14>
H(1A')	1.074(5)	0.952(3)	0.261(5)	6.2(11)
H(1B')	0.906(4)	0.938(3)	0.182(5)	4.9(10)
H(1C')	1.036(4)	0.852(3)	0.127(6)	5.6(11)
H(4A')	1.028(4)	0.611(3)	0.952(6)	4.9(10)
H(4B')	0.914(5)	0.536(3)	0.821(5)	6.1(11)
H(5')	1.138(4)	0.765(2)	0.848(5)	4.0(8)
H(6')	1.145(4)	0.897(3)	0.570(4)	3.6(8)
H(1)	0.783(3)	0.537(2)	0.490(3)	1.0(5)
H(2A)	0.718(3)	0.609(2)	0.183(4)	1.4(6)
H(2B)	0.594(3)	0.564(2)	0.035(4)	2.9(7)
H(8)	0.464(3)	0.107(2)	0.582(4)	2.2(6)
H(10A)	0.333(3)	0.132(2)	0.263(4)	1.7(6)
H(10B)	0.289(3)	0.258(2)	0.176(4)	1.6(6)
H(11A)	0.396(3)	0.155(2)	-0.048(4)	2.3(6)
H(11B)	0.506(3)	0.248(2)	0.013(3)	1.0(5)
H(14)	0.661(4)	0.148(3)	-0.120(5)	5.3(9)

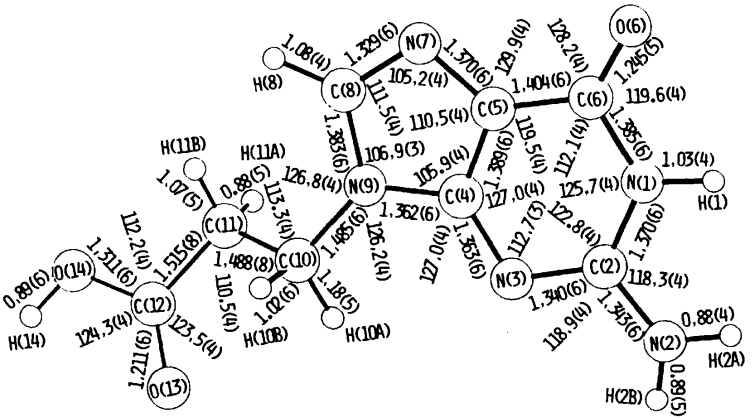

Fig. 1. Bond distances (l/Å) and angles (ϕ/°) in 9-(2-carboxyethyl) guanine. E.s.d.'s are shown in parentheses.

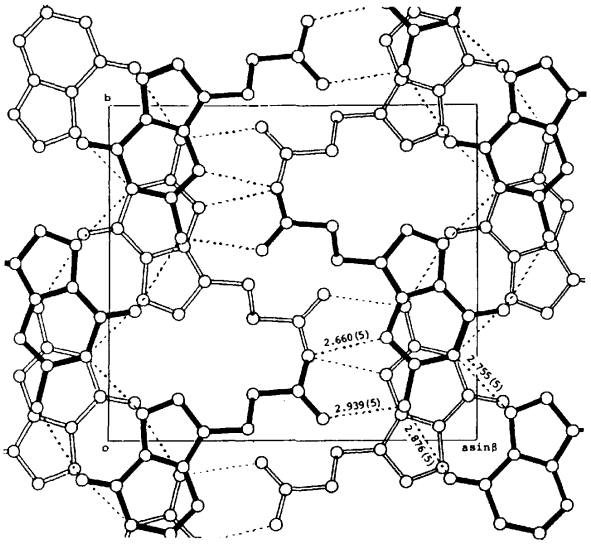

Fig. 2. Crystal structure of 9-(2-carboxyethyl) guanine, projected along the c axis. The broken lines indicate the hydrogen bonds, distances (l/Å) being added.

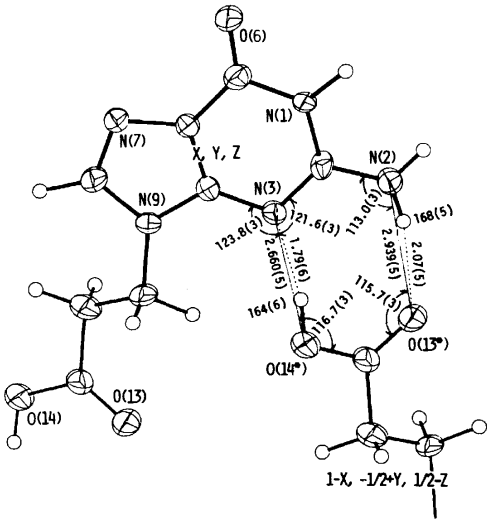

Fig. 3. A projective view of binding mode of the carboxyl group to the guanine moiety. Hydrogen bond distances (l/Å) and angles (ϕ/°) are shown with e.s.d.'s in parentheses. Thermal ellipsoids are drawn at 50% probability level.

guanosine.[15] As in guanine hemihydrate crystal,[16] the C(5)-N(7)-C(8) angle is slightly expanded due to the hydrogen bond to N(7). The torsion angles are 184.2(4)° for C(5)-C(4)-N(9)-C(10), 215.2(5)° for C(4)-N(9)-C(10)-C(11), 184.1(4)° for N(9)-C(10)-C(11)-C(12), and 162.4(4)° for C(10)-C(11)-C(12)-O(14).

The crystal structure and the hydrogen bond geometry are shown in Figs. 2 and 3. The carboxyl group of the adjacent molecule interacts with N(2) and N(3) of the guanine moiety through O···H-N and O-H···N hydrogen bonds. The dihedral angle between the least-squares planes of the purine ring and carboxyl group is 24.6(2)°. The guanine ring related by the 2_1 screw symmetry are linked by hydrogen bonds between N(1) and N(7) and between N(2) and O(6). These hydrogen bonds form a sheet parallel to the ab plane. There is no hydrogen bonds between the sheets.

Molecular and Crystal Structure of the Complex of 9-(2-Carboxyethyl)guanine and 1-Methylcytosine. The bond distances and angles are shown in Fig. 4. The carboxyl group takes an antiperiplanar O=C-O-H conformation.[17] This conformation is less stable by 2—4 kcal mol^{-1} than the synperiplanar form[18] and is usually found when the hydroxyl group participates in the intramolecular hydrogen bond.[19] The present crystal is a rare case where the hydroxyl group is hydrogen-bonded to the adjacent molecule. The bond distances of C=O and C-O of the carboxyl group are significantly different. The O=C-O angle is slightly contracted and the C-C-O angle is slightly expanded, in contrast to the synperiplanar O=C-O-H form. The geometry may be typical of the antiperiplanar carboxyl group without constrain of intramolecular hydrogen bonding.

The purine ring is planar within 0.030 Å. The bond distances and angles of the guanine moiety are similar to those of cx^{9}G in the preceding section. The torsion angles are 185.2(2)° for C(5)-C(4)-N(9)-C(10), 60.4(3)° for C(4)-N(9)-C(10)-C(11), 59.4(2)° for N(9)-C(10)-C(11)-C(12) and 12.7(3)° for C(10)-C(11)-C(12)-O(14).

1 cal=4.186 J

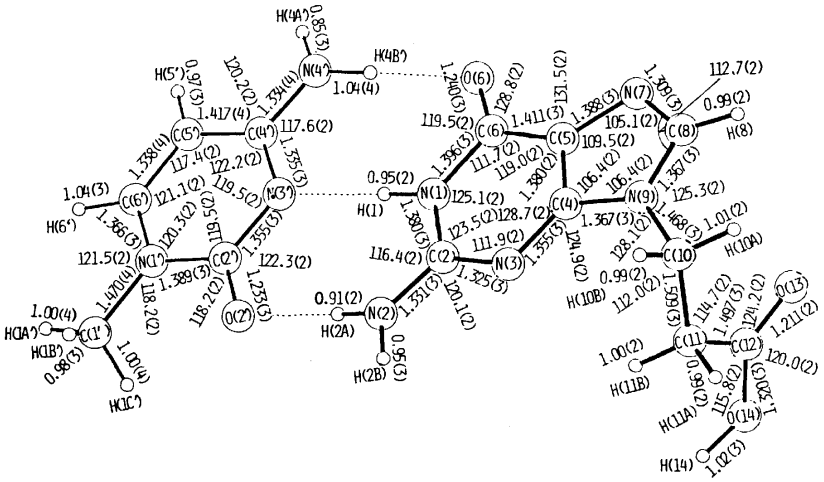

Fig. 4. Bond distances (l/Å) and angles (ϕ/°) in 9-(2-carboxyethyl)guanine : 1-methylcytosine complex. E.s.d.'s are shown in parentheses.

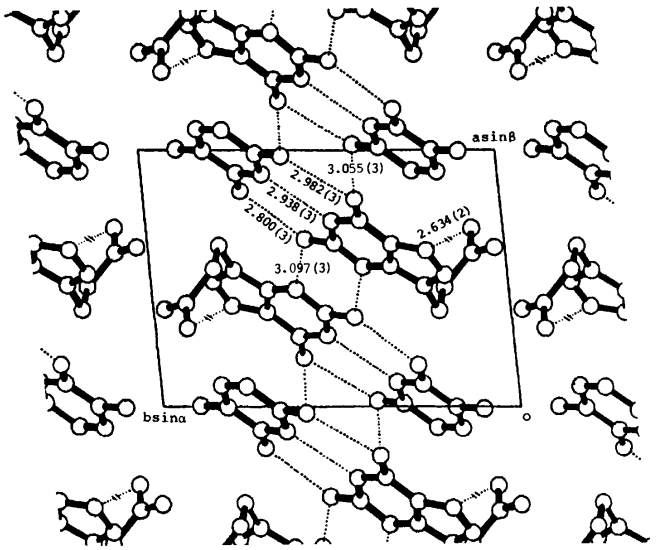

Fig. 5. Crystal structure of 9-(2-carboxyethyl) guanine: 1-methylcytosine complex projected along the c axis. Hydrogen bond distances (l/Å) are indicated.

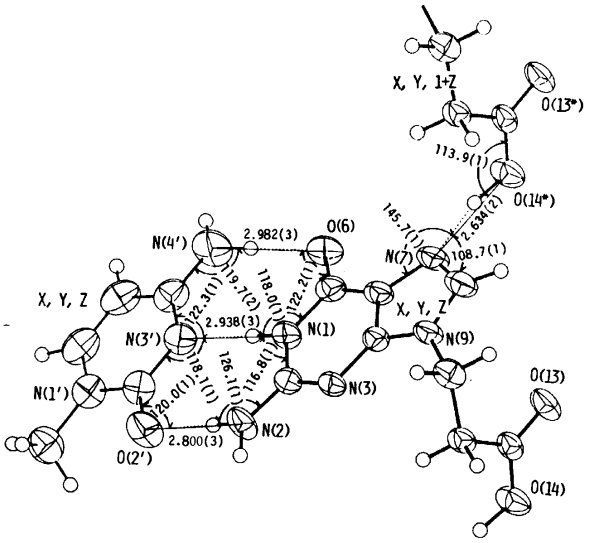

Fig. 6. A projective view of binding mode of the carboxyl group to the guanine-cytosine Watson-Crick base pair. Hydrogen bond distances (l/Å) and angles (ϕ/°) are shown with e.s.d.'s in parentheses. Thermal ellipsoids are drawn at 50% probability level.

The methylene chain is folded in contrast to that of cx^{9}G.

The bond distances and angles of 1-methylcytosine in the present complex are in good agreement with those of 1-methylcytosine[20] and cytidine.[21] The pyrimidine ring is essentially planar.

The crystal structure and hydrogen bond geometry are shown in Figs. 5 and 6. The guanine moiety and 1-methylcytosine form a Watson-Crick base pair through N(2)-H···O(2'), N(1)-H···N(3'), and O(6)···H-N(4') hydrogen bonds. The hydrogen bond distances are similar to those found in the complexes of 9-ethylguanine: 1-methylcytosine,[22] 9-ethylguanine: 1-methyl-5-fluorocytosine,[22] 9-ethylguanine: 1-methyl-5-bromocytosine,[23] deoxyguanosine: 5-bromocytidine,[24] and some salts of guaninyl-3',5'-cytidine.[25] The carboxyl group of the adjacent molecule interacts with N(7) of guanine in the Watson-Crick pair by O-H···N hydrogen bond. The hydrogen bond distance is very short, although the carboxyl group takes an unfavorable conformaion. This suggests that there is a marked preference between the carboxyl group and N(7) of guanine.

The carbonyl oxygen O(13) does not participate in any hydrogen bond; the closest contact 2.23(3) Å is observed with H(8) of the guanine moiety at ($-x$, $-y$, $1-z$). The base pairs form a ribbon extending along the [102] axis by the hydrogen bonds N(2)-H···N(3) and N(4')-H···O(6) around inversion centers at (1/2, 1/2, 0) and (1, 1/2, 1). The O(2') atom of 1-methylcytosine points to C(11) at ($1-x$, $1-y$, $-z$), the distance being 3.147(4) Å.

Hydrogen Bonding between the Watson-Crick Base Pair and Acidic Side Chain of Amino Acid. The present X-ray analyses of the model crystals are the first study on the interaction of amino acid side chain with guanine base, especially with guanine-cytosine Watson-

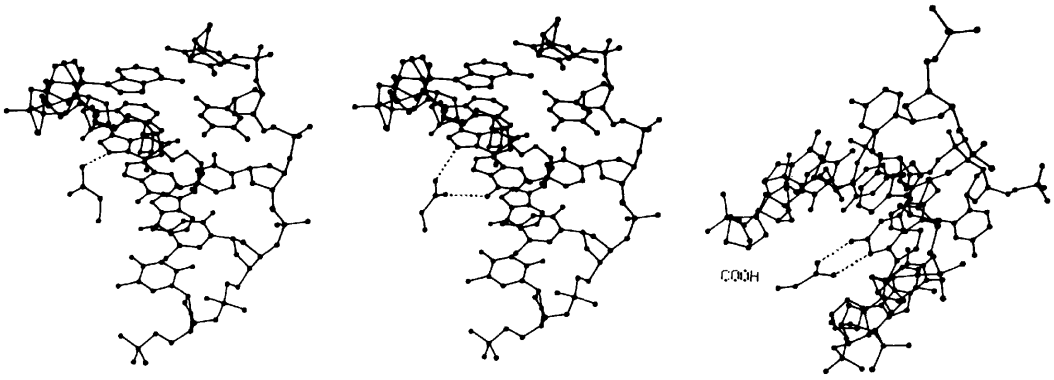

Fig. 7. Possible model fitting for the binding of the carboxyl group with guanine in the major and minor grooves of B-DNA. a) The carboxyl group takes an antiperiplanar conformation in the major groove, b) it is hydrogen-bonded with two adjacent base pairs in the major groove, and c) it is doubly hydrogen-bonded with guanine in the minor groove.

Crick pair. The model compound cx^{9}G contains the guanine moiety (p*K*a=2.5) and propionic acid moiety (p*K*a=4.1), the dissociation constants of which are comparable to those of guanosine nucleotide derivatives[26] and acidic side chains in the derivatives of amino acid or peptide,[27] respectively. So, the chemical behavior of each part of the present model compound is similar to that of the corresponding derivatives. Thus, the interaction found in this study may be realized in the protein-nucleic acid interactions.

The specificity in protein-nucleic acid interactions would arise from suitable combination of preferred hydrogen bonds between their components which are supported by the three-dimensional structure of macromolecules. It is important to examine if the hydrogen bonding found in the model crystals could be permitted for the bases in the particular secondary or tertiary structure of nucleic acids.

The carboxyl group was inserted in the major groove of B-DNA using the interaction geometry found here. Model fitting has been done successfully with the antiperiplanar O=C-O-H conformation (Fig. 7a). By the rotation of the carboxyl group around the O-C bond followed by slight translation, the other oxygen atom can form a hydrogen bond with the adjacent base in the same strand, as shown in Fig. 7b where adenine amino group is a binding site. Thus, the present hydrogen bond geometry may be an interaction model of guanine-cytosine base pair in the major groove with acidic side chain of proteins.

As the model for binding of the carboxyl group in the minor groove, the double hydrogen bonds with N(2) and N(3) of guanine, found in the crystal of cx^{9}G, might be useful, because the formation energy of this type is greater than any other double hydrogen bonds (ΔH_f= -15.0 kcal mol^{-1} calculated by the CNDO/2 method[28] while that for the Watson-Crick pairing is -18.2 kcal mol^{-1}). Although this groove is rather tight, the model fitting was also successful with slight changes of the binding geometry, as shown in Fig. 7c. As any double hydrogen bonds of carboxyl group in the minor groove can not be set up for the other nucleic acid bases, the present model could take a part in recognition of particular base sequences.

The present work was supported in part by a Grant-in-Aid for Scientific Research No. 57380026 from the Ministry of Education, Science and Culture, and Kawakami Foundation, to which the authors' thanks are due.

References

1) M. Ohki, A. Takenaka, H. Shimanouchi, and Y. Sasada, *Bull. Chem. Soc. Jpn.*, **48**, 848 (1975).
2) M. Ohki, A. Takenaka, H. Shimanouchi, and Y. Sasada. *Bull. Chem. Soc. Jpn.*, **50**, 2573 (1977).
3) A. Takenaka and Y. Sasada, 38th National Meeting of the Chemical Society of Japan, Nagoya, October 1978, Abstr. 1004.
4) A. Takenaka, M. Ohki, and Y. Sasada, *Bull. Chem. Soc. Jpn.*, **53**, 2724 (1980).
5) M. Takimoto, A. Takenaka, and Y. Sasada, *Bull. Chem. Soc. Jpn.*, **54**, 1635 (1981).
6) A. Takenaka and Y. Sasada, *Bull. Chem. Soc. Jpn.*, **55**, 680 (1982).
7) A. Takenaka, M. Takimoto, and Y. Sasada, *Biochim, Biophys. Acta*, **797**, 239 (1984).
8) M. Takimoto, A. Takenaka, and Y. Sasada, *Bull. Chem. Soc. Jpn.*, **55**, 2734 (1982).
9) S. Fujita, A. Takenaka, and Y. Sasada, *Bull. Chem. Soc. Jpn.*, **56**, 2234 (1983).
10) L. E. McCandlish and G. H. Stout, *Acta Crystallogr., Sect. A*, **31**, 245 (1975).
11) P. Main, S. E. Hull, L. Lessinger, G. Germain, J. P. Declercq, and M. M. Woolfson, "MULTAN 78. A System of Computer Programs for the Automatic Solution of Crystal Structures from X-Ray Diffraction Data," Univs. of York, England, and Louvain, Belgium (1978).
12) Lists of structure factors, anisotropic thermal parameters and least-squares plane equations and deviations of atoms from these planes have been deposited as Document No. 8426, at the office of the Chemical Society of Japan.
13) "International Tables for X-ray Crystallography," Kynoch Press, Birmingham (1974), Vol. IV, p. 71.

14) R. Destro, T. J. Kistenmacher, and R. E. Marsh, *Acta Crystallogr., Sect. B*, **30**, 79 (1974).
15) U. Thewalt, C. E. Bugg, and R. E. Marsh, *Acta Crystallogr., Sect. B*, **26**, 1089 (1970).
16) G. S. Mandel and R. E. Marsh, *Acta Crystallogr., Sect. B*, **31**, 2862 (1975).
17) L. Leiserowitz, *Acta Crystallogr., Sect. B*, **32**, 775 (1976).
18) T. Miyazawa and K. S. Pitzer, *J. Chem. Phys.* **30**, 1076 (1959); D. R. Jr Lide, *Ann. Rev. Phys. Chem.*, **15**, 225 (1964).
19) E. M. Gopalakrishna and L. Kartz, *Acta Crystallogr., Sect. B*, **28**, 2917 (1972); M. N. G. James and G. J. B. Williams, *Acta Crystallogr., Sect. B*, **30**, 1249 (1974).
20) M. Rossi and T. J. Kistenmacher, *Acta Crystallogr., Sect. B*, **33**, 3962 (1977).
21) S. Furberg, C. S. Peterson, and C. Rϕmming, *Acta Crystallogr.*, **18**, 313 (1965).
22) E. J. O'Brien, *Acta Crystallogr.*, **23**, 92 (1967).
23) H. M. Sobell, K. Tomita, and A. Rich, *Proc. Natl. Acad. Sci. U.S.A.*, **49**, 885 (1963).
24) A. E. Haschemeyer and H. M. Sobell, *Acta Crystallogr.*, **19**, 125 (1965).
25) J. M. Rosenberg, N. C. Seeman, R. O. Day, and A. Rich, *J. Mol. Biol.*, **104**, 145 (1976); B. Hingerty, E. Subramanian, S. D. Stellman, T. Sato, S. B. Broyde, and R. Langridge, *Acta Crystallogr., Sect. B*, **32**, 2998 (1976); A. Aggarwal, S. A. Islam, R. Kuroda, M. R. Sanderson, and S. Neidle, *Acta Crystallogr., Sect. B*, **39**, 98 (1983).
26) W. Pfleiderer, *Justus Liebigs Ann. Chem.* **647**, 167 (1961).
27) T. Miyazawa, private communication.
28) J. A. Pople and G. A. Segal, *J. Chem. Phys.*, **44**, 3289 (1966).

Solvent Effects on Optical and ESR Spectra of One-Electron Reduced Species of Cobalt(III) and Manganese(III) Tetraphenylporphyrins Produced by γ-Radiolysis at 77 K

Mikio Hoshino,* Shiro Konishi, and Masashi Imamura
Solar Energy Research Group, The Institute of Physical and Chemical Research, Wako, Saitama 351
(Received October 31, 1983)

One-electron reduction by γ-ray irradiation of cobalt(III) and manganese(III) tetraphenylporphyrins (ClCo(III)TPP, ClMn(III)TPP, and IMn(III)TPP) in ethanol and MTHF(2-methyltetrahydrofuran) solutions at 77 K results in the reduction of the central metals of these porphyrins. From the optical and ESR measurements, the reduced species are found to retain the axial anion, Cl^- or I^-, in MTHF but not in ethanol. The absorption spectroscopic studies of these porphyrins in ethanol solutions indicate that the axial halide ion is displaced by an ethanol molecule prior to γ-ray irradiation.

Reduced and oxidized porphyrins generated chemically and electrochemically have been subjected to numerous spectroscopic studies because of their importance as key intermediates in biological reactions.[1] In particular, optical absorption and ESR spectroscopic studies provide useful information on thir electronic structures and chemical properties. However, chemical reduction and oxidation and electrolysis techniques are unable to be applied to observation of unstable reduced and oxidized species in fluid solutions.

Radiation chemical techniques have been successfully applied to the detection of one-electron oxidation and reduction products of inorganic compounds,[2-7] metalloporphyrins,[8,9] and biologically important substances.[10,11] Recently we have systematically carried out optical and ESR measurements of one-electron reduced and oxidized products of metalloporphyrins and cobaloximes formed by γ-radiolysis of rigid solutions at 77 K.[12-19] Since molecules are immobilized in the low-temperature rigid solutions, the reduced or oxidized species are trapped as stable products and are subjected to the conventional spectroscopic measuremens.

In previous papers[12,16] we have shown that ClCo(III)TPP and ClMn(III)TPP in a less-polar solvent, MTHF, are reduced upon γ-ray irradiation at 77 K to from $Cl^-\cdots$Co(II)TPP and $Cl^-\cdots$Mn(II)TPP in which the anion Cl^- is confined in the axial position. These results imply that ClCo(III)TPP and ClMn(III)TPP hardly undergo ionic dissociation in MTHF.

In a preliminary experiment, we found that the absorption spectra of ClCo(III)TPP, ClMn(III)TPP, and IMn(III)TPP in ethanol solutions distinctly differ from those in MTHF solutions. The purpose of the present study is to investigate the one-electron reduced species of ClCo(III)TPP, ClMn(III)TPP, and IMn(III)TPP, produced by γ-ray irradiation at 77 K in a polar solvent, ethanol. The optical absorption and ESR spectra of the reduced species in ethanol are presented for the comparison with those in MTHF.

Experimental

Metalloporphyrins, ClCo(III)TPP, ClMn(III)TPP, and IMn(III)TPP, were prepared according to literature[20,21] and purified by column chromatography on Sephadex LH 20. 2-Methyltetrahydrofuran was purified by fractional distillation and stored on Na-K alloy to remove traces of water. Ethanol was used as supplied.

Optical absorption and ESR spectra were recorded on a Cary 14 spectrophotometer and a JEOL JES FE-3AX X-band spectrometer, respectively.

High-purity quartz cells having an optical pathlength of 0.1 mm were used for optical measurements. Two Kinds of ESR tubes were used: one is made of high-purity quartz and the other, specially prepared glass in which no hydrogen atoms are formed upon γ-ray irradiation at 77 K. A 1.2 kCi ^{60}Co source was used for γ-ray irradiation at a dose rate of *ca.* 53 kr min^{-1}.

Sample solutions containing 10^{-3} M (1 M=1 mol dm^{-3}) porphyrins were degassed and frozen in a Dewar vessel before γ-ray irradiation. A broad absorption due to trapped electrons formed by irradiation was eliminated by photobleaching before optical measurements of the reduced species. For the study of chemical reactions occurring in the irradiated solutions at elevated temperatures, the sample cells and tubes were warmed slightly by withdrawing them from liquid nitrogen for suitable time.

Results

Absorption Spectra. Figure 1 shows the absorption spectra of ClCo(III)TPP in ethanol solution before and after γ-ray irradiation at 77 K. The absorption

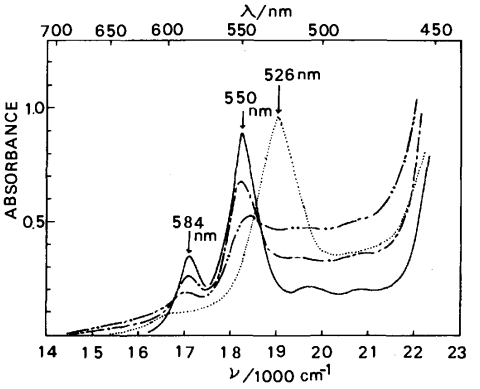

Fig. 1. Absorption spectra of ClCo(III)TPP in ethanol solution at 77K before γ-ray irradiation (——), after γ-ray irradiation for 60 min (— — —) and 150 min (— · —), and after once warming the irradiated solution for 2.0 min (·····).

peaks of ClCo(III)TPP are located at 550 and 584 nm. Except for band narrowing, the spectrum at 77 K is in good accord with that measured at room temperature. Upon γ-ray irradiation the intensities of these peaks decrease and a broad absorption appears over the wavelength region from 450 to 700 nm; the spectral change shows isosbestic points at 595 and 537 nm. The spectrum measured after irradiation for 150 min still indicates the presence of ClCo(III)TPP. Warming of the irradiated solution for 2 min gives the spectrum at 77 K shown by a dotted line in Fig. 1. Since the spectrum is the same as that of authentic Co(II)TPP in ethanol solution at 77 K, the broad absorption in 450—700 nm observed after irradiation is considered to be due to the one-electron reduced species of ClCo(III)TPP, which is transformed to Co(II)TPP at elevated temperatures. The absorption spectrum of the warmed solution shows the absence of ClCo(III)TPP, indicating that the remaining ClCo(III)TPP is reduced by solvent radicals formed upon γ-ray irradiation at 77 K.

An MTHF solution of ClCo(III)TPP at 77 K gives absorption peaks at 557 and 598 nm. The spectrum measured after γ-ray irradiation for 50 min shows the formation of a reduced species having an absorption peak at 513 nm. The reduced species changed to Co(III)TPP after warming the irradiated solution to room temperature.[12] It is noted that the reduced species of ClCo(III)TPP in MTHF exhibits a clear absorption peak at 513 nm, while that in ethanol, a broad band in the Q band region.

Figure 2 shows the absorption spectra of IMn(III)-TPP in MTHF measured before and after γ-ray irradiation at 77 K. The spectrum of IMn(III)TPP at 77 K closely resembles that at room temperature; the peak maxima are located at 550, 568, 602, and 646 nm in the Q band region. After γ-ray irradiation for 30 min the solution gives a new spectrum at 77 K. Since the spectrum measured at 77 K after once warming the irradiated solution for 1.0 min was identical with that of Mn(II)TPP prepared chemically, the new band is ascribed to the one-electron reduced species of IMn-(III)TPP, which is transformend to Mn(II)TPP at elevated temperatures.

Figure 3 shows the absorption spectra of IMn(III)-

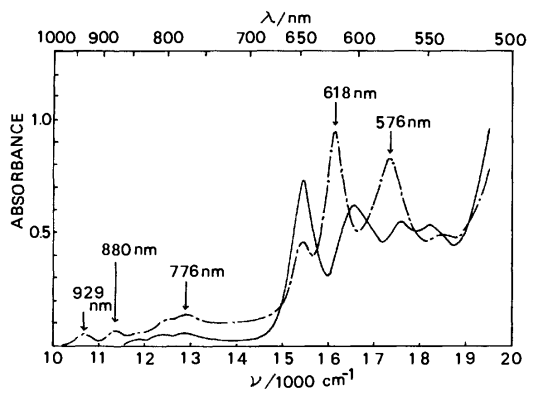

Fig. 2. Absorption spectra of IMn(III)TPP in MTHF solution at 77 K before (——) and after γ-ray irradiation for 30 min (— - —).

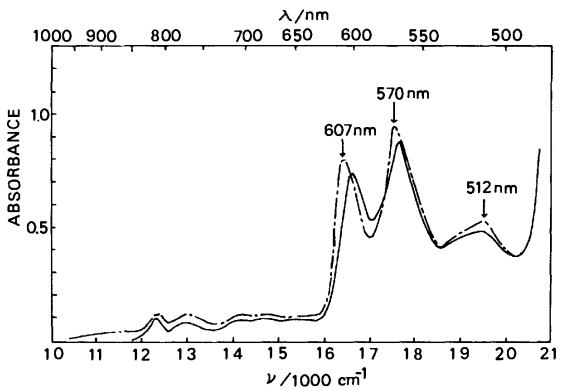

Fig. 3. Absorption spectra of IMn (III)TPP in ethanol solution at 77K before (——) and after γ-ray irradiation for 30 min (— - —).

TPP in ethanol solution before and after γ-ray irradiation at 77 K. No marked differences were observed between the two spectra of IMn(III)TPP at room temperature and 77 K. The location of the major absorption peaks in ethanol solution is fairly different from that in MTHF solution. γ-Ray irradiation of the solution gives rise to a new spectrum having major absorption peaks at 570 and 607 nm. The spectrum measured after once warming the irradiated solution shows the absorption maxima at 568 and 606 nm at 77 K, indicating the formation of Mn(II)TPP.

The absorption spectrum of ClMn(III)TPP in MTHF solution markedly differs from that of IMn-(III)TPP in MTHF, probably due to the effects of the different axial ions, Cl^- and I^-. Contrary to the MTHF solutions, ethanol solutions of ClMn(III)TPP and IMn(III)TPP give the same absorption spectrum. This result is interpreted by assuming that both ClMn-(III)TPP and IMn(III)TPP undergo ionic dissociation in ethanol solutions to from a common species, $Mn(III)TPP^+(EtOH)_2$, in which the axial positions are occupied by two ethanol molecules.[22,23]

ESR Spectra of γ-Irradiated Solutions. Figure 4A shows the ESR spectrum observed for ethanol solution of ClCo(III)TPP γ-irradiated at 77 K. The hyperfine structure of a cobalt atom (I=7/2) appearing in the parallel component reveals that the central metal, Co(III), in ClCo(III)TPP is reduced to Co(II). The ESR parameters determined for the reduced species are $g_{/\!/}=2.010\pm0.005$, $A_{/\!/}=105\pm5\times10^{-4}$ cm^{-1}, $g_\perp\simeq2.45$, and $A_\perp\simeq57\times10^{-4}$ cm^{-1}. Figure 4B shows the ESR spectrum measured at 77 K after warming the irradiated solution for 1.0 min. This spectrum is identical with that of authentic Co(II)TPP which is expected to have a structure of $Co(II)TPP(EtOH)_2$ in ethanol solution at 77 K. The ESR parameters are $g_{/\!/}=2.024\pm0.005$, $A_{/\!/}=99\pm5\times10^{-4}$ cm^{-1}, $g_\perp\simeq2.45$, and $A_\perp\simeq57\times10^{-4}$ cm^{-1}.

Figure 5A shows the ESR spectrum observed for the γ-irradiated MTHF solution of IMn(III)TPP at 77 K. The spectrum shows well-resolved six hyperfine lines due to ^{55}Mn (I=5/2) at the g=6 region in addition to an intense signal from solvent radicals at g=2.0. The absence of the hyperfine coupling due to the iodine

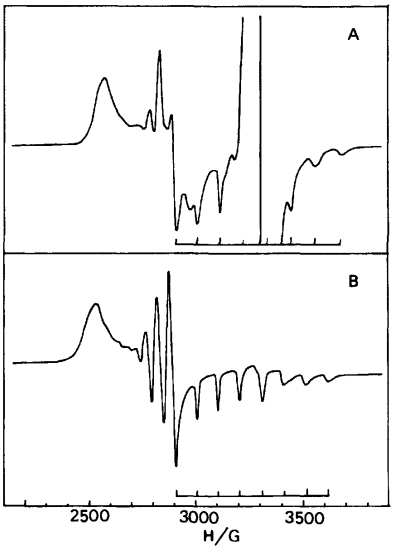

Fig. 4. ESR spectra of ClCo(III)TPP solution in ethanol measured at 77K after 20 min γ-irradiation (A), followed by 2.0 min warming of the irradiated solution (B).

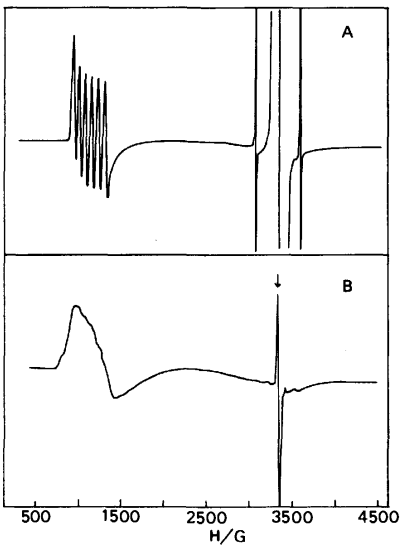

Fig. 5. ESR spectra IMn(III)TPP solution in MTHF measured at 77K after 20 min γ-irradiation (A), followed by 2.0 min warming of the irradiated solution (B). An arrow in B indicates the signal from color centers in quartz tube.

atom implies that the I-Mn bond in IMnTPP is dissociated by the dissociative electron attachment. Figure 5B shows the ESR spectrum measured for the γ-irradiated solution at 77 K after once warming it to remove signals due to solvent radicals. The low-field signal at g=6 becomes broad and the high field signals becomes observable by warming the irradiated sample. The ESR spectrum is the same as that of authentic Mn(II)TPP in MTHF solution at 77 K.

Figure 6A shows the ESR spectrum of a γ-irradiated ethanol solution of IMn(III)TPP at 77 K. The spectrum shows less-resolved six hyperfine lines at g=6. When the irradiated solution is warmed for 1.0 min

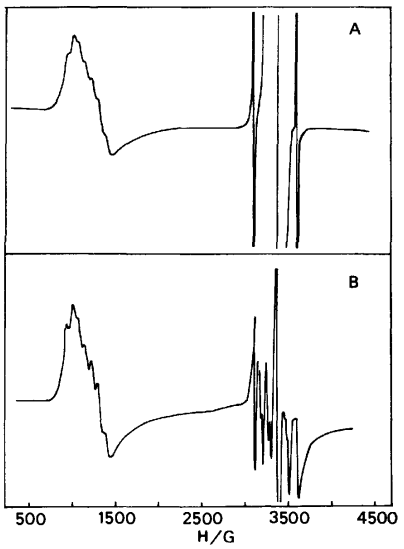

Fig. 6. ESR spectra of IMn(III)TPP solution in ethanol measured at 77K after 20 min γ-irradiation (A), followed by 2.0 min warming of the irradiated solution.

and recooled to 77 K, the signal intensity at g=6 slightly decreases and a new signal due to unidentified manganese(II) species appears at $g\simeq2$. The line shape of the low-field signals is invariant even after warming the irradiated solution. These results are in good accord with those obtained for the γ-irradiated Mn(III)TPP solution in deuterated methanol at 77 K.[9]

A γ-irradiated ethanol solution of ClMn(III)TPP gives the same ESR spectra, both before and after warming, as those shown in Fig. 6A and 6B. This result implies that the common species is produced from the ethanol solutions of ClMn(III)TPP and IMn(III)TPP upon γ-ray irradiation. Taking account of the optical measurements, $Mn(III)TPP^+(EtOH)_2$ is considered to be a precursor of the reduced species in the ethanol solutions.

Discussion

Formation of One-electron Reduced Species by γ-Ray Irradiation. Solid ethanol solutions exposed to γ-rays at 77 K release mobile electrons (e_m^-) according to:

$$CH_3CH_2OH \longrightarrow CH_3CH_2OH^+ + e_m^-$$

The ethanol cation radical, $CH_3CH_2OH^+$, undergoes ion-molecular reaction with a parent ethanol molecule to form a 2-hydroxyethyl or ethoxyl radical and a protonated ethanol.[13] The mobile electrons are either trapped in the solution or captured by solute molecules (S) if any to form trapped electrons (e_t) or solute anions (S^-), respectively:

$$e_m^- \longrightarrow e_t^-$$

$$e_m^- + S \longrightarrow S^-.$$

The similar processes take place in MTHF solution, too. γ-Irradiation of metalloporphyrin solutions in ethanol or MTHF at 77 K, therefore, produces one-electron reduced metalloporphyrins along with e_t^- and radicals originated from ethanol or MTHF molecules. The absorption spectra of one-electron reduced

metalloporhyrins in ethanol are measured after photobleaching of e_t which has a broad absorption band centered around 530 nm.[25,26]

Identification of One-electron Reduced Species at 77 K. The one-electron reduced product of ClCo(III)TPP in MTHF at 77 K has a structure of a constrained complex in which the anion, Cl^-, is confined in the axial position of Co(II)TPP.[12] The ESR spectrum of the constrained complex is characteristically different from that of authentic Co(II)TPP in MTHF solution at 77 K. The ESR parameters of the constrained complex are qualitatively interpreted by assuming that A_1^2 state of Co(II)TPP is mixed with the higher excited states[27] such as E^4 by electrostatic interaction due to the axial anion.

The one-electron reduced species of ClCo(III)TPP in ethanol solution at 77 K, on the other hand, does not form the constrained complex. The fact that the ESR parameters of the one-electron reduced species in ethanol considerably resemble those of authentic Co(II)TPP suggests that Cl^- is located far from the cobalt atom in Co(II)TPP. The paperelectrophoresis studies revealed that ClCo(III)TPP in alcohol solution is dissociated as[28]

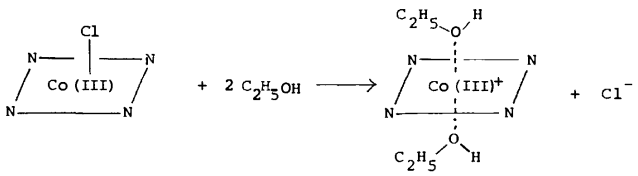

Consequently ClCo(III)TPP in ethanol solution at 77 K is regarded as having a form of $Co(III)TPP^+(EtOH)_2$. When the ethanol solution is exposed to γ-rays, $Co(III)TPP^+(EtOH)_2$ is reduced by a mobile electron to form $Co(II)TPP(EtOH)_2'$ which is transformed to $Co(II)TPP(EtOH)_2$ by warming the irradiated solution. Since $Co(III)TPP^+(EtOH)_2$ may accept a mobile electon without accompanying displacement of axial ethanol molecules owing to high viscosity of the solvent at 77 K, the distance, $Co-O\begin{smallmatrix}H\\ \diagdown C_2H_5\end{smallmatrix}$, in $Co(III)TPP^+(EtOH)_2'$ is expected to be almost the same as that in $Co(III)TPP^+(EtOH)_2$. Taking account of the electrostatic interaction between a positively charged Co(III) atom and an oxygen atom of axial ethanol, the Co-O distance in $Co(III)TPP^+(EtOH)_2$ is reasonably assumed to be shorter than that in $Co(II)TPP(EtOH)_2$. We therefore conclude that the Co-O distance in $Co(II)TPP(EtOH)_2'$ is shorter than that in $Co(II)TPP(EtOH)_2$. The transformation of $CO(II)TPP(EtOH)_2'$ to $Co(II)TPP(EtOH)_2$ by warming presumably results in a small displacement of axial ethanol molecules and, therefore, in the absorption and ESR spectral change of the one-electron reduced product of ClCo(III)TPP in ethanol at elevated temperatures.

The ESR spectrum observed for the γ-irradiated ethanol solutions of IMn(III)TPP at 77 K shows six hyperfine lines due to ^{55}Mn at $g=6$, indicating the formation of high-spin Mn(II)TPP which has a d^5-electron configuration. For MTHF solution, the structure of the reduced species is concluded to be $I^-\cdots Mn(II)TPP$ on the basis of the previous ESR studies on one-electron reduced species of ClMn(II)-TPP and BrMn(III)TPP; the two species give well-resolved ESR spectrum at $g=6$ owing to the effects of the axial anions.[16] Warmig the irradiated IMn(III)-TPP solution gives the same ESR spectrum at 77 K as that for chemically prepared Mn(II)TPP. This result indicates that liberation of I^- from $I^-\cdots$ Mn(II)TPP occurs by warming. The one-electron reduced species of IMn(III)TPP in ethanol solution, on the other hand, gives less resolved ESR spectrum at $g=6$, which is in good accord with that of chemically prepared Mn(II)TPP. We concluded that axial anion I^- is located far from the central Mn atom in the ethanol solution.

Conclusion

The absorpion spectra of ClCo(III)TPP and IMn(III)TPP in ethanol solutions are essentially different from those in MTHF solutions. The optical and ESR studies on their one-electron reduced species produced by γ-ray irradiation at 77 K show that these species retain axial anions in MTHF whereas not in ethanol. This fact leads to the conclusion that ClCo(III)TPP or IMn(III)TPP has already been dissociated in ethanol solutions into $Co(III)TPP^+(EtOH)_2$ and Cl^- or $Mn(III)TPP^+(EtOH)_2$ and I^- prior to acceptance of an electron ejected from solvent molecules by γ-ray irradiation.

References

1) J. Faier and M. S. Davis, "The Prophyrins", ed by D. Dorphin, Academic Press: New York (1979), Vol. IV part B, p. 167.
2) M. Nakamura and S. Fujiwara, *J. Coord. Chem.*, **1**, 221 (1971).
3) H. Kawazoe, H. Hosono, J. Nishii, and T. Kanazawa, *J. Chem. Phys.*, **76**, 3429 (1982).
4) O. P. Anderson and M. C. R. Symons. *J. Chem. Soc. Commun.*, **1972**, 1020.
5) J. R. Shock and M. T. Rogers, *J. Chem. Phys.*, **62**, 2640 (1975).
6) W. C. Lin, C. A. McDowell, and D. J. Ward, *J. Chem. Phys.*, **49**, 2883 (1968).
7) M. Hoshino S. Konishi, M. Nakajima, and M. Imamura, *Bull. Chem. Soc. Jpn.*, **56**, 1233 (1983).
8) P. Neta, *J. Phys. Chem.*, **85**, 3678 (1981).
9) R. Rao and M. C. R. Symons, *J. Chem. Soc. Faraday Trans.*, **78**, 3393 (1982).
10) M. C. R. Symons and R. L. Peterson, *Biochim. Biophys. Acta*, **535**, 241 (1978).
11) L. C. Dickinson and M. C. R. Symnons, *J. Phys. Chem.*, **86**, 917 (1982).
12) S. Konishi, M. Hoshino, and M. Imamura, *Chem. Phys. Lett.*, **72**, 459 (1980).
13) S. Konishi, M. Hoshino, and M. Imamura, *J. Phys. Chem.*, **84**, 3437 (1980).
14) M. Hoshino, K. Ikehara, M. Imamura, H. Seki, and Y. Hama, *Photochem. Photobiol.*, **34**, 75 (1981).
15) M. Hoshino, S. Konishi, Y. Terai, and M. Imamura, *Inorg. Chem.*, **21**, 89 (1982).

16) S. Konishi, M. Hoshino, and M. Imamura, *J. Phys. Chem.*, **86**, 1412 (1982).
17) M. Hoshino, S. Konishi, K.Ito, and M.Imamura, *Chem. Phys. Lett.* **88**, 138 (1982).
18) S. Konishi, M. Hoshino, and M. Imamura, *J. Am. Chem. Soc.*, **104**, 2057 (1982).
19) S. Konishi, M. Hoshino, and M. Imamura *J. Phys. Chem.*, **86**, 4537 (1982).
20) T. Sakurai, K. Yamamoto, H. Naito, and M. Nakamoto, *Bull. Chem. Soc. Jpn.*, **49**, 3042 (1976).
21) A. D. Alder, F. R. Long, F. Kampas, and J. Kim, *J. Inorg. Nucl. Chem.*, **32**, 2443 (1970).
22) L. J. Boucher, *J. Am. Chem. Soc.*, **90**, 6640 (1968).
23) L. J. Boucher, *Coord. Chem. Rev.*, **7**, 289 (1972).
24) M. Hoshino, S. Arai, M. Imamura, K. Ikehara, and Y. Hama, *J. Phys. Chem.*, **84**, 2576 (1980).
25) T. Shida and M. Imamura, *J. Phys. Chem.*, **78**, 232 (1974).
26) M. J. Blandamer, L. Shields, and M. C. R. Symons, *J. Chem. Soc.*, 1127 (1965).
27) B. R. McGarvy, *Can. J. Chem.*, **53**, 2498 (1975).
28) K. Yamamoto, *Sci. Papers Inst. Phys. Chem. Res.*, **71**, 111 (1977).

The Crystal Structure of a New Thiosilicate of Thallium, $TlInSiS_4$

Yuji NAKAMURA,* Atsushi ARUGA, Izumi NAKAI, and Kozo NAGASHIMA
Department of Chemistry, The University of Tsukuba, Ibaraki, 305
(Received November 1, 1983)

The crystal structure of a new synthetic compound with the composition of $TlInSiS_4$ has been determined. The crystal is orthorhombic, and the space group is *Pbnm* with $Z=8$. The cell dimensions are $a=11.74(1)$, $b=17.038(7)$, and $c=7.285(3)$ Å. The structure was solved by the Patterson method and refined to a final R-value of 0.074 for all the observed reflections. The structure is characterized by a sheet structure built up from alternating infinite $(InS_3)_n$ chains and dimeric Si_2S_6 groups. The Si_2S_6 groups consist of two SiS_4 tetrahedra sharing an edge. The thallium atoms are situated between the sheets and are surrounded by nine sulfur atoms at distances between 3.293 and 3.957 Å.

Studies of ternary and quaternary chalcogenides containing 4B elements in the periodic table have been extensively carried out during the last two decades. Numerous phases have been found, and the determinations of their crystal structures have provided evidence for the existence of various anionic groups formed by arrangements of thioanions. For example, it is well known that there are SiS_4^{4-},[1] GeS_4^{4-}[1-3], and SnS_4^{4-}[4] (isolated tetrahedral anions), $Ge_2S_7^{6-}$[5] and $Sn_2S_7^{6-}$[5] (dimeric anions consisting of two tetrahedra sharing one corner), $Ge_2S_6^{4-}$[6,7], and $Sn_2S_6^{4-}$[7] (dimeric isolated anions consisting of edge-sharing tetrahedra), $Si_4S_{10}^{4-}$[8] and $Ge_4S_{10}^{4-}$[8-10] (adamantane-like anions), and $(GeS_3)_n^{2n-}$[11,12] (infinite chains).

In order to elucidate systematically the crystal chemistry of those chalcogenides, we have undertaken the preparation of Tl-III-IV-S_4 type compounds with III=Al, Ga, In; IV=Si, Ge by the conventional evacuated-silica-tube method. This study produced single crystals of five new compounds with a quaternary composition.[13] The crystal structure of $TlInSiS_4$ is described in the present paper.

Experimental

A tabular crystal with approximate dimensions of 0.050×0.175×0.125 mm was used for the X-ray investigations. The rotation and Weissenberg photographs with Cu $K\alpha$ radiation showed an orthorhombic symmetry with systematic absences of $h+l=2n+1$ for $(h0l)$ reflections and of $k=2n+1$ for $(0kl)$ reflections, so that possible space groups are non-centrosymmetric $Pbn2_1$ and centrosymmetric *Pbnm*; the latter was subsequently established by the crystal-structure analysis.

The lattice parameters were determined by a least-squares refinement using the 2θ values of 22 reflections in the range of 21—34° centered automatically on a Rigaku AFC-5 four-circle diffractometer with Mo $K\alpha$ radiation ($\lambda=0.71068$ Å); they led to these orthorhombic cell constants: $a=11.74(1)$, $b=17.038(6)$, and $c=7.285(3)$ Å.

The chemical composition was determined by means of electron-probe X-ray microanalysis (JEOL JXA-50A X-ray microanalyzer automated by the ELIONIX ACPS-XR control system at the Chemical Analysis Center of the University of Tsukuba). The result of analysis gave the following values: Tl=41.1(42.98), In=25.1(24.15), Si=5.7(5.90), S=27.1(26.97), $\sum$ 99.0(100.00) wt%, The theoretical values for $TlInSiS_4$ are given in brackets. The density calculated for $TlInSiS_4$, $D_x=4.34\,g\cdot cm^{-3}$ for eight formula units in the unit cell, agrees well with the measured density of $4.37\,g\cdot cm^{-3}$. Table 1 summarizes the crystallographic data of $TlInSiS_4$.

Table 1. Crystallographic data

Formula	$TlInSiS_4$
Formula weight	475.52
Decomposition point	300 °C
Crystal system	Orthorhombic
Space group	*Pbnm*
a	11.74(1) Å
b	17.038(7) Å
c	7.285(3) Å
V	1457(2) Å^3
Z	8
D_m	$4.37\,g\cdot cm^{-3}$
D_x	$4.34\,g\cdot cm^{-3}$
μ(Mo $K\alpha$)	$266.72\,cm^{-1}$

The intensity data were collected on a Rigaku Rotaflex four-circle diffractometer operated at 50 kV and 160 mA with graphite monochromated Mo $K\alpha$ radiation, 2θ-ω scan technique, and a scan speed of 2° per minute. The scanning widths and offset values were determined by the following formulae; $\Delta\omega=1.0+0.5\times tan\theta$ and $\delta=0.5\times\Delta\omega$ respectively. The intensity measurements were repeated up to two times for each reflection until $\sigma(|Fo|)/|Fo|$ became less than 0.05. The intensities of three standard reflections, (122), (0, 10, 0) and (004), were measured every 50 reflections. No significant fluctuation in the intensities could be observed during the data collection. A total of 2383 independent reflections below $2\theta=61°$ were measured, of which 940 reflections with $|Fo|\geqq 3\sigma(|Fo|)$ were considered as observed and used for the structure determination. The intensity data were corrected for Lorentz, polarization, and absorption factors (μ(Mo $K\alpha$)=266.72 cm^{-1}). The absorption corrections were made by the use of the computer program ACACA.[14] The transmission factors varied from 0.079 to 0.278.

Determination and Refinement of the Structure

The positions of one independent thallium atom and the indium atom were determined from the Patterson maps. The positions of the other thallium atom, six sulfur atoms, and two silicon atoms were determined by successive Fourier and difference Fourier syntheses. The full-matrix least-squares refinements, including all atoms with isotropic temperature factors using RFINE-2,[15] yielded the $R(=\sum||Fo|-|Fc||/\sum|Fo|)$ value of 0.234 and $R_w(=\{\sum w(|Fo|-|Fc|)^2/\sum w|Fo|^2\}^{1/2}$,

where $w=1/\sigma^2(|Fo|)$) of 0.241 for all observed reflections. The difference Fourier synthesis at this stage indicated that the assumed silicon sites with high positive residual peaks seemed to be partly occupied by indium atoms. In a similar way, the indium site showed a negative residual peak, suggesting that the site is partly replaced by the silicon atoms. Then, the site occupancies were refined with the program RFINE-2 on the basis of the assumption that the total occupancy of the site is 1. The occupancies of the silicon atoms at the Si(1) and Si(2) sites were 0.42 and 0.91 respectively, and the partial occupancy of the indium atom at the In site could be determined to be 0.67. Further refinement with anisotropic temperature factors and anomalous dispersion correction reduced the R-value to 0.074 and the R_w-value to 0.059 for all the observed reflections. The maximum shift of the atomic parameters in the last cycle was less than 0.01 times the corresponding standard deviations. A difference Fourier synthesis using the final atomic parameters showed no significant residual peaks. The scattering factors for neutral atoms tabulated by Cromer and Mann[16] were used in the calculations. The anomalous dispersion correction factors were taken from the International Tables for X-ray Crystallography.[17] The computations were performed on a FACOM M-200 computer at the Information Center of the University of Tsukuba.

The final atomic coordinates and thermal parameters are given in Table 2, while Table 3 shows the site occupancies of the indium and silicon atoms. Lists of the anisotropic temperature factors and the observed and calculated structure factors are deposited as Document No. 8419 at the Chemical Society of Japan.

Table 2. Atomic coordinates and isotropic thermal parameters[a)]

Atom	x	y	z	B_{eq}/Å^2
Tl(1)	0.0578(2)	0.1555(1)	0.25	7.3
Tl(2)	0.3817(2)	0.0572(1)	0.25	6.6
In	0.7395(2)	0.1538(1)	−0.0021(3)	2.9
Si(1)	0.8076(3)	0.3229(2)	0.25	2.8
Si(2)	0.6899(6)	0.4831(4)	0.25	2.8
S(1)	0.8591(6)	0.0411(4)	0.0064(9)	4.5
S(2)	0.8626(7)	0.2622(5)	−0.0064(11)	5.8
S(3)	0.1190(9)	0.3511(6)	0.25	4.9
S(4)	0.6177(9)	0.1618(5)	0.25	4.4
S(5)	0.6177(8)	0.3693(5)	0.25	4.1
S(6)	0.8719(9)	0.4543(6)	0.25	4.9

a) Estimated standard deviations are shown in parentheses.

Description and Discussion of the Structure

The crystal structure of $TlInSiS_4$ is presented in Fig. 1-(a) (projected along the c axis) and Fig. 1-(b) (projected on to the (100) plane). In the structure, In, S(1), and S(2) are located in the general positions at nearly $z=0$, while all the remaining atoms are in the special positions at $z=0.25$.

Table 3. Site occupancies of indium and silicon atoms

Site	In	Si	Position
In	0.67	0.33	8 *d*
Si(1)	0.58	0.42	4 *c*
Si(2)	0.09	0.91	4 *c*

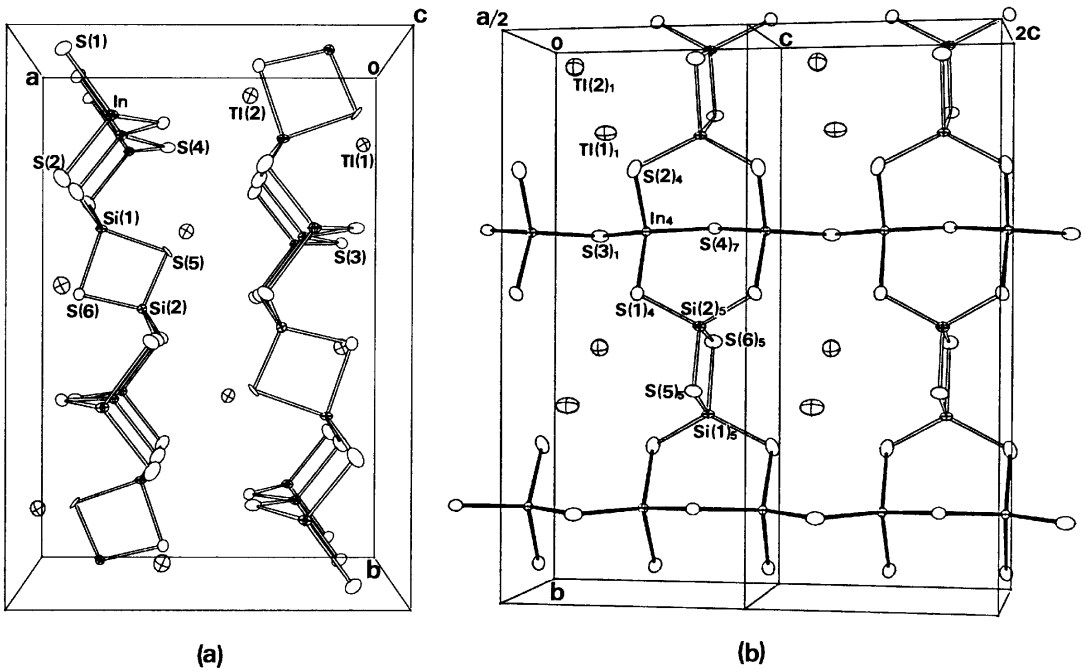

Fig. 1. Structure of $TlInSiS_4$ with the numbering scheme of atoms. (a) Projection along the c axis. (b) Projection along the a axis.

The two silicon atoms, Si(1) and Si(2), are essentially four-coordinated by sulfur atoms forming the SiS_4 tetrahedra. The two tetrahedra share an edge to form dimeric Si_2S_6 groups. Similarly, the indium atom is tetrahedrally coordinated by four sulfur atoms. The InS_4 tetrahedra are linked together to form an infinite chain by sharing one vertex along the *c* axis, as is shown in Fig. 1-(b). The chains are connected with the dimeric Si_2S_6 groups by sharing two sulfur atoms at the apexes to form an infinite two-dimensional sheet. The sheet extends parallel to the (100) plane. Individual layers are held together by the electrostatic forces of the thallium ions lying between them. It may be worth mentioning that the temperature factors of all the atoms in the structure have unusually large values in comparison with those of any compound including these atoms.

The interatomic distances and bond angles are listed in Tables 4 and 5 respectively. The atomic configuration of the Si_2S_6 group is illustrated in Fig. 2, along with the calculated bond lengths. The Si_2S_6 groups consist of two tetrahedra joined by a common edge, where two silicon atoms, Si(1) and Si(2), and two sulfur atoms, S(5) and S(6), in the four-membered ring lie on the same plane. The S(1) and S(2) atoms in the Si_2S_6 group seem to imply some terminal character due to comparatively weak bonding with indium atoms. Such atoms will be called "terminal" in the present paper. The terminal Si-S bond distances are shorter than the bridging Si-S bond distances. This feature is especially remarkable in the configuration of sulfur atoms bonded with Si(1). In the dimer, the mean Si(1)-S bond distance is longer than the mean Si(2)-S bond distance. This difference can be ascribed to the partial substitution of indium atoms for silicon atoms. The Si(1)-S distances for distorted $Si(1)S_4$ tetrahedron range from 2.230 to 2.365 Å, with an average of 2.297 Å, which is close to the value for the sum of the covalent radii, 2.30 Å, estimated by considering the occupancies of silicon and indium atoms at the Si(1) site. The terminal bonds have a definite π-content, while the bridging Si(1)-S bonds correspond approximately to single bonds. On the other

Table 4. Bond distances (*l*/Å), with estimated standard deviations in parentheses, An asterisk (*) indicates an atom related by the two-fold symmetry

$Si(1)-S(2)_1$	2.230(8)	$In-S(3)_7$	2.296(7)
$Si(1)-S(2)_6$	2.230(8)	$In-S(4)_1$	2.331(7)
$Si(1)-S(6)_1$	2.362(10)	$In-S(2)_1$	2.346(9)
$Si(1)-S(5)_1$	2.365(10)	$In-S(1)_1$	2.379(7)
Mean:	2.297	Mean:	2.338
$Si(2)-S(1)_3$	2.111(7)		
$Si(2)-S(1)_8$	2.111(7)		
$Si(2)-S(5)_1$	2.117(11)		
$Si(2)-S(6)_1$	2.191(13)		
Mean:	2.133		
$Tl(1)-S(3)_1$	3.410(10)	$Tl(2)-S(4)_1$	3.293(11)
$Tl(1)-S(2)_1$*	3.471(9)	$Tl(2)-S(6)_3$*	3.382(11)
$Tl(1)-S(2)_6$*	3.471(9)	$Tl(2)-S(3)_3$*	3.512(10)
$Tl(1)-S(1)_1$*	3.519(7)	$Tl(2)-S(2)_4$	3.559(8)
$Tl(1)-S(1)_6$*	3.519(7)	$Tl(2)-S(2)_7$	3.559(8)
$Tl(1)-S(5)_7$	3.734(3)	$Tl(2)-S(6)_7$	3.650(2)
$Tl(1)-S(5)_7$*	3.734(3)	$Tl(2)-S(6)_7$*	3.650(2)
$Tl(1)-S(1)_2$*	3.957(7)	$Tl(2)-S(1)_2$*	3.780(7)
$Tl(1)-S(1)_5$*	3.957(7)	$Tl(2)-S(1)_5$*	3.780(7)
Mean:	3.641	Mean:	3.574

Code	Symmetry operator	Code	Symmetry operator
1	x, y, z	5	$-x$, $-y$, $1/2+z$
2	$-x$, $-y$, $-z$	6	x, y, $1/2-z$
3	$1/2-x$, $1/2+y$, $1/2-z$	7	$1/2+x$, $1/2-y$, $-z$
4	$1/2+x$, $1/2-y$, $1/2+z$	8	$1/2-x$, $1/2+y$, z

Table 5. Bond angles (ϕ/°) for silicon and indium atoms, with estimated standard deviations in parentheses

$S(2)_1-Si(1)-S(2)_6$	113.8(4)
$S(2)_1-Si(1)-S(5)_1$	115.3(3)
$S(2)_1-Si(1)-S(6)_1$	110.3(3)
$S(2)_6-Si(1)-S(5)_1$	115.3(3)
$S(2)_6-Si(1)-S(6)_1$	110.3(3)
$S(5)_1-Si(1)-S(6)_1$	89.1(3)
Mean:	109.0
$S(1)_3-Si(2)-S(1)_8$	114.4(5)
$S(1)_3-Si(2)-S(5)_1$	108.7(3)
$S(1)_3-Si(2)-S(6)_1$	111.8(3)
$S(1)_8-Si(2)-S(5)_1$	108.7(3)
$S(1)_8-Si(2)-S(6)_1$	111.8(3)
$S(5)_1-Si(2)-S(6)_1$	100.6(5)
Mean:	109.3
$Si(1)_1-S(5)-Si(2)_1$	85.9(4)
$Si(1)_1-S(6)-Si(2)_1$	84.4(4)
$S(1)_1-In-S(2)_1$	105.8(3)
$S(1)_1-In-S(3)_7$	110.8(3)
$S(1)_1-In-S(4)_1$	112.9(3)
$S(2)_1-In-S(3)_7$	113.4(3)
$S(2)_1-In-S(4)_1$	110.0(3)
$S(3)_7-In-S(4)_1$	104.1(3)
Mean:	109.5
$In_4-S(3)-In_7$	103.8(4)
$In_1-S(4)-In_6$	104.0(4)

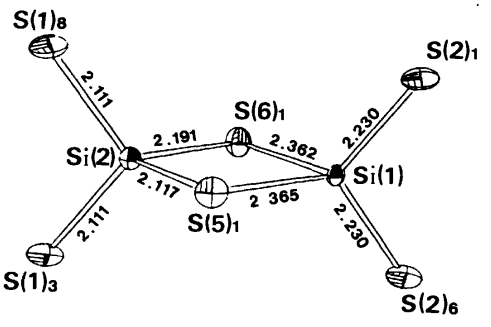

Fig. 2. Atomic configuration of dimeric Si_2S_6 group.

hand, in the distorted $Si(2)S_4$ tetrahedron, the partial substitution of the indium atom for the Si(2) site seems to have no influence on the Si(2)-S bond lengths, which range from 2.111 to 2.191 Å. The mean Si(2)-S bond length of 2.133 Å is closely related to the mean bond lengths observed in other thiosilicates, e.g., Fe_2SiS_4 (2.130 Å),[18] Ba_2SiS_4 (2.17 Å),[1] $Na_4Si_4S_{10}$ (2.107 Å; bridge, 2.144 Å; terminal, 2.035 Å),[8] and SiS_2 (2.13 Å).[19] The S(terminal)-Si-S(bridge) bond angles are in the 108.7—115.3° range; also, the S(terminal)-Si-S(terminal) bond angles are 113.8° for Si(1) and 114.4° for Si(2). These bond angles are larger than the regular tetrahedral angle of 109.28′. On the other hand, the S(bridge)-Si-S(bridge) bond angles within the four-membered ring, 89.1° for Si(1) and 100.6° for Si(2), are significantly smaller than those in the regular tetrahedron. The distortion from the regular tetrahedral angle must be due to the repulsion between the two positively charged silicon atoms. The formation of such dimers is, therefore, attributable to the tendency of the configuration of the four-membered ring to minimize repulsions by electrostatic force: the repulsions between the two positively charged silicon atoms and those between the two negatively charged sulfur atoms. This unexpected atomic configuration of the Si_2S_6 group, which is novel for thio- and oxo-anions, is similar to the structure of Al_2Cl_6 (in the gas phase) and Al_2Br_6, and is very similar to configurations of, *e.g.*, the $Ge_2S_6^{4-}$ anions in $Tl_4Ge_2S_6$[6] and $Na_4Ge_2S_6 \cdot 14H_2O$,[7] the $Ge_2Se_6^{4-}$ anion in $Na_4Ge_2Se_6 \cdot 16H_2O$,[20] and the $Sn_2S_6^{4-}$ anion in $Na_4Sn_2S_6 \cdot 14H_2O$.[7] On the contrary, taking into account the substitution of the indium atom for the Si(1) site, it appears that the SiS_4 tetrahedron combines with the InS_4 tetrahedron by means of a common edge to form a dimeric (SiS_3-InS_3) group. This is the first example of a dimer composed of both silicon and indium tetrahedra.

The indium atom is bonded to the four nearest sulfur atoms, thus forming an almost regular tetrahedron, as is shown in Fig. 3. The S-In-S bond angles range from 104.1 to 113.4°, with an average value of 109.5°. These values are in agreement with the regular tetrahedral angle of 109°28′. The In-S bond lengths in the range from 2.296 to 2.379 Å are significantly less than the values found in β-In_2S_3 (tetrahedron: 2.44—2.48 Å; octahedron: 2.54—2.68 Å).[21] These values are in accord with the value for the sum of the covalent radii, 2.32 Å, calculated on the basis of the occupancies of the indium atom and the silicon atom in the In site. The sharing of two sulfur atoms for each InS_4 tetrahedron may result in simple infinite chains with the formula of $(InS_3)_n$, as is shown in Fig. 1-(b). The In-S(1) and In-S(2) bond lengths, 2.346 and 2.379 Å, are somewhat longer than the In-S(3) and In-S(4) bond lengths, 2.296 and 2.331 Å. The dimeric Si_2S_6 groups hold the parallel chains by sharing two edges to form a two-dimensional sheet-like network (see Fig. 1).

Two thallium atoms which are nonequivalent in the cell are located between these sheets, bonded weakly to their nearest neighbours. One of them, Tl(1), forms a 7+2 irregular coordination polyhedron (Fig. 4). Seven sulfur atoms are closer to the thallium atom at distances from 3.410 to 3.734 Å, while two sulfur atoms are further away, at distances of 3.957 Å. The average Tl-S distance for Tl(1) is 3.641 Å in the nine-fold coordination polyhedron. The arrangement of sulfur atoms around the other thallium atom, Tl(2), shows no systematic coordination geometry (Fig. 5), with nine Tl-(2)-S contacts ranging from 3.293 to 3.780 Å, with the mean of 3.574 Å.

The mean Tl-S bond distances for the Tl(1) and Tl(2) atoms in the nine-fold coordination polyhedron are considerably longer than the mean bond distances for the similar coordination polyhedra found in $Tl_4Ge_4S_{10}$ (Tl-S: 3.43 Å)[10] and in thallium sulfosalts, *e.g.*, simo-

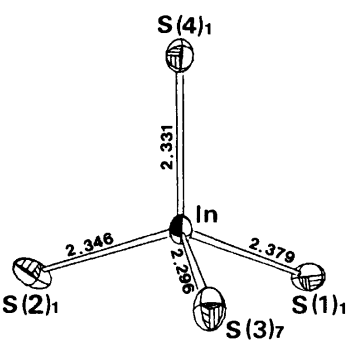

Fig. 3. Atomic arrangement in the InS_4 tetrahedron.

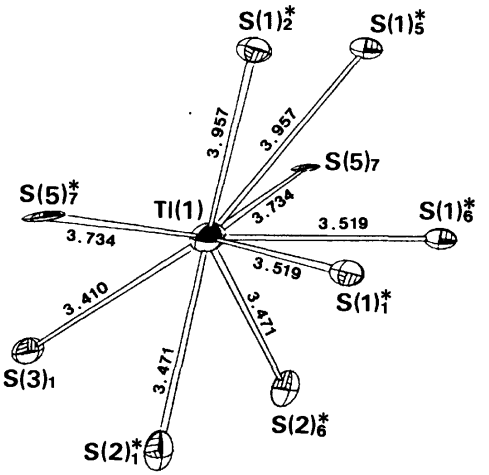

Fig. 4. Coordination of the sulfur atoms about the Tl(1) atom.

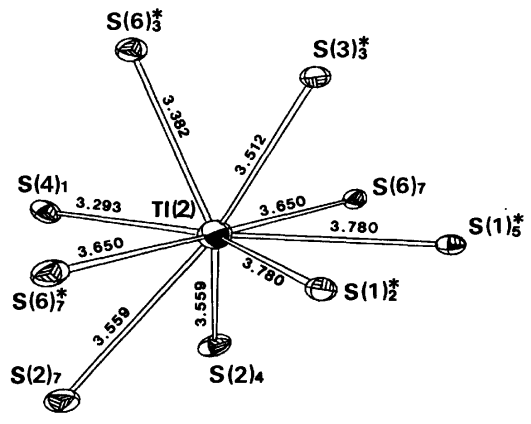

Fig. 5. Coordination polyhedron of the Tl(2) atom.

nite, $TlHgAs_3S_6$ (Tl-S: 3.43 Å)[22] and synthetic parapierrotite, $TlSb_5S_8$ (Tl-S: 3.39 Å).[23] Because those long bond distances represent relatively weak bonding interactions, such substances might be expected to cleave most readily in directions parallel to the sheets, as is observed in micas. In fact, this expectation is confirmed in a series of quaternary chalcogenides having the formulae of $TlInSiS_4$, $TlInGeS_4$, $TlGaSiS_4$, $TlGaGeS_4$, and $TlAlGeS_4$.[13]

The authors are grateful to Professors Masaaki Ohmasa and Shigeho Sueno, the University of Tsukuba, for their helpful advice and for reading the paper.

Reference

1) R. Dumail, M. Ribes, and E. Philippot, *C. R. Acad. Sci., Ser. C*, **272**, 303 (1971).
2) K. Susa and H. Steinfink, *J. Solid State Chem.*, **3**, 75 (1971).
3) E. Philippot, M. Ribes, and M. Maurin, *Rev. Chim. Miner.*, **8**, 99 (1971).
4) W. Schiwy, S. Pohl, and B. Krebs, *Z. Anorg. Allg. Chem.* **402**, 77 (1973).
5) J. C. Jumas, J. Olivier-Fourcade, F. Vermot-Gaud-Daniel, E. Philippot, and M. Maurin, *Rev. Chim. Miner.*, **11**, 13 (1974).
6) G. Eulenberger, *Acta Crystallogr., Sect. B*, **34**, 2614 (1978).
7) B. Krebs, S. Pohl, and W. Schiwy, *Z. Anorg. Allg. Chem.*, **393**, 241 (1972).
8) M. Ribes, J. Olivier-Fourcade, E. Philippot, and M. Maurin, *J. Solid State Chem.*, **8**, 195 (1973).
9) B. Krebs and S. Pohl, *Z. Naturforsch. B*, **26**, 853 (1971).
10) G. Eulenberger, *Acta Crystallogr., Sect. B*, **32**, 3059 (1976).
11) J. Olivier-Fourcade, E. Philippot, M. Ribes, and M. Maurin, *Rev. Chim. Miner.*, **9**, 757 (1972).
12) M. Ribes, J. Olivier-Fourcade, E. Philippot, and M. Maurin, *Acta Crystallogr., Sect. B*, **30**, 1391 (1974).
13) Y. Nakamura, I. Nakai, and K. Nagashima, *Mater. Res. Bull.*, (in press).
14) B. J. Wuensch and C. T. Prewitt, *Z. Kristallogr.*, **122**, 24 (1965).
15) L. W. Finger, RFINE-2, Geophysical Lab. Carnegie Institution, Washington, D. C. (1972).
16) D. T. Cromer and J. B. Mann, *Acta Crystallogr., Sect. A*, **24**, 321 (1968).
17) "International Tables for X-ray Crystallography," Vol. IV, Kynoch Press, Birmingham (1974), pp. 72—75.
18) H. Vincent and E. F. Bertaut, *Acta Crystallogr. Sect. B*, **32**, 1749 (1976).
19) C. T. Prewitt and H. S. Young, *Science*, **149**, 535 (1965).
20) B. Krebs and H. Müller, *Z. Anorg. Allg. Chem.*, **496**, 47 (1983).
21) G. A. Steigmann, H. H. Sutherland, and J. Goodyear, *Acta Crystallogr.*, **19**, 967 (1965).
22) P. Engel, W. Nowacki, T. Balić-Zunić, and S. Ščavnićar, *Z. Kristallogr.*, **161**, 159 (1982).
23) P. Engel, *Z. Kristallogr.*, **151**, 203 (1980).

 © 1984 The Chemical Society of Japan Bull. Chem. Soc. Jpn., 57, 1723—1730 (1984)

Excited-state Reactions of Coumarins in Aqueous Solutions. II. The Fluorescence Quenching of 7-Ethoxycoumarins by Halide Ions

Tetsuo MORIYA

Electrotechnical Laboratory, 1-1-4 Umezono, Sakura-mura, Niihari-gun, Ibaraki, 305

(Received November 2, 1983)

The fluorescence yield and the fluorescence lifetime of 7-ethoxycoumarins in aqueous solutions are reduced with the increase in the temperature and in the concentration of the quenching agents. The radiationless deactivation of the excited state in the absence of quenchers is temperature-dependent; its activation energy has been determined to be 32.5—34.8 kJ mol^{-1}. The quenching reaction due to halide ions proceeds *via* both a diffusional and a static process. The rate constant for the diffusional process has a value of $(9.7—10.2)\times10^9$ mol^{-1} dm^3 s^{-1} in the case of I^- as a quencher. The static quenching component can be approximately described by the $V[Q]$ expression, with the static quenching constant, V, being 1.6—1.8 mol^{-1} dm^3. The quenching efficiencies that represent the probability leading to real quenching reactions by an encounter of the molecule and the halide ion are unity for I^-, 0.39—0.42 for Br^-, and almost zero for Cl^-. The possible physical interpretation of the quenching mechanism is discussed in relation to the electron transfer between colliding species.

Although a considerable volume of data has been accumulated on the luminescence properties of various coumarin derivatives,[1] few works have appeared on the fluorescence-quenching of the molecule in solution by unlike molecules or by inorganic ions. We have already examined in detail the fluorescent behavior of 7-hydroxycoumarins,[2] and our study has revealed that the molecules have several molecular species in the optically excited state, depending on the pH of the solution. This situation has made it very difficult to investigate the fluorescence-quenching effects of these molecules because of the complexity of the fluorescence spectrum itself in the absence of quenchers. If the hydroxyl group of 7-hydroxycoumarins is replaced by the ethoxyl group, then the neutral species becomes the only species existing in the excited state as well as in the ground state, and the fluorescence spectrum becomes a very simple one over a wide pH range in aqueous solutions, in contrast to the case of 7-hydroxy-substituted coumarins. Accordingly, 7-ethoxy-substituted coumarins are a convenient group for a fundamental study of fluorescence-quenching reactions of coumarins.

The quantum yield of molecules in solution is known to be affected by a variety of factors, such as the temperature, the viscosity, and the concentration of the quenching agents. In this paper, halide ions have been chosen as quenchers, and the fluorescence intensities of 7-ethoxycoumarin (**1**) and 7-ethoxy-4-methylcoumarin (**2**) in aqueous solutions have been measured as a function of the concentration of the quencher and the temperature of the solution. The reaction-rate constant for fluorescence quenching by halide ions and the several activation energies related to it will be derived by means of the obtained data, and the quenching mechanism will be discussed in detail.

Experimental

Materials. The high-purity-grade reagents of 7-ethoxycoumarin (**1**) and 7-ethoxy-4-methylcoumarin (**2**) were obtained from Molecular Probes, Inc., and used as purchased. Their melting points were determined distinctly by means of differential thermal analysis (DTA); the purity was revealed to be very high by the measured DTA curves:[3] **1**, mp 84.8 °C **2**, mp 115.5 °C. The sodium chloride, sodium bromide, sodium iodide, and sodium thiosulfate were pure and were obtained from Wako Pure Chemical Ind. The water was permeated and distilled.

Methods. The UV absorption spectra at the ambient temperature were obtained on a Hitachi 323 spectrophotometer. The fluorescence-intensity measurements were done on a Hitachi MPF 4 spectrofluorometer with an S-5 type photomultiplier tube. For the temperature-dependence studies, we used a hollow cell holder, through which water from a constant-temperature bath was circulated. The temperature in the cuvette could be controlled to within ±0.5° between 10 and 50 °C, and was monitored directly by means of a thermocouple immediately after the fluorescence measurement.

The wavelengths of the excitation light were chosen to be 324 nm for **1** and 321 nm for **2**, which corresponded to the absorption maxima. The concentrations of the fluorescent molecules in the aqueous solution were $\approx5\times10^{-5}$ mol dm^{-3} for **1** and $\approx4\times10^{-5}$ mol dm^{-3} for **2**, with which the reliable and stable recording of the fluorescence spectra was ensured.[4] Since the shape and position of the emission spectrum were not noticeably altered by either the change in the temperature or by the addition of a quencher, the fluorescence intensity was usually determined by the measurement of the relative intensity at the emission maxima, which were found at 390 nm and 382 nm for **1** and **2** respectively.

In the quenching experiment, the fluorescence of a series of samples, containing a constant amount of a fluorescent compound and a graduated amount of a quencher, was measured. The stocked solutions of quenchers used to vary the concentration of the halide ions were 4M NaCl, 2M NaBr, and 0.2M NaI (containing $\approx10^{-4}$ M $Na_2S_2O_3$ to prevent I_3^- formation; 1 M=1 mol dm^{-3}). The quenchers had no disturbing absorption in the wavelength region of interest.

The fluorescence lifetime measurements were performed by using a time-correlated single-photon-counting fluorometer similar to the one described in Ref. 5. Because the determined lifetime becomes less accurate for lifetimes shorter than 2 ns when our apparatus was used, the supplemental relationship:

$$\tau_0(t) = \tau_0^{20}\frac{I_0(t)}{I_0^{20}}, \tag{1}$$

was used to obtain the temperature dependence of the lifetime at higher temperatures, where τ_0^{20} and $\tau_0(t)$, I_0^{20} and $I_0(t)$ are the lifetimes and the emission intensities at 20 °C and t °C in the absence of a quencher. The viscosity of water was taken from

the literature.

Results and Discussion

Temperature Dependence of the Fluorescence Lifetime. A frequently postulated kinetic scheme for the fluorescence-quenching process is as follows:

$$A + h\nu_A \xrightarrow{I_{abs}} A^*$$

$$A^* + Q \underset{k_2}{\overset{k_1}{\rightleftharpoons}} (AQ)^* \xrightarrow{k_3} A + Q$$

$$(AQ)^* \xrightarrow{n_1} A + h\nu_F \qquad (AQ)^* \xrightarrow{n_2} A$$

Here, A, Q, and $h\nu$ represent the fluorophore, the quencher, and the light quantum; A* and (AQ)* are the excited states of the fluorophore and of the encounter complex between A and Q respectively; the k's are the reaction-rate constants, and the n's are the transition probabilities. When the quencher is absent, the lifetime, τ_0, and the quantum yield, ϕ_0, of the excited molecule at t °C are given by:

$$\tau_0(t) = \frac{1}{n_1+n_2(t)} \text{ and } \phi_0(t) = \frac{n_1}{n_1+n_2(t)}, \qquad (2)$$

where n_1 and n_2 are the radiative and radiationless transition probabilities respectively. The temperature dependence of the lifetime or the quantum yield of **1** and **2** in an aqueous solution is quite large, as may be seen from Fig. 1. Because of the effect of the slight broadening of the emission spectra at higher temperatures, the integrated area of the spectrum was used to estimate the rigorous quantum yield. No shift in the wavelength of the emission maximum was observed upon raising the temperature, suggesting that the fluorescing state itself is not altered at all.

If the reasonable assumptions are made that n_1 is independent of the temperature (at least in the region between 10 to 50 °C) and that only one radiationless deactivation process is significant, then the temperature dependence of the lifetime may be expressed by:

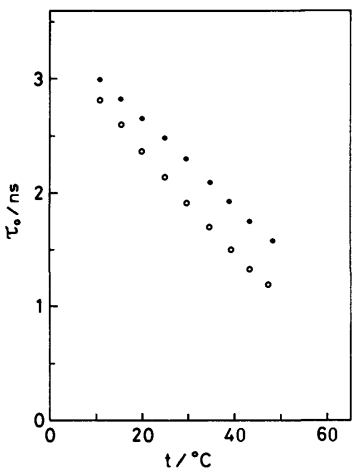

Fig. 1. Temperature dependence of the fluorescence lifetimes of 7-ethoxycoumarins in aqueous solution. ○, 7-ethoxycoumarin (**1**); ●, 7-ethoxy-4-methylcoumarin (**2**).

$$\frac{1}{\tau_0(t)} - n_1 = n_2(t) = n_2^0 \exp\left(-\frac{E_2}{RT}\right), \qquad (3)$$

where n_2^0 is the frequency factor for the deactivation process and involves the entropic component of the corresponding free energy of activation, E_2 is the activation energy for the deactivation process, R is the gas constant, and T is the absolute temperature. By means of the numerical fitting of Eq. 3 with the data in Fig. 1, the value of n_1 can be determined; Fig. 2 shows the logarithmic plots of $(1/\tau_0)-n_1$ *vs.* $1/T$, from the slope of which we have obtained the E_2 of Eq. 3. The actual lifetime, τ_0, at 20 °C, the radiative lifetime, $\tau_1(=1/n_1)$, and the activation energy, E_2, are listed in Table 1. It is known from the obtained values that the radiative and radiationless transition probabilities are of the same order at around 20 °C. The activation energies of 32.5—34.8 kJ mol^{-1} are similar to those for tryptophan derivatives in water;[6] this similarity may be related to the activation of a "tunneling" process from the excited to the ground state or, alternatively, of an electron-ejecting process of the molecule to the solvent. It may be noted here that the assumption of only one deactivation process is an expedient one because the examined temperature range is not so wide as to exclude completely the existence of the temperature-independent term or other types of temperature-dependent terms. In contrast to the case of an organic solvent,[7] the quenching by dissolved dioxygen in an aqueous solution has been shown by the lifetime measurement to be unimportant.

Fluorescence Quenching by Halide Ions. In the quenching reaction between an excited state of a fluoro-

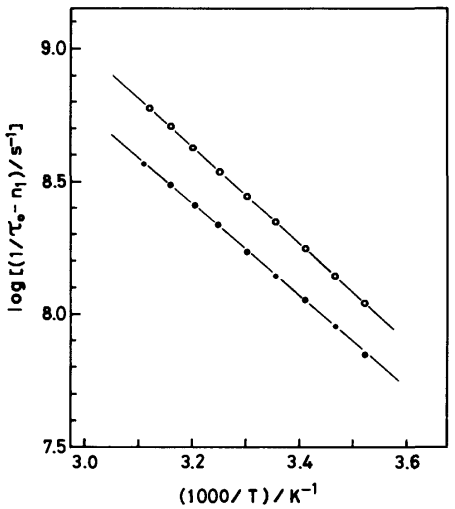

Fig. 2. Logarithmic plots of $(1/\tau_0)-n_1$ *vs.* 1/T. n_1 is chosen to be 2.92×10^8 s^{-1} for **1** and 3.11×10^8 s^{-1} for **2**: ○, **1**; ●, **2**.

Table 1. Actual and radiative lifetimes, and activation energies for the radiationless transition process

Substance	τ_0/ns[a]	n_1^{-1}/ns	E_2/kJ mol^{-1}
1	2.0_0	3.4_3	34.8
2	2.2_5	3.2_2	32.5

a) The values at 20 °C.

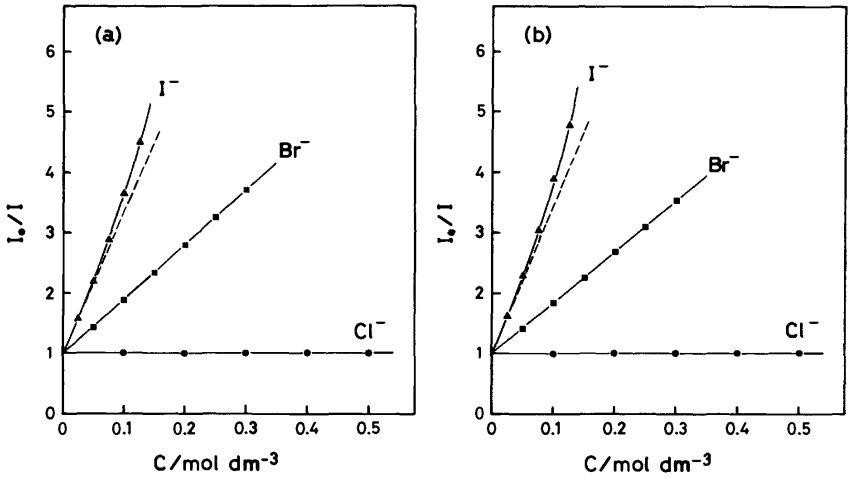

Fig. 3. Stern-Volmer plots for the fluorescence quenching by I^- (▲), Br^- (■), and Cl^- (●) in aqueous solution at 20°C. (a), 7-ethoxycoumarin (**1**); (b), 7-ethoxy-4-methylcoumarin (**2**).

phore, A*, and a quencher, Q, the encounter complex, (AQ)*, that is formed with a diffusion-controlled rate constant, k_1, reacts to dissipate the electronic energy by some internal-mechanism rate constant, k_3. For such a case, the Stern-Volmer relationship under steady-state conditions is described by:[8]

$$\frac{\phi_0}{\phi} = 1 + K_{sv}[Q] = \frac{I_0}{I}, \tag{4}$$

where ϕ_0 and ϕ, I_0 and I, are the quantum yields and the emission intensities in the absence and in the presence of Q, respectively. K_{sv} is the collisional quenching constant, which is equal to $k_q\tau_0$; k_q is the apparent rate constant for the collisional quenching process; it is given by:

$$k_q = \gamma k_1 \text{ and } \gamma = \frac{k_3}{k_2+k_3}. \tag{5}$$

Here, γ represents the efficiency of the quenching reaction, which approaches unity if $k_2 \ll k_3$. When not every encounter between Q and A* results in quenching, the efficiency of the reaction becomes less than unity, and k_q is approximately equal to k_1k_3/k_2 if $k_2 \gg k_3$.

The data in Figs. 3(a) and 3(b) are the Stern-Volmer plots obtained when Cl^-, Br^-, and I^- were used as quenchers. Cl^- had no effect on the fluorescence intensity when $[Cl^-] \lesssim 0.5$ mol dm^{-3}. Br^- and I^- drastically quenched the fluorescence of both **1** and **2**. When I^- is used as a quencher, it may be seen from Fig. 3 that the plots are apparently curved upwards in a fashion similar to those found in many other detailed quenching studies.[9] This type of deviation from the expected linear plot can be explained by the fact that only a certain fraction, W, of the excited state is actually quenched by the collisional mechanism. Some molecules in the excited state, the fraction of which is $1-W$, are deactivated almost instantaneously after being formed because a quencher happens to be randomly positioned in the proximity at the time the molecules are excited and interacts very strongly with them. Several models can be employed to describe this instantaneous or "static" quenching process, all leading to the following modified form of the Stern-Volmer equation:

$$\frac{\phi_0}{\phi} = \frac{1+K_{sv}[Q]}{W} = \frac{I_0}{I}. \tag{6}$$

Model 1. The complete Smolchowski equation for diffusion-controlled reactions contains an often neglected transient term:[10,11]

$$k_1 = 4\pi N'RD + 4R^2(\pi D)^{1/2}t^{-1/2}$$
$$= (\text{steady state term}) + (\text{transient term}) \tag{7}$$

where N′ is Avogadro's number per millimole, R is the encounter distance between the reactants, D is the sum of the individual diffusion coefficients of the reactants, and t is the time. The retention of the latter term leads to an additional factor, W, in the Stern-Volmer equation which is approximately equal to $\exp(-V[Q])$, where V is the static quenching constant.[10]

Model 2. Frank and Vavilov[12] have suggested that instantaneous quenching results at those instances in a randomly distributed system when a quencher happens to reside within a "sphere of action" with a volume of V/N' and a radius of r, *i.e.*, $V/N' = 4\pi r^3/3$, surrounding a fluorophore at the time of excitation. In this case, W is also given by this expression: $\exp(-V[Q])$.

Model 3. In the model of Moon *et al.*,[13] instantaneous quenching follows the excitation of the ground-state complex, (AQ). Such a situation can be described by adding the following reactions to the primary scheme:

$$\begin{array}{ccc} A + h\nu_A & \xrightarrow{I_{abs}\delta} & A^* \\ {\scriptstyle K^0}\Big\| & & \\ (AQ) + h\nu_A & \xrightarrow{I_{abs}(1-\delta)} & (AQ) \end{array}$$

where:

$$\delta = \frac{1}{1+(\varepsilon_{AQ}/\varepsilon_A)K^0[Q]} \text{ and } K^0 = \frac{[AQ]}{[A][Q]}, \tag{8}$$

ε_{AQ} and ε_A being the molar extinction coefficients of (AQ) and A respectively at the excitation wavelength. Then the fraction, W, is given by:

$$W = \frac{\delta+k_2/k_3}{1+k_2/k_3} = \gamma\left(\delta+\frac{k_2}{k_3}\right). \tag{9}$$

If the dark complex, (AQ), is really formed in the solution, δ decreases from unity and, therefore, W decreases, leading to the decrease in the quantum yield.

Because the fraction, W, depends on the concentration of Q in all the cases mentioned above, the Stern-Volmer plots for a quencher with high quenching ability generally deviate from a linear plot. In order to extract more tractable information from these models, it is sensible to calculate the value of $\{1-(I/I_0)\}/[Q]$, that is:

$$\frac{1-(I/I_0)}{[Q]} = K_{sv}\frac{I}{I_0} + \frac{1-W}{[Q]}. \quad (10)$$

For Models 1 and 2, when $V[Q] \ll 1$ is satisfied, $W \approx 1-V[Q]$ and Eq. 10 is written as:

$$\frac{1-(I/I_0)}{[Q]} = K_{sv}\frac{I}{I_0} + V. \quad (11)$$

For Model 3, when $(\varepsilon_{AQ}/\varepsilon_A)K^0[Q] \ll 1$ is satisfied, $W \approx 1-\gamma(\varepsilon_{AQ}/\varepsilon_A)K^0[Q]$ and Eq. 10 is written as:

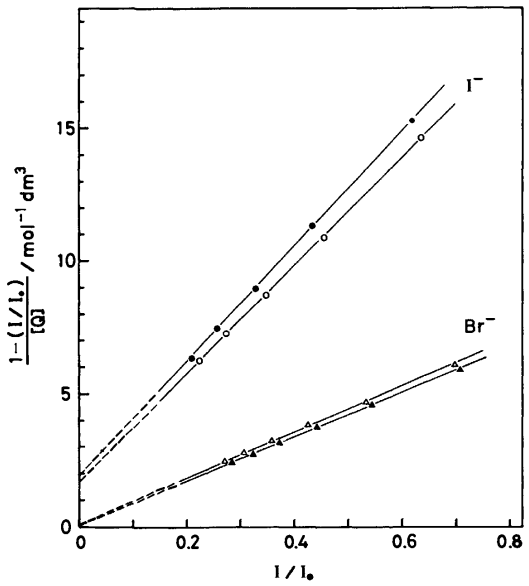

Fig. 4. Plots of $[1-(I/I_0)]/[Q]$ *vs.* I/I_0 at 20°C. I^- as a quencher: ○, **1**; ●, **2**. Br^- as a quencher: △, **1**; ▲, **2**.

$$\frac{1-(I/I_0)}{[Q]} = K_{sv}\frac{I}{I_0} + \gamma\frac{\varepsilon_{AQ}}{\varepsilon_A}K^0. \quad (12)$$

In any case, $\{1-(I/I_0)\}/[Q]$ is described by the form of $a(I/I_0)+b$ when the concentration of quenchers is relatively low. Naturally, the second term, b, of Eq. 10 becomes strictly zero if the linear condition, *i.e.*, $W=1$, is satisfied. The plot of $\{1-(I/I_0)\}/[Q]$ *vs.* I/I_0, therefore, becomes linear in this approximation, the slope, a, of which is K_{sv}, and the intercept, b, of which at $I/I_0 \to 0$ becomes V or $\gamma(\varepsilon_{AQ}/\varepsilon_A)K^0$, depending upon the model being used.

Fig. 4 shows the plots of $\{1-(I/I_0)\}/[Q]$ *vs.* I/I_0 for Compounds **1** and **2** in an aqueous solution at 20 °C. The quenching effects by two halide ions, *i.e.*, Br^- and I^-, have been examined. As can readily be seen from Fig. 4, the effect of varying the fluorescent molecule on the slope and intercept is rather small, but that of varying the quenching ion from Br^- to I^- is large; the values of K_{sv} ($=k_q\tau_0$) and b at 20 °C are listed in Table 2. As for the case of Br^-, the deviation from the linear Stern-Volmer relation is small, because b is very small; this is also known from the plots in Fig. 3. On the other hand, b is much larger for I^-, and the deviation becomes quite large. It may be noted that, in spite of such a deviation from the Stern-Volmer plot, the approximations made in Eqs. 11 and 12 are fully appropriate, as the expansion inacuracy is less than 4% over the concentration range of the quencher used. Accordingly, the newly derived relation of Eqs. 11 and 12 turns out to be a more powerful equation for the analysis of strongly quenching processes than the usual Stern-Volmer equation.

Table 2. Values of the quenching constant K_{sv} and the constant b at 20 °C

Substance	Quencher	K_{sv}/mol^{-1} dm^3	b/mol^{-1} dm^3 a)
1	Br^-	8.5_9	0.1
	I^-	20.3_0	1.7
2	Br^-	8.4_6	0.0_4
	I^-	21.7_2	1.9

a) b is the value for the second term of Eq. 11 or 12.

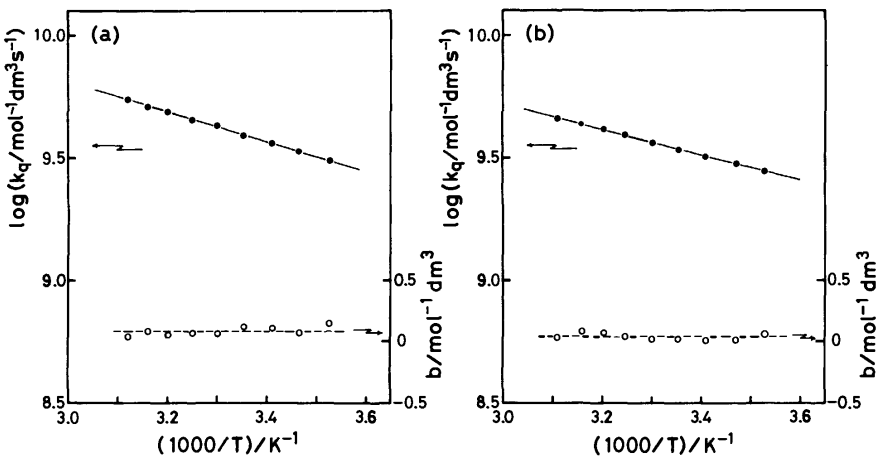

Fig. 5. Arrhenius plots of the rate constants for the collisional quenching, and plots of the static quenching constants *vs.* $1/T$. Br^- as a quencher: (a), **1**; (b), **2**.

Temperature Dependence of the Rate Constant. The collisional quenching constant, K_{SV}, depends, of course, on the temperature through the temperature dependence of the quenching-rate constant, k_q, and the lifetime, τ_0. The values of K_{SV} and τ_0 at temperatures between 10 and 50 °C could be known by independent measurements, so that the temperature dependence of k_q was readily estimated from these values; the logarithm of k_q is plotted against the inverse of the absolute temperature in Figs. 5 and 6. It is clear that the plots of log k_q *vs.* $1/T$ are linear in the temperature range measured. Assuming $k_q \propto \exp(-E_q/RT)$, the activation energy, E_q, for the collisional quenching process was obtained from the slope of this plot; it is listed in Table 3. It seems that E_q is dominated mainly by the species of quenchers, since Compounds **1** and **2** have very similar values of E_q for Br^- and I^- respectively.

Concerning the case of I^-, E_q has been found to be 16.3 and 15.6 kJ mol^{-1} for **1** and **2** respectively; these values are very similar to the value obtained for indole derivatives in water, *i.e.*, 15.5 kJ mol^{-1}.[14] As will be mentioned later, these values are also very near the activation energy for the viscosity of water; this suggests that the rate of reaction is limited only by the diffusion of the reactants through the aqueous solution. E_q for Br^- is somewhat less than these values; the reason for such a difference will be discussed below.

The plots of b in Figs. 5 and 6 show no indication of the temperature dependence in any case. Model 3 predicts that b is temperature-dependent, for the equilibrium constant, K^0, contained in the expression of b varies with the temperature. This fact would contradict the experimental result, although the small possibility that K^0, as well as b, varies very slowly with the temperature cannot be denied. Furthermore, no trace of the ground-state complex, (AQ), could be found by means of the absorption measurement, even if the concentration of a halide ion was set extremely high. Therefore, the deviation from the linear Stern-Volmer relation is not due to the process described by Model 3. Model 1 also predicts the dependece of b on the temperature through the temperature dependence of the diffusion coefficient, which is contained in the transient term of Eq. 7.

On the other hand, Model 2 uses only the statistical nature of the quenchers distributed around the fluorescent molecule, so that no dependence on the temperature is predicted in accordance with the experimental result. For these reasons, it seems most reasonable, in the case of the coumarin derivatives in an aqueous solution, to discuss the quenching phenomena in terms of Model 2, *i.e.*, the sphere-of-action model. By equating b with V, the values of V averaged over temperatures shown in Table 3 are obtained. Using the relation: $V/N' = 4\pi r^3/3$, the radius of the sphere of action for the quenching by I^- is estimated to be 8.6 Å for **1** and 9.0 Å for **2**. These radii are slightly larger than the value, 6—7 Å, which can be estimated as the sum of the radii of the coumarin and the iodide ion. This clearly shows that the instantaneous quenching can occur if the quencher is very near to, or in contact with, the fluorescent molecule at the exact moment that it becomes excited. In the case of Br^-, the active volume element,

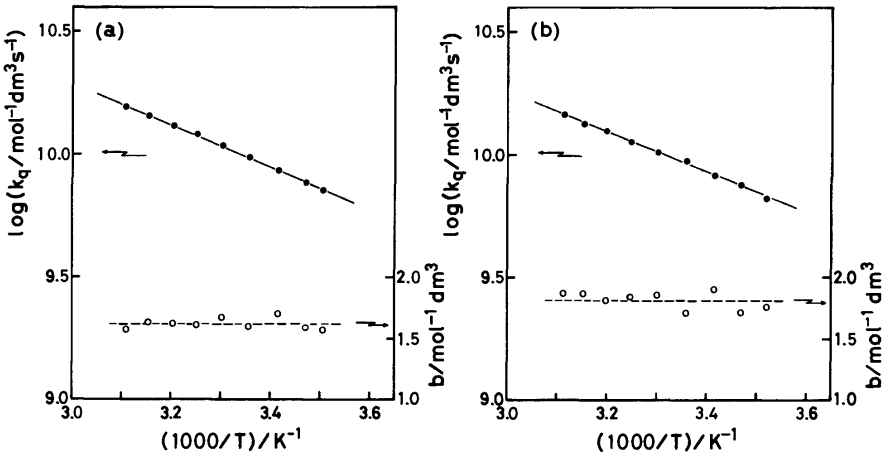

Fig. 6. Arrhenius plots of the rate constants for the collisional quenching, and plots of the static quenching constants *vs.* $1/T$. I^- as a quencher: (a), **1**; (b), **2**.

TABLE 3. RATE CONSTANTS FOR THE COLLISIONAL QUENCHING PROCESS AT 20 °C, ACTIVATION ENERGIES FOR THE COLLISIONAL QUENCHING, STATIC QUENCHING CONSTANTS, AND RADII OF THE SPHERE OF ACTION

Substance	Quencher	$k_q \times 10^{-9}$ / mol^{-1} dm^3 s^{-1}	E_q / kJ mol^{-1}	V / mol^{-1} dm^3	r / Å
1	Br^-	4.3_0	11.7	0.0_8	3.2
	I^-	10.1_5	16.3	1.6_2	8.6
2	Br^-	3.7_6	9.9	0.0_4	2.5
	I^-	9.6_5	15.6	1.8_1	9.0

V/N', is much smaller and r is less than 4 Å (see Table 3). This is attributable to the weakness in the quenching ability of Br^-, in comparison with that of I^-, because the contact of the quencher with the fluorophore does not always lead to subsequent fluorescence quenching.

Quenching Efficiency. If the values of R and D are reasonably assigned as 7 Å and 1.5×10^{-5} cm^2 s^{-1}, based on the molecular and ionic volumes and the Stokes-Einstein relation,[8] the diffusion-limited value of the quenching-rate constant, k_1, can be calculated to be 7.9×10^9 mol^{-1} dm^3 s^{-1} by using the steady-state portion of Eq. 7, *i.e.*, $k_1=4\pi N'RD$. It was previously mentioned that the actual quenching rate, k_q, is given by $k_q=\gamma k_1$, where γ is the efficiency of the quenching reaction. Although the value obtained above is only a rough estimation, it is close to the experimental values for I^- which are shown in Table 3; the quenching-rate constants for Br^- are somewhat smaller. This indicates that the efficiency of the quenching reaction by I^- is almost unity, while that of the reaction by Br^- is less than unity. The diffusion coefficients of Br^- and I^- in water do not differ very much; therefore, assuming $\gamma=1$ for I^-, the value of γ for Br^- is estimated by means of Eq. 5 to be 0.42 for **1** and 0.39 for **2**, which means more than half of the encounter events between the coumarin and Br^- do not result in the fluorescence quenching. In other words, the encounter distance, R, is shortened effectively to γR for inefficient quenchers such as Br^-.

It has become clear that the efficiency of the collisional deactivation depends on the strength of the quenching ability of each quencher, which is represented by the value "γ". For an efficient quencher like I^-, the efficiency of the quenching reaction is unity, and the magnitude of k_q can be interpreted as the frequency of the collisional encounter between A* and Q. In the case of $\gamma=1$, the temperature behavior of k_q coincides with that of the diffusion-controlled rate constant, k_1 ($=4\pi N'RD$); the temperature dependence of k_1 is due to that of the diffusion coefficient, D. When a relatively narrow region of temperature is considered, D is approximately written as:[15]

$$D = D'\exp(-E_d/RT), \tag{13}$$

where E_d is the activation energy of diffusion and D' is the value at $T=\infty$. Therefore, the obtained value of E_q is equivalent to the activation energy of diffusion.

If γ happens to be less than unity, as in the case of Br^-, the expression for k_q becomes more complicated; in particular, the magnitudes of k_2 and k_3, which may depend on the temperature, become significant. Nevertheless, if the dependence of γ on the temperature is roughly represented by an activation energy, E_γ, *i.e.*, $\gamma\propto\exp(E_\gamma/RT)$, the discussion proceeds parallel to that for the case of $\gamma=1$. The activation energy of k_q for Br^- is smaller than that for I^- by 4.6—5.7 kJ mol^{-1}, as may be seen in Table 3. Considering $k_q\propto\gamma D$, the activation energy of k_q for Br^- may be said to correspond with E_d-E_γ. If such an idea of "efficiency" is also applicable to the radius of the sphere of action, and if r is replaced by γr, then the value of V for Br^- becomes smaller by an order of magnitude than that for I^- due to the factor of γ^3. This prediction agrees well with the experimental results shown in Table 3.

Relation between the Rate Constant and the Viscosity. As has been mentioned previously, $k_1\propto D$, and, as a first approximation, D is obtained by the Stokes-Einstein relation, $D=kT/6\pi R\eta$, where η is the viscosity of water; the plot of k_q *vs.* T/η should be linear if $\gamma=1$. Fig. 7 shows such plots for Br^- and I^-. In reality, k_q for I^- is linearly dependent on T/η, as is to be expected from a diffusion-controlled reaction; in addition, the plot for Br^- is also linear, but the slope is more gentle than that for I^-. Although linear dependence is obtained for both cases, a curious point remains that k_q at a low T/η does not go exactly to zero, which contradicts the simple Stokes-Einstein relation. The deviation from this relationship is due to the inapplicability of the Stokes coefficients of viscous friction, which are introduced by the assumption that the solute molecules are moving in a solvent continuum. Taking proper account of the relative size of the solute and solvent molecules, the expression for the diffusion coefficient sufficient to describe experiments is given by:[8]

$$D = A\frac{T}{\eta} + b\eta^x\frac{T}{\eta}, \tag{14}$$

where A, b and x are constants and the rate constant of diffusional quenching is written as:

$$k_q = \gamma k_1 = \gamma\cdot 4\pi N'RD$$
$$= A'\gamma\frac{T}{\eta} + b'\gamma\eta^x\frac{T}{\eta}. \tag{15}$$

By using the activation energy of the quenching efficiency and of the fluidity, γ and η can be described by:

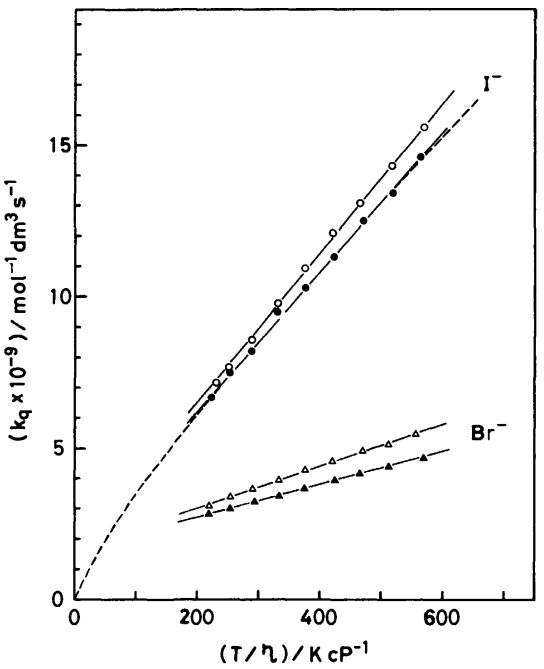

Fig. 7. Dependence of the rate constants for the collisional quenching upon T/η. I^- as a quencher: ○, **1**; ●, **2**. Br^- as a quencher: △, **1**; ▲, **2**. The dashed curve indicates the variation of k_q according to Eq. 17 without any approximation.

Table 4. Parameters obtained for the modified Stokes-Einstein relation and for the quenching efficiency

Substance	Quencher	$A' \times 10^{-7}$ / mol^{-1} dm^3 s^{-1} cP K^{-1}	$B' \times 10^{-4}$ / mol^{-1} dm^3 s^{-1} cP K^{-1}	E_γ / kJ mol^{-1}	$\gamma' \times 10^2$
1	Br^-	2.6_0	8.5_4	4.6_0	6.6_8
	I^-			0	1
2	Br^-	2.3_9	8.4_9	5.7_3	3.8_4
	I^-			0	1

$$\gamma = \gamma' \exp(E_\gamma/RT) \text{ and } \eta = \eta' \exp(E_\eta/RT), \quad (16)$$

in the temperature range of 10—50 °C used; in the case of water, $\eta' \approx 1.2 \times 10^{-3}$ cP and $E_\eta \approx 16.4$ kJ mol^{-1} in the neighborhood of 30 °C, the mean temperature of the measured region; the values of E_γ are already known as $E_\gamma \approx 0$ ($\gamma' = 1$) in the case of I^- and 4.60 and 5.73 kJ mol^{-1} for **1** and **2** respectively in the case of Br^-. The value of x was presumed to be 0.7 by plotting $k_q\eta/T$ *vs.* η^x in the case of I^- for various values of x and by searching for a linear dependency. Then, Eq. 15 is rewritten as:

$$k_q = A'\gamma' \exp(E_\gamma/RT)\frac{T}{\eta} + B'\gamma' \exp\{(E_\gamma + xE_\eta)/RT\}\frac{T}{\eta}, \quad (17)$$

where A', B' and γ' are constants. Regarding $\exp(E_\gamma/RT)$ and $\exp\{(E_\gamma+xE_\eta)/RT\}$ as functions of η/T, and by expanding them around $(\eta/T)_{30}$, the value of η/T at 30 °C, we obtain approximately this relation:

$$\begin{aligned} k_q = {} & \gamma' \exp(E_\gamma/RT_0)\left\{A'\frac{E_\eta + RT_0 - E_\gamma}{E_\eta + RT_0}\right. \\ & \left. + B' \exp(xE_\eta/RT_0)\frac{E_\eta + RT_0 - (E_\gamma + xE_\eta)}{E_\eta + RT_0}\right\}\frac{T}{\eta} \\ & + \gamma' \exp(E_\gamma/RT_0)\left(\frac{T}{\eta}\right)_{30}\left\{A'\frac{E_\gamma}{E_\eta + RT_0}\right. \\ & \left. + B' \exp(xE_\eta/RT_0)\frac{E_\gamma + xE_\eta}{E_\eta + RT_0}\right\}, \end{aligned} \quad (18)$$

where $T_0 = 303.15$ K. Eq. 18 is valid in the neighborhood of 30 °C; this explains very well the experimental relationship of $k_q = a(T/\eta) + b$. By substituting all known parameters and by using the data in Fig. 7, the unknown constants, A', B', and γ', can be obtained as listed in Table 4. It can be recognized from Fig. 7 that the k_q values for both Br^- and I^- have a linear dependence on T/η in the measured region, as is to be expected from Eq. 18. The difference in the slopes for Br^- and I^- is due to the lower quenching efficiency of Br^-; it is interesting that the intercepts at $T/\eta = 0$ are unexpectedly nearly equal in all cases.

In conclusion, the quenching-rate constant of the coumarin derivatives by halide ions is reasonably well described by means of the diffusion-controlled mechanism of the quenching reaction. I^- has been shown to be an "efficient" quencher; Br^- is rather an "inefficient" quencher; Cl^- is a very weak quencher and has no effect on the fluorescence under the conditions examined. Such an order of quenching ability is parallel with the order of the ionization energies of halide anions.[16] Therefore, the initiation of the quenching process is perhaps related with the electron transfer from the ion to the fluorescent molecule in the excited

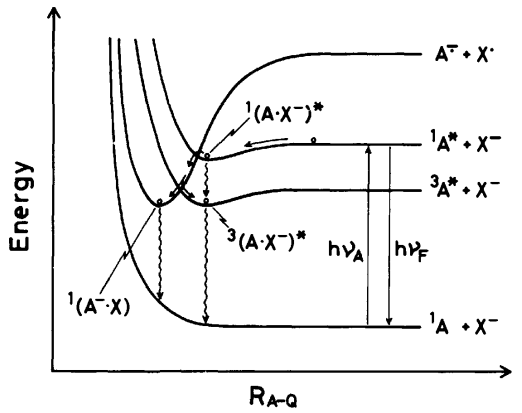

Fig. 8. Schematic potential energy curves of the colliding species and presumable pathways for the fluorescence quenching. R_{A-Q} is the distance between the fluorescent molecule and the halide anion. $^1A^*$ and $^3A^*$ are the singlet and triplet state of the excited molecule, and A^- is the anion radical generated by the electron transfer from the halide anion, X^-. The upward and downward arrows describe the radiative transition, and the downward wavy arrows represent the radiationless transition caused by the collisional reaction.

state.[18] Fig. 8 shows a schematic drawing of the energy levels of the interacting species; it takes account of all the results discussed so far. At an infinite distance, the energy differences between the singlet ground and excited states of 7-ethoxycoumarins are 338—343 kJ mol^{-1}, and the ionization energies of Cl^-, Br^-, and I^- in an aqueous solution are 678, 623, and 544 kJ mol^{-1}.[16] If the crossing of the energy curves of $^1A^*+X^-$ and $A^-+X\cdot$ resides near the encounter distance, the electron transfer from a halide anion to an excited molecule will easily occur, which results in an efficient conversion of the singlet state of the encounter complex, $^1(AX^-)^*$, to its triplet state or, alternatively, to the charge-transferred singlet state, $^1(A^-X\cdot)$. Because the stability of the charge-transferred complex, $(A^-X\cdot)$, is altered by the magnitude of the ionization energy of halide anions, and because its energy position goes lower as the ionization energy decreases, the above-mentioned conversion induced by the electron-transfer process may become a main quenching pathway for I^- and Br^-, but not for Cl^-. However, from a consideration of only the information obtained here, the so-called heavy-atom effect of halide anions, which directly converts the singlet state of the encounter complex to its triplet state, *i.e.*, $^1(AX^-)^* \rightarrow {}^3(AX^-)^*$, cannot be excluded completely. This point is dis-

cussed fully in Refs. 17 and 18, where it is concluded that the main pathway for the fluorescence quenching by diamagnetic inorganic anions is strongly related to the electron-transfer process. It is also revealed that the Stokes-Einstein relation must be somewhat modified in order to explain the dependence of the quenching-rate constants on the viscosity and temperature of the solution.

The author wish to thank Dr. Hiroyuki Anzai of this laboratory for his helpful advice and stimulating discussions during the course of this work.

References

1) O. S. Wolfbeis, E. Lippert, and H. Schwarz, *Ber. Bunsenges. Phys. Chem.*, **84**, 1115 (1980), and the references cited therein.
2) T. Moriya, *Bull. Chem. Soc. Jpn.*, **56**, 6 (1983).
3) T. Moriya and H. Anzai, *Bull. Electrotech. Lab.*, **46**, 431 (1982).
4) T. Moriya, *Bull. Electrotech. Lab.*, **47**, 81 (1983).
5) C. Lewis, W. R. Ware, L. J. Doemeny, and T. L. Nemzek, *Rev. Sci. Instrum.*, **44**, 107 (1973).
6) E. P. Kirby and R. F. Steiner, *J. Phys. Chem.*, **74**, 4480 (1970).
7) W. R. Ware, *J. Phys. Chem.*, **66**, 455 (1962).
8) A. H. Alwattar, M. D. Lumb, and J. B. Birks, "Organic Molecular Photophysics," Vol. 1, ed by J. B. Birks, Wiley, New York (1973), p. 403.
9) T. L. Nemzek and W. R. Ware, *J. Chem. Phys.*, **62**, 477 (1975).
10) A. Weller, *Z. Phys. Chem. N. F.*, **13**, 335 (1957).
11) W. R. Ware and J. S. Novros, *J. Phys. Chem.*, **70**, 3246 (1966).
12) J. M. Frank and S. J. Wawilow, *Z. Phys.*, **69**, 100 (1931).
13) A. Y. Moon, D. C. Poland, and H. A. Scheraga, *J. Phys. Chem.*, **69**, 2960 (1965).
14) M. R. Eftink and C. A. Ghiron, *J. Phys. Chem.*, **80**, 486 (1976).
15) S. G. Glasstone, K. J. Laidler, and H. Eyring, "The Theory of Rate Processes," McGraw-Hill, New York and London (1941).
16) A. Treinin and E. Hayon, *J. Am. Chem. Soc.*, **98**, 3884 (1976).
17) A. R. Watkins, *J. Phys. Chem.*, **78**, 2555 (1974).
18) R. Beer, K. M. C. Davis, and R. Hodgson, *J. Chem. Soc., Chem. Commun.*, **1970**, 840.

Saw-toothed Distributions of Deuterium in Butenes Formed by 1,3-Butadiene Deuteration on a Pt/Al_2O_3 Catalyst in D_2SO_4

Katsuaki SHIMAZU and Hideaki KITA*
Department of Chemistry, Faculty of Science, Hokkaido University, Sapporo 060
(Received November 28, 1983)

Saw-toothed distributions of deuterium are observed in butenes produced by the deuteration of 1,3-butadiene on Pt/Al_2O_3 catalysts suspended in 0.5 M D_2SO_4. The nature of the saw-tooth is sensitive to the purity of the solution and to the deuterium content of the solution. On the basis of the N-profiles (the distributions of hydrogen equilibrated with surface H/D pool) deduced from the observed distributions of deuterium in butenes, the saw-tooth distribution is explained by the reaction mechanism where *cis*- and *trans*-1-methyl-π-allyls are reaction intermediates for the formation of *cis*-2-butene and the other isomers of 1-and *trans*-2-butenes respectively.

The heterogeneous catalytic hydrogenation of 1,3-butadiene in the gas phase has widely been studied on various transition-metal catalysts from the 1960's, for example, on Pt,[1-4] Pd,[1-3,5] other noble metals,[1-4] Co[6-8], and Ni.[6,8,9] However, only a few of these studies have used an isotopic tracer method. The deuteration of 1,3-butadiene on Pt catalysts has been reported only by Bates *et al.*[3] Their reaction mechanism includes mono- and di-π-bonded butadiene as the raction intermediates. 1,3-Butadiene is first chemisorbed in the mono-π-bonded form and then some of the adsorbed 1,3-butadiene becomes the di-π-bonded one in an irreversible way. Thereafter, these adsorbed butadienes, in equilibrium with the corresponding adsorbed butenyl intermediates, are converted to butenes. Their discussion was based on the N-profiles calculated from the distribution of the deuterium in the products.

One must mention that in gaseous catalytic deuteration, deuterium up-take is limited to a lower extent because of the lower deuterium-fraction in adsorbed hydrogen atoms, f_D, due to both the slow rate of the exchange reaction of the adsorbed hydrogen with D_2[3,10] and the smaller ratio, D in D_2 gas/H in butadiene. This limitation is entirely removed in the case of the reaction in a deuterated acid solution.[11] That is, f_D is raised nearly to unity through the fast equilibrium step; $D(a) \rightleftharpoons D^+ + e^-$ on Pt, and the ratio of D in solution/H in butadiene is extremely large. Thus, the reaction products in a solution of deuterated acid are expected to acquire many more deuterium atoms and to provide more concrete information for the elucidation of the reaction mechanism. We have already reported the deuteration of 1,3-butadiene on Pt/graphite[11] and Pt-net,[12] of ethylene[13] and propene[14] on Pt in a 0.5 M D_2SO_4 solution. The deuteration of cyclopentene in solutions of tetrahydrofuran (THF) containing D_2O with and without 5% D_2SO_4 or in the other solutions of CH_3COOD, CH_3OD, $(CH_3)_3COD$, and $DOCH_2CH_2ND_2$-CH_3OD has been studied by Phillipson and Burwell,[15] but here the f_D's are lower than that in a deuterated acid solution, and hence the average number of deuterium atoms taken up in the product cyclopentane was much smaller, even though the addition of D_2O to THF accelerated the deuterium-exchange reaction.

In the present investigation, the deuteration of 1,3-butadiene on a Pt/Al_2O_3 catalyst was conducted in 0.5 M D_2SO_4 purified by the preelectrolysis. We will present a new saw-toothed distribution of deuterium in butenes and discuss the reaction mechanism.

Experimental

Catalysts. The Pt/Al_2O_3 (0.5 wt% Pt) used in this study was a *reference catalyst* supplied by the Catalysis Society of Japan and was prepared as follows.[16] The γ-alumina (BET surface area, 174 m^2/g; pore volume, 0.66 ml/g) was impregnated in an aqueous solution of H_2PtCl_6 and then dried overnight. After calcination at 450 °C for 3 h in O_2, the catalyst was reduced in a H_2 stream at 300 °C for 3 h and then recalcinated at 600 °C for 3 h. The dispersion of Pt has been measured by means of the CO, H_2, and O_2 adsorption methods by several investigators and found to be *ca.* 0.6, though slightly scattered.[16]

Reaction Procedure. The catalyst (0.1—0.2 g), heated at 250 °C for 1 h in a H_2 stream, was suspended in 0.5 M D_2SO_4 and rereduced by bubbling D_2 (Showa Denko, 7N-purity, 99.97D%, P_D=13 mmHg, 1 mmHg=133.3 $N \cdot m^{-2}$) through the solution. The reaction gas was mixture of 1,3-butadiene (4N-purity, P_R=14 mmHg), D_2(P_D=7 or 28 mmHg) and He (7N-purity) at a total pressure of 1 atm. The reaction was conducted by circulating the reaction gas through the solution at 20±1 °C. Our previous work has shown that, under these conditions, the diffusion of D_2 to the catalyst surface is rate-determining.[11,12] No reaction occurred under these conditions without the catalyst.

Solution. The solution of 0.5 M D_2SO_4 was prepared from D_2O (Showa Denko, 99.75D%) and sulfuric acid-d_2 (Merck 99D%). The deuterium content of the solution was estimated from its specific gravity. Unless otherwise stated, the solution was subjected to preelectrolysis overnight (anodically and then cathodically, several mA). The AES and XPS of the Pt electrode used for the preelectrolysis were run on an ESCA 3 Electron Spectrometer (VG Scientific, Ltd.) to detect any impurity picked up from the solution. Both the purity and the deuterium content of the solution greatly influenced the results. These effects will be discussed in the text.

Analysis. The analyses of the products were conducted gas-chromatographically and mass-spectrometerically, as has been described previously.[11]

† 1 M=1 mol dm^{-3}.

Results and Discussion

Saw-toothed Distribution. Table 1 presents the saw-toothed distributions of deuterium in butenes produced from 1,3-butadiene on 0.5 wt%Pt/Al_2O_3 in pre-electrolyzed 0.5 M D_2SO_4 with a high deuterium content (99.7D%). The saw-toothed shape is most clear in *trans*-2-butene and least clear in *cis*-2-butene, while the latter product shows the most enhanced deuterium-exchange among the three isomers. Such saw-toothed distributions are independent of the conversion, at least up to 20%. As has been stated above, each butene takes up much more deuterium atoms than it does in gaseous deuteration on Pt catalysts. For example, the average deuterium number, DN, ($\sum_{i=1}^{8} i \cdot X_i$, X_i is the fraction of the d_i-species) of *cis*-2-butene in Table 1 is 5.2, while, it is 2.1 in the gaseous deuteration.[3] However, the product distributions are very close to each other; butane: 1-butene: *trans*-2-butene: *cis*-2-butene=44:34:11:12 in this work and 44:36:10:10 at 15 °C in a gaseous reaction.[1] This fact indicates that the reaction mechanism is almost the same for both systems. The present saw-toothed distributions have also been observed in our separate experiments on such other catalysts as 5 wt% Pt/Al_2O_3, 0.5 wt% Pt/SiO_2, Pt/TiO_2, and Pt/Nb_2O_5 in a deuterated solution.[17] Therefore, it is concluded that the kind of supports and the amount of doped Pt have no effect on the reaction mechanism.

The saw-toothed shape is sensitive to the solution purity and the deuterium content of the solution. When the solution is used repeatedly without the pre-electrolysis (this was the case in our previous work on Pt/graphite[11]), the saw-tooth becomes less clear. Such a situation is reproduced in the present catalyst as exemplified by the distribution of deuterium in *trans*-2-butene in Fig. 1 (-○-). The overnight pre-electrolysis of the same solution makes the saw-toothed shape clearer, as is shown in Fig. 1 (-△-), indicating that a trace of impurity interferes with the appearance of the saw-toothed shape. In order to check on the impurities removed, the surface of the Pt electrode used for the preelectrolysis was examined by means of the AES and XPS. Both spectra show the peaks of carbon, oxygen, and sulfur. Since the peak intensity of carbon and oxygen is much the same as that on clean Pt foil, neither kind of atom comes from the solution. The presence of sulfur is easily understood, as it comes from SO_4^{2-} in the solution, not from the impurity. The complete absence of the other kinds of atoms in the spectra leads us to assume organic compounds as the impurities in the solution, since organic compounds will be decomposed during the anodic polarization, while inorganic compounds will be deposited through discharge during the cathodic polarization. However, a possibility would remain that the impurity is so small an amount of the inorganic compound that it cannot be detected by means of the AES and XPS. Further

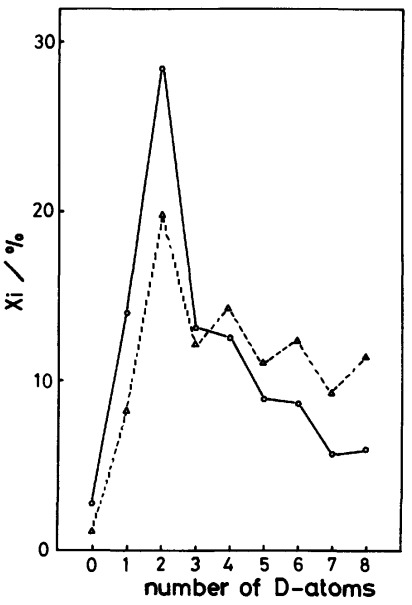

Fig. 1. Distribution of deuterium in *trans*-2-butene formed by the deuteration of 1,3-butadiene on Pt/Al_2O_3 in 0.5M D_2SO_4 of 98.5D%.
The solution; without (○) and with (△) preelectrolysis. P_R=14 mmHg, P_D=28 mmHg. Total conversions are 5.1% for ○ and 7.8% for △.

TABLE 1. DISTRIBUTION OF DEUTERIUM IN BUTENES OBTAINED BY THE HYDROGENATION OF 1,3-BUTADIENE ON Pt/Al_2O_3 IN 0.5 M D_2SO_4 OF 99.7 D%, CALCULATED DISTRIBUTIONS AND N-PROFILES
P_R=14 mmHg, P_D=7 mmHg, total conversion; 2.0%

Product	i=	0	1	2	3	4	5	6	7	8	DN	f_D
1-butene	found (X_i)	0.8	5.9	22.5	15.6	15.9	12.4	9.6	7.8	9.4	4.1	
	calcd (X_i)	0.2	4.6	22.7	15.6	16.7	12.6	9.5	8.0	9.0		
	N-profile (N_i)	0.0	0.0	23.0	13.0	17.0	13.0	12.0	0.0	21.0		0.90
trans-2-butene	found (X_i)	1.2	6.4	21.0	11.9	14.4	10.9	12.8	8.5	12.9	4.4	
	calcd (X_i)	0.2	4.0	22.0	12.5	14.9	11.0	12.6	10.0	12.7		
	N-profile (N_i)	0.0	0.0	23.0	10.0	16.0	8.0	16.0	0.0	27.0		0.91
cis-2-butene	found (X_i)	1.6	3.7	12.9	9.3	10.7	11.2	13.1	14.2	23.4	5.2	
	calcd (X_i)	0.0	1.8	13.0	8.9	10.0	11.2	13.4	14.2	23.5		
	N-profile (N_i)	0.0	0.0	13.0	8.0	9.0	9.0	15.0	0.0	42.0		0.93

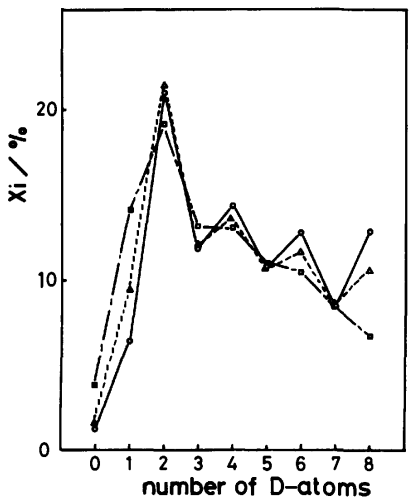

Fig. 2. Distribution of deuterium in *trans*-2-butene formed by the deuteration of 1,3-butadiene on Pt/Al_2O_3 in 0.5M D_2SO_4 of 99.7 D% (○), 97.6 D% (△), and 94.2 D% (□). All the solutions were subjected to the preelectrolysis overnight. P_R=14 mmHg, P_D= 7 mmHg. Total conversions are 2.0% for ○ and 2.5 % for △ and □.

examination is required for the solution of this problem.

The saw-tooth also tends to be smoothed by decreasing the deuterium content of the solution (Fig. 2). In the solution of 94.2 D%, only the shoulders can be seen at butene-d_4 and -d_6. Though both factors - the solution purity and deuterium content of the solution- influence the saw-toothed shape very much, the lack of the saw-toothed shape in the previous work is taken predominantly as being due to the impurity factor, for the decrease in the deuterium content upon repeated use is not large enough to smoothen out the saw-toothed shape.

Isotopically exchanged 1,3-butadiene was not detected after the reaction. Therefore, it is concluded that there is an irreversible adsorption of 1,3-butadiene on the Pt surface.

Simulation by N-profile. The N-profiles of butenes were calculated in order to discuss the reaction mechanism. The N-profile consists of N_0, N_1, ···, N_8, where N_i represents the fraction of the butene in which i hydrogen positions have been equilibrated with the surface H/D pool. The fraction of molecules in which m out of i equilibrated atoms are deuterium, $X_m(i)$, is given by the standard binomial formula as;

$$X_m(i) = {}_iC_m f_D^m (1-f_D)^{i-m}$$

Thus, the fraction of d_m-species, X_m, is calculated as;

$$X_m = \sum_{i=m}^{8} X_m(i) \cdot N_i$$

The N-profile is determined so that X_m, m=0, 1, ···, 8, can best fit the observed distribution of deuterium by adjusting N_2, N_3, ···, N_8 (N_0=N_1=0 because the two hydrogen or deuterium atoms are necessarily taken up in butenes).

The N-profiles thus calculated are shown in Table 1, together with the experimental and the calculated X_m distributions of deuterium. The first thing to notice is that each experimental distribution is satisfactorily reproduced by the X_m calculated based on the N-profile listed in the third row for each butene. The N-profiles of 1-butene and *trans*-2-butene resemble each other. Maxima appear at N_2, N_4, and N_8. N_6 appears as a clear maximum for *trans*-2-butene, but only as a shoulder for 1-butene. N_7 is exceptionally small in both cases. Thus, the N-profiles of 1-butene and *trans*-2-butene also reflect the characteristic features of the maxima (or shoulder) at N_2, N_4, N_6, and N_8. On the other hand, the N-profile of *cis*-2-butene presents three maxima, at N_2, N_6, and N_8, without N_4.

N-profile and Reaction Mechanism. The above features of N-profiles are explained by the following reaction mechanism including the reaction intermediates, **3** and **4** proposed by Bates *et al.*[3] for the same reaction, but on Pd/Al_2O_3 in the gas phase;

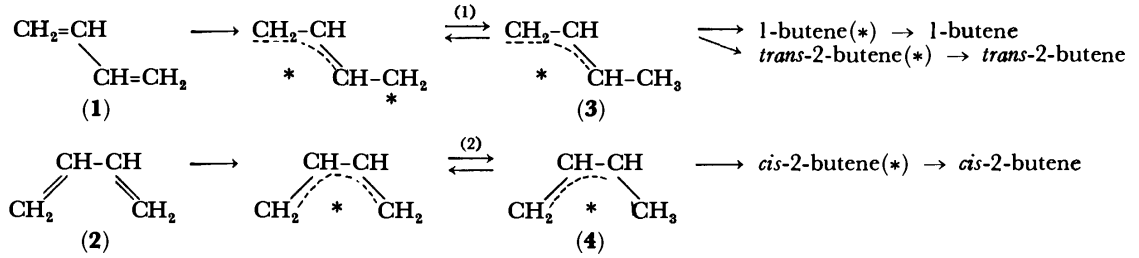

A molecule of 1,3-butadiene in the gas phase which exists in the *s-trans* **1** or *s-cis* **2** form is adsorbed irreversibly on the surface by delocalizing its π-electrons with the same geometrical configuration. The adsorbed *s-trans*-butadiene is converted to either 1-butene or *trans*-2-butene through *trans*-1-methyl-π-allyl **3**, whereas the *s-cis*-butadiene is converted only to *cis*-2-butene through *cis*-1-methyl-π-allyl **4**. Interconversions between the two kinds of adsorbed butadienes and between *trans*- and *cis*-1-methyl-π-allyls are not allowed because of the double-bond-like nature of the internal C-C bond. The lack of these interconversions is in accordance with the clear difference in the distribution of deuterium between *trans*- and *cis*-2-butene. This difference can not be accounted for by either σ- or π-bonded butadiene, since these adsorbed butadienes allow a rotation of the other vinyl group around the axis of the internal C-C bond and, hence, mutual interconversion between the *trans* and *cis* forms. The σ-bonded butadiene is not likely to be present, as is seen from the negative shift of the work function caused by the butadiene adsorp-

tion on Pt(100) and Pt(111).[18]

It must be expected on the basis of the above mechanism that a good correlation exists between the molar fraction of *cis*-2-butene in the products and that of *s-cis*-1,3-butadiene in the gas phase, because *cis*-2-butene is the only product from *s-cis*-1,3-butadiene (butane comes from the *s-trans via* 1-butene[11]). The former molar fraction is 12%, while the latter has been reported to be 3—7%.[19] The correlation is not bad if one takes into account the small modification in the stability of *s-cis*-1, 3-butadiene at the adsorption.

In the above mechanism, the *s-trans* route produces d_4 species by H/D exchange only through Step (1) and d_6 species through Step (1) and also the following Step (3), first proposed by Bates *et al.*[3];

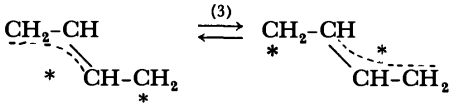

The relative rate of the hydrogenation of species **3** to the reverse of Step (1) for 1-butene formation is somewhat faster than the case of *trans*-2-butene formation. Thus, no distinct maximum is observed at N_6 for 1-butene.

On the other hand, the *s-cis* route gives the N_6-species of *cis*-2-butene through the single step of the reversible Step (2), because the two terminal methylenes in the adsorbed *s-cis*-butadiene are equivalent. Thus, the maximum at N_4 for *cis*-2-butene is diminished.

In addition to N_4 and N_6, considerable amounts of N_3 and N_5 are obtained. This can be readily explained by the slowness of the reverse rates of Steps (1) and (2).

The high fraction of N_8 and the zero amounts of N_7 for all the butenes suggest the presence of another sequence which causes an extremely fast H/D exchange over a molecule. The above mechanism can not explain the formation of N_8-species. One possible explanation could be that the butyl intermediate accelerates the H/D exchange by the following, reversible step;

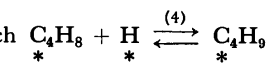

where $\overset{*}{C_4H_9}$ includes the two possible butyls bonded at either of the carbon atoms of the double bond. Thus, all the hydrogen atoms in the molecule become H/D exchangeable through Steps (1) to (4). The admission of the adsorbed butyl, however, will undoubtedly cause the hydroisomerization of butenes, which is not the case in the hydrogenation of 1,3-butadiene.[11] Further investigation of the details will be required.

The above mechanism is different from that on Pt/Al_2O_3 in the gas phase proposed by Bates *et al.*[3], where *mono-* and *di-*π-bonded butadienes were proposed. Interconversion between these two π-bonded butadienes was taken not to be readily reversible. Their discussion was based on the N-profiles, which differed for the respective butenes, though the observed distribution of deuterium in 1-butene was very similar to that of *trans*-2-butene, but different from that of *cis*-2-butene, as in our results. Therefore, their N-profiles had to lead to a different mechanism. Since the f_D in the gas-phase deuteration is rather low, it is essentially difficult to calculate the N-profile accurately from the distribution of deuterium in less deuterated products, though a somewhat saw-toothed figure can be noticed in their N-profile calculated for *trans*-2-butene. On the other hand, the present system can provide highly deuterium-exchanged products which ensure an accurate N-profile, and it enables us to elucidate the reaction mechanism more precisely.

The authors wish to thank Professor I. Toyoshima of Hokkaido University for the measurements of the XPS and AES. The present work was partly supported by a Grant-in-Aid for Scientific Research, No 57470001, from the Ministry of Education.

References

1) G. C. Bond, G. Webb, P. B. Wells, and J. M. Winterbottom, *J. Chem. Soc.*, **1965**, 3218.
2) P. B. Wells and A. J. Bates, *J. Chem. Soc.*, **1968**, 3064.
3) A. J. Bates, Z. K. Leszczyński, J. J. Phillipson, P. B. Wells, and G. R. Wilson, *J. Chem. Soc. (A)*, **1970**, 2435.
4) P. B. Wells, *J. Catal.*, **52**, 498 (1978).
5) E. F. Meyer and R. L. Burwell, Jr., *J. Am. Chem. Soc.*, **85**, 2881 (1963).
6) J. J. Phillipson, P. B. Wells, and G. R. Wilson, *J. Chem. Soc. (A)*, **1969**, 1351.
7) B. J. Joice, J. J. Rooney, P. B. Wells, and G. R. Wilson, *Discuss. Faraday Soc.*, **1966**, 223.
8) M. George, R. B. Moyes, D. Ramanarao, and P. B. Wells, *J. Catal.*, **52**, 486 (1978).
9) Y. Okamoto, K. Fukino, T. Imanaka, and S. Teranishi, *J. Catal.*, **74**, 173 (1982).
10) G. C. Bond, J. J. Phillipson, P. B. Wells, and J. M. Winterbottom, *Trans. Faraday Soc.*, **60**, 1847 (1964).
11) H. Kita, K. Shimazu, Y. Kakuno, and A. Katayama-Aramata, *J. Catal.*, **74**, 323 (1982).
12) H. Kita, N. Kubota, and K. Shimazu, *Electrochim. Acta*, **26**, 1185 (1981).
13) K. Fujikawa, H. Kita, K. Miyahara, and S. Sato, *J. Chem. Soc. Faraday I*, **71**, 1573 (1975).
14) K. Shimazu and H. Kita, *J. Catal.*, **86**, 129 (1984).
15) J. J. Phillipson and R. L. Burwell, Jr., *J. Am. Chem. Soc.*, **92**, 6125 (1970).
16) Committee on Reference Catalysts, Catalyst Society of Japan, "Reports of 4th Meeting of Reference Catalysts," 1982.
17) H. Kita, R. Yoneda, K. Shimazu, H. Hattori, and K. Tanabe, to be published.
18) A. E. Morgan and G. A. Somorjai, *J. Chem. Phys.*, **51**, 3309 (1969); G. A. Somorjai, *Catal Rev.*, **7**, 87 (1972).
19) L. B. Smith and J. L. Massingil, *J. Am. Chem. Soc.*, **83**, 4301 (1961).

A Kinetic Study on the Chemiluminescence of 9-Alkylacridines upon Air Oxidation in Alkaline Aprotic Solvents

Isao KAMIYA,* Takashi SUGIMOTO, and Kuniaki YAMABE†
Department of Chemistry, College of General Education, Nagoya University, Chikusa-ku, Nagoya 464
†*Department of Industrial Chemistry, Sasebo Technical College, Sasebo 857-11*
(Received November 28, 1983)

9-Methyl- (**1a**), 9-benzyl- (**1b**), 9-(diphenylmethyl)- (**1c**), and 9-ethylacridine (**1d**) were employed to obtain luminescent features of the acridines. The decay of chemiluminescence (CL) exhibits a pseudo-first order behavior with apparent rate constants 0.10, 3.30, 4.10, and 0.07 min^{-1} at 312 K for **1a**, **1b**, **1c**, and **1d**, respectively. A relatively high CL quantum yield (6.3×10^{-3}) is provided for **1a**, in contrast to low yields for **1b**, **1c**, and **1d** (1.5×10^{-6}, 1.1×10^{-5}, and 1.3×10^{-4}, respectively). A reaction mechanism involving a cleavage of a dioxetane intermediate to give excited singlet acridone anion is plausible for the luminescent reaction. In view of the fact that several dioxetanes decompose to give excited singlet products in high yields, the CL appears to arise from a minor reaction.

A number of acridines and acridinium salts have been reported to chemiluminesce in various reactions.[1] However, there exists little information as to the chemiluminescence (CL) of 9-alkylacridines on base-catalyzed air oxidation except a short description by White and Harding.[2] They observed a CL of 9-methylacridine (**1a**) on reaction with potassium *t*-butoxide (*t*-BuOK) and oxygen in dimethyl sulfoxide and proposed a reaction scheme involving a cleavage of a dioxetane intermediate to give the excited singlet acridone anion. Recently, such 1,2-dioxetanes as **2a**, **2b**, and **2c** have been derived and shown to decompose

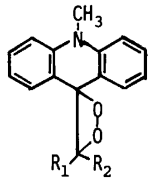

2a: $R_1=R_2=H$
2b: $R_1=H$, $R_2=C_6H_5$
2c: $R_1=R_2=C_6H_5$

thermally to give excited singlet 10-methylacridone.[3] According to Lee and Singer,[3c] the chemiexcitation yield for the generation of excited singlet 10-methylacridone changes with a structural variation at R_1 and R_2 in the dioxetanes, increasing in the order **2a**<**2b**<**2c**. Thus, we anticipated that if dioxetane intermediates like **2b** and **2c** were generated, the CL from air oxidation of 9-benzyl- (**1b**) or 9-(diphenylmethyl)acridine (**1c**) would be more intense than that from **1a**. A preliminary experiment, however, showed that the pattern of the substituent effect was contrary to our expectation; only feeble emission could be detected from **1b** and **1c** in spite of a high yield of ground state of acridone anion being obtained.

In order to study the effect of 9-alkyl substituents on the CL intensity of 9-alkylacridines **1a**—**1c** and 9-ethylacridine (**1d**), we investigated the kinetics for the luminescent air oxidation and determined the CL quantum and chemiexcitation yields for the generation of the excited singlet acridone anion.

Results and Discussion

The luminescent reaction was initiated by adding 0.3 cm^3 of a solution of *t*-BuOK in *t*-butyl alcohol (*t*-BuOK/*t*-BuOH solution, 2×10^{-2} mol/dm^3) to 2.0 cm^3 of an aerated solution of **1a**, **1b**, **1c**, or **1d** in DMF (1×10^{-4} mol/dm^3). CL emissions from each acridine show the same spectral distribution, matching the fluorescence (FL) spectra of the spent reaction mixtures and the FL spectrum of acridone anion under the identical experimental conditions,[4] as shown in Fig. 1. Actually, 9-acridone was detected and identified by a comparison with an authentic sample (Tokyo Kasei, guaranteed reagent) by means of thin layer chromatography on silica gel.

Under the experimental conditions employed, CL decays showed a pseudo-first order behavior to about 3 half-lives. From the decays, apparent rate constants at several different temperatures were determined. Rates of reactions were also determined by following the increase in the concentration of acridone anion through measurement of its FL-emission intensity at 465 nm. The FL-increasing curves obtained from **1a** and **1b** are illustrated together with the corresponding CL-decay curves in Fig. 2. The rate constants determined from the FL-increasing curves and those from CL-decay curves are shown in Table 1. A fairly good

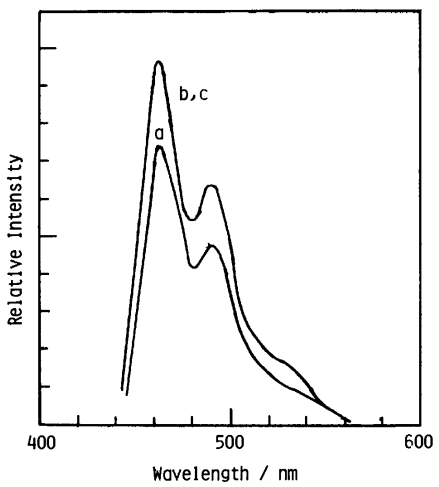

Fig. 1. The CL spectrum of **1a** in DMF (a), and FL spectra of the spent reaction mextures (b) and acridone anion under the identical conditions (c).

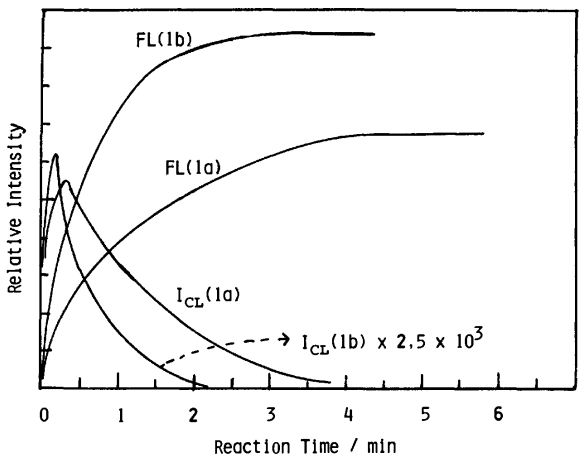

Fig. 2. FL-increasing curves (FL) and CL-decay curves (I_{CL}) in systems of **1a** and **1b** at 307K.

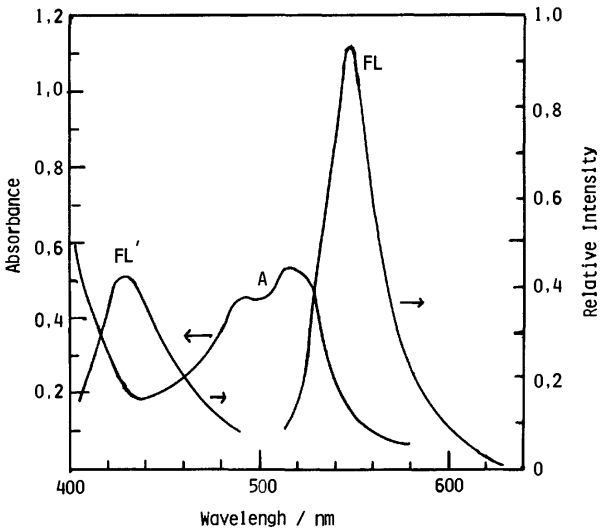

Fig. 3. The spectra of absorption and FL emission of orange-red intermediate in a system of **1b**. A: Absorption; FL: FL emission; FL': FL emission of **1b**.

TABLE 1. APPARENT PSEUDO-FIRST ORDER RATE CONSTANTS (k_{obsd}/min^{-1}) FOR THE CHEMILUMINESCENT REACTIONS OF **1a—d** AT SEVERAL DIFFERENT TEMPERATURES

Method of measurement	CL decay	FL curve	CL decay	FL curve
Acridine	**1a**		**1b**	
293 K	0.21	0.23	0.78	0.77
289 K	0.34	0.34	0.91	0.91
303 K	0.48	0.51	1.59	1.53
307 K	0.75	0.78	1.95	1.85
312 K	1.00	1.01	3.30	3.26
Acridine	**1c**		**1d**	
312 K	4.10	4.05	0.07	0.07
316 K			0.10	0.10
321 K			0.14	0.16

TABLE 2. APPARENT ACTIVATION ENERGIES (E_a) AND PREEXPONENTIAL FACTORS (A) FOR THE CHEMILUMINESCENT REACTIONS OF **1a**, **1b**, AND **1d**

Acridine	E_a / kJ mol^{-1}	A / min^{-1}
1a	65.2	8.8×10^{10}
1b	58.9	2.4×10^{10}
1d	70.8	4.2×10^{10}

agreement is found between the two, which indicates that the rate of the luminescent reaction is parallel to the rate of generation of acridone anion. The rate constants yield rather good Arrhenius plots, from which apparent activation energies and preexponential factors for **1a**, **1b**, and **1d** were determined. These kinetic data are tabulated in Table 2.

When *t*-BuOK/*t*-BuOH solution was added to a degassed solution of **1a** or **1b** *in vacuo*, no CL emission was observed and an orange-red intermediate was found, which was stable in the absence of oxygen. The absorption and FL spectra of this intermediate in a system with **1b** are shown Fig. 3. An admission of air to the system caused CL to appear progressively. Mason and Roberts[5] observed a similar orange-red intermediate when they added aqueous sodium hydroxide to a degassed solution of 4,5-dihydropyrazino[2,1-a:3,4-a']diisoquinolinediium dibromide in methanol, which chemiluminesced on reaction with oxygen due to generation of excited singlet 1,2-di[2-(1-isoquinolonyl)]-ethane. Heller and coworkers[6] reported that the orange-red color is attributable to a formation of electron-rich olefin *via* a cation radical, which reacts with oxygen to produce excited singlet 1,2-di[2-(1-isoquinolonyl)]ethane, and that the initial step of the change is the abstraction of a proton from the pyrazinodiisoquinolinediium salt.

On the analogy of the luminescent reaction of the pyradinodiisoquinolinediium salt, it seems likely that an electron-rich olefin is generated at the initial stage by loss of a proton from acridines. The extremely low magnitude of reaction rate for **1d** is probably due to low concentration of the olefin since no appreciable formation of the orange-red intermidiate was observed.

In view of the experimental results described above, the following reaction scheme, analogous to the one outlined by White and Harding,[2] would be plausible for the luminescent reaction.

(1) Proton transfer from acridine (AH) to *t*-BuO$^-$ to form an electron-rich olefin (A$^-$):

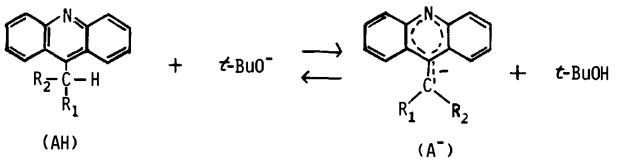

(2) Reaction of A$^-$ with oxygen to produce a peroxide anion (AO_2^-):

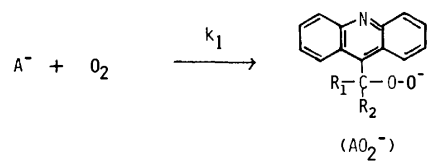

(3) Of the decomposition processes of AO_2^-, one is a cleavage *via* a dioxetane intermediate (X) to give excited singlet acridone anion ($P^*(S_1)$):

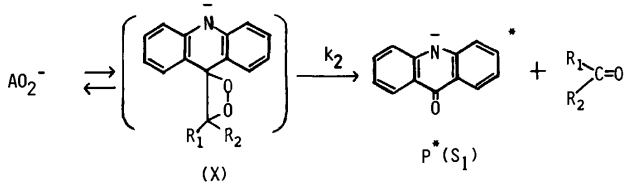

or to give the ground state of acridone anion ($P(S_0)$):

$$AO_2^- \rightleftarrows (X) \xrightarrow{k_3} P(S_0) + R_1R_2C{=}O.$$

(4) The cleavage processes of AO_2^- *via* acyclic pathways to give $P(S_0)$ and other products (Q) will compete with the above processes:

$$AO_2^- \xrightarrow{k_4} P(S_0),$$

$$AO_2^- \xrightarrow{k_5} Q.$$

(5) FL emission from $P^*(S_1)$:

$$P^*(S_1) \xrightarrow{k_6} P(S_0) + h\nu.$$

(6) Radiationless deactivation of $P^*(S_1)$:

$$P^*(S_1) \xrightarrow{k_7} P(S_0).$$

(7) Intersystem crossing to excited triplet acridone anion ($P^*(T_1)$) followed by radiationless deactivation:

$$P^*(S_1) \xrightarrow{k_8} P^*(T_1) \longrightarrow P(S_0).$$

According to the scheme, the intensity of CL emission is given by

$$I_{CL} = k_6[P^*(S_1)].$$

Using the steady-state approximation formulations $d[P^*(S_1)]/dt=0$ and $d[AO_2^-]/dt=0$, I_{CL} can be written as

$$I_{CL} = (k_2/(k_2+k_3+k_4+k_5))\Phi_F k_1[A^-][O_2],$$

where Φ_F is the apparent FL quantum yield of acridone anion in aerated DMF-*t*-BuOK systems and is given by

$$\Phi_F = k_6/(k_6+k_7+k_8).$$

If $[O_2]$ and $[t\text{-BuO}^-]$ are assumed to be maintained constant during the CL emission, I_{CL} is given by

$$I_{CL} = (k_2/(k_2+k_3+k_4+k_5))\Phi_F k_{obsd}[AH],$$

where

$$k_{obsd} = k_1[O_2]K[t\text{-BuO}^-]/[t\text{-BuOH}]$$

and

$$K = [A^-][t\text{-BuOH}]/[AH][t\text{-BuO}^-].$$

Figure 4 shows plots of the logarithm of emission intensity *vs.* time for the CL of **1a** (1.0×10^{-4} mol/dm^3) for different concentrations of *t*-BuOK, which indicates that the apparent first-order rate constant for the CL decay (k_{obsd}) is a function of $[t\text{-BuO}^-]$ as assumed above.

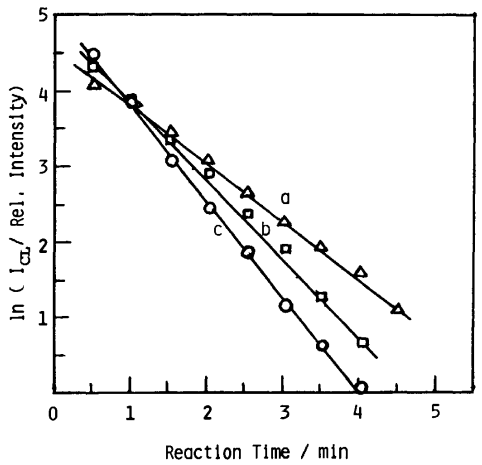

Fig. 4. The plots of ln (CL intensities of **1a** with different *t*-BuOK concentrations) *vs.* reaction time at 321K.
a: $[t\text{-BuOK}]=2.5\times10^{-3}$ mol/dm^3, $k_{obsd}=0.28$ min^{-1}; b: 4.0×10^{-3} mol/dm^3, 1.00 min^{-1}; c: 5.0×10^{-3} mol/dm^3, 1.30 min^{-1}.

The scheme further gives the following relation:

$$d[P(S_0)]/dt = ((k_2+k_3+k_4)/(k_2+k_3+k_4+k_5))k_{obsd}[AH].$$

Because of the low concentration of A^-, $d[P(S_0)]/dt$ is approximately written as

$$d[P(S_0)]/dt = ((k_2+k_3+k_4)/(k_2+k_3+k_4+k_5)) \times(-d[AH]/dt),$$

so that $[AH]=[AH]_0\exp(-k_{obsd}t)$, where $[AH]_0$ is the initial concentration of acridine.

Thus, I_{CL} is given by

$$I_{CL} = (k_2/(k_2+k_3+k_4+k_5))\Phi_F k_{obsd}[AH]_0 \exp(-k_{obsd}t), \quad (1)$$

and the concentration of acridone anion at reaction time *t* is given by

$$[P(S_0)]_t = ((k_2+k_3+k_4)/(k_2+k_3+k_4+k_5))[AH]_0 \times(1-\exp(-k_{obsd}t)). \quad (2)$$

From Eqs. 1 and 2, the overall CL quantum yield defined by

$$\Phi_{CL} = \int_0^{t_e} I_{CL}dt/[AH]_0$$

is given by

$$\Phi_{CL} = \Phi^*\Phi_F\Phi_r,$$

where t_e is the duration of CL emission, Φ^* is the chemiexcitation yield for the generation of excited singlet acridone anion from acridine, given by

$$\Phi^* = k_2/(k_2+k_3+k_4+k_5),$$

and Φ_r is the yield of acridone anion from acridine, given by

$$\Phi_r = [P(S_0)]_{t_e}/[AH]_0.$$

Φ_{CL} was determined from the ratio of the total light emitted from the CL of acridine to that from a standard luminol solution in dimethyl sulfoxide containing *t*-BuOK ($\Phi^S_{CL}=1.28\times10^{-2}$)[7] by the same method as described in our previous paper.[8] Φ_r was determined from

TABLE 3. CHEMILUMINESCENCE QUANTUM YIELD (Φ_{CL}), YIELDS OF ACRIDONE ANION FROM ACRIDINES (Φ_r), AND CHEMIEXCITATION YIELDS FOR THE GENERATION OF EXCITED SINGLET ACRIDONE ANION FROM DIOXETANE INTERMEDIATES (Φ^*) AT SEVERAL DIFFERENT TEMPERATURES

	Φ_{CL}	Φ_r	Φ^*	Φ_{CL}	Φ_r	Φ^*
	1a			**1b**		
293 K	6.3×10^{-3}	0.40	7.5×10^{-2}	1.6×10^{-6}	0.625	1.2×10^{-6}
298 K	6.8×10^{-3}	0.43	7.5×10^{-2}	1.5×10^{-6}	0.63	1.1×10^{-6}
303 K	6.9×10^{-3}	0.43	7.6×10^{-2}	1.5×10^{-6}	0.66	1.1×10^{-6}
307 K	6.3×10^{-3}	0.40	7.5×10^{-2}	1.5×10^{-6}	0.62	1.1×10^{-6}
312 K	6.3×10^{-3}	0.425	7.1×10^{-2}	1.4×10^{-6}	0.625	1.1×10^{-6}
	1c			**1d**		
312 K	1.1×10^{-5}	0.60	7.8×10^{-5}	1.1×10^{-4}	0.21	2.5×10^{-3}
316 K				1.3×10^{-4}	0.24	2.6×10^{-3}
321 K				1.45×10^{-4}	0.34	2.2×10^{-3}

($\Phi_F=0.21$ over the temperature range)

FL assay with known concentrations of acridone anion as internal standard by the method reported by Lee and coworkers (the method of standard addition).[9] Φ_F was determined by comparison of the FL emission of acridone anion in basic DMF[4] with that from a standard solution of quinine sulfate in 0.50 mol/dm^3 H_2SO_4 ($\Phi_F^S=0.50$)[10] and obtained to be 0.21, which was maintained almost constant over the temperature range of 289—321 K. The values of Φ_{CL} and Φ_r at several different temperatures and of Φ^* calculated from Eq. 3 are tabulated in Table 3. The results indicate that neither k_{obsd} nor Φ_r but Φ^* contributes to Φ_{CL}, which means that the ratio of k_2 to $k_3+k_4+k_5$ governs the CL quantum yield. The little dependence of Φ^* (and thus Φ_{CL}) on temperature may be interpreted in terms of the little dependence of k_2, k_3, k_4, and k_5 on temperature due to the low activation energy for the decomposition of unstable peroxide anion (AO_2^-). Our present experimental data do not allow us to decide whether k_3 or k_4+k_5 contributes predominantly to the lowering of the value of Φ_{CL} since the net chemiexcitation yield from dioxetane intermediate, $k_2/(k_2+k_3)$, cannot be determined. In view of the fact that several isolated dioxetanes decompose to give excited singlet product in high yields,[3a,c] it seems likely that the decomposition path *via* the dioxetane intermediate is a minor one, and thus, the extremely high magnitude of k_4 or k_5 lowers the Φ_{CL}-values of **1b** and **1c**.

Two other possibilities to lower the Φ_{CL}-values of **1b** and **1c** are conceivable. One is the direct generation of excited triplet acetophenone (from **1b**) or benzophenone (from **1c**), and the other is the generation of some quenching products. These, however, seem unlikely because neither indirect CL with 9,10-dibromoanthracence (one of triplet monitors) nor cis isomerization of added *trans*-stilbene could be observed, and because the CL of **1a** was not quenched by the addition of **1b** or **1c**. Further investigation is required to clarify the reason why the CL emissions from **1b** and **1c** are by far lower than the one from **1a**.

Experimental

Preparation of 9-Alkylacridines. The acridines were synthesized by heating a mixture of a carboxylic acid and diphenylamine with zinc chloride. The following procedure is representative of the syntheses. A mixture of diphenylamine (5.0 g), acetic acid (5.0 g), and zinc chloride (2.0 g) was heated at 210—220 °C for 10 h. While warm, the mixture was mixed with water (200 cm^3) and the product was extracted with benzene (3×200 cm^3). Evaporation of the extract and subsequent crystallization from benzene gave 9-methylacridine (**1a**) as pale yellow needles (49% yield): mp 117.5—118.5 °C [O. Blum, *Chem. Ber.*, **62**, 881 (1929): mp 117—118 °C]; MS *m/z* 193 (M^+). Found: C, 87.05; H, 5.68; N, 7.20. Calcd for $C_{14}H_{11}N$: C, 87.01; H, 5.74; N, 7.25. In a similar way, the following compounds were synthesized. 9-ethylacridine (**1d**) (58% yield): mp 115.5—116.5 °C [O. Tsuge, M. Nishinohara, and K. Sadano, *Bull. Chem. Soc. Jpn.*, **38**, 2037 (1965): mp 116 °C]; MS *m/z* 207 (M^+). Found: C, 86.59; H, 6.38; N, 6.62. Calcd for $C_{15}H_{13}N$: C, 86.92; H, 6.32; N, 6.76. 9-benzylacridine (**1b**) (58% yield): mp 173—174 °C [E. H. Huntress and E. N. Show, *J. Org. Chem.*, **13**, 674 (1948): mp 173 °C]; MS *m/z* 269 (M^+). Found: C, 88.93; H, 5.59; N, 5.27. Calcd for $C_{20}H_{15}N$: C, 88.18; H, 5.61; N, 5.20. 9-(diphenylmethyl)acridine (**1c**) (30% yield): mp 195—197 °C (from a 1.1 mixture of benzene and hexane); MS *m/z* 345 (M^+). Found: C, 89.95; H, 5.60; N, 4.15. Calcd for $C_{26}H_{19}N$: C, 90.39; H, 5.55; N, 4.06.

Measurements of Intensity and Spectra of CL and FL Emissions. The reactions were conducted in a quartz cell (1.0×1.0×4.5 cm), which was kept at a constant temperature by means of thermostated cell holder. The intensity and spectrum of CL emission were measured on a Hitachi MPF-2A fluorescence spectrophotometer, with the excitation source off. The intensity and spectrum of FL emission were also measured on the same apparatus.

References

1) F. McCapra and D. G. Richardson, *Tetrahedron Lett.*, **1964**, 3167; F. McCapra, D. G. Richardson, and Y. C. Chang, *Photochem. Photobiol.*, **4**, 1111 (1965); M. M. Rauhut, D. Sheehan, R. A. Clark, B. G. Roberts, and A. M. Semsel, *J. Org. Chem.*, **30**, 3587 (1965); E. Rapaport, M. W. Cass, and E. H. White, *J. Am. Chem. Soc.*, **94**, 3160 (1972); J. Gaglias and J. Nikokavouras, *Monatsch. Chem.*, **110**, 763 (1979); G. Perkizas and J. Nikokavouras, *ibid.*, **114**, 3 (1983).

2) E. H. White and M. J. Harding, *Photochem. Photobiol.*, **4**, 1129 (1965).

3) a) F. McCapra, I. Beheshti, A. Burford, R. A. Hann, and K. A. Zaklika, *J. Chem. Soc., Chem. Commun.*, **1977**, 944; b) E. H. White, N. Suzuki, and W. H. Hendrickson, *Chem. Lett.*, **1979**, 1491; c) C. Lee and L. A. Singer, *J. Am. Chem. Soc.*, **102**, 3823 (1980).

4) The solution of acridone anion was prepared by adding 0.3 cm^3 of a *t*-BuOK/*t*-BuOH solution (2×10^{-2} mol/dm^3) to a solution of 9-acridone in DMF (1.0×10^{-4} mol/dm^3).

5) S. F. Mason and D. R. Roberts, *Chem. commun.*, **1967**, 476.

6) C. A. Heller, R. A. Henry, and J. M. Fritsh, "Chemiluminescence and Bioluminescence," ed by M. J. Cormier, D. M. Hercules, and J. Lee, Plenum Press, New York (1973), p. 249.

7) J. Lee, A. S. Wesley, J. F. Ferguson III, and H. H. Seliger, "Bioluminescence in Progress," ed by F. H. Johnson and Y. Haneda, Princetone Univ. Press, Princetone (1966), p. 35.

8) I. Kamiya and T. Sugimoto, *Bull. Chem. Soc. Jpn.*, **54**, 25 (1981).

9) K.-M. Lee, L. A. Singer, and K. D. Legg, *J. Org. Chem.*, **41**, 2685 (1976).

10) J. N. Demas and G. A. Crosby, *J. Phys. Chem.*, **75**, 991 (1971).

The Effect of 4-Hydroxyl Substituent on the Singlet Chemiexcitation Yield in Base-catalyzed Air Oxidation of 3,5-Dichlorophenylpyruvic Acids

Isao KAMIYA,* Shizuaki MURATA, and Kuniaki YAMABE†
Department of Chemistry, College of General Education, Nagoya University, Chikusa-ku, Nagoya 464
†*Department of Industrial Chemistry, Sasebo Technical College, Sasebo 857-11*
(Received January 20, 1984)

In base-catalyzed air oxidation of substituted phenylpyruvic acids, an excited singlet product is generated from 3,5-dichloro-4-hydroxyphenylpyruvic acid (**1**) but excited triplet products from 3,5-dichlorophenyl- (**2**) and 3,5-dichloro-4-methoxyphenylpyruvic acid (**3**). According to the reaction scheme proposed, the singlet chemiexcitation yield from **1** and the triplet yields from **2** and **3** are 1.2×10^{-4}, 8.3×10^{-4}, and 6.7×10^{-4}, respectively. A discussion is made on the difference in spin state selectivity between **1** and **2** or **3**.

By studying the chemiluminescence (CL) in air oxidation of -CO-CH- containing molecules, we have revealed that excited triplet products are generated from simple molecules such as 3-methyl-2-butanone and isopropyl phenyl ketone.[1] We have further observed a direct CL due to generation of excited singlet products in similar air oxidations of 9, 10-diacylanthracenes[2] and 3-acyl-9-methylcarbazoles.[3]

In view of the evidence that simple isolated 1,2-dioxetanes predominantly give excited triplet products by homolytic cleavage,[4] whereas several 1,2-dioxetanes bearing easily oxidizable substituents decompose to give excited singlet products in high yield by intramolecular electron-transfer mechanism,[5] it seemed likely that the difference in spin states of products is attributable to different decomposition paths of 1,2-dioxetane intermediates.

In the present study on the chemiexcitation in base-catalyzed air oxidation of substituted phenylpyruvic acids,[6] a remarkable difference in spin state selectivity has been found between 3,5-dichloro-4-hydroxyphenyl- (**1**) and 3,5-dichlorophenyl- (**2**) or 3,5-dichloro-4-methoxyphenylpyruvic acid (**3**); an excited singlet product is generated from **1** but excited triplet products from **2** and **3**. Details of the experimental results and a discussion based on the results will be presented in this paper.

Results and Discussion

The reaction was initiated at 40 °C by adding 0.1 cm^3 of a solution of potassium *t*-butoxide in *t*-butyl alcohol (*t*-BuOK/*t*-BuOH solution, 2×10^{-2} mol/dm^3) to 2.0 cm^3 of an aerated solution of **1**, **2**, or **3** (5.0×10^{-4} mol/dm^3) in *N*,*N*-dimethylformamide (DMF). Direct CL was exhibited from **1**, whose spectral distribution has a peak at 390 nm and is similar to the fluorescence (FL) spectrum of 3,5-dichloro-4-hydroxybenzaldehyde (**4**) (Fig. 1(a,c)). This finding indicates that the emitting species is excited singlet **4**. Upon adding 9,10-diphenylanthracence (DPA) or 9,10-dibromoanthracence (DBA), there appeared indirect CL, whose spectrum comprises a peak at 430 nm (FL from DPA or DBA) and a shoulder at 390 nm (emission from **4**) as shown in Fig. 1 (b,d).

In contrast to **1**, neither direct CL nor indirect CL with DPA could be detected from **2** or **3** to any significant degree, whereas indirect CL with DBA was exhibited. These results strongly suggest a generation of excited triplet products (presumably, 3,5-dichlorobenzaldehyde (**5**) from **2**, and 3,5-dichloro-4-methoxybenzaldehyde (**6**) from **3**) since DBA is more capable of accepting the energy of excited triplet species than DPA due to the heavy-atom effect, the energy being released in the form of FL emission.[7]

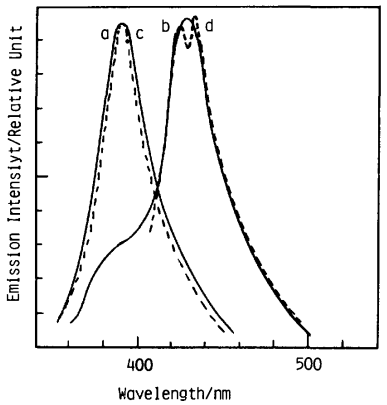

Fig. 1. Emission spectra: direct CL of **1** (—— a), indirect CL with DPA (—— b), FL of **4** (---- c), FL of DPA (----d).

The base-catalyzed air oxidation of such enolizable carbonyl compounds as **1**, **2**, and **3** would follow the same reaction pathways as the one proposed for the luminescent air oxidation of simple ketones,[1] 9,10-diacylanthracences,[2] and 3-acyl-9-methylcarbazoles,[3] which is quite similar to the mechanism for the base-catalyzed autoxidation of carbonyl compounds.[8]

(1) Anion A could be formed from pyruvic acid, **1**, **2**, or **3** by the action of strong basic *t*-BuOK.

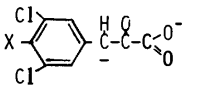

A X = O^- (from 1)
X = H (from 2)
X = OCH_3 (from 3)

(2) Reaction of A with oxygen produce peroxides AO_2:

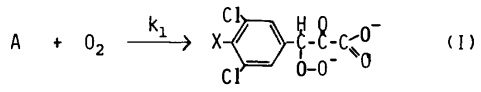

AO_2 (I)

(3) Of decomposition processes of AO_2, one is a cleavage *via* 1,2-dioxetane intermediates (M) to give excited singlet **4** ($P^*(S_1)$) from **1** or excited triplet **5** and **6** ($P(T_1)$) from **2** and **3**, respectivey:

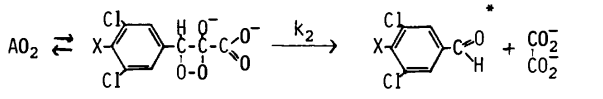

M $P^*(S_1)$: X=O⁻ $P^*(T_1)$: X=H, OCH_3 (II)

or to give the ground state of **4**, **5**, or **6** ($P(S_0)$):

$$AO_2 \rightleftarrows M \xrightarrow{k_3} P(S_0). \quad \text{(III)}$$

(4) The cleavage of AO_2 *via* acyclic pathways to give $P(S_0)$) and other products Q will compete with the above processes:

$$AO_2 \xrightarrow{k_4} P(S_0), \quad \text{(IV)}$$

$$AO_2 \xrightarrow{k_5} Q. \quad \text{(V)}$$

(5) FL emission from $P^*(S_1)$:

$$P^*(S_1) \xrightarrow{k_6} P(S_0) + h\nu_0. \quad \text{(VI)}$$

(6) Radiationless deactivation of $P^*(S_1)$:

$$P^*(S_1) \xrightarrow{k_7} P(S_0). \quad \text{(VII)}$$

(7) Intersystem crossing to excited triplet state ($P^*(T_1)$) followed by radiationless deactivation:

$$P^*(S_1) \xrightarrow{k_8} P^*(T_1) \longrightarrow P(S_0). \quad \text{(VIII)}$$

According to the scheme, the intensity of direct CL of **1** is given by

$$I^0_{CD} = \Phi^*_S \Phi^0_F k_1 [A][O_2],$$

where Φ^*_S is the singlet chemiexcitation yield for the generation of $P^*(S_1)$ from **1** and Φ^0_F is the apparent FL quantum yield of **4**, which are respectively given by

$$\Phi^*_S = k_2/(k_2+k_3+k_4+k_5) \text{ and } \Phi^0_F = k_6/(k_6+k_7+k_8).$$

Assuming that $\Phi^*_S \Phi^0_F$ is maintained constant during the reaction, the total light emission is given by

$$\int I^0_{CL} dt = \Phi^*_S \Phi^0_F k_1 \int [A][O_2] dt.$$

From the reaction scheme, the following relation is obtained:

$$k_1 \int [A][O_2] dt = [\mathbf{1}]_0,$$

where $[\mathbf{1}]_0$ is the initial concentration of **1**. The same relations are also obtained for **2** and **3**.

Thus, the overall CL quantum yield of direct CL of **1** is given by

$$\Phi^0_{CL} = \int I^0_{CL} dt / [\mathbf{1}]_0 = \Phi^*_S \Phi^0_F. \quad (1)$$

When fluorescer D (DPA or DBA) is added, the following steps IX—XI are to be taken into account.

Singlet-singlet energy transfer from $P^*(S_1)$ to D:

$$P^*(S_1) + D(S_0) \xrightarrow{k_{SS}} P(S_0) + D^*(S_1). \quad \text{(IX)}$$

FL emission from $D^*(S_1)$:

$$D^*(S_1) \xrightarrow{k_F} D(S_0) + h\nu_1, \quad \text{(X)}$$

Radiationless deactivation processes:

$$D^*(S_1) \xrightarrow{\Sigma k_Q} D(S_0). \quad \text{(XI)}$$

Taking all of the steps into account allows us to formulate the quantum yield of indirect CL of **1** with D as

$$\Phi^D_{CL} = \frac{\Phi^0_F + (k_{SS}/(k_6+k_7+k_8))\Phi^D_F[D]}{1+(k_{SS}/(k_6+k_7+k_8))[D]} \Phi^*_S, \quad (2)$$

where Φ^D_F is the apparent FL quantum yield of *D*, given by

$$\Phi^D_F = k_F/(k_F + \Sigma k_Q).$$

From Eqs. **1** and **2**, we obtain

$$\frac{\Phi^0_{CL}}{\Phi^D_{CL}-\Phi^0_{CL}} = \frac{\Phi^0_F}{\Phi^D_F-\Phi^0_F}\left(1+\frac{k_6+k_7+k_8}{k_{SS}} \cdot \frac{1}{[D]}\right). \quad (3)$$

Φ^0_{CL} and Φ^D_{CL} for several different concentrations of DPA were evaluated by a comporison of the total light emission from the systems with that from a standard luminol solution in dimethyl sulfoxide containing *t*-BuOK ($\Phi^S_{CL}=1.28\times10^{-2}$)[9] by the same method as that described in our previous peper.[3] The results are tabulated in Table 1. The quantum yield of indirect CL of **1** when [DBA] is 5×10^{-4} mol/dm³ ($\Phi^{DBA}_{CL}(\mathbf{1})$) was determined to be 1.3×10^{-6}. By a comparison of the FL-emission intensities of **4**, DPA, and DBA with that of a standard solution of quinine sulfate in 0.50

Table 1. Values of Φ^0_{CL} and Φ^{DPA}_{CL} for different concentrations of DPA

[DPA] / 10^{-4} mol dm^{-3}	20	10	5.0	1.1	0.65	0
Φ^{DPA}_{CL} / 10^{-6}	18.9	9.3	6.6	1.8	1.1	0.8 (Φ^0_{CL})

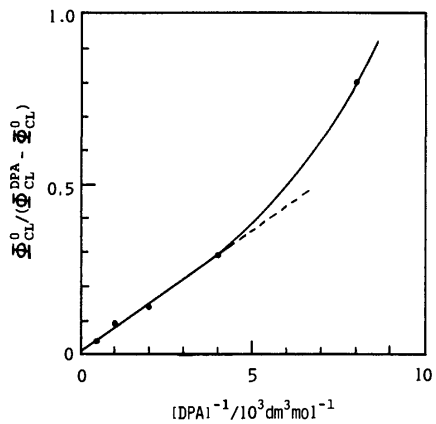

Fig. 2. Plot of $\Phi^0_{CL}/(\Phi^{DPA}_{CL}-\Phi^0_{CL})$ *vs.* 1/[DPA].

mol/dm³ H_2SO_4 (Φ_F^S=0.50),[10] the values of Φ_F^0, Φ_F^{DPA}, and Φ_F^{DBA} were determined to be 6.7×10^{-3}, 1.0, and 0.12, at 40 °C, respectively.

As shown in Fig. 2, linear plots of $\Phi_{CL}^0/(\Phi_{CL}^{DPA}-\Phi_{CL}^0)$ *vs.* 1/[DPA] can be obtained except for the systems with dilute concentrations of DPA, indicating that Eq. 3 is plausible when [DPA] is higher than 2.5×10^{-4} mol/dm³. The value of the *abscissa* intercept in Fig. 3, $\Phi_F^0/(\Phi_F^{DPA}-\Phi_F^0)$ is 7×10^{-3}. A direct calculation with the values of Φ_F^0 (6.7×10^{-3}) and Φ_F^{DPA}(1.0) gives a similar value of 6.7×10^{-3}. From the ratio of the line slope to the *abscissa* intercept, the magnitude of $k_{SS}/(k_6+k_7+k_8)$ is estimated to be 95 dm³/mol. If it is assumed that only P*(S_1) is generated from **1** and the magnitude of $k_{SS}/(k_6+k_7+k_8)$ for DBA is comparable to that for DPA, the value of Φ_{CL}^{DBA}(**1**) when [DBA] is 5.0×10^{-4} mol/dm³ may be calculated by the equation (see Eq. 3)

$$\frac{8\times10^{-7}}{\Phi_{CL}^{DBA}(\mathbf{1})-8\times10^{-7}} = \frac{6.7\times10^{-3}}{0.12-6.7\times10^{-3}}\left(1+\frac{1}{95}\frac{1}{5\times10^{-4}}\right),$$

from which Φ_{CL}^{DBA}(**1**) is obtained to be 1.4×10^{-6}. The calculated value is in fairly good agreement with the observed value (1.3×10^{-6}).

From Eq. 1 and the values of Φ_{CL}^0 (8×10^{-7}) and Φ_F^0 (6.7×10^{-3}), the singlet chemiexcitation yield (Φ_S^*) from **1** is estimated to be 1.2×10^{-4}.

In the systems of **2** and **3**, where excited triplet **5** and **6** (P*(T_1)) may be generated from phenylpyruvate anion, the steps I—V and the following steps VI′—XI′ will be taken into account.

Radiationless deactivation of P*(T_1):

$$P^*(T_1) \xrightarrow{k_6'} P(S_0), \qquad \text{(VI′)}$$

Quenching of P*(T_1) by oxygen:

$$P^*(T_1) + O_2 \xrightarrow{k_7'} P(S_0) + O_2(\Delta), \qquad \text{(VII′)}$$

Triplet-singlet energy transfer from P*(T_1) to DBA:

$$P^*(T_1) + DBA(S_0) \xrightarrow{k_{TS}} P(S_0) + DBA^*(S_1), \qquad \text{(VIII′)}$$

Triplet-triplet energy transfer:

$$P^*(T_1) + DBA(S_0) \xrightarrow{k_{TT}} P(S_0) + DBA^*(T_1), \qquad \text{(IX′)}$$

FL emission from DBA*(S_1):

$$DBA^*(S_1) \xrightarrow{k_F'} DBA(S_0) + h\nu_2, \qquad \text{(X′)}$$

Radiationless deactivation of DBA*(S_1):

$$DBA^*(S_1) \xrightarrow{\Sigma k_Q'} DBA(S_0). \qquad \text{(XI′)}$$

Then, the quantum yield of indirect CL of **2** (or **3**) with DBA is written by

$$\Phi_{CL}^{DBA}(\mathbf{2}) = \int I_{CL}^{DBA}(\mathbf{2})dt/[\mathbf{2}]_0 = \frac{\Phi_T^*k_{TS}\Phi_F^{DBA}[DBA]}{(k_{TS}+k_{TT})[DBA]+k_6'+k_7'[O_2]}$$

or

$$\frac{1}{\Phi_{CL}^{DBA}(\mathbf{2})} = \frac{1}{\Phi_F^{DBA}\Phi_T^*\Phi_{TS}}\left(1+\frac{k_6'+k_7'[O_2]}{(k_{TS}+k_{TT})[DBA]}\right), \qquad (4)$$

where $\Phi_F^{DBA}=k_F'/(k_F'+\Sigma k_Q')$, $\Phi_{TS}=k_{TS}/(k_{TS}+k_{TT})$, and $\Phi_T^*=k_2/(k_2+k_3+k_4+k_5)$. The observed values of Φ_{CL}^{DBA}(**2**) and Φ_{CL}^{DBA}(**3**) are shown in Tables 2 and 3, respectively. The plots of $1/\Phi_{CL}^{DBA}$(**2**) *vs.* 1/[DBA] and of $1/\Phi_{CL}^{DBA}$(**3**) *vs.* 1/[DBA] are shown in Figs. 3 and 4, respectively. The results indicate that Eq. 4 is plausible except for the systems with low concentrations of DBA. From the values of the *abscissa* intercepts in Figs. 3 and 4 and the values of Φ_F^{DBA}(0.12) and

Table 2. Values of Φ_{CL}^{DBA}(**2**) for different concentrations of DBA

[DBA] / 10^{-4} mol dm^{-3}	20	10	5.0	3.3	2.5	1.3
Φ_{CL}^{DBA}(**2**) / 10^{-6}	11	7.2	4.3	2.5	1.5	0.4

Table 3. Values of Φ_{CL}^{DBA}(**3**) for different concentrations of DBA

[DBA] / 10^{-4} mol dm^{-3}	20	10	5.0	2.5	1.3
Φ_{CL}^{DBA}(**3**) / 10^{-6}	5.9	3.3	1.8	0.9	0.4

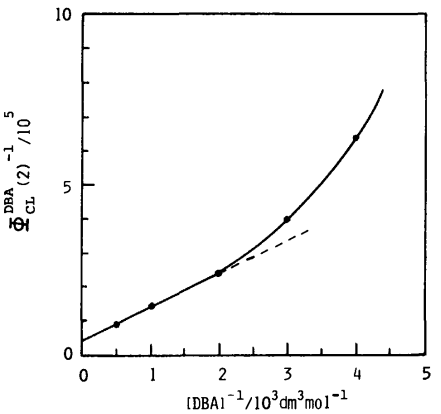

Fig. 3. Plot of $1/\Phi_{CL}^{DBA}$(**2**) *vs.* 1/[DBA].

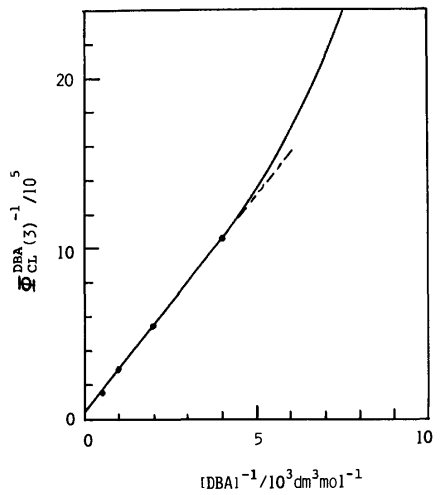

Fig. 4. Plot of $1/\Phi_{CL}^{DBA}$(**3**) *vs.* 1/[DBA].

Φ_{TS} (0.25),[11] the triplet chemiexcitation yields from **2** and **3** are estimated to be 8.3×10^{-4} and 6.7×10^{-4}, respectively.

Schaap and Gagnon[12] have reported noticeable chemiexcitation features about the spin state selectivity in the thermolysis of 1,2-dioxetanes **7a—7d**. Hy-

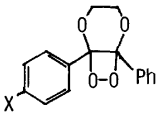

7 a: X = OH; b: X = OCH_3; c: X = H; d: X = O^-

droxy-substituted (**7a**), methoxy-substituted (**7b**), and unsubstituted one (**7c**) decomposed to give excited triplet products, which are typical of most simple 1,2-dioxetanes, while the very unstable phenoxide one (**7d**) decomposed with high singlet chemiexitation yield. Moreover, the deprotonation of **7a** to give **7d** with a base resulted in a flash of brilliant luminescence. White *et al.*[13] also showed that only the cases of the

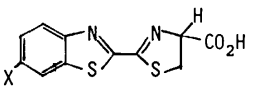

8 a: X = OCH_3; b: X = $NHCOCH_3$; c: X = NH_2; d: X = O^-

natural oxido-substituted luciferin (**8d**) and amino-substituted luciferin (**8c**) exhibited bioluminescence, although the luciferins **8a—8d** were oxidized to give carbonyl products *via* the corresponding 1,2-dioxetanes. The high singlet chemiexcitation yields have nicely been explained by the intramolucular electron-transfer mechanism.[14]

On the analogy of the chemiexcitation features of the 1,2-dioxetanes, the cleavage of an oxido-substituted 1,2-dioxetane intermediate by the intramolecular electron-transfer mechanism would be plausible for the generation of an excited singlet product from **1**. The low values of both Φ_S^* and Φ_T^* are presumably due to the fact that the chemiexcitation *via* the 1,2-dioxetane intermediate arises from a minor reaction.

More examples of -CO-CH- containing molecules as this type should be investigated to confirm this trend.

Experimental

Instruments. IR spectra were recorded on a JASCO A-102 spectrophotometer in the noted phase. ^1H NMR and ^{13}C NMR spectra were determined on a JEOL FX-90 spectrometer. Chemical shifts are reported as δ values in parts per million relative to the central signal of DMSO-d_6 (2.43 for ^1H and 29.50 for ^{13}C). The intensity and specta of CL emission were determined by measuring the output of R44 photomutiplier-photometer (Opelecs CLS-1 spectrophotometer). The intensity and spectra of FL emission were measured on a Hitachi MPF-2A fluorescence spectrophotometer.

Materials. For the preparation of **1**, **2**, and **3**, 4-hydroxy- and 4-methoxybenzaldehyde, *N*-acetylglycine (Nakarai Kagaku), sulfonyl chloride (Wako Junyaku), 3,5-dichlorobenzaldehyde (Aldrich), and various solvents were used without further purification. For the measurement of CL and FL emissions, *t*-BuOK (Merck, for synthesis), *t*-BuOH (Tokyo Kasei, extra pure grade), DPA (Nakarai Kagaku, specially prepared reagent), and quinine sulfate (Nakarai Kagaku, extra pure reagent) were used as received. DBA (Tokyo Kasei, guaranteed reagent) and luminol (Nakarai Kagaku, guaranteed reagent) were purified by recrystallization from xylene and dilute hydrochloric acid, respectively. DMF (Wako Junyaku, extra pure reagent) was distilled prior to use.[15]

Preparation of 3,5-Dichloro-4-hydroxyphenylpyruvic Acid (1). Following reported procedures,[16] **1** was prepared from 4-hydroxybenzaldehyde *via* chlorination, condensation with *N*-acetylglycine, and acid hydrolysis. Recrystallization from acetic acid gave pure **1** as colorless crystals (mp 208—210 °C decomp. uncorr.).

Preparation of Dichlorophenylpyruvic Acid (2). A mixture of 3,5-dichlorobenzaldehyde (1 g), *N*-acetylglycine (0.8 g), and sodium acetate (0.6 g) in acetic anhydride (7 cm^3) was heated under reflux for 4 h, and then allowed to stand overnight in a refrigerator. The crystals were filtered, washed with boiling water, and dried under vacuum. The crude product was heated under reflux with 3 cm^3 of 30% hydrochloric acid and 10 cm^3 of acetic acid for 4 h. The solvents were removed off on a rotary evaporator. Recrystallization from acetic acid with activated carbon gave a pale brown powder (0.33 g). The crude product was purified by a column of C_{18} reversed phase silica (10 g, Silica Gel ODS-Q3, 75 Å, 30—50 μm, purchased from Fuji Gel Co.) with a mixture of methanol, water, and acetic acid (50:50:1) as an eluant. Pure **2** (0.27 g, 23% overall yield) was obtained as colorless crystals (mp 153—155 °C, uncorr.): IR (KBr disk) 3500(OH) and 1695 (C=O) cm^{-1}; ^1H NMR (CD_3SOCD_3) 7.72 (2H, d, J=2.0 Hz, H-C(2) and H-C(6) of arom.), 7.32 (1H, t, J=2.0 Hz, H-C(4) of arom.), and 6.30 (1H, s, ArCH= enol form); ^{13}C NMR (CD_3SOCD_3) 165.52 (COOH), 144.28 (C(1) of arom.), 138.60 (C(4) of arom.), 133.83 (C(3) and C(5) of arom.), 127.11 (C(2) and C(6) of arom.), 125.97 (=COH enol from), and 106.30 (ArC= enol form). Found: C, 46.31; H, 2.51. Calcd for $C_9H_6Cl_2O_3$: C, 46.38; H, 2.59.[17]

Preparation of 3,5-Dichloro-4-methoxyphenylpyruvic Acid (3). To 13.6 g of 4-methoxybenzaldehyde, 122 g of sulfonyl chloride was added by distillation and the mixture was allowed to stand for 3 d at room temperature. After the sulfonyl chloride was removed by evaporation, the residue was distilled under reduced pressure (2 Torr, 140°C) (1 Torr= 133.322 Pa). The yellow oil obtained, which solidfied into white powder by cooling, was recrystallized from methanol. Pure 3,5-dichloro-4-methoxybenzaldehyde (15 g, 73% yield, mp 58—61 °C) was obtained as colorless crystals. A mixture of 3,5-dichloro-4-methoxybenzaldehyde (4.3 g), *N*-acetylglycine (4.3 g), and sodium acetate (3.1 g) was dissolved in 35 cm^3 of acetic anhydride, and the solution was warmed on a water bath for 2 h, and then cooled. A 1:1 mixture of water and petroleum (10 cm^3) was added and the resulting precipitate was triturated, filtered, and dried. Recrystallization from chloroform gave 1.98 g (18.3% yield) of pale yellow crystals of 4-(4-methoxy-3,5-dichlorobenzylidene)-2-methyl-5-oxazolone (mp 190—195 °C). The oxazolone (1.5 g) obtained was dissolved in a mixture of acetic acid (40 cm^3) and 6 mol/dm^3 hydrochloric acid (14 cm^3), and the solution was heated at 140—160 °C under reflux for 2 h, and then the mixture was allowed to stand overnight at room temperature. The resulting white precipitate was

filtered, washed with water, and dried. Recrystallization from acetic acid gave 0.89 g (64.5% yield) of **3** (mp 190 °C): IR (KBr disk) 3460(OH), and 1685(C=O) cm^{-1}: ^1H NMR (CD_3SOCD_3) 9.80 (2H, br, OH), 7.84 (2H, s, arom.), 6.33 (1H, s, ArCH= enol form), and 3.79 (3H, s, OCH_3); ^{13}C NMR (CD_3SOCD_3) 165.7 (COOH), 149.9 (C(1) of arom.), 143.3 (C(3) and C(5) of arom.), 133.2 (C(4) of arom.), 129.2 (=C-OH enol form), 128.1 (C(2) and C(5) of arom.), 106.3 (ArCH= enol form and 60.6 (CH_3O). Found: C, 45.54; H, 3.30. Calcd for $C_{10}H_8Cl_2O_4$: C, 45.63; H, 3.04.[18]

References

1) I. Kamiya and T. Sugimoto, *Chem. Lett.*, **1976**, 33; *Bull. Chem. Soc., Jpn.*, **50**, 2442 (1977); I. Kamiya, *ibid.*, **50**, 2447 (1977).

2) I. Kamiya and T. Sugimoto, *Chem. Lett.*, **1978**. 335; *Photochem. Photobiol.*, **30**, 49 (1979).

3) I. Kamiya and T. Sugimoto, *Bull. Chem. Soc. Jpn.*, **54**, 25 (1981).

4) W. Adam, "Chemical and Biological Generation of Excited States," ed by W. Adam and G. Cilento, Acad. Press, New York (1982), p. 115, and references cited therein.

5) K. A. Zaklika, A. L. Thayer, and A. P.Schaap, *J. Am. Chem. Soc.*, **100**, 4916 (1978); F. McCapra, I. Beheshti, A. Burford, R. A. Hann, and K. A. Zaklika, *J. Chem. Soc., Chem. Commun.*, **1977**, 944; C. Lee and L. A. Singer, *J. Am. Chem. Soc.*, **102**, 3823 (1980).

6) G. Cilento, M. Nakano, H. Fukuyama, K. Suwa, and I. Kamiya, *Biochem. Biophys. Res. Commun.*, **58**, 296 (1974).

7) V. A. Belyakov and R. F. Vassilèv, *Photochem. Photobiol.*,**11**, 179 (1970); T. Wilson and A. P. Schaap, *J. Am. Chem. Soc.*, **93**, 4216 (1971); N. J. Turro, P. Lechtken, G. Schuster, J. Orell, H.-C. Steinmetzer, and W. Adam, *ibid.*, **96**, 1627 (1974); M. A. Umgreit and E. H. White, *J. Org. Chem.*, **41**, 479 (1976); T. Wilson, D. E. Golan, M. S. Harris, and A. L. Baumstark, *J. Am. Chem. Soc.*, **98**, 1086 (1976).

8) W. von E. Doering and R. M. Haines, *J. Am. Chem Soc.*, **76**, 482 (1954).

9) J. Lee, A. S. Weley, J. F. Ferguson III, and H. H. Seliger, " Bioluminescence in Progress," ed by F. H. Johnson and Y. Haneda, Princeton Univ. Press Princetone (1966), p. 35.

10) J. N. Demas and G. A. Crosby, *J. Phys. Chem.*, **75**, 991 (1971).

11) Φ_{TS} for DBA is found to take the value between 2.0 and 3.0 (see Ref. 3).

12) A. P. Schaap and S. D. Gagnon *J. Am. Chem. Soc.*, **104**, 3504 (1982).

13) E. H. White, H. Worther, H. H. Siliger, and W. D. McElroy, *J. Am. Chem. Soc.*, **88**, 2015 (1966); E. H. White and H. Worther, *J. Org. Chem.*, **31**, 1484 (1966).

14) F. McCapra, *J. Chem. Soc., Chem. Commun.*, **1977**, 946; G. B. Schuster, B. Dixon, J.-Y. Koo, S. P. Schmidt and J. P. Smith, *Photochem. Photobiol.*, **30**, 17 (1979).

15) The solutions of DPA and DBA in DMF are not so stable, so that both solutions should be made before use.

16) A. Nishinaga, H. Kon, H. J. Cohmann, and T. Matsuura, *J. Org. Chem.*, **30**, 157 (1968).

17) The elementary analysis was conducted at the Elementary Analytical Center of Kyoto University.

18) The elementary analysis was conducted at the Analytical Section, Research Institute of Industrial Science, Kyushu University.

Flash Photolysis Study for Substituent and Solvent Effects on Spin-trapping Rates of Phenylthiyl Radicals with Nitrones

Osamu ITO* and Minoru MATSUDA
Chemical Research Institute of Nonaqueous Solutions, Tohoku University, Katahira, Sendai, Miyagi, 980
(Received December 10, 1983)

The spin-trapping rates for the reactions of para-substituted phenylthiyl radicals with nitrones have been determined by flash photolysis. For the phenylthiyl radical, the rate constant (in $mol^{-1}\,dm^3\,s^{-1}$) in benzene for a cyclic nitrone, 5,5-dimethyl-1-pyrroline *N*-oxide, is 5.2×10^8, which is greater than that for acyclic one, *N*-*t*-butyl-α-toluenimine *N*-oxide (1.1×10^7). The rates decrease with the solvent polarity and with the hydrogen-bonding ability; the maximum ratio of *ca.* 30 is observed for the rates between cyclohexane and methanol. Combined with the observed substituent effects, the mechanisms of the reactions and properties of the transition states are discussed.

The spin-trapping rates can be relatively determined from the stationary ESR signal intensities of the stable spin adducts,[1-4] while, for the reactions producing the unstable spin adducts, the time dependences of decays of the attacking radicals or formations of the spin adducts must be directly followed.[5-7] In the previous paper we have shown that the absolute rates for spin trapping of the thiyl radicals with nitroso spin-traps were determined from decay of the thiyl radicals generated by flash photolysis;[8] however, in these reaction rates we could not find the solvent effects which were reported in the literature.[4b] We can expect the solvent effects in polar and hydrogen-bonding solvents for more polar spin traps, nitrones ($-C{=}N^+{-}O^-$). In this study we investigate the thiyl radical-trapping reactions with 5,5-dimethyl-1-pyrroline *N*-oxide (DMPO) as a cyclic nitrone and *N*-*t*-butyl-α-toluenimine *N*-oxide (PBN, α-phenyl-*N*-*t*-butylnitrone) as an acyclic nitrone. From both solvent and substituent effects, the property and structure of the transition state are discussed.

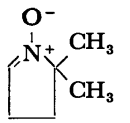

DMPO

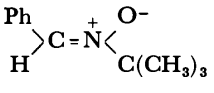

PBN

Experimental

Commercially available DMPO (Aldrich) and PBN (Aldrich) were used without further purification. Diphenyl disulfides were purified by recrystallization from ethanol. Solvents were distilled when spectrophotometric grade ones were not available. Samplings and measurements were made in the dark to prevent inadvertent photolysis.

The ESR spectra of the spin adducts were measured with a Varian E4 ESR spectrometer during the photolysis of disulfides (*ca.* 10^{-3} mol dm^{-3}) with the light between 350 and 450 nm (500 W high pressure Hg lamp) in the presence of nitrones (*ca.* 10^{-3} mol dm^{-3}) in degassed solution (*ca.* 10^{-1} Pa). Decay of the ESR signals after cutting off the light was followed by a fast recorder or by a transient memory.

The xenon flash photolysis apparatus was of standard design;[8] input energy was 150 J and the half-duration of xenon flash lamp (Xenon Corp. N-851 C) was *ca.* 10 μs. By the use of light filter, disulfides were flash photodecomposed with the light between 350 and 450 nm so as to avoid the photolysis of nitrones.

Results and Discussion

ESR Measurements. ESR spectra were observed during the photolysis of disulfides in the presence of nitrones as shown in Fig. 1. The hyperfine splitting constants of the nitrogen atom (a_N) and the α-hydrogen atom (a_H) are summarized in Table 1. The spin adducts with PBN can be ascribed to the nitroxides, **1**, as shown in Scheme 1, since both a_N and a_H are in good agreement

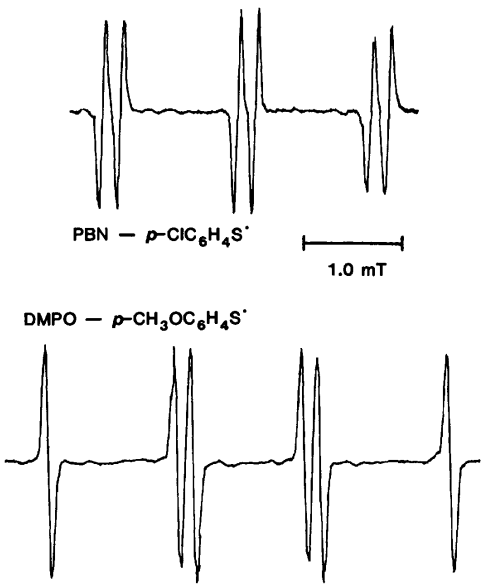

Fig. 1. ESR spectra of spin adducts produced by light illumination of diphenyl disulfides (*ca.* 10^{-3} mol dm^{-3}) in the presence of nitrones (*ca.* 10^{-3} mol dm^{-3}) in degassed benzene.

TABLE 1. ESR PARAMETERS AND HALF-LIFE ($\tau_{1/2}$) OF SPIN ADDUCTS IN BENZENE AT 23 °C

	DMPO			PBN		
	a_N / mT	a_H / mT	$\tau_{1/2}$ / s	a_N / mT	a_H / mT	$\tau_{1/2}$ / s
p-ClC_6H_4S·	1.36	1.43	3.3	1.38	0.18	0.38
p-$CH_3OC_6H_4S$·	1.33	1.45	1.7	1.39	0.18	0.15

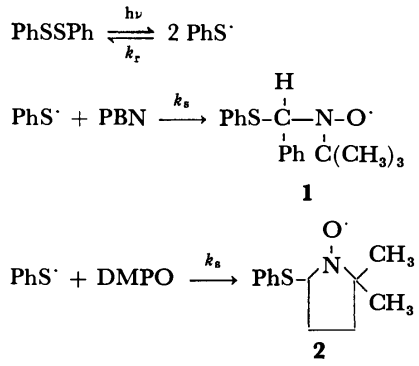

Scheme 1.

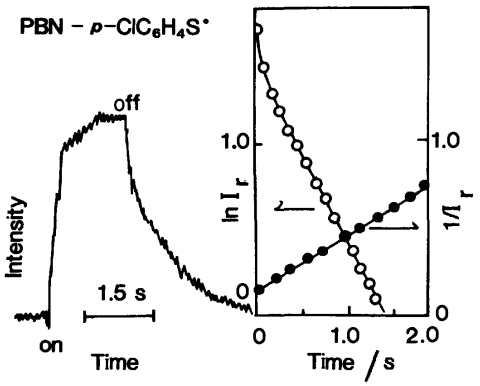

Fig. 2. Time dependence of ESR signal of the spin adduct produced by light illumination of disulfide in the presence of PBN at 23°C. The decay is plotted with the first-order (ln I_r *vs.* time; I_r refers to the relative signal intensity) and with the second-order ($1/I_r$).

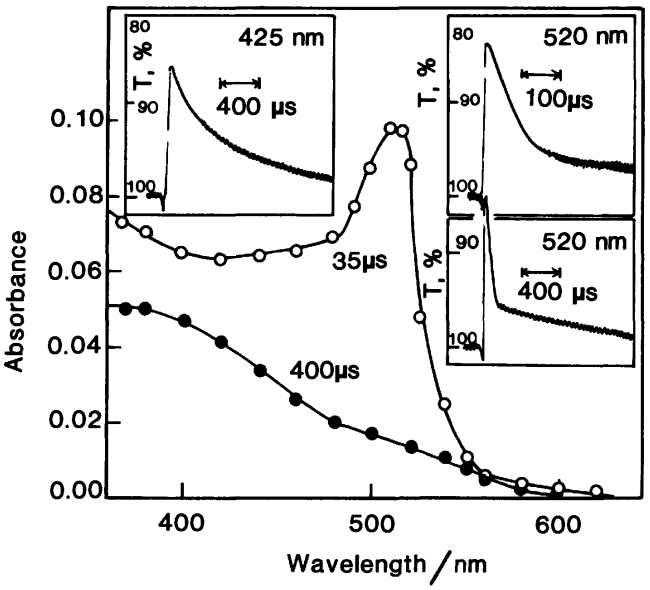

Fig. 3. Transient absorption spectra observed by flash photolysis of bis (*p-t*-butylphenyl) disulfide (*ca.* 10^{-4} mol dm^{-3}) in the presence of PBN (3.0×10^{-3} mol dm^{-3}) in benzene. The absorption band at 510 nm observed 35 μs after flash is ascribed to the *p-t*-butylphenylthiyl radical and the band of 400 μs after flash is ascribed to the spin adduct. Insert: The fast decay and the slow decay at 520 and 425 nm.

with the reported ones.[9] The spin adducts with DMPO have large a_H value characteristic to cyclic nitroxides, **2**; such large a_H values come from both conformational and electronic reasons.[10]

Figure 2 shows that the growth of the ESR signal intensity reaches at the maximum within *ca.* 1 s and that the signal decays rapidly after cutting off the light. The decay curves seem to obey either one second-order kinetics or two first-order kinetics. The half-life of the spin adduct is approximately estimated from the initial part of the decay curves (Table 1). The spin adducts with DMPO are more stable than those with PBN. The substituent effects of the phenylthiyl moiety on a_N, a_H, and half-life of the nitrone adducts are smaller than those of the nitroso adducts;[8] this finding is reasonably interpreted because the C-S bond is formed at the α-carbon in the former, whereas the S atom bonds directly to the nitrogen atom in the latter.

Transient Absorption Spectra. Figure 3 shows transient absorption spectra observed by the flash photodecomposition of bis(*p-t*-butylphenyl) disulfide in the presence of PBN. The absorption band at *ca.* 510 nm observed immediately after flash (35 μs) is attributed to the *p-t*-butylphenylthiyl radical.[8] Similar absorption bands were observed for other phenylthiyl radicals. The decay rate of the thiyl radical in the presence of PBN (decay curve at 520 nm of Fig. 3) is faster than that without PBN. The decay curve at 520 nm is composed of the fast and slow decay parts; the slow part yielded a spectrum which is depicted with the absorbances at 400 μs after flash. This spectrum may be attributed to the spin adduct. The decay profile at 425 nm shown in a long time scale in Fig. 3 seems to obey second-order kinetics rather than first-order kinetics. The half-life evaluated from the decay at 425 nm is *ca.* 1 ms which is considerably shorter than that evaluated from the ESR signal. This suggests the presence of the fast decay process which did not appear in the decay of the ESR signal; otherwise, there may be inadvertent photolysis of the spin adducts with the monitoring light of the flash photolysis experiment. The second-order decay of the spin adducts indicates that the decomposition mechanism of the spin adducts may include the dimerization process to the diamagnetic dimers before the fission of the bonds as Grillan and Ingold suggested.[11] Similar phenomena were observed for DMPO.

Determination of Rate Constants. The decay rate of the thiyl radical can be evaluated from the first order plots for the decay of the absorption band of the thiyl radical by the addition of nitrones (Fig. 4). The rate can be expressed as Eq. 1:

$$-d[PhS^{\cdot}]/dt = 2k_r[PhS^{\cdot}]^2 + k_s[PhS^{\cdot}][\text{nitrone}] \quad (1)$$

The processes for the reproduction of the thiyl radical with the decomposition of the adduct and the reaction of the thiyl radical with the spin adduct are omitted from the rate expression because of their small contribution.[8] By the addition of nitrones in large excess

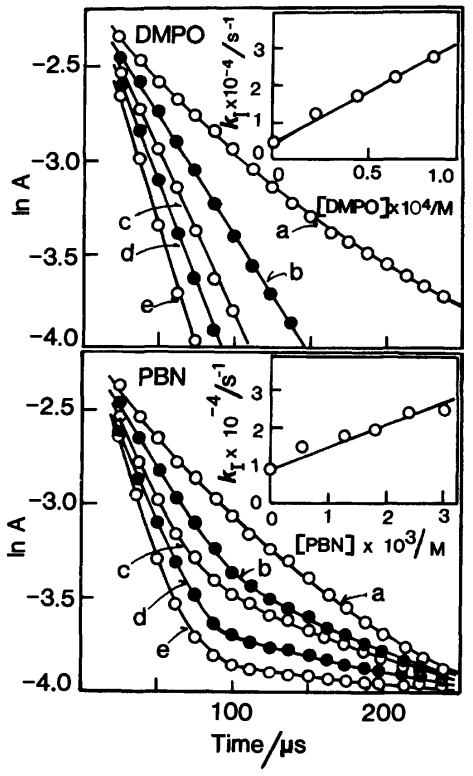

Fig. 4. The first-order plots for decay of *p*-t-butylphenylthiyl radical. [DMPO] × 10^5 mol dm^{-3}: a, 0; b, 2.2; c, 4.4; d, 6.6; and e, 8.8. [PBN] × 10^3 mol dm^{-3}: a, 0; b, 0.55, c, 1.3; d, 2.4; and e, 3.0. Insert: Pseudo-first-order plots; 1 M = 1 mol dm^{-3}.

compared with the concentration of the thiyl radical generated by one flash exposure which was estimated to be *ca.* 10^{-6} mol dm^{-3},[8] decay kinetics approaches first order (Fig. 4). In Fig. 4, the slopes of the first-order plots (k_1) are plotted against [nitrone]; fairly good pseudo-first-order relationships are found. The slopes yield the rate constants for spin trapping (k_S). In the case of PBN, although the slow decay part disturbs the analysis, the k_S values can be estimated from the slopes of the initial parts.

Substituent Effect. In order to clarify the contribution of the polar transition state to the reactivity, we at first examined the substituent effect of the phenylthiyl radicals. In Table 2 the rate constants for the phenylthiyl radicals with both electron-donating and withdrawing substituents are summarized. For each nitrone, the electron-withdrawing substituents accelerate the rates and *vice versa*. The Hammett plots *vs.* σ^+ (Fig. 5) yielded straight lines, whereas the plots *vs.* σ yielded curves. This suggests that the resonance factors contribute to the reactivities in addition to the inductive effects and that, in the Yukawa-Tsuno equation, $\log(k/k_0)=\rho(\sigma^\circ+r\Delta_{R^+})$, the r value is about 1.[12] The slopes for the k_S values in benzene yielded $\rho^+=0.98\pm0.02$ for DMPO and $\rho^+=1.14\pm0.02$ for PBN. The observed interval between both lines is the difference in the reactivities of two nitrones.

Although the rates decrease in methanol (Table 2), a straight line is also found in the Hammett plot for DMPO (Fig. 5); $\rho^+=1.15\pm0.02$ which is slightly greater

Table 2. Substituent effect on spin-trapping rate constants (k_S) of *p*-$XC_6H_4S^\cdot$ with DMPO and PBN in benzene or in methanol at 23 °C

X	$k_S \times 10^{-6}$ / $mol^{-1}\,dm^3\,s^{-1}$ DMPO[a] In benzene	DMPO[a] In methanol	PBN[b] In benzene
Br	750	72	17
Cl	700	60	12
H	520	54	11
t-C_4H_9	260	26	5.6
CH_3	300	19	5.0
CH_3O	110	5.4	1.1

a) Estimation error is *ca.* 10%. b) Estimation error is *ca.* 20%.

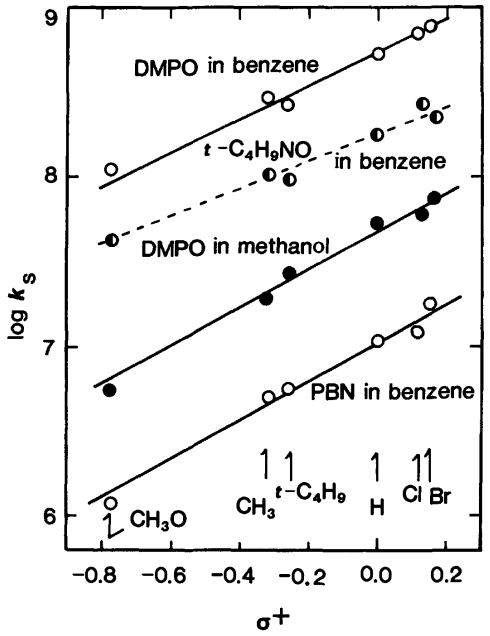

Fig. 5. The Hammett plots of $\log k_S$ *vs.* σ^+. Data for *t*-C_4H_9NO are cited from ref. 8.

than that in benzene. Positive ρ^+ values, in general, indicate that there is a contribution of the polar resonance structures to the transition state such as [PhS^-, $nitrone^{+}\cdot$]. In the case of the phenylthiyl radicals, however, since the thermodynamic stabilities vary with the change of the para substituents,[13] some parts of the observed ρ^+ value for the reactivities may come from the linear free-energy relationship and remaining parts can be attributable to the polar transition state.

The slope of the Hammett plot for 2-methyl-2-nitrosopropane (Fig. 5)[8] is less than those for nitrones; this indicates that the contribution of the polar resonance structure for nitrones is greater than that for nitroso compounds. The polar structures anticipated for nitrones are shown below (**3a**—**3c**), in which **3c** reasonably represents the charge transfer from nitrone to the thiyl radical. On the other hand, the polar resonance structures for the nitroso spin-trapping reactions are not so stable as nitrones. For a highly electro-

philic benzoyloxyl radical-trapping with PBN, a similar tendency was reported,[1a] whereas the opposite tendency was reported for less electrophilic attacking radicals such as *t*-butoxyl radical and primary radical.[1c,4a]

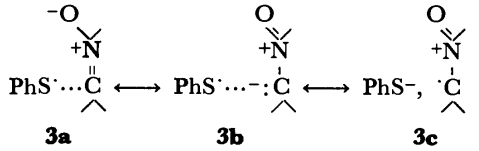

3a **3b** **3c**

Solvent Effect. The k_S values for the reaction of *p*-*t*-butylphenylthiyl radical with DMPO in nonpolar, polar, and alcoholic solvents are summarized in Table 3. The k_S values decrease with the solvent polarity; the ratio of k_S in cyclohexane to k_S in 1,2-dichloroethane is *ca.* 5. Alcoholic solvents reduce the k_S values in a great extent; the ratio of k_S in cyclohexane to that in methanol is *ca.* 30. A similar tendency was found for the reaction system with PBN. Figure 6 shows a plot of log k_S *vs.* the Kirkwood parameter, $(\varepsilon-1)/(2\varepsilon+1)$, which is one of solvent polarity parameters.[14] The points are divided into two groups; the upper group includes nonpolar and polar solvents and the lower one includes alcoholic solvents. The upper group shows a linear correlation with a slope of −2.48, which corresponds to the coefficient of the following equation derived by Steam and Eyring.[15]

$$\ln k_s = \ln k_s^\circ - \frac{1}{kT}\cdot\frac{\varepsilon-1}{2\varepsilon+1}\cdot\left(\frac{\mu_s^2}{r_s^3}+\frac{\mu_n^2}{r_n^3}-\frac{\mu_{\neq}^2}{r_{\neq}^3}\right) \qquad (2)$$

where k_s° refers to the rate constant at $\varepsilon=1$; μ and r refer to the dipole moment and radius, respectively. Subscripts s, n, and $\neq$ refer to the thiyl radical, nitrone, and activated complex, respectively. The component of the dipole moment of the thiyl radical parallel to the C-N-O bonds of nitrone can be assumed to be zero when the thiyl radical approaches perpendiculary the C-N-O bonds as shown in **3**. Thus, by substituting $r_s=r_n=3.0$ Å, $r_{\neq}=3.5$ Å, and $\mu_n=3.55$ D,[16] we can calculated $\mu_{\neq}$ to be 3.1 D. The activated complex becomes less polar than nitrone in the reactant; this suggests that there is a contribution of the resonance structures as would be anticipated from the substituent effect, **3b** and **3c**, which do not play any important role in nitrone alone in the reactant.

Table 3. Solvent effect on spin-trapping rate constants (k_s) of t-$C_4H_9C_6H_4S^\cdot$ with DMPO at 23 °C

Solvent	$k_s\times10^{-7}$	Solvent	$k_s\times10^{-7}$
c-C_6H_{12}	79	C_5H_5N	21
CCl_4	52	CH_3CN	23
(*n*-$C_3H_7)_2O$	43	$(CH_3)_2SO$	19
(*i*-$C_3H_7)_2O$	42	CH_2ClCH_2Cl	16
$CH_3CO_2C_2H_5$	30	$(C_2H_5)_2CHOH$	4.3
FC_6H_5	23	C_2H_5OH	3.0
$(CH_2)_4O$	22		

Unit of k_s; $mol^{-1}\,dm^3\,s^{-1}$.

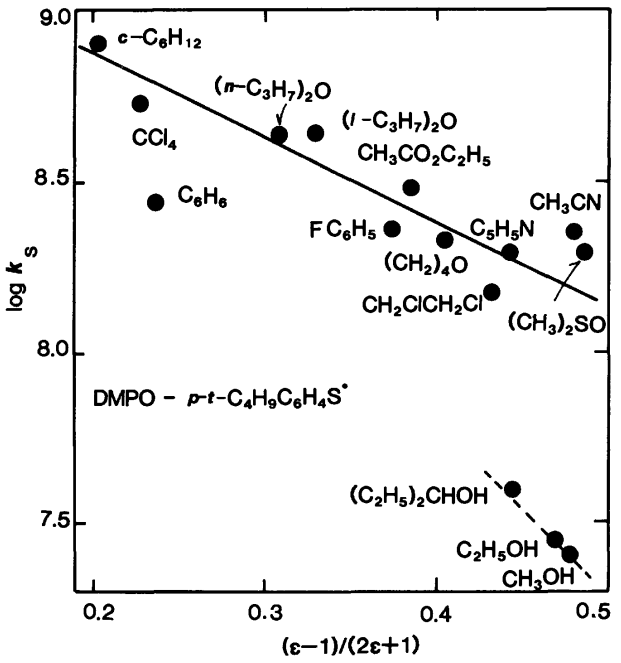

Fig. 6. Plots of log k_s *vs.* the Kirkwood parameter, $(\varepsilon-1)/(2\varepsilon+1)$.

On the other hand, the thiyl radical-trapping rates with nitroso compounds did not show appreciable solvent polarity effect,[8] although the dipole moments of nitroso compounds (*ca.* 3.2 D)[17] are only slightly smaller than those of nitrones (*ca.* 3.6 D).[16] One of the reasons is that the resonance structure ($-\ddot{N}^+-O^-$) in the reactant can not be changed by the approach of the thiyl radical in the transition state.

Alcoholic solvents reduce the rates more than the rates expected only from the solvent polarity (Fig. 6). Since such a decrease in the rates was not observed for nitroso compounds,[8] this can be attributd to the strong hydrogen bonding with nitrone, not but with the thiyl radical. Hydrogen bonding may stabilize nitrone in the reactant more than that in the activated complex, because the interaction of hydrogen atom of alcohols with the anionic oxygen atom of nitrone in the former is greater than that with the neutral oxygen atom in the latter (**3b** and **3c**). The order of a decrease in the rates among three alcoholic solvents seems to correlate with the Kirkwood parameter as seen in Fig. 6, suggesting that such interaction is cooperating with the solvent polarity effect. On the other hand, the solvent effect was not observed for the rates of nitroso spin-trapping reactions even in methanol;[8] this suggests that the hydrogen-bonding ability of the nitroso group is considerably smaller than that of nitrone.

Relative Reactivity. Since the solvent effect on the rates was observed for nitrones but not for nitroso compounds, the order of the reactivities among various spin traps depends upon solvents. In benzene, the order toward each thiyl radical is DMPO>nitrosobenzene>*t*-C_4H_9NO>PBN, whereas in methanol the order changes as nitrosobenzene>*t*-C_4H_9NO>DMPO>PBN. The order may also change with the electrophilicity of the attacking radical; *i.e.*, the slopes of the Hammett plots for nitrones are steeper than that of nitroso compound. For less electrophilic radicals such as the primary alkyl radical, the reported order differs from that of the thiyl radical (in benzene, nitroso-

benzene>t-C_4H_9NO>DMPO>PBN).[4b] The ratio of the rates for DMPO to PBN for the thiyl radical (*ca.* 50) varies with the attacking radicals; the ratio increases with the electrophilicity of the attacking radicals (primary alkyl radical (*ca.* 20)[1b] and t-butoxyl radical (*ca.* 90)).[4a] The higher reactivity of DMPO can be attributed to the strain energy released with the change from cyclic double bond to cyclic single bond.[18,19]

We would like to thank Professor Y. Ikegami and Dr. S. Tero-Kubota of Tohoku University for helpful discussion.

References

1) a) E. G. Janzen, C. A. Evans, and Y. Nishi, *J. Am. Chem. Soc.*, **94**, 8236 (1972); b) E. G. Janzen and C. A. Evans, *ibid.*, **95**, 8205 (1973); c) E. G. Janzen and C. A. Evans, *ibid.*, **97**, 205 (1975).
2) F. P. Sargent, *J. Phys. Chem.*, **81**, 89 (1977).
3) a) T. Doba, T. Ichikawa, and H. Yoshida, *Bull. Chem. Soc. Jpn.*, **50**, 3158 (1977); b) T. Doba and H. Yoshida, *ibid.*, **55**, 1753 (1982).
4) a) P. Schmid and K. U. Ingold, *J. Am. Chem. Soc.*, **100**, 2493 (1978); b) Y. Maeda, P. Schmid, D. Griller, and K. U. Ingold, *J. Chem. Soc., Chem. Commun.*, **1978**, 525; c) Y. Maeda and K. U. Ingold, *J. Am. Chem. Soc.*, **101**, 4975 (1979).
5) E. Finkelstein, G. M. Rosen, and E. J. Rauckman, *J. Am. Chem. Soc.* **102**, 4994 (1980).
6) P. Neta, S. Steenken, E. G. Janzen, and R. V. Shetty, *J. Phys. Chem.*, **84**, 532 (1980).
7) C. L. Greenstock and R. H. Wiebe, *Can. J. Chem.*, **60**, 1560 (1982).
8) O. Ito and M. Matsuda, *J. Am. Chem. Soc.*, **105**, 1937 (1983).
9) C. Chatgilialoglu, B. C. Gilbert, B. Gill, and M. D. Sexton, *J. Chem. Soc., Perkin Trans. 2*, **1980**, 1141.
10) E. G. Janzen and J. I.-P. Liu, *J. Magn. Reson.* **9**, 510 (1973).
11) T. Grillan and K. U. Ingold, *J. Am. Chem. Soc.*, **93**, 6555 (1971).
12) Y. Yukawa, Y. Tsuno, and M. Sawada, *Bull. Chem. Soc. Jpn.*, **39**, 2274 (1966).
13) O. Ito and M. Matsuda, *J. Am. Chem. Soc.* **101**, 5732 (1979).
14) J. G. Kirkwood, *Chem. Rev.*, **24**, 233 (1934).
15) A. E. Stearn and H. Eyring, *J. Chem. Phys.*, **5**, 113 (1937).
16) J. Hamer and A. Maculuso, *Chem. Rev.*, **1964**, 473.
17) B. G. Gowenlock and W. Luttke, *Quart. Rev.*, **12**, 321 (1958).
18) J. Gresser, A. Rajbenbach, and M. Szwarc, *J. Am. Chem. Soc.*, **83**, 3005 (1961).
19) O. Ito and M. Matsuda, *J. Org. Chem.* **49**, 17 (1984).

Corrections for Intensity Data in Energy-dispersive X-Ray Diffractometry of Liquids. Application to Carbon Tetrachloride

Keiko NISHIKAWA* and Takao IIJIMA
Department of Chemistry, Faculty of Science, Gakushuin University, Mejiro, Toshima-ku, Tokyo 171
(Received December 13, 1983)

The procedure of the analysis of the diffraction intensity of liquids obtained by the energy-dispersive method has been revised and improved. A new method for determining the energy spectrum of the primary beam is presented. The escape correction, the slit correction and the correction for multiple scattering have been newly applied. Scattering of X-rays from liquid CCl_4 has been measured and its structure function has been obtained by an improved procedure.

The intensity measurement of scattered X-rays by the use of energy-dispersive method has been carried out in various experiments since it was introduced by Giessen and Gordon.[1] In the energy-dispersive method, white X-rays are used as the primary beam and the scattered photons are detected and energy-analyzed by a solid state detector (SSD) connected with a multichannel pulse height analyzer (MCA). The energies of detected photons are distributed over the whole energy-region of the primary beam, so the scattering intensities of a certain range of the scattering parameters s, ($s=(4\pi\sin\theta/hc)E$, 2θ: scattering angle, E: photon energy), are accumulated in parallel.

This method has various advantages[2-4] over the conventional angle-dispersive method. However, the rather complex procedure of the data analysis is a drawback. The problems in the data analysis for quantitative intensity studies are as follows:

1) the determination of the properties of the primary beam, namely, the energy spectrum and the energy dependence of polarizaion of the primary beam,

2) the corrections for the effects originating from the detector, the slit system and the sample, namely, the escape correction when pure Ge or Ge(Li) detector is used, the slit correction and the absorption correction,

3) the correction for multiple scattering and the theoretical estimation of the intensity of Compton scattering.

Prober and Schultz performed the first quantitative measurement of the diffraction intensity from a sample which gives a halo pattern by the use of the energy-dispersive technique.[5] Three years later, Murata and one of the present authors (K. N.),[2] and Egami[3] reported the construction of their energy-dispersive diffractometers and the procedures of data analysis. In recent years, the energy-dispersive technique was also applied to the measurement of scattering intensities from gases.[6]

Prober and Schultz determined the energy spectrum of the primary beam by comparing the observed scattering intensity of the sample itself at high s-values, where the curve of the diffraction intensity is smooth without any particular structure, with the theoretical scattering intensity of mercury atoms.[5] However, they neglected the Compton shift in this procedure. This negligence seems to lead to a serious error. Egami followed the method by Prober and Schultz in determination of the primary energy spectrum, and developed this method considering the Compton shift.[3] For the determination of not only the primary energy spectrum but also the absorption coefficient of the sample, Egami proposed a self-consistent analysis.[3,4,7] However, it seems unreliable because too many parameters have to be determined simultaneously. Egami did not make the escape correction and the slit correction.

Murata and Nishikawa directly observed the energy spectrum of the primary beam by the use of the same slit system as in the measurement of scattered X-rays from samples, reducing the radiation intensity by decreasing the tube current to a few micro-amperes.[2] However, there has been anxiety about whether or not the decrease of the tube current produces distortion of the energy spectrum of the primary beam. In the data analysis of Ref. 2, the recoil factor for free electrons was used and the band-width ratio in the Compton shift was ignored. The polarization of the primary beam was neglected. Actually the effect has been found to be small in the energy region they used.

In the present paper, we report a procedure of improved data analysis of the energy-dispersive method and the structure function of liquid CCl_4 obtained by the improved procedure.

Experimental

Diffractometer. Since the main constitution of the apparatus is the same as that in Ref. 2, only the outline is given in the following. The geometry of the diffractometer is shown in Fig. 1. A horizontal goniometer system is adopted, in which an X-ray source and a detector are set in a horizontal plane. Although measurement by the energy-dispersive tech-

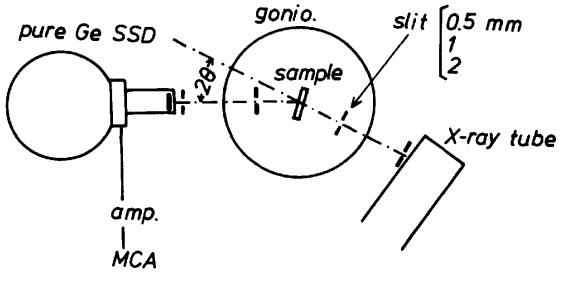

Fig. 1. Schematic diagram of the energy-dispersive diffractometer.

nique is carried out at a fixed scattering angle, such measurement must be repeated at different angles in order to cover a sufficiently wide region of s-space. To change the scattering angle, the X-ray tube is rotated around the vertical axis of the goniometer, which has a θ-2θ scanning system, while the detector (SSD) with a heavy cryostat is fixed.

A fine focus Phillips tube with a tungsten target is used, because strong white X-rays can be obtained without disturbance by characteristic X-rays, and the applicable power is large. The high voltage power supply for X-rays (Rigaku Denki Co.) is used. The stability of the high voltage is better than 0.1%. The X-ray tube is usually operated at 47.5 kV and 30 mA. The scattered X-rays are detected by a pure Ge SSD (ORTEC, Model 1513-10190). A pair of slits made of lead is used for both the incident and the detecting collimators. The separation of the two slits is about 150 mm. The width of the slit is varied: 0.5, 1, and 2 mm, and the height is 6 mm. The sample holder reported previously[8] is attached at the center of the goniometer. The transmission geometry is employed in order to make absorption correction easier.

Measurement of CCl_4. The diffracted X-ray photons from liquid CCl_4 at room temperature were collected at the scattering angles of 2θ=2.5, 4, 6, 10, 16, 28, 40, and 56°, by operating the X-ray tube at 47.5 kV and 30 mA. The spectrum in the energy-region 12—38 keV (λ=1.03—0.326 Å) is used for the analysis. The settings of 2θ=2.5, 4, 6, 10, 16, 28, 40, and 56° correspond to the regions of s=0.27—0.84, 0.42—1.34, 0.64—2.02 1.06—3.36, 1.69—5.36, 2.94—9.32, 4.16—13.18 and 5.71—18.09 Å^{-1}, respectively. In usual structure studies it is not necessary to measure the intensities at so many scattering angles. However, in the present experiment it is desired to obtain justification of a procedure of an analysis that includes several corrections. This is ascertained by checking the consistency of the data in the same s-regions which have been collected at different settings of the scattering angles and analyzed independently.

The scattering from Myler films, 5 μm thick, of the windows of the sample holder, was also measured. The measurement includes the scattering intensity from air, too. The thickness of the sample was 0.50 mm.

In order to obtain the relation of the photon energy *vs.* the channel number in the MCA, the fluorescent X-rays from Ba, Ag, Mo, Cu, and Cr were observed. The channel numbers of these peaks in the MCA were fitted to the energies of the corresponding characteristic X-rays by using a table by Bearden.[9] The linear relationship between the photon energy and the channel number is good.

The Properties of the Primary Beam

The Energy Spectrum of the Primary Beam. The energy spectrum of the primary beam was determined by measuring the scattering from air at low scattering angle with the same slit system and the same operating conditions of the tube as in the measurement of the sample. This method requires no particular preparation, because the diffraction measurement without the sample holder gives the scattering intensity from air. The scattering intensity of air at low scattering angles is strong enough to measure by the use of a usual sealed-off tube, because the effective volume of air which scatters X-rays is fairly large. In the analysis of the data of low scattering angles, it is permissible to neglect the Compton shift and the polarization of the primary beam. Moreover, the scattering amplitudes of light atoms such as N and O can be theoretically calculated with high accuracy.[10]

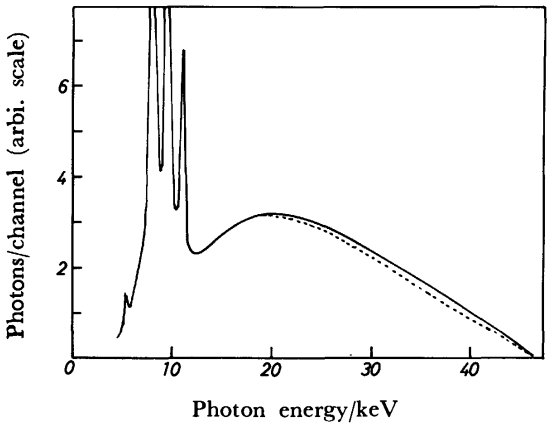

Fig. 2. The energy spectra of the primary beam. The solid curve is the spectrum determined by measuring scattering intensities of air. The broken curve is the one obtained by direct measurement by decreasing the tube current to a few micro-amperes.

The spectrum of the primary beam obtained from the scattering intensity of air is shown in Fig. 2, where it is compared with the spectrum measured directly at a tube current of a few micro-amperes. As is shown in Fig. 2, the intensity at high energy region obtained from air is stronger than that from the direct measurement. This seems to be caused by the difference between the amplitude of the ripples of the imperfectly smoothed voltage applied to the X-ray tube for the tube current of milli-amperes and that for the tube current of micro-amperes. In the former case the amplitude of the ripples is greater than that in the latter. The number of photons of radiated X-rays in a channel is not simply proportional to the applied voltage. So the intensity at the high energy region may become stronger in the case of the operation at milli-amperes. Another origin of the difference in the energy spectrum of the primary beam may be the difference of the size of the focus of the electron beam on the target.

The Polarization of the Primary Beam. It is known that the white X-ray radiation is polarized in the direction parallel to the electron beam at the high energy limit of the Bremsstrahlung spectrum.[11] The polarization $\Pi(E)$ of the primary beam is defined by

$$\Pi(E) = (I_{p,n}(E) - I_{p,p}(E))/(I_{p,n}(E) + I_{p,p}(E)), \quad (1)$$

where $I_{p,n}$ and $I_{p,p}$ are the intensities of the normal and parallel polarization components, respectively, with respect to the scattering plane. It is known that the polarization $\Pi(E)$ of white X-rays from a thin target is very large, and some experiments of such samples have been reported. However, there have been very few measurements for the polarization $\Pi(E)$ from such thick targets as those used in commercial sealed-off tubes. One recent example was the experiment carried out by Olsen *et al.*[12]

We also measured the polarization $\Pi(E)$ of our X-ray tube with a tungsten target (Phillips fine focus) at 47.5 kV. Two scattering intensities from silica glass were measured at a fixed scattering angle with

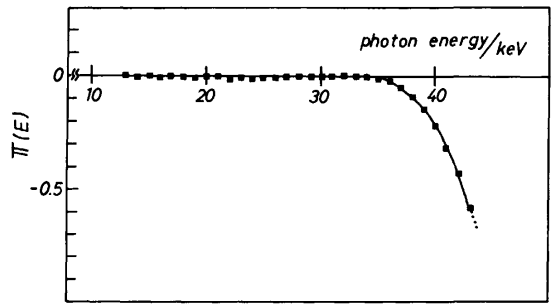

Fig. 3. The measured polarization $\Pi(E)$ of the used tungsten tube at 47.5 kV.

point focus collimators. One of them was the intensity measured in the ordinary condition where the X-ray tube was set on the scattering plane, and the other was that where the X-ray tube was set perpendicular to the scattering plane. From these two intensities, the polarization $\Pi(E)$ was obtained as shown in Fig. 3. The result is in fairly good agreement with that of Olsen *et al.*[12] However, the present result contains large uncertainties, because $\Pi(E)$ is computed from the differences of the two intensities which are nearly equal.

The $\Pi(E)$ amounts to almost -0.5 at the high energy limit, but up to the energy of 38 keV which is 0.8× (incident electron energy), absolute value of $\Pi(E)$ is below 0.1. So, in order to make the error caused by the polarization of the primary beam small, it is preferable to use the data whose energy region is below 0.8×(incident electron energy). By the use of this energy region, the errors due to the polarization contained in the data which are obtained at the scattering angle below 25° are less than 1%. But at high angles, for example, 2θ=56°, they amount to 5% if the polarization correction is not made. In our data, which are corrected by the use of the measured polarization, $\Pi(E)$, the estimated uncertainties are about 1% even at high scattering angles (2θ=40 and 56°).

In order to cancel the effect of polarization, Olsen *et al.*[12] and Egami[3] proposed the use of a diffractometer with an X-ray tube tilted away from the diffraction plane by 45°. In aperture collimator systems, this method may be used. However, it is not suitable in the case of slit systems, because the projection of the slit height on the scattering plane becomes large and the resolution of the scattering angle becomes low.

Correction for the Effects Originating from the Detector, the Slit System and the Sample

The Escape Correction. When a pure Ge or Li drifted Ge SSD is used, escape peaks are observed.[13] Some photons which come into the detector excite K electrons of Ge atoms and produce $K\alpha$ or $K\beta$ fluorescent X-rays characteristic of Ge. If the fluorescent X-ray photon is instantly re-absorbed in the crystal of the SSD, the output pulse height from the detector has a value corresponding to the energy of the original photon that entered the detector. However, if the fluorescent X-ray photon escapes from the detector

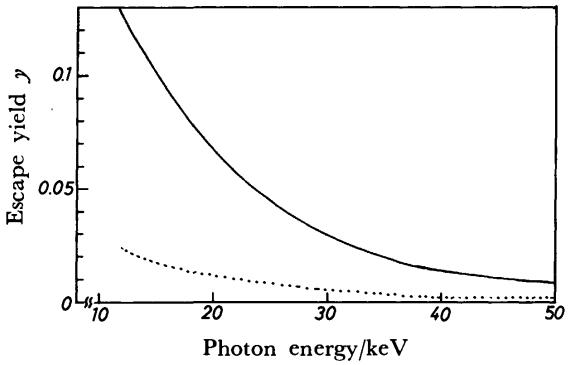

Fig. 4. The escape yield, $y(E)$, of the Ge SSD.[14] The solid curve is the yield for $K\alpha$ photons, and the broken curve for $K\beta$ photons.

crystal, the pulse height from the detector decreases to the value corresponding to the original photon energy minus E_k, the energy of Ge $K\alpha$ or $K\beta$ photons. Thus the number of photons counted at the energy E becomes less, and that at the energy $E-E_k$ becomes more, than the values they shoud be, where E_k is about 10 keV.

The yield of the escape, $y(E)$, of the Ge SSD used in the present work was measured by Mitsuhashi *et al.*, by the use of a single crystal of Si.[6,14] It is shown in Fig. 4.

With a little manipulation, we obtain the following formula for the true intensity I_0 at energy E:

$$I_0 = J_0 - \frac{y_1}{1-y_1}J_1 + \frac{y_1y_2}{(1-y_1)(1-y_2)}J_2 - \frac{y_1y_2y_3}{(1-y_1)(1-y_2)(1-y_3)}J_3 + \cdots\cdots \quad (\text{for } E<E_k) \quad (2)$$

and

$$I_0 = \frac{1}{1-y_0}\left[J_0 - \frac{y_1}{1-y_1}J_1 + \frac{y_1y_2}{(1-y_1)(1-y_2)}J_2 - \frac{y_1y_2y_3}{(1-y_1)(1-y_2)(1-y_3)}J_3 + \cdots\cdots\right] \quad (\text{for } E\geq E_k) \quad (3)$$

where J_n is the apparent intensity observed by the Ge SSD at the energy $E+nE_k$; y_n is the escape yield at the energy $E+nE_k$. The progression in Eq. 2 or 3 is terminated at the n-th term where the energy of $(E+(n+1)E_k)$ becomes for the first time greater than the high energy limit which is determined by the applied tube voltage. By the use of the measured values of y_n and J_n, we can make the escape correction with sufficient accuracy.

Slit Correction. The peaks and valleys of the observed intensity curve are smeared by the convolution due to the dispersion of the scattering angle, which is determined by the geometrical arrangement and widths of the slits. For liquid CCl_4, which gives a sharp peak at small s-values, the reduction of the peak height caused by this convolution is a serious problem.

According to the method of the slit correction in the experiment of small angle scattering[15] the deconvoluted intensity $I(s)$ is approximately given by

$$I(s) = 2\tilde{I}(s) - [\tilde{I}(s+\Delta s)+\tilde{I}(s-\Delta s)]/2, \quad (4)$$

where $\tilde{I}(s)$ is the observed intensity at s and Δs is the dispersion of the scattering parameter s, which is related to the angle dispersion ξ by the following formula:

$$\Delta s = \frac{4\pi}{hc} E \sin(\theta+\xi) - \frac{4\pi}{hc} E \sin\theta. \quad (5)$$

The parameter ξ is the dispersion of the angle caused by the width of slits. The values of ξ are estimated to be 0.125, 0.250, and 0.50° for the slits with the widths of 0.5, 1, and 2 mm, respectively, in the geometrical arrangement of the present work. The details of the estimation of ξ are given in Appendix 1. The first peak at $s \simeq 1.3 \text{Å}^{-1}$ for liquid CCl_4 becomes 5% higher than that without the slit correction, when the data were obtained at the scattering angle of $2\theta=6°$ and 0.5 mm slit systems with 150 mm separation were used.

Absorption Correction. The most important correction in energy-dispersive diffractometry is the absorption correction, because the linear absorption coefficient, μ, changes to a great extent with the energy of the X-rays. The values of $\mu(E)$ were experimentally determined from the measurements of the transmittance of the sample at $\theta=0°$ with the primary beam. The tube was operated at a few micro-amperes, after being stabilized well before the measurement. The observed values are shown in Fig. 5, together with the calculated ones. The calculation of $\mu(E)$ was performed according to the International Tables.[16] A good agreement was obtained except in the high-energy region and the low-energy region. In the former region, the calculated absorption coefficients are somewhat smaller than the observed ones, while in the latter region, the calculated absorption coefficients are larger. The observed absorption coefficients were used for the data analysis.

In the present work, the transmission geometry is adopted and the absorption factor $A_{coh}(E,\theta)$ is given simply by

$$A_{coh}(E,\theta) = \exp(-\mu(E) l \sec\theta), \quad (6)$$

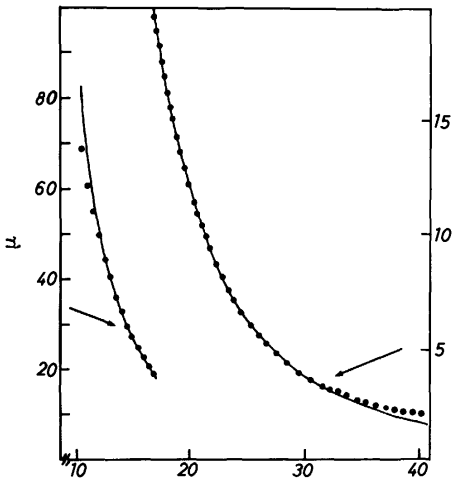

Fig. 5. The observed (dots) and calculated (solid curve) linear absorption coefficient, μ, of liquid CCl_4.

where l is the thickness of the sample.[2] The incoherent absorption factor $A_{inc}(E,E',\theta)$ is given by

$$A_{inc}(E,E',\theta) = \int_0^l \exp[-\mu(E)x\sec\theta - \mu(E')(l-x)\sec\theta]dx/l$$
$$= \frac{\exp(-\mu(E')l\sec\theta)}{l\mu(E)\sec\theta(1-\mu(E')/\mu(E))} \times [1-\exp\{-\mu(E)l\sec\theta(1-\mu(E')/\mu(E))\}], \quad (7)$$

if Compton scattering is assumed to occur with equal probability at any place inside the sample.

Egami proposed the reflection geometry as the optical system,[7] because the absorption factor $A(E,\theta)$ is proportional to $\mu(E)^{-1}$ in this arrangement. However, this is valid only when the incident beam is completely absorbed by the sample and when all the X-rays scattered at a particular angle from the sample are collected by the detector. In order to satisfy these conditions, it is necessary to use a wide detector slit on the side of the sample. This results in loss of angular resolution, which causes a serious error, as mentioned in the section of the slit correction. Moreover, the reflection geometry makes it difficult to measure scattering intensities at low angles.

Problems in the Scattering Process

Multiple Scattering. We have considered the kinematical double scattering, following the method by Warren and Mozzi,[17] who reported the correction for the double scattering of an amorphous sample in the case of reflection geometry and for the angle-dispersive method. We have calculated the effect of the double scattering for the transmission geometry and for the used region of the photon energy. The details are given in Appendix 2. In the case of the reflection method, Warren and Mozzi[17] and Egami[7] reported that the ratio of the double scattering intensity to the single scattering intensity amounts to 8% and 10%, respectively. However, in the case of transmission method, the maximum value of this ratio is 1.5%. This is because the sample is very thin (0.5 mm in the present experiment) in the transmission method. The energy-dependence of the ratio is rather small, but the ratio becomes larger as the scattering angle increases, as is shown in Appendix 2 (Fig. 13).

Compton Scattering. In the energy-dispersive method, the observed intensities are the sum of the intensities of incoherent scattering or Compton scattering and coherent scattering. The accumulated counts at a certain channel corresponding to the photon energy E contain the counts of incoherently scattered photons which have the incident energy E'. E' is larger than E by the Compton shift ΔE, which is given by

$$\Delta E = \frac{2E^2\sin^2\theta}{mc^2} \frac{1}{\left(1-\frac{2E}{mc^2}\sin^2\theta\right)}. \quad (8)$$

Since it is difficult to measure the incoherent scattering of the sample separately, we used the sum of

atomic incoherent scattering factors of the constituent atoms for the stoichiometric unit of the sample, denoted by I_{inc} multiplied by the recoil factor K, in the analysis. The atomic incoherent scattering factors are calculated by Cromer.[18] The Breit-Dirac recoil factor K is $(E/E')^2$ in the case of free electrons, and the ratio of the band width, $(dE'/dE)=(E'/E)^2$, cancels out the recoil factor, as pointed out by Egami[3] (see Eq. 9). However, for a system with bound electrons, the recoil factor is (E/E'),[19] and accordingly the product $K(dE'/dE)$ becomes (E'/E). Compton scattering has a profile with a width due to the momentum distribution of electrons, but it is permissible to neglect this width in the analysis.

Reduction to the Structure Function

After we measured the energy spectrum of X-rays from the sample, the structure function is obtained according to the following processes.

First the escape correction and the slit correction are performed. After these corrections, the observed spectrum $I_{obsd}(E,\theta)$ is expressed as

$$\begin{aligned} I_{obsd}(E,\theta) = k[&A_{coh}(E,\theta)P(E,\theta)I_p(E)I_{coh}(E,\theta) \\ &+ K(dE'/dE)A_{inc}(E,E',\theta)P(E',\theta)I_p(E')I_{inc}(E',\theta) \\ &+ A_{coh}(E,\theta)P(E,\theta)I_p(E)D(E,\theta)] \\ &+ A_{coh}(E,\theta)I_{back}(E,\theta) \end{aligned} \quad (9)$$

In Eq. 9, A is the absorption factor, P the polarization factor, I_{coh} and KI_{inc} are the coherent and incoherent scattering intensities of the sample, respectively. D is the double scattering intensity. I_{back} is the experimentally obtained background intensity, which includes the scattering from windows of the sample holder and that from air, and the intensity of parasitic scattering. $I_p(E)$ is the energy spectrum of the primary beam, obtained experimentally as mentioned in previous Chapter, including the attenuation due to the X-ray absorption by air and the detector efficiency. For I_p and I_{back} described in Eq. 9, the escape correction and the slit correction are already performed. The scale factor k normalizes the observed intensity to the absolute scale of the stoichiometric unit of the liquid. E' is the initial photon energy which is reduced to E after Compton scattering. The polarization factor, P, in Eq. 9 is given by

$$P(E,\theta) = (1+\cos^2 2\theta)/2 + (1-\cos^2 2\theta)\Pi(E)/2, \quad (10)$$

in terms of the polarization $\Pi(E)$, which has been determined experimentally as mentioned in the previous section.

Second, with the use of the absorption factor $A_{coh}(E,\theta)$ calculated by the use of the measured values of $\mu(E)$ and Eq. 6, the fourth term in Eq. 9 is subtracted easily. Dividing the remaining term by the factor $A_{coh}(E,\theta)P(E,\theta)I_p(E)$, we obtain the following quantity:

$$\begin{aligned} I'_{obsd}(E,\theta) = k\Big\{&I_{coh}(E,\theta) + \frac{(E'/E)A_{inc}(E,E',\theta)P(E',\theta)I_p(E')}{A_{coh}(E,\theta)P(E,\theta)I_p(E)} \\ &\times I_{inc}(E',\theta) + D(E,\theta)\Big\} \end{aligned} \quad (11)$$

The product $K(dE'/dE)$ has been replaced by (E'/E) as discussed in the preceding section. All the factors in the second term in Eq. 11 are known. The double scattering intensity, $D(E,\theta)$ has been estimated as described in Appendix 2.

Next, we should determine the scale factor k as in the following process. The total coherent intensity I_{coh} is composed of three terms; that is,

$$I_{coh}(E,\theta) = \sum_n f_n(s)^2 + i_1 + i_2 \quad (12)$$

where the first term is the self-scattering intensity from the constituent atoms, the second term i_1 represents the molecular term which is the result of the interference from each atom pair within a molecule, and the third term i_2 represents the interference from atom pairs between different molecules. Since the term i_2 in Eq. 12 vanishes at large s-values, I_{coh} is given by the first and second terms in Eq. 12. The scale factor k to normalize the experimental intensity to the absolute intensity is obtained by comparing the experimental intensity with the calculated absolute intensity, which is composed of I_{coh} and the second and third terms in Eq. 11. The scale factor k was easily obtained for the data at 2θ=28, 40, and 56°.

For the data which are obtained at smaller scattering angles, the approximation of $i_2 \simeq 0$ is not valid. Utilizing the values of $I_{coh}(s)$ obtained by the data at 2θ=28° for the overlapping s-region of 2θ=28° and the next lower angle 2θ=16°, we can calculate the absolute intensity for 2θ=16°, because $I_{coh}(E,\theta)$ is simply a function of s, and the second and the third terms of Eq. 11 are known. By comparing the calculated absolute intensity and $I'_{obsd}(E,2\theta=16°)$, the scale factor k for 2θ=16° is determined. This procedure is repeated for the data obtained at lower scattering angles, and both k and $I_{coh}(s)$ can be determined.

The obtained total coherent intensity $I_{coh}(s)$ for liquid CCl_4 at room temperature is shown in Fig. 6 by a solid curve, together with the calculated values of the self-scattering intensity from the individual atoms, *i.e.*, $\sum_n f_n(s)^2$ by broken curve. The weighted structure function, $si(s)$, is shown in Fig. 7, where $i(s)$

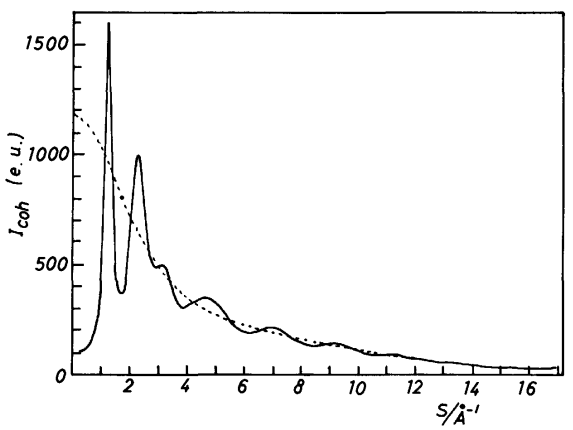

Fig. 6. The observed total coherent intensity $I_{coh}(s)$ for liquid CCl_4 (solid curve) and self-scattering intensity from the constituent atoms (broken curve).

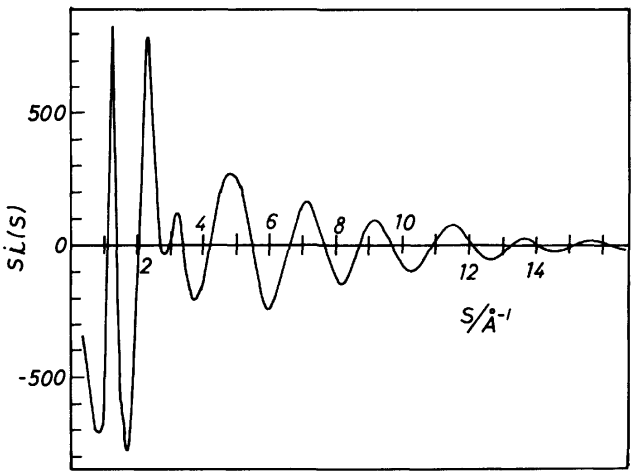

Fig. 7. Weighted structure function $si(s)$ for liquid CCl_4 at room temperature.

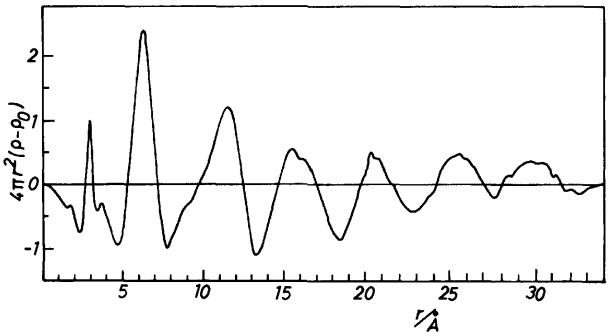

Fig. 8. The electronic distribution function of liquid CCl_4 containing the distribution of electron cloud, $4\pi r^2(\rho-\rho_0)$.

is the reduced intensity defined by

$$i(s) = I_{\text{coh}} - \sum_n f_n(s)^2 = i_1 + i_2. \quad (13)$$

The weighted structure function contains the information on the molecular structure and on the arrangement of molecules in the liquid.

The distribution function containing the distribution of electron cloud is shown in Fig. 8. It is defined by the Fourier transform of the weighted structure function, $si(s)$,

$$4\pi r^2(\rho-\rho_0) = \frac{2r}{\pi\sum_n Z_n^2}\int si(s)\sin sr ds, \quad (14)$$

where ρ_0 is the bulk number density of the liquid and Z_n is the atomic number of the n-th component atom.

Discussion

We have enumerated many factors which affect the accuracy of the intensity data obtained by the energy-dispersive method and taken them into account in the analysis. Whether or not the corrections have improved the experimental results is ascertained in the following two ways. First, we can check the consistency of the data in the same s-region which

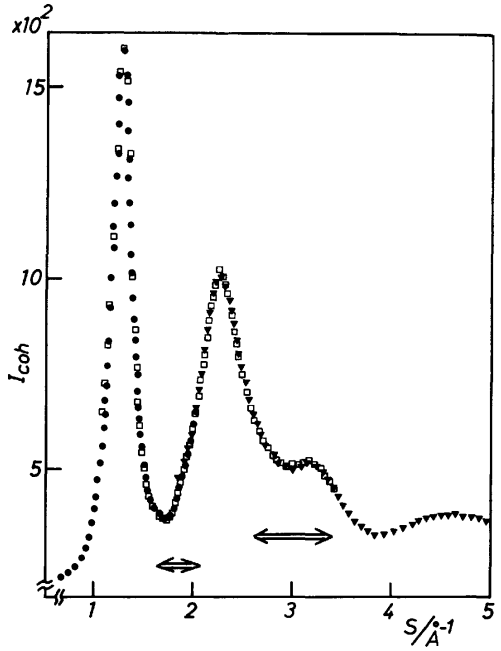

Fig. 9. The total coherent intensity for liquid CCl_4 to show the consistency of the data obtained by different angle-setting. The marks such as ●, □, and ▼ show the data obtained by the angle-setting at $2\theta = 6$, 10, and 16°, respectively. The arrows show the region used for determining the scale factor k.

are collected at different scattering angles and analyzed independently. This consistency is very good as is shown in Fig. 9, when the energy region ranging from 10 to 38 keV is used. In the energy region lower than 10 keV, the absorption by liquid is very strong, and the uncertainty of the observed transmittance becomes large. In the energy region higher than 38 keV, the uncertainty of the polarization of the primary beam becomes large. In the case of liquid CCl_4, the energy region of 10—38 keV is suitable to use for the measurement of scattering intensities.

Second, in order to evaluate the procedure of the present work, the intensity data obtained by the present experiment may be compared with data obtained by the angle-dispersive method. The diffraction intensity of this sample (liquid CCl_4) has been measured by several authors.[20-23] However, only Narten presented the numerical values of the intensity data in the table.[23] Our experiment has been carried out at room temperature and Narten reported the data at 20°C. So, our data obtained by energy-dispersive method have been compared with those of Narten in the form of the molecular structure function $H(s)$, where $H(s)$ is defined by

$$H(s) = i(s)/(\sum_n f_n(s))^2. \quad (15)$$

As is shown in Fig. 10, the present structure function is in fairly good agreement with the one by Narten[23] except for the small s-region. In Fig. 10, our data are shown by a solid curve and Narten's data by dots. A large difference is observed at the small s-region (s= 0—1.3 Å^{-1}). For the region of s less than 1 Å^{-1}, the values of $H(s)$ by Narten are too small, because for

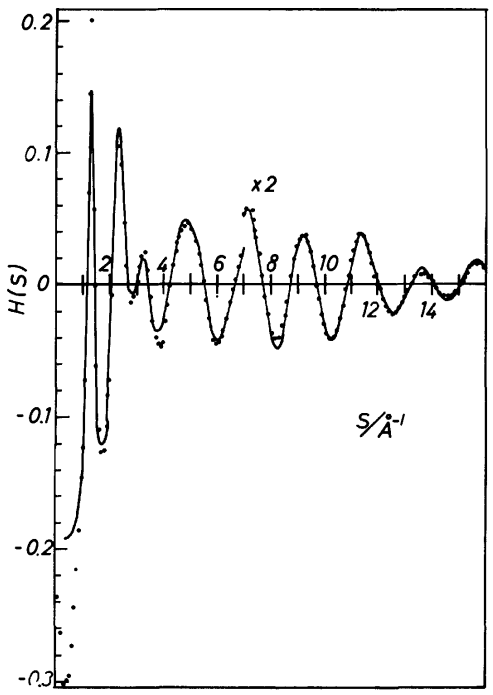

Fig. 10. The comparison of the structure function $H(s)$ of the present work and Narten's.[23] Solid curve is the present data and dots show Narten's.

liquid CCl_4 the structure function $H(s)$ can never be less than -0.217, even if the total coherent intensity I_{coh} were equal to zero at $s\simeq 0$ Å^{-1}. For the peak-height at $s\simeq 1.3$ Å^{-1}, Narten's value is much higher than our data. We can not understand why these discrepancies in $H(s)$ exist in the small s-region, because the total coherent intensity obtained by Narten[23] shows very good agreement with ours (Fig. 6) in the region $s\simeq 0$ Å^{-1} and also for the peak-height at $s\simeq 1.3$ Å^{-1}.

The results mentioned above seem to show the need of the corrections discussed in the present paper.

The diffraction intensity of liquid CCl_4 was also measured as the first sample when Murata and Nishikawa constructed an energy-dispersive diffractometer.[2] The main difference between the previous and the present data is the peak-height of the first peak at $s\simeq 1.3$ Å^{-1}. The first peak of the present data is much higher than that of the previous data, because in the previous analysis the slit correction was not made. In the data corrections which we have newly made, the effect of the slit correction is the largest. Especially for liquid CCl_4, whose diffraction pattern has a very sharp peak at small s-region, the divergence of the scattering angle in the experimental condition is very sensitive to the peak-height.

We believe that solutions have been given to the problems in the analysis of the diffraction data obtained by the energy-dispersive method. One of the remaining problems may be the anomalous dispersion. In the case of CCl_4, this effect is rather small in the energy range used in the experiment. However, this effect should be taken into account for samples containing heavier atoms.

By the revision and improvement of the analysis for the data obtained by the energy-dispersive method, the intensity data of liquid CCl_4 have been improved, but the structure model is unchanged. The model of the bcc local structure[24] has turned out to be still valid with better agreement between the observed and the simulated curves of the structure function. The discussion on the structure of liquid CCl_4 will be reported in detail in a succeeding paper.

The authors wish to express their thanks to Messrs. Masayoshi Hamano, Hiroshi Miyagi, and Yuzi Shimokawa of the machine shop of Gakushuin University for the construction of the vertical tube holder to measure the polarization of the primary beam. Their thanks are also due to Professor Hideki Morikawa of Tokyo Institute of Technology for offering the sample of silica glass. The present work is a continuation to the research project initiated by Professor Yoshitada Murata of the Institute for Solid State Physics, the University of Tokyo.

Appendix 1

Slit Correction. For middle or large angle scattering experiments, the widths of the slits which are ordinarily used have a smearing effect on the observed intensity data. It is also permissible to neglect the effect of the finite slit height. We describe the slit correction for the diffraction data which are smeared due to the width of the slits.

The experimental scattered intensity $\tilde{I}(E,\theta)$ for a scattering angle 2θ is related to the scattered intensity of the perfect collimation, $I(E,\theta)$, by the equation

$$\begin{aligned}\tilde{I}(E,\theta) &= \iiint I(E,\theta+\delta\theta)W(w,z,u)\mathrm{d}w\mathrm{d}z\mathrm{d}u \\ &\quad / \iiint W(w,z,u)\mathrm{d}w\mathrm{d}z\mathrm{d}u \\ &= \iiint [I(E,\theta)+I'(E,\theta)\delta\theta+\tfrac{1}{2}I''(E,\theta)\delta\theta^2] \\ &\quad \times W\mathrm{d}w\mathrm{d}z\mathrm{d}u / \iiint W\mathrm{d}w\mathrm{d}z\mathrm{d}u. \qquad \text{(A1.1)}\end{aligned}$$

where $W(w,z,u)$ is a weight function, the form of which depends on the collimation system. The parameters w, z, and u are the deviations of a path of X-rays from the central line (chained line in Fig. 11) in the collimator, on the side of the incident slit, on the sample and on the detector slit, respectively, as is shown in Fig. 11. The central lines

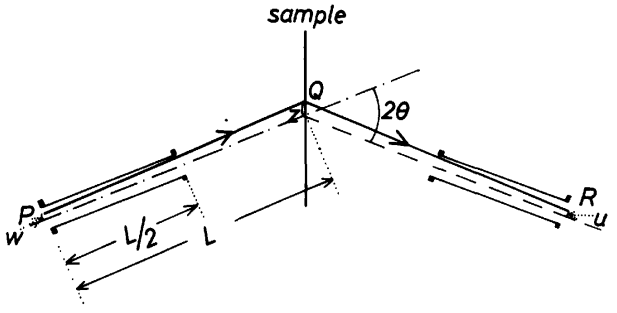

Fig. 11. Geometry of the slit system. We consider the angle dispersion for the X-rays which pass through P, Q and R.

determine the scattering angle 2θ. The notations I' and I'' show the first and second derivatives of the intensity I. In Eq. A1.1, the angular deviation $\delta\theta$ is a function of w, z, and u. Equation A1.1 is rewritten as

$$\tilde{I}(E,\theta) = I(E,\theta) + I'(E,\theta)\iiint \delta\theta W \mathrm{d}w\mathrm{d}z\mathrm{d}u \Big/ \iiint W \mathrm{d}w\mathrm{d}z\mathrm{d}u + \frac{1}{2}I''(E,\theta)\iiint \delta\theta^2 W \mathrm{d}w\mathrm{d}z\mathrm{d}u \Big/ \iiint W \mathrm{d}w\mathrm{d}z\mathrm{d}u \quad \text{(A1.2)}$$

The second term in Eq. A1.2 vanishes, because it is possible to assume that the function $(\delta\theta W)$ is an odd function of the parameters w, z, and u. Let us define the angle dispersion ξ by the following relation:

$$\xi = (\overline{\delta\theta^2})^{1/2} = \left[\iiint \delta\theta^2 W \mathrm{d}w\mathrm{d}z\mathrm{d}u \Big/ \iiint W \mathrm{d}w\mathrm{d}z\mathrm{d}u\right]^{1/2}. \quad \text{(A1.3)}$$

We have

$$\tilde{I}(E,\theta) = I(E,\theta) + \frac{1}{2}I''(E,\theta)\xi^2. \quad \text{(A1.4)}$$

On the other hand,

$$\tilde{I}(E,\theta+\xi) = \tilde{I}(E,\theta) + \tilde{I}'(E,\theta)\xi + \frac{1}{2}\tilde{I}''(E,\theta)\xi^2 \quad \text{(A1.5)}$$

$$\tilde{I}(E,\theta-\xi) = \tilde{I}(E,\theta) - \tilde{I}'(E,\theta)\xi + \frac{1}{2}\tilde{I}''(E,\theta)\xi^2 \quad \text{(A1.6)}$$

By the summation of Eq. A1.5 and Eq. A1.6, we obtain

$$\tilde{I}''(E,\theta)\xi^2 = \tilde{I}(E,\theta+\xi) + \tilde{I}(E,\theta-\xi) - 2\tilde{I}(E,\theta). \quad \text{(A1.7)}$$

Now, we make an appriximation,

$$\tilde{I}''(E,\theta) = I''(E,\theta), \quad \text{(A1.8)}$$

then we have

$$I(E,\theta) = 2\tilde{I}(E,\theta) - \frac{1}{2}[\tilde{I}(E,\theta+\xi) + \tilde{I}(E,\theta-\xi)], \quad \text{(A1.9)}$$

from Eq. A1.4 and Eq. A1.7. This equation corresponds to Eq. 4 in the text. With enough accuracy, we can approximate the intensity $\tilde{I}(E,\theta+\xi)$ by $\tilde{I}(E+\delta E,\theta)$, where the pair of parameters $E+\delta E$ and θ gives the same s-value as the pair of E and $\theta+\xi$.

The angle dispersion must be estimated for a particular optical geometry. Let us consider a path of X-rays which pass through the points P, Q, and R (see Fig. 11). Let the incident collimator be placed symmetrically to the detecting collimator. For low scattering angles, we have

$$\delta(2\theta) = (z-w)/L + (z-u)/L$$

or

$$\delta\theta = [2z-(w+u)]/2L \quad \text{(A1.10)}$$

where L is the distance between the slit on the side of the X-ray tube (or the detector) and the sample, and $\cos\theta$ is approximated by unity. For the gentle peaks obtained at large scattering angles, the angle dispersion causes little smearing effect. We consider the slit correction only for the case of low scattering angles. Let us derive the expressions of ξ for some optical systems.

Case 1: The incident beam is perfectly parallel and u is fixed to zero. In this case,

$$\delta\theta = z/2L$$
$$W(w,z,u)\mathrm{d}w\mathrm{d}z\mathrm{d}u = Q(z)\mathrm{d}z.$$

where $Q(z)$ is simply a constant for the slit system, and is given by

$$Q(z) = 1/2d. \quad \text{(A1.11)}$$

Accordingly,

$$\xi^2 = \int_{-d}^{d}\left(\frac{z}{2L}\right)^2\frac{1}{2d}\mathrm{d}z \Big/ \int_{-d}^{d}\left(\frac{1}{2d}\right)\mathrm{d}z = d^2/12L^2 \quad \text{(A1.12)}$$

Case 2: The incident beam is perfectly parallel and u is not fixed to zero. This case gives the following relations:

$$\delta\theta = (z-u)/2L$$
$$W(w,z,u)\mathrm{d}w\mathrm{d}z\mathrm{d}u = V(z,u)\mathrm{d}z\mathrm{d}u$$

where

$$\text{if } |z| \geq |u|, \quad \text{then } V(z,u) = Q(z)$$

and

$$\text{if } |z| < |u|, \quad \text{then } V(z,u) = Q(u).$$

Considering the symmetrical property of the beam around the central lines, we can omit the cross term of u and z, and we have

$$\begin{aligned}\xi^2 &= \iint\left(\frac{z-u}{2L}\right)^2 V(z,u)\mathrm{d}z\mathrm{d}u \Big/ \iint V(z,u)\mathrm{d}z\mathrm{d}u \\ &= \frac{1}{4L^2}\iint(z^2+u^2)V(z,u)\mathrm{d}z\mathrm{d}u \Big/ \iint V(z,u)\mathrm{d}z\mathrm{d}u \\ &= \frac{1}{4L^2}\left\{2\left[\int_{z=0}^{d}\int_{u=0}^{z}\left(\frac{z^2+u^2}{2d}\right)\mathrm{d}u\mathrm{d}z + \int_{u=0}^{d}\int_{z=0}^{u}\left(\frac{z^2+u^2}{2d}\right)\mathrm{d}z\mathrm{d}u\right]\right. \\ &\quad \left./2\left[\int_{z=0}^{d}\int_{u=0}^{z}\mathrm{d}uQ(z)\mathrm{d}z + \int_{u=0}^{d}\int_{z=0}^{u}\mathrm{d}zQ(u)\mathrm{d}u\right]\right\} \\ &= d^2/6L^2 \end{aligned} \quad \text{(A1.13)}$$

Case 3: Let the length of the collimator be L; namely, there is no separation between the collimators and the sample. In this case, we find

$$\delta\theta = [2z-(\omega+u)]/2L$$
$$W(w,z,u)\mathrm{d}w\mathrm{d}z\mathrm{d}u = Q(q)\mathrm{d}w\mathrm{d}z\mathrm{d}u$$

where q is the maximum among $|u|$, $|z|$, and $|w|$. By the same reason as in Case 2, the cross terms of w, z, and u vanish, and we obtain the following relation:

$$\begin{aligned}\xi^2 &= \iiint\left[\frac{2z-(w+u)}{2L}\right]^2 Q(q)\mathrm{d}w\mathrm{d}z\mathrm{d}u \Big/ \iiint Q(q)\mathrm{d}w\mathrm{d}z\mathrm{d}u \\ &= \frac{1}{4L^2}\iiint(4z^2+w^2+u^2)Q(q)\mathrm{d}w\mathrm{d}z\mathrm{d}u \\ &\quad \Big/ \iiint Q(q)\mathrm{d}w\mathrm{d}z\mathrm{d}u.\end{aligned}$$

The integration can be analytically performed to give

$$\xi^2 = d^2/2L^2 \quad \text{(A1.14)}$$

Case 4: In the optical geometry of the present work the length of the collimator is $L/2$. In this most realistic case,

$$\delta\theta = [2z-(w+u)]/2L$$
$$W(w,z,u)\mathrm{d}w\mathrm{d}u\mathrm{d}z = Q(q)\mathrm{d}w\mathrm{d}z\mathrm{d}u$$

where q is the maximum among $|w|$, $|w+z|/2$, $|u+z|/2$, and $|u|$. By the consideration of the symmetrical property of W, the region of the integration is reduced to

$$-d \leq w \leq d,$$
$$0 \leq u \leq d,$$

and

$$-3d \leq z \leq 2d.$$

TABLE 1. THE MEAN SQUARES OF ANGLE DISPERSION, ξ^2, FOR SLIT AND APERTURE SYSTEMS

L is the distance between the detector and the sample. The notations d and r refer to half of the slit width and the radius of the aperture, respectively.

	Slit	Aperture
Case 1	$d^2/12L^2$	$r^2/16L^2$
Case 2	$d^2/6L^2$	$2r^2/15L^2$
Case 3	$d^2/2L^2$	$5r^2/12L^2$
Case 4	$1.706\times d^2/L^2$	$1.404\times r^2/L^2$

In this case, we can not integrate Eq. A1.3 analytically. The result obtained by numerical integration is

$$\xi^2 = \iiint\left[\frac{2z-(w+u)}{2L}\right]^2 Q(q)\mathrm{d}w\mathrm{d}z\mathrm{d}u \Big/ \iiint Q(q)\mathrm{d}w\mathrm{d}z\mathrm{d}u = 1.706\times d^2/L^2 \quad \text{(A1.15)}$$

For the aperture systems with the radius r, the weight function becomes

$$Q_A(x) = 2\sqrt{r^2-x^2}/\pi r^2 \quad \text{(A1.16)}$$

in place of Eq. A1.11, and ξ^2 can be calculated by replacing $Q(x)$ by $Q_A(x)$. For comparison, the expressions of ξ^2 for both slit systems and aperture systems are listed in Table 1, for cases 1 to 4.

Appendix 2

Multiple scattering. The following calculation was made with reference to the work by Warren and Mozzi.[17] Let us consider the double scattering from the sample for the transmission geometry. The power of the primary beam is given by I_0S_0, where I_0 is the intensity of the primary beam per unit area and S_0 is the cross section area of the primary beam. Let n be the number density of the units of composition, and $J(2\theta)$ be the intensity of the single scattering per unit of composition for the scattering angle 2θ. Let $\mathrm{d}I_r$ be the intensity at distance r from the volume element $\mathrm{d}V_1$ due to the scattering of the primary beam by $\mathrm{d}V_1$, then

$$\mathrm{d}I_r = A_1P_1I_0\frac{e^4}{m^2c^4r^2}J(2\theta_1)nS_0\mathrm{d}t \quad \text{(A2.1)}$$

where A_1 is the absorption factor, P_1 the polarization factor and r is the distance between volume element $\mathrm{d}V_1$ and $\mathrm{d}V_2$. Let $\mathrm{d}I(2)$ be the intensity at the point of observation at distance R from the sample, due to the scattering of the intensity $\mathrm{d}I_r$ by the volume element $\mathrm{d}V_2$.

$$\mathrm{d}I(2) = A_2P_2\mathrm{d}I_r\frac{e^4}{m^2c^4R^2}J(2\theta_2)n\mathrm{d}V_2. \quad \text{(A2.2)}$$

Here, the volume element $\mathrm{d}V_2$ is given by

$$\mathrm{d}V_2 = r^2\cos\varepsilon\,\mathrm{d}\varepsilon\mathrm{d}\varphi\mathrm{d}r, \quad \text{(A2.3)}$$

(see Fig. 12 for the definitions of the angles θ, $2\theta_1$, $2\theta_2$, ε, and φ and of the distances t and r). By Eq. A2.1 for $\mathrm{d}I_r$, we have

$$\mathrm{d}I(2) = I_0S_0AP\left(\frac{e^4}{m^2c^4}\right)^2\frac{n^2}{R^2}J(2\theta_1)J(2\theta_2)\cos\varepsilon\,\mathrm{d}\varepsilon\mathrm{d}\varphi\mathrm{d}t\mathrm{d}r. \quad \text{(A2.4)}$$

The absorption factor A in Eq. A2.4 is given by

$$A = \exp(-\mu f(r))$$

where μ is the linear absorption coefficient and $f(r)$ is the path length of the X-ray beam in the sample and given by

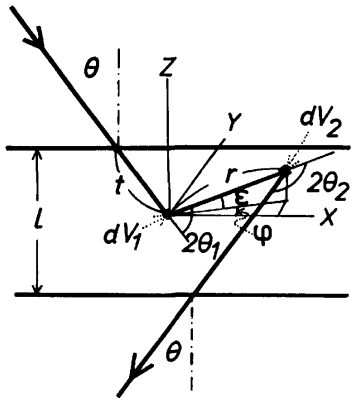

Fig. 12. Geometry of the double scattering process for the transmission method.

$$f(r) = r + l/\cos\theta + r\sin\varepsilon/\cos\theta \quad \text{(A2.5)}$$

where l is the thickness of the sample. The polarization factor P is given by

$$P = \cos^2 2\theta_1 + \cos^2 2\theta_2 + (\cos 2\theta_1\cos 2\theta_2 - \cos 2\theta)^2/2. \quad \text{(A2.6)}$$

The polarization of the primary beam is neglected, because it is small in the energy region we used. The double scattering $I(2)$ is given by the integration of Eq. A2.4 by the parameters t, r, ε, and φ.

First let us consider the integration by the parameters t and r. In the integrand in Eq. A2.4 only the absorption factor A is a function of the parameters t and r. We define A' by

$$A' = \iint \exp(-\mu f(r))\mathrm{d}r\mathrm{d}t.$$

The region of the integration by r for the case of forward scattering ($\varepsilon\leq 0$) is different from that for back scattering ($\varepsilon>0$). For the former, r goes from 0 to $(l-t\cos\theta)/(-\sin\varepsilon)$ and for the latter, r goes from 0 to $t\cos\theta/\sin\varepsilon$. The region of the integration for t is the same for the two cases and becomes from 0 to $l\sec\theta$. For the forward scattering, we obtain

$$A' = \int_{t=0}^{l\sec\theta}\int_{r=0}^{\frac{-l+t\cos\theta}{\sin\varepsilon}} \exp\{-\mu f(r)\}\mathrm{d}r\mathrm{d}t = \exp(-\mu l\sec\theta)\left[\frac{\cos\theta\cdot\sin\varepsilon}{\mu^2(\cos\theta+\sin\varepsilon)^2} \times\{1-\exp[\mu l(\sec\theta+\operatorname{cosec}\varepsilon)]\}+\frac{l}{\mu(\cos\theta+\sin\varepsilon)}\right] \quad \text{(A2.7)}$$

For the back scattering, we have

$$A'' = \int_{t=0}^{l\sec\theta}\int_{r=0}^{\frac{t\cos\theta}{\sin\varepsilon}} \exp\{-\mu f(r)\}\mathrm{d}r\mathrm{d}t = \exp(-\mu l\sec\theta)\left[\frac{\cos\theta\sin\varepsilon}{\mu^2(\cos\theta+\sin\varepsilon)^2} \times\{\exp[-\mu l(\sec\theta+\operatorname{cosec}\varepsilon)]-1\}+\frac{l}{\mu(\cos\theta+\sin\varepsilon)}\right] \quad \text{(A2.8)}$$

Next, we relate the scattering angles $2\theta_1$ and $2\theta_2$ to the angles θ, ε, and φ. By a simple calculation, we obtain

$$\cos 2\theta_1 = \cos\varepsilon\cos\varphi\sin\theta - \sin\varepsilon\cos\theta$$

and

$$\cos 2\theta_2 = -\cos\varepsilon\cos\varphi\sin\theta - \sin\varepsilon\cos\theta. \quad \text{(A2.9)}$$

We have

$$I(2) = I_0 S_0 \left(\frac{e^4}{m^2c^4}\right)^2 \frac{n^2}{R^2} \times \left[\int_{\varphi=-\pi}^{\pi}\int_{\varepsilon=-\frac{\pi}{2}}^{0} A'\cdot P\cdot J(2\theta_1)J(2\theta_2)\cos\varepsilon\, d\varepsilon d\varphi + \int_{\varphi=-\pi}^{\pi}\int_{\varepsilon=0}^{\frac{\pi}{2}} A''\cdot P\cdot J(2\theta_1)J(2\theta_2)\cos\varepsilon\, d\varepsilon d\varphi\right]$$
$$= I_0 S_0 \left(\frac{e^4}{m^2c^4}\right)^2 \frac{n^2}{R^2} \times 2\left[\int_{\varphi=0}^{\pi}\int_{\varepsilon=\frac{\pi}{2}}^{0} A'\cdot P\cdot J(2\theta_1)J(2\theta_2)\cos\varepsilon\, d\varepsilon d\varphi + \int_{\varphi=0}^{\pi}\int_{\varepsilon=0}^{\frac{\pi}{2}} A''\cdot P\cdot J(2\theta_1)J(2\theta_2)\cos\varepsilon\, d\varepsilon d\varphi\right] \quad \text{(A2.10)}$$

On the other hand, the corresponding intensity of the single scattering is given by

$$I(1) = I_0\left(\frac{e^4}{m^2c^4}\right)\frac{nl\sec\theta S_0}{R^2}\left(\frac{1+\cos^2\theta}{2}\right)J(2\theta)\exp(-\mu l\sec\theta) \quad \text{(A2.11)}$$

The double scattering ratio to the single scattering is $I(2)/I(1)$ and is calculated by Eq. A2.10 and A2.11. In the calculation of Eq. A2.10, numerical integration is made for the parameters ε and φ. The intensity $J(2\theta)$ (and $J(2\theta_1)$, $J(2\theta_2)$) is approximated by

$$J(2\theta) = \sum_n f_n(E,\theta)^2 + I_{inc}(E,\theta). \quad \text{(A.12)}$$

This approximation is good enough because the double scattering is averaged over all directions and shows a smooth change for the scattering parameter s.

For each energy used for the experiment, we have calculated the ratio of the double scattering intensity to the single scattering intensity. The result is shown in Fig. 13 for the scattering angles 2θ=2.5, 28, and 55°. The double scattering intensity $D(E,\theta)$ in the text is estimated by $(I(2)/I(1))\,J(2\theta)$.

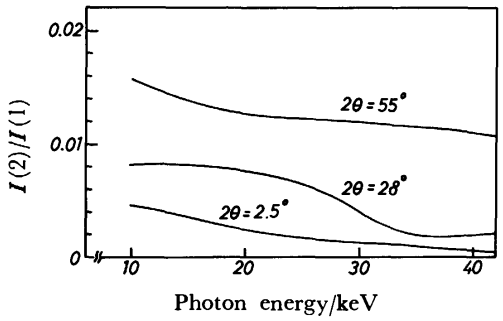

Fig. 13. The double scattering ratios to the single scattering *vs.* photon energies. The ratios are shown for the scattering angles 2θ=2.5, 28, and 55°.

References

1) B. C. Giessen and G. E. Gordon, *Science*, **159**, 973 (1968).
2) Y. Murata and K. Nishikawa, *Bull. Chem. Soc. Jpn .*, **51**, 411 (1978).
3) T. Egami, *J. Mater. Sci .*, **13**, 2587 (1978).
4) T. Egami, *J. Appl. Phys .*, **50**, 1564 (1979).
5) J. M. Prober and J. M. Schultz, *J. Appl. Crystallogr .*, **8**, 405 (1975).
6) T. Iijima and T. Mitsuhashi, "X-ray Instrumentation for Photon Factory," ed by Hosoya, KTK Publishing Co., Tokyo (in press).
7) T. Egami, *Topics in applied Physics* , **46**, 25 (1981).
8) K. Nishikawa and N. Kitagawa, *Bull. Chem. Soc. Jpn .*, **53**, 2804 (1980).
9) J. A. Bearden, *Rev. Mod. Phys.*, **39**, 78 (1967).
10) J. H. Hubbell, Wm. J. Veigele, E. A. Briggs, R. T. Brown, D. T. Cromer, and R. J. Howerton, *J. Phys. Chem. Ref. Data.*, **4**, 471 (1975).
11) A. H. Compton and S. K. Allison, "X-rays in Theory and Experiment," D. Van Nostrand Company, Toronto (1949).
12) J. S. Olsen, B. Buras, and T. Jensen, *Acta Crystallogr .*, **A34**, 84 (1978).
13) T. Fukamachi, S. Togawa, and S. Hosoya, *J. Appl. Crystallogr.*, **6**, 297 (1973).
14) T. Mitsuhashi, J. Nagao, and T. Iijima, Annual Meeting of the Crystallographic Society of Japan, Tokyo (1982).
15) O. Kratky, G. Porod, and Z. Skala, *Acta Phys. Austriaca*, **13**, 76 (1960).
16) "International Tables for X-ray Crystallography," Vol III, Kynoch Press, Birmingham (1962).
17) B. E. Warren and R. L. Mozzi, *Acta Crystallogr.*, **21**, 459 (1966).
18) D. T. Cromer, *J. Chem. Phys.*, **50**, 4857 (1967).
19) R. A. Bonham, *Phys. Rev.*, **A23**, 2950 (1981).
20) R. U. Gruebel and G. T. Clayton, *J. Chem. Phys.*, **46**, 639 (1967).
21) A. H. Narten, M. D. Danford, and H. A. Levy, *J. Chem. Phys.*, **46**, 4875 (1967).
22) G. Reichelt, J. U. Weidner, and W. Zimmermann, *Ber. Bunsenges. Phys. Chem.*, **78**, 1050 (1974).
23) A. H. Narten, *J. Chem. Phys.*, **65**, 573 (1976).
24) K. Nishikawa and Y. Murata, *Bull. Chem. Soc. Jpn.*, **52**, 293 (1979).

Electron Spin Distributions and g-Value Shifts in the Novel Electron Donors with 1,3-Dithiole Rings

Atsushi TERAHARA,* Hiroaki OHYA-NISHIGUCHI, Noboru HIROTA, Hiroshi AWAJI,† Tokuzo KAWASE,† Shigeo YONEDA,† Toyonari SUGIMOTO,† and Zen-ichi YOSHIDA†

Department of Chemistry, Faculty of Science, Kyoto University, Kyoto 606

†*Department of Synthetic Chemistry, Faculty of Engineering, Kyoto University, Kyoto 606*

(Received December 22, 1983)

The ESR spectra of the cation radicals of TTF and its related compounds in which two 1,3-dithiole rings are connected by conjugated carbon and cumulene chains are measured. The spin distributions obtained from the *hfcc* due to the protons and sulfur atoms agree well with the results of the MINDO/3 calculations. The spin densities on the sulfur and central carbon atoms decreases as the central chain length increases. A linear relationship, $g=2.00379+0.00108\ a(S)$, between the *g*-values and the sulfur *hfcc* is noted and explained in terms of the Stone's theory. The *g*-values of the cation radicals with cumulene chains deviate from this relation and a possible cause is suggested.

The cation radical states of π electron donors play essential roles in making the organic metals such as tetrathiafuluvalene-tetracyanoquinodimethan(TTF-TCNQ) highly conductive[1] or in producing superconductivity in the salts of tetramethyltetraselenafuluvalene $(TMTSF)_2^{+\cdot}X^-(X^-=PF_6^-, ClO_4)$.[2] In order to understand the electronic band structures and the conduction mechanisms of these salts, it is desirable to know the details of the wave function and the orbital energies of the highest occupied molecular orbitals (HOMO). Electron spin resonance (ESR) and cyclic voltammetry measurements can provide information about them.

We have synthesized the compounds **2** to **5** shown in Fig. 1 in order to find electron donors better than TTF (**1**) and investigated their properties with various experimental techniques.[3] From the cyclic voltammetry measurements it was found that all these compounds have oxidation potentials ($E_{1/2}^{ox}$) lower than TTF and that they can be novel electron donors. Here we have studied the cation radicals of these compounds by ESR and examined the results in comparison with those predicted by the MINDO/3 calculation.

In this paper we first describe the results of the ESR investigation on the cation radicals of these compounds **1** to **5** in solution. From the hyperfine coupling constants (*hfcc*) of protons and sulfur atoms (^{33}S isotopes), the spin density distributions of the HOMO are determined in detail. The ESR spectra of the cation radicals of the several derivatives of **1**—**5** shown in Fig. 1 are also studied to examine the effects of substitution on the spin distributions.

Secondly, we compare the spin distributions obtained by ESR measurements with those calculated by the MINDO/3 method. We discuss how the HOMO changes as the central carbon chain in TTF becomes longer with conjugated or cumulene groups. In the case of **3**, there is an ambiguity whether the structure is *cis*- or *trans*-conformer. We investigated the compounds **6** and **7** shown in Fig. 1 in order to answer this question.

Finally, we discuss the relationship between the *g*-values and the sulfur *hfcc* noted for a series of compounds **1** to **3** using the Stone's theory. The *g*-values of **4** and **5**, however, deviate from this relationship. The origin of this deviation is discussed.

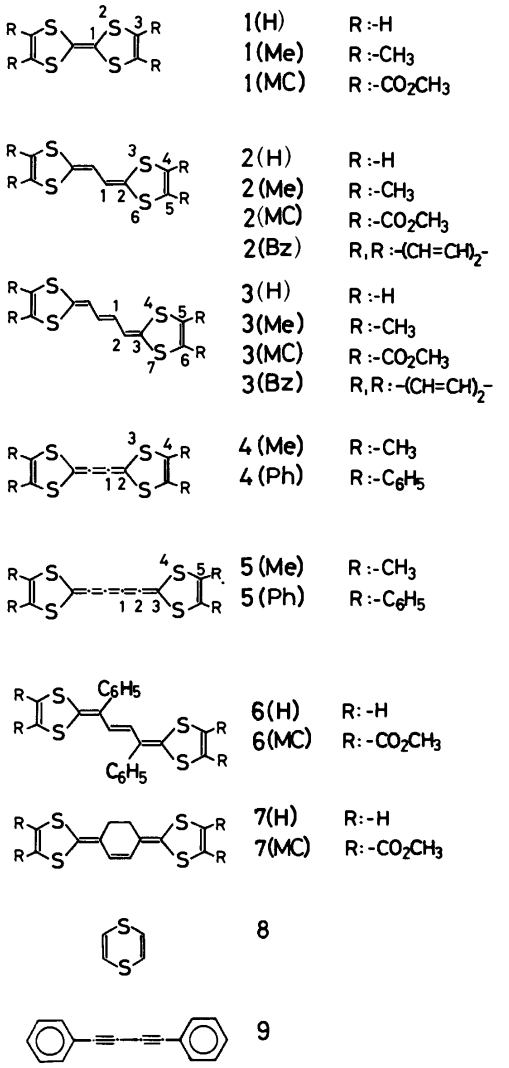

Fig. 1. Molecular structures investigated. The numbers distinguish the π-system and its derivatives are denoted by their abbreviations in last parenthes.

Experimental

The synthesis of the compounds **2**, **3**, and their derivatives was described elsewhere.[3] The series of compounds with cumulene skeletons are very unstable in the neutral states and we have not yet succeeded in synthesis. However the dication states of their tetramethyl and tetraphenyl derivatives are stable enough to be obtained in the form of perchlorate salts $\mathbf{4}^{2+}$ $2ClO_4^-$ and $\mathbf{5}^{2+}$ $2ClO_4^-$.[4] The generation of the cation radicals and the ESR measurements were carried out by using an electrochemical ESR system based on a JEOL-FE3X spectrometer.[5] The cation radicals of **1**, **2**, and **3** were generated by one-electron oxidation, while those of **4** and **5** were obtained by one-electron reduction of corresponding dications. Dry dichloromethane of spectroscopic grade was used as the solvent and tetrabutylammonium tetrafluoroborate was used as the supporting electrolyte. Potassiumn nitrosilbis(sulfate) was used as a standard sample for calibration of the magnetic field, the accuracy being within ±0.005 G†. *g*-Values were measured in reference to the signal of Cr(III) diluted in MgO (g=1.9800), the accuracy being within ±0.0001.

Results and Discussion

The ESR Spectra of $\mathbf{1}^{+\cdot}$, $\mathbf{2}^{+\cdot}$, *and* $\mathbf{3}^{+\cdot}$. The cation radicals of **1**(H), **2**(H), and their derivatives are stable but that of **3**(H) is a little unstable when it is oxidized at room temperature. The ESR spectra of these compounds do not change over the entire range of the temperature from −80 °C to room temperature. The proton *hfcc* and *g*-values of the cation radicals of **1**(H) and **1**(Me) are very close to those reported previously.[6] The ESR spectra of compounds $\mathbf{2}(H)^{+\cdot}$ and $\mathbf{3}(H)^{+\cdot}$ are shown in Figs. 2a and 3a, respectively, as examples. All of these ESR spectra have the linewidths of about 0.2 G and are easily analyzed and reconstructed by computer simulation (Figs. 2b and 3b).

The *hfcc* due to the isotopic sulfur atoms, ^{33}S (I=3/2) were observed as satellite lines in some cases. Especially, in the case of tetrakis (methoxycarbonyl) derivatives of $\mathbf{2}(MC)^{+\cdot}$ and $\mathbf{3}(MC)^{+\cdot}$, it was easy to observe the ^{33}S satellites because of the simplification of the ESR spectra by methoxycarbonyl substitution. As a typical example, the satellite lines of $\mathbf{2}(MC)^{+\cdot}$ are shown in Fig. 4. Two kinds of ^{33}S satellites are expected for **2** and **3** from the molecular symmetries, but only one is expected in **1** because four sulfur atoms are equivalent. Two kinds of ^{33}S satellites were observed for most of **2** and **3** as expected. In the spectrum of $\mathbf{2}(H)^{+\cdot}$, however, only one ^{33}S satellite (3.98 G) was resolved because the ^{33}S satellite due to the *hfcc* smaller than 3.98 G overlapps with the other lines.

In Table 1 are listed the obtained *g*-values and the *hfcc* of the protons and ^{33}S. The assignment of the

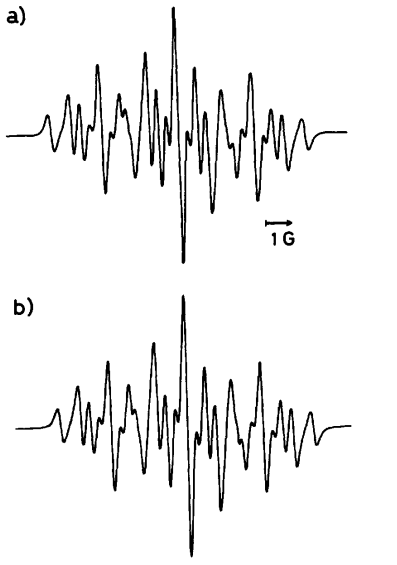

Fig. 2. The observed (a) and simulated (b) ESR spectra of $\mathbf{2}(H)^{+\cdot}$.

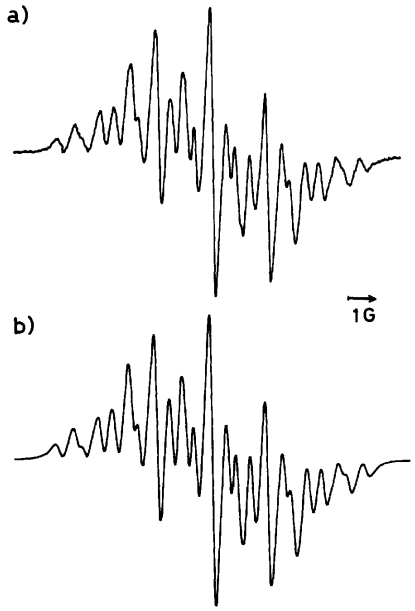

Fig. 3. The observed (a) and simulated (b) ESR spectra of $\mathbf{3}(H)^{+\cdot}$.

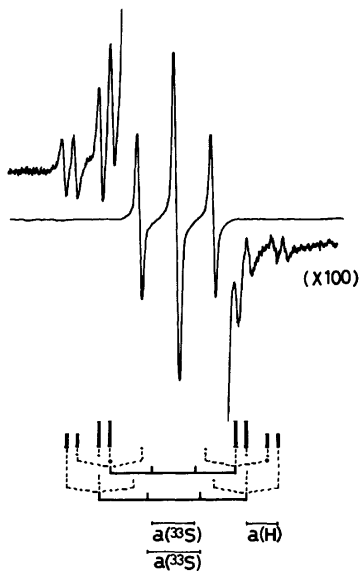

Fig. 4. The main splitting and ^{33}S satellite lines observed for $\mathbf{2}(MC)^{-\cdot}$; the analysis of the satellite lines indicated lower.

† 1 G=10^{-4} T.

hfcc due to protons and ^{33}S is based on the results of MINDO/3 calculation. Comparing the *hfcc* due to the central protons and the ^{33}S and the *g*-values of derivatives with those of the parent compounds, it is found that there is no substantial effect of substitution by tetramethyl, tetrakis(methoxycarbonyl), and dibenzo groups on the spin distribution. This is because the spin densities on the carbon atoms attached by substituent groups are relatively small. It is also noticeable that both the *g*-values and ^{33}S *hfcc* decrease in the order of **1**, **2**, and **3**. The same trend holds for the *hfcc* of the side protons and the central protons in **2** and **3**.

The ESR Spectra of $4^{+\cdot}$ *and* $5^{+\cdot}$. **4**(Me)$^{+\cdot}$ and **5**(Me)$^{+\cdot}$ are stable when they are generated by one-electron reduction at the temperature below −40 °C. The ESR spectrum of **4**(Me)$^{+\cdot}$ shown in Fig. 5a indicates a clear splitting of 0.69 G due to the twelve methyl protons, while in the spectrum of **5**(Me)$^{+\cdot}$ shown in Fig. 5b only a sign of about 0.5 G splitting due to the methyl protons is observed. The satellite ^{33}S splittings of **4**(Me)$^{+\cdot}$ and **5**(ph)$^{+\cdot}$ were observed but that of **5**(Me)$^{+\cdot}$ was not observed because of low intensity of the ESR signal. The four sulfur atoms are all equivalent in **4** and **5**.

Comparing the *hfcc* due to the methyl protons of **4**(Me)$^{+\cdot}$ and **5**(Me)$^{+\cdot}$ and the *hfcc* due to ^{33}S of **4**(Me)$^{+\cdot}$ and **5**(Ph)$^{+\cdot}$ with those of **1**(Me)$^{+\cdot}$, it is seen that the *hfcc* also decrease in the order of **1**, **4**, and **5**, as observed in the series of **2** and **3**. On the other hand, the *g*-value does not follow the same order. This point will be discussed later in detail.

Comparison with MO Calculation. We calculated the spin density distributions of these compounds using the MINDO/3 method which is capable of handling sulfur atoms.[7] The atomic coordinates of **1** were taken from the crystallographic data of **1**(H)[8] and those of the other compounds **2** to **5** were obtained based on the structure of **1** by using the bond lengths and bond angles adopted widely. For the methyl derivatives we carried out the calculation by fixing configurations of the methyl groups.

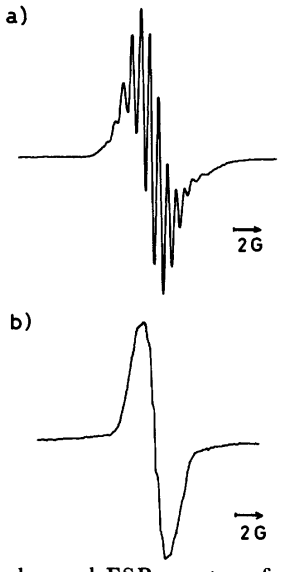

Fig. 5. The observed ESR spectra of **4**(Me)$^{+\cdot}$ (a) and **5**(Me)$^{+\cdot}$ (b).

The *hfcc* of the protons and ^{33}S obtained by the ESR study are compared with those estimated from the spin densities calculated by MINDO/3 method by using the following equations;

$$a(\mathrm{H}) = -24.0 \cdot \rho(C) \quad \text{for aromatic protons,} \tag{1}$$

$$a(\mathrm{Me}) = 507 \cdot \rho(H) \quad \text{for methyl protons,} \tag{2}$$

$$a(^{33}\mathrm{S}) = 33.0 \cdot \rho(S) \quad \text{for } ^{33}S, \tag{3}$$

here $\rho(C)$ is the $2p\pi$ spin densities on the carbon atoms attached by the aromatic protons. For methyl protons a(Me) are obtained from the averaged spin densities on the 1*s* orbitals of three methyl protons $\rho(H)$ by Eq. (2). The ^{33}S *hfcc* is estimated from the spin densities of $3p\pi$ of sulfur atoms $\rho(S)$ by using Eq. (3) proposed previousely.[9]

The calculated *hfcc* are also listed in Table 1. The correlation between the observed and calculated *hfcc* is shown in Fig. 6. From this figure it is seen that the agreement between the observed and calculated *hfcc* is satisfactory. We also note that there is a fair linear relationship between the calculated energy of the HOMO and the $E_{1/2}^{\circ}$ measured by the cyclic voltammetry as shown in Fig. 7. Based on these results it is concluded that the HOMO calculated by the MINDO/3 method represents the actual orbital quite well.

The trend that the *hfcc* of ^{33}S and protons decrease in the order of **1**, **2**, and **3** is reproduced by this calculation. This trend is seen clearly from Fig. 8, which indicates the HOMO schematically. It is also seen from this picture that the spin is localized on the four sulfur atoms and central conjugated carbon chains. In the compounds with cumulene chains the situation is similar (Fig. 8), though the spin densities on the cumulene chains are slightly different from those on the normal conjugated chains.

The Structure of **3**. There are two possibilities for the structure of **3**, namely, *trans* and *cis* conformers. According to the chromatographic study, there is only one species for **3**. We tried to determine the structure of **3** by comparing the NMR and UV spectra of **3** with those of **6** and **7**, which are regarded as the rigid model compounds for the *trans* and *cis* forms of **3**, respectively. However, this attempt was in failure because there were no significant differences in the spectra between **6** and **7**. Then we compared the ESR parameters. It is also interesting to examine whether the spin density distribution changes by conformational change of *cis* and *trans* form, since the spin distribution in stilbene is known to depend on the conformation.[10]

The *hfcc* of both the central and side protons listed in Table 2 are almost the same for *trans* **6**(H)$^{+\cdot}$ and *cis* **7**(H)$^{+\cdot}$ (the difference between the two groups of the side protons was not seen in spectra). However the *g*-value of **6**(H)$^{+\cdot}$ is larger than that of **7**(H)$^{+\cdot}$ by 0.0004, which agree with the difference between **6**-(MC)$^{+\cdot}$ and **7**(MC)$^{+\cdot}$. The *g*-value of **3**(H)$^{+\cdot}$ is very close to that of **6**(H)$^{+\cdot}$. Therefore, **3**(H)$^{+\cdot}$ is likely to be the *trans* form.

The Relationship Between The g-values and The ^{33}S

hfcc. As was described before, both the *g*-value and ^{33}S *hfcc* of the compounds **1**, **2**, and **3** decrease in the order of **1**, **2**, and **3**. Figure 9 shows the plots of the *g*-value *vs.* ^{33}S *hfcc* for all the compounds containing only C, H, and S atoms for which the ^{33}S splittings was observed in this study. The solid straight line obtained by a least square fit to the experimental points of five compounds is expressed by

$$g = 2.00379 + 0.00108 \cdot a(^{33}S) \quad (4)$$

The above relationship indicates that there is a linear

Table 1. The ESR parameters obtained in this study for the compounds **1** to **5** with the *hfcc* calculated by MINDO/3 method

Compound	$E_{1/2}°$/v	*g*-value	*hfcc*/G Obsd		Calcd	
1(H)	0.32	2.0084	1.26	(4H)	−0.99	(3)
			4.27	(^{33}S)	4.18	(2)
1(Me)	0.25	2.0081	0.78	(12H)	0.53	(3)
			3.99	(^{33}S)	4.06	(2)
1(Mc)	—	2.0081	4.52	(^{33}S)	—	
2(H)	0.24	2.0081	3.13	(2H)	−3.24	(1)
			1.23	(2H)	−0.78	(4)
			0.82	(2H)	−0.78	(5)
			3.98	(^{33}S)	3.62	(6)
					2.96	(3)
2(Me)	0.10	2.0072	2.90	(2H)	−3.10	(1)
			0.84	(6H)	0.42	(4)
			0.38	(6H)	0.36	(5)
				(^{33}S)	3.55	(6)
				(^{33}S)	2.91	(3)
2(Mc)	—	2.0080	2.93	(2H)		
			4.89	(^{33}S)		
			4.26	(^{33}S)		
2(Bz)	—	2.0076	2.92	(2H)	−3.13	(1)
			0.50	(2H)	−0.32	(8)
			0.28	(2H)	−0.26	(9)
			0.24	(4H)	−0.09	(10)
					−0.05	(7)
			4.07	(^{33}S)	3.59	(6)
			3.03	(^{33}S)	2.71	(3)
3(H)	0.26	2.0072	2.14	(4H)	−2.65	(2)
					−2.45	(1)
			0.99	(2H)	−0.57	(5)
			0.63	(2H)	−0.51	(6)
				(^{33}S)	2.81	(7)
				(^{33}S)	2.27	(4)
3(Me)	0.14	2.0070	2.32	(2H)	−2.56	(2)
			1.99	(2H)	−2.45	(1)
			0.99	(6H)	0.30	(5)
			0.33	(6H)	0.26	(6)
				(^{33}S)	2.80	(7)
				(^{33}S)	2.27	(4)
3(MC)	—	2.0072	2.21	(2H)		
			2.70	(^{33}S)		
3(Bz)	—	2.0067	2.10	(4H)		
4(Me)	0.09	2.0087	0.69	(12H)	0.40	(4)
			3.93	(^{33}S)	3.16	(3)
4(Ph)	—	2.0085	—		—	
5(Me)	−0.12	2.0066	0.5	(12H)	0.15	(5)
				(^{33}S)	3.16	(5)
5(Ph)	—	2.0053	3.69	(^{33}S)	—	

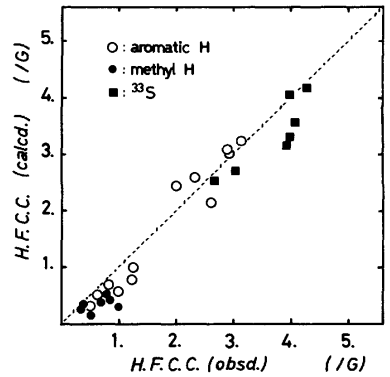

Fig. 6. The correlation between observed *hfcc* and calculated ones by MINDO/3 method for both protons and ^{33}S.

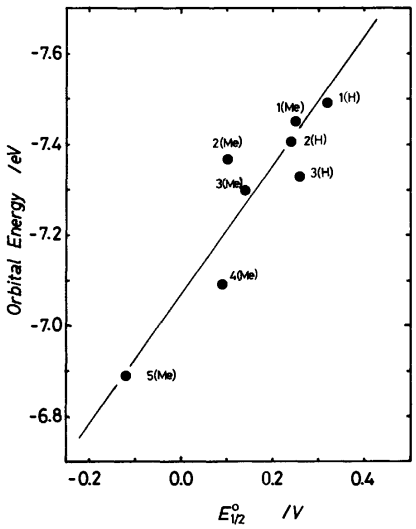

Fig. 7. The correlation between oxidation potentials ($E_{1/2}$) and calculated orbital energies of HOMO.

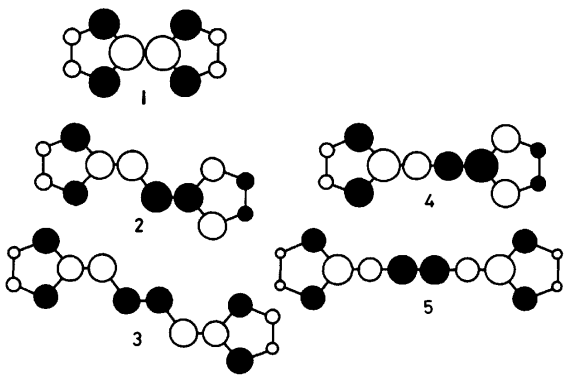

Fig. 8. Schematic view of the HOMO, the area of circle corresponds to the spin density and open circle indicates the positive sign of the coefficient of HOMO.

Table 2. The observed ESR parameters for **3**(H)$^{+\cdot}$, **6**(H)$^{+\cdot}$, **7**(H)$^{+\cdot}$, and their tetrakis(methoxycarbonyl) derivatives

	g-value	*hfcc*/G			*g*-value	*hfcc*/G	
3(H)	2.0072	2.14	(4H)	**3**(MC)	2.0072	2.21	(2H)
						1.78	(2H)
		0.99	(2H)				
		0.63	(2H)				
						3.19	(^{33}S)
						2.70	(^{33}S)
6(H)	2.0072	1.91	(2H)	**6**(MC)	2.0070	2.04	(2H)
		0.92	(4H)				
		2.66	(^{33}S)			2.96	(^{33}S)
						2.59	(^{33}S)
7(H)	2.0068	1.89	(6H)	**7**(MC)	2.0066	2.03	(2H)
						1.67	(4H)
		0.86	(4H)				
						2.89	(^{33}S)
						2.52	(^{33}S)

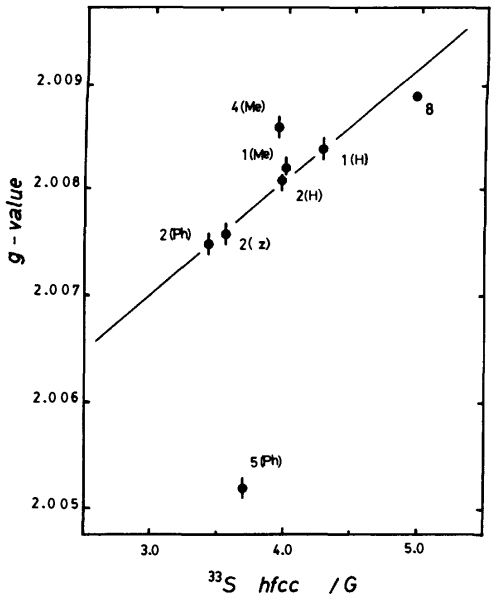

Fig. 9. The correlation between *g*-values and ^{33}S *hfcc* observed for the compounds containing only C, H, and S atoms. The solid line is a least square fitting line of Eq. (4) for five compounds without cumulene chain.

relation between the *g*-values and the π spin densities on the sulfur atoms. This means that the variation of the spin density on the sulfur atoms is the main cause of the *g* shift. In the following, we discuss this correlation by using the Stone's theory.[11]

One of the principal components of the *g* tensor can be derived by using the second order perturbation theory as

$$g^{\alpha\alpha} = g_e - 2\Sigma_n \frac{\langle \Psi_0 | \Sigma_\mu \zeta_\mu l_{\alpha\mu} | \Psi_n \rangle \langle \Psi_n | \Sigma_\nu l_{\alpha\nu} | \Psi_0 \rangle}{E_n - E_0}, \quad (5)$$

where the notations in Eq. 5 have usual meanings.[12] Stone[11] has shown that the deviation of *g*-value from the free electron *g*-value $\Delta g = g - g_e$ for the radicals of

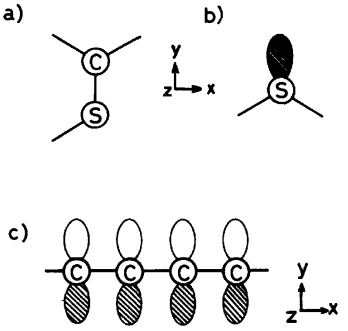

Fig. 10. The local axes for a) C-S bond, b) non-bonding orbital on sulfur atom, and c) cumulene or acetylene carbon chain. π orbital is along to z axis.

conjugated aromatic hydrocarbons can be expressed by the sum of the contributions from the σ-orbitals localized on C-C and C-H fragments. We formulate the contributions to Δg from the C-S fragment and nonbonding orbital on the sulfur atom in a similar way.

We first consider the contribution from the C-S bond. If the local axes are chosen as shown in Fig. 10a, bonding and antibonding orbitals of the C-S bond, $\psi(\sigma)$ and $\psi(\sigma^*)$, with the energy of E_σ and E_{σ^*}, respectively, can be written by linear combinations of two sp^2 orbitals belonging to the C and S atoms as

$$\psi(\sigma) = c_1\{\sqrt{1/3}\, S(\mathrm{C}) - \sqrt{2/3}\, P_y(\mathrm{C})\} + c_2\{\sqrt{1/3}\, S(\mathrm{S}) + \sqrt{2/3}\, P_y(\mathrm{S})\} \quad (6)$$

$$\psi(\sigma^*) = c_2\{\sqrt{1/3}\, S(\mathrm{C}) - \sqrt{2/3}\, P_y(\mathrm{C})\} - c_1\{\sqrt{1/3}\, S(\mathrm{S}) + \sqrt{2/3}\, P_y(\mathrm{S})\}. \quad (7)$$

Here, c_1 and c_2 are the normalization constants. On the other hand, the π orbital $\psi(\pi)$ (HOMO) with the energy E_π on the C-S fragment is expressd by

$$\psi(\pi) = c_C P_z(C) + c_S P_z(S), \quad (8)$$

where c_C and c_S are the coefficients of the singly occupied π orbital normalized over all atoms in the molecule. By substituting Eqs. (6), (7), and (8) to Eq. (5), we obtain

$$\Delta g^{xx} = \frac{4}{3}\frac{(c_1c_C - c_2c_S)(c_1\zeta_C c_C - c_2\zeta_S c_S)}{E_\pi - E_\sigma} + \frac{4}{3}\frac{(c_2c_C + c_1c_S)(c_2\zeta_C c_C + c_1\zeta_S c_S)}{E_\pi - E_{\sigma^*}}. \quad (9)$$

In order to simplify Eq. (9), we assume that $c_1 = c_2 = 1/\sqrt{2}$ and that the spin-orbit coupling constant of carbon atom ($\zeta_C = 29\ \mathrm{cm}^{-1}$) can be neglected compared with that of sulfur atom ($\zeta_S = 382\ \mathrm{cm}^{-1}$). Taking into account that c_C is the same order of magnitude as c_S and has an opposite sign to c_S in HOMO as seen in Fig. 8, we obtain the following simple relation between Δg^{xx} and c_S^2;

$$\Delta g^{xx} = \frac{4}{3}\frac{c_S^2\zeta_S}{E_\pi - E_\sigma} \quad (10)$$

Next, we treat the contribution from the non-bonding orbital on the S atom (Fig. 10b) in a similar way.

The non-bonding orbital on S atom, $\psi(n)$, with the energy of E_n is given by one of the three sp^2 orbitals;

$$\psi(n) = \sqrt{1/3}\,S(S) + \sqrt{2/3}\,P_y(S), \quad (11)$$

and we obtain the contribution for Δg^{xx} as well;

$$\Delta g^{xx} = \frac{4}{3}\frac{c_S^2\zeta_S}{E_\pi - E_n} \quad (12)$$

where, c_S^2 is the coefficient of $P_z(S)$ π orbital. The Δg due to the S atom is given after averaged for the three principal values as,

$$\Delta g = \frac{4}{9}\zeta_S\left(\frac{n_{C-S}}{E_\pi - E_\sigma} + \frac{n_S}{E_\pi - E_n}\right)c_S^2, \quad (13)$$

where n_{C-S} and n_s represent the number of C-S bond and the number of non-bonding orbital, respectively.

Consequently, the g-value is expected to correlate with the spin density on the sulfur atom by Eq. (13). Here, the coefficient of c_S^2 corresponds to the slope of the straight line of Eg. (4). We can roughly estimate this coefficient to be 0.00136 by taking the energy differences to be 3 eV and 10 eV for $(E_\pi - E_n)$ and $(E_\pi - E_\sigma)$, respectively, and by converting the c_S^2 to $a(^{33}S)$ by Eg. (3). This value is in reasonable agreement with the value of 0.00108 obtained experimentally. On the other hand, the intercept of the line at $a(^{33}S)=0$ corresponds to the total contribution from the residual C-C and C-H fragments. The obtained intercept 2.00379 is close to the g-values of the radicals of aromatic hydrocarbons. Therefore, it is concluded that the main cause of the g shift in our case is attributed to the variation of the spin densities on the sulfur atom.

To examine the validity of our formulation further we plot the data for the cation radical of dithin (**8**) (g=2.0089; $a(^{33}S)$=9.84 G),[13] which has a very different π system from that of TTF. When we take account of the fact that there are only two sulfur atom in **8** instead of four in TTF, the correlation between g and $a(^{33}S)$ agrees with that predicted by the line in Fig. 9. This indicates that Eq. (13) is also applicable to other compounds with similar sigma structure.

The Anomaly in g*-Value of* $4^{+\cdot}$ *and* $5^{+\cdot}$. The plots of g-value *vs.* ^{33}S *hfcc* for $4(Me)^{+\cdot}$ and $5(ph)^{+\cdot}$ shown in Fig. 9 deviate from the correlation line; the g-value of $4(Me)^{+\cdot}$ is larger than the line by 0.0004 and that of $5(ph)^{+\cdot}$ is smaller by 0.0027. A similar decrease of the g-value was reported by Goldberg and Bard[14] in the case of the anion radical of 1,4-diphenyl-1,3-butadiyne (**9**); g=2.00216 is smaller than that of 1,4-diphenyl-1,3-butadiene anion radical by 0.00054 and smaller than g_e. They suggested that the cause of this decrease can be attributed to the decrease of the energy difference between the π_z-orbital and the lowest unoccupied π_y-orbital, the latter being localized on the central acetylene carbons and perpendicular to the π_z-orbital shown in Fig. 10c. The anomalous g shift in our case may also be explained in a similar way.

The contribution of the acetylene or cumulene carbon chain to the g shift can be calculated by Eq. (5) as follows. The π_y-orbitals are expressed by the linear combination of P_y orbitals;

$$\phi^{(n)}(\pi_y) = \sum_i b_i^{(n)} P_{yi}(C), \quad (14)$$

and the π_z-orbital (HOMO) is also expressed by

$$\phi(\pi_z) = \sum_i c_i P_{zi}(C) \quad (15)$$

Substituting Egs. (14) and (15) to Eg. (5), we obtain

$$\Delta g = \frac{2}{3}\zeta_C \sum_n \frac{\{\sum_i c_i b_i^{(n)}\}^2}{E_{\pi z} - E_{\pi y}^{(n)}}. \quad (16)$$

Small energy denominators in Eq. (16) lead to a large Δg.

Therefore, the anomaly in g-value of $4^{+\cdot}$ and $5^{+\cdot}$ are likely due to the closeness of π_y and π_z orbitals. We estimate the energy differences by using Eq. (16). If the Hückel orbitals of butadiene with β=2.5 eV are used for the energies and the coefficients $b_i^{(n)}$ of π_y-orbitals, the energy differences between the π_z-orbital and the lowest unoccupied π_y-orbital are estimated to be 0.026 eV and 0.26 eV for $5(ph)^{+\cdot}$ and $9^{-\cdot}$, respectively.

On the other hand, when the energy of the π_z-orbital is very close to the energy of the doubly occupied orbital of π_y-orbital, the g-value becomes large. The slightly large g-value of $4(Me)^{+\cdot}$ is considered to be due to this effect. The energy difference in $4(Me)^{+\cdot}$ is estimated to be 0.30 eV by a similar argument.

Investigation on the electronic conductivities of the organic metals containing radical cations of the present compounds are in progress.

References

1) J. P. Ferraris, D. O. Cowan, V. Walatka, Jr., and J. H. Perlstein, *J. Am. Chem. Soc.*, **95**, 948 (1973); L. B. Colemen, M. J. Cohen, D. J. Sandman, F. G. Yamagishi, A. F. Garito, and A. G. Heeger, *Solid State Commun.*, **12**, 1125 (1973).

2) K. Bechgaard, C. S. Jacobsen, H. J. Pedersen, and N. Thorup, *Solid State Commun.*, **33**, 1119 (1980); D. Jerome, A. Mazaud, M. Ribault, and K. Bechgaard, *J. Phys., Lett.*, 41, L95 (1980); K. Andres, F. Wudl, D. B. McWhan, G. A. Thomas, D. Nalewajek, and A. L. Stevens, *Phys. Rev. Lett.*, **45**, 1449 (1980).

3) Z. Yoshida, T. Kawase, H. Awaji, I. Sugimoto, T. Sugimoto, and S. Yoneda, *Tetrahedron Lett.*, **1983**, 3469; Z. Yoshida, T. Kawase, H. Awaji, and S. Yoneda, *ibid.*, **1983**, 3473.

4) Z. Yoshida, H. Awaji, T. Sugimoto, and S. Yoneda, in preparation.

5) H. Ohya-Nishiguchi, *Bull. Chem. Soc. Jpn.*, **52**, 2064 (1979).

6) S. Hunig, G. Kielich, H. Quast, and D. Scheutzow, Liebigs *Ann. Chem.*, **1973**, 310; F. Wudl, A. A. Kruger, M. L. Kaplan, and R. S. Hutton, *J. Org. Chem.*, **42**, 768 (1977).

7) R. C. Bingham, M. J. S. Dewar, and D. H. Lo, *J. Am. Chem. Soc.*, **97**, 1285 (1975).

8) W. F. Cooper, N. C. Kenny, J. W. Edmons, A. Nagel, F. Wudl, and P. Coppens, *Chem. Commun.*, **1971**, 889.

9) F. B. Bramwell, R. C. Haddon, F. Wudl, M. L. Kaplan, and J. H. Marshall, *J. Am. Chem. Soc.*, **100**, 4612 (1978).

10) F. Gerson, H. Ohya-Nishiguchi, M. Szwarc, and G. Levin, *Chem. Phys. Lett.*, **52**, 587 (1977).

11) A. J. Stone, *Mol. Phys.*, **6**, 509 (1963).

12) For Example, see N. M. Atherton, "Electron Spin Resonance, Theory and Applications," John Wily and Sons Inc., p. 207 (1973).

13) P. D. Sullivan, *J. Am. Chem. Soc.*, **90**, 3618 (1968).

14) I. B. Goldberg and A. J. Bard, *Chem. Phys. Lett.*, **7**, 139 (1970).

Kinetic Studies of Fast Equilibrium by Means of High-performance Liquid Chromatography. VI. Separation of Rotamers of Formanilide

Masataka MORIYASU,* Kazuko KAWANISHI, Atsushi KATO, and Yohei HASHIMOTO
Kobe Women's College of Pharmacy, Motoyamakita-machi, Higashinada-ku, Kobe 658
(Received December 26, 1983)

The restricted rotation about the carbon-nitrogen bond of formanilide has been investigated by high-performance liquid chromatography. At lower temperatures, two peaks corresponding to two dynamic rotamers (*E*- and *Z*-form) have appeared on chromatograms, whereas at higher temperatures they have not been separated and a single peak has appeared on chromatograms, due to rapid bond rotation. The equilibrium concentration ratio of *E*- to *Z*-form has been found to vary in different solvents, suggesting the presence of solute-solvent and solute-solute interactions such as hydrogen bond formation. Determination of kinetic characteristics such as rate constant and activation energy of fast reactions has been established by high-performance liquid chromatography. The authors have named the present method "dynamic high-performance liquid chromatography," in imitation of "dynamic nuclear magnetic resonance spectroscopy" which traces fast equilibrium.

In this research series[1-5] a method has been devised to investigate fast equilibrium by means of high-performance liquid chromatography(HPLC). In part IV of this series,[4] the restricted rotation about carbon-nitrogen bonds of unsymmetrical palladium(II) dithiocarbamate chelates was examined. The carbon-nitrogen bonds of these compounds have the double-bond character shown in the following cannonical forms, and these compounds gave two peaks in

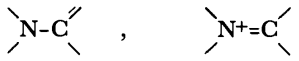

HPLC chromatograms at lower temperatures due to the separation of two labile rotamers. On the other hand, at higher temperatures rotamers were not separated and only one peak appeared.

There exist numerous substances which have a partially double-bond character on carbon-nitrogen bonds. Amides fall under this category. The present report deals with a kinetic study of intramolecular bond rotation of formanilide.

Experimental

Reagents. Formanilide was purchased commercially and was recrystallized from hexane-diethyl ether. Acetanilide was also obtained commercially and was used without further purification.

Apparatus. The HPLC apparatus described in our previous report[4] was modified as depicted in Figs. 1 and 2. Bathcooler (Model Cryocool CC-80f, Neslab Instrument Inc.), thermoregulator, heater, stirrer and HPLC column were plunged into the bath filled with methanol. The temperature of the bath was controlled from 25 to −60 °C. HPLC was possible up to −60 °C with a gradual decrease of column efficiency. Satisfactory separation of two rotamers was attained when temperature was below −30 °C. Two injectors (both Model 7125, Rheodyne), a six-way valve (Model 7010, Rheodyne), and a three-way valve (Model 7010, Rheodyne) were fixed on the plastic board which was placed on the upper part of the bath. Thus, most of the flow paths in stainless steel tubes were immersed in the cooled bath.

In order to obtain kinetically unstable species and to observe its change into other species, the following procedures were carried out. The equilibrated solution of two isomers (X⇌Y) was supplied to HPLC from injector I, and the portion corresponding to the retention time of X (or Y) was collected into the reservoir, which was controlled at various temperatures(−30—0 °C) by a freezing mixture composed of methanol-water. The collected portion was stirred and then kept standing for a few minutes. After the flow paths were changed by the six-way valve, the solution in the reservoir was sucked in from injector II. The injection was repeated for a definite interval. With the lapse of time, the peak of Y (or X) grew, while that of X (or Y) fell. Thus, the progress of the reaction X→Y (or Y→X) at lower temperatures was traced by HPLC.

Nuclear magnetic resonance (NMR) spectra were measured on a Varian Model XL-200 instrument, using tetramethylsilane as an internal reference.

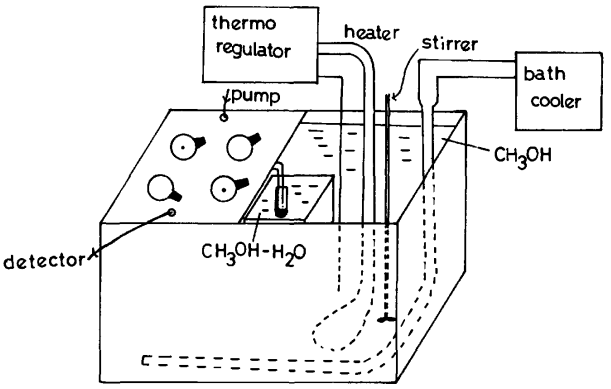

Fig. 1. HPLC apparatus for low temperature measurements.

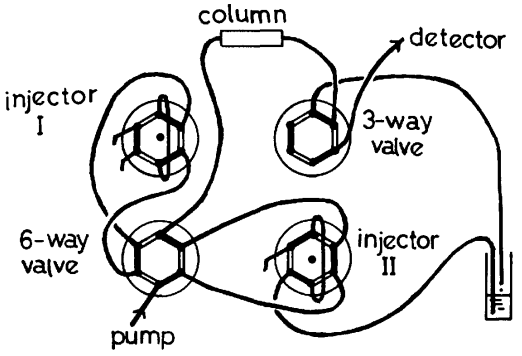

Fig. 2. Flow path of HPLC sampling system.

Results and Discussion

HPLC of Formanilide at Lower Temperatures. The theoretical treatment for analyzing a fast unimolecular reaction by HPLC was detailed in our previous report.[4]

Figure 3 shows chromatograms of the mixture of formanilide and acetanilide on silica gel packings at various temperatures. A slight broad peak of formanilide at room temperature splits into two sharp peaks at −30 °C *via* complicated chromatograms at intermediate temperatures. Contrary to this, acetanilide gives only one peak at all temperatures. This phenomenon is explained as follows. It has been established from NMR study that amide compouds can exist as the equilibrated mixture of two dynamic rotamers.[6] Thus, the NMR study[7] has demonstrated that formanilide exists as the mixture of two rotamers (*E*- and *Z*-form), while acetanilide exists exclusively as the *Z*-form.

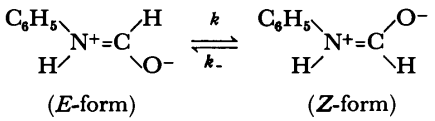

(1)

Since the carbon-nitrogen bond has a strong double-bond character, the intramolecular bond rotation around this carbon-nitrogen bond is seriously restricted. Figure 3 suggests that this bond rotation does not occur during chromatography at lower temperatures and then two rotamers are separated. On the other hand, at higher temperatures, since partial or complete bond rotation occurs during chromatography, two rotamers are not separated.

Equilibrium Ratio of Two Rotamers. Since the bond rotation practically does not occur during chromatography when HPLC is operated under −30 °C, it follows that chromatograms obtained at this temperature directly indicate the equilibrium concentrations of two isomers prior to HPLC. Thus, when samples of formanilide dissolved in different conditions, such as concentration, solvent and temperature, are submitted to HPLC, chromatogram patterns will vary due to the differences of the equilibrium ratios of the two isomers.

Formanilide was dissolved in 22 different solvents and these solutions were submitted to HPLC at −30 °C. Figure 4 exemplifies chromatograms of 0.5% formanilide solutions in different solvents. Here the temperatures of the sample solutions were controlled to be 25 °C. The ratio of two peak heights was found to vary markedly. Now, since it was elucidated that the equilibrium ratio of two isomers really varied in different solvents, an attempt was made to determine the equilibrium ratio of two isomers in different conditions; the procedure was carried out as follows, similar to that described in our previous report.[4] The equilibrated sample solution was submitted to HPLC and the portions corresponding to the former and the latter peaks were collected. The solution was then diluted to a definite volume by HPLC solvent. Each solution reached equilibrium promptly at room temperature according to Eq. 1. Thus, when the aliquot of these solutions was submitted to HPLC once more, two equilibrated peaks appeared on chromatograms again. Thus, from the measurements of two peak heights (or areas), the ratio of two isomers was determined. It should be noted here that direct measurements of two peak areas in Fig. 4 do not give the ratio of two isomers due to the difference in their absorption coefficients.

In order to identify the peaks which appeared on chromatograms, we compared present HPLC results with NMR results reported by other authors.[7] It was demonstrated in Ref. 7 that in chloroform the ratio of *Z*-form of formanilide increased with increase of form-

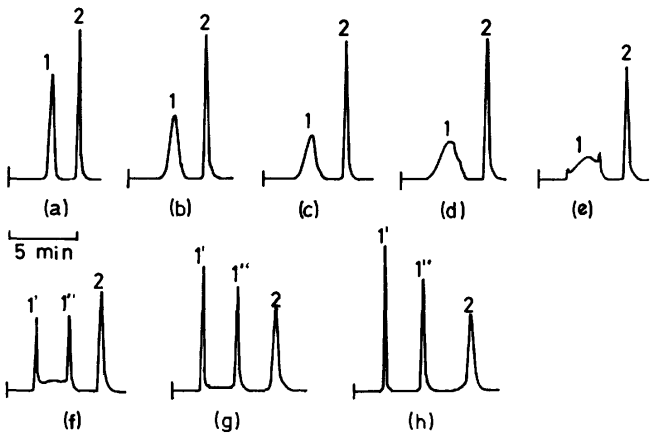

Fig. 3. HPLC chromatograms of the mixture of formanilide and acetanilide at various temperatures. Column: Polygosil 60-5 (4.6 mm × 25 cm). Eluent: hexane: isopropyl acetate: acetic acid = 100: 47: 3. Flow rate: 2.5 cm³/min. Detector: UV 254 nm. (a) 25°C, (b) 15°C, (c) 10°C, (d) 5°C, (e) 0°C, (f) −10°C, (g) −20°C, (h) −30°C. 1 formanilide (1′ *E*-form, 1″ *Z*-form), 2 acetoanilide.

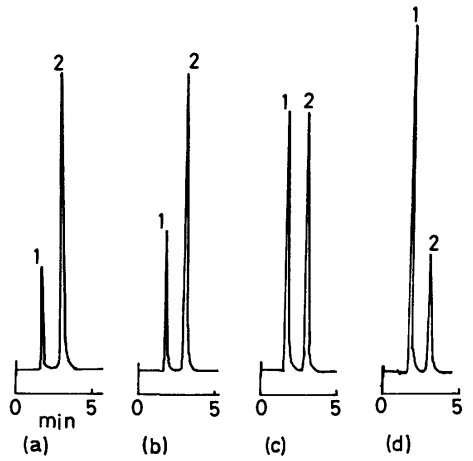

Fig. 4. HPLC chromatograms of 0.5% solution of formanilide dissolved in different solvents. Colum: Polygosil 60-5 (4.6 mm × 25 cm). Eluent: hexane: ethyl acetate: acetic acid = 100: 57: 3. Flow rate: 2.5 cm³/min. Detector: UV 254 nm. Column temperature: −30 °C. (a) in 2-propanol, (b) in methanol, (c) in acetic acid, (d) in carbon tetrachloride. 1 *E*-form of formanilide, 2 *Z*-from of formanilide.

anilide concentration. Formanilide was dissolved in chloroform at various concentrations to be submitted to HPLC. The ratio of the two peak areas was found to vary according to the concentration of formanilide, and the ratio of the latter peak was large when concentration of formanilide was high. The latter peak was thus identified as *Z*-form by NMR study, as shown in Table 1.

Now that the method to determine the ratio of two isomers was established and the problem of peak identification was resolved, equilibrium ratios of two isomers in 22 different solvents were determined; the results are summarized in Table 2. Interesting is the fact that when formanilide is dissolved in polar solvents such as methanol and water, the percentage of *Z*-form is high, while in nonpolar solvents such as chloroform and carbon tetrachloride, *E*-form is the predominant species. The latter phenomenon will be interpreted in terms of solute-solute hydrogen bond formation; *E*-form of formanilide exists as a ring dimer in chloroform or carbon tetrachloride.[7-10] This effect seems to result in a more stable structure of *E*-form in these solvents. In the former, polar solvents such as methanol and water will interact with formanilide strongly by solute-solvent hydrogen bond formation. When *Z*-form of formanilide enters into the tetrahedral lattice in solvent water, this species will be stabilized by hydrogen bond formation, as shown in the following

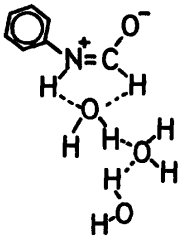

chart. A similar discussion will hold for several other polar solvents, such as methanol and ethanol.

Table 1. Percentage of formaniliide existing as *Z*-form *vs.* concentration in chloroform

mol%	HPLC(25 °C)* *Z*-form %	mol%	NMR(35 °C)** *Z*-form %
		31.3	64
28.7	63		
		23.3	62
16.7	60		
		9.7	58
9.1	54		
		5.1	50
4.8	47		
		2.9	48
2.5	46		
		1.5	45

* This work. ** Ref. 7. These data are values in deuterated chloroform.

Table 2. Percentage of formanilide existing as *Z*-form in different solvents

Solvent	*Z*-form %	Solvent	*Z*-form %
2-propanol	81	dimethyl sulfoxide	65
1-butanol	79	benzene	58
ethanol	78	hexane*	57
N,*N*-dimethyl formamide	74	formamide	57
water	73	1,4-dioxane	57
pyridine	71	cyclohexane*	54
methanol	71	dichloromethane	53
acetonitrile	70	acetic acid	49
tetrahydrofuran	70	acetone	48
ethyl acetate	68	chloroform	46
diethyl ether	66	carbon tetrachloride	28

0.5% solution, 25 °C. * 0.1% solution.

Rate of Interconversion and Energy Barrier for Bond Rotation. The rate constant k in Eq. 1 was determined by HPLC with similar procedures as described in our previous report.[4] The equilibrated solution of formanilide was supplied to HPLC through injector I, and the portion corresponding to the former peak (*E*-form) was collected into a reservoir thermostated at low temperatures. The collected portion was stirred and then left standing for a few minutes. After changing the flow path by the six-way valve, the solution in the reservoir was sucked into the column from injector II repeatedly at a definite intervals. With the lapse of time, the peak of *Z*-form appeared and grew gradually, while the peak of *E*-form fell. The rate constant k was calculated according to the following equation assuming a unimolecular process:[4]

$$k = \{y_e/x_0(t'+\Delta t)\}\ln\{y_e/(y_e-y'-\Delta y)\}, \quad (2)$$

where x_o, y_e and $y'+\Delta y$ were the initial concentration of *E*-form, the equilibrium concentration of *Z*-form and the concentration of *Z*-form at a definite time, $t'+\Delta t$, respectively. Thus, from the growth of peak height of *Z*-form, k was calculated. The value at −27.6 °C was determined to be $(1.27\pm0.05)\times10^{-3}$ s^{-1}.

In order to determine the energy barrier(E_a) for the

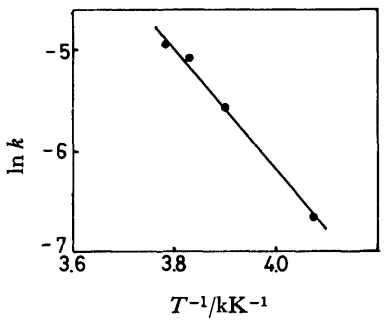

Fig. 5. Activation energy of the carbon–nitrogen bond rotation. Chromatographic conditions were similar to those shown in Fig. 4. The values of k were determined at various temperatuers according to Eq. 3. The value E_a was determined from the follwoing equation: $k=A_0\exp(-E_a/RT)$

carbon-nitrogen bond rotation, k was measured at different temperatures. Thus, from Arrhenius' plot shown in Fig. 5, E_a was determined to be (54.2±5.0) kJ mol^{-1}. From this plot the rate constant k at room temperature was estimated to be 9.5×10^{-2} s^{-1} (at 25 °C). Thus, it follows that the bond rotation occurs several times in a minute at room temperature.

Comparison of HPLC and NMR Results. The ^{1}H NMR spectra of formanilide were measured in deuterated dimethyl sulfoxide at various temperatures. A part of the spectra concerning the C-H protons near 8.3 and 8.8 ppm, assigned as *Z*- and *E*-form, respectively, is depicted in Fig. 6. The lower field band of *E*-form gave triplet-like signals at room temperature, which were analyzed as a mixture of doublet and singlet signals; the former was coupled with N-H proton (J=11.2 Hz) and the latter was not because of being replaced by deuteron in the solvent. When the temperature was increased to 60 °C, the "triplet" signals coalesced into a broad signal. A similar discussion will hold for the *Z*-form signal of C-H (8.3 ppm), though due to small spin-spin coupling constant, this band gave a singlet peak with deuteron exchanged partially. The spectral pattern from 60 to 150 °C shown in Fig. 6 resembles that of HPLC chromatograms depicted in Fig. 3, though the temperature range differs. This can reasonably be interpreted as follows. NMR has been well known to be a powerful tool for investigating fast equilibrium in solution, because two conformers which undergo interconversion promptly can be detected as different two species. Thus, two isomers of formanilide can be distinguished by NMR at room temperature. With increasing temperature, since the rate of interconversion increases rapidly, the two signals will commence to coalesce. A similar phenomenon should also occur in HPLC. Since a kinetically unstable species whose lifetime is a few seconds cannot be distinguished by HPLC, only one peak appears on chromatograms at room temperature. With decreasing temperature, lifetimes of two rotamers are prolonged and consequently two peaks corresponding to each rotamer appear on chromatograms. Thus, both Figs. 3 and 6 reflect identical phenomenon, *i.e.*, carbon-nitrogen bond rotation.

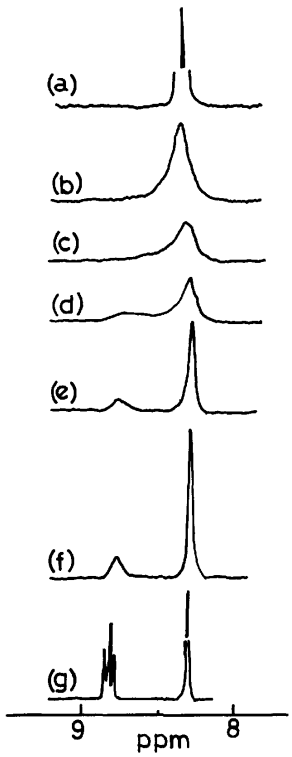

Fig. 6. The ^{1}H NMR spectra of formanilide in dimethylsulfoxide at different temperatures.
(a) 150 °C, (b) 100 °C, (c) 90 °C, (d) 80 °C, (e) 70 °C, (f) 60 °C, (g) 24 °C

The method has been well established for examining fast equilibrium of two dynamic isomers by means of NMR, which has been called dynamic nuclear magnetic resonance spectroscopy (DNMR). The energy barrier of carbon-nitrogen bond rotation has been well examined on various amides by DNMR. This method is based on the measurements of signal width at different temperatures, which is broadened due to fast interconversion of two conformers. Thus, from the signal shape analysis, the energy barrier has been determined to be from 13 to 30 kcal mol^{-1} (1 kcal mol^{-1}=4.18 kJ mol^{-1}) for various amides, mainly for *N*,*N*-disubstituted amides.[6] Determination of the energy barrier for *N*-monosubstitutued amides by ^{1}H NMR is difficult because intermolecular hydrogen bond formation complicates signal shape. Two isomers of *o*-methylformanilide were separated with careful treatment[11] and their ^{1}H NMR spectra were measured at low temperatures;[12] the E_a and k for this amide were 15.7 kcal mol^{-1} and $(2.7—4.4)\times10^{-3}$ s^{-1}, respectively, at −40 °C. Since two isomers of nonsubstitutued formanilide would rotate rapidly, while the *o*-methyl-substitutued one would not due to steric hindrance, the present value of E_a (54.2 kJ mol^{-1}=13.0 kcal mol^{-1}) of the former seems to be a reasonable one. DNMR study of ^{13}C NMR of formanilide demonstrated[13] that E_a was about 20 kcal mol^{-1} at high temperatures under the assumption that the effect of hydrogen-bond formation on signal shape was negligible in ^{13}C NMR study. The discrepancy between the ^{13}C NMR and present HPLC results might be interpreted at least partially in terms of the temperature difference of the measurements.

Conclusions

In this rsearch series, it has been demonstrated that rather fast equilibria can be traced by means of HPLC based on conventional principles. For this purpose, DNMR method has been used exclusively. The present HPLC method is comparable with the DNMR method. Since the time scale of detection for HPLC differs from that for NMR, kinetic data obtainable by DNMR method are not always obtained by HPLC method. The authors, however, consider that the HPLC method have some advantages over the DNMR method. First, undesirable effects such as hydrogen-bond formation, which tends to broaden the signal shape in NMR, can be neglected in HPLC. Second, in HPLC method, kinetically unstable species can be obtained, so determination of physicochemical properties of labile species will be possible by combining HPLC

with other suitable apparatus. The authors propose here to call this HPLC method dynamic high-performance liquid chromatography, in imitation of DNMR which traces fast equilibria in solution.

This work was partially supported by a Grant-in-Aid for scientific research from the Ministry of Education, Science and Culture. The authors are grateful to Miss T. Sai, Kobe Women's College of Pharmacy, for NMR measurements.

References

1) M. Moriyasu and Y. Hashimoto, *Bull. Chem. Soc. Jpn.*, **53**, 3590 (1980).
2) M. Moriyasu and Y. Hashimoto,*Bull. Chem. Soc. Jpn.*, **54**, 2470 (1981).
3) M. Moriyasu and Y. Hashimoto, *Bull. Chem. Soc. Jpn.*, **54**, 3374 (1981).
4) M. Moriyasu, Y. Hashimoto, and M. Endo, *Bull. Chem. Soc. Jpn.*, **56**, 1972 (1983).
5) M. Moriyasu and Y. Hashimoto, *Bull. Chem. Soc. Jpn.*, **57**, 1823 (1984).
6) W. E. Stewart and T. H. Siddall, III, *Chem. Rev.*, **70**, 517 (1970).
7) A. J. R. Bourn, D. G. Gillies, and E. W. Randall, *Tetrahedron*, **20**, 1811 (1964).
8) P. R. Andrews, *Aust. J. Chem.*, **25**, 2243 (1972).
9) L. G. Belinskaya and A. V. Lukashov, Mater. Vses. Konf. Vopr. Method. Tekh. Ul'trazvuk. Spektrosk., 2nd, 101 (1973). *Chem. Abstr.*, **84**, 58418t (1976).
10) L. G. Belinskaya, A. V. Lukashov, and E. S. Efremov, *Izv. Timiryazev. S-kh. Akad.*, **1974**, 162. *Chem. Abstr.*, **81**, 119752j (1974).
11) A. Mannschreck, *Tetrahedron Lett.*, **1965**, 1341.
12) T. H. Siddall, III, W. E. Stewart, and A. L. Marston, *J. Phys. Chem.*, **72**, 2135 (1968).
13) H. Nakanishi and O. Yamamoto, *Chem. Lett.*, **1974**, 521.

Far Ultraviolet Electric Linear Dichroism. II. Pulsed Electric Dichroism Apparatus and Dichroic Spectra of Collagen in Aqueous Solution in the 230—187 nm Wavelength Region

Kiwamu YAMAOKA,* Manabu ASATO, Koichiro MATSUDA, and Kazuyoshi UEDA
Faculty of Science, Hiroshima University, Higashisenda-machi, Naka-ku, Hiroshima 730
(Received January 17, 1984)

A Pulsed electric linear dichroism (ELD) apparatus is described for studying the optical properties and solution conformation of biologically important macromolecules whose chromophores absorb light in the far ultraviolet region. This apparatus is capable of generating a rectangular-wave electric pulse field with a duration of 5 μs—5 ms and an amplitude of 0.2—8 kV over the 360—185 nm region. A special feature to this apparatus is its ability to record both parallel and perpendicular dichroism signals simultaneously and independently. To prove the instrumental performance, some dichroic spectra of calfskin collagen solution (pH 3.16 and concentration 0.03 g dm^{-3}) in 0.001 mol dm^{-3} H_3PO_4 were measured in the 230—187 nm region, where the peptide chromophore shows a broad absorption spectrum. The reduced dichroism of collagen was positive but not constant throughout the wavelength region. A detailed analysis revealed that the peptide spectrum contains three overlapping absorption bands centered at 219, 200, and 189 nm. These transition moments were found to be inclined at ±(50.6—51.0°) (219 nm), ±(48.8—49.5°) (200 nm), and ±(56.0—55.8°) (189 nm) relative to the orientation axis of a triple-stranded collagen helix.

When a homogeneous electric field is externally applied to a macromolecular solution, the solute molecules tend to orient toward the direction of the electric field. If these molecules contain chromophoric groups, they absorb linearly-polarized light selectively. The difference in absorbances $\Delta A(=A_{/\!/}^{E}-A_{\perp}^{E})$ between the light component polarized parallel ($A_{/\!/}^{E}$) and perpendicular ($A_{\perp}^{E}$) to the direction of the electric field is a negative or positive quantity, which is termed the electric linear dichroism (ELD).[1-3] By examining the wavelength dependence of reduced dichroism, $\Delta A/A$, inside an absorption band, where A is the isotropic absorbance in the absence of electric field, useful information may be extracted on the relative arrangement between a particular chromophore and the polymer backbone chain and on the overall polymer conformation in solution.

Although natural and synthetic polymers often contain characteristic chromophores in the ultraviolet and far ultraviolet regions, the dependence of $\Delta A/A$ on wavelength has been studied only in a few cases.[1-13] (Related subjects have been reviewed prior to 1973 in Refs. 1—5.) This is mostly because technical difficulties are involved in measuring the electric dichroism spectra; for instance, no commercial instruments are available as yet. The instrumentation of electric dichroism in the visible and near ultraviolet regions has been reported with particular emphasis on a fast and high-voltage square-wave pulse, a widely covered wavelength region, and a high spectral resolution.[6,14] With such a pulsed electric field, the transient dichroic signal of an ionic solution can be measured. This in turn makes it possible to determine the relaxation time and to estimate the overall macromolecular shape.

Such vital biopolymers as nucleic acids, polypeptides, proteins, and polysaccharides all have intrinsic chromophores in the far ultraviolet region. Hence, for the purpose of clarifying the optical properties and solution conformation of these biopolymers, we initiated a series of the far ultraviolet ELD studies. In this paper, we will briefly describe a new ELD apparatus, which can cover 360—185 nm and allow an independent and simultaneous detection of both parallel and perpendicular signals. This procedure is essential to detect any anomalous electrochromic effect,[15] although it has been often ignored. With this apparatus, we will demonstrate some important features associated with ELD spectra of collagen in an acid solution, together with an analytical procedure for observed data.

Apparatus and Data Analysis

Apparatus. A transient ELD apparatus consists of four major parts; the electric, optical, signal-detecting, and measuring-cell systems. The principles and design procedure for such an apparatus have been discussed elsewhere.[1,2,6,14] A new feature was added to the present far ultraviolet ELD apparatus, in such a way that both parallel and perpendcular signals can be recorded by applying a single high-voltage pulse to a sample cell. Figure 1 shows the block diagram of this apparatus. The electric system is unchanged from that previously described in detail.[14] It consists of a pulse generator, a homemade pulse amplifier, a 10 kV DC high-voltage power supply, and a homemade high-voltage pulse discharge network. The single square-wave pulse applied to a measuring "Kerr" cell was attenuated with a Tektronix 1000:1 P6013A probe and fed to a 7A18 plug-in amplifier of a Sony-Tektronix 7844 dual beam oscilloscope. The rise and decay times of a high voltage pulse were confirmed to be less than 1 μs under optimum conditions.[14]

Figure 2 shows the optical system schematically; this was newly designed and constructed for the present purpose. The light source is a water-cooled 200 watt deuterium discharge arc lamp D_2 (D-200F, Original Hanau, West Germany) operated on a 100 volt DC power in the 400—185 nm region. This lamp is about four times as intense as the conventional 40—30 watt deuterium lamp. The monochromatic light from a 25 cm grating double monochromator with low stray light and high wavelength accuracy (0.1 nm) (Japan

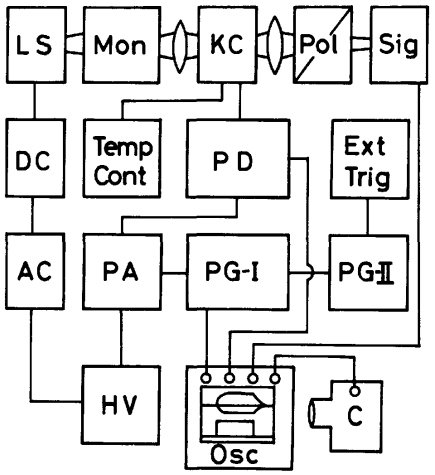

Fig. 1. Block diagram of pulsed linear electric dichroism apparatus. AC, Yamabishi Electric Co. NAC-1.5K voltage regulator; DC, Ewig & Co. HS-D200F starter-power supply; LS, light source; Mon, 25-cm tandem double monochromator; KC, "Kerr" cell and holder; Pol, magnesium fluoride polarizer; Sig, signal detector; HV, Kawaguchi Electric Works Model V-710 high-voltage DC power supply (0–10 kV); PA, homemade pulse amplifier; PD, pulse discharge network;[14] PG-I, Anritsu Electric Co. Model MG411B pulse generator; PG-II, Toyo Telesonic Co. Model 7103C pulse generator for baseline triggering; Ext Trig, homemade external trigger to activate the whole measuring system; C, Polaroid camera; Osc, 7844 dual beam oscilloscope; Temp Cont, regulated temperature bath.

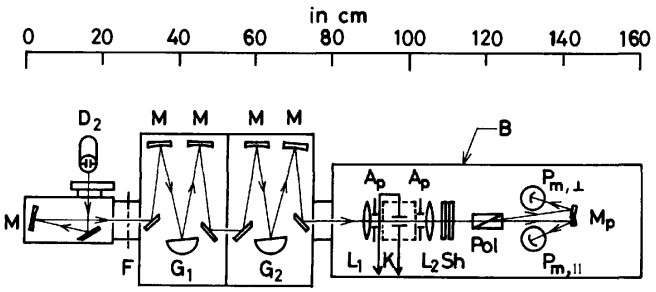

Fig. 2. Schematic diagram of optical system. D_2, deuterium lamp (see text); F, cut-off filter, M, concave mirror; G_1 and G_2, diffraction gratings; B, blackened aluminum enclosure; L_1 and L_2, quartz lenses; K, "Kerr" cell; A_p, rectangular aperture; Pol, polarizer; Sh, shutter; $P_{m,//}$ and $P_{m,\perp}$, photomultipliers; M_p, front-faced reflecting mirrors.

Spectroscopic Co. Model CT-25ND) is collimated by the first double-convex lens L_1 to the center of a "Kerr" cell K. The diverging beam is again converged onto the front of photomultipliers $P_{m,//}$ and $P_{m,\perp}$ by the second double-convex lens L_2. These lenses are made of strain-free far ultraviolet transmitting quartz (Extrasil grade), the focal length and the diameter being 55 mm and 33 mm respectively. A screen with a 4×10 mm rectangular aperture is placed behind L_1 and another with a 2×8 mm aperture is in front of L_2. A Rochon-type

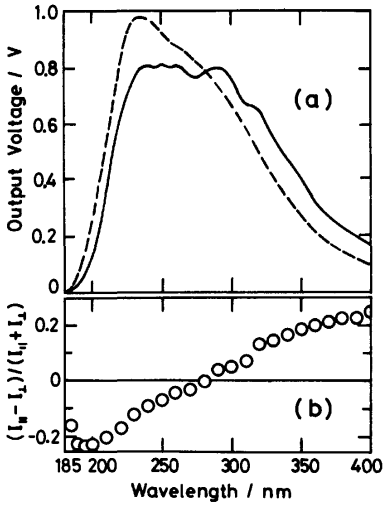

Fig. 3. The overall spectral intensity distribution of deuterium lamp in the ELD apparatus (a) and the wavelength dependence of the degree of polarization p (b). In (a), the light intensities, $I_{//}$ (——) and $I_\perp$ (----), were detected as the photomultiplier output voltage. In (b), $p=(I_{//}-I_\perp)/(I_{//}+I_\perp)$, where $I_{//}$ and $I_\perp$ are the intensities of light polarized parallel and perpendicular to the direction of electric field in the absence of a "Kerr" cell assembly.

magnesium fluoride beam-splitting polarizer Pol (MFR-9, Karl Lambrecht, Inc., Chicago, USA) is inserted. This prism is set in such a way that the emerging light is separated into two components; one, polarized parallel to the pulsed electric field, traveling straight and the other, polarized perpendicular to the field, traveling obliquely at an angle of 4.5° at 200 nm. Thus, both parallel- and perpendicularly-polarized emerging light beams can be detected *independently* and *simultaneously* without rotating the prism. Each of these beams is further separated and converged by placing a rectangular concave mirror M_p (11×42 mm) with a focal length of 60 mm, which reflects light from the front surface coated with aluminum and protected with magnesium fluoride.

The signal-detecting system consists of two matched side-on type R106UH photomultipliers (Hamamatsu TV Co.), each detecting the linearly polarized beam. The voltage generated by each P_m tube is led to either of the separate channels of the dual beam oscilloscope. Two signals and an attenuated pulse are all displayed simultaneously on a cathode-ray tube (CRT) and photographed with a Tektronix C-53 oscilloscope camera. Figure 3a shows the spectral characteristics of the photomultiplier output voltage with a 200 watt deuterium lamp in the 400—185 nm region. In the present optical system, the transmitted light intensity is both wavelength- and polarization-dependent. Figure 3b shows the degree of polarization for the overall optical system. In practice, however, these features do not interfere with the signal measurement at discrete wavelengths, since the instrument is operated manually.

A cylindrical high-voltage-resistant "Kerr" cell was made of either Kel-F or Acrylite plastics for the far ultraviolet region. The design of the cell is essentially

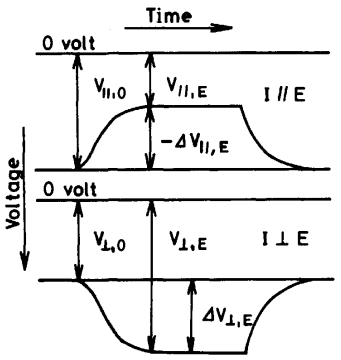

Fig. 4. Parallel- and perpendicular-polarized dichroism signals for data analysis. Notations are given in Eqs. 1–3 in text.

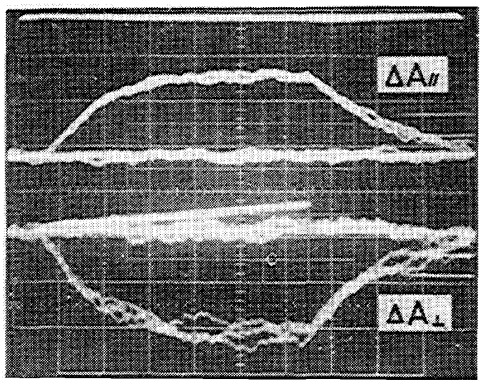

Fig. 5. Simultaneous display of transient dichroism signals for a collagen solution. Wavelength, 200 nm; field strength, 12.8 kV/cm; sweep timp, 100 μs/division.

the same as the one described previously;[6,14] the gap between two highly polished electrode plates (stainless steel) is 0.327 cm and the optical path length is 0.60 cm. The volume of a sample solution is 0.2—0.3 ml. The Kerr cell is set inside the blackened brass block, through which a temperature-controlled fluid circulates with an accuracy of ±0.05 °C. The temperature of a sample is recorded with a small thermistor probe which is in direct contact wih the solution.

Data Analysis. Figure 4 schematically shows the dichroic signals displayed on a CRT screen. Let $I_{//,E}$ and $I_{//,0}$ be the parallel-polarized light intensities transmitting through the solution and the polarizer and falling onto a detecting tube in the presence and the absence of an external electric field. The difference in absorbances $\Delta A_{//}(=A^E_{//}-A)$ is given as[13,14]

$$\Delta A_{//} = \Delta\varepsilon_{//}Cl = (\varepsilon^E_{//}-\varepsilon)Cl = -\log\left(1+\frac{\Delta I_{//,E}}{I_{//,0}}\right) = -\log\left(1+\frac{\Delta V_{//,E}}{V_{//,0}}\right), \quad (1)$$

where C is the molar concentration of solute, l is the path length in cm, $\varepsilon^E_{//}$ and ε are the molar absorption coefficients of the solute, and $V_{//,E}$ and $V_{//,0}$ are the voltages generated across a load resistor in the presence and the absence of the external field. $\Delta V_{//,E}(=V_{//,E}-V_{//,0})$ should be determined within the range, in which the light intensity is linearly proportional to the voltage generated.[14] Similarly, for the perpendicularly-polarized light,

$$\Delta A_{\perp} = \Delta\varepsilon_{\perp}Cl = (\varepsilon^E_{\perp}-\varepsilon)Cl = -\log\left(1+\frac{\Delta I_{\perp,E}}{I_{\perp,0}}\right) = -\log\left(1+\frac{\Delta V_{\perp,E}}{V_{\perp,0}}\right). \quad (2)$$

The reduced dichroism is given from Eqs. 1 and 2 as

$$\frac{\Delta A}{A} = \frac{A^E_{//}-A^E_{\perp}}{A} = \frac{1}{A}\log\left(\frac{1+\dfrac{\Delta V_{\perp,E}}{V_{\perp,0}}}{1+\dfrac{\Delta V_{//,E}}{V_{//,0}}}\right). \quad (3)$$

If the applied electric pulse field orients solute molecules, but does not deform the molecular shape, then the following relation should hold:[15]

$$\frac{\Delta A_{//}}{A} = -\frac{2\Delta A_{\perp}}{A} \quad \text{and} \quad 3A = A^E_{//} + 2A^E_{\perp}. \quad (4)$$

Experimental

Materials and Measurements. Collagen (type III, acid soluble from calfskin) was purchased from Sigma Co. The sample was kindly purified by Dr. K. Gekko of Nagoya University by dissolving it in 0.5 M (1 M=1 mol dm^{-3}) acetic acid and centrifuging at 4 °C to remove precipitates. After repeating this procedure, the supernatant was dialyzed against distilled water and then freeze-dried. The collagen solution was prepared by dissolving the dried sample in 1 mM H_3PO_4 aqueous solution (pH=3.16), the concentration being 0.28 mM (=0.03 g dm^{-3}).[16,17] The isotropic spectrum was measured on a Hitachi EPS-3T spectrophotometer with a pair of 0.5 cm quartz cells. The electric dichroism was measured on the present apparatus with two Kerr cells; one (l=2.00 cm with a gap of 0.330 cm[14]) the 230—208 nm region and the other (l=0.60 cm with a gap of 0.327 cm) in the 206.5—187 nm region. The slit widths were adjusted manually, so that the half-intensity width was less than 2 nm at 200 nm. All measurements were performed at 20 °C under nitrogen gas purge (3 L/min).

Figure 5 shows an oscillogram of a collagen solution. Both $\Delta A_{//}$ and $\Delta A_{\perp}$ were traced three times to illustrate the reproducibility.

Results and Discussion

Dependence of Electric Dichroism on Field Strength. Figure 6 shows the dependence of the observed dichroism of collagen on the applied electric field at 200 nm. Parallel and perpendicular specific dichroic signals ($\Delta A_{//}/A$ and $\Delta A_{\perp}/A$) are plotted against the square of the field strength, E^2, together with the reduced dichroism ($\Delta A/A$) which was calculated with the aid of Eq. 3. The first relation in Eq. 4 holds up to 19 kV/cm, which indicates that no anomalous effect is induced by the applied field. The $\Delta A/A$ values tend to saturate at high fields. By extrapolating these values to infinitely high field, the saturated value, $(\Delta A/A)_s$, was estimated with due consideration for curvature.[18,19] This procedure is shown in Fig. 7, where $\Delta A/A$ values at 200 nm were plotted against E^{-1} and E^{-2} and the intercepts were determined to be 0.333 and 0.291 by linear least-square fitting. These values correspond to the upper and lower limits for the true value of $(\Delta A/A)_s$; the value of 0.333

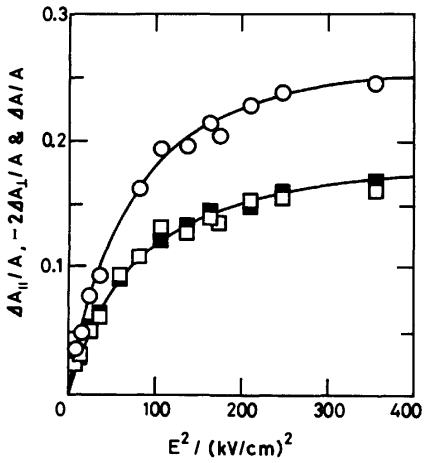

Fig. 6. Dependence of dichroism for a collagen solution on applied electric field. $\Delta A_{//}/A$ (□), $-2\Delta A_\perp/A$ (■), and $\Delta A/A$ (○) at 200 nm.

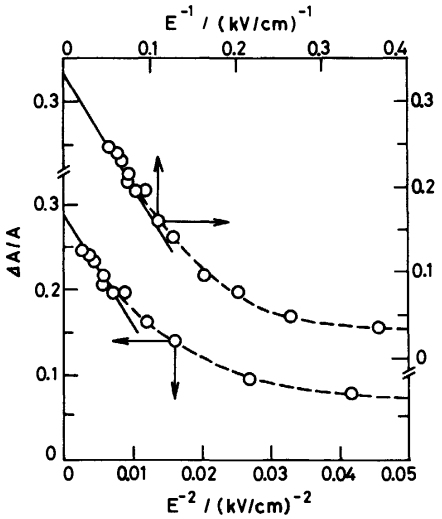

Fig. 7. Extrapolation of reduced dichroism to infinitely high field strength. The data were the same as those in Fig. 6. Solid lines represent the least-square fitting. Other details are given in text.

would be reached if the orientation of the collagen helices results from the pure permanent dipole moment, while the estimated value would be 0.291 if the orientation is solely due to the polarizability anisotropy.[18,19]

Dependence of Electric Dichroism on Wavelengh. Figure 8 shows the dependence of dichroism on wavelength (upper half) and the anisotropic spectra, $A_{//}^E$ and $A_\perp^E$, at a constant field strength of 16.3 kV/cm, together with the isotropic spectrum of collagen, A, in the absence of the field (lower half). The reduced dichroism is positive but not constant throughout the 230—187 nm region, indicating that the broad single-peaked isotropic spectrum is only apparent and contains several transition moments directed at different angles relative to the orientation axis of a collagen molecule. These dichroic spectra of the peptide chromophore of collagen in solution could be determined, for the first time, with the present ELD apparatus. The $A_{//}^E$-spectrum with the maximum at 192 nm is always more

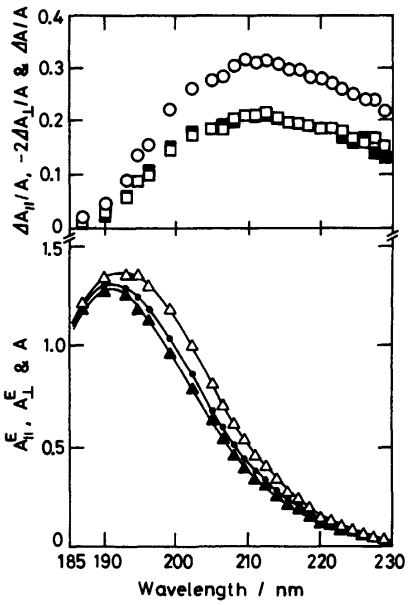

Fig. 8. The dependence of reduced dichroism on wavelength (upper half)and the anisotropic spectra (lower half) of collagen in an acid solution at 16.3 kV/cm. Upper half: $\Delta A_{//}/A$ (□), $-2\Delta A_\perp/A$ (■), and $\Delta A/A$ (○). Lower half: $A_{//}^E$ (-△-), $A_\perp^E$ (-▲-); the observed isotropic spectrum (——) and the isotropic absorbance calculated with $3A=A_{//}^E+2A_\perp^E$ (●). The path lengths are normalized to 0.60 cm in all cases.

intense than the $A_\perp^E$-spectrum with the maximum at 190 nm, both spectra coinciding with each other below 188 nm. It should be noted that these absorption maxima are shifted relative to the maximum of the isotropic spectrum at 191 nm. A similar trend was observed for a stroked collagen film.[20] Equation 4 holds over the entire wavelength region; the isotropic spectrum calculated with the relation, $3A=A_{//}^E+2A_\perp^E$, was indicated with dots (lower half).

Simulation of Reduced Dichroism. Collagen in a triple-stranded helix conformation is known to be oriented by a pulsed electric field, owing to the interaction predominantly with the permanent dipole moment borne on the polypeptide chains.[21-23] The orientation axis of collagen toward the electric field is the longitudinal axis of the triple helix. The degree of orientation (denoted as Φ) of collagen molecules in solution at a given orienting field strength of E is related to the reduced dichroism observed at E and the saturated dichroism as $\Delta A/A=(\Delta A/A)_s\times\Phi$,[15] Φ being independent of wavelength inasmuch as the value of E is specified. For example, $\Phi=0.72$ at $E=16.3$ kV/cm, since at 200 nm $\Delta A/A=0.240$ and $(\Delta A/A)_s=0.333$ (the last was estimated from the extrapolation of $\Delta A/A$ against E^{-1}). The value of $(\Delta A/A)_s$ may be calculated at any wavelength, once the value of Φ is known. It is related to the absorption transition moment by the following expression:[13]

$$\left(\frac{\Delta A}{A}\right)_s=\left(\frac{\Delta A}{A}\right)\left(\frac{1}{\Phi}\right)=\frac{3}{2}\frac{\sum_i(3\cos^2\theta_i-1)A_i}{\sum_i A_i}, \qquad (5)$$

where θ_i is the angle between the transition dipole

moment direction of the ith absorption band with absorbance A_i and the orientation axis of a collagen molecule, *i. e.*, the long axis of the triple-stranded helix.

From the variation of $\Delta A/A$ with wavelength in Fig. 8, at least three overlapping component bands must be present in the peptide band; approximately the first is at 230—210 nm, the second at 210—200 nm, and the third at 200—185 nm. In order to simulate the wavelength dependence of $\Delta A/A$ with these bands, the isotropic spectrum must be decomposed into these three component bands. In this work, the profile of each band was assumed to be Gaussian as

$$A_i(\tilde{\nu}) = A_{i,\max}\exp\left[-(4\ln 2)\left(\frac{\tilde{\nu}-\tilde{\nu}_{i,\max}}{\delta_i(\tilde{\nu})}\right)^2\right], \quad (6)$$

where $A_i(\tilde{\nu})$ is the absorbance at a given wave number $\tilde{\nu}$, $A_{i,\max}$ is the maximum absorbance at the peak position $\tilde{\nu}_{i,\max}$, and $\delta_i(\tilde{\nu})$ is the half-intensity band width where $A_i/A_{i,\max}=0.5$.

Figure 9 shows a decomposition of the observed isotropic spectrum (circles) into three component bands (dashed lines) centered at 219 nm, 200 nm, and 189 nm. The resultant spectrum (solid line), composed of these three bands, is in excellent agreement with the observed spectrum. With the characteristic parameters for $A_{i,\max}$ (i=1—3) given in Table 1, the experimentally obtained values of $\Delta A/A$ were fitted by adjusting the angle θ_i with the aid of Eq. 5. The best values of θ_i (i=1—3) are given in Table 1. The agreement between the experimental and simulated values of $\Delta A/A$ is good throughout the 230—187 nm region. Since collagen is a complex protein consisting of many different amino acid residues, it would not be relevant further to refine the simulated

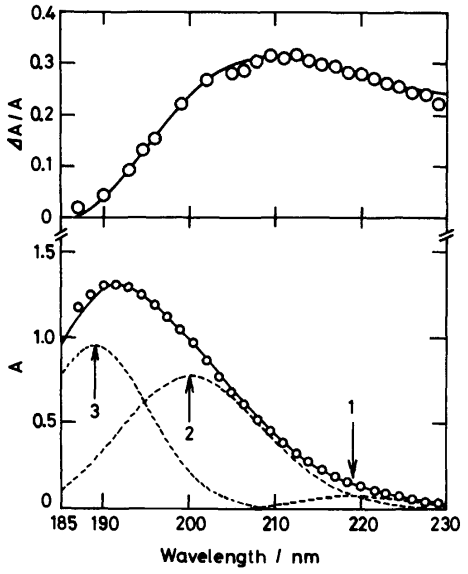

Fig. 9. Decomposition and simulation of the isotropic spectrum and the wavelength dependence of $\Delta A/A$ of collagen. Upper half: observed values of $\Delta A/A$ (O) and the simulated dependence of $\Delta A/A$ (——) on wavelength. Lower half: observed (O) and simulated (——) isotropic spectra, together with three component bands (----). These are: (1) the 219 nm band, (2) the 200 nm band, and (3) the 189 nm band. The experimental data are taken from Fig. 8.

wavelength dependence of $\Delta A/A$ values by decomposing the isotropic spectrum into four or more component bands.

The Peptide Chromophore in Collagen. There have been two reports, one by Mandel and Holzwarth[20] and the other by Jenness *et al.*,[17] in which the optical properties of collagen were quantitatively studied in solutions and in stroked films. These workers, however, failed to identify the first component band at 219 nm that was detected in this work. This transition may be assigned to the n-π^* transition on the carbonyl oxygen because of its weak intensity and long wavelength peak.[17,20] It is the wavelength dependence of the reduced dichroism, but not of the dichroism, $\Delta A_{/\!/}$ or $\Delta A_{\perp}$,[20] itself that reveals the hidden features in an isotropic spectrum, such as the number of transition moments and the angles, in a tangible fashion. Since Eq. 5 yields only the absolute magnitude for the angle θ_i, it may be said that the direction of the n-π^* transition makes an angle +(50.6—51.0°) or −(50.6—51.0°) (θ_1) with respect to the orientation axis of a collagen molecule.

The second component band at 200 nm is associated with a positive dichroism with an angle +(48.8—49.5°) or −(48.8—49.5°) (θ_2), while the third band at 189 nm is associated with a negative dichroism with an angle of +(56.0—55.8°) or −(56.0—55.8°) (θ_3). The presence of these bands has been noted both in the isotropic spectrum and in the anisotropic spectra of collagen films.[20] On the basis of Moffitt's prediction,[24] Mandel and Holzwarth have assigned these bands to the exciton-split π-π^* transitions which are expected for a single-stranded helix.[20,24] The allowed exciton bands are polarized parallel and perpendicular to the axis of the helix. According to the prediction, the positive 200-nm band is the parallel (//) band, while the negative 189-nm band is the perpendicular (⊥) band. As mentioned above, the wavelength dependence of $\Delta A/A$ can afford the angle relative to the orientation axis which is the axis of the triple-stranded helix of collagen. The estimated angles are about ±49°, but not 0°, for the "//-band" and about ±56°, but not 90°, for the "⊥-band". This discrepancy between the observed and theoretically expected values for angles θ_2 and θ_3 may be

Table 1. The optical property of collagen in acid solution

i	$\frac{\tilde{\nu}_{i,\max}\times 10^{-4}}{\text{cm}^{-1}}$	$A_{i,\max}$	$\frac{\delta_i\times 10^{-4}}{\text{cm}^{-1}}$	$\frac{\lvert\theta_i\rvert}{\text{deg}}$
1	4.57 (219)[a]	0.07	0.33	50.6[b] (51.0)[c]
2	5.00 (200)[a]	0.77	0.48	48.8[b] (49.5)[c]
3	5.29 (189)[a]	0.95	0.40	56.0[b] (55.8)[c]

a) Values in parentheses are the peak positions expressed with wavelength in nm. b) Angles calculated from $(\Delta A/A)_s$ which were obtained by the E^{-1} extrapolation. c) The same obtained by the E^{-2} extrapolation.

attributed to three possibilities which remain to be resolved.

The first possibility is that the exciton band is not formed over the collagen helix which consists of three intermolecular hydrogen-bonded helix chains. The second is that the exciton splitting does occur, but it is limited only to each single-stranded helix chain which is coiled around the collagen axis. The third is that the Moffitt-type splitting does not actually occur, and the observed component bands all belong to the intrinsic peptide chromophore. These are interesting poins for future investigations, which must be deferred until the geometry of the collagen helix and the optical property of small-molecular-weight amide compounds are more thoroughly clarified.

Conclusion

We have constructed a high-voltage pulsed electric linear dichroism apparatus with the aim of unraveling the optical properties of the chromophores involved in biologically important macromolecules, which absorb light in the far ultraviolet region. Using this apparatus, we have measured the dichroic spectra of collagen in an acid solution over the 230—187 nm region, in which the reduced dichroism was found to be wavelength-dependent. We have presented a detailed, analytical procedure for electric dichroism data. On the basis of this analysis, we concluded that the isotropic absorption spectrum of collagen contains at least three transition moments, which make different angles with respect to the orientation axis of the collagen helix.

We are deeply indebted to Dr. E. Charney of the National Institutes of Health (Bethesda, Md., USA) for kindly lending us a magnesium fluoride polarizer in the initial stage of this work. This work was in part supported by a Grant-in-Aid for Scientific Research (No. 347009) from the Ministry of Education, Science, and Culture.

References

1) E. Fredericq and C. Houssier, "Electric Dichroism and Electric Birefringence," Clarendon Press, Oxford (1973).
2) K. Yamaoka, "Polyelectrolytes" (in Japanese), vol. 13, "Kobunshi Jikkengaku," ed by M. Kaneko, S. Sugai, and M. Nagasawa, Kyoritsu Press, Tokyo (1978), Chap. 9. pp. 230—255.
3) C. M. Paulson, Jr., "Molecular Electro-Optics," Part 1, ed by C. T. O'Konski, Marcel Dekker, New York (1976), Chap. 7, pp. 243—273.
4) K. Yoshioka, "Molecular Electro-Optics," Part 2, ed by C. T. O'Konski, Marcel Dekker, New York (1978), Chap. 17, pp. 601—643.
5) M. Shirai, "Molecular Electro-Optics," Part 2, ed by C. T. O'Konski, Marcel Dekker, New York (1978), Chap. 19, pp. 685—711.
6) K. Yamaoka and E. Charney, *Macromolecules*, **6**, 66 (1973).
7) J. Bontemps, C. Houssier, and E. Fredericq, *Biophys. Chem.*, **2**, 301 (1974).
8) C. Houssier, B. Hardy, and E. Fredericq, *Biopolymers*, **13**, 1141 (1974).
9) M. Tricot, C. Houssier, and V. Desreux, *Biophys. Chem.*, **3**, 291 (1975).
10) N. E. Geacintov, A. Gagliano, V. Ivanovic, and I. B. Weinstein, *Biochemistry*, **17**, 5256 (1978).
11) H. H. Chen and E. Charney, *Biopolymers*, **19**, 2123 (1980).
12) K. Yamaoka and K. Matsuda, *Macromolecules*, **14**, 595 (1981).
13) K. Matsuda and K. Yamaoka, *Bull. Chem. Soc. Jpn.*, **55**, 69 (1982).
14) K. Yamaoka and K. Matsuda, *J. Sci. Hiroshima Univ. Ser. A*, **43**, 185 (1980).
15) K. Yamaoka and E. Charney, *J. Am. Chem. Soc.*, **94**, 8963 (1972).
16) W. B. Gratzer, W. Rhodes, and G. D. Fasman, *Biopolymers*, **1**, 319 (1963).
17) D. D. Jenness, C. Sprecher, and W. C. Johnson, Jr., *Biopolymers*, **15**, 513 (1976).
18) E. Charnery and K. Yamaoka, *Biochemistry*, **21**, 834 (1982).
19) K. Yamaoka and K. Fukudome, *Bull. Chem. Soc. Jpn.*, **56**, 60 (1983).
20) R. Mandel and G. Holzwarth, *Biopolymers*, **12**, 655 (1973).
21) K. Yoshioka and C. T. O'Konski, *Biopolymers*, **4**, 499 (1966).
22) J. C. Bernengo, B. Roux, and D. Herbage, *Biopolymers*, **13**, 641 (1974).
23) S. Umemura, M. Sakamoto, R. Hayakawa, and Y. Wada, *Biopolymers*, **18**, 25 (1979).
24) W. Moffitt, *Proc. Natl. Acad. Sci. U.S.A.*, **42**, 736 (1956).

Dispersibility of Magnetic and Nonmagnetic Iron(III) Oxides in Cyclohexane and Effect of Water on the Stability

Kazuhiko KANDORI,* Akio KAZAMA, Kijiro KON-NO, and Ayao KITAHARA
Department of Industrial Chemistry, Science University of Tokyo, Kagurazaka, Shinjuku-ku, Tokyo 162
(Received January 24, 1984)

The dispersion stability of needlelike and octahedral iron(III) oxides of magnetic or nonmagnetic particles in cyclohexane solutions of sodium 1,2-bis(2-ethylhexyloxycarbonyl)ethanesulfonate (Aerosol OT or AOT) was studied on anhydrous and hydrous systems. The dispersion stability of the anhydrous system was examined for seven kinds of oxides. The sedimentation velocity of dispersions, the histograms of particle distribution, the adsorption of Aerosol OT on the particles and zeta potential were measured. Potential energies of the interaction between a pair of particles were calculated for the anhydrous system. It was suggested from the calculation of potential energies that the magnetic attractive force, which is a function of the strength of the saturation magnetization and the volume of particle, is a main factor affecting the flocculation of the magnetic particles in cyclohexane as well as in 2-butanone reported in the previous papers. The study of the dispersion stability of the hydrous system was done for three kinds of needlelike oxides. The relatively stable region appeared in the lower concentration range of water. The stability decreased at the fixed water concentration followed by marked flocculation ("floc formation" region). It was considered that the appearance of the "floc formation" is caused by the formation of thick hydration layer on the oxide surface and the decrease of zeta potential.

Many data on the stability of colloidal dispersions in nonpolar organic media as well as in water have been accumulated. The stability of colloidal dispersions discussed in water by the DLVO theory[1] has been extended to that in nonpolar organic media.[2-5] The effect of zeta potential of carbon black and titanium oxides on the dispersibility in nonpolar organic media has been discussed.[4,6,7]

The important role of a small quantity of water had also been indicated in nonpolar media. For example, the effect of water on the dispersion of TiO_2 in surfactant solutions in nonpolar media has been reported by Parfitt *et al.*.[7] The effect of water on the dispersibility and the zeta potential for carbon black particles has been also shown in Aerosol OT/cyclohexane solution.[8,9]

On the other hand, the dispersion stability of pigments in polar organic media has recently drawn much attention as seen in paints used for magnetic tapes in the industrial field. However, the fundamental studies of pigment in polar organic media are very rare.[10] The authors have reported the dispersibility of the magnetic particles by two kinds of copolymer dispersants for the anhydrous and the hydrous systems[11-13] and that of the carbon black particles by Aerosol OT[14] in 2-butanone. Hence it seems to be interesting that the dispersibility of the magnetic particles in nonpolar organic media is compared with that in polar organic media published already.[11-13]

In this paper, the dispersions of needlelike and octahedral iron(III) oxides of the magnetic or nonmagnetic particles are prepared in cyclohexane. The sedimentation experiments of dispersions and measurements of adsorption and zeta potential are carried out to study the dispersibility. The characteristic behavior of the sedimentation experiment in the anhydrous system is compared with the calculated data of the potential energies and with the results of the dispersibility in polar organic media. Further study is mainly focussed the effect of water on the stability. Interesting behavior of the dispersibility is compared with the system of the dispersion of carbon black in cyclohexane in the previous paper.

Experimental

Materials. Seven kinds of iron(III) oxides were prepared according to the references.[15-17] Each property of these iron(III) oxides is shown in Table 1. The oxides of Nos. 1—5 were the same samples as used in the previous papers[11-13] and purified similarly.

Cyclohexane used as a solvent was purified and dried from GR-grade material as usual and treated finally with Molecular Sieve 4A to remove any trace of water. Aerosol OT used as a dispersant was commercial grade and was purified according to the previous method.[18]

Preparation of Dispersions. The dispersion was prepared by mixing the particles (0.2 wt%) and the solution of a fixed concentrations of the dispersant(AOT) and water under irradiation with ultrasonic apparatus (Kaijo Denki Co. Model TA-4015, Power Supply 150 W, 20 kHz) for 5 min. No precipitation was observed immidiately after this procedure.

Estimation of Dispersion Stability. The stability of the dispersion was estimated for the anhydrous and hydrous systems by two kinds of sedimentation experiments stated in the previous papers.[11-13] One was the experiment to obtain the sedimentation velocity in sedimentation tubes of the diameter of 1 cm. The other was done with a sedimentation balance in order to verify the dispersion stability obtained by sedimentation tube. The particles were almost distributed over the range of the diameter 0—1 μm in the particle distribution histograms obtained by the latter. So that the median diameter, which seems to be the most partinent parameter to indicate the dispersion stability, was determined from the histograms.[12]

Measurements of Adsorption of Aerosol OT or Water and Zeta Potential. The dispersions of the oxides involving a fixed amount of AOT and/or water(the molar ratio of water to AOT, R=[water]/[AOT], was fixed; that was R=0.5, 1, 2, 3) were shaken for 16 hr at 30±0.1 °C. The concentration of the oxide was 4 wt% for the adsorption of AOT and 0.2 wt% for that of water. The equilibrium concentrations of AOT and water in the supernatant after centrifugation were determined

TABLE 1. PROPERTIES OF IRON(III) OXIDES

No.	Class	Specific surface area (m^2/g)	Saturation magnetization (emu/g)	Saturation magnetization (gauss)	Size Å	Density (g/cm^3)	Volume of a particles (m^3)
1	γ-Fe_2O_3	37.6	68	3674	1470×160	4.3	2.96×10^{-23}
2	α-Fe_2O_3	108	1	46.5	1610×142	3.9	2.55×10^{-23}
3	α-Fe_2O_3	33.1	33[a]	1659	1400×178	4.0	3.48×10^{-23}
4	γ-Fe_2O_3	9.3	62	3400	1820	4.5	3.16×10^{-21}
5	α-Fe_2O_3	8.6	29[a]	1674	1820	4.6	3.16×10^{-21}
6	γ-Fe_2O_3	14.8	72	4072	6736×773	4.5	3.16×10^{-21}
7	α-Fe_2O_3	10.3	0.3	14.7	6770×765	3.9	3.11×10^{-21}

a) α-Fe_2O_3 keeps its magnetization.

by an ultraviolet spectrometer (UV-200 S, Shimadzu Co.) and a Karl-Fischer apparatus, respectively, to calculate the amount of adsorption.

Electrophotoretic mobility was measured by microelectrophoresis with Laser Zee TM Model 500 (PEN KEM Co.) as stated in the previous papers.[11,13,14]

Calculation of Potential Energy. Potential energies between particles were calculated in the anhydrous system according to the methods published in previous paper[12] in order to evaluate the result of the dispersibility of seven kinds of oxides. The octahedral and needlelike particles used in this paper were assumed to be spherical and cylindrical, respectively. The parallel interaction was only considered for the needlelike particles, because it is clear from the previous paper that the parallel interaction is more predominant than the head-tail interaction between the needlelike particles.[12]

Four kinds of potential energies of the interaction between a pair of particles were considered: Steric repulsion between adsorbed layers(V_R^{en}), electrostatic double layer repulsion(V_R^{el}), van der Waals attraction (V_A^{δ} or V_A^{L}) and magnetic attraction (V_A^{M}). They are expressed in following equations (1)—(8).

For Octahedral Particles: i) Steric repulsion between adsorbed layers; Here Ottewill-Walker's equation was utilized:[19]

$$V_R^{en} = \frac{4\pi kTC_v^2}{3v_1^2\rho_2^2}\cdot(\psi_1-\kappa_1)\left(\delta-\frac{H}{2}\right)^2\left(3a+2\delta+\frac{H}{2}\right) \quad (1)$$

where C_v is the concentration of AOT in the adsorbed layer, v_1 is the molecular volume of a solvent, δ is the thickness of an adsorbed layer, ρ_2 is the density of AOT, a is the radius of a particle, H is the shortest distance between the particle surfaces and ψ_1 and κ_1 are entropic and enthalpic parameters of mixing proposed Flory.

ii) Electrostatic double layer repulsion:[20]

$$V_R^{el} = \frac{\varepsilon a^2\zeta^2}{2a+H} \quad (2)$$

where ε is the dielectric constant of a medium and ζ is zeta potential.

iii) Van der Waals attraction; Here Vold's equation was used, considering the effect of adsorbed layer:[21]

$$V_A^{\delta} = -\frac{1}{12}\left\{(\sqrt{A_{22}}-\sqrt{A_{33}})^2\cdot\frac{a+\delta}{H}+(\sqrt{A_{33}}-\sqrt{A_{11}})^2\cdot\frac{a}{H+2\delta}+4a(\sqrt{A_{22}}-\sqrt{A_{33}})(\sqrt{A_{33}}-\sqrt{A_{11}})\cdot\frac{a+\delta}{(H+\delta)(2a+\delta)}\right\} \quad (3)$$

where A_{11}, A_{22} and A_{33} are the Hamaker constants of the oxide, a solvent and AOT adsorbed, respectively.

iv) Magnetic attraction:[22]

$$V_A^{M} = -2\left(\frac{M}{4\pi}\right)^2\frac{v^2}{(2a+H)^3} \quad (4)$$

where M is the saturation magnetization (gauss) and v is the volume of a particle.

For Needlelike Particles: i) Steric repulsion between adsorbed layers:[19]

$$V_R^{en} = \frac{2kTC_v^2}{v_1\rho_2^2}\cdot(\psi_1-\kappa_1)\cdot V \quad (5)$$

where V is the total volume of the overlapping zone of the adsorbed layer.

ii) Electrostatic double layer repulsion:[12]

$$V_R^{el} = \frac{\varepsilon\sqrt{h\kappa}\psi_0^2}{2\pi}\left[\frac{2}{3}\left(\frac{1}{\exp(\kappa H+1)+1}\right)-\frac{1}{\exp(\kappa H)+1}\right)\cdot\times(1+3\kappa H)+2\left\{\left(\frac{1}{\exp(\kappa H)+1}-\frac{1}{\exp(\kappa H+1)+1}\right)\kappa H+\frac{1}{\exp(\kappa H)+1}\right\}+1.142\exp(-\kappa H)-2\exp(-\kappa H-1)\right] \quad (6)$$

where h is the radius of the cylinder of a needlelike particle, H is the shortest distance between the particle surface and κ is the reciprocal Debye length expressed as follows:

$$\kappa = \sqrt{\frac{8\pi nz^2e^2}{\varepsilon kT}} \quad (6')$$

The equation (6) introduced under an assumption of $\kappa h>1$ in the previous paper[12] was approximately used for the cyclohexane system($\kappa h<1$). This approximation can be allowed, because the contribution of this repulsion is comparatively small as seen in Table 3-2.

iii) Van der Waals attraction:[1]

$$V_A^{L} = -\frac{A}{48}\left\{\frac{1}{(H/2)^2}+\frac{1}{(H/2+h)^2}-\frac{2}{(H/2+h/2)^2}\right\} \quad (7)$$

where A is the Hamaker constant of the oxide in cyclohexane. Here the effect of adsorbed layer was neglected.

iv) Magnetic attraction:[12]

$$V_A^{M} = -\left(\frac{M}{4\pi}\right)^2\frac{v^2}{(2h+H)^3} \quad (8)$$

Total potential energy (V_T) of the octahedral and the needlelike particles are calculated by summing the contributions of Eqs. (1)—(4) and Eqs. (5)—(8), respectively.

Results

Effect of AOT on the Stability. The change of the boundary lines between the supernatant and the dispersion (the sediment height) in the sedimentation tube are shown as a function of time for seven kinds of oxides in Fig. 1. Here AOT of 20 mM was used as a dispersant. In

the absence of AOT, all of the dispersions sedimented rapider than Nos. 4, 5, 6 in Fig. 1. This shows the effectiveness of AOT on the stability of iron oxides in cyclohexane. The sedimentation velocity, that is, the gradient of the lines in Fig. 1 was used to discussed the dispersion stability.

In order to examine the effect of AOT concentration on the dispersibility and zeta potential, measurements of the sedimentation and zeta potential were carried out for the magnetic needlelike particle (No. 1). The dependence of the sedimentation velocity and zeta potential on the AOT concentration is indicated in Fig. 2. The amount of adsorbed AOT is also shown in Fig. 2. The dispersion stability is markedly improved by the addition of a small amount of AOT (2—3 mM), as seen in Fig. 2. This concentration is the similar order to the critical micellar concentration of AOT in cyclohexane (1.4 mM).[23] Moreover, at this concentration of AOT, the adsorption reaches approximately the saturation. This correspondence illustrates the effect of AOT molecules adsorbed on the dispersibility of the oxide.

Comparison of the Dispersibility of Seven Kinds of Oxides in Anhydrous System. The following result is seen from Fig. 1. The effect of AOT on the stabilization of the dispersions is remarkable in the system of the needlelike nonmagnetic oxide(No. 2). The dispersibility of the needlelike and magnetic oxides (Nos. 1 and 3) and needlelike and nonmagnetic oxide (No. 7) is considerably improved by the addition of AOT of 20 mM. On the other hand, the dispersibility of the octahedral oxides(Nos. 4 and 5) and the needlelike and magnetic oxide in which particles have large volume(No. 6) is scarcely improved.

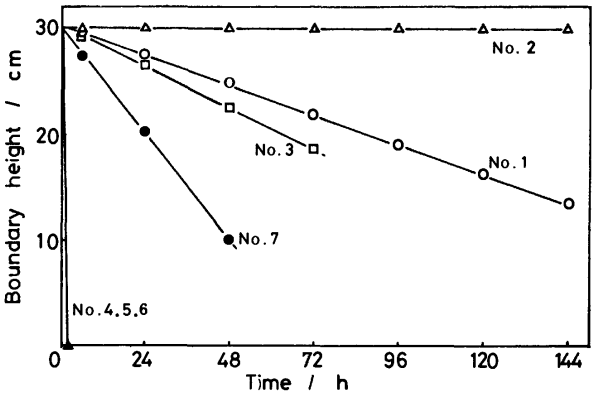

Fig. 1. Plots of Boundary height *vs.* Time. [AOT]=20 mM

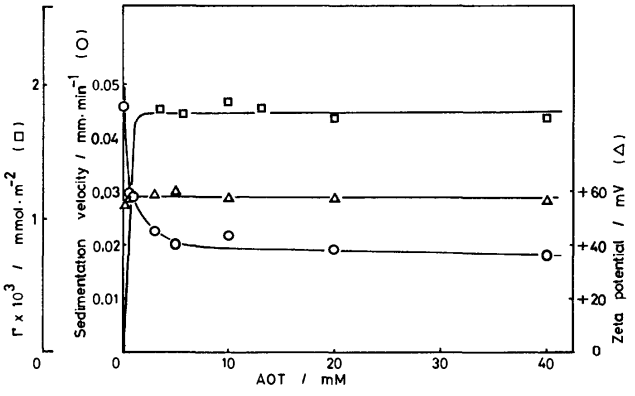

Fig. 2. Relation of the sedimentation velocity (○), zeta potential (△) and amount of adsorbed AOT (□) with Aerosol OT concentration for No. 1 sample.

The result of each measurement for seven kinds of oxides was listed in Table 2 to estimate the dispersibility. Here adsorption isotherms were the Langmuirian type and their Langmuir plots were linear in all cases. The saturation values of adsorption (Γ_m) listed in Table 2 for seven kinds of oxides were obtained from these Langmuir plots. Table 2 shows that the order of the magnitude of the sedimentation velocity is as follows;

$$\text{No. } 6 \simeq 4 > \text{No. } 5 \gg \text{No. } 7 > \text{No. } 3 > \text{No. } 1 > \text{No. } 2 \qquad \text{(A)}$$

The result of (A) agrees with the result of the dispersibility in 2-butanone for Nos. 1—5 oxides stabilized by two kinds of copolymer dispersants,[11] except for the order between No. 3 and No. 1, though the difference between them is minor.

The order of the magnitude of the median diameter in Table 2 obtained by the sedimentation balance is as follows;

$$\text{No. } 6 > \text{No. } 4 > \text{No. } 5 > \text{No. } 3 > \text{No. } 7 > \text{No. } 1 > \text{No. } 2 \qquad \text{(B)}$$

The result of (B) agrees with the result of (A) except for the order between No. 3 and No. 7, though the difference between them is minor.

It is seen in Table 2 that there are not so much differences among the zeta potential of each particle, and the order of the value does not agree with that of the sedimentation velocity. Moreover, the order of the saturation amount of adsorbed AOT does not also agree with that of the sedimentation velocity.

Potential Energy in Anhydrous System. The dispersibility of seven kinds of oxides might be evaluated quantitatively from the magnitude of the total potential energy consisting of repulsive (V_R^n, V_R^l) and attractive (V_A^δ or V_A^L, V_A^M) energies between particles which were expressed by Eqs. (1)—(8).

Numerical values used for each equation were as follows: In Eqs. (1) and (5), $\psi_1-\kappa_1=0.1$[24], $a=1000$ Å, $\rho_1=$

Table 2. Results of each measurement of iron(III) oxides

No.	Sedimentation velocity (mm/min)	ζ-potential (mV)	$\Gamma_m \times 10^3$ (mmol/m²)	D_{med} (μm)
1	0.019	+55.7	1.74	0.898
2	0	+60.0	1.45	0.649
3	0.027	+43.2	1.75	1.65
4	3.00	+40.8	2.06	15.3
5	2.00	+37.5	1.89	9.78
6	3.00	+53.7	1.74	23.5
7	0.068	+57.7	1.44	1.06

1.0 g/cm^3 [25] and C_v was calculated from the following equation for each particle, $C_v=\Gamma_m/\delta \cdot So$, where Γ_m is the saturation amount of adsorbed AOT, δ is the thickness of the adsorbed surfactant molecules(15 Å)[25] and So is the specific surface area of each particle.

In Eqs. (2) and (6), ε=2.02[26] and ζ was listed in Table 2. κ=3132 cm^{-1} was calculated for 20 mM AOT/cyclohexane solution from Eq. (6)′ with the ion concentration(n) obtained by the electric conductivity method described before.[27] In Eqs. (3) and (7), the Hamaker constants were as follows: A_{11}= 2.1×10^{-19} J for particles,[12] A_{22}=5.9×10^{-20} J for solvent,[12] A_{33}=2.5×10^{-20} J for adsorbed layer.[24] The value of A, 4.6×10^{-20} J, in Eg. (7) was calculated from the following equation, $A=(\sqrt{A_{11}}-\sqrt{A_{22}})^2$.

Table 3-1. The potential energy for octahedral particles (unit: kT)

	H/Å	10	20	100
No. 4	V_A^M	-7.76×10^4	-7.55×10^4	-6.7×10^4
	V_A^L	−19.5	−14.6	−6.60
	V_R^{el}	4.51	4.49	4.32
	V_R^{en}	265	66.4	0
	V_T	-7.63×10^4	-7.54×10^4	-6.7×10^4
No. 5	V_A^M	-1.86×10^4	-1.83×10^4	-1.63×10^4
	V_A^L	−19.5	−14.6	−6.60
	V_R^{el}	3.81	3.79	3.65
	V_R^{en}	223	55.8	0
	V_T	-1.84×10^4	-1.83×10^4	-1.63×10^4

Table 3-2. The potential energy of parallel interaction for needlelike particles (unit: kT)

	H/Å	10	20	100
No. 1	V_A^M	−3691	−3109	−1032
	V_A^L	−1068	−254	−5.78
	V_R^{el}	0.246	0.246	0.246
	V_R^{en}	499	178	0
	V_T	−4260	−3180	−1040
No. 2	V_A^M	−0.60	−0.50	−0.15
	V_A^L	−1033	−240	−5.04
	V_R^{el}	0.293	0.293	0.292
	V_R^{en}	361	129	0
	V_T	−672	−111	−4.90
No. 3	V_A^M	−769	−658	−238
	V_A^L	−1136	−278	−6.59
	V_R^{el}	0.149	0.149	0.149
	V_R^{en}	506	180	0
	V_T	−1400	−751	−244
No. 6	V_A^M	-5.3×10^5	-5.1×10^5	-3.8×10^5
	V_A^L	-2.41×10^4	−5914	−234
	V_R^{el}	2.30	2.30	2.30
	V_R^{en}	4769	1689	0
	V_T	-5.49×10^5	-5.14×10^5	-3.80×10^5
No. 7	V_A^M	−6.88	−6.62	−4.95
	V_A^L	-2.40×10^4	−5914	−223
	V_R^{el}	2.66	2.66	2.66
	V_R^{en}	3282	1159	0
	V_T	-2.07×10^4	−4760	−225

In Eqs. (4) and (8), the values in Table 1 (gauss) were used for the saturation magnetization(M).

The results of the calculation for the octahedral particles obtained from Eqs. (1)—(4) and for the needlelike Eqs. (5)—(8) are listed in Tables 3-1 and 3-2, respectively. The dispersibility of the seven kinds of oxides can be discussed quantitatively from the results.

As seen in Table 3-1 for the octahedral particles (Nos. 4, 5), the orders of the energy of the magnetic attractive force(V_A^M) are about -10^4kT, though the orders of the energy of steric repulsion(V_R^{st}) and electric repulsion(V_R^{el}) are about 2×10^2—$5\times10kT$ and below $5kT$, respectively. Therefore, it can be considered that the total potential energies(V_T) are mainly dominated by the magnetic attractive force.

As seen in Table 3-2 for the needlelike particles, the orders of the energy of magnetic attractive force(V_A^M) are about -10^2—-10^3kT for No. 1 and No. 3 oxides. The energy of van der Waals attractive force(V_A^L) is also high, similarly to the magnetic attractive force in the range of the short distance. But it drastically decreases with increase of the distance. The energies of steric repulsion(V_R^{st}) and electric repulsion(V_R^{el}) are relatively low. Hence the total potential energies(V_T) for the highly magnetic and needlelike particles(Nos. 1, 3 and 6) are dominated by both the energies of magnetic attractive force and those of van der Waals attractive force in the region of the short distance between two particles. But they are only dominated by the energy of the magnetic attractive force in the region of the long distance. Fig. 3 shows the potential energy curves for Nos. 1, 2 and 3 oxides as examples.

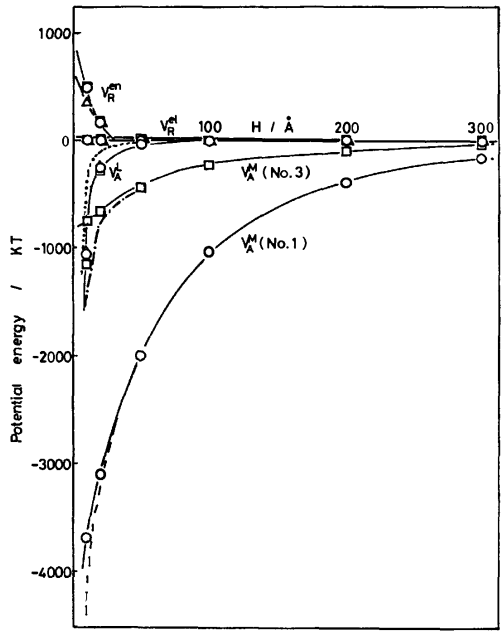

Fig. 3. The potential energy curves of the parallel interaction for three kinds of needlelike particles.

Sample	V_T
○; No. 1	— — — — —
△; No. 2	—— - —— -
□; No. 3	- - - - - - - -

On the other hand, the energy of the magnetic attractive force(V_A^M) for nonmagnetic and needlelike particles(Nos. 2 and 7) is low. So that they are only dominated by the van der Waals attractive force.

Effect of Water on Dispersibility. The effect of water on the stability of dispersions in cyclohexane was investigated in the presence of 20 mM of AOT. The needlelike particles of Nos. 1, 2 and 7 were selected for the study.

The sedimentation velocity, zeta potential and the amount of water adsorbed on the oxide surface are shown as a function of water concentration for Nos. 1, 2 and 7 oxides in Fig. 4. As shown in Fig. 4 the stable region(lower sedimentation velocity) appeared in the lower concentration range of water and the sedimentation velocity suddenly increases in a fixed concentration range. The latter behavior shows the occurrence of rapid flocculation for three kinds of oxides. The concentration region is named the "floc formation" region. Water concentrations of about 60, 100 and 80 mM are the "floc formation" regions for Nos. 1, 2 and 7 oxides, respectively. The similar "floc formation" due to the presence of water was already observed for the hydrophobic carbon black particles [9] and for the iron oxide particles. [13] Zeta potential gradually decreases with increase of the concentration of water.

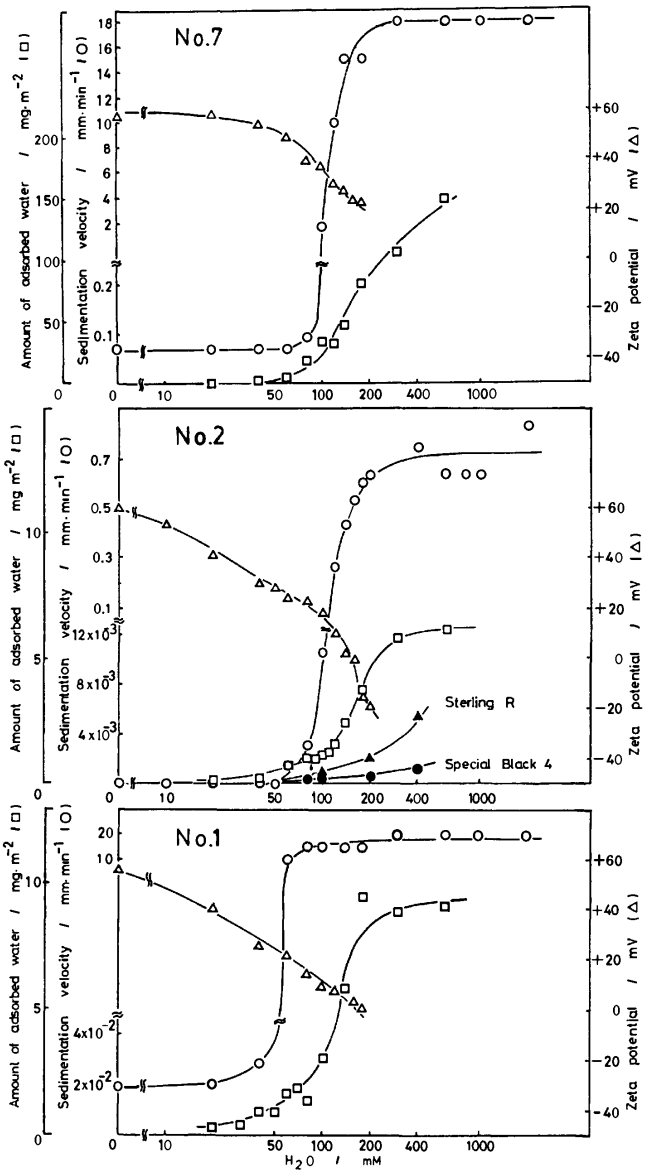

Fig. 4. Change of the sedimentation velocity (○), zeta potential (△) and amount of adsorbed water (□) of Nos. 1,2 and 7 samples with water concentration. [AOT]=20 mM. Fulled mark in the figure is expressing the amount of adsorbed water of carbon black particles (Sterling R and Special Black-4) from Ref. (9). Sterling R: Cabot Co. pH=5.5, Specific surface area=25 m²/g. Special black-4: Degussa Co. pH=2.0, Specific surface area=180 m²/g.

The median diameter(D_{med}), determined from the particle distribution histograms, was shown in Fig. 5 as a function of concentration of water for three kinds of oxides. These results are well correspondent with the results of Fig. 4, though the increase of the median diameter of No. 2 oxide is relatively low.

The amount of adsorbed AOT was shown in Fig. 6 as a function of concentration of water under the constant concentration of AOT(20 mM). The amount of adsorbed AOT gradually decrease with increase of water concentration.

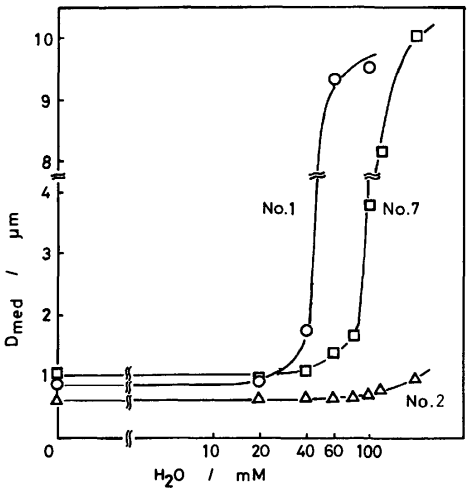

Fig. 5. Change of the median diameter of No. 1, 2 and 7 samples with water concentration.

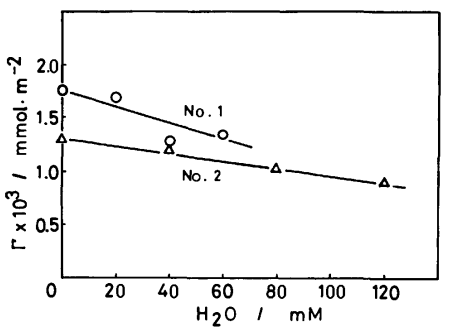

Fig. 6. Change of the amount of adsorbed Aerosol OT for No. 1 and No. 2 samples with water concentration. [AOT]=20 mM.

Discussion

Dispersibility of the Anhydrous Systems. The dispersibility of iron oxides in cyclohexane is stabilized by the addition of AOT as shown in Figs. 1 and 2. However, the difference in the dispersibility of seven kinds of oxides as seen in series (A) or (B) does not correspond with the difference of zeta potential and the amount of adsorbed AOT of each particle in Table 2. This fact was seen in the dispersibility in 2-butanone.[11] It was discussed from the difference in the saturation magnetization and the size of particles. In order to check the applicability of the discussion to this study, the potential energies between the particles were calculate.

The order of the magnitude of the total potential energy, by comparison at the same distance(*i.e.* H=20 Å) in Table 3-1 and 3-2, is as follows:

No. 6>No. 4>No. 5>No. 7>No. 1>No. 3>No. 2 (C)

It is clear that this result of (C) agrees with the results of (A) and (B) expressing the order of the dispersibility except for the No. 3 oxide. This fact shows that the magnetic attractive force, which depends on the strength of the magnetization and the volume of particle, is the main factor affecting the dispersibility of the iron oxides in cyclohexane similarly in 2-butanone.[11,12]

Effect of Water on the Dispersibility. The amount of adsorbed water, as shown in Fig. 4, remarkably increased from a fixed concentration range of water which is approximately coincident with the region of the "floc formation". Hence the occurrence of the "floc formation" is discussed as follows: The thickness of water molecules in hydration layer was calculated from Fig. 4, under an assumption that water molecules would be uniformly adsorbed on the particle surface. The thickness was above 6 molecules for all systems in the region of the "floc formation" from the calculation. So that it can be estimated that the water forms thick hydration layer above this region. The hydration layers formed at the oxide surface would work as a binder between the particles by the strong hydrogen bond among water molecules and would cause the "floc formation". The occurrence of the "floc formation" would be also due to the decrease of the energy of the electric repulsive force, because zeta potential decreases with increase of water concentration as shown in Fig. 4.

The mechanism of the effect of water on the dispersibility as seen in Fig. 4 is considered from the following discussion. In the anhydrous system, AOT molecules would be adsorbed on the oxide surface orienting nonpolar group outside and at the same time excess counter ions(Na^+) are prefferentially adsorbed on the oxide surface to cause the zeta potential positive. On the addition of a small amount of water, a part of water molecules would be adsorbed on the oxide surface and the others would be solubilized in AOT micelles in the bulk solution. With increase of the concentration of water, AOT on the oxide surface would be desorbed and transferred to the swollen micelles due to their strong ion-dipole interaction with water molecules as shown in Fig. 6. The counter ions would be also transferred to the water solubilized in reversed micelles to decrease the zeta potential. Further increase of the concentration of water increases the adsorption of water on the particle surface as well as the increase of the water core in reversed micelles. Zeta potential furthermore decreases by the shift of the slipping plane from the particle surface caused by the formation of the thick hydration layer. So that the dispersion is destabilized by the thick hydration layer and the decreased zeta potential to form "floc formation" region.

It is considered that the difference in "floc formation" regions of Nos. 1 and 2 which was seen in Fig. 4 is caused by the difference of the degree of hydrophilicity. It was described in the previous paper that the degree of hydrophilicity of No. 1 particle is higher than No. 2 particle.[13] The formation of the thicker hydration layer on No.1 particle at lower water concentration is also evidently seen in Fig. 4 for cyclohexane system. This hydration layer works as the attractive force between particles. Moreover, it was also described in the previous papers[12,13] that the energy of magnetic attractive force would not be influenced by the kind of solvents. Hence the magnetic attractive force would operate between No. 1 particles in cyclohexane as well as in 2-butanone. So that No. 1 paticle having higher saturation magnetization will be also causes the strong magnetic attractive forces between the particles in cyclohexane as shown in Fig. 3. Therefore, No. 1 particle flocculate at the lower water concentration than No. 2 particle.

It was reported in the previous paper[9] that carbon black particles (Sterling R and Special Black-4) are restabilized in the water concentration of 800—1000 mM by formation of the weak network structure among carbon black particles and AOT microemulsion. This behavior was not observed for the iron oxide particles in this study. This difference would be due to the difference of the amount of the adsorbed water, the density and the size of each particle. The amount of adsorbed water on the oxide surface is much higer than that on carbon black surface as seen in Fig. 4, due to the difference of the hydrophilicity. This may lead restabilization of the iron oxide difficult.

References

1) E. J. W. Verwey and J. Th. G. Overbeek, "Theory of Stability of Lyophobic Colloids," Elsevier, Amsterdam (1948).

2) J. L. van der Minne and P. H. J. Hermanie, *J. Colloid Sci.*, **7**, 600 (1952).

3) H. Koelmans and J. Th. G. Overbeek, *Discuss. Faraday Chem. Soc.*, **18**, 52 (1954).

4) J. L. van der Minne and P. H. J. Hermanie, *J. Colloid Sci.*, **8**, 38 (1953).

5) D. N. L. McGown and G. D. Parfitt, *Kolloid Z. Z. Polym.*, **220**, 56(1967).

6) J. Briant and B. Bernelin, *Rev. Inst. France Petrole.*, **16**, 1767 (1961).

7) D. N. L. McGown and G. D. Parfitt, *J. Colloid Interface Sci.*, **20**, 650 (1965); D. N. L. McGown and G. D. Parfitt, *Discuss. Faraday Soc.*, **42**, 225 (1966).

8) A .Kitahara, S.Karasawa and H. Yamada, *J. Colloid Interface Sci.*, **25**, 490 (1967).
9) A. Kitahara, T. Tamura and K. Kon-no, *Separation Sci. & Technology.*,**15**, 249 (1981).
10) N. de Rooy, P. L. de Bruyn and J. Th. G. Overbeek, *J. Colloid Interface Sci.*, **75**, 542 (1980).
11) K. Kandori, A. Kitahara and K. Kon-no, *Bull. Chem. Soc. Jpn .*, **56**, 1581 (1983).
12) K. Kandori, K. Kon-no and A. Kitahara, *Nippon Kagaku Kaishi.*, **1983** 963.
13) K. Kandori, A. Kitahara and K. Kon-no, *J. Colloid Interface Sci.,(in print).*
14) K. Kandori, A. Kazama, K. Kon-no and A. Kitahara, *Nippon Kagaku Kaishi* , **1983**, 1562.
15) M. Kiyama, *Funtai oyobi Funmatsu Yakin.*, **23**, 77 (1976).
16) M. Camras, U. S. Patent 2694656 (1954).
17) M. Camras, Kokai Tokkyo Koho, 26-7776 (1951).
18) A. Kitahara and K. Kon-no, *J. Phys. Chem.*, **70**, 3394 (1966).
19) R. H. Ottewill and T. Walker, *Kolloid Z. Z. Polym.*, **227**, 108 (1967).
20) J. Lyklema, *Adv. Colloid Interface Sci.*, **2**, 65 (1968).
21) M. J. Vold, *J. Colloid Sci.*, **16**, 1 (1961).
22) R. E. Rosensweig, J. W. Netor and R. Timmins, AIChE. Symp. Ser., 5, 104 (1965).
23) K. Kon-no and A. Kitahara, *Kogyo Kagaku Kaishi.*, **68**, 56 (1965).
24) D. H. Napper, *Trans. Faraday Soc.*, **64**, 1701 (1968).
25) M. Gobe, K. Kon-no, K. Kandori and A. Kitahara, *J. Colloid Interface Sci.*, **93**, 293 (1983).
26) C. Marsden B. Sc., "Solvent Guide," Cleaver-Hume Press, London, 395 (1963).
27) A. Kitahara, T .Komatsuzawa and K. Kon-no, Proc. Inter. Congr. Surface Active Substances, vol. II, 135 (1968).

 © 1984 The Chemical Society of Japan Bull. Chem. Soc. Jpn., 57, 1784—1788 (1984) [Vol. 57, No. 7

Photoelectron Angular Distribution and Assignment of Photoelectron Spectrum of Ozone

Shunji KATSUMATA,* Haruo SHIROMARU, and Toshiaki KIMURA
Physical Chemistry Laboratory, Institute of Applied Electricity, Hokkaido University, Sapporo 060
(Received February 3, 1984)

For the first three ionized states of ozone the ordering of $^2A_1$, $^2B_2$ and $^2A_2$ states has so far been controversial both experimentally and theoretically. The present work establishes assignment of the $^2A_2$ state by using the characteristic of electron energy dependence of an asymmetry parameter (β) of photoelectron angular distribution measured with NeI, HeI, and NeII resonance radiation. From measurements of photoelectron spectra of ozone with NeI, HeI, and HeII radiation, we newly find that two bands centered at 16.50 and 17.6 eV exhibit vibrational structures with the spacings of about 850 and about 1000 cm^{-1}, respectively. Furthermore abnormally weak bands are also confirmed at 22.7, 24.1, and 26.8 eV in the HeII spectrum.

Three studies of ozone by a high resolution VUV photoelectron (PE) spectroscopy have so far been reported in the literature,[1-3] except a work performed at a low resolution.[4] There appears disagreement concerning the identification of PE bands and vibrational spacings and orbital assignment of bands. For example, Frost *et al.*[1] and Brundle[2] reported four and five bands in the HeI spectrum, respectively, but Dyke *et al.*[3] identified eight bands including weak bands. Furthermore, Dyke *et al.* estimated the adiabatic ionization energy (IE) of the first band to be 12.44 eV, whereas other workers assigned it to 12.53,[1] 12.56[2] and 12.519 eV[5] as the corresponding value, respectively. For a vibrational structure of the third band at 13.57 eV, Frost *et al.* and Dyke *et al.* suggested that the bending mode is excited, but their values for the vibrational spacing are not equal. Brundle, on the other hand, concluded that the stretch mode is excited in the band.

We suppose that sources inducing the disagreement may be as follows; i) the sample of ozone was mainly contaminated with oxygen, ii) some PE bands due to ozone are weak and diffuse, and iii) the π biradical nature (predicted to be about 23% theoretically[6,7]) of the ground state of ozone makes the orbital assignment of bands difficult.

In order to explain the PE spectrum of ozone, various theoretical calculations[8-15] which go beyond the single-configuration SCF approximation have so far been carried out, but the calculated results are not always consistent, as described by Cederbaum *et al.*[13] Particularly for the first two PE bands at 12.75 and 13.02 eV,[3] the energy difference is so small that the assignment of the ionic states could not be deduced definitely even if the most reliable theoretical calculation is carried out. Therefore, Cederbaum *et al.*[13] and Maloquist *et al.*[15] calculated each vibrational structure of the first three PE bands to assign by comparison with the experimental PE bands. However, the calculated vibrational structures by them disagree for the $^2A_1$ and $^2B_2$ states and the proposed assignments also differ. In addition to the first three PE bands, observation of some shake-up or CI bands is predicted from the theoretical calculations taking account of configuration interaction (CI).

In the present study, we measured NeI, HeI, and HeII PE spectra at a high resolution using a very pure sample of ozone in order to establish the PE bands of ozone. For the first three PE bands, measurements of the photoelectron angular distribution parameter (β) were also carried out at NeI, HeI, and NeII radiation in order to determine the nature of their bands unambiguously by using the characteristics of the photon energy dependence of β.

Experimental

The photoelectron angular distribution of free molecules for unpolarized radiation is given by

$$J(\theta) \propto 1 + \frac{1}{2}\beta\left(\frac{3}{2}\sin^2\theta - 1\right) \quad (1)$$

where $J(\theta)$ is the photoelectron intensity, θ is the angle between the incoming photons and the outgoing photoelectrons, and β is the asymmetry parameter ranging between -1 and 2. In order to obtain β values, the photoelectron spectra were measured at θ=90° and 135° using NeI, HeI, and NeII radiation, with a photoelectron spectrometer (VG Scientific Ltd., model ADES-400), as described previously.[16,17] The energy resolution of about 120 meV was used to increase photoelectron counts and to measure in the short time for avoiding a variation of a sample pressure. On the other hand, NeI, HeI, and HeII spectra of ozone were recorded using a PE spectrometer (JASCO Ltd., model PE-1A) described elsewhere.[18] An energy resolution was about 25 meV for NeI and HeI spectra and about 70 meV for HeII spectrum. A full spectrum was usually measured with a scan voltage of 5 or 7 mV per one channel. Each of two PE spectrometers mentioned above was connected to a microcomputer system in order to control a scan voltage, a sample pressure and rotation of a turn table putting an analyzer for angular distribution measurement, automatically. Data were stored in a multichannel scaler and processed by use of a microcomputer (NEC COMPO BS/80) equipped with a floppy disk drive, an X-Y plotter and a printer. The multichannel scaler and the controller for driving pulse motors were home-made.

The ozone used in this work was produced from oxygen in a commercial ozonizer (NIPPON OZONE Ltd., type 0-1-2), stored by adsorbing on nonindicating silica gel at −196 °C (liq. N_2) and purified by pumping off oxygen. The glass vessel containing the adsorbed ozone, equipped with a teflon needle valve, was then connected to the spectrometer. The ozone was introduced into the spectrometer at the required pressure through the teflon needle valve, by raising the temperature of the vessel to about −80 °C by ethanol-liq. N_2. In the case of using the JASCO spectrometer, the ozone encounters no metal except for an ionization chamber coated

by an aquadag, but little amount of the residual oxygen was measured all the time. In the case of using the VG spectrometer equipped with a stainless steel needle valve and a copper inlet tube, the decomposition of ozone was also found not to affect the value. Argon was used for the energy calibration.

Results

Figure 1A shows the HeI photoelectron spectrum of ozone obtained here which is partially contaminated by a little amount of the residual oxygen. The oxygen contamination was easily identified since more amount of oxygen was observed at early stage of measurement. Fig. 1C exhibits the PE spectrum of pure ozone obtained by subtracting the pure oxygen spectrum (Fig. 1B) from Fig. 1A. We tentatively classified the PE bands into two types by their intensities. Individual ionization bands in Fig. 1C are indicated by solid lines with the numerals or alphabet at their band maxima which correspond to vertical ionization energies. Numerals are used for the bands with normal intensity in the spectrum while alphabet is used for the abnormally weak band which must be shake-up or CI band.

The first three bands in the 12—14 eV region are known to exhibit complex vibrational structures. The interpretation of the vibrational spacing and the orbital assignmet for these bands have so far been controversial. Figure 2 shows the first three bands measured with a scan voltage of 1 mV per one channel. Then, analyses of the vibrational separations elucidate that there are three ionized states in the 12—14 eV region. Furthermore, the adiabatic IE value of the first ionized state is confirmed to be 12.43 eV as shown in Fig. 2, in agreement with the value of Dyke *et al.*[3] The vibrational structures will be discussed in detail later.

It should be noted that the vibrational structure centered at 16.5 eV (band 4) is fairly resolved in this work, which was not reported in the previous papers.[1-4] Figure 3 exhibits the expanded PE bands measured with a scan voltage of 1 mV, and there the two vibrational structures are identified with the spacings

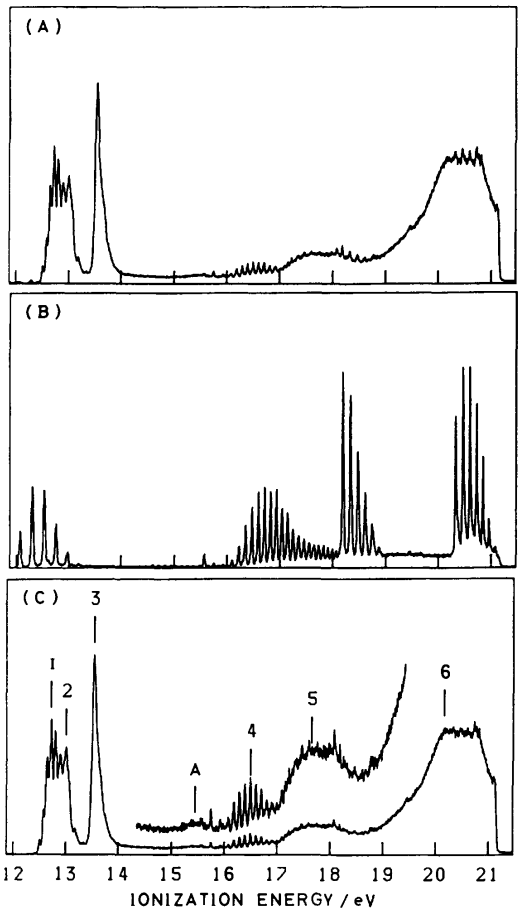

Fig. 1. HeI photoelectron spectrum of (A) ozone sample, (B) oxygen and (C) ozone obtaind by subtracting (B) from (A). Solid line indicates the maximum of the band.

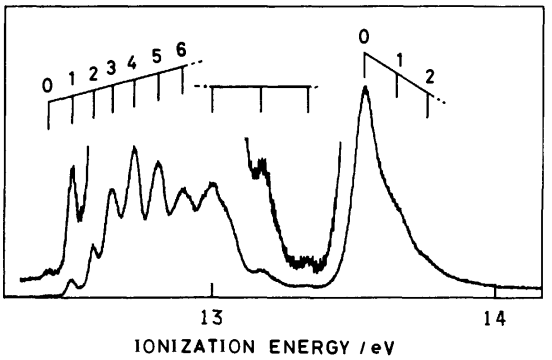

Fig. 2. Expanded scale spectrum of the first three bands 1 to 3 in the HeI spectrum of ozone.

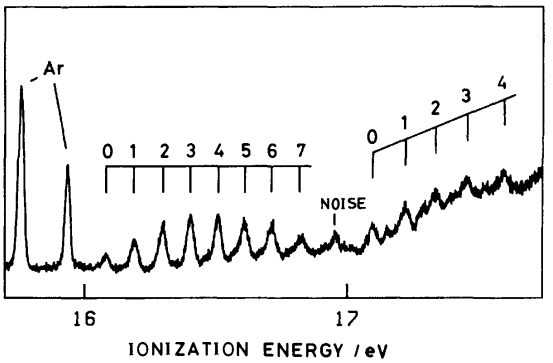

Fig. 3. Expanded scale spectrum of the bands 4 and 5 in the HeI spectrum of ozone.

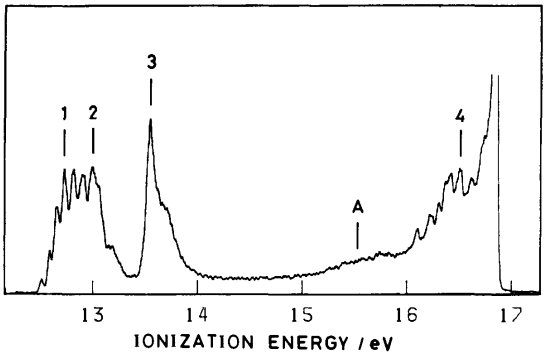

Fig. 4. NeI photoelectron spectrum of ozone.

TABLE 1. ASYMMETRY PARAMETER (β) AND ASSIGNMENT OF THE FIRST THREE PHOTOELECTRON BANDS OF OZONE

Band	Experimental I_v (eV)	Ionic state	β value NeI	β value HeI	β value NeII	Theoretical assignments References [8,9,11,14]	[10,13]	[12,15]
1	12.73[a]	1^2A_1	0.31	0.15	0.69	1^2A_1	1^2A_1	1^2B_2
2	13.00	1^2B_2	0.29	0.11	0.69	1^2B_2	1^2A_2	1^2A_1
3	13.54	1^2A_2	−0.31	0.10	0.87	1^2A_2	1^2B_2	1^2A_2

a) The adiabatic ionization energy is 12.43 eV.

TABLE 2. COMPARISON OF EXPERIMENTAL IONIZATION ENERGIES WITH THEORETICAL RESULTS FOR THE PE BANDS IN THE REGION BETWEEN 14 AND 28 eV

Band	Experimental I_v (eV)	Theoretical results[d] Ref. 14		Ref. 10	
A	15.6	2^2B_2	15.19 (1.6)	$^2B_2$	16.45 (1.2)
4	16.50[a]	2^2B_1	17.17 (44.9)	$^2B_1$	15.91 (44.4)
5	17.6[b]	3^2A_1	18.20 (28.1)	$^2A_1$	17.61 (39.3)
		4^2B_2	18.67 (15.6)	$^2B_2$	19.02 (13.2)
				$^2B_2$	19.40 (29.9)
6	19.4[c]	5^2B_2	20.13 (6.4)	$^2A_1$	20.34 (2.3)
		5^2A_1	20.35 (24.5)	$^2A_1$	21.69 (6.2)
		6^2A_1	21.57 (2.5)	$^2B_2$	22.08 (33.2)
	20.00	6^2B_2	21.65 (47.1)	$^2A_1$	22.58 (14.4)
		5^2B_1	22.28 (42.6)	$^2B_1$	22.95 (33.2)
	20.8[c]	7^2B_2	22.42 (22.3)	$^2A_1$	23.12 (22.9)
		7^2A_1	22.56 (31.9)	$^2A_1$	23.84 (5.3)
B	22.7				
C	24.1				
D	26.8				

a) The adiabatic IE is 16.09 eV. b) The adiabatic IE is 17.10 eV. c) Shoulders of band 6. d) The ionic states and the I_v's (eV) are shown with the monopole intensities multiplied by one hundred in the parentheses.

of about 850 and 1000 cm^{-1}, respectively. The NeI spectrum shown in Fig. 4 also displays the vibrational structure near 16.5 eV although the spectrum is complicated by NeI (16.67 and 16.85 eV) resonance lines. The weak and diffuse band at 15.6 eV (band A) indicated by Dyke *et al.* could be also certified in the NeI and HeI spectra in this work. Concerning other bands, our HeI and NeI spectra are in good agreement with the previous ones.

The HeII spectrum of ozone shown in Fig. 5 is in fair agreement with that reported by Dyke *et al.*[3] They however suggested only a very weak band at 24.7 eV (corresponding to the band C) in the region between 21 and 28 eV. As can be seen in Fig. 5, the bands B and D were found as well as the band C. The ionization energies determined in this work are listed in Tables 1 and 2.

Concerning photoelectron angular distribution, the experimental NeI and HeI β values for the first three bands are plotted against ionization energy in Fig. 6, together with the HeI spectrum obtained at θ=90°. The HeI β values for the three vertical IE peaks are commonly about 0.1, and the NeI β values for the first and second peaks are also about 0.3 similarly. However,

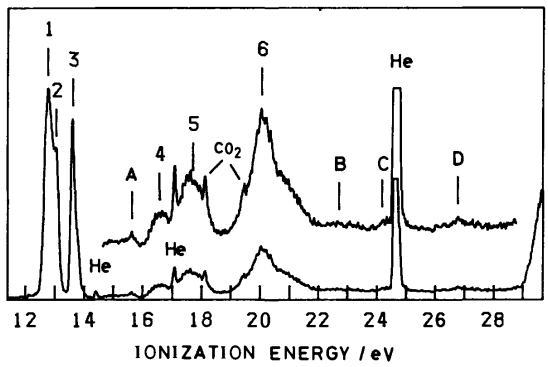

Fig. 5. HeII photoelectron spectrum of ozone.

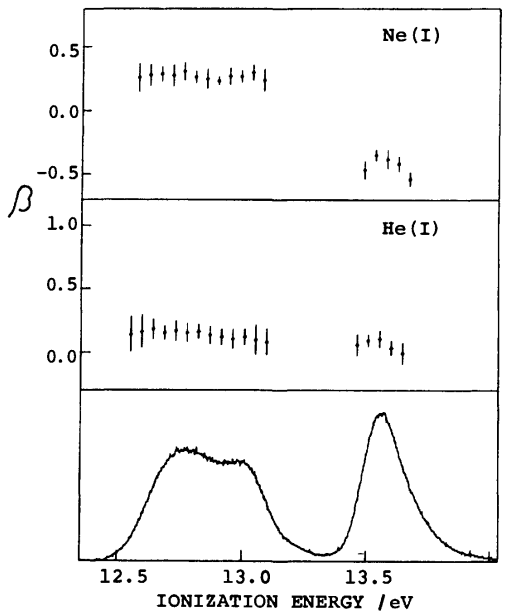

Fig. 6. Plots of experimental β values of ozone obtained for NeI and HeI radiation in the first three bands, and HeI photoelectron spectrum obtained at θ=90°.

the NeI β value (−0.31) for the third peak is quite different from those of them.

Discussion

The PE Bands in the 12—14 eV Region. It is of no doubt from the PE spectra mentioned above that there are three bands in the 12—14 eV region. The assignment for the first three ionic states of ozone presents an interesting problem for theoretical

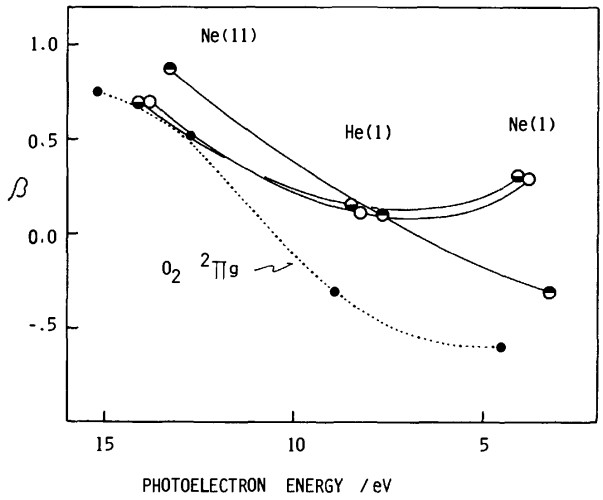

Fig. 7. Photoelectron energy dependence of β for (◒) band 1, (○) band 2 and (◓) band 3 of ozone and for (●) the $^2\Pi_g$ band of oxygen.

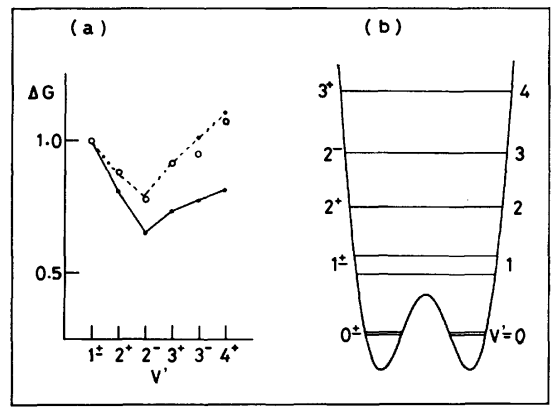

Fig. 8. (a) Plots of the relative vibrational spacing against vibrational quantum number for the first ionized state. Open circle shows the experimental value; solid line, the theoretical value taken from Ref. 23 in the case of $\rho=0.6$ and $B=1.2$; dotted line, corrected with anharmonicity. (b) Potential curve and vibrational levels in the case of solid line in (a).

treatments of correlation and/or reorganization effects. If Koopmans' theorem[19] is assumed, the order of increasing ionization energy would be $1a_2$ (13.24 eV), $6a_1$ (15.01 eV) and $4b_2$ (15.39 eV) from *ab initio* SCF MO calculation.[14] However, the order of the ionic states suggested previously by both experimental and theoretical studies is either the $^2A_1$, $^2B_2$, and $^2A_2$ state or the $^2A_1$, $^2A_2$, and $^2B_2$ state, predicting a breakdown of Koopmans' theorem because of the π biradical nature of the initial state.

The a_2 orbital of ozone consists of a simple combination of the p_π terminal oxygen orbitals and it is very similar to the $1\pi_g$ orbital of oxygen molecule. Our aim is to determine the a_2 orbital by using the characteristic of the photoelectron energy dependence of β. Fig. 7 shows plots of β values obtained at NeI, HeI, and NeII radiation for the three vertical IE peaks, together with that of β for the $v'=1$ peak of the $1\,^2\Pi_g$ ionic state of oxygen molecule.[20,21] The peak of $v'=1$ for oxygen involves no autoionization effect at NeI radiation.[20] It is found from Fig. 7 that the β curve for the third peak of ozone has higher slope than those for others and is quite similar to that for the $^2\Pi_g$ state of oxygen molecule. Therefore, the third ionized state of ozone must be assigned to the $^2A_2$. Next problem is the order of the first two ionized states which should be either the $^2A_1$ and $^2B_2$ or the $^2B_2$ and $^2A_1$. It should be determined by analysis of the vibrational spacing.

Concerning the vibrational structure of the two bands in the 12—13.4 eV region, Fig. 2 exhibits easily distinguishable two vibrational progressions which consist of seven peaks in the low region of 12.43 up to 12.91 eV and three peaks in the high region of 13.00 to 13.34 eV. For the first progression, the relative vibrational spacing (ΔG) between the adjacent peaks from $v'=0$ up to 6 is irregular as shown by open circle in Fig. 8a, which exhibits the minimum value of 540 cm^{-1} at the third spacing and gradually increases toward higher quanta. The averaged separation is about 640 cm^{-1} and assigned to the bending mode, ν_2, which is 719 cm^{-1} in neutral ozone.[22] The irregular spacing obtained in this work is in good agreement with that reported by Dyke *et al.*[3] who suggested that the Renner-Teller effect contributes to the irregularity.

We investigated the irregular spacing on the basis of the double-minimum potential method proposed by Coon *et al.*[23] If parameters $\rho=0.6$ and $B=1.2$ are used, individual spacings are displayed by a solid line in Fig. 8a according to the notation of v' by Coon *et al.* Furthermore, the experimental spacings are better reproduced by taking account of an anharmonicity of $2X'h\nu(v'+1)$, as shown by dotted line in Fig. 8a. Then the estimated separation, $h\nu$, is 690 cm^{-1} and assigned to the bending mode ν_2. Figure 8b shows the double-minimum potential and the vibrational levels obtained here by use of $\rho=0.6$ and $B=1.2$. The barrier height at $\phi=180°$ (linear ozone) is about 830 cm^{-1} corresponding to about one vibrational energy. The positions of the minima give the angle of an equilibrium geometry of the ionized state of ozone. The angle was obtained as about 170° and is very different from that (116.8°) of the neutral ozone.[22] This fact clearly predicts that Franck-Condon factors between the ionized state and the neutral ground state do not reproduce the experimental results at all, in spite of the satisfactory reproducibility of vibrational spacing. As the result, we must conclude that the irregular spacing can not be explained by the model such as the Renner-Teller effect but possibly results from an anharmonicity such as some potential change near an equilibrium geometry of the cation.

For the second band, the peak at 13.00 eV displaying a shoulder in the high energy side allows us to predict the partial overlap of the progression belonging to the first band. The first two spacings between the adjacent peaks at 13.00 up to 13.34 eV are 1380 and 1330 cm^{-1}, respectively, and assigned to the symmetric stretch mode, ν_1 (1124 cm^{-1} in neutral[22]). The vertical IE value of the second ionic state is naturally assigned to be 13.00 eV. The adiabatic IE value however seems not to be the same as the vertical one because the spectral pattern of the first band exhibits such change as an

increase of the background in the region above the peak of $v'=5$.

Concerning the third band at 13.54 eV, the vibrational structure is badly broadened but is still resolved as a faint structure. The broadening may be brought about by a predissociation[5] as one of some possibilities. The averaged separation is about 900 cm^{-1}, being in better agreement with the value (900 cm^{-1}) of Brundle[2] than that (800 cm^{-1}) of Dyke *et al.*[3] The vibration may be assigned to the ν_1.

Considering the vibrational structure of the first three ionic states, the excitation of the bending mode must be due to ionization from the angle-determining a_1 orbital, so that the first band may be assigned to the $^2A_1$ state. Since the third band is assigned to the $^2A_2$ state from the result of the photoelectron angular distribution, the second band must be the $^2B_2$ state. Experimental asymmetry parameters and assignment for these bands are summarized in Table 1 in comparison with theoretical assignments.

The PE Bands in the 14—28 eV Region. The bands observed in the region above 14 eV can be classified into two types by their intensities. First, the bands 4—6 with normal intensity are obtained at 16.5, 17.6, and 20.0 eV, respectively, and secondly, the CI bands *A*—*D* with abnormally weak intensity appear at 15.6, 22.7, 24.1, and 26.8 eV, respectively. In order to interpret these bands, we consider it most useful to refer to available theoretical results calculated by *ab initio* CI methods.[10,14] Their results are compared in Table 2. The theoretical calculations by Basch[10] and Kosugi *et al.*[14] presented both the ionization energies and the monopole intensities which wholly seem to be in good agreement with the experimental results.

Let's consider the bands 4 and 5. According to the calculated results by Refs. 10 and 14, the band 4 corresponds to the $^2B_1$ ionic state. As can be seen from Fig. 3, this band has the vibrational spacing of about 850 cm^{-1} of which value is almost constant over the eight vibrational peaks. Hence, the vibration may be predicted to be the stretch mode ν_1 weakened by ionization from the strong bonding orbital of $1b_1$, rather than a bending mode. The band 5 exhibits a faint vibrational structure of about 1000 cm^{-1} associated with stretch mode in the low energy region, as shown in Fig. 3. The band seems to consist of overlapping bands due to two ionized states at least since it is broad and intense. This expectation is in good agreement with the theoretical results, one of which predicts two ionized states of $^2A_1$ and $^2B_2$, as listed in Table 2.

The band 6 centered at 20.00 eV exhibits two shoulders at 19.4 and 20.8 eV. According to the theoretical results, this band must correspond to many ionized states. Two theoretical results available are not consistent with each other and definite assignment of this band will be also impossible experimentally.

Concerning the abnormally weak CI bands, the band A at 15.6 eV may be assigned to the $^2B_2$ state as predicted by the theoretical results.[10,14] The other CI bands B—D must be interpreted by some theoretical calculations involving configuration interaction.

We would like to thank Mr. Y. Shindo in this Institute for his cooperation in constructing controllers and interfaces for the micro computer system. We also thank Professor S. Iwata in Keio University for drawing our attention to this work.

References

1) D. C. Frost, S. T. Lee and C. A. McDowell, *Chem. Phys. Lett.*, **24**, 149 (1974).
2) C. R. Brundle, *Chem. Phys. Lett.*, **26**, 25 (1974).
3) J. M. Dyke, L. Golob, N. Jonathan, A. Morris, and M. Okuda, *J. Chem. Soc. Faraday Trans. 2*, **70**, 1828 (1974).
4) T. N. Radwan and D. W. Turner, *J. Chem. Soc. A*, **1966**, 85.
5) M. J. Weiss, J. Berkowitz, and E. H. Appelman, *J. Chem. Phys.*, **66**, 2049 (1977).
6) J. Hay and T. H. Dunning Jr, *J. Chem. Phys.*, **67**, 2290 (1977).
7) W. D. Laidig and H. F. Schaefer III, *J. Chem. Phys.*, **74**, 3411 (1981).
8) H. Sambe and R. H. Felton, *J. Chem. Phys.*, **61**, 3862 (1974).
9) D. P. Chong, F. G. Herring, and D. McWilliams, *J. Electron Spectrosc. Relat. Phenom.*, **7**, 445 (1975).
10) H. Basch, *J. Am. Chem. Soc.*, **97**, 6047 (1975).
11) P. J. Hay, T. H. Dunning Jr., and W. A. Goddard III, *J. Chem. Phys.*, **62**, 3912 (1975).
12) R. P. Messmer and D. R. Salahub, *J. Chem. Phys.*, **65**, 779 (1976).
13) L. S. Cederbaum, W. Domcke, W. Von Niessen, and W. P. Kraemer, *Mol. Phys.*, **34**, 381 (1977).
14) N. Kosugi, H. Kuroda, and S. Iwata, *Chem. Phys.*, **58**, 267 (1981).
15) P-A. Malquist. H. Agren, and B. O. Roos, *Chem. Phys. Lett.*, **98**, 444 (1983).
16) S. Katsumata, K. Mitani, and H. Shiromaru, *Chem. Phys. Lett.*, **75**, 196 (1980).
17) S. Katsumata, H. Shiromaru, K. Mitani, S. Iwata, and K. Kimura, *Chem. Phys.*, **69**, 423 (1982).
18) K. Kimura, S. Katsumata, Y. Achiba, T. Yamazaki, and S. Iwata, "Handbook of HeI photoelectron spectra of fundamental organic molecules," (Japan Scientific Societies, Tokyo, 1981).
19) T. Koopmans, *Physica*, **1**, 104 (1934).
20) T. A. Carlson, *Chem. Phys. Lett.*, **9**, 23 (1971).
21) D. G. McCoy, J. M. Morton, and G. V. Marr, *J. Phys. B*, **11**, L547 (1978).
22) T. Tanaka and Y. Morino, *J. Mol. Spectrosc.*, **33**, 538 (1970).
23) J. B. Coon, N. W. Naugle, and R. D. McKenzie, *J. Mol. Spectrosc.*, **20**, 107 (1966).

Simple Estimation of Ionization Energies. An Improvement of Koopmans' Approximation by Scaling

Makoto ISIHARA
Department of General Education, Shotoku-Gakuen Women's Junior College, Nakauzura 1-38, Gifu 500
(Received February 13, 1984)

A simple method of estimating ionization energies is proposed, formulation being made for atomic systems. The method aims at improving Koopmans' approximation by incorporating a scale factor into Koopmans' variation problem for the hole state in the space built of the occupied Hartree-Fock manifold of the parent state. The shrinking of the electronic cloud through ionization is effectively taken into account with the scale factor; the scaling makes the hole state fulfil the virial theorem. Numerical examples are given for valence-shell and core ionizations of several atomic systems. The results are encouraging on the whole. The attendant concepts, the quasiparticle ejection energy and the global correction, seem to be helpful in understanding the electronic behavior through ionization.

The ionization energy can be obtained, in principle, by subtracting the parent state energy from the hole state one calculated separately;[1] the problem is thus ascribed to the calculation of state energies with sufficient accuracy. Surely this way of thinking is orthodox, but we have to endure two disadvantages. One is not essential but practical; the laboriousness to keep high accuracy through subtraction of two nearly equal large numbers. The other is conceptual; the loss of intuitive and intimate understanding of the ionization energy as a physical quantity. Here it is neither suitable nor possible to give an adequate bibliography of state energy calculations;[2] we only list a few interesting devisals[3,4] and a practical approximate method based on the Rayleigh-Schrödinger perturbation theory[5] in references.

Nowadays we already have several elaborate methods of directly evaluating ionization energies of atoms and molecules, the Green's function methods,[6-10] the equation-of-motion methods,[11,12] and so on.[13,14] The perturbation analysis has arrived at a fairly high stage.[13,15,16] All of these elaborate methods, however, require relevant knowledge of unoccupied orbitals in order to display their own superior abilities; the knowledge is almost exclusively unavailable from the Hartree-Fock (HF) calculation for the parent state.

As a standard method without use of explicit knowledge of unoccupied orbitals we have what is called ΔSCF method.[17,18] Subtraction of two nearly equal large numbers being avoided in its variant the transition operator method for the ΔSCF calculation,[19] we must still perform separate self-consistent-field (SCF) calculations for each hole state of interest besides the parent state. Though ΔSCF method is a natural approximation to "separate energy calculations for individual states" mentioned above, its essential consists in meticulous consideration of the electronic reorganization effect with complete neglect of the correlation energy change; we can sometimes obtain rather comfortable estimates from Koopmans' relation[20] because of fortunate cancellation between the reorganization and correlation corrections.

Of course, we should rely on elaborate methods to reproduce or to predict experimental values accurately.[10] Simple or, in another word, handy estimations are, nevertheless, not to be despised from both practical and conceptual points of view. Especially, those of clear physical grounds advance our knowledge of both the quantity and the system under consideration.

Koopmans' relation results from the variation problem within the hole state space built of the occupied HF manifold of the parent state.[20-22] An extension to the case of the correlated parent state has been attempted[22] and analyzed.[23] Now cannot we effectively enrich Koopmans' variation problem only by introducing some additional variation parameter?

In this paper, confining ourselves to atomic systems, we propose a simple method of estimating ionization energies, where a scale factor[24] is incorporated into Koopmans' variation problem as an additional variation parameter. The motivation stems from the observation that the hole state in Koopmans' treatment does not fulfil the virial theorem[24,25] which we think a fundamental requisite for approximate states to be well-behaved. The scaling to make the virial theorem hold in the hole state is a key of the present method. Our confinement to atomic systems should not be regarded as an intrinsic restriction but is a setting for the compact presentation of the essential of the method.

Method

Throughout this section we work within the spin unrestricted picture, calling spinorbitals merely orbitals. Let $\{\phi_p\}$ be canonical orbitals obtained from the HF calculation for the parent state. The scaled orbitals $\{\phi_p^\lambda\}$ are constructed with a real scale factor λ as

$$\phi_p^\lambda(\boldsymbol{r}) = \lambda^{3/2}\phi_p(\lambda\boldsymbol{r}), \tag{1}$$

where $\boldsymbol{r}$ stands for the spatial coordinate. The orthonormality is preserved in the sense that

$$\int \phi_p^{\lambda *}\phi_q^\lambda \mathrm{d}\tau = \delta_{pq}, \tag{2}$$

the integration running over the spin and spatial coordinates. Denoting the creation and annihilation operators for ϕ_p^λ as $a_p^{\lambda\dagger}$ and a_p^λ, respectively, we can write the electronic Hamiltonian in the second quantized form as

$$H = \sum_{pq} (\lambda^2 t_{pq} + \lambda v_{pq}) a_p^{\lambda\dagger} a_q^{\lambda} + \frac{\lambda}{2} \sum_{pqrs} v_{qs}^{pr} a_p^{\lambda\dagger} a_r^{\lambda\dagger} a_s^{\lambda} a_q^{\lambda}, \tag{3}$$

where

$$t_{pq} = \int \phi_p^*(-\Delta/2)\phi_q d\tau, \tag{4}$$

$$v_{pq} = \int \phi_p^*(-Z/|\boldsymbol{r}|)\phi_q d\tau, \tag{5}$$

and

$$v_{qs}^{pr} = \iint \phi_p^*(\boldsymbol{r})\phi_r^*(\boldsymbol{r}')(1/|\boldsymbol{r}-\boldsymbol{r}'|)\phi_s(\boldsymbol{r}')\phi_q(\boldsymbol{r}) d\tau d\tau'. \tag{6}$$

Here Z is the atomic number.

Let us label the occupied orbitals in the parent state with the indices $\{i, j, k, l\}$ and introduce the notation for the scaled HF state

$$|N,\lambda\rangle = \prod_j a_j^{\lambda\dagger} |\text{vacuum}\rangle. \tag{7}$$

The parent state, written in the above notation as $|N,1\rangle$, has the energy

$$E_N = \langle N,1|H|N,1\rangle = T + V \tag{8}$$

with

$$T = \sum_j t_{jj} \tag{9}$$

and

$$V = \sum_j (v_{jj} + \sum_k (v_{jk}^{jk} - v_{kj}^{jk})/2). \tag{10}$$

We postulate that the parent state already satisfies the virial theorem;[25]

$$2T + V = 0. \tag{11}$$

On the other hand, our trial hole state is prepared in the form

$$|N-1,\lambda,\boldsymbol{C}\rangle = \sum_j c_j^* a_j^{\lambda} |N,\lambda\rangle, \tag{12}$$

where $\boldsymbol{C}$ stands for $\{c_j\}$. This trial state is, of course, orthogonal to the parent state $|N,1\rangle$, since they are different eigenstates of the number of electrons. Regarding λ and $\boldsymbol{C}$ as variation parameters, we would like to minimize the expectation value

$$\begin{aligned} E_{N-1}(\lambda,\boldsymbol{C}) &= \langle N-1,\lambda,\boldsymbol{C}|H|N-1,\lambda,\boldsymbol{C}\rangle \\ &= \lambda^2(T - \sum_{jk} c_j^* c_k t_{jk}) + \lambda(V - \sum_{jk} c_j^* c_k u_{jk}) \end{aligned} \tag{13}$$

with

$$u_{jk} = v_{jk} + \sum_i (v_{ki}^{ji} - v_{ik}^{ji}) \tag{14}$$

under the normalization constraint

$$\langle N-1,\lambda,\boldsymbol{C}|N-1,\lambda,\boldsymbol{C}\rangle = \sum_j c_j^* c_j = 1. \tag{15}$$

This conditional extremum problem can be treated easily as an unconditional one by Lagrange's undetermined multiplier method. Noting that $\{t_{jk}\}$ and $\{u_{jk}\}$ are hermitian, we resultantly arrive at the following system of equations with a real multiplier ω.

$$\begin{cases} \lambda = \left(-\frac{1}{2}\right)(V - \sum_{jk} c_j^* c_k u_{jk})/(T - \sum_{jk} c_j^* c_k t_{jk}) & (16) \\ \sum_k (\lambda^2 t_{jk} + \lambda u_{jk}) c_k = \omega c_j & (17) \end{cases}$$

together with the normalization condition given by Eq. 15.

Because λ contains $\boldsymbol{C}$, Eq. 17 does not form a genuine eigenvalue problem. It is, however, impractical to work out the problem by substituting Eq. 16 into Eq. 17. We had better solve the system of Eqs. 16 and 17 iteratively, treating Eq. 17 as an eigenvalue problem with λ given:

[0] For certain i, assume the mixing coefficients as

$$c_j = \delta_{ji}. \tag{18}$$

[1] Compute λ by Eq. 16 with the assumed $\boldsymbol{C}$.

[2] Solve the eigenvalue problem Eq. 17 for the computed λ, obtaining the computed $\boldsymbol{C}$ through the normalization of Eq. 15.

[3] Go back to the process 1 with the computed $\boldsymbol{C}$ as the assumed $\boldsymbol{C}$ until the computed $\boldsymbol{C}$ coincides with the assumed $\boldsymbol{C}$.

As to usual ionization energies we may choose the index of the highest occupied orbital as i in the initial setting (Eq. 18). Other choices of i lead us to inner valence-shell and core ionization energies.

Our hole state thus obtained fulfils the virial theorem; Eq. 16 is nothing other than the virial condition.[25] After substitution of the determined λ and $\boldsymbol{C}$, Eq. 13 gives the hole state energy

$$E_{N-1} = \lambda^2 T + \lambda V - \omega \tag{19}$$

by virtue of Eq. 17. From Eqs. 8 and 19, using the virial theorem for the parent state (Eq. 11), we have the ionization energy

$$I = E_{N-1} - E_N = -\omega + \Lambda \tag{20}$$

with

$$\Lambda = -(\lambda-1)^2 E_N. \tag{21}$$

In the form of Eq. 20 a characteristic of our method is clearly seen. Our ionization energy consists of two parts: $-\omega$, the ejection energy of the quasiparticle for the ionization considered, literally of quasiparticle nature, and Λ, the residual correction, of global nature. It may be suitable and convenient to refer to the former as the quasiparticle ejection energy and to the latter as the global correction. Note that the scaling affects not only Λ of the explicit λ-dependence but also ω. Roughly speaking, the scale factor greater than unity shrinks the electronic cloud closer to the nucleus. This contraction conserves the "shape" of the electronic cloud for the constituent hole state $a_j^{\lambda}|N,\lambda\rangle$ individually, but the image of the shape-conservative contraction fails in the hole state $|N-1,\lambda,\boldsymbol{C}\rangle$ in general, because λ and $\boldsymbol{C}$ interrelate to each other.

Without scaling, that is, in Koopmans' treatment, we have Eq. 17 with $\lambda=1$, which is just the canonical HF equation in the canonical orbital representation; ω becomes the canonical orbital energy and Λ vanishes. Still Koopmans' approximation is not to be confused with a "limiting case" of making λ tend to unity in our method. The approximation inherently violates the virial theorem for the hole state.

Numerical Examples

The present method has been applied to valence-shell and core ionizations of several atomic systems of which parent states have single configurations in Roothaan's

Table 1. Dependence on the size of a basis set

System	B_N[a]	E_N^{SCF}[b]/a.u.	1s-ionization		2p-ionization	
			I/a.u.	λ	I/a.u.	λ
He	1	−2.84766	0.8477	1.18519		
	2	−2.86167	0.8720	1.17922		
	5	−2.86168	0.8720	1.17921		
Ne	1, 1[1]	−127.812	32.144	1.07603	0.5358	1.01449
	2, 2[2]	−128.535	32.247	1.07540	0.8179	1.01375
	2, 3[4]	−128.547	32.261	1.07536	0.8270	1.01374
	2, 4[4]	−128.547	32.261	1.07536	0.8270	1.01374
Ar	1, 1, 1[1, 1]	−525.765	117.77	1.04165	9.211	1.01452
	2, 2, 2[2, 2]	−526.815	117.83	1.04377	9.468	1.01414
	2, 2, 3[2, 3]	−526.817	117.83	1.04378	9.469	1.01415
	1, 0, 7[1, 0, 7]	−526.817	117.83	1.04379	9.470	1.01416

a) The number of the basis functions for the parent state SCF calculation; $n_1,n_2,\cdots[n_3,n_4,\cdots]$ means $n_1\times 1s+n_2\times 2s+\cdots n_3\times 2p+n_4\times 3p+\cdots$. b) The SCF parent state energy.

Table 2. Dependence on the basis set of the similar size

System		Na^+		Cl^-			
Ionization		1s	2p	1s	2s	2p	3s
$B^{a,b)}$	K[d]/a.u.	40.760	1.7929	104.51	10.229	7.6956	0.7332
	I/a.u.	40.231	1.7701	103.74	10.150	7.6007	0.7305
	λ	1.06768	1.01319	1.04652	1.01376	1.01465	1.00246
	C 1s	0.99947		0.99969	−0.00682		0.00031
	2s [2p]	0.03261	[1.00000]	0.02408	0.99992	[0.99995]	−0.00187
	3s [3p]			−0.00625	0.01074	[0.00965]	1.00000
$CR^{b,c)}$	K/a.u.	40.760	1.7972	104.51	10.229	7.6953	0.7330
	I/a.u.	40.232	1.7700	103.74	10.150	7.6004	0.7302
	λ	1.06768	1.01319	1.04652	1.01376	1.01464	1.00245
	C 1s	0.99947		0.99969	−0.00682		0.00031
	2s [2p]	0.03262	[1.00000]	0.02408	0.99992	[0.99995]	−0.00184
	3s [3p]			−0.00625	0.01072	[0.00965]	1.00000

a) The case of Bagus' bases: B_N=2,2,1[4] for Na^+ and 1,2,4[3,2,2] for Cl^-. b) Both of Bagus' and CR's bases give E_N^{SCF}/a.u. = −161.677 for Na^+ and −459.577 for Cl^-. c) The case of CR's bases: B_N=2,3[4] for Na^+ and 2,2,3[2,4] for Cl^-. d) Koopmans' value.

HF calculation.[26] The results are summarized in Tables 1—5.

Tables 1 and 2 concern preliminary examination of the basis set dependence. The dependence on the size of a basis set is examined in Table 1 using Clementi and Roetti (CR)'s bases.[27] As the result of SCF calculation settles down, that of our calculation also does. There is an obvious gap between the single and double zeta results; the former seems of no use. Table 2 compares the cases using CR's and Bagus'[17] bases of the similar size. The results are almost identical. As the SCF calculation tends to the HF limit, this identity is expected to become complete. What is shown in Tables 1 and 2 is rather natural, since our method does not work upon basis functions themselves but work upon occupied HF orbitals.

Table 3 presents the results for usual valence-shell ionizations. CR's occupied SCF orbitals are used as a starting point of our calculation. Koopmans' and the ΔSCF values for the sake of comparison are quoted also from CR's SCF calculation. For the closed-shell systems, that is, for He-, Ne-, and Ar-isoelectronic systems, our values of ionization energies are variously lower than Koopmans' ones, nearing the experimental; the lowering ranges from about eighty to a few percent of that attained by ΔSCF method. On the other hand, for what we call the semiclosed-shell systems, Be- and Mg-isoelectronic systems, our values are only little depressed from and remain approximately equal to Koopmans' values in spite of the obvious lowering of the ΔSCF values. The ionization energies of these systems are, as is well known, rather considerably larger than Koopmans' estimates; our method can be said to work fairly well. The results for the open-shell systems, N and O^+, are moderate and we may draw no outstanding feature from them; our estimates are a little more agreeable than Koopmans' ones.

Tables 4 and 5 show the results for core ionizations.

Table 3. Ionization energies of atomic systems[a]

System	He	Li^+	Be	B^+	N[b]	O^+ [b]	F^-
B_N	5	4	2, 4	2, 3	2, 4[4]	2, 3[4]	2, 3[5]
B_{N-1}[c]	hy.[d]	hy.	2, 2	2, 2	2, 3[4]	2, 3[4]	2, 4[4]
Δ[e]/a.u.	0.8617	2.736	0.296	0.862	0.513	1.273	0.050
K/a.u.	0.9180	2.7924	0.3093	0.8738	0.5676	1.3269	0.1809
X[e,f]/a.u.	0.90354	2.7796	0.3426	0.92437	0.53410	1.2905	0.129†
I/a.u.	0.8720	2.7453	0.3086	0.8728	0.5594	1.3166	0.1622
ω/a.u.	0.7801	2.6510	0.3079	0.8718	0.5509	1.3058	0.1430
Λ/a.u.	0.0919	0.0943	0.0007	0.0010	0.0085	0.0108	0.0192
λ	1.17921	1.11414	1.00709	1.00664	1.01246	1.01204	1.01389
C 1s	1.00000	1.00000	−0.00246	−0.00271			
2s [2p]			1.00000	1.00000	[1.00000]	[1.00000]	[1.00000]
R[g]	81.7	83.5	5.3	8.5	15.0	19.1	14.3
$D\Delta$[h]/a.u.	−0.0418	−0.044	−0.047	−0.062	−0.021	−0.018	−0.079
DK[h]/a.u.	0.0145	0.0128	−0.0333	−0.0506	0.0335	0.0364	0.052
DI[h]/a.u.	−0.0315	−0.0343	−0.0340	−0.0516	0.0253	0.0261	0.033

System	Ne	Na^+	Mg	Al^+	Cl^-	Ar	K^+
B_N	2, 4[4]	2, 3[4]	2, 2, 3[3]	2, 2, 3[3]	2, 2, 3[2, 4]	2, 2, 3[2, 3]	2, 2, 3[2, 3]
B_{N-1}	2, 3[4]	2, 3[4]	2, 2, 3[3]	2, 2, 3[3]	2, 2, 3[2, 3]	2, 2, 3[2, 3]	2, 2, 3[2, 3]
Δ/a.u.	0.729	1.680	0.242	0.644	0.095	0.543	1.126
K/a.u.	0.8504	1.7972	0.2530	0.6521	0.1499	0.5906	1.1711
X/a.u.	0.79244	1.7377	0.2810	0.69190	0.136†	0.57912	1.1622
I/a.u.	0.8270	1.7700	0.2529	0.6519	0.1481	0.5885	1.1680
ω/a.u.	0.8028	1.7419	0.2528	0.6517	0.1462	0.5860	1.1648
Λ/a.u.	0.0242	0.0281	0.0001	0.0002	0.0019	0.0025	0.0032
λ	1.01374	1.01319	1.00073	1.00092	1.00202	1.00219	1.00229
C 1s			0.00005	0.00010			
2s [2p]	[1.00000]	[1.00000]	−0.00040	−0.00061	[−0.00130]	[−0.00158]	[−0.00170]
3s [3p]			1.00000	1.00000	[1.00000]	[1.00000]	[1.00000]
R	19.3	23.2	0.9	2.5	3.3	4.4	6.9
$D\Delta$/a.u.	−0.063	−0.058	−0.039	−0.048	−0.041	−0.036	−0.036
DK/a.u.	0.0580	0.0595	−0.0280	−0.0398	0.014	0.0115	0.0089
DI/a.u.	0.0346	0.0323	−0.0281	−0.0400	0.012	0.0094	0.0058

a) The valence-shell ionization concerning the highest occupied orbital is meant. b) The ^4S state is used as the parent state. c) The number of the basis functions for the hole state SCF calculation in ΔSCF method. d) The hydrogen-like orbital. e) Δ and X stand for the ΔSCF and experimental values, respectively. f) All values are taken from the table in Ref. 28 except for the values with a dagger, which are from the data of electron affinities (Ref. 29). g) The percentage of the lowering from Koopmans' value by the present method in that by ΔSCF method; $R=100(K-I)/(K-\Delta)$. h) The deviations from the experimental value; $D\Delta=\Delta-X$, $DK=K-X$, and $DI=I-X$.

Occupied orbitals for our calculation as well as Koopmans' and the ΔSCF values are taken from Bagus' SCF calculation. Certainly ΔSCF method gives much more excellent results than Koopmans' relation as to core ionizations in which the reorganization effect is primary.[17,18] The present method works satisfactorily as well for inner core ionizations. For outer core ionizations,[18] however, our values are not so favorable, being better than Koopmans' to some extent.

The global correction is generally small and about few percent or less of the ionization energy, yet the magnitude is usually comparable with the difference between Koopmans' and experimental values of the ionization energy. We have the slight global corrections due to the scale factors very close to unity for the valence-shell ionizations of the semiclosed-shell systems. This seems, so to speak, to represent the "stiffness" of the electronic cloud characteristic of these systems. Another general feature is observed in the results of the isoelectronic sequence: While the quasiparticle ejection energy changes distinctly according to the atomic number in a sequence, the global correction as well as the scale factor varies comparatively slowly. As the atomic number increases, the scale factor becomes small little by little remaining similar. This may be well understood from the image that the larger nuclear charge forms the tighter electronic cloud with the similar shape in the parent

Table 4. The 1s-ionization energies of Ne- and Ar-isoelectronic systems

System	F^-	Ne	Na^+	Cl^-	Ar	K^+
B_N	2, 3, 1[5]	2, 2, 1[4]	2, 2, 1[4]	1, 2, 4[3, 2, 2]	1, 2, 4[3, 2, 2]	1, 2, 4[3, 2, 2]
B_{N-1}	2, 2, 1[4]	2, 2, 1[4]	2, 2, 1[4]	1, 2, 4[3, 2, 2]	1, 2, 4[3, 2, 2]	1, 2, 4[3, 2, 2]
Δ/a.u.	24.935	31.921	39.935	103.29	117.43	132.59
K/a.u.	25.830	32.772	40.760	104.51	118.61	133.75
$X^{a)}$/a.u.	24.992	31.985*	40.000	103.60	117.81*	133.10
I/a.u.	25.345	32.261	40.231	103.74	117.83	132.96
ω/a.u.	24.640	31.531	39.491	102.75	116.82	131.94
Δ/a.u.	0.705	0.730	0.740	0.99	1.01	1.02
λ	1.08421	1.07536	1.06768	1.04652	1.04379	1.04127
C 1s	0.99924	0.99937	0.99947	0.99969	0.99972	0.99975
2s	0.03894	0.03559	0.03261	0.02408	0.02278	0.02155
3s				−0.00625	−0.00624	−0.00621
R	54.2	60.1	64.1	63.1	66.1	68.1
$D\Delta$/a.u.	−0.057	−0.064	−0.065	−0.31	−0.38	−0.51
DK/a.u.	0.838	0.787	0.760	0.91	0.80	0.65
DI/a.u.	0.353	0.276	0.231	0.14	0.02	−0.14

a) The values with an asterisk are taken from the table in Ref. 30; others are from Bagus' paper, Ref. 17.

Table 5. The 2s-ionization energies of Ne- and Ar-isoelectronic systems

System	F^-	Ne	Na^+	Cl^-	Ar	K^+
B_N	2, 3, 1[5]	2, 2, 1[4]	2, 2, 1[4]	1, 2, 4[3, 2, 2]	1, 2, 4[3, 2, 2]	1, 2, 4[3, 2, 2]
B_{N-1}	2, 2, 1[4]	2, 2, 1[4]	2, 2, 1[4]	1, 2, 4[3, 2, 2]	1, 2, 4[3, 2, 2]	1, 2, 4[3, 2, 1]
Δ/a.u.	0.9282	1.8123	2.9682	9.811	11.938	14.346
K/a.u.	1.0746	1.9303	3.0737	10.229	12.322	14.708
X/a.u.	0.8947	1.7812*	2.9434	9.7?	11.99*	14.4?
I/a.u.	1.0529	1.9075	3.0496	10.150	12.237	14.620
ω/a.u.	1.0293	1.8824	3.0232	10.063	12.145	14.523
Δ/a.u.	0.0236	0.0251	0.0264	0.087	0.092	0.097
λ	1.01541	1.01397	1.01279	1.01376	1.01325	1.01271
C 1s	−0.00646	−0.00606	−0.00572	−0.00682	−0.00662	−0.00639
2s	0.99998	0.99998	0.99998	0.99992	0.99992	0.99992
3s				0.01074	0.01083	0.01076
R	14.8	19.3	22.8	18.9	22.1	24.3
$D\Delta$/a.u.	0.0335	0.0331	0.0248	0.1	−0.05	−0.1
DK/a.u.	0.1799	0.1491	0.1303	0.5	0.33	0.3
DI/a.u.	0.1582	0.1263	0.1062	0.4	0.25	0.2

state. The scale factor and the global correction reflect a nature of the electronic cloud of the system considered.

Concluding Remarks

The method proposed is a natural improvement of Koopmans' approximation but stands on a much more sound ground. The numerical examples in the previous section show the usefulness of the method in both qualitative and quantitative aspects. Though the method, intended for a handy estimation, should not be expected to reproduce experimental values accurately, the obtained values are almost always better than Koopmans' and sometimes surprisingly appropriate. The method allows us to get some feel about the electronic behavior through ionization. Above all it should be emphasized that our method requires little additional work to the parent state HF calculation, the laboriousness being incomparable with that of the HF calculation for each hole state of interest. We believe that the present method is promising as a simple estimation in place of Koopmans' relation.

The idea of the present work has two obvious direction of development: One is, of course, an extension to molecular systems. We have somewhat more to be done, but there seems to exist no essential difficulty. The other is an application to estimating electron affinities, which is straightforward in principle. Still the virtual orbitals supplied by the parent state HF calculation are unphysical or poor-physical; we must improve the virtual orbitals[31] relevantly at a time.

References

1) There is some semantic problem about the usage of the terms: ground, ionic, hole states, and so on. The definition of the ground state is arbitrary depending on whether or not the number of electrons are specified (Specified: The usual ionization $He \rightarrow He^+$ is the process from the two-electron ground state to the one-electron ground state. Nonspecified: In the process $Be^+ \rightarrow Be^{++}$ we cannot call Be^+ the ground state, the ground state being Be.), but the tractable N-electron state may be referred to as the ground state concerning the transition to the $N-1$-electron state. When the N-electron state is ionic, the $N-1$-electron state is not necessarily ionic. Though the "ionized" state matches the word "ionization", it is suitable to call the $N-1$-electron state the ionized state only if the N-electron state is neutral. We use "parent" for "N-electron" and "hole" for "$N-1$-electron"; the word "hole" does not always fit literally into the $N-1$-electron state. The term "ionization energy" is undoubtedly inappropriate for the ionic parent state, yet it has been used traditionally too long to be replaced by others. Here we use it reluctantly.

2) Some fundamental, important works are cited in Ref. 10b.

3) S. F. Boys and N. C. Handy, *Proc. R. Soc. London, Ser. A*, **310**, 43 (1969); *ibid.*, **310**, 63 (1969).

4) A. W. Weiss, *Phys. Rev. A*, **3**, 126 (1971); C. M. Moser and R. K. Nesbet, *ibid.*, **4**, 1336 (1971); *ibid.*, **6**, 1710 (1972).

5) D. P. Chong, F. G. Herring, and D. McWilliams, *J. Chem. Phys*, **61**, 78 (1974); their subsequent works with great attention to basis sets are cited in Ref. 10b up to 1977; D. P. Chong and S. R. Langhoff, *Chem. Phys.*, **67**, 153 (1982). For the use of energy-shifted perturbation theory, D. P. Chong and Y. Takahata, *Int. J. Quantum Chem.*, **12**, 549 (1977). For the use of effective core potentials, S. R. Langhoff and D. P. Chong, *Int. J. Quantum Chem.*, **23**, 875 (1983); *Chem. Phys. Lett.*, **100**, 259 (1983).

6) W. P. Reinhardt and J. D. Doll, *J. Chem. Phys.*, **50**, 2767 (1969); F. Ecker and G. Hohlneicher, *Theor. Chim. Acta*, **25**, 289 (1972); J. D. Doll and W. P. Reinhardt, *J. Chem. Phys.*, **57**, 1169 (1972); L. S. Cederbaum, G. Hohlneicher, and S. Peyerimhoff, *Chem. Phys. Lett.*, **11**, 421 (1971); W. P. Reinhardt and J. B. Smith, *J. Chem. Phys.*, **58**, 2148 (1973). These are pioneering works but may be said to have become rather primitive today.

7) B. Schneider, H. S. Taylor and R. Yaris, *Phys. Rev. A*, **1**, 855 (1970); B. S. Yarlagadda, G. Csanak, H. S. Taylor, B. Schneider, and R. Yaris, *ibid.*, **7**, 146 (1973); P.-O. Nerbrant, *Int. J. Quantum Chem.*, **9**, 901 (1975).

8) L. S. Cederbaum, *Theor. Chim. Acta*, **31**, 239 (1973); *J. Chem. Phys.*, **62**, 2160 (1975); *J. Phys. B*, **8**, 290 (1975). His method has produced a dominant number of applicative works, on which we refer to review articles in Ref. 10. A new approximation scheme has been proposed on Green's functions; J. Schirmer, L. S. Cederbaum, and O. Walter, *Phys. Rev. A*, **28**, 1237 (1983).

9) G. D. Purvis and Y. Öhrn, *J. Chem. Phys.*, **60**. 4063 (1974); *ibid.*, **62**, 2045 (1975).

10) a) L. S. Cederbaum and W. Domcke, *Adv. Chem. Phys.*, **36**, 205 (1977); b) W. von Niessen, G. H. F. Diercksen, and L. S. Cederbaum, *J. Chem. Phys.*, **67**, 4124 (1977).

11) J. Simons and W. D. Smith, *J. Chem. Phys.*, **58**, 4899 (1973); J. Simons, *Chem. Phys. Lett.*, **25**, 122 (1974). See the references of Ref. 10b as to its applications.

12) D. L. Yeager, Ph. D. Thesis, California Institute of Technology, 1975; M. F. Herman, K. F. Freed, and D. L. Yeager, *Adv. Chem. Phys.*, **48**, 1 (1981).

13) B. T. Pickup and O. Goscinski, *Mol. Phys.*, **26**, 1013 (1973).

14) I. Hubač, V. Kvasnička, and A. Holubec, *Chem. Phys. Lett.*, **23**, 381 (1973); V. Kvasnička and I. Hubač, *J. Chem. Phys.*, **60**, 4483 (1974).

15) A. J. Hernández and P. W. Langhoff, *Chem. Phys. Lett.*, **49**, 421 (1977).

16) G. Born, H. A. Kurtz, and Y. Öhrn, *J. Chem. Phys.*, **68**, 74 (1978).

17) P. S. Bagus, *Phys. Rev.*, **139**, A619 (1965).

18) L. Hedin and A. Johansson, *J. Phys. B*, **2**, 1336 (1969).

19) O. Goscinski, B. T. Pickup, and G. Purvis, *Chem. Phys. Lett.*, **22**, 167 (1973); O. Goscinski, M. Hehenberger, B. Roos, and P. Siegbahn, *ibid.*, **33**, 427 (1975).

20) T. Koopmans, *Physica*, **1**, 104 (1933).

21) R. K. Nesbet, *Adv. Chem. Phys.*, **9**, 321 (1965); M. D. Newton, *J. Chem. Phys.*, **48**, 2825 (1968); M. Isihara, *Bull. Chem. Soc. Jpn.*, **55**, 1392 (1982); correction, *ibid.*, **55**, 2692 (1982).

22) D. W. Smith and O. W. Day, *J. Chem. Phys.*, **62**, 113 (1975); O. W. Day and K. W. Smith, *ibid.*, **62**, 155 (1975); M. M. Morrell, R. G. Parr, and M. Levy, *ibid.*, **62**, 549 (1975).

23) B. T. Pickup, *Chem. Phys. Lett.*, **33**, 422 (1975); E. Andersen and J. Simons, *J. Chem. Phys.*, **66**, 1067 (1977).

24) P.-O. Löwdin, *J. Mol. Spectrosc.*, **3**, 46 (1959); this contains a complete bibliography of the fundamental works on the subject up to 1958; A. D. McLean, *J. Chem. Phys.*, **40**, 2774 (1964).

25) S. T. Epstein, "The Variation Method in Quantum Chemistry," Academic Press, New York (1974), Section 20.

26) C. C. J. Roothaan, *Rev. Mod. Phys.*, **23**, 69 (1951); *ibid.*, **32**, 179 (1960).

27) E. Clementi and C. Roetti, *At. Data Nucl. Data Tables*, **14**, 177 (1974).

28) C. E. Moore, "Ionization Potentials and Ionization Limits Derived from Analyses of Optical Spectra," NSRDS-NBS 34, U. S. Government Printing Office, Washington, D. C. (1970).

29) L. M. Branscombe, "Atomic and Molecular Processes," ed by D. R. Bates, Academic Press, New York (1962), p. 135.

30) D. A. Shirley, R. L. Martin, S. P. Kowalczyk, F. R. McFeely, and L. Ley, *Phys. Rev. B*, **15**, 544 (1977).

31) For example, S. Huzinaga and C. Arnau, *Phys. Rev. A*, **1**, 1285 (1970); *J. Chem. Phys.*, **54**, 1948 (1971); E. R. Davidson, *ibid.*, **57**, 1999 (1972); K. Morokuma and S. Iwata, *Chem. Phys. Lett.*, **16**, 192 (1972); S. Huzinaga and K. Hirao, *J. Chem. Phys.*, **66**, 2157 (1977).

Carbon-13 Nuclear Magnetic Relaxation Studies of Benzene Molecules Adsorbed on the Pillar Interlayered Montmorillonite

Mutsuyoshi MATSUMOTO,*,† Sumio SHINODA, (the late) Hiroshi TAKAHASHI, and Yasukazu SAITO
Institute of Industrial Science, The University of Tokyo,
22-1, Roppongi 7 Chome, Minato-ku, Tokyo 106
(Received February 14, 1984)

Carbon-13 nuclear magnetic relaxation times of ^{13}C-enriched benzene have been determined in order to elucidate the adsorption properties of PILM (pillar interlayered montmorillonite) by varying temperatures and coverages. The activation energy of diffusion as small as 6.5 kJ mol^{-1} indicates that the majority of PILM adsorption sites exhibits a weak interaction with benzene. The pre-exponential factor of correlation time was exceptionally large, probably because the two-dimensional pore structure of PILM, in contrast to the three-dimentional zeolite or the open surfaces of graphitized carbon black and silica gel, restricts the chance for the adsorbate to diffuse. In the spin-lattice relaxation spectra at low temperatures, the internal and the external surfaces of PILM were discriminated, since the two adsorbed states on these surfaces give different T_1 and chemical shift values.

In recent years, there has been a growing interest in sheet silicates or aluminosilicates such as montmorillonite, vermiculite, kaolinite, and halloysite. The advantage of using montmorillonite is the easiness to accept an intercalating substance and to control the size of the generated interlayer (micropore) compared with the other clay minerals. Thus organic reactant molecules introduced into the interlayer space may undergo novel types of chemical reactions.[1]

The basic layer structure of montmorillonite is threefold, consisting of a gibbsite Al_2O_3 layer (the octahedral layer) sandwiched by two $Si_2O_5^{2-}$ sheets (the tetrahedral layer). In the octahedral layer a part of the Al^{3+} ions are randomly substituted with Fe^{3+} or Mg^{2+} ions, the lack of the lattice charge being balanced with exchangeable cations (usually Na^+).

Thermal stability is endowed by substituting the exchangeable Na^+ with $[Al_{13}O_4(OH)_{24+x}(OH_2)_{12-x}]^{7-x}$ followed by a calcination treatment, since this polynuclear inorganic cation acts as a pillar substance and forms an interlayer network. Extensive investigations have been made on catalytic[2] and adsorption[3] properties of this new type of compound, *i.e.*, pillar interlayered montmorillonite (PILM).

As well established by the diffusion and shape-selective properties of zeolite,[4] the mobility of molecules inside the pore is essentially important for catalysis and adsorption. Not only the mobility of molecules but also various interactions of the adsorbed molecules with the surfaces and other neighboring molecules are well elucidated by NMR relaxation measurements.[5–9] In the present work ^{13}C nuclear magnetic relaxation study has been performed for the molecular dynamics of benzene adsorbed on PILM in order to gain a deeper insight into the characteristics of intercalation compounds.

Experimental

Montmorillonite. Otay montmorillonite, supplied from Ward's Natural Science Establishment, Inc., was used; the fraction less than 2 μm in diameter was separated by gravity sedimentation in water dispersion.

Intercalation. An aqueous solution of $AlCl_3$ (0.3 mol dm^{-3}) was vigorously stirred under reflux, followed by a slow dropwise addition of NaOH (1.0 mol dm^{-3}), until the OH/Al ratio of the solution became 2.37;[10–12] by this procedure the polynuclear cation, $[Al_{13}O_4(OH)_{24}(OH_2)_{12}]^{7+}$,[13] was formed. The resultant solution was added dropwise to the refluxing water suspension of montmorillonite (3%) upto about five times as much as the total cation exchange capacity (*ca.* 1 meq. g^{-1}) of montmorillonite. The boiling slurry was aged for 2 h, filtered, and washed with distilled water until Cl^- ions were undetected by the $AgNO_3$ test. The product was dried in an oven overnight at 393 K, calcined in air at 673 K for 2 h, and then kept in a desiccator containing the saturated aqueous solution of NH_4Cl. A schematic view of pillar interlayered montmorillonite (PILM) is shown in Fig. 1.

Nitrogen adsorption isotherm obeyed the Langmuir-type equation at 77 K for PILM, which was pretreated overnight under vacuum (<10^{-1} pa) at 393 K. The surface area of 290 m^2 g^{-1} thus obtained was much larger than the external surface area of 40 m^2 g^{-1}, determined with the α_s-plot.[14] The d-spacing (c_0) of PILM was 1.80 nm, whereas the interlayer spacing was 0.84 nm.[3] This magnitude is acceptable because the pillar diameter is *ca.* 0.9 nm.[10] These results support the view of PILM microporosity, with the structure shown in Fig. 1.

NMR Measurements. 0.4 g (dry basis) of PILM was placed in a Pyrex NMR sample tube (10 mm O. D.) and fixed with a Teflon plug. After the heat treatment at 393 K under vacuum (<10^{-3} Pa) overnight, a given amount of gaseous dosage of ^{13}C-enriched (89%) benzene, supplied from Molécules Marquées France, was introduced to the sample at room temperature; the monolayer capacity of benzene on PILM (1.81 mmol g^{-1} at θ=1) was determined from the adsorption isotherm at 298 K. In order to seal off the sample tube without losing any benzene molecule present in the vapor phase, the sample was frozen with liquid nitrogen.

^{13}C-NMR measurements were carried out at 15.04 MHz using a pulsed Fourier-transform spectrometer (Jeol JNX-FX60Q). The spectra of phisically adsorbed benzene were obtained as easily as liquid benzene with, however, about 100 times broader line width. Spin-lattice relaxation times T_1 were determined by the inversion recovery method following a π-t-$\pi/2$ pulse sequence.[15] Spin-spin relaxation times T_2 were measured by means of the Carr-Purcell-Meiboom-Gill method under conditions of non-spinning and non-^1H-decoupling, which are required for this type of measurements.[16] The absolute value spectra, $(u^2+v^2)^{1/2}$, instead of the conventional absorption ones, v,

† Present address: National Chemical Laboratory for Industry, 1-1, Higashi, Yatabe-machi, Tsukuba-gun, Ibaraki 305.

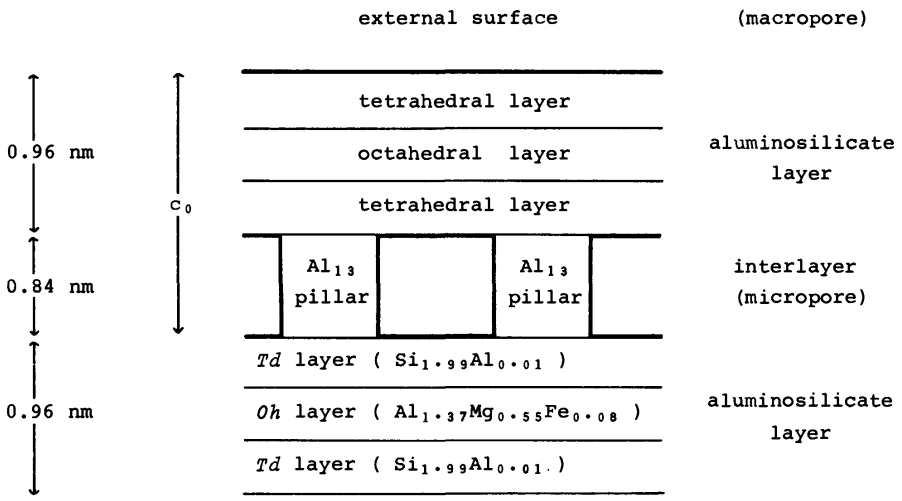

Fig. 1. Schematic view of pillar interlayered montmorillonite (PILM).

were adopted in determining T_2.[17] If not otherwise stated, the longitudinal and transversal relaxation were treated as purely exponential. The sample temperature was stabilized within the range of ±1 K (181—327 K).

Results and Discussion

NOE and Relaxation Mechanism. It was confirmed that the NOE (nuclear Overhauser enhancement) was unity (no enhancement of signal intensity under conditions of ^1H decoupling) for all the studied samples of benzene adsorbed on PILM. This fact clearly indicates that the ^1H-^{13}C dipolar interaction is completely ineffective[18] for the ^{13}C relaxation of the adsorbed benzene. Although high ^{13}C-enrichment in benzene (89%) may bring about the ^{13}C-^{13}C dipolar interaction, this interaction is much weaker than the ^1H-^{13}C dipolar interaction owing to a lower gyromagnetic ratio and a longer internuclear distance. Thus, the dominant mechanism for the relaxation is ascribed to the dipolar interaction with paramagnetic species. This view is supported by the quite high level of Fe^{3+} impurities in the aluminosilicate layer of PILM (13,000 ppm); it was pointed out for propene adsorbed on cation-exchanged X and Y type zeolites that NOE fell down to unity, when the Fe^{3+} content became beyond 700 ppm.[19]

Chemical Shift and Line Width. Figure 2 shows typical temperature dependence of the spectra (θ=0.23) for benzene adsorbed on PILM. Small resonance shift for the adsorbed benzene (about 1 ppm to higher field referred to the liquid) was observed for the adsorption coverage of $0.016 \leqq \theta \leqq 1.0$ within the limits of experimental error (±0.5 ppm). Since the order of magnitude of this shift is covered within the range of necessary corrections for medium effects, no further remarks will be given. It is apparent from Fig. 2 that the higher the temperature is, the narrower the width of the ^{13}C resonance is. This phenomenon is in accord with "motional narrowing",[18] and commonly observed for all other samples (θ=0.016, 1.0, and 1.9).

Figure 3 presents the effect of adsorption coverage (θ) on the spectra at 302 K.

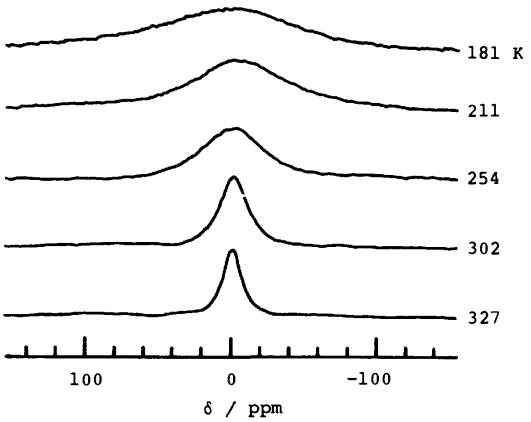

Fig. 2. ^{13}C-NMR spectra of benzene adsorbed on PILM (θ=0.23) as a function of temperature. Resonance frequency: 15.04 MHz. Standard for δ: liquid benzene.

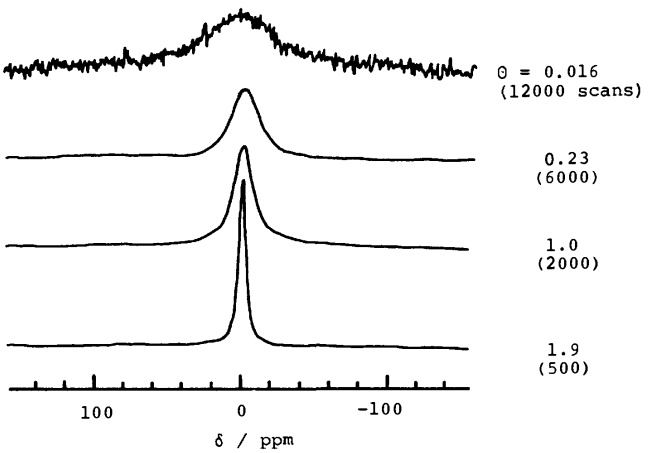

Fig. 3. ^{13}C-NMR spectra of benzene adsorbed on PILM as a function of coverage. Temperature: 302 K. Resonance frequency: 15.04 MHz. Standard for δ: liquid benzene.

The trend of marked broadening of the resonance peak caused by the decrease of θ was noticed at all the

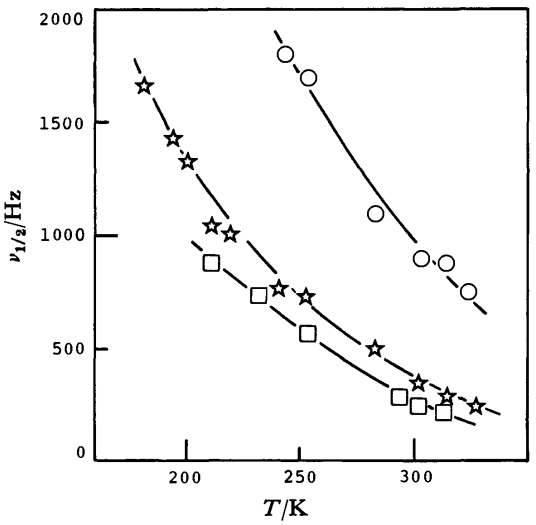

Fig. 4. Temperature dependence of ^{13}C-NMR half-height width ($\nu_{1/2}$) for benzene adsorbed on PILM. ○: θ=0.016, ☆: θ=0.23, □: θ=1.0.

temperature studied. Referred to the temperature dependence described above, the translational motion is considered to become more restricted as θ decreases (*vide infra*). The half-height width data are shown in Fig. 4.

Longitudinal and Transverse Relaxation Times. In order to consider the motional behavior of benzene adsorbed on PILM more precisely, we measured T_1 and T_2 varying both temperature and adsorption coverage θ. At higher coverage (θ=1.0, 1.9) T_1's were determined from the beginning of the decay ($0 \leqq t \leqq 2T_1$), since the relaxation functions were deviated from the exponential type at the later stage of the decay. The results of these measurements are summarized in Fig. 5.

Longitudinal and transverse relaxation times for the dipolar relaxations of ^{13}C near a paramagnetic center are given by[5,6,20,21]

$$\frac{1}{T_1} = \frac{\gamma_I^2\gamma_S^2\hbar^2 S(S+1)}{15r_{IS}^6}\left(\frac{6\tau_c}{1+\omega_I^2\tau_c^2}\right) \quad (1)$$

$$\frac{1}{T_2} = \frac{\gamma_I^2\gamma_S^2\hbar^2 S(S+1)}{15r_{IS}^6}\left(4\tau_c+\frac{3\tau_c}{1+\omega_I^2\tau_c^2}\right) \quad (2)$$

where γ is gyromagnetic ratio, $\omega_I=\gamma_I H_0$ resonance frequency of nuclear spin I, r_{IS} distance between the spins I and S, and τ_c correlation time for the diffusion of the adsorbate (the time between molecular jumps). Eqs. (1) and (2) imply $\omega_S \gg \omega_I$ and $\tau_{Si}(\simeq 10^{-6}\ \mathrm{s}) \gg \tau_c$ (i=1,2), where $\omega_S=\gamma_S H_0$ is resonance frequency of electron spin S and τ_{Si} means the electron spin relaxation time.

Scalar interaction is prohibited, because Fe^{3+} ions are included only in the octahedral layer which is separated from the interlayer (micropore) by the tetrahedral layer.

As revealed in the systematic change of T_1 with adsorption coverage (Fig. 5), the mobility of benzene molecule is more restricted at a given temperature as the coverage is lowered, indicating the presence of strong adsorption sites on PILM. The amount of this site is

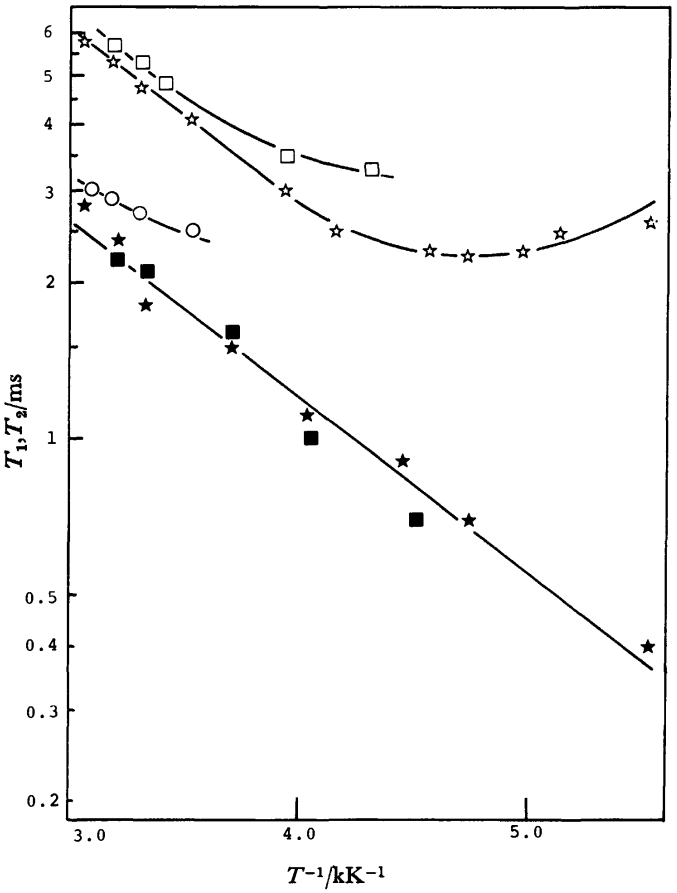

Fig. 5. Temperature dependence of ^{13}C relaxation times of benzene adsorbed on PILM; T_1 and T_2 indicated by open and solid symbols, respectively. ○: θ=0.016, ☆,★: θ=0.23, □,■: θ=1.0.

certainly limited, since the change of T_1 is larger for θ=0.23→0.016 than for θ=1.0→0.23.

A similar behavior was reported for benzene adsorbed on silica gel.[22] However, an inverse trend was pointed out for cyclohexane adsorbed on NaY-zeolite, where intermolecular hindrance between cyclohexane molecules became dominant rather than particular interactions with adsorption sites, as the pore filling factor increased.[21]

Low-temperature T_1 measurements for θ=0.016 and θ=1.0 were encountered with experimental difficulties due to severe line broadening and peak separation (*vide infra*), respectively. However, a rather flat minimum of T_1 is clearly seen for θ=0.23 (Fig. 5), which suggest a distribution of correlation times.[6] Resing showed that many experimental data were put in order by the assumption of correlation times with a logarithmic Gaussian distribution:[5]

$$\tau_c' = \tau_c \exp\{(E'-\langle E\rangle)/RT\}$$

with

$$\tau_c = \tau_0 \exp(\langle E\rangle/RT)$$

and

$$\beta = [2\langle\{(E'-\langle E\rangle)/RT\}^2\rangle]^{1/2}$$

where E' is the activation energy of the motional pro-

TABLE 1. TRANSLATIONAL MOBILITIES OF BENZENE IN ADSORBED AND LIQUID STATES

System or adsorbent		$E^{a)}$/kJ mol^{-1}	$10^{8}\tau_c{}^{b)}$/s	$10^{12}\tau_0{}^{c)}$/s	Ref.
liquid	—	13	0.0015[d)]	0.0089	26
graphitized carbon black	$\theta=1$	15	0.089	0.17	23
NaY-zeolite	$\theta=0.2$	16	40	42	25
	$\theta=0.83$	23	260	4.9	
silica gel	A site (4%)	13.4	3.0	14	27
	B site (15%)	7.7	0.16	19	
	C site (81%)	1.5	0.014	59	
PILM	$\theta=0.23$	6.5	1.1	270	this study

a) Activation energy for translational diffusion. b) Correlation time for translational diffusion at 210 K. c) Pre-exponential factor of τ_c. d) Extrapolated to 210 K in the equation for liquid benzene: $\tau_c=8.9\times10^{-15}\exp(1.3\times10^{4}/RT)$.

cess, $\langle E\rangle$ is the average value of E', R is the gas constant, and T is the absolute temperature. A theoretical curve was given for the relationship between β and the ratio T_1/T_2 at the minimum of T_1.[6] $T_1/T_2=1.83$ corresponds to $\beta=0$ with one correlation time. On the other hand, the value of 3.3 observed in this case leads to $\beta=1.3$, which supports the view that the correlation times are distributed within a certain range. On the basis of $\omega_I\tau_c=1$ at the minimum of T_1, τ_c was obtained as 1.1×10^{-8} s at 210 K.

As shown in Fig. 5, a linear relationship was observed between T_1 or T_2 and the reciprocal absolute temperature in the high temperature range ($\omega_I^2\tau_c^2\ll1$). Since T_1 and T_2 are inversely proportional to τ_c in this region, the activation energy for diffusion $\langle E\rangle$ ($=E$) is therefore able to be determined from the temperature dependence of the relaxation times. From the T_1 measurements for $\theta=0.23$, the value of 6.5 kJ mol^{-1} was obtained. The validity of this value was confirmed, for the same value was obtained from the T_2 measurements in the whole temperature range studied.

Translational Mobilities of Benzene Molecules in the Adsorbed and the Liquid States. Table 1 summarizes translational mobilities of benzene molecules in the adsorbed and the liquid states. Benzene molecules adsorbed on the graphitized carbon black ($\theta=1$) are as mobile as liquid, probably due to the geometrical and electronic similarities between benzene and graphite.[23] Difference in the pre-exponential factor τ_0 may reflect the spatial limitation of motion in the adsorbed state.

Benzene molecules adsorbed in the supercage of NaY-zeolite are known to be extremely restricted in mobility. The adsorption center for benzene has been ascribed to the sodium ions at the S_{II}-sites (maximam number of 4 per supercage).[8,24] As a consequence of mutual hindrance between the adsorbed molecules, E increases with θ, exhibiting the largest E value of 23 kJ mol^{-1} at $\theta=0.83$.[25]

The activation energy of 6.5 kJ mol^{-1} for PILM at $\theta=0.23$ is small, probably because the interaction of benzene with the surface sites is weak comparable to those for B and C sites of silica gel.[27]

On the contrary, the observed pre-exponential factor τ_0 for benzene molecules absorbed on PILM was exceptionally larger than those on silica gel and NaY-zeolite. With regard to NaY-zeolite, a similar value was obtained for cyclohexane (1.5×10^{-12} s) as small as benzene (4.9×10^{-12} s), reflecting its geometrical structure.

The activation energy and the pre-exponential factor of diffusion for benzene adsorbed on NaX-zeolite were reported as 25 ± 7 kJ mol^{-1} and 8.2×10^{-4} cm^2 s^{-1}, respectively.[28]

The pre-exponential factor of the correlation time τ_0 is known to be related to that of diffusion D_0 by

$$\tau_0 = \langle l^2\rangle/6D_0$$

where $\langle l^2\rangle$ is the mean square jump length in diffusion. From the references of τ_0[25] and D_0[28], the value of $(\langle l^2\rangle)^{1/2}$ was deduced to be 1.5 nm, which is reasonable in magnitude from the geometrical viewpoint of NaX and NaY-zeolites. Provided that the magnitude of $\langle l^2\rangle$ of benzene on PILM is similar to that on NaY (NaX)-zeolite, the value of D_0 would become obviously smaller for PILM than for the zeolite. The two-dimensional lamellar structure of PILM seems to afford less chance for the adsorbed molecules to diffuse in contrast to the three-dimensional framework structure of NaY-zeolite.

Adsorption Sites on PILM. Besides the silanol and the abundant siloxane groups, possible candidates to be mentioned as the surface adsorption sites of PILM are as follows: (i) the exchangeable cations such as Na^+ and Ca^{2+} in the interlayer, (ii) the hydroxyl groups on the alumina pillar surface, (iii) the Al^{3+} ions as the substituting elements of the $Si_2O_5^{2-}$ network in the tetrahedral layer, and (iv) Lewis acid sites generated as the oxygen vacancies on the alumina pillar surface. The amounts of the exchangeable cations (i) and the hydroxyl groups on the pillar surface (ii) were estimated as 0.19 and 5 mmol g^{-1}, respectively, whereas the Al^{3+} ions in the tetrahedral layer (iii) amounted only to 0.049 mmol g^{-1}.[3] Since the amount of the strong adsorption sites is a little larger or smaller than $\theta=0.016$ (0.029 mmol g^{-1}) and at least far smaller than $\theta=0.23$ (0.42 mmol g^{-1}) (*vide ante*), the Al^{3+} ions in the tetrahedral layer as well as the oxygen vacancies on the alumina pillar surface introduced by the heat treatment could be the candidates of the strong adsorption sites. It is also highly probable that all these adsorption sites on PILM are related to the distribution pattern of the observed E and τ_c values.

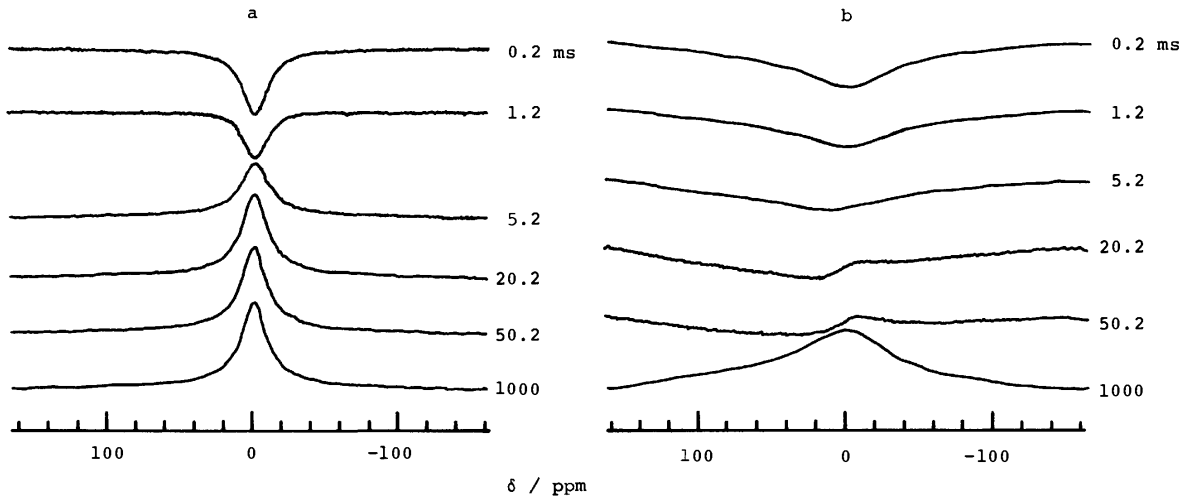

Fig. 6. ^{13}C spin-lattice relaxation spectra of benzene adsorbed on PILM (θ=1.9) at the temperatures of 282 K (a) and 220 K (b).
Resonance frequency: 15.04 MHz. Pulse sequenne: π-t-$\pi/2$. Standard for δ: liquid benzene.

Discrimination of Internal and External Surfaces. For lamellar adsorbents, discrimination of internal surface (micropore) and external surface (macropore) under dynamic conditions is important especially in relation to catalytic properties. Difference in T_1 between the adsorbed states enables peak discrimination in the spin-lattice relaxation spectra, which were observed for the samples with θ=1.0 under 203 K and θ=1.9 under 234 K. Illustrative spectra are presented in Fig. 6 (θ=1.9). It is apparent from Fig. 6 that there exist two peaks with different relaxation rates at 220 K, and that they are coalesced at 282 K into a single peak at the middle position. Accurate chemical shifts were determined from the absolute-value display of the spectra.

The high-field peak ($\delta\simeq-2$ ppm) exhibited shorter T_1 ($\simeq$7 ms) and narrower $\nu_{1/2}$ ($\simeq$1000 Hz) than the low-field peak ($\delta\simeq$8 ppm, $T_1>$100 ms, $\nu_{1/2}\simeq$1700 Hz). We assign the former to benzene molecules adsorbed in the micropore, and the latter to those adsorbed on the external surface on the basis of the following results. In the case of θ=1.0, the intensity of the low-field peak were very similar to those obtained for θ=0.23, whereas the pattern of exceedingly long T_1 and large $\nu_{1/2}$ exhibited in the low-field peak was quite exceptional.

Since long T_1 is indicative of high mobility, the low-field peak is naturally assigned to the external surface adsorption. At higher temperature than 254 K, discrimination of the two adsorbed states became difficult due to the onset of free exchange.

We consider that the NMR spin-lattice relaxation spectra of adsorbed molecules on intercalation compounds are useful to characterize the adsorbate mobility as well as the adsorption sites.

References

1) J. M. Thomas, "Intercalation Chemistry," ed by M. S. Whittingham and A. J. Jacobson, Academic Press, New York (1982), Chap. 3.
2) J. Shabtai, R. Lazar, and A. G. Oblad, "Proc. 7th Intern. Congr. Catal.," ed by T. Seiyama and K. Tanabe, Kodansha Ltd., Tokyo (1980), p. 828.
3) M. Matsumoto, M. Suzuki, H. Takahashi, and Y. Saito, to be submitted.
4) J. A. Rabo, *Catal. Rev.-Sci. Eng.*, **23**, 293 (1981).
5) H. A. Resing, *Adv. Mol. Relaxation Processes*, **3**, 199 (1972).
6) H. Pfeifer, "NMR-Basic Principles and Progress," Springer-Verlag, Berlin (1972), Vol. 7, p. 53.
7) H. Lechert, *Catal. Rev.-Sci. Eng.*, **14**, 1 (1976).
8) H. Pfeifer, "Magnetic Resonance in Colloid and Interface Science," ed by H. A. Resing and C. G. Wade, ACS Symposium Series, **34**, 36 (1976).
9) "Magnetic Resonance in Colloid and Interface Science," ed by J. P. Fraissard and H. A. Resing, D. Reidel Publishing Co., Boston (1980).
10) D. E. W. Vaughan, "Proc. 5th Intern. Conf. Zeolite," ed by L. V. Rees, Heyden & Son Ltd., London (1980), p. 94.
11) N. Lahav, U. Shani, and J. Shabtai, *Clays Clay Miner.*, **26**, 107 (1978).
12) J. W. Akitt, N. N. Greenwood, B. L. Khandelwal, and G. D. Lester, *J. Chem. Soc. Dalton Trans.*, **1972**, 604.
13) G. Johansson, G. Lundgren, L. G. Sillén, and R. Söderquist, *Acta Chem. Scand.*, **14**, 769 (1960).
14) M. R. Bhambhani, P. A. Cutting, K. S. W. Sing, and D. H. Turk, *J. Colloid Interface Sci.*, **38**, 109 (1972).
15) T. C. Farrar and E. D. Becker, "Pulse and Fourier Transform NMR," Academic Press, New York (1971), Chap. 2.
16) R. Freeman and H. D. W. Hill, "Dynamic Nuclear Magnetic Resonance Spectroscopy," ed by L. M. Jackman and F. A. Cotton, Academic Press, New York (1975), Chap. 5.
17) M. L. Martin, G. J. Martin, and J.-J. Delpuech, "Practical NMR Spectroscopy," Heyden & Son Ltd., London (1980), Chap. 7.
18) J. R. Lyerla Jr. and G. C. Levy, "Topics in Carbon-13 NMR Spectroscopy," ed by G. C. Levy, Wiley-Interscince, New York (1974), Vol. 1, Chap. 3.
19) A. D. H. Clague, I. E. Maxwell, J. P. C. M. van Dongen, and J. Binsma, *Appl. Surface Sci.*, **1**, 288 (1978).
20) A. Abragam, "The Principles of Nuclear Magnetism," Oxford Univ. Press, London (1961), Chap. 8.
21) D. Michel and J. Thöring, *Z. Phys. Chem. (Leipzig)*, **247**, 85 (1971).
22) H. Winkler, M. Nagel, D. Michel, and H. Pfeifer, *Z.*

Phys. Chem. (Leipzig), **248**, 17 (1971).
23) B. Boddenberg and J. A. Moreno, *Ber. Bunsenges. Phys. Chem.*, **87**, 83 (1983).
24) H. Lechert and K. P. Whittern, *Ber. Bunsenges. Phys. Chem.*, **82**, 1054 (1978).
25) M. Nagel, D. Michel, and D. Geschke, *J. Colloid Interface Sci.*, **36**, 254 (1971).
26) W. Dietrich, B. Gross, and R. Kosfeld, *Z. Naturforsch., Teil A*, **25**, 40 (1970).
27) E. M. Peterson, D. E. O'Reilly, and T. Tsang, *J. Chem. Phys.*, **70**, 3409 (1979).
28) M. Bülow, W. Mietk, P. Struve, and P. Lorenz, *J. Chem. Soc. Faraday Trans. I*, **79**, 2457 (1983).

The Theory of Liquid Ion-exchange Membrane Ion-selective Electrodes Based on the Concept of the Mixed Ion-transfer Potential**

Takashi KAKIUCHI and Mitsugi SENDA*
Department of Agricultural Chemistry and Research Center for Cell and Tissue Culture, Faculty of Agriculture, Kyoto University, Sakyo-ku, Kyoto 606
(Received October 17, 1983)

The theory of liquid ion-exchange membrane ion-selective electrodes has been developed on the basis of the concept of the zero-current potential, or the mixed potential in the presence of interfering ions, of ion transfer at the interface between a liquid membrane and a sample solution. Under the assumptions of the reversible ion transfer at the interface, the presence of supporting electrolytes in both phases, and the monovalency of all relevant ions, theoretical equations for the mixed potential are derived for two cases; the primary and interfering ions have 1) the same charge sign and 2) the opposite sign. The selectivity coefficients of the ion-selective electrodes can be expressed as a function of the difference between the standard ion-transfer potentials of the primary and interfering ions, the ratios of the mass-transfer coefficients of the ions, and the ratios of the concentrations of the ions. The theoretical prediction has been shown to be applicable to an interpretation of the response of liquid-membrane ion-selective electrodes.

The theory of the ion transport in liquid ion-exchange membrane proposed by Sandblom *et al.*[1] has been widely used for the interpretation of the response of ion-selective electrodes with the liquid ion-exchange membrane. This theory can predict the observed linear relationship between the selectivity coefficient of the ion-selective electrodes and the ion-distribution coefficients. However, the theory seems unsuccessful in explaining the observed fact that the experimental selectivity coefficients vary with the experimental conditions under which the selectivity coefficients are determined.[2-5] Such variation of the selectivity coefficients is one of the puzzles in the field of ion-selective electrodes which have not yet been fully solved.[6] Several attempts have been made to interpret this fact in terms of the concentration polarization of the ions in the solution just outside the membrane.[5,7-12] Most of these treatments presume the validity of the basic assumption implied in the Sandblom *et al.* theory,[1] that of the steady state of the ion transport throughout the liquid-membrane. This assumption, however, is not realistic when the membrane is not thin enough, *e.g.*, in the case of the experiments using a U-shaped cell.[13] Moreover, this theory is obviously not applicable to the ion-selective electrodes with a blocked interface, *e.g.*, coated wire electrodes.[14]

When a relatively thick membrane is brought into contact with a sample solution, the compositions of the inner solution and of the membrane in the vicinity of the membrane-inner solution interface or membrane-electronic conductor interface would remain unchanged unless a sufficiently long time elapses, while the compositions in the vicinity of the membrane-sample solution interface generally change with the time due to the ion-transfer reactions across the interface, resulting in the concentration polarization on both sides of the interface. Therefore, it seems necessary to examine the ion-transfer processes occurring at the membrane-sample solution interface for the understanding of the response of the liquid-membrane ion-selective electrodes.

In the last decade, ion transfer processes between two immiscible electrolyte solutions have been intensively studied using various electrochemical techniques.[15] Since the solvents used for liquid membranes are usually only poorly miscible with aqueous solutions and since the interface between them can be considered as an interface between two immiscible electrolyte solutions, the electrochemistry of the ion transfer at such interfaces has an immediate significance in elucidating the ion-transfer processes occurring at the membrane-solution interface of ion-selective electrodes of the liquid-membrane type. Cammann[16] first suggested the importance of the mixed potential concept[17] at the membrane-solution interface. Koryta[18] has pointed out that the current *vs.* potential curves of the ion transfer at the membrane-solution interface are of fundamental importance in interpreting the response of the ion-selective electrodes and showed that the Nernstian, sub-Nernstian, and super-Nernstian responses can be deduced from the zero current potential of the appropriate "anodic and cathodic waves" of the ion transfers of the relevant ions. Fujinaga and his co-workers[19,20] have advanced this approach and applied it to several types of ion-selective electrodes.

The aim of this study is to present a quantitative theory of the zero-current potential of ion transfer, which we call the mixed potential of ion-transfer in the case of the presence of interfering ions, at the interface between a liquid membrane and a sample solution, and to apply the theory to the interpretation of the response of the ion-selective electrodes with the liquid ion-exchange membrane. The mixed ion-transfer potential can be easily formulated using the current *vs.* potential curves for the transfer of primary and interfering ions when the supporting electrolytes exist in both the liquid membrane and the sample solution. The model system consisting of a liquid membrane and a sample solution, both containing supporting electrolytes, provides us with the characteristics of the ion distribution

** The main results of the present paper were presented at the 28th Annual Meeting on Polarography, November 11—12, 1982, Sapporo.[31]

processes with mass transfer *per si* at the membrane-solution interface, knowledge which seems essential for understanding the response of the liquid-membrane ion-selective electrodes to various ionic species. The ion-transfer processes at the membrane-sample solution interface should play an essential role in determining the potential response also in the liquid-membrane ion-selective electrode of the type with no such supporting electrolyte, like most of the ion-selective electrodes with liquid ion-exchangers so far studied. The ion-transfer processes are also important in the solid-membrane ion-selective electrodes.

Theoretical

We consider a liquid-membrane ion-selective electrode immersed in a sample solution. The electrochemical cell thus formed may be represented by:

Ref. 1	Liquid Membrane	Sample Solution	Ref. 2	(I)

where Ref. 1 and Ref. 2 are the reference electrodes. Ref. 2 may be a conventional reference electrode, whereas Ref. 1 may consist of an internal solution with a conventional reference electrode, or it may be an electronic conductor in the case of a coated wire electrode. Below, we assume that the potential difference between Ref. 1 and the membrane and that between the sample solution and Ref. 2 are invariant, irrespective of the composition of the membrane and of the sample solution.

When a liquid membrane and a sample solution, both containing electrolytes, are brought into contact to form a membrane-solution interface, ions will generally move across the interface according to the difference in their electrochemical potentials in the two phases. The transfer of ions across the interface is associated with the flow of the current. The net ion-transfer current I across the interface is the sum of the partial ion-transfer currents, I_j, due to the transfer of the j ion across the interface:

$$I = \sum_j I_j \tag{1}$$

The potential of an ion-selective electrode is usually measured under zero-current conditions:

$$I = \sum_j I_j = 0 \tag{2}$$

The inner potential of the sample solution phase, referred to that of the membrane phase, *i.e.*, the liquid junction potential between the two phases, at zero current, $\Delta_O^W\varphi(I=0)$, may generally be composed of an interfacial potential and two diffusion potentials:

$$\Delta_O^W\varphi(I=0) = \Delta\varphi_{diff}^0(I=0) + \Delta_O^W\varphi_{Interfacial}(I=0) + \Delta\varphi_{diff}^W(I=0) \tag{3}$$

In Eq. 3, $\Delta_{diff}^\alpha\varphi(I=0)$ is the diffusion potential in the α phase(α=O or W), where the superscripts O and W denote the membrane and solution phases respectively, and where $\Delta_O^W\varphi_{interfacial}(I=0)$ is the interfacial potential, which is also called the "phase-boundary potential"[21] or the "Donnan potential".[22] The interfacial potential is determined by the kinetics of ion transfer, which is represented by I_j and which is generally different from the interfacial potential at the distribution equilibrium at which all I_j's are zero and the interfacial potential is identical with the distribution potential.[23] When the partial ion-transfer current is not zero, the diffusion potentials are generally present, even at I=0.

The potential of an ion-selective electrode in the cell(I) at zero current, $E(I=0)$, is related to the liquid-junction potential, $\Delta_O^W\varphi(I=0)$, by:

$$E(I=0) = E_{mix} = \Delta_O^W\varphi(I=0) + \Delta E_{ref} \tag{4}$$

where $E(I=0)$ is the potential of Ref. 2 with respect to Ref. 1 in the cell(I) at I=0 and is identical with the mixed ion-transfer potential, E_{mix}, in the presence of interfering ions, and where ΔE_{ref} is the potential difference associated with the reference electrodes in the cell(I), which may include possible liquid-junction potentials at the sample solution-reference electrode and the membrane-reference electrode junctions. We will confine the following treatment to the cases where both the membrane and the sample solution contain a sufficient amount of the supporting electrolytes, so that the migration of the ions becomes negligible. This condition also ensures that the two diffusion potential terms in Eq. 3 are negligibly small;[24] hence:

$$\Delta_O^W\varphi(I=0) \fallingdotseq \Delta_O^W\varphi_{Interfacial}(I=0) \tag{5}$$

We assume that the rate of the transfer of ions across the interface is so fast that the Nernst equation:

$$\Delta_O^W\varphi_{Interfacial} = \Delta_O^W\varphi_j^0 + \frac{RT}{z_jF}\ln\frac{\gamma_j^{W,0}}{\gamma_j^{O,0}} + \frac{RT}{z_jF}\ln\frac{c_j^{W,0}}{c_j^{O,0}} \tag{6}$$

holds for every ion passing through the interface, *i.e.*, that the ion-transfer processes are reversible or Nernstain. In Eq. 6, $\Delta_O^W\varphi_j^0$ is the standard potential of the ion transfer of the ion j from the membrane phase to the sample solution phase;[23] z_j is the electric charge of the ion j; $c_j^{\alpha,0}$(α=O or W) is the surface concentration of the ion j, which is usually considered as the concentration of the ion j just outside the diffuse double layer in the phase α,[25] and $\gamma_j^{\alpha,0}$(α=O or W) is the corresponding activity coefficient of the ion j. R, T, and F have the usual meanings. We also assume that the diffusion coefficients of the ions are independent of the ion concentrations.

When the membrane is so thick that the ion transfer in the membrane phase as well as that in the solution phase meet the condition of semi-infinite mass transfer, the partial current I_j due to the transfer of the ion j through the interface can be written as:

$$\frac{I_j}{z_jFA} = \frac{D_j^W}{\delta_j^W}(c_j^W - c_j^{W,0}) = k_j^W(c_j^W - c_j^{W,0}) \tag{7}$$

$$= -\frac{D_j^O}{\delta_j^O}(c_j^O - c_j^{O,0}) = -k_j^O(c_j^O - c_j^{O,0}) \tag{8}$$

where A is the surface area of the interface; D_j^α, δ_j^α and k_j^α are the diffusion coefficient, the diffusion layer thickness, and the mass-transfer coefficient of the ion j in the phase α(α=O or W) respectively, and c_j^α is the concentration of the ion j in the bulk of the phase α(α=O or W) δ_j^O and δ_j^W have the forms of $1/(\pi D_j^O t)^{1/2}$ and $1/(\pi D_j^W t)^{1/2}$ respectively in the case of a semi-infinite linear diffu-

sion of the ions at a stationary planar interface, where t is the time elapsed from the instant of the contact of the membrane with the sample solution. In Eqs. 7 and 8, the sign of the current is taken as positive(negative) when the positively(negatively) charged ion transfers from the sample solution to the membrane. Equations 7 and 8 hold also in the presence of the convective transport of ions if one chooses appropriate expressions for δ_j^0 and δ_j^W. From Eqs. 6—8 we obtain the equation of a current *vs.* potential curve for the reversible transfer of the ion j through the interface:

$$I_j = \frac{I_{j,\mathrm{lim}}^{\mathrm{o}} + I_{j,\mathrm{lim}}^{\mathrm{w}} \exp(f_j)}{1+\exp(f_j)} \tag{9}$$

where

$$f_j = \frac{z_j F}{RT}(E - E_{1/2,j}^{\mathrm{r}}) \tag{10}$$

and where $I_{j,\mathrm{lim}}^{\alpha}(\alpha = \mathrm{W}$ or $\mathrm{O})$ is the limiting current for the transfer of the ion j from the phase α to the other; it is defined by

$$\frac{I_{j,\mathrm{lim}}^{\mathrm{w}}}{z_j F A} = k_j^{\mathrm{w}} c_j^{\mathrm{w}} \tag{11}$$

and

$$\frac{I_{j,\mathrm{lim}}^{\mathrm{o}}}{z_j F A} = -k_j^{\mathrm{o}} c_j^{\mathrm{o}} \tag{12}$$

In Eq. 10, E is the potential of Ref 2 with respect to Ref 1 in the cell(I), while $E_{1/2,j}^{\mathrm{r}}$ is the reversible half-wave potential of the transfer of the ion j and is defined by

$$E_{1/2,j}^{\mathrm{r}} = \Delta_{\mathrm{o}}^{\mathrm{w}}\varphi_j^0 + \frac{RT}{z_j F} \ln \frac{\gamma_j^{\mathrm{w},0} k_j^{\mathrm{w}}}{\gamma_j^{\mathrm{o},0} k_j^{\mathrm{o}}} + \Delta E_{\mathrm{ref}} \tag{13}$$

By substituting Eq. 9 into Eq. 2, we obtain:

$$\sum_j \frac{I_{j,\mathrm{lim}}^{\mathrm{o}} + I_{j,\mathrm{lim}}^{\mathrm{w}} \exp(f_j^0)}{1+\exp(f_j^0)} = 0 \tag{14}$$

where f_j^0 is the f_j at $I=0$. The potential which satisfies Eq. 14, *i.e.*, $E(I=0)$, gives the zero-current ion-transfer potential, or the mixed ion-transfer potential in the case of simultaneous ion transfers of more than two ions.

Below we will consider the mixed ion-transfer potential and the selectivity coefficient for two cases, *i.e.*, the primary and interfering ions have (1) the same charge sign and (2) the opposite charge sign. It is assumed that the electrolytes are completely dissociated in both the membrane and the sample solution, that all the ions are monovalent, and that $\gamma_j^{\mathrm{o},0} = \gamma_j^{\mathrm{w},0} = 1$.

Primary and Interfering Ions with the Same Charge Sign. Consider the case where the membrane that contains three cations, K1, K2, and K4, and an anion, A4, is brought into contact with a sample solution containing two cations, K1 and K3, and an anion, A3. Then, the electrochemical cell can be represented by

Ref. 1	K1 K3, A3	K1, K2 K4, A4	Ref. 2	(II)
	Membrane	Sample solution		

Suppose also that, among these ions, only K1 and K2 ions can pass through the interface. Such a condition may be fulfilled when the values of the standard ion-transfer potentials for K3 and A4, $\Delta_{\mathrm{O}}^{\mathrm{W}}\varphi_{\mathrm{K3}}^0$ and $\Delta_{\mathrm{O}}^{\mathrm{W}}\varphi_{\mathrm{K4}}^0$, are very negative, while those of K4 and A3, $\Delta_{\mathrm{O}}^{\mathrm{W}}\varphi_{\mathrm{K4}}^0$ and $\Delta_{\mathrm{O}}^{\mathrm{W}}\varphi_{\mathrm{K3}}^0$, are very positive, compared with those of K1 and K2, $\Delta_{\mathrm{O}}^{\mathrm{W}}\varphi_{\mathrm{K1}}^0$ and $\Delta_{\mathrm{O}}^{\mathrm{W}}\varphi_{\mathrm{K2}}^0$. If we regard K1 and K2, as a primary ion and an interfering ion respectively, the electrolytes, K3A3 in the membrane and K4A4 in the sample solution, may be considered to be supporting electrolytes.

The current *vs.* potential curve for the transfer of K1 is schematically represented by Curve 1 in Fig. 1. If $\Delta_{\mathrm{O}}^{\mathrm{W}}\varphi_{\mathrm{K2}}^0 \gg \Delta_{\mathrm{O}}^{\mathrm{W}}\varphi_{\mathrm{K1}}^0$, the partial ion-transfer current of K2, I_{K2}, is negligibly small around the equilibrium potential of K1, as is shown by Curve 2 in Fig. 1. Then, the potential where the current I becomes zero corresponds to the equilibrium potential for the distribution of K1 between the two phases:

$$E(I=0) = \Delta_{\mathrm{O}}^{\mathrm{W}}\varphi_{\mathrm{K1}}^0 - \frac{RT}{F} \ln (c_{\mathrm{K1}}^{\mathrm{W}}/c_{\mathrm{K1}}^{\mathrm{O}}) + \Delta E_{\mathrm{ref}} \tag{15}$$

When the value of the standard ion-transfer potential of K2 is close to that of K1, as shown by Curve 3 in Fig. 1, the potential at zero current deviates from the equilib-

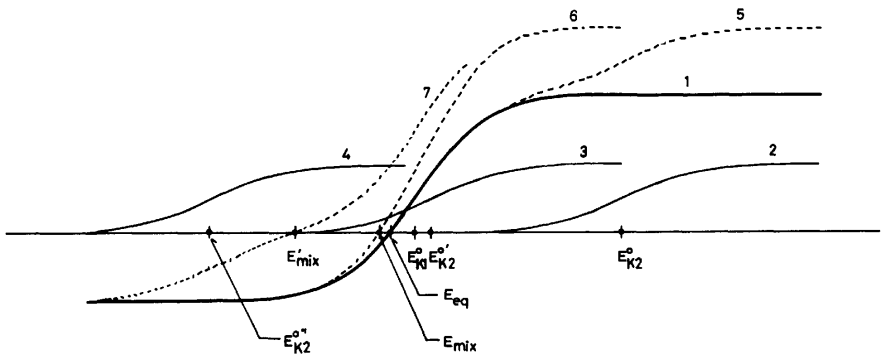

Fig. 1. Schematic representation of current *vs.* potential curves for the ion transfers between a liquid membrane and a sample solution for a primary ion K1 (curve 1), for an interfering ion K2 when $\Delta_{\mathrm{O}}^{\mathrm{W}}\varphi_{\mathrm{K2}}^0 \gg \Delta_{\mathrm{O}}^{\mathrm{W}}\varphi_{\mathrm{K1}}^0$(2), for K2 when $\Delta_{\mathrm{O}}^{\mathrm{W}}\varphi_{\mathrm{K2}}^0 \fallingdotseq \Delta_{\mathrm{O}}^{\mathrm{W}}\varphi_{\mathrm{K1}}^0$(3), and for K2 when $\Delta_{\mathrm{O}}^{\mathrm{W}}\varphi_{\mathrm{K2}}^0 \ll \Delta_{\mathrm{O}}^{\mathrm{W}}\varphi_{\mathrm{K1}}^0$(4). Curves 5, 6, and 7 show the total current *vs.* potential curves when the partial currents for K2 are given by (2), (3), and (4), respectively. Standard ion transfer potentials and the mixed ion transfer potentials are indicated on the potential axis.

rium potential of Eq. 15 to the negative direction because of the deformation of the total current *vs.* potential curve (Curve 6 in Fig. 1). Accordingly, the potential at zero current is not the equilibrium potential, but an mixed ion-transfer potential, E_{mix}, in which the ion transfers of both K1 and K2 participate. When $\Delta^{W}_{O}\varphi^{0}_{K2} \ll \Delta^{W}_{O}\varphi^{0}_{K1}$, the interference by the K2 ion becomes enormous, as is shown by Curve 7 in Fig. 1.

From Eq. 14, the mixed ion-transfer potential for the cell(II) is given by

$$E_{mix} = E^{0}_{K1} + \frac{RT}{F}\ln J \tag{16}$$

where

$$J = \frac{1}{2}[-(A+B\xi)+\{(A+B\xi)^2+C\xi\}^{1/2}] \tag{17}$$

$$\xi = \exp\left[\frac{F}{RT}\Delta E^{0}_{K2,K1}\right] \tag{18}$$

$$A = \left(\frac{k^{W}_{K2}}{k^{O}_{K1}}\frac{c^{W}_{K2}}{c^{W}_{K1}} - \frac{c^{O}_{K1}}{c^{W}_{K1}}\right)\Big/\left(1+\frac{k^{W}_{K2}}{k^{W}_{K1}}\frac{c^{W}_{K2}}{c^{W}_{K1}}\right) \tag{19}$$

$$B = \frac{k^{W}_{K2}}{k^{O}_{K2}}\Big/\left(1+\frac{k^{W}_{K2}}{k^{W}_{K1}}\frac{c^{W}_{K2}}{c^{W}_{K1}}\right) \tag{20}$$

$$C = 4\frac{k^{W}_{K2}}{k^{O}_{K2}}\frac{c^{O}_{K1}}{c^{W}_{K1}}\Big/\left(1+\frac{k^{W}_{K2}}{k^{W}_{K1}}\frac{c^{W}_{K2}}{c^{W}_{K1}}\right) \tag{21}$$

and

$$E^{0}_{K1} = \Delta^{W}_{O}\varphi^{0}_{K1} + \Delta E_{rlf}$$

In Eq. 18, $\Delta E^{0}_{K2,K1}$ is defined by

$$\Delta E^{0}_{K2,K1} = \Delta^{W}_{O}\varphi^{0}_{K2} - \Delta^{W}_{O}\varphi^{0}_{K1} \tag{22}$$

Usually, the selectivity of ion-selective electrodes for the ion i over the ion j is evaluated through the selectivity coefficient, $k^{pot}_{i,j}$, defined by the Nicolsky equation,[26] which may be written for the present case as:

$$E = E^{0}_{K1} - \frac{RT}{F}\ln\frac{c^{W}_{K1}+k^{pot}_{K1,K2}c^{W}_{K2}}{c^{O}_{K1}} \tag{23}$$

We have introduced the c^{O}_{K1} term in the denominator of the argument of the logarithm in Eq. 23 in order for the limiting behavior of E at infinitely small $k^{pot}_{K1,K2}$ values or at infinitely small c^{W}_{K2} values to coincide with that of Eq. 15. By equating E of Eq. 23 with E_{mix} of Eq. 16, one obtains

$$k^{pot}_{K1,K2} = (c^{W}_{K1}/c^{W}_{K2})(c^{O}_{K1}/c^{W}_{K1}-J)/J \tag{24}$$

Equations 16—24 are applicable to the cases where the primary ion as well as the interfering ion are anions, A1 and A2, in place of K1 and K2 in the cell(II), if one replaces, respectively, the subscripts K1 and K2 with A1 and A2, and if

$$\xi=\exp[(F/RT)\Delta E^{0}_{K2,K1}] \text{ and } \Delta E^{0}_{K2,K1} = \Delta^{W}_{O}\varphi^{0}_{K2}-\Delta^{W}_{O}\varphi^{0}_{K1}$$

with

$$\xi=\exp[(F/RT)\Delta E^{0}_{A1,A2}] \text{ and } \Delta E^{0}_{A1,A2} = \Delta^{W}_{O}\varphi^{0}_{A1}-\Delta^{W}_{O}\varphi^{0}_{A2}$$

in these equations.

Primary and Interfering Ions with the Opposite Charge Sign. When the interfering ion has a charge whose sign is opposite to that of the primary ion, the response of the ion-selective electrodes is significantly different from the cases described above. Let us first consider the case in which the primary ion and the interfering ion are a cation K1 and an anion A2 respectively. In this case, the cell may be represented by:

Ref. 1	K1 / K3, A3 (Membrane)	K1, A2 / K4, A4 (Sample solution)	Ref. 2	(III)

Figure 2 schematically represents the effect of the interfering anion A2 on the current *vs.* potential curve of the primary ion K1. When $\Delta^{W}_{O}\varphi^{0}_{A2} \ll \Delta^{W}_{O}\varphi^{0}_{K1}$ (Curve 2), there is no significant interference. The interference becomes appreciable, however, when $\Delta^{W}_{O}\varphi^{0}_{A2}$ is close to $\Delta^{W}_{O}\varphi^{0}_{K1}$, as is shown by Curve 5 in Fig. 2. In contrast to

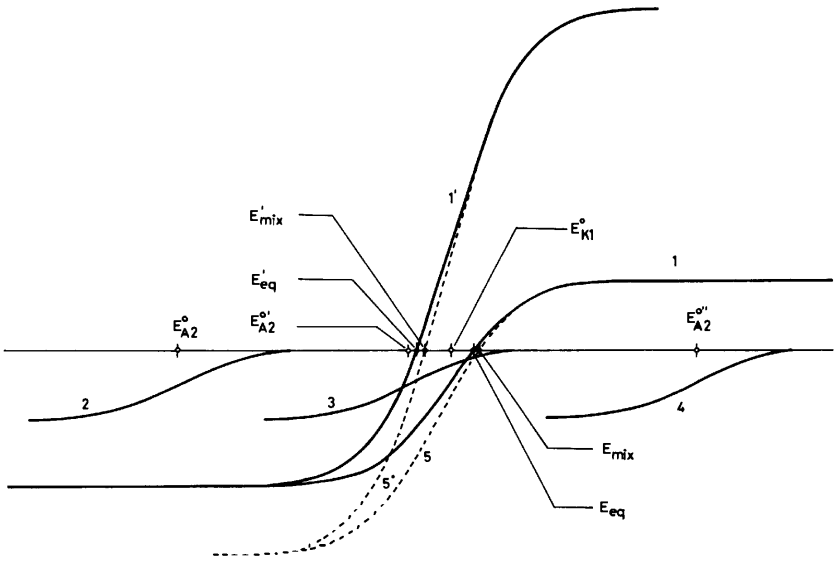

Fig. 2. Schematic representation of current *vs.* potential curves when an interfering ion is an anion A2: the curves for K1 (curves 1 and 1'), for A2 when $\Delta^{W}_{O}\varphi^{0}_{A2} \ll \Delta^{W}_{O}\varphi^{0}_{K1}$(2), $\Delta^{W}_{O}\varphi^{0}_{A2} \fallingdotseq \Delta^{W}_{O}\varphi^{0}_{K1}$(3), and $\Delta^{W}_{O}\varphi^{0}_{A2} \gg \Delta^{W}_{O}\varphi^{0}_{K1}$(4). Curves 1' represents the current potential curve when c^{W}_{K1} is four times larger than that of curve 1. Curves 5 and 5' are the total current *vs.* potential curves for these two cases.

the interference by a cation K2, the presence of the interfering anion shifts the zero-current ion-transfer potential to the positive direction (Curve 5 in Fig. 2). Another distinctive feature of the anion interference is that the degree of the interference becomes greater with the increase in c^{W}_{K1} at a given concentration of A2 in the sample solution, as can be seen from a comparison of Curve 5 with 5′ and of E_{mix} with E'_{mix} in Fig. 2.

Equations 16 and 17 are also valid for the mixed ion-transfer potential for the cell (III), if one defines the terms ξ, A, B, and C in Eqs. 16 and 17 as follows:

$$\xi = \exp\left[\frac{F}{RT}\Delta E^{0}_{A2,K1}\right] \tag{25}$$

$$A = -\frac{c^{O}_{K1}}{c^{W}_{K1}} \tag{26}$$

$$B = \frac{k^{O}_{A2}}{k^{W}_{A2}}\left(1-\frac{k^{W}_{A2}}{k^{W}_{K1}}\frac{c^{W}_{A2}}{c^{W}_{K1}}\right) \tag{27}$$

$$C = 4\left(\frac{k^{O}_{A2}}{k^{O}_{K1}}\frac{c^{W}_{A2}}{c^{W}_{K1}}+\frac{k^{O}_{A2}}{k^{W}_{A2}}\frac{c^{O}_{K1}}{c^{W}_{K1}}\right) \tag{28}$$

where

$$\Delta E^{0}_{A2,K1} = \Delta^{W}_{O}\varphi^{0}_{A2} - \Delta^{W}_{O}\varphi^{0}_{K1} \tag{29}$$

Equations 16, 17, and 25—29 are applicable to the cases where the primary ion is an anion A1 and the interfering ion is a cation K2, in place of K1 and A2 in the cell (III), if one replaces, respectively, the subscripts K1 and A2 with A1 and K2, and if $\xi=\exp[(F/RT)\Delta E^{0}_{A2,K1}]$ and $\Delta E^{0}_{A2,K1}=\Delta^{W}_{O}\varphi^{0}_{A2}-\Delta^{W}_{O}\varphi^{0}_{K1}$ with $\xi=\exp[(F/RT)\Delta E^{0}_{A1,K2}]$ and $\Delta E^{0}_{A1,K2}=\Delta^{W}_{O}\varphi^{0}_{A1}-\Delta^{W}_{O}\varphi^{0}_{K2}$ in these equations.

Discussion

Equations 16—22 explicitly relate the mixed ion-transfer potential with the various parameters: the difference between the standard ion-transfer potentials for K1 and K2, $\Delta E^{0}_{K2,K1}$; the ratios of the mass-transfer coefficients, k^{O}_{K1}/k^{W}_{K1}, k^{O}_{K2}/k^{W}_{K2}, and k^{W}_{K2}/k^{W}_{K1}, and the ratios of the concentrations, c^{W}_{K2}/c^{W}_{K1} and c^{O}_{K1}/c^{W}_{K1}. E_{mix} is solely determined by the properties of the primary and interfering ions as well as by those of the two solvents and has nothing to do with the nature of the A3 ion, which is usually called the liquid "ion-exchanger" in the membrane. Therefore, for the ion-selective electrode of the type represented by the cell (II) (and also (III)), the term liquid "ion-exchanger" membrane is obviously inadequate.

Figure 3 shows the mixed ion-transfer potentials as a function of c^{W}_{K2}/c^{W}_{K1} at different values of $\Delta E^{0}_{K2,K1}$ and at $c^{O}_{K1}/c^{W}_{K1}=1$, $k^{W}_{K1}/k^{O}_{K1}=k^{W}_{K2}/k^{O}_{K2}=\sqrt{2}$, and $k^{W}_{K2}/k^{W}_{K1}=1$. This figure indicates that E_{mix} shows a Nernstian response to c^{W}_{K1} at the higher values of c^{W}_{K1} at given values of c^{W}_{K2} and c^{O}_{K1}, but E_{mix} deviates from the Nernstian slope at the lower values of c^{W}_{K1}. The interference of K2 becomes significant as the difference between the standard ion-transfer potentials for K1 and K2 becomes negative.

Equation 24 expresses $k^{pot}_{K1,K2}$ as a function of the difference between the standard ion-transfer potentials of the ions K1 and K2, $\Delta E^{0}_{K2,K1}$; the concentration ratios, c^{W}_{K2}/c^{W}_{K1} and c^{O}_{K1}/c^{W}_{K2}, and the ratios of the mass-transfer

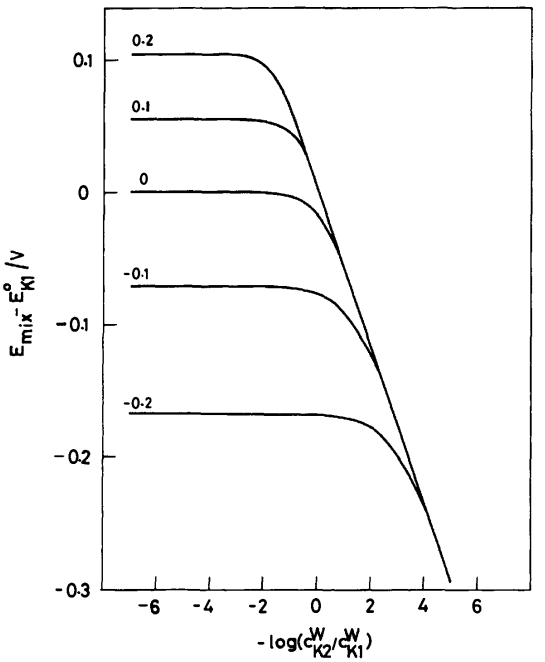

Fig. 3. Dependence of mixed ion transfer potentials on $\log(c^{W}_{K2}/c^{W}_{K1})$ at $k^{W}_{K1}/k^{W}_{K1}=k^{O}_{K2}/k^{W}_{K2}=\sqrt{2}$, $k^{W}_{K2}/k^{W}_{K1}=1$ and $c^{O}_{K1}/c^{W}_{K1}=1$ calculated from Eq. 16. Labels indicate the values of $\Delta E^{0}_{K2,K1}$.

coefficients, k^{O}_{K1}/k^{W}_{K1}, k^{O}_{K2}/k^{W}_{K2}, and k^{W}_{K2}/k^{W}_{K1}; the selectivity coefficient depends upon these parameters. Among these factors, the difference in the standard ion-transfer potentials $\Delta E^{0}_{K2,K1}$ is intrinsic for a given set of ions and solvents, whereas the ratios of the maas-transfer coefficients and of the concentrations vary with the experimental conditions. When there is no convective transport of the ions, the ratio of the mass-transfer coefficients is reduced to the square root of the ratio of the diffusion coefficients, for example, $k^{O}_{K1}/k^{W}_{K1}=(D^{O}_{K1}/D^{W}_{K1})^{1/2}$; then the ratios of the mass-transfer coefficient are also constants for a given set of ions and solvents.

The values of $k^{pot}_{K1,K2}$ were calculated from Eq. 24 and are plotted in Fig. 4 as a function of $\Delta E^{0}_{K2,K1}$ at different values of k^{W}_{K2}/k^{W}_{K1} when $k^{O}_{K1}/k^{W}_{K1}=k^{O}_{K2}/k^{W}_{K2}=\sqrt{2}$ and $c^{O}_{K1}/c^{W}_{K1}=c^{W}_{K2}/c^{W}_{K1}=1$. When the value of k^{W}_{K2}/k^{W}_{K1} is larger than unity, the logarithm of $k^{pot}_{K1,K2}$ changes almost linearly with $\Delta E^{0}_{K2,K1}$. On the other hand, when k^{W}_{K2}/k^{W}_{K1} is less than unity, the plots deviate from the straight lines at large negative values of $\Delta E^{0}_{K2,K1}$. The approximate linear relationship between $\log k^{pot}_{K1,K2}$ and $\Delta E^{0}_{K2,K1}$ in the positive range of $\Delta E^{0}_{K2,K1}$ at the lower values of k^{W}_{K2}/k^{W}_{K1} and in both the positive and negative ranges of $\Delta E^{0}_{K2,K1}$ at higher values of k^{W}_{K2}/k^{W}_{K1} is in line with the experimental finding that the logarithm of the selectivity coefficients of the liquid ion-exchange membrane electrodes correlates linearly with the logarithm of the ion-exchange equilibrium constants.[11]

Figure 4 shows that the selectivity coefficient depends markedly on the value of k^{W}_{K2}/k^{W}_{K1}, especially at the

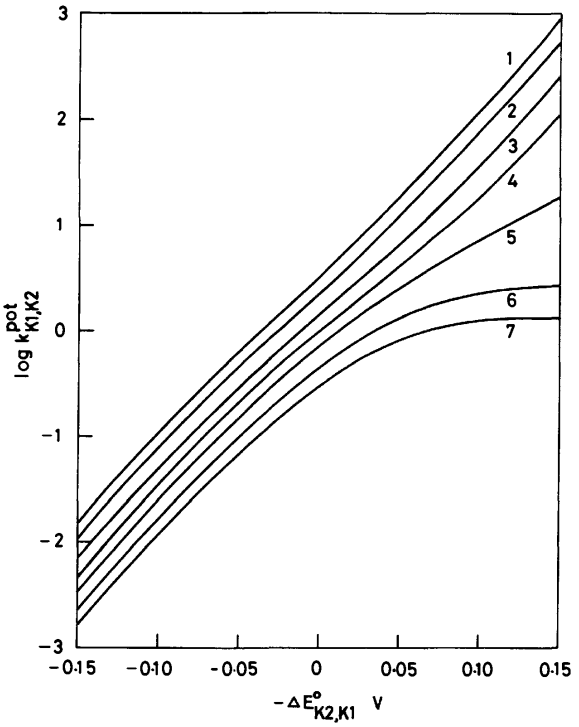

Fig. 4. $\log(k^{pot}_{K1,K2})$ *vs.* $\Delta E^{0}_{K2,K1}$ curves at $k^{w}_{K2}/k^{w}_{K1}=\sqrt{10}$ (curve 1), $\sqrt{5}$ (2), $\sqrt{2}$ (3), 1(4), $\sqrt{0.5}$(5), $\sqrt{0.2}$(6), and $\sqrt{0.1}$(7), when $k^{o}_{K1}/k^{w}_{K1}=k^{o}_{K2}/k^{w}_{K2}=\sqrt{2}$ and $c^{w}_{K2}/c^{w}_{K1}=c^{o}_{K1}/c^{w}_{K1}=1$, calculated from Eq. 24.

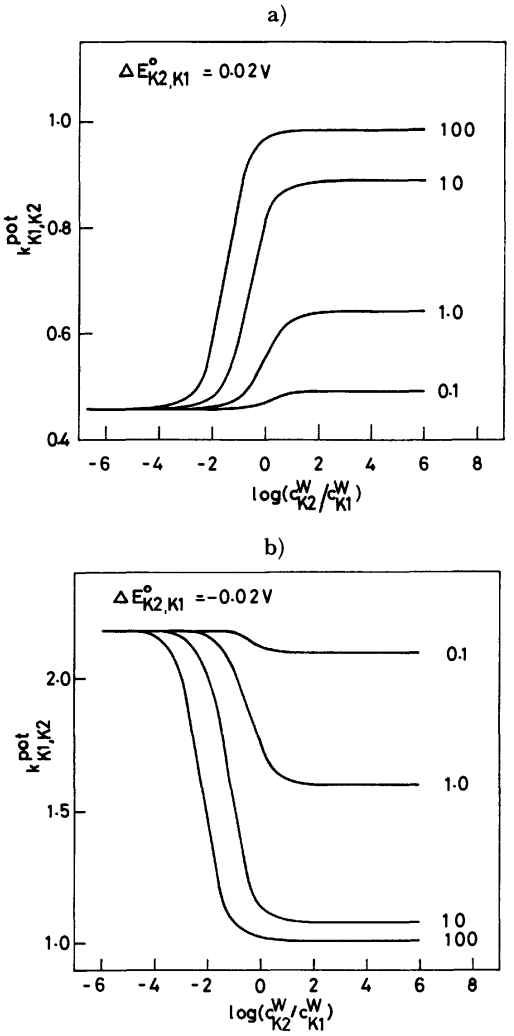

Fig. 5. Change of $k^{pot}_{K1,K2}$ with $\log(c^{w}_{K2}/c^{w}_{K1})$ calculated from Eq. 24 for $\Delta E^{0}_{K2,K1}=0.02$ V (Fig. 5a) and -0.02 V (Fig. 5b). Labels indicate the values of c^{o}_{K1}/c^{w}_{K2}.

negative extreme of $\Delta E^{0}_{K2,K1}$. This means that, in the absence of convection in both the membrane and the sample solution, the selectivity coefficient depends upon the relative magnitude of the diffusion coefficients of the primary and interfering ions. The dependence of the mixed potential and the selectivity coefficient on the ratio of the mass-transfer coefficients accounts for the effect of the convection on the potential response and the value of the selectivity coefficient of the ion-selective electrodes. The effect of stirring the sample solutions on the potential response of the ion-selective electrodes has been reported.[27] The often observed irreproducible values of the experimental selectivity coefficients may be attributed to such an effect of the mass-transfer coefficients on the selectivity coefficients, since the mass-transfer coefficient is generally not well reproducible under natural convection, which can be caused by the density gradient, accompanied by ion transfers across the membrane-solution interface.

The dependence of $k^{pot}_{K1,K2}$ on the concentration ratios, c^{w}_{K2}/c^{w}_{K1} and c^{o}_{K1}/c^{w}_{K2}, at several values of c^{o}_{K1}/c^{w}_{K2} was calculated from Eq. 24 for $\Delta E^{0}_{K2,K1}=0.02$ V (Fig. 5a) and -0.02 V (Fig. 5b). These conditions correspond to those in experiments for the determination of the selectivity coefficients using the procedure in which the concentration of the primary ion in the sample solution is changed while keeping the concentration of the primary ion in the membrane and that of the interfering ion in the sample solution constant.[26] Figures 5a and 5b show that the value of $k^{pot}_{K1,K2}$ depends markedly upon both c^{w}_{K2}/c^{w}_{K1} and c^{o}_{K1}/c^{w}_{K2}, except at the small extreme of c^{w}_{K2}/c^{w}_{K1}. The trend of the change in the $k^{pot}_{K1,K2}$ value depends upon the sign of $\Delta E^{0}_{K2,K1}$. For a positive value of $\Delta E^{0}_{K2,K1}$, $k^{pot}_{K1,K2}$ increases with the increae in c^{w}_{K2}/c^{w}_{K1}, whereas it decreases with the increase in c^{w}_{K2}/c^{w}_{K1} for a negative value of $\Delta E^{0}_{K2,K1}$. In both cases, the larger the value of c^{o}_{K1}/c^{w}_{K2}, the greater the change in $k^{pot}_{K1,K2}$ with the change in c^{w}_{K2}/c^{w}_{K2}. At the large extreme of c^{w}_{K2}/c^{w}_{K1}, $k^{pot}_{K1,K2}$ reaches a constant value whose magnitude depends upon c^{o}_{K1}/c^{w}_{K2}. These figures clearly illustrate that the experimental $k^{pot}_{K1,K2}$ values can vary with the experimental conditions.[2-6] For example, the selectivity coefficients are often determined from the intersection of the extrapolation of the two linear portions of a curve similar to those shown in Fig. 3.[28] This $k^{pot}_{K1,K2}$ value corresponds to the limiting value of $k^{pot}_{K1,K2}$ at the large extreme of c^{w}_{K2}/c^{w}_{K1} in Figs. 5a and 5b, that is, at the infinitely small concentration of the primary ion. This means that, at a given value of c^{o}_{K1}, the selectivity coefficient depends on the concentration level of the interfering ion in the sample solution.[6] The theoretical prediction of the dependence of the selectivity coefficient

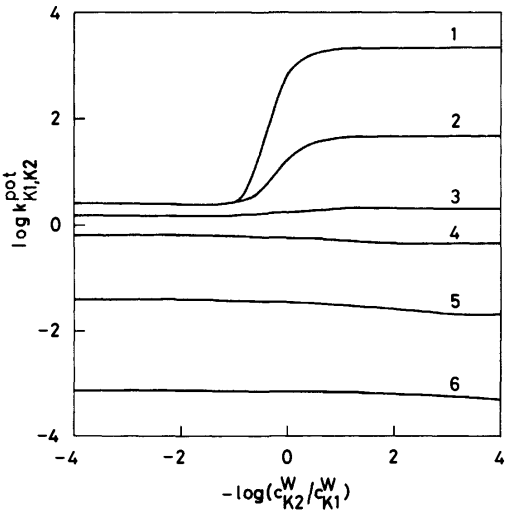

Fig. 6. $\log(k^{pot}_{K1,K2})$ *vs.* $\log(c^W_{K2}/c^W_{K1})$ curves calculated from Eq. 24 at $\Delta E^0_{K2,K1}=-0.2(1)$, $-0.1(2)$, $-0.02(3)$, $0.02(4)$, $0.1(5)$, and $0.2\,V(6)$, when $k^W_{K1}/k^0_{K1}=\sqrt{2}$, $k^W_{K2}/k^W_{K1}=1$ and $c^0_{K1}/c^W_{K1}=1$.

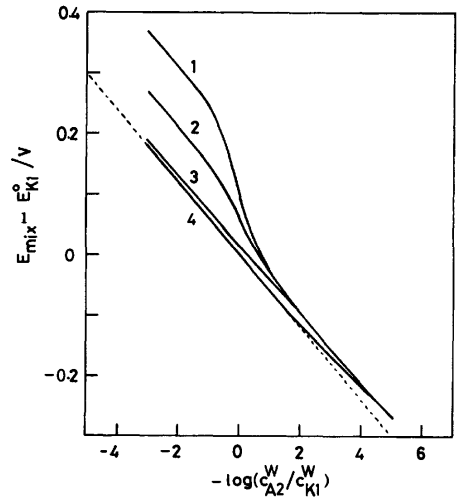

Fig. 7. Variation of E_{mix} with $\log(c^W_{A2}/c^W_{K1})$ at $\Delta E^0_{A2,K1}=0.2(1)$, $0.1(2)$, $0(3)$, and $-0.1\,V(4)$, when $k^W_{K1}/k^0_{K1}=k^W_{A2}/k^0_{A2}=\sqrt{2}$, $k^W_{A2}/k^W_{K1}=1$ and $c^0_{K1}/c^W_{A2}=1$.

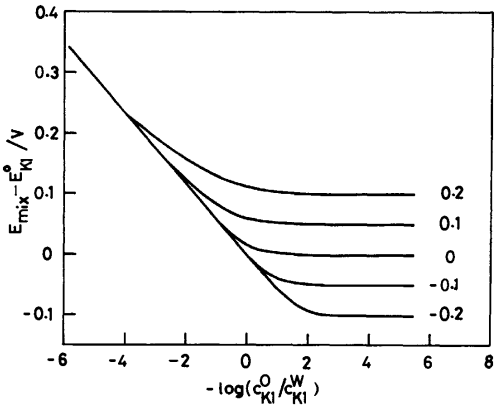

Fig. 8. Variation of E_{mix} with $\log(c^0_{K1}/c^W_{K1})$ at $\Delta E^0_{A2,K1}=0.2(1)$, $0.1(2)$, $0(3)$, $-0.1(4)$, and $-0.2\,V(5)$, when $k^W_{K1}/k^0_{K1}=k^W_{A2}/k^0_{A2}=\sqrt{2}$, $k^W_{A2}/k^W_{K1}=1$ and $c^W_{A2}/c^W_{K1}=1$.

on the concentrations of the ions, as exemplified in Figs. 5a and 5b, apparently conforms to the trends of the experimental observations found by Srinivasan and Rechnitz[2] for several anion-selective electrodes.

The selectivity coefficient is sometimes determined using the procedure in which the concentration of an interfering ion in a sample solution is changed, while the primary ion concentrations both in the sample solution and in the membrane are kept constant.[3,29] The selectivity coefficients corresponding to such experimental conditions were calculated from Eq. 24 at several different values of $\Delta E^0_{K2,K1}$; they are shown in Fig. 6 as a function of $\log(c^W_{K2}/c^W_{K1})$ at $c^O_{K1}/c^W_{K1}=1$. For the large positive values of $\Delta E^0_{K2,K1}$, $\log k^{pot}_{K1,K2}$ is almost independent of $\log(c^W_{K2}/c^W_{K1})$, whereas it varies drastically at the large negative values of $\Delta E^0_{K2,K1}$. In the small values of c^W_{K2}/c^W_{K1}, $k^{pot}_{K1,K2}$ reaches a constant value whose magnitude is dependent on the value of $\Delta E^0_{K2,K1}$. Such behavior of $k^{pot}_{K1,K2}$ has also been found experimentally for anion-selective electrodes of the liquid-membrane type.[3,9,11] Senkyr and Petr[9] and Morf[11] have suggested that the selectivity coefficients of anion-selective electrodes with respect to several different interfering ions converge to unity with the decrease in the activity of the interfering ions. However, this is not in conformity with the present theory, as is shown in Fig. 6.

Figure 7 shows the mixed ion-transfer potentials of the cell(III) for several different values of $\Delta E^0_{A2,K1}$ when c^W_{A2}/c^W_{K1} is changed, while keeping the c^O_{K1}/c^W_{A2} ratio constant. The effect of anion interference is quite different from that of cation interference. When $\Delta E^0_{A2,K1}$ has a large positive value, E_{mix} shows a so-called "super-Nernstian" response in the middle range of c^W_{A2}/c^W_{K1}. At the large extreme of c^W_{A2}/c^W_{K1}, E_{mix} *vs.* $\log(c^W_{A2}/c^W_{K1})$ curves exhibit the Nernstian response. At the small extreme of c^W_{A2}/c^W_{K1}, all the curves merge into a single curve with a sub-Nernstian slope.

Figure 8 shows the mixed ion-transfer potential of the cell(III) as a function of $\log(c^O_{K1}/c^W_{K1})$ at $c^W_{A2}/c^W_{K1}=1$ for several different values of $\Delta E^0_{A2,K1}$. Experimentally, such conditions may be met when the concentrations of K1 and A2 in the sample solution are changed by adding a salt K1A2 to the sample solution, *i.e.*, in the case of the so-called co-ion interference.[30] In such cases, the deviation of the potential from the Nernstian behavior becomes significant at the lower values of c^O_{K1}/c^W_{K1}, *i.e.*, at the larger values of c^W_{K1} at a constant c^O_{K1} value. A similar change in the potential has been found for a co-ion interference with the nitrate-selective electrodes.[30]

The present theory is limited to the case of the presence of supporting electrolytes in both membrane and solution phases and of the semi-infinite mass-transport of ions. However the above results indicate that the ion transfer across the membrane-sample solution interface plays an essential role in determining the potential of ion-selective electrodes through the interfacial potential and that the concepts of the zero-current potential

and the mixed ion-transfer potential are satisfactorily applicable for interpreting the behavior of the ion-selective electrodes with liquid membranes and also with solid membranes.

The present treatment can also be extended to more general cases, *e.g.*, simultaneous ion transfers of more than two ions and arbitrary valencies of the ions, and also to the presence of association between ions and between ions and ligands(ionophores).

References

1) J. Sandblom, G. Eisenman, and J. L. Walker, Jr., *J. Phys. Chem.*, **71**, 3862 (1967).
2) K. Srinivasan and G. A. Rechnitz, *Anal. Chem.*, **41**, 1203 (1969).
3) A. Hulanicki and R. Lewandowski, *Chem. Anal. (Warsaw)*, **19**, 53 (1974).
4) J. Senkyr and J. Petr, *Chem. Listy*, **73**, 1079 (1979).
5) N. Yoshida and N. Ishibashi, *Bull. Chem. Soc. Jpn.*, **50**, 3189 (1977).
6) L. Cunningham and H. Freiser, *Anal. Chim. Acta*, **132**, 43 (1981).
7) D. Midgley, *Anal. Chem.*, **49**, 1211 (1977).
8) A. Hulanicki and A. Lewenstem, *Talanta*, **24**, 171 (1977).
9) J. Senkyr and J. Petr, "Ion-Selective Electrodes 3," ed by E. Pungor, Elsevier, Amsterdam (1981), p. 237.
10) A. Jyo and N. Ishibashi, cited in Ref. 11, p. 246 ff.
11) W. E. Morf, "The Principles of Ion-Selective Electrodes and of Membrane Transport," Elsevier, Amsterdam (1981).
12) W. E. Morf, "Ion-Selective Electrodes 3," ed by E. Pungor, Elsevier, Amsterdam (1981), p. 267.
13) See, for example, A. Jyo, M. Torikai, and N. Ishibashi, *Bull. Chem. Soc. Jpn.*, **47**, 2862 (1974).
14) H. James, G. Carmack, and H. Freiser, *Anal. Chem.*, **44**, 856 (1972).
15) For a review, see J. Koryta and P. Vanysek, "Advances in Electrocemistry and Electrochemical Engineering," ed by H. Gerischer and C. W. Tobias, John Wiley, New York (1981), Vol. 12, p. 113.
16) K. Cammann, "Ion-Selective Electrodes," ed by E. Pungor and I. Buzas, Elsevier, Amsterdam (1978), p. 297.
17) I. M. Kolthoff and C. S. Millar, *J. Am. Chem. Soc.*, **62**, 2171 (1940).
18) J. Koryta, *Anal. Chim. Acta*, **111**, 1 (1979); J. Koryta, Proceedings of the J. Heyrovsky Memorial Congress on Polarography, Prague, Czechoslovakia, August 25—29, 1980, p. 38.
19) T. Fujinaga. *Phil. Trans. Roy. Soc.*, London, **A305**, 631 (1982).
20) T. Fujinaga, S. Kihara, and Z. Yoshida, *Bunseki Kagaku*, **31**, E301, (1982).
21) Ref. 11, p. 35.
22) J. Koryta, "Ion-Selective Electrodes," Cambridge Univ. Press, Cambridge (1975), p. 18.
23) L. Q. Hung, *J. Electroanal. Chem. Interfacial Electrochem.*, **115**, 159 (1980).
24) I. Tachi and M. Senda, *Denki Kagaku*, **21**, 575 (1953).
25) T. Kakiuchi and M. Senda, *Bull. Chem. Soc. Jpn.*, **56**, 1753 (1983).
26) B. P. Nicolsky, *Zh. Fiz. Khim.*, **10**, 495 (1937).
27) Ref. 11, pp. 255, 391.
28) G. G. Guilbault, IUPAC Inf. Bull., 1978, No. 1, p. 69.
29) Ref. 11, p. 246.
30) A. Jyo, K. Fukamachi, W. Koga, and N. Ishibashi, *Bull. Chem. Soc. Jpn.*, **50**, 670 (1977).
31) T. Kakiuchi, T. Kakutani and M. Senda, paper presented at the 28th Annual Meeting on Polarography, November 11—12. 1983, Sapporo; abstract, *Rev. Polarogr. (Kyoto)*, **28**, 38 (1982).

Syntheses and Crystal Structures of Diaquatris(*m*-hydroxybenzoato)-lanthanoid(III) *m*-Hydroxybenzoic Acid Dihydrate (M=La, Ce, Pr, and Nd), and Di-μ-(*m*-hydroxybenzoato)bis-{triaquabis(*m*-hydroxybenzoato)lanthanoid(III)} Dihydrate (M=Sm, Gd, Dy, Er, and Yb)

Yukio Koizumi,† Hiroshi Sawase,† Yasuo Suzuki,† Toshio Takeuchi,††
Mamoru Shimoi, and Akira Ouchi*
Department of Chemistry, College of Arts and Sciences, The University of Tokyo, Komaba 3-8-1, Meguro-ku, Tokyo 153
†*Department of Industrial Chemistry, Faculty of Engineering, Meiji University, Higashi-Mita, Tama-ku, Kawasaki-shi, Kanagawa 214*
††*Department of General Sciences, Faculty of Science and Technology, Sophia University, Kioi-cho, Chiyoda-ku, Tokyo 102*
(Received November 28, 1983)

Two types of lanthanoid(III) *m*-hydroxybenzoates, indicated in the title, have been synthesized, and the crystal and molecular structures of four representative complexes, where M=La (**1**), Nd (**2**), Sm (**3**), and Er (**4**), were determined by the single-crystal X-ray diffraction method. They are all triclinic, space group $P\bar{1}$, and the cell constants are as follows: (**1**) a=12.351(11), b=15.533(10), c=9.250(4) Å, α=109.86(4), β=101.40(6), γ=62.95(6)°; (**2**) a=12.287(4), b=15.542(7), c=9.194(3) Å, α=109.64(3), β=101.46(3), γ=62.83(3)°; (**3**) a=10.580(1), b=12.006(5), c=10.105(2) Å, α=111.14(2), β=90.27(1), γ=97.16(2)°; (**4**) a=10.586(4), b=11.943(6), c=10.027(5) Å, α=111.11(3), β=90.53(4), γ=97.26(4)°. The final R values obtained were (**1**) 0.039, (**2**) 0.038, (**3**) 0.030, and (**4**) 0.039. The central metal atoms of both types of complexes are octa-coordinated, and each is in a square-antiprism geometry. In **1** and **2**, one free acid molecule is present, and the molecule is hydrogen-bonded to the oxygen atoms of the coordinated water molecules through its carboxyl oxygen atoms. **1** and **2** have linear polymeric structure, and each pair of the metal atoms is bridged by a pair of the carboxylate ligands, while **3** and **4** have a dimeric structure, where metal atoms are bridged by two carboxylate ligands.

Several examples of the complicated structures of lanthanoid(III) carboxylates have already been elucidated.[1-7] Among them, the tetraacetato complex of cerium(III) has the most interesting structure; four acetate ions are coordinated to the central metal atom by both of the carboxyl oxygen atoms, forming four-membered chelate rings.[1] Although the structures of lanthanoid(III) aromatic carboxylates are expected to be different from those of the aliphatic ones, only a few results have been published thus far.[5,8-10] This is probably due to the difficulty in obtaining good crystals for the X-ray analysis, as their solubilities are generally low. To raise the solubility of the complexes, it is thought to be effective to introduce hydroxyl groups on the phenyl group of the ligand; however, *o*- and *p*-hydroxybenzoates of lanthanoids(III) are hardly soluble in water. On the other hand, *m*-hydroxybenzoates of lanthanoid(III) are soluble enough into water, and their crystals were obtained easily. Indeed, their tetracarboxylato complexes of some lanthanoid(III), with the formula of $HML_4 \cdot 4H_2O$ (where M=La, Ce, and Nd, HL=*m*-hydroxybenzoic acid) have been reported,[11] though their structure has not been solved. We could obtain the tetracarboxylates of La, Ce, Pr, and Nd from an aqueous solution containing an excess of the acid: moreover, new tricarboxylate-type complexes were obtained for the heavier lanthanoids: Sm, Gd, Dy, Er, and Yb, under similar experimental conditions.

It was found, from the results of the preliminary structural studies, that the coordination geometry of both types of complexes resemble each other. It was thought to be interesting to check the variation in the bond lengths and some detailed structures of the complexes, depending on the change in the atomic number of the central metal atom. Therefore, the lanthanum(III) (**1**) and neodymium(III) (**2**) complexes of the tetracarboxylate type, as well as the samarium(III) (**3**), and erbium(III) (**4**) complexes of the tricarboxylate type, were chosen, and their structures were fully determined by the single-crystal X-ray diffraction method.

Experimental

*Synthesis of Diaquatris(*m*-hydroxybenzoato)lanthanum(III)-(*m*-hydroxybenzoic acid) dihydrate polymer (**1**).* About 1.3 g (9.4 mmol) of *m*-hydroxybenzoic acid and fresh lanthanum(III) hydroxide, prepared from 0.75 g (2.0 mmol) of lanthanum(III) chloride heptahydrate, were mixed in hot water (about 20 cm^3). The solution was then cooled and left standing in a silica-gel desiccator overnight; the crystalline product was thus obtained. The product was washed with water and diethyl ether successively to remove the excess free acid. The crude product thus obtained could be recrystallized from the aqueous solution by leaving it in a silica-gel desiccator for several days. The yield was about 0.9 g (about 60%).

A similar synthetic technique is applicable to obtain the isomorphous cerium(III), and praseodymium(III) complexes; their yields were about the same. In the case of neodymium(III) **2**, as the tetracarboxylate is hardly precipitated at all, a little more free acid was added to the more dilute aqueous solution, and it was left standing in the desiccator longer. The coprecipitated free acid was removed by washing the product with diethyl ether repeatedly.

*Synthesis of Di-*μ*-(*m*-hydroxybenzoato)bis{triaquabis-(*m*-hydroxybenzoato)erbium(III)} Dihydrate (**4**).* When the

procedure used for the former type of complexes was applied to erbium(III) hydroxide, the titled complex was obtained as single crystals; even when the mole ratio of the added acid to the metal salt was increased, the precipitate obtained was a mixture of the titled tricarboxylate complex and the free acid. Similarly, this type of tricarboxylate complex was obtained for samarium(III) (**3**), gadolinium(III), dysprosium(III), and ytterbium(III). The yields were all about 60%.

The results of the elemental analyses of the products are shown in Table 1.

Table 1. Analyses of the complexes

Type[a)]	Ln		Ln(%)	C(%)	H(%)
1	La	Found	18.05	43.96	3.82
		Calcd	18.27	44.23	3.84
1	Ce	Found	18.10	43.91	3.81
		Calcd	18.40	44.16	3.84
1	Pr	Found	18.78	43.89	3.81
		Calcd	18.48	44.11	3.83
1	Nd	Found	19.02	43.67	3.78
		Calcd	18.84	43.92	3.82
2	Sm	Found	24.00	39.84	3.60
		Calcd	23.72	39.80	3.66
2	Gd	Found	24.80	39.43	3.58
		Calcd	24.55	39.37	3.62
2	Dy	Found	25.49	39.30	3.58
		Calcd	25.16	39.05	3.59
2	Er	Found	25.91	38.77	3.50
		Calcd	25.71	38.77	3.56
2	Yb	Found	26.63	38.61	3.41
		Calcd	26.63	38.42	3.53

a) The chemical formulae of the complexes: Type 1: $[LnL_3(H_2O)_2]\cdot HL\cdot 2H_2O$; Type 2: $[LnL_3(H_2O)_3]_2\cdot 2H_2O$ (where HL = *m*-hydroxybenzoic acid).

Single-crystal X-Ray Analysis. Crystals 0.4×0.3×0.3 mm³ in size were used as the samples of **1**, **2**, and **3**, while a crystal 0.3×0.3×0.3 mm³ in size was used as the sample of **4**. The reflections were collected on a Rigaku AFC-6A automated four-circle diffractometer with graphite monochromated Mo $K\alpha$ radiation (0.7107 Å), the θ-2θ scan technique being employed (scan speed 4° min^{-1}; scan width 1.03+0.5tanθ°). These crystals are all triclinic, space group $P\bar{1}$; their crystallographic data are shown in Table 2. The intensities were corrected for Lorentz and polarization factors, but no correction was made for absorption and extinction. All the calculations were carried out on a HITAC M-200H computer of the Computer Center of the University of Tokyo, using the local version of the UNICS program.[12] The atomic-scattering factors were taken from the tables.[13]

Structure Determination. The structure of each complex was solved by the heavy-atom method. In the case of the **1** and **4** complexes, the central metal and some oxygen atoms were deduced from the three-dimensional Patterson maps, while all the other non-hydrogen atoms were located by means of successive Fourier syntheses and refined by the block-diagonal least-squares method. The final R values obtained by applying the anisotropic temperature factors are shown in Table 2.[14] As **2** and **3** were found to be isomorphous with **1**, and **4** respectively, from their X-ray crystallographic data, the positional and thermal parameters of the latter complexes were tentatively applied to the former ones as the starting data, and they were then refined as usual.

Other Measurements. The X-ray powder patterns of these complexes were obtained by the use of a diffractometer, Model DX-GO-F JEOL, using Cu $K\alpha$ radiation, in the range from 6° to 50° in 2θ. The infrared absorption spectra of the samples were obtained by means of a JASCO A-202 grating infrared spectrophotometer, using Nujol and hexachloro-1,3-butadiene mull. The simultaneous thermogravimetric(TG) and differential thermal analyses(DTA) were carried out with a Rigaku Denki "Thermoflex" M-8075, using a sample of about 10 mg in each run, referring to Al_2O_3, at the heating rate of 2.5 K min^{-1}. The pH of the titrated solution was measured by the use of a Toa-Dempa glass electrode pH meter, model HM-5A.

Table 2. Crystallographic data and X-ray-measurement conditions of the complexes

Ln[a)]	La	Nd	Sm	Er
$a(l/\text{Å})$	12.351(11)	12.287(4)	10.580(1)	10.586(4)
$b(l/\text{Å})$	15.533(10)	15.542(7)	12.006(5)	11.943(6)
$c(l/\text{Å})$	9.250(4)	9.194(3)	10.105(2)	10.027(5)
$\alpha(\phi/°)$	109.86(4)	109.64(3)	111.14(2)	111.11(3)
$\beta(\phi/°)$	101.40(6)	101.46(3)	90.27(1)	90.53(4)
$\gamma(\phi/°)$	62.95(6)	62.83(3)	97.16(2)	97.26(4)
$U(v/\text{Å}^3)$	1484.6(20)	1469.0(11)	1186.1(6)	1171.0(10)
D_m(d/Mg m^{-3})	1.69(3)	1.71(3)	1.78(3)	1.82(3)
D_x(d/Mg m^{-3})	1.70	1.73	1.78	1.85
Z	4	4	4	4
μ(Mo Kα)(n/mm^{-1})	1.56	1.87	2.57	3.79
F.W.[b)]	760.4	765.8	633.8	650.7
Scanned range(2θ/°)	3—42	3—42	3—44	3—43.5
Measured reflections	3473	3426	3142	3007
Reflections used for calculation[c)]	3087	3022	2958	2925
R	0.039	0.038	0.030	0.039

a) The central metal atom of the complexes. Their formulae are shown in Table 1. b) For the formulae containing one atom of the central metal. c) The reflections of $|F_o| > 3\sigma(|F_o|)$ were selected and used.

Results and Discussion

The final atomic parameters of the complexes are listed in Table 3.[15] The perspective drawings of **1** and **4** around each central metal atom, together with their numbering scheme are shown in Figs. 1 and 2. Their crystal packing diagrams are shown in Figs. 3 and 4.

Table 3. Final atomic coordinates ($\times 10^4$) and equivalent isotropic temperature factors (B_{eq}/Å^2), with estimated standard deviations in parentheses

(1) Diaquatris(*m*-hydroxybenzoato)lanthanum(III) *m*-hydroxybenzoic acid dihydrate				
Atom	*x*	*y*	*z*	B_{eq}/Å$^{2a)}$
La	4935.4(4)	4635.0(4)	2143(1)	1.7
O(11)	3575(5)	4129(4)	3074(6)	2.6
O(12)	4003(5)	4753(4)	5522(6)	2.8
O(13)	706(5)	4971(5)	8245(7)	4.3
O(21)	5508(5)	6744(4)	4(6)	3.0
O(22)	5148(5)	5876(4)	1139(6)	2.5
O(23)	4312(6)	8317(4)	6557(7)	4.3
O(31)	3167(5)	6280(4)	3611(6)	2.6
O(32)	2758(4)	5643(4)	1181(6)	2.2
O(33)	-1797(5)	7632(4)	421(7)	3.7
O(41)	8571(5)	1340(5)	2322(7)	4.4
O(42)	9169(5)	2349(5)	1799(8)	4.7
O(43)	13506(5)	188(5)	498(8)	4.7
C(11)	3400(7)	4371(6)	4474(9)	2.3
C(12)	2442(7)	4166(6)	4917(9)	2.4
C(13)	1983(8)	3524(6)	3830(10)	3.1
C(14)	1041(8)	3391(7)	4242(11)	3.8
C(15)	613(8)	3863(7)	5723(10)	3.5
C(16)	1113(7)	4499(6)	6794(9)	2.6
C(17)	2013(7)	4643(6)	6371(9)	2.3
C(21)	5359(7)	6625(6)	1204(9)	2.3
C(22)	5457(7)	7344(6)	2724(9)	2.0
C(23)	6223(8)	7817(7)	2896(10)	3.5
C(24)	6304(9)	8498(8)	4308(11)	4.6
C(25)	5653(9)	8688(7)	5555(10)	4.0
C(26)	4942(8)	8173(6)	5334(10)	3.0
C(27)	4814(7)	7504(6)	3928(9)	2.1
C(31)	2437(7)	6298(6)	2438(9)	2.0
C(32)	1151(7)	7106(6)	2551(9)	2.5
C(33)	858(8)	7965(6)	3857(10)	3.2
C(34)	-344(8)	8708(7)	3884(11)	3.9
C(35)	-1219(8)	8612(7)	2752(10)	3.4
C(36)	-906(7)	7732(7)	1530(10)	2.9
C(37)	281(7)	6988(6)	1395(9)	2.6
C(41)	9391(8)	1540(7)	1937(10)	3.4
C(42)	10624(7)	678(6)	1686(9)	2.6
C(43)	10861(8)	-226(7)	1928(11)	4.0
C(44)	12009(9)	-994(7)	1704(12)	4.6
C(45)	12910(8)	-870(7)	1216(11)	4.2
C(46)	12655(7)	20(6)	973(11)	3.1
C(47)	11521(7)	814(7)	1225(10)	3.0
O(W1)	6993(5)	3676(4)	1028(6)	2.9
O(W2)	6373(5)	3080(4)	3278(6)	2.8
O(W3)	5537(5)	8417(4)	9376(7)	3.3
O(W4)	1580(5)	4289(4)	890(7)	3.6

(2) Diaquatris(*m*-hydroxybenzoato)neodymium(III) *m*-hydroxybenzoic acid dihydrate				
Atom	*x*	*y*	*z*	B_{eq}/Å$^{2a)}$
Nd	4934.7(4)	4636.8(3)	2128.9(5)	1.7
O(11)	3621(5)	4160(4)	3107(6)	2.6
O(12)	4019(5)	4780(4)	5603(6)	2.6
O(13)	695(5)	4959(5)	8235(7)	3.9
O(21)	5486(5)	6706(4)	-47(6)	2.6
O(22)	5137(5)	5858(4)	1150(6)	2.3
O(23)	4303(6)	8310(5)	6554(7)	4.1
O(31)	3226(4)	6249(4)	3592(6)	2.2
O(32)	2799(4)	5604(4)	1159(6)	2.1
O(33)	-1784(5)	7610(4)	399(7)	3.4
O(41)	8544(5)	1371(5)	2337(7)	4.2
O(42)	9153(5)	2366(5)	1797(8)	4.5
O(43)	13534(5)	174(5)	492(8)	4.6
C(11)	3429(7)	4387(6)	4522(9)	1.9
C(12)	2459(7)	4180(6)	4924(9)	1.9
C(13)	2022(7)	3519(6)	3804(10)	2.7
C(14)	1086(8)	3377(7)	4200(11)	3.4
C(15)	623(7)	3849(6)	5681(10)	3.1
C(16)	1108(7)	4481(6)	6752(9)	2.5
C(17)	2021(7)	4649(6)	6391(9)	2.5
C(21)	5353(7)	6586(6)	1195(9)	1.9
C(22)	5447(7)	7327(5)	2710(9)	1.8
C(23)	6206(8)	7809(6)	2858(10)	3.1
C(24)	6288(9)	8488(7)	4270(11)	4.4
C(25)	5639(8)	8681(7)	5533(10)	3.3
C(26)	4923(7)	8167(6)	5339(10)	2.8
C(27)	4799(7)	7501(6)	3938(9)	2.1
C(31)	2470(7)	6269(6)	2439(9)	2.0
C(32)	1190(7)	7078(6)	2562(9)	2.2
C(33)	895(8)	7942(6)	3845(10)	2.8
C(34)	-304(8)	8700(7)	3888(11)	3.5
C(35)	-1198(8)	8597(6)	2739(11)	3.2
C(36)	-886(7)	7706(6)	1516(10)	2.7
C(37)	311(7)	6960(6)	1360(9)	2.6
C(41)	9382(8)	1552(7)	1946(10)	3.1
C(42)	10610(7)	698(6)	1702(10)	2.4
C(43)	10826(8)	-209(7)	1940(11)	3.4
C(44)	11999(9)	-993(7)	1708(12)	4.6
C(45)	12923(8)	-884(7)	1218(11)	3.6
C(46)	12654(8)	39(7)	977(10)	3.2
C(47)	11506(8)	845(7)	1228(10)	3.0
O(W1)	6957(5)	3696(4)	1021(6)	2.5
O(W2)	6339(4)	3117(4)	3255(6)	2.4
O(W3)	5546(5)	8397(4)	9376(7)	3.2
O(W4)	1615(5)	4276(4)	880(7)	3.5

Table 3. Continued

(3) Di-μ-(*m*-hydroxybenzoato)bis{triaquabis(*m*-hydroxybenzoato)samarium(III)}·dihydrate.[b]

Atom	*x*	*y*	*z*	B_{eq}/Å²[a]
Sm	4934.5(3)	4297.0(2)	2544.2(3)	1.9
O(11)	2147(4)	3593(4)	-908(5)	3.4
O(12)	3341(4)	3486(4)	819(5)	3.6
O(13)	2329(5)	-687(5)	712(8)	7.4
O(21)	3148(4)	6090(4)	6599(4)	3.3
O(22)	3659(4)	5228(4)	4372(5)	3.2
O(23)	158(4)	6023(5)	1552(5)	4.9
O(31)	6119(4)	6343(3)	3640(4)	2.5
O(32)	4594(4)	6163(4)	2069(4)	2.7
O(33)	4472(5)	10410(4)	2217(6)	5.2
C(11)	2484(5)	3024(5)	-190(6)	2.5
C(12)	1934(5)	1735(5)	-535(7)	2.6
C(13)	1046(7)	1174(6)	-1669(7)	3.7
C(14)	592(8)	-45(7)	-2009(8)	4.7
C(15)	1011(7)	-690(6)	-1240(8)	4.2
C(16)	1884(7)	-101(6)	-106(9)	4.3
C(17)	2339(6)	1111(6)	278(8)	3.7
C(21)	2925(5)	5776(5)	5274(7)	2.5
C(22)	1703(5)	6088(5)	4803(6)	2.1
C(23)	793(6)	6470(5)	5783(7)	2.7
C(24)	-360(6)	6698(6)	5324(7)	3.3
C(25)	-591(6)	6557(6)	3915(7)	3.2
C(26)	346(6)	6180(6)	2959(7)	3.1
C(27)	1501(6)	5936(6)	3378(7)	2.9
C(31)	5478(5)	6828(5)	2978(6)	2.1
C(32)	5735(6)	8125(5)	3257(6)	2.3
C(33)	6774(6)	8817(6)	4173(7)	3.3
C(34)	7000(7)	10046(6)	4423(8)	4.1
C(35)	6233(7)	10567(6)	3754(8)	4.0
C(36)	5221(7)	9855(6)	2854(7)	3.7
C(37)	4943(6)	8633(5)	2581(7)	3.0
O(W1)	3988(4)	2805(4)	3519(4)	2.9
O(W2)	5505(4)	2189(4)	1013(5)	3.7
O(W3)	6335(4)	4406(4)	653(4)	2.6
O(W4)	8425(5)	2999(5)	163(8)	7.1

(4) Di-μ-(*m*-hydroxybenzoato)bis{triaquabis(*m*-hydroxybenzoato)erbium(III)}·dihydrate[b]

Atom	*x*	*y*	*z*	B_{eq}/Å²[a]
Er	4941.5(3)	4295.2(2)	2510.5(3)	1.6
O(11)	2194(5)	3590(5)	-927(6)	3.1
O(12)	3411(5)	3490(5)	810(6)	3.1
O(13)	2335(7)	-663(6)	820(9)	6.4
O(21)	3260(5)	6042(5)	6503(6)	2.8
O(22)	3676(5)	5185(4)	4229(6)	2.7
O(23)	115(6)	6033(3)	1553(6)	4.5
O(31)	6105(5)	6284(4)	3641(5)	2.2
O(32)	4606(5)	6132(4)	2032(6)	2.9
O(33)	4531(7)	10421(5)	2218(7)	4.5
C(11)	2545(7)	3029(7)	-193(8)	2.3
C(12)	1968(7)	1735(7)	-518(8)	2.4
C(13)	1086(8)	1153(7)	-1683(9)	3.1
C(14)	618(10)	-60(8)	-1987(10)	4.3
C(15)	1039(9)	-695(8)	-1200(10)	3.9
C(16)	1896(8)	-96(7)	-48(11)	3.9
C(17)	2361(8)	1130(7)	331(10)	3.5
C(21)	2984(7)	5733(6)	5183(8)	2.0
C(22)	1750(7)	6076(6)	4764(8)	2.0
C(23)	890(7)	6467(7)	5801(9)	2.6
C(24)	-289(8)	6702(7)	5382(9)	3.2
C(25)	-569(8)	6562(7)	3956(9)	3.2
C(26)	341(8)	6180(7)	2957(9)	2.8
C(27)	1504(7)	5929(7)	3346(8)	2.5
C(31)	5476(7)	6767(6)	2953(7)	1.6
C(32)	5742(7)	8087(7)	3266(8)	2.5
C(33)	6773(8)	8808(7)	4236(9)	2.9
C(34)	7023(9)	10026(7)	4492(11)	3.8
C(35)	6269(9)	10560(8)	3822(10)	3.8
C(36)	5264(8)	9847(7)	2868(9)	3.3
C(37)	4980(8)	8627(7)	2580(8)	2.6
O(W1)	4027(5)	2851(4)	3490(5)	2.6
O(W2)	5523(6)	2231(5)	1032(6)	3.5
O(W3)	6314(5)	4405(4)	691(5)	2.3
O(W4)	8399(7)	3008(6)	144(9)	6.0

a) The equivalent isotropic temperature factors were computed using the following expression: $B_{eq}=4/3(B_{11}a^2+B_{22}b^2+B_{33}c^2+B_{12}ab\cos\gamma+B_{13}ac\cos\beta+B_{23}bc\cos\alpha)$. The B_{ij}'s are defined by: $\exp[-(h^2B_{11}+k^2B_{22}+l^2B_{33}+2klB_{23}+2hlB_{13}+2hkB_{12})]$.

The Structure of Lanthanum(III) Complex (1). The central lanthanum(III) atom of **1** is octa-coordinated and is in a square-antiprism geometry, being coordinated to eight oxygen atoms. The La atom is bridged to La^{i} as well as to La^{ii} with a couple of the respective carboxylate ligands, to form a linear polymeric structure (where the keys to the symmetry operations are: i: 1.0−*x*, 1.0−*y*, 1.0−*z*; ii: 1.0−*x*, 1.0−*y*, −*z*). Therefore, the zig-zag chain of the polymeric complex is parallel to *z*-axis. The center of symmetry of **1** exists at the mid-point of La and La^{i}, as well as of La and La^{ii}. Each oxygen atom of the carboxylate ligand, which bridge La and La^{i} atoms, is coordinated to a respective metal atom, forming a La-O-C-O-La^{i}-type bridge. In the case of the ligand, which bridges La and La^{ii}, O(21) and O(22) are coordinated to La^{ii} and La respectively; moreover, the O(22) takes a position not very far from La^{ii} (3.074(8) Å). Taking this additional weak bonding, La···O(22^{ii}), into consideration, the La atom can be said to be ennea-coordinated and to be in a capped square-antiprism geometry. Another carboxylate ligand forms a four-membered chelate ring, coordinated to the metal atom through both of the carboxylate oxygen atoms, O(31) and O(32). Two water oxygen atoms, O(W1) and O(W2), are also coordinated to the metal atom, and the fourth acid molecule forms hydrogen bondings with the water oxygen atoms O(W1)···O(42), 2.698(8) Å, and O(W2)···O(41), 2.860(7) Å, where the former bonding is

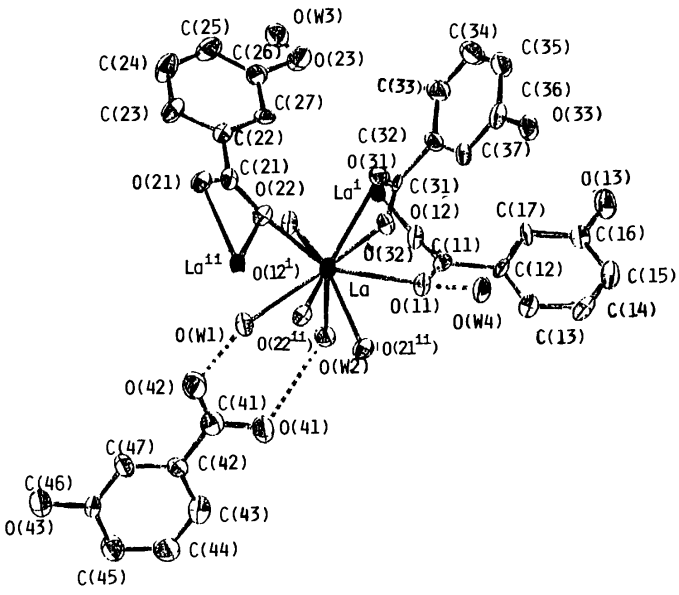

Fig. 1. A perspective drawing of diaquatris(*m*-hydroxybenzoato)lanthanum(III)(*m*-hydroxybenzoic acid)·dihydrate, and the numbering scheme of atoms.

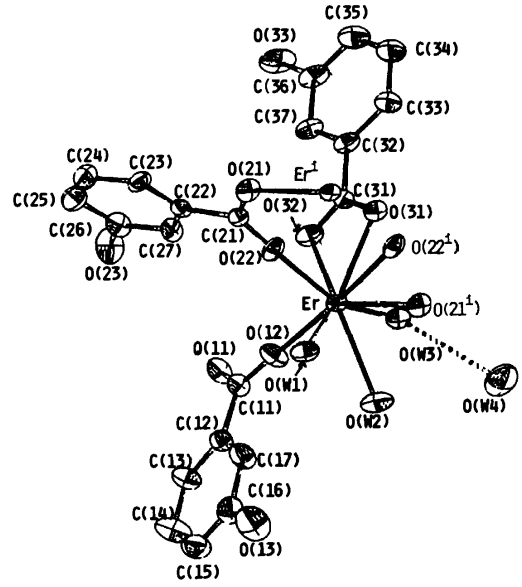

Fig. 2. A perspective drawing of di-μ-(*m*-hydroxybenzoato) bis{triaquabis(*m*-hydroxybenzoato) erbium(III)}·dihydrate, and the numbering scheme of atoms.

through the water hydrogen and the latter one through the acid hydrogen atom. The other water oxygen atoms, O(W3) and O(W4), are not coordinated to the lanthanoid atom. The phenol hydroxyl oxygen atoms of the ligands are not coordinated to the metal atom, either. Possible hydrogen bondings between the oxygen atoms are summarized in Table 4 (less than 2.95 Å). Thus, a polymer chain of the complex is weakly bonded to other chains.

The two C-O bond lengths of each carboxyl group which acts as a ligand are not very different from each other; the differences are O(11), O(12)-C(11), 0.056; O(21), O(22)-C(21), 0.043; and O(31), O(32)-C(31), 0.013 Å. However, that of the fourth acid molecule is a

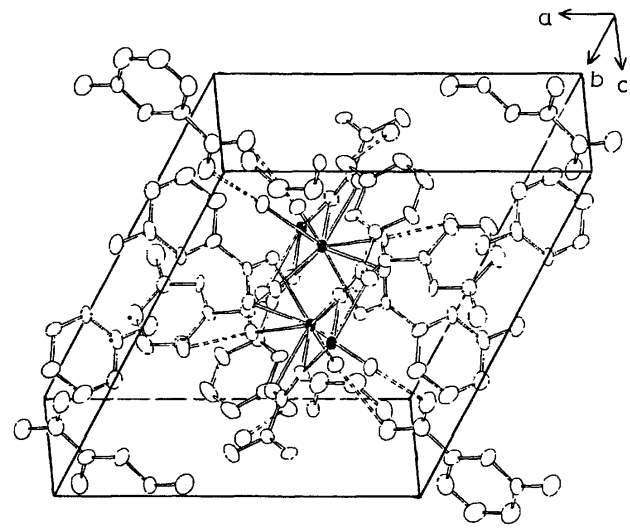

Fig. 3. Crystal packing diagram of the lanthanum(III) complex.

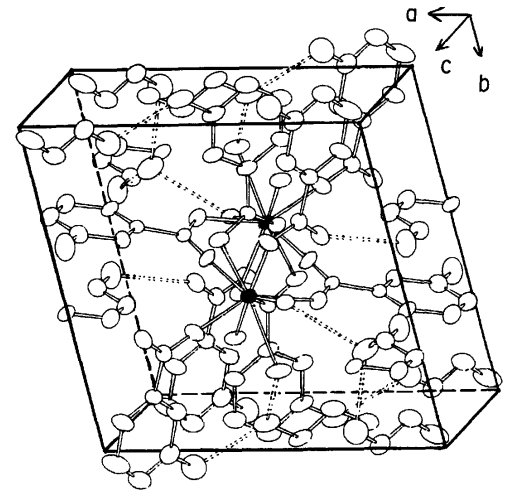

Fig. 4. Crystal packing diagram of the erbium(III) complex.

little large, 0.130 Å, like that of a free acid molecule.

The Structure of the Neodymium(III) Complex (2). The **2** complex is isomorphous with **1**, and both structures resemble each other. Every Nd-O length in **2** (2.491 Å in average) is shorter than the corresponding La-O ones in **1** (2.606 Å in average) by about 0.11 Å, and among them, M-O(12^{i}), M-O(22^{ii}), and M-O(21^{ii}) are especially shortened; the reductions of the above-mentioned distances are much larger than those to be expected from the decrease in the central-metal-atom radius (the atomic radii are: La, 1.877; Nd, 1.821 Å[16a]). They are all bridging ligand ones, and the inter-metal-atom distances, M···M^{i} as well as M···M^{ii}, also decrease, as is shown in Table 4. The hydrogen bond lengths, O(W1)···O(42) and O(W2)···O(41), of **2** are slightly shorter than the respective ones of **1**.

The Structure of the Samarium(III) Complex (3). The central samarium(III) atom of **3** is octa-coordinated and is in a square-antiprism geometry, being coordi-

Table 4. Interatomic distances and bond angles of the complexes

M[a)]	La(l/Å)	Nd(l/Å)	M[a)]	Sm(l/Å)	Er(l/Å)
M-O(22)	2.580(8)	2.479(7)	M-O(22)	2.322(4)	2.231(5)
M-O(32)	2.601(5)	2.512(5)	M-O(31)	2.467(4)	2.396(5)
M-O(21^{II})	2.634(6)	2.488(6)	M-O(21^{I})	2.364(5)	2.283(6)
M-O(W1)	2.541(6)	2.457(5)	M-O(W1)	2.452(5)	2.386(6)
M-O(12^{I})	2.536(6)	2.356(5)	M-O(12)	2.273(4)	2.198(5)
M-O(31)	2.660(5)	2.559(4)	M-O(32)	2.521(5)	2.474(6)
M-O(11)	2.570(8)	2.466(8)	M-O(W3)	2.455(4)	2.372(6)
M-O(W2)	2.723(6)	2.615(6)	M-O(W2)	2.594(4)	2.534(5)
M-O(22^{II})	3.074(6)	2.843(6)	M···O(22^{I})	3.273(5)	3.382(6)
O(11)-C(11)	1.346(11)	1.268(10)	O(11)-C(11)	1.239(9)	1.241(11)
O(12)-C(11)	1.290(10)	1.263(10)	O(12)-C(11)	1.276(7)	1.269(9)
O(13)-C(16)	1.450(11)	1.385(10)	O(13)-C(16)	1.378(12)	1.389(15)
C(11)-C(12)	1.530(16)	1.506(15)	C(11)-C(12)	1.496(9)	1.503(11)
C(12)-C(13)	1.422(13)	1.405(12)	C(12)-C(13)	1.388(9)	1.396(11)
C(13)-C(14)	1.432(17)	1.400(17)	C(13)-C(14)	1.397(10)	1.391(13)
C(14)-C(15)	1.483(14)	1.404(13)	C(14)-C(15)	1.384(13)	1.381(16)
C(15)-C(16)	1.439(12)	1.393(13)	C(15)-C(16)	1.381(10)	1.375(12)
C(16)-C(17)	1.392(16)	1.383(15)	C(16)-C(17)	1.384(9)	1.395(12)
C(17)-C(12)	1.460(12)	1.382(11)	C(17)-C(12)	1.393(12)	1.390(15)
O(21)-C(21)	1.325(13)	1.269(12)	O(21)-C(21)	1.266(8)	1.260(9)
O(22)-C(21)	1.282(13)	1.261(13)	O(22)-C(21)	1.252(7)	1.250(9)
O(23)-C(26)	1.469(13)	1.376(13)	O(23)-C(26)	1.376(9)	1.369(11)
O(31)-C(31)	1.324(10)	1.262(9)	O(31)-C(31)	1.274(8)	1.275(10)
O(32)-C(31)	1.311(9)	1.267(8)	O(32)-C(31)	1.278(6)	1.257(8)
O(33)-C(36)	1.417(10)	1.375(10)	O(33)-C(36)	1.386(10)	1.395(13)
O(41)-C(41)	1.338(15)	1.322(15)			
O(42)-C(41)	1.208(14)	1.214(13)			
O(43)-C(46)	1.387(15)	1.369(15)			
M···M^{II}	4.811(3)	4.473(2)	M···M^{I}	4.625(2)	4.654(3)
M···M^{I}	5.379(3)	4.999(2)	M···M^{II}	5.959(2)	5.853(3)
O(W1)···O(42)	2.698(8)	2.682(7)			
O(W2)···O(41)	2.860(7)	2.841(7)	O(W2)···O(W3)	2.847(7)	2.767(8)
O(W1)···O(W2)	3.027(11)	2.844(10)	O(W1)···O(W2)	2.919(6)	2.860(8)
O(W1)···O(32^{II})	2.858(10)	2.700(10)	O(W1)···O(31^{I})	2.686(6)	2.696(7)
O(W2)···O(23^{I})	2.723(12)	2.738(11)	O(W2)···O(21^{I})	2.786(5)	2.760(7)
O(W3)···O(23)	2.898(9)	2.732(8)	O(W2)···O(33^{III})	2.923(8)	2.913(10)
O(W3)···O(21^{III})	2.887(11)	2.886(11)	O(W4)···O(13^{IV})	2.606(8)	2.621(9)
O(W4)···O(11)	2.921(8)	2.853(8)	O(33)···O(13^{V})	2.640(8)	2.630(9)
O(W4)···O(13^{IV})	2.713(10)	2.706(9)	O(23)···O(11^{VI})	2.658(7)	2.650(9)
O(33)···O($W4^{V}$)	2.727(9)	2.692(9)	O(W3)···O(W4)	2.884(7)	2.872(9)
O(43)···O($W3^{VI}$)	2.863(12)	2.878(12)			

Bond Angles

M	La(ϕ/°)	Nd(ϕ/°)	M	Sm(ϕ/°)	Er(ϕ/°)
O(22)-M-O(32)	74.71(19)	76.06(20)	O(22)-M-O(31)	77.39(13)	77.56(17)
O(32)-M-O(21^{II})	76.59(16)	77.78(16)	O(31)-M-O(21^{I})	77.96(14)	76.37(18)
O(21^{II})-M-O(W1)	80.34(17)	81.72(17)	O(21^{I})-M-O(W1)	82.40(16)	80.05(20)
O(W1)-M-O(22)	74.69(21)	76.24(21)	O(W1)-M-O(22)	71.39(15)	71.20(19)
O(31)-M-O(11)	70.29(19)	71.62(20)	O(32)-M-O(W3)	72.75(15)	73.01(19)
O(11)-M-O(W2)	71.01(21)	71.49(21)	O(W3)-M-O(W2)	68.59(13)	68.56(17)
O(W2)-M-O(12^{I})	69.65(17)	71.78(17)	O(W2)-M-O(12)	74.84(14)	75.10(18)
O(12^{I})-M-O(31)	75.73(16)	77.15(16)	O(12)-M-O(32)	80.72(16)	80.93(20)
O(32)-M-O(31)	52.44(14)	51.14(14)	O(31)-M-O(32)	52.17(14)	53.57(17)
O(W1)-M-O(W2)	70.12(17)	68.12(17)	O(W1)-M-O(W2)	70.61(14)	71.02(18)
M-O(11)-C(11)	123.2(5)	124.8(5)	M-O(12)-C(11)	177.5(3)	178.7(4)
M^{I}-O(12)-C(11)	169.2(5)	170.0(5)			

Table 4. Continued

M	La(ϕ/°)	Nd(ϕ/°)	M	Sm(ϕ/°)	Er(ϕ/°)
O(11)-C(11)-O(12)	125.4(9)	122.6(9)	O(11)-C(11)-O(12)	122.0(5)	122.6(7)
O(11)-C(11)-C(12)	119.5(7)	118.5(7)	O(11)-C(11)-C(12)	120.3(5)	119.7(6)
O(12)-C(11)-C(12)	115.1(8)	118.9(8)	O(12)-C(11)-C(12)	117.6(6)	117.6(7)
C(11)-C(12)-C(13)	116.3(8)	119.5(7)	C(11)-C(12)-C(13)	119.8(6)	119.9(7)
C(11)-C(12)-C(17)	123.3(9)	121.8(8)	C(11)-C(12)-C(17)	119.3(5)	118.8(7)
M^{ii}-O(21)-C(21)	107.3(5)	104.3(5)	M^{i}-O(21)-C(21)	119.5(4)	125.7(4)
M-O(22)-C(21)	155.7(6)	157.9(6)	M-O(22)-C(21)	174.1(4)	177.1(4)
O(21)-C(21)-O(22)	119.3(7)	120.1(7)	O(21)-C(21)-O(22)	123.0(5)	123.6(7)
M-O(31)-C(31)	90.4(4)	93.4(4)	M-O(31)-C(31)	95.9(3)	94.7(4)
M-O(32)-C(31)	93.3(4)	95.5(4)	M-O(32)-C(31)	93.3(3)	91.5(4)
O(31)-C(31)-O(32)	123.9(5)	119.9(5)	O(31)-C(31)-O(32)	118.6(5)	120.2(6)
O(W2)···O(41)-C(41)	114.0(6)	113.8(6)			
O(W1)···O(42)-C(41)	126.7(6)	126.4(6)			
O(41)-C(41)-O(42)	123.4(8)	121.9(8)			

a) The central metal atom of each complex is shown. The chemical formulae of the first two differ from those of the latter two (see Table 1, footnoot).
Keys to the symmetry operations: For the lanthanum(III) and neodymium(III) complexes: i: $1.0-x$, $1.0-y$, $1.0-z$; ii: $1.0-x$, $1.0-y$, $-z$; iii: x, y, $1.0+z$; iv: $-x$, $1.0-y$, $1.0-z$; v: $-x$, $1.0-y$, $-z$; vi: $2.0-x$, $1.0-y$, $1.0-z$. For the samarium(III) and erbium(III) complexes: i: $1.0-x$, $1.0-y$, $1.0-z$; ii: $1.0-x$, $1.0-y$, $-z$; iii: x, $-1.0+y$, z; iv: $1.0-x$, $-y$, $-z$; v: x, $1.0+y$, z; vi: $-x$, $1.0-y$, $-z$.

nated to eight oxygen atoms, as is shown in Fig. 2 (Er-(III) analogue). The metal atom Sm is bridged to Sm^{i} with a couple of the carboxylato ligands (where the keys to the symmetry operations are: i: $1.0-x$, $1.0-y$, and $1.0-z$, and Sm···Sm^{i} is 4.625 Å). As the shortest interatomic distance from an oxygen atom of the complex around Sm to Sm^{ii} is O(II)···Sm^{ii}=4.451(5) Å, there is no bridging between Sm and Sm^{ii} (where the keys to the symmetry operations are: ii: $1.0-x$, $1.0-y$, $-z$, and Sm···Sm^{ii} is 5.959 Å). Therefore, **3** should be regarded as having a dimeric structure, but the complex molecules are approximately lined to the *z*-axis, as in the case of **1**. Between Sm and Sm^{i}, there are two Sm-O-C-O-Sm^{i}-type bridges, where O(21)-Sm^{i} and O(22)-Sm are 2.364(5) and 2.322(4) Å respectively. As O(22)···Sm^{i} is 3.273(5) Å, it is too far to be considered as a-bonding. The eight Sm-O coordination bond distances are in the range of 2.273(4) and 2.594(4) Å (2.431 Å on the average). The difference between a pair of C-O bond lengths of each carboxyl group of the ligands are: O(11), O(12)-C(11), 0.037; O(21), O(22)-C(21), 0.014; O(31), O(32)-C(31), 0.004 Å. They are not large, not even the first one, where the ligand is in a unidentate form. As in the case of **1**, the short O···O distances around O(W4), and the phenyl hydroxyl oxygen atoms are summarized in Table 4; some of them are expected to form the hydrogen bonds.

The Structure of the Erbium(III) Complex (4). The **4** complex is isomorphous with **3**, although the bond distances around the central metal atom are a little different. As the Er-O bond lengths are in the range of 2.198(5) and 2.534(5) Å (2.359 Å on the average), the difference in the average M-O lengths of **3** and **4** is a little longer than that in the metal atomic radii (the atomic radii are: Sm, 1.802; Er, 1.757 Å [16a]). The interatomic distance, Er···$O(22^{i})$, is 3.382(6) Å, which is longer than the corresponding Sm···$O(22^{i})$ distance, 3.273(5) Å, in spite of the fact that the former metal atomic radius is smaller than the latter. The interatomic distances, Er···Er^{i} or Er^{ii}, are not much different from those of the corresponding distances of **3**; the differences are smaller than those between **1** and **2**.

The comparison of 1,2-Type and 3,4-Type Complexes. The respective interatomic distances and the bond angles of **1**, **2**, **3**, and **4** are shown in Table 4, while their atomic coordination geometries are shown in Fig. 5.

There are some similarities between **1** and **3**-type complexes. They are triclinic, with the space group $P\bar{1}$; the central metal atom is octa-coordinatated and is in a square-antiprism geometry. Both types of complexes are lined almost parallel to the *z*-axis, although the **3**-type is discrete between M and M^{ii} and is dimer. In the **1**-type, the M···M^{i} distance is about 0.5 Å longer than that of the M···M^{ii}; and therefore, the long and short M···M′ distances appear alternatively in the polymeric chain of the **1**-type complexes. In the **3**-type complexes, an additional water oxygen atom, O(W3), is coordinated to the metal atom in place of one bridging oxygen atom, O(11), of the **1**-type complexes. The positions of the other ligating atoms are almost the same as in both types of complexes.

The differences between **1** and **3** may be summarized as follows:

1) The **3**-type complexes do not have the free acid molecule in the crystal.

2) The **3**-type complexes are in the dimeric structure.

3) The interatomic distances, M···$O(22^{i})$, of **3** is much longer than the corresponding one of **2**, M···$O(22^{ii})$, and the former complex can not be considered as having the ennea-coordination.

4) When are compared **3** and **2**, the Sm-O(22) and Sm-$O(21^{i})$ (2.322(4) and 2.364(5) Å) distances are much

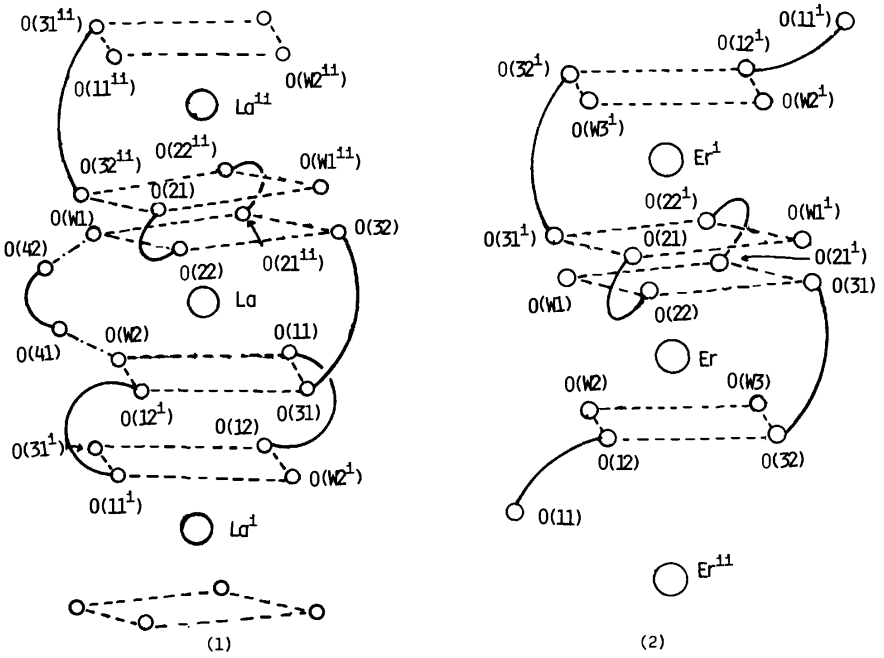

Fig. 5. Arrangement of the coordinating atoms around the central metal atoms of (1) the lanthanum(III) and (2) the erbium(III) complexes. (Key to the symmetric operations: i: 1.0—x, 1.0—y, 1.0—z; ii: 1.0—x, 1.0—y, —z.)

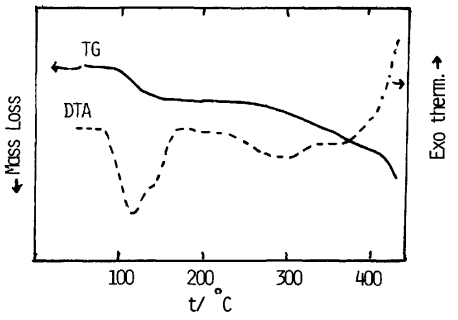

Fig. 6. TG(——) and DTA (----) curves of the lanthanum (III) complex. Mass loss of TG was taken downwards, and the exothermal change of DTA was taken upwards.

shorter than the corresponding Nd-O(22) and Nd-O(21^{ii}) (2.479(7) and 2.488(6) Å) distances of **2**, even the difference of their metal atomic radii is considered (Sm, 1.802 and Nd, 1.821 Å). Nevertheless, the interatomic distance, Sm···Sm^{i} of **3** is longer than the Nd···Nd^{ii} distance of **2** by 0.15 Å.

Although it was already known that the complexes of light and heavy lanthanoid(III) with the same ligand are sometimes different from each other in their chemical compositions,[16b,17,18] only a few comparisons of their structures have been published.[18]

The radii of lanthanoid atoms decrease with the increase in their atomic number. When the reduction of the radius is not large, only the bond lengths between the central metal and the coordinated atoms decrease, and the crystal is kept in an isomorphous state. However, when the radius decreases more, the ligand molecules must approach too near each other if the same configuration in the crystal is kept. Then they are rearranged to another structure, as in the present case.

Results of Other Measurements. As the four water molecules in **1** are divided into two groups, the coordinated ones and the crystalline ones, they can be expected to be distinguished by the thermal analysis. However, as is shown in Fig. 6, even when a relatively slow temperature-raising speed was applied (2.5 K min^{-1}), the dehydration peak of the DTA curve did not show any clear separation. Only a shoulder was found on the higher-temperature side of the peak, which means that there are two different types of water molecules and that they are removed at slightly different temperatures.

The fourth acid molecule in **1** is bonded only indirectly to the lanthanoid atom in the solid. This molecule can be expected to be liberated in its aqueous solution; this was ascertained by the measurement of the pH variation in the solution during titration with sodium hydroxide. The concentration of the complex used was [La^{III}]=3.01×10^{-3} mol dm^{-3}, and that of NaOH was 0.1 mol dm^{-3}. The results are shown in Fig. 7. An inflection point was observed when an equimol of NaOH was added, and the metal hydroxide began to precipitate after that point.

The infrared absorption spectra of the free acid, **1**, and of **4** are shown in Fig. 8. The spectra of the other lanthanoid complexes are almost the same as those of the two representative complexes. Although the free acid has two peaks in the ν_{as}(COO) region, at 1675 and 1598 cm^{-1}, the latter one is likely to be mixed with those of the phenyl group or of the hydroxyl group vibration. As the spectra of **1** has a peak at 1690 cm^{-1}, the fourth acid molecule in the complex is expected to act almost as a free acid. Although they may be overlapped, or mixed with other vibrations, the peaks at 1590 and 1502 cm^{-1} are expected to contain the ν_{as}(COO) mode of the coordinated ligand. In the spectra of **4**, one strong

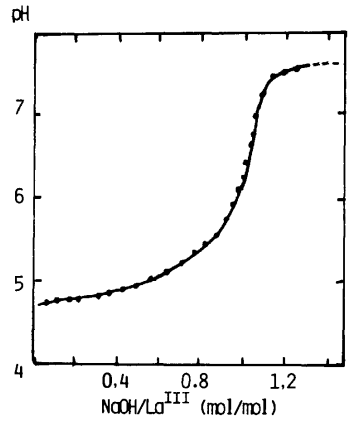

Fig. 7. The titration curve of the lanthanum(III) complex, using sodium hydroxide. ([La^{III}]=3.01×10^{-3} mol dm^{-3}; [NaOH]=0.1 mol dm^{-3}, in aqueous solution).

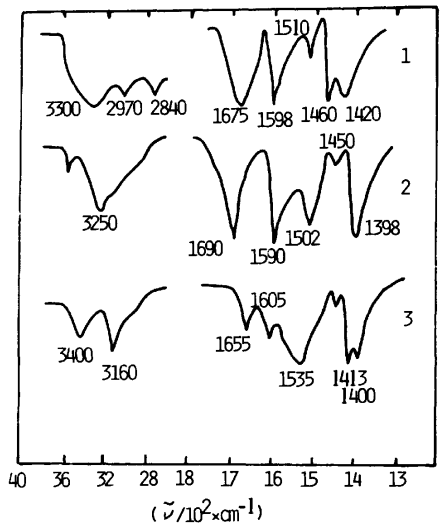

Fig. 8. Infrared absorption spectra of 1) *m*-hydroxybenzoic acid, 2) the lanthanum(III) complex (**1**), and 3) the erbium(III) copmlex (**4**).

peak is found at 1535 cm^{-1}, which is thought to be the ν_{as}(COO) mode of the coordinated ligand. The other peaks in the region, 1655 and 1605 cm^{-1}, may correspond with some modes of the other coordinated ligands in the complex; however, the exact assignment is difficult.

The authors wish to thank heartily The Shin-Etsu Chemical Co., Ltd., for aiding this study by presenting the highly pure lanthanoid oxides. The present work was partly supported by a Grant-in-Aid for Scientific Researches (No. 57430011) from the Ministry of Education, Science, and Culture. The helpful discussions about this research by Mr. Kiyofumi Nagai and Miss Reiko Nakamura are also deeply acknowledged.

References

1) G. C. Sadikov, G. A. Kukina, and M. A. Porai-Koshits, *Zh. Strukt. Khim.*, **12**, 859 (1971).
2) G. C. Sadikov, G. A. Kukina, M. A. Porai-Koshits, and L. A. Pospelova, *Zh. Strukt. Khim.*, **9**, 145 (1968).
3) L. A. Aslanov, I. K. Abdul'minev, M. A. Porai-Koshits, and V. I. Ivanov, *Dokl. Akad. Nauk SSSR*, **205**, 343 (1972).
4) M. C. Favas, D. L. Kepert, B. W. Skelton, and A. H. White, *J. Chem. Soc. Dalton Trans.*, **1980**, 454.
5) M. S. Khiyalov, I. R. Amiraslanov, Kh. S. Mamedov, and E. M. Movsumov, *Koord. Khim.*, **7**, 445 (1981).
6) H. R. Wenk, *Z. Krystallogr.*, **154**, 137 (1981).
7) L. A. Aslanov, V. M. Ionov, and I. D. Kiekaev, *Koord. Khim.*, **2**, 1674 (1976).
8) Y. Koizumi, H. Sawase, Y. Suzuki, M. Shimoi, and A. Ouchi, *Bull. Chem. Soc. Jpn.*, **57**, 1677 (1984).
9) L. A. Aslanov, I. K. Abdul'minev, and M. A. Porai-Koshits, *Zh. Fiz. Khim.*, **47**, 1055 (1973).
10) H. B. Kerfoot, G. R. Choppin, and T. J. Kistenmacher, *Inorg. Chem.*, **18**, 787 (1979).
11) K. Kimura, "Muki-Kagaku-Zensho IX-2," Maruzen, Tokyo (1949), p. 535.
12) "The Universal Crystallographic Computation Program System (UNICS)," ed by T. Sakurai, Crystallographic Society of Japan, Tokyo (1967).
13) "International Tables for X-Ray Crystallography," Kynoch Press, Birmingham (1974), Vol. IV.
14) $R=\Sigma||F_o|-|F_c||/\Sigma|F_o|$
15) The final thermal parameters and the F_o–F_c tables are deposited as Document No.8422 at the office of the Editor of the Bull. Chem. Soc. Jpn.
16) T. Moeller, "The Lanthanides," in "Comprehensive Inorganic Chemistry," ed by J. C. Bailer and others, Pergamon Press, New York, N. Y. (1973), Vol. 4, a) p. 7, b) p. 94.
17) S. Kondo, M. Shimoi, A. Ouchi, and T. Takeuchi, *Bull. Chem. Soc. Jpn.*, **55**, 2840 (1982).
18) A. A. Pinkerton, and D. Schwarzenbach, *J. Chem. Soc. Dalton Trans.*, **1976**, 2466.

 © 1984 The Chemical Society of Japan Bull. Chem. Soc. Jpn., 57, 1818—1822 (1984)

Kinetic and Thermodynamic Characterization of Thermal Pyridine Liberation-Anation Reactions of Bis(2,3-alkanedione dioximato)dipyridinecobalt(III) Iodide in the Solid State

Setsuko KINOSHITA,* Hisanobu WAKITA, and Isao MASUDA
Department of Chemistry, Faculty of Science, Fukuoka University, Nanakuma, Jonan-ku, Fukuoka 814-01
(Received November 29, 1983)

Thermodynamic and kinetic characterizations were carried out on the thermal, pyridine liberation-anation reactions, $[Co^{III}(R,CH_3\text{-dioxH})_2(py)_2]I \xrightarrow{\Delta} [Co^{III}(R,CH_3\text{-dioxH})_2(py)I]+py\uparrow$.* These occurred endothermally in the solid state of the complexes. The ΔH values of the reactions were determined. A large increment in the entropy was found to be indispensable for the progress of the reactions; it could be brought about by the liberation of gaseous pyridine from the solid system of the complexes. The kinetic analyses revealed that the reaction rates were increased by the substitution of R with the longer-carbon-chain alkyl groups. The activation enthalpies and activation free energies were shown to be decreased by the above substitutions. The Co^{III}-pyridine bond was observed to be weakened by the electron-donating inductive effect of R to the central cobalt atom and by the steric interference of R toward axial pyridine coordination.

Tsuchiya *et al.* have revealed that the complexes, $[Ni(H_2O)_2(N,N'\text{-deen})_2]Cl_2$* and $[Cr(NH_3)_6]X_3$ ($X=Cl^-$, Br^-), thermally liberate the volatile ligands in the coordination sphere such as H_2O or NH_3 accompaning anation reactions, in the solid state.[1] Analogous anation reactions which occur in the solid state were investigated by Zsakó *et al.* using complexes of the type, $[Co(DH)_2B_2]X$ [DH=dimethylglyoximato and (*E,E*)-(benzil dioximato); B=pyridine, aniline and their derivatives; $X=Cl^-$, Br^-, I^-, and SCN^-]; these thermally eliminated B to produce complexes of the type, $[Co(DH)_2(B)X]$.[2] Although they carried out kinetic analyses on these reactions, they only achieved ambiguous conclusions, probably due to their indiscriminate choice of the compounds.

In the present article, complexes of 2,3-alkanedione dioximes, $[Co(R,CH_3\text{-dioxH})_2(py)_2]I$,* with a series of extended alkyl groups R on the dioximato moiety, have been subjected to thermal investigation. The steric effect on the reactions arising from the alkyl groups will be discussed. In our previous investigation, it was revealed that the thermally induced one-electron transfer reactions from ligand L to Co^{III} in the solid $[Co^{III}(salen)L]$ complexes (L=2,4-alkanedionato ligand) were controlled dominantly by the activation entropies which were increased by the substitution of alkyl groups on the carbon atom at the 4-position of L.[3]

Experimental

Materials. The ligands, $R,CH_3\text{-dioxH}_2$, were prepared as described elsewhere.[4] The series of $[Co(R,CH_3\text{-dioxH})_2(py)_2]I$ complexes, including newly prepared ones with R= C_2H_5, n-C_3H_7, and n-C_4H_9, were prepared by following the method reported in the literature.[5] The complexes were recrystallized from dichloromethane solution by addition of petroleum ether to the solution. The analytical data of the complexes are given in Table 1. As Table 1 shows, the complexes were obtained in an anhydrous state when they included R=CH_3 and C_2H_5, but were obtained dihydrate and tetrahydrate when they included R=n-C_3H_7 and n-C_4H_9, respectively.

Table 1. Analytical data of the complexes, $[Co(R, CH_3\text{-dioxH})_2(py)_2]I$[a]

R	C %	H %	N %	Co %
CH_3	37.61	4.14	14.48	10.38
	(37.66)	(4.18)	(14.65)	(10.26)
C_2H_5	40.04	4.53	13.94	9.89
	(39.87)	(4.32)	(13.96)	(9.79)
n-C_3H_7; dihydrate	39.65	5.41	12.62	8.84
	(39.46)	(5.79)	(12.15)	(8.80)
n-C_4H_9; tetrahydrate	39.46	6.03	11.51	8.07
	(39.76)	(5.94)	(11.19)	(8.03)

a) Calculated values are given in parentheses.

The ^1H NMR spectra in DMSO-d_6 solution showed that all the complexes obtained here have a peak at 18.18 ppm which could be ascribed to the hydrogen atom in the =N-O-H-O-N= group formed by an intramolecular hydrogen bond in the complex molecules.[6] This is consistent with the assumption that the two dioximate monoanion molecules are coordinated symmetrically in the equatorial plane and the two pyridine molecules, in the axial positions.

Measurements. TG-DSC and powder X-ray diffraction measurements were carried out as described previously.[4] The kinetic analyses under isothermal conditions were carried out on the TG curves. The particle size of the samples provided for the thermal analyses was under 200 mesh.

Results

Pyrolysis. The TG-DSC curves are shown in Fig. 1. For the $[Co(CH_3,CH_3\text{-dioxH})_2(py)_2]I$ complex, an endothermic DSC peak appeared with a maximum at 158 °C, and a weight-loss corresponded to this change was 13.7%, being in agreement with calculated 13.8% for the elimination of one mole of pyridine per mole of complex. The powder X-ray diffraction of the product which was left behind after the above weight-loss was coincident with that of authentic $[Co(CH_3,CH_3$-

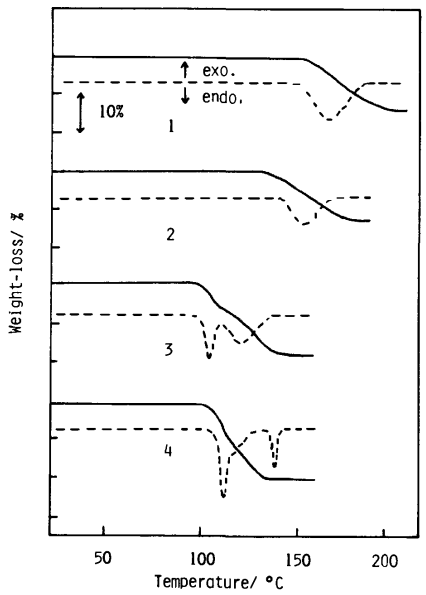

Fig. 1. TG(——) and DSC(----) curves of the complexes, $[Co(R,CH_3\text{-dioxH})_2(py)_2]I$, in a flowing N_2 atmosphere. Heating rate: 10 °C/min.
1, R=CH_3; 2, R=C_2H_5; 3, R=n-C_3H_7 (dihydrate); 4, R=n-C_4H_9 (tetrahydrate).

dioxH)$_2$(py)I].[7] Similarly, $[Co(C_2H_5,CH_3\text{-dioxH})_2(py)_2]I$ released pyridine leaving behind $[Co(C_2H_5, CH_3\text{-dioxH})_2(py)I]$. The observed weight-loss, 13.1%, corresponded to the calculated value, 13.1%. For $[Co(n\text{-}C_3H_7,CH_3\text{-dioxH})_2(py)_2]I\cdot 2H_2O$, dehydration occurred at *ca.* 100 °C, the weight-loss was 5.7% (Calcd, 5.4%). Then, pyridine was liberated; the weight-loss was 12.8% (Calcd, 12.5%). In the case of $[Co(n\text{-}C_4H_9,CH_3\text{-dioxH})_2(py)_2]I\cdot 4H_2O$, dehydration occurred accompanied by subsequent pyridine liberation; the total weight-loss was 21.2% (Calcd, 20.7%). A DSC peak at 143 °C is due to the melting of the resulting $[Co(n\text{-}C_4H_9,CH_3\text{-dioxH})_2(py)I]$. The results of the above thermal analyses are consistent with the following reaction scheme:

$$[Co(R, CH_3\text{-dioxH})_2(py)_2]I \xrightarrow{\Delta} [Co(R, CH_3\text{-dioxH})_2(py)I] + py\uparrow. \quad (1)$$

The reactions all proceeded endothermally. The enthalpy changes, ΔH values, determined by means of the DSC peak area measurement,[4] are given in Table 2.

Kinetic Analysis. As seen in Fig. 1, the pyridine liberation-anation reactions (Eq. 1) tend to occur at lower temperatures when the complexes include R having longer-carbon-chains. In order to reveal the kinetic character of the reactions, the kinetic analyses were carried out under isothermal conditions. It was found that the rate plots were linear. This is exemplyfied in Fig. 2 by the results obtained for $[Co(CH_3,CH_3\text{-dioxH})_2(py)_2]I$; similar linear relations were also obtained for the other complexes. These rate plots indicated that the reactions proceeded following the Avrami-Erofeev equation (Eq. 2),[8] for all the complexes.

$$\alpha/1-\alpha = kt^n \quad (n=1) \quad (2)$$

Table 2. Thermodynamic data of pyridine liberation-anation reactions of the complexes, $[Co(R, CH_3\text{-dioxH})_2(py)_2]I$

R	DSC peak maximum temp/K	ΔH kJ mol^{-1}	ΔS JK^{-1} mol^{-1}
CH_3	431	50±2	>116±5
C_2H_5	427	47±3	>110±7
n-C_3H_7	393	39±2	> 99±5

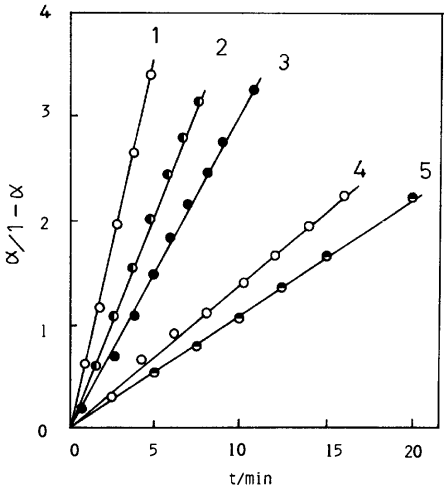

Fig. 2. Rate plots for pyridine liberation-anation reactions of $[Co(R,CH_3\text{-dioxH})_2(py)_2]I$; R=$CH_3$, under isothermal conditions.
1, 422.7 K; 2, 419.0 K; 3, 416.7 K; 4, 413.9 K; 5, 411.6 K.

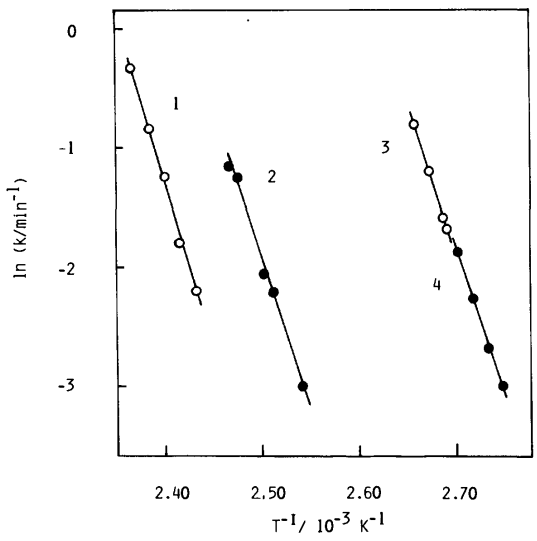

Fig. 3. Arrhenius plots for pyridine liberation-anation reactions of $[Co(R,CH_3\text{-dioxH})_2(py)_2]I$.
1, R=CH_3; 2, R=C_2H_5; 3, R=n-C_3H_7; 4, R=n-C_4H_9.

In Eq. 2, α is the molar fraction of $[Co(R,CH_3\text{-dioxH})_2(py)I]$ produced in the system by the reaction (Eq. 1); k, the rate constant; t, the reaction time. The k values at several different temperatures were determined from the slopes of the straight lines in the rate plots. Then, the Arrhenius plots gave good linear relations as shown in Fig. 3. According to the Arrhenius

equation, $k=A\exp(-E/RT)$, the activation energies, E values, and the pre-exponential factors, A valuse, were calculated from these Arrhenius plots. In order to disclose the reaction character more extensively, the activation enthalpies, ΔH^* values, and the activation entropies, ΔS^* values, were calculated by Eqs. 3 and 4, respectively:[3]

$$\Delta H^* = E - RT \quad (3)$$

$$\Delta S^* = R[\ln(Ah/kT) - 1]. \quad (4)$$

The E value, 266±9 kJ mol^{-1}, obtained for [Co(CH$_3$,CH$_3$-dioxH)$_2$(py)$_2$]I is larger as compared with E=227 kJ mol^{-1} reported by Zsacó *et al.*,[2] who determined it under non-isothermal conditions.

Discussion

Thermodynamics. As described in the results section, the [Co(R,CH$_3$-dioxH)$_2$(py)$_2$]I complexes thermally liberated pyridine in the solid state to produce the [Co(R,CH$_3$-dioxH)$_2$(py)I] complexes (*cf.* Eq. 1). A thermodynamic cycle regarding the reactions is delineated in Fig. 4. As is seen in Fig. 4, the observed ΔH value is composed of those due to the three energy terms given in Eq. 5:

$$\Delta H = \Delta H_{\text{subst}} + (\Delta H_{\text{lattice}} - \Delta H'_{\text{lattice}}). \quad (5)$$

The ΔH_{subst} values are expected to be positive because the basicity of iodide ion is appreciably weaker than pyridine. And $\Delta H_{\text{lattice}} - \Delta H'_{\text{lattice}}$ values are also expected to be positive, as the $\Delta H_{\text{lattice}}$ values of the ionic crystals of [Co(R,CH$_3$-dioxH)$_2$(py)$_2$]I are considered to be larger than those of the molecular crystals of [Co(R,CH$_3$-dioxH)$_2$(py)I]. Hence, it is reasonable that ΔH values are found to be positive as given in Table 2.

Furthermore, judging from the positive ΔH values and with $\Delta G=\Delta H-T\Delta S<0$ for the occurrence of reaction, large increases in the S values are indispensable in the present reactions. The ΔS values calculated for the present reactions are given in Table 2. Such large increments in the S values, as seen in Table 2, would be brought about by elimination of gaseous pyridine from the solid system. An evaluated ΔS value of the reaction, pyridine(solid)→pyridine(gas) at 431 K was *ca.* 125 J K^{-1} mol^{-1} when C_p (molar heat capacity at constant pressure) was assumed to be 106 J K^{-1} mol^{-1} in the gas phase and 133 J K^{-1} mol^{-1} in the liquid and solid phases.

Kinetics. The reactions (Eq. 1) fitted well the Avrami-Erofeev equation, Eq. 2, wherein n=1; it would be interpreted as that the reactions proceeded one-dimensionally after nucleation had occurred. For comparison, the rate constants, k values, of the reactions are normalized to those at 400 K. These values, as seen in Table 3, increase in the following order of R; CH$_3$<C$_2$H$_5$<n-C$_3$H$_7$<n-C$_4$H$_9$. Therefore, it is generally expected that the activation enthalpies ΔH^* values, increase in the inverse order of R in the above. In fact, this trend is seen in Table 3. If the ΔH^* value were considered to reflect mostly the strength of the Co^{III}-pyridine bonding, the increase in the ΔH^* value could be explained as follows: the electron donating alkyl groups behave to increase the electron density on the dioximato moiety, and hence, to decrease the Lewis acidity of the cobalt atom; these resulted in a weakening of the Co^{III}-pyridine bonding. A longer-carbon-chain alkyl group may weaken the Co^{III}- pyridine bonding more extensively.

The activation entropies, ΔS^* values, are positive and rather large, as given in Table 3. This fact is in line with the assumption that the reaction follows the S_N1 mechanism, that is, the reaction rate is controlled not by the anation, but by the pyridine dissociation process.[3] The fact that the k values increase in the above order of R also supports the S_N1 reaction mechanism.

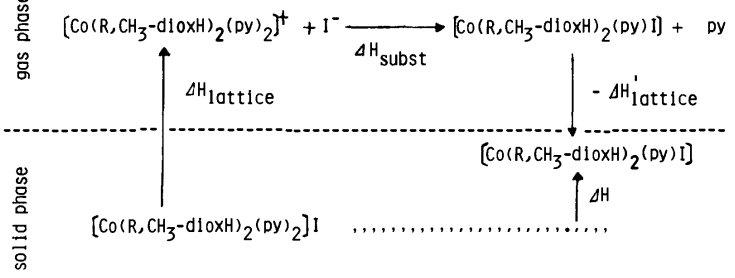

Fig. 4. Thermodynamic cycle proposed for the reaction given in Eq. 1. ΔH_{subst}; energy for substitution reaction in the gas phase, $\Delta H_{\text{lattice}}$ and $\Delta H'_{\text{lattice}}$; lattice energy.

TABLE 3. KINETIC DATA OF PYRIDINE LIBERATION-ANATION REACTIONS OF THE COMPLEXES, [Co(R, CH$_3$-dioxH)$_2$(py)$_2$]I

R	E / kJ mol^{-1}	log (A/s^{-1})	k(400K) / s^{-1}	ΔH^*(400K) / kJ mol^{-1}	ΔS^*(400K) / J K^{-1} mol^{-1}
CH$_3$	266± 9	31.0±1.1	(1.78±0.21)×10^{-4}	263± 9	338±21
C$_2$H$_5$	232±15	27.7±1.9	(2.04±0.23)×10^{-3}	229±15	275±36
n-C$_3$H$_7$	214± 8	27.5±1.1	(3.39±0.30)×10^{-1}	211± 8	271±21
n-C$_4$H$_9$	210± 7	27.1±1.0	(4.16±0.40)×10^{-1}	207± 7	263±19

As mentioned above, when the complexes included R groups with longer-carbon-chains, they underwent reaction with smaller ΔH^* values. In order to disclose the contribution of the entropic term to the reactions, the ΔG^* values are calculated by the relation, $\Delta G^* = \Delta H^* - T\Delta S^*$, and are plotted against the ΔH^* values in Fig. 5-A. The relation in Fig. 5-A indicates that the ΔG^* values decrease with decreasing ΔH^* values, *i.e.*, ΔG^* values decrease in the order of R as CH_3> C_2H_5>*n*-C_3H_7>*n*-C_4H_9. This relation indicates that the ΔS^* values are almost definite for the reactions of the series of the complexes examined here. By taking into account the relation, $k = \frac{kT}{h}\exp(-\Delta G^*/RT)$, it is expected that the k values increase in the above order of R. The relation between ΔG^* and ΔH^* values, disclosed above, is in contrast to that known for the thermal, [Co^{III}(salen)L]→[Co^{II}(salen)] reactions; in the latter case, the extended alkyl groups on L resulted in the decrease in the ΔG^* values and the increase in the ΔH^* values, indicating that the reaction is dominated by the entropy term.[3] It is demonstrated in Fig. 5-B.

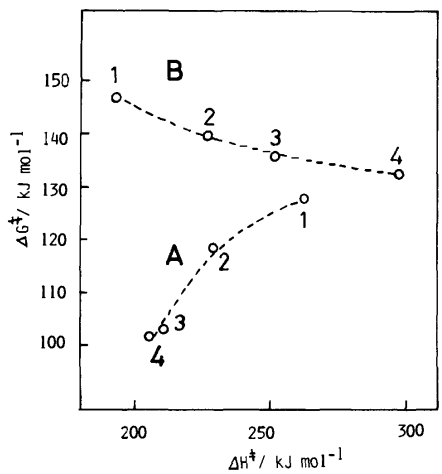

Fig. 5. Relation between ΔG^* and ΔH^* values.
A, [Co(R,CH_3-dioxH)$_2$(py)$_2$]I: 1, R=CH_3; 2, R=C_2H_5; 3, R=*n*-C_3H_7; 4, R=*n*-C_4H_9.
B, [Co(salen)L]: 1, L=pentanedionato; 2, L=hexanedionato; 3, L=heptanedionato; 4, L=nonanedionato.

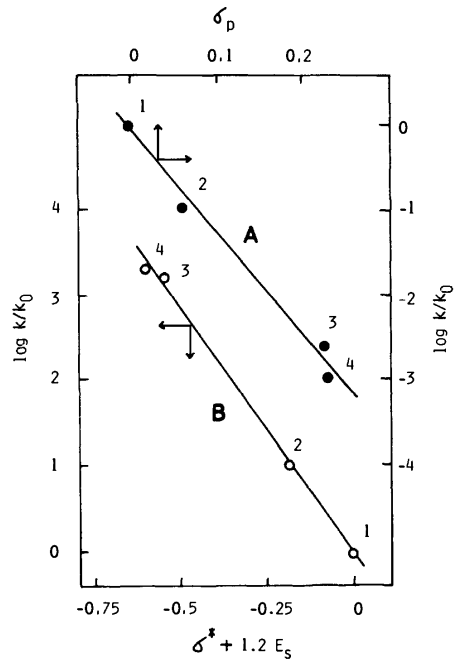

Fig. 6. A; Hammett's plots for pyridine liberation reactions of Ni[*N*-(R-C_6H_4)salam]$_2$(py)$_2$: 1, R=H; 2, R=*p*-F; 3, R=*p*-Cl; 4, R=*p*-Br.
B; Taft's plots for pyridine liberation-anation reactions of [Co(R,CH_3-dioxH)$_2$(py)$_2$]I: 1, R=CH_3; 2, R=C_2H_5; 3, R=*n*-C_3H_7; 4, R=*n*-C_4H_9.

For the thermal pyridine liberation reactions of Ni[*N*-(R-C_6H_4)salam]$_2$(py)$_2$* (R=H, *p*-F, *p*-Cl and *p*-Br),[9] Hammett's plots of the log k/k_0 (400 K) against σ_p are shown in Fig. 6-A. The linear relation, seen in Fig. 6-A, indicates that the rate constant k is controlled dominantly by the electron-donating inductive effect of the substituent, R. Similar plots were attempted for the present series of the complexes. However, no linear relation was found. An inspection of a stereo model of these complex molecules implies steric interference which might exist beween the extended R groups and the axial pyridine ligands. Evidence for the above type of interference can be obtained by applying the following Taft's relation for the analyses of the reactions:

$$\log k/k_0 = \rho^*\sigma^* + \delta E_s = \rho^*\left(\sigma^* + \frac{\delta}{\rho^*}E_s\right). \quad (6)$$

In Eq. 6, σ^* and E_s are, as have been defined by Taft, polar and steric substituent constants, respectively; ρ^* and δ are definite value with respect to a series of analogous reactions and these are parameters susceptible, respectively, to the polar and steric effects of the substituents. The relation given by Eq. 6 has been observed extensively for the organic reactions; for example, the methanolysis reactions of 1-mentyl esters of a series of aliphatic carboxylic acid, $RCO_2C_{10}H_{19}$, are clearly shown to be affected by both steric and electronic effects of R groups with extended-carbon-chains.[10] The fact that the ΔS^* values are nearly definite for the reactions of the present complexes is considered to support the application of the Taft equation. For, if the ΔS^* values were remarkably differed from each other in the series of reactions, the ρ^* and δ values would vary appreciably with temperature. As Fig. 6-B shows, a good linear relation is observed when log k/k_0 is plotted against $\sigma^*+1.2\,E_s$; ρ^* and δ are calculated to be −5.7 and −7.0, respectively. This result indicates that a steric effect due to the R groups as well as the electronic one, can contribute to the pyridine liberation reaction. That is, the Co^{III}-pyridine bonding can be weakened both by steric interference between the R and pyridine groups and by the inductive effect due to R. Thus, the substitution of the R groups having longer-carbon-chains into the complexes causes the decrease both in the ΔH^* and ΔG^* values, hence it causes the increase in the k value.[11]

In summary, the [Co(R,CH_3-dioxH)$_2$(py)$_2$]I complexes tend to liberate pyridine at lower temperature by including the R groups with longer-carbon-chain; this is in line with the case of the reactions, [Co^{III}-

(salen)L]→[Co^{II}(salen)]. However, it is noticeable that in the former case, the R groups behave to decrease the activation enthalpy ΔH^*, whereas in the latter case, the R groups substituted on L behave to increase activation entropy ΔS^*.

References

* R,CH_3-dioxH$_2$: CH_3-C(=NOH)-C(=NOH)-R, py: pyridine, *N,N'*-deen: *N,N'*-diethylethylenediamine, salamH: salicylideneamine.

1) H. Ueno, A. Uehara, and R. Tsuchiya, *Bull. Chem. Soc. Jpn.*, **54**, 1821 (1981); Y. Ihara, E. Izumi, A. Uehara, R. Tsuchiya, S. Nakagawa, E. Kyuno, *ibid.*, **55**,1028 (1982).

2) J. Zsakó, Cs. Várhelyi and E. Kékedy, *J. Inorg. Nucl. Chem.*, **28**, 2637 (1966); **32**, 2999 (1970).

3) S. Kinoshita, K. Miyokawa, H. Wakita, and I. Masuda, *polyhedron*, **2**, 125 (1983); *Bull. Chem. Soc. Jpn.*, **57**, 381 (1984).

4) M. I, H. Wakita and I. Masuda, *Bull. Chem. Soc. Jpn.*, **56**, 1627 (1983).

5) Y. Nakatsuka and K. Iinuma, *Nippon Kagaku Kaishi*, **55**, 630 (1934).

6) Y. Yamano, I. Masuda, and K. Shinra, *J. Inorg. Nucl. Chem.*, **33**, 521 (1971), and the references therein.

7) H. A. O. Hill and K. G. Morallee, *J. Chem. Soc., A*, **1969**, 554.

8) M. Avrami, *J. Chem. Phys.*, **7**, 1103 (1939); *ibid*, **8**, 212 (1940); *ibid*, **9**, 177 (1941); B. V. Erofeev, *Dokl. Akad. Nauk. SSSR*, **52**, 511 (1946).

9) K. Miyokawa, H. Hirashima, and I. Masuda, *Bull. Chem. Soc. Jpn.*, **55**, 104 (1982).

10) W. A. Pavelich and R. W. Taft, Jr., *J. Am. Chem. Soc.*, **79**, 4935 (1957).

11) When 2,3-alkanedione dioxime with R=$CH_2CH(CH_3)_2$ was used, only the mono(pyridine) adduct of [Co{$CH_2CH(CH_3)_2$,CH_3-dioxH}$_2$(py)I] was isolated. It is speculated that if the bis(pyridine) adduct were isolated, its pyridine liberation-anation reaction in the solid state would be very fast; the rate constant k(400 K) is evaluated to be 1.7×10^7 times larger than that of [Co(CH_3,CH_3-dioxH)$_2$(py)$_2$]I.

Kinetic Studies of Fast Equilibrium by Means of High-performance Liquid Chromatography. V. Stepwise Complex Formation of the Nickel(II) Ion with 2,2′-Bipyridine and 1,10-Phenanthroline

Masataka MORIYASU* and Yohei HASHIMOTO
Kobe Women's College of Pharmacy, Motoyamakita-machi, Higashinada-ku, Kobe 658
(Received December 6, 1983)

The stepwise complex formation of the nickel(II) ion (M^{2+}) with 2,2′-bipyridine(bpy) and 1,10-phenanthroline(phen) ($M_{n-1}^{2+}+L \rightleftharpoons ML_n^{2+}$ with $K_n=[ML_n^{2+}]/[ML_{n-1}^{2+}][L]$, where $n=1-3$), has been investigated by means of high-performance liquid chromatography. Peaks of the labile partially ligand substituted complexes, ML^{2+} and ML_2^{2+}, have appeared on chromatograms, along with peaks of the ML_3^{2+} and excess free ligands, on reverse phase ion-pair chromatography using sodium dodecyl sulfate in acidic media. Each labile species has been found to be eluted without any noticeable change, such as ligand addition, dissociation, or disproportionation, during chromatography. Thus, the chromatograms obtained have directly indicated the equilibrium concentrations of each species in the solutions prior to chromatography. The stepwise complex formation constants of nickel(II) with bpy or phen have been determined by means of high-performance liquid chromatography.

In this series of papers[1-4] it has been demonstrated that a considerably fast reaction can be traced by means of high-performance liquid chromatography(HPLC) based on conventional principles. The present report deals with the complex formation of the nickel(II) ion (M^{2+}) with 2,2′-bipyridine(bpy) and 1,10-phenanthroline(phen) in aqueous media.

The representative stepwise complex formation of M^{2+} with these *N,N*-coordinates chelating reagents(L) is expressed by the following equations:

$$M^{2+} + L \underset{k_{-1}}{\overset{k_1}{\rightleftharpoons}} ML^{2+} \quad (1)$$

$$ML^{2+} + L \underset{k_{-2}}{\overset{k_2}{\rightleftharpoons}} ML_2^{2+} \quad (2)$$

$$ML_2^{2+} + L \underset{k_{-3}}{\overset{k_3}{\rightleftharpoons}} ML_3^{2+} \quad (3)$$

$$K_1 = [ML^{2+}]/[M^{2+}][L] \quad (4)$$

$$K_2 = [ML_2^{2+}]/[ML^{2+}][L] \quad (5)$$

$$K_3 = [ML_3^{2+}]/[ML_2^{2+}][L] \quad (6)$$

The rate constant k_1, which was determined by several authors by means of the stopped-flow method,[5-10] is a bimolecular rate constant of the order of 10^3 mol^{-1} dm^3 s^{-1}, suggesting that mono-complex formation proceeds promptly. In strongly acidic conditions, since bpy and phen exist as the protonated form HL^+, another path for complex formation has been proposed:[8]

$$L + H^+ \underset{k_-}{\overset{k}{\rightleftharpoons}} HL^+ \quad (7)$$

$$K = [HL^+]/[H^+][L] \quad (8)$$

$$M^{2+} + HL^+ \underset{k'_{-1}}{\overset{k'_1}{\rightleftharpoons}} ML^{2+} + H^+ \quad (9)$$

$$ML^{2+} + HL^+ \underset{k'_{-2}}{\overset{k'_2}{\rightleftharpoons}} ML_2^{2+} + H^+ \quad (10)$$

$$ML_2^{2+} + HL^+ \underset{k'_{-3}}{\overset{k'_3}{\rightleftharpoons}} ML_3^{2+} + H^+ \quad (11)$$

The rate constant k'_1 has been reported to be of the order of 10^0—10^1 mol^{-1} dm^3 s^{-1},[8-10] much smaller than k_1. When M^{2+} and L are mixed, the complex formation reaches equilibrium almost instantaneously, except in strong acidic conditions. If the equilibrated solution is supplied to HPLC, it seems that the equilibrium prior to HPLC is displaced rapidly and that each labile species undergoes some reactions in the column promptly. This, however, is not always true for the following reasons. Among the various equilibrium equations mentioned above, the acid-base equilibrium shown in Eq. 7 will reach the equilibrium fastest. Thus, the rate constants k and k_- will be large, and when L (or HL^+) is chromatographed, it will reach equilibrium ($L^+ + H^+ \rightleftharpoons HL^+$) in the eluent almost instantaneously. The progress of other reactions in the column is not so fast. Since the forward reaction of Eq. 1 is a bimolecular one, the progress of the reaction is retarded during chromatography because of the decrease in the probability of collision between M^{2+} and L. Furthermore, mono-complex formation will be suppressed in an acidic eluent because, in acidic media, almost all ligands exist as the protonated form HL^+, which reacts with M^{2+} only slowly. The backward reaction of Eq. 1 is also slow. The dissociation rate constant, k_{-1}, of the $[Ni(bpy)]^{2+}$ complex has been reported to be of the order of 10^{-4} s^{-1}.[11] Our previous report[4] demonstrated that the progress of a unimolecular reaction during chromatography could be suppressed when the rate constant was of the order of 10^{-4} s^{-1}.

A similar discussion might hold for the second and the third steps of complex formation described in Eqs. 2, 3, 10, and 11. Aside from the reactions mentioned above, another type of reaction of ML^{2+} and ML_2^{2+} should be taken into consideration.

$$2ML^{2+} \underset{k_{-d}}{\overset{k_d}{\rightleftharpoons}} ML_2^{2+} + M^{2+} \quad (12)$$

This type of "disproportionation" reaction is not always negligible because the "reactants" are not separated by HPLC. We ourselves have previously described the disproportionation reaction for the sys-

tem of nickel(II) dithiocarbamate chelates[1] and demonstrated that the disproportionation did not occur during chromatography. Similarly, it might safely be concluded that disproportionation can also be neglected in the present case.

When all the above premises are fulfilled, each labile species is eluted without any change in the column. In this case, since the concentrations of each species prior to HPLC can be determined from the peak height (or area) appearing on chromatograms, the equilibrium constants, K_1, K_2, and K_3 in Eqs. 4, 5, and 6 will be determined.

Experimental

Reagents. A standard solution of nickel(II) was prepared by dissolving $NiCl_2 \cdot 6H_2O$ in water. The chelating reagents (bpy and phen) were also dissolved in water.

Apparatus. The HPLC apparatus used in this study is similar to the one described previously.[1] Several reverse phase packings (Nucleosil 5C18 (5 μm), LiChrosorb RP 18 (5 μm), Hypersil ODS (5 μm), Nucleosil 5C8 (5 μm), and LiChrosorb RP 8 (5 μm)) were slurry packed into stainless steel columns. A digital pH meter (Model 225, Iwaki Glass Co., Ltd.) was used to measure the accurate pH of the equilibrated solutions prior to HPLC.

Results and Discussion

Optimum Conditions of Reverse Phase Ion-pair Chromatography. The separation of some heavy metal chelates of bpy[12] and phen[13,14] has been reported by several authors using a proper ion-pair reagent such as sodium 1-pentanesulfonate. We here chose sodium dodecyl sulfate as an ion-pair reagent. The ion-pair reagent was dissolved in the mixed solvent system of water-acetonitrile, and the pH of the solution was controlled by adding a suitable quantity of salt. A satisfactory separation was attained when the solvent system was strongly acidic. Among the several acids tested, tartaric acid gave best results, and so we here chose this solvent system. The elution behavior varied markedly when different packings were used. Among these, Nucleosil 5C18 gave satisfactory results. Other packings gave a poor resolution due to either serious tailing or the overlap of two peaks. When free bpy or phen was injected into the column, a peak corresponding to red-colored $[Fe(bpy)_3]^{2+}$ or $[Fe(phen)_3]^{2+}$ appeared on chromatograms, along with the peak of free bpy or phen because of the contamination of iron ion from the HPLC apparatus. In order to eliminate the contamination, a minute amount of ethylenediaminetetraacetic acid(EDTA,H_4edta) was added to the eluent.[15] Thus treated, the peak of $[Fe(bpy)_3]^{2+}$ or $[Fe(phen)_3]^{2+}$ disappeared and the enlarged peak of free bpy or phen alone appeared on chromatograms. This treatment, which permits the quantitative elution of free bpy (or phen), is not always preferred because there exists some possibility that coordinated bpy (or phen) might be substituted for edta during chromatography. As will be shown in the following section, this ligand exchange is negligible when the concentration of EDTA added is small. Therefore, the content of EDTA should be so chosen that free bpy (or phen) may be eluted quantitatively and the peak heights of ML^{2+}, ML_2^{2+}, and ML_3^{2+} may not be affected by EDTA addition.

The best conditions for HPLC were as follows: solvent system: acetonitrile: 0.05 mol dm^{-3} tartaric acid: 0.001 mol dm^{-3} EDTA: sodium dodecyl sulfate =80: 50:0.3:0.5 g; Column: Nucleosil 5C18 (4.6 mm×15 cm); Column temperature: 25 °C (for phen chelate) or 10 °C (for bpy chelate); Flow rate: 1.5 cm^3 min^{-1}; Detector: UV 254 nm. Hereafter, the experiments were carried out under these conditions.

HPLC of Ni^{2+}-bpy System. Two solutions of Ni^{2+} and bpy were mixed, and after the pH had been adjusted to 1.9—2.0 by $HClO_4$-$NaClO_4$, the solutions were made up to a definite volume. The concentrations of the total nickel(II) ion [M_t] and ClO_4^- were chosen to be 1.0×10^{-3} mol dm^{-3} and 1.0×10^{-1} mol dm^{-3}. The ratio of the [M_t] to the total bpy [L_t] was changed from 0.25 to 3.5 consecutively in the molar ratio. Then, the aliquots of these samples was submitted to HPLC; the chromatograms are shown in Fig. 1. Several peaks appeared on the chromatograms. Peak 2, which was

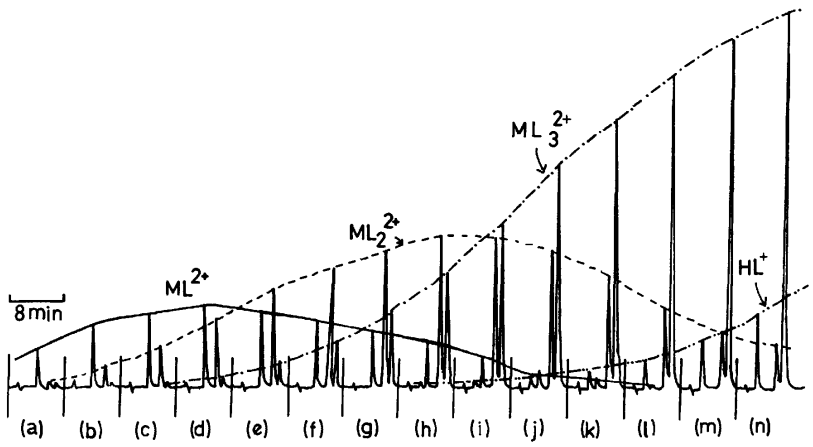

Fig. 1. Chromatograms of nickel(II)-bpy system in acidic media. For chromatographic conditions, see text.
[M_t]=1.0 mM, pH=1.93—1.99($HClO_4$-$NaClO_4$, ClO_4^-=0.1 M)
[L_t]/[M_t] 0.25(a), 0.50(b), 0.75(c), 1.00(d), 1.25(e), 1.50(f), 1.75(g), 2.00(h), 2.25(i), 2.50(j), 2.75(k), 3.00(l), 3.25(m), 3.50(n).

relatively large when the $[L_t]/[M_t]$ ratio was small and which reached the maximum under the condition $[L_t]/[M_t]=1.0$, corresponds to the 1:1 complex ML^{2+}. Peak 3, which gave highest peak when $[L_t]/[M_t]$ was equal to 2.0, is the peak of the 1:2 complex ML_2^{2+}. The last peak (Peak 4), which increased gradually with the increase in $[L_t]$, corresponds to the 1:3 complex ML_3^{2+}. When $[L_t]/[M_t]$ exceeded 2.0, a new peak (Peak 5) appeared on chromatograms. This peak, which grew with the increase in $[L_t]/[M_t]$ is attributed to the peak of free bpy. Near the present HPLC conditions, free ligands should be chromatographed as the protonated form HL^+, because the eluent is strongly acidic. In Fig. 1, the peak of the aquanickel(II) ion M^{2+} did not appear on chromatograms because the aqua ion does not have any absorption in the UV range. When the portion corresponding to the solvent front was collected and sodium diethyldithiocarbamate was added to the portion, a brownish yellow color of nickel(II) diethyldithiocarbamate chelate appeared, suggesting that the aquanickel(II) ion was eluted without retention.

It seems that the elution sequence, M^{2+}, ML^{2+}, ML_2^{2+}, and ML_3^{2+}, is reasonable for the following reason. With an increase in the coordination number of the hydrophobic bulky bpy ligand, the hydrophobicity of the chelate increases. Thus, the 1:3 complex will form a very hydrophobic ion pair with the dodecyl sulfate ion, which has a strong affinity with the hydrophobic ODS stationary phase. Thus, the retention time of the 1:3 complex will be the longest, and the elution sequence described above will result. Since the aquanickel(II) ion is very hydrophilic, it is not retained on the stationary phase at all.

The addition of EDTA to the eluent was necessary for the quantitative elution of free ligands. In order to investigate the effect of EDTA on other peaks, HPLC was carried out in the presence and absence of EDTA. Each peak height was found to be indifferent to the addition of EDTA, with the exception of the peak of free bpy. This result suggests that the bpy ligand coordinated with ML^{2+}, ML_2^{2+}, and ML_3^{2+} is not replaced by edta during chromatography when the EDTA concentration is low.

Determination of the Stepwise Complex Formation Constants of the Ni^{2+}-bpy System. Two solutions of Ni^{2+} and bpy were mixed so that $[L_t]/[M_t]$ was equal to 2.0. Then the pH of the solution was changed from 1 to 8 by the use of $HClO_4$-$NaClO_4$ or $NaClO_4$-NaOH. The concentration of $[M_t]$ was chosen as 1.0×10^{-3} mol dm^{-3}. Figures 2(a) and (b) depict examples of chromatograms near acidic and almost neutral conditions. These two chromatograms suggest that some difference in chromatograms exists when the pH values of the sample solutions are different. This can be explained in terms of the "protonation reaction" of bpy. The concentration of ligands effective on complex formation is smaller in acidic media than in basic or neutral media, because in acidic conditions most of the bpy exists as the protonated form HL^+. Thus, the ratio of the 1:3 complex is smaller in acidic media than in neutral media because of the low effective concentration of bpy available for complex formation.

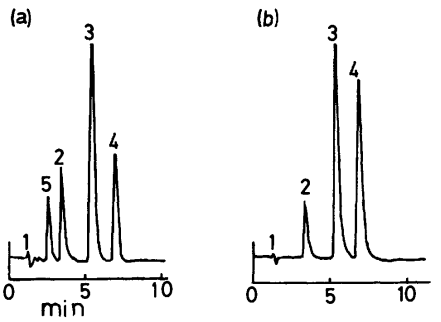

Fig. 2. Chromatograms of nickel(II)-bpy system at $[L_t]/[M_t]=2.0$. For chromatographic conditions, see text.
$[M_t]=1.0$ mM, $[L_t]=2.0$ mM, pH=1.2(a), 5.1(b) ($HClO_4$-$NaClO_4$, $ClO_4^-=0.1$ M)
1 M^{2+}(solvent front), 2 ML^{2+}, 3 ML_2^{2+}, 4 ML_3^{2+}, 5 HL^+.

Now peaks of HL^+, ML_3^{2+}, ML_2^{2+}, ML^{2+}, and possibly M^{2+} appeared on chromatograms in acidic conditions, as is shown in Fig. 2(a), the determination of the stepwise complex formation constants, K_1, K_2, and K_3, is, therefore, possible provided that the equilibrium concentrations of each species are known. For this purpose, the following facts are noteworthy: (1) The chromatograms shown in Fig. 2 should directly indicate the equilibrium concentration of each species prior to HPLC. The ion-pair formation of these metal chelates with the dodecyl sulfate ion might result in a displacement of the equilibrium. If this phenomenon really occurs, the reaction proceeds instantaneously in the column. The fast separation speed of HPLC and the moderate lability of these chelates suggest that this reaction is unlikely to occur. Furthermore, when the content of SDS in the eluent was chosen as 0.1 and 1.0 g instead of 0.5 g, the percentage of ML_3^{2+} in the sample shown in Fig. 2(a) was not changed. (2) Calibration graphs of each species are necessary, the procedure being carried out as follows: First, a linear calibration graph of bpy is obtained. Second, a calibration graph of ML_3^{2+} is obtained by mixing nickel(II) and bpy so that the $[L_t]/[M_t]$ ratio is 4.0 or higher near neutral pH conditions and by supplying the sample to HPLC. This sample gave only two peaks of ML_3^{2+} and excess free ligands, suggesting the complete 1:3 complex formation. The calibration graph of ML_3^{2+} was also linear. Calibration curves of other species could not be obtained directly because of either the lack of absorption(M^{2+}) or the lability of the chelates(ML^{2+} and ML_2^{2+}). It is noteworthy here that the measurements of each peak area in Fig. 2(a) do not give the concentrations of each species because of the difference in the absorption coefficients of the species. The absorption coefficients were found to decrease in this order: $ML_3^{2+}>ML_2^{2+}>ML^{2+}$, which was parallel to the coordination numbers of bpy. Calibration graphs of these labile species were obtained by the following procedures. Fractions corresponding to M^{2+}, ML^{2+}, and ML_2^{2+} were collected, and a slight excess of bpy was added. After the pH was adjusted to approximately neutral, each portion was diluted to a definite volume

Table 1. Stepwise complex formation constants of the nickel(II)-bpy system at 25 °C

$\log K_1$	$\log K_2$	$\log K_3$	Ref.
6.92±0.11	6.81±0.07	6.25±0.06	This work*
6.80	6.46	5.20	17
7.13	6.88	6.53	18
7.07	6.86	6.20	19
6.9	6.8	5.9	20
6.95	6.83	6.35	21

* Chromatograms are shown in Fig. 2(a).
The concentrations of each species are as follows: $[M]_t=1.00$ mM (1M=1 mol dm^{-3}); $[L]_t=2.00$ mM; $[M^{2+}]=(0.16\pm0.02)$ mM; $[ML^{2+}]=(0.29\pm0.01)$ mM; $[ML_2^{2+}]=(0.41\pm0.01)$ mM; $[ML_3^{2+}]=(0.16\pm0.005)$ mM; $[L]+[HL^+]\fallingdotseq[HL^+]=(0.35\pm0.03)$ mM; pH=1.21.
From the measurements of the peak height, the total concentration of $[M_t]$ was calculated to be (1.02±0.045) mM.

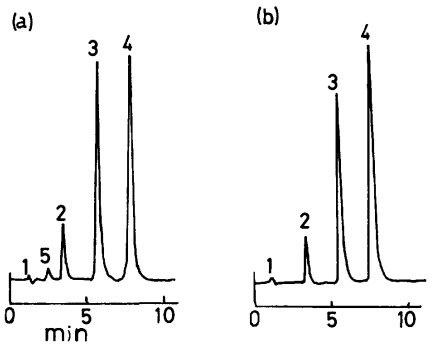

Fig. 3. Chromatograms of nickel(II)-phen system at $[L_t]/[M_t]=2.0$. For chromatographic conditions, see text.
$[M_t]=0.5$ mM, $[L_t]=1.0$ mM, pH=1.3(a), 6.2(b) (HCl–NaCl, $Cl^-=0.05$ M)
1 M^{2+} (solvent front), 2 ML^{2+}, 3 ML_2^{2+}, 4 ML_3^{3+}, 5 HL^+.

by the use of the HPLC solvent. Each sample solution was left to stand at least 2 h and then submitted to HPLC. From the peak heights (or areas) of ML_3^{2+} which then appeared on chromatograms, the initial concentrations of ML_2^{2+}, ML^{2+}, and M^{2+} were calculated. In order to confirm that each species was converted into the 1:3 complex thoroughly, the following experiments were carried out. The aquanickel(II) ion (M^{2+}) was dissolved in the HPLC solvent in the presence and absence of EDTA and tartaric acid. A slight excess of bpy was added to these solutions and pH was adjusted to be almost neutral. These two solutions were then diluted to a definite volume and were submitted to HPLC. The peak heights of ML_3^{2+} were similar for these two sample solutions, suggesting the complete 1:3 complex formation.

Now, the concentrations of M^{2+}, ML^{2+}, ML_2^{2+}, ML_3^{2+}, and HL^+ were determined by HPLC, K_1, K_2, and K_3 can be determined if the dissociation constant of bpy (K in Eq. 8) is known. Table 1 indicates these values by assuming log K=4.4.[16] The stepwise complex formation constants reported by other authors[17–21] are also included in this table. The present values agree very well with the results of other authors, suggesting the reliability of the present HPLC method.

Table 2. Stepwise complex formation constants of the nickel(II)-phen system at 25 °C

$\log K_1$	$\log K_2$	$\log K_3$	Ref.
8.97±0.35	8.82±0.16	8.40±0.15	This work*
8.60	8.10	7.55	22
8.80	8.30	7.70	23
8.8	8.3	7.7	18
8.0	8.0	7.9	19
8.65	8.43	7.83	24

* Chromatograms are shown in Fig. 3(a).
The concentrations of each species are as follows: $[M]_t=0.50$ mM; $[L]_t=1.00$ mM; $[M^{2+}]=(0.03\pm0.01)$ mM; $[ML^{2+}]=(0.10\pm0.01)$ mM; $[ML_2^{2+}]=(0.21\pm0.01)$ mM; $[ML_3^{2+}]=(0.17\pm0.01)$ mM; $[L]+[HL^+]\fallingdotseq[HL^+]=(0.015\pm0.003]$ mM; pH=1.33.
The concentration of $[M_t]$ was calculated to be (0.51±0.04) mM.

Ni^{2+}-phen System. Similar experiments were carried out for the Ni^{2+}-phen system. The chromatogram patterns obtained resembled those for the Ni^{2+}-bpy system. The results at $[L_t]/[M_t]=2.0$ are exemplified in Figs. 3(a) and (b) under acidic and almost neutral conditions. The equilibrium concentrations of M^{2+}, ML^{2+}, ML_2^{2+}, ML_3^{2+}, and HL^+ were determined by HPLC with similar procedures; thus, the stepwise complex formation constants were calculated. The results are tabulated in Table 2, assuming that log K=5.0.[16] The results reported by other authors[18,19,22–24] are also appended in this table. The present results agree fairly well with those of other authors, though the present data are slightly larger. A comparison of Table I and Table II indicates that the ratio of HL^+ and ML^{2+} is smaller in the Ni^{2+}-phen system than in the Ni^{2+}-bpy system. This may be attributed to the fact that the stepwise complex formation constants are larger for the Ni^{2+}-phen system than for the Ni^{2+}-bpy system.

References

1) M. Moriyasu and Y. Hashimoto, *Bull. Chem. Soc. Jpn.*, **53**, 3590 (1980).
2) M. Moriyasu and Y. Hashimoto, *Bull. Chem. Soc. Jpn.*, **54**, 2470 (1981).
3) M. Moriyasu and Y. Hashimoto, *Bull. Chem. Soc. Jpn.*, **54**, 3374 (1981).
4) M. Moriyasu, Y. Hashimoto, and M. Endo, *Bull. Chem. Soc. Jpn.*, **56**, 1972 (1983).
5) H. P. Bennetto and E. F. Caldin, *J. Chem. Soc.*, **1971**, 2191.
6) W. S. Melvin, D. P. Rablen, and G. Gorden, *Inorg. Chem.*, **11**, 488 (1972).
7) R. H. Holyer, C. D. Hubbard, S. F. A. Kettle, and R. G. Wilkins, *Inorg. Chem.*, **4**, 929 (1965).
8) J. C. Cassatte, W. A. Johnson, L. M. Smith, and R. G. Wilkins, *J. Am. Chem. Soc.*, **94**, 8399 (1972).
9) M. L. Sanduja and W. M. Smith, *Can. J. Chem.*, **47**, 3773 (1969).

10) I. Ando, N. Nishijima, K. Ujimoto, and H. Kurihara, *Bull. Chem. Soc. Jpn.*, **55**, 2881 (1982).
11) G. A. Melson and R. G. Wilkins, *J. Chem. Soc.*, **1962**, 4208.
12) S. J. Valenty and P. E. Behnken, *Anal. Chem.*, **50**, 835 (1978).
13) J. W. O'Laughin and R. S. Hanson, *Anal. Chem.*, **52**, 2263 (1980).
14) J. W. O'Laughin, *Anal. Chem.*, **54**, 178 (1982).
15) H. Hoshino, T. Yotsuyanagi, and K. Aomura, *Bunseki Kagaku*, **27**, 315 (1978).
16) The Chemical Society, "Stability Constants of Metal-Ion Complexes, Special Publications No. 17 and No. 25," The Chemical Society, London (1964) and (1971).
17) G. Atkinson and J. E. Bauman, Jr., *Inorg. Chem.*, **1**, 900 (1962).
18) G. Anderegg, *Helv. Chim. Acta*, **46**, 2397 (1963).
19) H. Irving and D. H. Meller, *J. Chem. Soc.*, **1962**, 5222.
20) S. Cabani and M. Landucci, *J. Chem. Soc.*, **1962**, 278.
21) R. L. Davies and K. W. Dunning, *J. Chem. Soc.*, **1965**, 1468.
22) C. V. Banks and R. C. Bystroff, *J. Am. Chem. Soc.*, **81**, 6153 (1959).
23) G. Anderegg, *Helv. Chim. Acta*, **42**, 344 (1959).
24) J. P. Scharff and M. R. Paris, *Bull. Soc. Chim. France*, **1967**, 1782.

 © 1984 The Chemical Society of Japan Bull. Chem. Soc. Jpn., 57, 1828—1832 (1984) [Vol. 57, No. 7

The Color Reaction of Purine Bases by Ternary-complex Formation with Eosin and Silver(I)†

Yoshikazu FUJITA, Itsuo MORI,* Shoko KITANO,
Hiroshi KAWABE, and Yoshiyuki KAMADA
Osaka College of Pharmacy, 2-10-65, Kawai, Matsubara, Osaka 580
(Received December 7, 1983)

A color reaction of purine bases utilizing a ternary-complex system among a purine base, a metal ion, and a xanthene dye was studied, and the fundamental conditions for the spectrophotometric determination of purine bases(as adenine) with eosin and silver(I) were established. The absorption maxima of the ternary-complexes lie at 550—560 nm against water. The optimum pH ranges for the color formation of the complexes are pH 4.8—5.4. Beer's law is obeyed over the range of 1—10 μg/10 cm³ of adenine, and the apparent molar absorptivity is 1.1×10^5 dm³ mol⁻¹ cm⁻¹ at 560 nm. In the determination of adenine, the coexistence of pyrimidine bases, such as uracil and cytosine, and nucleotides containing adenine, such as 5′-adenosine triphosphate(ATP) and β-nicotinamide-adenine dinucleotide(NAD), scarcely interfere.

Various photometries and fluorometries of ions and substances utilizing the ternary-complex system (metal ion-electronegative ligand-organic base system) have been reported[1-8]; for example, the ionic-association complex system between a metal ion-1,10-phenanthroline(phen) cation and the anion of a dyestuff such as a xanthene derivative have been studied.

Eosin(2,4,5,7-tetrabromofluorescein) as a xanthene derivative is already used for the determination of such metal ions as silver(I), cadmium(II), iron(III), and cobalt(II).[9-15] However, the method for the determination of organic compounds by using eosin and a metal ion have not been reported entirely.

On the other hand, we recognized that the addition of a purine base to an eosin-silver(I) solution (Solution C) showed a red shift compared with that of Solution C or eosin solution (Solution B), and that the magnitude of the increase in the absorbance of this mixed solution at around 550—560 nm was proportional to the concentration of a purine base.

In this paper, therefore, the fundamental conditions for a new color reaction of purine bases by ternary-complex formation with eosin and silver(I) were studied, and the spectrophotometric determination of purine bases(as adenine) using this color reaction has been established.

Experimental

Reagents and Materials. Stock solutions (1.0×10^{-2} mol dm⁻³) of purine bases were prepared by dissolving proper quantities of purine bases in 2 cm³ of 10% sulfuric acid and diluting the mixtures to 100 cm³ with water. The working solution was made up to the suitable dilution by the use of this stock solution as required. A stock solution (1.0×10^{-1} mol dm⁻³) of silver(I) was prepared by dissolving silver nitrate in water, and then corrected by potentiometry. The working solution (1.0×10^{-3} mol dm⁻³) was made by the suitable dilution of this stock solution. A solution (1.0×10^{-3} mol dm⁻³) of eosin was prepared by dissolving eosin ($C_{20}H_6O_5Br_4Na_2$, Tokyo Kasei Kogyo Co., Ltd., Tokyo) in water. A 2.0% poly(*N*-vinylpyrrolidone)(PVP) solution was prepared by dissolving PVP (K-15, Tokyo Kasei Kogyo, Co., Ltd.) in water. A buffer solution (pH 5.0) was prepared by mixing 0.2 mol dm⁻³ acetic acid and 0.2 mol dm⁻³ sodium acetate solutions. All the other reagents and materials were of an analytical grade and were used without further purification. Doubly distilled water was used.

Apparatus. A Shimadzu Model UV-240 recording spectrophotometer with 1.0-cm quartz cells was used for the absorption spectra and absorbance measurements. A Hitachi-Horiba Model F-7 AD glass electrode pH meter was used for the pH measurements. A Metrohm Model E336A potentiograph was employed for the potentiometric titrations.

Standard Procedure for the Determination of Adenine. A solution containing 1—10 μg adenine was transferred to a 10 cm³ volumetric flask; to this solution 1.0 cm³ of a 2.0% PVP solution, 3.0 cm³ of the buffer (pH 5.0) solution, 0.5 cm³ of a 1.0×10^{-3} mol dm⁻³ eosin solution and 1.0 cm³ of a 1.0×10^{-3} mol dm⁻³ silver(I) solution were added. The mixture was diluted to 10 cm³ with water, kept at 45 °C for 20 min, and then cooled for 10 min in water. The absorbance of the eosin-silver(I)-adenine solution (Solution A) was measured at 560 nm against a eosin solution (Solution B).

Results and Discussion

Color Reaction and Absorption Spectra. On the addition of adenine, a purine base, to the eosin-silver(I) solution (Solution C), the maximum absorption of the eosin-silver(I)-adenine ternary complex solution (Solution A) at around 560 nm was distinctly observed; its absorbance was proportional to the concentration of adenine. Solution A without a surfactant was unstable, and it gradually precipitated on standing. The use of a nonionic surfactant was effective as a dispersion agent. By the way, no difference in absorption spectra between Solution C and the eosin solution (Solution B) in the absence of adenine was observed. The absorption spectra of Solutions A, B, and C in the presence of PVP at pH 5.0 are shown in Fig. 1.

On the other hand, other purine bases, such as guanine or phen, also formed the colored complexes, but the difference in absorbance between Solution B and its ternary complex solution was small as compared with that of the adenine complex solution. The absorption spectrum of the eosin-silver(I)-guanine solution or the eosin-silver(I)-phen solution under the same condi-

† Application of Xanthene Derivatives for Analytical Chemistry. Part XXXVIII. Part XXXVII: M. Yamazaki, I. Mori, Y. Fujita, S. Kitano, and Y. Kamada, *Bunseki Kagaku*, **33**, 170 (1984).

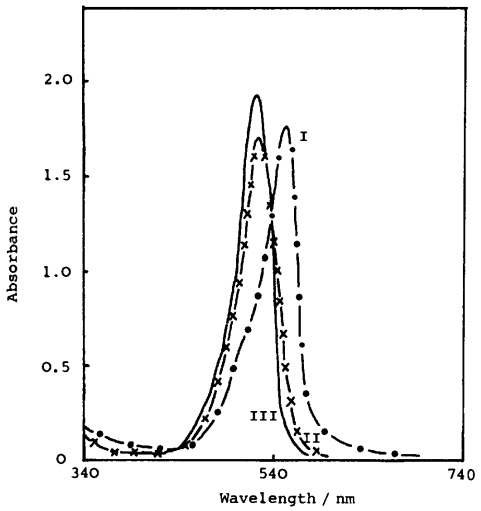

Fig. 1. Absorption spectra of eosin, eosin-silver(I), eosin-silver(I)-adenine, eosin-silver(I)-guanine, and eosin-silver(I)-phen solutions at pH 5.0.
Eosin: 2.5×10^{-5} mol dm^{-3}; silver(I): 5.0×10^{-5} mol dm^{-3}; adenine, guanine, and phen: 5.0×10^{-5} mol dm^{-3}; PVP: 1.0 cm^3 of 2.0% PVP solution/10 cm^3; Reference: water; curve I: eosin-silver(I)-adenine solution; curve II: eosin-silver(I)-guanine and eosin-silver(I)-phen solutions; curve III: eosin-silver(I) and eosin solution.

tions is also shown in Fig. 1.

The effect of dyes was studied by measuring the absorbance of Solution A against a dye solution. Eosin was superior to the other dyes tested in terms of sensitivity. The results are given in Table 1.

Only silver(I) was effective among the various metal ions: silver(I), cadmium(II), copper(II), zinc(II), iron (III), manganese(II), cobalt(II), cerium(III), lanthanum(III), thorium(IV), paladium(II), *etc.* The eosin-silver(I)-purine base ternary complex solution was fairly stable and was scarcely affected by any metal ions.

In the ternary complex systems among eosin, silver(I), and purine bases, the color reactions of various purine bases were examined. The difference in absorbance between the eosin-silver(I)-adenine solution and Solution B was larger than that of the other purine bases tested. The results are given in Table 2.

From the results described above, adenine was chosen for the purpose of fundamental investigations of the determination of purine bases, and the absorbance of Solution A at 560 nm against Solution B was measured in order to allow the determination of adenine.

Effect of pH. The effect of the pH on the color development was investigated with a solution containing 6.8 μg/10 cm^3 adenine. As is shown in Fig. 2, the ranges in which the maximum and nearly constant absorbance was observed at pH 4.8—5.4. Hence, the pH value of 5.0 with a 0.2 mol dm^{-3} acetic acid —0.2 mol dm^{-3} sodium acetate buffer solution was used for the pH adjustment.

Effect of Surfactants. Among the various surfactants tested, PVP(K-15), a nonionic surfactant, was best as a dispersion agent; the maximum and constant absorbance of Solution A was observed upon the addition of more than 0.75 cm^3 of a 2.0% PVP solution to the final volume of 10 cm^3. The results are given in Table 3.

Effect of Eosin and Silver(I) Concentrations. The effect of the amounts of eosin and silver(I) was exam-

Table 1. Effect of dyes

Dyes	Absorbance	at λ_{max}
Eosin	0.490	560
Erythrosine**	0.123	570
Phloxine**	0.153	575
Rose Bengal**	0.106	585
2,4,5,7-Tetrachlorofluorescein*	0.026	555
3′,4′,5′,6′-Tetrachlorofluorescein*	0	—
2,7-Dichlorofluorescein*	0.020	530
Fluorescein*	0	—
Pyrogallol Red**	0	—
Bromopyrogallol Red**	0.020	585
o-Hydroxyhydroquinonephthalein*	0	—
2,4,5,7-Tetrabromophenol-sulfonphthalein*	0	—
2,4,5,7-Tetrabromophenolphthalein*	0	—

Adenine taken: 6.8 μg/10 cm^3; dye: 5.0×10^{-5} mol dm^{-3}; silver(I): 1.0×10^{-4} mol dm^{-3}; PVP: 1.0 cm^3 of 2.0% PVP solution/10 cm^3; pH: 5.0; Reference: dye solution. * Synthesized by the published procedure[19]. ** Pure grade materials available commercially.

Table 2. Color reaction between some purine bases and solution B

Purine bases	(mol dm^{-3})	Absorbance	at λ_{max}
Adenine	5.0×10^{-6}	0.490	560
Guanine	2.0×10^{-5}	0.330	555
Hypoxanthine	5.0×10^{-5}	0.135	550
Purine	5.0×10^{-5}	0.140	555
6-Iodopurine	5.0×10^{-6}	0.310	560
6-Mercaptopurine	5.0×10^{-6}	0.125	555
1-Methyladenine	5.0×10^{-5}	0.015	555

Eosin: 5.0×10^{-5} mol dm^{-3}; silver(I): 1.0×10^{-4} mol dm^{-3}; PVP: 1.0 cm^3 of 2.0% PVP solution/10 cm^3; pH: 5.0; Reference: Solution B.

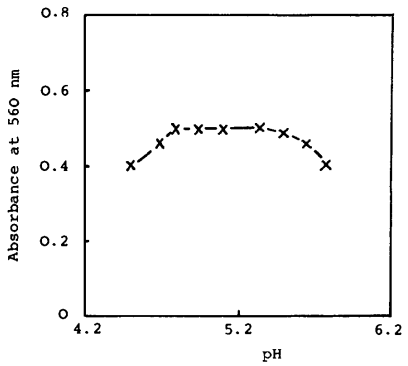

Fig. 2. Effect of pH.
Adenine: 6.8 μg/10 cm^3(5.0×10^{-6} mol dm^{-3}); silver (I): 1.0×10^{-4} mol dm^{-3}; eosin: 5.0×10^{-5} mol dm^{-3}; PVP: 1.0 cm^3 of 2,0% PVP solution/10 cm^3; Reference: Solution B.

TABLE 3. EFFECT OF SURFACTANTS

Surfactants	Absorbance at λ_{max}	
PVP(K-15)	0.490	560
PVP(K-30)	0.475	560
PVP(K-90)	0.438	560
Polyvinyl alcohol(n: 500)	0.370	555
Polyvinyl alcohol(n: 2000)	0.413	555
Poly(oxyethylene) sorbitan monolaurate	0.336	560
Gum arabic	0.320	550
Gelatin	0.257	550
Sodium dodecyl sulfate	0.124	545
Hexadecyltrimethylammonium chloride	0	—

Adenine taken: 6.8 μg/10 cm^3; eosin: 5.0×10^{-5} mol dm^{-3}; silver(I): 1.0×10^{-4} mol dm^{-3}; surfactant: 1.0 cm^3 of 2.0% surfactant solution/10 cm^3; pH: 5.0; Reference: Solution B.

ined by varying the molar ratio of eosin to silver(I), the amount of adenine being kept constant. A maximum and almost constant absorbance was observed upon the addition of a 0.5—1.5 cm^3 of 1.0×10^{-3} mol dm^{-3} silver(I) solution. The molar ratio of silver(I) to eosin in the complex was found by the molar-ratio method to be 2:1 in the presence of adenine.

Accordingly, all further work was carried out with 5.0×10^{-5} mol dm^{-3} eosin and 1.0×10^{-4} mol dm^{-3} silver(I) in the final volume.

Sequence of Addition and Stability. The maximum absorbance was obtained when silver(I) was finally added to an eosin-adenine solution. The color formation of the ternary complex did not occur instantaneously at room temperature (15—25 °C), about more than 120 min being required for a complete color reaction. The effect of the temperature on the color formation was examined by heating the mixed solution for 10—60 min at various temperature (30°, 45°, or 60 °C); the maximum and constant absorbance was obtained by heating for 20 min at 45 °C and cooling for 10 min in water. The absorbance was constant for at least 2 h at room temperature.

Calibration Curve. The calibration curve for adenine was constructed according to the standard procedure. It was found that Beer's law held in the concentration range of 1—10 μg of adenine in the final volume of 10 cm^3. The apparent molar absorptivity at 560 nm was estimated to be 1.1×10^5 dm^3 mol^{-1} cm^{-1}. The sensitivity, according to Sandell's scale, was 0.0013 μg cm^{-2} for adenine. The relative standard deviation for five replicate determinations was 0.68% for 6.8 μg of adenine.

Effects of Foreign Substances. The effects of foreign substances on the determination of adenine were also examined. The coexistence of most metal ions did not interfere in a 100-fold excess over adenine. Among the various anions tested, the coexistence of small amounts of thiosulfate, thiocyanate, cyanide, and iodide, and the presence of large amounts of chloride gave negative errors because of reacting with silver(I). These anions could be conveniently eliminated by the addition of a silver nitrate solution as a preliminary step. Anions such as phosphate, nitrate, and organic acid ions did not interfere. The presence of small amounts of such purine bases as guanine, hypoxanthine, 6-mercaptopurine, and 6-iodopurine, and the coexistence of large amounts of such purine bases as purine, 1-methyladenine, and uric acid did interfere, though, xanthine derivatives such as caffeine and theophilline, and pyrimidine bases such as uracil and cytosine, did not affect the determination of adenine. Moreover, nucleosides and nucleotides, such as adenosine, 5′-adenine triphosphate (ATP), β-nicotinamide-adenine dinucleotide (NAD) and adenosine cyclic 3′,

TABLE 4. EFFECT OF FOREIGN SUBSTANCES

Substances	Added (μg/10 cm^3)	Mole ratio (Substance/Adenine)	Absorbance at 560 nm
—	—	—	0.490
Fe(III), Sulfate	279.3	100	0.419
Cd(II), Nitrate	281.0	50	0.546
Zn(II), Nitrate	326.9	100	0.490
Mg(II), Nitrate	274.7	100	0.490
Cl^-, Sodium	35.5	20	0.327
I^-, Potassium	12.7	2	0.356
CN^-, Potassium	6.5	5	0.440
SCN^-, Potassium	5.8	2	0.417
$S_2O_3^{2-}$, Sodium	1.4	1/5	0.398
$H_2PO_4^-$, Potassium	485.0	100	0.490
Tartaric acid	750.5	100	0.490
Citric acid	960.6	100	0.490
Guanine	1.5	1/5	0.320
Hypoxanthine	3.4	1/2	0.400
6-Iodopurine	2.5	1/5	0.268
6-Mercaptopurine	1.5	1/5	0.395
Purine	12.0	2	0.450
1-Methyladenine	37.5	5	0.450
Uric acid	42.0	5	0.384
Theophylline	900.8	100	0.490
Uracil	560.5	100	0.490
Cytosine	555.5	100	0.490
Adenosine	1336.2	100	0.490
ATP	3025.0	100	0.490
NAD	3317.5	100	0.490
Cyclic AMP	1646.0	100	0.490
FAD*	865.6	20	0.417
Putrescine hydrochloride	44.1	10	0.343
Spermidine hydrochloride	36.3	5	0.410
Glutamine	730.8	100	0.490
L-Ascorbic acid	880.6	100	0.490
D-Glucose	900.8	100	0.490
Albumin(Human)	50.0	—	0.438
DNA(Herring)**	20.0	—	0.388

Adenine taken: 6.8 μg/10 cm^3; eosin: 5.0×10^{-5} mol dm^{-3}; silver(I): 1.0×10^{-4} mol dm^{-3}; PVP: 1.0 cm^3 of 2.0% PVP solution/10 cm^3; pH: 5.0; Reference: Solution B.
* FAD, Flavin adenine dinucleotide; ** DNA, Deoxyribonucleic acid.

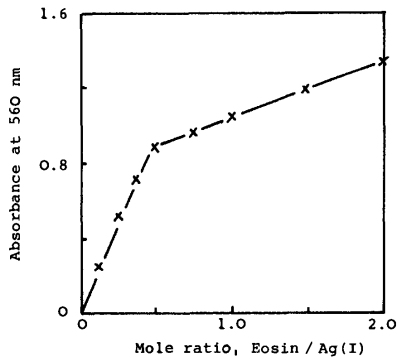

Fig. 3. Composition of [eosin: silver(I)] in the presence of adenine obtained by the molar-ratio method. Silver(I): 2.0×10^{-5} mol dm^{-3}; eosin: 2.0×10^{-4} mol dm$^{-3}\times$X cm^3/10 cm^3; adenine: 1.0×10^{-4} mol dm^{-3}; PVP: 1.0 cm^3 of 2.0% PVP solution/10 cm^3; pH: 5.0; Reference: Solution B.

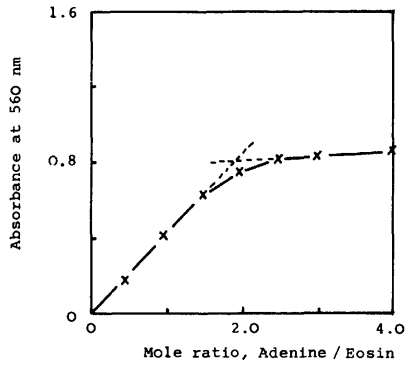

Fig. 4. Composition of [adenine: eosin] in the presence of silver(I) obtained by the molar-ratio method. Silver(I): 2.0×10^{-5} mol dm^{-3}; eosin: 1.0×10^{-5} mol dm^{-3}; adenine: 1.0×10^{-4} mol dm$^{-3}\times$X cm^3/10 cm^3; PVP: 1.0 cm^3 of 2.0% PVP solution/10 cm^3; pH:5.0; Reference: Solution B.

5′-monophosphate (cyclic AMP), also did not interfere in a 100-fold excess. Though such amines as putrescine, spermidine and tryptamine interfered in large amounts, amino acids, D-glucose, L-ascorbic acid, *etc.* did not interfere. The results are summarized in Table 4.

The Composition of the Complex. The mole ratio of silver(I) to eosin was established by the molar-ratio and continuous-variation methods. The results indicated that the mole ratio of silver(I) to eosin was 2:1. The results obtained by the molar-ratio method are shown in Fig. 3.

It was found that the adenine-to-eosin ratio obtained by the molar-ratio method was 2:1, as is shown in Fig. 4.

From these results, it is deduced that the ternary complex formed in this reaction system may be expressed as (adenine)$_2$(Ag)$_2$(eosin).

Color Reaction between Substances Containing Adenine and Solution C. The color reactions between some substances containing adenine and Solution C were also studied. No difference in color between these substances containing adenine and Solution C was observed. Therefore, liberated adenine was determined by the standard procedure after these substances containing adenine had been treated with acid-hydrolysis as a preliminary step. The results are given in Table 5.

TABLE 5. ANALYTICAL RESULTS OF SUBSTANCES CONTAINING ADENINE AS OBTAINED BY THE STANDARD PROCEDURE AFTER ACID-HYDROLYSIS

Substances	Recovery* (%)	
	Method A	Method B
Adenosine	99.1	—
ATP	98.7	—
NAD	84.0	—
Cyclic AMP	52.5	70.0
FAD	0	76.6

Eosin: 5.0×10^{-5} mol dm^{-3}; silver(I): 1.0×10^{-4} mol dm^{-3}; PVP: 1.0 cm^3 of 2.0% PVP solution/10 cm^3; pH 5.0; Reference: Solution B.

* Mean of 3 determinations; method A, boiled gently for 20 min in a 10% H_2SO_4 solution; method B, refluxed for 1 h in a 5% H_2SO_4 solution.

Though further investigation is necessary, this proposed method may also be useful in the determination of nucleosides and nucleotides.

Conclusion

The fundamental conditions for the color reaction of purine bases by ternary-complex formation with eosin and silver(I) have been discussed, and a spectrophotometric method for the determination of adenine, a purine base, utilizing this ternary complex has been established. This method could be used in the concentration range of 1—10 μg/10 cm^3 adenine at 560 nm. The apparent molar absorptivity in this procedure was estimated to be 1.1×10^5 dm^3 mol^{-1} cm^{-1} for adenine. The method is inferior to the fluorometric methods[16,17] in sensitivity, but it is about 10 times more sensitive than the method[18] utilizing the diazo-coupling reaction with the Brotton-Marshall reagent. This method is superior to those methods in terms of rapidity, simplicity, and reproducibility. In addition, this proposed method for the determination of adenine is scarcely affected by the coexistence of pyrimidine bases, such as uracil and cytosine, and the substances containing adenine, such as adenosine, ATP and NAD. The application to the determination of these nucleosides or nucleotides with a suitable preliminary treatment may be feasible. Therefore, the application to high-performance liquid chromatography for purine bases can also be expected.

References

1) A. K. Babko, *Talanta*, **15**, 721 (1968).
2) A. T. Pilipenko and M. M. Tananaiko, *Talanta*, **21**, 501 (1974).
3) T. Sakaguchi, *Kagaku no Ryoiki*, **30**, 36 (1976).
4) K. Ueno, *Bunseki Kagaku*, **19**, 736 (1971).
5) H. Nishida, *Bunseki*, **1977**, 33.

6) S. Motomizu, T. Iwachido, and T. Toei, *Bunseki*, **1980**, 234.
7) P. R. Haddad, *Talanta*, **24**, 1 (1977).
8) Z. Marczenko, *Chem. Anal. (Warsaw)*, **24**, 551 (1979).
9) Chongyang Fan and Wei Li, *Hua Hsueh Tung Pao*, **212**, 247 (1980); *Anal. Abstr.*, **39**, 5B46 (1980).
10) J. Pancl, *Chem. Prum.*, **31**, 421 (1981); *Anal. Abstr.*, **42**, 3B56 (1982).
11) K. A. Idriss, M. M. Seleim, and M. S. Abu-Bukr, *Proc.-Indian Acad. Sci., Sect. A*, **89**, 519 (1980); *Anal. Abstr.*, **41**, 3B56 (1981).
12) M. A. Matveets, S. D. Akhmetova, and D. P. Shcherbov, *Zh. Anal. Khim.*, **35**, 1640 (1980).
13) D. N. Lisitsyna and D. P. Shcherbov, *Zh. Anal. Khim.*, **25**, 2310 (1970).
14) M. T. El-Gharmy, R. W. Frei, and G. W. Higgs, *Anal. Chim. Acta*, **47**, 41 (1969).
15) D. N. Lisitsyna and D. P. Shcherbov, *Zh. Anal. Khim.*, **28**, 1203 (1973).
16) H. Yuki, C. Sempuku, M. Park, and K. Takiura, *Anal. Biochem.*, **46**, 123 (1972).
17) G. Arigad and S. Damle, *Anal. Biochem.*, **50**, 321 (1972).
18) D. L. Woodhouse, *Arch. Biochem.*, **22**, 347 (1950).
19) I. Mori, *Yakugaku Zasshi*, **85**, 481 (1965).

Reactions of Metal Complexes with Carbohydrates. Synthesis and Structure of (2-[(2-Aminoethyl)amino]-2-deoxy-L-sorbose)(ethylenediamine)-nickel(II) Dichloride Hemi Methanol Solvate: [Ni(en)(L-sor-en)]$Cl_2 \cdot 1/2CH_3OH$ (en=ethylenediamine and sor=sorbose)

Taro Tsubomura, Shigenobu Yano,* Koshiro Toriumi,† Tasuku Ito,† and Sadao Yoshikawa*

Department of Synthetic Chemistry, Faculty of Engineering, The University of Tokyo, Hongo, Bunkyo-ku, Tokyo 113

†*Division of Applied Molecular Science, Institute for Molecular Science, Okazaki National Reserch Institute, Okazaki 444*

(Received January 24, 1984)

The synthesis and crystal structure of the complex [Ni(en)(L-sor-en)]$Cl_2 \cdot 1/2CH_3OH$ which was derived from the reaction of tris(ethylenediamine)nickel(II) dichloride dihydrate with L-sorbose are described. Crystallographic details for the complex are follows: space group C2 (monoclinic); a=17.862(2) Å, b=8.212(1) Å, c=12.644(2) Å, β=90.89(1)°; Z=4; D_{calcd}=1.53 gcm^{-3}. The structure was solved by heavy atom methods, and the structure parameters including almost all hydrogen atoms were refined by least-squares methods. The final R factor was 0.032 for 2680 independent reflections. The nickel atom is octahedrally coordinated with a bidentate ethylenediamine and a tetradentate glycosylamine ligand of L-sor-en. L-Sorbose moiety adopts the six-membered α-$^2C_5$ chair conformation. In addition to the synthesis and structure of this complex, we report the results of absorption and circular dichroism spectroscopy.

Carbohydrates have long been known to form complexes with metal ions. The interactions between metal and carbohydrates in solution have been much studied; by potentiometric titration,[1] electrophoresis,[2] circular dichroism,[3] NMR spectroscopy,[4] ESR spectroscopy,[5] and chromatography,[6] *etc.* There are many complexes of alkaline earth metals with carbohydrates, some of which were analyzed by X-ray crystallography,[7] however only a few transition metal complexes, which were confirmed to have sugar chelates, have been reported.[8]

Recently the structure of both complexes [Ni(en)(D-fru-en)]$CL_2 \cdot CH_3OH$[9] (**1**) and [Ni(L-rham-tn)$_2$]$Br_2 \cdot 2H_2O \cdot CH_3OH$[10] (en=ethylenediamine, D-fru-en=2-[(2-aminoethyl)amino]-2-deoxy-D-fructose, tn=trimethylenediamine, L-rham=tn=1-[(3-aminopropyl)amino]-1-deoxy-L-rhamnose) was determined by X-ray crystallography. The crystal structure of complex **1** suggested that an *N*-glycoside derived from a ketose and a diamine coordinates to the nickel atom through the two oxygen atoms of the hydroxyl groups on C-1 and C-3 of the sugar moiety and through the two nitrogen atoms of the diamine. It also indicated that the coordination structure of a ketose will depend on the orientation of the C-3 hydroxyl group and this makes a significant contribution to the circular dichroism.

In the course of our study to clarify the interactions between transition metals and carbohydrates,[9,10] we have prepared and characterized a new nickel(II) complex containing an *N*-glycoside which was derived from the reaction of tris(ethylenediamine)nickel(II) ion with L-sorbose. Since L-sorbose is C-5 epimer of D-fructose, the absolute configurations around other asymmetric carbon atoms are the same as those of D-fructose in the pyranose form (Fig. 1). Consequently the coordination behaviour of *N*-glycosides derived from L-sorbose, and the circular dichroism of their complexes are expected to be similar to those for complexes

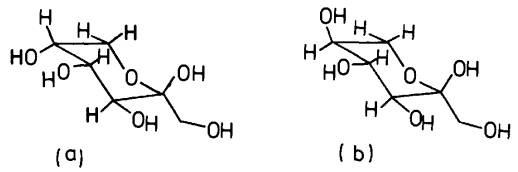

Fig. 1. The structure of ketohexoses in the pyranose form: (a) α-L-sorbose and (b) β-D-fructose.

of D-fructose. However, the CD curves of the complexes are different, as is shown later in this report. To clarify the stereochemistry of this complex, we have undertaken a crystal and molecular structure determination. A preliminary account of this work has already appeared.[11]

Experimental

All materials were reagent grade. L-Sorbose was purchased from Tokyo Kasei Co., [Ni(en)$_3$]$Cl_2 \cdot 2H_2O$[12] was prepared by the ordinary method.

Preparation of [Ni(en)(L-sor-en)]$Cl_2 \cdot 1/2CH_3OH$ (2)

This complex was prepared from tris(ethylenediamine)-nickel(II) complex and L-sorbose by a similar method described previously[9] with slight modifications, as follows. To a solution of 8.8 mmol [Ni(en)$_3$]$Cl_2 \cdot H_2O$ in 80 mL of methanol was added 17.6 mmol of L-sorbose and 8.8 mmol of NH_4Cl, and heated to reflux for 1 h. The color of the solution changed from violet to blue. Then it was concentrated to about 30 mL by a rotary evaporator and poured on to a column of Sephadex LH-20 gel (4 cm×90 cm), and the material was eluted with methanol. The colored material was separated into violet, blue, yellow, and orange bands. The blue fractions were collected and concentrated to about 15 mL and kept at 5 °C. Blue crystals (520 mg) were obtained, they were recrystallized from a minimum amount of hot methanol. Found: Ni, 14.3; C, 29.19; H, 6.86; N, 13.36; Cl, 16.56; Calcd. for $C_{10.5}H_{28}N_4O_{5.5}Cl_2Ni$: Ni, 13.7; C, 29.46;

H, 6.61; N, 13.09; Cl, 16.56.

Measurements Visible and near infrared absorption spectra were measured with a Hitachi model 340 recording spectrophotometer. Reflectance spectra were recorded on this instrument equipped with a reflectance attachment. Circular dichroism spectra were recorded on a Jasco J-500 recording spectropolarimeter. Magnetic susceptibility was measured at room temperature using a Shimadzu MB-100 magnetic balance (Faraday method). Diamagnetic corrections were calculated from Pascal's constants.[13]

Crystal Data and Intensity Data Collection of [Ni(en)(L-sor-en)]Cl$_2$·1/2CH$_3$OH. A block-shaped blue crystal (0.56×0.50×0.35 mm), which was coated with epoxy cement, was used to collect diffraction data on a Rigaku AFC-5 four-circle automated diffractometer controlled by a Facom U-100 computer and the Rigaku FOS program system, equipped with Mo $K\alpha$ radiation (λ=0.71073 Å). The accurate unit cell dimentions were determined by least-squares methods from θ values for 40 reflections in the range of 25°—31° measured on the diffractometer. Crystal data are as follows.

[Ni(en)(L-sor-en)]Cl$_2$·1/2CH$_3$OH, $C_{10.5}H_{28}N_4O_{5.5}Cl_2Ni$, M.W.=428.02, Monoclinic, space group C2, a=17.862(2), b=8.212(1), c=12.644(2) Å, β=90.89(1)°, D(obsd)=1.55 g cm^{-3} (by flotation in 1,2-dichloroethane and 1,2-dibromoethane mixture), D(calcd)=1.53 g cm^{-3}, Z=4.

Intensity data were collected by θ-2θ method (2$\theta \leqq 60°$), scan speed=3°/min, scan width=(1.2+tanθ)°. Backgrounds were measured both at the beginning and the end of the scan, each for half time of the scan. Three standard reflections were monitored for every fifty reflections, and no significant changes were found. Of the 2997 reflections collected, 2680 independent reflections with $|F_o|>3\sigma(|F_o|)$ were used in the structure analysis. The intensity data were corrected for standard Lorentz-polarization effects. An absorption correction with a numerical integration procedure was applied; μ=13.92 cm^{-1} (Mo $K\alpha$).

Structure Solution and Refinement. All calculations were carried out on a HITAC M-200H system of The Computer Center of The Institute for Molecular Science with a universal computing program UNICS-III.[14] The initial coordinates of the nickel atom were determined by a three dimensional Patterson synthesis. The positions and isotropic temperature factors of other nonhydrogen atoms were determined by means of mutual cycles of Fourier synthesis and block-diagonal least squares refinement. Atomic scattering factors were taken from Ref. 15. A methanol molecule was found to be located close to a special position on the twofold axis. A weighting scheme $1/w=\sigma_{count}^2+(0.015|F_o|)^2$ was employed and anomalous scattering factors[16] for non hydrogen atoms were introduced in F_c. Least-squares refinement of the atomic parameters with isotropic temperature factors of the nonhydrogen atoms gave convergence at R=10.16%. ($R=\sum||F_o|-|F_c||/\sum|F_o|$). The absolute configuration of this complex was determined from the known configuration of L-sorbose. When the f'' values of Ni, Cl, O, N, and C atoms were reversed in sign to test the structure, the convergence was reached to R=10.34%. At this stage, anisotropic temperature factors were introduced for all nonhydrogen atoms. Difference Fourier synthesis made clear the locations of all hydrogen atoms of the complex cation except for H(C9)1, the coordinates of this H(C9)1 were calculated by assuming a tetrahedral coordination with C-H bond distance of 1.08 Å. The positional parameters and isotropic temperature factors of all hydrogen atoms are also refined. The final R factor was 0.032, and R_w was 0.042 ($R_w=[\sum w(|F_o|-|F_c|)^2/\sum w\cdot|F_o|^2]^{1/2}$). The final difference Fourier synthesis revealed no unusual features with the highest peak being 0.71 Å^{-3}. The anisotropic thermal parameters and complete list of the $|F_o|$ and $|F_c|$ values have been preserved by the Chemical Society of Japan (Document No. 8425).

Results and Discussion

Synthesis. The reaction of L-sorbose with [Ni(en)$_3$]Cl$_2$·H$_2$O was studied and the new complex containing glycosylamine ligand (L-sor-en) was isolated. The method of preparation was almost the same as described previously to prepare the glycosylamine complex containing another monosaccharides.[9] When tris diamine nickel(II) complex and L-sorbose are refluxed in methanol, the solution becomes blue. This solution is separated into four bands by gel permeation chromatography. The first violet band consists of the starting nickel-diamine complex, the second blue band contains glycosylamine complex, and the contents of the third and the fourth fractions (yellow and orange) are not clear. Blue crystals are obtained from blue fractions. When NH_4Cl is not added to the reactant, more reaction time is necessary and about half of the yield of glycosylamine complex is obtained. Consequently NH_4Cl appears to act as a general acid base catalyst similar to the formation of glycosylamine without metal.[17] Analytical data indicated that this complex has a glycosylamine and a diamine similar to [Ni(en)(D-fru-en)]Cl$_2$·CH$_3$OH.[9] This complex is soluble in methanol and water, but it decomposes in a few days in water.

Magnetic Moments and Absorption Spectra. Magnetic moments and absorption spectra were measured to investigate the coordination geometry of the nickel complex. The effective magnetic moment at room temperature of this complex **2** is 3.17 μ_B, which is normal for octahedral nickel(II) complexes.[18] Near-infrared and visible absorption spectra and CD spectra of this complex together with complex **1** in methanolic solution are given in Fig. 2. Table 1 lists their spectral data. Both of these absorption spectra possess three peaks in the near-infrared and visible region

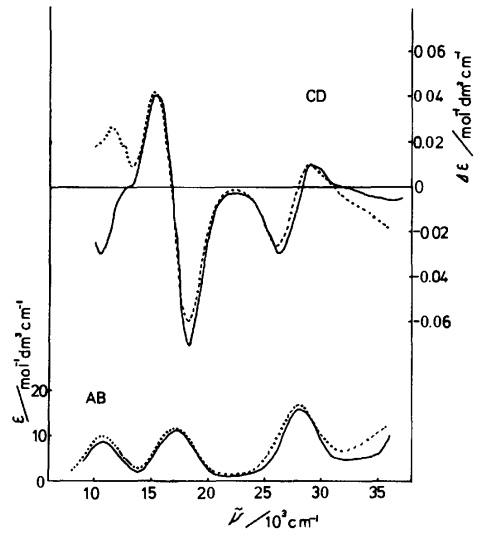

Fig. 2. Absorption and circular dichroism spectra of complexes: [Ni(en)(L-sor-en)]$^{2+}$ (——) and [Ni(en)-(D-fru-en)]$^{2+}$ (----).

TABLE 1. ABSORPTION, CIRCULAR DICHROISM, AND REFLECTANCE SPECTRAL DATA OF COMPLEX [Ni(en)(L-sor-en)]$Cl_2 \cdot 1/2CH_3OH$

Abs. max.[a]	ε	CD. max.[a]	$\Delta\varepsilon$	Ref. max.
10^3 cm^{-1}	dm^3 mol^{-1} cm^{-1}	10^3 cm^{-1}	10^{-2} dm^3 mol^{-1} cm^{-1}	10^3 cm^{-1}
10.7	8.7	10.4	−3.14	10.6
12.8[sh]	3.8			
17.2	11.1	15.3	+4.16	17.5
		18.3	−7.02	
28.0	15.8	26.2	−2.89	27.7
		29.2	+1.02	

a) Absorption and circular dichroism spectra were recorded in methanol solution.

TABLE 2. ATOMIC PARAMETERS AND ESTIMATED STANDARD DEVIATIONS FOR NON-HYDROGEN ATOMS

Atom	x[a]	y[a]	z[a]	B_{eq}[b]
Ni	8012(1)	5000(0)	2232(1)	2.6
Cl(1)	6958(1)	4822(2)	−985(1)	4.6
Cl(2)	6191(1)	1661(2)	3697(1)	6.0
O(1)	9037(1)	5970(3)	2857(2)	3.7
O(2)	9708(1)	1939(3)	3364(2)	3.7
O(3)	7895(1)	3880(3)	3729(2)	2.8
O(4)	7666(1)	851(4)	4793(2)	3.7
O(5)	8686(2)	−1706(3)	4203(2)	4.2
N(1)	8772(1)	3041(4)	2131(2)	2.7
N(2)	8362(2)	5545(4)	722(2)	4.0
N(3)	7395(2)	7023(4)	2626(2)	3.7
N(4)	6980(2)	4059(5)	1761(2)	3.9
C(1)	9491(2)	4740(5)	3368(3)	3.8
C(2)	9121(2)	3077(4)	3187(3)	2.9
C(3)	8491(2)	2799(4)	4001(2)	2.5
C(4)	8225(2)	1050(4)	3999(2)	2.7
C(5)	8895(2)	−35(6)	4235(2)	3.2
C(6)	9474(2)	264(5)	3383(3)	3.5
C(7)	9262(2)	3364(6)	1216(3)	4.2
C(8)	8788(3)	4097(7)	342(3)	4.9
C(9)	6596(3)	6603(9)	2590(5)	6.7
C(10)	6425(3)	5349(10)	1838(6)	7.9
C(M)	5000(0)	3234(23)	0(0)	14.7
O(M)	5190(15)	4076(53)	−366(19)	28.7

a) Positional parameters are multiplied by 10^4. b) Thermal parameters are given by the equivalent temperature factors.

TABLE 3. BOND DISTANCES AND THEIR ESTIMATED STANDARD DEVIATIONS FOR NON-HYDROGEN ATOMS

Atom A	Atom B	Distances l/Å	Atom A	Atom B	Distances l/Å
Ni	-O(1)	2.137(3)	Ni	-O(3)	2.118(2)
Ni	-N(1)	2.109(3)	Ni	-N(2)	2.068(3)
Ni	-N(3)	2.059(3)	Ni	-N(4)	2.078(3)
O(1)	-C(1)	1.441(5)	O(3)	-C(3)	1.425(4)
O(4)	-C(4)	1.436(4)	O(5)	-C(5)	1.422(5)
O(2)	-C(2)	1.419(4)	O(2)	-C(6)	1.438(5)
N(1)	-C(2)	1.466(4)	N(1)	-C(7)	1.485(5)
N(2)	-C(8)	1.496(6)	N(3)	-C(9)	1.470(6)
N(4)	-C(10)	1.456(8)	C(1)	-C(2)	1.532(5)
C(2)	-C(3)	1.553(4)	C(3)	-C(4)	1.513(5)
C(4)	-C(5)	1.519(5)	C(5)	-C(6)	1.524(5)
C(7)	-C(8)	1.507(6)	C(9)	-C(10)	1.431(10)
O(M)	-C(M)	0.902(40)			

and the molar absorption coefficient of these peaks are comparatively small. These spectral features are typical for octahedral nickel(II) complexes.[19] The $10D_q$ value of complex **2**, which is equal to the energy of the first absorption peak in the case of d^8 octahedral complex, is 10.7 kcm^{-1}, that is normal for N_4O_2 nickel(II) octahedral complex.[19] The absorption spectra of the complexes **1** and **2** are almost identical, so it is deduced that these complexes have similar ligand fields around the nickel atoms.

Crystal and Molecular Structure of [Ni(en)(L-sor-en)]-$Cl_2 \cdot 1/2CH_3OH$. Since this structure analysis yielded a high degree of convergence of parameters for a sugar-containing complex (R=0.032), the coordinates of all atoms including hydrogen atoms of the complex cation were determined. The final atomic coordinates, bond distances, and bond angles are listed in Tables 2, 3, and 4, respectively.

Fig. 3 shows an ORTEP drawing[20] of the complex cation $[Ni(en)(L\text{-sor-en})]^{2+}$. The nickel atom is coordinated with four nitrogen atoms and two oxygen atoms. The coordination geometry of this complex resembles that of the D-fructose complex **1**. The nickel atom is coordinated with a tetradentate glycosylamine (L-sor-en) and a bidentate diamine (en).

The glycosylamine coordinates to the nickel atom at four points through the two hydroxyl groups on carbon 1, and carbon 3 of the sugar moiety, and the two nitrogen atoms of the ethylenediamine residue. In the glycosylamine, L-sorbose moiety has the usual α-$^2C_5$ pyranose form. This form is the most stable in the solution of L-sorbose alone,[21] and it is known that crystalline α-L-sorbose also takes this form.[22] This anomeric structure is equivalent to the case of the D-fru-en complex **1**, although the nomenclature of the anomeric form in the complex **1** is β because the nomenclature of the anomeric form is reversed whether the absolute configuration of the ketose is D or L. In the tetradentate glycosylamine ligand, five membered chelate ring of the ethylenediamine moiety adopts a symmetrical gauche conformation, but other five membered chelates (Ni-N(1)-C(2)-C(3)-O(3)) and

Table 4. Bond angles and their estimated standard deviations for non-hydrogen atoms

Atom B	Atom A	Atom C	Angle ϕ/°	Atom B	Atom A	Atom C	Angle ϕ/°
O(1)-	Ni	-O(3)	85.9(1)	O(1)-	Ni	-N(1)	76.1(1)
O(1)-	Ni	-N(2)	89.5(1)	O(1)-	Ni	-N(3)	93.9(1)
O(1)-	Ni	-N(4)	174.9(1)	O(3)-	Ni	-N(1)	78.2(1)
O(3)-	Ni	-N(2)	162.8(1)	O(3)-	Ni	-N(3)	94.2(1)
O(3)-	Ni	-N(4)	89.7(1)	N(1)-	Ni	-N(2)	84.6(1)
N(1)-	Ni	-N(3)	167.7(1)	N(1)-	Ni	-N(4)	105.5(1)
N(2)-	Ni	-N(3)	102.7(1)	N(2)-	Ni	-N(4)	95.5(1)
N(3)-	Ni	-N(4)	83.9(1)	Ni	-O(1)-	C(1)	112.1(2)
Ni	-O(3)	-C(3)	113.7(2)	C(2)-	O(2)-	C(6)	114.8(2)
Ni	-N(1)	-C(2)	101.2(2)	Ni	-N(1)-	C(7)	107.4(2)
C(2)-	N(1)	-C(7)	117.3(3)	Ni	-N(2)-	C(8)	106.7(3)
Ni	-N(3)	-C(9)	109.1(3)	Ni	-N(4)-	C(10)	108.2(3)
O(1)-	C(1)	-C(2)	108.7(3)	O(2)-	C(2)-	N(1)	115.7(3)
O(2)-	C(2)	-C(1)	104.4(2)	O(2)-	C(2)-	C(3)	109.9(3)
N(1)-	C(2)	-C(1)	109.3(3)	N(1)-	C(2)-	C(3)	107.3(2)
C(1)-	C(2)	-C(3)	110.3(3)	O(3)-	C(3)-	C(2)	107.2(2)
O(3)-	C(3)	-C(4)	110.9(2)	C(2)-	C(3)-	C(4)	111.7(3)
O(4)-	C(4)	-C(3)	109.2(3)	O(4)-	C(4)-	C(5)	110.5(3)
C(3)-	C(4)	-C(5)	108.1(3)	O(5)-	C(5)-	C(4)	110.8(3)
O(5)-	C(5)	-C(6)	108.4(3)	C(4)-	C(5)-	C(6)	108.0(3)
O(2)-	C(6)	-C(5)	111.5(3)	N(1)-	C(7)-	C(8)	108.2(3)
N(2)-	C(8)	-C(7)	111.4(3)	N(3)-	C(9)-	C(10)	112.8(5)
N(4)-	C(10)	-C(9)	115.5(4)				

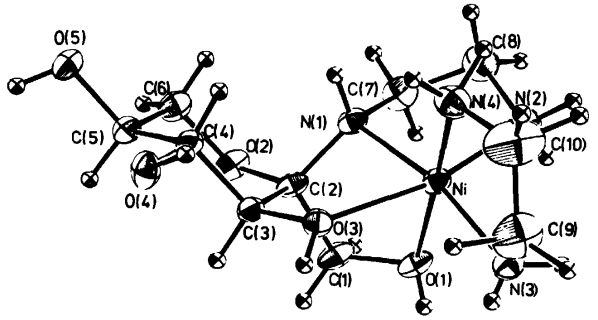

Fig. 3. A perspective drawing of the complex cation $[Ni(en)(L\text{-sor-en})]^{2+}$.

(Ni-N(1)-C(2)-C(1)-O(1)) are in the asymmetrical ones. The absolute configuration of the secondary nitrogen atom is *S*. These structural features around the nickel atom are common to complex **1** and **2**. The bidentate ethylenediamine chelate has the δ-gauche conformation (Fig. 4), although the corresponding ethylenediamine chelate ring of the complex **1** has the λ-gauche conformation. This is the most conspicuous difference of the structure around the nickel atom between complex **1** and **2**.

The coordination geometry around the nickel atom of the complex **2** is distorted octahedral symmetry. The least cis angle around the nickel atom is 76.1° (O(1)-Ni-N(1)), and the largest cis angle is 105.5° (N(1)-Ni-N(4)). Furthermore, the least trans angle around the nickel atom is 162.8° (Table 4). This tendency for distortion from an octahedron is similar to the

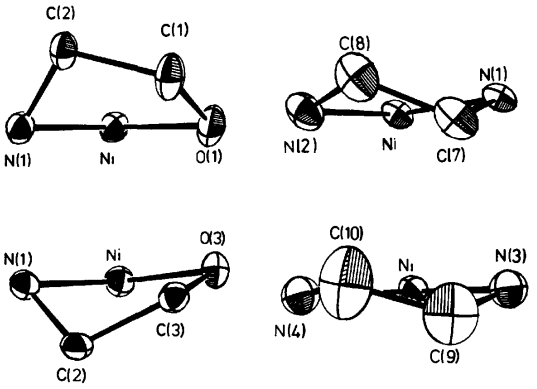

Fig. 4. Perspective drawings of the chelate rings.

case of complex **1**. The bite angle of the five membered chelate rings are smaller than ninety degrees, and they are normal.[24] The conformation of L-sorbose moiety is the typical chair form. The angles of C-C-C and C-O-C in the pyranose ring are within 110°±2.1° similar to α-L-sorbose crystals.[22]

The average nickel-nitrogen bond distance of 2.08 Å is very close to that in the complex **1** (2.07 Å), and they are normal values in comparison with the reported nickel-nitrogen bond distances. The average nickel-oxygen bond distance of 2.13 Å is slightly shorter than that in the complex **1** (2.17 Å), however these values are considerably longer compared with the reported nickel-oxygen distances of carboxylate complexes.[23] These results show that the coordinate bond between the nickel and the hydroxyl groups is comparatively weak. In this structure analysis the coordinates of all hydrogen atoms of the complex cation were refined by least squares methods. The average oxygen-hydrogen bond distance of the coordinated hydroxyl groups is 0.76(4) Å, which is shorter than that of free hydroxyl groups (0.88(4) Å). The average angle around the coordinated oxygen atoms is 114(2)°. As mentioned above, the coordination structure of the hydroxyl groups to the nickel ion is revealed. This is one of the important results of this structure analysis, since the orientation of hydroxyl groups can not be estimated by geometric considerations. This is a rare sample to clarify the coordination geometry of hydroxyl groups to the nickel ion.

The unit cell contains four complex cations, eight Cl^- anions and two methanol molecules of solvation. The carbon atom of this methanol molecule is located at a special position on the twofold axis, so that the oxygen atom of this methanol is disordered to two positions, each of which has a population of 0.5. The stereoview of the unit cell is shown in Fig. 5. Hydrogen bonds of the type O-H···Cl and N-H···Cl probably exist between O(4)···Cl(2), O(5)···Cl(2), N(1)···Cl(1), and N(3)···Cl(1). Since the interatomic distance of O(3)···O(4) between two molecules is short (2.68 Å), they are probably linked by hydrogen bonding. The hydrogen bonding distances are listed in Table 5.

Circular Dichroism. In the octahedral ligand field, only the lowest energy transition $^3A_{2g} \rightarrow {}^3T_{2g}$ is magnetic dipole allowed in the case of nickel(II) com-

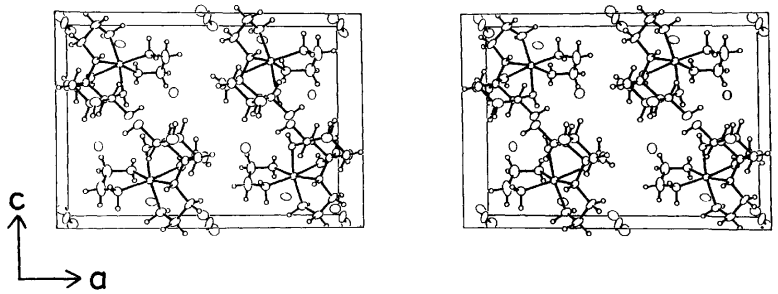

Fig. 5. A stereo view of the unit cell.

TABLE 5. INTERATOMIC DISTANCES<3.5 Å OUTSIDE THE COMPLEX CATION AND ESTIMATED STANDARD DEVIATIONS: A-H···B

Atom A	Atom B	A-H Distance l/Å	A···B Distance l/Å	Symmetry of Atom B
O(4)	Cl(2)	0.90(5)	3.032(2)	x, y, z
O(5)	Cl(2)	0.86(3)	2.980(3)	$1.5-x$, $-0.5+y$, $1-z$
O(3)	O(4)	0.90(5)	2.678(4)	$1.5-x$, $0.5+y$, $1-z$
N(3)	Cl(1)	0.88(4)	3.275(3)	$1.5-x$, $-0.5+y$, $1-z$
N(3)	Cl(1)	0.93(5)	3.316(3)	$1.5-x$, $-0.5+y$, $1-z$

plex. The two higher energy spin allowed transitions are magnetic dipole forbidden and are expected for CD bands significantly weaker than the allowed transitions. It is often observed that the CD pattern of the first transition band is too much influenced by stereochemical features of dissymmetric nickel(II) complexes.[25] The CD spectra of $[Ni(en)(D\text{-fru-en})]^{2+}$ and $[Ni(en)(L\text{-sor-en})]^{2+}$ in methanol are shown in Fig. 2. They have CD curves of opposite sign in the first absorption region. The X-ray crystal structure analysis for both the complexes revealed that the structure of the two complex cations are similar except for the orientation of each C-5 atom and the conformation of each bidentate ethylenediamine. In this case the contributions of these stereochemical differences mentioned above can be ruled out, since each C-5 atom is far from the central metal atom to effect the circular dichroism in the d-d bands, and an ethylenediamine chelate makes a rapid interconversion between δ and λ in solution. Therefore it is an unusual fact that the CD curves of the complexes are dissimilar. On the other hand it is interesting to note that their CD spectra are nearly identical in the second and third absorption region. These results indicate that detailed stereochemical examinations using many kinds of diamines and ketoses are necessary to establish the relationships between the structure of the complexes and their CD spectra.

The results obtained in this study revealed that L-sorbose reacts with $[Ni(en)_3]^{2+}$ to yield the octahedral nickel(II) complex which is surrounded with a bidentate ethylenediamine and a tetradentate *N*-glycoside. The X-ray crystallographic study of this complex revealed the coordination structures of hydroxyl groups to the nickel atom. The results of the crystal structure of $[Ni(en)(D\text{-fru-en})]Cl_2 \cdot CH_3OH$[9] and $[Ni(en)(L\text{-sor-en})]Cl_2 \cdot 1/2CH_3OH$ confirmed that the coordination geometry of these complexes is almost the same, and that the coordination pattern of an *N*-glycoside ligand derived from a ketose and a diamine depends on the orientation of the C-3 hydroxyl groups of the sugar. Unusual features were observed in the CD spectra of these complexes.

The authors wish to thank Prof. Kozo Sone and Dr. Yutaka Fukuda of Ochanomizu University for help in obtaining the magnetic data. The present work was partially supported by a Grant-in-aid for Scientific Research (No. 58540380) from the ministry of Education, Science and Culture.

References

1) M. Miyazaki, S. Nishimura, A. Yoshida, and N. Okubo, *Chem. Pharm. Bull.*, **27**, 532 (1979).
2) S. J. Angyal and J. A. Mills, *Aust. J. Chem.*, **32**, 1993 (1979).
3) W. Voelter, G. Kuhfittig, G. Schneider, and E. Bayer, *Liebigs Ann. Chem.*, **734**, 126 (1970).
4) S. Hanessian and G. Patil, *Tetrahedron Lett.*, **1978**, 1031.
5) Y. H. Chao and D. R. Kearns, *J. Am. Chem. Soc.*, **99**, 6425 (1977); M. J. Adam and L. D. Hall, *Can. J. Chem.*, **60**, 2229 (1982).
6) J. Briggs, P. Finch, M. C. Matulewicz, and H. Weigel, *Carbohydr. Res.*, **97**, 181 (1981).
7) S. J. Angyal, *Chem. Soc. Rev.*, **9**, 415 (1980).
8) For example; J. F. Conn, J. J. Kim, F. L. Suddath, P. Blattman, and A. Rich, *J. Am. Chem. Soc.*, **96**, 7152 (1974); G. E. Tailor and J. M. Waters, *Tetrahedron Lett.*, **22**, 1277 (1981).
9) S. Takizawa, H. Sugita, S. Yano, and S. Yoshikawa, *J. Am. Chem. Soc.*, **102**, 7969 (1980).
10) H. Shioi, S. Yano, K. Toriumi, T. Ito, and S. Yoshikawa, *J. Chem. Soc. Chem. Comm.*, **1983** 201.
11) T. Tsubomura, S. Yano, K. Toriumi, T. Ito, and S. Yoshikawa *Polyhedron*, **2**, 123 (1983).
12) A. Werner, *Z. Anorg. Chem.*, **21**, 210 (1899).
13) "Landolt-Boernstein Tabellen," Neue Serie, Springer-Verlag (1966), II Band, 2 Teil.
14) T. Sakurai and K. Kobayashi, *Rikagaku Kenkyusho*

Hokoku, **55**, 69 (1979).
15) For Ni, Cl, O, N, C atoms, "International Tables for X-ray Crystallography," Kynoch press, Birmingham, England (1962), Vol. III, pp. 270—276; for H atoms, R. F. Stewart, E. R. Davidson, and W. T. Simpson *J. Chem. Phys.*, **42**, 3175 (1965).
16) D. T. Cromer, *Acta. Crystallogr.*, **18**, 17 (1965).
17) C. P. Barry and J. Haneyman, *J. Chem. Soc.*, **1952**, 4147.
18) F. A. Cotton and G. Wilkinson, "Advanced Inorganic Chemistry 4th. Ed.," John Wiley Sons, New York (1980), p. 787.
19) L. Sacconi, *Transition Metal Chem. Ser. Advan.*, **4**, 199 (1968).
20) C. K. Johnson, "ORTEPII," USAEC Report ORNL-3794, Oak Ridge National Laboratory, Tennessee 1971.
21) A. S. Perlin, P. Herve Du Penhoat, and H. S. Isbell, "Carbohydrates in Solution," ed by H. S. Isbell, ACS Advances in Chemistry Series 117, American Chemical Society, Washington (1973), p. 40.
22) S. H. Kim and R. D. Rosenstein, *Acta. Crystallogr.*, **22**, 648 (1967).
23) C. F. Campana, D. F. Shepard, and W. M. Litchman, *Inorg. Chem.*, **20**, 4039 (1981).
24) For example; Y. Saito, "Inorganic Molecular Dissymmetry," Springer-Verlag, Berlin (1979), Chap. 4.
25) S. Kitagawa, T. Murakami, and M. Hatano, *Inorg. Chem.*, **14**, 2347 (1975); M. J. Harding, S. F. Mason, and B. J. Peart, *J. Chem. Soc. Dalton*, **1973**, 955.

Inductively Coupled Plasma Atomic Emission Spectrometry Utilizing a Direct Graphite Cup Insertion Technique

Hiroki HARAGUCHI,* Mohammad ABDULLAH, Tetsuya HASEGAWA, Masao KUROSAWA, and Keiichiro FUWA

Department of Chemistry, Faculty of Science, The University of Tokyo, Hongo, Bunkyo-ku, Tokyo 113

(Received January 18, 1984)

A preliminary study on analytical performances of graphite sample cups is described for an instrumental assembly to carry out microliter volumes of liquid sample analysis. The graphite cup with a graphite rod and an insulating handle is inserted axially *via* the injector tube of a quartz torch into a low power operated inductively coupled argon plasma. Univariate search method has been employed for optimization of cup size, rod height and plasma operating parameters for manganese ionic line at 257.6 nm to obtain the most favorable net signal-to-background ratio. Detection limits, reproducibilities and dynamic ranges are also reported for manganese, zinc, lead, chromium, and nickel in solution.

In addition to conventional pneumatic nebulization, sample introduction into an inductively coupled plasma (ICP) for atomic emission spectrometry has been concerned with external vaporization using electrothermal heating,[1,2] spark excitation,[3] or laser ablation.[4] In these introduction techniques, the generated aerosol is transported into the plasma with a stream of the carrier gas.

Recently, Salin and Horlick[5] described a method in which samples were introduced directly into a 2.5 kW argon ICP using a graphite electrode inserted axially *via* the injector tube of a Fassel type torch. In their experiments, the plasma had to be ignited and extinguished on each insertion. Continuous operation of the plasma was achieved by Sommer and Ohls[6] who inserted samples into a Greenfield type torch supporting an argon-nitrogen ICP at a continuous RF power of 3 kW. Kirkbright and Walton[7] as well as Kirkbright and Zhang Li-Xing[8] were also able to introduce sample solutions into a low power (<1.5 kW), continuously running argon ICP supported on a demountable torch described by Bombelka.[9] Kirk-bright and his coworkers used an axial flat-ended graphite rod onto which only 5 μl of sample solution could be applied with a micropipet.

The present study reports an attempt to develop a technique for direct insertion of the graphite cup into a continuously running argon ICP with low power *via* the injector tube of a quartz torch. In these experiments, the graphite rod with graphite sample cup into which 10 μl of sample solution can be applied with a micropipet are designed to overcome the limitations encountered by the previous papers.[5-8]

Experimental

Chemicals and Materials. All standard solutions for calibration curves were prepared by diluting the standard stock solutions (1000 μg/ml) of the respective elements with 1% nitric acid. The sample solution (5—10 μl) was transferred in the graphite sample cup with a micropipet, and dried by an IR lamp prior to its insertion into the plasma.

The graphite rods (Tokai H. P. G. Spectroscopic Electrodes) were obtained from Tokai Carbon Co., Ltd., and the graphite sample cups and graphite rods of required dimensions were constructed in our laboratory. The graphite cup was burnt 5 times in the plasma to minimize the impurity levels prior to analyte vaporization. One graphite cup was available more than 20 times for sample insertion into the plasma.

Instrumentation. An ICP atomic emission spectrometer (Model Plasma Atomcomp Mk II) and a standard quartz torch from Jarrell-Ash Co. were used in our experiments. The instrumental components and operating conditions are summarized in Table 1. The central injector tube of the ICP quartz torch with 20 mm o. d. was replaced with a 3.7 mm i. d. quartz tube, which had no constriction at the tip. The torch was supported with a magnetic stand and a clamp.

The schematic diagram of the torch assembly is shown in Fig. 1. The insertion device consisted of a graphite sample cup with a graphite rod and a Teflon insulating handle, all of which were of 3.3 mm o.d. The inner diameter and the depth of the graphite cup were 2.5 mm and 2 mm, respectively. An adjustable Teflon stopper, which was equipped at the bottom end of the Teflon insulating handle, controlled the final position of the cup in the plasma.

Both of the polychromator (Paschen-Runge type) and the monochromator (Ebert type) were available for the emission

Table 1. Instrumentations and operating conditions

ICP spectrometer	Jarrell-Ash model Plasma Atomcomp Mk II
RF generator	Plasma Therm Inc. model HFP 2000 D
Frequency	27.12 MHz
Max output power	2.0 kW
Polychromator	Paschen-Runge type (75 cm focal length)
Grating	2400 grooves/mm
Reciprocal linear dispersion	0.54 nm/mm at 270 nm
Entrance slit width	25 μm
Exit slit width	50 μm (Na & K 100 μm)
Monochromator	Jarrell-Ash model 82-00 Ebert type (50 cm focal length)
Amplifier	Keithley model 472
High voltage power supply	Hamamatsu Photonics model HTV-C665
Multipen Recorder	Rikadenki model R-10.

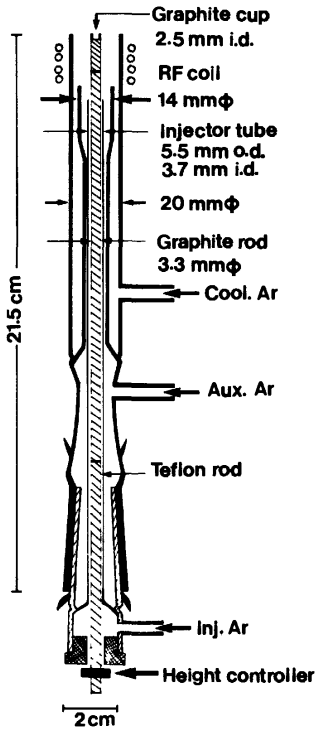

Fig. 1. A schematic diagram of the plasma torch assembly for direct graphite cup insertion device.

signal detection. The analog signal measurements were performed by using a dc amplifier (Model 472 from Keithley) and a strip chart recorder.

Procedure. For simplicity of the experimental procedure, no carrier argon gas was used in the injector tube. The plasma was ignited well with closing the bottom of the injector tube. When the plasma was ignited, the flow rate of the auxiliary argon gas was initially about 1 l/min, and then it was increased at the optimum flow rate of 1.4 l/min. Under these conditions, the plasma was kept sustained even when the graphite sample cup was inserted and taken out, although Salin and Horlick extinguished the plasma during the sample cup operation. Thereafter the plasma could be sustained with the injector tube of the open bottom.

The sample solution of 5—10 μl was applied in the graphite sample cup and dried with an IR lamp prior to insertion. The sample cup assembled with the graphite rod and insulating handle was manually raised through the injector tube until it was fixed at the final position in the plasma. A spark-like discharge occurred momentarily near the load coil when the graphite sample cup was inserted along the injector tube. No change of background signal level was observed at this time. Immediately after the graphite sample cup was inserted into the plasma, the brightness of the plasma decreased. This may be due to the coupling change of RF power with the graphite cup, *i.e*, matching shift of RF power, which was accompanied by significant baseline drift on the recorder. The cup was held in the plasma for 30 s, and after a few seconds the emission signal of the element was observed.

Results and Discussion

Optimization of Experimental Parameters and Conditions. After the preliminary operating conditions of the ICP instrument and the graphite cup insertion device were examined, the following experimental conditions for the ICP-AES measurements were optimized

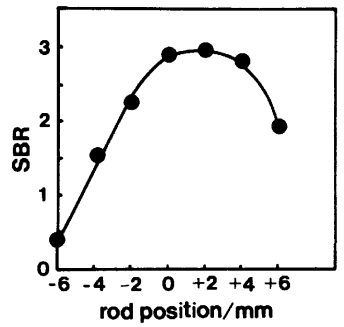

Fig. 2. Optimization of rod position in the plasma relative to the top of the load coil. Power 1.09 kW, observation height 16 mm, coolant argon flow rate 19 l/min, auxiliary argon flow rate 2 l/min, lateral viewing position plasma central channel.

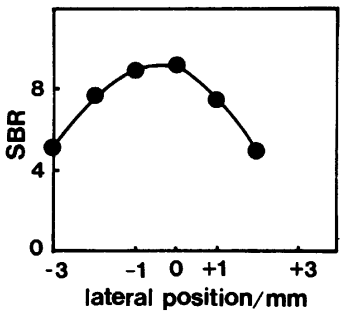

Fig. 3. Variation of net SBR with lateral viewing position of the plasma. Rod position 2 mm above the load coil, power 1.09 kW, observation height 16 mm, coolant argon flow rate 19 l/min, auxiliary argon flow rate 2 l/min.

by using an univariate search method; cup position relative to the top of the load coil, depth of the recess in the graphite cups, RF power, observation height above the load coil, viewing position in the plasma, and flow rates of coolant and auxiliary argon gases. According to the univariate search method, the experimental conditions are optimized by obtaining the maximum signal-to-background ratio (SBR) when one variable is change at a time. Net SBR for manganese ionic line at 257.6 nm obtained from the recorder signals were taken as response. In the following experiments, 5 μl aliquot of 50 ng/ml manganese solution is applied on the graphite sample cup, if no statement is given.

The rod position (from the bottom of the cup) relative to the top of the load coil was optimized under the operating conditions of RF power 1.09 kW, observation height 16 mm, coolant argon flow rate 19 l/min, and auxiliary argon flow rate 2 l/min. The graphite cups used were 1 mm in depth. The optimum rod (cup) height for best SBR was found to be 2 mm (Fig. 2) above the load coil. Under the same operating conditions, a lateral scan was carried out at a rod height of 2 mm to ensure the observation area of the plasma tail flame. The result is shown in Fig. 3. The region of best SBR was almost near the plasma central channel.

Effect of depth in the graphite sample cups on SBR at a rod height of 2 mm is shown in Fig. 4. In the experi-

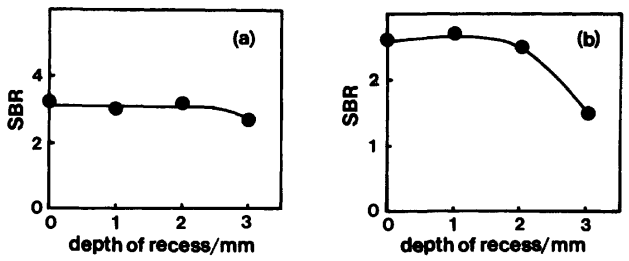

Fig. 4 a) Variation of net SBR with depth of recess in graphite sample cups (rod height was taken from the bottom of the cup). b) Variation of net SBR with depth of recess in graphite sample cups (rod height was taken from the top rim of the cup). Rod position 2 mm above the load coil, power 1.09 kW, observation height 16 mm, coolant argon flow rate 19 l/min, auxiliary argon flow rate 2 l/min, lateral viewing position plasma central channel.

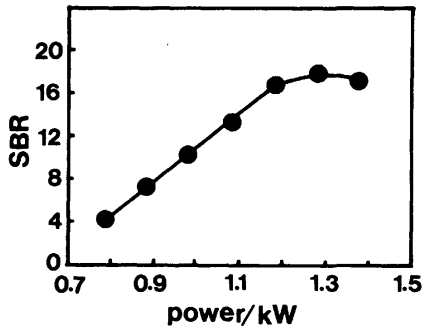

Fig. 5. Univariate search for power of operation. Rod position 2 mm, observation height 16 mm, lateral position plasma central channel, coolant argon flow rate 19 l/min, auxiliary argon flow rate 2 l/min.

ments, the cups of different depths were used, and the rod height of 2 mm was maintained in two different ways: The first one was taken from the bottom of the cup relative to the top of the load coil (Fig. 4a), in which SBR was almost constant up to 2 mm depth in the cup. The second one was taken from the top rim of the cup relative to the top of the load coil (Fig. 4b), in which SBR gradually decreased with increasing the depths of the cups. Consequently, the graphite cup of 2 mm depth was used in the subsequent experiments. Ten μl of solution can be also applied to this cup.

For optimization of RF power (Fig. 5), it was necessary to stabilize the system at least for 30 min after each increase of RF power. Here RF power was defined as "the forward power minus the reflected power." As for RF power, the optimun power of operation for the best SBR appeared to be 1.18 kW.

Effect of observation height above the load coil on SBR of manganese ionic line at 257.6 nm is shown in Fig. 6. It was clearly observed that the optimum observation height was 16 mm above the load coil.

The flow rates of coolant and auxiliary argon gases were also optimized, and they were 18 l/min and 2 l/min, respectively. These gas flow rates provided little effect on SBR compared to other plasma operating parameters. It should be noted that in the present system continuous operation of the plasma with the

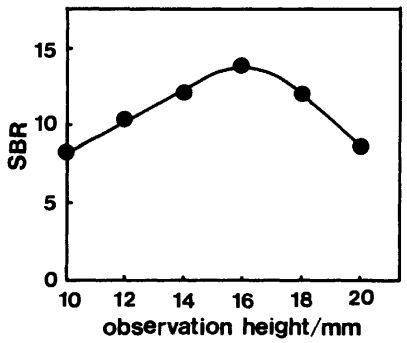

Fig. 6. Univariate search for optimum observation height above the load coil. Rod position 2 mm, power 1.18 kW, coolant argon flow rate 19 l/min, auxiliary argon flow rate 2 l/min, lateral position plasma central channel.

Table 2. Optimum operating conditions for ICP-AES utilizing direct graphite cup insertion technique

Graphite sample cup	Inner diameter 2.5 mm depth 2 mm
Rod position in the plasma	4 mm above load coil
RF Power	0.9 kW
Observation height	16 mm above load coil
Lateral viewing position	Plasma center
Coolant Ar-flow rate	17 l/min
Auxiliary Ar-flow rate	1.4 l/min.

injector tube of opened bottom required the coolant argon gas flow rate more than 15 l/min, and the auxiliary argon gas flow rate more than 1.4 l/min.

The optimum operating conditions for the best SBR obtained for manganese ionic line at 257.6 nm after 5 times repeats of the optimization procedure cycle are summarized in Table 2. Precise establishment of optimum plasma operating conditions by univariate search method is rather difficult because of the interdependent and complex plasma parameter variables. So the optimum operating conditions shown in Table 2 are the compromized ones among all the variables examined for stable operation of the plasma with the injector tube of open bottom.

Time-dependent Signal Profile. Under the optimum operating conditions shown in Table 2, some typical time-dependent emission signal profiles, obtained with 10 μl aliquot of each element utilizing the direct graphite cup insertion technique are shown in Figs.7 and 8. As can be seen in these figures, immediately after insertion of the graphite cup into the plasma, large baseline drift occurred with Pb, Cr, and Ni, while as for Mn and Zn the baseline drift was not so significant. The baseline drift and the emission signal peak are well separated for all the elements studied. In addition, after insertion of the cup into the plasma, the elements are completely vaporized within 10 s with an exception of Zn an Pb which complete vaporization within 4 s.

Durability of Graphite Cup. A single graphite cup could be used up to 20 times of insertion into the

plasma without deteriorating the emission intensity of the analyte. After then the emission intensity (peak height as well as integrated intensity) was gradually decreased with repeated use of the cup, and diffusion of analyte vapor took place through the side wall of the porous graphite cup, resulting in lower emission intensity. Due to this short durability of the graphite cup, multicups were used throughout the experiments.

Detection Limits, Reproducibilities and Linear Dynamic Ranges. Although the system was optimized for manganese ionic line at 257.6 nm, detection limits, relative standard deviations (RSDs) and linear dynamic ranges were evaluated for manganese, zinc, lead, chromium, and nickel with each of the elements in 1% nitric acid solution by using multicups under the same operating conditions. The results are summarized in Table 3. In the experiments, ten integrated signals (each 10 s integration) were measured for each of these elements using 10 μl aliquot of the analyte (50 ng/ml) with the detection system of a polychromator. Corresponding ten integrated background signals were also measured for 1% nitric acid as a blank. The detection limit was then calculated as the concentration of the analyte which was equivalent to three times of the standard deviation(3σ) of the background signals. RSD is expressed in percent. The linear dynamic ranges obtained were linear over the concentration range of 4.0—5.7 orders of magnitude. The detection limits and RSD from peak height measurement are also presented in the same table. As can be seen from Table 3, the detection limits obtained are comparable to those reported by Kirkbright *et al.*[7,8]

Conclusion

The sensitivity, precision and linear dynamic ranges obtained by ICP-AES utilizing direct graphite cup insertion technique are comparable to those obtained

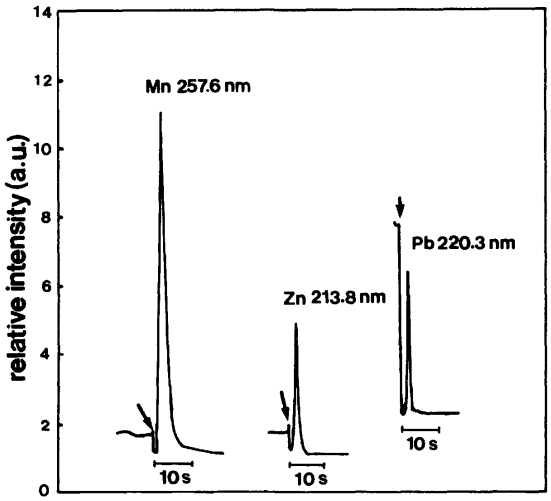

Fig. 7. Time-dependent emission signal profiles obtained for 0.1 μg/ml of manganese, zinc, and lead by ICP-AES utilizing direct graphite cup insertion technique. The arrow lines indicate insertion of the cup into the plasma.

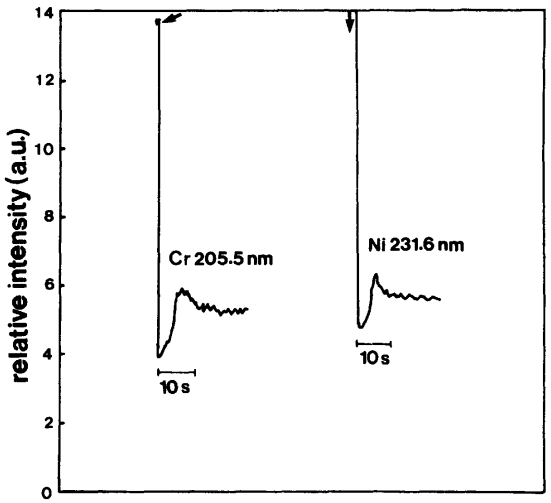

Fig. 8. Time-dependent emission signal profiles obtained for 0.1 μg/ml of chromium, and nickel by ICP-AES utilizing direct graphite cup insertion technique. The arrow lines indicate insertion of the cup into the plasma.

Table 3. Detection limits, relative standard deviations and linear dynamic ranges obtained by ICP-AES utilizing the direct graphite cup insertion technique

Element	Wavelength[a] (nm)	Detection limit (3σ) concentration (ng/ml)	Detection limit (3σ) absolute amount (pg)	RSD[c] (%)	log(LDR)[d]	Detection limit (2σ)[e] (ng/ml)
Mn	257.6 II	0.84	8.4	4.1	5.0	—
		0.40[b]	4.0[b]	11.0[b]		1.2[b]
Zn	213.8 I×2	18.0	180	15.4	4.0	
		1.8[b]	18.0[b]	13.0[b]		0.7[b]
Pb	220.3 II	5.8	58.0	6.0	4.7	
		10.5[b]	105[b]	18.0[b]		7.0[b]
Cr	205.5 II×2	9.7	97.0	6.4	5.7	4.8[b]
Ni	231.6 II×2	14.8	148	12.0	5.7	12.7[b]

a) I and II indicate the atomic and ionic lines, respectively, and (×2) shows the use of the second order lines. b) Peak height measurement. c) Relative standard deviation. d) Linear dynamic range in log unit. e) Reported by Kirkbright and Walton[7], and Kirkbright and Zhang Li-Xing.[8]

by any other sample introduction techniques. In addition the system is almost free from the interferences due to variation in sample transport efficiency which is known for sample introduction through tubing by eletrothermal vaporization. Further, the use of a polychromator for signal detection and integration for direct graphite cup insertion technique shows its potential feasibility for multielement analysis of trace elements in small volume liquid samples. Optimization for individual element, use of more sensitive analytical lines, and automation of the rod insertion device using a stepping motor may improve the analytical figures of merit such as the detection limits and precision.

References

1) D. E. Nixon, V. A. Fassel, and R. N. Kniseley, *Anal. Chem.*, **146**, 210 (1974).
2) A. M. Gunn, D. L. Millard, and G. F. Kirkbright, *Analyst*, **103**, 1066 (1978).
3) H. G. C. Human, R. H. Scott, A. R. Oakes, and C. D. West, *Analyst*, **101**, 265 (1976).
4) M. Thompson, J. E. Goulter, and F. Sieper, *Analyst*, **106**, 32 (1981).
5) E. D. Salin, and G. Horlick, *Anal. Chem.*, **51**, 2284 (1979).
6) D. Sommer, and K. Ohls, *Fresenius' Z. Anal. Chem.*, **304**, 97 (1980).
7) G. F. Kirkbright, and S. J. Walton, *Analyst*, **107**, 276 (1982).
8) G. F. Kirkbright, and Zhang Li-Xing, *Analyst*, **107**, 617 (1982).
9) R. Bombelka, Ph. D. Thesis, University of London (1978).

Electrode Kinetics of Viologen Polymers Attached on Graphite Surfaces

Takeo OHSAKA, Hisao YAMAMOTO, Masao KANEKO,† Akira YAMADA,†
Michiko NAKAMURA,†† Setsuko NAKAMURA,†† and Noboru OYAMA*
Department of Applied Chemistry for Resources, Tokyo University of Agriculture and Technology, Koganei, Tokyo 184
†*The Institute of Physical and Chemical Research, Wako-shi, Saitama 351*
††*Department of Chemistry, Japan Women's University, Mejirodai, Bunkyo-ku, Tokyo 112*
(Received January 20, 1984)

A "heterogeneous" electron-transfer process of three kinds of viologen polymers, *i.e.*, *N,N'*-dimethyl-4,4'-bipyridinium (methylviologen, MV)-Nafion®, poly(xylylviologen) (PXV)-poly(*p*-styrenesulfonate) (PSS) and poly(methylviologen) (PMV), in which MV and PXV were electrostatically trapped in Nafion and PSS, respectively, on a basal-plane pyrolytic graphite (BPG) electrode and PMV was directly attached to the BPG electrode surface, was examined by normal pulse voltammetry. The relevant kinetic parameters (*i.e.*, the standard rate constant, k°_{el} and the cathodic transfer coefficient, α) of the electrode reaction and the apparent diffusion coefficients, D_{app}, for the "homogeneous" charge transport within these polymer films were determined at the various surface concentrations ($\Gamma_{MV^{2+}}$ in units of mol cm^{-2}) of viologen dication site. With the PMV and PXV-PSS systems, both k°_{el} and D_{app} were independent of $\Gamma_{MV^{2+}}$, while with the MV-Nafion system both k°_{el} and D_{app} decreased with an increase in $\Gamma_{MV^{2+}}$ under the constant concentration of Nafion. The values of α were independent of $\Gamma_{MV^{2+}}$ and constant (*i.e.*, 0.56, 0.58, and 0.20 for the PMV, MV-Nafion and PXV-PSS systems, respectively).

In a series of papers concerning the "polymer-coated electrodes,"[1-4] we have examined the "heterogeneous" electron-transfer reactions between the electrode and the electroactive species confined to the polymer films on the electrode surfaces as well as the "homogeneous" charge transport process within the polymer films incorporating the electroactive species by means of the normal pulse voltammetry (Scheme 1). It has become apparent that the "heterogeneous" electron-transfer reaction (process I) at the electrode/film interface obeys the conventional Butler-Volmer equation[5] which characterizes the electrode reaction at an uncoated, ordinary electrode in a solution and that the "homogeneous" charge transport process (process II) within the films obeys the Fick's law relations which are the same as those in thin layer electrochemistry[6] except that the polymer film is *ca.* 10^3 thinner than the usual thin layer electrochemical cell. The process II can be treated as a semi-infinite diffusion process when the distance of charge transport δ ($\approx 2(D_{app} \cdot t)^{1/2}$) is smaller than the thickness of the film (ϕ) (D_{app}: the apparent diffusion coefficient for the diffusion-like charge transport process within the film, t: time). Furthermore, from the previous data with respect to the $[Mo(CN)_8]^{4-/3-}$,[1,2] $[Fe(CN)_6]^{4-/3-}$,[3] $[W(CN)_8]^{4-/3-}$ and $[IrCl_6]^{3-/2-}$ [4] incorporated electrostatically into the protonated poly(4-vinylpyridine) (PVP) films and the $[Fe(CN)_5]^{3-/2-}$ [3] coordinated to the unprotonated PVP films, we have also found that the kinetic parameters (*i.e.*, the standard rate constant, k°_{el}, and the transfer coefficient, α) of "heterogeneous" electron transfer reaction and D_{app} depend upon the molar ratio of the incorporated

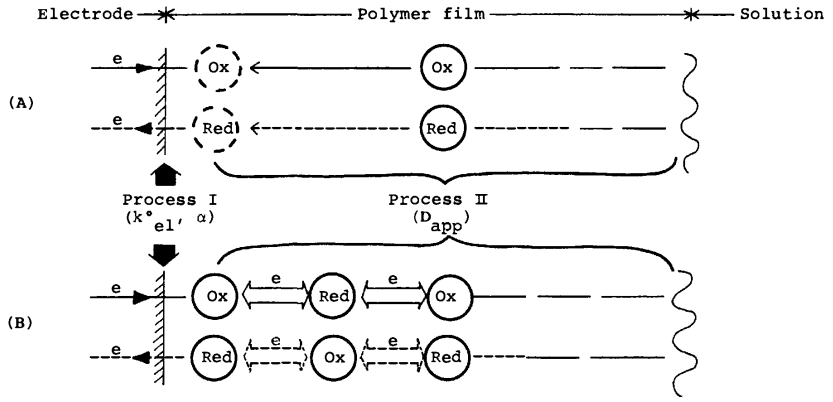

Scheme 1. Schematic depiction of charge transfer process on electrodes coated with polymers containing electroactive species.
Processes I and II represent heterogeneous electron transfer process and homogeneous charge transfer process, respectively. k°_{el} and α are the standard rate constant and the transfer coefficient respectively, of process I. D_{app} is the apparent diffusion coefficient for process II. Overall electrode reaction: (——) reduction, (----) oxidation. Charge can be transported through polymer films *via* (A) physical diffusion of electroactive species itself and (B) electron self-exchange between the redox couples. Note that process II (A and B) is associated with charge-compensating counter ion motion.

electroactive species to pyridine group of PVP. Such a concentration dependence of k°_{el}, α and D_{app} is worthy of remark, since this behavior has been rarely observed in the case of ordinary electrode reaction with an uncoated electrode and the physical diffusion in the solution phase except for special cases.[7-9]

In this paper, we will extend the normal pulse voltammetric study concerning "heterogeneous" electron-transfer reaction and "homogeneous" charge transport process on polymer-coated electrodes for the *N,N'*-dimethyl-4,4'-bipyridinium (methylviologen, MV)-Nafion (perfluorinated ion exchange polymer), poly(xylylviologen) (PXV)-poly(*p*-styrenesulfonate) (PSS) and poly(methylviologen) (PMV) systems. The MV and PXV are electrostatically trapped in the anionic polymer coatings, *i.e.*, Nafion and PSS, respectively, on a basal-plane pyrolytic graphite (BPG) electrode and PMV is directly attached to the BPG electrode surfaces owing to the water insolubility of PMV itself (Fig. 1). In these three systems, the viologen dication group is the common electroactive site. In each system, the dependence of k°_{el}, α and D_{app} upon the concentration of viologen dication site in polymer coatings will be examined and compared with the previous results[1-4] obtained with the highly charged anionic redox species confined in cationic polymer films on electrodes.

Experimental

Materials. *N,N'*-Dimethyl-4,4'-bipyridinium dichloride (methylviologen, $MVCl_2$) (Wako Chemical Co.) was recrystallized twice from methanol-acetone. The polymer pendant methylviologen (PMV) and poly(xylylviologen) (PXV) with average molecular weight 9.8×10^3 and 8×10^3, respectively, were prepared as described elsewhere.[10-13] Nafion membrane 125^R which was obtained from Du Pont de Nemours and Company (Wilmington, DE) was used as an electrode-coating film of polyelectrolyte. The stock solution of Nafion was prepared as described previously[10-13] and the concentration was 2.55 mg ml^{-1}. The preparation of sodium poly(*p*-styrenesulfonate) (PSS) was carried out according to the same procedure as described previously.[13] The average molecular weight of the PSS was 5×10^4. The concentration of styrenesulfonate as PSS was 2.4 mM (1M=1 mol dm^{-3}). The basal-plane pyrolytic graphite (BPG) (Union Carbide Co.) disk electrodes (area: 0.17 cm^2) were prepared and mounted into glass tube with heat-shrinkable polyolefin tube.[14,15] Sodium perchlorate was used as a supporting electrolyte in sample solution (pH 3.4). All other chemicals were reagent grade and were used without further purification.

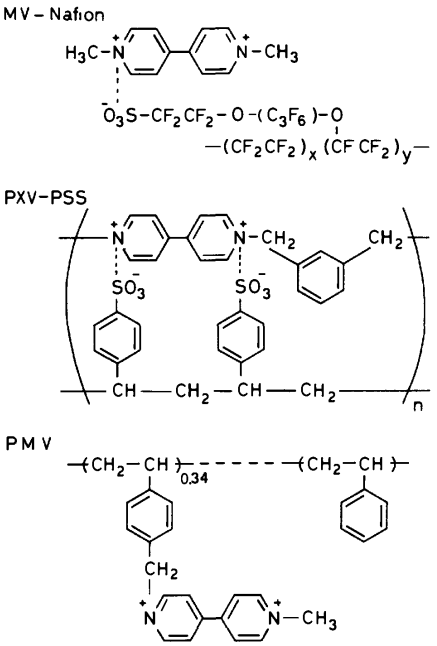

Fig. 1. Structures of the viologen polymers used.

Apparatus and Procedures. Aliquots of the stock solution of Nafion were spread by a microsyringe on the freshly cleaved electrode surface of BPG and then the solvent was evaporated at room temperature. The resulting electrode was soaked in a 0.2 to 10 mM solution of MV for 1 to 60 min in order to achieve the incorporation of desired quantities of MV in Nafion coatings. Adherent coatings of intermolecular complex of PXV and PSS (PXV-PSS) were produced by transferring aliquots (1—6 μl) of an aqueous stock solution containing 1.2 mM of viologen as PXV and of an aqueous stock solution containing 2.4 mM styrenesulfonate as PSS to the surface of a freshly cleaved BPG electrode, mixing them on it, and then evaporating the solvent at room temperature. With PMV film coating, aliquots of methanolic solution containing 3 mM methylviologen as PMV were spread by a microsyringe on the freshly cleaved BPG surface and air-dried to remove methanol. The quantity of the electroactive reactants (*i.e.*, viologen dication) existing in polymer coatings on electrodes was determined by measuring the charge required in a potential-step experiment[15] to quantitatively reduce the dications (MV^{2+}) of MV, PXV of PMV to the corresponding radical monocations (MV^{+}) and/or measuring the area of cyclic voltammograms (for the oxidation-reduction reaction of the $MV^{2+/+}$ redox couple) obtained at slow potential scan rates. The quantity of incorporated reactant estimated by two procedures was the same within an experimental error.

Normal pulse voltammograms were obtained with instruments which were constructed in our laboratory and were recorded with an X-Y recorder (Watanabe Corp.). Positive feedback circuitry was employed to provide as much compensation as possible of the additional resistance (20—80Ω) associated with the polymer coatings. Measurements were confined to times sufficiently short to ensure that semi-infinite linear diffusion prevailed.[1-4,16] Solutions were deaerated with prepurified nitrogen and experiments were conducted at 25 °C. Potentials were measured and are quoted with respect to a sodium chloride saturated calomel electrode (SSCE).

Results and Discussion

Homogeneous Charge Transport Process within the Coatings Incorporating Electroactive Species. A set of normal pulse voltammograms for the reduction of MV^{2+} (to MV^{+}) as PXV-PSS complex or PMV coated on BPG or as MV incorporated into Nafion film on BPG at various sampling times is shown in Fig. 2. The electrode was scanned only over the first of the two reduction waves (*i.e.*, MV^{2+} to MV^{+} and MV^{+} to MV^{0}), because the salt of the PXV-PSS, MV in Nafion and PMV become water soluble when the charge of the viologen is reduced to zero.[13] Thus, the responses observed arise from reduction of the viologen dication

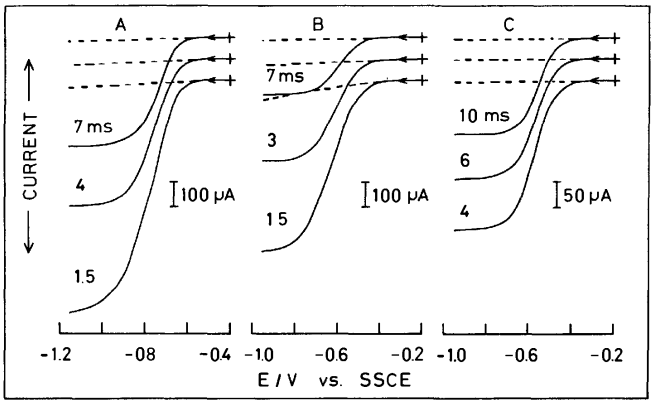

Fig. 2. Typical normal pulse voltammograms for the reduction of viologen dication as (A) MV incorporated into Nafion film on BPG electrodes and (B) PXV-PSS and (C) PMV coated on BPG electrodes at various sampling times in a 0.2 M $NaClO_4$ solution (pH= 3.4). (A): $\Gamma_{MV^{2+}}=9.2\times10^{-9}$ mol cm^{-2}, $\Gamma_{Nafion}=1.5\times10^{-7}$ mol cm^{-2}, (B): $\Gamma_{MV^{2+}}=5.6\times10^{-8}$ mol cm^{-2}, $\Gamma_{PSS}=1.1\times10^{-7}$ mol cm^{-2}, (C): $\Gamma_{MV^{2+}}=7.3\times10^{-9}$ mol cm^{-2}. Sampling times (ms) are given on each voltammogram. Dotted lines show residual current.

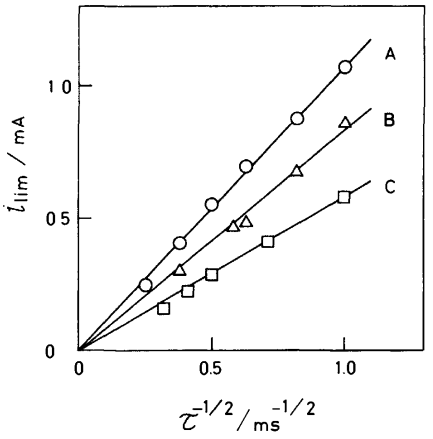

Fig. 3. Plots of limiting current, i_{lim}, *vs.* (sampling time)$^{-1/2}$ for the reduction of viologen dication as (A) MV-Nafion, (B) PXV-PSS, and (C) PMV on BPG electrodes. Other experimental conditions are the same as in Fig. 2.

to the radical cation.

The wave shapes are similar to those observed for solution-phase redox species at an uncoated electrode.[17-19] The half-wave potentials of the first waves obtained with MV-Nafion, PXV-PSS and PMV coated BPG electrodes are observed at −0.74, −0.52, and −0.57 V *vs.* SSCE, respectively at sampling time of 6 ms. This indicates differences in the spatial distribution and the electrostatic interaction of the redox centers and differences in the degree of porosity and hydrophobic nature of the coating film (*i.e.*, changes in the chemical environment of the coating film).[13,20,21] At any rate, the half-wave potential of the normal pulse voltammograms shifted to more positive values with increasing sampling times. Plots of the cathodic limiting current (i_{lim}) of these normal pulse voltammograms against the inverse square root of the sampling time (τ) were found to be linear as expected for the diffusion-controlled limiting current (Fig. 3).[1-4,17-19] Thus, the values of the apparent diffusion coefficients, D_{app}, for the process of the charge transport within the films were obtained from the slopes of the i_{lim} *vs.* $\tau^{-1/2}$ plots by using the Cottrell equation:[22]

$$(i_d)^C_{Cott} = nFAC^\circ\sqrt{D_{app}/\pi\tau} \quad (1)$$

where $(i_d)^C_{Cott}$ denotes the cathodic limiting diffusion current, n the number of electrons involved in the "heterogeneous" electron transfer reaction, F the Faraday constant, A the electrode area and C° the bulk concentration of the redox sites confined in polymeric coatings.

It has been generally recognized that the values of the apparent diffusion coefficients for the charge transport process within the polymeric films depend upon the kind and the concentration of the incorporated redox species, the kind of the film confining the redox species, the kind of the soaking solution, *etc.*[1-4,16,23-32] So far, the three types of dependences of D_{app} on the volume concentration (C°_M in units of mol cm^{-3}) of the incorporated electroactive species in polymeric films, that is, (1) D_{app} decreases with an increase in C°_M,[1-4,16,26-29] (2) D_{app} increases with an increase in C°_M,[29] and (3) D_{app} is independent of C°_M[28,30-32] have been reported and some possible models of the physical meaning of the D_{app} obtained have been ever proposed for the individual cases. In this study, the dependence of D_{app} upon the surface concentration of electroactive sites in polymer films (*i.e.*, $\Gamma_{MV^{2+}}$ in units of mol cm^{-2}) was examined. The results obtained are shown in Fig. 5, together with the dependence of k°_{el} and α upon $\Gamma_{MV^{2+}}$. With PMV and PXV-PSS systems, D_{app} is independent of $\Gamma_{MV^{2+}}$, while with MV-Nafion system D_{app} decreases with increasing $\Gamma_{MV^{2+}}$.

When the "homogeneous" charge transport process within the coatings follows the electron-exchange mechanism which was originally proposed by Kaufman and Engler,[33,34] electrons are removed from MV^{2+} sites that are remote from the BPG electrode by successive electron transfers between neighbor MV^{2+} and MV^{+} sites in the coating. D_{app} will be determined by the process limiting charge transport, which may be the intrinsic electron-transfer rate between adjacent sites, the rate of charge compensating counter ion motion which is necessarily coupled to electron transfer, or the rate of segmental motions of the polymer backbone. Translation of D_{app} into an electron transfer rate constant is of interest. If every "collision" in fact results in electron self-exchange, then the reaction is truly diffusion-controlled, D_{app} represents the diffusion rate, and D_{app} can be converted to an effective electron-transfer rate constant, k^{diff}_{ex}, by using a conventional formula for collision-controlled reaction rates:[4,29,35]

$$k^{diff}_{ex} = \frac{4\pi NRD}{10^3} \quad (2)$$

where N is Avogadro's number, R and D are the sum of the radii and of the diffusion coefficients, respectively, of the reactants. For $D_{app}=1\times10^{-9}$ cm^2

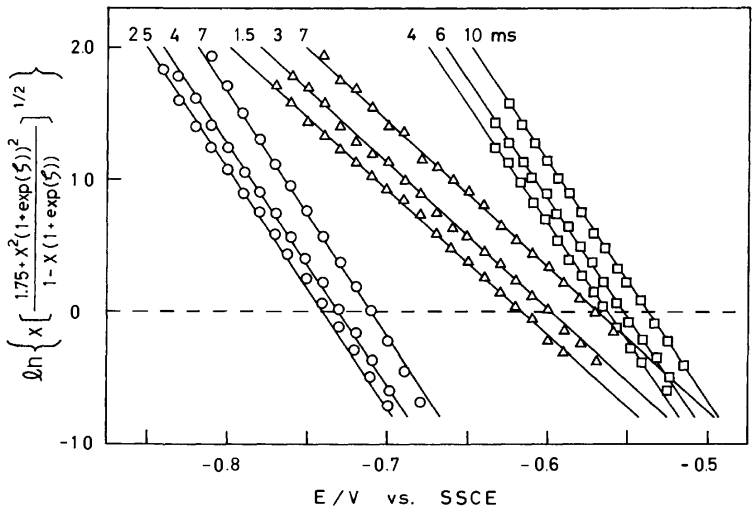

Fig. 4. Modified log plots of normal pulse voltammograms for the reduction of viologen dication as MV-Nafion, PXV-PSS and PMV on BPG electrodes. (○): MV-Nafion, (△): PXV-PSS, (□): PMV. Sampling times (ms) are indicated on each straight line. Other experimental conditions are the same as in Fig. 2.

s^{-1} and R=10Å,[29] with the assumption of $D=2\,D_{app}$, $k_{ex}^{diff}=1.5\times10^{6}\,M^{-1}\,s^{-1}$ which is ~5 times smaller than the self-exchange rate constant of the $MV^{2+/+}$ redox couple ($k_{ex}=8\times10^{6}\,M^{-1}\,s^{-1}$).[36] If we assume that the electron transfer is itself the slow step, then $D_{app}\approx\pi k_{ex}^{act}\,\delta^{2}C/4$ (δ: the distance between the centers of the reactants when the electron transfer occurs, C: the sum of the volume concentrations of the oxidized and reduced forms of the redox couple, k_{ex}^{act}: the second-order self-exchange rate constant for the redox couple).[7,8,28-30,32] In this case, for $D_{app}=1\times10^{-9}\,cm^{2}\,s^{-1}$, δ=10Å[29,32] and $C_{MV^{2+}}=\Gamma_{MV^{2+}}/\phi$ (film thickness)$=1.1\times10^{-4}$ mol cm^{-3}, $k_{ex}^{act}=1.1\times10^{6}\,M^{-1}\,s^{-1}$. This is also smaller than the self-exchange rate constant of the $MV^{2+/+}$ couple.[36] From these calculations, it is likely that the process limiting charge transport may be the rate of charge compensating counter ion motion and/or the rate of segmental motions of the polymer film.[1-4,15,16,23-26,33,34]

Heterogeneous Electron-transfer Reactions between the Electrodes and Electroactive Sites Confined in the Polymer Coatings on Electrode Surfaces. An analysis of the rising part of the current-potential curves shown in Fig. 2 allows us to estimate the kinetic parameters (*i.e.*, the standard rate constant and the cathodic transfer coefficient) of the heterogeneous electron-transfer reaction. The relevant current-potential relationship[1-4,17-19] for normal pulse voltammograms for the simple electrode process, Red⇌Ox+ne, has already been derived and is given for the reduction by

$$E = E_{1/2}^{r} + \frac{RT}{\alpha nF}\ln\left\{\frac{4}{\sqrt{3}}\frac{k^{\circ}_{el}\sqrt{\tau}}{\sqrt{D}}\right\} - \frac{RT}{\alpha nF}\ln\left\{x\left[\frac{1.75+x^{2}(1+\exp(\zeta))^{2}}{1-x(1+\exp(\zeta))}\right]^{1/2}\right\} \qquad (3)$$

where E is the electrode potential, $E_{1/2}^{r}$ the reversible half-wave potential, α the cathodic transfer coefficient, k°_{el} the standard rate constant, τ the sampling time, R the gas constant, T the absolute temperature, ζ the dimensionless parameter expressed as $\{(nF/RT)(E-E_{1/2}^{r})\}$, and D the diffusion coefficient expressed as $\{(D_{app}$(for cathodic process))$^{\alpha}(D_{app}$(for anodic process))$^{1-\alpha}\}$. The x is the ratio of the current at potential E to the cathodic limiting diffusion current, $(i_d)_{Cott}^{C}$, expressed by the Cottrell equation (Eq. 1).

Figure 4 shows the typical examples of the modified log plots of normal pulse voltammograms in which the logarithm of the third term on r.h.s. of Eq. 3 is plotted against E for the reduction of viologen dications to the corresponding radical monocations in polymer coatings. These plots gave the straight lines the slopes of which were constant at the different sampling times ranging from 1 to 10 ms in each system. From the slope of the straight lines shown in Fig. 4 and the intersect of these lines with the zero-line the values of k°_{el} and α were estimated by using the known values of $E_{1/2}^{r}$, D*1, and τ. For doing this, the values of $E_{1/2}^{r}$ were estimated as the average of the anodic and cathodic peak potentials of the cyclic voltammograms for the oxidation-reduction of the $MV^{2+/+}$ redox couple in coatings on BPG electrodes in a solution containing only supporting electrolyte.

Figure 5 shows the dependence of k°_{el} and α upon $\Gamma_{MV^{2+}}$. With the PMV and PXV-PSS systems, the values of k°_{el} were independent of $\Gamma_{MV^{2+}}$ and were $(3.9\pm0.4)\times10^{-5}$ and $(1.1\pm0.3)\times10^{-4}$ cm s^{-1}, respectively. The difference in k°_{el} values may be primarily attributed to the difference in the molecular polymer-structure of PMV and PXV-PSS and their overall film-morphology. On the other hand, with the MV-Nafion system the values of k°_{el} decreased gradually with increasing $\Gamma_{MV^{2+}}$. The similar dependence of k°_{el} upon the concentration of electroactive species in coatings has been previously observed for several other systems (*e.g.*, the $[Mo(CN)_8]^{4-/3-}$, $[Fe(CN)_6]^{4-/3-}$, and $[IrCl_6]^{3-/2-}$ redox couples incorporated into the proto-

*1 With the assumption that D_{app} (for cathodic process)$\approx D_{app}$ (for anodic process), the values of D were estimated as those of D_{app} (for cathodic process).

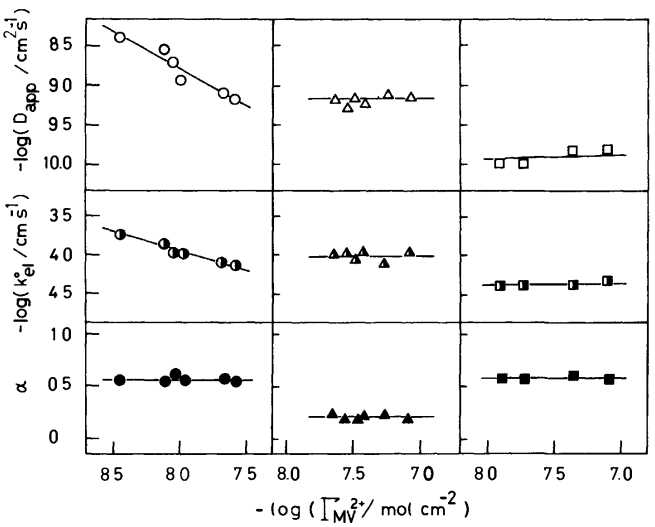

Fig. 5. Dependence of k°_{el}, α and D_{app} upon $\Gamma_{MV^{2+}}$. (○,◑,●): MV-Nafion ($\Gamma_{Nafion}=1.5\times10^{-7}$ mol cm^{-2}), (△,◭,▲,): PXV-PSS ($C_{MV^{2+}}=1.1\times10^{-4}$ mol cm^{-3} and $C_{pss}=2.2\times10^{-4}$ mol cm^{-3}), (□,◨,■): PMV ($C_{MV^{2+}}=1.1\times10^{-4}$ mol cm^{-3}). Other experimental conditions are the same as in Fig. 2.

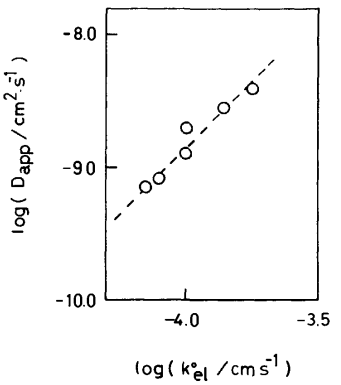

Fig. 6. Linear relationship between log k°_{el} and log D_{app} in the MV-Nafion system. The values of k°_{el} and D_{app} were taken from Fig. 5.

nated poly(4-vinylpyridine) (PVP) film on BPG electrodes.[1-4]

In the case of the PMV and PXV-PSS systems, the volume concentration ($C_{MV^{2+}}$) of MV^{2+} is constant ($C_{MV^{2+}}=1.5\times10^{-4}$ and 1.1×10^{-4} mol cm^{-3} for the PMV and PXV-PSS systems, respectively), because the thickness of the coating film can be assumed to be proportional to the amount of coating on the electrode surfaces. The independence of D_{app} against $\Gamma_{MV^{2+}}$ indicates that the degree of the solvent swelling and the porosity of the coating film, the spatial distribution of the viologen sites and the supporting electrolytic ions, the electrostatic interaction of the viologen sites, *etc.* do not change substantially with the thickness (ϕ) of coatings in the range examined of ϕ (1.9×10^{-4} to 7.5×10^{-4} cm). On the other hand, in the case of the MV-Nafion system, the values of $\Gamma_{MV^{2+}}$ were changed deliberately (see Experimental Section) under the constant amount coated of Nafion ($\Gamma_{Nafion}=1.5\times10^{-7}$ mol cm^{-2}), so that $C_{MV^{2+}}$ increases with an increase in $\Gamma_{MV^{2+}}$. As can readily be seen from the essential ground (*i.e.*, electrostatic interaction[1-4,16,26]) of the incorporation of methylviologen dication (MV) into anionic Nafion film, MV is strongly interacting with its surroundings. As the $\Gamma_{MV^{2+}}$ increases, the degree of electrostatic cross-linking of the film by the dication, *i.e.*, multiple ion pairing of dications with the sulfonyl groups of Nafion becomes to be large. It is thus thought that the free energy required to reorganize the surrounding medium prior to the electron transfer becomes to be large with an increase in $\Gamma_{MV^{2+}}$.[3,4] On the basis of such a consideration, the dependence of k°_{el} on $\Gamma_{MV^{2+}}$ shown in Fig. 5 appears to arise from the change of the solvent reorganization energy by changing $\Gamma_{MV^{2+}}$.

The values of cathodic transfer coefficient (α) were independent of $\Gamma_{MV^{2+}}$ in the systems studied. Note that the values (0.56 and 0.58) of α obtained with PMV and MV-Nafion coated BPG electrodes are almost the same and largely different from that (0.20) obtained with PXV-PSS coated BPG electrode. Such a significant small value of α has been obtained in the PMV system when the polyelectrolyte such as sodium poly(*p*-styrenesulfonate) was used as a supporting electrolyte.[37] Such different α-values may reflect the different reaction positions of the viologen dication sites (*e.g.*, with respect to the outer Helmholtz plane) in the transition state of the electron-transfer reaction and/or the existence of the potential-independent chemical reaction preceding the electron-transfer reaction proper.[4,38-41]

Comparison with Previous Results. As mentioned above, in the MV-Nafion system, the values of both D_{app} and k°_{el} decreased with increasing concentration of viologen dication in Nafion coatings. A similar dependence of both D_{app} and k°_{el} upon the concentration of the incorporated species has been previously observed with the $[Fe(CN)_6]^{4-/3-}$, $[Mo(CN)_8]^{4-/3-}$, and $[IrCl_6]^{3-/2-}$ incorporated into the protonated PVP film coated on BPG electrodes.[1-4] Furthermore, it has been found in these redox systems that there is a linear relationship between log k°_{el} and log D_{app}, even though the theoretical explanation for this relationship has not been given yet. For the MV-Nafion system also, we can see the establishment of this linear relationship (see Fig. 6). Such a linear relationship may suggest that the increase of the concentration of the redox sites (or species) confined in polymer coatings causes an increase in the degree of electrostatic cross-linking[1-4,16,26,42] and/or the electrostatic repulsions[4,43] between the highly charged redox sites (or species) and these result in the decrease in the rates of both heterogeneous electron transfer reaction at the electrode/film interfaces and homogeneous charge transfer process within the coatings. Additional work is required to make this point clearer.

This work was partly supported by the Grant of the Shimadzu Foundation for Science and Technology.

References

1) N. Oyama, K. Sato, S. Yamaguchi, and H. Matsuda,

Denki Kagaku, **51**, 91 (1983).
2) K. Sato, S. Yamaguchi, H. Matsuda, T. Ohsaka, and N. Oyama, *Bull. Chem. Soc. Jpn.*, **56**, 2004 (1983).
3) N. Oyama, T. Ohsaka, M. Kaneko, K. Sato, and H. Matsuda, *J. Am. Chem. Soc.*, **105**, 6003 (1983).
4) N. Oyama, T. Ohsaka, and T. Ushirogouchi, *J. Phys. Chem.*, in press (1984).
5) For example, A. J. Bard and L. R. Faulkner, "Electrochemical Methods, Fundamentals and Applications," Wiley, New York (1980), Chap. 3.
6) D. M. Oglesby, S. H. Omang, and C. N. Reilley, *Anal. Chem.*, **37**, 1312 (1965).
7) I. Ruff, *Electrochimica Acta*, **15**, 1059 (1970).
8) I. Ruff, V. G. Friedrich, K. Demeter, and K. Csillag, *J. Phys. Chem.*, **75**, 3303 (1971).
9) K. Suga, T. Yorifuji, S. Aoyagui, and T. Saji, *Electrochimica Acta*, **27**, 1259 (1982).
10) N. Oyama, S. Yamaguchi, M. Kaneko, and A. Yamada, *J. Electroanal.Chem.*, **139**, 215 (1982).
11) M. Kaneko, A. Yamada, N. Oyama, and S. Yamaguchi, *Makromol. Chem. Rapid Commun.*, **3**, 769 (1982).
12) N. Oyama, T. Ohsaka, K. Sato, and H. Yamamoto, *Anal. Chem.*, **55**, 1429 (1983).
13) N. Oyama, N. Oki, H. Ohno, Y. Ohnuki, H. Matsuda, and E. Tsuchida, *J. Phys. Chem.*, **87**, 3642 (1983).
14) N. Oyama and F. C. Anson, *Anal. Chem.*, **52**, 1192 (1980).
15) N. Oyama and F. C. Anson, *J. Electrochem. Soc.*, **127**, 640 (1980).
16) N. Oyama, S. Yamaguchi, Y. Nishiki, K. Tokuda, H. Matsuda, and F. C. Anson, *J. Electroanal. Chem.*, **139**, 371 (1982).
17) S. Yamaguchi, H. Matsuda, T. Ohsaka, and N. Oyama, *Bull. Chem. Soc. Jpn.*, **56**, 2952 (1983).
18) T. Ohsaka, N. Oyama, S. Yamaguchi, and H. Matsuda, *Bull. Chem. Soc. Jpn.*, **54**, 2475 (1981).
19) H. Matsuda, *Bull. Chem. Soc. Jpn.*, **53**, 3439 (1980).
20) I. Rubinstein and A. J. Bard, *J. Am. Chem. Soc.*, **102**, 6641 (1980).
21) I. Rubinstein and A. J. Bard, *J. Am. Chem. Soc.*, **103**, 5007 (1981).
22) F. G. Cottrell, *Z. Phys. Chem.*, **42**, 385 (1903).
23) A. H. Schroeder, F. B. Kaufman, V. Patel, and E. M. Engler, *J. Electroanal. Chem.*, **113**, 193 (1980).
24) A. H. Schroeder and F. B. Kaufman, *J. Electroanal. Chem.*, **113**, 209 (1980).
25) J. Q. Chambers, F. B. Kaufman, and K. H. Nichols, *J. Electroanal. Chem.*, **142**, 277 (1982).
26) J. Facci and R. W. Murray, *J. Electroanal. Chem.*, **124** 339 (1981).
27) F. C. Anson, T. Ohsaka, and J. M. Savéant, *J. Am. Chem. Soc.*, **105**, 4883 (1983).
28) D. A. Buttry and F. C. Anson, *J. Electroanal. Chem.*, **130**, 333 (1981).
29) D. A. Buttry and F. C. Anson, *J. Am. Chem. Soc.*, **105**, 685 (1983).
30) H. S. White, J. Leddy, and A. J. Bard, *J. Am. Chem. Soc.*, **104**, 4811 (1982).
31) C. R. Martin, I. Rubinstein, and A. J. Bard, *J. Am. Chem. Soc.*, **104**, 4817 (1982).
32) J. Facci and R. W. Murray, *J. Phys. Chem.*, **85**, 2870 (1981).
33) F. B. Kaufman and E. M. Engler, *J. Am. Chem. Soc.*, **101**, 547 (1979).
34) F. B. Kaufman, A. H. Schroeder, E. M. Engler, S. R. Kramer, and J. Q. Chambers, *J. Am. Chem. Soc.*, **102**, 483 (1980).
35) G. G. Hammers, "Principles of Chemical Kinetics," Academic Press, New York (1978), p. 62.
36) C. R. Bock, J. A. Connor, A. R. Gutierrez, J. J. Meyer, D. G. Whitten, B. P. Sullivan, and J. K. Nagle, *Chem. Phys. Lett.*, **61**, 522 (1979).
37) T. Ohsaka, K. Sato, H. Matsuda, and N. Oyama, *J. Electrochem. Soc.*, submitted (1984).
38) A. S. Baranski and W. R. Fawcett, *J. Electroanal. Chem.*, **100**, 185 (1979).
39) A. S. Baranski and W. R. Fawcett, *J. Chem. Soc. Faraday I*, **76**, 1962 (1980).
40) W. R. Fawcett, *J. Electroanal. Chem.*, **22**, 19 (1969).
41) M. J. Weaver, *J. Phys. Chem.*, **83**, 1748 (1979).
42) K-N. Kuo and R. W. Murray, *J. Electroanal. Chem.*, **131**, 37 (1982).
43) K. Shigehara, N. Oyama, and F. C. Anson, *Inorg. Chem.*, **20**, 518 (1981).

 © 1984 The Chemical Society of Japan Bull. Chem. Soc. Jpn., 57, 1850—1855 (1984)

Some Palladium(II) Complexes Containing Both the *O*-Unidentate β-Diketonato and 2-, 3-, or 4-Pyridyl Ligands. Dynamic Behaviors of *trans*-[Pd(β-dik-*O*)-(C_5H_3(6-Cl)N-C^2)(PEt_3)$_2$] in Solution

Hiroshi TANAKA, Kiyoshi ISOBE, Shinichi KAWAGUCHI,* and Seichi OKEYA†
Department of Chemistry, Faculty of Science, Osaka City University, Sumiyoshiku, Osaka 558
†*Faculty of Education, Wakayama University, Fukiage, Wakayama 640*
(Received February 2, 1984)

Palladium(II) complexes of the [Pd(β-dik-*O*)(pyridyl)(PEt_3)$_2$] type containing an *O*-unidentate acetylacetonate, trifluoroacetylacetonate, or hexafluoroacetylacetonate anion and a 2-, 3-, 4-pyridyl or 6-chloro-2-pyridyl group as ligands were prepared and characterized mainly by ^{1}H and ^{13}C NMR spectroscopy. The acetylacetonate and hexafluoroacetylacetonate ligands in the [Pd(β-dik-*O*)(C_5H_3(6-Cl)N-C^2)(PEt_3)$_2$] complexes undergo the head-to-tail donor-atom exchange reaction, to which an intramolecular mechanism is proposed.

In a previous paper[1] a number of palladium(II) complexes containing an *O*,*O*′-chelating β-diketonate anion and a 2-, 3-, or 4-pyridyl group as ligands were prepared and characterized mainly by ^{1}H and ^{13}C NMR spectroscopy. Among these complexes [Pd(acac)-(C_5H_3(6-Cl)N-C^2)(PPh_3)] was found to undergo coordination site exchange catalyzed not only by usual free ligands such as tertiary phosphines, pyridine and its derivatives, but also by various donor solvents. Although the 6-chloro-2-pyridyl complex is stereochemically rigid by itself, the corresponding 2-pyridyl complex [Pd(acac)(C_5H_4N-C^2)(PPh_3)] partially dissociates in solution to liberate triphenylphosphine, which catalyzes the coordination-site exchange reaction of the parent complex, averaging the environments of two methyl groups of the acetylacetonate ligand (autocatalysis). Furthermore molecules of [Pd(acac)(C_5H_4N-C^3 or -C^4)(PPh_3)] were found to catalyze mutually their own coordination-site exchange (self-catalysis).

In the course of this investigation various pyridylpalladium(II) complexes containing an *O*-unidentate β-diketonate anion as a ligand were obtained. This paper reports on the preparation and characterization of these interesting compounds as well as dynamic behaviors of some of them in solution.

Experimental

Preparation of Complexes. The starting complexes [Pd(β-dik)(pyridyl)(PPh_3)] (β-dik=chelating anion of β-diketone (β-dikH) such as acetylacetone (acacH), trifluoroacetylacetone (tfacH), and hexafluoroacetylacetone (hfacH); pyridyl=C_5H_4N-C^2, C_5H_4N-C^3, C_5H_4N-C^4, or C_5H_3(6-Cl)-N-C^2) were prepared according to the methods reported previously.[1] Preparation of [PdBr(pyridyl)(PEt_3)$_2$] was also reported.[2] The present complexes [Pd(β-dik-*O*)(pyridyl)-(PEt_3)$_2$] containing an *O*-unidentate β-diketonate anion were prepared by two methods both in dichloromethane: (A) reactions of [Pd(β-dik)(pyridyl)(PPh_3)] with excess triethylphosphine, and (B) reactions of [PdBr(pyridyl)(PEt_3)$_2$] with Tl(β-dik). Here is described only a favorable method for each complex.

*[Pd(acac-O)(C_5H_4N-C²)(PEt_3)$_2$] (**a1**): (Method A)*; Triethylphosphine (0.087 cm³, 0.596 mmol) was added to a solution of [Pd(acac)(C_5H_4N-C^2)(PPh_3)] (0.109 g, 0.199 mmol) in dichloromethane (5 cm³) and the mixture was stirred at room temperature for 30 min. After concentration to *ca.* 1 cm³ by evaporation under reduced pressure, diethyl ether was added to the concentrate to deposit a white precipitate, which was filtered, washed with the ether and dried *in vacuo*. The product was purified by dissolution in dichloromethane followed by reprecipitation on addition of diethyl ether. The yield was 0.075 g (71.9%).

*[Pd(tfac-O)(C_5H_4N-C²)(PEt_3)$_2$] (**a2**): (Method A)*; Complex **a2** was obtained in a 76.4% yield by the reaction between [Pd(tfac)(C_5H_4N-C^2)(PPh_3)] and PEt_3.

*[Pd(hfac-O)(C_5H_4N-C²)(PEt_3)$_2$](**a3**): (Method B)*; A mixture of [PdBr(C_5H_4N-C^2)(PEt_3)$_2$] (0.309 g, 0.616 mmol) and Tl(hfac) (0.262 g, 0.636 mmol) in dichloromethane (10 cm³) was stirred at room temperature for 50 min. After separation of thallium(I) bromide by filtration, the filtrate was concentrated to *ca.* 1 cm³. On addition of petroleum ether (bp<60 °C) to the concentrate a precipitate appeared, which was filtered, washed with petroleum ether, and dried *in vacuo*. The yield was 0.272 g (68.1%).

*[Pd(acac-O)(C_5H_4N-C³)(PEt_3)$_2$] (**b1**), [Pd(tfac-O)(C_5H_4N-C³)(PEt_3)$_2$] (**b2**), and [Pd(hfac-O)(C_5H_4N-C³)(PEt_3)$_2$] (**b3**)*: These complexes were similarly prepared by methods A, A, and B in 88.5, 88.0, and 37.7% yields, respectively. Complex **b3** is insoluble in usual organic solvents and precludes purification.

*[Pd(acac-O)(C_5H_4N-C⁴)(PEt_3)$_2$] (**c1**), [Pd(tfac-O)(C_5H_4N-C⁴)(PEt_3)$_2$] (**c2**), and [Pd(hfac-O)(C_5H_4N-C⁴)(PEt_3)$_2$] (**c3**)*: Methods A, A, and B gave these complexes in 84.9, 91.9, and 42.6% yields, respectively.

*[Pd(acac-O)(C_5H_3(6-Cl)N-C²)(PEt_3)$_2$] (**d1**), [Pd(tfac-O)(C_5H_3-(6-Cl)N-C²)(PEt_3)$_2$](**d2**), and [Pd(hfac-O)(C_5H_3(6-Cl)N-C²)-(PEt_3)$_2$](**d3**)*: Complexes **d1** and **d2** were obtained by method A in 72.3 and 75.1% yields, respectively, while method B is preferable for compound **d3**. After filtration of thallium(I) chloride produced by the reaction between [PdCl(C_5H_3(6-Cl)N-C^2)PEt_3)$_2$] (0.269 g, 0.549 mmol) and Tl(hfac) (0.248 g, 0.603 mmol) in dichloromethane (10 cm³) at room temperature, the solvent was vaporized *in vacuo* as far as possible. The residual mass was extracted with heptane. On standing the extract deposited a small additional amount of thallium(I) chloride, which was separated by filtration. The solvent was evaporated to dryness and the residue was dried at 50 °C *in vacuo*. The yield of **d3** was 0.261 g (71.8%).

Measurements. Infrared spectra were obtained in Nujol mull on a JASCO DS 701G spectrophotometer. The NMR spectra were recorded with JEOL JNM-MH100 (for ^{1}H) and FX 60Q (for ^{13}C and ^{31}P) spectrometers. Molecular weight was determined by vapor pressure osmometry with an instrument manufactured by Knauer in West Berlin, West Germany.

Results and Discussion

In recent years two of the present authors (S. K. and S. O.) and their coworkers studied extensively the reactions of [M(β-dik)$_2$] (M=Pd and Pt) with a variety of nitrogen bases,[3] tertiary phosphines,[4] and arsines.[4c] Among many kinds of products, some palladium(II) and platinum(II) complexes, [M(β-dik)(β-dik-*O*)L][4a] and [Pt(β-dik-*O*)$_2$L$_2$],[3c,4a] containing the *O*-unidentate β-diketonate ligand were obtained. Kinetics and equilibrium of the reaction between [Pd(tfac)$_2$] and P(*o*-tolyl)$_3$ to form [Pd(tfac)(tfac-*O*){P(*o*-tolyl)$_3$}] (Eq. 1)[5] and the crystal and molecular structure of the product[6] were also reported.

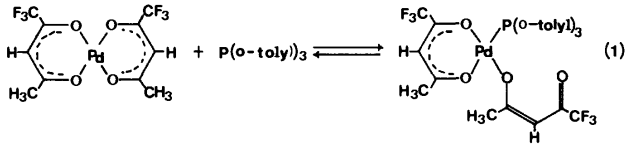

(1)

Now triethylphosphine reacted with [Pd(β-dik)(pyridyl)(PPh$_3$)] to convert the *O*,*O*′-chelated β-dik ligand into the *O*-unidentate state besides displacement of triphenylphosphine (Eq. 2, where R=pyridyl).

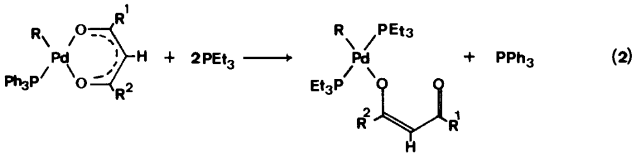

(2)

Although triethylphosphine was used in excess, other products such as [Pd(pyridyl)(PEt$_3$)$_3$](β-dik) and [Pd(pyridyl)(β-dik-*C*^{3})(PEt$_3$)$_2$] were not produced, but only the *O*-unidentate β-diketonato complexes were obtained in good yields. These complexes were also prepared by the reactions of [PdX(pyridyl)(PEt$_3$)$_2$] with Tl(β-dik) (Eq. 3), whereas the corresponding triphenylphosphine complexes [PdX(pyridyl)(PPh$_3$)$_2$] reacted with Tl(β-dik) to afford the β-dik chelates (Eq. 4).

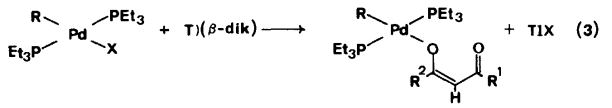

(3)

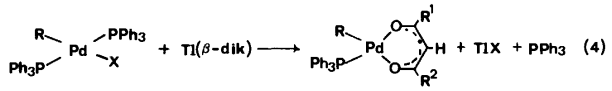

(4)

The Pd-PEt$_3$ bond seems to be stronger than Pd-PPh$_3$ and not cleaved by the intramolecular attack of the dangling carbonyl end of the *O*-unidentate β-diketonate ligand. It is worth noting that the β-diketonate anion is accepted as an *O*-unidentate ligand in the substitution reaction 3 irrespective of the nature of β-diketone (β-dik=acac, tfac, and hfac), whereas the central carbon bonding is prefered in many other reactions such as those exemplified by Eqs. 5[7] and 6 (β-dik=acac, tfac, or hfac).[8]

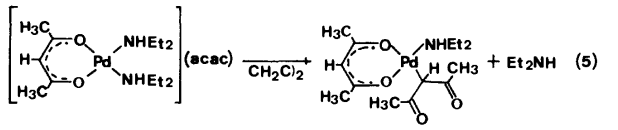

(5)

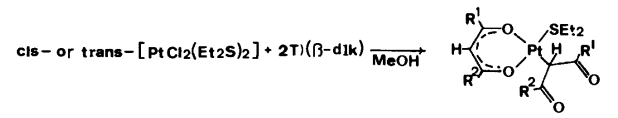

(6)

In the case of reaction 3 the carbon-bonded pyridyl ligand may exert trans influence to favor the *O*-bonding over the *C*-bonding of the β-diketonate anion. The PEt$_3$ ligands positioned mutually trans (*vide infra*) may also exert a steric influence on the entering β-diketonate ligand to favor the less bulky *O*-bonding. Results of elemental analysis and molecular weight determination of the newly prepared complexes are listed in Table 1.

^{1}H and ^{13}C NMR Spectra. The ^{1}H and ^{13}C{^{1}H} NMR data are collected in Tables 2 and 3, respectively. The latter data were obtained only for the 6-

Table 1. Analytical data for complexes [Pd(β-dik-*O*)(pyridyl)(PEt$_3$)$_2$]

No	β-dik	pyridyl	Found (Calcd)			
			C(%)	H(%)	N(%)	Mol wt[a]
a1	acac	C_5H_4N-*C*^{2}	50.44(50.82)	7.90(7.95)	2.71(2.69)	528(519.9)
a2	tfac	C_5H_4N-*C*^{2}	46.07(46.04)	6.62(6.67)	2.42(2.44)	582(573.9)
a3	hfac	C_5H_4N-*C*^{2}	41.50(42.09)	5.54(5.62)	2.24(2.23)	631(627.9)
b1	acac	C_5H_4N-*C*^{3}	50.69(50.82)	7.94(7.95)	2.63(2.69)	533(519.9)
b2	tfac	C_5H_4N-*C*^{3}	45.68(46.04)	6.63(6.67)	2.37(2.44)	589(573.9)
b3	hfac	C_5H_4N-*C*^{3}	41.24(42.09)	5.39(5.62)	2.28(2.23)	b)
c1	acac	C_5H_4N-*C*^{4}	50.87(50.82)	7.91(7.95)	2.72(2.69)	530(519.9)
c2	tfac	C_5H_4N-*C*^{4}	45.74(46.04)	6.54(6.67)	2.41(2.44)	575(573.9)
c3	hfac	C_5H_4N-*C*^{4}	41.37(42.09)	5.49(5.62)	2.23(2.23)	b)
d1	acac	C_5H_3(6-Cl)N-*C*^{2}	47.67(47.67)	7.28(7.27)	2.52(2.53)	550(554.4)
d2	tfac	C_5H_3(6-Cl)N-*C*^{2}	43.46(43.44)	6.12(6.13)	2.29(2.30)	613(608.3)
d3	hfac	C_5H_3(6-Cl)N-*C*^{2}	38.85(39.90)	5.15(5.17)	2.10(2.11)	663(662.3)

a) Determined in dichloromethane at 27 °C. b) Insoluble in organic solvents.

Table 2. ^{1}H NMR data in $CDCl_3$ at room temperature[a)]

Complex	β-dik		Pyridyl	PEt_3	
	CH_3	CH		CH_3	CH_2
a1	2.02, 2.36	5.87	6.68—7.26, 8.48 d	1.09 q	1.36 m
a2	2.43	5.95	6.65—7.36, 8.44 d	1.08 q	1.33 m
a3		5.54	6.65—7.35, 8.45 d	1.08 q	1.35 m
b1	2.01, 2.35	5.82	6.95 dd, 7.57 dd, 8.10 d, 8.50 s	1.10 q	1.37 m
b2	2.45	5.91	7.00 dd, 7.59 dd, 8.15 d, 8.51 s	1.10 q	1.35 m
c1	2.01, 2.34	5.79	7.30 d, 8.06 d	1.11 q	1.40 m
c2	2.45	5.91	7.33 d, 8.09 d	1.10 q	1.40 m
d1	2.03, 2.36	5.84	6.74—7.24	1.12 q	1.40 m
d2	2.42	5.92	6.72—7.20	1.09 q	1.34 m
d3		5.64	6.76 d, 7.04 t, 7.56 d	1.08 br	1.36 br

a) Chemical shifts in ppm from internal Me_4Si. s=singlet, d=doublet, t=triplet, q=1:4:6:4:1 quintet, m=multiplet, br=broad.

Table 3. $^{13}C\{^1H\}$ NMR data for $[Pd(\beta\text{-dik})(C_5H_3(6\text{-Cl})N\text{-}C^2)(PEt_3)_2]$[a)]

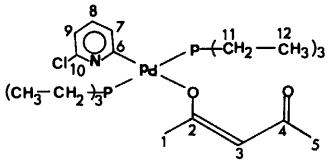

Complex	C (1)	C (2)	C (3)	C (4)	C (5)	C (6)	C (7)	C (8)	C (9)	C(10)	C(11)	C(12)
d1[b)]	25.2	187.5	103.3	192.7	30.5	177.0 (5)	130.7 (6)	134.7	117.2	149.4	13.4 (12)	7.7
d2[b)]	27.3	195.9	96.1	174.2 [23]	119.1 [293]	175.0 (4)	130.6 (7)	135.0	117.6	149.6	13.4 (13)	7.6
d3[b)]	118.5 [289]	174.1 [32]	86.0	174.1 [32]	118.5 [289]	d)	130.4 (4)	134.5	117.4	149.1	13.8 (br)	7.3
d3[c)]	118.2 [290]	174.0 [30]	85.7	174.0 [30]	118.2 [290]	173.9 (4)	131.1 (7)	135.5	117.7	149.4	13.3 (12)	7.5

a) Chemical shifts in ppm from internal Me_4Si. Figures in parentheses and brackets give N(C-P) and J(C-F) in Hz, br=broad. b) Measured in $CDCl_3$ at room temperature. c) Measured in CD_2Cl_2 at −30 °C. d) Indiscernible because of a weak intensity and overlapping with signals from C(2).

chloro-2-pyridyl complexes which are sufficiently soluble in chloroform to allow the ^{13}C NMR measurements. The methyl-proton signal from the PEt_3 ligands in each complex appears as a 1:4:6:4:1 quintet and the methylene protons resonate as a multiplet. This spectral pattern is characteristic of the PEt_3 ligands situated mutually trans.[9)] The methylene carbons of the PEt_3 ligands in each of complexes **d1**, **d2**, and **d3** exhibit a triplet signal owing to coupling to the phosphorus atoms which are situated trans to each other and virtually coupling. In fact the $^{31}P\{^1H\}$ NMR spectra of **d1** and **d2** in $CDCl_3$ and of **d3** in CD_2Cl_2 show a singlet at 11.9, 12.0, and 9.5 ppm, respectively, downfield from external 85% H_3PO_4. The signal from **d3** is broad at room temperature (half-height width *ca.* 7 Hz) and becomes broader at higher temperature (half-height width at 60 °C *ca.* 14 Hz), while it sharpens at lower temperatures (half-height width at −30 °C *ca.* 2 Hz).

Figures 1, 2, and 3 compare the ^1H and $^{13}C\{^1H\}$ signals from the β-diketonate ligands in **d1**, **d2**, and **d3**. Of the two methyl-proton signals from complex **d1**, the lower-field one (δ2.36) is assigned to the methyl adjacent to the coordinated carbonyl group by reference to the data for $[Pt(acac\text{-}O)_2(piperidine)_2]$ which exhibits two methyl signals, one at 2.25 ppm[3c)] and the other flanked by ^{195}Pt satellites at 2.34 ppm.[3c)] The ^{13}C NMR data for the acac ligand in this platinum(II) complex (C^1 23.9, C^2 188.7, C^3 103.3, C^4 196.8, and C^5 30.6 ppm) are quite helpful for assignment of ^{13}C signals from **d1** (Table 3). The ^1H and ^{13}C NMR spectra of the *O*-unidentate tfac in **d2** (Fig. 2) also bear a close resemblance to those of the tfac-*O* ligands in $[Pt(\beta\text{-dik})(tfac\text{-}O)L]$ (β-dik=acac or tfac, L=PPh_3, P(*o*-tolyl)$_3$, or PEt_3), $[Pd(tfac)(tfac\text{-}O)L]$ (L=P(*o*-tolyl)$_3$ or P(cyclohexyl)$_3$), and $[Pt(tfac\text{-}O)_2(PEt_3)_2]$.[4a)]

Head-to-Tail Intramolecular Donor Atom Exchange of the O-Unidentate β-dik Ligands. Although the NMR spectra of **d1** and **d2** are satisfactorily interpreted on the basis that these complexes are stereochemically rigid in solution, complex **d3** shows only one set of signals from CF_3 and CO carbons (Fig. 3), indicating that **d3** is fluxional and the environments of both halves

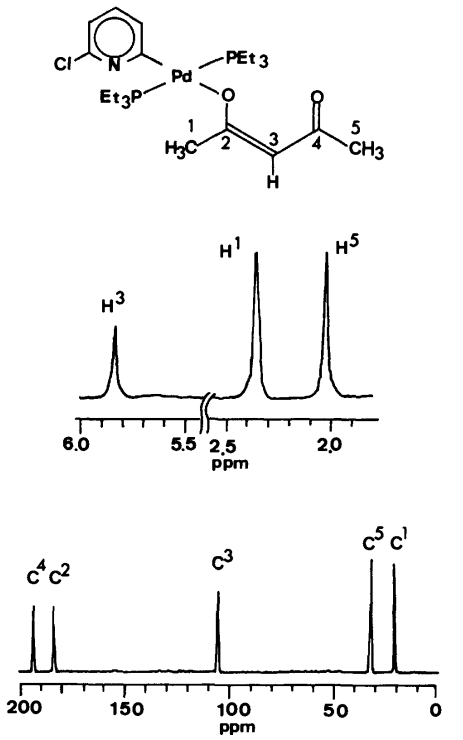

Fig. 1. ^{1}H and $^{13}C\{^{1}H\}$ NMR signals from the acetylacetonate ligand in [Pd(acac-*O*)(C_5H_3(6-Cl)N-*C*^{2})-(PEt_3)$_2$] (**d1**) in $CDCl_3$ at room temperature. Chemical shifts are shown in ppm from internal Me_4Si.

of the *O*-unidentate hfac ligand are averaged rapidly on the NMR time scale. Unfortunately solubility of **d3** in dichloromethane is so poor at lower temperatures as to preclude the spectral determination below −30 °C, but the ^{13}C signals from the hfac-*O* ligand become broader with decreasing temperature and the carbonyl carbon signals show some indication of splitting.

As is seen in Fig. 4, the methyl-proton signals from the acac ligand in **d1** become sharper at 0 °C and broader at 50 °C, suggesting fluxional motion similar to that exhibited by **d3**. Complex **d1** as well as **d3** seems to undergo the head-to-tail intramolecular donor-atom exchange (Eq. 7), since no other change in spectrum is observed in this temperature range.

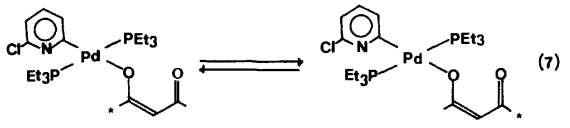

(7)

In order to study the fluxional motion of **d1** at higher temperatures *o*-dichlorobenzene was employed as solvent. A minor methyl signal appeared at 1.92 ppm besides the 2.11 and 2.56 ppm ones in this solvent at room temperature (Fig. 4). The chemical shift of this additional signal corresponds to average of methyl signals (1.90 and 1.94 ppm) of complex **d4**[1)] in Eq. 8. In a previous paper triphenylphosphine was found to be a very effective catalyst for the coordination-site exchange reaction of [Pd(acac)(C_5H_3(6-Cl)N-*C*^{2})(PPh_3)].[1)] Triethylphosphine liberated by the chelate ring closure reaction (Eq. 8) seems to catalyze the coordination-site exchange of **d4**.

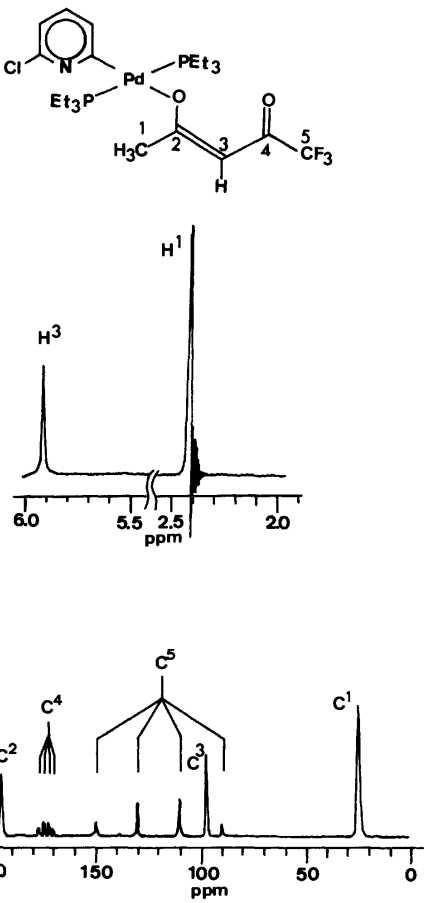

Fig. 2. ^{1}H and $^{13}C\{^{1}H\}$ NMR signals from the trifluoroacetylacetonate ligand in [Pd(tfac-*O*)(C_5H_3-(6-Cl)N-*C*^{2})(PEt_3)$_2$] (**d2**) in $CDCl_3$ at room temperature. Chemical shifts are shown in ppm from internal Me_4Si.

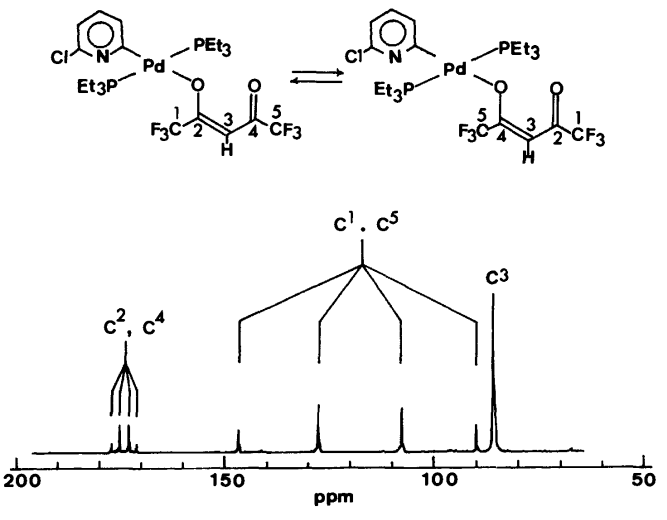

Fig. 3. $^{13}C\{^{1}H\}$ NMR signals from the hexafluoroacetylacetonate ligand in [Pd(hfac-*O*)(C_5H_3(6-Cl)N-*C*^{2})-(PEt_3)$_2$] (**d3**) in $CDCl_3$ at room temperature. Chemical shifts are shown in ppm from internal Me_4Si.

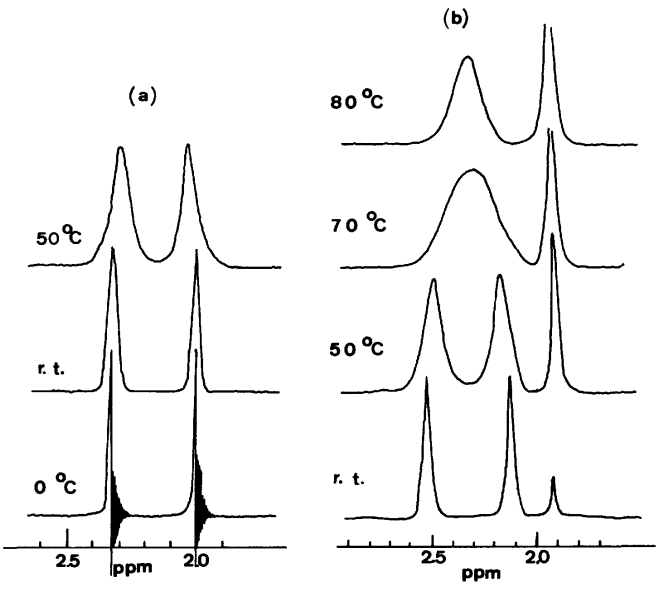

Fig. 4. ^{1}H NMR signals from the acetylacetonate ligand in [Pd(acac-*O*)(C_5H_3(C_5H_3(6-Cl)N-*C*^{2})(PEt_3)$_2$] (**d1**) in $CDCl_3$ (a) and *o*-dichlorobenzene (b) at several temperatures.

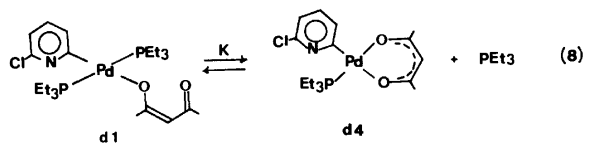

The equilibrium quotient K of reaction 8 was determined from the signal-area ratio to be 7.0×10^{-3} mol dm^{-3} at 33 °C. As is seen in Fig. 4, the δ1.92 signal becomes larger remarkably with temperature, K being 1.7×10^{-2}, 4.5×10^{-2}, 1.0×10^{-1}, and 2.2×10^{-1} mol dm^{-3} at 60, 70, 90, and 120 °C, respectively, and ΔH was obtained as 40.2 kJ mol^{-1}. Reaction 8 does not occur appreciably in chloroform and dichloromethane.

The ^{1}H NMR spectrum of R_3Si(acac-*O*) was found by Pinnavaia and his collaborators to be composed of signals from both cis and trans isomers.[10]

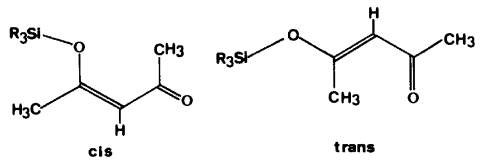

The trans isomer exhibits two methyl doublets and a methine multiplet owing to the spin-spin coupling between the methine and methyl protons, while the cis isomer shows a methyl singlet and a methine singlet without coupling. Equivalence of the two methyl groups in the cis isomer was thought to be caused by the intramolecular rearrangement *via* a trigonal-bipyramidal transition state involving the *O,O'*-chelated acetylacetonate anion.[10]

Complex **d1** shows only one methine singlet and two methyl signals with no sign of coupling indicating that the dangling acetyl group of the acac ligand is positioned cis to the coordinating oxygen atom with respect to the C=C bond. The same structure was also assigned to *trans*-[Pt(acac-*O*)$_2$(PEt_3)$_2$].[11] As is seen in Fig. 4 methyl signals become broader with increasing temperature and collapse at 70 °C. Above 80 °C one broad signal is observed. As a mechanism for the head-to-tail donor-atom exchange of the *O*-unidentate β-diketonate ligand in the present case, a simple oscillatory motion of the β-diketonate ligand spanning the apical and basal coordination sites in the square-pyramidal intermediate (Eq. 9) is proposed.

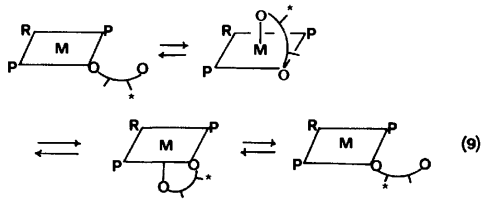

This kind of motion of a potentially bidentate ligand was previously assumed to explain the environmental equivalence of both halves of the essentially unidentate 1,10-phenanthroline in *cis*-[PtCl(phen)(PEt_3)$_2$]BF_4.[12] The X-ray molecular structures and solution behaviors of square-pyramidal complexes [Pt(hfac)$_2$(PCy_3)] and [Pd(hfac)$_2${P(*o*-tolyl)$_3$}] were reported and the oscillatory motion depicted above was proposed as one of the two fluxional modes to average the environments of four CF_3 groups involved in the palladium(II) complex.[13]

Although the hfac anion gives these stable square-pyramidal platinum(II) and palladium(II) complexes in which one hfac anion spans the apical and basal coordination sites, the analogous reaction between [Pd(tfac)$_2$] and P(*o*-tolyl)$_3$ proceeds reversibly to afford [Pd(tfac)(tfac-*O*){P(*o*-tolyl)$_3$}] (Eq. 1), exhibiting no spectral evidence for the five-coordinate intermediate.[5] No examples of square-pyramidal platinum(II) and palladium(II) complexes containing the acac ligand have been obtained either. These results suggest that the five-coordinate square-pyramidal intermediate as postulated in Eq. 9 will be most favorable for the hfac complex. It may be the reason why complex **d3** undergoes the fluxional motion much more readily than **d1** does.

We wish to thank Mr. Junichi Gohda for elemental analyses.

References

1) H. Tanaka, K. Isobe, and S. Kawaguchi, *Chem. Lett.*, **1981**, 769; H. Tanaka, K. Isobe, S. Kawaguchi, and S. Okeya, *Bull. Chem. Soc. Jpn.*, **57**, 456 (1984).

2) K. Isobe, E. Kai, Y. Nakamura, K. Nishimoto, T. Miwa, S. Kawaguchi, K. Kinoshita, and K. Nakatsu, *J. Am. Chem. Soc.*, **102**, 2745 (1980); a full paper will appear in *Bull. Chem. Soc. Jpn.*

3) a) S. Okeya, H. Sazaki, M. Ogita, T. Takemoto, Y. Onuki, Y. Nakamura, B. K. Mohapatra, and S. Kawaguchi, *Bull. Chem. Soc. Jpn.*, **54**, 1978 (1981); b) S. Okeya, H. Yoshimatsu, Y. Nakamura, and S. Kawaguchi, *ibid.*, **55**, 483 (1982); c) S. Okeya, Y. Nakamura, and S. Kawaguchi, *ibid.*, **55**, 1460 (1982).

4) a) S. Okeya, Y. Nakamura, and S. Kawaguchi, *Bull. Chem. Soc. Jpn.*, **54**, 3396 (1981); b) S. Okeya, Y. Nakamura, S. Kawaguchi, and T. Hinomoto, *ibid.*, **55**, 477 (1982). c) S. Okeya, Y. Nakamura, S. Kawaguchi, and T. Hinomoto, *Inorg. Chem.*, **20**, 1576 (1981).

5) S. Matsumoto and S. Kawaguchi, *Bull. Chem. Soc. Jpn.*, **54**, 1704 (1981).

6) S. Ooi, T. Matsushita, K. Nishimoto, Y. Nakamura, S. Kawaguchi, and S. Okeya, *Inorg. Chim. Acta*, **76**, L55 (1983); *Bull. Chem. Soc. Jpn.*, **56**, 3297 (1983).

7) S. Matsumoto and S. Kawaguchi, *Bull. Chem. Soc. Jpn.*, **54**, 150 (1981).

8) F. Sasakura, K. Isobe, and S. kawaguchi, in preparation.

9) W. J. Louw, *Inorg. Chem.*, **9**, 2147 (1977).

10) J. J. Howe and T. J. Pinnavaia, *J. Am. Chem. Soc.*, **91**, 5378 (1969); T. J. Pinnavaia, W. J. Collins, and J. J. Howe, *ibid.*, **92**, 4544 (1970).

11) T. Ito, T. Kiriyama, and A. Yamamoto, *Chem. Lett.*, **1976**, 835.

12) K. R. Dixon, *Inorg. Chem.*, **16**, 2618 (1977).

13) S. Okeya, T. Miyamoto, S. Ooi, Y. Nakamura, and S. Kawaguchi, *Inorg. Chim. Acta*, **45**, L135 (1980); *Bull. Chem. Soc. Jpn.*, **57**, 395 (1984).

 © 1984 The Chemical Society of Japan Bull. Chem. Soc. Jpn., 57, 1856—1858 (1984) [Vol. 57, No. 7

Comparison of the Experimental Zone Mobility-pH Curves of the Bases of Nucleic Acid on the Pure Cellulose Paper with the Calculated Ones[1)]

Yoshinori KITAOKA

Research Reactor Institute, Kyoto University, Kumatori-cho, Sennan-gun, Osaka 590-04

(Received February 2, 1984)

Comparison of the experimental zone mobility-pH curves of nucleic acid bases with the calculated ones was made over acidic and basic regions using a pure cellulose paper as a support after correction of the capillary action and the endoosmotic flow. The mobilities in the acid region agreed with the calculated ones but those in the basic region did not. Some unknown factors affect the mobilities in the basic region.

Paper electrophoretic behavior of weak acids or bases is strongly affected by the pH-value of a supporting solution, which controls the ratios of ionization of a migrant.[2)] Several workers have studied the mobilities and the pH-values of the supporting solution. Smith[3,4)] discussed the relationship between the mobility and the dissociations of amino and phosphonoxy groups of nucleotides. Wade and Morgan[5)] separated nucleoside and bases using a borate buffer. Kiso and coworkers[6)] derived an equation for the relationship between mobility and pH-value and applied it to phosphorus compounds. If we know the mobility of each species and the dissociation constant of a given compound, the zone mobility-pH curves[6)] could be drawn theoretically. However, in the actual electrophoresis using a support, the observed mobilities are affected by electroosmosis, capillary action, and so on of the support in addition to the chemical nature of the supporting solution.[7)] Thus, the good agreement between the observed and the calculated mobilities will be made only under well defined conditions. In this experiment, in order to lessen the chemical effect of a support on the mobility, a pure cellulose paper was used as a support. Although electrophoretic separation at fixed and narrow pH-range has often been reported, this is not so for the electrophoretic behavior over an extended acid and alkaline range in the same experiment. In this experiment, the pH-values were continuously varied over a range of pH=2.0—13 in the same system. The theoretical mobility-pH curves were calculated by a microcomputer.

In this report, we discuss the differences between the observed and the calculated mobilities of nucleic acid bases on pure cellulose paper (A=adenine, G=guanine, T=thymine, U=uracil, and C=cytosine). The observed mobilities of the bases were found to be in good agreement with the calculated ones in the acid region, but not in the alkaline region.

Reagent and Procedures

The procedures and apparatus used were similar to those described previously.[8)] All the nucleic acid bases (A, G, T, U, C) were purchased from Sigma (St. Louis, Mo., U. S. A.). Sørensen's buffer solutions[9)] were used as a supporting solution: citrate buffer; pH=2.0—6.0, phosphate buffer; pH6.0—8.0, glycine buffer; pH=9.0—13.0. A 5 μl volume of sample solution (10^{-2} M (1 M=1 mol dm^{-3})) was spotted at the center of the filter paper (Toyoroshi, No. 51A, pure cellulose paper) wetted with a supporting solution. The spotting paper was immersed in hexane and a constant voltage (1000 V/30 cm) applied to it for 30 min at 20 °C. The position of the bases on the paper was detected by irradiation with ultraviolet light (253 nm). In order to estimate the electroosmotic flow, glucose was migrated under the same electrophoretic conditions as for the bases. The glucose was detected by spraying with *o*-aminophenol solution.[10)]

Results and Discussion

The observed electrophoretic behaviors of the bases against pH-values are shown in Fig. 1. The migration distances shown were not corrected for the electroosmotic flow which was estimated from the movement of glucose under conditions similar to those of electrophoresis. Thus, the observed migration distances include the movements by the electroosmotic flow. The average electroosmotic flow (-1.0 ± 0.3 cm, pK_i=4.0) in this experiment is shown in Fig. 2. The effects of a capillary action on the migrations are negligible because the sample solutions were spotted at the center of the filter paper.[7)]

Generally, the zone mobility is the weighted mean value of the mobility of each species present in a given solution. In an ideal solution where only C_i and C_{i+1} species are present, the zone mobility U_{zi} is expressed by the Eq. 1

$$U_{zi} = (U_i[C_i] + U_{i+1}[C_{i+1}])/([C_i] + [C_{i+1}]), \quad (1)$$

where U_i and U_{i+1} are the mobility of C_i and C_{i+1} ions, and $[C_i]$ and $[C_{i+1}]$ the concentration of C_i and C_{i+1} ions in a given system. The concentration of each chemical species is related to the dissociation constant (K_i)

$$K_i = [C_{i+1}][H^+]/[C_i]. \quad (2)$$

Then, by substituting Eq. 2 into Eq. 1, we obtain

$$U_{zi} = \frac{U_i + U_{i+1} \cdot K_i/[H^+]}{1 + K_i/[H^+]}. \quad (3)$$

Thus, if we know the values of U_i, U_{i+1}, and K_i respectively, the value of U_{zi} against the pH value will be calculated. The curves in Fig. 2 are drawn by substituting the most suitable values obtained by the actual

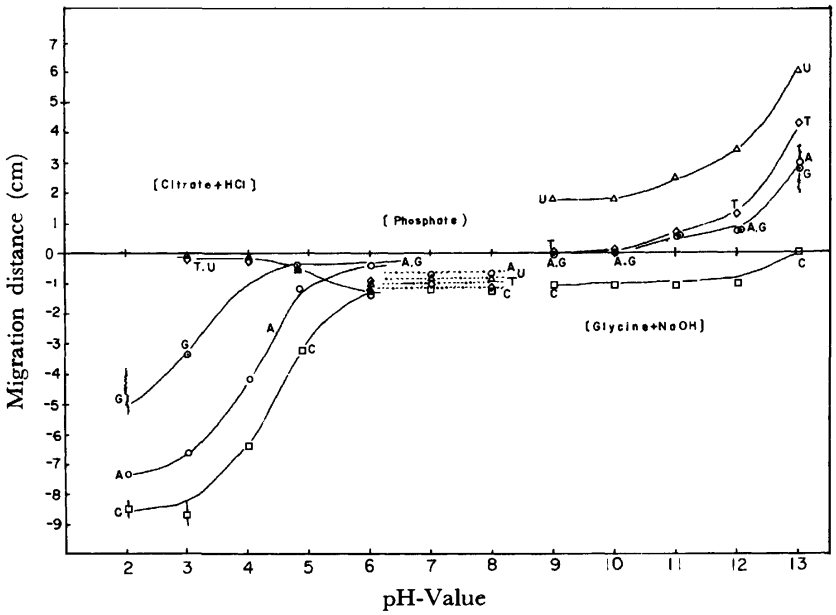

Fig. 1. Observed electrophoretic behaviors of the bases of the nucleic acid against pH-values.
Sample solutions: ○, adenine (A); ⊙, guanine (G); △, uracil (U); ◇, thymine (T); □, cytosine (C). Electrophoresis conditions: 1000 V per 30 cm, 30 min, at 20 °C. Supporting solutions, citric acid buffer (pH=2.0—6.0); phosphoric acid buffer (pH=6.0—8.0); glycine+NaOH buffer (pH=9.0—13.0). Support, pure cellulose paper (Toyoroshi No. 51 A). Spotting position, the centre of a support. Positive movement is towards the anode, negative movement towards the cathode.

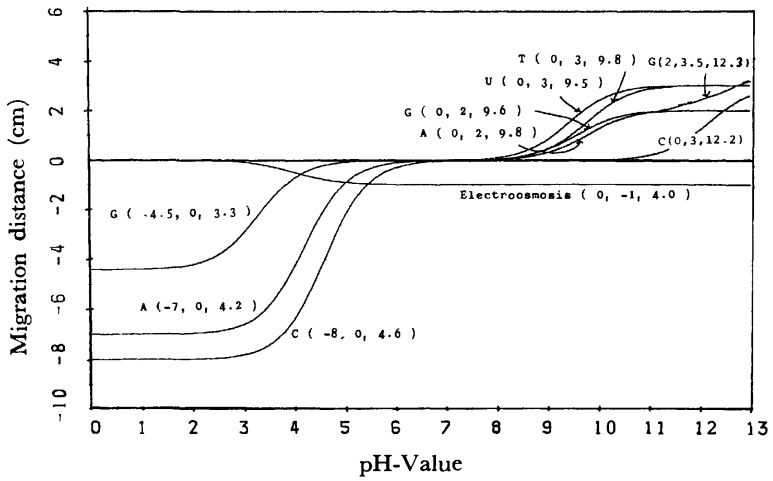

Fig. 2. Calculated migration curves of the bases of the nucleic acid.
Electrophoresis conditions and symbols used are the same as in Fig. 1. The three figures in the parenthesis are migration distances (cm) of C_i, C_{i+1}, and pK_i-value in this order.

experiment for equation 3. The zone mobility-pH curves shown in Fig. 2 are drawn by a microcomputer (Model, NEC PC-9801) equipped with a plotter (Watanabe multi myplot).* The three figures in the parenthesis in Fig. 2 show U_i, U_{i+1}, and pK_i (negative logarithm of K_i) in this order. U_i and U_{i+1} are the mobilities of each species, they varies with the charge, the molecular weight, the hydration, the shape, the size etc. The U_i and U_{i+1} in Fig. 2 were taken from this experiment. The pK_i values were referred to the data[11] which are determined by the chemical methods other than the electrophoresis. The electroosmotic flows were measured by the movement of glucose. The main cause of the flows seems to be due to the carboxyl groups in cellulose paper introduced during the manufacturing of the filter paper.[12] As the inflection point of the electroosmotic flow was estimated to be around pH=4.0 from this experiment, the pK_i value are assumed to be 4.0, and the calculated curve was drawn by the microcomputer. In acid region, movements due to the protonated amino groups of the bases are expected. Three bases (A, G, C) moved towards the cathode while two bases (T, U) having no amino group did not. Compar-

* The computer program is available on application to the author.

ing the actual results with the calculated ones in the acid region, we find a good agreement. In the neutral region, as all the bases have no charge on the molecule, it is assumed that they do not migrate. The observed small migrations of all the bases towards the cathodic side were within the range of the electroosmotic flow. In alkaline region, the dissociation of the hydrogen of the phenolic hydroxyl groups or of the imino group is expected. The p$K$is of the phenolic groups of U, G, and T or of the imino group of A are reported to be within pH=9—10.[11] In this experiment, no inflextion point was found within pH=9—10. Furthermore, the movement of U at pH=9.0 is too large, comparing with that of G or T. In the strongly alkaline region (pH=12—13), the dissociation of the hydrogen atom of the imino groups of G or of phenolic hydroxyl group of C is expected. The high migration distances of U and T may be due to the dissociation (pK>13[13]) of the hydrogen of the second phenolic hydroxy group. Although we tried to select the most appropriate mobility for the anions obtained from actual experiment, agreement between observed and calculated values were never obtained. The inflection points of the experimental curves were not definite and the inflection point seemed to be shifted to a more alkaline region. The data for migration at pH=13 may not be reliable because of the possibility of partial decomposition of the sample and the support. The migration of C in the cathodic side is due to the electroosmosis. The discrepancy between the calculated and observed curves are much large in alkaline region. The cause of the discrepancy seems to be some unknown factors other than electroosmosis and capillary action. Some chemically specific interaction between a migrant and a supporting solution or the structual change of a filter paper in alkaline region might be considered. Further studies on the cause of the discrepancy in alkaline region is needed.

From the chemical isolation point of view, A, G, and C could be separated from T and U in acid region, and U and T could be separated from each other in alkaline region. The neutral region is not good for the separation of any bases.

In conclusin, it is found that the electrophoretic behavior in the acid region could be explained satisfactorily but not in the alkaline region.

References

1) Part XVII of "Study on the separation mechanism of electrophoresis." Part XVI; Lit. 7.
2) J. R. Whitaker, "Paper Chromatography and Electrophoresis," Academic Press, New York, London (1967), Vol. 1.
3) J. D. Smith, in "Nucleic Acid" (E. Chargaff and J. N. Davidson, eds.), Academic Press, New York (1955), Vol. 1, p. 267.
4) R. Markham and J. D. Smith, *Biochem. J.*, **52**, 558 (1952).
5) H. E. Wade and D. M. Morgan, *Biochem. J.*, **60**, 264 (1955).
6) Y. Kiso, M. Kobayashi, Y. Kitaoka, K. Kawamoto, and J. Takada, *J. Chromatogr.*, **35**, 215 (1968).
7) Y. Kitaoka, *Bull. Chem. Soc. Jpn.*, **55**, 2281 (1982).
8) Y. Kitaoka, *J. Chromatogr.*, **252**, 301 (1982).
9) S. P. L. Sørensen, *Erg. Physiol.*, **12**, 393 (1912).
10) V. B. Kupressova, *Izv. Sibirsk Otd. Akad. Nauk SSSR, Ser. Biol. Med. Nauk*, **141** (1965).
11) R. M. C. Dawson, D. C. Elliott, W. H. Elliott and K. M. Jones (Editors), "Data for Biochemical Research," Clarendon Press. Oxford (1959).
12) Y. Kitaoka, *Bull. Chem. Soc. Jpn.*, **54**, 757 (1981).
13) "Handbook of Biochemistry," 2nd edition, ed by H. A. Sober and R. A. Hart, The Chemical Rubber Co., Ohio (1968).

Cation Ordering in (NaLa)(MgW)O_6 with the Perovskite Structure

Tadashi Sekiya, Tetsuo Yamamoto, and Yasuyoshi Torii*
Government Industrial Research Institute, Nagoya Hirate-machi, Kita-ku, Nagoya 462
(Received November 11, 1983)

The title compound with an ordered monoclinic (pseudotetragonal) perovskite structure has been prepared. The lattice constants are a=5.5239(5), b=5.5253(4), c=7.8936(6) Å, β=90.16(1)°, and Z=2. The superstructure was found to be due to a layer-like ordering of Na^+ and La^{3+} ions along alternate c-planes as well as a NaCl-type ordering of Mg^{2+} and W^{6+} ions in the octahedral sites. This new compound is the first example for the occurence of cation ordering in the A site. The origin of the superstructure was discussed.

There are many examples of ABO_3-type perovskites where cation ordering occurs in the B site when ions of different size and charge substitute for a single B atom. Generally, cation ordering is unlikely to occur in the A site. An ordering of A-site vacancies, however, has been found only in some compounds such as $La_{0.33}NbO_3$[1,2] and $La_{0.67}TiO_3$[3]. Recently we have reported that $La_{1.33}(MgW)O_6$ crystallized in an orthorhombically distorted perovskite structure, showing a NaCl-type ordering of B ions as well as an ordering of A-site vacancies along alternate c-planes.[4] Our attempt to prepare a new perovskite of (NaLa)(MgW)O_6 composition was successful. The X-ray diffraction pattern was highly similar to that of $La_{1.33}(MgW)O_6$ in general features. This new compound is therefore considered having a layer-like ordering of Na^+ and La^{3+} ions in the A site. This remarkable ordering phenomenon at the larger cation sublattice has been observed in the perovskite-related compounds (NaLn)TiO_4 (Ln=lanthanoids.[5] The superstructure of Na^+ and La^{3+} ions may result in a poor charge compensation in the octahedral surroundings. The new compound (NaLa)-(MgW)O_6 is challenging for a crystal chemical investigation. The purpose of the present work is to examine the cation distribution in this compound and to interpret the origin of the superstructure.

Experimental

The title compound was prepared from Na_2CO_3, La_2O_3, MgO and WO_3 of high purity. 2.5 Mol% of excess Na_2CO_3 was added to a stoichiometric composition for vaporization of Na_2O at elevated temperatures. The weighed batch was heated at 950 °C for 4 h in air. The reacted mixture was further ground, pressed into disks and reheated twice at 1100 °C for 6 hrs on a Pt foil in a closed alumina crucible. As shown in Fig. 1(a), the X-ray diffraction analysis of the product showed that the phase crystallized well and that it did not contain any additional compound. The reflections were measured at a scanning speed of (1/8)° 2θ/min and the Bragg angles were corrected with a silicon standard. The lattice constants were refined by the least-squares method.[6] The observed intensities were measured by cutting out and weighing tracings of the peaks. Infrared absorption measurements between 1200—250 cm^{-1} were made for powder specimens dispersed in a pressed KBr disk, using a Perkin-Elmer infrared spectrophotometer model 180.

Results and Discussion

The title compound (NaLa)(MgW)O_6 shows an X-ray powder pattern characteristic of the perovskite

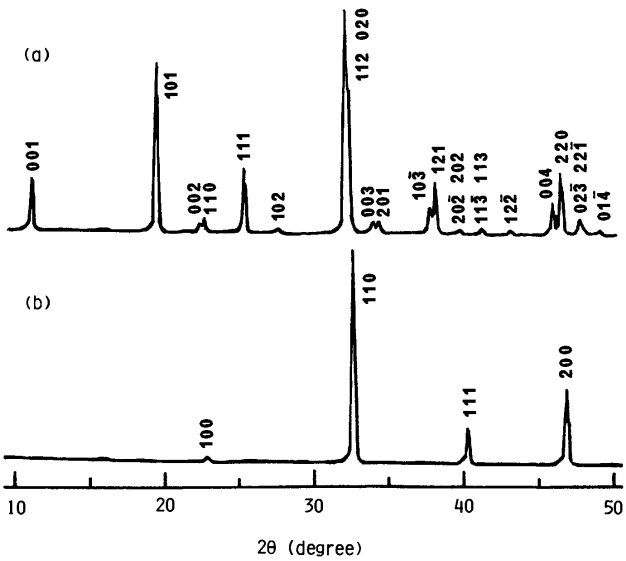

Fig. 1. X-Ray powder patterns of perovskites (NaLa)(MgW)O_6 (a) and (NaLa)Ti_2O_6 (b).

structure, as can be seen by comparison with that of a simple perovskite (NaLa)Ti_2O_6[7] in Fig. 1(b). The X-ray diffraction data for (NaLa)(MgW)O_6 are given in Table 1. The superstructural reflections marked by an asterisk arise from a NaCl-type ordering of Mg^{2+} and W^{6+} ions in the oxygen-octahedral sites. In addition to their reflections, extra reflections marked by double asterisks are observed in the X-ray powder pattern of (NaLa)(MgW)O_6. Various kinds of line-splitting phenomena indicate appreciable distortion from ideally cubic symmetry. All the reflections in Table 1 could be satisfactorily indexed on the basis of a monoclinic unit cell with β close to 90°. Its lattice constants were refined for selected 41 observed reflections by the least-squares method. This gave a=5.5239(5), b=5.5253(4), c=7.8936(6) Å, and β=90.16(1)°. The cell-edges are approximately $\sqrt{2}a'$ for the a- and b-axis and $2a'$ for the c-axis, where a' is the length of the perovskite-like subcell edge. Since the a and b dimensions are very nearly equal, the monoclinic unit cell is considered to be pseudotetragonal. The pycnometrically measured density of 6.46 g/cm^3 was in good agreement with the calculated value of 6.42 g/cm^3 for two formula units of (NaLa)(MgW)O_6 per cell. This result supports that the new compound has the chemical formula of (NaLa)-(MgW)O_6.

The reflections given in Table 1 show no systematic

Table 1. X-Ray diffraction data for (NaLa)(MgW)O_6

h k l	d_{obsd}	d_{cal}	I_{obsd}	I_{cal}	h k l	d_{obsd}	d_{cal}	I_{obsd}	I_{cal}
0 0 1**	7.88	7.89	17	25	1 3 $\bar{1}$**	1.7060	1.7062	5	4
1 0 1*	4.52	4.52	50	54	3 1 1**	1.7046	1.7046		
0 0 2	3.95	3.95	7	3	0 2 4	1.6051	1.6058	38	53
1 1 0	3.90	3.91			3 1 $\bar{2}$	1.5986	1.5990		
1 1 1**	3.50	3.50	20	16	1 3 $\bar{2}$	1.5981	1.5982		
1 0 2**	3.21	3.21	1	6	2 2 $\bar{3}$**	1.5696	1.5698	2	2
1 1 $\bar{2}$		2.779			2 2 3**	1.5672	1.5669		
1 1 2	2.775	2.774	100	100	2 1 $\bar{4}$**	1.5436	1.5438	1	1
0 2 0	2.762	2.763			2 1 4**	1.5398	1.5400		
0 0 3**	2.631	2.631	4	2	1 0 $\bar{5}$*	1.5188	1.5191	8	13
2 0 1**	2.606	2.605	4	7	2 3 $\bar{1}$*	1.5049	1.5047		
1 0 $\bar{3}$*	2.376	2.378			2 3 1*	1.5041	1.5038		
1 0 3*	2.374	2.376	26	35	1 1 $\bar{5}$**	1.4651	1.4649	4	1
1 2 1*	2.357	2.357			2 2 $\bar{4}$	1.3894	1.3896	15	26
2 0 $\bar{2}$	2.264	2.266	1	3	2 2 4	1.3868	1.3868		
2 0 2	2.261	2.263			0 4 0	1.3818	1.3813		
1 1 $\bar{3}$**	2.184	2.184	2	4	1 2 $\bar{5}$*	1.3296	1.3296	7	13
1 1 3**	2.179	2.180			3 2 $\bar{3}$*	1.3255	1.3254		
1 2 $\bar{2}$**	2.095	2.096	1	3	3 2 3*	1.3223	1.3227		
2 1 2**	2.090	2.092			4 0 $\bar{2}$	1.3045	1.3046	1	1
0 0 4	1.9738	1.9734	11	15	3 3 $\bar{1}$**	1.2850	1.2852	1	1
2 2 0	1.9530	1.9532	23	28	3 3 1**	1.2839	1.2844		
0 2 $\bar{3}$**	1.9058	1.9053	8	6	1 0 $\bar{6}$**	1.2809	1.2806		
2 0 3**	1.9039	1.9024			1 1 $\bar{6}$	1.2479	1.2475	14	11
2 2 $\bar{1}$**	1.8970	1.8969			3 3 $\bar{2}$	1.2369	1.2373		
0 1 $\bar{4}$**	1.8591	1.8584	1	1	2 4 0	1.2356	1.2354		
1 2 $\bar{3}$*	1.8023	1.8023	10	16	4 0 3**	1.2217	1.2214	1	1
1 2 3*		1.8001			4 1 $\bar{3}$*	1.1953	1.1952	2	5
2 1 3*	1.7990	1.7988			3 1 $\bar{5}$**	1.1729	1.1728	4	1
3 0 $\bar{1}$*	1.7944	1.7943			1 3 5**	1.1711	1.1709		
0 3 $\bar{1}$*	1.7932	1.7936			4 0 $\bar{4}$	1.1329	1.1329	5	9
1 1 $\bar{4}$	1.7633	1.7628	3	2	0 4 4	1.1314	1.1316		
2 2 $\bar{2}$	1.7515	1.7520			4 2 $\bar{3}$**	1.1190	1.1192	2	1
2 2 2		1.7492			2 4 3**	1.1180	1.1178		
1 3 0	1.7476	1.7472			4 2 3**	1.1169	1.1171		

* Superstructural reflection due to a NaCl-type ordering of B-site ions. ** Superstructural reflection due to a layer-like ordering of A-site ions.

absences for general reflections of *hkl* type, and the monoclinic cell is therefore primitive. This X-ray pattern, except the additional reflections marked by double asterisks, obeys a body-centered absence rule. On the other hand, the additional reflections marked by double asterisks occur with only $h+k=2n$ for (hkl) planes, if a few reflections of very weak intensity are ignored. This indicates that (NaLa)(MgW)O_6 has a C-face-centered lattice for special atoms. Especially, the appearance of relatively strong *001* reflection at about 7.88 Å, which can not be assigned to the NaCl-type ordering of the B ions, points to a doubling of the c'-axis in the small perovskite subcell, as found in $La_{0.33}NbO_3$[2] and $La_{0.67}TiO_3$.[3] In the compound (NaLa)(MgW)O_6, a cation ordering of Na^+ and La^{3+} ions is therefore considered to occur along alternate c-planes. Thus a superstructure model based on cation ordering is proposed as shown in Fig. 2. The perovskite subcell is designated by dotted outlines.

The extinction rule deduced from the observed reflections in Table 1 is as follows; *0k0*: ($k=2n$). So two space groups, $P2_1$ (No. 4) and $P2_1/m$ (No. 11), satisfy the extinction rule and simultaneously give

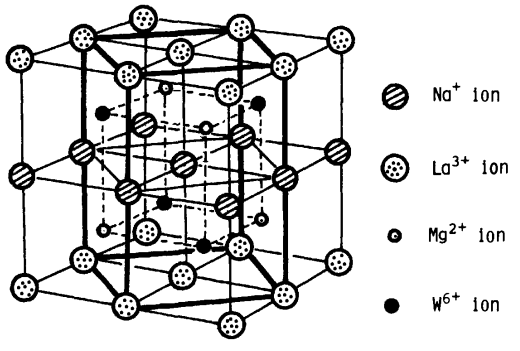

Fig. 2. Superstructure of (NaLa)(MgW)O_6, where oxygen ions are not shown.
Monoclinic unit cell: heavy solid line. Perovskite-like subcell: dotted line,

the monoclinic crystal system[8]. The space group of monoclinic (NaLa)(MgW)O_6 probably belongs to $P2_1$, judging from the three-dimensional symmetry of the B ions in the NaCl-type ordering. The c-axis in (NaLa)(MgW)O_6 is regarded as a characteristic axis of the pseudotetragonal (actually monoclinic) cell.

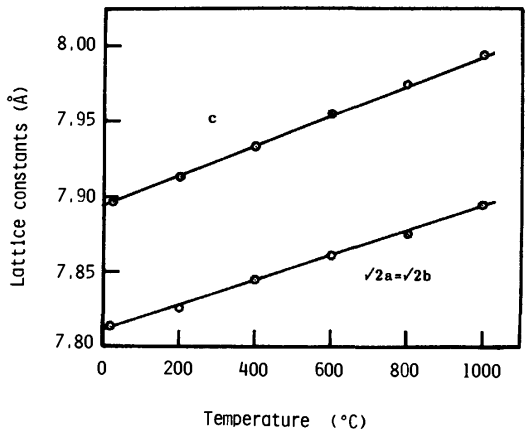

Fig. 3. Temperature dependence of lattice constants for (NaLa)(MgW)O_6.

Figure 3 shows the variation of the lattice constants of monoclinic (NaLa)(MgW)O_6 with temperature. The unit cell was tetragonal at 200 °C, and phase transitions were absent up to 1000 °C. The marked change in the cell dimensions with temperature is not accompanied by any appreciable change in the degree of tetragonality, and the superstructural reflections marked by double asterisks did not disappear even at 1000 °C. This result shows a crystallographic tendency similar to $La_{0.33}NbO_3$,[9] $La_{0.67}TiO_3$,[3] and $La_{1.33}(MgW)O_6$,[10] in which the A-site vacancies are ordered along alternate c-planes. Generally, the low symmetry of ordinary perovskites is expected to improve at high temperatures. The title compound (NaLa)(MgW)O_6 also differs from ordinary perovskites in the nature of tetragonal distortion. Hence the basic cell distortion in this compound is concluded to be tetragonal. The monoclinic distortion deviated from the tetragonal symmetry probably arises from atomic displacements in the neighboring perovskite subcells.

In order to confirm the proposed superstructure (Fig. 2), the theoretical intensities for (NaLa)(MgW)O_6 were calculated using ideal position parameters on the assumption of a tetragonal cell and were compared with the observed intensities in Table 1. In intensity calculations, the effects of atomic displacements and crystal distortion (actually monoclinic) on reflection intensity were neglected to avoid troublesome position parameters. In such a rough test, however, a qualitatively good agreement between the observed and calculated intensities was obtained as shown on the right side of each reflection in Table 1. The reliability factor R for the intensities of 36 peaks was 28%. This result gives good evidence for the general correctness of the proposed structure. Consequently the basic superstructure of (NaLa)(MgW)O_6 is concluded to arise from the NaCl-type ordering of the B ions as well as the layer-like ordering of the A ions, although cation ordering is unlikely to occur among the A-site ions in the perovskite structure. In this respect, the new compound (NaLa)(MgW)O_6 is an exceptional case.

Figure 4 gives the infrared absorption spectra of perovskites (NaLa)(MgW)O_6 and (NaLa)Ti_2O_6. In the case of cubic (NaLa)Ti_2O_6, two strong absorption band

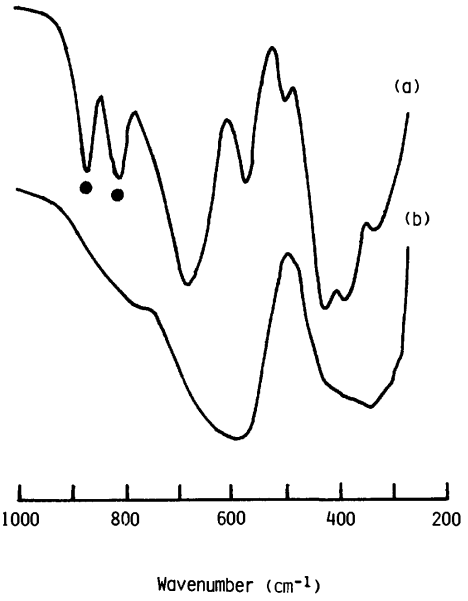

Fig. 4. Infrared absorption spectra of perovskites (NaLa)(MgW)O_6 (a) and (NaLa)Ti_2O_6 (b).

peaks were observed at 600 and about 340 cm^{-1}. On the basis of Last's mode assignment[11] on the perovskites, the high frequency band corresponds to the Ti-O stretching mode, while the lower frequency band does to the Ti-O bending mode. On the other hand, the spectrum of monoclinic (NaLa)(MgW)O_6 is more complicated. Two strong absorption bands at 685 and about 400 cm^{-1} are assigned to the internal modes of oxygen octahedra. The extra bands probably arises from the monoclinic distortion from ideal cubic symmetry, which would split degenerate modes to give additional frequencies as mentioned by some investigators.[12–14] However, it should be noted that two strong bands (marked a black circle) were found at 870 and 820 cm^{-1}. In view of the spectral positions, the two bands must be due to the B-O vibrational mode. The strong bands at very high wavenumbers, which are not expected for a regular octahedron, indicate a strong deviation from cubic symmetry. Such a remarkable spectrum[15] has been found in perovskite-related compounds (NaLn)TiO_4, where the Na^+ and Ln^{3+} ions are ordered on the larger cation sublattice. In the case of (NaLn)TiO_4, a strong band is located around 900 cm^{-1} in addition to the normal vibrations. This striking band is absent in Sr_2TiO_4. This fact that this mode was observed at very high wavenumbers has been concluded to be due to the superstructure of Na^+ and Ln^{3+} ions which results in a poor charge compensation in the octahedral surroundings. Consequently the infrared spectrum of (NaLa)(MgW)O_6 supports that a layer-like ordering of Na^+ and La^{3+} ions occurs on the A site.

Our attempt to prepare the corresponding Ni and Zn compounds to (NaLa)(MgW)O_6 was unsuccessful. A similar result[4] has been obtained for the replacements of Ni^{2+} and Zn^{2+} ions for Mg^{2+} ion in cation-deficient perovskite $La_{1.33}(MgW)O_6$. Since these three cations are roughly equal in size, the failure of the preparation is not thought to be mainly due to the ionic size effect.

Thus the Mg/W combination not only contributes to the framework as constituent ions, but also plays an important role in the stabilization of the perculiarly ordered perovskite structure.

According to the X-ray structure analysis[2] of orthorhombic (pseudotetragonal) $La_{0.33}NbO_3$, the Nb^{5+} ions are displaced from the centers of the oxygen octahedra which themselves suffer distortion so as to retain only one of their four-fold axes. The particular displacement of the Nb^{5+} ions must be connected with the ordering of A-site vacancies along alternate c-planes. Recently we have reported that A-site vacancies are randomly distributed in the cubic $La_{0.33}NbO_3$ phase crystallized by rapid quenching of its melt.[16] Further, the pseudotetragonal perovskites $La_{0.33}NbO_3$ and $(NaLa)(MgW)O_6$ show the temperature-independent tetragonality, in addition to the layer-like ordering of A-site ions. Consequently, $(NaLa)(MgW)O_6$ is also considered to have similar off-centered octahedra to $La_{0.33}NbO_3$. This conclusion is supported by the infrared data of $(NaLa)(MgW)O_6$. Such a severly distorted octahedral-site seems to be unfavorable surroundings for Ni^{2+} and Zn^{2+} ions owing to strong crystal field effect of Ni^{2+} ($3d^8$) ion and tetrahedral site-preference of Zn^{2+} ($3d^{10}$) ion. This situation is reflected in the nonexistence of $NiSiO_3$ and $ZnSiO_3$ pyroxenes (the existence of $MgSiO_3$ pyroxene), since the pyroxene structure[17] consists of severely distorted octahedra and single chains of SiO_4 tetrahedra. Thus the Mg^{2+} ion makes no small contribution to the stabilization of this type of superstructure. The origin of the superstructure is represented as follows: The difference in charge between the Na^+ and La^{3+} ions is enough to cause cation ordering to occur among the A-site ions. The electrostatic imbalance due to the layer-like ordering of Na^+ and La^{3+} ions is compensated by the particular displacement of the Mg^{2+} and W^{6+} ions for the c direction, and such an electrostatic interaction gives rise to the pseudotetragonal distortion. In consequence, two strong absorption bands at very high wavenumbers were observed in the infrared spectrum of $(NaLa)(MgW)O_6$. The temperature-independent tetragonality shown in Fig. 3 is closely related with the layer-like ordering of A-site ions along alternate c-planes.

References

1) H. P. Rooksby, E. A. D. White, and S. A. Langston, *J. Am. Ceram. Soc.*, **48**, 447 (1965).
2) P. N. Iyer and A. J. Smith, *Acta Crystallogr.*, **23**, 740 (1967).
3) M. Abe and K. Uchino, *Mater. Res. Bull.*, **9**, 147 (1974).
4) Y. Torii, *Chem. Lett.*, **1979**, 1215.
5) G. Blasse, *J. Inorg. Nucl. Chem.*, **30**, 656 (1968).
6) T. Sakurai, UNICS (Crystallographic Soc. Japan, 1967).
7) A. I. Agranovskaya, *Bull. Acad. Sci. USSR Phys. Ser.*, **24**, 1271 (1960).
8) "International Tables for X-ray Crystallography," Vol I, Kynoch Press, Birmingham, England, 1969.
9) Y. Torii, *Bull. Chem. Soc. Jpn.*, **52**, 245 (1979).
10) Y. Torii and T. Sekiya, *Mater. Res. Bull.*, **16**, 1153 (1981).
11) J. T. Last, *Phys. Rev.*, **105**, 1740 (1957).
12) A. F. Yatsenko, *Izv. Akad. Nauk SSSR, Ser. Fiz.*, **22**, 1456 (1958).
13) C. H. Perry and D. J. MacCarthy, *Phys. Rev.*, **138**, A1537 (1965).
14) G. Blasse and A. F. Corsmit, *J. Solid State Chem.*, **10**, 39 (1974).
15) G. Blasse and G. P. M. Van Den Heuvel, *J. Solid State Chem.*, **10**, 206 (1974).
16) Y. Torii, T. Sekiya and T. Yamamoto, *Mater. Res. Bull.*, **17**, 727 (1982).
17) Y. Matsui, Y. Syono, S. Akimoto, and K. Kitayama, *Geochem. J.*, **2**, 61 (1968).

Preparation and Reaction of 1-(Methylthio- and phenylthio)-vinyllithium Reagents

Takeshi TAKEDA,* Hiroyuki FURUKAWA, Mizue FUJIMORI, Kouichi SUZUKI, and Tooru FUJIWARA
Department of Industrial Chemistry, Faculty of Technology, Tokyo University of Agriculture and Technology, Koganei, Tokyo 184
(Received August 6, 1983)

An improved procedure for the preparation of 1-(methylthio- and phenylthio)vinyllithium reagents utilizing 2-methoxyalkyl sulfides was developed and their reactions with ketones, aldehydes, oxiranes, and alkyl halides were studied.

The utilization of various heteroatom-stabilized vinyl anions in organic synthesis has become increasingly important in recent years.[1] The α-lithiated alkenyl sulfide (**3**) is one of these anions, and usefulness of **3** in the synthesis of certain organic compounds has well been demonstrated. For example, Oshima *et al.* showed that **3**, which are useful intermediates for the synthesis of ketones,[2] could be considered as acyl anion equivalents. It was also reported that the adducts of **3** with aldehydes might be valuable intermediates for the preparation of furans and 1,4-dicarbonyl compounds.[3]

Since **3** is generally prepared by the treatment of alkenlyl sulfide (**2**) with strong base, such as *s*-butyllithium, *t*-butyllithium, or lithium diisopropylamide (LDA), the preparation of alkenyl sulfides (**2**) is required at the first step of the aforementioned synthesis. However, the synthesis of **2** may not be straightforward in some cases.[4] We have thus investigated an improved procedure for the preparation of **3**. Recently, we found that the reaction of 2-methoxyalkyl sulfides (**1**) with two molar butyllithium in the presence of *N,N,N′,N′*-tetramethylethylenediamine (TMEDA) directly produced **3**, probably *via* **2**.[5]

Concerning the formation of alkenyl sulfide from 2-methoxyalkyl sulfide and subsequent lithiation, Corey *et al.* reported that 1,3-bis(methylthio)propene (**4**) was obtained by the reaction of 1,3-bis(methylthio)-2-methoxypropane (**5**) with an equimolar amount of LDA, and 1,3-bis(methylthio)allyl anion (**6**) was directly produced when **5** was treated with two equivalents of LDA.[6] Unlike the above-mentioned result of us, the formation of vinyllithium (**3**) was not observed in the lithiation of **4** with LDA. This selective formation of the allyl anion (**6**) is apparently due to the presence of methylthio group attached to the allylic position of **4**.

In this paper, we wish to report the scope and limitation for the generation of **3** with our method, and the results obtained in the reaction of **3** with carbonyl compounds, oxiranes, and alkyl halides are described.

Results and Discussion

1-(Methylthio- and phenylthio)vinyllithiums (**3**) were prepared by the reaction of the corresponding 2-methoxyalkyl sulfides (**1**) with butyllithium or LDA as indicated in Eq. 1. The yield of **3** was estimated on the basis of the isolated yield of adduct with benzaldehyde (Table 1). Satisfactory results were obtained when **1** was treated with butyllitium at −30 °C or higher for 1 to 3 h in the presence of TMEDA. At −78 °C, the yield of **3a**

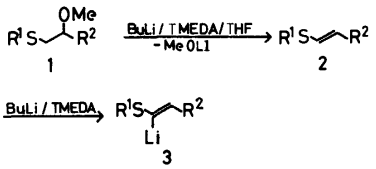

1a R¹=Me R²=H
1b R¹=Me R²=Ph(CH₂)₂
1c R¹=Me R²=(CH₃)₂CHCH₂
1d R¹=Me R²=Ph
1e R¹=Ph R²=Ph(CH₂)₂
1f R¹=Ph R²=(CH₃)₂CHCH₂
1g R¹=Ph R²=CH₃(CH₂)₄ (1)

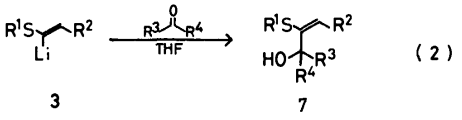

(2)

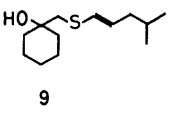

Table 1. The reaction of **3** with benzaldehyde

Run	2-Methoxyalkyl sulfide	Temp °C	Time h	Product	(Yield/%)
1	**1a**	−78	1	**7a-1**	(Trace)[a]
2	**1a**	−78	1	**7a-1**	(11)
3	**1a**	−30	1	**7a-1**	(80)
4	**1a**	0	0.5	**7a-1**	(74)
5	**1d**	0	1	**7d-1**	(0)
6	**1d**	−30	2	**7d-1**	(0)[b]
7	**1d**	−60	2.5	**7d-1**	(55)[b]
8	**1d**	−30	1	**7d-1**	(22)[c]
9	**1e**	−30	2	**7e-1**	(84)
10	**1e**	−23	3	**7e-1**	(74)
11	**1e**	0	0.5	**7e-1**	(82)
12	**1f**	0	0.5	**7f-1**	(66)
13	**1f**	−30	3	**7f-1**	(69)
14	**1f**	−23	3	**7f-1**	(74)

a) The reaction was carried out without TMEDA. b) The reaction was carried out in the presence of HMPA (0.6 ml/mmol) using LDA as a base. c) LDA was used as a base.

Table 2. The reaction of **3** with aldehydes and ketones

2-Methoxy-alkyl sulfide	Aldehyde or ketone R^3	Aldehyde or ketone R^4	Product (Yield/%)	2-Methoxy-alkyl sulfide	Aldehyde or ketone R^3	Aldehyde or ketone R^4	Product (Yield/%)
1a	Ph	H	**7a-1** (80)	**1e**	CH_3CH_2	H	**7e-2** (64)
1a	$Ph(CH_2)_2$	H	**7a-2** (81)	**1e**	$(CH_3)_2CHCH_2$	H	**7e-3** (58)
1a	PhCH=CH	H	**7a-3** (88)	**1e**	Ph	CH_3	**7e-4** (44)
1a	CH_3CH_2	H	**7a-4** (65)	**1f**	Ph	H	**7f-1** (74)
1a	$(CH_3)_2CHCH_2$	H	**7a-5** (70)	**1f**	$Ph(CH_2)_2$	H	**7f-2** (77)
1a	Ph	CH_3	**7a-6** (68)[a]	**1f**	PhCH=CH	H	**7f-3** (84)
1c	$-(CH_2)_5-$		**7c-1** (15)[b]	**1f**	CH_3CH_2	H	**7f-4** (72)
1d	Ph	H	**7d-1** (55)	**1f**	$(CH_3)_2CHCH_2$	H	**7f-5** (75)
1d	$Ph(CH_2)_2$	H	**7d-2** (40)	**1f**	$-(CH_2)_5-$		**7f-6** (57)
1d	PhCH=CH	H	**7d-3** (67)	**1f**	Ph	CH_3	**7f-7** (60)
1d	CH_3CH_2	H	**7d-4** (28)	**1g**	Ph	H	**7g-1** (61)
1d	$(CH_3)_2CHCH_2$	H	**7d-5** (33)	**1g**	$-(CH_2)_5-$		**7g-2** (50)[a]
1e	Ph	H	**7e-1** (84)	**1g**	Ph	CH_3	**7g-3** (59)

a) The reaction was carried out at −78 °C. b) 1-[(4-Methyl-1-pentenylthio)methyl]-1-cyclohexanol (**9**) was isolated in 14% yield as a by-product.

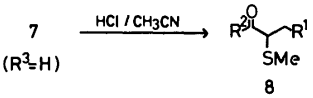

(3)

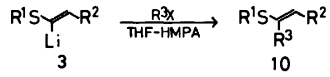

(4)

Table 3. The reaction of **3b** and **3c** with aldehydes

R^1	R^2	Product	(Yield/%)
$Ph(CH_2)_2$	Ph	**8b-1**	(47)
$Ph(CH_2)_2$	$Ph(CH_2)_2$	**8b-2**	(39)
$Ph(CH_2)_2$	CH_3CH_2	**8b-3**	(27)
$(CH_3)_2CHCH_2$	Ph	**8c-1**	(32)

Table 4. The reaction of **3** with alkyl halides

2-Methoxy-alkyl sulfide	RX	Product	(Yield/%)
1a	$CH_3(CH_2)_7I$	**10a-1**	(77)
1e	CH_3I	**10e-1**	(76)
1e	$CH_3(CH_2)_7I$	**10e-2**	(64)
1e	$PhCH_2Br$	**10e-3**	(34)
1f	CH_3I	**10f-1**	(92)[a]
1f	$CH_3(CH_2)_7I$	**10f-2**	(82)
1f	$PhCH_2Br$	**10f-3**	(32)
1f	$CH_2=CHCH_2Br$	**10f-4**	(43)
1f	$(CH_3)_3SiCl$	**10f-5**	(84)
1g	CH_3I	**10g-1**	(84)
1g	CH_3CH_2I	**10g-2**	(85)
1g	$CH_3(CH_2)_7I$	**10g-3**	(67)
1g	$PhCH_2Br$	**10g-4**	(31)

a) The reaction was carried out at −50 °C without HMPA.

was only 11% after 1 h. In the absence of TMEDA, only a trace amount of **3a** was produced under similar reaction conditions. In contrast to the reactions of **1a**, **1e**, and **1f**, the treatment of 2-methoxy-2-phenylethyl sulfide (**1d**) with butyllithium did not afford **3**, but produced the Michael type adduct of the intermediate alkenyl sulfide (**2**). When LDA was used as a base, however, this side reaction was suppressed.

The reaction of **3** with various aldehydes and ketones proceeded smoothly and produced β-methylthio and phenylthio β,γ-unsaturated alcohols (**7**) in good yields (Table 2). When allylic hydrogen was present in the intermediate methl alkenyl sulfide (**2**), **7** was contaminated by some by-products. Since the purification of **7** was not successful in these cases, a mixture of the products was treated with hydrochloric acid in CH_3CN,[7] and the formation of **7** was proved by the isolation of the α-methylthio ketone (**8**) (Table 3). The NMR spectra of the by-products produced along with **7** suggested that not only α-lithiation but also lithiation of γ-position and the methylthio group proceeded in this case. In fact 2-hydroxyalkyl vinyl sulfide (**9**), which originated from the lithiation of methylthio group, was isolated in 14% yield in addition to α-adduct (**7c-1**) in the reaction of **1c** with cyclohexanone.

The alkylation of 1-(pheylthio)vinyllithium (**3**) was also examined. When **3f** was allowed to react with octyl iodide at −30 °C, the alkylated product (**10f-2**) was isolated only in 15% yield. On the other hand, **10f-2** was obtained in 67% yield by the reaction carried out at −78 °C. Furthermore, it was found that the yield of **10f-2** increased by the use of hexamethylphosphoric triamide (HMPA) as an additive. Accordingly, the reactions of **3** with various alkyl halides were performed in the presence of HMPA (Table 4).

When primary alkyl halides were employed, the corresponding 1-alkyl-1-alkenyl sulfides (**10**) were produced in good yields. On the other hand, the reactions with benzyl bromide or allyl bromide resulted in the formation of **10** only in moderate yields. The coupl-

Table 5. The reaction of 3 with oxiranes

2-Methoxyalkyl sulfide	Oxirane R	Product	(Yield/%)
1a	Ph	**11a-1**	(27)[a]
1a	Ph	**11a-1**	(74)
1f	Ph	**11f-1**	(72)
1f	CH_3CH_2	**11f-2**	(64)
1g	Ph	**11g-1**	(58)
1g	CH_3CH_2	**11g-2**	(54)

a) The reaction was carried out without HMPA.

ing reactions of halides appeared to reduce the yield of **10**. Finally, it should be pointed out that the reaction of **3** with *s*-alkyl halide, such as isopropyl iodide or *s*-butyl bromide, gave no alkylated product.

The reaction of **3** with oxiranes also took place smoothly and γ-alkylthio γ,δ-unsaturated alcohols (**11**) were obtained in good yields (Table 5). In this reaction, the addition of HMPA markedly increased the yield of **11** as well.

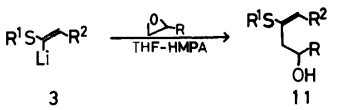

(5)

The first step of the present preparation of **3** may be the formation of alkenyl sulfide (**2**). In fact, the corresponding alkenyl sulfide (**2**) were isolated in high yields (**2e**; 90%, **2f**;95%, **2g**; 85%) when 2-methoxyalkyl sulfides (**1**) were treated with an equimolar amount of butyllithium in the presence of TMEDA. The NMR spectra of the isolated alkenyl sulfides (**2**) suggested that they were *E*-isomers. In order to check the stereochemical purity of the resultant **2g**, we synthesized the authentic (*Z*)-**2f** by the following procedures. The alkenyl sulfide (**2f**) prepared by the present reaction was photoisomerized by the irradiation with high pressure mercury lamp to yield a mixture of (*Z*)- and (*E*)-**2f**. Although the separation of stereoisomers of **2f** was unsuccessful, the corresponding sulfoxides (**12-1**) were separated by TLC. The oxidation of **2f** was carried out by the treatment with *m*-chloroperbenzoic acid (MCPBA) in CH_2Cl_2 at −23 °C. The stereochemically pure alkenyl sulfoxides ((*E*)- and (*Z*)-**12-1**) were reduced with ethylmagnesium bromide in the presence of CuI[8] to give the authentic (*E*)- and (*Z*)-**2f**. The examination of the ^1H NMR spectra of these alkenyl sulfides showed that **2f** of the *E*-configuration was produced stereoselectively by the reaction of **1f** with butyllithium. Further, it was confirmed that **12-1** prepared by the oxidation of **2f** without photolysis contained no *Z*-isomer by its NMR spectrum.

Since alkenyl anions generally exhibit very high degree of retention of configuration,[9] we expected that the present reactions gave the 1-substituted alkenyl sulfides (**7**, **10**, and **11**) stereoselectively. Actually, the obtained alkenyl sulfides seemed to be pure *E*-isomers on the basis of their NMR spectra. In order to determine the configuration of alkenyl sulfides, we prepared several authentic *E*-alkenyl sulfides ((*E*)-**7f-1**, (*E*)-**7f-4**, (*E*)-**10f-1**, and (*E*)-**10f-2**) from the alkenyl sulfoxide (**12-1**) by the method reported by Takei *et al.*[10] The NMR spectra of the authentic alkenyl sulfides were identical with those of the alkenyl sulfides obtained by the present reactions. Further, we concluded that the alkenyl sulfides (**7f-1**, **7f-4**, **10f-1**, and **10f-2**) contained no *Z*-isomer on the basis of the following experimental results. The alkenyl sulfides (**7f-1**, **7f-4**, **10f-1**, and **10f-2**) prepared by the reaction of **3f** with electrophiles were irradiated with high pressure mercury lamp to give the mixtures of two stereoisomers. The two isomers were separated each other by TLC with exception of **7f-4**. The structures of the stereoisomers produced by the photolysis were determined to be *Z*-alkenyl sulfides by the comparison of their IR and NMR spectra with those of the authentic *E*-isomers. It was confirmed that NMR signals characteristic to the *Z*-isomers were absent in the NMR spectra of the starting alkenyl sulfides. (*E*)- and (*Z*)-**10f-1** obtained by the above-mentioned procedure were oxidized with MCPBA to the corresponding sulfoxides (**12-2**). The NMR signal of vinyl proton of (*E*)-**12-2** appeared at δ=6.40 and that of (*Z*)-**12-2** appeared at δ=5.94. On the other hand, the NMR spectrum of the sulfoxide derived from **10f-1** without photolysis showed only one signal for the vinyl proton at δ=6.40.

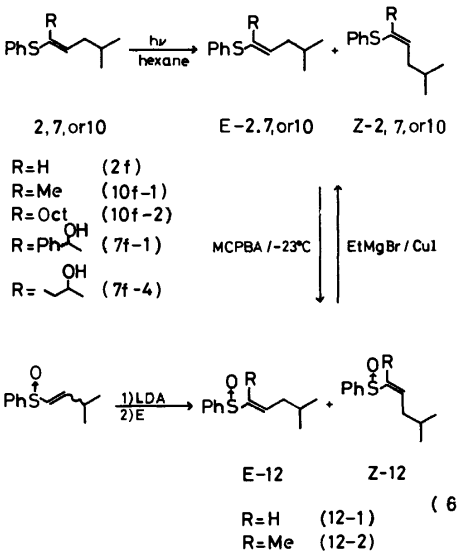

(6)

In conclusion, it is demonstrated that various alkenyl sulfides with β-substituents were easily synthesized in good to high yields by the use of 1-(methylthio- and phenylthio)vinyllithium reagents (**3**) prepared by the treatment of 2-methoxyalkyl sulfides (**1**) with two molar butyllithium in the presence of TMEDA and the reactions of **3** with some electrophiles proceeded stereoselectively to give the *E*-isomers in all cases examined. The present method for the preparation of **3** would extend the applicability of α-lithiated alkenyl sulfides in organic synthesis.

Experimental

Measurements. The boiling points and melting point

were uncorrected. NMR spectra were recorded with JEOL JNM-C-60HL spectrometer. IR spectra were measured with a JASCO DS-403G spectrometer.

2-Methoxyalkyl Sulfide (1). Phenyl (or methyl) 2-methoxyalkyl sulfides (**1b, c, d, e, f,** and **g**) were synthesized by the methylation (MeI/NaH/THF) of the corresponding 2-hydroxyalkyl sulfides prepared from aldehydes by the methods reported by Corey and Seebach,[11] and Peterson.[12] The boiling points, spectral data, and overall yields from aldehydes were as follows: 2-Methoxy-4-phenylbutyl methyl sulfide (**1b**); 45%, 102—105 °C/1 Torr (1 Torr=133.322 Pa), IR (neat): 3040, 2920, 1603, 1496, 1455, 1100, 744, and 700 cm^{-1}. ^1H NMR (CCl_4): δ=1.59—2.11 (2H, m), 2.02 (3H, s), 2.38—2.80 (4H, m), 3.03—3.37 (1H, m), 3.27 (3H, s), and 7.08 (5H, s). 2-Methoxy-4-methylpentyl methyl sulfide (**1c**); 52%, 89—92 °C/30 Torr, IR (neat): 2960, 1467, 1368, and 1096 cm^{-1}. ^1H NMR (CCl_4): δ=0.92 (6H, d, J=6 Hz), 1.15—1.88 (3H, m), 2.10 (3H, s), 2.28—2.52 (2H, m), 2.98—3.34 (1H, m), and 3.31 (3H, s). 2-Methoxy-2-phenylethyl methyl sulfide (**1d**); 64%, 85—87 °C/2 Torr, IR (neat): 2900, 1602, 1495, 1455, 1105, 742, and 702 cm^{-1}. ^1H NMR (CCl_4): δ=1.98 (3H, s), 2.58 and 2.69 (2H, 2d, J=6 and 7 Hz), 3.18 (3H, s), 4.09 and 4.21 (1H, 2d, J=6 and 7 Hz), and 7.24 (5H, s). 2-Methoxy-4-phenylbutyl phenyl sulfide (**1e**); 84%, 150—152 °C/0.6 Torr, IR (neat): 3030, 2930, 1583, 1480, 1438, 1097, 1026, 737, and 695 cm^{-1}. ^1H NMR (CCl_4): δ=1.54—2.06 (2H, m), 2.38—3.33 (5H, m), 3.24 (3H, s) and 6.72—7.37 (10H, m). 2-Methoxy-4-methylpentyl phenyl sulfide (**1f**); 69%, 98 °C/0.7 Torr, IR (neat): 2960, 1586, 1481, 1438, 1027, 737, and 692 cm^{-1}. ^1H NMR (CCl_4): δ=0.89 (6H, d, J=6 Hz), 1.13—1.97 (3H, m), 2.67 and 2.94 (2H, 2d, J=8 and 5 Hz), 3.03—3.41 (1H, m), 3.23 (3H, s), and 6.86—7.41 (5H, m). 2-Methoxyheptyl phenyl sulfide (**1g**); 83%, 94 °C/0.2 Torr, IR (neat): 2940, 1586, 1481, 1439, 1097, 1026, 738, and 692 cm^{-1}. ^1H NMR (CCl_4): δ=0.60—1.73 (11H, m), 2.72—3.00 (2H, m), 3.12—3.36 (1H, m), 3.24 (3H, s), and 6.83—7.40 (5H, m). 2-Methoxyethyl methyl sulfide (**1a**) (70%, bp 129—131 °C, lit.[13], 132 °C) was prepared by the alkylation of 2-mercaptoethanol.

Preparation of 1-(Alkylthio)vinyllithium (3). 1-(Methylthio)vinyllithium (3a): To a THF (5 ml) solution of **1a** (212 mg, 2 mmol) and TMEDA (511 mg, 4.4 mmol) was added dropwise a hexane solution of butyllithium (4.4 mmol) at −30 °C. After stirring for 1 h, the resultant pale yellow solution of **3a** was used for the subsequent reactions.

1-Methylthio-2-phenylvinyllithium (3d). To a THF (0.5 ml) solution of LDA prepared from diisopropylamine (101 mg, 1 mmol) and butyllithium (1 mmol) was added a THF (1 ml) solution of **1d** (182 mg, 1 mmol) at −30 °C. After stirring for 40 min, HMPA (0.6 ml) and an additional THF (0.5 ml) solution of LDA (diisopropylamine; 121 mg, 1.2 mmol, butyllithium; 1.2 mmol) were successively added to the reaction mixture at −60 °C and stirring was continued for 2.5 h. The resultant dark green solution of **3d** was used in the subsequent steps.

4-Phenyl-1-phenylthio-1-butenyllithium (3e). To a THF (1 ml) solution of TMEDA (244 mg, 2.1 mmol) were added a hexane solution of butyllithium (2.1 mmol) and a THF (1 ml) solution of 2-methoxy-4-phenylbutyl phenyl sulfide (**1e**) (272 mg, 1 mmol) successively at −30 °C. After stirring for 2 h, the reddish purple solution of **3e** was obtained. By a similar procedure, the THF solutions of other vinyllithiums (**3b** and **c**; 0 °C, 30 min, **3f** and **g**; −23 °C, 3 h) were prepared.

The Reaction of 1-(Methylthio)vinyllithium (3a) with Benzaldehyde. To a THF solution of **3a** prepared from **1a** (212 mg, 2 mmol) by the above-mentioned procedure was added a THF (2 ml) solution of benzaldehyde (233 mg, 2.2 mmol) at −30 °C and the reaction mixture was allowed to warm up to r.t. The reaction was quenched by the addition of a phosphate buffer solution (pH 7). The organic material was extracted with AcOEt and dried over Na_2SO_4. The extract was condensed under reduced pressure. The residue was chromatographed on silica gel (AcOEt–hexane) and 2-methylthio-1-phenyl-2-propen-1-ol (**7a-1**) was isolated (289 mg) in 80% yield. **7a-1**; a viscous oil. IR (neat): 3420, 1602, 1494, 1040, 861, 755, and 702 cm^{-1}. ^1H NMR (CCl_4): δ=2.12 (3H, s), 2.54 (1H, br s), 4.70 (1H, s), 5.08 (1H, s), 5.31 (1H, s), and 7.21 (5H, s). Found: C, 66.50; H, 6.70; S, 17.61%. Calcd for $C_{10}H_{12}OS$: C, 66.62; H, 6.71; S, 17.79%.

In a similar manner, the following β-alkylthio β,γ-unsaturated alcohols (**7**) and 2-hydroxyalkyl vinyl sulfide (**9**) were obtained. 2-Methylthio-5-phenyl-1-penten-3-ol (**7a-2**); a viscous oil. IR (neat): 3420, 1604, 1497, 1047, 861, 754, and 704 cm^{-1}. ^1H NMR (CCl_4): δ=1.63—2.10 (3H, m), 2.17 (3H, s), 2.44—2.89 (2H, m), 3.84—4.26 (1H, m), 4.56 (1H, s), 5.20 (1H, s), and 7.08 (5H, s). Found: C, 69.23; H, 7.77; S, 15.19%. Calcd for $C_{12}H_{16}OS$: C, 69.19; H, 7.74; S, 15.39%. 2-Methylthio-5-phenyl-1,4-pentadien-3-ol (**7a-3**); a viscous oil. IR (neat): 3410, 1601, 1497, 1030, 967, 863, 757, and 698 cm^{-1}. ^1H NMR (CCl_4): 2.18 (3H, s), 2.18—2.40 (1H, br s), 4.47 (1H, s), 4.47—4.83 (1H, br s), 5.31 (1H, s), 6.06 (1H, dd, J=16 and 6 Hz), 6.57 (1H, d, J=16 Hz), and 6.97—7.42 (10H, m). Found: C, 69.64; H, 6.84; S, 15.29%. Calcd for $C_{12}H_{14}OS$: C, 69.86; H, 6.84; S, 15.54%. 2-Methylthio-1-penten-3-ol (**7a-4**); a viscous oil. IR (neat): 3420, 1602, 1100, 983, and 859 cm^{-1}. ^1H NMR (CCl_4): δ=0.70—1.11 (3H, m), 1.36—1.80 (2H, m), 2.02—2.15 (1H, m), 2.20 (3H, s), 3.98 (1H, t, J=6 Hz), 4.67 (1H, s), and 5.20 (1H, s). Found: C, 54.39; H, 9.17; S, 24.11%. Calcd for $C_6H_{12}OS$: C, 54.51; H, 9.14; S, 24.25%. 5-Methyl-2-methylthio-1-hexen-3-ol (**7a-5**); a viscous oil. IR (neat): 3400, 2960, 1600, 1063, and 855 cm^{-1}. ^1H NMR (CCl_4): δ=0.94 (6H, d, J=6 Hz), 1.27—1.93 (3H, m), 1.93—2.15 (1H, m), 2.19 (3H, s), 4.11 (1H, t, J=6 Hz), 4.53 (1H, s), and 5.21 (1H, s). Found: C, 59.57; H, 10.09; S, 19.64%. Calcd for $C_8H_{16}OS$: C, 59.96; H, 10.06; S, 20.00%. 3-Methylthio-1-phenyl-3-buten-2-ol (**7a-6**); a viscous oil. IR (neat): 3450, 1597, 1496, 1070, 864, 718, and 701 cm^{-1}. ^1H NMR (CCl_4): δ=1.69 (3H, s), 2.13 (3H, s), 2.31 (1H, s), 4.78 (1H, s), 5.39 (1H, s), and 7.01—7.54 (5H, m). Found: C, 67.90; H, 7.30; S, 16.26%. Calcd for $C_{11}H_{14}OS$: C, 68.00; H, 7.26; S, 16.50%. 1-(4-Methyl-1-methylthio-2-pentenyl)-1-cyclohexanol (**7c-1**); a viscous oil. IR (neat): 3460, 2940, 1605, 1447, 1060, 982, and 913 cm^{-1}. ^1H NMR (CCl_4): δ=0.94 (6H, d, J=6 Hz), 1.14—2.14 (12H, m), 2.15 (3H, s), 2.14—2.60 (2H, m), and 5.18 (1H, t, J=7 Hz). Found: C, 67.97; H, 10.51; S, 13.66%. Calcd for $C_{13}H_{24}OS$: C, 68.37; H, 10.59; S, 14.04%. 1-[(4-Methyl-1-pentenylthio)methyl]-1-cyclohexanol (**9**); a viscous oil. IR (neat): 3450, 2940, 1613, 1448, 1056, 978, and 948 cm^{-1}. ^1H NMR (CCl_4): δ=0.88 (6H, d, J=6 Hz), 1.10—2.26 (14H, m), 2.68 (2H, s), 5.58 (1H, dt, J=15 and 6 Hz), and 5.93 (1H, d, J=15 Hz). Found: C, 68.40; H, 10.70; S, 13.95%. Calcd for $C_{13}H_{24}OS$: C, 68.37; H, 10.59; S, 14.04%. 2-Methylthio-1,3-diphenyl-2-propen-1-ol (**7d-1**); mp 63—64 °C (hexane-benzene). IR (neat): 3400, 1599, 1494, 1030, 753, and 698 cm^{-1}. ^1H NMR (CCl_4): δ=2.10 (3H, s), 2.85—3.27 (1H, br s), 5.65—5.95 (1H, br s), 6.32 (1H, s), and 6.88—7.42 (10H, m). Found: C, 74.81; H, 6.29; S, 12.50%. Calcd for $C_{16}H_{16}OS$: C, 74.96; H, 6.29; S, 12.51%. 2-Methylthio-1,5-diphenyl-1-penten-3-ol (**7d-2**); a viscous oil. IR (neat): 3400, 1602, 1497, 1053, 787, 756, and 699 cm^{-1}. ^1H NMR (CCl_4): δ=1.61—2.14 (2H, m), 2.18 (3H, s), 2.31—2.82 (3H, m), 4.51—4.84 (1H, m), 6.05 (1H, s), and 7.07 (10H, s). Found: C, 76.19; H, 7.11; S, 10.51%. Calcd for $C_{18}H_{20}OS$: C, 76.01; H, 7.09; S, 11.27%. 2-Methylthio-1,5-diphenyl-1,4-pentadien-3-ol (**7d-3**); a viscous oil. IR (neat): 3400, 1599, 1495, 1068, 964, 784, 750, and 694 cm^{-1}. ^1H NMR (CCl_4): δ=1.94—2.17 (1H, br s), 2.32 (3H, s), 5.21—5.47 (1H, br s), 6.30 (1H, s), 6.13 (1H, dd, J=16 and 4 Hz), 6.61 (1H, d, J=16 Hz), and 6.77—7.46 (10H, m). Found: C, 75.97; H, 6.51;

S, 11.02%. Calcd for $C_{18}H_{18}OS$: C, 76.56; H, 6.42; S, 11.35%. 2-Methylthio-1-phenyl-1-penten-3-ol (**7d-4**); a viscous oil. IR (neat): 3390, 2950, 1598, 1493, 1028, 753, and 697 cm^{-1}. ^1H NMR (CCl_4): δ=0.85 (3H, t, J=7 Hz), 1.38—1.90 (2H, m), 2.25 (3H, s), 4.17—4.73 (1H, m), 6.10 (1H, s), and 7.13 (5H, s). Found: C, 69.08; H, 7.82; S, 14.90%. Calcd for $C_{12}H_{16}OS$: C, 69.19; H, 7.74; S, 15.39%. 5-Methyl-2-methylthio-1-phenyl-1-hexen-3-ol (**7d-5**); a viscous oil. IR (neat): 3380, 2950, 1600, 1029, 755, and 694 cm^{-1}. ^1H NMR (CCl_4): δ=0.59—1.03 (6H, m), 1.13—1.84 (3H, m), 1.97—2.22 (1H, br s), 2.25 (3H, s), 4.52—4.90 (1H, m), 6.09 (1H, s), and 7.16 (5H, s). Found: C, 71.15; H, 8.58; S, 13.15%. Calcd for $C_{14}H_{20}OS$: C, 71.14; H, 8.53; S, 13.56%. 1,5-Diphenyl-2-phenylthio-2-penten-1-ol (**7e-1**); a viscous oil. IR (neat): 3430, 3020, 1601, 1582, 1496, 1479, 1025, 743, and 698 cm^{-1}. ^1H NMR (CCl_4): δ=2.19—2.97 (4H, m), 2.78 (1H, s), 5.52 (1H, s), 5.76 (1H, t, J=7 Hz), and 6.59—7.70 (15H, m). Found: C, 79.70; H, 6.33; S, 9.22%. Calcd for $C_{23}H_{22}OS$: C, 79.73; H, 6.40; S, 9.25%. 7-Phenyl-4-phenylthio-4-hepten-3-ol (**7e-2**); a viscous oil. IR (neat): 3420, 1602, 1582, 1496, 1478, 1086, 1024, 743, and 697 cm^{-1}. ^1H NMR (CCl_4): δ=0.84 (3H, t, J=7 Hz), 1.20—1.78 (3H, m), 2.26—2.83 (4H, m), 4.02—4.45 (1H, m), 5.74 (1H, t, J=7 Hz), and 6.97—7.38 (10H, m). Found: C, 76.38; H, 7.49; S, 10.52%. Calcd for $C_{19}H_{22}OS$: C, 76.47; H, 7.43; S, 10.74%. 2-Methyl-8-phenyl-5-phenylthio-5-octen-4-ol (**7e-3**); a viscous oil. IR (neat): 3420, 2960, 1603, 1583, 1497, 1480, 1068, 1026, 744, and 698 cm^{-1}. ^1H NMR (CCl_4): δ=0.84 and 0.88 (6H, 2d, J=6 and 7 Hz), 1.03—1.92 (4H, m), 2.33—2.86 (4H, m), 4.39 (1H, dd, J=8 and 5 Hz), 5.60 (1H, t, J=8 Hz), and 6.80—7.33 (10H, m). Found: C, 76.91; H, 8.15; S, 9.45%. Calcd for $C_{21}H_{26}OS$: C, 77.25; H, 8.03; S, 9.82%. 2,6-Diphenyl-3-phenylthio-3-hexen-2-ol (**7e-4**); a viscous oil. IR (neat): 3450, 1597, 1580, 1495, 1477, 1024, 743, and 696 cm^{-1}. ^1H NMR (CCl_4): δ=1.64 (3H, s), 2.08 (1H, s), 2.15—2.38 (4H, m), 5.64 (1H, t, J=7 Hz), and 6.58—7.48 (15H, m). Found: C, 79.94; H, 6.71; S, 8.77%. Calcd for $C_{24}H_{24}OS$: C, 79.96; H, 6.71; S, 8.89%. 5-Methyl-1-phenyl-2-phenylthio-2-hexen-1-ol (**7f-1**); a viscous oil. IR (neat): 3420, 2950, 1581, 1479, 1025, 740, and 697 cm^{-1}. ^1H NMR (CCl_4): δ=0.91 (6H, d, J=7 Hz), 1.17—1.92 (1H, m), 2.16 (2H, t, J=8 Hz), 2.59 (1H, d, J=7 Hz), 5.54 (1H, d, J=7 Hz), 5.79 (1H, t, J=8 Hz), and 6.70—7.37 (10H, m). Found: C, 76.60; H, 7.51; S, 10.51%. Calcd for $C_{19}H_{22}OS$: C, 76.47; H, 7.43; S, 10.74%. 7-Methyl-1-phenyl-4-phenylthio-4-octen-3-ol (**7f-2**); a viscous oil. IR (neat): 3420, 2950, 1601, 1581, 1497, 1478, 1024, 744, and 697 cm^{-1}. ^1H NMR (CCl_4): δ=0.85 (6H, d, J=7 Hz), 1.11—2.12 (6H, m), 2.60 (2H, t, J=7 Hz), 4.14—4.56 (1H, m), 5.69 (1H, t, J=8 Hz), and 6.77—7.38 (10H, m). Found: C, 77.01; H, 8.10; S, 9.52%. Calcd for $C_{21}H_{26}OS$: C, 77.25; H, 8.03; S, 9.82%. 7-Methyl-1-phenyl-4-phenylthio-1,4-octadien-3-ol (**7f-3**); a viscous oil. IR (neat): 3400, 2950, 1580, 1478, 1024, 966, 750, and 692 cm^{-1}. ^1H NMR (CCl_4): δ=0.95 (6H, d, J=6 Hz), 1.20—1.92 (1H, m), 2.19 (2H, t, J=7 Hz), 4.93—5.27 (1H, m), 5.88 (1H, t, J=7 Hz), 5.97 (1H, dd, J=16 and 5 Hz), 6.48 (1H, d, J=16 Hz), and 6.96—7.43 (10H, m). Found: C, 77.49; H, 7.47; S, 9.58%. Calcd for $C_{21}H_{24}OS$: C, 77.73; H, 7.46; S, 9.88%. 7-Methyl-4-phenylthio-4-octen-3-ol (**7f-4**); a viscous oil. IR (neat): 3420, 2960, 1582, 1480, 1024, 739, and 690 cm^{-1}. ^1H NMR (CCl_4): δ=0.68—1.11 (3H, m), 0.91 (6H, d, J=7 Hz), 1.11—2.30 (6H, m), 4.18—4.66 (1H, m), 5.81 (1H, t, J=8 Hz), and 6.98—7.57 (5H, m). Found: C, 71.45; H, 8.77; S, 12.42%. Calcd for $C_{15}H_{22}OS$: C, 71.96; H, 8.85; S, 12.80%. 2,8-Dimethyl-5-phenylthio-5-nonen-4-ol (**7f-5**); a viscous oil. IR (neat): 3420, 2950, 1579, 1477, 1022, 736, and 687 cm^{-1}. ^1H NMR (CCl_4): δ=0.93 (12H, d, J=7 Hz), 1.16—2.25 (7H, m), 4.28—4.62 (1H, m), 5.69 (1H, t, J=8 Hz), and 6.89—7.41 (5H, m). Found: C, 73.38; H, 9.48; S, 11.14%. Calcd for $C_{17}H_{26}OS$: C, 73.33; H, 9.41; S, 11.51%. 1-(4-Methyl-1-phenylthio-1-pentenyl)-1-cyclohexanol (**7f-6**); a viscous oil. IR (neat): 3480, 2940, 2870, 1582, 1479, 1024, 738, and 690 cm^{-1}. ^1H NMR (CCl_4): δ=0.93 (6H, d, J=7 Hz), 1.06—2.03 (12H, m), 2.39 (2H, t, J=7 Hz), 5.81 (1H, t, J=7 Hz), and 7.00—7.50 (5H, m). Found: 74.23; H, 8.98; S, 10.84%. Calcd for $C_{18}H_{26}OS$: C, 74.43; H, 9.02; S, 11.04%. 6-Methyl-2-phenyl-3-phenylthio-3-hepten-2-ol (**7f-7**); a viscous oil. IR (neat): 3450, 1598, 1580, 1495, 1478, 1066, 1024, 743, and 694 cm^{-1}. ^1H NMR (CCl_4): δ=0.65 and 0.70 (6H, 2d, J=7 Hz), 1.10—2.00 (3H, m), 1.70 (3H, s), 2.31 (1H, s), 5.70 (1H, t, J=8 Hz), and 6.84—7.51 (10H, m). Found: C, 76.86; H, 7.83; S, 10.09%. Calcd for $C_{20}H_{24}OS$: C, 76.88; H, 7.74; S, 10.26%. 1-Phenyl-2-phenylthio-2-octen-1-ol (**7g-1**); a viscous oil. IR (neat): 3400, 3020, 2880, 1575, 1470, 1430, 1015, 725, and 685 cm^{-1}. ^1H NMR (CCl_4): δ=0.55—1.61 (9H, m), 1.96—2.50 (2H, m), 2.93 (1H, s), 5.61 (1H, s), 5.84 (1H, t, J=7 Hz), and 6.88—7.49 (10H, m). Found: C, 76.91; H, 7.84; S, 9.96%. Calcd for $C_{20}H_{24}OS$: C, 76.88; H, 7.74; S, 10.26%. 1-(1-Phenylthio-1-heptenyl)-1-cyclohexanol (**7g-2**); a viscous oil. IR (neat): 3490, 2930, 1584, 1482, 1432, 1028, 742, and 693 cm^{-1}. ^1H NMR (CCl_4): δ=0.70—2.03 (20H, m), 2.25—2.73 (2H, m), 5.84 (1H, t, J=7 Hz), and 7.00—7.48 (5H, m). Found: C, 74.95; H, 9.42; S, 10.44%. Calcd for $C_{19}H_{28}OS$: C, 74.95; H, 9.27; S, 10.53%. 2-Phenyl-3-phenylthio-3-nonen-2-ol (**7g-3**); a viscous oil. IR (neat): 3460, 2920, 1598, 1580, 1493, 1478, 1439, 1024, 739, and 699 cm^{-1}. ^1H NMR (CCl_4): δ=0.53—1.40 (9H, m), 1.68 (3H, s), 1.60—2.30 (2H, m), 2,56 (1H, s). 5.80 (1H, t, J=7 Hz) and 7.03—7.67 (10H, m). Found: C, 77.47; H, 8.13; S, 9.58%. Calcd for $C_{21}H_{26}OS$: C, 77.25; H, 8.03; S, 9.82%. The following α-methylthio ketones were obtained by the reaction of **3b** and **3c** with aldehydes followded by the isomerization by hydrochloric acid. 2-Methylthio-1,5-diphenyl-1-pentanone (**8b-1**); a viscous oil. IR (neat): 3020, 2920, 1673, 1498, 1449, 742, and 699 cm^{-}. ^1H NMR (CCl_4): δ=1.41—2.06 (4H, m), 1.81 (3H, s), 2.41—2.78 (2H, m), 3.94 (1H, t, J=7 Hz), 7.09 (5H, s), 7.17—7.48 (3H, m), and 7.67—8.02 (2H, m). Found: C, 76.04; H, 7.18; S, 11.18%. Calcd for $C_{18}H_{20}OS$: C, 76.01; H, 7.09; S, 11.27%. 4-Methylthio-1,7-diphenyl-3-heptanone (**8b-2**); a viscous oil. IR (neat): 3020, 2920, 1700, 1453, 746, and 697 cm^{-1}. ^1H NMR (CCl_4): δ=1.30—1.87 (4H, m), 1.70 (3H, s), 2.27—3.12 (7H, m), and 7.12 (10H, s). Found: C, 76.49; H, 7.70; S, 10.07%. Calcd for $C_{20}H_{24}OS$: C, 76.88; H, 7.74; S, 10.26%. 4-Methylthio-7-phenyl-3-heptanone (**8b-3**); a viscous oil. IR (neat): 3020, 2940, 1703, 1453, 747, and 698 cm^{-1}. ^1H NMR (CCl_4): δ=1.04 (3H, t, J=8 Hz), 1.35—1.88 (4H, m), 1.82 (3H, s), 2.10—2.79 (4H, m), and 7.11 (5H, s). Found: C, 71.32; H, 8.61; S, 13.14%. Calcd for $C_{14}H_{20}OS$: C, 71.14; H, 8.53; S, 13.56%. 5-Methyl-2-methylthio-1-phenyl-1-hexanone (**8c-1**); a viscous oil. IR (neat): 3020, 2940, 1672, 1448, 739, and 695 cm^{-1}. ^1H NMR (CCl_4): δ=0.92 (6H, d, J=6 Hz), 1.03—2.13 (5H, m), 1.85 (3H, s), 3.92 (1H, t, J=7 Hz), 7.08—7.51 (3H, m), and 7.73—8.02 (2H, m). Found: C, 71.20; H, 8.55; S, 13.38%. Calcd for $C_{14}H_{20}OS$: C, 71.14; H, 8.53; S, 13.56%.

Reaction of 4-Phenyl-1-phenylthio-1-butenyllithium (3e) with Octyl Iodide. To a THF solution of **3e** prepared from **1e** (272 mg, 1 mmol) was added an HMPA (0.6 ml) solution of octyl iodide (360 mg, 1.5 mmol) at −78 °C. After stirring for 30 min at −78 °C, the reaction mixture was warmed up to r.t. The reaction was quenched by the addition of aqueous NH_4Cl. The usual work up gave 1-phenyl-4-phenylthio-3-dodecene (**10e-2**) (439 mg, 64%). **10e-2**; an oil. IR (neat): 2930, 1602, 1598, 1583, 1480, 1455, 1440, 1027, 742, and 699 cm^{-1}. ^1H NMR (CCl_4): δ=0.60—1.67 (15H, m), 1.82—2.90 (6H, m), 5.77 (1H, t, J=7 Hz), and 7.17 (10H, s). Found: C, 81.55; H, 9.25; S, 8.90%. Calcd for $C_{24}H_{32}S$: C, 81.76; H, 9.15; S, 9.09%. In a similar manner, the following alkenyl sulfides (**10**) were obtained. 2-Methylthio-1-decene (**10a-1**); an oil. IR (neat): 2920, 1710, 1598, and 840 cm^{-1}. ^1H NMR (CCl_4): δ=0.62—1.88 (15H, m),

1.92—2.40 (2H, m), 2.16 (3H, s), 4.50 (1H, s), and 4.94 (1H, s). Found: C, 70.92; H, 11.87; S, 16.80%. Calcd for $C_{11}H_{22}S$: C, 70.90; H, 11.90; S, 17.20%. 5-Phenyl-2-phenylthio-2-pentene (**10e-1**)[10]; an oil. IR (neat): 2920, 1601, 1582, 1496, 1478, 1453, 1439, 1026, 745, and 697 cm^{-1}. ^{1}H NMR (CCl_4): δ=1.72 (3H, s), 2.08—2.85 (4H, m), 5.81 (1H, t, J=6 Hz), and 7.15 (10H, s). Found: C, 80.41; H, 7.26; S, 12.27%. Calcd for $C_{17}H_{18}S$: C, 80.27; H, 7.13; S, 12.60%. 1,5-Diphenyl-2-phenylthio-2-pentene (**10e-3**); an oil. IR (neat): 3020, 2920, 1600, 1582, 1497, 1476, 1453, 1438, 1024, 742, and 698 cm^{-1}. ^{1}H NMR (CCl_4): δ=2.22—2.86 (4H, m), 3.36 (2H, s), 5.85 (1H, t, J=7 Hz), and 6.74—7.41 (15H, m). Found: C, 83.52; H, 6.80; S, 9.51%. Calcd for $C_{23}H_{22}S$: C, 83.59; H, 6.71; S, 9.70%. 5-Methyl-2-phenylthio-2-hexene (**10f-1**); an oil. IR (neat): 2950, 1581, 1476, 1437, 1023, 737, and 688 cm^{-1}. ^{1}H NMR (CCl_4): δ=0.95 (6H, d, J=6 Hz), 1.07—2.43 (3H, m), 1.88 (3H, br s), 5.79 (1H, br t, J=7 Hz), and 7.21 (5H, s). Found: C, 75.81; H, 8.96; S, 15.36%. Calcd for $C_{13}H_{18}S$: C, 75.67; H, 8.79; S, 15.54%. 2-Methyl-5-phenylthio-4-tridecene (**10f-2**); an oil. IR (neat): 2920, 1582, 1479, 1467, 1439, 1025, 737, and 690 cm^{-1}. ^{1}H NMR (CCl_4): δ=0.65—2.44 (20H, m), 0.93 (6H, d, J=6 Hz), 5.79 (1H, t, J=7 Hz), and 7.26 (5H, s). Found: C, 78.81; H, 10.65; S, 10.34%. Calcd for $C_{20}H_{32}S$: C, 78.88; H, 10.59; S, 10.53%. 5-Methyl-1-phenyl-2-phenylthio-2-hexene (**10f-3**); an oil. IR (neat): 2950, 1598, 1581, 1495, 1475, 1452, 1438, 1024, 740, and 695 cm^{-1}. ^{1}H NMR (CCl_4): δ=0.93 (6H, d, J=6 Hz), 1.43—2.28 (3H, m), 3.47 (2H, s), 5.88 (1H, t, J=7 Hz), and 6.81—7.38 (10H, m). Found: C, 80.94; H, 7.98; S, 11.19%. Calcd for $C_{19}H_{22}S$: C, 80.80; H, 7.85; S, 11.35%. 7-Methyl-4-phenylthio-1,4-octadiene (**10f-4**); an oil. IR (neat): 2900, 1647, 1593, 1490, 1037, 922, 752, and 702 cm^{-1}. ^{1}H NMR (CCl_4): δ=0.92 (6H, d, J=6 Hz), 1.43—2.25 (3H, m), 2.93 (2H, d, J=6 Hz), 4.76—5.22 (2H, m), 6.13—5.45 (2H, m), and 7.05—7.47 (5H, m). Found: C, 77.50; H, 8.80; S, 13.67%. Calcd for $C_{15}H_{20}S$: C, 77.52; H, 8.68; S, 13.80%. 4-Methyl-1-phenylthio-1-trimethylsilyl-1-pentene (**10f-5**); an oil. IR (neat): 2960, 1582, 1477, 1440, 1249, 841, 740, and 692 cm^{-1}. ^{1}H NMR (CCl_4): δ=0.11 (9H, s), 0.93 (6H, d, J=6 Hz), 1.35—1.89 (1H, m), 2.16 (2H, t, J=7 Hz), 6.42 (1H, t, J=7 Hz), and 6.93—7.42 (5H, m). Found: C, 68.46: H, 9.21; S, 12.32%. Calcd for $C_{15}H_{24}SSi$: C, 68.11; H, 9.15; S, 12.12%. 2-Phenylthio-2-octene (**10g-1**); an oil. IR (neat): 2960, 1593, 1487, 1449, 1035, 750, and 701 cm^{-1}. ^{1}H NMR (CCl_4): δ=0.60—1.72 (9H, m), 1.82—2.01 (3H, m), 2.01—2.60 (2H, m), 5.63—6.02 (1H, m), and 7.01—7.62 (5H, m). Found: C, 76.25; H, 9.25; S, 14.34%. Calcd for $C_{14}H_{20}S$: C, 76.30; H, 9.15; S, 14.55%. 3-Phenylthio-3-nonene (**10g-2**); an oil. IR (neat): 2980, 1593, 1489, 1474, 1449, 1036, 748, and 701 cm^{-1}. ^{1}H NMR (CCl_4): δ=0.67—1.70 (9H, m), 1.04 (3H, t, J=7 Hz), 1.88—2.45 (4H, m), 5.81 (1H, t, J=7 Hz), and 6.92—7.53 (5H, m). Found: C, 76.83; H, 9.65; S, 13.39%. Calcd for $C_{15}H_{22}S$: C, 76.86; H, 9.46; S, 13.68%. 7-Phenylthio-6-pentadecene (**10g-3**); an oil. IR (neat): 2930, 1583, 1480, 1468, 1441, 1027, 762, 740, and 692 cm^{-1}. ^{1}H NMR (CCl_4): δ=0.50—1.75 (24H, m), 1.85—2.48 (4H, m), 5.78 (1H, t, J=7 Hz), and 6.95—7.42 (5H, m). Found: C, 79.33; H, 10.81; S, 10.06%. Calcd for $C_{21}H_{34}S$: C, 79.18; H, 10.76; S, 10.06%. 1-Phenyl-2-phenylthio-2-octene (**10g-4**); an oil. IR (neat): 3030, 2930, 1600, 1582, 1498, 1476, 1453, 1440, 1026, 742, and 695 cm^{-1}. ^{1}H NMR (CCl_4): δ=0.68—1.64 (9H, m), 1.96—2.48 (2H, m), 3.52 (2H, s), 5.93 (1H, t, J=7 Hz), and 7.16 and 7.25 (10H, 2s). Found: C, 81.07; H, 8.20; S, 10.76%. Calcd for $C_{20}H_{24}S$: C, 81.03; H, 8.16; S, 10.81%.

*The Reaction of 1-Phenylthio-1-heptenyllithium (**3g**) with 1,2-Epoxybutane.* To a THF solution of **3g** prepared from **1g** (477 mg, 2 mmol) was added an HMPA (0.6 ml) solution of 1,2-epoxybutane (216 mg, 3 mmol) at −78 °C. After stirring for 30 min, the reaction mixture was warmed up to r.t. The reaction was quenched by the addition of a phosphate buffer solution (pH 7). The usual work up gave 5-phenylthio-5-undecen-3-ol (**11g-2**) (301 mg, 54%). **11g-2**; a viscous oil. IR (neat): 3420, 3070, 2930, 1584, 1477, 1440, 1105, 744, and 692 cm^{-1}. ^{1}H NMR (CCl_4): δ=0.62—1.70 (14H, m), 1.90—2.43 (5H. m), 3.53—3.90 (1H, m), 5.96 (1H, t, J=7 Hz), and 6.94—7.45 (5H, m). Found: C, 73.02; H, 9.43; S, 11.36%. Calcd for $C_{17}H_{26}OS$: C, 73.33; H, 9.41; S, 11.51%. In a similar manner, the following γ-phenylthio γ,δ-unsaturated alcohols (**11**) were obtained. 3-Methylthio-1-phenyl-3-buten-1-ol (**11a-1**); a viscous oil. IR (neat): 3400, 1600, 1582, 1053, 854, 757, and 700 cm^{-1}. ^{1}H NMR (CCl_4): δ=2.16 (3H, s), 252 (2, d, J=6 Hz), 2.64—2.87 (1H, br s), 4.53 (1H, s), 4.80 (1H, t, J=6 Hz), 5.01 (1H, s), and 7.28 (5H, s). Found: C, 68.10; H, 7.20; S, 16.49%. Calcd for $C_{11}H_{14}OS$: C, 68.00; H, 7.26; S, 16.50%. 6-Methyl-1-phenyl-3-phenylthio-3-hepten-1-ol (**11f-1**); a viscous oil. IR (neat): 3400, 1600, 1582, 1053, 854, 757, and 700 cm^{-1}. ^{1}H NMR (CCl_4): δ=0.80 and 0.85 (6H, 2d, J=6 Hz), 1.24—2.09 (4H, m), 2.43 and 2.53 (2H, 2d, J=5 and 7 Hz), 4.90 (1H, dd, J=5 and 7 Hz), 5.94 (1H, t, J=7 Hz), and 6.93—7.45 (10H, m). Found: C, 76.86; H, 7.79; S, 10.14%. Calcd for $C_{20}H_{24}OS$: C, 76.88; H, 7.74; S, 10.26%. 8-Methyl-5-phenylthio-5-nonen-3-ol (**11f-2**); a viscous oil. IR (neat): 3390, 2950, 1584, 1480, 1072, 1028, 743, and 696 cm^{-1}. ^{1}H NMR (CCl_4): δ=0.60—1.08 (3H, m), 0.93 (6H, d, J=6 Hz), 1.13—1.77 (3H, m), 1.86—2.63 (5H, m), 3.48—3.97 (1H, m), 5.96 (1H, t, J=7 Hz), and 7.29 (5H, s). Found: C, 72.46; H, 9.12; S, 12.15%. Calcd for $C_{16}H_{24}OS$: C, 72.68; H, 9.15; S, 12.12%. 1-Phenyl-3-phenylthio-3-nonen-1-ol (**11g-1**); a viscous oil. IR (neat): 3410, 3050, 3020, 2920, 1582, 1478, 1050, 1024, 742, and 699 cm^{-1}. ^{1}H NMR (CCl_4): δ=0.66—1.53 (9H, m), 1.60—2.34 (3H, m), 2.46 and 2.56 (2H, 2d, J=5 and 8 Hz), 4.94 (1H, dd, J=5 and 8 Hz), 5.97 (1H, t, J=8Hz), and 7.23 and 7.28 (10H, 2s). Found: C, 76.64; H, 8.02; S, 9.68%. Calcd for $C_{21}H_{26}OS$: C, 77.25; H, 8.03; S, 9.80%.

*Preparation of (E)-4-Methyl-1-phenylthio-1-pentene (**2f**) and (Z)-**2f**.* A hexane (4 ml) solution of **2f** (364 mg, 1.9 mmol) prepared by the reaction of **1f** with an equimolar amount of butyllithium was irradiated by high pressure mercury lamp (400 W) for 40 min. After evaporation of the solvent, the residue was dissolved in CH_2Cl_2 (6 ml) and was added to a CH_2Cl_2 (6 ml) solution of MCPBA (327 mg, 1.9 mmol) at −23 °C. The reaction mixture was stirred for 1 h. Then, the reaction was quenched by the addition of 5% aqueous $NaHCO_3$ and the crude sulfoxides were extracted with CH_2Cl_2. The extract was dried over Na_2SO_4 and condensed under reduced pressure. The residue was chromatographed on silica gel (AcOEt-hexane) and (*E*)-4-methyl-1-phenylsulfinyl-1-pentene (**12-1**) (136 mg, 34%) and (*Z*)-**12-1** (96 mg, 24%) were obtained. The reduction of the sulfoxides were carried out by the method reported by Posner and Tang.[8] To a suspension of CuI (37 mg, 0.19 mmol) in ether (0.7 ml) was added an ethereal solution of ethylmagnesium bromide (1.9 mmol) at 0 °C. After stirring for 1 h, (*E*)-**12-1** (135 mg, 0.65 mmol) in ether (0.7 ml) was added to the solution and the reaction mixture was stirred for 1 h. The reaction was quenched by the addition of aqueous NH_4Cl and the organic substance was extracted with ether. The extract was dried over Na_2SO_4 and condensed under reduced pressure. The crude sulfide was purified by TLC (hexane) and (*E*)-**2f** (61 mg) was isolated in 49% yield. In a similar manner, (*Z*)-**2f** was also obtained by the reduction of (*Z*)-**12-1** in 33% yield. (*E*)-**12-1**; a viscous oil. IR (neat): 2950, 1623, 1580, 1466, 1444, 1086, 1047, 968, 746, and 690 cm^{-1}. ^{1}H NMR (CCl_4): δ=0.90 (6H, d, J=6 Hz), 1.43—2.28 (3H, m), 6.18 (1H, d, J=15 Hz), 6.57 (1H, dt, J=15 and 7 Hz), and 7.37—7.82 (5H, m). (*Z*)-**12-1**; a viscous oil. IR (neat): 2950, 1614, 1580, 1465, 1443, 1083,

1040, 745, 715, and 690 cm^{-1}. ^1H NMR (CCl_4): δ=1.00 (6H, d, J=6 Hz), 1.47—2.07 (1H, m), 2.36—2.68 (2H, m), 5.86—6.42 (2H, m), and 7.35—7.73 (5H, m). (*E*)-**2f**; an oil. IR (neat): 2950, 1582, 1480, 1440, 1080, 1025, 953, 738, and 689 cm^{-1}. ^1H NMR (CCl_4): δ=0.93 (6H, d, J=6 Hz), 1.07—1.93 (1H, m), 1.93—2.20 (2H, m), 5.83 (1H, dt, J=14 and 6 Hz), 6.15 (1H, d, J=14 Hz), and 7.21 (5H, s). (*Z*)-**2f**; an oil. IR (neat): 2940, 1584, 1479, 1438, 1080, 1023, 762, 733, and 685 cm^{-1}. ^1H NMR (CCl_4): δ=0.97 (6H, d, J=6 Hz), 1.37—2.02 (1H, m), 2.16 (2H, t, J=7 Hz), 5.77 (1H, dt, J=10 and 7 Hz), 6.20 (1H, d, J=10 Hz), and 7.23 (5H, s).

*Photoisomerization of 5-Methyl-2-phenylthio-2-hexene (**10f-1**).* A hexane (2.8 ml) solution of **10f-1** (305 mg, 1.47 mmol) was irradiated with high pressure mercury lamp (400 W) for 2 h. After evaporation of the solvent, the residue was chromatographed on silica gel (hexane) and (*E*)-**10f-1** (100 mg) and (*Z*)-**10f-1** (164 mg) were obtained in 33% and 54% yields, respectively. (*Z*)-**10f-1**; an oil. IR (neat): 2960, 1583, 1479, 1441, 1026, 739, and 690 cm^{-1}. ^1H NMR (CCl_4): δ=0.93 (6H, d, J=7 Hz), 1.09—2.42 (3H, m), 1.86 (3H, br s), 5.83 (1H, br t, J=7 Hz), and 7.25 (5H, s). In a similar manner, the photoisomerization of **7f-1** (0.7 h, *E*; 16%, *Z*; 33%), **7f-4** (0.7 h, 78%, *E*:*Z*=40:60), and **10f-2** (2 h, *E*; 35%, *Z*; 38%) were carried out and the following *Z*-isomers were obtained. (*Z*)-5-Methyl-1-phenyl-2-phenylthio-2-hexene-1-ol (**7f-1**); a viscous oil. IR (neat): 3380, 2950, 1582, 1479, 1025, 740, and 698 cm^{-1}. ^1H NMR (CCl_4): δ=0.91 (6H, d, J=7 Hz), 1.20—1.98 (1H, m), 2.26 (3H, br t, J=7 Hz), 5.08 (1H, br s), 6.33 (1H, t, J=7 Hz), 7.21 and 7.27 (10H, 2s) (*E* and *Z*)-7-methyl-4-phenylthio-4-octen-3-ol (**7f-4**); a viscous oil. IR (neat): 3400, 2960, 1583, 1480, 1024, 739, and 690 cm^{-1}. ^1H NMR (CCl_4): δ=0.91 (6H, d, J=7 Hz), 0.68—1.12 (3H, m), 1.12—2.46 (6H, m), 3.99 and 4.44 (1H, 2t, J=7 Hz), 5.81 and 6.33 (1H, 2t, J=7 Hz), and 6.99—7.56 (5H, m). (*Z*)-2-Methyl-5-phenylthio-4-tridecene (**10f-2**); an oil. IR (neat): 2920, 1582, 1479, 1438, 1027, 739, and 690 cm^{-1}. ^1H NMR (CCl_4): δ=0.64—2.48 (20H, m), 0.93 (6H, d, J=6 Hz), 5.85 (1H, t, J=7 Hz), and 7.22 (5H, s).

*Preparation of (Z)-5-Methyl-2-phenylsulfinyl-2-hexene (**12-2**).* To a CH_2Cl_2 (3 ml) solution of MCPBA (134 mg, 0.78 mmol) was added a CH_2Cl_2 (3 ml) solution of (*Z*)-5-methyl-2-phenylthio-2-hexene (**10f-1**) (160 mg, 0.78 mmol) at −23 °C. After stirring for 1 h, 5% aqueous $NaHCO_3$ was added to the reaction mixture and the usual work up gave (*Z*)-**12-2** (102 mg) in 59% yield. (*Z*)-**12-2**; a viscous oil. IR (neat): 2950, 1580, 1464, 1443, 1083, 1041, 748, and 693 cm^{-1}. ^1H NMR (CCl_4): δ=1.03 (6H, d, J=5 Hz), 1.45—2.86 (3H, m), 1.64 (3H, br s), 5.94 (1H, br t, J=8 Hz), and 7.49 (5H, m). In a similar manner, (*E*)-**12-2** was obtained by the oxidation of (*E*)-**10f-1**. (*E*)-5-Methyl-2-phenylsulfinyl-2-hexene (**12-2**) (55%); a viscous oil. IR (neat): 2950, 1580, 1466, 1443, 1086, 1043, 749, and 692 cm^{-1}. ^1H NMR (CCl_4): δ=0.97 (6H, d, J=5 Hz), 1.16—2.28 (3H, m), 1.56 (3H, br s), 6.40 (1H, br t, J=8 Hz), and 7.25—7.72 (5H, m).

References

1) H. W. Gschwend and H. R. Rodriguez, *Org. React.*, **26**, 32 (1979).

2) K. Oshima, K. Shimozi, H. Takahashi, H. Yamamoto, and H. Nozaki, *J. Am. Chem. Soc.*, **95**, 2694 (1973).

3) R. C. Cookson and P. J. Persons, *J. Chem. Soc., Chem. Commun.*, **1976**, 990; T. Takeda and T. Fujiwara, *Chem. Lett.*, **1982**, 1113.

4) I. Shahak and J. Almog, *Synthesis*, **1969**, 170; T. Mukaiyama, T. Kumamoto, S. Fukuyama, and T. Taguchi, *Bull. Chem. Soc. Jpn.*, **43**, 2870 (1970); E. J. Corey and J. I. Shulman, *J. Org. Chem.*, **35**, 777 (1970); J. I. Grayson and S. Warren, *J. Chem. Soc., Perkin Trans. 1*, 2263 (1977); T. Mukaiyama and K. Saigo, *Chem. Lett.*, **1973**, 479; and references cited therein; T. Oida, S. Tanimoto, H. Ikehira, and M. Okano, *Bull. Chem. Soc. Jpn.*, **56**, 959 (1983); W. Dumont and A. Krief, *J. Chem. Soc., Chem. Commun.*, **1980**, 673; T. Mukaiyama, M. Shiono, and T. Sato, *Chem. Lett.*, **1974**, 37.

5) T. Takeda, H. Furukawa, and T. Fujiwara, *Chem. Lett.*, **1982**, 593.

6) E. J. Corey, B. W. Erickson, and R. Noyori, *J. Am. Chem. Soc.*, **93**, 1724 (1971).

7) R. C. Cookson and P. J. Persons, *J. Chem. Soc., Chem. Commun.*, **1978**, 821.

8) G. H. Posner and P.-W. Tang, *J. Org. Chem.*, **43**, 4131 (1978).

9) D. Y. Curtin and J. W. Crump, *J. Am. Chem. Soc.*, **80**, 1922 (1958); H. M. Walborsky and L. M. Turner, *ibid.*, **94**, 2273 (1972), and references cited therein.

10) H. Takei, H. Sugimura, M. Miura, and H. Okamura, *Chem. Lett.*, **1980**, 1209.

11) E. J. Corey and D. Seebach, *J. Org. Chem.*, **31**, 4097 (1966).

12) D. J. Peterson, *J. Org. Chem.*, **32**, 1717 (1967).

13) W. V. E. Doering and K. C. Schreiber, *J. Am. Chem. Soc.*, **77**, 514 (1955).

Photooxygenation Reactions of 4-Flavanols and Benzylic-type Alcohols

Morio SUZUKI,* Eiji YAMAZAKI, Fumiaki TAKABE, Motonobu MORIOKA, Hideo MIZUNO, and Ryoka MATSUSHIMA

Department of Industrial Chemistry, Faculty of Engineering, Shizuoka University, Hamamatsu 432

(Received August 31, 1983)

On irradiation in benzene under oxygen atmosphere *cis*- and *trans*-4-flavanols gave flavanones with significant structural effects on the yield: A high cis/trans selectivity and enhancement effect by electron-donating substituents. A series of benzylic-type alcohols showed similar substituent effects. The structure-reactivity relationships were explained in terms of the stereoelectronic requirements for favorable overlapping of intermediates. In order to infer the active oxidant species, the above photoreactions were compared with the oxidations by singlet oxygen and superoxide ion. The involvement of superoxide ion or its related species such as electron transfer complex $R^{+\cdot}\cdots O_2^{-\cdot}$ was suggested. The effects of additives and solvents were also investigated.

A detailed study has been reported on the photooxidation reaction of a series of benzylic-type alcohols in DMSO under oxygen atmosphere, showing a special effects of DMSO or the formation of a charge transfer complex.[1] On the other hand, a high stereoselectivity has been observed for the thermal oxidations of secondary alcohols[2] and a series of 4-chromanols[3] with chromium trioxide, which has been attributed to both the stereoelectronic effect and the strain relief. A significant cis/trans selectivity has also been observed in the oxidation of cis and trans isomers of 4-flavanols with the triplet state benzophenone, which has been explained in terms of the stereoelectronic requirements or favorable overlapping of the radical intermediates.[4]

The present paper reports on the structural effects in the photooxygenation reactions of 4-flavanols **1**—**3** and the related benzylic-type alcohols **4**—**11** (Chart 1).

Results and Discussion

Photooxygenation Reactions. Table 1 summarizes the yields of flavanones formed in the photooxidations of 4-flavanols under oxygen atmosphere, in benzene (benzene/O_2), in benzene-diphenyl sulfone (benzene-DPSO/O_2), and in dimethyl sulfoxide (DMSO/O_2), respectively. No reaction products were detected from a benzene solution of **1a** after bubbling through with oxygen gas for 8.5 h in the dark, while only a trace amount of flavanone was detected by TLC analysis on irradiation under nitrogen atmosphere in place of oxygen.

In the above photoreactions two points may be noted as to the structural effects of the substrates: (i) the cis isomers (**1a**, **2a**, **3a**) show higher reactivities compared with the corresponding trans isomers (**1b**, **2b**, **3b**), (ii) electron donating substituents at the 7-position facilitate the reaction. The latter (ii) implies the electrophilic nature of the intermediates while the former (i) suggests the conformational requirements for the substrates and/or intermediates.

Table 2 shows relative reactivities of a series of benzylic-type alcohols (hereafter denoted as benzylic alcohols) in the photooxidations in benzene/O_2, in benzene-DPSO/O_2, and in DMSO/O_2, respectively.

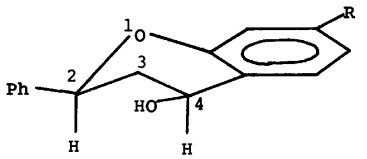

2,4-cis-4-Flavanols

1a R = H
2a R = Cl
3a R = OMe

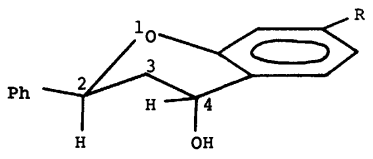

2,4-trans-4-Flavanols

1b R = H
2b R = Cl
3b R = OMe

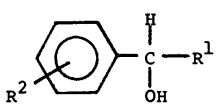

Benzylic alcohols

4	R^1 = Me	R^2 = H	8	R^1 = Me	R^2 = o-OMe
5	R^1 = Me	R^2 = p-Cl	9	R^1 = Me	R^2 = o,p-$(OMe)_2$
6	R^1 = Me	R^2 = p-OMe	10	R^1 = H	R^2 = H
7	R^1 = Me	R^2 = m-OMe	11	R^1 = t-Bu	R^2 = H

Chart 1.

Table 1. Photooxidations of 4-flavanols under different conditions

4-Flavanol	Percent yield of flavanone		
	Benzene/O_2[a]	Benzene-DPSO/O_2[b]	DMSO/O_2[c]
1a	22	34	20
1b	Trace	Trace	Trace
2a	35	44	22
2b	4	Trace	Trace
3a	53	d)	71
3b	12	d)	11

a) 4-Flavanol 0.04 mol dm^{-3} in benzene, under O_2 atomsphere, irradiation time 8 h. b) 4-Flavanol 0.04 mol dm^{-3}, diphenyl sulfone (DPSO) 0.04 mol dm^{-3} in benzene, under O_2 atmosphere, irradiation time 8 h. c) 4-Flavanol 0.025 mol dm^{-3} in dimethyl sulfoxide, under O_2 atmosphere, irradiation time 15 h. d) Photolyzed mixture solutions were too complex to analyze.

Table 2. Photooxidations of benzylic alcohols

Photooxidation system	Benzylic alcohol	Consumption of alcohol/%	Yield of acetophenone/%
Benzene/O_2[a]	**4**	12	12
	5	20	10
	6	32	29
	7	16	8
	8	10	8
	9	19	10
Benzene-DPSO/O_2[b]	**4**	51	45
	5	58	27
	6	98	19
DMSO/O_2[c]	**4**	10	10
	10	29	23[d]
	11	0	0

a) Benzylic alcohol 0.04 mol dm^3 in benzene, under O_2 atmosphere, irradiation time 10 h. b) Benzylic alcohol 0.04 mol dm^{-3}, diphenyl sulfone (DPSO) 0.04 mol dm^3 in benzene, under O_2 atmosphere, irradiation time 10 h. c) Benzylic alcohol 0.025 mol dm^{-3} in dimethyl sulfoxide, under O_2 atmosphere, irradiation time 15 h. d) Benzoic acid was also formed in 6% yield.

Relative reactivities of the *p*-substituted benzylic alcohols in benzene/O_2 show similar tendency (**4**<**5**<**6**) to that of 4-flavanols (**1a**<**2a**<**3a**). Although relative consumption rates in benzene-DPSO/O_2 also show similar tendency, the large gaps between the consumption of the substrates and the yield of acetophenones prevent detailed inspection.

On the other hand, ortho and meta substituents tend to lower the reactivity (**8**, **9** compared with **4**, **6**). Comparison of **4**, **10**, and **11** in DMSO/O_2 shows that bulky groups on the benzylic carbon depress the reaction in spite of the electron-donating ability, implying predominant role of steric factors over the stabilities of intermediates (*e.g.*, benzylic radicals).

Oxidations with Singlet Oxygen and Superoxide Ion. In order to infer the active oxidant species involved in the photooxygenation reactions, it seemed reasonable to compare the reactivities with those in the oxidations by singlet oxygen and superoxide ion, respectively. Oxidation of 4-flavanols by singlet oxygen gave the corresponding flavanones with high cis/trans selectivities (Table 4) which are comparable with those in Table 1. However, the substituent effect of the reactiviy order (**1a**>**2a**>**3a**) is the reverse to that in Table 1, thus suggesting different mechanisms. In the oxidation of 4-flavanols (R) with singlet oxygen in *t*-butyl alcohol, which is fairly polar solvent, superoxide ion may be generated from singlet oxygen *via* CT interaction[5,6] and act as the oxidant species, *e.g.*,

$$R + {}^1O_2 \rightleftharpoons R^{+\cdot} + O_2^{-\cdot} \longrightarrow RO_2 \rightarrow \rightarrow \text{products.}$$

Then, the difference in the reactivity order (Tables 1 and 4) may be due to the difference in the active oxidant species between superoxide ion (in *t*-butyl alcohol) and polar CT complexes (in benzene).

No sufficient data were available for the oxidation of 4-flavanols with superoxide ion (Table 4); the reaction in benzene gave mixtures too complex to analyze, except for **1a** and **1b** which show rather low cis/trans selectivity. In addition, reactions weie complicated by the concomitant rearrangement reaction (ring opening). Thus, **1a**, **1b**, **2a**, and **2b** gave the corresponding 2′-hydroxychalcones stoichiometrically while **3a** and **3b** led to highly complex mixtures incapable of analysis.

As alternatives to the 4-flavanols, a series of benzylic alcohols may serve to see the structure-reactivity relationships in the superoxide ion oxidation. Table 3 illustrates the yields of acetophenone produced in the superoxide oxidation in benzene, showing that the reaction is fairly clean. The substituent effects on the reactivity are comparable to those in the photooxygenation reaction in benzene (Table 2). Thus, electron-donating substituents at the *p*-position facilitate the reaction (**4**—**6** and **5**/**6**), whereas the substituents at the ortho or meta position retard (**7**—**9**). From the similarities in the structure-reactivity relationships (Tables 1—3), it seems probable that the active oxidant species,

Table 3. Yields of acetophenones in the oxidation of benzylic alcohols with $O_2^{-\cdot}$[a]

Benzylic alcohol	Percent yield of acetophenone at				
	1 h	2 h	4 h	8 h	16 h
4	4	6	12	16	21
5	4	5	7	13	16
6	16	22	32	45	64
7			12		15
8			2		3
9			5		6
5/**6**[b]			6/37		13/55

a) Benzylic alcohol 3.3×10^{-2} mol dm^{-3}, KO_2 0.19 mol dm^{-3}, 18-Crown-6 3.3×10^{-2} mol dm^{-3} in benzene, under N_2 atmosphere, for 16 h at room temperature. b) A mixture solution of **5** and **6** each in 3.3×10^{-2} mol dm^{-3} were oxidized with $O_2^{-\cdot}$.

Table 4. Oxidations of 4-flavanols with $O_2^{-\cdot}$ and $^1O_2$

Oxidant and solvent	4-Flavanol	Consumption of flavanol/%	Yield of flavanone/%	Yield of chalcone/%
$O_2^{-\cdot}$/Benzene[a]	**1a**	17	7	5
	1b	10	3	4
$O_2^{-\cdot}$/DMSO[b]	**1a**	12	Trace	12
	1b	14	Trace	14
	2a	15	Trace	15
	2b	15	Trace	15
$^1O_2$/*t*-BuOH[c]	**1a**		53	
	1b		Trace	
	2a		34	
	2b		Trace	
	3a		28	
	3b		Trace	

a) 4-Flavanol 0.025 mol dm^{-3}, KO_2 0.25 mol dm^{-3}, 18-Crown-6 0.025 mol dm^{-3} in benzene, for 2 h at room temperature. b) 4-Flavanol 0.025 mol dm^{-3}, KO_2 0.08 mol dm^{-3}, 18-Crown-6 0.025 mol dm^{-3} in dimethyl sulfoxide, for 3 h at room temperature. c) 4-Flavanol 0.13 mol dm^{-3}, Rose Bengal 3.3×10^{-4} mol dm^{-3} in *t*-butyl alcohol, irradiated with a W-lamp (300 W) for 5 h. Similar results were obtained with thionine sensitizer in place of Rose Bengal.

Table 5. Photooxidation of **4** in the presence of DPSO[a]

DPSO added $\times10^3$ mol dm^{-3}	Consumption of alcohol/%	Yield of acetophenone/%
0	4	4
2	9	9
4	11	11
8	17	17
10	22	19
20	20	20
40	25	25
80	40	32

a) 1-Phenylethanol 0.04 mol dm^{-3} in benzene, under O_2 atmosphere, irradiated for 10 h. A fairly worn-out light source (100-W Hg lamp) was employed in this irradiation and the intensity was much lower than that of the one used elsewhere in the present study.

Table 6. Effects of additives on the yield of flavanone in the photooxidation of **1a** under oxygen atmosphere[a]

Additive mol dm^{-3}	Percent yield of flavanone[b] at 2 h	4 h	6 h	8 h	10 h
Nil	Trace	10	19	29	41
		12	24	30	
DABCO/0.02	0	0	0	Trace	
DTBP/0.02	Trace	22	37	58	
DMB/0.02	Trace	Trace	13	26	
TNM/0.02	76	100	100		
DPSO/0.04	24	43			
DPSO/0.04+DTBP/0.02	47				
DPSO/0.04+DMB/0.02	38				

a) In benzene solution of **1a** 0.02 mol dm^{-3}. DABCO: 1,4-diazabicyclo[2.2.2]octane, DTBP: 2,6-di-*t*-butylphenol, DMB: *p*-dimethoxybenzene, TNM: tetranitromethane, DPSO: diphenyl sulfone. b) Determined from the ^{1}H-NMR signal intensities at $\delta=5$.

involved in the photooxygenation reaction in benzene, is superoxide ion or its related species such as CT complexes. In fact 4-flavanols (**1a**, **3a**, and **3b**) in methanol under oxygen atmosphere showed broad enhancements of the UV-absorption in the region of 220—350 nm, which are ascribable to the charge transfer absorption.

Effects of Solvent and Additives. Photooxygenation of **1a** in different solvents under comparable conditions showed a wide variation in the yield of flavanone (%); ethyl acetate (100%), acetonitrile (61%), benzene (54%), DMSO (45%), 1,2-dimehoxyethane (13%), *t*-butyl alcohol (8%), DMF (trace).

Solvent polarity has been shown to play the key role in partitioning active species between the types of ion pairs and CT cmplexes present in solution.[6-9] The reactivity order shown here is not in the order of solvent polarity, hence superoxide ion mechanism is of minor importance at least in less polar solvents.

Photooxidation of **4** in benzene/O_2 was significantly facilitated by the addition of small amounts of diphenyl sulfone (DPSO). Both the consumption of **4** and the yield of acetophenone were increased with increasing addition of DPSO (Table 5). The enhancement effect may be relevant to charge transfer phenomena as has been implied earlier in the photooxidation of benzylic alcohols in DMSO/O_2.[1]

The effects of other additives were also examined including 1,4-diazabicyclo[2. 2. 2]octane (DABCO) as a powerful detector for singlet oxygen,[5] 2,6-di-*t*-butylphenol (DTBP) for free radicals,[10] tetranitromethane (TNM) for superoxide ion,[11] and *p*-dimethoxybenzene (DMB) as a competitor for the presumed CT complex formation of **1a** with O_2.[6] Table 6 shows the additive effects on the percent yield of flavanone formed in the photooxidation of **1a** in O_2-saturated benzene. Insufficient supply of O_2 during photolysis gave somewhat different results. Thus, comparable irradiation

of **1a** in sealed ampuls, after bubbling through with O_2 gas for 30 min, gave flavanone in 19% (additive/nil), 16% (DABCO/0.02 mol dm^{-3}), a trace (DMB/0.02 mol dm^{-3}), a trace (DTBP/0.02 mol dm^{-3}), respectively. Further, irradiation under air, in place of O_2 gas, led to no significant amount of the product.

The remarkable enhancement effect by TNM implies the important role of CT interaction, while the strong depression by DABCO suggests the involvement of singlet oxygen. However, the photoreaction in sealed ampuls (O_2-insufficient conditions) was little subject to DABCO, hence singlet oxygen does not necessarily act as the oxidant species in its own form. The presence or absence of the depression by DABCO, depending on excess or deficiency of O_2, also implies that singlet oxygen is formed indirectly, *via* equilibria including complex formation which would become significant only in the presence of a large excess of O_2 (Scheme 1). The depression effect by DMB can be explained in terms of the competitive complex formation with oxygen species, which would be more significant in O_2-insufficient solution (Scheme 2). Also, it is notable that the photoreaction was enhanced by the combined addition of DPSO and DMB, as compared to the single addition of either, suggesting electron transfer sensitization by the additives.

Speculation on the Mechanism. Direct evidence has been reported for the generation of radical ions in electron transfer photooxygenation reactions in highly polar solvents.[7] In nonpolar solvents such as benzene, however, no such ion pair formation seems to occur but highly polar CT complexes are often formed.[6,12] The present photooxygenation reactions in benzene/O_2 can be explained in terms of Scheme 1, which is essentially similar to those proposed for the electron transfer photooxygenations of ethers,[13] amines,[12,14] and alkylbenzenes,[14,15] except for the inefficient generation of ion pairs in the present photoreaction. Here, ArRCHOH $\cdots O_2$ represents a contact pair between the substrate and oxygen in their ground states which is implied by the enhanced UV-absorption(250—300 nm). On excitation this will lead to a CT complex ($ArRCHOH^{+\cdot}\cdots O_2^{-\cdot}$), which will then undergo back electron transfer (k_2), proton transfer (k_1) to give the substrate radicals ArRĊOH, or the reversible formation of singlet oxygen (k_3, k_4). In the presence of DABCO efficient quenching of $^1O_2$ would occur to depress the photoreaction. The overall reaction efficiency will be governed by the ratio k_1/k_2 which in turn depends on the structure of the relative stability of ArRĊOH, if the subsequent processes (k_5, k_6) occur irreversibly. The in-cage radical coupling reaction (k_5) would proceed rapidly and little scavenged by added radical inhibitors such as DTBP.

In the presence of excess O_2 the out-of-cage reaction (k_6) would also occur efficiently before scavenged by DTBP. Disproportionation of the peroxyl radical (k_8) and decomposition of the hydroperoxide (k_7) will lead to the final products. The reactivity ratio of **3a**/**1a** or **4**/**6** is in the range of 2-3 (Tables 1 and 2), which corresponds to the Hammet reaction constant of $-0.6 \leqq \rho \leqq 1.4$, being consistent with the intermediacy of the substrate radicals.

The structure-reactivity relationships may be explained in terms of the stereoelectronic effects of the radical intermediates, assuming that the reaction efficiency is mainly determined by the ratio k_1/k_2 or the stability of the radical intermediate. Since the hydrogen atom on the 4-position is assigned to quasi-axial for the *cis*-4-flavanols **1a—3a** and quasi-equatorial for the trans isomers **1b—3b**,[16] the transition states or the 4-hydroxy-4-flavanyl radical intermediates would have conformations as [A] and [B], respectively (Chart 2). For the conformer [A] the *p*-type orbital on the 4-position is capable of overlapping with both the hydroxyl and phenoxyl groups. The conformer [B] is incapable of such coplanar overapping and less stable. Thus the cis/trans selectivity in Table 1 can be explained by the stereoelectronic effects of the intermediates. The substituent effects of benzylic alcohols (Table 2) may be explained in a similar manner. Thus, in the absence of ortho substituents the benzylic radicals can have the coplanar configuration [C] to allow favorable overapping with both the aryl and the hydroxyl groups. In the presence of ortho substituents such coplanarity would be sterically hindered, leading to unstable intermediates [D]. The methoxyl group at the meta position would destabilize the benzylic radicals due to its inductive effect while incapable of resonance effect, resulting in the slight depression of the product formation (**7** in Table 2). Photooxidations in DMSO/O_2 and in benzene-DPSO/O_2 show structure-reactivity relationships apparently similar to those in benzene/O_2, suggesting similar intermediates, ArRĊOH.

Highly complicated features are suggested for the

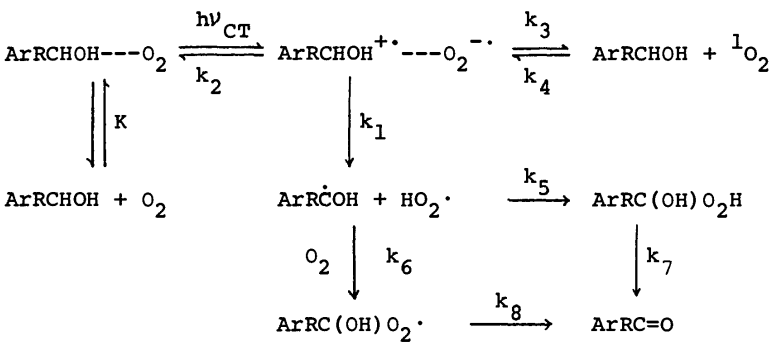

Scheme 1.

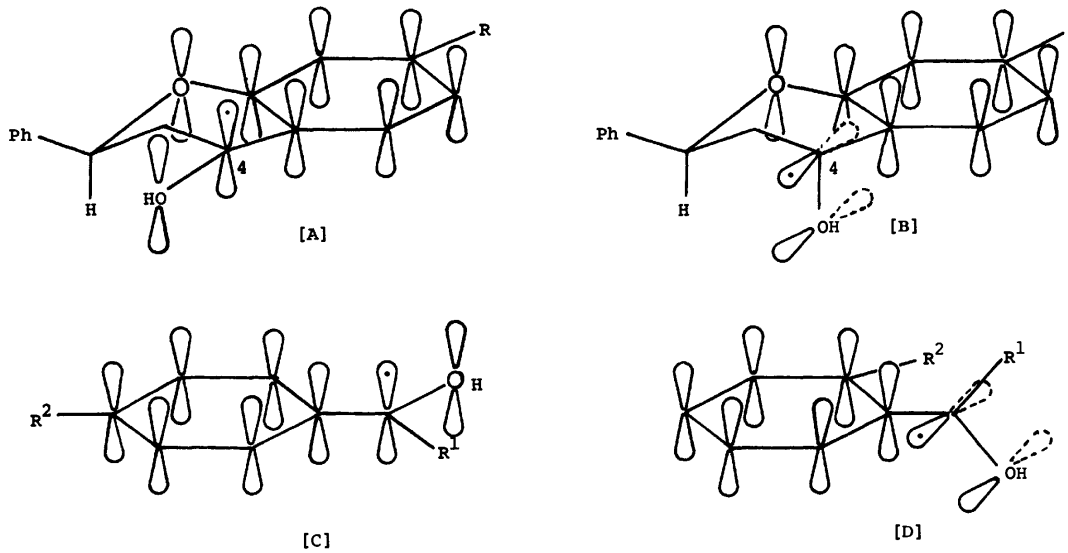

Chart 2.

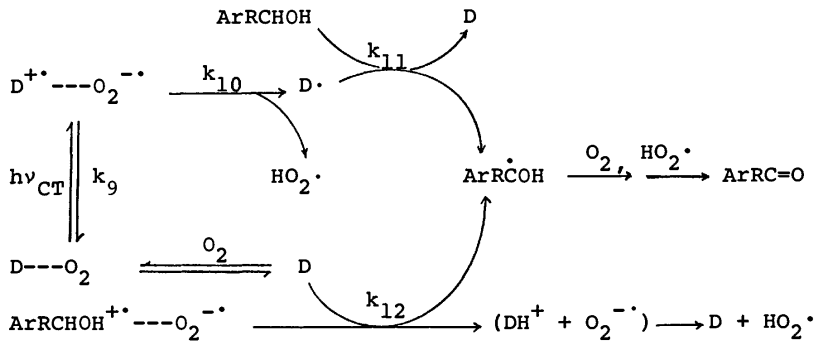

Scheme 2.

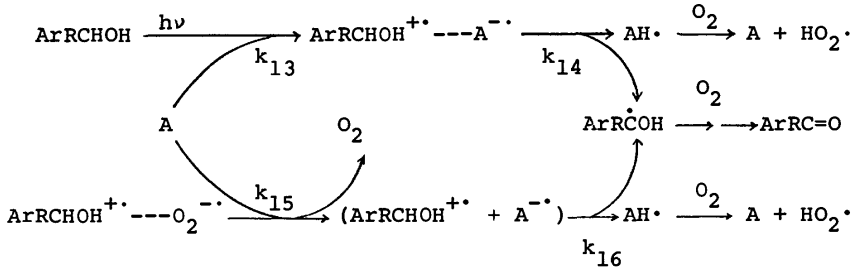

Scheme 3.

effects of additives, since many of the additives can act on the various species present in the systems. For example, DTBP can be a good competitor for electron transfer interaction as well as a powerful scavenger of free radicals. It may also act as a carrier and/or initiator in free radical reactions.

Crude mechanisms are tentatively proposed for the effects of electron donors (Scheme 2) and electron acceptors (Scheme 3), respectively. In the presence of a good electron donor (D) such as DMB or DTBP, a CT complex of D ($D^{+\cdot}\cdots O_2^{-\cdot}$) may be formed on CT excitation of a contact pair ($D\cdots O_2$). These processes would not seriously affect the formation of $ArRCHOH\cdots O_2$ and $ArRCHOH^{+\cdot}\cdots O_2^{-\cdot}$, in the presence of excess O_2.

Subsequent proton transfer (k_{10}) will give radical D· which may undergo hydrogen abstraction from the substrates (k_{11}) to give the radical ArRĊOH. Alternatively, proton transfer from $ArRCHOH^{+\cdot}\cdots O_2^{-\cdot}$ to D may proceed (k_{12}) to facilitate the formation of ArRĊOH, thus eventually enhancing the product formation. The enhancement effects of D may be also due to the increased solubility or concentration of O_2 gas *via* contact pair formation.

In the presence of a good electron acceptor (A) such as TNM or DPSO, on the other hand, another type of CT complex ($ArRCHOH^{+\cdot}\cdots A^{-\cdot}$) may be formed ($k_{13}$), followed by proton transfer (k_{14}) to give ArRĊOH (Scheme 3). Alternatively, electron transfer from $ArRCHOH^{+\cdot}\cdots O_2^{-\cdot}$ to A may occur (k_{15}).

Subsequent proton transfer (k_{16}) will lead to ArRĊOH, thus eventually facilitating the photoreaction.

Experimental

Apparatus and Procedure. The light source for irradiation was a 100-W high pressure mercury lamp (Rico). The UV absorption and proton NMR spectra were measured with a Hitachi 200-10 UV-spectrophotometer and a Hitachi R-24 NMR spectrometer (60 MH_z), respectively. The product mixtures were chromatographed over Caster wax or PEG-20 M on 60—80 mesh Chromosorb WAW (3 mm×3 m), by the use of a Shimadzu GC-4CM-PF with a FID deteactor and nitrogen carrier gas. All melting points and boiling points were uncorrected.

Materials. While 2,4-*cis*-4-flavanols **1a**, **2a**, and **3a** were prepared by the reduction of the corresponding flavanones with sodium borohydride,[17,18] 2,4-*trans*-4-flavanols **1b**, **2b**, and **3b** were obtained from **1a**, **2a**, and **3a**, respectively, by treatment with phosphorous tribromide followed by alkaline hydrolysis.[18] **1a**: Colorless needles from methanol, mp 147.5—148 °C; **1b**: colorless needles from benzene-petroleum benzine, mp 115—116 °C; **2a**: colorless needles from ethanol-water, mp 103—103.5 °C; **2b**: colorless needles from hexane-benzene, mp 49.5—51.5 °C; **3a**: colorless needles from methanol, mp 100—101 °C; **3b**: colorless needles from benzene-petroleum benzine, mp 110—111 °C. 1-Phenylethanol **4** was of guaranteed grade commercially available (Wako Chemicals), while **5**—**9** were prepared by the reduction of the corresponding *p*-substituted acetophenones with sodium borohydride.[9] The purities were confirmed by GLC analysis. **5**: Bp 96.5—97 °C/5 mmHg†; **6**: bp 110.5 °C/4 mmHg; **7**: bp 94 °C/2.5 mmHg; **8**: bp 100 °C/5 mmHg; **9**: colorless needles from ether-petroleum ether, mp 41.5—42.5°C. Diphenyl sulfone, acetophenone, DABCO and DTBP were of the purest grade commercially available. Benzene and other solvents were distilled before use.

Photooxygenation Reactions. Typical procedures will be described below. A 25 ml benzene solution containing 0.04 mol dm^{-3} substrate was bubbled through with oxygen gas for 30 min, then irradiated at room temperature while stirring with a magnetic stirrer under oxygen atmosphere for 8—10 h. The photolyzed mixtures from 4-flavanols were analyzed by ^1H NMR spectroscopy after the removal of the solvent. Relative yields of flavanones and 4-flavanols recovered were calculated from the relative intensities of the protons at the C-2 position of flavanones and those at the C-4 or C-2 positions of 4-flavanols. Besides flavanones, trace amounts of 2′-hydroxychalcones were detected by TLC analysis on silica gel-benzene. The photoproducts from benzylic alcohols (**4**—**11**) were determined on GLC by comparing with corresponding acetophenones commercially available (acetophenone, 4′-chloro- and 4′-methoxyacetophenones) or prepared by known methods.[20] 3′-Methoxyacetophenone: Bp 134—135.5 °C/24 mmHg; 2′,4′-dimethoxyacetophenone: Colorless needles from benzene, mp 39—40 °C; 2′-methoxyacetophenone: Bp 132—135 °C/25 mmHg.

Oxidation by Superoxide Ion. A 30 ml benzene solution containing 18-Crown-6 (0.25 g, 1.0 mmol) and a benzylic alcohol (1.0 mmol) was mechanically stirred while bubbling through with nitrogen gas, then added potassium peroxide (0.40 g, 5.3 mmol) and continued stirring until the color changed into orange (*ca.* 15 h). Water was added and shaken, then the organic layer was condensed and analyzed on GLC as described above. Similarly, 4-flavanols were oxidized under nitrogen atmosphere in a 20 ml benzene solution containing a 4-flavanol (1.0 mmol), 18-Crown-6 (1.0 mmol), and potassium peroxide (10 mmol) for 2 h, or in a 20 ml DMSO solution containing a 4-flavanol (1.0 mmol), 18-Crown-6 (0.76 mmol), and potassium peroxide (2.8 mmol) for 3—5 h. The products were analyzed by NMR spectroscopy as described above.

Oxidation of 4-Flavanols by Singlet Oxygen. A 15 ml solution of *t*-butyl alcohol containing a 4-flavanol (2 mmol) and Rose Bengal or thionine (5 mg) as a sensitizer was irradiated with a 300-W tungsten lamp for 5 h while stirring with magnetic stirrer under oxygen atmosphere.

The authors would like to express their thanks to Mr. Jiro Amano and Tsukasa Uei for discussion.

† 1 mm Hg≈133.322 Pa

References

1) T. Sato, H. Inoue, and K. Hata, *Bull. Chem. Soc. Jpn.*, **40**, 1502 (1967).
2) H. Kwart and P. S. Francis, *J. Am. Chem. Soc.*, **81**, 2116 (1959).
3) S. Yamaguchi, K. Kabuto, Y. Kikuchi, and N. Inoue, *Bull. Chem. Soc. Jpn.*, **44**, 3487 (1971).
4) M. Suzuki, J. Amano, M. Morioka, H. Mizuno, and R. Matsushima, *Bull. Chem. Soc. Jpn.*, **50**, 1169 (1977).
5) C. Quannes and T. Wilson, *J. Am. Chem. Soc.*, **90**, 6527 (1968); C. S. Foote, E. R. Peterson, and K. W. Lee, *ibid.*, **94**, 1032 (1972); C. F. Denke and N. I. Krinsky, *ibid.*, **98**, 3041 (1976); T. Thomas and C. S. Foote, *Photochem. Photobiol.*, **27**, 683 (1978).
6) J. Eriksen and C. S. Foote, *J. Am. Chem. Soc.*, **102**, 6083 (1980).
7) I. Saito and T. Matsuura, *J. Am. Chem. Soc.*, **103**, 188 (1981).
8) A. P. Schaap, K. A. Zaklika, B. Kaskar, and L. W. M. Fung, *J. Am. Chem. Soc.*, **102**, 389 (1980).
9) L. T. Spada and C. S. Foote, *J. Am. Chem. Soc.*, **103**, 391 (1981).
10) C. S. Foote, S. Wexler, and W. Ando, *Tetrahedron Lett.*, **1965**, 4111.
11) W. Bors, M. Saran, E. Lengfelder, C. Michel, C. Fuchs, and C. Frenzel, *Photochem. Photobiol.*, **28**, 629 (1978).
12) H. Tsubomura, T. Yagishita, and H. Toi, *Bull. Chem. Soc. Jpn.*, **46**, 3051 (1973).
13) C. von Sonntag, K. Neuwald, H. P. Schuchmann, F. Weeke, and E. Janssen, *J. Chem. Soc., Perkin. Trans. 2*, **1975**, 171.
14) M. Kojima, H. Sakuragi, and K. Tokumaru, *Tetrahedron Lett.*, **22**, 2889 (1981).
15) K. Onodera, H. Sakuragi, and K. Tokumaru, *Tetrahedron Lett.*, **21**, 2831 (1980).
16) H. L. Tökes and R. Bognar, *Tetrahedron*, **29**, 909 (1973); J. W. C. Lewis, *Aust. J. Chem.*, **21**, 2059 (1968).
17) A. Löbenwein, *Ber.*, **57**, 1515 (1924).
18) A. B. Kulkarni, *Indian J. Chem.*, **8**, 119 (1970).
19) K. B. Wiberg and T. M. Shryne, *J. Am. Chem. Soc.*, **77**, 2774 (1955); A. C. Davies, E. E. Edwin, J. Kenyon, and A. Walsh, *J. Chem. Soc.*, **1957**, 3158.
20) R. N. Goel, A. C. Jain, and T. R. Seshadr, *Proc. Indian Acad. Sci.*, **48**, 180 (1958).

Reaction of Enamines with Acetals or Trialkyl Orthoformates Activated by Lewis Acids

Osamu TAKAZAWA,* Kunio KOGAMI, and Kazuo HAYASHI
Kawasaki Research Laboratories, T. Hasegawa Co., Ltd., 335 Kariyado, Nakahara-ku, Kawasaki 211
(Received October 13, 1983)

Enamines, prepared readily from various carbonyl compounds, react with acetals or trialkyl orthoformates in the presence of Lewis acids such as $BF_3 \cdot OEt_2$ to give corresponding β-alkoxy carbonyl compounds or α-dialkoxymethyl carbonyl compounds in good yields. The reaction of dienamines with acetals or trialkyl orthoformates also selectively gives corresponding β,γ-unsaturated α-(α-alkoxyalkyl) carbonyl compounds or β,γ-unsaturated α-diakoxymethyl carbonyl compounds in good yields.

The reaction of enamines with trialkyl orthoformates was briefly reported in our previous paper.[1] In this report, the above reaction is investigated in detail.

In the preceding paper,[2] it was shown that the β-alkoxy carbonyl compounds or α-dimethoxymethyl carbonyl compounds are obtained by the reaction of enol silyl ethers with acetals or trimethyl orthoformate in the presence of $TiCl_4$. In the present investigation, it has been found that enamines react with acetals or trialkyl orthoformates in the presence of Lewis acids similarly to enol silyl ethers. For example, to a dichloromethane solution of a 1.2 molar amount of acetaldehyde diethyl acetal (**2**) was added a 1.3 molar amount of $BF_3 \cdot OEt_2$ at −40 °C in argon atmosphere. Then 1-morpholino-1-cyclohexene (**1**) was added and the reaction mixture was stirred for 1 h at room temperature. After hydrolysis, the resulting organic layer was concentrated. The reaction product, 2-(1-ethoxyethyl)-1-cyclohexanone (**3**), was obtained in 76% yield after distillation under reduced pressure, the reaction concerned being summarized as:

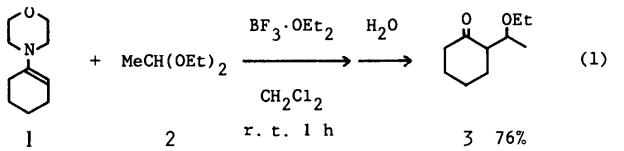

1 2 3 76%

(Erythro and threo mixture)

In order to investigate the effect of Lewis acids, reactions of **1** with **2** in the presence of various Lewis acids were tried according to the procedure mentioned above (Table 1). The results described in Table 1 demonstrate that, of the Lewis acids examined, $BF_3 \cdot OEt_2$ exhibits a remarkable effect as compared with the others. In case $TiCl_4$ was employed, 2-ethylidenecyclohexanone was obtained as a major product along with **3**.

The effect of the amount of $BF_3 \cdot OEt_2$ upon the yield of **3** was then investigated by using the reaction between **1** and a 1.2 molar amount of **2** at room temperature for 1 h as a reference reaction. It was found that the product **3** was obtained in the highest yield when a 1.3 or 1.5 molar amount of $BF_3 \cdot OEt_2$ was applied (Table 2).

Furthermore, the effect of amines used in enamine synthesis was studied by treating enamines derived from various amines and cyclohexanone with a 1.2 and 1.3 molar amount of **2** and $BF_3 \cdot OEt_2$, respectively, under similar conditions as described above. The results shown herein indicate that morpholine enamine (**1**) is significantly favored in this reaction to afford the best yield (Table 3).

Reactions of **1**, 3,7-dimethyl-1-morpholino-1,6-octadiene (**11**), or 1-piperidino-1-hexene (**14**) with a variety of acetals were tried in the presence of $BF_3 \cdot OEt_2$ according to the typical procedure, and the corresponding β-alkoxy carbonyl compounds were obtained in good yields as shown in Table 4.

The reaction of crotonaldehyde dimethyl acetal with **1** gave a Michael type adduct (**18**) in 13% yield

TABLE 1. REACTION OF THE ENAMINE **1** WITH THE ACETAL **2** IN THE PRESENCE OF VARIOUS LEWIS ACIDS

Lewis acid	Reaction conditions		Yield[a] of **3**[b]
	Temp./°C	Time/h	%
$BF_3 \cdot OEt_2$	0	3	68
$BF_3 \cdot OEt_2$	r. t.	1	76
$TiCl_4$	r. t.	1	21 (52)[c]
$SnCl_4$	r. t.	2	trace
$AlCl_3$	r. t.	24	15 (6)[c]
$ZnCl_2$	r. t.	24	trace
$ZnBr_2$	r. t.	24	trace
$FeCl_3$	r. t.	24	trace
$MgCl_2$	r. t.	24	0

a) Isolated yield. b) An erythro and threo mixture. c) Yield of 2-ethylidenecyclohexanone.

TABLE 2. EFFECT OF THE AMOUNT OF $BF_3 \cdot OEt_2$ ON THE YIELD

Molar ratio of $BF_3 \cdot OEt_2$	0.1	0.5	1.0	1.2	1.3	1.5	2.0
Yield[a] of **3**[b]/%	Trace	16	48	72	76	76	55

a) Isolated yield. b) An erythro and threo mixture.

TABLE 3. EFFECT OF AMINES USED IN ENAMINE SYNTHESIS

Enamine	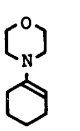	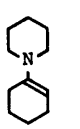	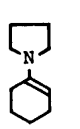	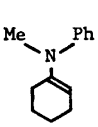
	1	4	5	6
Yield[a] of **3**[b]/%	76	32	Trace	44

a) Isolated yield. b) An erythro and threo mixture.

together with β-methoxy ketone (**17**) in 53% yield:[3]

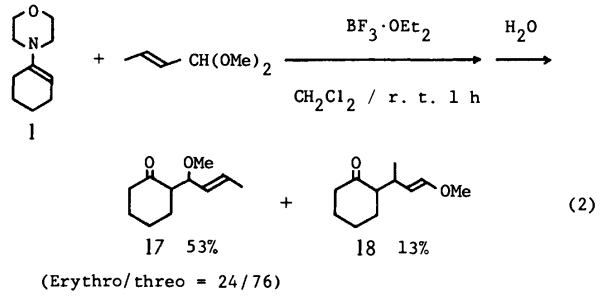

In contrast to the result[4] that the reaction of dienyloxysilanes with acetals gave α,β-unsaturated γ-(α-alkoxyalkyl) carbonyl compounds, the present reaction of a dienamine, 2-methyl-5-morpholino-2,4-hexadiene (**19**), with acetals selectively afforded β,γ-unsaturated α-(α-alkoxyalkyl) carbonyl compounds, **20**, or **22**, as shown by the following equation:

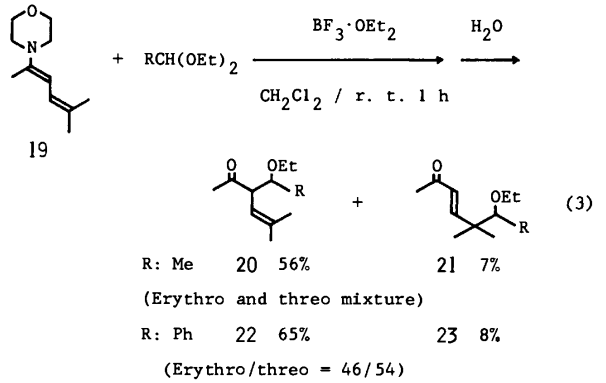

It is known that the reaction of enamines with alkyl halomethyl ethers affords α-alkoxymethyl carbonyl compounds.[5] In contrast to this finding, the present reaction gives α-(1-alkoxyalkyl) carbonyl compounds in good yields.

On the other hand, α-dialkoxymethyl carbonyl compounds are obtained by the reaction of enamines with trialkyl orthoformates. For example, to a dichloromethane solution of **1** and a 1.3 molar amount of triethyl orthoformate was added a 1.3 molar amount of $BF_3 \cdot OEt_2$ at −40 °C in argon atmosphere. Then the reaction mixture was stirred for 1 h at 0 °C. After hydrolysis, the resulting organic layer was concentrated. The reaction product, 2-diethoxymethyl-1-cyclohexanone (**24**), was obtained in 85% yield after distillation under reduced pressure, the reaction concerned being summarized as:

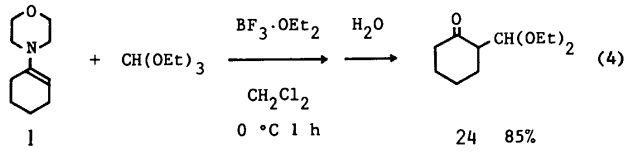

In a similar manner, the reaction of enamines derived from various carbonyl compounds with trialkyl orthoformates afforded the corresponding α-dialkoxymethyl carbonyl compounds as listed in Table 5.

Table 4. Synthesis of β-alkoxy carbonyl compounds from enamines and acetals in the presence of $BF_3 \cdot OEt_2$

Enamine	Acetal		Product	Isolated yield/%	Isomer ratio[a] a/b
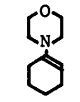 1	$MeCH(OBu^n)_2$	7	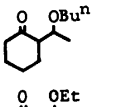	81	-
	$PhCH(OEt)_2$	8	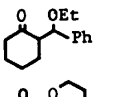	89	38/62[b]
		9	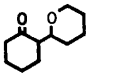	57	59/41[c]
		10	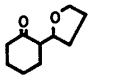	70	55/45[c]
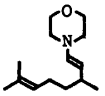 11	$PhCH(OEt)_2$	12	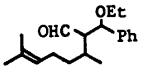	81	48/52[b]
		13	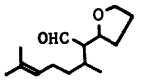	79	54/46[c]
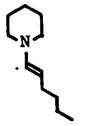 14	$PhCH(OEt)_2$	15	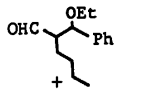	56	30/70[b,d]
		16	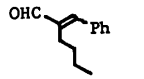	12	-

a) Erythro and threo isomers. Determined by GLC analysis. b) a/b = erythro/threo. c) The stereochemistries of a and b are not determined. d) Determined by NMR analysis.

Since the reactivity of trialkyl orthoformates toward enamines is higher than that of acetals, α-dialkoxymethyl carbonyl compounds were obtained in good yields in the presence of $TiCl_4$, $SnCl_4$, or $ZnCl_2$.

In contrast to the result that the reaction of dienoxysilanes with trialkyl orthoformates gave α,β-unsaturated γ-dialkoxymethyl carbonyl compounds,[4] the present reaction of dienamine **19** with trimethyl orthoformate afforded β,γ-unsaturated α-dimethoxymethyl ketone (**28**).

It is known that the reaction of enamines with a mixed anhydride of formic acid and acetic acid[5c] or the Vilsmeier reagent ($POCl_3$-DMF)[6] affords 2-formyl ketones. In comparison with the above reaction, the present reaction has an advantage in that α-dialkoxymethyl carbonyl compounds, having the protected formyl and carbonyl groups in the same molecule, is exclusively formed by a one-step procedure.

Experimental

Spectra. ^1H NMR spectra were recorded on a Hitachi R-24A spectrometer. Chemical shifts are reported on the δ scale relative to tetramethylsilane as an internal standard. IR spectra were taken with a JASCO IRA-2 spectrometer. Products were identified by NMR and IR spectra and elemental analyses.

Materials. Commercially available $BF_3 \cdot OEt_2$, $TiCl_4$,

Table 5. Reaction of enamines with methyl or ethyl orthoformate

Enamine	Methyl or ethyl orthoformate	Lewis acid	Reaction conditions		Product	Isolated yield
			Temp/°C	Time/h		%
1	$CH(OEt)_3$	$BF_3 \cdot OEt_2$	0	1	24	85
		$SnCl_4$	0	1		90
		$ZnCl_2$	r.t.	14		54
1	$CH(OMe)_3$	$BF_3 \cdot OEt_2$	0	1	25	74
		$TiCl_4$	-40	1		64
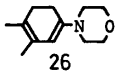 26	$CH(OMe)_3$	$TiCl_4$	-78	0.5	27	70
19	$CH(OMe)_3$	$BF_3 \cdot OEt_2$	0	1	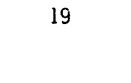 28	75
		$SnCl_4$	0	1		68
		$TiCl_4$	0	1		63
11	$CH(OEt)_3$	$BF_3 \cdot OEt_2$	-40	1	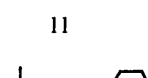 29	78
		$ZnCl_2$	r.t.	3		43
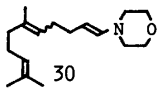 30	$CH(OMe)_3$	$BF_3 \cdot OEt_2$	-40	1	31	61
14	$CH(OEt)_3$	$BF_3 \cdot OEt_2$	-40	1	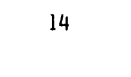 32	71
		$SnCl_4$	-40	1		70

and $SnCl_4$ were distilled in argon atmosphere before use. Anhydrous $AlCl_3$, $ZnCl_2$, $ZnBr_2$, $FeCl_3$, and $MgCl_2$ were used without purification. Enamines of carbonyl compounds, 1-morpholino-1-cyclohexene (**1**), 1-pyrrolidino-1-cyclohexene (**5**), and *N*-(1-cyclohexenyl)-*N*-methylaniline (**6**), were prepared according to literature procedures[5c,7] and purified by distillation. **1**: bp 116—117 °C/10 mmHg (1 mmHg≈133.322 Pa) (lit,[7] 118—120 °C/10 mmHg); **5**: bp 103—104 °C/10 mmHg (lit,[5c] 105—107 °C/13 mmHg); **6**: bp 95—97 °C/1 mmHg (lit,[5c] 148—153 °C/12 mmHg). In a similar manner, 1-piperidino-1-cyclohexene (**4**), 3,7-dimethyl-1-morpholino-1,6-octadiene (**11**), 1-piperidino-1-hexene (**14**), 5-methyl-2-morpholino-2,4-hexadiene (**19**), 3,4-dimethyl-1-morpholino-1,3-cyclohexadiene (**26**), and 6,10-dimethyl-1-morpholino-1,5,9-undecatriene (5*E*:5*Z*=1:1) (**30**) were prepared from the corresponding carbonyl compounds and amines, and the physical data are as follows. **4**: bp 109—110 °C/10 mmHg; NMR ($CDCl_3$) δ=1.52 (10H, m), 2.04 (4H, m), 2.74 (4H, m), and 4.66 (1H, t, J=3.0 Hz). **11**: bp 113 °C/2 mmg; NMR ($CDCl_3$) δ=1.00 (3H, d, J=6.0 Hz), 1.2—2.3 (5H, m), 1.61 (3H, s), 1.70 (3H, s), 2.75 (4H, m), 4.30 (1H, dd, J=14.5 and 8.5 Hz), 5.10 (1H, t, J=7.0 Hz), and 5.75 (1H, d, J=14.5 Hz). **14**: bp 103 °C/13 mmHg; NMR ($CDCl_3$) δ=0.90 (3H, t, J=5.5 Hz), 1.1—1.8 (10H, m), 1.97 (2H, q, J=7.0 Hz), 2.75 (4H, m), 4.38 (1H, dt, J=14.0 and 7.0 Hz), and 5.80 (1H, d, J=14.0 Hz). **19**: bp 125—127 °C/9 mmHg; NMR ($CDCl_3$) δ=1.72 (3H, s), 1.80 (3H, s), 1.88 (3H, s), 2.88 (4H, m), 3.75 (4H, m), 5.30 (1H, d, J=11.5 Hz), and 5.96 (1H, d, J=11.5 Hz). **26**: bp 97—98 °C/0.6 mmHg; NMR ($CDCl_3$) δ=1.70 (6H, s), 2.15 (4H, s), 2.82 (4H, m), 3.69 (4H, m), and 4.76 (1H, s). **30**: NMR ($CDCl_3$) δ=1.60 and 1.68 (9H, s), 1.8—2.2 (8H, m), 2.70 (4H, m), 3.65 (4H, m), 4.45 (1H, m), 5.10 (2H, m), and 5.80 (1H, d, J=14.0 Hz).

Reaction of 1-Morpholino-1-cyclohexene (1) with Acetaldehyde Diethyl Acetal (2) in the Presence of $BF_3 \cdot OEt_2$. To a dichloromethane (50 ml) solution of 7.08 g (60 mmol) of acetaldehyde diethyl acetal (**2**) was added 9.23 g (65 mmol) of $BF_3 \cdot OEt_2$ at −40 °C in argon atmosphere. Then 8.35 g (50 mmol) of 1-morpholino-1-cyclohexene (**1**) was added immediately and the reaction mixture was stirred for 1 h at room temperture. The mixture was quenched with water and stirred for 1 h at room temperature. After hydrolysis, the organic layer was washed with a saturated solution of $NaHCO_3$ and dried over $MgSO_4$. After removal of the solvent, the residue was distilled under reduced pressure to give a mixture of diastereomers (**3a** and **3b**) of 2-(1-ethoxyethyl)cyclohexanone (**3**) (6.50 g, 93—94 °C/10 mmHg, 76%). **3a** and **3b** were in the ratio 46:54 as found by means of gas chromatography (PEG-20 M). Analytically pure samples of **3a** and **3b** were prepared by preparative gas chromatography (20% PEG-20 M).

Reactions of enamines, such as 1-morpholino-1-cyclohexene (**1**), 1-piperidino-1-cyclohexene (*4*), 1-pyrrolidino-1-cyclohexene (**5**), *N*-(1-cyclohexenyl)-*N*-methylaniline (**6**), 3,7-dimethyl-1-morpholino-1,6-octadiene (**11**), and 1-piperidino-1-hexene (**14**), with various acetals were carrid out according to the same procedure, and the yields of the corresponding β-alkoxy carbonyl compounds are listed in Tables 3 and 4. The physical properties and analytical data of the products are shown in Table 6.

Reaction of 1-Morpholino-1-cyclohexene (1) with Acetaldehyde Diethyl Acetel (2) in the Presence of Various Lewis Acids. To a dichloromethane (50 ml) solution of 7.08 g (60 mmol) of acetaldehyde diethyl acetal (**2**) was added a Lewis acid (65 mmol) at −40 °C in argon atmosphere. Then 8.35 g (50 mmol) of 1-morpholino-1-cyclohexene (1) was added immediately. The reaction mixture was worked up as described above and purified by distillation. The reaction conditions and the yields of **3** are listed in Table 1.

Reaction of 1-Morpholino-1-cyclohexene (1) with Crotonaldehyde Dimethyl Acetal. Into a mixture of 8.35 g (50 mmol) of **1** and 6.96 g (60 mmol) of crotonaldehyde dimethyl acetal in dichloromethane (50 ml) was added 8.52 g (60 mmol) of $BF_3 \cdot OEt_2$ at −40°C in argon atmosphere and the reaction mixture was stirred for 1 h at room temperature. The reaction mixture was worked up as described above and the resulting residue was distilled under reduced pressure to give a mixture of diastereomers (**17a** and **17b**) of 2-(*trans*-1-methoxy-2-butenyl)-1-cyclohexanone (**17**) and 2-(*trans*-3-

Table 6. Physical properties and analytical data of products

Product	Bp θ_b/°C(mmHg)	Isomer[a]	IR cm^{-1}	NMR (δ, $CDCl_3$, J/Hz)	Found(Calcd)/% C	H
3	93—94(10)[b]	a	1710 1105	1.14(3H, t, J=7.0), 1.14(3H, d, J=6.0), 1.4—2.1(6H, m), 2.1—2.5(3H, m), 3.47(2H, m), 3.76 (1H, quint, J=6.0).	70.40 (70.55)	10.69 (10.66)
		b	1710 1105	1.10(3H, d, J=6.0), 1.16(3H, t, J=7.0), 1.4—2.2(6H, m), 2.2—2.7(3H, m), 3.48(2H, m), 3.90 (1H, quint, J=6.0).	70.40 (70.55)	10.58 (10.66)
7	82—83(1.0)[b]	Mixture	1710 1105	0.88(3H, t, J=7.0), 1.06 and 1.08(3H, d, J=6.0), 1.2—2.1(10H, m), 2.1—2.5(3H, m), 3.37(2H, m), 3.82(1H, quint, J=6.0).	72.62 (72.68)	11.14 (11.18)
8	117—118 (1.0)[b]	a (erythro)	1710 1100 700	1.13(3H, t, J=7.0), 1.4—2.1(6H, m), 2.1—2.6 (3H, m), 3.37(2H, q, J=7.0), 4.84(1H, d, J=4.4), 7.26(5H, s).	77.56 (77.55)	8.68 (8.68)
		b (threo)	1713 1095 700	1.10(3H, t, J=7.0), 1.3—2.1(6H, m), 2.2—2.9 (3H, m), 3.35(2H, q, J=7.0), 4.67(1H, d, J=8.0), 7.26(5H, s).	77.59 (77.55)	8.68 (8.68)
9	87—88(1.2)[b]	a	1710 1090	1.2—2.1(12H, m), 2.1—2.5(3H, m), 3.2—4.2(3H, m).	72.22 (72.49)	9.90 (9.95)
		b	1710 1090	1.2—2.2(12H, m), 2.2—2.7(3H, m), 3.2—4.1(3H, m).	72.46 (72.49)	9.96 (9.95)
10	80—81(1.2)[b]	a	1710 1053	1.2—2.2(10H, m), 2.2—2.6(3H, m), 3.72(2H, m), 3.98(1H, q, J=7.0).	71.21 (71.39)	9.72 (9.59)
		b	1710	1.3—2.2(10H, m), 2.2—2.8(3H, m), 3.78(2H, m), 4.17(1H, q, J=7.0).	71.25 (71.39)	9.61 (9.59)
12	144—145 (1.0)[b]	a (erythro)	1722 1100 698	1.06(3H, d, J=6.0), 1.12(3H, t, J=7.0), 1.60(3H, s), 1.67(3H, s), 1.3—2.4(5H, m), 2.75(1H, m), 3.32(2H, q, J=7.0), 4.66(1H, d, J=8.0), 5.08 (1H, m), 7.28(5H, s), 9.52 and 9.57(1H, d, J=3.2).	78.92 (79.12)	9.72 (9.78)
		b (threo)	1723 1090 698	0.95(3H, d, J=6.0), 1.10(3H, t, J=7.0), 1.53 (3H, s), 1.57(3H, s),1.3—2.1(5H, m), 2.52(1H, m), 3.32(2H, q, J=7.0), 4.72(1H, d, J=9.2), 4.80(1H, m), 7.31(5H, s), 9.83 and 9.86(1H, d, J=4.5).	78.85 (79.12)	9.70 (9.78)
13	109—111 (1.0)[b]	a	1720 1068	1.02(3H, d, J=6.0), 1.60(3H, s), 1.67(3H, s), 1.2—2.3(9H, m), 2.47(1H, m), 3.72(2H, m), 4.12 (1H, q, J=7.0), 5.10(1H, t, J=6.0), 9.72 and 9.76(1H, d, J=2.4).	74.81 (74.95)	10.93 (10.78)
		b	1725 1060	1.00 and 1.03(3H, d, J=6.0), 1.60(3H, s), 1.67 (3H, s), 1.2—2.3(10H, m), 3.75(2H, m), 4.20(1H, m), 5.50(1H, t, J=6.0), 9.70 and 9.75 (1H, d, J=4.4).	74.78 (74.95)	10.71 (10.78)
15		Mixture (e/t=30/70)[c]	1727 1095 700	0.7—1.6(12H, m), 2.50(1H, m), 3.28(2H, m), 4.42 (1H, d, J=9.0, CH-O threo), 4.58(1H, d, J=5.7, CH-O erythro), 7.25 and 7.28(5H, s), 9.63 (1H, d, J=2.7, CHO erythro), 9.70(1H, d, J=4.0, CHO threo).	76.72 (76.88)	9.53 (9.46)
16			1680 1620	0.92(3H, m), 1.2—1.7(4H, m), 2.50(2H, m), 7.11 (1H, s), 7.37(5H, s), 9.45(1H, s).		
17		a (erythro)	1710 1090 970	1.72(3H, d, J=5.5), 1.5—2.1(6H, m), 2.2—2.6(3H, m), 3.25(3H, s), 3.99(1H, dd, J=7.0, 4.4), 5.42 (1H, dd, J=15.5, 7.0), 5.68(1H, dq, J=15.5, 5.5).	72.54 (72.49)	10.02 (9.95)
		b (threo)	1713 1090 970	1.75(3H, d, J=6.0), 1.4—2.2(6H, m), 2.2—2.7 (3H, m), 3.24(3H, s), 3.92(1H, t, J=8.0), 5.27 (1H, dd, J=16.0, 8.0), 5.68(1H, dq, J=16.0, 6.0).	72.43 (72.49)	10.06 (9.95)
18			1710 1650	1.03(3H, dd, J=6.4, 1.0), 1.4—2.8(10H, m), 3.48 (3H, s), 4.75(1H, dd, J=12.6, 8.4), 6.30(1H, d,	72.55 (72.49)	10.03 (9.95)

Table 6. Continued

Product	Bp θ_b/°C(mmHg)	Isomer[a]	IR cm^{-1}	NMR (δ, $CDCl_3$, J/Hz)	Found(Calcd)/% C	H
			1205	J=12.6).		
			935			
20		Mixture	1713	1.08(3H, d, J=6.0), 1.11 and 1.13(3H, t, J=	71.66	10.86
			1100	7.0), 1.64—1.78(6H, m), 3.16—3.95(4H, m), 4.95 and 5.23(1H, d, J=9.0).	(71.70)	(10.94)
21			1700	1.02(3H, d, J=6.0), 1.05(6H, s), 1.15(3H, t, J=	71.75	10.88
			1680	7.0), 2.23(3H, s), 3.15(1H, q, J=6.0), 3.47(2H,	(71.70)	(10.94)
			1620	m), 6.03(1H, d, J=16.0), 6.88(1H, d, J=16.0).		
			1100			
22		Mixture	1715	1.08 and 1.13(3H, t, J=7.0), 1.22 and 1.39(3H,	77.98	9.14
		(e/t=46/54)[c]	1095	d, J=1.5), 1.53 and 1.74(3H, d, J=1.5), 2.02	(78.01)	(9.00)
			698	(3H, s, $COCH_3$ erythro), 2.22(3H, s, $COCH_3$ threo), 3.10—3.83(3H, m), 4.46(1H, d, J=10.0, CH-O threo), 4.67(1H, d, J=5.6, CH-O erythro), 4.93 and 5.48(1H, d, J=10.0), 7.24(5H, s).		
23			1700	1.01(3H, s), 1.09(3H, s), 1.14(3H, t, J=7.0), 2.23	78.10	9.07
			1677	(3H, s), 3.32(2H, m), 4.02(1H, s), 5.92(1H, d,	(78.01)	(9.00)
			1623	J=16.0), 6.93(1H, d, J=16.0), 7.23(5H, s).		
			1100			
			1070			
24	76(0.9)		1713	1.17(6H, t, J=7.0), 1.4—2.5(8H, m), 2.60(1H,	65.88	10.05
			1105	m), 3.62(4H, m), 4.82(1H, d, J=6.0).	(65.97)	(10.07)
			1060			
25	67(1.0)		1713	1.4—2.5(8H, m), 2.60(1H, m), 3.37(6H, s), 4.65	62.57	9.25
			1105	(1H, d, J=6.0).	(62.77)	(9.36)
			1070			
27	77/0.7		1720	1.75(6H, s), 2.1—2.8(4H, m), 2.92(1H, d, J=6.0),	66.58	9.08
			1100	3.40(6H, s), 4.63(1H, d, J=6.0).	(66.64)	(9.15)
			1070			
28	62/1.2		1710	1.75(6H, m), 2.12(3H, s), 3.28(3H, s), 3.35(3H,	64.52	9.69
			1120	s), 3.66(1H, dd, J=10.0, 8.4), 4.60(1H, d, J=	(64.49)	(9.74)
			1080	8.4), 5.14(1H, d, J=10.0).		
			1060			
29	111—112		1725	1.05(3H, t, J=7.0), 1.17(3H, t, J=7.0), 1.19(3H,	70.21	10.95
	(1.0)		1120	t, J=7.0), 1.60(3H, s), 1.68(3H, s), 1.3—2.3(5H,	(70.27)	(11.01)
			1060	m), 2.50(1H, m), 3.57(4H, m), 4.87(1H, m), 5.08 (1H, t, J=6.0), 9.71(1H, d, J=4.0).		
31			1725	1.60 and 1.68(9H, s), 1.6—2.2(8H, m), 2.65(1H,		
			1120	m), 3.38(6H, s), 4.50(1H, d, J=6.0), 5.10(2H,		
			1070	m), 9.67(1H, d, J=3.0).		
32	70/1.2		1727	0.88(3H, t, J=6.0), 1.18(3H, t, J=7.0), 1.20(3H,	65.20	10.87
			1120	t, J=7.0), 1.0—1.8(6H, m), 2.55(1H, m), 3.60	(65.31)	(10.96)
			1060	(4H, m), 4.64(1H, d, J=6.0), 9.68(1H, d, J= 3.0).		

a) Erythro and threo isomers. b) An erythro and threo mixture. c) e stands for erythro and t for threo.

methoxy-1-methyl-2-propenyl)-1-cyclohexanone (**18**) (6.00 g, 77—84 °C/2.0 mmHg, 66%). **17a** (erythro), **17b** (threo), and **18** were found to be in the ratio 13:40:13 by means of gas chromatography (PEG 20 M). Analytically pure samples of products were prepared by silica-gel column chromatography (hexane-ether) and preparative gas chromatography (20% PEG-20 M).

Reaction of 5-Methyl-2-morpholino-2,4-hexadiene (19) with Acetals. To a dichloromethane (50 ml) solution of 10.8 g (60 mmol) of benzaldehyde diethyl acetal was added 9.23 g (65 mmol) of $BF_3 \cdot OEt_2$ at −40 °C in argon atmosphere. Then 9.05 g (50 mmol) of 5-methyl-2-morpholino-2,4-hexadiene (**19**) was added immediately and the reaction mixture was stirred for 1 h at room temperature. The reaction mixture was worked up as described above and purified by silica-gel column chromatography. Elution with hexane and ether afforded 8.01 g (65%) of a mixture of diastereomers (**22a** and **22b**) of 3-(α-ethoxybenzyl)-5-methyl-4-hexen-2-one (**22**) and 0.98 g (8%) of 5-(α-ethoxybenzyl)-5-methyl-3-hexen-2-one (**23**). **22a** (erythro) and **22b** (threo) were in the ratio 46:54 as

Table 7. NMR signals of methylene protons in β-alkoxy carbonyl compounds

Product			Ha/δ	Jab/Hz	Solvent
8	a	(erythro)	4.84	4.4 (2.5)[a]	$CDCl_3$
	b	(threo)	4.67	8.0 (9.0)[a]	$CDCl_3$
12	a	(erythro)	4.66	8.0	$CDCl_3$
	b	(threo)	4.72	9.3	$CDCl_3$
15	a	(erythro)	4.58	5.7	$CDCl_3$
	b	(threo)	4.42	9.0	$CDCl_3$
17	a	(erythro)	3.99	4.4 (3.7)[a]	$CDCl_3$
	b	(threo)	3.92	8.0 (7.0)[a]	$CDCl_3$
22	a	(erythro)	4.67	5.6	$CDCl_3$
	b	(threo)	4.46	10.0	$CDCl_3$

a) The value of the corresponding aldol.

found by means of NMR.

Similarly, the reaction of **19** (9.05 g, 50 mmol) and acetaldehyde diethyl acetal (7.08 g, 60 mmol) in the presence of $BF_3 \cdot OEt_2$ (9.23 g, 65 mmol) gave 5.15 g (56%) of a mixture of diastereomers of 3-(1-ethoxyethyl)-5-methyl-4-hexen-2-one (**20**) and 0.65 g (7%) of *trans*-5-(1-ethoxyethyl)-5-methyl-3-hexen-2-one (**21**).

Stereochemistry of β-Alkoxy Carbonyl Compounds. The diastereomers **8a** and **8b** were stereospecifically converted into the corresponding *O*-methyloximes **33a** and **33b** by treatment with *O*-methylhydroxylamine (1.5 equiv., H_2O–MeOH, r. t, quant.). Then, it was found that **33a** and **33b** were erythro and threo isomers, respectively, by comparison with authentic samples prepared stereospecifically from the corresponding aldols[8] by treatment with *O*-methylhydroxylamine (1.5 equiv., H_2O–MeOH, r. t.) and NaH–EtI (THF, reflux, 30—50% yields). Therefore, it was determined that **8a** and **8b** were erythro and threo isomers, respectively. The stereochemistry of the diastereomers **17a** and **17b** was determined in a similar manner as above.

The stereochemistry of the diastereomers of **12**, **15**, and **22** was assigned on the basis of NMR spectra (shown in Table 7). Each of the diastereomers of **12**, **15**, and **22** has an absorption due to the proton (Ha) of the O–CH group or the other tertiary hydrogen (Hb), and a comparison of the coupling constant (*J*ab) of the isomers suggests the assigned stereochemistry.

Reaction of 1-Morpholino-1-cyclohexene (1) with Triethyl Orthoformate in the Presence of $SnCl_4$. To a mixture of 8.35 g (50 mmol) of 1-morpholino-1-cyclohexene (**1**) and 9.62 g (65 mmol) of triethyl orthoformate in dichloromethane (50 ml) was added 16.9 g (65 mmol) of $SnCl_4$ at −40 °C in argon atmosphere. Then the reaction mixture was stirred for 1 h at 0 °C. The mixture was quenched with water and stirred for 1 h at room temperature. After hydrolysis, the resulting organic layer was washed with a saturated solution of $NaHCO_3$ and dried over $MgSO_4$. After removal of the solvent, the residue was distilled to afford 9.00 g (90%) of 2-diethoxymethyl-1-cyclohexanone (**24**) (76 °C/0.9 mmHg).

The reaction of enamines, such as **1**, **11**, **14**, **19**, 3,4-dimethyl-1-morpholino-1,3-cyclohexadiene (**26**), and 1-morpholino-6,10-dimethyl-1,5,9-undecatriene (5*E*:5*Z*=1:1) (**30**), with triethyl or trimethyl orthoformate in the presence of various Lewis acids were carried out according to the same procedure, and the yields of the corresponding α-dialkoxymethyl carbonyl compounds are listed in Table 5. The physical properties and analytical data of the products are shown in Table 6.

The authors wish to express their thanks to Professor Teruaki Mukaiyama, the University of Tokyo for his helpful discussions.

Reference

1) O. Takazawa and T. Mukaiyama, *Chem. Lett.*, **1982**, 1307.
2) T. Mukaiyama and M. Hayashi, *Chem. Lett.*, **1974**, 15.
3) K. Narasaka, K. Soai, Y. Aikawa, and T. Mukaiyama, *Bull. Chem. Soc. Jpn.*, **49**, 779 (1976).
4) a) T. Mukaiyama and A. Ishida, *Chem. Lett.*, **1975**, 319; b) M. Asaoka, N. Sugimura, and H. Takei, *Bull. Chem. Soc. Jpn.*, **52**, 1953 (1979); c) I. Fleming, J. Goldhill, and I. Paterson, *Tetrahedron Lett.*, **1979**, 3209; d) O. Takazawa, H. Tamura, K. Kogami, and K. Hayashi, *Bull. Chem. Soc. Jpn.*, **55**, 1907 (1982).
5) a) A. T. Blomquist and E. Moriconi, *J. Org. Chem.*, **26**, 3761 (1961); b) G. Opitz, H. Hellmann, H. Mildenberger, and H. Suhr, *Justus Liebigs Ann. Chem.*, **649**, 39 (1961); c) G. Stork, A. Brizzolara, H. Landesman, J. Szmuszkovicz, and R. Terrell, *J. Am. Chem. Soc.*, **85**, 207 (1963).
6) W. Ziegenbein, *Angew. Chem.*, **77**, 380 (1965).
7) S. Hünig, E. Lücke, and W. Brenniger, *Org. Synth.*, Coll. Vol. V, 808 (1973).
8) T. Mukaiyama, K. Banno, and K. Narasaka, *J. Am. Chem. Soc.*, **96**, 7503 (1974).

Atmosphere Dependent Photoreaction of 4-Pyridinecarboxylic Ester in Acidic Methanolic Solutions

Toru SUGIYAMA,* Yukari KUSANO, Kazuya YAGI,
Yoko ITO, and Akira SUGIMORI*
Department of Chemistry, Faculty of Science and Technology, Sophia University, Kioi-cho 7-1, Chiyoda-ku, Tokyo 102
(Received October 26, 1983)

The UV-irradiation of methyl 4-pyridinecarboxylate (**1**) in methanol under oxygen in the presence of sulfuric acid brings about methoxylation at the 3-position of the pyridine ring, while under nitrogen methoxylation and hydroxymethylation occur at the 2-position. The change of photoreactions of **1** caused by oxygen can not be explained either by the promotion of intersystem crossing by O_2 or by the charge transfer interactions between **1** and O_2.

The UV-irradiation of pyridinecarboxylic acid derivatives in acidic alcoholic solutions generally leads to alkylation, hydroxyalkylation, and alkoxylation at the α-and γ-positions of the pyridine ring.[1-5] In the course of our studies on the photoreactions of pyridinecarboxylic acid derivatives, we have observed a remarkable effect of oxygen in the photoreaction of 4-pyridinecarboxylic ester in alcohols in the presence of sulfuric acid.[6]

Although the photoreactions in the presence of oxygen have been extensively investigated, the roles of oxygen in the photoreactions have not yet been fully clarified. Besides the well-investigated reactions *via* singlet oxygen, the interest in the effects of oxygen *via* electron transfer interactions is increasing.[7] Pac *et al.* reported a marked increase in the quantum yields by oxygen on the sensitized retro-cycloaddition of dimethylthymine dimers.[8] Mizuno *et al.* have recently reported that the photoisomerization of 1,2-diarylcyclopropanes in the presence of 9,10-dicyanoanthracene is promoted by the addition of air.[9] The acceleration by oxygen in these photoreactions has been ascribed to the electron transfer interactions between the excited substrates and oxygen.

There remain, however, several interesting effects of oxygen, the roles of which have not yet been elucidated. Among them is promotion of the photochemical alcoholysis of organic halides by oxygen.[10]

In this paper we report the analysis of the effects of oxygen in the photoreactions of methyl 4-pyridinecarboxylate in acidic methanolic solutions.

Results and Discussion

Types of Photoreactions under N_2 and O_2 Atmosphere. The UV-irradiation of methyl 4-pyridinecarboxylate(**1**) in methanol under nitrogen atmosphere in the presence of sulfuric acid brings about methoxylation and hydroxymethylation at the 2-position of the pyridine ring accompanied by the formation of trace amounts of dimethyl 3,3′-bipyridine-4,4′-dicarboxylate and 4-pyridylmethanol (Table 1).

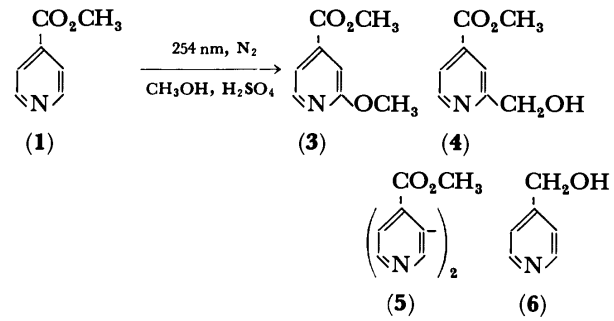

Under oxygen atmosphere, these reactions are inhibited and **1** gives the methoxylation product at the 3-position selectively (Table 1).

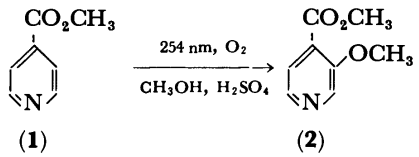

The photoreaction of **1** is characterized by the fact that the presence of oxygen causes a dramatic change in the position of the methoxylation Such a remarkable oxygen effect was not observed in the photoreactions of 2- and 3-pyridinecarboxylic esters.

Photoreactions under N_2. The photoreactions of methyl 4-pyridinecarboxylate (**1**) in an acidic methanolic solution under nitrogen are essentially similar to those of 2- and 3-pyridinecarboxylic esters:[3,4] ionic methoxylation and hydroxymethylation in radical reaction occur in parallel. The difference of the photo-

Table 1. Photoreactions of methyl 4-pyridinecarboxylate (**1**) in methanol in the presence of H_2SO_4.[a]

Atmosphere	Conversion of **1** / %	(Yield of product)[b] / %				
		2	**3**	**4**	**5**	**6**
N_2	47.5	Trace	14	5.5	Trace	Trace
O_2	14	88	Trace	0.0	0.0	0.0

a) [**1**] = 0.02 mol dm^{-3}; [H_2SO_4] = 0.25 mol dm^{-3}; Irradiation time, 25 min; Temp., 30 °C. b) Yields were determined by means of GLC and/or HPLC, and were calculated on the basis of **1** consumed.

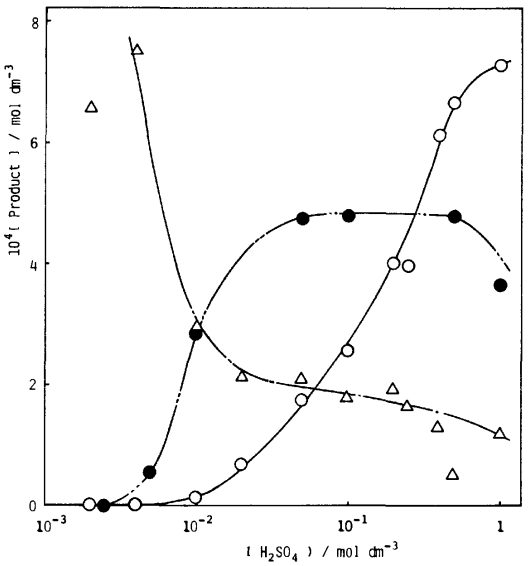

Fig. 1. Dependence of photo-methoxylation and -hydroxymethylation at the 2-position under N_2 and photo-methoxylation at the 3-position under O_2 on the concentration of sulfuric acid.
[**1**]=0.01 mol dm^{-3}, —○—: **3**, —△— — —: **4** (under N_2), —●— — —: **2** (under O_2).

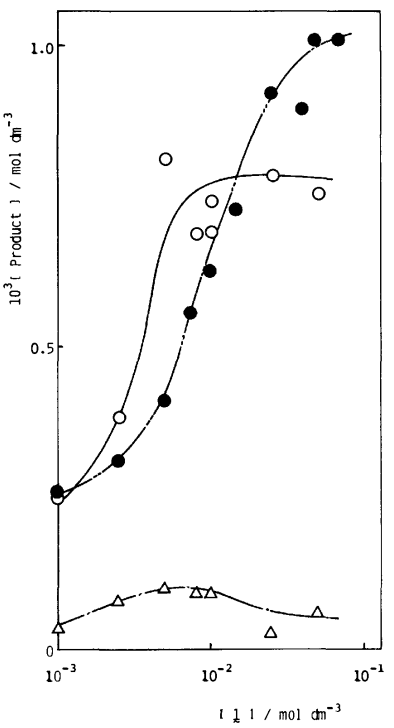

Fig. 2. Dependence of yields of **3** and **4** under N_2 and **2** under O_2 on the concentration of **1**.
[H_2SO_4]=1.0 mol dm^{-3}, —○—: **3**, —△— — —: **4** (under N_2), —●— — —: **2** (under O_2).

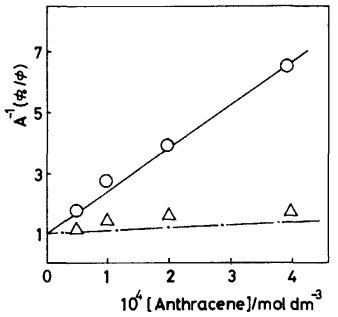

Fig. 3. Effects of anthracene on the photo-methoxylation and -hydroxymethylation at the 2-position of **1**.
[**1**]=0.01 mol dm^{-3}, [H_2SO_4]=0.05 mol dm^{-3}, —○—: **3**, —△— — —: **4**.

reactions of 4-pyridinecarboxylic ester from those of 2- and 3-isomers are: 1) the occurrence of hydroxymethylation in place of methylation which occurs in 2- and 3-pyridinecarboxylic esters and 2) the formation of dimethyl 3,3′-bipyridine-4,4′-dicarboxylate (dimerization) and 4-pyridylmethanol (reduction).

The photoreaction of **1** is dependent on the concentration of added sulfuric acid and on the concentration of the substrate itself.

Figure 1 shows the effect of the concentration of sulfuric acid on the photoreaction. In the lower concentrations of sulfuric acid, hydroxymethylation occurs exclusively. As the concentration of sulfuric acid increases, hydroxymethylation is suppressed and methoxylation becomes dominant. This shows that non-protonated **1** undergoes only hydroxymethylation and protonated **1** undergoes methoxylation and hydroxymethylation.

The photo-methoxylation of **1** shows a remarkable concentration dependence of the substrate (Fig. 2). A similar concentration dependence was observed in the photo-methoxylation of methyl 2-pyridinecarboxylate and a kinetic analysis revealed that the photo-methoxylation of 2-pyridinecarboxylic ester proceeds *via* an excimer of the substrate.[3] The similarity of the concentration dependences in the photo-methoxylations of 2- and 4-pyridinecarboxylic esters suggests the participation of an excited dimer in the formation of **3**.

The inhibition of photo-methoxylation of **1** by aromatic hydrocarbons is very similar to that of 2-pyridinecarboxylic ester.[3] Photo-methoxylation at the 2-position under nitrogen atmosphere is inhibited by anthracene effectively as is shown in a Stern-Volmer plot in Fig. 3.[11] Similar inhibitions are observed for *trans*-1,3-pentadiene, naphthalene, triphenylene, azulene, and even for benzene which is considered as a triplet sensitizer. The efficiencies for the quenching of the formation of **3** by the additives correlate very well with the ionization potentials of the additives (Fig. 4). These facts can be explained by the quenching of an excimer *via* an electron transfer (from aromatic hydrocarbons to **1**) mechanism proposed by Caldwell *et al.*[12]

Hydroxymethylation should originate from an excited monomer in the singlet excited state, because it is not inhibited by anthracene as is shown in Fig. 3.

Photo-hydroxymethylation should be initiated by the hydrogen abstraction by an excited **1** from methanol. The radical pair thus formed combines to give an addition product which is converted to 4-pyridylmethanol either *via* disproportionation or *via* a kind of oxidation.

Mechanism for the photo-methoxylation and the hydroxymethylation of **1** is summarized in Scheme 1.

Although the bipyridine formation (a kind of dimerization) and the reduction of the ester carbonyl to alcohol are characteristic for the photoreaction of **1**, the detailed analyses of the mechanism for the formation of these products could not be done, because their yields are very low.

Photo-methoxylation at the 3-Position under O_2. The UV-irradiation of **1** in methanol in the presence of sulfuric acid under O_2 gives methyl 3-methoxy-4-pyridinecarboxylate (**2**) selectively. The results summarized in Table 2 indicate that the yields of the products are changed by the addition of oxygen. When the solution is deoxyganated by bubbling nitrogen, the methoxylation at the 2-position becomes dominant. As the partial pressure of oxygen becomes higher, the methoxylation at the 3-position remarkably increases, while the methoxylation and the hydroxymethylation at the 2-position as well as the rate of decomposition of **1** are suppressed.

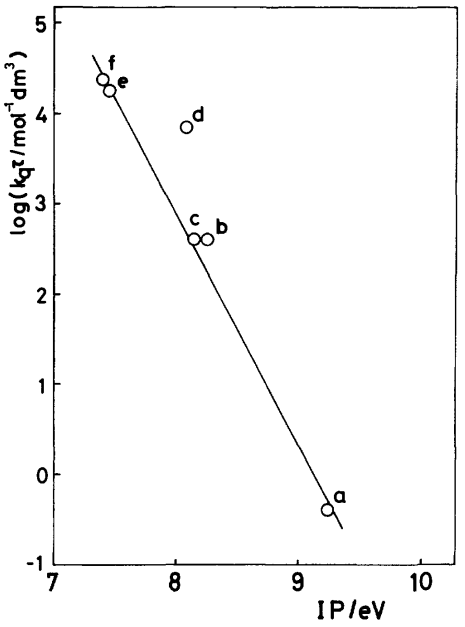

Fig. 4. Relation between $k_q\tau$ for the quenching of photo-methoxylation at the 2-position and ionization potentials of quenchers. a) benzene, b) *trans*-1,3-pentadiene, c) naphthalene, d) triphenylene, e) anthracene, f) azulene.

Oxygen does not serve as an oxidizing agent of a precursor of **2**, because the addition of $K_3[Fe(CN)_6]$ as an oxidizing agent after the irradiation of **1** under N_2 does not increase the yield of **2** (Table 2). The bubbling of oxygen through the solution which has been irradiated under N_2 causes no increase in the yield of **2**.

Such a dramatic change of photoreactions by oxygen has not been observed in the cases of 2- and 3-pyridinecarboxylic esters for which oxygen only inhibits the photoreactions.[3,4]

As is shown on Figs. 1 and 2 the methoxylation at the 3-position under O_2 shows dependence on the concentrations of sulfuric acid and **1**. These facts are somewhat similar to the methoxylation at the 2-position under N_2 described in the preceeding section.

However, the effects of additives on the methoxylation at the 3-position are different from those of the methoxylation at the 2-position under N_2. Methoxylation under O_2 is not inhibited by anthracene and by *trans*-1,3-pentadiene, while that under N_2 are inhibited by aromatic hydrocarbons. This fact indicates that the excited states responsible for the two kinds of methoxylation are different in character.

Role of Oxygen in the Photo-methoxylation at the 3-Position. In order to explore the role of oxygen in the promotion of the photo-methoxylation at the 3-position, we have tested the following possibilities for the role of oxygen: 1) the acceleration of intersystem crossing and 2) charge transfer interaction between **1** and oxygen resulting in the electron transfer.

Unexpectedly, no evidence in support of the role of oxygen is observed as described in the following sections.

Possibility of Acceleration of Intersystem Crossing. Oxygen could accelerate intersystem crossing of an excited singlet state of **1** to a triplet state and the triplet would give the methoxylation product at the

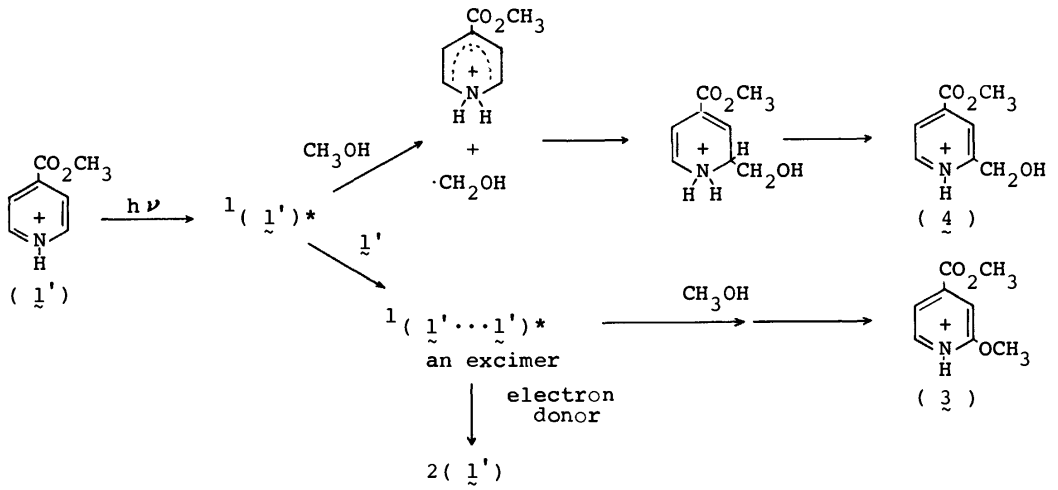

Scheme 1. Mechanism of photoreactions of **1** under N_2.

Table 2. Photoreactions of **1** in methanol in the presence of H_2SO_4[a]

Atmosphere[b]	Additive	Conversion of **1** %	10^4[Product]/mol dm^{-3}		
			2	**3**	**4**
N_2	—	24	0.35	4.12	2.31
Air	—	17	6.25	1.82	0.90
O_2	—	10	5.69	0.00	0.00
NO	—	0	0.00	0.00	0.00
N_2	O_2[c]	22	0.27	4.01	1.69
N_2	$[Fe(CN)_6]^{3-}$[d]	21	0.25	2.67	3.20
N_2	Ph_2CO[e]	0	0.00	0.00	0.00
O_2	Ph_2CO[e]	0	0.00	0.00	0.00

a) [**1**]=0.01 mol dm^{-3}; [H_2SO_4]=0.25 mol dm^{-3}; Irradiation time, 1 h; Temp., 20 °C. b) The solution was purged with gas for 50 min before irradiation. c) O_2 was bubbled after irradiation. d) $K_3[Fe(CN)_6]$ was added after irradiation. e) [**1**]=5×10^{-3} mol dm^{-3}; [H_2SO_4]=1×10^{-1} mol dm^{-3}; Irradiation time, 48 h; Temp., 25.5 °C; Irradiated with monochromatic light of 365 nm.

3-position (**2**). This possibility can be tested by examining the contribution of a triplet state of **2** for the formation of **2**.

Triplet quenchers such as anthracene and *trans*-1,3-pentadiene have little effect on the formation of **2**, as mentioned before. When the irradiation is carried out in the presence of benzophenone, no reaction occurs under either O_2 or N_2. The irradiation is carried out under NO, a paramagnetic gas, but no reaction occurs, as is shown in Table 2.

Possibility of Effect via Charge Transfer Interaction between Substrate and Oxygen. Oxygen is an efficient electron acceptor and can affect the photoreactions *via* charge transfer interaction either in the ground[13-16] or in the excited state. Oxygen could abstract an electron from the substrate and the irradiation of **1** under O_2 may give an electron-deficient intermediate (the postulated intermediate formed in the above process should easily undergo the necleophilic methoxylation). If this process actually occurs, electron acceptors other than oxygen could show the same effect as oxygen. To test this possibility, the irradiation in the presence of several typical electron acceptors in place of oxygen (reduction potential, $E_{1/2}$=−0.94 V *vs.* SCE in CH_3CN)[7] are carried out under N_2 atmosphere. *p*-Dicyanobenzene ($E_{1/2}$=−1.97 V *vs.* Ag/$AgClO_4$ (0.1 mol dm^{-3}) in DMF)[17] and 1,2,4,5-tetracyanobenzene ($E_{1/2}$=−1.02 V *vs.* Ag/$AgClO_4$ (0.1 mol dm^{-3}) in DMF)[17] have almost no effect on the photoreaction of **1**: the electron acceptors neither promote the methoxylation at the 3-position nor inhibit the methoxylation at the 2-position (Table 3).[11]

The above results indicate that the remarkable change of the photoreactivity of **1** by oxygen is not due to the charge transfer interactions between the substrate and oxygen.

Since the concentration dependence curves of the methoxylations under N_2 and O_2 are somewhat different as shown in Fig. 2, it seems that the excimer leading to the methoxylation at the 3-position under O_2 is different in character from that leading to the methoxylation at the 2-position under N_2.

The present study revealed that the oxygen effect observed in the photoreaction of **1** in acidic methanolic solutions can not be categorized as types of oxygen effect which have been generally accepted. The processes of the photo-methoxylation of 4-pyridinecarboxylic ester at the 3-position should contain a novel type of the interaction between oxygen and the excited molecule.

Table 3. Effects of electron acceptors on the photo-methoxylations of **1** under N_2[a]

Acceptor	[Acceptor] mol dm^{-3}	Relative yield[b]	
		2	**3**
None	—	0.12	1.00
DCNB[c]	8.0×10^{-4}	0.05	0.99
TCNB[d]	1.6×10^{-4}	0.08	0.99
TCNB[d]	3.2×10^{-4}	0.11	1.01

a) [**1**]=0.01 mol dm^{-3}; [H_2SO_4]=0.05 mol dm^{-3}; Irradiation time, 1 h; Temp., 20 °C. b) Relative yields based on the A value of **3**.[11] c) *p*-Dicyanobenzene. d) 1,2,4,5-Tetracyanobenzene.

Experimental

Materials. Commercial methly 4-pyridinecarboxylate (GR grade reagent of Tokyo Kasei Co) was purified by vacuum distillation; bp, 94—95 °C/16.5 mmHg (1 mmHg≈133.322 Pa). Anthracene (standard reagent for elemental analysis made by E. Merck Co.), triphenylene (GR grade reagent of Tokyo Kasei Co.), *trans*-1,3-pentadiene (GR grade reagent of Wako Junyaku Co.), and azulene (GR grade reagent of Tokyo Kasei Co.) were used without further purification. Commercial *p*-dicyanobenzene was purified by recrystallization; mp, 228—229 °C. 1,2,4,5-tetracyanobenzene was kindly supplied by Mr. Haruhiko Tomoda of Shibaura Institute of Technology.

UV-Irradiation for Preparation of Products. Through the solutions of **1** (0.02 mol dm^{-3}, 50 cm^3) containing sulfuric acaid (0.25 mol dm^{-3}) oxygen or nitrogen were bubbled for 50 min before irradiation. The solutions were irradiated with a 17 W low pressure mercury lamp for 25 min at 30 °C.

UV-Irradiation for Study of Mechanism. The solutions of **1** (20 cm^3) containing sulfuric acid and the additives, if necessary, were purged with a gas (O_2, air, or N_2) for 50 min before irradiation. The solutions were irradiated with a 17 W low pressure mercury lamp in a merry-go-round type ap-

paratus at 20°C.

For wavelength effect experiments the irradiation was carried out by using a Shimadzu-Bausch-Lomb Co. monochrometer equipped with a 200 W super high pressure mercury lamp.

Isolation and Identification of Photo-products. After the irradiation the solution was concentrated with a rotary evaporator and neutralized with sodium carbonate solution. The neutralized solution was extracted with ethyl acetate. The products were separated by means of TLC (Plate, GF_{254} Type 60 of E. Merck Co.; developing solvent, ethyl acetate-dichloromethane 3:7 v/v).

Methyl 3-methoxy-4-pyridinecarboxylate (**2**): Mp 55—56.5 °C; IR (KBr disk) 1720 (ester C=O) and 1220 cm^{-1} (C-O-C); ^1H NMR ($CDCl_3$) δ=8.44 (1 H, s), 8.29 (1 H, d, J=4 Hz), 7.55 (1 H, d, J=4 Hz), 4.02 (3H,s), and 3.91 (3H,s); MS (70 ev), m/z (rel intensity) 167 (M^+; 77), 152 (14), 138 (18), 137 (9), 136 (100), 135 (18), 134 (79), 106 (31), 93 (36), and 78 (74), Found: m/z 167.0585. Calcd for $C_8H_9NO_3$: M, 167.0583.

Methyl 2-methoxy-4-pyridinecarboxylate (**3**) was identified by the accordance of its ^1H NMR spectra with those obtained by Deady *et al.*[18]

Methyl 2-hydroxymethyl-4-pyridinecarboxylate(**4**) (mp 67.5—68 °C; lit,[19] 68—69 °C) was identified by means of spectral analyses.

Dimethyl 3,3′-bipyridine-4,4′-dicarboxylate(**5**): Mp 184—187 °C(sub); IR (KBr disk), 1720 cm^{-1} (ester C=O); ^1H NMR ($CDCl_3$) δ=8.95 (1 H, d. J=1.6 Hz), 8.85 (1 H, d, J=5 Hz), 7.87 (1 H, dd, J=1.6 and 5 Hz), and 4.00 (3H, s); Found: C, 61.7; H, 4.7; N, 10.2% M^+, 272. Calcd for $C_{14}H_{12}N_2O_4$: C, 61.76; H, 4.44; N, 10.29%; M, 272.

4-Pyridylmethanol (**6**) was identified by the accordance of gas-chromatographic and spectral properties with those of authentic sample.

Quantitative Analyses of Photo-products. The yields of the products were determined by means of GLC (1.5 m column of 10% PEG 20M on 60—80 mesh Celite 545) with a Shimadzu gas chromatograph model GC 6A and/or by means of HPLC with Shimadzu liquid chromatograph model LC 1 and LC 3A (4.6 mm×25 cm column of Zorbax ODS; eluent, H_2O-MeOH 4:6 v/v).

Spectral Measurments. IR spectra were measured on a Hitachi 215 spectrometer, and ^1H NMR spectra were determined with Hitachi R 22 NMR spectrometer (90M Hz) with tetramethylsilane as an internal standard. MS spectra were recorded on a JEOL D-300 spectrometer.

The authors wish to thanks to Professor L. W. Deady of La Trobe University in Australia and Professor Ichiya Ninomiya of Kobe Women's College of Pharmacy for sending them the spectral data of pyridinecarboxylic esters and Mr. Haruhiko Tomoda of Shibaura Institute of Technology for a gift of 1,2,4,5-tetracyanobenzene.

References

1) A. Sugimori, *Yuki Gosei Kagaku Kyokai Shi*, **39**, 712 (1981).
2) T. Sugiyama, E. Tobita, K. Takagi, M. Sato, Y. Kumagai, G. P. Satô, and A. Sugimori, *Chem. Lett.*, **1980**, 131.
3) T. Sugiyama, T. Furihata, K. Takagi, M. Sato, S. Akiyama, G. P. Satô, and A. Sugimori, *Bull. Chem. Soc. Jpn.*, **54**, 3785 (1981).
4) A. Sugimori, E. Tobita, Y. Kumagai, and G. P. Satô, *Bull. Chem. Soc. Jpn.*, **54**, 1761 (1981).
5) A. Sugimori, T. Furihata, S. Mikayama, M. Yoshida, and Y. Nakanishi, *Bull. Chem. Soc. Jpn.*, **55**, 2906 (1982).
6) Preliminary report, T. Sugiyama, K. Yagi, Y. Ito, and A. Sugimori, *Chem. Lett.*, **1982**, 917.
7) J. Eriksen and C. S. Foote, *J. Am. Chem. Soc.*, **102**, 6083 (1980); D. S. Steichen and C. S. Foote, *ibid.*, **103**, 1855 (1981).
8) T. Majima, C. Pac, J. Kubo, and H. Sakurai, *Tetrahedron Lett.*, **21**, 377 (1980), C. Pac, J. Kubo, T. Majima, and H. Sakurai, *Photochem. Photoboil.*, **36**, 273 (1982).
9) K. Mizuno, Z.Hiromoto, K. Ohnishi, and Y. Otsuji, *Chem. Lett.*, **1983**, 1059.
10) Y. Izawa, H. Tomioka, M. Natsume, S. Beppu, and H. Tsujii, *J. Org. Chem.*, **45**, 4835 (1980).
11) In this case, the effects of additives were analyzed by means of an index A, the relative quantum yield calculated on the basis of the light absorbed by **1**, because the additives absorb the 254 nm light competitively with **1**. A^{-1} corresponds ϕ_0/ϕ in the Stern-Volmer plots for the quenching experiments. A=Y/L, Y=(Yield in the presence of additive (**Q**))/(Yield in the absence of additive (**Q**)), $L=\varepsilon_1[\mathbf{1}]/(\varepsilon_1[\mathbf{1}]+\varepsilon_Q[\mathbf{Q}])$, where ε_1 and ε_Q are the molar absorption coefficients of **1** and **Q** at 254 nm, respectively.
12) R. A. Caldwell, D. Creed, D. C. DeMarco, L. A. Melton, H. Ohta, and P. H. Wine, *J. Am. Chem. Soc.*, **102**, 2369 (1980).
13) C. von Sonntag, K. Neuwald, H. -P. Schuchmann, F.Weeke, E. Janssen, *J. Chem. Soc. Perkin Trans., 2*, **1975**, 171.
14) K. S. Wei and A. H. Adelman, *Tetrahedron Lett.*, **1969**, 3297.
15) M. Kojima and H. Sakuragi, and K. Tokumaru, *Tetrahedron Lett.*, **22**, 2889 (1981).
16) T. Ishigami, Y. Kinoshita, and A. Sugimori, *Chem. Lett.*, **1974**, 149; Y. Izawa, K.Ishiguro, and H. Tomioka, *Bull. Chem. Soc. Jpn.*, **56**, 1490 (1983).
17) P. H. Rieger, I. Bernal, W. H. Reinmuth, and G. K. Fraenkel, *J. Am. Chem. Soc.*, **85**, 683 (1963).
18) L. W. Deady, P. M. Harrison, and R. D. Topsom, *Org. Magn. Reson.*, **7**, 41 (1975); L. W. Deady, private communication.
19) I. Ninomiya, private communication.

 © 1984 The Chemical Society of Japan Bull. Chem. Soc. Jpn., 57, 1887—1890 (1984)

Ni(0)-Trialkylphosphine Complexes. Efficient Homo-coupling Catalyst for Aryl, Alkenyl, and Heteroaromatic Halides

Kentaro TAKAGI,* Naomi HAYAMA, and Ken SASAKI†

College of Liberal Arts and Science, Okayama University, Tsushima, Okayama 700

†*Department of Polymer Science and Engineering, Kyoto Technical University, Matsugasaki, Kyoto 606*

(Received October 29, 1983)

Bis(trialkylphosphine)nickel(0) generated *in situ* from bis(trialkylphosphine)nickel(II) chloride was found to be an effective catalyst for a homo-coupling of aryl, alkenyl, or heteroaromatic halides with zinc powder. The catalytic reaction proceeded very well in NMP or HMPA solvent under mild conditions to afford dehalogenative-coupling products in good yields.

It has been shown recently that several zerovalent nickel complexes exhibit specific ability in a reductive coupling of aryl or alkenyl halides.[1] These nickel (0) complexes may be divided into two groups according to the kinds of coordinated ligands: One group is characterized by the presence of phosphorus ligands, especially triphenylphosphine, while another is characterized by the absence of them.

$$2\,ArX + NiL_n \longrightarrow Ar\text{-}Ar + NiX_2L_m$$

L=PPh_3,[2-5] 1,5-COD,[2,6] none (or solvent)[7-9] n,m= 2—4

Although the reactivities of nickel(0) complexes containing trialkylphosphine ligands in the coupling reaction have been little reported,[1] the complexes are much more reactive than triarylphosphine analogs in certain organometallic reactions, such as oxidative additions of aryl or alkenyl halides.[10] It is also known that trialkylphosphine ligands impart better thermal stability to some organometallics than triarylphosphine ligands do.[11] Thus, nickel(0) complexes containing trialkylphosphine ligands are expected to show interesting reactivities in the title reaction. In this paper, we will describe a facile homo-coupling of aryl, alkenyl, and heteroaromatic halides with zinc powder in the presence of catalytic amounts of bis(trialkylphosphine)nickels(0) which are generated *in situ* by a reduction of bis(trialkylphosphine)nickel(II) chlorides, with zinc powder.

Results and Discussion

General Survey of Reaction Conditions and Homo-coupling of Aryl Halides. All zerovalent nickel used in this study were prepared *in situ* by the reduction of divalent nickel complexes with zinc powder.[12] 2—10 mol% of the nickel(II) precursor was used together with an excess of zinc powder intending to render the reaction catalytic in nickel as shown in Scheme 1 (*vide infra*).

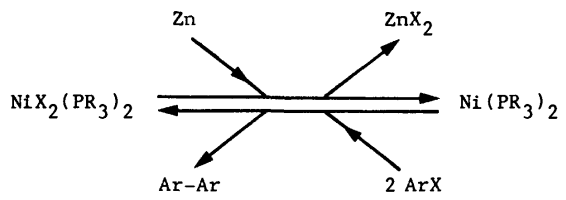

Scheme 1.

Following this convenient method, bis(triphenylphosphine)-, bis(triethylphosphine)-, or metallic nickel(0) was generated *in situ*, and their catalytic activities in the homo-coupling of bromobenzene with zinc powder were compared with one other. Hexamethylphosphoric triamide (HMPA) was used as a solvent since *in situ* generated metallic nickel is known to work in the solvent.[7] Runs 1—3 in Table 1 clearly show that bis(triethylphosphine)nickel(0) is the most favorable judging from the turnover number of the catalyst. Encouraged by this result, the catalytic activities of nickel(0)-trialkylphosphine complexes toward various organic halides containing an otherwise inert sp^2-carbon-halogen bond were investigated in detail.

Among the bis(trialkylphosphine)nickel(II)-chloride precursors examined, both triethylphosphine (PEt_3) and tributylphosphine (PBu_3) complexes gave biphenyl in better yields than either 1,2-bis(diethylphosphino)ethane ($Et_2PCH_2CH_2PEt_2$) or tricyclohexylphosphine (PCy_3) complex (Runs 7, 12, 14—16). The addition of two molar equivalents of tributylphosphine retarded the reaction with bis(tributylphosphine)nickel(II) chloride considerably (Runs 12 and 13).[13] As solvent for this reaction, *N*-methyl-2-pyrrolidone (NMP) as well as HMPA were effective, whereas other solvents like 1,1,2,2-tetramethylurea (TMU), *N*,*N*-dimethylformamide (DMF), acetonitrile (AN), or tetrahydrofuran (THF) were less effective (Runs 3, 7—11). Throughout the entire research, we prefered to use NMP unless otherwise noted since no special care need in the handling of this solvent in contrast with HMPA.[14] The addition of potassium iodide was effective for a smooth catalytic reaction (Runs 5 and 6).

The reaction of iodobenzene proceeded more readily than that of bromobenzene (Runs 5 and 7), whereas that of chlorobenzene did not react to completion even at elevated temperatures like 80 °C (Runs 17 and 18). Several functional groups such as ester, ketone, or alkyl were compatible with this reaction and a bulky substituent did not much alter the total reactivity (Runs 19—21). Thus, 2,2′-dibenzoylbiphenyl was readily obtained from 2-iodobenzophenone at 30 °C in a good yield.

Homo-coupling of Alkenyl Halides. The reaction of alkenyl bromides also proceeded very well under mild conditions to afford conjugated alkadienes in good yields as shown in Table 2. Interesting stereochemistry was observed in the reaction of (*E*)- or (*Z*)-β-bromostyrene: Only one of the two double bonds in the produced alkadiene retained the configuration of the

alkenyl halide (Runs 26 and 27). Thus, for example, (*E*)-β-bromostyrene afforded (*E,E*)-1,4-diphenyl-1,3-butadiene mainly with a small amount of (*E,Z*)-isomer, but no (*Z,Z*)-isomer. The fact that third isomers ((*E,E*)-isomer from (Z)-alkenyl halide and (*Z,Z*)-isomer from (*E*)-alkenyl halide) were obtained from neither (*E*)- nor (*Z*)-β-bromostyrene seems to indicate that cis,trans-isomerization of the alkenyl group does not occur on nickel. Therefore, it may be speculated that the isomerization happened on the transfered-alkenyl ligand at

TABLE 1. NICKEL(0)-CATALYZED HOMO-COUPLING OF ARYL HALIDES[a]

Run	Aryl halide	Nickel(II) complex	Solvent	Temp °C	Time h	Biaryl[b] %
1	C_6H_5Br	$NiBr_2(PPh_3)_2$	HMPA	30	2	25
2	C_6H_5Br	$NiBr_2$	HMPA	30	2	34[c]
3	C_6H_5Br	$NiCl_2(PEt_3)_2$	HMPA	30	2	95
4	C_6H_5I	$NiCl_2(PEt_3)_2$	HMPA	25	3	93
5	C_6H_5I	$NiCl_2(PEt_3)_2$	NMP	25	1	88
6[d]	C_6H_5I	$NiCl_2(PEt_3)_2$	NMP	25	12	19
7	C_6H_5Br	$NiCl_2(PEt_3)_2$	NMP	30	2	74
8	C_6H_5Br	$NiCl_2(PEt_3)_2$	TMU	30	2	61
9	C_6H_5Br	$NiCl_2(PEt_3)_2$	DMF	50	12	15
10	C_6H_5Br	$NiCl_2(PEt_3)_2$	AN	50	12	0
11	C_6H_5Br	$NiCl_2(PEt_3)_2$	THF	50	12	0
12	C_6H_5Br	$NiCl_2(PBu_3)_2$	NMP	30	2	81
13[e]	C_6H_5Br	$NiCl_2(PBu_3)_2$	NMP	30	4	35[f]
14	C_6H_5Br	$NiCl_2(Et_2PCH_2CH_2PEt_2)$	NMP	30	4	7[g]
15	C_6H_5Br	$NiCl_2(PCy_3)_2$	NMP	30	4	0
16	C_6H_5Br	$NiCl_2(PCy_3)_2$	NMP	80	4	75
17	C_6H_5Cl	$NiCl_2(PBu_3)_2$	HMPA	80	10	18
18	C_6H_5Cl	$NiCl_2(PEt_3)_2$	HMPA	80	10	25
19	*p*-$CH_3C_6H_4I$	$NiCl_2(PEt_3)_2$	NMP	30	2	(87)
20	*m*-$CH_3O_2CC_6H_4Br$	$NiCl_2(PEt_3)_2$	NMP	30	3	(91)
21	*o*-$C_6H_5COC_6H_4I$	$NiCl_2(PEt_3)_2$	NMP	30	6	(67)

a) In the presence of 0.25 mmol (Runs 1—18) or 2 mmol (Runs 19—21) of aryl halide in 0.3 ml (Runs 1—18) or 4 ml (Runs 19—21) of solvent under nitrogen. The molar ratio of the component was as follows: ArX/Ni(II)/Zn/KI=1.0/0.04/1.0/2.0 (Runs 1—16, 20, and 21), 1.0/0.08/1.0/2.0 (Run 17), 1.0/0.25/1.0/2.0 (Run 18), or 1.0/0.02/0.5/1.0 (Run 19). b) Yields were determined by GLC using internal standards. Yields in parentheses were isolated ones. c) 50% of iodobenzene was obtained. d) Run without potassium iodide. e) Run with 0.02 mmol of tributylphosphine. f) 38% of iodobenzene was obtained. g) 34% of iodobenzene was obtained.

TABLE 2. NICKEL(0)-CATALYZED HOMO-COUPLING OF ALKENYL AND HETEROAROMATIC HALIDES[a]

Run	RX	Solvent	Temp °C	Time h	*R-R*[b] %
22	2-Bromo-1,1-diphenylethene	NMP	50	1	97
23	2-Bromo-1,1-diphenylethene	NMP	30	1.5	(96)
24	2,Bromo-1,1-diphenylethene	HMPA	50	1	97
25	1-Bromo-2-methylpropene	HMPA	50	1	83
26	(*Z*)-β-Bromostyrene[c]	NMP	50	1	76 (3/20/77)[d]
27	(*E*)-β-Bromostyrene[e]	NMP	50	1	85 (95/5/0)[d]
28	3-Bromofuran	HMPA	40	3	80
29	Methyl 2-bromo-5-furancarboxylate	HMPA	40	24	(90)
30	3-Iodothiophene	HMPA	40	1	(83)
31	2-Iodothiophene	HMPA	40	2	(87)
32	2-Bromothiophene	HMPA	40	4	7
33	3-Iodopyridine	HMPA	40	4	0
34	2-Iodopyridine	HMPA	40	4	0

a) In the presence of 0.25 mmol (Runs 22, 24—28, 32—34) or 2 mmol (Runs 23, 29—31) of organic halide in 0.3 ml (Runs 22, 24—28, 32—34) or 4 ml (Runs 23, 29—31) of solvent under nitrogen. The molar ratio of the component was as follows: RX/$NiCl_2(PEt_3)_2$/Zn/KI=1.0/0.04/1.0/2.0 (Runs 22—27) or 1.0/0.1/1.5/2.0 (Runs 28—34). b) Yields were determined by GLC using internal standards. Yields in parentheses were isolated ones. c) *Z*/*E*=98/2. d) (*E,E*) : (*E,Z*) : (*Z,Z*). e) *Z*/*E*<1/99.

the stage of disproportionation between two oxidative-addition adducts to produce a diorganonickel species (*vide infra*).

Homo-coupling of Heteroaromatic Halides. The homo-coupling of 2- or 3-bromofuran proceeded well in HMPA solvent to afford the corresponding dimer in good yield (Runs 28 and 29). On the other hand, neither reactions of 2- nor 3-bromothiophene proceeded to completion under conditions similar to those adopted above; however both iodothiophenes afforded dimers in good yields (Runs 30—32). In the case of 2- or 3-halopyridine, neither bromo nor iodo compounds afforded any of the corresponding dimers (Runs 33 and 34). Thus, the order of decreasing reactivities of heteroaromatic halides in the nickel(0)-catalyzed homo-coupling with zinc powder is 3-furyl≧2-furyl>2-thienyl, 3-thienyl>2-pyridyl, 3-pyridyl. Since, in a series of substituted halobenzenes, electron-withdrawing substituents usually enhance the reactivities in the nickel(0)-promoted homo-coupling,[2,4,7,9] the least reactivities of halopyridines were unexpected judging from the fact that halopyridines have the most electron deficient heterocycles among the examined compounds.[15] The observed difference in reactivities might suggest that not only a term of electron density but also other terms such as coordinating abilities of hetero atoms to nickel(0) and/or -(II) species must be considered as well when the reactivities of a series of heteroaromatic halides are compared.

Reaction Path. The results presented above lead to the following equations as the most plausible sequences of the reaction. The bis(trialkylphosphine)-nickel(0) which comes from the reduction of bis(trialkylphosphine)nickel(II) chloride with zinc powder

$$NiCl_2(PR'_3)_2 + Zn \longrightarrow Ni(PR'_3)_2 + ZnCl_2 \quad (1)$$

$$Ni(PR'_3)_2 + RX \rightleftarrows \underset{\mathbf{1}}{NiX(R)(PR'_3)_2} \quad (2)$$

$$2\,NiX(R)(PR'_3)_2 \longrightarrow \underset{\mathbf{2}}{Ni(R)_2(PR'_3)_2} + NiX_2(PR'_3)_2 \quad (3)$$

$$Ni(R)_2(PR'_3)_2 \longrightarrow R_2 + Ni(PR'_3)_2 \quad (4)$$

(Eq. 1) readily reacts with aryl, alkenyl, or some heteroaromatic halides to give an oxidative-addition adduct (**1**) (Eq. 2). Following this, the disproportionation between the two adducts occurs to give a nickel(II)-halide complex and a diorganonickel(II) species (**2**) (Eq. 3) which subsequently yields a dimer (Eq. 4). This type of decomposition is well-established and is not catalytic by nature.[16] To ensure the catalytic cycle, the original nickel(0) must be regenerated from the nickel(II) thus formed, and zinc powder in at least a stoichiometric quantity is required.

It is well-known that oxidative addition of alkenyl halides towards various low valent transition metal complexes proceeds with retention of configuration[17] and it is also believed that reductive elimination from various organometallic compounds proceeds again with retention of configuration of the alkenyl ligands.[18] Thus, observed partial cis,trans-isomerization in the reaction of alkenyl halides probably happened at the stage of disproportionation on the trans-

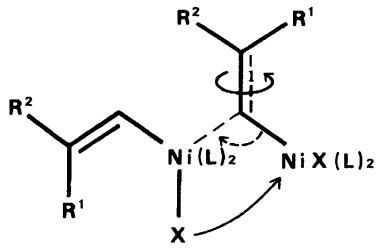

fered alkenyl ligand (*vide ante*).[19]

Experimental

All reagents including zinc powder (purchased from Kanto Chemicals) were used directly as obtained commercially, unless otherwise noted. The solvents were distilled and were dried over a Molecular Sieve (3A). The bis(trialkylphosphine)-nickel(II) chlorides were prepared by previously reported method.[20] 2-Iodobenzophenone,[21] (*E*)-,[22] or (*Z*)-β-bromostyrene,[23] 2-bromo-1,1-diphenylethene,[24] 2-,[25] or 3-iodopyridine,[26] and 3-iodothiophene[27] were prepared according to procedures in the literatures. A Hitachi 160 gas chromatograph was used for the GLC analysis. ^{1}H NMR spectra were obtained on a JOEL PMX 60 spectrometer.

General Procedure for Homo-coupling. Preparation of Dimethyl 3,3′-Biphenyldicarboxylate: A mixture of methyl *m*-bromobenzoate (430 mg, 2 mmol), bis(triethylphosphine)-nickel(II) chloride (29.3 mg, 0.08 mmol), zinc powder (134 mg, 2 mmol), potassium iodide (664 mg, 4 mmol), and NMP (4 ml) was evacuated, flushed with nitrogen, and kept at 30 °C for 3 h with stirring. To the resulting mixture, dilute hydrochloric acid (0.1 mol dm^{-3}, 30 ml) was added. The organic materials were extracted with two 20 ml portions of ether, washed with three 30 ml portions of aqueous sodium chloride, and dried over anhydrous sodium sulfate. Evaporation of the solvent gave 247 mg of dimethyl 3,3′-biphenyldicarboxylate (91%) which was proved to be essentially pure and not contaminated by triethylphosphine by NMR and GLC analysis. Mp 99.5—101 °C (lit,[28] 104 °C). Recrystallization from ethanol gave 217 mg (80%) of the biaryl. Mp 102—103 °C. Found: C, 71.03; H, 5.26%. Calcd for $C_{16}H_{14}O_4$: C, 71.10; H, 5.22%.

4,4′-Dimethylbiphenyl: Mp 121—121.5 °C (lit,[29] 121 °C). Found: C, 92.36; H, 7.82%. Calcd for $C_{14}H_{14}$: C, 92.26; H, 7.74%.

2,2′-Dibenzoylbiphenyl: Mp 169.5—170.5 °C (lit,[30] 171 °C). Found: C, 86.15; H, 5.18%. Calcd for $C_{26}H_{18}O_2$: C, 86.15; H, 5.02%.

1,1,4,4-Tetraphenyl-1,3-butadiene: Mp 198.5—199.5 °C (lit,[31] 207—210 °C). Found: C, 93.96; H, 6.31%. Calcd for $C_{28}H_{22}$: C, 93.81; H, 6.19%

Dimethyl 2,2′-Bifuryl-5,5′dicarboxylate: Mp 228—229 °C (lit,[32] 233—234 °C). Found: C, 57.42; H, 3.98%. Calcd for $C_{12}H_{10}O_6$: C, 57.61; H, 4.03%.

3,3′-Bithienyl: Mp 133—134 °C (lit,[33] 130—132 °C). Found: C, 58.17; H, 3.69%. Calcd for $C_8H_6S_2$: C, 57.80; H, 3.64%.

2,2′-Bithienyl: Mp 28—29 °C (lit,[34] 33 °C). Found: C, 57.68; H, 3.67%. Calcd for $C_8H_6S_2$: C, 57.80; H, 3.64%.

References

1) P. W. Jolly, "Nickel Catalyzed Coupling of Organic Halides and Related Reactions," in "Comprehensive Organometallic Chemistry," ed by G. Wilkinson, Pergamon Press, Oxford (1982), Vol. 8, p. 723.

2) M. F. Semmelhack, P. M. Helquist, and J. D.

Gorzynski, *J. Am. Chem. Soc.*, **94**, 9234 (1972); M. F. Semmelhack, P. Helquist, L. D. Jones, L. Keller, L. Mendelson, L. S. Ryono, J. G. Smith, and R. D. Stauff, *ibid.*, **103**, 6460 (1981).

3) A. S. Kende, L. S. Liebeskind, and D. M. Braitsch, *Tetrahedron Lett.*, **1975**, 3375.

4) M. Zembayashi, K. Tamao, J. Yoshida, and M. Kumada, *Tetrahedron Lett.*, **1977**, 4089.

5) M. Mori, Y. Hashimoto, and Y. Ban, *Tetrahedron Lett.*, **21**, 631 (1980).

6) M. F. Semmelhack, P. M. Helquist, and L. D. Jones, *J. Am. Chem. Soc.*, **93**, 5908 (1971).

7) K. Takagi, N. Hayama, and S. Inokawa, *Chem. Lett.*, **1979**, 917; *Bull. Chem. Soc. Jpn.*, **53**, 3691 (1980); K. Takagi and N. Hayama, *Chem. Lett.*, **1983**, 637.

8) R. G. Gastinger, B. B. Anderson, and K. J. Klabunde, *J. Am. Chem. Soc.*, **102**, 4959 (1980).

9) S. Inaba, H. Matsumoto, and R. D. Rieke, *Tetrahedron Lett.*, **23**, 4215 (1982); H. Matsumoto, S. Inaba, and R. D. Rieke, *J. Org. Chem.*, **48**, 840 (1983).

10) G. W. Parshall, *J. Am. Chem. Soc.*, **96**, 2360 (1974); R. D. Rieke, W. J. Wolf, N. Kujundzic, and A. V. Kavaliunas, *ibid.*, **99**, 4159 (1977).

11) D. F. Fahey and J. E. Mahan, *J. Am. Chem. Soc.*, **99**, 2501 (1977); L. Cassar and A. Giarrusso, *Gazz. Chim. Ital.*, **103**, 793 (1973).

12) C. A. Tolman, W. C. Seidel, and D. H. Gerlach, *J. Am. Chem. Soc.*, **94**, 2669 (1972).

13) This result is in marked contrast with that with bis(triphenylphosphine)nickel(II) chloride where excess triphenylphosphine ligand had been added, presumably to prevent the decomposition of an active catalyst.[4]

14) M. Fieser and L. F. Fieser, "Reagents for Organic Synthesis, "Wiley-Interscience Publication, New York (1976), Vol. 6, p. 273.

15) R. T. Morrison and R. N. Boyd, "Organic Chemistry," 2nd ed, Allyn and Bacon, Boston (1969), p. 1073.

16) A. Nakamura and S. Otsuka, *Tetrahedron Lett.*, **1974**, 463; See also T. T. Tsou and J. K. Kochi, *J. Am. Chem. Soc.*, **101**, 7547 (1979).

17) J. K. Stille and K. S. Y. Lau, *Acc. Chem. Res.*, **10**, 434 (1977).

18) T. T. Tsou and J. K. Kochi, *J. Org. Chem.*, **45**, 1930 (1980); M. K. Loar and J. K. Stille, *J. Am. Chem. Soc.*, **103**, 4174 (1981); M. Zembayashi, K. Tamao, and M. Kumada, *Tetrahedron Lett.*, **1975**, 1719; J. W. Labadie and J. K. Stille, *J. Am. Chem. Soc.*, **105**, 6129 (1983).

19) An iodide bridge may bring two nickel centers close together to facilitate the metathetical transfer of an organo ligand. See Ref. 4.

20) K. A. Jensen, P. H. Nielsen, and C. T. Pedersen, *Acta Chem. Scand.*, **17**, 1115 (1963).

21) F. G. Mann and E. J. Chaplin, *J. Chem. Soc.*, **1937**, 527.

22) L. J. Dolby, C. Wilkins, and T. G. Frey, *J. Org. Chem.*, **31**, 1114 (1966).

23) S. J. Cristol and W. P. Norris, *J. Am. Chem. Soc.*, **75**, 2645 (1953).

24) P. Lipp, *Ber.*, **56**, 567 (1923).

25) W. Baker, R. F. Curtis, and E. G. Edwards, *J. Chem. Soc.*, **1951**, 85.

26) E. Gergely and T. Iredale, *J. Chem. Soc.*, **1953**, 3226.

27) K. Takagi, N. Hayama, and T. Okamoto, *Chem. Lett.*, **1978**, 191.

28) F. Ullmann and O. Lowenthal, *Justus Liebigs Ann. Chem.*, **332**, 72 (1904).

29) T. Zincke, *Ber.*, **4**, 396 (1871).

30) R. G. R. Bacon and W. S. Lindsay, *J. Chem. Soc.*, **1958**, 1382.

31) C. D. Hurd and C. N. Webb, *J. Am. Chem. Soc.*, **49**, 546 (1927).

32) R. Grigg, J. A. Knight, and M. V. Sargent, *J. Chem. Soc., C*, **1966**, 976.

33) S. Gronowitz and H. Karlsonn, *Arkiv Kemi*, **17**, 89 (1961).

34) H. Wynberg and A. Logothetis, *J. Am. Chem. Soc.*, **78**, 1958 (1956).

 © 1984 The Chemical Society of Japan Bull. Chem. Soc. Jpn., 57, 1891—1896 (1984)

Differential Scanning Calorimetric Studies on the Thermal Denaturation of Ribonuclease A in Aqueous 2-Methyl-2,4-pentanediol

Yukihisa FUJITA* and Yukinao NODA

Department of Chemistry, Hyogo College of Medicine, Mukogawa, Nishinomiya, Hyogo 663

(Received October 31, 1983)

The thermal denaturation of ribonuclease A in aqueous solutions of 2-methyl-2,4-pentanediol(MPD) was investigated by differential scanning calorimetry at pH 5.8, *i.e.*, conditions similar to those used to crystallize the protein, and also at pH 3. A two-state reversible denaturation occurred in aqueous MPD up to 50%(v/v) MPD. Under both conditions the denaturation temperature, T_d, decreased almost linearly with increasing MPD concentration; there was a slightly greater effect at pH 5.8. The calorimetric enthalpy, ΔH_d, first increased with increasing MPD concentration and then decreased slightly at MPD concentrations above 20—30%. This behavior is analogous to that observed for organic additives, such as ethanol and dimethyl sulfoxide, with denaturing agents. The plot of ΔH_d against ΔS_d, the denaturation entropy at T_d, gave a linear correlation between these parameters, indicating a close relationship between the MPD-induced unstabilization of the protein and the water structure around the protein molecule. The standard thermodynamic parameters for denaturation, $\Delta G°$, $\Delta H°$, and $\Delta S°$, were calculated from T_d and ΔH_d, assuming a constant heat capacity change. The unstabilizing effect of MPD on the thermal stability of the protein results from that the increase in $\Delta H°$, induced by MPD, is compensated by a large increase in $\Delta S°$, with a resulting decrease in $\Delta G°$; it is in accord with an effect on solvent ordering around the exposed nonpolar groups of the protein. It also indicates a temperature dependence of the MPD effect on the protein stability.

Differential scanning calorimetry(DSC)** is a useful tool for measuring the thermally induced conformational transition of biopolymers such as proteins and nucleic acids. Application of DSC to the study of protein denaturation has increased the available thermodynamic information on the unfolding process of protein; this has been recently reviewed by Biltonen and Freire[1] and Privalov.[2] The thermogram can be used to calculate the van't Hoff enthalpy[3] or an effective enthalpy[4] for comparison with the calorimetric enthalpy to determine the cooperativity and nature of the denaturation. Furthermore, the other thermodynamic parameters for denaturation, as well as the denaturation temperature and enthalpy, can be calculated without any ambiguous assumptions.[2,5] These studies may lead to an understanding of the nature and magnitude of the forces that stabilize the native conformation of proteins, which has been a major focus of protein research.

Organic solvents such as alcohols and sulfoxides alter the conformation of proteins when added to aqueous protein solutions as result of solvent effects on the local Gibbs energy of conformational stability of the amino acid residues exposed to the surface.[6,7] 2-Methyl-2,4-pentanediol(MPD) is well known as a crystallizing reagent for proteins. For the purpose of X-ray crystal-structure analysis, bovine pancreatic ribonuclease A(RNase A) was crystallized from a mixture of 55% MPD and 45%(v/v) water and the crystals equilibrated with 75% MPD were used.[8] The water-MPD solvent system has a partially hydrophobic character, since the MPD molecule contains six methylene groups, and one might expect it to unstabilize the native structure of a protein. Indeed, monohydric alcohols depress the denaturation temperature of RNase A, a reflection of their unstabilizing action on the native structure, and the unstabilizing effect becomes more effective with an increase in their hydrophobic character.[9] We have observed that ethylene glycol also lowers the denaturation temperature of RNase A at pH 5.[10] In addition, solubility measurements of amino acids in 55% MPD have shown a favorable Gibbs energy of transfer of most amino acid side chains to this medium.[11] This suggests that MPD has a denaturing rather than a crystallizing action.

On the other hand, Bello and Nowoswiat[12,13] have reported that RNase A crystals in 75% MPD possess enzymatic activity and that the same histidine residues are carboxymethylated in the crystal as in aqueous solution, suggesting that the structure of crystalline RNase A appears to be similar to that in aqueous solution. They have further shown from the solubility data of amino acids that the unfolding of RNase A in 55% MPD would have a positive Gibbs energy change at 25 °C.[11] The CD spectra of RNase A in water and 50% MPD are indistinguishable in the far-and near-UV regions.[11,14] Pittz and Timasheff[14] have reported that RNase A is preferentially hydrated in mixtures of water and MPD. According to Bull and Breese,[15] any substance which trends to maintain or increase the hydration of proteins stablize a protein. Indeed, sugars and polyhydric alcohols which induce the preferential hydration of proteins stabilize them against thermal denaturation.[16-19] Therefore, it is of interest to study the effect of MPD on the thermal stability of RNase A.

In this paper, the thermal denaturation of ribonuclease A in aqueous MPD solutions at MPD concentrations up to 50%(v/v) was investigated by DSC at pH 5.8, *i.e.*, conditions similar to those used to crystallize the protein, and at pH 3 and the results are reported.

** Abbreviations used: DSC,differential scanning calorimetry; MPD, 2-methyl-2,4-pentanediol; RNase A, ribonuclease A(bovine pancreatic, EC 3.1.4.22).

Experimental

Materials. Bovine pancreatic ribonuclease A (EC 3.1.4.22) was purchased from Sigma Chemical Co.(type I-A,five-times recrystallized). 2-Methyl-2,4-pentanediol was purified by the method of Bello and Nowoswiat.[12] Other chemicals were reagent grade products from Wako Pure Chemical Industries. The experiments were carried out in either 0.05 mol dm^{-3} acetate or glycine buffer adjusted respectively to pH 5.8 and 3 with 1 mol dm^{-3} HCl. Protein concentrations were determined spectrophotometrically on a Hitachi 323 automatic recording spectrophotometer. The extinction coefficient was assumed to be 7.1 at 277 nm for a 10 mg cm^{-3} RNase A solution.[20] The same value was used at all solvent compositions, since it has been shown that variation of solvent composition from water to 50% MPD does not significantly affect the position of the absorption maximum nor the extinction coefficient of this protein.[21]

DSC Measurements. The thermal denaturation of RNase A was measured on a Seiko Instruments & Electronics SSC-560U differential scanning calorimeter(conduction type) at a heating rate of 1 K min^{-1} and at protein concentrations of 5—10 mg cm^{-3}. The sample solutions were extensively dialyzed at 4 °C against the solvent which was used as reference material, and then hermetically sealed in a silver vessel (0.06 cm^3). The DSC apparatus was calibrated using gallium, benzophenone, palmitic acid, and naphthalene. The area between the transition peak and a base line fitted by inspection was measured with a planimeter and converted to the calorimetric enthalpy of denaturation, ΔH_d, using the calibration constant, 2.29 mJ $mV^{-1}s^{-1}$, and the molecular weight of 13700 for RNase A. The denaturation temperature, T_d, was estimated from the temperature at which the area of the transition peak was divided into halves by assuming that the area under the peak was proportional to the amount denatured. The difference between the obtained T_d and the temperature of maximal heat flow, T_p, did not exceed 0.5 K in every measurement because of the nearly symmetrical nature of the transition peak. Privalov and Khechinashivili[4] have reported that T_d was lower than T_p by approximately 0.7 K. For each solvent composition, these thermodynamic parameters were evaluated as the averaged value of five or more experiments. Temperatures have experiment errors of ±0.1 °C. The ΔH_d values have maximum expected errors of ±5% including errors in sample preparation, calibration constant, and reproduciblity.

Results and Discussion

Representative DSC scans for the thermal denaturation of RNase A in aqueous MPD solutions at pH 5.8 are shown in Fig. 1. The DSC curves shown correspond to denaturation of a protein solution of 8 mg cm^{-3} and MPD concentrations of 0, 20, and 50%(v/v). In every measurement, a reproducible endothermic peak was observed occurring over a temperature width of 19—22 K. The increase in MPD content leads to a shift of the transition peak towards lower temperature and variation of the peak area. The endothermal slope of the base line in the pre- and post-transition regions which was observed in the DSC curves obtained at MPD concentrations below 40% were typical features of globular proteins, indicating that the temperature coefficients of the heat capacities of the native and denatured states are positive. As can be seen from this figure, the DSC curve obtained at 50% MPD exhibited only a slightly exothermal slope

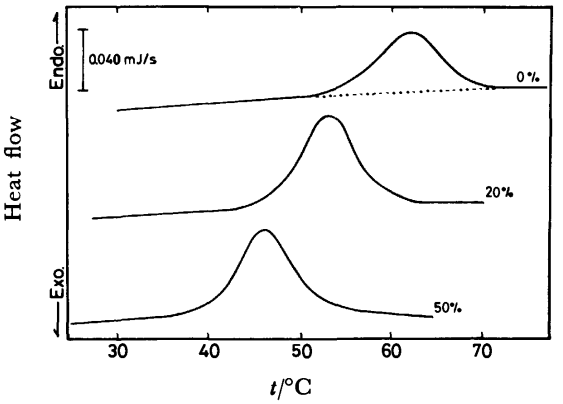

Fig. 1. DSC curves for the thermal denaturation of RNase A in aqueous MPD solutions at pH 5.8. Protein concentration is a 8 mg cm^{-3} and MPD concentrations are 0, 20, and 50% (v/v). The dotted line in the top figure shows the base line assumed in the transition region for the determination of the thermodynamic parameters of denaturation.

of the base line in the post-transition region; this was probably a reflection of partial aggregation of the denatured protein. A further addition of MPD brought about a remarkable increase in the exothermal slope of the base line and an extreme decrease in the solubility of the protein. At MPD contents more than 50%, therefore, the thermodynamic parameters for denaturation could not be estimated exactly.

The reversibility of the thermal denaturation of RNase A in MPD-water mixtures was confirmed by reheating the protein solution after rapidly cooling from the first scan, although the reversible nature of the denaturation of RNase A in aqueous solution has been well established.[4,22-25] The thermal denaturation was almost completely reversible, 98±5%, in aqueous MPD solutions at MPD concentrations up to 50%. The denaturation temperature was scarcely influenced by heating rates slower than 1 K min^{-1}, allowing equilibrium analysis of the data. The ΔH_d values obtained in aqueous buffer solutions were 370±9 kJ mol^{-1} at pH 3 and 428±17 kJ mol^{-1} at pH 5.8. These values are in very good agreement with those reported by Tsong *et al.*[24] and Privalov *et al.*[25] from calorimetric experiments at similar pH values. However, the T_d value in glycine buffer at pH 3, 53.5±0.1 °C, is considerably higher compared to the data of Tsong *et al.*[24] and Privalov *et al.*[25] The value obtained in acetate buffer at pH 5.8, 61.5±0.1 °C, is in good accord with those obtained by Tsong *et al.*,[24] Crescenzi and Delben[26] from DSC measurements, and Konishi and Scheraga[27] from spectrophotometric measurements at similar pH, but it is slightly lower than those reported by Privalov *et al.*[25] at pH 5.5 and Jacobson and Turner[28] from DSC measurements at pH 5. Although the reason for the differences in T_d is not clear, a number of factors such as protein concentration, ionic strength, specific buffer effect, purity of the protein sample (contamination), and heating rate could contribute to the differences. For example, Tsong *et al.*[24] have shown that the T_d of RNase A in aqueous buffer at pH 2.8 increases by 4.2 K when the protein con-

centration is increased from 0.1 to 2.7%(w/w).

The calorimetric transition profile permits assessment of the validity of the two-state theory of denaturation for this protein. If the transition does not involve the formation of thermodynamically stable intermediates, the shape of the transition profile is dictated by the van't Hoff equation. In this case, the effective enthalpy of denaturation, ΔH_{eff}, was evaluated by applying an approximated expression,[25]

$$\Delta H_{eff} = 4RT_d^2/\Delta T_{1/2}$$

where $\Delta T_{1/2}$ is the half-width of the transition peak. The ratio of calorimetric to effective enthalpies of denaturation, $\Delta H_d/\Delta H_{eff}$, showed near-unity value, 1.02±0.04, meaning that the thermal denaturation of RNase A in aqueous MPD solutions is very nearly a two-state process.

Figure 2 shows the dependence of the denaturation temperature on the MPD concentration at pH 3 and at pH 5.8. Under both conditions the T_d decreases monotonously with an increase in the MPD concentration. It is evident that MPD unstabilizes RNase A against thermal denaturation. This is consistant with the expectation based on the hydrophobic character of MPD and on the results of our investigation with ethylene glycol.[10] Therefore, the thermal unstabilization of RNase A by MPD appears to be responsible for the hydrophobic character of solvent induced by the addition of MPD. Needless to say, the T_d values at pH 5.8 which is the pH near the isoelectric point of this protein are higher than those at pH 3. The lowering of T_d by MPD is slightly larger at pH 5.8 than at pH 3, suggesting the temperature dependence of the thermally unstabilizing effect of MPD on the protein. The dependence of the calorimetric enthalpy of denaturation on the MPD concentration is shown in Fig. 3. The error bar shown in the figure is the standard deviation of the data. The denaturation enthalpy exhibits a maximum, that is, the ΔH_d first increases with increasing the concentration of MPD and then decreases slightly at MPD concentrations above approximately 30%(v/v), corresponding to about 2.3 mol dm^{-3}. A similar trend of ΔH_d has been observed for the thermal denaturation of RNase A with dimethylsulfoxide[28] and lysozyme with monohydric alcohols[3,29] and with sulfoxides.[30] These organic solvents strongly unstabilize these proteins against thermal denaturation.

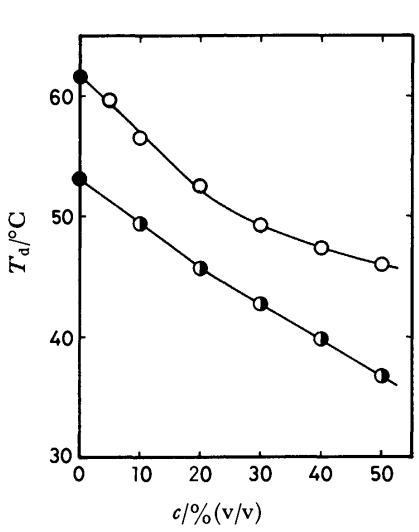

Fig. 2. Variation of the denaturation temperature, T_d, with the concentration of MPD at pH 5.8 (○) and at pH 3 (◑).
The symbol ● refers to the buffer solution without MPD.

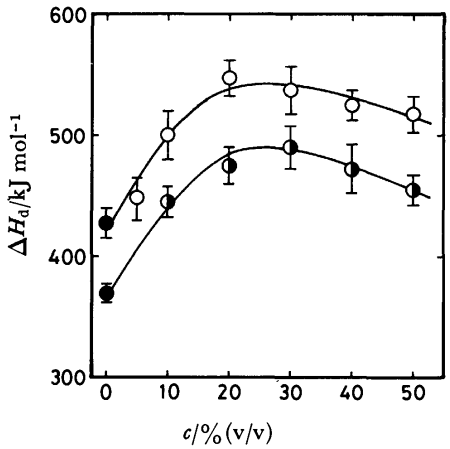

Fig. 3. Variation of the calorimetric enthalpy of denaturation, ΔH_d, with the concentration of MPD. The symbols used are identical with those in Fig. 2. The error bar shows the standard deviation of the data.

As is evident from Figs. 2 and 3, the dependence of ΔH_d on T_d is analogous to each other under both conditions; ΔH_d passes through a maximum with increasing temperature. The similarity of the temperature dependences of ΔH_d under both conditions, pH 5.8 and 3, suggests that the thermal unstabilization of RNase A induced by MPD is not directly dependent on the pH. Furthermore, the dependence of ΔH_d on T_d in the presence of MPD differs drastically from that described by Privalov[2] for variation of T_d induced by variation of the pH and addition of guanidine hydrochloride. He has shown that the denaturation enthalpy is a linear function of the denaturation temperature under all conditions. This means that the mechanism of the MPD-induced unstabilization is different, at least, from that induced by denaturants such as guanidine hydrochloride and urea.

In Fig. 4, the denaturation enthalpy is plotted against the denaturation entropy at the denaturation temperature, $\Delta S_d(=\Delta H_d/T_d)$. A linear correlation between these thermodynamic parameters suggests that the unstabilization by MPD on the thermal stability of RNase A is closely related to the water structure around the protein molecule.[31] The compensation temperature, which is defined as the slope of the graph, is about 300 K. This value is within the temperature range of 250 to 320 K observed for many processes.

The equilibrium constant of denaturation can also be obtained directly from the thermogram, since the area under the transition peak is proportional to the amount of the protein denatured. The equilibrium constant, K, at temperature T may be taken as $Q_T/(Q-Q_T)$, where Q is the total area of the transition peak and Q_T is the partial area up to temperature T. For

the present three-component system, the dependence of the equilibrium constant of denaturation on the solvent variables is ascribed to the difference in the preferential binding of solvent compositions between the native and denatured states.[32,33] The logarithm of K obtained at pH 5.8 thus is plotted against the logarithm of the MPD concentration in Fig. 5. The molarity unit was used instead of activity on the assumption that the activity coefficient is unity, since there is no activity datum for MPD in water. The slope of the lines is a positive, 3.09±0.07, and nearly temperature independent within the experiment error. This indicates that the binding of MPD to the protein increases upon denaturation. In fact, the increase in the protein surface on denaturation is generated by exposing the nonpolar residues buried in the interior of the native protein and by breaking peptide-peptide hydrogen bonds in the native state and replacing them by peptide-water hydrogen bonds. The resultant increase in the surface area of the denatured protein probably contributes to an increase in the extent of the hydrophobic interactions between the nonpolar groups of the protein and the nonpolar moiety of MPD.

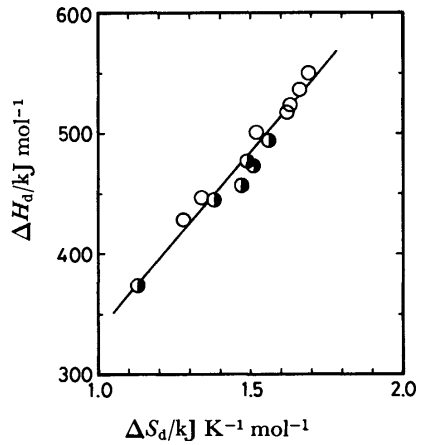

Fig. 4. Enthalpy-entropy compensation plot for the thermal denaturation of RNase A in MPD-water mixtures at pH 5.8 (○) and at pH 3 (◑).

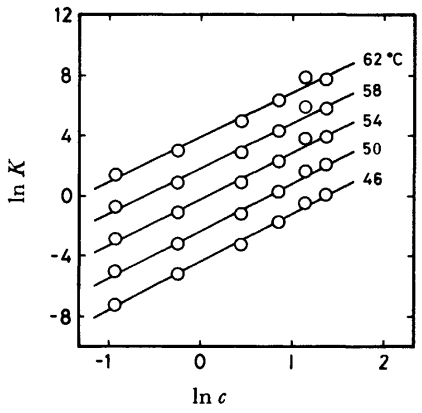

Fig. 5. Wyman plots of the effect of MPD on the thermal denaturation of RNase A at several temperatures.
The number at the right end of each line shows the temperature.

A more quantitative estimation of the MPD effect on the thermal stability of RNase A may be given by comparison of the thermodynamic parameters of denaturation, $\Delta G°$, $\Delta H°$, and $\Delta S°$, at identical temperatures. These have not been reported previously for this solvent system. Assuming that the heat capacity change of denaturation, ΔC_p, is independent of temperature, standard thermodynamic parameters at any temperature, T, can be calculated by the equations.[3,4]

$$\Delta H° = \Delta H_d - \Delta C_p(T_d - T)$$
$$\Delta S° = \Delta H_d/T_d - \Delta C_p \ln(T_d/T)$$
$$\Delta G° = \Delta H° - T\Delta S°$$

For the calculation, ΔC_p in MPD-water mixtures was assumed to be identical with that in aqueous buffer, 5.02 kJ K^{-1} mol^{-1}, since, unfortunately it can not be determined accurately in the present study. This assumption will not cause significant error in the standard thermodynamic parameters when T is close to T_d. Using the data obtained at pH 5.8, therefore, the standard thermodynamic parameters of denaturation were calculated at 53 °C, which is near the midpoint of the range, 46.0 to 61.5 °C, of the T_d obtained at pH 5.8 and were plotted as a function of the MPD concentration in Fig. 6. It is evident that $\Delta G°$ decreases monotonously with increasing MPD concentration. On the other hand, $\Delta H°$ and $\Delta S°$ increase gradually with an increase in the MPD content and tend to flatter at the MPD concentrations above 20%(v/v). In the thermal denaturation of RNase A, the increase in $\Delta H°$ induced by MPD is compensated by a large increase in $\Delta S°$, with a resulting decrease in $\Delta G°$. Therefore, the thermal unstabilization of RNase A by MPD seems to be dominantly produced by an entropic rather than an enthalpic effect, suggesting the possibility of some kind of solvent-disordering effect around the protein. These

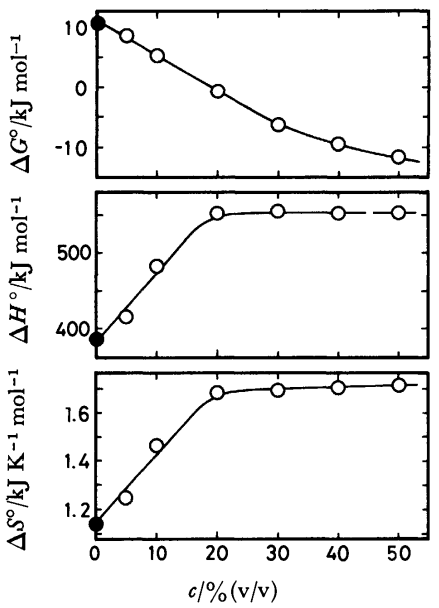

Fig. 6. Variation of the standard thermodynamic parameters of denaturation, $\Delta G°$, $\Delta H°$, and $\Delta S°$, with the concentration of MPD at 53°C.
The symbols ● and ○ refer to the aqueous and the mixed solvents at pH 5.8, respectively.

results are similar to the observation by Brandts[34] that, at a given temperature, $\Delta H°$ and $\Delta S°$ are much larger for the denaturation of chymotrypsinogen in ethanol -water mixtures than in water. Brandts and Hunt[22] have also shown that $\Delta H°$ of the thermal denaturation of RNase in the same solvent system increases with increasing ethanol content, with a maximum around an ethanol concentration of 20%(v/v). At present, the unstabilization of proteins by the addition of alcohols has been explained in terms of their effect on the structure of the water in contact with the nonpolar residues and the direct interaction of alcohol with the protein, which cause weakening the hydrophobic interactions between the nonpolar residue of protein.[7,22] Although RNase A is preferentially hydrated in MPD-water mixtures at low temperature near room temperature,[14] it is not clear at present whether MPD is preferentially bound to the protein or not at elevated temperatures which the thermal denaturation occurs, but, at least, the binding of MPD to the protein increases upon denaturation. A decrease in solvent ordering around the protein and the consequent reduction of the hydrophobic effect when MPD is added to the medium would render more favorable the exposure to solvent of hydrophobic groups buried in the interior of the native protein.

The unstabilizing effect of MPD is consistent with our expectation based on previous studies of the thermal denaturation of lysozyme in aqueous solutions of monohydric alcohols[29] and ethylene glycol[19] and RNase A in aqueous ethylene glycol.[10] However, Pittz and Bello[11] have concluded from the solubility data of amino acids that the unfolding of RNase A in 55% MPD has a positive Gibbs energy change at 25 °C, that is, a stabilizing effect of MPD on the protein. The study of the interactions between RNase A and solvent components in MPD-water mixtures at pH 5.8 by differential refractometry and light scattering has shown that the protein is preferentially hydrated at all solvent compositions up to 50%(v/v) MPD.[14] According to Bull and Breese,[15] any substance which trends to increase the hydration of proteins stabilize a protein. These findings suggests the stabilization of the native protein by MPD at low temperatures near room temperature and the temperature dependence of the MPD effect on solvent ordering around the protein. Thus, in order to examine the temperature dependence of the MPD effect on the thermal stability of RNase A, the $\Delta G°$ at each solvent composition was calculated at several temperatures in the transition region. As expected, it was found that the $\Delta G°$ value increased with a decrease in temperature and further that the decrease in $\Delta G°$ by MPD became reduced with decreasing temperature. Therefore, the temperature dependence of $\Delta G°$ at each MPD content was extrapolated to 25 °C and the resulting value of $\Delta G°$ was plotted against the MPD concentration in Fig. 7. At high temperature, as shown in Fig. 6, MPD is quite effective in decreasing the Gibbs energy change of denaturation. However, at low temperature, MPD acts differently even at a qualitative level, *i.e.*, it behaves as a rather stabilizing agent for native RNase A at low MPD concentrations, almost independent of the pH. Although this conclusion depends to some extent on the validity of the extrapolation, this qualitative

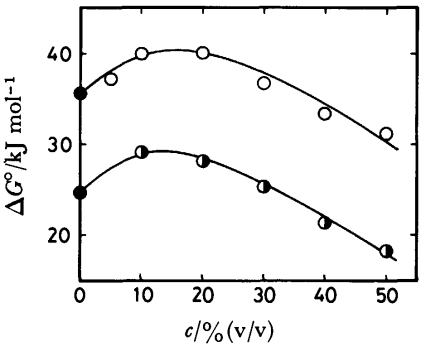

Fig. 7. Variation of $\Delta G°$ with MPD concentration at 25°C.
The symbols used are identical with those in Fig. 2.

conclusion appears to be justified, as the temperature range of extrapolation is short and the effect is large. Moreover, the native protein is too stable at 25 °C and pH 3 to permit direct measurement of the denaturation. Such behavior of $\Delta G°$ has also been found for the denaturation of RNase A in aqueous ethanol solution.[22] This implies that relatively nonpolar organic additives, which have hitherto been considered to be only denaturing agents, might show somewhat the same behavior at low temperature. Indeed, we observed for the thermal denaturation of RNase A in aqueous solutions of ethylene glycol at different pH values that ethylene glycol decreased the denaturation temperature at high temperature, near 60 °C, but increased it at lower temperature, near 40 °C.

These results may be explained on the basis of solvent ordering effect, similarly to that proposed by Brandts and Hunt[22] for the stabilizing effect of ethanol at low temperature and at low ethanol concentration. According to their hypothesis, ethanol replaces ordered water molecules around exposed hydrophobic groups, both solvent components becoming part of the solvent sheath which surrounds the nonpolar side chains of the protein.[34-36] In the case of ethanol, this structure is disrupted at temperatures near room temperature, permitting the formation of hydrophobic contacts between the nonpolar moiety of the alcohol and the nonpolar groups of the protein and leading to the unstabilization of the protein. In the case of MPD, such a solvation sheath around the exposed nonpolar groups of the protein should remain intact up to relatively high temperature, at least, near 25 °C, since the hydrophobicity of MPD appears to be smaller than that of ethanol.

References

1) R. L. Biltonen and E. Freire, *CRC Crit. Rev. Biochem.*, **1978**, 85.
2) P. L. Privalov, *Adv. Protein Chem.*, **33**, 167 (1978).
3) G. Velicelebi and J. M. Sturtevant, *Biochemistry*, **18**, 1180 (1979).
4) P. L. Privalov and N. N. Khechinashivili, *J. Mol. Biol.*, **86**, 665 (1974).
5) J. F. Chlebowski and S. Mabrey, *J. Biol. Chem.*, **252**, 7042 (1977).
6) C. Tanford, *Adv. Protein Chem.*, **33**, 122 (1968).
7) F. Franks and D. Eagland, *CRC Crit. Rev. Biochem.*,

1975, 165.
8) M. V. King, B. S. Magdoff, M. B. Adelman, and D. Harker, *Acta Crystallogr.*, **9**, 460 (1956).
9) E. E. Schrier, R. T. Ingwall, and H. A. Scheraga, *J. Phys. Chem.*, **69**, 298 (1965).
10) Y. Fujita and Y. Noda, 29th Kinki Local Meeting of the Biochemical Society of Japan, Kyoto, May 1982, Abstr. p. 23.
11) E. P. Pittz and J. Bello, *Arch. Biochem. Biophys.*, **146**, 513 (1971).
12) J. Bello and E. F. Nowoswiat, *Biochim. Biophys. Acta*, **105**, 325 (1965).
13) J. Bello and E. F. Nowoswiat, *Biochemistry*, **8**, 2628 (1968).
14) E. P. Pittz and S. N. Timasheff, *Biochemistry*, **17**, 615 (1978).
15) H. B. Bull and K. Breese, *Biopolymers*, **17**, 2121 (1978).
16) T. Arakawa and S. N. Timasheff, *Biochemistry*, **21**, 6536 (1982).
17) K. Gekko and T. Morikawa, *J. Biochem. (Tokyo)*, **90**, 51 (1981).
18) H. Uedaira and H. Uedaira, *Bull. Chem. Soc. Jpn.*, **53**, 2451 (1980).
19) Y. Fujita, Y. Iwasa, and Y. Noda, *Bull. Chem. Soc. Jpn.*, **55**, 1896 (1982).
20) W. F. Harrington and J. A. Schellman, *C. R. Trav. Lab. Carlsberg*, **30**, 21 (1956).
21) E. P. Pittz and J. Bello, *Arch. Biochem. Biophys.*, **156**, 437 (1973).
22) J. F. Brandts and L. Hunt, *J. Am. Chem. Soc.*, **89**, 4826 (1967).
23) F. Delben, V. Crescenzi, and F. Quadrifoglio, *Int. J. Protein Res.*, **1**, 145 (1969).
24) T. Y. Tsong, R. P. Hearn, D. P. Wrathall, and J. M. Sturtevant, *Biochemistry*, **9**, 2666 (1970).
25) P. L. Privalov, E. I. Tiktopulo, and N. N. Khechinashvili, *Int. J. Pept. Protein Res.*, **5**, 229 (1973).
26) V. Crescenzi and F. Delben, *Int. J. Protein Res.*, **3**, 57 (1971).
27) Y. Konishi and H. A. Scheraga, *Biochemistry*, **19**, 1308 (1980).
28) A. L. Jacobson and C. L. Turner, *Biochemistry*, **19**, 4534 (1980).
29) Y. Fujita, A. Miyanaga, and Y. Noda, *Bull. Chem. Soc. Jpn.*, **52**, 3659 (1979).
30) Y. Fujita, S. Izumiguchi, and Y. Noda, *Int. J. Pept. Protein Res.*, **19**, 25 (1982).
31) R. Lumry and S. Rajender, *Biopolymers*, **9**, 1125 (1970).
32) J. Wyman, *Adv. Protein Chem.*, **19**, 223 (1964).
33) C. Tanford, *J. Mol. Biol.*, **39**, 539 (1969).
34) J. F. Brandts, *J. Am. Chem. Soc.*, **86**, 429, 4302 (1964).
35) F. M. Pohl, *Eur. J. Biochem.*, **7**, 146 (1968).
36) D. Eagland, "Water: A Comprehensive Treatise," ed by F. Franks, Plenum Press, N. Y. (1975), Vol. 4, Chap. 5.

Asymmetric Hydrogenation of Dehydroamino Acids and Dehydrodipeptides with Rhodium(I)-modified DIOP Catalysts

Takamichi YAMAGISHI,* Masanobu YATAGAI, Hidetoshi HATAKEYAMA, and Mitsuhiko HIDA
Department of Industrial Chemistry, Faculty of Technology, Tokyo Metropolitan University, Fukasawa, Setagaya-ku, Tokyo 158
(Received November 9, 1983)

(−)-DIOP was modified in two ways: i), Introduction of a large aromatic substituent at the dioxolane ring of (-)-DIOP and ii), replacement of one diphenylphosphino group by diarylphosphino group to give unsymmetrical DIOPs. Modification at the dioxolane ring had a small effect on the asymmetric induction by DIOP in the hydrogenation. Modification at the phosphino group affected the stereocontrol by the ligand and the unsymmetrical DIOP with di-2-naphthylphosphino group gave higher optical yields than (−)-DIOP for the hydrogenation of α-acetamidocinnamic acid and dehydrodipeptides.

Asymmetric hydrogenation of dehydroamino acid derivatives has been intensively studied using many chiral diphosphine or diphosphinite ligands. DIOP, the first chiral diphosphine reported in the literature,[1] has been widely used because of its ease of preparation and its effectiveness for asymmetric hydrogenation of various substrates, but the optical yields of hydrogenation reported are about 80% e.e. at most.[1,2] Many modifications of DIOP have been reported;[2a,3] only a few ligands could give a little higher stereoselectivity than the DIOP in the hydrogenation of α-acetamidocinnamic acid.

The authors have modified (−)-DIOP in two ways (Scheme 1):

i) Introduction of a large aromatic substituent on the dioxolane ring of (−)-DIOP (compound **1**).

ii) Modification at the phosphino group of (−)-DIOP (compound **3**). The former would cause a change in face and edge conformation of the phenyl groups on phosphorus atoms of the ligand by steric repulsion between the aromatic substituent and the methylene unit adjacent to the phosphino group. The latter affords unsymmetrical DIOPs with a diphenylphosphino group at one side and a diarylphosphino group at the other side. This modification would provide a significant change in the steric and electronic factors of the bidentate ligand. The unsymmetrical DIOP coordinated onto Rh(I) would provide different degrees of congestion at two apical sites of the complex,[4] while prochiral substrates will generally coordinate unsymmetrically onto rhodium. Therefore, the unsymmetrical DIOP may allow more preferable fitting of the prochiral substrate than symmetrical DIOP[5] at the step of face-selection of the substrate.

Using two types of modifiefd DIOPs, the asymmetric hydrogenation of dehydroamino acid derivatives and dehydrodipeptides was studied. The effect of modification was large in the case of unsymmetrical DIOP with 2-naphthyl substituent.

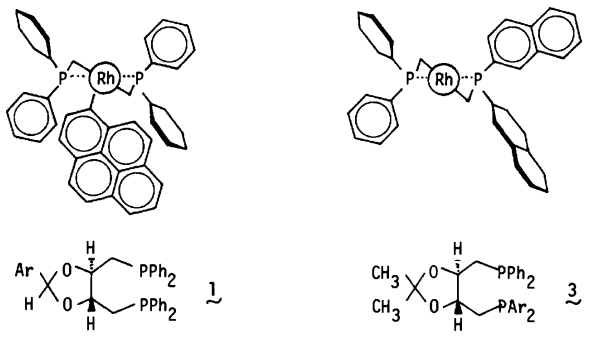

Scheme 1.

Results and Discussion

The modified DIOPs examined in this paper are listed in Table 1. As DIOP derivatives modified at the dioxolane ring, two derivatives (**1a** and **1b**) were prepared by the phosphination of acetals derived from corresponding aromatic aldehydes and 1,4-di-*O*-tosyl-L-threitol. In the hydrogenation, cationic rhodium(I) complexes, [Rh(diphosphine)(nbd)]$^+BF_4^-$ (nbd: norbornadiene), were used as catalysts.

Unsymmetrical DIOPs (**3a—3d**) were prepared by two-step phosphination of 2,3-*O*-isopropylidene-1,4-di-*O*-tosyl-L-threitol (ditosylate) using $LiPPh_2$ and $LiPAr_2$ successively (Scheme 2). For the monophosphination of ditosylate, lithium diphenylphosphide was

Table 1. Modified DIOPs

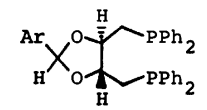

1 **1a**: Ar=2-naphthyl
1b: Ar=1-pyrenyl

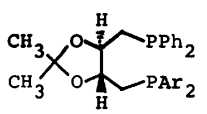

3 **3a**: Ar=*p*-tolyl
3b: Ar=*p*-methoxyphenyl
3c: Ar=1-naphthyl
3d: Ar=2-naphthyl

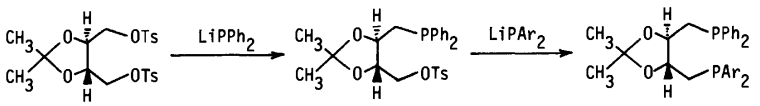

Scheme 2.

used in 0.5 molar excess to ditosylate in order to consume ditosylate completely. Extraction of by-products such as (−)-DIOP or tetraphenyldiphosphane (Ph_2P-PPh_2) from the reaction products with hot hexane left monophosphine **2** as a viscous oil. Monophosphine **2** was phosphinated by lithium diarylphosphide to give unsymmetrical DIOPs. As these DIOPs were viscous oil, they were converted to cationic rhodium(I) complexes and purified by recrystallization.

Circular Dichroism Spectra. The circular dichroism (CD) spectra for [Rh(diphosphine)(nbd)]$^+BF_4^-$ complexes are shown in Figs. 1 and 2. Though modification at the dioxolane ring of (−)-DIOP gave a relatively small change in the CD spectra (Fig. 1), CD spectra of unsymmetrical DIOP complexes were strongly dependent on the aryl substituent in the phosphino group. The intensity of CD spectra near 350 nm

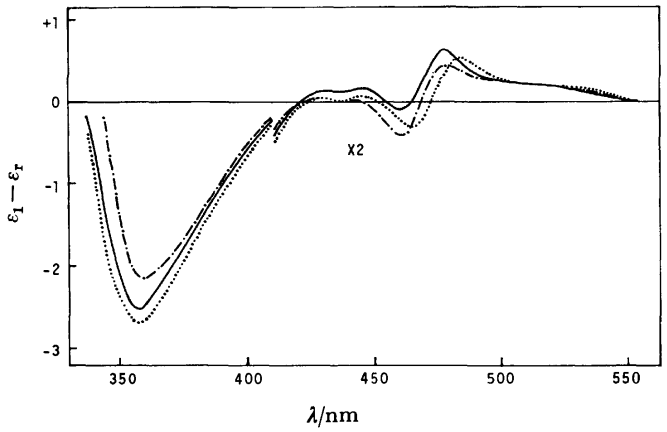

Fig. 1. CD spectra of cationic Rh(I) complexes of DIOP derivatives modified at the dioxolane ring in methanol solution.
——: [Rh((−)-DIOP)(nbd)]$^+BF_4^-$; ·····: [Rh(**1a**)(nbd)]$^+BF_4^-$; —·—: [Rh(**1b**)(nbd)]$^+BF_4^-$.

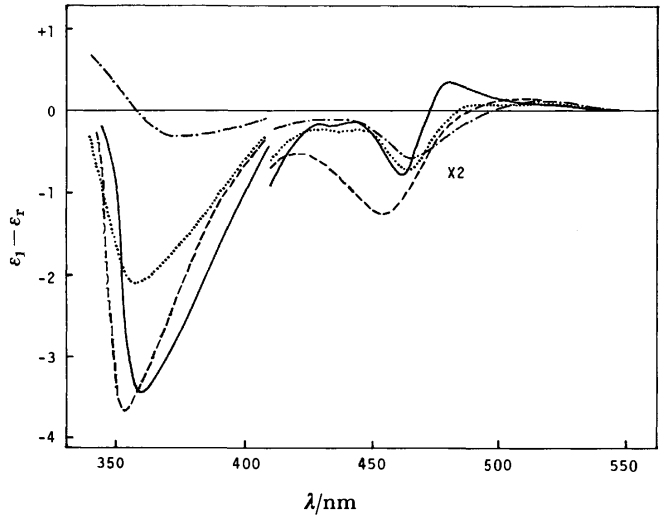

Fig. 2. CD spectra of cationic Rh(I) complexes of unsymmetrical DIOPs in methanol solution.
——: [Rh(**3a**)(nbd)]$^+BF_4^-$; ·····: [Rh(**3b**)(nbd)]$^+BF_4^-$; ----: [Rh(**3c**)(nbd)]$^+BF_4^-$; —·—: [Rh(**3d**)(nbd)]$^+BF_4^-$.

of the complexes of **3a**—**3d** was strongest for the complex of **3c** and least strong for the complex of **3d**, thus suggesting a different stereoelectronic effect of the aryl substituent in the ligands.

Hydrogenation with Modified DIOPs. Asymmetric hydrogenations of dehydroamino acid derivatives using cationic complex of **1a** or **1b** were compared with those by (−)-DIOP complex. As for the reaction rate, no apparent difference was observed between (−)-DIOP and **1a** or **1b**. The optical yields were decreased slightly in the order of (−)-DIOP, **1a** and **1b** (for example, optical yields for the reaction of α-acetamidocinnamic acid were 79, 79, and 70% e.e., respectively). A CPK model of the cationic complex coordinated by **1a** or **1b** suggested a steric repulsion between the aromatic substituent and the methylene unit adjacent to the phosphino group. It will cause a change of the face and edge conformation of phenyl groups of the ligand to alter the steric control, but the obtained results would indicate that the change in the face and edge conformation was not so large even in the case of **1b** with a pyrene ring. In the reactions of methyl esters of α-acetamidocinnamic acid and α-benzamidocinnamic acid, however, **1a** gave higher optical yields than those by DIOP.

In the case of cationic rhodium complexes, modification at the dioxolane ring of DIOP gave generally a small negative effect on the stereoselection. On the other hand, neutral rhodium(I) complexes prepared from $[Rh(cod)Cl]_2$ and modified DIOPs (**1a** and **1b**) *in situ* gave higher optical yields in the reaction of α-acetamidocinnamic acid than the catalyst from $[Rh(cod)Cl]_2$ and (−)-DIOP (Optical yields were 77, 77 and 72% e.e., respectively). This result would indicate that the structures of neutral chlororhodium-diphosphine complexes are different from the square planar cationic complexes.[6] Cationic rhodium(I)-**1a**-α-acetamidocinnamic acid and neutral chlororhodium(I)-**1a**-α-acetamidocinnamic acid systems showed different absorption maxima corresponding to d-d transition in ethanol-benzene(2:1) solution (Fig. 3).

The introduction of aromatic substituent on the dioxolane ring of DIOP had a small effect on the steric control by DIOP in the hydrogenation of dehydroamino

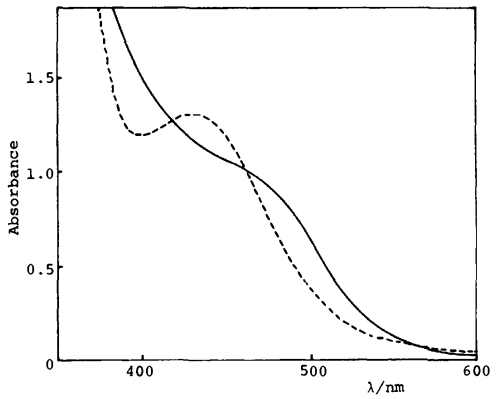

Fig. 3. Absorption spectra of Rh(I)-**1a**-α-acetamidocinnamic acid in ethanol-benzene(2/1).
——: cationic Rh(I)-**1a**-α-acetamidocinnamic acid; ----: neutral Rh(I)Cl-**1a**-α-acetamidocinnamic acid.

acid derivatives. Therefore, it will be necessary to introduce larger ring systems to cause a significant change in the face and edge conformation of the phenyl groups of the ligand.[7]

Results of hydrogenation of dehydroamino acids using unsymmetrical DIOPs (**3a—3d**) are summarized in Table 2. As shown in the Table, modification at the phosphino group influenced the optical yields depending on the combination of the ligand and substrate, though the (*R*)-selectivity held for all ligands. As for α-acetamidocinnamic acid, **3a** and **3d** afforded higher optical yields than DIOP did; **3d** gave an especially high yield about 90% e.e., suggesting the increased stereocontrol by the 2-naphthyl group. For isopropyl α-acetamidocinnamate, however, **3d** was less effective than (−)-DIOP. It is likely that the less electron-donating di-2-naphthylphosphino group favors the coordination of carbonyl oxygen in amido group of the substrate in the trans position on the rhodium complex, thus olefinic double bond occupying the cis position to the di-2-naphthylphosphino group.[4] So, bulky isopropyl group of ester would lower the stereoselectivity by the steric repulsion between naphthyl substituent of **3d** and isopropyl group of ester. For α-acetamidoacrylic acid **3d** gave only low optical yield. **3b** with *p*-methoxyphenyl group gave generally low optical yields, though the hydrogenation itself proceeded faster than the reaction with DIOP or **3a**. Using Rh(I)-DIOP catalysts, α-benzamidocinnamic acid was reduced with much lower optical yields than α-acetamidocinnamic acid, and the decrease in optical yields was large with **3a** or **3b** catalysts. In the case of **3a** or **3b** with an electron-donating substituent carbonyl oxygen in amido group of the substrate would occupy the cis position to the diarylphosphino group of **3a** or **3b**. Thus, substituent on the phenyl group of **3a** or **3b** would increase the steric repulsion with benzoyl group of the substrate. In the case of α-acetamidoacrylic acid, the difference between the steric factors by **3a** and **3b** seems to be not so large. Therefore, the large difference in optical yields between **3a** and **3b** for α-acetamidoacrylic acid would suggest that not only the steric effect but also the electronic effect by electron-donating substituent on the phenyl group played a role in the stereoselection.

Table 2. Asymmetric hydrogenation of dehydroamino acid derivatives with Rh(I)-unsymmetrical DIOP catalysts[a]

Substrate[b]	% e.e.[c]				
	(−)-DIOP	**3a**	**3b**	**3c**	**3d**
C_6H_5, $NHCOCH_3$, H, $COOH$	79	83	68	63	88
C_6H_5, $NHCOCH_3$, H, $COOCH(CH_3)_2$	85	84	71	59	78
C_6H_5, $NHCOC_6H_5$, H, $COOH$	62	55	40	—	—
H, $NHCOCH_3$, H, $COOH$	77	64	55	—	47

a) Hydrogenations were performed with cationic Rh(I) complexes in ethanol-benzene (2/1) under atmospheric hydrogen pressure at 20 °C. b) Substrate/Rh=200. c) Optical yields (% e.e.) were determined from the specific rotation of the product and that of optically pure substance.[2e,9] Absolute configuration of the products was (*R*) in every case.

In the CD spectra of the Rh(I)-unsymmetrical DIOP complexes, **3c** with 1-naphthyl groups showed the strongest CD spectra, suggesting a large stereoelectronic effect by 1-naphthyl substituent on the rhodium complex, but the rate of hydrogenation using **3c** was slow and the stereoselectivity was poor, presumably because of a very crowded structure around the phosphorus atom of the ligand.

The results of dehydrodipeptide reductions using modified DIOPs (**1a**, **1b**, and **3a—3d**) are shown in Table 3. In the reaction of Ac-ΔPhe-(*S*)-Phe-OH, which has a large steric factor, **1b** with a pyrene ring at the dioxolane ring gave a higher optical yield (64% d.e.) than DIOP (58% d.e.) and the reaction with **1b** pro-

Table 3. Asymmetric hydrogenation of dehydrodipeptides with Rh(I)-modified DIOP catalysts[a]

Dehydrodipeptide[b]	Diphosphine	Time / min	Conv. / %	(*S,S*)/(*R,S*) or (*S,R*)/(*R,R*)	% d.e.
Ac-ΔPhe-(*S*)-Phe-OH	(−)-DIOP	10	100	21/79	58
	1a	10	100	24/76	52
	1b	8	100	18/82	64
	3a	10	100	22/78	56
	3b	8	100	23/77	54
	3d	5	100	14/86	72
Ac-ΔPhe-(*S*)-Ala-OMe	(−)-DIOP	3	100	3/97	94
	3d	5	100	3/97	94
Ac-ΔPhe-(*R*)-Phe-OMe	(−)-DIOP	5	100	6/94	88
	3d	5	100	3/97	94

a) Hydrogenations were performed with cationic Rh(I) complexes in ethanol under atmospheric hydrogen pressure at 20 °C. b) Dehydrodipeptide/Rh=50.

ceeded faster than that with DIOP or **1a**, though **1b** was less effective than DIOP or **1a** for the reactions of dehydroamino acid derivatives. In the case of dehydrodipeptides, carboxyl group in the substrate would weakly occupy the apical site of the complex, and this will favor the stereoselection.[8] For Ac-ΔPhe-(*R*)-Phe-OH, DIOP and **1b** gave almost the same optical yields (92 and 90% d.e., respectively). Unsymmetrical **3a** and **3b** showed similar stereoselectivities to that by DIOP. It is noted that **3d** with 2-naphthyl groups afforded a higher optical yield (72% d.e.). We think that the di-2-naphthylphosphino group caused different congestions at two apical sites of the complex and had a different electronic effect on rhodium from that caused by the diphenylphosphino group. This would affect the fitting of dehydrodipeptide onto rhodium and the succeeding reactions on the complex. The effectiveness of **3d** was observed also in the cases of Ac-ΔPhe-(*S*)-Ala-OMe and Ac-ΔPhe-(*R*)-Phe-OMe to give high optical yields, more than 90% d.e..

Among the modified DIOPs, unsymmetrical DIOPs affected the stereocontrol in the asymmetric hydrogenation and the unsymmetrical DIOP with 2-naphthyl groups was effective for the hydrogenation of α-acetamidocinnamic acid and dehydrodipeptides. It will be possible to widen the applicability of the unsymmetrical ligands for other catalytic asymmetric reactions by selecting the diarylphosphino group.

Experimental

General Procedures. ^{1}H NMR spectra were recorded on a HITACHI R-24 spectrometer. Absorption spectra and CD spectra were recorded on a HITACHI 220A spectrophotometer and on a JASCO J-40A spectropolarimeter, respectively. Optical rotations were measured with a UNION P 101 automatic digital polarimeter.

Materials. α-Acetamidoacrylic and α-acetamidocinnamic acids were commercial products. α-Acylaminocinnamic acid derivatives and *N*-acetyldehydrodipeptides were prepared according to the literature.[2e,11-13] Chlorodiarylphosphines (aryl=*p*-tolyl, *p*-methoxyphenyl, 1-naphthyl, and 2-naphthyl) were prepared by the reaction of sodium diethyl phosphonite with corresponding Grignard reagent[14] followed by the reaction with PCl_3.[15] 2,3-*O*-Isopropylidene-1,4-di-*O*-tosyl-L-threitol,[16] 1,4-di-*O*-tosyl-L-threitol,[17] and (−)-DIOP[1b] were prepared by the methods reported. [Rh(nbd)(acac)] was prepared according to the literature.[18]

*Preparation of DIOP Derivatives Modified at the Dioxolane Ring (**1a** and **1b**).* 1,4-Di-*O*-tosyl-L-threitol was reacted with aromatic aldehyde (2-formylnaphthalene or 1-formylpyrene) in the presence of *p*-toluenesulfonic acid in dry benzene under reflux using a Dean-Stark trap.[17] Recrystallization of the product gave the acetal as white crystals. Phosphination of the acetal was performed in a THF solution using lithium diphenylphosphide. Solvent was evaporated and the residue was recrystallized from THF-ethanol after washing with ethanol to give white needles.

2,3-O-(2-Naphthylmethylene)-1,4-di-O-tosyl-L-thretiol: White crystals from THF-ethanol (42% yield). Mp 120.0—120.8 °C (corr.). ^{1}H NMR($CDCl_3$) δ=7.1—7.9 (15H, m, aromatic H), 5.1 (1H, s, CH), 4.3 (6H, bs, CH and CH_2), 2.36 (3H, s, CH_3), 2.31 (3H, s, CH_3).

2,3-O-(1-Pyrenylmethylene)-1,4-di-O-tosyl-L-threitol: White crystals from benzene-ethanol (55% yield). Mp 54.2—55.0 °C (corr.). ^{1}H NMR($CDCl_3$) δ=6.7—8.1 (22H, m, aromatic H and CH), 4.3 (6H, m, CH and CH_2), 2.3 (3H, s, CH_3), 2.2 (3H, s, CH_3).

*(−)-2,3-O-(2-Naphthylmethylene)-1,4-bis(diphenylphosphino)-2,3-butanediol (**1a**)*: White needles (66% yield). Mp 122—123 °C (corr., sealed tube). $[\alpha]_D^{25}$ −48.8° (*c* 0.48, C_6H_6). ^{1}H NMR($CDCl_3$) δ=7.2—7.9 (27H, m, aromatic H), 6.0 (1H, s, CH), 4.0—4.4 (2H, m, CH), 2.55 (4H, d, CH_2).

*(−)-2,3-O-(1-Pyrenylmethylene)-1,4-bis(diphenylphosphino)-2,3-butanediol (**1b**)*: White needles (66% yield). Mp 158.5—159.1 °C (corr., sealed tube). $[\alpha]_D^{25}$ −70.0° (*c* 0.55, C_6H_6). ^{1}H NMR($CDCl_3$) δ=7.8—8.3 (9H, m, aromatic H), 7.1—7.6 (20H, m, aromatic H), 6.8 (1H, s, CH), 4.1—4.6 (2H, m, CH), 2.5—2.7 (4H, q, CH_2).

*Preparation of Unsymmetrical DIOPs (**3a**—**3d**).* *(−)-2,3-O-Isopropylidene-4-diphenylphosphino-1-O-tosyl-1,2,3-butanetriol (**2**)*: To a THF solution of 2,3-*O*-isopropylidene-1,4-di-*O*-tosyl-L-threitol (ditosylate), 0.5 molar excess of lithium diphenylphosphide in THF was added slowly over 8 h and the mixture was stirred for another 12 h. Evaporation of solvent and extraction of the residue with dry benzene gave an oily crude product. Extraction of by-products (DIOP and tetraphenyldiphosphane) from the oily product with hot hexane gave monophosphine **2** as a very viscous oil containing a small amount of ditosylate (less than 5 mol%). 49% yield. ^{1}H NMR($CDCl_3$) δ=7.2—7.9 (14H, m, aromatic H), 3.6—4.2 (4H, m, CH and CH_2), 2.3—2.5 (5H, d, CH_2 and CH_3), 1.4 (3H, s, CH_3), 1.2 (3H, s, CH_3).

Phosphination of **2** was performed by adding a THF solution of **2** slowly to 0.2—0.4 molar excess of lithium diarylphosphide in THF. Solvent was evaporated and the residue was extracted with ether. The ether extract was concentrated. After removing tetraaryldiphosphane (Ar_2P-PAr_2) and unreacted **2** by cooling at −20 °C, unsymmetrical DIOP was precipitated by adding hexane to the ethereal mother liquor and cooling at −20 °C.

*(−)-2,3-O-Isopropylidene-1-diphenylphosphino-4-(di-p-tolylphosphino)-2,3-butanediol (**3a**)*: Viscous oil (68% yield). $[\alpha]_D^{25}$ −6.6° (*c* 0.7, C_6H_6). ^{1}H NMR($CDCl_3$) δ=6.9—7.6(18H, m, aromatic H), 3.7—4.2 (2H, m, CH), 2.2—2.5 (10H, m, CH_2 and CH_3), 1.3 (6H, s, CH_3).

*(−)-2,3-O-Isopropylidene-1-diphenylphosphino-4-[bis(p-methoxyphenyl)phosphino]-2,3-butanediol (**3b**)*: Viscous oil (*ca.* 40% yield). ^{1}H NMR ($CDCl_3$) δ=6.8—7.7 (18H, m, aromatic H), 3.7—4.0 (2H, m, CH), 3.8 (6H, s, OCH_3), 2.9 (4H, m, CH_2), 1.35 (3H, s, CH_3), 1.25 (3H, s, CH_3).

*(−)-2,3-O-Isopropylidene-1-diphenylphosphino-4-(di-1-naphthylphosphino)-2,3-butanediol (**3c**)*: Pale yellow solid (*ca.* 25% yield). ^{1}H NMR($CDCl_3$) δ=7.0—8.8 (25H, m, aromatic H), 4.0—4.3 (2H, m, CH), 2.4—2.6 (4H, m, CH_2), 1.35 (6H, bs, CH_3).

*(−)-2,3-O-Isopropylidene-1-diphenylphosphino-4-(di-2-naphthylphosphino)-2,3-butanediol (**3d**)*: Viscous oil (*ca.* 25% yield). ^{1}H NMR($CDCl_3$) δ=7.0—8.2 (25H, m, aromatic H), 4.0—4.3 (2H, m, CH), 2.4—2.5 (4H, m, CH_2), 1.4 (3H, s, CH_3), 1.3 (3H, s, CH_3).

TLC analysis and NMR spectra showed that **3c** and **3d** contained corresponding tetranaphthyldiphosphane (about 10%).

Preparation of Cationic Rhodium(I) Complexes. Cationic Rh(I) complexes [Rh(diphosphine)(nbd)]$^+BF_4^-$ were prepared from [Rh(nbd)(acac)], modified DIOP and $NaBF_4$ in CH_2Cl_2-H_2O two phase system,[19] and the complexes were recrystallized from methanol-ether.

*[Rh(**1a**)(nbd)]$^+BF_4^-$*: Orange-red crystals (60% yield). ^{1}H NMR($CDCl_3$) δ=7.3—7.8 (27H, m, aromatic H), 5.9 (1H, s, CH), 4.5 (4H, m, olefinic H), 3.9—4.1 (4H, m, CH), 2.8—3.1 (4H, m, CH_2), 1.5 (2H, m, CH_2).

*[Rh(**1b**)(nbd)]$^+BF_4^-$*: Bright red crystals (82% yield). ^{1}H NMR($CDCl_3$) δ=7.2—8.0 (29H, m, aromtic H), 6.8 (1H,

s, CH), 4.4—4.6 (4H, m, olefinic H), 3.8—4.1 (4H, m, CH), 2.9—3.2 (4H, m, CH_2), 1.4 (2H, m, CH_2).

[Rh(3a)(nbd)]$^+BF_4^-$: Orange-red crystals (60% yield). ^1H NMR($CDCl_3$) δ=7.2—7.8 (18H, m, aromatic H), 4.4—4.7 (4H, m, olefinic H), 3.5—4.2 (4H, m, CH), 2.4—3.0 (4H, m, CH_2), 2.45 (3H, s, CH_3), 2.50 (3H, s, CH_3), 1.55 (2H, m, CH_2), 1.2 (6H, s, CH_3).

[Rh(3b)(nbd)]$^+BF_4^-$: Orange crystals (69% yield). ^1H NMR($CDCl_3$) δ=7.0—7.8 (18H, m, aromatic H), 4.3—4.6 (4H, m, olefinic H), 3.7—4.0 (4H, m, CH), 3.85 (3H, s, OCH_3), 3.90 (3H, s, OCH_3), 2.2—2.8 (4H, m, CH_2), 1.5 (2H, m, CH_2), 1.2 (6H, s, CH_3).

[Rh(3c)(nbd)]$^+BF_4^-$: Orange crystals (39% yield). ^1H NMR($CDCl_3$) δ=7.0—8.5 (24H, m, aromatic H), 4.3—4.8 (4H, m, olefinic H), 3.8—4.2 (4H, m, CH), 2.5 (4H, m, CH_2), 1.4 (2H, m, CH_2), 1.2 (3H, s, CH_3), 1.1 (3H, s, CH_3).

[Rh(3d)(nbd)]$^+BF_4^-$: Orange crystals (32% yield). ^1H NMR($CDCl_3$) δ=7.2—8.2 (24H, m, aromatic H), 4.5—4.9 (4H, m, olefinic H), 3.8—4.2 (4H, m, CH), 2.3—2.4 (4H, m, CH_2), 1.6 (2H, m, CH_2), 1.3 (3H, s, CH_3), 1.2 (3H, s, CH_3).

Hydrogenations. Typically, dehydroamino acid derivatives (2 mmol) was hydrogenated using 0.01 mmol of cationic Rh(I) catalyst in 10 cm^3 benzene-ethanol(2/1). Optical yields were determined polarimetrically. In the case of dehydrodipeptides, 1 mmol of dehydrodipeptide was hydrogenated with 0.02 mmol of Rh(I) catalyst in 3 cm^3 ethanol. Diastereomeric excess and the chirality, newly formed, were determined by ^1H NMR with shift reagent.

Absorption Spectra Measurements. Hydrogen was introduced to a 10 mm cell containing [Rh(**1a**)(nbd)]$^+BF_4^-$ or neutral chlororhodium complex from $[Rh(nbd)Cl]_2$ and **1a** (**1a**/Rh=1.1) in ethanol-benzene. The cell was shaken until the absorption of coordinated olefin disappeared. Then the cell was evacuated and α-acetamidocinnamic acid solution was added under nitrogen (Rh: 0.5 mmol/dm^3).

CD Spectra Measurements. CD spectra of cationic Rh(I) complexes [Rh(diphosphine)(nbd)]$^+BF_4^-$ were recorded in methanol solution (0.5 mmol/dm^3) using a 10 mm cell under nitrogen.

The authors express their gratitude to Professor M. Kobayashi and Dr. N. Kamigata, Tokyo Metropolitan University, for CD spectroscopy.

References

1) a) T. P. Dang and H. B. Kagan, *J. Chem. Soc., Chem. Commun.*, **1971**, 481; b) H. B. Kagan and T. P. Dang, *J. Am. Chem. Soc.*, **94**, 6429 (1972).

2) a) T. P. Dang, J. C. Poulin, and H. B. Kagan, *J. Organomet. Chem.*, **91**, 105 (1975); b) A. Levi, G. Modena, and G. Scorrano, *J. Chem. Soc., Chem. Commun.*, **1975**, 6; c) G. Gelbard and H. B. Kagan, *Tetrahedron*, **32**, 233 (1976); d) R. Glaser, S. Geresh, and J. Blumenfeld, *J. Organomet. Chem.*, **112**, 355 (1976); e) R. Glaser and B. Vainas, *ibid.*, **121**, 249 (1976); f) Y. Chauvin, D. Commereuc, and R. Stern, *ibid.*, **146**, 311 (1978).

3) R. Glaser, M. Twaik, S. Geresh, and J. Blumenfeld, *Tetrahedron Lett.*, **1977**, 4635; H. B. Kagan, T. Yamagishi, J. C. Motte, and R. Setton, *Israel J. Chem.*, **17**, 274 (1978); U. Hengartner, D. Valentine, Jr., K. K. Johnson, M. E. Larsheid, F. Pigott, F. Scheidl, J. W. Scott, R. C. Sun, J. M. Townsend, and T. H. Williams, *J. Org. Chem.*, **44**, 3741 (1979); J. M. Brown and B. A. Murrer, *Tetrahedron Lett.*, **21**, 581 (1980); C. F. Hobbs and W. S. Knowles, *J. Org. Chem.*, **46**, 4422 (1981); E. C. Alyea and D. W. Meek, *Adv. Chem. Ser.*, **196**, 324 (1982).

4) I. Ojima, T. Kogure, and N. Yoda, *J. Org. Chem.*, **45**, 4728 (1980).

5) G. Valavoine, S. Brunie, and H. B. Kagan, *J. Organomet. Chem.*, **187**, 125 (1980).

6) By X-ray structural determination, neutral chloroiridium-DIOP complex [IrCl((+)-DIOP)(cod)] has been shown to have a distorted trigonal bipyramid structure, where DIOP occupies apical and equatorial positions and chlorine occupies an equatorial position: S. Brunie, J. Mazan, N. Langlois, and H. B. Kagan, *J. Organomet. Chem.*, **114**, 225 (1976).

7) S. Gladialli, G. Faeda, M. Marchetti, and C. Botteghi, *J. Organomet. Chem.*, **244**, 289 (1983).

8) I. Ojima, T. Kogure, N. Yoda, T. Suzuki, M. Yatabe, and T. Tanaka, *J. Org. Chem.*, **47**, 1329 (1982).

9) M. D. Fryzuk and B. Bosnich, *J. Am. Chem. Soc.*, **99**, 6262 (1977).

10) R. Glaser an S. Geresh, *Tetrahedron*, **35**, 2381 (1979).

11) R. M. Herbst and D. S. Shemin, *Org. Synth.*, Coll. Vol. II, 1, 406 (1943).

12) D. G. Doherty, J. E. Tietzman, and M. Bergmann, *J. Biol. Chem.*, **147**, 617 (1943).

13) D. Meyer, J. C. Poulin, and H. B. Kagan, *J. Org. Chem.*, **45**, 4680 (1980).

14) B. B. Hunt and B. C. Saunders, *J. Chem. Soc.*, **1957**, 2413.

15) R. E. Montgomery and L. D. Qurn, *J. Am. Chem. Soc.*, **87**, 2393 (1965).

16) H. Carmack and C. J. Kelly, *J. Org. Chem.*, **33**, 2171 (1968).

17) W. Dumont, J. C. Poulin, T. P. Dang, and H. B. Kagan, *J. Am. Chem. Soc.*, **95**, 8295 (1973).

18) R. Cramer, *J. Chem. Soc.*, **1964**, 217.

19) R. R. Schrock and J. A. Osborn, *J. Am. Chem. Soc.*, **93**, 2397 (1971).

 © 1984 The Chemical Society of Japan Bull. Chem. Soc. Jpn., 57, 1902—1907 (1984) [Vol. 57, No. 7

Total Synthesis of Racemic and Optically Active Coronafacic Acids

Susumu OHIRA
Department of Chemistry, Faculty of Science, Hiroshima University, Higashisenda-machi, Naka-ku, Hiroshima 730
(Received November 17, 1983)

(±)-Methyl 3-ethyl-4-oxotricyclo[4.3.0.0^{1,5}]nonane-5-carboxylate (**4**), prepared by the stereoselective alkylation of methyl 4-oxotricyclo[4.3.0.0^{1,5}]nonane-5-carboxylate, was reduced with zinc borohydride, and the resultant hydroxy ester was treated with *p*-toluenesulfonyl chloride to give a mixture of α,β-unsaturated esters, having hydrindan skeletons. The mixture was submitted to hydroboration-oxidation to afford a keto ester, which was hydrolyzed to (±)-coronafacic acid (**2**). A diastereomeric mixture of *l*-menthyl 3-ethyl-4-oxotricyclo-[4.3.0.0^{1,5}]nonane-5-carboxylates, prepared by a modification of the synthesis of (±)-**4**, was resolved by column chromatography on silica gel, and each diastereomer was converted into (+)-**2** and (−)-**2** in a similar way as (±)-**2**.

Coronatine (**1**), a phytotoxin produced by *Pseudomonas syringae pv. atropurpurea*, induces chlorosis on the leaves of Italian ryegrass and a hypertrophy on potato tuber tissues at a very low concentration.[1] The structure of **1** was established by the combination of a single-crystal X-ray analysis of coronafacic acid (**2**)[2a] and partial synthesis of **1**, which was achieved from natural **2** and synthesized coronamic acid (**3**).[2b] Determination of the absolute configuration of **1** was based on the ORD measurement of **2**[2b] and X-ray diffraction analysis of the *N*-acetyl derivative of the enantiomer of **3**.[2c] The first synthesis of (±)-**2**,[3a] which means the total synthesis of coronatine in a formal sense, was reported by Ichihara *et al.* in 1977. Since then many different syntheses have been accomplished constructing the hydrindan skeleton by characteristic methods, namely the intermolecular or intramolecular Diels-Alder reaction,[3,4b] the anionic oxy-Cope rearrangement,[4a] and the palladium-catalyzed cyclization followed by the Dieckmann condensation.[5] In this paper, I describe the total synthesis of racemic and optically active coronafacic acids,[6] including the transformation of the tricyclo[4.3.0.0^{1,5}]nonane system to the hydrindan skeleton *via* the cleavage of the cyclopropane ring.

Synthesis of (±)-Coronafacic Acid.[6a] As C_{7a}-epimer of **2** is easily convertible to **2**,[2-4] the major stereochemical problem in the synthesis of (±)-**2** was the introduction of the C_6-ethyl group *trans* to the C_{3a}-proton. A tricyclo[4.3.0.0^{1,5}]nonane derivative (**4**) appeared to be a suitable synthetic intermediate, because (±)-**4** was expected to be thermodynamically more stable than its C_3-epimer (**5**), which may have a significant interaction between the ethyl group and the cyclopropane ring. Transformation of the similar tricyclic compound to the fused bicyclic one was reported by Ruppert and White,[7] although there has been no application to the synthesis of the natural product.

1-Cyclopentenecarbaldehyde (**6**)[8] was reduced with lithium aluminium hydride to give an alcohol (**7**). Treatment of **7** with *p*-toluenesulfonyl chloride (TsCl) under the phase-transfer catalyzed conditions (benzene-aqueous sodium hydroxide)[9] gave a sensitive sulfonate (**8**), which was not obtainable in the standard way (TsCl–pyridine). Without purification, **8** was subjected to reaction with the dianion of methyl acetoacetate, giving a β-keto ester (**9**)[10] in 66% yield from **6**. Treatment of **9** with *p*-toluenesulfonyl azide in acetonitrile in the presence of triethylamine afforded a diazo compound, which was heated in refluxing toluene with a catalytic amount of trimethyl phosphite-copper(I) iodide complex to give a 60% yield of the cycloadduct (±)-**10**.

Alkylation of (±)-**10** with 1 equiv of lithium diisopropylamide (LDA) and ethyl bromide in tetrahydrofuran provided a mixture of the monoalkylation product (±)-**4** and the dialkylation product (±)-**11** in various ratios depending on the reaction conditions. Although (±)-**5** was not produced as was expected, the yield of (±)-**4** was generally unsatisfactory due to production of (±)-**11** and recovery of (±)-**10**. After some considerable investigation, a 68% yield of (±)-**4** was obtained using a small excess of LDA, 4 equiv of hexamethylphosphoric triamide (HMPA) as a cosolvent, and 5 equiv of ethyl iodide in place of the bromide. The stereochemistry of (±)-**4** was confirmed by single-crystal X-ray analysis as shown in Fig 1.[11]

(±)-**4** was reduced with sodium borohydride in methanol to give an epimeric mixtur (*a* 3:1 ratio) of the hydroxy ester (±)-**12** and (±)-**13**; these were separated by chromatography on silica gel. The major product was assumed to be (±)-**12**, produced by the attack of the hydride from the less hindered side. Evidently, the ^{1}H NMR spectrum of the minor product (**13**) showed the CHOH proton at δ 4.06 as a double doublet, coupled with the adjacent methine proton (J= 3.5 Hz) and the OH proton (J=6.5 Hz), suggesting the intramolecular hydrogen bonding between the hydroxyl group and the ester carbonyl group. On

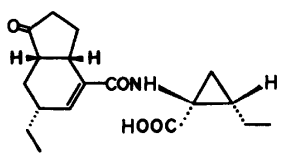

(1)

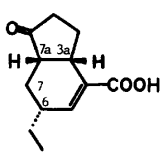

(2)

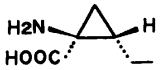

(3)

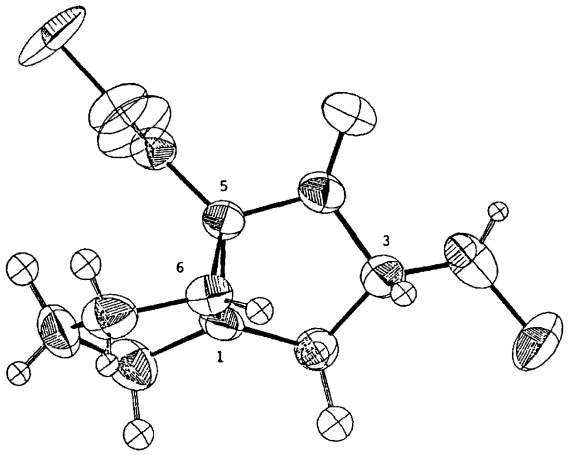

Fig. 1. Computer-generated perspective drawing of compound **4**.

the other hand, the ^{1}H NMR spectrum of the major product (**12**) showed the CHOH proton at δ 4.16 as a doublet with a larger coupling (J=6.5 Hz) than that of the minor product. Reduction of (±)-**4** with zinc borohydride gave a 86% yield of (±)-**12** as a single isolated product by the attack of the hydride from the same side as the ester carbonyl group.[11]

Transformation of (±)-**12** to the fused bicyclic system was attempted using HMPA or TsCl. Treatment with refluxing HMPA for a few minutes, or a large excess of TsCl for a few days at room temperature, afforded an unseparable mixture of α,β-unsaturated esters (±)-**14a—c**, contaminated with the aromatized product (**15**). Their structures were determined by GC-MS spectra and the ^{1}H NMR spectrum of the mixture, which showed the C_1-proton of (±)-**14a** and the C_7-proton of (±)-**14b** at δ 5.17 and 5.40 (each bs), the C_5-proton of (±)-**14a—c** at δ 6.5—6.9 (m), and two aromatic protons of **15** at δ 7.15 and 7.56 (each bs). After standing for a week at room temperature, almost all of the (±)-**14a—c** changed to **15**. When (±)-**12** was treated with 2—3 equiv of TsCl in pyridine at 90 °C for 1 h, a 1:1:1 mixture (glc analysis) of (±)-**14a—c** was obtained without **15**.

The unseparable mixture was then submitted to hydroboration and subsequent oxidation with pyridinium chlorochromate to give a complex mixture, from which a methyl ester of (±)-coronafacic acid (**16**) was isolated in 8% yield based on (±)-**12**. The ^{1}H NMR spectrum of (±)-**16** was identical with that of the methyl ester derived from the natural product. The hydroboration-oxidation process was investigated under various reaction conditions; but the yield of (±)-**16** could not be improved. Epoxidation of (±)-**14a—c** with *m*-chloroperbenzoic acid and subsequent treatment with boron trifluoride etherate afforded an undesired mixture, from which (±)-**16** could not be isolated.

Hydrolysis of (±)-**16** with refluxing aqueous hydrochloric acid[4] gave an 80% yield of (±)-**2**, whose spectral and analytical properties were identical with those of the natural product.[12]

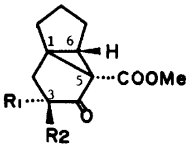

(4) R_1=Et, R2=H
(5) R_1=H, R2=Et
(10) R_1=R2=H
(11) R_1=R2=Et

(6) R=CHO
(7) R=CH2OH
(8) R=CH2OTs
(9) R=CH2CH2COCH2COOMe

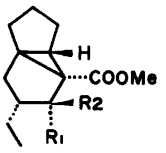

(12) R_1=H, R2=OH
(13) R_1=OH, R2=H

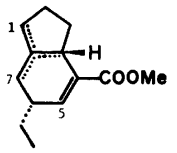

(14a) $\Delta^{1,7a}$
(14b) $\Delta^{7,7a}$
(14c) $\Delta^{3a,7a}$

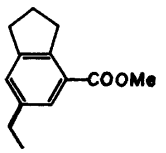

(15)

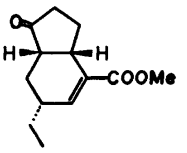

(16)

Synthesis of Optically Active Coronafacic Acids.[6b] Although the overall yield of (±)-**2** (0.9% from **6**) was not very satisfactory, the short process fror. (±)-**4** was attractive for the synthesis of optically active coronafacic acids, as there has been no approach to (+)- and/or (−)-**2** in contrast to (+)- and (−)-**3** which were prepared by resolution of the racemate.[2b] It was decided to try the resolution of the *l*-menthyl ester derivative[14] corresponding to (±)-**4**.

To circumvent the late alkylation step (**10**→**4**) in this study, the dianion of *l*-menthyl acetoacetate was first alkylated with 1 equiv of ethyl bromide to give the 3-oxohexanoate (**17**) in 88% yield. Reaction of **8** with the dianion of **17** afforded a 75% yield of a β-keto ester (**18**), whose diazotization and subsequent carbenoid addition gave a stereoisomeric mixture of the desired diastereomers (**19**) and its isomers (**20**) in 56% yield. Isolation of each isomer was difficult; however treatment of the mixture with sodium methoxide in refluxing methanol caused epimerization of **20** to afford only **19**. Fortunately, it could be resolved cleanly by column chromatography on silica gel and recrystallization from methanol gave **19a** and **19b** in a 1:1 ratio. The absolute configurations of **19a** and **19b** became clear after completion of the synthesis of (+)- and (−)-**2**.

Although **19a** could be converted to *l*-menthyl ester of (+)-**2** in three steps as described above, the ester resisted hydrolysis under mild acidic conditions (aqueous hydrochloric acid, aqueous sulfuric acid-acetic acid. To avoid the possibility of epimerization at the C_6-

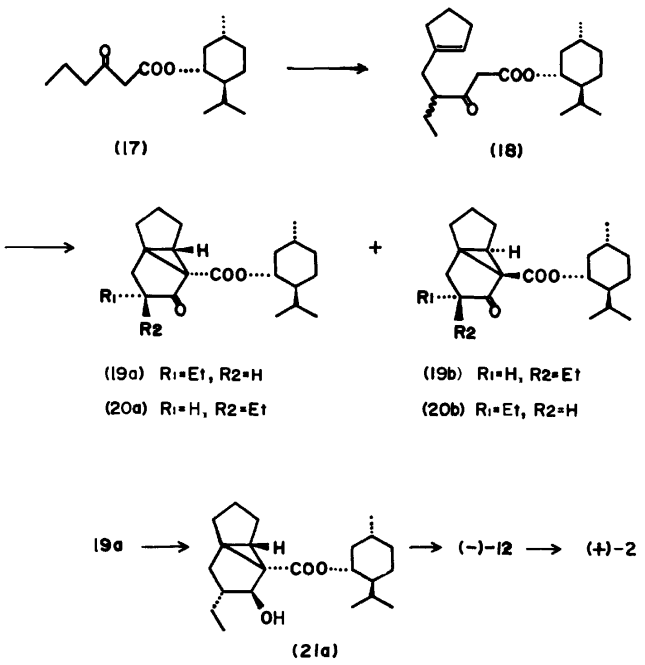

position under vigorous conditions of hydrolysis, the hydroxy ester (**21a**), which was obtained by reduction of **19a** with zinc borohydride in 90% yield, was converted beforehand into the corresponding methyl ester. Hydrolysis of **21a** was not achieved by refluxing in aqueous sodium hydroxide-methanol or ethanol, but was effected on refluxing with aqueous sodium hydroxide-dimethyl sulfoxide. The resultant carboxylic acid was esterified with ethereal diazomethane to give (−)-**12** in 88% yield from **21a**. By a similar transformation as described for the synthesis of (±)-**2**, (−)-**12** was led to (+)-**2** ($[\alpha]_D^{20}$+109°, lit,[2a] +119°) whose optical rotation showed the same sign as the natural product. (−)-**2** ($[\alpha]_D^{20}$−119°) was obtained from **19b** on a similar four-step process.

Experimental

All melting points were uncorrected. IR spectra were recorded on a Hitachi EPI-G3 spectrometer. The ordinary mass spectra were determined on a Hitachi RMU-6L mass spectrometer, using a direct inlet system with a prove temperature of 60—100 °C, an ionizing energy 70 eV and an accelerating voltage 3.2 kV. The high resolution mass spectra were taken using a Hitachi RMU-7L double focussing mass spectrometer. ^{1}H NMR spectra were recorded on Varian T-60 (60 MHz) and Hitachi R-22 (90 MHz), employing tetramethylsilane as an internal standard. Optical rotations were measured on a Yanako OR-50 polarimeter. Column chromatography and preparative TLC were performed on Merck silica gel 60 (70—230 mesh ASTM) and 60 PF_{254}, respectively.

*Methyl 3-Oxo-5-(1-cyclopentenyl)pentanoate (**9**).* 1-Cyclopentenecarbaldehyde (**6**)[8] (6.79 g, 70.6 mmol) was added to a suspension of lithium aluminium hydride (1.0 g, 26.4 mmol) in anhydrous ether (100 ml), and the reaction mixture was stirred at room temperature for 2 h. After the excess reagent was destroyed with ethyl acetate, aqueous sodium hydroxide was added to the mixture until aluminium oxide separated. The organic layer was washed with brine, and dried ($MgSO_4$). Removal of the solvent gave **7** (6.59 g) as a colorless oil, which was used directly in the next reaction: IR ($CHCl_3$) 3620, 3420 (OH), and 1670 cm^{-1} (-CH=C-); ^{1}H NMR (CCl_4) δ=3.76 (1H, bs, OH), 4.07 (2H, bs, $C\underline{H}_2OH$), and 5.55 (1H, bs, -CH=C-); MS *m/z* (rel intensity) 98 (M^+; 64), 80 (29), 70 (86), 67 (100), 57 (63), and 31 (85).

To a solution of **7** (6.59 g, 67.1 mmol) and *p*-toluenesulfonyl chloride (15.4 g, 80.6 mmol) in benzene (100 ml), was added 30% aqueous sodium hydroxide (100 ml) and benzyltriethylammonium chloride (0.8 g), with vigorous stirring at 20 °C (water bath). After the heterogeneous mixture was stirred for 5 h, the organic layer was washed with water, dil hydrochloric acid and brine, and dried (Na_2SO_4). The solvent was carefully evaporated *in vacuo* at *ca.* 30 °C to give the sensitive *p*-toluenesulfonate **8** as a colorless oil, which was used immediately in the next reaction: ^{1}H NMR (CCl_4) δ=2.43 (3H, s, CH_3), 4.54 (2H, bs, $C\underline{H}_2OTs$), and 5.65 (1H, bs, -CH=C-).

To a suspension of 55% sodium hydride (4.85 g, 111 mmol) in tetrahydrofuran (100 ml), was added a solution of methyl acetoacetate (11.7 g, 101 mmol) in tetrahydrofuran (300 ml) at 0—20 °C, and subsequently 1.6 M (1M=1 mol dm^{-3}) butyllithium in hexane (69 ml, 110 mmol) under nitrogen at −5—0 °C (ice-ethanol bath). To the yellow solution of the dianion, was added a solution of the sulfonate **8** in tetrahydrofuran (200 ml) at 0 °C, and the reaction mixture was stirred for 3 h. After quenching with aqueous ammonium chloride, the solvent was evaporated and the residue was extracted with ether. The organic layer was dried (Na_2SO_4) and evaporated *in vacuo* to give a crude product. Purification of the mixture by column chromatography on silica gel (300 g) using ethyl acetate-hexane (1:3) as eluent, gave **9** (9.09 g, 66% yield from **6**) as an oil: IR ($CHCl_3$) 1740 (ester C=O) and 1710 cm^{-1} (C=O); ^{1}H NMR (CCl_4) δ=3.33 (2H, s, $COCH_2CO$), 3.71 (3H, s, $COOCH_3$), and 5.32 (1H, bs, -CH=C-); MS *m/z* (rel intensity) 196 (M^+; 17), 178 (26), 122 (60), 95 (80), 94 (70), 80 (97), and 79 (100). Found: C, 67.14; H, 8.44%. Calcd for $C_{11}H_{16}O_3$: C, 67.32; H, 8.22%.

*(±)-Methyl 4-Oxoticyclo[4.3.0.0^{1,5}]nonane-5-carboxylate (**10**).* The keto ester **9** (3.39 g, 17.3 mmol) was dissolved in acetonitrile (70 ml) and mixed with triethylamine (2.62 g, 25.9 mmol) and *p*-toluenesulfonyl azide (3.57 g, 19.0 mmol) at room temperature. After standing overnight, the solvent was removed and the residue was treated with ether and water. The organic layer was washed with aqueous sodium hydroxide, water, and brine, and dried (Na_2SO_4). Removal of the solvent gave a crude product as an oil which was dissolved in toluene (200 ml) and refluxed for 5 h with trimethyl phosphite-copper (I) iodide complex (0.5 g). After cooling, the mixture was filtered and evaporated *in vacuo* to give a dark brown oil. Purification of the mixture by column chromatography on silica gel (160 g) using ethyl acetate-hexane (1:3) as eluent, gave (±)-**10** (2.02 g, 60% yield), which was recrystallized from ether-hexane as colorless prisms: Mp 68.5—69.5 °C; IR ($CHCl_3$) 1735 (ester C=O) and 1710 cm^{-1} (C=O); ^{1}H NMR (CCl_4) δ=0.6—1.4 (1H, brm, -CH-) and 3.68 (3H, s, $COOCH_3$); MS *m/z* (rel intensity) 194 (M^+; 10), 166 (36), 162 (100), 152 (48), 135 (28), and 93 (77). Found: C, 67.81; H, 7.38%. Calcd for $C_{11}H_{14}O_3$: C, 68.02; H, 7.27%.

*(±)-Methyl 3-Ethyl-4-oxotricyclo[4.3.0.0^{1,5}]nonane-5-carboxylate (**4**).* To a solution of lithium diisopropylamide in tetrahydrofuran (20 ml), prepared from diisopropylamine (450 mg, 4.38 mmol) and 1.6 M butyllithium in hexane (2.0 ml, 3.2 mmol) at 0 °C, was added a solution of (±)-**10** (567 mg, 2.93 mmol) and hexamethylphosphoric triamide (2.1 g, 11.7 mmol) in tetrahydrofuran (5 ml). The mixture was stirred for 15 min and ethyl iodide (2.3 g, 16 mmol) was

added to the solution. After stirring at 0 °C for 3 h, the reaction mixture was quenched with aqueous ammonium chloride. The solvent was evaporated *in vacuo* and the residue was extracted with ether. The organic layer was dried (Na_2SO_4) and evaporated *in vacuo* to give a crude product. Purification by column chromatography on silica gel (30 g) using ethyl acetate–hexane (1:5) as eluent, gave (±)-**4** (442 mg, 68% yield), which was recrystallized from ether–hexane as colorless prisms: Mp 71.5—73 °C; IR ($CHCl_3$) 1740 (ester C=O) and 1715 cm^{-1} (C=O); ^1H NMR (CCl_4) δ=0.87 (3H, t, J=7 Hz, $CH_2C\underline{H}_3$) and 3.66 (3H, s, $COOCH_3$); MS *m/z* (rel intensity) 222 (M^+; 12), 194 (80), 166 (100), 152 (54), 134 (36), and 93 (70). Found: C, 69.96; H, 8.12%. Calcd for $C_{13}H_{18}O_3$: C, 70.24; H, 8.16%.

A mixture from less polar fractions was purified by preparative TLC, using ethyl acetate–hexane (1:10) as solvent, to give the dialkylation product (±)-**11** (99 mg) as a colorless oil: IR ($CHCl_3$) 1735 (ester C=O) and 1710 cm^{-1} (C=O); ^1H NMR (CCl_4) δ=0.78 (3H, t, J=6.5 Hz, $CH_2C\underline{H}_3$), 0.83 (3H, t, J=6.5 Hz, $CH_2C\underline{H}_3$), and 3.67 (3H, s, $COOCH_3$); MS *m/z* (rel intensity) 250 (M^+; 3), 222 (19), 190 (10), 166 (100), and 98 (78). Found: C, 72.00; H, 9.10%. Calcd for $C_{15}H_{22}O_3$: C, 71.97; H, 8.86%.

X-Ray Analysis of (±)-4. (±)-**4** crystallized as a monoclinic crystal with a=8.617(2), b=9.737(3), c=15.070(6) Å, β=103.19(3)°. All unique diffraction intensities with $2\theta<50.0°$ were collected in a variable speed ω-scan mode on a Syntex R3 four-circle diffractometer with graphite-monochromated Mo $K\alpha$ radiation (0.7107 A). 1420 were judged to be observed after correction for Lorentz, polarization, and background effects. A phasing model which was obtained from the program MALTAN[14] was defined using Syntex XTL program system. Full-matrix least-squares refinements with anisotropic temperature factors for the nonhydrogen atoms and isotropic ones for the hydrogen atoms converged to a final R factor of 0.082 for 1420 reflections.

Reduction of (±)-4 with Sodium Borohydride. A stirred solution of (±)-**4** (78 mg, 0.35 mmol) in methanol (3 ml) was treated with sodium borohydride (67 mg, 1.8 mmol) for 2 h at room temperature. After the solvent was removed *in vacuo*, the residue was taken up in ether, washed with dil hydrochloric acid, aqueous sodium hydrogencarbonate and brine, and dried (Na_2SO_4). Removal of the solvent *in vacuo* gave a crude product, which was purified by preparative TLC, developed twice, using ethyl acetate–hexane (1:5) as solvent, to give (±)-**12** (47 mg, 60% yield) and (±)-**13** (17 mg, 22% yield). (±)-**12**: a colorless oil; R_f 0.45 (ethyl acetate–hexane=1:2); IR ($CHCl_3$) 3600 (OH) and 1710 cm^{-1} (ester C=O); ^1H NMR (CCl_4) δ=0.90 (3H, t, J=6 Hz, $CH_2C\underline{H}_3$), 2.61 (1H, bs, OH), 3.71 (3H, s, $COOCH_3$), and 4.16 (1H, d, J=6.5 Hz, $-C\underline{H}OH$); MS *m/z* (rel intensity) 224 (M^+; 14), 206 (18), 191 (25), 177 (43), 165 (48), 147 (56), and 136 (100). Found: C, 69.33; H, 9.16%. Calcd for $C_{13}H_{20}O_3$: C, 69.61; H, 8.99%. (±)-**13**: a colorless oil; R_f 0.52 (ethyl acetate–hexane=1:2); IR ($CHCl_3$) 3600 (OH) and 1710 cm^{-1} (C=O); ^1H NMR (CCl_4) δ=2.57 (1H, d, J=6.5 Hz, OH), 3.70 (3H, s, $COOCH_3$), and 4.06 (1H, dd, J=6.5, 3.5 Hz, $-C\underline{H}OH$). Found: C, 69.23; H, 9.12%. Calcd for $C_{13}H_{20}O_3$: C, 69.01; H, 8.99%.

Reduction of (±)-4 with Zinc Borohydride. To a solution of (±)-**4** (155 mg, 0.697 mmol) in ether (5 ml), was added 0.33 M zinc borohydride in ether (2.1 ml, 0.69 mmol) at 0 °C. After stirring for 2 h, the reaction mixture was quenched with ice and dil hydrochloric acid. The organic layer was washed with aqueous sodium hydrogencarbonate and brine, and dried (Na_2SO_4). Removal of the solvent gave a crude product which was purified by preparative TLC, developed twice, using ethyl acetate–hexane (1:5) as solvent, to give (±)-**12** (135 mg, 86% yield).

Methyl Ester of (±)-Coronafacic Acid (16). A solution of (±)-**12** (135 mg, 0.602 mmol) and *p*-toluenesulfonyl chloride (344 mg, 1.80 mmol) in pyridine (2 ml) was stirred at 90 °C under nitrogen for 1 h. The solvent was removed *in vacuo*, and the residue was treated with ether and water. The organic layer was washed with dil hydrochloric acid and brine, and dried (Na_2SO_4). Removal of the solvent gave a crude product, which was purified by preparative TLC, using ethyl acetate–hexane (1:5) as solvent, to give the unseparable mixture of (±)-**14a—c** (93 mg) as a colorless oil: IR ($CHCl_3$) 1710 (ester C=O) and 1630 ($-CH=\overset{1}{C}-$); ^1H NMR (CCl_4) δ=3.66, 3.67 (3H totally, each s, $COOCH_3$), 5.17, 5.40 (each *ca.* 0.3H, bs, C_1-or C_7-olefin proton), and 6.5—6.9 (1H, m, C_5-olefin proton).

To a solution of (±)-**14a—c** (93 mg, 0.46 mmol) in tetrahydrofuran (5 ml) was added 2.6 M borane in tetrahydrofuran (0.6 ml, 1.56 mmol) at 0 °C under nitrogen. The reaction mixture was stirred for 1 h at 0 °C and excess borane was destroyed with a small portion of water. Dichloromethane (10 ml) and pyridinium chlorochromate (0.8 g, 3.6 mmol) was added to the mixture succesively at 0—20 °C, and the mixture was stirred at room temperature for 2 h. The dark brown solution was passed over silica gel using ethyl acetate as eluent. After removal of the solvent, the residue was treated with ether and water. The organic layer was dried (Na_2SO_4) and evaporated *in vacuo* to give a complex mixture of many products. Isolation by preparative TLC, developed three times, using ethyl acetate–hexane (1:8) as solvent, and further purification by preparative TLC, developed twice, using ether–hexane (1:5) as solvent, provided (±)-**16** (11 mg, 8% yield from (±)-**12**), as a colorless oil: IR ($CHCl_3$) 1740 (ester C=O), 1710 (C=O), and 1640 cm^{-1} ($-CH=\overset{1}{C}-$); ^1H NMR ($CDCl_3$: 90 MHz) δ=0.99 (3H, t, J=7 Hz, $CH_2C\underline{H}_3$), and 6.93 (1H, bs, $-CH=\overset{1}{C}-$); MS *m/z* (rel intensity) 222 (M^+; 100), 193 (14), 190 (26), 145 (20), 133 (28), and 119 (74). Found: *m/z* 222.1272. Calcd for $C_{13}H_{18}O_3$: M, 222.1255. The ^1H NMR spectrum of (±)-**16** was identical with that of the methyl ester of natural coronafacic acid.

(±)-Coronafacic Acid (2). A suspension of (±)-**16** (12 mg, 0.054 mmol) in 2.4 M hydrochloric acid (10 ml) was refluxed for 2 h with vigorous stirring. After cooling, the mixture was extracted with dichloromethane and the organic layer was dried (Na_2SO_4). The solvent was removed *in vacuo* and the residue was purified by preparative TLC, developed twice, using ethyl acetate–hexane (1:2) as solvent, to give (±)-**2** (9 mg, 80% yield), which was recrystallized from diisopropyl ether as colorless prisms: mp 130—132 °C (lit,[3b] 115—127 °C); IR ($CHCl_3$) 3400—2500 (COOH), 1735 (C=O), 1685 (COOH), and 1635 cm^{-1} ($-CH=\overset{1}{C}-CO$); ^1H NMR ($CDCl_3$: 90 MHz) δ=0.99 (3H, t, J=7 Hz, $CH_2C\underline{H}_3$), 2.96—3.23 (1H, m, $-\overset{1}{C}=CHC\underline{H}-$), 7.11 (1H, bs, $-\overset{1}{C}=CH-$), and 10.28 (1H, bs, COOH); MS *m/z* (rel intensity) 208 (M^+; 100), 190 (20), 163 (29), 151 (33), 133 (48), 119 (71), 105 (47), 91 (64), and 79 (88). Found: C, 69.13; H, 7.66%. Calcd for $C_{12}H_{16}O_3$: C, 69.21; H, 7.74%. The ^1H NMR spectrum of (±)-**2** was identical with that of the natural product. The IR spectrum of (±)-**2** was identical with that of an authentic sample.[12]

l-Menthyl 3-Oxohexanoate (17). A similar procedure to the preparation of **9**, using *l*-menthyl acetoacetate[13] (13.94 g, 58 mmol), 55% sodium hydride (3.04 g, 70 mmol), 1.6 M butyllithium in hexane (40 ml, 64 mmol), and ethyl bromide (7.6 g, 69.7 mmol), gave a crude product, which was chromatographed on silica gel (400 g), using ethyl acetate–hexane (1:30) as eluent, to give **17** (13.7 g, 88% yield) as an oil; $[\alpha]_D^{20}$ −63.5 ° (*c* 0.85, $CHCl_3$); IR ($CHCl_3$) 1730 (ester C=O) and 1705 cm^{-1} (C=O); ^1H NMR (CCl_4) δ=2.47 (2H, t, J=7 Hz, $CH_2C\underline{H}_2CO$), 3.28 (2H, s, $COCH_2CO$), and 4.64 (1H, dt,

J=10, 4 Hz, COOCH–); MS m/z (rel intensity) 268 (M^+; 1), 155 (5), 138 (76), 123 (30), 113 (15), 95 (68), 71 (72), and 43 (100). Found: C, 71.67; H, 10.73%. Calcd for $C_{16}H_{28}O_3$: C, 71.60; H, 10.52%.

1-Menthyl 3-Oxo-4-(1-cyclopentenylmethyl)hexanoate (18). A similar procedure to the preparation of **9**, using **17** (1.29 g, 4.81 mmol), 55% sodium hydride (230 mg, 5.27 mmol), 1.6 M butyllithium in hexane (3.3 ml, 5.3 mmol), and **8** prepared from **7** (380 mg, 3.88 mmol) gave a crude product, which was chromatographed on silica gel (60 g), using ethyl acetate-hexane (1:50) as eluent, to give **18** (1.016 g, 75% yield from **7**) as an oil: IR ($CHCl_3$) 1735 (ester C=O), 1710 (C=O), and 1645 cm^{-1} (–CH=C–), ^1H NMR (CCl_4) δ=2.70 (1H, m, COCH–), 3.27 (2H, s, $COCH_2CO$), 4.67 (1H, m, COOCH–), and 5.35 (1H, bs, –CH=C–); MS m/z (rel intensity) 348 (M^+; 3), 210 (56), 192 (33), 130 (40), 123 (87), 83 (65), and 81 (100). Found: C, 75.51; H, 10.53%. Calcd for $C_{22}H_{36}O_3$: C, 75.81; H, 10.41%.

Preparation of 1-Menthyl 3-Ethyl-4-oxotricyclo[4.3.0.0^{1,5}]-nonane-5-carboxylates (19) and (20). A similar procedure to the preparation of (±)-**10**, using **18** (8.21 g, 23.6 mmol), triethylamine (2.86 g, 28.3mmol), *p*-toluenesulfonyl azide (4.88 g, 24.8 mmol), and a catalytic amount of trimethyl phosphite-copper(I) iodide complex, gave a crude product, which was chromatographed on silica gel (300 g), using ethyl acetate-hexane (1:15) as eluent, to give a mixture of cycloadducts **19** and **20** (4.54 g, 56% yield).

Epimerization of 20 and Resolution of 19. To a solution of sodium methoxide in methanol, prepared by addition of sodium (0.5 g, 22 mmol) into methanol (200 ml), was added the mixture of **19** and **20** (4.20 g, 12.1 mmol), and refluxed for 2 h. After cooling, aqueous ammonium chloride was added to the mixture and the methanol was evaporated *in vacuo*. The residue was extracted with ether and the organic layer was dried (Na_2SO_4). Removal of the solvent gave the mixture of **19a** and **19b**, which was chromatographed on silica gel (200 g) using ether-hexane (1:10) as eluent. Repeated column chromatography on silica gel and final purification by recrystallization from methanol gave pure **19a** (1.65 g, 21% yield from **18**) and **19b** (1.61 g, 21% yield from **18**). **19a**: Mp 70—71 °C (colorless prisms); R_f 0.26 (ether-hexane=1:5); $[\alpha]_D^{20}$ −86.7° (c 4.65, $CHCl_3$); IR (CCl_4) 1740 (ester C=O) and 1720 cm^{-1} (C=O); ^1H NMR (CCl_4) δ=4.65 (1H, dt, J=10, 4 Hz, COOCH–); MS m/z (rel intensity) 346 (M^+; 1), 209 (52), 191 (100), 180 (21), 164 (44), 152 (20), 138 (40), 123 (19), and 95 (45). Found: C, 76.54; H, 10.19%. Calcd for $C_{22}H_{34}O_3$: C, 76.26; H, 9.89%. **19b**: mp 100—101.5 °C (colorless prisms); R_f 0.31 (ether-hexane=1:5); $[\alpha]_D^{20}$ +5.4° (c 3.68, $CHCl_3$); IR (CCl_4) 1740 (ester C=O) and 1715 cm^{-1} (C=O); ^1H NMR (CCl_4) δ=4.62 (1H, dt, J=10, 4 Hz, COOCH–). Found: C, 76.54; H, 9.96%. Calcd for $C_{22}H_{34}O_3$: C, 76.26; H, 9.89%.

Reduction of 19 with Zinc Borohydride. A similar procedure to the reduction of (±)-**4**, using **19a** (1.016 g, 2.93 mmol) and 0.33 M zinc borohydride in ether (6.8 ml, 2.24 mmol), gave a crude product, which was chromatographed on silica gel (50 g), using ethyl acetate-hexane (1:8) as eluent, to give **21a** (0.918 g, 90% yield) as a colorless oil: $[\alpha]_D^{20}$ −67.5° (c 1.53, $CHCl_3$); IR (CCl_4) 3600 (OH) and 1705 cm^{-1} (ester C=O); ^1H NMR (CCl_4) δ=2.26 (1H, s, OH), 4.05 (1H, d, J=6.5 Hz, –CHOH), and 4.68 (1H, dt, J=10, 4 Hz, COOCH–); Found: C, 75.64; H, 10.69%. Calcd for $C_{22}H_{36}O_3$: C, 75.82; H, 10.41%.

Hydrolysis of 21a and Subsequent Esterification. A solution of **21a** (769 mg, 2.21 mmol) in 2.5 M aqueous sodium hydroxide (15 ml) and dimethyl sulfoxide (30 ml) was refluxed for 3 h. After addition of water, the mixture was extracted with ether. The aqueous layer was acidified with crashed ice and 6 M hydrochloric acid, and extracted with ether. The organic layer was washed with brine and dried (Na_2SO_4). Removal of the solvent gave a crude carboxylic acid, which was treated with ethereal diazomethane. After evaporation of the solvent, the residue was purified by column chromatography on silica gel (60 g), using ethyl acetate-hexane (1:5) as eluent, to give (−)-**12** (436 mg, 88% yield) as a colorless oil: $[\alpha]_D^{20}$ −43.5° (c 1.82, $CHCl_3$); the physical data (IR, ^1H NMR, and TLC analysis) of (−)-**12** were identical with those of (±)-**12**. Found: C, 69.72; H, 9.08%. Calcd for $C_{13}H_{20}O_3$: C, 69.61; H, 8.99%.

(+)-Coronafacic Acid (2). A similar three-step procedure to the preparation of (±)-**2** from (±)-**12**, using (−)-**12** (1.22 g), gave (+)-**2** (15 mg), which was recrystallized from diisopropyl ether: Mp 142—143 °C (colorless prisms) (authentic sample[12]: 142—143 °C, mmp 142—143 °C, lit,[2a] 125—126 °C); $[\alpha]_D^{20}$ +109° (c 0.75, MeOH, lit,[2a] +119.1°); IR and ^1H NMR spectra were identical with those of the natural product and (±)-**2**. Found: C, 69.09; H, 7.81%. Calcd for $C_{12}H_{16}O_3$: C, 69.21; H, 7.74%.

(−)-Coronafacic Acid (2). A similar five-step procedure to the preparation of (+)-**2** from **19a**, using **19b** (1.151 g), gave (−)-**2** (17 mg), which was recrystallized from diisopropyl ether: Mp 142—143 °C (colorless prisms); $[\alpha]_D^{20}$ −119° (c 0.86, MeOH); IR and ^1H NMR spectra were identical with those of the natural product and (±)-**2**. Found: C, 69.31; H, 7.93%. Calcd for $C_{12}H_{16}O_3$: C, 69.21; H, 7.74%.

The author wishes to express his hearty thanks to Associate Professor Mitsuru Nakayama of Hiroshima University for his encouragement and guidance during the course of this research. The author is grateful to his laboratory staff, for useful suggestions and continual encouragement, and also to Professor Akitami Ichihara, Hokkaido University, for kindly providing him with an authentic sample, as well as spectral data of natural coronafacic acid and its methyl ester. Thanks are also due to Dr. Shizuko Eguchi (MS) and Dr. Sachihiko Imai (NMR), Hiroshima University, for the spectral measurement. The author is grateful to Dr. Hiroshi Nozaki, Okayama University of Science, for the help and advice with X-ray analysis.†

References

1) K. Nishiyama, R. Sakai, A. Ezuka, A. Ichihara, K. Shiraishi, M. Ogasawara, H. Sato, and S. Sakamura, *Ann. Phytopath. Soc. Jpn.*, **42**, 613 (1976); K. Nishiyama, R. Sakai, A. Ezuka, A. Ichihara, K. Shiraishi, and S. Sakamura, *ibid.*, **43**, 219 (1977).

2) a) A. Ichihara, K. Shiraishi, H. Sato, S. Sakamura, K. Nishiyama, R. Sakai, A. Furusaki, and T. Matsumoto, *J. Am. Chem. Soc.*, **99**, 636 (1977); b) A. Ichihara, K. Shiraishi, S. Sakamura, K. Nishiyama, and R. Sakai, *Tetrahedron Lett.*, **1977**, 269; c) A. Ichihara, K. Shiraishi, S. Sakamura, A. Furusaki, N. Hashiba, and T. Matsumoto, *ibid.*, **1979**, 365.

3) a) A. Ichihara, R. Kimura, K. Moriyasu, and S. Sakamura, *Tetrahedron Lett.*, **1977**, 4331; b) A. Ichihara, R. Kimura, S. Yamada, and S. Sakamura, *J. Am. Chem. Soc.*, **102**, 6353 (1980).

4) a) M. E. Jung and J. P. Hudspeth, *J. Am. Chem. Soc.*, **102**, 2463 (1980); b) M. E. Jung and K. M. Halweg, *Tetrahedron Lett.*, **22**, 2735 (1981).

† The complete F_o–F_c data are deposited as Document No. 8412 at the Office of the Editor of Bull. Chem. Soc. Jpn.

5) J. Tsuji, *Pure Appl. Chem.*, **53**, 2371 (1981).
6) A part of this work has already been briefly communicated: a) M. Nakayama, S. Ohira, Y. Okamura, and S. Soga, *Chem. Lett.*, **1981**, 731; b) M. Nakayama and S. Ohira, *Agric. Biol. Chem.*, **47**, 1689 (1983).
7) J. F. Ruppert and J. D. White *J. Am. Chem. Soc.*, **103**, 1808 (1981).
8) J. B. Brown, H. B. Henbest, and E. R. H. Jones, *J. Chem. Soc.*, **1950**, 3634.
9) W. Szeja, *Synthesis*, **1979**, 822.
10) M. J. Bullivant and G. Pattenden, *J. Chem. Soc., Perkin Trans. 1*, **1976**, 249.
11) T. Nakata and T. Oishi, *Tetrahedron Lett.*, **1980**, 1641.
12) The authentic sample of (+)-**2** was supplied by Professor A. Ichihara, Hokkaido University, and the characteristics (mp, TLC, IR) were measured in this laboratory.
13) D. F. Taber, S. A. Saheh, and R. W. Korsmeyer, *J. Org. Chem.*, **45**, 4699 (1980).
14) G. Germain, P. Main, and M. M. Woolfson, *Acta Crystallogr., Sect. B*, **24**, 274 (1970).

Palladium(II) Sulfate-Heteropoly Acid-catalyzed Oxidation of Cycloolefins in Liquid Phase

Haruo OGAWA,* Hideharu FUJINAMI, Kazuo TAYA, and Shousuke TERATANI†
Department of Chemistry, Tokyo Gakugei University, Koganei-shi, Tokyo 184
†*The Institute of Physical and Chemical Research, Wako-shi, Saitama 351*
(Received November 17, 1983)

Heteropoly acid (HPA) was used as an oxidant in the Wacker catalyst system. Among the catalyst systems examined, the $PdSO_4$-$H_3PMo_6W_6O_{40}$ catalyst system showed the highest activity with regard to the oxidation of cycloolefins, particularly cyclopentene and cyclohexene, to the corresponding cyclic ketones. The largest total turnover number with respect to Pd^{2+} was found to be 85 in water containing 20% *N*-methylformamide by volume. The initial rate of cyclohexene oxidation was expressed as

$$V_0 = k[\text{Cyclohexene}]^{1.0}[PdSO_4]^{1.0}[\text{HPA}]^0[O_2]^0.$$

The rate-determining step was suggested as being where cyclohexene was oxidized to cyclohexanone by Pd(II) salt. The apparent activation energy was 7.8 kcal mol^{-1} (1 cal=4.18 J). In the catalytic oxidation of cycloolefins (C_nH_{2n-2}: n=5, 6, 7, and 8), the yield of alicyclic ketone decreased as the carbon number n increased. Methyl-substituted cyclohexenes exhibited lower reactivities than cyclohexene.

The Wacker catalyst ($PdCl_2$-$CuCl_2$) is the well-established homogeneous catalyst for olefin oxidation. But there is still the need to improve the conventional Wacker catalyst, because the Cl^- anion in aqueous media causes reactor corrosion and the undesirable formation of chlorinated by-products, particularly from higher olefins. An improvement could be attained by replacing $CuCl_2$ with an oxidant which is easily reoxidized under the reaction conditions.

One candidate for the oxidant is 12-heteropoly acid, because the electrochemical reduction and oxidation of the 12-heteropolyanion proceed reversibly in acidic solutions. They are accompanied by transfer of 2,4,or 6 electrons and retention of the Keggin structure.[1] It has been reported that the redox potential of the 12-heteropoly acid which can play the role of the oxidant in the Wacker catalyst system must be in the range of 0.59—1.229 V[2] or 0.19—1.116 V[3] (*vs.* NHE); *i.e.*, the redox potential of the 12-heteropolyanion should be higher than that of the palladium redox couple Pd^{2+}/Pd^0 and lower than that of the oxygen redox couple O_2/H_2O. The highest redox potentials were measured to be 0.3 V[1] or 0.32 V[3,4] (*vs.* SCE) for $PMo_{12}O_{40}^{3-}$, and 0.50 V[3] (*vs.* SCE) for $PMo_6W_6O_{40}^{3-}$, and 0.28 V[5] (*vs.* SCE) for $PMoW_{11}O_{40}^{3-}$. These values suggest that one can substitute one of the above heteropolyanions for $CuCl_2$ as the oxidant in the Wacker catalyst system.

Recently, it was found that the 12-heteropoly acids can oxidize palladium atoms and that Pd(II) salt-heteropoly acid systems can be used as catalysts for the oxidation of ethylene[2] and 1-butene.[6] We have reported a successful attempt to obtain alicyclic ketones from cycloolefins using a $PdSO_4$-$H_3PMo_6W_6O_{40}$ catalyst system under mild conditions.[7] In this paper, details of the results are described.

Results and Discussion

Catalyst System. Figure 1 shows the initial rates of cyclohexene oxidation and amounts of cyclohexanone produced after 20 h from the start of the reaction as a function of Mo content in the $PdSO_4$-$H_3PMo_nW_{12-n}O_{40}$ catalyst series. The mixed-coordinated heteropoly acid, $H_3PMo_6W_6O_{40}$, was found to be the most active oxidant judging from the initial rate and the amount of cyclohexanone produced.

Figure 2 shows the changes of IR absorption spectra of the heteropoly acid during the oxidation. Each band is assigned according to the literature[8] as follows: 1070 cm^{-1} to P-O stretching (O_p band), 970 cm^{-1} to M=O (M: Mo and W) stretching (O_t band), and 790, 870 cm^{-1} to M-O-M vibration (O_b band). After the reaction proceeded for 20 h, the intensities of the O_p band and the O_b band decreased significantly, while the intensity of the O_t band was almost unchanged. Similar behavior in IR absorption was reported by other wokers[9-11] who concluded that these decreases in intnsity were caused by the reduction of the heteropoly compounds but the Keggin structure was still retained. The IR spectrum of the heteropoly acid used for the reaction is clearly different from those

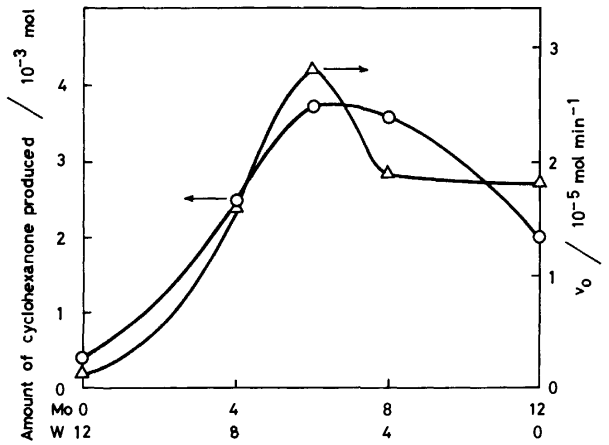

Fig. 1. Activity of $PdSO_4$-$H_3PMo_nW_{12-n}O_{40}$ catalyst system for cyclohexanone production. Each experiment was carried out at 303K for 20h under oxygen at 1 atm using cyclohexene (2.9×10^{-2} mol), $PdSO_4$ (8.3×10^{-3} mol), $H_3PMo_nW_{12-n}O_{40}$ (2.0×10^{-4} mol), and H_2O (10 ml).

of WO_3 and MoO_3. It is unlikely that the heteropoly acid decomposed to the WO_3 and MoO_3 units.

Various Pd(II) salts were tested in the oxidation of cyclohexene and 3-methylcyclohexene using $H_3PMo_6W_6O_{40}$ as the oxidant. Yields of cyclic ketones and total turnover numbers with respect to Pd^{2+} are listed in Table 1. The reaction time in Table 1 means the period of time after which no further oxidation occurred. From the standpoint of the total turnover number and the initial rate, $PdSO_4$ is the most active salt among the Pd(II) salts tested. The amount of cyclohexanone produced decreased in the following order depending upon the kind of counter anion of Pd^{2+};

$$SO_4^{2-} > NO_3^- > CH_3COO^- \geqslant Cl^-.$$

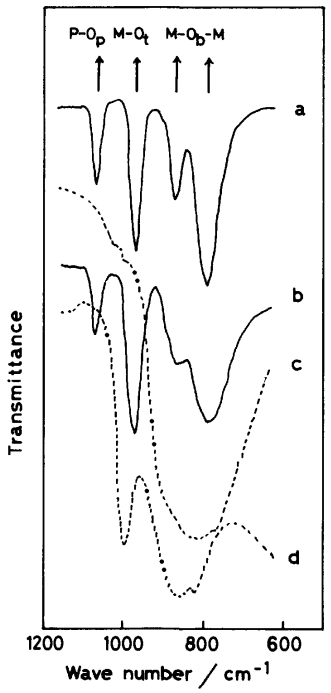

Fig. 2. IR spectra of heteropoly acid and related oxides:
a, Synthesized $H_3PMo_6W_6O_{40}$; b, $H_3PMo_6W_6O_{40}$ after 20 h of reaction; c, authentic WO_3; d, authentic MoO_3.

A similar order was observed in the oxidation of 1-butene.[6] We then adopted $PdSO_4$-$H_3PMo_6W_6O_{40}$ as a pertinent catalyst system for the oxidation of various cycloolefins.

Rate Expression. The amount of cyclohexanone produced was equal to that of cyclohexene consumed and to half of the oxygen uptake. The material balance indicates that the overall reaction is written as

$$\text{Cyclohexene} + 1/2\ O_2 = \text{Cyclohexanone}.$$

From the temperature dependence of the initial rate, the apparent activation energy was found to be 7.8 kcal·mol.$^{-1}$ The dependence of the initial rate of cyclohexanone production on the concentrations of cyclohexene and $PdSO_4$ is shown in Figs. 3 and 4, respectively. The slopes of the lines indicate that the oxidation of cyclohexene was first-order in both cyclohexene and $PdSO_4$. Under the present conditions, the initial rate was independent of the concentration of the heteropoly acid (see Fig. 5) and the partial pressure of oxygen. Accordingly, the following rate expression was obtained:

$$V_o = k[\text{Cyclohexene}]^{1.0}[PdSO_4]^{1.0}[HPA]^0[O_2]^0.$$

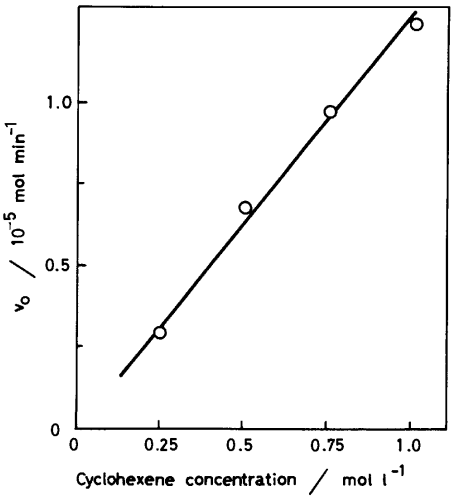

Fig. 3. Dependence of the initial rate of cyclohexanone production on cyclohexene concentration. Reaction conditions: $PdSO_4$ (5.0×10^{-5} mol) and $H_3PMo_6W_6O_{40}$ (2.0×10^{-4} mol) in H_2O (10 ml); and cyclohexene-cyclohexane solution (6 ml).

Table 1. Activity of Pd(II) salt-$H_3PMo_6W_6O_{40}$ catalyst[a)]

Olefin	Pd(II) salt	Time/h	Yield/%	Total turnover number[b)]	$V_o/10^{-5}$ mol min^{-1}
3-methylcyclohexene[c)]	$PdSO_4$	16	20.5	4	0.1
	$PdCl_2$	22	1.7	0.3	—
	$Pd(NO_3)_2$	21	15.2	3	—
Cyclohexene[d)]	$PdSO_4$	10	70.3	21	0.37
	$PdCl_2$	24	4.1	1	0.02
	$Pd(NO_3)_2$	23	63.9	19	0.29
	$Pd(CH_3COO)_2$	24	12.1	4	0.05

a) All oxidations were carried out at 303 K under 1 atm oxygen using both cyclohexane (3 ml) and H_2O (10 ml) as solvents. b) With respect to Pd^{2+}. c) 3-Methylcyclohexene (6.6×10^{-3} mol), Pd(II) salt (8.3×10^{-5} mol), and $H_3PMo_6W_6O_{40}$ (2×10^{-4} mol). d) Cyclohexene (1.5×10^{-3} mol), Pd(II) salt (5×10^{-5} mol), and $H_3PMo_6W_6O_{40}$ (2×10^{-4} mol).

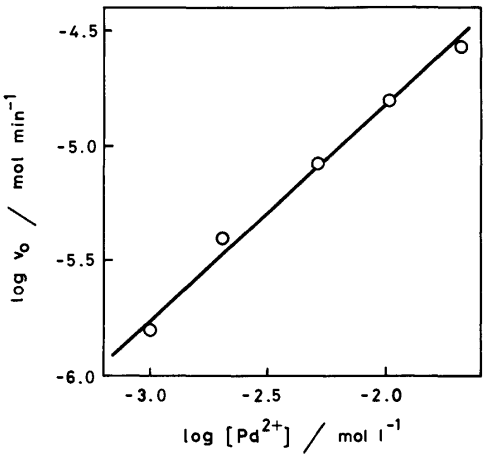

Fig. 4. Dependence of the initial rate of cyclohexanone production on $PdSO_4$ concentration. Reaction conditions: $PdSO_4$ in H_2O (10 ml), $H_3PMo_6W_6O_{40}$ (2.0×10^{-4} mol), cyclohexene (3.0×10^{-3} mol) in cyclohexane (6 ml).

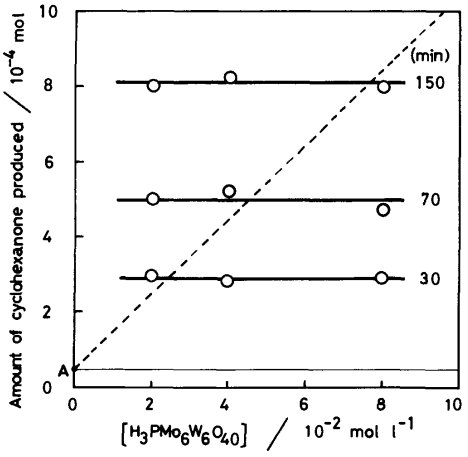

Fig. 5. Dependence of cyclohexanone production on heteropoly acid concentration. Reaction conditions: cyclohexene (3.0×10^{-3} mol) in cyclohexane (3 ml), heteropoly acid and $PdSO_4$ (5.0×10^{-5} mol) in H_2O (10 ml).

Redox Cycle in the Catalyst System. In order to clarify the role of the heteropoly acid and oxygen in the oxidation of cyclohexene, the reaction was carried out under nitrogen at atmospheric pressure. The aqueous reaction mixture was degassed by bubbling nitrogen gas through it for 15 min. The reaction was then conducted for 3 h at room temperature. As shown in Fig. 6, 0.27×10^{-3} mol of cyclohexanone was produced. The amount is very close to the amount (0.25×10^{-3} mol) calculated under the assumption that all heteropoly acid molecules act as oxidants which accept two electrons each from a Pd^0 atom. When nitrogen gas was replaced by oxygen gas at this reaction stage, the oxidation started again. These facts indicate that a heteropoly acid molecule of the oxidized form oxidized a Pd^0 atom to a Pd^{2+} ion and was accompanied by transfer of two electrons. A heteropoly acid molecule of the reduced form was then easily reoxidized by molecular oxygen. From the measurements of the redox potential

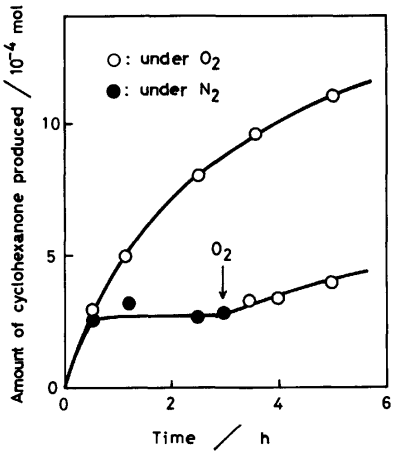

Fig. 6. Oxidation of cyclohexene under O_2 or N_2 at 1 atm. Reaction conditions cyclohexene (3.0×10^{-3} mol), $PdSO_4$ (5.0×10^{-5} mol), and $H_3PMo_6W_6O_{40}$ (2.0×10^{-4} mol) in H_2O (10 ml); cyclohexane (3 ml).

of $H_3PMo_6W_6O_{40}$, Izumi *et al.* concluded that two electrons were transferred in the oxidation and reduction processes.[3]

The oxidation of cyclohexene can be written as follows:

$$\text{Cyclohexene} + Pd^{2+} + H_2O \rightarrow \text{Cyclohexanone} + 2H^+ + Pd^0 \quad (1)$$

$$Pd^0 + HPA_{ox} \longrightarrow Pd^{2+} + HPA_{red} \quad (2)$$

$$HPA_{red} + 1/2O_2 + 2H^+ \longrightarrow HPA_{ox} + H_2O, \quad (3)$$

the subscripts ox and red stand for the oxidized and reduced forms, respectively. The oxidation proceeds catalytically through the redox cycles consisting of processes (1), (2), and (3).

One can confirm the passage through the redox cycles using the data shown in Fig. 5. The horizontal line through point A indicates the amount of cyclohexanone (0.05×10^{-3} mol) expected from the stoichiometric oxidation by $PdSO_4$ alone according to process (1). The dotted line indicates the amount of cyclohexanone expected from the amount of the oxidant heteropoly acid added under the assumption that processes (1) and (2) are operating. Figure 5 clearly shows that the amounts of cyclohexanone produced were above the horizontal line and exceeded the dotted line as the reaction proceeded when smaller amounts of heteropoly acid were used. These observations evidence that the redox cycles consisting of the processes (1), (2), and (3) were all operating effectively under the present conditions.

The system, $PdSO_4$(0.05×10^{-3} mol)-$H_3Mo_6W_6O_{40}$-(0.2×10^{-3} mol), gave about 0.8×10^{-3} mol of cyclohexanone after 150 min of reaction. It was deduced from the values that the redox cycle of $H_3PMo_6W_6O_{40}$,

turned at least 3 times. In a H_2O-*N*-methylformamide solvent, the cycle turned at least 21 times (see Table 3).

Table 2. Oxidation of cycloolefins in H_2O-cyclohexane mixture[a)]

Olefin	Time/h	Yield/%	Total turnover number[b)]	$V_0/10^{-5}$ mol min^{-1}
Cyclohexene[c)]	10	0.0[d)]	0	0
Cyclohexene[e)]	10	0.0[d)]	0	0
Cyclopentene[f)]	6	100	30	1.25
Cyclohexene[f)]	10	70.3	21	0.37
Cycloheptene[f)]	22	10.0	3	0.01
Cyclooctene[f)]	6	Trace	0	0
1-Methylcyclohexene[g)]	8	0	0	0
3-Methylcyclohexene[g)]	16	20.5[h)]	4	0.1
4-Methylcyclohexene[g)]	18	2.5[i)]	0.5	0.003
1-Hexene[f)]	10	85.9[j)]	25.8	0.67

a) Each experiment was carried out at 303 K using a mixture of cyclohexane (3 ml) and H_2O (10 ml) under 1 atm oxygen. b) With respect to Pd^{2+}. c) Cyclohexene (1.5×10^{-3} mol), $H_3PMo_{12}O_{40}$ (2×10^{-4} mol), and concd. H_2SO_4 were added to the aqueous solution in order to make the pH similar to that for the conditions of footnote e (pH 1.3). d) No oxygen was absorbed during the reaction. e) Cyclohexene (1.5×10^{-3} mol), $H_3PMo_6W_6O_{40}$ (2×10^{-4} mol), and concd. H_2SO_4 (trace). f) Olefin (1.5×10^{-3} mol), $PdSO_4$ (5×10^{-5} mol), and $H_3PMo_6W_6O_{40}$ (2×10^{-4} mol). g) Olefin (6.6×10^{-3} mol), $PdSO_4$ (8.3×10^{-5} mol), and $H_3PMo_6W_6O_{40}$ (2×10^{-4} mol). h) 2-Methylcyclohexanone, 7.6%; 3-methylcyclohexanone, 12.9%. i) 3-Methylcyclohexanone, 1.7%; 4-methylcyclohexanone, 0.8%. j) 2-Hexanone, 75%; hexanal, 10.9%.

Oxidation of Cycloolefins. The results of the oxidation of cycloolefins were listed in Table 2. The yields of ketones in an H_2O-cyclohexane mixture decreased in the following order:

Cyclopentene > Cyclohexene > Cycloheptene > Cyclooctene,

Cyclohexene > 3-Methylcyclohexene > 4-Methylcyclohexene > 1-Methylcyclohexene.

The increase in the carbon number of the cycloolefins caused the yield of the cyclic ketones to decrease. Relative reactivities of the cycloolefins were measured by their competitive oxidation. Figure 7 shows the result of the competitive oxidation of a cyclopentene-cyclohexene equimolar mixture together with the results of the individual oxidation of cyclopentene and cyclohexene. The production of cyclopentanone was not affected by the presence of cyclohexene; while the production of cyclohexanone was inhibited by cyclopentene. After an induction period of about 3 h, cyclohexanone began to form. Competitive reactions of a cyclohexene-cycloheptene equimolar mixture and a cyclohexene-cyclooctene equimolar mixture behaved similarly; *i.e.*, the oxidation of olefin having a smaller number of carbon atoms was not retarded by the higher olefin, while the oxidation of olefin having a larger number of carbon atoms was retarded by the lower olefin.

Rate-determining Step. In the oxidation of 1-butene, Izumi *et al.*[3] suggested that process(3)determines the rate in the $PdSO_4$-$H_3PMo_6W_6O_{40}$ catalyst system. The rate expression for the cyclohexene oxidation described before suggests that process (1) is rate-determining. The shift of the rate-determining process from (3) to (1) may be due to the very low reactivities of the cycloolefins toward Pd^{2+}. This consideration is supported by the facts that the rate of process (1) decreases as the carbon number of the straight-chain olefins[12] increases and that the oxidation rate of cyclohexene was slower than that of 1-hexene (see Table 2).

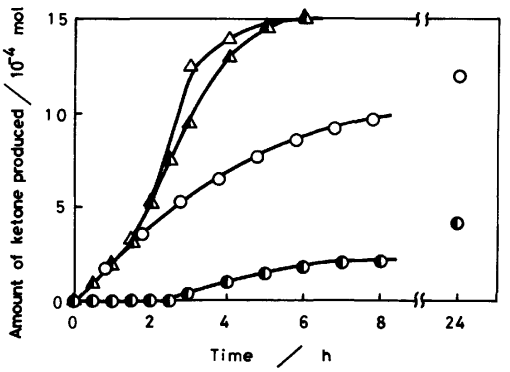

Fig. 7. Reaction profiles of oxidation of cyclopentene and cyclohexene and competive oxidation of a cyclopentene-cyclohexene equimolecular mixture: △, cyclopentanone; ○, cyclohexanone; ▲ and ◐, cyclopentanone and cyclohexanone produced in the competitive oxidation, respectively. Reaction conditions; olefin (1.5×10^{-3} mol), $PdSO_4$ (5.0×10^{-5} mol), and $H_3PMo_6W_6O_{40}$ (2.0×10^{-4} mol) in H_2O (10 ml); cyclohexane (3 ml).

Cyclohexene Oxidation in Various Solvents. The oxidation of olefin with the Wacker catalyst is affected by solvating forces. Clement and Selwitz[13] described a convenient synthesis of 2-dodecanone from 1-dodecene using aqueous *N,N*-dimethylformamide solvent, and suggested that *N,N*-dimethylformamide provided more intimate contact between the olefin and the catalyst solution and also might exert a solvent effect which promoted reaction. Lloyd *et al.*[14] reported that the oxidation of cyclohexene with $PdCl_2$-$CuCl_2$ catalyst proceeded more readily in alcoholic media and most readily in media containing little or no water because of

Table 3. Oxidation of cyclohexene in various solvents[a)]

Solvent system	Catalyst	Time/h	Yield/%	Total turnover number[b)]
H_2O-cyclohexane[c)]	$PdSO_4$-$H_3PMo_6W_6O_{40}$	10	70.3	21
Ethanol[d)]		7	7.3	7
H_2O-Et_2O[c)]		18	90.0	27
H_2O-$Pr^i{}_2O$[c)]		20	84.9	26
H_2O-$Bu^n{}_2O$[c)]		22	40.1	12
H_2O-formamide[c)]		5	23.3	7
H_2O-DMF[c)]		23	88.1	26
H_2O-*N*-methylformamide[c)]		5	96.7	29
H_2O-*N*-methylformamide[e)]		24	84.7	85
Ethanol[d)]	$PdCl_2$-$CuCl_2$	22	73.8	74

a) Each experiment was carried out at 303 K, except at 293 K in H_2O-Et_2O solvent, using Pd(II) salt (5×10^{-5} mol) and $H_3PMo_6W_6O_{40}$ (2×10^{-4} mol) or Cu(II) salt (2×10^{-4} mol) under 1 atm oxygen. b) With respect to Pd^{2+}. c) Cyclohexene (1.5×10^{-3} mol), H_2O (10 ml), and organic solvent (3 ml). d) Cyclohexene (5×10^{-3} mol) and ethanol (10 ml). e) Cyclohexene (5×10^{-3} mol), H_2O (8 ml), and *N*-methylformamide (2 ml).

the greater reactivity of the alcohol-solvated Pd(II) species.

Various solvents were used for the oxidation of cyclohexene with $PdSO_4$-$H_3PMo_6W_6O_{40}$ catalyst in order to obtain cyclohexanone in good yields. The results are shown in Table 3. Each run was stopped after the time denoted in Table 3 because no further oxidation occurred thereafter. Methanol, ethanol, 2-propanol, and *t*-butyl alcohol were examined, but oxidation took place only in ethanol giving a low yield of 7.3 %. Alcohols are not suitable solvents for the present catalyst system, although $PdCl_2$-$CuCl_2$ catalyst prefers ethanol as a solvent.

In H_2O-ether solvent systems, the oxidation proceeded readily in the following order:

diethyl ether>diisopropyl ether>dibutyl ether.

Interestingly, the larger the dielectric constant of solvent is, the higher the yield of cyclohexanone becomes.

In the H_2O-formamide solvent systems examined, the H_2O-*N*-methylformamide system was the most efficient. Figure 8 shows the effect of the addition of *N*-methylformamide to water on the yield of cyclohexanone. The best yield was obtained with water containing 20% *N*-methylformamide (by volume) and the total turnover number with respect to Pd^{2+} reached 85 after 24 h of reaction. When equal volumes of *N*-methylformamide and water were employed, the yield dropped drastically. Tetrahydrofuran, sulfolane, and dimethyl sulfoxide, which are not listed in Table 3, were highly inferior to *N*-methylformamide.

Life of the $PdSO_4$-$H_3PMo_6W_6O_{40}$ Catalyst. The oxidation proceeded catalytically within a certain reaction period. The reaction was inhibited by deposition of palladium metal. $PdSO_4$ or $H_3PMo_6W_6O_{40}$ was added to the reaction mixture after the inhibition, but the reaction did not proceed any more. To start the oxidation again, simultaneous addition of both $PdSO_4$ and $H_3PMo_6W_6O_{40}$ was required. The change of the IR spectra in Fig. 2 suggests that the $H_3PMo_6W_6O_{40}$ was in the reduced state after the inhibition. Calcination of the heteropoly acid in air at 673 K for 1 h restored about half of its activity. To produce a longer life for the present catalyst system, it is required that the reoxidation of the reduced heteropoly acid be activated in the course of the reaction.

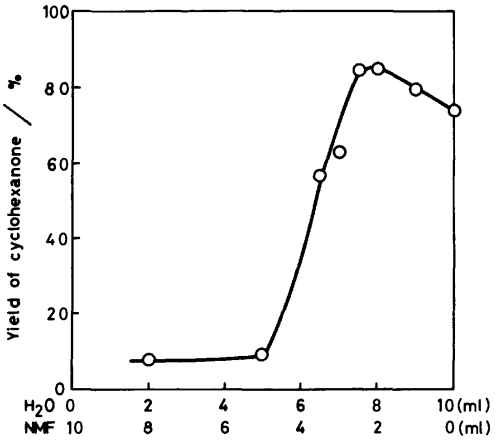

Fig. 8. Effect of addition of *N*-methylformamide (NMF) to water on the yield of cyclohexanone. Each experiment was carried out at 303K using cyclohexene (1.5×10^{-3} mol), $PdSO_4$ (5.0×10^{-4} mol), and $H_3PMo_6W_6O_{40}$ (2.0×10^{-4} mol) under oxygen at 1 atm over a 24 h period.

Experimental

Materials. *Catalysts*: Pd(II) salts were used as received; $PdSO_4$ (Mitsuwa Chemicals; assay(Pd) 52.5%), Pd-$(NO_3)_2$ (Wako Chemicals; assay(Pd) 45.5%) and $PdCl_2$ (Wako Chemicals; assay(Pd) 59.0%).

$H_3PMo_{12}O_{40}$ and $H_3PW_{12}O_{40}$ were purchased from Ventron Alfa Products, and used as received. Various mixed-coordinated heteropoly acids, $H_3PMo_nW_{12-n}O_{40}$ were synthesized according to the method reported.[15] It was confirmed by thermogravimetric analysis that a $H_3PMo_6W_6O_{40}$ molecule contained 10.8 molecules of water of crystallization.

Cycloolefins: Reagent grade cyclopentene, cyclohexene, cycloheptene, cyclooctene, 1-methylcyclohexene, 3-methyl-

cyclohexene, 4-methylcyclohexene, and 1-hexene were purchased from Wako Chemicals and Tokyo Kasei, and used without further purification.

Solvent: Organic solvents were all guaranteed grade except ethers (reagent grade) and were used as received.

Apparatus and Procedure. The oxidation was carried out under oxygen at atmospheric pressure using a 20 ml glass vessel reactor surrounded by a jacket in which thermostated water at 303±0.1 K was circulated. A wrist-action shaker was used to achieve vigorous agitation of the reaction solution. A typical example of the oxidation of cycloolefin is illustrative. $PdSO_4$ (0.05×10^{-3} mol) and heteropoly acid (0.2×10^{-3} mol) were dissolved in water (10 ml) and the resulting mixture was allowed to settle for a day at room temperature to obtain a homogeneous solution. The solution was stirred with a magnetic stirrer under oxygen at atmospheric pressure and 303 K for 1 h in order to activate the catalyst in the solution. After the treatment, cyclohexene (1.5×10^{-3} mol) in cyclohexane (3 ml) which contained *trans*-decalin (0.3×10^{-3} mol) as an internal standard was injected into the reaction solution. The oxidation was then carried out with vigorous agitation.

Analysis of Reaction Products and Catalysts. The reaction mixtures were analyzed with a Yanagimoto Model G80 gas chromatograph. The progress of reaction was followed by glc analysis of aliquot samples and by oxygen-uptake measurements. Reaction products were identified by comparing their retention times with those of the authentic samples. To confirm the identification, gas chromatographically separated samples of the reaction products were analyzed with a JASCO infrared spectrometer, a Hitachi RMS-4 mass spectrometer, and a JEOL FX-90Q ^1H NMR spectrometer. Spectroscopic data are listed as below: Cyclopentanone; IR (neat) ν=1745 cm^{-1} (C=O); ^1H NMR ($CDCl_3$) δ=2.07 (8H, m, cyclopentyl); MS (8 ev) *m/z* (rel intensity), 84 (M^+;100), 85 (5.2), 56 (4.3). Cyclohexanone; IR (neat) ν=1703 cm^{-1} (C=O); ^1H NMR ($CDCl_3$) δ=1.74 (6H, m, cyclohexyl), δ=2.30 (4H, m, cyclohexyl); MS (8 ev) *m/z* (rel intensity), 98 (M^+;100), 99 (6.4), 80 (3.7). Cycloheptanone; IR (neat) ν=1703 cm^{-1} (C=O); ^1H NMR ($CDCl_3$) δ=1.63 (8H, m, cycloheptyl), δ=2.46 (4H, m, cycloheptyl).

Synthesized heteropoly acids were analyzed with the IR spectrometer and a Rigaku-Denki 8076D TG-DTA analyzer.

This work was partially supported by a Grant-in-Aid for Science Research No 57740258 from the Ministry of Education, Science and Culture, Japan.

Refereres

1) G. A. Tsigdinos and C. J. Hallada, *J. Less-Common Met.* **36**, 79 (1974).
2) K. I. Matveev, *Kinet. Katal.*, **18**, 862 (1977). K. I. Matveev, E. G. Zhizhna, N. B. Shitova, and L. I. Kuznetsova, *ibid.*, **18**, 380 (1977).
3) K. Urabe, F. Kimura, and Y. Izumi, "Shokubai" (Catalyst), Catalysis Society of Japan, **22**, 10P. (1980).
4) J. J. Altenau, M. T. Pope, R. A. Prados, and H. So, *Inorg, Chem*, **14**, 417 (1975).
5) R. Massart, R. Contant, J. M. Fruchart, J. P. Ciabrini, and M. Fournier, *Inorg. Chem.*, **16**, 2916 (1977).
6) K. Urabe, F. Kimura, and Y. Izumi, Proc. 7th Intern. Cong. Catalysis, Tokyo (1980), Part B, p. 1418.
7) H. Ogawa, H. Fujinami, H. Taya, and S. Teratani, *J. Chem. Soc., Chem. Commun*, **1981**, 1274.
8) C. Rocchiccioli-Deltcheff, R. Thouvenot, and R. Franck, *Spectrochim. Acta*, **32A**, 587 (1976).
9) M. Misono, K. Sakata, and Y. Yoneda, Proc. 7th Intern. Cong. Catalysis, Tokyo (1980), Part B, p. 1047; K. Katayama, T. Nakamura, M. Misono and Y. Yoneda, Chem. Lett., **1981**, 89.
10) K. Eguchi, Y. Toyozawa, K. Furuta, N. Yamazoe, and T. Seiyama, *Chem. Lett.*, **1981**, 1253.
11) M. Akimoto and E. Echigoya, *Chem. Lett.*, **1981**, 1759.
12) P. M. Henry, *J. Am. Chem. Soc.*, **88**, 1595 (1966).
13) W. H. Clement and C. M. Selwitz, *J. Org. Chem.*, **29**, 241 (1964).
14) W. G. Lloyd and B. J. Luberoff, *J. Org. Chem.*, **34**, 3949 (1969).
15) J. C. Bailar, *Inorg. Chem.*, **1**, 132 (1937).

The Oxidation of Biphenylene and Its Derivatives with $Mn(OAc)_3$ and $Pb(OAc)_4$

Kazu KUROSAWA,* Tetsuya TAKAMURA, Yasunari UENO,
John F. W. McOMIE†, and N. D. PEARSON†
Department of Chemistry, Faculty of Science, Kumamoto University, Kurokami 2-39-1, Kumamoto 860
†*School of Chemistry, The University, Bristol BS 8 1TS England*
(Received November 18, 1983)

The reaction of biphenylene with $Pb(OAc)_4$ gave 2-substituted biphenylenes and 2,3-biphenylenedione. The reaction of 2-methylbiphenylene and 2,3-dimethylbiphenylene with $Mn(OAc)_3$ yielded products in which the methyl substituent had been oxidized. The reaction of 2-methoxybiphenylene with $Pb(OAc)_4$ gave 2-acetoxy-3-methoxybiphenylene and *r*-2,*c*-3-diacetoxy-2-methoxy-2,3-dihydrobiphenylene, which is the first example of a 2,3-dihydrobiphenylene. The reactions of 2-carboxy-, 2-methoxycarbonyl- and 2,7-dibromobiphenylene with $Mn(OAc)_3$ and (in part) with $Pb(OAc)_4$ yielded nuclear acetoxymethylated products. The conversion of *r*-2,*c*-3-diacetoxy-2-methoxy-2,3-dihydrobiphenylene into 5,10-diacetoxy-7(8*H*)-benzocyclooctenone was observed.

A previous study on the oxidation of biphenylene (**1**) with $Mn(OAc)_3$ resulted in the formation of a propellane, 7-oxa-10,11-benzotricyclo[4.3.2.$0^{1,6}$]undeca-2,4,10-triene-8-one.[1] This led us to investigate the reactions of mono- and disubstituted biphenylenes in the hope of obtaining further evidence on the anomalous reactivity of biphenylene towards $Mn(OAc)_3$. The reaction of biphenylene with $Pb(OAc)_4$ was also studied, since this reagent should show a similar reactivity under certain reaction conditions,[2] although one of the authors has already reported that the reaction of biphenylene (**1**) with $Pd(OAc)_4$, followed by hydrolysis gave 2-hydroxybiphenylene.[3]

Results

When biphenylene (**1**) was oxidized with $Pb(OAc)_4$ in a 1:2 molar ratio, it gave 2-acetoxybiphenylene (**2**) and 2,3-biphenylenedione (**3**) (Table 1, Entry 2). When the molar ratio of the oxidant to substrate was increased, the yields were not very much affected, but a third product, 2-formylbiphenylene (**4**), was obtained (Entries 3 and 4). 2-Acetoxymethylbiphenylene (**5**) was detected by its CH_2 and CH_3 peaks in the ^{1}H-NMR spectrum of the crude product.

When 2-methylbiphenylene[4] (**7**) was oxidized with $Mn(OAc)_3$ and with $Pb(OAc)_4$, the products were found to be **4** and **5**. When acetic anhydride was added to the reaction mixture of $Mn(OAc)_3$, **5** was the major product, while the yield of **4** decreased, and compounds **6**, **8a**, and **8b** were isolated. The structures of **8a** and **8b** were determined by comparison with the corresponding authentic samples (see Experimental). The results are summarized in Table 2. It was shown that the recovery of **7** was much less than that of **1** in the oxidation with $Pb(OAc)_4$.

When the reaction of 2-methoxybiphenylene[5] (**11**) with $Mn(OAc)_3$ was examined in molar ratios of 1:2 and 1:4 in acetic acid at room temperature, it gave a complex mixture which could not be separated. The reaction of **11** with $Pb(OAc)_4$, in a molar ratio of 1:1 under similar reaction conditions gave two com-

TABLE 1. OXIDATION OF BIPHENYLENE (**1**) WITH $Pb(OAc)_4$ IN ACETIC ACID

Entry	Molar ratio of substrate :oxidant	Time / min	Temp / °C	Recovered substrate (%)	Product(yield/%)[a]		
					2	**3**	**4**
1	1 : 2	180	100	42	7	2	
2	1 : 2	20	Reflux	39	12	1	
3	1 : 3	20	Reflux	29	13	2	2
4	1 : 4	20	Reflux	25	10	3	1

a) Yields are based on the amount of the substrate used.

TABLE 2. OXIDATION OF 2-METHYLBIPHENYLENE (**7**) WITH $Pb(OAc)_4$ AND $Mn(OAc)_3$ IN ACETIC ACID AT THE REFLUX TEMPERATURE

Entry	Oxidant	Molar ratio	Time / min	Recovered substrate (%)	Product(yield/%)[a]				
					4[b]	**5**[b]	**6**	**8a**	**8b**
1	$Pb(OAc)_4$	1 : 2	20	11	21	15			
2	$Mn(OAc)_3$	1 : 4	35		27	21			
3	$Mn(OAc)_3$	1 : 4[c]	8	2	4	35	1	2	2

a) Yields are based on the amount of the substrate used. b) Yields were estimated from their ^{1}H-NMR spectra.
c) Acetic anhydride (10 ml) was added.

pounds; **12** (5%) and **13** (9%). Spectroscopic properties of **13** indicate that the structure of **13** could be either 2,3-diacetoxy-2-methoxy-2,3-dihydrobiphenylene (**13a**) or 2,4a-diacetoxy-3-methoxy-2,4a-dihydrobiphenylene (**13b**). However, the structure **13a** is preferred because compound **13** showed a symmetrical A_2B_2 pattern due to aromatic protons in the ^{1}H-NMR spectrum. Also, the δ values calculated[6] for H-1 and H-4 in **13a** are the same (6.0) and they agree with the experimental value (6.0), whereas the values calculated for H-1 and H-4 in **13b** (4.95 and 6.0 respectively) differ by about 1 ppm. The compound **13** was stable in $CDCl_3$ solution, but when the solution contained HCl (or DCl), it was converted to a new compound, **14**, which showed a new carbonyl carbon at δ 197.722 and a methylene carbon at δ 41.164 in its ^{13}C-NMR spectrum. The ^{1}H-NMR spectrum indicated the presence of =CH-CO-CH_2-CH=unit. These spectroscopic properties suggest the structure of 5,10-diacetoxy-7(8*H*)-benzocyclooctenone (**14**) (Scheme 1).

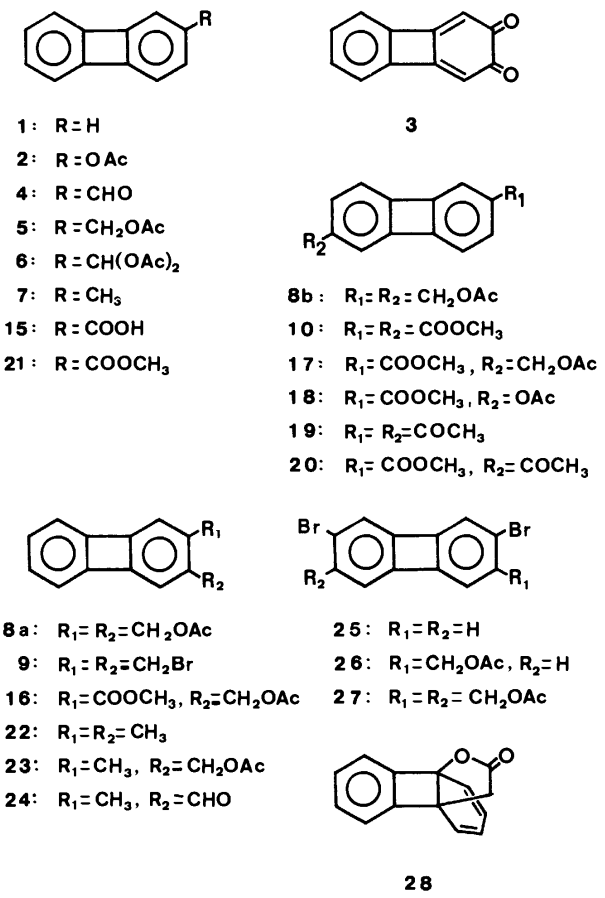

Fig. 1.

When 2-carboxybiphenylene[3] (15) was oxidized with $Pb(OAc)_4$ and $Mn(OAc)_3$, followed by treatment with diazomethane, three compounds, **16**, **17**, and **18**, were obtained (Table 3, Entries 1—4). The structures of these compounds were elucidated by spectroscopic evidence, by conversion to a known compound, and by synthesis. The structure of **16** was confirmed by reducing it with $LiAlH_4$ and then acetylating it to give a bis(acetoxymethyl)biphenylene which was identical with **8a**. In the same way, the structure of compound **17** was confirmed by converting it into the bis(acetoxymethyl) compound **8b**. The structure of **18**, which could not be obtained as a pure substance, was confirmed by an unambiguous synthesis. The Baeyer-Villiger oxidation of 2-acetyl-6-(methoxycarbonyl)biphenylene (**20**) which was obtained from 2,6-diacetylbiphenylene (**19**) gave **18**. When 2-(methoxycarbonyl)biphenylene[3] (**21**) was oxidized with $Pb(OAc)_4$ and with $Mn(OAc)_3$, it gave again **16**, **17**, and **18** in slightly modified yields (Table 3, Entries 5 and 6).

Oxidation of 2,3-dimethylbiphenylene[4] (**22**) with $Mn(OAc)_3$ in the molar ratio of 1:2 gave 2-acetoxymethyl-3-methylbiphenylene (**23**) and 2-formyl-3-methylbiphenylene[4] (**24**) (Table 4, Entry 1). When the molar ratio was increased to 1:4, the products were **23**, **24**, and **8a** together with very small amounts of the other substitution products which could not be separated. The structure of **23** was proved by its ^{1}H-NMR spectrum which showed the presence of six aromatic protons, one $ArCH_2$ and $ArCH_3$ group.

Bromination of biphenylene with *N*-bromosuccinimide (molar ratio 1:2) in *N*,*N*-dimethylformamide gave a mixture of dibromobiphenylenes. 2,7-Dibromobiphenylene (**25**) (the less soluble isomer) was obtained by fractional crystallization of the mixture. However, it is easier to isolate **25** if the bromination of biphenylene is carried out in two steps, *i.e. via* monobromobiphenylene. The orientation of **25** was proved by treatment with butyllithium and then with methyl iodide, which gave 2,7-dimethylbiphenylene. Oxidation of 2,7-dibromobiphenylene (**25**) with $Mn(OAc)_3$ gave mono(acetoxymethyl) compound **26** and a much lower yield of the bis(acetoxymethyl) compound **27** (Table 4, Entry 3). The structures of **26** and **27** were

Table 3. Oxidations of 2-carboxybiphenylene (**15**) and 2-(methoxycarbonyl)biphenylene (**21**) with $Pb(OAc)_4$ and $Mn(OAc)_3$ in acetic acid at the reflux temperature

Entry	Substrate	Oxidant	Molar ratio	Time / min	Recovered substrate (%)	Product(yield/%)[a]		
						16	**17**	**18**
1	**15**	$Pb(OAc)_4$	1 : 1	30	56[b]	5	4	3
2	**15**	$Pb(OAc)_4$	1 : 2	30	33[b]	4	4	4
3	**15**	$Pb(OAc)_4$	1 : 3	20	23[b]	6	4	4
4	**15**	$Mn(OAc)_3$	1 : 6	50	31[b]	2	2	6
5	**21**	$Pb(OAc)_4$	1 : 2	35	39	10	4	7
6	**21**	$Mn(OAc)_3$	1 : 4	180	51	11	7	4

a) Yields are based on the amount of the substrate used. b) Isolated as methyl ester.

TABLE 4. OXIDATIONS OF 2,3-DIMETHYLBIPHENYLENE (**22**) AND 2,7-DIBROMOBIPHENYLENE (**25**) WITH $Mn(OAc)_3$ AT THE REFLUX TEMPERATURE

Entry	Substrate	Molar ratio of substrate : oxidant : Ac_2O	Recovered substrate (%)	Product (yield/%)[a]
1	**22**	1 : 2 : 100	15	**23**(33), **24**(10)
2	**22**	1 : 4 : 100	0	**23**(4), **24**(14), **8a**(14)[b]
3	**25**	1 : 3.7 : 90	29	**26**(23), **27**(2)
4	**25**	1 : 5.5 : 90	21	**26**(28), **27**(4)

a) Yields are based on the amount of the substrate used. b) Yield was estimated from its ^{1}H-NMR spectrum.

determined by their ^{1}H-NMR spectra. In each experiment, there were many unidentified products which could not be separated.

Discussion

The oxidation of biphenylene (**1**) with $Mn(OAc)_3$ gives a mixture of 2-substituted biphenylenes and an addition product, namely the propellane **28** (0—10% yield).[1] The latter is presumably formed by attack of the $^{\cdot}CH_2COOH$ radical at position 4a of biphenylene, followed by cyclization. The formation of **4** and **5** in the reaction of **1** with $Pb(OAc)_4$ indicates that this acetate also yielded the $^{\cdot}CH_2COOH$ radical in minor quantity, but it could not afford any of the propellane **28**. The reaction of **5** with $Pb(OAc)_4$ gave **4** in a 35% yield, together with 2-(diacetoxymethyl)biphenylene **6** (14%). It seemed that **2** might be a precursor for **3**; therefore, the reaction of **2** with $Pb(OAc)_4$ was also carried out, but it gave **3** (3%) and unchanged **2** (19%). The result indicates that **2** cannot be the major precursor because of the poor yield of **3** from **2**. We hoped that $Mn(OAc)_3$ oxidation of biphenylene containing either electron-donating (CH_3) or electron-withdrawing substituents (COOH, $COOCH_3$, and Br) would give higher yields of propellane. However, we were not able to detect any propellane type of products from the substituted biphenylenes, but we obtained acetoxymethylated-biphenylenes as the major product in each case. Our results show that the incoming groups, OAc and CH_2COOH (and thence CH_2OAc, $CH(OAc)_2$, CHO),[7] always enter at β-positions (2,3,6,7) of the biphenylene nucleus. This is further evidence of the unreactivity of the α-positions (1,4,5,8) towards substitution by free radicals, by electron-transfer mechanism, and by electrophilic reagents. On the other hand, the reactions of **7** and **22** with $Mn(OAc)_3$ occurred at the methyl group rather than in the biphenylene nucleus, giving acetoxymetyl- and formyl-derivatives.

Several reactions have been reported in which X-Y reagents add to biphenylene and give products with ring-enlargement, for example in the reaction of biphenylene with HNO_3 and Ac_2O[8] and in the reaction of methoxybiphenylene with Br_2.[9] However, as far as we know, compound **13a** is the first example of a stable 2,3-adduct isolated from an addition reaction of biphenylene. It has been reported that aliphatic vinyl ether, CH_2=CHOR, reacts with $Pb(OAc)_4$ at room temperature to give diacetate, *e.g.* CH_2=CHOR gives $AcOCH_2CH(OR)OAc$.[10] In 2-methoxybiphenylene (**11**), the $C_{(2)}$-$C_{(3)}$ bond is more like a double-bond than the $C_{(1)}$-$C_{(2)}$ bond is, and the CH_3O-$C_{(2)}$-$C_{(3)}$ system may behave like a vinyl ether. The proposed rearrangement of **13a** to A involves the 1,3-migration of two acetoxyl groups. Similar [3,3] sigmatropic changes have been recorded, *e.g.* the reversible isomerization of 6-acyloxy-2,4-cyclohexadienes into 4-acyloxy-2,5-cyclohexadienes by heating them in chloroform or pyridine.[11] Now the thermal [3,3] sigmatropic rearrangement of allylic acetates proceeds suprafacially *via* a 6-membered transition state;[11] hence the two acetoxyl groups in **13a** must be *cis* as shown.[12] The rearrangement of **13a** into A could take place either in two-steps, *e.g.* *via* **13b**, or in one step *via* simultaneous 1,3-migration of two acetoxyl groups. However both paths (one-step and two-step) have the same stereochemical requirements and lead to the same conclusion concerning the relative stereochemistry of **13a** and A. The intermediate, B, is an enol ether and, as expected,[8] undergoes very rapid acid-catalyzed hydrolysis to the ketone **14**. In conclusion, it was shown that the reaction of biphenylenes having electron-withdrawing groups

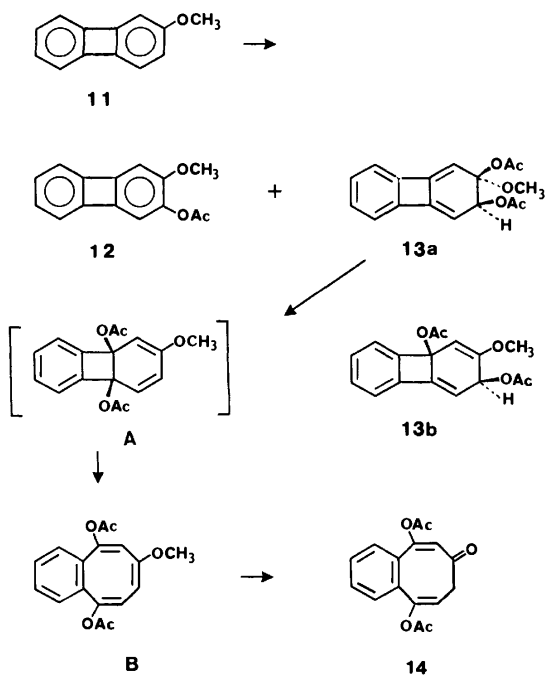

Scheme 1.

with $Mn(OAc)_3$ and $Pb(OAc)_4$ yielded acetoxymethylated derivatives, whereas the methyl group was oxidized in the reaction of methyl substituted biphenylenes. The reaction of 2-methoxybiphenylene with $Pb(OAc)_4$ provided the first example of a stable 2,3-adduct in the addition reaction of biphenylene.

Experimental

The ^{1}H-NMR spectra at 60 MHz and 200 MHz were recorded with a Hitachi-Perkin-Elmer R 24 (or JEOL PMX 60) and with a JEOL FX 200 spectrometer, respectively, with TMS as internal reference. The ^{13}C-NMR spectra at 22.5 MHz were obtained on a JEOL FX 90Q spectrometer. The IR spectra were taken on a JASCO IR A-1 grating spectrometer. The high-resolution Mass spectra were recorded on an A.E.I. MS 902 spectrometer (VG2AB electronics and ion source) with direct inlet at 75 ev. The melting points were determined with a Yanagimoto micro-melting point apparatus and were not corrected.

Oxidation with $Pb(OAc)_4$. The typical procedure for the oxidations of biphenylene[13] and its derivatives was as follows. A mixture of a biphenylene (1 mmol) and $Pb(OAc)_4$ in acetic acid (15 ml) was heated or stirred until the solution became negative to a wet KI-starch paper. The reaction mixture was then diluted with water (15 ml) and extracted with chloroform. After removal of the chloroform *in vacuo*, the resulting mixture was separated on TLC (Wakogel B10) with chloroform as the developing solvent. In the case of the oxidation of 2-carboxybiphenylene, the products were treated with diazomethane in diethyl ether and then separated. Yields are summarized in Tables 1, 2, 3, and 4.

Oxidation Products of Biphenylene (1). 2-Acetoxybiphenylene (**2**), mp 91—92 °C (lit,[5] mp 91—92 °C), 2,3-biphenylenedione (**3**), mp 213—216 °C (from light petroleum) (lit,[14] 216—217 °C), and 2-formylbiphenylene (**4**), mp 80—82 °C (light petrolem) (lit,[15] mp 78—79 °C). The ^{1}H-NMR and IR spectra were identical with those of authentic samples.[1,16]

Oxidation Products of 2-Acetoxymethylphenylene[1] (5). *2-Formylbiphenylene (4)*: **4** (35%) was obtained as a mixture with **5** (28%); the yields were estimated from its ^{1}H-NMR spectrum.

2-(Diacetoxymethyl)biphenylene (6): Mp 154—155 °C (CCl_4); 14%; IR($CHCl_3$) 1760 cm^{-1} (OAc); ^{1}H-NMR ($CDCl_3$) δ=2.00 (6H, s, 2×OAc), 6.5—6.7 (7H, m, aromatic), and 7.42 (1H, s, -CH<); MS *m/z* (rel intensity) 43 (40), 151 (37), 179 (48), 180 (78), 181 (100), 223 (3), and 282.0890 (64, M^+). Calcd for $C_{17}H_{14}O_4$: M, 282.0892.

Oxidation Products of 2-Methylbiphenylene[4] (7). 2-Formylbiphenylene (**4**) and 2-acetoxymethylbiphenylene (**5**) were obtained as a mixture.

Oxidation Products of 2-Methoxybiphenylene[3] (11). *2-Acetoxy-3-methoxybiphenylene (12)*: Mp 125.4—126.4 °C (hexane) (lit,[17] mp 111—112 °C); 5%; IR ($CHCl_3$) 1760 cm^{-1} (OAc); ^{1}H-NMR ($CDCl_3$) δ=2.23 (3H, s, OAc), 3.77 (3H, s, OCH_3), 6.26 (1H, s, $H_{(1)}$ or $H_{(4)}$), 6.40 (1H, s, $H_{(4)}$ or $H_{(1)}$), and 6.2—6.7 (4H, m, $H_{(5)}$-$H_{(8)}$); MS *m/z* (rel intensity) 126.0476 (22), 180.0443 (91), 198.9746 (100), 240.0834 (28, M^+). Calcd for $C_{15}H_{12}O_3$: M, 240.0774.

r-*2*,c-*3-Diacetoxy-2-methoxy-2,3-dihydrobiphenylene (13a)*: Mp 137.5—138.5 °C (methanol); 9%; IR ($CHCl_3$) 1640 (C=C) and 1760 cm^{-1} (OAc); ^{1}H-NMR ($CDCl_3$) δ=2.15 (6H, s, 2×OAc), 3.50 (3H, s, OCH_3), 4.95 (1H, d, *J*=6.0 Hz, -CH<), 6.0 (2H, m, 2×-CH=), and 7.2—7.4 (4H, m, aromatic). The doublet at δ 4.95 collapsed to a singlet on irradiation of the signals at δ 6.0; ^{13}C-NMR ($CDCl_3$) δ=21.126 (2×$OCO\underline{C}H_3$), 55.281 (OCH_3), 96.615 (-CH<), 116.789 (=CH-), 119.000 (=CH-), 127.709 (=CH-), 127.913 (=CH-), 128.594 (=CH-), 128.866 (=CH-), 135.874, 136.044, 145.672, 149.218 153.394, 168.941 ($O\underline{C}OCH_3$), and 169.723 ($O\underline{C}OCH_3$); MS *m/z* (rel intensity, formula) 182.0413 (20, $C_{12}H_6O_2$), 183.0433 (32, $C_{12}H_7O_2$), 197.0589 (30, $C_{13}H_9O_2$), 198.0637 (100, $C_{13}H_{10}O_2$), 199.0704 (20, $C_{13}H_{11}O_2$), 201.0507 (16, $C_{12}H_9O_3$), 215.0721 (35, $C_{13}H_{11}O_3$), 216.0789 (27, $C_{13}H_{12}O_3$), and 258.0941 (10, $C_{15}H_{14}O_4$). Found: C, 67.86; H, 5.41%. Calcd for $C_{17}H_{16}O_5$: C, 67.99; H, 5.37%.

5,10-Diacetoxy-7(8H)-benzocyclooctenone (14): IR (CH_2Cl_2) 1670, 1690, 1725, and 1775 cm^{-1} (OAc); ^{1}H-NMR (200 MHz, $CDCl_3$) δ=2.192 (6H, s, 2×OAc), 2.769 (1H, dd, *J*=12.94 and 10.36 Hz, -$\underline{H}$CH-), 3.019 (1H, ddd, *J*=12.94, 7.42, and 1.71 Hz, -$\underline{H}$CH-), 5.813 (1H, dd, *J*=10.36 and 7.42 Hz, $H_{(9)}$), 6.290 (1H, d, *J*=1.71 Hz, $H_{(6)}$), and 7.492 (4H, m, aromatic); ^{13}C-NMR ($CDCl_3$) δ=20.956 (q, $OCO\underline{C}H_3$), 21.160 (q, $OCO\underline{C}H_3$), 41.162 (t, $-CH_2-$), 115.700 (d, =CH-), 123.457 (d, =CH-), 126.859 (d, =CH-), 128.492 (d, =CH-), 129.206 (d, =CH-), 130.023 (d, =CH-), 133.527 (s, =$\underline{C}$-), 134.071 (s, =$\underline{C}$-), 147.815 (s, =$\underline{C}$-), 156.422 (s, =$\underline{C}$-), 168.125 (s, $O\underline{C}OCH_3$), 169.111 (s, $O\underline{C}OCH_3$), and 197.722 (s, >C=O); MS *m/z* (rel intensity) 43 (100), 128 (17), 156 (23), 157 (20), 159 (86), 160 (76), 174 (22), 184 (24), 202.0622 (51, calcd for $C_{12}H_{10}O_3$: 202.0630), and 244.0738 (25, calcd for $C_{14}H_{12}O_4$: 244.0735).

Oxidation Products of 2-Carboxy-[3] (15) and 2-(Methoxycarbonyl)biphenylene[3] (21). *2-Acetoxymethyl-3-(methoxycarbonyl)biphenylene (16)*: Mp 96.7—97.7 °C (methanol); IR ($CHCl_3$) 1710 (-$COOCH_3$) and 1725 cm^{-1} (OAc); ^{1}H-NMR ($CDCl_3$) δ=2.10 (3H, s, OAc), 3.82 (3H, s, OCH_3), 5.33 (2H, s, $-CH_2O-$), 6.75 (5H, m, $H_{(4)}$-$H_{(8)}$), and 7.12 (1H, s, $H_{(1)}$); MS *m/z* (rel intensity) 43 (11), 151 (18), 179 (17), 207 (100), 239 (10), 282.0899 (37, M^+). Calcd for $C_{17}H_{14}O_4$: M, 282.0892.

2-Acetoxymethyl-6-(methoxycarbonyl)biphenylene (17): Mp 95.5—96.6 °C (methanol); IR ($CHCl_3$) 1710 (-$COOCH_3$) and 1735 cm^{-1} (OAc): ^{1}H-NMR ($CDCl_3$) δ=2.05 (3H, s, OAc), 3.80 (3H, s, OCH_3), 4.88 (2H, s, $-CH_2O-$), 6.5—6.9 (4H, m, $H_{(4)}$, $H_{(5)}$, $H_{(7)}$, and $H_{(8)}$), 7.20 (1H, d, *J*=1.0 Hz, $H_{(1)}$), and 7.52 (1H, dd, *J*=6.0 and 1.0 Hz, $H_{(3)}$); MS *m/z* (rel intensity) 43 (14), 223 (70), 240 (25), and 282.0894 (100, M^+). Calcd for $C_{17}H_{14}O_4$: M, 282.0892.

2-Acetoxy-6-(methoxycarbonyl)biphenylene (18): Mp 134—137 °C (metanol); IR ($CHCl_3$) 1725 (-$COOCH_3$) and 1760 cm^{-1} (OAc); ^{1}H-NMR ($CDCl_3$) δ=2.25 (3H, s, OAc), 3.80 (3H, s, OCH_3), 6.5—6.8 (4H, m, $H_{(4)}$, $H_{(5)}$, $H_{(7)}$, and $H_{(8)}$), 7.20 (1H, d, *J*=1.0 Hz, $H_{(1)}$), and 7.60 (1H, dd, *J*=6.0 and 1.0 Hz, $H_{(3)}$); MS *m/z* (rel intensity) 167 (14), 195 (22), 226.0642 (100, M^+ −42, calcd for $C_{14}H_{10}O_3$: 226.0630), and 268.0733 (13, M^+). Calcd for $C_{16}H_{12}O_4$: M, 268.0735.

Oxidation of 2-Methylbiphenylene (7) with $Mn(OAc)_3$. A mixture of **7** (1 mmol) and $Mn(OAc)_3\,2H_2O$[18] in acetic acid (20 ml) was heated under reflux for the time shown in Table 2 until the color of the Mn(III) ions disappeared. The reaction mixture was worked up in a manner similar to that described in the oxidation with $Pb(OAc)_4$. 2-Formylbiphenylene (**4**) and 2-acetoxymethylbiphenylene (**5**) were obtained as a mixture, yields of which were estimated from the ^{1}H-NMR as shown in Table 2.

2-(Diacetoxymethyl)biphenylene (6): Mp 154—155 °C

2,3-Bis(acetoxymethyl)biphenylene (8a): Mp 88—89 °C (ethanol); IR (CCl_4) 1742 cm^{-1} (OAc); ^{1}H-NMR ($CDCl_3$) δ=2.00 (6H, s, 2×OAc); 4.91 (4, s, 2×$-CH_2O-$), and 6.62 (6H, br. s, aromatic); MS *m/z* (rel intensity) 43 (22), 165 (26), 194 (100), 296.1038 (17, M^+). Calcd for $C_{18}H_{16}O_4$: M, 296.1048.

2,6-Bis(acetoxymethyl)biphenylene (8b): Mp 104—105.5 °C (ethanol); IR ($CHCl_3$) 1742 cm^{-1} (OAc); ^{1}H-NMR (CCl_4) δ=2.00 (6H, s, 2×OAc), 4.74 (4H, s, 2×$-CH_2O-$), 6.56 (6H, m, aromatic); MS *m/z* (rel intensity) 43 (23), 152 (10), 165 (28), 178

(19), 195 (12), 237 (77), 254 (11), and 296.1030 (100, M^+). Calcd for $C_{18}H_{16}O_4$: M, 296.1048.

Preparation of 2,3-Bis(acetoxymethyl)biphenylene (8a). *a) From 2,3-bis(bromomethyl)biphenylene (9)*: A mixture of 2,3-bis(bromomethyl)biphenylene[17] (258 mg) and anhydrous sodium acetate (205 mg) in acetic acid was refluxed for 3 h, then allowed to stand for 60 h. Water (50 ml) was added and the mixture was extracted with toluene (2×25 ml). The toluene was evaporated and the residue was separated by TLC on silica gel with chloroform as eluent. The major component was collected and recrystallized from aqueous ethanol. The product (162 mg, 55%), mp 88—89 °C was identical (IR, ^{1}H-NMR and Mass) with compound **8a**.

b) From 2-acetoxymethyl-3-(methoxycarbonyl)biphenylene (16): A mixture of **16** (60 mg), anhydrous tetrahydrofuran (10 ml), and lithium aluminium hydride (200 mg) was stirred at room temperature for 2 h. After ethyl acetate (1 ml) and 3M (1M=1 mol dm^{-3}) hydrochloric acid (100 ml) had been added to the mixture, it was extracted with ethyl acetate. After removal of the ethyl acetate, the resulting liquid was treated with acetic anhydride (1 ml) in pyridine (1 ml) overnight. The mixture was poured into water and the precipitate was collected, and recrystallized from methanol, giving **8a** (45 mg, 72%), mp 89—90 °C.

Oxidation of 2,6-Diacetylbiphenylene (19) by King's Method.[19] A mixture of 2,6-diacetylbiphenylene[20] (**19**) (460 mg, 2 mmol), iodine (1.1 g, 4 mmol), and pyridine (30 ml) was heated on a steam bath for 1 h, then kept at room temperature for 12 h. The brown precipitate was collected by filtration and washed with water. The solid was boiled for 2 h with water (10 ml) and 10% sodium hydroxide (15 ml), then poured into water (50 ml). The mixture was extracted with diethyl ether to remove non-acidic material. The aqueous solution was acidified with hydrochloric acid and the yellow precipitate was collected and dried at 100 °C. This solid (275 mg) did not melt below 350 °C. A mixture of the solid (250 mg) and boron trifluoride-methanol complex (14% BF_3, 12 ml) in methanol (20 ml) was refluxed for 6 h. The solution was cooled, poured into a saturated aqueous solution of sodium hydrogencarbonate, then extracted with diethyl ether. Evaporation of the ethereal solution gave a yellow solid (130 mg) which was separated by preparative TLC (silica gel) in benzene, the plate being eluted four times to achieve good separation. The band with lowest R_f value gave a yellow solid (6 mg, 1.5%) mp 256 °C identified as 2,6-diacetylbiphenylene (mixed mp and IR spectrum). The middle band gave 2-acetyl-6-(methoxycarbonyl)biphenylene (**20**) as a yellow solid (93 mg, 20% overall), mp 180—181 °C; IR (Nujol mull) 1670 and 1722 cm^{-1}; UV (C_2H_5OH) λ_{max} (log ε) 216 (3.76), 266 (4.32), 279 (4.42), 326^{sh} (3.04), 339^{sh} (3.34), 342 (3.34), 354^{sh} (3.61), 357 (3.62), and 374 nm (3.87); ^{1}H-NMR ($CDCl_3$) δ=2.42 (3H, s, $COCH_3$), 3.79 (3H, s, OCH_3), 6.69 (2H, d, $H_{(4)}$ and $H_{(8)}$), 7.19 (1H, d, $H_{(1)}$), 7.24 (1H, d, $H_{(5)}$), 7.45 (1H, dd, $J_{1,3}$=1.0 and $J_{4,5}$=7.5 Hz, $H_{(3)}$), and 7.58 (1H, dd, $J_{5,7}$=1.0 and $J_{7,8}$=7.5 Hz, $H_{(7)}$). Found: C, 75.98; H, 4.68%. Calcd for $C_{16}H_{12}O_3$: C, 76.19; H, 4.76%. The band with the highest R_f value gave 2,6-bis(methoxycarbonyl)biphenylene (**10**) (30 mg, 6% overall) as a yellow solid, mp 210—212 °C (lit,[21] mp 223—225 °C); IR (Nujol mull) 852, 902, and 1715 cm^{-1}; UV (C_2H_5OH) λ_{max} log ε) 216 (4.16), 262^{sh} (4.67), 269 (4.75), 277^{sh} (4.62), 322^{sh} (3.25), 330^{sh} (3.38), 334 (3.51), 338 (3.52), 347 (3.78), 3.52 (3.79), and 369 nm (3.98); ^{1}H-NMR ($CDCl_3$) δ=3.77 (6H, s, 2×OCH_3), 6.76 (2H, d, $H_{(4)}$ and $H_{(8)}$), 7.31 (2H, d, $H_{(1)}$ and $H_{(5)}$), and 7.65 (2H, dd, $J_{1,3}$=1.0 and $J_{3,4}$=7.5 Hz, $H_{(3)}$ and $H_{(7)}$).

Preparation of 2,6-Bis(acetoxymethyl)biphenylene (8b). *a) From 2,6-bis(methoxycarbonyl)biphenylene[21] (10)*: 2,6-Bis-(methoxycarbonyl)biphenylene (100 mg), when reduced and acetylated in a manner similar to the above, yielded **8b** (86 mg, 78%), mp 105—106.4 °C.

b) From 2-acetoxymethyl-6-(methoxycarbonyl)biphenylene (17): 2-Acetoxymethyl-6-(methoxycarbonyl)biphenylene (**17**) (80 mg) was similarly treated with lithium aluminium hydride and then acetic anhydride to give **8b** (40 mg, 47%), mp 104—106 °C.

Preparation of 2-Acetoxy-6-(methoxycarbonyl)biphenylene (18) from 2-Acetyl-6-(methoxycarbonyl)biphenylene (20). A mixture of **20** (10.4 mg) and *m*-chloroperbenzoic acid (22 mg) in deuteriochloroform (0.3 ml) was kept at 36 °C for 6.5 h. The reaction mixture was passed through a short alumina column eluting with chloroform. After removal of the chloroform, the resulting solid was recrystallized from methanol, giving **18** (7.6 mg, 69%), mp 147—148 °C.

Oxidation of 2,3-Dimethylbiphenylene[4] (22) with Mn(OAc)$_3$. A mixture of **22** (170 mg, 0.94 mmol) and $Mn(OAc)_3 2H_2O$ (500 mg, 1.86 mmol) in acetic acid (20 ml) and acetic anhydride (10 ml) was heated under reflux until the brown color of the solution had changed to yellow. Water (150 ml) was added and the mixture was allowed to stand overnight. The mixture was extracted with toluene (2×100 ml). The toluene extracts were evaporated to dryness. TLC on silica gel, with chloroform as eluent, showed two components, whose R_f values were 0.75 and 0.59, and a third component, R_f 0.55 (visible under UV light), which overlapped the component with R_f value 0.59. The mixture was partially separated on a column of silica gel (35 g) using chloroform as eluent. The fractions corresponding to R_f values 0.59—0.55 were separated by chromatography several times on TLC plates (0.5 mm thickness of silica gel). The compound with R_f value 0.75 was unchanged compound **22**.

When the experiment was repeated using 1.01 g instead of 500 mg of $Mn(OAc)_3$, a new component (with R_f value 0.38) was obtained. The results are summarized in Table 4.

2-Acetoxymethyl-3-methylbiphenylene (23): R_f value 0.59; mp 62—64 °C (from aqueous ethanol); ^{1}H-NMR ($CDCl_3$) δ= 2.02 (3H, s, OAc), 2.10 (3H, s, CH_3), 4.82 (2H, s, -CH_2O-), and 6.30—6.80 (6H, m, aromatic); MS *m/z* (rel intensity) 165 (12), 178 (100), 179 (60), 238.0976 (45, M^+). Calcd for $C_{16}H_{14}O_2$: M, 238.0994.

2-Formyl-3-methylbiphenylene (24): R_f value 0.55; mp 141—143 °C (lit,[4] 136—138 °C), identified by its ^{1}H-NMR spectrum.[4]

2,3-Bis(acetoxymethyl)biphenylene (8a): R_f value 0.38; This was not obtained pure, but its ^{1}H-NMR spectrum (apart from impurities) was identical with that of an authentic sample.

Preparation of 2,7-Dibromobiphenylene (25). (In collaboration with Dr. M. E. Cracknell) A mixture of biphenylene (4.57 g) and *N*-bromosuccinimide (4.50 g) in dry *N,N*-dimethylformamide (50 ml) was stirred at room temperature for 3 h. The mixture was diluted with water (100 ml) and stirred for 3 h more. The crude product was collected, dried, and sublimed at 90 °C/0.5 mmHg (1 mmHg≈133.322 Pa) and gave 2-bromobiphenylene (5.55 g, 80%) as yellow crystals, mp 63—65 °C (lit,[20] mp 64—65 °C). A mixture of 2-bromobiphenylene (2 g) and *N*-bromosuccinimide (1.54 g) in *N,N*-dimethylformamide (50 ml) was stirred at room temperature for 20 h. The mixture was poured into ice water, and the solid was collected and dried in a vacuum desiccator. The crude product was fractionally crystallized from methanol and gave 2,7-dibromobiphenylene (**25**) (0.28 g, 10%) as yellow plates, mp 137—138 °C; ^{1}H-NMR ($CDCl_3$) δ=6.37 (2H, dd, $H_{(4)}$ and $H_{(5)}$), 6.65 (2H, m, $J_{1,3}$=1.2 and $J_{1,4}$= 0.8 Hz, $H_{(1)}$ and $H_{(8)}$), and 6.83 (2H, dd, $J_{3,4}$=6.8 Hz, $H_{(3)}$, $H_{(6)}$). Found: C, 46.39; H, 2.13%. Calcd for $C_{12}H_6Br_2$: C, 46.49; H, 1.95%.

Conversion of 2,7-Dibromobiphenylene (25) into 2,7-Dimethylbiphenylene. 2,7-Dibromobiphenylene (1 g) was dissolved in sodium-dried diethyl ether (40 ml) and cooled to 0

°C under an atmosphere of nitrogen. Butyllithium (10 ml) was added and the solution was stirred for 5 min. Methyl iodide (4.6 g) was added to the solution, giving some precipitates. The uncovered reaction mixture was left stirring overnight. Water was added and the solution was extracted with diethyl ether. The organic layer was washed with a saturated solution of sodium chloride and dried over anhydrous sodium sulfate. The solution was filtered and then the solvent was evaporated off. The resulting solid was recrystallized from ethanol to give 2,7-dimethylbiphenylene (197 mg, 34%), mp 113—114 °C (lit,[22] mp 115 °C). The ^{1}H-NMR spectrum was identical with that reported.

Oxidation of 2,7-Dibromobiphenylene (25) with Mn(OAc)$_3$. A mixture of **25** (340 mg) and $Mn(OAc)_32H_2O$ (1.08 g) in acetic acid (20 ml) and acetic anhydride (9.3 ml) was heated under reflux until the color of the solution had changed from brown to yellow. The products were isolated and separated as described for the oxidation of 2,3-dimethylbiphenylene. The experiment was repeated using 1.62 g in place of 1.08 g $Mn(OAc)_32H_2O$. The yields for both experiments are shown in Table 4.

2-Acetoxymethyl-3,6-dibromobiphenylene (26): Mp 133—134 °C (ethanol); ^{1}H-NMR δ=2.14 (3H, s, CH_3), 5.01 (2H, s, -CH_2O-), 6.55 (1H, dd, $H_{(8)}$), 6.72 (1H, d, $J_{1,4}$=0.4 Hz, $H_{(1)}$), 6.79 (1H, dd, $J_{5,7}$=1.5 and $J_{5,8}$=0.7 Hz, $H_{(5)}$), 6.87 (1H, br. s, $H_{(4)}$), and 6.97 (1H, dd, $J_{7,8}$=7.4 Hz, $H_{(7)}$). Found: C, 47.59; H, 2.82: Br, 41.56%. Calcd for $C_{15}H_{10}Br_2O_2$: C, 47.16; H, 2.64; Br, 41.83%.

2,7-Bis(acetoxymethyl)-3,6-dibromobiphenylene (27): Mp153—154 °C (ethanol); ^{1}H-NMR ($CDCl_3$) δ=2.08 (6H, s, 2×CH_3), 4.97 (4H, s, 2×-CH_2O-), 6.67 (2H, s, $H_{(1)}$ and $H_{(8)}$), and 6.77 (2H, s, $H_{(4)}$ and $H_{(5)}$); MS *m/z* (rel intensity) 43 (27), 163 (11), 209 (11), 331 (98), 332 (19), 333 (100), 334 (18), 395 (18), 452 (18, M^+), 453.9235 (45, M^+), and 456 (19, M^+). Calcd for $C_{18}H_{14}O_4$ $^{79}Br^{81}Br$: M, 453.9238.

We are indepted to Dr. B. E. Ayres for performing the oxidation of 2,6-diacetylbiphenylene.

References

1) K. Kurosawa and J. F. W. McOmie, *Bull. Chem. Soc. Jpn.*, **54**, 3877 (1981).
2) E. I. Heiba, R. M. Dessau, and W. J. Koehl, Jr., *J. Am. Chem. Soc.*, **90**, 2706 (1968).
3) W. Baker, M. P. V. Boarland, and J. F. W. McOmie, *J. Chem. Soc.*, **1954**, 1476.
4) P. R. Buckland and J. F. W. McOmie, *Tetrahedron*, **33**, 1797 (1977).
5) J. M. Blatchly, D. V. Gardner, and J. F. W. McOmie, *J. Chem. Soc. (C)*, **1967**, 272.
6) U. E. Matter, C. Pascual, E. Pretsch, A. Pross, W. Simon, and S. Sternhell, *Tetrahedron*, **25**, 691 (1969).
7) E. I. Heiba, R. M. Dessau, and W. J. Koehl, Jr., *J. Am. Chem. Soc.*, **91**, 138 (1969).
8) J. W. Barton and K. E. Whitaker, *J. Chem. Soc. (C)*, **1968**, 1663.
9) H. Kidokoro, M. Sato, and S. Ebine, *Chem. Lett.*, **1981**, 1269; *Bull. Chem. Soc. Jpn.*, **55**, 3204 (1982).
10) R. Criegee, P. Dimroth, K. Noll, R. Simon, and U. Weis, *Chem. Ber.*, **90**, 1070 (1957).
11) D. H. R. Barton, P. D. Magnus, and M. J. Pearson, *J. Chem. Soc. (C)*, **1971**, 2231.
12) Structures **13a** and A show the relative stereochemistry of the asymmetric carbon atoms. Compound **13a** is obtained in the racemic form.
13) F. M. Logullo, A. H. Seitz, and L. Friedman, *Org. Synth.*, Coll. Vol., V, 54 (1973).
14) J. M. Blatchly, J. F. W. McOmie, and S. D. Thatte, *J. Chem. Soc.*, **1962**, 5090.
15) J. F. W. McOmie and S. D. Thatte, *J. Chem. Soc.*, **1962**, 5298.
16) M. Sato, H. Fujino, S. Ebine, and J. Tsunetsugu, *Bull. Chem. Soc. Jpn.*, **50**, 3076 (1977).
17) P. R. Buckland, N. P. Hacker, and J. F. W. McOmie, *J. Chem. Soc., Perkin Trans. 1*, **1983**, 1443.
18) P. J. Andrulis, Jr., M. J. S. Dewar, R. Dietz, and L. Hunt, *J. Am. Chem. Soc.*, **88**, 5473 (1966).
19) L. C. King, *J. Am. Chem. Soc.*, **66**, 894 (1944).
20) W. Baker, J. W. Barton, and J. F. W. McOmie, *J. Chem. Soc.*, **1958**, 2666.
21) A. Recca and J. K. Stille, *Macromolecules*, **11**, 79 (1978).
22) P. R. Constantine, G. E. Hall, C. R. Harrison, J. F. W. McOmie, and R. J. G. Searle, *J. Chem. Soc (C)*, **1966**, 1767.

Asymmetric Hydrogenation Catalyzed by (Achiral Base)bis(dimethylglyoximato)cobalt(II)-Chiral Cocatalyst System[1)]

Seiji TAKEUCHI* and Yoshiaki OHGO
Niigata College of Pharmacy, 5829 Kamishinei-cho, Niigata 950-21
(Received November 28, 1983)

Chiral tertiary amines with a secondary amide group at α- or β-carbon were prepared, and an asymmetric hydrogenation of methyl 2-(acetylamino)acrylate and *N,N'*-dimethyl-5-benzylidenehydantoin catalyzed by achiral base-coordinated bis(dimethylglyoximato)cobalt(II)-chiral cocatalyst system was examined by using each of them as the cocatalyst. The enantiomeric excess of *N,N'*-dimethyl-5-benzylhydantoin reached 79.1% with (*S*)-*N*-[(*R*)-1-phenylethyl]-2-quinuclidinecarboxamide as the cocatalyst. Remarkable differences were observed in the enantioselectivities between the two substrates for the same cocatalysts. Discussion about the conformations of the cocatalysts and substrates led to proposed models of chirality-recognizing transition states.

The authors have previously reported the asymmetric hydrogenation catalyzed by the achiral base-coordinated bis(dimethylglyoximato)cabalt(II)-chiral base(cocatalyst) system(hereafter abbreviated as Co(dmgH)$_2$·B-B*; B and B* are achiral and chiral bases respectively). Co(dmgH)$_2$·B-quinine resulted in high optical yields (up to 78%) for α-diketones such as benzil, but in low optical yields (up to 19%) for dehydro amino acid derivatives. A hydrogen bond between the hydroxyl group of cocatalyst(quinine) and the carbonyl group of substrate(benzil) in the chirality-recognizing transition state extremely enhances the enantioselectivity of this system.[2)]

In the preceding paper, the authors reported the asymmetric hydrogenation of methyl 2-(acetylamino)-acrylate with 34.5%ee(enantiomeric excess) using (2*S*, 3*S*)-2-acetoxy-3-dimethylamino-3-pheny-*N*-[(*R*)-1-phenylethyl]propionamide as the cocatalyst and deduced that the hydrogen bond between the amide groups of the substrate and cocatalyst acts as an attractive force to enhance the enantioselectivity.[3)]

Here, we would like to describe the preparation of other new cocatalysts and the asymmetric hydrogenation of 2-(acetylamino)acrylate and *N,N'*-dimethyl-5-benzylidenehydantoin using them as the cocatalysts.

Results and Discussion

Preparation of Cocatalysts. Four diastereoisomers of 2-acetoxy-3-dimethylamino-3-phenyl-[(*S*)-1-phenylethyl]propionamide [**12**(DHP-*OAc*-(2*R*,3*R*)*S*), **13**(DHP-*OAc*-(2*S*,3*S*)*S*), **14**(DHP-*OAc*-(2*R*,3*S*)*S*), and **15**(DHP-*OAc*-(2*S*,3*R*)*S*)] were prepared from (*S*)-1-phenylethylammonium 2,3-epoxy-3-phenylpropionate by the route shown in Scheme 1. Four enantiomers of them [**12'**(DHP-*OAc*-(2*S*,3*S*)*R*), **13'**(DHP-*OAc*-(2*R*, 3*R*)*R*), **14'**(DHP-*OAc*-(2*S*,3*R*)*R*), and **15'**(DHP-*OAc*-(2*R*,3*S*)*R*)] were prepared from (*R*)-1-phenylethyl-

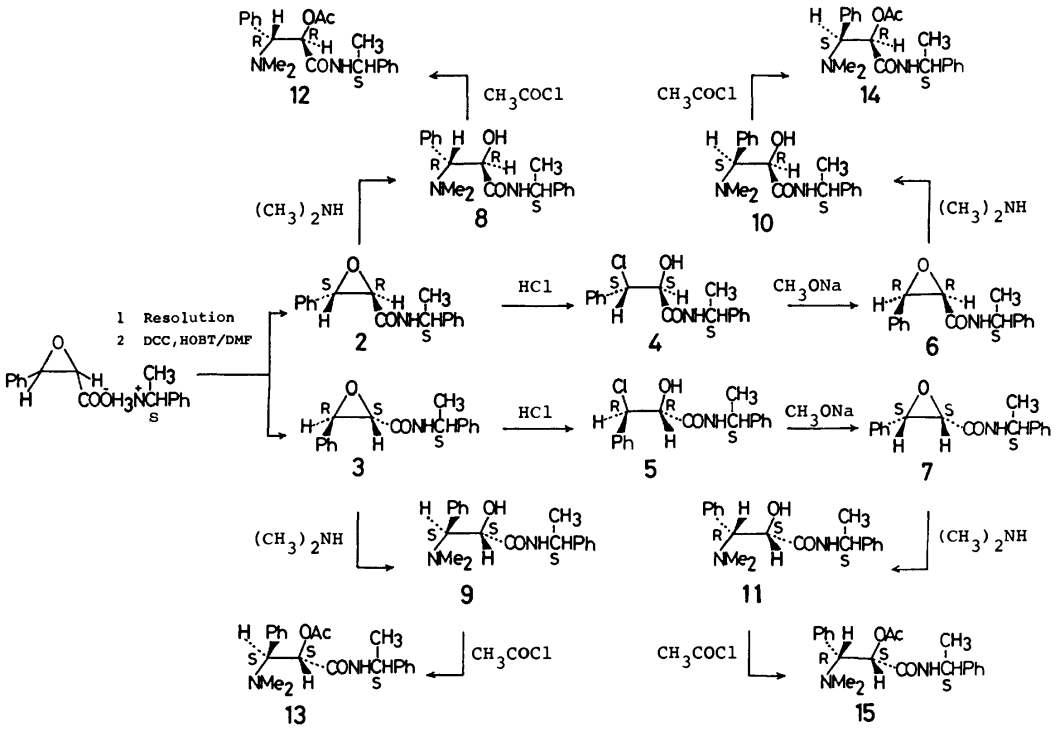

Scheme 1.

ammonium 2,3-epoxy-3-phenylpropionate by the same procedures (each enantiomer of the compounds in Scheme 1 is expressed as the same number with prime). O-Benzoyl derivative DHP-*OBz*-(2*S*,3*S*)*R* was obtained by benzoylation of **8′**.

Two diastereoisomers of *N*-[(*R*)-1-phenylethyl]-2-quinuclidinecarboxamide [**18**(QC-(*S*)*R*) and **19**(QC-(*R*)*R*)] were prepared from (*S*)- and (*R*)-2-quinuclidinecarboxylic acids (**16** and **17**, respectively) by the route shown in Scheme 2.

(Details are described in the Experimental section).

Asymmetric Hydrogenation of Methyl 2-(acetylamino)-acrylate and N,N′-Dimethyl-5-Benzylidenehydantoin with $Co(dmgH)_2$·B-chiral Amino Amides. The asymmetric hydrogenation of methyl 2-(acetylamino)acrylate and *N,N′*-dimethyl-5-benzylidenehydantoin with $Co(dmgH)_2$·B-B* was carried out in benzene under an atmospheric pressure of hydrogen at room temperature.

The chiral α- and β-amino amides prepared above were used as the cocatalysts(B*), and quinine and (*S*)-

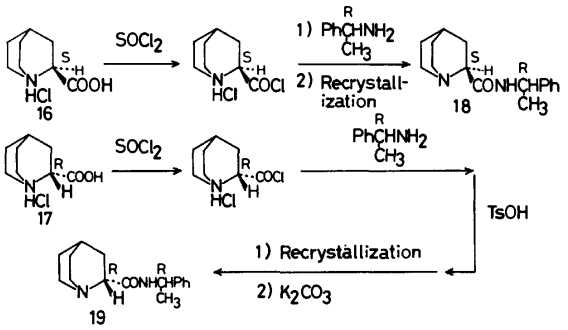

Scheme 2.

Table 1. The asymmetric hydrogenation of 2-(acetylamino)acrylate with $Co(dmgH)_2$·PPh_3-chiral amino amides[a]

Run	B*	Methyl *N*-acetylalaninate			
		Yield/%	$[\alpha]_D$/°	Config.[b]	% e.e.[c]
1	DHP-*OAc*-(2*S*,3*R*)*R*	60.0	+2.4	*R*	2.6
2	DHP-*OAc*-(2*R*,3*S*)*S*	45.5	−0.5[d]	*S*	0.5
3	DHP-*OAc*-(2*R*,3*S*)*R*	59.3	−0.9	*S*	1.0
4	DHP-*OAc*-(2*S*,3*R*)*S*	43.6	+0.6	*R*	0.7
5	DHP-*OAc*-(2*S*,3*S*)*S*	53.3	+31.3	*R*	34.1
6	DHP-*OAc*-(2*R*,3*R*)*R*	48.6	−33.4	*S*	36.4
7	DHP-*OAc*-(2*S*,3*S*)*R*	45.5	+31.6	*R*	34.5
8	DHP-*OAc*-(2*R*,3*R*)*S*	40.7	−36.0	*S*	39.3
9	DHP-*OBz*-(2*S*,3*S*)*R*	45.5	+39.7	*R*	43.3
10	QC-(*S*)*R*	45.5	+38.0	*R*	41.4
11	QC-(*R*)*R*	65.3	−38.7	*S*	42.2

a) The molar ratio of substrate to cobalt was 10 : 1, while those of PPh_3, the chiral amino amide and its hydrochloride to cobalt were all 1 : 1. Solvent was benzene. b) Configuration. c) See Reference 4). d) Optically pure *S* isomer: $[\alpha]_D$ −91.7° (*c* 2, water).

Table 2. The asymmetric hydrogenation of *N,N′*-dimethyl-5-benzylidenehydantion with $Co(dmgH)_2$·B-chiral bases[a]

Run	B	B*	*N,N′*-dimethyl-5-benzylhydantoin			
			Yield/%	$[\alpha]_D$/°	Config.[b]	% e.e.[c]
1	BA	Quinine	93.0	−12.7	*S*	14.8
2	PPh_3	Quinine	91.0	−49.4	*S*	57.4
3	PPh_3	Pha-*S,R*[d]	93.5	−0.8	*S*	0.9
4	PPh_3	Pha-*S,S*	93.5	−2.0	*S*	2.3
5	PPh_3	DHP-*OAc*-(2*R*,3*S*)*S*	94.4	−10.0	*S*	11.6
6	PPh_3	DHP-*OAc*-(2*S*,3*R*)*S*	95.0	+10.0	*R*	11.6
7	PPh_3	DHP-*OAc*-(2*R*,3*R*)*R*	91.5	+31.9	*R*	37.1
8	PPh_3	DHP-*OAc*-(2*R*,3*R*)*S*	93.5	+35.5	*R*	41.3
9	PPh_3	DHP-*OBz*-(2*S*,3*S*)*R*	91.0	−37.0	*S*	43.0
10	BA	QC-(*S*)*R*	98.0	−15.6	*S*	18.1
11	PPh_3	QC-(*S*)*R*	93.0	−68.0	*S*	79.1
12	PPh_3	QC-(*R*)*R*	96.5	+60.7	*R*	70.6

a) The molar ratio of substrate to cobalt was 9.3 : 1, while those of PPh_3, BA, the chiral bases and their hydrochlorides to cobalt were all 1 : 1. Solvent was benzene. b) Configuration. c) Optical purity. d) $PhCH_2$-$\overset{S}{C}H(N(CH_3)_2)$-CONH$\overset{R}{C}H(CH_3)$Ph.

N^{α},N^{α}-dimethyl-*N*-[(*R*)-1-phenylethyl]phenylalaninamide(Pha-*S*,*R*) were also used as B* for comparison in the case of *N*,*N*′-dimethyl-5-benzylidenehydantoin. Benzylamine(BA) and triphenylphosphine(PPh_3) were used as the achiral bases(B).

As the specific rotation of enantiomerically pure *N*,*N*′-dimethyl-5-benzylhydantoin was unknown, the enantiomeric excesses shown in Table 2 were determined by the method described in the Experimental section.

The results of the asymmetric hydrogenation are summarized in Table 1 and Table 2.

As can be seen in Table 1, the enantiomeric excesses[4] in runs 5—9 are much higher than those in runs 1—4, and the enantioselectivities are affected by the configurations of the C-2 and C-3 chiral centers of DHP-*OAc* and DHP-*OBz* (the cocatalysts are erythro isomers in runs 5—9 and threo isomers in runs 1—4) but are little affected by that of the chiral center of 1-phenylethylamine moiety.

The most stable conformations of the erythro and the threo isomers may exist as shown in Fig. 1.

In the chirality-recognizing step (*i.e.*, the protonation by the protonated chiral cocatalyst to the carbanion formed through the hydrogenation with $Co(dmgH)_2 \cdot B$[2]), a hydrogen bonding between the amide group of cocatalyst and the functional group of carbanion is possible in the erythro isomer but not in the threo isomer, since in the threo isomer the protonated dimethylamino group and the amide group exist in anti position and cannot interact with the carbanion simultaneously. This explains the difference between enantioselectivity in runs 5—9 and runs 1—4.

As can be seen in Table 2, the enantiomeric excess of *N*,*N*′-dimethyl-5-benzylhydantoin reached 79.1% (run 11), which is the highest value so far attained in the asymmetric hydrogenation of olefinic compounds with $Co(dmgH)_2 \cdot B$-B* system. The configuration of the predominant isomer in every case coincides with that of the chiral center bearing a tertiary amino group of the cocatalyst and the enantioselectivity is not so largely affected by the configuration of the 1-phenylethylamine moiety.

A comparison of Tables 1 and 2 shows that the configurations of *N*,*N*′-dimethyl-5-benzylhydantoin in runs 7, 8, 9, 11 and 12 of Table 2 are opposite to those of methyl *N*-acetylalaninate in runs 6, 8, 9, 10 and 11 of Table 1, respectively, and the enantioselectivities are remarkably increased in runs 11 and 12 of Table 2. The reason for the difference in the enantioselectivity

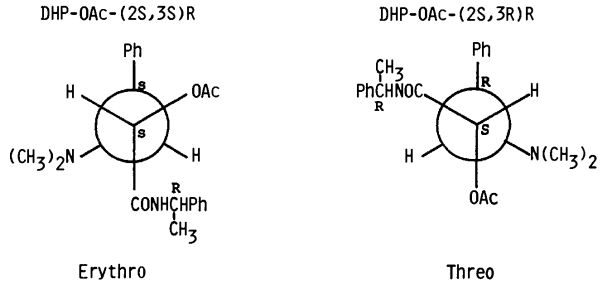

Fig. 1. Conformations of DHP-*OAc*.

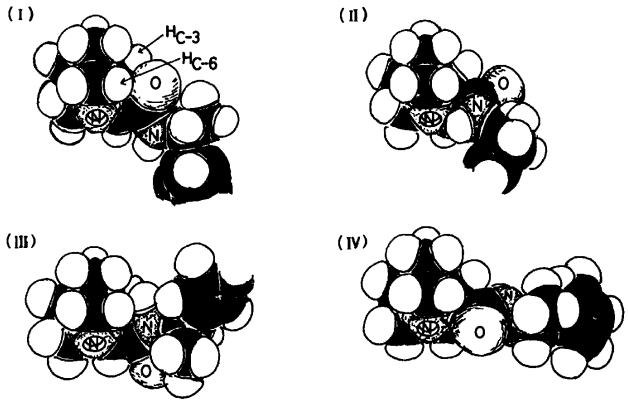

Fig. 2. Conformations of QC-(*S*)*R*.

between the two substrates will be discussed below in the cases of run 10 of Table 1 and run 11 of Table 2.

As the enantioselective recognition is made through the protonation to the carbanions formed from the two substrates by the protonated QC-(*S*)*R*, it is necessary to discuss the interactions between the conformers of the protonated QC-(*S*)*R* and the carbanions. The conformations of QC-(*S*)*R* and the carbanions were considered with CPK's space-filling models.

As C=O and N-H of amide group lie in coplanar anti position, the possible conformers of QC-(*S*)*R* are shown in Fig. 2.

The conformer **III** is very unstable because of a large steric repulsion between the hydrogen atoms attached to C-3 and C-6 of the quinuclidine ($H_{C\text{-}3}$ and $H_{C\text{-}6}$, respectively) and that of N-H of amide group (N-**H**). The conformer **II** and the protonated conformer **IV** are stable because of intramolecular hydrogen bonds (between N-**H** and the nitrogen atom of quinuclidine, and between the carbonyl oxygen and the hydrogen attached to the nitrogen atom of quinuclidine, respectively) and because of small steric repulsions between $H_{C\text{-}3}$, $H_{C\text{-}6}$ and the amide group. Their stabilities, however, will decrease their proton-accepting and proton-donating activities respectively, and will moreover lower their abilities to make an intermolecular hydrogen bond. The protonated conformer **I** (HQC-(*S*)*R*-I) is relatively stable because the steric repulsion between $H_{C\text{-}3}$, $H_{C\text{-}6}$ and the carbonyl oxygen is not so large, and thus can make an intermolecular hydrogen bond between N-**H** of HQC-(*S*)*R*-I and the carbonyl oxygen of the carbanions (the intramolecular hydrogen bonding is impossible).

Therefore, HQC-(*S*)*R*-I is regarded as the best conformer with which to determine the chirality of the carbanions through the intermolecular hydrogen bond in the protonation step.

The possible conformations of the carbanions of (*S*)-*N*,*N*′-dimethyl-5-benzylhydantoin ((*S*)-$DMBH_a$ and (*S*)-$DMBH_b$) and methyl (*R*)-*N*-acetylalaninate ((*R*)-AA) are shown in Fig. 3.

The conformer (*S*)-$DMBH_a$ is more stable irrespective of the relatively large steric repulsion between the hydantoin and benzene rings and is more likely to react with HQC-(*S*)*R*-I than (*S*)-$DMBH_b$, because the electrostatic repulsion between the lone pair on the asym-

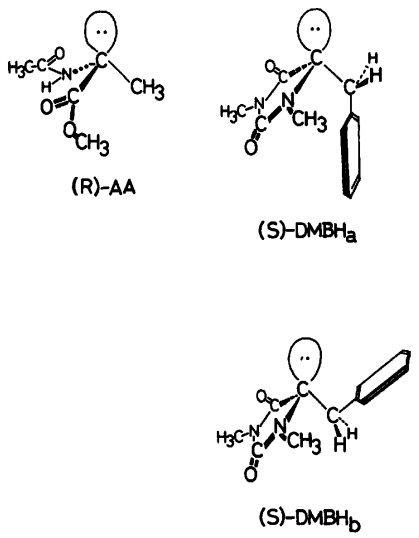

Fig. 3. Conformations of (*R*)-*N*-acetylalaninate and (*S*)-*N*,*N*′-dimethyl-5-benzylhydantoin.

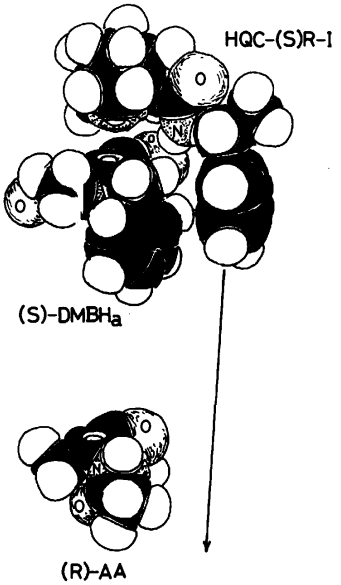

Fig. 4. Models of the protonation by HQC-(*S*)*R*-I to (*S*)-$DMBH_a$ and (*R*)-AA.

metric carbon atom of (*S*)-$DMBH_b$ and the π-electron on the benzene ring is more serious and/or the benzene ring of (*S*)-$DMBH_b$ prevents HQC-(*S*)*R*-I from approaching to the reaction center of (*S*)-$DMBH_b$.

As shown in Fig. 4, HQC-(*S*)*R*-I can approach (*S*)-$DMBH_a$ to make the intermolecular hydrogen bond between N-**H** of HQC-(*S*)*R*-I and the C-4 carbonyl oxygen of (*S*)-$DMBH_a$ without any substantial overlap of their substituents (in Fig. 4, the hydrogen atom attached to the nitrogen atom of quinuclidine and the lone pair on the asymmetric carbon atom of (*S*)-$DMBH_a$ and (*R*)-AA are not depicted for convenience).

On the other hand, if HQC-(*S*)*R*-I approaches (*R*)-$DMBH_a$ without the overlap of their substituents, the intermolecular hydrogen bonding becomes impossible.

Consequently, HQC-(*S*)*R*-I can selectively protonate (*S*)-$DMBH_a$ to give (*S*)-*N*,*N*′-dimethyl-5-benzylhydantoin predominantly with relatively high enantioselectivity.

As can be seen in Fig. 4, HQC-(*S*)*R*-I can approach (*R*)-AA to make the intermolecular hydrogen bond between N-**H** of HQC-(*S*)*R*-I and the carbonyl oxygen of ester group of (*R*)-AA without any substantial overlap of their substituents (if HQC-(*S*)*R*-I in Fig. 4 is shifted in the direction of the arrow and is so placed as to make the hydrogen bond, a plausible model of the transition state of protonation to (*R*)-AA by HQC-(*S*)*R*-I will be made). HQC-(*S*)*R*-I can also approach (*S*)-AA to make the hydrogen bond without a significant overlap of their substituents. However, the approach of HQC-(*S*)*R*-I may occur preferentially to (*R*)-AA rather than to (S)-AA, since the space between $COOCH_3$ and $NHCOCH_3$ is larger than that between CH_3 and $COOCH_3$.

This may explain the opposite and lower enantioselectivity in run 10 of Table 1 in comparison with that of run 11 of Table 2.

Experimental

The melting points were determined by Yanagimoto micro-melting point apparatus and were uncorrected. The IR spectra were recorded on a JASCO A-3 spectrometer. The ^1H NMR spectra were obtained on JEOL-FX 200 spectrometer. The optical rotations were measured with a Perkin Elmer 241 polarimeter.

Preparation of Stereoisomers of DHP-OAc and DHP-OBz. As the preparations of **12** and **12′** were described in the preceding paper,[3] the preparation procedures of the other three diastereoisomers and their enantiomers are described below.

*(2R,3S)-2,3-Epoxy-3-phenyl-*N*-[(R)-1-phenylethyl]propionamide (3′) and Its Enantiomer (3).* Starting from 72.1 g of ethyl 2,3-epoxy-3-phenylpropionate, 40.0 g of crystalline (*R*)-1-phenylethylammonium (2*S*,3*R*)-2,3-epoxy-3-phenylpropionate was obtained by Harada's method.[5] The filtrate which contained (*R*)-1-phenylethylammonium (2*R*,3*S*)-2,3-epoxy-3-phenylpropionate(**1′**) was concentrated to dryness *in vacuo* to afford 34.0 g of sirupy residue. This was dissolved in DMF (200 ml) and to the solution was added a solution of DCC (24.6 g, 119 mmol) and 1-hydroxybenzotriazole (16.0 g, 119 mmol) in DMF (150 ml) during 1.5 h on ice-cooling with stirring. Stirring was continued overnight at room tempetature. After filtration of the precipitate, the filtrate was concentrated *in vacuo* at 30—40 °C. The residue was dissolved in ethyl acetate (*ca.* 1300 ml), and the solution was washed successively with a 10% citric acid solution (200 ml), a 4% sodium hydrogencarbonate solution (200 ml), and a sodium chloride solution (300 ml) and then dried (Na_2SO_4). The solution was concentrated to 150—200 ml and the crystals which separated out were dissolved thoroughly on heating. To the solution petroleum ether was added carefully. Crystals (prisms, 17.1 g) were obtained: $[\alpha]_D^{17.5}$ −2.1°; $[\alpha]_{365}^{17.5}$ +46.2° (*c* 0.999, $CHCl_3$).

Its enantiomer(**3**) was likewise prepared from the sirupy residue (33.8 g) containing **1** to give 12.7 g of crystals (prisms): $[\alpha]_D^{25.5}$ +1.6°; $[\alpha]_{365}^{25.5}$ −47.9° (*c* 0.988, $CHCl_3$).

*(2S,3S)-3-Dimethylamino-2-hydroxy-3-phenyl-*N*-[(S)-1-phenylethyl]propionamide (9) and Its Enantiomer (9′).* A suspension of **3** (5.0 g) in a 50% aqueous dimethylamine solution (200 ml) was stirred for 2.5 h at room temperature. The homogeneous solution obtained was evaporated *in vacuo*. A crystalline mass was separated out when water began to evaporate and then was filtered off after water was

added to the solution. After drying, the crystals (5.7 g) were recrystallized from benzene to give 4.2 g of needles: $[\alpha]_D^{20.0}$ −56.1° (*c* 1.016, $CHCl_3$).

Its enantiomer was likewise prepared from **3′** (7.0 g) to give 2.47 g (first crop) and 4.36 g (second crop) of crystals (needles): $[\alpha]_D^{26.0}$ +54.2° (*c* 0.994, $CHCl_3$) and $[\alpha]_D^{21.0}$ +56.1° (*c* 1.007, $CHCl_3$), respectively.

(2S,3S)-2-Acetoxy-3-dimethylamino-3-phenyl-N-[(S)-1-phenylethyl]propionamide (13) and Its Enantiomer (13′). To a solution of **9** (3.8 g, 12.2 mmol) in dry ethyl acetate (200 ml) was added acetyl chloride (1.0 g, 12.2 mmol). The solution was allowed to stand overnight at room temperature. The amorphous solid which separated out was dissolved in water after ethyl acetate was decanted. The aqueous solution was washed with ether, and the aqueous layer was made basic with a sodium hydrogencarbonate solution. The solution was extracted with ethyl acetate. The ethyl acetate layer was dried(Na_2SO_4) and concentrated to yield 3.7 g of crystalline material. This was recrystallized from ethyl acetate-petroleum ether to give 3.23 g of needles: $[\alpha]_D^{27.5}$ −66.8° (*c* 1.003, $CHCl_3$).

Its enantiomer was likewise prepared from **9′** (5.0 g) to give 3.97 g of needles: $[\alpha]_D^{27.0}$ +66.6° (*c* 0.998, $CHCl_3$).

(2S,3S)-3-Chloro-2-hydroxy-3-phenyl-N-[(S)-1-phenylethyl]propionamide (4) and Its Enantiomer (4′). Into a solution of **2** (1.2 g) in 1000 ml of dry benzene was bubbled dry hydrogen chloride gas for 30 min at room temperature with stirring. Stirring was continued for 1 h and then concentrated to dryness to yield 1.2 g of crystalline material.[6] 14.4 g of the crystalline material thus obtained was recrystallized from ethyl acetate (150 ml)- petroleum ether (158 ml) to give 7.7 g of needles: $[\alpha]_D^{20.0}$ +40.8° (*c* 0.500, $CHCl_3$).

Its enantiomer was likewise prepared from **2′** *via* 10.7 g of crystalline material to give 6.1 g of needles: $[\alpha]_D^{27.0}$ −41.1° (*c* 0.506, $CHCl_3$).

(2R,3R)-2,3-Epoxy-3-phenyl-N-[(S)-1-phenylethyl]propionamide (6) and Its Enantiomer (6′). 6.45 g (21.2 mmol) of **4** was dissolved in ethanol (200 ml) while heating. After cooling, 2.12 mol dm^{-1} sodium methoxide solution (10.0 ml) was added dropwise to the solution during 2—3 min with stirring. The solution was allowed to stand for 1.5 h at room temperature and then concentrated. The residue was extracted with chloroform. The chloroform layer was dried (Na_2SO_4) and concentrated to yield 5.5 g of crystalline material. This was recrystallized from ethyl acetate-petroleum ether to give 4.3 g of needles: $[\alpha]_D^{24.0}$ −59.7° (*c* 1.003, $CHCl_3$).

Its enantiomer was likewise prepared from **4′** (5.0 g) to give 4.4 g of needles: $[\alpha]_D^{24.0}$ +60.6° (*c* 1.019, $CHCl_3$).

(2R,3S)-3-Dimethylamino-2-hydroxy-3-phenyl-N-[(S)-1-phenylethyl]propionamide (10) and Its Enantiomer (10′). A suspension of 4.2 g of **6** in a 50% aqueous dimethylamine solution (140 ml) was stirred for 1.5 h at room temperature. The homogeneous solution was treated and purified by the same procedure as **9** to give 4.28 g of needles: $[\alpha]_D^{21.0}$ −125.6° (*c* 1.022, $CHCl_3$).

Its enantiomer was likewise prepared from **6′** (3.5 g) to give 3.2 g of needles: $[\alpha]_D^{20.0}$ +127.1° (*c* 1.036, $CHCl_3$).

(2R,3S)-2-Acetoxy-3-dimethylamino-3-phenyl-N-[(S)-1-phenylethyl]propionamide (14) and Its Enantiomer (14′). These were prepared from **10** (3.6 g) and **10′** (2.9 g) by the same procedure as **13** to give needles (3.4 g and 2.5 g): $[\alpha]_D^{25.0}$ −12.0° (*c* 1.002, $CHCl_3$) and $[\alpha]_D^{27.5}$ +11.9° (*c* 1.003, $CHCl_3$), respectively.

(2R,3R)-3-Chloro-2-hydroxy-3-phenyl-N-[(S)-1-phenylethyl]propionamide (5) and Its Enantiomer (5′). This was prepared from **3** by the same procedure as **4**. The crystalline material (14.5 g) thus obtained was recrystallized from ethyl acetate (100 ml)-petroleum ether (126 ml) to give 5.56 g of prisms. This was again recrystallized from ethyl acetate (25 ml)-petroleum ether (43 ml) to give 4.4 g of prisms: $[\alpha]_D^{20.0}$ −158.3° (*c* 0.504, $CHCl_3$).

Its enantiomer was likewise prepared from **3′**. The product (12.5 g) was recrystallized from ethyl acetate-petroleum ether to give 4.4 g of prisms: $[\alpha]_D^{20.0}$ +156.6° (*c* 0.516, $CHCl_3$).

(2S,3S)-2,3-Epoxy-3-phenyl-N-[(S)-1-phenylethyl]propionamide (7) and Its Enantiomer (7′). These were prepared from **5** (4.1 g) and **5′** (4.0 g) by the same procedure as **6** to give needles (2.5 g and 2.5 g): $[\alpha]_D^{20.5}$ −0.0°; $[\alpha]_{365}^{20.5}$ −16.3° (*c* 1.003, $CHCl_3$) and $[\alpha]_D^{20.5}$ +0.0°; $[\alpha]_{365}^{20.5}$ +15.8° (*c* 1.006, $CHCl_3$), respectively.

(2S,3R)-3-Dimethylamino-2-hydroxy-3-phenyl-N[(S)-1-phenylethyl]propionamide (11) and Its Enantiomer (11′). These were prepared from **7** (3.2 g) and **7′** (3.0 g) by the same procedure as **10** except for recryatallization from ethyl acetate-petroleum ether to give needles (1.82 g and 2.5 g): $[\alpha]_D^{21.0}$ −81.6° (*c* 1.000, $CHCl_3$) and $[\alpha]_D^{20.0}$ +81.6° (*c* 1.002, $CHCl_3$), respectively.

(2S,3R)-2-Acetoxy-3-dimethylamino-3-phenyl-N-[(S)-1-phenylethyl]propionamide (15) and Its Enantiomer (15′). These were prepared from **11** (2.0 g) and **11′** (2.1 g) by the same procedure as **13** except for recrystallization from ether to give needles (1.37 g and 1.25 g): $[\alpha]_D^{27.0}$ −109.8° (*c* 1.001, $CHCl_3$) and $[\alpha]_D^{26.0}$ +110.0° (*c* 1.003, $CHCl_3$), respectively.

(2S,3S)-2-Benzoyloxy-3-dimethylamino-3-phenyl-N-[(R)-1-phenylethyl]propionamide. To a solution of **8′** (1.2 g, 3.8 mmol) in dry ethyl actate (200 ml) was added benzoyl chloride (0.59 g, 4.2 mmol). The solution was allowed to stand for 2 d and then concentrated. The residue was solidified with ether. The solid material was filtered off and recrystallized from methanol-ether to give 0.69 g of prisms: $[\alpha]_D^{15.0}$ +103.3° (*c* 1.002, CH_3OH); IR(KBr) 3500, 3200, 3100, 2800—2400 (amide NH and N^+–H), 1720 (ester C=O) and 1690 cm^{-1} (amide C=O). Found: C, 66.31; H, 6.63; N, 5.95%. Calcd for $C_{26}H_{29}N_2O_3Cl \cdot H_2O$: C, 66.17; H, 6.68; N, 5.80%.

Melting points, elemental analyses, IR spectra and ^1H NMR spectra of the compounds **2**—**15** and their enantiomers **2′**—**15′** are summarized in Tables 3, 4, 5 and 6.

Preparation of QC-(S)R and QC-(R)R. 2-Quinuclidinecarboxylic acid was prepared from 4-pyridinecarbaldehyde and diethyl malonate by the method reported by Långström.[7] Optical resolution of ethyl 2-quinuclidinecarboxylate was caried out by the method reported by Pracejus and Kohl.[8] (*S*)- and (*R*)- quinuclidinecarboxylic acid hydrochlorides, whose optical rotations were $[\alpha]_D^{21.0}$ −96.5° (1.073, water) and $[\alpha]_D^{24.0}$ +97.5° (*c* 1.012, water), respectivety (literature[7]: $[\alpha]_D$ −96.2° (*c* 1, water)) were obtained by hydrolysis of their ethyl esters. QC-(*S*)*R* and QC-(*R*)*R* were prepared by a condensation of **16** and **17** with (*R*)-1-phenylethylamine by the following procedures.[9]

(S)-N-[(R)-1-Phenylethyl]-2-quinuclidinecarboxamide (18).[10] Thionyl chloride (31.5 ml) and **16** (2.95 g, 15.4 mmol) were refluxed for 20 min and the homogeneous solution was concentrated to remove the excess thionyl chloride. To the residue was added dry ether (60 ml) and (*R*)-1-phenylethylamine (8.0 ml, 62 mmol) on ice cooling with stirring. Stirring was continued for 3 h and to the solution was added 50% aqueous potassium carbonate solution untill the water layer became basic. The water layer was extracted with ether three times (300 ml). The ether layer was dried(Na_2SO_4) and concentrated to remove also the excess (*R*)-1-phenylethylamine and to give 3.1 g of oily material which soon crystallized. This was recrystallized from petroleum ether to give 2.33 g of plates: mp 97.0—99.0 °C; $[\alpha]_D^{22.5}$ −3.5°, $[\alpha]_{365}^{22.5}$ +41.1° (*c* 1.004, $CHCl_3$); IR (KBr) 3350 (NH) and 1650 cm^{-1} (amide C=O); ^1H NMR ($CDCl_3$) δ=1.47 (3H, d, *J*=7.1 Hz, $C\underline{H}_3$), 1.47 (4H, m), 1.82 (3H, m), 2.62 (2H, q), 2.88 (2H, m), 3.31 (1H, t, *J*= 8.8 Hz, C-2 methine proton), 5.14 (1H, quintet, *J*=7.1 Hz, CH_3-$C\underline{H}$) and 7.30 (6H, m, Ph and $N\underline{H}$). Found: C, 74.38;

Table 3. 2,3-Epoxy-3-phenyl-*N*-(1-phenylethyl)propionamide

No.[a]	mp/°C	Found(Calcd)/% C (76.38)	H (6.41)	N (5.24)[b]	IR, ν/cm^{-1} NH	C=O (amide)	^{1}HNMR, δ in $CDCl_3$ CH_3-CH (J_{Hz})	CHCONH (J_{Hz})	CHPh (J_{Hz})	CH-CH_3
2	169.0—170.0	76.36	6.54	5.57	3280	1670	1.53 d	3.54 d	3.80 d	5.15 q[c]
2′	168.0—169.0	76.12	6.66	5.83			(6.84)	(1.96)	(1.96)	
3	165.0—166.0	76.27	6.42	5.61	3300	1660	1.52 d	3.51 d	3.91 d	5.15 q
3′	166.0—167.0	76.12	6.65	5.71			(6.84)	(1.96)	(1.96)	
6	97.0— 98.0	76.47	6.44	5.50	3340	1640	1.39 d	3.80 d	4.31 d	4.83 q
6′	97.5— 98.0	76.44	6.40	5.32			(6.84)	(4.90)	(4.90)	
7	124.0—126.0	76.37	6.46	5.36	3350	1640	0.81 d	3.78 d	4.35 d	4.82 q
7′	125.0—127.0	76.35	6.44	5.39			(6.84)	(4.90)	(4.90)	

a) Compound number. b) Calculated for $C_{17}H_{17}NO_2$. c) Quintet.

Table 4. 3-Chloro-2-hydroxy-3-phenyl-*N*-(1-phenylethyl)propionamide

No.[a]	mp/°C	Found(Calcd)/% C (67.21)	H (5.97)	N (4.61)[b]	IR, ν/cm^{-1} NH	OH	C=O (amide)	^{1}HNMR, δ in $CDCl_3$ CH_3-CH (J_{Hz})	CHCONH (J_{Hz})	OH (J_{Hz})	CHPh (J_{Hz})	CH-CH_3
4	166.0—168.0	67.40	6.30	4.99	3400	3280	1640	1.50 d	4.40 dd	3.00 d	5.59 d	5.13 q[c]
4′	164.5—166.5	67.42	6.28	4.96				(6.84)	(6.86, 2.44)	(6.86)	(2.44)	
5	127.0—130.0	67.44	6.02	4.62	3400	3250	1650	1.52 d	4.29 dd	3.10 d	5.55 d	5.13 q
5′	131.0—132.0	67.31	6.00	4.55				(6.84)	(6.86, 2.46)	(6.86)	(2.46)	

a) Compound number. b) Calculated for $C_{17}H_{18}NO_2Cl$. c) Quintet.

Table 5. 3-Dimethylamino-2-hydroxy-3-phenyl-*N*-(1-phenylethyl)propionamide

No.[a]	mp/°C	Found(Calcd)/% C (73.04)	H (7.74)	N (8.97)[b]	IR, ν/cm^{-1} NH	OH	C=O (amide)	^{1}HNMR, δ in $CDCl_3$ CH_3-CH (J_{Hz})	$N(CH_3)_2$	CHCONH (J_{Hz})	CHPh (J_{Hz})	CH-CH_3
8	156.5—157.5	73.18	7.87	8.83	3400	3300	1650	1.40 d	2.26 s	3.59 d	4.59 d	4.89 q[c]
8′	157.0—157.5	73.23	7.77	8.97				(6.86)		(5.62)	(5.62)	
9	100.5—102.0	71.28	8.05	8.64[d]	3400	3300	1635	0.93 d	2.26 s	3.54 d	4.56 d	4.82 q
9′	100.0—101.0	71.12	8.01	8.63[d]				(6.86)		(5.40)	(5.40)	
10	140.0—142.0	73.01	7.94	8.90	3380	3280	1650	1.46 d	2.12 s	3.60 d	4.34 d	5.05 q
10′	142.0—143.0	73.17	7.91	8.89				(6.96)		(7.34)	(7.34)	
11	100.0—101.0	72.93	7.89	8.81	3280		1658	1.46 d	2.18 s	3.66 d	4.32 d	5.04 q
11′	100.0—101.0	73.10	7.84	8.84				(7.10)		(7.76)	(7.76)	

a) Compound number. b) Calculated for $C_{19}H_{24}N_2O_2$. c) Quintet. d) Calculated for $C_{19}H_{24}N_2O_2 \cdot 1/2H_2O$: C, 71.00; H, 7.84; N, 8.72%.

Table 6. 2-Acetoxy-3-dimethylamino-3-phenyl-*N*-(1-phenylethyl)propionamide

No.[a]	mp/°C	Found(Calcd)(%) C (71.16)	H (7.39)	N (7.90)[b]	IR, ν/cm^{-1} NH	C=O (ester)	C=O (amide)	^{1}HNMR, δ in $CDCl_3$ CH_3-CH (J_{Hz})	$N(CH_3)_2$	$COOCH_3$	CHCONH (J_{Hz})	CHPh (J_{Hz})	CH-CH_3
12	78.0— 82.0	71.14	7.59	7.85	3400	1725	1675	1.44 d	2.21 s	2.02 s	3.88 d	5.79 d	5.02 q[c]
12′	83.0— 84.0	71.28	7.61	7.78				(6.86)			(7.58)	(7.58)	
13	153.0—154.5	71.38	7.57	7.87	3300	1740	1660	1.25 d	2.19 s	1.99 s	3.81 d	5.76 d	5.00 q
13′	152.0—153.5	71.34	7.54	7.86				(6.96)			(7.58)	(7.58)	
14	144.0—145.0	71.30	7.55	7.75	3350, 3300	1750	1650, 1680	1.23 d	2.26 s	2.14 s	3.78 d	5.60 d	4.97 q
14′	144.0—146.0	71.26	7.60	7.79				(6.86)			(7.10)	(7.10)	
15	127.5—129.0	71.22	7.57	7.86	3300	1740	1650	1.41 d	2.28 s	2.13 s	3.73 d	5.63 d	5.00 q
15′	128.0—130.0	71.25	7.59	7.78				(6.98)			(6.84)	(6.84)	

a) Compound number. b) Calculated for $C_{21}H_{26}N_2O_3$. c) Quintet.

H. 8.58; N, 10.84%. Calcd for $C_{16}H_{22}N_2O$: C, 74.26; H, 8.81; N, 10.76%.

(R)-N[(R)-1-Phenylethyl]-2-quinuclidinecarboxamide (19).[10] This was prepared from **17** (2.3 g) by the procedure used for **20** to yield 2.6 g of oily material which did not crystallize. *p*-Toluenesulfonic acid (1.54 g, 8.1 mmol) and 2.1 g (8.1 mmol) of the oily material were dissolved in methanol (20 ml) and then the solution was concentrated to dryness. To the residue was added dry benzene and the mixture was concentrated (this was repeated 2—3 times). The crystalline material obtained was recrystallized from ethyl acetate (1200 ml) to give 2.2 g of thin plates, which were further recrystallized from ethyl acetate (700 ml) to give 1.8 g of thin plates. These crystals were dissolved in a small amount of water and to the solution was added enough 50% potassium carbonate solution to make the water layer basic. The solution was extracted with ether 2—3 times. The ether layer was dried (Na_2SO_4) and concentrated to give 1.1 g of oil: $[\alpha]_D^{21.5}$ +121.6° (*c* 1.017, $CHCl_3$); IR (NaCl) 3350 (NH) and 1770 cm^{-1} (amide C=O); ^1H NMR ($CDCl_3$) δ=1.49 (3H, d, *J*= 6.84 Hz, CH_3), 1.49 (4H, m), 1.78 (3H, m), 2.75 (2H, t), 2.88 (2H, q), 3.27 (1H, t, *J*=7.8 Hz, C-2 methine proton), 5.51 (1H, quintet, *J*=6.84 Hz, CH_3-CH), 7.30 (6H, m, Ph and NH).

Asymmetric Hydrogenation of Methyl 2-(acetylamino)acrylate and N,N'-Dimethyl-5-benzylidenehydantoin with Co(dmgH)$_2$·B-B.* As the procedures of the hydrogenation of methyl 2-(acetylamino)acrylate and the isolation of the hydrogenated product were described in the preceding paper,[3] only those of *N,N'*-dimethyl-5-benzylidenehydantoin in run 11 of Table 2 are given below.

To a methanol solution (10 ml) of $CoCl_2·6H_2O$ (0.25 g, 1.05 mmol) was added a hot solution of dimethylglyoxime (0.24 g, 1.05 mmol) in methanol (15 ml) under nitrogen atmosphere with stirring. The solution was stirred for 2—3 min and then 1.0 ml of 2.12 mol dm^{-1} sodium methoxide solution was added to the solution. After 1—2 min, triphenylphosphine (0.275 g, 1.05 mmol) in hot methanol (15 ml) and a methanol solution of equimolar mixture of **18** (0.27 g, 1.05 mmol) and its hydrochloride were added to the solution.

Methanol in the resulting catalyst solution was evaporated *in vacuo*; stirring was continued untill the sample became a wet paste. To this paste 15 ml of degassed benzene was added by a syringe under atmospheric pressure of hydrogen, and the mixture was then evaporated again to wet paste *in vacuo*. To the resulting catalyst was added a degassed benzene solution (60 ml) of *N,N'*-dimethyl-5-benzylidenehydantoin (2.0 g, 9.26 mmol) again with a syringe.

After a theoretical amount of hydrogen was absorbed (for about 3 d), 100 ml of benzene was added to the reaction mixture. Then the solution was washed successively with water, sodium chloride solution, 3 mol dm^{-1} hydrochloric acid solution (100 ml), sodium chloride solution and sodium hydrogencarbonate solution. The benzene layer was dried (Na_2SO_4) and concentrated to give an oily material.

The oily material was adsorbed on a silica-gel column (Wako Gel C-300, 20 g, 1.8ϕ×23 cm), and eluted by benzene (100—150 ml) and then by a mixture of benzene and ethyl acetate (10:1, 200 ml; and then 5:1, 100 ml). Triphenylphosphine was eluted out with 100—150 ml of benzene and 1.89 g of oily material was obtained from the eluates of the mixture of benzene and ethyl acetete (10:1 and 5:1, 300 ml). The oily material was soon crystallized.

When benzylamine was used as the achiral base, the purification of the product through silica-gel column was not necessary.

Determination of the Specific Rotation of an Enantiomerically Pure (S)-N,N'-Dimethyl-5-benzylhydantoin. (*S*)-5-benzylhydantoin[$[\alpha]_D^{21.0}$ −102.2° (*c* 0.508, 50% C_2H_5OH), literature[11]: $[\alpha]_D$ −96.3° (50% C_2H_5OH)] prepared from (*S*)-phenylalanine was dimethylated by Shin's method[12] as follows.

To a mixture of (*S*)-5-benzylhydantoin (6.0 g) and potassium carbonate (43.8 g) in DMF (180 ml) was added methyl iodide (33 ml) with vigorous stirring; the stirring was continued for 2 d at room temperature. The reaction mixture was poured into water (200 ml) and the solution was extracted with ethyl acetate twice (400 ml). The ethyl acetate layer was washed with sodium chloride solution (200 ml) three times, dried(Na_2SO_4) and then concentrated to give oily material.

The oily material was adsorbed on a silica-gel column (Wako Gel C-300, 60 g, 3.5ϕ×20 cm), and eluted by benzene (600 ml) and then by a mixture of benzene and ethyl acetate (5:1, 700 ml). The eluate of the mixture of benzene and ethyl

TABLE 7. RECRYSTALLIZATION OF *N,N'*-DIMETHYL-5-BENZYLHYDANTOIN OF $[\alpha]_D$ −62.3°

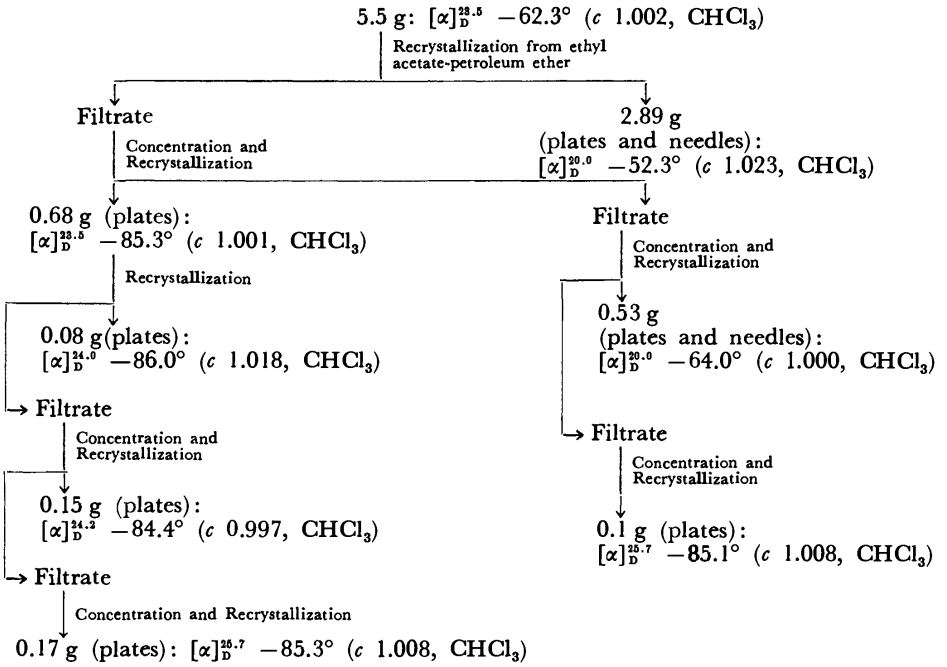

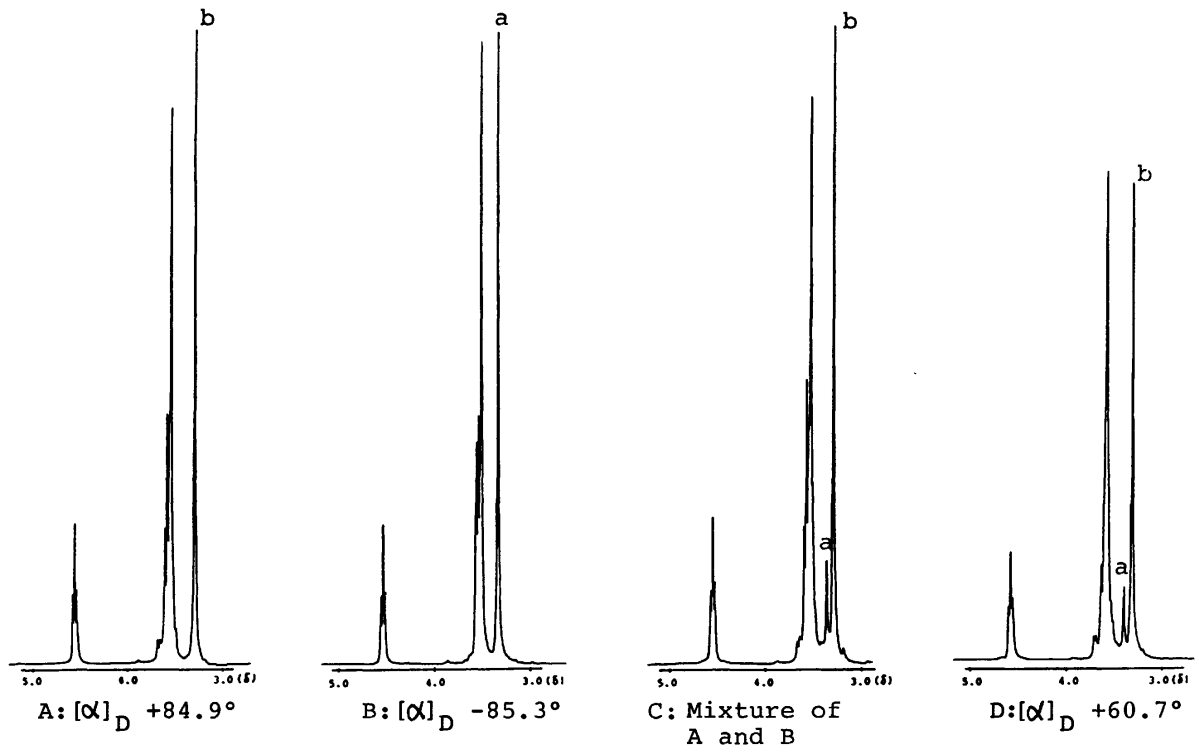

Fig. 5. ^1H NMR spectra of *N,N'*-dimethyl-5-benzylhydantoin in the presence of chiral shift reagent. In each case 45.0—46.0 mg of the sample was dissolved in 860—875 mg of $CDCl_3$ and to the solution 16.0—17.0 mg of the chiral shift reagent was added.

acetate was concentrated to give 5.78 g of oily material which crystallized gradually: $[\alpha]_D^{23.5}$ −62.3° (*c* 1.022, $CHCl_3$).

This was recrystallized from ethyl acetate-petroleum ether to give 2.89 g of crystals in which plates were covered with needles: $[\alpha]_D^{20.0}$ −52.3° (*c* 1.004, $CHCl_3$). The filtrate was concentrated and the crystals obtained were recrystallized from ethyl acetate-petroleum ether to give 0.68 g of long plates: $[\alpha]_D^{23.5}$ −85.3° (*c* 1.001, $CHCl_3$). The long plates were recrystallized repeatedly, as shown in Table 7.

The highest value thus obtained was $[\alpha]_D^{24.0}$ −86.0° (*c* 1.018, $CHCl_3$).

N,N'-dimethyl-5-benzylhydantoin (1.5 g) in run 12 of Table 2 ($[\alpha]_D^{24.0}$+60.7° (*c* 1.004, $CHCl_3$)) was similarly recrystallized from ethyl acetate-petroleum ether to give 0.19 g of long plates as a second crop: $[\alpha]_D^{22.0}$ +84.9° (*c* 1.002, $CHCl_3$).

The ^1H NMR spectra of the samples of $[\alpha]_D$ +84.9° (A), $[\alpha]_D$ −85.3° (B), $[\alpha]_D$ +60.7° (D; of run 12 in Table 2) and the mixture (C) of (A, 39.1 mg) and (B, 6.6 mg) in the presence of tris(3-trifluoroacetyl-d-camphorato)europium(III)[13] are shown in Fig. 5. These ^1H NMR spectra show that signals a and b of each spectrum are those of *S* and *R* enantiomers respectively and that the samples (A) and (B) are approximately enantiomerically pure.[14] Therefore, the highest value detected above ($[\alpha]_D$ −86.0°) must be the one of the enantiomerically pure sample; the enantiomeric excesses in Table 2 were thus calculated from this value.

The authors wish to express their thanks to Professor Chung-gi Shin, Kanagawa University, for his valuable discussions; to Miss Tatsuko Sakai, Meijho University, for her elemental analyses; and to Mr. Katsuhiko Sotomaru, Gasukuro Kogyo Co. Ltd., for his GLC analyses. We also would like to thank Mr. Akira Ohtaki and Miss Satoko Ohkura for the preparation of 2-quinuclidinecarboxylic acid and its derivatives.

References

1) Part XII on Asymmetric Reactions.

2) Part X on Asymmetric Reactions: Y. Ohgo, S. Takeuchi, Y. Natori, and J. Yoshimura, *Bull. Chem. Soc. Jpn.*, **54**, 2124 (1981).

3) Part XI on Asymmetric Reactions: S. Takeuchi and Y. Ohgo, *Bull. Chem. Soc. Jpn.*, **54**, 2136 (1981).

4) The values calculated from the specific rotation were in approximate agreement with those determined using a capillary column packed with a chiral liquid phase (OA-200, 30 m). The GLC analysis was performed at Gasukuro Kogyo Co.,Ltd..

5) K. Harada, *J. Org. Chem.*, **31**, 1407 (1966).

6) The epoxide ring opening of both **2** and **3** with dry hydrogen chloride gave mixtures of the corresponding threo (**4** and **5** respectively; 70%) and erythro (30%) isomers, which were determined from intensities of ^1H NMR signals of C-CH_3 (threo δ=1.50, erythro δ=1.40; threo δ=1.52, erythro δ=1.03, respectively). See: C. C. Tung and A. J. Speziale, *J. Chem. Soc.*, **28**, 2009 (1963).

7) B. Långström, *Chimica Scripta*, **5**, 170 (1974).

8) H. Pracejus and G. Kohl, *Ann.*, **722**, 1 (1969).

9) H. Pracejus, F. W. Wilcke, amd K. Hanemann, *J. Prak. Chem.*, **319**, 219 (1977).

10) When a crystal of **18** was added as seed to the petroleum ether solution saturated with (*RS*)-*N*-[(*R*)-1-phenylethyl]-2-quinuclidinecarboxamide (3.6 g), crystals (1.0 g) contaminated by a trace amount of **19** were separated out. Thus **18** and **19** (from the filtrate) could also be obtained by the same purification procedures described in the Experi-

mental section.
11) J. P. Greenstein and M. Winitz, "Chemistry of Amino Acids," John Wiley & Sons Inc., New York (1961), Vol 1, p 94.
12) C. Shin, Y. Sato, M. Hayakawa, and M. Kondo, *Heterocycles*, **16**, 1573 (1981).
13) G. R. Sullivan, "Topics in Stereochemistry," ed by E. L. Eliel and N. L. Allinger, John Wiley & Sons Inc., New York (1978), Vol 10, pp 287—329.
14) Signals (a and b) having nearly equal intensities were observed in the case of the racemate.

Syntheses of Polythia[*n*]ferrocenophanes and Polythia[*n.n*]-ferrocenophanes. Marocyclic Polysulfide Ligands Containing a Ferrocene Nucleus

Masaru SATO,* Sinsuke TANAKA, Seiji EBINE,† and Sadatoshi AKABORI††
Chemical Analysis Center, Saitama University, Urawa, Saitama 338
†*Department of Chemistry, Faculty of Science, Saitama University, Urawa, Saitama 338*
††*Department of Chemistry, Faculty of Science, Toho University, Funabashi, Chiba 274*
(Received December 1, 1983)

1,1′-Bis(2-chloroethylthio)ferrocene reacted with disodium 1,2-ethanedithiolate to give 1,4,7,10-tetrathia-[10]ferrocenophane and 1,4,7,10,22,25,28,31-octathia[10.10]ferrocenophane, along with unexpected 1,4,7-trithia-[7]ferrocenophane, 1,4,7,10,13-pentathia[13]ferrocenophane and 1,4,7,10,13,25,28,31,34-nonathia[10.13]ferrocenophane. The reaction of 1,1′-bis(2-chloroethylthio)ferrocene with disodium 1,3-propanedithiolate gave 1,4,-8,11-tetrathia[11]ferrocneophane. 1,1′-Bis(3-chloropropylthio)ferrocene reacted with disodium 1,2-ethanedithiolate and 1,3-propanedithiolate to afford 1,5,8,12-tetrathia[12]ferrocenophane and 1,5,8,12,24,27,31,34-octathia-[12.12]ferrocenophane, and 1,5,9,13-tetrathia[13]ferrocenophane, respectively. The structural features of the above polythia[*n*]ferrocenophanes are also discussed on the bases of their spectral data.

Various types of crown ethers have been prepared and their functionalities investigated.[1] The first thia-crown ether was synthesized in 1934[2] and thereafter some thia-macrocyclic compounds have been prepared[3-6] and shown to have a high affinity toward transition metal cations.[3,7-9] Especially, the complex with a copper atom has attracted much attention as a model of the blue copper protein,[8] nevertheless, the modified thia-crown ethers have scarcely been reported. Polythiaferrocenophanes, in which a ferrocene nucleus is incorporated in the framework of a thia-crown ether ring, is a new type of these modified thia-crown compounds. We now report on the preparation of several polythia[*n*]ferrocenophanes and polythia[*n.n*]-ferrocenophanes.[10]

Disodium 1,1′-ferrocenedithiolate (**1**), which was prepared from 1,1′-ferrocenedithiol[11] and sodium hydroxide in ethanol, reacted with 1,2-dibromoethane in ethanol at room temperature to give 1,4-dithia[4]-ferrocenophane (**2**) as orange crystals in 37% yield. Although a polymeric compound was produced, no dimer of **2** was isolated. In the ^{1}H-NMR spectrum of **2**, the α- and β-protons of ferrocene rings appeared as two well-separated doublets at δ 4.41 and 4.19, suggesting the presence of a little tilt-deformation in the two cyclopentadienyl rings of the ferrocene nucleus.[12] The bridging methylene protons resonated downfield, δ 3.33; this would be explained by the fact that they are rigidly held in a deshielding zone between two cyclopentadienyl rings.[13]

Compound **1** reacted with 1-bromo-2-chloroethane in ethanol to give 1,1′-bis(2-chloroethylthio)ferrocene (**3**) as yellow crystals in 67% yield, along with a small amount of **2**. The ^{1}H-NMR spectrum of **3** showed the methylene protons as a A_2X_2 pattern at δ 2.86 (t, 4H, J=8.7 Hz) and 3.57 (t, 4H, J=8.7 Hz), supporting the assigned structure. Similarly, **1** reacted with 1-bromo-3-chloropropane to give 1,1′-bis(3-chloropropylthio)ferrocene (**4**) as an orange oil in 71% yield. The ^{1}H-NMR spectrum, which showed the methylene protons as two triplets at δ 2.71 (4H, J=6.5 Hz, CH_2S) and 3.61 (4H, J=6.5 Hz, CH_2Cl) and a pentuplet at δ 1.94 (4H, $CH_2C\underline{H}_2CH_2$) and the ring protons as a multiplet at δ 4.24, confirmed the proposed structure.

A solution of dichloride **3** in dry tetrahydrofuran (THF) was added all at once to a solution of sodium sulfide nonahydrate in ethanol and the resulting solution was refluxed for 10 h. After the usual work-up, the reaction mixture was chromatographed on silica gel to give a moderate yield (27.5%) of 1,4,7-trithia[7]-ferrocenophane (**5**) and a trace amount of the dimer, 1,4,7,19,22,25-hexathia[7.7]ferrocenophane (**6**), along with unexpected 1,4-dithia[4]ferrocenophane (**2**) (5.0%)

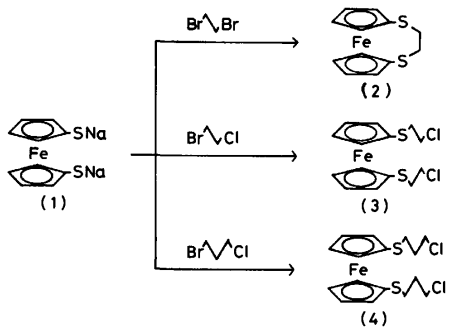

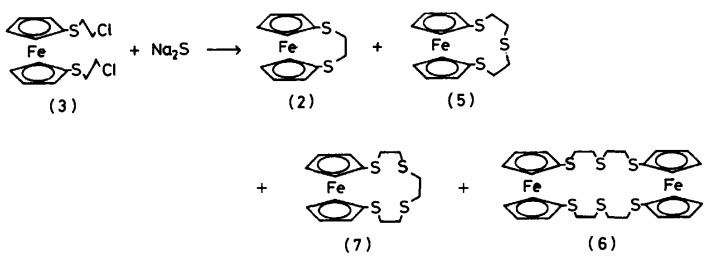

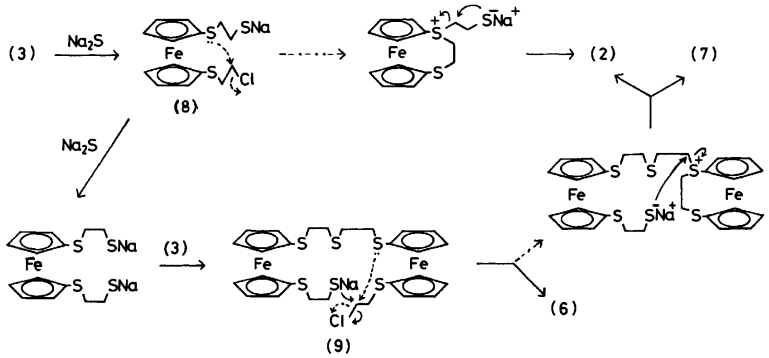

Scheme 1.

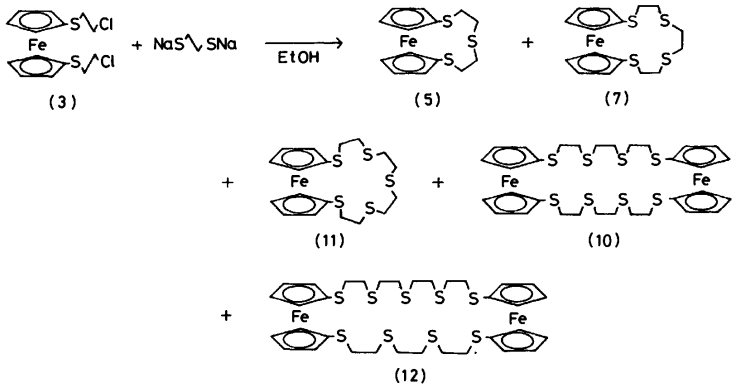

and 1,4,7,10-tetrathia[10]ferrocenophane (**7**) (3.1%). The formation of the abnormal products **2** and **7** may be rationalized in terms of the formation of the intermediate monochloride (**8**) or the dimeric monochloride (**9**) and the following cyclic sulfonium ions as shown in Scheme 1. Similar propagation products are reported in the reaction of bis(2-chloroethyl) ether with sodium sulfide.[14] The replacement of the reaction solvent from ethanol to *N*,*N*-dimethylformamide caused no enhancement of the yield of **5** and **6**. The structure of **5** was confirmed by its ^{1}H-NMR and mass spectra [*m*/*z* 336 (M^+)]. In the ^{1}H-NMR spectrum of **5**, the ring protons and the methylene protons appeared as a pair of triplets at δ 4.25 (4H) and 4.33 (4H), and as a multiplet at δ 2.9—3.5 (8H), respectively. The close appearance of the α- and β-ring protons suggests little tilt-deformation caused by the seven-membered (three sulfur and four carbon atoms) bridging chain. The structure of the dimer **6** was similarly assigned by its mass spectrum [*m*/*z* 672 (M^+)] and ^{1}H-NMR spectrum [δ 4.28 (s, 8H) and δ 2.6—3.2 (m, 8H)]. The methylene protons of the former were observed at somewhat lower field than that of the latter; this is probably because the former methylene portons were held in a deshielding zone between the two cyclopentadienyl rings as described above.

The dichloride **3** reacted with four equivalents of disodium 1,2-ethanedithiolate by refluxing in ethanol-tetrahydrofuran for 2 h. After the usual work-up, the reaction mixture was chromatographed on silica gel by elution with hexane-toluene to give 1,4,7,10-tetrathia[10]-ferrocenophane (**7**) and 1,4,7,10,22,25,28,31-octathia[10.10]-ferrocenophane (**10**) in 50.4 and 3.6% yields, respectively. Moreover, the unexpected products, 1,4,7-trithia[7]ferrocenophane (**5**) (1.7%), 1,4,7,-10,13-pentathia[13]ferrocenophane (**11**) (11.6%), and 1,-4,7,10,13,25,28,31,34-nonathia[10.13]ferrocenophane (**12**) (1.6%) were isolated. Treatment of **3** with one equivalent of disodium 1,2-ethanedithiolate under similar conditions gave all compounds described above (**5**, **7**, **10**, **11**, and **12**) in yields slightly different from the above experiment. The structure of these compounds was assigned by their elemental analyses, mass, and ^{1}H-NMR spectra. For example, **11** showed the molecular ion (M^+) at *m*/*z* 456 in the mass spectrum. The ^{1}H-NMR spectrum of **11** had the resonances at δ 4.26 (m, 8H) and 2.7—3.2 (m, 16H). The formation of **5** can be rationalized by the intermediate formation of a monochloride followed by a cyclic sulfonium ion as described above (Scheme 2). A similar process was presumed in the reaction of bis(2-chloroethyl) sulfide with the sodium salt of 1,2-ethanedithiol.[5] A possible mechanism for the unexpected formation of **11** and **12** is proposed in Scheme 2. A similar type of reaction has been observed only in the reaction of 1,1′-bis-(2-chloroethoxy)ferrocene with disodium 1,2-ethanedithiolate.[15] The initial reaction would be a nucleophilic attack of two moles of disodium 1,2-ethanedithiolate on the halogenated carbons of **3** to form the dithiolate (**13**). Subsequently, one proton elimination from the methylene carbon next to a sulfur atom takes place and is followed by elimination of S^{2-} to give a vinyl sulfide intermediate (**14**). Thus, the formation of **11** can be interpreted by an intramolecular attack of $-S^-$ to the double bond of **14** followed by addition of proton to the resulting sulfur-stabi-

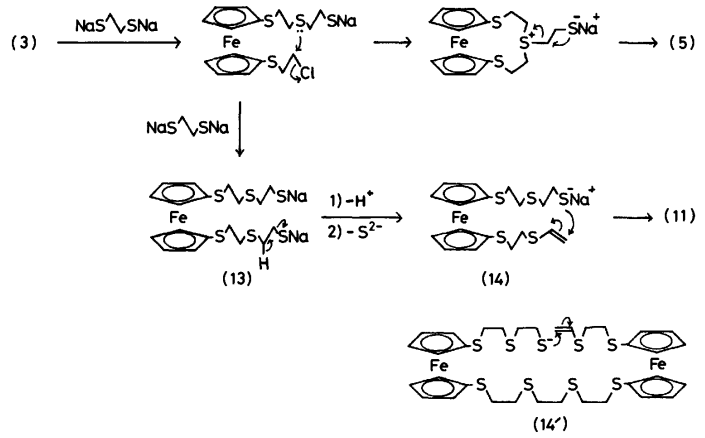

Scheme 2.

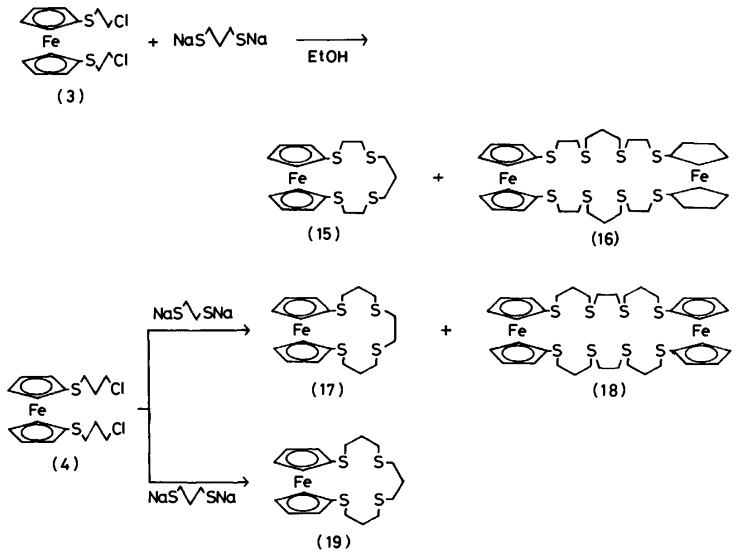

lized anion. The formation of **12** can be similarly explained *via* the intermediate (**14'**). The driving force of the unusual propagation reaction may be an easy formation of the sulfur-stabilized carbanion from **13**.

The chloride **3** was treated with four equivalents of disodium 1,3-propanedithiolate in refluxing ethanol-tetrahydrofuran for 2 h under nitrogen. After the usual work-up, the reaction mixture was chromatographed on silica gel to give 1,4,8,11-tetrathia[11]ferrocenophane (**15**) in 57% yield. The ^{1}H-NMR spectrum of **15** showed ferrocene ring protons as a singlet at δ 4.27 (8H), the methylene protons next to a sulfur atom as multiplets at δ 2.7—3.0 (8H) and 3.0—3.2 (4H), and the methylene protons as a quintet at δ 2.02, confirming the assigned structure. On addition to **15**, the compound (**16**), assumed to be the dimer of **15** by its mass and ^{1}H-NMR spectra, was isolated, although the final assignment was unsuccessful because of insufficient product.

1,1'-bis(3-chloropropylthio)ferrocene (**4**) reacted with four molar equivalents of disodium 1,2-ethanedithiolate in similar conditions to those described above, affording 1,5,8,12-tetrathia[12]ferrocenophane (**17**) and 1,5,8,12,24,28,31,35-octathia[12.12]ferrocenophane (**18**) in 47.8% and 11.2% yields, respectively. The reaction with one equivalent of the sodium salt gave considerably decreased yields of the products and no dimer **18**. The reaction of **4** with one equivalent of disodium 1,3-propanedithiolate gave 1,5,9,13-tetrathia[13]ferrocenophane (**19**) in 64.6% yields. The reaction with 4 equivalents of the sodium salt resulted in no increase of the yield of **19** and no isolation of the corresponding dimer.

The electronic and ^{13}C-NMR spectral data of the mononuclear derivatives **2**, **5**, **7**, **11**, **15**, **17**, and **19** were summarized in Tables 1 and 2. As shown in Table 1, 1,4,7-trithia[7]ferrocenophane (**5**) showed an abnormally bathochromic shift ($\Delta\lambda$ *ca.* 20 nm) and an increase in the absorbance ($\Delta\varepsilon$ *ca.* 40) of an absorption band near 440 nm characteristic of ferrocene, which was assigned to d-d transition from the HOMO to the LUMO.[16] In its ^{13}C-NMR spectrum, **5** showed a

Table 1. Electronic spectral data of mononuclear ferrocenophanes **2**, **5**, **7**, **11**, **15**, **17**, and **19**

Compd	**2**	**5**	**7**	**11**	**15**	**17**	**19**
λ_{max} (nm)	438	461	442	442	443	443	443
ε	138	272	223	195	196	191	190

Table 2. ^{13}C-NMR Spectral data of mononuclear ferrocenophanes **2**, **5**, **7**, **11**, **15**, **17**, and **19** (22.5 MHz, $CDCl_3$)

Compd	^{13}C-NMR (δ)
2	85.0 (C_b), 70.0 (C_α), 68.7 (C_β), 31.1 (SCH_2)
5	89.7 (C_b), 70.6 (C_α), 67.5 (C_β), 37.2, 32.8 (SCH_2)
7	85.3 (C_b), 72.1 (C_α), 68.9 (C_β), 38.3, 32.6, 31.1 (SCH_2)
11	84.4 (C_b), 72.4 (C_α), 69.2 (C_β), 37.2, 33.4, 32.7, 32.3 (SCH_2)
15	85.3 (C_b), 72.0 (C_α), 68.8 (C_β), 36.8, 31.9, 31.3, 30.4 (SCH_2)
17	84.3 (C_b), 72.9 (C_α), 68.9 (C_β), 34.9, 32.1, 30.0, 29.1 (SCH_2)
19	84.1 (C_b), 72.9 (C_α), 68.9 (C_β), 35.0, 30.8, 30.2, 28.9 (SCH_2)

down-field shift of the bridgehead carbon resonance ($\Delta\delta$ *ca.* 4 ppm) and an up-field shift of the α- and β-ring carbon resonances ($\Delta\delta$ 0.6—2.3 ppm) of the ferrocene necleus, compared with those of other cyclophanes. There seems to be no tilting strain of the two cyclopentadienyl rings in this molecule, since only a slight splitting of the chemical shifts of the α- and β-ring protons was observed as described previously. The stereomolecular model also evidenced the absence of a tilting strain in **5**. The abnormal shifts observed in the electronic and ^{13}C-NMR spectra therefore may be interpreted by an interaction either between a ferrocene nucleus and a sulfur atom in the 4-position or between a ferrocene nucleus and sulfur atoms in the 1- and 7-positions of **5**. The former possibility, however, is excluded by the fact that such an abnormal shift was not observed in the electronic and ^{13}C-NMR spectra of 1,7-dioxa-4-thia[7]ferrocenophane.[17] From consideration of the stereomolecular model of **5**, the hybrid orbital of the lone pair of the sulfur atom attached to the cyclopentadienyl rings is held to be perpendicular to the plane of cyclopentadienyl rings. Two possible interactions, therefore, remain to explain the spectroscopic characteristics observed in **5**: an interaction between the nonbonding d-orbital on the iron atom and the lone pair of a sulfur atom and an interaction between the lone pair of a sulfur atom and the Fe-C bond connecting a cyclopentadienyl ring to an iron atom (σ-π conjugation).[18] The detailed study on this phenomena will be discussed in another paper.[19]

Experimental

Materials. 1,1′-Ferrocenedithiol was prepared from 1,2,3-trithia[3]ferrocenophane.[11] 1,2-Dibromoethane, 1-bromo-2-chloroethane, 1-bromo-3-chloropropane, 1,2-ethanedithiol and 1,3-propanedithiol were all commercially available; the purity of the last two was checked by GLC. All reactions were done under an atmosphere of nitrogen.

1,4-Dithia[4]ferrocenophane (2). To a suspension of 1,1′-ferrocenedithiol (0.34 g, 1.4 mmol) in ethanol (50 ml) was added a 40% aq solution of sodium hydroxide (0.23 ml) under stirring. The resulting red solution of disodium 1,1′-ferrocenedithiolate (**1**) and a solution of 1,2-dibromoethane (0.12 ml, 1.4 mmol) in ethanol (50 ml) were added dropwise at the same rate to N_2-saturated ethanol (100 ml) for a period of 3 h under stirring at room temperature, and then further stirred overnight. After the reaction had been completed, the mixture was evaporated under vacuum, the residue was dissolved in benzene and the undissolved material was filtered off. Chromatography of the condensed filtrate on silica gel gave 1,4-dithia[4]ferrocenophane (**2**) (0.14 g, 37%) as orange cubes, mp 138—139 °C. Found: C, 52.18; H, 4.34%. Calcd for $C_{12}H_{12}S_2Fe$: C, 52.18; H, 4.38%. MS (75 eV); *m/z* 276 (M^+, 100%) and 248 ($M^+-CH_2CH_2$, 57%). IR (KBr): 3080, 1410, 1160, 1020, 890, and 810 cm^{-1}. ^{1}H-NMR ($CDCl_3$): δ=3.33 (s, 4H, CH_2CH_2), 4.19 (t, 4H, J= 1.9 Hz, H_α), and 4.41 (t, 4H, J=1.9 Hz, H_β).

1,1′-Bis(2-chloroethylthio)ferrocene (3). To a solution of disodium 1,1′-ferrocenedithiolate (**1**), prepared from 1,1′-ferrocenedithiol (0.50 g, 2 mmol) and 40% aq sodium hydroxide (0.4 ml) in ethanol (40 ml), was all at once added a solution of 1-bromo-2-chloroethane (0.63 g, 4.4 mmol) in ethanol (2 ml). The solution was stirred for 4 h at room temperature. After the reaction mixture had been evaporated under vacuum, the residue was chromatographed on silica gel by elution of hexane-toluene (2:1), giving 1,1′-bis(2-chloroethylthio)ferrocene (**3**) as orange crystals (0.45 g, 61%), mp 90.5—91 °C, along with a trace amount (4%) of 1,4-dithia[4]-ferrocenophane (**2**). Found: C, 45.05; H, 4.10%. Calcd for $C_{14}H_{16}Cl_2S_2Fe$: C, 44.82; H, 4.30%. MS (75 eV):*m/z* 375 (M^+, 100%) and 276 ($M^+-C_2H_4Cl_2$, 32%). IR (KBr): 3080, 1438, 1210, 1020, 983, 828, and 690 cm^{-1}. ^{1}H-NMR ($CDCl_3$): δ= 2.86 (t, 4H, J=8.7 Hz, CH_2S), 3.57 (t, 4H, J=8.7 Hz, CH_2Cl) 4.29 (t, 4H, J=1.7 Hz), 4.35 (t, 4H, J=1.7 Hz).

1,1′-Bis(3-chloropropylthio)ferrocene (4). A similar reaction of 1,1′-ferrocenedithiol (3.83 g, 15.3 mmol), 40% aq sqlution of sodium hydroxide (2.3 ml), and 1-bromo-3-chloropropane (5.78 g, 36.7 mmol) gave 1,1′-bis(3-chloropropylthio)ferrocene (**4**) (4.36 g, 70.7%) as an orange oil. Found: C, 47.59; H, 5.00%. Calcd for $C_{16}H_{20}Cl_2S_2Fe$: C, 47.66; H, 5.01%. MS (75 eV): *m/z* 402 (M^+, 100%). IR (Neat): 3080, 2950, 1440, 1420, 1268, 1020, and 825 cm^{-1}. ^{1}H-NMR ($CDCl_3$): δ= 1.94 (m, 4H, CH_2), 2.71 (t, 4H, J=6.8 Hz, CH_2S), 3.61 (t, 4H, J=6.4 Hz, CH_2Cl), 4.24 (t, 4H, J=1.8 Hz), and 4.30 (t, 4H, J=1.8 Hz).

Reaction of 1,1′-Bis(2-chloroethylthio)ferrocene (3) with Sodium Sulfide. To a solution of sodium sulfide nonahydrate (0.54 g, 2.2 mmol) in anhyd. ethanol (250 ml) was added a solution of 1,1′-bis(2-chloroethylthio)ferrocene (**3**) (0.67 g, 1.8 mmol) in tetrahydrofuran (THF) (45 ml). The solution was refluxed for 10 h under nitrogen. After the reaction had been completed, the reaction mixture was evaporated under vacuum, the residue was dissolved in benzene and the yellow precipitate was filtered off. The filtrate was condensed and chromatographed on silica gel by elution with hexane-toluene, the following products being separated and purified by recrystallization. 1,4-Dithia[4]ferrocenophane (**2**) (0.025 g, 5%). 1,4,7-Trithia[7]ferrocenophane (**5**) (0.17 g, 28%) as red plates, mp 120 °C. Found: C, 50.10; H, 4.89%. Calcd for $C_{14}H_{16}S_3Fe$: C, 50.00; H, 4.80%. MS (75 ev): *m/z* 336 (M^+, 100%), 280 ($M^+-2C_2H_4$, 44%), 248 (24%), and 184 (44%). IR (KBr): 3080, 1418, 1160, 1020, and 806 cm^{-1}.

^{1}H-NMR ($CDCl_3$): δ=3.0—3.5 (m, 8H, CH_2S), 4.28 (m, 8H, ring-H). 1,4,7,10-Tetrathia[10]ferrocenophane (**7**) (0.22 g, 3.1%) (See later.). 1,4,7,19,22,25-Hexathia-[7.7]ferrocenophane (**6**) (0.039 g, 6.5%) as yellow orange crystals, mp 185—185.5 °C. Found: 50.13; H, 4.79%. Calcd for $C_{28}H_{32}S_6Fe_2$: C, 50.00; H, 4.80%. MS (75 eV): *m/z* 672 (M^+, 14%), 336 ($M^+/2$, 23%), and 304 ($M^+/2$-S, 100%). IR (KBr) 3080, 1418, 1190, 1022, and 810 cm^{-1}. ^{1}H-NMR ($CDCl_3$):δ=2.6—3.2 (m, 16H, CH_2S) and 4.28 (s, 16H).

The same reaction was carried out using *N,N*-dimethylformamide in the place of ethanol-THF as a solvent to give **5** and **6** in 27.2 and 9.1% yields, respectively.

Reaction of 1,1′-Bis(2-chloroethylthio)ferrocene (3) with Disodium 1,2-Ethanedithiolate. To a solution of sodium hydroxide (1.2 g, 30 mml) in anhyd ethanol (400 ml) was added 1,2-ethanedithiol (1.0 ml, 12 mmol), and then all at once a solution of 1,1′-bis(2-chloroethylthio)ferrocene (**3**) (1.12 g, 3 mmol) in anhyd THF (75 ml). The resulting solution was gently refluxed for 2 h and then evaporated under vacuum. Water was added, the mixture was extracted with benzene and the benzene extract was dried over anhyd. sodium sulfate and evaporated. The residue was chromatographed on silica gel to give the following products: 1,4,7-Trithia[7]ferroceneophane (**5**) (0.017 g, 1.7%). 1,4,7,10-Tetrathia[10]ferrocenophane (**7**) (0.60 g, 50.5%) as orange crystals, mp 116 °C. Found: C, 48.61; H, 4.97%. Calcd for $C_{16}H_{20}S_4Fe$: C, 48.48; H, 5.09%. MS (75 eV): *m/z* 396 (M^+, 100%), 272 (M^+—124, 61%) and 184 (18%). IR (KBr): 3075, 1420, 1268, 1020, 800, and 688 cm^{-1}. ^{1}H-NMR ($CDCl_3$): δ=2.7—3.0 (m, 4H, CH_2S), 3.0—3.3 (m, 4H, CH_2S), 3.10 (s, 4H, SCH_2-CH_2S), and 4.25 (m, 8H, ring-H).

1,4,7,10,13-Pentathia[13]ferrocenophane (**11**)(0.159 g, 11.6%) as orange needles, mp 100.5—102 °C. Found: C, 47.49; H, 5.44%. Calcd for $C_{18}H_{24}S_5Fe$: C, 47.36; H, 5.30%. MS (75 eV): *m/z* 456 (M^+, 100%), 332 (M^+—124), 272 (13%), and 184 (11%). IR (KBr): 3070, 1420, 1195, 1025, and 820 cm^{-1}. ^{1}H-NMR ($CDCl_3$): δ=2.7—3.2 (m, 16H, CH_2S) and 4.26 (s, 8H, ring-H).

1,4,7,10,22,24,27,30-Octathia[10,10]ferrocenophane (**10**) (0.043 g, 3.6%) as reddish orange crystals, mp 152.5—153.5 °C. Found: C, 48.48; H, 5.25%. Calcd for $C_{32}H_{40}S_8Fe_2$: C, 48.48; H, 5.09%. MS (25 eV): *m/z* 792 (M^+, 100%) and 272 (59%). IR (KBr): 3080, 2920, 1422, 1200, 1020 and 820 cm^{-1}. ^{1}H-NMR ($CDCl_3$): δ=2.5—3.0 (m, 16H, CH_2S), 2.66 (s, 8H, SCH_2CH_2S), and 4.34 (m, 16H, ring-H).

1,4,7,10,13,25,28,31,34-nonathia[10.13]ferrocenophane (**12**) (0.022 g, 1.6%) as orange crystals, mp 114.5 °C. Found: C, 47.74; H, 5.53%. Calcd for $C_{34}H_{44}S_9Fe_2$: C, 47.88; H, 5.20%. MS (35 eV): *m/z* 852 (M^+, 7%) and 272 (100%). IR (KBr): 3080, 2920, 1424, 1188, 1018, and 805 cm^{-1}. ^{1}H-NMR ($CDCl_3$): δ= 2.5—3.0 (m, 28H, CH_2S) and 4.35 (m, 16H, ring-H).

When one equivalent of disodium 1,2-ethanedithiolate was used in the above reaction, the yields of **5**, **7**, **11**, **10**, and **12** were 6.0, 32.7, 8.6, 2.6, and 1.4%, respectively.

Reaction of 1,1′-Bis(2-chloroethylthio)ferrocene (3) with 1,3-Propanedithiol. To a solution of sodium hydroxide (0.855 g) in anhydrous ethanol (280 ml) was added 1,3-propanedithiol (0.84 ml, 8.4 mmol) and then a solution of 1,1′-bis(2-chloroethylthio) ferrocene (0.748 g, 2 mmol) in anhyd. THF (50 ml) under an atmosphere of nitrogen. The solution was refluxed for 2 h and then evaporated. The residue was chromatographed on silica gel to give two products: 1,4,8,11-tetrathia[11]ferrocenophane (**15**) (0.462 g, 56.3%) as orange plates, mp 75 °C. Found: C, 49.79; H, 5.15%. Calcd for $C_{17}H_{22}S_4Fe$: C, 49.75; H, 5.40%. MS (75 eV): m/z 410 (M^+, 96%), 286 (M^+ —124, 100%), 248 (35%), and 184 (16%). IR (KBr): 3080, 2895, 1432, 1262. 1160, 1024, 886, and 805 cm^{-1}. ^{1}H-NMR ($CDCl_3$): δ=2.02 (p, 2H, J=7.5 Hz, CH_2), 2.7—3.0 (m, 8H, CH_2S), 3.0—3.2 (m, 4H, CH_2S), and 4.27 (s, 8H, ring-H).

1,4,8,11,23,26,30,33-Octathia[11.11]ferrocenophane (**16**) as yellow crystals, mp 132 °C. MS (35 eV): *m/z* 820 (M^+, 4%), 410 ($M^+/2$, 14%), and 286 (100%). IR (KBr): 3085, 2930, 1622, 1430, 1204, 1025, 895, and 835 cm^{-1}. ^{1}H-NMR ($CDCl_3$): δ=1.75 (p, 4H, J=7.3 Hz, CH_2), 2.56 (t, 8H, J=7.3 Hz, SCH_2), 3.0—2.5 (m, 16H, SCH_2), and 4.34 (m, 16H, ring-H).

Reaction of 1,1′-Bis(3-chloropropylthio)ferrocene(4) with 1,2-Ethanedithiol. To a solution of disodium 1,2-ethanedithiolate, prepared from 1,2-ethanedithiol (1.0 ml, 12 mmol) and sodium hydroxide (1.2 g, 30 mmol) in anhyd. ethanol (400 ml) was added a solution of 1,1′-bis(3-chloropropylthio) ferrocene (**4**) (1.21 g, 3 mmol) in anhyd THF (75 ml) under an atmosphere of nitrogen. After being refluxed for 2 h, the solution was evaporated under vacuum, the residue was dissolved in water, the mixture was extracted with benzene, the extract was dried over anhyd. sodium sulfate and then evaporated. From the residue, two crystalline products were isolated by chromatography on silica gel:

1,5,8,12-Tetrathia[12]ferrocenophane (**17**) (0.608 g, 47.8%) as orange crystals, mp 98 °C. Found: C, 51.25; H, 5.70%. Calcd for $C_{18}H_{24}S_4Fe$: C, 50.93; H, 5.70%. MS (75 eV): *m/z* 424 (M^+, 100%) and 184 (19%). IR (KBr): 3080, 2900, 1410, 1248, 1165, 1020, and 812 cm^{-1}. ^{1}H-NMR ($CDCl_3$): δ=1.91 (m, 4H, CH_2), 2.7—3.0 (m, 8H, CH_2S), 2.80 (s, 4H, SCH_2CH_2S), and 4.25 (s, 8H, ring-H).

1,5,8,12,24,28,31,35-Octathia[12.12]ferrocenophane (**18**) (0.143 g, 11,2%) as yellow fine needles, mp 82—83 °C. Found: 51.17; H, 5.79%. Calcd for $C_{36}H_{48}S_8Fe_2$: C, 50.93; H, 5.70%. MS(35 eV): *m/z* 848 (M^+, 18%) and 424 ($M^+/2$, 100%). IR (KBr): 2900, 1422, 1240, 1020, and 830 cm^{-1}. ^{1}H-NMR ($CDCl_3$): δ=1.82 (p, 8H, J=7.3 Hz, CH_2), 2.66 (t, 8H, J= 7.5 Hz, CH_2S), 2.69 (s, 8H, SCH_2CH_2S), 2.73 (t, 8H, J=7.1 Hz, CH_2S), 4.2—4.37 (m, 16H, ring-H).

When one equivalent of disodium 1,2-ethanedithiolate was used in the above reaction, **17** was obtained in 35% yield and the dimer **18** was not isolated.

1,5,9,13-Tetrathia[13]ferrocenophane (19). To a solution of disodium 1,3-propanedithiolate, prepared from 1,3-propanedithiol (0.10 ml, 1 mmol) and sodium hydroxide (0.089 g, 2.2 mmol) in anhyd. ethanol (125 ml), was all at once added a solution of 1,1′-bis(3-chloropropylthio)ferrocene (**4**) (0.403 g, 1.0 mmol) in anhyd. THF (26 ml) under nitrogen. The solution was gently refluxed for 5 h and then evaporated under vacuum. The residue was chromatographed on silica gal by elution with hexane-toluene (3:1) to give 1,5,9,13-tetrathia[13]ferrocenophane (**19**) (0.283 g, 64.6%) as orange needles, mp 60 °C. Found: C, 52.20; H, 5.81%. Calcd for $C_{19}H_{26}S_4Fe$: C, 52.04; H, 5.98%. MS (75 eV): *m/z* 438 (M^+, 100%) and 184 (5%). IR (KBr): 3100, 2900, 1415, 1255, 1168, 1020, and 818 cm^{-1}. ^{1}H-NMR ($CDCl_3$): δ= 1.7—2.2 (m, 6H, CH_2), 2.5—3.0 (m, 12H, SCH_2), and 4.25 (s, 8H, ring-H).

Application of 4 equivalents of disodium 1,3-propandithiolate in the above reaction resulted in no increase in the yield of the monomer **19** and no detection of the corresponding dimer.

References

1) R. M. Izatt and J. J. Christensen, "*Synthetic Multidentate Macrocyclic Compound*", Academic Press, New York (1974).

2) J. R. Meadow and E. E. Reid, *J. Am. Chem. Soc.*, **56**, 2177 (1934).

3) W. Rosen and D. H. Busch, *Inorg. Chem.*, **9**, 262 (1970); idem, *J. Am. Chem. Soc.*, **91**, 4694 (1969).

4) D. St. C. Black and I. A. Malean, *Tetrahedron Lett.*, **1969**, 3961.

5) L. A. Ochrymowycz, C.-P. Mark, and J. D. Michna, *J. Org. Chem.*, **39**, 2079 (1974).
6) J. S. Bradshaw and J. Y. K. Hui, *J. Heterocycl. Chem.*, **11**, 649 (1974).
7) K. Travis and D. H. Busch, *Inorg. Chem.*, **13**, 2591 (1974).
8) T. E. Jones, L. L. Zimmer, L. L. Diaddario, D. B. Rorabacker, and L. A. Ochrymowycz, *J. Am. Chem. Soc.*, **97**, 7163 (1975); T. E. Jones, D. B. Rorabacker, and L. A. Ochrymowycz, *ibid.*, **97**, 7485 (1975); E. R. Dockal, T. E. Jones, W. F. Sokol, R. J. Engerer, D. B. Rorabacker, and L. A. Ochrymowycz, *ibid.*, **98**, 4324 (1976).
9) T.-F. Lai and C.-K. Poon, *J. Chem. Soc. Dalton, Trans*, **1982**, 1465.
10) A Preliminary report: M. Sato, H. Watanabe, S. Ebine, and S. Akabori, *Chem. Lett.*, **1982**, 1753.
11) J. J. Bishop, A. Davison, M. L. Katcher, D. W. Lichtenberg, R. E. Merrill, and J. C. Smart, *J. Organomet. Chem.*, **27**, 241 (1971).
12) T. H. Barr and W. E. Watts, *Tetrahedron*, **24**, 6111 (1968).
13) L. N. Mulay and M. E. Fox, *J. Chem. Phys.*, **38**, 760 (1963).
14) L. Mortillaro, M. Russo, L. Credali, C. De. Checchi, *J. Chem. Soc. (C)*, **1966**, 428.
15) S. Akabaori, S. Shibahara, Y. Habata, and M. Sato, *Bull. Chem. Soc. Jpn.*, in press.
16) D. R. Scott and R. S. Becker, *J. Chem. Phys.*, **35**, 516 (1961).
17) S. Akabori, Y. Habata, M. Sato, and S. Ebine, *Bull. Chem. Soc. Jpn.*, **56**, 1459 (1983).
18) The σ-π conjugation was used in order to explain the abnormal stability of α,α-disubstituted ferrocenylmethylium ion. T. G. Traylor, and J. C. Ware, *J. Am. Chem. Soc.*, **89**, 2304 (1967).
19) M. Sato, S. Tanaka, S. Ebine, and S. Akabori, to be submitted.

1-Bromo-2-ethoxycyclopropyllithium: A Synthetic Equivalent of 2-Lithio- or 3-Lithiopropenal. Application to the Synthesis of Juvenile Hormone (JH-II), β-Sinensal, and Jasmonoids

Yoshitomi MORIZAWA, Akihiro KANAKURA, Hajime YAMAMOTO, Tamejiro HIYAMA,*,† and Hitosi NOZAKI

Department of Industrial Chemistry, Faculty of Engineering, Kyoto University, Yoshida, Kyoto 606

(Received December 2, 1983)

The ethyl vinyl ether-dibromocarbene adduct was lithiated with butyllithium at −95 °C in tetrahydrofuran. The resulting lithium carbenoid **3** was allowed to react with various electrophiles to give 1-substituted *trans*-1-bromo-2-ethoxycyclopropanes (**1**) in good yields. The trans relationship of Br and OEt groups was found particularly pertinent to the ethanolysis of **1** producing 2-substituted propenal diethyl acetal derivatives. The reaction has been applied to 1-methoxycyclohexene-dibromocarbene adducts, giving rise hereby 2-substituted 2-cyclohepten-1-one dimethyl acetals under ring enlargement. The transformation has been utilized in the synthesis of a homoterpenoid (JH-II) or a terpenoid (β-sinensal) structure by S_N2' substitution of allylic acetates with lithium dimethylcuprate(I) or iron pentacarbonyl respectively. The reaction products of **3** with aldehydes are oxidized with dimethyl sulfoxide to give cyclopropyl ketones whose ethanolysis in the presence of boron trifluoride ether complex gives β-bromo γ-keto aldehyde acetals. Debromination followed by acidic hydrolysis produces γ-keto aldehydes serving as precursors of dihydrojasmone and *cis*-jasmone.

Cyclopropane ring cleavage provides highly efficient methods for stereoselective and often stereospecific transformation.[1] The synthetic application heavily depends on the accessibility of appropriately substituted cyclopropanes, which are often prepared *via* lithium carbenoids.[2] Lithium-halogen exchange reaction of *gem*- dihalocyclopropanes at low temperature provides the requisite carbenoids. The present paper deals with the chemistry of a lithium carbenoid derived from the ethyl vinyl ether-dibromocarbene adduct as applied to the synthesis of some terpenoids and related compounds.[3]

Reaction of 1-Bromo-2-ethoxycyclopropyllithium. Thermal rearrangement of 1,1-dihalo-2-alkoxycyclopropanes to 2-halopropenal derivatives is well-documented,[4] although the stereo-electronic aspect of the ring opening still remains unsolved. *trans*- and *cis*-1-Bromo-2-ethoxycyclopropanes (**1a**), (**1a'**) are prepared by reducing 1,1-dibromo-2-ethoxycyclopropane (**1b**) with tributyltin hydride.[5] As shown in Scheme 1 each isomer (1 mol dm^{-3}) was dissolved in ethanol and heated at 70 °C in the presence of potassium carbonate. The reaction was monitored by GLC assay. Pseudo first order rate constant for the trans isomer (**1a**) was 9.2×10^{-2} min^{-1}, whereas that for the cis isomer (**1a'**) was 7.8×10^{-4} min^{-1}. Thus, the transformation of **1a** to propenal diethyl acetal (**2a**) (93% GLC yield) proceeded about 100 times faster than the cis isomer (**1a'**). The difference of the reaction rate is attributed to the one of the energy-barrier of the ring-opening to give ethoxyallyl cation of W-form and sickle one, since the cyclopropyl halide-allyl cation transformation proceeds under orbital control.[11]

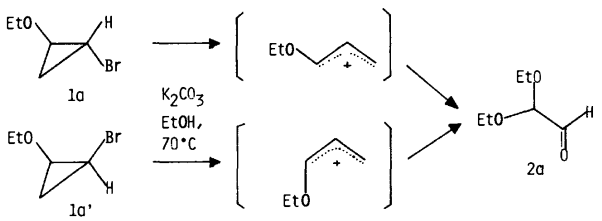

Scheme 1.

The favored isomers **1**[6] (Scheme 2) are prepared by means of the carbenoid **3** obtained by bromine–lithium exchange reaction of 1,1-dibromo-2-ethoxycyclopropane[7] **1b** with butyllithium. Treatment of the resulting carbenoid **3** at −95 °C with an electrophile gave the corresponding adduct **1**, which was successively heated in ethanol in the presence of potassium carbonate to afford a diethyl acetal **2**. Acidic hydrolysis gave the aldehyde **4**. The results are summarized in Table 1. According to the present two-step procedure, the carbenoid **3** is synthetically equivalent to 2-lithiopropenal[8] and provides 2-substituted propenal derivatives which themselves are potentially useful synthetic intermediates.[9]

The methodology described herein has been applicable to cyclic enol ether-dibromocarbene adducts (Scheme 3). For example, lithiation of 1-methoxy-7,7-dibromonorcarane **5** with butyllithium at −95 °C and treatment of the resulting carbenoid **6**[10] with an electro-

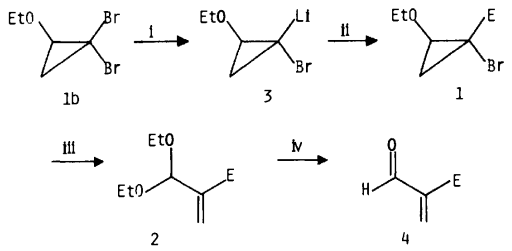

Scheme 2.

† Address correspondence: Sagami Chemical Research Center, 4-4-1 Nishiohnuma, Sagamihara, Kanagawa 229.

Table 1. Synthesis of 2-substituted propenal diethyl acetals and 2-substituted propenals

Entry	Electrophile	Yield (%)[a] of 2		Yield (%)[a] of 4	
1	H_2O	**2a**	93[b]		—
2	Br_2[c]	**2b**	93		—
3	Me_3SiCl	**2c**	87	**4c**	80[d]
4	PhSSPh	**2d**	74		—
5	n-$C_6H_{13}CHO$	**2e**	77[e]	**4e**	100

a) Isolated yield. b) GLC yield (5% Apieson L, 6% KOH). c) **2b** was prepared from **1b** under the ethanolysis conditions. d) Transformed into its 2,4-dinitrophenylhydrazone. e) Based on the consumed heptanal.

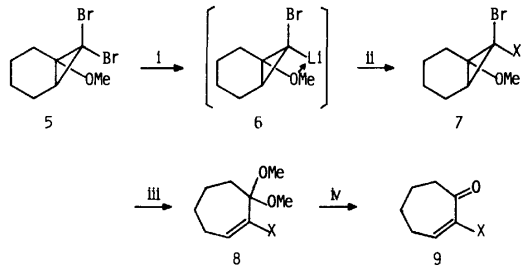

a: X = $SiMe_3$
b: X = CH(OH)n-C_6H_{13}
c: X = $CH_2CH{=}CMe_2$
d: X = n-C_5H_{11}
e: X = Me

i: n-BuLi, THF, -95°C, ii : Electrophile,
iii: MeOH, K_2CO_3, reflux, iv : H_3O^+.

Scheme 3.

phile afforded **7** whose substituents were appropriately disposed for the subsequent rearrangement.[11] Solvolysis of **7** in methanol in the presence of potassium carbonate gave cycloheptenone dimethyl acetal (**8**) under ring-enlargement. Although the reaction of **6** with trimethylsilyl chloride and heptanal took place with no difficulty, alkylation of the carbenoid turned out rather arduous. By employing hexamethylphosphoric triamide (HMPA) as the cosolvent,[1b] the alkylated products **9c—9e** were obtained. The results are shown in Table 2.

Synthesis of JH-II and β-Sinensal. The allylic acetate of type **10** is useful for the synthesis of α, β-unsaturated aldehyde moiety of homoterpenoid and terpenoid structure, such as **11** and **13** as shown in Scheme 4. For example, the allylic acetate **10** derived from **2e** was treated with lithium dimethylcuprate(I) in ether at −18 °C[12] to give, after acid-hydrolysis, (*E*)-2-ethyl-2-nonenal (**11**).[13] Selective S_N2' type methyl introduction is the key of the present synthesis.

As shown in Scheme 5, this result has been successfully applied to the synthesis of juvenile hormone (JH-II).[14] The aldehyde **20** (Scheme 6) was allowed to react with the carbenoid **3**, and the adduct was subjected to the two-step transformation of Scheme 2 to afford the acetal which was isolated as the acetate **14** in 84% overall

Table 2. Transformation of 1-methoxycyclohexene-dibromocarbene adducts into 2-substituted 2-cycloheptenones

Entry	Electrophile	Yield (%)	
1	$ClSiMe_3$	**9a**	57
2	n-$C_6H_{13}CHO$	**9b**	57
3	$Me_2C{=}CHCH_2Br$	**9c**	46[a]
4	n-$C_5H_{11}I$	**9d**	40[a]
5	MeI	**9e**	41[a]

a) HMPA : THF = 10 : 1 was used as a solvent for the alkylation step.

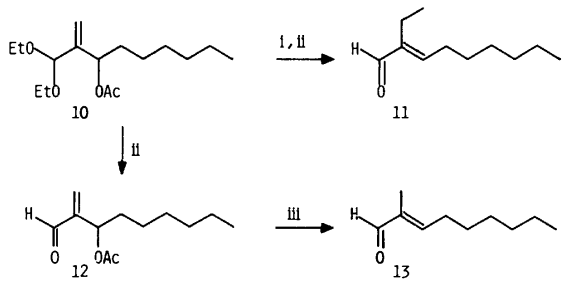

i: Me_2CuLi, ii: H_3O^+, iii: $NaBCNH_3$ or $Fe(CO)_5$-DABCO-DMF.

Scheme 4.

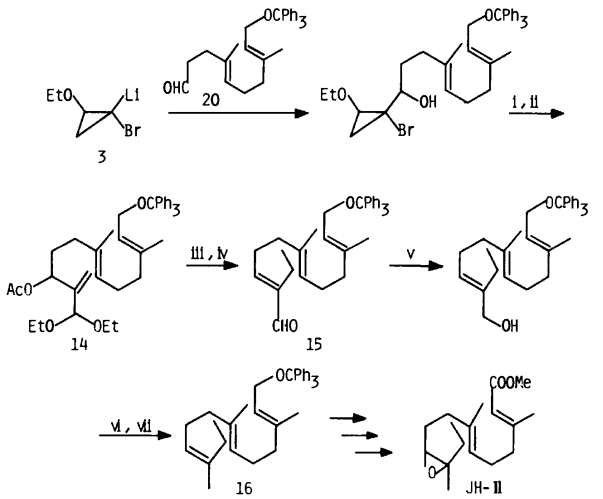

i: K_2CO_3, EtOH, 70°C, ii: Ac_2O, pyr., iii: Me_2CuLi,
iv: H_3O^+, v: $NaBH_4$, vi: SO_3-pyr., vii: $LiAlH_4$, reflux.

Scheme 5.

yield. Treatment of **14** with lithium dimethylcuprate(I) and then with 5% aq sulfuric acid in THF gave an aldehyde **15** in 83% yield. Deoxygenation of **15** was accomplished by sodium borohydride reduction followed by removal of the produced allylic hydroxyl group[15] to afford **16** (78% yield). Cleavage of the protecting trityl group[14c] and the subsequent route[14a] to the target molecule are already established.

As Shown in Scheme 4, the aldehyde **12** is also transformed into (*E*)-α,β-unsaturated aldehyde **13** by a formal S_N2' type introduction of hydride and elimination of acetoxyl group. For example, when **12** was mixed with 0.5 mol of sodium cyanotrihydroborate in metha-

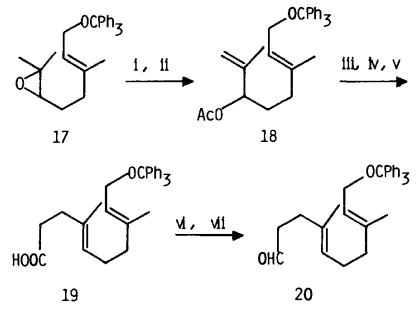

i: $LiNEt_2$, ii: Ac_2O-Py, iii: $LiN(i\text{-}Pr)(C_6H_{11})$, t-$BuMe_2SiCl$, iv: 70°C, v: AcOH, vi: $LiAlH_4$, vii, PCC.

Scheme 6.

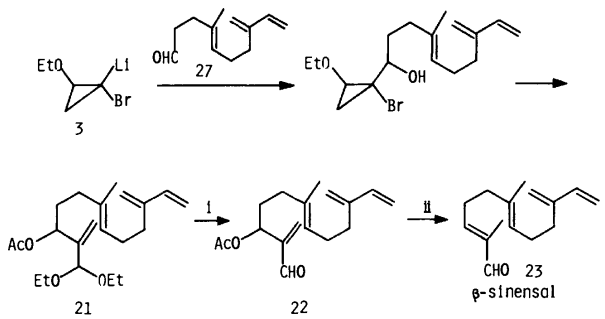

Scheme 7.

nol-acetic acid 10:1 at 0 °C, saturation of the olefinic bond occurred preferentially to afford the aldehyde **13** in 61% yield. The reduction is much more efficiently performed by means of iron pentacarbonyl and 1,4-diazabicyclo[2.2.2]octane (DABCO) in wet *N,N*-dimethylformamide (DMF) (96% yield).[16] It should be noted that the incipient 1,1-disubstituted ethylenic linkage is reduced to produce a new, triply substituted one which remains intact under the conditions.

The applicability of the new method has been demonstrated in the synthesis of β-sinensal (**23**) (Scheme 7), an important constituent of the odor and taste of Chinese orange oil (*Citrus sinensus L.*).[17] A triene aldehyde **27** (Scheme 8) was subjected to the carbenoid reaction as described in Scheme 2 to give the acetal acetate **21**. Deprotection of the aldehyde group with 5% aq sulfuric acid in THF resulted in polymerization of the large part of the product due to the acid-sensitive 1,3-diene moiety. The hydrolysis with silica gel-10% aq oxalic acid (10:1) suspended in dichloromethane[18] at room temperature gave the aldehyde **22** in 87% yield. Reductive removal of the acetoxyl group was selectively attained with iron pentacarbonyl-DABCO in wet DMF and β-sinensal (**23**) was produced in 95% yield.

Transformation of the Adducts of the Carbenoid 3 with Aldehydes into γ-Keto Aldehydes. Synthesis of Dihydrojasmone and cis-Jasmone. Ring-cleavage reaction of cyclopropyl ketone derivatives[19] has been also applicable to the homologation of carbon skeleton as shown in Scheme 9. Oxidation of **1e** type adducts of Scheme 2 was best carried out to give acid-lable *r*-1-bromo-*t*-2-ethoxy-1-heptanoyl-cyclopropane (**28a**) by the Swern's method.[20] Without isolation, **28a** was treated with

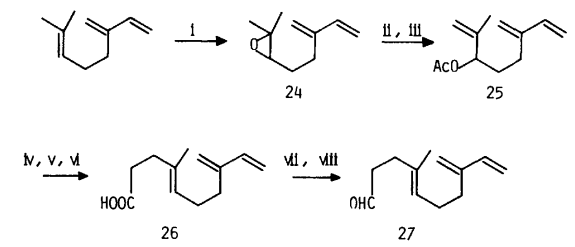

i: MCPBA, ii: LiNi-Pr_2, iii: Ac_2O-pyr., iv: LiNi-Pr_2, t-$BuMe_2SiCl$, v: 70°C, vi: $PhCH_2NMe_3F$, aq MeOH, vii: $LiAlH_4$, viii: PCC.

Scheme 8.

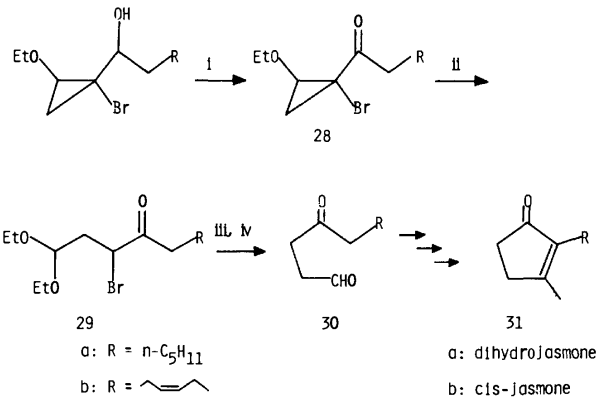

i: DMSO, $(CF_3CO)_2O$, Et_3N, ii: EtOH, BF_3:OEt_2 or AcOH, iii: $CrCl_3$-$LiAlH_4$, iv: H_3O^+

Scheme 9.

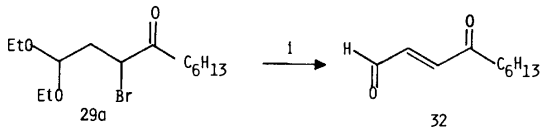

i: 15% H_2SO_4-THF

Scheme 10.

catalytic amount of boron trifluoride ether complex at room temperature to give a bromo acetal ketone **29a**. Reductive debromination with $CrCl_3$-$LiAlH_4$[21] followed by hydrolysis gave 4-oxodecanal (**30a**)[22], which was readily transformed into dihydrojasmone (**31a**)[23].

Starting with (*Z*)-4-heptenal,[24] *cis*-jasmone was prepared by the similar sequence of reactions. The ring-opening of the cyclopropyl ketone **28b** with BF_3-OEt_2 proceeded very slowly and gave complex mixture. On treatment with a catalytic amount of acetic acid, however, **28b** was converted to a bromo acetal ketone **29b** at room temperature in fairly good yield. The compound **29b** was reduced to give the γ-keto aldehyde **30b**,[22] a key precursor of *cis*-jasmone (**31b**).[25]

Acid hydrolysis of **29a** resulted in the formation of an α, β-unsaturated γ-keto aldehyde **32** (56% yield) (Scheme 10).

In conclusion, 1-bromo-2-ethoxycyclopropyllithium (**3**) is found to be a useful C_3 homologation reagent. The sequence shown in Scheme 2 clearly demonstrates that the lithium carbenoid **3** is a synthetic equivalent of 2-lithiopropenal or its acetal. In contrast, Scheme 9

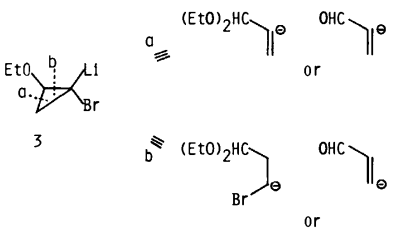

together with Scheme 10 shows that **3** is attached to an aldehyde at the carbon (3) of propenal or 3-bromopropanal. This ambient reactivity of **3** is controlled by the ring-opening operation (*a* or *b*) of **1** derived from **3**, and the applicability of the reagent has been illustrated in the synthesis of terpenoids and jasmonoids.

Experimental

All temperatures recorded are uncorrected. Distillation of small amount of samples (less than 1 g) was carried out with Kugelrohr. ^{1}H-NMR spectra (tetramethylsilane as an internal standard unless otherwise noted) were obtained on a Varian EM 390 spectrometer or JOEL PMX-60 spectrometer, chemical shifts being given in ppm unit. IR spectra of neat liquid film samples (unless otherwise noted) on a Shimadzu IR-27G spectrometer, MS on a Hitachi RMU-6L spectrometer, and exact mass on a Hitachi M-80 spectrometer, Gas-liquid phase chromatography (GLC) analyses were performed with a Yanagimoto GCG-550F chromatograph. Preparative TLC plates were prepared with Merck Kiesel-gel PF_{254}. Column chromatography was carried out with silica gel (Wakogel C-100) at atmospheric pressure.

*Synthesis of 2-(Diethoxymethyl)-1-nonen-3-ol (**2e**) and 3-Hydroxy-2-methylenenonanal (**4e**). A Typical Procedure for the Reaction of 1-Bromo-2-ethoxycyclopropyllithium (**3**) with an Electrophile*: Butyllithium (1.67 M† hexane solution, 7.2 ml, 12.0 mmol) was added to a THF (50 ml) solution of 1,1-dibromo-2-ethoxycyclopropane (2.93 g, 12.0 mmol) at −95 °C over a period of 5 min. After stirring for 10 min heptanal (1.12 g, 9.8 mmol) was added at −95 °C, and the reaction mixture was stirred at −95 °C for 30 min, then at room temperature for 20 min. Workup gave **1e** which was dissolved in ethanol (15 ml), and the mixture was stirred with potassium carbonate (6.90 g, 50 mmol) for 1 h under reflux. Workup and purification by column chromatography (hexane-ether=3:1) gave **2e** (1.84 g, 77% yield): bp 100—105 °C (bath temperature)/14 Torr**; ^{1}H-NMR (CCl_4) δ=0.6—1.6 (m+t, 19 H), 2.20 (br s, 1H), 3.2—3.8 (m, 4H, $CH_3C\underline{H}_2O$), 4.05 (t, J=5 Hz, 1H, C$\underline{H}$-OH), 4.80 (br s, 1H), 5.17 (br s, 2H, =C$\underline{H}_2$); IR 3450, 2940, 2870, 1460, 1365, 1105, 1050, 923 cm^{-1}; MS *m/z* (rel intensity) 199 (9), 154 (4), 115 (56), 103 (53), 85 (100), 55 (47), 43 (69).

A mixture of the acetal **2e** in THF (5 ml) and 5% aq sulfuric acid (5 ml) was stirred at room temperature for 5 min. Workup followed by purification by column chromatography gave **4e** (1.32 g, quantitative yield): bp 115—120 °C (bath temperature)/20 Torr; ^{1}H-NMR δ=0.7—1.6 (m. 13H), 2.20 (br s, 1H), 4.37 (t, J=6 Hz, 1H), 5.95 (d, J=1 Hz, 1H), 6.38 (d, J=1 Hz, 1H), 9.52 (s, 1H); IR 3450, 1685, 955, 908, 790 cm^{-1}; MS *m/z* (rel intensity) 170 (M$^+$, 2), 123 (7), 100 (13), 85 (100), 55 (40), 43 (80). Found: C, 70.63; H, 10.86%. Calcd for $C_{10}H_{18}O_2$: C, 70.54; H, 10.66%.

r-*1-Bromo-t-2-ethoxy-1-trimethylsilylcyclopropane (**1c**)*: Bp 61—63 °C (bath temperature)/2 Torr; ^{1}H-NMR (CCl_4, internal standard CH_2Cl_2) δ=0.15 (s, 9H), 1.04—1.26 (m+t(δ=1.15, J=7.1 Hz), 5H), 3.52 (q, J=7.1 Hz, 2H), 3.68 (dd, J=6.5, 4.5 Hz, 1H); IR 2980, 2890, 1335, 1240, 1120. 1050, 840 cm^{-1}; MS *m/z* (rel intensity) 209 (4), 207 (4), 157 (24), 139 (10), 137 (10), 113 (45), 75 (24), 73 (100).

*2-Bromo-3,3-diethoxypropene (**2b**)*[26]: Bp 120—130 °C (bath temperature)/20 Torr; ^{1}H-NMR (CCl_4, internal standard, $CHCl_3$) δ=0.95 (t, J=7 Hz, 6H), 3.1—3.5 (m, 4H), 4.57 (br, s, 1H), 5.43 (br, s, 1H), 5.87 (br, s, 1H); IR 2980, 2880, 1630, 1370, 1050, 905 cm^{-1}; MS *m/z* (rel intensity) 165 (32), 163 (34), 137 (88), 135 (99), 109 (21), 108 (26), 103 (100), 75 (52).

*2-Trimethylsilyl-3,3-diethoxypropene (**2c**)*: Bp 88—90 °C/26 Torr; ^{1}H-NMR (CCl_4, $CHCl_3$ internal standard) δ=0.03 (s, 9H), 1.10 (t, J=6.5 Hz, 6H), 3.2—3.7 (m, 4H), 4.80 (br s, 1H), 5.45 (m, 1H), 5.80 (m, 1H); IR 2980, 2880, 1240, 1110, 940, 840 cm^{-1}; MS *m/z* (rel intensity) 157 (17), 113 (28), 103 (100), 75 (51), 73 (44). Hydrolysis of **2c** with aq sulfuric acid gave 2-trimethylsilylpropenal (*4c*) which was characterized as the 2,4-dinitrophenylhydrazone: mp 153.5—154 °C (orange needle, 95% ethanol-ethyl acetate); ^{1}H-NMR ($CDCl_3$, $CHCl_3$ internal standard); δ=0.12 (s, 9H), 5.88 (d, J=1.8 Hz, 1H), 6.03 (d, J=1.8 Hz, 1H), 7.70 (d, J=10 Hz, 1H), 7.79 (br s, 1H), 8.21 (dd, J=10, 3 Hz, 1H), 9.00 (d, J=3 Hz, 1H), 11.0 (br s, 1H); IR 3280, 2930, 2850, 1615, 1595, 1510, 1315, 1130, 1080, 840 cm^{-1}; MS *m/z* (rel intensity) 308 (M$^+$, 1), 148 (17), 147 (100), 75 (24), 73 (26), 66 (12). Found: C, 46.94; H, 5.23, N, 18.36%. Calcd for $C_{12}H_{16}N_4O_4$: C, 46.74; H, 5.23; N, 18.17%.

*2-Phenylthio-3,3-diethoxypropene (**2d**)*: Bp 115—125 °C (bath temperature)/0.06 Torr; ^{1}H-NMR (CCl_4) δ=1.16 (t, J=7 Hz, 6H), 3.3—3.7 (m, 4H), 4.85 (s, 2H), 5.51 (s, 1H), 7.2—7.5 (m, 5H); IR 3060, 2980, 2880, 1610, 1480, 1445, 1380, 1110, 1010, 880, 750 cm^{-1}; MS *m/z* (rel intensity) 238 (M$^+$, 11), 194 (25), 147 (25), 185 (31), 103 (100), 91 (29), 75 (74); Found: C, 65.54; H, 7.50%. Calcd for $C_{13}H_{18}O_2S$: C, 65.51; H, 7.61%.

*2-Trimethylsilyl-2-cyclohepten-1-one (**9a**)*. A hexane solution (1.7 M) of butyllithium (1.64 ml, 2.8 mmol) was added drop by drop to 7,7-dibromo-1-methoxynorcarane[27] (0.71 g, 2.5 mmol) in THF (10 ml) at −95 °C. After 10 min's aging chlorotrimethylsilane (1 ml, *ca.* 8 mmol) was added and the reaction mixture was stirred for 2 h at −95 °C, allowed to warm up to room temperature and treated with water. The organic layer was extracted with ether, dried (sodium sulfate) and concentrated *in vacuo*. The residue was heated in methanol (7 ml) to reflux with potassium carbonate (2.1 g, 15 mmol) for 2 h. Usual workup gave **8a**, which was dissolved in a mixture of THF (5 ml) and 5% aq sulfuric acid (5 ml) and stirred at room temperature for 20 min. Workup followed by purification by column chromatography gave **9a** (0.31 g, 57% yield): bp 147—150 °C (bath temperature)/15 Torr; ^{1}H-NMR (CCl_4, CH_2Cl_2 internal standard) δ=0.07 (s, 9H), 1.6—1.8 (m, 4H), 2.4—2.6 (m, 4H), 6.58 (t, J=6 Hz, 1H); IR 2940, 2865, 1660, 1595, 1450, 1235, 945, 840 cm^{-1}; MS *m/z* (rel intensity) 182 (M$^+$, 82), 167 (1), 155 (4), 137 (3), 75 (11), 73 (8), 40 (100). Found: C, 65.93; H, 10.09%. Calcd for $C_{10}H_{18}OSi$: C, 65.87; H, 9.95%.

*2-(1-Hydroxyheptyl)-2-cyclohepten-1-one (**9b**)*: Bp 90—110 °C (bath temperature)/1 Torr; ^{1}H-NMR (CCl_4) δ=0.88 (t, J=6 Hz, 3H), 1.1—1.6 (m, 10H), 1.6—2.0 (m. 4H), 2.3—3.0 (m, 5H), 4.0—4.3 (m, 1H), 6.52 (t, J=6 Hz, 1H); IR 3450, 2930, 2860, 1660, 1460, 1370, 900 cm^{-1}; MS *m/z* (rel intensity) 224 (M$^+$, 2), 206 (9), 149 (16), 139 (100), 121 (10), 111 (13), 97 (17), 93 (15), 83 (14), 79 (16). Found: C, 74.78; H, 10.86%. Calcd for $C_{14}H_{24}O_2$: C, 74.95; H, 10.78%.

*2-(3-Methyl-2-butenyl)-2-cyclohepten-1-one (**9c**)*: Bp 115—125 °C (bath temperature)/0.15 Torr; ^{1}H-NMR (CCl_4) δ=1.6—1.9 (m+s (δ=1.60)+s (δ=1.70), 10H), 2.2—2.6 (m, 4H), 2.83 (d, J=7.8 Hz, 2H), 5.02 (t, J=7.8 Hz, 1H), 6.30 (t,

† 1 M=1 mol dm^{-3}; ** Torr=133.322 Pa.

J=6.3 Hz, 1H); IR 2920, 2850, 1665, 1455, 1370, 850 cm^{-1}; MS m/z (rel intensity) 178 (M^+, 33), 163 (100), 135 (53), 107 (33), 95 (40), 93 (45), 79 (47). Found: C, 81.05; H, 10.44%. Calcd for $C_{12}H_{18}O$: C, 80.85; H, 10.18%.

*2-Pentyl-2-cyclohepten-1-one (**9d**)*: Bp 160—170 °C (bath temperature)/0.3 Torr; ^{1}H-NMR (CCl_4) δ=0.90 (t, J=6 Hz, 3H), 1.0—1.5 (m, 6H), 1.5—2.0 (m, 4H), 2.0—2.6 (m, 6H), 6.33 (t, J=6 Hz, 1H); IR 2970, 1665, 1270, 885 cm^{-1}; MS m/z (rel intensity) 180 (M^+, 14), 151 (40), 133 (30), 112 (40), 95 (100), 81 (37), 67 (100). Found: C, 79.89; H, 11.44%. Calcd for $C_{12}H_{20}O$: C, 79.94; H, 11.18%.

*2-Methyl-2-cyclohepten-1-one (**9e**)*[28]: Bp 135—140 °C (bath temperature)/12 Torr; ^{1}H-NMR (CCl_4) δ=1.6—1.8 (m+d (δ=1.76, J=1.5 Hz), 7H), 2.2—2.6 (m, 4H), 6.44 (tq, J=1.5, 6 Hz, 1H); IR 2950, 1660, 1050, 850, 790 cm^{-1}; MS m/z (rel intensity) 125 (M^++1, 7), 124 (M^+, 53), 95 (58), 81 (46), 67 (100), 55 (31).

*3-Acetoxy-2-diethoxymethyl-1-nonene (**10**).* Acetal alcohol **2e** was acetylated with excess acetic anhydride and pyridine at room temperature for 12 h: bp 110—116 °C (bath temperature)/0.5 Torr; ^{1}H-NMR (CCl_4) δ=0.7—1.8 (m, 19H), 1.98 (s, 3H), 3.2—3.6 (m, 4H), 4.80 (br s, 1H), 5.0—5.3 (m, 3H); IR 2950, 2880, 1740, 1360, 1226, 1050 cm^{-1}; MS m/z (rel intensity) 181 (52), 103 (100), 85 (20), 75 (45), 43 (82). Found: C, 67.09; H, 10.51%. Calcd for $C_{16}H_{30}O_4$: C, 67.09; H, 10.56%.

*(E)-2-Ethyl-2-nonenal (**11**).* To lithium dimethylcuprate(I) (1.2 mmol) in ether (5 ml), **10** dissolved in ether (1 ml) was added at −18 °C and stirred for 30 min. The reaction mixture was poured into aq ammonium chloride and extracted with ether. The organic layer was concentrated and treated with aq 5% sulfuric acid (5 ml)-THF (5 ml) at room temperature for 5 min. Workup and purification by preparative TLC (hexane-ether=5:1) gave (*E*)-2-ethyl-2-nonenal (**11**) (82 mg, 61% yield) along with the (*Z*)-isomer (less than 5%). **11** gave: bp 118—120 °C (bath temperature)/18 Torr; ^{1}H-NMR (CCl_4) δ=0.90 (t, J=6.0 Hz, 3H), 0.94 (t, J=7.6 Hz, 3H), 1.1—1.8 (m, 7H), 2.0—2.6 (m, 4H), 6.28 (t, J=7.6 Hz, 1H), 9.28 (s, 1H); IR 2950, 2875, 2730, 1685, 1640, 1460, 1080, 792 cm^{-1}; MS m/z (rel intensity) 168 (M^+, 8), 149 (6), 139 (12), 111 (33), 85 (37), 79 (33), 55 (74), 41 (100). Found: m/z 168.1540. Calcd for $C_{11}H_{20}O$: M^+ 168.1514. (*Z*)-2-Ethyl-2-nonenal gave ^{1}H-NMR (CCl_4) δ=0.6—1.8 (m, 13H), 1.9—2.8 (m, 4H), 6.30 (t, J=8.0 Hz, 1H), 10.06 (s, 1H).

*Hydrolysis of **10** to 3-Acetoxy-2-methylenenonenal (**12**).* Diethyl acetal **10** (1.43 g, 5.0 mmol) was treated with THF (15 ml)-aq 5% sulfuric acid (15 ml) at room temperature for 80 min. Workup gave pure aldehyde **12** (1.06 g, quantitative yield): ^{1}H-NMR (CCl_4) δ=0.87 (t, J=5.9 Hz, 3H), 1.1—1.8 (m, 10H), 2.00 (s, 3H), 5.47 (t, J=7.5 Hz, 1H), 5.98 (s, 1H), 6.25 (s, 1H), 9.48 (s, 1H).

*Synthesis of (E)-2-Methyl-2-nonenal (**13**).*[29] *Procedure A*: To the compound **12** (50 mg, 0.23 mmol) dissolved in methanol (1 ml)-acetic acid (0.1 ml), sodium cyanotrihydroborate (11 mg, 0.18 mmol) was added at room temperature for 2 h. Workup with brine and purification by preparative TLC gave **13** (22 mg, 61% yield).

Procedure B: Iron pentacarbonyl (0.25 ml, 1.9 mmol) was added to DABCO (0.11 g, 0.94 mmol) in wet *N,N*-dimethylformamide (DMF:H_2O=98:2) (1 ml). To the resulting dark-brown solution, the compound **12** (0.10 g, 0.46 mmol) was added and allowed to react for 1 h. Quenching was effected by addition of satd ethereal solution of iodine and water. Workup and purification by preparative TLC (hexane-ether=7:1, R_f 0.40—0.55) gave **13** (67 mg, 96% yield): ^{1}H-NMR (CCl_4) δ=0.90 (t, J=6.0 Hz, 3H), 1.2—1.7 (m, 8H), 1.71 (s, 3H), 2.32 (q, J=7.0 Hz, 2H), 6.34 (t, J=7.5 Hz, 1H), 9.31 (s, 1H), IR 2940, 2730, 1685, 1640, 1465, 1225, 1070, 820, 790, 725 cm^{-1}; MS m/z (rel intensity) 154 (M^+, 5), 135 (5), 97 (50), 84 (46), 71 (68), 55 (75), 43 (100).

*Synthesis of (E)-4-Methyl-8-methylene-4,9-decadienal (**27**).* Myrcene (10.0 g, 73 mmol) was transformed with *m*-chloroperbenzoic acid (15.9 g, 73.5 mmol) in chloroform (150 ml) at 0 °C for 5 h into 6,7-epoxy-7-methyl-3-methylene-1-octene (**24**) (6.7 g, 60% yield): bp 79—81 °C/9 Torr; ^{1}H-NMR (CCl_4) δ=1.22 (s, 3H), 1.26 (s, 3H), 1.63 (dt, J=6.0, 7.6 Hz, 2H), 2.34 (dt, J=4.5, 7.6 Hz, 2H), 2.57 (t, J=6.0 Hz, 1H), 4.9—5.4 (m, 4H), 6.33 (dd, J=11.4, 18.0 Hz, 1H); IR 3090, 2930, 1595, 1465, 1240, 1115, 990, 895 cm^{-1}; MS m/z (rel intensity) 152 (M^+, 5), 137 (8), 134 (8), 119 (16), 109 (18), 93 (29), 79 (100), 71 (57), 59 (57). Found: C, 78.99; H, 10.76%. Calcd for $C_{10}H_{16}O$: C, 78.90; H, 10.59%. The epoxide **24** (0.16 g, 1.05 mmol) was added to lithium diisopropylamide (1.5 mmol) in ether (4 ml) at 0 °C, and the reaction mixture was stirred for 15 h. To this solution, acetic anhydride (1 ml) and pyridine (0.5 ml) were added and stirred at room temperature for 2 h. Workup and purification by preparative TLC (hexane-ethyl acetate=5:1, R_f 0.55—0.65) gave an acetate **25** (0.13 g, 70% yield): bp 75—85 °C (bath temperature)/11 Torr; ^{1}H-NMR (CCl_4) δ=1.6—2.3 (m+d (δ=1.72, J=0.9 Hz), 7H), 1.99 (s, 3H), 4.8—5.3 (m, 7H), 6.27 (dd, J=11.4, 17.4 Hz, 1H); IR 3030, 2935, 1735, 1650, 1595, 1225, 1020, 900 cm^{-1}; MS m/z (rel intensity) 194 (M^+, 0.3), 152 (4), 134 (8), 119 (17), 105 (11), 93 (14), 91 (16), 79 (17), 43 (100). Found: C, 74.30; H, 9.45. Calcd for $C_{12}H_{18}O_2$: C, 74.19: H, 9.34%.

The acetate **25** (3.37 g, 17.3 mmol) was added to lithium diisopropylamide (34.7 mmol) at −78 °C and stirred for 1 h at −78 °C. To this solution, *t*-butylchlorodimethylsilane (5.22 g, 34.7 mmol) dissolved in THF (10 ml)-hexamethylphosphoric triamide (3 ml) was added, and the reaction mixture was warmed up gradually to room temperature, then heated at 70 °C for 2.5 h, after cooling poured into water and extracted with ether. The organic layer was concentrated. The residue was dissolved in methanol (20 ml) and treated with aq trimethylbenzylammonium fluoride (*ca.* 0.5 ml). Workup and purification by column chromatography gave a carboxylic acid **26** (2.76 g, 82% yield): bp 70—80 °C (bath temperature)/1 Torr; ^{1}H-NMR (CCl_4) δ=1.62 (br s, 3H), 2.1—2.5 (m, 8H), 4.9—5.3 (m, 5H), 6.27 (dd, J=11.4, 17.4 Hz, 1H), 11.10 (br s, 1H); IR 3100, 2650, 1710, 1595, 1450, 990, 895 cm^{-1}; MS m/z (rel intensity) 194 (M^+, 4), 134 (7), 121 (9), 109 (12), 93 (100), 81 (46), 67 (24). Found: C, 73.93; H, 9.49%. Calcd for $C_{12}H_{18}O_2$: C, 74.19; H, 9.34%.

The carboxylic acid **26** (0.075 g, 0.38 mmol) was reduced with lithium aluminum hydride (0.026 g, 0.67 mmol) in ether. Workup and purification by preparative TLC (hexane-ether=1:2, R_f 0.40—0.50) gave an alcohol (0.058 g, 84% yield): bp 70—80 °C (bath temperature)/1 Torr; ^{1}H-NMR (CCl_4) δ=1.60 (br s, 3H), 1.9—2.3 (m, 8H), 2.70 (br s, 1H), 3.50 (t, J=6.5 Hz, 2H), 4.8—5.3 (m, 5H), 6.27 (dd, J=11.4, 17.4 Hz, 1H); IR 3350, 3090, 2980, 1595, 1445, 1060, 990 cm^{-1}; MS m/z (rel intensity) 180 (M^+, 3), 121 (9), 119 (9), 93 (100), 75 (100).

The alcohol (1.57 g, 8.7 mmol) was converted into the aldehyde **27** with pyridinium chlorochromate (PCC)[30] (5.65 g, 17.5 mmol) in 77% yield. Bp 95—105 °C (bath temperature)/15 Torr; ^{1}H-NMR (CCl_4) δ=1.61 (br s, 3H), 2.1—2.5 (m, 8H), 4.8—5.3 (m, 5H), 6.27 (dd, J=11.4, 17.4 Hz, 1H), 9.65 (s, 1H); IR 3090, 2910, 2730, 1725, 1595, 990, 895 cm^{-1}; MS m/z (rel intensity) 178 (M^+, 2), 160 (2), 145 (4), 134 (10), 119 (16), 93 (100), 85 (37). Found: C, 81.13; H, 10.33%. Calcd for $C_{12}H_{18}O$: C, 80.85; H, 10.18%.

*(E)-3-Acetoxy-2-diethoxymethyl-6-methyl-10-methylene-1,6,11-dodecatriene (**21**).* The lithium carbenoid was produced from 1,1-dibromocyclopropane (0.85 g, 3.5 mmol) and allowed to react with the aldehyde **27** (0.36 g, 2.0 mmol) to give cyclopropylmethanol, which was without purification treated with ethanol (10 ml) in the presence of potassium carbonate (1.4 g, 10 mmol). The resulting alcohol was directly acetylated to give **21** (0.59 g, 83% yield): bp 132—134

°C (bath temperature)/1 Torr; ^{1}H-NMR (CCl_4) δ=1.18 (t, J=7.4 Hz, 6H), 1.60 (br s, 3H), 1.7—2.2 (m+s (δ=1.99), 11H), 3.2—3.7 (m, 4H), 4.7—5.3 (m, 7H), 6.27 (dd, J=11.4, 17.4 Hz, 1H); IR 2990, 1740, 1595, 1450, 1230, 1115, 1050, 890 cm^{-1}; MS m/z (rel intensity) 244 (21), 217 (23), 198 (14), 183 (11), 151 (22), 149 (23), 131 (28), 123 (31), 105 (33), 93 (75), 79 (38), 43 (100). Found: C, 71.88; H, 9.96%. Calcd for $C_{21}H_{34}O_4$: C, 71.96; H, 9.78%.

(E)-3-Acetoxy-2,10-dimethylene-6-methyl-6,11-dodecadienal (22). The diethyl acetal (**21**) (0.45 g, 1.29 mmol) dissolved in dichloromethane (1 ml) was treated with silica gel (Wakogel C-100) (1.36 g) and 10% aq oxalic acid (0.14 ml) in dichloromethane (3 ml) at room temperature for 1 h. The reaction mixture was neutralized with sodium hydrogencarbonate (0.045 g), and then filtered. Concentration of the filtrate and purification by column chromatography gave the desired aldehyde (**22**) (0.31 g, 87% yield): bp 120 °C (bath temperature)/1 Torr; ^{1}H-NMR (CCl_4) δ=1.60 (br s, 3H), 1.6—2.3 (m+s (δ=2.03), 11H), 4.9—5.6 (m, 6H), 5.97 (br s, 1H), 6.21 (dd, J=11.4, 17.4 Hz, 1H), 6.24 (br s, 1H), 9.50 (s, 1H); IR 3080, 2700, 1740, 1690, 1595, 1440, 1220, 1050, 1020, 895 cm^{-1}; MS m/z (rel intensity) 221 (5), 188 (6), 173 (5), 145 (8), 133 (19), 119 (19), 105 (20), 93 (100), 79 (37). Found: C, 73.99; H, 8.84%. Calcd for $C_{17}H_{24}O_3$: C, 73.88; H, 8.75%.

Transformation of 22 into β-Sinensal (23). Iron pentacarbonyl (0.91 ml, 1.45 mmol) was added to **22** (90 mg, 0.33 mmol) dissolved in a mixture of DABCO (81 mg, 0.72 mmol) and DMF-water (98:2, 1 ml), and the whole was stirred at room temperature for 1 h. Workup gave **23**[17] in 95% yield: ^{1}H-NMR (CCl_4) δ=1.63 (br s, 3H), 1.71 (br s, 3H), 1.9—2.6 (m, 8H), 4.8—5.3 (m, 5H), 6.1—6.5 (m, 2H), 9.28 (s, 3H); IR 2940, 2740, 1680, 1655, 1595, 990, 893 cm^{-1}; MS m/z (rel intensity) 218 (M^+, 5), 203 (3), 190 (10), 133 (26), 93 (100), 81 (39).

Preparation of (4E,8E)-4,8-Dimethyl-10-triphenylmethoxy-4,8-decadienal (20). A pyridine (100 ml) solution of geraniol (15.4 g, 0.10 mol) and triphenylmethyl chloride (35.0 g, 0.12 mol) was refluxed for 15 h. Evaporation of the pyridine under reduced pressure followed by column chromatography gave the geranyl triphenylmethyl ether in 33% yield: ^{1}H-NMR (CCl_4) δ=1.46 (s, 3H), 1.61 (s, 3H), 1.67 (s, 3H), 1.9—2.1 (m, 4H), 3.52 (d, J=6 Hz, 2H), 4.9—5.1 (m, 1H), 5.2—5.5 (m, 1H), 7.0—7.5 (m, 15H); IR 3080, 3050, 2950, 1670, 1600, 1495, 1455, 1050, 900, 765, 748, 710 cm^{-1}.

The geranyl triphenylmethyl ether (13.0 g, 32.7 mmol) was treated with *m*-chloroperbenzoic acid (7.1 g, 32.7 mmol) in chloroform (30 ml) at 0 °C for 2.5 h. Purification by column chromatography gave the epoxide **17** (7.9 g, 58% yield): ^{1}H-NMR (CCl_4) δ=1.22 (s, 3H), 1.25 (s, 3H), 1.47 (s, 3H), 1.5—1.6 (m, 2H), 2.13 (d, J=8 Hz, 2H), 2.50 (t, J=6 Hz, 1H), 3.53 (d, J=6 Hz, 2H), 5.42 (t, J=7 Hz, 1H), 7.0—7.5 (m, 15H); IR 3080, 2980, 1672, 1598, 1495, 1454, 1050, 900, 765, 750, 710 cm^{-1}.

The epoxide **17** (8.0 g, 19 mmol) was isomerized with lithium diethylamide (20 mmol) in ether for 48 h to an allylic alcohol (4.5 g, 57% yield) which showed: ^{1}H-NMR (CCl_4) δ=1.3—1.8 (m+s (δ=1.47, 3H)+d (δ=1.70, J=1.2 Hz, 3H), totally 9H), 1.9—2.2 (m, 2H), 3.53 (d, J=6 Hz, 2H), 3.93 (t, J=6 Hz, 1H), 4.74 (t, J=2 Hz, 1H), 4.87 (quintet, J=1.2 Hz, 1H), 5.41 (t, J=6 Hz, 1H), 7.0—7.5 (m, 15H); IR 3400, 3080, 1650, 1600, 1495, 1453, 1045, 900, 765, 712 cm^{-1}.

The alcohol (4.0 g, 9.8 mmol) was treated with acetic anhydride (10 ml) and pyridine (10 ml) at room temperature for 12 h to give **18** in 93% yield: ^{1}H-NMR (CCl_4) δ=1.47 (s, 3H), 1.5—1.8 (m+d (δ=1.72, J=1.2 Hz), 5H), 1.8—2.1 (m+s (δ=1.97), 5H), 3.53 (d, J=6 Hz, 2H), 4.83 (t, J=2 Hz, 1H), 4.91 (quintet, J=1.2 Hz, 1H), 5.09 (t, J=6 Hz, 1H), 5.39 (t, J=6 Hz, 1H), 7.0—7.5 (m, 15H); IR 3070, 2940, 1738, 1649, 1595, 1490, 1450, 1225, 1042, 895, 763 cm^{-1}.

The acetate **18** was converted into a carboxylic acid **19** in 85% yield as described for the transformation of **25** into **26**. ^{1}H-NMR ($CDCl_3$) δ=1.45 (s, 3H), 1.61 (s, 3H), 1.9—2.1 (m, 4H), 2.2—2.5 (m, 4H), 3.53 (d, J=6 Hz, 2H), 5.0—5.2 (m, 1H), 5.33 (t, J=6 Hz, 1H), 7.0—7.5 (m, 15H), 10.0—10.2 (m, 1H); IR 3080, 2950, 1710, 1598, 1494, 1453, 1045, 765, 710 cm^{-1}.

The carboxylic acid **19** was reduced with lithium aluminum hydride to give an alcohol, which was converted into the aldehyde **20** with pyridinium chlorochromate in 80% yield: ^{1}H-NMR (CCl_4) δ=1.43 (s, 3H), 1.61 (s, 3H), 1.9—2.0 (m, 4H), 2.1—2.4 (m, 4H), 3.56 (d, J=6 Hz, 2H), 5.0—5.2 (m, 1H), 5.40 (t, J=6 Hz, 1H), 7.0—7.5 (m, 15H), 9.53 (t, J=0.6 Hz, 1H); IR 3080, 2940, 2740, 1725, 1672, 1596, 1492, 1450, 1048, 900, 765, 750, 710 cm^{-1}. Found: C, 85.02; H, 7.96%. Calcd for $C_{31}H_{34}O_2$: C, 84.89; H, 7.81%.

(6E,10E)-3-Acetoxy-2-diethoxymethyl-6,10-dimethyl-12-triphenylmethoxy-1,6,10-dodecatriene (14): ^{1}H-NMR (CCl_4) δ=1.17 (t, J=7.2 Hz, 6H), 1.46 (s, 3H), 1.5—2.1 (m+s (δ=1.60, 3H)+s (δ=1.93, 3H), totally 14H), 3.2—3.6 (m, 6H), 4.78 (s, 1H), 5.0—5.5 (m, 5H), 7.0—7.5 (m, 15H); IR 2990, 1740, 1452, 1230, 1115, 1050, 765, 710 cm^{-1}.

(2E,6E,10E)-2-Ethyl-6,10-dimethyl-12-triphenylmethoxy-2,6,10-dodecatrienal (15). To lithium dimethylcuprate(I) (0.6 mmol) in ether (3 ml), allylic acetate (**14**) (0.12 g, 0.20 mmol) was added at −18 °C and the resulting mixture was stirred for 30 min at −18 °C. Workup followed by hydrolysis with aq 5% sulfuric acid-THF (1:1) and isomerization with potassium carbonate (8 mg) in methanol (12 ml) at 40 °C for 15 h gave **15** (0.072 g, 73% yield): ^{1}H-NMR (CCl_4) δ= 0.92 (t, J=7.5 Hz, 3H), 1.47 (s, 3H), 1.63 (s, 3H), 2.0—2.5 (m, 10H), 3.52, (d, J=7.2 Hz, 2H), 5.0—5.2 (m, 1H), 5.37 (t, J=7.0 Hz, 1H), 6.22 (t, J=7.2 Hz, 1H), 7.0—7.5 (m, 15H), 9.23 (s, 1H); IR 3080, 3000, 2950, 2740, 1688, 1644, 1598, 1494, 1453, 1046 710 cm^{-1}.

(2E,6E,10E)-2-Ethyl-6,10-dimethyl-12-triphenylmethoxy-2,6,10-dodecatrien-1-ol. The aldehyde **15** was reduced with sodium borohydride (quantitative yield): ^{1}H-NMR (CCl_4) δ= 0.97 (t, J=7 Hz, 3H), 1.47 (s, 3H), 1.62 (s, 3H), 1.8—2.2 (m, 10H), 3.52 (d, J=6 Hz, 2H), 3.88 (s, 2H), 5.0—5.5 (m, 3H), 7.0—7.5 (m, 15H); IR 3320, 3080, 2930, 1665, 1596, 1494, 1452, 1050, 900, 750, 710 cm^{-1}. Found: C, 85.15; H. 8.72%. Calcd for $C_{35}H_{42}O_2$: C, 84.97; H, 8.56%.

(2E,6E,10Z)-3,7,11-Trimethyl-2,6,10-tridecatriene-1-ol triphenyl methyl Ether (16). To the above alcohol (77 mg, 0.16 mmol) dissolved in THF (2 ml), sulfur trioxide-pyridine complex (49 mg, 0.31 mmol) was added at 0 °C. After 3 h, lithium aluminum hydride (*ca.* 50 mg) was added and the reaction was heated to reflux for 3 h. Workup and purification by preparative TLC (hexane-ether=5:1, R_f 0.80) gave **16**[31] 58 mg, 78% yield): ^{1}H-NMR (CCl_4) δ=0.94 (t, J=7.5 Hz, 3H), 1.48 (s, 3H), 1.61 (s, 3H), 1.64 (s, 3H), 1.7—2.1 (m, 10H), 3.52 (d, J=6.0 Hz, 2H), 4.9—5.1 (m, 2H), 5.39 (d, J=6.0 Hz, 1H), 7.0—7.5 (m, 15H); IR 3080, 2990, 2940, 1665, 1596, 1494, 1453, 1050, 900, 745, 710 cm^{-1}.

Preparation of 3-Bromo-1,1-diethoxy-4-decanone (29a). To dimethyl sulfoxide (DMSO) (1.56 g, 20.0 mmol) dissolved in dichloromethane (20 ml), trifluoroacetic anhydride (3.15 g, 15.0 mmol) in dichloromethane (5 ml) was added over 10 min at −78 °C. After 10 min, a dichloromethane solution (5 ml) of the alcohol **1e** (prepared from **3** (15 mmol) and heptanal (9.65 mmol), and used without purification) was added over a period of 10 min at −78 °C, and the resulting solution was stirred for 70 min before quenching with triethylamine (4 ml), then warmed up and stirred for 70 min at room temperature. Workup gave a crude cyclopropyl ketone **28a** which was dissolved in ethanol (15 ml) containing a catalytic amount of boron trifluoride ether complex (*ca.* 50 mg) for 2 h at room temperature. Workup and purification by column chromatography (hexane-ether=10:1) gave **29a** (2.32g, 74% yield): ^{1}H-NMR (CCl_4) δ=0.89 (t, J=5.6 Hz, 3H), 1.13 (t,

J=7.1 Hz, 3H), 1.17 (t, J=7.1 Hz, 3H), 1.3—1.8 (m, 8H), 1.9—2.9 (m, 4H), 3.2—4.1 (m, 4H), 4.27 (t, J=7.4 Hz, 1H), 4.47 (dd, J=4.7, 6.3 Hz, 1H); IR 2940, 1715, 1460, 1360, 1120, 1155 cm^{-1}; MS m/z (rel intensity) 280 (5), 279 (4), 278 (5), 277 (5), 197 (24), 113 (17), 103 (100), 97 (33), 85 (70), 75 (43).

Synthesis of 4-Oxodecanal (30a). Lithium aluminum hydride (48 mg, 1.25 mmol) was added to the suspension of chromium(III) chloride (0.40 g, 2.50 mmol) in THF (2 ml) at 0 °C. To the resulting dark brown reagent[21], the α-bromo ketone **29a** (0.17 g, 0.52 mmol) was added, and the whole was stirred for 1 h at room temperature. Workup gave a crude keto acetal (0.13 g) which was stirred in a mixture of THF (3 ml) and aq 15% sulfuric acid (1 ml) at room temperature for 1.5 h. Workup and purification by column chromatography (hexane-ether=3:1) gave **30a**[22] (70 mg, 80% yield): ^{1}H-NMR (CCl_4) δ=0.7—1.1 (m, 3H), 1.1—1.8 (m, 8H), 2.38 (t, J=7.4 Hz, 2H), 2.63 (s, 4H), 9.72 (s, 1H); IR 2940, 2740, 1705, 1460, 1405, 1125, 865 cm^{-1}; MS m/z (rel intensity) 170 (M^+, 1), 113 (35), 100 (24), 85 (79), 72 (52), 57 (47), 43 (100).

Preparation of (Z)-3-Bromo-1,1-diethoxy-7-decen-4-one (29b). The lithium carbenoid **3** was prepared from 1,1-dibromo-2-ethoxycyclopropane (0.44 g, 1.79 mmol), butyllithium (1.98 M hexane solution, 0.88 ml, 1.75 mmol) and allowed to react with (Z)-heptenal (0.12 g, 1.04 mmol). The produced alcohol was oxidized without purification by the Swern's method as described for the oxidation of **1e** to give **28b** which was stirred in ethanol (5 ml) containing acetic acid (*ca.* 15 mg) at room temperature for 4 h. Workup gave **29b** (0.26 g, 77% yield): ^{1}H-NMR (CCl_4) δ=0.98 (t, J=8.4 Hz, 3H), 1.16 (t, J=6.6 Hz, 3H), 1.19 (t, J=6.6 Hz, 3H), 1.9—3.0 (m, 8H), 3.3—3.8 (m, 4H), 4.33 (t, J=6.6 Hz, 1H), 4.52 (dd, J=9.6, 15.6 Hz, 1H), 5.1—5.5 (m, 2H); IR 2980, 1720, 1450, 1380, 1125, 1160, 790 cm^{-1}; MS m/z (rel intensity) 277 (8), 275 (8), 195 (66), 167 (22), 149 (22), 103 (98), 85 (61), 75 (88), 55 (88), 47 (100). Found: m/z 275.0616. Calcd for $C_{12}H_{20}O_2Br$ (M-OEt): M 275.0646.

Synthesis of (Z)-4-Oxo-7-decenal (30b). Reduction of **29b** with the $CrCl_3$-$LiAlH_4$ reagent[21] gave **30b** in 91% yield: ^{1}H-NMR (CCl_4) δ=0.97 (t, J=7.2 Hz, 3H), 1.7—2.8 (m+s (δ=2.65, 4H), totally 10H), 5.0—5.5 (m, 2H), 9.73 (s, 1H); IR 3055, 2960, 1720, 1415, 1095, 1020, 865, 720 cm^{-1}; MS m/z (rel intensity) 168 (M^+, 3), 149 (7), 123 (35), 95 (37), 85 (91), 69 (51), 68 (53), 55 (86), 41 (100).

(E)-4-Oxo-2-decenal (32). The bromo acetal **29a** (0.17 g, 0.52 mmol) was treated with THF (3 ml)-aq 15% sulfuric acid (2 ml) at room temperature for 5 h. Workup and purification by preparative TLC (hexane-ethyl acetate=10:1, double development) gave **32** (56 mg, 64% yield): ^{1}H-NMR (CCl_4) δ=0.91 (t, J=5.7 Hz, 3H), 1.1—1.9 (m, 8H), 2.65 (t, J=6.9 Hz, 2H), 6.7—6.9 (m, 2H), 9.75 (dd, J=1.8, 5.4 Hz, 1H); IR 2950, 2750, 1700, 1625, 1115, 1080, 980 cm^{-1}; MS m/z (rel intensity) 168 (M^+, 6), 139 (47), 125 (15), 111 (20), 98 (83), 83 (77), 70 (58), 55 (94), 43 (100). Found: m/z 168.1158. Calcd for $C_{10}H_{16}O_2$: M 168.1149.

References

1) a) R. Wenkert, *Acc. Chem. Res.*, **13**, 27 (1980); b) T. Hiyama and H. Nozaki, *J. Synth. Org. Chem. Jpn.*, **35**, 979 (1977); c) D. Tunemoto and K. Kondo, *ibid.*, **35**, 1070 (1977); d) M. Murakami and S. Nishida, *ibid.*, **41**, 22 (1983); e) M. Demuth and G. Mikhail, *Tetrahedron*, **39**, 991 (1983).

2) a) G. Köbrich, *Angew. Chem., Int. Ed. Engl.*, **11**, 473 (1972); b) K. Kitatani, T. Hiyama, and H. Nozaki, *Bull. Chem. Soc. Jpn.*, **50**, 3288 (1977); c) T. Hiyama, S. Takehara, K. Kitatani, and H. Nozaki, *Tetrahedron Lett.*, **1974**, 3295; d) K. Kitatani, H. Yamamoto, T. Hiyama, and H. Nozaki, *Bull. Chem. Soc. Jpn.*, **50**, 2158 (1977); e) H. Taguchi, H. Yamamoto, and H. Nozaki, *ibid.*, **50**, 1588 (1977); f) K. G. Taylor, *Tetrahedron*, **38**, 2751 (1982).

3) A part of this work was published in a communication form: T. Hiyama, A. Kanakura, H. Yamamoto, and H. Nozaki, *Tetrahedron Lett.*, **1978**, 3047 and 3051.

4) a) Y. Bessière, D. N. Savary, and M. Schlosser, *Helv. Chim. Acta*, **60**, 1739 (1977); b) L. Skatteböl, *J. Org. Chem.*, **31**, 1554 (1966); c) G. Stork, M. Nussim, and B. August, *Tetrahedron*, Suppl. 8, Part I, pp 105 (1966); d) G. Stork and T. L. Macdonald, *J. Am. Chem. Soc.*, **97**, 1264 (1975); e) P. Amice, L. Blanco, and J. M. Conia, *Synthesis*, **1976**, 196; f) E. Wenkert, D. A. Berges, N. F. Gollob, *J. Am. Chem. Soc.*, **100**, 1263 (1978); g) E. Wenkert and D. A. Berges, ibid., **89**, 2507 (1967); h) Y. Ito, S. Fujii, and T. Saegusa, *J. Org. Chem.*, **41**, 2073 (1976); i) T. Hiyama, T. Mishima, K. Kitatani, and H. Nozaki, *Tetrahedron Lett.*, **1974**, 3297; j) M. S. Baird and P. D. Slowey, *ibid.*, **23**, 3795 (1982); k) L. Blanco, P. Amice, and J.-M. Conia, *Synthesis*, **1981**, 289, 291; l) F. Camps, J. Coll, G. Fabriás, A Gurrero, and M. Riba, *Tetrahedron Lett.*, **24**, 3387 (1983).

5) a) K. Hayashi, J. Iyoda, and I. Shiihara, *J. Organomet. Chem.*, **10**, 81 (1967); b) D. Seyferth, H. Yamazaki, and D. L. Alleston, *J. Org. Chem.*, **28**, 703 (1963).

6) a) K. G. Taylor, W. E. Hobbs, M. S. Clark, and J. Chaney, *J. Org. Chem.*, **37**, 2436 (1972); b) K. G. Taylor, W. E. Hobbs, and M. Saquet, *ibid.*, **36**, 369 (1971); c) J. D. White and L. G. Wade, Jr., *ibid.*, **40**, 118 (1975).

7) E. J. Corey and P. Ulrich., *Tetrahedron Lett.*, **1975**, 3685.

8) a) J. Ficini and J.-C. Depezay, *Tetrahedron Lett.*, **1969**, 4797; b) J.-C. Depezay and Y. Le Merrer, *ibid.*, **1974**, 2751, 2755; c) J. P. Marino and J. S. Farima, *ibid.*, **1975**, 3901; d) P. A. Grieco, C.-L. J. Wang, and G. Majetich, *J. Org. Chem.*, **41**, 726 (1976).

9) For example 3-trialkylsilyl-3-buten-2-one is a useful annulation reagent: a) G. M. Ksander, J. E. McMurry, and M. Johnson, *J. Org. Chem.*, **42**, 1180 (1977); b) G. Stork and B. Ganem, *J. Am. Chem. Soc.*, **95**, 6152 (1973); c) G. Stork and J. Singh, *ibid.*, **96**, 6181 (1974); d) R. K. Boeckman, Jr., *ibid.*, **95**, 6867 (1973); e) idem, ibid., **96**, 6179 (1974).

10) The configuration of the carbenoid is discussed by Taylor (ref 6a) and lithium ion is found to occupy the exo position cis to methoxyl group. The intramolecular coordination effect by the adjacent methoxyl group seems extremely remarkable to reverse the configuration of the carbenoid predominating in the absence of the methoxyl group. See Ref. 2b.

11) Orbital symmetry rule suggests 7-*endo*-halonorcarane is amenable to ring opening reaction under solvolytic conditions, while 7-*exo*-halo isomer remains unchanged. See R. B. Woodward and R. Hoffmann, "The Conservation of Orbital Symmetry," Verlag Chemie GmbH, Weinheim, Germany, 1970, p 56.

12) R. J. Anderson, C. A. Henrick, and J. B. Siddall, *J. Am. Chem. Soc.*, **92**, 735 (1970).

13) The cuprate reactions are explained (Ref. 12) to proceed through one-electron transfer yielding an allyl radical i of the thermodynamically favorable W form. Subseqent methyl transfer, therefore, should give (Z)-olefin ii and hence iii. In fact iii [NMR (CCl_4): δ=6.30 (t, J=8 Hz, 1H), 10.06 (s, 1H)] was the major product when deacetalization was performed carefully, but isomerization to **11** occurred rapidly and completely upon purification on silica gel. Formation of an S_N2 type product iv was less than 5%.

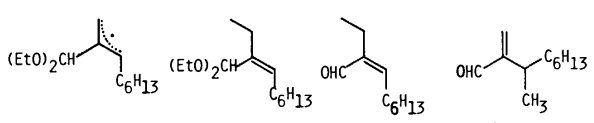

i ii iii iv

14) a) E. J. Corey, J. A. Katzenellenbogen, N. W. Gilman, S. A. Roman, and B. W. Erickson, *J. Am. Chem. Soc.*, **90**, 5618

(1968); b) E. J. Corey and H. Yamamoto, *ibid.*, **92**, 6637 (1970); c) S. Tanaka, H. Yamamoto, H. Nozaki, K. B. Sharpless, R. C. Michaelson, and J. D. Cutting, *ibid.*, **96**, 5254 (1974); d) Synthesis of a cyclic analog: C. Wawrzenczyk and A. Zabza, *Tetrahedron*, **36**, 3091 (1980).

15) E. J. Corey and K. Achiwa, *J. Org. Chem.*, **34**, 3667 (1969).

16) R. Noyori, I. Umeda, and T. Ishigami, *J. Org. Chem.*, **37**, 1542 (1972).

17) a) A. F. Thomas, *J. Chem. Soc., Chem. Commun.*, **1967**, 947. *idem*, *J. Am. Chem. Soc.*, **91**, 3281 (1969); b) G. Büchi and H. Wüest, *Helv. Chim. Acta*, **50**, 2440 (1967); c) E. Bertele and P. Schudel, *ibid.*, **50**, 2445 (1967); d) M. Baumann, W. Hoffmann, H. Pommer, *Liebigs Ann. Chem.*, **1976**, 1626; e) β-sinensal synthesis: G. Büchi and H. Wüest, *J. Am. Chem. Soc.*, **96**, 7573 (1974); O. P. Vig, R. C. Aggarwal, S. S. Bari, and S. D. Sharma, *Indian J. Chem., Sect. B* **1979**, 33; *Chem. Abstr.*, **92**, 22622f; T. Mimura, Y. Kimura, and T. Nakai, *Chem. Lett.*, **1979**, 1361. K. Sato, S. Inoue, and K. Watanabe, *J. Chem. Soc. Perkin Trans I*, **1981**, 2411.

18) F. Huet, A. Lechevallier, M. Pellet, and J. M. Conia, *Synthesis*, **1978**, 63.

19) S. Danishefsky, R. Mckee, and R. K. Singh, *J. Am. Chem. Soc.*, **99**, 4783 (1977).

20) a) K. Omura, A. K. Sharma, and D. Swern, *J. Org. Chem.*, **41**, 957 (1976); b) S. L. Huang, K. Omura, and D. Swern, *Synthesis*, **1978**, 297.

21) a) Y. Okude, S. Hirano, T. Hiyama, and H. Nozaki, *J. Am. Chem. Soc.*, **99**, 3179 (1977); b) Y. Okude, T. Hiyama, and H. Nozaki, *Tetrahedron Lett.*, **1977**, 3829; c) T. Hiyama, K. Kimura, and H. Nozaki, *ibid.*, **22**, 1037 (1981); d) T. Hiyama, Y. Okude, K. Kimura, and H. Nozaki, *Bull. Chem. Soc. Jpn.*, **55**, 561 (1982).

22) K. Oshima, H. Yamamoto, and H. Nozaki, *J. Am. Chem. Soc.*, **95**, 4446 (1973).

23) a) T. Mukaiyama, K. Narasaka, and M. Furusato, *J. Am. Chem. Soc.*, **94**, 8641 (1972); b) P. A. Grieco, *J. Org. Chem.*, **37**, 2363 (1972).

24) A. I. Meyers, A. Nabeya, H. W. Adickes, I. R. Politzer, G. R. Malone, A. C. Koveleskey, R. L. Nolen, and R. C. Portnoy, *J. Org. Chem.*, **38**, 36 (1973).

25) G. Büchi and B. Egger, *J. Org. Chem.*, **36**, 2021 (1971).

26) C. Broquet and A.-M. Touzin, *Bull. Soc. Chim. Fr.*, **1972**, 2488.

27) a) D. G. Lindsay and C. B. Rese, Tetraheron, **21**, 1673 (1965); b) K. G. Taylar, W. E. Hobbs, M. S. Clark, and J. Chaney, *J. Org. Chem.*, **37**, 2436 (1972).

28) T. Shono, J. Hayashi, H. Omoto, and Y. Matsumura, *Tetrahedron Lett.*, **1977**, 2667.

29) M. Dedieu and Y.-L. Pascal, *Bull. Soc. Chim. Fr.*, **1978**, 593.

30) E. J. Corey and J. W. Suggs, *Tetrahedron Lett.*, **1975**, 2647.

31) A. Yasuda, S. Tanaka, H. Yamamoto and H. Nozaki, *Bull. Chem. Soc. Jpn.*, **52**, 1701 (1979).

The Asymmetric Ullmann Coupling Reaction of Chiral Diol Diesters of 1-Bromo-2-naphthoic Acid and 2-Halo-3-nitrobenzoic Acids: Highly Diastereoselective Synthesis of Atropisomeric 6,6'-Dinitrodiphenic Acids[1)]

Sotaro MIYANO,* Shigeru HANDA, Kunitoshi SHIMIZU,
Katsuya TAGAMI, and Harukichi HASHIMOTO
Department of Applied Chemistry, Faculty of Engineering, Tohoku University, Aramaki-Aoba, Sendai 980
(Received December 5, 1983)

The copper-promoted Ullmann reaction of chiral diol diesters of 1-bromo-2-naphthoic acid induced axial dissymmetry into the newly formed 1,1'-binaphthyl bond: chiral diol, apparent net optical yield for the joining of two naphthyl units, and axial chirality induced are as follows: (*S*)-1,1'-binaphthyl-2,2'-diol, 71%, *S*; (1*S*,2*S*)-1,2-diphenyl-1,2-ethanediol, 32%, *S*; (1*R*,2*R*)-1,2-bis(ethoxycarbonyl)-1,2-ethanediol, 33%, *S*; (4*S*,5*S*)-bis(hydroxymethyl)-2,2-dimethyl-1,3-dioxolane, 3.7%, *R*. The reaction of (*R*)-1,1'-binaphthyl-2,2'-diol esters of 2-halo-3-nitrobenzoic acids gave up to 85% net optical yield for the coupling; the intramolecular cyclization proceeded with virtually complete diastereoselectivity to give cyclic diester of *R*,*R*-configuration in a 42% isolated yield. This remarkable stereocontrol is ascribed to the steric requirement of the 12-membered cyclic diester structure containing rigid 1,1'-binaphthyl and 1,1'-biphenyl moiety.

Although axially dissymmetric biaryl skeletons have been successfully utilized in the asymmetric recognition,[2)] direct route to the requisite chiral biaryls are limited.[3)] Thus, the construction of atropisomeric biaryls by asymmetric induction represents a potential value. Recently two groups disclosed elegant synthesis of chiral binaphthyls through nucleophilic aromatic displacement using oxazolines as the activating substituents for the naphthalene nucleus.[4,5)]

In the previous paper,[1)] we have reported asymmetric synthesis of atropisomeric 1,1'-binaphthyl derivatives (**3** and **4**) *via* the Ullmann reaction of chiral 1,1'-binaphthyl-2,2'-diol esters (**1a**) of 1-bromo-2-naphthoic acid followed by cleavage of the ester linkage (Scheme 1).

Herein we wish to report the effects of the diol structure on the induction of axial dissymmetry in the asymmetric Ullmann reaction, and an extention to a highly diastereoselective synthesis of chiral 6,6'-dinitrodiphenic acids.

Results and Discussion

Induction of Axial Dissymmetry into 1,1'-Binaphthyl Bond. Chiral diols (**2a—2d**) were converted into respective diesters **1a—1d** by the reaction with 1-bromo-2-naphthoyl chloride in benzene-pyridine. These bifunctional substrates were treated with activated copper powder in gently-refluxing DMF to give thoroughly debrominated products. As evidenced by TLC and HPLC, these mixtures were comprised of many components containing intramolecularly coupled cyclic diester **7**, the reduction product **8**, and various oligomers formed *via* intermolecular reactions. The ester linkage of the reaction products was reductively cleaved to hydroxymethyl function by the treatment with lithium aluminum hydride (LAH). The apparent net optical yields for the induction of axial dissymmetry in joining two naphthyl units by the asymmetric Ullmann reaction were estimated from the optical rotations of the 2,2'-bis(hydroxymethyl)-1,1'-binaphthyls **4** thus obtained (Table 1).

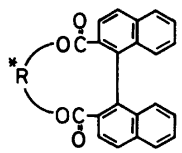

7

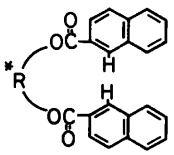

8

It is noted that axially dissymmetric 1,1'-binaphthyl-2,2'-diol (*S*)-**2a** gave relatively high optical yields of up to 71% under dilution conditions. In the previous paper,[1)] we reported that the intramolecular coupling of (*S*)-**1a** proceeds with complete diastereoselectivity to

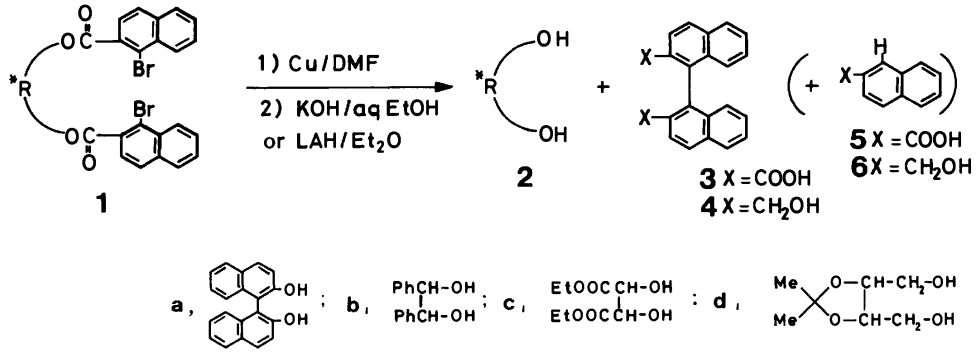

Scheme 1.

Table 1. Asymmetric ullmann coupling of chiral diol diesters of 1-bromo-2-naphthoic acid[a)]

1	Reaction conditions: 1 (mmol)	Cu (g)	DMF (ml)	Addn time/h	4: Optical purity/%[b)]	Config
(*S*)-**1a**	0.401	1.0	10	—[c)]	45	*S*
	1.25	2.0	80	5	57	*S*
	0.864	2.0	60	8	71	*S*
(*S*)-**1b**	2.92	2.0	60	1	23	*S*
	2.78	2.0	100	5	32	*S*
(*R*)-**1c**	2.86	2.0	80	5	33	*S*
(*S*)-**1d**	1.99	3.0	50	5	3.7	*R*

a) A solution of **1** in DMF was added to a gently-refluxing suspension of copper powder in DMF. After the addition, the reaction was continued for another 2 h. b) Calculated on the basis of the value for optically pure (*S*)-**4**; $[\alpha]_{546}^{23}$ —86.0° (*c* 1.43, acetone). See Ref. 1. c) Result from Ref. 1 where a mixture of diester and copper powder in DMF was heated at 120—130 °C for 10 h.

give cyclic diester (*S,S*)-**7a** with no detectable amount of (*S,R*)-isomer. This remarkable stereocontrol is ascribed to the steric requirement in assembling 12-membered cyclic diester which contains two sets of 1,1′-binaphthyl residues. However, competing intermolecular coupling of **1** to oligomeric products seems hardly to induce axial dissymmetry in the joining of two naphthyl moieties,[1,6] thus reducing the overall optical yield for the synthesis of chiral binaphthyls *via* the route depicted in Scheme 1. Thus, the substantial improvement of the optical yields under dilution reaction conditions should be attributed to the enhancement of the unimolecular process.

C-Chiral 1,4-diol (*S*)-**2d** was almost ineffective to cause asymmetric induction, while 1,2-diols such as (1*S*,2*S*)-1,2-diphenyl-1,2-ethanediol ((*S*)-**2b**) and (1*R*, 2*R*)-1,2-bis(ethoxycarbonyl)-1,2-ethanediol ((*R*)-**2c**) induced *S* chirality into the binaphthyl linkage with moderate optical yields. As was stated above, intermolecular coupling of chiral 1-bromo-2-naphthoates seems not so effective in asymmetric induction, the monocyclization step to **7** is critical for determining the overall optical yield in Scheme 1. In this respect, 1,2-ethanediol **2b** and **2c** seem not so strictly control the stereochemistry of monocyclization as binaphthol **2a**. Actually, (*S*)-**1b** gave the cycle **7b** as a mixture of (*S,S*)- and (*S,R*)-isomer in a ratio of 5.2:1 (*i.e.* 68% diastereomeric excess) based on HPLC of the crude reaction mixture (5-h addition reaction in Table 1).

Examination of CPK molecular models does not show so much difference in steric distortions between the diastereomeric cycles (*S,S*)- and (*S,R*)-**7b**, showing sharp contrast to the possible cycles (*S,S*)- and (*S,R*)-**7a** from (*S*)-**1a**.[1] In the case of (*S,R*)-**7b**, however, the lone pair electrons on one of the ester oxygen seem to strongly interact with one naphthalene ring plane. Another explanation for the preferential formation of (*S,S*)-**7b** over (*S,R*)-counterpart may involve the inspection of plausible conformers of (*S*)-**1b** which may lead

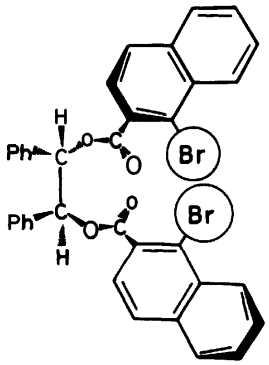

Fig. 1. Conformer (*S*)-**1b**-*S* to (*S,S*)-**7b**.

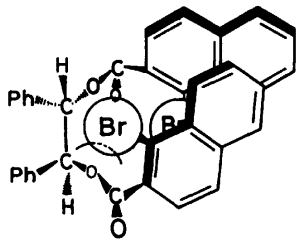

Fig. 2. Conformer (*S*)-**1b**-*R* to (*S,R*)-**7b**.

to the coupling stages and thus may reflect transition states. As schematically shown in Figs. 1 and 2, the conformer (*S*)-**1b**-*S* which may lead to *S,S*-coupling will be significantly favored over (*S*)-**1b**-*R* conformer to *S,R*-coupling because of the severe steric distortion in the latter caused by inwardly directed bromine and one ester oxygen atom. This reasoning is based on the assumption that the central mechanistic feature of the Ullmann coupling reaction involves intermediary of organocopper species and free radicals do not play critical role, thus imposing relatively high steric requirements in the coupling process.[7,8]

Although we have been unable to resolve reaction products from (*R*)-**1c**, similar rationalization as above may be applied to explain the preferential formation of (*S*)-binaphthyl (*S*)-**4**: Phenyl and ethoxycarbonyl substituents do not exert meaningful differences on the plausible conformers depicted in Fig. 1 and 2. This may explain the similarity of the magnitudes of asymmetric induction and the sense of chirality with (*S*)-**2b** and (*R*)-**2c**.

Highly Asymmetric Synthesis of Chiral 6,6′-Dinitrodiphenic Acids. Knowing that 1,1′-binaphthyl-2,2′-diol is the best chiral auxiliary among the diols examined, we tried the reaction of diether **9**, but did not observe any sign of debromination after an elongated treatment with activated copper powder at reflux in DMF.[9]

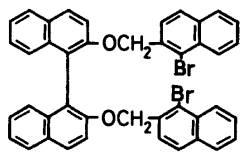

9

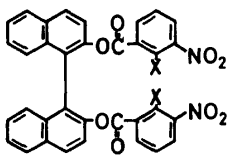

10 X = I
11 X = Cl
12 X = H

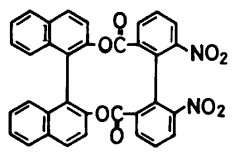

13

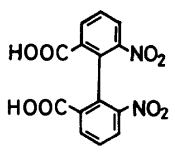

14

It is well known that electron-withdrawing substituents activate aromatic nucleus toward the Ullmann reaction.[8] Hoping to enhance the key unimolecular coupling, we tried the reaction of 2-halo-3-nitrobenzoic acid esters (**10** and **11**). A reaction of (*R*)-2,2′-bis(2-iodo-3-nitrobenzoyloxy)-1,1′-binaphthyl ((*R*)-**10**) was carried out as above. HPLC of the reaction mixture showed the presence of, in the order of elution, the cyclic diester (*R,R*)-**13** as the major component as expected (*ca.* 70% of the HPLC peak area by UV absorption at 254 nm), the reduction product (*R*)-**12** (*ca.* 10%), and others. It has been our general experience that monomeric cyclic diesters **7** are more mobile than the open chain counterparts **8** on chromatography. After a hydrolytic treatment and standard extractive workup followed by TLC, a sample of (*R*)-6,6′-dinitrodiphenic acid ((*R*)-**14**) was recovered in *ca.* 50% chemical yield, with $[\alpha]_D^{22}$+116° in 95% EtOH, indicating a 85% optical yield based on the rotation of enantiomerically pure (*R*)-**14** (*vide infra*). It should be noted that the chiral source (*R*)-**2a** was recovered without appreciable loss of optical activity. Similarly, (*S*)-diacid ((*S*)-**14**) was obtainable by the reaction of (*S*)-**10**.

The dichloro ester (*R*)-**11**, prepared from commercially available 2-chloro-3-nitrobenzoic acid, gave analogous results but with slightly reduced overall optical yield (80%). The Ullmann product was subjected to a silica-gel chromatography to give a pure sample of (*R,R*)-**13** as an yellow-orange powder in a 42% isolated yield, $[\alpha]_D^{22}$+226° in $CHCl_3$. The enantiomeric purity of the sample was confirmed by the optical rotations of the recovered (*R*)-**2a** and (*R*)-**14** obtained after hydrolytic cleavage of the ester linkage. The specific rotation of the recovered diacid (*R*)-**14** was $[\alpha]_D^{22}$ +136.6° (95% EtOH), while that claimed for enantiomerically pure (*R*)-**14** is $[\alpha]_D$ +133.7° (95% EtOH).[10]

Here again, high steric requirement in assembling 12-membered cyclic diester **13** which contains rigid binaphthyl and biphenyl skeleton explains the exclusive formation of (*R,R*)-**13** without (*R,S*)-isomer. Moreover, two sets of nitro substituents in (*R,S*)-**13** can not lie on the attaching benzene planes, further disfavoring the formation of it (Figs. 3 and 4).

Although the scope and limitations of the asymmetric Ullmann coupling reaction remains to be examined,[11] the method presented here, that is the intramolecular coupling of two aryl moieties attached to a chiral 1,1′-binaphthyl residue, is likely to provide an entry into the asymmetric synthesis of chiral biaryls.

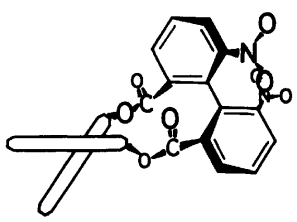

Fig. 3. (*R,R*)-**13**.

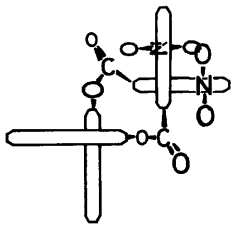

Fig. 4. (*R,S*)-**13**.

Experimental

Melting points are uncorrected. Measurements and materials were similar to those described in the previous paper unless otherwise noted.[1]

The following compounds were prepared as described in the literature; 2-iodo-3-nitrobenzoic acid,[12,13] mp 205—209 °C (lit,[13] 210—212 °C), IR (KBr) 1710, 1540, and 1370 cm^{-1}; (4*S*,5*S*)-4,5-bis(hydroxymethyl)-2,2-dimethyl-1,3-dioxolane ((*S*)-**2d**),[14] bp 112 °C/1.5 mmHg.†

Racemic 1,2-diphenyl-1,2-ethanediol was resolved into *R*- and *S*-isomer by direct crystallization from ether solution.[15] Crystals which showed levorotation in $CHCl_3$ were collected[16]; mp 148—149 °C (lit,[16b] 148—149 °C), $[\alpha]_D^{22}$ −95.0° (*c* 1.00, EtOH) (lit,[16b] $[\alpha]_D^{22}$−94.5° (*c* 0.998, EtOH)). Commercial 2-chloro-3-nitrobenzoic acid and (1*R*,2*R*)-1,2-bis(ethoxycarbonyl)-1,2-ethanediol were used as received. 2-Halo-3-nitrobenzoic acids were converted to acid chlorides by the treatment with thionyl chloride.

Synthesis of Diol Diesters. To a stirred, water-chilled solution of a chiral diol **2** (5—6 mmol) in PhH(100 ml)-pyridine(10 ml) was slowly added slightly excess amount of an acid chloride (12—14 mmol). The mixture was stirred overnight at ambient temperature and finally heated under reflux for 3 h. The reaction mixture was diluted with PhH (50 ml), and then 50 ml of 2 M†† HCl was added. The aqueous layer was extracted with PhH (30 ml×3). The combined organic extracts were washed successively with 2 M HCl, 1 M Na_2CO_3, and water, and then dried over Na_2SO_4 in the presence of activated charcoal. After volatiles were removed under a reduced pressure, the crude diester was purified by column chromatography and/or recrystallization. Yields were generally good to excellent (65—95%).

*(S)-2,2′-Bis(1-bromo-2-naphthoyloxy)-1,1′-binaphthyl ((S)-**1a**)*: This compound was the same as was used in the previous work.[1]

*(1S,2S)-1,2-Bis(1-bromo-2-naphthoyloxy)-1,2-diphenylethane ((S,S)-**1b**)*: The crude material was chromatographed on a silica-gel column with toluene as the eluent to yield white solids: mp 177—179 °C; $[\alpha]_D^{22}$ +12.3° (*c* 1.63, $CHCl_3$); IR (KBr) 3500—3300, 3050—2950, 1730, 1260, 1220, 1110, 960, 808, 750, and 690 cm^{-1}; ^1H NMR ($CDCl_3$) δ=6.47, (2H, s, -CH<×2), 7.20 (10H, s, $-C_6H_5$×2), 7.30—7.80 (10H, m), and 8.15—8.45 (2H, m). Found: C, 63.60; H, 3.43; Br, 23.27%. Calcd for $C_{36}H_{24}Br_2O_4$: C, 63.55; H, 3.56; Br, 23.49%.

*Diethyl (2R,3R)-2,3-Bis(1-bromo-2-naphthoyloxy)-1,4-butanedioate ((R,R)-**1c**)*: The crude material was chromatographed on a silica-gel column with $CHCl_3$ (1% EtOH) as the eluent, and then recrystallized from MeOH: mp 127—129 °C; $[\alpha]_D^{22}$

† 1 mmHg≈133.322 Pa.

†† 1 M=1 mol dm^{-3}.

−79.1° (*c* 0.923, $CHCl_3$); IR (KBr) 3500—3300, 3000—2850, 1765—1740, 1250, 1220—1195, 1110, 805, and 755 cm^{-1}; ^1H NMR ($CDCl_3$) δ=1.1—1.33 (6H, t, *J*=7 Hz, $-CH_3\times2$), 4.06—4.41 (4H, q, *J*=7 Hz, $-CH_2-\times2$), 6.03 (2H, s, $-CH<\times2$), 7.33—7.80 (10H, m), and 8.15—8.40 (2H, m). Found: C, 53.51; H, 3.45; Br, 24.04%. Calcd for $C_{30}H_{24}Br_2O_8$: C, 53.59; H, 3.60; Br, 23.77%.

*(4S,5S)-4,5-Bis(1-bromo-2-naphthoyloxymethyl)-2,2-dimethyl-1,3-dioxolane ((S)-**1d**)*: The crude material was recrystallized from acetone: mp 136—138 °C; $[\alpha]_D^{22}$ −15.3° (*c* 0.979, acetone); IR (KBr) 3500—3300, 3000—2850, 1730, 1460, 1370, 1260, 1220, 1120, 990, and 750 cm^{-1}; ^1H NMR ($CDCl_3$) δ=1.40, (6H, s, $-CH_3\times2$), 4.2—4.6 (6H, m), 7.3—7.8 (10H, m), and 8.2—8.4(2H, m). Found: C, 55.54; H, 3.63; Br, 25.20%. Calcd for $C_{29}H_{24}Br_2O_6$: C, 55.44; H, 3.85; Br, 25.43%.

*(R)-2,2′-Bis(2-iodo-3-nitrobenzoyloxy)-1,1′-binaphthyl ((R)-**10**)*: The crude material was chromatographed on a silica-gel column with toluene as the eluent: mp 99—106 °C; $[\alpha]_D^{22}$ +22.3° (*c* 1.03, $CHCl_3$); IR (KBr) 3500—3300, 1750, 1530, 1350, 1250, 1190, 1110, 1090, 805, 760—720, and 690 cm^{-1}; ^1H NMR ($CDCl_3$) δ=6.55—8.00 (m). Found: C, 49.15; H, 2.04; N, 3.19; I, 29.98%. Calcd for $C_{34}H_{18}I_2N_2O_8$: C, 48.83; H, 2.17; N, 3.35; I, 30.35%.

*(S)-**10***: $[\alpha]_D^{22}$ −23.1° (*c* 0.997, $CHCl_3$). Found: C, 49.18; H, 2.08; N, 3.35; I, 29.82%.

*(R)-2,2′-Bis(2-chloro-3-nitrobenzoyloxy)-1,1′-binaphthyl ((R)-**11**)*: The crude material was chromatographed on a silica-gel column with toluene as the eluent: mp 77—80 °C; $[\alpha]_D^{22}$ +43.2° (*c* 1.46, $CHCl_3$); IR (KBr) 1755, 1535, 1350, 1280—1240, 1190, 1120—1080, 805, 735, and 680 cm^{-1}; ^1H NMR ($CDCl_3$) δ=6.90—8.00 (m). Found: C, 62.58; H, 2.73; N, 4.13; Cl, 10.43%. Calcd for $C_{34}H_{18}Cl_2N_2O_8$: C,62.50; H, 2.78; N, 4.29; Cl, 10.85%.

*(±)-2,2′-Bis(3-nitrobenzoyloxy)-1,1′-binaphthyl (**12**)*: The crude material was chromatographed on a silica-gel column with toluene as the eluent: mp 174—177 °C; IR (KBr) 3500—3300, 1750—1740, 1530, 1345, 1240, 1200, 1100, 805, 750, and 705 cm^{-1}; MS (70 eV), *m/z* (%) 584 (M^+, 18.4), 268 (4.32), 150 (44.9), and 104 (12.3). Found: C, 70.06; H, 3.31; N, 4.44% Calcd for $C_{34}H_{20}N_2O_8$: C, 69.86; H, 3.45; N, 4.79%.

*(±)-2,2′-Bis(1-bromo-2-naphthylmethoxy)-1,1′-binaphthyl (**9**)*: (±)-1,1′-Binaphthyl-2,2′-diol (5.74 g, 20.0 mmol) was added to a sodium methoxide (prepared from 1.1 g (48 mmol) of sodium) in 50 ml of DMF. To the mixture was slowly added 1-bromo-2-bromomethylnaphthalene (12.0 g, 40 mmol), and the mixture was diluted with 50 ml of toluene. The reaction was stirred overnight at room temperature, and worked up as usual. The crude material was recrystallized from $CHCl_3$-EtOH (2/1), 8.8 g (61%): mp 177—178 °C; IR (KBr) 1620, 1590, 1500, 1340, 1290, 1235, 1120, 1100, 840, 830, and 765 cm^{-1}; ^1H NMR (CCl_4) δ=5.6(4H, s, $-CH_2-\times2$), and 7.2—8.0 (24H, m). Found: C, 69.89; H, 3.77; Br, 22.31%. Calcd for $C_{42}H_{28}O_2Br_2$: C, 69.63; H, 3.90; Br, 22.06%.

Ullmann Reaction of Bifunctional Substrates. The reaction of (*S*)-**1a** is representative. See Table 1 for the reaction conditions.

*Ullmann Reaction of (S)-**1a***: In a 200-ml, two-necked, round-bottomed flask, copper powder (2.0 g) was pretreated for activation just prior to use.[1] Under a nitrogen atmosphere, to the flask were attached a reflux condenser topped with nitrogen inlet and a pressure-equilibrating Hershberg-type dropping funnel.[17] The funnel was charged with 0.650 g (0.864 mmol) of (*S*)-**1a**, which was then dissolved in 30 ml of DMF. The copper powder was stirred vigorously in 30 ml of DMF and heated to a gentle reflux. To the suspension was added the ester over 8 h period. After the addition had been completed, the reaction mixture was stirred under reflux for another 2 h. After the reaction, the mixture was allowed to cool to room temperature, diluted with 50 ml of PhH, and then filtered. Solids were washed well with portions of PhH. Combined organic layer was washed successively with 2 M HCl and then water (×3), and dried over Na_2SO_4 in the presence of activated charcoal. Evaporation of the solvent *in vacuo* left a pale yellow residue (0.482 g); $[\alpha]_D^{22}$ −201° (*c* 1.03, PhH). A portion of the residue (0.30 g) was boiled with 0.2 g of LAH in ether (40 ml) for 4 h. The reaction was quenched with cautious addition of ethyl acetate and then water, and worked up as usual. Preparative TLC on silica gel with $CHCl_3$-ethyl acetate (4/1) afforded (*S*)-**4** (80 mg), $[\alpha]_{546}^{22}$ −61.1° (*c* 0.973, acetone), and (*S*)-**2a** (127 mg), $[\alpha]_D^{22}$ −35.0° (*c* 1.06, THF).

When the addition time of (*S*)-**1a** was reduced to 5 h, the Ullmann product showed $[\alpha]_D^{22}$ −170° (*c* 1.30, PhH), and the optical rotation of recovered **4** was reduced to $[\alpha]_{546}^{22}$ −49.2° (*c* 0.955, acetone).

*Ullmann Reaction of (S)-**1b***: The addition time of (*S*)-**1b**, optical rotation of the Ullmann product, and that of recovered **4** were as follows; 1 h, $[\alpha]_D^{22}$ +10.1° (*c* 1.19, $CHCl_3$), $[\alpha]_{546}^{22}$ −19.7° (*c* 1.02, acetone); 5 h, $[\alpha]_D^{22}$ −42.3° (*c* 1.40, $CHCl_3$), $[\alpha]_{546}^{22}$ −27.5° (*c* 1.16, acetone).

Among the products of these Ullmann reactions, the component eluted third on HPLC (ODS column, CH_3CN-H_2O (20/1)) was assigned as the reduction product **8b** by comparing the retention volume with that of authentic sample. The most mobile component was assigned as (*S,R*)-**7b**, and the second as (*S,S*)-**7b** on the basis of the peak areas of these two components on HPLC (UV absorption at 254 nm) and optical purity of the **4** obtained after LAH reduction of mixtures of these two components. The HPLC peak areas were calibrated to mole fractions of (*S,S*)- and (*S,R*)-**7b** using the formula

$$\text{O.P.} \times (1/100) \approx (fP_{S,S}-P_{S,R})/(fP_{S,S}+P_{S,R}) = (M_{S,S}-M_{S,R})/(M_{S,S}+M_{S,R})$$

where O.P.=% optical purity of the recovered **4**, $M_{S,S}$=moles of (*S,S*)-**7b**, $M_{S,R}$=moles of (*S,R*)-**7b**, $P_{S,S}$=peak area of (*S,S*)-**7b** on HPLC, $P_{S,R}$=peak area of (*S,R*)-**7b**, and f= a correspondence factor (2.86, r=0.995) experimentally determined from different mixtures of (*S,S*)- and (*S,R*)-**7b** and the optical rotations of recovered **4**.

In an example, a fraction from the column chromatography which contained (*S,R*)- and (*S,S*)-**7b** (0.170 g, HPLC peak area ratio $P_{S,R}/P_{S,S}$=0.202) was treated with LAH to give (*S*)-**4**, 89 mg (86%), $[\alpha]_{546}^{22}$ −73.7° (*c* 1.02, acetone) and (*S*)-**2b**, 68 mg (97%), $[\alpha]_D^{22}$ −91.3° (*c* 1.03, EtOH).

*Ullmann Reaction of (R)-**1c***: The Ullmann product showed $[\alpha]_D^{22}$ −1.9° (*c* 1.08, $CHCl_3$), and the optical rotation of recovered **4** was $[\alpha]_{546}^{23}$ −28.1° (*c* 1.27, acetone).

*Ullmann Reaction of (S)-**1d***: The Ullmann product showed $[\alpha]_D^{23}$ +13.7° (*c* 1.69, acetone), and the optical rotation of recovered **4** was $[\alpha]_{546}^{22}$ +3.2° (*c* 1.89, acetone).

*Attempted Ullmann Reaction of (±)-2,2′-Bis(1-bromo-2-naphthylmethoxy)-1,1′-binaphthyl (**9**)*: A mixture of **9** (2.50 g, 3.45 mmol) and activated copper powder (prepared from 2.0 g of Cu) in 30 ml of DMF was refluxed for 10 h with vigorous stirring under nitrogen. HPLC showed the presence of only starting material; the organic residue weighed 2.20 g (88%), and the IR absorption spectra (KBr) were superimposable to those of **9**.

When an intimate mixture of **9** (2.40 g, 3.31 mmol) and copper powder (1.5 g) was heated to 250 °C for 4 h in a sand bath, an intractable tarry matter resulted.

*Ullmann Reaction of (R)-2,2′-Bis(2-iodo-3-nitrobenzoyloxy)-1,1′-binaphthyl ((R)-**10**)*: A solution of (*R*)-**10** (1.26 g, 1.51 mmol) in 40 ml of DMF was added to a gently-refluxing suspension of copper powder (1.5 g) in 60 ml of DMF over 5 h period, and then the reaction was continued for another 2 h. The organic residue weighed 0.824 g, $[\alpha]_D^{22}$ +166° (*c* 1.37, $CHCl_3$).

Part of the residue (0.787 g) was refluxed with KOH (1.5 g) in EtOH(80 ml)-H_2O (10 ml) for 3 h. After solvents were removed *in vacuo*, the mixture was diluted with H_2O (20 ml) and 2 M HCl (10 ml), and then extracted with ethyl acetate (30 ml×3). Combined organic layer was extracted with 1 M Na_2CO_3 (30 ml×3) and then H_2O (30 ml×3), and dried over Na_2SO_4. Removal of the solvent left (*R*)-**2a**, 0.323 g (84%), $[\alpha]_D^{22}$ +36.3° (*c* 1.85, THF). The combined aq extracts were made acidic with conc. HCl, and then extracted with ethyl acetate (30 ml×3). The organic extracts were treated as usual. Evaporation of the solvent left a mixture of *m*-nitrobenzoic acid and 6,6'-dinitrodiphenic acid **14**, 0.381 g, *ca.* 85% yield. A preparative TLC with PhH-ethyl acetate-acetic acid (5/2/trace) gave (*R*)-**14**, 0.211 g (55.4%); $[\alpha]_D^{22}$+116° (*c* 1.18, 95% EtOH); IR (KBr) 3500—2500, 1730, 1690, 1530, 1340, 1260, 1105, 890, 770, 740, and 690 cm^{-1}; ^1H NMR (acetone-d_6) δ= 7.48—7.77 (2H, m), 8.15—8.30 (4H, m), and 10.85 (2H, s, -COOH×2).

Ullmann Reaction of (S)-10: Similar reaction of (*S*)-**10** (0.972 g, 1.16 mmol) with copper powder (1.5 g) in 100 ml of DMF gave the Ullmann product, 0.573 g, $[\alpha]_D^{22}$ −164° (*c* 0.923, $CHCl_3$). The diacid (*S*)-**14** was recovered in a 50% yield and showed $[\alpha]_D^{22}$ −114° (*c* 1.08, 95% EtOH).

Ullmann Reaction of (R)-2,2'-Bis(2-chloro-3-nitrobenzoyloxy)-1,1'-binaphthyl ((R)-11): The chloro ester (*R*)-**11** (1.24 g, 1.90 mmol) was allowed to react with copper powder (2.5 g) using 100 ml of DMF. The organic residue weighed 1.05 g (*ca.* 95%), $[\alpha]_D^{22}$ +159° (*c* 1.24, $CHCl_3$). From the residue, a 0.483 g of sample was chromatographed on a silica-gel column with toluene as the eluent to give (*R,R*)-**13**, 0.213 g (42% yield based on the (*R*)-**11** used); $[\alpha]_D^{22}$ +226° (*c* 0.989, $CHCl_3$); mp 211—215 °C; MS (70 eV), *m/z* (%) 582 (M^+, 34.6), 283 (6.02), 282 (3.69), 269 (6.21), 268 (25.9), 255 (4.85), 239 (4.56), 226 (3.20), 198 (3.10), 138 (4.17), and 134 (3.69); IR (KBr) 3500—3300, 3000—2850, 1755, 1530, 1345, 1260, 1210, 1190, 1090, 850, 805, 745, and 700 cm^{-1}. Found: C, 69.92; H, 3.29; N, 4.88%. Calcd for $C_{34}H_{18}N_2O_8$: C, 70.10; H, 3.11; N, 4.81%.

The cyclic diester (0.189 g, 0.324 mmol) was treated with KOH in aq EtOH as above, affording (*R*)-**14**, 70 mg (65%), $[\alpha]_D^{22}$ +136.6° (*c* 0.915, 95% EtOH), mp 222—225 °C (lit,[9] 231—231.5 °C), and (*R*)-**2a**, 68 mg (73%), $[\alpha]_D^{22}$ +34.6° (*c* 1.10, THF).

We thank Associate Professor Junzo Yamashita and Dr. Yoshio Inoue of our laboratory for their encouragement for this work. We are also grateful to Professor Shozo Yamaguchi of our university for kind gift of 2-chloro-3-nitrobenzoic acid. The present work was partially supported by a Grant-in-Aid for Scientific Research No. 57550526 from the Ministry of Education, Science and Culture.

References

1) Previous report in this series of investigation; S. Miyano, M. Tobita, and H. Hashimoto, *Bull. Chem. Soc. Jpn.*, **54**, 3522 (1981).

2) For recent examples; a) K. Tani, T. Yamagata, S. Otsuka, S. Akutagawa, H. Kumobayashi, T. Taketomi, H. Takaya, A. Miyashita, and R. Noyori, *J. Chem. Soc., Chem. Commun.*, **1982**, 600; b) S. Sakane, J. Fujiwara, K. Maruoka, and H. Yamamoto, *J. Am. Chem. Soc.*, **105**, 6154 (1983); c) W. Arnold, J. J. Daly, R. Imhof, and E. Kyburz, *Tetrahedron Lett.*, **24**, 343 (1983).

3) J. Brussee and A. C. A. Jansen, *Tetrahedron Lett.*, **24**, 3261 (1983). See also references cited in Ref. 1.

4) A. I. Meyers and K. A. Lutomski, *J. Am. Chem. Soc.*, **104**, 879 (1982).

5) J. M. Wilson and D. J. Cram, *J. Am. Chem. Soc.*, **104**, 881 (1982).

6) S. Miyano, M. Tobita, S. Suzuki, Y. Nishikawa, and H. Hashimoto, *Chem. Lett.*, **1980**, 1027.

7) a) T. Cohen and I. Cristea, *J. Am. Chem. Soc.*, **98**, 748 (1976); b) G. van Koten, J. T. B. H. Jastrzebski, and J. G. Noltes, *J. Org. Chem.*, **42**, 2047 (1977); c) Y. Mugnier and E. Laviron, *J. Chem. Soc., Perkin Trans. 2*, **1979**, 1264; d) F. E. Ziegler, I. Chliwner, K. W. Fowler, S. J. Kanfer, S. J. Kuo, and N. D. Sinha, *J. Am. Chem. Soc.*, **102**, 790 (1980), and references cited therein.

8) Reviews of the Ullmann reaction: a) P. E. Fanta, *Synthesis*, **1974**, 9; b) M. Sainsbury, *Tetrahedron*, **36**, 3327 (1980).

9) *Cf.* F. E. Ziegler and J. A. Schwartz, *J. Org. Chem.*, **43**, 985 (1978).

10) A. W. Ingersoll and J. R. Little, *J. Am. Chem. Soc.*, **56**, 2123 (1934). See also, P. Newman, P. Rutkin, K. Mislow, *ibid.*, **80**, 465 (1958).

11) Intramolecular Ullmann coupling of achiral substrates; a) M. S. Newman and J. A. Cella, *J. Org. Chem.*, **39**, 2084 (1974); b) M. S. Newman and M. W. Logue, *ibid.*, **36**, 1398 (1971); c) *Cf.* G. van Koten and J. G. Noltes, *J. Organomet. Chem.*, **104**, 127 (1976).

12) a) F. C. Whitmore, P. J. Culhane, and H. T. Neher, *Org. Synth.*, Coll. Vol. 1, 56 (1976); b) P. J. Culhane, *ibid.*, Coll. Vol. 1, 125 (1967).

13) D. C. Iffland and H. Siegel, *J. Am. Chem. Soc.*, **80**, 1947 (1958).

14) P. W. Feit, *J. Med. Chem.*, **7**, 14 (1964).

15) J. Yamashita, M. Minagawa, A. Sonobe, S. Ohashi, M. Kawamura, K. Shimizu, and H. Hashimoto, *Chem. Lett.*, **1982**, 1409.

16) a) J. Read, J. G. M. Campbell, and T. V. Barker, *J. Chem. Soc.*, **1930**, 2305; b) G. Berti and F. Bottari, *J. Org. Chem.*, **25**, 1286 (1960).

17) R. E. Benson and B. C. McKusick, *Org. Synth.*, Coll. Voll. 4, 746 (1963).

 © 1984 The Chemical Society of Japan Bull. Chem. Soc. Jpn., 57, 1948—1953 (1984) [Vol. 57, No. 7

Practical Procedure for the Chemoselective Reduction of Esters by Sodium Borohydride. Effect of the Slow Addition of Methanol[1)]

Kenso SOAI,* Hidekazu OYAMADA, Masako TAKASE, and Atushiro OOKAWA
Department of Applied Chemistry, Faculty of Science, Science University of Tokyo, Kagurazaka, Shinjuku-ku, Tokyo 162
(Received December 8, 1983)

The effect of solvents on the reduction of esters was examined with readily available sodium borohydride which is known to be incapable of reducing such functional groups. In mixed solvents of *t*-butyl alcohol-methanol or tetrahydrofuran-methanol, various carboxylic esters and lactones were found to be reduced by sodium borohydride to the corresponding alcohols or diols in high yields. Slow addition of methanol to the refluxing mixture of ester and sodium borohydride in *t*-butyl alcohol or tetrahydrofuran was essential to achieve effective reduction. On the other hand, each individual solvent, methanol or *t*-butyl alcohol, was not effective for the reduction. The procedure provided a practical method for the functional group selective reduction of esters in the presence of chloro, cyano, carboxylato, carbamoyl, carboxy or nitro groups, which can not usually be performed by lithium aluminium hydride.

We wish to report here a practical and selective reduction of esters and lactones with sodium borohydride ($NaBH_4$) in mixed solvent of *t*-butyl alcohol(*t*-BuOH)-methanol(MeOH), and in tetrahydrofuran(THF)-MeOH.

$NaBH_4$, since its discovery by Schlesinger, Brown and co-workers,[2)] has enjoyed extensive use in the reduction of ketones and aldehydes. $NaBH_4$ is presently one of the most easily available among many complex metal hydrides, it is easier to manipulate than lithium aluminium hydride($LiAlH_4$) and lithium borohydride because of its lower sensitivity towards moisture.[3)]

Though selective reduction of esters is an important method in organic synthesis,[4)] $LiAlH_4$ can not usually be used for the purpose because of its excessive reducing power.[3)] On the other hand, it is generally accepted that $NaBH_4$, a mild reducing agent, does not effectively reduce carboxylic esters.[5)] If the reduction of esters with $NaBH_4$ is realized, the procedure may open the route to the reduction of esters with excellent functional group selectivities. Reduction of esters with $NaBH_4$ in ethanol(EtOH)[6)] or MeOH[7)] result in the formation of alcohols only in low yields. High reaction temperature (300 °C),[8)] use of polyethylene glycol (PEG 400) of high boiling point[9)] or metal salt additive[10)] is required for the reduction of esters with $NaBH_4$.

We recently reported that $NaBH_4$ in mixed solvent of THF and a protic solvent shows much higher stereoselectivity than in each individual solvent in asymmetric reduction of chiral α-keto amides.[11)] We describe in this paper the details of the study on solvents and the scope and limitations of the selective reduction of esters with $NaBH_4$ in mixed solvents.

Results and Discussion

In order to study the effect of mixed solvents (solvent A and solvent B) on the reduction of esters by $NaBH_4$, methyl benzoate (**1**) was chosen as a model compound. Solvent B (0.8 ml) was added slowly (1 h) to the mixture of **1** (1 mmol) and $NaBH_4$ (2.1—2.6 mmol) in solvent A (4 ml) at various temperatures. The reactions were quenched by the addition of water or dil. HCl,[12)] and the yields of the resulting benzyl alcohol (**2**) were determined by GLC. For comparison, reductions in single solvents, MeOH or *t*-BuOH, were also run. The results are summarized in Table 1.

$$\underset{(1)}{PhCO_2Me} \xrightarrow[\text{solvent A and solvent B}]{NaBH_4} \underset{(2)}{PhCH_2OH}$$

The following conclusions and comments may be drawn from the data in Table 1: (1) Reduction in a single solvent of MeOH afforded **2** in only 11% yield (Entry 1) and vigorous evolution of gas (probably hydrogen) was observed when $NaBH_4$ and MeOH were mixed. This low yield of the alcohol was in accord with the previously reported result of the reduction of ester with $NaBH_4$ in MeOH.[7)] (2) The yield of **2** was only 6% when reaction was run in a single solvent of *t*-BuOH (Entry 2). *t*-BuOH seemed to be almost inert to $NaBH_4$.[10c)] (3) A dramatic result was obtained when MeOH was added to the refluxing mixture of $NaBH_4$ and **1** in *t*-BuOH. The yield of **2** increased 88% (Entry 3).[13)] (4) Furthermore, combination of THF and MeOH was found to be more effective. The yield of **2** reached 97% (Entry 6). (5) Reduction at refluxing

Table 1. Effect of solvent and temperature on the reduction of methyl benzoate (**1**) by sodium borohydride[a)]

$$\underset{(1)}{PhCO_2Me} \xrightarrow[\text{solvent A and solvent B}]{NaBH_4} \underset{(2)}{FhCH_2OH}$$

Entry	Solvent[b)] A-B	Temp. /°C	Time /h	Yield of **2**, %[c)]
1	MeOH	reflux	2.0	11
2	*t*-BuOH	reflux	2.0	6
3	*t*-BuOH-MeOH	reflux	2.0	88
4	*t*-BuOH-MeOH	r.t.	2.0	3
5	*t*-BuOH-*i*-PrOH	reflux	2.5	20
6	THF-MeOH	reflux	2.0	97
7	*i*-PrOH-MeOH	reflux	2.0	38
8	Et_2O-MeOH	reflux	2.0	38
9	Benzene-MeOH	reflux	3.0	11
10	Diglyme-MeOH	50	4.5	60

a) Molar ratio $NaBH_4$: ester=2.5 : 1.0. b) Volumetric ratio of solvent A : B=5 : 1. c) Yields determined by G.L.C.

temperature (88%, Entry 3) afforded a higher yield of **2** than that at room temperature (3%, Entry 4). (6) As co-solvent, MeOH (88%, Entry 3) was more effective than 2-propanol (20%, Entry 5). (7) $NaBH_4$ is known to be soluble in diglyme.[3c] Reduction at 50 °C gave a moderate yield (60%) of **2** (Entry 10). However there remains a possibility of a higher yield in the reduction run at a higher temperature. (8) $NaBH_4$ was not soluble in the mixed solvent of benzene and MeOH and the yield of **2** was low (Entry 9). (9) Low yield (38%) of **2** in ether and MeOH (Entry 8) was probably due to the lower reaction temperature than that of THF–MeOH (Entry 6). (10) *t*-BuOH was more effective than 2-propanol (Entries 3 and 7).

As described, the addition of MeOH to the refluxing mixture of methyl benzoate (**1**) and $NaBH_4$ in *t*-BuOH or THF was very effective for the conversion of **1** to benzyl alcohol (**2**). It is also of interest that the mixed solvent of *t*-BuOH and MeOH (Table 1, Entry 3) was much more effective than the separate individual solvents, *t*-BuOH (Entry 2) or MeOH (Entry 1).

From the standpoint of synthesis, the present method has the following advantages over the procedure using PEG 400[9] (1) High yields using lesser amount of $NaBH_4$. (2) Shorter reaction time. (3) An easier working-up procedure because of the use of solvents of lower boiling points (MeOH, *t*-BuOH, THF). (4) Easier control of the rate of evolution of the hydrogen formed by the reaction between MeOH and $NaBH_4$. In the case of PEG 400, evolution of hydrogen, formed by reaction between PEG and $NaBH_4$, is reported during the warming of the reaction mixture.[9] On the other hand, the present procedure includes the slow addition of MeOH to the refluxing mixture of $NaBH_4$ and ester in THF or *t*-BuOH. Therefore, the rate of the evolution of gas by the reaction of MeOH and $NaBH_4$ is limited by the amount of MeOH added (reaction between *t*-BuOH and $NaBH_4$ is negligible,[10c] Table 1, Entry 2).

We then examined if the present procedure of the reduction of **1** is applicable to other esters and lactones. In a similar manner, reduction of various esters and lactones by $NaBH_4$ was performed either in mixed solvents of *t*-BuOH–MeOH or THF–MeOH. As clearly seen from the data summarized in Table 2, aliphatic, aromatic, heterocyclic mono- and diesters, in all cases, gave the corresponding alcohols in high yields. Diesters such as diethyl phthalate gave 1,2-benzenedimethanol in 91% yield and phthalide in 8% yield (Entry 14). Lactones afforded the corresponding diols in high yield, too (Entries 15 and 16). Even esters of sterically hindered carboxylic acids such as methyl 2-ethylbutanoate and methyl 2,2-dimethylpropanoate were reduced in high yields (Entries 3 and 4). The effect of the structure of the alcohol moiety of the esters was examined using various kinds of benzoates (Entries 5—12). Methl and ethyl benzoates were reduced in high yields (Entries 5, 6 and 7), and isopropyl benzoate afforded a moderate yield of **2** (Entries 8 and 9). However *t*-butyl benzoate was reduced only in low yield (Entries 10 and 11) Reduction of an α,β-unsaturated ester was accompanied by the reduction of the carbon-carbon double bond (Entry 17).[6] Methyl *p*-hydroxybenzoate was not reduced and was recovered unchange (Entry 18).[14]

The results of the preceding paragraphs suggested the possibility of a selective reduction of esters by the reducing system used. In fact, when compounds other than esters such as benzamide, *N,N*-dimethylbenzamide or 1-chlorodecane (**3**) were treated with $NaBH_4$ in refluxing *t*-BuOH–MeOH, no reduction products were obtained and all the substrates were recovered in 100%, 98%, and 93% yield respectively. In order to establish the synthetic utility of the reduction of esters by $NaBH_4$ in mixed solvents, we examined the competitive or selective reduction of esters in the presence of other groups.[15] The results are shown in Table 3.

A mixture of equimolar amounts of methyl benzoate (1) and 1-chlorodecane (**3**) was treated with $NaBH_4$ in refluxing *t*-BuOH–MeOH. **1** was reduced selectively to afford benzyl alcohol(2) in the yield of 82%, whereas 88% of **3** was recovered (Entry 1). Similarly, in the competitive reduction carried out in THF–MeOH, **2** was obtained in 88% yield and the recovery of **3** was 88% (Entry 2). Similarly, in the competitive reduction of esters in the presence of benzonitrile (Entries 3 and 4), sodium benzoate (Entry 5) benzamide (Entry 6) or benzoylglycine (Entry 9), esters were reduced selectively in moderate to high yields (49—97%). Whereas substrates other than esters were recovered in high yields (84—97%). Sodium benzoate was recovered as benzoic acid (85%, Entry 5). The ethoxycarbonyl group of ethyl *p*-nitrobenzoate was reduced selectively to afford *p*-nitrobenzyl alcohol in high yields (Entries 7 and 8). As described above, reduction by $NaBH_4$ in mixed solvents is useful for the selective reduction of esters in the presence of other functional groups such as chloro, cyano, carboxylato, carbamoyl, carboxy or nitro.

It is reported that hydroxylic solvents play an important role in the reduction of ketones with $NaBH_4$.[16] Hydroxylic solvents are incorporated in the mechanism of the reduction.[16] In inert solvents such as diglyme, reductions of ketones by $NaBH_4$ do not proceed to any appreciable extent.[17] Though it is not yet clear, we tentatively assume the following possibilities, (1) and/or (2), for the unusually high yields of the reduction of esters by the addition of MeOH to the refluxing mixture of $NaBH_4$ and esters in *t*-BuOH or THF. (1) MeOH as a protic solvent may play the same role as in the reductions of ketones by $NaBH_4$ in hydroxylic solvent.[16] (2) When MeOH reacts with $NaBH_4$, various alkoxyhydroborate(−1) are formed, *i.e.* $BH_3(OMe)^-$, $BH_2(OMe)_2^-$, $BH(OMe)_3^-$. These species or their aggregated form may show higher reducing power than $NaBH_4$, and may be capable of reducing esters.[18,22] Detailed discussion of the mechanistic aspects of the reduction of esters with $NaBH_4$ in mixed solvents must await further investigation. Low yields of the reduction of esters with $NaBH_4$ in single solvents of MeOH(Table 1, Entry 1) or EtOH[6] may be attributed to the high concentration of protic solvents. When a large amount of MeOH or EtOH exists, hydrides of $NaBH_4$ are rapidly consumed by the reaction with hydroxylic solvents especially at reflux temperatures. On the other hand, slow addition of MeOH to the mixture of $NaBH_4$ and ester in the present study may suppress this side reaction because the concentration of MeOH is much

Table 2. Reduction of esters and lactones by $NaBH_4$[a] in mixed solvents of *t*-BuOH-MeOH or THF-MeOH

Entry	Ester or lactone	Mixed solvent[b]	Product	Yield/%[c]
1	$CH_3(CH_2)_8CO_2CH_3$	THF-MeOH	$CH_3(CH_2)_8CH_2OH$	90
2	$CH_3(CH_2)_{16}CO_2CH_3$	*t*-BuOH-MeOH	$CH_3(CH_2)_{16}CH_2OH$	79
3	$(C_2H_5)_2CHCO_2CH_3$	*t*-BuOH-MeOH	$(C_2H_5)_2CHCH_2OH$	84[e]
4	$(CH_3)_3CCO_2CH_3$	*t*-BuOH-MeOH	$(CH_3)_3CCH_2OH$	76[e]
5	$PhCO_2CH_3$ (**1**)	THF-MeOH	$PhCH_2OH$ (**2**)	97[e]
6	$PhCO_2CH_2CH_3$[d]	*t*-BuOH-MeOH	**2**	83[e]
7	$PhCO_2CH_2CH_3$[d]	THF-MeOH	**2**	83[e]
8	$PhCO_2i\text{-}Pr$[d]	*t*-BuOH-MeOH	**2**	60[e]
9	$PhCO_2i\text{-}Pr$[d]	THF-MeOH	**2**	63[e]
10	$PhCO_2t\text{-}Bu$[d]	*t*-BuOH-MeOH	**2**	17[e]
11	$PhCO_2t\text{-}Bu$[d]	THF-MeOH	**2**	24[e]
12	$PhCO_2CH_2Ph$[d]	*t*-BuOH-MeOH	**2**	98[e,f]
13	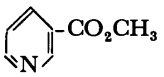	*t*-BuOH-MeOH	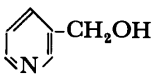	78
14	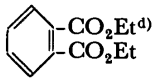	*t*-BuOH-MeOH	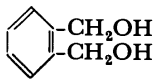 mp 61—62 °C [lit,[i] 63—65 °C]	91
			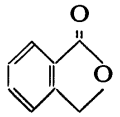	8
15	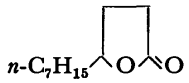	*t*-BuOH-MeOH	$n\text{-}C_7H_{15}CH(OH)(CH_2)_2CH_2OH$	91
16	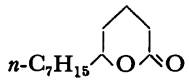	*t*-BuOH-MeOH	$n\text{-}C_7H_{15}CH(OH)(CH_2)_3CH_2OH$	89
17	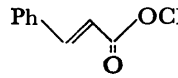	THF-MeOH	$PhCH{=}CH\text{-}CH_2OH$	29[g]
18	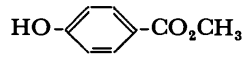	*t*-BuOH-MeOH	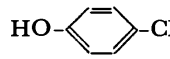	0[h]

a) Molar ratio $NaBH_4$: ester = 2.5 : 1.0, unless otherwise noted. b) Refluxing temperature. c) Yields of isolated pure products unless otherwise noted. d) Molar ratio $NaBH_4$: ester = 5.0 : 1.0. e) Yields determined by GLC. f) Two moles of **2** were produced by the reduction of benzyl benzoate. g) Cinnamyl alcohol (29%), 3-phenylpropanol (50%) and methyl 3-phenylpropanoate (11%). Yields determined by NMR analysis. h) Recovery of the ester was 70%. i) Ref. 24.

Table 3. Selective or competitive reduction of esters in the presence of other groups (A) by $NaBH_4$ in mixed solvents[a]

$$\text{Ester} + \text{A} \xrightarrow[t\text{-BuOH-MeOH or THF-MeOH}]{NaBH_4} \text{Alcohol} + \text{A}$$

Entry	Ester	Compound of other group (A)	Solvent	Product yield/%[b]		Recovery A/%[c]
1	$PhCO_2CH_3$ (**1**)	$n\text{-}C_9H_{19}CH_2Cl$ (**3**)	*t*-BuOH-MeOH	$PhCH_2OH$ (**2**)	82	88
2	**1**	$n\text{-}C_9H_{19}CH_2Cl$ (**3**)	THF-MeOH	**2**	81	88
3	**1**	PhCN	*t*-BuOH-MeOH	**2**	61[d]	87[d]
4	**1**	PhCN	THF-MeOH	**2**	72[d]	84[d]
5	$n\text{-}C_9H_{19}CO_2CH_3$	$PhCO_2Na$	*t*-BuOH-MeOH	$n\text{-}C_9H_{19}CH_2OH$	74	85[e]
6	$n\text{-}C_9H_{19}CO_2CH_3$	$PhCONH_2$	*t*-BuOH-MeOH	$n\text{-}C_9H_{19}CH_2OH$	75	97
7	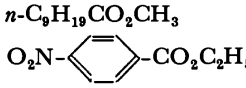		*t*-BuOH-MeOH	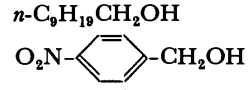	89	
8	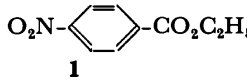		THF-MeOH	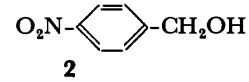	88	
9	**1**	$PhCONHCH_2CO_2H$	*t*-BuOH-MeOH	**2**	49	87

a) Molar ratio (ester : A : $NaBH_4$ = 1.0 : 1.0 : 2.5), at refluxing temperature. b) Isolated yields unless otherwise noted. c) Isolated recovery. d) Determined by GLC. e) Recovered as benzoic acid after acidic treatment.

lower than that in single solvent of MeOH.

Conclusion

The addition of MeOH to a refluxing mixture of $NaBH_4$ and esters or lactones in *t*-BuOH or THF enabled the reduction of carboxylic esters or lactones to the corresponding alcohols or diols in high yields. The method provided synthetically useful selective reduction of esters in the presence of other reducible groups. Advantages of the method are the availability and easy manipulation of the reagents ($NaBH_4$, *t*-BuOH, THF, MeOH) and easy working-up because of the low boiling points of the solvents.

Experimental

Melting points were not corrected. IR spectra were recorded with a Hitachi 260-10 spectrophotometer. ^{1}H-NMR spectra (60 MHz) were recorded by using either a Varian EM-360A NMR spectrometer or a JEOL JNM- PMX-60 NMR spectrometer. GLC analyses were carried out with a Shimadzu Gas Chromatograph either model GC-4C or model GC-4A. All of the reaction were run under an atmosphere of argon.

Materials. 2-Propanol and benzene were stored over 4 Å molecular sieves. Methanol was stored over 3Å molecular sieves. *t*-Butyl alcohol was purchased from Kanto and was used without further purification. Tetrahydrofuran and diglyme were distilled from lithium aluminum hydride prior to use.

$NaBH_4$ (Nakarai) was used without further purification. Its activity (99%) was determined following a similar procedure described in the literature.[22] Most of the organic compounds utilized in this study were commercial products of high purity (Tokyo Kasei, Nakarai), but they were further purified by distillation when necessary. Methyl 2-ethylbutanoate was synthesized from the corresponding acid and MeOH using a catalytic amount of sulfuric acid according to the standard procedure: bp. 131—132 °C, lit,[23] bp. 135—137 °C (736 mm) .

Procedure for The Study of The Effect of Mixed Solvents and Temperature on The Reduction of Methyl Benzoate (1) by $NaBH_4$ (Table 1) Solvent B (0.8 ml) was added over a period of 1 h to the refluxing mixture of **1** (0.136 g, 1 mmol) and $NaBH_4$ (0.079—0.098 g, 2.1—2.6 mmol) in solvent A (4 ml). The reaction mixture was refluxed for an additional 1 h or more, and then 1—2 ml of diluted HCl or water was added. Most of the organic solvents of A and B were evaporated on a rotary evaporator. Naphthalene in ether was added to the residue. The yields of benzyl alcohol (**2**) were determined by GLC using naphthalene as internal standard (2 m glass column of 10% PEG 20M (1 M=1 mol dm^{-3}) on Chromosorb W AW, column temperature 140—170 °C, carrier gas He, TC detector).

General Procedure for The Reduction of Esters or Lactones by $NaBH_4$ in Mixed Solvents of t-BuOH-MeOH or THF-MeOH (Table 2). Methanol (0.8 ml) was added over a period of 1 h to the refluxing mixture of $NaBH_4$ (1 mmol) and ester or lactone (1 mmol) in *t*-BuOH (4 ml) or THF (4 ml). After the addition of MeOH, the reaction mixture was refluxed for an appropriate period. The reaction was quenched by the addition of diluted HCl or H_2O.

(1) The resulting alcohols were isolated according to the following procedure. Most of the organic solvents were evaporated on a rotary evaporator, and the residue was extracted with dichloromethane (6×5 ml). The combined extracts were dried over anhydrous sodium sulfate. After the evaporation of the solvent under reduced pressure, the residue was purified on preparative silica gel TLC. The NMR and IR spectra were identical with those of authentic samples.[24]

1,4-Undecanediol (Entry 15): NMR ($CDCl_3$) 0.6—1.8 (m, 19H), 3.3—3.75 (m, 3H), 4.0 (broad, 2H); IR (neat) 3320, 2950, 2870, 1470, 1070 cm^{-1}. Found: C, 70.12; H, 12.81%. Calcd for $C_{11}H_{24}O_2$: C, 70.16; H, 12.85%.

1,5-Dodecanediol (Entry 16): Mp 43.5—44.2 °C; NMR ($CDCl_3$) 0.6—1.9 (m, 21H), 3.0 (s, 2H), 3.4—3.8 (m, 3H); IR (KBr) 3280, 2920, 2850, 1460, 1380, 1138, 1108, 1065, 920 cm^{-1}. Found: C, 71.27; H, 12.88%. Calcd for $C_{12}H_{26}O_2$: C, 71.23; H, 12.95%.

(2) In the determination of the yields by gas chromatography, appropriate internal standards were added to the quenched reaction mixture and GLC analyses then carried out. The conditions of GLC analyses were as follows: for benzyl alcohol (**2**) (Entries 5—12), 2-m glass column of 10% PEG 20M on Chromosorb W AW, column temp. 145 °C, internal standard: naphthalene, TC detector; for 2-ethyl 1-butanol (Entry 3), capillary column SE-30, column temp. 45 °C, 2,2-dimethyl 1-propanol (internal standard), FI detector; for 2,2-dimethyl 1-propanol (Entry 4), capillary column SE-30, column temp. 45 °C, 2-ethyl 1-butanol (internal standard), FI detector.

Competitive Reduction of The Mixture of Methyl Benzoate (1) and 1-Chlorodecane or Benzonitrile (Table 3, Entry 1—4). Equimolar mixtures of methyl benzoate (**1**) (1 mmol) and 1-chlorodecane (1 mmol) or benzonitrile (1 mmol) were reduced with $NaBH_4$ in *t*-BuOH-MeOH or THF-MeOH according to the procedure described in the preceding paraph. Benzyl alcohol (**2**) (81—82%) and 1-chlorodecane (88%) (Entries 1 and 2) were purified on preparative silica gel TLC using dichloromethane as developing solvent. Yield of **2** (61—72%) and recoveries of benzonitrile (84—87%) (Entries 3 and 4) were determined by GLC analyses (2-m glass column of 10% PEG 20M on Chromosorb W AW, column temperature 140 °C, FI detector, with naphthalene as internal standard).

Competitive Reduction of The Mixture of Methyl Decanoate and Sodium Benzoate (Table 3, Entry 5). An equimolar mixture of methyl decanoate (1 mmol) and sodium benzoate (1 mmol) was reduced with $NaBH_4$ in *t*-BuOH-MeOH as described above. The reaction was quenched with water, and the solution made alkaline by adding 1M aq NaOH. The mixture was extracted with dichloromethane. The extracts were dried over anhydrous sodium sulfate, and evaporated on a rotary evaporator. Purification on silica gel TLC [developing solvent dichloromethane:ether (6:1)] gave 1-decanol in 74% yield. The 1-decanol synthesized was identical with an authentic sample in GLC analysis. Benzoic acid was recovered according to the following procedure. The water layer was acidified by diluted HCl, and extracted with dichloromethane and evaporated on a rotary evaporator. Purification on silica gel TLC [developing solvent dichloromethane:ether (6:1)] gave benzoic acid in 85% recovery.

Competitive Reduction of The Mixture of Methyl Decanoate and Benzamide (Table 3, Entry 6). An equimolar mixture of methyl decanoate and benzamide was reduced with $NaBH_4$ in t-BuOH-MeOH as described above. Purification on silica gel TLC [developing solvent CH_2Cl_2:MeOH (20:1)] afforded 1-decanol in 75% yield and benzamide in 97% recovery.

Reduction of Ethyl p-Nitrobenzoate (Table 3, Entries 7, 8). Ethyl *p*-nitrobenzoate was reduced with $NaBH_4$ in *t*-BuOH-MeOH or THF-MeOH. Silica gel TLC purification [developing solvent CH_2Cl_2:MeOH (10:1)] gave *p*-nitrobenzyl alcohol in 88—89% yield. mp 90—91 °C (lit,[22] mp 92—93 °C); ^{1}H NMR ($CDCl_3$) 2.15 (s, 1H, OH), 4.8 (s, 2H, CH_2), 7.4—8.3 (dd, 4H, aromatic protones); IR (KBr) 3540, 1610, 1518, 1345, 1065, 748 cm^{-1}.

Effect of The Molar Ratio of $NaBH_4$ and Methyl Benzoate (1) **1** was reduced in THF-MeOH using various amounts of $NaBH_4$ according to the procedure described in preceding paragraphs. Yields are those of the benzyl alcohol (**2**) isolated.

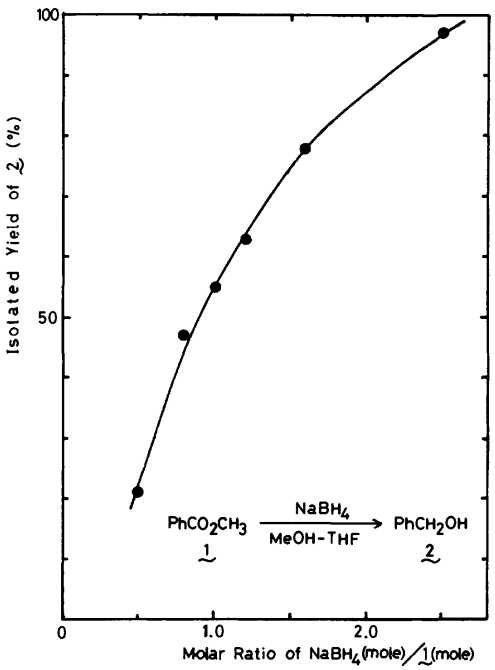

Fig. 1. Effect of Molar Ratio.

References

1) Preliminary communication, K. Soai, H. Oyamada, and A. Ookawa, *Synth. Commun.*, **12**, 463 (1982).

2) H. I. Schlesinger, H. C. Brown, H. R. Hoekstra, and L. R. Rapp, *J. Am. Chem. Soc.*, **75**, 199 (1953).

3) For recent reviews of complex metal hydrides, see a) E. R. H. Walker, *Chem. Soc. Rev.*, **5**, 23 (1976); b) H. C. Brown, and S. Krishnamurthy, *Tetrahedron*, **35**, 567 (1979); c) A. Hajós, "Complex Hydrides," Akademiai Kiado, Budapest, (1979).

4) H. O. House, "Modern Synthetic Reactions," 2nd ed., Benjamin Inc., California, 1972.

5) Exceptions are the esters with complex forming neighbouring functional groups, for example oxo and hydroxy esters, and R^1COOR^2 esters with an electron withdrawing R^2 group. a) V. Boekelheide and R. J. Windgassen, Jr., *J. Am. Chem. Soc.*, **81**, 1456 (1959); b) J. E. G. Barnett and P. W. Kent, *J. Chem. Soc.*, **1963**, 2743; c) S. Takahashi and L. A. Cohen, *J. Org. Chem.*, **35**, 1505 (1970); d) P. L. Hall and R. B. Perfetti, *ibid.*, **39**, 111 (1974).

6) H. C. Brown, S. Narasimhan, and Y. M. Choi, *J. Org. Chem.*, **47**, 4702 (1982).

7) M. S. Brown, and H. Rapoport, *J. Org. Chem.*, **28**, 3261 (1963).

8) A. Nose and T. Kudo, *Yakugaku Zasshi*, **96**, 1401 (1976).

9) E. Santaniello, P. Ferraboschi, and P. Sozzani, *J. Org. Chem.*, **46**, 4584 (1981).

10) a) H. C. Brown, and B. C. S. Rao, *J. Am. Chem. Soc.*, **78**, 2582 (1956); b) G. R. Pettit and T. R. Kasturi, *J. Org. Chem.*, **26**, 4557 (1961); c) H. C. Brown, E. J. Mead, and B. C. S. Rao., *J. Am. Chem. Soc.*, **77**, 6209 (1955).

11) K. Soai, K. Komiya, Y. Shigematsu, H. Hasegawa, and A. Ookawa, *J. Chem. Soc., Chem. Commun.*, **1982**, 1282.

12) No significant difference in the yield of benzyl alcohol (**2**) was observed between the methods of quenching. Yields of **2** by the addition of water or dil. HCl were 63% and 62% respectively in comparative reductions of **1**.

13) Slow addition of MeOH was more effective than rapid addition. When MeOH (12 mmol) was added to the mixture of ($NaBH_4$ 2.5 mmol) and **1** (1 mmol) before heating, the yield of **2** dropped to 64%. Interestingly, hydride of the reagent remained even after reflux. Despite this molar ratio of $NaBH_4$ and MeOH (1.0:4.8), evolution of gas (hydrogen) was observed when the reaction was quenched with dil. HCl.

14) Methyl *p*-hydroxybenzoate is known to resist reduction. See ref. 9.

15) When different groups are attached to the same molecule, the selectivity may be changed by neighbouring group participation. On the other hand, even pairs of groups of the same type have been differentiated by virtue of their steric environment in the molecule which has a rather rigid skeleton. Therefore we assume that competitive reduction is on a suitable scale for the functional group selectivity of the reaction. a) F. C. Huang, L. F. H. Lee, R. S. D. Mittal, P. R. Ravikumar, J. A. Chan, C. J. Sih, E. Caspi, and C. R. Eck, *J. Am. Chem. Soc.*, **97**, 4144 (1975); b) P. A. Bell and M. B. Gravestock, *Can. J. Chem.*, **47**, 2099 (1969).

16) D. C. Wigfield and F. W. Gowland, *Tetrahedron Lett.*, **1976**, 3373.

17) H. C. Brown and K. Ichikawa, *J. Am. Chem. Soc.*, **83**, 4372 (1961).

18) Sodium hydrotrimethoxyborate [$NaBH(OCH_3)_3$] is known to undergo rapid disproportionation into $NaBH_4$ and sodium tetramethoxyborate in THF.[19]

$$4\,NaBH(OCH_3)_3 \xrightarrow[THF]{} NaBH_4 + 3\,NaB(OCH_3)_4$$

Though reduction of esters with $NaBH(OCH_3)_3$ is reported, $NaBH(OCH_3)_3$ reduces the esters only slowly in ether at reflux or in dibutyl ether at high temperatures(100—140 °C)[20] with the exception of the reduction in dimethoxyethane at reflux.[15b]

To clarify whether all the reducing species are formed *in situ* $NaBH(OCH_3)_3$ in the reduction of esters by $NaBH_4$ in THF-MeOH, effect of the molar ratio of $NaBH_4$ and ethyl benzoate (**1**) was studied in the mixed solvent of THF and MeOH. Results are shown in Fig. 1. The yield of benzyl alcohol (**2**) increased with increase of $NaBH_4$. It become clear that $NaBH(OCH_3)_3$ is not the only reducing species, at least when the molar ratio of $NaBH_4$ to ester (**1**) is between 0.8—1.2. The reason is as follows: $NaBH(OCH_3)_3$ has only one active hydride[21] and one ester needs two active hydrides to be reduced to the corresponding alcohol. If $NaBH(OCH_3)_3$ were the only reducing species and if the reduction proceeded quantitatively, the yield of **2** could not exceed 50% when equimolar amounts of $NaBH_4$ and **1** were used. However, the actual isolated yield of **2** was 55% using equimolar amounts of $NaBH_4$ in mixed solvent of THF and MeOH.

19) H. C. Brown, E. J. Mead, and P. A. Tierney, *J. Am. Chem. Soc.*, **79**, 5400 (1957).

20) H. C. Brown, and E. J. Mead, *J. Am. Chem. Soc.*, **75**, 6263 (1953).

21) It is not meant in this text that "active hydride" is the actual species. The term is used only for the purpose of easy counting.

22) The reducing power of lithium borohydride is enhanced by the presence of MeOH. K. Soai, A. Ookawa, and H. Hayashi, *J. Chem. Soc., Chem. Commun.*, **1983**, 668.

23) H. C. Brown, G. W. Kramer, A. B. Levy, and M. M. Midland, "Organic Synthesis via Boranes," Wiley Interscience, New York, 1975.
24) "Dictionary of Organic Compounds," ed by J. Buckingham, Chapman and Hall, New York (1982).
25) C. J. Pouchert, and J. R. Campbell, "The Aldrich Library of NMR Spectra," Aldrich Chemical Co. Inc., Wisconsin, (1974).

Syntheses of the Sex-Attractant of Pine Sawflies

Tadashi KIKUKAWA, Motomasa IMAIDA, and Akira TAI*
Institute for Protein Research, Osaka University, Yamada-oka, Suita, Osaka 565
(Received December 15, 1983)

In order to establish the stereochemistry of the sex attractant of various species of pine sawflies, (2*S*,3*R*,7*R*)-, (2*S*,3*R*,7*S*)- and (2*S*,3*S*,7*S*)-2-acetoxy- and 2-propionyloxy-3,7-dimethylpentadecane were synthesized. The alcohol moiety of each pheromone was prepared by the coupling of Grignard reagent of C_{12} block with tosylate of C_5 block. The C_{12} blocks, (*R*)- and (*S*)-1-bromo-2-methylundecane, were prepared from (*R*)-(+)-pulegone. The C_5 blocks, (2*R*,3*S*)- or (2*S*,3*S*)-2-methyl-3-tetrahydropyranyloxy-1-(tosyloxy)butane, were derived from (2*S*,3*S*)- or (2*R*,3*S*)-2-methyl-3-hydroxybutyric acid prepared by the enantio-differentiating hydrogenation of methyl 2-methyl-3-oxobutyrate over the asymmetrically modified nickel catalyst.

Virgin females of pine sawflies (*Hymenoptera, Diprionidae*) utilize a powerful sex pheromone to attract males. In 1967, Jewett *et al.*[1] reported that the chemical structure of *N. lecontei* (red headed pine sawfly) was an acetate of (2*R**,3*R**)-3,7-dimethyl-2-pentadecanol (*erythro*-**1**). At the same time, it was proposed that the pheromones of various sawflies were either acetates or propionates of **1**.

The acetate or propionate of the synthesized racemic **1**[2] (a mixture of all possible isomers) was, however, much less active than the natural pheromone and could not discriminate a difference among species. These data suggested that not only a sort of ester moiety but also stereochemistry of **1** were essential factors to distinguish the many sympatric species of sawflies.

In order to clarify the stereochemistry of the pheromones, we have synthesized optically active *erythro*-isomers, (2*S*,3*S*,7*R*/*S*)- and (2*R*,3*R*,7*R*/*S*)-**1**, and *threo*-isomers, (2*S**,3*R**,7*R*/*S*)-, (2*S*,3*R*,7*R*/*S*)- and (2*R*,3*S*,7*R*/*S*)-**1**.[3,4] The field assay of these compounds against *N. lecontei* clearly showed that the natural pheromone must be erythro (2*S*,3*S*)-configuration.[5,6] Later, K. Mori *et al.*[7] synthesized the four *erythro*-isomers: (2*R*,3*R*,7*R*)-, (2*R*,3*R*,7*S*)-, (2*S*,3*S*,7*R*)- and (2*S*,3*S*,7*S*)-**1**. The field assay carried out by Kraemer *et al.*[8] showed that only the acetate of (2*S*,3*S*,7*S*)-1 was highly active against *N. lecontei*. Thus the pheromone of *N. lecontei* was expected to be a single component and its structure was established to be (2*S*,3*S*,7*S*)-**1**. Although (2*S*,3*S*)- or (2*S*,3*S*,7*S*)-**1** attracted many other *Neodiprion* families in the field, its potency for attraction was very weak compared to that of the natural pheromone of each species.

In the course of the field assay by using *erythro*-and *threo*-isomers, we have found that the pheromone of various species other than *N. lecontei* was not a single component but a mixture of *threo*-and *erythro*-isomers. For example, a mixture of (2*S*,3*S*,7*S*)- and (2*S*,3*R*,7*R*/*S*)-**1** in a different ratio functioned for the discrimination of two closely related species, *N. sertifer* and *N. banksianae*.[9] On carrying out the stereochemical studies of this pheromone in detail, the syntheses of optically pure *threo*-isomer as well as *erythro*-isomer were absolutely necessary. Although the synthetic methods of four possible *erythro*-isomers have been reported,[7,10,11] the methods were not applicable for the synthesis of the optically pure *threo*-isomers. This report describes the method for the syntheses of optically pure three essential stereoisomers for the biological study of the pheromone of sawfly: (2*S*,3*R*,7*R*)-, (2*S*,3*R*,7*S*)- and (2*S*,3*S*,7*S*)-**1**.

Results and Discussion

The most reliable procedure to prepare an optically pure stereoisomer is to assemble optically pure building blocks by a method which does not involve the bond breaking and bond forming process at the chiral center of each block. Our synthetic procedure was designed in line with the above mentioned policy. The procedure consists of the preparation of optically pure C_{12} blocks and C_5 blocks and their couplings,as shown in Fig. 1.

Optically pure C_{12} blocks, (*R*)- and (*S*)-1-bromo-3-methylundecane (**9**), were prepared from (*R*)-(+)-citronellic acid (**3**) ($[\alpha]_D^{20}$+8.89° (neat), lit,[12] $[\alpha]_D^{25}$+8.48° (neat)) derived from (*R*)-(+)-pulegone (**2**) ($[\alpha]_D^{20}$+21.97° (neat)) supplied by courtesy of Takasago Perfume Industry Co. The resulting (*R*)-3 was determined to be essentially optically pure by the GLC method developed in this study. A diastereomeric mixture of amides

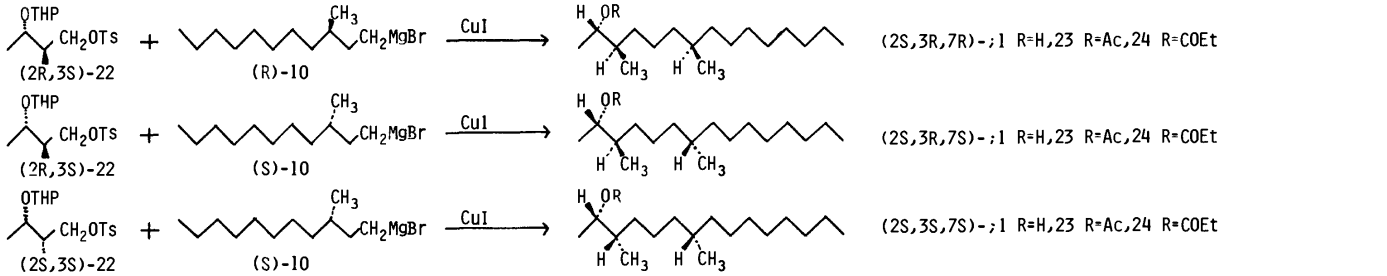

Fig. 1. Preparation of 3,7-dimethyl-2-pentadecanol (**1**) and its derivatives, (**23**) and (**24**).

from citronellic acid and α-methylbenzylamine was found to be completely resolved by capillary GLC (OV-101, 50 m (L)×0.25 mm (I.D)). When the **3** used for this study was converted to its amide with (*S*)-α-methylbenzylamline ($[\alpha]_D^{20}$ −39° (neat), Aldrich Co.), the diastereomeric excess (d.e.) of the resulting amide was 98%. However, the (*S*)-α-methylbenzylamine[13] was found to be not optically pure. The GLC analysis with a chiral capillary column (OA-500, 40 m (L)×0.25 mm (I.D)) indicated that the enantiomeric excess (e.e.) of this amine was 98%. If our citronellic acid had been contaminated with some antipode, the d.e. value of amide would have been less than 98%.

From the fact that the d.e. value of amide and the e.e. value of amine were identical, and that the optical rotation of our citronellic acid was slightly higher than the reported value[12], it was concluded that the (*R*)-citronellic acid must be optically pure.

The procedure for the preparation of (*R*)-**9** is shown in Fig. 2. (*R*)-Ethyl citronellate (**4**) prepared by the esterification of (*R*)-**3** was ozonized in methanol.[14] The hydrogenolysis of the ozonide over Pd/C gave ethyl (*R*)-3-methyl-6-oxohexanoate (**5**). The reaction of (*R*)-**5** with Wittig reagent[15] prepared from pentyltriphenylphosphonium bromide and butyllithium gave ethyl (*R*)-3-methyl-6-undecenoate (**6**). Hydrogenation of (*R*)-**6** over Pt(Adam's) gave ethyl (*R*)-3-methylundecanoate (**7**), which was reduced with lithium aluminum hydride to give (*R*)-3-methyl-1-undecanol (**8**). The bromination[16] of (*R*)-**8** gave (*R*)-**9**: $[\alpha]_D^{20}$ −4.07° (*c* 4.9, hexane). The (*R*)-**9** was converted to Grignard reagent ((*R*)-**10**) ((*R*)-C_{12} block) in ether right before the use for the coupling reaction.

The procedure for the preparation of (*S*)-**9** is shown in Fig. 3. The reduction of (*R*)-**4** with lithium aluminum hydride gave the corresponding alcohol(**11**), which was then converted to a tosylate ((*R*)-**12**). The coupling of (*R*)-**12** with hexylmagnesium chloride in the presence of copper(I) iodide[17] gave (*R*)-2,6-dimethyl-2-tetradecene (**13**). The ozonolysis of (*R*)-**13** in dichloromethane and oxidative cleavage of the ozonide with hydrogen peroxide in formic acid[14] gave (*S*)-4-methyldodecanoic acid (**14**). The Hunsdiecker reaction[18] of (*S*)-**14** gave (*S*)-**9**: $[\alpha]_D^{20}$ +4.04° (*c* 4.5, hexane). The (*S*)-**9** was converted to Grignard reagent ((*S*)-**10**) ((*S*)-C_{12} block) in ether right before the use for the coupling reaction.

As the optical rotations of (*R*)-and of (*S*)-**9** were the same value within experimental error, it was concluded that no racemization took places in each step of the reaction process. Therefore, these bromides (**9**) must be optically pure.

The preparation of C_5 blocks is shown in Fig. 4.

The hydrogenation of methyl 2-methyl-3-oxobutyrate (**15**) over the nickel catalyst modified with (*S,S*)-tartaric acid, ((*S,S*)-TA-MHNi) gave a mixture of methyl *threo*-and *erythro*-3-hydroxy-2-methylbutyrate (**16**) in a ratio of 25 to 75[19,20]. The effective isolation of *threo*-and *erythro*-isomer on a practical scale was successfully achieved by the crystallization method. The procedure shown in Fig. 4 enabled us to isolate *threo*-isomer with 55% recovery and *erythro*-isomer with 54% recovery. The advantage of this method is that *threo*-and *erythro*-isomers were obtained at once; furthermore the optical purity of each diastereomer was approximately 60%.

The mixture of *threo*-and *erythro*-**16** was saponified to sodium 3-hydroxy-2-methylbutyrate (**17**). The sodium salt thus obtained was dissolved in a minimum amount of methanol. By the slow addition of acetone to the solution, sodium salt of *threo*-isomer was preferentially precipitated as crystals. The recrystallization of the sodium salt from methanol-acetone gave pure *threo*-**17** (optical purity 60%, (2*S*,3*S*) in excess). *Erythro*-isomer enriched in the mother liquid of the first crystallization converted to cyclohexylammonium salt (**19**). Three succesive recrystallizations from EtOH gave pure *erythro*-**19** (optical purity 60%, (2*R*,3*S*) in excess).

Enrichments of optical purity of *threo*-and *erythro*-2-

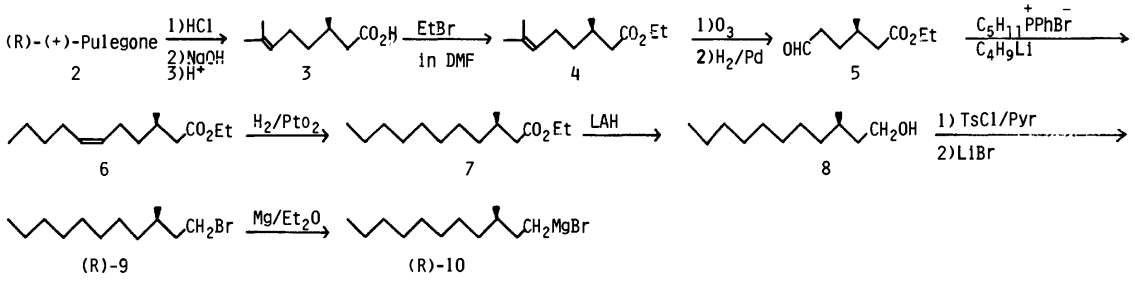

Fig. 2. Preparation of (R)-C_{12} building block.

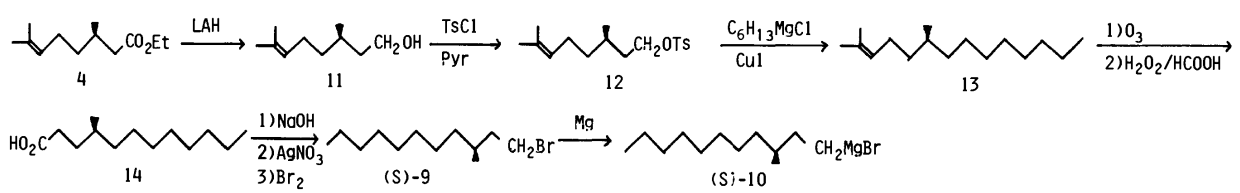

Fig. 3. Preparation of (*S*)-C_{12} building block.

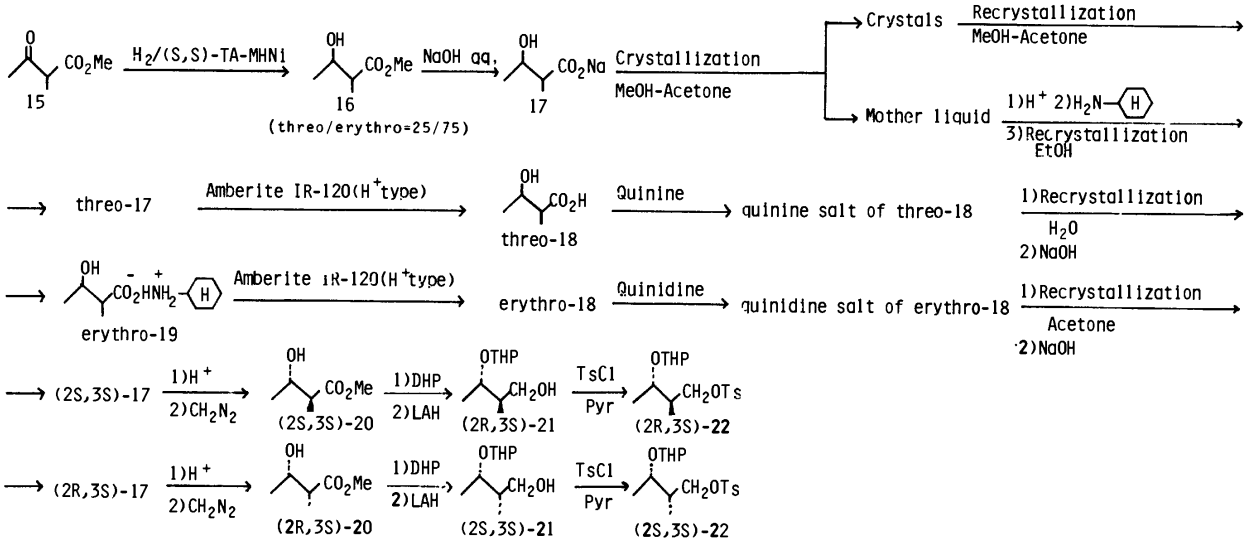

Fig. 4. Preparation of C_5 building blocks.

hydroxy-3-methylbutyric acid (**18**) were carried out by the recrystallization of quinine (*threo*-) and quinidine (*erythro*-) salt respectively. Removal of base by sodium hydroxide gave pure (2*S*,3*S*)-and (2*R*,3*S*)-**17**. The **17** was esterified to the corresponding methyl ester (**20**). After the protection of hydroxyl group of **20** by the treatment of dihydropyran, the resulting compounds were reduced with lithium aluminum hydride to give 2-methyl-3-tetrahydropyranyloxy-1-butanol (**21**). Tosylation of **21** by the conventional procedure gave 2-methyl-3-tetrahydropyranyloxy-1-(tosyloxy)butane (**22**), as shown in Fig. 4.

The coupling reaction of **22** with **10** was carried out by the reported method[17] to give the corresponding alcohol, as shown in Fig. 1. The stereochemical purity at the 2 and 3 position of the resulting (2*S*,3*S*, 7*S*)-, (2*S*,3*R*,7*S*)- and (2*S*,3*R*,7*R*)-**1** were determined by the analytical GLC (Capillary column PEG 20M, 50 m (L)×0.25 mm (I.D)) which can detect at least 0.2% of contaminated epimer. The optical purity of these compounds were also proved by the ^{1}H-NMR.

Each alcohol was converted to the acetate and propionate by the conventional procedure and the resulting esters were employed for the field assays. The synergistic effect of the acetate of (2*S*,3*R*,7*R*)-**1** on the acetate of (2*S*,3*S*,7*S*)-**1** in *N. sertifer* was clearly demonstrated.[21] For other species, the highly biological activity of the mixture of the acetate of (2*S*,3*R*,7*R*)- or (2*S*,3*R*,7*S*)-**1** and acetate of (2*S*,3*S*,7*S*)-**1** has been observed.[9] Details of the biological studies will be published elsewhere.

Experimental

All melting and boiling points are uncorrected. IR spectra were recorded on a Shimadzu IR-420 spectrometer. ^{1}H-NMR spectra were recorded in $CDCl_3$ solution at 200 MHz with TMS as an internal standard on a JOEL FX-200 spectrometer. Optical rotations were measured on a Perkin-Elmer 241 polarimeter. The analytical GLC and preparative GLC were carried out on a Shimadzu GC-6A gas chromatograph.

(R)-(+)- *Citronellic Acid (3).* This was prepared from (*R*)-(+)-pulegone (**2**), $[\alpha]_D^{20}$ +21.97° (neat), supplied by Takasago Perfume Industry Co., in 80% yield by the reported method[12]: bp 98.5 °C/1.5 mmHg†; $[\alpha]_D^{20}$ +8.89° (neat), lit,[12] $[\alpha]_D^{20}$ +8.48° (neat); GLC (3% OV-17 on Chromosorb W, 2 m×3 mm, at 150—220°, temperature gradient, 8 °C/min, carrier gas N_2, 1.4 kg/cm^{-2}), Rt 11 min (a single peak).

Determination of the Optical Purity of (R)-(+)-citronellic Acid. To the (*R*)-**3** (0.1 ml) in a test tube was added dicyclohexylcarbodiimide (DCC) (0.2 g) in ethyl acetate (0.5 ml) and then (*S*)-α-methylbenzylamine (0.2 ml) (Aldrich Co. $[\alpha]_D^{20}$—39° (neat), the e.e. was 98%, which was determined by the method described in the following section). After the mixture was allowed to stand for 1 h, acetic acid was added to this to decompose excess DCC. The white crystals which precipitated were removed by using a centrifuge. The supernatant was subjected to GLC analysis (capillary column OV-101, 50 m (L)×0.25 mm (I.D), at 160 °C, carrier gas N_2, 1.4 kg/cm^2). Under these conditions, (*R**,*S**)- and (*R**,*R**)-amide were completely resolved at the retention times of 69.4 min and 71.4 min respectively at 160 °C. The d.e. of the (*R*,*S*)-amide obtained above was calculated to be 98% from the ratio of the two peaks. The d.e. value was identical with the e.e. value of the (*S*)-α-methylbenzylamine employed. When the same **3** as above was allowed to react with (*R*)-α-methylbenzylamine (Aldrich Co. $[\alpha]_D^{20}$+38° (neat), the e.e. was determined to be 97%), the d.e. of (*R*,*R*)-amide was calculated to be 97% from the ratio of the two peaks. Since the d.e. values of these amides corresponded to the e.e. values of the α-methylbenzylamine employed for analyses, (*R*)-**3** was expected to be optically pure.

Determination of Optical Purity of (R)- and (S)-α-Methylbenzylamine. To (*R*)- or (*S*)-amine (0.1 ml) dissolved in ether (2 ml), trifluoroacetic anhydride (2 ml) was added. After removing the water soluble matter by washing with water, the ether solution was dried over $MgSO_4$. The resulting ethereal solution of *N*-trifluoroacetyl-α-methylbenzylamine was subjected to GLC analysis on OA-500 (Sumitomo Chemical Co. Ltd; capillary column coated with chiral compound, 40 m (L)×0.25 mm (I.D), at 150 °C, carrier gas N_2, 1.4 kg/cm^2). The (*R*)- and (*S*)-*N*-trifluoroacetamide were completely resolved at the retention time of 17.9 and 19.3 min at 150 °C respectively.

† 1 mmHg≈133.322 Pa.

Ethyl Citronellate (4). This was prepared from sodium salt of (*R*)-**3** and ethyl bromide in DMF. From 150 g of 3, 166 g (94.4%) of **4** was obtained: bp 66—68°C/1.5 mmHg; $[\alpha]_D^{20}$+2.6° (*c* 4.5, hexane); GLC(3% OV-17 on Chromosorb W, 2 m×3 mm, at 140 °C, carrier gas N_2, 1.4 kg/cm²), Rt 7 min (a single peak).

Ethyl (R)-3-Methyl-6-oxohexanoate (5). Ozone (4% in carrier gas) was introduced into 25 g of **4** dissolved in methanol (20 ml) in a carrier gas (O_2) (flow rate 0.2 l/min) at −70 °C. After the excess ozone in the reaction mixture was blown off by N_2 gas, the residue was transferred into a flask which contained a suspension of the preactivated Pd/C (100 mg) in methanol (20 ml). The reaction was continued until the theoretical amount of hydrogen was absorbed under atmospheric pressure at room temperature. After removal of Pd/C by filtration, and evaporation of methanol from the filtrate, the residue was distilled *in vacuo* to give 14.5 g (67%) of **5**: bp 124 °C/20 mmHg; $[\alpha]_D^{20}$ +4.0° (*c* 5.1, hexane); GLC (2.5% PEG 20M+3% $AgNO_3$ on Uniport B, 2 m×3 mm, at 150 °C, carrier gas N_2, 1.4 kg/cm²), Rt 5 min (a single peak); NMR ($CDCl_3$, TMS), δ=9.79 (1H for -CHO, s); IR (neat), 1720 and 1740 cm⁻¹ for aldehyde and ester groups. Found: C, 61.31; H, 9.48%. Calcd for $C_9H_{16}O_3$: C,62.76; H, 9.36%.

Ethyl (R)-3-Methyl-6-undecenoate (6). Pentyltriphenylphosphonium bromide was prepared from triphenylphosphine and 1-bromopentane in dry benzene.[15]

Butyllithium (4.28 g in 40 ml of hexane) was added dropwise into a suspension of the above pentyltriphenylphosphonium bromide (27.6 g) in anhydrous ether (200 ml) under nitrogen at room temperature. Into the solution of the ylide thus obtained, a solution of (*R*)-**5** (11.5 g) in ether (20 ml) was added dropwise at room temperature. The mixture was refluxed for 2 h and allowed to stand overnight at room temperature. After removal of insoluble matter by filtration, the ether in the filtrate was evaporated under reduced pressure. The residue was eluted with a 1 to 1 mixture of hexane and ether on a silica gel column (Wakogel C-100). The eluate was concentrated *in vacuo* and the residue was distilled to give 9.6 g (63.6%) of **6**: bp 91—92 °C/1.5 mmHg; $[\alpha]_D^{20}$+0.24° (*c* 5.4, hexane). Found: C, 72.34; H, 11.34%. Calcd for $C_{14}H_{26}O_2$: C, 74.28; H, 11.58%.

Ethyl (R)-3-Methylundecanoate (7). The **6** (9.6 g) was hydrogenated over Pt-black (60 mg) in methanol (20 ml). The distillation of the reaction product gave 9.3 g of (*R*)-**7**: bp 107—109 °C/5 mmHg; $[\alpha]_D^{20}$ +1.83° (*c* 5, hexane); GLC (2.5% PEG-20M+3% $AgNO_3$ on Uniport B, 2 m×3 mm, at 180 °C, carrier gas N_2, 1.4 kg/cm²), Rt 3.8 min (a single peak); IR (neat), 1738 cm⁻¹ for ester group.

(R)-3-Methyl-1-undecanol (8). The **7** (9.3 g) in dry ether (20 ml) was reduced with lithium aluminum hydride (2.3 g) in dry ether (100 ml). The reaction mixture was worked up by conventional procedures to give 7.6 g (>99%) of (*R*)-**8**: bp 137—140 °C/15 mmHg; $[\alpha]_D^{20}$ +4.8° (*c* 5.1, hexane); GLC (3% OV-17 on Chromosorb W, 2 m×3 mm, at 160 °C, carrier gas N_2, 1.4 kg/cm²), Rt 8 min (a single peak); IR (neat), 3300, 2900, 2840, 1450, 1380, 1050 cm⁻¹; NMR ($CDCl_3$, TMS), δ=0.92 (6H, overlapped t and d, 2×C<u>H</u>$_3$-), 1.26 (17H, br s, -(C<u>H</u>$_2$)$_8$- and -C<u>H</u>-), 3.69 (2H, t, -C<u>H</u>$_2$OH). Fond: C, 77.26; H, 14.15%. Calcd for $C_{12}H_{26}O$: C, 77.35; H, 14.07%.

(R)-1-Bromo-3-methylundecane (9). *p*-Toluenesulfonyl chloride (11.7 g) was added to (*R*)-**8** (7.6 g) in dry pyridine (40 ml) under stirring and ice-cooling. The mixture was stirred for 2 h and allowed to stand overnight in a refrigerator. Then it was poured onto ice-water and extracted with ether. The extract was washed with water, aqueous $CuSO_4$, $NaHCO_3$ and brine, dried over $MgSO_4$ and concentrated *in vacuo* to give the tosylate of **8** as viscous oil: IR (neat), 2900, 1600, 1450, 1360, 1180, 1100, 940 cm⁻¹. Anhydrous lithium bromide (3.6 g) was added to a stirred solution of the tosylate (7 g) in acetone (20 ml) at once. The reaction mixture was kept at around 40 °C for 1 h. The resulting insoluble matter was separated by filtration and washed with ether. The filtrate and washing were combined and concentrated *in vacuo*. The residue was chromatographed over silica gel (Wacogel C-100). Elution with hexane gave 7.2 g (70.6%) of (*R*)-**9**: bp 99—105 °C/5 mmHg; GLC (3% OV-17 on Chromosorb W, 2 m×3 mm, at 170 °C, carrier gas N_2, 1.4 kg/cm²), Rt 9 min (96% purity with 4% unidentified impurity, Rt 7 min). The analytical sample is purified by a preparative GLC (10% OV-17 on Chromosorb W , 5 m×4 mm, at 210 °C), $[\alpha]_D^{20}$ −4.07° (*c* 4.9,hexane); IR (neat), 2900, 2850, 1450, 1370, 1255, 720, 645 cm⁻¹; NMR ($CDCl_3$, TMS), δ=0.89 (6H, overlapped t and d, 2×C<u>H</u>$_3$-), 1.27 (14H, s, -(C<u>H</u>$_2$)$_7$-), 1.5—1.93 (3H, m, BrCH$_2$C<u>H</u>$_2$C<u>H</u>(CH$_3$)-), 3.41 (2H, t, BrC<u>H</u>$_2$-). Found: C, 57.95; H, 10.21%. Calcd for $C_{12}H_{25}Br$: C, 57.83; H, 10.11%.

(R)-Citronellol (11). The reduction of (*R*)-**4** with lithium aluminum hydride gave (*R*)-**11** in 96% yield: bp 117 °C/18 mmHg; $[\alpha]_D^{20}$ +6.16° (*c* 4.9, hexane); GLC (3% OV-17 on Chromosorb W, 2 m×3 mm, at 150 °C, carrier gas N_2, 1.4 kg/cm²), Rt 2.5 min (a single peak).

(R)-Citronellyl Tosylate (12). This was prepared by the reaction between **11** and *p*-toluenesulfonyl chloride in dry pridine. From 31.5 g of (*R*)-**11**, 55 g (87.8%) of crude (*R*)-**12** was obtained as a viscous oil. The product was used for the next step without further purification.

(R)-2,6-Dimethyl-2-tetradecene (13). Grignard reagent was prepared from Mg (10.7 g) and 1-chlorohexane (53 g) in dry ether (200 ml). To this reagent, cooled at −70 °C, a solution of (*R*)-**12** (55 g) in ether (100 ml) was added gradually. Then well pulverized CuI (4.2 g) was added to the mixture at once. The temperature of the reaction mixture was kept at −70 °C for 1 h, then gradually raised to room temperature. The mixture was allowed to stand over night, refluxed for 1 h and then poured into aqueous NH_4Cl, and extracted three times with ether. The combined extract was washed with aqueous NH_4Cl, $NaHCO_3$ and brine and dried over $MgSO_4$. After removal of the ether *in vacuo*, the residue was chromatographed over silica gel (Wakogel C-100). The fraction eluted with 1% ether in hexane (150 ml) was concentrated *in vacuo* and distilled to give 35 g (80.1% from **12**) of the pure **13**: bp 134—140 °C/13 mmHg; $[\alpha]_D^{20}$−1.67° (*c* 5.5, hexane); GLC (3% OV-17 on Chromosorb W, 2 m×3 mm, at 160 °C, carrier gas N_2, 1.4 kg/cm²), Rt 9 min (a single peak); IR (neat), 2900, 2840, 1450, 1370, 820 720 cm⁻¹; NMR ($CDCl_3$, TMS), δ=0.87 (6H, overlapped t and d, 2×C<u>H</u>$_3$-), 1.26 (17H, br s, -(C<u>H</u>$_2$)$_8$- and -C<u>H</u>-), 1.64 (6H, d, =C(C<u>H</u>$_3$)$_2$), 1.9 (2H, m, -C<u>H</u>$_2$-CH=C-), 5.11 (1H, t, -C<u>H</u>=C-).

(S)-4-Methyldodecanoic Acid (14). The ozonolysis of **13** (35 g) in CH_2Cl_2 (50 ml) at −70 °C and the oxidative cleavage of the resulting ozonide with 35% H_2O_2/HCOOH by the reported procedur[14] gave 25 g (89.5%) of **14**: bp 130—140 °C/1.5 mmHg; $[\alpha]_D^{20}$−0.6° (*c* 5.3, hexane); IR (neat), 3000, 2890, 2840, 2600, 1710, 1700, 1450, 1420, 1280, 1210, 915 cm⁻¹. Found: C, 72.00; H, 12.58%. Calcd for $C_{13}H_{26}O_2$: C, 72.84; H, 12.23%. A small portion of the product was converted to methyl ester. NMR ($CDCl_3$, TMS) of the ester showed signals as follows: δ=0.88 (6H, overlapped t and d, 2×C<u>H</u>$_3$-), 1.26 (17H, br s, -(C<u>H</u>$_2$)$_8$ -and -C<u>H</u>-), 2.38 (2H, m, -C<u>H</u>$_2$CO$_2$-), 3,66 (3H, s, -COOC<u>H</u>$_3$).

(S)-Bromo-3-methylundecane (9). To a solution of potassium hydroxide (6.6 g) in water (300 ml) was added (*S*)-**14** (25 g) with stirring. The solution of potassium salt of **14** thus obtained and the solution of $AgNO_3$ (19.9 g) were added simultaneously into 100 ml of hot water (60 °C) at about the same rate. The resulting white precipitate was filtered, washed with water and acetone, and dried over P_2O_5 to give 33.6 g of silver salt of **14**. To a suspension of silver salt of **14**

(33.6 g) in CCl_4 (200 ml, dried over molecular sieves) was slowly added dried bromine (16.75 g) in CCl_4 (50 ml) with stirring and cooling. The mixture was kept under ice-cooling for 1 h and allowed to stand for 2 h at room temperature. After that, the temperature of the mixture was gradually increased to refluxing temperature. The reaction was continued until no more generation of carbon dioxide was observed. The insoluble matter in the reaction mixture was filtered off and washed with hexane (200 ml). The combined filtrate and washing were concentrated *in vacuo*. The residue was distilled to give 22 g (84.6%) of (*S*)-**9**: bp 90—93 °C/3 mmHg; GLC (3% OV-17 on Chromosorb W, 2 m×3 mm, at 165 °C, carrier gas N_2, 1.4 kg/cm²), Rt 13 min (95% purity with unidentified impurity, Rt 8 min). The analytical sample is purified by a preparative GLC (10% OV-17 on Chromosorb W, 5 m×4 mm, at 210 °C: $[\alpha]_D^{20}$ +4.04° (*c* 4.5, hexane); Found: C, 57.45; H, 10.01%. Calcd for $C_{12}H_{25}Br$: C, 57.83; H, 10.11%. The IR and NMR spectra were identical with those of (*R*)-**9**.

Methyl threo-*and* erythro-*3-Hydroxy-2-methylbutyrate (16).* Methyl 2-methyl-3-oxobutyrate (**15**) (120 g) dissolved in THF (300 ml) was hydrogenated over reduced nickel (7.6 g) modified with (*S,S*)-tartaric acid (MHNi) in an autoclave (1000 ml capacity) by the procedure reported before[19,20] to give 116 g (95%) of crude methyl 3-hydroxy-2-methylbutyrate (**16**): bp 79—81 °C/18 mmHg. GLC (5% NPGS on Chromosorb W, 2 m×3 mm, at 90 °C, carrier gas N_2, 1.4 kg/cm²) indicated that the products consisted of 25% of *threo*-**16** (retention time 12.8 min) and 75% of *erythro*-**16** (retention time 14.1 min). Seven repeated runs gave 833 g of crude **16**.

The Separation of threo-*and erythro-3-Hydroxy-2-methylbutyric Acid (18).* The **16** obtained above was saponified with 30% aqueous sodium hydroxide at 0 °C to give sodium 3-hydroxy-2-methylbutyrate (**17**). The aqueous solution of **17** was concentrated *in vacuo* at 40 °C to give 800 g of white crystalline **17**. A 200 g part of the crystals was dissolved in hot methanol (*ca.* 800 ml), and acetone (*ca.* 600 ml) was gradually added to the solution at room temperature until crystals of the sodium salt appeared. The crystals thus obtained were filtered to give 56.4 g of crude *threo*-**17**. Four repeated runs of this procedure gave 216 g of the salt. Three recrystallizations from methanol–acetone gave 108.8 g (13.6% from **16**) of pure *threo*-**17**. A small portion of the salt was acidified and the resulting acid was converted to methyl ester by the treatment of diazomethane. The GLC (5% NPGS on Chromosorb W, 2 m×3 mm, at 90 °C, carrier gas N_2, 1.4 kg/cm²) of the methyl ester showed a single peak of the *threo*-isomer; Rt 12.8 min: $[\alpha]_D^{20}$ +22.4° (*c* 5, MeOH). The optical purity of the ester was calculated to be 61% based on the reported value ($[\alpha]_D^{20}$ +36.80° (*c* 5, MeOH)) for optically pure (2*S*,3*S*)-**20**.[22]

The mother liquids obtained from the original crystallization and the first recrystallization, as mentioned before, were combined and concentrated to dryness. The residue (534 g) was acidified with hydrochloric acid and was extracted with three 150 ml portions of ether. The evaporation of the extracts under reduced pressure gave 448.4 g (95% recovery from **17**) of 3-hydroxy-2-methylbutyric acid (**18**) enriched with *erythro*-isomer. The resulting **18** was dissolved in ethanol (650 ml) and then the solution was mixed with cyclohexylamine (380 g) under nitrogen. The mixture was allowed to stand overnight in a refrigerator. The crystals which precipitated were collected and recrystallized twice from ethanol to give 494.4 g (40% from **16**) of pure cyclohexylammonium salt (*erythro*-**19**). A small portion of the salt was acidified, and the free acid was converted to methyl ester with diazomethane. The GLC (5% NPGS on Chromosorb W, 2 m×3 mm, at 90 °C, carrier gas N_2, 1.4 kg/cm²) of the ester showed a single peak corresponding to the *erythro*-isomer; Rt 14.1 min: $[\alpha]_D^{20}$ −8.5° (*c* 5, MeOH). The optical purity of the ester was calculated to be 60% based on the reported value ($[\alpha]_D^{20}$ +14.32° (*c* 5, MeOH)) for optically pure (2*S*, 3*R*)-**20**.[22]

Enrichment of Optical Purity of threo-*18.* *Threo*-**17** (90 g) dissolved in water (1000 ml) was passed through the column of Amberlite IR-120 (H^+ type) and the resulting solution of acid was converted to quinine salt with quinine (210 g) by the procedure reported before.[22] The quinine salt was recrystallized from water three times to give 144 g (51% from *threo*-**17**) of pure crystals of quinine salt: mp 154 °C; $[\alpha]_D^{20}$ −163° (*c* 2, 50% aq EtOH). The crystals were dissolved in water (200 ml) and the solution was mixed with 5% aqueous solution of NaOH until the pH of the mixture became 10. After removal of quinine precipitated by filteration, the filtrate was concentrated to dryness. Crystallization of the residue from ethanol–acetone gave 45 g (98% from quinine salt) of (2*S*,3*S*)-**17**: $[\alpha]_D^{20}$ +10.6° (*c* 10, H_2O).

Enrichment of Optical Purity of erythro-*18.* *Erythro*-**19** (100 g) in water (1000 ml) was passed through the column packed with Amberlite IR-120 (H^+ type) and the eluted acid was treated with 149 g of quinidine. The resulting quinidine salt was recrystallized three times from acetone.[22]

The purified quinidine salt thus obtained amounted to 101.8 g (58% from *erythro*-**19**): mp 100 °C; $[\alpha]_D^{20}$ +172° (*c* 1, H_2O). The quinidine salt dissolved in water was treated with 5% aqueous solution of NaOH while stirring. After removal of the quinidine which precipitated, the filtrate was concentrated to dryness. Crystallization of the residue from ethanol–acetone gave 30.0 g (93.2% from quinidine salt) of (2*R*,3*S*)-**17** as crystals: $[\alpha]_D^{20}$ +7.5° (*c* 10, H_2O).

Methyl (2S,3S)-3-Hydroxy-2-methylbutyrate ((2S,3S)-20). The **18** liberated from (2*S*,3*S*)-**17** (20 g) by the treatment with 12M[††] HCl (48 ml) was extracted with three 40 ml portions of ether. After the extract was concentrated to *ca.* 80 ml, an excess amount of ethereal diazomethane was added to the solution. After removal of the ether, the residue was distilled *in vacuo* to give 17.6 g (95.2%) of (2*S*,3*S*)-**20**: bp 75 °C/13 mmHg; $[\alpha]_D^{20}$ +36.80° (*c* 5, MeOH); GLC (5% NPGS on Chromosorb W, 2 m×3 mm, at 90 °C, carrier gas N_2, 1.4 kg/cm²), Rt 12.8 min. (a single peak); NMR ($CDCl_3$, TMS), δ=1.17 (3H, d, J=7.1 Hz, $C\underline{H}_3$- at C-2), 1.24 (3H, d, J=6.4 Hz, $C\underline{H}_3$- at C_3), 2.47 (1H, quintet, -C$\underline{H}$(CH_3)-CO_2-CH_3), 2.64—2.72 (1H, br, -O$\underline{H}$), 3.72 (3H, s, -$CO_2C\underline{H}_3$), 3.85 (1H, quintet, $CH_3C\underline{H}$(OH)-). Found: C, 54.45; H, 9.16%. Calcd for $C_6H_{12}O_3$: C, 54.53; H, 9.15%. In the NMR, methyl protons of ester group of (2*S*,3*S*)-**20** and that of (2*R*,3*R*)-**20** showed different chemical shift in the presence of chiral shift reagent. As for the sample of (2*S*,3*S*)-**20**, no detectable signals of antipode was observed when the spectra was measured with 17.5 mg of the sample and 45 mg of Eu(hfc)₃ in $CDCl_3$ (0.4 ml).

Methyl (2R,3S)-3-Hydroxy-2-methylbutyrate ((2R,3S)-20). By the procedure mentioned above, 20 g of (2*R*,3*S*)-**17** was converted into 17 g (92%) of (2*R*,3*S*)-**20**: bp 75 °C/15 mmHg; $[\alpha]_D^{20}$ −14.3° (*c* 5, MeOH); GLC (5% NPGS on Chromosorb W, 2 m×3 mm, at 90 °C, carrier gas N_2, 1.4 kg/cm²), Rt 14.0 min. (a single peak); NMR ($CDCl_3$, TMS), δ=1.18 (3H, d, J=6.4 Hz, $C\underline{H}_3$- at C_3), 1.19 (3H, d, J=7.6 Hz, $C\underline{H}_3$- at C_2), 2.3—2.7 (2H, m, -C$\underline{H}$(CH_3)CO_2CH_3 and -O$\underline{H}$), 3.71 (3H, s, $-CO_2C\underline{H}_3$), 3.2—4.2 (1H, m, $CH_3C\underline{H}$(OH)-). Found: C, 54.60; H, 9.46%. Calcd for $C_6H_{12}O_3$: C, 54.53; H, 9.15%. In the NMR, methyl protons of ester group of (2*R*,3*S*)-**20** and that of (2*S*,3*R*)-**20** showed different chemical shifts in the presence of chiral shift reagent. As for the present sample, no detectable signals of antipode was observed when the spectra were measured with the sample (19.2 mg) and Eu(hfc)₃ (100 mg) in $CDCl_3$ (0.4 ml).

(2R,3S)-2-Methyl-3-tetrahydropyranyloxy-1-butanol ((2R,3S)-21). To the solution (2*S*,3*S*)-**20** (13.5 g) and dihydro-

[††] 1M=1 mol dm^{-3}.

pyran (7.8 g) in dry ether (20 ml) was added *p*-toluenesulfonic acid (0.1 g) with stirring at room temperature. The reaction mixture was allowed to stand overnight at room temperature and washed with aqueous $NaHCO_3$, and dried over K_2CO_3. This material was employed for the next step without further purification. To a stirred and ice-cooled suspension of lithium aluminum hydride (5.7 g) in dry ether (200 ml) was added dropwise the above ester in dry ether (30 ml). The mixture was refluxed for 3 h, cooled down to room temperature and hydrolyzed with the theoretical amount of water (10.8 g). The white precipitate was filtered on Celite and washed with ether. The combined filtrate was concentrated *in vacuo*. The distillation of the residue gave 12.2 g (83.7%) of (2*R*,3*S*)-**21**: bp 86.6 °C/2 mmHg; IR (neat), 3600—3800, 2800, 2700, 1430—1450, 1370, 1110—1120, 1010, 970, 930, 900, 870, 800 cm^{-1}. Found: C, 64.00; H, 10.91%. Calcd for $C_{10}H_{20}O_3$: C, 63.79; H, 10.71%.

(2S,3S)-2-Methyl-3-tetrahydropyranyloxy-1-butanol ((2*S*,3*S*)-**21**). By the same method as discribed above, (2*R*,3*S*)-**20** (20 g) was converted to 15.1 g (68%) of (2*S*,3*S*)-**21**: bp 93 °C/3 mmHg. Found: C, 63.60; H, 10.82%. Calcd for $C_{10}H_{20}O_3$: C, 63.79; H, 10.71%.

(2R,3S)-2-Methyl-3-tetrahydropyranyloxy-1-(tosyloxy)butane ((2R,3*S*)-**22**). The (2*R*,3*S*)-**21** (12.2 g) was added dropwise to the solution of *p*-toluenesulfonyl chloride (14.9 g) in dry pyridine (50 ml) cooled on an ice bath. After the reaction mixture was allowed to stand in a refrigerator overnight, it was poured into ice-water (100 ml), and extracted with three 20 ml portions of ether. The combined extract was washed with water, aqueous $CuSO_4$, $NaHCO_3$, and then brine, dried over $MgSO_4$ and concentrated *in vacuo* to give 21 g (95.4%) of crude (2*R*,3*S*)-**22**.

(2S,3S)-2-Methyl-3-tetrahydropyranyloxy-1-(tosyloxy)butane ((2*S*,3*S*)-**22**). The (2*S*,3*S*)-**21** (12.2 g) was treated with 14.9 g of *p*-toluenesulfonyl chloride. The reaction product was worked up by the same procedure as before to give 18.3 g (83%) of crude (2*R*,3*S*)-**22**.

(2S,3R,7R)-3,7-Dimethyl-2-pentadecanol ((2*S*,3R,7R)-**1**). Grignard reagent, (*R*)-**10** was prepared from magnesium (0.43 g) and (*R*)-**9** (4.4 g) in well dried ether (30 ml). After the solution of (*R*)-**10** was cooled down to −70 °C in a Dry Ice-acetone bath, (2*R*,3*S*)-**21** (3 g) dissolved in ether (10 ml) and CuI (0.2 g) were added to the solution with stirring. The temperature of the reaction mixture was gradually raised to 5 °C and kept at 5 °C for 3 h and then overnight at room temperature. After the reaction mixture was refluxed and cooled down, the resulting ether solution was poured into ice-cooled NH_4Cl and the ethereal layer separated out. The aqueous layer was extracted with three 10 ml portions of ether. The combined ethereal solution was washed with aqueous NH_4Cl, $NaHCO_3$ and brine and then evaporated *in vacuo*. The remaining material was treated with *p*-toluenesulfonic acid (0.2 g) in methanol (20 ml) to give crude (2*S*,3*R*,7*R*)-**1**. The crude **1** was purified on a column (Wacogel C-100) with hexane (120 ml) and then 50% ether in hexane (100 ml). The (2*S*,3*R*,7*R*)-**1** was eluted in the second fraction. After removal of the solvent *in vacuo*, the distillation of the residue gave 1.9 g (84.4% from (2*R*,3*S*)-**22**) of (2*S*,3*R*,7*R*)-**1**: bp 116 °C/0.5 mmHg; $[\alpha]_D^{20}$ +16.03° (*c* 5.2, hexane); GLC (capillary column PEG 20M, 50 m (L)×0.25 mm (I.D), at 140 °C, carrier gas N_2, 1.2 kg/cm^2), Rt 15.5 min (a single peak); IR (neat) 3300, 2900, 2850, 1465, 1377, 1095 cm^{-1}; NMR ($CDCl_3$, TMS), δ=0.85 (9H, overlapped t and d, CH_3- at C-3, C-7 and terminal), 1.12 (3H, d, *J*=6.4 Hz, CH_3- at C-2), 1.26 (22H, br s, -$(CH_2)_{10}$-and 2×-CH-), 3.6 (1H, m, -CH(OH)-). Found: C, 79.04; H, 14.30%. Calcd for $C_{17}H_{36}O$: C, 79.61; ,H, 14.15%. (2*S*,3*R*)-**1** and (2*S*,3*S*)-**1** can be distinguished in the capillary GLC and ^{1}H-NMR. The capillary GLC (PEG 20M) results showed that the retention times of the former and the later were 15.5 min and 15.2 min, respectively. The present sample showed a single peak (Rt 15.5) and no peak of (2*S*,3*S*)-**1** (Rt. 15.2 min) was observed. By NMR, only doublet splitting of C-1 methyl signals was observed. Those analyses indicated that the sample was completely free from (2*S*,3*S*)-**1**.

(2S,3R,7S)-3,7-Dimethyl-2-pentadecanol ((2*S*,3R,7*S*)-**1**). This was obtained from (*S*)-**10** and (2*R*,3*S*)-**22** in 80% yield by the procedure mentioned before: bp 106.5—108 °C/0.4 mmHg; $[\alpha]_D^{20}$ +16.36° (*c* 3.5, hexane), GLC (capillary column PEG 20M, 50 m (L)×0.25 mm (I.D), at 130 °C, carrier gas N_2, 1.2 kg/cm^2), Rt 15.5 min (a single peak); IR (neat), 3300, 2900, 2850, 1465, 1377, 1095 cm^{-1}; NMR ($CDCl_3$, TMS), δ=0.85 (9H, overlapped t and d, CH_3-at C-3, C-7 and terminal), 1.16 (3H, d, *J*=6.4 Hz, CH_3- at C-2), 1.26 (22H, br s, -$(CH_2)_{10}$- and 2×-CH-), 3.6 (1H, m, -CH(OH)-). Found: C, 78.76; H, 14.29%. Calcd for $C_{17}H_{36}O$: C, 79.61; H, 14.15%. It was shown that the product was completely free from (2*S*,3*S*)-**1** in the capillary GLC and NMR analyses of this sample under the same conditions as mentioned before.

(2S,3S,7S)-3,7-Dimethyl-2-pentadecanol ((2*S*,3*S*,7*S*)-**1**). This was obtained from (*S*)-**10** and (2*S*,3*S*)-**22** in 52% yield by the method mentioned before: bp 110—117 °C/0.5 mmHg; $[\alpha]_D^{20}$ −10.4° (*c* 3.7, hexane); GLC (capillary column PEG 20M, 50 m (L)×0.25 mm (I.D), at 130 °C, carrier gas N_2, 1.2 kg/cm^2), Rt 15.2 min (a single peak); IR (neat) 3300, 2900, 2850, 1450, 1370, 1400, 920, 715 cm^{-1}; NMR ($CDCl_3$, TMS), δ=0.86 (9H, overlapped t and d, CH_3- at C-3, C-7 and terminal), 1.15 (3H, d, *J*=6.4 Hz, CH_3- at C-2), 1.26 (22H, br s, -$(CH_2)_{10}$- and 2×-CH-), 3.6 (1H, m, -CH(OH)-). Found: C, 78.95; H, 14.32%. Calcd for $C_{17}H_{36}O$: C, 79.61; H, 14.15%.

It was shown that the sample was completely free from (2*R*,3*S*)-isomer in the capillary GLC and NMR analyses

Table 1. Analytical date of (2*S*,3*R*,7*R*)-, (2*S*,3*R*,7*S*)-, or (2*S*,3*S*,7*S*)-2-acetoxy- and 2-propionyloxy-3,7-dimethylpentadecane

Compounds	r.t. of GLC[a)]	$[\alpha]_D^{20}$ in hexane	Elemental analysis	
			Calcd for $C_{19}H_{38}O_2$	Found
(2*S*,3*R*,7*R*)-**23**	16.1 min	+6.97±0.06 (*c* 1.4)	C, 76.45; H, 12.83	C, 76.03; H, 13.52
(2*S*,3*R*,7*S*)-**23**	16.1 min	+6.39±0.04 (*c* 4.9)		C, 76.39; H, 13.13
(2*S*,3*S*,7*S*)-**23**	15.8 min	−6.05±0.04 (*c* 4.3)		C, 75.98; H, 13.44
			Calcd for $C_{20}H_{40}O_2$	Found
(2*S*,3*R*,7*R*)-**24**	18.6 min	+7.03±0.03 (*c* 7.2)	C, 76.86; H, 12.90	C, 76.09; H, 13.00
(2*S*,3*R*,7*S*)-**24**	18.6 min	+6.67±0.04 (*c* 4.5)		C, 76.28; H, 12.92
(2*S*,3*S*,7*S*)-**24**	18.1 min	−6.16±0.03 (*c* 6.6)		C, 76.75; H, 13.07

a) Retention times at 130 °C on capillary column (PEG 20 M, 50 m(L) × 0.25 mm(I.D), carrier gas N_2, 1.4 kg/cm^2).

as mentioned before.

The Preparation of Pheromone. (2*S*,3*R*,7*R*)-, (2*S*,3*R*,7*S*)- and (2*S*,3*S*,7*S*)-3,7-dimethyl-2-pentadecanol were converted to the corresponding acetates and propionates by the conventional method respectively. The analytical data of the products are summarized in Table 1.

We wish to express our appreciation to Mr. S. Muraki of Takasago Perfume Inderstry Co., for the gift of optically pure (+)-pulegone. We also wish to thank Professor Yoshiharu Izumi, Dr. Tadao Harada, and Dr. Hiroshi Ozaki of Institute for Protein Research, Osaka University for their helpful suggestions on the synthetic study, and Professor Fumio Matsumura and Mr. Julius Olaifa of Pesticide Research Center, Michigan State University, and Professor Harry C. Coppel and Dr. Mark Kraemer of the University of Wisconsin for their detailed information about the biological study. Thanks are also due to Mr. Tsutomu Osawa for NMR analysis and Mrs. Aiko Kobatake for elemental analysis.

References

1) D. M. Jewett, F. Matsumura, and H. C. Coppel, *Science*, **192**, 51 (1976).
2) D. M. Jewett, F. Matsumura, and H. C. Coppel, *J. Chem. Ecol.*, **4**, 277 (1978).
3) A. Tai, M. Imaida, T. Oda, and H. Watanabe., *Chem. Lett.*, **1978**, 61.
4) T. Kikukawa, F. Matsumura, M. Kraemer, and H. C. Coppel, *J. Chem. Ecol.*, **8**, 301 (1982).
5) F. Matsumura, A. Tai, and H. C. Coppel, *Univ. Wisc. For. Res. Note* No. **216**, 4 (1978).
6) F. Matsumura, A. Tai, H. C. Coppel, and M. Imaida, *J. Chem. Ecol.*, **5**, 237 (1979).
7) K. Mori, S. Tamada, and M. Matsui, *Tetrahedron Lett.*, **1978**, 901.
8) M. Kraemer, H. C. Coppel, F. Matsumura, R. C. Wilkinson, and T. Kikukawa., *J. Chem. Ecol.*, **7**, 1063 (1981).
9) T. Kikukawa, A. Tai, F. Matsumura, J. Olaifa, M. Kraemer, and H.C. Coppel, The Fifth International Congress of Pesticide Chemistry (IUPAC) Kyoto, Japan, **1982**, III C-18.
10) S. Bystrom, H. Hogberg, and T. Norin, *Tetrahedron*, **37**, 2249 (1981).
11) G. Magnusson, *Tetrahedron Lett.*, **1977**, 2713.
12) C. G. Overberger and H. Kaye, *J. Am. Chem. Soc.*, **89**, 5640 (1967).
13) H. D. Dewitt and A. W. Iupersoll., *J. Am. Chem. Soc.*, **73**, 5782 (1951).
14) R. H. Perry. Jr., *J. Org. Chem.*, **24**, 829 (1959).
15) G. Wittig and U. Schoellkopf, *Org. Syn.*, Coll. Vol. **5**, 5719.
16) K. B. Wiberg and B. R. Lowry, *J. Am. Chem. Soc.*, **85**, 3188 (1963).
17) G. Fouquet and M. Schlosser, *Angew. Chem., Int. Ed. Engl.*, **13**, 82 (1974).
18) C. V. Wilson, *Org. Rec.*, **9**, 332 (1957).
19) A. Tai, H. Watanabe, and T. Harada, *Bull. Chem. Soc. Jpn.*, **52**, 1468 (1979).
20) T. Harada, S. Onaka, A. Tai, and Y. Izumi, *Chem. Lett.*, **1977**, 1131.
21) T. Kikukawa, F. Matsumura, J. Olaifa, M. Kraemer, H. C. Coppel, and A. Tai, *J. Chem. Ecol.*, **9**, 673 (1983).
22) A. Tai and M. Imaida, *Bull. Chem. Soc. Jpn.*, **51**, 1114 (1978).

3,5-Dinitro-1-(4-nitrophenyl)-4-pyridone, A Novel and Convenient Protecting Reagent for Primary Amines[1)]

Eizo MATSUMURA,† Hironori KOBAYASHI, Tomomi NISHIKAWA, Masahiro ARIGA, Yasuo TOHDA, and Toshihide KAWASHIMA*

Department of Chemistry, Osaka Kyoiku University, Minamikawahori-cho 4-88, Tennoji-ku, Osaka 543

(Received December 19, 1983)

Crystalline derivatives of the following L-amino acids modified by 3,5-dinitro-4-pyridone have been prepared: glycine, alanine, valine, leucine, isoleucine, phenylalanine, serine, threonine, tyrosine, aspartic acid, asparagine, glutamic acid, glutamine, tryptophan, histidine, arginine, methionine and lysine. The modified L-amino acids (DNPY-L-amino acids) could be purified by recrystallization and were characterized by ^{1}H-NMR, IR and UV spectral data. The molar rotation of the DNPY-L-amino acids varied from 2 to 100 times those of the parent amino acids. The effectiveness of 3,5-dinitro-1-(4-nitrophenyl)-4-pyridone as an amino-protecting reagent of L-amino acids is described.

We have previously reported that 1-substituted 3,5-dinitro-2- and 4-pyridones reacted with some carbon nucleophiles. In the reaction, a new ring transformation was found by action of alkali salts of β-keto esters and vinyl ethers.[2)]

We have recently shown that the treatment of the 4-pyridone with a primary amine leads to another type of ring transformation reaction. Thus 3,5-dinitro-1-(4-nitrophenyl)-4-pyridone(DNPY[3)]-C_6H_4-NO_2-4) and 1.1 equimolar amounts of propylamine in pyridine medium gave 3,5-dinitro-1-propyl-4-pyridone and 4-nitroaniline in nearly quantitative yields at room temperature.[4)] The reaction involves the nucleophilic attack of the amine in sequence at C-2 and C-6 positions on the 4-pyridone and exchanges of the amine moiety in the pyridone ring, as shown in Scheme 1.

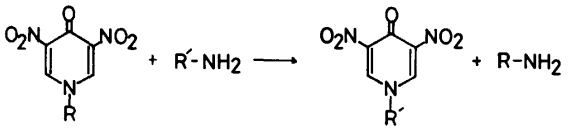

Scheme 1.

The reaction may be referred to the difference in nucleophilicity between the introduced amines and the liberated ones. Therefore the 4-pyridone derivative with an electron-withdrawing substituent at the 1-position should be one of the best protecting reagents for primary amines.

In synthetic organic chemistry, a variety of protective reagents (*e.g.*, urethane-type, acyl-type and alkyl-type), have been developed and utilized.[5)] Here we propose the 1-substituted 3,5-dinitro-4-pyridone as a novel reagent for blocking of the amino function, since the 4-pyridone reacts easily under very mild conditions.

The present paper describes the first application of the reagent to amino acids and the properties of the resulting modified amino acids(DNPY-L-amino acids).

Results and Discussion

Preparation of 1-Substituted 3,5-Dinitro-4-Pyridones. 1-Substituted 3,5-dinitro-4-pyridones (**2a**—**2c**) were prepared by two step reactions from 4-pyridinol, as shown in Scheme 2.

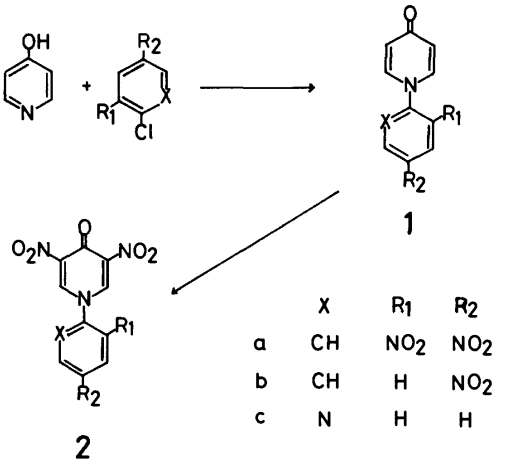

Scheme 2.

Table 1. Yield of 1-substituted 3,5-dinitro-4-pyridones

4-Pyridone	**2a**	**2b**	**2c**
Overall yield[a)]	13%	70%	24%

a) Based on 4-pyridinol.

As has been pointed out, the 4-pyridone with a stronger electron-withdrawing group at the 1-position would be more favorable for a protective reagent. However, the strongest electron-withdrawing group does not always make the pyridone the best reagent for protecting. Tetranitro compound, **2a** is indeed the most electron-deficient, but its precursor **1a** is too electron-poor to give the nitration product **2a** in good yield, as Table 1 shows. Among the three pyridones, **2b** was chosen as the suitable substrate for our purpose in view of the yield obtained and the cost for preparation.

Syntheses of Modified L-Amino Acids (DNPY-L-Amino Acids). In aqueous pyridine, **2b** reacted with eighteen kinds of L-amino acids in high yield, as follows.

The reaction was accomplished in 2—24 h at room

† Emeritus professor of Osaka Kyoiku University.

TABLE 2. PHYSICAL PROPERTIES OF THE DNPY-L-AMINO ACIDS (DNPY-A)

DNPY-A A=L-Amino acid	Reaction time (h)	Decomposition Point (°C)	Shape of Crystals	Yield/%
Gly	4.0	220.0	prisms	quant.
Ala	4.0	195.0	needles	quant.
Val	4.0	237.5—239.0	columns	82
Leu	4.0	210.0—212.0	prisms	80
Ile	4.0	240.0—245.0	plates	86
Phe	4.0	105.0—107.0	needles	55
Ser	5.0	184.5—185.5	needles	quant.
Thr	3.0	203.0	needles	75
Tyr	3.0	234.0—235.0	needles	quant.
Asp	5.0	112.0	needles	89
Asn	2.5	130.0—131.5	needles	81
Glu	5.5	218.0—221.0	columns	quant.
Gln	2.0	225.0—226.0	prisms	90
Trp	3.0	191.0—193.0	needles	55
His	3.0	255.0—257.0	plates	quant.
Arg	2.0	175.5—176.0	needles	77
Met	3.0	149.0—151.0	prisms	98
Lys[a)]	23.0	190.5—191.5	needles	87

a) Bis-DNPY-L-Lys

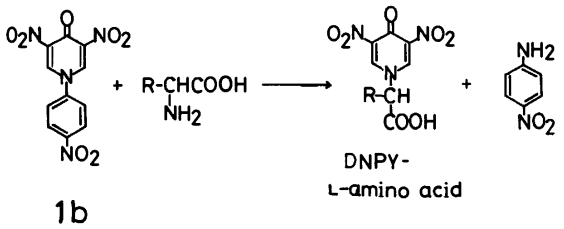

Scheme 3.

temperature when all reactants had been dissolved completely.

The solvent was evaporated *in vacuo* and then the residue was extracted with chloroform to remove 4-nitroaniline. The aqueous layer was condensed to give a DNPY L-amino acid. All the L-amino acids except L-lysine could be converted to α-amino-protected compounds. In the case of L-lysine, which had two amino functions, it reacted with an equimolar amount of **2b** to give a mixture of mono-DNPY-L-lysine, bis-DNPY-L-lysine and L-lysine. From L-arginine, on the other hand, α-amino-protected product was only obtained in 77% yield. The results can be explained by the suggestion that the latter's ω-amino function is a part of the amidine structure and is less nucleophilic to **2b** under the conditions used. In the former, however, its ω-amino function reacts easily with **2b** because its p*K*a value is 10.28.[6] Thus treatment of L-lysine with 2 equimolar amounts of **2b** gave bis-DNPY-L-lysine in good yield. In both cases, the reactions under nitrogen atmosphere led to better results.

All of the modified L-amino acids were yellow solids because of the DNPY-protection and could be purified by recrystallization from aqueous ethanol. The DNPY-protection caused the amino function to become tertiarized and the modified L-amino acids to become less hygroscopic. Thus the DNPY-L-amino acids could be handled more easily. Their structures were determined based upon the spectroscopic data, as follows.

The Spectroscopic Properties of the DNPY-L-amino Acids. The spectral characteristics of the DNPY-L-amino acids are summarized in Table 3. In the ^{1}H-NMR spectrum, the aromatic protons on the pyridone ring appear as a sharp singlet at *ca.* δ=9.1. In addition, the α-methine proton of the modified L-amino acid moiety is shifted downfield compared with that of the parent L-amino acid, due to the electron-withdrawing effect of the DNPY group. The infrared spectra of the DNPY-L-amino acids show the stretching vibration of the pyridone carbonyl at *ca.* 1670 cm^{-1} characteristically. Furthermore, the asymmetrical and the symmetrical stretching vibration of the nitro group are present at about 1510 and 1340 cm^{-1}, respectively.

In the ultraviolet spectrum, the absorption identified as the π-π* transition of the pyridone ring appears at *ca.* 340 nm with ε=*ca.* 4.5×10^3 characteristically.

The Optical Property of The DNPY-L-amino Acids. The values of the optical rotation have been used as a quantification of the modified amino acids, so those of the DNPY-L-amino acids determined in DMF are listed in Table 4.

The molar rotation of the DNPY-L-amino acids, $[M]_D$ are in general higher and in some cases very much higher than those of the parent L-amino acids. Furthermore, the values are comparable with or superior to those of well-known DNP-L-amino acids, of which the molar rotations vary from 2 to 100 times those of the parent amino acids.[7] The results may permit the identification and the optical characterization of a small quantity of an amino acid enantiomorph, so the DNPY group would be useful for amino-protection.

Removal of the DNPY Group. For the removal

Table 3. Spectroscopic properties of the DNPY-L-amino acids (DNPY-A)

DNPY-A A=L-Amino acid	IR $\tilde{\nu}$/cm^{-1}		^{1}H-NMR δ/ppm[1]		UV[2]	
	$\nu_{C=O}$[3]	ν_{NO_2}	H_2 & H_6	α-methine	λ_{max}/nm	ε(at max)$\times 10^3$
Gly	1674	1510, 1345	9.13	—	342	6.92
Ala	1673	1510, 1342	9.15	5.34(q)	341	4.23
Val	1675	1512, 1346	9.12	4.92(d)	342	4.65
Leu	1676	1512, 1345	9.16	5.23(dd)	340	4.17
Ile	1670	1512, 1345	9.13	4.97(d)	342	5.16
Phe	1672	1510, 1340	9.10	5.63(t)	342	2.74
Ser	1675	1505, 1336	9.14	5.36(dd)	341	4.83
Thr	1675	1510, 1340	9.09	5.22(d)	340	4.67
Tyr	1670	1508, 1335	9.03	5.53(t)	340	3.96
Asp	1670	1510, 1340	9.24	5.63(t)	340	3.72
Asn	1670	1513, 1340	9.19	5.46(t)	340	4.45
Glu	1677	1510, 1340	9.15	5.20(m)	342	4.30
Gln	1677	1510, 1340	9.11	5.24(t)	354	4.17[4]
Trp	1670	1510, 1325	9.01	5.62(t)	340	4.64
His	1680	1510, 1325	9.04	5.35(t)	—	—[5]
Arg	1673	1510, 1335	9.12	5.30(m)[6]	346[7]	3.97
Met	1665	1526, 1352	9.15	5.30(m)	339	4.17
Lys[8]	1688 1678	1511, 1320	9.15 9.11	5.25(t)	358	8.10[4]

1) In DMSO-d_6. 2) In EtOH. 3) On pyridone ring. 4) In DMF. 5) Slightly soluble in every solvent. 6) In CF_3COOD. 7) In 6 M-HCl (1 M=1 mol dm^{-3}). 8) Bis-DNPY-L-Lys.

Table 4. Optical properties of the DNPY-L-amino acids (DNPY-A)

DNPY-A A=L-Amino acid	Molecular formula	Found (%)			Calcd (%)			$[\alpha]_D^{15}$ in DMF	$[M]_D$	$[M]_D$ of parent amino acid[b]
		C	H	N	C	H	N			
Gly	$C_7H_5N_3O_7$	34.82	2.09	17.50	34.58	2.07	17.28	—	—	—
Ala	$C_8H_7N_3O_7$	37.32	2.73	16.46	37.36	2.74	16.34	−26.2°	−67.4°	+13.0°
Val	$C_{10}H_{11}N_3O_7$	42.07	3.83	14.80	42.11	3.89	14.73	−127.5°	−269.2°	+33.7°
Leu	$C_{11}H_{13}N_3O_7$	44.15	4.35	14.07	44.15	4.38	14.04	−53.5°	−118.5°	+30.0°
Ile	$C_{11}H_{13}N_3O_7$	43.94	4.19	14.12	44.15	4.38	14.04	−114.0°	−252.5°	+53.1°
Phe	$C_{14}H_{11}N_3O_7$	50.70	3.50	12.39	50.45	3.33	12.61	−150.0°	−370.0°	−7.4°
Ser	$C_8H_7N_3O_8$	35.20	2.60	15.49	35.17	2.58	15.38	−0.87°	−1.8°	+15.9°
Thr	$C_9H_9N_3O_8$	37.48	3.09	14.64	37.64	3.16	14.63	+25.0°	+53.1°	−17.9°
Tyr	$C_{14}H_{11}N_3O_8$	48.27	3.03	12.02	48.14	3.17	12.03	−208.0°	−537.7°	−21.4°
Asp	$C_9H_7N_3O_9$	35.44	2.43	13.87	35.89	2.34	13.95	−69.5°	−154.9°	+34.9°
Asn	$C_9H_8N_4O_8$	35.91	2.88	18.37	36.01	2.69	18.67	+30.5°	+67.8°	+45.3°[e]
Glu	$C_{10}H_9H_3O_9$	42.02	3.34	13.66	42.20	3.26	13.78[a]	−71.5°	−166.8°	+47.4°
Gln	$C_{10}H_{10}N_4O_8$	38.34	3.21	17.83	38.22	3.21	17.83	−83.5°	−194.2°	+57.3°[f]
Trp	$C_{16}H_{12}N_4O_7$	51.38	3.22	14.84	51.62	3.25	15.05	−190.8°	−525.7°	+5.7°
Arg	$C_{11}H_{14}N_6O_7$	38.47	4.10	24.67	38.60	4.12	24.56[b]	−3.5°	−8.9°	+48.0°
Met	$C_{10}H_{11}N_3O_7S$	37.76	3.53	13.10	37.86	3.49	13.24	−61.5°	−143.2°	+36.0°
Lys[c]	$C_{16}H_{14}N_6O_{12}$	39.70	3.08	17.41	39.84	2.93	17.43	−52.3°	−186.7°	+38.0°
His	$C_{11}H_9N_5O_7$	40.60	2.80	21.59	40.88	2.81	21.67	—[d]	—	+19.2°

a) Calcd for $C_{10}H_9N_3O_9\cdot 1/2C_5H_5N$. b) In 5 M-HCl. c) Bis-DNPY-L-Lys. d) Slightly soluble in every solvent. e) In 3 M-HCl. f) In 1 M-HCl.

of the DNPY group from the modified L-amino acid, a deblocking reagent must be more nucleophilic than the corresponding L-amino acid, of which the α-amino function generally has a p*K*a value of 9.1—9.8.[6] In addition, on the deblocking reaction, the liberated L-amino acid has to be easily separated from the DNPY-derivative formed. Thus hexylamine, whose p*K*a value was 10.64[8] was selected as a deblocking reagent. The removal reaction also proceeded in aqueous pyridine medium at room temperature for 0.5—2.5 h similar to the blocking process. The liberated L-amino acid was recovered in good yield after the same post-treatment as used for the blocking procedure. The results are shown in Table 5, along with the specific

TABLE 5. YIELD AND SPECIFIC ROTATION OF RECOVERED L-AMINO ACIDS

L-Amino acid	Yield/%	$[\alpha]_D^{15}$ in 5 M-HCl (lit,)[a]
Ala	91.7	+14.9° (+14.7°)
Leu	97.0	+14.7° (+14.7°)
Phe	85.7	−4.5° (−4.5°)
Ser	90.9	+14.9° (+15.1°)
Thr	83.8	−14.6° (−15.1°)
Tyr	88.3	−11.3° (−11.8°)
Glu	84.0	+32.3° (+32.2°)
Asn	96.2	+34.8° (+34.3°)
His	92.0	+12.4° (+12.4°)
Met	85.1	+25.3° (+24.1°)

a) Reference 6).

rotation.

No change in specific rotation of the L-amino acid throughout the DNPY-modification was found, within an uncertainty of about four percent. The results indicate that racemization does not occur; this is an important advantage of the DNPY-modification.

Subsequently, the DNPY-modification is very utilizable for amino-protection of amino acids in following aspects.

(1) 3,5-Dinitro-1-(4-nitrophenyl)-4-pyridone, the protecting reagent is easily prepared from pyridine with a sequence of only three reactions.

(2) The blocking and deblocking processes proceed under very mild conditions, in aqueous pyridine and at room temperature with stirring.

(3) The tertiarization by DNPY-protection makes an amino acid less hygroscopic and the modified L-amino acid can be handled more easily.

(4) The DNPY-L-amino acids are identified very easily by the spectroscopic data of the characteristic DNPY group.

(5) No racemization takes place throughout the modification.

The DNPY-modification tertiarized the nitrogen of the α-amino group on every L-amino acids like phthaloyl-masking.

The latter, however, has not been applied to tryptophan.[9] Furthermore, its blocking-deblocking processes are more complicated and drastic than the DNPY-method. In these aspects, the DNPY-protecting is superior to the phthaloyl-modification.

Further work is in progress, and the data of esterification and of peptide synthesis with the DNPY-L-amino acid will be reported elsewhere.

Experimental

Measurements. All melting points were determined on a Yanako Melting Point Apparatus and are uncorrected. ^{1}H-NMR, IR and UV spectra were obtained on a HITACHI R-20B High Resolution Spectrometer, a HITACHI 225 Grating Infrared Spectrophotometer, and a HITACHI EPS-3 Recording Spectrophotometer, respectively. Optical rotation was determined on a Jasco DIP-180 automatic polarimeter.

*3,5-Dinitro-(4-nitrophenyl)-4-pyridone (**2b**).* Two and a half grams of sodium metal was dissolved in 100 ml of absolute ethanol and then 10 g of 4-pyridinol was added gradually. After 30 min, the mixture was evaporated and the residue was dissolved in 50 ml of DMF.

To the solution, a DMF (50 ml) solution of 18 g of 1-chloro-4-nitrobenzene was added dropwise and the resulting mixture was heated at 150 °C for 10 h. After cooling, the mixture was evaporated *in vacuo*, and water was added to the residue. The aqueous solution was acidified till pH 5. Yellow crystalline precipitates were collected and recrystallized from water to give 1-(4-nitrophenyl)-4-pyridone (**1b**) quantitatively, mp 191—192 °C; IR (as Nujol mulls): 1675 cm^{-1} (C=O), 1530, 1350 (NO_2); ^{1}H-NMR (DMSO-d_6): δ=6.29 (2H, d, J=8 Hz, β-protons of pyridone ring), 8.13 (2H, d, J=8 Hz, α-protons of pyridone ring), and 7.86 and 8.37 (4H, AA'BB', J=9 Hz, aromatic protons of 1,4-disubstituted benzene ring).

One gram of 1-(4-nitrophenyl)-4-pyridone (**1b**) was dissolved in 20 ml of concentrated sulfuric acid (d=1.84), and then 5.8g of fuming nitric acid (d=1.52) was added gradually with ice cooling. The mixture was poured over crushed ice. The yellow crystalline solid was collected and washed with cold water. The solid was recrystallized from aqueous acetic acid (*ca.* 50%) to give **2b** as yellow needles in 70% yield; mp 264—265 °C; IR (as Nujol mulls): 1680 cm^{-1} (C=O), 1600, 1540, 1500, 1345, 850; ^{1}H-NMR (DMSO-d_6): δ=9.36 (2H, sharp s, α-protons of pyridone ring), and 8.47 and 8.06 (4H, AA'BB', J=9 Hz, aromatic protons of 1,4-disubstituted benzene ring); Found: C, 42.84; H, 2.15; N, 18.39%. Calcd for $C_{11}H_6N_4O_7$: C, 43.15; H, 1.98; N, 18.30%.

The other 1-substituted 3,5-dinitro-4-pyridones, **2a** and **2c** were prepared in a way similar to that used for **2b**.

L-Amino acids were supplied by Wako Pure Chemical Industries, Ltd. The protecting reaction by **2b** was carried out as follows.

In a round-bottomed flask were placed **2b** (2.0 mmol), L-amino acid (2.2 mmol) and 60 ml of water–pyridine (3:1). The mixture was stirred with a magnetic stirrer at room temperature. (In the cases of L-Arg and L-Lys, under nitrogen stream.) After all reactants had dissolved, the solvent was removed below 30 °C *in vacuo*. A yellow residue was obtained, to which water was added. The resulting mixture was extracted with chloroform to remove 4-nitroaniline. The aqueous layer was acidified with dilute hydrochloric acid till pH 1—2 and then evaporated under reduced pressure to give a yellow crystalline solid. The crude product was collected and washed with water, and recrystallized from aqueous ethanol.

The purified DNPY-L-amino acid was dried over phosphorus pentaoxide at 100 °C for 5—6 h *in vacuo*.

Deblocking Reaction of The DNPY-L-amino Acid. In a round-bottomed flask were placed DNPY-L-Ala (1 mmol), hexylamine (1.1 mmol) and 15 ml of pyridine. The mixture was stirred at room temperature for 1.5 h. The solvent was evaporated *in vacuo* and water was added to the residue. The mixture was extracted with chloroform. The water layer was neutralized and condensed to give L-Ala in 92% yield. After dryness, L-Ala was identified by the spectroscopic data and its specific rotation. The organic layer was evaporated to give 1-hexyl-3,5-dinitro-4-pyridone[4] quantitatively, which was identified by comparing with an authentic sample. The other DNPY-L-amino acids were treated similarly to give the parent L-amino acids.

The authors are grateful to the Ministry of Education, Science and Culture for Grant-in-Aid for Scientific Research No. 56740212 for partial support of this work.

References

1) Nucleophilic reaction upon electron-deficient pyridone derivatives. VI.

2) E. Matsumura, M. Ariga, and Y. Tohda, *Bull. Chem. Soc. Jpn.*, **53**, 2891 (1980).

3) "DNPY" represents "3,5-dinitro-4-oxo-1,4-dihydro-1-pyridyl".

4) E. Matsumura, M. Ariga, Y. Tohda, and T. Kawashima, *Tetrahedron Lett.*, **22**, 757 (1981).

5) Extensive references on amino-protecting groups are here: a) Y. Wolman, "The Chemistry of the Amino Group", ed by S. Patai, Wiley-Interscience, London (1968), Chap. 11; b) R. A. Boissonnas, *Advan. Org. Chem.*, **3**, 159 (1963); c) J. F. W. McOmie, "Protective Groups in Organic Chemistry", William Clowes & Sons Limited, London (1973), Chap. 2; d) E. Weunsch, "Methoden der Organischen Chemie" (Huben-Weyl), Band XI (1974).

6) "Seikagaku Data Book", ed by Biochemical Society of Japan, Tokyo Kagaku Dohjin Co., Tokyo (1979), p 31.

7) K. R. Rao and H. A. Sober, *J. Am. Chem. Soc.*, **76**, 1328 (1954).

8) C. W. Hoerr, M. R. McCorkle, and A. W. Ralston, *J. Am. Chem. Soc.*, **65**, 328 (1943).

9) G. H. L. Nefkens, G. L. Tesser, and R. J. F. Nivard, *Recl. Trav. Chim. Pay-Bas*, **79**, 688 (1960).

Liquid Crystal Materials with Sulfur Atoms Incorporated in the Principal Structure 1. New Liquid Crystal Compounds with 1,3-Dithiane Ring

Yuichiro HARAMOTO,* Atushi NOBE, and Hiroyoshi KAMOGAWA
Department of Applied Chemistry, Yamanashi University, Takeda 4, Kofu 400
(Received December 19, 1983)

2-(*p*-Substituted phenyl)-5-alkyl-1,3-dithianes, new liquid crystals, were synthesized by the thioacetalization of the corresponding aldehydes and dithiols. These compounds have characteristic supercooling states, exhibit monotropic liquid crystal phases even in the case of long terminal alkyl substituents. The mesomorphic characteristics of these compounds were different from those of the corresponding 1,3-dioxanes, this must originate in the difference in the molecular width caused by the difference in the atomic volume between sulfur and oxygen.

In a previous communication,[1] 2,5-disubstituted 1,3-dithianes and 1,3-oxathianes as novel types of liquid crystal were reported. Since only 2,5-disubstituted 1,3-dioxanes are known as structurally related liquid crystal materials,[2] we wish to report here in more detail the synthesis and properties of these novel 1,3-dithiane type liquid crystals prepared by us.

Results and Discussion

2-(*p*-Substituted phenyl)-5-alkyl-1,3-dithianes were synthesized *via* the following route.

Compounds **2** and **3** were obtained in good yields. In step **3**→**4**, the reaction temperature was crucial. If the reaction temperature was 70—75 °C, the main product was a mono substituted bromide contrary to our purpose. Therefore, the reaction temperature must be kept at 95—100 °C. As compound **5** was susceptible to oxidation, step **4**→**5** required a nitrogen atomosphere. In **5**→**7**, both axial (cis) and equatorial (trans) isomers were produced differing at the C-5 position of the 1,3-dithiane ring. Repeated recrystallization was necessary to obtain the purified equatorial isomers. In the case of 2-(*p*-cyanophenyl)-5-alkyl-1,3-dithianes, the production ratios of the axial isomers were higher than those for other 1,3-dithianes, so that purification of the equatorial isomers by recrystallization was unsuccessful.

Centrifugal liquid chromatography and T.L.C. were used to purify these compounds. As the axial and equatorial isomers exhibited different patterns of ^{1}H-NMR, the existance of the axial isomer can be detected by the examination of proton signals at δ=2.3—3.5: proton signals of the equatorial isomer are located only in a narrow range of ^{1}H-NMR chemical shift (δ=2.6—2.9), whereas those of the axial isomer cover a wide range (δ=2.3—3.5). Synthesized compounds **7** are all colorless and odorless crystals or powders, which are soluble in common organic solvents. They all exhibited remarkable supercooled states (about 15—70 °C below the melting point). This property seems to originate from the steric structure of the 1,3-dithiane ring bearing bulky sulfur and its dominant role in the lateral interactions between molecules, since the corresponding 1,3-dioxane-type compounds mostly indicate enantiotropic liquid crystal behavior. (Table 1)

Mesomorphic ranges determined for compounds **7** are given in Table 1, together with those for the corresponding 1,3-dioxanes.

Measurement of the mesomorphic ranges and assignment of the mesophases were carried out by means of a differential scanning calorimeter (D.S.C.) and a micro melting point apparatus equipped with polarizers.

In the alkyl-chain length ranging from R=C_2 to C_4 (**7-1**—**7-17**), any mesomorphic phases could not be observed under the polarization microscope. These compounds only exhibited the supercooled state. In the alkyl chain length from R=C_5 to C_7 (**7-18**—**7-32**), monotropic nematic phases were observed under the

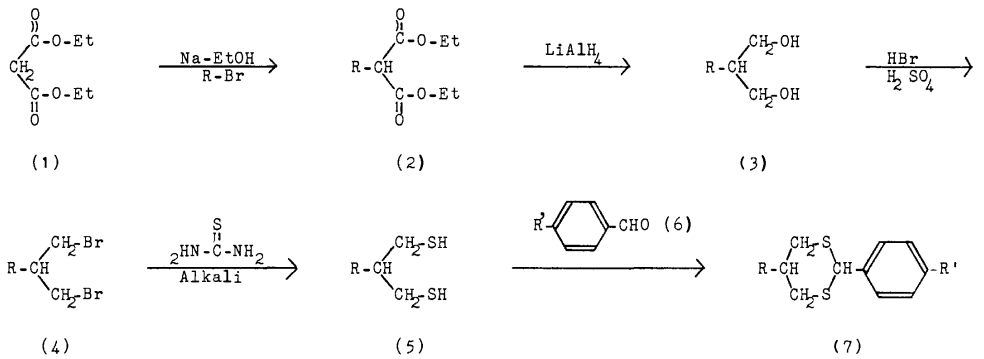

R: -C_2H_5, *n*-C_3H_7, *n*-C_4H_9, *n*-C_5H_{11}, *n*-C_6H_{13}, *n*-C_7H_{15}, *n*-C_8H_{17}.
R′: -OCH_3, -OC_2H_5, *n*-OC_3H_7, *n*-OC_4H_9, *n*-OC_5H_{11}, *n*-OC_6H_{13}, *n*-OC_7H_{15}, -CH_3, -CN.

Fig. 1.

TABLE 1. TRANSITION TEMPERATURE OF COMPOUNDS **7** AND THE CORRESPONDING 1,3-DIOXANES

	R	R′	Transition temp./°C[a]
7—1	C_2H_5	OC H_3	C $\underset{34}{\overset{69}{\rightleftharpoons}}$ I
7—2	C_2H_5	*n*-OC_4H_4	C $\underset{10}{\overset{50}{\rightleftharpoons}}$ I
7—3	C_2H_5	CH_3	C $\underset{55}{\overset{95}{\rightleftharpoons}}$ I
7—4	C_2H_5	C N	C $\underset{90}{\overset{130}{\rightleftharpoons}}$ I
7—5	*n*-C_3H_7	OC H_3	C $\underset{34}{\overset{97}{\rightleftharpoons}}$ I
7—6	*n*-C_3H_7	*n*-OC_4H_9	C $\underset{25}{\overset{46}{\rightleftharpoons}}$ I
7—7	*n*-C_3H_7	CH_3	C $\underset{45}{\overset{87}{\rightleftharpoons}}$ I
7—8	*n*-C_3H_7	C N	C $\underset{78}{\overset{133}{\rightleftharpoons}}$ I
7—9	*n*-C_4H_9	OC H_3	C $\underset{35}{\overset{85}{\rightleftharpoons}}$ I
7—10	*n*-C_4H_9	OC_2H_5	C $\underset{35}{\overset{75}{\rightleftharpoons}}$ I
7—11	*n*-C_4H_9	*n*-OC_3H_7	C $\underset{32}{\overset{65}{\rightleftharpoons}}$ I
7—12	*n*-C_4H_9	*n*-OC_4H_9	C $\underset{27}{\overset{68}{\rightleftharpoons}}$ I
7—13	*n*-C_4H_9	*n*-OC_5H_{11}	C $\underset{33}{\overset{64}{\rightleftharpoons}}$ I
7—14	*n*-C_4H_9	*n*-OC_6H_{13}	C $\underset{40}{\overset{70}{\rightleftharpoons}}$ I
7—15	*n*-C_4H_9	*n*-OC_7H_{15}	C $\underset{37}{\overset{65}{\rightleftharpoons}}$ I
7—16	*n*-C_4H_9	CH_3	C $\underset{42}{\overset{67}{\rightleftharpoons}}$ I
7—17	*n*-C_4H_9	C N	C $\underset{30}{\overset{88}{\rightleftharpoons}}$ I
7—18	*n*-C_5H_{11}	OC_2H_5	C $\underset{35}{\overset{57}{\rightleftharpoons}}$ I
7—19	*n*-C_5H_{11}	*n*-OC_3H_7	C $\underset{40}{\overset{55}{\rightleftharpoons}}$ I
7—20	*n*-C_5H_{11}	*n*-OC_4H_9	C $\overset{46}{\longrightarrow}$ N $\underset{26}{\overset{43}{\rightleftharpoons}}$ I
7—21	*n*-C_5H_{11}	*n*-OC_5H_{11}	C $\overset{61}{\longrightarrow}$ N $\underset{40}{\overset{45}{\rightleftharpoons}}$ I
7—22	*n*-C_5H_{11}	C N	C $\underset{28}{\overset{98}{\rightleftharpoons}}$ I
7—23	*n*-C_6H_{13}	OC_2H_5	C $\overset{61}{\longrightarrow}$ N $\underset{32}{\overset{43}{\rightleftharpoons}}$ I
7—24	*n*-C_6H_{13}	*n*-OC_3H_7	C $\underset{38}{\overset{75}{\rightleftharpoons}}$ I
7—25	*n*-C_6H_{13}	*n*-OC_4H_9	C $\overset{55}{\longrightarrow}$ N $\underset{34}{\overset{44}{\rightleftharpoons}}$ I
7—26	*n*-C_6H_{13}	*n*-OC_5H_{11}	C $\overset{60}{\longrightarrow}$ N $\underset{38}{\overset{47}{\rightleftharpoons}}$ I
7—27	*n*-C_6H_{13}	C N	C $\underset{36}{\overset{90}{\rightleftharpoons}}$ I
7—28	*n*-C_7H_{15}	OC_2H_5	C $\overset{70}{\longrightarrow}$ N $\underset{48}{\overset{57}{\rightleftharpoons}}$ I
7—29	*n*-C_7H_{15}	*n*-OC_3H_7	C $\overset{60}{\longrightarrow}$ N $\underset{35}{\overset{50}{\rightleftharpoons}}$ I
7—30	*n*-C_7H_{15}	*n*-OC_4H_9	C $\overset{59}{\longrightarrow}$ N $\underset{42}{\overset{56}{\rightleftharpoons}}$ I
7—31	*n*-C_7H_{15}	*n*-OC_5H_{11}	C $\overset{67}{\longrightarrow}$ N $\underset{52}{\overset{58}{\rightleftharpoons}}$ I
7—32	*n*-C_7H_{15}	C N	C $\underset{43}{\overset{98}{\rightleftharpoons}}$ I
7—33	*n*-C_8H_{17}	*n*-OC_3H_7	C $\overset{56}{\longrightarrow}$ S $\underset{31}{\overset{56}{\rightleftharpoons}}$ I
7—34	*n*-C_8H_{17}	*n*-OC_4H_9	C $\overset{57}{\longrightarrow}$ S $\underset{26}{\overset{57}{\rightleftharpoons}}$ I
7—35	*n*-C_8H_{17}	*n*-OC_5H_{11}	C $\overset{55}{\longrightarrow}$ S $\underset{34}{\overset{55}{\rightleftharpoons}}$ I
7—36	*n*-C_8H_{17}	C N	C $\underset{39}{\overset{93}{\rightleftharpoons}}$ I

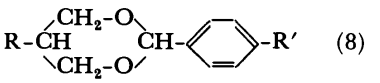

(8)

b)

8—1	*n*-C_5H_{11}	*n*-OC_4H_9	C $\overset{40}{\longrightarrow}$ N $\overset{53}{\longrightarrow}$ I
8—2	*n*-C_5H_{11}	*n*-OC_5H_{11}	C $\overset{38}{\longrightarrow}$ N $\overset{50.5}{\longrightarrow}$ I
8—3	*n*-C_6H_{13}	*n*-OC_4H_9	C $\overset{35.5}{\longrightarrow}$ S $\overset{44}{\longrightarrow}$ N $\overset{50}{\longrightarrow}$ I
8—4	*n*-C_6H_{13}	C N	C $\overset{47}{\longrightarrow}$ N $\underset{40.5}{\rightleftharpoons}$ I
8—5	*n*-C_7H_{15}	*n*-OC_4H_9	C $\overset{49}{\longrightarrow}$ S $\overset{59.5}{\longrightarrow}$ I
8—6	*n*-C_7H_{15}	*n*-OC_6H_{13}	C $\overset{37.5}{\longrightarrow}$ S $\overset{62}{\longrightarrow}$ I
8—7	*n*-C_7H_{15}	C N	C $\overset{54}{\longrightarrow}$ N $\underset{52}{\rightleftharpoons}$ I
8—8	*n*-C_8H_{17}	*n*-OC_5H_{11}	C $\overset{38}{\longrightarrow}$ S $\overset{60}{\longrightarrow}$ I

a) C=crystal; N=nematic; I=isotropic; S=smectic. b) Cited from Ref. 2.

polarization microscope. In compounds of R=C_8 (**7-33—7-35**), monotropic smectic phases were observed.

In the case of 2-(*p*-alkoxyphenyl)-5-butyl-1,3-dithianes (**7-9—7-15**), increasing the carbon number of the *p*-alkoxyl group (R′) did not afford any mesophases, but in 2-(*p*-butoxyphenyl)-5-alkyl-1,3-dithianes, increasing the length of the alkyl group (R) brought about the appearance of mesophases (**7-20**, **-25**, **-30**, **-34**). Therefore, the effect of the chain length of the alkyl substituent (R) at the C-5 position of the 1,3-dithiane ring on the appearance of mesophases is more marked than that of the *p*-alkoxyl substituent (R′) of the 2-phenyl group.

While, for R=C_5 to C_8, all 1,3-dithiane compounds indicated monotropic liquid crystal behavior, the corresponding 1,3-dioxane compounds became enantiotropic liquid crystals.

This suggests that the increased width of the 1,3-dithiane molecule caused by the bulky sulfur atoms decreases attractive interactions between the molecules. This strong tendency to exhibit monotropic mesophases is a feature of this 2-(*p*-substituted phenyl)-5-alkyl-1,3-dithiane liquid crystal group.

Experimental

IR, ^{1}H-NMR, ^{13}C-NMR, and mass spectra were obtained with a Hitachi 215 spectrophotometer, a JNM-PMX 60 spectrometer, a JNM FX 90Q FT-NMR spectrometer, and a Hitachi RMU-6 MG spectrometer, respectively. Elemental analyses were carried out with a Perkin-Elmer 250 instrument. Centrifugal liquid chromatography was made with a Hitachi CLC-5 apparatus. Mesomorphic phases and transition temperatures were determined more precisely and in detail than in the communication[1] by means of both a Mitamura Riken micro melting point apparatus equipped with polarizers and D.S.C., with satisfactory coincidences of the results. The rate of cooling was fixed to 1 °C/min.

Diethyl n-*Alkylmalonates (2).* A conventional procedure[3] was used for the syntheses of **2**. Yields ranged from 80 to 90%. Bp: 82—84 °C/3—5 mmHg† (R=C_2H_5), 90—92 °C/3—5 mmHg (R=C_3H_7), 94—97 °C/3—5 mmHg (R=C_4H_9), 110—113 °C/4—6 mmHg (R=C_5H_{11}), 113—115 °C/3—5 mmHg (R=C_6H_{13}), 120—123 °C/3—5 mmHg (C_7H_{15}), 124—128 °C/3—5 mmHg (R=H_8H_{17}). IR ($CHCl_3$) 2800—3000 (Alkyl), 1740 (C=O) cm^{-1}. ^{1}H-NMR ($CDCl_3$) δ=0.7—2.1 (m, Alkyl), 3.25 (t, 1H, CH), 4.2 (q, 4H, $2CH_2$-O).

2-*Alkyl*-1,3-*propanediol (3).* $LiAlH_4$-reduction of 2 in ether at 35 °C for 18 h provided **3**. Yields ranged from 90 to 95%. IR ($CHCl_3$) 3600 (OH), 2800—3000 (Alkyl) cm^{-1}. ^{1}H-NMR ($CDCl_3$) δ=0.6—2.1 (m, R-CH), 3.1—4.3 (m, 6H, $2CH_2$-OH).

2-*Alkyl*-1,3-*dibromopropane (4).* To a solution of 48% HBr (50g) and conc. H_2SO_4 (15 g) cooled in an ice bath were added successively compound **3** (0.1 mol) and conc. H_2SO_4 (25g). The solution was kept at 95—100 °C, for 18 h. The reaction mixture was then poured into ice water (200g). The mixture was stirred and extracted twice with ether (each 400 ml). The extract was washed with cold 10% aq $NaHCO_3$, and concentrated on a rotary evaporator at 30 °C. The residue was distilled *in vacuo* to afford transparent liquid in a 30—50% yield. Bp: 60—65 °C/1—2 mmHg (R=C_2H_5), 65—69 °C/1—2 mmHg (R=C_3H_7), 73—74 °C/1—2 mmHg (R=C_4H_9), 76—79 °C/1—2 mmHg (R=C_5H_{11}), 91—92 °C/2—3 mmHg (R=C_6H_{13}), 97—100 °C/1—2 mmHg (R=C_7H_{15}), 105—108 °C/1—2 mmHg (R=C_8H_{17}). IR ($CHCl_3$) 2800—3000 (Alkyl) cm^{-1}. ^{1}H-NMR ($CDCl_3$) δ=0.7—2.1 (m, R-CH), 3.45—3.75 (m, 4H, $2CH_2$-Br).

2-Alkyl-1,3-propanedithiol (5). To a solution of thiourea (0.064 mol, 4.9 g) in triethylene glycol (8 ml) kept at 75 °C was added compound **4** (0.016 mol) in a nitrogen atmosphere, followed by stirring at 75 °C for 18 h.

Tetraethylenepentamine (0.016 mol, 3.03 g) was then added, and the mixture was stirred at 75 °C for 2 h under a nitrogen atmosphere. The reaction mixture was fractionated *in vacuo* to afford a transparent oily product in a 70—80% yields. Bp: 55—57 °C/1—2 mmHg (R=C_2H_5), 64—66 °C/1—2 mmHg (R=C_3H_7), 82—85 °C/1—2 mmHg (C_4H_9), 95—98 °C/1—2 mmHg (R=C_5H_{11}), 108—110 °C/1—2 mmHg (R=C_6H_{13}), 109—113 °C/1 mmHg (R=C_7H_{15}, 116—121 °C/1—2 mmHg (R=C_8H_{17}). IR ($CHCl_3$) 2800—3000 (Alkyl) cm^{-1}. ^{1}H-NMR ($CDCl_3$) δ=0.7—2.1 (m, R-CH, 2SH), 2.5—2.9 (m, 4H, $2CH_2$-S).

*2-(*p*-Substituted phenyl)-5-alkyl-1,3-dithiane (7).* To a solution of compound **5** (0.004 mol) and *p*-substituted benzaldehyde **6** (0.004 mol) in anhyd. $CHCl_3$ (200 ml) cooled in an ice bath were added $BF_3 \cdot (C_2H_5)_2O$ (0.5 g) and molecular sieves (3A, 1/5; 3g). The mixture was stirred at 0—5 °C for 8 h and then at 20—25 °C for 18 h. The solution was washed with 10% $NaHCO_3$(400 ml), then with water (400 ml), dried over anhyd. Na_2SO_4, and evaporated *in vacuo* at 40 °C. The crude product was purified by recrystallizations from hexane-ether (5:1, v/v), then if necessary, by centrifugal liquid chromatography to separate the trans isomers.

*2-(*p*-Alkoxyphenyl)-5-Alkyl-1,3-dithianes.* IR ($CHCl_3$) 2800—3000 (Alkyl), 1600 (Ar), 1240 (Ether) cm^{-1}. ^{1}H-NMR ($CDCl_3$) 7-1, 7-5, 7-9: δ=0.7—2.1 (m, R-CH), 2.6—2.9 (m, 4H, CH_2-S), 3.8 (s, 3H, OCH_3), 5.05 (s, 1H, $\overset{S}{S}$>CH-), 6.7—7.5 (q, 4H, ArH); Others: δ=0.7—2.1 (m, R-CH, O-CH_2-C_n-$\underline{H}_{2n+1}$), 2.6—2.9 (m, 4H, $2CH_2$-S), 3.9 (t, 2H, OCH_2, 5.05 (s, 1H, $\overset{S}{S}$>CH-), 6.7—7.6 (q, 4H, ArH).

*[2-(*p*-Methoxyphenyl)-5-ethyl-1,3-dithiane (7-1)]*: Yield, 49%.

Found: C, 64.40; H, 8.21. Calcd for $C_{13}H_{18}S_2O_1$: C, 61.37; H, 7.13. MS (*m/z*) 254 (M^+).

*[2-(*p*-Butoxyphenyl)-5-ethyl-1,3-dithiane (7-2)]*: Yield, 76%.

Found: C, 64.40; H, 8.21. Calcd for $C_{14}H_{24}S_2O_1$: C, 64.82; H, 8.16 MS (*m/z*) 296 (M^+).

*[2-(*p*-Methoxyphenyl)-5-propyl-1,3-dithiane (7-5)]*: Yield, 70%.

Found: C, 62.32; H, 7.51. Calcd for $S_{14}H_{20}S_2O_1$: C, 62.64; H, 7.51. MS (*m/z*) 268 (M^+).

*[2-(*p*-Butoxyphenyl)-5-propyl-1,3-dithiane (7-6)]*: Yield, 72%.

Found: C, 65.89; H, 8.59. Calcd for $C_{17}H_{26}S_2O_1$: C, 65.76; H, 8.44. MS (*m/z*) 310 (M^+).

*[2-(*p*-Methoxyphenyl)-5-butyl-1,3-dithiane (7-9)]*: Yield, 62%.

Found: C, 63.59; H, 7.80. Calcd for $C_{15}H_{22}S_2O_1$: C, 63.78; H, 7.85. MS (*m/z*) 282 (M^+).

*[2-(*p*-Ethoxyphenyl)-5-butyl-1,3-dithiane (7-10)]*: Yield, 70%.

Found: C, 64.66; H, 8.14. Calcd for $C_{16}H_{24}S_2O_1$: C, 64.82; H, 8.16. MS (*m/z*) 296 (M^+).

*[2-(*p*-Propoxyphenyl)-5-butyl-1,3-dithiane (7-11)]*: Yield, 62%.

Found: C, 65.96; H, 8.38. Calcd for $C_{17}H_{26}S_2O_1$: C, 65.76; H, 8.44. MS (*m/z*) 310 (M^+).

*[2-(*p*-Butoxyphenyl)-5-butyl-1,3-dithiane (7-12)]*: Yield, 61%.

Found: C, 66.56 ; H, 8.72. Calcd for $C_{18}H_{28}S_2O_1$: C, 66.62; H, 8.70. MS (*m/z*) 324 (M^+).

*[2-(*p*-Pentyloxyphenyl)-5-butyl-1,3-dithiane (7-13)]*: Yield,

† 1 mmHg≈133.322 Pa.

69%.

Found: C, 67.49; H, 8.95. Calcd for $C_{19}H_{30}S_2O_1$: C, 67.40; H, 8.93. MS (*m/z*) 338 (M^+).

*[2-(p-Hexyloxyphenyl)-5-butyl-1,3-dithiane (**7-14**)]*: Yield, 66%.

Found: C, 68.07; H, 9.21. Calcd for $C_{20}H_{32}S_2O_1$: C, 68.13; H, 9.15. MS (*m/z*) 352 (M^+).

*[2-(p-Heptyloxyphenyl)-5-butyl-1,3-dithiane (**7-15**)]*: Yield, 67%.

Found: C, 68.88; H, 9.29. Calcd for $C_{21}H_{34}S_2O_1$: C, 68.80; H, 9.35. MS (*m/z*) 366 (M^+).

*[2-(p-Ethoxyphenyl)-5-pentyl-1,3-dithiane (**7-18**)]*: Yield, 63%.

Found: C, 65.80; H, 8.43. Calcd for $C_{17}H_{26}S_2O_1$: C, 65.76; H, 8.44. MS (*m/z*) 310 (M^+).

*[2-(p-Propoxyphenyl)-5-pentyl-1,3-dithiane (**7-19**)]*: Yield, 69%.

Found: C, 66.71; H, 8.71. Calcd for $C_{18}H_{28}S_2O_1$: C, 66.62; H, 8.70. MS (*m/z*) 324 (M^+).

*[2-(p-Butoxyphenyl)-5-pentyl-1,3-dithiane (**7-20**)]*: Yield, 64%.

Found: C, 67.28; H, 8.95. Calcd for $C_{19}H_{30}S_2O_1$: C, 67.40; H, 8.93. MS (*m/z*) 338 (M^+).

*[2-(p-Pentyloxyphenyl)-5-pentyl-1,3-dithiane (**7-21**)]*: Yield, 66%.

Found: C, 68.12; H, 9.29. Calcd for $C_{20}H_{32}S_2O_1$: C, 68.13; H, 9.15. MS (*m/z*) 352 (M^+).

*[2-(p-Ethoxyphenyl)-5-hexyl-1,3-dithiane (**7-23**)]*: Yield, 56%.

Found: C, 66.79; H, 8.68. Calcd for $C_{18}H_{28}S_2O_1$: C, 66.62; H, 8.70. MS (*m/z*) 324 (M^+).

*[2-(p-Propoxyphenyl)-5-hexyl-1,3-dithiane (**7-24**)]*: Yield, 68%.

Found: C, 67.49; H, 8.92. Calcd for $C_{19}H_{30}S_2O_1$: C, 67.40; H, 8.93. MS (*m/z*) 338 (M^+).

*[2-(p-Butoxyphenyl)-5-hexyl-1,3-dithiane (**7-25**)]*: Yield, 71%.

Found: C, 68.19; H, 9.14. Calcd for $C_{20}H_{32}S_2O_1$: C, 68.13; H, 9.15. MS (*m/z*) 352 (M^+).

*[2-(p-Pentyloxyphenyl)-5-hexyl-1,3-dithiane (**7-26**)]*: Yield, 68%.

Found: C, 68.64; H, 9.37. Calcd for $C_{21}H_{34}S_2O_1$: C, 68.80; H, 9.35. MS (*m/z*) 366 (M^+).

*[2-(p-Ethoxyphenyl)-5-heptyl-1,3-dithiane (**7-28**)]*: Yield, 67%.

Found: C, 67.45; H, 8.92. Calcd for $C_{19}H_{30}S_2O_1$: C, 67.40; H, 8.93. MS (*m/z*) 338 (M^+).

*[2-(p-Propocyphenyl)-5-heptyl-1,3-dithiane (**7-29**)]*: Yield, 70%.

Found: C, 68.21 ; H, 9.14. Calcd for $C_{20}H_{32}S_2O_1$: C, 68.13; H, 19.15 MS (*m/z*) 352 (M^+).

*[2-(p-Butoxyphenyl)-5-heptyl-1,3-dithiane (**7-30**)]*: Yield, 55%.

Found: C, 68.75; H, 9.32. Calcd for $C_{21}H_{34}S_2O_1$: C, 68.80; H, 9.35. MS (*m/z*) 366 (M^+).

*[2-(p-Pentyloxyphenyl)-5-heptyl-1,3-dithiane (**7-31**)]*: Yield, 66%.

Found: C, 69.46; H, 9.69. Calcd for $C_{22}H_{36}S_2O_1$: C, 69.42; H, 9.53. MS (*m/z*) 380 (M^+).

*[2-(p-Propoxyphenyl)-5-octyl-1,3-dithiane (**7-33**)]*: Yield, 61%.

Found: C, 68.60; H, 9.38. Calcd for $C_{21}H_{34}S_2O_1$: C, 68.80; H, 9.35. MS (*m/z*) 366 (M^+).

*[2-(p-Butoxyphenyl)-5-octyl-1,3-dithiane (**7-34**)]*: Yield, 53%.

Found: C, 69.20; H, 9.60. Calcd for $C_{22}H_{36}S_2O_1$: C, 69.42; H, 9.53. MS (*m/z*) 380 (M^+).

*[2-(p-Pentyloxyphenyl)-5-octyl-1,3-dithiane (**7-35**)]*: Yield, 70%.

Found: C, 69.89; H, 9.72. Calcd for $C_{23}H_{38}S_2O_1$: C, 69.99; H, 9.71. MS (*m/z*) 394 (M^+).

2-(p-Methylphenyl)-5-alkyl-1,3-dithianes. IR ($CHCl_3$) 2800—3000 (Alkyl), 1600 (Ar) cm^{-1}. ^{1}H-NMR ($CDCl_3$) δ=0.7—2.1 (m, R-CH), 2.25 (s, 3H, CH_3), 2.6—2.9 (m, 4H, $2CH_2$-S), 5.05 (s, 1H, $\overset{S}{S}$>CH-), 6.95—7.5 (q, 4H, ArH).

*[2-(p-Methylphenyl)-5-ethyl-1,3-dithiane (**7-3**)]*: Yield, 63%.

Found: C, 65.58; H, 7.49. Calcd for $C_{13}H_{18}S_2$: C, 65.49; H, 7.60. MS (*m/z*) 238 (M^+).

*[2-(p-Methylphenyl)-5-propyl-1,3-dithiane (**7-7**)]*: Yield, 61%.

Found: C, 66.58; H, 7.73. Calcd for $C_{14}H_{20}S_2$: C, 66.61; H, 7.99. MS (*m/z*) 252 (M^+).

*[2-(p-Methylphenyl)-5-butyl-1,3-dithiane (**7-16**)]*: Yield, 72%.

Found: C, 67.99; H, 8.25. Calcd for $C_{15}H_{22}S_2$: C, 67.61; H, 8.32. MS (*m/z*) 266 (M^+).

2-(p-Cyanophenyl)-5-alkyl-1,3-dithianes. IR ($CHCl_3$) 2800—3000 (Alkyl), 2215 (CN), 1600 (Ar) cm^{-1}. ^{1}H-NMR ($CDCl_3$) Trans: δ=0.7—2.0 (m, R-CH), 2.6—2.9 (m, 4H, $2CH_2$-S), 5.10 (s, 1H, $\overset{S}{S}$>CH-), 7.60 (s, 4H, ArH). Cis: δ=0.7—2.0 (m, R-CH), 2.4—3.5 (m, 4H, CH_2-S), 5.08 (s, 1H, $\overset{S}{S}$>CH-), 7.65 (s, 4H, ArH).

*[2-(p-Cyanophenyl)-5-ethyl-1,3-dithiane (**7-4**)]*: Yield, 53%.

Found: C, 62.97; H, 6.06; N, 5.64 Calcd for $C_{13}H_{15}N_1S_2$: C, 62.61; H, 6.06; N, 5.62 ^{13}C-NMR ($CDCl_3$). Trans: δ=50.77 (C2 of the 1,3-dithiane ring), 37.06 (C4, C6), 37.22 (C5). Cis: δ=50.15 (C2), 35.27 (C4, C6), 30.83 (C5). MS (*m/z*) 249 (M^+).

*[2-(p-Cyanophenyl)-5-propyl-1,3-dithiane (**7-8**)]*: Yield, 52%.

Found: C, 64.03; H, 6.54; N, 5.44 Calcd for $C_{14}H_{17}N_1S_2$: C, 68.83; H, 6.51; N, 5.32. ^{13}C-NMR ($CDCl_3$). Trans: δ=50.77 (C2), 37.38 (C4, C6), 35.22 (C5). Cis: δ=50.06 (C2), 35.60 (C4, C6), 28.88 (C5). MS (*m/z*) 263 (M^+).

*[2-(p-Cyanophenyl)-5-butyl-1,3-dithiane (**7-17**)]*: Yield, 50%.

Found: C, 64.80; H, 6.97; N, 5.15. Calcd for $C_{15}H_{19}N_1S_2$: C, 64.94; H, 6.90; N, 5.05. ^{13}C-NMR ($CDCl_3$). *Trans:* δ=50.66 (C2), 37.33 (C4, C6), 36.14 (C5). Cis: δ=49.96 (C2), 35.60 (C4, C6), 29.80 (C5). MS (*m/z*) 277 (M^+).

*[2-(p-Cyanophenyl)-5-pentyl-1,3-dithiane (**7-22**)]*: Yield, 56%.

Found: C, 66.00; H, 7.16; N, 4.89 Calcd for $C_{16}H_{21}N_1S_2$: C, 65.93; H, 7.26; N, 4.81. ^{13}C-NMR ($CDCl_3$). Trans: δ=50.82 (C2), 37.38 (C4, C6), 36.46 (C5). Cis: δ=50.01 (C2), 35.49 (C4, C6), 30.12 (C5). MS (*m/z*) 291 (M^+).

*[2-(p-Cyanophenyl)-5-hexyl-1,3-dithiane (**7-27**)]*: Yield, 47%.

Found: C, 66.47; H, 7.51; N, 4.69. Calcd for $C_{17}H_{23}N_1S_2$: C, 66.83; H, 7.59; N, 4.59 MS (*m/z*) 305 (M^+).

*[2-(p-Cyanophenyl)-5-heptyl-1,3-dithiane (**7-32**)]*: Yield, 42%.

Found: C, 67.58; H, 7.90; N, 4.35. Calcd for $C_{18}H_{25}N_1S_2$: C, 67.66; H, 7.89; N, 4.38. MS (*m/z*) 319 (M^+).

*[2-(p-Cyanopenyl)-5-octyl-1,3-dithane (**7-36**)]*: Yield, 49%.

Found: C, 68.72; H, 8.06; N, 4.12. Calcd for $C_{19}H_{27}N_1S_2$: C, 68.42; H, 8.16; N, 4.20. MS (*m/z*) 333 (M^+).

References

1) Y. Haramoto and H. Kamogawa, *J. Chem. Soc., Chem. Commun.*, **1983**, 75.

2) D. Demus and H. Zaschke (to V. E. W. Kombinat Microelectonic), *Japan Pat. Appl. No. 54-160916*, Dec. 1979.

3) A. H. Blatt. *Org. Synth.*, Coll. Vol. I, 250 (1967).

Restricted Rotation Involving the Tetrahedral Carbon. LIV. The Effects of 1-Substituents on the Barriers to Rotation in 9-(2-Methyl-1-naphthyl)fluorenes[1,2]

Shigeru MURATA, Teruo MORI, and Michinori ŌKI*
Department of Chemistry, Faculty of Science, The University of Tokyo, Bunkyo-ku, Tokyo 113
(Received December 20, 1983)

A series of 1-substituted 9-(2-methyl-1-naphthyl)fluorenes, where the substituent is fluoro, chloro, bromo, or methyl, has been prepared and barriers to rotation in these compounds have been examined to investigate the substituent effects. The barrier is enhanced generally, if we go from the 1-substituent of a small size to that of a large size with an exception of the fluorine case: the 1-fluoro compound exhibits a lower barrier to rotation than the unsubstituted compound by *ca.* 0.5 kcal mol^{-1}. X-Ray crystallographic analysis suggests that, in the fluoro compound, the C_9(fluorene)-to-C_1(naphthalene) bond is abnormally long, although other compounds possess bonds of normal lengths. The low barrier to rotation in the fluoro compound relative to the unsubstituted is thus attributed to the raise of the ground state energy and insufficient raise of the transition state energy in the former compound.

Although various stable rotamers of 9-arylfluorenes are isolated at room temperature, their barriers to rotation are usually less than 30 kcal mol^{-1} (1 cal=4.184 J).[3,4] The only exceptions to these are the reports by Ford *et al.*[5] and by Kajigaeshi and associates.[6] The former authors pointed out that the barrier to rotation in 1-methyl-9-(2-methyl-1-naphthyl)-fluorene (**2b**) was 33.3±0.3 kcal/mol at 166 °C, and the latters that of 32.8 kcal mol^{-1} at 170 °C in 1,2-benzoannelated 9-(2-methyl-1-naphthyl)fluorene. These reports certainly suggest that the transition state for rotation about the C_9(fluorene)-to-C_1(naphthalene) bond is raised relative to the ground state because the substituent in the 1-position of the fluorene ring interacts strongly with the 2-methyl-1-naphthyl group in the transition state for rotation.

In this context, it will be of interest to see the effect of the 1-substituent in the fluorene ring on the barrier to rotation. At the outset, we prepared 1-fluoro-9-(1-naphthyl)fluorene and surprisingly found that the introduction of the fluoro substituent into the 1-position of the fluorene moiety reduced the barrier to rotation. This finding prompted us to reexamine the barriers to rotation in the parent compound, 9-(1-naphthyl)fluorene. The results shown in Table 1 clearly indicate that the barriers reported by others[7,8] were reproducible and confirm that the introduction of a fluorine atom to the 1-position of fluorene reduces the barrier height in the system of 9-(1-naphthyl)-fluorene.

In order to find generality of the trend in the barrier heights, we examined the barrier to rotation in 1-fluoro-9-(2-methyl-1-naphthyl)fluorene (**2c**). The barrier to rotation in **2c** was again lower than that reported for the parent compound.[7] Thus the reduction of the barrier height on introduction of a fluorine atom to the 1-position of fluorene seems to be a general practice.

Then it became of interest to examine the barriers in a series of 1-substituted 9-(2-methyl-1-naphthyl)fluorenes (**2**): what is the general tendency in affecting the barrier heights due to the presence of a 1-substituent in these compounds? This paper reports the results of the investigation and discusses the origin of the anomalous barrier heights in the fluoro compounds from the X-ray crystallographic data of **2c** and two related compounds.

The syntheses of the compounds in question were straightforward. 1-Substituted 9-fluorenones (**1**) were treated with 2-methyl-1-naphthyllithium or the corresponding Grignard reagent and the products were reduced to the desired compound (**2**). The rotational isomers of **2** were separated by chromatography. The stereochemistry of each rotamer was assigned by considering the chemical shifts of the methyl protons which is

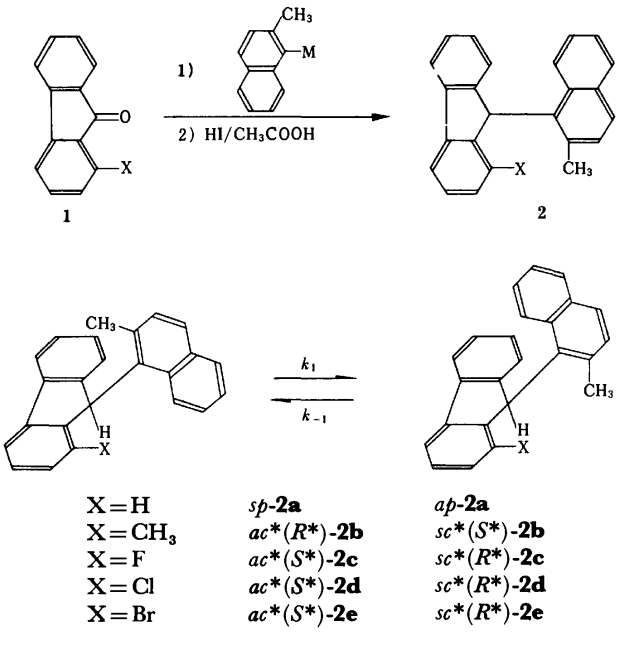

X=H	*sp*-**2a**	*ap*-**2a**
X=CH_3	*ac**(*R**)-**2b**	*sc**(*S**)-**2b**
X=F	*ac**(*S**)-**2c**	*sc**(*R**)-**2c**
X=Cl	*ac**(*S**)-**2d**	*sc**(*R**)-**2d**
X=Br	*ac**(*S**)-**2e**	*sc**(*R**)-**2e**

TABLE 1. BARRIERS TO ROTATION IN 1-SUBSTITUTED 9-(1-NAPHTHYL)FLUORENES

1-substituent	T_c/°C	$\Delta G_c^{\ddagger}$/kcal mol^{-1} [a]	K[b]
H	96	19.0	0.50
F	84	18.5	0.45

a) For the process from the more populated isomer to the less populated. b) Equilibrium constants at coalescence temperature: *ap*/*sp* for the unsubstituted compound and *sc*/*ac* for the fluoro compound.

attached to the naphthalene nucleus in ^{1}H NMR spectra as are customarily done in other cases.

The rates of rotation in **2** together with equilibrium constants at various temperatures are summarized in Table 2 and activation parameters with relative rates of rotation in Table 3.

The equilibrium constants are very close to unity when **2** is a hydrocarbon irrespective of the substituent (H or methyl) in the 1-position of the fluorene ring. In contrast, if the 1-substituent is a halogen, a rotamer in which the 2-methyl group (in naphthalene) is over the fluorene ring is disfavored to some extent. This tendency is the largest when X is fluorine and equilibrium constants become closer to unity as the halogens become larger. The reason for this phenomenon is not well understood at the moment but could be a repulsive interaction between the 2-methyl (in naphthalene) and the fluorene groups and consequently the large deformation, as discussed in the crystal structure section.

The barriers to rotation about the C_9(fluorene)-to-C_1(naphthalene) bond indicate that they are enhanced as the bulkiness of the 1-substituent in the fluorene ring increases, except the case of fluorine. Therefore, the series of X=H, Cl, Br, and CH_3 is quite normal in the sense that the bulkier 1-substituent in the fluorene ring affects more the transition state of rotation than the ground state.

To shed light to the reason for the anomaly in the fluorine compound (**2c**), X-ray crystallography of *ac**(*S**)-**2c**[9] was carried out. The X-ray structures of **2a** and **2b** were also examined for comparison. Unfortunately, however, only *sc**(*S**) form of **2b** gave suitable crystals for the X-ray investigation, whereas *sp*-**2a** and *ac**(*S**)-**2c**, in which the 2-methyl groups are over the fluorene moiety, gave suitable crystals. Therefore, we may have to discuss with some reservations if we really compare the structures. The results are given in Tables 4 through 7. The nonhydrogen atoms are numbered or designated as shown below.

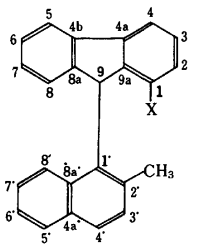

The first feature in the structures which we wish to discuss is the dihedral angles made by the naphthyl group and the C_9-H bond. Since we neglect the positions of hydrogens, the dihedral angles are given by the C-C-C planes in Table 6. The most apparent feature is that the naphthyl group does not bisect the C(8a)-C(9)-C(9a) angle, thus does not eclipse the C_9-H. This is interesting because, in solution chemistry, the eclipsing conformation about a C_{ar}-C_{aliph} bond is supposed to be often the energy minimum due to the fact that two equivalent groups in the geminal position give equivalent ^{1}H NMR chemical shifts when the internal rotation is frozen.[10] Although we have to discuss the difference carefully, because the conformation in the solid state is not nec-

Table 2. Rate constants of rotation and equilibrium constants in 1-substituted 9-(2-methyl-1-naphthyl)-fluorenes (**2**) in *o*-dichlorobenzene

1-substituent	Temp/°C	k_1/s^{-1}	K[a]
H	69.6	1.48×10^{-6}	1.14±0.02
	81.3	5.47×10^{-6}	
	102.0	4.15×10^{-5}	
	111.8	1.01×10^{-4}	
F	69.5	2.88×10^{-6}	1.52±0.04
	81.0	1.06×10^{-5}	
	102.0	7.76×10^{-5}	
	111.9	1.83×10^{-4}	
Cl	102.0	2.49×10^{-6}	1.43±0.03
	111.9	7.36×10^{-6}	
	132.6	2.82×10^{-5}	
	144.7	1.29×10^{-4}	
Br	111.6	3.68×10^{-6}	1.37±0.02
	132.6	2.82×10^{-5}	
	144.8	8.01×10^{-5}	
	156.4	1.86×10^{-4}	
CH_3	111.9	1.95×10^{-6}	1.12±0.02
	132.7	1.53×10^{-5}	
	144.7	4.31×10^{-5}	
	155.9	9.22×10^{-5}	

a) The equilibrium constants were constant within the error limit shown in the temperature range examined. K is *ap*/*sp*, *ac**(*R**)/*sc**(*S**), and *ac**(*S**)/*sc**(*R**), for **2a**, **2b**, and **2c**—**2e**, respectively.

Table 3. Activation parameters and relative rates of internal rotation in 1-substituted 9-(2-methyl-1-naphthyl)fluorenes (**2**) in *o*-dichlorobenzene

Substituent	ΔH^* / kcal mol^{-1}	ΔS^* / e.u.	ΔG^*(383 K) / kcal mol^{-1}	k(383 K) / s^{-1}	k_{rel}(383 K)
H	25.5±0.2	−11.2±0.6	29.7	8.53×10^{-5}	1.0
F	24.8±0.5	−11.6±1.5	29.3	1.54×10^{-4}	1.8
Cl	27.9±0.8	−10.3±0.8	31.8	5.70×10^{-6}	0.067
Br	28.1±0.9	−10.8±0.9	32.2	3.24×10^{-6}	0.038
CH_3[a]	28.2±1.5	−11.7±3.8	32.7	1.66×10^{-6}	0.019

a) These data give a free energy of activation which is in good agreement with that given by Ford *et al.* at 166 °C.[5]

TABLE 4. ATOMIC POSITIONAL PARAMETERS ($\times 10^4$) WITH ESTIMATED STANDARD DEVIATIONS IN PARENTHESES AND EQUIVALENT ISOTROPIC THERMAL PARAMETERS OF 1-SUBSTITUTED 9-(2-METHYL-1-NAPHTHYL)FLUORENES (**2**)

Atom	x	y	z	B_{eq}/Å^2
		***sp*-2a** (X=H)		
C(1)	11106(5)	3176(5)	4806(2)	4.6
C(2)	12107(6)	3553(5)	5282(2)	5.5
C(3)	13166(5)	2502(6)	5485(2)	5.1
C(4)	13238(5)	1034(5)	5209(2)	4.5
C(4a)	12226(4)	642(4)	4733(2)	3.6
C(4b)	11996(4)	-802(4)	4380(2)	3.6
C(5)	12754(5)	-2203(5)	4403(2)	4.4
C(6)	12259(6)	-3408(5)	4014(2)	5.2
C(7)	11086(6)	-3235(5)	3609(2)	5.5
C(8)	10317(5)	-1817(5)	3578(2)	4.0
C(8a)	10809(4)	-621(4)	3966(2)	3.6
C(9)	10145(4)	988(4)	4045(2)	3.4
C(9a)	11159(4)	1701(4)	4542(2)	3.4
C(1')	9799(4)	1989(4)	3748(2)	3.6
C(2')	10823(5)	2259(5)	3021(2)	4.2
C(3')	10459(6)	3212(5)	2484(2)	5.2
C(4')	9164(6)	3944(5)	2426(2)	5.1
C(4a')	8118(5)	3741(5)	2890(2)	4.3
C(5')	6777(6)	5741(5)	2845(2)	4.5
C(6')	5727(6)	4306(6)	3218(3)	6.0
C(7')	5992(5)	3298(6)	3793(2)	5.6
C(8')	7295(5)	2531(5)	3857(2)	4.4
C(8a')	8420(4)	2745(4)	3416(3)	3.5
CH_3	12326(6)	1586(6)	3064(3)	6.0
		***sc**(*S**)-2b** (X=CH_3)		
X	613(2)	6780(6)	393(2)	7.4
C(1)	1059(2)	5090(6)	420(1)	5.5
C(2)	1416(2)	4373(7)	-8(1)	7.3
C(3)	1855(2)	2840(7)	24(2)	7.8
C(4)	1972(2)	1973(6)	475(2)	6.7
C(4a)	1625(2)	2636(5)	903(1)	4.6
C(4b)	1649(2)	2003(4)	1426(1)	4.3
C(5)	2037(2)	592(5)	1654(2)	5.6
C(6)	1959(2)	319(5)	2165(2)	6.0
C(7)	1508(2)	1404(5)	2453(1)	5.5
C(8)	1111(2)	2814(4)	2233(1)	4.3
C(8a)	1194(2)	3102(4)	1719(1)	3.7
C(9)	875(2)	4618(4)	1395(1)	3.5
C(9a)	1165(2)	4165(5)	872(1)	4.1
C(1')	52(2)	4944(4)	1464(1)	3.4
C(2')	-185(2)	6524(4)	1685(1)	4.2
C(3')	-947(2)	6815(5)	1759(1)	5.1
C(4')	-1453(2)	5588(5)	1611(1)	5.2
C(4a')	-1234(2)	3978(5)	1373(1)	4.2
C(5')	-1758(2)	2703(5)	1201(1)	5.5
C(6')	-1549(2)	1162(5)	970(1)	5.8
C(7')	-794(2)	772(5)	907(1)	5.1
C(8')	-276(2)	1976(4)	1069(1)	4.2
C(8a')	-470(2)	3631(4)	1303(1)	3.4
CH_3	341(2)	8003(5)	1853(1)	5.7
		***ac**(*S**)-2c** (X=F)		
X	7949(2)	5816(2)	1602(2)	7.3
C(1)	6481(4)	6045(2)	1266(3)	4.4
C(2)	6081(4)	6827(2)	705(3)	5.3
C(3)	4592(4)	7059(2)	365(3)	5.3
C(4)	3527(4)	6523(2)	560(3)	4.7
C(4a)	3973(4)	5740(2)	1118(3)	4.1
C(4b)	3111(4)	5046(2)	1427(3)	4.3
C(5)	1593(4)	4978(2)	1272(3)	5.3
C(6)	1071(4)	4234(3)	1642(3)	6.4
C(7)	2040(5)	3563(3)	2158(3)	6.3
C(8)	3560(4)	3638(2)	2334(3)	5.5
C(8a)	4083(4)	4385(2)	1973(3)	4.3
C(9)	5676(4)	4612(2)	2053(3)	4.1
C(9a)	5477(4)	5501(2)	1496(3)	4.0
C(1')	6790(4)	4528(2)	3286(3)	4.2
C(2')	6795(4)	5098(2)	4163(3)	4.9
C(3')	7848(4)	4990(3)	5292(3)	5.9
C(4')	8855(4)	4343(3)	5515(3)	5.8
C(4a')	8870(4)	3734(2)	4663(3)	5.0
C(5')	9901(4)	3044(3)	4892(4)	6.3
C(6')	9877(4)	2437(3)	4080(5)	7.3
C(7')	8836(5)	2497(3)	2967(4)	7.3
C(8')	7838(4)	3172(2)	2701(3)	5.7
C(8a')	7815(4)	3814(2)	3515(3)	4.4
CH_3	5729(5)	5842(3)	4040(3)	6.3

TABLE 5. BOND LENGTHS AND BOND ANGLES

	***sp*-2a**	***sc**(*S**)-2b**	***ac**(*S**)-2c**
Bond length l/Å			
C(1)-X	——	1.494(6)	1.367(9)
C(1)-C(2)	1.416(6)	1.407(5)	1.383(9)
C(1)-C(9a)	1.385(8)	1.392(5)	1.358(6)
C(2)-C(3)	1.372(15)	1.392(7)	1.386(10)
C(3)-C(4)	1.394(8)	1.370(6)	1.379(6)
C(4)-C(4a)	1.397(6)	1.385(5)	1.389(6)
C(4a)-C(4b)	1.463(6)	1.460(5)	1.464(6)
C(4a)-C(9a)	1.395(15)	1.411(5)	1.402(10)
C(4b)-C(5)	1.397(15)	1.399(5)	1.391(6)
C(4b)-C(8a)	1.397(8)	1.395(4)	1.400(10)
C(5)-C(6)	1.395(6)	1.374(6)	1.380(7)
C(6)-C(7)	1.394(9)	1.376(5)	1.400(10)
C(7)-C(8)	1.386(15)	1.396(4)	1.390(7)
C(8)-C(8a)	1.389(6)	1.385(4)	1.381(6)
C(8a)-C(9)	1.505(13)	1.527(4)	1.518(5)
C(9)-C(9a)	1.531(7)	1.517(4)	1.520(5)
C(9)-C(1')	1.518(7)	1.516(4)	1.539(20)
C(1')-C(2')	1.390(1)	1.381(4)	1.377(5)
C(1')-C(8a')	1.437(6)	1.431(4)	1.441(6)
C(2')-C(3')	1.432(8)	1.415(5)	1.427(19)
C(2')-CH_3	1.509(7)	1.520(5)	1.508(6)
C(3')-C(4')	1.358(7)	1.352(5)	1.352(7)
C(4')-C(4a')	1.406(15)	1.407(5)	1.397(6)
C(4a')-C(5')	1.432(7)	1.417(5)	1.416(6)
C(4a')-C(8a')	1.423(7)	1.423(4)	1.440(20)
C(5')-C(6')	1.371(15)	1.350(5)	1.352(7)
C(6')-C(7')	1.403(8)	1.410(5)	1.405(20)
C(7')-C(8')	1.380(7)	1.366(5)	1.379(7)
C(8')-C(8a')	1.428(15)	1.419(4)	1.402(5)
Bond angle ϕ/°			
C(2)-C(1)-X	——	121.9(3)	118.2(6)
C(2)-C(1)-C(9a)	117.3(7)	116.2(4)	122.8(5)
C(9a)-C(1)-X	——	121.9(3)	119.0(3)
C(1)-C(2)-C(3)	120.8(4)	121.5(4)	118.2(6)
C(2)-C(3)-C(4)	121.9(6)	121.7(4)	121.3(3)
C(3)-C(4)-C(4a)	117.8(7)	118.2(4)	118.7(5)
C(4)-C(4a)-C(4b)	130.7(6)	130.2(3)	130.9(4)
C(4)-C(4a)-C(9a)	120.4(4)	120.6(3)	121.0(6)
C(4b)-C(4a)-C(9a)	109.0(5)	109.2(3)	108.0(3)
C(4a)-C(4b)-C(5)	131.1(4)	131.6(3)	130.7(4)
C(4a)-C(4b)-C(8a)	108.5(7)	108.7(3)	108.8(3)
C(5)-C(4b)-C(8a)	120.3(6)	119.7(3)	120.5(6)
C(4b)-C(5)-C(6)	118.7(4)	118.8(3)	118.4(5)
C(5)-C(6)-C(7)	120.2(6)	121.3(4)	121.1(4)
C(6)-C(7)-C(8)	121.5(6)	121.0(3)	120.6(6)
C(7)-C(8)-C(8a)	118.2(4)	117.9(3)	118.3(5)
C(4b)-C(8a)-C(8)	121.1(6)	121.3(3)	121.2(3)
C(4b)-C(8a)-C(9)	110.7(6)	110.1(2)	110.7(5)

Table 5. Continued

	sp-**2a**	*sc**(*S**)-**2b**	*ac**(*S**)-**2c**
Bond angle ϕ/°			
C(8)-C(8a)-C(9)	128.2(3)	128.5(3)	128.1(5)
C(8a)-C(9)-C(9a)	102.0(4)	102.4(2)	101.4(6)
C(8a)-C(9)-C(1')	115.4(6)	115.0(2)	114.4(9)
C(9a)-C(9)-C(1')	119.5(4)	119.0(2)	117.3(3)
C(9)-C(1')-C(2')	121.1(5)	119.9(3)	121.7(4)
C(9)-C(1')-C(8a')	120.0(9)	120.8(3)	118.1(6)
C(2')-C(1')-C(8a')	118.8(6)	119.3(3)	120.2(8)
C(1')-C(2')-C(3')	119.6(5)	120.0(3)	119.5(4)
C(1')-C(2')-CH_3	122.7(6)	122.4(3)	124.8(8)
C(3')-C(2')-CH_3	117.7(9)	117.6(3)	115.6(6)
C(2')-C(3')-C(4')	121.8(9)	121.5(3)	121.2(6)
C(3')-C(4')-C(4a')	120.2(6)	120.5(3)	121.4(8)
C(4')-C(4a')-C(5')	120.7(6)	121.3(3)	121.9(8)
C(4')-C(4a')-C(8a')	119.5(5)	119.2(3)	119.1(4)
C(5')-C(4a')-C(8a')	119.9(9)	119.5(3)	118.9(6)
C(4a')-C(5')-C(6')	121.2(6)	121.4(3)	121.8(9)
C(5')-C(6')-C(7')	119.7(6)	120.0(3)	119.8(4)
C(6')-C(7')-C(8')	120.5(9)	120.0(3)	119.9(7)
C(7')-C(8')-C(8a')	121.7(6)	122.0(3)	122.3(8)
C(1')-C(8a')-C(8')	122.9(5)	123.5(3)	124.4(8)
C(1')-C(8a')-C(4a')	120.1(9)	119.4(3)	118.5(6)
C(8')-C(8a')-C(4a')	117.0(5)	117.1(3)	117.1(4)

essarily retained in solution, it is possible that, by ^{1}H NMR, the rapid exchange $+ap \rightleftharpoons -ap$ *or* $+sp \rightleftharpoons -sp$ cannot be detected.[11] Another common feature of interest in the structures is concerned with C(9) and its vicinity: the C(8a)-C(9) and C(9)-C(9a) distances are very long and the C(8a)-C(9)-C(9a) bond angle is very small relative to those in fluorene.[12] These must be the results of steric strain which is eased by lengthening the bonds and by sharpening the angle.

The conformations about the C(9)-C(1') bond in *ac**(*S**)-**2c** are interesting. The methyl group which is over the fluorene ring is close to C(1), which bears the 1-substituent, rather than to C(8a). The cause for this phenomenon is not clear at the moment.

The molecular structures of *sp*-**2a** and *sc**(*S**)-**2b** are quite normal, except the atomic positions close to C(9), as pointed out above. The bond distances and bond angles are very close to those reported for fluorene[12] and 1,5-dimethylnaphthalene[13] except some points discussed above and below. The abnormality is caused because of the presence of the 2'-methyl group over the fluorene ring and also because of the fact that the naphthyl group does not eclipse the C(9)-H bond. The steric congestion in *sp*-**2a** is relieved by lengthening the C(9)-C(9a) bond which is close to the 2'-methyl group. Thus the C(9)-C(9a) bond in *sp*-**2a** is longer than the C(8a)-C(9) (Table 5). This explanation is partially supported by the fact that the lengths of C(8a)-C(9) and C(9)-C(9a) bonds in *sc**(*S**)-**2b** are close to each other. Due to the small size of the π-system relative to the methyl, the congestion in *sc**(*S**)-**2b** must be small.

Table 7. Some distances (Å) between nonbonded atoms in proximity of steric crowding

Atom 1	Atom 2	*sp*-**2a**	*sc**(*S**)-**2b**	*ac**(*S**)-**2c**
X	C(1')	—	3.299(5)	3.263(14)
CH_3[a]	C(8a)	3.328(21)	3.284(4)	3.369(23)
CH_3[a]	C(9a)	3.058(19)	3.123(4)	3.044(7)
CH_3[a]	C(1)	3.654(13)	3.762(5)	3.632(15)
CH_3[a]	C(8)	4.108(21)	4.026(5)	4.188(21)

a) Atom 1 is C(8a') in the case of *sc**(*S**)-**2b**.

Some nonbonded distances between atoms in the congested sites are compiled in Table 7. The X-C(1') distances in *sc**(*S**)-**2b** and *ac**(*S**)-**2c** are shorter than or very close to the sum of the van der Waals radii of the atom and/or the groups concerned. This strain seems to be distributed widely over the molecules. The small difference in distances CH_3-C(8a) and CH_3-C(9a) together with the same trend in the dihedral angle in *sc**(*S**)-**2b** relative to others is a reflection of the fact that a π-system is smaller in size than a methyl. As far as these nonbonded distances concern, *sp*-**2a** and *ac**(*S**)-**2c** take similar structures.

The structure of the fluoro compound, *ac**(*S**)-**2c**, shows some interesting features. The bond distance of C(1)-C(9a) is abnormally short, compared with those in other compounds, and that of C(9)-C(1') abnormally long, although the latter involves a large error. It is tempting to consider that, due to the electronic effect of the fluorine substituent, the bond C(1)-C(9a) is shortened and this effect also restricts the lengthening of the C(9)-C(9a) bond: the latter bond is very long in *sp*-**2a** because of the steric effect but is almost normal in *ac**(*S**)-**2c**. The strain caused by these bond distances seems to be released by lengthening the C(9)-C(1') bond together with widening the C(9)-C(1')-C(2') and C(1')-C(2')-CH_3 angles and contracting the C(9)-C(1')-C(8a') and C(3')-C(2')-CH_3 angles. We therefore conclude that the relatively low barrier to rotation in **2c** is caused by the strain in the ground state, whereas the transition state energy is not raised to a great extent.

Experimental

9-(2-Methyl-1-naphthyl)fluorene (2a). Rotamers were obtained as reported in a previous paper.[14]

1-Fluoro-9-(2-methyl-1-naphthyl)fluorene (2c). To a stirred solution of 2-methyl-1-naphthylmagnesium bromide, prepared from 1.3 g (5.9 mmol) of 1-bromo-2-methylnaphthalene, 0.14 g (5.8 mmol) of magnesium, and 9 mL of dry tetrahydrofuran under a nitrogen atmosphere, 0.97 g (4.9 mmol) of 1-fluoro-9-fluorenone (**1**:X=F)[15] was added at room temperature. The mixture was heated under reflux for 1.5 h with stirring, cooled and decomposed with

Table 6. Dihedral angles (degree) involving the naphthyl group in **2**

Plane 1	Plane 2	*sp*-**2a**	*sc**(*S**)-**2b**	*ac**(*S**)-**2c**
C(2')-C(1')-C(9)	C(1')-C(9)-C(8a)	71.7	67.7	71.3
C(2')-C(1')-C(9)	C(1')-C(9)-C(9a)	50.7	54.3	47.1

18 mL of 25% aqueous ammonium chloride. The organic layer was separated and the aqueous layer was extracted with ether. The combined organic layer was washed with water and dried over magnesium sulfate. After evaporation of the solvent, the residue was submitted to chromatography on silica gel (3:1 hexane-benzene eluent). The product was dissolved in 35 mL of acetic acid and heated with 8.7 mL of 57% hydriodic acid for 3 h at 60 °C. The mixture was poured into a cold solution of sodium hydrogensulfite. The organic product was extracted with dichloromethane. The extract was washed with aqueous sodium hydrogencarbonate and dried over magnesium sulfate. After evaporation of the solvent, the product was separated by silica gel chromatography (hexane eluent). The *ac**(*S**) form was eluted first and then *sc**(*R**) form followed. The combined yield of the both forms was 0.91 g (57% based on the amount of 1-fluoro-9-fluorenone).

*ac**(*S**), mp 159—160 °C. Found: C, 89.02; H, 5.16%. Calcd for $C_{24}H_{17}F$: C, 88.86; H, 5.28%. ^{1}H NMR ($CDCl_3$) δ =1.38 (3H, s), 6.27 (1H, s), 6.9—7.9 (12H, m), 8.53 (1H, d, J=8 Hz). ^{19}F NMR ($CDCl_3$, ppm from C_6F_6): 44.2 (dd, J=9.3 and 4.5 Hz).

*sc**(*R**), mp 140—141 °C. Found: C, 89.15; H, 5.07%. Calcd for $C_{24}H_{17}F$: C, 88.86; H, 5.28%. ^{1}H NMR ($CDCl_3$), δ=2.86 (3H, s), 5.86 (1H, s), 6.44 (1H, d, J=9 Hz), 6.8—8.0 (12H, m). ^{19}F NMR ($CDCl_3$, ppm from C_6F_6): 42.7 (dd, J=9.3 and 4.5 Hz).

*1-Chloro-9-(2-methyl-1-naphthyl)fluorene (**2d**).* A solution of 2-methyl-1-naphthyllithium was prepared from 3.71 g (16.8 mmol) of 1-bromo-2-methylnaphthalene and 0.29 g of lithium in 16.8 mL of ether by stirring the mixture for 1 h at room temperature. To a 7.3 mL portion of the solution was added 1.25 g (5.8 mmol) of 1-chloro-9-fluorenone (**1**:X=Cl)[16] and the mixture was heated under reflux for 1 h with stirring. After the mixture was coold, it was treated similarly as above. The product was reduced with hydriodic acid by stirring a solution prepared as above for 15 h at room temperature. The total yield of **2d** was 57% based on the amount of 1-chloro-9-fluorenone used.

*ac**(*S**), mp 197—198 °C. Found: C, 84.29; H, 4.79; Cl, 10.49%. Calcd for $C_{24}H_{17}Cl$: C, 84.57; H, 5.03; Cl, 10.40%. ^{1}H NMR ($CDCl_3$) δ=1.35 (3H, s), 6.22 (1H, s), 7.0—7.9 (12H, m), 8.55 (1H, d, J=8 Hz).

*sc**(*R**), mp 186—187 °C. Found: C, 84.82; H, 4.79; Cl, 10.29%. Calcd for $C_{24}H_{17}Cl$: C, 84.57; H, 5.03; Cl, 10.40%. ^{1}H NMR ($CDCl_3$): δ=2.91 (3H, s), 5.80 (1H, s), 6.42 (1H, d, J=9 Hz), 6.8—8.0 (12H, m).

*1-Bromo-9-(2-methyl-1-naphthyl)fluorene (**2e**)* was prepared similarly as described in the preparation of the 1-chloro compound (**2d**). The yield was 32% based on the amount of 1-bromo-9-fluorenone (**1**:X=Br).[16]

*ac**(*S**), mp 192—193 °C. Found: C, 74.96; H, 4.39; Br, 21.06%. Calcd for $C_{24}H_{17}Br$: C, 74.82; H, 4.45; Br, 20.74%. ^{1}H NMR ($CDCl_3$) δ=1.34 (3H, s), 6.16 (1H, s), 6.9—8.0 (12H, m), 8.57 (1H, d, J=9 Hz).

*sc**(*R**), mp 189—190 °C. Found: C, 74.88; H, 4.36; Br, 21.02%. Calcd for $C_{24}H_{17}Br$: C, 74.82; H, 4.45; Br, 20.74%. ^{1}H NMR ($CDCl_3$) δ=2.74 (3H, s), 5.74 (1H, s), 6.42 (1H, d, J=9 Hz), 6.8—8.0 (12H, m).

*1-Methyl-9-(2-methyl-1-naphthyl)fluorene (**2b**)* rotamers were already prepared by Ford *et al.*[5] with a different method from that described above. These were also prepared as above in 56% yield based on 1-methyl-9-fluorenone (**1**:X=CH_3)[5,17] used.

*ac**(*R**), mp 152—153 °C (lit,[5] 152—153.5 °C). Found: C, 93.63; H, 6.03%. Calcd for $C_{25}H_{20}$: C, 93.71; H, 6.29%. ^{1}H NMR ($CDCl_3$) δ=1.28 (3H, s), 1.72 (3H, s), 6.12 (1H, s), 6.9—7.9 (12H, m), 8.58 (1H, d, J=9 Hz).

*sc**(*S**), mp 195—196 °C (lit,[5] 189—191 °C). Found: C, 93.77; H, 6.11%. Calcd for $C_{25}H_{20}$: C, 93.71; H, 6.29%. ^{1}H NMR ($CDCl_3$) δ=1.71 (3H, s), 2.84 (3H, s), 5.70 (1H, s), 6.47 (1H, d, J=8 Hz), 6.8—8.0 (12H, m).

1-Fluoro-9-(1-naphthyl)fluorene, mp 109.0—110.5 °C, was prepared similarly as described in the preparation of **2c**. Found: C, 89.27; H, 4.71%. Calcd for $C_{23}H_{15}F$: C, 89.01; H, 4.87%. ^{1}H NMR ($CDCl_3$) δ=5.40 (2/3H, s), 6.06 (1/3H, s), 6.5—7.9 (13 1/3H, m), 8.43 (2/3H, br d).

9-(1-Naphthyl)fluorene was prepared according to the published method.[7]

Kinetic Measurement of Internal Rotation by Dynamic NMR. A sample was dissolved in hexachlorobutadiene to make up a *ca.* 5% solution. The temperature was read by the chemical shift differences of the ethylene glycol protons. The free energy of activation was calculated by the graphical method.[18]

Kinetic Measurement of Internal Rotation by Classical Method. Each pure rotamer (25—30 mg), *sp*-**2a** and other corresponding forms, was dissolved in 0.45 mL of *o*-dichlorobenzene. The solution was placed in an NMR sample tube and oxygen was purged from the solution by bubbling dry nitrogen gas for some time. The tube was sealed and was heated by immersing the tube in an appropriate boiling-solvent bath. The ratio of rotational isomers was determined by ^{1}H NMR spectroscopy at appropriate intervals and the equilibrium constant was obtained by heating the solution for a long enough time. The rate constants were calculated by assuming reversible first order kinetics. Activation parameters were obtained by putting these rate constants into the Eyring equation.

Spectral Measurement. ^{1}H NMR spectra were recorded either on a Hitachi R-20B, which operates at 60 MHz, or a Varian EM-390 spectrometer which operates at 90 MHz. ^{19}F NMR spectra were obtained with the Varian EM-390 spectrometer operating at 84.67 MHz.

X-Ray Crystallography. Crystals of *sp*-9-(2-methyl-1-naphthyl)fluorene (**2a**), *ac**(*S**)-1-fluoro-9-(2-methyl-1-naphthyl)fluorene (**2c**), and *sc**(*S**)-1-methyl-9-(2-methyl-1-naphthyl)fluorene (**2b**) were grown from hexane-benzene. The suitable crystals were mounted on a Rigaku AFC-M diffractometer and the intensity data of $|F_o| \geq 3\sigma|F_o|$ were collected using Cu $K\alpha$ radiation of 1.54180 Å wave length within the range of $2\theta \leq 57°$. Total reflections used for the analysis were 2011, 2335, and 2352 for *sp*-**2a**, *sc**(*S**)-**2b**, and *ac**(*S**)-**2c**, respectively.

The crystal data were as follows. *sp*-9-(2-Methyl-1-naphthyl)fluorene: $C_{24}H_{18}$, F. W. 306.41, monoclinic, space group $P2_1/N$, a=9.264(2) Å, b=8.621(2) Å, c=21.083(7) Å, β=91.53(2)°, z=4, D_C=1.21 g/cm^3.

*ac**(*S**)-1-Fluoro-9-(2-methyl-1-naphthyl)fluorene: $C_{24}H_{17}F$, F. W.=324.40, monoclinic, space group $P2_1/C$, a=9.438(4) Å, b=15.514(6) Å, c=12.032(6) Å, β=107.79(2)°, z=4, D_C= 1.28 g/cm^3.

*sc**(*S**)-1-Methyl-9-(2-methyl-1-naphthyl)fluorene: $C_{25}H_{20}$, F. W. 320.41, primitive orthorhombic, space group Pbcn, a=18.164(4) Å, b=7.414(2) Å, c=26.431(6) Å, z=8, D_C= 1.20 g/cm^3.

The structures were solved by the direct method. All the positional and thermal parameters were refined by the least-squares method. The final R values for *sp*-**2a**, *sc**(*S**)-**2b**, and *ac**(*S**)-**2c** were 7.6, 6.5, and 7.0%, respectively.

We wish to thank Rigaku Denki Company for the rent of an AFC-M machine which made this study possible. We also thank Mr. Toshihiko Hori and Miss Yukiko Takagi of the same company for the technical assistance.

References

1) For Part LIII, see G. Yamamoto and M. Ōki, *Chem. Lett.*, **1984**, 97.
2) A preliminary note has been published: S. Murata, T. Mori, and M. Ōki, *Chem. Lett.*, **1982**, 271.
3) M. Ōki, *Angew. Chem., Int. Ed. Engl.*, **15**, 87 (1976).
4) M. Ōki, *Top. Stereochem.*, **14**, 1 (1983).
5) W. T. Ford, T. B. Thompson, K. A. J. Snoble, and J. M. Timco, *J. Am. Chem. Soc.*, **97**, 95 (1975).
6) S. Fujisaki, M. Fujimoto, N. Fujii, M. Umemoto, and S. Kajigaeshi, *Nippon Kagaku Kaishi*, **1979**, 739.
7) T. H. Siddall, III, and W. E. Stewart, *J. Org. Chem.*, **34**, 233 (1969).
8) K. D. Bartle, P. H. G. Bavin, D. W. Jones, and R. L'Amie, *Tetrahedron*, **26**, 911 (1970).
9) Since the nomenclature of stereochemistry recommended by IUPAC (L. C. Cross and W. Klyne, *Pure Appl. Chem.*, **45**, 11 (1976)) does not cover conformations involving chiral centers, we wish to use symbols proposed by one of the authors.[4] *ac**(*S**) means a racemic mixture of +*ac*(*S*) and −*ac*(*R*), and *sc**(*R**) a racemic mixture of +*sc*(*R*) and −*sc*(*S*). Others will be clear as well from these examples.
10) S. Sternhell, "Rotation about Single Bonds in Organic Molecules" in "Dynamic Nuclear Magnetic Resonance Spectroscopy" ed by L. M. Jackman and F. A. Cotton, Academic Press, New York (1975), pp. 163—201.
11) Ōki briefly commented that a ^{1}H NMR signal due to the methylene protons in a 9-(2-bromomethyl-6-methylphenyl)fluorene rotamer became broad at low temperatures.[3] This must mean that the eclipsing form of the C_9–H with the 2-bromomethyl-6-methylphenyl group is not the energy minimum but there are two potential minima within the *sp* or the *ap* zone. The ^{1}H NMR spectra of these compounds in 1:1 CF_2ClH–$CFCl_2H$ are now reexamined at 250 MHz. The *sp* form showed broadening of the methylene proton signal at 120 K whereas the *ap* form showed no significant broadening at the temperature. The results at least support the assumption that the potential is of the double-minimum type. We wish to thank Professor C. H. Bushweller, The University of Vermont, for the measurement of the ^{1}H NMR spectra at 250 MHz at low temperatures.
12) D. M. Burns and J. Iball, *Proc. R. Soc. London, Ser. A*, **227**, 200 (1954).
13) G. Ferraris, D. W. Jones, J. Yerkes, and K. D. Bartle, *J. Chem. Soc., Perkin Trans. 2*, **1972**, 1628.
14) M. Nakamura, N. Nakamura, and M. Ōki, *Bull. Chem. Soc. Jpn.*, **50**, 1097 (1977).
15) T. L. Fletcher and M. J. Namkung, *Chem. Ind.*, **1961**, 179.
16) E. H. Huntress, K. Pfister, III, and K. H. Pfister, *J. Am. Chem. Soc.*, **64**, 2845 (1942).
17) T. Mori and M. Ōki, *Bull. Chem. Soc. Jpn.*, **54**, 1199 (1981).
18) A. Jaeschke, H. Muensch, H. G. Schmid, H. Friebolin, and A. Mannschreck, *J. Mol. Spectrosc.*, **31**, 14 (1969).

The Synthesis of Li^+-selective Polyether Carriers and Thier Behavior in Cation Transport through Liquid Membranes[1)]

Kazuhisa HIRATANI,* Kazuhiro TAGUCHI, Hideki SUGIHARA, and Kokoro IIO
Industrial Products Research Institute, Higashi 1-chome, Yatabe-machi, Tsukuba-gun, Ibaraki 305
(Received November 18, 1983)

Noncyclic polyethers exhibiting lithium ion selectivity have been synthesized. Their competitive alkali-metal-ion transport through liquid membranes has been investigated, and the influence of their structures on the rates and selectivities of cation transport has been demonstrated. It has been found that the introduction of the oxytrimethylene chain on the polyethers is significant for the appearance of a high selectivity for the lithium ion, and also that the kind of terminal group might play an important role either in determining the rates of cation transport or the selectivity for the lithium ion. The introduction of a methyl group at the 2-position on the quinolyl terminal group of the polyether increased largely the selectivity for the lithium ion compared with that of the polyether having an unsubstituted quinolyl group. The cause of this was discussed on the basis of the NMR spectroscopic method and the CPK-model building.

The lithium ion has the smallest naked ionic radius (0.66 Å) among the alkali metal ions, whereas it has the largest hydrated one (3.40 Å) and also the strongest hydrated energy (ΔH=124 kcal/mol) among them.[2)] Therefore, it is not easy to design a compound with lithium ion-selectivity, and there have been few reports about available compounds which exhibit lithium ion-selective transport through liquid membranes or which extract the lithium ion into organic solvents, compared with the cases of other alkali metal ions.[3)] In addition, the lithium is an important cation practically, and its selective separation and concentration from a diluted aqueous solution will become of significance in the future. For example, there is a possibility that large amounts of lithium are required for the production of tritium, which is used as a reactant in the nuclear-fusion reaction. Thus, the synthesis of lithium ion-selective compounds is a very interesting target.

In a previous paper, one of the present authors has reported that 1-[3-(*o*-carboxyphenoxy)propoxy]-2-[3-(8-quinolyloxy)propoxy]-4(or 5)-*t*-butylbenzene (**1**) can transport the lithium ion selectively through liquid membranes and against its concentration gradient.[4)] So far, there has been no report of a noncyclic polyether carrier exhibiting uphill transport for the lithium ion selectively.[5)] Though some cyclic polyethers, *e.g.*, 12-crown-4 and its derivatives, and cryptand[211], can take up the lithium ion selectively, they do not always transport it selectively and efficiently.[6)]

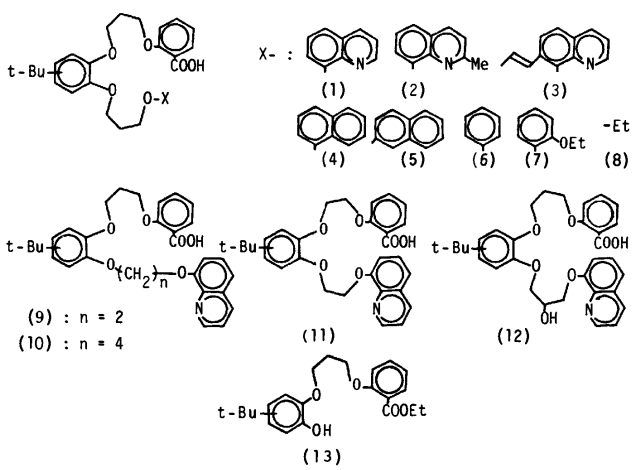

In this paper, we wish to report that analogues of **1**, **2**—**12**, were newly synthesized in order to investigate the effects of their structural modification on the transport rates and selectivities. In the cation-transport experiments, the competitive cation transport of alkali metal ions from an alkaline aqueous solution (source phase) through a chloroform phase to an acidic aqueous solution (receiving phase) by these noncyclic polyethers was examined.

Results and Discussion

Dependence of the Cocentration of Cations in Aqueous Phases on the Li^+-Selectivity of 1. The competitive ion transport of alkali metal ions (Li^+, Na^+, and K^+) by **1** against their concentration gradient was examined by changing the concentration of cations in both aqueous solutions under a constant concentration (1.5×10^{-4} mol in 30 ml of chloroform) of polyether (**1**) and a constant pH gradient. The results are shown in Figs. 1,2, and 3. Table 1 shows the amounts of cation transported after 2 d and the selectivities. Under these conditions, no cation could be transported without a carrier. In the membrane system (0.15 M† LiOH+0.15 M NaOH+0.15 M KOH+0.175 MH_2SO_4, 15 ml/1.5×10^{-4} mol of **1**, 30 ml of chloroform/0.15 M LiOH+0.15 M NaOH+0.15 M KOH+0.275 M H_2SO_4, 15 ml), which initially contained a sufficient cation concentration in comparison with the magnitude of the pH gradient between the two aqueous phases, the selectivity for the lithium ion was much higher than in the system which had an initial concentration of 0.1 M for each cation. That is, the transport ratios, Li/Na and Li/K, reach 6.6 and >10 respectively in this system, and the amount of the lithium ion transported reaches 0.795 mmol after 2 d. On the other hand, when the initial concentration of each cation was 0.033 M and the magnitude of the initial pH gradient was the same as above, 82% of the lithium ion in the source phase was trans-

† 1 M=1 mol dm^{-3}.

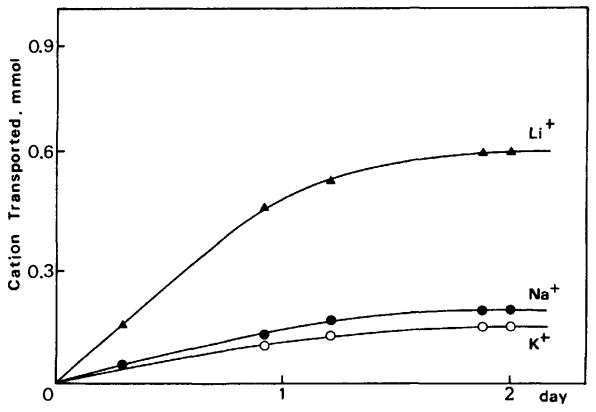

Fig. 1. Cation transport by (**1**) for lithium, sodium, and potassium ion species existing together. Initial transport conditions (25 °C) ; Source phase : 15 ml of 0.1M LiOH+0.1 M NaOH+0.1 M KOH+0.1 M H_2SO_4 aqueous solution, Chloroform membrane : 30 ml of chloroform containing 1.5×10^{-4} mole of (**1**), Receiving phase : 15 ml of 0.1 M LiOH+0.1 M NaOH+0.1 M KOH+0.2 M H_2SO_4 aqueous solution.

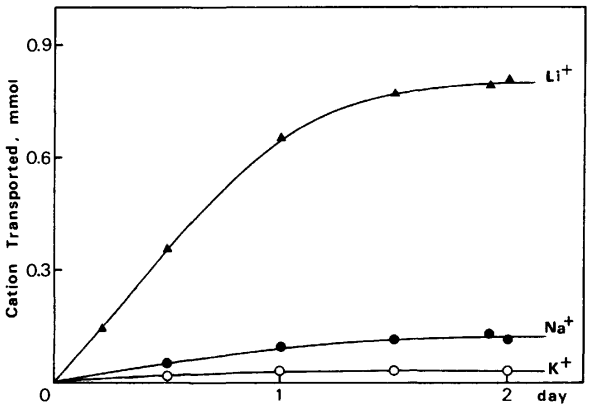

Fig. 2. Cation transport by (**1**) for lithium, sodium, and potassium ion species existing together. Initial transport conditions (25 °C); Sourcephase: 15 ml of 0.15 M LiOH+0.15 M NaOH+0.15 M KOH+0.175 M H_2SO_4 aqueous solution, Chloroform membrane: 30 ml of chloroform containing 1.5×10^{-4} mole of (**1**), Receiving phase: 15 ml of 0.15 M LiOH+0.15 M NaOH+0.15 M KOH+0.275 M H_2SO_4 aqueous solution.

ported by **1** after 2 d, although the selectivity (Li/Na) became fairly low. In this system, both sodium and potassium ions were transported gradually with the time, as is shown in Fig. 3, making a sigmoidal shape. This could be attributed to the excessive pH gradient, which is not exhausted by the transport of the lithium ion, between the two aqueous phases. Interestingly, this trend is in line with the results observed in the case of the potassium ion-selective polyether, 1-[2-[2-(8-quinolyloxy)-ethoxy]ethoxy]-2[2-[2-(*o*-carboxyphenoxy)ethoxy]ethoxy]-4(or 5)-*t*-butylbenzene, as has been reported recently.[7] These results mean that the selectivity for a cation can be changed greatly by changing the con-

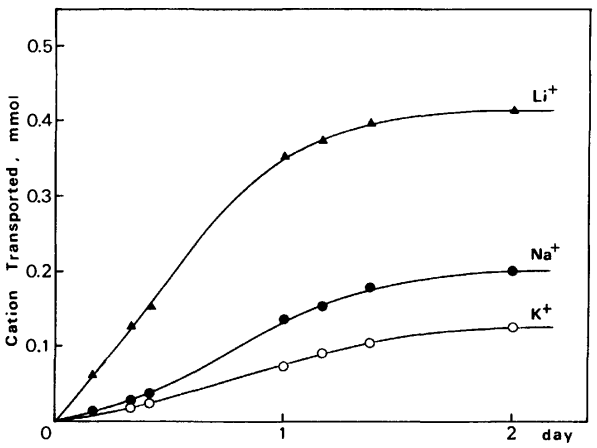

Fig. 3. Cation transport by (**1**) lithium, sodium, and potassium ion species existing together. Initial transport conditions (25 °C); Source phase: 15 ml of 0.033 M LiOH+0.033 M NaOH+0.033 M KOH aqueous solution, Chloroform membrane : 30 ml of chloroform containing 1.5×10^{-4} mole of (**1**), Receiving phase : 15 ml of 0.033 M LiOH+0.033 M NaOH+0.033 M KOH+0.1 M H_2SO_4 aqueous solution.

Table 1. Influence of initial cation concentration on the amounts of cation transported by (**1**)

Initial conc. of each cation*	Cation transported after 2 d (mmol)			Selectivity	
	Li	Na	K	Li/Na	Li/K
0.033 M	0.410	0.205	0.125	2.0	3.3
0.10 M	0.615	0.180	0.120	3.4	5.1
0.15 M	0.795	0.120	0.030	6.6	$\gg$10

* Other conditions: see the footnotes in Figures 1,2, and 3 respectively.

centration of cations in the aqueous phases under a constant pH gradient. Therefore, it is suggested that the lithium ion can be separated and concentrated with a high selectivity from other alkali ions against their concentration gradient when adequate transport conditions are chosen in the system.

Effects of the Kind of Oxyalkylene Chain on the Selectivity. As has been described above, we have found that the noncyclic polyether (**1**), with both *o*-carboxyphenyl and 8-quinolyl terminal groups, exhibits the ability of the selective uphill transport of the lithium ion. Then, what structure of the noncyclic polyethers which exhibit lithium ion-selectivity is essentially required? In order to clarify this question, firstly, the effects of the kind of oxyalkylene chain on the selectivity were examined.

Some noncyclic polyethers which contain oxyethylene, oxytrimethylene, and/or oxytetramethylene chains were prepared and used as carriers in the cation transport through liquid membranes. The results are shown in Table 2. In Table 2, polyether (**1**) which contains two oxytrimethylene chains, exhibits the best selectivity for the lithium ion between them. The selectivity is lowered when the oxyalkylene chain

TABLE 2. INFLUENCE OF KINDS OF ALKYLENE CHAIN ON THE CATION-SELECTIVE TRANSPORT

Polyether	Cations transported after 2 d (%)				Selectivity		
	Li	Na	K	Total	Li/Na	Li/K	Na/K
(**1**)	41	12	8	61	3.4	5.1	1.5
(**9**)	34	17	11	62	2.0	3.1	1.5
(**10**)	36	16	11	63	2.2	3.3	1.5
(**11**)	28	21	13	62	1.3	2.1	1.6

Initial transport conditions (25 °C):

(Source phase)	(Chloroform membrane)	(Receiving phase)
0.1 M LiOH 0.1 M NaOH 0.1 M KOH 0.1 M H_2SO_4 15 ml	Polyether 1.5×10^{-4} mol $CHCl_3$ 30 ml	0.1 M LiOH 0.1 M NaOH 0.1 M KOH 0.2 M H_2SO_4 15 ml

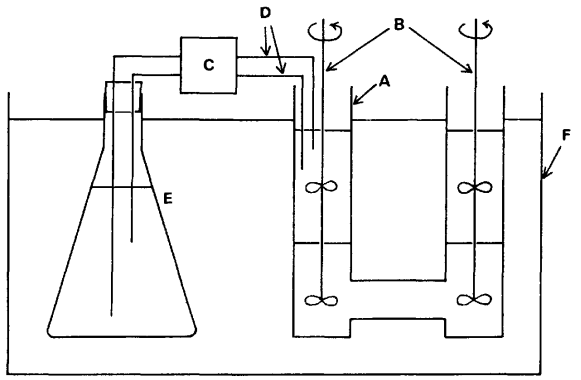

Fig. 4. Apparatus for measuring cation transport ; (A) U-type glass tube, (B) glass stirrer (200 min^{-1}.), (C) circulating pump, (D) polypropylene tube (diameter 2 mm) for circulating aqueous solution in the source phase, (E) 100-ml Erlenmeyer flask, (F) water bath controlled temperature (25 °C).

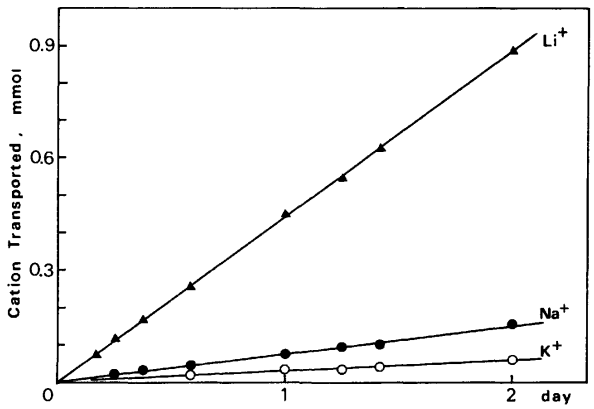

Fig. 5. Cation transport by (**2**) for lithium, sodium, and potassium ion species existing together. Initial transport conditions (25 °C) ; Source phase : 115 ml of 0.1 M LiOH+0.1 M NaOH+0.1 M KOH+0.1 M H_2SO_4 aqueous solution, Chloroform membrane : 30 ml of chloroform containing 1.5×10^{-4} mole of (**2**), Receiving phase : 15 ml of 0.05 M H_2SO_4 aqueous solution.

of polyether is either longer or shorter than oxytrimethylene. The structural significance of the oxytrimethylene-chain unit is noted for the appearance of a high selectivity for the lithium ion.

Effects of Terminal Groups on the Selectivity. Next, the effects of the kind of terminal groups on the selectivity were examined using polyethers containing other substituent groups in place of the 8-quinolyl terminal group of **1**. The other groups of **1** are not changed because the two trimethylene groups are important for the appearance of the high selectivity for the lithium ion and the other terminal group, the *o*-carboxyphenyl group, is required for cation-catching. In this study, as is shown in Fig. 4, a large amount of the solution in the source phase is circulated to keep the concentration of the cations constant, and the receiving phase contains only 15 ml of the 0.05 M sulfuric acid solution. Under these transport conditions, the amounts of each cation transported increased linearly with the running time for 2 d at least. Figure 5 summarizes the results obtained in the case of polyehter (**2**), while Table 3 shows the results of the transport rates (μmol/hr), which were calculated from the linear slopes of the amounts of each cation transported *vs.* the running time, and the selectivities of polyethers, (**1**)—(**8**) and (**12**). The values of the selectivities of **1** in Table 3 are a little different from those in Table 2 because of the different transport conditions. The values in Tables 1 and 2 were calculated from the amounts of the cation transported after 2 d, whereas the values in Table 3 were calculated from the transport rates of the cations. Here, it may be noted that the selectivity ratios, Li/Na and Li/K, change greatly with the change in the position of the substituent group introduced to the quinoline skelton. Polyether (**2**), which contains the 2-methyl-8-quinolyl group, gives a selectivity for the lithium ion superior to the (**1**) and (**3**) polyethers, whereas the (**3**) polyether which contains the 7-(1-propenyl)-8-quinolyl group,[8] gives a worse selectivity for the lithium ion than **1**. It is suggested that the structure of the terminal group and the position of the group introduced into the terminal group are important in order to increase the selectivity for the lithium ion. Furthermore, although there is little difference of selectivity for the lithium ion between **1** and the polyethers, (**4**) and (**5**), the significance of the heteroatom on the terminal

Table 3. Influence of substituents of the carriers on the cation-selective transport

Polyether	Transport rate (μ mol/hr)			Selectivity		
	Li	Na	K	Li/Na	Li/K	Na/K
(**1**)	20	6.2	3.4	3.2	5.9	1.8
(**2**)	18	3.1	1.3	5.8	14	2.5
(**3**)	18	6.9	5.6	2.6	3.2	1.2
(**4**)	19	6.3	5.3	3.0	3.6	1.2
(**5**)	19	6.1	5.0	3.1	3.8	1.2
(**6**)	19	6.9	5.0	2.8	3.8	1.4
(**7**)	19	5.3	4.1	3.6	4.7	1.3
(**8**)	10	3.4	2.2	2.9	4.6	1.6
(**12**)	13	11	10	1.2	1.3	1.1

Initial transport conditions (25 °C):

(Source phase)	(Chloroform membrane)	(Receiving phase)
0.1 M LiOH 0.1 M NaOH 0.1 M KOH 0.1 M H_2SO_4 115 ml	Polyether 1.5×10^{-4} mol $CHCl_3$ 30 ml	0.05 M H_2SO_4 15 ml

group may be presumed from the enhancement of the selectivity in the case of **7** containing the *o*-ethoxyphenyl terminal group compared with that of **6** containing the phenyl group.[9] In the case of **8**, which contains an ethyl terminal group, the selectivity is not much different from that in the case of the polyethers containing a phenyl or naphthyl group, but the transport rates of each cation using **8** as a carrier decrease apparently in spite of stirring mechanically at 200 min^{-1} in every case, in comparison with those in the case of the polyethers containing aromatic substituents. The transport rates may depend on the difference in hydrophobicity between them. Thus, no large difference in selectivities between polyethers, (**4**)—(**6**) and (**8**), is observed. These results suggest that the more important factor affecting the selectivities for a cation is the introduction of the oxytrimethylene chain, as is shown in Table 2, rather than the kinds of terminal group. By the way, polyether (**12**), with the 2-hydroxy-1,3-propanediyl group, with which 8-quinolyloxy and *t*-butyl-*o*-phenyleneoxy groups are bound, exhibits a much lower selectivity for the lithium ion than **1**. The cause of this will be discussed later.

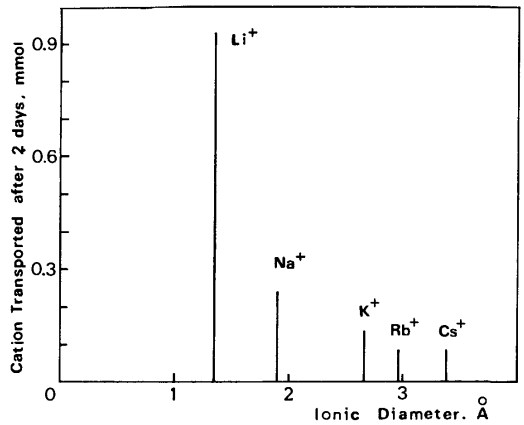

Fig. 6. Dependence of ionic diameter on the amounts of cation transported by (**1**) after 2 d. Initial transport conditions (25 °C) ; Source phase : 115 ml of 0.1 M LiOH+0.1 M NaOH+0.1 M KOH+0.1 M RbOH+0.1 M CsOH+0.2 M H_2SO_4 aqueous solution, Chloroform membrane : 30 ml of chloroform containing 1.5×10^{-4} mole of (**1**), Receiving phase : 15 ml of 0.05 M H_2SO_4 aqueous solution.

Structures of the Polyethers with Li^+-Selective Transport. From the results obtained, the structural significance of noncyclic polyethers may be pointed out. How can these polyethers exhibit Li^+-selective transport through liquid membranes?

Figure 6 shows the results of cation transport by **1** for five alkali metal ion species existing together in the source phese. Apparently, the smaller the ionic diameter, the larger the transport rates: $Li^+ \gg Na^+ > K^+ > Rb^+ \approx Cs^+$. Although the ionic diameter of a naked lithium ion is the smallest (1.32 Å) among alkali metal ions, its hydrated diameter (total hydration number =25) is the largest (6.80 Å) among them. The uptake of hydrated lithium ions by the polyethers does not occur, probably because the proton signal assigned to water does not appear in the NMR spectrum of Li-salt of **1** in $CDCl_3$. Furthermore, if the hydrated lithium ion can be transported, it can not be explained why the transport rates decrease in the order of the naked ionic diameter from the smallest Li^+ to the largest Cs^+. Additionally, in the case of the polyether containing the *p*-carboxyphenyl terminal group substituted for the *o*-carboxyphenyl one, its alkali salt can not be soluble in chloroform and can not be mobile through liquid membranes.[10] This means that the hydrated lithium ion is insoluble in chloroform. Therefore, it is reasonable to consider that the naked lithium ion becomes incorporated into the polyether carrier by means of the electrostatic interaction between ether-oxygens of the polyether and the lithium ion in a manner similar to cyclic polyethers, the so-called crown ethers.[11]

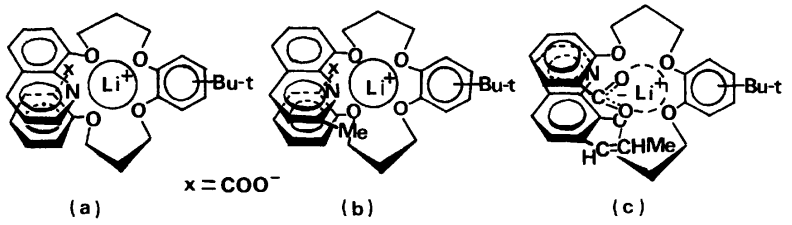

Fig. 7. Pseudocyclic structures Li-salts of polyethers on the basis of the CPK model; (a) Li—(**1**), (b) Li—(**2**), (c) Li—(**3**).

Here, if one looks at the molecular models of the carboxylate salt of the polyether with the lithium ion, it can be understood that these polyethers can transport the lithium ion selectively. As is shown in Fig. 7, the polyether (**1**) can form a pseudocyclic structure (a), the cavity of which has a diameter of 1.4—1.6 Å, and then the terminal aromatic rings overlap one another plainly to form a stacking structure,[12] when both ether-oxygen and nitrogen atoms are spatially directed to the inside. This indicates that the lithium ion best fits the size of the cavity formed. The other compounds with two oxytrimethylene chains, (**2**)—(**8**), also form the size of cavity which the lithium ion best fits among alkali metal ions. The stacking structure between terminal aromatic rings is suggested on the basis of the CPK-model building when the lithium ion becomes incorporated into the cavity of the polyethers.

The NMR spectra of polyether (**1**)-cation salts have been measured in order to get information concerning the stacking structure. Figure 8 shows the NMR spectra of the polyether (**1**), its Li^+ salt, and its K^+ salt. Especially notable is the proton at the 2-position of the quinolyl group; the proton (δ=8.96 ppm) in the case of Li^+ salt shifts to a higher magnetic field than that (δ=9.09 ppm) of the free polyether, while the proton (δ=9.08 ppm) in the case of the K^+ salt shifts hardly at all. It is presumed that the shift to the higher magnetic field in the case of Li^+ salt is to be attributed to the shielding effect (ring-current effect) of the aromatic rings on account of the stacking structure between them. If the nitrogen atom on the quinolyl group participates in the coordination to cations, the proton at the 2-position of the quinolyl group should shift to the lower magnetic field rather than that of free polyether (**1**). On the other hand, the size of the potassium ion is large, so that the terminal aromatic rings can not completely overlap each other. This can be confirmed from the CPK-model building.

The (**2**) polyether exhibits the most excellent selectivity for the lithium ion among the polyethers, whereas the (**3**) polyether exhibits a worse selectivity for it than even **1**. The difference in selectivity among the polyethers, (**1**)—(**3**), can not be explained by their lipophilicity because it increases in the following order: **1**<**2**<**3**. The difference in selectivity between **2** and **3** was also inferred on the basis of the CPK-model building (Fig. 7-b and 7-c). The CPK model indicates that the methyl moiety of **2** fills a space of the hydrophobic exterior which the (**1**) polyether forms around the cavity when aromatic terminal groups are stacked parallel to each other, playing a

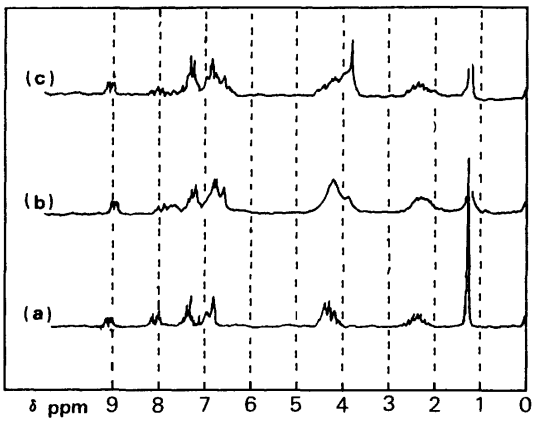

Fig. 8. NMR spectrum of (**1**) and its alkali salts ; (a) (**1**), (b) the Li salt, (c) the K salt.

part in the hydrophobic wall around the cavity (see, Fig. 7-b), whereas the 1-propenyl moiety of **3** can not act as a hydrophobic wall around the cavity, unlike the methyl moiety of **2**, but 1-propenyl and carboxylato groups on the two terminal aromatics could, rather, collide with each other when the complex with the lithium ion forms,to interfere a little with the favorable structure for the lithium ion (Fig. 7-c).

The small difference in selectivity for the lithium ion between **1** and **4** is not always reflected by the participation of the nitrogen atom,[9] which may be suggested from the CPK-model building, in the uptake of the lithium ion. On the contrary, the difference in selectivity dependent on the length of the oxyalkylene chain is reflected by the size of the cavity formed on the basis of the CPK-model building. The selective transport for the lithium ion by **12** is greatly lowered compared with that by **1**. It is presumed that the ability to wrap favorably around the lithium ion is decreased because the hydrophilic OH group on the trimethylene chain tends to be oriented inside the cavity in a nonpolar solvent (liquid membranes), resulting in the deformation of the cavity. From these considerations, we can reach the conclusion that the essential point in the structure of a noncyclic polyether for exhibiting lithium ion-selective transport is to contain the 1,2-bis(3-oxytrimethyleneoxy)phenyl group.

The schematic mechanism of cation transport by **1** as an example is proposed in Fig. 9. Thus, when the structure of the polyether can enoughly satisfy every process as follows: i) a selective uptake of cations at the boundary between phases (a) and (b), ii) solubility into the chloroform liquid membrane (b) and mobility

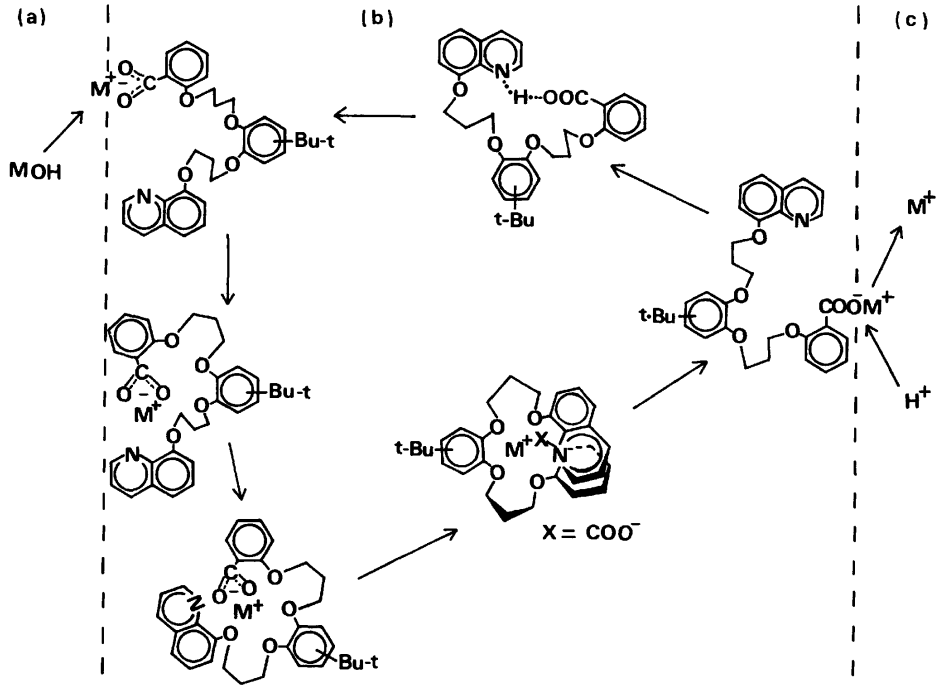

Fig. 9. Posturated cation transport sheme; (a) Source phase, (b) Chloroform membrane, (c) Receiving phase.

through it, and a smooth and rapid release of cations at the boundary between phases (b) and (c), the cation transport by the polyether is considered to proceed most effectively and selectively.

Experimental

General. The IR spectra were recorded with a JASCO A-3 Infrared spectrophotometer. The ^{1}HNMR (60 MHz) spectra were recorded with a Varian EM-360 spectrometer. The chemical shifts for $CDCl_3$ solutions are reported from internal tetramethylsilane.

1-[3-(o-Carboxyphenoxy)propoxy]-2-[3-(8-quinolyloxy)propoxy]-4-(or 5)-t-butylbenzene (1). *Method 1*: Under a nitrogen atmosphere, to a solution of 33.2 g (0.2 mol) of 4-*t*-butylcatechol in 150 ml of DMF was added 55.2 g of powdered potassium carbonate, after which the reaction mixture was stirred at 70 °C for 2 h. Then, 40 g (0.21 mol) of 3-chloro-1-propanol and a small amount of KI were added to it, and the mixture was stirred at 70 °C for 24 h. The solvent was evaporated under reduced pressure, and the residue was added to an aqueous hydrochloric acid solution to neutralize it and then extracted with chloroform. The chloroform extract was washed with water, dried with anhydrous magnesium sulfate, and evaporated to give an oily residue. The residue was purified by Kugelrohr distillation at 190 °C (0.3 mmHg[††]) to give 43 g (76%) of 1,2-bis(3-hydroxypropoxy)-4-*t*-butylbenzene as a colorless liquid.

To the solution of 31.7 g of 1,2-bis(3-hydroxypropoxy)4-*t*-butylbenzene and 30 g of pyridine in 150 ml of benzene was added dropwise 20 g of thionyl chloride. After refluxing for 10 h, the benzene solution was washed twice with water, then with diluted aqueous K_2CO_3 and with water. After the solution had been dried with anhydrous $MgSO_4$, the benzene was removed and the residue was purified by Kugelrohr distillation at 186 °C (1.3 mmHg) to give 27 g (76%) of 1,2-bis(3-chloropropoxy)-4-*t*-butylbenzene as a colorless liquid.

The reaction mixture of 3.4 g (0.02 mol) of ethyl salicylate and 2.3 g (0.02 mol) of *t*-BuOK in 50 ml of DMF was stirred until it became homogeneous. To the solution was then added 15 g (0.047 mol) of 1,2-bis(3-chloropropoxy)-4-*t*-butylbenzene, and the mixture was stirred at 70 °C for 42 h. After cooling to room temperature, the reaction mixture was poured into water and extracted with benzene. The benzene layer was washed with water three times and dried with anhydrous $MgSO_4$. After the solvent and the excess reactants had been removed under reduced pressure, the residue was submitted to column chromatography on activated alumina (Wako gel, 300 mesh) with a chloroform eluent to give 5.1 g (57%) of 1-[3-(*o*-ethoxycarbonylphenoxy)propoxy]-2-(3-chloropropoxy)-4(or 5)-*t*-butylbenzene as a colorless liquid.

The reaction mixture of 2.0 g of 8-quinolinol and 0.30 g of NaH in 30 ml of DMF was stirred until it became homogeneous. To the solution was then added 4.8 g (0.011 mol) of 1-[3-(*o*-ethoxycarbonylphenoxy)propoxy]-2-(3-chloropropoxy)-4(or 5)-*t*-butylbenzene, and the mixture was stirred at 70 °C for 48 h. After cooling to room temperature, the reaction mixture was poured into water and extracted with benzene. The benzene layer was washed with water three times and dried with $MgSO_4$. After the solvent had been evaporated, the residue was submitted to column chromatography on activated alumina (Wako gel, 300 mesh) with a chloroform eluent to give 3.7 g (62%) of 1-[3-(*o*-ethoxycarbonylphenoxy)-propoxy]-2-[3-(8-quinolyloxy)propoxy]-4(or 5)-*t*-butylbenzene. This ethyl ester (2.8 g) and 1 g of KOH in 30 ml of ethanol were refluxed under stirring overnight. After the ethanol had been evaporated, water was added to the residue, and the solution was slightly acidified with glacial acetic acid and extracted with chloroform two times. The chloroform layer was washed with water two times and dried with $MgSO_4$. After the removal of chloroform, the residue was submitted to column chromatography on silica gel (Wako gel, 300 mesh)

[††] 1 mmHg≈133.322 Pa.

with a chloroform eluent to give 2.1 g (79%) of **1** as a pale yellow glassy solid. ^{1}H NMR ($CDCl_3$) δ=1.27 (9H, s, $C(CH_3)_3$), 2.0—2.8 (4H, m, $OCH_2C\underline{H}_2CH_2O$), 4.1—4.7 (8H, m, $OC\underline{H}_2$-$CH_2C\underline{H}_2O$), 6.8—7.7 (10H, m, aromatic), 8.1—8.4 (2H, m, aromatic), 9.09 (1H, m, aromatic), *ca.* 8—9 (1H, broad, COOH); IR(KBr): 3280 and 2500 (COOH), 1705 (C=O), 1600 and 1580 cm^{-1} (aromatic C=C). Found: C 72.03, H 6.51, N 2.55%. Calcd for $C_{32}H_{35}NO_6$: C 72.57, H 6.66, N 2.64%.

Method 2: The reaction mixture of 33 g (0.2 mol) of ethyl salicylate and 5 g (0.2 mol) of NaH in 150 ml of DMF was stirred until it became homogeneous. To the solution was added 40 g of 2-(3-chloropropoxy)tetrahydropyran, which had been obtained quantitatively by the reaction of 3-chloro-1-propanol with 3,4-dihydro-2*H*-pyran, and the mixture was stirred at 70 °C for 24 h. After it was cooled to room temperature, the reaction mixture was poured into water and extracted with benzene. The benzene layer was washed with water and dried with $MgSO_4$. After the benzene had been removed, 100 ml of ethanol and a few drops of conc. HCl were added to the residue, and the solution was stirred at room temperature overnight. After the removal of the solvent, water was added to the residue, and the solution was extracted with chloroform. The chloroform layer was washed with water and dried with $MgSO_4$. After the removal of the chloroform, the residue was purified by Kugelrohr distillation at 180 °C (0.5 mmHg) to give 36.0 g (80%) of ethyl 2-(3-hydroxypropoxy)benzoate. To the reaction mixture of 33 g (0.15 mol) of ethyl 2-(3-hydroxypropoxy)benzoate and 15 g of pyridine in 300 ml of benzene was then added 20 g of thionyl chloride, drop by drop, and then the mixture was refluxed under stirring for 17 h. After cooling to room temperature, the solution was washed with water three times, then with diluted aqueous K_2CO_3 and with water, and dried with $MgSO_4$. After the removal of the benzene, the residue was purified by Kugelrohr distillation at 150 °C (0.4 mmHg) to give 30 g (83%) of ethyl 2-(3-chloropropoxy)benzoate.

The reaction mixture of 50 g (0.3 mol) of 4-*t*-butylcatechol and 6.0 g (0.054 mol) of *t*-BuOK in 150 ml of DMF was stirred under a nitrogen atmosphere until it became homogeneous. To the solution was added 13 g (0.054 mol) of ethyl 2-(3-chloropropoxy)benzoate, and the mixture was stirred at 70 °C for 48 h. After cooling to room temperature, 200 ml of benzene was added to the solution, and it was washed with water three times and dried with $MgSO_4$. After the removal of the benzene, the excess *t*-butylcatechol was removed from the residue at 130 °C under reduced pressure (0.5 mmHg). The residue was submitted to column chromatography on activated alumina with a chloroform eluent to give 14.5 g (76%) of 2-[3-(*o*-ethoxycarbonylphenoxy)propoxy]-4(or 5)-*t*-butylphenol (**13**) as a colorless liquid. ^{1}H NMR ($CDCl_3$) δ=1.30 (9H, s, $C(CH_3)_3$), 1.37 (3H, t (7.2 Hz), $OCH_2C\underline{H}_3$), 2.0—2.6 (2H, m, $OCH_2C\underline{H}_2CH_2O$), 4.05—4.60 (4H, m, $OC\underline{H}_2CH_2C\underline{H}_2O$), 4.35 (2H, q (7.2 Hz), $OC\underline{H}_2CH_3$), *ca.* 5.7 (1H, broad, OH), 6.8—8.0 (7H, m, aromatic); IR (neat): 3440 (OH), 1720 (C=O), 1600 and 1580 cm^{-1} (aromatic C=C). Found: C 71.28, H 7.65%. Calcd for $C_{22}H_{28}O_5$: C 70.94, H 7.58%.

The mixture of 36 g (0.25 mol) of 8-quinolinol and 28 g (0.25 mol) of *t*-BuOK in 70 ml of DMSO was stirred until it became homogeneous. To the solution 24 g (0.25 mol) of 3-chloro-1-propanol was added, and the mixture was stirred at 70 °C for 38 h. The solution was then poured into 500 ml of water, and the solid, which was precipitated in water, was separated from the solution by filtration, washed with water three times, and dried under a vacuum to give 33 g (66%) of 3-(8-quinolyloxy)-1-propanol. To the solution of 23 g (0.11 mol) of 3-(8-quinolyloxy)-1-propanol in 100 ml of benzene was added 16 g (0.13 mol) of thionyl chloride, drop by drop, after which the solution was refluxed for 5 h under stirring. After cooling to room temperature, diluted aqueous K_2CO_3 was slowly added to the solution until it became slightly basic. The benzene layer was washed with water two times and dried with $MgSO_4$. After the removal of the benzene, the crude product was purified by recrystallization from hexane to give 17 g (68%) of 1-chloro-3-(8-quinolyloxy)propane as a white solid; mp 68—69 °C.

The reaction mixture of 7.3 g (0.02 mol) of **13** and 2.2 g (0.02 mol) of *t*-BuOK in 50 ml of DMSO was stirred until it became homogeneous. To the solution was then added 4.4 g (0.02 mol) of 1-chloro-3-(8-quinolyloxy)propane and a small amount of KI, and the mixture was stirred at 70 °C for 4 d. Then, benzene and water were added to the solution, and the benzene layer was washed with water and dried with $MgSO_4$. After the removal of the benzene, the residue was submitted to column chromatography on activated alumina with a chloroform eluent to give 9.4 g (85%) of 1-[3-(*o*-ethoxycarbonylphenoxy)propoxy]-2-[3-(8-quinolyloxy)propoxy]-4(or 5)-*t*-butylbenzene as a pale yellow liquid. The polyether (**1**) was obtained in a manner similar to that described in Method 1.

The polyethers, (**2**)—(**8**) and (**10**), were obtained by the reaction of **13** with the corresponding 3-substituted 1-chloropropane in a manner similar to that described in Method 2.

1-[3-(o-Carboxyphenoxy)propoxy]-2-[3-(2-methyl-8-quinolyloxy)-propoxy]-4(or 5)-t-butylbenzene (2). The above procedure was followed, using **13** and 1-chloro-3-(2-methyl-8-quinolyloxy)propane; a pale yellow glassy solid. ^{1}H NMR ($CDCl_3$) δ=1.27 (9H, s, $C(CH_3)_3$), 2.0—2.7 (4H, m, OCH_2-$C\underline{H}_2CH_2O$), 2.77 (3H, s, CH_3-Ar), 4.05—4.65 (8H, m, $OC\underline{H}_2$-$CH_2C\underline{H}_2O$), 6.8—7.6 (10H, m, aromatic), 7.9—8.3 (2H, m, aromatic), *ca.* 8.9 (1H, broad, COOH); IR (KBr): 3280 and 2550 (COOH), 1710 (C=O), 1605, 1580, and 1575 cm^{-1} (aromatic C=C). Found: C 72.26, H 6.81, N 2.49%. Calcd for $C_{33}H_{37}NO_6$: C 72.91, H 6.86, N 2.57%.

1-[3-(o-Carboxyphenoxy)propoxy]-2-[3-[7-(1-propenyl)-8-quinolyloxy]propoxy]-4(or 5)-t-butylbenzene (3). The above procedure was followed, using **13** and 1-chloro-3-[7-(1-propenyl)-8-quinolyloxy]propane, which had been obtained by the reaction of 7-allyl-8-quinolinol with 3-chloro-1-propanol, followed by treatment with thionyl chloride. 7-Allyl-8-quinolinol was obtained in a good yield by the Claisen rearrangement of 8-(allyloxy)quinoline. Polyether (**3**): a pale yellow glassy solid. ^{1}H NMR ($CDCl_3$) δ=1.32 (9H, s, C (CH_3)$_3$), 1.78 (3H, d, $C\underline{H}_3$-CH=CH-Ar), 2.0—2.6 (4H, m, $OCH_2C\underline{H}_2CH_2O$), 4.0—4.6 (8H, m, $OC\underline{H}_2CH_2C\underline{H}_2O$), 6.0—6.6 (1H, m, CH_3-C$\underline{H}$=CH-Ar), 6.7—7.8 (10H, m, aromatic and CH_3-CH=C$\underline{H}$-Ar), 8.10 (2H, m, aromatic), 8.87 (1H, m, aromatic), *ca.* 8.8 (1H, broad, COOH); IR (KBr): 3270 and 2450 (COOH), 1725 and 1700 (C=O), 1645 (CH=CH), 1600 and 1580 cm^{-1} (aromatic C=C). Found: C 73.07, H 6.71, N 2.38%. Calcd for $C_{35}H_{39}NO_6$: C 73.79, H 6.90, N 2.46%.

1-[3-(o-Carboxyphenoxy)propoxy]-2-[3-(1-naphthyloxy)propoxy]-4(or 5)-t-butylbenzene (4). The above procedure was followed, using **13** and 1-chloro-3-(1-naphthyloxy)propane, which had been obtained by the reaction of 1-naphthol with 1,3-dichloropropane: colorless liquid. ^{1}H NMR ($CDCl_3$) δ=1.28 (9H, s, C (CH_3)$_3$), 2.0—2.7 (4H, m, OCH_2-$C\underline{H}_2CH_2O$), 4.0—4.55 (8H, m, $OC\underline{H}_2CH_2C\underline{H}_2O$), 6.7—8.5 (14H, m, aromatic), *ca.* 9—10 (1H, broad, COOH); IR (neat): 3300 (COOH), 1740 and 1700 (C=O), 1630, 1605, and 1580 cm^{-1} (aromatic C=C). Found: C 75.40, H 6.72%. Calcd for $C_{33}H_{36}O_6$: C 74.98, H 6.86%.

1-[3-(o-Carboxyphenoxy)propoxy]-2-[3-(2-naphthyloxy)propoxy]-4(or 5)-t-butylbenzene (5). The above procedure was followed, using **13** and 1-chloro-3-(2-naphthyloxy)propane: colorless liquid. ^{1}H NMR ($CDCl_3$) δ=1.31 (9H, s, $C(CH_3)_3$), 2.0—2.6 (4H, m, $OCH_2C\underline{H}_2CH_2O$), 4.05—4.55 (8H, m, $OC\underline{H}_2CH_2C\underline{H}_2O$), 6.83—7.97 (13H, m, aromatic),

8.22 (1H, m, aromatic), *ca.* 9—10 (1H, broad, COOH); IR (neat): 3300 (COOH), 1740 and 1700 (C=O), 1630, 1600, and 1580 cm^{-1} (aromatic C=C). Found: C 74.41, H 6.95%. Calcd. for $C_{33}H_{36}O_6$: C 74.98, H 6.86%.

1-[3-(o-Carboxyphenoxy)propoxy]-2-(3-phenoxypropoxy)-4(or 5)-t-butylbenzene (6). The above procedure was followed using **13** and 1-chloro-3-phenoxypropane: colorless liquid. ^1H NMR ($CDCl_3$) δ=1.30(9H, s, $C(CH_3)_3$), 2.0—2.6 (4H, m, $OCH_2C\underline{H}_2CH_2O$), 3.95—4.65 (8H, m, $OC\underline{H}_2CH_2$-$C\underline{H}_2O$), 6.7—7.7 (1H, m, aromatic), 8.05—8.30 (1H, m, aromatic), *ca.* 9—10 (1H, broad, COOH); IR (neat): 3290 (COOH), 1740 and 1695 (C=O), 1605 and 1590 cm^{-1} (aromatic C=C). Found: C 73.56, H 7.03%. Calcd for $C_{29}H_{34}O_6$: 72.78, H 7.16%.

1-[3-(o-Carboxyphenoxy)propoxy]-2-[3-(o-ethoxyphenoxy)propoxy]-4(or 5)-t-butylbenzene (7). The above procedure was followed, using **13** and 1-chloro-3-(*o*-ethoxyphenoxy)-propane which was obtained by the reaction of *o*-ethoxyphenol with 1,3-dichloropropnane: pale yellow liquid. ^1H NMR ($CDCl_3$) δ=1.30 (9H, s, $C(CH_3)_3$), 1.40 (3H, t, OCH_2-$C\underline{H}_3$), 2.0—2.6 (4H, m, $OCH_2C\underline{H}_2CH_2O$), 4.06 (2H, q, $OC\underline{H}_2CH_3$), 4.1—4.7 (8H, m, $OC\underline{H}_2CH_2C\underline{H}_2O$), 6.93 (4H, s, aromatic), 6.8—7.8 (6H, m, aromatic), 8.22 (1H, m, aromatic), *ca.* 9—10 (1H, broad, COOH); IR (neat): 3300 (COOH), 1740 and 1700 (C=O), 1605 and 1580 cm^{-1} (aromatic C=C). Found: C 70.73, H 7.02%. Calcd for $C_{31}H_{38}O_7$: C 71.26, H 7.33 %.

1-[3-(o-Carboxyphenoxy)propoxy]-2-(3-ethoxypropoxy)-4(or 5)-t-butylbenzene (8). The above procedure was followed, using **13** and 1-chloro-3-ethoxypropane, which had been obtained by the reaction of 3-ethoxypropionic acid with $LiAlH_4$ following chlorination: colorless liquid. ^1H NMR ($CDCl_3$) δ=1.17 (3H, t, $OCH_2C\underline{H}_3$), 1.31 (9H, s, $C(CH_3)_3$), 1.75—2.65 (4H, m, $OCH_2C\underline{H}_2CH_2O$), 3.47 (2H, q, $OC\underline{H}_2CH_3$), 3.59 (2H, t, $OCH_2CH_2C\underline{H}_2O$-$CH_2CH_3$), 3.95—4.70 (6H, m, $OC\underline{H}_2CH_2C\underline{H}_2O$), 6.87—7.80 (6H, m, aromatic), 8.22 (1H, m, aromatic), *ca.* 9 (1H, broad, COOH); IR (neat): 3290 (COOH), 1740 and 1700 (C=O), 1605 and 1580 cm^{-1} (aromatic C=C). Found: C 70.30, H 7.63%. Calcd for $C_{25}H_{34}O_6$: C 69.74, H 7.96%.

1-[3-(o-Carboxyphenoxy)propoxy]-2-[4-(8-quinolyloxy)butoxy]-4(or 5)-t-butylbenzene (10). The above procedure was followed, using **13** and 1-chloro-4-(8-quinolyloxy)butane, which had been obtained by the reaction of 8-quinolinol with 4-chloro-1-butanol, following chlorination: a pale yellow glassy solid. ^1H NMR ($CDCl_3$) δ=1.28 (9H, s, $C(CH_3)_3$), 1.9—2.5 (6H, m, $OCH_2C\underline{H}_2CH_2O$ and $OCH_2C\underline{H}_2C\underline{H}_2$-$CH_2O$), 3.85—4.65 (8H, m, $OC\underline{H}_2CH_2C\underline{H}_2O$ and $OC\underline{H}_2$-$CH_2CH_2C\underline{H}_2O$), 6.85—7.65 (10H, m, aromatic), 8.0—8.3 (2H, m, aromatic), 9.00 (1H, m, aromatic), *ca.* 8—9 (1H, broad, COOH); IR (KBr): 3290 and 2500 (COOH), 1710 (C=O), 1600 and 1580 cm^{-1} (aromatic C=C) Found: C 72.11, H 7.05, N 2.43%. Calcd for $C_{33}H_{37}NO_6$: 72.91, H 6.86, N 2.58%.

1-[3-(o-Carboxyphenoxy)propoxy]-2-[2-(8-quinolyloxy)ethoxy]-4(or 5)-t-butylbenzene (9). The reaction mixture of 3.7 g (0.01 mol) of **13** and 1.2 g of *t*-BuOK in 50 ml of DMSO was stirred until it became homogeneous. To the solution was then added 3.0 g of 2-(2-chloroethoxy)tetrahydropyran, and the mixture was stirred at 70 °C for 90 h. The solution was then poured into water and extracted with benzene. The benzene layer was washed with water three times and dried with $MgSO_4$. After the removal of the benzene, 50 ml of EtOH and a few drops of conc. HCl were added to the residue and the mixture was stirred overnight at room temperature. After the removal of the ethanol, the residue was extracted with chloroform, washed with water, and dried with $MgSO_4$. After the removal of the chloroform, the residue was submitted to column chromatography on activated alumina with $CHCl_3$–EtOH (9:1) eluents to give 2.9 g (70%) of 1-[3-(*o*-ethoxycarbonylphenoxy)propoxy]-2-(2-hydroxyethoxy)-4(or 5)-*t*-butylbenzene as a colorless liqued.

To the solution of 2.8 g of 1-[3-(*o*-ethoxycarbonylphenoxy)-propoxy]-2-(2-hydroxyethoxy)-4(or 5)-*t*-butylbenzene and 0.60 g of pyridine in 30 ml of benzene was added 0.9 g of thionyl chloride, and the mixture was refluxed overnight. The benzene layer was washed with water and then with aqueous K_2CO_3, and dried with $MgSO_4$. After the removal of the benzene, the residue was submitted to column chromatography on activated alumina with a chloroform eluent to give 2.3 g (78%) of 1-[3-(*o*-ethoxycarbonylphenoxy)propoxy]-2-(2-chloroethoxy)-4(or 5)-*t*-butylbenzene as a colorless liquid.

The reaction mixture of 1.0 g of 8-quinolinol and 0.65 g of *t*-BuOK in 15 ml of DMSO was stirred until it became homogeneous. To the solution was then added 2.3 g of 1-[3-(*o*-ethoxycarbonylphenoxy)propoxyl-2-(2-chloroethoxy)-4(or 5)-*t*-butylbenzene, and the mixture was stirred at 70 °C for 4 h. After it had cooled to room temperature, 100 ml of benzene was added to the solution, and it was washed with water three times and dried with $MgSO_4$. After the removal of the benzene, the residue was submitted to column chromatography on activated alumina with a chloroform eluent to give 1.9 g (66%) of 1-[3-(*o*-ethoxycarbonylphenoxy)propoxy]-2-[2-(8-quinolyloxy]ethoxy]-4(or 5)-*t*-butylbenzene as a pale yellow liquid. The solution of 1.1 g of this ethyl ester and 0.5 g of KOH in 30 ml of ethanol was refluxed overnight. After the removal of the ethanol, water was poured into the residue, and the solution was slightly acidified with glacial acetic acid and extracted with chloroform two times. The chloroform layer was washed with water two times and dried with $MgSO_4$. After the removal of the chloroform, the residue was submitted to column chromatography on silica gel (300 mesh) with a chloroform eluent to give 0.8 g (80%) of **9**: a pale yellow glassy solid. ^1H NMR ($CDCl_3$) δ=1.28 (9H, s, $C(CH_3)_3$), 2.0—2.5 (2H, m, $OCH_2C\underline{H}_2CH_2O$), 4.25 (2H, t, $OC\underline{H}_2CH_2CH_2O$-$C_6H_4$(*o*-COOH)), 4.37 (2H, t, $OCH_2CH_2C\underline{H}_2O$-$C_6H_4$(*o*-COOH)), 4.63 (4H, s, $OC\underline{H}_2C\underline{H}_2O$), 6.8—7.65 (10H, m, aromatic), 8.0—8.3 (2H, m, aromatic), 8.3 (1H, broad, COOH), 9.03 (1H, m, aromatic); IR (KBr): 3260 and 2500 (COOH), 1705 (C=O), 1600 and 1580 cm^{-1} (atomatic C=C). Found: C 71.88, H 6.62, N 2.85%. Calcd for $C_{31}H_{33}NO_6$: C 72.21, H 6.45, N 2.71%.

1-[2-(o-Carboxyphenoxy)ethoxy]-2-[2-(8-quinolyloxy)ethoxy]-4(or 5)-t-butylbenzene (11). A procedure similar to that described above (Method 1 for **1**) was used for the preparation of **11**: a pale yellow glassy solid. ^1H NMR ($CDCl_3$) δ= 1.30 (9H, s, $C(CH_3)_3$), 4.43 (4H, s, $OC\underline{H}_2C\underline{H}_2O$-quinolyl), 4.65 (4H, m, $OC\underline{H}_2C\underline{H}_2O$-$C_6H_4$(*o*-COOH)), 6.7—7.7 (10H, m, aromatic), 7.9—8.3 (2H, m, aromatic), 9.07 (1H, m, aromatic), 10.07 (1H, broad, COOH); IR (KBr): 3280 and 2500 (COOH), 1730 and 1710 (C=O), 1605 and 1580 cm^{-1} (aromatic C=C). Found: C 71.88, H 6.49, N 2.76%. Calcd for $C_{30}H_{31}NO_6$: C 71.98, H 6.24, N 2.80%.

1-[3-(o-Carboxyphenoxy)propoxy]-2-[3-(8-quinolyloxy)-2-hydroxypropoxy]-4(or 5)-t-butylbenzene (12). The reaction mixture of 7.4 g 0.02 mol) of **13** and 2.3 g (0.02 mol) of *t*-BuOK in 30 ml of benzene was stirred at room temperature until it became homogeneous. After the removal of the benzene, 24 g of epichlorohydrin was added to the residue, and then the mixture was stirred at 70 °C for 19 h. After cooling to room temperature, the mixture was poured into water and extracted with benzene. The benzene layer was washed with water three times and dried with $MgSO_4$. After the removal of the benzene and excess epichlorohydrin under a vacuum, 7.9 g (93%) of the crude product, 1-[3-(*o*-ethoxycarbonylphenoxy)-propoxy]-2-glycidyl-4(or 5)-*t*-butylbenzene, was obtained. This product was used for the following reaction without further purification.

After the reaction mixture of 3.0 g (0.02 mol) of 8-quinolinol and 2.0 g (0.018 mol) of *t*-BuOK in 50 ml of dioxane had been stirred at 70 °C for 2 h, 7.5 g (0.018 mol) of 1-[3-(*o*-ethoxycarbonylphenoxy)propoxy]-2-glycidyl-4(or 5)-*t*-butylbenzene was added to it, and the mixture was stirred at 70 °C for 46 h. Then, after the removal of the dioxane, to the residue was added water and the solution was slightly acidified with glacial acetic acid and extracted with benzene. The benzene layer was washed with water three times and dried with $MgSO_4$. After the removal of the benzene, the residue was submitted to column chromatography on activated alumina with a chloroform eluent to give 5.6 g (53%) of 1-[3-(*o*-ethoxycarbonylphenoxy)propoxy]-2-[3-(8-quinolyloxy)-2-hydroxypropoxy]-4(or 5)-*t*-butylbenzene as a pale yellow liquid. The solution of 2.0 g of this ethyl ester and 1.0 g of KOH in 50 ml of ethanol was refluxed overnight. After the removal of the ethanol, water was poured into the residue, and the solution was slightly acidified with glacial acetic acid and extracted with chloroform. The chloroform layer was washed with water two times and dried with $MgSO_4$. After the removal of the chloroform, the residue was submitted to column chromatography on silica gel (300 mesh) with chloroform-ethanol (9:1) eluents to give 1.1 g (58%) of **12**: a pale yellow glassy solid. ^{1}H NMR ($CDCl_3$) δ=1.26 (9H, s, $C(CH_3)_3$), 2.0—2.6 (2H, m, $OCH_2C\underline{H}_2CH_2O$), 4.0—4.7 (9H, m, $OC\underline{H}_2$-$CH_2C\underline{H}_2O$ and $OC\underline{H}_2C\underline{H}(OH)C\underline{H}_2O$), 6.8—7.7 (12H, m, aromatic, $OCH_2CH(O\underline{H})CH_2O$, and $COO\underline{H}$), 7.94—8.40 (2H, m, aromatic), 9.06 (1H, m, aromatic); IR (KBr): 3450 (OH), 3290 and 2500 (COOH), 1720 (C=O), 1605 and 1580 cm^{-1} (aromatic C=C). Found: C 71.09, H 6.31, N 2.77%. Calcd for $C_{32}H_{35}HO_7$: C 70.44, H 6.47, N 2.57%.

General Procedure of Cation Transport. Reagents: Chloroform (extra-pure grade) was used without further purification. Each aqueous solution which was used in either the source or receiving phase was prepared by the dilution of one normal alkali hydroxide and/or one normal acid.

Procedure: A U-type glass tube as previously reported[7] was used for measuring the transport of the alkali-metal ions. In the first case (*cf.* Table 1 and Table 2), the same volumes of an aqueous solution which initially contained the same amounts of alkali-metal ions were used as both aqueous phases. First, 30 ml of chloroform containing 1.5×10^{-4} mol of a carrier was placed in the tube. Two kinds of the aqueous solution used for the source phase and the receiving phase were subsequently poured into both sides. The tube was then placed in a water bath whose temperature was kept at 25±0.2 °C. Each phase was agitated at 200 min^{-1} mechanically with a pair of glass stirrers.

In the second case (*cf.* Table 3), a large amount of the aqueous solution (115 ml) was used for the source phase, while 15 ml of a 0.05 M sulfuric acid solution was used for the receiving phase. As is shown in Fig. 4, the solution for the source phase was circulated by means of a circulating pump (circulating velocity, 2.5 ml/ min.). Under these conditions, the concentration of each cation in the receiving phase was confirmed to increase linearly with the running time (less than 2 d), and the apparent transport rates of cations were calculated.

The transport of alkali-metal ions was initiated by the addition of the aqueous solutions. At each time point, 50 μl of the solution was withdrawn from each aqueous phase, and the concentration of the cation was adjusted by using a measuring flask and determined by means of a Shimadzu AA-646 atomic absorption spectrometer. The transport of cations in the blank systems was negligible. The detailed conditions are shown in the tables.

References

1) Part VII: "Synthesis and Properties of Noncyclic Polyether Compounds." Part VI; K. Hiratani, H. Sugihara, K. Taguchi, and K. Iio, *Chem. Lett.*, **1983**, 1657.

2) W. Wierenga, "The Total Synthesis of Natural Products," ed by J. ApSimon, Wiley-Interscience, New York (1981), Vol. 4, p. 265.

3) "Host Guest Complex Chemistry, I and II," ed by F. Vögtle, Springer-Verlag, Berlin (1981(I) and 1982(II)); K. Nakashima, S. Nakatsuji, S. Akiyama, T. Kaneda, and S. Misumi, *Chem. Lett.*, **1982**, 1781.

4) K. Hiratani, *Chem. Lett.*, **1982**, 1021.

5) It has been reported that a neutral diglycolic diamide can be used as a carrier of an electrode with Li^+-selectivity: N. N. L. Kirsch, R. J. J. Funck, E. Pretsch, and W. Simon, *Helv. Chim. Acta*, **60**, 2326 (1977).

6) For example, Y. Kobuke, K. Hanji, K. Horiguchi, M. Asada,.Y. Nakayama, and J. Furukawa, *J. Amer. Chem. Soc.*, **98**, 7414 (1976); M. Kirch and J.-M. Lehn, *Angew. Chem. Int. Ed.Engl.*, **14**, 555 (1975); J. D. Lamb, R. M. Izatt, D. G. Garrick, J. S. Bradshaw, and J. J. Christensen,*J. Membr. Sci.*, **9**, 83 (1981).

7) K. Hiratani, I. Nozawa, T. Nakagawa, and S. Yamada,*J. Membr. Sci.*, **12**, 207 (1982).

8) During the reaction of 3-chloro-1-propanol with 7-allyl-8-quinolinol, the 7-allyl group on the quinoline ring changed to a 7-propenyl one as a result of the base used.

9) B. Tümmler, G. Maass, F. Vögtle, H. Sieger, U. Heimann, and E. Weber, *J. Amer. Chem. Soc.*, **101**, 2588 (1979).

10) H. Kuboniwa, K. Yamaguchi, A. Hirao, S. Nakahama, and N. Yamazaki, *Chem. Lett.*, **1982**, 1937.

11) Also in natural noncyclic polyethers, *e.g.*, monensin and nigericin, the periphery of the complex consists of lipophilic regions making the complex *exo*-lipophilic and thus soluble in lipophilic media: M. Dobler, "Ionophores and Their Structures," John Wiley&Sons, New York (1981), Chap. 7, pp. 77—120.

12) In the complex of 1,11-bis(2-methyl-8-quinolyloxy)-3,6,9-trioxaundecane with RbI, the polyether has been reported by X-ray structure analysis to display a herical configuration with both heterocycles stacked parallel to each other at 3.4 Å: G. Weber and W. Saenger, *Acta Crystallogr, Sect. B*, **35**, 1346 (1979).

 © 1984 The Chemical Society of Japan Bull. Chem. Soc. Jpn., 57, 1985—1989 (1984)

Crystal and Molecular Structure of 4-*t*-Butyl-5-cyano-2-phenyl-1-thioxo-7-thia-1-phosphabicyclo[2.2.1]hept-2-ene

Tokiko UCHIDA,* Kozo KOZAWA, Takao SAITO,† and Shinichi MOTOKI†

Department of Industrial and Engineering Chemistry, Faculty of Science and Technology, Science University of Tokyo, Noda, Chiba 278

†*Department of Chemistry, Faculty of Science, Science University of Tokyo, Kagurazaka, Shinjuku-ku, Tokyo 162*

(Received December 22, 1983)

The crystal and molecular structures of the title compound were determined by means of X-ray diffraction. Crystal data: $C_{16}H_{18}NS_2P$, M_r=319.4, triclinic, a=12.731(2), b=13.143(1), c=12.483(1) Å, α=102.39(1), β=104.34(1), γ=117.96(1)°, V=1648.6 Å^3, space group P$\bar{1}$, D_m=1.30, D_x=1.287 g cm^{-3}, Z=4, μ=4.02 cm^{-1} (Mo $K\alpha$). The structure was solved by the direct method and refined by the block-diagonal least-squares method to R=0.082 for 4495 observed reflections. The bond distances and angles are in good agreement with the ordinary values except for the P-S-C bridged angle of 82.5°. An asymmetric unit contains two crystallographically independent molecules, which are rotational isomers along the P-C bond.

The title compound (**3**) was formed by the reaction of acrylonitrile and 3,8-di-*t*-butyl-5,6-diphenyl-1-thioxo-2,9-dithia-1-phosphabicyclo[4.3.0]nona-3,7-diene (**2**) prepared from 4,4-dimethyl-1-phenyl-1-pentene-3-thione (**1**).[1,2] Compound **3** has a unique norbornene-like skeleton in which one of the sulfur atoms bridges between phosphorus and carbon atoms. The present study was performed to confirm the structure and establish the total geometry of the molecule.

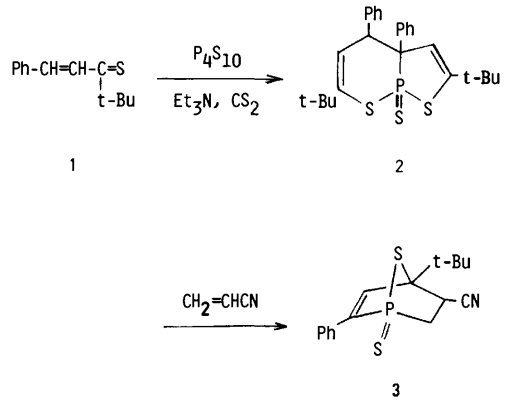

Experimental

The compound was prepared by the method described previously.[1] Colorless crystals were obtained by recrystallization from chloroform with a well-developed (112) face.

After determining preliminary cell constants and space group from Weissenberg photographs, a crytal with dimensions of 0.40×0.25×0.15 mm was mounted with the (112) face perpendicular to the ϕ axis on a Hilger & Watts diffractometer with Zr-filtered Mo$K\alpha$ radiation. Lattice constants were determined by a least-squares procedure for setting angles of 12 reflections with $16.5° < \theta < 21.4°$. The intensities were recorded with an θ-2θ step scan mode at every 0.01° of θ step up to $2\theta \leqq 55°$. The scan width of θ was 0.8° for all the reflections. Counting time was 1 s per step for peak measurements, and backgrounds were measured for 10 s at both ends of a scan.

Three standard reflections, monitored every 50 measurements, showed no significant change throughout the data collection. Of the 7545 independent reflections measured, 4495 with $F_o \geqq 3\sigma(F)$ were used for further calculations. Lorentz and polarization corrections were applied but no absorption correction was made. No systematical absent spectra was observed. Density was determined by the flotation method with K_2HgI_4 aqueous solution.

Crystal Data: $C_{16}H_{18}NS_2P$, M_r=319.4, triclinic, a=12.731(2), b=13.143(1), c=12.483(1) Å, α=102.39(1), β=104.34(1), γ=117.96(1)°, V=1648.6 Å^3, space group P$\bar{1}$, D_m=1.30, D_x=1.287 g cm^{-3}, Z=4, μ=4.02 cm^{-1} (Mo $K\alpha$).

Solution and Refinement of the Structure

The structure was solved by the direct method.[3] After several cycles of block-diagonal least-squares refinement, all the H atoms were located on the difference Fourier map. The final cycle was calculated with the anisotropic thermal parameters for non-H atoms, a fixed isotropic thermal parameter for H atoms, B=4.0 Å^2, and anomalous scattering factors for S and P atoms. The quantity minimized was $\sum w(|F_o|-|F_c|)^2$, where $w=[\sigma^2(F)+0.0011|F_o|^2]^{-1}$. In the final cycle, the maximum parameter shift/error was less than 0.07. Final R and R_w were 0.082 and 0.084, respectively. A final difference Fourier synthesis showed no significant features. The atomic scattering factors were adopted from "International Tables for X-ray Crystallography."[4] All the computations were carried out on a HITAC M-200H computer at the Computer Center of Tokyo University with the *UNICS* program system.[5]

Results and Discussion

The asymmetric unit contains two crystallographically independent molecules, hereafter referred to as molecule A and molecule B. Table 1 lists the final fractional coordinates and the equivalent thermal parameters.[6] The bond distances with the numbering scheme of atoms are given in Fig. 1, and the bond angles in Table 2. The bond distances and angles including P and S atoms almost agree with the literature values[7] except for the P-S(2)-C(3) angle. Differences between corresponding bond distances and bond angles in molecules A and B are not so significant. Figure 2 shows an *ORTEP* drawing of molecule A.[8] Each of two five-membered rings takes an envelope conformation, commonly possessing the P-S(2)-C(3) bridge. A

Table 1. The final fractional coordinates and equivalent isotropic thermal parameters
Estimated standard deviations are given in parentheses. The equivalent isotropic thermal parameters for non-hydrogen atoms are calculated using the expression: $B_{eq}=4/3\Sigma_i\Sigma_j\mathbf{a}_i\mathbf{a}_j\beta_{ij}$, where the $\mathbf{a}_i$'s are the unit cell edges in direct space. The isotropic thermal parameter of hydrogen atoms is fixed, $B=4.0$ Å^2.

Atom	x	y	z	B_{eq}/Å^2	Atom	x	y	z	B_{eq}/Å^2
Molecule A					Molecule B				
S(1)	0.6055(2)	0.4028(2)	0.4939(2)	6.3(1)	S(1)	1.0933(2)	0.3502(1)	−0.0343(2)	5.59(8)
S(2)	0.3256(2)	0.2740(2)	0.5516(1)	4.84(8)	S(2)	1.0084(1)	0.3933(1)	0.2047(1)	4.63(6)
P	0.5236(2)	0.3489(1)	0.5991(1)	4.09(7)	P	0.9594(1)	0.2978(1)	0.0264(1)	3.64(6)
N	0.5896(5)	0.4276(5)	1.0068(4)	5.2(2)	N	0.5170(4)	0.1198(4)	−0.0591(4)	5.2(2)
C(1)	0.5220(5)	0.2283(4)	0.6516(4)	3.1(2)	C(1)	0.8637(4)	0.1412(4)	0.0266(4)	3.1(2)
C(2)	0.4371(5)	0.1986(4)	0.7018(4)	3.1(2)	C(2)	0.8085(5)	0.1509(5)	0.1029(4)	3.4(2)
C(3)	0.3633(5)	0.2625(5)	0.7006(4)	3.5(2)	C(3)	0.8328(5)	0.2780(4)	0.1640(4)	3.6(2)
C(4)	0.4684(5)	0.4034(5)	0.7916(5)	4.1(3)	C(4)	0.7608(5)	0.3032(4)	0.0600(5)	3.5(2)
C(5)	0.5701(6)	0.4672(5)	0.7410(6)	5.0(3)	C(5)	0.8252(5)	0.3161(5)	−0.0308(5)	3.9(2)
C(61)	0.6063(5)	0.1817(5)	0.6489(4)	3.3(2)	C(61)	0.8329(5)	0.0254(4)	−0.0605(4)	3.2(2)
C(62)	0.7280(5)	0.2531(6)	0.6467(5)	4.6(3)	C(62)	0.9198(5)	0.0208(5)	−0.1077(5)	4.3(3)
C(63)	0.8059(6)	0.2062(7)	0.6488(6)	5.8(4)	C(63)	0.8880(6)	−0.0897(6)	−0.1879(5)	5.0(3)
C(64)	0.7643(7)	0.0900(7)	0.6507(6)	6.2(4)	C(64)	0.7688(7)	−0.1971(5)	−0.2259(6)	5.4(3)
C(65)	0.6440(6)	0.0182(6)	0.6507(5)	5.1(3)	C(65)	0.6809(6)	−0.1940(5)	−0.1800(6)	5.9(3)
C(66)	0.5649(5)	0.0641(5)	0.6508(5)	3.9(2)	C(66)	0.7115(5)	−0.0854(5)	−0.0990(5)	4.6(3)
C(7)	0.2364(5)	0.1938(6)	0.7207(5)	4.4(3)	C(7)	0.8030(6)	0.2964(6)	0.2788(5)	5.1(3)
C(71)	0.1526(6)	0.0569(6)	0.6291(6)	6.7(3)	C(71)	0.6561(7)	0.2087(6)	0.2450(6)	7.4(4)
C(72)	0.2645(6)	0.1964(6)	0.8479(5)	5.4(3)	C(72)	0.8833(8)	0.2698(8)	0.3698(6)	8.0(5)
C(73)	0.1578(7)	0.2519(8)	0.6989(7)	6.9(4)	C(73)	0.8434(7)	0.4306(6)	0.3361(6)	7.0(4)
C(8)	0.5350(5)	0.4143(5)	0.9128(5)	4.2(3)	C(8)	0.6216(5)	0.2000(5)	−0.0053(5)	3.9(3)
H(2)	0.433(5)	0.149(5)	0.751(5)		H(2)	0.745(5)	0.079(5)	0.111(5)	
H(4)	0.427(5)	0.445(5)	0.805(5)		H(4)	0.768(5)	0.384(5)	0.098(5)	
H(51)	0.578(6)	0.536(5)	0.732(5)		H(51)	0.858(6)	0.392(5)	−0.036(5)	
H(52)	0.661(6)	0.499(5)	0.801(5)		H(52)	0.769(5)	0.251(5)	−0.111(5)	
H(62)	0.755(5)	0.330(5)	0.648(5)		H(62)	1.001(5)	0.095(5)	−0.076(5)	
H(63)	0.881(5)	0.250(5)	0.638(5)		H(63)	0.948(5)	−0.090(5)	−0.221(5)	
H(64)	0.815(5)	0.054(5)	0.648(5)		H(64)	0.747(5)	−0.273(5)	−0.280(5)	
H(65)	0.609(5)	−0.070(5)	0.644(5)		H(65)	0.603(5)	−0.263(5)	−0.205(5)	
H(66)	0.477(5)	0.006(5)	0.641(5)		H(66)	0.651(5)	−0.081(5)	−0.073(5)	
H(71a)	0.134(5)	0.045(5)	0.548(5)		H(71a)	0.644(5)	0.135(5)	0.222(5)	
H(71b)	0.080(5)	0.025(5)	0.645(5)		H(71b)	0.645(5)	0.215(5)	0.313(5)	
H(71c)	0.194(5)	0.018(5)	0.647(5)		H(71c)	0.606(5)	0.235(5)	0.194(5)	
H(72a)	0.310(5)	0.158(5)	0.860(5)		H(72a)	0.832(5)	0.185(5)	0.336(5)	
H(72b)	0.190(5)	0.137(5)	0.860(5)		H(72b)	0.863(6)	0.276(5)	0.445(5)	
H(72c)	0.314(5)	0.289(5)	0.915(5)		H(72c)	0.984(5)	0.325(5)	0.388(5)	
H(73a)	0.084(5)	0.210(5)	0.716(5)		H(73a)	0.780(5)	0.441(5)	0.284(5)	
H(73b)	0.206(5)	0.334(5)	0.742(5)		H(73b)	0.831(5)	0.443(5)	0.399(5)	
H(73c)	0.129(5)	0.248(5)	0.618(5)		H(73c)	0.938(5)	0.482(5)	0.363(5)	

considerable decrease in bond angle is observed at the bridged S atom [P-S(2)-C(3) of average 82.5°], which indicates the steric strain about the bicyclo skeleton. Table 3 gives bond angles of bridged S atom in several bicyclo compounds,[9-12] though the value of the P-S-C bridge angle has not been reported other than in the present study. As expected, the more the number of ring atoms increases, the larger the bridge C-S-C angle changes.

Figure 3, the Newman projection along the P-C(1) bond, shows that the torsion angles of S(1)-P-C(1)-C(61) are appreciably different for molecule A and molecule B. The conformational difference between molecules A and B is obviously illustrated in Fig. 4, which is the projection of phenyl group and its neighboring atoms onto the plane perpendicular to the C(1)=C(2) double bond. Although the S(1)···H(62) and H(2)···H(66) separations keep the van der Waals distances, their relative orientations are distinct from one another in the two molecules. In other words, molecule A and molecule B are rotational isomers to each other, because the C(1)-C(61) bond is kept from free rotation by the steric hindrance of ortho hydrogens, H(62) and H(66).

Planarity of the plane defined by atoms around the C(1)=C(2) double bond [C(1), C(2), C(3), C(61) and P] is

not so good: the maximum deviation from the least-squares plane reaches to 0.09 Å of C(1) in molecule B.[6] That is because of the strain of bicyclo skeleton and the overcrowding effect of bulky substituents, namely *t*-

Table 2. Bond angles of molecule A and molecule B with their estimated standard deviations in parentheses

Bond angle	ϕ/°	
	Melecule A	Molecule B
P-S(2)-C(3)	82.3(2)	82.6(2)
S(1)-P-S(2)	121.3(1)	118.6(1)
S(1)-P-C(1)	123.4(2)	124.9(2)
S(1)-P-C(5)	118.2(3)	119.2(2)
S(2)-P-C(1)	94.7(2)	95.5(2)
S(2)-P-C(5)	93.0(3)	94.4(2)
C(1)-P-C(5)	99.7(3)	97.8(3)
P-C(1)-C(2)	106.5(4)	106.6(4)
P-C(1)-C(61)	127.0(5)	124.9(4)
C(2)-C(1)-C(61)	126.3(6)	127.2(5)
C(1)-C(2)-C(3)	118.2(5)	117.9(5)
C(2)-C(3)-C(4)	105.3(5)	105.1(5)
C(2)-C(3)-S(2)	105.6(4)	105.3(4)
C(2)-C(3)-C(7)	114.9(5)	116.1(5)
S(2)-C(3)-C(4)	103.7(4)	103.3(4)
S(2)-C(3)-C(7)	110.2(4)	109.5(4)
C(4)-C(3)-C(7)	116.1(5)	116.3(5)
C(3)-C(4)-C(5)	109.1(5)	110.5(5)
C(3)-C(4)-C(8)	113.0(5)	111.2(5)
C(5)-C(4)-C(8)	109.5(6)	108.5(5)
C(4)-C(8)-N	177.3(7)	176.9(7)
C(4)-C(5)-P	106.7(5)	105.5(4)
C(1)-C(61)-C(62)	121.9(6)	122.8(6)
C(1)-C(61)-C(66)	119.0(6)	119.4(5)
C(61)-C(62)-C(63)	119.5(7)	121.0(6)
C(62)-C(63)-C(64)	121.1(8)	120.8(7)
C(63)-C(64)-C(65)	119.8(8)	118.9(8)
C(64)-C(65)-C(66)	120.2(7)	121.1(7)
C(65)-C(66)-C(61)	120.4(6)	120.4(6)
C(66)-C(61)-C(62)	119.0(6)	117.8(6)
C(3)-C(7)-C(71)	107.7(6)	110.2(6)
C(3)-C(7)-C(72)	111.9(6)	108.5(6)
C(3)-C(7)-C(73)	111.6(6)	110.0(6)
C(71)-C(7)-C(72)	109.7(6)	111.2(7)
C(71)-C(7)-C(73)	108.1(7)	108.6(7)
C(72)-C(7)-C(73)	107.9(7)	108.4(7)

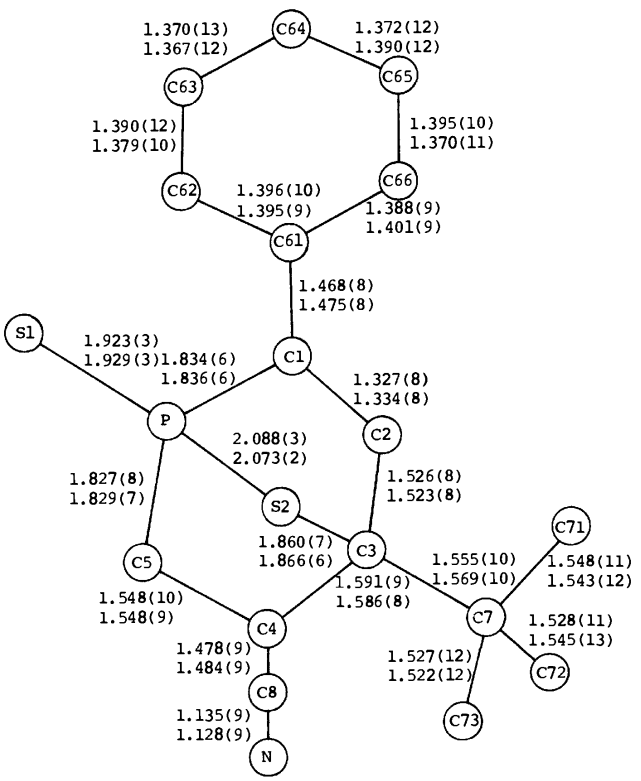

Fig. 1. Atom numbering and bond distances (Å) of molecule A (upper values) and molecule B (lower values). E.s.d.'s are in parentheses.

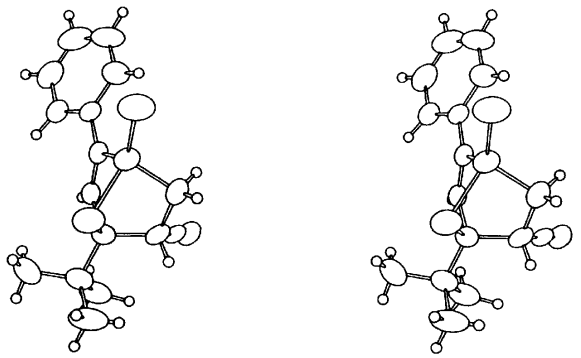

Fig. 2. Stereoscopic view of the molecule A. The thermal ellipsoids for non-H atoms are at the 50 % probability level, while H atoms are represented by spheres of arbitrary radius.

Table 3. Bond angle of bridged S atom in several bicyclo compounds

Bond	Angle ϕ/°	Skeleton of compound	Reference
P-S-C	82.5(2)[a]	7-Thia-1-phosphabicyclo[2.2.1]hept-2-ene	This work
C-S-C	81.4(1)	7-Thiabicyclo[2.2.1]hept-5-en-2-one	9
C-S-C	81.2(1)	7-Thiabicyclo[2.2.1]hepta-2,5-diene	10
C-S-C	84.9	8-Thia-2-azabicyclo[3.2.1]oct-3-ene	11
C-S-C	94.6(6)	9-Thiabicyclo[3.3.1]nonane-2,6-dione	12

a) Average value of molecule A and molecule B.

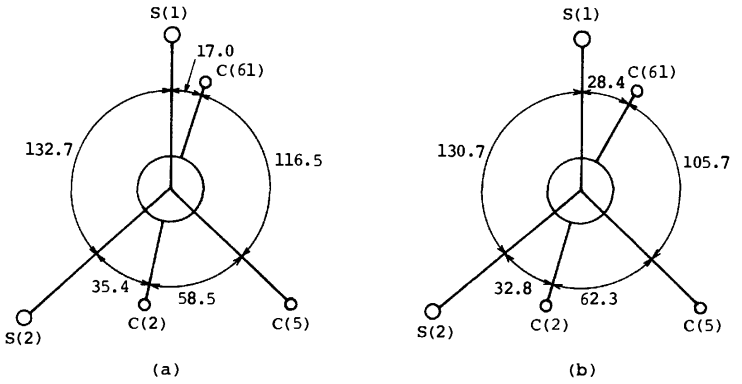

Fig. 3. Newman projections along the P-C(1) bond with torsion angles (°). (a) Molecule A, and (b) molecule B.

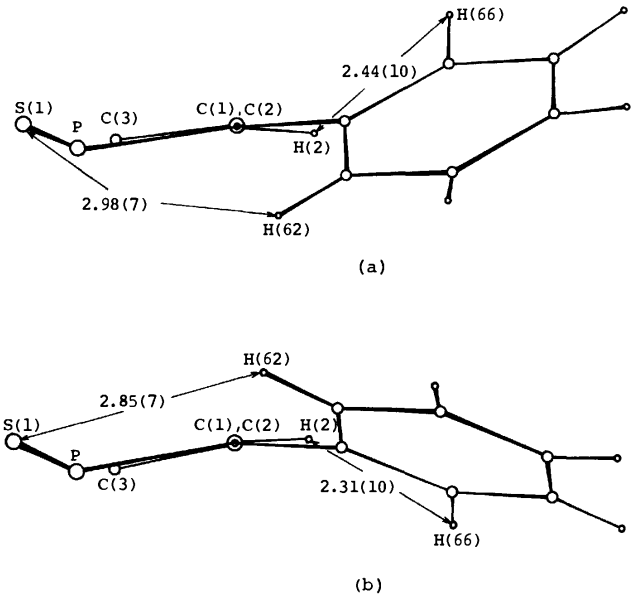

Fig. 4. Projections of several atoms along the C(1)=C(2) bond with several atomic distances (Å). (a) Molecule A, and (b) molecule B.

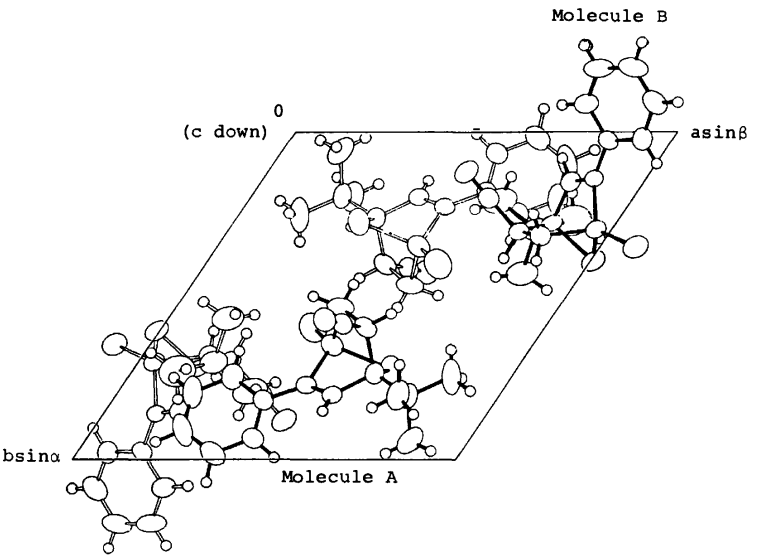

Fig. 5. The crystal structure projected along the *c* axis. The thermal ellipsoids for non-H atoms are at the 50% probability level, while H atoms are represented by spheres of arbitrary radius.

butyl and phenyl groups. Similar effects were observed in several substituted ethylenes, in which the ethylenic C=C double bonds were twisted owing to the steric interactions.[13] The dihedral angles between the above-mentioned plane and phenyl group, that composes a faily good plane, are 26.9° and −29.6° for molecule A and molecule B, respectively.[6] Figure 5 shows the packing arrangement of the molecules in a unit cell.[8] There is no particular interaction, for example hydrogen bonding between molecules, since all the intermolecular atomic distances are considered to be van der Waals contacts.

The authors express their hearty thanks to Mr. Hiroshi Taguchi for his technical assistance.

References

1) H. Yamaguchi, S. Kametani, T. Karakusa, T. Saito, and S. Motoki, *Tetrahedron Lett.*, **23**, 1263 (1982).

2) T. Uchida, K. Kozawa, T. Saito, and S. Motoki, *Bull. Chem. Soc. Jpn.*, **57**, 1990 (1984).

3) P. Main, S. E. Hull, L. Lessinger, G. Germain, J. P. Declercq, and M. M. Woolfson, *MULTAN* 78. "A system of Computer Programs for the Automatic Solution of Crystal Structures from X-ray Diffraction Data," University of York, England (1978).

4) "International Tables for X-Ray Crystallography," The Kynoch Press, Birmingham (1974), Vol. IV.

5) "Universal Crystallographic Computation Program System," ed by T. Sakurai, Crystallographic Society of Japan, Tokyo (1967).

6) Tables of structure factors, anisotropic temperature parameters, and least-squares planes, have been deposited at the office of the Chemical Society of Japan (Document No. 8423).

7) A. Grand, J. B. Robert, and A. Filhol, *Acta Crystallogr. Sect. B*, **33**, 1526 (1977); J. Martin and J. B. Robert, *ibid.*, **35**, 1623 (1979); Z. Galdecki, *ibid.*, **36**, 2807 (1980).

8) C. K. Johnson, *ORTEP*. "Oak Ridge Thermal Ellipsoid Plot Program," ORNL-3794, Oak Ridge National Laboratory, Oak Ridge, Tenessee, U. S. A. (1965).

9) R. K. Murray, Jr., J. S. Polley, S. S. Abdel-Meguid, and V. W. Day, *J. Org. Chem.*, **42**, 2127 (1977).

10) S. K. Obendorf, M. E. Leonowicz, and R. E. Hughes, *Acta Crystallogr., Sect. B*, **32**, 718 (1976).

11) J. L. Flippen, *Acta Crystallogr. Sect. B*, **28**, 1519 (1972).

12) M. J. Bovill, P. J. Cox, H. P. Flitman, M. H. P. Guy, A. D. U. Hardy, P. H. McCabe, M. A. Macdonald, G. A. Sim, and D. N. J. White, *Acta Crystallogr. Sect. B*, **35**, 669 (1979).

13) D. Adhikesavalu and K. Venkatesan, *Acta Crystallogr. Sect. B*, **37**, 2048 (1981); *ibid., Sect. C*, **39**, 589 (1983).

Crystal and Molecular Structure of 3,8-Di-*t*-butyl-5,6-diphenyl-1-thioxo-2,9-dithia-1-phosphabicyclo[4.3.0]nona-3,7-diene

Tokiko UCHIDA,* Kozo KOZAWA, Takao SAITO,† and Shinichi MOTOKI†

Department of Industrial and Engineering Chemistry, Faculty of Science and Technology, Science University of Tokyo, Noda, Chiba 278

†*Department of Chemistry, Faculty of Science, Science University of Tokyo, Kagurazaka, Shinjuku-ku, Tokyo 162*

(Received December 22, 1983)

The crystal and molecular structures of the title compound were determined by means of X-ray diffraction. Crystal data: $C_{26}H_{31}S_3P$, M_r=470.68, orthorhombic, a=17.116(4), b=19.798(4), c=14.898(3) Å, V=5048.4 Å^3 (21 °C), space group Pbca, D_m=1.23, D_x=1.239 g cm^{-3}, Z=8, μ=3.58 cm^{-1} (Mo $K\alpha$). The structure was solved by the direct method and refined by the full-matrix least-squares method to R=0.083 for 3318 observed reflections. The bicyclo skeleton is so highly strained that abnormal bond distances [P-C of 1.895(5) and C-C of 1.594(6) Å] were observed. Conformation of six-membered ring is a boat-form.

Previously, we found that treatment of α,β-unsaturated thioketones (**1**) with P_4S_{10} gave 1-thioxo-2,9-dithia-1-phosphabicyclo[4.3.0]nona-3,7-dienes (**2**).[1,2] They possess a characteristic heterocyclic skeleton, and are useful starting materials of the synthesis of various new heterocycles. The X-ray analysis of the title compound (**3**) has been performed to confirm its exact structure, since the arrangement of phosphorus and sulfur atoms in the molecule are difficult to elucidate by spectroscopic methods (IR, ^{1}H-, and ^{13}C-NMR spectra).

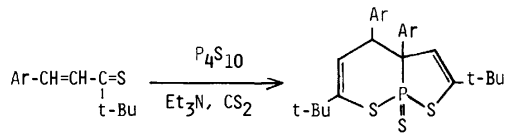

1 **2**

3 : Ar = Ph

Experimental

The synthesis of the compound was described previously.[1] Crystals were obtained from chloroform as colorless hexagonal platelets with a well-developed(010) cleavage plane.

After determining preliminary cell parameters and space group from Weissenberg photographs, a crystal with dimensions of 0.35×0.40×0.50 mm was mounted with the c axis parallel to the ϕ-axis on a Hilger & Watts diffractometer. Lattice parameters were determined by a least-squares procedure with setting angles of 12 reflections with $20.9°<\theta<25.9°$ (Zr-filtered Mo $K\alpha$ radiation, λ=0.7107 Å). The intensities were recorded with a θ-2θ step scan mode at every 0.02° of θ step up to $2\theta\leq55°$. The scan width of θ was 0.8° for all the reflections. Counting time was 1 s count at each 40 steps of 0.04° in 2θ, background count of 5 s at each end of the scan range. Three standard reflections, (040, 021, and 210) monitored every 50 measurements, showed changes within ±3% of $|F|$'s throughout the data collection. Of the 6408 independent reflections measured, 3320 with $F_o\geq3\sigma(F)$ were used for further calculations. Lorentz and polarization corrections were applied as usual, but the absorption correction was not made. Density was observed by the flotation method with K_2HgI_4 aqueous solution.

Crystal Data: $C_{26}H_{31}S_3P$, M_r=470.68, orthorhombic, a=17.116(4), b=19.798(4), c=14.898(3) Å, V=5048.4 Å^3 (21 °C); absent spectra: $0kl$ k odd, $h0l$ l odd, $hk0$ h odd; Space group Pbca; D_m=1.23, D_x=1.239 g cm^{-3}; Z=8; μ=3.58 cm^{-1} (Mo $K\alpha$).

Solution and Refinement of the Structure

The structure was solved by the direct method.[3] After several cycles of block-diagonal least-squares refinement, 19 H atoms were located on a difference Fourier map. The next cycles with anisotropic non-H atoms and isotropic 19 H atoms reduced R to 0.090. Then, difference Fourier map revealed the remaining 12 H atoms. The final refinement was carried out with the full-matrix least-squares with the anisotropic thermal parameters for non-H atoms, a fixed isotropic thermal parameter for H atoms, B=4.0 Å^2, and anomalous dispersion corrections for S and P atoms. The quantity minimized was $\sum w(|F_o|-|F_c|)^2$, where $w=[\sigma^2(F_o)]^{-1}$ and $\sigma(F_o)$ is the standard deviation in the observed amplitudes based on counting statistics.

In the final cycle, the maximum parameter shft/error was less than 0.5. Final R and $R_w=[\sum w(|F_o|-|F_c|)^2/\sum w|F_o|^2]^{1/2}$ were 0.083 and 0.038, respectively, where two reflections (040 and 021) were given zero weight because they were seriously affected by extinction. A final difference synthesis showed no significant feature. The atomic scattering factors with anomalous corrections were adopted from "International Tables for X-ray Crystallography."[4] All the computations were performed on a HITAC M-200H computer at the Compurter Center of Tokyo University with the *UNICS* program system.[5]

Discussion

The final atomic coordinates and equivalent temperature parameters are listed in Table 1. The numbering scheme is given in Fig. 1 with the bond distances, and Table 2 shows the bond angles.[6] Figure 2 gives the stereoscopic view of the molecule drawn by *ORTEP*.[7]

The bicyclo skeleton has a shallow envelope thiaphosphacyclopentene ring and a boat-form thiaphosphacyclohexene ring, which are cis-fused together with the bridging P-C(4) bond that is the side of the boat of the six-membered ring.

The molecule possesses three stereochemically char-

TABLE 1. THE FINAL FRACTIONAL COORDINATES AND EQUIVALENT ISOTROPIC THERMAL PARAMETERS

Estimated standard deviations are given in parentheses. The equivalent isotropic thermal parameters for non-hydrogen atoms are calculated using the expression: $B_{eq}=4/3\sum_i\sum_j \mathbf{a}_i\mathbf{a}_j\beta_{ij}$, where the $\mathbf{a}_i$'s are the unit cell edges in direct space. The isotropic thermal parameter of hydrogen atoms is fixed, $B=4.0$ Å^2.

Atom	x	y	z	B_{eq}/Å^2	Atom	x	y	z
P	0.10993(7)	0.37035(7)	0.30978(9)	3.35(8)	H(2)	0.158(3)	0.343(3)	0.566(3)
S(1)	0.18690(8)	0.43856(7)	0.37048(9)	3.73(8)	H(3)	0.059(3)	0.430(2)	0.488(3)
S(2)	0.16903(8)	0.27822(7)	0.29822(9)	4.23(9)	H(32)	−0.062(3)	0.435(2)	0.556(3)
S(3)	0.07438(8)	0.40783(8)	0.19788(9)	5.4(1)	H(33)	−0.148(3)	0.406(2)	0.665(3)
C(1)	0.2085(3)	0.3920(2)	0.4710(3)	2.9(3)	H(34)	−0.130(3)	0.297(2)	0.739(3)
C(2)	0.1492(3)	0.3649(2)	0.5157(3)	2.9(3)	H(35)	−0.028(3)	0.230(2)	0.705(3)
C(3)	0.0639(3)	0.3775(2)	0.4924(3)	2.7(3)	H(36)	0.057(3)	0.266(3)	0.596(3)
C(4)	0.0376(3)	0.3443(2)	0.3997(3)	2.7(3)	H(42)	−0.098(3)	0.280(2)	0.384(3)
C(5)	0.0442(3)	0.2688(2)	0.4062(3)	2.9(3)	H(43)	−0.224(3)	0.317(3)	0.354(3)
C(6)	0.1006(3)	0.2345(2)	0.3694(3)	3.0(3)	H(44)	−0.244(3)	0.440(3)	0.339(3)
C(7)	0.2950(3)	0.3875(3)	0.4946(4)	3.6(3)	H(45)	−0.135(3)	0.510(2)	0.347(3)
C(8)	0.3301(4)	0.4579(4)	0.4963(6)	7.4(5)	H(46)	−0.012(3)	0.472(2)	0.369(3)
C(9)	0.3384(4)	0.3442(5)	0.4268(6)	7.9(6)	H(5)	0.003(3)	0.249(3)	0.445(3)
C(10)	0.3055(4)	0.3559(5)	0.5858(6)	8.5(6)	H(81)	0.387(3)	0.457(3)	0.507(3)
C(11)	0.1202(3)	0.1594(3)	0.3842(3)	3.6(3)	H(82)	0.298(3)	0.475(3)	0.551(3)
C(12)	0.0500(4)	0.1237(3)	0.4251(5)	5.8(4)	H(83)	0.331(3)	0.472(3)	0.433(3)
C(13)	0.1431(4)	0.1250(3)	0.2957(5)	6.7(5)	H(91)	0.339(4)	0.367(3)	0.373(3)
C(14)	0.1892(4)	0.1556(3)	0.4498(5)	5.6(4)	H(92)	0.322(3)	0.300(3)	0.447(4)
C(31)	0.0089(3)	0.3553(2)	0.5673(3)	2.5(3)	H(93)	0.393(3)	0.348(3)	0.442(3)
C(32)	−0.0533(3)	0.3961(3)	0.5905(3)	3.5(3)	H(101)	0.360(3)	0.365(3)	0.606(3)
C(33)	−0.1056(3)	0.3758(3)	0.6561(4)	4.4(4)	H(102)	0.287(3)	0.315(3)	0.592(4)
C(34)	−0.0977(3)	0.3145(3)	0.6974(4)	4.5(4)	H(103)	0.280(3)	0.389(3)	0.632(3)
C(35)	−0.0354(3)	0.2730(3)	0.6759(3)	3.6(3)	H(121)	0.060(3)	0.076(2)	0.433(3)
C(36)	0.0180(3)	0.2933(3)	0.6111(3)	3.2(3)	H(122)	0.000(3)	0.130(3)	0.380(3)
C(41)	−0.0434(3)	0.3699(2)	0.3761(3)	3.0(3)	H(123)	0.033(3)	0.140(3)	0.492(3)
C(42)	−0.1063(3)	0.3269(3)	0.3705(3)	3.5(3)	H(131)	0.152(3)	0.075(2)	0.315(3)
C(43)	−0.1811(4)	0.3514(3)	0.3555(4)	4.8(4)	H(132)	0.193(3)	0.143(3)	0.267(4)
C(44)	−0.1942(3)	0.4195(4)	0.3465(4)	5.1(4)	H(133)	0.085(3)	0.120(2)	0.264(3)
C(45)	−0.1315(4)	0.4631(3)	0.3507(4)	4.8(4)	H(141)	0.241(3)	0.184(3)	0.428(3)
C(46)	−0.0561(3)	0.4386(3)	0.3654(4)	4.0(3)	H(142)	0.208(3)	0.108(2)	0.469(3)
					H(143)	0.171(3)	0.175(3)	0.512(3)

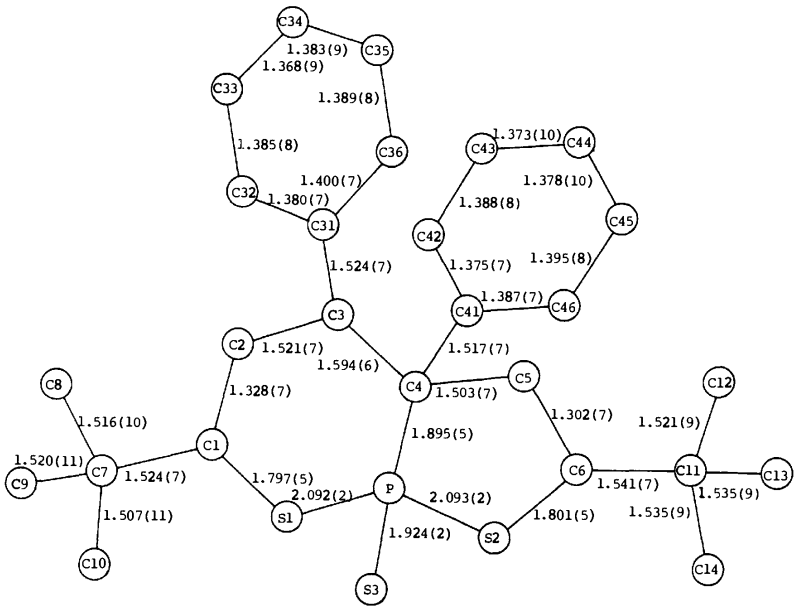

Fig. 1. Atom numbering and bond distaces (Å) of **3**. E.s.d.'s are in parentheses.

acteristic features. (i) The conformation of six-membered ring is a boat-form, as mentioned above. (ii) Several abnormal bond distances and bond angles are observed about the bridgehead P and C(4) atoms. The C(3)-C(4) bond distance of 1.594(6) Å is apparently longer than the commonly accepted C-C bond distance, and the observed P-C(4) bond distance of 1.895 (5)Å is longer than the average P-C bond distance of 1.832(7) Å in 4-*t*-butyl-5-cyano-2-phenyl-1-thioxo-7-thia-1-phosphabicyclo[2.2.1]hept-2-ene,[2] which was synthesized by using **3** as the starting material.[1] (iii) Though C(3) is a chiral atom, the conformational isomer has not been found in the present study.

These features can be elucidated by positing the existence of two double bonds in the ring system and the four bulky substituents, especially two neighboring phenyl groups. *cis*-8-Azabicyclo[4.3.0]non-3-ene methiodide[8] possesses a boat-form cyclohexene ring, which consists of six ring carbon atoms with no substituents except for hydrogen atoms. It has a similar bicyclo skeleton to that of **3** and has no abnormal bond distances in the ring system. So, if both bridgehead atoms are tetrahedrally bonded, the most stable conformation of *cis*-fused bicyclo[4.3.0]non-3-ene ring must be a boat-form. In the case of the present compound (**3**), moreover, the second ethylenic group in the five-membered ring, makes the *trans*-fusing of two rings impossible. The elongation of P-C(4) and C(3)-C(4) bonds are due to the strain caused by the neighboring phenyl groups: such a situation is often observed in fused ring systems with bulky substituents.[9] The phenyl group attached to the C(3) takes a position eclipsed to the H(2), while it is staggered (gauche) to the other phenyl group attached to

Table 2. The bond angles with their e.s.d.'s in parentheses

Bond angle	ϕ/°	Bond angle	ϕ/°
S(1)-P-S(2)	107.08(8)	C(1)-C(7)-C(10)	110.4(5)
S(1)-P-S(3)	108.95(9)	C(8)-C(7)-C(9)	109.6(6)
S(1)-P-C(4)	106.3(2)	C(8)-C(7)-C(10)	108.6(6)
S(2)-P-S(3)	114.70(9)	C(9)-C(7)-C(10)	107.8(6)
S(2)-P-C(4)	97.9(2)	C(6)-C(11)-C(12)	109.5(5)
S(3)-P-C(4)	120.7(2)	C(6)-C(11)-C(13)	111.1(5)
P-S(1)-C(1)	99.2(2)	C(6)-C(11)-C(14)	107.8(4)
S(1)-C(1)-C(2)	117.9(4)	C(12)-C(11)-C(13)	109.9(5)
S(1)-C(1)-C(7)	115.0(3)	C(12)-C(11)-C(14)	109.3(5)
C(7)-C(1)-C(2)	127.1(5)	C(13)-C(11)-C(14)	109.1(5)
C(1)-C(2)-C(3)	123.6(5)	C(3)-C(31)-C(32)	119.5(4)
C(2)-C(3)-C(4)	113.7(4)	C(3)-C(31)-C(36)	121.7(4)
C(2)-C(3)-C(31)	112.2(4)	C(31)-C(32)-C(33)	120.4(5)
C(4)-C(3)-C(31)	110.0(4)	C(32)-C(33)-C(34)	120.7(6)
C(3)-C(4)-P	108.4(3)	C(33)-C(34)-C(35)	119.9(6)
C(3)-C(4)-C(41)	108.8(4)	C(34)-C(35)-C(36)	119.8(5)
P-C(4)-C(41)	110.0(3)	C(35)-C(36)-C(31)	120.3(5)
C(3)-C(4)-C(5)	109.4(4)	C(36)-C(31)-C(32)	118.8(5)
P-C(4)-C(3)	108.4(3)	C(4)-C(41)-C(42)	121.5(4)
P-C(4)-C(5)	105.5(3)	C(4)-C(41)-C(46)	119.9(4)
C(4)-C(5)-C(6)	123.2(5)	C(41)-C(42)-C(43)	121.0(5)
C(5)-C(6)-S(2)	118.7(4)	C(42)-C(43)-C(44)	120.6(6)
C(5)-C(6)-C(11)	127.2(5)	C(43)-C(44)-C(45)	119.0(7)
C(11)-C(6)-S(2)	114.0(3)	C(44)-C(45)-C(46)	120.6(6)
P-S(2)-C(6)	93.2(2)	C(45)-C(46)-C(41)	120.3(5)
C(1)-C(7)-C(8)	109.5(5)	C(46)-C(41)-C(42)	118.5(5)
C(1)-C(7)-C(9)	110.8(5)		

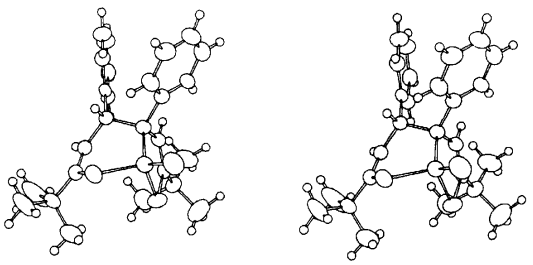

Fig. 2. Stereoscopic view of molecule **3**. The thermal ellipsoids for non-H atoms are at the 50 % probability level, while H atoms are represented by spheres of arbitrary radius.

Table 3. Torsion angles about six-membered ring

Bond	Angle θ/°
P-S(1)-C(1)-C(2)	46.5
S(1)-C(1)-C(2)-C(3)	7.0
C(1)-C(2)-C(3)-C(4)	68.9
C(2)-C(3)-C(4)-P	50.9
C(3)-C(4)-P-S(1)	5.0
C(4)-P-S(1)-C(1)	47.6
C(31)-C(3)-C(4)-C(41)	62.7
C(41)-C(4)-C(3)-H(3)	54.2
C(31)-C(3)-C(2)-H(2)	5.5

Table 4. Deviations of atoms from least-squares planes (l/Å)

Plane E1:	$0.0496X-0.8442Y-0.5337Z+10.1282=0$			
	S (1)	0.01	C (3)	−0.04
	C (1)	0.01	C (7)	−0.03
	C (2)	0.06		
Plane E2:	$-0.5988X-0.1855Y-0.7791Z+6.2238=0$			
	S (2)	0.01	C (6)	0.04
	C (4)	−0.07	C (11)	−0.05
	C (5)	0.07	P*	0.14
Plane P1:	$-0.5585X-0.4365Y-0.7054Z+9.1227=0$			
	C (31)	0.005	C (35)	−0.001
	C (32)	0.003	C (36)	−0.006
	C (33)	−0.011	C (3)*	0.075
Plane P2:	$0.1363X-0.0855Y-0.9870Z+6.2504=0$			
	C (41)	−0.007	C (45)	0.003
	C (42)	0.001	C (46)	0.005
	C (43)	0.006	C (4)*	−0.122
	C (44)	−0.008		

Average e.s.d.'s are 0.04 Å for Planes E1 and E2, and 0.007 Å for Planes P1 and P2. Orthogonal coordinates X, Y, and Z (Å) are parallel to the crystal axes a, b and c.

Atoms marked with asterisk were excluded from the calculations.

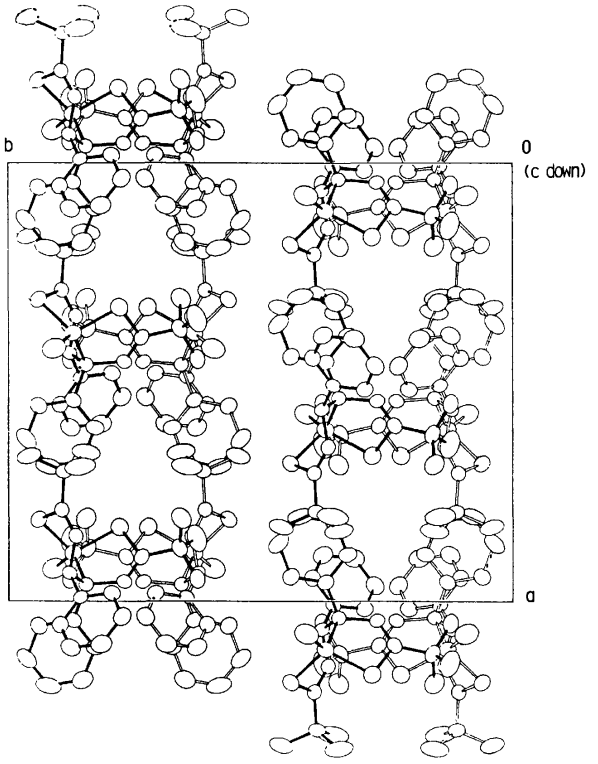

Fig. 3. Crystal structure of **3** projected along the *c* axis. The thermal ellipsoids for non-H atoms are at the 50% probability level. H atoms are omitted.

the C(4). Since this stereochemical feature gives the minimum Pitzer strain, the formation of a conformational isomer about C(3) must be difficult. Several torsion angles related to the six-membered ring are listed in Table 3.

The two ethylenic groups and the two phenyl groups each form fairly good planes. Table 4 gives their least-squares planes with deviations of atoms from them. The dihedral angles between the planes are as follows: E1-P1, 44.2°; E2-P2, 45.3°, and P1-P2, 48.9°.

The crystal structure of **3** is shown in Fig. 3.[7] There are no special interactions between the molecules, since all the intermolecular atomic distances are considered to be van der Waals contacts.

References

1) H. Yamaguchi, S. Kametani, T. Karakusa, T. Saito, and S. Motoki, *Tetrahedron Lett.*, **23**, 1263 (1982).

2) T. Uchida, K. Kozawa, T. Saito, and S. Motoki, *Bull. Chem. Soc. Jpn.*, **57**, 1985 (1984).

3) P. Main, S. E. Hull, L. Lessinger, G. Germain, J. P. Declercq, and M. M. Woolfson, *MULTAN* 78. "A System of Computer Programs for the Automatic Solution of Crystal Structures from X-ray Diffraction Data," University of York, England (1978).

4) "International Tables for X-Ray Crystallography," The Kynoch Press, Birmingham (1974), Vol. IV.

5) "Universal Crystallographic Computation Program System," ed by T. Sakurai, Crystallographic Society of Japan, Tokyo (1967).

6) Tables of structure factors and anisotropic temperature parameters have been deposited in the office of the Chemical Society of Japan (Document No. 8424).

7) C. K. Johnson, *ORTEP*. "Oak Ridge Thermal Ellipsoid Plot Program," ORNL-3794, Oak Ridge National Laboratory, Oak Ridge, Tennessee, U. S. A. (1965).

8) G. D. Smith, R. D. Otzenberger, B. P. Mundy, and C. N. Caughlan, *J. Org. Chem.*, **39**, 321 (1974).

9) A. Dondoni, A. Medici, and C. Venturoli, *J. Org. Chem.*, **45**, 621 (1980); K. Go and G. Kartha, *Acta Crystallogr., Sect. C*, **39**, 376 (1983).

A Convenient Method for the Regioselective Synthesis of 4-Alkyl(aryl)pyridines Using Pyridinium Salts

Kin-ya AKIBA,* Yūji ISEKI, and Makoto WADA
Department of Chemistry, Faculty of Science, Hiroshima University, Higashisenda-machi, Hiroshima 730
(Received December 24, 1983)

$RCu \cdot BF_3$ reacted with 1-ethoxycarbonylpyridinium chloride at the 4-position with almost complete regioselectivity (>99%) to afford the corresponding 1,4-dihydropyridine derivatives in high yields (81—94%). The dihydropyridines were oxidized by oxygen to give 4-alkyl(aryl)pyridines (38—68%). Grignard reagents also reacted with 1-*t*-butyldimethylsilylpyridinium triflate with almost complete regioselectivity (>99%) to afford the corresponding 1,4-dihydropyridines, which were easily oxidized by oxygen to give 4-substituted pyridines in higher yields than above (58—70%).

Considerable efforts have been directed at the introduction of substituents directly onto pyridine using organometallic reagents.[1] Organolithiums were shown to add to the 2-position selectively in high yields[2] and Grignard reagents to the 2- and 4-positions under forceful conditions in low yields.[3] 2-Lithio-1,3-dithiane adds to the 4-position and 4-formylpyridine is obtained after hydrolysis and air-oxidation.[4] However, it is necessary to activate pyridine as the pyridinium salt for facile reaction with organometalloids. Grignard and organocadmium reagents afford 2-substituted 1-acyl-1,2-dihydropyridines in good yields under mild conditions.[5]

Lithium dialkylcuprate (I) is the only organometallic reagent known which adds to the 4-position of a pyridinium salt predominantly,[6] but one half of the alkyl group of the reagent is inevitably wasted. Therefore, it still remains to devise some pertinent method to introduce substituents selectively into the 4-position of pyridine. Recently, Katritzky and co-workers challenged this problem successfully and reported the synthesis of 4-substituted pyridines in good yields starting with 1-(2,6-dimethyl-4-oxo-1,4-dihydro-1-pyridyl)pyridinium salt (**1**), where the 2,6-positions of the pyridinium moiety is sterically shielded.[7]

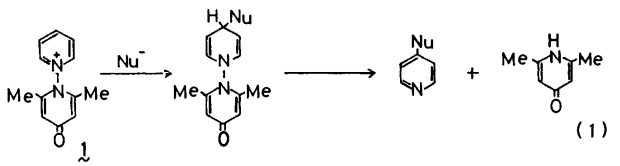

(1)

In order to circumvent the preparation of the special starting material **1** and to start with pyridine itself, we investigated successfully the following two methods (Scheme 1) with the objective to, *i.e.*, i) use softer and maybe bulkier nucleophiles to increase the regioselectivity of attack at the 4-position of 1-ethoxycarbonylpyridinium chloride (Method A), ii) use the most versatile nucleophile, Grignard reagents, and choose bulky quaternizing reagents to shield the 2- and 6-positions sterically, which can readily be eliminated to give the pyridine nucleus (Method B).

Both methods showed better than a 99% selective nucleophilic attack at the 4-position relative to the 2-position.[8]

Quite recently after our research had been completed, we became aware of the results of Comins and Abdullah[9] which is closely related to Method A. This fact prompted us to publish our results in full.

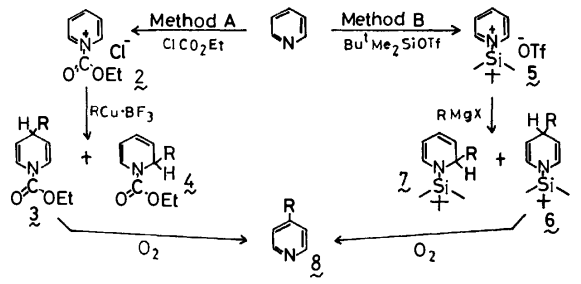

Scheme 1.

Results and Discussion

Regioselective Synthesis of 4-Alkyl(aryl)pyridines by Method A. We examined the reaction of ethoxycarbonylpyridinium chloride with butylmagnesium bromide in tetrahydrofuran (THF) at 0 °C first in order to find a convenient procedure to convert the 1,2-dihydropyridine into the 2-substituted pyridine. While Fraenkel *et al.* obtained only 1,2-dihydropyridine (**4a**) in a moderate yield,[5a] a mixture (80% total yield) of 1,2-dihydropyridine (**4a**) and 1,4-dihydropyridine (**3a**) was obtained in a ratio of 65 to 35. A similar result was obtained with hexylmagnesium bromide. Furthermore, our result was confirmed recently by Comins *et al.*[9] and Yamaguchi *et al.*[10]

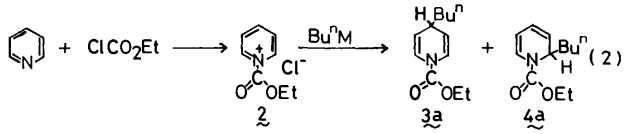

(2)

We then examined the reaction of **2** with butyllithium in ether, in which case the corresponding dihydropyridine was not obtained but the original pyridine was recovered. On the other hand, the reaction of **2** with $Bu^nLi \cdot BBu^n_3$ in ether afforded a mixture of **3a** and **4a** in a ratio of 75 to 25 with a total yield of 42%. Accordingly, we investigated the reaction of $Bu^nMgBr \cdot BBu^n_3$, Bu^nCu, and $Bu^nCu \cdot BF_3$[11] with **2** and the results are summarized in Table 1. Exclusive attack at the 4-position was achieved with Bu^nCu and $Bu^nCu \cdot$

Table 1. Reaction of various organometallic reagents with **2**

Nucleophile		Yield of **3a** and **4a**(%)[3]	Ratio=1,4-(**3a**)/1,2-(**4a**)[4]	Solvent
Bu^nMgBr		80	35/65	THF
HexMgBr		90	30/70	THF
Bu^nLi		0	—	ether
$Bu^nLi \cdot BBu^n_3$ [1]		42	75/25	ether
$Bu^nMgBr \cdot BBu^n_3$ [1]		58	62/38	THF
Bu^nCu	(Bu^nLi+CuI)	35	—	ether
	(Bu^nMgBr+CuI)	78	99.5/0.5	THF
$Bu^nCu \cdot BF_3$[2]	(Bu^nLi+CuI)	48	98.0/2.0	ether
	(Bu^nMgBr+CuI)	59	99.2/0.8	ether
	(Bu^nMgBr+CuI)	89	99.5/0.5	THF

1) Tributylborane complex was prepared by addition of the borane to Bu^nLi or Bu^nMgBr at −78 °C. 2) This reagent was prepared following the procedure of Maruyama and Yamamoto.[11] 3) Isolated yield by Kugelrohr distillation. 4) Product ratio was determined by GLC analysis (5% Apiezon Grease L on Chromosorb WAW DMCS, 100 °C→230 °C).

Table 2. Regioselective synthesis of **3** and **8**

	R	Total yield of **3** and **4**[1](%)	Ratio: 1,4-(**3**)/1,2-(**4**)[2]	Oxidation time (h)	Yield of **8**[3] (%)	Overall yield from Py (%)
a	$CH_3(CH_2)_3$-	89	99.5/0.5	1	68	61
b	$CH_3(CH_2)_5$-	85	99.7/0.3	1	66	56
c	$PhCH_2CH_2$-	81	100/0	19	55[4]	45
d	CH_3CH_2(CH$_3$)CH-	83	99.7/0.3	7	38[4]	32
e	Ph-	94	99.0/1.0	12	59	55

1) Isolated yield by Kugelrohr distillation. Satisfactory IR and ^1H NMR data were obtained for these compounds and satisfactory MS data was obtained for **3a**. 2) By GLC analysis (5% Apiezon Grease L on Chromosorb WAW DMCS, 100 °C⟶230 °C). 3) Isolated yield by Kugelrohr distillation. Identified by IR and ^1H NMR spectroscopy and MS. 4) Lower yields may be due to over-oxidation.

BF_3 in high yield in THF (**3a**:**4a**=~99.5:~0.5). The total yields were about 10% higher with $Bu^nCu \cdot BF_3$ than with Bu^nCu under the same conditions as shown in Table 1. This can probably be ascribed to the relative stability of the copper reagents.

It was also found that the yield of **3a** was higher when butylmagnesium bromide was used as a source of organocopper reagent compared with that using butyllithium.

Therefore, we examined the reaction of various $RCu \cdot BF_3$ reagents with **2** in THF and some of the results are summarized in Table 2. Evidently this method is superior to that with lithium dialkylcuprate (I),[6] because one equivalent of an alkyl group is transferred to the pyridine nucleus stoichiometrically. Moreover, the ratio (99.0:1.0) remains high even with $PhCu \cdot BF_3$, whereas it lowered to 90:10 with lithium diphenylcuprate (I).

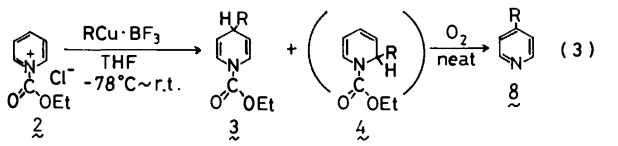

(3)

It is noteworthy that 1,4-dihydropyridines (**3**) can be obtained pure and stable by distillation with quick work-up in the air. 1,4-Dihydropyridines (**3**) were fully characterized as described in Experimental Section. The ^1H NMR of **3a** in $CDCl_3$ (δ) showed the 4-H at 2.72—3.10 as a multiplet, the 3-H and 5-H at 4.77 as a broad double of doublet (J=8 and 3 Hz), and the 2-H and 6-H at 6.79 as a broad doublet (J=8 Hz). The characteristic ^1H NMR signals are almost identical to all **3**.

On the other hand, it is well known that dihydropyridine derivatives are susceptible to oxidation and a small amount of oxidized product **8** was often detected by ^1H NMR. Therefore, oxidation of **3a** in solution (CH_2Cl_2 and THF) was effected by bubbling dry air or oxygen during 10—15 h, but the yield of **8a** was 40—50%. The product **8a** was obtained in 68% yield by oxidation of the neat liquid **3a** under an oxygen atmosphere with stirring for 1 h followed by distillation. Others were oxidized similarly as shown in Table 2. Oxidation of **3e** proceeds sluggishly. The lower yield of **8c** and **8d** may be ascribed to overoxidation. Other oxidations of **3a** were less successful, *i.e.*, i) with H_2O_2-NaOH in THF for 3 d at r.t., 24%; ii) with MCPBA in CH_2Cl_2 for 12 h at r.t., 9%; iii) MCPBA in CH_2Cl_2 for 3 h at reflux, 10%; iv) with *p*-benzoquinone in CH_2Cl_2 at r.t., no reaction took place and at reflux for 3 h, only a tarry residue was obtained. Although oxidation of **3a** to **8a** was performed with silver nitrate in THF at r.t. in 67% yield and that with sulfur has been reported,[12] we adopted the above mentioned procedure mainly due to its simplicity.

We next demonstrated the utility of this method to some of substituted pyridines to investigate the limitation of this method. First, reaction of the 3-bromopyridinium salt (**10a**) with $Bu^nCu \cdot BF_3$ was carried out by the same procedure as described above where 3-bromo-4-butyl-1-ethoxycarbonyl-1,4-dihydropyridine (**11a**) was obtained in 42% yield after Kugelrohr distillation. In a similar manner, reaction of the 3-methoxycarbonylpyridinium salt (**10b**) was tried, however, the reaction mixture was very complicated. Purification of the mixture by flash column chromatography afforded 4-butyl-1-ethoxycarbonyl-3-methoxycarbonyl-1,4-dihydropyridine (**11b**, 19%) and its oxidized product, 4-butyl-3-methoxycarbonylpyridine (12%).

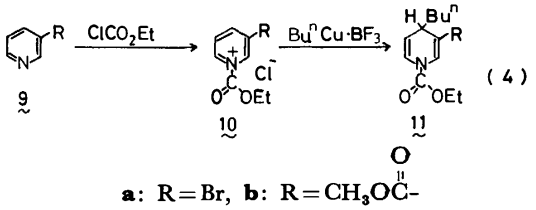

(4)

a: R=Br, **b**: R=CH_3OC(=O)-

On the other hand, when α-picoline was used the desired product was not obtained because the α-picolinium salt was not prepared in a pure state at 0 °C with or without solvent and a dark brown viscous oil was gradually produced. It was reported that the α-picolinium salt can be prepared below −20 °C and used for the reaction with a Grignard reagent in the presence of CuI, although the yields were low.[9]

Regioselective Synthesis of 4-Alkylpyridines by Method B. In the regioselective synthesis of 4-alkylpyridines *via* Method A, the total yield was not so high as desired due to the moderate yield in the oxidation step. We now describe a more facile and handy method for the regioselective synthesis of 4-alkylpyridines using Grignard reagents as the nucleophile and a silyl triflate as a quaternizing reagent. The silyl group is electron-donating and the resulting 1,4-dihydropyridines can be oxidized more easily.

The reaction of pyridine with trimethysilyl chloride was carried out first, however, the corresponding pyridinium salt was not obtained under several conditions since the chloride anion seemed to attack the silicon to dissociate the pyridinium salt. Trimethylsilyl trifluoromethanesulfonate (**12′**) was then used as a quaternizing reagent because trifluoromethanesulfonate anion has a low nucleophilicity. The reaction of pyridine with **12′** in CH_2Cl_2 at 0 °C afforded the trimethylsilylpyridinium triflate (**5′**) as a white solid after removal of the solvent. When **5′** was allowed to react with a couple of $RCu \cdot BF_3$ in THF, no desired product was obtained after the oxidation procedure and pyridine was recovered. This result suggests that the trimethylsilyl group does not activate the pyridinium moiety sufficiently, compared to the ethoxycarbonyl group, for $RCu \cdot BF_3$ to add to **5′**. Phenethylmagnesium bromide in THF was then added to a suspension of **5′** in THF at room temperature. After oxidative work-up phenethylpyridine was obtained in 29% yield where the ratio of the 4- to 2-derivative was 99 to 1. Trimethylphenethylsilane and pyridine were the major products.

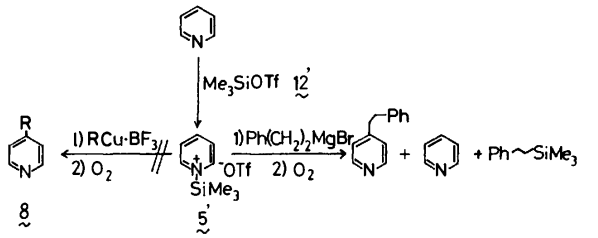

Scheme 2.

Since reaction of *t*-butyldimethylsilyl chloride with nucleophiles is 10^4 times slower relative to trimethylsilyl chloride,[13] we used *t*-butyldimethylsilyl triflate (**12**) as a quaternizing reagent. When *t*-butyldimethylsilylpyridinium triflate (**5**), prepared from **12** and pyridine, was reacted with phenethylmagnesium bromide followed by oxidation of **6** and **7** using oxygen, 4- and 2-phenethylpyridines were obtained (67%, **8c**:**8′c**= 98.9:1.1). The reaction of various Grignard reagents with **5** was attempted and some of results are summarized in Table 3.

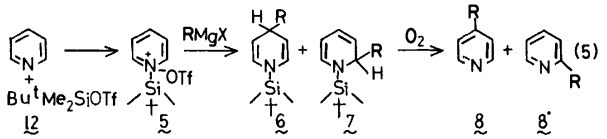

(5)

When the entire process is carried out in one-pot, *i.e.*, oxygen was bubbled through a mixture of THF and aq $NaHCO_3$ solution, the yields of 4-alkylpyridines were 10—20% lower than the results shown in Table 3.

It should be noted that there is definitely a limitation to this method depending on the nature of the nucleophiles. When butyllithium was used instead of butylmagnesium bromide, the total yield of butylpyridine was 58% according to the standard procedure and the ratio of 4- to 2-substitution was 85 to 15, showing poorer selectivity. The lithium enolate of acetophe-

Table 3. Regioselective synthesis of 4-alkylpyridines (**8**)

	R	Yield (%)	Ratio (**8** : **8′**)[4]
a	$CH_3(CH_2)_3$-	68[1] (79)[3]	99.6 : 0.4
b	$CH_3(CH_2)_5$-	62[1] (72)[3]	99.5 : 0.5
c	$PhCH_2CH_2$-	64[2] (71)[3]	98.9 : 1.1
d	CH_3CH_2(CH$_3$)CH-	58[1] (72)[3]	98.8 : 1.2
e	Ph-	59[2] (73)[3]	99.7 : 0.3
f	$CH_3(CH_2)_2$-	61[1] (78)[3]	99.4 : 0.6
g	CH_3(CH$_3$)CH-	65[1] (73)[3]	99.0 : 1.0
h	$CH_3(CH_2)_4$-	63[1] (75)[3]	99.5 : 0.5
i	$CH_3(CH_2)_7$-	69[1] (78)[3]	99.7 : 0.3

1) Isolated yield based on pyridine after Kugelrohr distillation. 2) Isolated yield after TLC (SiO_2, $MeCO_2Et$) purification. 3) Yield after ether extraction (pure by ^1H NMR). 4) Determined by GLC (5% Apiezon Grease L on Chromosorb WAW DMCS, 150—200 °C).

none and Grignard type reagent of 2-mercaptoacetate attacked the silicon of **5** almost exclusively. On the other hand, no reaction took place with **5** when dibutylboron enolate and trimethylsilyl enol ether of acetophenone and the Reformatzky reagent of ethyl bromoacetate were used.

We also applied this reaction to introduce functional groups other than alkyl and aryl groups into the 4-position of the pyridine ring. First, the reaction of **5** with the Grignard reagent **13**, prepared from 2-bromopropionaldehyde ethylene acetal, afforded 3-(4-pyridyl)propionaldehyde ethylene acetal (**14**) in 50% yield after oxidation under a stream of oxygen followed by purification. In a similar fashion, **5** reacted with 1-(trimethylsilylmethyl)vinylmagnesium bromide[14] (**15**) to give **16** in 38% yield after standard work-up. Thus, it was demonstrated that almost any Grignard reagent containing some functional group can be introduced selectively at the 4-position of pyridine.

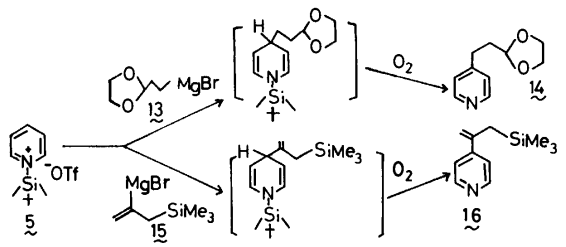

Scheme 3.

Attempted Reactions of 1,4-Dihydropyridines as Enamines. Since 1-ethoxycarbonyl-1,4-dihydropyridines (**3**) can be obtained easily after distillation and 1-*t*-butyldimethylsilyl-1,4-dihydropyridines (**6**) can be generated *in situ* in high yield, we investigated their use as enamines to introduce a second substituent into the 3-position. There is only one such a report by Shōno *et al.* where the Vilsmeier reaction of 1-methoxycarbonyl-1,4-dihydropyridine gave 3-formyl-1-methoxycarbonyl-1,4-dihydropyridine in 75% yield.[15] When acetylation of **3a** was carried out in dichloromethane at −78 °C in the presence of a ten molar excess of acetyl chloride and tin tetrachloride, the expected **11c** was obtained in 21% yield after separation by flash column chromatography. Although **11c** gave correct ^{1}H NMR and IR spectra, it gradually deteriorated under careful handling. At r.t., **3a** was oxidized by tin tetrachloride to **8a** in low yield (*ca.* 30%) together with tarry material.

Since the silyl group is electron-donating, acylation of **6a** generated *in situ* by Method B was attempted. However, exchange of the silyl group for the acyl group occurred unexpectedly in moderate yield (R=EtO, 57%; R=Me, 65%).[16] Although the mechanism of this exchange is not clear, electron transfer from **6a** to the acylating reagent may take place at the initial stage of the reaction, because nucleophilic attack at the N-Si bond should not take place due to the steric effects of the silyl group as exemplified by the inertness of the bond to methylmagnesium iodide and sodium ethoxide. Desilylation by TBAF (tetrabutylammonium fluoride) took place to give **8a** in high yield after usual work-up in the air.

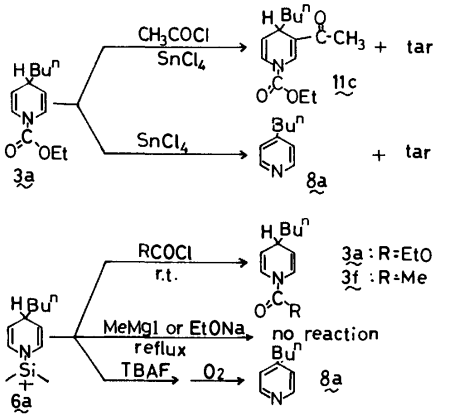

Scheme 4.

Experimental

Infrared spectra were recorded with a Hitachi 215 spectrophotometer. ^{1}H NMR spectra were recorded with a Varian T-60 spectrometer and chemical shifts (δ) were reported in ppm using internal tetramethylsilane. Mass spectra were measured with a Hitachi RMU-6L spectrometer. Boiling points quoted for products distilled in a Kugelrohr apparatus refer to the oven temperature. Melting points were measured using a Yanagimoto micro melting point apparatus and are uncorrected. GLC was performed with a Yanagimoto gas chromatograph G-180 equipped with a 3.0 m×4 mm column, packed with 5% Apiezon Grease L on Chromosorb WAW DMCS. Merck 230—400 mesh silica gel (art 9385) was used for flash column chromatography. All reactions were carried out under a nitrogen atmosphere using syringe and septum techniques.[17] THF and diethyl ether were freshly distilled from Na/benzophenone. Pyridine, α-picoline, and alkyl halides were distilled from CaH_2 under nitrogen. Ethyl chloroformate and boron trifluoride etherate were used after simple distillation under nitrogen. Trimethylsilyl chloride was used after distillation in the presence of a small amount of quinoline. Trimethylsilyl triflate and *t*-butyldimethylsilyl triflate were prepared according to the literature.[18] Butyllithium in hexane was carefully standardized prior to use.

Preparation of 4-Alkyl-1-ethoxycarbonyl-1,4-dihydropyridines (3) by the Reaction of 1-Ethoxycarbonylpyridinium Chloride (2) with RCu·BF$_3$. Method A. 4-Butyl-1-ethoxycarbonyl-1,4-dihydropyridine (3a). General Procedure: Butylmagnesium bromide, prepared from butyl bromide (1.90 ml, 17.6 mmol) and magnesium (0.43 g, 17.6 mmol) in THF (30 ml), was added to a suspension of CuI (3.36 g, 17.6 mmol) in THF (60 ml) at −20 °C under nitrogen through a double-ended needle and the mixture was stirred for 10 min at that temperature. The mixture was then cooled to −78 °C and $BF_3 \cdot OEt_2$ (2.17 ml, 17.6 mmol) was added slowly. After stirring for 10 min at −78 °C, the resulting dark brown mixture was transferred through a double-ended needle to a suspension of the pyridinium salt, which was prepared from pyridine (1.22 ml, 15.0 mmol) and ethyl chloroformate (1.44 ml, 15.0 mmol) in THF (60 ml) at 0 °C, and the mixture was allowed to warm to room temperature with stirring. The color changed from dark brown to dark gray. After the reaction mixture was stirred for 3 h at room temperature, aq 5% $NaHCO_3$ (100 ml) was added and the THF was evaporated under reduced pressure. The following procedure must be carried out quickly because the 1,4-dihydropyridine is easily oxidized. The product was extracted with ether (30 ml×3) and the solvent was evaporated under reduced pressure after drying ($MgSO_4$). The

crude product was purified by Kugelrohr distillation to afford 4-butyl-1-ethoxycarbonyl-1,4-dihydropyridine (2.80 g) in 89% yield. bp 125—135 °C/1.0 mmHg (by Kugelrohr distillation); ^{1}H NMR ($CDCl_3$) δ=0.60—1.50 (m, 12H), 2.72—3.10 (m, 1H), 4.19 (q, 2H, J=7 Hz), 4.77 (br. dd, 2H, J=8, 3 Hz), and 6.79 (br. d, 2H, J=8 Hz); IR (neat) 2940, 1720, 1690. 1635, 1470, 1415, 1400, 1375, 1335, 1310, 1210, 1120, 970, 950, 760, and 740 cm^{-1}; MS (m/z) 209 (M^+, 14.7%), 152 (100), 135 (32.2), 108 (58.0), and 83 (76.7); Ratio: **3a**/**4a**=99.5/0.5 (by GLC analysis); Calcd for $C_{12}H_{19}NO_2$: C, 68.86; H, 9.15; N, 6.69%; Found: C, 68.60; H, 9.45; N, 6.61%.

*1-Ethoxycarbonyl-4-hexyl-1,4-dihydropyridine (**3b**).* Yield 81%; bp 140—165 °C/0.15 mmHg (by Kugelrohr distillation); ^{1}H NMR ($CDCl_3$) δ=0.90—1.70 (m, 16H), 2.76—3.10 (m, 1H), 4.11 (q, 2H, J=7 Hz), 4.81 (br. dd, 2H, J=8, 3 Hz), and 6.74 (br. d, 2H, J=8 Hz); IR (neat) 2930, 1720, 1690, 1635, 1465, 1415, 1395, 1375, 1335, 1310, 1205, 1110, 955, 760, 740 cm^{-1}; Ratio: **3b**/**4b**=99.7/0.3 (by GLC analysis).

*1-Ethoxycarbonyl-4-phenethyl-1,4-dihydropyridine (**3c**).* Yield 81%; bp 140—150 °C/0.50 mmHg (by Kugelrohr distillation); ^{1}H NMR ($CDCl_3$) δ=1.28 (t, 3H, J=7 Hz), 1.50—1.90 (m, 2H), 2.40—2.80 (m, 2H), 2.80—3.20 (m, 1H), 4.22 (q, 2H, J=7 Hz), 4.84 (br. dd, 2H, J=8, 3 Hz), 6.79 (br. d, 2H, J=8 Hz), and 7.17 (s, 5H); IR (neat) 2940, 1730, 1635, 1400, 1380, 1340, 1315, 1215, 1120, 960, 740, and 700 cm^{-1}; Ratio: **3c**/**4c**=100/0 (by GLC analysis).

*4-s-Butyl-1-ethoxycarbonyl-1,4-dihydropyridine (**3d**).* Yield 83%; bp 115—125 °C/0.35 mmHg (by Kugelrohr distillation); ^{1}H NMR ($CDCl_3$) δ=0.60—1.60 (m, 12H), 2.85—3.13 (m, 1H), 4.21 (q, 2H, J=7 Hz), 4.77 (br. dd, 2H, J=8, 3 Hz), and 6.80 (br. d, 2H, J=8 Hz); IR (neat) 2950, 1720, 1690, 1635, 1465, 1415, 1330, 1310, 1210, 1110, 975, 760, and 730 cm^{-1}; Ratio: **3d**/**4d**=99.7/0.3 (by GLC analysis).

*1-Ethoxycarbonyl-4-phenyl-1,4-dihydropyridine (**3e**).* Yield 94%; bp 185—195 °C/0.70 mmHg (by Kugelrohr distillation); ^{1}H NMR ($CDCl_3$) δ=1.29 (t, 3H, J=7 Hz), 4.25 (q, 2H, J=7 Hz), 4.10—4.30 (m, 1H), 4.89 (br. dd, 2H, J=8, 3 Hz), 6.85 (br. d, 2H, J=8, 3 Hz), and 7.10—7.60 (m, 5H); IR (neat) 2980, 1720, 1690, 1630, 1415, 1375, 1335, 1310, 1205, 1115, 980, 840, 725, and 695 cm^{-1}; Ratio: **3e**/**4e**=99.0/1.0 (by GLC analysis).

*The Conversion of **3** into 4-Alkylpyridine (**8**). 4-Butylpyridine (**8a**). General Procedure*: The dihydropyridine (**3a**: 0.338 g, 1.62 mmol) was placed in a flask under an atmosphere of oxygen without solvent. Stirring was continued until TLC analysis indicated that the starting material was consumed (*ca.* for 6 h). Aqueous 5 M HCl (1 M=1 mol dm^{-3}) was added to the mixture until a pH of 2 was obtained and the organic layer was extracted with water (20 ml×3). The acidic solution was then treated with aqueous 3M NaOH until a pH of 11 was obtained. The product was extracted with CH_2Cl_2 (50 ml×2) and the extracts were dried over anhydrous $MgSO_4$, filtered, concentrated under reduced pressure, and distilled by Kugelrohr to give 0.149 g (68%) of 4-butylpyridine (**8a**), which gave correct elemental analysis. Bp 90—100 °C/12 mmHg (lit,[20] bp 98 °C/20 mmHg).

*4-Hexylpyridine (**8b**).* Yield 66%; bp 120—140 °C/18 mmHg (by Kugelrohr distillation) (lit,[9] bp 130—132 °C/16 mmHg).

*4-Phenethylpyridine (**8c**).* Yield 55%; mp 68.5—70.0 °C (from hexane); (lit,[21] mp 70—71 °C).

*4-s-Butylpyridine (**8d**).* Yield 38%; bp 125—145 °C/25 mmHg (by Kugelrohr distillation) (lit,[22] bp 90—150 °C/20 mmHg; bp 194—195 °C/740 mmHg).

*4-Phenylpyridine (**8e**).* Yield 59%; mp 75.5—76 °C (lit,[9]mp 73—74 °C).

*Preparation of 4-Alkylpyridines (**8**) by the Reaction of the N-Silylpyridinium Salts (**5**) with Grignard Reagent: Method B. 4-Butylpyridine (**8a**). General Procedure*: A solution of pyridine (0.38 ml, 4.70 mmol) in CH_2Cl_2 (5 ml) was cooled to 0 °C and *t*-butyldimethylsilyl triflate (**12**) (1.24 ml, 4.69 mmol) was added. After stirring for 5 min, the solvent was evaporated under reduced pressure to give the pyridinium salt as a white solid. The pyridinium salt can be also prepared without solvent. THF (7 ml) was added to the pyridinium salt and then cooled to ice bath temperature. Butylmagnesium bromide, prepared from butyl bromide (0.62 ml, 5.77 mmol) and magnesium (0.14 g, 5.76 mmol) in THF (20 ml), was added to a suspension of the pyridinium salt and the mixture was stirred for 2—3 h at room temperature under a nitrogen atmosphere. The crude product, which contained 20—40% of 4-butylpyridine due to air-oxidation, was obtained by ether extraction (15 ml×3) after quenching the mixture with 5% aq $NaHCO_3$ (30 ml). The mixture of crude product was placed in a flask and stirred for 3 h under an atmosphere of oxygen. The method of purification was the same as described for the synthesis of 4-alkylpyridine from 4-alkyl-1-ethoxycarbonyl-1,4-dihydropyridine (**3**). 4-Butylpyridine was obtained in 68% yield (**8a**:**8′a**=97.6:0.4, by GLC analysis). Overall yields of 4-alkylpyridines and ratios (4-alkylpyridine/2-alkylpyridine) were

*Hexylpyridine (**8b**).* :62% :99.5/0.5
*Phenethylpyridine (**8c**).* :64% :98.9/1.1
s-*Butylpyridine (**8d**).* :58% :98.8/1.2
*Phenylpyridine (**8e**).* :59% :99.7/0.3
*Propylpyridine (**8f**).* :61% :99.4/0.6

bp 70—85 °C/18 mmHg (by Kugelrohr distillation) (lit,[20] bp 80 °C/20 mmHg).

s-*Propylpyridine (**8g**).* :65% :99.0/1.0

bp 170 °C (by Kugelrohr distillation) (lit,[23] bp 173 °C).

*Pentylpyridine (**8h**).* :63% :99.5/0.5

bp 110—122 °C/15 mmHg (by Kugelrohr distillation) (lit,[20] bp 114 °C/20 mmHg).

*Octylpyridine (**8i**).* :69% :99.7/0.3

bp 103—115 °C/1 mmHg (by Kugelrohr distillation) (lit,[20] bp 91 °C/0.1 mmHg).

*3-(4-Pyridyl)propionaldehyde Ethylene Acetal (**14**).* Yield 50%; ratio: 4-substituted pyridine (**14**)/2-substituted pyridine (**14′**)=98.3/1.7; ^{1}H NMR (CCl_4) δ=1.69—2.12 (m, 2H), 2.52—2.88 (m, 2H), 3.68—4.03 (m, 4H), 4.76 (t, 1H, J=4.5 Hz), 7.01 (dd, 2H, J=4, 2 Hz), and 8.33 (dd, 2H, J=4, 2 Hz); IR (neat) 1605, 1410, 1135, and 1025 cm^{-1}.

*2-(4-Pyridyl)-3-trimethylsilyl-1-propene (**16**).* Yield 38%; ^{1}H NMR (CCl_4) δ=−0.07 (s, 9H), 1.98 (s, 2H), 4.95 (d, 1H, J=1 Hz), 5.25 (d, 1H, J=1 Hz), 7.17 (dd, 2H, J=5, 1.5 Hz), and 8.43 (dd, 2H, J=5, 1.5 Hz); IR (neat) 2960, 1595, 1405, 1245, 845, and 825 cm^{-1}.

Introduction of a Butyl Group into the 4-Position of 3-Substiteud Pyridines (3-Bromopyridine, Methyl nicotinate). The procedure for the synthesis of these compounds was the same as described above in the synthesis of 4-alkylpyridines by Method A.

*3-Bromo-4-butyl-1-ethoxycarbonyl-1,4-dihydropyridine (**11a**).* Attempts to purify **11a** by Kugelrohr distillation was not so successful as much residue was produced by polymerization during distillation. Almost pure **11a** was obtained after extraction as indicated by ^{1}H NMR in which case the yield was about 80%.

Yield 42%; bp 150—160 °C/0.5 mmHg (by Kugelrohr distillation); ^{1}H NMR ($CDCl_3$) δ=0.70—1.72 (m, 12H), 3.04—3.36 (m, 1H), 4.22 (q, 2H, J=7 Hz), 4.77 (dd, 1H, J=8, 4 Hz), 6.73 (d, 1H, J=8 Hz), and 7.07 (s, 1H).

*4-Butyl-1-ethoxycarbonyl-3-methoxycarbonyl-1,4-dihydropyridine (**11b**).* A portion of **11b** was oxidized to 4-butyl-3-methoxycarbonylpyridine during purification by flash

† 1 mm Hg≈133.322 Pa.

column chromatography.

Yield 19% (purified by flash column chromatography, SiO_2: hexane/AcOEt=9/1): ^1H NMR ($CDCl_3$) δ=0.65—1.90 (m, 12H), 3.04—3.36 (m, 1H), 3.77 (s, 3H), 4.34 (q, 2H, J=7 Hz), 5.10 (dd, 1H, J=8, 5 Hz), 6.87 (d, 1H, J=8 Hz), and 7.95 (s, 1H); IR (neat) 2960, 1730, 1710, 1625, 1470, 1400, 1375, 1330, 1230, 1175, 765, and 735 cm^{-1}.

4-Butyl-3-methoxycarbonylpyridine. Yield 12% (purified by flash column chromatography, SiO_2: hexane/AcOEt=9/1): ^1H NMR ($CDCl_3$) δ=0.75—1.85 (m, 7H), 2.98 (t, 2H, J=8 Hz), 3.94 (s, 3H), 7.17 (d, 1H, J=5 Hz), 8.42 (d, 1H, J=5 Hz), and 8.88 (s, 1H); IR (neat) 2950, 1720, 1585, 1275, and 1100 cm^{-1}.

*Reaction of 4-Butyl-1-t-butyldimethylsilyl-1,4-dihydropyridine (**6a**) with Acetyl Chloride and Ethyl Chloroformate. 1-Acetyl-4-butyl-1,4-dihydropyridine (**3f**)*: To the reaction mixture containing **6a**, prepared from **5** (2.47 mmol) and butylmagnesium bromide, was added acetyl chloride (0.23 ml, 3.23 mmol) at room temperature with stirring. After stirring for 2 h, the reaction mixture was quenched with 20 ml of 5% aqueous sodium hydrogencarbonate. The crude product was extracted with ether (15 ml×3), dried over anhydrous $MgSO_4$, filtered, and the solvent was removed under reduced pressure. Flash column chromatography (SiO_2, hexane/AcOEt=9/1) afforded 1-acetyl-4-butyl-1,4-dihydropyridine (**3f**) in a 65% yield (0.288 g). This compound is susceptible to be oxidized by oxygen.

^1H NMR (CCl_4) δ=0.87—1.55 (m, 9H), 2.11 (s, 3H), 2.80—3.07 (m, 1H), 4.60—5.00 (m, 2H), 6.30—6.60 (m, 1H), and 6.87—7.17 (m, 1H); IR (neat): 2920, 1670, 1375, 1325, and 1310 cm^{-1}.

*4-Butyl-1-ethoxycarbonyl-1,4-dihydropyridine (**3a**).* Yield 57% (flash column chromatography: SiO_2 hexane/AcOEt=9/1), spectral data were identical to those described before.

Partial support of this work was provided by Grant-in-Aid for Scientific Research (No. 554139) and that for Special Project Research (No. 56109002) administered by Ministry of Education, Science and Culture. Kind gift of silylating reagents is sincerely acknowledged for Chisso Co. Ltd.

References

1) a) U. Eisner and J. Kuthan, *Chem. Rev.*, **72**, 1 (1972); b) D. M. Stout and A. I. Meyers, *ibid.*, **82**, 223 (1982).

2) a) C. S. Giam and J. L. Stout, *J. Chem. Soc., Chem. Commun.*, **1969**, 142; b) C. S. Giam and J. L. Stout. *ibid.*, **1970**, 478; c) C. S. Giam, E. E. Knaus, and F. M. Pasutto, *J. Org. Chem.*, **39**, 3565 (1974).

3) a) W. von E. Doering and V. Z. Pasternak, *J. Am. Chem. Soc.*, **72**, 143 (1950); b) R. A. Benkeser and D. S. Holtar, *ibid.*, **73**, 5861 (1951).

4) T. Taguchi, M. Nishi, K. Watanabe, and T. Mukaiyama, *Chem. Lett.*, **1973**, 1307.

5) a) G. Fraenkel, J. W. Cooper, and C. M. Fink, *Angew. Chem. Int. Ed. Engl.*, **9**, 523 (1970); b) R. E. Lyle, J. L. Marshall, and D. J. Comins, *Tetrahedron Lett.*, **1977**, 1015.

6) E. Piers and M. Soucy, *Can. J. Chem.*, **52**, 3563 (1974).

7) a) A. R. Katritzky, H. Beltrami, and M. P. Sammes, *J. Chem. Soc., Chem. Commun.*, **1979**, 137; b) A. R. Katritzky, H. Beltrami, J. G. Keay, D. N. Rogerss, M. P. Sammes, C. W. G. Leung, and C. M. Lee, *Angew. Chem. Int. Ed. Engl.*, **18**, 792 (1979); c) A. R. Katritzky, J. G. Keay, and M. P. Sammes, *J. Chem. Soc., Perkin Trans. I.*, **1981**, 668; d) A. R. Katritzky, H. Bertrami, and M. P. Sammes, *J. Chem. Res. (s)* **1981**, 133.

8) For preliminary report, see: K. Akiba, Y. Iseki, and M. Wada, *Tetrahedron Lett.*, **23**, 429, 3935 (1982).

9) Very recently, Comins, *et al.* reported a convenient method for the synthesis of 4-alkylpyridines via regioselective addition of Grignard reagents to 1-acylpyridinium salts in the presence of a catalytic amount of copper(I) iodide. D. L. Comins and A. H. Abdullah, *J. Org. Chem.*, **47**, 4315 (1982).

10) R. Yamaguchi, Y. Nakazono, and M. Kawanishi, *Tetrahedron Lett.*, **24**, 1801 (1983).

11) K. Maruyama and Y. Yamamoto, *J. Am. Chem. Soc.*, **99**, 8068 (1977).

12) R. E. Lyle and D. L. Comins, *J. Org. Chem.*, **41**, 3250 (1976).

13) E. Akerman, *Acta Chem. Scand.*, **10**, 298 (1956), **11**, 373 (1957).

14) a) H. Nishiyama, S. Narimatsu, and K. Itoh, *Tetrahedron Lett.*, **22**, 5289 (1981); b) H. Nishiyama, H. Yokoyama, S. Narimatsu, and K. Itoh, *ibid.*, **23**, 1267 (1982).

15) T. Shōno, Y. Matsumura, K. Tsubata, Y. Sugihara, S. Yamane, T. Kanazawa, and T. Aoki *J. Am. Chem. Soc.*, **104**, 6697 (1982).

16) The *N*-acylation of enaminosilanes with a trimethylsilyl group has been reported. W. Ando and H. Tsumaki, *Tetrahedron Lett.*, **23**, 3073 (1982).

17) See: G. W. Kramer, A. B. Levy, and M. M. Midland, "Organic Syntheses via Boranes" ed by H. C. Brown, John-Wiley, New York, 1975, Chapter 9.

18) H. C. Marsman and H. G. Horn, *Z. Naturforsch. B*, **27**, 1448 (1972).

19) S. C. Watson and J. F. Eastham, *J. Organomet. Chem.*, **9**, 165 (1967).

20) J. R. Wibaut and J. W. Hey, *Recl. Trav. Chim. Pays-Bas*, **72**, 513 (1953).

21) F. W. Bergstrom, T. R. Norton, and R. A. Seibert, *J. Org. Chem.*, **10**, 452 (1945).

22) A. E. Tchitchibabine, *Bull. Soc. Chim. France.*, **5**, 429 (1938).

23) G. R. Clemo and E. Hoggarth, *J. Chem. Soc.*, **1941**, 41.

Effects of Pore Size Distribution on the Catalytic Performance for Coal Liquefaction. I. The Activity and Selectivity of the Catalyst

Hiromichi SHIMADA,* Minoru KURITA, Toshio SATO, Yuji YOSHIMURA, Tomohiro KAWAKAMI,† Suehiko YOSHITOMI,† and Akio NISHIJIMA
National Chemical Laboratory for Industry, Yatabe, Ibaraki 305
†*Shibaura Institute of Technology, 3-9-14, Shibaura, Minato-ku, Tokyo 108*
(Received December 1, 1983)

Coal liquefaction experiments were carried out by using seven catalysts with different pore structures. As for the unimodal catalysts, the total conversion increased with the pore radius of the catalyst because of the lesser pore-diffusional limitation. However, the ratio of oil to oil-plus-asphaltene decreased with the pore radius. In the case of a large-pore catalyst, heavy components with a large molecular size and a low reactivity can approach the intra-particle active sites and occupy them to prevent the hydrocracking of asphaltene to oil. Bimodal catalysts with micropores ($r<10$ nm) and macropores ($r>300$ nm) gave higher values of both the coal liquefaction and the oil yields than did the unimodal catalysts. The presence of macropores seems to enhance the pore diffusion and increase the efficiency of the micropore use, while mesopores with radii between 10 nm and 300 nm did not make such a high contribution to the pore diffusion as was shown for the macropores. For the removal of heteroatoms, there was little difference in the performance among the catalysts with different pore structures. It is suggested that the active sites for the heteroatom removal are deactivated easily by the heavy components.

Molybdenum alumina catalysts have long been used for the hydrodesulfurization (HDS) of gas oil and the refining of the petroleum residue. Recently serious attention has been paied to the use of these catalysts for the direct liquefaction of coal in a fixed bed or an ebullated bed. However, since there are many differences in properties between coal (or coal derived liquids) and petroleum, MoO_3/Al_2O_3 catalysts designed for petroleum refining cannot show a high activity or favorable selectivity for the direct liquefaction of coal. Further, the catalytic activity, especially the hydrogenation activity, declines rapidly during the hydrotreatment of coal because of coke build-up and metal deposition on the surface of the catalyst.[1,2]

During the course of the development of molybdenum catalysts for coal liquefaction, a deliberate designing of the catalyst is absolutely necessary. For this purpose, it is necessary to clarify the effects of the properties of the catalyst on its activity, selectivity, and life. The present paper will describe the effects of the pore size distribution (PSD) on the activity and selectivity of the supported catalyst.

Recently, in the petroleum hydrotreating process the feedstocks have become heavier, and many kinds of functions besides HDS and hydrocracking activity, such as asphaltene conversion and demetallation, have come to be required for the catalyst. Furthermore, large amounts of poisoning materials contained in heavy feedstocaks deactivate the conventional HDS catalysts rapidly. One of the solutions to these problems can be found in designing the proper pore structure of catalyst support. Numerous catalysts with different pore structures have been tested and reported in many patents[3-10] and papers.[11-13] As a result of these investigations, some effects of the PSD on the catalytic activity and life have become obvious. They are;

1. The pore-diffusional limitation of the reaction rates is serious in the hydrotreating of heavy feedstocks than in the light gas oil.
2. The optimal pore structure may not be the same for every hydrotreating reaction, desulfurization, denitrogenation, asphaltene conversion, and demetallation.
3. Carbonaceous and metal deposition from the feedstocks on the catalysts varies as a function of the pore structure.

On the contrary, a few fundamental studies have been undertaken on the effects of the PSD of the catalyst used for coal liquefaction. Weller and his co-workers[14-16], by using several kinds of supports which have different average pore diameters, demonstrated that the catalysts with large pores showed a higher performance than those with small pores. Bertolacini *et al.*[17,18] indicated that a bimodal PSD is required for high performance, especially in terms of aging. As has been shown above, it has become somewhat clear that the PSD of the catalyst support plays an important role in the performance of the catalyst for coal liquefaction. However, the proper PSD of the catalyst for coal liquefaction will differ with the starting materials and with the products aimed at. Process conditions, such as the type of reactor, will also change the most favorable PSD. Accordingly, further practical studies have to be undertaken on the effects of the PSD on the catalytic activity, selectivity, and life in order to develop practical catalysts with high performance.

In the present study, the effects of the PSD on the activity and selectivity of the catalyst will be investigated by using both unimodal and bimodal catalysts. Moreover, the roles of micro-, meso-, and macropores in the catalytic activity will also be clarified. Seven catalysts with different PSD values, with the same weight loading of molybdenum, were prepared and screened for coal liquefaction in a batch autoclave. From the results of the product distribution and the removal of nitrogen and sulfur, the proper pore structure for each reaction will be discussed.

Experimental

Equipment. A 500-cm^3 autoclave with a magnedrive stirrer was used for all runs of coal liquefaction. The auto-

clave was equipped with a wire basket to prevent the catalysts from being crushed. The hydrogenation of 1-methylnaphthalene (1-MN) was carried out using a 50-cm³ autoclave in order to examine the activity of the catalysts.

Catalysts. Seven kinds of Al_2O_3 (sphere with a diameter of 1.6 mm) with different PSD values were chosen as catalyst supports (prepared by Sumitomo Aluminum Smelting Co., Ltd.). Figures 1—3 show the PSD curves of the catalyst supports (before impregnation with active components) as measured by using a mercury porosimeter (AMINCO 60,000 psi). The MoO_3/Al_2O_3 catalysts were prepared by impregnating the Al_2O_3 supports with an ammoniacal solution of ammonium heptamolybdate, and the $NiO-MoO_3/Al_2O_3$ catalysts with an ammoniacal solution of ammonium heptamolybdate and nickel nitrate. All the operations of the impregnation procedure were performed at pH values over 9.0 for 42 h (at 27 °C) using the equilibrium adsorption method.[19] The samples were subsequently dried (at 110 °C, 16 h) and calcined (at 300 °C, 50 min; subsequently at 500 °C, 3 h).

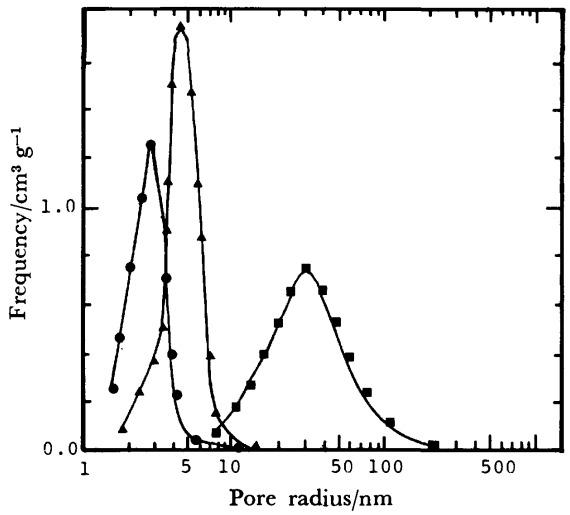

Fig. 1. Pore size distributions of catalysts.
●: Catalyst A, ▲: catalyst B, ■: catalyst C

The loading of molybdenum was determined by chemical analysis, and that of nickel, by the use of an X-ray fluorescence analyzer (Rigaku, Ultra Trace System). The specific surface areas and pore volumes of all the catalysts were measured by using the mercury porosimeter. The properties and the chemical components of the catalysts are summarized in Tables 1 and 2. Reductive sulfiding was carried out in a stream of 10 vol% of H_2S (balance H_2) at 350 °C for 2 h before liquefaction.

Procedures. *Coal Liquefaction*: The coal used was a subbituminous Taiheiyo coal containing 16.1% ash (dry base). The rersults of the elemental analysis of the coal were: C, 74.9; H, 6.2; N, 1.3; S, 0.4; O, 17.2% (moisture and ash free base). The powdered coal with a diameter smaller than 150 μm was dried at 110 °C in a nitrogen atmosphere before use. The solvent used was hydrogenated anthracene oil (HAO), which contained: C, 91.8; H, 7.0; N, 0.6; S, 0.1; O, 0.5%.

The autoclave was charged with coal (60 g), a solvent (140 g), and a catalyst (5 g), and then pressurized with H_2 to an initial pressure of 100 kg cm^{-2} at room temperature. The temperature of the unit was increased to 400 °C over a period of 2 h and then held at this temperature for 1 h. The stirring rate was 900 min^{-1} for all runs.

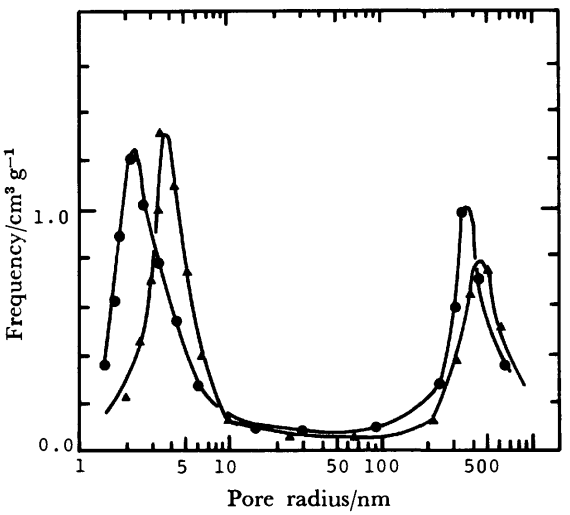

Fig. 2. Pore size distributions of catalysts.
●: Catalyst D, ▲: catalyst E

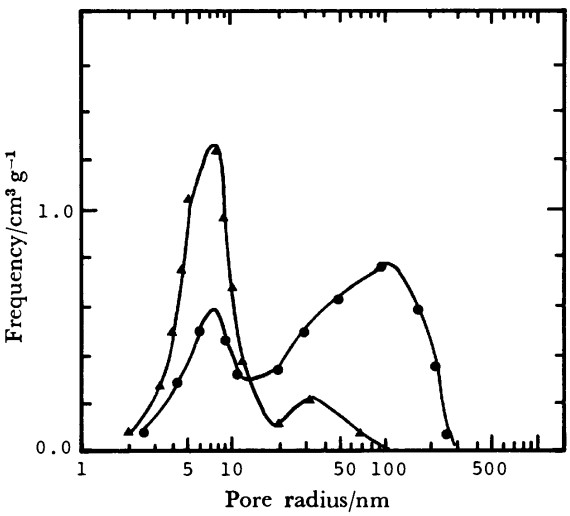

Fig. 3. Pore size distributions of catalysts.
▲: Catalyst F, ●: catalyst G

Table 1. Properties of molybdenum catalysts

Catalyst	A	B	C	D	E	F	G
Phase of Al_2O_3[a]	γ	γ	α	γ	γ	γ	γ
S. A.[b]/m² g⁻¹	276	211	39	316	261	175	120
P. V.[c]/cm³ g⁻¹	0.37	0.48	0.55	0.76	0.84	0.63	1.25
MoO_3/wt%	3.4	3.2	2.8	3.5	2.9	2.8	3.4
SiO_2/wt%	tr.[d]	tr.	3.8	tr.	tr.	4.0	tr.

a) Decided by using X-ray diffraction. b) Surface area. c) Pore volume. d) Less than 0.5.

Table 2. Properties of nickel molybdenum catalysts

Catalyst	P[a]	Q[b]	R[c]
S.A.[d]/$m^2\ g^{-1}$	252	34	188
P.V.[e]/$cm^3\ g^{-1}$	0.36	0.50	0.74
MoO_3/wt%	11.7	11.0	15.3
NiO/wt%	3.3	3.3	3.6
SiO_2/wt%	tr.[f]	3.8	tr.

a) The same support was used as for the catalyst A. b) The same support was used as for the catalyst B. c) The same support was used as for the catalyst C. d) Surface area. e) Pore volume. f) Less than 0.5.

After cooling to room temperature, the gas was slowly discharged through a wet gas meter. During this letdown, a sample of the gas was collected in a syringe in order to determine the gas composition. The liquid and solid products were separated into "toluene insolubles," "asphaltene (toluene soluble and hexane insoluble)," and "oil (hexane soluble)" portions using a Soxhlet extractor. The nitrogen and sulfur contents in the liquid products were determined by means of a nitrogen and sulfur analyzer (Mitsubishi Kasei, MCI-TN-02).

Hydrogenation of 1-Methylnaphthalene (1-MN): The hydrogenation activity of the catalysts was examined using 1-MN as a reactant. The autoclave was charged with 10 cm^3 of 1-MN and 0.5 g of a catalyst, and then pressurized with H_2 to an initial pressure of 70 kg cm^{-2}. The unit was then heated to 375 °C over a 10-min period and then held at this temperature for 90 min. The analysis of the liquid product was done using a gas chromatograph equipped with a FFAP fused silica capillary column (25 m).

Results and Discussion

Conversion and Oil Yields. The results of the coal liquefaction and hydrogenation of 1-MN on molybdenum catalysts are summarized in Table 3. In the liquefaction of coal, the total conversion (oil-plus-asphaltene yields) and the oil yields for a blank run were much lower than those for runs with a catalyst. 1-MN did not react without a catalyst. These results made it clear that the catalysts accelerated the reaction rates.

In the liquefaction test, the gas composition for the blank run was: CO_2, 5.9; CO, 1.3; CH_4, 4.0; C_2H_6, 1.1% (in addition, trace amounts of H_2S and NH_3 were detected), whereas that for the runs with a catalyst was: CO_2, 6.0—6.4; CO, 1.5—1.6; CH_4, 4.0—4.2; C_2H_6, 1.5%. There was little difference in gas composition among runs with a catalyst. A small difference in the gas composition was found between runs with and without a catalyst. In catalytic runs the concentrations of CH_4 and C_2H_6 (hydrocarbons) were a little higher than those in the run without a catalyst. The hydrocracking activity of the catalyst seems to result in this difference.

Unimodal Catalysts: The total conversion increased with the pore size of the catalyst (A<B<C) despite the smaller surface area of the large-pore catalysts. In the case of the catalyst C, which has an eminently small surface area, the loading of MoO_3 exceeded the monolayer coverage. Therefore, the catalyst C showed a much lower activity for the hydrogenation of 1-MN. However, a higher total conversion was given for coal liquefaction by the catalyst C than by the catalysts A and B. This tendency shows that the production of asphaltene from coal was greatly affected by the pore structure of the catalyst because the pore diffusion limited the reaction rates seriously. On the other hand, with an increase in the pore diameter of the catalyst, the production of oil remained constant, or even decreased, the ratio of oil to oil-plus-asphaltene decreasing obviously.

Ho *et al.*[16] also reported that the total coal liquefaction was seriously limited by the pore diffusion, and that the ratio of oil to oil-plus-asphaltene decreased with an increase in the diameter of the catalyst pore. They explained that this phenomenon was due to the low reaction temperature (400 °C) when the oil production rate was small. In the present study, however, a high oil yield was given by some catalysts (D and E) in spite of a low reaction temperature. This result suggests that the pore structure of the catalyst also affected the production rate of oil from asphaltene.

It has been known that the molecular weight of the asphaltene derived from coal, although always much lower than that from petroleum, ranges from 400 to 800.[20-22] Considering the fact that the coal-derived asphaltene has a polyaromatic ring structure, its molecular size might be larger than 1 nm. In addition, large molecules with polyaromatic rings are known to have a tendency to aggregate with each other and to give a micell-like structure. It may thus be assumed that there exists a pore-diffusional limitation in the production of oil from asphaltene.

Mass-transfer theory for porous catalysts indicates that, in a series reaction, poor yields of intermediate

Table 3. Activity tests of molybdenum catalysts

Catalyst	None	A	B	C	D	E	F	G
Most probable pore radius/nm	—	2.5	4.5	30	2.5, 350	4.5, 450	7, 35	7, 100
Coal liquefaction								
Total conversion/wt%[a]	83.3	89.9	93.2	94.4	94.7	95.7	92.8	93.4
Oil yields/wt%	52.7	65.7	65.6	64.2	71.9	70.0	64.5	66.7
Oil/(oil+asp.)[b]	0.63	0.73	0.70	0.68	0.76	0.73	0.70	0.71
Hydrogenation of 1-methylnaphthalene								
Conversion/%[c]	0.0	13.5	14.8	7.2	12.2	16.4	15.2	12.2

a) Oil plus asphaltene yields (toluene solubles). b) Oil yields/Total conversion. c) (1-MT*+5-MT)/(1-MT+5-MT+1-Methylnaphthalene). *MT: Methyltetralin.

products are obtained for a catalyst with a low effectiveness factor.[23] In the case of coal liquefaction, asphaltene is an intermediate product, when coal is the starting material and oil is the final product of a series reaction, indicating that a small-pore catalyst with a low effectiveness factor gives a higher ratio of oil to asphaltene than dose a large-pore catalyst.

On the other hand, it is considered that heavy components with a low reactivity (heavier than preasphaltene) can reach the intra-particle active sites of large-pore catalysts and occupy them easily, thus preventing the hydrocracking of asphaltene to oil. In fact, the analysis of the aged catalyst showed that the carbonaceous materials deposited on the catalyst were heavy components with a lower H/C ratio than asphaltene.[24]

The contribution of the catalyst to coal liquefaction is considered to be smaller than that of the hydrogen-donor solvent at the first stage of liquefaction.[25,26] The effects of catalysts on the product distribution are reflected in the increase in light components, such as the oil or distillate fraction, especially in the case of molybdenum catalysts.[27,28] In the present study, all of the catalysts gave a higher ratio of oil to oil-plus-asphaltene than was observed in the blank run. This result shows that the production of oil was more accelerated by the catalysts than that of asphaltene. However, as has been shown above, the product distribution changes with the pore size distribution of the catalyst. This result suggests that an elaborate designing of the proper pore size distribution of the catalyst is required to get a desirable product distribution.

Bimodal Catalysts: Bimodal catalysts with micropores with radii smaller than 10 nm and macropores with radii larger than 300 nm (D and E) gave a much higher value in both total conversion and oil yields than did the unimodal catalysts (Table 3). When the physical properties of bimodal catalysts were compared with those of unimodal catalysts, the pore volume of the former was found to be approximately twice as large as that of the latter in spite of the small difference in surface area between them (Table 1). This fact suggests that the macropores did not increase the number of the active sites, but enhanced the diffusion rates of the molecules inside the catalyst particle. In fact, in the case of the hydrogenation of 1-MN, which has a small molecular size, no effect of the macroporosity was observed.

A higher total conversion and lower oil yields were given in the catalyst E, with large micropores, than in the catalyst D, with small micropores. Micropores with small radii were favorable for the production of light components, even in the case of the bimodal catalysts, this result being in keeping with that obtained for the unimodal catalysts.

The catalysts with large micropores ($r \sim 7$ nm) and mesopores ($10\text{ nm} < r < 300\text{ nm}$) (F and G) gave lower values both in total conversion and oil yields than the catalysts D and E. The catalyst G, with a large volume of mesopores with a large diameter, gave a higher total conversion and higher oil yields than the catalyst F. However, even in the case of the catalyst G, mesoporosity did not enhance the catalytic activity as compared with the macroporosity.

Table 4. Coal liquefaction with nickel molybdenum catalysts

Catalyst	P	Q	R
Pore radius[a]/nm	2.5	30	4.5, 450
Total conversion/wt%[b]	87.9	95.9	95.1
Oil yields/wt%	59.5	71.8	78.1
Oil/(oil+asp.)[c]	0.68	0.75	0.81

a) Most probable pore radius. b) Oil plus asphaltene yields (toluene solubles). c) Oil yields/total conversion.

Nickel Molybdenum Catalysts: The results of coal liquefaction with nickel molybdenum catalysts are shown in Table 4. Higher oil yields were given for the catalysts Q and R as compared with the catalysts C and E. This result is due to the high loading of molybdenum and the additional loading of nickel. However, the catalyst P, with only microporosity, gave a lower total conversion and lower oil yields than the catalyst A. This result indicates that the high loading of the active components decreased the effective pore size of the catalyst if the catalyst has only microporosity.

The effects of the pore structure observed for NiO–MoO_3/Al_2O_3 catalysts were similar to those obtained for MoO_3/Al_2O_3 catalysts; a high total conversion was given by the large-pore or bimodal catalysts, and high oil yields, by the bimodal catalyst. These results support our previous discussion and show that, in the case of industrial catalysts, the pore size distribution of the support also affects the activity and selectivity of the catalyst. It may also be suggested that a high loading of active metal components cannot enhance the performance of the small-pore catalyst because of the pore-diffusional limitation.

Heteroatom Removals. The contents of nitrogen and sulfur in each fraction of the products are given in Table 5. Excepet for the catalysts F and G, higher contents of nitrogen were given in the runs with a catalyst than in the run without a catalyst. In most cases, the hexane-soluble fraction gave a higher concentration of nitrogen compounds than the toluene-soluble fraction. These results suggest that the catalysts do not very much accelerate the hydrodenitrogenation (HDN) of light components during the hydrogenation of coal. One reason for this phenomenon is that the strong adsorption of heavy components on the catalyst reduced the catalytic activity for HDN. As has been mentioned above, coal derived oil obtained by the catalytic hydrogenation of coal contains fairly large amounts of heteroatoms. However, it may be useful as a liquefaction solvent because of its polar interaction with coal molecules.[29,30]

In the runs with catalysts having meso- or macropores, lower nitrogen contents were given in spite of the high total conversion and oil yields, as compared with the runs with micropore catalysts or without a catalyst. This suggests that large pores are preferable to small pores for nitrogen-removal reaction from coal molecules.

In terms of HDS, although the sulfur contents in the products of the runs with catalysts were smaller than those without a catalyst, there was little difference

TABLE 5. CONTENTS OF NITROGEN AND SURFUR IN LIQUEFACTION PRODUCTS

Catalyst	None	A	B	C	D	E	F	G
Most probable pore radius/nm	—	2.5	4.5	30	2.5, 350	4.5, 450	7, 35	7, 100
Nitrogen								
Hexane solubles/wt%	0.62	0.76	0.78	0.64	0.63	0.62	0.57	0.53
Toluene solubles/wt%	0.64	0.73	0.70	0.64	0.62	0.62	0.47	0.50
Sulfur								
Hexane solubles/wt. ppm.	1210	750	850	760	730	620	830	820
Toluene solubles/wt. ppm.	1200	810	710	790	720	820	740	730

among catalysts. Plumail *et al.*[13] reported that smaller pores were more favorable for HDS than asphaltene conversion in the case of petroleum refining, while Ho *et al.*[16] indicated that in the case of coal liquefaction the bimodal PSD, which was most favorable for a total conversion, also gave the highest HDS performance. In the present study, the concentration of sulfur in the starting material was extremely low. Therefore, it may be difficult to discuss the HDS activity of the catalyst.

As has been described above, the pore size distribution has great effects on the activity and the selectivity of the catalyst, because the pore diffusion limits the reaction rates seriously. Large pores are more advantageous in the production of asphaltene than small pores. On the other hand, small pores are required for the production of light components. In fact, mesopores are superior to micropores in terms of total conversion, while inferior in the production of oil. Bimodal catalysts with macroporosity ($r>300$ nm) and microporosity ($r<10$ nm) performed excellently in terms of both total conversion and oil yields. Macropores enhance the efficiency of the catalyst, while micropores are useful for the production of oil. Mesopores, as compared with macropores, have no great effect on the increase in the pore-diffusional limitation.

Finally, these results show that the design of the pore structure is very important in getting a favorable product distribution. On the other hand, the pore structure of the catalyst support is also known to have great effects on the life of the catalyst. The effects of the pore size distribution of the support on the aging behavior of the catalyst during coal liquefaction will be discussed in the following work.

References

1) A. Nishijima *et al.*, Proc. Pan-Pacific Synfuels Conference, Tokyo, Japan (1982) / C-4.

2) T. L. Cable, F. E. Massoth, and M. G. Thomas, *Fuel Processing Technol.*, **4**, 265 (1981).

3) T. Kuwata, Y. Ohguchi, and H. Nomura, U. S. Patent 3530066 (1970); *Chem. Abstr.*, **77**, 103825s (1972).

4) A. L. Hensley, Jr., U. S. Patent 3766058 (1971); *Chem. Abstr.*, **79**, 33394r (1973).

5) J. A. Frayer, D. Y. Ko, and J. A. Paraskos, U. S. Patent 3876530; *Chem. Abstr.*, **83**, 63255w (1975).

6) S. M. Oleck *et al.*, U. S. Patent 3891541 (1975); *Chem. Abstr.*, **83**, 150185s (1975).

7) G. R. Wilson, U. S. Patent 3907668 (1975); *Chem. Abstr.*, **84**, 46989s (1976).

8) M. Donaldo, U. S. Patent 3985643 (1976).

9) E. J. Rosinski *et al.*, U. S. Patent 4082695 (1978); *Chem. Abstr.*, **89**, 77547d (1978).

10) Y. Fukui *et al.*, U. S. Patent 4166026 (1979); *Chem. Abstr.*, **90**, 139984a (1979).

11) T. Ono, O. Togari, and M. Nakamura, *J. Japan Petrol. Inst.*, **23**, 110 (1980).

12) K. Nomura *et al.*, *J. Japan Petrol. Inst.*, **24**, 253 (1981).

13) J. C. Plumail *et al.*, *Prepr. Div. Pet.. Chem., Am. Chem. Soc.*, 562 (1983).

14) Y. K. Yen, D. E. Furlani, and S. W. Weller, *Ind. Eng. Chem., Prod. Res. Dev.*, **15**, 24 (1976).

15) J. Scinta and S. W. Weller, *Fuel Processing Technol.*, **1** 279 (1977/1978).

16) P. N. Ho and S. W. Weller, *Fuel Processing Technol.*, **4**, 21 (1981).

17) R. J. BertoLacini *et al.*, EPRI Report, AF-574 (1977).

18) R. J. BertoLacini *et al.*, EPRI Report, AF-1084 (1980).

19) L. Wang and W. K. Hall, *J. Catal.*, **66**, 251 (1980).

20) R. Yoshida *et al. Bull. Chem. Soc. Jpn.*, **52**, 1464 (1979).

21) T. Aczel and H. E. Lumpkin, *Adv. Chem. Ser.*, **179**, 13 (1979).

22) I. Schwager *et al.*, *Fuel*, **57**, 100 (1978).

23) C. N. Satterfield, "Mass Transfer in Heterogeneous Catalysis," M. I. T. Press, London (1970). p. 214.

24) H. Shimada *et al.*, *J. Japan. Petrol. Inst.*, in press.

25) Y. Kamiya *et al.*, *Fuel*, **61**, 906 (1982).

26) Y. Kitaoka *et al.*, *Fuel*, **61**, 919 (1982).

27) B. Granoff *et al.*, *Prepr. Div. Fuel Chem.*, **23**, 23 (1978).

28) Y. Miki and Y. Sugimoto, *Nenryo Kyokaishi*, **62**, 408 (1983).

29) J. W. Hellgeth, L. T. Taylor, and A. M. Squires, Proc. 1983 International Conference on Coal Science, Pittsburgh, USA (1983), p. 172.

30) D. C. Cronauer and R. I. McNeil, Proc. 1983 International Conterence on Coal Science Pittsburgh, USA (1983) p. 176.

The Adsorption Behavior of Monoionic Dyes at the Aqueous Solution/Air Interface

Yorie UCHIZONO,* Emiko SHIMADA, Yuuko OKAYAMA, Yuuzo HARADA, Makoto ARATONO,† and Kinsi MOTOMURA†

Faculty of Home Life Science, Fukuoka Women's University, Fukuoka 813

†*Department of Chemistry, Faculty of Science, Kyushu University 33, Fukuoka 812*

(Received January 5, 1984)

Synopsis. The surface tension of the aqueous solutions of six dyes have been measured as a function of dye concentration at 298.15 K under atmospheric pressure. The adsorbed films of four azo dyes have been found to transform from the gaseous phase to the expanded phase. The relation between the molecular structure of dye and the state of the adsorbed film has been discussed by making use of the surface pressure *vs.* mean area curve.

It is necessary to have a detailed knowledge of the adsorption behavior of dyes at interfaces in order to understand the dyeing process on fibers. Properties of the adsorbed films of dyes, however, have been scarcely clarified. The purpose of this paper is to obtain information about the adsorption behavior of dyes at their aqueous solution/air interface and about the effect of the molecular structure of dyes on it. The surface tension of the aqueous solutions of dyes, which have different molecular structures, was measured and analyzed by making use of thermodynamic equations.

Experimental

The dyes used in the present study are summarized in Table 1. The commercially available dyes, except for Ethyl Orange and 2,4-diamino-4′-methylazobenzene chloride (DAM), were used by the recrystallization from distilled water and then ethanol several times. Ethyl Orange was prepared by coupling diazotized sulfanilic acid with *N*,*N*-diethylaniline and then recrystallized from distilled water and ethanol. DAM was synthesized by the coupling of *m*-phenylenediamine and diazotized *p*-toluidine according to the usual way and recrystallized from the aqueous solution of 1% hydrochloric acid. Water was twice distilled from alkaline permanganate solution.

The surface tension was measured by the drop volume method with a precision better than 0.05 mN m^{-1}.[1] The drop was stood for about 15 min to reach the adsorption equilibrium.

TABLE 1. C. I. NUMBER AND STRUCTURAL FORMULA OF DYE

Dye	C. I. Number	Structural formula
(1) C. I. Acid Yellow 36	C. I. 13065	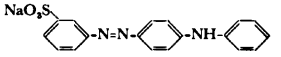
(2) Ethyl Orange		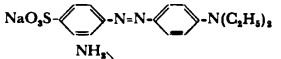
(3) C. I. Basic Orange 2	C. I. 11270	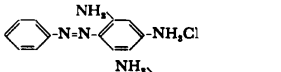
(4) DAM[a]		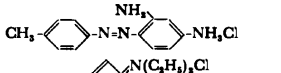
(5) C. I. Basic Green 1	C. I. 42040	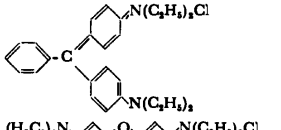
(6) C. I. Basic Violet 10	C. I. 45170	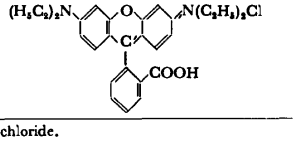

a) 2,4-Diamino-4′-methylazobenzene monohydrochloride.

Results and Discussion

The surface tension γ *vs.* molality of dye m_1 curves are shown in Fig. 1. It is seen that γ decreases with increasing m_1. However, it should be noted that the γ *vs.* m_1 curves of Ethyl Orange, C. I. Basic Orange 2, DAM, and C. I. Acid Yellow 36 consist of two portions, *i.e.*, the linear one with a small slope and the curved one with a relatively large slope. Such a break point on the curve has been observed in the cases of various surfactants.[1,2] It has been proved thermodynamically that the adsorbed film of the surfactant transforms from a gaseous to an expanded phase at the concentration of the break point.[1,2] It may be said, therefore, that the phase transition takes place in the adsorbed films of these azo dyes.

On the other hand, the γ values of the aqueous solutions of C. I. Basic Green 1 and C. I. Basic Violet 10 decrease monotonously with increase in m_1. Moreover, the γ *vs.* m_1 curve of C. I. Basic Violet 10 seems to approach a constant value. Taking into account that a large number of dyes associate to form aggregates in their aqueous solution,[3-6] the shape of the γ *vs.* m_1 curves can be attributed to the formation of aggregates. It is concluded, therefore, that the adsorbed films of C. I. Basic Green 1 and C. I. Basic Violet 10 are not attended by the phase transition within the present concentration range.

To clarify the state of adsorbed films, it is advantageous to evaluate the surface density of dye molecules. According to the thermodynamics,[1] the surface excess number of moles per unit area of a dye Γ_1^H can be

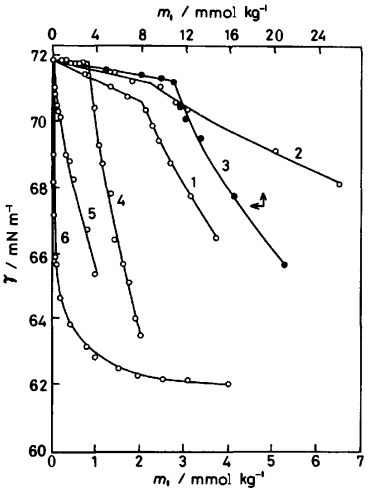

Fig. 1. Surface tension *vs.* molality curves of six dyes at 298.15 K.
1: C. I. Acid Yellow 36, 2: Ethyl Orange, 3: C. I. Basic Orange 2, 4: DAM, 5: C. I. Basic Green 1, 6: C. I. Basic Violet 10.

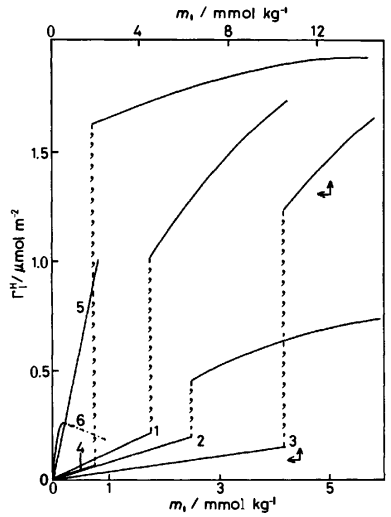

Fig. 2. Surface density *vs.* molality curves of six dyes at 298.15 K.
1: C. I. Acid Yellow 36, 2: Ethyl Orange, 3: C. I. Basic Orange 2, 4: DAM, 5: C. I. Basic Green 1, 6: C. I. Basic Violet 10.

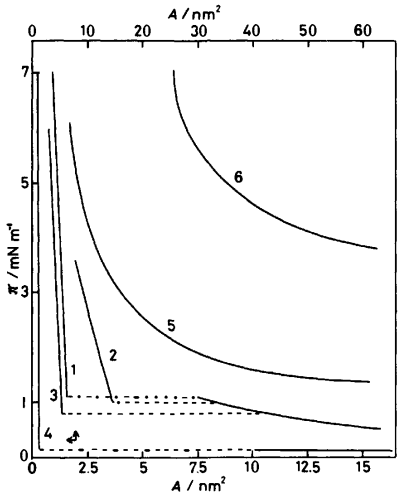

Fig. 3. Surface pressure *vs.* mean area curves of six dyes at 298.15 K.
1: C. I. Acid Yellow 36, 2: Ethyl Orange, 3: C. I. Basic Orange 2, 4: DAM, 5: C. I. Basic Green 1, 6: C. I. Basic Violet 10.

calculated by the following equation:

$$\Gamma_1^H = -m_1(\partial\gamma/\partial m_1)_{T,p}/2RT, \quad (1)$$

where R is the gas constant. Shown in Fig. 2 are the surface density *vs.* molality curves at 298.15 K under atmospheric pressure. It is seen that the values of Γ_1^H increase with increasing m_1 except for C. I. Basic Violet 10. The fact that the Γ_1^H *vs.* m_1 curve of C. I. Basic Violet 10 has a maximum is explicable by the nonideality of its aqueous solution,[7] which results from the formation of the aggregates. As is expected, the discontinuous change in Γ_1^H is observed for the dye which has the break point on γ *vs.* m_1 curve in Fig. 1. This fact confirms that the phase transition takes place in the adsorbed films and, taking into account that the surface tension is equivalent to the Gibbs free energy, it is the first order. The surface pressure π *vs.* the area per adsorbed molecule A curve is useful to elucidate the state of adsorbed film. Here, $\pi=\gamma^0-\gamma$ and $A=1/N_A\Gamma_1^H$, where γ^0 is the surface tension of pure water and N_A Avogadro's number. The results are shown in Fig. 3. It is seen that the π *vs.* A curves of the azo dyes are a typical one attended by the phase transition. Taking into account that the values of the transition pressure and area are comparable to those of the surfactants,[1,2] the phase transition can be said to take place from a gaseous state to an expanded state. On the other hand, the π *vs.* A curves of C. I. Basic Green 1 and C. I. Basic Violet 10 at 298.15 K are found to be a two-dimensional isotherm at a temperature higher than the critical temperature of the phase transition between gaseous and expanded states.

It should be noted that the azo dyes differ significantly from one another in the A value of the expanded film. However, the order of the A value is found to be the same as that of the transition pressure value except for Ethyl Orange. Taking into account that the molecules of these dyes are linear and similar in cross sections, this order represents that of the strength of the intermolecular interaction in the adsorbed film. A large value of A for Ethyl Orange may be attributable to the bulky diethylamino substituent. On the other hand, since the molecules of C. I. Basic Green 1 and C. I. Basic Violet 10 have nonlinear structures, their intermolecular interactions at the surface are too weak to cause the phase transition from the gaseous film to the expanded film.

References

1) K. Motomura, S. Iwanaga, Y. Hayami, S. Uryu, and R. Matuura, *J. Colloid Interface Sci.*, **80**, 32 (1981).
2) M. Aratono, S. Uryu, Y. Hayami, K. Motomura, and R. Matuura, *J. Colloid Interface Sci.*, **98**, 33 (1984).
3) P. Mukerjee and A. K. Ghosh, *J. Am. Chem. Soc.*, **92**, 6403 (1970).
4) D. Pugh, C. H. Giles and D. G. Duff, *Trans. Faraday Soc.*, **67**, 563 (1971).
5) B. H. Robinson, A. Löffler and G. Schwarz, *J. Chem. Soc., Faraday Trans. 1*, **69**, 56 (1973).
6) R. L. Reeves and S. A. Harkaway, *J. Colloid Interface Sci.*, **64**, 342 (1978).
7) R. Aveyard, B. J. Briscoe, and J. Chapman, *J. Colloid Interface Sci.*, **44**, 282 (1973).

Ab Initio MO Study on the 1,2-Hydrogen Migration from the Twisted Propene

Osamu KIKUCHI
Department of Chemistry, The University of Tsukuba, Sakura, Ibaraki 305
(Received January 21, 1984)

Synopsis. The 1,2-hydrogen migration from the 90°-twisted propene to the corresponding carbenes was examined on the basis of *ab initio* MO CI calculations. It was predicted that, in the polarized zwitterionic states of the twisted propene, the 1,2-hydrogen migration occurs from the negatively-charged carbon atom to the positively-charged one.

There is experimental evidence[1] that photochemical reactions of olefins involve the carbene intermediates.

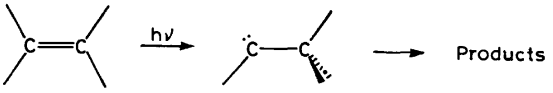

Also, it is well known that the excited state of an olefin is stabilized by a double-bond rotation which gives the twisted structure.[2] Thus a working hypothesis is used that the intermediate carbene is formed by the 1,2-hydrogen migration from the twisted structure.[3] Evleth and Sevin[4] have investigated theoretically the photodecomposition processes of ethylene and have shown that the 1,2-hydrogen migration occurs from the zwitterionic state of the 90°-twisted ethylene.

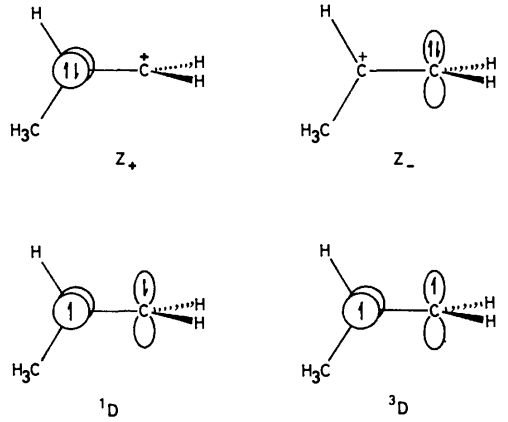

In the case of the 90°-twisted propene, there are two lower-lying zwitterionic states, Z_+ and Z_-, which have different polarizations. In each zwitterionic state, two different 1,2-hydrogen migrations are possible: the H^a-migration to form isopropylidene and the H^b-migration to form propylidene. This note intends to compare these two reaction paths on the basis of *ab initio* MO CI calculations and to predict the reactivity of the twisted unsymmetric olefins.

First, the 1,2-hydrogen migration of the twisted ethylene is described. The energy diagrams for the twisted ethylene, ethylidene, and the half-reacted species are shown in Fig. 1. Each energy level in Fig. 1 was calculated by means of the closed-shell or restricted open-shell SCF method with the 4-31G basis set[5] by using the molecular structure which was optimized with the STO-3G basis set.[6] The overall shape of Fig. 1

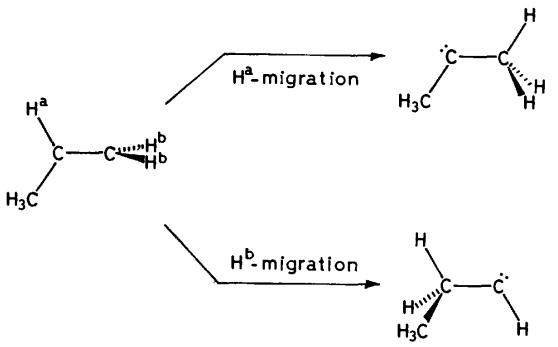

is similar to that observed in the energy variations reported by Evleth and Sevin.[3]

In the calculation of the propene system, the molecular structures of the twisted propene, propylidene, isopropylidene, and the half-reacted species were obtained by introducing a methyl group into the optimized structure of the ^1D state of the ethylene–ethylidene system. Moreover, the intermediate structures were estimated by interpolation. The MO basis set used in the CI calculation[7] was the open-shell SCF solution for the ^1D state. In the CI calculation, 41 singly- and doubly-excited configurations were selected. The potential energy curves obtained with the 4-31G basis set are shown in Fig. 2.

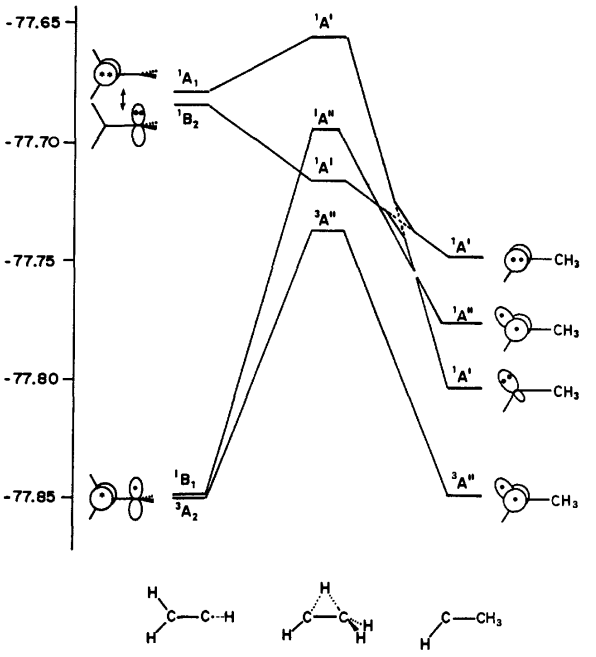

Fig. 1. Energy diagrams for the twisted (D_{2h}) ethylene, the half-reacted species, and ethylidene. The electronic structures of the twisted ethylene and ethylidene are shown schematically on both sides of the diagrams. The energies are in a.u.

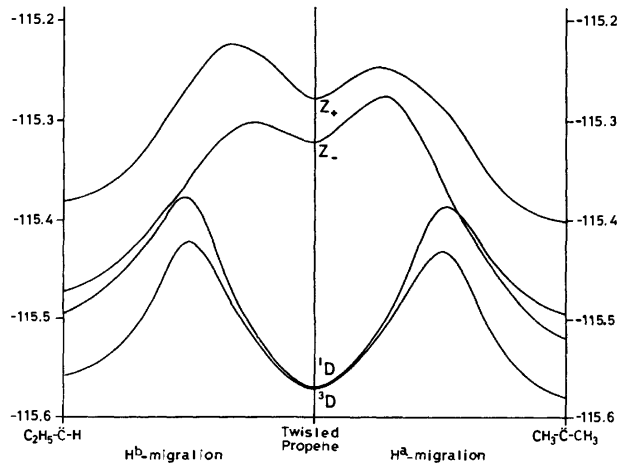

Fig. 2. Potential energy (in a.u.) curves along the hydrogen migrations from the twisted propene. The electron configurations of the twisted propene are shown in the text. The electron configurations at the carbene centers in four electronic states of propylidene and isopropylidene are same as those of ethylidene which are shown in Fig. 1.

The Z_+ and Z_- zwitterionic states of propene are largely polarized. In the Z_- state, for example, the negative charge on the C^- atom was calculated to be -1.04 and the positive charge on the C^+ atom to be $+0.69$. The Z_- state was found to be lower in energy than the Z_+ state. This may be understood simply from the electron-donating character of the methyl group.

Figure 2 indicates the preferable path for the hydrogen migration from the zwitterionic states. From the Z_- state, the H^b-migration is expected to occur easily more than the H^a-migration, while the H^a-migration is expected to occur from the Z_+ state. These two different results give a common conclusion that the 1,2-hydrogen migration from the zwitterionic states of the twisted non-symmetric olefins occurs from the negatively-charged carbon atom to the positively-charged carbon atom. Figure 2 also indicates that the singlet diradical (^1D) and the triplet diradical (^3D) of twisted olefins might not undergo the 1,2-hydrogen

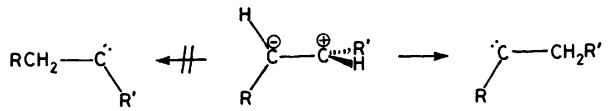

migration, since the activation energy is very large.

The preferential migration, which occurs to the positive center, involves 2 electrons (4N+2) in the C···H···C bond of the transition state, while the migration to the negative center involves 4 electrons (4N) in it. This is quite parallel to the ground state 1,2-migrations in carbonium ions and carbanions: the 1,2-migration occurs very easily in carbonium ions (2 electron transition state), while it is absent in carbanions (4 electron transition state).[8] Although the present study treats the excited states, the conclusion obtained is equivalent to the ground state reactivity which is widely accepted.

References

1) P. J. Kropp, *Pure Appl. Chem.*, **24**, 585 (1970); S. S. Hixson, *J. Am. Chem. Soc.*, **97**, 1981 (1975); Y. Inoue, S. Takamuku, and H. Sakurai, *J. Chem. Soc., Perkin Trans. 2*, **1977**, 1635; R. Srinivasan and K. H. Brown, *J. Am. Chem. Soc.*, **100**, 4602 (1978); P. J. Kropp and F. P. Tise, *ibid.*, **103**, 7293 (1981).

2) The electronic structure of twisted olefins has been discussed in connection with the sudden polarization phenomenon: L. Salem and C. Rowland, *Angew. Chem., Int. Ed. Engl.*, **11**, 92 (1972); L. Salem, *Acc. Chem. Res.*, **12**, 87 (1979); J.-P. Malrieu, *Theoret. Chim. Acta*, **59**, 251 (1981); I. Nebot-Gil and J. P. Malrieu, *J. Am. Chem. Soc.*, **104**, 3320 (1982).

3) Another model to address the 1,2-migration is the reaction from the Rydberg state of the planar olefin: P. J. Kropp, *J. Org. Photochem.*, **4**, 1 (1979).

4) E. M. Evleth and A. Savin, *J. Am. Chem. Soc.*, **103**, 7414 (1981).

5) R. Ditchfield, W. J. Hehre, and J. A. Pople, *J. Chem. Phys.*, **54**, 724 (1971).

6) R. F. Stewart, *J. Chem. Phys.*, **52**, 431 (1970).

7) Since the symmetry property of the system is not preserved during the H^b-migration and the excited singlet state can not be obtained by usual SCF calculations, the CI method was used for the propene system.

8) H. E. Zimmerman, *Acc. Chem. Res.*, **5**, 393 (1972).

Studies of Cyanamide Derivatives. Part 110. A Facile Synthesis of 2,4,6-Triureido-1,3,5-triazine and 2-Amino-4,6-diureido-1,3,5-triazine

Kokoro Iio* and Eiichi Ichikawa†

Industrial Products Research Institute, Yatabe-machi Higashi, Tsukuba-gun, Ibaraki 305

†*Faculty of Engineering, Tokyo Institute of Technology, Ookayama, Meguro-ku, Tokyo 152*

(Received December 24, 1983)

Synopsis. 2,4,6-Triureido-1,3,5-triazine and 2-amino-4,6-diureido-1,3,5-triazine were readily synthesized in high yields, 94 and 85% respectively, by the alcoholysis of 2,4,6-tris(cyanoamino)-1,3,5-triazine and 2-amino-4,6-bis(cyanoamino)-1,3,5-triazine in the presence of hydrogen chloride.

There are numerous reports[1-7] on preparations and uses of ureido-1,3,5-triazines such as 2,4-diamino-6-ureido-1,3,5-triazine (**1**), 2-amino-4,6-diureido-1,3,5-triazine (**2**), and 2,4,6-triureido-1,3,5-triazine (**3**). However, there are still problems with the preparations of these compounds.[8,9] In our previous paper,[10,11] we reported the preparation of **1** and its properties. This paper will describe a facile method of synthesizing **2** and **3** from the corresponding cyanoamino-1,3,5-triazines and will clarify their properties in acidic and alkaline aqueous solutions.

An attempted cyclotrimerization of linear cyanoureido compounds such as cyanourea and *N*-cyano-*O*-ethylisourea did not give **3**. Cyanourea, however, gave 1-carbamoyl-3-cyanoguanidine and 1-cyanobiuret,[12] and *N*-cyano-*O*-ethylisoures gave 2-amino-4-ethoxy-6-ureido-1,3,5-triazine (**4**) in the presence of hydrogen chloride, using sulfolane as a solvent. The isoureido group attached to 1,3,5-triazine ring might be converted into the ureido group by the action of hydrogen chloride. Furthermore, acid hydration of cyanoamino-1,3,5-triazines failed to give the corresponding ureido-1,3,5-triazines, except for **1**.[10]

Alcoholysis of 2,4,6-tris(cyanoamino)-1,3,5-triazine in the presence of hydrogen chloride gave **3** hydrochloride. During the reaction, methyl chloride was evolved and identified by its mass spectrum. The free **3** was given in 94% yield by the treatment of its hydrochloride with a dilute sodium hydroxide solution. **3** was slightly soluble in water and ordinary organic solvents, but could be recrystallized from a hot dilute nitric acid solution as the nitrate.

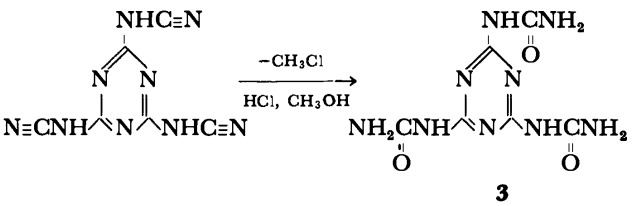

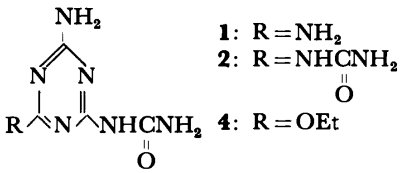

1: R = NH_2
2: R = $NHCNH_2$ (O)
4: R = OEt

In a similar manner, **2** was synthesized from 2-amino-4,6-bis(cyanoamino)-1,3,5-triazine in 85% yield. **2** was also slightly soluble in water and organic solvents, but could be recrystallized from a hot dilute sulfuric acid solution as the sulfate.

It was reported[10] that the alkaline hydrolysis of **1** gave melamine, carbon dioxide, and ammonia in high yields. The similar alkaline hydrolysis of **3**, however, gave ammeline instead of melamine, along with carbon dioxide and ammonia. In the case of **2**, melamine, ammeline, carbon dioxide, and ammonia were all obtained.

Acid hydrolyses of **2** and **3** with 2 mol dm^{-3} of hydrochloric acid were examined. The reaction was followed by the IR spectrum of the reaction mixture. Small amounts of the solution were taken out at 30 min intervals and evaporated to dryness. In the case of **3**, cyanuric acid was readily detected after 30 min refluxing the solution. Cyanuric acid and urea were obtained in 95 and 26% yields respectively after 4 h. In the case of **2**, cyanuric acid was detected after 1 h. Cyanuric acid, ammelide and urea were obtained in 74, 2 and 34% yields respectively after 2 h. These results suggest that the hydrolysis of **2** and **3** is liable to take place on the carbon atom of the 1,3,5-triazine ring attached with ureido group, and that the preparation of **2** and **3** by the acid hydration of corresponding cyanoamino-1,3,5-triazines is very difficult.

Experimental

The melting points are uncorrected. The IR spectra were taken with a Hitachi EPI-2 spectrometer. The UV spectra were taken with a Hitachi 624 spectrometer. The NMR spectra were measured with a Hitachi R-24A spectrometer using TMS as an internal standard. The mass spectra were taken with a JEOL JMS-D100 mass spectrometer.

2-Amino-4-ethoxy-6-ureido-1,3,5-triazine (4). Hydrogen chloride (1.82 g, 0.05 mol) was introduced into a stirred solution on *N*-cyano-*O*-ethylisourea (5.66 g, 0.05 mol) in 20 mol of sulfolane at room temperature. After 2 h at 70 °C, the solution was poured into a large amount of water. The precipitate of **4** was filtered and recrystallized from water. The yield was 2.52 g (51%). Mp 220 °C. Found: C, 36.10; H, 4.99; N, 42.10%; M^+, 198. Calcd for $C_6H_{10}N_6O_2$: C, 36.36; H, 5.09; N, 42.42%; M^+, 198. IR (KBr) 1700 (C=O) and 815 cm^{-1} (1,3,5-triazine ring). UV (H_2O) 212.4 nm (log ε 4.55). NMR (DMSO-d_6) δ=1.24 (3H, CH_3), 4.25 (2H, CH_2), 7.10, 7.36, 8.60, and 9.67 (5H, m).

2,4,6-Triureido-1,3,5-triazine (3). Hydrogen chloride (7.29 g, 0.2 mol) was introduced into a suspension of the trisodium salt of 2,4,6-tris(cyanoamino)-1,3,5-triazine[13] (5.34 g, 166 mmol) in 40 ml of methanol under cooling below 5 °C. The reaction mixture was stirred for 2 h at room temperature, and then heated to reflux for 2 h, evolving methyl

chloride, which was identified by the mass spectrometer, MS m/z 52 and 50 (M^+). After cooling, the precipitate was filtered and washed with a dilute sodium hydroxide solution and water. The yield of **3** was 4.52 g (94%). **3** was recrystallized from a hot dilute nitric acid solution (0.50 g of **3**/4 mol dm^{-3} HNO_3 180 ml) as the nitrate: mp>360 °C; Found: C, 21.19; H, 3.56; N, 41.62; H_2O, 5.87%. Calcd for $C_6H_9N_9O_3 \cdot HNO_3 \cdot H_2O$: C, 21.43; H, 3.60; N, 41.66; H_2O, 5.36%. IR (KBr) 1720, 1700 (C=O), and 795 cm^{-1} (1,3,5-triazine ring). UV (H_2O) 215.5 (log ε 4.86) and *ca.* 247.0 nm (sh, 4.08).

2-Amino-4,6-diureido-1,3,5-triazine (2). **2** was synthesized from 2-amino-4,6-bis(cyanoamino)-1,3,5-triazine[14] by the same method as above, in 85% yield. **2** was recrystallized from the hot dilute sulfuric acid solution (0.50 g of **2**/10% H_2SO_4 100 ml) as the sulfate: mp>360 °C; Found: C, 19.07; H, 3.43; N, 36.40%. Calcd for $C_5H_8N_8O_2 \cdot H_2SO_4$: C, 19.36; H, 3.23; N, 36.12%. IR (KBr) 1715 (C=O) and 790 cm^{-1} (1,3,5-triazine ring). UV (H_2O) 216.0 (log ε 4.62) and *ca.* 242.5 nm (sh, 3.86).

Alkaline Hydrolysis. According to the previously reported method,[10] **3** gave ammeline (43%), barium carbonate (83%), and ammonia (82%).

Similarly **2** gave melamine (33%), ammeline (9%), barium carbonate (62%), and ammonia (57%).

Acid Hydrolysis. **3** (0.97 g, 1/300 mol) was refluxed in 40 ml of 2 mol dm^{-3} of hydrochloric acid for 4 h. After the reaction mixture had been evaporated to dryness under reduced pressure, the residue was washed with a small amount of water to give 3.30 g (77%) of cyanuric acid. The filtrate was neutralized with dilute sodium hydroxide solution and the saturated melamine solution was added to give 0.13 g (18%) of melamine cyanurate. The filtrate was evaporated and extracted with ethanol to give 0.32 g (26%) of urea as the nitrate. Ammonia was detected in the solution.

In a similar manner, **2** was refluxed in 2 mol dm^{-3} of hydrochloric acid for 2 h, and gave cyanuric acid (70%), melamine cyanurate (4%), urea nitrate (34%), and ammelide (2%). Ammonia was also detected in the solution. Products were confirmed by comparing their IR spectrum and melting points with those of an authentic sample.

References

1) K. Muraoka, I. Sugaya, H. Noda, K. Horie, S. Suda, and Y. Ooya, Jpn. Patent 70-27835 (1970).
2) H. H. Grossmann, K. H. Burg, and G. Sextro, Ger. Offen. 2348808 (1975).
3) M. Taguchi and M. Aramaki, Jpn. Patent 69-04656 (1969).
4) A. Hantzsch and H. Bauer, *Chem. Ber.*, **38**, 1005, (1905).
5) G. F. D'Alelio, U. S. Patent 2394042 (1946).
6) F. L. Scott and H. Q. Smith, U. S. Dept. Com., Office Tech. Serv. PB Rept., 152012 (1960); U. S. Patent 3101335 (1963).
7) H. Bieling, M. Radüchel, G. Wenzel, and H. Beyer, *J. Prakt. Chem.*, **28**, 325, (1965).
8) E. A. Werner, *J. Chem. Soc.*, **103**, 2275, (1913).
9) I. Honda, A. Murata, A. Nisikawa, M. Maekawa, and Y. Oshima, *Kogyo Kagaku Zasshi*, **71**, 529, (1968); Jpn. Patent 12429 (1967).
10) E. Ichikawa, T. Takizawa, and K. Odo, *Yuki Gosei Kagaku Kyokai Shi*, **32**, 936, (1974).
11) K. Iio, E. Ichikawa, and K. Odo, *Yuki Gosei Kagaku Kyokai Shi*, **32**, 513, (1974).
12) K. Iio, *Bull. Chem. Soc. Jpn.*, **57**, 625, (1984).
13) W. Madelung and E. Kern, *Justus Liebigs Ann. Chem.*, **427**, 26, (1922).
14) T. Suyama and K. Odo, *Yuki Gosei Kagaku Kyokai Shi*, **29**, 298, (1971).

Reaction of *N*-Aroyl-*N*-*t*-butylhydroxylamines with Thionyl Chloride. Synthesis of Substituted Benzohydroximoyl Chlorides

Yuzuru UCHIDA* and Seizi KOZUKA†

Department of Applied Chemistry, Osaka Institute of Technology, Asahi-ku, Osaka 535

†*Department of Applied Chemistry, Faculty of Engineering, Osaka City University, Sumiyoshi-ku, Osaka 558*

(Received December 28, 1983)

Synopsis. The reaction of *N*-benzoyl-*N*-*t*-butylhydroxylamine with thionyl chloride in carbon tetrachloride gave *O*-chlorosulfinylbenzohydroximoyl chloride as the main product. On treating with ethanol, the compound gave benzohydroximoyl chloride in good yield. The reaction was applied to the synthesis of substituted benzohydroximoyl chlorides.

We have previously shown that *N*-[2-(methylthio)-benzoyl]-*N*-alkylhydroxylamines gave 2-substituted 1,2-benzisothiazol-3(2*H*)-ones in good yields on treating with thionyl chloride and pyridine.[1] In the course of our study on the reaction of the hydroxylamine derivatives, the reaction of *N*-benzoyl-*N*-*t*-butylhydroxylamine with thionyl chloride was found to give benzohydroximoyl chloride in good yield. Benzohydroximoyl chloride and its derivatives have been exensively used for the synthesis of heterocyclic compounds as precursors of benzonitrile oxides.[2] We wish to report here an efficient method for the synthesis of substituted benzohydroximoyl chlorides.

Results and Discussion

N-Aroyl-*N*-*t*-butylhydroxylamines (**1**) were prepared by hydrolysis of *N*-aroyl-*O*-benzoyl-*N*-*t*-butylhydroxylamines with sodium hydroxide in methanol, as reported previously.[3] The reaction of **1** with thionyl chloride was carried out at −30 °C. A detailed product analysis was performed for the reaction of **1a** with thionyl chloride in carbon tetrachloride. After removal of the solvent and the excess thionyl chloride, the IR spectrum of the reaction product showed the characteristic bands of *O*-chlorosulfinylbenzohydroximoyl chloride (**4a**) together with weak bands at 1770 cm^{-1} and 1330 cm^{-1}. On treating with ethanol, the product gave benzohydroximoyl chloride (**5a**) (78%), benzohydroxamic acid (**7a**) (8%) ethyl benzoate (**8a**) (4%), and diethyl sulfite. The results suggest that the reaction product is a mixture of **4a**, 5-phenyl-1,3,2,4-dioxathiazole 2-oxide (**6a**), and benzoyl chloride. *t*-Butyl chloride was detected by ^{1}H-NMR spectrum of the reaction mixture. Chloride **4a** was difficult to isolate from the reaction mixture, because **4a** was sensitive to heat and moisture. The compound **4a** and **6a**[4] were prepared by the reactions of **5a** and **7a** with thionyl chloride, respectively, and the reactions of **4a** were examined. On heating of **4a** in boiling toluene, benzonitrile was formed in 82% yield. When **4a** was treated with aqueous acetone, benzohydroximoyl chloride was obtained in 90% yield. On treating **4a** with ethanol, **5a** and diethyl sulfite were formed in 90 and 70% yields, respectively.

The reaction of **1a** with thionyl chloride was carried out in various solvents, and the reaction mixture was treated with ethanol. Benzohyxroximoyl chloride (**5a**) was obtained as the main product, together with small amounts of **7a**, **8a**, and diethyl sulfite. No significant difference was observed in the yields of **5a**, except for the reaction in acetonitrile. When the reaction of **1a** with thionyl chloride was carried out in acetonitrile, **5a** and **7a** were formed in 20 and 45% yields, respectively after treatment of the reaction mixture with ethanol. Ethyl phenylcarbamate (**9a**) and 3-phenyl-5-methyl-1,2,4-oxadiazole (**10a**) were also obtained in 9 and 27% yields, respectively, by the reaction in acetonitrile.

Similarly, the reaction of *N*-aroyl-*N*-*t*-butylhydroxylamines (**1b—h**) with thionyl chloride in carbon tetrachloride gave *m*- and *p*-substituted benzohydroximoyl chlorides (**5b—h**) after treatment with ethanol. The results are summarized in Table 1. On the other hand, *N*-(*o*-methoxybenzoyl)-*N*-*t*-butylhydroxylamine (**1i**) and *N*-(*o*-chlorobenzoyl)-*N*-*t*-butylhydroxylamine (**1j**) did not give the corresponding benzohydroximoyl chlorides under the same reaction conditions.

Although benzohydroximoyl chlorides are usually prepared by chlorination of benzaldehyde oximes,[5-8] *p*-methoxybenzohydroximoyl chloride is difficult to obtain by chlorination of *p*-methoxybenzaldehyde oxime. In the chlorination, the strong electron-donating substituent facilitates chlorination on the aromatic ring, giving a mixture of chlorinated products.[9,10] As given in Table 1, the present reaction is successfully applied to the synthesis of *m*- and *p*-substituted benzohydroximoyl chlorides bearing both electron-donating and electron-withdrawing substituents. In addition, the present method is useful for the synthesis of **5e**, which has a sulfide group which is usually oxidized during the chlorination.

The most probable mechanism for the present reaction is shown in Scheme 1. The reaction proceeds through intermediates, *N*-aroyl-*O*-chlorosulfinyl-*N*-*t*-

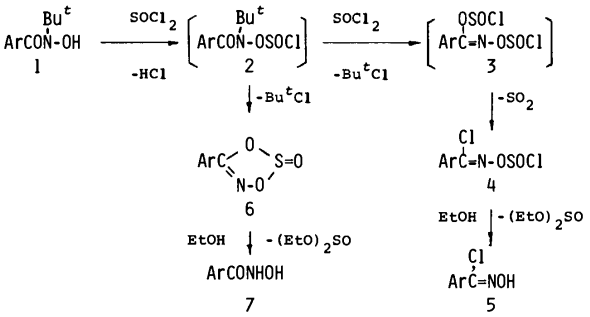

Scheme 1.

Table 1. Yields of substituted benzohydroximoyl chlorides

Substrate 1	Ar	Solvent	Product	Yield[a] %	Mp θ_m/°C
1a	C_6H_5	CCl_4	**5a**	78	51—52 (lit,[5] 48—52)
1a		CH_2Cl_2	**5a**	66	
1a		CS_2	**5a**	78	
1a		C_6H_6[b]	**5a**	77	
1a		Hexane	**5a**	66	
1a		CH_3CN	**5a**	20[c]	
1b	*p*-$CH_3C_6H_4$	CCl_4	**5b**	66	71—72 (lit,[6] 68—69)
1c	*p*-$CH_3OC_6H_4$	CCl_4	**5c**	62	88—89 (lit,[9] 88—89)
1d	*m*-$CH_3OC_6H_4$	CCl_4	**5d**	88	66—67
1e	*p*-$CH_3SC_6H_4$	CCl_4	**5e**	73	91.5—92.5
1f	*p*-ClC_6H_4	CCl_4	**5f**	88	91.5—92.5 (lit,[7] 88.5—89.5)
1g	*m*-ClC_6H_4	CCl_4	**5g**	74	68—69 (lit,[7] 69—70)
1h	*p*-$NO_2C_6H_4$	CCl_4[d]	**5h**	87	125.5—126.5 (lit,[7] 124—125)

a) Isolated yields. b) The reaction was carried out at 5 °C for 5 h and allowed to stand overnight. c) Compounds **7a**, **8a**, and **10a** were obtained in 45, 9, and 27% yields, respectively. d) The reaction was carried out at 25 °C for 15 h.

butylhydroxylamines (**2**), and bis(chlorosulfinyl) compound (**3**). The intermediates **2** and **3** are transformed to **6** and **4** by the subsequent eliminations of *t*-butyl chloride and sulfur dioxide, respectively. In the reaction of **1** with thionyl chloride in acetonitrile, oxadiazole **10** would be formed by cycloaddition of acetonitrile and benzonitrile oxides.

Experimental

Preparation of N-*Aroyl*-N-*t*-*butylhydroxylamines (1).* *N*-Aroyl-*N*-*t*-butylhydroxylamines (**1**) were prepared by hydrolysis of the corresponding *N*-aroyl-*O*-benzoyl-*N*-*t*-butylhydroxylamines with sodium hydroxide in methanol, as reported previously.[3]

Reaction of N-*Aroyl*-N-*t*-*butylhydroxylamines (1) with Thionyl Chloride.* A typical run was as follows: Thionyl chloride (10 g, 84 mmol) was added to a stirred mixture of *N*-benzoyl-*N*-*t*-butylhydroxylamine (**1a**) (1.932 g, 10 mmol) and carbon tetrachloride (30 cm³) at −30 °C. The mixture was stirred at −30 °C for 5 h, and allowed to stand overnight at room temperature. The solvent and excess thionyl chloride were evaporated under reduced pressure. Ethanol (10 cm³) was added to the residue, and the mixture was stirred at room temperature for 2 h. After removal of the ethanol, the residue was separated by column chromatography on silica gel, using dichloromethane and ethyl acetate as the eluents. The fractions obtained by dichloromethane as the eluent gave **5a** (1.218 g, 78%) and **8a** (0.062 g, 4%). Benzohydroxamic acid (**7a**) (0.110 g, 8%) was obtained with the chromatography with ethyl acetate as the eluent. Similarly, the reaction of **1b**—h with thionyl chloride gave **5b**—h. **5d**; Found: C, 51.78; H, 4.24; N, 7.54%. Calcd for $C_8H_8ClNO_2$: C, 51.77; H, 4.34; N, 7.55%. **5e**; Found: C, 47.64; H, 3.84; N, 6.87%. Calcd for C_8H_8ClNOS: C, 47.64; H, 4.00; N, 6.95%.

Preparation of O-Chlorosulfinylbenzohydroximoyl Chloride (4a). Thionyl chloride (5.0 g, 42 mmol) was added to a solution of benzohydroximoyl chloride (1.555 g, 10 mmol) in dichloromethane (30 cm³) and the mixture was allowed to stand overnight. Removal of the solvent and excess thionyl chloride *in vacuo* gave *O*-chlorosulfinylbenzohydroximoyl chloride (**4a**) (2.303 g, 97%) as a colorless oil. IR (neat) 1590, 1580, 1240, 880, 760, 690, and 600 cm⁻¹.

Preparation of 5-Phenyl-1,3,2,4-dioxathiazole 2-oxide (6a). A mixture of benzohydroxamic acid (**7a**) (2.742 g, 20 mmol) and thionyl chloride (10 g, 84 mmol) in dichloromethane (30 cm³) was allowed to stand for 6 h at 30 °C. The excess thionyl chloride and the solvent were evaporated under reduced pressure to give (**6a**) (3.554 g, 97%). IR (neat) 1605, 1325, 1240, 1060, 850, and 720 cm⁻¹.

Thermal Decomposition of 4a A solution of **4a** (0.246 g, 1.03 mmol) in toluene (10 cm³) was refluxed for 4 h. The products were analyzed by GLC.

Hydrolysis of 4a. A solution of **4a** (0.463 g, 1.95 mmol) in acetone (8 cm³) and water (2 cm³) was allowed to stand overnight. After evaporation of acetone, the residue was extracted with diethyl ether. The extract was washed with water and dried over anhydrous calcium chloride. Removal of the ether gave **5a** (0.272 g, 90%).

Alcoholysis of 4a. A solution of **4a** (0.463 g, 1.95 mmol) in ethanol (10 cm³) was allowed to stand for 2 h. The reaction mixture was subjected to GLC analysis, and the remainder was chromatographed on silica gel to isolate the products. Diethyl sulfite (70%, GLC) and **5a** (0.272 g, 90%) were obtained.

References

1) Y. Uchida and S. Kozuka, *Bull. Chem. Soc. Jpn.*, **55**, 1183 (1982).
2) For example: R. Huisgen, *Angew. Chem.*, **75**, 604 (1963).
3) Y. Uchida, Y. Hashimoto, and S. Kozuka, *Bull. Chem. Soc. Jpn.*, **53**, 2309.
4) J. Sauer and K. K. Mayer, *Tetrahedron Lett.*, **1968**, 319.
5) P. Rajagopalan, B. G. Advani, and C. N. Talaty, *Org. Synth.*, Coll. Vol. V, 504 (1973).
6) R. H. Wiley and B. J. Wakefield. *J. Org. Chem.*, **25**, 546 (1960).
7) K. J. Dignam, A. F. Hegary, and P. L. Quain, *J. Chem. Soc., Perkin Trans. 2*, **1977**, 1457.
8) A. Werner and H. Buss, *Ber. Dtsch. Chem. Ges.*, **27**, 2197 (1894).
9) C. R. Kinney, E. W. Smith, B. L. Woolley, and A. R. Willey, *J. Am. Chem. Soc.*, **55**, 3418 (1933).
10) Y. H. Chiang, *J. Org. Chem.*, **36**, 2146 (1971).

Shinjulactones G and H, New Bitter Principles of *Ailanthus altissima* SWINGLE

Masami ISHIBASHI, Shin YOSHIMURA, Takahiko TSUYUKI, Takeyoshi TAKAHASHI,* and Kazuhiro MATSUSHITA†

Department of Chemistry, Faculty of Science, The University of Tokyo, Hongo, Bunkyo-ku, Tokyo 113

†*Application Center, Scientific Instrument Project, JEOL Ltd., Nakagami, Akishima, Tokyo 196*

(Received February 3, 1984)

Synopsis. Two bitter quassinoids, shinjulactones G and H were isolated from *Ailanthus altissima* SWINGLE and their structures were determined to be 1β,11β,12α,20-tetrahydroxypicras-3-ene-2,16-dione and 2α,12β-dihydroxypicrasane-1,11,16-trione, respectively, by spectral and chemical means.

In the continuation of our studies on the bitter principles of Simaroubaceous plants, the structure determination of six quassinoids isolated from *Ailanthus altissima* SWINGLE (Japanese name: Shinju or Niwaurushi) has been reported.[1] Two new bitter principles named shinjulactones G and H (**1** and **2**), have been isolated from the same plant. This paper describes the structure determination of **1** and **2**.

Aqueous extract of the root bark of *A. altissima* was continuously extracted with dichloromethane. The organic layer was subjected to separation by a silica-gel column chromatography and then further purified by a partition column chromatography on silicic acid to afford two minor bitter quassinoids, shinjulactone G (**1**, *ca.* 0.0003% yield) and shinjulactone H (**2**, *ca.* 0.001% yield) together with other quassinoids.

Shinjulactone G (**1**), mp 274—277 °C, gave a weak molecular ion peak in high resolution mass spectrum, leading to the molecular formula, $C_{20}H_{28}O_7$, for **1**. IR and ^{1}H NMR spectra of **1** revealed the presence of a vinyl methyl, a tertiary methyl, a secondary methyl, a hydroxymethyl, and an α,β-unsaturated carbonyl, and a lactone grouping. ^{1}H NMR decoupling experiment suggested that the structure of shinjulactone G (**1**) might be formulated as 20-hydroxyklaineanone. Configuration of the hydroxyl groups at C-11 and C-12 was determined by coupling constants ($J_{11,12}$=3 and $J_{12,13}$=2.5 Hz). The structure of shinjulactone G (**1**) was further confirmed by chemical conversion of **1** into chaparrinone triacetate (**3**).[2] According to the procedure described for klaineanone[2] and 15-hydroxyklaineanone,[3] shinjulactone G (**1**) was acetylated to give a triacetate (**4**), which showed an IR absorption band at 3450 cm^{-1} and a doublet signal at δ 7.84 (J=5 Hz) due to a hydroxyl group in the ^{1}H NMR of **4**. Since the doublet signal coupled with a broad singlet signal due to $C_{(11)}$-H at δ 5.05 with the coupling constant J=5 Hz, the hydroxyl group was concluded to exist at C-11. Jones oxidation of **4** afforded chaparrinone triacetate (**3**), which was completely identical with an authentic sample. Thus, the structure of shinjulactone G (**1**) was determined to be 1β,11β,12α,20-tetrahydroxypicras-3-ene-2,16-dione.

Shinjulactone H (**2**), mp 135—139 °C, was shown to have a molecular formula, $C_{20}H_{28}O_6$, by high resolution mass spectrum. ^{1}H (Table 1) and ^{13}C NMR spectra indicated the presence of two tertiary methyls, two secondary methyls, two isolated carbonyls, and a lactone grouping. The IR absorption band at 3450 cm^{-1} and two doublet signals at δ 81.9 and 69.9 in the ^{13}C NMR spectrum of **2** indicated that the remaining two oxygen atoms are ascribed to hydroxyl groups. These spectral features are very similar to those of amarolide (**5**).[4,5] Acetylation of shinjulactone H (**2**) gave a diacetate (**6**) which was not identical with amarolide diacetate (**7**).[5] The ^{1}H NMR spectral comparison between shinjulactone H (**2**) and amarolide (**5**) could reveal a difference in the relative position of hydroxyl and carbonyl groups in ring C. Shinjulactone H (**2**) showed a double doublet at δ 4.01 with coupling constants J=11 and 3 Hz and a multiplet at δ 2.16, assignable to $C_{(12)}$-H and $C_{(13)}$-H, respectively. On irradiation at δ 4.01, the multiplet signal resulted in a change of its shape. When D_2O was added, the double doublet was changed into a doublet with a coupling constant J=11 Hz, which implies the protons at C-12 and C-13 are in trans-diaxial relationship and the former was coupled with the hydroxyl proton at C-12. From these observations together with a singlet signal at δ 2.94 due to $C_{(9)}$-H, the structure (**2**) was proposed for shinjulactone H. The proposed structure (**2**) was firmly established by a preparation of shinjulactone H diacetate (**6**) from known chaparrolide (**8**).[6] Acetylation of chaparrolide (**8**) afforded two diacetates (**9** and **10**) and a known triacetate, 1,2,12-tri-*O*-acetylchaparrolide (**11**).[6] From the ^{1}H NMR spectra, the diacetates (**9** and **10**) were assigned to be 2,12- and 1,2-di-*O*-acetyl derivatives, respectively. 2,12-Di-*O*-acetylchaparrolide (**9**) was oxidized with Jones reagent to give a keto acetate (**6**), which was completely identical with the diacetate (**6**) derived from shinjulactone H (**2**). The structure of shinjulactone H (**2**) was, therfore, concluded to be 2α,12β-dihydroxypicrasane-1,11,16-trione.[7]

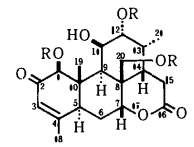

1 R=H
4 R=Ac

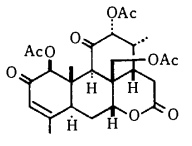

3

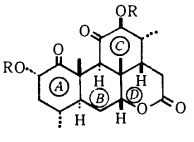

2 R=H
6 R=Ac

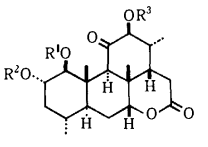

8 R^1=H, R^2=H, R^3=H
9 R^1=H, R^2=Ac, R^3=Ac
10 R^1=Ac, R^2=Ac, R^3=H
11 R^1=Ac, R^2=Ac, R^3=Ac

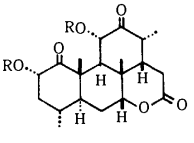

5 R=H
7 R=Ac

Table 1. ^{1}H NMR Spectra at 400 MHz of Shinjulactones G and H (**1** and **2**)[a,b]

	1		**2**	
	δ	J	δ	J
1-H	4.18 s			
2-H			4.77 ddd	12, 7.5, 4.5
3-H	6.15 br s		1.92—2.05[c]	
3-H′			2.45 ddd	13, 7.5, 3.5
4-H			1.92—2.05[c]	
5-H	3.15—3.18[c]		1.39 ddd	12.5, 12.5, 3
6-H	2.22 ddd	15, 3.5, 3.5	2.04 ddd	15, 3, 3
6-H′	2.27 ddd	15, 12.5, 2.5	1.87 ddd	15, 12.5, 2.5
7-H	5.34 dd	3.5, 2.5	4.31 dd	3, 2.5
9-H	2.85 d	2.5	2.94 s	
11-H	5.87 br s[d]			
12-H	4.14 br s[d]		4.01 dd	11, 3
13-H	2.93 m[d]		2.16 m	
14-H	3.15—3.18[c,d]		1.92—2.05[c]	
15-H	4.33 dd	19, 11.5	2.70 dd	19, 13
15-H′	2.97 dd	19, 7	2.84 dd	19, 7
4-CH_3	1.76 br s		0.95 d	6.5
8-CH_3			1.13 s[e]	
10-CH_3	1.53 s		1.58 s[e]	
13-CH_3	1.23 d	7	1.20 d	7
20-H	5.55 d	12		
20-H′	4.38 d	12		
2-OH			3.43 d	4.5
12-OH			3.53 d	3

a) δ and J are expressed in ppm and Hz, respectively. b) Measured in C_5D_5N for **1** and in $CDCl_3$ for **2**. c) Signals were overlapped. d) Coupling constants were determined by decoupling experiment; $J_{9,11}=2.5$, $J_{11,12}=3$, $J_{12,13}=2.5$, and $J_{13,14}=4.5$ Hz. e) Signals may be reversed.

Experimental[8]

Shinjulactone G (1). Mp 274—277 °C; $[\alpha]_D^{26}$ +6.5° (*c* 1.2, pyridine); IR (KBr) 3470, 1730, 1700, 1675, and 1280 cm^{-1}; UV (ethanol) 237 nm (ε 5300); ^{1}H NMR (Table 1); ^{13}C NMR (pyridine-d_5) δ 12.4q, 15.5q, 22.4q, 26.4t, 27.9d, 29.4t, 36.2d, 41.7d, 42.4s, 43.3d, 48.8s, 61.8t, 74.2d, 77.7d, 79.7d, 85.0d, 124.8d, 165.1s, 172.2s, and 199.6s; MS *m/z* (%) 380 (M$^+$), 362 (100), 347 (27), and 151 (50); Found: *m/z* 380.1824. Calcd for $C_{20}H_{28}O_7$: M, 380.1834.

1,12,20-Tri-O-acetylshinjulactone G (4). Shinjulactone G (**1**; 7 mg) was acetylated in the usual manner to afford **4** (8 mg), mp 130—134 °C, IR (film) 3450, 1735, 1680, and 1235 cm^{-1}; ^{1}H NMR (pyridine-d_5) δ 0.94 (3H, d, J=7 Hz), 1.65 (3H, s), 1.80 (3H, br s), 1.90, 2.07, and 2.18 (each 3H, s), 5.05 (1H, br s), 5.73 (1H, s), 5.96 (1H, d, J=13 Hz), 6.10 (1H, br s), and 7.84 (1H, d, J=5 Hz); MS *m/z* (%) 506 (M$^+$; 7), 488 (9), 446 (70), and 404 (100); Found: *m/z* 506.2104. Calcd for $C_{26}H_{34}O_{10}$: M, 506.2150.

Oxidation of 4 with Jones Reagent. 1,12,20-Tri-*O*-acetylshinjulactone G (**4**; 7.5 mg) was treated with Jones reagent (in excess) in acetone (6 mL) at room temperature for 8 h. The usual work-up afforded chaparrionone triacetate (**3**; 5 mg), which was identified with an authentic sample by TLC, ^{1}H NMR, IR, and mass spectra.

Shinjulactone H (2). Mp 135—139 °C; $[\alpha]_D^{21}$ −14° (*c* 3.9, ethanol); IR (KBr) 3450, 1720, and 1230 cm^{-1}; ^{1}H NMR (Table 1); ^{13}C NMR ($CDCl_3$) δ 15.2q, 15.2q, 18.2q, 23.8q, 26.7t, 27.6t, 27.9d, 39.2s, 39.4d, 45.3d, 46.6t, 46.8d, 47.0d, 48.8s, 69.9d, 76.2d, 81.9d, 169.3s, 208.2s, and 213.0s; MS *m/z* (%) 364 (M$^+$; 23), 346 (43), 321 (46), and 57 (100); Found: *m/z* 364.1877. Calcd for $C_{20}H_{28}O_6$: M, 364.1884.

2,12-Di-O-acetylshinjulactone H (6). Acetylation of shinjulactone H (**2**; 10 mg) gave **6** (12 mg), mp 146—150 °C; IR (KBr) 1745, 1730, and 1230 cm^{-1}; ^{1}H NMR ($CDCl_3$) δ 0.96 (3H, d, J=6.5 Hz), 1.04 (3H, d, J=6 Hz), 1.17 (3H, s), 1.60 (3H, s), 2.11 and 2.17 (each 3H, s), 4.26 (1H, t, J=3 Hz), 5.12 (1H, d, J=12.5 Hz), and 5.77 (1H, dd, J=13 and 7 Hz); MS *m/z* (%) 448 (M$^+$; 9), 406 (10), 388 (100), and 328 (21); Found: *m/z* 448.2089. Calcd for $C_{24}H_{32}O_8$: M, 448.2096.

Acetylation of Chaparrolide (8). Chaparrolide (**8**; 61 mg) was acetylated with acetic anhydride (1 mL) in pyridine (2 mL) at room temperature for 6 h. After the usual work-up, the reaction mixture was separated by a column chromatography (silica gel; 30 g). Elution with benzene–acetone (9:1) afforded **11** (*ca.* 30 mg), **10** (*ca.* 25 mg), and **9** (16 mg) in succession. **9**: mp 152—154 °C; IR (KBr) 3450, 1735, and 1250 cm^{-1}; ^{1}H NMR ($CDCl_3$) δ 0.88 (3H, d, J=6.5 Hz), 1.06 (3H, d, J=6 Hz), 1.15 (3H, s), 1.36 (3H, s), 2.03 and 2.16 (each 3H, s), 3.17 (1H, dd, J=9 and 5 Hz), 4.31 (1H, t, J=3 Hz), 4.87 (1H, m), and 4.89 (1H, d, J=11.5 Hz); MS *m/z* (%) 450 (M$^+$; 7), 390 (100), 348 (43), and 330 (54); Found *m/z* 450.2226. Calcd for $C_{24}H_{34}O_8$: M, 450.2253. **10**: mp 167—168 °C; IR (KBr) 3450, 1735, and 1235 cm^{-1}; ^{1}H NMR ($CDCl_3$) δ 0.90 (3H, d, J=6 Hz), 1.06 (3H, s), 1.12 (3H, d, J=6.5 Hz), 1.46 (3H, s), 1.86 and 1.97 (each 3H, s), 3.27 (1H, d, J=5 Hz), 3.80 (1H, dd, J=10.5 and 5 Hz), 4.28 (1H, t, J=2.5 Hz), 4.62 (1H, d, J=10 Hz), and 5.06 (1H, m); MS *m/z* (%) 450 (M$^+$; 24), 390 (84), 348 (57), and 330 (100); Found: *m/z* 450.2238. Calcd for $C_{24}H_{34}O_8$: M, 450.2253.

Oxidation of 9 with Jones Reagent. 2,12-Di-*O*-acetylchaparrolide (**9**; 16 mg) was treated with Jones reagent (in excess) at 0 °C for 1.5 h. After the usual work-up, a keto acetate (**6**; 12.5 mg) was obtained and was identified with 2,12-di-*O*-acetylshinjulactone H (**6**) by TLC, ^{1}H NMR, IR, and mass spectra.

References

1) M. Ishibashi, T. Tsuyuki, T. Murae, H. Hirota, T. Takahashi, A. Itai, and Y. Iitaka, *Bull. Chem. Soc. Jpn.*, **56**, 3683 (1983); H. Naora, M. Ishibashi, T. Furuno, T. Tsuyuki, T. Murae, H. Hirota, T. Takahashi, A. Itai, and Y. Iitaka, *ibid.*, **56**, 3694 (1983).

2) J. Polonsky and N. Bourguignon-Zylber, *Bull. Soc. Chim. Fr.*, **1965**, 2793.

3) J. Polonsky, Z. Baskevitch-Varon, and M. Debray, *C. R. Acad. Sci., Ser. C*, **280**, 1149 (1975).

4) C. G. Casinovi, V. Bellavita, G. Grandolini, and P. Ceccherelli, *Tetrahedron Lett.*, **1965**, 2273.

5) W. Stöcklin, M. Stefanović, T. A. Geissman, and C. G. Casinovi, *Tetrahedron Lett.*, **1970**, 2399.

6) R. E. Mitchell, W. Stöcklin, M. Stefanović, and T. A. Geissman, *Phytochemistry*, **10**, 411 (1971).

7) This structure had been previously proposed for amarolide by Casinovi *et al.*[4] but the structure of amarolide was later revised to **5**.[5]

8) General Procedures are the same as described in the previous papers.[1] Root bark of *A. altissima* was collected at the Botanical Gardens, Faculty of Science, the University of Tokyo in August 1982.

Synthesis of *cis*-12-Nonadecen-9-one, *cis*-13-Icosen-10-one, the Pheromone of Peach Fruit Moth, and *cis*-15-Henicosen-11-one, the Pheromone of Douglas Fir Tussock Moth

Shota Ito,* Norio Saito, Kiyotaka Hatakeda, Tomio Goto, Yutaka Ikushima, and Takashi Asano
Government Industrial Research Institute, Tohoku, 4-2-1 Nigatake, Sendai 983
(Received January 5, 1984)

Synopsis. A convenient synthesis of *cis*-12-nonadecen-9-one (**4a**), *cis*-13-icosen-10-one (**4b**), the pheromone of peach fruit moth, and *cis*-15-henicosen-11-one (**4c**), the pheromone of Douglas fir tussock moth, is described. **4a** was synthesized from methyl 3-oxoundecanoate and 1-bromo-2-nonyne (**2a**) *via* 12-nonadecyn-9-one. The higher homolog **4b** could be obtained from methyl-3-oxododecanoate and **2a**. Similarly, **4c** was prepared from methyl 3-oxotridecanoate and 1-bromo-3-nonyne (**2b**).

cis-12-Nonadecen-9-one (**4a**) and *cis*-13-icosen-10-one (**4b**) have been recognized as the principles of sex pheromone of Japanese peach fruit moth (*Carposina niponensis* Walsingham), a major economic pest of peach, apple and other fruits in Japan.[1] It is pointed out that a mixture of **4a** and **4b** in a ratio 1:20 shows the strongest biological activity.[1,2] On the other hand, *cis*-15-henicosen-11-one (**4c**) is known as the sex pheromone of Douglas fir tussock moth (*Orgyia pseudotsugata* McDunnough), a severe defoliator of Douglas fir and other fir forests in western North America.[3] These three compounds are unusual in that most lepidopterous sex pheromones are characterized as unsaturated fatty alcohols, acetates or aldehydes of C_{12}, C_{14}, or C_{16} chain length.[4]

Since above mentioned pheromones are potent male attractants, and might be of practical interests, a variety of synthetic methods of **4a**, **4b**,[1,5] and **4c**[6] have been reported. However no example for the preparation of these unsaturated ketones by the same technique has been explored.

Recently general and practical methods for the synthesis of arbitrary β-keto esters, versatile intermediates in organic synthesis, have been developed.[7] Thus we wish to report here a convenient synthesis of **4a**, **4b**, and **4c** starting from β-keto esters (**1**) which could be obtained easily accoding to Yonemitsu *et al.*[7a]

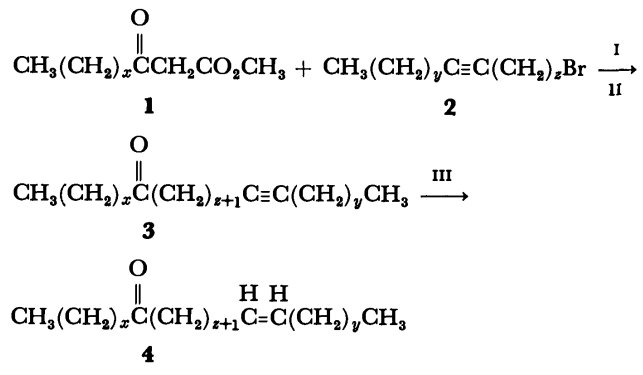

1 a: $x=7$, b: $x=8$, c: $x=9$; **2** a: $y=5$, $z=1$, b: $y=4$, $z=2$; **3,4** a: $x=7$, $y=5$, $z=1$, b: $x=8$, $y=5$, $z=1$, c: $x=9$, $y=4$, $z=2$
I: NaH in Toluene; II: wet DMSO; III: H_2/Pd-$BaSO_4$

Scheme 1.

The high stereoselectivity and chemical yield anticipated for the reduction of acetylenic bond to corresponding *cis*-olefin suggested 12-nonadecyn-9-one (**3a**), 13-icosyn-10-one (**3b**) and 15-henicosyn-11-one (**3c**) as the primary synthetic goal.[8] Thus the synthesis of title compounds **4a**, **4b**, and **4c** was carried out according to Scheme 1.

Methyl 3-oxoundecanoate (**1a**) was alkylated with 1-brom-2-nonyne (**2a**) in toluene in the presence of sodium hydride. The porduct, without isolation, was then heated in wet dimethyl sulfoxide (DMSO)[9] to be demethoxycarbonylated to 12-nonadecyn-9-one (**3a**) in a good yield (80%). **3b** was also prepared in the same manner from methyl 3-oxododecanoate (**1b**). **3c** could be obtained by the same procedure from methyl 3-oxotridecanoate (**1c**) and 1-bromo-3-nonyne (**2b**) in a low yield (≈40%). However, the yield of **3c** was improved upon (78%) by carrying out the alkylation in the presence of *N*,*N*-dimethylformamide (DMF). These acetylenic ketones were partially hydrogenated over palladium/barium sulfate catalyst to give desired compounds in 89—91% yields. The resulting products, **4a**, **4b**, and **4c** showed no infrared absorption band in the neighborhood of 970 cm^{-1} due to disubstituted *trans*-alkene. The structure of these products were identified by comparing IR and NMR spectra with those of reported data.[5,6]

Experimental

The IR and NMR spectra were recorded on Hitachi 285 and JEOL/FX-100 spectrometer respectively.

12-Nonadecyn-9-one (3a), 13-Icosyn-10-one (3b), and *15-Henicosyn-11-one (3c).* To a stirred suspension of sodium hydride (50% mineral oil dispersion 1.49 g, 31 mmol) in dry toluene (150 ml) a solution of methyl 3-oxoundecanoate (**1a**) (6.42 g, 30 mmol) in dry toluene (20 ml) was added dropwise over a period of 20 min at room temperature. Stirring was continued for 1 h. Then 1-bromo-2-nonyne (**2a**)[10] (6.7 g, 32 mmol) and powdered sodium iodide (2 g) were added. The mixture was refluxed for 11 h and then poured onto cold hydrochloric acid. The toluene layer was separated and the solvent was distilled off *in vacuo*. The residue was dissolved in a mixture of DMSO (50 ml) and water (5 ml) then the solution was heated (150 °C, bath temp) for 3.5 h. The mixture was poured onto ice water and extracted with ether (100 ml×2). The ether solution was washed with brine and dried over anhydrous magnesium sulfate, concentrated *in vacuo* to give crude **3a** as a pale yellow liquid. This crude **3a** was chromatographed over silicagel with hexane-benzene (6:4) as eluent to give 6.66 g (80%) of **3a**. IR (neat): 2940, 2860, 1720, 1460, 1090 cm^{-1}. NMR ($CDCl_3$): δ 0.87 (6H, distored t, J=6 Hz), 1.08—

1.66 (20H, br s), 1.97—2.23 (4H, m), 2.25—2.63 (4H, m). *13-Icosyn-10-one (3b)* was obtained from methyl 3-oxododecanoate (**1b**) and **2a** by the same procedure in 78% yield. IR (neat): 2960, 2860, 1720, 1460, 1090 cm^{-1}. NMR ($CDCl_3$): δ 0.90 (6H, distored t, J=6 Hz), 1.05—1.73 (22H, br s), 1.96—2.22 (4H, m), 2.27—2.63 (4H, m). *15-Henicosyn-11-one (3c)* could be prepared from methyl 3-oxotridecanoate (**1c**) and 1-bromo-3-nonyne (**2b**)[11] in 78% yield by using a mixture of toluene and DMF (10—15% of toluene)[12] as the solvent of the alkylation. IR (neat): 2920, 2840, 1715, 1460, 1090 cm^{-1}. NMR ($CDCl_3$): δ 0.93 (6H, distored t, J=6 Hz), 1.10—1.80 (24H, br s), 1.98—2.23 (4H, m), 2.26—2.60 (4H, m).

cis-*12-Nonadecen-9-one (4a)*, cis-*13-Icosen-10-one (4b)*, and cis-*15-Henicosen-11-one (4c)*. A methanol solution (35 ml) of **3a** (1.60 g, 5.8 mmol) containing two drops of quinoline was hydrogenated over 5% Pd-$BaSO_4$ (120 mg) under atmospheric pressure for 3 h. The solid was filtered off and the filtrate was concentrated *in vacuo*. The residue was dissolved in ether and washed with 5% hydrochloric acid, brine, dried over magnesium sulfate. Concentration of ether gave crude **4a** which was chromatographed over silica gel with hexane-benzene (6:4) as eluent to obtain 1.48 g (91%) of **4a**. IR (neat): 2960, 1710, 1460, 1370 cm^{-1}. NMR ($CDCl_3$): δ 0.88 (6H, distored t, J=6 Hz), 1.10—1.70 (20H, br s), 1.90—2.12 (2H, m), 2.20—2.42 (6H, m), 5.17—5.40 (2H, m). cis-*13-Icosen-10-one (4b)* was obtained by the same manner from **3b** in 89% yield. IR (neat): 2930, 1710, 1470, 1370 cm^{-1}. NMR ($CDCl_3$): δ 0.90 (6H, distored t, J=6 Hz), 1.10—1.70 (22H, br s), 1.90—2.10 (4H, m), 2.20—2.40 (6H, m), 5.15—5.40 (2H, m). cis-*Henicosen-11-one (4c)* was prepared from **3c** by the same procedure in 91% yield. IR (neat): 3000, 1715, 1460, 1370 cm^{-1}. NMR ($CDCl_3$): δ 0.98 (6H, distored t, J=6 Hz), 1.05—1.75 (24H, br s), 1.90—2.15 (4H, m), 2.35 (4H, t, J=7 Hz), 5.26—5.32 (2H, m).

References

1) Y. Tamaki, K. Honma, and K. Kawasaki, *Appl. Entmol. Zool.* **12**, 60 (1977).

2) S. Shirasaki, M. Yamada, R. Saito, K. Yanaginuma, M. Kumakura, and Y. Tamaki, *Nippon Oyo Dobutsu Konchu Gakkai Shi*, **23**, 240 (1979).

3) R. G. Smith, G. E. Daterman, and G. D. Davis, Jr., *Science*, **188**, 63 (1975).

4) J. M. Brand, J. C. Young, and R. M. Silverstein, *Fortsch. Chem. Org. Natur.*, **37**, 1 (1979).

5) T. Yoshida and S. Saito, *Bull. Chem. Soc. Jpn.*, **55**, 3047 (1982) and references cited therein.

6) M. Fetizon and C. Lazare, *J. Chem. Soc., Perkin Trans. 1*, **1978**, 842; O. P. Vig, M. L. Sharma, N. K. Verma, and N. Malik, *Indian J. Chem.*, **19B**, 950 (1980); Y. Murata, K. Inomata, H. Kinoshita, and H. Kotake, *Bull. Chem. Soc. Jpn.*, **56**, 2539 (1983) and references cited therein.

7) a) Y. Oikawa, K. Suzuki, and O. Yonemitsu, *J. Org. Chem.*, **43**, 2088 (1978); b) W. Wierenga and H. I. Skulnik, *ibid.*, **44**, 310 (1979); c) R. P. Houghton and D. J. Lapham, *Synthesis*, **1982**, 451.

8) Another reason for choosing **3** as key intermediate for **4** is the fact that *trans*-olefin can also be obtained easily by reduction of acetylene with Na/NH_3. It is known that the trans isomer of **4c** is also biologically active (see Ref. 3).

9) A. P. Krapcho, J. F. Weinmaster, J. M. Eldridge, E. G. E. Jahngen, Jr., A. J. Lovey, and W. P. Stephens, *J. Org. Chem.*, **43**, 138 (1978).

10) W. W. Christie and R. T. Holman, *Chem. Phys. Lipids*, **1**, 407 (1967).

11) R. W. Bradshaw, A. C. Day, E. R. H. Jones, C. B. Page, V. Thaller, and R. A. Hodge, *J. Chem. Soc., C*, **1971**, 1156

12) When a large quantity of DMF was used the yield of **3c** was lower (≈66%).

Studies on Nucleosides and Nucleotides. XI.[1] Synthesis of 5′-Deoxypyrimidine Nucleosides

Junji KIMURA, Yoshiyuki NISHIKUBO, and Oyo MITSUNOBU
College of Science and Engineering, Aoyama Gakuin University, Chitosedai, Setagaya-ku, Tokyo 157
(Received January 14, 1984)

Synopsis. When 2′,3′-*O*-(triphenylphosphoranediyl)-O^2,5′-cyclouridine and N^4-benzoyl-2′,3′-*O*-(triphenylphosphoranediyl)-O^2,5′-cyclocytidine were allowed to react with tributyltin hydride in the presence of azobisisobutyronitrile under reflux, 5′-deoxyuridine (84% yield) and N^4-benzoyl-5′-deoxycytidine (71% yield) were obtained.

Tributyltin hydride (**1**) has been widely used as a reducing agent for organic compounds which include alkyl halides,[2a] nitro compounds,[2b] and xanthates.[2c]

In this paper we wish to report the reaction of 2′,3′-*O*-(triphenylphosphoranediyl)cyclonucleosides with **1**.

When 2′,3′-*O*-(triphenylphosphoranediyl)-O^2,5′-cyclouridine (**2**) was allowed to react with two molar amounts of **1** in the presence of azobisisobutyronitrile (AIBN) in THF under reflux for 6 h, 5′-deoxyuridine (**3**)[3] was obtained in 84% yield. When three molar amounts of **1** were used, a minor, more polar product was isolated by preparative layer chromatography ($CHCl_3$:MeOH=10:1). Based on ^{1}H-NMR spectroscopy, the structure of the side product was assigned to be N^3-methyl-5′-deoxyuridine (**4**) which would be formed during work-up. Thus, **2** was first reacted with **1** in THF as above, followed by addition of methanol, and the resulting solution was refluxed for 8 h. Compound **4** was expectedly isolated in 40% yield along with **3** (60%). Reduction of N^4-benzoyl-2′,3′-*O*-(triphenylphosphoranediyl)-O^2,5′-cyclocytidine (**5**) by the use of two molar amounts of **1** in the presence of AIBN afforded N^4-benzoyl-5′-deoxycytidine (**6**) in 71% yield. Products **3**, **4**, and **6** were readily converted into the corresponding acetonides, indicating that the 2′- and 3′-hydroxyl groups have the original cis configuration.

Contrary to the case of pyrimidine nucleosides, 3′,5′-*O*-(triphenylphosphoranediyl)adenosine or 2′,3′-*O*-(triphenylphosphoranediyl)-N^3,5′-cycloguanosine did not react with **1**.

From these results, it is proved that **1** does not react at the phosphoranediyl group but induces cleavage of the O^2,5′-anhydro bond of **2** or **5**.

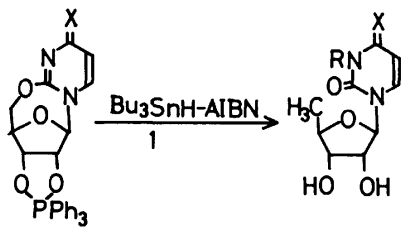

2 X=O
5 X=NBz

3 X=O R=H
4 X=O R=Me
6 X=NBz R=H

We next examined the reaction of 2′,3′-*O*-isopropylidene-O^2,5′-cyclouridine (**7**) under the same conditions where 5′-deoxy-2′,3′-*O*-isopropylideneuridine was obtained in only 31% yield with 63% recovery of **7**. On the other hand, O^2-methyluridine, 5′-*O*-benzoyl-O^2,2′-cyclouridine, and O^2,2′-cyclocytidine hydrochloride were not reduced by **1** and starting materials were quantitatively recovered.

It is generally known that the O^2,2′-anhydro bond of pyrimidine nucleosides is more stable than the O^2,5′-anhydro bond.[4] The difference of reactivity between **2** and **7** might be due to 2′,3′-*O*-protecting group which exerts influence on the stability of O^2,5′-anhydro bond. Thus the phosphoranediyl group activate the O^2,5′-anhydro bond of **2** or **5** to some extent compared to isopropylidene group.

Experimental

5′-Deoxyuridine (3) and N³-Methyl-5′-deoxyuridine (4). A suspended solution of **2** (486 mg, 1 mmol),[5] **1** (582 mg, 2 mmol), and AIBN (40 mg) in THF (15 ml) was refluxed under nitrogen atmosphere for 6 h. As the reaction proceeded, the solution became homogeneous. The reaction solution was evaporated and 191 mg (84% yield) of the product **3** was obtained by column chromatography (Merck Kieselgel 60, solvent; $CHCl_3$: MeOH=5:1), followed by recrystallization from CH_3CN and had mp 187—189 °C (lit,[3] mp 182—184 °C); UV_{max}^{MeOH} 264 (ε 9800) nm; UV_{min} 232 nm. Found: C, 47.32; H, 5.30; N, 12.29%. Calcd for $C_9H_{12}O_5N_2$: C, 47.37; H, 5.30; N, 12.28%. NMR (DMSO-d_6) δ=1.28 (d, 3H, C$_5$′H), 5.63 (d, 1H, C$_5$H), 5.69 (d, 1H, C$_1$′H), and 7.55 ppm (d, 1H, C$_6$H).

Similarly, the reaction of **2** with three molar amounts of **1** in the presence of AIBN in THF was carried out under reflux for 6 h and methanol (20 ml) was added to the resulting mixture. The solution was successively refluxed for 8 h and evaporated. The products were separated by column chromatography (solvent; $CHCl_3$: MeOH=10:1) to give **3** and **4** in 60% and 40% yields, respectively. Compound **4** recrystallized from benzene had mp 107—109 °C; UV_{max}^{MeOH} 263 nm; UV_{min} 234 nm. Found: C, 49.48; H, 5.81; N, 11.55%. Calcd for $C_{10}H_{14}O_5N_2$: C, 49.48; H, 5.83; N, 11.57%. NMR ($CDCl_3$) δ=1.43 (d, 3H, C$_5$′H), 3.30 (s, 3H, CH_3), 5.65 (d, 1H, C$_1$′H), 5.78 (d, 1H, C$_5$H), and 7.43 ppm (d, 1H, C$_6$H).

N⁴-Benzoyl-5′-deoxycytidine (6). The reaction of **5**[5] with two molar amounts of **1** in the presence of AIBN in THF under reflux for 6 h gave **6** in 71% yield. The **6** recrystallized from methanol had mp 201—202 °C; UV_{max}^{MeOH} 261 (ε 22200); 306 nm, UV_{min} 232, 287 nm. Found; C, 57.66; H, 5.12; N, 12.61%. Calcd for $C_{16}H_{17}O_5N_3$: C, 58.00; H, 5.17; N, 12.68%. NMR (DMSO-d_6) δ=1.39 (d, 3H, C$_5$′H) and 5.81 ppm (d, 1H, C$_1$′H).

N³-Methyl-5′-deoxy-2′,3′-O-isopropylideneuridine. A solution of **4** in 2,2-dimethoxypropane-acetone in the presence of *p*-toluenesulfonic acid was stirred at room temperature for 5 h. The title compound was quantitatively iso-

lated as an oil by preparative TLC (developing solvent; ethyl acetate). NMR ($CDCl_3$) δ=1.38 (d, 3H, $C_{5'}H$), 1.32, 1.55 (s, 6H, $(CH_3)_2C$), 3.30 (s, 3H, CH_3), 5.56 (d, 1H, $C_{1'}H$), 5.70 (d, 1H, C_5H), and 7.20 ppm (d, 1H, C_6H).

N^4-*Benzoyl-5'-deoxy-2',3'-O-isopropylidenecytidine.* A solution of **6** in 2,2-dimethoxypropane-acetone in the presence of *p*-toluenesulfonic acid was stirred at room temperature for 2 h. The product was isolated in 61% yield by preparative TLC ($CHCl_3$:MeOH=10:1) and had mp 184—186 °C. NMR (DMSO-d_6) δ=1.38 (d, 3H, $C_{5'}H$), 1.31, 1.45 (s, 6H, $(CH_3)_2C$), and 5.83 ppm (d, 1H, $C_{1'}H$).

References

1) Part X: O. Mitsunobu, N. Ito, S. Saita, T. Ogihara, H. Tamaoki, H. Nagasawa, H. Suzuki, and J. Kimura, *Tetrahedron Lett.*, **23**, 517 (1982).

2) a) H. G. Kuivila and L. W. Menepace, *J. Org. Chem.*, **28**, 2165 (1963). E. J. Corey and J. W. Suggs, *ibid.*, **40**, 2554 (1975); b) N. Ono, H. Miyake, R. Tamura, and A. Kaji, *Tetrahedron Lett.*, **22**, 1705 (1981); c) D. H. R. Barton and S. W. McCombie, *J. Chem. Soc., Perkin Trans. 1*, **1975**, 1574.

3) B. Schwarz, D. Cech, A. Holy, and J. Skoda, *Coll. Czech. Chem. Commun.*, **45**, 3217 (1980).

4) M. Ikehara and T. Ueda, *Yuki Gosei Kagaku Kyokai Shi*, **32**, 403 (1974).

5) J. Kimura, K. Yagi, H. Suzuki, and O. Mitsunobu, *Bull. Chem. Soc. Jpn.*, **53**, 3670 (1980).

Pyridinium Fluorochromate or Benzyltrimethylammonium Chlorochromate for Selective Oxidation of Alcohols

Tsuyoshi NONAKA, Shigekazu KANEMOTO, Koichiro OSHIMA,* and Hitosi NOZAKI
Department of Industrial Chemistry, Faculty of Engineering, Kyoto University, Yoshida, Kyoto 606
(Received January 20, 1984)

Synopsis. Selective oxidation of secondary alcohols in the presence of primary ones has been achieved by the following sequences, (1) selective protection of primary alcohols with *t*-BuMe$_2$SiCl, (2) oxidation of secondary alcohols with title reagents, and (3) deprotection of primary hydroxyls.

The reagents containing the chromium(VI) as a key atom are most commonly used for the oxidation of alcohols to carbonyl compounds because of their ready accessibility and operational simplicity.[1] A large number of them, however, cannot be applied to modern organic synthesis and there still exists a need for new methods for the oxidation of complex or highly sensitive substrates. Here we wish to describe the preparation and reaction of several chromium(VI) reagents which oxidize alcohols under slightly acidic or neutral conditions.

Among many reagents examined, only pyridinium fluorochromate (PFC)[2] was as reactive as pyridinium chlorochromate (PCC) and oxidation took place at 25 °C. The reaction with benzyltrimethylammonium chlorochromate (BTMACC) proceeded very sluggishly at 25 °C and the completion of oxidation required heating at 80 °C in 1,2-dichloroethane. Tetrabutylammonium chlorochromate (TBACC) was marginal and tetramethylammonium chlorochromate, tetramethylammonium fluorochromate, and tetrabutylammonium fluorochromate were inert for the oxidation of alcohols. The results of representative experiments by means of PFC together with those by BTMACC and TBACC are summarized in Table 1.

It is worth noting that PFC is less acidic than PCC, thus even such acid-labile compounds as SiMe$_2$Bu^t ethers or trityl ethers survive without buffering the reaction mixture with bases. Combination of this oxidation procedure with selective protection of primary hydroxyl groups provides us with a simple route to the selective oxidation of primary, secondary diols at the secondary positions.[3]

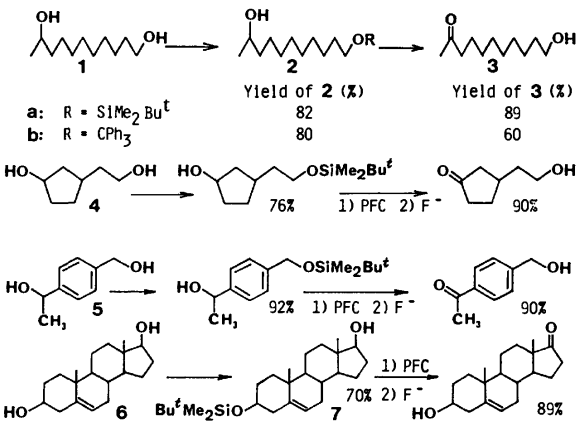

Treatment of 1,10-undecanediol with Bu^{t}Me$_2$SiCl and Et$_3$N in the presence of a catalytic amount of 4-dimethylaminopyridine gave monosilyl ether **2a** in 82% yield. Similarly, the diols **4** and **5** could be transformed into their monoethers. Oxidation of monosilyl ether **2a** with PFC or BTMACC followed by desilylation (Bu$^n_4$NF) provided 11-hydroxy-2-undecanone (**3**) in 89% or 90%, respectively. In contrast, the reaction of **2a** with PCC gave *t*-butyldimethylsilyl ether of keto alcohol (**3**) (68%) along with 10-oxoundecanal (20%). Trityl ether **2b** was also converted into the ketone **3** with PFC followed by deprotection (*p*-TsOH).[4] As exemplified below, the selective oxidation of secondary, secondary

Table 1. Oxidation of alcohols with PFC, BTMACC, or TBACC

Alcohol	Oxidant	Conditions		Yield/%[a] of carbonyl compound
		Temp °C	Time h	
4-*t*-Butylcyclohexanol	PFC[b]	25	6	92
Cyclododecanol	PFC	25	6	93
	BTMACC[c]	80	10	97
	TBACC[c]	80	30	68
PhCH(OH)Me	PFC	25	6	88
4-Dodecanol	PFC	25	8	96
1-Dodecanol	PFC	25	6	78
	BTMACC	80	10	92
	TBACC	80	30	58
Carveol	PFC	25	2	96
	BTMACC	80	4	87
	TBACC	80	2	72
Geraniol	PFC	25	2	80[d]
	BTMACC	80	6	83[e]
	TBACC	80	3	58[f]
Nerol	PFC	25	2	82[g]
Borneol	PFC	25	8	77
3β-Cholestanol	PFC	25	6	96
	BTMACC	80	10	98
p-Bromobenzyl alcohol	PFC	25	2	97
l-Menthol	PFC	25	6	92
2-Cyclododecen-1-ol	PFC	25	4	87
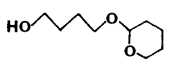	PFC	25	4	78[h]

a) Yields represent isolated purified products. b) 2 mmol of alcohols and 4 mmol of PFC were employed. c) 2 mmol of alcohols and 6 mmol of BTMACC or TBACC were employed. d) A mixture of *cis* and *trans* citral was obtained. The ratio of *cis*:*trans* was 15:85. e) *cis*:*trans*=29:71. f) *cis*:*trans*=13:87. g) *cis*:*trans*=68:32. h) THP ether remained untouched.

diol, 5-androstene-3β,17β-diol to the 17-keto steroid, has been also achieved.

Experimental

Distillation was carried out in Kugelrohr (Büchi) and boiling points were determined by mesuring the bath temperature. All mp and bp are not corrected. All ^{1}H-NMR spectra (tetramethylsilane as an internal standard) were obtained in ppm units. The IR spectra of neat liquid film samples were measured on a Shimadzu IR-27 or Hitachi IR-215 spectrometer. Microanalysis was performed at the Elemental Analyses Center of Kyoto University. Preparative TLC plates were prepared with Merck Kiesel-gel PF_{254}. Column chromatography was carried out with silica gel (Wakogel C-200) at atmospheric pressure.

Preparation of Benzyltrimethylammonium Chlorochromate (BTMACC). Anhydrous chromium trioxide (5.0 g, 50 mmol) was dissolved in 6 M† HCl (9.0 ml, 55 mmol) at 0 °C. After stirring for 5 min, a solution of benzyltrimethylammonium hydroxide (40% in H_2O, 23 g, 55 mmol) was carefully added over 10 min to give an orange solid which was collected, washed, and dried for 5 h *in vacuo* (yield 13.1 g, 96%, mp 85 °C (decomp)). Found: C, 41.69; H, 5.43; N, 4.80%. Calcd for $C_{10}H_{16}ClNO_3Cr$: C, 42.11; H, 5.61; N, 4.91%. Other chromium(VI) reagents were prepared in a similar fashion.

Oxidation of 4-t-Butylcyclohexanol to 4-t-Butylcyclohexanone. A Typical Procedure for the Oxidation of Alcohols with PFC, BTMACC, or TBACC: A solution of 4-*t*-butylcyclohexanol (0.31 g, 2.0 mmol) in CH_2Cl_2 (2.0 ml) was added in one portion to the CH_2Cl_2 (8.0 ml) suspension of PFC (0.80 g, 4.0 mmol). After stirring for 6 h at 25 °C, the resulting mixture was diluted with ether (20 ml) and the supernatant was decanted. The residue was washed twice with 10 ml portions of ether. The combined organic solution was washed with $NaHSO_3$ and brine. Purification by silica gel column chromatography gave 4-*t*-butylcyclohexanone (0.28 g) in 92% yield.

General Procedure for the Preparation of Mono Ethers. According to the reported method,[5] diols **1**, **4**, and **5** were transformed into their monosilyl ethers on treatment with Bu^tMe_2SiCl and Et_3N in the presence of 4-dimethylaminopyridine. Similarly, trityl ether **2b** was prepared from diol **1** and Ph_3CCl instead of Bu^tMe_2SiCl.[6]

11-(t-Butyldimethylsiloxy)-2-undecanone. A dichloromethane solution of 11-(*t*-butyldimethylsiloxy)-2-undecanol (0.6 g, 2.0 mmol) was combined with PFC (0.8 g, 4.0 mmol) and the whole was stirred for 3 h at 25 °C. Workup (Et_2O, $NaHSO_3$) and purification by preparative TLC gave the title compound (0.53 g, 89% yield) as an oil: Bp 116—118 °C (bath temp, 1 Torr‖); IR (neat) 2890, 2820, 1705, 1250, 1090, 830 cm^{-1}; NMR ($CDCl_3$) δ 0.03 (s, 6H), 0.91 (s, 9H), 1.2—1.4 (m, 10H), 1.4—1.6 (m, 4H), 2.13 (s, 3H), 2.40 (t, *J*=7.4 Hz, 2H), 3.57 (t, *J*=6.5 Hz, 2H). Found: C, 67.78; H, 12.32%. Calcd for $C_{17}H_{36}O_2Si$: C, 67.94; H, 12.07%.

11-Hydroxy-2-undecanone (3). A THF solution of siloxyl ketone (0.30 g, 1.0 mmol) was treated with Bu^n_4NF (1.0 M THF solution, 1.1 ml) for 30 min at 25 °C to give the hydroxy ketone (0.30 g) quantitatively: Mp 42—43 °C; IR (neat) 3424, 1709, 1358, 1042 cm^{-1}; NMR (CCl_4) δ 1.1—1.8 (m, 14H), 2.09 (s, 3H), 2.36 (t, *J*=6.6 Hz, 2H), 3.58 (t, *J*=6.8 Hz, 2H), 3.78 (b, 1H). Found: C, 70.65; H, 11.90%. Calcd for $C_{11}H_{22}O_2$: C, 70.92; H, 11.90%.

3-[2-(t-Butyldimethylsiloxy)ethyl]cyclopentanone: Bp 137 °C (bath temp, 1 Torr); IR (neat) 1730, 1250, 1100, 830, 770 cm^{-1}; NMR ($CDCl_3$) δ 0.03 (s, 6H), 0.85 (s, 9H), 1.2—2.5 (m, 11H), 3.62 (t, *J*=5.8 Hz, 2H). Found: C, 64.51; H, 10.96%. Calcd for $C_{13}H_{26}O_2Si$: C, 64.46; H, 10.74%.

p-[(t-Butyldimethylsiloxy)methyl]phenyl Methyl Ketone: Bp 103 °C (bath temp, 1 Torr); IR (neat) 2900, 1670, 1600, 1266, 1092 cm^{-1}; NMR ($CDCl_3$) δ 0.05 (s, 6H), 0.85 (s, 9H), 2.44 (s, 3H), 4.64 (s, 2H), 7.2—7.9 (m, 4H). Found: C, 68.10; H, 9.35%. Calcd for $C_{15}H_{24}O_2Si$: C, 68.18; H. 9.09%.

Conversion of 5-Androstene-3β,17β-diol (6) to 3β-Hydroxy-5-androsten-17-one. Following the Hosoda's prodcedure,[7] diol **6** was converted into monosilyl ether **7** in 70% yield. This compound (0.20 g, 0.5 mmol) was treated successively with PFC (0.20 g, 1.0 mmol) and Bu^n_4NF (5.5 mmol) to give 17-keto steroid (0.13 g, 89% yield) which was identifical with an authentic sample.

Financial supports by the Asahi Glass Foundation for Industrial Technology and a Grant-in-Aid for Scientific Research No. 58550566 from the Ministry of Education, Science and Culture is acknowledged.

References

1) CrO_3·2py: J. C. Collins, W. W. Hess, and F. J. Frank, *Tetrahedron Lett.*, **1968**, 3363; R. Ratcliffe and R. Rodehorst, *J. Org. Chem.*, **35**, 4000, (1970); CrO_2Cl_2: K. B. Sharpless and K. Akashi, *J. Am. Chem. Soc.*, **97**, 5927 (1975); PCC: E. J. Corey and J. W. Suggs, *Tetrahedron Lett.*, **1975**, 2647; PDC: E. J. Corey and G. Schmidt, *ibid.*, **1979**, 399: PDC-$Me_3SiOOSiMe_3$: S. Kanemoto, K. Oshima, S. Matsubara, K. Takai, and H. Nozaki, *ibid.*, **24**, 2185 (1983).

2) PFC has been independently introduced for an efficient oxidant. Reported data have been omitted in this paper. M. N. Bhattacharjee, M. K. Chaudhuri, H. S. Dasgupta, N. Roy, and D. T. Khathing, *Synthesis*, **1982**, 588.

3) Several methods are known for the preferential oxidation of secondary over primary hydroxyls, see Y. Ueno and M. Okawara, *Tetrahedron Lett.*, **1976**, 4597; M. E. Jung and R. W. Brown, *ibid.*, **1978**, 2771; G. H. Posner, R. B. Perfetti, and A. W. Runquist, *ibid.*, **1976**, 3499; M. A. Neirabeyeh, J.-C. Ziegler, and B. Gross, *Synthesis*, **1976**, 811; H. Tomioka, K. Oshima, and H. Nozaki, *Tetrahedron Lett.*, **23**, 539 (1982).

4) Oxidation of trityl ether **2b** with PCC gave a mixture of the desired trityl ether of 11-hydroxy-2-undecanone (39%), 10-oxoundecanal (27%), and Ph_3COH (39%).

5) S. K. Chandhary and O. Hernandez, *Tetrahedron Lett.*, **1979**, 99.

6) S. Hanessian and A. P. A. Staub, *Tetrahedron Lett.*, **1973**, 3555; S. K. Chaudhary and O. Hernandez, *ibid.*, **1979**, 95.

7) H. Hosoda, D. K. Fukushima, and J. Fishman, *J, Org, Chem.*, **38**, 4209 (1973).

† 1 M=1 mol dm^{-3}.

‖ 1 Torr=133.322 Pa.

Equilibria in Aqueous Ternary System Containing Na^+, $CH_3CO_2^-$, and HPO_4^{2-} between 38 and 75 °C

Takahiro WADA,* Fumiko YOKOTANI, and Yoshihiro MATSUO
Central Research Laboratory, Matsushita Electric Industrial Co., Ltd., 1006 Kadoma, Osaka 571
(Received September 1, 1983)

Synopsis. Ternary system CH_3CO_2Na–Na_2HPO_4–H_2O was investigated between 38 and 75 °C. No double salt formation occurs in this temperature range. Saturated CH_3CO_2Na solution has a strong dehydrating influence on $Na_2HPO_4 \cdot 2H_2O$ and $Na_2HPO_4 \cdot 7H_2O$. The lowest formation temperature for anhydrous Na_2HPO_4 is about 57 °C.

Recently, Kimura[1] reported that addition of a small amount of a mixture of disodium hydrogenphosphate and anhydrous sodium acetate to a sodium acetate solution is very effective for the crystal nucleation of sodium acetate trihydrate from the solution. Wada and Matsuo[2] have studied the influence of preheating on the crystallization of sodium acetate trihydrate from its aqueous solution with a small amount of disodium hydrogenphosphate added, proposing an adsorption model to account for the crystal nucleation catalytic effect. To complete the investigation, knowledge is required of the ternary system, sodium acetate–disodium hydrogenphosphate–water. Phase diagrams of the binary systems, sodium acetate–water and disodium hydrogenphosphate–water, based on data from Seidell's compilation,[3] are shown in Fig. 1. In this figure, W_a and W_b are the mass fractions of sodium acetate and disodium hydrogenphosphate, respectively.

This paper reports results from an investigation using disodium hydrogenphosphate together with sodium acetate aqueous solution.

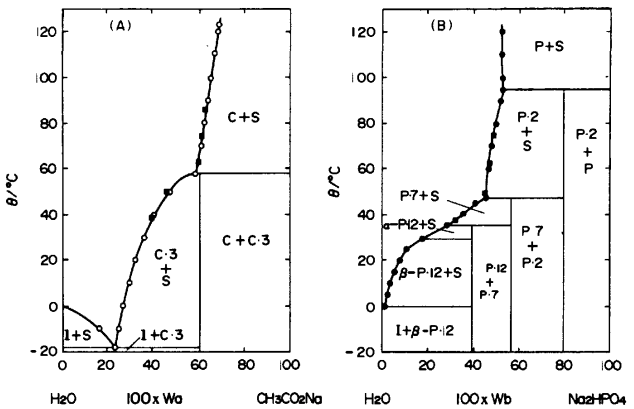

Fig. 1. Phase diagrams of the binary systems, CH_3CO_2Na–H_2O (A) and Na_2HPO_4–H_2O (B). Symbols: I = ICE, C = CH_3CO_2Na, C·3 = $CH_3CO_2Na \cdot 3H_2O$, P = Na_2HPO_4, P·2 = $Na_2HPO_4 \cdot 2H_2O$, P·7 = $Na_2HPO_4 \cdot 7H_2O$, P·12 = $Na_2HPO_4 \cdot 12H_2O$, S = Solution.
○: the data obtained by Green,[4] ●: the average of the reported data (the transition temperature between α-P·12 and β-P·12 in the presence of P·7 is not unkown),[3] ■: the data obtained by the present experiment.

Experimental

Sodium acetate trihydrate, anhydrous sodium acetate, and disodium hydrogenphosphate were guaranteed grade reagents. Experiments were conducted as previously described.[5] Phosphate ion was analyzed colorimetrically. The concentration of dissolved total salts was determined by drying the supernatant solution. The sodium acetate concentration was calculated from the difference in concentration between total salts and disodium hydrogenphosphate. The redidual solid existing in equilibrium with the saturated solution was separated out and identified by the X-ray diffraction. The solution in equilibrium with two solid phases was confirmed by analyzing the solution with those solids added.

Results

For the ternary system sodium acetate–disodium hydrogenphosphate–water, four sets of data for isotherms between 38 and 75 °C are shown in Table 1. Solubilities of the binary systems, sodium acetate–water and disodium hydrogenphosphate–water, determined by the present experiment, are plotted in Fig. 1. From Fig. 1, it is clear that the solubilities determined here are in good agreement with the reported data.

There is no formation of double salt in the present system between 38 and 75 °C. It is noteworthy that the saturated sodium acetate solutions contain only a small amount of disodium hydrogenphosphate and that they have a very strong dehydrating influence on the disodium hydrogenphosphate hydrates. The outline of the ternary system below 75 °C is given in Fig. 2, with

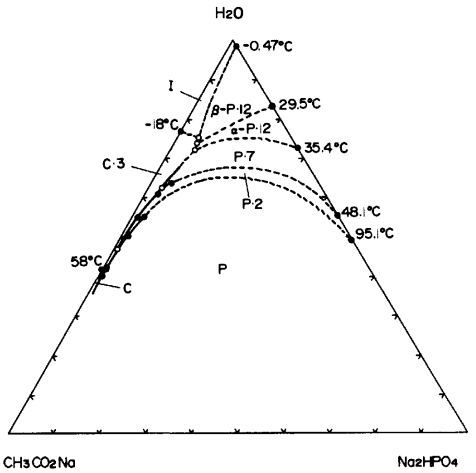

Fig. 2. Synopsis of the composition of the solution at the invariant and univariant equilibria of the ternary system CH_3CO_2Na–Na_2HPO_4–H_2O. The symbols in this figure indicate the same phases as those in Fig. 1.
●: the data obtained by the present experiment,
○: the invariant point.

Table 1. Data for isotherms for ternary system CH_3CO_2Na-Na_2HPO_4-H_2O at 38, 50, 62, and 75 °C

θ/°C	Solution		Solid[c] phase	θ/°C	Solution		Solid[c] phase
	$100\times W_a$[a]	$100\times W_b$[b]			$100\times W_a$[a]	$100\times W_b$[b]	
38	0	31.9	P·7	62	0	45.4	P·2
	5.3	24.2	P·7		9.2	30.5	P·2
	11.5	16.1	P·7		21.0	14.7	P·2
	18.0	10.3	P·7		34.4	4.4	P·2
	23.6	7.3	P·7		40.4	2.5	P·2
	27.9	6.0	P·7		46.1	1.6	P·2
	32.0	4.4	P·7+P2		48.4	1.3	P·2+P
	34.0	3.6	P·2		52.9	1.0	P
	37.0	2.6	P·2+C3		57.5	0.69	P+C
	38.5	0	C·3		58.2	0	C
50	0	44.4	P·2	75	0	47.4	P·2
	7.6	32.6	P·2		9.1	32.6	P·2
	12.1	22.7	P·2		20.0	17.3	P·2
	20.6	14.2	P·2		32.1	6.5	P·2
	29.6	6.3	P·2		40.0	3.3	P·2
	34.8	3.6	P·2		42.2	2.8	P·2+P
	38.5	2.7	P·2		48.1	1.6	P
	42.3	1.7	P·2		53.0	0.97	P
	43.6	1.4	P·2+C·3		59.2	0.60	P+C
	44.5	0	C·3		59.6	0	C

a) W_a is the mass fraction of CH_3CO_2Na in the system. b) W_b is the mass fraction of Na_2HPO_4 in the system. c) Symbols: C=CH_3CO_2Na, C·3=$CH_3CO_2Na\cdot 3H_2O$, P=Na_2HPO_4, P·2=$Na_2HPO_4\cdot 2H_2O$, and P·7=$Na_2HPO_4\cdot 7H_2O$.

some assumptions applied for the lowest temperature. This figure gives a survey of the formation of the solid.

Isothermally invariant points were plotted with temperature on the ordinate and disodium hydrogenphosphate concentration on the abscissa. The lowest formation temperature for anhydrous disodium hydrogenphosphate is determined as about 57 °C from the point of intersection of the curves on which the solution is in equilibrium with two solid phases.

The authors wish to express their thanks to Dr. Ryoichi Kiriyama for his useful discussions and to Drs. Tsuneharu Nitta, Eiichi Hirota, and Masanari Mikoda for their continuous encouragement. They are grateful to Miss Shoko Ueno for the colorimetric analyses and also to Dr. Ryoichi Yamamoto for his discussions throughout this work.

References

1) H. Kimura, *J. Jpn. Assoc. Cryst. Growth*, No.3, 73 (1982).
2) T. Wada and Y. Matsuo, *Bull. Chem. Soc. Jpn.*, **57**, 561 (1984).
3) A. Seidell, "Solubilities of Inorganic and Metal-Organic Compounds," 4th ed, ACS, (1965), Vol. II, pp.854, and 1102.
4) W. F. Green, *J. Phys. Chem.*, **12**, 555 (1908).
5) T. Wada, F. Yokotani, and Y. Matsuo, *Bull. Chem. Soc. Jpn.*, **57**, 1671 (1984).

Effect of M-series PRBS Modulation on the Time Resolution in Correlation Photoacoustics

Yoshinori SUGITANI* and Akinori UEJIMA
Institute of Chemistry, The University of Tsukuba, Sakura-mura, Ibaraki 305
(Received September 5, 1983)

Synopsis. Time resolution in the first kind correlation photoacoustics using the M-series PRBS mechanical light modulator was experimentally checked. It was found that the time resolution limited by the mechanical chopper was more determinative than that by the microphone detector or the time delay unit in the experimental system used.

It has been demonstrated[1,2] that the introduction of the cross-correlation technique into photoacoustic spectroscopy enables a new kind of experiment such as measuring the delay time of photoacoustic output signal with respect to the exciting light, or recording the absorption spectra of a definite layer lying deep in a layered material. The delay time measurement is conducted by the correlation photoacoustics of the first kind, where the spectra are obtained from the measurement of cross-correlation function $C(\tau)$ between an exciting input and the resultant photoacoustic output as a function of delay time τ. The measurement of the absorption spectra of a layer is referred to as the correlation photoacoustics of the second kind, where the cross-correlation function is recorded as a function of the exciting wavelength λ at the fixed delay time τ_0 of the reference signal.

In the first kind correlation photoacoustics we are interested in the shortest limit of the delay time measurable by the present experimental system. A similar problem occurs in the measurement of the second kind correlation spectra in the sense that one would be interested in the shortest distance between layers which can be resolved from each other by the present system. Both of these problems are reduced to the same term of "time resolution", since the distance between layers can be converted into time scale if the thermal conductivity of the material is known, and *vice versa*.

Experimental

A block diagram for the first and second kind correlation photoacoustics is shown in Fig. 1. In the present work only the first kind correlation spectra have been measured. The exciting light from the He-Ne laser source(NEC, 50 mw) was mechanically modulated by the chopper which gives a pseudo random binary sequence(PRBS) modulaton based on the M-series (maximum-length linear shift register) binary sequence. The modulated light was introduced into a photoacoustic cell to irradiate the carbon black sample. The output was detected by a microphone (SONY, electret condenser type, FET buffer included, No. 8-814-196-50) and was fed into a correlator, essentially an integral circuit. The reference signal detected by a photo-diode was delayed by the variable amount of τ at T. D. U. (Time Delay Unit) and led into the correlator, the output of which was recorded as a function of τ.

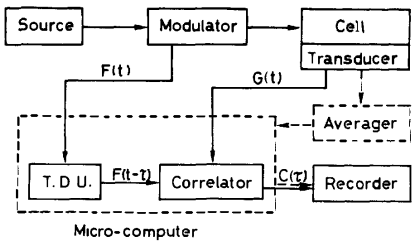

Fig. 1. Block diagram showing the experimental setup for the measurement of the first kind correlation photoacoustic spectra.

Results and Discussion

There are many factors which will influence the limit of experimental time resolution. Some are concerned with the characteristics of the sample measured. One of the major factors coming from the measuring system would be the way of modulating input signal.

Figure 2 shows the power spectrum of the input signal produced by a PRBS chopper with $63(=2^6-1)$ binary bit in a sequence, when rotated at 390 rpm. The upper limit of the modulation frequency contained in the spectrum is around 410 Hz neglecting the higher order components, so that the time resolution attainable by this chopping system would be about 2.5 ms(=1/400 s) at highest. To improve time resolution, or to increase the highest component of modulating frequecy contained, one has to either raise the rotating speed of the chopper or use other choppers which have larger number of binary bits of the M-series. Figure 3 shows the first kind correlation spectra by the use of the $31(=2^5-1)$ bit and $127(=2^7-1)$ bit PRBS choppers at the rotating speed of 396 rpm. The delay time of about 0.5 ms obtained from the peak position of curve A is considerably smaller than that

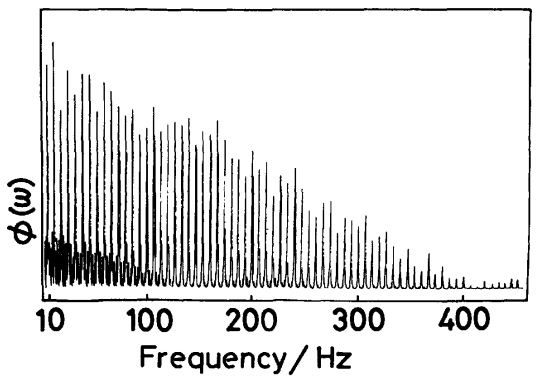

Fig. 2. Power spectrum of the M-series 63 bit PRBS chopper rotated at 396 rpm. Higher frequency part of the spectrum starting from about 410Hz is omitted in the figure.

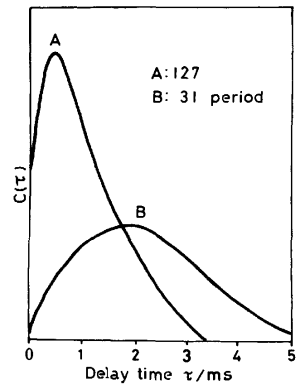

Fig. 3. The first kind correlation photoacoustic spectra of carbon black sample with the use of the 127 bit (A) and 31 bit (B) choppers rotated at 396 rpm.

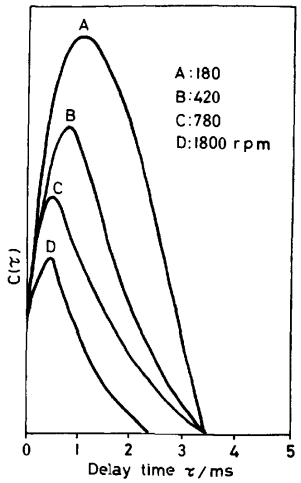

Fig. 4. The first kind correlation photoacoustic spectra of the carbon black sample recorded at the different rotating speeds of the 127 bit PRBS chopper; A: 180, B: 420, C: 780, and D: 1800rpm.

from curve B(about 2 ms), showing that the 127 bit chopper gives much closer value to the delay time of carbon black. Similar experiments using the 255 bit PRBS chopper showed the same line shape and peak position as curve A, indicating that the delay time 0.5ms obtained by the 127 bit chopper gives the lowest τ value when the choppers are rotated at 396 rpm.

Figure 4 shows the change of the first kind correlation spectra of the carbon black at different rotating speeds of the 127 bit PRBS chopper. The peak position of curve D agrees with that of curve C within the experimental error. Similar results have been obtained with the use of a 255 bit chopper at lower rotating speeds (approximately at half speeds). A 511 ($=2^9-1$) bit chopper which comes next to the 255 bit one would be the biggest possible one in view of manufacturing and/or stability of rotation at high speeds. We are not yet successful in driving the 511 bit chopper at a sufficient stability probably due to the lack of driving power. The time resolution practically obtainable with the use of the 127 bit chopper would be $(1/127\times1/30)s\fallingdotseq260\ \mu s$ at highest when rotated at 1800 rpm.

The ways of signal detection and signal processing are other important factors which determine the limit of time resolution. The microphone used in the present experiment has the working range up to about 15 kHz. Consequently the time resolution with the use of this microphone could reach to 70 μs which is sufficiently shorter than 260 μs, the time resolution limited by the 127 bit chopper.

The slowest part of the signal processing of the present system lies in the time delay unit(T. D. U., Fig.1) which digitally delays the reference signal by certain amount of τ by a microcomputer(NEC, TK-80) program. The limit of time resolution of this unit is determined by the speed of the microprocessor(D8080-AFC) of TK-80 as tens of microseconds[3], which is a comparable order of magnitude to that limited by the microphone. The correlator in our system is made by the analog unit which works much faster than the TK-80 digital unit, so that no limit of time resolution from the correlator unit will be put in the present system of signal processing.

Great improvements in time resolution would be expected by the use of a laser source in place of the xenon lamp source, an acousto-optic modulating system in place of the mechanical PRBS chopping system, or a piezoelectric detecting system in place of the microphonic detection. Effect of these replacements will be studied on conditions developed.

Authors wish to thank Professor Kozo Nagashima, The University of Tsukuba, Institute of Chemistry, for his kind support and encouragement during the course of this work.

References

1) K. Kato, S. Ishino and Y. Sugitani: *Chem. Lett.* **1980**, 783.

2) Y. Sugitani: *Kagaku no Ryoiki* **35**, 8 (1981); Y. Sugitani, A. Uejima and K. Kato: *J. Photoacoustics* **1**, 217 (1982).

3) TK-80E/80 USER'S MANUAL, IEM-560D (NEC), (1978).

The Crystal Structure of $(TMTTF)_2ReO_4$

Hayao KOBAYASHI,* Akiko KOBAYASHI,† Yukiyoshi SASAKI,† Gunzi SAITO,†† and Hiroo INOKUCHI††
Department of Chemistry, Faculty of Science, Toho University, Funabashi, Chiba 274
†*Department of Chemistry, Faculty of Science, The University of Tokyo, Hongo, Bunkyo-ku, Tokyo 113*
Institute for Molecular Science, Okazaki 444
(Received October 19, 1983)

Synopsis. The crystal of $(TMTTF)_2ReO_4$ is isomorphous with the other $(TMTTF)_2X$ compounds($X=ClO_4$, PF_6, Br,···). TMTTF molecules are stacked face-to face to form a zig-zag column. Although the structure of $(TMTTF)_2ReO_4$ closely resembles that of the analogous compound, $(TMTSF)_2ReO_4$, the loose intermolecular contacts in $(TMTTF)_2ReO_4$ suggest that the intermolecular interaction appears to be much weaker than that in $(TMTSF)_2ReO_4$.

It is well-known that tetramethyltetraselenafulvalene(TMTSF) forms a number of 2:1 salts with a variety of monovalent inorganic anions (Bechgaard salt). They exhibit a superconducting-phase transition and the charge (or spin)-density wave instability characteristic of one-dimensional metal systems.[1] Although the Bechgaard salts are isomorphic with each other, their physical properties are different from salt to salt and are sensitive to the small structural change induced by the variation in the anions. The sulfur analog, tetramethyltetrathiafulvalene (TMTTF), also form the isostructural series of $(TMTTF)_2X$ salts ($X=ClO_4$, PF_6, Br,···).[2] The band-structure calculation[3] shows that the Fermi surface of $(TMTTF)_2X$ is composed of distorted planes, quite similar to that of $(TMTSF)_2X$.[4] However, unlike $(TMTSF)_2X$, $(TMTTF)_2X$ undegoes a metal-insulator transition at a comparatively high temperature.[5] Recent studies have shown that $(TMTTF)_2Br$ and $(TMTTF)_2SCN$ take the antiferromagnetic ground states.[6,7]

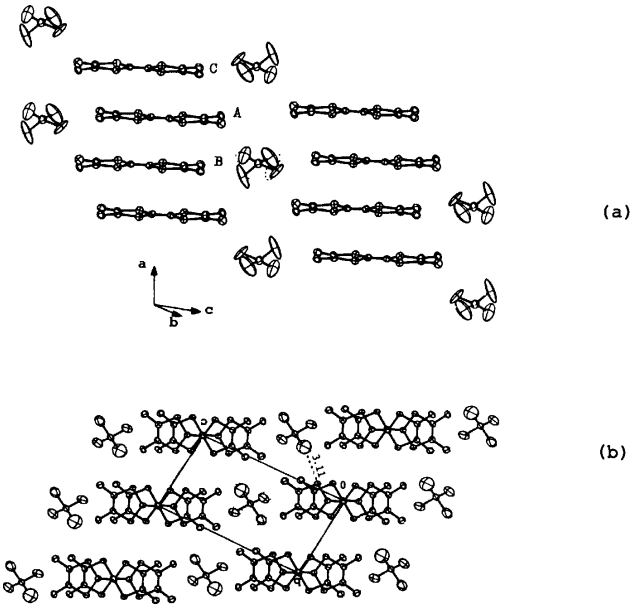

Fig. 1. (a) Side view of stack (tilted 10 °). The ReO_4 anions show disorder, taking one of the two possible positions randomly.
(b) View along *a*.

TABLE 1. FRACTIONAL COORDINATES AND ISOTROPIC TEMPERATURE FACTORS FOR $(TMTTF)_2ReO_4$

Atom	*x*	*y*	*z*	B_{eq}/Å²
Re	0.0	0.5	0.5	4.8
S (1)	0.3539(5)	0.3122(4)	0.1073(2)	3.7
S (2)	0.2410(5)	−0.0639(4)	0.2105(2)	3.5
S (3)	0.2827(5)	0.1451(4)	−0.1111(2)	3.7
S (4)	0.1766(5)	−0.2306(4)	−0.0084(2)	3.7
C (1)	0.2756(17)	0.0750(15)	0.0957(9)	3.2
C (2)	0.2517(17)	0.0073(15)	0.0022(9)	3.1
C (3)	0.3621(19)	0.2915(16)	0.2393(10)	4.2
C (4)	0.3079(18)	0.1148(17)	0.2895(10)	3.9
C (5)	0.2232(17)	−0.0331(16)	−0.1914(9)	3.7
C (6)	0.1729(18)	−0.2093(16)	−0.1399(10)	3.8
C (7)	0.4297(20)	0.4665(18)	0.2920(10)	4.6
C (8)	0.3083(23)	0.0703(21)	0.4019(11)	5.1
C (9)	0.2317(20)	0.0206(19)	−0.3018(10)	4.3
C (10)	0.1157(19)	−0.3865(17)	−0.1913(11)	4.5
O (1)	0.0517(51)	0.3185(34)	0.4540(24)	16.1
O (2)	0.1463(82)	0.6313(42)	0.5670(28)	19.6
O (3)	0.0310(88)	0.4271(74)	0.5775(42)	16.7
O (4)	−0.0679(68)	0.3748(46)	0.6242(28)	16.2

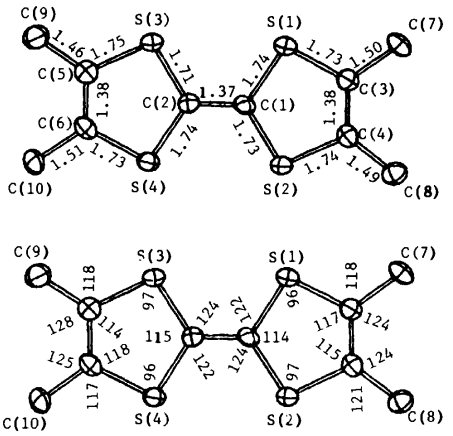

Fig. 2. The bond lengths (Å) and angles (°) of TMTTF. The averaged standard deviations of the bond lengths and angles are 0.02 Å and 1.3 °, respectively.

We also made structure analyses of $(TMTTF)_2X$ ($X=ClO_4$, ReO_4) and $(TMTSF)_2X$ ($X=BF_4$, ReO_4), $(TMTSF)_2BF_4$ structure of which has been previously reported.[8] However, we found that the structural description has been made on $(TMTSF)_2ReO_4$ and $(TMTTF)_2ClO_4$.[2,9] In this paper, we wish to report on the crystal structure of $(TMTTF)_2ReO_4$.

The black needle crystals were prepared electrochemically. The crystal data are: $(TMTTF)_2ReO_4$, $(C_{10}H_{12}S_4)_2ReO_4$, F.W.=771.1, triclinic, $P\bar{1}$, a=7.166(2), b=7.621(2), c=13.230(3) Å, α=86.62(2), β=95.56(2), γ=108.20(2)°, U=679.5(3) Å^3, Z=1, d_c=1.88 gcm^{-3}. The intensities were measured on a Rigaku automated diffractometer with Mo $K\alpha$ radiation up to 2θ=60°. The structure refinement gave a conventional R value of 0.066. The structure is shown in Fig. 1. The bond lengths and angles are given in Fig. 2. The atomic coordinates are given in Table 1. The table of the anisotropic temperature factors and F_o-F_c table are kept at the Chemical Society of Japan (Document No. 8421).

As has been mentioned before, $(TMTTF)_2ReO_4$ is isostructural with the other compounds of the $(TMTTF)_2X$ and $(TMTSF)_2X$ series. The planar TMTTF molecules are stacked face-to-face to from a zig-zag column along the a axis. Two independent interplanar distances are 3.57 (A···B) and 3.59 Å (A···C) (see Fig. 1). These values are somewhat larger than those of the other $(TMTTF)_2X$ salts:[2] 3.50, 3.53 Å (x=Br); 3.50, 3.57 (NO_3); 3.50, 3.54 (I); 3.54, 3.56 (BF_4); 3.49, 3.56 (SCN); 3.52, 3.59 (ClO_4); 3.53, 3.62 (PF_6). There appears to be a good correlation between the size of the anions and the interplanar distances. Although the $(TMTTF)_2X$ compound is considred to be a one-dimensional metal around room temperature, there is no short intermolecular contact along the columns. The shortest S···S distance in $(TMTTF)_2ReO_4$ (3.74 Å) is longer than the van der Waals distance of S···S (3.70 Å). Similarly, in the perchrolate salt, the shortest S···S distance is 3.73 Å.[10]

The short contact between Se stoms and the atoms of the anions is a common structural feature in $(TMTSF)_2X$ systems.[11] The shortest Se···O distance in $(TMTSF)_2ReO_4$ is 3.10 Å,[10] indicating a strong coupling between the TMTSF columns and the ReO_4 anions. This is consistent with the occurence of a sharp metal-insulator transition in $(TMTSF)_2ReO_4$, where the distortion of TMTSF columns and the displacement of ReO_4 anions take place cooperatively.[12] However, the shortest S···O contact in $(TMTTF)_2ReO_4$ is 3.12 Å, which is only slightly shorter than the corresponding van der Waals distance. The generous metal-insulator transition in $(TMTTF)_2X$[5] ($X=BF_4$, ClO_4, SCN,···) may be attributable to the loose contact between TMTTF columns and the anions. The preliminary resistivity measurement of $(TMTTF)_2ReO_4$ suggests the existence of a metal-insulator transition around 230 K, with the room-temperature resistivity of 0.03 Ω cm.

References

1) D. Jerome, *Mol. Cryst. Liq. Cryst.*, **79**, 155 (1982).
2) B. Liautard, S. Peytavin, G. Brun, and M. Maurin, *J. Physique*, **43**, 1453 (1982).
3) T. Mori, A. Kobayashi, Y. Sasaki, H. Kobayashi, G. Saito, and H. Inokuchi, *Bull. Chem. Soc. Jpn.*, **57**, 627 (1984).
4) T. Mori, A. Kobayashi, Y. Sasaki, H. Kobayashi, *Chem. Lett.*, **1982**, 1923.
5) P. Delhaes, C. Coulon, J. Amiell, and S. Flandrois, *Mol. Cryst. Liq. Cryst.*, **50**, 43 (1979).
6) S. S. Parkin, J. C. Scott, J. B. Torrance, and E. M. Engler, *Phys. Rev.*, **B26**, 6319 (1982).
7) C. Coulon, A. Maaroufi, J. Amiell, E. Dupart, S. Flandrois, P. Delhaes, P. Moret, J. P. Pouget, and J. P. Morand, *Phy. Rev.*, **B26**, 6322 (1982).
8) H. Kobayashi, A. Kobayashi, G. Saito, and H. Inokuchi, *Chem. Lett.*, **1982**, 245.
9) K. Bechgaard, *Mol. Cryst. Liq. Cryst.*, **79**, 1, (1982).
10) H. Kobayashi, unpublished work.
11) F. Wudl, *Mol. Cryst. Liq. Cryst.*, **79**, 67 (1982).
12) R. Moret, J. P. Pouget, R. Comes, and K. Bechgaard, *Phys. Rev. Lett.*, **49**, 1008 (1982).

The Partial Molar Volume of 1-Alkanols in a Sodium Dodecylsulfate Solution around Its Critical Micelle Concentration

Masahiro MANABE,* Sumiyoshi KIKUCHI, Shingo KATAYAMA, Susumu TOKUNAGA, and Masaharu KODA
Department of Industrical Chemistry, Niihama Technical College Niihama, Ehime 792
(Received October 20, 1983)

Synopsis. The partial molar volume (V_a) of 1-alkanols (C_6–C_8) was determined at 25 °C in a solution of sodium dodecylsulfate up to its critical micelle concentration in water. The V_a in micellar solutions is higher than that in non-micellar ones. This increase in V_a has been explained in terms of the promotion of micellization by the addition of alkanol.

The partial molar volume of 1-alkanols[1,2] and alkanes[3,4] in a micellar solution of surfactants has been reported to be higher than that in water. The higher value has been attributed to the incorpotation of the solubilizate in micelles, their inside having an oil-like character.

On the other hand, the higher value can possibly be explained in terms of the transformation of the monomer surfactant species into a micellar one on the addition of the solubilizate, judging from the following well-known facts. One is the lowering of the critical micelle concentration (cmc) of the surfactants in the presence of alkanols.[5] Another is the higher partial molar volume of the micellar surfactant species than that of the monomer one in water.[6] No quantitative explanation derived from the viewpoint of micellization has, however, been proposed until now.

In order to confirm the validity of this explanation, the partial molar volume of 1-alkanols (C_6–C_8) was determined in solutions of sodium dodecylsulfate (SDS), up to 8 mmol kg^{-1}, just around cmc_0 (cmc in water) at 25 °C. The method of determination was the same dilatometric one as was used in previous studies[1,7]: a small amount of alkanol was successively injected into a dilatometer filled with a SDS solution.

The dependence of the experimentally determined partial molar volume (V_a) on the concentration of alkanol (C_a) for heptanol is illustrated in Fig. 1. In SDS solutions with very low concentrations as well as in water, V_a continues to be constant up to the solubility of the alkanol, followed by higher constant V_a values obtained in a turbid solution. When the SDS concentration (C_s) exceeds a certain value (C_s=2 mmol kg^{-1} for heptanol), an abrupt increase in V_a from a lower constant value to a higher one appears, without turbidity, at an alkanol concentration (C_a^*). Thereafter, the solution is saturated with the alkanol. The trend is obvious that C_a^* decreases and the solubility increases as C_s increases. As may be seen in Fig. 1, the respective concentrations, C_a^*, and the solubility coincide reasonably well with the alkanol concentration at the cmc of SDS, as determined by a surface-tension method.[8] The consistency shows that the abrupt increase in V_a at C_a^* is due to the beginning of micelle formation upon the addition of alkanol.

As for each SDS solution, the values of V_a below C_a^*, between C_a^* and the solubility, and above the solubility are averaged to give the respective mean values, V_a^f, V_a^m, and V_a^s, which are then plotted in Fig. 2 against C_s, together with the literature data.[1] It may be seen that each value has little dependence on C_s. V_a^f is close to the V_a in water: V_a^f corresponds to the partial molar volume of monomerically dissolving alkanol. V_a^m reflects the partial molar volume of alkanol in the presence of micelles, and V_a^s corresponds to that of alkanol in the separated phase. The values for each state of alkanol are averaged again, denoted by $\overline{V}_a^f$, $\overline{V}_a^m$, and $\overline{V}_a^s$, and listed in Table 1. It may be noticed that $\overline{V}_a^m$ is in agreement with the partial molar volume of each alkanol determined above the cmc_0 of SDS (Fig. 1). This fact suggests that the partial molar volume of alkanol at just cmc_0 must be equal to $\overline{V}_a^m$. $\overline{V}_a^s$ is close to the molar volume of pure liquid alkanol[1] (see Table 1), although the alkanol in the separated phase is not pure, but saturated with water.

In order to simplify the discussion, we will consider the volumetric behavior under the particular condition that the concentrations of both the micelle and the added alkanol are extremely low. If a small amount of alkanol (ΔC_a mol) is added to such a SDS solution (1 dm^3) with a very low concentration of the micelle (at cmc_0), it is probable that almost the entire amount of the added alkanol will dissolve monomerically in the aqueous bulk phase and cause the volume-increase by

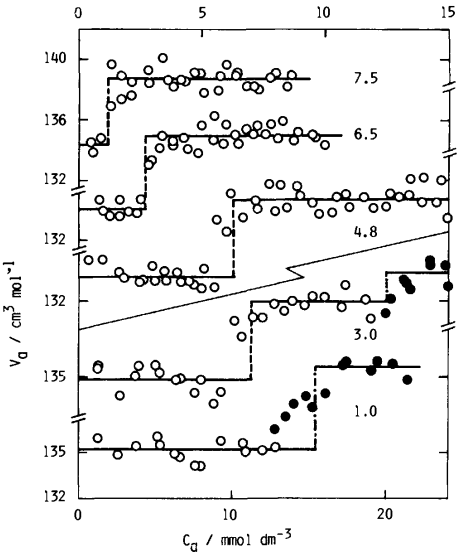

Fig. 1. The dependence of partial molar volume of 1-heptanol on its concentration in SDS solution at 25 °C. Closed circle indicates appearance of turbidity. Broken line and chain one indicate the concentration of the alkanol at cmc of SDS and solubility of the alkanol, respectively, taken from Ref. (1). Number represents C_s (mmol kg^{-1}).

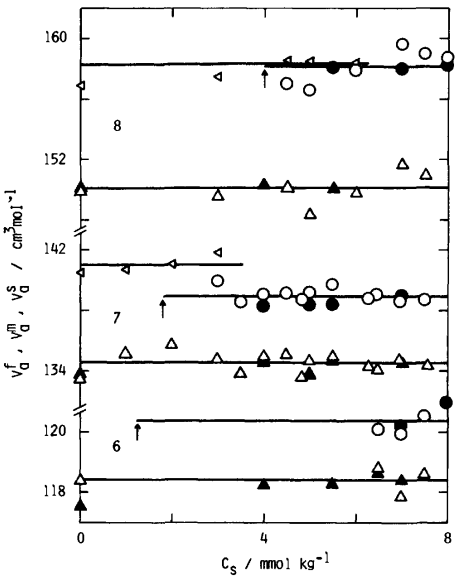

Fig. 2. The dependence of partial molar volume of 1-alkanols on the concentration of SDS at 25 °C. Large triangle, circle, and small triangle represent V_a^f, V_a^m, and V_a^s, respectively. Closed mark is from Ref.(1). Number indicated the number of carbon atoms in the alkanol molecule. Arrow indicates C_s below which micelle formation is impposible, described in Ref. (8).

Table 1. Partial molar volume of 1-alkanols in an SDS solution at 25 °C

	Partial molar volume/cm^3 mol^{-1}				
	$\overline{V}_a^f$	$\overline{V}_a^m$		$\overline{V}_a^s$	Molar volume[b]
		Below cmc_0	Above cmc_0[b]		
N[a]	—	—	—	—	—
6	118.36	120.38	120.93		124.70
7	134.50	138.87	139.04	141.02	141.59
8	150.12	158.11	157.53	158.21	157.91

a) Number of carbon atoms in an alkanol molecule.
b) Taken from Ref. (1).

$\Delta\overline{V}_s$ ($-\Delta$cmc) resulting from the micellization of Δcmc mol of SDS, since the increase in the concentration of alkanol (ΔC_a mol dm^{-3}) leads to the decrease in cmc (Δcmc mol dm^{-3}), where $\Delta\overline{V}_s$ indicates the partial molar volume increment of SDS on its micellization. Therefore, the total volume increment of the whole solution is $\overline{V}_a^f\,\Delta C_a+\Delta\overline{V}_s$ ($-\Delta$cmc). On the basis of the general definition of the partial molar volume, the volume increment per mole of alkanol added to the micellar solution, $\overline{V}_a^m$, corresponds to $\overline{V}_a^f+\Delta\overline{V}_s$ ($-\Delta$cmc/ΔC_a) *i.e.* $\overline{V}_a^m-\overline{V}_a^f=\Delta\overline{V}_s$ ($-\Delta$cmc/ΔC_a). The validity of the equation can be checked in Fig. 3, by using the literature data of the rate of cmc-lowering, Δcmc/ΔC_a, of 1-alkanols in an SDS solution[5] and of the $\Delta\overline{V}_s$ for SDS in water (11 cm^3 mol^{-1}).[6] It can be recoginzed that the point ($\overline{V}_a^m-\overline{V}_a^f$, $-\Delta$cmc/ΔC_a) for each alkanol falls on a straight curve with a slope of unity and passing through 11 cm^3 mol^{-1} ($\Delta\overline{V}_a$) at the unity of $-\Delta$cmc/ΔC_a, taking the experimental errors of each term into account. The result gives the conclusion that the gain in the partial molar volume, $V_a^m-V_a^f$, is essentially to be attributed, no to the solubilization of the added alkanol,[1,2] but to the promotion of the micellization of SDS alone.

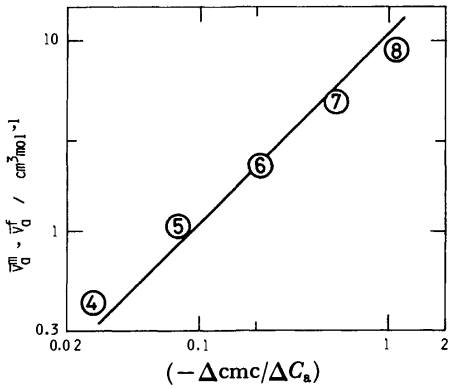

Fig. 3. The relation between log ($\overline{V}_a^m-\overline{V}_a^f$) and log ($-\Delta$cmc/$\Delta C_a$) in 1-alkanol $-$SDS system at 25 °C. Number indicates the number of carbon atoms in alkanol molecule. For the straight curve, see in text. $\overline{V}_a^m$ and $\overline{V}_a^f$ of 1-butanol and 1-pentanol are taken from Ref.(1).

Above cmc_0, V_a^m must be correlated in a complicated manner with the amount of solubilized alkanol. If we can estimate the quantity corresponding to Δcmc/ΔC_a at any concentration of the surfactant, the further analysis of V_a^m will be possible.

References

1) M. Manabe, K. Shirahama, and M. Koda, *Bull. Chem. Soc. Jpn.*, **49**, 2904 (1976).
2) E. Vikingstad, *J. Colloid Interface Sci.*, **72**, 75 (1979).
3) E. Vikingstad and H. Hoiland, *J. Colloid Interface Sci.*, **64**, 510 (1978).
4) E. Vikingstad, *J. Colloid Interface Sci.*, **68**, 287 (1979).
5) M. Manabe and M. Koda, *Bull. Chem. Soc. Jpn.*, **51**, 1599 (1978).
6) K. Shinoda and T. Soda, *J. Phys. Chem.*, **67**, 2072 (1963).
7) M. Manabe and M. Koda, *Bull. Chem. Soc. Jpn.*, **48**, 2367 (1975).
8) M. Manabe, Y. Tanizaki, H. Watanabe, S. Tokunaga, and M. Koda, *Memoirs of the Niihama Technical College (Science and Engineering)*, **19**, 50 (1983).

Selective Formation of Solute Radicals in the Radiolysis of Neopentane-Cyclopentane Mixtures at 4 and 77 K as Studied by Capillary Gas Chromatography and ESR Spectroscopy

Bernard TILQUIN, Catherine GOURDIN-SERVENIERE, Tetsuo MIYAZAKI,*,† Kenji FUEKI†
Laboratoire de Chimie Inorganique et Analytique, Universite Catholique de Louvain, Place Louis Pasteur 1, B-1348 Louvain-la-Neuve, Belgium
†*Department of Synthetic Chemistry, Faculty of Engineering, Nagoya University, Chikusa-ku, Nagoya 464*
(Received November 1, 1983)

Synopsis. The dimer yields in the radiolysis of the *neo*-C_5H_{12}-*cyclo*-C_5H_{10} (1 mol%) mixtures at 77 and 4 K have been measured by capillary gas chromatography. Analysis of the results indicates that cyclopentyl radicals are produced selectively at 77 K, while their selective formation is suppressed at 4 K. This result coincides well with the data obtained by ESR spectroscopy.

When neopentane containing a small amount of other alkane is γ-irradiated at 77 K, solute alkyl radicals are formed selectively.[1] H atoms, produced by the radiolysis of neopentane, abstract hydrogen atoms much more efficiently from the alkane solute than the neopentane solvent to form the solute radicals selectively.[2] This phenomenon was also found in several solid alkanes.[3] The selective formation of radicals was studied by ESR spectroscopy which can only detect trapped reaction intermediates. Since it has been generally accepted that the radiation effect is not selective, the selective formation of the solute radicals should be verified by the product analysis which gives information about overall radiation effects.

Recently the selective formation of the $C_{10}H_{21}$ radicals in the radiolysis of the n-$C_{10}D_{22}$-n-$C_{10}H_{22}$ mixtures was verified by the analysis of dimer products.[4]

Here, we report the results on dimer products in the radiolysis of the neopentane-cyclopentane mixtures as measured by a capillary gas chromatography, and compare them with the results of ESR measurement.

Experimental

The details of the experimental procedure were described in a previous paper.[5] Neopentane and cyclopentane were the same as those used previously.[5] In order to cool the sample completely, helium gas at 400 mmHg was sealed in a cell for the γ-irradiation at 4 K. The total dose for experiments on product analysis at 4 and 77 K was fixed at 0.24 Mrad. The dose rate of γ-rays was 0.14 Mrad h^{-1}.

Product analysis was performed by means of Varian Aerograph 1440 and 3700 gas chromatographs with a FID detector. The capillary column (25 m×1.25 mm) was coated with squalane. A typical chromatogram of the heavy products in the radiolysis of neopentane was shown in a previous paper.[5]

The radicals produced in the irradiated samples were measured with a JEOL ESR spectrometer at microwave power levels of 200 μW at 77 K and 10 μW at 4 K.

Results and Discussion

When pure neopentane is γ-irradiated at 77 K, neopentyl radicals are the main radicals observed by ESR spectroscopy.[2] Figure 1A shows the ESR spectrum of the *neo*-C_5H_{12}-*cyclo*-C_5H_{10} (1 mol%) mixture γ-irradiated at 77 K. The spectrum consists of the spectrum of cyclopentyl radicals, denoted by arrows (↑), and that of neopentyl radicals, denoted by arrows (↑). The relative yield of the cyclopentyl radicals, measured by a double integration of the spectrum, amounts to 26% of the total radical yields, which is much higher than the concentration (1 mol%) of cyclopentane in the mixture. The selective formation of the solute radicals was reported previously by Miyazaki *et al.*[1] Figure 1B shows the ESR spectrum of the *neo*-C_5H_{12}-*cyclo*-C_5H_{10} (1 mol%) mixture containing He, γ-irradiated at 4 K and measured at 4 K. It is seen that cyclopentyl radicals are not observed at all, but neopentyl radicals, denoted by arrows (↕), are formed, exclusively.[6,7]

In order to measure the dimer products in the radiolysis of the *neo*-C_5H_{12}-*cyclo*-C_5H_{10} mixture by gas chromatography, 2,2,5,5-tetramethylhexane (bineopentyl), neopentylcyclopentane, and bicyclopentyl were synthesized and their structures were determined by ^{13}C NMR spectroscopy. The chromatographic retention of the radiolysis products was compared with that of the

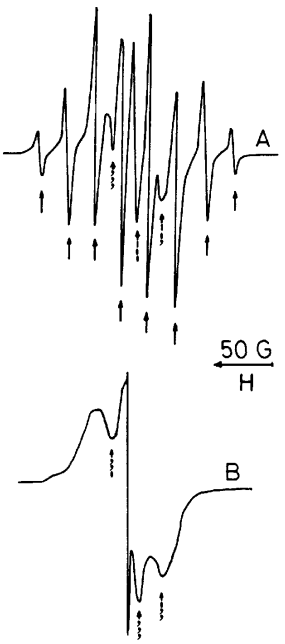

Fig. 1. ESR spectra of γ-irradiated *neo*-C_5H_{12}-cyclo-C_5H_{10} (1 mol%). A, Spectrum measured at 77 K after γ-irradiation at 77 K; B, Spectrum measured at 4 K after γ-irradiation at 4 K. Total doses at 77 and 4 K are 0.24 and 0.06 Mrad, respectively.

Table 1. Relative yields of dimer products in the radiolysis of neopentane at 77 K and 4 K[a]

Product[b]		*neo*-C_5H_{12}	*neo*-C_5H_{12}-*cyclo*-C_5H_{10} (1 mol%)	
		77 K	77 K	4 K
2233TeMC$_4$	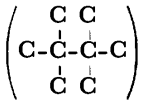	—	—	0.23
2244TeMC$_5$	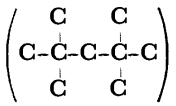	0.03	0.04	—
225TMC$_6$	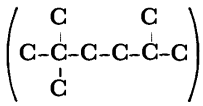	0.05		0.02
C_9H_{18}[c]		0.19	0.20	0.15
bineopentyl	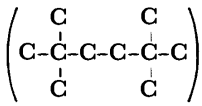	1.0	1.0	1.0
$C_{10}H_{22}$		0.08	0.07	0.08
neopentyl-cyclopentane	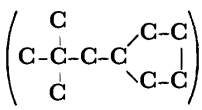	—	0.63	0.07
bicyclopentyl	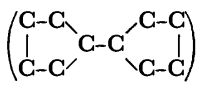	—	0.13	0.003

a) Yield of bineopentyl is taken as 1. *G*-values of bineopentyl at 77 and 4 K are approximately 0.3. b) T, Te, and M represent tri, tetra, and methyl, respectively. For example, 2233TeMC$_4$ means 2,2,3,3-tetramethylbutane. c) C_9H_{18} represents a mixture of isomers. (*cf.* Ref. 5)

synthesized one. The relative yields of dimer products are shown in Table 1. Bineopentyl, neopentylcyclopentane and bicyclopentyl are all formed in the radiolysis of the *neo*-C_5H_{12}-*cyclo*-C_5H_{10}(1 mol%) mixture at 77 K. In the radiolysis at 4 K, however, the formation of neopentylcyclopentane and bicyclopentyl is suppressed drastically, but bineopentyl is still a main product.

The relative yields of neopentyl and cyclopentyl radicals can be estimated from the dimer yields by the following assumptions: (1) the dimer formation is due to the recombination of radicals; (2) neopentyl and cyclopentyl radicals have the same dispropotionation-combination rate constant ratio, k_d/k_c. Then, the relative yields of neopentyl and cyclopentyl radicals can be obtained as follows:[8]

$$\text{Yield of } \textit{neo}\text{-}C_5H_{11} = 2 \times (\text{bineopentyl yield}) + (\text{neopentylcyclopentane yield})$$

$$\text{Yield of } \textit{cyclo}\text{-}C_5H_9 = 2 \times (\text{bicyclopentyl yield}) + (\text{neopentylcyclopentane yield})$$

The relative yields of neopentyl and cyclopentyl radicals in the radiolysis of the *neo*-C_5H_{12}-*cyclo*-C_5H_{10} (1 mol%) mixture at 77 and 4 K are summarized in Table 2. Since k_d/k_c for secondary radicals, such as cyclopentyl radicals, may be larger than that for primary radicals, such as neopentyl radicals,[9] the relative yields of the cyclopentyl radicals may be somewhat underestimated. The radical yields obtained by the product analysis coincide well with those by ESR spectroscopy. The yields of cyclopentyl radicals at 77 K are much higher than expected from the mole fraction of cyclopentane in the mixture. Thus, it has been confirmed from product analysis as well as ESR measurement that the cyclopentyl radicals, *i.e.*, solute radicals, are selectively formed in the radiolysis of the *neo*-C_5H_{12}-*cyclo*-C_5H_{10} (1 mol%) mixture at 77 K.

Table 2. Relative yields of neopentyl and cyclopentyl radicals in the radiolysis of *neo*-C_5H_{12}-*cyclo*-C_5H_{10} (1 mol%) at 77 and 4 K[a]

Radicals	77 K		4 K	
	Prod. Anal.[b]	ESR[c]	Prod. Anal.[b]	ESR[c]
neo-C_5H_{11}	1.00	1.00	1.00	1.00
cyclo-C_5H_9	0.33	0.35	0.03	<0.05

a) Yield of *neo*-C_5H_{11} radicals is taken as 1.00. b) Yield of radicals were obtained by analysis of dimer products. c) Yield of radicals were obtained by ESR measurements. The ratio of concentration of *cyclo*-C_5H_9 radicals to that of *neo*-C_5H_{11} radicals did not change after annealing the γ-irradiated sample to 77 K.

References

1) T. Miyazaki, T. Wakayama, M. Fukaya, Y. Saitake, and Z. Kuri, *Bull Chem. Soc. Jpn.*, **46**, 1030 (1973).

2) T. Miyazaki and T. Hirayama, *J. Phys. Chem.*, **79**, 566 (1975).

3) T. Miyazaki, J. Kasugai, M. Wada, and K. Kinugawa, *Bull. Chem. Soc. Jpn.*, **51**, 1676 (1978).

4) a) B. Tilquin, Th. Baudson, P. Claes, O. Claesson, and A. Lund, *Radiat. Phys. Chem.*, **17**, 235 (1981); b) B. Tilquin, Th. Baudson, P. Claes, A. Lund, and O. Claesson, *J. Phys. Chem.*,**86**, 3324 (1982).

5) B. Tilquin, L. M. Fontaine, P. Claes, T. Miyazaki, A. Wakahara, and K. Fueki, *Radition Effects*, **66**, 9 (1982).

6) a) K. Kinugawa, T. Miyazaki, and H. Hase, *Radiat. Phys. Chem.*,**10**, 341 (1977); b) M. Iwasaki, K. Toriyama, K. Nunome, M. Fukaya, and H. Muto, *J. Phys. Chem.*, **81**, 1410 (1977).

7) The ESR spectrum in the radiolysis of the neopentane system at 4 K is independent of an irradiation dose in the range of 0.06—0.24 Mrad. (*cf.* Ref. 5 and 6).

8) Isobutene is one of the main stable products in the radiolysis of neopentane. Since a product of C_4H_9-C was not formed in the radiolysis of *neo*-C_5H_{12}-*cyclo*-C_5H_{10} at 77 K, the reaction of free radicals with stable producs, such as isobutene, may play a minor role.

9) a) B. Tilquin, J. Allaet, and P. Claes, *J. Phys. Chem.*, **78**, 462 (1974); b) P. Tilman, P. Claes, and B. Tilquin, *Radiat. Phys. Chem.*, **15**, 465 (1980).

Interionic Charge Transfer Enhanced by Hydrophobic Interaction

Koichi HIRANO* and Masahiko TOKUHARA
Department of Chemistry, Miyagi University of Education, Aramaki-aoba, Sendai 980
(Received November 10, 1983)

Synopsis. A water solution containing Rhodamine 6G and Na-tetraphenylborate exhbits a new absorption band at 540 nm, which has the characteristics of a charge-transfer (CT) band. In organic solvents, however, such a CT band is not found. This indicates that hydrophobic interactions enhance the charge transfer interaction.

Spectroscopic studies on the charge transfer interaction in water solution have been made in connection with the biological interest.[1-6] However, very little has been reported about the effect of hydrophobic interactions on the charge transfer interaction.

In the present report we show evidence to support the view that hydrophobic interactions play an important role in the formation of the charge transfer (CT) complex.

Experimental and Results

When the sodium salts of tetraphenylborate (BPh_4^-) is added to a water solution of Rhodamine 6G (Rhod $6G^+$), a purple color appears instantaneously. At the same time, the characteristic fluorescence of the Rhod $6G^+$ ion decreases on adding the BPh_4^- solution. On the contrary, no evidence of any CT interactions with BPh_4^- was found for Rhod $6G^+$ in organic solvents such as ethanol, acetonitrile, and *N*-methylformamide. These results indicate that water enhances the CT interaction between the organic ions both possessing large hydrophobic groups.

The UV/VIS absorption spectra of the water solutions of mixtures of Rhod 6G and Na-tetraphenylborate were examined on a Shimadzu UV 200S double beam spectrophotometer at 25 C°. The results are shown in Fig. 1. The appearance of isosbestic points confirms the presence of a new complex. The absorption maximum of the new band was determined as λ=540 nm from the concentration dependence of the peak position of the spectra. We analysed the spectra on the basis of a modified Rose-Drago equation[7]:

$$\frac{ab}{d-d_0} = \left(a+b-\frac{d-d_0}{\varepsilon_C-\varepsilon_A}\right)\frac{1}{\varepsilon_C-\varepsilon_A} + \frac{1}{K(\varepsilon_C-\varepsilon_A)} \qquad (1)$$

where d_0, d, ε_A, ε_C, a, b and K denote the absorbances of Rhod $6G^+$ and mixtures, the molar absorptivites of Rhod $6G^+$ and complex, the initial concentrations of Rhod $6G^+$ and BPh_4^-, and the equilibrium constant for the complex. By means of an iterative method, the constant was determined as $K=1.02\times10^5$ l/mol at 25 C°. This is fairly comparable with the K values of the ion pair of $[(i\text{-}C_5H_{11})_3(n\text{-}C_4H_9)N]^+BPh_4^-$ determined by conductometry[8] or of fluorenylsodium by spectrophotometry.[9] These facts strongly suggest the new entity to be an interionic CT complex with 1:1 stoichiometry. Therefore, equlibrium (2) should be considered;

$$\text{Rhod } 6G^+ + BPh_4^- \rightleftharpoons \text{Rhod } 6G^+ \leftarrow BPh_4^- \qquad (2)$$

Thus the new absorption at 540 nm is ascribable to the CT band arising from the excitation of the complex.

Discussion

From Table 1, it is evident that the CT interaction between Rhod $6G^+$ and BPh_4^- is not affected by the solvent polarity, but it is storongly dependent upon the nature of the solvent, the lipophilicity or hydrophobic solvation capability. In organic solvents, the solvent-solute pairs must be formed predominantly in comparison with the solute-solute pairs, because of their relatively strong hydrophobicity. Hence, it is difficult to form the tight binding donor-acceptor ion pairs. This leads to the interuption of the subsequent charge

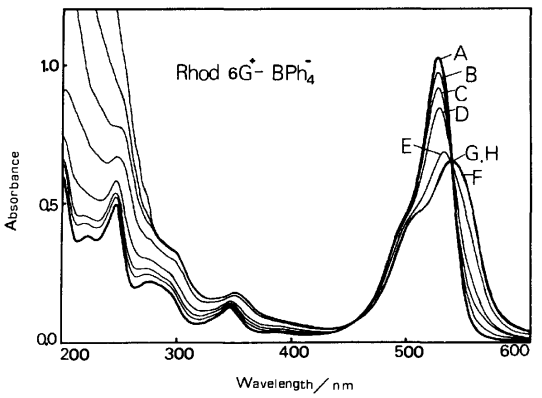

Fig. 1. Absorption spectra of Rhod $6G^+$ (1.12×10^{-5} mol/l) in water with various amounts of BPh_4^- at 25 °C. A none, B 1.06×10^{-6} mol/l, C 0.19×10^{-5} mol/l, D 0.38×10^{-5} mol/l, E 0.76×10^{-5} mol/l, F 1.52×10^{-5} mol/l, G 3.42×10^{-5} mol/l, H 6.83×10^{-5} mol/l.

TABLE 1. SOLVENT DEPENDENCE ON THE CT-COMPLEX FORMATION BETWEEN Rhod $6G^+$ AND BPh_4^- IONS

Solvent	Dielectric constant	Spectral evidence	Complex formation
Water	78.54[a]	A new band appears at 540 nm.	yes
Ethanol	24.30[b]	A shift in the Rhod $6G^+$ spectrum is observed.	no
Acetonitrile	37.45[b]	A shift in the Rhod $6G^+$ spectrum is observed.	no
N-Methylformamide	182.4[b]	A shift in the Rhod $6G^+$ spectrum is observed.	no

a) The Chemical Society of Japan, Ed. "Kagaku Binran, Kiso-hen II", Maruzen (1957) p. 1166. b) A. J. Bard, Ed. "Electroanalytical Chemistry", Marcel Dekker, Inc., New York (1969) Vol. 3, Appendix 1.

transfer since CT interaction involves short range forces, so that the formation of the CT complex is reduced. This explains why the CT band is not found in solvents such as ethanol, acetonitrile and *N*-methylformamide. On the contrary, when water is used as a solvent the stacking between the donor and acceptor ions must be promoted, for solvent water enhances the hydrophobic interactions between the two ions.[10-11] Once stacking take place between two pi-elctron systems, the charge transfer from donor to acceptor occurs easily, because intermolecular charge transfer is most strongly favored in the case where "active orbital" overlapping between donnor and scceptor is possible.[12] This is the main reason why Rhod $6G^+$ forms a CT complex with BPh_4^- in water solution.

Subsequently, we have estimated the overall free energy change on complex formation as $\Delta G=-26$ kJ/mol. Let ΔG_{HI} be the free energy change due to the hydrophobic interaction we can split ΔG into two contributions;

$$\Delta G = \Delta G_{E,C} + \Delta G_{HI} \quad (3)$$

where $\Delta G_{E,C}$ is the contributions from electrostatic and CT interactions. Sheraga[13] calculated ΔG_{HI} values for various types of hydrophobic interactions; $\Delta G_{HI}=-1.3\sim-6.3$ kJ/mol were determined. These values are relatively small in comparison with the ΔG. In spite of the fact, the hydrophobic effect on the CT interaction must be significant, because ΔG_{HI} describes the tendency to form the tight binding ion pairs, and only a fraction of the pairs yield the CT complex.

References

1) H. A. Harbury and K. A. Foley, *Proc. Natl. Acad. Sci. U.S.A*, **44**, 662 (1958).
2) I. Isenberg and A. Szent-Györgyi, *Proc. Natl. Acad. Sci. U.S.A*, **44**, 857 (1958).
3) G. Cilento and M. Berenholc, *Biochim. Biophys Acta*, **271**, 94 (1965).
4) T. Sasaki and H. Hosoya, *Biochim. Biophys. Acta*, **112**, 459 (1966).
5) J. Mauchamp and M. Shimitzky, *Biochim.*, **8**, 1554 (1969).
6) A. Szent-Györgyi and .J. McLaughlin, *Proc. Natl. Acad. Sci. U.S.A*, **69**, 3510 (1972).
7) J. N. Rose and S. R. Drago, *J. Am. Chem. Soc.*, **81**, 6138 (1959).
8) C. Carvazal, K. J. Töle, J. Smid, and M. Szwarc, *J. Am. Chem. Soc.*, **87**, 5548 (1965).
9) T. E. Hogen-Esch and J. Smid, *J. Am. Chem. Soc.*, **88**, 307 (1966).
10) B. E. Fischer and H. Sigel, *J. Am. Chem. Soc.*, **102**, 2998 (1980).
11) F. Zuccarello, A. Randino, G. Buemi, and C. Rigano, *Bull. Chem. Soc. Jpn.*, **56**, 1837 (1983).
12) S. P. McGlynn, *Chem. Rev.*, **58**, 1113 (1958).
13) H. A. Scheraga, *Accounts Chem. Res.*, **12**, 7 (1979).

Dependence of Efficiency of Photoinduced Electron Transfer from Pyrene to Copper(II) Ion on Copper(II)-Ion Fraction on Dodecyl-Sulfate-Micelle Surface

Takashi NAKAMURA, Akira KIRA,* and Masashi IMAMURA
The Institute of Physical and Chemical Research Wako-shi, Saitama 351-01
(Received November 24, 1983)

Synopis. In quenching of the pyrene fluorescence by copper(II) ions in dodecyl sulfate micelles whose surface is covered by sodium and copper(II) ions, the pyrene-cation quantum yield decreases, after reaching a certain maximum yield, with increasing copper(II)-ion fraction. The decrease suggests that the micellar structure becomes unfavorable for electron transfer quenching as copper(II) ions displace sodium ions on the micellar surface.

Pyrene cations are produced in quenching of the pyrene singlet excited state by copper(II) ions in sodium dodecyl sulfate (SDS) micelle solutions.[1] Previous studies of fluorescence measurement[2] as well as our early laser photolysis study[1] have been made at low concentrations of both surfactant and quencher in order to avoid possible complexities caused by the change in the micellar size and shape. Recently, remarkable surfactant-concentration effects have been found in this electron transfer at SDS concentrations of 0.05—1 M (1 M=1 mol dm^{-3}).[3] The present note deals with the seemingly unusual dependence of the pyrene-cation quantum yield on the fraction of copper(II) dodecyl sulfate (CUDS) in mixed solutions of SDS and CUDS. This mixture provides dodecyl sulfate micelles covered by sodium and copper(II) ions. Considering the importance of comparison of the data for the same total dodecyl sulfate (DS^-) concentration, it is convenient to define the copper(II)-ion fraction on the micellar surface, $F(Cu^{2+})$, by

$$F(Cu^{2+}) = 2[CUDS]/(2[CUDS]+[SDS]) \quad (1)$$

where the denominator represents the total dodecyl sulfate concentration, and the value of $F(Cu^{2+})$ thus defined equals unity for CUDS solutions without SDS.

Experimental

Deaerated solutions containing 0.2 mM pyrene were subjected to laser photolysis, where a 20-ns pulse of a frequency-doubled ruby laser (347 nm) was used for excitation.[1,3] In order to prevent biphotonic ionization, the excitation intensity was adjusted so that the sample absorbed an energy of about 2 mJ cm^{-2} per pulse. The numbers of absorbed photons were estimated using the anthracene T-T absorption as a reference.[1]

Results

The pyrene fluorescence lifetime in the presence of 10 mM CUDS is 43 ns for an SDS concentration of 1.0 M and becomes shorter with decreasing SDS concentration.[3] In CUDS micelles the pyrene fluorescence vanishes within the duration of the laser pulse, indicating a lifetime shorter than 20 ns. These lifetimes are much shorter than the natural fluorescence lifetime in SDS micelles, 340 ns for SDS concentrations of 0.05 to 1.0 M. Thus, practically all the excited pyrene molecules were quenched by copper(II) ions under the present experimental conditions. The absorption spectra of pyrene cations with a peak at 450 nm were practically unchanged in shape and position under various conditions used in the experiments. The cation quantum yield, Φ, was determined from the absorbance at 450 nm where the molar absorption coefficient is 20500 $M^{-1}\,cm^{-1}$.[4]

Figure 1A exhibits the cation quantum yield as a function of the copper(II)-ion fraction in SDS/CUDS mixture solutions where the total dodecyl sulfate concentraion was kept at 0.5 M. The cation yield increases as expected with the CUDS concentration up to Φ=0.56 at a copper(II)-ion fraction of 0.2 (the data in such a region are presented elsewhere[3]) but then decreaes to converge finally to about 0.45. Such decrease in the cation yield with increasing reactant concentration is rather unusual in the chemical-kinetic point of view. The cation quantum yields in CUDS solutions containing no SDS are plotted in Fig. 2A for several CUDS concentrations. The dependence of the yield on the CUDS concentration in this plot cannot be ascribed to the difference in the copper(II)-ion fraction on the micellar surface, for $F(Cu^{2+})$=1 for all these solutions, but to the change in the micellar size, as has been discussed in our preceding paper.[3] The cation quantum yields in mixture solutions of SDS (0.05—1.0 M) and

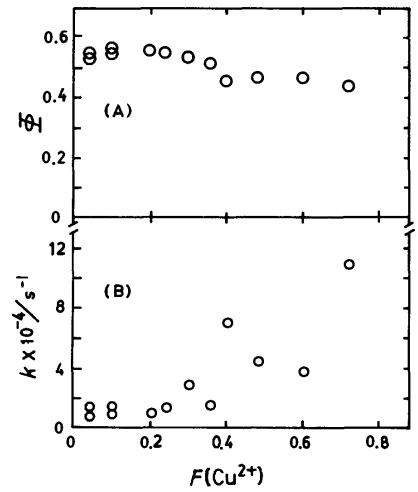

Fig. 1. The pyrene cation quantum yields (A) and the decay rate constants (B) plotted as a function of the copper(II)-ion fraction in CUDS/SDS mixture solutions where the total DS^- concentration is kept at 0.5 M.

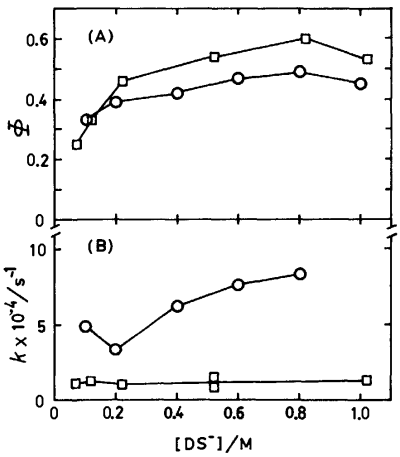

Fig. 2. The pyrene cation quantum yields (A) and the cation decay rate constants (B) in CUDS solutions (○) and in SDS solutions containing 10 mM CUDS (□) plotted as a function of the DS^- concentration.

CUDS (10 mM) are also plotted, for comparison, as a function of the total dodecyl sulfate concentration in Fig. 2A. When the two plots are compared at the same DS^- concentration, the yield for a CUDS solution is lower than that for a SDS/10 mM-CUDS mixture solution, that is, the decrease in the cation yield in the region of high copper(II)-ion fraction occurs, except in the low DS^- concentration region near 0.05 M.

The decay of pyrene cations obeyed the first-order rate law in contrast to a previous result for *N*-methylphenothiazine ions in CUDS micelles.[5] The apparent decay rate constants as plotted in Fig. 1B and 2B indicate that the decay is too slow to compete with the cation formation whose apparent rate constants exceed $2\times10^7\ s^{-1}$ (=1/(43 ns)) and that it does not affect the observed cation yield. It is interesting that the cation decay is not affected by sodium ions but enhanced by copper(II) ions, as suggested by the results shown in Fig. 2B, although this finding will not be subjected to discussion in this note.

Discussion

Phenomenologically, the pyrene cation quantum yield is given by

$$\Phi = \frac{k_{qe}[\mathrm{CUDS}]}{k_s + (k_{qe}+k_{qd})[\mathrm{CUDS}]} \qquad (2)$$

where k_s is the rate constant for the spontaneous fluorescence decay in the absence of copper(II) ions, k_{qe} is the one for electron transfer on quenching, and k_{qd} is the one for quenching processes other than the electron transfer. The electron-transfer efficiency defined by $k_{qe}/(k_{qe}+k_{qd})$ practically equals the observed cation yield, if $k_s \ll (k_{qe}+k_{qd})[\mathrm{CUDS}]$. The fluorescence decay data indicate that this condition is met in CUDS solutions. In SDS/10-mMCUDS mixture solutions, certain portions, which is less than 13% (=43 ns/340 ns), of the singlet excited pyrene molecules fail to react with copper(II) ions; therefore, the electron-transfer efficiency is higher than the observed cation yield. Thus, the decrease in the cation yield observed at high CUDS concentrations indicates the decrease in the electron-transfer efficiency. The concentration dependence of the electron-transfer efficiency is most likely connected with the change in the micellar structure, as will be discussed below.

In our preceding paper on surfactant concentration effects on electron transfer,[3] we have proposed a hypothesis that the electron-transfer efficiency is larger for a densely packed structure of the surfactant layer than for a porous structure. According to this hypothesis, the decrease in the cation yield in the region of high copper(II)-ion fraction is interpreted as that the increase in the copper(II)-ion fraction disturbs a densely packed structure attained in SDS micelles. The densely packed structure is probably peculiar to large rod-like micelles which are believed to exist in solutions of high (above about 0.5 M for SDS) surfactant concentrations.[6] The finding that the decrease in the cation yield at high copper(II)-ion fractions occurs for DS^- concentrations above 0.2 M supports the above explanation based on the densely packed structure of rod-like micelles. The exceptional agreement in the cation yield between a 50 mM-SDS/10 mM-CUDS solution and a 50 mM CUDS solution as shown in Fig. 2A is understood, if it is assumed that porous spherical micelles which lack the densely packed structure are mainly involved in the reaction at these low surfactant concentrations. Incidentally, spherical micelles of CUDS and SDS are similar in size, as suggested by the aggregation numbers (of dodecyl sulfate ions): 85 for CUDS[7] and 62 for SDS.[8]

References

1) T. Nakamura, A. Kira, and M. Imamura, *J. Phys. Chem.*, **87**, 3122 (1983).

2) M. A. J. Rodgers and M. E. DaSilva e Wheeler, *Chem. Phys. Lett.*, **53**, 165 (1978); F. Grieser and R. Tausch-Treml, *J. Am. Chem. Soc.*, **102**, 7258 (1980); J. C. Dederen, M. Van der Ausweaer, and F. C. DeSchryver, *J. Phys. Chem.*, **85**, 1198 (1981).

3) T. Nakamura, A. Kira, and M. Imamura, *J. Phys. Chem.*, in press.

4) G. E. Hall and G. A. Kenney-Wallace, *Chem. Phys.*, **32**, 313 (1978).

5) Y. Moroi, A. M. Braun, and M. Graetzel, *J. Am. Chem. Soc.*, **101**, 567 (1979).

6) For example, J. K. Thomas, *Chem. Rev.*, **80**, 23 (1980).

7) I. Satake, I. Iwamatsu, S. Hosokawa, and R. Matuura, *Bull. Chem. Soc. Jpn.*, **36**, 204 (1963).

8) K. J. Mysels and L. H. Princen, *J. Phys. Chem.*, **63**, 1696 (1959).

Reactions of Dipyridylacetylenes and Carbon Disulfide under High Pressure. Synthesis of Tetra-2-pyridyltetrathiafulvalene

Takahiro NAGAWA, Yoshiaki ZAMA, and Yoshiyuki OKAMOTO*

Department of Chemistry, Polytechnic Institute of New York, Brooklyn, New York 11201, U.S.A.

(Received August 23, 1983)

Synopsis The reaction of di-2-pyridylacetylene with CS_2 at 100 °C under 4500 atm for 12 h. gave tetra-2-pyridyltetrathiafulvalene in 80% yield.

Electron-rich tetrathiafulvalene (TTF) reacts with tetra cyanoquinodimethan (TCNQ) to form a charge transfer complex which has unusually high electrical conductivity.[1] Recently certain planar transition metal organic macrocyclic solids were also found to be conductive.[2] Thus, it would be interesting to couple the electron-rich TTF π-systen with a metal complex into a single conjugated and repeating framework. Engler and his coworkers recently synthesized polymers based on TTF and a metal 1,3-dithiolene complex and found they were highly conductive.[3]

We have shown previously that TTF derivatives can be readily synthesized by the reactions between acetylenic compounds substituted with strong electron-withdrawing groups and CS_2 under high pressure.[4] In exploring a simple synthetic route for the TTF compounds which are capable of forming metal complexes, we have initiated the preparation of pyridyl-substituted TTF compounds from the reaction between a corresponding acetylene compound and CS_2 under high pressure.

Di-2-, 3- and 4-pyridylacetylenes were synthesized according to the reported methods[5-7] and reactions of these pyridyl compounds with CS_2 under pressure were carried out. Di-2-pyridylacetylene was dissolved in CS_2 and the solution was pressurized to 4500 atm and heated at 100 °C for 12 h. Tetra-2-pyridyltetrathiafulvalene was obtained in 80% yield based on the dipyridylacetylene used.

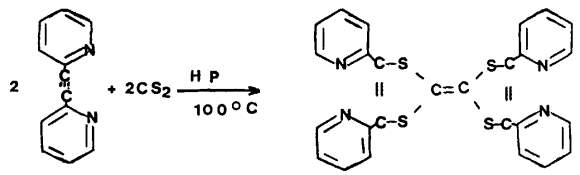

The reactions of di-3- and 4-pyridylacetylene with CS_2 were carried out using similar and more severe conditions (~6000 atm, at 110 °C). However, the corresponding TTF derivatives were not obtained and most of the starting dipyridyl compounds were recovered.

The mechanism for the formation of TTF derivatives under high pressure was proposed to be the dimerization of the 1,3-dithiolium carbene formed from the reaction between an acetylenic compound and CS_2.[4]

Apparently the electronegative nitrogens of di-2-pyridylacetylene make the acetylenic carbon more reactive to CS_2 as compared with those of di-3- and 4-pyridyl compounds. Since pyridinium compounds are highly electron-withdrawing, reactions of di-3- and 4-pyridylacetylenes with CS_2 in the presence of excess

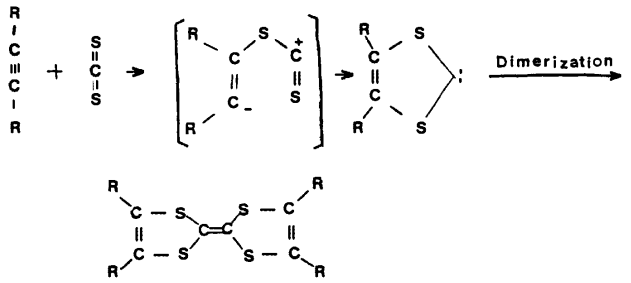

CH_3COOH or CF_3COOH were carried out at a pressure of 5000 atm for 12 h at 100 °C. The reactions yielded a brown solid which was found to contain several components, but the corresponding TTF derivatives could not be isolated.

The charge transfer complexes of the tetra-2-pyridyl-TTF synthesized with I_2 and TCNQ were prepared and the electrical conductivities were in the range of 10^{-5}—10^{-4} Ω^{-1} cm^{-1}.

Experimental

Infrared spectra were recorded on a Perkin-Elmer Model 457 grating infrared spectrophotometer. Nuclear Magnetic Resonance spectra were recorded on a Varian A-60 NMR spectrometer or a JEOL JNM-FX 90Q. Ultraviolet spectra were recorded on a Cary 15 UV-VIS spectrophotometer. Mass spectra were obtained at the Rockefeller University Mass Spectrometric Lab. using chemical ionization. Melting points were measured on an electrothermal apparatus and are uncorrected. Elemental analyses were performed by Schwarzkopf Microanalytical Laboratory, New York.

High pressure experiments were performed in Teflon capsules (3 ml capacity) in a stainless steel die and compressed *via* a piston with a Clifton 200 ton hydraulic press.

Materials. Di-2-pyridylacetylene was prepared in a manner identical to that described in the literature[5] in 90% yield, mp 70—73 °C (lit,[5] mp 69—70 °C). Di-3-pyridylacetylene was synthesized in a manner similar to that reported, mp 61—62 °C (lit,[6] mp 60—62 °C). Di-4-pyridylacetylene was also prepared by the method reported, mp 115—116 °C (lit,[7] mp 114 °C).

Synthesis. A typical reaction procedure at high pressure is as follows: Di-2-pyridylacetylene (1.0 g, 5.7 mmol) was dissolved in carbon disulfide (3 ml) and then placed in a Teflon capsule. Pressure was applied at 4500—5000 atm and the capsule was heated at 100 °C for 12 h. Pressure was controlled within 200 atm. After cooling, the capsule was opened and a dark red material was isolated (1.1 g). A brown solid was recrystallized from tetrahydrofuran, mp 287—290 °C. (0.80 g, yield 56%) IR (KBr) 1572, 1442, 1258, 1020, 962, 935 cm^{-1}; λ_{max} 355 nm (ε 8000), 385 (9150), 425 (2000) *m/z* 512. Calcd for $C_{26}H_{16}N_4S_4$: C, 60.94; H, 3.10; N, 10.94%. Found: C, 61.10; H, 3.40; N, 11.10%.

TCNQ and I_2 Complexes. To the acetonitrile solution, 20 ml of tetra-2-pyridyl-TTF (1.0 g, 0.02 mol) was added 1 equiv mol of a TCNQ solution (20 ml) in acetonitrile. Upon evaporating the solvent, a dark brown complex was

obtained. Tetra-2-pyridyl-TTF powder was exposed to I_2 vapor for 2—4 h and the complex obtained (mol ratio of the TTF to I_2 was 1:0.3, respectively). The electrical conductivities of these compounds were measured on compressed pellets using nickel electrodes with a Keithley electrometer.

This research was partly supported by a generous grant from Koppers Company, Inc.

References

1) J. Ferrais, D. D. Cowan, V. Walalka, Jr., and J. H. Perlstein, *J. Am. Chem. Soc.*, **95**, 948 (1973); M. Narita and C. U. Pittman, Jr., *Synthesis*, **1976**, 486.

2) "Highly Conductive One-Dimensional Solids," ed by J. T. Devreese, R. P. Evrard, and V. E. Van Doren, Plenum Press, New York (1979).

3) E. M. Egler, N. Martinez-Rivera, and R. R. Schumaker, Org. Coating and Plastics Chemistry, Vol. 41, ACS 178th Meeting, September 1979.

4) J. E. Rice and Y. Okamoto, *J. Org. Chem.*, **46**, 446 (1981); J. E. Rice, P. Wojciechowski, and Y. Okamoto, *Heterocycles*, **18**, 191 (1982).

5) D. Jerchel and J. N. Bridson, *J. Chem. Soc.*, **1969**, 1143.

6) T. Teitei, D. Wells, and W. H. F. Sasse, *Aust. J. Chem.*, **26**, 2129 (1973).

7) T. Martin and L. Andreas, *Chimia*, **34**, 23 (1980).

 © 1984 The Chemical Society of Japan Bull. Chem. Soc. Jpn., 57, 2037—2039 (1984)

Adsorption Measurements during Catalytic Isomerization of Pentenes and 2-Methyl-1-pentene over KC_{24}

Susumu TSUCHIYA,* Shinji YAMAMOTO, and Hayao IMAMURA
Department of Industrial Chemistry, Faculty of Engineering, Yamaguchi University, Tokiwadai, Ube 755
(Received June 1, 1983)

The catalytic isomerization of pentenes over KC_{24} has been investigated. The double-bond-migration and the *cis-trans* isomerization took place over KC_{24}, but the skeletal isomerization was not observed. From the rates of reactions and the selectivity ratios, all six of the relative rate constants and the activation energies of reactions were determined. The reaction paths on the triangular graph calculated from the rate constants show the *cis*-convex type profile. The competitive isomerization of 1-pentene and 2-methyl-1-pentene has also been investigated. The rate of isomerization of 1-pentene was greater than that of 2-methyl-1-pentene, which can be explained on the basis that the amount of chemisorption of 1-pentene during the competitive reaction is greater than that of 2-methyl-1-pentene.

Great attention has been paid to all the characteristic properties of graphite intercalation compounds, and the catalytic properties of the compounds have been extensively investigated in various reactions.[1-2] In heterogeneous catalysis, adsorption plays an important role, and measuring the adsorption during the reaction has been fruitful in many investigations.[3] In this work, the interest has centered on the catalytic characteristics of KC_{24} for the isomerization of pentenes; the adsorption during the course of reaction was measured.

Experimental

Materials. The KC_{24} samples used as catalysts were prepared in the manner described elsewhere.[4] Graphite (1.25 g of Union Carbide Spectroscopic Grade powder) and 0.44 g of potassium metal were used for each preparation. The preparation vessel was heated in a electric heater for 24 h under *ca.* 10^{-3} Pa at 620 K to form KC_{24}, and then evacuated for 30 min. The X-ray diffraction data of the samples formed agreed quite well with those reported by Rüdorff and Schultze.[5] The color of the KC_{24} obtained was deep blue.

Pentenes used as the reactants were obtained from Tokyo Kasei Co., Ltd., and were purified by repeated distillation *in vacuo*. The purity was confirmed by gas chromatography to be more than 99%.

Helium (99.995%) and nitrogen (99.99%) were obtained from the Seitetsu Kagaku Co., Ltd.

Procedure. The apparatus used for the present study was essentially the same as that used previously.[6] A closed circulating system with greaseless stopcocks and with a U-shaped reactor, connected to a conventional vacuum line and a gas chromatograph, was used to follow the reaction. The volume of the reaction system corresponded to about 288 cm^3 at a reaction temperature of 373 K.

Known amounts of reactant and an inert gas, *e.g.* nitrogen, were introduced into the reaction system, and the reaction was started by circulating. The ambient pressure and the composition of circulating gas were measured at suitable time intervals by a gas chromatograph with a column of 2,4-dimethylsulfolane on Uniport C. Inert gases were useful for effective circulation and accurate analysis.

The amounts of adsorption were obtained from the material balance. When 1-pentene was the reactant, amounts of adsorption were estimated from the amount of 1-pentene introduced and the pressure and the composition of the circulating gas at the suitable time. The sum of pentenes adsorbed could only be estimated.

Before each run, the catalyst was evacuated under *ca.* 10^{-3} Pa for 3 h at 573 K, and helium was introduced into the reactor. The evacuation temperature was selected as about 50 K lower than the preparation temperature of the catalyst; care was taken to avoid changes of KC_{24}. The reactor was then cooled to the reaction temperature and evacuated for a few minutes. The experimental results were well reproducible.

Results and Discussion

Isomerization of Pentenes. The double-bond-migration and the *cis-trans* isomerization of pentenes took place over KC_{24}, of which BET surface area was 50 m^2/g. The graphite did not show any catalytic activity for the reaction under the same experimental conditions. No skeletal isomerization occurred. No gase-

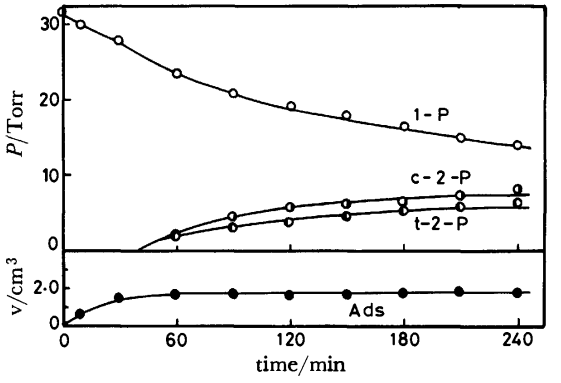

Fig. 1. Adsorption measurement during the isomerization of 1-pentene over KC_{24} at 440 K. (1 Torr= 133.322 Pa)

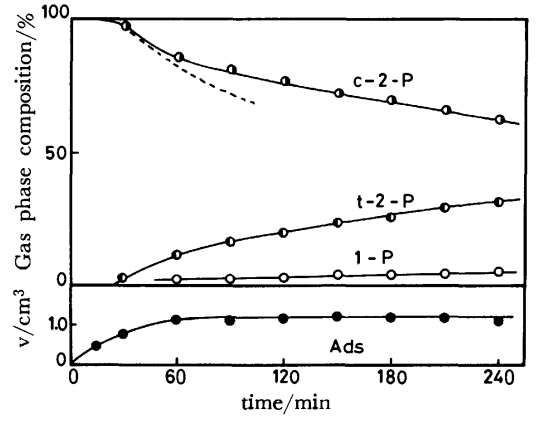

Fig. 2. Adsorption measurement during the isomerization of *cis*-2-pentene over KC_{24} at 513 K.

ous hydrocarbon other than pentenes was detected in the reaction mixtures under the present experimental conditions.

Figure 1 shows a typical result for the isomerization of 1-pentene over KC_{24} at 440 K, together with those of adsorption measurements. The adsorption measured appears to be chemical in nature, in view of the high adsorption temperature as 440 K. An induction period is observed at the initial stage of reaction. This may arise from the fact that at the initial stage the rate of adsorption of the reactant is much higher than that of desorption of the reactant as well as of the product. Accordingly, the decrease in the pressure of the reactant observed after the induction period is attributable to the progress of isomerization alone.

Figure 2 shows a typical result of the isomerization of *cis*-2-pentene over KC_{24} at 513 K. A similar induction period of the reaction is also observed. Instead of pressure, the composition in the gas phase is shown, as a function of time. The rate of the isomerization of *cis*-2-pentene is lower than that of 1-pentene (the broken line) under the same initial pressure.

The amounts of pentenes adsorbed appear to be almost constant; at the later stage of the reaction, the sums of the amount of reactant adsorbed and that of product adsorbed are constant. If the adsorption of reactant were the rate-determining step, the amounts of adsorption of reactant and of product would increase with increasing the pressure of product. If the desorption of product were the rate-determining step, the amounts of adsorption of reactant and of product would decrease with decreasing the pressure of reactant. In both cases, the sums of the adsorption of the reactant and product are not constant. The present result can be explained on the basis that the surface reaction is the rate-determining step. After the induction period the amount of reactant adsorbed depends on the ambient pressure of reactant, and will decrease with time. The rate of isomerization may be proportional to the amount of adsorbed reactant, since the surface reaction in the rate-determining step. Thus, the decrease in the rate of isomerization with its progress is explicable.

Ottmers *et al.*[7] reported that the catalytic activity of KC_n (n=8, 24, 36) for the isomerization of 1-pentene sharply declined with time on stream. The activity was estimated from the per pass conversion in the flow system. In the closed circulating system, a conversion is integrated with reaction time. Therefore, if the initial rapid decrease in catalytic activity actually takes place, the effect would be diluted. It was accordingly impossible in the present experiment to observe the clear deactivation process. As Ottmers *et al.*[7] suggested, the deactivation process might be due to traces of oxygen in the flow system.

The good reproducibility of the experimental results in the present work, however, suggests that the deactivation process during the course of the reaction, if it exists, is not permanent, and that the catalytic activity can be easily regenerated by evacuation.

The isomerization of pentenes was almost first order with respect to the pressure of reactant, ranging from 2×10^3 to 1.3×10^4 Pa, after the induction period. From the rates of reaction and the selectivity ratios: *cis/trans*, *trans*/1, and 1/*cis*, all six of the relative rate constants expressed by Scheme 1 and the activation energies of reaction were determined.

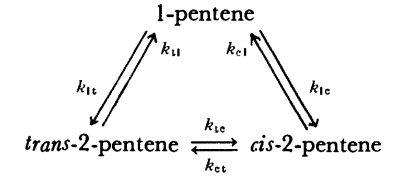

Scheme 1.

The relative rate constants at 440 K and the activation energies (bracketed) are shown in Fig. 3.

When the isomerization of 1-pentene takes place with the allyl anion mechanism, the initial *cis/trans* ratio is greater than unity.[8,9] The selectivity ratios obtained in the present study satisfy the condition of the allyl anion mechanism.

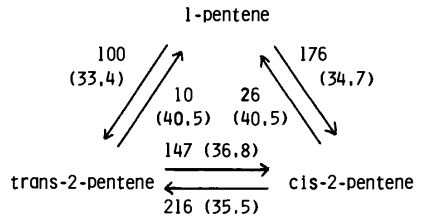

Fig. 3. Relative rate constants at 440 K and activation energies (kJ/mol) bracketed.

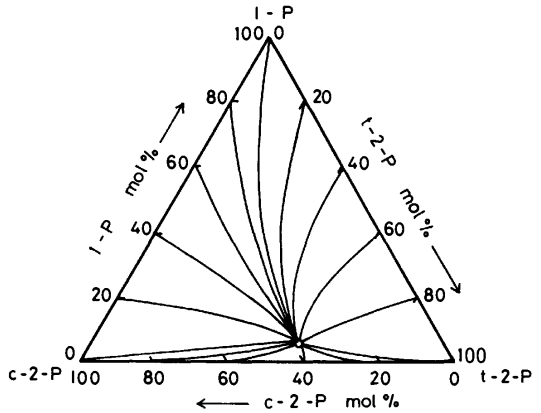

Fig. 4a. Reaction profile of isomerization of pentenes over KC_{24} at 440 K.

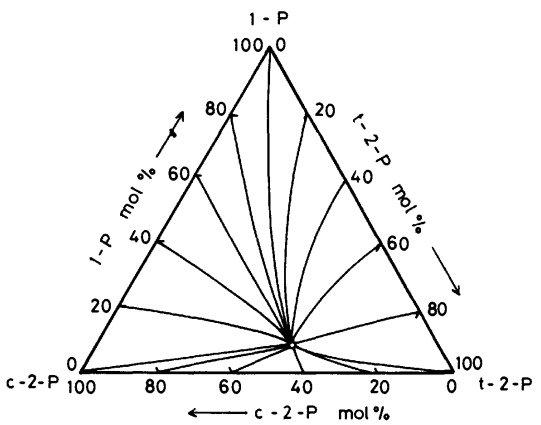

Fig. 4b. Reaction profile of isomerization of pentenes over KC_{24} at 513 K.

When the isomerization of pentenes proceeds, the composition of pentenes in the gas phase varies with time. The mol% of 1-pentene, *cis*-2-pentene, and *trans*-2-pentene corresponding to reaction time can be calculated from the relative rate constants, k_{ij}.[4,10,11] Figures 4a and 4b show the reaction paths calculated at 440 K and 513 K, respectively. These triangular graphs thus represent one of the catalytic characteristics of KC_{24} for the isomerization of pentenes. The curves, which originate from the left side of the triangle, bend in a convex manner to the left. The *cis*-convexity increased at a lower temperature, as shown in Fig. 4. These characteristics of pentenes are similar to those of butenes previously reported.[4]

Competitive Isomerization of 1-Pentene and 2-Methyl-1-Pentene. The reactivities of 1-pentene and 2-methyl-1-pentene have been studied. Figure 5 shows a typical result of the competitive isomerization of 1-pentene and 2-methyl-1-pentene over KC_{24} at 440 K. *cis*-2-Pentene, *trans*-2-pentene, and 2-methyl-2-pentene were observed as the products. The induction period is also observed both for 1-pentene and 2-methyl-1-pentene. The rate of adsorption of 1-pentene at initial state is larger than that of 2-methyl-1-pentene, which may be due to the structure effect of KC_{24}. 2-Methyl-1-pentene has a larger cross-sectional area than 1-pentene, and finds it more difficult to penetrate into the KC_{24} lattice. The amount of adsorption of 1-pentene at a later time is more than that of 2-methyl-1-pentene. The rate of isomerization of 1-pentene after the induction period is also more than that of 2-methyl-1-pentene. These results suggest that the higher rate of isomerization of 1-pentene than 2-methyl-1-pentene is due to either the larger rate of adsorption or the larger amount of adsorption of 1-pentene or both.

The degree of adsorption of 1-pentene in the presence of 2-methyl-1-pentene shown in Fig. 1 is less than that in the absence of 2-methyl-1-pentene shown in Fig. 5. This suggests that the adsorption of 1-pentene is disturbed by the presence of 2-methyl-1-pentene, and that 1-pentene is more strongly adsorbed on the same kind of sites than is 2-methyl-1-pentene in the competitive adsorption during the reaction.

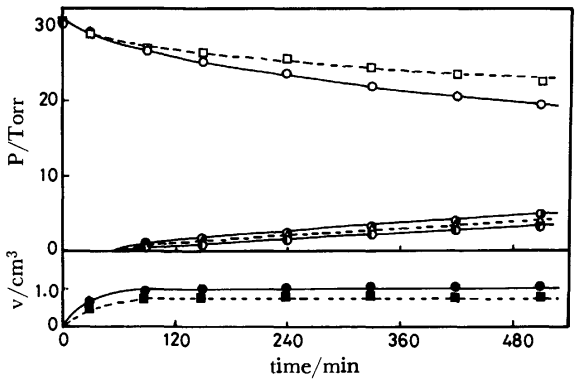

Fig. 5. Adsorption measurement during the competitive isomerization of 1-pentene and of 2-methyl-1-pentene over KC_{24} at 440 K.
Gaseous olefins: 1-pentene (-○-), 2-methyl-1-pentene (--□--), *cis*-2-pentene (-◑-), *trans*-2-pentene (-◐-), 2-methyl-2-pentene (--△--), Adsorbed olefins: *n*-pentenes adsorbed (-●-), methylpentenes adsorbed (--■--).

Conclusion

The catalytic selectivity of KC_{24} for the isomerization of pentenes is similar to that of butenes. The initial *cis/trans* ratio can be explained on the basis that the reaction may proceed *via* an allyl anion mechanism. One of the catalytic characteristics is thus shown in Fig. 5. Competitive isomerization revealed that 1-pentene is more reactive than 2-methyl-1-pentene over KC_{24}. This fact can be explained on the basis that the rate and/or the amount of adsorption of 1-pentene during the competitive reaction are larger than those of 2-methyl-1-pentene.

The authors are grateful to Professor T. Mizota of the Department of Mining and Mineral Engineering of this faculty for his X-ray analysis. This work was supported by a Grant-in-Aid for Scientific Research from the Ministry of Education, for which the authors' thanks are due.

References

1) M. A. M. Boersma, "Catal. Rev.-Sci. Eng.," ed by H. Heinemann and J. J. Carberry, Marcel Dekker, New York (1974), Vol. 10, p. 243.
2) M. A. M. Boersma, "Advanced Materials in Catalysis," ed by J. J. Burton and R. L. Garten, Academic Press, New York (1977), p. 67.
3) K. Tamaru, "Adv. Catal.," ed by D. D. Eley, H. Pines, and P. B. Weisz, Academic Press, New York (1964), Vol. 15, p. 63.
4) S. Tsuchiya, T. Misumi, N. Ohuye, and H. Imamura, *Bull. Chem. Soc. Jpn.*, **55**, 3089 (1982).
5) W. Rüdorff and E. Schulze, *Z. Anorg. Allg. Chem.*, **277**, 156 (1954).
6) S. Tsuchiya and T. Shiba, *Bull. Chem. Soc. Jpn.*, **38**, 1726 (1965).
7) D. M. Ottmers and H. F. Rase, *Ind. Eng. Chem., Fundam.* **5**, 302 (1966).
8) J. Goldwasser and W. K. Hall, *J. Catal.*, **71**, 53 (1981).
9) H. Hattori, N. Yoshii, and K. Tanabe, *Proc. 5th Int. Congr. Catal. (Miami)*, **10**, 233 (1973).
10) J. Wei and C. D. Prater, "Adv. Catal.,"ed by D. D. Eley, P. W. Selwood, and P. B. Weisz, Academic Press, New York (1962), Vol. 13, p. 203.
11) W. O. Haag and H. Pines., *J. Am. Chem. Soc.*, **82**, 378, 2488 (1960).

 © 1984 The Chemical Society of Japan Bull. Chem. Soc. Jpn., 57, 2040—2045 (1984) [Vol. 57, No. 8

Vibrational Level Populations of Hydrogen Fluoride Produced in Infrared Multiple-photon Decompositon of C_2H_5F

Yo-ichi ISHIKAWA* and Shigeyoshi ARAI
The Institute of Physical and Chemical Research, Wako-shi, Saitama 351-01
(Received July 30, 1983)

CO_2 TEA laser-induced photolysis of C_2H_5F was studied by using a time-resolved infrared fluorescence technique. Molecular elimination of vibrationally excited hydrogen fluoride (HF*) from C_2H_5F* occurs in the process. Rotational temperatures and vibrational level populations of HF* are estimated from observed fluorescence spectra by computational fitting. Higher vibrational levels are populated to a less extent in the decomposition under a collisionless condition. When the pressure of C_2H_5F is increased, however, population inversion is allowed among some levels. Possible reaction mechanism is discussed for the production of HF* at extraordinarily high vibrational levels.

Infrared multiple-photon decomposition (IRMPD) is usually considered to be a unimolecular decomposition of a molecule excited vibrationally above its decomposition threshold under a collisionless condition. However, it has been pointed out that the decomposition induced by collisions between highly vibrationally excited molecules occurs significantly even in a relatively low pressure region.[1-3] Previous time-resolved luminescence studies show that both instantaneous and delayed emissions are observable in IRMPD.[1,3,4] The latter has been ascribed to radiative species produced in collisions between highly vibrationally excited molecules. The collision-induced decomposition was estimated to contribute over 90% to the total decomposition at a pressure as low as 0.07 Torr (1 Torr≈133.322 Pa), where excited molecules can not collide with each other at least within a laser pulse duration.[3] On the other hand, Danen and Jang[5] have suggested that the decomposition *via* collisional V-V ladder climbing is not significant in IRMPD of large molecules.

The time-resolved infrared spectroscopic technique has been applied to UV photolysis by an excimer laser[6] or IRMPD by a CO_2 TEA laser.[7-9] This method affords dynamic information on rotation-vibration states of decomposition fragments and parent molecules. Quick and Wittig[8] measured infrared fluorescence spectra of HF* produced in IRMPD of fluorinated ethanes and ethylenes and estimated the rotational temperatures and vibrational distributions from spectral simulation. They found $N_v/N_{v+1}>1$ under a collisionless condition, where N_v and N_{v+1} denote the vibrational level populations at levels v and $v+1$, respectively. The addition of inert gas does not influence the vibrational distribution, while it lowers the rotational temperature.

Our previous study has shown that the energy transfer from highly vibrationally excited molecules is a main cause for isotope scrambling in IRMPD of mixtures of trifluoromethane-d_1 and -d_0 (CDF_3 and CHF_3).[9] However, the kinetic behavior of highly vibrationally excited molecule has not yet been well understood except for its unimolecular decomposition channel.[4,10] In this paper, we report time-resolved infrared fluorescence spectra observed in IRMPD of C_2H_5F, where the pressure of reactant is varied from 0.025 Torr, a collisionless condition, to 10 Torr. The fluorescence in the wavelength region of 2.2—3.2 μm is due to the HF* produced in a molecular elimination process. The role of highly vibrationally excited parent molecule in IRMPD will be discussed on the basis of the estimate of rotational temperatures and vibrational distributions of HF*.

Experimental

The experimental apparatus and procedure are similar to the previous ones.[9] The laser used for irradiation was a CO_2 TEA laser (Lumonics 103-2). The pulse duration was about 80 ns fwhm when the laser was operated without nitrogen gas in the cavity. All samples were irradiated with the P(20) line (1046.85 cm^{-1}) of the 9.6 μm CO_2 band at a repetition rate of 0.7 Hz. Laser energy was measured with a pyroelectric detector. The laser beam was truncated through a 9.9 mm diameter iris and focused onto the center of irradiation cell with a BaF_2 lens ($f.l.$=20 cm). The beam area at focus was estimated to be 5×10^{-3} cm^2 from a beam divergence of about 2 mrad. Laser fluences at focus were calculated from the beam area and laser energies. The cell with two KBr windows at both ends was 36 cm in length in the laser beam direction and 2 cm in inner diameter. The infrared fluorescence light at a focal regime, *i.e.*, in the vicinity of the center of cell, was made parallel by a parabolic mirror and then focused on the entrance slit of the infrared spectrometer (Ritsu Oyo Kogaku, MC-20L) by a CaF_2 lens ($f.l.$=20 cm). The focal point of laser beam was adjusted to fit the focal point of the parabolic mirror in the optical arrangement. More than 70% of the emission light at focus is converted into a parallel beam by reflection on the parabolic mirror. The maximum field of view of the detection system is limited to a 2 cm range along the laser beam within the enclosure of mirror. The fluence variation may be milder than 40% of the fluence at focus because the optical setup was designed to pick up most efficiently the emission in the vicinity of the focus. The infrared light was detected with an InSb detector mounted behind the exit slit of spectrometer. The current signal from the detector, after converted into a voltage signal, was amplified by a preamplifier (PAR Model 115) and then averaged by a boxcar system (a PAR Model 162 boxcar averager and a PAR Model 155 gated integrator). The aperture duration τ_g, aperture delay τ_d,, and time constant τ_c used for the boxcar averager will be described in the table and figure legends. The overall rise time was about 2 μs. The signal picked up by a photon drag detector was used as the trigger for the boxcar averager. The flow rate of a reactant gas in the cell was set between 1 and 10 Torr ml min^{-1} according to the pressure used. Pressures were measured with a capacitance-type manometer (MKS Baratron Model 220 BH).

Fluoroethane was synthesized through reaction of potassium fluoride with ethyl tosylate and purified by low temperature distillation.[11] Its purity was found to be higher

than 99% in an infrared absorption measurement. Argon purchased from Takachiho Kagaku Kogyo Co. (research grade) was used without further purification.

Results

The laser irradiation of 9.0 Torr C_2H_5F at a fluence of 40 J cm^{-2} yielded infrared fluorescence in a wide wavelength region of 2.2—3.8 μm. The spectrum of Fig. 1 (a) in the region of 2.2—3.2 μm (solid curve) is attributed to vibrationally excited HF*. The observed spectrum was simulated according to the method reported by Quick and Wittig.[8] The rotation-vibration terms of HF* were calculated by using the equation[12]

$$F_{vJ} = \sum_{lm} Y_{lm}(v+1/2)^l[J(J+1)]^m, \quad (1)$$

where Y_{lm} is a constant related to the molecular constants of HF; J and v are a rotational quantum number and a vibrational quantum number, respectively. On the other hand, the emission intensity of the v', $J'\rightarrow v''$, J'' transition I_{em} was calcualted by using the equation

$$I_{em} \propto \frac{C_{em}\,\nu^4\,F\,S_{J'}}{Q_r}\exp\left[-(F_{v'J'} - F_{v'0})(hc)/(kT)\right], \quad (2)$$

where $S_{J'}$ is $J'+1$ for P branch, *i.e.* $\Delta J = J'-J'' = -1 (J' = 0, 1, 2, \cdots)$ and J' for R branch, *i.e.*, $\Delta J = +1$ ($J' = 1, 2, 3, \cdots$); C_{em} is a constant proportional to the square of a transition dipole moment, values for various vibrational transitions being given in the paper by Herblin and Emanuel;[13] the symbol ν is a transition frequency; Q_r is the rotational partition function defined by a certain rotational temperature T; the Boltzmann distribution being assumed for the rotational level populations; F is a relative vibrationa level population, which may be regarded as a fitting parameter in this simulation; the symbols h and k are the Planck and Boltzmann constants, respectivery; and c is the light speed. Finally, each profile of emission line was determined from the slit function and the simulation spectrum was constructed by superposing the emission lines. The

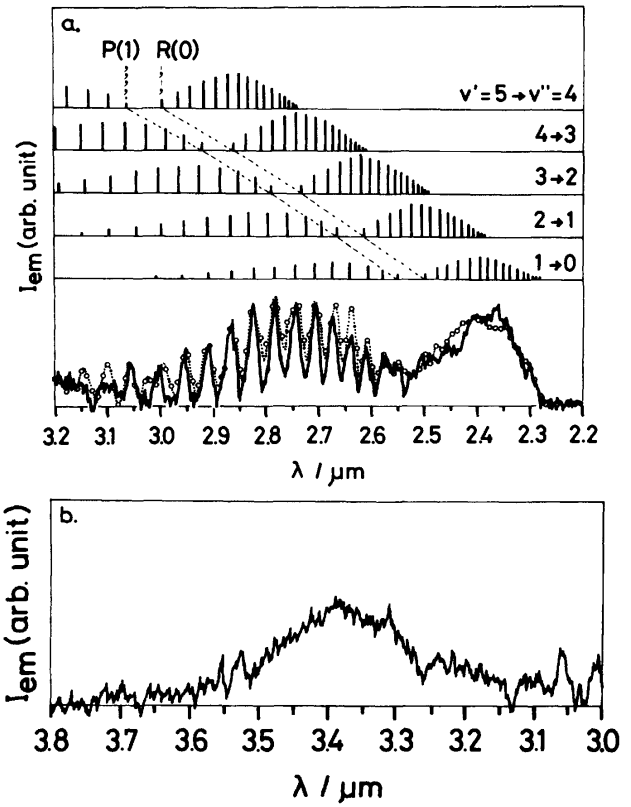

Fig. 1. Infrared fluorescence spectra obtained with CO_2 TEA laser irradiation of 9.0-Torr C_2H_5F in the wavelength regions of 2.2—3.2 (a) and 3.0—3.8 μm (b). Irradiation wavenumber, 1046.85 cm^{-1}; laser fluence, 40 J cm^{-2}; wavelength resolution, 0.016 μm fwhm; τ_d, 1 μs; τ_g, 10 μs (see Experimental). Relative emission intensities of rotation-vibration transitions ($\Delta v = 1$ and $v' \leqq 5$) are shown in the upper part, where T_{rot} is assumed to be 1800 K. O, calculated point (see text).

Table 1. Pressure effects on rotational temperatures and vibrational level populations of HF* produced in IRMPD of C_2H_5F[a]

C_2H_5F	Ar	T_{rot}	N_{vib}				
Torr	Torr	K	$v'=1$	2	3	4	5
0.025	1.5	300	1	0.50	0.40	0.10	0
0.05	3.0	300	1	0.50	0.40	0.10	0.10
0.10	5.9	300	1	0.60	0.40	0.10	0.10
0.17	9.8	300	1	0.50	0.30	0.10	0
0.28		800	1	0.60	0.40	0.20	0
0.40		800	1	0.60	0.40	0.10	0
0.50		900	1	0.50	0.30	0.10	0
1.0		900	1	0.40	0.15	0.30	0.05
2.0		1000	1	0.30	0.05	0.30	0
5.0		1500	1	0.33	0.13	0.25	0.19
		(±300)		(±0.08)	(±0.08)	(±0.11)	(±0.11)
6.0		1800	1	0.35	0.05	0.30	0
9.0		1800	1	0.25	0.05	0.35	0.25
0.20[b]	12(He)	450	1	0.60	0.25	0.10	0
				(±0.1)	(±0.05)		
0.20[b]		800	1	0.55	0.2	0.1	0

a) Laser line, 9.6 μm P(20) at 1046.85 cm^{-1}; laser fluence, approximately 40 J cm^{-2} (E_{in}=0.23 J pulse^{-1} and focal length=20 cm); τ_d=1 μs; τ_g=10 μs. b) Ref. 8.

calculated intensity distributions of the rotational lines due to the rotation-vibration transitions ($\Delta v=1$ and $v' \leqq 5$) with a common rotational temperature of 1800 K are illustrated in the upper part of Fig. 1(a), where each vibrational level has the same total population. Then, the fluorescence intensities through the actual slit function, which had a triangular shape with 0.016 μm fwhm, were calculated at wavelength intervals of 0.01 μm, as shown by the open circles in Fig. 1(a). The vibrational level populations were selected so that the simulated spectrum gave the best fit. The dotted curve represents a smooth connection of the calculated points. Figure 1(b) is the fluorescence spectrum in the region of 3.0—3.8 μm, which may originate from vibrationally excited parent molecules $C_2H_5F^*$ because the emission center at about 3.4 μm coincides in wavelength with the $v'=1 \leftarrow v''=0$ transition in the C-H stretching mode of C_2H_5F. The ratio of the emission peak intensity of HF* (at 2.35 μm) to that of $C_2H_5F^*$ (at 3.4 μm) is about 1.3.

The variation in pressure influences the rotational temperature T_{rot} and vibrational level populations N_{vib} of HF*; the pressure effects on T_{rot} and N_{vib} are summarized in Table 1. These data were obtained from the spectral simulation where N_{vib} ($v'=1$) was always normalized to unity in each case. Both T_{rot} and N_{vib} are fitting parameters in the present treatment. T_{rot} can be estimated directly from the spectral shape in the wavelength region below 2.36 μm since the rotational lines of the $v'=1 \rightarrow v''=0$ transition are isolated from those of the other transitions. For 5.0-Torr C_2H_5F the simulation was performed for four spectra observed independently under the same experimental conditions. The error limit in Table 1 shows the range of the scatter of T_{rot} or N_{vib} in the simulation. In practice, we could not satisfactorily reproduce the spectrum obtained with 5.0-Torr C_2H_5F by using the values out of the error limits. Quick and Wittig[8] gave error limits, which are included in Table 1 for the vibrational level populations calculated in a similar manner. The rotational temperature increases with an increase in C_2H_5F pressure. When the partial pressure of C_2H_5F was lower than 0.17 Torr, argon approximately 60 times was added to the system. The addition of argon to a reaction mixture lowers T_{rot} to room temperature and enhances the signal intensity, *i.e.*, the dissociation probability, while N_{vib} at each vibrational level is scarcely affected by the addition of argon. The effect of argon is also shown in Table 1, where $N_{v/b}$ at each vibrational level has similar values for C_2H_5F at 0.025—0.50 Torr with and without argon, although T_{rot} changes between 300 and 900 K. For comparison, the populations reported by Quick and Wittig[8] are included in the same table; their result is consistent with ours.

Figure 2 presents four typical HF* fluorescence spectra obtained at different pressures, where open circles are calculated in the above-mentioned method. The wavelength resolution was sacrificed for the measurements at low pressures because the emission intensity decreased with decreasing pressure. The spectrum apparently becomes broader with increasing pressure above 0.5 Torr. The relative fluorescence intensities due to HF* at $v'=2$ and 3 decrease with increasing pressure, while those due to $v'=4$ and 5 increase. T_{rot} also increases with pressure. It is worth noting that the absolute fluorescence intensities due to HF* and $C_2H_5F^*$ increase markedly with an increase in C_2H_5F pressure. However, the intensity due to $C_2H_5F^*$ grows more rapidly as compared with that due to HF*.

The infrared fluorescence spectra determined at 3, 10, 20, 30, and 50 μs after the laser pulse are shown in

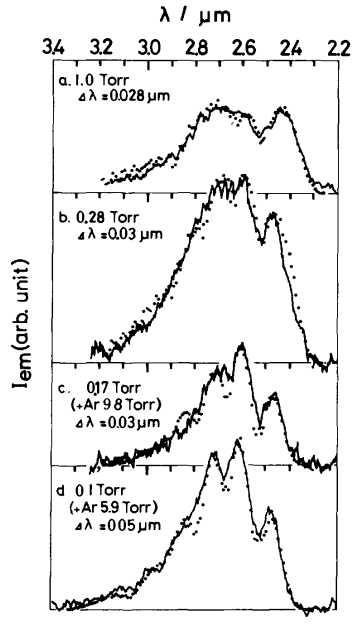

Fig. 2. Infrared fluorescence spectra obtained with 1.0-Torr (a), 0.28-Torr (b), 0.17-Torr (c), and 0.1-Torr (d) C_2H_5F. Argon was added in (c) and (d). Laser fluence, 40 J cm^{-2}; τ_d, 1 μs; τ_g, 10 μs; O, calculated point. Wavelength resolution Δλ is shown in the figure.

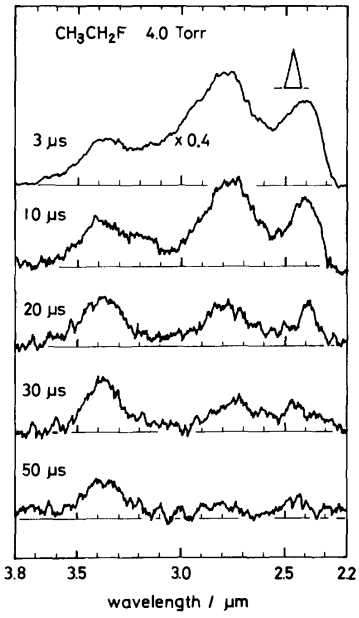

Fig. 3. Infrared fluorescence spectra obtained with 4.0-Torr C_2H_5F. The spectra were determined at 3, 10, 20, 30, and 50 μs after the laser pulse. Wavelength resolution is shown in the figure. Laser fluence, 40 J cm^{-2}; τ_d, 1 μs; τ_g, 10 μs.

TABLE 2. TRANSIENT VIBRATIONAL POPULATIONS OF HF* PRODUCED IN IRMPD OF C_2H_5F[a)]

τ_d	T_{rot}	N_{vib}				
μs	K	$v'=1$	2	3	4	5
2	1800	1	0.4	0.2	0.2	0.3
3	1800	1	0.4	0.2	0.1	0.3
6	1200	1	0.3	0.05	0.4	0.1
10	1200	1	0.2	0.05	0.3	0.05
15	1200	1	0.2	0.05	0.15	0.05
20	1200	1	0.2	0.05	0.15	0.05

a) Laser line, 9.6 μm P(20) (1046.85 cm^{-1}); laser fluence, about 40 J cm^{-2}; τ_g=1 μs; C_2H_5F pressure, 5.0±0.1 Torr.

Fig. 3. The pressure of C_2H_5F is 4.0 Torr. The time dependences of the vibrational level populations obtained with 5.0-Torr C_2H_5F are summarized in Table 2. The vibrational level populations at v'=2, 3, and 5 decrease with a lapse of time; the higher the level is, the larger is the decrease. The population at v'=4 reaches a maximum at 6 μs and then decreases.

Table 3 presents the fluence effect on the fluorescence. The production of HF* at high vibrational levels tends to increase with increasing fluence. This tendency can be seen with 5-Torr C_2H_5F alone and with the mixture of 0.17-Torr C_2H_5F and 9.83-Torr Ar. However, the change in vibrational level population is not evident in the present study because a possible fluence variation is restricted within a narrow range.

Figure 4 shows the fluorescence intensity *vs.* time curve observed at 2.4, 2.8, and 3.4 μm for 4-Torr C_2H_5F. The fluorescence monitored at 2.4 μm corresponds mainly to the R branch of the HF* ($v'=1\rightarrow HF(v''=0)$ transition, while that at 2.8 μm includes several transitions of $\Delta v=1$ from various vibrational levels. Parent molecules fluoresce at the vicinity of 3.4 μm. The fluoresce due to HF* grows almost completely within the response time of the detection system, *i.e.*, 3 μs. The following decay consists of the rapid component with a lifetime of 10 μs and the slow component lasting for 30—40 μs. The whole temporal behavior is invariant against C_2H_5F pressure if it is higher than 0.5 Torr. In contrast, only the slow component is observed for the decay curve if the pressure is lower than 0.2 Torr. Moreover, the decay rate tends to decrease with decreasing pressure in the low pressure region.

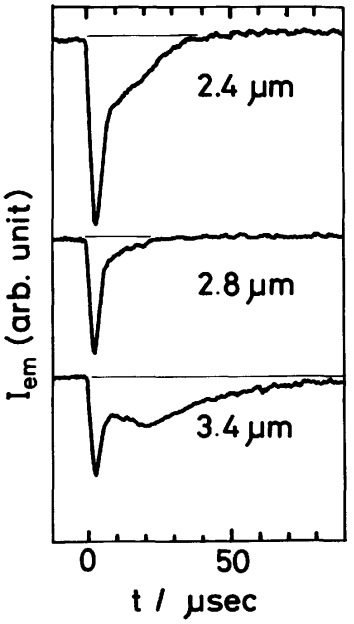

Fig. 4. Fluorescence intensity *vs.* time curves obtained with 4.0-Torr C_2H_5F. Laser fluence, 40 J cm^{-2}.

Discussion

Setser and coworkers[14)] and Quick and Wittig[8)] have reported that the molecular elimination of HF occurs in IRMPD of C_2H_5F:

$$C_2H_5F + nh\nu \longrightarrow C_2H_4 + HF \qquad \Delta H = 10 \text{ kcal mol}^{-1}. \quad (4)$$

The activation energy of this reaction has been found to be approximately 57 kcal mol^{-1}. The dissociation energies of bonds C-C, C-H, and C-F in ethane-type molecules are estimated to be 85, 100, and 100 kcal mol, respectively. Therefore, the molecular elimination of HF should be the most favorable reaction channel in IRMPD of C_2H_5F. When 4.0 Torr C_2H_5F was irradiated with a CO_2 TEA laser (1000 pulses), three new bands attributable to products appeared near 1030, 950, and 730 cm^{-1} in the infrared absorption spectrum. The first band corresponds to the ν_3 mode (SiF deg. stretch) of SiF_4,[15)] the second to the ν_7 mode (CH_2 wag) of C_2H_4,[16)] and the third to the ν_5 mode (CH bend) of C_2H_2.[16)] Acetylene may be formed secondarily by the

TABLE 3. LASER FLUENCE EFFECT ON THE VIBRATIONAL POPULATIONS OF HF* IN IRMPD OF C_2H_5F[a)]

Laser fluence	T_{rot}	N_{vib}					
J cm^{-2}	K	$v'=1$	2	3	4	5	6
$[C_2H_5F]$=5.0±0.1 Torr[b)]							
20	1800	1	0.7	0.1	0.4	0	0
23	2000	1	0.7	0.1	0.2	0.2	0
24	2000	1	0.8	0.2	0.3	0.3	0
29	2000	1	0.4	0.05	0.2	0.4	0
40	2000	1	0.4	0.05	0.1	0.5	0.2
$[C_2H_5F]$=0.17 Torr and [Ar]=9.8 Torr[c)]							
30	300	1	0.2	0.4	0.2	0	
36	300	1	0.8	0.6	0.1	0	
41	300	1	0.8	0.6	0.1	0.1	
46	300	1	0.8	0.6	0.3	0.2	

a) Laser line, 9.6 μm P(20) (1046.85 cm^{-1}). b) τ_d=3 μs and τ_g=1 μs. c) τ_d=1 μs and τ_g=5 μs.

decomposition of ethylene.[17] The production of SiF_4 implies that hydrogen fluoride reacts with the glass wall. These results support the previous conclusion that Reaction (4) proceeds most efficiently in IRMPD of C_2H_5F. We could not find the infrared emission due to vibrationally excited DF* in IRMPD of a mixture of 1-Torr C_2H_5F and 2-Torr D_2. This fact suggests that no fluorine atom is produced in the primary process of IRMPD of C_2H_5F.

Vibrational level populations have been estimated for hydrogen halides produced from halogenated hydrocarbons activated in various processes. Steady-state infrared fluorescences of hydrogen halides were measured in chemical activation[18] and mercury sensitized photolysis.[19] Transient fluorescences were measured in UV laser photolysis.[20] Throughout these measurements, N_v was always larger than N_{v+1}. In the present study, however, we found the extraordinary population distribution of HF* at C_2H_5F pressures higher than 1.0-Torr. The extraordinary population distribution might be explained in the following ways: (a) some vibrational levels of HF* are overpopulated in the so-called Treanor distribution *via* collisional V-V ladder climbing;[21] (b) the energy transfer from highly vibrationally excited C_2H_5F* yields preferentially HF* at some particular vibrational levels. Fürsich and Kompa[22] could not observe any inverted vibrational population when hydrogen fluoride at 30—60 Torr was directly excited with pulses from a high power HF laser. This result denies item (a) above as a reasonable cause for the extraordinary population distribution. In our experiment, pressures of C_2H_5F are lower than 10 Torr. Since HF is produced from excited C_2H_5F*, the partial pressure of vibrationally excited hydrogen fluoride HF* should be much lower than 10 Torr. It is highly improbable that the Treanor distribution of HF* is accomplished at low partial pressures of HF. Vibrationally excited C_2H_5F* was found to fluoresce in the wavelength region of 3.1—3.6 μm. As shown in Figs. 3 and 4, the fluorescence was observed over 100 μs after the pulse, although the fluorescence due to HF* terminated within 40 μs. The clear difference between the transient behavior of C_2H_5F* and HF* seems to rule out item (b) above for the production of HF*.

The fluorescence intensity *vs.* time curve observed at 2.4 μm for 0.17-Torr of C_2H_5F exhibits only one decay component, which fits a first-order kinetic low. The origin of HF* at such a low pressure may be the laser-induced multiple-photon decomposition of C_2H_5F. The collision-induced process can be ignored for the production of HF*. Assuming that HF* is fully produced within the pulse duration, one can estimate the rate constant for the collisional deactivation of HF* to be $3\times10^5\,s^{-1}\,Torr^{-1}$. The fluorescence monitored at 2.4 μm is due to HF* in a vibrational state of $v'=1$. Hancock and Green[23] have measured rate constants of deactivation of HF* ($v'=1$) by several hydrocarbons by use of the laser-induced vibrational fluorescence technique. Of the rate constants, cyclopropane has the same value as C_2H_5F.

The HF* fluorescence intensity *vs.* time curves obtained with C_2H_5F at pressures higher than 0.5 Torr show a fast rise followed by fast and slow decays. The qeunching lifetime of HF* is expected to be shorter than 1 μs if the pressure of C_2H_5F is higher than 3 Torr. The initial fluorescence spike is mainly due to the HF* molecules produced in IRMPD of C_2H_5F. The fast rise is limited by the response time of the detection system since the production of HF* in IRMPD terminates at the end of pulse. The fast decay is caused by the collisional deactivation of the fraction of HF* produced in IRMPD. The slow decay suggests that HF* is also produced in a slow process after the termination of pulse. One possible mechanism for the slow formation of HF* is the decomposition of excited C_2H_5F molecules produced in the collision induced process. The direct IRMPE of C_2H_5F results in the distribution of excited molecules over a wide range of internal energy. Those C_2H_5F molecules which have energies much higher than the threshold energy undergo immediate decomposition. On the other hand, those molecules which have energies almost euqal to or a little higher than the threshold energy persist for a long time after the laser pulse irradiation. It should be noted that the reaction zone in IRMPD is limited to a small volume around a focal point and that most molecules in the reaction zone are in highly vibrationally excited states. Collisions among vibrationally excited molecules with long lifetimes may produce excited molecules above the dissociation threshold. The excited HF* molecules formed in the subsequent decomposition may show the inverted vibrational level populations. The energy distribution of excited C_2H_5F molecules approaches the Boltzmann distribution defined by temperature with a lapse of time. However, the fraction of excited molecules produced above the threshold during the relaxation process undergoes the decomposition leading to the formation of HF*. The temperature inside a reaction zone is usually high enough to induce thermal decomposition in IRMPD at high fluences or high pressures. However, the temperature gradually decreases as excited molecules diffuse from the reaction zone or cold molecules diffuse into the reaction zone.

A pressure is expected to affect IRMPD through hole filling and energy transfer. These phenomena couple together to influence the absorption and decomposition processes. Richardson and Setser[14] have studied IRMPD of binary mixtures, where one component does not absorb the laser energy but does possess the decomposition channel with the threshold energy comparable to that of the other component. The decomposition yields of both components were measured as a function of total pressure. They found that for pressures $\geq$1 Torr the intermolecular energy transfer is sufficiently rapid that the collision-induced decomposition of the non-absorbing molecule is prominent. In our experiment, the collision-induced decomposition seems to become important for pressures $\geq$1 Torr.

The response time and sensitivity of the present detection system are not satisfactory for transient infrared fluorescence observation. Therefore, it is exceedingly difficult to separate out the effects of the collision-induced process on the observed vibrational level populations from those arising from the laser-induced multiple-photon excitation process itself. However, we observed the distribution of HF* with $N_v/N_{v+1}\geq1$ at low pres-

sures of C_2H_5F where IRMPD occurs mainly. The extraordinary distribution becomes more prominent with increasing pressure or a lapse of time. These facts are consistent with the above-mentioned mechanism.

References

1) R. V. Ambartzumian, N. V. Chekalin, V. S. Dolzhikov, V. S. Letokhov, and E. A. Ryabov, *Chem. Phys. Lett.*, **25**, 515 (1974); R. V. Ambartzumian, V. S. Dolzhikov, V. S. Letokhov, E. A. Ryabov, and N. V. Chekalin, *Sov. Phys.-JETP*, **42**, 36 (1976).

2) R. Corkum, C. Willis, and R. A. Back, *Chem. Phys.*, **24**, 13 (1977).

3) Y. Haas and G. Yahav, *Chem. Phys. Lett.*, **48**, 63 (1977); G. Yahav and Y. Haas, *Chem. Phys.*, **35**, 41 (1978).

4) C. R.Quick, Jr., J. J. Tiee, T. A. Fischer, and C. Wittig, *Chem. Phys. Lett.*, **62**, 435 (1979).

5) W. C. Danen and J. C. Jang, "Multiphoton Infrared Excitation and Reaction of Organic Compounds," in "Laser-Induced Chemical Processes," ed by J. L. Steinfeld, Plenum Press, New York (1981), p. 117.

6) S. L. Baughcum and S. R. Leone, *J. Chem. Phys.*, **72**, 6531 (1980); M. G. Moss, M. D. Ensminger, and J. D. McDonald, *J. Chem. Phys.*, **74**, 6631 (1981).

7) G. A. West, R. E. Weston, Jr., and G..W. Flynn, *Chem. Phys.*, **35**, 275 (1978); C. R. Quick, Jr. and C. Wittig, *ibid.*, **32**, 75 (1978); C. R. Quick, Jr. and C. Wittig, *J. Chem. Phys.*, **69**, 4201 (1978).

8) C. R. Quick, Jr. and C. Wittig, *J. Chem. Phys.*, **72**, 1694 (1980).

9) Y. Ishikawa, H. Yamazaki, Y. Hama, and S. Arai, *Appl. Phys.*, **B32**, 85 (1983).

10) C. M. Miller and R. N. Zare, *Chem. Phys. Lett.*, **71**, 376 (1980).

11) W. F. Edgell and L. Parbs, *J. Am. Chem. Soc.*, **77**, 4899 (1955).

12) D. U. Webb and K. N. Rao, *J. Mol. Spectrosc.*, **28**, 121 (1968).

13) J. M. Herbelin and G. Emanuel, *J. Chem. Phys.*, **60**, 687 (1974).

14) T. H. Richardson and D. W. Setser, *J. Phys. Chem.*, **81**, 2301 (1977); J. C. Jang and D. W. Setser, *J. Phys. Chem.*, **83**, 2809 (1979).

15) E. A. Jones, J. S. Kirby-Smith, P. J. H. Woltz, and A. M. Nielsen, *J. Chem. Phys.*, **19**, 242 (1951).

16) T. Shimanouchi, "Tables of Molecular Vibrational Frequencies Consolidated Volume I," NSRDS-NBS 39, (1972).

17) N. C. Peterson, R. G. Manning, and W. Braun, *J. Res. NBS*, **83**, 117 (1977).

18) M. J. Berry and G. C. Pimentel, *J. Chem. Phys.*, **49**, 5190 (1968); M. J. Berry and G. C. Pimentel, *IEEE J. Quantum Electron.*, **QE-6**, 176 (1970); P. N. Clough, J. C. Polanyi, and R. T. Taguchi, *Can. J. Chem.*, **48**, 2919 (1970).

19) H. Watanabe, H. Horiguchi, and S. Tsuchiya, *Bull. Chem. Soc. Jpn.*, **53**, 1530 (1980).

20) M. J. Berry, *J. Chem. Phys.*, **61**, 3114 (1974).

21) C. E. Treanor, J. W. Rich, and R. G. Rehm, *J. Chem. Phys.*, **48**, 1798 (1968).

22) M. Fürsich and K. L. Kompa, *J. Chem. Phys.*, **75**, 763 (1981).

23) J. K. Hancock and W. H. Green, *J. Chem. Phys.*, **59**, 6350 (1973).

Disproportionation reaction of Nitrogen Monoxide on CaHY-type Zeolite

Yoshinori KANNO* and Hisao IMAI†

*Government Industrial Research Institute, Nagoya, Hirate-cho, Kita-ku, Nagoya 462

†Research Laboratory of Engineering Materials, Tokyo Institute of Technology, Nagatsuta-cho, Midori-ku, Yokohama 227

(Received August 12, 1983)

The disproportionation reaction of NO was investigated on CaHY-type zeolite. The relation between pretreatment temperature and activity was determined by the pulse reaction technique, and the dependence of the initial formation rate of N_2O on NO pressure was investigated with a gas circulation system. The rate of initial formation of N_2O is third order in NO pressure in the lower pressure region (*ca.* 30 Torr, 1 Torr≈133.322 Pa) and 2.2th order in NO pressure in the higher pressure region (*ca.* 200 Torr). TPD spectra are composed mainly of three peaks: The first peak is assigned to the unreactive adsorbed NO, the second to the NO produced by the decomposition of N_2O_3 and left on the zeolite surface, and the third to the N_2O remaining. On the basis of the reaction mechanism proposed by Chao and Lunsford, the rate equation for the initial formation of N_2O has been derived as $\alpha=\bar{k}_2K_1P^3/(1+K_1P^2)$, where P, K_1, and $\bar{k}_2$ are the pressure of NO, an equilibrium constant, and a rate constant, respectively. This equation is in good agreement with experimental results obtained with the gas circulation system.

In a study on sorption and reactivity of NO, Addison and Barrer[1] found that the disproportionation reaction of NO, $4NO=N_2O+N_2O_3$, occurs on chabazite, faujasite, and A-type zeolites at 0 °C or lower temperatures; the resulting N_2O can be removed quantitatively, whereas the N_2O_3 stays occluded in the zeolites. Later, Alekseyev *et al.*[2] studied infrared spectra of NO adsorbed on A- and X-type zeolites. Chao and Lunsford[3] also studied those on NaY- and CaY-type zeolites and proposed a mechanism for the disproportionation reaction.

Recently, the disproportionation reaction on MgHY-type zeolites with different degrees of ion exchange was studied by use of a pulsed microreactor, and it was revealed that active sites for this reaction are Mg^{2+} located on Site II.[4] This reaction on alkaline earth metal oxides[5,6] has further been investigated, with a result that the activity order is MgO>CaO>SrO>BaO. Pulse technique studies[7–9] of this reaction on Y-type zeolites with various metal ions exchanged disclosed that alkaline earth Y-type zeolites possess higher activities, whereas the zinc family, alkali metals, and LaY-type zeolites possess lower activities, as detailed by the activity sequence: CaY>CdY>MgY>ZnY>LaY>BeY>NaY>LiY>KY≫SrY>BaY, AgY, HgY, FeY, AlY=0.

Understanding the reactivity of NO, on the other hand, is of great value for studies on the transformation and elimination of atmospheric pollutants.[10–18] The disproportionation reaction, therefore, is important not only from a fundamental viewpoint but also from a practical aspect.

The present study has been carried out to collect kinetic information on the disproportionation reaction of NO. Measurements for activity and TPD chromatogram were made on CaHY-type zeolites.

Experimental

Materials and Reagents. A synthetic Y-type zeolite (Union Carbide Co.) in the sodium form (SK-40) was ion-exchanged 16 times at 90 °C with 10 wt% solution of ammonium nitrate. A $CaNH_4Y$-type zeolite was prepared *via* ion-exchange of the resultant NH_4Y-type zeolite with a solution of calcium nitrate at 90 °C. The resultant $CaNH_4Y$-type zeolite was washed 3 times with 0.05 mol dm^{-3} calcium nitrate solution and dried overnight at 110 °C. The composition of the $CaNH_4Y$-type zeolite prepared in this way corresponds to $Ca_{24}(NH_4)_8Na(AlO_2)_{57}(SiO_2)_{135}\cdot nH_2O$ per unit cell. A chemical analysis of samples was done by flame spectrophotometry (Na^+) and atomic absorption spectrophotometry (Ca^{2+} and Al^{3+}); the sample was pressed at about 10 ton/cm^2 and ground into pieces of 32 to 60 mesh and of 1 to 2 mm.

Powder X-ray diffraction patterns and values of specific surface area measured with a BET apparatus confirmed that no structual damages were caused during the sample preparation. Prior to various measurements, a CaHY-type zeolite was prepared by a treatment for ammonia removal of the $CaNH_4Y$-type zeolite. Details of the treatment will be described in the following section. The helium used (for the pulsed microreactor and TPD experiment) was passed through a Yanagimoto RT003 purifier. NO was obtained from a commercial cylinder (Takachiho Chemical Industry, Ltd.) and purified first by passage through a dry NaOH-packed column (for the pulse method and TPD experiment) and then by a repetition of distillations at −196 °C (for the closed gas circulation system).

Apparatus and Procedure. *1. Pulsed Microreactor*: After a treatment at 150 °C for 3 h in a stream of dry CO_2-free air, the temperature of a sample of *ca.* 10 mg was increased up to the desired temperature (this temperature will be called the pretreatment temperature) at a constant rate of 0.5 °C/min, where the sample was kept for 4 h before being annealed in a stream of He for 2 h. After the temperature of the sample was lowered down to the reaction temperature, 2.26 cm^3 of NO was injected onto the zeolite in a stream (10.0 cm^3/min) of He.

2. Temperature-programmed Desorption: TPD studies were carried out as follows: After a run of the pulsed reaction described above was finished, the temperature of reaction vessel was raised at a constant rate of 7.14 °C/min in a stream of He (10 cm^3/min). The effluent gas was periodically analyzed with a gas chromatograph, equipped with a Porapak T and Molecular Sieve 13X column at 50 °C and using He as carrier gas, for contents of NO, N_2O, O_2, and N_2.

3. Closed Gas Circulation System: A closed gas circulation system (*ca.* 705 cm^3) equipped with a pyrex reaction vessel was used to study the kinetics of the disproportionation reaction of NO. A zeolite (*ca.* 2 cm^3) was treated at 500 °C in acoordance with the procedure described above under the heading in

"Pulsed Microreactor" and was evacuated (10^{-6} Torr) at a constant temperature (500 °C) for 2 h. After a series of these treatments, the temperature of vessel was adjusted to the reaction temperature and NO gas was introduced into the reaction system. The amount of products was measured by gas chromatography.

Results

Activity and Pretreatment Temperature. The activity was measured at 15 °C with a pulsed microreactor. Since the activity decreased markedly with increasing number of pulses, it is expressed by the rate of N_2O formation in the first pulse, which is taken to indicate the activity for the disproportionation reaction of NO. The gas analysis showed that the only gaseous product is N_2O, in agreement with the result of Addison and Barrer.[1]

Figure 1 shows the relation between activity and pretreatment temperature in the range 400—900 °C. The activity increases with an increase in pretreatment temperature, reaches a broad maximum at 700 °C, and decreases gradually with a further increase in pretreatment temperature. A powder X-ray diffraction examination of zeolites activated at each pretreatment temperature revealed that this gradual decrease in activity is caused by a collapse of the crystalline structure of zeolite pretreated at 800 or 900 °C.

TPD Profile. Addison and Barrer[7] insisted that the N_2O_3 produced by the disproportionation reaction of NO would be stabilized in the zeolite. On the other hand, Chao and Lunsford[2] suggested that the adsorbed N_2O_3 will decompose to give NO and NO_2 when the excess NO gas is removed by evacuation from the reaction mixture. In the procedure described above for temperature-programmed desorption, therefore, the NO_2 gas desorbed by raising temperature was removed by a dry NaOH-packed column in order to avoid complexity. TPD profiles were measured after the first pulse reaction. The change in TPD profile with pretreatment temperature was disclosed. Figure 2 shows the TPD profile of zeolites treated at 700 °C, the numerical values indicating the desorption temperature.

The TPD profile is composed of five signals α, β, γ, δ, and ε arranged in parallel with the increasing temperature scale, of which signals δ and ε are negligibly small. One can consider that peaks α, β, and γ offer information about adsorbed species staying on the zeolite surface after the disproportionation reaction of NO. According to an analysis of desorbed gases, peak α consists of NO, *ca.* 90% of peak β is composed of NO with the residual portion as N_2O, and *ca.* 90% of peak γ is N_2O with the rest as NO.

TPD profiles of zeolites treated at various pretreatment temperatures are also composed of five signals and the area of each peak (α, β, γ) varied independently of the others. In spite of the low resolution of TPD peaks (α, β, γ), the area of each peak (α, β, γ) was determined by drawing a supplementary line in order to separate the three peaks. Figure 3 shows the relation between the area of each peak (α, β, γ) and the pretreatment temperature. The plot breadth in Fig. 3 indicates the experimental error range in connection with the arbitrariness of the method to draw the supplementary lines. The area of peak α decreases gradually with an increase in pretreatment temperature, and those of peaks β and γ increase with increasing pretreatment temperature, reach a broad maximum at *ca.* 700 °C, and decrease with a further increase in pretreatment temperature. The variation in peak areas of β and γ showed a tendency similar to the variation in the activity illustrated in Fig. 1, hence it follows that peaks β and γ reflect the activity. The desorption temperatures for peaks α, β, and γ were approximately constant in all experiments, indicating that the respective adsorp-

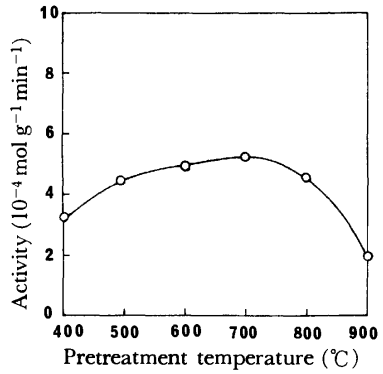

Fig. 1. Activity plotted against pretreatment temperature.

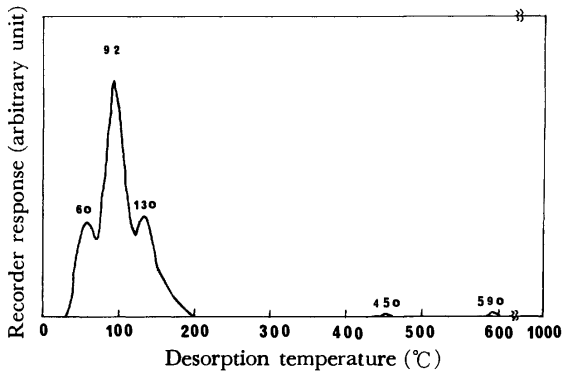

Fig. 2. TPD spectrum of CaHY zeolite heat treated at 700 °C.

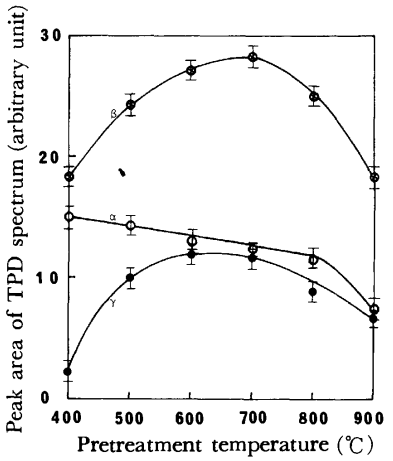

Fig. 3. Peak area of TPD spectrum plotted against pretreatment temperature.

tion states are almost independent of pretreatment temperature.

Reaction Kinetics. The desorption peak of N_2O was recognized in the TPD experiment after a pulse reaction, indicating that readsorption of N_2O formed by the disproportionation of NO will occur. However, we assume for convenience in this paper that irreversible adsorption of N_2O should occur only in the initial stage of reaction, so that the formation rate of N_2O may be expressed as the rate of Reaction 2, specified in the following section, for a comparatively prolonged stage of reaction pass time.

The Elovich equation in wide use is one of the most convenient ways of describing chemisorption kinetics, especially when the chemisorption is slow. The Elovich equation is written in its differential form as $dQ/dt=\alpha \exp(-\beta Q)$ where Q (mol g^{-1}) is the amount of N_2O produced at a reaction pass time t (min) and α and β are constants for each system at a fixed temperature. In its integrated form, the equation can be written as $Q=(1/\beta)\ln(t+t_o)-(1/\beta)\ln t_o$, $t_o=1/\alpha\beta$ (constant) where α (mol g^{-1} min^{-1}) is the initial formation rate of N_2O, *i.e.*, the formation rate of N_2O taken when the reaction pass time t approaches zero.

The dependence of the initial formation rate of N_2O on NO pressure was studied on zeolites pretreated at 500 °C by using a closed gas circulation system at reaction temperature 0 °C. Figure 4 shows the relation

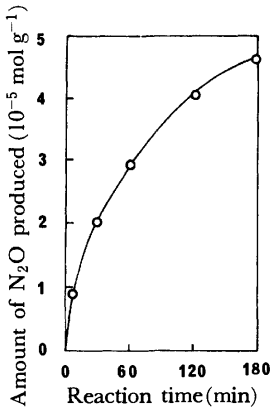

Fig. 4. Amount of N_2O produced plotted against reaction time.
P_0=110.2 Torr: Reaction temp. 0 °C

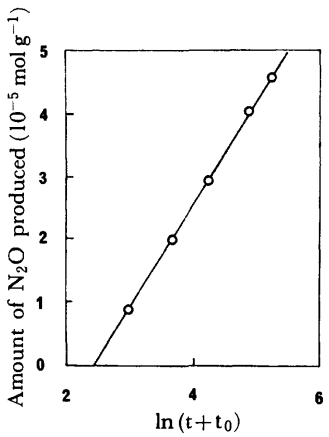

Fig. 5. Relationship between Q and $\ln(t+t_0)$.
$Q=1/\beta \ln(t+t_0)-1/\beta \ln t_0$, $t_0=1/\alpha\beta$, t_0=9.87 min

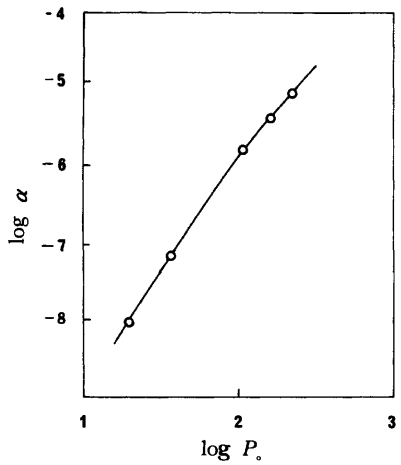

Fig. 6. Relationship between $\log\alpha$ and $\log P_o$.

between the amount of N_2O produced and the reaction pass time t obtained when the pressure P_o of introduced NO is equal to 110 Torr. The curve in Fig. 4 shows an initial rapid upturn, in good correspondence to the Elovich equation. The best-fit value of t_o as obtained by using the integrated formula of Elovich equation is given in Fig. 5 as 9.87 min, which in turn evaluates α as 1.58×10^{-6} mol g^{-1} min^{-1}. In accordance with this procedure, the relation between the introduced-NO pressure P_o and the initial formation rate α was determined. Figure 6 shows the relation between log P_o and log α. The reaction order of the initial formation rate of N_2O was determined from the slope of the curve in Fig. 6; α is proportional to the third order of P_o in the lower pressure region (*ca.* 30 Torr). In an intermediate pressure region, the slope of the curve in Fig. 6 gradually decreases with an increase in NO pressure and α obeys the 2.2th order of P_o in the higher pressure region (*ca.* 200 Torr). Therefore, it is concluded that the initial formation rate of N_2O is third order with respect to NO pressure, and that the reaction order gradually decreases with an increase in NO pressure.

Discussion

Rate Equation for Initial Formation of N_2O. The mechanism proposed by Chao and Lunsford for the disproportionation reaction of NO,[3] is

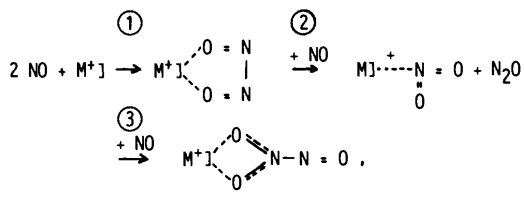

(from Chao and Lunsford's model[3])

where M^+ refers to Na^+ and Ca^{2+} for NaY- and CaY-type zeolites, respectively. For derivation of the initial formation rate of N_2O, we assume that the backward reaction of step ② is negligible. On this assumption, *i.e.*, the rate determining step is step ②, we have the following effective reaction sequence for the initial formation of N_2O:

$$[\quad] + 2NO \overset{K_1}{=} [N_2O_2], \qquad (1)$$

$$[N_2O_2] + NO \xrightarrow{\vec{k}_2} [NO_2] + N_2O, \quad (2)$$

$$[N_2O_2] + [\quad] = 1, \quad (3)$$

where [ ] denotes vacant adsorption sites, $[N_2O_2]$ denotes N_2O_2 adsorption sites, K_1 is the equilibrium constant for Eq. 1, and $\vec{k}_2$ is the rate constant for Eq. 2. By using Eqs. 1, 2, and 3, the initial formation rate α is formulated as

$$\alpha = \vec{k}_2[N_2O_2]\,P = \vec{k}_2K_1P^3/(1+K_1P^2), \quad (4)$$

where P is the pressure of NO. Therefore, the reaction order n is given by

$$n = \partial \ln \alpha/\partial \ln P = 3 - 2K_1P^2/(1+K_1P^2). \quad (5)$$

Equations 4 or 5 indicates that the initial formation rate of N_2O is expected to obey a third-order relation with respect to NO pressure at the lower pressure region if K_1P^2 is negligibly smaller than 1, and that the reaction order will decrease with an increase in NO pressure. On the other hand, a first-order relation is available if K_1P^2 is so large as to make 1 negligible. These characteristics may interpret the relation between log P_o and log α shown in Fig. 6.

Active Sites. Figure 1 shows that the activity increases with an increase in pretreatment temperature. In a study on the relation between the cation destribution and the residual water content in faujasites with metal cations exchanged, Dempsey and Olson[19] found that the occupancy of Sites I′ and II′[20] increase with an increase in the residual water content. Yamada *et al.*[21] studied chemisorptions of two kinds of gases having different adsorption properties, CO and NO, on NiHY-type zeolites, and concluded that the distribution of Ni^{2+} in the cation Site II increase with an increase in pretreatment temperature. From a study on the disproportionation reaction of NO on MgHY-type zeolites with different degrees of ion exchange, we derived[4] that the concentration of Mg^{2+} serving as active sites increases with an increase in pretreatment temperature. Thus, the effect of pretreatment temperature, shown in Fig. 1,may be considered to originate from an increase in Ca^{2+} distributed in Site II on Y-type zeolite.

In relation to activity and pretreatment temperature, we have described that the activity decreases markedly with increasing number of pulses. This drastic decrease in activity may be interpreted as follows: Most of the active sites or Ca^{2+} distributed in Site II are covered with N_2O_3 produced by the disproportionation reaction immediately after the NO in the first pulse has been introduced onto a CaHY-type zeolite, so that the resulting drastic decrease in the number of active sites will lead to the disappearance of catalytic activity. We[6] formerly reported that the apparent activation energy for the disproportionation of NO on CaY-type zeolite in the temperature range between −24 and 45 °C is −6.9 kcal/mol. Therefore, even if the disproportionation reaction of NO were carried out at 200 °C where NO, N_2O_3, and N_2O once adsorbed are desorbed, it would be most probable that nobody should be able to get a steady state activity of catalyst.

Reaction Mechanisms. On the basis of infrared spectra relating to NO adsorbed on CaY-type zeolite, Chao and Lunsford[3] deduced that the infrared peak assignable to N_2O disappears after the reaction mixture has been pumped out. In our study, however, peak γ of TPD profile has been assigned to N_2O. This discrepancy seems to be due to the fact that the TPD experiment was carried out in a He carrier gas flow with no pumping applied after the activity had been measured according to the pulse method. In addition, an experiment in which N_2O instead of NO was pulsed into the reactor has led to a conclusion that most of induced N_2O molecules remain adsorbed on a CaHY-type zeolite, without being allowed to desorb out into the gas phase. This experimental information is in support of the idea that the adsorptive power of N_2O is stronger than that of NO.

In accordance with the reaction mechanism proposed by Chao and Lunsford,[3] an N_2O_2 adsorbed at a cationic active site causes a rearrangement by reaction with a gas phase NO molecule to produce N_2O and NO_2, and the resulting NO_2 reacts rapidly with an NO molecule in the gas phase, leaving the spieces N_2O_3 on the zeolite surface. This reaction stage is step③ in Chao and Lunsford's model.

A comparison of Figs. 1 and 3 leads us to notice that peaks β and γ have a certain relation in activity. The results can be explained as follows: As is well known, N_2O_3 dissociates easily into NO and NO_2 and thus, the N_2O_3, formed by the disproportionation reaction and left on the surface, is caused to dissociate into NO and NO_2 when heated in the TPD experiment, the resulting NO corresponding to peak β in the TPD profile, whereas the resulting NO_2 is removed during passage through the dry NaOH-packed column before entering the detector.

Peak γ in the TPD profile is expected to be composed of a part of the N_2O formed by disproportionation and still remaining in the zeolite. The diameter of N_2O molecule is larger than that of NO molecule, hence it may follow that N_2O molecule is harder to desorb than NO molecule. This may be the reason for the observation that peak γ appears in a higher temperature region than peak β. On the other hand, peak α may be regarded as corresponding to the unreactive NO which is weakly adsorbed on the zeolite surface.

As seen from Fig. 3 for the pretreatment temperature range 600—700 °C, the areas of TPD peaks β and γ are *ca.* 1.5 and 4 times as large as those for the pretreatment temperature 400 °C. On the basis of these facts, the effect of pretreatment temperature on the area of TPD peak may be deduced as follows: As the pretreatment temperature is increased, *i.e.*, the number of water molecules in the zeolite structure is decreased, the amount of empty sites increases so that the N_2O produced by the disproportionation reaction of NO is made liable to adsorb on empty sites.

References

1) W. E. Addison and R. M. Barrer, *J. Chem. Soc.*, **1955**, 757.

2) A. V. Alekseyev, V. N. Filimonov, and A. N. Terenin, *Dokl. Akad. Nauk SSSR*, **147**, 1392 (1962).

3) C.-C. Chao and J. H. Lunsford, *J. Am. Chem. Soc.*, **93**, 71 (1971).

4) Y. Kanno and H. Imai, *Nippon Kagaku Kaishi*, **1982**,

1559.
5) M. J. D. Low and R. T. Yang, *J. Catal.*, **34**, 479 (1974).
6) Y. Kanno and H. Imai, *Chem. Lett.*, **1982**, 723.
7) Y. Kanno and H. Imai, *Mater. Res. Bull.*, **17**, 1161 (1982).
8) Y. Kanno and H. Imai, *Mater. Res. Bull.*, **18**, 269 (1983).
9) Y. Kanno and H. Imai, *Mater. Res. Bull.*, **18**, 945 (1983).
10) M. Shelef and K. J. Otto, *J. Catal.*, **18**, 184 (1970).
11) M. Shelef and J. T. Kummer, *Chem. Eng. Prog.*, **67**, 74 (1971).
12) J. P. Contour, *Pollut. Atom.*, **1975**, 65.
13) T. Seiyama, T. Arakawa, T. Matsuda, N. Yamazoe, and Y. Takita, *Chem. Lett.*, **1975**, 781.
14) K. A. Windhorst and J. H. Lunsford, *J. Am. Chem. Soc.*, **97**, 1407 (1975).
15) K. A. Windhorst and J. H. Lunsford, *J. Chem. Soc., Chem. Commun.*, **1975**, 852.
16) A. Kato, S. Matsuda, F. Nakajima, M. Imanari, and Y. Watanabe, *J. Phys. Chem.*, **85**, 1710 (1981).
17) S. Okazaki and T. Okuyama, *Bull. Chem. Soc. Jpn.*, **56**, 2159 (1983).
18) Y. Kanno, *J. Jpn. Petrol. Inst.*, **26**, 377 (1983).
19) E. Dempsey and D. H. Olson, *J. Phys. Chem.*, **74**, 305 (1970).
20) The nomenclature adopted in this paper is based on that used by Breck (D. W. Breck, "Zeolite Molecular Sieves," John Wiley and Sons, New York (1974), p. 97). Site I is at the center of a hexagonal prism and Site I′ is in the sodalite cage and on the other side of the 6-membered ring of the hexagonal prism. Site II and II′ are associated with the 6-memberered ring of sodalite cage, which lead to super cages. Site II is displaced towards the center of the super cage, whereas Site II′ is displaced towards the inside of the sodalite cage.
21) H. Yamada, H. Kuronuma, and H. Imai, *Nippon Kagaku Kaishi*, **1977**, 481.

 © 1984 The Chemical Society of Japan Bull. Chem. Soc. Jpn., 57, 2051—2054 (1984)

Adsorptions of Organic Compounds in Basic Solutions

Kohei URANO* and Hisanao KANO
Department of Safety and Environmental Engineering, Yokohama National University, 156 Tokiwadai, Hodogaya-ku, Yokohama 240
(Received October 12, 1983)

The adsorption isotherms of various aromatic compounds on an activated carbon or a polystyrene adsorbent in aqueous solutions and basic solutions were investigated. The adsorption isotherms of nonionic compounds and strong anionic electrolytes in the basic solutions were equal to the isotherms in the aqueous solutions. However, the adsorbed amounts of weak anionic electrolytes decreased with ionization in the basic solutions, and the adsorption isotherms of the non-ionized form and the ionized form of all these compounds except phenol could be expressed by the Freundlich equations with the same values of n. The amounts of those weak anionic electrolytes adsorbed at a desired pH could be calculated from the adsorption isotherms of the non-ionized form and the ionized form and the ionization constants.

Applications of adsorption from solutions on solid adsorbents have been considerably developed and become very important in many fields, such as in purification processes, water-treatment processes, and analytical methods.[1]

Adsorptions are now carried out at various pH values in those adsorption processes, and regenerations by desorption with a basic solution are applied in several processes. However, the influence of the pH on the adsorptions of organic compounds in water has not been made clear.[2] In this study, the adsorption isotherms of 7 aromatic compounds on an activated carbon or a polystyrene adsorbent were obtained in basic solutions, and they were compared with the isotherms in aqueous solutions.

Experimental

Three nonionic and four anionic compounds, whose properties are shown in Table 1, were tested as adsorbates in this study. A granular activated carbon and a polystyrene adsorbent whose properties are shown in Table 2 were used as adsorbents.

The adsorption isotherms at 25 °C were obtained by means of a batch-adsorption method as same in the previous paper.[3]

Results and Discussion

The adsorption isotherms in the aqueous solutions are shown in Figs. 1 and 2 as the Freundlich expression, logarithmic relationships between the adsorbed amount Q(mol g^{-1}) and the equilibrium concentration C(mol dm^{-3}). Most of them show linearity, and most could be expressed by the Freundlich equation; $Q = kC^{1/n}$. However, the isotherms for several anionic compounds, such as benzoic acid and nitrobenzoic acid fell lower in the concentration range than about 10^{-4} mol dm^{-3}. Further, the amount of the benzenesulfonic acid adsorbed for the activated carbon was much smaller than those of the other compounds, and it was negligibly small for the polystyrene adsorbent. Since benzoic acid and nitrobenzoic acid are ionized partially in the concentration range lower than about 10^{-4} mol dm^{-3} and since benzensulfonic acid is ionized completely throughout the concentration range, it can be presumed that the adsorbed amounts decrease with the ionization of the adsorbates.

Then the adsorption isotherms in sodium hydroxide solutions were obtained. The adsorption isotherms of the nonionic compounds and benzenesulfonic acid in the 1 mol dm^{-3} sodium hydroxide solution are shown

TABLE 1. PROPERTIES OF THE ADSORBATES TESTED

Adsorbate	Molecular weight	Solubility / mol dm^{-3}	Ionization constant K_a
Nitrobenzene	123.1	1.6×10^{-2}	—
Benzaldehyde	106.1	2.8×10^{-2}	—
Benzonitrile	103.1	2.1×10^{-2}	—
Benzoic acid	122.1	2.8×10^{-2}	6.1×10^{-5}
m-Nitrobenzoic acid	167.1	2.1×10^{-2}	3.6×10^{-4}
Phenol	94.1	9.2×10^{-1}	1.0×10^{-10}
Benzenesulfonic acid	158.2	∞	2×10^{-1}

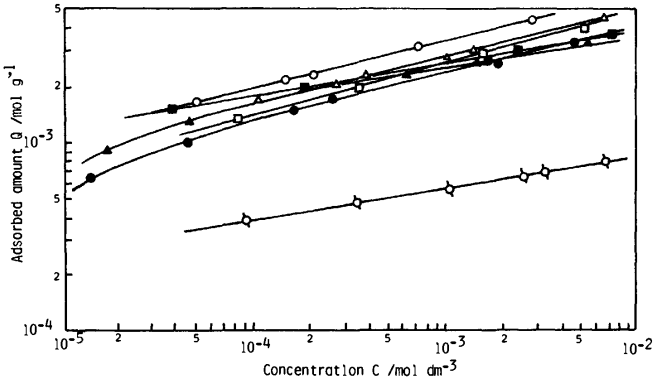

Fig. 1. Adsorption isotherms of organic compounds on activated carbon in aqueous solutions at 25 °C.
○: Nitrobenzene, △: benzaldehyde, □: benzonitrile, ●: benzoic acid, ▲: *m*-nitrobenzoic acid, ■: phenol, ⍜: benzenesulfonic acid.

TABLE 2. PROPERTIES OF THE ADSORBENTS USED

Adsorbent	Name	Surface area / m^2 g^{-1}	Pore volume/cm^3 g^{-1} Total	<20 nm
Activated Carbon	Filtrasorb 400	1030	0.84	0.52
Polystyrene	XAD-4	640	1.48	1.07

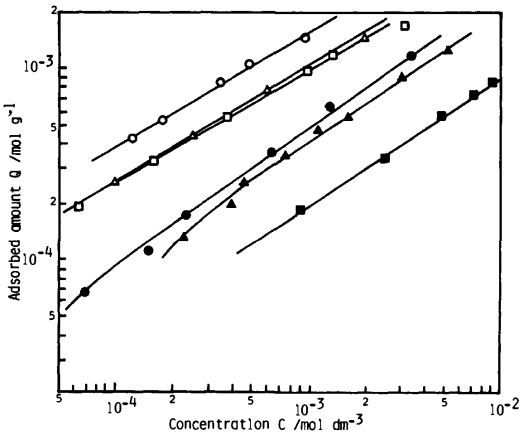

Fig. 2. Adsorption isotherms of organic compounds on polystyrene adsorbent in aqueous solutions at 25°C.
(Symbols are same as in Fig. 1)

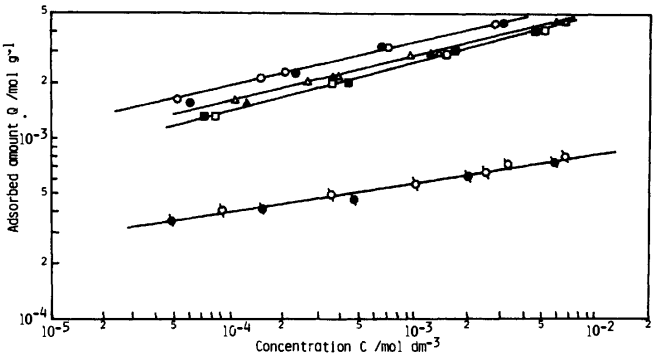

Fig. 3. Adsorption isotherms of nonionic compounds and benzenesulfonic acid on activated carbon in sodium hydroxide solutions at 25°C.
○ △ □ ◌: Aqueous solution, ● ▲ ■ ◉: 1 mol dm^{-3} NaOH solution, ○ ●: nitrobenzene, △ ▲: benzaldehyde, □ ■: benzonitrile, ◌ ◉: benzenesulfonic acid.

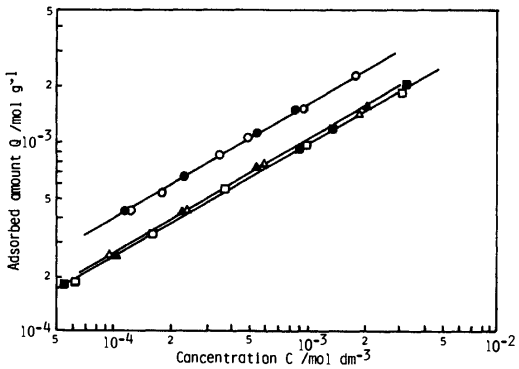

Fig. 4. Adsorption isotherms of nonionic compounds on polystyrene adsorbent in sodium hydroxide solutions at 25°C.
○ △ □: Aqueous solution, ● ▲ ■: 1 mol dm^{-3} NaOH solution ○ ●: nitrobenzene, △ ▲: benzaldehyde, □ ■: benzonitrile.

in Figs. 3 and 4. The adsorption isotherms for these compounds in the basic solutions were almost equal to those in the aqueous solutions. Therefore, sodium hydroxide did not influence the adsorptions of the nonionic compounds and the strong anionic electrolytes.

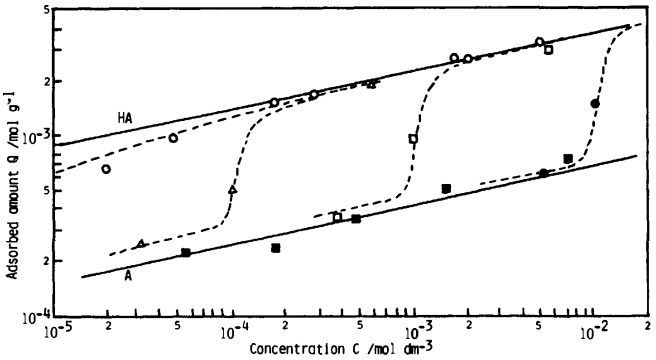

Fig. 5. Adsorption isotherms of benzoic acid on activated carbon in sodium hydroxide solutions at 25°C.
○: Aqueous solution, △: 10^{-4} mol dm^{-3} NaOH solution, □: 10^{-3} mol dm^{-3} NaOH solution, ●: 10^{-2} mol dm^{-3} NaOH solution, ■: 1 mol dm^{-3} NaOH solution.

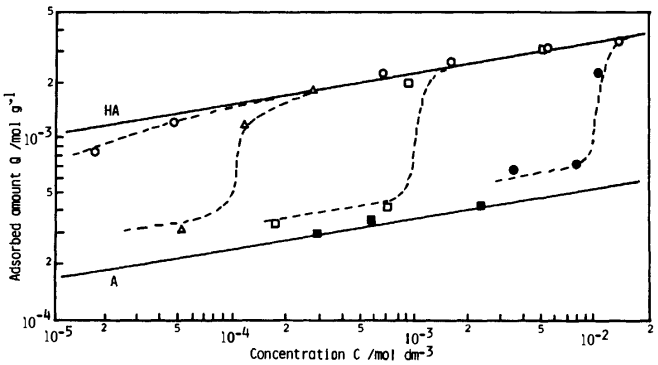

Fig. 6. Adsorption isotherms of nitrobenzoic acid on activated carbon in sodium hydroxide solutions at 25°C.
(Symbols are same as in Fig. 5)

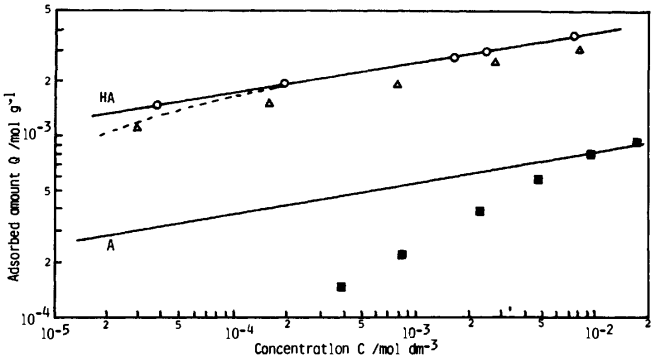

Fig. 7. Adsorption isotherms of phenol on activated carbon in sodium hydroxide solutions at 25°C.
(Symbols are same as in Fig. 5)

The adsorption isotherms of the weak anionic electrolytes in sodium hydroxide solutions from 10^{-4} to 1 mol dm^{-3} are shown in Figs. 5—10. The amounts of these weak anionic electrolytes adsorbed in the 1 mol dm^{-3} sodium hydroxide solutions, in which those compounds were completely ionized, were much smaller than those in the aqueous solutions for the activated carbon. Their amounts adsorbed on the polystyrene adsorbent were negligibly small in the solutions of 1 mol dm^{-3} sodium hydroxide.

However, the adsorption isotherms of the completely ionized form for the activated carbon were parallel to their isotherms of the non-ionized form in the aqueous solutions, except for phenol. That, the values of n of the Freundlich equation were equal to one another. Urano *et al.*[3] reported that the distribution function of the adsorption energy could be obtained from the modified Freundlich isotherm equation; $Q=k'(C/C_s)^{1/n}$, and that the values of k' and n related, respectively, to adsorption space and mechanism, where C_s is the saturated concentration of the adsorbate. The fact that the values of n for the non-ionized form and the ionized form were equal to one another shows that the adsorption mechanisms of both forms are equal and that only the solubilities C_s are different. That, it can be thought that the adsorption amounts for those compounds except phenol decrease with the ionization in the basic solutions, because the apparent solubilities C_s of the ionized forms increase much more than those of the non-ionized forms.

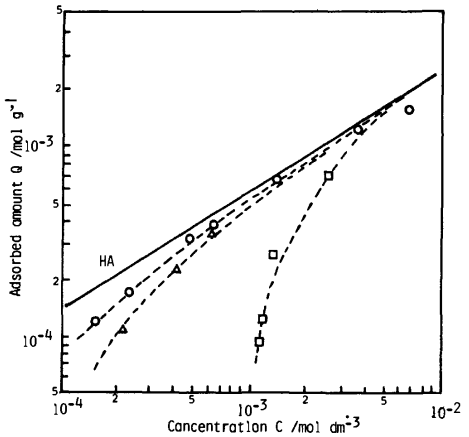

Fig. 8. Adsorption isotherms of benzoic acid on polystyrene adsorbent in sodium hydroxide solutions at 25 °C.
(Symbols are same as in Fig. 5)

The adsorptions of those weak anionic electrolytes in a basic solution seem to be examples of the adsorption of the dual-components, the non-ionized form (HA) and the ionized form (A). Getzen and Ward[4] reported a method of estimating the adsorption of several substituted benzoic acids by the application of the Langmuir equation for dual-components. However, it is difficult to determine the parameters of the Langmuir equation for application over a wide concentration range. Radke and Prausnitz[5] also proposed a method of predicting the adsorption of multi-components by means of a thermodynamic consideration. The total amounts Q of benzoic acid adsorbed under several conditions were calculated by the Radke-Prausnitz method for the forms of HA and A; they are compared with the observed data in Table 3. The calculated values are different from the observed data. Therefore, the Radke-Prausnitz method cannot be applied for the adsorption of the ionic compounds.

Now, assuming that the adsorptions of the non-ionized and the ionized forms are independent of one another, the total adsorbed amounts Q can be calculated as follows from the sum of the two Freundlich equations for HA and A;

$$Q = Q_{HA} + Q_A = k_{HA}C_{HA}^{1/n} + k_AC_H^{1/n} \quad (1)$$

The values of k_{HA}, k_A, and n can be obtained from the adsorption isotherms in aqueous solutions and sodium hydroxide solutions of 1 mol dm^{-3}; they are summarized in Table 4. The concentrations of the non-ionized and the ionized forms, C_{HA} and C_A, can be calculated from

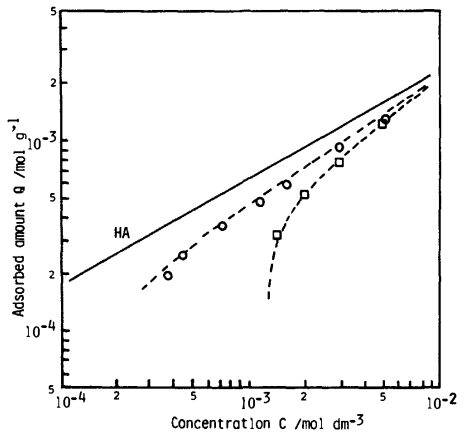

Fig. 9. Adsorption isotherms of nitrobenzoic acid on polystyrene adsorbent in sodium hydroxide solutions at 25 °C.
(Symbols are same as in Fig. 5)

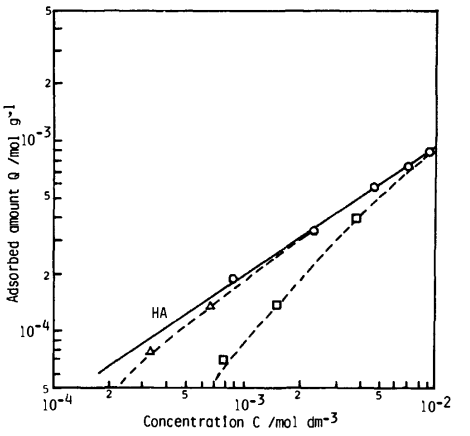

Fig. 10. Adsorption isotherms of phenol on polystyrene adsorbent in sodium hydroxide solutions at 25 °C.
(Symbols are same as in Fig. 5)

Table 3. Comparison of Q calculated by the Radke-Prausnitz method and observed data for benzoic acid

C_{Na}	C	C_{HA}	C_A	Q/mol g^{-1}	
mol dm^{-3}	mol dm^{-3}	mol dm^{-3}	mol dm^{-3}	Calculated	Observed
1.0×10^{-2}	5.0×10^{-3}	6.0×10^{-10}	5.0×10^{-3}	2.0×10^{-4}	6.0×10^{-4}
1.0×10^{-2}	1.0×10^{-2}	1.2×10^{-6}	1.0×10^{-2}	7.4×10^{-4}	1.5×10^{-3}
1.0×10^{-2}	2.6×10^{-2}	1.6×10^{-2}	1.0×10^{-2}	1.4×10^{-3}	5.2×10^{-3}

TABLE 4. PARAMETERS OF FREUNDLICH EQUATION FOR THE NON-IONIZED FORM AND THE IONIZED FORM

	Activated Carbon			Polystyrene		
	k_{HA}	k_A	n	k_{HA}	k_A	n
Nitrobenzene	1.9×10^{-2}	—	4.0	9.1×10^{-2}	—	1.7
Benzaldehyde	1.6×10^{-2}	—	3.9	6.2×10^{-2}	—	1.7
Benzonitrile	1.7×10^{-2}	—	3.7	4.5×10^{-2}	—	1.8
Benzoic acid	9.4×10^{-3}	1.8×10^{-3}	4.8	6.7×10^{-2}	$<10^{-4}$	1.5
m-Nitrobenzoic acid	7.9×10^{-3}	1.2×10^{-3}	5.7	2.8×10^{-2}	$<10^{-4}$	1.8
Phenol	8.3×10^{-3}	—	5.7	1.9×10^{-2}	$<10^{-4}$	1.5
Benzenesulfonic acid	—	1.6×10^{-3}	6.7	—	$<10^{-4}$	—

the total concentration of the organic compound C, the concentration of the sodium ion C_{Na}, and the ionization constant K_a by means of the following equations;

$$C = C_{HA} + C_A \quad (2)$$

$$C_H + C_{Na} = C_A + C_{OH} = C_A + 10^{-14}/C_H \quad (3)$$

$$K_a = C_H C_A / C_{HA} \quad (4)$$

The adsorption isotherms in 10^{-4}, 10^{-3}, and 10^{-2} mol dm^{-3} of sodium hydroxide solutions were calculated by means of Eqs. 1—4; they all shown as broken lines in Figs. 5—10. The calculated lines approximately fit the observed plots for the various systems of a weak anionic compound and an adsorbent except for the adsorption of phenol on the activated carbon. Therefore, the adsorptions of the non-ionized form and the ionized form of those compounds seem to be practically independent of one another.

Consequently, the total adsorbed amount at a desired pH (or C_H) for the weak anionic electrolytes, except for several phenolic compounds,[6] can be predicted by the use of Eq. 1 from the adsorption isotherms of the non-ionized form and the ionized form and the ionization constant, because the concentrations of both forms, C_{HA} and C_A, can be given as Eqs. 5 and 6 from Eqs. 2—4 at the desired pH;

$$C_{HA} = 10^{-pH}C/(10^{-pH} + K_a) \quad (5)$$

$$C_A = K_a C/(10^{-pH} + K_a) \quad (6)$$

The amounts of phenol adsorbed on the activated carbon decreased much in the lower concentration ranges in basic solutions, as shown in Fig. 7. It was shown in previous papers[3,6] that several phenolic compounds combined with the carbon surface by means of the π-electron combination. Therefore, the deviation of phenol for the activated carbon may be due to the combination of the hydroxide ion with the electrophilic groups on the surface of activated carbon.[3,6]

References

1) K. Urano, *Industrial Water*, No. 232, 33 (1978).
2) J. S. Mattson and H. B. Mark, Jr., "Activated Carbon," Marcel Dekker, New York (1971).
3) K. Urano, Y. Koichi, and Y. Nakazawa, *J. Colloid and Interface Sci.*, **81**, 477 (1981).
4) F. W. Getzen and T. M. Ward, *J. Colloid and Interface Sci.*, **31**, 441 (1969).
5) C. J. Radke and J. M. Prausnitz, *AIChE J.*, **18**, 761 (1972).
6) K. Urano, H. Kano, and T. Tabata, *Bull. Chem. Soc. Jpn.*, **57**, 2307 (1984).

Applicability of a New Adsorption Isotherm Equation and Adsorption Abilities of Commercial Chelating Resins for Single Metal Ions in Acidic Solution

Kohei URANO,* Veerapan CHANYASAK, Nobuhiko FUJII, and Toshiaki YUKAWA
Department of Safety and Environmental Engineering, Yokohama National University, 156 Tokiwadai, Hodogaya-ku, Yokohama 240
(Received December 8, 1983)

Adsorption isotherms for single metal ions (Ca^{2+}, Fe^{3+}, Cu^{2+}, Zn^{2+}, Cd^{2+}, or Pb^{2+}) in acidic solutions at 25 °C on 9 types of commercial chelating resins were obtained. The results could all be expressed by the isotherm equation, $Q=Q_{max}/(1+AC_M^{-\alpha}C_H^{\beta})$, reported in the preceding paper. The parameters α and β, which indicate respectively the influences of concentrations of metal ion (C_M) and hydrogen ion (C_H) on the adsorption capacities (Q), were discussed in relation to the properties of the chelating resins and the metal ions.

Chelating resins have been used for the removal and the recovery of metals from water and also for the concentration and analysis of trace metals.[1-4] Conventional studies on chelating resins, however, related only to those involving syntheses and examples of application under specific conditions.[5] In a previous study,[6] competitive adsorptions of metal ion and of hydrogen ion on chelating resin were investigated, and it was shown that the adsorption isotherms of single heavy metal ion in acidic solution on several systems of metal ion and chelating resin could be represented by the following equation;

$$Q = Q_{max}/(1+AC_M^{-\alpha}C_H^{\beta}). \quad (1)$$

Here Q is an adsorption amount (m mol/g-dry resin), Q_{max} is the maximum adsorption amount which can be determined from the total ion-exchange capacity of the resin, A is a correction factor, C_M is the concentration (mol dm^{-3}) of metal ion, and C_H is the concentration (mol dm^{-3}) of hydrogen ion. α and β are parameters such that the values of $1-\alpha$ and β show the exponents of the distribution function of ligands which have various dissociation constants. However, this isotherm equation is semi-theoretical and its applicability to many systems of chelating resin and metal ion over wide concentration ranges of metal ion and hydrogen ion needs to be confirmed experimentally.

The objectives of this study are to establish the validity of the above equation for various systems of commercial chelating resins and heavy metal ions, and to estimate the adsorption abilities of commercial chelating resins for various metal ions by the values of α and β in Eq.1.

Experimental

Nine types of chelating resins were employed in this study. They were UR-10, UR-20, UR-30, UR-40, UR-50, which are

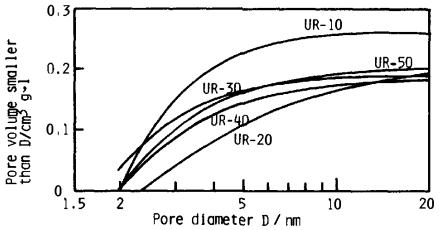

Fig. 1. Pore-size distribution of chelating resins used (I).

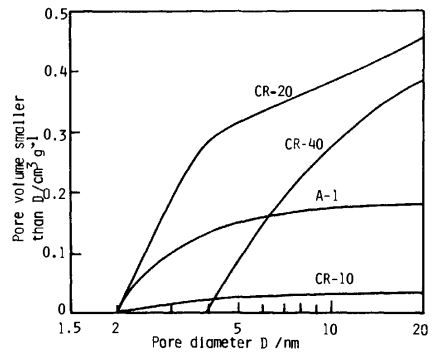

Fig. 2. Pore-size distribution of chelating resins used (II).

TABLE 1. PROPERTIES OF THE CHELATING RESINS USED

Symbol	Maker	Matrix	Main functional group	Phenolic OH / meq g^{-1}	Swelling ratio (Na/H)	Surface area / m^2 g^{-1}
UR-10	Unitika	Polyphenol	$-N(CH_2COOH)_2$	1.94	1.4	350
UR-20		Polyphenol		1.84	1.8	170
UR-30		Polyphenol		1.97	2.0	260
UR-40		Polyphenol		0.0	1.6	220
UR-50		Polyphenol		1.17	2.1	260
CR-10	Mitsubishi Chem.	Polystyrene	$-N(CH_2COOH)_2$	—	2.0	40
CR-20		Polystyrene	$-NH(C_2H_4NH)_nH$	—	—	—
CR-40*		Polyethylene	$-CH_2CH_2NH-$	—	—	—
A-1	Dow Chem.	Polystyrene	$-N(CH_2COOH)_2$	—	2.2	280

* gel type

products of Unitika Ltd. in Japan, CR-10, CR-20, CR-40 of Mitsubishi Chemical Industry Ltd. in Japan, and Dowex A-1 of Dow Chemical Ltd. in USA. They have various functional groups to chelate with metal ions. The properties of these resins are shown in Table 1. Their pore-size distributions which were measured by the methanol adsoption method[7]

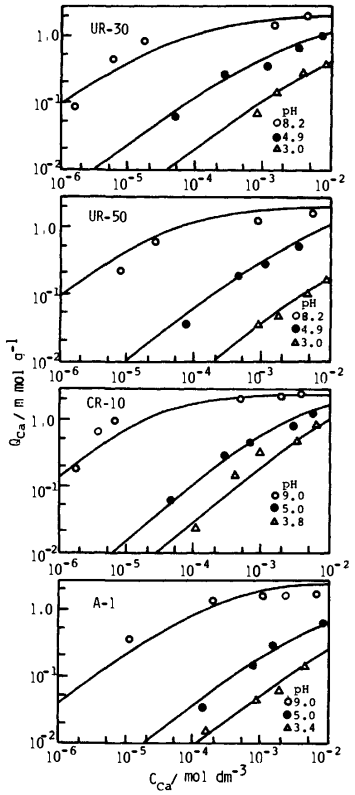

Fig. 3. Adsorption isotherms of Ca^{2+} for various resins and pH.
(Curves in Figs. 3—8 calculated by Eq. [1].)

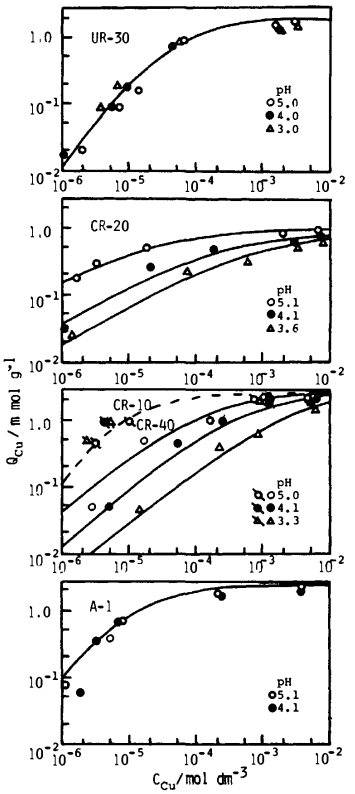

Fig. 5. Adsorption isotherms of Cu^{2+} for various resins and pH.

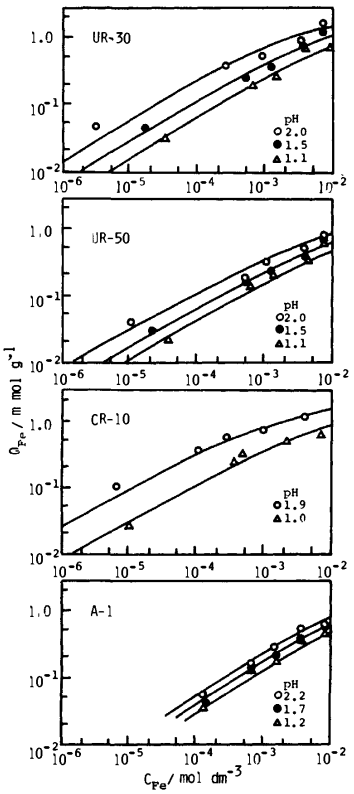

Fig. 4. Adsorption isotherms of Fe^{3+} for various resins and pH.

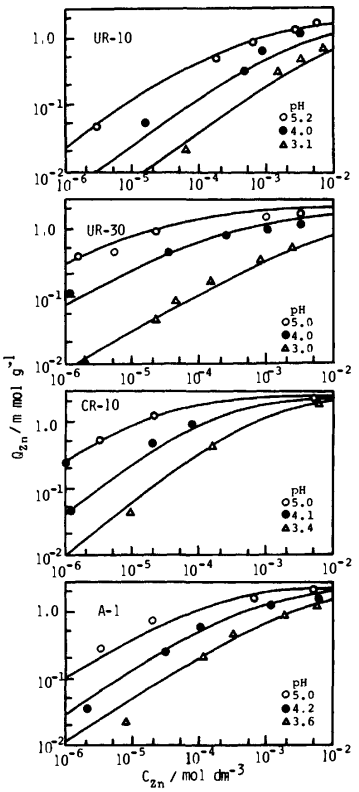

Fig. 6. Adsorption isotherms of Zn^{2+} for various resins and pH.

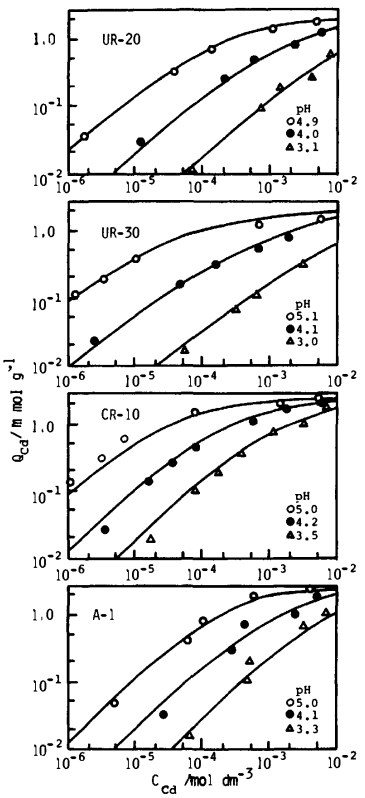

Fig. 7. Adsorption isotherms of Cd^{2+} for various resins and pH.

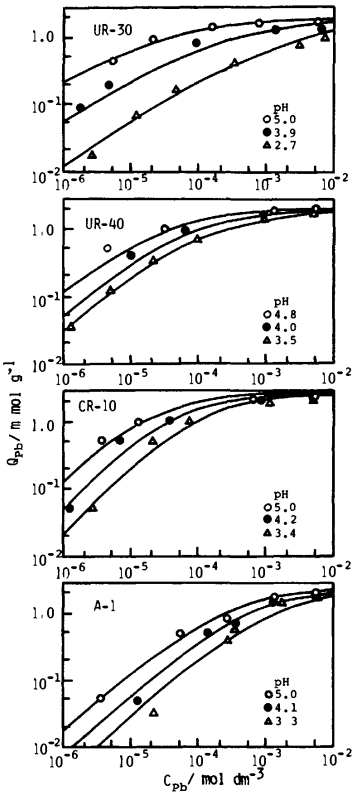

Fig. 8. Adsorption isotherms of Pb^{2+} for various resins and pH.

are shown in Figs.1 and 2. The swelling ratio corresponds to the degree of crosslinkage of the resin. Three types of UR-20 and UR-30, namely H, Ca, and Na types, were used in the experiments, but only the H type of the other resins was used.

Metal salts employed for adsorption tests were nitrates of Ca(II), Fe(III), Cu(II), Zn(II), Cd(II), and Pb(II) of reagent grade.

The methods for the pretreatments of the resins and the batchwise adsorption tests have been described in the previous paper.[6] The pH was controlled at about 3, 4, 5, 8, or 9 for the adsorption tests of Ca^{2+} about 1 or 2 for Fe^{3+}, and about 3, 4, or 5 for Cu^{2+}, Zn^{2+}, Cd^{2+}, and Pb^{2+}. The concentrations of Ca^{2+} and Fe^{3+} were measured by an atomic absorption flame spectrophotometer, Model AA-610 of Shimadzu Co., and the concentrations of Cu^{2+}, Zn^{2+}, Cd^{2+}, and Pb^{2+} were measured by an anodic stripping voltametric analyzer, Model AS-01 of Mitsubishi Chemical Industry Ltd.

Results and Discussion

Applicability of the Adsorption Isotherm Equation. Adsorption isotherms of each metal at 25 °C are shown in Figs. 3—8, respectively. The curves in these figures were calculated from Eq.1, and the plots show the measured data. All the measured data fitted approximately on the calculated curves. Consequently, it is confirmed that the isotherm Eq.1 can be applied generally for the various systems of commercial chelating resin and metal ion over a wide ranges of pH and concentration of the metal ion. The values of the parameters of Eq.1 for all the tested systems are listed in Table 2.

Variation of α and β with Systems of Chelating Resin and Metal Ion. Variations of the values of α and β, which show respectively the influences of C_M and C_H on Q, with the chelating resins, are discussed for each metal ion.

Calcium Adsorption: The α values of UR-10, UR-20, and UR-30 which have many phenolic OH groups are 0.66 ± 0.03 for Ca^{2+}, whereas for UR-40, UR-50, CR-10, and Dowex A-1 which have few or no phenolic OH group, the α values are 0.81 ± 0.06. The influence of the phenolic OH group on the adsorption of Ca^{2+} was greater than on the adsorption of the other heavy metal ions. This difference may be attributed to the high ionization ratio of the phenolic OH group at the higher pH values in the adsorption tests of Ca^{2+}. The β values for Ca^{2+} show only a small variation among the chelating resins. However, resins with higher degrees of crosslinkage tend to have smaller β values.

Iron (III) Adsorption: Fe^{3+} adsorbed slightly on CR-20 and CR-40 which have amino groups. For all the other resins, the α values for Fe^{3+} are 0.60 ± 0.06. Except for Dowex A-1 whose β value is 0.30, the β values of Fe^{3+} are 0.57 ± 0.09. The reason for the small β for Dowex A-1 may be because Dowex A-1 has various functional groups. Compared to CR-10, which has similar resin matrix to Dowex A-1 but only iminodiacetate functional group, Dowex A-1 has also smaller β values for other metals. In other words, more metals adsorbed on Dowex A-1 at low pH, though less adsorbed on Dowex A-1 than on CR-10 at normal pH.

Copper Adsorption: The adsorption of Cu^{2+} was specific and different from those of the other heavy metal ions. Many chelating resins could adsorb much Cu^{2+} at concentration higher than 10^{-3} mol dm^{-3}, but the adsorptions at the lower concentration range varied

TABLE 2. PARAMENTERS OF Eq. [1] OBTAINED BY EXPERIMENTS

Metal	Resin	Q_{max}	A	α	β
Ca^{2+}	UR-10	2.0	4.6	0.64	0.30
	UR-20	2.0	1.8	0.66	0.36
	UR-30	2.0	2.6	0.69	0.40
	UR-40	2.0	0.87	0.80	0.41
	UR-50	2.0	13	0.75	0.53
	CR-10	2.5	1.6	0.87	0.47
	A-1	2.5	5.1	0.75	0.38
Fe^{3+}	UR-30	2.0	0.46	0.63	0.65
	UR-50	2.0	0.73	0.58	0.48
	CR-10	2.5	0.48	0.55	0.53
	A-1	2.5	0.43	0.66	0.30
Cu^{2+}	UR-10	2.0	0.19	0.67	0.28
	UR-20(H)	2.0	2.0×10^{-7}	1.6	0.0
	UR-20(Ca)	2.0	5.0×10^{-6}	1.6	0.0
	UR-30(H)	2.0	1.0×10^{-5}	1.2	0.0
	UR-30(Na)	2.0	1.0×10^{-5}	1.2	0.0
	UR-40	2.0	2.3×10^{-3}	0.56	0.0
	UR-50	2.0	2.0×10^{-2}	0.62	0.26
	CR-10	2.5	1.7×10^{-7}	1.4	0.0
	CR-20	1.0	6.8	0.56	0.68
	CR-40	2.5	0.44	0.80	0.53
	A-1	2.5	3.4×10^{-6}	1.2	0.0
Zn^{2+}	UR-10	2.0	2.7	0.70	0.52
	UR-20(H)	2.0	7.0	0.82	0.95
	UR-20(Ca)	2.0	1.2	0.80	0.60
	UR-30(H)	2.0	18	0.57	0.78
	UR-30(Na)	2.0	24	0.58	0.71
	UR-40	2.0	0.96	0.28	0.23
	UR-50	2.0	17	0.67	0.85
	CR-10	2.5	6.0	0.76	0.87
	CR-40	2.5	116	0.49	0.51
	A-1	2.5	8.6	0.65	0.69
Cd^{2+}	UR-10	2.0	44	0.72	0.69
	UR-20(H)	2.0	46	0.84	0.97
	UR-20(Ca)	2.0	61	0.84	0.94
	UR-30(H)	2.0	27	0.71	0.88
	UR-30(Na)	2.0	80	0.72	0.80
	UR-40	2.0	24	0.86	1.0
	UR-50	2.0	47	0.68	0.80
	CR-10	2.5	20	0.86	1.0
	CR-20	1.0	0.23	0.86	0.20
	CR-40	2.5	3.1	0.91	0.50
	A-1	2.5	24	0.88	0.89
Pb^{2+}	UR-10	2.0	0.90	0.56	0.31
	UR-20(H)	2.0	7.3×10^{-2}	0.96	0.68
	UR-20(Ca)	2.0	1.2×10^{-2}	0.96	0.40
	UR-30(H)	2.0	0.76	0.63	0.55
	UR-30(Na)	2.0	1.3	0.62	0.50
	UR-40	2.0	5.0×10^{-2}	0.80	0.48
	UR-50	2.0	0.64	0.66	0.56
	CR-10	2.5	8.4×10^{-3}	0.94	0.46
	CR-20	1.7	4.9	0.99	0.55
	CR-40	0.7	0.45	1.1	0.47
	A-1	2.5	9.0×10^{-2}	0.84	0.38

widely with different resins. Therefore, the α values for Cu^{2+} vary widely with the chelating resins. The β values for Cu^{2+} are very small for most of the resins except for CR-20 and CR-40 which have amino functional groups. Two resins, CR-20 and CR-40, adsorb Cu^{2+} selectively, because N-O ligands form complexes with Cu^{2+} easily. However, the values of the parameters A, α, and β for CR-20 and CR-40, which have different a resin matrix but similar functional group, are very different form each other. Further, it was found that the α values of UR-20 for Cu^{2+}, Zn^{2+}, Cd^{2+}, and Pb^{2+} were larger than those of the other resins of the UR series. The reason is unknown, though the pore-size distribution of UR-20 was different from those of the other resins.

Zinc Adsorption: The α and β values for Zn^{2+} show

large variations with the chelating resins. The α values of the UR series resins for Zn^{2+} do not depend on the amount of phenolic OH group. The α values of UR-20 or UR-30 of different ion types, namely H, Na, and Ca types, for Zn^{2+} are slightly different, but the β values of these different type resins decreased in the following order: H type>Na type>Ca type. In the cases of the Ca type resins, Ca^{2+} ion which was released with adsorption of H^+ might be adsorbed competitively with Zn^{2+}, as a result, the apparent β values are smaller than those of the other types. However, in the cases of the Na type resins, the released Na^+ might be adsorbed much less than Zn^{2+}. The reason for the smaller β values of the Na type resins than the H type resins might be that Na^+ in the resins became difficult to release due to shrinking of the Na type resins with the adsorption of H^+. It was also found that the β values for Cd^{2+} and Pb^{2+} of different type resins varied in the same order as in the case of Zn^{2+}.

Cadmium Adsorption: The α values of the UR series resins for Cd^{2+} do not depend on the amounts of phenolic OH group, but the α values of UR-40 having no phenolic OH group are larger than the other resins of UR series. The β values of CR-20 and CR-40, which have amino group, for Cd^{2+} are smaller than those of the other resins. The β value of UR-10 with high degree of crosslinkage for Cd^{2+} is slightly smaller than those of the other resins of UR series.

Lead Adsorption: As is in the case of Cd^{2+}, the α values for Pb^{2+} can be divided into two groups; (1) UR-10, UR-30, and UR-50 and (2) the other resins. The β value of UR-10 for Pb^{2+} is also smaller than the values of the other resins, this is similar to the case of Cd^{2+}. As mentioned previously, the β value of UR-20 is larger than the values of the other resins.

Order of β Values: The β values of various chelating resins increase in the order: $Cu^{2+}<Ca^{2+}<Pb^{2+}<Fe^{3+}<Zn^{2+}<Cd^{2+}$. This order, except for Ca^{2+} whose adsorption tests were carried out at higher pH than the others, is in opposite order to the stability constants of ethylenediaminetetraacetate with these metal ions. The reason for the deviation of Ca^{2+} adsorption may be that the phenolic OH group of the resins of UR series influences the adsorption at the higher pH range.

References

1) M. I. Abdullah and L. G. Royle, *Anal. Chim. Acta*, **58**, 283 (1972).
2) J. Digman Jr., K. M. Gloss, E. A. Milano, and S. Sigga, *Anal. Chem.*, **46**, 774 (1974).
3) P. Burba and K. H. Lieser, *Angew. Makromol. Chem.*, **64**, 197 (1977).
4) K. Urano and N. Fujii, *Mizushorigijutsu*, **22**, 1031 (1981).
5) K. Urano and N. Fujii, *Mizushorigijutsu*, **23**, 3 (1982).
6) K. Urano, V. Chanyasak, and N. Fujii, *J. Colloid Interface Sci.*, **82**, 251 (1981).
7) K. Urano, *Hyomen*, **13**, 738 (1975).

Adsorption Isotherm Equation for Coexistence of Two Kinds of Metal Ions in Acidic Solution on Chelating Resin

Kohei URANO* and Nobuhiko FUJII
Department of Safety and Environmental Engineering, Yokohama National University, 156 Tokiwadai, Hodogaya-ku, Yokohama, 240
(Received December 8, 1983)

Adsorption isotherms for the coexistence of two metal ions (combinations of Zn^{2+}, Cd^{2+}, and Pb^{2+}) in acidic solutions on chelating resins were measured at 25 °C. They were analyzed in relation to the adsorption isotherm equation of a single metal ion, $Q=Q_{max}/(1+AC_M^{-\alpha}C_H^{\beta})$, as was reported in the preceding paper. It is found that the adsorption isotherms of two metal ions (i and j) in acidic solution on chelating resins can be generally expressed by the equation;

$$Q_{i,j}=Q_{max}/\{1+A_iC_i^{-\alpha_i}C_H^{\beta_i}(1+K_{i,j}C_j^{\alpha_j}C_H^{-\beta_j})\}$$

over wide ranges of concentrations of the metal ion, C, and the hydrogen ion, C_H (mol dm^{-3}). Where Q_i and $Q_{i,j}$ are the adsorption amounts (m mol/g-dry resin) of i metal ion in the absence and in the coexistence of j metal ion. Q_{max} is the maximum adsorption amount, α and β are parameters in the adsorption of single metal solution, A and K are correction factors, and subscripts i and j identifing i and j metal ions. The adsorption capacities of two metal ions in acidic solution can be obtained from the isotherms parameters A_i, α_i, α_j, β_i and β_j for an individual single metal ion and only one additional parameter $K_{i,j}$ is needed.

Chelating resins are used to separate a specific metal ion from many coexisting ions in water for removal and analysis of the ion. However, there are few studies on selective adsorption of metal ions on chelating resins under various conditions. In the previous papers,[1,2] the general adsorption isotherm equation and its parameter were given for many systems of chelating resin and single-component heavy metal ion in acidic solution, but no general isotherm equation has been reported for the competitive adsorption of three adsorbates, two metal ions and hydrogen ion. In this study, adsorption isotherms for coexistence of two metal ions (combinations of Zn^{2+}, Cd^{2+}, and Pb^{2+}) in acidic solution on several chelating resins, which have iminodiacetate groups, were measured. They were analyzed by using the adsorption isotherm equation of each single-component heavy metal ion to give a general isotherm equation for selective adsorption of a heavy metal ion in competition with another coexisting metal ion and hydrogen ion.

Experimental

The tested systems of chelating resin and metal ions are shown in Table 1. The chelating resins of UR-40, CR-10, and Dowex A-1 are products of Unitika Ltd., Mitsubishi Chemical Industry Ltd., and Dow Chemical Ltd., respectively. Their properties were described in the preceding paper.[2] The methods for the pretreatments of the resins and the batchwise adsorption tests were similar to those described in the previous paper.[1]

Solutions containing two metal nitrates of various concentrations ranging from 5×10^{-4} to 1×10^{-2} mol dm^{-3} and at constant pH were used for the adsorption tests. The analytical method for determining the metal ions was also similar to that described in the previous papers.[1,2]

TABLE 1. TESTED SYSTEMS OF CHELATING RESIN, METALS, AND pH

Resin	Metals	pH
UR-40	Cd^{2+}-Pb^{2+}	5.1, 3.6
CR-10	Zn^{2+}-Cd^{2+}	5.0, 3.6
CR-10	Zn^{2+}-Pb^{2+}	5.0, 3.6
A-1	Zn^{2+}-Pb^{2+}	5.0, 3.4

Results and Discussion

The adsorbed amount of single i metal ion in acidic solution, Q_i, can be given by the following equation reported in the previous paper.[1]

TABLE 2. PARAMETERS OF Eq. (1) FOR TESTED SYSTEMS

Resin	Metal	Q_{max}	A_i	α_i	β_i
UR-40	Cd^{2+}	2.0	24	0.86	1.0
UR-40	Pb^{2+}	2.0	5.0×10^{-2}	0.80	0.48
CR-10	Zn^{2+}	2.5	6.0	0.76	0.87
CR-10	Cd^{2+}	2.5	20	0.86	1.0
CR-10	Pb^{2+}	2.5	8.4×10^{-3}	0.94	0.46
A-1	Zn^{2+}	2.5	8.6	0.65	0.69
A-1	Pb^{2+}	2.5	9.0×10^{-2}	0.84	0.38

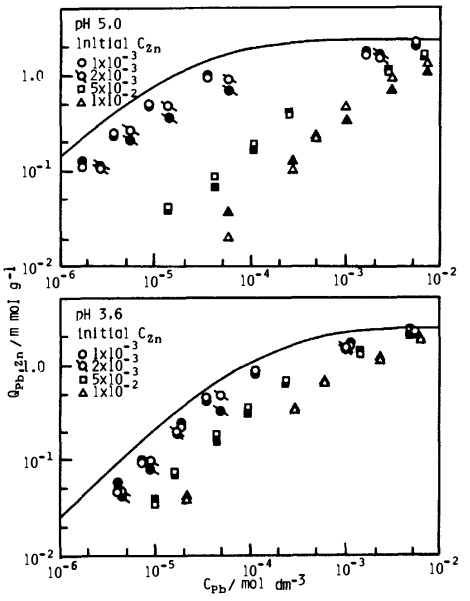

Fig. 1. Adsorption equilibria of Pb^{2+} under coexistence of Zn^{2+} on CR-10 at 25 °C (In all Figs. 1 and 3—9, curves show adsorption isotherms of single metal ion i by Eq. [1], open marks show observed data, and black marks show calculated $Q_{i,j}$ by Eq. [6] for the observed C_i and C_j).

$$Q_i = Q_{max}/(1+A_iC_i^{-\alpha_i}C_H^{\beta_i}) \quad (1)$$

Here, Q_{max} is the maximum adsorption amount which can be given by total ion-exchange capacity of the resin, and C_i and C_H are the concentrations of the i metal ion and hydrogen ion. α_i and β_i are parameters which indicate the degree of influences of C_i and C_H on Q_i. In other words, they show adsorbabilities of i metal ion and hydrogen ion, hence $A_iC_i^{-\alpha_i}C_H^{\beta_i}$ actually means an interfering factor for Q_i. The values of A_i, α_i, and β_i for all the tested systems of chelating resin and metal ion had been obtained in the preceding study.[2] They are listed again in Table 2 because they are needed for the analyses of the results in this study.

Adsorption equilibria of Pb^{2+} under the coexistence of Zn^{2+} on CR-10 at a pH of 5.0 and 3.6 are shown in Fig.1. The adsorbed amount of Pb^{2+} under the coexistence of Zn^{2+} in the acidic solution, $Q_{Pb,Zn}$, was smaller at higher initial concentration of Zn^{2+} and approached Q_{Pb} for a single Pb^{2+} solution at lower concentration of Zn^{2+}.

The interferences of the j metal ion and hydrogen ion to the adsorption of i metal ion were assumed to be represented by Eq. 2 as in the case of the adsorption of a single metal ion.

$$Q_{i,j} = Q_{max}/\{1+A_iC_i^{-\alpha_i}C_H^{\beta_i}(1+K_{i,j}C_j^{\gamma}C_H^{-\delta})\} \quad (2)$$

The interfering factor $K_{i,j}C_j^{\gamma}C_H^{-\delta}$ could be expressed by Eq. 3 from Eq. 2.

$$K_{i,j}C_j^{\gamma}C_H^{-\delta} = (Q_{max}-Q_{i,j})/Q_{i,j}A_iC_i^{-\alpha_i}C_H^{\beta_i} - 1 \quad (3)$$

Therefore, both logarithmic relationships between the values of the righthand side of Eq. 3 and C_j at a constant pH (C_H) and between the values of the righthand side of Eq. 3 and C_H at a constant C_j should be linear. For the adsorption of Pb^{2+} under the coexistence of Zn^{2+} at the constant pH, the former relationships were plotted on a log-log graph as shown in Fig. 2. Straight parallel lines with a slope, γ, of 0.76 were obtained. Also, the log-log plots of the latter relationship at fixed C_{Zn} for the same system showed straight lines with a slope, $-\delta$, of -0.87 as is also shown in Fig. 2. Therefore, the following equation can be obtained for the system of CR-10, Pb^{2+} and Zn^{2+}.

$$Q_{Pb,Zn} = 2.5/\{1+8.4\times10^{-3}C_{Pb}^{-0.94}C_H^{0.46} \times(1+0.44C_{Zn}^{0.76}C_H^{-0.87})\} \quad (4)$$

The calculated values of $Q_{Pb,Zn}$ by Eq. 4 for the same C_{Pb} and C_{Zn} as the observed data were plotted also in the Fig. 1 as black marks, and they are approximately equal to the observed data as open marks. Consequently, the adsorption amount of Pb^{2+} under the coexistence of Zn^{2+} could be obtained by Eq. 4.

The values of $\gamma=0.76$ and $\delta=0.87$ for this system were equal to the values of α_i and β_i for Zn^{2+} adsorption in the single solution on CR-10. Furthermore, the adsorption amount of Zn^{2+}, $Q_{Zn,Pb}$, for the same system could be given by Eq. 5.

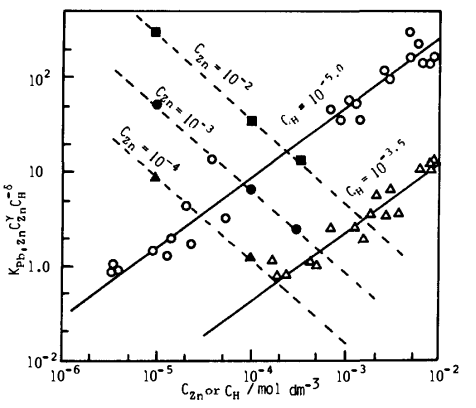

Fig. 2. Logarithmic plots of $K_{Pb,Zn}C_{Zn}{}^{\gamma}C_H{}^{-\delta}$ against C_{Zn} at constant C_H or against C_H at constant C_{Zn} for adsorption of Pb^{2+} on CR-10 under coexistence of Zn^{2+}.

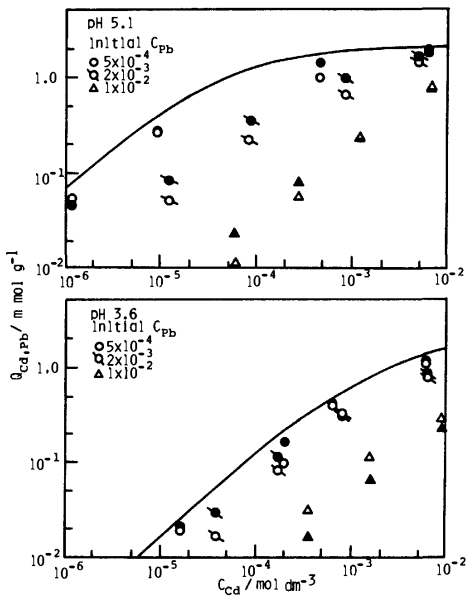

Fig. 3. Adsorption equilibria of Cd^{2+} under coexistence of Pb^{2+} on UR-40 at 25°C.

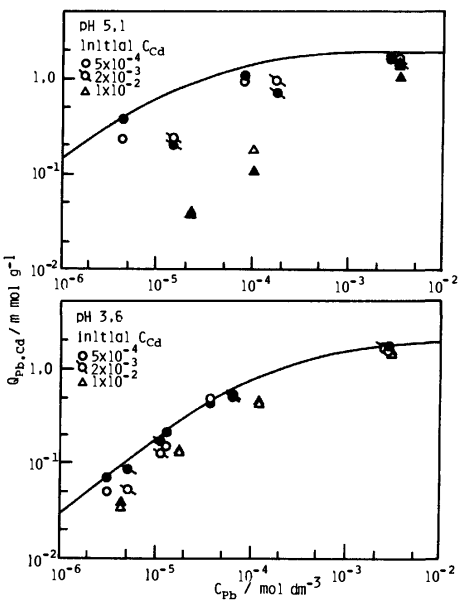

Fig. 4. Adsorption equilibria of Pb^{2+} under coexistence of Cd^{2+} on UR-40 at 25°C.

$$Q_{Zn,Pb} = 2.5/\{1+6.0C_{Zn}^{-0.76}C_H^{0.87}(1+50C_{Pb}^{0.94}C_H^{-0.46})\} \quad (5)$$

The values of $\gamma=0.94$ and $\delta=0.46$ were also equal to the values of α_i and β_i for Pb^{2+} adsorption in the single solution on CR-10.

Therefore, the following equation seems to be valid over a wide concentration range for two metal ions and hydrogen ion.

$$Q_{i,j} = Q_{max}/\{1+A_iC_i^{-\alpha_i}C_H^{\beta_i}(1+K_{i,j}C^{\alpha_j}C_H^{-\beta_j})\} \quad (6)$$

For the other tested systems of chelating resin and metal ions, the calculated values of $Q_{i,j}$ by Eq. 6 are compared with the observed data in Figs. 3—9. In these figures, curves show the adsorption isotherms of a single i ion by Eq. 1, open marks show the observed data, and black marks show the calculated $Q_{i,j}$ for the observed C_i and C_j. The computed values of $K_{i,j}$ for all the system are shown in Table 3. Almost all the observed data for the various systems were closely equal to the calculated values over a wide range of conditions. The small deviations of a few data from the calculat-

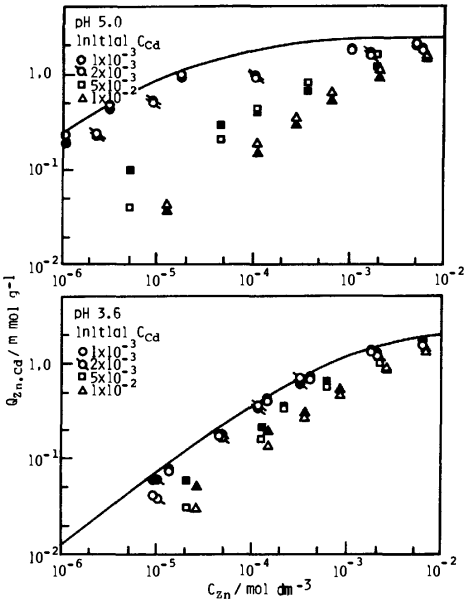

Fig. 5. Adsorption equilibria of Zn^{2+} under coexistence of Cd^{2+} on CR-10 at 25°C.

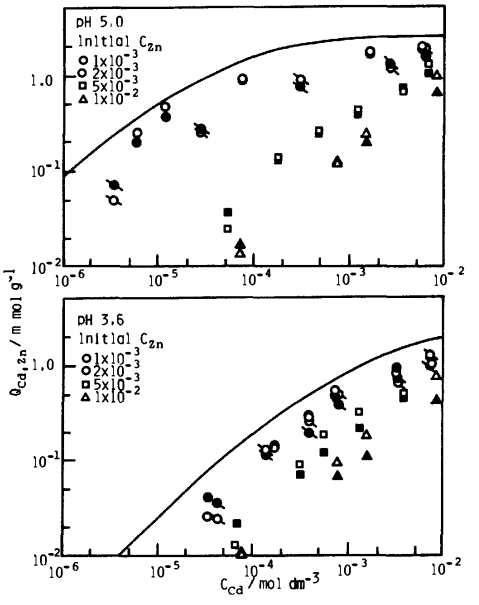

Fig. 6. Adsorption equilibria of Cd^{2+} under coexistence of Zn^{2+} on CR-10 at 25°C.

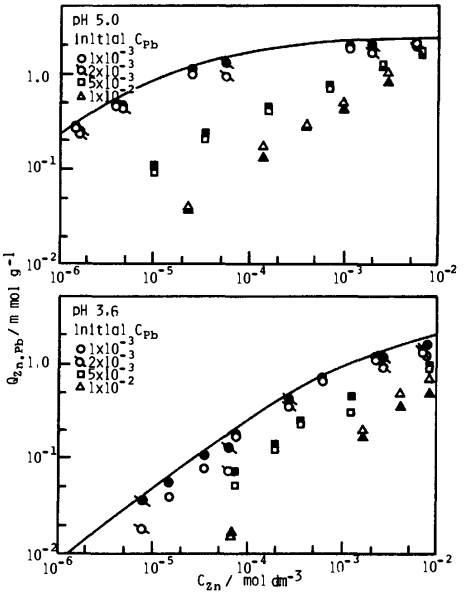

Fig. 7. Adsorption equilibria of Zn^{2+} under coexistence of Pb^{2+} on CR-10 at 25°C.

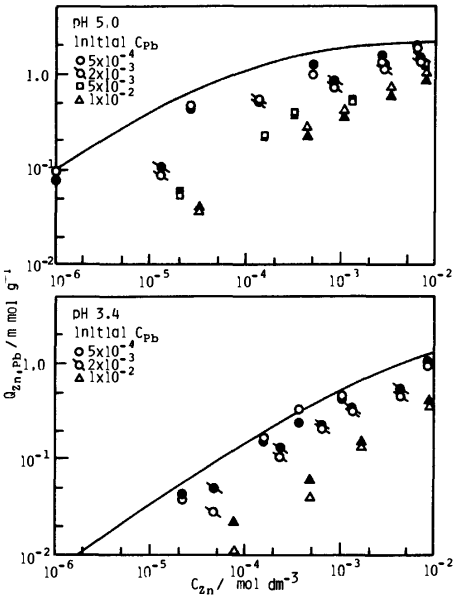

Fig. 8. Adsorption equilibria of Zn^{2+} under coexistence of Pb^{2+} on Dowex A-1 at 25°C.

TABLE 3. PARAMETER $K_{i,j}$ OF EQ. (6) OBTAINED BY EXPERIMENTS

Resin	Metal i-j	$K_{i,j}$
UR-40	Cd^{2+}-Pb^{2+}	2.7×10^{-2}
	Pb^{2+}-Cd^{2+}	44
CR-10	Zn^{2+}-Cd^{2+}	0.47
	Cd^{2+}-Zn^{2+}	4.3×10^{-2}
	Zn^{2+}-Pb^{2+}	50
	Pb^{2+}-Zn^{2}	0.44
A-1	Zn^{2+}-Pb^{2+}	0.29
	Pb^{2+}-Zn^{2+}	18

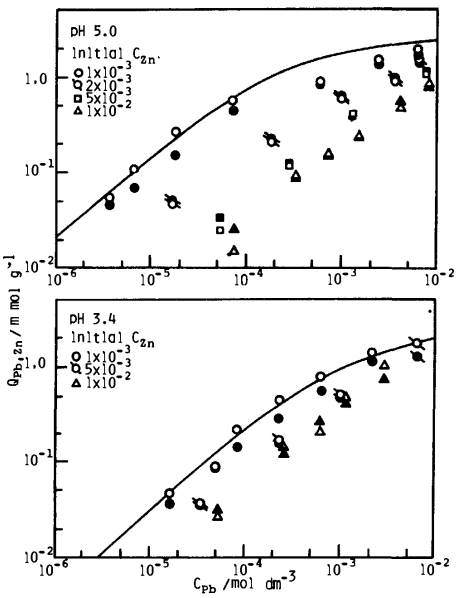

Fig. 9. Adsorption equilibria of Pb^{2+} under coexistence of Zn^{2+} on Dowex A-1 at 25°C.

ed values will be due to errors of analysis of C_i and of the values of α and β. Consequently, it was confirmed that the selective adsorption isotherm of i ion under coexistence of j ion and hydrogen ion is given by Eq. 6 which contained only one additional correction parameter $K_{i,j}$ with the parameters of the adsorption isotherms for single i and j metal ions. The fact that the adsorption isotherm equation for dual metal ions could be generally expressed by application of the adsorption isotherm equation of single metal ion proves that those adsorption isotherm equations well describe adsorption phenomena on chelating resins.

References

1) K. Urano, V. Chanyasak, and N. Fujii, *J. Colloid Interface Sci.*, **82**, 251 (1981).

2) K. Urano, V. Chanyasak, and N. Fujii, *Bull. Chem. Soc. Japan*, **57**, 2055 (1984).

The Volume, Adiabatic Compressibility, and Viscosity of Amino Acids in Aqueous Alkali-chloride Solutions

Toshio OGAWA, Kiyoshi MIZUTANI, and Motoo YASUDA*
Department of Chemistry, College of General Education, Nagoya University, Chikusa-ku, Nagoya 464
(Received January 5, 1984)

The apparent molal volumes (ϕ_V), apparent molal adiabatic compressibilities (ϕ_{KS}), and relative viscosities (n_r) at 25 °C have been obtained for the following amino acids in aqueous alkali-chloride solutions from measurements of the density, the ultrasonic velocity, and the flow time: glycine, L-alanine, β-alanine, α-aminoisobutyric acid, L-serine, and L-threonine. Viscosity measurements were also carried out in water for reference. The alkali chlorides used were lithium, sodium, and potassium chlorides. The limiting values ϕ_V°, ϕ_{KS}°, and the extended Jones-Dole viscosity coefficients, B and D, were calculated by a linear extrapolation using the least-squares method. All the ϕ_V°, ϕ_{KS}°, and B values obtained in the mixed solvents were larger than the corresponding ones in water, except in a few cases of the B coefficient. The results are discussed in terms of the dehydration effect of the electrolytes upon the amino acids.

Much attention has been given recently to the effects of electrolytes and nonelectrolytes on the structure of water. A quantitative interpretation of the factors which govern the structure remains difficult notwithstanding numerous remarkable investigations. We ourselves carried out volume and compressibility measurements of several amino acids in urea–water mixtures in order to understand the effect of urea upon the hydration of the amino acids.[1] The results showed that both the apparent molal volumes and the apparent molal adiabatic compressibilities of the amino acids increased upon the addition of urea in aqueous amino-acid solutions. This was explained in terms of the dehydration effect of urea upon the amino-acid molecules. Although the influence of salts on the activity coefficients of nonelectrolytes in aqueous solutions and on kinetic problems was examined carefully for a long time, there was no systematic study of the influence of salts upon the volume, compressibility, and viscosity of nonelectrolytes. Recently, as with cyclic amino acids, proline and hydroxyproline, we carried out a volume, compressibility, and viscosity study in aqueous alkali-chloride solutions.[2] For a better understanding of the behavior of the amino acids in mixed aqueous solvents, the densities, ultrasonic velocities, and viscosities were measured at 25 °C for six amino acids in amino acid-water-alkali chloride ternary systems at various concentrations. The apparent molal volumes and apparent molal adiabatic compressibilities, and the viscosity B- and D-coefficients were calculated from these data.

Experimental

The amino acids and alkali chlorides used in this study were guaranteed reagents from Wako Chemical Industries, Ltd., and were used without further purification except the lithium chloride, which was used after having been dried for several hours at *ca.* 150 °C. The densities and efflux times were measured in 1 and 2 mol kg^{-1} aqueous alkali-chloride solutions. Viscosity measurements in water were also carried out. The ultrasonic velocities were determined in 2 mol kg^{-1} alkali-chloride solutions.

All the amino-acid solutions were prepared by weight in the concentration range of 0.2—1 mol kg^{-1} (the number of moles of amino acid per kg of the mixed solvent whenever the mixed solvents were used) ; the highest concentration of the respective amino acid depended on the solubility of the amino acid.

The density and ultrasonic velocity measurements have been described previously.[1] The viscosities were measured by means of two Cannon-Fenske capillary viscometers with efflux times of *ca.* 210 and 240 s for distilled water; the kinetic-energy correction needed was negligibly small. The temperature control of the thermostated bath systems regulating the densimeter, ultrasonic interferometer, and viscometers was better than ±0.005 °C.

The pH values of all the amino-acid solutions, both in water and in aqueous alkali-chloride solutions, were very close to the isoelectric point of the respective amino acid; thus, no appreciable change in the structure of dipolar molecules can be considered.

Results

The densities, ultrasonic velocities, and efflux times were measured at 25 °C for the following amino-acid solutions; glycine (Gly), L-alanine (Ala), β-alanine (β-Ala), α-aminoisobutyric acid (Me-ala), L-serine (Ser), and L-threonine (Thr). The apparent molal volumes were obtained from Eq. 1:

$$\phi_V = \frac{M}{d} + \frac{1000(d_\circ - d)}{m\, d_\circ\, d}, \tag{1}$$

where M is the molecular weight of the amino acid; m, its molal concentration, and $d_\circ$ and d, the densities of the solvent and the solution respectively. The adiabatic compressibilities, β_S, and the apparent molal adiabatic compressibilities, ϕ_{KS}, were obtained using Eq. 2 and Eq. 3 respectively, where β_S is expressed in bar^{-1}:

$$\beta_S = -\frac{1}{V}\left(\frac{\partial V}{\partial P}\right)_s = \frac{100}{d\,u^2}, \tag{2}$$

and:

$$\phi_{KS} = -\left(\frac{\partial \phi_V}{\partial P}\right)_s = \frac{\beta_S M}{d} + \frac{1000(\beta_S d_\circ - \beta_S^\circ d)}{m\, d_\circ\, d}, \tag{3}$$

where u is the velocity of sound (m s^{-1}) and where β_S° is the adiabatic compressibility of the solvent. The limiting values of the apparent molal volumes and the apparent molal adiabatic compressibilities were calculated by a linear extrapolation using the least-squared fit to these equations:

$$\phi_V = \phi_V^\circ + S_V m, \tag{4}$$

and:

$$\phi_{KS} = \phi_{KS}^{\circ} + S_K m, \quad (5)$$

where ϕ_V° and ϕ_{KS}° are the infinite dilution apparent molal volume and the apparent molal adiabatic compressibility respectively, and where S_V and S_K are the experimental slopes. At an infinite dilution, $\phi_V^{\circ}=\overline{V}^{\circ}$ (the infinite dilution partial molal volume) and $\phi_{KS}^{\circ}=\overline{K}_S^{\circ}$ (infinite dilution partial molal adiabatic compressibility). The derived values for ϕ_V° are summarized in Table 1, with the literature data on proline and hydroxyproline.[2] The standard deviations are mostly less than 0.02 $cm^3 mol^{-1}$. The values for ϕ_{KS}° and the standard deviations, σ, in water and 2 mol kg^{-1} aqueous alkali-chloride solutions are listed in Table 2.

The viscosity, η, of dilute solutions of nonelectrolytes is represented by:[3]

$$\eta = \eta_0(1+Bc), \quad (6)$$

Table 1. Limiting apparent molal volumes ϕ_V°

Amino acid	ϕ_V° / $cm^3 mol^{-1}$						
	H_2O	LiCl		NaCl		KCl	
		1*m*	2*m*	1*m*	2*m*	1*m*	2*m*
Gly	43.23	44.68	45.63	45.05	46.24	44.89	46.12
Ala	60.50	61.59	62.48	62.08	63.19	61.97	63.14
β-Ala	58.25	59.91	60.67	60.12	61.36	60.13	61.21
Me-ala	77.54	78.45	79.18	78.86	79.97	78.78	79.98
Ser	60.72	62.15	63.27	62.74	64.12	62.76	64.08
Thr	76.94	78.10	79.00	78.73	80.11	78.73	79.95
Pro[a]	82.87		84.37		85.30	84.22	85.00
Hyp[b]	84.45		86.54		87.34	86.09	87.10

a) Ref. 2. b) Hyp: hydroxyproline, Ref. 2.

Table 2. Limiting apparent molal adiabatic compressibilities with their estimated standard deviations σ in parentheses

Amino acid	ϕ_{KS}° / $10^{-4} cm^3 mol^{-1} bar^{-1}$			
	H_2O	2*m* LiCl	2*m* NaCl	2*m* KCl
Gly	−27.16(36)	−11.80(14)	−10.30(06)	−11.03(11)
Ala	−24.74(18)	−10.99(04)	−8.69(25)	−9.46(11)
β-Ala	−26.36(11)	−10.46(10)	−9.38(23)	−10.47(09)
Me-ala	−23.46(27)	−9.39(13)	−5.38(07)	−6.72(07)
Ser	−29.88(10)	−13.80(07)	−11.92(16)	−12.04(13)
Thr	−31.23(10)	−14.26(02)	−11.05(07)	−12.02(13)
Pro[a]	−24.19(09)	−7.85(04)	−4.55(19)	−6.86(26)
Hyp[a]	−22.27(08)	−7.23(12)	−4.74(09)	−6.70(13)

a) Ref. 2.

Table 3. Viscosity *B* and *D* coefficients

Amino acid		H_2O	LiCl		NaCl		KCl	
			1*m*	2*m*	1*m*	2*m*	1*m*	2*m*
Gly	$B/dm^3 mol^{-1}$	0.135	0.134	0.151	0.147	0.156	0.138	0.158
	$D/dm^6 mol^{-2}$	0.024	0.031	0.023	0.024	0.024	0.032	0.021
Ala	$B/dm^3 mol^{-1}$	0.247	0.255	0.262	0.256	0.263	0.248	0.253
	$D/dm^6 mol^{-2}$	0.050	0.055	0.060	0.056	0.059	0.061	0.065
β-Ala	$B/dm^3 mol^{-1}$	0.216	0.219	0.230	0.227	0.236	0.217	0.229
	$D/dm^6 mol^{-2}$	0.042	0.048	0.051	0.043	0.044	0.050	0.049
Me-ala	$B/dm^3 mol^{-1}$	0.346	0.359	0.369	0.354	0.366	0.352	0.354
	$D/dm^6 mol^{-2}$	0.112	0.111	0.115	0.114	0.113	0.112	0.118
Ser	$B/dm^3 mol^{-1}$	0.225	0.235	0.249	0.242	0.253	0.241	0.247
	$D/dm^6 mol^{-2}$	0.053	0.056	0.057	0.060	0.063	0.058	0.062
Thr	$B/dm^3 mol^{-1}$	0.335	0.337	0.348	0.336	0.352	0.324	0.343
	$D/dm^6 mol^{-2}$	0.084	0.106	0.113	0.111	0.108	0.124	0.108
Pro[a]	$B/dm^3 mol^{-1}$	0.279		0.306		0.304	0.293	0.304
	$D/dm^6 mol^{-2}$	0.07		0.08		0.07	0.07	0.07
Hyp[a]	$B/dm^3 mol^{-1}$	0.281		0.309		0.311	0.297	0.306
	$D/dm^6 mol^{-2}$	0.08		0.10		0.09	0.08	0.09

a) Ref. 2.

where η_0 is the viscosity of the solvent, c is the molar concentration of the solute, and B is an empirical constant which is called usually the Jones-Dole viscosity B-coefficient. This is known to depend on the size of the solute particle and also on the interaction between the solute and solvent molecules. The B-coefficient is expressed in molar concentration units; thus, the molar concentrations were calculated using the density data. For the more concentrated solutions of the amino acid used in this study, the relative viscosity is given by Eq. 7, in which D is an another empirical constant.[4] Desnoyers and Perron examined the D-coefficients and concluded that they cannot be interpreted unambiguously.[5]

$$\eta_r = 1 + Bc + Dc^2 \quad (7)$$

By rearranging this equation, we obtain:

$$(\eta_r - 1)/c = B + Dc. \quad (8)$$

The viscosity coefficients, B and D, were calculated by linear extrapolation using the least-squares fit to Eq. 8. Table 3 shows the viscosity in terms of the parameters of Eq. 7.

Discussion

Volume Results. The volume behavior of a solute in an infinite dilution is independent of the solute-solute interactions and thus can provide information concerning solute-solvent interactions. As may be seen from Table 1, the limiting apparent molal volumes of the amino acids in mixed solvents are larger than those of the corresponding ones in water. This was also observed for the data in aqueous urea solutions and was discussed in terms of the dehydration effect of urea upon the amino acids.[1] In order to ascertain the influence of the sodium-chloride concentration on the ϕ_V° of the amino acids, the transfer volumes, $\Delta\bar{V}_{tr}^\circ$, are plotted *vs.* the concentration of sodium chloride in Fig. 1;

$$\Delta\bar{V}_{tr}^\circ = \phi_V^\circ(\mathrm{NaCl}) - \phi_V^\circ(\mathrm{water}). \quad (9)$$

The transfer functions increase with the concentration, as in aqueous urea solutions.[1,6]

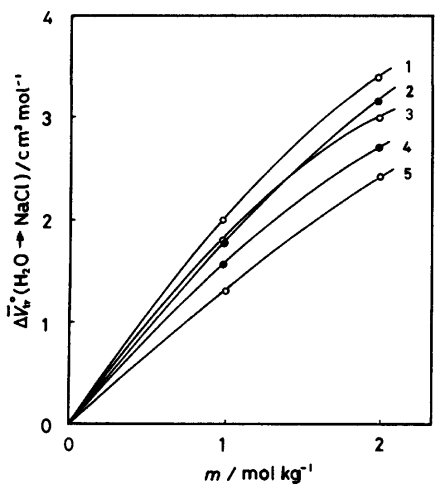

Fig. 1. Plot of $\Delta\bar{V}_{tr}^\circ$ *vs.* m for NaCl.
1: Ser, 2: Thr, 3: Gly, 4: Ala, 5: Me-ala.

The transfer volumes of the six amino acids studied decrease in the following order:

$$\mathrm{Ser} > \mathrm{Thr} > \beta\text{-Ala} > \mathrm{Gly} > \mathrm{Ala} > \mathrm{Me\text{-}ala},$$

for both water→aq NaCl and water→aq KCl transfers. The water→aq LiCl transfer volumes are in the same sequence except the Thr, which occurs between Gly and Ala. Our earlier study of the water→aqueous urea-transfer volumes gave a similar sequence:

$$\mathrm{Ser} > \mathrm{Thr} > \mathrm{Gly} > \beta\text{-Ala} \approx \mathrm{Ala} > \mathrm{Me\text{-}ala}.$$

The positive sign of the transfer volumes can be ascribed mainly to the fact that the hydration number of the amino acids is reduced by the addition of alkali chloride or urea: *i.e.*, the electrostriction effect which brings about the diminution in the volume of the solvent caused by the electrical fields of the dipolar solutes is reduced in the mixed solvents as compared with that in pure water. Ser and Thr, which contain an OH group, have larger transfer volumes; this was also observed in the case of hydroxyproline, *i.e.*, it has the larger transfer volume than proline, as may be seen from Table 1. In water-urea mixtures, the transfer volume of β-alanine was almost the same as that of alanine and less than that of glycine at a particular urea concentration.[1] In aqueous alkali-chloride solutions, β-Ala has a larger transfer volume than that of Gly. This may result from the fact that β-Ala has a larger dipole moment than that of Ala; thus, the former interacts more with the alkali and chloride ions than does Ala, which has a smaller dipole moment. The more the ion-dipole interaction, the more the dehydration effect. On the other hand, there may be no difference, or a very small one, as with the interaction of the amino acids with urea.

Compressibility Results. The infinite-dilution data for the compressibility can also give information concerning solute-solvent interactions. The limiting partial molal adiabatic compressibilities of the amino acids can be expressed by a simple model:[7]

$$\bar{K}_S^\circ = \bar{K}_S^\circ(\mathrm{int}) + \bar{K}_S^\circ(\mathrm{elect}), \quad (10)$$

where $\bar{K}_S^\circ$ (int) is the intrinsic partial molal adiabatic compressibility of the amino acid and where $\bar{K}_S^\circ$ (elect) is the electrostriction partial molal adiabatic compressibility due to the hydration of the amino acid. As has been noted by Millero *et al.*, as a first approximation, one can assume that $\bar{K}_S^\circ$ (int)≈0, since one would expect $\bar{K}_S^\circ$ (int) to be very small.[7] Thus, $\bar{K}_S^\circ$ may be thought to represent $\bar{K}_S^\circ$ (elect). The $\bar{K}_S^\circ$ values of the amino acids in water are all negative; this must come from the hydration of the charged centers of the amino acids, as the hydrated water molecules are already compressed and thus less compressible than that in the bulk. For the amino acids, the order of increasing (less negative) $\bar{K}_S^\circ$ values in water is:

$$\mathrm{Thr} < \mathrm{Ser} < \mathrm{Gly} < \beta\text{-Ala} < \mathrm{Ala} < \mathrm{Me\text{-}ala}.$$

This sequence may be considered to show a decreasing order of hydration, as a first approximation, particularly for the amino acids without the OH group, as will be mentioned below. If all the amino acids

were subjected to the dehydration effect by the addition of alkali chloride in the same proportion, the $\overline{K}_S^\circ$ (MCl)/$\overline{K}_S^\circ$ (water) ratios of the amino acids may be almost the same. The ratios decrease in the following order in 2*m* NaCl:

$$\text{Ser} > \text{Gly} > \beta\text{-Ala} \approx \text{Thr} > \text{Ala} > \text{Me-ala},$$

and in 2*m* KCl:

$$\text{Gly} \approx \text{Ser} > \beta\text{-Ala} > \text{Thr} \approx \text{Ala} > \text{Me-ala}.$$

The order in 2*m* LiCl differs a little compared with those in NaCl and in KCl, but the difference in ratios is rather small; therefore, the series is probably less reliable. The ratios in 3*m* aqueous urea show almost the same order as in NaCl and in the KCl solutions.[1] Thr and Ser are the amino acids with an OH group. As has been noted by Mathieson and Conway, ions which hydrogen-bond with water have unusual compressibilities.[8] Some have anomalously high compressibilities, while the OH^- ion exhibits a low compressibility. Thus, these two amino acids may be assumed to behave differently with the four other amino acids with no OH group. At any rate, however, Ser has a larger compressibility ratios than Thr in all the solvents studied. Of the four amino acids with no OH group, Gly has the largest value, and Me-ala , the smallest; β-Ala and Ala are in between in each solvent. This corresponds to the order of increasing absolute values of $\overline{K}_S^\circ$ in water, which answers to the order of increasing hydration numbers. Thus, the less hydrated amino acid in water has the lower compressibility ratio in the mixed solvent and then loses the hydrated water molecules more easily in the transfer from water to the mixed solvent. In this connection, it is very interesting to note that the compressibility ratios of proline and hydroxyproline with cyclic secondary amine group are very small (Table 2). These two amino acids must be supposed to lose their hydrated water molecules very easily in the transfer from water to the mixed solvent. However, from another point of view, as seen from the volume data, the number of dehydrated water molecules involved in the transfer increase in the order of increasing hydration number in water; in general, the more hydrated amino acid loses the more hydrated water molecules are involved in the transfer.

Viscosity Results. The viscosity coefficients of several amino acids at 25 °C have been reported by Devine and Lowe;[4] the *B*-coefficients of Gly and β-Ala were 0.143 and 0.220 respectively, while the *D*-coefficients were 0.010 and 0.040 respectively. However, the viscosity datum for the lowest concentration for each amino acid appears to be rather erroneous. If it is omitted, the recalculated coefficients were B= 0.139 and D=0.020 for Gly and B=0.216 and D= 0.051 for β-Ala. These values are in good agreement with the respective data listed in Table 3. In Table 3, though the solvent concentration is indicated in the molal concentration, the viscosity coefficients were calculated in molar concentration units, as has been mentioned above. The *B*-coefficients in the mixed solvents are larger than the corresponding values in water, particularly in 2*m* alkali-chloride solutions. However, the *B* values of Thr in 1*m* LiCl and 1*m* NaCl are almost the same as those in water and are rather small in 1*m* KCl. The reason for this is not clear at present. Concerning the effects of the salts on the *B*-coefficient of each amino acid, there seems to exist no regularity. The *D*-coefficients in the mixed solvents have almost the same value as the corresponding values in water.

For a dilute solution of unsolvated spherical colloidal suspensions, Einstein has derived this relation:

$$\eta_r = 1 + 2.5\phi, \tag{11}$$

where ϕ is the volume fraction of the solute.[9] If this equation is valid for the amino acids, Eq. 11 becomes:

$$\eta_r = 1 + 0.0025\, V_h\, c, \tag{12}$$

where V_h is the hydrodynamic volume in $cm^3 mol^{-1}$. Since the Dc^2 term in Eq. 7 can be assumed to be negligible in a dilute solution, the following relation holds:

$$B = 0.0025\, V_h. \tag{13}$$

As has been noted by Desnoyers and Perron, V_h may be assumed to be the partial molal volume of the unsolvated solute particle in a continuum solvent.[5] Thus, if the amino-acid molecule has no interaction with the solvent molecules, the larger *B* value in the mixed solvent might mean a larger hydrodynamic volume in the mixed solvent. However, as has been mentioned above, judging from both the volume and the compressibility data, it must be concluded that, in the mixed solvents, the amino-acid molecules are less hydrated than in water. One possible explanation may be as follows: the hydrated amino-acid molecules interact with the solvent molecules, reducing the structure of water and thus bringing about a dimunution of the *B* value; this effect must be larger in water than in the mixed solvents, for in the mixed solvents the structure of water is already broken to some extent by the cosolvent alkali chloride. Another explanation may be the ion-dipolar pair formation between the amino-acid molecule and the ions. However, since there is no definite relationship among the effects of ions upon the *B* values of the amino acids, it is not possible at present to conclude the reason why the *B* coefficients in the mixed solvents are larger than in water, notwithstanding the less hydration.

Alkali-metal-cation Effects. As may be seen from Tables 1 and 2, for the alkali-metal ions the order of decreasing dehydration effect is:

$$Na^+ > K^+ > Li^+.$$

This sequence is not that of either the increasing or decreasing crystal ionic radii of the alkali metals. The main factor determining the order may be the difference in the interaction of the alkali cations with the amino-acid molecules. Having a rather large dipole moment, the amino-acid molecules should have a rather large interaction with the ions. According to Frank and Wen, a small ion in aqueous solutions is surrounded by three concentric regions.[10] The innermost (Region A) is immobilized; the second (Region B) one is a less ice-like water structure, and the third (Region C) contains normal water. If some hydrated water molecules are lost by the interaction, the electrostric-

tion effect should decrease, and the volume and also the compressibility of the amino acid should increase, in the mixed solvent. Li^+ should have water molecules firmly bounded in Region A because of its small crystal radius. On the other hand, Na^+ and K^+ have larger radii; thus, they should have the water molecules held less firmly than Li^+. If only Na^+ and K^+ ions lose their water molecules in Region A when these three alkali cations interact strongly with the amino acid, this order of increasing effective radius: $Na^+ > K^+ > Li^+$ may result. This accounts for this order of decreasing dehydration effect $Na^+ > K^+ > Li^+$. However, for a further discussion the difference in the hydration number of the alkali cations must be taken into consideration.

References

1) T. Ogawa, M. Yasuda, and K. Mizutani, *Bull. Chem. Soc. Jpn.*, **57**, 662 (1984).
2) T. Ogawa, K. Mizutani, and M. Yasuda, *Nagoya Daigaku Kyoyobu Kiyo* (in Japanese), in press.
3) H. J. V. Tyrrell and M. Kennerley, *J. Chem. Soc., A*, **1968**, 2724.
4) W. Devine and B. M. Lowe, *J. Chem. Soc., A*, **1971**, 2113.
5) J. E. Desnoyers and G. Perron, *J. Solution Chem.*, **1**, 199 (1972).
6) O. Enea and C. Jolicoeur, *J. Phys. Chem.*, **86**, 3870 (1982).
7) F. J. Millero, A. Lo Surdo, and C. Shin, *J. Phys. Chem.*, **82**, 784 (1978).
8) J. G. Mathieson and B. E. Conway, *J. Solution Chem.*, **3**, 781 (1974).
9) A. Einstein, *Ann. Phys. (N. Y.)*, **19**, 289 (1906); **34**, 591 (1911).
10) H. S. Frank and W. Y. Wen, *Disc. Faraday Soc.*, **24**, 133 (1957).

 © 1984 The Chemical Society of Japan Bull. Chem. Soc. Jpn., 57, 2069—2074 (1984)

The Electrical and Structural Features of Vanadium-oxide Films as Formed by the Thermal Decomposition of Vanadium Naphthenate

Yoshiya KERA,* Hisateru IMORI, Shigeharu KIDA, and Katsumi DEGAWA
Department of Applied Chemistry, Faculty of Science and Engineering, Kinki University, Higashiosaka, Osaka 577
(Received January 17, 1984)

Vanadium-oxide thin film, which was amorphous, brownish, and transparent, was prepared more conveniently by improving Sekiya-Matsushita's method by, for instance, decomposing vanadium naphthenate thermally; that is, 10 wt% of a 1-butanol solution of vanadium naphthenate was dropped on slide glass, dried in air, decomposed at 600 °C for 20 min under 0.5 l/min of a N_2 stream which was equilibrated with water at 21.5 °C, and then taken out rapidly into the air for cooling. The VO thin film thus prepared usually showed an abrupt change in electric conductivity from 2×10^{-5} to 1×10^{-4} Ω^{-1} at about 60 °C. The electrical feature was greatly affected by the addition of other metal oxides, such as Na_2O, TiO_2, Cr_2O_3, MoO_3, and ZrO_2. Both the conductivity and the gap tended to decrease in the cases of TiO_2, Cr_2O_3, and MoO_3, and to increase in ZrO_2. On the addition of Na_2O, however, the conductivity increased only at temperatures lower than the transition point; thus, the gap decreased greatly, almost disappearing. It was concluded from these facts that the electrical feature of the vanadium-oxide film must be controlled to a great extent by the addition of some compounds of vanadium oxide with the other metal oxides formed at the grain boundary of the VO_2 amorphous particles. That is, the larger the conductivity of the compound in the boundary layer, the more clearly the intrinsic feature of the VO_2 particles appears, and *vice versa*.

Many vanadium-oxide compounds show a metal insulator or semiconductor transition, accompanied by a small change in the crystal structure.[1] Because big changes in not only the electrical property, but also the magnetic and optical properties, occur at the transition point, many solid-state physicists and chemists have worked on these subjects.[2-9] In order to investigate in detail such solid-state properties, the single crystal[10,11] and the thin film of the compounds have been prepared. With respect to the preparation of those thin films, the methods of the chemical deposition of the compounds from the vapor phase and the oxidation of the metal particles sputtered on substrates have mainly been applied,[12-16] but the procedures seem to be too complicated and it seems to be difficult to obtain a good film constantly. Recently, Sekiya and Matsushita[17] have reported a convenient method for the preparation of a vanadium-oxide thin film with a conductivity gap of one order of magnitude at about 60 °C. We have taken notice of the Sekiya-Matsushita method because the film may be used for studying the catalytic property of vanadium-oxide compounds in connection with their solid-state properties. In the present experiment, the method of preparing the vanadium-oxide thin film (VO thin film) was re-examined in order to make the procedure of Sekiya-Matsushita more convenient; further, the method of preparing VO thin films containing other metal oxides, such as Na_2O, TiO_2, Cr_2O_3, MoO_3, and ZrO_2, was examined. The electrical and structural features of the VO thin films thus prepared were discussed.

Experimental

1) Materials and Procedures. Vanadium naphthenate (containing *ca.* 3 wt% of the vanadium(IV) ion, Harima Kasei Co., Ltd.) was dissolved in 1-butanol to prepare 10 wt% of the solution. A thin film of vanadium oxide (VO thin film) was formed on a Pyrex glass plate by the following procedures. The glass plate was cut in the size of 11×24 mm^2; on both ends there had previously been deposited gold film (7 mm in width) as an electrode in order to keep a good ohmic contact during the conductivity measurements. Three droplets of the vanadium-naphthenate solution were placed on the plate, and it was dried at 20 °C in air for 1 h. The plate was then inserted into a furnace kept at 600 °C for 20 min to decompose the vanadium naphthenate and then rapidly taken out into the air for cooling. A nitrogen gas stream, bubbled in water kept exactly at 21.5 °C, was introduced into the furnace during the decomposition.

Upon the preparation of the VO thin films containing other metal oxides, such as Na_2O, TiO_2, Cr_2O_3, MoO_3, and ZrO_2, these oxides (CH_3ONa in the case of Na_2O) were weighed exactly and were then ground well with 10 wt% of a 1-butanol solution of vanadium naphthenate in an agate mortar in order to dissolve them fully. Then, the solution containing the metal oxides was dropped on the glass plate with the gold electrodes and subsequently decomposed by the procedures used in the case of the pure VO thin film. The concentrations of these metal oxides added to vanadium oxide were changed in the range of 10—60 atom%; (M)/(V).

2) Measurements. The electric conductivity was measured by the usual two-probe method. In the measurements of the conductivity, the temperature was elevated from 20 to 200 °C at the constant speed of 4.5 °C/min by the use of a programable controller, Yokogawa Model PC-182. In order to determine exactly the relationship between the conductivity and the temperature, an automatic-measurement system was constructed; both the potential difference between the ends of the VO thin film and the thermoelectric power generated in the CA-thermocouple attached to the film were amplified simultaneously by means of microvoltmeters, Ookura Denki Model AM-2002, and then introduced, at intervals of 1 °C into a microcomputer, Sharp Model MZ-80K2E, *via* a 12-bit A/D-convertor, Hoowa Sangiyo Model ADL-1224. The X-ray analyses of the thin films were done in the range of $2\theta=4$—60° by setting the glass plate with the VO thin film deposited directly in the sample holder. The diffractometer used was Rigaku Denki Model GF-Rad-γA. Cu $K\alpha$ radiation and nickel filter were used.

Results

1) Preparation Conditions of Vanadium-oxide Thin

Film. The VO thin films were prepared by decomposing the vanadium naphthenate for 10—20 min at 600 °C in a nitrogen stream equilibrated with water kept exactly at 21.5 °C. As a result, the VO thin film, transparent, was found to be formed only by decomposition for 20 min; its conductivity and the conductivity gap at the transition point were similar in extent with those shown in Fig. 1. In the VO thin films formed by decomposition for 10 and 15 min, however, both the conductivity and the gap were quite small. The VO thin films were also prepared by decomposing the vanadium naphthenate in a nitrogen stream equilibrated with water kept at 20—25 °C at 600 °C for 20 min. In the VO thin films formed in the N_2 stream equilibrated with water kept at 21 and 22 °C, an electrical feature similar to that shown in Fig. 1 was found. However, in the films formed in the stream equilibrated with water kept at 20 °C, both the conductivity and the gap became very small, and in those formed at 23—25 °C the transparency disappeared completely. Therefore, it was make clear that the VO thin film, which is transparent and which, further, shows the conductivity change of one order of magnitude accompanied by a phase transition at about 60 °C, could easily be prepared under the following conditions: vanadium-naphthenate film formed by dropping 10 wt% of the 1-butanol solution on a Pyrex glass plate and then by drying should be decomposed at 600 °C for 20 min in a nitrogen stream equilibrated with water kept at exactly at 21.5 °C.

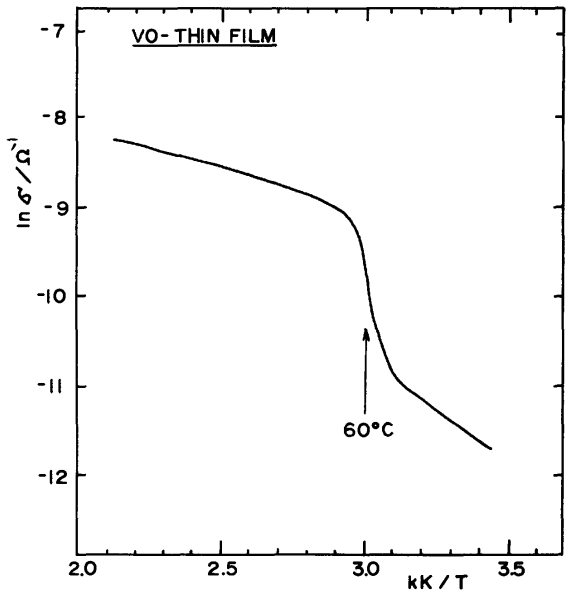

Fig. 1. The electric conductivity-temperature relation for the vanadium oxide thin film prepared by thermal decomposition of vanadium naphthenate solution; The plot of $\ln\sigma$ against $1/T$.

The thickness of the VO thin film thus prepared was evaluated roughly as 1—2 μm from the amounts of the vanadiun-naphthenate solution dropped on the substrate. The activation energies for the conductivity were estimated as 0.08 and 0.21 eV for above and below the transition temperature respectively, as shown in Table 1. Furthermore, the larger the conductivity, the smaller the activation energy tended generally to become, especially at temperatures above the transition point.

2) The Lnσ-1/T Curves of the VO Thin Films Containing Other Metal Oxides. With respect to the VO thin films formed from the vanadium-naphthenate solution, in which 10 and 40 atom% of sodium to vanadium were mixed, the conductivity-temperature curves ($\ln\sigma$-$1/T$) are shown in Figs. 2-a and b respectively. The conductivity of the film at 10 atom% was kept at the same level with that of the pure VO thin film above the transition temperature, but it became much higher than the pure VO film below that temperature. Thus, the conductivity gap at the transition point apparently decreased; further, in the film at 40 atom%, the conductivity gap almost disappeared. With respect to the VO thin films containing TiO_2, at 10 atom%, the $\ln\sigma$-$1/T$ curve was sim-

TABLE 1. THE CONDUCTIVITIES JUST ABOVE AND BELOW THE TRANSITION POINT FOR THE VO-THIN FILM WITHOUT AND WITH OTHER METAL OXIDES MIXED, AND THE ACTIVATION ENERGIES FOR THE ELECTRIC CONDUCTION AT TEMPERATURES HIGHER AND LOWER THAN THE TRANSITION POINT

Sample	$\sigma_h/\times10^{-4}\Omega^{-1}$	$E_a(h)$/eV	$\sigma_l/10^{-4}\Omega^{-1}$	$E_a(l)$/eV
Pure VO-film	1.23	0.08	0.22	0.21
$NaOCH_3$				
10 atom%	1.19	0.05	0.89	0.13
40 atom%	0.84	0.07	0.64	0.15
TiO_2				
10 atom%	1.28	0.09	0.26	0.24
20 atom%	0.42	0.08	0.29	0.20
30 atom%	0.14	0.13	0.12	0.31
Cr_2O_3				
10 atom%	0.32	0.12	0.15	0.23
40 atom%	0.21	0.12	0.17	0.21
MoO_3				
20 atom%	1.15	0.13	0.31	0.15
40 atom%	0.29	0.16	0.13	0.21
ZrO_2				
30 atom%	0.79	0.11	0.21	0.28
60 atom%	3.08	0.03	0.85	0.33

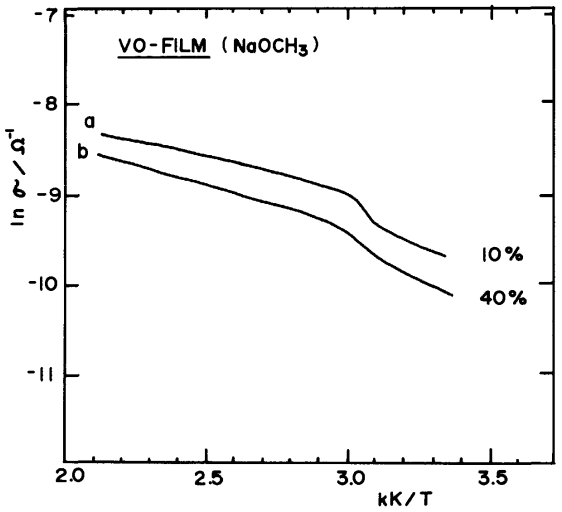

Fig. 2. The $\ln\sigma$-$1/T$ curves for the VO thin films containing 10 and 40 atom% of Na_2O.

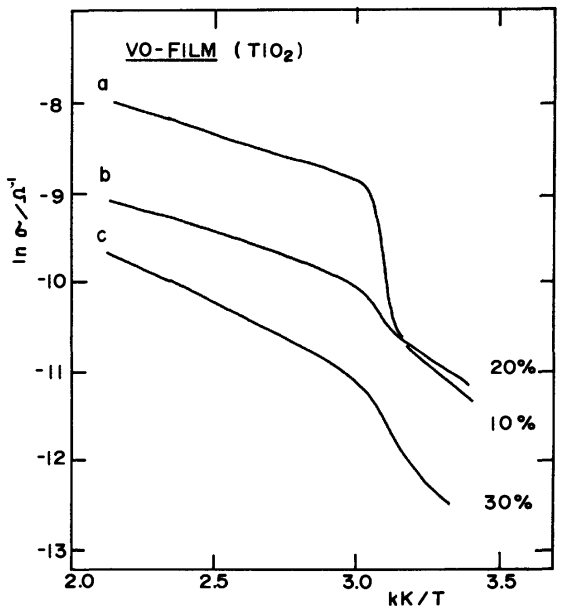

Fig. 3. The $\ln\sigma$-$1/T$ curves for the VO thin films containing 10, 20, and 30 atom% of TiO_2.

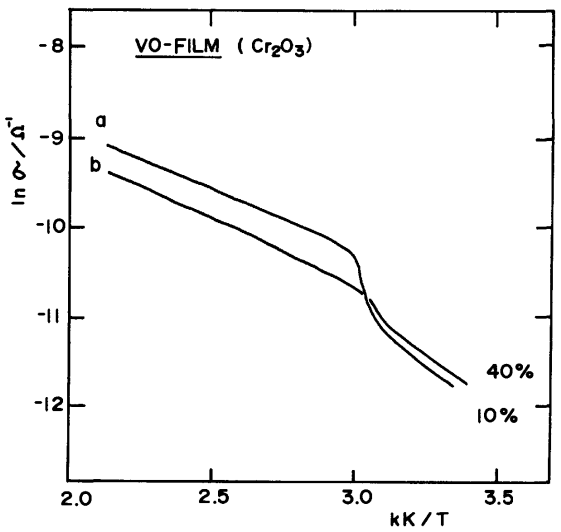

Fig. 4. The $\ln\sigma$-$1/T$ curves for the VO thin films containing 10 and 40 atom% of Cr_2O_3.

ilar to that of the pure VO thin film, as can be seen by comparing Fig. 3-a with Fig. 1, but at 20 atom% the σ-values considerably decreased only above the transition temperature, and thus the conductivity gap almost disappeared, as can be seen in Fig. 3-b. At 30 atom%, however, the conductivity decreased throughout the temperature region, as is shown in Fig. 3-c. With the VO thin films containing Cr_2O_3, both the conductivity and the gap considerably decreased at 10 atom%, and the gap almost disappeared at 40 atom%, as Fig. 4 shows. With the VO thin films containing MoO_3, the feature of the $\ln\sigma$-$1/T$ curve did not change, even at 20 atom%, but both the conductivity and the gap decreased considerably at 40 atom%,

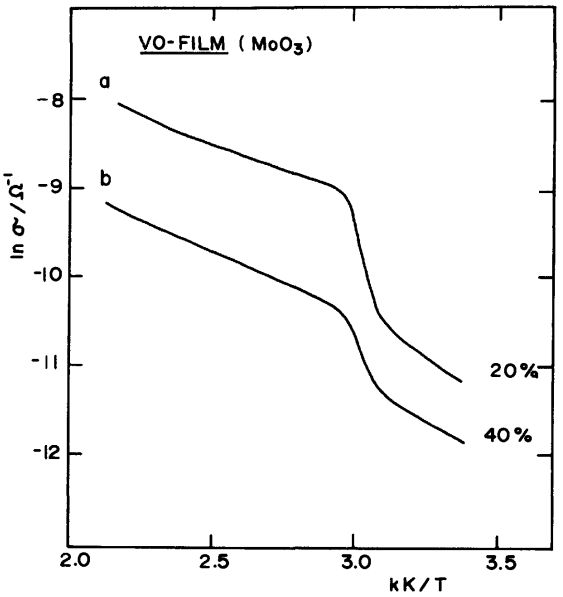

Fig. 5. The $\ln\sigma$-$1/T$ curves for the VO thin films containing 20 and 40 atom% of MoO_3.

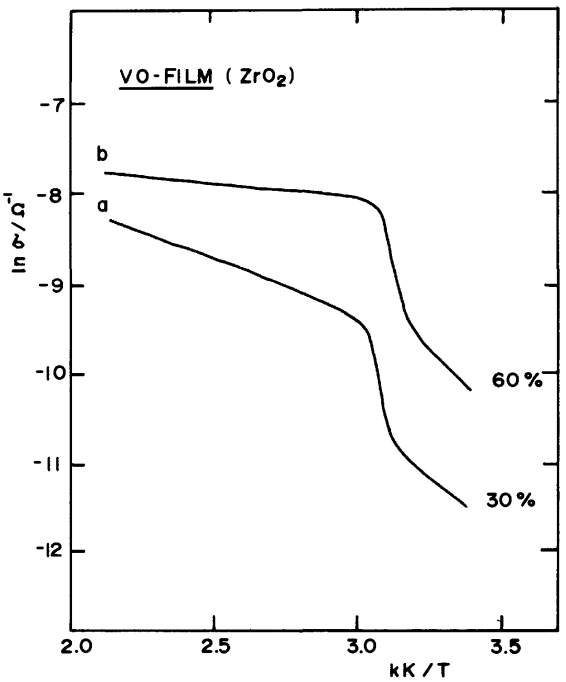

Fig. 6. The $\ln\sigma$-$1/T$ curves for the VO thin films containing 30 and 60 atom% of ZrO_2.

as Fig. 5 shows. With respect to the VO thin film containing ZrO_2, however, the conductivity and the gap tend to increase with an increase in the content of ZrO_2, especially at 60 atom%. Furthermore, it is known form Fig. 6-b and Fig. 1 and in Table 1 that the inclination of the $\ln\sigma$–$1/T$ curve increases greatly above the transition temperature, while it decreases below that temperature.

3) X-Ray Analyses of the VO Thin Films. The X-ray diffraction patterns of the pure VO thin film are shown in Fig. 7-a, where the strong lines at 2θ=38.65 and 44.95° are those caused by the gold electrodes deposited on both ends of the glass plate. Only rather weak peaks are seen at 2θ=12.2, 19.3, 28.0, and 29.2° in Fig. 7-a, except for a very broad unsplit line. These data suggest that the pure VO thin film is composed of very small crystalline particles or amorphous particles. X-Ray diffraction patterns similar to those of the pure VO thin film were also found in all the VO thin films containing TiO_2, Cr_2O_3, and MoO_3 except for the very weak peaks which appeared at angles differing a little from sample to sample, as Figs. 7-b—f show. However, no compounds corresponding to those weak peaks were found in any ASTM card. On the other hand, many sharp peaks were found in the X-ray diffraction patterns for the VO thin film containing ZrO_2, as Fig. 7-f shows; they are summarized in Fig. 8. Thus, it has to be emphasized that, only in ZrO_2 is the VO thin film composed of rather large crystalline particles. However, no compounds corresponding to those peaks were found in the ASTM cards.

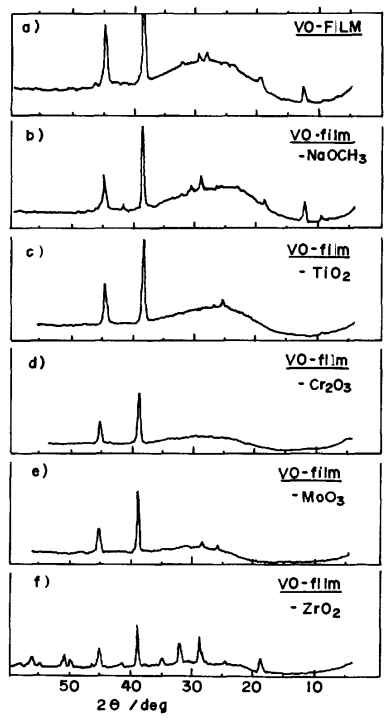

Fig. 7. X-Ray powder diffraction spectra for the vanadium oxide films: a) The pure VO-film, b) the VO-film containing 40 atom% of Na_2O, c) 30 atom% of TiO_2, d) 40 atom% of Cr_2O_3, e) 40 atom% of MoO_3, and f) 60 atom% of ZrO_2.

Discussion

1) Preparation Conditions of the Vanadium-oxide Thin Film. Sekiya and Matsushita successfully prepared a vanadium-oxide thin film by the thermal decomposition of vanadium naphthenate on a slide glass and a quartz plate.[17] The VO thin film showed a crystalline state and a conductivity change of about one order of magnitude at about 60 °C. To obtain a conductivity gap of such an extent, a thermal decomposition procedure must be repeated four times while the temperature is elevated at the speed of 5 °C/min from 25 up to 600 °C. The present paper proposes a more convenient procedure for the preparation of a VO thin film which showed a conductivity and a gap almost identical in extent with those of Sekiya and Matsushita; that is, the vanadium-naphthenate film formed by drying 10 wt% of the 1-butanol solution on a Pyrex glass plate needs to be decomposed thermally only once at 600 °C for 20 min under 0.5 l/min of a nitrogen stream equilibrated with water kept

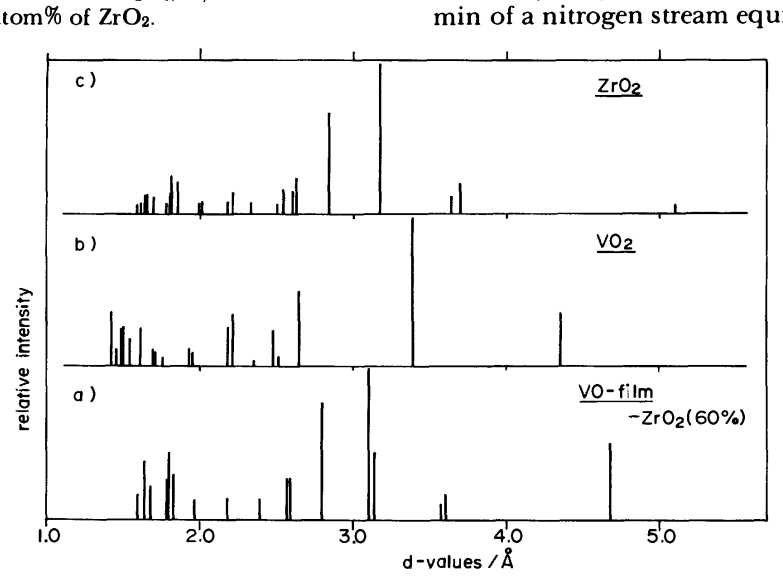

Fig. 8. X-Ray powder diffraction patterns for a) the VO-film, containing 60 atom% of ZrO_2, b) VO_2 crystalline powder,[19] and c) the original ZrO_2 powder.

at 21.5 °C and then to be rapidly taken out into the air. Sekiya and Matsushita suggested that the water vapor contained in the N_2 stream might affect the hydrolysis process of the vanadium naphthenate during the decomposition and might thus be an important factor in the formation of the VO thin film.[17] In the present study, the water vapor was confirmed to play a very important role in the formation process of the VO thin film; that is, under saturated water vapor at 21.0 and 22.0 °C, a favorable conductivity was obtained, but under that at 20.0 °C, both the conductivity and the gap became quite small, and under that at 23—25 °C, the transparency disappeared completely and the color changed to dark blue, as has been mentioned above. These results suggest that, under a rather high vapor pressure, the rates of the decomposition and the growth of the vanadium-oxide particles are accelerated to a great extent, and that thus, the VO_2 particles grown become so large as to block the transmission of visible light, while, on the contrary, under a lower vapor pressure, the decomposition and the growth of the particles cannot occur rapidly, so that both the conductivity and the gap become small.

2) The Conductivity Changes in the VO Thin Films Containing Other Metal Oxides. The VO_2 single crystal showed a metal semiconductor phase transition at 340±2 K (67±2 °C), and the specific conductivity changed abruptly from 10^{-3} to 10^{1} $\Omega^{-1}cm^{-1}$ at the transition point.[1,18] In fact, the inclination of the ln σ–$1/T$ curve changed from a positive to a negative value in the VO_2 single crystal. The conductivities, σ_l and σ_h, which were estimated by extrapolating the ln σ–$1/T$ curves from the temperatures below and above the transition point to the transition temperature in Fig. 1, were 2.2×10^{-5} and 1.2×10^{-4} Ω^{-1} respectively, as Table 1 shows. In the vanadium-oxide film of Sekiya and Matsushita,[17] 6.7×10^{-5} and 1×10^{-3} Ω^{-1} have been obtained as the values corresponding to σ_l and σ_h respectively. The conductivities of the thin films prepared by Sekiya *et al.* and by us at the transition point are very small relative to those of the VO_2 single crystal. Such a large difference in the conductivity is probably caused by the difference in dimensions. The difference might also arise from the difference in the extent of the contribution of the grain boundary to the conductivity; the conductivity is affected by the boundary layer to a much greater extent in the polycrystalline and amorphous films than in the single crystal. The VO thin film of Sekiya *et al.* is probably thicker than the present film because the former has been prepared repeatedly and is composed of rather large crystalline particles, while the present film is composed of amorphous or polycrystalline particles too small to be detected by X-ray diffraction analysis. In fact, both the conductivity and the gap are larger in Sekiya and Matsushita's film rather than in the present one. It can be expected, therefore, that the properties would be affected by those in the boundary layer to a much lesser extent in the former film than in the latter. Based on such an understanding with regard to the the apparent conductivity of the VO thin film, the electrical and structural features of the VO thin films containing the other metal oxides will be discussed below.

The conductivity gap at the transition point almost disappeared in the ln σ–$1/T$ curves of the VO thin films, containing 10 and 40 atom% of Na, as shown in Figs. 2-a and b. These films, brown and transparent, are composed of amorphous particles, as is known from the X-ray diffraction paterns in Fig. 7-b, although several minor peaks are seen in the patterns. By comparing the ln σ–$1/T$ curves of the VO thin film containing Na_2O with that of the pure VO thin film, the conductivity gap can apparently be seen to decrease because the conductivity increases considerably below the transition temperature upon the addition of Na_2O. Such changes may be caused by some sodium vanadium oxides formed in the grain boundary of the vanadiun-oxide particles. Upon the addition of TiO_2, the ln σ–$1/T$ curve was not affected at such rather low contents as 10 atom%, but at a high content, such as 20 or 30 atom%, it decreases as a whole, and also the conductivity gap becomes small, as shown in Figs. 3-a—c and in Table 1. These result might also be caused by the change in the conductivity of the grain boundary, accompanied by the formation of some titanium vanadium oxides. The additions of Cr_2O_3 and MoO_3 similarly affected the ln σ–$1/T$ curves, as shown in Figs. 4-a and b Figs. 5-a and b, and also in Table 1, although the effects seem to be relatively small upon the addition of MoO_3.

On the other hand, the conductivities of the VO thin films containing ZrO_2, especially at 60 atom%, generally increase relative to the pure VO thin film. Furthermore, the conductivity gap becomes large, and the inclination of the ln σ–$1/T$ curve tends to decrease above the transition point, while, on the contrary, it increases below the transition. That is, the activation energies for the electron conduction were estimated from the inclinations as 0.03 eV above the transition and as 0.33 eV below the transition, while the corresponding values for the pure VO thin film were similarly estimated as 0.08 and 0.21 eV respectively, as shown in Table 1. By comparing these corresponding values, therefore, we can make it clear that the activation energies decrease about 1/3 times at higher temperatures, while, on the contrary, they increase about 1.6 times at lower temperatures, upon the addition of ZrO_2. The change in the electrical property is probably connected with the facts that only in the addition of ZrO_2 did the transparency disappear completely, that the color changed dark blue from brown, and, further, that the crystalline part increased considerably relative to the amorphous part, as is shown by the X-ray powder patterns in Fig. 7-f.

3) The Electrical and Structural Features of the VO Thin Films. The X-ray diffraction patterns of the VO thin film containing 60 atom% of Zr are given in Fig. 8-a, while those of the pure VO_2 crystalline powder[19] and of the original ZrO_2 powder are shown in Figs. 8-b and c respectively for the sake of comparison. Since no peaks in Fig. 8-a are consistent with those in Fig. 8-b, the VO thin film containing ZrO_2 may not be composed of VO_2 crystalline particles, but of amorphous particles. On the other hand, the main peaks in Fig. 8-a, for instance, d=3.100, 2.797, 1.800, and 1.791 A, correspond well to those in Fig.

8-c: d=3.165, 2.842, 1.848, and 1.818 A respectively, although the d-values always shift a little relative to one another. Therefore, the diffraction peaks may be ascribed to some ZrO_2 crystallines, dissolving a little of the vanadium oxide, which are growing at the grain boundary. Thus, a large increase in the conductivity gap and a large decrease in the activation energy above the transition temperature can be understood if this Zr-V-O coumpound formed at the boundary layer has a large conductivity relative to the grain boundary of the pure VO thin film. The findings that the conductivities of the VO thin films containing TiO_2, Cr_2O_3, and MoO_3 became apparently smaller than that of the pure VO thin film, could similarly be understood if some compounds of vanadium oxide with the metal oxides were formed in the boundary layer and if, further, their conductivities were quite small. In the addition of Na_2O, the conductivity increased to a great extent below the transition temperature, while it changed almost not at all above the transition point, as has been mentioned above. This would suggest that the conductivities of some compounds of sodium vanadium oxide formed at the boundary layer are quite large.

Only in the addition of ZrO_2, did both the conductivity and the gap increase greatly; that is, the electrical feature of the VO_2 particle itself appeared more clearly, because the compounds of the vanadium oxide with ZrO_2 formed at the boundary showed quite a high conductivity. Upon the addition of Na_2O and ZrO_2, the corresponding compounds formed at the grain boundary of the vanadium-oxide particles showed a high conductivity relative to the boundary of the pure vanadium oxide itself, but the conductivity gap decreased greatly in the former and increased in the latter. Therefore, it can be expected that, upon the addition of Na_2O, almost no pure VO_2 particles are formed, but, rather, some sodium oxide particles are, while, on the contrary, almost all the pure VO_2 particles remain, without mixing with ZrO_2, on the addition of ZrO_2, except the boundary layer.

The authors wish to express their appreciation to Drs. Tadashi Sekiya and Osamu Kondo for their gift of the vanadium naphthenate and to Mr. Hideji Yonekawa for his help in the construction of the automatic measurement system by means of a microcomputer.

References

1) S. Kachi, T. Takada, Y. Bando, K. Kosuge, H. Okinaka, and K. Nagasawa, FELITES: *Proc. Intern. Conf., Japan*, 563 (1970).
2) N. F. Mott, *Proc. Phys. Soc. London, Sec A.*, **62**, 416 (1949); *Rev. Modern Phys.*, **40**, 677 (1968).
3) J. B. Goodenough, *Phys. Rev.*, **117**, 1442 (1960).
4) S. Westman, *Acta Chem. Scand.* **15**, 217 (1961).
5) H. W. Verleur, A. S. Barker, Jr.,and C. N. Berglund, *Phys. Rev.*, **172**, 172 (1968).
6) D. Adler, *Rev. Modern Phys.*, **40**, 714 (1968).
7) D. B. Mcwhan, T. M. Rice, and J. P. Remeika, *Phys. Rev. Lett.*, **23**, 1384 (1969).
8) G. J. Hyland, *J. Solid State Chem.*, **2**, 318 (1970).
9) C. J. Hearn, *J. Phys. C: Solid State Phys.*, **5**, 1317 (1972).
10) H. Takei, *Jpn. J. Appl. Phys.*, **7**, 827 (1968).
11) K. Nagasawa, Y. Bando, and T. Takada, *Bull. Inst. Chem. Res., Kyoto Univ.*, **49**, 322 (1971).
12) E. N. Fuls, D. H. Heusler, and A. R. Ross, *Appl. Phys. Lett.*, **10**, 199 (1967).
13) D. H. Hensler, *J. Appl. Phys.*, **39**, 2354 (1968).
14) J. B. MacChesney, J. F. Potter, and H. J Guggenheim, *J. Electrochem. Soc.*, **115**, 52 (1968).
15) G. A. Rozgonyi and W. J. Polito, *J. Electrochem.*, **115**, 56 (1968).
16) L. A. Ryabova, I. A. Serbinov, and A. S. Darevsky, *J. Electrochem.*, **119**, 427 (1972).
17) T. Sekiya and T. Matsushita, *Yogyo-Kyokaishi* (Japan), **85**, 13 (1977); *Report Gov. Ind. Res. Inst., Nagoya*, **27**, 92 (1978).
18) F. J. Morin, *Bell Syst. Tech. J.*, **37**, 1047 (1958).
19) ASTM-card No. 25-1003; ref. Evans and Morse, *Amer. Mineral.*, **40**, 861 (1955).

 © 1984 The Chemical Society of Japan Bull. Chem. Soc. Jpn., 57, 2075—2081 (1984)

The Three-dimensional Structure of Plasminostreptin, a Bacterial Protein Protease Inhibitor, at 2.8Å Resolution

Nobuo KAMIYA, Masaaki MATSUSHIMA,*,† and Hiromu SUGINO††

Department of Chemistry, Faculty of Science, Nagoya University, Chikusa-ku, Nagoya, Aichi 464

†*Department of Anatomy, Osaka Medical College, Takatsuki, Osaka 569*

††*Central Research Division, Takeda Chemical Industries, Ltd., Jusohonmachi, Yodogawa-ku, Osaka 532*

(Received March 8, 1984)

The three-dimensional structure of plasminostreptin, a bacterial protein protease inhibitor from *Streptomyces antifibrinolyticus*, was determined at 2.8Å resolution by the multiple isomorphous replacement technique. A dimer with the molecular weight of 11,402×2 was included in an asymmetric unit of the crystal. The monomer, composed of 109 amino acid residues, consisted of an antiparallel twisted β-sheet with five strands, two short helices, and irregular polypeptide-chain segments. The reactive site of plasminostreptin belonged to one of these irregular polypeptide-chain segments. The two monomers in the dimer were related by a non-crystallographic pseudo-two-fold axis, and the two β-sheets were arranged face-to-face with each other. The averaged angle between the strands of the two β-sheets was approximately 30° clockwise. In spite of 37 amino acid substitutions including the reactive site residues, the tertiary and quaternary structures of plasminostreptin were similar to those of *Streptomyces* subtilisin inhibitor (SSI). The main-chain conformations of the reactive site of plasminostreptin were similar to those of SSI and other protease inhibitors analysed previously. Moreover, the conformations of the side chain of the evolutionarily conservative asparagine in the so-called "secondary contact region" resembled those found in the inhibitors of the pancreatic secretory trypsin inhibitor family.

Plasminostreptin is a bacterial protein protease inhibitor, isolated from a culture fluid of *Streptomyces antifibrinolyticus* IFO** 13298; it was crystallized by Kakinuma *et al.*[1] It inhibits the proteolytic activities of plasmin, trypsin, and several microbial alkaline proteases (for example, subtilisin) by forming enzyme-inhibitor complexes with the inhibition constants of approximately 10^{-8}M (1M=1 mol dm^{-3}).[1] Two identical monomers are dimerized in a solution. The sequence of 109 amino acid residues comprising the monomer was determined by Sugino *et al.*[2] (Fig. 1), and the molecular weight of the monomer was calculated to be 11,402. The scissile peptide bond of the reactive site was located at Lys69-Gln70.[3] On the basis of the fact that 66% of the amino acid residues, and also the disulfide bonds, are identical with those of *Streptomyces* subtilisin inhibitor (SSI***),[4] plasminostreptin was classified in the SSI family of protein protease inhibitors by Laskowski and Kato.[5] However, the inhibition spectra of plasminostreptin are markedly different from those of SSI.[1,6] Compared with SSI, a total of 37 out of 109 amino acid residues are substituted in plasminostreptin, and Mitsui *et al.*[7] pointed out that some of these residues were inside the SSI molecule. From the preliminary X-ray work for the crystal of plasminostreptin, two monomers were expected in an asymmetric unit. In the case of SSI, however, only one monomer is included in the asymmetric unit. The crystallographic studies of plasminostreptin might reveal the similarities and differences between the structures of plasminostreptin and SSI.

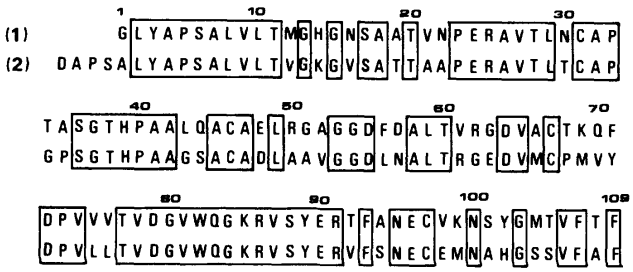

Fig. 1. The amino acid sequences of plasminostreptin[2] and SSI.[4] The residues enclosed by squares are identical between plasminostreptin (1) and SSI (2). To get the sequence number of SSI, four should be added to the number shown here. The scissile peptide bond of plasminostreptin is between Lys69 and Gln70.

The three-dimensional structures of the proteinaceous inhibitors of serine proteases have been studied about the bovine pancreatic trypsin inhibitor [Kunitz] (BPTI),[8] the complex of trypsin with BPTI,[9] and that of trypsin with the soybean trypsin inhibitor [Kunitz] (STI).[10] In addition, the structures of SSI and its complex with subtilisin BPN′ have been determined.[7,11] Recently, three inhibitors of the pancreatic secretory trypsin inhibitor [Kazal] (PSTI) family have also been analysed. These are the third domain of the Japanese quail ovomucoid inhibitor (OMJPQ3),[12] the third domain of the ovomucoid inhibitor from turkey (OMTKY3) complexed with *Streptomyces griseus* protease B,[13] and PSTI complexed with trypsin.[14] In this paper, we wish to report the three-dimensional structure of plasminostreptin at 2.8Å resolution and to compare it with those of SSI and other inhibitors previously analysed.

Experimental

The Crystals of Plasminostreptin. Plasminostreptin was purified by the method of Kakinuma *et al.*[1] The elongated octahedral crystals of plasminostreptin were prepared at 4°C in a solution in the absence of any buffer reagent. The typical dimensions of the crystals were 0.6×1.0×1.2 mm^3. The preliminary X-ray photographs revealed that the crystals belonged to the orthorhombic

††Present address: Department of Biochemistry and Molecular Biology, University of Texas, Houston, Texas 77030, U.S.A.

** Institute for Fermentation, Osaka, Japan.

*** Hereafter, the abbreviations for the proteins will be shown in parentheses on their first appearances.

TABLE 1. THE DATA SETS OF THE CRYSTALS OF PLASMINOSTREPTIN

Crystal	Condition	Resolution	Number of reflections	R_M
Native	Non-buffered	2.0Å	14,964(2σ)	0.040
	Phosphate-buffered	2.8Å	6,102(3σ)	0.024
Heavy-atom	0.5 mM $K_2[PtCl_4]$ for 7 days	2.8Å	6,000(3σ)	0.031
Derivatives	1.0 mM $HgBr_2$(2KBr) for 7 days	2.8Å	5,988(3σ)	0.033
	5.0 mM $K[Au(CN)_2]$ for 7 days	2.8Å	5,542(3σ)	0.023

There are two kinds of native crystals. One of them, non-buffered, was grown by the method of Kakinuma *et al.*[1], while the other, phosphate-buffered, was transferred into the phosphate-buffer solution for the MIR technique. The three heavy-atom derivatives were soaked in phosphate-buffer solutions containing the heavy-atom compounds. The reflections whose intensities were more than the values in parentheses (σ was the standard deviation of the reflection intensity) were taken into account in this analysis. The merging R factor, R_M, is defined as follows: $R_M=\sum||F^+|-|F^-||/\sum||F^+|+|F^-||$, where $|F^+|$ and $|F^-|$ are the amplitudes of a Friedel pair.

TABLE 2. THE HEAVY-ATOM PARAMETERS

Derivative	Atom	Occupancy	x	y	z	B
$K_2[PtCl_4]$	Pt1	32e	0.0204	−0.0145	0.1349	23 Å^2
	Pt2	26	−0.0149	0.2392	0.2540	27
$HgBr_2$	Hg1	26	0.0546	−0.0232	0.1293	31
	Hg2	18	−0.0166	0.2492	0.2690	41
$K[Au(CN)_2]$	Au1	19	−0.0598	0.1606	0.2316	19
	Au2	11	0.0639	0.1493	0.2486	8

The occupancies are converted to the electron unit by using the absolute scale factor, which was calculated through a Wilson plot.[21] (x, y, z) are the fractional coordinates of the atom. The isotropic temperature factors, B, of the Pt and Hg atoms are calculated from the anisotropic temperature factors.

system and that the space group was $P2_12_12_1$. The unit cell dimensions were a=56.88 Å, b=88.87 Å, and c=46.40 Å. Two monomers were expected in an asymmetric unit, which would give the packing density[15] of 2.6 Å^{3}u^{-1}. The crystals were transferred into a phosphate buffer (1.0 M, pH 6.8) for the structure determination by means of the multiple isomorphous replacement (MIR) technique[16] at 2.8 Å resolution. These crystals were regarded as the native crystals. Some of them were soaked in phosphate buffer solutions containing heavy-atom compounds at room temperature. The three heavy-atom derivatives listed in Table 1 were useful in this structure determination.

Data Collection. The X-ray diffraction intensities, including their Friedel pairs, were measured by the use of a computer-controlled four-circle diffractometer, Rigaku AFC-V, set on a rotating anode X-ray generator, Rigaku RU-200. The focus size on the anode was 0.3×3.0 mm^2, and the take-off angle was 6°. The incident X-ray beam was Cu$K\alpha$ radiation monochromatized with a graphite plate, and it was passed through a collimator with the diameter of 0.3 or 0.5 mm. The distance from the crystal to the receiving aperture (3×3 mm^2) was 40 cm. An evacuated beam tunnel was used to avoid X-ray absorption by the air. One of the computer programs for the data collection was modified by Associate Prof. Kyoyu Sasaki of Nagoya University to allow for ordinate analysis.[17] The continuous ω-scan was carried out at a scan speed of 0.04 degree s^{-1} over an angle of 0.72°. The counting time for each reflection was divided into 18 steps. In the ordinate analysis, the extreme three steps on both sides of the scan were regarded as the background, and the remaining twelve steps, as the reflected X-ray peak. In order to monitor the X-ray damage to the crystals, the intensities of four standard reflections were measured every 200 reflection measurements; the damages remained less than 10%. Two crystals were consumed for the data collection of each of the native and heavy-atom derivatives in the MIR technique. Another set of 2.0 Å -resolution data were collected with five original non-buffered crystals and used for the systematic checking of the molecular models.

The Structure Determination. Lorentz-polarization factors, the X-ray-absorption[18] factor, and the damage factor upon X-ray exposure were applied to each of the data sets. The scales between the two or five crystals were calculated using the intensities of the overlapped reflections. The intensity data are summerized in Table 1. After the Kraut scaling,[19] the difference Patterson maps of the derivatives were computed with the coefficients of $(|F_{PH}|-|F_P|)^2$.**** The coordinates of the heavy-atom sites were estimated from these maps. The parameters of these heavy atoms were refined by the phase-refinement procedure[20] (Table 2). The anomalous terms of the heavy atoms contributed only to the inner reflections. The handedness of the heavy-atom parameters were consistent with the calculation of the negative correlation coefficients[22] between the observed and calculated anomalous differences. The refined parameters were used for the calculation of the MIR phases.[23] The averaged figure of merit was 0.61 for the 6,102 reflections. The statistics for the phasing are shown in Table 3.

The MIR electron-density map was calculated at 2.8 Å resolution. The preliminary models of the two independent monomers in an asymmetric unit were built according to the Diamond procedure.[24] The corresponding C$^\alpha$ atoms of each monomer were superposed,[25] and the two monomers could be related by a linear transformation. In order to reduce possible errors in the MIR electron-density map, the electron densities of the two independent monomers were averaged according to the following procedures. (1) Summations of the squared differences between the electron densities at the grid points in one monomer and those at the corresponding points in the other monomer were calculated around the translational vector elements and the angular values estimated from the rotational matrix. (2) Based on the matrix and vector which gave the minimum value of the summation, the MIR electron densities of the two monomers could be averaged. Into this

**** F_{PH} and F_P are structure factors of the heavy-atom derivatives and the native crystal in the MIR technique respectively.

TABLE 3. STATISTICS IN THE MIR PHASING AT 2.8Å RESOLUTION

Crystal	Rc	Rk	Range($4\sin^2\theta/\lambda^2$)	0.016	0.032	0.048	0.064	0.080	0.096	0.112	0.128
Native			$\langle\|F_P\|\rangle$	635	469	516	509	416	328	262	223
			⟨f.o.m.⟩	0.54	0.76	0.70	0.65	0.60	0.59	0.55	0.52
$K_2[PtCl_4]$	0.55	0.109	R_F	0.34	0.20	0.13	0.13	0.13	0.14	0.16	0.16
Derivative			$\langle\|f_H\|\rangle$	80	77	69	62	54	48	44	39
			RMS E	173	66	49	48	43	35	32	30
$HgBr_2$	0.57	0.077	R_F	0.24	0.15	0.09	0.08	0.08	0.09	0.11	0.12
Derivative			$\langle\|f_H\|\rangle$	63	55	47	41	34	30	25	23
			RMS E	86	41	33	31	30	27	24	22
$K[Au(CN)_2]$	0.51	0.087	R_F	0.13	0.09	0.10	0.10	0.10	0.11	0.12	0.15
Derivative			$\langle\|f_H\|\rangle$	48	46	42	36	33	32	30	26
			RMS E	68	34	40	41	34	32	28	30

A total of 6,102 reflection data was divided into eight shells by the range of $4\sin^2\theta/\lambda^2$. The definitions are as follows:
$\langle|F_P|\rangle$; the averaged observed reflection amplitude of the native crystal. ⟨f.o.m⟩; the averaged figure of merit. R_F; $\sum||F_{PH}|-|F_P||/\sum|F_P|$. $\langle|f_H|\rangle$; the averaged calculated structure factor amplitudes of the heavy atoms in the derivative. Rc; $\sum|F_{PH}-F_P|-|f_H||/\sum|F_{PH}-F_P|$ for the centric data. Rk; $\sum||F_{PH}|-|F_P+f_H||/\sum|F_{PH}|$ for all of the reflections whose f.o.m. values are more than 0.85. RMS E; $\{\sum(|F_{PH}|-|F_P+f_H|)^2/n\}^{1/2}$ where n is the number of reflections.

averaged electron-density distribution, a Nicholson model (on a scale of 1 cm/ Å) of one monomer was fitted by using the half-mirror device of Richards.[26] A set of the atomic coordinates was measured on this device. The coordinates for the other monomer in the asymmetric unit were calculated with the linear transformation obtained by the procedure mentioned above. For the systematic checking of the atomic coordinate sets thus obtained, "removed maps"[27] ($|F_o|\exp^{i\alpha c}$) were calculated. The structure factor amplitudes ($|F_o|$) used were the observed 2.0 Å data, and the phases (αc) were those of the structure factors calculated from the atomic-coordinate sets where some atoms were systematically subtracted from the total atoms of the two independent monomers. Some parts of the models were fitted into the electron-density distributions of the "removed maps." The corrected atomic coordinates were refined energetically,[28] and the molecular models were more accurately adjusted to the electron-density distribution according to the Diamond real-space refinement procedure.[29] We believe that the resolution of this structure determination should be regarded as 2.8 Å, since the refinement of the structure with the 2.0 Å resolution data has not yet been completed. Hereafter we will describe the structure of plasminostreptin based on the corrected models.

Results and Discussion

The Monomer Structure. Figure 2 is a schematic illustration of the main chain of the plasminostreptin monomer. The monomer is composed of an antiparallel twisted β-pleated sheet with five strands and two short helices. The five strands of the β-sheet are those of Pro5–Gly15, Arg25–Cys31, Ser36–Thr38, Pro73–Gln83, and Lys85–Phe93. The two helices are defined as the α_1-helix (Ala42–Gly53) and the α_2-helix (Asn95–Gly103), like those of SSI.[7] These helices in the same side of the β-sheet are almost parallel to the sheet and are nearly perpendicular to each other. These secondary structural units are connected by the two disulfide bonds and irregular polypeptide-chain segments. One of the disulfide bonds (Cys31–Cys46) links the α_1-helix to the β-sheet, and the other (Cys67–Cys97) links a part of one of the irregular polypeptide-chain segments to the α_2-helix. The irregular polypeptide-chain segments are in the regions of the N-terminus (Gly1–Ala4), two loops (Asn16–Glu24, Gly54–Asp72), and the C-terminus (Gly103–Phe109). All these regions exist on the surface of the monomer, except for the C-terminal region, which is a part of the hydrophobic core of the monomer. One of the loops (Asn16–Glu24) protrudes from the β-sheet to the interspace between the monomers of the dimer structure (see the following section). The reactive site (Cys67–Phe71) belongs to the other loop (Gly54–Asp72). The site is proximate to the β-sheet and is linked to the α_2-helix by the disulfide bond (Cys67–Cys97). The four residues of Cys31–Thr34 constitute a β-turn, and Pro33 in this turn is in the *cis*-form.[30]

The Dimer Structure. The non-crystallographic relationship between the two monomers in the asymmetric unit is determined by the superposing procedure[25] of the corrected coordinates of the corresponding C^α atoms of each monomer. The rotational matrix and translational vector which relate the two monomers are listed in Table 4. Hereafter, the two monomers will be denoted as the I and II monomers. The centers of gravity calculated from the coordinates of the C^α atoms in angstrom units are (42.2 Å, 25.6 Å, 14.2 Å) and (31.5 Å, 42.4 Å, 25.9 Å) for the I and II monomers respectively. The spherical polar coordinates[31] of the

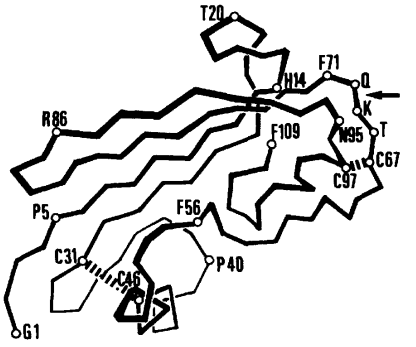

Fig. 2. A schematic drawing of the main chain of the monomer of plasminostreptin. The C^α atoms of 109 amino acid residues are at the creases, and the important positions are identified by open circles together with one letter codes of amino acid residues followed by the sequence number. The arrow represents the scissile peptide bond. The marks (IIIIII) denote the disulfide bonds.

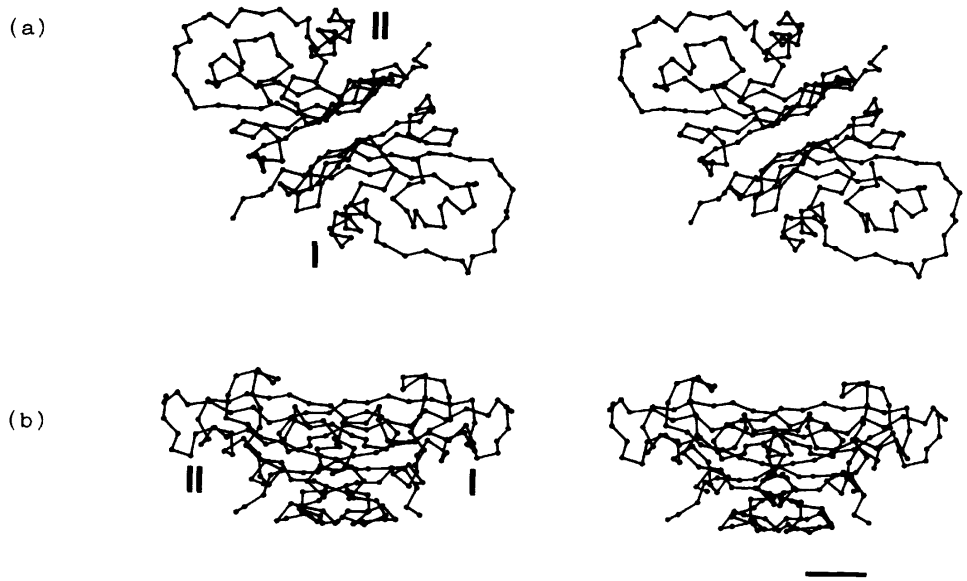

Fig. 3. Stereographic drawings of the plasminostreptin dimer.
The dimer is viewed parallel (a) and perpendicular (b) to the non-crystallographic pseudo-two-fold axis. The models are drawn with the C^{α} atoms. In (a), the lower-right model is the I monomer, and the upper-left is the II monomer. The scale bar in the bottom-right represents 10 Å.

TABLE 4. THE ROTATIONAL MATRIX AND THE TRANSLATIONAL VECTOR OF THE NON-CRYSTALLOGRAPHIC RELATIONSHIP BETWEEN THE I AND II MONOMERS

Rotational matrix			Translational vector
−0.038	−0.133	0.990	22.4
−0.079	−0.988	−0.136	73.0
0.996	−0.083	0.027	−14.4

The atomic coordinates (X, Y, Z) of the II monomer in angstrom units are related to those of the I monomer by this rotational matrix and translational vector: $X = 56.88 \times x$, $Y = 88.87 \times y$, and $Z = 46.40 \times z$, where (x, y, z) are the fractional coordinates.

rotation axis, calculated from the rotational matrix, are 83.7° (from the $-y$-axis of the unit cell in the x-y plane), 44.2° (from the z-axis), and 182.2° (rotational angle around the rotation axis). The root-mean-square (RMS) deviation is 1.4 Å between the superposed C^{α} atoms. Figure 3 shows the stereo-drawings viewed parallel and perpendicular to the rotational axis. It is possible to conclude that the I and II monomers may be related by a pseudo-two-fold symmetry and may form a dimer. The β-sheet of the I monomer is faced to that of the II monomer in the dimer structure. The topology of stacking β-sheets has been studied by several workers.[32-36] Cohen *et al.*[36] have pointed out that the averaged angle between the strands of the two twisted β-sheets (inter-sheet angle) is from 20° to 50° anticlockwise for the fragments of the immunoglobulin, the Bence-Jones protein, human prealbumin, CuZn superoxide dismutase, and Jack-bean concanavalin A, and that the nonpolar side chains are packed in the interspace between the β-sheets. In the dimer structure of plasminostreptin, the inter-sheet angle was about 30° clockwise, as shown in Fig. 3, and the direction of the rotation is opposite from those studied by Cohen *et al.* Figure 4 shows schematically the arrangement of side chains in between the two β-sheets. In the amino

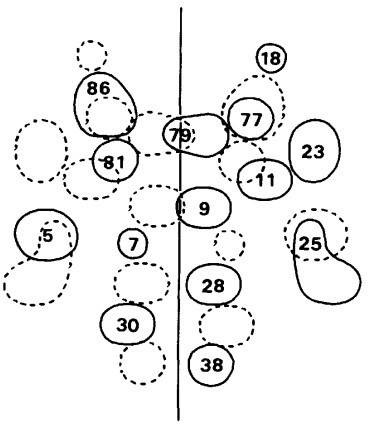

Fig. 4. The arrangement of the side chains between the β-sheets in the dimer. The vertical solid line represents the pseudo-two-fold axis. The side chains which belong to the I monomer are enclosed by the solid lines, and their sequence numbers are given in the circles. The side chains which belong to the II monomer are indicated by the broken circles. The broken circles are related to the solid circles by the pseudo-two-fold symmetry.

acid residues which are in the interspace between the two monomers, the side chains of Pro5, Val9, and Val81 are nonpolar, while those of Asp79 and Arg86 are polar. The side chains of Thr11, Thr28, Asn30, Thr38, and Thr77 are intermediate and can contribute to hydrogen bonds. The Thr11, Thr28, Asn30, Thr38, Thr77, Asp79, and Arg86 of both of the monomers either can be formally charged or can contribute to hydrogen bonds. The side chains of Val9 and Thr28 are close to the pseudo-two-fold axis which related the I and II monomers, and these side chains of the two monomers were in contact with each other. The side chain of Arg86 in one monomer could be expected to interact with the side chains of Thr11, Thr77, and

Asp79 in the other monomer. The side chain of Arg86 would not, however, interact with those of Thr11, Thr77, and Asp79 in an orientation of β-sheets where the inter-sheet angle was 20° to 50° anticlockwise, as in the proteins studied by Cohen *et al.*,[36] but it could interact with them in the orientation of the two monomers of plasminostreptin where the inter-sheet angle was about 30° clockwise.

Comparisons between the Main Chains of Plasminostreptin and SSI. According to the superposing procedure[25] of the corresponding C^{α} atoms, the RMS deviations are 1.4 Å for all the following combinations: the I monomer and the SSI subunit, the II monomer and the SSI subunit, and dimeric plasminostreptin and dimeric SSI. Therefore, the overall structure of plasminostreptin resembles that of SSI not only in the tertiary structure of the monomer, but also in the quaternary structure of the dimer. Compared with the sequence of SSI, a total of 37 out of 109 amino acid residues of plasminostreptin are substituted (see Fig. 1). Eight of these substituted residues are Met12, Val21, Ala52, Phe56, Val75, Val76, Lys99, and Thr108, whose side chains are buried in the monomer. The side chains of the other substituted residues are exposed to the solvent. Mitsui *et al.*[7] expected that the buried side chains could be accommodated in the SSI structure. Their expectations are, in fact, confirmed in the plasminostreptin structure. The residue of Phe56 may be noteworthy in these substitutions, since the total volume of the side chain is considerably larger than that of the corresponding residue, Leu60, of SSI. In the plasminostreptin structure, the benzene moiety of the phenylalanine is packed between the β-sheet and the α_1-helix, and it is nearly parallel to the β-sheet. The torsion angle around the C^{α}–C^{β} bond, χ_1, is similar to that of SSI. This kind of substitution is also found between the structures of the complexes of *Streptomyces griseus* protease A with Ac-Pro-Ala-Pro-Phe-H or -Phe-OH[37] and of *Streptomyces griseus* protease B with OMTKY3.[13] The P_1 residue is substituted from the phenylalanine of the tetrapeptides to the leucine residue in OMTKY3. The side chains are inserted between a β-sheet and a polypeptide chain, and they exist at almost the same position as the specific binding pocket of the enzyme. The substitution only slightly affects the conformations around them. Between the structures of plasminostreptin and SSI, no significant movement of the α_1-helix could be detected. However, the substitution might cause small conformational changes in the side chains around the phenylalanine residue.

Comparisons of the Reactive Site Region with the Inhibitors Already Analysed by X-Ray Crystallography. According to the classification of Laskowski and Kato[5], the six inhibitors which have already been analysed by X-ray crystallography may be classified into four families: the BPTI [Kunitz], STI [Kunitz], PSTI [Kazal], and SSI families. These four families are genetically different, and their main-chain foldings are also different from each other. It is, however, noticeable that the main-chain conformations of the reactive sites (the residues from P3 to P2′[38]) are homologous.[7] Their main-chain torsion angles, phi and psi, are listed in Table 5. The angles of the reactive site of plasminostreptin are similar, in spite of the differences in the amino acid sequences and their inhibitory specificities. These similarities can be expected as examples of convergent evolution.[39] Figure 5 shows the structures around the reactive site regions of plasminostreptin, SSI, and OMJPQ3. The structure of OMJPQ3 can be deemed as representing the inhibitors of the PSTI [Kazal] family, since the three inhibitors, OMJPQ3, OMTKY3, and PSTI, belonging the same inhibitor family turned out to have very similar overall structures.[12–14] The structure around the reactive site of plasminostreptin closely resembles those of SSI and OMJPQ3. (The benzene moiety of Phe71 in plasminostreptin extends to a different direction from those of the phenol moieties of Tyr75 in SSI and Tyr20 in OMJPQ3. This difference may be caused by the crystal packing, because the side chains of Phe71 and Asp72 are in close contact with the residues of Phe71 and Asn16 respectively of a neighboring monomer in the present crystal.) It is interesting to note that an asparagine residue in the secondary contact region[39] is evolutionarily conservative. The residues are Asn95 in plas-

Table 5. The main-chain conformations of the reactive sites of BPTI,[8] STI,[10] SSI,[a] OMJPQ3,[12] and plasminostreptin, and their residues

	P3		P2		P1		P1′		P2′	
	phi	psi	phi	psi	phi	psi	phi	psi	phi	psi
BPTI	−86°	−7°	−89°	165°	−127°	32°	−77°	178°	−134°	88°
STI	−46	−21	−77	136	−89	85	−135	−115	−175	−179
SSI	−123	144	−55	130	−74	76	−103	170	−117	96
OMJPQ3	−121	153	−64	160	−102	18	−61	138	−105	92
Plasminostreptin (tentative)	−120	168	−78	166	−127	29	−78	133	−95	72

BPTI	Pro	Cys	Lys(15)	Ala	Arg
STI	Ser	Tyr	Arg(63)	Ile	Arg
SSI	Cys	Pro	Met(73)	Val	Tyr
OMJPQ3	Cys	Pro	Lys(18)	Val	Tyr
Plasminostreptin	Cys	Thr	Lys(69)	Gln	Phe

The angles of plasminostreptin are those of the I monomer and should be regarded as tentative, since the structure refinement is not yet finished. a) The angles of SSI are those partially refined with the 2.3Å resolution data (R=27%; private communication from Dr. Yukio Mitsui).

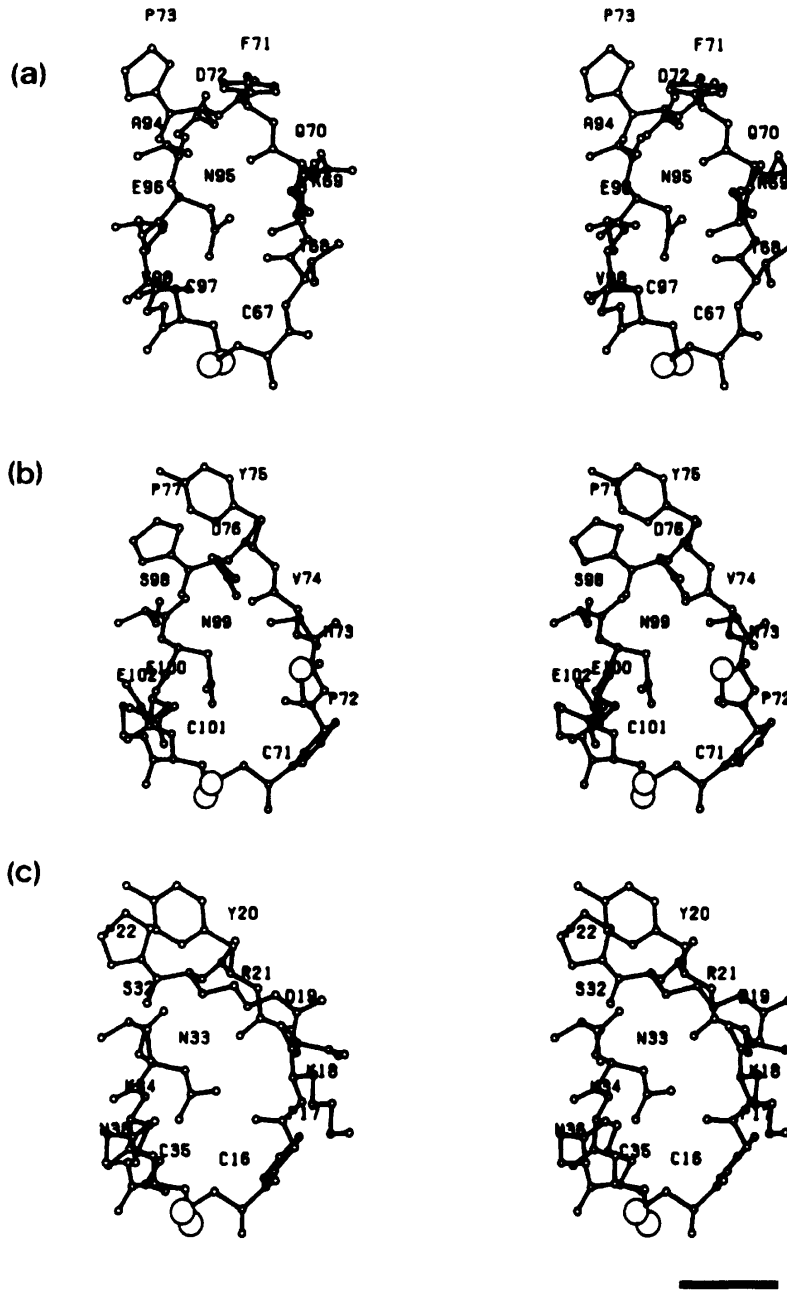

Fig. 5. Similarities of the structures around the reactive sites of plasminostreptin (a), SSI (b), and OMJPQ3 (c).
The reactive site of plasminostreptin is drawn with the coordinate set of the I monomer. The coordinate set of SSI was taken from the Protein Data Bank. The structure of OMJPQ3 is based on the coordinates kindly provided by Prof. Dr. Robert Huber. These structures are viewed from the nearly equivalent direction which was determined by means of the superpositions of the corresponding C^{α} atoms. The large open circles are the sulfur atoms. The residue names are represented by one letter codes followed by the sequence numbers. The scale bar in the bottom-right corner represents 5 Å.

minostreptin, Asn99 in SSI, and Asn33 in OMJPQ3. In all of the three inhibitors of the PSTI [Kazal] family, the side chain of the asparagine residue exists between the reactive site loop and the inner α-helix, connecting them with hydrogen-bonding networks.[12-14] Such a network in the OMJPQ3 structure consists of three hydrogen bonds between the N^{δ} atom of Asn33 and the main-chain carbonyl oxygen atoms of Pro17 and Asp19 in the reactive site, and between the O^{δ} atom of Asn33 and the peptide nitrogen atom of Asn36 in the α-helix.[12] Fujinaga *et al.*[13] considered this network to be essential for the inhibitory mechanism. It resists the formation of the tetrahedral intermediate of the proteolysis at the carbonyl-carbon atom of the scissile peptide bond.

This network has not been found in the SSI structure[7], but it seems likely to exist in the plasminostreptin structure, as shown in Fig. 5. The structure of plasminostreptin is being refined, and the conformations of Asn95 can be defined more precisely after the refinements.

The authors wish to thank Associate Professor Noriyoshi Sakabe, Dr. Kiwako Sakabe, and Associate Professor Kyoyu Sasaki of Nagoya University for their helpful suggestions in studying this structure and their critical advice in the preparation of this manuscript. We are also greatly thankful for the help of Professor Dr. Robert Huber of the Max-Planck-Institut für Biochemie in kindly informing us of the OMJPQ3 and PSTI structures. We also wish to thank Drs. Masao Nishikawa and Atsushi Kakinuma of Takeda Chemical Industries, Ltd., for their support and encouragement throughout this work. One of us (M. M.) is especially grateful to Professor Takashi Kihara of Osaka Medical College for his great encouragement during this study, and one of us (N. K.) is a holder of a scholarship from the Toyoda Physical and Chemical Research Institute. The computations were done at the Nagoya University Computation Center and Computer Center of the Institute for Molecular Science.

References

1) A. Kakinuma, H. Sugino, N. Moriya, and M. Isono, *J. Biol. Chem.*, **253**, 1529 (1978).
2) H. Sugino, A. Kakinuma, and S. Iwanaga, *J. Biol. Chem.*, **253**, 1546 (1978).
3) H. Sugino, S. Nakagawa, and A. Kakinuma, *J. Biol. Chem.*, **253**, 1538 (1978).
4) T. Ikenaka, S. Odani, M. Sakai, Y. Nabeshima, S. Sato, and S. Murao, *J. Biochem.*, **76**, 1191 (1974)
5) M. Laskowski, Jr. and I. Kato, *Annu. Rev. Biochem.*, **49**, 593 (1980).
6) S. Sato and S. Murao, *Agric. Biol. Chem.*, **37**, 1067 (1973).
7) Y. Mitsui, Y. Satow, Y. Watanabe, and Y. Iitaka, *J. Mol. Biol.*, **131**, 697 (1979).
8) J. Deisenhofer and W. Steigemann, *Acta Crystallogr., Sect. B*, **31**, 238 (1975).
9) R. Huber, D. Kukla, W. Bode, P. Schwager, K. Bartels, J. Deisenhofer, and W. Steigemann, *J. Mol. Biol.*, **89**, 73 (1974).
10) R. M. Sweet, H. T. Wright, J. Janin, C. H. Chothia, and D. M. Blow, *Biochemistry*, **13**, 4212 (1974).
11) S. Hirono, K. T. Nakamura, Y. Iitaka, and Y. Mitsui, *J. Mol. Biol.*, **131**, 855 (1979).
12) E. Papamokos, E. Weber, W. Bode, R. Huber, M. W. Empie, I. Kato, and M. Laskowski, Jr., *J. Mol. Biol.*, **158**, 515 (1982).
13) M. Fujinaga, R. J. Read, A. Sielecki, W. Ardelt, M. Laskowski, Jr., and M. N. G. James, *Proc. Natl. Acad. Sci. U. S. A.*, **79**, 4868 (1982).
14) M. Bolognesi, G. Gatti, E. Menegatti, M. Guarneri, M. Marquart, E. Papamokos, and R. Huber, *J. Mol. Biol.*, **162**, 839 (1982).
15) B. W. Matthews, *J. Mol. Biol.*, **33**, 491 (1968).
16) D. Harker, *Acta Crystallogr.*, **9**, 1 (1956).
17) I. J. Tickel, *Acta Crystallogr., Sect. B* **31**, 329 (1975).
18) A. C. T. North, D. C. Phillips, and F. S. Mathews, *Acta Crystallogr., Sect. A*, **24**, 351 (1968).
19) J. Kraut, L. C. Sieker, D. F. High, and S. T. Freer, *Proc. Natl. Acad. Sci. U. S. A.*, **48**, 1417 (1962).
20) H. Müirhead, J. M. Cox, L. Mazzarella, and M. F. Perutz, *J. Mol. Biol.*, **28**, 117 (1967).
21) A. J. C. Wilson, *Acta Crystallogr.*, **2**, 318 (1949)
22) P. M. Colman, J. N. Jasonius, and B. W. Matthews, *J. Mol. Biol.*,**70**, 710 (1972).
23) D. M. Blow and F. H. C. Crick, *Acta Crystallogr.*, **12**, 794 (1956).
24) R. Diamond, *Acta Crystallogr.*, **21**, 253 (1966).
25) K. Nishikawa and T. Ooi, "Program System for Protein Conformation Study II," Report of PSPCS Group for a Grant-in-Aid for Scientific Reseach from Ministry of Education (1978), p. 49.
26) F. M. Richards, *J. Mol. Biol.*, **37**, 225 (1968).
27) M. Vijayan, "Computing in Crystallography," ed by R. Diamond, S. Ramaseshan, and K. Vankatesan, Bangalore, Indian Academy of Sciences for the International Union of Crystallography (1980), 19.01—19.26.
28) M. Levitt, *J. Mol. Biol.*, **82**, 393 (1974).
29) R. Diamond, *Acta Crystallogr., Sect. A*, **27**, 436 (1971).
30) P. N. Lewis, F. A. Momany, and H. A. Scheraga, *Biochem. Biophys. Acta*, **303**, 211 (1973).
31) N. Tanaka, *Acta Crystallogr., Sect. A*, **33**, 191 (1977).
32) M. Levitt and C. Chothia, *Nature (London)*, **261**, 552 (1976).
33) M. J. E. Sternberg and J. M. Thornton, *J. Mol. Biol.*, **110**, 285 (1977).
34) J. S. Richardson, *Nature (London)*, **268**, 495 (1977).
35) C. Chothia, M. Levitt, and D. Richardson, *Proc. Natl. Acad. Sci. U. S. A.*, **74**, 4130 (1977).
36) F. E. Cohen, M. J. E. Sternberg, and W. R. Taylar, *J. Mol. Biol.*, **148**, 253 (1981).
37) M. N. G. James, A. R. Sielecki, G. D. Brayer, L. T. J. Delbaere, and C. A. Bauer, *J. Mol. Biol.*, **144**, 43 (1980).
38) I. Schechter and A. Berger, *Biochem. Biophys. Res. Commun.*, **27**, 157 (1967).
39) Y. Mitsui, Y. Satow, Y. Watanabe, S. Hirono and Y. Iitaka, *Nature (London)*, **277**, 447 (1979).

The Oxidation of Iron(II) Sulfate with Sulfur Dioxide and Oxygen Mixtures

Tsugio SATO,* Takashi GOTO, Taijiro OKABE, and Frank LAWSON†
Department of Applied Chemistry, Faculty of Engineering, Tohoku University, Sendai 980
†*Department of Chemical Engineering, Monash University, Clayton, Victoria 3168, Australia*
(Received August 25, 1983)

The oxidation of iron(II) sulfate with SO_2/O_2 (sulfur dioxide and oxygen mixtures) was carried out using an air-lift percolator in the temperature range of 25—50 °C and over the pH range of 0—3. Under conditions in which sulfur dioxide is immediately oxidized, the rate of the oxidation of iron(II) is proportional to the flow rate of sulfur dioxide and independent of the flow rate and partial pressure of oxygen, and the concentration of iron(II). The molar ratio of Fe^{2+} oxidized/SO_2 oxidized is 1.3—2 in the pH range of 0.5—2.0. A free-radical chain reaction in which HSO_5^- oxidizes iron(II) is proposed as the reaction mechanism.

Although the oxidation of iron(II) with oxygen according to Eq. (1):

$$Fe^{2+} + 1/4\,O_2 + 1/2\,H_2O \longrightarrow Fe^{3+} + OH^-, \quad (1)$$

is thermodynamically possible, practical rates of oxidation are so slow in acidic solutions that the oxidation is frequently performed with the aid of manganese dioxide, hydrogen peroxide, pressurized oxygen, iron-oxidizing bacteria, *etc.* Recently, it was reported that, although sulfur dioxide by itself reduces iron(III) to iron(II), a mixture of sulfur dioxide with oxygen oxidizes iron(II) to iron(III).[1,2] It was suggested that this reaction might be used for the separation of iron from a zinc-containing solution,[1] the selective recovery of zinc and copper from iron-containing lead slags,[3] and the leaching of metal-sulfide concentrates.[2] However, no systematic study of this reaction has yet been made, and the details are not clear. In the present study, a series of tests was carried out to investigate specifically the oxidation behavior of iron(II) with SO_2/O_2 in acidic solutions.

Experimental

Materials. All the chemicals were of an analytical reagent grade and were used without further purification.

Apparatus and Procedure. The apparatus used for the oxidation study is shown diagramatically in Fig. 1. In each test, 400 cm^3 of redistilled water was transferred to a Pyrex-glass air-lift percolator (50 $mm^{\phi} \times 650\,mm^{H}$) fitted with an unglazed pottery gas-ditributor plate. After the removal of the dissolved oxygen by passing nitrogen gas through for 20 min, a known quantity of iron(II) sulfate, sodium perchlorate, and 10 mol/dm^3 perchloric acid were added to adjust the concentration of iron(II), the ionic strength, and the pH, and then SO_2/O_2 was introduced to start the reaction. The pH of the solution was maintained at a preselected value by the addition of a 0.5 mol/dm^3 sodium hydroxide solution by means of a peristaltic pump; the temperature was maintained at a set temperature ± 0.5 °C by circulating temperature-controlled water through the jacket.

Unless otherwise stated, the general experimental conditions used were: temperature, 25 °C; pH, 1.7; ionic strength, 1.0 mol/dm^3; flow rate of oxygen, 200 cm^3/min; flow rate of sulfur dioxide, 5 cm^3/min; initial iron(II) concentration, 0.08 mol/dm^3.

Analysis. The concentration of iron(II) was determined by the modified 1,10-phenanthroline method proposed previously.[4] The concentration of sulfurous acid was determined iodimetrically after the addition of an acidified sodium cyclo-hexaphosphate solution to mask the iron(II) and iron(III), while the sulfate and dithionate concentrations were estimated gravimetrically as barium sulfate. The concentration of sulfur dioxide in the outlet gas was determined by the back-titration of the excess iodine with a sodium thiosulfate solution after the absorption of the sulfur dioxide in the iodine solution for 15 min.

Results and Discussion

Oxidation of Iron(II) with Oxygen. Experiments were conducted at two different temperatures, 25 and 50 °C, in the presence of 0.02 mol/dm^3 of different foreign substrates. The results of these tests are shown in Fig. 2. The oxidation of iron(II) with oxygen at both temperatures was very slow. However, in the presence of ethylenediaminetetraacetic acid (EDTA=H_4edta) and sodium triphosphate, the oxidation proceeded rapidly until the amount of resulting iron(III) reached about 0.02 mol/dm^3, the rates then fell, and the reaction stopped essentially. Copper(II) sulfate, known as a catalyst for iron(II) oxidation with oxygen,[5,6] increased the reaction rate, but the catalytic effect was substantially less than that seen with the complex-forming species, EDTA and triphosphate. On the other hand, the addition of catechol ($C_6H_4(OH)_2$) show-

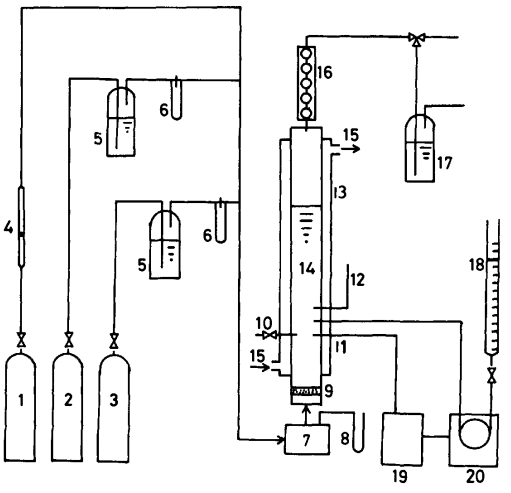

Fig. 1. Schematic diagram of the equipment used.
1. Sulfur dioxide cylinder, 2. Oxygen cylinder, 3. Nitrogen cylinder, 4. Flow meter, 5. Presaturater (H_2O), 6. Orifice, 7. Gas chamber, 8. Manometer, 9. Unglazed pottery plate, 10. Sample tap, 11. pH electrode, 12. Thermometer, 13. Water jacket, 14. Reaction solution, 15. Constant temperature water, 16. Condenser, 17. Iodine solution, 18. Sodium hydroxide solution, 19. pH controller, 20. Peristaltic pump.

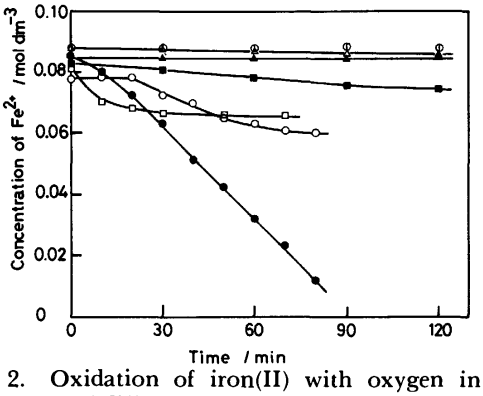

Fig. 2. Oxidation of iron(II) with oxygen in the presence of different foreign substrates.
■: 0.02 mol/dm^3 $CuSO_4$, ○: 0.02 mol/dm^3 $Na_5P_3O_{10}$, □: 0.02 mol/dm^3 EDTA-2Na, Φ: 0.02 mol/dm^3 $C_6H_4(OH)_2$, ●: SO_2 was introduced at a rate of 5 cm^3-NTP/min, △ ▲: None, Temperature (°C)---- ○, ●, □, ▲, Φ: 25, ■, △: 50.

ed no effect. These results indicated that the increase in the oxidation rate with EDTA and triphosphate was probably due to the reduction in redox potentials. The redox potentials of the metal ion and metal-complex ion couples are related through Eq. (2):

$$E^\circ_{ML} = E^\circ_M + \frac{RT}{nF} \ln \frac{K_{M(R)L}}{K_{M(O)L}}, \quad (2)$$

where E°_M and E°_{ML} are the standard redox potentials of metal aquaions and metal-complex ions, and where $K_{M(R)L}$ and $K_{M(O)L}$ are the stability constants of the reduced form and the oxidized form of metal-complex ions respectively. If $K_{M(O)L}$ is larger than $K_{M(R)L}$, E°_{ML} is smaller than E°_M, and the metal-complex ion is thermodynamically less stable than the aquaion under oxidizing conditions. Such an effect was in accord with the test results. When iron was complexed with EDTA and triphosphate ligands with large values of $K_{M(O)L}$, the oxidation rate of iron(II) was increased, whereas the rate was not affected in the presence of catechol, which has a smaller value. The fall-off in the reaction rate observed in the presence of EDTA and triphosphate (Fig. 2) seemed to be due to the consumption of the complex-forming species:[7]

$$Fe^{3+} + edta^{4-} = Fe(edta)^-, \quad (3)$$

$$Fe^{3+} + H_2P_3O_{10}^{3-} = FeH_2P_3O_{10}, \quad (4)$$

$$Fe^{3+} + H_3P_3O_{10}^{2-} = FeH_3P_3O_{10}^+. \quad (5)$$

When sulfur dioxide was introduced together with oxygen, iron(II) was rapidly oxidized at a constant rate. In addition, more than 99% of the sulfur dioxide introduced was converted in the solution to be oxidized to sulfate. The yield of dithionate was less than 1%, so that the reaction of iron(III) and hydrogen sulfite shown as Eq. (6)[8-10] was not significant under the reaction conditions used.

$$2Fe^{3+} + 2HSO_3^- \longrightarrow 2Fe^{2+} + S_2O_6^{2-} + 2H^+, \quad (6)$$

Therefore, the reactions occurring in the presence of SO_2 may be represented by Eqs. (1), (7), and (8):

$$SO_2 + H_2O = HSO_3^- + H^+, \quad (7)$$

$$HSO_3^- + 1/2\,O_2 \longrightarrow SO_4^{2-} + H^+. \quad (8)$$

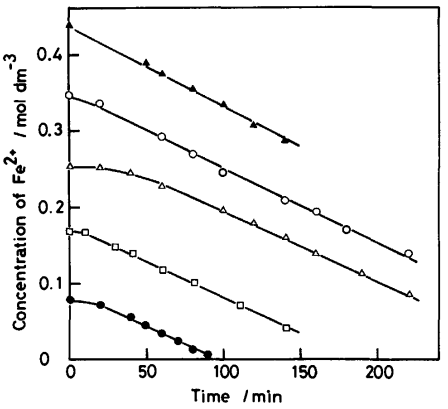

Fig. 3. Oxidation of different concentration of iron(II) with SO_2/O_2 at 50°C.
Solution pH: 0.9.

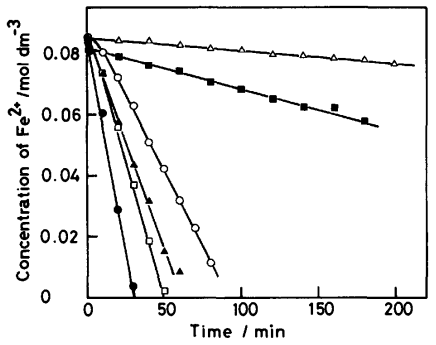

Fig. 4. Oxidation of iron(II) with SO_2/O_2 at different flow rate of sulfur dioxide.
Flow rate of sulfur dioxide (cm^3-NTP/min)----△: 0.39, ■: 0.77, ○: 5.0, ▲: 10, □: 15, ●: 20.

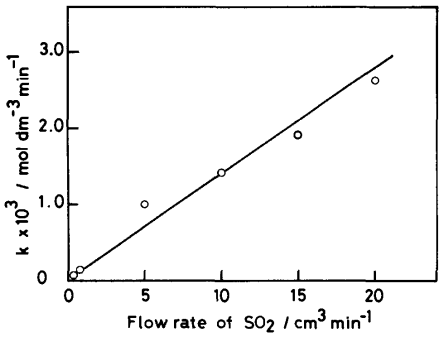

Fig. 5. Rate of oxidation as a function of sulfur dioxide flow rate.

Oxidation of Different Concentrations of Iron(II) with SO_2/O_2. A series of experiments was conducted in which the initial concentration of iron(II) was varied from 0.08 to 0.44 mol/dm^3. As is shown in Fig. 3, the plots of the concentration of iron(II) *versus* the time were all linear, with the same gradient. The reaction rate, therefore, was zeroth-order with respect to the iron(II) concentration. The lag period found in all experiments seems to be attributable to the time necessary for the sulfur dioxide to get to the solution from the cylinder rather than to some induction period.

In addition, a constant rate of oxidation was found even when the oxygen-flow rate and the partial pressure were varied over the ranges of 100—300 cm^3-NTP/min and 0.14—0.98 atm respectively. The mass transfer of oxygen, therefore, does not control the reaction under these experimental conditions.

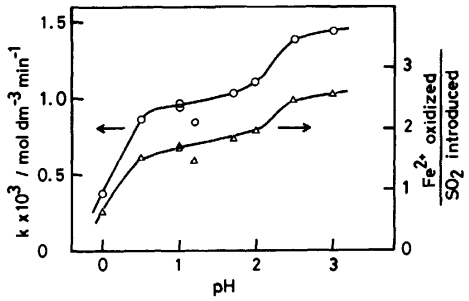

Fig. 6. Oxidation of iron(II) with SO_2/O_2 at different solution pH.

Oxidation of Iron(II) with SO_2/O_2 at Different Flow Rates of SO_2. The effect of changes in the flow rate of sulfur dioxide on the rate of oxidation of iron(II) is shown in Figs. 4 and 5. It is significant to note that the rate of oxidation increased linearly with the flow rate of sulfur dioxide over the range of 0.38—20 cm^3-NTP/min. The average value of the molar ratio of Fe^{2+} oxidized/SO_2 oxidized, calculated from the slope of the straight line shown in Fig. 5, is 1.3.

Oxidation of Iron(II) with SO_2/O_2 at Different Solution pHs. A series of oxidation experiments was carried out in which the solution pH was varied from 0 to 3.0. The results, shown in Fig. 6, indicated that there was no significant pH effect in the pH range of 0.5—2.0 with values of 1.3—2.0 for the molar ratio of Fe^{2+} oxidized/SO_2 introduced. However, the oxidation rate decreased dramatically below pH 0.5 and increased appreciably above pH 2.5. Since a significant amount of SO_2 was detected in the outlet gas at low-pH experiments, the reduction in the rate at low pHs may be due to the decreases in the solubility of sulfur dioxide[11] and in the oxidation rate of sulfurous acid with oxygen.[12,13] On the other hand, the rate increase at higher pHs seems to be attributable to the reduction of the oxidation potential of iron by the formation of a complex between iron and the hydroxide ions, as shown in Eqs. (9)—(14):[14]

$$Fe^{2+} + OH^- = FeOH^+, \quad (9)$$

$$Fe^{2+} + 2OH^- = Fe(OH)_2, \quad (10)$$

$$Fe^{3+} + OH^- \overset{K_I}{=} FeOH^{2+} \qquad pK_I = 11.1, \quad (11)$$

$$Fe^{3+} + 2OH^- \overset{K_{II}}{=} Fe(OH)_2^+ \qquad pK_{II} = 21.69, \quad (12)$$

$$2Fe^{3+} + 2OH^- \overset{K_d}{=} Fe_2(OH)_2^{4+} \qquad pK_d = 25.10, \quad (13)$$

$$Fe^{3+} + 3OH^- \overset{K_{sp}}{=} Fe(OH)_3 \qquad pK_{sp} = 37.20, \quad (14)$$

It has been reported that the reactive species of iron(II) with oxygen is Fe^{2+} in an acidic solution but $FeOH^+$ above a pH of about 3.[15] Further, the main iron(III) species above pH 2.5 is insoluble $Fe(OH)_3$; under these conditions, iron(II) becomes more easily oxidized.[15] Therefore, the direct oxidation of iron(II) with oxygen also proceeds at high pHs.

Oxidation of Iron(II) with SO_2/O_2 in the Presence of Different Foreign Substrates. A series of experiments was conducted in which different foreign substrates were added. Specifically, EDTA, sodium triphosphate, copper(II) sulfate, and catechol were used as these materials, all were known as accelrators or inhibitors for the oxidation of iron(II) and sulfite with oxygen, as shown in Table 1. Since the same reaction behavior was observed when the concentration of additives were changed from 0.01 to 0.03 mol/dm^3, the results of the tests using 0.02 mol/dm^3 of additives are given in Figs. 7 and 8. There was no noticeable influence on the reaction rate with the addition of copper(II) sulfate. In the presence of catechol, the oxidation did not proceed at all. On the other hand, EDTA and sodium triphosphate showed a limited inhibition; that is, the inhibition continued until the amount of iron(III) formed rose to about 0.02 mol/dm^3, but thereafter the rate was constant. When those results are compared with those shown in Fig. 2, it can be said that, while inhibition persists, the rates of oxidation in the presence of EDTA and triphosphate were

TABLE 1. CHARACTERIZATION OF ADDITIVES

Reaction	Acceleration	Inhibition
Oxidation of Fe^{2+} with O_2	EDTA $Na_3P_3O_{10}$ $CuSO_4$	$C_6H_4(OH)_2$
Oxidation of HSO_3^- with O_2	$CuSO_4$	EDTA $Na_5P_3O_{10}$ $C_6H_4(OH)_2$

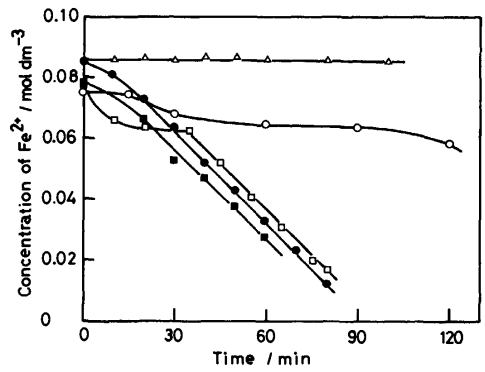

Fig. 7. Oxidation of iron(II) with SO_2/O_2 in the presence of different foreign substrates.
△: 0.02 mol/dm^3 $C_6H_4(OH)_2$, ■: 0.02 mol/dm^3 $CuSO_4$, ○: 0.02 mol/dm^3 $Na_5P_3O_{10}$, □: 0.02 mol/dm^3 EDTA-2Na, ●: None.

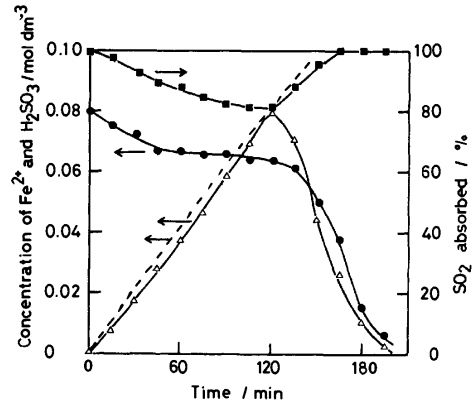

Fig. 8. Oxidation of iron(II) with SO_2/O_2 in the presence of 0.02 mol/dm^3 $Na_5P_3O_{10}$.
●: Fe^{2+}, △: H_2SO_3 found, ----: SO_2 absorbed (Calculated using analytical results of sulfur dioxide concentration in outlet gas).

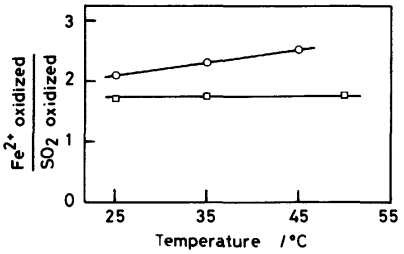

Fig. 9. Effect of temperature on the oxidation of iron(II) with SO_2/O_2.
□: pH 1.0, ○: pH 2.0.

almost the same as those found when oxygen alone was used with those compounds. It is of interest to note that the oxidation of sulfite did not proceed during this inhibition period, but that afterwards sulfurous acid and iron(II) both were rapidly oxidized (Fig. 8). It is considered, therefore, that complex-forming species, such as EDTA, triphosphate, and catechol, inhibit the oxidation of sulfurous acid with oxygen by masking iron(III), which acts as an oxidation catalyst. Such a process is known to inhibit sulfite oxidation.[16] It is also considered that some reactive intermediate produced in the reaction of sulfurous acid and oxygen plays a significant role in the oxidation of iron(II) to iron(III). The anions of HSO_5^-[17] and SO_5^{2-}[18] have, in fact, been postulated as intermediates in the oxidation of sulfite with oxygen, and SO_5^{2-} is known to be a strong oxidant in alkaline media.[19]

Oxidation of Iron(II) with SO_2/O_2 at Various Temperatures. The effect on the oxidation of the temperature over the 25—50 °C range at two different pHs, pH 1.0 and pH 2.0, is shown in Fig. 9. The Fe^{2+} oxidized/SO_2 oxidized molar ratio increased slightly with the increase in the temperature at pH 2.0, but there was no appreciable temperature effect at pH 1.0. The results obtained at pH 1.0 are not inconsistent with the idea that iron(II) is oxidized by an intermediate produced in the oxidation of sulfurous acid with oxygen. On the other hand, the results obtained at pH 2.0 showed that the direct oxidation of iron(II) with oxygen also occurred at higher temperatures.

General Discussion

The experimental results presented above have shown that; (a) the rate of the oxidation of iron(II) with SO_2/O_2 mixtures is independent of the concentrations of oxygen and iron(II), but is directly proportional to the amount of sulfurous acid oxidized; (b) the effects of changes in the pH and the temperature on the reaction rate are not significant; (c) the value of the Fe^{2+} oxidized/SO_2 oxidized molar ratio is 1.3—2.0; (d) some reactive intermediate produced in the reaction of sulfurous acid and oxygen plays a significant role in the oxidation of iron(II), and (e) the reaction between iron(III) and hydrogen sulfite does not occur under the reaction conditions used.

There have been many studies of the oxidation of sulfite with oxygen, and the free-radical-chain reactions shown by Eq. (A), proposed by Bäckstrom,[18] are the accepted oxidation mechanism for diluted sulfite solutions in the neutral and alkaline regions:

$$\left.\begin{aligned} &SO_3^{2-} + Cu^{2+} \longrightarrow \cdot SO_3^- + Cu^+,\\ &\cdot SO_3^- + O_2 \longrightarrow \cdot SO_5^-,\\ &\cdot SO_5^- + SO_3^{2-} \longrightarrow \cdot SO_3^- + SO_5^{2-},\\ &SO_5^{2-} + SO_3^{2-} \longrightarrow 2SO_4^{2-} + O_2,\\ &2\cdot SO_5^- \longrightarrow 2SO_4^{2-} + O_2. \end{aligned}\right\} \quad (A)$$

On the other hand, Schroeter has postulated the anion of HSO_5^- as an intermediate in the oxidation of a sulfite solution.[16] Since the tetravalent sulfur exists as $SO_2 \cdot H_2O$ and HSO_3^- below pH 4.5,[15] the postulation of HSO_5^- as an oxidation intermediate seems reasonable. Therefore, the following mechanism containing free-radical-chain reactions similar to that proposed for sulfite oxidation by Bäckstrom[18] was considered to be in reasonable agreement with the reaction results:

Equilibria:

$$SO_2 + H_2O \overset{K_1}{=} HSO_3^- + H^+, \quad (7)$$

$$Fe^{2+} + HSO_3^- \overset{K_2}{=} FeHSO_3^+, \quad (15)$$

$$Fe^{3+} + HSO_3^- \overset{K_3}{=} FeSO_3^+ + H^+. \quad (16)$$

Initiation:

$$FeHSO_3^+ + 1/4\, O_2 \xrightarrow{k_1} FeSO_3^+ + 1/2\, H_2O, \quad (17)$$

$$FeSO_3^+ \xrightarrow{k_2} \cdot SO_3^- + Fe^{2+}. \quad (18)$$

Propagation:

$$\cdot SO_3^- + O_2 \xrightarrow{k_3} \cdot SO_5^-, \quad (19)$$

$$\cdot SO_5^- + HSO_3^- \xrightarrow{k_4} HSO_5^- + \cdot SO_3^-. \quad (20)$$

Termination:

$$HSO_5^- + HSO_3^- \xrightarrow{k_5} 2SO_4^{2-} + 2H^+, \quad (21)$$

$$HSO_5^- + 2Fe^{2+} + H^+ \xrightarrow{k_6} SO_4^{2-} + 2Fe^{3+} + H_2O, \quad (22)$$

$$\cdot SO_5^- + \cdot SO_5^- \xrightarrow{\text{slow}} 2SO_4^{2-} + O_2. \quad (23)$$

The derived Fe^{2+} oxidized/SO_2 oxidized molar ratio based on this postulated mechanism is:

$$\frac{d[Fe^{3+}]/dt}{d[SO_4^{2-}]/dt} = \frac{2k_6[Fe^{2+}]^2[H^+]}{2k_5[HSO_3^-] + k_6[Fe^{2+}]^2[H^+]}$$

which would approach 2, since $2k_5[HSO_3^-]$ should be very small; this value is in agreement with the experimentally determined values of between 1.3—2.0 at pH 0.5—2.0. The assumption of a small value for $2k_5[HSO_3^-]$ seems reasonable because the sulfur dioxide introduced into the solution is immediately oxidized under the experimental conditions used. If the effect of the concentration of HSO_3^- on the oxidation of iron(II) could be investigated, it should be quite useful in confirming the propriety of this oxidation mechanism. However, it is important to remember that, in the presence of appreciable amounts of sulfurous acid, iron(III) reacts with HSO_3^- to form dithionate according to Eq. (6). In order to prevent this side reaction, the oxidaiton with SO_2/O_2 needs to be conducted in the absence of hydrogen sulfite ions in high concentrations at all time. Further, this mecha-

nism may also elucidate the strong oxidation power of SO_2/O_2 mixtures that was shown for the leaching of ZnS.[2)]

References

1) K. N. Subramanian and D. B. W. Yawney, British Patent 1494564 (1977).
2) W. A. Robert and I. G. Matthew, *Proc. Australas. Inst. Min. Met.*, **No. 280**, 41 (1981).
3) T. Sato and F. Lawson, *Hydrometallurgy*, **11**, 371 (1983).
4) T. Sato, *Ryusan to Kogyo*, **32**, 1 (1979).
5) R. E. Huffman and N. Davidson, *J. Am. Chem. Soc.*, **78**, 4836 (1956).
6) C. T. Mathews and R. G. Robins, *Proc. Australas. Inst. Min. Met.*, **No. 242**, 47 (1972).
7) L. G. Sillen, "Stability Constants of Metal Ion Complexes," Chem. Soc. Burlington House, London (1964), p. 116.
8) W. C. E. Higginson and J. W. Marshall, *J. Chem. Soc.*, 447 (1973).
9) D. W. Carlyle and D. F. Zeck, Jr., *Inorg. Chem.*, **12**, 2973 (1973).
10) T. Sato, T. Shimizu, and T. Okabe, *Nippon Kagaku Kaishi*, 361 (1978).
11) W. M. Latimer, "The Oxidation States of the Elements and Their Potentials in Aqueous Solutions (Oxidation Potentials)," 2nd Ed., Prentice Hall (1952), p. 74.
12) T. Sato and T. Okabe, *Nippon Kagaku Kaishi*, 1124 (1977).
13) R. J. Meyer, "Gmelins Handbook of Inorganic Chemistry," 8th Ed., Verlag Chemie, Weinheim, Germany, Vol. 9 (1965), p. 1454.
14) K. B. Yatsimirskii and V. P. Vasil'ev, "Instability Constants of Complex Compounds," Pergamon Press (1960), p. 113.
15) M. Nagayama, "Oxidation of Iron(II) Ion in Aqueous Solution with Oxygen," Symposium on the Characteristics of Waste Water and Its Treatment, Sendai, Japan (1973), p. 38.
16) A. Huss, Jr., P. K. Lim, and C. A. Eckert, *J. Phys. Chem.*, **86**, 4224 (1982).
17) L. C. Schroeter, "Sulfur Dioxide," Pergamon Press, New York (1966), p. 44.
18) L. C. Bäckstrom, *Z. Phys. Chem.*, **B25**, 122 (1934).
19) V. A. Etell, M. A. Mosiu, and E. A. Devuyst, *Hydrometallurgy*, **4**, 247 (1979).

The Synthesis and Thermal Decomposition of Magnesium Phosphoramidate

Makoto WATANABE,* Yoshio MORII, and Shoji SATO
Department of Industrial Chemistry, Chubu University, Matsumoto-cho, Kasugai, Aichi 487
(Received January 23, 1984)

Magnesium phosphoramidate-water (1/7) was made by adding an aqueous magnesium chloride solution to an aqueous potassium hydrogenphosphoramidate solution at pH 9.0—9.5. The product was stable at room temperature, while it decomposed on heating. The product decomposed to produce polyphosphates when it was heated in air. The decomposition product heated above 600 °C was magnesium diphosphate. A small amount of imidodiphosphate was made when the phosphoramidate was heated in dried N_2.

Phosphoramidates with P-N covalent bonds have potential as new chemical fertilizers and as flame-proof materials because they produce polyphosphates containing imino and amino groups when they are heated. There have been many papers on phosphoric triamide and several papers concerning synthesis, thermal decomposition, or hydrolysis of ammonium and alkali-metal salts of phosphoramidic or phosphorodiamidic acid have been published.[1] Other salts of these phosphoramidic and phosphorodiamidic acids have not been studied. The present authors investigated the syntheses and thermal decompositions of magnesium and calcium bis(hydrogenphosphoramidate).[2,3] This paper describes the synthesis and thermal decomposition of magnesium phosphoramidate.

Experimental

Materials and Procedure. Potassium hydrogenphosphoramidate was prepared by the method described in a textbook.[4] About 0.1 mol of the phosphoramidate was dissolved in 100 cm^3 of water. Magnesium chloride hexahydrate was dissolved in 100 cm^3 of water by 0.1 mol. The magnesium chloride solution was added slowly to the phosphoramidate solution below 5 °C to prevent the hydrolysis of the latter. The resulting mixture was stirred for about 15 min. The pH of the solution was kept at 9.0—9.5 with aqueous ammonia during the treatment. A white precipitate was produced and was filtered off, washed with cooled water, ethanol, and then acetone. The product was dried under 5330 Pa at 20—25 °C for 2 d.

Chemical Analysis. About 0.2 g of the product was dissolved in 20 cm^3 of 6-mol dm^{-3} nitric acid and the solution was heated on a water bath for 1 h. The orthophosphate in the solution was determined to be $Mg_2P_2O_7$ by the gravimetric method.[5] Nitrogen and magnesium in the product were determined by the Kjeldahl method and by the EDTA (disodium dihydrogen ethylenediaminetetraacetate dihydrate) titration technique respectively.

Paper Chromatography and Colorimetry of Phosphates. One-dimensional paper chromatographic separation was run for the separation of the phosphate species in a sample with acidic (for the separation of chain phosphates) and basic (for the separation of ring phosphates) solvents.[6] A sample was dissolved in a 2% EDTA aqueous solution and the pH of the solution was adjusted to about 7 with an aqueous sodium hydroxide solution. The resulting solution was spotted on Toyo No. 51A filter paper (2 by 50 cm). The development was run at 5 °C for 2 d. Phosphates on the chromatogram were extracted with a 0.1-mol dm^{-3} aqueous ammonia and determined colorimetrically by means of the molybdenum-blue method with Lucena-Conde and Prat's reagent.[7]

X-Ray Diffractometry. An X-ray diffraction pattern of a powder sample was taken with nickel-filtered Cu $K\alpha$ radiation by using a Toshiba X-ray diffractometer, ADG-102.

IR Measurement. An IR spectrum of a sample was recorded on a JASCO IR spectrophotometer, model A-3, using a KBr disc method.

DTA and TG. A sample was heated at the heating rate of 5 °C min^{-1} in air and in dried N_2 by using a Cho Balance TRDA$_1$-H-type apparatus.

^{31}P NMR. A sample was dissolved in a 6% EDTA deuterated-water solution. The ^{31}P NMR spectrum of the solution was taken by a JEOL-FX-60-FT-NMR instrument.

Determination of Bound Water. The amount of bound water in a sample was determined by the Karl Fisher method with an MK-AII apparatus made by Kyoto Denshi.

Results and Discussion

Composition of the Product. The yield of the product was about 18 g. Found: P, 12.5; N, 5.7; Mg, 9.8%. Calcd for $MgPO_3NH_2 \cdot 7H_2O$: P, 12.6; N, 5.7; Mg, 9.9%. Accordingly, the product is magnesium phosphoramidate heptahydrate. The product was stable in air at room temperature.

DTA and TG in Air. DTA and TG curves of $MgPO_3NH_2 \cdot 7H_2O$ are shown in Fig. 1. The samples as numbered on Fig. 1 were removed from a furnace, cooled in a silica-gel desiccator, and then subjected to further analysis. The results are presented in Table 1 and Fig. 2. As Table 1 shows, the first large endo-

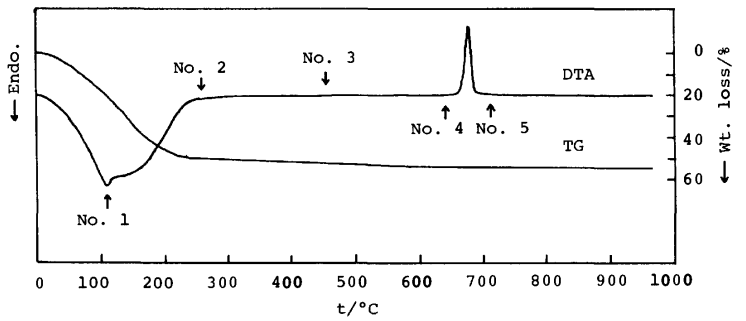

Fig. 1. DTA and TG curves of $MgPO_3NH_2 \cdot 7H_2O$ in air.

Table 1. Weight loss of the product and composition of the thermal decomposition products

Sample	Total N/%	Water/%	Wt. loss/%	Phosphates/P%			
				Ortho & Amido	Di & Imidodi	Tri	Higher
Product	5.7	51.4	—	100	0.0	0.0	0.0
No. 1	6.1	32.2	20.8	85.6	8.0	6.3	0.0
No. 2	3.5	6.1	49.9	61.0	35.0	4.0	0.0
No. 3	0.6	1.9	53.3	28.6	46.3	15.1	10.0
No. 4	0.0	0.0	54.7	—	—	—	—

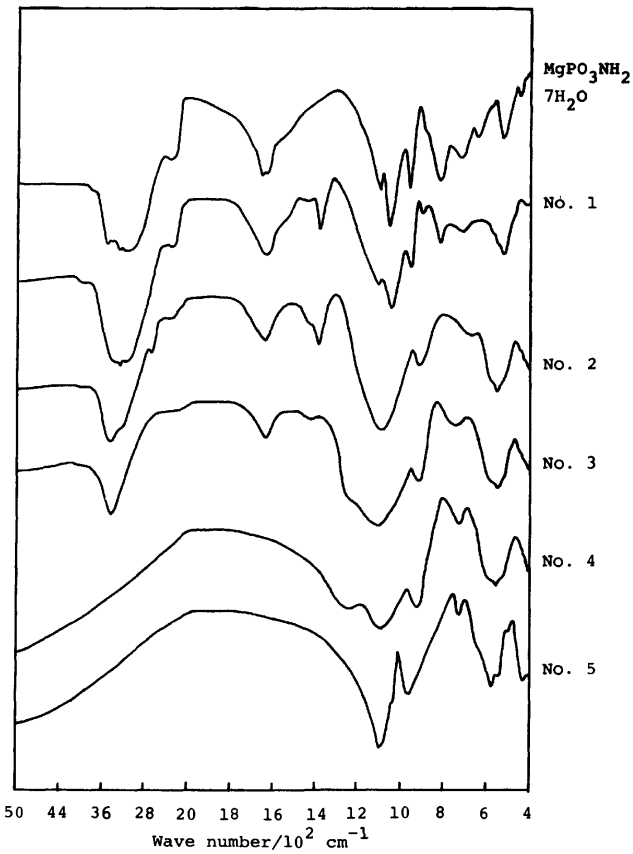

Fig. 2. IR spectra of the thermal decomposition products of $MgPO_3NH_2 \cdot 7H_2O$ in air.

thermic peak, with an accompanying rapid weight loss, seemed to be due to the elimination of bound water, and the endothermic reaction between 120 and 250 °C also included the elimination of ammonia. IR spectra of Nos. 1 and 2 showed the absorption of NH_4^+ at 1400 cm^{-1} and those of a P-O-P or a P-NH-P linkage at 940 and 740 cm^{-1}. Sample No. 1 gave X-ray diffraction peaks of $MgPO_3NH_2 \cdot 7H_2O$. Samples Nos. 2—4 were X-ray diffractometrically amorphous. After the large endothermic peaks, the weights of the samples gradually decreased until about 600 °C. The IR spectra of Nos. 3 and 4 had a large absorption due to a $(PO_3)^{2-}$ group at 1100 cm^{-1}. The absorptions of the two samples at 940 and 720 cm^{-1} seemed to be associated with a P-O-P linkage because, as Table 1 shows, the samples contained only a slight amount of nitrogen or did not contain any nitrogen at all. The two samples also exhibited an absorption at around 1250 cm^{-1}. Table 1 shows that sample No. 3 involves tri- and higher polyphosphates. So the absorption at 1250 cm^{-1} may be caused by the middle-PO_4 group of these polyphosphates. Samples Nos. 4 and 5 were insoluble in water or an aqueous EDTA solution and it was impossible to check the composition of the phosphates in the samples by the paper chromatography. The absorption of No. 4 at 1250 cm^{-1} may be due to a middle-PO_4 group of polyphosphates with chain lengths longer than that of diphosphate. The sample No. 5 did not show the absorption of a middle-PO_4 group and exhibited an X-ray diffraction diagram of $Mg_2P_2O_7$ (ASTM card, No. 8—38). So the exothermic peak at about 670 °C seemed to be due to crystallization of the amorphous phosphates to the diphosphate. According to stoichiometric considerations and the results obtained above, one can write the following thermal decomposition and condensation equations for the product:

$$O\text{-}P(=O)(Mg_{1/2})\text{-}NH_2 + H_2O \longrightarrow O\text{-}P(=O)(Mg_{1/2})\text{-}ONH_4, \quad (1)$$

$$2\ O\text{-}P(=O)(Mg_{1/2})\text{-}ONH_4 \longrightarrow O\text{-}P(=O)(Mg_{1/2})\text{-}O\text{-}P(=O)(Mg_{1/2})\text{-}O + 2NH_3 + H_2O. \quad (2)$$

The above equations show it is unreasonable for tri- and higher polyphosphates to be produced as intermediates of the thermal decomposition products. The following condensation reaction is considered to be difficult to occur at the relatively low temperature range of 100—600 °C; it has not been known to take place in this temperature range:

$$O\text{-}P(=O)(Mg_{1/2})\text{-}O\text{-}P(=O)(Mg_{1/2})\text{-}O + NH_4O\text{-}P(=O)(Mg_{1/2})\text{-}O \longrightarrow O\text{-}P(=O)(Mg_{1/2})\text{-}O\text{-}P(=O)(Mg_{1/2})\text{-}O\text{-}P(=O)(Mg_{1/2})\text{-}O + 1/2Mg(OH)_2 + NH_3. \quad (3)$$

The conflict can be resolved by the consideration that the following disproportionation reaction is taking place in the amorphous thermal decomposition products:

$$2\ O\text{-}P(=O)(Mg_{1/2})\text{-}ONH_4 \longrightarrow Mg_{1/2}O\text{-}P(=O)(NH_4)\text{-}O + O\text{-}P(=O)(Mg_{1/2})\text{-}OMg_{1/2}. \quad (4)$$

The species, $Mg_{1/2}(NH_4)_2PO_4$, is bifunctional for thermal condensation and can produce tri- and higher polyphosphates. As the final thermal decomposition product of $MgPO_3NH_2 \cdot 7H_2O$ showed an X-ray diffraction diagram of magnesium diphosphate and did not show an IR absorption of a $(PO_2)^-$ group, the following overall-thermal decomposition reaction can be written for the phosphoramidate:

$$2MgPO_3NH_2 \cdot 7H_2O \longrightarrow Mg_2P_2O_7 + 2NH_3 + 13H_2O. \quad (5)$$

The experimental final weight loss of the product showed a value very close to the calculated one for this decomposition reaction. The disappearance of polyphosphates with chain lengths longer than that of diphosphate in the thermal product can be explained by the following reorganization or degradation of the amorphous phosphates to diphosphate:

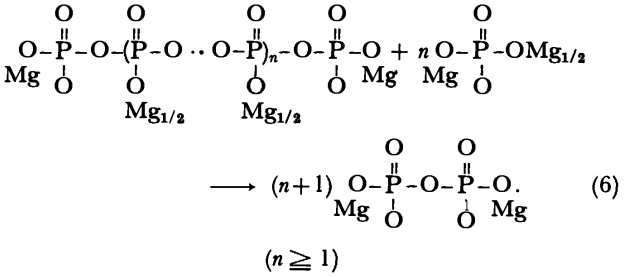

$$\longrightarrow (n+1)\ \text{Mg}\left[\text{O-P(=O)(O)-O-P(=O)(O)-O}\right]\text{Mg} \quad (6)$$

$$(n \geqq 1)$$

According to these results, it is not definitive yet that P-NH_2 linkages thermally decompose to form P-NH-P linkages by the elimination of ammonia. To obtain the data about this point, ^{31}P NMR spectrum of No. 2 was taken, because the thermal reaction seemed active at the temerature range and the sample still contained 3.5% of nitrogen. The sample indicated the ^{31}P NMR peaks of orthophosphate, phosphoramidate, and diphosphate, and did not show any peak of phosphates with an imino group. Therefore, magnesium phosphoramidate-water (1/7) did not decompose to make P-NH-P linkages thermally in air.

Isothermal Reaction at 150 °C. To obtain more detailed data about the thermal decomposition of the phosphoramidate, the isothermal decomposition of the phosphoramidate was carried out in air at 150 °C. This temperature is suitable for the analysis because the thermal reaction of the product was active and the elimination of ammonia from the decomposition product was not so rapid at this temperature. IR spectra of the isothermal decomposition products are presented in Fig. 3. With the passage of heating time, the

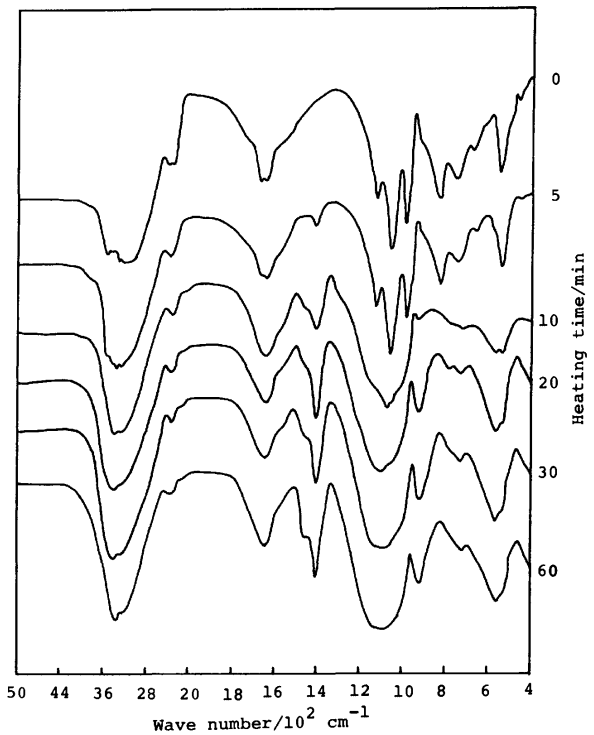

Fig. 3. IR spectra of the thermal decomposition products in air at 150 °C.

absorption of NH_4^+ at 1400 cm^{-1} and of a P-O-P or a P-NH-P linkage at 940 and 740 cm^{-1} appeared and their intensity increased, while the intensity of the absorption of a P-N linkage at 820 cm^{-1} decreased and disappeared after 10 min. These data show that Reactions 1 and 2 are taking place in the isothermal reaction of the phosphoramidate. The result listed in Table 2 well explains the change in the IR spectra of the decomposition products. The separation between orthophosphate and phosphoramidate and between di- and imidodiphosphate was not clear, but the result well agrees with the appearance of a P-O-P or a P-NH-P linkage in the IR spectra of the decomposition products. The above results do not indicate clearly that P-NH_2 linkages thermally decompose to form P-NH-P linkages with the elimination of ammonia at 150 °C. The ^{31}P NMR spectrum of the isothermal decomposition product at the reaction time of 30 min was taken. The sample did not show any peaks other than those of ortho-, monoamido-, and diphosphates. Therefore, magnesium phosphoramidate-water (1/7) may isothermally decompose at 150 °C according to

Table 2. Weight loss of the product and composition of the thermal decomposition products in air at 150 °C

Reaction time/min	Total N/%	N/% as NH_4^+	Water/%	Wt. loss/%	Phosphates/P%		
					Ortho & Amido	Di & Imidodi	Tri
0	5.7	—	51.4	—	100	0.0	0.0
5	5.6	1.2	40.4	8.3	84.1	12.4	3.5
10	5.5	2.2	31.2	19.9	70.8	22.9	6.3
20	5.4	2.3	15.5	37.7	68.7	26.4	4.9
30	5.2	2.5	8.9	44.8	68.2	27.4	4.4
60	4.4	2.8	5.9	48.4	68.1	28.2	3.7
120	3.8	2.7	4.6	49.3	66.1	30.2	3.7

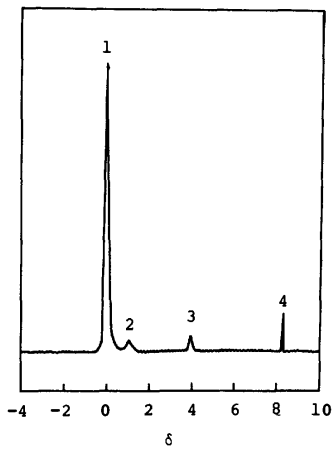

Fig. 4. ^{31}P NMR spectrum of the thermal decomposition product in dried N_2.
1: Orthophosphate, 2: imidodiphosphate, 3: phosphoramidate, 4: diphosphate.[10]

Reactions 1 and 2, and does not decompose to form a P-NH-P linkage. The result in Table 2 also seems to show that Reaction 4 and a condensation reaction of the product made by the disproportionation are taking place at the same time.

DTA and TG in Dried N_2. In dried N_2, $MgPO_3NH_2 \cdot 7H_2O$ gave quite similar DTA and TG curves to those in air and the decomposition products showed the same IR and X-ray diffraction data as those in air. It could be concluded that the product decomposes in dried N_2 according to a process analogous to that in air. A ^{31}P NMR spectrum of the decomposition product which was produced by heating the phosphoramidate by 250 °C by the DTA-TG instrument in dried N_2 is shown in Fig. 4. The small peak at 1.1 ppm was considered to be caused by imidodiphosphate. A small amount of the phosphoramidate may decompose in dried N_2 to make a P-NH-P linkage by the elimination of ammonia according to the following reaction:

$$2\ \mathrm{O{-}\overset{\overset{\mathrm{O}}{\|}}{P}{-}NH_2} \longrightarrow \mathrm{O{-}\overset{\overset{\mathrm{O}}{\|}}{P}{-}NH{-}\overset{\overset{\mathrm{O}}{\|}}{P}{-}O} + NH_3. \qquad (7)$$

(Mg, O)

References

1) D. E. C. Corbridge, "Phosphorus," Elsevier, Amsterdam (1980), p. 219 and the references cited there.
2) M. Watanabe, T. Inagaki, and S. Sato, *Bull. Chem. Soc. Jpn.*, **56**, 458 (1983).
3) M. Watanabe, T. Inagaki, Y. Morii, and T. Yamada, *Setsuko To Setsukai*, No. 184, 111 (1983).
4) "Shin Zitsuken Kagaku Koza," ed by the Chemical Society of Japan, Maruzen, Tokyo (1976), Vol. 8-[I], p. 354.
5) "Bunseki Kagaku Binran," ed by the Chemical Society of Japan, Maruzen, Tokyo (1971), pp. 204 and 1492.
6) S. Ohashi, *Kagaku To Kogyo*, **21**, 878 (1968). The A_2 and B_2 solvents in Table 3 were used.
7) F. Lucena-Conde and L. Prat, *Anal. Chim. Acta*, **16**, 473 (1957).
8) M. Grayson and E. J. Griffith, "Topics in Phosphorus Chemistry," John Wiley & Sons, New York (1969), Vol. 6, p. 235.
9) K. Nakanishi, "Sekigai Kyushu Supekutoru," Nankodo, Tokyo (1960).
10) M. M. Crutchfield, C. H. Dungan, J. H. Letcher, V. Mark, and J. R. Van Wazer, "Topics in Phosphorus Chemistry," Interscience Publishers, New York (1967), Vol. 5, p. 227; and the references cited there.

 © 1984 The Chemical Society of Japan Bull. Chem. Soc. Jpn., 57, 2091—2097 (1984)

Hydrophobic Vitamin B_{12}. III. Incorporation of Hydrophobic Vitamin B_{12} Derivatives into Single-Compartment Vesicles and Their Alkylation in Various Molecular Aggregates†

Yukito MURAKAMI,* Yoshio HISAEDA, and Teruhisa OHNO
Department of Organic Synthesis, Faculty of Engineering, Kyushu University, Hakozaki, Higashi-ku, Fukuoka 812
(Received February 16, 1984)

The incorporation of hydrophobic vitamin B_{12} derivatives into the single-compartment vesicles of *N,N*-didodecyl-N^{α}-[6-(tyimethylammonio)hexanoyl]-L-alaninamide bromide ($N^+C_5Ala2C_{12}$) was found to be primarily concerned with the extent of insolubility of the cobalt complexes in the aqueous bulk phase, while such incorporation into the single-walled vesicles of *N,N*-ditetradecyl-N^{α}-[6-(trimethylammonio)hexanoyl]-L-histidinamide bromide ($N^+C_5His2C_{14}$) was enhanced by the coordination interaction between the cobalt complex and the imidazolyl group of the lipid. In molecular aggregates formed with hexadecyltrimethylammonium bromide, α-[4-(1,1,3,3-tetramethylbutyl)phenyl]-ω-hydroxypoly(oxyethylene), or $N^+C_5Ala2C_{12}$, the alkylation rates of a hydrophobic vitamin B_{12} with 1-bromo-2-methylpropane and methyl 2-methyl-3-bromopropanoate were much enhanced relative to those in methanol. In the $N^+C_5Ala2C_{12}$ vesicle, a two-step mechanism was observed for the alkylation with the latter reagent. The possible origin of such rate enhancement was discussed.

It is of great interest to evaluate the microenvironmental effects on reactions of vitamin B_{12} in order to simulate the functions of apoproteins concerned in biological systems. Such enzymatic microenvironments for vitamin B_{12} seem to be concerned with the extents of integrated mode of hydrogen-bonding, hydrophobic, and other weak interactions effective in the active sites of enzymes. On the other hand, the physicochemical properties of hydrophobic vitamin B_{12} are subjected to change by the nature of reaction media as reported previously.[1,2] On the basis of the above viewpoints, the association behavior between micelles and the base-on and base-off methylcobalamin,[3] the interactions of vitamin B_{12a} with cysteine and *N*-alkanoylcysteines,[4] the formation of glycine, imidazole, and azide adducts of vitamin B_{12a},[5] and the methyl transfer reaction between methylcobalamin and mercuric acetate[6] have been investigated in aqueous and/or reversed micellar phases. The extents of these interactions and reactions have been discussed in connection with microenvironmental properties of the reaction sites concerned.

We have reported previously that amphiphiles involving an amino acid residue interposed between a polar head group and an aliphatic double-chain segment constitute stable single-compartment vesicles in aqueous media due to formation of the hydrogen-belt domain in the intramembrane region.[7] In this regard, these stable single-compartment vesicles have been utilized as media for various reactions to mimic the functions of apoproteins.[8] Futhermore, we have investigated the binding behavior of bilayer vesicles, formed with $N^+C_5Ala2C_{12}$, toward a hydrophobic cobalt complex, dicyano(8,12-diethyl-1,2,3,7,13,17,18,19-octamethyltetradehydrocorrinato)cobalt(III), and clarified that the bilayer vesicles may provide two binding sites which are largely different from each other in microenvironmental polarity.[9] Such previous studies prompted us to carry out various reactions of hydrophobic vitamin B_{12} derivatives in single-compartment vesicles of the peptide amphiphiles in order to obtain a clue to understanding microenvironmental effects characteristic of apoproteins. In this work, we investigated incorporation of the hydrophobic vitamin B_{12} derivatives into single-compartment vesicles formed with $N^+C_5Ala2C_{12}$ and $N^+C_5His2C_{14}$ and alkylation of the vitamin B_{12s} analogs in aqueous molecular aggregates as well as in methanol.

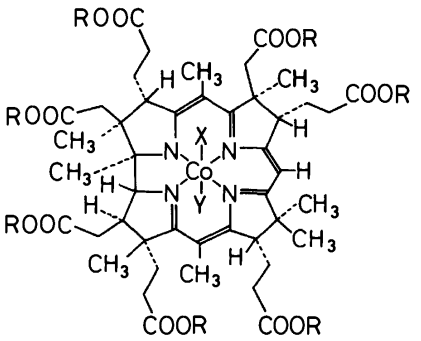

X=Y=CN
R=CH_3 : $(CN)_2$Cob(III)C_1ester
R=C_2H_5 : $(CN)_2$Cob(III)C_2ester
R=n-C_3H_7 : $(CN)_2$Cob(III)C_3ester
R=n-C_4H_9 : $(CN)_2$Cob(III)C_4ester

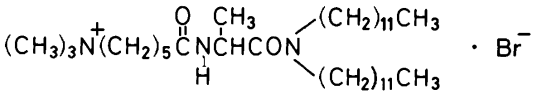

$N^+C_5Ala2C_{12}$

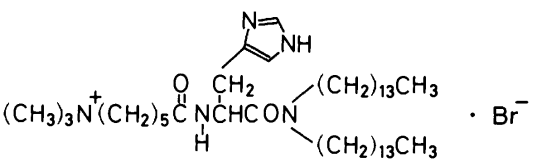

$N^+C_5His2C_{14}$

Experimental

General Analyses and Measurements. Elemental analyses were performed at the Microanalysis Center of Kyushu University. IR spectra were taken on a JASCO DS-

†Contribution No. 724 from this Department.

403G grating spectrophotometer, while electronic absorption spectra were recorded on a Hitachi 340 or a Hitachi 220A spectrophotometer. pH-Measurements were carried out with a Beckman expandomatic SS-2 pH meter equipped with a Metrohm EA-125 combined electrode after calibration with a combination of appropriate standard aqueous buffers. A JEOL JEM-200B electron microscope, installed at the Research Laboratory for High Voltage Electron Microscopy of Kyushu University, was used for morphological measurements of the aggregates.[7b] Circular dichroism (CD) spectra were recorded on a JASCO J-500C spectropolarimeter.

Materials. Cyanocobalamin was purchased from Nakarai Chemicals and used for its modifications without further purification. Hexadecyltrimethylammonium bromide (CTAB) was purchased from Nakarai Chemicals and recrystallized from ethanol. Sodium dodecyl sulfate (SDS) of Nakarai Chemicals and α-[4-(1,1,3,3-tetramethylbutyl)phenyl]-ω-hydroxypoly(oxyethylene) (n=9—10) (Triton X-100) of Rohm and Haas were used without further purification. 1-Bromo-2-methylpropane was obtained commercially from Nakarai Chemicals as extra pure grade and fractionally distilled just before use. Methyl 2-methyl-3-bromopropanoate was synthesized from the corresponding carboxylic acid: bp 73.0 °C/2.53×10³ Pa; IR (neat) 1735 cm^{-1} (ester C=O); ^{1}H-NMR ($CDCl_3$, TMS) δ=1.28 (3H, d, CH_3), 2.84 (1H, m, CH), 3.47 (2H, dd, CH_2) and 3.66 (3H, s, $COOCH_3$). These alkyl bromides were confirmed to be sufficiently pure by GLC. *N,N*-Didodecyl-*N*$^{\alpha}$-[6-trimethylammonio)hexanoyl]-L-alaninamide bromide ($N^+C_5Ala2C_{12}$) was synthesized according to the method described previously.[7b] *N,N*-Ditetradecyl-*N*$^{\alpha}$-[6-(trimethylammonio)-hexanoyl]-L-histidinamide bromide ($N^+C_5His2C_{14}$) was prepared in a manner similar to that reported previously by utilizing the benzyl group in place of the tosyl as an imidazole-protecting moiety.[8c]

Preparation of heptamethyl dicyanocobyrinate, $(CN)_2$-Cob(III)C$_1$ester, and heptamethyl cobyrinate perchlorate, [Cob(II)C$_1$ester]ClO_4, has been described previously.[1] Heptaethyl dicyanocobyrinate, $(CN)_2$Cob(III)C$_2$ester, heptapropyl dicyanocobyrinate, $(CN)_2$Cob(III)C$_3$ester, and heptabutyl dicyanocobyrinate, $(CN)_2$Cob(III)C$_4$ester, were prepared from cyanocobalamin according to the method of Werthemann *et al.*,[10] adopted for the preparation of $(CN)_2$Cob(III)C$_1$ester, with some modification as typically described below.

Heptapropyl Dicyanocobyrinate, $(CN)_2$Cob(III)C$_3$ester. Cyanocobalamin (500 mg, 0.37 mmol) in 333 ml of dry 1-propanol was mixed with 33 ml of cold conc. sulfuric acid and 167 ml of dry 1-propanol. The solution was deoxygenated by bubbling nitrogen gas through it for 1 h, and heated to 60—62 °C for 250 h in the dark under nitrogen atmosphere.[11] The solution was concentrated to *ca.* 100 ml, diluted with 250 ml of cold water, and quickly neutralized with sodium carbonate. After addition of 2.5 g of potassium cyanide, the reaction mixture was extracted with carbon tetrachloride (70 ml×3) and dichloromethane (70 ml×3). The dichloromethane extract, which contained partially esterified corrins, was used for the above esterification reaction. The carbon tetrachloride extract was evaporated to dryness, and the residue was purified by TLC on silica gel (Kiesel gel 60H) with dichloromethane–methanol (10:1 v/v). The TLC analysis showed the presence of 5 components: A purple one with the highest R_f was collected and dissolved in carbon tetrachloride. This solution was treated with aqueous potassium cyanide and evaporated to dryness to afford a dark purple solid: yield 190 mg (40%); λ_{max} (C_6H_6) 316, 372, 426, 520 sh, 550, and 590 nm; IR (neat) 2130 (C≡N) and 1730 cm^{-1} (ester C=O).

Found: C, 63.38; H, 7.98; N, 6.32. Calcd for $C_{68}H_{101}CoN_6O_{14}$: C, 63.53; H, 7.92; N, 6.54.

Heptaethyl Dicyanocobyrinate. Found: C, 61.31; H, 7.43; N, 6.83. Calcd for $C_{61}H_{87}CoN_6O_{14}$: C, 61.71; H, 7.39; N, 7.08.

Heptabutyl Dicyanocobyrinate. Found: C, 65.19; H, 8.40; N, 5.62. Calcd for $C_{75}H_{115}CoN_6O_{14}$: C, 65.10; H, 8.38; N, 6.07.

Heptapropyl Cobyrinate Perchlorate, [Cob(II)C$_3$ester]ClO_4. This complex was prepared after the method employed for the preparation of [Cob(II)C$_1$ester]ClO_4.[1] Found: C, 59.17; H, 7.70; N, 4.42. Calcd for $C_{66}H_{101}ClCoN_4O_{18}$: C, 59.47; H, 7.64; N, 4.20.

Equilibrium Measurements for Incorporation of $(CN)_2$Cob(III)C$_n$ester into Single-compartment Vesicles. A dichloromethane solution (1.1 ml) containing $N^+C_5Ala2C_{12}$ (1.0×10^{-5} mol) and $(CN)_2$Cob(III)C$_n$ester (n=1,2,3,4; 1.0×10^{-7} mol) was evaporated *in vacuo* to remove the solvent completely, and an aqueous potassium cyanide solution (1 ml, 5.0×10^{-4} mol dm^{-3}) was added to the residue. The resulting mixture was sonicated for 30 s with a probe-type sonicator at 30 W to give a clear solution. An extent of incorporation of a hydrophobic vitamin B_{12} into single-compartment vesicles was examined by gel-filtration chromatography on a column of Sephadex G-50 with an aqueous potassium cyanide solution (5.0×10^{-4} mol dm^{-3}) as an eluant; the bound complex was eluted first in the column void volume. An amount of the incorporated complex was determined by electronic spectroscopy.

Kinetic Measurements. A 3-ml sample of an aqueous buffer (5.00×10^{-3} mol dm^{-3} phosphate–4.75×10^{-2} mol dm^{-3} borate, pH 9.18) containing CTAB (5.0×10^{-3} mol dm^{-3}) was placed in a spectrophotometric cell thermostated at 21.5± 0.1 °C. The sample was deoxygenated by bubbling argon gas through it for 10 min. To this solution were added 10 µl of a methanol solution of [Cob(II)C$_3$ester]ClO_4 (final concentration, *ca.* 2×10^{-5} mol dm^{-3}) and 10 µl of the aqueous buffer containing sodium tetrahydroborate (final concentration, *ca.* 1—2×10^{-4} mol dm^{-3}) under argon atmosphere. The reduction of the complex to the cobalt(I) state took place instantaneously. A methanol solution of an alkyl bromide was injected into the medium containing the cobalt(I) complex under argon atmosphere to initiate the reaction. The mixture was quickly shaken, and the decrease in absorbance at 392 nm, characteristic of Cob(I)C$_3$ester, was monitored. In all kinetic runs, an alkyl bromide was used in excess to assure the pseudo-first-order conditions and clear isosbestic points were observed along the progress of conversion of the cobalt(I) complex to the corresponding alkylated complex. All the kinetic runs under the pseudo-first-order conditions provided linear correlations for ln (OD_t-OD_∞) *vs.* time, and the slopes (pseudo-first-order rate constants) were divided by the initial concentrations of alkyl bromides to give the corresponding second-order rate constants. The resulting alkylated complexes were confirmed by means of identification of their photolysis products obtained under aerobic conditions. The kinetic measurements in aqueous single-compartment vesicles were carried out as follows: an amphiphile (2.0×10^{-3} mol dm^{-3}) dispersed in the aqueous buffer was sonicated for 1 min with a probe-type sonicator at 30 W; [Cob(II)C$_3$ester]-ClO_4, sodium tetrahydroborate, and an alkyl halide were added to the resulting clear vesicle solution in a manner as stated above.

Results and Discussion

Incorporation of Hydrophobic Vitamin B_{12} into Single-compartment Vesicles. As shown in Table 1, the hydrophobic vitamin B_{12} derivatives, $(CN)_2$Cob(III)C$_n$ester, are readily incorporated into the $N^+C_5Ala2C_{12}$ vesicle when the n-value of C$_n$ is equal to 2 or larger.

Table 1. Incorporation of hydrophobic vitamin B_{12} derivatives into single-compartment vesicles[a]

Vesicle[b]	Complex[c]	Incorporated amount,[d] mol
$N^+C_5Ala2C_{12}$	$(CN)_2Cob(III)C_1ester$	0
$N^+C_5Ala2C_{12}$	$(CN)_2Cob(III)C_2ester$	2.4×10^{-7}
$N^+C_5Ala2C_{12}$	$(CN)_2Cob(III)C_3ester$	5.0×10^{-7}
$N^+C_5Ala2C_{12}$	$(CN)_2Cob(III)C_4ester$	5.0×10^{-7}
$N^+C_5His2C_{14}$	$[Cob(II)C_1ester]ClO_4$[e]	4.5×10^{-7}

a) Incorporation was examined by gel-filtration chromatography on a column (ϕ0.9×21 cm) of Sephadex G-50 with aqueous KCN solution (5×10^{-4} mol dm^{-3}) as an eluant. b) Quantity used, 1.0×10^{-5} mol. c) Qunatity used, 5.0×10^{-7} mol. d) Incorporated quantity was determined by electronic spectroscopy. e) Aqueous $NaClO_4$ solution (5×10^{-4} mol dm^{-3}) was used as an eluant.

$(CN)_2Cob(III)C_1ester$ is slightly soluble in water (*ca.* 10^{-4} mol dm^{-3}), but $(CN)_2Cob(III)C_3ester$ and $(CN)_2Cob(III)C_4ester$ are almost insoluble. Thus, the partitioning trend of $(CN)_2Cob(III)C_nester$ to the membrane phase is subjected to change by the hydrophobicity of the ester groups placed in the peripheral positions of the corrinoid skeleton. On the other hand, when a membrane-forming amphiphile involves a functional group capable of coordinating to the cobalt complex, such a coordination effect acts to enhance the incorporation of $[Cob(II)C_1ester]ClO_4$ having some limited solubility in water (*ca.* 10^{-3} mol dm^{-3}); this cobalt complex is largely incorporated into the $N^+C_5His2C_{14}$ vesicle (Table 1). The stability constant (K) for the coordination of the imidazolyl moiety of $N^+C_5His2C_{14}$ to the nuclear cobalt of $[Cob(II)C_1ester]ClO_4$ at one of its axial sites was measured in dichloromethane at 26.5 °C by the method described previously:[1] $\log K=5.5$. Consequently, the incorporation of $[Cob(II)C_1ester]ClO_4$ into the vesicles of $N^+C_5His2C_{14}$ originates in the axial coordination of the amphiphile to the complex. The experimental method for the equilibrium measurements (see Experimental) was not applied to the evaluation of an extent of incorporation of $[Cob(II)C_1ester]ClO_4$ into the $N^+C_5His2C_{14}$ vesicle since the complex was converted into the corresponding cobalt(III) complex during the sonication (see Fig. 1). Alternatively, a methanol solution of $[Cob(II)C_1ester]ClO_4$ was added to the single-compartment vesicles of $N^+C_5His2C_{14}$, and the cobalt(II) complex was confirmed to be bound to the vesicle in the base-on form in the light of our previous study[1] (Fig. 1). This clearly indicates that the imidazolyl moiety of $N^+C_5His2C_{14}$ in the vesicular state coordinates to the nuclear cobalt of $Cob(II)C_1ester$. The microenvironmental polarity for $(CN)_2Cob(III)C_3ester$ was evaluated when the complex was incorporated into the micelles or the vesicle in reference to the α- and γ-bands of the complex measured in various organic media (Table 2 and Fig. 2). The CTAB and Triton X-100 micelles provide a microenvironment comparable to acetonitrile, while the $N^+C_5Ala2C_{12}$ vesicle provides one equivalent to dichloromethane.

The structure of molecular aggregates composed of $N^+C_5Ala2C_{12}$, when $(CN)_2Cob(III)C_3ester$ was incorporated into them, was measured directly by electron

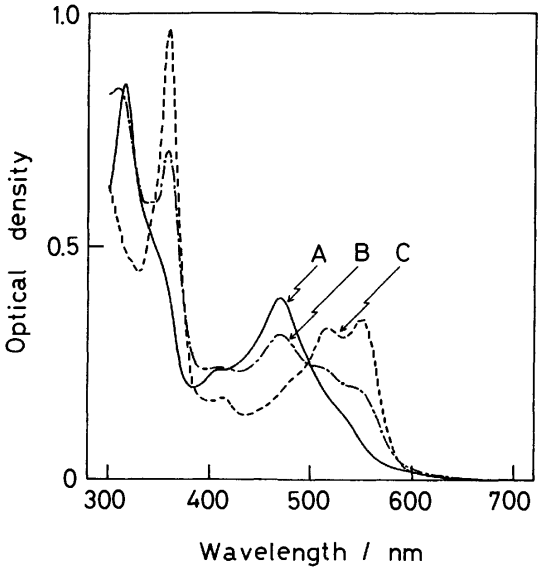

Fig. 1. Electronic spectra of $[Cob(II)C_1ester]ClO_4$ in aqueous phosphate (5.00×10^{-3} mol dm^{-3})-borate (4.75×10^{-2} mol dm^{-3}) buffer (pH 9.18) at 19.6±0.1 °C: A, $[Cob(II)C_1ester]ClO_4$, 3.16×10^{-5} mol dm^{-3}: B, $[Cob(II)C_1ester]ClO_4$, 3.16×10^{-5} mol dm^{-3}; $N^+C_5His2C_{14}$, 2.0×10^{-3} mol dm^{-3} (sonicated for 1 min at 30 W): C, sample B was sonicated for 1 min at 30 W.

Table 2. Characteristic absorption bands of $(CN)_2Cob(III)C_3ester$ in various media

Medium	Solvent parameters		α-Band,[c] nm	γ-Band,[c] nm
	Z[a]	$E_T(30)$[b]		
Benzene	54.0	34.5	590.4	372.0
Dichloromethane	64.2	41.1	588.8	371.0
Acetonitrile	71.3	46.0	587.2	370.2
Ethanol	79.6	51.9	584.8	368.8
Methanol	83.6	55.5	584.0	368.4
CTAB micelle	75[d]	48[d]	586.1	370.2
Triton X-100 micelle	71[d]	46[d]	587.2	370.5
$N^+C_5Ala2C_{12}$ vesicle	64[d]	41[d]	588.8	372.0

a) E. M. Kosower, "An Introduction to Physical Organic Chemistry," John Wiley and Sons, New York (1968), Part 2. b) C. Reichardt, "Solvent Effects in Organic Chemistry," Verlag Chemie, Weinheim (1979). c) Electronic absorption bands characteristic of the corrinoid complex are named α-, β-, and γ-bands by going from lower to higher energy regions. d) Numerical value was evaluated approximately in reference to the correlations given in Fig. 2.

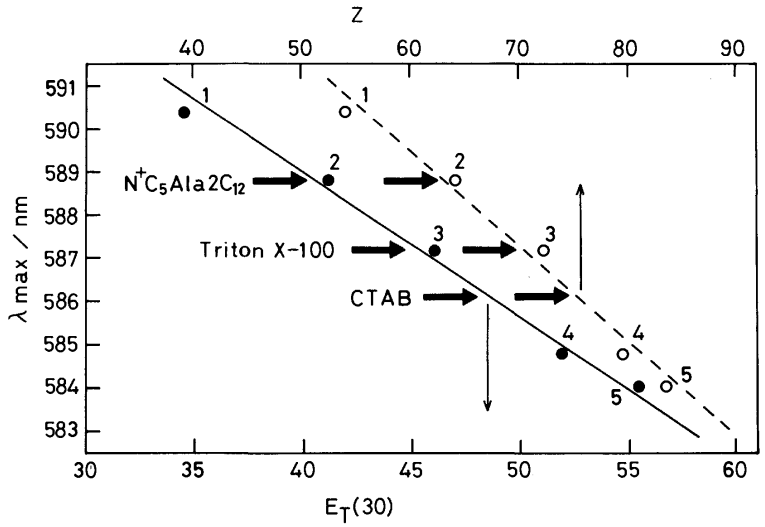

Fig. 2. Correlation of α-band of $(CN)_2$Cob(III)C_3ester with solvent polarity parameters, Z and $E_T(30)$: 1, benzene; 2, dichloromethane; 3, acetonitrile; 4, ethanol; 5, methanol. α-Bands of $(CN)_2$Cob(III)C_3ester in molecular aggregates are shown by arrows.

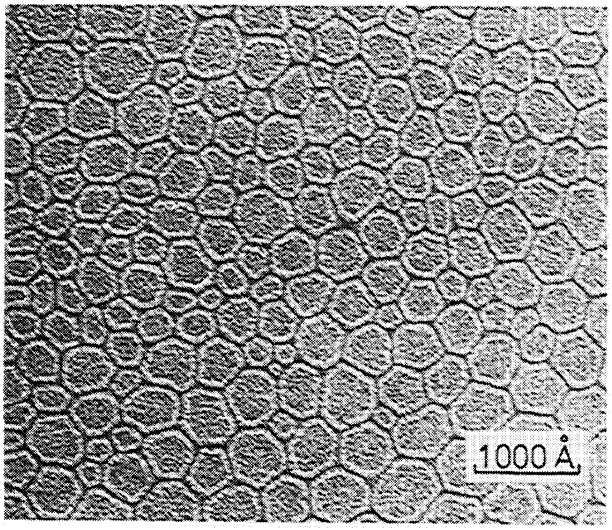

Fig. 3. Electron micrograph of single-compartment vesicles of N^+C_5Ala2C_{12} entrapping $(CN)_2$Cob(III)C_3ester: N^+C_5Ala2C_{12}, 5.0×10^{-3} mol dm^{-3}; $(CN)_2$Cob(III)C_3ester, 1.0×10^{-4} mol dm^{-3}: negatively stained with uranyl acetate, sonicated for 1 min with a probe-type sonicator at 30 W, and allowed to stand for 10 min at 5 °C.

microscopy (Fig. 3). A large number of single-compartment vesicles ranging from 200 through 700 Å in diameter are observable, and the layer thickness is evaluated to be 40—50 Å, approximately twice the length of the hydrophobic double-chain segment. This means that the incorporation of a hydrophobic vitamin B_{12}, does not disturb the aggregate morphology of such peptite lipid.

The CD spectra of $(CN)_2$Cob(III)C_1ester and [Cob(II)C_1ester]ClO_4 are shown in Fig. 4 as typical examples. The spectral pattern of $(CN)_2$Cob(III)C_1ester is comparable to that of cyanocobalamin.[12] [Cob(II)C_1ester]ClO_4 was gradually oxidized upon addition of potassium cyanide under aerobic conditions and finally converted to $(CN)_2$Cob(III)C_1ester as confirmed by CD spectroscopy. In the light of these observations, $(CN)_2$Cob(III)$C_n$ester and [Cob(II)$C_n$ester]ClO_4 prepared in the present study retain the same enantiomeric configurations as the naturally occurring vitamin B_{12}'s even after the hydrophobic modifications.

Alkylation of Hydrophobic Vitamin B_{12} in Various Media. The alkylation reactions of hydrophobic vitamin B_{12} derivatives with alkyl halides in various media were followed by the spectrophotometric method. Figure 5 shows a typical spectral change observed along the progress of alkylation in the CTAB micelle under the conditions: in the aqueous phosphate–borate buffer at pH 9.18 and 21.5±0.1 °C under argon. Pseudo-first-order plots for these reactions gave satisfactory straight lines, and the corresponding second-order rate constants for the reaction of Cob(I)C_3ester with 1-bromo-2-methylpropane and methyl 2-methyl-3-bromopropanoate in various media are summarized in Table 3.

The same kinetic runs were also carried out in the anionic micelles of sodium dodecyl sulfate (SDS). However, Cob(I)C_3ester was not formed instantaneously, different from the above runs. The electrostatic repulsion between the anionic micellar surface and the tetrahydroborate ion does not seem to allow the effective permeation of the latter into the micellar interior and acts to lower the reactivity of the reductant toward Cob(II)C_3ester.

In order to characterize the reactivity of the hydrophobic vitamin B_{12} derivatives toward alkyl halides relative to that of cobalamin in the cobalt(I) state, the second-order rate constants for the reactions of some hydrophobic vitamin B_{12}'s with 1-bromo-2-methylpropane were obtained in the same medium, methanol, as summarized in Table 4. The reactivity of the hydrophobic vitamin B_{12}'s in the alkylation decreases by 1/4- to 1/5-fold as compared with that of cobalamin. The reactivity of corrinoid complexes must be subjected to change by the nature of intramolecular cage, provided

with the peripheral substituents, at the axial sites of the nuclear cobalt(I). Since the axial sites of the hydrophobic vitamin B_{12}'s containing ester groups are apolar as compared with those of cobalamin bearing the amide moieties as well as the nucleotide group, the nucleophilicity of the present hydrophobic complexes is lowered relative to that of the latter natural complex in the light of the solvent effect on the Co^{II}/Co^{I} redox potential observed for Cob(II)C$_1$ester.[2] Furthermore, the transition state of alkylation becomes polar relative to the original state, so that the microenvironmental property of cobalamin provided at the cobalt(I) site would be in favor of such reaction. This environmental effect is reflected on the large stability of Cob(II)-

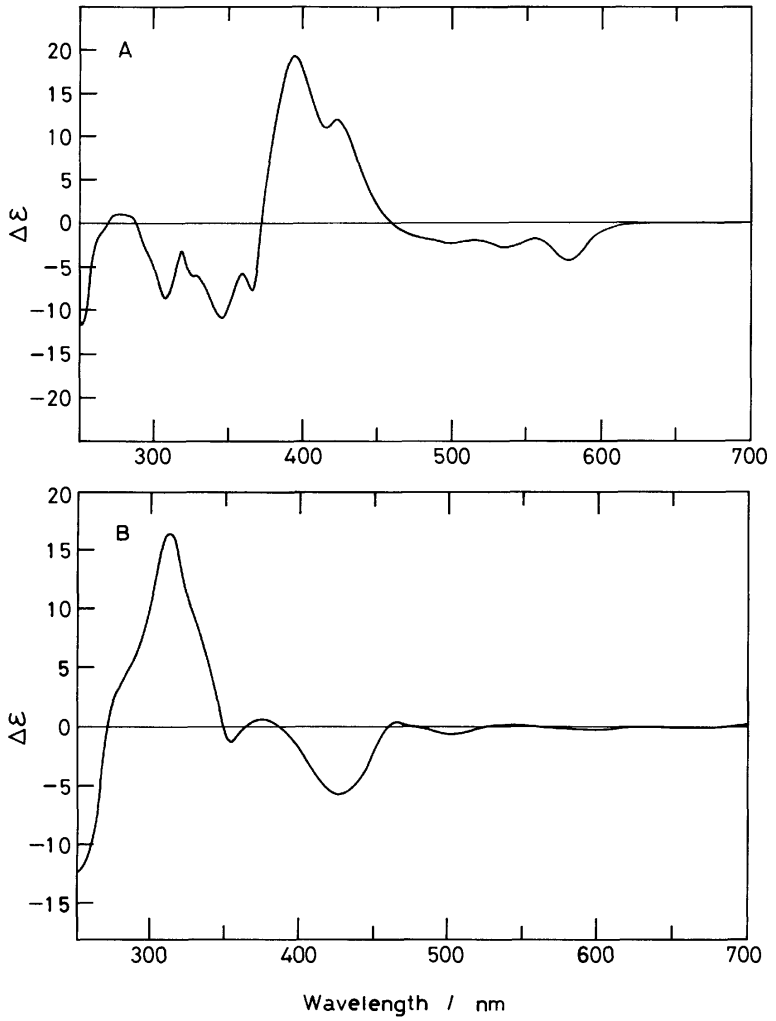

Fig. 4. CD spectra of $(CN)_2$Cob(III)C$_1$ester (A) and [Cob(II)C$_1$ester]-ClO_4 (B) in methanol at 20.0±0.1 °C.

Table 3. Second-order rate constants for the reactions of Cob(I)C$_3$ester with alkyl bromides in various media at 21.5±0.1 °C

Medium[a,b]	k_2/mol^{-1} dm^3 s^{-1}	
	$(CH_3)_2CHCH_2Br$	$(CH_3OOC)(CH_3)CHCH_2Br$
Methanol	0.21±0.03	0.87±0.05
Triton X-100 micelle	5.50±0.13	9.30±0.20
CTAB micelle	12.6±0.3	24.2±0.4
$N^+C_5Ala2C_{12}$ vesicle	10.8±0.2	39.0±0.8[c] (two steps)[d]

a) [Cob(I)C$_3$ester]=2.0×10^{-5} mol dm^{-3}. b) Amphiphile concentrations for molecular aggregates in phosphate (5.00×10^{-3} mol dm^{-3})-borate (4.75×10^{-2} mol dm^{-3}) buffer: Triton X-100,5.0×10^{-3} mol dm^{-3}; CTAB, 5.0×10^{-3} mol dm^{-3}; $N^+C_5Ala2C_{12}$, 2.0×10^{-3} mol dm^{-3}. c) Rate constant for the first step of two-step kinetics. d) Pseudo-first-order rate constants (k_{obsd}) for the two steps were measured by changing the concentration of the alkyl bromide (RX): first step, k_{obsd}=(2.46±0.15)×10^{-2} s^{-1} with [RX]=6.31×10^{-4} mol dm^{-3}; second step, k_{obsd}=(2.41±0.16)×10^{-2} s^{-1} with [RX]=5.32×10^{-3} mol dm^{-3} (k_{obsd} for the first step under this condition was too large to evaluate accurately and the stopped-flow technique was not applicable due to the foam-forming property of $N^+C_5Ala2C_{12}$).

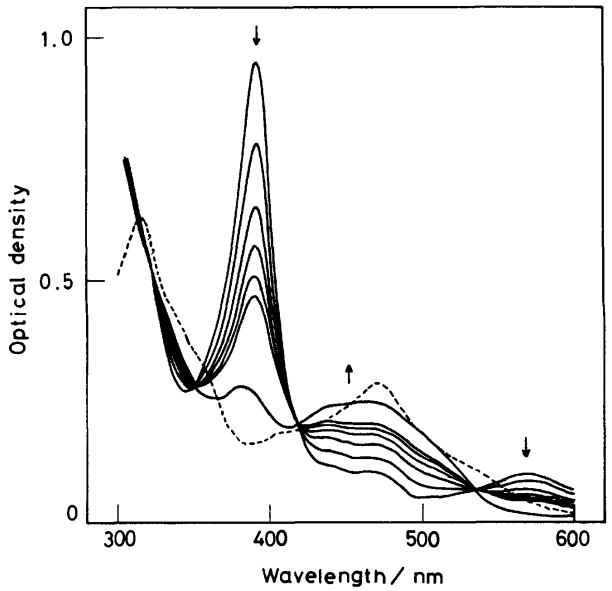

Fig. 5. Spectral change for the reaction of Cob(I)C3ester (2.1×10^{-5} mol dm^{-3}) with 1-bromo-2-methylpropane (2.1×10^{-4} mol dm^{-3}) in the presence of CTAB micelles (5.0×10^{-3} mol dm^{-3}) in aqueous phosphate-borate buffer (pH 9.18) at 21.5±0.1 °C. Trends of spectral change with time are shown by arrows. Broken line represents the spectrum for [Cob(II)C3ester]ClO_4 before reduced with $NaBH_4$.

Table 4. Second-order rate constants for the reactions of corrinoid Co^I complexes with 1-bromo-2-methylpropane[a] in methanol at 21.5±0.1 °C

Corrinoid complex[b]	k_2/mol^{-1} dm^3 s^{-1}
Cob(I)alamin	1.12±0.12
Cob(I)C1ester	0.27±0.08
Cob(I)C3ester	0.21±0.04

a) Concentration range for the alkyl bromide: 1.0×10^{-3}—2.1×10^{-3} mol dm^{-3}. b) Aquacobalamin, [Cob(II)C1ester]ClO_4, and [Cob(II)C3ester]ClO_4 were used as starting materials and reduced with sodium tetrahydroborate (*ca.* 6×10^{-4} mol dm^{-3}) to the corresponding cobalt(I) complexes under argon atmosphere.

$C_n$ester under aerobic conditions, while Cob(II)alamin is readily oxidized under the identical conditions. Even though the dioxygen adduct of Cob(II)$C_n$ester is formed to a limited extent, the oxidation of the hydrophobic vitamin B_{12r} does not take place readily. This is plausibly due to the following effect. In order that the electron transfer from Cob(II)$C_n$ester to dioxygen takes place, the coordinated oxygen molecule needs to be much polarized in the transition state. The apolar microenvironment provided at the cobalt site of Cob(II)$C_n$ester would not be favorable for the formation of such polarized structure.

The second-order rate constants for the reactions in the micellar and vesicular phases are 10—60 times greater than the corresponding values in methanol (Table 3). When methyl 2-methyl-3-bromopropanoate having an electron-withdrawing ester group is used as a substrate, the second-order rate constants are somewhat larger than the corresponding values for the reactions with 1-bromo-2-methylpropane. On the other hand, the rate enhancements in the molecular aggregates, relative to the reactivity in methanol, are much larger for the reaction with 1-bromo-2-methylpropane than those for the reaction with methyl 2-methyl-3-bromopropanoate. This would be due to the difference in hydrophobicity between the two substrates. The former substrate is to be more favorably incorporated into the hydrophobic interior of the molecular aggregates.

When 1-bromo-2-methylpropane is used as substrate, the second-order rate constant measured in the N^+C_5Ala2C_{12} vesicle is comparable to or even slightly less than that in the CTAB micelle, while the rate constant in the nonionic Triton X-100 micelle is smaller than both of the above values. This must originate in the difference in polarizing power, acting on the transition state, between the cationic and nonionic molecular aggregates; *i.e.*, the transition state is more effectively stabilized in the cationic aggregates.

In the single-compartment vesicles of N^+C_5Ala2C_{12}, the reaction behavior between Cob(I)C3ester and methyl 2-methyl-3-bromopropanoate was somewhat different from that in the micelles or in methanol. The reaction proceeded through a two-step mechanism; a faster step was followed by a slow one. The substrate-binding property of single-walled vesicles formed with *N,N*-ditetradecyl-N^{α}-[6-(trimethylammonio)hexanoyl]-L-alaninamide bromide has been investigated previously from both static and dynamic viewpoints, hexyl *p*-nitrophenyl ether being used as a pseudo-substrate. The substrate-binding equilibrium was achieved through a two-step mechanism: the substrate molecules located in the bulk phase are incorporated readily into the surface area as the first step and such incorporated guest molecules penetrate rather slowly from the surface area into the hydrophobic interior of vesicular assembly.[7g] This feature is consistent with the presence of a potential barrier between the surface and interior hydrophobic regions of the vesicular system for translocation of such a substrate. This barrier must be identical with the so-called hydrogen-belt domain located in the intramembrane region which has been identified by the use of dicyano(8,12-diethyl-1,2,3,7,13,17,18,19-octamethyltetradehydrocorrinato)cobalt(III) as a probe.[9] In the light of these previous studies, the two kinetic steps observed for the alkylation with methyl 2-methyl-3-bromopropanoate may be defined as follows: (i) The first-step reaction takes place quite readily in the relatively polar domain near the vesicular surface; (ii) the second-step reaction occurs in the hydrophobic domain after permeation of the substrate into it. Under the experimental conditions for measurements of the first step ([RX]=6.31×10^{-4} mol dm^{-3}, RX being methyl 2-methyl-3-bromopropanoate), the absorbance at 392 nm characteristic of Cob(I)C3ester decayed to about a 40% level of the initial one by following the pseudo-first-order kinetics; a further decay was extremely slow for accurate evaluation of the rate. Under the experimental conditions for measurements of the second step ([RX]=5.32×10^{-3} mol dm^{-3}), the 392 nm absorbance instantaneously decreased to about a 40% level of the initial one, followed by a slow decay in the pseudo-first-order kinetics. This result clearly indicates that the

molar ratio of Cob(I)C_3ester distributing between the relatively polar and apolar domains is approximately 6:4. The second-order rate constant for the reaction of Cob(I)C_3ester with 1-bromo-2-methylpropane in the $N^+C_5Ala2C_{12}$ vesicle is more or less comparable to that measured in the CTAB micelle, while the rate constant for the reaction of the same complex with methyl 2-methyl-3-bromopropanoate in the former vesicle is significantly larger than that in the CTAB micelle. The rate enhancement would originate in the effective entrapment of the latter substrate into the hydrogen-belt domain of the vesicle due to the hydrogen-bonding interaction of the methoxycarbonyl group with the domain.

The net volume occupied by the CTAB micelle is determined on the basis of the partial molar volume of the surfactant monomer in the micellar state; $\bar{V}=0.32-0.37\ dm^3\ mol^{-1}$.[13] The intrinsic volume occupied by the $N^+C_5Ala2C_{12}$ vesicle is assumed to be approximately equal to that by egg phosphatidylcholine; $\bar{V}=0.75\ dm^3\ mol^{-1}$.[14] Thus, the molecular aggregates under the present experimental conditions hold about 1/600 of the total solution volume. Since Cob(I)C_3ester, being insoluble in water, is completely encapsulated in the aggregates, the micro-concentration effect exercised by the molecular aggregates on Cob(I)C_3ester is undoubtedly responsible for the rate enhancement. Since the extents of incorporation of the alkyl bromides were not determined by the gel-filtration chromatography applied to the hydrophobic vitamin B_{12}'s for their chemical instability, a conventional extraction method was employed here to evaluate them;[15] at least 25% of the total amount of the substrates was entrapped into the aggregates. In conclusion, multiple hydrophobic materials can be incorporated into the hydrophobic intramembrane region, the extents being dependent on their hydrophobic properties. The entrapped substances may undergo reactions in the significantly small compartments of molecular aggregates, and the apparent rate enhancement is attained at least by the micro-concentration effect.

The present work was supported in part Grant-in-Aid for Scientific Research No. 58430016 from the Ministry of Education, Science and Culture.

References

1) Y. Murakami, Y. Hisaeda, and A. Kajihara, *Bull. Chem. Soc. Jpn.*, **56**, 3642 (1983).
2) Y. Murakami, Y. Hisaeda, A. Kajihara, and T. Ohno, *Bull. Chem. Soc. Jpn.*, **57**, 405 (1984).
3) L. S. Beckmann and D. G. Brown, *Biochim. Biophys. Acta*, **428**, 720 (1976).
4) F. Nome and J. H. Fendler, *J. Am. Chem. Soc.*, **99**, 1557 (1977).
5) J. H. Fendler, F. Nome, and H. C. Van Woert, *J. Am. Chem. Soc.*, **96**, 6745 (1974).
6) G. C. Robinson, F. Nome, and J. H. Fendler *J. Am. Chem. Soc.*, **99**, 4969 (1977).
7) a) Y. Murakami, A. Nakano, and K. Fukuya, *J. Am. Chem. Soc.*, **102**, 4253 (1980); b) Y. Murakami, A. Nakano, and H. Ikeda, *J. Org. Chem.*, **47**, 2137 (1982); c) Y. Murakami, A. Nakano, and A. Yoshimatsu, *Chem. Lett.*, **1984**, 13.
8) a) Y. Murakami, A. Nakano, A. Yoshimatsu, and K. Fukuya, *J. Am. Chem. Soc.*, **103**, 728 (1981); b) Y. Murakami, Y. Aoyama, J. Kikuchi, K. Nishida, and A. Nakano, *ibid.*, **104**, 2937 (1982); c) Y. Murakami, A. Nakano, K. Akiyoshi, *Bull. Chem. Soc. Jpn.*, **55**, 3004 (1982).
9) Y. Murakami, Y. Aoyama, A. Nakano, T. Tada, and K. Fukuya, *J. Am. Chem. Soc.*, **103**, 3951 (1981).
10) L. Werthemann, R. Keese, and A. Eschenmoser, unpublished results; see, L. Werthemann, Dissertation, ETH Zürich (Nr. 4097), Juris Druck and Verlag, Zürich (1968).
11) When heated above 65 °C, the lactonization proceeded in part at the peripheral site of the B ring; IR (neat) 1790 cm^{-1} (lactone C=O).
12) R. Bonnett, J. M. Godfrey, V. B. Math, P. M. Scopes, and R. N. Thomas, *J. Chem. Soc., Perkin Trans. 1*, **1973**, 252.
13) J. H. Fendler and W. L. Hinze, *J. Am. Chem. Soc.*, **103**, 5439 (1981).
14) C. Huang and J. T. Mason, *Proc. Natl. Acad. Sci. USA*, **75**, 308 (1978).
15) Diethyl ether ($E_T(30)=34.6$) was used as an extractant in the present work for technical reasons. $N^+C_5Ala2C_{12}$ in the vesicular state is hardly extracted with diethyl ether, while the present alkyl bromides present in the bulk aqueous phase were readily extracted. The extracted bromides were analyzed quantitatively by GLC. The fraction of the entrapped bromides was evaluated under consideration that those bromides bound to the vesicle are not readily extracted with diethyl ether.

Synthesis, Spectral and Magnetic Properties and Crystal Structures of Alkoxo-oxygen Coordinated Copper(II) Complexes of *N,N'*-Disubstituted Malonamide and Oxamide Derivatives

Takashi Toki, Masahiro Mikuriya,* Hisashi Ōkawa, Ichiro Murase,† and Sigeo Kida
Department of Chemistry, Faculty of Science, Kyushu University 33, Hakozaki, Higashi-ku, Fukuoka 812
†*Laboratory of Chemistry, College of General Education, Kyushu University 01, Ropponmatsu, Chuo-ku, Fukuoka 810*
(Received February 25, 1984)

1:1 Copper(II) complexes with *N,N'*-bis(2-hydroxyethyl)malonamide (abbreviated as H_4maae), MCu(maae) (M=Ca, Sr, Ba), and 2:1 copper(II) complexes with *N,N'*-bis(5-amino-3-hydroxypentyl)malonamide and *N,N'*-bis(5-amino-3-hydroxypentyl)oxamide (abbreviated as H_4madpl and H_4oxdpl, respectively),[Cu_2(madpl)]·$3H_2O$ and [Cu_2(oxdpl)]·$2H_2O$, were prepared and characterized by elemental analyses, infrared and electronic spectra, and magnetic susceptibilities. The 2:1 complexes exhibit a band at 23.3—27.0×10^3 cm^{-1} characteristic of alkoxo-oxygen bridged structure and show a very strong antiferromagnetic interaction, whereas the 1:1 complexes show no such band and their magnetic moments fall in the range of those for ordinary mononuclear copper(II) complexes. The crystal structures of [Cu_2(madpl)]·$3H_2O$ and BaCu(maae)·$7H_2O$ were determined by the single-crystal X-ray diffraction method. The structure of [Cu_2(madpl)]·$3H_2O$ consists of alkoxo-oxygen bridged binuclear molecules, where $madpl^{4-}$ functions as a sexadentate binucleating ligand with an $N_2O_2N_2$ donor set. In BaCu(maae)·$7H_2O$, the basic unit is a hetero-metal tetranuclear entity $(H_2O)_2${Ba$(H_2O)_4$Cu(maae)}$_2$ in which the two Ba^{2+} are linked sharing two H_2O and are also bound to alkoxo oxygens of $Cu(maae)^{2-}$. On the basis of the crystal structures, their spectral properties were discussed.

Although a great number of binuclear copper(II) complexes have been prepared, only few examples containing amide nitrogen coordination are known. Recently, we reported the preparation, crystal structure, spectra and magnetic properties of binuclear copper(II) complexes of amides derived from 3-amino-1-propanol and various amino acids.[1] The deprotonated amide coordination resulted in a marked increase in the planarity of the molecule. The magnetic and spectral properties of these complexes are consistent with the planar structure. As the continuation, in this study, we have prepared new sexadentate binucleating ligands derived from the reaction of 1,5-diamino-3-pentanol and diethyl malonate or diethyl oxalate (abbreviated as H_4madpl and H_4oxdpl, respectively) and isolated their 2:1 copper(II) complexes,[Cu_2(madpl)] (**1**) and [Cu_2(oxdpl)] (**2**), respectively. We have also prepared 1:1 copper(II) complexes with *N,N'*-bis(2-hydroxyethyl)malonamide (abbreviated as H_4maae),[2] MCu(maae) (M=Ca, Sr, Ba) (**3**). These complexes were characterized by spectral and magnetic measurements. The determination of X-ray crystal structures have been carried out for [Cu_2(madpl)]·$3H_2O$ and BaCu(maae)·$7H_2O$. The former complex has been found to have an alkoxo-oxygen bridged binuclear structure as expected. On the other hand, the latter has been revealed to be composed of novel type linearly linked Cu–Ba–Ba–Cu tetranuclear entities.

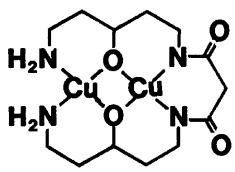

1

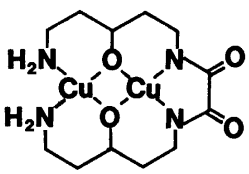

2

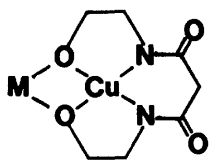

3

Experimental

Preparation of the Ligands. 1,5-Diamino-3-pentanol was prepared according to the method reported by Murase *et al.*[3] The preparative methods for H_4maae,[2] H_4madpl, and H_4oxdpl are all similar and exemplified by that for H_4oxdpl.

A 2:1 mixture of 1,5-diamino-3-pentanol and diethyl oxalate in ethanol was refluxed for 2 h. A white precipitate resulted was collected by filtration and washed with ethanol. This was used for synthesis of the complex without further purification.

Preparation of the Complexes. BaCu(maae)·$7H_2O$: To a mixture of copper(II) hydroxide (250 mg), H_4maae (500 mg) and sodium hydroxide (410 mg) in 100 ml of water was added 630 mg of barium chloride dihydrate under nitrogen atmosphere. The resulting reddish purple solution was filtered and allowed to stand overnight at room temperature. Red crystals separated were collected by filtration and dried in an open air. Anal. Found: C, 16.47; H, 4.62; N, 5.56%. Calcd for BaCu(maae)·$7H_2O$: C, 16.38; H, 4.71; N, 5.46%. The crystals lost all of the crystal water in a P_2O_5 desiccator under reduced pressure. Found: C, 21.57; H, 2.76; N, 7.16; Cu, 16.84%. Calcd for BaCu(maae): C, 21.72; H, 2.60; N, 7.24; Cu, 16.42%.

SrCu(maae): This complex was obtained as purple powder in the same way as that of BaCu(maae) except for using strontium chloride hexahydrate in place of barium chloride dihydrate. Found: C, 24.63; H, 3.07; N, 8.20; Cu, 19.12%. Calcd for SrCu(maae): C, 24.92; H, 2.99; N, 8.30; Cu, 18.84%.

CaCu(maae)·$3H_2O$: This complex was obtained as purple powder in the same way as that of BaCu(maae) except for using calcium chloride dihydrate instead of barium chloride dihydrate. The product was dried in a P_2O_5 desiccator under reduced pressure for two days. Found: C, 24.47; H, 4.74; N, 8.17; Cu, 20.50%. Calcd for CaCu(maae)·$3H_2O$: C, 24.45; H, 4.69; N, 8.15; Cu, 20.38%.

[Cu_2(madpl)]·$3H_2O$: To a mixture of copper(II) hydroxide (510 mg) and H_4madpl (800 mg) in 40 ml of water was added 840 mg of sodium hydroxide to give a reddish brown solution.

The solution was filtered and concentrated under reduced pressure to precipitate a red solid. It was recrystallized from ethanol to give red plates. Found: C, 32.45; H, 6.23; N, 11.48%. Calcd for $[Cu_2(madpl)]\cdot 3H_2O$: C, 32.43; H, 6.28; N, 11.64%.

$[Cu_2(oxdpl)]\cdot 2H_2O$: This complex was obtained as brown powder in a similar manner to the above but could not be recrystallized because of its low solubility in conventional solvents. Found: C, 31.99; H, 5.77; N, 12.39; Cu, 28.16%. Calcd for $[Cu_2(oxdpl)]\cdot 2H_2O$: C, 32.07; H, 5.83; N, 12.47; Cu, 28.28%.

Measurements. Cabon, hydrogen, and nitrogen analyses were carried out at the Service Center of Elemental Analysis, Kyushu University. Copper analysis was carried out with a Shimadzu Atomic Absorption-Flame Spectrophotometer Model AA-610. Infrared spectra were measured with a Hitachi Grating Infrared Spectrophotometer Model 215 in the region 4000—650 cm^{-1} on a KBr disk. Electronic spectra were measured with a Shimadzu Multipurpose Spectrophotometer Model MSP-5000 at room temperature. Magnetic susceptibility was measured by the Faraday method over the temperature range 80—300 K. The apparatus was calibrated by the use of $[Ni(en)_3]S_2O_3$. The susceptibilities were corrected for the diamagnetism of the constituent atoms by the use of Pascal's constants. Effective magnetic moments were calculated from the equation, $\mu_{eff}=2.828\sqrt{(\chi_A-N\alpha)T}$, where χ_A is the atomic magnetic susceptibility and $N\alpha$ is the

Table 1. Fractional positional parameters ($\times 10^4$) and thermal parameters of non-hydrogen atoms with their estimated standard deviations in parentheses

Atom	x	y	z	B_{eq}/Å^2
(1) $[Cu_2(madpl)]\cdot 3H_2O$				
Cu(1)	1228(1)	3001(1)	657(1)	2.7
Cu(2)	2541(1)	2306(1)	841(1)	2.4
O(1)	1860(3)	2387(8)	−490(5)	3.2
O(2)	4018(3)	2172(9)	−1401(6)	3.8
O(3)	4075(3)	2474(8)	3314(6)	3.2
O(4)	1896(2)	2901(8)	1969(5)	3.0
OW(1)	391(4)	233(11)	1153(8)	6.1
OW(2)	5037(3)	5897(10)	1219(8)	5.3
OW(3)	4395(3)	1440(9)	5993(7)	3.8
N(1)	609(3)	3037(11)	−894(8)	3.9
N(2)	3098(3)	1856(9)	−573(7)	2.6
N(3)	3119(3)	2253(9)	2423(6)	2.5
N(4)	685(3)	3952(10)	1981(8)	3.3
C(1)	758(4)	2484(14)	−2307(9)	3.8
C(2)	1207(4)	1247(13)	−2250(9)	3.6
C(3)	1830(4)	1763(11)	−1878(8)	2.8
C(4)	2292(4)	527(11)	−1968(9)	2.9
C(5)	2911(4)	1132(11)	−1915(8)	2.9
C(6)	3646(4)	2315(10)	−452(8)	2.4
C(7)	3879(4)	3091(11)	918(9)	3.2
C(8)	3674(4)	2551(10)	2315(8)	2.5
C(9)	2958(4)	1841(12)	3863(8)	3.5
C(10)	2320(5)	1541(14)	3964(10)	4.3
C(11)	1907(4)	2806(11)	3466(8)	3.0
C(12)	1298(5)	2678(10)	3945(11)	5.2
C(13)	868(5)	3938(13)	3534(10)	4.2
(2) $BaCu(maae)\cdot 7H_2O$				
Ba	708(1)	772(1)	−2161(1)	1.9
Cu	1235(2)	3822(2)	−2908(2)	1.9
O(1)	−668(12)	2568(10)	−3376(15)	2.5
O(2)	−40(13)	6900(10)	−1727(16)	2.7
O(3)	4700(13)	6978(10)	−2106(15)	2.5
O(4)	2280(14)	2582(10)	−3213(15)	2.5
OW(1)	−1251(13)	786(9)	−356(14)	2.5
OW(2)	−1421(14)	−1590(10)	−3637(15)	2.6
OW(3)	1711(15)	−552(11)	−4258(16)	3.3
OW(4)	2157(15)	2847(13)	463(17)	3.8
OW(5)	3858(14)	841(11)	−304(16)	3.2
OW(6)	4341(16)	1535(12)	3986(18)	3.6
OW(7)	5063(21)	576(14)	−2979(20)	4.8
N(1)	180(16)	5020(13)	−2518(19)	2.6
N(2)	3127(14)	5043(12)	−2556(19)	2.3
C(1)	−1733(24)	3039(17)	−3011(38)	5.2
C(2)	−1426(21)	4351(16)	−2811(33)	4.4
C(3)	716(18)	6177(14)	−2061(20)	2.1
C(4)	2350(20)	6867(16)	−1830(28)	3.4
C(5)	3464(18)	6236(14)	−2204(20)	2.2
C(6)	4285(20)	4504(14)	−2808(25)	2.9
C(7)	3917(18)	3218(14)	−2453(22)	2.4

temperature-independent paramagnetism in cgs emu.

X-Ray Crystal Structure Analysis. *[Cu₂(madpl)]·3H₂O*: A crystal with dimensions of 0.37×0.31×0.09 mm was used for the X-ray analysis. The unit-cell parameters and intensities were measured on a Rigaku AFC-5 automated four-circle diffractometer with graphite-monochromated Mo *Kα* radiation (λ=0.71069 Å) at 19±1°C. Intensity data were collected by the 2θ-ω scan technique with a scan rate of 8°min^{-1}. For weak reflections the peak scan was repeated up to four times depending on their intensities. Three standard reflections were monitored after every 100 reflections, and their intensities showed a good stability. The intensity data were corrected for the Lorentz and the polarization effects, but not for absorption.

Crystal Data: $Cu_2(C_{13}H_{24}N_4O_4)\cdot 3H_2O$, F. W.=481.5, monoclinic, space group $P2_1/n$, a=22.613(21), b=8.890(7), c=9.496(5) Å, β=93.00(8)°, D_m=1.66, D_c=1.68 g cm^{-3}, Z=4.

A total of 4200 reflections with $2\theta \leq 52°$ were collected, of

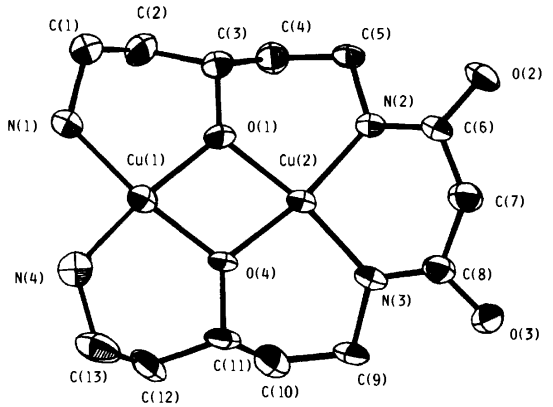

Fig. 1. Molecular structure of $[Cu_2(madpl)]\cdot 3H_2O$ with thermal ellipsoids (50% probability level). Water molecules are not shown.

Table 2. Interatomic distances (l/Å) and bond angles (ϕ/°) with their estimated standard deviations in parentheses

(1) $[Cu_2(madpl)]\cdot 3H_2O$			
(a) Copper coordination spheres			
Cu(1)···Cu(2)	3.029(3)	Cu(2)-O(1)	1.940(6)
Cu(1)-O(1)	1.922(6)	Cu(2)-O(4)	1.927(6)
Cu(1)-O(4)	1.910(6)	Cu(2)-N(2)	1.930(7)
Cu(1)-N(1)	1.978(8)	Cu(2)-N(3)	1.940(6)
Cu(1)-N(4)	1.990(8)		
Cu(1)-O(1)-Cu(2)	103.3(3)	N(1)-Cu(1)-N(4)	91.6(3)
Cu(1)-O(4)-Cu(2)	104.3(2)	O(1)-Cu(2)-O(4)	75.8(2)
O(1)-Cu(1)-O(4)	76.7(2)	O(1)-Cu(2)-N(2)	94.5(3)
O(1)-Cu(1)-N(1)	95.8(3)	O(4)-Cu(2)-N(3)	94.3(3)
O(4)-Cu(1)-N(4)	95.8(3)	N(2)-Cu(2)-N(3)	95.5(3)
(b) Madpl moiety			
N(1)-C(1)	1.484(12)	C(7)-C(8)	1.506(12)
C(1)-C(2)	1.496(15)	O(3)-C(8)	1.280(10)
C(2)-C(3)	1.506(13)	N(3)-C(8)	1.292(11)
O(1)-C(3)	1.428(10)	N(3)-C(9)	1.480(11)
C(3)-C(4)	1.522(13)	C(9)-C(10)	1.474(15)
C(4)-C(5)	1.499(13)	C(10)-C(11)	1.521(15)
N(2)-C(5)	1.469(11)	O(4)-C(11)	1.423(9)
N(2)-C(6)	1.306(11)	C(11)-C(12)	1.477(14)
O(2)-C(6)	1.270(10)	C(12)-C(13)	1.522(17)
C(6)-C(7)	1.541(12)	N(4)-C(13)	1.511(12)
Cu(1)-N(1)-C(1)	118.9(6)	N(3)-C(8)-C(7)	118.8(7)
N(1)-C(1)-C(2)	113.3(8)	O(3)-C(8)-C(7)	115.5(7)
C(1)-C(2)-C(3)	114.1(9)	O(3)-C(8)-N(3)	125.7(7)
O(1)-C(3)-C(2)	109.5(7)	Cu(2)-N(3)-C(8)	123.5(5)
Cu(1)-O(1)-C(3)	129.2(5)	Cu(2)-N(3)-C(9)	122.3(6)
C(2)-C(3)-C(4)	113.8(8)	C(8)-N(3)-C(9)	114.3(7)
O(1)-C(3)-C(4)	109.4(7)	N(3)-C(9)-C(10)	113.2(7)
Cu(2)-O(1)-C(3)	125.8(5)	C(9)-C(10)-C(11)	115.7(9)
C(3)-C(4)-C(5)	112.4(8)	O(4)-C(11)-C(10)	109.4(7)
N(2)-C(5)-C(4)	114.3(7)	Cu(2)-O(4)-C(11)	124.4(5)
Cu(2)-N(2)-C(5)	121.7(5)	C(10)-C(11)-C(12)	114.5(9)
C(5)-N(2)-C(6)	116.2(7)	O(4)-C(11)-C(12)	110.2(7)
Cu(2)-N(2)-C(6)	121.7(5)	Cu(1)-O(4)-C(11)	128.8(5)
N(2)-C(6)-C(7)	119.7(7)	C(11)-C(12)-C(13)	117.3(10)
O(2)-C(6)-N(2)	124.6(7)	N(4)-C(13)-C(12)	113.3(9)
O(2)-C(6)-C(7)	115.8(7)	Cu(1)-N(4)-C(13)	117.9(6)
C(6)-C(7)-C(8)	119.6(8)		
(c) Hydrogen bonds			
OW(1)···OW(1)$^{ia)}$	2.774(12)	OW(1)···N(1)	3.215(13)
OW(1)···OW(3)^{ii}	2.493(12)	OW(1)···N(4)	3.455(13)
OW(1)···O(3)^{iii}	2.728(12)	OW(2)···N(4)^{v}	2.429(11)
OW(1)···OW(3)$^{ii)}$	2.589(11)		
OW(2)···O(2)^{iv}	2.739(11)		
OW(2)···OW(2)^{iv}	2.809(12)		

TABLE 2. (Continued)

(2) BaCu(maae)·$7H_2O$			
(a) Barium coordination spheres			
Cu···Ba	3.569(2)	Ba-OW(2)	2.794(10)
Ba-O(1)	2.777(12)	Ba-OW(3)	2.811(16)
Ba-O(4)	2.741(13)	Ba-OW(4)	2.757(12)
Ba-OW(1)	2.889(15)	Ba-OW(5)	2.827(13)
Ba-OW(1)$^{ia)}$	2.960(12)		
O(1)-Ba-O(4)	60.6(4)	OW(1)-Ba-OW(2)	79.4(4)
O(1)-Ba-OW(1)	80.3(4)	OW(1)-Ba-OW(3)	149.5(3)
O(1)-Ba-OW(2)	110.8(3)	OW(1)-Ba-OW(4)	72.7(4)
O(1)-Ba-OW(3)	117.1(4)	OW(1)-Ba-OW(5)	117.8(4)
O(1)-Ba-OW(4)	74.6(4)	OW(2)-Ba-OW(3)	71.1(4)
O(1)-Ba-OW(5)	132.4(3)	OW(2)-Ba-OW(4)	150.2(5)
O(4)-Ba-OW(1)	132.9(4)	OW(2)-Ba-OW(5)	115.6(4)
O(4)-Ba-OW(2)	136.6(4)	OW(3)-Ba-OW(4)	131.1(4)
O(4)-Ba-OW(3)	76.5(4)	OW(3)-Ba-OW(5)	70.5(4)
O(4)-Ba-OW(4)	72.4(4)	OW(4)-Ba-OW(5)	70.8(4)
O(4)-Ba-OW(5)	78.2(4)	OW(1)^{i}-Ba-OW(5)	63.8(4)
OW(1)-Ba-OW(1)^{i}	67.1(4)	Ba-OW(1)-Ba^{i}	112.9(4)
(b) Copper coordination spheres			
Cu-O(1)	1.918(11)	Cu-N(1)	1.943(17)
Cu-O(4)	1.955(14)	Cu-N(2)	1.923(13)
O(1)-Cu-O(4)	91.8(5)	O(4)-Cu-N(2)	86.6(6)
O(1)-Cu-N(1)	86.7(6)	N(1)-Cu-N(2)	94.9(6)
(c) Maae moiety			
O(1)-C(1)	1.382(31)	C(4)-C(5)	1.526(30)
C(1)-C(2)	1.431(26)	O(3)-C(5)	1.265(20)
N(1)-C(2)	1.473(25)	N(2)-C(5)	1.292(20)
N(1)-C(3)	1.254(20)	N(2)-C(6)	1.457(27)
O(2)-C(3)	1.289(24)	C(6)-C(7)	1.528(24)
C(3)-C(4)	1.520(25)	O(4)-C(7)	1.428(18)
Cu-O(1)-Ba	97.3(4)	N(2)-C(5)-C(4)	120.6(16)
Cu-O(1)-C(1)	112.8(9)	O(3)-C(5)-N(2)	125.3(18)
Ba-O(1)-C(1)	130.2(14)	O(3)-C(5)-C(4)	114.1(14)
O(1)-C(1)-C(2)	114.5(21)	Cu-N(2)-C(5)	129.1(14)
N(1)-C(2)-C(1)	114.7(19)	Cu-N(2)-C(6)	113.3(10)
Cu-N(1)-C(2)	108.8(11)	C(5)-N(2)-C(6)	117.5(14)
Cu-N(1)-C(3)	128.4(14)	N(2)-C(6)-C(7)	104.8(16)
C(2)-N(1)-C(3)	122.8(17)	O(4)-C(7)-C(6)	112.9(13)
N(1)-C(3)-C(4)	122.7(18)	Cu-O(4)-Ba	97.5(6)
O(2)-C(3)-N(1)	124.2(17)	Ba-O(4)-C(7)	127.6(10)
O(2)-C(3)-C(4)	113.1(13)	Cu-O(4)-C(7)	106.0(9)

a) Symmetry code

Superscript	
i	$-x, -y, -z$
ii	$x-1/2, y, z-1/2$
iii	$1/2-x, -y, 1/2-z$
iv	$1-x, 1-y, -z$
v	$1/2-x, 1-y, 1/2-z$

which independent 2596 reflections had $|F_o| \geq 3\sigma(F_o)$ and were employed in the solution and refinement of the structure.

The structure was solved by the heavy-atom method. Refinement was carried out by the block-diagonal least-squares method. All the hydrogen atoms except for those of the water molecules were located from the difference Fourier map and included in the refinement. The final R value was 0.067.

BaCu(maae)·7H₂O: Data collection from a crystal of dimensions of 0.40×0.30×0.28 mm was carried out in a fashion similar to that employed for $Cu_2(madpl)\cdot 3H_2O$.

Crystal Data: $BaCu(C_7H_{10}N_2O_4)\cdot 7H_2O$, F. W.=513.2, triclinic space group $P\bar{1}$, a=9.642(3), b=11.374(3), c=8.761(3) Å, α=96.93(2), β=112.27(2), γ=102.83(2)°, D_m=2.02, D_c=2.02 g cm^{-3}, Z=2.

A total of 3746 reflections with $2\theta \leq 52°$ were collected, of which independent 3184 reflections had $|F_o| \geq 3\sigma(F_o)$ and were used in the solution and refinement of the structure. The structure was solved by the heavy-atom method and refined by the block-diagonal least-squares method. All the hydrogen atoms except for those bound to the water oxygen atoms, OW(2), OW(3), OW(4), and OW(5), were located from the difference Fourier map and included in the refinement. The final R value was 0.080.

All the calculations were carried out on the FACOM M-200 computer in the Computer Center of Kyushu University by the use of a local version[4] of the UNICS-III and the ORTEP programs. The final positional and thermal parameters with their estimated standard deviations are given in Table 1. The coordinates and isotropic temperature factors of the hydrogen atoms, the anisotropic thermal parameters of the nonhydrogen atoms, and the F_o-F_c tables have been deposited as a Document No. 8428 at the Office of the Editor.

Results and Discussion

Description of the Structure. *[Cu_2(madpl)]·3H_2O*: The crystal consists of alkoxo-oxygen bridged binuclear molecules, [Cu_2(madpl)], and crystal water. A perspective drawing of the binuclear molecule and the numbering system are illustrated in Fig. 1. Bond lengths and angles are listed in Table 2.

The two copper atoms, Cu(1) and Cu(2), are bridged by two alkoxo-oxygen atoms of madpl, O(1) and O(4). The N_2O_2 donor sets are planar and Cu(1) and Cu(2) deviate from the relevant N_2O_2 planes only by 0.081 and 0.018 Å, respectively. The dihedral angle of the planes is 7.4°. The Cu–O bond lengths (1.910—1.940 Å) and the Cu–N (amine) bond lengths (1.978(8) and 1.990(8) Å) are normal for in-plane coordination.[5-7] The Cu–N (amide) distances (1.930(7) and 1.940(6) Å) are substantially shorter than the Cu–N (amine) distances and fall in the range of those of deprotonated amide complexes (1.89—1.99 Å, average 1.92 Å).[8]

In the madpl moiety, the C–N bond lengths of the amide bonds (1.306(11) and 1.292(11) Å) are shorter than the other C–N bond distances (1.469—1.511 Å) as found in many copper(II) complexes with deprotonated amides.[8] The madpl ligand forms five six-membered chelate rings with two copper atoms. All these chelate rings assume a boat conformation (Table 3). The bonds attached to the bridging oxygen atom are almost coplanar (sums of the bond angles subtended at O(1) and O(3) are 358.3 and 357.5°, respectively).

The water molecules are located in the vicinity of

Table 3. Coefficients of equations of mean planes and deviations of atoms from the planes

	l	*m*	*n*	*d*	Distances from the planes (*l*/Å)			
(1) [Cu_2(madpl)]·3H_2O								
(a) Plane through	0.2703	0.9328	−0.2521	3.1635	O(1)	0.070	O(4)	−0.071
O(1), O(4), N(1), N(4)					N(1)	−0.059	N(4)	0.059
					Cu(1)	−0.081		
(b) Plane through	0.1926	0.9708	−0.1531	2.9921	O(1)	−0.051	O(4)	0.051
O(1), O(4), N(2), N(3)					N(2)	0.042	N(3)	−0.042
					Cu(2)	−0.018		
(c) Plane through	0.2324	0.9523	0.1853	3.8878	O(4)	−0.089	N(3)	0.085
O(4), N(3), C(9), C(11)					C(9)	−0.095	C(11)	0.100
					Cu(2)	−0.453	C(10)	−0.666
(d) Plane through	0.3542	0.9352	−0.0236	3.8371	O(4)	0.049	N(4)	−0.047
O(4), N(4), C(11), C(13)					C(11)	−0.055	C(13)	0.053
					Cu(1)	−0.373	C(12)	−0.659
(e) Plane through	0.1633	0.8864	−0.4412	2.8100	O(1)	−0.037	N(2)	0.036
O(1), N(2), C(3), C(5)					C(3)	0.042	C(5)	−0.041
					Cu(2)	−0.408	C(4)	−0.724
(f) Plane through	0.2592	0.9117	−0.3319	3.1394	O(1)	0.040	N(1)	−0.039
O(1), N(1), C(1), C(3)					C(1)	0.045	C(3)	−0.046
					Cu(1)	−0.194	C(2)	−0.713
(g) Plane through	−0.2586	0.9599	−0.0944	−0.1475	N(2)	−0.029	N(3)	0.029
N(2), N(3), C(6), C(8)					C(6)	0.031	C(8)	−0.032
					Cu(2)	0.554	C(7)	0.434
(h) Plane through	0.2121	0.9316	−0.3060	2.8835	Cu(1)	0.000	Cu(2)	0.000
Cu(1), Cu(2), C(3)					C(3)	0.000	O(1)	0.128
(i) Plane through	0.2069	0.9773	−0.0554	3.1476	Cu(1)	0.000	Cu(2)	0.000
Cu(1), Cu(2), C(11)					C(11)	0.000	O(4)	0.156
(j) Plane through	0.2114	0.9599	−0.1950	3.0218	Cu(1)	0.005	Cu(2)	0.005
Cu(1), Cu(2), O(1), O(4)					O(1)	−0.005	O(4)	−0.005
					C(3)	−0.294	C(11)	−0.358
(2) BaCu(maae)·7H_2O								
(a) Plane through	−0.0162	−0.2165	0.9314	−3.3350	O(1)	−0.042	O(4)	0.042
O(1), O(4), N(1), N(2)					N(1)	0.041	N(2)	−0.041
					Cu	0.001	Ba	1.370
(b) Plane through	−0.0170	−0.2461	0.9313	−3.4629	Cu	0.000	O(1)	0.000
Cu, O(1), N(1)					N(1)	0.000	C(1)	0.184
					C(2)	−0.026		
(c) Plane through	−0.0153	−0.1869	0.9306	−3.2018	Cu	0.000	O(4)	0.000
Cu, O(4), N(2)					N(2)	0.000	C(6)	−0.109
					C(7)	0.460		
(d) Plane through	0.0300	−0.2540	0.9133	−3.4206	Cu	0.025	N(1)	−0.039
Cu, N(1), N(2), C(3),					N(2)	0.010	C(3)	0.008
C(4), C(5)					C(4)	0.040	C(5)	−0.044
					O(2)	0.044	O(3)	−0.144
(e) Plane through	−0.0834	0.1787	0.8829	−1.5721	Ba	0.000	Cu	0.000
Ba, Cu, C(1)					C(1)	0.000	O(1)	−0.465
(f) Plane through	−0.0887	0.1798	0.8846	−1.5778	Ba	0.000	Cu	0.000
Ba, Cu, C(7)					C(7)	0.000	O(4)	−0.579

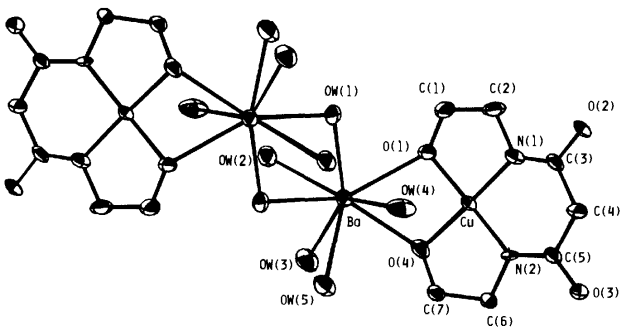

Fig. 2. A perspective view of $BaCu(maae)\cdot 7H_2O$ with thermal ellipsoids (50% probability level).

the amino and carbonyl groups of the madpl ligand by hydrogen bonding (Table 2) and do not coordinate to the copper atoms.

$BaCu(maae)\cdot 7H_2O$: The molecular structure of $BaCu(maae)\cdot 7H_2O$ is shown in Fig. 2. The unit cell contains two $BaCu(maae)\cdot 5H_2O$ units and crystal water molecules. Two water molecules intervene between two barium atoms to form a Cu-Ba-Ba-Cu tetranuclear entity as shown in Fig. 2. This unit is located at the crystallographic inversion center.

Each copper atom is coordinated by two alkoxo-oxygen and two amide nitrogen atoms in a square-planar geometry. These donor atoms are almost coplanar with the largest deviation of 0.042 Å, and the copper atom deviates from this plane by 0.001 Å. The Cu-O bond lengths (1.918(11) and 1.955(14) Å) fall in the range of those of the alkoxo-oxygen bridged binuclear copper(II) complexes.[1,5-7] The Cu-N (1.943(17) and 1.923(13) Å), C=O (1.289(24) and 1.265(20) Å) and C-N 1.254(20) and 1.292(20) Å) distances of the amide bonds are normal for the bond lengths of copper(II) complexes with deprotonated amides.[8] In the IR spectrum, the amide I (at≈1630 cm^{-1}) and amide II[9] (at≈1560 cm^{-1}) bands of the H_4maae are replaced by the band at≈1595 cm^{-1} on coordination. This is in accord with the general rule for the deprotonated amide coordination.[1]

The six-membered Cu-N(1)-C(3)-C(4)-C(5)-N(2) chelate ring is planar, the maximum deviation from the least-squares plane being 0.044 Å. The two five-membered Cu-O(1)-C(1)-C(2)-N(1) and Cu-O(4)-C(7)-C(6)-N(2) chelate rings assume a gauche conformation as is usually observed for saturated five-membered chelate rings.

The coordination around the barium atom is a distorted square antiprism with two alkoxo-oxygen atoms from the maae ligand and six water oxygen atoms. The barium-oxygen distances vary from 2.741 to 2.960 Å. These values are in the normal range for an eight-coordinated barium ion.[10] The Ba-O(1) and Ba-O(4) bond lengths are substantially shorter than the Ba-O (water oxygen) distances. The barium atom is not in the coordination plane of Cu(maae), the deviation from the O(1)-O(4)-N(1)-N(2) plane being 1.37 Å (Table 3). The geometries around the alkoxo-oxygen atoms considerably deviate from planar arrangement (sums of the bond angles subtended at O(1) and O(4) are 340.3 and 331.1 °, respectively).

Electronic Spectra. Some examples of the electronic spectra in nujol mull are shown in Fig. 3. The band maxima are given in Table 4.

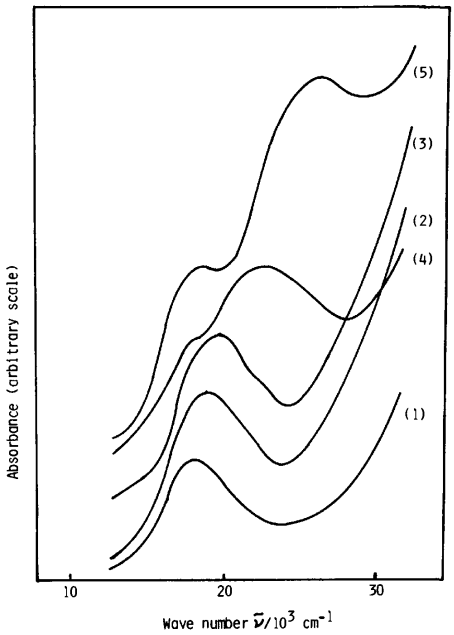

Fig. 3. Electronic spectra of (1) $CaCu(maae)\cdot 3H_2O$, (2) SrCu(maae), (3) BaCu(maae), (4) $[Cu_2(oxdpl)]\cdot 2H_2O$, and (5) $[Cu_2(madpl)]\cdot 3H_2O$ in nujol mull.

Table 4. Spectral data

Complex	Nujol mull spectra $\tilde{\nu}_{max}/10^3$ cm^{-1}	
$[Cu_2(madpl)]\cdot 3H_2O$	19.0	27.0
	18.2(97)	27.8(1260)[a]
$[Cu_2(oxdpl)]\cdot 2H_2O$	18 sh[b]	23.3
BaCu(maae)	19.8	
$BaCu(maae)\cdot 7H_2O$	18.8	
SrCu(maae)	19.2	
$CaCu(maae)\cdot 3H_2O$	18.5	

a) Absorption spectra in aqueous solution($\tilde{\nu}_{max}/10^3$ cm^{-1} (ε)). b) sh=shoulder.

All the complexes show a band assignable to d-d transitions at 18.5—19.8×10^3 cm^{-1}. The relatively high values of $\tilde{\nu}_{max}$ considered from the N_2O_2 coordination environment may be attributed to the square-planar coordination free from the axial perturbation.[1] More intense bands were observed at 27.0×10^3 and 23.3×10^3 cm^{-1} for $[Cu_2(madpl)]\cdot 3H_2O$ and $[Cu_2(oxdpl)]\cdot 2H_2O$, respectively. On the other hand, in the MCu(maae) complexes, no such bands were observed in this region. It is known that alkoxo-oxygen bridged binuclear copper(II) complexes always show an absorption at 22—29×10^3 cm^{-1}. This band is characteristic of alkoxo-oxygen bridged structure and may be assigned to $p_\pi(O)\rightarrow d(Cu)$ charge transfer transition.[11-13] The absence and presence of the characteristic CT band in the present complexes are understandable in terms of their bonding mode of the bridging oxygen atoms. The X-ray structure analyses of $[Cu_2(madpl)]\cdot 3H_2O$ and $BaCu(maae)\cdot$

Table 5. Magnetic data

Complex	μ_{eff}/B.M. (T/K)	θ/K	$2J$/cm^{-1} [a]	$N\alpha\times10^6$/cgs emu	P
$[Cu_2(madpl)]\cdot3H_2O$	0.36 (293)		−1075	27	0.017
$[Cu_2(oxdpl)]\cdot2H_2O$	0.55 (298)		−855	60	0.020
BaCu(maae)	1.71 (291)	−5			
SrCu(maae)	1.75 (288)	−5			
$CaCu(maae)\cdot3H_2O$	1.83 (295)	−12			

a) For all the complexes g=2.10 was assumed.

$7H_2O$ show that both complexes have alkoxo-oxygen bridged structures, but the two structures differ in their bridging mode: in $[Cu_2(madpl)]\cdot3H_2O$ the bonds attached to the bridging oxygen are almost coplanar as found for alkoxo-oxygen bridged binuclear copper(II) complexes so far reported,[1,5-7] whereas in BaCu(maae)·$7H_2O$ the geometry around the alkoxo-oxygen atom considerably deviates from planar arrangement. This fact suggests that a planar structure of the bridging oxygen may be responsible for the appearence of the characteristic band. Kida *et al.* interpreted the $p_\pi(O)\rightarrow$ d(Cu) charge transfer band in the visible region in the following way.[12] Usually the nonbonding orbital on the alkoxo-oxygen atom should be regarded to be sp^3 hybridized orbital rather than a p_z orbital. However, in the case of the bridging oxygen in a planar binuclear-structure, the good planarity of the Cu O Cu bond would

result in a pure p-character of the nonbonding orbital of the alkoxo-oxygen atom. Since optical electronegativity of the nonbonding electrons is dependent on the degree of hybridization of 2s and 2p orbitals, the O→Cu charge transfer band for the planar binuclear-structure would be lower in frequency compared with those of the usual nonplanar alkoxo complexes such as BaCu(maae)·$7H_2O$.

Magnetic Susceptibilities. The magnetic moments of the MCu(maae) complexes are 1.71—1.83 B. M. at room temperature. These complexes obey the Curie-Weiss law, $\chi_A=C/(T-\theta)$, in the temperature range 80—300 K. The Weiss constants, θ, are given in Table 5. The small negative θ values indicate that a weak antiferromagnetic interaction is operative between the copper(II) ions.

The magnetic moments per copper atom of $[Cu_2(madpl)]\cdot3H_2O$ and $[Cu_2(oxdpl)]\cdot2H_2O$ are 0.36 and 0.55 B. M., respectively, at room temperature, indicating a strong antiferromagnetic interaction is operating between the copper (II) ions. The temperature dependence of magnetic susceptibilities for these complexes can be interpreted by the modified Bleaney-Bowers equation[14]

$$\chi_A=\frac{Ng^2\beta^2}{3kT}\left[1+\frac{1}{3}\exp(-2J/kT)\right]^{-1}(1-P)+\frac{0.45P}{T}+N\alpha \quad (1)$$

where χ_A is a susceptibility per copper atom, P is the mole fraction of the mononuclear copper(II) impurity, and other symbols have the usual meanings. The second term in Eq. 1 was added to account for the presence of a small amount of paramagnetic impurity. The parameters, $-2J$, $N\alpha$, and P were evaluated from the best fit of the experimental data to Eq. 1 and are listed in Table 5. It is notable that the $-2J$ values, the energy separation between the spin-singlet ground state and the lowest spin-triplet state, for the present binuclear complexes are very large. Generally an antiferromagnetic spin-exchange interaction between two copper(II) ions becomes stronger when the tetragonal planes of the two copper(II) ions become more coplanar. In $[Cu_2(madpl)]\cdot3H_2O$, the two copper(II) ions and the donating atoms are almost coplanar, and there is no axial coordination which is a factor of depressing the antiferromagnetic interaction. Therefore, the very strong antiferromagnetic interaction observed for the present binuclear copper(II) complexes is attributable to the planar skeleton.[1]

The present work was partially supported by a Grant-in-Aid for Scientific Research No. 57740319 from the Ministry of Education, Science and Culture.

References

1) M. Mikuriya, T. Harada, H. Ōkawa, and S. Kida, *Inorg. Chim. Acta*, **75**, 1 (1983).
2) H. Ojima, *Kagaku No Ryoiki*, **26**, 937 (1972).
3) I. Murase, M. Hatano, M. Tanaka, S. Ueno H. Ōkawa, and S. Kida, *Bull. Chem. Soc. Jpn.*, **55**, 2404 (1982).
4) S. Kawano, *Rep. Comp. Cent. Kyushu Univ.*, **16**, 113 (1983); T. Sakurai and K. Kobayashi, *Rep. Inst. Phys. Chem. Res.*, **55**, 69 (1979); C. K. Johnson, Report No. 3794, Oak Ridge National Laboratotry, Oak Ridge, Tennessee (1965).
5) K. Nieminen and M. Näsäkkälä, *Acta Chem. Scand., Ser. A*, **34**, 375 (1980); K. Nieminen, *Acta Chem. Scand., Ser. A*, **35**, 753 (1981).
6) A. C. Villa, L. Coghi, A. G. Manfredotti, and C. Guastini, *Cryst. Struct. Commun.*, **3**, 543 (1974); N. Matsumoto, S. Kida, and I. Ueda, *J. Coord. Chem.*, **9**, 133 (1979).
7) M. Mikuriya, H. Ōkawa, and S. Kida, *Inorg. Chim. Acta*, **42**, 233 (1980); *ibid.*, **68**, 111 (1983); *Bull. Chem. Soc. Jpn.*, **53**, 2871 (1980); *ibid.*, **55**, 1086 (1982).
8) H. C. Freeman, *Adv. Protein Chem.*, **22**, 257 (1967); H. Sigel and R. B. Martin, *Chem. Rev.*, **82**, 385 (1982).
9) L. J. Bellamy, "The Infra-red Spectra of Complex Molecules," 3rd ed., Chapman and Hall, London (1975) p. 231.
10) E. Dubler, P. Korber, and H. R. Oswald, *Acta Crystallogr., Sect. B*, **29**, 1929 (1973); R. D. Shannon, *Acta Crystallogr., Sect. A*, **32**, 751 (1976); K. Mereiter and A. Preisinger, *Acta Crystallogr., Sect. B*, **38**, 382 (1982).
11) Y. Ishimura, Y. Nonaka, Y. Nishida, and S. Kida, *Bull. Chem. Soc. Jpn.*, **46**, 3728 (1973); Y. Nishida and S. Kida, *Chem. Lett.*, **1974**, 339; Y. Nishida, F. Numata, and S. Kida, *Inorg. Chim. Acta*, **11**, 189 (1974); Y. Nishida and S. Kida, *J. Inorg. Nucl. Chem.*, **38**, 451 (1976).
12) S. Kida, Y. Nishida, and M. Sakamoto, *Bull. Chem.*

Soc. Jpn., **46**, 2428 (1973).
13) M. Mikuriya, H. Ōkawa, and S. Kida, *Inorg. Chim. Acta*, **34**, 13 (1979); *Bull. Chem. Soc. Jpn.*, **53**, 3717 (1980); M. Nakamura, M. Mikuriya, H. Ōkawa, and S. Kida, *Bull. Chem. Soc. Jpn.*, **54**, 1825 (1981); M. Mikuriya, H. Ōkawa, and S. Kida, *Bull. Chem. Soc. Jpn.*, **54**, 2943 (1981); M. Mikuriya, M. Nakamura, H. Ōkawa, and S. Kida, *Inorg. Chim. Acta*, **70**, 223 (1983).
14) K. E. Hyde, G. Gordon, and G. F. Kokoszka, *J. Inorg. Nucl. Chem.*, **30**, 2155 (1968).

Photochemistry of Dihalogenobis(diamine)chromium(III) Complexes in Methanol

Masanori SAWANO, Hideki YOSHIFUJI, Akira UEHARA,* and Ryokichi TSUCHIYA
Department of Chemistry, Faculty of Science, Kanazawa University, Kanazawa 920
(Received February 29, 1984)

The photochemical reactions of *trans*- and *cis*-$[CrX_2(AA)_2]X$ in methanol were investigated under the ligand-field band irradiation, where X is Cl^- or Br^- ion and AA is en, pn or tn. In the earlier step of irradiation, only trans-to-cis photoisomerization was observed irrespective of diamines. The process of the photoisomerization was reasonably explained in terms of the bond indices calculated on the basis of VC theory. The quantum yields for dichloro complexes were larger than those for dibromo complexes, and the yields increased in the order of pn<en<tn complexes. The photochemistry of *cis*-$[CrCl_2(pn)_2]Cl$ was also studied and the difference of the photochemical reactions from the thermochemical reactions was discussed.

We have systematically studied the thermal cis-trans isomerization of $[CrX_2(AA)_2]X$ type complexes in a solid phase since ten years ago, where X is Cl^- or Br^- ion and AA is a diamine selected from ethylenediamine (en), *dl*-1,2-propanediamine (pn) and 1,3-propanediamine (tn).[1-4] In these studies, cis-to-trans isomerization was detected in the complexes containing tn which forms six-membered chelate ring with chromium(III) ion, whereas trans-to-cis isomerization was recognized in the complexes containing en or pn which forms five-membered chelate ring. The mechanism of the thermal isomerization was verified to be bond rupture.[1c,4]

The isomerization takes place not only in thermal environment, but also under sunlight. We have actually noticed that the exposure of *trans*-$[CrCl_2(pn)_2]Cl$ to sunlight readily causes trans-to-cis isomerization in a solid state. However, the photochemical reaction is difficult to be traced quantitatively in the solid because the reaction takes place just on the surface of the compound. Therefore, few studies have been devoted to the photochemistry in a solid state.[5]

In recent years, on the other hand, the photochemistries of transition metal complexes have extensively been investigated in solution.[6] Whether photochemical reactions are allowed or forbidden have reasonably been discussed on the basis of the orbital symmetries of reactants, products and intermediates.[7]

In the present study, the isomerization and subsequent reactions of $[CrX_2(AA)_2]X$ type complexes in methanol were investigated under the ligand-field band irradiation, where X is Cl^- or Br^- ion and AA is en, pn, or tn.

Experimental

Preparation of Complexes. *trans*-$[CrCl_2(en)_2]Cl$,[8] *cis*-$[CrCl_2(en)_2]Cl$,[9] *trans*-$[CrCl_2(pn)_2]Cl\cdot 1.5H_2O$,[10] *cis*-$[CrCl_2(pn)_2]Cl$,[11] *cis*- and *trans*-$[CrCl_2(tn)_2]Cl$,[12] *trans*-$[CrBr_2(en)_2]Br$,[13] *cis*-$[CrBr_2(en)_2]Br$,[14] *cis*- and *trans*-$[CrBr_2(pn)_2]Br$,[1b] and *cis*- and *trans*-$[CrBr_2(tn)_2]Br$[2b] were prepared by the known methods partially modified. The crude products were purified by the recrystallization from dry methanol and ether several times.

Isolation of Products during Photochemical Reactions. *fac-*$[CrCl_2(CH_3OH)(pn)_2]Cl\cdot H_2O$ *and cis-*$[CrBr(CH_3OH)(pn)_2]Br_2$: They were isolated during photochemical reaction of *cis*-$[CrCl_2(pn)_2]Cl$ and *cis*-$[CrBr_2(pn)_2]Br$, respectively. The light of 400 nm was irradiated for more than 600 min on the solution (methanol) containing appropriate amounts of *cis*-$[CrCl_2(pn)_2]Cl$ or *cis*-$[CrBr_2(pn)_2]Br$. The resulting solutions were evaporated to about a half of its volume, and thereto an appropriate amount of ether was added to precipitate the desired materials. The precipitates thus obtained were recrystallized from dry methanol–ether (1:1). The products were identified by means of elemental analyses, TLC, UV- and far-IR spectrophotometry, and molar conductivity measurements. Details will be mentioned in the later section.

Found for the former complex: C, 23.57; H, 7.61; N, 15.25%. Calcd for *fac*-$[CrCl_2(CH_3OH)(pn)_2]Cl\cdot H_2O$: C, 23.87; H, 7.34; N, 15.71%. Found for the latter complex: C, 17.61; H, 4.95; N, 11.36; Cr^{3+}, 11.03%. Calcd for *cis*-$[CrBr(CH_3OH)(pn)_2]Br_2$: C, 17.81; H, 5.12; N, 11.87; Cr^{3+}, 11.02%.

Preparation of Materials Used as Actinometer. Potassium tris(oxalato)ferrate(III), $K_3[Fe(C_2O_4)_3]$ was prepared by the literature method,[15] and Reinecke's salt, $K[Cr(NCS)_4(NH_3)_2]$ was derived from the corresponding ammonium salt[16] by metathesis.

Measurements. The apparatus used for the photochemical reactions was the lamp house (Model UI-501C) by Ushio Denki Co., Ltd. The light source was a 500 W Ushio short arc xenon lamp (Model UXL-500D-O). The monochromatized beams of 400, 530, and 580 nm were obtained with Toshiba interference filters, KL-40, KL-53 and KL-58, respectively.

The sample solution for photochemical reactions was prepared by dissolving either one of the complexes in absolute methanol. The solution was irradiated in a thermostated spectrophotometric cell of 10 cm length with a continuous mechanical stirring. A part of the beam for irradiation to the sample was simultaneously reflected by quartz plate and introduced into the cell setting the actinometer. The wavelengths used for irradiation were 400 and 580 nm for trans-complexes and 400 and 530 nm for cis-complexes. As the actinometer potassium tris(oxalato)ferrate(III)[17] was used for 400 nm, and Reinecke's salt, for 530 and 580 nm.[18] The temperature applied were 22 and 32 °C. The change in absorbances of the sample solution was measured at each relevant wavelength and the extents of photoconversion were determined. They were corrected by measuring the dark reaction under the same conditions as those for the sample solution.

The photochemical products were identified by measuring electronic spectra, far-IR spectra and molar conductivities, and by means of TLC and thermal analyses. The instruments used for the measurement of spectra were a JASCO UVIDEC-505 UV/VIS recording digital spectrophotometer and a JASCO Model IR-F far infrared spectrophotometer. The measurement of molar conductivities was carried out with a Yokogawa Universal Bridge BV-Z-12A. The plates used for TLC were those of silica gel G 250 made by Merck Ltd. Thermal analyses were performed with a MOM Typ-OD-102 Derivatograph and with a Chyo

Thermobalance.

Results

First, it should be noted for clarification of the following discussion that only trans-to-cis isomerization was detected for all the trans complexes, and no isomerization was found for the cis complexes, but instead the coordination of solvent was recognized.

Photochemical Reactions. trans-*[CrCl$_2$(pn)$_2$]Cl·1.5H$_2$O*: The photochemical behavior of the complex was basically the same irrespective of the irradiation wavelengths (580 and 400 nm) used for excitation. Figure 1 shows the electronic spectral changes with time on 580 nm irradiation in methanol at 22 °C. As seen from the figure, the absorption peaks of the complex shift with time toward those of the corresponding cis complex. Any isosbestic point is not detectable in the spectra. However, the application of TLC to the sample solution after irradiation for about thirty minutes evidenced the presence of *trans-* and *cis-*[$CrCl_2(pn)_2$]Cl. Table 1 summarized the R_f values. The R_f's (0.54 and 0.33) for the sample solution are quite close to those of the reference trans-form (0.54) and cis-form (0.34). Thus, the first photochemical reaction within thirty minutes is trans-to-cis photoisomerization.

Further irradiation brought about subsequent spectral changes, suggesting that a secondary photochemical reaction occurs besides the trans-to-cis isomerization. The secondary photochemical reaction was found to be parallel to the reaction of *cis-*[$CrCl_2(pn)_2$]Cl as described later.

trans-*[CrCl$_2$(en)$_2$]Cl*, trans-*[CrBr$_2$(en)$_2$]Br*, trans-*[CrBr$_2$(pn)$_2$]Br*, trans-*[CrCl$_2$(tn)$_2$]Cl and* trans-*[CrBr$_2$(tn)$_2$]Br*: The photochemical behaviors of the complexes were monitored on 580 and 400 nm irradiations in methanol at 22 and 32 °C. In all cases, the absorption spectra of the trans complexes shifted to those of the corresponding cis complexes. After the irradiation for about thirty minutes, the sample solutions were checked by TLC. Inspection of the R_f values in Table 1 reveals that all the sample solutions contain both trans and cis complexes. Thus, the photochemical reaction within 30 min is trans-to-cis isomerization. Interesting is that the direction of photo-isomerization (trans-to-cis) of the tn complexes is contrast to that of the thermal isomerization (cis-to-trans).

Further irradiation on the solution of *trans-*[$CrBr_2(pn)_2$]Br causes an additional reaction other than iso-

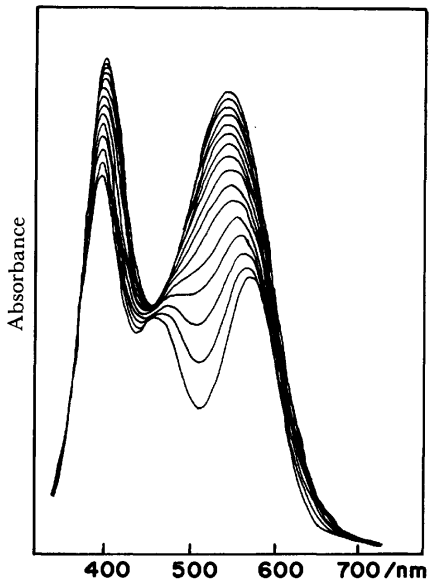

Fig. 1. Electronic spectral changes with time of *trans-*[$CrCl_2(pn)_2$]Cl·1.5H$_2$O in methanol on 580 nm irradiation at 22 °C. The spectra were monitored every ten minutes.

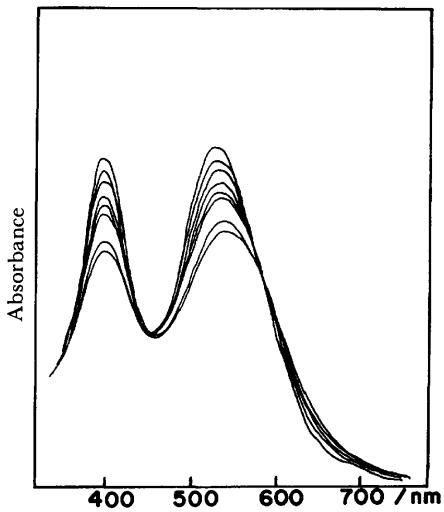

Fig. 2. Electronic spectral changes with time of *cis-*[$CrCl_2(pn)_2$]Cl in methanol on 530 nm irradiation at 22 °C. The spectra were monitored every twenty minutes.

Table 1. R_f Values by thin layer chromatography(TLC)[a]

Starting complex	Sample solution[b]		Reference complex	
			trans-form	*cis*-form
trans-[$CrCl_2(pn)_2$]Cl·1.5H$_2$O	0.54	0.33	0.54	0.34
trans-[$CrCl_2(en)_2$]Cl	0.60	0.41	0.60	0.40
trans-[$CrCl_2(tn)_2$]Cl	0.47	0.17	0.47	0.18
trans-[$CrBr_2(pn)_2$]Br	0.63	0.43	0.63	0.43
trans-[$CrBr_2(en)_2$]Br	0.70	0.34	0.70	0.33
trans-[$CrBr_2(tn)_2$]Br	0.55	0.22	0.55	0.22
cis-[$CrCl_2(pn)_2$]Cl	0.32	0.09[c]		0.34
cis-[$CrBr_2(pn)_2$]Br		0.13[c]		0.32

a) The mixture of 1-butanol, methanol, and acetic acid (7:2:1) was used as the developer. b) The sample solutions were irradiated for about 30 min and checked by TLC. c) The value is that for the secondary photochemical product.

merization, which is a reaction similar to that of *cis*-$[CrBr_2(pn)_2]Br$ as mentioned later.

cis-[CrCl₂(pn)₂]Cl: When the cis complex is irradiated, an isosbestic point appears at 587 nm in the spectra irrespective of the irradiation wavelengths (530 and 400 nm). Figure 2 shows the spectral changes with time on 530 nm irradiation at 22 °C. After appropriate irradiation times, aliquot of the sample solution was taken out to be analyzed by TLC. Two R_f values were obtained: one (0.32) is due to the cis complex and the other (0.09) may come from another product. We then tried to isolate the product as mentioned in Experimental section.

The molar conductivity of the product was 80.78 $\Omega^{-1}cm^{-1}$ in methanol at 25 °C, suggesting that the compound is 1-1 valence type. Far-IR spectra of the product showed the absorption peaks due to Cr–O (530 and 395 cm^{-1}), Cr–N (575 cm^{-1}) and Cr–Cl (490 and 290 cm^{-1}) stretching vibrations. The weight loss (13.9%) observed upon heating the compound at 180 °C corresponds to the evolution of one mole of H_2O (5.1%) plus one mole of CH_3OH (8.9%). These results support that the photoproduct has the formula of $[CrCl_2(CH_3OH)(pn)_2]Cl$. Two isomers are feasible for the configuration of the product: one is facial and the other, meridional with respect to the position of two chloride ions and methanol. The electronic spectrum of the product is illustrated in Fig. 3 together with those of *fac*- and *mer*-$[CrCl_2(H_2O)(dien)]^+$ (dien: diethylenetriamine). Comparison of these spectra readily reveals that the products has *fac*-configuration.

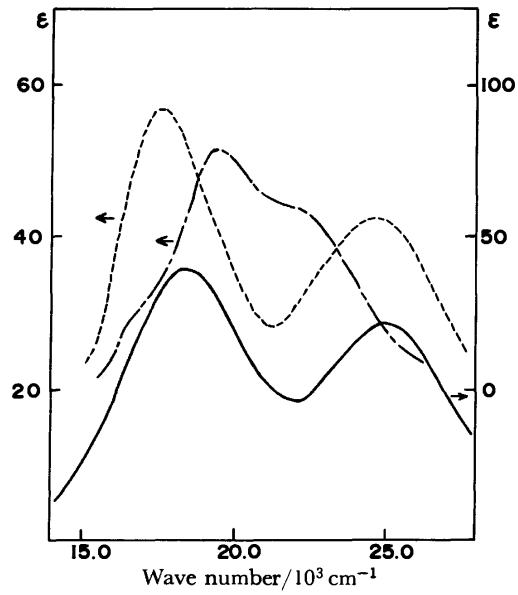

Fig. 3. Electronic spectra of *fac*-$[CrCl_2(CH_3OH)(pn)_2]$-Cl in methanol (——), *fac*-$[CrCl_2(H_2O)(dien)]^+$ in 0.6 M $HClO_4$ (1 M=1 mol dm^{-3}) (----), and *mer*-$[CrCl_2(H_2O)(dien)]^+$ in 1 M $HClO_4$ (——).

cis-[CrBr₂(pn)₂]Br: The spectral changes with time under 530 and 400 nm irradiations gave isosbestic points at 593, 483, and 442 nm for about 200 min. The first photoproduct giving these isosbestic points is assumed to be *fac*-$[CrBr_2(CH_3OH)(pn)_2]^+$, but the complex were unable to be isolated. After the irradiation for more than 600 min, the isosbestic points disappeared because of the formation of the secondary photoproduct. Details of the product are still unkown. We tentatively speculate from the electronic spectrum that the product is *fac*-$[CrBr(CH_3OH)_2(pn)_2]^{2+}$. Attempt to isolate the product was carried out as mentioned in Experimental section. However, the material isolated was always identified to be *cis*-$[CrBr(CH_3OH)(pn)_2]Br_2$ by TLC, elemental analysis, molar conductivity, far-IR spectra and thermal analysis. This is probably because upon crystallization, a unidentate pn contained in *fac*-$[CrBr(CH_3OH)_2(pn)_2]^{2+}$ functions as bidentate accompanied by the expulsion of one mole of CH_3OH from coordination sphere.

Quantum Yields. The photochemical product of each trans complex was the corresponding cis complex in the earlier step of irradiation. The ratios of the starting trans- to the cis-isomers produced were calculated from the absorbances of the resulting solution and those of the reference trans- and cis-isomers as reported previously.[1] The quantum yields were estimated by the use of those of the actinometers. Table 2 summarizes the quantum yields.

Discussion

Photochemistry of trans Complexes. (1) Labilization Mode: Gaussian analyses of the electronic spectra of the trans complexes gave four resolved curves. Figure 4 shows four Gaussian curves obtained for *trans*-$[CrCl_2$-

Table 2. Quantum yields (ϕ) for trans-to-cis isomerization of *trans*-$[CrX_2(AA)_2]X$

Starting complex AA	Irradiation wavelength (nm)	Temp. /°C	Quantum yield (ϕ) X=Cl	Quantum yield (ϕ) X=Br
pn	580	22	0.229±0.006	0.0453±0.0007
		32	0.194±0.005	0.0394±0.0003
	400	22	0.200±0.002	0.0182±0.0003
		32	0.149±0.002	0.0140±0.0006
en	580	22	0.302±0.003	0.0581±0.0004
		32	0.351±0.003	0.0671±0.0007
	400	22	0.276±0.004	0.0213±0.0003
		32	0.313±0.003	0.0254±0.0005
tn	580	22	0.346±0.005	0.135±0.002
		32	0.403±0.002	0.169±0.002
	400	22	0.308±0.008	0.0565±0.0004
		32	0.390±0.008	0.0721±0.0003

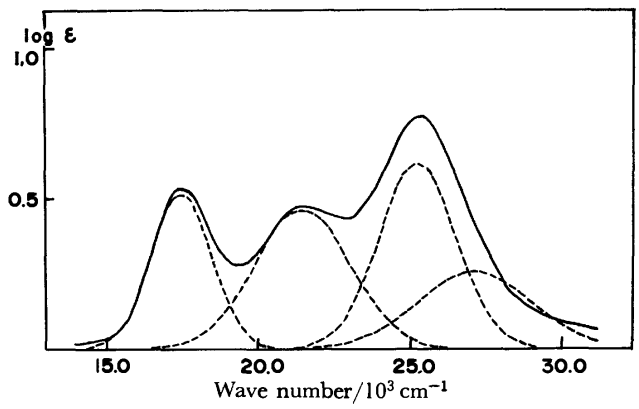

Fig. 4. Electronic spectrum of *trans*-$[CrCl_2(pn)_2]Cl \cdot 1.5H_2O$ with four Gaussian curves.

$(pn)_2]Cl \cdot 1.5H_2O$. These four peaks are assigned to the transition to excited states, $^4E_g{}^a$, $^4B_{2g}$, $^4A_{2g}$ and $^4E_g{}^b$ from the ground state $^4B_{1g}$ in D_{4h} symmetry of the trans complexes; the irradiation at 580 nm populates $^4E_g{}^a$ state, while the irradiation at 400 nm populates $^4A_{2g}$ state.[19]

Adamson *et al.* reported that the quartet excited state is inherently short-lived, but the state is labile enough for reaction to take place because it is in nearly pentagonal pyramid with a lengthened metal-ligand bond.[20]

The ratios of quantum yields at 580 and 400 nm are approximately constant for chlorides (*ca.* 1.1) and the bromides (2.4—2.8). This suggests that the photochemical reactions are related to either one of two excited states, $^4E_g{}^a$ and $^4B_{2g}$.

Table 3. Bond indices I* (Cr-L)(μm^{-1}) in the excited state for *trans*-$[CrX_2(AA)_2]X$

State	I*	X=Cl	X=Br
$^4E_g{}^a$	Cr-X	0.90	0.81
	Cr-N	1.21	1.22
$^4B_{2g}$	Cr-X	1.39	1.27
	Cr-N	0.90	0.90

The bond indices I* in the excited $^4E_g{}^a$ and $^4B_{2g}$ states were estimated according to VC theory[21], which are listed in Table 3. It may be deduced from the table that the bond Cr-X is ruptured in $^4E_g{}^a$ state and the bond Cr-N is ruptured in $^4B_{2g}$ state. MO theory gives the same results for the trans complexes.[22] In $^4E_g{}^a$ state, the axial π bond is strengthened and the σ bond is weakened; so the bond Cr-X is relatively activated. On the other hand, in $^4B_{2g}$ state, the equatorial π bond is weakened and σ bond, strengthened, the bond Cr-N being activated. It may therefore be concluded that the bond labilized in the trans complexes is Cr-X rather than Cr-N and the photoactive state which can undergo photoisomerization is $^4E_g{}^a$. The energies of 580 and 400 nm (206 and 299 kJ mol^{-1}) are enough to rupture the coordination bond.

(2) Photochemical Processes: Assuming that the photoactive state is ^4E_a and the reaction proceeds *via* five-coordinated intermediate, the allowed processes can be expressed as follows:

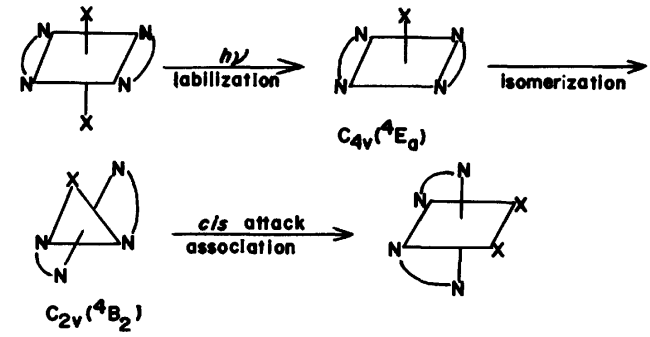

Scheme 1.

The first process is photolabilization expelling a halogeno ligand to form a five-coordinated intermediate of tetragonal pyramid (TP) with C_{4v} symmetry in ^4E_a state. The second process involves isomerization from TP to trigonal bipyramid (TBP) with X^- in equatorial position (C_{2v}) which is more energetically favored than with X^- in axial position (C_{3v}) d_{yz} is empty in the $^4B_2$ state of TBP, making cis attack easy. Therefore, exclusive production of the cis complexes from the corresponding trans complexes is reasonably explained by VC theory using five-coordinated intermediate.[22,23]

(3) Comparison of Quantum Yields: The quantum yields of the trans-dichloro complexes are larger than those of the trans-dibromo complexes as seen in Table 2. This may depend upon the small ionic radius of Cl^- (1.81 Å) compared with that of Br^- (1.96 Å). The yields increase in the following order of the diamines contained, pn<en<tn. The difference may depend upon the isomerization step in Scheme 1. Above all, the intermediate in the tn complexes is more stereomobile than those in the en or pn complexes, since the six-membered chelate ring in the tn complexes can be more easily elongated in the intermediates than the five-membered chelate ring in the en and pn complexes.

(4) Activation Energies: The quantum yields exhibit temperature dependence at two wavelengths at 22 and 32 °C. The apparent activation energies (E_a) were estimated from the plots of log ϕ *vs.* $1/T$, which are listed in Table 4. The values for each complex are roughly the same for both wavelengths. Thus, the photochemical reactions may occur from the same excited state, *i. e.*, the thermally equilibrated excited state (thexi state) $^4E_g{}^\circ$.[20]

Table 4. Apparent activation energies (Ea) for photoisomerization of *trans*-$[CrX_2(AA)_2]X$

AA	Irradiation wavelength(nm)	Ea (kJ mol^{-1})	
		X=Cl	X=Br
pn	580	−12.6±3.8	−10.4±1.7
	400	−22.5±1.7	−19.6±4.4
en	580	11.2±1.4	10.8±1.3
	400	11.9±1.8	13.2±2.5
tn	580	11.3±1.7	16.8±2.0
	400	17.6±3.3	18.2±0.8

The negative activation energies in the pn complexes are explainable by assuming that the electrons excited under irradiation relax to the $^4E_g{}^\circ$ state, but a part of the electrons are excited to the $^4E_g{}^a$ state by thermal energy to be deactivated instantly. Thus, the energy difference between $^4E_g{}^a$ and $^4E_g{}^\circ$ states may be small in the

Table 5. Quantum yields (ϕ) for the photochemical reaction of *cis*-$[CrCl_2(pn)_2]Cl$

Irradiation wavelength (nm)	Temp./°C	Quantum yield (ϕ)
530	22	0.049±0.001
	32	0.052±0.001
400	22	0.051±0.001
	32	0.050±0.001

Table 6. Bond indices I* (Cr–L)(μm^{-1}) in the excited state for *cis*-$[CrX_2(AA)_2]X$

State	I*	X=Cl	X=Br
$^4B_2$	Cr–N_{ax}	1.44	1.44
	Cr–N_{eq}	0.90	0.90
	Cr–X	0.97	0.89
^4E_a	Cr–N_{ax}	0.95	0.97
	Cr–N_{eq}	1.14	1.13
	Cr–X	1.11	1.01

case of the pn complexes. On the other hand, the activation energies in the en and tn complexes are positive because of the energy difference between $^4E_g{}^a$ and $^4E_g{}^\circ$ states being large, and so the energy enough for reaction to occur is thermally supplied.

Photochemistry of cis Complexes. The excited energy levels become higher in the following order: $^4B_2 < {}^4E_a < {}^4E_b < {}^4A_2$ in C_{2v} symmetry for the cis complexes. Since the quantum yields under 530 and 400 nm irradiations are nearly the same as seen in Table 5, the reaction is considered to take place from either one of $^4B_2$ and ^4E_a states.[24] On the basis of VC theory, the bond indices were estimated as listed in Table 6. Comparison of the bond indices reveals that the bond Cr–N_{eq} may be ruptured in the $^4B_2$ state and the bond Cr–N_{ax}, in the ^4E_a state. However, it is not so easy to determine from which excited state the photochemical reaction of *cis*-$[CrX_2(AA)_2]X$ takes place.

Comparison of Photochemical Reaction with Thermochemical Reaction. The mechanisms in the photochemical and thermochemical reactions can not be discussed on the same basis because the photochemical reaction occurs at the excited state, whereas the thermochemical reaction occurs at the ground state. However, the apparent difference was found in the direction of the isomerization. In thermal environment, the complexes containing five-membered chelate diamines such as en and pn undergo trans-to-cis isomerization and the complexes containing six-membered chelate diamine tn undergo cis-to-trans isomerization.[1c] In the ligand-field photochemistry, on the other hand, only trans-to-cis isomerization was observed irrespective of the diamines contained. Accordingly, in the case of $[CrX_2(tn)_2]X$, the direction of the isomerization is mutually reverse between photochemical and thermochemical reactions as follows:

$$trans\text{-}[CrX_2(tn)_2]X \underset{\triangle}{\overset{h\nu}{\rightleftharpoons}} cis\text{-}[CrX_2(tn)_2]X$$

References

1) a) T. Yoshikuni, R. Tsuchiya, A. Uehara, and E. Kyuno, *Bull. Chem. Soc. Jpn.*, **51**, 113 (1978); b) R. Tsuchiya, T. Ohki, A. Uehara, and E. Kyuno, *Thermochim. Acta*, **12**, 413 (1975); c) R. Tsuchiya, A. Uehara, and T. Yoshikuni, *Inorg. Chem.*, **21**, 590 (1982).

2) a) T. Yoshikuni, R. Tsuchiya, A. Uehara, and E. Kyuno, *Bull. Chem. Soc. Jpn.*, **50**, 883 (1979); b) S. Mitra, A. Uehara, and R. Tsuchiya, *Thermochim. Acta*, **34**, 189 (1979).

3) R. Tsuchiya and A. Uehara, *Thermochim. Acta*, **50**, 93 (1981).

4) R. Tsuchiya, T. Yoshikuni, S. Nakagawa, A. Uehara, and E. Kyuno, *Chem. Lett.*, **1977**, 339.

5) T. Takeuchi and A. Ohuchi, *Nippon Kagaku Zasshi*, **1974**, 1486; **1975**, 1175.

6) a) E. Zinato, "Concept of Inorganic Photochemistry," John Wiley & Sons, New York, 1975, Chapter 4; b) A. D. Kirk, *Coord. Chem. Rev.*, **39**, 225 (1981).

7) R. B. Woodward and R. Hoffmann, *Angew. Chem.*, **8**, 871 (1969).

8) J. Glerup, J. Josephsen, K. Michelven, E. Pedersen, and C. S. Schäffer, *Acta Chem. Scand.*, **24**, 247 (1970).

9) C. L. Rollinson and J. C. Bailar, Jr., *J. Am. Chem. Soc.*, **66**, 641 (1944).

10) J. W. Vaughn, O. J. Stvan, Jr., and V. E. Magnuson, *Inorg. Chem.*, **7**, 736 (1968).

11) J. A. Mclean, Jr. and N. A. Maes, *Inorg. Nucl. Chem. Lett.*, **8**, 147 (1972).

12) a) E. Pedersen, *Acta Chem. Scand.*, **24**, 3362 (1970); b) D. A. House, *Inorg. Nucl. Chem. Lett.*, **6**, 741 (1970).

13) L. Quinn and L. S. Garner, *Inorg. Chem.*, **3**, 1348 (1964).

14) P. Pfeiffer, *Z. Anorg. Chem.*, **56**, 279 (1908).

15) H. S. Booth, "Inorg. Synth.", Vol. 1 (1939), p. 36.

16) H. D. Dakin, "Org. Synth.", Collect. Vol. 2 (1943), p. 555.

17) C. G. Hatchard and C. A. Parker, *Proc. R. Soc. London, Ser. A*, **235**, 518 (1956).

18) E. E. Wegner and A. W. Adamson, *J. Am. Chem. Soc.*, **88**, 394 (1966).

19) L. M. Schwartz, *Anal. Chem.*, **43**, 1336 (1971).

20) A. W. Adamson, W. L. Waltz, E. Zinato, D. W. Watts, P. D. Fleischauer, and R. D. Linnholm, *Chem. Rev.*, **68**, 541 (1968).

21) L. G. Vanquickenborne and A. Ceulemans, *J. Am. Chem. Soc.*, **99**, 2208 (1977).

22) J. I. Zink, *J. Am. Chem. Soc.*, **94**, 8039 (1972).

23) L. G. Vanquickenborne and A. Ceulemans, *Inorg. Chem.*, **18**, 3475 (1979); *Inorg. Chem.*, **20**, 110 (1981); *Coord. Chem. Revs.*, **48**, 101 (1983).

24) E. Zinato, P. Riccieri, and M. Prelati, *Inorg. Chem.*, **20**, 1432 (1981).

 © 1984 The Chemical Society of Japan Bull. Chem. Soc. Jpn., 57, 2111—2115 (1984)

Bromochlorination of Alkenes with Dichlorobromate(1−) Ion. I

Takeshi NEGORO* and Yoshitsugu IKEDA
Department of Chemistry, Faculty of Education, Wakayama University, Fukiage, Wakayama 640
(Received October 12, 1983)

In the reaction of styrene with chlorine, the added bromide ions were mostly incorporated into the adduct, giving a bromo chloro compound. Tetrabutylammonium dichlorobromate(1−) was found to be an efficient bromochlorinating agent. The reactions of 2-butenes and stilbenes were completely *anti* stereospecific.

The reactions of alkenes with *N*-chlorosuccinimide (NCS) in the presence of a bromide ion have been know to proceed by prior formation of bromine chloride (BrCl) and its addition to alkenes.[1] Bromine chloride (BrCl) may presumably be produced from the reaction of molecular chlorine and a bromide ion.[2] On the other hand, quaternary ammonium dichlorobromate(1−) (R_4NBrCl_2) was prepared by treatment of quaternary ammonium bromide with chlorine.[3,4] The structure of R_4NBrCl_2 have been confirmed by IR and other spectral evidence.[4] No chemical reaction with R_4NBrCl_2, however, has been tried although a dichlorobromate(1−) ion has been accepted as an intermediate of the bromochlorination of alkenes.[1,5]

The reaction of alkene with R_4NBrCl_2 may proceed *via* BrCl as a possible intermediate, on assuming the following equilibrium (Scheme 1):

$$R_4N^+Br^- + Cl_2 \rightleftharpoons R_4N^+BrCl_2^- \rightleftharpoons R_4N^+Cl^- + BrCl$$

Scheme 1.

We investigated the reactions of alkenes with chlorine in the presence of tetrabutylammonium bromide and found that this system would be a convenient new bromochlorinating agent. We describe here the details of the reaction products obtained from reaction with styrene, the synthetic utility for bromochlorination, and also the mechanistic aspects of this reaction.

Results and Discussion

A solution of an excess amount of styrene (**1a**) in chloroform was treated at 15 °C with a chloroform solution of chlorine containing various amounts of tetrabutylammonium bromide. The reaction mixture was directly subjected to GLC analysis. The reaction products were a mixture of 1-chloro-2-phenylethylene (**2**), 1,2-dichloro-1-phenylethane (**3**), 2-bromo-1-chloro-1-phenylethane (**4a**), and 1,2-dibromo-1-phenylethane (**5**) with recovery of **1a**.

$$\underset{\mathbf{1a}}{C_6H_5CH{=}CH_2} \xrightarrow{Cl_2/Br^-} C_6H_5CH{=}CHCl\ (\mathbf{2}) + C_6H_5CHClCH_2Cl\ (\mathbf{3}) + C_6H_5CHClCH_2Br\ (\mathbf{4a}) + C_6H_5CHBrCH_2Br\ (\mathbf{5})$$

Scheme 2.

As was expected, the formation of the bromo chloro compound (**4a**) was markedly dependent on the amount of a bromide ion added (Table 1). The amount of **4a** increased proportionally with the increase of bromide ions until the number of bromide ions reached that of chlorine. Further addition of bromide ions moderately decreased the amount of **4a** with the formation of the dibromoalkane (**5**). Consequently, it is apparent that almost all the added bromide ions were incorporated into the adduct up to the equimolar amounts of bromide ions to that of chlorine. It is important to note that the ratios of **2** to **3** were nearly constant regardless of the numbers of bromide ions, and pretty close to that of the addition product of chlorine in the absence of bromide ions (Entry 1, Table 1).[6] In addition, only the bromo chloro adduct (**4a**) was formed in a regiospecific manner without contamination with 1-bromo-2-chloro-1-phenylethane, regardless of the number of bromide ions. The structure of the adduct (**4a**) was identified by comparison of its ^{13}C- and ^1H-NMR spectra with those of an authentic sample prepared from 1,2-dibromo-1-phenylethane and $SnCl_4$.[7]

If the bromochloroalkane (**4a**) was formed by the initial attack of chlorine, giving dichloride (**3**), and

TABLE 1. THE PRODUCT DISTRIBUTION[a] IN THE REACTION OF STYRENE (**1a**) WITH CHLORINE IN THE PRESENCE OF A BROMIDE ION[b] IN CHLOROFORM (50 ml) AT 15 °C

Entry	Added salt	Mol. ratio	%Composition[c]			
	mmol	Br^-/Cl_2	**2**	**3**	**4a**	**5**
1	no		45.7	54.3		
2	0.55	0.17	35.2	49.3	15.5	
3	0.80	0.25	34.4	42.5	23.1	
4	1.28	0.40	23.5	36.0	40.5	
5	1.95	0.61	14.1	23.1	62.8	
6	2.88	0.90	2.50	5.20	92.3	
7	3.22	1.01			100	
8	4.73	1.48			83.7	16.3

a) Determined by GLC analysis. b) Tetrabutylammonium bromide. c) Percentages are normalized to 100%. Values are not corrected for TCD response factors.

followed by either subsequent attack of a bromide ion on **3** or a 2-chloro-1-phenylethyl cation[8] as an intermediate, the ratios of **2** to **3** would be dependent on the amount of ammonium bromide. The present observations are inconsistent with the above mechanism and strongly suggest that the formation of **4a** is through a quite different mechanism from that of the process giving **2** and **3**. The most plausible process giving **4a** would involve an electrophilic attack of BrCl or dichlorobromate(1−) ion ($BrCl_2^-$) instead of chlorine. In fact, the reaction of BrCl to the same alkene has been found to yield only **4a** in a regiospecific manner.[9]

On the other hand, it is well known that the addition of molecular BrCl to alkene gives bromochloroalkane together with considerable amounts of dibromo and dichloro adducts formed by the attacks of Br_2 and Cl_2, which are in equilibrium with BrCl.[9,10] No dibromo and dichloro adducts were found in the present reaction by using an equimolar mixture of chlorine and bromide ion (Entry 7, Table 1). The results suggest that this reaction involves a different attacking species, not molecular BrCl. A similar result was also observed for the reaction of 3-β-trifluoroacetoxy-5-cholestene with BrCl in the presence of tetraphenylarsonium chloride, which gave the bromo chloro adduct in good yields without the formation of the dibromo and dichloro adducts.[11] In addition, kinetic data for the addition reaction of bromine to alkenes in the presence of a chloride ion have suggested a dichlorobromate(1−) ion as the reacting species.[5] Thus, a dichlorobromate(1−) ion would be the reactant and bromine chloride would not be involved in the process giving **4a**. A dichlorobromate(1−) ion was also suggested to be involved in the bromochlorination of cyclohexene with NCS and a bromide ion.[1]

As mentioned above, an equimolar mixture of chlorine and bromide ions would be a very effective and convenient bromochlorinating agent. Furthermore, several quaternary ammonium dichlorobromates(1−) were found to be easily isolable. The bromochlorinations of alkenes were also tried with the isolated salts. The reaction of styrene (**1a**) with tetrabutylammonium dichlorobromate(1−) (**6**) in chloroform completed within a few minutes at 0 °C, giving **4a** in nearly quantitative yield. Tetramethylammonium and phenyltrimethylammonium dichlorobromates(1−) (**7** and **8**) were also useful for the bromochlorination of alkenes, regardless of their lower solubilities. The reaction of **1a** with **6** was examined in several different solvents with a wide variety of polarities. Reactions in dioxane, carbon tetrachloride, ethyl acetate, dichloromethane, 1,2-dichloroethane, and acetic anhydride gave **4a** in similar yields. Thus, the usual aprotic solvents can be employed as the reaction medium. On the other hand, the reaction of **1a** in acetic acid gave **4a** (65%) and 1-acetoxy-2-bromo-1-phenylethane (**9**, 35%). In methanol, the major product was 2-bromo-1-methoxy-1-phenylethane (**10**, 80%). These results have also been found in the reaction of 1-hexene with BrCl in methanol.[12]

In order to obtain some information on the mechanistic aspects, the reactions of **6** with a variety of alkenes were examined. The results are given in Table 2. In analogy with the reaction of **1a**, reactions with methyl *trans*-cinnamate (**1b**) and vinyl acetate (**1c**) gave the corresponding regiospecific products. Addition to such alkenes as propene (**1d**) and 3-chloropropene (**1e**) gave both Markownikoff and *anti*-Markownikoff adducts. The reason for the formation of *anti*-Markownikoff adducts is uncertain; however, it may be attributed to the combined effects of polar and steric effects. Similar orientation have also been found in the reactions of these alkenes with other bromochlorinating agents.[13,14]

The additions to *cis*- and *trans*-2-butenes (**1f** and **1f'**), cyclohexene (**1g**), and methyl *trans*-cinnamate (**1b**) with **6** gave completely *anti* stereospecific products. Similarly, *anti* stereospecific products, *threo*- and *erythro*-1-bromo-2-chloro-1,2-diphenylethanes (**4h** and **4h'**) were obtained from *cis*- and *trans*-stilbenes (**1h** and **1h'**), respectively. The solvent effect on *anti*

Table 2. Bromochlorination of alkenes with **6** in $CHCl_3$[a]

Alkenes	Temp / °C	Products	Yield/%[b]
1a	0	$C_6H_5CHClCH_2Br$ (**4a**)	85(97)
1a	15	**4a**	84(98)[c]
1a	15	**4a**	86(95)[d]
1b	70	$C_6H_5CHClCHBrCOOMe$ (**4b**)	85[e]
1c	−5	$CH_2BrCHClOCOCH_3$ (**4c**)	82
1d	0	$CH_2BrCHClCH_3$ (**4d**) $CH_2ClCHBrCH_3$ (**4d'**)	85[f]
1e	50	$CH_2BrCHClCH_2Cl$ (**4e**) $CH_2ClCHBrCH_2Cl$ (**4e'**)	82[g]
1f	−10	$CH_3CHBrCHClCH_3$ (**4f**)	84[h]
1f'	−10	$CH_3CHBrCHClCH_3$ (**4f'**)	85[e]
1g	0	$C_6H_{10}BrCl$ (**4g**)	85[i]
1h	20	$C_6H_5CHBrCHClC_6H_5$ (**4h**)	95[h]
1h'	20	$C_6H_5CHBrCHClC_6H_5$ (**4h'**)	97[e]
1i	70	EtOOCCHBrCHClCOOEt (**4i'**)	66[e]
1i'	70	EtOOCCHBrCHClCOOEt (**4i'**)	71[e]

a) Reactions were carried out with 30 mmol of **6**, 30 mmol of alkene, and 100 ml of $CHCl_3$. b) Isolated yield. Figures in parentheses represent product yields determined by ^1H NMR before isolation using ethylbenzene as the internal standard. c) **7** as bromochlorinating agent. d) **8** as bromochlorinating agent. e) *erythro*. f) **4d**:**4d'**=56:44. g) **4e**:**4e'**=31:69. h) *threo*. i) *trans*.

stereospecific addition was examined. The reactions of **1h** in dichloromethane, 1,2-dichloroethane, acetic anhydride, and nitromethane gave *threo* isomer (**4h**) free from *erythro* isomer (**4h'**). In contrast, it has previously been reported that the addition of molecular BrCl to **1h'** in chloroform is *anti* stereospecific, while that of **1h** gives considerable amounts of **4h'**.[9] Furthermore, the stereochemistry of bromine addition to **1h** has been known to be dependent on the solvents.[15] Thus, the mode of the reaction is very different in the additions to **1h** with **6** and with BrCl (and Br_2). Therefore, the present results cannot be explained on the basis of any accepted mechanism for the additions of bromine and bromine chloride.[15,16] The completely *anti* stereospecific addition with **6** can be explained by assuming an $AdEC_2$-type mechanism involving a rate- and product-determining attack of a chloride ion to a three-center bound π complex-type intermediate (**11**)[17], as shown in Scheme 3. A similar mechanism has been suggested for the additions of Br_3^- and Br_2Cl^- to alkenes and dienes.[16,18]

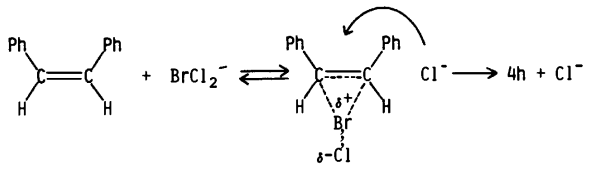

11

Scheme 3.

The product obtained from diethyl maleate (**1i**) and fumarate (**1i'**) was the same compound, diethyl *erythro*-2-bromo-3-chlorosuccinate (**4i'**). The reactions with these electron-deficient alkenes proceeded only on heating and the maleate (**1i**) was found to isomerize to the fumarate (**1i'**) under the reaction conditions. On the other hand, fumaric and maleic acids have been known to react with BrCl, yielding *erythro*- and *threo*-2-bromo-3-chlorosuccinic acids, respectively.[19] The difference would be additional evidence to support the conclusion that the reactant in the reaction of **6** is not BrCl but $BrCl_2^-$.

When compared with other bromochlorinating agents, the merits of ammonium dichlorobromate(1−) become evident. Although the formation of bromochloroalkanes by the use of a mixture of Br_2 and Cl_2 has been well known,[9] the yields appeared to be lower due to contaminations of dichloro and dibromoalkanes. Certain olefinic substances with BrCl prepared *in situ* from *N*-bromoacetamide and hydrogen chloride also give undesired by-products,[7] as was the case for a mixture of NCS and a bromide ion.[1] Although pyridine-BrCl complex[16,20] and a mixture of Br_2 and $SbCl_5$ (or $SbCl_3$)[13] were reported to be effective bromochlorinating agents, the products were usually complex. Tetraalkylammonium dichlorobromate(1−) can be handled easily and can be used as a very convenient bromochlorinating agent. Simple purification of the product provides pure bromochloroalkane in nearly quantitative yield.

Experimental

All the melting points and boiling points are uncorrected. NMR spectra were recorded on a JEOL JNM FX-60Q and a JEOL C-60HL spectrometer, using TMS as an internal standard. Mass spectra were recorded on a JMS-D-300 Mass spectrometer. The GLC analyses were performed on a Yanako GCG-550T with a Silicon DC 550 (25%)-Celite 545 (2 m) column (A) or Yanako G-180 Gas Chromatograph with a High vacuum silicon grease (25%)-Celite 545 (2 m) column (B). All the organic starting materials, including the solvents, were distilled or recrystallized before use. Chlorine was passed through water and sulfuric acid. Tetrabutylammonium dichlorobromate(1−) (**6**), tetramethylammonium dichlorobromate(1−) (**7**), and phenyltrimethylammonium dichlorobromate(1−) (**8**) were prepared by the literature procedure.[3]

The Reaction of Styrene (1a) with Chlorine in the Presence of Tetrabutylammonium Bromide. Experiments were carried out by adding 20 ml of chlorine solution in chloroform (0.16 mol dm^{-3}) in the presence of various amounts of tetrabutylammonium bromide (0.55—4.73 mmol) to 6.4 mmol of **1a** (in 30 ml of the same solvent) at 15 °C with stirring for 10 min. After the reaction completed, the mixture was washed with aq Na_2CO_3 and water, and dried over $MgSO_4$. The solvent was removed by evaporation. The relative amounts of products were determined by the peak areas of GLC on the column (A) at 100 °C with hydrogen as a carrier gas (50 ml/min). Retention times (in minutes) were: **1a**, 1; **2**, 3.2; **3**, 7.8; **4a**, 12.8; **5**, 14. The results are given in Table 1.

The Reaction of Styrene (1a) with 6. General Procedure: To a solution of **1a** (3.12 g, 30 mmol) in chloroform (100 ml), was added **6** (11.8 g, 30 mmol) at 0 °C over 20 min with stirring. The mixture was stirred for an additional 10—20 min, then washed with five 100-ml portions of water to remove the ammonium salt, dried over Na_2SO_4, and the solvent was evaporated. Distillation afforded 5.6 g (85%) of pure **4a**: bp 80—81 °C/1 mmHg (1 mmHg≈133.322 Pa) (lit,[7] 106—107 °C/6 mmHg); ^1H NMR ($CDCl_3$) δ=3.82, 3.83 (2H, 2d, J=8.3 and 6.6 Hz, CH_2Br), 5.03 (1H, q, J=8.3 and 6.6 Hz, CHCl), 7.36 (5H, s, C_6H_5); ^{13}C NMR ($CDCl_3$) δ=35.9, 61.3, 127.2, 128.6, 129.0, 138.3; MS M^+ at m/z=218, 220, 222 (100: 129:34); Found: m/z 217.9494. Calcd for C_8H_8BrCl: M, 217.9499. Yields in other aprotic solvents were: in dioxane, 78%; CCl_4, 80%; $CH_3COOC_2H_5$, 79%; CH_2Cl_2, 85%; CH_2ClCH_2Cl, 83%; $(CH_3CO)_2O$, 80%.

In Acetic Acid as the Solvent. To a solution of **1a** (1.04 g, 10 mmol) in acetic acid (30 ml) was added **6** (3.93 g, 10 mmol) at 20 °C over 5 min with stirring. The product was isolated by pouring the reaction mixture into cold saturated aq NaCl, followed by extraction with ether (200 ml) and washing with aq $NaHCO_3$ and water. The ethereal extract was dried over $MgSO_4$ and concentrated. The residue (2.00 g) was analyzed by GLC and ^1H-NMR. The composition analyzed by GLC was: **4a**, 65.4 and 1-acetoxy-2-bromo-1-phenylethane (**9**), 34.6%. ^1H-NMR shows 67:33 mixture of **4a** and **9**, respectively (by integration of methine protons). The ^1H-NMR spectrum of **9** corresponds well with that reported in the literature.[21]

In Methanol as the Solvent. To a solution of **1a** (1.04 g, 10 mmol) in methanol (30 ml) was added **6** (3.93 g, 10 mmol) at 0 °C over 5 min with stirring. The solvent was removed by evaporation, and ether (150 ml) was added to the residue. The ether solution was washed with aq $NaHCO_3$ and water. The ethereal extract was dried over $MgSO_4$ and concentrated. ^1H-NMR spectrum of the residue shows a 80:20 mixture of 2-bromo-1-methoxy-1-phenylethane (**10**) and **4a**, respectively (by integration of methine protons). Column chromatography of the residual oil (1.85 g) on silica gel with hexane as the eluent gave 1.10 g of pure **10** and 0.2 g of **4a**. The data for **10** are as follows: bp 65—66 °C/2 mmHg (lit,[22] 57 °C/0.40 mmHg); ^1H NMR ($CDCl_3$) δ=3.32 (3H, s, CH_3), 3.49,

3.50 (2H, 2d, J=5.7 and 7.0 Hz, CH_2Br), 4.37 (1H, approx. triplet, CH), 7.35 (5H, s, C_6H_5); ^{13}C NMR ($CDCl_3$) δ=36.2, 57.2, 83.4, 126.7, 128.4, 128.6, 139.0; MS M^+ at m/z=214, 216 (100:96); Found: m/z 213. 9981. Calcd for $C_9H_{11}BrO$: M, 213.9994.

Syntheses of Bromochloroalkanes by 6 in Chloroform. The procedure was the same as that described for that of **1a**, except for the reaction temperature and period. The results are given in Table 2.

Methyl erythro-*2-bromo-3-chloro-3-phenylpropanate (4b).* Mp 118—120 °C (from pentane). ^1H NMR ($CDCl_3$) δ=3.89 (3H, s, CH_3), 4.62 (1H, d, J=11.3 Hz, CHBr), 5.27 (1H, d, J=11.3 Hz, CHCl), 7.39 (5H, s, C_6H_5). Found: C, 43.51; H, 3.37%. Calcd for $C_{10}H_{10}BrClO_2$: C, 43.27; H, 3.63%.

1-Acetoxy-2-bromo-1-chloroethane (4c). Bp 80—81 °C/25 mmHg (lit,[13] 64—65 °C/10 mmHg). ^1H NMR ($CDCl_3$) δ=2.17 (3H, s, CH_3), 3.70 (2H, d, J=6.0 Hz, CH_2Br), 6.53 (1H, t, J=6.0 Hz, CHCl). ^{13}C NMR ($CDCl_3$) δ=20.6, 32.7, 80.0, 168.0.

1-Bromo-2-chloropropane (4d) and 2-Bromo-1-chloropropane (4d'). Gaseous propene (**1d**) from a cylinder was passed through the chloroform solution of **6** at 0 °C until the yellow color disappeared. After the usual work-up procedure, mixed bromochloroalkanes (**4d** and **4d'**) were obtained: bp 53—55 °C/70 mmHg. ^1H-NMR shows a 56:44 mixture of **4d** and **4d'**, respectively. ^1H NMR ($CDCl_3$) (an asterisk indicates **4d**) δ=1.65* (d, J=6.35 Hz, CH_3), 1.79 (d, J=6.34 Hz, CH_3), 3.3—4.4 (m). ^{13}C NMR ($CDCl_3$) (an asterisk indicates **4d**) δ=23.2, 37.5*, 46.3, 49.6, 55.4*. Although attempts to separate two regioisomers were unsuccessful, these assignments were supported for dibromo and dichloro analogs.[23]

1-Bromo-2,3-dichloropropane (4e) and 2-Bromo-1,3-dichloropropane (4e'). A mixture of two isomeric bromodichloropropanes (**4e** and **4e'**) was obtained from 3-chloropropene (**1e**): bp 60—62 °C/22 mmHg. ^{13}C NMR shows a 31:69 mixture of **4e** and **4e'**, respectively. The ratio was obtained by comparison of the spectra of each pure sample as follows: **4e**, ^{13}C NMR ($CDCl_3$) δ=33.1, 46.0, 57.9; **4e'**, ^{13}C NMR ($CDCl_3$) δ=45.2, 49.1.

threo-*2-Bromo-3-chlorobutane (4f).* Bp 45—48 °C/30 mmHg (lit,[24] 50—52 °C/30 mmHg). ^1H NMR ($CDCl_3$) δ=1.60 (3H, d, J=6.6 Hz, CH_3), 1.74 (3H, d, J=6.6 Hz, CH_3), 4.0—4.8 (2H, m, CHCl and CHBr). ^{13}C NMR ($CDCl_3$) δ=20.3, 20.4, 52.5, 60.5. MS M^+ at m/z=170, 172, 174 (100:129:31). Found: m/z 169.9490. Calcd for C_4H_8BrCl: M, 169.9498.

erythro-*2-Bromo-3-chlorobutane (4f').* Bp 51—52 °C/50 mmHg (lit,[24] 50—52 °C/51 mmHg). ^1H NMR ($CDCl_3$) δ=1.65 (3H, d, J=6.3 Hz, CH_3), 1.80 (3H, d, J=6.5 Hz, CH_3), 4.0—4.3 (2H, m, CHBr and CHCl). ^{13}C NMR ($CDCl_3$) δ=23.5, 53.8, 61.8. MS M^+ at m/z=170, 172, 174 (100:131:33). Found: m/z 169.9495. Calcd for C_4H_8BrCl: M, 169.9498.

trans-*1-Bromo-2-chlorocyclohexane (4g).* Bp 91—92 °C/18 mmHg (lit,[13] 90—95 °/17 mmHg). ^{13}C NMR ($CDCl_3$) δ=22.5, 23.3, 32.8, 33.3, 55.5, 62.9. MS M^+ at m/z=196, 198, 200 (100:129:32). Found: m/z 195.9640. Calcd for $C_6H_{10}BrCl$: M, 195.9655. The ^1H-NMR spectrum corresponds well with that reported in the literature.[25]

threo-*1-Bromo-2-chloro-1,2-diphenylethane (4h).* Mp 102.5—103 °C (from 95% ethanol) (lit,[9] 99—100 °C). ^1H NMR ($CDCl_3$) δ=5.34 (2H, s, CHBr and CHCl), 7.18 (10H, s, $2C_6H_5$). MS M^+ at m/z=294, 296, 298 (100:127:32). Found: m/z 293.9819. Calcd for $C_{14}H_{12}BrCl$: M, 293.9811.

erythro-*1-Bromo-2-chloro-1,2-diphenylethane (4h').* Mp 218—221 °C (from ligroine) (lit,[9] 220—221 °C). ^1H NMR ($CDCl_3$) δ=5.32 (2H, s, CHBr and CHCl), 7.42 (10H, m, $2C_6H_5$). MS M^+ at m/z=294, 296, 298 (100:132:34). Found: m/z 293.9809. Calcd for $C_{14}H_{12}BrCl$: M, 293.9811.

The Reactions of Diethyl Fumarate (1i') and Maleate (1i) with 6. The mixture of **6** (11.8 g, 30 mmol) and **1i'** (5.16 g, 30 mmol) in 100 ml of $CHCl_3$ was stirred at refluxing temperature for 50 h. The reaction mixture was washed with aq Na_2SO_3 and water. After the usual work-up procedure, the solid residue was recrystallized from ligroine to give 6.15 g (71%) of diethyl *erythro*-2-bromo-3-chlorosuccinate (**4i'**, mp 56—57 °C). The structure was confirmed by comparison of the ^1H-NMR spectra with that reported in the literature.[13]

In a similar way, analysis of the residue from the reaction of **1i** with **6** by ^1H-NMR revealed a mixture of **4i'** and unreacted alkenes. The solid residue was recrystallized from ligroine to give 5.7 g (66%) of product (mp 56—57 °C) (not depressed on admixture with the product obtained from **1i'**). ^1H-NMR analysis of the recovered alkene indicated 77% of **1i'** and 23% of **1i** on the basis of relative areas of the signals at δ=6.84 and 6.25 for olefinic protons, respectively.

Reaction of cis-*Stilbene (1h) with 6 in Various Solvents.* The reactions were carried out by the addition of 2 mmol of **6** to 2 mmol of **1h** in 50 ml of the solvents at 20 °C with stirring. After the yellow color disappeared, the reaction mixture was washed with water and dried over Na_2SO_4. The product of the reaction in acetic anhydride was isolated by extraction with ether. After the solvent was removed under reduced pressure, the residue was analyzed by GLC and ^1H-NMR. Reactions in $CHCl_3$, CH_2Cl_2, CH_2ClCH_2Cl, $(CH_3CO)_2O$, and CH_3NO_2 gave *threo* isomer (**4h**) free from *erythro* isomer (**4h'**). Yields in the solvents were: in $CHCl_3$, 95%; CH_2Cl_2, 98%; CH_2ClCH_2Cl, 96%; $(CH_3CO)_2O$, 95%; CH_3NO_2, 95%. The GLC analysis was performed on the column (B) at 150 °C with helium as a carrier gas (50 ml/min).

The authors wish to thank Dr. Seizi Kozuka of Osaka City University for helpful discussions.

References

1) D. S. Wilbur and K. W. Anderson, *J. Org. Chem.*, **47**, 358 (1982).

2) A. J. Downs and C. J. Adams, "Comprehensive Inorganic Chemistry," ed by J. C. Bailor, H. J. Emeleus, S. R. Nyholm, and A. F. Trotman-Dickenson, Pergamon Press, Oxford (1973), Vol. 2, p. 1192.

3) A. I. Popov and R. E. Buckles, *Inorg. Synth.*, Vol. V, 172 (1957).

4) W. B. Person, G. R. Anderson, J. N. Fordemwalt, H. Stammreich, and R. Forneris, *J. Chem. Phys.*, **35**, 908 (1961); J. C. Evans and G. Y.-S. Lo, *ibid.*, **44**, 4356 (1966).

5) R. P. Bell and M. Pring, *J. Chem. Soc., B*, **1966**, 1119.

6) The addition of chlorine to styrene has been reported although the detailed ratio of the products was not given: see W. S. Emerson and E. P. Agnew, *J. Am. Chem. Soc.*, **67**, 518 (1945).

7) R. E. Buckles and J. W. Long, *J. Am. Chem. Soc.*, **73**, 998 (1951).

8) R. C. Fahey and C. Schubert, *J. Am. Chem. Soc.*, **87**, 5172 (1965).

9) R. E. Buckles, J. L. Forrester, R. L. Burham, and T. W. McGee, *J. Org. Chem.*, **25**, 24 (1960).

10) A. I. Popov and J. J. Mannion, *J. Am. Chem. Soc.*, **74**, 222 (1952).

11) P. B. D. de la Mare and R. D. Wilson, *J. Chem. Soc., Perkin Trans. 2*, **1977**, 2048.

12) V. L. Heasley, D. F. Shellhamer, J. A. Iskikian, D. L. Street, and G. E. Heasley, *J. Org. Chem.*, **43**, 3139 (1978).

13) S. Uemura, A. Onoe, and M. Okano, *Bull. Chem. Soc. Jpn.*, **47**, 143 (1974).

14) P. B. D. de la Mare and S. Galandauer, *J. Chem. Soc.*, **1958**, 36.

15) R. E. Buckles, J. M. Bader, and R. J. Thurmaier, *J. Org.*

Chem., **27**, 4523 (1962).
16) G. E. Heasley, J. McCall Bundy, V. L. Heasley, S. Arnold, A. Gipe, D. McKee, R. Orr, S. L. Rodgers, and D. F. Shellhamer, *J. Org. Chem.*, **43**, 2793 (1978).
17) G. A. Olah and T. R. Hockswender, Jr, *J. Am. Chem. Soc.*, **96**, 3574 (1974); G. A. Olah, P. Schilling, P. W. Westerman, and H. C. Lin, *ibid.*, **96**, 3581 (1974).
18) G. Bellucci, G. Berti, R. Bianchini, G. Ingrosso, and K. Yates, *J. Org. Chem.*, **46**, 2315 (1981).
19) G. H. Schmid and D. G. Garratt, "The Chemistry of Double-Bonded Functional Groups,", ed by S. Patai, John Wiley and Sons, London (1977), Supplement A, part 2, p. 794; P. Walden, *Ber.*, **30**, 2883 (1897).
20) G. Bellucci, G. Ingrosso, F. Marioni, E. Mastrorilli, and I. Morelli, *J. Org. Chem.*, **39**, 2562 (1974).
21) J. H. Rolston and K. Yates, *J. Am. Chem. Soc.*, **91**, 1469 (1969).
22) V. L. Heasley, R. A. Skidgel, G. E. Heasley, and D. Strickland, *J. Org. Chem.*, **39**, 3953 (1974).
23) J. G. Grasselli and W. M. Ritchey, "Atlas of Spectral Data and Physical Constants for Organic Compounds," 2nd ed., C R C Press, Ohio (1975) Vol. IV, p. 209.
24) P. S. Skell, R. R. Pavlis, D. C. Lewis, and K. J. Shea, *J. Am. Chem. Soc.*, **95**, 6735 (1973).
25) H. M. van Dort and Th. J. Sekuur, *Tetrahedron Lett.*, **1963**, 1301.

Bromochlorination of Alkenes with Dichlorobromate(1−) Ion. II.[1] Regio- and Stereochemistry for the Bromochlorination of 1-Phenylpropenes with Dichlorobromate(1−) Ion

Takeshi NEGORO* and Yoshitsugu IKEDA
Department of Chemistry, Faculty of Education, Wakayama University, Fukiage, Wakayama 640
(Received October 12, 1983)

The bromochlorinations of 1-phenylpropenes with tetrabutylammonium dichlorobromate(1−) in aprotic solvents (dielectric constants 5—36) were found to be completely *anti* stereospecific and nonregiospecific, although Markownikoff adduct was mainly formed. In marked contrast, addition of molecular bromine chloride to the same alkenes was found to give nonstereospecific and regiospecific adducts. These results suggest that the addition of bromine chloride in the form of $(n\text{-}C_4H_9)_4NBrCl_2$ involves a rate- and product-determining attack of a chloride ion to a three-center bound π complex.

The stereochemistry of bromine addition to aryl-substituted alkenes has been shown to be markedly dependent both on the brominating agents and on the solvents employed.[2] The *anti* stereospecific additions were observed for the reaction with a tribromide ion[3,4] or with pyridine–bromine complex[4] as brominating agents. However, only a few systematic studies have been carried out on reaction with a dichlorobromate-(1−) ion as a bromochlorinating agent. It has been reported that 1-phenylpropenes give bromochlorinated adducts by reaction with $(CH_3)_4NBr_2Cl$ and pyridine–bromine chloride in a completely *trans* manner, while addition of molecular bromine chloride gives significant amounts of *cis*-adduct.[4] We have reported that tetrabutylammonium dichlorobromate(1−) reacted with stilbenes and 2-butenes to give the corresponding bromo chloro adducts in almost quantitative yields, and that the additions were in a completely *anti*-stereospecific manner.[1] In an attempt to gather more detailed information on bromochlorination with a dichlorobromate(1−) ion, we have investigated the regio- and stereochemistry of the addition to 1-phenylpropenes in solvents with widely different polarities. The reactions of 1-phenylpropenes with molecular bromine chloride were also carried out for comparison with the reactions of a dichlorobromate(1−) ion. This paper will describe reaction features of bromochlorination of 1-phenylpropenes with a dichlorobromate(1−) ion.

Results and Discussion

The reaction of tetrabutylammonium dichlorobromate(1−) [$(n\text{-}C_4H_9)_4NBrCl_2$, **1**] with *cis*-1-phenylpropene (**2a**) in chloroform gave a mixture of *threo*-2-bromo-1-chloro-1-phenylpropane (**3a**) and *threo*-1-bromo-2-chloro-1-phenylpropane (**4a**) in almost quantitative yield. *trans*-1-Phenylpropene (**2b**) was reacted with **1** to give a mixture of *erythro*-2-bromo-1-chloro and *erythro*-1-bromo-2-chloro adducts (**3b** and **4b**, respectively).

$$PhCH=CHCH_3 + \mathbf{1} \longrightarrow PhCHClCHBrCH_3 + PhCHBrCHClCH_3$$

2a	**3a**, 76%	**4a**, 24%
2b	**3b**, 95%	**4b**, 5%

Fig. 1.

Structural assignments of the bromo chloro compounds **3a** and **4a** were deduced by dehydrohalogenation to haloalkenes (Fig. 2). When a mixture of **3a** and **4a** was treated with 0.78 equivalent of potassium *t*-butoxide in *t*-butyl alcohol, the alkene (**5**) with recovery of the unreacted bromo chloro compound (**4a**) was obtained in good yield.

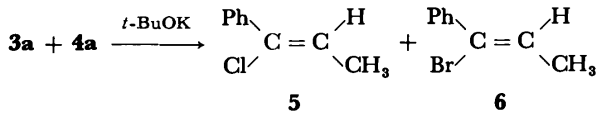

5 **6**

Fig. 2.

^{1}H-NMR analysis of the reaction mixture revealed that one isomer (**3a**), which gives **5**, was consumed faster than the other (**4a**); this other isomer (**4a**), which gives **6**, disappeared slowly. Thus, the more facile elimination of **3a** (than that of **4a**) would be due to either differences in eclipsing effect of the bulky substituents or in the ability of the leaving groups. The relative reactivities of **3a** and **4a** are in accordance with the usual reactivities of hydrogen halide eliminations.[5]

The structures of the major and minor products from **2a** and **2b** were also determined by comparisons of their ^{13}C- and ^{1}H-NMR spectra with those of the corresponding dibromo and dichloro adducts. Selected ^{1}C- and ^{1}H-NMR spectra of *threo*- and *erythro*-1,2-dihalo-1-phenylpropanes are listed in Tables 1 and 2, respectively. NMR analysis of the mixture of two regioisomers could be used to determine the amounts of each isomer.

TABLE 1. ^{13}C CHEMICAL SHIFTS FOR *threo*- AND *erythro*-1,2-DIHALO-1-PHENYLPROPANES IN $CDCl_3$ (δ VALUE)

$C_6H_5\text{-}C^1H(X)\text{-}C^2H(Y)\text{-}CH_3$

X	Y	C^1	C^2	CH_3
threo				
Br	Br	58.9	52.7	22.3
Cl	Cl	67.4	61.2	21.6
Br	Cl	59.2	61.0	22.0
Cl	Br	67.4	53.0	22.4
erythro				
Br	Br	59.1	51.1	25.7
Cl	Cl	67.4	60.1	22.1
Br	Cl	58.8	59.6	24.0
Cl	Br	67.5	51.5	23.4

Table 2. ^1H chemical shifts for *threo*- and *erythro*-1,2-dihalo-1-phenylpropanes in $CDCl_3$ (δ value)

C_6H_5-CX(H_a)-CY(H_b)-CH_3

X	Y	CH_3	H_a	H_b
threo				
Br	Br	1.67	5.22	4.59
Cl	Cl	1.44	5.00	4.38
Br	Cl	1.46	5.06	4.45
Cl	Br	1.62	5.06	4.47
erythro				
Br	Br	2.03	5.05	4.57
Cl	Cl	1.67	4.91	4.38
Br	Cl	1.80		
Cl	Br	1.90	4.98	4.45

The present addition reaction appeared to be stereospecific but not regiospecific. The lack of regiospecificity cannot be ascribed to the subsequent isomerization of the bromochloroalkanes, since prolonged reaction time did not cause a change of the isomer ratio of the products. Interconversions between two regioisomers (pure **3a** or the mixed isomers; **3a**:**4a**=60:40) were examined. However, no isomerization was observed in chloroform at room temperature for 3 h by using either 2 equivalents of **1** or of tetrabutylammonium chloride. Another possibility for the formation of *anti*-Markownikoff adduct (**4a** or **4b**) from dichloro adduct of alkenes can also be excluded, since no dichloroalkane was found in the reaction product.

When the reaction was carried out in the presence of a free radical inhibitor, 2,6-di-*t*-butyl-4-methylphenol, the product composition did not change within experimental error. Moreover, the same product ratio was obtained under either an oxygen or nitrogen atmosphere. These results indicate that the reaction proceeds in an electrophilic process rather than in a free radical one.

The regio- and stereochemistry of the reactions of **2a** and **2b** were investigated in solvents with widely different polarities in order to determine the mechanism of the reaction. Table 3 presents data for the effect of solvents on the regiochemistry of the addition to **2a** and **2b**. The reactions were completely *anti* stereospecific and nonregiospecific in all the aprotic solvents employed. No solvent effects on the regiochemistry have been observed (Table 3). A similar stereochemical result has been previously observed for the reaction of *cis*-stilbene with **1**.[1]

In contrast to the present results, Heasley *et al.*[4] have reported that the reactions of **2a** and **2b** with molecular bromine chloride (BrCl) in dichloromethane and carbon tetrachloride occurred in a nonstereospecific manner, although *anti* additions were favored. We have reinvestigated the reaction of the same alkenes with BrCl in various solvents to compare the results with that of **1**. Although the bromo chloro adducts were the major products in all cases, as expected, substantial amounts of dichloro and dibromo adducts were also found in the product. None of the *anti*-Markownikoff adducts were detected by ^1H- and ^{13}C-NMR analyses of the product mixtures in any of the solvents employed. The results are shown in Table 4.

Table 3. Solvent dependency on regiochemistry of the reactions of **2a** and **2b** with **1** at 0 °C

Solvent	Dielectric constant[a]	Product composition/%[b]			
		from **2a**		from **2b**	
		% **3a**	% **4a**	% **3b**	% **4b**
$CHCl_3$	4.81	76.0(76.8)	24.0(23.2)	94.5(95.8)	5.5(4.2)
$CH_3COOC_2H_5$	6.02	77.1	22.9	94.6	5.4
CH_2Cl_2	9.08	77.5(77.9)	22.5(22.1)	95.5(93.9)	4.5(6.1)
CH_2ClCH_2Cl	10.36	78.4	21.6	93.2	6.8
$(CH_3CO)_2O$	20.7	75.2(75.9)	24.8(24.1)	94.1(94.6)	5.9(5.4)
CH_3NO_2	35.87	78.0(76.2)	22.0(23.8)	92.2(92.9)	7.8(7.1)

a) J.A.Riddick and E.E.Toops,"Technique of Organic Chemistry," ed by A. Weissberger, Interscience, New York (1955), Vol. VII. b) Percentages are normalized to 100%. Determined by ^1H-NHR analysis. Figures in parentheses represent the product distributions determined by ^{13}C-NMR analysis.

Table 4. Solvent dependency on stereochemistry of bromo chloro compounds obtained from the addition of molecular bromine chloride to **2a** and **2b** at 0 °C

Solvent	Dielectric constant[b]	Product composition/%[a]			
		from **2a**		from **2b**	
		% **3a**	% **3b**	% **3a**	% **3b**
Dioxane[c]	2.21	21.4	78.6	18.3	81.7
CCl_4	2.23	76.1(75.5)[d]	23.9(24.5)[d]	11.8	88.2
$CHCl_3$	4.81	75.2	24.8	9.8	90.2
CH_2Cl_2	9.08	75.7(79)[d]	24.3(21)[d]	6.3(8.5)[d]	93.7(91.5)[d]
$(CH_3CO)_2O$	20.7	51.4	48.6	14.5	85.5
CH_3NO_2	35.87	49.8	50.2	9.1	90.9

a) Based on the amount of bromo chloro compounds, as determined by GLC analysis. Values were not corrected for FID response factors. Percentages are normalized to 100%. Yields of bromo chloro compounds were determined by GLC and found to be more than 70% in all runs. Other products were 5—10% of the dichloride and 12—20% of the dibromide. b) See footnote a in Table 3. c) At 20 °C. d) Data from Ref. 4.

These results show that the stereochemistry of the addition to *cis*-alkene (**2a**) is dependent on the polarity of the solvent. The addition in acetic anhydride or in nitromethane was nonstereospecific. The results of *trans*-alkene (**2b**) showed a much smaller dependency on the nature of the solvent. All the additions to **2b** were found to be *anti* stereoselective. A similar stereochemistry has been observed for the addition of bromine to these alkenes.[2] Since it is quite reasonable to consider that the process is the same for both bromine and bromine chloride additions,[4,6] a mechanism such as that illustrated in Fig. 3, similar to bromine addition, would be involved in the addition with bromine chloride.

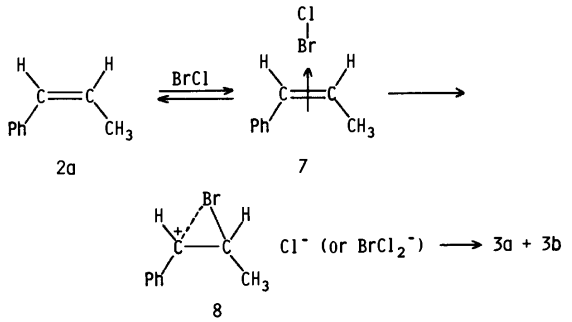

2a 7 8

Fig. 3.

The solvent dependency of the stereochemistry and the regiospecific addition observed for the reaction with these alkenes are fully in accordance with the mechanism involving a very weakly bridged benzylic carbonium ion intermediate (**8**) prior to the product-determining step.[2] The fact that the stereochemistry of the addition to **2a** is more sensitive to solvent polarity than that of the addition to **2b** gives strong evidence for the presence of the intermediate (**8**). The intermediate (**8**) for the reaction of **2a** tends to take a more energetically favored conformation due to the eclipsing effect of the adjacent methyl and phenyl groups. Furthermore, the peculiarity of stereochemistry observed in dioxane is easily explained in terms of specific solvation for the carbonium ion intermediate.[2]

As has been described above, the additions to alkenes appeared to be strikingly different in reactions with **1** and with BrCl in all aprotic solvents employed. These marked differences in the reactions of **1** and BrCl suggest that these two reactions are quite different in their mechanisms. The formation of completely *anti* stereospecific and *anti*-Markownikoff adducts in reaction with **1** rules out a weakly bridged benzylic-like ion intermediate (**8**), such as is shown in Fig. 3. If an intermediate such as **8** was involved, the complete formation of Markownikoff adduct would be expected.

The large differences of product distribution obtained by the reaction with **1** are consistent with the previous proposal that this reagent is an independent electrophile rather than a precursor of BrCl.[1] The reactions of $BrCl_2^-$ presently studied and Br_2Cl^- (or Br_3^-) reported by Heasley *et al.*[4] seem to involve similar mechanisms. Two possible mechanisms have been proposed by them, involving attack of a halide ion on a three-center bound π complex (**9**)[7] or on the bromonium ion intermediate (**10**).

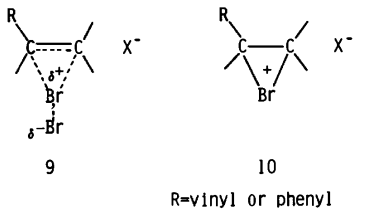

9 10

R=vinyl or phenyl

The bromonium ion intermediate (**10**), however, is hardly acceptable for the reaction of $BrCl_2^-$ since the present reaction gave nonregiospecific products. Thus, the $AdEC_2$ process involving an intermediate like **9** at the product-determining step would be applicable to the reaction of $BrCl_2^-$, as depicted in Fig. 4.

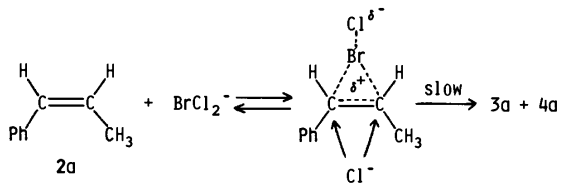

2a 11

Fig. 4.

The regiochemistry of the reaction of **1** would be dependent on the electronic effect of the phenyl ring which stabilizes the developing cationic character on the carbon in the complex (**11**). The *cis*- and *trans*-alkenes gave somewhat different regiochemical results. Markownikoff adducts were obtained mainly from both *cis*- and *trans*-alkenes (**2a** and **2b**) as given in Table 3. The *cis*-alkene gave less regioselectivity than the *trans*-alkene. The differences may be ascribed to the ability of stabilization of a cationic center by phenyl groups. The phenyl ring of the intermediate (**12**) formed from the *cis*-alkene would be skewed by the eclipsing effect.

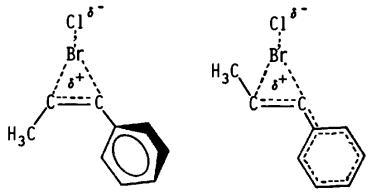

12 13

The intermediate (**13**) formed from the *trans*-alkene would be free from such an eclipsing effect and the developing cationic character would be delocalized over the phenyl ring. This type of stabilization may develop the cationic character on the carbon adjacent to the phenyl ring. Thus, attack of a chloride ion to the benzylic carbon atom would be more favored in the intermediate from *trans*-alkene than in that from *cis*-alkene. In fact, the *trans*-alkene (**2b**) was found to react faster than the *cis*-alkene (**2a**).[8]

Experimental

NMR spectra were recorded on a JEOL JNM FX-60Q and a JEOL C-60HL spectrometer using TMS as an internal standard. Mass spectra were recorded on a JMS-D-300 Mass

spectrometer. The GLC analyses were performed on a Yanako G-180 Gas Chromatograph. Tetrabutylammonium dichlorobromate(1-) (**1**) was prepared by the literature procedure.[9] All the organic starting materials, including the solvents, were distilled before use. Bromine chloride was prepared by adding an equimolar amount of bromine to a chlorine-carbon tetrachloride solution.

Reaction of cis-*1-Phenylpropene (**2a**) with 1.* Details of the reaction have been reported previously.[1] The mixture of **2a** (5.90 g, 50 mmol) and **1** (19.7 g, 50 mmol) in 100 ml of chloroform was stirred at 0 °C for 10 min. After the usual work-up procedure, distillation afforded 9.3 g (80%) of a mixture of two isomeric bromochloroalkanes (**3a** and **4a**): bp 90—91 °C/1 mmHg (1 mmHg≈133.322 Pa); MS M^+ at m/z= 232, 234, 236 (100:128:32); Found: m/z 231.9649. Calcd for $C_9H_{10}BrCl$: M, 231.9655. Although attempts to separate **3a** and **4a** by GLC were unsuccessful, ^{1}H-NMR analysis by integration of methyl protons revealed the product composition to be 76% of **3a** and 24% of **4a**. The major product was characterized as **3a** on the basis of the ^{1}H- and ^{13}C-NMR spectra of an authentic sample.[4]

Reaction of trans-*1-Phenylpropene (**2b**) with 1.* The reaction was carried out similarly to that of **2a**. Distillation afforded 9.6 g (82%) of mixed bromochloroalkanes (**3b** and **4b**): bp 91—92 °C/1 mmHg; MS M^+ at m/z=232, 234, 236 (100:128:32); Found: m/z 231.9648. Calcd for $C_9H_{10}BrCl$: M, 231.9655. ^{1}H-NMR analysis established the product composition as 96% of **3b** and 4% of **4b**. The major product was also characterized as **3b** on the basis of the ^{1}H- and ^{13}C-NMR spectra of an authentic sample.[4]

*Dehydrohalogenation of Regioisomers (**3a** and **4a**).* To 2.34 g (10 mmol) of the mixture composed of **3a** (76%) and **4a** (24%) in *t*-butyl alcohol (50 ml) was added 6 ml (2.23 mmol) of potassium *t*-butoxide in *t*-butyl alcohol (0.372 mol dm^{-3}); the mixture was stirred at 20 °C. After 30 min, 1 ml of the solution was taken up, shaken with water, and extracted with pentane. The pentane layer was washed with dilute acid and dried over $MgSO_4$. Evaporation of the pentane and analysis of the residue by ^{1}H NMR showed the composition to be: **3a**, 53.3%; **4a**, 25%; **5**, 21.7%; and **6**, 0%. The reaction was carried out further by the addition of 15 ml (5.58 mmol) of potassium *t*-butoxide solution (0.372 mol dm^{-3}); this mixture was stirred for 1 h. The reaction mixture was then worked up in a fashion similar to that described above. Evaporation of the pentane gave 1.58 g of the crude product. ^{1}H NMR showed the composition to be: **3a**, 0.5%; **4a**, 23%; **5**, 76.5%; and **6**, 0%. Column chromatography of this residue on silica gel with hexane as the eluent gave almost pure **4a** (150 mg) and **5** (711 mg). The data for **4a** are as follows: ^{1}H NMR ($CDCl_3$) δ=1.46 (3H, d, J=6.6 Hz, CH_3), 4.45 (1H, approx. quintet, CHCl), 5.06 (1H, d, J=6.6 Hz, CHBr), and 7.32 (5H, m, C_6H_5); MS M^+ at m/z=232, 234, 236 (100:127:32); Found: m/z 231.9649. Calcd for $C_9H_{10}BrCl$: M, 231.9655. The data for **5** are as follows: ^{1}H NMR (CCl_4) δ=1.90 (3H, d, J=6.7 Hz, CH_3), 6.31 (1H, d, J=6.7 Hz, CHCl), and 7.28—7.62 (5H, m, C_6H_5); MS M^+ at m/z=152, 154 (100:32); Found: m/z 152.0388. Calcd for C_9H_9Cl: M, 152.0393. The ^{1}H-NMR spectrum for **5** corresponds well with that reported in the literature.[10]

*Dehydrochlorination of Pure Regioisomer (**4a**).* To 120 mg (0.51 mmol) of **4a** in *t*-butyl alcohol (5 ml) was added 2 ml (0.74 mmol) of potassium *t*-butoxide solution (0.372 mol dm^{-3}); this mixture was stirred at 20 °C. After 30 min, the reaction mixture was worked up as described above. Evaporation of pentane gave 75 mg of crude product **6** as a colorless oil: ^{1}H NMR (CCl_4) δ=2.00 (3H, d, J=7.5 Hz, CH_3), 6.40 (1H, d, J=7.5 Hz, CHBr), and 7.35—7.80 (5H, m, C_6H_5); MS M^+ at m/z=196, 198 (100:97); Found: m/z 195.9898. Calcd for C_9H_9Br: M, 195.9888. The spectral patterns of this product were identical with those of a sample prepared by dehydromination of *threo*-1,2-dibromo-1-phenylpropane.

*Reaction of 1 with **2a** or **2b** in Various Solvents.* To 2 mmol of the alkene in 20 ml of the solvent was added 2 mmol of **1** at 0 °C over 5 min with stirring. After the yellow color disappeared, the mixture was washed with water and dried over Na_2SO_4. The product of the reaction in acetic anhydride was isolated by pouring the reaction mixture into water, followed by extraction with ether and washing with aq $NaHCO_3$ then water. After the solvent was removed under reduced pressure, the residues were analyzed by ^{1}H NMR and ^{13}C NMR in some cases. The relative amounts of products were determined from the ratio of the peak areas of the methyl protons of the bromo chloro compounds (**3a** and **4a** or **3b** and **4b**), and also from the ratio of peak heights of aliphatic carbons (^{13}C NMR). The results are given in Table 3.

*Reaction of Bromine Chloride with **2a** or **2b** in Various Solvents.* To 2.1 mmol of the solvent, was added 1.7 ml of BrCl solution in CCl_4(1.2 mol dm^{-3}) at 0 °C with stirring. Products of the reactions in acetic anhydride and dioxane were isolated by extraction with ether as described above. Products of the reactions in carbon tetrachloride, chloroform, dichloromethane, and nitromethane were obtained by direct evaporation of the solvent. GLC analysis of the residue gave six peaks with retention times of 12.3, 13.7, 18.9, 21.1, 27.6, and 32.8 min. These were assigned to be *erythro*-1,2-dichloro-, *threo*-1,2-dichloro-, *erythro*-2-bromo-1-chloro-, *threo*-2-bromo-1-chloro-, *erythro*-1,2-dibromo-, and *threo*-1,2-dibromo-1-phenylpropanes, except for unreacted alkene, respectively. GLC analyses were performed on a High vacuum silicon grease (25%)-Celite 545 (2 m) column at 120 °C with helium as a carrier gas (35 ml/min). The results are given in Table 4.

*The Reaction of 1 with **2a** in the Presence of a Radical Inhibitor.* When **2a** was treated with **1** in chloroform as described above, O_2 was bubbled during the reaction. The product ratio of 76.5:23.5 was obtained by ^{1}H-NMR analysis for **3a** and **4a**, respectively. The reaction was carried out with 1.18 g (10 mmol) of **2a**, 3.93 g (10 mmol) of **1**, and 0.70 g (0.3 mmol) of 2.6-di-*t*-butyl-4-methylphenol in chloroform (30 ml). After the usual work-up, the product ratio of 77.8: 22.2 was obtained by ^{1}H-NMR analysis for **3a** and **4a**, respectively. ^{13}C-NMR analysis also showed a 76.5:23.5 mixture of **3a** and **4a**, respectively.

Stability of the Bromo Chloro Compounds under the Reaction Conditions. To 1 mmol of the two regioisomers (**3a** and **4a**) in chloroform (10 ml) was added 2 mmol of **1** and allowed to stand for 3 h at room temperature with stirring. The mixture was shaken with aq sodium sulfite. The chloroform layer was separated, washed with water, and dried over $MgSO_4$. After the solvent was removed, the residue was analyzed by ^{1}H-NMR spectrum. No interconversion was observed. Namely, the same isomer compositions were observed within experimental error: Starting from a 60:40 mixture of **3a** and **4a** recovered a 59:41 mixture of **3a** and **4a**, and only **3a** was recovered from **3a** without contamination with **4a**.

The authors wish to thank Dr. Seizi Kozuka of Osaka City University for helpful discussions.

References

1) T. Negoro and Y. Ikeda, *Bull. Chem. Soc. Jpn.*, **57**, 2111 (1984).

2) J. H. Rolston and K. Yates, *J. Am. Chem. Soc.*, **91**, 1477 (1969).

3) R. E. Buckles, J. M. Bader, and R. J. Thurmaier, *J. Org. Chem.*, **27**, 4532 (1962).

4) G. E. Heasley, J. M. Bundy, V. L. Heasley, S. Arnold, A.

Gipe, D. McKee, R. Orr, S. L. Rodgers, and D. F. Shellhamer, *J. Org. Chem.*, **43**, 2793 (1978).

5) C. H. Depuy and C. A. Bishop, *J. Am. Chem. Soc.*, **82**, 2535 (1960).

6) a) V. L. Heasley, D. F. Shellhamer, J. A. Iskikian, D. L. Street, and G. E. Heasley, *J. Org. Chem.*, **43**, 3139 (1978); b) V. L. Heasley, D. W. Spaite, D. F. Shellhamer, and G. E. Heasley, *J. Org. Chem.*, **44**, 2608 (1979).

7) G. A. Olah and T. R. Hockswender, Jr, *J. Am. Chem. Soc.*, **96**, 3574 (1974); G. A. Olah, P. Schilling, P. W. Westerman, and H. C. Lin, *ibid.*, **96**, 3581 (1974).

8) The rates of the reactions of **2a** and **2b** with **1** were determined in chloroform relative to the rate of the reaction of styrene. Relative rates were measured at 0 °C by the competition method using ^{1}H-NMR analysis. The relative rates were found to be: styrene, 1.00; **2a**, 1.27±0.05; **2b**, 1.54±0.05.

9) A. I. Popov and R. E. Buckles, *Inorg. Synth.*, Vol. V, 172 (1957).

10) R. C, Fahey and Schubert, *J. Am. Chem. Soc.*, **87**, 5172 (1965).

 © 1984 The Chemical Society of Japan Bull. Chem. Soc. Jpn., 57, 2121—2126 (1984)

The Changes in Conformation and Complexability of 6,6′-Diamino-2,2′-bipyridine by Protonation

Noriyuki KISHII, Koji ARAKI, and Shinsaku SHIRAISHI*
Institute of Industrial Science, The University of Tokyo, Roppongi, Minato-ku, Tokyo 106
(Received November 30, 1983)

The reaction of 6,6′-dibromo-2,2′-bipyridine with ammonia in an autoclave gave 6,6′-diamino-2,2′-bipyridine (DABP) in more than 80% yields. DABP behaved as a diacidic base in the pH range of 0 to 10 with the conformational changes. DABP formed complexes with Cu(II), Ni(II), Co(II), and Zn(II). The amino groups at 6 and 6′ positions play a role as strong electron-donationg groups and not as coordination sites. p*K*a values and complex formation constants were estimated.

2,2′-Bipyridine (bpy) is well known as a typical ligand that forms stable complexes[1] with various transition metal ions in a wide pH range. Particularly, in last 15 years, tris(bpy) ruthenium complex has been extensively studied because of its potential applicability to photolysis of water in coupling with an electron acceptor such as methylviologen.[2] Various kinds of bpy derivatives have been synthesized and examined as to the effects of substituents on the complexing properties and on the physical properties of the complexes.[3,4] Among these derivatives, 6,6′-dimethyl-2,2′-bipyridine (Mbpy) exhibits an unique behavior in the complex formation due to the steric hindrance of the substituents at 6- and 6′- positions.[5] Mbpy forms almost exclusively mono or bis complex with various metals, while many other bpy derivatives usually form stable tris-bpy complexes. In a few tris complexes of Mbpy exceptionally known, the methyl substituents were reported to affect on the wavelength and/or life time of luminescence of ruthenium(II) complexes.[6] The recent interest in this field seems to be focussed on the examination of the effect of the substituents on bpy or analougus complexes with various metal ions.[7,8] 6,6′-Diamino-2,2′-bipyridine (DABP) is expected to exhibit interesting properties as a metal ligand. There was, however, no paper reported as to the properties of DABP and its complexing ability with metal ions except only two reports on the synthesis of DABP.[9,10] In this paper, we wish to report an improved synthesis and some physical properties of DABP along with complex formation. The influence of the amino group at 6,6′-positions on the ability of complex formation with some transition metal ions will be discussed.

Results

Preparation of 6,6′-Diamino-2,2′-bipyridine. 2,2′-Bipyridine (bpy) is rarely susceptible to either electrophilic or nucleophilic substitution reactions.[11] The usual Chichibabin reaction using sodium amide gave only a trace amount of amino derivatives.[10] Burstall reported that 6,6′-dibromo-2,2′-bipyridine (DBBP) was easily converted to DABP by the reaction with aqueous ammonia in a sealed tube for 14h,[9] but attempted preparation according to the report resulted in unsatisfactory results. An improved amination method was explored.

An unsealed glass ampoule containing DBBP was placed in an autoclave, into which liquid ammonia was added. DBBP was allowed to react with ammonia at 220 °C under a pressure of 100 kgf cm^{-2} (kgf= 9.80665N) for 6 h. After the reaction, the solid in the ampoule was dissolved in dilute aqueous HCl and filtered. Basification of the filtrate with aqueous ammonia gave crude DABP as a precipitate. Purification was effected by sublimation and the total yield was 80%. In these reaction conditions, there was no recovery of DBBP nor char formation and DBBP was considered to be fully converted into DABP. The remainder of DABP might be left unprecipitated in the bacified solution though its limited solubility. The reaction conditions described above were fairly optimized one. Three hours' reaction was not enough fully to convert DBBP into DABP, and longer reaction time more than 10 h also reduced the yield of DABP by noticeable char formation. The presence of metals diminished the yield of DABP, which is the reason why DBBP was placed in a glass ampoule. Imperfect purification of DBBP, especially residual copper, deteriorated the DABP formation and resulted in char formation. This may be due to the catalytic degradation of DBBP or DABP with copper or other metals.

Acid-base Properties of DABP. 2,2′-Bipyridine (bpy) and 1,10-phenanthrorine (phen) have been thought to be monoacidic base though they have two sites for potonation.[12] The second protonation occurs, however, only in a strong acid such as concentrated sulfuric acide.[13,14] The acid-base properties of DABP, which has four potentially basic nitrogen atoms in the molecule, were examined and it was found to act as a diacidic base in the pH range from 0 to 10.

The absorption spectra of DABP changed with pH (Fig. 1). Stepwise protonation is suggested. Figure 1-A shows the spectral change of DABP with isosbestic points due to the first protonation step, where DABP changed from free form to monoprotonated form with isosbestic points. Figure 1-B shows the spectral change of DABP with different isosbestic points from monoprotonated form to diprotonated form. The pattern of the spectral change in the first step is very similar to that of bpy, suggesting that this is due to monoprotonation step. This was confirmed by acid-base titration. The second step is diprotonation process. This

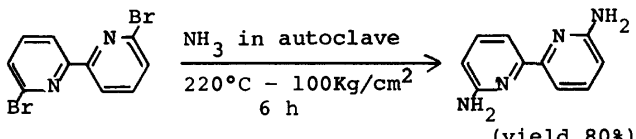

Scheme 1.

is not experimentally confirmed but plausibly considered to be so by the exsistence of isosbestic points in the spectral change. As shown in Fig. 1, DABP showed two stages of equilibrium substantially separated from each other, suggesting that the proton dissociation constants for mono and diprotonated forms of DABP were greatly different from each other. The pKa_4 for the first protonation stage and pKa_3 for the second protonation stage of DABP were determined to be 6.72 and 2.2 respectively by plotting the absorbances at 360 nm for the first stage protonation, and at 350 and 250 nm for the second stage protonation against pH (Fig. 2). The values are larger than those of bpy (4.5 and −0.5).[15,13] The pKa_4 was very close to 6.86 of 2-aminopyridine (Ampy),[16] where the amino group effects to strengthen the basicity of pyridine ring by its strong electron donating property.

The chemical shifts of ^{1}H-NMR spectra of DABP and related compounds in various media are listed in Table 1. The assignment was according to the literature.[17,18] The chemical shifts of DABP in DMSO were nearly close to those of Ampy except 3-H, and were shifted to upper field comparing with those of bpy. This indicates that the electron distribution on pyridine ring of DABP is similar to that of Ampy and their electron density are higher than that of bpy, being consistent with the pKa data described above.

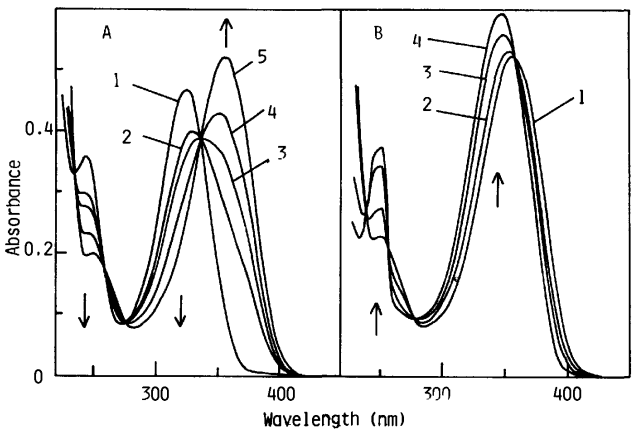

Fig. 1. The spectral Change of DABP (3.33×10^{-5} mol dm^{-3}).
A:Change from free to monoprotonated form 1) pH 10.00, 2) pH 7.00, 3) pH 6.57, 4) pH 6.00, 5) pH 4.90.
B: Change from mono to diprotonated form 1) pH 3.63, 2) pH 2.35, 3) pH 1.46, 5) pH 0.60.

Complex Formation. DABP showed the spectral change by complexation with metal ions. Figure 3 shows the spectral change of DABP as a function of Cu(II) concentration.

Continuous variation method was applied to the DABP-metal systems in a buffer solution of pH 9.3. The total concentration of metal and ligand employed was 2.00×10^{-5} mol dm^{-3}. The result confirmed the 1:1 stoichiometry of the DABP-metal systems except with Zn(II) (Fig. 4). There was nothing observed to indicate the formation of DABP tris complexes. In this respect, DABP resembles Mbpy in the pattern of the complex formation,[5] suggesting that the amino groups at 6 or 6′-positions act like methyl groups of Mbpy. The formation constants of 1:1 complexes ($\log K_1$) were obtained at pH 4.0 and 9.3 by the Rose-Drago method (Table 2). Typical examples are shown in Fig. 5. The constant for Zn(II) at pH 9.3 was not obtained, because Zn(II) forms only 2:1 complex (DABP:Metal) at the

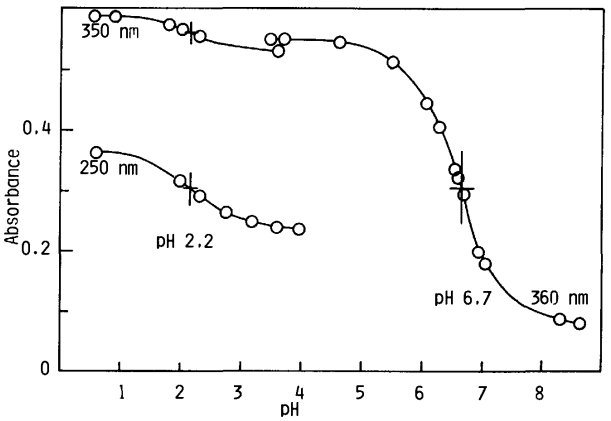

Fig. 2. The Absorbance of DABP (3.33×10^{-5} mol dm^{-3}) as a Function of pH.

TABLE 2. THE COMPLEX FORMATION CONSTANTS ($\log K_1$)

Metal ion	$\log K_1$		$\log K_{ex}$ calcd	
	pH 4.0	pH 9.3	pH 4.0	pH 9.3
Cu(II)	4.82	6.67	0.82	−0.05
Ni(II)	3.30	5.82	−0.70	−0.90
Co(II)	1.82	4.96	−2.18	−1.76
Zn(II)	2.17	—*	−1.83	—
Cu(I)	4.07	6.00	−0.10	−0.70

*) $\log K_2=11.7$

TABLE 1. CHEMICAL SHIFTS OF DABP AND RELATED COMPOUNDS

	Solvent	Position				$\delta_3-\delta_5$
		3	4	5	6	
Ampy	: DMSO	6.35	7.18	6.27	7.74	0.08
+1/2 eq. mol D_2SO_4	: D_2O	6.87	7.70	6.77	7.61	0.10
	: D_2SO_4	8.04	8.63	7.99	8.54	0.05
bpy	: DMSO	8.15	7.72	7.24	8.43	0.91
+1/2 eq. mol D_2SO_4	: D_2O	8.07	8.07	7.65	8.48	0.42
	: D_2SO_4	8.26	8.66	8.14	8.72	0.12
DABP	: DMSO	7.36	7.36	6.38		0.98
+1/2 eq. mol D_2SO_4	: D_2O	6.78	7.33	6.48		0.30
+ eq. mol D_2SO_4	: D_2O	7.05	7.64	6.80		0.25
	: D_2SO_4	7.49	8.21	7.41		0.08

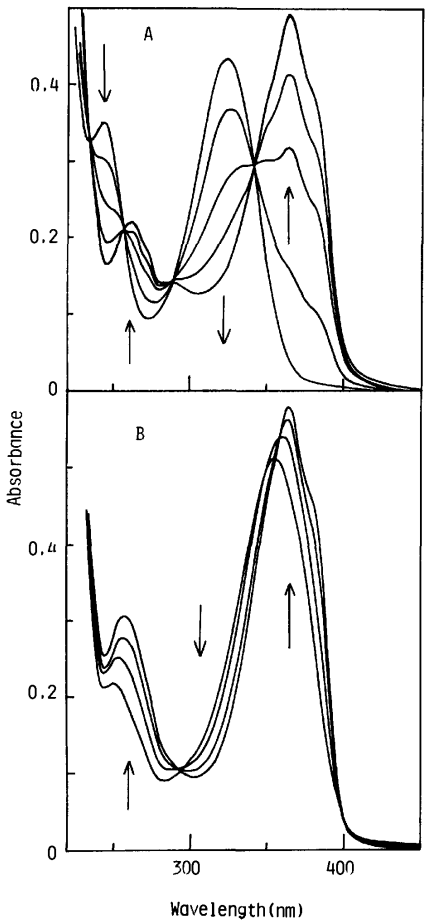

Fig. 3. The Spectral Change of DABP (3.33×10^{-5} mol dm^{-3}) as a Function of Cu(II) Concentration.
A: In pH 9.3 buffer solution
B: In pH 4.0 buffer solution.

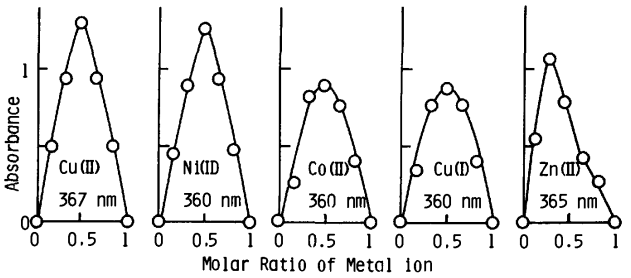

Fig. 4. Continuous Variation Method in pH 9.3 Buffer Solution at 20 °C.
[M]+[DABP]=2.0×10^{-4} mol dm^{-3}.

pH. At pH 1.0, the spectral changes of DABP was too small to estimate the complex formation constants. Cu(II) had the highest complexability at pH 9.0 among the metal ions employed and the order of abilities of complexation were Cu(II)>Cu(I)>Ni(II)>Co(II). This order was the same as for bpy.[19] The log K_1 values of DABP were smaller than those of bpy but larger than those of Mbpy.[20] The complex formation constants observed at pH 4.0 were smaller than those at pH 9.3. The order of the ability of complexation of metals with DABP at pH 4.0 was the same as that at pH 9.3 and also the same as that of bpy except Zn(II).

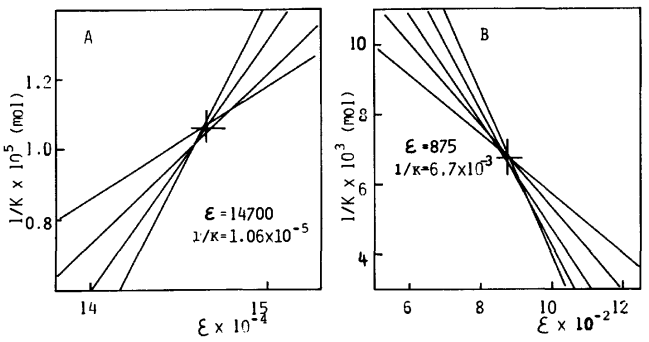

Fig. 5. Rose-Dorago Plots of Metal-DABP Systems at 20 °C.
A: Co(II)-DABP system in pH 9.3 buffer solution
B: Zn(II)-DABP system in pH 4.0 buffer solution.

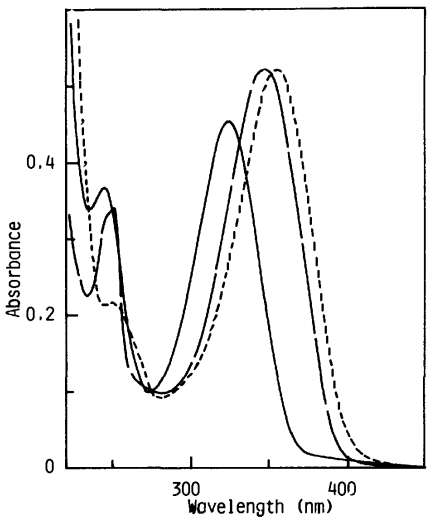

Fig. 6. Comparison of the Spectra of DABP (3.33×10^{-5} mol dm^{-3}) in Buffer Solutions of Different pH.
—— pH 9.3, ------ pH 4.0, ——pH 1.0.

Discussion

The Protonation Site and the Conformation of Protonated DABP. ^{1}H NMR spectrum of DABP in DMSO showed nearly the same chemical shifts as that of Ampy except the signal due to the ring proton at 3 position. The proton at 3 position of bpy in either protic or aprotic solvent is known to show an anomalous chemical shift comparing to the proton at 5 position due to the effect of diamagnetic anisotropy of neighbouring pyridine ring, and the conformation of bpy in solution is predicted by the relative chemical shift of the proton at 3 position to that at 5 postion $\delta_{H\text{-}3}-\delta_{H\text{-}5}$).[18] The relative chemical shifts of DABP in DMSO were 0.98, which is almost the same as that (0.91) of bpy. Bpy in solution is known to have transoidal conformation,[15,18] suggesting that the free form of DABP has transoidal conformation in the solution.

The UV absorption spectrum also supports transoidal conformation of free DABP. Figure 6 shows the absorption spectra of DABP in buffer solutions of pH 9.3, pH 4.0, and pH 1.0 corresponding to free, monoprotonated, and diprotonated form of DABP. Bpy has two bands at 232 nm and 279 nm in basic

solution.[15] Free form of DABP also has two bands at 244 and 325 nm. The spectral shapes of bpy and DABP resembles each other except that the two peaks of DABP are at longer wave lengths than those of bpy.

Monoprotonated DABP seems to have a cisoidal conformation, and the site for protonation seems to be on the ring nitrogen and not on the amino groups. Two bands of monoprotonated DABP appeared at 251 nm and 357 nm, being red-shifted in comparison with those of the free form. The monoprotonation of bpy is known to cause the red-shift comparing with free form.[15] The relative chemical shift ($\delta_{H\text{-}3}-\delta_{H\text{-}5}$) of monoprotonated DABP is 0.30 ppm and is near to 0.40 ppm of monoprotonated bpy. This also suggests that the monoprotonated DABP has the same conformation as that of monoprotonated bpy, which is known to have cisoidal conformation.[15] Thus monoprotonated DABP is concluded to have the cisoidal conformation to form chelation ring and the bacisity of the pyridine ring is increased as 100 times large as that of bpy by introduction of amino groups at 6- and 6'- positions.

The second protonation seems to be different from that of bpy. Two bands still appeared at 252 nm and 348 nm in the absorption spectrum of diprotonated DABP, whereas the second protonation on bpy leads to loss of one of the two peaks to exhibit only one absorption at 290 nm.[13] The second protonation on bpy at the other pyridine ring causes repulsive interaction between the two protonated sites and makes two pyridine rings twisted.[15] The disappearance of one of the two peaks observed in bpy seems to be due to the destruction of the coplanarity of the linked aromatic rings and is not observed in the case of 1,10-phenanthrorine,[13] nor in the dication of bpy formed by *N*-alkylation with 1,2-dichloroethane.[18] The second protonation on DABP is suggested not to destroy the conjugation so much as in the case of bpy. ^{1}H-NMR spectra also suport the consideration. The relative chemical shift of proton at 3 position to that at 5 position was 0.25 ppm, and being close to 0.3 ppm of monoprotonated DABP. Thus the secondly protonated DABP has still cisoidal conformation, and therefore, the second protonation is plausively considered to occur at amino group.

In a strong acid, however, the destruction of cisoidal conformation seems to be caused by the third and fourth protonation.[21] The relative chemical shifts of 3 position to that of 5 position in D_2SO_4 were 0.12, 0.08, and 0.05 ppm respectively for bpy, DABP, and Ampy. The value of DABP is intermediate between those of bpy and Ampy. In these conditions, bpy has twisted conformation and the proton at 3 position is not affected so much by the neighbouring aromatic rings. Thus the first and second stage protonation of DABP were suggested to occur as shown in scheme 2. It may be plausible from the electrostatic point of view too.

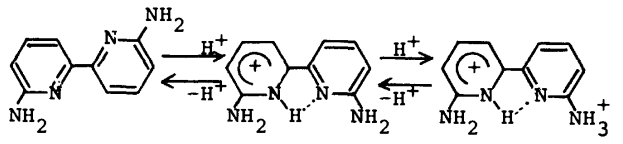

Scheme 2.

This may be the reason that the *K*a for the second protonation of DABP became larger about 1000 times than that of bpy.

Exchange of Proton with Metal Ion and the Effects of the Amino Group. Absorption spectra of Ni(II) complex with DABP in buffer solutions of pH 9.3 and 4.0 are shown in Fig. 7 along with that of monoprotonated DABP. Spectra of Ni(II) complex at pH 9.3 and pH 4.0 were almost the same as each other and very close to that of monoprotonated DABP, suggesting that complexing site for metal ions is the site where protonation occurs, and that proton and metal ion compete with each other in coordination. Supposing an equilibrium of ternary system among L, LH, and LM (Scheme 3), the equilibrium constants of the exchange between proton and metal ions (K_{ex}) can be estimated either by using the values of log K_1 at pH 9.3 and p*K*a or by using log K_1 at pH 4.0 for any of the metal ions forming 1 : 1 complex with DABP. The two independently obtained values of K_{ex} were nearly the same for Ni(II) and Co(II). Therefore, there is considered to exsit the ternary equilibrium among L, LH, and LM in moderate pH region and the metal decomplexation at lower pH region is also considered to be

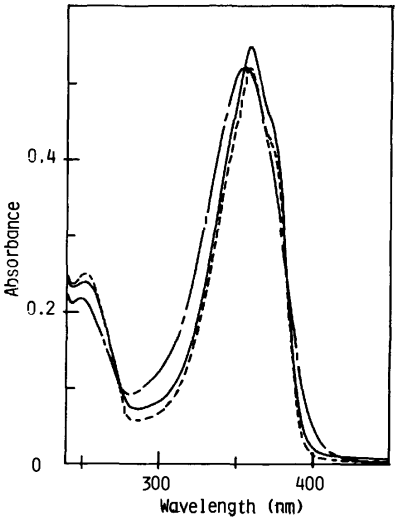

Fig. 7. Comparison of the Spectra of DABP (3.33×10^{-5} mol dm^{-3}) and DABP-Ni Systems in Different Buffer Solutions.
------ with excess amounts of Ni(II) in pH 9.3, —— with excess amounts of Ni(II) in pH 4.0, —·— in pH 4.0 without metal ion.

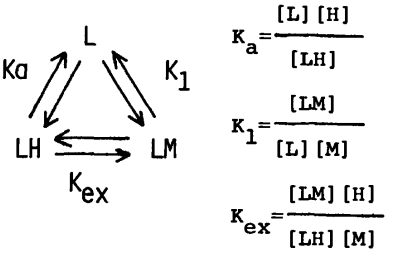

Scheme 3.

due to the exchange of metal ion with proton.

As discussed above, the sites for protonation and metal complexation of DABP are the ring nitrogen atoms. Electron donation by amino groups increases the basicity of ring nitrogen atoms of DABP and influences the complex formation properties. However, basicity is not directly related to complex formation ability. The ability of complex formation of DABP was less than that of bpy, although DABP has higher basicity than bpy. Mbpy which has higher bacicity than bpy is known to have less complexability than bpy. The substituents at 6- and 6′- positions decrease the complexability. For the compounds having similar steric effects, however, the basicity of the complexing site determines the complexability. The complex formation constants of DABP (log K_1=6.7 for Cu(II)) is larger than that of Mbpy (4.23) according to the higher basicity of DABP (pKa=6.7) than that of Mbpy (4.88). The differences in log K_1 and pKa are found to be almost parallel.

DABP forms only 1:1 complex with metal ions such as Cu(II), Ni(II), and Co(II) and no bis nor tris complexes due to the steric hindrance of the amino groups. Therefore, the complexes of DABP are more pH-sensitive than tris complexes of other bipyridine derivatives. Although pKa of 2,2′-bipyrazine is 0.5, tris-(bipyrazine)ruthenium is stable in concentrated sulfuric acid.[7] And tris(bipyridine) complex with Fe(II) is stable in the pH region of 1.0—9.0, though pKa of bipyridine is 4.5.[22] Whereas, the stability constant of DABP drastically changes between pH 4.0 and pH 9.3 about 100 times. This pH-sensitive properties of DABP for complex formation can be used as a pH- swich for selective uptake and release of metal ions.[24]

Experimental

6,6′-Dibromo-2,2′-bipyridine (DBBP). To a suspension of 2,6-dibromopyridine(50 g, 0.21 mol) in diethyl ether (350 cm^3), which was cooled under −60 °C in liquid nitrogen-hexane bath, butyllithium (2.2 mol dm^{-3} in hexane, 130 cm^3, 0.29 mol) was added slowly. Then the reaction mixture was cooled to −90 °C and a fine powder of anhydrous copper(II) (14.2 g, 1.04 mol) was added. The mixture was allowed to warm to −70 °C with efficient stirring. After 30 min, oxygen was bubbled slowly through the solution at −50 °C for 30 min. The reaction mixture was poured into aqueous HCl (6N, 500 cm^3) with stirring. The solid part was collected by filtration, washed with water and dried under vacuum. The dried solid was extracted with hot benzene. The benzene extract was evaporated. The residue was recrystallized from benzene to give colorless needles of DBBP in pure form, 20.2 g (61%). Mp 225—226 °C (lit.[23] 226—227 °C).

6,6′-Diamino-2,2′-bipyridine (DABP). DBBP (3.0 g, 9.6 mmol) was placed in a glass ampoule. Liquid ammonia (30 g) was also placed in another ampoule. The unsealed ampoules were placed in an 500 cm^3 autoclave, and heated up to 220 °C. The inner pressure rised up to 100 kgf cm^{-2}. Heating was continued for 6 h. After the reaction, the solid in the glass ampoule was dissolved in dilute aqueous HCl (50 cm^3) and filtered in order to remove insoluble matters, and unreacted starting material. Aqueous ammonia was added into the filtrate to precipitate a solid , which was collected by filtration, washed with aqueous ammonia and water, and dried under vacuum. The crude products were sublimated under vacuum (2 mmHg (270 Pa)-150—200 °C) to give 1.42 g (80%) of purified DABP, mp 185—186 °C (lit,[9] 186 °C). Found C, 64.67; H, 5.19; N, 30.21%. Calcd for $C_{10}H_{10}N_4$ C, 64.50; H, 5.41; N, 30.09%. The reaction for 3 h gave unreacted starting material (0.81 g, 27%) and DABP (0.93 g, 52%).

Spectral Measurements. The absorption spectra were recorded with a JASCO UVIDEC-505 spectrophotometer at 20 °C. The buffer solutions used were as follows: pH 1.0, HCl-KCl buffer; pH 4.0, 0.2 mol dm^{-3} acetic acid-sodium acetate buffer; pH 9.3, 0.2 mol dm^{-3} potassium borate buffer. The ionic strength was not adjusted. ^{1}H-NMR spectra were recorded with JEOL JMN-MH 100 spectrometer. The chemical shifts were determined by 10 mmol of substance in 0.4 cm^3 DMSO-d_6 with tetramethylsilane (TMS) as internal standard or in 0.4 cm^3 D_2O with TMS as external standard, and reported in ppm from TMS.

Determination of Complex Formation Constants. Metal salts used were, Cu(II)$Cl_2\cdot 2H_2O$, Ni(II)$Cl_2\cdot 6H_2O$, Co(II)$Cl_2\cdot 6H_2O$, Zn(II)$(CH_3COO)_2\cdot 2H_2O$, and Cu(I)Cl of Special grade quality (Wako Pure Chemical Co). Typical procedure is as follows: 0.01 cm^3 of metal solution (0.01—1.0 mol dm^{-3}) was added to 3 cm^3 of buffer solution containing 1.00×10^{-7} mol of DABP. The changes of absorbance and composition of the solution were plotted according to Rose-Dorago Method. Wavelengths used for the determination were as follows. Cu(II), 367 nm; Ni(II), 360 nm; Co(II), 360 nm; Zn(II), 365 nm; Cu(I), 360 nm.

Continuous variation method. The total concentration of metal ions and DABP was 2.00×10^{-5} mol dm^{-3}. The differences in absorbance were plotted against the composition of the solutions (metal ion/DABP). The wavelengths used for the measurement were the same ones used in the experiment described above.

References

1) F. A. Cotton and G. Wilkinson, "Advanced Inorganic Chemistry," 3rd ed, John Wiley and Sons, New York (1966).
2) K. Kalyanasundarum, *Coord. Chem. Rev.*, **46**, 159 (1979).
3) Wm. M. Banick and G. F. Smith, *Anal. Chim. Acta*, **19**, 304 (1958).
4) G. F. Smith and Wm. M. Banick, *Analyst (London)*, **83**, 661 (1958).
5) E. Bielli, P. M. Gidney, R. D. Gillard, B. T. Heaton, *J. Chem. Soc., Dalton Trans.*, **1974**, 2133.
6) R. N. Fabian, D. M. Klassen and R. W. Sonntag, *Inorg. Chem.*, **19**, 1977 (1980).
7) R. J. Crutchley, N. Kress, and A. B. P. Lever, *J. Am. Chem. Soc.*, **105**, 1170, (1983).
8) E. C. Constable and K. R. Sedden, *Tetrahedron*, **39**, 291 (1983).
9) F. H. Burstall, *J. Chem. Soc.*, **1938**, 1662.
10) M. T. Leffler, *Org. React.*, **1**, 91.
11) J. Haginiwa, *Yakugaku Zassi*, **75**, 731 (1956).
12) J. H. Baxendale and P. George, *Nature (London)*, **162**, 777 (1948).
13) F. H. Westheimer and O. T. Benefey, *J. Am. Chem. Soc.*, **78**, 5309 (1956).
14) W. A. E. McBryde, *Can. J. Chem.*, **43**, 3472 (1965).
15) K. Nakamoto, *J. Phys. Chem.*, **64**, 1420 (1960).
16) A. Albert, R. Goldadre, and J. Phillips, *J. Chem. Soc.*, **1948**, 2240.
17) G. R. Newkome, A. Nayak, F. Fronczek, T. Kawato, H. C. R. Taylor, L. Meade, and W. Mattice, *J. Am. Chem. Soc.*, **101**, 4472 (1979).
18) I. C. Calder, T. McL. Spotswood, and C. I. Tanzer, *Aust. J. Chem.*, **20**, 1195 (1967); T. McL. Spotswood and C. I. Tanzer, *ibid.*, **20**, 1213 (1967); T. McL. Spotswood and C. I. Tanzer, *ibid.*, **20**, 1227 (1967).

19) G. Anderegg, *Helv. Chim. Acta*, **46**, 2397 (1963).
20) B. R. James and R. J. P. Williams, *J. Chem. Soc.*, **1961**, 2007.
21) The ^{1}H-NMR spectrum of DABP in concentrated sulfuric acid did not suffer from downfield so much as that of Ampy in concentrated sulfuric acid, though the chemical shifts of free DABP and diprotonated DABP were close to those of free Ampy and monoprotonated Ampy. DABP may be exist as triprotonted form in concentrated sulfuric acid.
22) A. A. Schilt and G. F. Smith, *Anal. Chim. Acta*, **16**, 410 (1957).
23) J. E. Parks, B. E. Wagner, and R. H. Holm, *J. Organomet. Chem.*, **56**, 53 (1973).
24) N. Kishii, K. Araki, and S. Shiraishi, *J. Chem. Soc., Chem. Commun.*, **1984**, 103.

The Reaction of Butadienylphosphonates with a Oxosulfonium Ylide, Phosphonium Ylides, and Ketone Enolates

Toru MINAMI,* Takenobu YAMANOUCHI, Shigehumi TOKUMASU, and Ichiro HIRAO
Department of Industrial Chemistry, Kyushu Institute of Technology, Sensuicho, Tobata, Kitakyushu 804
(Received December 23, 1983)

The condensation of diethyl (ethoxycarbonylmethyl)phosphonate (**1a**) with cinnamaldehyde in the presence of piperidine gave a 1:1 mixture of diethyl (1*E*,3*E*)- (**2a**) and (1*Z*,3*E*)-(1-ethoxycarbonyl-4-phenyl-1,3-butadienyl)phosphonates (**2b**) in 82% yield, while a similar reaction using diethyl [cyanomethyl- (**1b**) and methylsulfonylmethyl]phosphonates (**1c**) exclusively gave diethyl (1*E*,3*E*)-[1-cyano- (**3**) and 1-methyl-sulfonyl-4-phenyl-1,3-butadienyl]phosphonates (**4**) in 78% and 93% yields, respectively. The reaction of the butadienylphosphonates **2**—**4** with dimethyloxosulfonium methylide (**5**) gave mixtures of (*E*)- and (*Z*)-(1-substituted 2-styrylcyclopropyl)phosphonates **7**—**9** in good yields. Similar treatment of the butadienylphosphonate **2** with phosphonium ylides **16a**—**c** led to (3-substituted 1-ethoxycarbonyl-2-styrylcyclopropyl)phosphonates **17a**—**c** in moderate yields. Reduction and oxidation of **7** were studied. The reaction of the phosphonates, **2** and **4**, with ketone enolates and ketones resulted in the formation of unexpected olefins **22**—**24** and dienes **20a, b**. The reaction mechanism is discussed.

In recent years, vinylphosphonates containing electronegative substituents on the α-carbon atom as well as vinylphosphonium salts have been extensively used as versatile reagents for the synthesis of a variety of heterocyclic and carbocyclic compounds, functionalized unsaturated systems such as olefins, dienes and their analogues, and benzene derivatives.[1] As a continuation of the studies on vinylphosphonates, we have previously reported the synthesis of diethyl 4-phenyl-1,3-butadienylphosphonates bearing electronegative substituents and their reactions with oxosulfonium and phosphonium ylides.[2] Since we incorrectly assigned the structures of the reaction products in an earlier communication, we wish to revise the structures and to report further details of the results in this paper. Some studies on the reaction of the phosphonates with nucleophiles such as ketone enolates are also described.

Results and Discussion

The Reaction with Dimethyloxosulfonium Methylide and Phosphonium Ylides. As described in previous communication,[2] the condensation of diethyl (ethoxycarbonylmethyl)phosphonate (**1a**) with cinnamaldehyde in the presence of piperidine gave a 1:1 mixture of diethyl (1*E*,3*E*)-(**2a**) and (1*Z*,3*E*)-(1-ethoxycarbonyl-4-phenyl-1,3-butadienyl)phosphonates (**2b**) in 82% yield, while the reaction using diethyl [cyanomethyl-(**1b**) and methylsulfonylmethyl]phosphonates (**1c**) afforded exclusively diethyl (1*E*,3*E*)-[1-cyano-(**3**) and 1-methylsulfonyl-4-phenyl-1,3-butadienyl]phosphonates (**4**) in 78% and 93% yields, respectively.

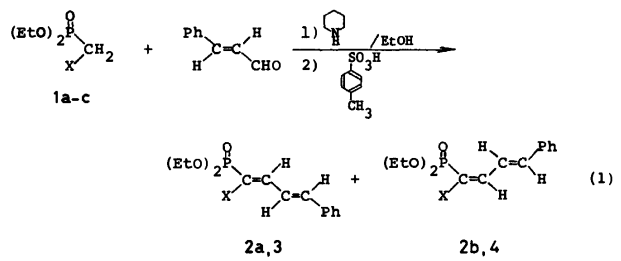

(1)

1a, 2a, 2b: X = CO_2Et
1b, 3: X = CN
1c, 4: X = SO_2Me

TABLE 1. THE REACTION OF DIETHYL (1-SUBSTITUTED 4-PHENYL-1,3-BUTADIENYL) PHOSPHONATES **2-4** WITH DIMETHYLOXOSULFONIUM METHYLIDE (**5**)

Butadienyl-phosphonates	Products (Product ratio)	Yields/%
2[a]	**7a**+**7b** (1:1)	91
3	**8a**+**8b** (9:1)	87
4	**9a**+**9b** (1:4)	41

a) A 1:1 mixture of **2a** and **2b**.

The reaction of these butadienylphosphonates with dimethyloxosulfonium methylide (**5**) gave mixtures of two isomeric products **7**—**9**, regardless of the stereochemistry of the starting butadienylphosphonates (Table 1). However, this reaction can be said to proceed nearly stereospecifically, since the reaction using single starting butadienylphosphonates **3** and **4** preferentially yielded **8a** and **9b**.

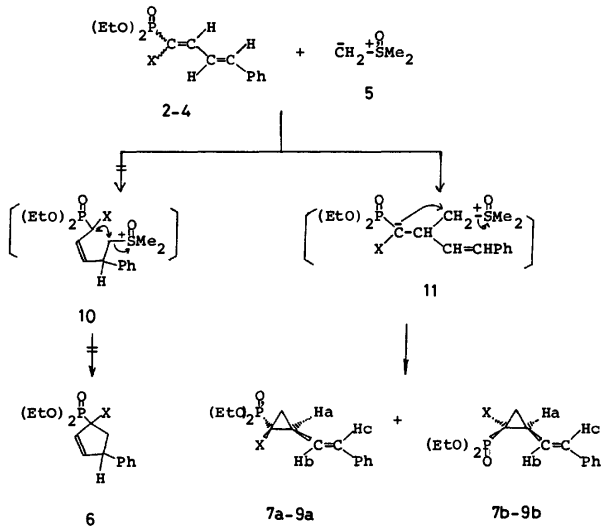

2, 7a, 7b: X = CO_2Et
3, 8a, 8b: X = CN
4, 9a, 9b: X = SO_2Me

Scheme 1.

Although we previously assigned the structures of the products to be diethyl (1-substituted 4-phenyl-2-cyclopentenyl)phosphonates **6**[2], we wish to revise them

here into structures **7**—**9**, since further study of the products indicated that our previous structural assignment was incorrect. The products are composed of mixtures of two stereoisomers, (*E*)- and (*Z*)-(1-substituted 2-styrylcyclopropyl)phosphonates **7**—**9**, whose structural assignment rests upon the following spectroscopic and chemical evidence.

The ^{1}H-NMR spectrum ($CDCl_3$) of **7a** shows methine Ha (m, 1H) at δ 2.15—3.0 and styryl Hb (dd, J=8.61, 15.93 Hz, 1H) and Hc (d, J=15.93 Hz, 1H) at δ 5.70—6.20 and at δ 6.68, while that of **7b** exhibits the corresponding peaks at δ 2.15—2.70 (m, Ha), 6.10—6.65 (dd, J=6.78, 15.93 Hz, Hb), and 6.71 (d, J=15.93 Hz, Hc). On the other hand, the ^{13}C-NMR spectra of **7a** and **7b** reveal a styryl β-carbon at δ 124.7 ppm (s) and at δ 126.7 ppm (d, $^3J_{P\text{-}C}$=4.3 Hz), respectively. Similarly, the styryl β-carbon of **8a** and **9a** resonates at δ 123.3 ppm (s) and at δ 123.1 ppm (s), whereas the corresponding carbon of **8b** and **9b** is found at δ 124.0 ppm (d, $^3J_{P\text{-}C}$=3.4 Hz) and at δ 124.3 ppm (d, $^3J_{P\text{-}C}$=3.4 Hz). Comparing the styryl β ^{13}C chemical shifts in **7a**—**9a** and **7b**—**9b**, it is observed that those in the latter are at 0.7 to 2.0 ppm lower fields from those in the former. It is also found that the compounds **7b**—**9b** have a coupling between phosphorus and the styryl β-carbon of 3.4 to 4.3 Hz, while the compounds **7a**—**9a** show none of the corresponding coupling. On the basis of these results, it can be said that the stereochemistry of **7a** and **7b** is correlated to that of the compounds **8a** and **9a**, and of their isomers **8b** and **9b**, respectively. Since treatment of the butadienylphosphonates **3** and **4** with the ylide **5** predominantly led to **8a** and **9b** as mentioned above, it would be reasonable to assign their structures as diethyl (*E*)-(1-cyano-2-styrylcyclopropyl)- and (*E*)-(1-methylsulfonyl-2-styrylcyclopropyl)-phosphonates rather than as the corresponding (*Z*)-isomers, due to more sterically favorable structures. Accordingly, the stereochemistry of **7a** and **7b** was assigned as (*E*)- and (*Z*)-form, respectively. Furthermore, that the products **7a** and **7b** are stereoisomeric with each other and contain the cyclopropyl moiety in the molecules was evident from the fact that catalytic hydrogenation of the mixture in ethanol over platinum catalyst at low hydrogen pressure gave only diethyl (1-ethoxycarbonyl-5-phenylpentyl)phosphate (**12**) in good yield. For it is well known that the cyclopropyl ring easily undergoes the ring opening in a catalytic hydrogenation.[3]

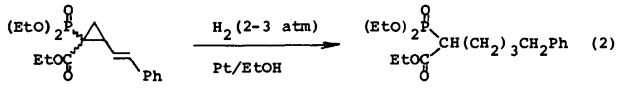

(2)

7 **12**

In addition, the structures of **7a** and **7b** were clearly established by their oxidations. Oxidation of **7a** with *m*-chloroperbenzoic acid converted into a lactone **13** in 91% yield, which would be formed *via* a cyclopropyloxirane **14**, while similar treatment of **7b** led to a cyclopropyloxirane **15** in 81% yield (Scheme 2). This result is obviously consistent with the above assigned structures **7a** and 7b, since only the *E*-isomer **7a** in which the ethoxycarbonyl and the styryl groups are located *cis* to each other can lead to **13**.

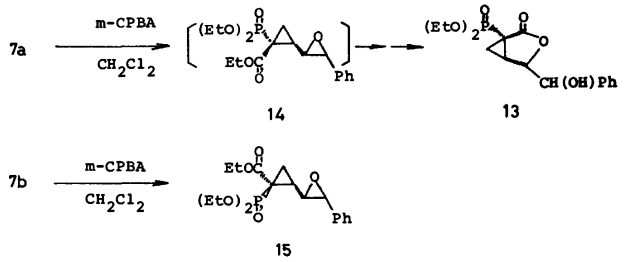

Scheme 2.

As shown in Scheme 1, these results imply that the ylide carbanion dose not attack on the δ-carbon of the butadienylphosphonates **2**—**4**, but on the β-carbon to give the intermediate **11**, followed by the elimination of dimethyl sulfoxide to lead to the cyclopropylphosphonates **7**—**9**.

The reaction of **2** with various phosphonium ylides **16a**—**c** similarly produced diethyl (3-substituted 1-ethoxycarbonyl-2-styrylcyclopropyl)phosphonates **17a**—**c** in rather low yields (45%—58%) along with comparable yields of triphenylphosphine.

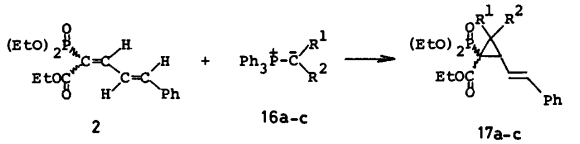

16a, 17a: $R^1 = R^2$ = Me
16b, 17b: R^1 = *p*-$MeOC_6H_4$, R^2 = H
16c, 17c: R^1 = *n*-C_5H_{11}, R^2 = H

+ Ph_3P (3)

The Reaction with Ketone Enolates. Darling and co-workers[4] reported that diethyl butadienylphosphonate containing no substituent undergoes the Michael addition of ketone enolate anions at the δ-position to give keto phosphonate carbanions (1,4-Michael adducts), but no Wittig-Horner reaction product was observed. On the other hand, Martin and Garrison[5] have recently reported that the reaction of [1-(methylthio)butadienyl]phosphonate with nucleophiles such as the enolate anion of formylcyclohexane and lithium dialkylcuprate(I)s similarly gives 1,4-Michael adducts, which subsequently undergo the Wittig-Horner reaction with ketones to yield dienes. Accordingly, it is of interest to examine the reactivity of the (4-phenylbutadienyl)phosphonates **2**—**4** bearing electronegative substituents toward ketone enolate anions, whether the phosphonates undergo 1,4-addition as previously reported or 1,2-addition as in the above-mentioned reaction with ylides. The reaction of **4** with equimolar amounts of the enolate anion of 4-methylacetophenone in the presence of excess 4-methylacetophenone unexpectedly gave 1-(4-methylphenyl)-5-phenyl-2,4-pentadien-1-one (**20b**), 1-methylsulfonyl-2-(4-methylphenyl)-1-propene (**23**), and 2-(4-methylphenyl)-3-methylsulfonyl-1-propene (**24**) in 41, 22, and 36% yields, respectively. Similar treatment of **2** with the enolate anion of acetophenone in the presence of acetophenone likewise led to 1,5-diphenyl-2,4-pentadien-1-one (**20a**), (*E*)- and (*Z*)-1-ethoxycarbonyl-2-phenyl-1-propene (**22a**) and (**22b**) in 51, 37, and 21% yields, respectively. On the other hand, the reaction of **4** with equimolar amounts of the enolate anion of 4-methylacetophenone resulted in the for-

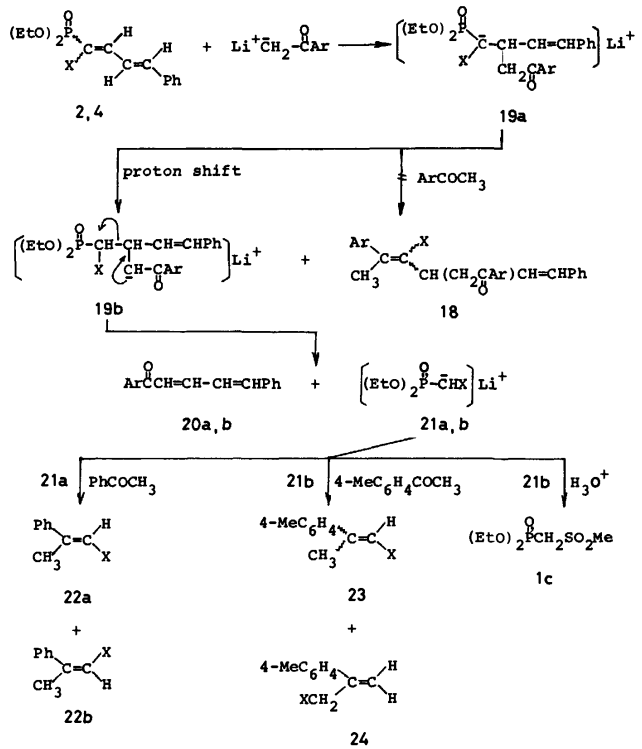

20a: Ar = Ph
20b: Ar = 4-MeC_6H_4
2, 21a, 22a, 22b: X = CO_2Et
4, 21b, 23, 24: X = SO_2Me

Scheme 3.

mation of **20b** (37%) and diethyl (methylsulfonylmethyl)phosphonate (**1c**) (26%). On the basis of these results, the reaction of the butadienylphosphonates **2**, **4** with ketone enolates in the presence of excess ketones can be accounted for by a sequence of a nucleophilic attack of the enolate anions on the β-carbon of the butadienylphosphonates, the proton shift from methylene adjacent to the aroyl group to phosphoryl-stabilized carbanions in **19a** and decomposition of the resultant **19b** to butadienes **20** and the phosphonate carbanions **21**, which react with excess ketones to afford the olefins **22—24** (Scheme 3).

Thus, in contrast to the results reported by Darling *et. al.*[4] and Martin *et. al.*[5] the above results show that butadienylphosphonates containing the phenyl group at the δ position undergo a Michael addition of nucleophiles to the β-carbon but not to the δ-carbon, primarily due to a large steric hindrance.

Studies on the effects of δ substituents on reactivities of butadienylphosphonates and their synthetic applications are in progress.

Experimental

General. ^{1}H-NMR and ^{13}C-NMR spectra were taken in $CDCl_3$ solution on a JEOL JNM-FX-60 operating at 60 and 15.04 MHz with Me_4Si as an internal standard. IR spectra were recorded with a Shimadzu IR-408 instrument. Mass spectra were taken with a JEOL DX-300 spectrometer. Melting points were measured in open capillary tubes and are uncorrected. Distillations of products were carried out with a Kugelrohr apparatus, and bath temperatures are reported.

General Procedure for the Preparation of Diethyl (1-Substituted 4-phenyl-1,3-butadienyl)phosphonates **2—4**. A solution of a phosphonate **1** (0.05 mol) and cinnamaldehyde (6.61 g, 0.05 mol) in 100 ml of dry ethanol containing catalytic amounts of piperidine was refluxed for *ca.* 30 h until disappearance of the carbonyl absorption at 1675 cm^{-1} in the IR spectrum. After removal of solvent ethanol, the residue was dissolved in 100 ml of dry benzene containing catalytic amounts of *p*-toluenesulfonic acid and the solution was refluxed for 3 h. After the usual work-up, bulb-to-bulb distillation of the residue gave a butadienylphosphonate.

*Diethyl (1E,3E)-(**2a**) and (1Z,3E)-(1-Ethoxycarbonyl-4-phenyl-1,3-butadienyl)phosphonate (**2b**).* The reaction was carried out as described above by using diethyl (ethoxycarbonylmethyl)phosphonate (**1a**) (11.21 g, 0.05 mol) to give 13.87 g (82%) yield of a 1:1 mixture of **2a** and **2b** [bp 178 °C/1 mmHg (1 mmHg≈133.322 Pa)]. Pure samples of each were obtained by preparative TLC. The product **2a** had the following properties: IR (neat): 1710, 1610, 1580, 1560, 1235, 1020 cm^{-1}; ^{1}H NMR δ=1.34 (6H, t, J=6.96 Hz, $POCH_2\underline{CH_3}$), 1.36 (3H, t, J=6.96 Hz, $OCH_2\underline{CH_3}$), 3.80—4.52 (6H, m, $PO\underline{CH_2}CH_3$ and $O\underline{CH_2}CH_3$), 6.80—8.10 (8H, m, olefinic and phenyl H); ^{13}C NMR δ=14.0, 16.1 (d, $^3J_{p\text{-}c}$=6.9 Hz), 60.8, 62.2 (d, $^2J_{p\text{-}c}$=6.0 Hz), 119.9 (d, $^1J_{p\text{-}c}$=186.5 Hz), 124.1 (d, $^3J_{p\text{-}c}$=19.8 Hz), 127.7, 128.6, 129.7, 135.3, 145.9, 154.6 (d, $^2J_{p\text{-}c}$=7.7 Hz), 164.4 (d, $^2J_{p\text{-}c}$=13.8 Hz); MS m/z 338 (M^+). The product **2b** had the following properties: IR (neat): 1710, 1610, 1580, 1560, 1235, 1020 cm^{-1}; ^{1}H NMR δ=1.34 (9H, t, J=6.96 Hz, $POCH_2\underline{CH_3}$ and $OCH_2\underline{CH_3}$), 3.80—4.50 (6H, m, $PO\underline{CH_2}CH_3$, and $O\underline{CH_2}CH_3$), 6.80—8.50 (8H, m, olefinic and phenyl H); ^{13}C NMR δ=14.2, 16.3 (d, $^3J_{p\text{-}c}$=6.9 Hz), 61.1, 62.2 (d, $^2J_{p\text{-}c}$=5.2 Hz), 119.4 (d, $^1J_{p\text{-}c}$=185.7 Hz), 124.9 (d, $^3J_{p\text{-}c}$=6.0 Hz), 128.1, 128.7, 129.9, 135.6, 146.7, 156.6 (d, $^2J_{p\text{-}c}$=7.7 Hz), 165.8 (d, $^2J_{p\text{-}c}$=13.8 Hz); MS m/z 338 (M^+).

Found (for a mixture of **2a** and **2b**): C, 60.05; H, 6.90. Calcd for $C_{17}H_{23}O_5P$: C, 60.35; H, 6.85%.

*Diethyl (1E,3E)-(1-Cyano-4-phenyl-1,3-butadienyl)phosphonate (**3**).* The reaction was carried out as described above by using diethyl cyanomethylphosphonate (**1b**) (8.86 g, 0.05 mol) to afford 11.36 g (78%) yield of **3** as a single product. Its structural assignment was made on the basis of the close similarity of its ^{1}H- and ^{13}C-NMR spectra to those of **2a**, as shown below. The product **3** had the following properties: bp 168 °C/2 mmHg; IR (neat): 2160, 1605, 1205 cm^{-1}; ^{1}H-NMR δ=1.39 (6H, dt, J=0.55 Hz, 6.96 Hz, $OCH_2\underline{CH_3}$), 3.80—4.45 (4H, m, $O\underline{CH_2}CH_3$), 7.0—8.05 (8H, m, olefinic and phenyl H); ^{13}C NMR δ=16.2 (d, $^3J_{p\text{-}c}$=6.0 Hz), 63.4 (d, $^2J_{p\text{-}c}$=6.0 Hz), 101.1 (d, $^1J_{p\text{-}c}$=202.0 Hz), 114.5 (d, $^2J_{p\text{-}c}$=12.0 Hz), 123.5 (d, $^3J_{p\text{-}c}$=18.1 Hz), 128.3, 129.0, 130.9, 134.5, 147.5, 159.4 (d, $^2J_{p\text{-}c}$=6.9 Hz); MS m/z 291 (M^+).

Found: C, 61.81; H, 6.20; N, 4.92. Calcd for $C_{15}H_{18}O_3NP$: C, 61.85; H, 6.23; N, 4.81%.

*Diethyl (1E,3E)-(1-Methylsulfonyl-4-phenyl-1,3-butadienyl)-phosphonate (**4**).* The reaction was carried out as described above by using diethyl (methylsulfonylmethyl)phosphonate (**1c**) (11.51 g, 0.05 mol) to produce 10.70 g (93%) yield of **4** as a sole product, whose structural assignment was similarly made by comparison of its ^{1}H- and ^{13}C-NMR spectra with those of **2b**. The compound **4** had the following properties: Mp 113—114 °C; IR (KBr) 1610, 1575, 1550, 1300, 1240, 1120 cm^{-1}; ^{1}H NMR δ=1.31 (6H, t, J=7.05 Hz, $OCH_2\underline{CH_3}$), 3.13 (3H, s, $SO_2\underline{Me}$), 3.80—4.50 (4H, quint., $O\underline{CH_2}CH_3$), 6.75—8.40 (8H, m, olefinic and phenyl H); ^{13}C NMR δ=16.0 (d, $^3J_{p\text{-}c}$=6.9 Hz), 42.9, 62.8 (d, $^2J_{p\text{-}c}$=5.2 Hz), 122.3 (d, $^3J_{p\text{-}c}$=6.0 Hz), 128.0, 128.7, 128.8 (d, $^1J_{p\text{-}c}$=179.7 Hz), 130.4, 134.7, 149.1, 154.5 (d, $^2J_{p\text{-}c}$=6.0 Hz) MS Found: m/z 344.0821. Calcd for $C_{15}H_{21}O_5SP$: 344.0846 (M^+).

General Procedure for the Synthesis of (1-Substituted 2-styrylcyclopropyl)phosphonates **7—9**. To a solution of dimethyloxosulfonium methylide (**5**) (5 mmol) in 15 ml of dry DMSO was added a butadienylphosphonate (5 mmol) in 5 ml of dry DMSO. The reaction mixture was then stirred at 50 °C for 5 h. After conventional work-up, distillation of the residue produced a mixture of two stereoisomers. Pure samples of each were obtained by preparative TLC.

Diethyl (E)-(1-ethoxycarbonyl-2-styrylcyclopropyl)phosphonate (7a): Yield 0.81 g (2.30 mmol, 46%); bp 190 °C/1 mmHg; IR (neat) 1705, 1580, 1240 cm^{-1}; ^1H NMR δ=0.90—2.10 (11H, m, CH_3 and cyclopropyl methylene H), 2.15—3.0 (1H, m, Ha), 3.60—4.50 (6H, m, $\underline{CH_2}CH_3$), 5.70—6.20 (1H, dd, J=8.61 Hz, 15.93 Hz, Hb), 6.68 (1H, d, J=15.93 Hz, Hc), 7.0—7.60 (5H, phenyl H); ^{13}C NMR δ=14.3, 16.5 (d, $^3J_{p\text{-}c}$=6.0 Hz), 19.4, 27.9 (d, $^1J_{p\text{-}c}$=187.4 Hz), 30.3, 61.7, 62.7 (d, $^2J_{p\text{-}c}$=5.2 Hz), 124.7, 126.1, 127.6, 128.6, 134.0, 136.8, 167.5; MS m/z 352 (M^+).

Diethyl (Z)-(1-ethoxycarbonyl-2-styrylcyclopropyl)phosphonate (7b): Yield 0.79 g (2.24 mmol, 45%); bp 190 °C/1 mmHg; IR (neat): 1705, 1580, 1240 cm^{-1}; ^1H NMR δ=0.90—1.50 (9H, m, Me), 1.50—2.15 (2H, m, cyclopropyl methylene H), 2.15—2.70 (1H, m, Ha), 3.75—4.50 (6H, m, $\underline{CH_2}CH_3$), 6.10—6.65 (1H, dd, J=6.78 Hz, 15.93 Hz, Hb), 6.71 (1H, d, J=15.93 Hz, Hc), 6.90—7.50 (5H, m, phenyl H); ^{13}C NMR δ=14.1, 16.4 (d, $^3J_{p\text{-}c}$=6.0 Hz), 21.2, 27.9 (d, $^1J_{p\text{-}c}$=187.4 Hz), 33.7 (d, $^2J_{p\text{-}c}$=2.6 Hz), 61.7, 62.4 (d, $^2J_{p\text{-}c}$=6.0 Hz), 126.1, 126.7 (d, $^3J_{p\text{-}c}$=4.3 Hz), 127.4, 128.5, 133.5, 136.9, 169.6; MS m/z 352 (M^+).

Found (for a mixture of **7a** and **7b**): C, 60.96; H, 7.39%. Calcd for $C_{15}H_{25}O_5P$: C, 61.36; H, 7.15%.

Diethyl (E)-(1-Cyano-2-styrylcyclopropyl)phosphonate (8a): Yield 1.19 g (3.9 mmol, 78.3%); bp 175 °C/2 mmHg; IR (neat): 2215, 1250 cm^{-1}; ^1H NMR δ=1.38 (6H, t, J=7.05 Hz, $CH_2\underline{CH_3}$), 1.55—2.20 (2H, m, cyclopropyl methylene H), 2.20—3.0 (1H, m, Ha), 3.90—4.50 (4H, m, $\underline{CH_2}CH_3$), 5.65—6.15 (1H, dd, J=8.61 Hz, 15.75 Hz, Hb), 6.76 (1H, d, J=15.75 Hz, Hc), 7.31 (5H, s, phenyl H); ^{13}C NMR δ=12.4 (d, $^1J_{p\text{-}c}$=196.0 Hz); 16.2 (d, $^3J_{p\text{-}c}$=6.0 Hz), 20.1, 28.5, 63.7 (d, $^2J_{p\text{-}c}$=6.9 Hz), 116.8 (d, $^2J_{p\text{-}c}$=3.4 Hz), 123.3, 126.1, 127.9, 128.4, 135.2, 135.7; MS m/z 305 (M^+).

Diethyl (Z)-(1-Cyano-2-styrylcyclopropyl)phosphonate (8b): Yield 0.133 g (0.44 mmol, 8.7%); bp 175 °C/2 mmHg; IR (neat): 2215, 1250 cm^{-1}; ^1H NMR δ=1.0—1.56 (6H, m, $CH_2\underline{CH_3}$), 1.56—2.20 (2H, m, cyclopropyl methylene H), 2.25—3.0 (1H, m, Ha), 3.70—4.55 (4H, m, $\underline{CH_2}CH_3$), 6.0—6.50 (1H, dd, J=8.70 Hz, 15.94 Hz, Hb), 6.78 (1H, d, J=15.94 Hz, Hc), 7.30 (5H, br.s, phenyl H); ^{13}C NMR δ=12.3 (d, $^1J_{p\text{-}c}$=197.7 Hz), 16.3 (d, $^3J_{p\text{-}c}$=6.0 Hz), 21.2, 32.3, 63.6 (d, $^2J_{p\text{-}c}$=6.0 Hz), 119.0 (d, $^2J_{p\text{-}c}$=4.3 Hz), 124.0 (d, $^3J_{p\text{-}c}$=3.4 Hz), 126.3, 128.3, 128.7, 135.1, 136.3; MS m/z 305 (M^+).

Found (for a mixture of **8a** and **8b**): C, 62.55; H, 6.68; N, 4.54%. Calcd for $C_{16}H_{20}O_3NP$: C, 62.94; H, 6.60; N, 4.59%.

Diethyl (Z)-(1-Methylsulfonyl-2-styrylcyclopropyl)phosphonate (9a): Yield 0.146 g (0.41 mmol, 8.2%); Oil; IR (neat): 1310, 1230, 1130 cm^{-1}; ^1H NMR δ=1.38 (6H, t, J=7.14 Hz, $CH_2\underline{CH_3}$), 1.55—2.40 (2H, m, cyclopropyl methylene H), 2.40—3.20 (1H, m, Ha), 3.08 (3H, s, $SO_2\underline{Me}$), 3.90—4.60 (4H, m, $\underline{CH_2}$-CH_3), 5.95—6.70 (1H, dd, J=8.79 Hz, 15.93 Hz, Hb), 6.81 (1H, d, J=15.93 Hz, Hc), 7.31 (5H, s, phenyl H); ^{13}C NMR δ=16.4 (d, $^3J_{p\text{-}c}$=6.0 Hz), 17.2, 30.0, 42.4, 42.5 (d, $^1J_{p\text{-}c}$=176.6 Hz), 63.5 (d, $^2J_{p\text{-}c}$=6.0 Hz), 64.2 (d, $^2J_{p\text{-}c}$=6.9 Hz), 123.1, 126.3, 128.1, 128.7, 136.0, 136.3; MS Found: m/z 358.1005. Calcd for $C_{16}H_{23}O_5SP$: 358.1004 (M^+).

Diethyl (E)-(1-Methylsulfonyl-2-styrylcyclopropyl)phosphonate (9b): Yield 0.582 g (1.62 mmol, 32.8%); mp 77 °C; IR (KBr) 1300, 1230, 1130 cm^{-1}; ^1H NMR δ=1.0—1.60 (6H, m, $CH_2\underline{CH_3}$), 1.60—2.30 (2H, m, cyclopropyl methylene H), 2.60—3.30 (1H, m, Ha), 3.15 (3H, s, $SO_2\underline{Me}$), 6.0—6.50 (1H, dd, J=8.42 Hz, 15.75 Hz, Hb), 6.75 (1H, d, J=15.75 Hz, Hc), 7.30 (5H, s, phenyl H); ^{13}C NMR δ=16.3 (d, $^3J_{p\text{-}c}$=6.0 Hz), 19.2, 28.8 (d, $^2J_{p\text{-}c}$=2.5 Hz), 41.3, 42.3 (d, $^1J_{p\text{-}c}$=183.2 Hz), 63.3 (d, $^2J_{p\text{-}c}$=6.9 Hz), 63.7 (d, $^2J_{p\text{-}c}$=6.1 Hz), 124.3 (d, $^3J_{p\text{-}c}$=3.4 Hz), 126.1, 127.7, 128.6, 134.6, 136.5; MS Found: m/z 358.0985. Calcd for $C_{16}H_{23}O_5SP$: 358.1004 (M^+).

Diethyl (1-Ethoxycarbonyl-3,3-dimethyl-2-styrylcyclopropyl)-phosphonate (17a). To a solution of isopropylidenetriphenylphosphorane (**16a**) (5 mmol), *in situ* generated from isopropyltriphenylphosphonium bromide (1.97 g, 5 mmol) and butyllithium (5.5 mmol), in 15 ml of THF was added **2** dissolved in 10 ml of THF at room temperature. The solution was then refluxed for 6 h. After conventional work-up, the residue was chromatographed on silica gel using benzene and chloroform as eluent. The first fraction gave 0.80 g (61%) yield of triphenylphosphine. Distillation of the oily product obtained from the second fraction gave **17a** (1.11 g, 58%), which is composed of two stereoisomers. The separation of the two isomers was not attempted. The compound **17a** had the following properties: bp 170 °C/1 mmHg; IR (neat): 1720, 1600, 1260 cm^{-1}, ^1H NMR δ=1.0—1.60 (15H, m, Me), 2.39—2.96 (1H, m, CH-), 3.85—4.55 (6H, m, OCH_2), 6.25—6.75 (1H, dd, J=8.42 Hz, 15.80 Hz, olefinic H), 6.75—7.0 (1H, 2xd, olefinic H), 7.20—7.55 (5H, m, phenyl H); MS Found: m/z 380.1773. Calcd for $C_{20}H_{29}O_5P$: 380.1771 (M^+).

Diethyl [1-Ethoxycarbonyl-3-(4-methoxyphenyl)-2-styrylcyclopropyl]phosphonate (17b). The reaction was carried out as described above using **2** (0.66 g, 2 mmol) and 4-methoxybenzylidenetriphenylphosphorane (**16b**) (2 mmol). After the usual work-up, the residue was similarly chromatographed on silica gel to give 0.26 g (50%) of triphenylphosphine and 0.41 g (45%) of **17b**: Oil; IR (neat): 1720, 1260 cm^{-1}; ^1H NMR δ=1.27 (9H, t, J=7.1 Hz, $CH_2\underline{CH_3}$), 1.1—2.45 (2H, m, CH-), 3.71 (3H, s, OCH_3), 3.75—4.40 (6H, m, $\underline{CH_2}CH_3$), 5.75—6.25 (1H, dd, olefinic H), 6.55—6.90 (1H, 2xd, olefinic H), 7.0—7.55 (9H, m, aromatic H); MS Found: m/z 458.1904. Calcd for $C_{25}H_{31}O_6P$: 458.1858 (M^+).

Diethyl (1-Ethoxycarbonyl-3-pentyl-2-styrylcyclopropyl)phosphonate (17c). The reaction was carried out as described above using **2** (0.66 g, 2 mmol) and *n*-hexylidenetriphenylphosphorane (**16c**). After the usual work-up, the residue was similarly chromatographed on silica gel to give 0.43 g (51%) of **17c**: Oil; IR (neat): 1710, 1610, 1250 cm^{-1}; ^1H NMR δ=0.85—2.20 (22H, m, CH_3, CH_2, CH-), 3.85—4.45 (6H, m, OCH_2), 6.05—6.40 (1H, m, olefinic H), 6.50—6.85 (1H, m, olefinic H), 7.27 (5H, s, phenyl H); MS Found: m/z 422.2269. Calcd for $C_{23}H_{35}O_5P$: 422.2222 (M^+).

Hydrogenation of **7**. The hydrogenation of **7** (1:1 mixture of **7a** and **7b**) (0.35 g, 1 mmol) was accomplished in 10 h in ethanol over Pt (PtO_2, 20 mg) to afford **12** (0.28 g, 79%) as a colorless oil: IR (neat): 1720, 1260 cm^{-1}; ^1H NMR δ=1.13—2.25 (15H, m, CH_3 and CH_2), 2.61 (2H, t, J=8.06 Hz, $CH_2\underline{CH_2}Ph$), 2.80—3.25 (1H, m, CH-), 3.85—4.40 (6H, quint. OCH_2), 7.19 (5H, s, phenyl H); MS Found: m/z 356.1717. Calcd for $C_{18}H_{29}O_5P$; 356.1751.

Oxidation of **7a**. A solution of a mixture of **7a** (0.16 g, 0.45 mmol) and *m*-chloroperbenzoic acid (70%, 0.19 g, 1.67 equiv) in 5 ml of CH_2Cl_2 was refluxed for 10 h. After the usual work-up, the residue was chromatographed on preparative TLC with ether as eluent to give 0.14 g (91%) of *1-diethoxyphosphinyl-4-(α-hydroxybenzyl)-3-oxabicyclo[3.1.0]-hexan-2-one* (**13**): Oil; IR (neat): 3300, 1770, 1260 cm^{-1}; ^1H NMR δ=1.35 (6H, t, J=6.96 Hz, CH_3), 1.02—2.18 (2H, m, cyclopropyl CH_2), 2.30—2.85 (1H, cyclopropyl CH-), 3.40—3.75 (1H, br., OH, D_2O exchangeable), 3.90—4.60 (5H, m, OCH_2 and lactone CH-), 4.85—5.10 (1H, br., -$\underline{CH}$ (OH)Ph), 7.37 (5H, s, phenyl H); ^{13}C NMR δ=16.2, 16.4 (d, $^3J_{p\text{-}c}$=6.9 Hz), 23.3 (d, $^1J_{p\text{-}c}$=200.3 Hz), 24.7, 63.2 (d, $^2J_{p\text{-}c}$=6.0 Hz), 63.6 (d, $^2J_{p\text{-}c}$=5.2 Hz), 73.5, 82.5, (d, $^3J_{p\text{-}c}$=2.6 Hz), 126.3, 128.0, 128.6, 138.7, 171.6 (d, $^2J_{p\text{-}c}$=10.3 Hz); MS Found: m/z 341.1175. Calcd for $C_{16}H_{22}O_6P$: 341.1154 (M^++1).

Oxidation of **7b**. A solution of **7b** (0.20 g, 0.568 mmol) and *m*-chloroperbenzoic acid (70%, 0.21 g, 1.50 equiv.) was treated under the same condition as **7a**. After a similar work-up, the residue was chromatographed on preparative TLC with ether as eluent to give 0.170 g (81%) of *(E)-2-[(Z)-1-ethoxycarbonyl-1-diethoxyphosphinylcyclopropyl]-3-phenyloxirane (15)*: Oil; IR (neat): 1720, 1260, 1020 cm^{-1}; ^1H NMR δ=0.80—2.10 (12H, m, CH_3, cyclopropyl CH_2 and CH-), 3.20—3.50 (1H, m, -CH(O)-CHPh), 3.50—4.50 (7H, m, OCH_2 and -CH(O)-CHPh), 7.28 (5H, s, phenyl H); ^{13}C NMR δ=13.9, 16.1 (d, $^3J_{p-c}$=5.2 Hz), 19.3, 24.6 (d, $^1J_{p-c}$=194.3 Hz), 30.4 (d, $^2J_{p-c}$=2.6 Hz), 58.6, 60.0 (d, $^3J_{p-c}$=3.4 Hz), 61.7, 62.4 (d, $^2J_{p-c}$=6.0 Hz), 125.6, 128.1, 136.5, 169.0 (d, $^2J_{p-c}$=7.7 Hz); MS Found: *m/z* 368.1359. Calcd for $C_{18}H_{27}O_7P$: 368.1362 (M^+).

Reaction of **4** *with 4-Methylacetophenone in the Presence of Lithium Diisopropylamide (LDA). A. The Reaction Using Excess Amounts of 4-Methylacetophenone*: To a cooled solution of LDA (1.1 mmol) in THF (15 ml) at −75 °C was added 4-methylacetophenone (0.30 g, 2.24 mmol). The solution was stirred for 1 h at this temperature. Then the butadienylphosphonate **4** (0.33 g, 0.96 mmol) was added to the solution and the mixture was stirred at −75 °C for 0.5 h and at refluxing temperature for 10 h. After a conventional work-up, the residue was chromatographed on preparative TLC with $CHCl_3$ as eluent to give **20b** (97 mg, 41%), **23** (44 mg, 22%) and **24** (73 mg, 36%), respectively.

1-(4-Methylphenyl)-5-phenyl-2,4-pentadien-1-one (20b): Mp 84—85 °C; IR (KBr): 1640 cm^{-1}; ^1H NMR δ=2.36 (3H, s, Me), 6.60—7.60 (11H, m, aromatic and olefinic H), 7.88 (2H, d, *J*=8.10 Hz, the other aromatic H); MS Found: *m/z* 248.1216. Calcd for $C_{18}H_{16}O$: 248.1201 (M^+).

1-Methylsulfonyl-2-(4-methylphenyl)-1-propene (23): Oil; IR (neat): 1300, 1120 cm^{-1}; ^1H NMR δ=2.38 (3H, s, Me), 2.56 (3H, d, *J*=1.17 Hz, Me(H)C=C(H)), 3.04 (3H, s, SO_2Me), 6.38—6.60 (1H, q, *J*=1.17 Hz, olefinic H), 6.80—7.50 (4H, m, aromatic H); MS Found: *m/z* 210.0746. Calcd for $C_{11}H_{14}O_2S$: 210.0715 (M^+). This compound was consistent with an authentic sample independently prepared from **1c** and 4-methylacetophenone.

2-(4-Methylphenyl)-3-methylsulfonyl-1-propene (24): Mp 56—57 °C; IR (KBr): 1300, 1120 cm^{-1}; ^1H NMR δ=2.35 (3H, s, Me), 2.71 (3H, s, SO_2Me), 4.17 (2H, s, CH_2SO_2Me), 5.50 (1H, s, olefinic H), 5.72 (1H, s, olefinic H), 6.90—7.50 (4H, m, phenyl H); MS Found: *m/z* 210.0738. Calcd for $C_{11}H_{14}O_2S$: 210.0715 (M^+). This compound was consistent with an authentic sample prepared from **1c** and 4-methylacetophenone.

B. The Reaction Using an Equimolar Amount of 4-Methylacetophenone. The reaction was similarly carried out at −75 °C for 1 h and at room temperature for 10 h using the procedure described above with **4** (0.34 g, 0.99 mmol), 4-methylacetophenone (0.15 g, 1.12 mmol) and LDA (1.1 mmol) in dry THF (20 ml). After the usual work-up, similar treatment of the residue gave **20b** (90 mg, 37%) and **1c** (60 mg, 26%).

Reaction of **2** *with Acetophenone in the Presence of LDA.* The reaction was carried out as described above using **2** (0.34 g, 1 mmol), acetophenone (0.24 g, 2 mmol) and LDA (1 mmol). After similar treatment, **20a**, **22a**, and **22b** were obtained in 0.12 g (51%), 0.07 g (37%), and 0.04 g (21%) yields, respectively.

1,5-Diphenyl-2,4-pentadien-1-one (20a): Oil; IR (neat): 1650 cm^{-1}; ^1H NMR δ=6.70—8.10 (14H, m, aromatic and olefinic H); MS Found: *m/z* 234.1035. Calcd for $C_{17}H_{14}O$: 234.1044 (M^+).

(E)-1-Ethoxycarbonyl-2-phenyl-1-propene (22a): Oil; IR (neat): 1720 cm^{-1}; ^1H NMR δ=1.07 (3H, t, *J*=7.14 Hz, CH_2CH_3), 2.17 (3H, d, *J*=1.47 Hz, CH_3(H)C=C(H)), 3.99 (2H, q, *J*=7.14 Hz, OCH_2CH_3), 5.90 (1H, q, *J*=1.47 Hz, CH_3(H)C=C(H)), 6.90—7.50 (5H, m, phenyl H); MS Found: *m/z* 190.1013. Calcd for $C_{12}H_{14}O_2$: 190.0994 (M^+). This compound was consistent with an authentic sample prepared from **1a** and acetophenone.

(Z)-1-Ethoxycarbonyl-2-phenyl-1-propene (22b): Oil; IR (neat): 1710 cm^{-1}; ^1H NMR δ=1.30 (3H, t, *J*=7.18 Hz, CH_2CH_3), 2.57 (3H, d, *J*=1.17 Hz, CH_3(H)C=C(H)), 4.42 (2H, q, *J*=7.18 Hz, OCH_2CH_3), 6.13 (1H, q, *J*=1.17 Hz, CH_3(H)C=C(H)), 7.10—7.60 (5H, m, phenyl H); MS *m/z* 190 (M^+). This compound was consistent with an authentic sample prepared from **1a** and acetophenone.

We are grateful for support of this work by a Grant-in-Aid for Scientific Research (No 58550548) from the Ministry of Education, Science and Culture.

References

1) a) T. Minami, H. Suganuma, and T. Agawa, *Chem. Lett.*, **1978**, 285; b) W. A. Kleschick and C. H. Heathcock, *J. Org. Chem.*, **43**, 1256 (1978); c) M. A. Semmelhack, J. C. Tomesch, M. Czarny, and S. Boettger, *ibid.*, **43**, 1259 (1978); d) J. Ide, R. Endo and S. Muramatsu, *Chem. Lett.*, **1978**, 401; e) M. Mikolajczyk, S. Grzejszczak, and K. Korbacz, *Tetrahedron Lett.*, **22**, 3097 (1981); f) B. Venugopalan, A. B. Hamlet, and T. Durst, *ibid.*, **22**, 191 (1981); g) T. Minami, K. Nishimura, I. Hirao, H. Suganuma, and T. Agawa, *J. Org. Chem.*, **47**, 2360 (1982) and references cited therein.

2) T. Minami, T. Yamanouchi, S. Takenaka, and I. Hirao, *Tetrahedron Lett.*, **24**, 767 (1983).

3) a) J. Newham, *Chem. Rev.*, **63**, 123 (1963); b) C. Gröger and H. Musso, *Angew. Chem.,Int. Ed. Engl.*, **15**, 373 (1976); c) M. Charton, "The Chemistry of Alkenes", ed. by J. Zabicky, Interscience, New York (1970), Vol. 2, p 588.

4) S. D. Darling, F. N. Muralidharan, and V. B. Muralidharan, *Tetrahedron Lett.*, **1979**, 2757, 2761.

5) S. F. Martin and P. J. Garrison, *Synthesis*, **1982**, 394.

Carbon-13 NMR Spectra of 5-(4-Substituted Benzylidene)-2,3,4,5-tetrahydropyridines

Yoshito TAKEUCHI,* Takashi BANDO, Shuji TOMODA, and Yujiro NOMURA
Department of Chemistry, College of Arts and Sciences, The University of Tokyo, Komaba, Meguro-ku, Tokyo 153
(Received December 26, 1983)

Carbon-13 chemical shifts for a series of 5-(4-substituted benzylidene)-2,3,4,5-tetrahydropyridines were determined. The substituent chemical shifts (SCS) were correlated with σ_I and σ_R° values by means of DSP and DSP-NLR analysis. It was found that as a substituent the C=C-C=N moiety is as mild as C=C and that the former can be approximated as a vinylogue of the C=N moiety. C-13 lanthanoid-induced shifts (LIS) of the parent compound were also discussed.

Numerous attempts have been made to correlate electronic substituent constants with C-13 chemical shifts of substituted aromatic systems.[1] Extention of these correlation to the aromatic systems with additional π-bonded side chains continue to interest several group of investigaters[2] in connection with the elucidation of the mechanism of transmission of the electronic substituent effect through the conjugated system.

Recently we prepared a series of 5-(4-substituted benzylidene)-2,3,4,5-tetrahydropyridine (**1a—1g**) by the reaction of 2,3,4,5-tetrahydropyridine trimer and appropriately substituted benzaldehydes.[3] These compounds are interesting in that the side chain C=C double bond is further conjugated with C=N double bond, and that the two double bonds are fixed in the *s-trans* conformation. In this study we compare C-13 substituent chemical shifts (SCS) of **1** with those of 4-substituted styrenes (**2**)[4] and 4-substituted phenylacetylenes (**3**),[5] in order to estimate the effect of additional conjugation by C=N bond upon the electronic property of styrene framework.

Comparison will also be made with SCS of *N*-(4-substituted benzylidene)-methylamines (**4**),[6] *N*-(4-substituted benzylidene)-*t*-butylamines (**5**)[6] and *N*-(4-substituted benzylidene)anilines (**6**),[7] and *N*-benzylidene(4-substituted aniline)s (**7**)[7] where C=N bond is directly bonded to the benzene ring.

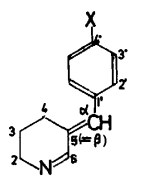

1

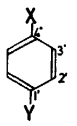

2~7

2 Y=-CH=CH$_2$
3 -C≡CH
4 -CH=N-Me
5 -CH=N-t-Bu
6 -CH=N-Ph
7 -N=CH-Ph

Experimental

The preparation of benzylidenetetrahydropyridines **1a—1g** were already reported.[3]

The solutions for NMR measurements were prepared by dissolving *ca.* 50 mg of the **1a—1g** into $CDCl_3$ (1.0 ml) containing 1% tetramethylsilane (TMS) which acts as the internal standard. For LIS (lanthanoid-induced shift) study, 54 mg (0.316 mmol) of 5-(4-substituted benzylidene)-2,3,4,5-tetrahydropyridine was dissolved in $CDCl_3$ (1.0 ml), and a weighed amount of Eu(fod)$_3$ was added. The molar ratio of shift reagent/solute varied from 0.023 to 0.297.

The instrument employed was JEOL FX-90Q spectrometer operating at 22.5 MHz with a 10 mm $^1H/^{13}C$ dual probe. The spectra were obtained with proton noise decoupling for 5KHz spectral width, collection of 8K data points in the FID, and 13 μs pulse width (45°). Usually 100 scans were accumlated with a 3.5s pulse interval after each pulse. C-13 NMR chemical shifts of **1a—1g** were listed in Table 1. Assignment of C-13 NMR signals of **1a** was already reported.[8] Assignments of signals for **1b—1g** were made by comparison with the data for corresponding styrenes (**2a—2g**).[4]

Results and Discussion

The Nature of C=C-C=N Moiety. Compounds **1** may be regarded as one of aromatic systems of the general type *p*-X-C_6H_4-Y which has been extensively investigated in view of the electronic interaction between the two substituents as manifested by C-13 SCS.[9] A comparison of SCS of **1** with those of **2** is expected to depend on the difference of the interactions, one between X (variable substituents) and C=C-C=N and the other between X and C=C moiety. If the additional C=N bond does not affect the interaction to any significant extent, the correlation of SCS of **1a—1g** with those of **2a—2g** for the equivalent positions should provide a linear correlation with a slope of unity. The result of correlations is listed in Table 2.

TABLE 1. C-13 CHEMICAL SHIFTS OF 5-(4-SUBSTITUTED BENZYLIDENE)-2,3,4,5-TETRAHYDROPYRIDINES[a]

Compd.	X	C6	C5(Cβ)	C4	C3	C2	Cα	Cl′	C2′	C3′	C4′	X[b]
1a	H	163.64	131.70	21.63	25.03	49.70	136.11	135.93	129.43	128.42	128.00	
1b	NMe_2	164.31	127.96	21.62	25.25	49.35	136.84	124.06	130.99	111.82	150.01	40.14
1c	OMe	163.64	129.66	21.37	24.88	49.31	135.71	128.44	130.78	113.72	159.26	55.06
1d	Me	163.66	130.89	21.56	25.03	49.57	136.09	133.11	129.10	129.42	137.93	21.23
1e	Cl	163.28	132.08	21.45	24.92	49.57	134.79	134.35	130.69	128.61	134.35	
1f	CN	162.74	134.14	21.40	24.97	49.68	133.81	140.47	129.68	132.08	111.17	118.64
1g	NO_2	162.57	134.56	21.33	24.93	49.70	133.22	142.39	128.61	123.65	146.68	

a) δ values b) ^{13}C nuclei of substituents

TABLE 2. CORRELATION BETWEEN SCS FOR 1 AND 2[a]

Carbon	a	b	r
C5(Cβ)	0.759	−0.443	0.993
Cα	1.932	0.885	0.975
Cl′	1.104	0.250	>0.999
C3′	1.040	0.266	0.998
C4′	1.024	−0.559	0.999

a) SCS(**1**)=a·SCS(**2**)+b; r, correlation coefficient.

Except for C2′ (meta to the substituent), a reasonable correlation (r>0.975) is always obtained. The slope of the correlation at Cl′ is larger than unity by 0.1, suggesting that the interaction of C=C-C=N moiety with X is a little larger than that of C=C moiety. The deviation of the slope from unity is much more enhanced at side-chain carbons (Cα and Cβ). This is consistent with the contribution of such a zwitterionic canonical structure as

$$>C=C-C=N- \cdots\cdots >C^{+}-C=C-N^{-}- \quad (1)$$
$$\alpha\ \beta\ 6 \qquad\qquad \alpha\ \beta\ 6$$

DSP and DSP-NLR Analysis. In order to clarify the nature of the interaction shown in Table 2, a DSP (dual substituent parameter) or a DSP-NLR (nonlinear resonance effect)[9,10] of **1** and **2** together with a variety of related systems **3**—**7** were attempted. DSP or DSP-NLR analyses were made on an identical sets of substituents, *i.e.*, NMe_2, OMe, Me, Cl, CN, and NO_2, wherever possible. In certain cases SCS data for one or two substituents were not available but from previous experiences, this will not likely to cause a serious error. According to Taft *et al.*[9] C-13 SCS of appropriate carbons of substituted aromatic system of the general type X-C_6H_4-Y where X and Y are variable and fixed substituent, respectively, can be correlated with the DSP and DSP-NLR based on the equation

$$\text{C-13 SCS} = \rho_I\sigma_I + \rho_R\sigma_R^{\circ}/(1-\varepsilon\sigma_R^{\circ}), \quad (2)$$

where σ_I and σ_R° are inductive and resonance substituent constants, respectively, and ρ_I and ρ_R are transmission coefficients determined by the least-square method. ε is null in DSP analysis by definition, while a constant for each fixed substituent Y in DSP-NLR analysis and characterizes the electron demand exerted by Y.

The results of the ayalyses for Cl′, Cα, and C5(Cβ), are summerized in Table 3. In this Table cases where f, the goodness of fit parameter, is above 0.06, the critical value for an acceptable fit, are also included for the sake of comparison. At Cl′, both ρ_I and ρ_R of **1** are larger than those of **2**, which corresponds to the slope (1.1) of the correlation given in Table 2. The ε value is small, comparable with that for **2**, to indicate that the C=C-C=N moiety is "mild" in the sense that there is no additional interaction with X through the π-frame. It is in sharp contrast with much larger ε values for **3**, **5**—**7**.

It is reported[9] that ε values in DSP-NLR analyses largely depend on the nature of terminal atoms with which Y is bonded to the benzene ring. In **1**—**6**, although the terminal atoms are all carbons, the termini can be subdivided into three types, *i.e.*, C=C, C≡C, or C=N. Our data indicate that a C=C terminal is milder than C≡C, C=N (**5**, **6**) or N=C (**7**) termini regardless of the presence of further conjugation.

A large deviation of the solpe from unity found in the correlation for Cα and Cβ given in Table 2 clearly shows that a considerable perturbation was invoked in the electronic properties of C=C bond in **1**. The slope for Cα is three times as large as that for Cβ probably because of the contribution of dipolar structure as shown in Eq. (1).

The DSP analyses of SCS for these side-chain carbons show that at Cα both ρ_I and ρ_R for **1** are larger than those for **2**. The increase is more significant for ρ_R. At Cβ, the contrary is the case. Thus, both ρ_I and ρ_R of **1** are smaller than those for **2**, and the decrease is larger for ρ_I. In view of the rather small difference between **1** and **2** of ρ_I and ρ_R at Cl′, it may be concluded that the side-chain carbon nuclei rather than the aromatic carbon atoms are much more affected by the elongation of conjugated system.

There remains one small problem. May **1** be ragarded as a vinylogue of **4**—**6**? ρ_I and ρ_R of **1** at C6 are −1.38 and −1.17, respectively, with f=0.16. The resonance effect of X is transmitted to C6 of **1** even more effectively than to Cα of **4**—**6**. Hence, **1** may be regarded as a vinylogue of such imines as **4**—**6** at least in a qualitative manner. The smaller ρ_I of **1** at C6 corresponds to the greater number of intervening bond or greater distance be-

TABLE 3. DSP AND DSP-NLR[a] ANALYSIS OF VARIOUS p-X-C_6H_4-Y SYSTEMS

Carbon	Parameter[b]	**1**	**2**	**3**	**4**	**5**	**6**	**7**
Cl′	ρ_I	5.03(5.18)	4.08(4.17)	4.20(4.57)	4.09	4.21(4.58)	3.95(4.32)	4.42(4.43)
	ρ_R	21.66(20.63)	20.01(19.40)	22.58(19.80)	20.52	20.43(17.54)	20.49(17.00)	20.01(17.41)
	f	0.03(0.02)	0.02(0.01)	0.05(0.02)	0.07	0.06(0.03)	0.07(0.03)	0.01
	ε	0(−0.11)	0(−0.07)	0(−0.28)	0	0(−0.32)	0(−0.38)	0(−0.34)
Cα	ρ_I	−3.87(−3.88)	−2.83	−2.75	−3.36	−3.21	−3.83	
	ρ_R	−1.66(0.18)	0.13	−1.80	−0.17	−0.39	−0.53	
	f	0.18(0.18)	0.13	0.13	0.13	0.06	0.14	
	ε	0(−0.05)	0	0	0	0	0	
C5	ρ_I	3.14	5.30(5.28)	5.59				2.96(3.12)
(Cβ)	ρ_R	7.23	8.47(8.65)	5.80				6.63(5.90)
	f	0.09	0.05(0.05)	0.16				0.09(0.08)
	ε	0	0(0.05)	0				0(−0.36)

a) Values in parentheses. In certain DSP-NLR analyses ε values did not converge on reasonables values.
b) For definition of parameters, see Eq(1).

tween X and C-6 while larger ρ_R of **1** indicates more effective transmission of resonance effect to C-6 through π-frame as compared with that between X and Cα.

Lanthanoid-induced Shifts. Lathanoid-induced shifts of C-13 nuclei are due to the combination of contact and pseudo contact shifts. The contact term, which is much more important in conjugated systems than in saturated systems, causes in certain cases an alternating sign along the carbon chain.[11]

The contact shift arises from the delocalization of the unpaired electron of the shift reagent to the substrate atoms. It occurred to us that there might be parallelism between the extent of spin delocalization and the transmission of substituent effect through the π-frame. Thus the sign of ρ values of **1** at C6 (both negative) clearly establishes the alternating nature of the ρ signs along the π-chain Cl'-Cα-Cβ-C6. This alternation has been pointed out[5] for side-chain C-13 shifts for **2** and chalcones (two carbon unit). Our system is, to the best of our knowledge, the longest π-chain with alternating ρ signs.

With this in mind, we measured LIS of **1a** by Eu(fod)$_3$. The result is summarized in Fig. 1, where the observed LIS are plotted against the molar ratio [Eu(fod)$_3$]/[solute]. Clearly, the sign of LIS does alternate along Cl'-Cα-Cβ-C6 chain. Negative LIS for Cβ and Cl' are associated with positive ρ values, and positive LIS for Cα and C6 with negative ρ values. This parallelism is another piece of evidence to the through conjugation in Ph-C=C-C=N moiety.

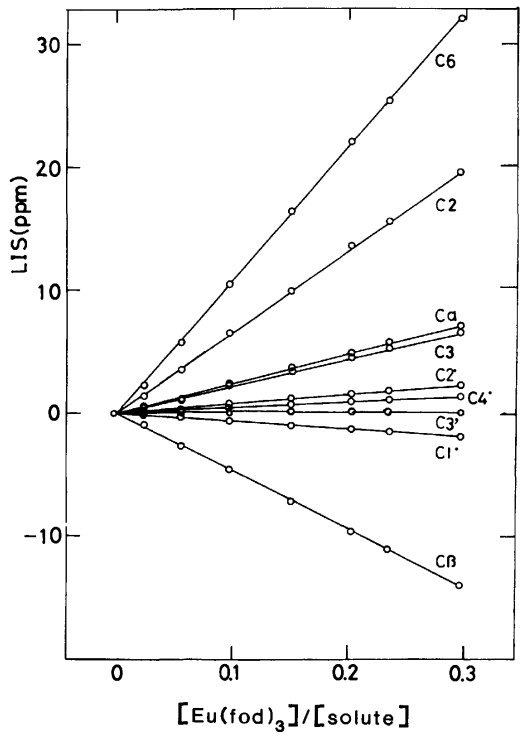

Fig. 1. Lanthanoid-induced shifts (LIS) in 5-benzylidene-2,3,4,5-tetrahydropyridine (**1a**).

Conclusion

The nature of C=C-C=N moiety in **1** as a substituent is mild and very close to the C=C moiety in respect to the magnitude of interaction with the variable substituent X attached to the same aromatic ring. The transmission of substituent effect of X to the side chain of **1** is somewhat different from that of compounds with -C=N or -N=C side-chains. The general behavior of **1** may, however, be regarded as a vinylogue of benzylideneamines. In **1**, the alternation of signs of ρ values in DSP analyses are parallel with that of LIS along Cl'-Cα-Cβ-C6 linkage. This phenomenon might be useful for theoretical treatment of the substituent effect in aromatic system.

The present work was partially suppoted by a Grant-in-Aid for Scientific Research No. 443007 from the Ministry of Education, Science and Culture.

References

1) For instance, G. E. Maciel, in G. C. Levy, ed. "Topics in Carbon-13 NMR Spectroscopy," Vol. 1, p. 53 (1974).
2) R. G. Jones and G. Allen, *Org. Magn. Reson.*, **19**, 196 (1982) and references therein.
3) Y. Nomura, T. Bando, Y. Takeuchi, and S. Tomoda, *Bull. Chem. Soc. Jpn*, **56**, 3199 (1983).
4) G. K. Hamer, I. R. Peat, and W. F. Reynolds, *Can. J. Chem.*, **51**, 897 (1973).
5) D. D. Dawson and W. F. Reynolds, *Can. J. Chem.*, **53**, 373 (1975).
6) W. B. Jennings, V. E. Wilson, D. R. Boyd, and P. B. Coulter, *Org. Magn. Reson.*, **21**, 279 (1983).
7) N. Inamoto, K. Kushida, S. Masuda, H. Ohta, S. Satoh, Y. Tamura, K. Tokumaru, K. Tori, and M. Yoshida, *Tetrahedron Lett.*, 3617 (1974).
8) Y. Nomura, T. Bando, Y. Takeuchi, and S. Tomoda, *Bull. Chem. Soc. Jpn.* **57**, 1271 (1984).
9) J. Bromilow, R. T. C. Brownlee, D. J. Craik, M. Sadek, and R. W. Taft, *J. Org. Chem.* **45**, 2429 (1980).
10) For a recent assessment of DSP analysis, see M. Charton, *Prog. Phys. Org. Chem.*, **13**, 119 (1981).
11) F. W. Wehrli and T. Wirthlin, "Interpretation of Carbon-13 NMR Spectra," Heyden & Sons, London (1978), p. 96.

Base-induced Cyclization of *N*-[Bis(ethoxycarbonyl)methyl]-2-bromo-3-hydroxybutyramide Derivatives

Masao Shiozaki,* Noboru Ishida, Tetsuo Hiraoka, and Hiroshi Maruyama
Chemical Research Laboratories of Sankyo Company Limited, Hiromachi 1-2-58, Shinagawa-ku, Tokyo 140
(Received December 24, 1983)

Treatment of (2*R*,3*R*)-*N*-(2,4-dimethoxybenzyl)-*N*-[bis(ethoxycarbonyl)methyl]-2-bromo-3-hydroxybutyramide (**5**) with DBU yielded the bicyclic β-lactam **13** by a direct cyclization, and its diastereoisomer **14** and the γ-lactam **15** *via* the *trans*-epoxide **6**. The same treatment of (2*S*,3*R*)-isomer (**11**) gave the direct cyclization product **14** in 93% yield. On the other hand, reaction of **5** and **11** with sodium hydride afforded the 2-azetidinone derivatives (mainly **14** (23%) from **5**, and **19** (75%) from **11**, respectively) *via* the corresponding epoxides **6** and **12**.

The first report on the discovery of thienamycin (isolation, structure, and biological activity) by the groups of Merck Sharp and Dohme Research Laboratories in 1976 produced a broad impact on organic chemists as well as medicinal chemists. This was because of the unique structure of thienamycin, different from that of traditional β-lactam antibiotics, and because of its powerful biological activity. Since its discovery, many congeners of thienamycin have been isolated as natural products and, at the same time, many attempts at syntheses of these carbapenems have been carried out by many groups. As one of such groups, we have reported on the stereocontrolled syntheses of monocyclic intermediates to carbapenems possessing a (1-hydroxy)ethyl side chain at the C-3 position.[1] Ahead of the cyclization of *N*-(2,4-dimethoxybenzyl)-*N*-(*t*-butoxycarbonylmethyl)-2-bromo-3-hydroxybutyramide[1b] obtained from L-threonine, the cyclization of 2-bromo-3-hydroxybutyramide derivatives (**5** and **11**) by means of bases was investigated in order to use the results in carbapenem synthesis.[2] As a result, it was confirmed that whether passing through the 2,3-epoxy derivatives (**6** or **12**) or not, base-induced intramolecular S_N2 cyclization occurred to give β-lactam derivatives as main products, together with the starting threonines (L-, L-*allo*, D-, and D-*allo*-). Thus we might be able to obtain the desired stereoisomer at the C-3 position and a hydroxyethyl side chain of β-lactam congeners.

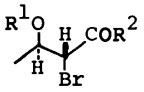

1 R^1 = H, R^2 = OH
2 R^1 = $SiMe_2Bu^t$, R^2 = OH
3 R^1 = $SiMe_2Bu^t$, R^2 = Cl
4 R^1 = $SiMe_2Bu^t$, R^2 = N(DMB)CH(COOEt)$_2$
5 R^1 = H, R^2 = N(DMB)CH(COOEt)$_2$

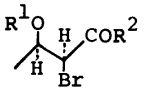

7 R^1 = H, R^2 = OH
8 R^1 = $SiMe_2Bu^t$, R^2 = OH
9 R^1 = $SiMe_2Bu^t$, R^2 = Cl
10 R^1 = $SiMe_2Bu^t$, R^2 = N(DMB)CH(COOEt)$_2$
11 R^1 = H, R^2 = N(DMB)CH(COOEt)$_2$

DMB = 2,4-dimethoxybenzyl

Scheme 1.

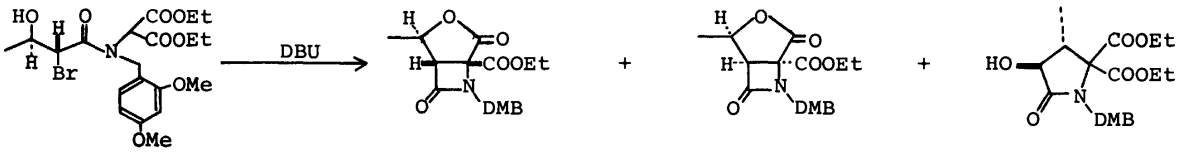

5 13 14 15

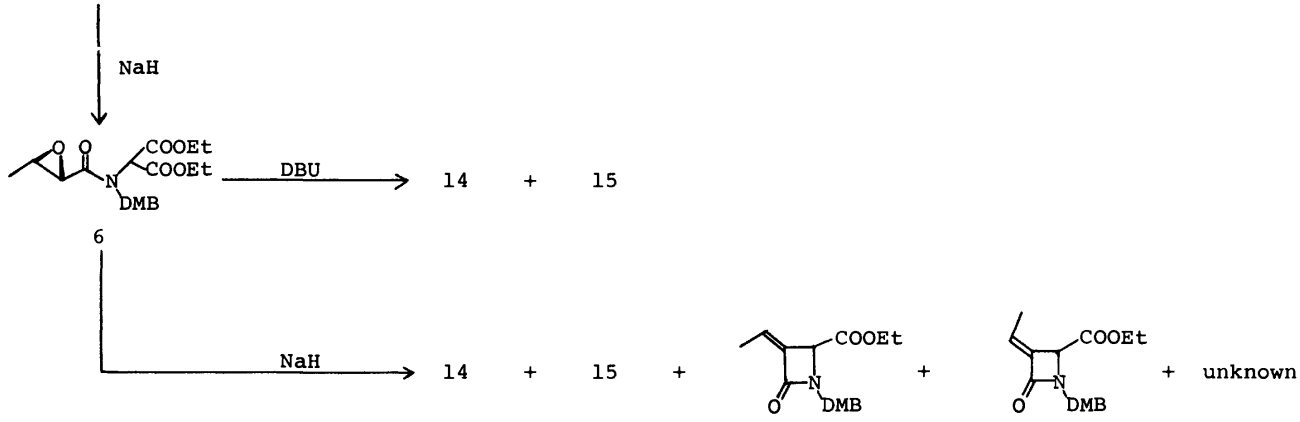

6

DMB = 2,4-dimethoxybenzyl

16 17 18

Scheme 2.

We wish here to report the results.

The starting **5** and **11** were synthesized as follows (Scheme 1). (2*R*,3*R*)-2-Bromo-3-hydroxybutyric acid (**1**) obtained from (2*R*,3*R*)-threonine (D-*allo*-threonine) was converted to the corresponding *t*-butyldimethylsilyl ether **2**, which was further treated with oxalyl dichloride in tetrahydrofuran (THF) at 20 °C for 3—16 h to give the acid chloride **3**. Treatment of **3** with diethyl (2,4-dimethoxybenzylamino)malonate in THF in the presence of Et_3N gave the *t*-butyldimethylsilyl ether **4**: Mp 90—91 °C: $[\alpha]_D^{25}$ −18.5° (*c*=2.00, $CHCl_3$). Desilylation of **4** with EtOH–H_2O–conc. HCl (9:2:1) gave **5**: Mp 74.5—75.5 °C: $[\alpha]_D^{24}$ −18.0° (*c*=2.00, $CHCl_3$). In addition, (2*S*,3*R*)-2-bromo-3-hydroxybutyric acid (**7**) obtained from (2*S*,3*R*)-threonine (L-threonine) was converted to **11** *via* **8**, **9**, and **10** according to the procedures described above. In the proton NMR of these *N*,*N*-disubstituted amides which contain a chiral part on the molecule, each of the methylene protons neighboring the nitrogen becomes non-equivalent. As a result, the methylene protons often show an AB-type coupling, and each part of the malonyl esters occasionally shows a different chemical shift.

Treatment of **5** with 2 equivalents of NaH in THF at 0 °C for 30 min gave the *trans*-epoxide **6** in 86% yield (Scheme 2). However, treatment of **5** with 1 equivalent of NaH resulted only in the recovery of the starting **5**. On the other hand, treatment of **5** with 2 equivalents of 1,8-diazabicyclo[5.4.0]undec-7-ene (DBU) in THF at 25 °C for 4 h gave mainly three products, a 6:1 mixture of bicyclic lactone azetidinones (**13** and **14**) in 75% yield (both were inseparable chromatographically and the ratio of **13** and **14** (6:1) was estimated by comparison with the authentic ^{1}H-NMR data of **13** and **14** obtained from **21** and **23**, respectively), and the hydroxy γ-lactam **15** in 7% yield. This result reveals that treatment of **5** with DBU incurs both direct 2-azetidinone formation to give **13** and epoxidation to give the intermediate **6**, and then successive ring closure of **6** branches off two pathways to give a normal ring closure product with a 4-membered ring and a 5-membered ring product, which results in a violation of Baldwin's ring closure rules.[3] As a matter of course, treatment of the epoxide **6** with DBU yielded two products, **14** and **15**, in 60% and 30% yields, respectively. On the other hand, treatment of **6** with 1.2 equivalents of NaH at 25 °C for 2 h gave **14** (23%) as a major product, and **15** (7.5%), **16** (6%), **17** (2%), and an unknown product (**18**) (mp 148—153 °C) as minor products. In this experiment, **14** was obtained *via* lactonization of the corresponding hydroxy carboxylic acid. The absolute configuration and the rate of racemization of **16** and **17** were not clear; however, the value of $[\alpha]_D^{25}$ of **16** was −2.7° in EtOH. The tendency for ring closure of the epoxide **6** by treatment with DBU or NaH was a little different, that is, the yields of **14** and **15** were 60% and 30% for use of DBU,

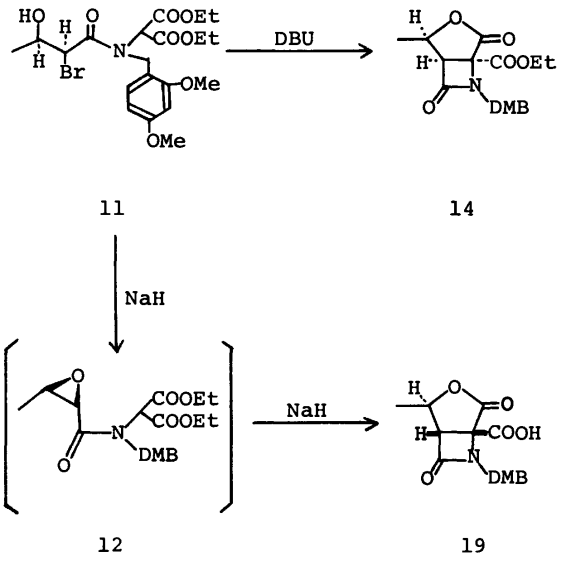

Scheme 3.

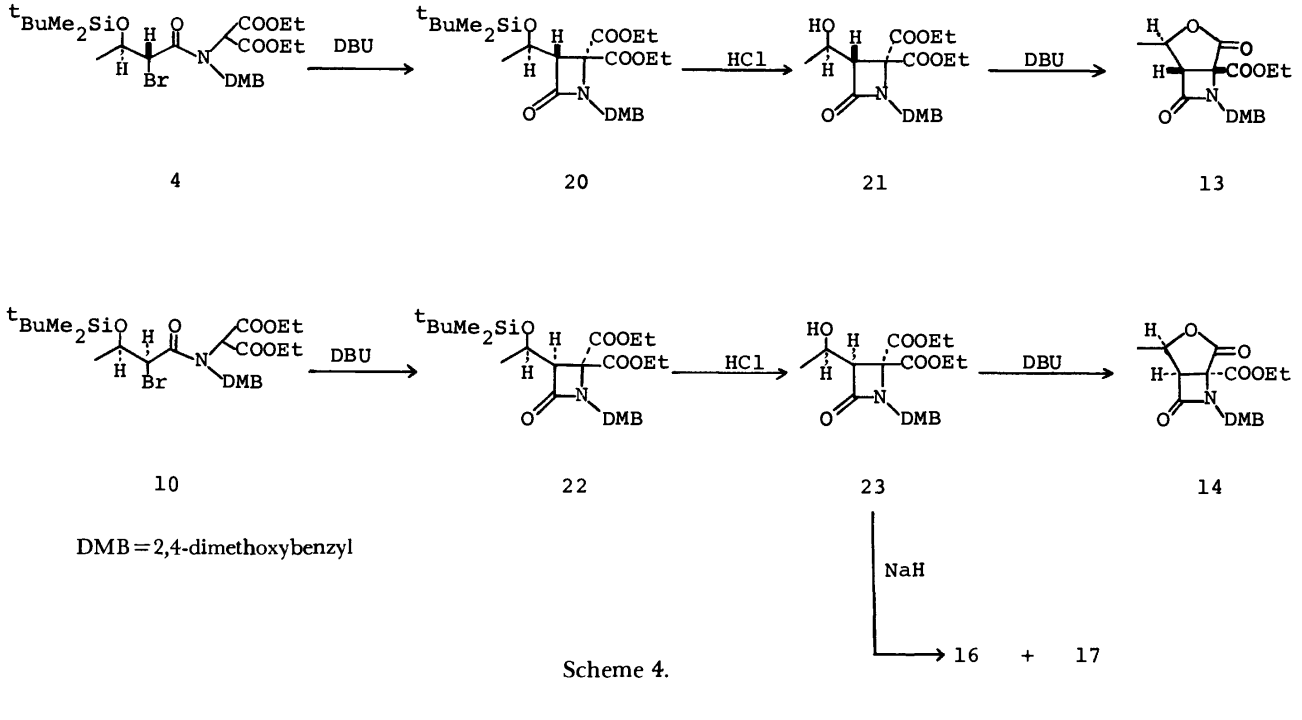

Scheme 4.

but 23% and 7% for use of NaH. In addition, it was obvious that the common intermediate to form **14**, **16**, and **17** was the compound **23**, as mentioned later.

We tried the cyclization of **11** with DBU and NaH (Scheme 3). Treatment of **11** with 2 equivalents of DBU in THF at 25 °C for 3 h gave **14** (93%), *via* a corresponding hydroxy carboxylic acid and by direct cyclization without passing through the epoxide **12**, as a single product. However, treatment of **11** with 3.7 equivalents of NaH in THF at 15 °C for 16 h gave a carboxylic acid **21** (76%) as a crystalline solid: Mp 180—184 °C; $[\alpha]_D^{25}$ −77.9° (*c*=2.00, THF), *via* the *cis*-epoxide **12**.

Alternatively, the compounds **13**, **14**, **15**, and **17** were synthesized from the O-protected compounds, **4** and **10** (Scheme 4). Treatment of **4** with DBU gave **20** (93%) as an oil: $[\alpha]_D^{25}$+28.5° (*c*=2.55, $CHCl_3$). Desilylation of **20** with EtOH–H_2O conc. HCl (9:2:1) at 20 °C for 16 h gave **21** (92%). Lactonization of **21** with DBU gave **13** (89%). In the same way, cyclization of **10** with DBU gave **22** (86%). Desilylation of **22** with EtOH–H_2O-conc. HCl (9:2:1) at 25 °C for 3 h gave **23** (60%) as a crystyalline solid: Mp 91—92 °C; $[\alpha]_D^{24}$ −75.6° (*c*=0.44, $CHCl_3$). Lactonization of **23** with DBU gave **14** in good yield. On the other hand, treatment of **23** with 1.56 equiv of NaH at 15 °C for 16 h gave **16** (13.9%), whose $[\alpha]_D^{24}$ value was −2.8° (*c*=0.47, EtOH), and **17** (7.5%).

Thus, we can obtain the required stereoisomers by use of the reaction of the O-protected or nonprotected 2-bromo-3-hydroxybutyramide derivatives or their corresponding epoxides[4] with alkaline metal or amine base.

Experimental

Melting points were determined on a Yanagimoto micromelting point apparatus and were uncorrected. Optical rotations were obtained by the use of a Perkin-Elmer 241 polarimeter. ^{1}H-NMR spectra were recorded at 60 MHz with a Varian T-60 spectrometer using tetramethylsilane as an internal standard. The IR absorption spectra were determined on a Jasco IR A-2 spectrophotometer. Mass spectra were obtained on a JMS-OlSG mass spectrometer. Preparative TLC was performed on silica gel plates (Merck 60 PF_{245}), and column chromatography was carried out on columns packed with Merck silica gel 60 using slightly increased pressure (1.5 atm) for elution. Elemental analyses were performed by the Analytical Centre of Analytical and Metabolic Research Laboratories, Sankyo Company, Limited.

(2R,3R)-2-Bromo-3-(t-butyldimethylsilyloxy)butyric Acid (2). To a solution of (2*R*,3*R*)-2-Bromo-3-hydroxybutyric acid[1c] (**1**, 18.3 g, 0.10 mol) in DMF (50 ml) was added *t*-butyldimethylsilyl chloride (45 g, 0.30 mol), Et_3N (30 g) and 4-dimethylaminopyridine (1.0 g). The mixture was stirred for 16 h at room temperature, then poured into water (300 ml), adjusted to pH 2 with dil HCl and then pH 8 with powdery $NaHCO_3$, and washed twice with Et_2O (each 200 ml). The aqueous layer was saturated with NaCl, and reacidified to pH 2 with dil HCl, and extracted with Et_2O (200 ml×3). The extract was washed with brine, dried over $MgSO_4$, and concentrated *in vacuo* to give 6.4 g (21.5%) of **2**, which was employed for the next reaction without further purificaiton. ^{1}H NMR ($CDCl_3$) δ=0.12 (6H, s), 0.90 (9H, s), 1.38 (3H, d, *J*=6 Hz), 4.01 (1H, d, *J*=8 Hz), 4.20 (1H, qd, *J*=6, 8 Hz), 9.62 (1H, bs, COOH). IR ν_{max} (film) 3600—2400, 1720 cm^{-1}. MS *m/z* 241 (M^+–Bu^t, ^{81}Br), 239.

(2S,3R)-2-Bromo-3-(t-butyldimethylsilyloxy)butyric Acid (8). (2*S*,3*R*)-2-Bromo-3-hydroxybutyric acid (**7**) was treated as described above to give **8** (30%) as an oil. IR ν_{max} (film) 3600—2400, 1723 cm^{-1}. NMR ($CDCl_3$) δ=0.12 (6H, s), 0.93 (9H, s), 1.21 (3H, d, *J*=6 Hz), 4.0—4.4 (2H, m), 9.51 (1H, bs, COOH). MS *m/z* 241 (M^+–Bu^t, ^{81}Br), 239.

(2R,3R)-2-Bromo-3-(t-butyldimethylsilyloxy)butyryl Chloride (3). To a solution of **2** (6.0 g, 20.2 mmol) in THF (30 ml) was added oxalyl dichloride (5.0 ml, 59 mmol) at 25 °C. After 3 h stirring, the reaction mixture was concentrated *in vacuo* to give 6.3 g (99%) of **3** as an oil, which was employed for the next reaction without purification. NMR ($CDCl_3$) δ=0.10 (6H, s), 0.88 (9H, s), 1.40 (3H, d, *J*=6 Hz), 4.1—4.5 (2H, m). IR ν_{max} (film) 1810 cm^{-1}.

(2S,3R)-2-Bromo-3-(t-butyldimethylsilyloxy)butyryl Chloride (9). The acid **8** was treated as described above to give an acid chloride **9** (quantitative), which was employed for the next reaction without purification. IR ν_{max} (film) 1815 cm^{-1}.

(2R,3R)-N-(2,4-Dimethoxybenzyl)-N-[bis(ethoxycarbonyl)methyl]-2-bromo-3-(t-butyldimethylsilyloxy)butyramide (4). To a solution of **3** (5.25 g, 16.6 mmol) and diethyl (2,4-dimethoxybenzylamino)malonate[1b] (5.40 g, 16.6 mmol) in THF (50 ml) was added a solution of Et_3N (1.70 g, 16.6 mmol) in THF (20 ml) at 5 °C with stirring over a period of 10 min. After the stirring was continued for 30 min at room temperature, the reaction mixture was extracted with EtOAc. The organic layer was washed with dil HCl, sat $NaHCO_3$ and brine, dried over $MgSO_4$, and concentrated *in vacuo* to give an oily residue which was chromatographed on a silica-gel (200 g) column. Elution with cyclohexane–EtOAc (4:1) gave 0.25 g of an unknown material at lower R_f value and 5.32 g (54%) of **4** as a crystalline solid: Mp 90—91 °C (from hexane). $[\alpha]_D^{25}$ −18.5° (*c*=2.0, $CHCl_3$). IR ν_{max} ($CHCl_3$) 1750 (shoulder), 1740, 1665, 1613, 1590 cm^{-1}. NMR ($CDCl_3$) δ=0.12 (6H, s), 0.90 9H, s), 1.05 3H, t, *J*=7 Hz), 1.26 (3H, t, *J*=7 Hz), 1.31 3H, d, *J*=6 Hz), 3.4—4.6 [12H, m, (containing 3H singlet at δ= 3.80 and 3H singlet at δ=3.83)], 4.70 (2H, s), 5.58 (1H, s), 6.28—6.48 (2H, m), 7.22 (1H, d, *J*=9 Hz).

Found: C, 51.97; H, 7.11; N, 2.27; Br, 13.17%. Calcd for $C_{26}H_{42}NO_8SiBr$: C, 51.60; H, 6.95; N, 2.32; Br, 13.21%.

(2S,3R)-N-(2,4-Dimethoxybenzyl)-N-[bis(ethoxycarbonyl)methyl]-2-bromo-3-(t-butyldimethylsilyloxy)butyramide (10). The acid chloride (**9**, 3.25 g) was treated as described above to give 1.62 g (26%) of **10**, 2.18 g of unknown material and 0.88 g of *N*-(2, 4-dimethoxybenzyl)-*N*-[bis(ethoxycarbonyl)methyl]-2-bromocrotonamide, which was due to the contamination of the corresponding acid chloride in the starting **9**. MS *m/z* 548 (M^+–Bu^t, ^{81}Br), 546. IR ν_{max} (film) 1750, 1662, 1612, 1588 cm^{-1}. NMR ($CDCl_3$) δ= 0.10 (3H, s), 0.14 (3H, S), 0.90 (9H, s), 1.20 (3H, t, *J*=7 Hz), 1.22 (3H, t, *J*=7 Hz), 1.25 (3H, d, *J*=6 Hz), 3.78 (3H, s), 3.80 (3H, s), 3.9—4.9 (9H, m), 6.40 (1H, d, *J*= 2 Hz), 6.40 (1H, dd, *J*=2, 9 Hz), 7.16 (1H, d, *J*=9 Hz).

Found: C, 51.83; H, 7.20; N, 2.30; Br, 13.14%. Calcd for $C_{26}H_{42}O_8NBrSi$: C, 51.60; H, 6.95; N, 2.32; Br, 13.21%.

(2R,3R)-N-(2,4-Dimethoxybenzyl)-N-[bis(ethoxycarbonyl)methyl]-2-bromo-3-hydroxybutyramide (5). A solution of **4** (4.26 g, 7.0 mmol) in EtOH (180 ml) and dil HCl (H_2O/conc. HCl=2/1, 60 ml) was stirred for 8 h at 20 °C, concentrated to a volume of 100 ml, and extracted with EtOAc (300 ml). The organic layer was washed with sat $NaHCO_3$ and brine, dried over $MgSO_4$ and concentrated to give an oily residue which was chromatographed on a silica-gel (100 g) column. Elution with cyclohexane–EtOAc (1:1) gave 3.45 g (quantitative) of **5** as a crystalline solid: Mp 74.5—75.5 °C (from EtOH). $[\alpha]_D^{24}$ −18.0° (*c*=2.00, $CHCl_3$). IR ν_{max} ($CHCl_3$) 3560, 1760—1740, 1650, 1613, 1590 cm^{-1}. NMR ($CDCl_3$) δ=1.17 (3H, t, *J*=7 Hz), 1.22 (3H, t, *J*=7 Hz), 1.40 (3H, d, *J*=6 Hz), 3.52 (1H, d, *J*= 4 Hz, OH), 3.78 (3H, s), 3.81 (3H, s), 4.08 (2H, q, *J*=7 Hz), 4.11 (2H, q, *J*=7 Hz), 4.40 (1H, d, *J*=3.5 Hz, C_2–H), 4.48, 4.85 (2H,

AB-q, J=16 Hz), 4.63 (1H, s), 6.28—6.47 (2H, m, olefinic), 7.02—7.17 (1H, m, olefinic).

Found: C, 48.88; H, 5.70; N, 2.77; Br, 16.12%. Calcd for $C_{20}H_{28}O_8NBr$: C, 48.95; H, 5.71; N, 2.85; Br, 16.30%.

(2S,3R)-N-(2,4-Dimethoxybenzyl)-N-[bis(ethoxycarbonyl)methyl]-2-bromo-3-hydroxybutyramide (11). The silyl ether **10** was treated with EtOH-H_2O-conc. HCl (9:2:1) for 1 h at 20 °C as described above to give **11** (81.5%) as a viscous oil. IR ν_{max} (film) 3475, 1750, 1739, 1655, 1610, 1587 cm^{-1}. NMR ($CDCl_3$) δ=1.20 (3H, t, J=7 Hz), 1.22 (3H, t, J=7 Hz), 1.26 (3H, d, J=7 Hz), 3.84 (6H, s), 3.97—5.05 (10H, m), 6.48 (1H, d, J=2 Hz), 6.48 (1H, dd, J=2, 9 Hz), 7.15 (1H, J=9 Hz).

Found: C, 48.76; H, 5.80; N, 2.81; Br, 16.17%. Calcd for $C_{20}H_{28}O_8NBr$: C, 48.95; H, 5.71; N, 2.85; Br, 16.30%.

(2S,3R)-N-(2,4-Dimethoxybenzyl)-N-[bis(ethoxycarbonyl)methyl]-2,3-epoxybutyramide (6). To a solution of **5** (490.3 mg, 1.0 mmol) in THF (4 ml) was added NaH (55% dispersion in mineral oil, 83 mg, 2.0 mmol) at 0 °C. After 30 min stirring, the starting **5** had disappeared completely. The reaction mixture was diluted with EtOAc, washed with 5% HCl, sat $NaHCO_3$ and brine, dried over $MgSO_4$, and concentrated *in vacuo* to give an oily residue which was chromatographed on preparative silica-gel TLC plates. Development with cyclohexane-EtOAc (1:1) gave 352 mg (86%) of **6** as a viscous oil. NMR ($CDCl_3$) δ=1.20 (6H, t, J=7 Hz), 1.22 (3H, d, J=5 Hz), 3.65 (1H, dq, J=2, 5 Hz), 3.38 (1H, d, J=2 Hz), 3.80 (3H, s), 3.81 (3H, s), 4.10 (2H, q, J=7 Hz), 4.13 (2H, q, J=7 Hz), 4.71 (2H, s), 5.29 (1H, s), 6.43 (2H, m), 7.17 (1H, d, J=9 Hz). IR ν_{max} (film) 1750—1730, 1672, 1612, 1590 cm^{-1}.

Found: C, 58.30; H, 6.51; N, 3.29%. Calcd for $C_{20}H_{27}O_8N$: C, 58.67; H, 6.65; N, 3.42%.

Reaciton of 5 with DBU. To a solution of **5** (245 mg, 0.5 mmol) in THF (4 ml) was added DBU (152 mg, 1 mmol) at 25 °C with stirring. After 4 h, the reaction mixture was diluted with EtOAc, then washed with 10% HCl, sat $NaHCO_3$ and brine, dried over $MgSO_4$, and concentrated *in vacuo* to give an oily mixture. The mixture was chromatographed on preparative silica-gel TLC plates. Development with EtOAc-cyclohexane (1:1) gave 136 mg (75%) of a 6:1 mixture of **13** and **14** which could not be separated because the R_f values of 0.40 were almost the same (The ratio of **13**:**14** was estimated by comparison with authentic ^{1}H-NMR data of **13** and **14** obtained from **21** and **22**, respectively.), and 14 mg (7%) of **15** (R_f=0.25). MS m/z 409 (M^+), 223, 167, 151. IR ν_{max} (film) 3360, 1750 (shoulder), 1730, 1695, 1612, 1590 cm^{-1}. NMR ($CDCl_3$) δ=1.07 (3H, t, J=7 Hz), 1.19 (3H, t, J=7 Hz), 1.25 (3H, d, J=7 Hz), 2.55—3.12 (1H, m), 3.6—4.3 [12H, m, (containing 6H singlet at δ=3.77)], 4.49, 4.78 (2H, AB-q, J=16 Hz), 6.35 (1H, d, J=2 Hz), 6.35 (1H, dd, J=2, 9 Hz), 6.90 (1H, d, J=9 Hz).

Found: C, 58.22; H, 6.99; N, 3.37%. Calcd for $C_{20}H_{27}O_8N$: C, 58.67; H, 6.65; N, 3.42%.

Reaction of 6 with DBU. A soluiton of 6 (205 mg, 0.5 mmol) and DBU (80 mg, 0.53 mmol) in THF (5 ml) was stirred for 6 h at 25 °C and concentrated *in vacuo* to give an oily mixture, which was chromatographed on preparative silica-gel TLC plates. Development with cyclohexane-EtOAc (1:1) gave 61 mg (29.8%) of **15** on R_f=0.25 as a viscous oil, and an acidic product on R_f=0, which was eluted off from the silica gel with MeOH. The MeOH solution was concentrated *in vacuo* to give an oily residue which was diluted with EtOAc. The EtOAc solution was washed with 5% HCl, H_2O and brine, dried over $MgSO_4$, and concentrated *in vacuo* to give 108 mg (59.5%) of the lactonized product **14** as a viscous oil. MS m/z 363 (M^+). IR ν_{max} (film) 1770, 1750 (shoulder), 1735 (shoulder), 1613, 1590 cm^{-1}. NMR ($CDCl_3$) δ=1.26 (3H, t, J=7 Hz), 1.55 (3H, d, J=6 Hz), 3.90 (1H, d, J=7 Hz, C_1-H), 4.22 (2H, q, J=7 Hz), 4.38, 4.63 (2H, AB-q, J=15 Hz), 4.76 (1H, quintaplet, J=7 Hz, C_2-H), 6.2—6.5 (2H, m), 7.12 (1H, d, J=9 Hz).

Found: C, 59.47; H, 5.86; N, 3.73%. Calcd for $C_{18}H_{21}O_7N$: C, 59.49; H, 5.83; N, 3.86%.

Raction of 6 with NaH. To a solution of **6** (150 mg, 0.367 mmol) in THF (2 ml) was added NaH (55% dispersion in mineral oil, 20 mg, 0.458 mmol) at 25 °C with strirring. After 2 h, the reaction mixture was diluted with EtOAc, washed with 5% HCl, H_2O, brine, dried over $MgSO_4$, and concentrated *in vacuo* to give an oily residue which was chromatographed on a preparative silica-gel TLC plate. Development with cyclohexane-EtOAc (1:1) gave 7 mg (6%) of **16** (R_f=0.683); $[\alpha]_D^{25}$ −2.7 ° (c=0.77, EtOH), 15 mg of a mixture of **17** and unknown **18** (R_f=0.583, Fractional crystallization of this mixture from *i*-Pr_2O gave 11 mg of **18** as a crystalline solid; mp 148—153 °C. The remaining mother liquor contained 4 mg of a 1:1 mixture of **17** and **18**. This was estimated by the comparison with the ^{1}H NMR of each authentic sample of **17**, obtained from **23**, and **18**.), 17 mg (7.5%) of **15** (R_f=0.283), and an acidic product (R_f=0) which was eluted off from the silica-gel with MeOH, and concentrated *in vacuo* to give an oily residue which was diluted with EtOAc (50 ml). The solution was washed with 10% HCl, H_2O and brine, dried over $MgSO_4$, and concentrated *in vacuo* to give 31 mg (23.3%) of **14**.

Reaction of 11 with DBU. A solution of **11** (120 mg, 0.245 mmol) and DBU (76 mg, 0.500 mmol) in THF (2 ml) was stirred for 1 h at 25 °C. The precipitated DBU-HBr salt was filtrated, and the filtrate was concentrated *in vacuo* to give an oily residue which was chromatographed on a preparative silica gel TLC plate. Development with cyclohexane-EtOAc (1:1) gave an acidic material of R_f=0. The silica gel layer of this part was eluted with MeOH which was concentrated *in vacuo* to give a residue. The residue was diluted with EtOAc which was washed with 10% HCl, H_2O and brine, and dried over $MgSO_4$, and then concentrated *in vacuo* to give 83 mg (93.4%) of **14** as a viscous oil.

Reaction of 11 with NaH. To a solution of **11** (120 mg, 0.245 mmol) in THF (2 ml) was added NaH (55% dispersion in mineral oil, 40 mg, 0.917 mmol) under cooling with ice bath.

The mixture was kept for 16 h at 15 °C, then diluted with EtOAc, washed with 10% HCl, H_2O and brine, dried over $MgSO_4$, and concentrated *in vacuo* to give a crude crystalline acid. The acid was suspended in a small amount of EtOAc, triturated in large excess of hexane, and then collected by suction filtration to give 62 mg (75.6%) of **19** as a crystalline solid: Mp 180—184 °C (from EtOAc). $[\alpha]_D^{23}$ −77.9 °C (c=2.00, THF). IR ν_{max} (Nujol) 3500—2400, 1780, 1740, 1730 (shoulder), 1613, 1588 cm^{-1}. NMR (DMF-d_7) δ=1.40 (3H, d, J=6 Hz), 3.78 (6H, s), 4.10 (1H, d, J=1 Hz), 4.47 (2H, s), 4.93 (1H, dq, J=1, 6 Hz), 6.55 (1H, dd, J=2, 9 Hz), 6.58 (1H, d, J=2 Hz), 7.18 (1H, d, J=9 Hz), 10.50 (1H, bs, COOH).

Found: C, 57.49; H, 5.22; N, 4.18%. Calcd for $C_{16}H_{17}O_7N$: C, 57.31; H, 5.11; 4.18%.

(3S)-1-(2,4-Dimethoxybenzyl)-3-[(R)-1-(t-butyldimethylsilyloxy)ethyl]-4,4-bis(ethoxycarbonyl)-2-azetidinone (20). To a solution of **4** (1.0 g, 1.65 mmol) in THF (20 ml) was added DBU (300 mg, 1.97 mmol) at 20 °C. After 16 h stirring at 20 °C, the reaction mixture was diluted with EtOAc, washed with a cold 5% HCl aqueous solution, sat $NaHCO_3$ and brine, dried over $MgSO_4$, and concentrated *in vacuo* to give 0.79 g (92.8%) of **20** as an oil. $[\alpha]_D^{25}$ +28.5 ° (c=2.55, $CHCl_3$). NMR ($CDCl_3$) δ=0.08 (6H, s), 0.88 (9H, s), 1.04 (3H, t, J=7 Hz), 1.26 (3H, t, J=7 Hz), 1.33 (3H, d, J=6 Hz), 3.6—4.5 [12H, m, (containing 6H singlet at δ=3.79)], 4.50, 4.79 (2H, AB-q, J=15 Hz), 6.39 (1H, d, J=2 Hz), 6.39 (1H, dd, J=2, 9 Hz), 7.09 (1H, d, J=9 Hz). IR ν_{max} (film) 1770, 1742, 1613, 1590 cm^{-1}. MS m/z 466 (M^+−C_4H_9).

Found: C, 58.84; H, 7.45; N, 2.58%. Calcd for $C_{26}H_{41}O_8NSi$: C, 59.58; H, 7.83; N, 2.67%.

(3S)-1-(2,4-Dimethoxybenzyl)-3-[(R)-1-(hydroxy)ethyl]-4,4-bis(ethoxycarbonyl)-2-azetidinone (21). A solution of **20** (523.7 mg, 1.0 mmol) in EtOH–H_2O–conc HCl (9:2:1, 24 ml) was allowed to stand for 16 h at 20 °C. The reaction mixture was diluted with EtOAc, washed with water, sat $NaHCO_3$ and brine, dried over $MgSO_4$, and concentrated *in vacuo* to give a crude mixture which was chromatographed on preparative silica-gel TLC plates. Development with cyclohexane–EtOAc (1:1) gave 376 mg (91.8%) of **21** (R_f=0.52) as a viscous oil. IR ν_{max} (film) 3475, 1765-1730, 1610, 1588 cm^{-1}. NMR ($CDCl_3$) δ=1.10 (3H, t, J=7 Hz), 1.28 (3H, t, J=7 Hz), 1.38 (3H, d, J=6 Hz), 3.18 (1H, bs, OH), 3.66 (1H, d, J=9 Hz), 3.78 (6H, s), 3.88 (2H, q, J=7 Hz), 4.27 (2H, q, J=7 Hz), 4.38, 4.72 (2H, AB-q, J=15 Hz), 4.0—4.5 (1H, m), 6.38 (1H, d, J=2 Hz), 6.38 (1H, dd, J=2, 9 Hz), 7.05 (1H, d, J=9 Hz). MS m/z 409 (M^+), 364.

Found: C, 58.61; H, 6.69; N, 3.40%. Calcd for $C_{20}H_{27}O_8N$: C, 58.67; H, 6.65; N, 3.42%.

(1S,2R,5S)-6-(2,4-Dimethoxybenzyl)-5-ethoxycarbonyl-2-methyl-4,7-dioxo-3-oxa-6-azabicyclo[3.2.0]heptane (13). A solution of **21** (107 mg, 0.261 mmol) in THF (2 ml) containing DBU (40 mg, 0.263 mmol) was stirred for 3 h at 24 °C. The reaction mixture was diluted with EtOAc, washed with 5% HCl, sat $NaHCO_3$ and brine, dried over $MgSO_4$, and concentrated *in vacuo* to give an oily residue which was chromatographed on a preparative silica-gel TLC plate. Development with cyclohexane–EtOAc (1:1) gave 85 mg (89%) of **13** (R_f=0.46). NMR ($CDCl_3$) δ=1.26 (3H, t, J=7.5 Hz), 1.45 (3H, d, J=6 Hz), 3.66 (1H, d, J=1 Hz), 3.81 (6H, s), 4.26 (2H, q, J=7.5 Hz), 4.51 (2H, s), 4.90 (1H, dq, J=1, 6 Hz), 6.43 (1H, d, J=2 Hz), 6.43 (1H, dd, J=2, 9 Hz), 7.15 (1H, d, J=9 Hz). IR ν_{max} (film) 1770, 1730 (shoulder), 1612, 1590 cm^{-1}. MS m/z 363 (M^+).

Found: C, 59.27; H, 5.94; N, 3.80%. Calcd for $C_{18}H_{21}O_7N$: C, 59.49; H, 5.83; N, 3.86%.

(3R)-1-(2,4-Dimethoxybenzyl)-3-[(R)-1-(t-butyldimethylsilyloxy)ethyl]-4,4-bis(ethoxycarbonyl)-2-azetidinone (22). A solution of **10** (485 mg, 0.80 mmol) in THF (5 ml) containing DBU (122 mg, 0.802 mmol) was refluxed for 30 min. After cooling, the reaction mixture was diluted with EtOAc, washed with 1% HCl, sat $NaHCO_3$ and brine, dried over $MgSO_4$, and concentrated *in vacuo* to give a crude oil which was chromatographed on silica-gel preparative TLC plates. Development with cyclohexane–EtOAc (3:1) gave 363 mg (86%) of **22** (the same R_f value as that of the starting **10**). NMR ($CDCl_3$) δ=0.05 (3H, s), 0.08 (3H, s), 0.88 (9H, s), 1.05 (3H, t, J=7 Hz), 1.24 (3H, t, J=7 Hz), 1.35 (3H, d, J=6 Hz), 3.62 (1H, d, J=3.5 Hz), 3.78 (6H, s), 3.78 (2H, q, J=7 Hz), 4.20 (2H, q, J=7 Hz), 4.33 (1H, dq, J=3.5, 6 Hz), 4.43, 4.72 (2H, AB-q, J=15 Hz), 6.36 (1H, d, J=2 Hz), 6.36 (1H, dd, J=2, 9 Hz), 7.16 (1H, d, J=9 Hz). IR ν_{max} (film) 1770, 1740, 1613, 1590 cm^{-1}. MS m/z 466 (M^+–Bu^t).

Found: C, 58.86; H, 7.44; N, 2.70%. Calcd for $C_{26}H_{41}O_8NSi$: C, 59.58; H, 7.83; N, 2.67%.

(3R)-1-(2,4-Dimethoxybenzyl)-3-[(R)-1-(hydroxy)ethyl]-4,4-bis(ethoxycarbonyl)-2-azetidinone (23). A solution of **22** (350 mg, 0.668 mmol) in EtOH–H_2O–conc HCl (9:2:1, 8 ml) was allowed to stand for 3 h at 25 °C. The reaction mixture was diluted with EtOAc, washed with water, sat $NaHCO_3$ and brine, dried over $MgSO_4$, and concentrated *in vacuo* to give a crude oily mixture which was chromatographed on silica-gel preparative TLC plates. Development with cyclohexane–EtOAc (1:1) gave 164 mg (60%) of **23** (R_f=0.367) as a crystalline solid: Mp 91—92 °C (from EtOAc-hexane). $[\alpha]_D^{24}$ −75.6 (c=0.44, $CHCl_3$). NMR ($CDCl_3$) δ= 1.08 (3H, t, J=7 Hz), 1.28 (3H, t, J=7 Hz), 1.43 (3H, d, J=6 Hz), 1.95 (1H, d, J=6 Hz, OH), 3.6—4.2 [8H, m, (containing 6H singlet at δ=3.81)], 4.25 (4H, q, J=7 Hz), 4.48, 4.81 (2H, AB-q, J=15 Hz), 6.39 (1H, d, J=2 Hz), 6.39 (1H, dd, J=2, 9 Hz), 7.13 (1H, d, J=9 Hz). IR ν_{max} (Nujol) 3390, 1760—1730, 1610, 1585 cm^{-1}.

Found: C, 58.70; 6.63; N, 3.44%. Calcd for $C_{20}H_{27}O_8N$: C, 58.67; H, 6.65; N, 3.42%.

(1R,2R,5R)-6-(2,4-Dimethoxybenzyl)-5-ethoxycarbonyl-2-methyl-4,7-dioxo-3-oxa-6-azabicyclo[3.2.0]heptane (14). Treatment of **23** with one equivalent of DBU as described above in the formation of **14** from **11** by DBU gave **14** in 72% yield.

(Z)- and (E)-1-(2,4-Dimethoxybenzyl)-3-ethylidene-4-ethoxycarbonyl-2-azetidinone (16) and (17). To a solution of **23** (120 mg, 0.293 mmol) in THF (2 ml) was added NaH (55% dispersion in mineral oil, 20 mg). The mixture was stirred for 16 h at 15 °C, and diluted with EtOAc. The solution was washed with H_2O and brine, dried over $MgSO_4$, and concentrated *in vacuo* to give an oily residue which was chromatographed on a silica-gel preparative TLC plate. Development with cyclohexane–EtOAc (4:1) gave 13 mg (13.9%) of **16** (R_f=0.17) and 7 mg (7.5%) of **17** (R_f=0.070). **16**: $[\alpha]_D^{25}$ −2.8° (c=0.47, EtOH). NMR ($CDCl_3$) δ=1.26 (3H, t, J=7 Hz), 2.00 (3H, d, J=7 Hz), 3.78 (3H, s), 3.81 (3H, s), 4.20 (2H, q, J=7 Hz), 4.21 (1H, d, J=1 Hz), 4.27, 4.72 (2H, AB-q, J=14.5 Hz), 5.66 (1H, dq, J=1, 7 Hz), 6.40 (2H, m), 7.10 (1H, d, J=9 Hz). IR ν_{max} (film) 1750, 1720 (shoulder, w), 1613,1590 cm^{-1}. MS m/z 319 (M^+), 290, 246, 218, 166, 151.

Found: C, 63.39; H, 6.54; N, 4.26%. Calcd for $C_{17}H_{21}O_5N$: C, 63.88; H, 6.57; N, 4.38%. **17**: NMR ($CDCl_3$) δ=1.27 (3H, t, J=7 Hz), 1.76 (3H, d, J=6.5 Hz), 3.80 (3H, s), 3.82 (3H, s), 4.22 (2H, q, J=7 Hz), 4.25, 4.70 (2H, AB-q, J=14 Hz), 4.38 (1H, d, J=1 Hz), 6.15 (1H, dq, J=1, 6.5 Hz), 6.41 (1H, dd, J=2, 9 Hz), 6.41 (1H, d, J=2 Hz), 7.12 (1H, d, J=9 Hz). IR ν_{max} (film) 1760—1740, 1612, 1590 cm^{-1}. MS m/z 319 (M^+), 290, 246, 218, 166, 151, 126, 121.

Found: C, 63.34; H, 6.49; N, 4.27%. Calcd. for $C_{17}H_{21}O_5N$: C, 63.88; H, 6.57; N, 4.38%.

References

1) a) M. Shiozaki and T. Hiraoka, *Tetrahedron*, **38**, 3457 (1982); b) M. Shiozaki, N. Ishida, H. Maruyama, and T. Hiraoka, *ibid.*, **39**, 2399 (1983); c) M. Shiozaki, N. Ishida, T. Hiraoka, and H. Maruyama, *Tetrahedron Lett.*, **22**, 5205 (1981).

2) M. Shiozaki, N. Ishida, T. Hiraoka, and H. Maruyama, *Chem. Lett.*, **1983**, 169.

3) a) J. E. Baldwin, *J. Chem. Soc., Chem. Commun.*, 734 (1976); b) J. E. Baldwin, J. Cutting, W. Dupont, L. I. Kruse, L. Silberman, and R. C. Thomas, *ibid*, 736 (1976); c) J. E. Baldwin, *ibid.*, 738 (1976); d) J. E. Baldwin and J. A. Reiss, *ibid*, 77 (1977); e) J. E. Baldwin and L. I. Kruse, *ibid.*, 233 (1977); f) J. E. Baldwin, R. C. Thomas, L. I. Kruse, and L. Silberman, *J. Org. Chem.*, **42**, 3846 (1977).

4) A. K. Bose, B. M. Bhawal, B. B. Shankar, and M. S. Manhas, In 186th ACS Natl Meet., Washington. DC. USA, Aug 28- Sep 2, 1983: Abstr. p. 86.

Photoinduced Addition Reaction of 1,4-Dibromo-2,5-piperazinedione with 1-Alkenes

Kuniaki ITOH,* Hiroshi YAMADA,† and Akira SERA†
Department of Science of Material Reactions, Division of Science of Materials, Graduate School of Science and Technology.
†*Department of Chemistry, Faculty of Science, Kobe University, Kobe 657*
(Received December 28, 1983)

Irradiation of 1,4-dibromo-2,5-piperazinedione (**1**) with olefins in acetonitrile gave mixtures of addition products (1:1-adducts and 1:2-adducts). Addition of 1,2-epoxybutane (a hydrogen bromide scavenger) resulted in enhanced yields of the adducts. Structures of the adducts were elucidated and a reaction mechanism is discussed.

The allylic bromination of olefins by *N*-bromosuccinimide (NBS) was believed to involve the bromide atom chain (the Goldfinger mechanism). However, Skell and his co-workers[1,2] showed that the reaction of NBS with cyclohexene in dichloromethane gave 3- and 4-bromocyclohexenes and 1-bromo-2-succinimidocyclohexane. Thus the substitution and the addition are competitive processes (substitution/addition= 0.17). Chow and his co-workers[3] similarly exemplified that in the photolysis of an acetonitrile solution of NBS in the presence of cyclohexene the succinimido radical preferentially added to the olefin double bond to give the same adduct. These findings suggest the intervention of the succinimido radical as the chain carrier where the concentration of NBS is kept high by using good NBS dissolving solvents and the concentration of the bromine molecule is kept low by added olefins. The addition reaction of acylaminyl radicals to olefins, however, has not been so thoroughly examined. Thouchard and Lessard[4] reported that the photochemical reaction of *N*-haloacetamides with olefins gave addition products in good yields, but *N*-halo-*N*-methylacetamides failed to add to simple olefins.[5] In a previous paper,[6] we described that irradiation of 1,4-dibromo-2,5-piperazinedione (**1**) with cyclohexene resulted in the radical addition of **1** to cyclohexene to give 1-(2-bromocyclohexyl)-2,5-piperazinediones (1:1-adducts) and 1,4-bis(2-bromocyclohexyl)-2,5-piperazinediones (1:2-adducts) in acetonitrile, dichloromethane, or chloroform, which are characterized as good solvents for **1**. This paper concerns the product distribution in photoaddition of **1** to 1-alkene isomers in acetonitrile. The structures of adducts and the reaction mechanism are also discussed.

Results and Discussion

The photoreaction of 1,4-dibromo-2,5-pipera-

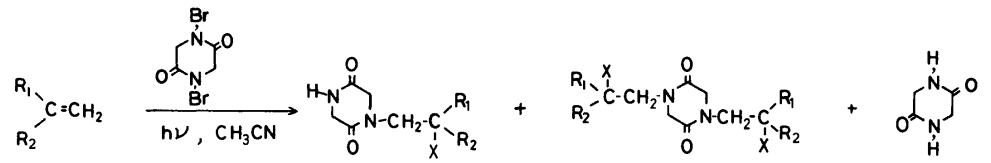

	R_1	R_2		R_1	R_2	X		R_1	R_2	X
2	n-C_4H_9	H	**2′(OH)**	n-C_4H_9	H	OH	**2″a,b**	n-C_4H_9	H	Br
							2″(OH)a,b	n-C_4H_9	H	OH
3	n-C_3H_7	CH_3	**3′**	n-C_3H_7	CH_3	Br	**3″a,b**	n-C_3H_7	CH_3	Br
4	i-C_3H_7	CH_3	**4′**	i-C_3H_7	CH_3	Br	**4″a,b**	i-C_3H_7	CH_3	Br
5	t-C_4H_9	H	**5′**	t-C_4H_9	H	Br	**5″a,b**	t-C_4H_9	H	Br

Scheme 1.

TABLE 1. PRODUCT DISTRIBUTION OF PHOTOREACTION OF 1,4-DIBROMO-2,5-PIPERAZINEDIONE WITH 1-ALKENES[a]

	Product distribution (yields/%)				
	1:1-Adduct		1:2-Adduct		2,5-Piperazinedione
1-Hexene(**2**)	**2′(OH)**	11	**2″a,b**	5[c]	54
			2″(OH)	7[c]	
1-Hexene(**2**)[b]	**2′(OH)**	16	**2″a,b**	21[c]	39
			2″(OH)a,b	9[c]	
2-Methyl-1-petene(**3**)	**3′**	5	**3″a,b**	45[c]	3
2,3-Dimethyl-1-butene(**4**)	**4′**	3	**4″a**	17	8
			4″b	11	
3,3-Dimethyl-1-butene(**5**)	**5′**	7	**5″a**	2	trace[d]
			5″b	2	

a) A mixture of **1** (2 mmol) and an olefin (20 mmol) in 10 cm^3 of acetonitrile was irradiated at ambient temperature for 5 h. Isolated yields are given based on **1** employed. b) 1,2-Epoxybutane (4 mmol) was added. c) A mixture of two stereoisomers. d) Unchanged **1** was recovered in 60% yield.

zinedione (**1**, 2 mmol) with isomeric 1-alkenes (**2**—**5**, 20 mmol) was carried out in acetonitrile using a high pressure mercury lamp at ambient temperature. The reaction gave mixtures of 1 : 1-adducts (**2′**—**5′**; characterized by ′) and 1 : 2-adducts (**2″**—**5″**; characterized by ″) in addition to allylic brominated products and dibromides. The adduct mixtures were separated by silica-gel column chromatography, and the structures were determined by elemental and spectroscopic analyses. The results are summarized in Scheme 1 and Table 1.

A chromatographic separation of the adduct mixtures obtained from the photoreaction of **1** with 1-hexene (**2**) gave an isomer mixture of bromine-containing 1 : 2-adducts (**2″**), an isomer mixture of hydroxyl group-containing 1 : 2-adducts (**2″(OH)**), and a hydroxyl group-containing 1 : 1-adduct (**2′(OH)**). No bromine-containing 1 : 1-adduct was obtained. Addition of 1,2-epoxybutane (a hydrogen bromide scavenger) resulted in increased yields of the adducts. The adduct mixture (**2″**) was re-chromatographed to give isomers **2″a** and **2″b**. Both **2″a** and **2″b** had two bromine atoms, and they gave similar NMR and IR spectra. Treatment of **2″a** and **2″b** by tributyltin hydride afforded identical 1,4-dihexyl-2,5-piperazinedione (**2″(H)**). NMR spectra of **2″a** and **2″b**, and their reduction product (**2″(H)**) indicated that the 2,5-dioxo-1-piperazinyl group added to the less substituted carbon atom of **2**, and that **2″a** and **2″b** are stereoisomers each other at the carbon atoms bearing bromine atoms. The hydroxyl group-containing adduct consisted of two isomers, **2″(OH)a** and **b** (in about a 3 : 4 ratio (NMR)); they hardly separated on TLC. IR spectra of **2″(OH)a**, **b** showed the presence of hydroxyl groups, and no bromine atom was contained as checked by MS; the distinct M^+-2H_2O was detected on MS spectra. The structure of **2′(OH)** was deduced by similar analysis.

The adduct mixtures obtained from the photoreactions of **1** with 2-methyl-1-pentene (**3**), 2,3-dimethyl-1-butene (**4**), and 3,3-dimethyl-1-butene (**5**) were also analyzed, and the structures of the corresponding 1 : 1-adducts (**3′**—**5′**) and 1 : 2-adducts (**3″**—**5″**) were similarly determined as given in Scheme 1. In these cases, adducts corresponding to **2′(OH)** and **2″(OH)** were not obtained.

For allylic brominations of alkenes with NBS, Goldfinger[7] pointed out that the bromine atom should be the hydrogen atom abstracting species of the chain sequence, and that the succinimido radical should be less reactive. However, evidence was reported that disclosed unexpected high reactivity of the succinimido radical in the addition reactions to olefinic double bonds.[1,3] We had also reported that the photoreaction of 1,4-dibromo-2,5-piperazinedione (**1**) with cyclohexene in acetonitrile gave a considerable amount of addition products.[6] The 1-alkenes employed in the present study gave similar adducts (Scheme 1 and Table 1). The respective bromine-containing 1 : 2-adduct consisted of two diasteromers. The 2,5-piperazinedione moieties were found to be attached to the less substituted carbon atoms of the original olefins. The direction of addition appears to be determined by the mode of addition of the 2,5-dioxo-1-piperazinyl radical (**7**) to the olefins to give more stable alkyl radicals. The stability of the

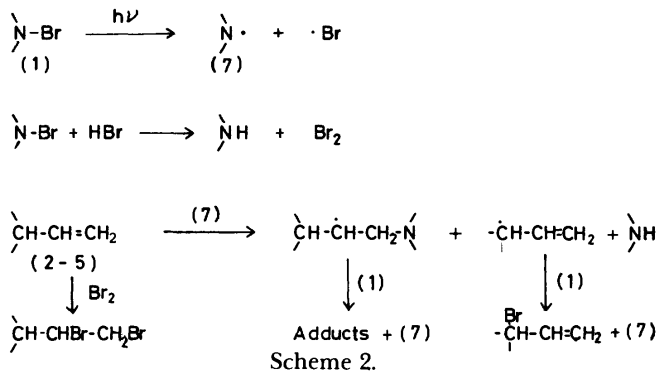

Scheme 2.

intermediate alkyl radicals is responsible for the amounts of the adducts produced (tertiary alkyl radicals from **3** and **4**, while secondary alkyl radicals from **2** and **5**). In the photoreaction with 5, no rearranged products such as 1-(3-bromo-2,3-dimethylbutyl)- or 1-(4-bromo-2,3-dimethyl-2-butyl)-2,5-piperazinedione were detected. This indicates that the addition proceeded through a radical mechanism. Steric inhibition to addition is also observed in the cases where methyl groups are present at the C_3 position of the olefins.

In the photoreaction of **1** with 1-hexene (**2**), 1-(2-hydroxyhexyl)-2,5-piperazinedione (**2′(OH)**) and a mixture of 1,4-bis(2-hydroxyhexyl)-2,5-piperazinediones (**2″(OH)a**, **b**) were produced as well as 1,4-bis(2-bromohexyl)-2,5-piperazinediones (**2″a**, **b**). Hydrolysis during chromatographic separation is considered to result in these hydroxyl group-containing adducts from corresponding bromine-containing adducts. Participation by the neighboring amide group may be responsible for facilitating the hydrolysis. Because of the bulk of the neighboring 2,5-piperazinedione moiety, this assisted hydrolysis works only in the case of the adducts produced from **2**. The presence of methyl substituents at the C_2 and/or C_3 positions of the side chains of **3″**, **4″**, and **5″** makes the *N*-participation impossible, so that no hydroxy group-containing adducts exist in the reactions with **3**, **4**, and **5**. A treatment of an acetone solution of **2″** with silica gel containing a small amount of hydrobromic acid actually yielded **2″(OH)**. To trap hydrogen bromide generated during the photoreaction, the reaction was examined in the presence of 1,2-epoxybutane. The addition of two mole equivalents of 1,2-epoxybutane results in an increased yield of the adducts, and the ratio of **2″(OH)** to **2″** is considerably reduced. This implies that the hydrolysis of **2″** is catalyzed by hydrogen bromide.

Photoreaction of **1** with electron poor olefins (methyl acrylate, stilbene, *etc*) gave few adducts even in the presence of 1,2-epoxybutane, but a considerable amount of polymers and dibromides were produced.

Experimental

The olefins and 1,2-epoxybutane were dried over Molecular Sieve 4A and distilled over copper(I) chloride prior to use. Acetonitrile was dried over calcium hydride and distilled. 1,4-Dibromo-2,5-piperazinedione (**1**) was prepared according to the procedure reported earlier.[8] IR spectra (KBr) were recorded with JASCO IR-A-1 and -3 spectrometers. NMR spectra were measured on JEOL JNM-PMX-60 and

PS-100 spectrometers using tetramethylsilane as the internal standard. Mass spectra were obtained by a Hitachi RMU-6MG and ESCO EMD-05A spectrometers. Irradiation was conducted through a Pyrex filter using an Ushio Model UI-50le high-pressure mecury arc lamp (500 W).

Reaction of 1,4-Dibromo-2,5-piperazinedione (1) with 1-Hexene (2) in the Presence of 1,2-Epoxybutane. A typical experimental procedure is described. Irradiation of a mixture containing 544 mg (2 mmol) of **1**, 1.68 g (20 mmol) of 1-hexene and 1,2-epoxybutane (288 mg, 4 mmol) in acetonitrile (10 cm^3) was carried out with stirring at the ambient temperature for 4 h. The mixture was filtered to give 2,5-piperazinedione in a 39% yield. The filtrates (2—3 runs) were combined, and after removal of the solvent the products were separated on a silica-gel column (benzene→benzene and acetone→acetone). The 1:2-adducts **2"a,b** were rechromatographed on a silica-gel column (benzene→benzene and acetone) to give a pure specimen. Yields are given in Table 1 on the basis of **1** employed. Physical constants of the isolated products are shown below.

1,4-Bis(2-bromohexyl)-2,5-piperazinedione (2"a): Mp 125—126 °C (from benzene). IR, 1670, 1490, 1430, 1340, 1250, 1190, and 950 cm^{-1}. ^1H NMR ($CDCl_3$), δ=0.9 (6H, m, CH_3), 1.0—2.0 (12H, m, $-(CH_2)_3-$), 3.1—3.8 (4H, m, $N-CH_2-$), 4.04 (2H, s, ring H), 4.12 (2H, s, ring H), and 4.2—4.5 (2H, m, -CHBr-).

Found: C, 43.43; H, 6.49%. Calcd for $C_{16}H_{28}Br_2N_2O_2$; C, 43.65; H, 6.14%.

2"b: Mp 92—93.5 °C (from benzene). IR, 1670, 1495, 1430, 1340, 1250, 1190, and 950 cm^{-1}. ^1H NMR($CDCl_3$), δ=0.9 (6H, m, CH_3), 1.0—2.1 (12H, m, $-(CH_2)_3-$), 3.1—3.8 (4H, m, $N-CH_2-$), 4.08 (2H, s, ring H), 4.19 (2H, s, ring H), and 4.3—4.6 (2H, m, -CHBr-).

Found: C, 43.05; H, 6.58%. Calcd see above.

1,4-Bis(2-hydroxyhexyl)-2,5-piperazinedione (2"(OH)a,b): A mixture of two isomers (*a*:*b*=3:4). Mp 213.5—215.0 °C (from ethanol-hexane). IR, 3400, 1650, 1510, 1425, 1345, and 1130 cm^{-1}. ^1H NMR ($CDCl_3$), δ=0.9 (6H, m, CH_3), 1.0—1.5 (12H, m, $-(CH_2)_3-$), 3.0—3.5 (4H, m, $N-CH_2-$), 3.5—3.9 (2H, m, $-C\underline{H}(OH)-$), 3.82 (2H, broad s, OH), and 4.01 (4H, s, ring H). MS (*m/z*), 278 (M^+-2H_2O), 223, 205, 145, 111, 84, and 56.

Found: C, 61.03; H, 9.83; N, 8.89%. Calcd for $C_{16}H_{30}N_2O_4$; C, 61.12; H, 9.62; N, 8.91%.

1-(2-Hydroxyhexyl)-2,5-piperazinedione (2'(OH)): Mp 219—220 °C (from ethanol-hexane). IR, 3400, 3230, 1650, 1495, 1425, 1330, and 1130 cm^{-1}. ^1H NMR ($CDCl_3$), δ=0.9 (3H, m, CH_3), 1.1—1.6 (6H, m, $-(CH_2)_3-$), 2.9—3.5 (2H, m, $N-CH_2-$), 3.5—3.9 (1H, m, $-C\underline{H}(OH)-$), 3.72 (2H, s, ring H), 3.88 (2H, s, ring H), 4.25 (1H, broad s, OH), and 7.85 (1H, s, NH). MS (*m/z*), 214 (M^+), 196 (M^+-H_2O), 157, 128, 115, and 99.

Found: C, 56.05; H, 8.65; N, 13.46%. Calcd for $C_{10}H_{18}N_2O_3$: C, 56.05; H, 8.47; N, 13.07%.

Hydrogenolysis of 1,4-Bis(2-bromohexyl)-2,5-piperazinedione (2"a, b) with Tributyltin Hydride. The compound (**2"a** or **2"b**) (149 mg, 0.34 mmol), tributyltin hydride (24 mg, 0.82 mmol), and AIBN (16 mg) were dissolved in 5 cm^3 of benzene, and the mixture was kept in an atmosphere of nitrogen at 80 °C for 3 h. The solvent was evaporated off and the residue was chromatographed on a silica-gel column using benzene-acetone (4:1) to give 1,4-dihexyl-2,5-piperazinedione (**2"(H)**) in 95% yield: Mp 85—86 °C (from benzene). IR, 1660, 1495, and 1335 cm^{-1}. ^1H NMR ($CDCl_3$), δ=0.9 (6H, m, CH_3), 0.9—2.0 (16H, m, $-(CH_2)_4-$), 3.34 (4H, t, *J*=7 Hz, $N-CH_2-$), and 3.88 (4H, s, ring H).

Found: C, 68.18; H, 10.87%. Calcd for $C_{16}H_{30}N_2O_2$: C, 68.04; H, 10.71%.

Photoadducts of 2-Methyl-1-pentene (3) with 1. 1,4-Bis(2-bromo-2-methylpentyl)-2,5-piperazinedione (3"a, b): A mixture of two isomers. Mp 111—113 °C (from benzene-hexane). IR, 1680, 1490, 1425, 1330, 1200, and 1190 cm^{-1}. ^1H NMR (C_6H_6), δ=0.9 (6H, m, CH_3), 1.2—2.1 (8H, m, $-(CH_2)_2-$), 1.70 (6H, s, $-CBr(CH_3)-$), 3.55—4.05 (4H, two AB quartets, *J*=14 and 16 Hz, $N-CH_2-$), and 4.10 (4H, s, ring H).

Found: C, 44.04; H, 6.67%. Calcd for $C_{16}H_{28}Br_2N_2O_2$: C, 43.65; H, 6.36%.

1-(2-Bromo-2-methylpentyl)-2,5-piperazinedione (3'): Mp 91.5—93 °C (from benzene-hexane). IR, 3210, 1670, 1475, 1325, and 1115 cm^{-1}. ^1H NMR ($CDCl_3$), δ=0.97 (3H, m, CH_3), 1.2—2.0 (4H, m, $-(CH_2)_2-$), 1.68 (3H, s, $CBr(CH_3)-$), 3.53 and 3.91 (center) (2H, AB quartet, *J*=15 Hz, $N-CH_2-$), 3.93 (2H, s, ring H), 4.16 and 4.31 (center) (2H, AB quartet, *J*=17 Hz, ring H), and 7.62 (1H, s, NH).

Found: C, 43.20; H, 6.15%. Calcd for $C_{10}H_{17}BrN_2O_2$: C, 43.33; H, 6.18%.

1,4-Bis(2-methylpentyl)-2,5-piperazinedione (3"(H)): Mp 88—89 °C (from hexane). IR, 1660, 1480, 1325, 1285, and 1190 cm^{-1}; ^1H NMR ($CDCl_3$), δ=0.9 (6H, m, CH_3), 0.94 (6H, s, $CH(C\underline{H}_3)-$), 1.0—1.9 (10H, m, $-(CH_2)_2-CH-$), 3.24 and 3.85 (center) (4H, AB quartet, *J*=7 Hz, $N-CH_2-$), and 3.92 (4H, s, ring H).

Found: C, 67.75; H, 10.61%. Calcd for $C_{16}H_{30}N_2O_2$: C, 68.04; H, 10.71%.

1-(2-Methylpentyl)-2,5-piperazinedione (3'(H)): Mp 121.5—123.0 °C (from hexane). IR, 3200, 1670, 1475, 1335, 1280, and 1015 cm^{-1}. ^1H NMR ($CDCl_3$), δ=0.9 (3H, m, CH_3), 0.93 (3H, s, $-CH(C\underline{H}_3)-$), 1.0—1.9 (5H, m, $-(CH_2)_2-CH-$), 3.21 and 3.83 (center) (2H, AB quartet, *J*=7 Hz, $N-CH_2-$), 3.95 (4H, s, ring H), and 7.48 (1H, s, NH).

Found: C, 60.61; H, 8.90%. Calcd for $C_{10}H_{18}N_2O_2$: C, 60.58; H, 9.15%.

Photoadducts of 2,3-Dimethyl-1-butene (4) with 1. 1,4-Bis(2-bromo-2,3-dimethylbutyl)-2,5-piperazinedione (4"a): Mp 104—105 °C (from benzene). IR, 1680, 1480, 1380, 1320, 1205, 1180, and 1030 cm^{-1}. ^1H NMR ($CDCl_3$), δ=1.10 (12H, d, *J*=6 Hz, $CH(C\underline{H}_3)_2$), 1.65 (6H, s, $CBr(CH_3)-$), 1.5—2.2 (2H, m, $-C\underline{H}(CH_3)_2$), 3.38 and 4.22 (center) (4H, AB quartet, *J*=15 Hz, $N-CH_2-$), and 4.10 and 4.58 (center) (4H, AB quartet, *J*=16 Hz, ring H).

Found: C, 43.67; H, 6.54%. Calcd for $C_{16}H_{28}Br_2N_2O_2$: C, 43.65; H, 6.36%.

4"b: Mp 109—110 °C (from benzene). IR, 1670, 1490, 1380, 1325, 1180, and 1030 cm^{-1}. ^1H NMR ($CDCl_3$), δ=1.12 (12H, d, *J*=6 Hz, $CH(C\underline{H}_3)_2$), 1.67 (6H, s, $CBr(CH_3)-$), 1.5—2.2 (2H, m, $C\underline{H}(CH_3)_2$), 3.26 and 4.23 (center) (4H, AB quartet, *J*=15 Hz, $N-CH_2-$), and 4.02 and 4.74 (center) (4H, AB quartet, *J*=17 Hz, ring H).

Found: C, 43.72; H, 6.37%. Calcd above see.

1-(2-Bromo-2,3-dimethylbutyl)-2,5-piperazinedione (4'): Mp 210 °C (dec.) (from benzene). IR, 3320, 3210, 1670, 1655, 1470, 1320, 1105, and 1020 cm^{-1}. ^1H NMR ($CDCl_3$), δ=1.08 (6H, d, *J*=6 Hz, $-CH(C\underline{H}_3)_2$), 1.66 (3H, s, $-CBr(CH_3)-$), 1.5—2.2 (1H, m, $-C\underline{H}(CH_3)_2$), 3.28 and 4.26 (center) (2H, AB quartet, *J*=15 Hz, $N-CH_2-$), 3.98 (2H, s, ring H), 3.99 and 4.61 (center) (2H, AB quartet, *J*=17 Hz, ring H), and 7.69 (1H, s, NH).

Found: C, 43.04; H, 6.18%. Calcd for $C_{10}H_{17}BrN_2O_2$: C, 43.33; H, 6.18%.

1,4-Bis(2,3-dimethylbutyl)-2,5-piperazinedione (4"(H)): Mp 70—72 °C (from benzene-hexane). IR, 1670, 1480, 1335, and 1180 cm^{-1}. ^1H NMR ($CDCl_3$), δ=0.87 (12H, m, $CH(C\underline{H}_3)_2$), 1.3—2.0 (4H, m, $-C\underline{H}(CH_3)-C\underline{H}(CH_3)_2$), 1.66 (6H, d, *J*=9 Hz, $CH(C\underline{H}_3)-$), 3.2—3.8 (4H, m, $N-CH_2-$), 3.88 (2H, s, ring H), and 4.07 (2H, s, ring H).

Found: C, 67.99; H, 10.26%. Calcd for $C_{16}H_{30}N_2O_2$: C, 68.04; H, 10.71%.

1-(2,3-Dimethylbutyl)-2,5-piperazinedione (4'(H)): Mp 163—165 °C (from benzene-hexane). IR, 3220, 1670, 1470, 1320, and 1110 cm^{-1}. ^1H NMR ($CDCl_3$), δ=0.87 (6H, m, $CH-(C\underline{H}_3)_2$), 1.3—2.1 (2H, m, $-C\underline{H}(CH_3)-C\underline{H}(CH_3)_2$), 1.63 (3H, d,

J=9 Hz, CH($C\underline{H}_3$)), 3.2—4.0 (2H, m, N-CH_2-), 3.85 (2H, s, ring H), 3.95 (2H, s, ring H), and 7.20 (1H, s, NH).

Found: C, 60.45; H, 8.80%. Calcd for $C_{10}H_{18}N_2O_2$: C, 60.58; H, 9.15%.

Photoadducts of 3,3-Dimethyl-1-butene (5) with **1**. *1,4-Bis(2-bromo-3,3-dimethylbutyl)-2,5-piperazinedione (5"a)*: Mp 226—227 °C (from benzene-acetone). IR, 1675, 1475, 1330, 1290, 1185, and 1110 cm^{-1}. ^1H NMR ($CDCl_3$), δ=1.11 (18H, s, $C(CH_3)_3$), 3.21 (2H, dd, J=11 and 15 Hz, N-CH_2-), 4.00 and 4.40 (center) (4H, AB quartet, J=16 Hz, ring H), 4.17 (2H, dd, J=2 and 15 Hz, N-CH_2-), and 4.26 (2H, dd, J=2 and 11 Hz, -CHBr-).

Found: C, 43.85; H, 6.46%. Calcd for $C_{16}H_{28}Br_2N_2O_2$: C, 43.65; H, 6.36%.

5"b: Mp 242—243 °C (from benzene-acetone). IR, 1670, 1475, 1335, 1280, 1185, and 1120 cm^{-1}. ^1H NMR ($CDCl_3$), δ=1.12 (18H, s, $C(CH_3)_3$), 3.29 (2H, dd, J=11 and 15 Hz, N-CH_2-), 3.98 and 4.42 (center) (4H, AB quartet, J=16 Hz, ring H), 4.18 (2H, dd, J=2 and 15 Hz, N-CH_2-), and 4.29 (2H, dd, J=2 and 11 Hz, -CHBr-).

Found: C, 43.85; H, 6.62%. Calcd see above.

1-(2-Bromo-3,3-dimethylbutyl)-2,5-piperazinedione (5'): Mp 177—178 °C (from benzene and acetone). IR, 3230, 1670, 1465, 1320, 1280, and 1120 cm^{-1}. ^1H NMR ($CDCl_3$), δ=1.11 (9H, s, $C(CH_3)_3$), 3.25 (1H, dd, J=11 and 15 Hz, N-CH_2-), 3.99 and 4.42 (center) (2H, AB quartet, J=17 Hz, ring H), 4.03 (2H, s, ring H), 4.23 (1H, dd, J=3 and 15 Hz, N-CH_2-), 4.31 (1H, dd, J=3 and 11 Hz, -CHBr-), and 7.00 (1H, s, NH).

Found: C, 43.84; H, 6.62%. Calcd for $C_{10}H_{17}BrN_2O_2$: C, 43.33; H, 6.18%.

1,4-Bis(3,3-dimethylbutyl)-2,5-piperazinedione (5"(H)): Mp 190—191.5 °C (from benzene-hexane). IR, 1675, 1480, 1317, and 1285 cm^{-1}. ^1H NMR ($CDCl_3$), δ=0.98 (18H, s, $C(CH_3)_3$), 1.43 (4H, m, N-CH_2-$C\underline{H}_2$-), 3.36 (4H, m, N-CH_2-), and 3.86 (4H, s, ring H).

Found: C, 67.82; H, 10.68%. Calcd for $C_{16}H_{30}N_2O_2$: C, 68.04; H, 10.71%.

1-(3,3-Dimethylbutyl)-2,5-piperazinedione (5'(H)): Mp 223.5—224.5 ° (from benzene-hexane). IR, 3240, 1670, 1475, 1320, 1285, and 1120 cm^{-1}. ^1H NMR ($CDCl_3$), δ=0.95 (9H, s, $C(CH_3)_3$), 1.42 (2H, m, N-CH_2-$C\underline{H}_2$-), 3.35 (2H, m, N-CH_2-), 3.88 (2H, s, ring H), 3.92 (2H, s, ring H), and 6.90 (1H, s, NH).

Found: C, 60.67; H, 8.94%. Calcd for $C_{10}H_{18}N_2O_2$: C, 60.58; H, 9.15%.

References

1) J. C. Day, M. G. Katsaros, W. D. Kocher, A. E. Scott, and P. S. Skell *J. Am. Chem. Soc.*, **100**, 1950 (1978).

2) R. L. Tlumak and P. S. Skell, *J. Am. Chem. Soc.*, **104**, 7267 (1982).

3) F. -L. Lu, Y. M. A. Naguib, M.Kitadani, and Y. L. Chow, *Can. J. Chem.*, **57**, 1967 (1979).

4) D. Touchard and J. Lessard, *Tetrahedron Lett.*, **1971**, 4425.

5) D.Touchard and J. Lessard, *Tetrahedron Lett.*, **1973**, 3827.

6) K. Itoh, *Bull.Chem.Soc.Jpn.*, **56**, 1705 (1983).

7) J. Adam, P. A. Gosselaim, and P. Goldfinger, *Nature* (London), **171**, 704 (1953).

8) A. Sera, H. Yamada, and K. Itoh, *Bull. Chem. Soc. Jpn.*, **53**, 219 (1980).

Photoresponsive Crown Ethers. 12. Photocontrol of Metal Ion Complexation with Thiacrown Ethers

Seiji SHINKAI,* Yoshihiro HONDA, Kaori UEDA, and Osamu MANABE*
Department of Industrial Chemistry, Faculty of Engineering, Nagasaki University, Nagasaki 852
(Received December 28, 1983)

Thiacrown ethers with a photofunctional azolinkage were synthesized to control their binding ability by an on-off light switch: They are the N_2S_4 crowns capped with 2,2′-azopyridine (**1**) or azobenzene (**2**). The cis-trans isomerism occurred reversibly by photoirradiation. The binding ability, evaluated by solvent extraction, showed that (i) the order of the affinity for Hg^{2+} is *N,N′*-dibenzoylated N_2S_4 crown (**4**)≈photoirradiated **1**>*trans*-**1**>photoirradiated **2**>*trans*-**2**, (ii) neither *trans*-**2** nor **4** shows significant affinity toward heavy metal ions such as Cu^{2+}, Co^{2+}, Ni^{2+}, and Pb^{2+}, (iii) *trans*-**1** has a slight affinity (Ex% 5.9%) for Cu^{2+},whereas photoisomerized **1** shows the remarkably enhanced affinity (Ex% 93.9%) with Cu^{2+}, and (iv) such light-induced improvement is not seen for **2**. The relatively poor binding ability of **2** and **4** is rationalized in terms of the unfavorable inside-out conformation of the N_2S_4 crown ring. The remarkable affinity change in *cis*-**1** is probably due to the cooperative contribution of the thiacrown and the azopyridine cap constructing a new ligand site. **1** was used as a carrier for Cu^{2+} transport through a liquid membrane. It was found that the rate is efficiently accelerated by UV-light irradiation.

Chemical substances which exhibit photoinduced structural changes are potential candidates not only for the storage of light energy but also as mediators for the conversion of light into other forms of energy. Further, if the structural changes occurring in the photoresponsive chromophores can be transmitted to functional molecules, the fundamental functions of photoresponsive systems in nature may be mimicked in artificial systems. Azobenzene derivatives which exhibit photoinduced reversible cis-trans isomerism have frequently been employed as photoantennae which trigger subsequent events of a number of functional molecules.[1-6]

The purpose of our investigation has been to control the functions of a crown ether family by an on-off light switch, which would lead to the photocontrol of ion-extraction and membrane transport.[7-12] We have developed two different techniques to change the binding ability of crown ethers by light. One method is to induce a conformational change in the crown ether moiety in conjugation with a photoinduced configurational change in the azobenzene moiety. A typical example is azobenzene-bridged crown ether.[7] The other method is associated with a change in the spatial position between two crown rings which leads to interconversion between 1:1 and 2:1 crown/cation complexes. The photoresponsiveness of azobis(benzocrown ether)s (so-called butterfly crown ethers) is a typical example.[8,11] It was shown that in these photoresponsive crown ethers, not only the binding ability but also the ion selectivity is markedly influenced by photoirradiation[7-14] and that in some cases an all-or-nothing change in the binding ability is observed.[15,16] By use of such photoresponsive crown ethers, we can control the ion-extraction and membrane-transport of alkali and alkaline earth metal cations by an on-off light switch. It is known that a thiacrown family exhibits an affinity toward heavy metal cations.[17,18] Thus, if one can extend the above concept to the thiacrown family, it would lead to photocontrol of the ion-binding ability toward heavy metal cations. With these objects in view, we synthesized thiacrown analogues **1**—**4** to test the photoresponsive binding of heavy metal cations.

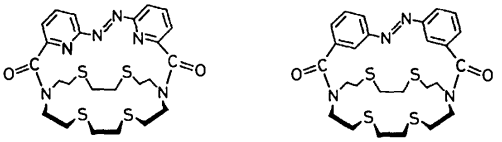
trans-1

trans-2

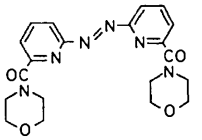
trans-3

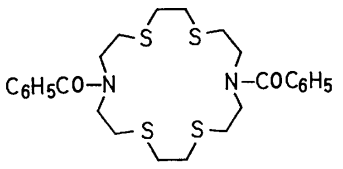
4

Results and Discussion

^{1}H-NMR Spectra of Capped Thiacrown Ethers. We previously synthesized azobenzene-capped and azopyridine-capped crown ethers (**5** and **6**, respectively) from 1,4,10,13-tetraoxa-7,16-diaza-18-crown-6(N_2O_4 crown).[7,12] It was found that in the ^{1}H-NMR spectra of these compounds the chemical shifts of the crown protons are sensitively affected by ring current of the aromatic rings. For example, *trans*-**5** gave two resolved peaks at 3.6—3.9 ppm (8H) and 4.1—4.8 ppm (16H), which were attributed to NCH_2 and OCH_2 of the crown ring, respectively.[7] Since the crown protons of N_2O_4 crown derivatives usually appear at 3.4—3.8 ppm as a broad single peak, the downfield shift in *trans*-**5** is ascribed to the anisotropic effect of the benzene rings.

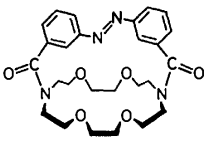
trans-5

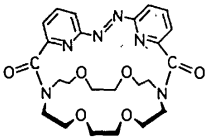
trans-6

A similar anisotropic effect was seen for *trans*-**1** and *trans*-**2**. In contrast to a broad single peak (2.80 ppm in $CDCl_3$) observed for the methylene protons of 1,4,10,13-tetrathia-7,16-diazacyclooctadecane (N_2S_4 crown), *trans*-**1** and *trans*-**2** gave the resolved, complex NMR spectra at 2.6—4.8 ppm (Fig. 1). The downfield chemical shifts observed at 4.6 ppm (2H) for *trans*-**1** and 3.8 ppm (4H) for *trans*-**2** would be attributed to the central methylene protons which most strongly undergo the anisotropic effect of the aromatic caps. As seen in Fig. 1, the NMR peaks of *trans*-**2** are significantly broad at 30°C and sharpened with increasing temperature. It is conceivable that the broadening effect is induced by the steric rigidity of the bicyclic *trans*-**2**. A similar temperature-dependence is seen for the crown ether analogue

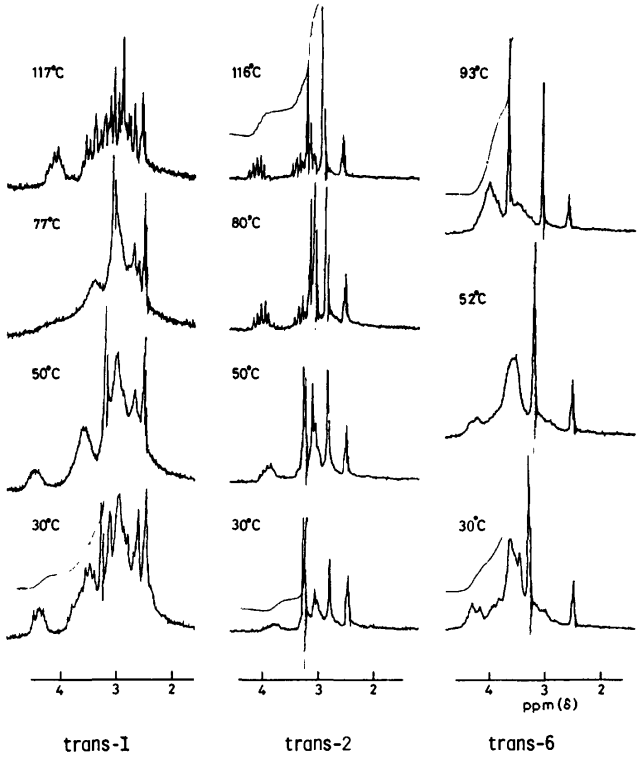

Fig. 1. Temperature dependence of the NMR spectra of *trans*-**1**, *trans*-**2**, and *trans*-**6** (solvent: Me_2SO-d_6).

trans-**6**. On the other hand, the NMR spectrum of *trans*-**1** had a peculiar temperature-dependence: The peaks at 30°C were very sharp, and with increasing temperature they once became broad at the intermediate temperature region, finally being sharpened again at 117°C. The intergral intensity of the downfield peak (around 4.6 ppm) at 30°C corresponds to two protons. The peak is once absorbed into the main absorption band at intermediate temperature and finally separated as four proton intensity at 117°C. According to recent X-ray crystallographic studies, most of thiacrown ethers show some disorder due to differences in the sulfide bond configuration.[19,20] It is likely on the basis of the above NMR data and the X-ray analysis[21] that the thiacrown ring of *trans*-**1** involves a few configurational isomers. We cannot explain readily, however, why the temperature dependences of the NMR spectra are so different between azopyridine-capped *trans*-**1** and azobenzene-capped *trans*-**2**.

Spectral Examination of Metal-Crown Interactions. In order to evaluate interactions between the thiacrown ethers and heavy metal ions, the absorption spectra were taken in methanol or *o*-dichlorobenzene(DCB)-1-butanol(*n*-BuOH) mixed solvent. The latter mixed solvent was used to compare the spectral data with the subsequent ion-extraction and thermal cis-to-trans isomerization under the consistent conditions. The results are summarized in Table 1. The absorption bands at around 325 nm and 450 nm in *trans*-**1**, *trans*-**2**, and *trans*-**3** are ascribed to π-π^* and n-π^* bands, respectively. Since **4** gives no appreciable absorption band at 300—600 nm and **2** gives no additional absorption band on the addition of heavy metal ions, a new absorption band (when it appears) can be attributed mainly to the interaction between the 2,2′-azopyridine cap with metal ions. Examination of the spectral data on *trans*-**1** and *trans*-**3** revealed that under the present conditions *trans*-**3** are capable of binding most heavy metal ions while *trans*-**1** interacts selectively with Cu^{2+} (in methanol and DCB–BuOH) and Hg^{2+} (in methanol). In these systems, the π-π^* bands shifted significantly to longer wavelength region (340—350 nm). The *trans*-**1**·Cu^{2+} complex afforded an additional, weak absorption band at around 550 nm only in

Table 1. Influence of heavy metal ions on the spectroscopic properties (30°C)[a]

Metal salt	Solvent	$\lambda_{max}(\varepsilon_{max})$			
		trans-**1**	*trans*-**2**	*trans*-**3**	**4**
None	MeOH	323(13200) 460(140)			
None	DCB(91):BuOH(9)	328(12700) 450(220)	325(17300) 440(370)	323(10800) 460(310)	
$CuCl_2$	MeOH	353 555		340	
$CuCl_2$	DCB(91):BuOH(9)	Sh	No	353	No
$HgCl_2$[b]	MeOH	342		335	
$HgCl_2$	DCB(91):BuOH(9)	No	No	341	No
$CoCl_2$	DCB(91):BuOH(9)	Weak Sh	No	Sh	No
$Ni(NO_3)_2$	DCB(91):BuOH(9)	No	No	330	No
$Pb(OCOCH_3)_2$[c]	DCB(91):BuOH(9)	No	No	Sh	No

a) [metal salt]=1.00×10^{-3} M, [**1**, **2**, **3** or **4**]=2.50×10^{-5} M. "Sh" denotes the shoulder at 350—400 nm. "No" means that the spectrum is scarcely affected by added metal ions. b) [$HgCl_2$]=0.30 M. c) [$Pb(OCOCH_3)_2$]=5.51×10^{-5} M.

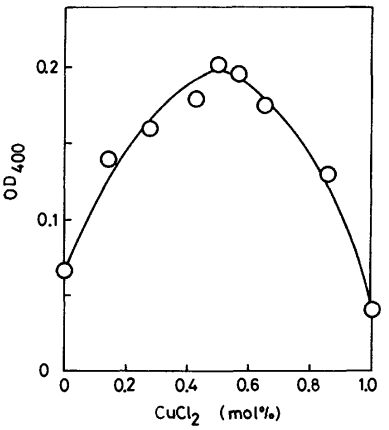

Fig. 2. Continuous variation plots of OD_{400}. 30°C, methanol (containing 9.1 vol% dioxane), [*trans*-**1**]+[$CuCl_2$]=5.01×10^{-4} M, 0.2 cm cell.

methanol. Since such an absorption band was scarcely detected for the *trans*-**3**·Cu^{2+} complex, the band may arise from the interaction of the thiacrown moiety with Cu^{2+} bound to the azopyridine moiety of *trans*-**1**. In fact, many thiacrown ethers we recently synthesized gave a new absorption band at 500—600 nm in the presence of Cu^{2+}.[22]

The binding of Cu^{2+} to *trans*-**1** was further estimated by a continuous variation method in methanol (Fig. 2). Clearly, the absorbance at 400 nm ascribable to the complex formation provided a maximum at 0.5 mol% of $CuCl_2$, indicating that *trans*-**1** forms the 1:1 complex with $CuCl_2$. Here, we tried to determine the association constants (K_t) for *trans*-**1** by a spectroscopic method. They were evaluated by using Eq. 1, which holds for the formation of a 1:1 complex under $[metal]_0 \gg [trans\text{-}1]_0$, where OD_0 and OD are the absorbances of *trans*-**1** in the absence and the presence of metal ions, respectively, and ε is the apparent molar absorption coefficient of the *trans*-**1**·metal complexes.

$$\frac{OD-OD_0}{[metal]_0} = \varepsilon K_t[trans\text{-}1]_0 - K_t OD \qquad (1)$$

In methanol solvent, new absorption maxima appeared on the addition of $CuCl_2$ and $HgCl_2$ at 353 and 342 nm, respectively (Table 1). Thus, the wavelengths at the maximum or near the maximum were used to follow the spectral changes in methanol. In DCB–BuOH mixed solvent, the addition of $CuCl_2$ developed a shoulder at around 400 nm, so that we chose the 380 nm band where the spectral change seemed most apparent. The plots of $[metal]_0$ *vs.* OD, which showed saturation curves (Fig. 3), were analyzed according to Eq. 1, resulting in good linear relationships between $(OD-OD_0)/[metal]_0$ and OD with $r>0.98$. We here assume that $HgCl_2$ also forms the 1:1 complex with *trans*-**1**. The K_t values were determined from the slopes (*i.e.*, $-K_t$) by least-squares analysis: For $CuCl_2$ K_t=8660 M^{-1} (methanol) and 686 M^{-1} (DCB-*n*-BuOH); for $HgCl_2$ 18 M^{-1} (methanol).†

Metal Ion Catalyses in the Thermal Cis-to-Trans Isomerization. **1**, **2**, and **3** in DCB-*n*-BuOH (9:1 by volume) could be isomerized to the *cis*-forms by UV-light ir-

† 1 M=1 mol dm^{-3}.

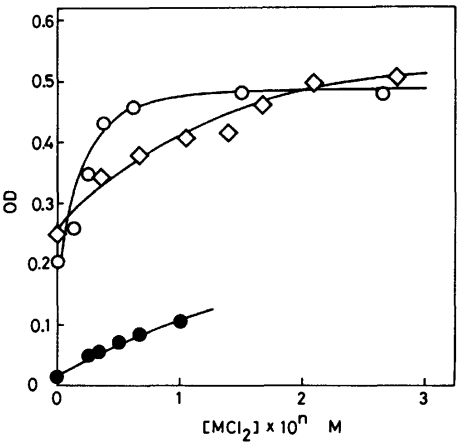

Fig. 3. OD of new absorption bands based on the complex formation with *trans*-**1** plotted against metal ion concentrations (30°C). ○ $CuCl_2$-MeOH, [*trans*-**1**]=4.14×10^{-5} M, *n* (in abscissa)=3 and OD (in ordinate) is at 353 nm; ● $CuCl_2$-DCB: *n*-BuOH (9:1 by volume), [*trans*-**1**]=3.88×10^{-5} M, *n* (in abscissa)=3 and OD (in ordinate) is at 380 nm; ◇ $HgCl_2$-MeOH, [*trans*-**1**]=4.14×10^{-5} M, *n* (in abscissa) =1 and OD (in ordinate) is at 350 nm.

TABLE 2. INFLUENCE OF HEAVY METAL IONS ON THE FIRST-ORDER RATE CONSTANTS (k, h^{-1}) FOR THE THERMAL CIS-TO-TRANS ISOMERIZATION(30°C)[a]

Metal salt	Azo compound		
	1	**2**	**3**
None	0.0765	0.0133	0.0921
$CuCl_2$	0.220	0.308	
$HgCl_2$	0.088	0.020	
$CoCl_2$	0.078	0.023	
$Ni(NO_3)_2$	0.080	0.068	
$Pb(OCOCH_3)_2$	0.075[b]	0.015[b]	

a) Solvent: *o*-dichlorobenzene : 1-butanol=91:9 by volume, [metal salt]=1.00×10^{-3} M, [**1**]=[**3**]=3.87×10^{-5} M, [**2**]=3.24×10^{-5} M. b) $[Pb(OCOCH_3)_2]=5.51\times10^{-5}$ M.

radiation (330 nm<λ<380 nm) without degradation. We found, however, that the *cis* concentration of **2** (azobenzene-capped) at the photostationary state is high (70%), whereas those of **1** (azopyridine-capped) and **3** are only 24 and 18%, respectively. We thus looked for other wavelengths which might improve the *cis* concentrations of **1** and **3**, but failed.

It is known that some heavy metal ions can catalyze the thermal isomerization of azo-linkages,[2,23] probably because of the stabilization of the transition-state through metal ion coordination to the azo linkages. In Table 2, typical first-order rate constants in the presence of metal ions are summarized. As the rate constant for **1** (0.0765 h^{-1}) is comparable with that for **3** (0.0921 h^{-1}), steric inhibition due to the rigidity arising from the thiacrown moiety is unlikely. Similarly, the rate constant for **2** (0.0133 h^{-1}) is comparable with that for the azobenzene-capped crown ether analog (0.0562 h^{-1} at 40°C in DCB)[7]. From Table 2, most of the heavy metal ions used are capable of catalyzing the thermal isomerization and, in particular, Cu^{2+} provides the greatest catalytic effect. We thus carried

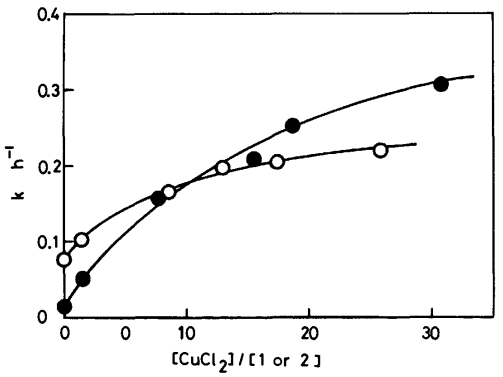

Fig. 4. Influence of added $CuCl_2$ on the thermal cis-to-trans isomerization in DCB-*n*-BuOH (9:1 by volume) at 30°C. ○ [**1**]=3.87×10⁻⁵M; ● [**2**]=3.24×10⁻⁵M.

out further detailed investigation on the Cu^{2+} catalysis. In Fig. 4, the first-order rate constants for **1** and **2** are plotted against the Cu^{2+} concentration. The plots for **1** and **2** seem to afford a simple saturation curve.

The Cu^{2+}-catalyzed isomerization in Fig. 4 is expressed by Scheme 1, where K_c is the association constant with the *cis*-forms and k_0 and k are the first-order rate constants in the absence and the presence of metal ions, respectively.

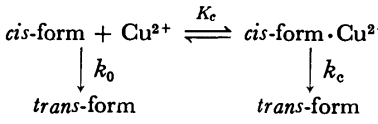

Scheme 1.

K_c and k_c can be evaluated by using Eq 2,[24] which holds for the formation of a 1:1 complex under $[Cu^{2+}] \gg [cis\text{-form}]$, where $q=(k_c/k_0)-1$ and k_c is the first-order rate constant for the complex.

$$\frac{k_0}{k-k_0} = \frac{1}{qK_c}\cdot\frac{1}{[Cu^{2+}]} + \frac{1}{q} \qquad (2)$$

From the plots of $k_0/(k-k_0)$ against $[Cu^{2+}]_0^{-1}$, we determind $(qK_c)^{-1}$ (slope) and q^{-1} (intercept) by the least-squares procedure ($r>0.99$). Thus, K_c and k_c were calculated from these two terms: K_c=2190 M^{-1} and k_c=0.294 h^{-1} for *cis*-**1**: K_c=1726 M^{-1} and k_c=0.472 h^{-1} for *cis*-**2**.

The rate values show that the rate constants for the Cu^{2+}-complexes of *cis*-**1** and *cis*-**2** are greater by 3.8-fold and 34.5-fold, respectively, than those for the uncomplexed *cis*-forms. On the other hand, the K_c value for *cis*-**1** is greater by 3.2-fold than the K_t value for *trans*-**1**. Previously, we estimated the K_c value for the azopyridine-capped crown ether analog (**6**) from a similar kinetic method.[12] In **6**, the azopyridine is the main association site with Cu^{2+}, so that we considered the K_c to be the true association constant with the *cis*-form. In **1**, however, one must take the another interaction with the thiacrown moiety (at least partially) into account which would not be reflected by the kinetics. Thus, the K_c values determined here mainly reflect the interaction with the azo moietics and should be considered to be the "kinetic" association constants.

Solvent Extraction of Heavy Metal Ions. The binding ability of **1**, **2**, and **4** was estimated by solvent extraction of heavy metal ions from water to an organic phase (DCB: *n*-BuOH=4:1 by volume). We employed picrate ion (Pic) which is one of the most convenient counteranions for solvent extraction. In the extraction of Cu^{2+} and Hg^{2+}, however, the aqueous phase after the treatment gave an absorption band at around 350 nm (*vide supra*), which partially overlapped with the absorption band of picrate ion. We thus employed Methyl Orange (MO: λ_{max} 466 nm) for Cu^{2+} and Hg^{2+}. To make all the extraction data comparable, we determined the extractability (Ex%) of Hg^{2+} with picrate ion by correcting the 350 nm band, but the accuracy of the Hg^{2+}-picrate system must be somewhat inferior to others. The results, together with the detailed extraction conditions, are summarized in Table 3.

The examination of Table 3 reveals that (i) except for Hg^{2+}, **4** generally acts as a poor ligand for heavy metal ions, (ii) Hg^{2+} is bound not only to **4** but also to **1** and **2**, and the Ex%'s for **1** (but not so much for **2**) are improved by UV-light irradiation, (iii) neither **2** nor **4** binds Cu^{2+} appreciably, indicating that the small Ex% of *trans*-**1** for Cu^{2+} is probably due to the interaction with the azopyridine moiety, (iv) most significantly, the Ex% of **1** for Cu^{2+} dramatically enhanced by UV-light irradiation (5.9%→93.9%). The binding ability of **4** with Hg^{2+} can be rationalized either by the

Table 3. Influence of photoirradiation on the extraction of heavy metal ions to the organic phase(*o*-dichlorobenzene: 1-butanol=4:1 by volume) with **1**, **2**, and **4** at 30°C[a]

Crown	Counteranion	Extracted counteranion/%				
		Cu^{2+}	Hg^{2+}	Co^{2+}	Ni^{2+}	Pb^{2+}
trans-**1**	Pic		18	1.7	0	5.5
	MO	5.9	13.8			
Photoirradiated **1**[b]	Pic		37	1.7	2.4	5.5
	MO	93.9	28.1			
trans-**2**	Pic		0—3	0	0	0
	MO	0	6.8			
Photoirradiated **2**[c]	Pic		0—3	0	2.7	1.4
	MO	0	8.2			
4	Pic		22	0	1.2	0
	MO	0	30.5			

a) Extraction conditions: aqueous phase, [metal salt]=0.010M, [Pic(picric acid)]=1.00×10⁻⁴M or [MO(Methyl Orange)]=8.90×10⁻⁵M, pH 4.2—4.3 with Et_4NOH(*ca.* 10⁻⁴M); organic phase, [crown]=1.00×10⁻³M. b) *cis*-Form 27%. c) *cis*-Form 53%.

general affinity between sulfur and Hg^{2+} or by the relatively large Hg^{2+} radius. The ion radius of Hg^{2+} (1.10—1.16 Å) is comparable with that of Na^+ (1.13—1.16 Å), whereas except for that of Pb^{2+} (1.32—1.63 Å), those of other metal ions (0.76—0.84 Å) are comparable with that of Li^+ (0.73—0.88 Å). Anyway, the absence of the significant affinity for other heavy metal ions (even for Cu^{2+}) is unexpected. Recently, the crystal structure of 1,4,7,10,13,16-hexathiacyclooctadecane (hexathia analog of 18-crown-6) was reported by Harman *et al.*[20] They found the sulfur atoms in a gauche configuration in the thiacrown ether at the position where the corresponding oxygens in the conventional crown ether would be anti. As a result, the thiacrown ether has both endo- and exodentate-sulfur atoms, resulting in a tendency for bridging two metal ions rather than chelating to one as conventional crown ethers do. If **4** adopts a similar conformation in solution (and probably it does[21]), it is unlikely that the four sulfur atoms coordinate to one metal ion. The examination of the CPK model suggests that, assuming sp^3 for the amide nitrogens, the boat-form of **4** in which the four sulfur atoms can coordinate to one metal ion is highly crowded, whereas the crowding is somewhat relaxed in the chair-form in which only two sulfur atoms can coordinate to one metal ion. It seems to us, therefore, that the coordination of the four sulfur atoms of the N_2S_4 crown to one metal would be energetically unfavorable. The low association tendency of **2** with Hg^{2+} relative to **4** would be ascribed to further deformation of the thiacrown ring by the azobenzene cap. Further details of the relation between the crown structure and the metal selectivity will be described elsewhere.[21]

Finally, we would like to consider the photoirradiation effect on **1**. Based on the spectral change in the azopyridine moiety (Fig. 3), we estimated the association constants of *trans*-**1** in methanol for Cu^{2+} and Hg^{2+} to be 8660 and 18 M^{-1}, respectively. Contrary to these association constants, Hg^{2+} gave the greater Ex% values than Cu^{2+} (Table 3). The discrepancy is accommodated by taking the contribution of the thiacrown moiety into account: that is, the spectroscopically-determined association constants mainly reflect the interaction with the azoarene caps, whereas the interaction with the thiacrown moiety, which is not detected by spectroscopy, is expected for Hg^{2+}.

For the Hg^{2+}-binding to *trans*-**1**, one may consider the cooperative coordination of the thiacrown and the azopyridine-cap, because the Ex% of *trans*-**1** (Pic 18%, MO 13.8%) is significantly higher than that for *trans*-**2** (Pic 0—3%, MO 6.8%). Interestingly, we found that the Ex% of **1** for Cu^{2+} is remarkably enhanced by UV-light irradiation and a similar improvement is also seen for Hg^{2+}. When taking the low *cis* concentration (27%) in the extraction solution into account, the improvement is quite dramatic. The results strongly suggest that in *cis*-**1** the thiacrown and the azopyridine cap cooperatively build a ligation site with a strong coordination ability. At present, we can only speculate on the structure from the CPK model: the azopyridine-cap in *trans*-**1** stands vertically over the thiacrown ether plane.[21] whereas that in *cis*-**1** is almost parallel to the thiacrown plane. Therefore, one (or two) pyridine nitrogen in the *cis*-cap is directed towards two adjacent sulfur atoms in the thiacrown ring. In this case, the metal cation undergoes the cooperative coordination both from the pyridine nitrogen and the sulfur atoms. Although further study is needed to clarify the structure of the binding site, the results indicate that **1** has a dramatic photoresponsiveness in the binding to Cu^{2+}.

Table 4. Photocontrol of Cu^{2+} transport across a liquid membrane (30 °C)[a]

Condition	Transport rate/mol h^{-1}	
	Method I[b]	Method II[c]
Dark	1.4×10^{-8}	*ca.* 2×10^{-10}
UV light[d]	6.3×10^{-9}	1.2×10^{-9}
UV and visible lights[e]	7.0×10^{-9}	1.2×10^{-9}

a) The membrane phase (10 ml, *o*-dichlorobenzene: 1-butanol=4:1 by volume) : [**1**]=3.00×10^{-4} M. b) IN aqueous phae: [$CuCl_2$]=0.010 M, [picrate]=1.00×10^{-3} M, [CH_3COONH_4]=0.010 M. OUT aqueous phase: water. The rate was estimated from the absorption maximum of picrate ion. c) IN aqueous phase: [$CuCl_2$]=0.010 M. OUT aqueous phase: water. The rate was estimated from the absorption band of Cu^{2+}-PAN complex (see Experimental). d) The membrane phase was irradiated through a color glass filter (330 nm<λ<380 nm) for 10 min at intervals of 60 min. e) UV(10 min)→dark(50 min)→visible(10 min)→dark (50 min)→repeated.

Photocontrol of Cu^{2+} Transport. Since the large difference in Ex% was found for the extraction of Cu^{2+} with **1**, we attempted the photocontrol of Cu^{2+} transport across a liquid membrane at 30 °C. The results are summarized in Table 4.

When picrate ion as a counteranion was added to the IN aqueous phase (method I), the rate under UV-light irradiation was smaller than that in the dark. We observed, however, that in the transport under UV-light irradiation the membrane phase rapidly colors yellow. This indicates that Cu^{2+}-picrate salt, which is efficiently extracted with *cis*-**1** into the membrane phase, is not released to the OUT aqueous phase. We found that *cis*-**1** can be isomerized to *trans*-**1** (half-life, *ca.* 2 min at 30 °C) by irradiation of a 200-W tungsten lamp even in the presence of Cu^{2+} ion. Therefore, we alternately irradiated the membrane phase by UV and visible lights in order to facilitate the ion-release by the isomerization to *trans*-**1**, but the rate was scarcely improved.

We previously experienced that hydrophobic counteranions facilitate the ion-extraction but rather decelerate the rate of the ion-release from the membrane phase.[8] We thus carried out the Cu^{2+} transport without any hydrophobic counteranions (method II). Although the absolute values of the Cu^{2+} transport were relatively small, the rate under UV-light irradiation was significantly enhanced compared with that in the dark. Visible light had no effect on the transport rate. Probably, the rate enhancement in method II is attributed to the improved extraction efficiency by photoisomerized *cis*-**1**. In other words, the extraction of Cu^{2+} to the membrane phase from the IN aqueous phase is rate-determining through the transport system.

Conclusions. In this article we have indicated that the concept to photocontrol the chemical and

physical functions of a crown ether family can be extended to a thiacrown ether family which acts as receptors for heavy metal ions. Being different from "inactive" alkali metal ions, some kinds of heavy metal ions show various catalytic activities as seen in metalloproteins. We thus consider that the catalytic activities of heavy metal ions could be photocontrolled by use of thiacrown ethers or azacrown ethers as photoresponsive mediators. Although the frameworks of the photoresponsive thiacrown ethers are still to be improved, the results indicate that the binding ability towards heavy metal ions can be controlled, in principle, by switching the light source on and off. Further investigation is currently in progress in this laboratory.

Experimental

Materials. The preparation of 6,6′-bis(morpholinocarbonyl)-2,2′-azopyridine (**3**) was described previously.[12]

1,4,10,13-Tetrathia-7,16-diazacyclooctadecane (N_2S_4 crown) was prepared from equimolar amounts of 1,2-ethanedithiol and bis(2-bromoethyl)amine hydrobromide in ethanol in the presence of sodium ethoxide; mp 128—129 °C (lit,[25] 124 °C), yield 14%, M^+ 326. ^{1}H-NMR ($CDCl_3$, δ): NH, 2.03, 2H; NCH_2 and SCH_2, 2.80, 24H. Found: C, 43.92; H, 7.97; N, 8.53%. Calcd for $C_{12}H_{26}N_2S_4$: C, 44.13; H, 8.02; N, 8.58%.

Compound **1** was synthesized from equimolar amounts of the N_2S_4 crown and 6,6′-bis(chloroformyl)-2,2′-azopyridine according to the high dilution method in chlorobenzene in the presence of excess triethylamine. The procedure is essentially similar to that described for the synthesis of *trans*-**6**[12]: mp 249—251 °C (dec), yield 33%, M^+ 562. ^{1}H-NMR ($CDCl_3$, δ): N_2S_4 crown protons, 2.4—4.0 and 4.4—4.8, 22H and 2H, respectively; pyridine protons, 7.8—8.2, 6H. Found: C, 51.16; H, 5.23; N, 14.80%. Calcd for $C_{24}H_{30}N_6S_2O_4$: C, 51.22; H, 5.37; N, 14.93%.

Compound **2** was synthesized from equimolar amounts of the N_2S_4 crown and 3,3′-bis(chloroformyl)azobenzene in chlorobenzene in the presence of excess triethylamine. The product was purified by a TLC method (silica gel and chloroform); mp 256—258 °C, yield 24%, M^+ 560. IR (KBr disk): $\nu_{C=O}$ 1635 cm^{-1}. ^{1}H-NMR (Me_2SO-d_6, δ): N_2S_4 crown protons, 2.6—3.4 and 3.6—4.0, 20H and 4H, respectively; benzene protons, 7.64 (4H), 7.96 (2H), and 8.12 (2H). Found: C, 55.51; H, 5.74; N, 10.00%. Calcd for $C_{26}H_{32}N_4O_2S_4$: C, 55.68; H, 5.75; N, 9.99%.

Compound **4** was obtained by the treatment of the N_2S_4 crown with benzoyl chloride in benzene in the presence of excess triethylamine. The product was recrystallized from benzene; mp 105—107 °C, yield 51%, M^+ 534. Found: C, 58.16; H, 6.51; N, 4.95%. Calcd for $C_{26}H_{34}N_2O_2S_4$: C, 58.39; H, 6.41; N, 5.24%.

Miscellaneous. The method of solvent extraction and the rate determination of thermal cis-to-trans isomerization were described previously.[7-12] As a UV-light source for the trans-to-cis isomerization, a 100-W high-pressure Hg-lamp with a color glass filter (330 nm$<\lambda<$380 nm) was used.

Transport of Cu^{2+} across a liquid (DCB: *n*-BuOH=4:1 by volume) membrane with the aid of **1** was examined with a U-tube. The U-tube (10 mm diameter) was immersed in a thermostated (30 °C) water bath. The transport system consisted of 10 ml of the liquid membrane and IN and OUT aqueous phases (5 ml each). The membrane phase was stirred at a constant speed (180 rpm). When required, the tube was irradiated either by a 100-W high-pressure Hg-lamp or by a 200-W tungsten lamp. In method I, the rate of Cu^{2+} transport was estimated from the absorption maximum of picrate ion. In method II, the aliquots of the OUT aqueous phase were treated with 1-(2-pyridylazo)-2-naphthol (PAN) and the rate was determined from the absorption band at 550 nm using a calibration curve. Further details of the transport methods are recorded in footnotes to Table 4.

This research was supported by a grant from the Ministry of Education of Japan. We thank the helpful discussions of Dr. H. L. Ammon, and Dr. K. T. Douglas.

References

1) D. Balasubramanian, S. Subramani, and S. Kumar, *Nature (London)*, **254**, 252 (1975).
2) K. Kano, Y. Tanaka, T. Ogawa, M. Shimomura, Y. Okahata, and T. Kunitake, *Chem. Lett.*, **1980**, 421.
3) A. Ueno, J. Anzai, T. Osa, and Y. Kodama, *Bull. Chem. Soc. Jpn.*, **50**, 2995 (1977).
4) A. Ueno, H. Yoshimura, R. Saka, and T. Osa, *J. Am. Chem. Soc.*, **101**, 2779 (1979).
5) M. Irie, and K. Hayashi, *J. Macromol. Sci. Chem.*, **A13**, 511 (1979).
6) C. D. Eisenbach, *Makromol. Chem.*, **179**, 2489 (1978).
7) S. Shinkai, T. Ogawa, T. Nakaji, Y. Kusano, and O. Manabe, *Tetrahedron Lett.*, **1979**, 4569; S. Shinkai, T. Nakaji, Y. Nishida, T. Ogawa, and O. Manabe, *J. Am. Chem. Soc.*, **102**, 5860 (1980).
8) S. Shinkai, T. Nakaji, T. Ogawa, K. Shigematsu, and O. Manabe, *J. Am. Chem. Soc.*, **103**, 111 (1981); A. Kumano, O. Niwa, T. Kajiyama, M. Takayanagi, K. Kano, and S. Shinkai, *Chem. Lett.*, **1983**, 1327.
9) S. Shinkai, K. Shigematsu, Y. Kusano, and O. Manabe, *J. Chem. Soc., Perkin Trans. 1*, **1981**, 3279.
10) S. Shinkai, T. Minami, Y. Kusano, and O. Manabe, *J. Am. Chem. Soc.*, **104**, 1967 (1982).
11) S. Shinkai, K. Shigematsu, M. Sato, and O. Manabe, *J. Chem. Soc., Perkin Trans. 1*, **1982**, 2735.
12) S. Shinkai, T. Kouno, Y. Kusano, and O. Manabe, *J. Chem. Soc., Perkin Trans. 1*, **1982**, 2741.
13) I. Yamashita, M. Fujii, T. Kaneda, S. Misumi, and T. Otsubo, *Tetrahedron Lett.*, **1980**, 541.
14) M. Shiga, M. Takagi, and K. Ueno, *Chem. Lett.*, **1980**, 1021.
15) S. Shinkai, T. Minami, Y. Kusano, and O. Manabe, *Tetrahedron Lett.*, **23**, 2581 (1982); *J. Am. Chem. Soc.*, **105**, 1851 (1983).
16) J.-P. Desvergne, and H. Bouas-Laurent, *J. Chem. Soc., Chem. Commun.*, **1978**, 403.
17) J. J. Christensen, D. J. Eatough, and R. M. Izatt, *Chem. Rev.*, **74**, 351 (1974).
18) J. D. Bradshaw, and P. E. Scott, *Tetrahedron*, **36**, 461 (1980).
19) R. E. DeSimone, and M. D. Glick, *J. Am. Chem. Soc.*, **98**, 762 (1976).
20) J. R. Harman, R. E. Wolf, B. M. Foxman, and S. R. Cooper, *J. Am. Chem. Soc.*, **105**, 131 (1983) and references cited therein.
21) X-Ray analysis showed that four of the eight C-S bonds of *trans*-**2** employ the anti conformation, whereas six of the eight C-O bonds of *trans*-**6** employ the anti conformation: H. L. Ammon, S. K. Bhattacharjee, S. Shinkai, and Y. Honda, *J. Am. Chem. Soc.*, **106**, 262 (1984).
22) S. Shinkai, K. Shigematsu, Y. Honda, and O. Manabe, to be submitted.
23) D. P. Fisher, V. Piermattie, and J. C. Dabrowiak, *J. Am. Chem. Soc.*, **99**, 2811 (1977).
24) J. A. Mollica, Jr., and K. A. Connors, *J. Am. Chem. Soc.*, **89**, 308 (1967).
25) D. S. C. Black, and I. A. McLean, *Aust, J. Chem.*, **24**, 1401 (1971).

Redox-Switched Crown Ethers. 1. Redox-Coupled Control of Metal-Ionophore Interactions and Their Application to Membrane Transport[1)]

Seiji SHINKAI,* Kenichi INUZUKA, Kenzo HARA, Takaaki SONE, and Osamu MANABE*
Department of Industrial Chemistry, Faculty of Engineering, Nagasaki University, Nagasaki 852
(Received January 14, 1984)

Polyether ionophores with redox-functional thiol groups were synthesized: they are a diaza-18-crown-6 with a disulfide cap that exhibits redox-responsive interconversion between crown($\mathbf{1}_{red}$) and cryptand($\mathbf{1}_{ox}$) and tri- and tetra(oxyethylene)s having a mercapto and an 8-quinolyl group as their terminal groups that feature redox-responsive interconversion between monopodands ($\mathbf{2}_{red}$) and dipodands ($\mathbf{2}_{ox}$). For Na^+ $\mathbf{1}_{red}$ and $\mathbf{1}_{ox}$ showed a similar ion affinity, but $\mathbf{1}_{ox}$ bound K^+, Rb^+, and Cs^+ more efficiently than $\mathbf{1}_{red}$ because of the coordination of the cap oxygens to the complexed metal cations. The difference was rationalized by such that "K^+ (Rb^+ and Cs^+ also) perches on the crown-ring whereas Na^+ nests in it," $\mathbf{2}_{ox}$ showed, in most cases, the ion affinity significantly higher than corresponding $\mathbf{2}_{red}$, indicating the cooperative action of the two poly(oxyethylene) chains on the ion-binding. The rate of K^+ transport with $\mathbf{2}_{red}$ across a liquid membrane was very slow but $\mathbf{2}_{ox}$ carried K^+ more efficiently. It was found that the rate of K^+ transport started with $\mathbf{2}_{red}$ is efficiently accelerated by the addition of I_2. This is due to the redox-switch of the carrier from $\mathbf{2}_{red}$ to $\mathbf{2}_{ox}$. These results suggest that the redox-functionalized ionophores provide novel applications of ion-extraction and ion-transport.

Macrocyclic polyethers contain intramolecular cavities delineated by molecular segments and are capable of specific chelation with alkali and alkaline earth metal ions. The specificity in the chelation stems from a host-guest relationship[2-4]: that is, the ion-selectivity is primarily subjected to the size and shape of the intramolecular cavities. One may thus expect that if the ring conformation or the topological ring shape can be reversibly changed in response to some input energy, it would lead to the "control" of ion-binding ability and ion-selectivity by an on-off switch. Furthermore, this is important in relation to the membrane transport phenomenon mediated by some antibiotic carriers where the reversible interconversion between the cyclic and the acyclic form of the antibiotics plays the crucial role.[5)] There are several synthetic ionophores that exhibit pH-dependent interconversion between the acyclic and the pseudo-cyclic form,[6-11)] but to the best of our knowledge there is no example for the redox-dependent acyclic-cyclic interconversion.[1)] We considered that the interconversion would be realized more directly by utilizing the reversible bond-formation and bond-scission. The most suitable candidate to this purpose would be the redox reaction of a thiol-disulfide couple, because the reversibility is excellent and the reaction occurs under mild conditions. Here, we wish to report such examples of "redox-switched" ionophores, the ion affinity of which changes in response to redox of a thiol-disulfide bond: that is, (i) a crown ether with a disulfide cap which features a crown ($\mathbf{1}_{red}$)–cryptand($\mathbf{1}_{ox}$) interconversion, and (ii) a monopodand($\mathbf{2}_{red}$)–dipodand($\mathbf{2}_{ox}$) interconversion in which two 8-quinolyl groups are linked by a disulfide bond *via* poly(oxyethylene) chains.

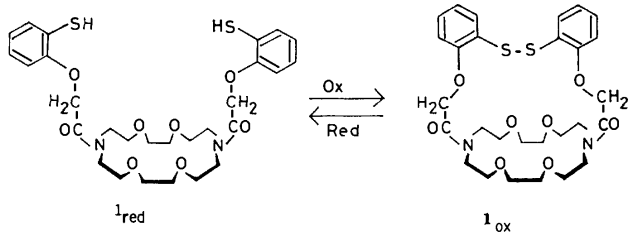

$\mathbf{1}_{red}$ $\mathbf{1}_{ox}$

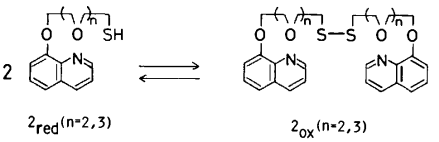

$\mathbf{2}_{red}$(n=2,3) $\mathbf{2}_{ox}$(n=2,3)

Experimental

Materials. $\mathbf{1}_{red}$ and $\mathbf{1}_{ox}$ were synthesized according to a following reaction Scheme 1.

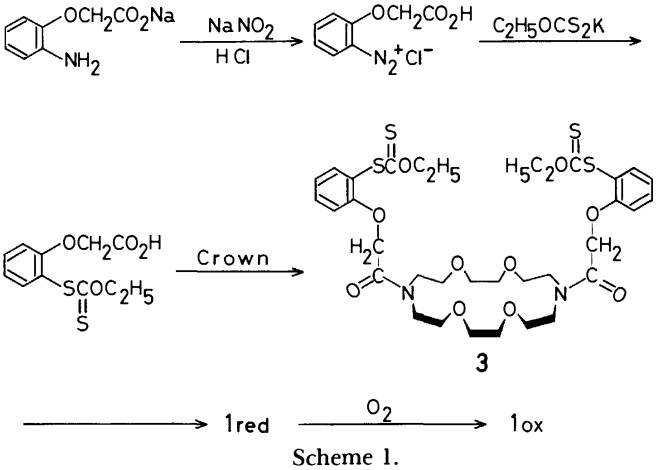

Scheme 1.

Sodium *o*-aminophenoxyacetate (18.9 g; 0.10 mol) and $NaNO_2$ (6.90 g; 0.10 mol) were dissolved in 100 ml of water. This solution was added dropwise to 60 ml of 6 M† HCl solution at 0—5 °C. After 5 min excess $NaNO_2$ was decomposed by sulfamic acid. The solution was mixed slowly with 200 ml of aqueous solution containing potassium ethyl xanthate (19.2 g; 0.12 mol) and sodium hydrogencarbonate (25.5 g; 0.30 mol) in an ice-water bath. The progress of the reaction was followed by a color test with H-acid. The solution was treated with active charcoal at room temperature. After filtration the solution was acidified to pH 1 with concd. HCl, the precipitate being recovered by filtration. The raw product (*o*-(ethoxythiocarbonylthio)phenoxyacetic acid) thus obtained was again dissolved in $NaHCO_3$ solution, treated with active charcoal, and recovered by acidification

† 1 M=1 mol dm^{-3}.

with concd. HCl; mp 119—120 °C, single spot on TLC, yield from sodium *o*-aminophenoxyacetate 30.9%. IR (KBr): $\nu_{C=O}$ 1750 cm^{-1}, ν_{C-O-C} 1090 and 1230 cm^{-1}; M$^+$ (*m/z*) 272; NMR (Me_2SO-d_6, δ): CH_3, 1.22, 3H; O-CH_2, 4.54, 2H; O-CH_2-CO, 4.73, 2H; benzene protons, 7.20, 4H. Found: C, 48.70; H, 4.46%. Calcd for $C_{11}H_{12}O_4S_2$: C, 48.51; H, 4.44%.

In 150 ml of anhydrous tetrahydrofuran (THF) *o*-(ethoxythiocarbonylthio)phenoxyacetic acid (7.20 g; 0.0264 mol) and pivaloyl chloride (3.72 g; 0.0309 mol) were reacted for 30 min at 0 °C. To the stirred solution was added dropwise a THF solution (100 ml) containing 1,4,10,13-tetraoxa-7,16-diazacyclooctadecane (3.0 g; 0.0114 mol) and triethylamine (4.8 ml; 0.034 mol). The reaction was continued for 2 h at room temperature and then refluxed for 1 h. The white precipitate formed on cooling was collected by filtration, and triethylamine hydrochloride was removed by washing with water. The remaining product (**3** in Scheme 1) was recrystallized from 1-butanol; mp 161—164 °C, yield 84.0%. IR (KBr): $\nu_{C=O}$ 1650 cm^{-1}, ν_{C-O-C} 1130 and 1230 cm^{-1}; NMR (Me_2SO-d_6, δ) CH_3, 1.19, 6H; crown protons, 3.36, 24H; O-CH_2, 4.53, 4H; O-CH_2-CO, 4.89, 4H; benzene protons, 7.20, 8H. Found: C, 53.14; H, 6.34; N, 3.50%. Calcd for $C_{34}H_{46}N_2O_{16}S_4$: C, 52.97; H, 6.01; N, 3.63%.

3 was hydrolyzed to $\mathbf{1}_{red}$. **3** (7.77 g; 0.0101 mol) was suspended in 600 ml of ethanol and mixed with 200 ml of 75 vol% ethanol solution containing NaOH (1.75 g; 0.0407 mol). The reaction mixture was refluxed under a nitrogen stream and the progress of the reaction was followed by a TLC method. After 1 h, 2-mercaptoethanol (2.0 g; 0.0256 mol) and then 3 ml of acetic acid were added. The white precipitate was obtained from the cooled solution; mp 166—168 °C, yield 85.1%. IR (KBr): $\nu_{C=O}$ 1650 cm^{-1}, ν_{C-O-C} 1130 and 1225 cm^{-1}, ν_{SH} 2580 cm^{-1}; NMR (Me_2SO-d_6, δ) SH, 3.24, 2H; crown protons, 3.54, 24H; CH_2, 4.93, 4H; benzene protons, 7.05, 8H. Found: C, 56.29; H, 6.69; N, 4.57%. Calcd for $C_{28}H_{38}N_2O_8S_2$: C, 56.55; H, 6.44; N, 4.71%.

$\mathbf{1}_{red}$ (1.0 g; 1.68×10^{-3} mol) was dissolved in 400 ml of 0.1 M KOH solution and an oxygen stream was introduced at room temperature. After 5 h, the white precipitate ($\mathbf{1}_{ox}$) was recovered by filtration and recrystallized from ethylene glycol monomethyl ether; mp 172—175 °C, yield 54.2%. IR (KBr): $\nu_{C=O}$ 1650 cm^{-1}, ν_{C-O-C} 1075 and 1220 cm^{-1}; M$^+$ (*m/z*) 592; NMR (Me_2SO-d_6, δ) crown protons, 3.51, 24H; CH_2, 4.89, 4H; benzene protons, 7.00, 8H. Found: C, 56.45; H, 6.65; N, 4.62%. Calcd for $C_{28}H_{36}N_2O_8S_2$: C, 56.74; H, 6.12; N, 4.73%.

$\mathbf{2}_{red}$ and $\mathbf{2}_{ox}$ were synthesized according to Scheme 2. Since the synthesis of **4** has been described by Hiratani *et al.*,[7,8] we here record only the analytical data.

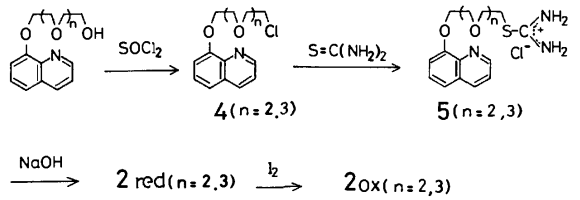

Scheme 2.

4 (n=2); oil, single spot on TLC, yield 90.9%. IR (neat) quinoline 1500 and 1600 cm^{-1}, ν_{C-O-C} 1120 cm^{-1}; NMR ($CDCl_3$, δ) methylene protons, 3.70 (8H), 4.04 (2H), and 4.40 (2H); quinoline protons, 7.05 (1H), 7.35 (3H), 8.05 (1H), and 8.85 (1H).

4 (n=3); oil, single spot on TLC, yield 59.6%. IR (neat) quinoline 1500 and 1600 cm^{-1}, ν_{C-O-C} 1120 cm^{-1}; NMR ($CDCl_3$, δ) methylene protons, 3.65 (12H), 4.10 (2H), and 4.45 (2H); quinoline protons, 7.15 (1H), 7.40 (3H), 8.10 (1H), and 8.90 (1H).

4 (n=2) (5.13 g; 0.0173 mol) was treated with thiourea (1.45 g; 0.0190 mol) in 30 ml of ethanol at boiling temperature. The progress of the reaction was followed by a TLC method. After 40 h, the solution was epavorated to dryness and the remaining solid (**5** (n=2)) was dissolved in 100 ml of water and washed with chloroform. The aqueous solution was mixed with 20 ml of NaOH (0.69 g) solution and heated at 80 °C. After cooling the solution was adjusted to pH 6—7 with 0.1 M HCl and extracted with chloroform. The chloroform solution of $\mathbf{2}_{red}$(n=2) thus obtained was treated with I_2 to give $\mathbf{2}_{ox}$(n=2). $\mathbf{2}_{ox}$(n=2) was isolated by a preparative TLC method (silica gel and chloroform); oil, single spot on TLC, yield 43.5%. IR (neat) quinoline 1500 and 1600 cm^{-1}, ν_{C-O-C} 1120 cm^{-1}; M$^+$ (*m/z*) 584; NMR ($CDCl_3$, δ) methylene protons, 2.80 (2H), 3.65 (6H), 4.02 (2H), and 4.38 (2H); quinoline protons, 7.10 (1H), 7.36 (3H), 8.10 (1H), and 8.85 (1H). Found: C, 57.49; H, 6.33; N, 4.44; S, 10.16%. Calcd for $C_{30}H_{36}N_2O_6S_2\cdot3.35\,H_2O$: C, 57.46; H, 6.12; N, 4.47; S, 10.23%.

$\mathbf{2}_{ox}$(n=3) was similarly synthesized from **4**(n=3) *via* **5**(n=3) and $\mathbf{2}_{red}$(n=3); oil, single spot on TLC, yield 59.6%. IR (neat) quinoline 1500 and 1600 cm^{-1}, ν_{C-O-C} 1100 cm^{-1}; NMR ($CDCl_3$, δ) methylene protons, 2.90 (2H), 3.65 (10H), 4.10 (2H), and 4.45 (2H); quinoline protons, 7.18 (1H), 7.39 (3H), 8.10 (1H), and 8.92 (1H). Found: C, 59.82; H, 6.54; N, 4.01%. Calcd for $C_{34}H_{44}N_2O_8S_2$: C, 60.69; H, 6.59; N, 4.16%.

Solvent Extraction. The method of solvent extraction has been described in detail previously.[12-14] In this study, 5 ml of organic solution containing the ionophore was agitated with 5 ml of buffered aqueous solution containing alkali metal salts of 8-anilinonaphthalene-1-sulfonate (ANS). The extractability (Ex%) was estimated from the partition of ANS between the organic and the aqueous phase. Since the isolation of $\mathbf{2}_{red}$(n=2, 3) was extremely difficult, $\mathbf{2}_{red}$(n=2, 3) reduced from $\mathbf{2}_{ox}$(n=2, 3) with $Na_2S_2O_4$ was directly used for extraction. The extraction with $\mathbf{1}_{red}$ and $\mathbf{2}_{red}$(n=2, 3) was carried out under anaerobic (N_2) conditions. After determining Ex% the contents of $\mathbf{1}_{ox}$ or $\mathbf{2}_{ox}$(n=2, 3) formed during the extraction were evaluated by a TLC method using a high-speed TLC scanner (Shimadzu CS-920): usually the amounts of concomitant $\mathbf{1}_{ox}$ or $\mathbf{2}_{ox}$(n=2, 3) were negligible (less than 2%).

Membrane Transport. Transport of Na^+ and K^+ across a liquid (chloroform) membrane was carried out in a U-tube which consisted of two (IN and OUT) aqueous phases (10 ml each) and a membrane phase (40 ml). The membrane phase was stirred at a constant speed (180 rpm) and thermostated to 30 °C. The rates of K^+-transport were estimated from the absorption band of ANS (350 nm) in the OUT aqueous phase.

Results and Discussion

Comments on the Oxidation Methods. We have found that iodine is the most suitable to the oxidation of $\mathbf{2}_{rex}$ to $\mathbf{2}_{ox}$ because the reaction is very fast and occurs under mild conditions. Furthermore, the progress of the reaction can be monitored by the color change. However, it turned out to be rather unsuitable to the oxidation of $\mathbf{1}_{red}$ to $\mathbf{1}_{ox}$ because the intermolecular disulfide formation significantly competed with the intramolecular one. The TLC analysis showed that the oxidation of $\mathbf{1}_{red}$(3.36×10^{-4} mol) by iodine in 50 ml of chloroform gave mainly the polymeric products and $\mathbf{1}_{ox}$ was a minor product. We attempted the isolation of $\mathbf{1}_{ox}$ by preparative TLC but the isolated product was always contaminated with some unknown materials

TABLE 1. EXTRACTION OF ALKALI METAL SALTS OF ANS WITH $\mathbf{1}_{red}$ AND $\mathbf{1}_{ox}$ AND THEIR ASSOCIATION CONSTANTS (K_c)[a]

Ionophore	Metal	Ex%	$K_e \cdot 10^{-3}/M^{-2}$ [b]	K_c/M^{-1} [c]
$\mathbf{1}_{red}$	Na^+	39.9	3.59	756
	K^+	39.0	3.95	697
	Rb^+	31.6	2.89	416
	Cs^+	26.5	2.92	284
$\mathbf{1}_{ox}$	Na^+	40.2	3.66	771
	K^+	53.3	12.8	2250
	Rb^+	46.7	9.55	1370
	Cs^+	35.6	6.53	635

a) 30°C. Organic phase: [$\mathbf{1}_{red}$ or $\mathbf{1}_{ox}$]=4.00×10^{-3}M in *o*-dichlorobenzene: 1-butanol=80:20 by volume. Aqueous phase: pH 4.0 with MOH(0.010 M)-H_3PO_4, [MCl]=0.10 M, [ANS]=5.00×10^{-5}M. b) K_e=[$M^+A^- \cdot \mathbf{1}^*$]/[$M^+$][$A^-$][$\mathbf{1}^*$] where the asterisk and A^- refer to the species in the organic phase and the counteranion, respectively. c) K_c=[$M^+A^- \cdot \mathbf{1}^*$]/[MA*][$\mathbf{1}^*$]=$K_e/K_d$ where K_d=[MA*]/[M^+][A^-].

(probably oligomeric oxidation products).

On the other hand, O_2-oxidation of $\mathbf{1}_{red}$ in the presence of KOH gave $\mathbf{1}_{ox}$ as a main product, although the reaction was not so fast. Pure $\mathbf{1}_{ox}$ could be isolated without using the preparative TLC method. As a control experiment, we oxidized $\mathbf{1}_{red}$ by O_2 in the presence of triethylamine. Although the main product was still $\mathbf{1}_{ox}$, a considerable amount of the polymeric products was formed. These results suggest that the "template effect" of K^+ which facilitates the intramolecular disulfide formation may be operative on the oxidation process.

Solvent Extraction of Alkali Metal Cations. The binding ability of $\mathbf{1}_{red}$ and $\mathbf{1}_{ox}$ was estimated by solvent extraction of alkali metal salts of 8-anilinonaphthalene-1-sulfonate (ANS) from water to the organic phase (*o*-dichlorobenzene: 1-butanol=80:20 by volume). Alkali picrates which are frequently used for solvent extraction were not employed in the present study, because the oxidative nature of picrate ion is unfavorable to the redox treatment of the ionophores. The extractability(Ex%) was estimated by the partition of ANS between the aqueous and the organic phases. The pH of the aqueous phase was buffered to 4.0 where ANS is fully dissociated while the thiol groups of $\mathbf{1}_{red}$ are undissociated. We confirmed that both $\mathbf{1}_{red}$ and $\mathbf{1}_{ox}$ do not leak into the aqueous phase under the extraction conditions. The results are summarized in Table 1.

Examination of Table 1 reveals that (i) $\mathbf{1}_{red}$ and $\mathbf{1}_{ox}$ have the similar Ex% values for Na^+, (ii) $\mathbf{1}_{ox}$ is capable of extracting K^+, Rb^+, and Cs^+ more efficiently than $\mathbf{1}_{red}$ and (iii) the maximum Ex% is observed for the extraction of K^+ with $\mathbf{1}_{ox}$. The inspection of CPK model of $\mathbf{1}_{ox}$ suggests that two phenolic oxygens can be directed towards the crown ring, indicating the coordination ability to metal ions complexed in the crown ring. However, the oxygens are apparently far from the crown ring plane as compared with those of crypt- and 222 which exhibits a high affinity with Na^+ and K^+.[2] The expansion of the intramolecular cavity of $\mathbf{1}_{ox}$ is due to six atoms (two sulfurs and four carbons) present between the two oxygens in the disulfide cap. Conceivably, small Na^+ is deeply bound to the diaza-18-crown-6 ring, so that the two oxygens are too far to coordinate to the complexed Na^+ ion. In contrast, other alkali metal ions with relatively large ion-radii would be able to interact with the oxygens owing to the shallow-binding to the crown ring. The situation would be well expressed by "K^+ (Rb^+ and Cs^+ also) perches on the crown ring whereas Na^+ nests in it."[15]

According to the established procedure,[16-18] we estimated K_e (extraction equilibrium constants) and K_c(complexation contants). The results in Table 1 indicate again that the K_c values of $\mathbf{1}_{ox}$ for K^+, Rb^+, and Cs^+ are greater by 2—3 fold than those of $\mathbf{1}_{red}$, whereas there is no difference in the K_c for Na^+. Conceivably, $\mathbf{1}_{ox}$ is expected to act as a cryptand analogue, whereas $\mathbf{1}_{red}$ is a simple crown ether (or at most, a lariat-type crown ether).[19,20]

The absolute K_c values in Table 1 are smaller by about two orders of magnitude than those of conventional 18-crown-6 analogues.[2-4] This is due to the two amide nitrogens present in the diaza-18-crown-6 ring. We thus attempted to reduce the carbonyls in $\mathbf{1}_{red}$ to the methylene groups with B_2H_6 or $LiAlH_4$. Although we confirmed the disappearance of the carbonyls with IR, the isolation was very difficult and unsuccessful.

The redox scheme for the interconversion between $\mathbf{2}_{red}$ and $\mathbf{2}_{ox}$ can be more simplified, because one need not take the competition between intra- and intermolecular oxidations into account. The results of solvent extraction between water and chloroform are summarized in Table 2. Neither $\mathbf{2}_{red}$ nor $\mathbf{2}_{ox}$ leaked into the aqueous phase under the extraction conditions. Unfortunately, the partition of ANS to the chloroform phase was so small that we could not determine the K_d values (see footnote c to Table 1) accurately. Therefore, we determined Ex% and K_e and summarized in Table 2.

It is seen from Table 2 that (i) $\mathbf{2}_{red}(n=2)$ and $\mathbf{2}_{ox}(n=2)$ have the highest selectivity towards Na^+ while $\mathbf{2}_{red}(n=3)$ and $\mathbf{2}_{ox}(n=3)$ show the highest selectivity towards K^+ (ii) when comparing the $n=2$ series with the $n=3$ series, there is little difference in Ex% for Na^+, but Ex%'s of the $n=3$ series for K^+, Rb^+, and Cs^+ are significantly higher than those of the $n=2$ series, and (iii) most importantly, Ex%'s of $\mathbf{2}_{ox}$ are higher than $\mathbf{2}_{red}$, indicating the cooperative ion-binding by two chains of $\mathbf{2}_{ox}$. It is well known that acyclic polyethers have a relatively good ion-selectivity like cyclic polyethers.[6-11] The selectivity is particularly associated with the length of the poly(oxyethylene) chain. For example, Hiratani *et al.*[7,8] demonstrated that **6** and **7** exhibit the selectivity for Li^+ and Na^+, respectively. $\mathbf{2}_{red}(n=2)$ and $\mathbf{2}_{red}(n=3)$ which have the chain length similar to **6** and

TABLE 2. EXTRACTION OF ALKALI METAL SALTS OF ANS WITH $2_{red}(n=2, 3)$ AND $2_{ox}(n=2, 3)$ AND THEIR EXTRACTION EQUILBRIUM CONNSTANTS (K_e)[a]

Ionophore	Metal	Ex%	K_e·[b]/M^{-2}
$2_{red}(n=2)$	Li^+	4.7	16.5
	Na^+	8.1	29.5
	K^+	4.8	17.0
	Rb^+	5.3	19.5
	Cs^+	2.5	8.5
$2_{ox}(n=2)$	Li^+	10.6	79.9(39.7)
	Na^+	11.9	92.0(45.7)
	K^+	11.0	84.2(41.9)
	Rb^+	9.8	73.1(36.3)
	Cs^+	6.8	49.8(24.5)
$2_{red}(n=3)$	Na^+	9.5	35.2
	K^+	10.3	38.1
	Rb^+	9.9	36.8
	Cs^+	5.9	21.0
$2_{ox}(n=3)$	Na^+	13.3	105(52.5)
	K^+	15.6	125(61.7)
	Rb^+	12.8	100(50.1)
	Cs^+	10.8	81.6(40.7)

a) 30°C. Organic phase: $[2_{red}(n=2, 3)]=2[2_{ox}(n=2, 3)]=1.00\times10^{-2}$ M in chloroform. Aqueous phase: pH 6.0 with MOH(0.010 M)-H_3PO_4, [MCl]=0.29 M, $[ANS]=5.00\times10^{-4}$ M. b) $K_e=[M^+A^-\cdot\mathbf{2}^*]/[M^+][A^-][\mathbf{2}^*]$. The values in the parenthesis are obtained by the same equation on the basis that one quinoline chain corresponds to one ligand (*i.e.*, [ligand]=2[**2**]).

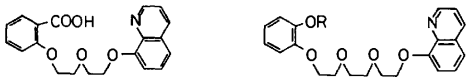

6 7

7, repectively, showed the ion-selectivity towards Na^+ and K^+, respectively. This implies that the maximum selectivity of $2_{red}(n=2)$ and $2_{red}(n=3)$ shifts a little to the larger metal cations. According to Hiratani *et al.*,[7,8] the pseudo-cyclic structures from **6** and **7** are formed so that the terminal benzene and quinoline can overlap each other. Such a stacking association of the aromatic terminal groups cannot be expected for 2_{red}. Conceivably, the sizes of the psuedo-cyclic structures of 2_{red} are somewhat greater than those of corresponding **6** and **7**.

The extraction data showed that Ex%'s of 2_{ox} are significantly greater than those of 2_{red}, indicating that the two chains in 2_{ox} act cooperatively on metal-binding. On the other hand, the ion-selectivities of 2_{ox} are similar to those of 2_{red}, indicating that the two chains in 2_{ox} would act rather independently. The apparently incompatible results may be rationalized in terms of the peculiar conformation of the central disulfide linkage. The azimuthal angle in the lowest energy conformation of diethyl disulfide is considered to be 90°, although the bulky substituents may enlarge the angle.[21] It is unconceivable, therefore, that the two chains in 2_{ox} enjoy the coplanarity around a metal ion. Probably, 2_{ox} wraps a metal cation by forming a helical structure. In fact, several podands having the coordinative terminal groups adopt helical structures to bind metal ions,[6-8,10] and the azimuthal angle of the central disulfide linkage would be rather advantageous to the helical structure. If one accepts the hypothesis, one can elucidate the enhanced Ex%'s of 2_{ox} relative to 2_{red} as well as the unchanged ion-selectivities. To obtain evidence for this, we took the NMR spectra of 2_{ox} in the presence of K^+ and Rb^+, but could not detect the appreciable change in chemical shifts probably because of the low association abilities.

TABLE 3. RATES (k) OF ION TRANSPORT THROUGH A LIQUID MEMBRANE (30°C)[a]

Run	Metal	Carrier	Transport rate / 10^{-6} mol h^{-1}
1	Na^+	$2_{red}(n=2)$	0.07
2	Na^+	$2_{ox}(n=2)$	0.09
3	Na^+	$2_{red}(n=3)$	0.06
4	Na^+	$2_{ox}(n=3)$	0.20
5	K^+	$2_{red}(n=2)$	0.10
6	K^+	$2_{ox}(n=2)$	0.18
7	K^+	$2_{red}(n=3)$	0.12
8	K^+	$2_{ox}(n=3)$	0.50
9[b]	K^+	$2_{red}(n=3)\rightarrow2_{ox}(n=3)$	0.10→0.75

a) In aqueous phase (10 ml): [MCl]=0.290 M, pH 6.0 with MOH (0.010 M)-H_3PO_4(0.011 M), $[ANS]=5.00\times10^{-3}$ M. OUT aqueous phase (10 ml): water. Membrane phase (40 ml $CHCl_3$): $[2_{red}]=2[2_{ox}]=2.00\times10^{-3}$ M. b) In order to suppress the pH change in the IN aqueous phase by added I_2 the buffer concentration is enhanced while $[K^+]$ is constant: [MCl]=0.100 M, pH 6.0 with MOH (0.200 M)-H_3PO_4 (0.114 M), $[ANS]=5.00\times10^{-3}$ M.

Ion-Transport across a Liquid Membrane. Various kinds of chemical and physical phenomena have been utilized to increase the rate of ion transport through membranes: redox energies,[22,23] light energies,[13,14,24-27] countercurrent of metal cations,[28] pH-dependent lactone cyclization,[29] *etc.*[30] Some of these systems have been applied to active transport. To the best of our knowledge, however, there exists no precedent for the ion-transport mediated by the redox interconversion of ionophores such as **1** or **2**.[31] We here demonstrate that the ion-transport rate can be changed by the redox interconversion between 2_{red} and 2_{ox}.

Table 3 shows the rates of Na^+ or K^+ transport across a liquid (chloroform) membrane. The leak of the metal ions was not detected in the absence of **2**. For $2_{red}(n=2)$ and $2_{ox}(n=2)$, the rates of Na^+ transport are similar but the rate of K^+ transport with $2_{red}(n=2)$ is significantly higher than that with 2_{red} $(n=2)$. The results are well compatible with the extraction data in Table 2: for example, Ex% of Na^+ with $2_{ox}(n=2)$(11.9%) is close to that with $2_{red}(n=2)$(8.1%), whereas Ex% of K^+ with $2_{ox}(n=2)$(11.0%) is more than two times greater than that with $2_{red}(n=2)$(4.8%). A similar trend was observed for the transport with $2_{red}(n=3)$ and $2_{ox}(n=3)$: that is $2_{ox}(n=3)$ exhibits the transport ability higher than $2_{red}(n=3)$. Figure 1 shows the plot of Ex% against the rate of ion-transport. It is clearly seen from Fig. 1 that the higher is the Ex%, the faster is the ion-transport rate. One can conclude on the basis of this fact that the ion-extraction step from the IN aqueous phase to the membrane phase, but not the ion-release step from the membrane phase to the OUT aqueous phase, is totally rate-determining.

The largest rate increase was observed for K^+ transport with $2_{ox}(n=3)/2_{red}(n=3)$(4.2-fold). We thus con-

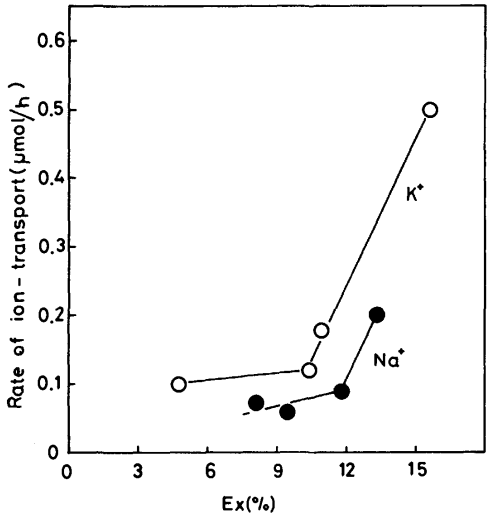

Fig. 1. Plots of rate of ion-transport *vs.* Ex%.

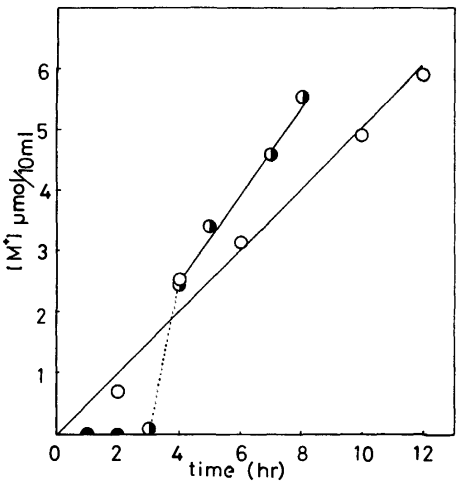

Fig. 2. Transport of K^+ across a liquid (chloroform) membrane. ○ with $\mathbf{2}_{ox}$ (n=3) (run 8 in Table 3); ●→◑ transport was started with $\mathbf{2}_{red}$ (n=3) and I_2 was added after 2 h (run 9 in Table 3).

ducted the "redox-switched" experiment with this combination. K^+ transport was started with $\mathbf{2}_{red}$ (n=3) as a carrier in the membrane phase, and iodine([I_2]= 0.5 [$\mathbf{2}_{red}$(n=3)] was added to the membrane phase after 2 h. As illustrated in Fig. 2, the rate of K^+ transport was enhanced to 7.5×10^{-7} mol h^{-1} from 1.0×10^{-7} mol h^{-1} after an induction period (about 1 h). In a separate study, we corroborated that $\mathbf{2}_{red}$(n=3) has been oxidized to $\mathbf{2}_{ox}$ (n=3) within 1 h in the membrane and that K^+ is not transported through the chloroform membrane containing only iodine. Therefore, the marked rate increase can be ascribed to the production of the capable ion-carrier (*i.e.*, $\mathbf{2}_{ox}$(n=3)) in the membrane phase by treatment with the oxidizing agent. The induction period after I_2 addition is ascribed either to the oxidation time of $\mathbf{2}_{red}$ to $\mathbf{2}_{ox}$ or to the diffusion of K^+ across the liquid membrane. The slightly greater transport rate after the oxidation relative to that with $\mathbf{2}_{ox}$ is probably due to the change in the buffer concentration. We also attempted the reverse control of K^+ transport by reducing $\mathbf{2}_{ox}$(n=3) to $\mathbf{2}_{red}$(n=3) by tributylphosphine (0.01 M=10[$\mathbf{2}_{ox}$(n=3)]). Although $\mathbf{2}_{ox}$(n=3) was reduced to $\mathbf{2}_{red}$(n=3) in 1.5 h, the K^+ increase in the OUT aqueous phase was scarcely affected for 4 h after the addition of tributylphosphine. The membrane phase contained a significant amount of K^+ extracted with $\mathbf{2}_{ox}$(n=3) before tributylphosphine addition. Conceivably, the K^+ ion was released gradually to the OUT aqueous phase even after $\mathbf{2}_{ox}$(n=3) being reduced to $\mathbf{2}_{red}$(n=3). At present, we consider that the "volume" of the membrane phase must be considerably reduced in order to achieve the rapid response of the reverse control.

Ion transport using the interconversion between $\mathbf{1}_{red}$ and $\mathbf{1}_{ox}$ may be also interesting. In this case, however, one has to pay additional attention to intra- *versus* intermolecular oxidation of $\mathbf{1}_{red}$ in the membrane phase. In addition, the difference in K_c values is not large enough to attain the efficient control of ion-transport by redox-switch. We thus did not perform the ion-transport with $\mathbf{1}_{red}$ and $\mathbf{1}_{ox}$.

Conclusions. The present system demonstrated that the ion-binding ability of redox-functionalized ionophores can be changed by the treatment with redox reagents. This is directly applicable to the control of ion transport across membranes. The novel phenomenon becomes possible because these synthetic ionophores have within the molecule both a redox-functional group and an ionophilic site. Although the framework of the present "redox-switched" functions must be further improved, we expect that this concept might be applied more generally to the control of the chemical and physical functions of synthetic ionophores by the redox energy source.

We thank Professor K. Sasaki and Dr. A. Kunai for helpful discussions. We are indebted to Miss T. Yamamichi for technical assistance.

References

1) Preliminary communication: S. Shinkai, K. Inuzuka, O. Manabe, *Chem. Lett.*, **1983**, 747.
2) J.-M. Lehn, *Acc. Chem. Res.*, **11**, 49 (1978).
3) D. J. Cram and J. M. Cram, *Acc. Chem. Res.*, **11**, 8 (1978).
4) F. Vögtle, "Host Guest Complex Chemistry I", Springer-Verlag, Berlin (1981).
5) E. M. Choy, D. F. Evans, and E. L. Cussler, *J. Am. Chem. Soc.*, **96**, 7085 (1974).
6) F. Vögtle and E. Weber, *Angew. Chem., Int. Ed. Engl.*, **18**, 753 (1979); G. Weber, W. Saenger, F. Vögtle, and H. Sieger, *Angew. Chem., Int. Ed. Engl.*, **18**, 226 (1979).
7) K. Hiratani, S. Aiba, and T. Nakagawa, *Chem. Lett.*, **1980**, 477.
8) K. Hiratani, *Chem. Lett.*, **1982**, 1021.
9) N. Yamazaki, S. Nakahama, A. Hirao, and S. Negi, *Tetrahedron Lett.*, **1978**, 2429.
10) H. Kuboniwa, K. Yamaguchi, A. Hirao, S. Nakahama, and N. Yamazaki, *Chem. Lett.*, **1982**, 1937.
11) B. Tümmler, G. Maass, E. Weber, W. Wehner, and F. Vögtle, *J. Am. Chem. Soc.*, **99**, 4683 (1977).
12) S. Shinkai, T. Nakaji, Y. Nishida, T. Ogawa, and O. Manabe, *J. Am. Chem. Soc.*, **102**, 5860 (1980).
13) S. Shinkai, T. Nakaji, T. Ogawa, K. Shigematsu, and O. Manabe, *J. Am. Chem. Soc.*, **103**, 111 (1981).
14) S. Shinkai, K. Shigematsu, Y. Kusano, and O. Manabe, *J. Chem. Soc., Perkin Trans. 1*, **1981**, 3279.
15) D. M. Dishong, C. J. Diamond, M. I. Cinoman, and G. W. Gokel, *J. Am. Chem. Soc.*, **105**, 586 (1983).

16) K. H. Wong, K. Yagi, and J. Smid, *J. Membr. Biol.*, **18**, 379 (1979).
17) J. M. Timko, S. S. Moore, D. M. Walba, P. C. Hiberty, and D. J. Cram, *J. Am. Chem. Soc.*, **99**, 4207 (1977).
18) T. Maeda, K. Kimura, and T. Shono, *Bull. Chem. Soc. Jpn.*, **55**, 3506 (1982).
19) R. A. Schultz, D. S. Dishong, and G. W. Gokel, *J. Am. Chem. Soc.*, **104**, 625 (1982).
20) A. Masuyama, Y. Nakatsuji, I. Ikeda, and M. Okahara, *Tetrahedron Lett.*, **22**, 4665 (1981).
21) D. W. Scott, H. L. Finke, M. E. Gross, G. B. Guthrise, and H. M. Huffman, *J. Am. Chem. Soc.*, **72**, 2424 (1950); D. W. Scott, H. L. Finke, J. P. McCullogh, M. E. Gross, R. E. Pennington, and G. Waddington, *ibid.*, **74**, 2478 (1952).
22) S. Matsuo, A. Ohki, M. Takagi, and K. Ueno, *Chem. Lett.*, **1981**, 1543.
23) J. J. Grimaldi and J.-M. Lehn, *J. Am. Chem. Soc.*, **101**, 1333 (1979); J.-M. Lehn, *Nature*, **265**, 229 (1977).
24) S. Shinkai, T. Minami, Y. Kusano, and O. Manabe, *J. Am. Chem. Soc.*, **104**, 1967 (1982).
25) S. Shinkai, T. Kouno, Y. Kusano, and O. Manabe, *J. Chem. Soc., Perkin Trans. 1*, **1982**, 2741.
26) J. Sunamoto, K. Iwamoto, Y. Mohri, and T. Kominato, *J. Am. Chem. Soc.*, **104**, 5502 (1982).
27) T. Shimidzu and M. Yoshikawa, *J. Membr. Sci.*, **13**, 1 (1983).
28) M. Sugiura and T. Shinbo, *Bull. Chem. Soc. Jpn.*, **52**, 684 (1979).
29) T. Shimidzu, M. Yoshikawa, M. Hasegawa, and H. Chiba, *Kobunshi Ronbunshu*, **34**, 753 (1977).
30) J. Rebek, Jr. and R. V. Wattley, *J. Am. Chem. Soc.*, **102**, 4853 (1980).
31) A Similar idea has recently been offered by M. Raban *et al.*: private communication.

 © 1984 The Chemical Society of Japan Bull. Chem. Soc. Jpn., 57, 2156—2161 (1984)

Phosphinyl- and Phosphinothioylamino Acids and Peptides. VIII. New Practical Removal Conditions for the *S*-Mpt Group and their Application for the Synthesis of Bis[*N,N*-diallyl-[D-Ala^2, L-Leu^5]-enkephalyl]cystine

Masaaki UEKI* and Kozo SHINOZAKI

Department of Applied Chemistry, Science University of Tokyo, 1-3 Kagurazaka, Shinjuku-ku, Tokyo 162

(Received January 10, 1984)

Synthesis of bis[*N,N*-diallyl-[D-Ala^2, L-Leu^5]-enkephalyl]cystine, which is expected to be a selective opioid δ-receptor antagonist, was studied. The mercapto group of cysteine was protected by the dimethylphosphinothioyl(Mpt) group. For the removal of this group without damaging the allyl moiety, new mild removal conditions by use of KF/18-crown-6 in a solvent mixture of acetonitrile-methanol are proposed. Bis[D-Ala^2, L-Leu^5]-enkephalyl]cystine was also prepared in a similar manner.

Since the discovery of enkephalins by Hughes and Kosterlitz,[1] chemistry and biochemistry of opioid peptides have attracted the attention of many reseachers. Many analogs and derivatives have been prepared in order to develop more potent, more selective and metabolically stable ligands and also to explain the structure-activity relationship and drug-receptor interactions.[2] Of these, *N,N*-diallyl-[L-Leu^5]-enkephalin methyl ester (ICI 139462, **1**) and its metabolically more stable analog (ICI 154129, **2**) are of special interest because they showed selective antagonistic activity toward the δ-receptor, but their affinity was not sufficiently high.[3] Another interesting recent finding is that a dimeric enkephalin **3** has increased affinity and selectivity for the δ-receptor as compared with the corresponding monomer.[4] We have tried to synthesize *N,N*-diallyl-[D-Ala^2, L-Leu^5]-enkephalin dimerized at extended *C*-terminal cystine **4**. This paper describes the synthetic procedures.

$(CH_2{=}CHCH_2)_2$L-Tyr-Gly-Gly-L-Phe-L-Leu-OMe **1**

$(CH_2{=}CHCH_2)_2$L-Tyr-Gly-$NHCH_2CH_2S$-$CH(CH_2C_6H_5)$-L-Leu-OH **2**

(H-L-Tyr-D-Ala-Gly-L-Phe-L-Leu-NH-CH_2-)$_2$ **3**

[$(CH_2{=}CHCH_2)_2$L-Tyr-D-Ala-Gly-L-Phe-L-Leu-L-Cys-OH]$_2$ **4**

Results and Discussion

In planning the synthesis of **4**, selection of a mercapto protecting group was important. Various kinds of protecting groups for the cysteine mercapto function are now available; most of these require liquid HF or heavy metal ions for removal.[5] In the latter case, cysteine-containing peptides are generated from their thiolates by treatment with thiols. Removal conditions that may damage the double bond of the allyl group should be avoided.

Recently, we found that diphenylphosphinothioyl (Ppt)[6] and dimethylphosphinothioyl (Mpt)[7] groups, which are removed by treatment with an aqueous alkali or $AgNO_3$ solution, could be used for the protection of the mercapto group of cysteine. Independently, Horner *et al.*[8] also reported the use of the Ppt group for the same purpose and recommended its removal by unsolvated fluoride ions in dichloromethane, chloroform or tetrahydrofuran. This removal method seemed to be attractive, but it was not shown whether more polar solvents, which dissolve large peptide molecules, could also be used. We have investigated solvent effects in the removal reactions of the *S*-phosphinothioyl groups by fluoride ions.

As a preliminary experiment, a comparison was made between Mpt and Ppt groups. When 2 equivalents of tetrabutylammonium fluoride trihydrate (**5**) were added at 30 °C to a solution of Boc-L-Ala-L-Cys(Mpt)-OMe (**6**) in dichloromethane the *S*-Mpt group was cleaved instantaneously. However, removal of the *S*-Ppt group of Boc-L-Ala-L-Cys(Ppt)-OMe in the same manner took about 15 min. Based on these results, further studies were made by use of compound **6**, which carries the *S*-Mpt group. As a source of fluoride ions, KF in the presence of an equimolar amount of 18-crown-6 was also used because tetrabutylammonium fluoride trihydrate was too hygroscopic. All results are summarized in the Table 1.

The removal of the *S*-Mpt group by **5** was almost instantaneous in all aprotic solvents examined. The deprotection by KF/18-crown-6 also took place rapidly. On the contrary, the reaction in methanol was slow because of solvation of fluoride ions. Since methanol is a good solvent for large peptides, we tried the use of methanol by mixing with acetonitrile or dichloromethane and found that these mixed solvents were effective for this reaction up to the methanol content of 50%. In these solvent mixtures, no difference of cleaving abilities of tetrabutylammonium fluoride and KF-crown ether was observed. It was also noted that methanol protonated rapidly to yield the thiol form product. From these results it was concluded that the *S*-Mpt group would be useful for the synthesis of large peptides containing cysteine or cystine.

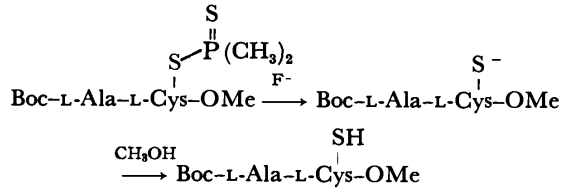

As the first application of the *S*-Mpt group involving the new removal conditions, synthesis of bis[*N,N*-diallyl-[D-Ala^2, L-Leu^5]-enkephalyl]cystine (**4**) was performed according to the scheme illustrated in Fig. 1

TABLE 1. SOLVENT EFFECTS IN REMOVAL OF *S*-PHOSPHINOTHIOYL GROUPS BY FLUORIDE IONS

Compound	Solvent	Time for complete removal (at 30°C) KF/18-crown-6	$(n\text{-}C_4H_9)_4N^+F^-$
Boc-L-Ala-L-Cys(Ppt)-OMe	CH_2Cl_2		15 min
Boc-L-Ala-L-Cys(Mpt)-OMe (**6**)	CH_2Cl_2	4 h	Instantaneous
6	$CHCl_3$	3 h	Instantaneous
6	THF*	>4 h	Instantaneous
6	CH_3CN	30 min	Instantaneous
6	CH_3OH	4 h	4 h
6	CH_3CN-CH_3OH (8:2)	30 min	
6	CH_3CN-CH_3OH (1:1)	1 h15 min	1 h
6	CH_2Cl_2-CH_3OH (1:1)	1 h15 min	1 h
6	CH_3CN-CH_2Cl_2-CH_3OH (1:1:1)	30 min	

* Tetrahydrofuran

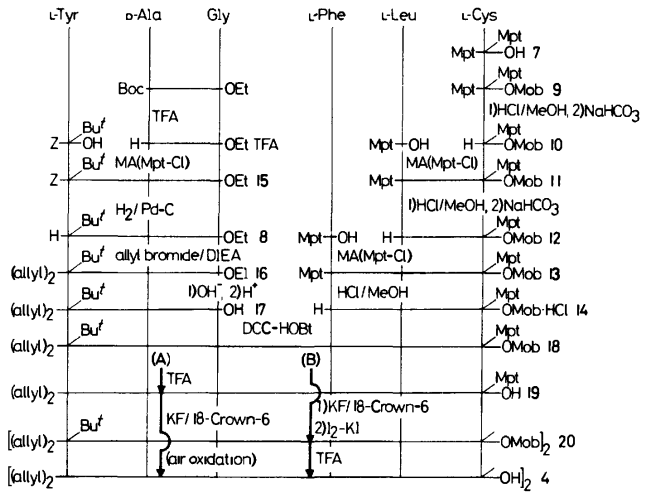

Fig. 1. Synthesis of Bis[*N*,*N*-diallyl-[D-Ala^2, L-Leu^5]-enkephalyl]cystine.

Synthesis was made by the classical method, starting with *N*,*S*-bis(Mpt)-L-cysteine (**7**).[7] **7** was esterified with *p*-methoxybenzyl alcohol in a 87% yield by use of 2 equivalents of *N*-(dimethylphosphinothioyl)imidazole.[9] From the *N*, *S*-bis-Mpt cysteine *p*-methoxybenzyl ester thus obtained, the *N*-Mpt group was selectively removed by treating with 0.4 M† HCl in methanol (3 equiv) at room temperature overnight. Succeeding couplings were performed by the Mpt-mixed anhydride method.[10] This method would allow incorporation of tyrosine moiety without protecting its phenolic hydroxyl group, but in this synthesis *t*-butyl group was introduced as a protecting group in order to avoid *O*-allylation in an *N*-allylation step. For the *N*-allylation, *N*-terminal tripeptide ester **8** was treated with excess allyl bromide in the presence of *N*,*N*-diisopropylethylamine in chloroform at room temperature for 2 d. After hydrolysis of the ethyl ester, *N*,*N*-diallyltripeptide acid **17** was coupled with *C*-terminal tripeptide ester **14** by the dicyclohexylcarbodiimide (DCC)-1-hydroxybenzotriazole (HOBt) method[11] to give protected, *N*,*N*-diallylhexapeptide ester **18** in a yield of 68%.

† 1 M=1 mol dm^{-3}.

Final deprotection required two steps: Treatment with trifluoroacetic acid (TFA) to cleave the *t*-butyl ether and *p*-methoxybenzyl ester bonds and treatment with KF/18-crown-6 to remove the *S*-Mpt group. When the *S*-Mpt group was removed at the first step, the removal conditions determined in the model experiments were effective, except that a somewhat longer reaction time (9 h) was required. After oxidation by iodine and final deprotection by TFA, the desired compound **4** was obtained. But in this case, purification by preparative thin-layer chromatography and gel chromatography in Sephadex LH-20 failed to give completely pure material, probably because of incomplete deprotection by TFA.

On the other hand, when the removal of the *S*-Mpt was performed at the final step, some difficulty was encountered, probably because the *S*-Mpt group was blocked conformationally. But when the excess reagents (10 equiv KF+4 equiv 18-crown-6) were used at higher temperature (50 °C), the removal was complete after 10 h. During these procedures, air oxidation of the product occurred to give **4** directly; this could be purified by preparative silica-gel thin-layer chromatography and gel chromatography on Sephadex LH-20.

Based on the success in the synthesis of **4**, we also prepared bis[D-Ala^2, L-Leu^5]-enkephalyl]cystine with free *N*-terminals in order to determine the effects of *N*-allylation on the pharmacological activity. In this case tyrosine was incorporated without protecting its phenolic hydroxyl group. Again, a better result was obtained when the *S*-Mpt group was removed before removal of *N*- and *C*-terminal protecting groups by TFA.

As expected, the compound **4** showed selective antagonistic activity toward the opioid δ-receptor. Additionally, the compound **4** was found to be approximately ten-fold more effective than ICI 154129 in antagonizing the δ-receptor agonists. Thus, as far as we know, the compound **4** seems to be the most potent δ antagonist.

Experimental

Thin-layer chromatography (TLC) was performed on

silica gel plates (Merck 60F_{254}) in the following solvent systems: Ether (R_f^1), ethyl acetate (R_f^2), chloroform-methanol (9:1, R_f^3), chloroform-methanol-acetic acid (95:5:3, R_f^4), chloroform-methanol-acetic acid (85:25:20, R_f^5), chloroform-methanol-water (65:25:4, R_f^6), chloroform-methanol -29% aqueous ammonia (60:30:5, R_f^7), 1-butanol-acetic acid-water (4:1:1, R_f^8).

N,S-*Bis(dimethylphosphinothioyl)*-L-*cysteine* p-*Methoxybenzyl Ester (Mpt*-L-*Cys(Mpt)*-*OMob) (9).* To a cooled solution of Mpt-L-Cys(Mpt)-OH[7] (1.53 g, 5 mmol) and *p*-methoxybenzyl alcohol (0.62 cm³, 5 mmol) in *N,N*-dimethylformamide (1 cm³) and chloroform (15 cm³), *N*-Mpt-imidazole (1.60 g, 10 mmol) was added; the solution was stirred at 0 °C for 4.5 h and at room temperature overnight. After removal of precipitates by filtration, the filtrate was evaporated *in vacuo*. The residue was dissolved in ethyl acetate. The solution was washed successively with water, an ice-cold 5% citric acid solution, water, a 5% sodium hydrogencarbonate solution, water, and a saturated sodium chloride solution, dried over anhydrous sodium sulfate, and evaporated. The oily residue was dissolved in dichloromethane and placed in a silica-gel column (2.5×37 cm). Elution with ether gave **9** as colorless oil; 1.86 g (87%). $[\alpha]_D^{26}$−5.12 ° (*c* 1, methanol); R_f^1 0.54, R_f^2 0.68. Found: C, 42.35; H, 5.93; N, 3.27; P, 14.49%. Calcd for $C_{15}H_{25}NO_3P_2S_3$: C, 42.34; H, 5.91; N, 3.29; P, 14.56%.

S-*Dimethylphosphinothioyl*-L-*cysteine* p-*Methoxybenzyl Ester Hydrochloride (H*-L-*Cys(Mpt)*-*OMob*·*HCl) (10*·*HCl).* Compound **9** (1.86 g, 4.37 mmol) was stirred with 0.4 M HCl in methanol (32.8 cm³) at 0 °C for 1 h and the mixture was kept standing at room temperature overnight. The solvent was evaporated *in vacuo* and the residue was triturated with ether. Crystalline precipitates were collected by filtration, washed with ether, and dried over P_2O_5; 1.56 g (95%). The sample was once changed to the free amine form and again precipitated from 3 M HCl in ethyl acetate (1.38 cm³); 1.17 g (72%). An analytical sample was recrystallized from hot methanol; mp 136—137 °C (decomp); $[\alpha]_D^{26}$+3.52 ° (*c* 1, methanol); R_f^4 0.23, R_f^5 0.64. Found: C, 42.38; H, 5.72; N, 3.79; P, 8.22%. Calcd for $C_{13}H_{21}NO_3PS_2Cl$: C, 42.22; H, 5.72; N, 3.79, P, 8.37%. This salt was dissolved in water and neutralized with sodium hydrogencarbonate. The solution was extracted with ethyl acetate several times. The extracts were dried and evaporated to give the free base **10** as colorless oil.

N-*Dimethylphosphinothioyl*-L-*leucyl*-S-*dimethylphosphinothioyl*-L-*cysteine* p-*Methoxybenzyl Ester (Mpt*-L-*Leu*-L-*Cys(Mpt)*-*OMob) (11).* Mpt-L-Leu-OH·DCHA[12] (1.16 g, 2.87 mmol) was dissolved in chloroform (3 cm³) and treated with Mpt-Cl (0.369 g, 2.87 mmol) at 0 °C for 40 min. To this **10** (0.957 g, 2.87 mmol) and *N,N*-diisopropylethylamine (0.50 cm³, 2.87 mmol) in chloroform (3 cm³) were added and the solution was stirred at 0 °C for 1 h. After the usual washing procedures,the product was obtained by silica-gel column chromatography as a colorless oil; 1.35 g (87%). $[\alpha]_D^{25}$−59.3 ° (*c* 1, methanol); R_f^2 0.30, R_f^3 0.67. Found: C, 46.63; H, 6.76; N, 5.15; P, 11.49%. Calcd for $C_{21}H_{36}N_2O_4P_2S_3$: C, 46.83; H, 6.74; N, 5.20; P, 11.50%.

L-*Leucyl*-S-*dimethylphosphinothioyl*-L-*cysteine* p-*Methoxybenzyl Ester (H*-L-*Leu*-L-*Cys(Mpt)*-*OMob) (12).* The Mpt group of **11** (1.23 g, 2.28 mmmol) was removed by 0.4 M HCl in methanol (28.8 cm³). After evaporation of the solvent, ether and water were added to the residue. The ether layer was separated and washed with water. The water layer and extracts were gathered, neutralized with sodium hydrogen-carbonate and extracted with ether. The extracts were dried over anhydrous sodium sulfate and evaporated to give a colorless oil; 0.967 g (95%).

N-Dimethylphosphinothioyl-L-*phenylalanyl*-L-*leucyl*-S-*dimethylphosphinothioyl*-L-*cysteine* p-*Methoxybenzyl Ester (Mpt*-L-*Phe*-L-*Leu*-L-*Cys(Mpt)*-*OMob) (13).* Mpt-L-Phe-OH·DCHA[12] (1.035 g, 2.36 mmol) was dissolved in chloroform (5 cm³) and treated with Mpt-Cl (0.303 g, 2.36 mmol) at 0 °C for 1 h. To this a solution of **12** (1.05 g, 2.36 mmol) and *N,N*-diisopropylethylamine (0.41 cm³, 2.36 mmol) in chloroform (3 cm³) was added. The solution was stirred at 0 °C for 1 h and then evaporated *in vacuo*. After the usual washing procedures the product was obtained by silica-gel column chromatography eluted by chloroform-methanol (98:2). Pure materials were obtained by recrystallization from ethyl acetate-ether as colorless crystals; 1.30 g (79%). $[\alpha]_D^{26}$−60.4 ° (*c* 1, methanol); R_f^1 0.18, R_f^2 0.67. Found: C, 52.21; H, 6.60; N, 6.11; P; 8.73%. Calcd for $C_{30}H_{45}N_3O_5P_2S_3 \cdot 1/2H_2O$: C, 52.08; H, 6.65; N, 6.07; P, 8.82%.

L-*Phenylalanyl*-L-*leucyl*-S-*dimethylphosphinothioyl*-L-*cysteine* p-*Methoxybenzyl Ester Hydrochloride (H*-L-*Phe*-L-*Leu*-L-*Cys(Mpt)*-*OMob. HCl) (14).* Compound **13** (1.43 g, 2.09 mmol) was stirred with 0.4 M HCl in methanol (15.7 cm³) at 0 °C for 1 h and the mixture was kept standing at room temperature overnight. The solvent was evaporated *in vacuo* and the residue was triturated with ether. Crystalline precipitates were collected by filtration, washed with ether and ethyl acetate and dried over P_2O_5; 1.089 g (82%). R_f^4 0.07, R_f^5 0.74.

N-*Benzyloxycarbonyl*-O-t-*butyl*-L-*tyrosyl*-D-*alanylglycine Ethyl Ester (Z*-L-*Tyr(Bu^t)*-D-*Ala*-*Gly*-*OEt) (15).* Mpt-Cl (0.257 g, 2 mmol) was added to an ice-cold stirred solution of Z-L-Tyr(Bu^t)-OH·DCHA[13] (1.105 g, 2 mmol) in chloroform (4 cm³), after which the mixture was stirred for 1 h. To this solution, a mixture of TFA·H-D-Ala-Gly-OEt (0.576 g, 2 mmol) and triethylamine (0.56 cm³, 4 mmol) in chloroform (2 cm³) and *N,N*-dimethylformamide (2 cm³) was added in several portions at 0 °C. After having been stirred at this temperature for 1 h, the solution was washed in the usual way, dried and evaporated *in vacuo*. The oily residue was dissolved in dichloromethane and placed in a silica-gel column (1.1×12 cm). Elution with ether gave **15** as a colorless oil; 0.899 g (85%).

N,N-*Diallyl*-O-t-*butyl*-L-*tyrosyl*-D-*alanylglycine Ethyl Ester ((allyl)$_2$*-L-*Tyr(Bu^t)*-D-*Ala*-*Gly*-*OEt) (16).* A mixture of **15** (0.899 g, 1.70 mmol), 10% palladium-charcoal (0.42 g), cyclohexene (15 cm³), and ethanol (30 cm³) was refluxed for 7 h. After removal of the catalyst by filtration the filtrate was evaporated *in vacuo*. The oily residue was dissolved in chloroform (15 cm³) and *N,N*-diisopropylethylamine (1.05 cm³, 6 mmol) and cooled to 0 °C. To this solution allyl bromide (8.65 cm³, 100 mmol) was added drop by drop over a period of 30 min at this temperature and the solution stirred at room temperature for 2 d. The solution was evaporated and the oily residue was shaken with ethyl acetate and water. The organic layer was separated and washed with water, a 5% sodium hydrogencarbonate solution, water and a saturated sodium chloride solution, dried over anhydrous sodium sulfate, and evaporated. The oily residue was purified by preparative silica-gel thin-layer chromatography using ether as a developing solvent. From the desired band (R_f=0.4—0.6) compound **15** was obtained as colorless oil; 0.544 g (67%). An analytical sample was obtained by rechromatography on Sephadex LH-20 (1.9×100 cm) eluted with methanol. The desired fractions were collected and evaported *in vacuo* to give **16** as colorless oil; 0.544 g (67%). $[\alpha]_D^{26}$−18.4 ° (*c* 1, methanol); R_f^2 0.45, R_f^3 0.49. Found: C, 65.92; H, 8.46; N, 8.82%. Calcd for $C_{26}H_{39}N_3O_5$: C, 65.94; H, 8.32; N, 8.87%.

N,N-*Diallyl*-O-t-*butyl*-L-*tyrosyl*-D-*alanylglycyl*-L-*phenylalanyl*-L-*leucyl*-S-*dimethylphosphinothioyl*-L-*cysteine* p-*Methoxybenzyl Ester ((allyl)$_2$*-L-*Tyr(Bu^t)*-D-*Ala*-*Gly*-L-*Phe*-L-*Leu*-L-*Cys(Mpt)*-*OMob) (18).* Compound **16** (0.492 g, 1.04 mmol) was dissolved in methanol (3 cm³). To this a 1 M aqueous NaOH solution (1.23 cm³) was added at 0 °C. After the solution had been stirred at this temperature for 30 min

and at room temperature overnight, methanol was removed *in vacuo*. The resulting solution was acidified to pH 4 by acetic acid at 0 °C. To this,Diaion HP-20 resin was added until no spot corresponding to (allyl)$_2$-L-Tyr(Bu^t)-D-Ala-Gly-OH (**17**) was detectable on TLC. The resin was filtered and washed with water until the filtrate became neutral. Elution of **16** was performed by methanol to give an amorphous solid: 0.448 g (100%).

To a suspension of **17** (0.298 g, 0.669 mmol) in chloroform (2 cm^3) and dissolved *N,N*-diisopropylethylamine (0.117 cm^3, 0.669 mmol) and **14** (0.442 g, 0.669 mmol), dicyclohexylcarbodiimide (0.138 g, 0.669 mmol) and 1-hydroxybenzotriazole (0.090 g, 0.669 mmol) were added at 0 °C. The mixture was stirred at this temperature for 1 h, and at room temperature overnight. Precipitates were filtered off and the filtrate was evaporated *in vacuo*. The solid residue was dissolved in dichloromethane and washed with water, a 5% sodium hydrogencarbonate solution, water and a saturated sodium chloride solution, dried over anhydrous sodium sulfate and evaporated. Crude materials were then purified by preparative silica-gel thin-layer chromatography using chloroform–methanol (100:1) as a developing solvent system. The desired band was eluted with dichloromethane–methanol (9:1) and the eluates evaporated *in vacuo*. The residue was again dissolved in a small volume of dichloromethane and placed in a Sephadex LH-20 column (1.9×100 cm) and eluted with methanol. The desired fractions were collected and evaporated *in vacuo* to give **18** as colorless crystals; 0.471 g (68%). An analytical sample was recrystallized from hot methanol; mp 188—190 °C; $[\alpha]_D^{26}$−20° (*c* 1, *N,N*-dimethylformamide); R_f^3 0.61, R_f^4 0.40. Found: C, 60.90; H, 7.17; N, 8.21; P, 2.63%. Calcd for $C_{52}H_{73}N_6O_9PS_2$: C, 61.16; H, 7.20; N, 8.23; P, 3.03%.

N,N-*Diallyl-*L*-tyrosyl-*D*-alanylglycyl-*L*-phenylalanyl-*L*-leucyl-S-dimethylphosphinothioyl-*L*-cysteine ((allyl)$_2$-L-Tyr-D-Ala-Gly-L-Phe-L-Leu-L-Cys(Mpt)-OH) (19).* Trifluoroacetic acid (4 cm^3) was added to an ice-cold solution of compound **18** (0.236 g, 0.23 mmol) in dichloromethane (4 cm^3) containing anisole (0.4 cm^3). After having been kept at room temperature for 6.5 h, the solution was evaporated *in vacuo*. The solid residue was washed with ether and dissolved in methanol (10 cm^3) and water (2 cm^3). The solution was neutralized to pH 7 by addition of solid sodium hydrogencarbonate at 0 °C, and then evaporated. The residual materials were submitted to preparative silica-gel thin-layer chromatography in a solvent system of chloroform–methanol–water (65:25:4). The desired band (R_f=0.5—0.7) was eluted with methanol and evaporated *in vacuo*. The residue was dissolved again in a small volume of methanol and placed in a Sephadex LH-20 column (1.9×100 cm) and eluted with methanol. The desired fractions were collected and evaporated *in vacuo* to give **19** as colorless crystals; 0.175 g (87%). An analytical sample was recrystallized from hot methanol; mp 169—172 °C; $[\alpha]_D^{26}$+7 °(*c* 1, acetic acid); R_f^6 0.54, R_f^7 0.64. Found: C, 55.08; H, 6.61; N, 9.56; P, 3.14%. Calcd for $C_{40}H_{57}N_6O_8PS_2 \cdot 4/3H_2O$: C, 55.28; H, 6.92; N, 9.67; P, 3.56%.

*Bis(*N,N-*diallyl-*O*-t-*butyl-*L*-tyrosyl-*D*-alanylglycyl-*L*-phenylalanyl-*L*-leucyl)-*L*-cystine Bis(*p*-methoxybenzyl Ester) ((allyl)$_2$-L-Tyr(Bu^t)-D-Ala-Gly-L-Phe-L-Leu-L-Cys-OMob)$_2$ (20).*

To a solution of compound **18** (0.294 g, 0.288 mmol) in methanol (3 cm^3) and acetonitrile (3 cm^3), KF (33.5 mg, 0.576 mmol) and 18-crown-6 (0.152 g, 0.576 mmol) were added. The mixture was stirred at room temperature for 9 h and treated with 0.1 M iodine–potassium iodide in 90% methanol solution (1.6 cm^3). The yellow solution was evaporated *in vacuo*. The residue was dissolved in ethyl acetate and washed with water, a sodium thiosulfate solution, water, a 5% citric acid solution, water, a saturated sodium chloride solution, dried over anhydrous sodium sulfate, and evaporated *in vacuo*. The residue was purified by preparative silica-gel thin-layer chromatography in a solvent system of chloroform–methanol (95:5). The desired band (R_f=0.6—0.7) was eluted with methanol and evaporated *in vacuo*. The residue was again purified by gel chromatography on Sephadex LH-20 (1.9×100 cm) eluted with methanol. The desired fractions were collected and eluates evaporated *in vacuo* to yield **20** as colorless crystals; 0.237 g (88%). Mp 196—199 °C; R_f^3 0.54, R_f^4 0.29. Found: C, 64.25; H, 7.25; N, 9.00%. Calcd for $C_{100}H_{134}N_{12}O_{18}S_2 \cdot CH_3OH$: C, 64.24; H, 7.37; N, 8.90%.

*Bis(*N,N-*diallyl-*L*-tyrosyl-*D*-alanylglycyl-*L*-phenylalanycyl-*L*-leucyl)-*L*-cystine ((allyl)$_2$-L-Tyr-D-Ala-Gly-L-Phe-L-Leu-L-Cys-OH)$_2$ (4).* *Method A*: To a solution of compound **19** (0.129 g, 0.149 mmol) in methanol (10 cm^3) and acetonitrile (10 cm^3), KF (0.083 g, 1.48 mmol) and 18-crown-6 (0.158 g, 0.595 mmol) were added. The mixture was stirred at 50 °C for 10 h and evaporated *in vacuo*. The residue was dissolved in a small volume of methanol and water and applied to a column (1.2×21 cm) of Dowex 50 W×2 (H^+ form). The resin was rinsed with water (150 cm^3) and then the desired material was eluted with a 1% aqueous ammonia solution. The crude peptide was purified by preparative silica-gel thin-layer chromatography in a solvent system of chloroform–methanol–water (65:25:4) and gel chromatography on Sephadex LH-20 (1.9×100 cm) eluted with methanol. The desired fractions were collected and evaporated *in vacuo* to yield **4** as colorless crystals; 58 mg (51%). An analytical sample was further purified by preparative silica-gel thin-layer chromatography in a solvent system of 1-butanol–acetic acid–water (4:1:1) and gel chromatography on Sephadex LH-20. Mp 198—208 °C (decomp); $[\alpha]_D^{26}$+6.7 (*c* 1, acetic acid); R_f^6 0.20, R_f^7 0.21, R_f^8 0.52. Found: C, 56.87; H, 6.67; N, 10.17%. Calcd for $C_{76}H_{102}N_{12}O_{16}S_2 \cdot 2H_2CO_3 \cdot H_2O$: C, 56.92; H, 6.61; N, 10.21%.

Method B: Compound **20** (0.236 g, 0.127 mmol) was stirred with trifluoroacetic acid (4 cm^3) containing anisole (0.8 cm^3) at 0 °C for 1 h and at room temperature over night. The solution was evaporated *in vacuo* and the residue was crystallized by triturating with ether. Crystalline precipitates were purified by preparative silica-gel thin-layer chromatopraphy using chloroform–methanol–29% aqueous ammonia (60:30:5). The desired band was eluted with methanol and the eluates were evaporated *in vacuo*. The residue was again purified by gel chromatography on Sephadex LH-20 (1.9×100 cm) eluted with methanol. The desired fractions were collected and eluates evaporated *in vacuo* to yield **4** as colorless crystals; 79 mg (41%). Mp 171—179 °C (decomp); R_f^6 0.19, R_f^7 0.22, R_f^8 0.53.

N-*(t-Butoxycarbonyl)-*L*-tyrosyl-*D*-alanylglycine Ethyl Ester (Boc-L-Tyr-D-Ala-Gly-OEt) (21).* Mpt-Cl (0.257 g, 2 mmol) was added to an ice-cold stirred solution of Boc-L-Tyr-OH (0.563 g, 2 mmol) and triethylamine (0.28 cm^3, 2 mmol) in chloroform (3 cm^3), after which the mixture was stirred for 1 h. To this solution a mixture of TFA·H-D-Ala-Gly-OEt (0.576 g, 2 mmol) and triethylamine (0.56 cm^3, 4 mmol) in *N,N*-dimethylformamide (2 cm^3) and chloroform (2 cm^3) was added in several portions at 0 °C. After having been stirred at this temperature for 1 h, the solution was washed in the usual way, dried and evaporated *in vacuo*. Solid residue was purified by preparative silica-gel thin-layer chromatography using chloroform–methanol (37:3) for development. The desired band (R_f=0.4—0.6) was eluted with chloroform–methanol (9:1) and eluates evaporated *in vacuo*. The residue was crystallized from hot ethyl acetate to give colorless crystals; 0.674 g (77%). Mp 164—166 °C; R_f^2 0.56, R_f^3 0.45.

N-*(t-Butoxycarbonyl)-*L*-tyrosyl-*D*-alanylglycine (Boc-L-Tyr-D-Ala-Gly-OH) (22).* To an ice-cold solution of **21** (0.479 g, 1.1 mmol) in methanol (3 cm^3), a 1 M aqueous NaOH solution (2.2 cm^3) was added and the solution was stirred at

0 °C for 30 min and at room temperature for 4 h. After removal of methanol *in vacuo*, the solution was acidified to pH 3 by solid citric acid at 0 °C. To this Diaion HP-20 resin was added until no spot corresponding to the product was detectable on TLC. The resin was filtered and washed with water until the filtrate became neutral. Elution of the resin with methanol and evaporation *in vacuo* of the eluates gave a chromatographically homogeneous amorphous solid; 0.430 g (95%). R_f^5 0.50, R_f^6 0.22.

N-(t-Butoxycarbonyl)-L-tyrosyl-D-alanylglycyl-L-phenylalanyl-L-leucyl-S-dimethylphosphinothioyl-L-cysteine p-Methoxybenzyl Ester (Boc-L-Tyr-D-Ala-Gly-L-Phe-L-Leu-L-Cys(Mpt)-OMob) (23). To a mixture of **22** (0.390 g, 0.742 mmol), *N,N*-diisopropylethylamine (0.129 cm³, 0.742 mmol) and **14** (0.468 g, 0.742 mmol) in chloroform (3 cm³) and *N,N*-dimethylformamide (3 cm³), dicyclohexylcarbodiimide (0.153 g, 0.742 mmol) and 1-hydroxybenzotriazole (0.100 g, 0.742 mmol) were added at 0 °C. After the mixture was stirred at room temperature overnight, all the solvents were removed *in vacuo*. To the solid residue, dichloromethane was added, and precipitates were removed by filtration and washed. The filtrate and washings were washed as usual, dried and evaporated to give an amorphous solid. This was purified by preparative silica-gel thin-layer chromatography, using chloroform–methanol (9:1) as a developing solvent. The desired band (R_f=0.5—0.7) was eluted with methanol and eluates were evaporated *in vacuo*. The residue was dissolved again in a small volume of methanol and this mixture was placed in a Sephadex LH-20 column (1.9×100 cm), which was eluted with methanol. The desired fractions were collected and evaporated *in vacuo* to give colorless crystals; 0.560 g (76%). Mp 141—145 °C; R_f^3 0.60, R_f^4 0.18. Found: C, 57.63; H, 6.70; N, 8.60%. Calcd for $C_{47}H_{65}N_6O_{11}PS_2$: C, 57.30; H, 6.65; N, 8.53%.

L-Tyrosyl-D-alanylglycyl-L-phenylalanyl-L-leucyl-S-dimethylphosphinothioyl-L-cysteine (H-L-Tyr-D-Ala-Gly-L-Phe-L-Leu-L-Cys(Mpt)-OH) (24). Trifluoroacetic acid (3 cm³) was added to an ice-cold solution of compound **23** (0.200 g, 0.203 mmol) in dichloromethane (2 cm³) containing anisole (0.3 cm³). After having been kept at room temperature overnight, the solution was evaporated *in vacuo*. The solid residue was washed with ether and purified by preparative silica-gel thin-layer chromatography using chloroform–methanol–29% aqueous ammonia (60:30:5). The desired band (R_f=0.3—0.5) was dissolved again in a small volume of acetic acid and the mixture was placed in a Sephadex LH-20 column (1.9×100 cm), which was eluted with methanol. The desired fractions were collected and evaporated *in vacuo* to give **24** as colorless crystals: 0.0991 g(63%). R_f^6 0.56, R_f^7 0.47. Found: C, 52.62; H, 6.57; N, 10.45%. Calcd for $C_{34}H_{49}N_6O_8PS_2 \cdot CH_3OH \cdot 1/4H_2O$: C, 52.45; H, 6.72; N, 10.49%.

Bis(N-(t-butoxycarbonyl)-L-tyrosyl-D-alanylglycyl-L-phenylalanyl-L-leucyl)-L-cystine Bis(p-methoxybenzyl Ester) (Boc-L-Tyr-D-Ala-Gly-L-Phe-L-Leu-L-Cys-OMob)₂ (25). To a solution of compound **23** (0.201 g, 0.204 mmol) in methanol (4 cm³) and acetonitrile (4 cm³), KF (0.0237 g, 0.407 mmol) and 18-crown-6 (0.108 g, 0.407 mmol) were added. After having been stirred at room temperature for 9 h, the mixture was treated with 0.1 M iodine–potassium iodide solution in 90% methanol (2.3 cm³) and evaporated *in vacuo*. The residue was dissolved in ethyl acetate and water. The organic layer was separated and washed with water, a sodium thiosulfate solution, water, a 5% citric acid solution, water and a saturated sodium chloride solution, dried over anhydrous sodium sulfate, and evaporated. The residue was purified by preparative silica-gel thin-layer chromatography by using chloroform–methanol (9:1). The desired band (R_f=0.5—0.6) was eluted with methanol and the eluates were evaporated *in vacuo*. The residue was further purified by preparative silica-gel thin-layer chromatography using chloroform–methanol (95:5) and gel chromatography on Sephadex LH-20 (1.9×100 cm) eluting with methanol. The desired fractions were collected and the eluates were evaporated *in vacuo* to yield **25** as colorless crystals; 0.136 g(74%). Mp 195—198 °C; R_f^3 0.55, R_f^4 0.07. Found: C, 58.83; H, 6.64; N, 9.14%. Calcd for $C_{90}H_{118}N_{12}O_{22}S_2 \cdot 3H_2O$; C, 58.80; H, 6.80; N, 9.14%.

Bis(L-tyrosyl-D-alanylglycyl-L-phenylalanyl-L-leucyl)-L-cystine (H-L-Tyr-D-Ala-Gly-L-Phe-L-Leu-L-Cys-OH)₂ (26). Method A: To a solution of compound **24** (0.136 g, 0.178 mmol) in methanol (10 cm³) and acetonitrile (10 cm³), KF (0.124 g, 2.135 mmol) and 18-crown-6 (0.282 g, 1.067 mmol) were added. The mixture was stirred at 50 °C for 9 h and then evaporated *in vacuo*. The residue was dissolved in water (20 cm³) and to this Diaion HP-20 resin was added. The resin was filtered and washed with water (200 cm³). Elution of **26** was performed by methanol and eluates were evaporated. The residue was subjected to preparative silica-gel thin-layer chromatography using chloroform–methanol–water (65:25:4). The desired band (R_f=0.2—0.3) was eluted with methanol and the eluates were evaporated *in vacuo*. The residue was dissolved in a small volume of methanol and placed in a Sephadex LH-20 column (1.9×100 cm), which was eluted with methanol. The desired fractions were collected and evaporated *in vacuo* to give **26** as colorless crystals; 55.3 mg(46%). R_f^6 0.25, R_f^7 0.07, R_f^8 0.54.

Method B: Compound 25 (0.129 g, 0.072 mmol) was dissolved in TFA (4 cm³) containing anisole (0.4 cm³). The solution was stirred at 0 °C for 4 h and evaporated *in vacuo*. The residue was triturated with ether to give crystals, which were dissolved in a small volume of methanol and subjected to preparative silica-gel thin-layer chromatography using chloroform–methanol–29% aqueous ammonia (60:30:5). The desired band was eluted with methanol and the eluates were evaporated *in vacuo*. The residue was again dissolved in a small volume of methanol and water and placed in a column (1.2×20 cm) of Dowex 1×2 ion-exchange resin (acetate form), which was eluted with a 1% acetic acid solution. The eluates were evaporated and the residue was purified by gel chromatograhy on Sephadex LH-20 (1.9×100 cm), eluting with methanol. The desired fractions were collected and evaporated *in vacuo* to give colorless crystals; 44.5 mg (45%). Mp 198—202 °C (decomp); R_f^6 0.25, R_f^7 0.06, R_f^8 0.56. Found: C, 53.52; H, 6.22; N, 11.49%. Calcd for $C_{64}H_{86}O_{16}N_{12}S_2 \cdot 1/2H_2O$: C, 53.68, H, 6.21; N, 11.38%.

The authors wish to thank Professor Tetsuo Oka (Tokai University) for the biological activity measurements and for his encouragement throughout this work.

References

1) J. Hughes, T. W. Smith, H. W. Kosterlitz, L A. Fothergill, B. A. Horgan, and H. R. Morris, *Nature (London)*, **258**, 577 (1975).
2) Reviews in *Br. Med. Bull.*, **39**, No 1 (1983).
3) J. S. Shaw, L. Miller, M. J. Turnbull, J. J. Gormley, and J. S. Morley, *Life Sci.*, **31**, 1259 (1982).
4) T. Costa, Y. Shimohigashi, S. A. Krumins, P. J. Munson, and D. Rodbard, *Life Sci.*, **31**, 1625 (1982).
5) R. G. Hiskey, "The Peptide," ed by E. Gross and J. Meienhofer, Academic Press, New York (1981), Vol. 3, Chap. 3, p. 137.
6) S. Ikeda, F. Tonegawa, E. Shikano, K. Shinozaki, and M. Ueki, *Bull. Chem. Soc. Jpn.*, **52**, 1431 (1979).
7) M. Ueki and K. Shinozaki, *Bull. Chem. Soc. Jpn.*, **56**, 1187 (1983).
8) L. Horner, R. Gehring, and H. Lindel, *Phosphorous*

and Sulfur, **11**, 349 (1981).
9) S. Ikeda, private communication. Ref: S. Ikeda and M. Ueki, 47th National Meeting of the Chemical Society of Japan, Osaka, April 1983, Abstr., No. 4H09.
10) M. Ueki and T. Inazu, *Chem. Lett.*, **1982**, 45.
11) W. König and R. Geiger, *Chem. Ber.*, **103**, 2024 (1970).
12) M. Ueki, T. Inazu, and S. Ikeda, *Bull. Chem. Soc. Jpn.*, **52**, 2424 (1979).
13) E. Wünsch and J. Jentsch, *Chem. Ber.*, **97**, 2490(1964).

Formations of Novel Dimeric Cyclohexanone Oxime Compounds

Haruyo SATO,* Shinzo IMAMURA, Yukishige KITANO,† Teruo KANDA,†† and Tamaichi ASHIDA††

Chemical Research Laboratory, Basic Research Laboratories, Toray Industries, Inc., 9-1, Ooe-cho, Minato-ku, Nagoya, 455-91

†*Toray Research Center, Inc., Sonoyama, Ohtsu, 520*

††*Faculty of Engineering, Nagoya University, Chikusa-ku, Nagoya, 464*

(Received January 9, 1984)

The structure of the dimeric oxime compound obtained by the reaction of 2-chlorocyclohexanone oxime or 1-chloro-2-nitrosocyclohexane dimer with stoichiometrical ammonia was established to be 14-oxa-7,15,16-triazatetracyclo[11.2.1.$0^{1,6}$.$0^{8,13}$]hexadecan-16-ol by spectroscopic methods and X-ray crystallography; the result leads to a revision of the previously proposed structure, bis(2-hydroxyiminocyclohexyl)amine.

2-Aminocycloalkanone oxime can be obtained by the reaction of 2-chlorocycloalkanone oxime or its dimer, 1-chloro-2-nitrosocycloalkane dimer, with a large excess of ammonia.[1] In the commercial chemico-enzymatic process[2] used to prepare L-lysine, 2-aminocyclohexanone oxime (**3**) is produced in large scale from 2-chlorocyclohexanone oxime (**1**) or 1-chloro-2-nitrosocyclohexane dimer (**2**). The structure of the principal by-product of the reaction (hereinafter named "compound **A**") was proposed to be bis(2-hydroxyiminocyclohexyl) amine (**4**) by Ohno *et al.*[3] and J. Beger *et al.*[4] (Scheme 1). However, while we were engaged in the further study of this reaction, we had some doubts about the chemical structure of compound **A**. Thus we have attempted the detailed instrumental analysis of compound **A** and its analog to elucidate the proper chemical structure.

The following experimental results may give support to assigning structure **4** to compound **A**. (i) In the reaction of **1** or **2** with ammonia, compound **A** increases with the decrease in the molar ratio of ammonia. Thus it is inferred from analogy with the reaction of alkyl halide and ammonia that compound **A** is an oxime having a imino group. (ii) 1,2,3,4,6,7,8,9-octahydrophenazine (**6**) was obtained as a major product when compound **A** was heated in acidic or alkaline aqueous solution. Moreover, bis(perhydro-2-oxo-3-azepinyl)amine (**5**), a plausible product from **4**, was formed as a major product by the Beckmann rearrangement of compound **A** in 100% sulfuric acid (Scheme 2). (iii) Compound **A** is obtainable in high yield by the reaction of **1** and **3**. (iv) The elemental analysis of compound **A** gave the empirical formula $C_{12}H_{21}N_3O_2$. However, when the properties of compound **A** are compared with those of **3**, the following different points are found: (v) The pattern of IR spectrum does not resemble to that of **3**. Particularly, the absorption at 1670 cm^{-1} arising from oxime group was missing in the spectrum of compound **A**. (vi) Compound **A** is only sparingly soluble in such solvents as chloroform and alcohols, while **3** is fairly soluble in them. (vii) The rate of the salt exchange reaction of compound **A** with ammonium chloride is lower than that of **3**. (viii) Compound **A** was formed by heating **3** with ammonia, but the reverse reaction did not proceed. Therefore, it is doubtful whether compound **A** and **3** have analogous functional groups or not.

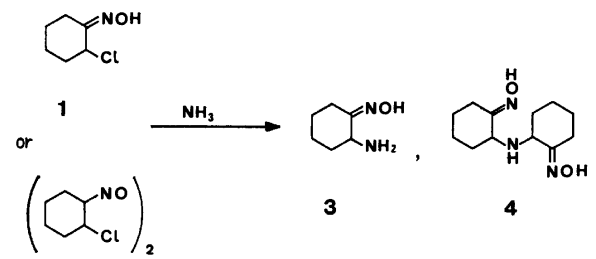

Scheme 1.

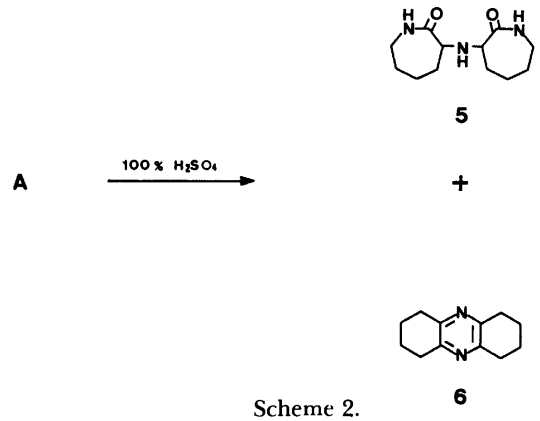

Scheme 2.

Accordingly, we synthesized a reference compound and compared the data from instrumental analyses of the compound with those of compound **A** to elucidate the proper structure. We found that the reaction of 2-chlorocyclohexanone oxime or 1-chloro-2-nitrosocyclohexane dimer with stoichiometrical ammonia yields dimeric cyclohexanone oxime, 14-oxa-7,15,16-triazatetracyclo[11.2.1.$0^{1,6}$.$0^{8,13}$]hexadecan-16-ol.

Results and Discussion

2-Chlorocyclohexanone oxime (**1**) or 1-chloro-2-nitrosocyclohexane dimer (**2**) was treated with stoichiometrical ammonium chloride in a two-phase solvent system containing organic and aqueous alkaline layers to produce compound **A**. **1** or **2** was also reacted with stoichiometrical methylamine hydrochloride to produce compound **B**. 2-(methylamino)cyclohexanone oxime was obtained by the reaction of **1** or **2** with excess methylamine in organic solvents such as benzene and chloroform.

The structures of compound **A** and **B** were studied in the following procedure.

The elemental analyses gave the empirical formulae $C_{12}H_{21}N_3O_2$ and $C_{13}H_{23}N_3O_2$ to compounds **A** and **B**, respectively. Though ^{1}H-NMR spectrum of compound

A was not obtained due to its poor solubility, two kinds of protons exchangeable with deuterium in deuterium oxide were observed at δ=6.1 and 7.8 in the spectrum of compound **B**. ^{13}C-NMR spectra of both compounds showed analogous peak-patterns, the peaks to be noticed being observed at δ=100, 86, 60 (2 carbon atoms) in compound **A** and at δ=99, 85, 68, 63 in compound **B**. The peaks at δ=99—100 and 85—86 are reasonably assigned to quarternary carbon atoms, and the remaining peaks at δ=60—68 are also reasonably assigned to carbon atoms adjacent to the amino group. Thus, it is inferred that both compounds have two quarternary carbon atoms of considerably different natures and two similar carbon atoms adjacent to the amino group. Moreover, since no peaks were observed in the field lower than 100, it is suggested that neither of them has an oxime group.

In the IR spectra of both compounds, no absorption at 1670 cm^{-1} arising from oxime group was observed, but the bands due to amino groups and hydroxyl groups were observed at 3200—3100 cm^{-1}. Mass spectra of both compounds showed the fragment peaks at m/z $(M-17)^+$ resulting from the elimination of a hydroxyl radical, but no other useful information was obtained from them.

From these observations, we assigned 14-oxa-7,15,16-triazatetracyclo[11.2.1.0^{1,6}.0^{8,13}]hexadecan-16-ol (**7**) and 7-methyl-14-oxa-7,15,16-triazatetracyclo[11.2.1.0^{1,6}.0^{8,13}] hexadecan-16-ol (**8**) to the structures of compounds **A** and **B**, and the structure of **7** was definitely confirmed by X-ray diffraction analysis.

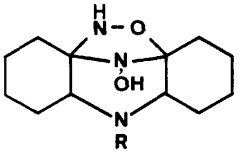

7 R = H
8 R = CH_3

The crystallographic structure of **7** is shown in Fig. 1. The atomic positional parameters are listed in Table 1 and Table 2 presents some of more important bond lengths and angles. The molecule has a fused ring structure. The two outer cyclohexane rings are attached equatorially to the central six-membered heterocyclic ring and is in a chair conformation. The bonding pattern within the three six-membered ring is normal with an average C–C bond length of 1.528 Å and C–N bond length of 1.471 Å. The longest of these, C(1)–C(6), 1.543 (3) Å and C(7)–C(12), 1.550(3) Å, can be ascribed to the high degree of substitution on these C atoms. The bond angle, C(1)–N(2)–C(12), is much less, 100.1(1)°, than expected as the effect of the ring strain of attached five-membered ring and has probably resulted in the long N(2)–O(2) length of 1.458(2) Å found at this point. The sum of the valency angles around N(2) is 314.6°. The dihedral angles between C(1)–C(6)–C(7)–C(12) and C(1)–C(3)–C(4)–C(6) and between C(1)–C(6)–C(7)–C(12)

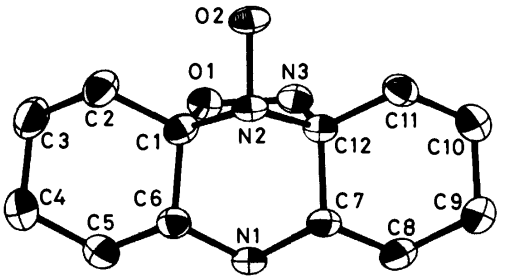

Fig. 1. Perspective view of the molecule **7** with atomic numbering scheme. The ellipsoids are drawn to enclose 50% probability.

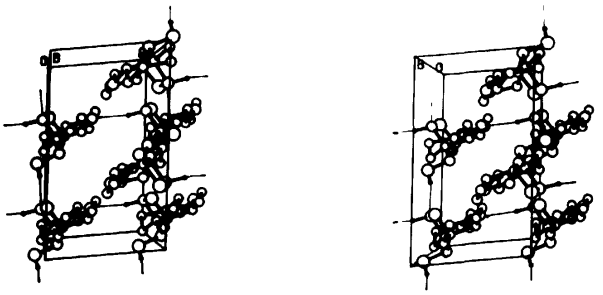

Fig. 2. Stereodrawing of the crystal structure. The hydrogen bonds are shown by fine lines. For H-atoms only the atoms contributed to the hydrogen bonds are drawn for clarity.

Table 1. Positional (×10^4) and thermal (×10) parameters

Atom	x	y	z	B_{eq}/Å$^{2a)}$
C(1)	1707(2)	1674(1)	4115(1)	23
C(2)	1295(3)	930(1)	4504(2)	31
C(3)	1953(4)	419(1)	3502(2)	38
C(4)	4378(4)	515(1)	3271(2)	43
C(5)	4787(3)	1256(1)	2834(2)	32
C(6)	4117(3)	1795(1)	3791(1)	25
C(7)	3295(2)	3031(1)	3947(1)	24
C(8)	3262(3)	3708(1)	3198(2)	31
C(9)	2118(3)	4290(1)	3875(2)	39
C(10)	−256(3)	4077(1)	4062(2)	36
C(11)	−276(3)	3408(1)	4839(1)	28
C(12)	915(2)	2817(1)	4233(1)	22
N(1)	4384(2)	2491(1)	3250(1)	26
N(2)	1253(2)	2195(1)	5061(1)	22
N(3)	−420(2)	2569(1)	3066(1)	23
O(1)	204(2)	1835(1)	2975(1)	24
O(2)	−894(2)	2021(1)	5499(1)	27

a) The equivalent isotropic temperature factor defined by W. C. Hamilton (*Acta Crystallogr.*, **12**, 609 (1959)).

TABLE 2. IMPORTANT BOND LENGTHS AND ANGLES

Bond length	l/Å		l/Å
C(1)-C(2)	1.517(2)	C(2)-C(3)	1.528(3)
C(3)-C(4)	1.517(3)	C(4)-C(5)	1.527(3)
C(5)-C(6)	1.532(2)	C(6)-C(1)	1.543(2)
C(7)-C(8)	1.524(2)	C(8)-C(9)	1.529(3)
C(9)-C(10)	1.520(3)	C(10)-C(11)	1.528(3)
C(11)-C(12)	1.522(2)	C(12)-C(7)	1.550(2)
N(1)-C(6)	1.470(2)	N(1)-C(7)	1.467(2)
N(2)-C(1)	1.461(2)	N(2)-C(12)	1.484(2)
N(2)-O(2)	1.458(2)	N(3)-C(12)	1.480(2)
N(3)-O(1)	1.467(2)	O(1)-C(1)	1.462(2)
Bond angle	ϕ/°		ϕ/°
C(2)-C(1)-C(6)	112.8(1)	C(1)-C(2)-C(3)	111.1(2)
C(2)-C(3)-C(4)	110.9(2)	C(3)-C(4)-C(5)	110.5(2)
C(4)-C(5)-C(6)	111.9(2)	C(5)-C(6)-C(1)	111.2(1)
C(8)-C(7)-C(12)	111.4(1)	C(7)-C(8)-C(9)	111.5(2)
C(8)-C(9)-C(10)	109.8(2)	C(9)-C(10)-C(11)	110.9(2)
C(10)-C(11)-C(12)	111.9(1)	C(11)-C(12)-C(7)	111.7(1)
C(6)-C(1)-N(2)	107.2(1)	C(1)-C(6)-N(1)	111.5(1)
C(7)-C(12)-N(2)	104.8(1)	C(12)-C(7)-N(1)	112.4(1)
C(6)-N(1)-C(7)	112.2(1)	C(1)-N(2)-C(12)	100.1(1)
N(2)-C(1)-O(1)	105.9(1)	N(2)-C(12)-N(3)	105.1(1)
C(1)-O(1)-N(3)	106.9(1)	C(12)-N(3)-O(1)	104.1(1)
C(6)-C(1)-O(1)	107.6(1)	C(2)-C(1)-O(1)	108.5(1)
C(7)-C(12)-N(3)	111.0(1)	C(11)-C(12)-N(3)	110.6(1)
C(2)-C(1)-N(2)	114.5(1)	C(11)-C(12)-N(2)	113.4(1)
C(5)-C(6)-N(1)	108.3(1)	C(8)-C(7)-N(1)	109.2(1)
C(1)-N(2)-O(2)	107.5(1)	C(12)-N(2)-O(2)	107.5(1)

and C(7)–C(9)–C(10)–C(12) are 11.5(1)° and 7.4(1)°, respectively. O(1) and N(3) atoms axially attached to the C(1) and C(12) atoms respectively make five membered ring with the atom N(2) by an envelope conformation, with this atom 0.610(5) Å out of plane of the remaining four ring atoms. Figure 2 displays the packing. The molecules are linked by two types of intermolecular hydrogen bonds, such that the crystal contains an infinite two-dimensional net perpendicular to the b axis. One hydrogen bond exists between N(3)–H(N3) and N(1) of the molecules related by the c glide plane in the direction of a, the second between O(2)–H(O2) and N(3) of the successive molecules along the c. Thus each molecule is hydrogen bonded to four neighboring molecules. The plate-like morphology of the crystal parallels the orientation of the hydrogen-bonded nets. The hydrogen bond distances and angles are: N(3)···N(1), 3.158(2); H(N3)···N(1), 2.22(2) Å; N(3)–H(N3)···N(1), 163(2)°; O(2)···N(3), 2.807(2); H(O2)···N(3), 1.85(3) Å; O(2)–H(O2)···N(3), 170(3)°.

We speculate that this moderately complicated compound was formed by the reaction mechanism shown in Scheme 3. Hydrogen chloride was eliminated from **1** or **2** to give nitrosocyclohexene, and this was converted to **3** by addition of ammonia. When the molar ratio of ammonia was low, **3** reacted with another intermediary nitrosocyclohexene to give **4**. Spontaneous intramolecular 1,3-dipolar addition reaction between two oxime groups gave 14-oxa-7,15,16-triazatetracyclo-[11.2.1.$0^{1,6}$.$0^{8,13}$] hexadecan-16-ol (**7**).

A plausible mechanism for the formation of bislactam (**5**) and octahydrophenazine (**6**) are also illustrated in Scheme 4. Compound **7** was protonated in an acidic medium to produce a common intermediate (**9**). In 100% sulfuric acid, bislactam (**5**) was obtained by the

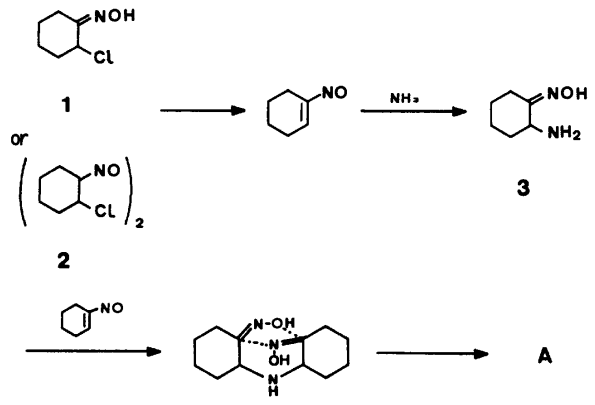

Scheme 3.

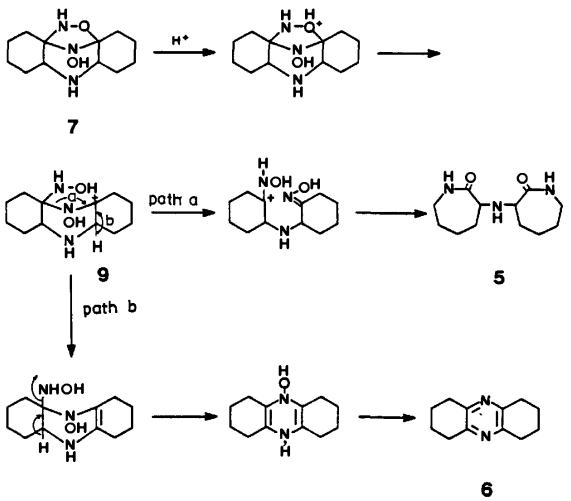

Scheme 4.

Beckmann rearrangement (path a). On the other hand, when **7** was heated in an acidic aqueous solution, **6** was formed by the elimination of hydroxylamino radical from **9** (path b).

Experimental

General. Melting points are uncorrected. The IR and mass spectra were recorded on Shimadzu IR-40 and Hitachi RMU-7M spectrometers respectively. ^{1}H-NMR and ^{13}C-NMR specra were recorded on Hitachi R-24B (60 MHz) spectrometer and JEOL FX-90Q pulse FT spectrometer (22.49 MHz) using TMS as internal standard.

Preparation of 2-Chlorocyclohexanone Oxime (1) and 1-Chloro-2-nitrosocyclohexane Dimer (2). **1** and **2** were prepared by the methods described in the patent.[5]

Preparation of 2-Aminocyclohexanone Oxime (3). In a 500 ml stainless steel autoclave, a mixture of 1-chloro-2-nitrosocyclohexane dimer (14.8 g, 0.05 mol), ammonia (170 g, 10 mol) and methanol 100 ml was heated at 70 °C. After 1 h, ammonia and methanol were removed under reduced pressure to give 15.7 g of crude 2-aminocyclohexanone oxime hydrochloride (95.3%). The crude product was purified by recrystallization from water to give (14.9 g, 90.6%) of 2-aminocyclohexanone oxime hydrochloride as white crystals; mp 212.0—213.0 °C. Found: C, 43.85; H, 8.00; N, 17.16; Cl, 21.49 %. Calcd for $C_6H_{13}N_2OCl$: C, 43.77; H, 8.02; N, 17.02; Cl, 21.53 %.

Preparation of 2-(Methylamino)cyclohexanone Oxime. To a solution of 1-chloro-2-nitrosocyclohexane dimer (14.8 g, 0.05 mol) in benzene (100 ml) was added dropwise at 60 °C a solution of methylamine (6.2 g, 0.2 mol) in benzene (50 ml) during 1 h, and the reaction mixture was heated at 60 °C for an additional 1 h. After the reaction, the mixture was cooled to room temperature and washed with a 100 ml portion of 10% sodium hydroxide. The benzene layer was dried over anhydrous magnesium sulfate, and benzene was removed under reduced pressure to give crude 13.5 g of 2-(methylamino)-cyclohexanone oxime (94.9%). The crude product was purified by recrystallization from methanol to give 10.8 g of 2-(methylamino)cyclohexanone oxime as white crystals (75.9%); mp 103—104 °C. Found: C, 59.18; H, 9.83; N, 19.75%. Calcd for $C_7H_{14}N_2O$: C, 59.12; H, 9.93; N, 19.71%.

Preparation of 14-Oxa-7,15,16-triazatetracyclo[11.2.1.0^{1,6}.0^{8,13}]-hexadecan-16-ol (7). To a mixture of 1-chloro-2-nitrosocyclohexane dimer (14.8 g, 0.05 mol), dichloromethane (200 ml), and 2 mol dm^{-3} sodium hydroxyde solution (100 ml) was added dropwise at room temperature a solution of ammonium chloride (5.4 g, 0.1 mol) in water (50 ml) during 30 min. The reaction mixture was stirred for an additional 2 h. A crystalline material suspended in the reaction mixture was filtered and washed with water. The crude product was purified by recrystallization from ethanol to give 11.3 g (94.6%) of **7** as a white solid; mp 186—187 °C. ^{1}H-NMR (CD_3COOD) δ=1.3—2.2 (m 12H), 2.2—2.6 (t 4H), 3.4—3.8 (m 2H). ^{13}C-NMR CD_3COOD δ=22.5, 23.1, 23.6, 24.3, 27.2, 27.6, 28.7, 60.3, 60.4, 85.6, 100.0. IR (KBr): 3280, 3120, 2940, 2870, 1480, 1450, 1120, 958, 942, 905, 898, 860, 820, 795 cm^{-1}. Found: C, 60.58; H, 8.81; N, 17.69%. Calcd for $C_{12}H_{21}N_3O_2$: C, 60.23; H, 8.85; N, 17.56%.

Preparation of 7-Methyl-14-oxa-7,15,16-triazatetracyclo[11.2.1.-0^{1,6}.0^{8,13}]hexadecan-16-ol (8). In a similar manner to the above, **8** was prepared from methylamine hydrochloride in 90.7% yield; white solid; mp 157—158 °C. ^{1}H-NMR (DMSO-d_6) δ=1.0—2.0 (m 16H), 2.0—2.3 (m 2H), 2.1 (s 3H), 5.9—6.1 (1H), 7.8 (1H). ^{13}C-NMR ($CDCl_3$) δ=22.5, 23.0, 24.1, 27.8, 28.1, 29.2, 29.6, 36.4, 37.9, 62.6, 67.9, 85.0, 99.1. IR (KBr): 3210, 3100, 2930, 2850, 2770, 1450, 1360, 1350, 1260, 1250, 1190, 1150, 1120, 1040, 980, 950, 930, 900, 870, 830, 790, 700 cm^{-1}. Found: C, 61.77; H, 9.03; N, 16.62%. Calcd for $C_{13}H_{23}N_3O_2$: C, 61.63; H, 9.15; N, 16.59%.

Preparation of 1,2,3,4,6,7,8,9-Octahydrophenazine (6). A mixture of 14-oxa-7,15,16-triazatetracyclo[11.2.1.0^{1,6}.0^{8,13}] hexadecan-16-ol (**7**) (23.9 g, 0.1 mol) and 1 mol dm^{-3} sulfuric acid (100 ml) was heated at 60 °C. After 3 h, the reaction mixture was cooled to room temperature and adjusted to pH 10 with 2 mol dm^{-3} sodium hydroxide solution. The solution was extracted with three 100 ml portions of benzene and then dried over anhydrous magnesium sulfate. After removal of the benzene, the residue was distilled under reduced pressure, and the fraction at 128 °C/1.6 mmHg was collected; mp 108—109 °C. ^{1}H-NMR ($CDCl_3$) δ=1.6—2.2 (8H), 2.6—3.1 (8H). IR (KBr): 2920, 2860, 1460, 1430, 1420, 1390, 1335, 1240, 1210, 1190, 1130, 1120, 1070, 1060, 980, 925, 890, 870, 816, 750 cm^{-1}. Found: C, 76.30; H, 8.43; N, 14.67%. Calcd for $C_{12}H_{16}N_2$: C, 76.56; H, 8.57; N, 14.88%.

Preparation of Bis(perhydro-2-oxo-3-azepinyl)amine (5). To 100% sulfuric acid (98 g, 1 mol) was added at 60 °C 14oxa-7, 15, 16-triazatetracyclo[11.2.1.0^{1,6}.0^{8,13}]hexadecan-16-ol (23.9 g, 0.1 mol) over 30 min. The reaction mixture was heated at 60 °C for an additional 1 h. After the reaction mixture was cooled to 10—20 °C, water (200 ml) was added at 0—5 °C. The resulting solution was adjusted to pH 10 with 30% sodium hydroxide solution and was extracted with three 300 ml portions of chloroform; then the chloroform extract was dried over anhydrous magnesium sulfate. After removal of the chloroform, the residue was distilled under reduced pressure, and the fraction at 220 °C/0.25 mmHg was collected. ^{1}H-NMR (DMSO-d_6) δ=1.2—2.4 (12H), 2.5 (NH), 2.9—3.4 (4H), 4.0—4.5 (2H), 8.0—8.6 (-NH-C(=O)-, 2H). IR (KBr): 3300, 3200, 3070, 2970, 2920, 2840, 1660, 1470, 1450, 1420, 1380, 1350, 1320, 1300, 1260, 1150, 1130, 1110, 980, 970, 820 cm^{-1}. Found: C, 60.56; H, 8.51; N, 17.79%. Calcd for $C_{12}H_{21}N_3O_2$: C, 60.23; H, 8.85; N, 17.56%.

X-Ray Crystal Structure Determination. Crystal data: $C_{12}H_{21}N_3O_2$, Mr=239.32, monoclinic, $P2_1/c$, a=6.022(1), b=19.245(4), c=10.560(1) Å, β=95.94(1)°, V=1217.4 Å^3, Dm=1.298, Dx=1.306 Mg m^{-3}, Z=4, F(000)=520, μ(Cu $K\alpha$)=0.74 mm^{-1}, the final R was 0.0464 for 2022 unique reflections.

Crystals of compound **7** suitable for X-ray diffraction were obtained upon recrystallization from an ethanol solution. Preliminary film work revealed the material to be monoclinic with systematic absences (h0l, $l=2n+1$; 0k0, $k=2n+1$) strongly indicative of the centrosymmetric space group C_{2h}^5 $-P2_1/c$. The density was measured by flotation in chloroform-cyclohexane solution. The unit cell parameters were obtained by least-squares from 2θ values for 15 reflections measured on a diffractometer. The intensities of 2022 (1990 non-zero) independent reflections were collected on a Rigaku automatic four-circle diffractometer up to an angle of 2θ=125° with graphite monochromated Cu $K\alpha$ radiation, using the $2\theta-\omega$ scan technique and scan range of $(0.8+0.142\tan\theta)°(\omega)$. The scan speed and the background counting time were 10°/min and 3s at each terminus of the scans for $0°<2\theta\leqq 80°$, 5°/min and 6s for $80°<2\theta\leqq 100°$, and 2°/min, 15s for $110°<2\theta\leqq 125°$. Three standard reflections were measured every 100 measurements with no significant deterioration in intensity. Lorentz and polarization correction were applied, but not that for absorption.

The structure was solved with the MULTAN 78 program[6] which located all the non-hydrogen atoms. Isotropic and anisotropic block-diagonal least-squares refinement with HBLS VI program[7] reduced R to 0.070. A difference synthesis at this stage clearly indicated all H atoms, which were included in the refinement with isotropic temperature factors. In the refinement, the function minimized was $\sum\omega(|F_o|-|F_c|)^2$

with $\omega=[\sigma^2(F_o)+a|F_o|+b|F_o|^2]^{-1}$ for $F_o\neq 0$ and $\omega=c$ for $F_o=0$, where $\sigma(F_o)$ is the standard deviation based on counting statistics. Final refinement ($a=0.0006$, $b=5.7428$ and $c=0.01379$) gave $R=0.0464$ ($\omega R=0.0639$) for all reflections and $R=0.0459$ for non-zero reflections. No significant peaks were observed in the final difference map, except for a few peaks of *ca* 0.3 eÅ^{-3}. All calculations were performed with the UNICS programs on a FACOM M-200 computer.[8]

References

1) Toray Industries, Inc., U. S. Patent. 3839448 (1974).
2) Y. Izumi, I. Chibata, and T. Itoh, *Angew. Chem., Int. Ed. Engl.*, **17**, 176 (1978).
3) M. Ohno, S. Torimitsu, N. Naruse, and M. Okamoto, *Bull. Chem. Soc. Jpn.*, **39**, 1129 (1966).
4) J. Beger, T. T. Luong, C. Thieleman, and P. D. Thong, *J. Prakt. Chem.* **320**, 433 (1978).
5) FMC corp, U. S. Patent 2485180 (1949); BASF, DE. Patent 1082253 (1960).
6) P. Main, S. E. Hull, L. Lessinger, G. Germain, J. P. Declercq, and M. M. Woolfson, "MULTAN 78, A System of Computer Programmes for the Automatic Solution of Crystal Structure from X-ray Diffraction Data", Univ. of York, England, and Louvain, Belgium (1978).
7) T. Ashida, "The Universal Crystallographic Computing System-Nagoya", The Computation Center, Nagoya University (1981).
8) The lists of structure factors, anisotropic thermal parameters for non-hydrogen atoms and atomic parameters for hydrogen atoms are deposited at the office of this Bulletin as Document No. 8420.

 © 1984 The Chemical Society of Japan Bull. Chem. Soc. Jpn., 57, 2167—2170 (1984)

Reactions of 2-Chloroacyltrimethylsilanes with Grignard Reagents. Preparation of 3-(Trimethylsilyl)-2-alkanones and 2-(Trimethylsilyl)-1-alkanols[1)]

Toshio SATO,† Kazuhisa MATSUMOTO, Toru ABE, and Isao KUWAJIMA*
Department of Chemistry, Tokyo Institute of Technology, Meguro, Tokyo 152, Japan
(Received January 11, 1984)

Reactions of 2-chloroacyltrimethylsilanes with Grignard reagents have been examined. Thus, treatment with methylmagnesium iodide affords the corresponding 3-(trimethylsilyl)-2-alkanones through an initial addition followed by removal of chloride anion and 1,2-rearrangement of silyl group. In contrast, the reaction proceeds with 2 equiv of the Grignard reagents bearing β-hydrogen to give 2-(trimethylsilyl)-1-alkanols, where initial reduction of the silylcarbonyl group followed by such rearrangement and addition of the Grignard reagents to the resulting 2-(trimethylsilyl)alkanals have been proposed.

Enol silyl ethers have recently been employed as one of the most promising nucleophiles in organic synthesis.[2)] Use of this class of compounds has allowed regioselective introduction of a variety of functional groups or carbon chain onto α-carbons of the carbonyl compounds. For regioselective preparation of enol silyl ethers from the corresponding ketones, difference of thermodynamically and kinetically favorable enolates has usually been utilized to reflect their geometries to those of enol silyl ethers.[3)] Based on these features, various methods have been developed for regioselective synthesis of enol silyl ethers, but there have been still encountered several difficulties on occasions where such difference is very small or negligible. In order to explore a new methodology for regioselective synthesis of enol silyl ethers,[4)] we have examined the reaction of 2-chloroacyltrimetylsilanes **1** with Grignard reagents, assuming that the initially formed adduct **2** undergoes 1,2-rearrangement[5)] of silyl group from carbon to oxygen to yield **3**. The resulting **3** may be converted to the corresponding enol silyl ethers regiospecifically through removal of magnesium halides as shown in Scheme 1.

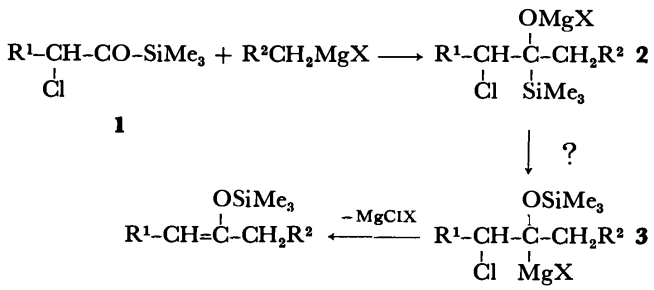

Scheme 1.

Results and Discussion

The requisite 2-chloroacyltrimethylsilanes **1** can be prepared in excellent yields by treating the corresponding enol silyl ethers of acyltrimethylsilanes[6)] with an equimolar amount of chlorine in carbon tetrachloride at ambident temperature (see Table 1). Direct chlorination of acyltrimethylsilanes is also employable, but formation of a small amount of dichlorides accompanies as by-products.[7)]

†Present address: Chemistry Department of Resources, Mie University, Tsu, Mie 514.

$$R^1\text{-CH=C(OSiMe}_3\text{)-SiMe}_3 + Cl_2 \longrightarrow R^1\text{CH(Cl)-CO-SiMe}_3$$

1

TABLE 1. PREPARATION OF 2-CHLORO- AND 2-BROMOACYLTRIMETHYLSILANES **1**

R¹	Yield/%	
	Chloride	Bromide
a) *n*-C_4H_9	83	81
b) *n*-C_6H_{13}	89	92
c) $C_6H_5CH_2$	87	87
d) CH_2=CH-$(CH_2)_7$	82	85

In contrary to our assumption, treatment of 2-chlorohexanoyltrimethylsilane with an equimolar amount of methylmagnesium iodide in tetrahydrofuran (THF) at −78 °C has never afforded the expected enol silyl ether, but its isomer, 3-trimethylsilyl-2-heptanone has been isolated in 91% yield (Eq. 1). Other chlorides also afforded the corresponding 3-(trimethylsilyl)-2-alkanones **4** in excellent yields (Table 2). Similar reactions were also examined with methyllithium, but afforded much less satisfactory results.

$$\mathbf{1} + CH_3MgI \longrightarrow \mathbf{2}(R^2\text{=H,X=I}) \longrightarrow R^1\text{CH(SiMe}_3\text{)-CO-CH}_3 \quad \mathbf{4} \quad (1)$$

TABLE 2. PREPARATION OF 3-(TRIMETHYLSILYL)-2-ALKANONES **4**

R¹	Yield/%
a) *n*-C_4H_9	91
b) *n*-C_6H_{13}	90
c) $C_6H_5CH_2$	98
d) CH_2=CH-$(CH_2)_7$	91

Similarly, 2-methyl-1-propenylmagnesium bromide afforded the corresponding unsaturated silyl ketone **4e** in 72% yield.

$$C_4H_9\text{-CH(Cl)-CO-SiMe}_3 + (CH_3)_2C\text{=CHMgBr} \longrightarrow C_4H_9\text{-CH(SiMe}_3\text{)-CO-CH=C(CH}_3\text{)}_2 \quad \mathbf{4e}$$

These results have clearly indicated that transfer of silyl group to the neighboring carbon atom takes place preferentially even under such mild reaction conditions. Intermediary formation of α,β-epoxysilane can

be ruled out because Mg^{2+} cation induced rearrangement of such material should afford the corresponding 2-halo-2-(trimethylsilyl)-3-alkanol as reported.[8] Instead, the reaction is considered to proceed through removal of chloride anion from the initially formed alkoxide **2** followed by rearrangement of trimethylsilyl group to the resulting cationic site to afford **4**. We have found no evidence on the question whether these processes occur successively or in concerted manner, but both of them are expected to be greatly favored. The first stage may be facilitated by σ-π interaction with the neighboring silyl group[9] and the second one may be accelerated by the aid of an anionic character of O–Mg bond. A combination of these three factors is considered to induce this characteristic transformation so efficiently.

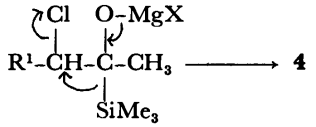

In contrast, on using Grignard reagents bearing β-hydrogen in the reaction with **1**, 2 equiv of the Grignard reagent are required to complete a conversion, and 2-(trimethylsilyl)-1-alkanol **5** has been obtained in place of **4**. For example, the reaction of **1** ($R^1=C_6H_5CH_2$) with 1 equiv of hexylmagnesium bromide resulted in formation of a mixture of **5** ($R^1=C_6H_5CH_2$, $R^2=C_4H_9$, 39%) and 3-phenylpropanal (18%) together with the recovered starting material (17%), whereas use of 2 equiv of the Grignard reagent led to the exclusive formation of the corresponding **5**.

In connection with this transformation, it has been reported by Brook *et al.*[10] that in stead of an addition reaction, acylsilanes undergo reduction preferentially to yield 2-(trimethylsilyl)-1-alkanols on treating with Grignard reagents bearing β-hydrogen. Similarly, it appears to be reasonable to assume that the corresponding alkoxide **6** is formed as an initial product in this case. Then, **6** may undergo the same type of transformation to yield the corresponding 2-(trimethylsilyl)alkanal **7**, which reacts further with the Grignard reagent to give **5** as shown in Eq. 2. Higher reactivity of an aldehyde function to such nucleophiles has made it very difficult to isolate 7. Although several attempts to isolate **7** have failed, formation of 3-phenylpropanal in the above experiment supports **7** as a plausible intermediate.

According to Cram's rule,[11,12] selective formation of erythro isomer **5** has been expected in the reaction of **7** with Grignard reagents because trimethylsilyl group should behave as much more bulky one than most of alkyl groups. Hudrlik *et al.* recently described threo selective reduction of 2-(trimethylsilyl)alkanones with

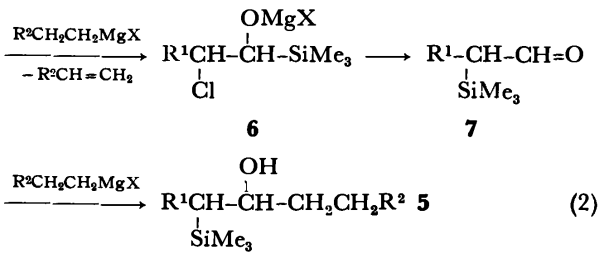

(2)

Table 3. Preparation of 2-(trimethylsilyl)-1-alkanols **5**

R^1	R^2	Yield/%
a) n-C_4H_9	n-C_2H_5	85
b) n-C_4H_9	n-C_4H_9	90
c) n-C_6H_{13}	n-C_4H_9	90
d) $C_6H_5CH_2$	n-C_2H_5	92
e) $C_6H_5CH_2$	n-C_4H_9	96
f) CH_2=CH-$(CH_2)_7$	n-C_4H_9	92

diisobutylaluminium hydride (DIBAL) and stereoselective conversion of the resulting alcohols to (*E*)- and (*Z*)-olefins under the influence of base and Lewis acid, respectively.[12a]

In order to confirm stereochemical outcome of this addition reaction, 2-chlorohexanoyltrimethylsilane was treated with 2.2 equiv of butylmagnesium bromide in THF at −78 °C for 30 min, and the corresponding **5** ($R^1=C_4H_9$, $R^2=C_2H_5$) was isolated in 85% yield. As expected, on treating with potassium hydride and boron trifluoride etherate, the resulting alcohol **5** afforded (*E*)- and (*Z*)-5-decene, respectively, in highly stereo-controlled manner as shown in the following equation. These results apparently verified highly selective formation of erythro isomer **5** in the present one-pot procedure.

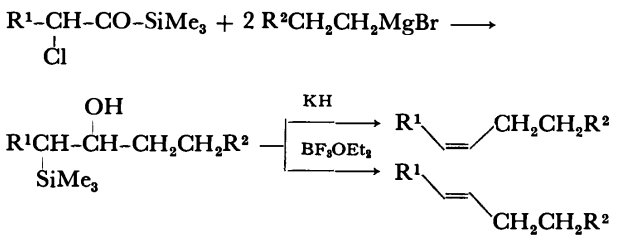

Yield of olefins/% ($Z:E$)

R^1	R^2	KH	$BF_3\cdot OEt_2$
C_4H_9	C_2H_5	82 (96:4)	85 (5:95)
C_2H_5	C_6H_5	89 (96:4)	78 (6:94)

In summary, use of 2-chloroacyltrimethylsilanes has made it feasible to prepare 3-(trimethylsilyl)-2-alkanones or 2-(trimethylsilyl)-1-alkanols, depending on the Grignard reagent employed, in completely regiocontrolled manner. The latter alcohols can be oxidized to the corresponding silyl ketones[12a] in good yield.

Although we failed to explore a method for regiospecific preparation of enol silyl ethers by a sequence described above,[13] these silyl ketones[12,14] obtained undergo a facile isomerization to the corresponding enol silyl ethers regiospecifically.[15] Further, these silyl ketones themselves have been proved to be especially useful for regioselective aldol formation because the silyl group has played dual roles for selective generation of two types of enolates as described already.[16]

Experimental

General Methods. Boiling points are uncorrected. Infrared (IR) spectra were recorded on a Hitachi EPI-G3 spectrometer; absorptions are reported in reciprocal centimeters. Proton nuclear magnetic resonance spectra (^1H NMR) were obtained on a Hitachi R-24B spectrometer; chemi-

cal shifts (δ) are expressed in part per million downfield from tetramethylsilane. Analytical gas-liquid chromatography (GLC) was performed on a Hitachi 163 instrument with a flame ionization detector and nitrogen carrier gas (1.0—1.3 kg/cm^2) using a OV-101 fused silica 20 m capillary column (Hitachi Chemi-Column). Microanalysis were performed with a Perkin-Elmer 240 at the Micro-analytical Laboratory, Tokyo Institute of Technology.

Reactions involving air- or moisture-sensitive compounds were carried out in appropriate round-bottomed flasks with stirring bars under nitrogen or argon atmosphere. Bulb-to-bulb distillation was performed with a Büchi Kugelrohr apparatus.

Preparative thin-layer chromatography (TLC) was carried out on glass plates (20×20 cm) coated with Merck silica gel PF 254 (1 mm thick).

Hexane was distilled from sodium. Ether and tetrahydrofuran (THF) were distilled from sodium-benzophenone ketyl immediately before use.

Materials. Enol trimethylsilyl ethers of acyltrimethylsilanes were prepared from the corresponding enol trimethylsilyl ethers of benzenethiol or methanethiol esters according to the procedure developed in our laboratory.[6]

Preparation of 2-Chloro- or 2-Bromoacyltrimethylsilanes. General Procedure: An enol trimethylsilyl ether of acyltrimethylsilane (1 mmol) in carbon tetrachloride (1.5 ml) was added to a carbon tetrachloride (4.5 ml) solution of chlorine or bromine (1.1 mmol) at −20 °C and it was stirred for 5—10 min at that temperature under argon. Then, the solvent was removed on a rotary evaporator, and the residual oil was separated by preparative TLC using a mixture of hexane and ether (5:1) as a solvent to give the title compound.

2-Chlorohexanoyltrimethylsilane **1a**: IR(neat): 1650, 1250, 855 cm^{-1}; NMR(CCl_4) δ=0.30 (s, 9H), 0.77—2.33 (m, 9H), 4.11 (t, J=6 Hz, 1H); Calcd for $C_9H_{19}OClSi$: C, 52.27; H, 9.26. Found: C, 52.40; H, 9.05.

2-Bromohexanoyltrimethylsilane **1a'**: IR (neat): 1652, 1250, 855 cm^{-1}; NMR(CCl_4) δ=0.40 (s, 9H), 0.76—2.33 (m, 9H), 4.33 (t, J=7 Hz, 1H); Calcd for $C_9H_{19}OBrSi$: C, 43.03; H, 7.62. Found: C, 43.21; H, 7.50.

2-Chlorooctanoyltrimethylsilane **1b**: IR (neat): 1650, 1250, 855 cm^{-1}; NMR(CCl_4) δ=0.33 (s, 9H), 0.66—2.43 (m, 13H), 4.15 (t, J=5 Hz, 1H); Calcd for $C_{11}H_{23}OClSi$: C, 52.26; H, 9.87. Found: 52.43; H, 9.59.

2-Bromooctanoyltrimethylsilane **1b'**: IR (neat): 1650, 1250, 855 cm^{-1}; NMR(CCl_4) δ=0.33 (s, 9H), 0.66—2.43 (m, 13H), 4.37 (t, J=7 Hz, 1H).

2-Chloro-3-phenylpropionyltrimethylsilane **1c**: IR (neat): 1645, 1250, 845 cm^{-1}; NMR(CCl_4) δ=0.33 (s, 9H), 2.99 (dd, J=14 and 8 Hz, 1H), 3.40 (dd, J=14 and 6 Hz, 1H), 4.50 (dd, J=8 and 6 Hz, 1H), 7.20 (s, 5H); Calcd for $C_{12}H_{17}OClSi$: C, 59.85; H, 7.12. Found: C, 60.06; H, 6.97.

2-Bromo-3-phenylpropionyltrimethylsilane **1c'**. IR (neat): 1640, 1250, 845 cm^{-1}; NMR (CCl_4) δ=0.20 (s, 9H), 3.05 (dd, J=14 and 7 Hz, 1H), 3.53 (dd, J=14 and 7 Hz, 1H), 4.70 (t, J=7 Hz, 1H), 7.23 (s, 5H).

2-Chloro-10-undecenoyltrimethylsilane **1d**: IR (neat): 1652, 1250, 855 cm^{-1}; NMR(CCl_4) δ=0.30 (s, 9H), 1.15—2.25 (m, 14H), 4.23 (t, J=6 Hz, 1H), 4.94 (d, J=13 Hz, 1H), 4.99 (d, J=17 Hz, 1H), 5.78 (m, 1H); Calcd for $C_{14}H_{27}OClSi$: C, 61.17; H, 9.90. Found: C, 61.05; H, 10.08.

2-Bromo-10-undecenoyltrimethylsilane **1d'**. IR (neat): 1651, 1250, 855 cm^{-1}; NMR(CCl_4) δ=0.30 (s, 9H), 1.00—2.50 (m, 14H), 4.40 (t, J=6 Hz, 1H), 4.94 (d, J=13 Hz, 1H), 4.99 (d, J=17 Hz, 1H), 5.78 (m, 1H).

The Reaction of 2-Chloroacyltrimethylsilane with Methylmagnesium Iodide. General Procedure: An ethereal solution of methylmagnesium iodide (21.8 ml of 0.95 M solution (1 M=1 mol dm^{-3})) was added to a THF (20 ml) solution of 2-chloroacyltrimethylsilane (20 mmol) at −78 °C and it was stirred for 30 min at that temperature under argon. Hexane (200 ml) pre-cooled to −60 °C was added directly to the reaction mixture and the resulting solution was washed with satd aq NH_4Cl (20 ml). After drying the organic layer with anhyd $MgSO_4$ and removal of the solvent, fractional distillation of the residual oil gave the corresponding 3-(trimethylsilyl)-2-alkanone.

3-(Trimethylsilyl)-2-heptanone **4a**: Bp 78—83 °C/5 mmHg (1 mmHg≈133.322 Pa); IR (neat): 2950, 2920, 2845, 1693, 1253, 843 cm^{-1}; NMR (CCl_4) δ=−0.11 (s, 9H), 1.63—4.70 (m, 9H), 1.83 (s, 3H), 2.06—2.43 (m, 1H); Calcd for $C_{10}H_{22}OSi$: C, 64.45; H, 11.90. Found: C, 64.28; H, 12.13.

3-(Trimethylsilyl)-2-nonanone **4b**: Bp 86—90 °C/2 mmHg; IR (neat): 2950, 2920, 2845, 1693, 1253, 843 cm^{-1}; NMR (CCl_4) δ=−0.10 (s, 9H), 0.57—1.60 (m, 16H), 1.87 (s, 3H), 2.13—2.50 (m, 1H); Calcd for $C_{12}H_{26}OSi$: C, 67.22; H, 12.22. Found: C, 67.09; H, 12.07.

4-Phenyl-3-(trimethylsilyl)-2-butanone **4c**: Bp 117—120 °C/1 mmHg; IR (neat): 3020, 1920, 1690, 1605, 1497, 1255, 845 cm^{-1}; NMR (CCl_4) δ=0.00 (s, 9H), 1.77 (s, 3H), 2.35—3.38 (m, 3H), 7.05 (s, 5H); Calcd for $C_{13}H_{20}OSi$: C, 70.85; H, 9.15. Found: C, 70.62; H, 9.03.

3-(Trimethylsilyl)-11-dodecen-2-one **4d**: Bp. 117—120 °C/1 mmHg; IR (neat): 3070, 2925, 2850, 1695, 1645, 1255, 985, 910, 840 cm^{-1}; NMR (CCl_4) δ=−0.11 (s, 9H), 0.90—1.40 (m, 12H), 1.75—2.40 (m, 3H), 4.87 (d, J=11 Hz, 1H), 4.92 (d, J=16 Hz, 1H), 5.12—6.00 (m, 1H); Calcd for $C_{15}H_{30}OSi$: C, 70.79; H, 11.88. Found: C, 70.92; H, 12.03.

2-Methyl-5-(trimethylsilyl)-2-nonen-4-one **4e**: IR (neat): 1670, 1620 cm^{-1}; NMR (CCl_4) δ=0.07 (s, 9H), 0.70—1.50 (m, 9H), 1.70—2.40 (m, 2H), 1.87 (s, 3H), 2.13 (s, 3H), 5.90 (m, 1H).

The Reaction of 2-Chloroacyltrimethylsilane with a Grignard Reagent Bearing β-Hydrogen. General Procedure: An ethereal solution of the Grignard reagent (5.2 mmol) was added to a THF (2.5 ml) solution of 2-chloroacyltrimethylsilane (2.5 mmol) at −78 °C and it was stirred for 30 min at that temperature. Then, the reaction mixture was quenched with satd aq NH_4Cl and the aqueous layer was extracted with ether. After drying the combined extracts over anhyd $MgSO_4$ and removal of the solvent, purification of the residual oil with TLC using a mixture of hexane and ether (20:1) afforded the corresponding 2-(trimethylsilyl)-1-alkanol.

5-(Trimethylsilyl)-6-dodecanol **5b**: IR (neat): 3440, 2950, 2920, 1240, 836 cm^{-1}; NMR (CCl_4) δ=−0.07 (s, 9H), 0.7—1.62 (m, 23H), 2.06 (br s, 1H), 3.63 (m, 1H); Calcd for $C_{15}H_{34}OSi$: C, 69.69; H, 13.26. Found: C, 69.42; H, 13.38.

6-(Trimethylsilyl)-7-tetradecanol **5c**: IR (neat): 3450, 2920, 2850, 1247, 836 cm^{-1}; NMR (CCl_4) δ=0.03 (s, 9H), 0.77—1.73 (m, 27H), 1.97 (br s, 1H), 3.77 (m, 1H); Calcd for $C_{17}H_{38}OSi$: C, 71.25; H, 13.37. Found: C, 71.07; H, 13.16.

1-Phenyl-2-(trimethylsilyl)-3-heptanol **5d**: IR (neat): 3430, 1250, 840 cm^{-1}; NMR (CCl_4) δ=0.10 (s, 9H), 0.90—1.80 (m, 11H), 2.83 (d, J=7 Hz, 2H), 3.85 (m, 1H), 7.26 (s, 5H).

1-Phenyl-2-(trimethylsilyl)-3-nonanol **5e**: IR (neat): 3450, 3060, 3030, 3000, 2940, 2900, 2835, 1600, 1490, 1245, 835 cm^{-1}; NMR (CCl_4) δ=0.03 (s, 9H), 0.7—1.9 (m, 14H), 2.01 (br s, 1H), 2.95 (d, J=7 Hz, 2H), 3.95 (m, 1H), 7.38 (s, 5H); Calcd for $C_{18}H_{32}OSi$: C, 73.90; H, 11.03. Found: C, 73.68; H, 10.89.

8-(Trimethylsilyl)-16-heptadecen-7-ol **5f**: IR (neat): 3420, 3070, 2925, 2850, 1645, 1255, 910, 840; NMR (CCl_4) δ=−0.07 (s, 9H), 0.6—1.67 (m, 26H), 1.67—2.17 (m, 2H), 2.83 (br s, 1H), 4.87 (d, J=11 Hz, 1H), 4.92 (d, J=16 Hz, 1H), 5.12—6.00 (m, 1H); Calcd for $C_{20}H_{42}OSi$: C, 73.54; H, 12.96. Found: C, 73.33; H, 13.04.

Conversion of 6-(Trimethylsilyl)-5-decanol to (E)- and (Z)-5-Decene. 2-Chlorohexanoyltrimethylsilane (412 mg, 2 mmol) was treated with butylmagnesium bromide (4.4 mmol) in a

similar manner as described above and 6-(trimethylsilyl)-5-decanol **5a** (462 mg, 85%) was obtained. IR (neat): 3450, 2960, 1680, 835 cm^{-1}; NMR(CCl_4) δ=−0.06 (s, 9H), 0.77—1.67 (m, 19H), 3.70 (m, 1H). To a THF (2 ml) solution of the alcohol **5a** (230 mg, 1 mmol) was added KH (3 mmol) in THF (1 ml) at 0 °C and it was stirred for 1 h at room temperature. Then, the reaction mixture was quenched with sat aq NH_4Cl and the aqueous layer was extracted with ether. The combined extracts were dried over anhyd $MgSO_4$, and the resulting solution was analyzed by GLC using decane as an internal standard, which showed formation of a mixture of (*E*)- and (*Z*)-5-decene in 82% yield. Ratio of (*E*)- to (*Z*)-isomer was determined to be 4:96 by comparison with the authentic sample.

The same alcohol (216 mg, 0.94 mmol) was treated with BF_3OEt_2 (0.4 ml) in dichloromethane (5 ml) at room temperature for 1 h. Similar analysis of the reaction mixture indicated formation of (*E*)- and (*Z*)-5-decene in 85% yield in a ratio of 95:5, respectively.

References

1) A preliminary report dealing with certain aspects of this work has appeared; T. Sato, T. Abe, and I. Kuwajima, *Tetrahedron Lett.*, 259 (1978).

2) a) E. W. Colvin, "Silicon in Organic Synthesis", Butterworths, London, 1981, chapter 17; b) W. P. Weber, "Silicon Reagents for Organic Synthesis", Springer-Verlag, Berlin, 1983, chapter 12; c) P. Brownbridge, *Synthesis*, 1, 85 (1983).

3) G. Stork and P. F. Hudrlik, *J. Am. Chem. Soc.*, **90**, 4462, 4464 (1968); H. O. House, L. J. Czuba, M. Gall, and H. D. Olmstead, *J. Org. Chem.*, **34**, 2324 (1969); See also ref 2b, chapter 16.

4) Other indirect methods for regiospecific preparation of enol silyl ethers, see: I. Kuwajima and M. Kato, *J. Chem. Soc., Chem. Commun.*, 708 (1979); I. Kuwajima and M. Kato, *Tetrahedron Lett.*, **21**, 2745 (1980); M. Kato, A. Mori, H. Oshino, J. Enda, K. Kobayashi, and I. Kuwajima, *J. Am. Chem. Soc.*, **106**, 1773 (1984).

5) A. G. Brook, *Acc. Chem. Res.*, **7**, 77 (1974).

6) I. Kuwajima, M. Arai, and T. Sato, *J. Am. Chem. Soc.*, **99**, 4181 (1977); I. Kuwajima, M. Kato, and T. Sato, *J. Chem. Soc., Chem. Commun.*, 478 (1978); I. Kuwajima, A. Mori, and M. Kato, *Bull. Chem. Soc. Jpn.*, **53**, 2368 (1980).

7) I. Kuwajima, T. Abe, and N. Minami, *Chem. Lett.*, 993 (1976).

8) P. F. Hudrlik, R. N. Misra, G. P. Withers, A. M. Hudrlik, and R. J. Rona, *Tetrahedron Lett.*, 1453 (1976).

9) A. W. P. Jarvie, *Organomet. Chem. Rev.*, **A6**, 153 (1970).

10) A. G. Brook, M. A. Quigley, G. J. D. Peddle, N. V. Schwartz, and C. M. Warner, *J. Am. Chem. Soc.*, **82**, 5102 (1960).

11) D. J. Cram and F. A. Abd Elhafez, *J. Am. Chem. Soc.*, **74**, 5828 (1952).

12) a) P. F. Hudrlik and D. Peterson, *J. Am. Chem. Soc.*, **97**, 1464 (1975); b) K. Utimoto, M. Obayashi, and H. Nozaki, *J. Org. Chem.*, **41**, 2940 (1976).

13) Reich and his collaborators reported a regioselective preparation of enol silyl ethers using acyltrimethylsilanes: H. J. Reich, J. J. Rusek, and R. E. Olson, *J. Am. Chem. Soc.*, **101**, 2225 (1979).

14) Other methods for the preparation of 2-silyl ketones, see: M. Obayashi, K. Utimoto, and H. Nozaki, *Tetrahedron Lett.*, 1805 (1977); M. Obayashi, K. Utimoto, and H. Nozaki, *Bull. Chem. Soc. Jpn.*, **52**, 2646 (1979); C. J. Kowalski, M. L. O'Dowd, M. C. Burke, and K. W. Fields, *J. Am. Chem. Soc.*, **102**, 5471 (1980); I. Kuwajima and R. Takeda, *Tetrahedron Lett.*, **22**, 2381 (1981); H. Beisswenger and M. Hanack, *ibid.*, **23**, 403 (1982).

15) On mercury(II) salt-catalyzed isomerization: I. F. Lutsenko, Y. I. Baukov, O. V. Dudukina, and E. N. Kramarova, *J. Organomet. Chem.*, **11**, 35 (1968). On thermal isomerization: A. G. Brook, D. M. Macrae, and W. W. Limburg, *J. Am. Chem. Soc.*, **89**, 5493 (1967), and Ref 5.

16) I. Kuwajima, T. Inoue, and T. Sato, *Tetrahedron Lett.*, 4887 (1978).

 © 1984 The Chemical Society of Japan Bull. Chem. Soc. Jpn., 57, 2171—2176 (1984)

Axially Dissymmetric Bis(aminophosphine)s Derived from 2,2′-Diamino-1,1′-binaphthyl. Synthesis and Application to Rhodium(I)-Catalyzed Asymmetric Hydrogenations[1)]

Sotaro MIYANO,* Masayoshi NAWA, Akira MORI, and Harukichi HASHIMOTO
Department of Applied Chemistry, Faculty of Engineering, Tohoku University, Aramaki-Aoba 980
(Received January 13, 1984)

Axially dissymmetric bisphosphine ligands, (*R*)- and (*S*)-2,2′-bis(diphenylphosphinoamino)-1,1′-binaphthyl (BDPAB) and (*R*)-2,2′-bis[*N*-(diphenylphosphino)methylamino]-1,1′-binaphthyl (Me-BDPAB) were conveniently prepared from 2,2′-diamino-1,1′-binaphthyl. The rhodium(I)-catalyzed asymmetric hydrogenation of α-acylamidoacrylic acids and esters gave the corresponding amino acids of up to 95% optical purity. The sign of the centro-chirality of the product amino acids was always the same to that of the axial chirality of the ligand in both cases of BDPAB and Me-BDPAB.

Asymmetric hydrogenation of prochiral olefins catalyzed by rhodium(I)-chiral phosphine complexes has been widely studied.[2)] Although the mechanism of the hydrogenation has recently been greatly clarified,[3)] there has still been continuing interest in the synthesis of novel chiral phosphine ligands,[4)] as subtle variations in ligand structure not only greatly affect the optical yields but sometimes alter even the absolute configuration of the preferential products. Some of these ligands have shown enantioselectivity which rivals that of enzymic reactions. However, the synthesis and isolation of many of chiral phosphines require tedious manipulations, imposing some restrictions to their wide use. In this regard, aminophosphines have recently attracting much interest because they can be readily prepared and show high stereoselectivity in the rhodium-catalyzed asymmetric hydrogenation.[5)]

Axially dissymmetric 1,1′-binaphthyl moiety has proved to be highly desirable asymmetry-inducing unit because of its structural rigidity and simplicity, resistance to racemization, and above all, effectiveness of chiral recognition.[6)] Three research groups have reported chiral bisphosphine ligands, **1a** (NAPHOS),[7)] **1b**,[8)] and **2** (BINAP),[9)] which contain the atropisomeric 1,1′-binaphthyl residue as the chiral element for use in the rhodium-catalyzed asymmetric hydrogenation of prochiral olefins. Recently a biphenyl phosphine **3** (MABP) has appeared.[10)]

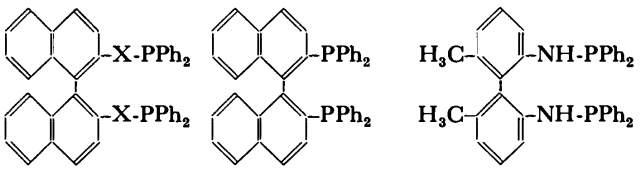

1 a -X- = $-CH_2-$ (NAPHOS)
b -X- = -O-
c -X- = -NH- (BDPAB)
d -X- = $-N(CH_3)-$ (Me-BDPAB)

2 (BINAP) **3** (MABP)

We ourselves have reported briefly a facile synthesis of (*R*)- and (*S*)-2,2′-bis(diphenylphosphinoamino)-1,1′-binaphthyl (**1c**, hereafter abbreviated as BDPAB) and asymmetric hydrogenation of α-acylamidoacrylic acids and esters by use of Rh(I)–BDPAB complexes.[1)] In this paper, we wish to report the results we have obtained in the course of this investigation including the synthesis of 2,2′-bis[*N*-(diphenylphosphino)methylamino]-1,1′-binaphthyl (**1d**, Me-BDPAB).

Results and Discussion

Synthesis of 2,2′-Diamino-1,1′-binaphthyls. According to the method reported briefly by Clemo and Dawson,[11)] 2-naphthol was converted to 2,2′-diamino-1,1′-binaphthyl (**4a**) by heating with hydrazine hydrate to 170—180 °C in a sealed vessel, and then treating with hot aq HCl. Although the yield of the diamine was not so much good (less than 40% at our hand) and the formation of carcinogenic 2-naphthylamine as a by-product requires careful handling of the reaction mixture, the procedure seems to be the one of choice because of operational simplicity and inexpensive starting materials.[12)] Both enantiomers of the diamine (**4a**) were readily obtained by the method of Kuhn and Goldfinger using *d*-camphorsulfonic acid as the resolving agent.[12)]

Preparation of 2,2′-bis(methylamino)- and 2,2′-bis(ethylamino)-1,1′-binaphthyl (**4b** and **4c**) is summarized in Eq. 1. Treatment of parent diamine **4a** with

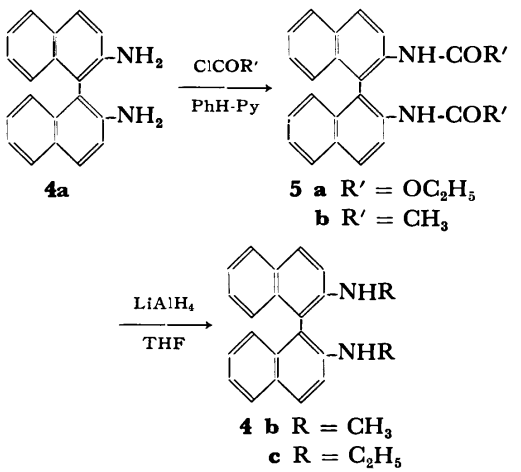

4a **5 a** R′ = OC_2H_5, **b** R′ = CH_3 **4 b** R = CH_3, **c** R = C_2H_5 (1)

ethyl chloroformate in benzene-pyridine gave 2,2′-bis(ethoxycarbonylamino)-1,1′-binaphthyl (**5a**), which was then boiled with lithium aluminium hydride (LAH) in THF to give **4b**. By using (*R*)- or (*S*)-**4a**, the corresponding atropisomeric **4b** was obtained. Similar treatment of diamine **4a** with acetyl chloride and then reduction with LAH gave *N*-ethyl analogue, **4c**.

Synthesis of 2,2′-Bis(diphenylphosphinoamino)-1,1′-binaphthyls. At first, diamine **4a** was treated with diphenylphosphinous chloride in THF in the presence of triethylamine or pyridine according to the conventional procedure,[5] but no detectable amount of phosphinated amine was resulted. Then, racemic **4a** was *N,N′*-dilithiated with stoichiometric amount of butyllithium in THF–hexane at −30 °C followed by treatment with diphenylphosphinous chloride; BDPAB **1c** was obtained as white crystals in a 75% yield (Eq. 2). Similar treatment of (*R*)- and (*S*)-**4a** gave the corresponding (*R*)- and (*S*)-BDPAB, respectively. The (*R*)-BDPAB was recrystallized twice from ethanol–benzene to show $[\alpha]_D^{23}$+27.2° in benzene. Significant racemization of the axial dissymmetry is ruled out considering the high asymmetric induction in the Rh(I)-catalyzed hydrogenation of (*Z*)-α-benzamidocinnamic acid (*vide infra*).

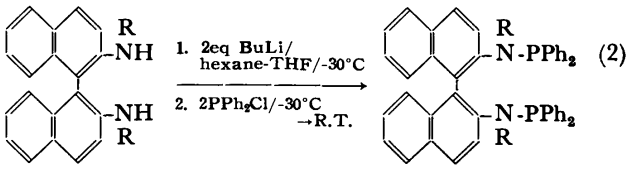

4 a R = H
b R = CH_3

1 c R = H (BDPAB)
d R = CH_3 (Me-BDPAB)

N-Methyl analogue of BDPAB, 2,2′-bis[*N*-(diphenylphosphino)methylamino]-1, 1′-binaphthyl (**1d**, Me-BDPAB), was prepared from **4b** by the similar procedure. (*R*)-Me-BDPAB was obtainable by use of (*R*)-**4b**. *N*-Ethylamine **4c**, however, did not afford the (ethylamino)phosphine (Et-BDPAB) even under somewhat forcing conditions. This was unexpected result at first, but inspection of CPK molecular models suggests that replacement of *N*-ethyl for *N*-methyl substituent imposes rather severe steric bulk on the amide anion due to the steric repulsion against naphthalene nucleus, and thus inhibits the nucleophilic attack to phosphorous center.

Asymmetric Hydrogenation. Generally, chiral catalysts were prepared just prior to the hydrogenation by mixing $[Rh(olefin)_2Cl]_2$ with 2.2 molar amount of one of the chiral bis(aminophosphine)s in the presence or absence of sodium tetraphenylborate under an inert atmosphere. Hydrogenation of several olefinic substrates was carried out in a glass tube placed in an autoclave. After the reaction, products were recovered according to the literature.[13] The optical yields were determined by comparing the rotations of the isolated products with those of the reported values for the pure enantiomers.

Table 1 shows the effects of reaction variables on the hydrogenation of (*Z*)-α-acetamidocinnamic acid using (*R*)- or (*S*)-BDPAB as the ligand. Reaction medium significantly affected the catalyst activity and optical yield. Solvent comprised of a 1:2 mixture of benzene and methanol or ethanol gave good results; the hydrogenation proceeded almost quantitatively at initial hydrogen pressure of 30 kg/cm² at ambient temperature with high optical yield. In such solvent system, the active catalyst seemed to be a cationic rhodium(I) species,[14] as was demonstrated from the fact that comparable result was obtained by using [Rh(COD)(*R*)-BDPAB]$^+BF_4^-$ as the catalyst. The optical yield was rather insensitive to the hydrogenation pressure, while addition of triethylamine was harmful to chiral recognition.[15]

Table 2 summarizes the results of the hydrogenation of several olefinic substrates. High optical yields (80—95%) were obtained with (*R*)- and (*S*)-BDPAB ligand in the hydrogenation of α-acetamidoacrylic acids **6a**—**6c**, ester **6e**, and itaconic acid **6g**. Comparison of these results with those reported by Tamao *et al.*[7] and by Grubbs and DeVries[8] shows that among bisphosphine ligands **1** which apparently form a nine-membered chelate ring, BDPAB (**1c**) is superior to NAPHOS (**1a**) or phosphite **1b** in chiral recognition in the hydrogenation of dehydroamino acids. Although the conversion was low, an appreciable optical yields were obtained with (*E*)-α-methylcinnamic acid. Simple olefin **6h** reacted completely but gave poor optical yields.

Recent studies on the mechanism of asymmetric hydrogenation of dehydroamino acids have demonstrated that thermodynamic and kinetic profiles of the process must be clarified before correlating catalyst structure to the product conformation.[3] It is widely accepted, however, that a chiral ligand which can fix rigid complex catalyst is essential for effective

Table 1. Asymmetric hydrogenation of (z)-α-acetamidocinnamic acid catalyzed by Rh(I)-BDPAB[a]

Catalyst[b]	Config. of BDPAB	Solvent /ml	Initial H_2 pres. /kg/cm²	Opt. yield[c] /%	Config. of product
A	R	EtOH(8)-PhH(4)	30	85	R
A	R	MeOH(8)-PhH(4)	30	89	R
A	R	EtOH(8)-PhH(4)	30	29[d]	R
A	R	*i*-PrOH(10)-PhH(5)	30	15	R
A	R	$PhCH_3$(12)-Me_2CO(12)	30	7[e]	R
A	S	THF(12)	80	9.5[f]	S
B	R	MeOH(8)-PhH(4)	5	87	R
B	R	MeOH(8)-PhH(4)	10	85	R
B	R	MeOH(8)-PhH(4)	30	90	R
B	R	MeOH(8)-PhH(4)	80	68	R
C	R	MeOH(6)-PhH(6)	30	91	R

a) Reaction conditions: Substrate **6b**, 0.45—0.50 g; [**6b**]/[Rh] (mol/mol)=50; 24—25 °C, 24 h. Conversion was 100% unless otherwise noted. b) A: 1/2[Rh(cycooctene)$_2$Cl]$_2$+1.1(p*—p) or 1/2[Rh(COD)Cl]$_2$+1.1(p*—p). B: 1/2[Rh(COD)Cl]$_2$+1.1(p*—p)+3$NaBPh_4$. C: [Rh(COD)(*R*)-BDPAB]$^+BF_4^-$. c) See footnote e) in Table 2. d) Et_3N was added ([Et_3N]/[Rh] (mol/mol)=4.7). e) Conversion, 20%. f) Conversion, 32%.

Table 2. Asymmetric hydrogenation of olefinic substrates[a]

Substrate	Catalyst[b]	Ligand[c]	Solvent[d]	Opt. yield/%[e]	Config. of product
$CH_2=C(NHCOCH_3)(COOH)$ (6a)	A	(*R*)	EtOH-PhH	86	*R*
	A	(*S*)	EtOH-PhH	88	*S*
	A	(*R*)-Me	EtOH-PhH	90	*R*
$Ph(H)C=C(NHCOCH_3)(COOH)$ (6b)	A	(*R*)	MeOH-PhH	89	*R*
	A	(*R*)-Me	EtOH-PhH	36	*R*
$Ph(H)C=C(NHCOPh)(COOH)$ (6c)	A	(*R*)	EtOH-PhH	95	*R*
	A	(*R*)-Me	EtOH-PhH	61	*R*
$Ph(H)C=C(NHCOCH_3)(COOCH_3)$ (6d)	A	(*R*)	MeOH-PhH	69	*R*
$Ph(H)C=C(NHCOPh)(COOCH_3)$ (6e)	A	(*R*)	MeOH-PhH	89	*R*
$Ph(H)C=C(CH_3)(COOH)$ (6f)	A	(*S*)	EtOH-PhH	47[f]	*S*
	B	(*R*)	MeOH-PhH	49[g]	*R*
$CH_2=C(CH_2COOH)(COOH)$ (6g)	B	(*R*)	MeOH-PhH	80	*S*
	B	(*S*)	MeOH-PhH	77	*R*
	B	(*R*)-Me	MeOH-PhH	40	*S*
$CH_2=C(Ph)(C_2H_5)$ (6h)	B	(*R*)	MeOH-PhH	2.4[h]	*S*
	B	(*R*)-Me	MeOH-PhH	1.3[h]	*S*

a) See footnote a) in Table 1; initial H_2 pressure, 30 kg/cm^2. b) See footnote b) in Table 1. c) (*R*): (*R*)-BDPAB. (*S*): (*S*)-BDPAB. (*R*)-Me: (*R*)-Me-BDPAB. d) ROH(8—10 ml)-PhH(4—5 ml). e) Optical yields were determined on the basis of the reported rotation for the optically pure enantiomers: (*R*)-*N*-acetylalanine,[25] $[\alpha]_D^{26}$+66.3°(*c* 2.0, H_2O); (*S*)-*N*-acetylphenylalanine,[25] $[\alpha]_D^{26}$+46.0°(*c* 1.0, EtOH); (*S*)-*N*-benzoylphenylalanine,[25] $[\alpha]_D^{27}$−40.3° (*c* 1.0, MeOH); (*S*)-2-methyl-3-phenylpropionic acid,[26] $[\alpha]_D^{25}$+27.06° (PhH); (*R*)-methylsuccinic acid,[25] $[\alpha]_D^{20}$+16.88° (*c* 2.16, EtOH); (*R*)-2-phenylbutane,[27] $[\alpha]_D^{20}$−27.31°(neat); (*S*)-*N*-acetylphenylalanine methyl ester,[14] $[\alpha]_D^{25}$+21.4° (*c* 1.9, MeOH); (*S*)-*N*-benzoylphenylalanine methyl ester,[14] $[\alpha]_D^{25}$−45.3° (*c* 1.3, EtOH). Values for the (*S*)-BDPAB were corrected for the 95% optical purity of the ligand. f) Conversion, 38%. g) Conversion, 54%. h) [Substrate]/[Rh] (mol/mol)=160.

dissymmetric discrimination, and here we would like to point out some structural features of the BDPAB ligand.

It is noted that the hydrogenation of (*Z*)-dehydroamino acids **6a**—**6e** using (*R*)-BDPAB ligand always gave (*R*)-α-amino acids preferentially, and (*S*)-BDPAB preferred (*S*)-counterparts. Similar ligand-product relationship in chirality is reported in the hydrogenation of **6b** with (*S*)-NAPHOS.[7] Examination of CPK molecular models suggests that (*R*)-BDPAB confines rigid nine-membered chelate ring with square planar Rh(I) containing hardly flexible 1,1′-binaphthyl skeleton, arraying four phenyl rings in an alternating edge-face manner as is observed in the seven-membered (*R*,*R*)-DIOP-Rh(I) complex of nearly δ-conformation.

On the other hand, Miyashita *et al.* have shown that BINAP ligand (**2**) fixes seven-membered chelate ring of λ-skew-boat conformation, and that (*R*)- and (*S*)-BINAP induce (*S*)- and (*R*)-chirality, respectively, in the Rh(I)-catalyzed hydrogenation of (*Z*)-α-acylamidoacrylic acids. That is, the sense of asymmetric induction is quite opposite between BDPAB and BINAP. It is surprising that MABP (**3**),[10] which seems to form closely related Rh(I)-complex to BDPAB, also gave opposite enantioselection in the hydrogenation of (*Z*)-α-acetamidoacrylic acid to *N*-acetylalanine, and at present we have no idea to explain these results.

It has been reported that *N*-methylation of 1,2-bis(diphenylphosphinoamino)ethane-type ligand such as **7a** to **7b** causes inversion of the chiral stereoselectivity on the Rh(I)-catalyzed hydrogenation of α-acetamidoacrylic acids.[5d,5e] This drastic change in stereoselectivity has been explained from the structural studies of the complexes including X-ray analysis that the helical orientation of the phenyl rings of the ligand would be inverted by *N*-methyl groups in the aminophosphine when coordinated to rhodium.[16]

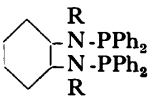

7 a R = H
b R = CH_3

In all cases examined, however, hydrogenation with (*R*)-Me-BDPAB ligand gave reduction products of the same chirality to those obtained with (*R*)-BDPAB ligand, although the effects of *N*-methylation on optical yields were different from substrate to substrate (Table 2). It seems that the rigid 1,1′-binaphthyl skeleton is mostly responsible for the overall structure

of BDPAB-type ligand regardless of the presence or absence of *N*-methyl substituents.

Experimental

Measurements. IR spectra were obtained on a Shimadzu IR 430 spectrophotometer. NMR spectra were determined on a Hitachi R-24A instrument using hexamethyldisiloxane as an internal standard. Mass spectra were recorded on a JEOR-D 300 double focussing mass spectrometer with direct sample injection. Optical rotations were recorded on a Union PM-101 automatic digital polarimeter. Melting points were corrected.

Materials. Following commercial materials were recrystallized or distilled before use; α-acetamidoacrylic acid (**6a**) (mp 185—186 °C), (*Z*)-α-acetamidocinnamic acid (**6b**) (mp 185—187 °C (H_2O)), and itaconic acid (**6g**) (mp 169.5—171.5 °C (EtOH)). (*Z*)-α-Benzamidocinnamic acid (**6c**) (mp 229—231 °C),[17] (*E*)-α-methylcinnamic acid (**6f**) (mp 81—81.5 °C),[18] 2-phenyl-1-butene (**6h**) (bp 66—67 °C/20 mmHg†)[19] were prepared by standard methods. Methyl (*Z*)-α-acetamidocinnamate (**6d**) (mp 122.5—124 °C (MeOH)) and methyl (*Z*)-α-benzamidocinnamate (**6e**) (mp 140—141 °C (MeOH)) were obtained by the reaction of diazomethane with **6b** and **6c**, respectively. $[Rh(cyclooctene)_2Cl]_2$[20] and $[Rh(COD)Cl]_2$[21] were prepared according to the literature. Commercial BuLi in hexane (*ca.* 15% solution) was titrated before use.[22] Solvents were purified as usual under nitrogen. All reactions involving phosphines were routinely performed under an inert atmosphere of nitrogen or argon.

2,2'-Diamino-1,1'-binaphthyl (4a). Clemo and Dawson's procedure[11] was utilized as follows: 2-Naphthol (40.0 g, 0.278 mol) and 8.8 ml of hydrazine hydrate (80% solution, *ca.* 0.14 mol) were heated in a *ca.* 90 ml inner-volume stainless steel autoclave at 170—180 °C for 48 h. After the vessel was cooled, it was opened and the contents were remelted by heating. The yellowish viscous material was poured into a 2-necked round-bottom flask containing 600 ml of 1:1 HCl. To the flask were attached mechanical stirrer and a reflux condenser. The stirred mixture was heated at reflux, during which time brown tarry matter appeared. After standing for a while, supernatant liquid was siphoned off. Similar hot extraction was repeated 3 times by using 300 ml of 1:1 HCl each time. The combined HCl extracts were made alkaline by cautious addition of NaOH pellets with ice-cooling. The mixture was boiled and filtered while hot. Then, the precipitate was boiled in 500 ml of water and filtered hot; the procedure was repeated several times to thoroughly remove 2-naphthylamine. The precipitate was dissolved in a 400 ml of 2 M†† HCl, filtered hot from activated charcoal. The filtrate was made alkaline with 10% NaOH; formed precipitate was filtered off and dried *in vacuo*, 14.4 g (36.6%), mp 187—188 °C. Recrystallization from ethanol-acetone gave a pure sample of mp 193.2—194.3 °C (lit,[23] mp 193 °C); IR (KBr): 3450, 3300, 3100, 1610, 1500, 1430, 1380, 1350, 1280, 810, and 750 cm^{-1}; ^1H NMR ($CDCl_3$) δ=3.5 (4H, br), 6.9—7.3 (8H, m), and 7.5—7.8 (4H, m). Found: C, 84.41; H, 5.67; N, 9.72%. Calcd for $C_{20}H_{16}N_2$: C, 84.48; H, 5.67; N, 9.85%.

Resolution of 4a. The method was Kuhn and Goldfinger's,[12] while control of temperature seemed important to obtain fine precipitate of the less soluble diastereomer salt. (±)-Diamine (**4a**) (10.5 g, 36.9 mmol) was dissolved in 300 ml of chlorobenzene with warming up to 70 °C. To the stirred solution kept at *ca.* 50 °C was added slowly a solution of *d*-camphorsulfonic acid monohydrate (8.4 g, 34 mmol) in ethanol (60 ml). By the end of the addition, fine white crystals began to deposit. The mixture was stirred till it reached to room temperature, and then allowed to stand overnight. The precipitate was filtered off, washed with chlorobenzene (50 ml×3), and dried *in vacuo* to give (*d*)-(*d*)-salt, $[\alpha]_D^{23}$+101 ° (*c* 0.86, py) (lit,[23] $[\alpha]_D^{19}$+103.6 ° (*c* 1.05, py)); IR (KBr): 3450, 3300, 1740, 1130, and 1030 cm^{-1}. The salt was dissolved in 60 ml of pyridine, and poured into 500 ml of water to give white suspension. Solid was collected by filtration, dissolved in 200 ml of 2 M HCl, decolorized with activated charcoal, and filtered. The filtrate was made alkaline with aq NH_3 to give white precipitate, which was recovered by filtration, dried, and recrystallized from ethanol-benzene to give 4.50 g (86%) of (*R*)-(+)-**4a**; mp 245—246 °C (lit,[24] mp 245 °C); $[\alpha]_D^{22}$+157.4 ° (*c* 0.712, py) (lit,[23] $[\alpha]_D^{21-22}$ +151.7 ° (*c* 0.5-1, py)). A weak, but somewhat broad IR absorption at 1105 cm^{-1} of (±)-**4a** was missing in (*R*)-**4a**. Found: C, 84.29; H, 5.63; N, 9.45%.

The above chlorobenzene-ethanol filtrate which contained more soluble (*d*)-(*l*)-salt was evaporated *in vacuo* to leave brown residue, which was treated as above to liberate free (*S*)-(−)-base. The crude material was recrystallized twice from ethanol-benzene, 2.5 g (48%), mp 244—246 °C, $[\alpha]_D^{23}$−153.0 ° (*c* 0.758, py). Found: C, 84.50; H, 5.77; N, 9.53%.

2,2'-Bis(ethoxycarbonylamino)-1,1'-binaphthyl (5a). To a stirred, water-chilled solution of racemic **4a** (3.95 g, 13.9 mmol) in benzene (80 ml) and pyridine (10 ml) was added dropwise a solution of ethyl chloroformate (3.75 g, 34.6 mmol) in benzene (20 ml). After the addition was complete, the mixture was stirred for 2 h at ambient temperature. The reaction was quenched by adding 100 ml of 10% NaOH. The resulting organic layer and benzene extracts (50 ml×2) from the aqueous layer were combined, washed with water and dried over $MgSO_4$. The solvents were evaporated *in vacuo*, and resulting residue was recrystallized from ethanol-acetone to give 3.77 g of diester **5a** (63.3%); mp 155—156 °C; IR (KBr): 3400, 3300, 2900, 1720, 1600, 1490, 1210, 1090, 820, and 740 cm^{-1}; ^1H NMR (acetone-d_6) δ=1.0 (6H, t, *J*=6.8 Hz), 2.7 (2H, s), 3.9 (4H, q, *J*=6.8 Hz), 6.8—7.5 (8H, m), and 7.6—8.3 (4H, m). Found: C, 72.95; H, 5.71; N, 6.20%. Calcd for $C_{26}H_{24}O_4N_2$: C, 72.88; H, 5.65; N, 6.54%.

(R)-(+)-5a: Similar treatment of (*R*)-(+)-**4a** (2.2 g, 7.7 mmol) gave (*R*)-(+)-**5a**, 2.2 g (67%), mp 70—72 °C, $[\alpha]_D^{23}$+68.5° (*c* 1.23, THF).

2,2'-Bis(methylamino)-1,1'-binaphthyl (4b). To a stirred suspension of LAH (4 g) in 100 ml of THF was added dropwise a solution of **5a** (7.6 g, 17.7 mmol) in 50 ml of THF. The mixture was heated at reflux for 3 h. The reaction mixture was cooled in an ice-bath and the remaining hydride was carefully quenched by dropwise addition of water (5 ml) and then 15% NaOH (5 ml). A white precipitate was filtered off and thoroughly washed with ether. The combined filtrate and ether washings were washed with water, dried over Na_2SO_4 overnight. After the solvents were evaporated under reduced pressure, the residue was recrystallized from ethanol-benzene, 4.5 g (81%); mp 149—151 °C; IR (KBr): 3400, 1620, 1600, 1500, 1420, 1340, 1300, 1170, 1150, 810, and 750 cm^{-1}. ^1H NMR (acetone-d_6) δ=2.7 (6H, d, *J*=6.0 Hz), 3.9 (2H, br), 6.5—7.3 (8H, m), and 7.3—8.0 (4H, m). Found: C, 84.37; H, 6.40; N, 8.96%. Calcd for $C_{22}H_{20}N_2$: C, 84.58; H, 6.45; N, 8.97%.

(R)-(+)-4b: The (*R*)-(+)−**5a** (1.53 g, 3.56 mmol) was treated with LAH (0.9 g) in 50 ml of THF and worked up as above. After removal of volatiles *in vacuo*, the residue was recrystallized from ethanol to give (*R*)-(+)-**4b**, 0.73 g (66%), mp 143—144 °C, $[\alpha]_D^{23}$+182 ° (*c* 1.09, PhH). Found: C, 84.21; H, 6.59; N, 8.82%.

2,2'-Bis(ethylamino)-1,1'-binaphthyl (4c). A mixture of diamine **4a** (1.2 g, 4.2 mmol) and acetyl chloride (1.1 g,

† 1 mmHg≈133.322 Pa.

†† 1 M=1 mol dm^{-3}

14 mmol) in benzene (40 ml) and pyridine (8 ml) was stirred overnight at ambient temperature. Organic residue obtained after usual workup was recrystallized from ethanol to give a 1.22 g sample (79% yield) of 2,2'-bis(acetamido)-1,1'-binaphthyl **5b**, mp 235—235.5 °C; IR (KBr): 3300, 1670, 1600, 1490, 1420, 1270, 820, and 740 cm^{-1}. ^1H NMR ($CDCl_3$+DMSO-d_6) δ=1.7 (6H, s) and 6.5—8.3 (14H, m); MS (70 eV), *m/z* (%) 369 (M+1, 3.0) and 368 (M^+, 10.5). Found: C, 78.13; H, 5.60; N, 7.65%. Calcd for $C_{24}H_{20}N_2O_2$: C, 78.24; H, 5.47; N, 7.60%.

A mixture of **5b** (0.50 g, 1.4 mmol) and LAH (0.3 g) was boiled in 35 ml of THF for 3 h. The mixture was worked up as was stated in the synthesis of **4b**. Recrystallization from ethanol gave 0.25 g of **4c** (54%), mp 127.5—128 °C; IR (KBr): 3400, 2900, 1610, 1600, 1480, 1410, 1320, 1290, 1140, 800, and 740 cm^{-1}: ^1H NMR ($CDCl_3$) δ=0.95 (6H, t, *J*=7.0 Hz), 3.1 (4H, q, *J*=7.0 Hz), 3.9 (2H, br), and 6.5—8.0 (12H, m); MS (70 eV), *m/z* (%), 341 (M+1, 8.8) and 340 (M^+, 29.8). Found: C, 84.21; H, 6.88; N, 8.03%. Calcd for $C_{24}H_{24}N_2$: C, 84.67; H, 7.11; N, 8.23%.

2,2'-Bis(diphenylphosphinoamino)-1,1'-binaphthyl (1c, BDPAB). In a 100 ml, three-necked round-bottom flask equipped with a magnetic stirrer, a thermometer, a pressure equilibrating dropping funnel, and a reflux condenser topped with nitrogen inlet was placed racemic **4a** (1.55 g, 5.45 mmol). The whole system was purged with nitrogen. After the amine had been dissolved in 50 ml of THF, the solution was cooled to −30—−32 °C in a methanol-Dry Ice bath. To the cooled solution was added dropwise a hexane solution (8.8 ml) of 1.30 M BuLi (11.4 mmol) over 40 min. After the addition, the mixture was stirred at −30 °C for 20 min. To the stirred mixture kept at −28—−30 °C was added dropwise a solution of diphenylphosphinous chloride (2.46 g, 11.2 mmol) dissolved in 10 ml of THF over 40 min. Stirring was continued for another 1 h. Then the cooling bath was removed, and the mixture was stirred overnight at ambient temperature. Lithium chloride precipitated was filtered off under nitrogen, and then volatiles were evaporated *in vacuo* to leave yellowish resinous residue. This was digested with portions of warm ethanol (*ca.* 30 ml×3) to give white solid. Recrystallization from ethanol-benzene gave white crystals, 2.58 g (72.6%); mp 164—165 °C; IR (KBr): 3330, 3030, 1610, 1590, 1500, 1460, 1430, 1390, 1340, 1270, 1240, 980, 810, 740, 730, and 690 cm^{-1}; ^1H NMR ($CDCl_3$) δ=4.4 and 4.6 (2H, br), and 6.6—7.4 and 6.5—7.9 (32H, m); MS (70 eV), *m/z* (%), 654 (M+2, 6.3), 653 (M+1, 26.5), and 652 (M^+, 52.2). Found: C, 80.48; H, 5.12; N, 4.33%. Calcd for $C_{44}H_{34}N_2P_2$: C, 80.97; H, 5.25; N, 4.29; P, 9.49%.

(R)-(+)-BDPAB: The diamine (*R*)-**4a** (2.16 g, 7.59 mmol) was treated as above to give (*R*)-(+)-BDPAB, 3.3 g (67%), mp 153—155 °C (PhH–EtOH); $[\alpha]_D^{23}$+26.1° (*c* 1.14, PhH). The product was again recrystallized from ethanol-benzene to increase the rotation to $[\alpha]_D^{23}$+27.2° (*c* 1.14, PhH), mp 154—155 °C. Subsequent recrystallization did not change the rotation. Found: C, 80.66; H, 5.19; N, 4.42%.

(S)-(−)-BDPAB: A sample of (*S*)-(−)-**4a** of $[\alpha]_D$ −153.0° gave diphosphine (*S*)-(−)-BDPAB of $[\alpha]_D^{23}$−25.8° (*c* 0.776, PhH) after two recrystallization from ethanol-benzene, mp 152—153 °C, the optical purity of which was estimated to be 95% on the basis of the maximum rotation of (*R*)-(+)-BDPAB of $[\alpha]_D$ +27.2°. Found: C, 80.93; H, 5.38; N, 4.59%.

2,2'-Bis[N-(diphenylphosphino)methylamino]-1,1'-binaphthyl (Me-BDPAB). According to the procedure used for the synthesis of BDPAB, **4b** (0.50 g, 1.6 mmol) was treated with BuLi (3.36 mmol), and then with diphenylphosphinous chloride (0.74 g, 3.3 mmol). Recrystallization from ethanol-benzene gave fine crystals, 0.60 g (56.2%), mp 159—161 °C; IR (KBr): 3050, 2800, 1615, 1590, 1500, 1470, 1430, 1350, 1325, 1270, 1240, 1090, 960, 930, 740, 695, and 495 cm^{-1}; ^1H NMR ($CDCl_3$) δ=2.5 (6H, s) and 6.6—8.0 (32H, m); MS (70 eV), *m/z* (%), 682 (M+2, 2.9), 681 (M+1, 9.7), and 680 (M^+, 33.8). Found: C, 81.05; H, 5.68; N, 3.99%. Calcd for $C_{46}H_{38}N_2P_2$: C, 81.16; H, 5.63; N, 4.12; P, 9.10%.

(R)-(−)-Me-BDPAB: A sample of (*R*)-(+)-**4b** of $[\alpha]_D$+182° (0.63 g, 2.0 mmol) was treated with BuLi (4.2 mmol) and then with diphenylphosphinous chloride (0.93 g, 4.2 mmol) as above. After the reaction, the filtrate was evaporated *in vacuo*; the residue was freed from LiCl by dissolution in benzene and filtration. The benzene filtrate was evaporated *in vacuo* to give yellowish powder, 0.65 g (48%), mp 68—71 °C, $[\alpha]_D^{23}$ −20.7° (*c* 1.26, PhH). IR and ^1H NMR spectra were identical to those of the racemic phosphine. Found: C, 80.62; H, 5.96; N, 3.51%. Attempts to recrystallize the optically active phosphine by varying solvents were unsuccesful.

Attempted Preparation of 2,2'-Bis[N-(diphenylphosphino)-ethylamino]-1,1'-binaphthyl (Et-BDPAB). Diamine **4c** (0.23 g, 0.68 mmol) was treated with BuLi (1.4 mmol), and then with diphenylphosphinous chloride (0.35 g, 1.6 mmol) as above. After usual workup, almost all of the diamine was recovered unchanged. In an another attempt, after the reaction mixture had been stirred overnight at ambient temperature, it was finally refluxed for 2 h, while no appreciable aminophosphine was obtained.

Preparation of Hydrogenation Catalysts. Catalyst A, (1/2 [Rh(olefin)$_2$Cl]$_2$+1.1BDPAB): The catalyst was prepared just prior to the hydrogenation by the reaction of [Rh(COD)Cl]$_2$ or [Rh(cyclooctene)$_2$Cl]$_2$ with a chiral diphosphine in benzene ([diphosphine]/[Rh] (mol/mol)=1.1). Typically, 17 mg (2.4×10^{-2} mmol) of [Rh(cyclooctene)$_2$Cl]$_2$ and 35 mg (5.4×10^{-2} mmol) of (*R*)-BDPAB in 4 ml of benzene was stirred at room temperature for 20 min under argon. The clear wine-red catalyst solution was transferred under rigorous exclusion of air to a reaction vessel, which contained an olefinic substrate (*vide infra*), by a hypodermic syringe.

Catalyst B, (1/2[Rh(COD)Cl]$_2$+1.1BDPAB+3NaBPh$_4$): Typically, (*R*)-BDPAB (35 mg, 5.4×10^{-2} mmol) in benzene (2 ml) was added to a methanol solution (2 ml) of [Rh(COD)Cl]$_2$ (12 mg, 2.4×10^{-2} mmol). The solution was stirred for 15 min, to which was added $NaBPh_4$ (48 mg, 14×10^{-2} mmol) in 2 ml of MeOH. The mixture was stirred for 10 min before it was transferred to a hydrogenation vessel.

Catalyst C, ([Rh(COD)(R)-BDPAB]$^+$BF$_4^-$): To a warm benzene solution (2 ml) of (*R*)-BDPAB (0.79 g, 1.2 mmol) was added [Rh(COD)Cl]$_2$ (0.28 g, 0.57 mmol) in MeOH (5 ml). After the mixture was stirred at 30—35 °C for 2 h, $NaBF_4$ (0.43 g, 3.9 mmol) in H_2O (4 ml) was added over 2 h period. The two-layer mixture was allowed to stand for 5 days at room temperature. Precipitated [Rh(COD)(*R*)-BDPAB]$^+BF_4^-$ was collected, 0.99 g (89%).

Hydrogenation Procedure. A reaction in a benzene-methanol solution is representative. The hydrogenation was carried out in a glass tube (*ca.* 30 ml volume) placed in a 100 ml inner-volume autoclave. After the glass tube was charged with an olefinic substrate (0.45—0.50 g), the whole system was evacuated and refilled with argon several times. The substrate was dissolved in 4 ml of methanol, and to the stirred solution was added a catalyst solution. If necessary, another benzene and/or methanol were added to adjust the solvent volume. The whole system was purged thoroughly with hydrogen, and it was charged to initial hydrogen pressure of 30 kg/cm^2. After the reaction mixture had been stirred at room temperature for 24 h, whole contents in the glass tube was transferred to a flask and solvents were removed *in vacuo*.

N-Acyl amino acids were recovered by the literature procedure.[13] 2-Methyl-3-phenylpropionic acid was isolated by preparative TLC (silica gel, ethyl acetate–aq NH_3 (trace)). *N*-Acyl amino acid esters were recovered by TLC (silica gel,

ethyl acetate–hexane (1.5/1). Hydrogenation products were characterized by IR and NMR spectra.[13]

References

1) Preliminary communication: S. Miyano, M. Nawa, and H. Hashimoto, *Chem. Lett.*, **1980**, 729.

2) Recent reviews: W. S. Knowles, *Acc. Chem. Res.*, **16**, 106 (1983); R. E. Merrill, *CHEMTECH*, **1981**, 118; V. Čaplar, G. Comisso, and V. Šunjić, *Synthesis*, **1981**, 85.

3) For example, a) A. S. C. Chan, J. J. Pluth, and J. Halpern, *J. Am. Chem. Soc.*, **102**, 5952 (1980); b) I. Ojima, T. Kogure, and N. Yoda, *J. Org. Chem.*, **45**, 4728 (1980); c) P. A. MacNeil, N. K. Roberts, and B. Bosnich, *J. Am. Chem. Soc.*, **103**, 2273 (1981); d) P. S. Chua, N. K. Roberts, B. Bosnich, S. J. Okrasinski, and J. Halpern, *J. Chem. Soc., Chem. Commun.*, **1981**, 1278; e) J. M. Brown and D. Parker, *Organometallics*, **1**, 950 (1982), and references cited therein.

4) For example, a) T. Yoshikuni and J. C. Bailar, Jr., *Inorg. Chem.*, **21**, 2129 (1982); b) K. Tani, K. Suwa, T. Yamagata, and S. Otsuka, *Chem. Lett.*, **1982**, 265; c) J. P. Amma and J. K. Stille, *J. Org. Chem.*, **47**, 468 (1982); d) D. L. Allen, V. C. Gibson, M. L. H. Green, J. F. Skinner, J. Bashkin, and P. D. Grebenik, *J. Chen. Soc., Chem. Commun.*, **1983**, 895.

5) a) M. Fiorini and G. M. Giongo, *J. Mol. Catal.*, **5**, 303 (1979) ; b) G. Pracejus and H. Pracejus, *Tetrahedron Lett.*, **1977**, 3497; c) W. Beck and H. Menzel, *J. Organomet. Chem.*, **133**, 307 (1977); d) K. Kashiwabara, K. Hanaki, and J. Fujita, *Bull. Chem. Soc. Jpn.*, **53**, 2275 (1980); e) K. Onuma, T. Ito, and A. Nakamura, *ibid.*, **53**, 2012 (1980); f) G. Markl, G. Y. Jin, and C. Schoerner, *Tetrahedron Lett.*, **1980**, 1845; g) K. Osakada, T. Ikariya, M. Saburi, and S. Yoshikawa, *Chem. Lett.*, **1981**, 1691.

6) a) S. Miyano, M. Tobita, and H. Hashimoto, *Bull. Chem. Soc. Jpn.*, **54**, 3522 (1981); b) J. Brussee and A. C. A. Jansen, *Tetrahedron Lett.*, **24**, 3261 (1983), and references cited therein.

7) K. Tamao, H. Yamamoto, H. Matsumoto, N. Miyake, T. Hayashi, and M. Kumada, *Tetrahedron Lett.*, **1977**, 1389.

8) R. H. Grubbs and R. A. DeVries, *Tetrahedron Lett.*, **1977**, 1879.

9) A. Miyashita, A. Yasuda, H. Takaya, K. Toriumi, T. Ito, T. Souchi, and R. Noyori, *J. Am. Chem. Soc.*, **102**, 7932 (1980).

10) A. Uehara, T. Kubota, and R. Tsuchiya, *Chem. Lett.*, **1983**, 441.

11) G. R. Clemo and E. C. Dawson, *J. Chem. Soc.*, **1939**, 1114.

12) *Cf.* R. Kuhn and P. Goldfinger, *Justus Liebigs Ann. Chem.*, **470**, 183 (1929).

13) a) H. B. Kagan and T.-P. Dang, *J. Am. Chem. Soc.*, **94**, 6429 (1972); b) B. D. Vineyard, W. S. Knowles, M. J. Sabacky, G. L. Bachman, and D. J. Weinkauff, *ibid.*, **99**, 5946 (1977); c) M. D. Fryzuk and B. Bosnich, *ibid.*, **99**, 6262 (1977).

14) D. Sinou and H. B. Kagan, *J. Organomet. Chem.*, **114**, 325 (1976).

15) *Cf.* See Ref. 3b).

16) K. Onuma and A. Nakamura, *Bull. Chem. Soc. Jpn.*, **54**, 761 (1981).

17) H. B. Gillespie and H. R. Snyder, *Org. Synth.*, Coll. Vol. II, 489 (1966).

18) J. R. Johnson, *Org. React.*, **1**, 210 (1960).

19) A. Maercker, *Org. React.*, **14**, 270 (1965).

20) A. van der Ent and A. L. Onderdelinden, *Inorg. Synth.*, **14**, 92 (1973).

21) R. B. King, Organometallic Synth, Vol. 1, 132 (1965).

22) S. C. Watson and J. F. Eastham, *J. Organomet. Chem.*, **9**, 165 (1967).

23) R. C. Schulz and R. H. Jung, *Makromol. Chem.*, **116**, 190 (1968).

24) K. Mislow and P. A. Grasemann, *J. Org. Chem.*, **23**, 2027 (1958).

25) See references cited in Ref. 3b) and 13c).

26) R. E. Radgett, R. L. Beamer, *J. Pharm. Sci.*, **53**, 689 (1964).

27) a) P. W. B. Harrison, J. Kenyon, and J. R. Shepherd, *J. Chem. Soc.*. **1926**, 658; b) D. J. Cram and J. Tadanier, *J. Am. Chem. Soc.*, **81**, 2737 (1959).

 © 1984 The Chemical Society of Japan Bull. Chem. Soc. Jpn., 57, 2177—2183 (1984)

The Effect of Ethylene Glycol on the Thermal Denaturation of Ribonuclease A and Chymotrypsinogen A as Measured by Differential Scanning Calorimetry

Yukihisa FUJITA* and Yukinao NODA

Department of Chemistry, Hyogo College of Medicine, Mukogawa, Nishinomiya, Hyogo 663

(Received January 21, 1984)

The thermal denaturation of ribonuclease A(RNase A) and chymotrypsinogen A in aqueous solutions of ethylene glycol (EG) was investigated by differential scanning calorimetry at several pH values in the acidic region. The calorimetric enthalpies of denaturation, ΔH_d, of these proteins increased monotonously with increasing the EG concentration under all the conditions studied. These proteins, however, differed from one another in the variation of the denaturation temperature, T_d, with the addition of EG. The T_d of chemotrypsinogen decreased slightly with an increase in EG concentration under all the conditions, producing a greater effect at high pH. The T_d of RNase A, on the other hand, was almost independent of the EG content at pH 3.8, while at pH 2 and 3, the T_d increased slightly with increasing the EG concentration and decreased slightly at pH 5. That is, EG stabilized or unstabilized these proteins against thermal denaturation, in a way which seemed to be dependent on temperature rather than the pH. The standard thermodynamic parameters for denaturation, $\Delta G°$, $\Delta H°$, and $\Delta S°$, which were calculated using T_d and ΔH_d and assuming a constant heat capacity change, suggested that the slight increase or decrease in $\Delta G°$ induced by EG is attributed to whether $\Delta H°$ increases as much as $\Delta S°$ does or not. These results may be explained on the basis of the effect of EG on the solvation around hydrophobic groups of the protein. The EG effect may depends on the structural properties of proteins such as hydrophobicity and polarity, as well as on temperature.

The structural stability of proteins is extensively controlled by the interactions between the protein and surrounding solvent molecules. Various substances stabilize or unstabilize the native structure of proteins when added to aqueous protein solutions as a reflection of their effect on the water structure around the protein.[1-4] Polyhydric alcohols such as glycerol and sorbitol prevent the lose of enzymatic activities[5,6] and raise the thermal transition temperature of proteins. This stabilizing effect had been attributed to a lessened hydrogen bond-rupturing capacities of the medium.[7] Recently, Gekko and coinvestigators[10-13] concluded from extensive studies that the protein stabilization by polyhydric alcohols is due to a preferential hydration effect which strengthens the hydrophobic interactions of the protein. The preferential hydration of proteins in the presence of polyhydric alcohols has been directly shown from equilibrium dialysis[14] and densimetric experiments.[12] On the other hand, monohydric alcohols unstabilize the native structure of proteins. This may be attributed to the perturbation of the characteristic water structure around the protein molecule and to the direct interactions with the protein.[1-3] These alcohols are preferentially bound to protein in alcohol-water mixtures, which is accompanied by a protein dehydration.[14,15] These studies imply that any substance which trends to maintain or increase the hydration of proteins stabilizes a protein and, to the contrary, any substance which is bound to and dehydrates the protein unstabilizes the native structure of proteins.

According to this hypothesis, ethylene glycol (EG)** would have a stabilizing effect on the native structure of proteins, since a number of proteins are preferentially hydrated in EG-water mixtures.[14,16] Actually there have been many observations which show the protein stabilization induced by EG. For example, we reported previously that the denaturation temperature and enthalpy of lysozyme are higher in aqueous EG solutions at pH 2 than in aqueous solution at the same pH.[17] The stabilization of ribonuclease A (RNase A) and lysozyme by the addition of EG has been also shown by Gerlsma and Stuur.[8] However, there have been some contradictory observations concerning the EG effect on the thermal stability of proteins. The thermal transition temperatures of chymotrypsinogen and ovalbumin were depressed by the addition of EG.[7,9] Furthermore, a lowering of the denaturation temperatures of RNase A and lysozyme by EG has been shown at high pH in the acidic region,[2,10] which is in contrast with Gerlsma and Stuur's and our observations for the same proteins. These observations attracted our attention to a systematic examination of the EG effect on the thermal stability of proteins.

Differential scanning calorimetry (DSC) is a useful tool for measuring the thermally induced conformational transition of biological macromolecules such as proteins and nucleic acids. An application of DSC to the study of protein denaturation provides the available thermodynamic information on the unfolding process of proteins. This may contribute greatly to an understanding of the nature and magnitude of the forces that stabilize the native structure of proteins. Recent studies have been reviewed by Biltonen and Freire[18] and by Privalov.[19] We have been investigating the effect of various substances on the thermal stability of globular proteins by means of DSC.

A study of the thermal denaturation of ribonuclease A (RNase A) and chymotrypsinogen A in aqueous EG solutions at several acidic pH values was carried out by DSC; this paper reports the results. These proteins were chosen because they differ greatly in hydrophobicity and polarity and because their thermal denaturation had been investigated extensively in the past.

Experimental

Materials. Bovine pancreatic ribonuclease A (five-times recrystallized, type I-A) and chymotrypsinogen A (six-

** Abbreviations used: DSC, differential scanning calorimetry; EG, ethylene glycol; RNase A, ribonuclease A (bovine pancreatic, EC 3.1.4.22).

times recrystallized, type II) were purchased from Sigma Chemical Co. Ethylene glycol was purified by distillation under reduced pressure. Other chemicals were reagent grade products from Wako Pure Chemical Industries. In the case of RNase A, the experiments were carried out in either 0.05 mol dm^{-3} glycine buffer–EG mixtures adjusted to pH 2, 3, and 3.8 or 0.05 mol dm^{-3} acetate buffer–EG mixtures adjusted to pH 5 with 1 mol dm^{-3} HCl as measured by a Horiba f-7ss pH meter standardized at pH 4 in aqueous solution. In the case of chymotrypsinogen A, either 0.01 mol dm^{-3} glycine (at pH 2 and 3) or 0.01 mol dm^{-3} acetate buffer (at pH 4) was used to minimize aggregation of the denatured protein. The protein solutions were subjected to extensive dialysis against the solvent at 4 °C prior to making DSC measurements. Protein concentrations were determined spectrophotometrically on a Hitachi 323 automatic spectrophotometer. The extinction coefficients were assumed to be 7.38 at 277 nm[20] and 20.3 at 282 nm[21] for a 10 mg cm^{-3} aueous solution of RNase A and chymotrypsinogen A, respectively. The coefficients were corrected for each mixed solvent by the method of Lee *et al.*[22]

DSC measurements. The thermal denaturation of these proteins was measured on a Seiko Instruments & Electronics SSC-560U differential scanning calorimeter (conduction type) at a heating rate of 1 K min^{-1} and at protein concentrations of 8—12 mg cm^{-3} for RNase A and 15—19 mg cm^{-3} for chymotrypsinogen A. The sample solutions (0.06 cm^3) were hermetically sealed in a silver vessel. An equal amount of the solvent was used as reference material. The DSC apparatus was calibrated using gallium, benzophenone, palmitic acid, and naphthalene. The area between the transition peak and a base line fitted by inspection was measured with a planimeter and converted to the calorimetric enthalpy of denaturation, ΔH_d, using the calibration constant, 2.29 mJ mV^{-1}s^{-1}, and the molecular weight of 13 700 for RNase A and 25 700 for chymotrypsinogen A. The denaturation temperature, T_d, was estimated from the temperature at which the area under the transition peak was divided into halves, since the area is proportional to the amount denatured. The difference between the T_d obtained and the temperature of maximal heat flow did not exceed 0.5 K in every measurement because of the symmetrical nature of the transition peak.

Results and Discussion

Representative DSC scans for the thermal denaturation of RNase A in aqueous EG solutions at pH 3 are shown in Fig. 1. The DSC curves shown correspond to denaturation of a protein solution of 10 mg cm^{-3} in EG concentrations of 0 and 4.64 mol dm^{-3}. At pH 3, the addition of EG to a aqueous solution of RNase A induces a slight shift of the transition peak toward high temperature and an increase of the peak area. In the case of RNase A, although the temperature width of the transition peak, 20—22 K, was hardly influenced by the variation of pH or by the addition of EG, the shift of the transition peak induced by EG was dependent on the pH. On the other hand, the transition peak of chymotrypsinogen A was slightly shifted a toward low temperature by the addition of EG and the peak area slightly increased under all the conditions studied. Moreover, the temperature width of the transition peak became smaller in going from low pH to high pH, consistent with the observation by Brandts[23] in the spectrophotometric experiments; the temperature width of 22—24 K at pH 2 decreased to 16—19 K at pH 4.

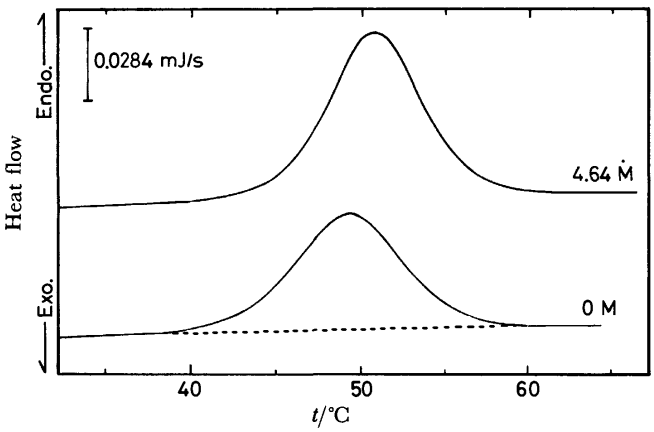

Fig. 1. DSC curves for the thermal denaturation of RNase A in aqueous EG solutions at pH 3. Protein concentration is a 10 mg cm^{-3} and EG concentrations are 0 and 4.64 mol dm^{-3}. The dotted line shows the base line assumed in the transition region for the determination of the thermodynamic parameters of denaturation.

As seen in the figure, the DSC curves obtained exhibit that there is a difference in the heat capacity between the native and denatured states of these proteins; this has been observed for many proteins including the proteins.[19] Therefore, one of the major problem for estimating exactly the thermodynamic parameters of denaturation is how to determine a suitable base line in the transition region. Some estimations of ΔH_d were made by using the base line obtained by extrapolation of the base lines for native and denatured states to the denaturation temperature. However, the ΔH_d obtained by such a procedure was not significntly different from that estimated using a linear base line fitted by inspection. Under our conditions, relatively low protein concentration, the exact heat capacity change upon denaturation seems to be considerably difficult for the DSC apparatus used to determine directly in the individual scan. In this experiment, therefore, we employed a linear base line fitted to the difference of the base lines before and after the transition. Although the thermal denaturation of these proteins has been shown to be a reversible two-state process in aqueous solution,[23–26] the reversibility for the denaturation in EG–water mixtures was checked by reheating the protein solution after rapidly cooling from the first scan. In each solvent composition, there were no significant variations in the position of the transition peak and in the peak area on reheating, indicating that the denaturation of these proteins is almost reversible in EG–water mixtures. In addition, the denaturation temperature was scarcely influenced by heating rates slower than 1 K min^{-1}, allowing equilibrium analysis of the data.

The values of T_d and ΔH_d obtained in EG–water mixtures at different pH values are listed in Table 1. These thermodynamic parameters were evaluated as the average value of five and more experiments. The T_d values have experimental errors of ± 0.1 °C and the ΔH_d values have maximum expected errors of $\pm 5\%$ including errors in sample preparation, calibration constant, and reproducibility. For RNase A, the ΔH_d values in aqueous buffers at different pH in the range

TABLE 1. THERMODYNAMIC PARAMETERS OF THERMAL DENATURATION OF PROTEINS IN AQUEOUS EG SOLUTIONS AT DIFFERENT pH VALUES

pH	c_{EG}	T_d	ΔH_d	ΔS_d
	mol dm^{-3}	°C	kJ mol^{-1}	kJ K^{-1} mol^{-1}
		RNase A		
2.0	0	38.0	348	1.12
	1.07	38.9	377	1.21
	2.45	39.5	410	1.31
	3.94	40.6	425	1.35
3.0	0	49.3	390	1.21
	1.01	49.5	401	1.24
	2.13	49.8	431	1.33
	3.43	50.2	465	1.44
	4.64	50.4	487	1.51
3.8	0	56.1	423	1.28
	0.99	56.1	428	1.30
	2.14	56.2	470	1.43
	3.43	56.1	485	1.47
	4.68	56.0	500	1.52
5.0	0	61.0	453	1.36
	0.99	60.7	472	1.41
	2.14	60.5	477	1.43
	3.42	60.2	506	1.52
	4.70	59.9	528	1.59
		Chymotrypsinogen A		
2.0	0	41.5	351	1.12
	1.06	41.0	367	1.17
	2.46	40.2	380	1.21
	4.03	39.6	406	1.30
3.0	0	51.4	498	1.53
	0.97	50.9	509	1.57
	2.24	50.2	520	1.61
	3.55	49.6	533	1.65
	4.70	49.0	547	1.70
4.0	0	61.9	637	1.90
	1.07	61.2	652	1.95
	2.44	60.2	660	1.98
	3.98	59.1	670	2.02

2 to 5 are in agreement with those obtained by Tsong *et al.*[24] and Privalov *et al.*[25] from calorimetric experiments at similar pH values, while the T_d values at low pH are higher than the data of theirs and those at high pH are slightly lower. However, Jacobson and Turner[26] have recently reported considerably higher T_d values from DSC measurements at pH 4.1 and 5.0. Although the reason for the differences in T_d is not clear at present, a number of factors such as protein concentration, ionic strength, buffer, purity of the protein sample (contamination), or heating rate could contribute to the differences. For example, the heating rate used by Jacobson and Turner[26] is considerably higher than that used in this experiment. In addition, Tsong *et al.*[24] have reported that the T_d of RNase A increases with an increase in protein concentration. The T_d and ΔH_d values of chymotrypsinogen A in aqueous buffer solutions at pH 2, 3, and 4 are in accord with previous values obtained by Jackson and Brandts[27] and Privalov *et al.*[28] at similar pH values. Figure 2 represents the temperature dependence of the denaturation enthalpy in aqueous buffer without EG. As has been pointed out by Privalov,[19] ΔH_d is a linear function of T_d, with slope equal to the heat capacity change, ΔC_p^d, on denaturation. The values of ΔC_p^d obtained from the slope of the graph, 4.57 kJ K^{-1} mol^{-1} for RNase A and 14.0 kJ K^{-1} mol^{-1} for chymotrypsinogen A, are in very good agreement with those calculated using the data of Privalov *et al.*[24,27] for the thermal denaturation of these proteins in aqueous solutions of varying the pH. A similar value for chymotrypsinogen has been obtained by Biltonen *et al.*[29] from the heat capacities of the native and denatured states of the protein.

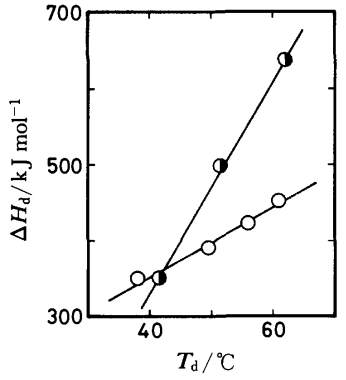

Fig. 2. Dependence of the denaturation enthalpies of RNase A(○) and chymotrypsinogen A(◑) in aqueous buffer without EG on the denaturation temperature.

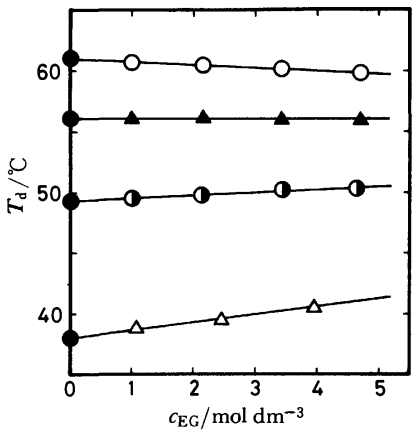

Fig. 3. Variation of the denaturation temperature of RNase A with the EG concentration at pH 2(△), 3(◑), 3.8(▲), and 5(○).
The symbol ● refers to the buffer solution without EG.

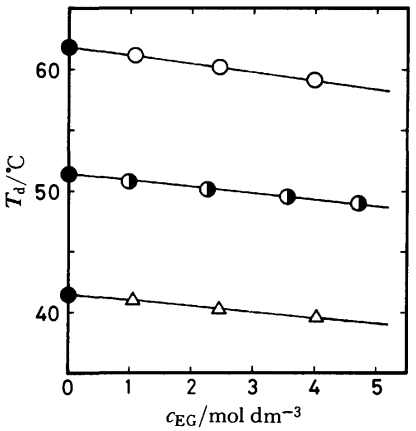

Fig. 4. Variation of the denaturation temperature of chymotrypsinogen A with the EG concentration at pH 2(△), 3(◑), and 4(○).

Figures 3 and 4 show the dependence of the denaturation temperature of RNase A and chymotrypsinogen A on the EG concentration, respectively. It is obvious from Fig. 3 that at pH 3.8 the T_d of RNase is almost independent of the EG content, while the T_d increases slightly with increasing the EG concentration at pH 2 and 3 and decreases slightly at pH 5. Similar results on the EG-induced change in T_d at low pH have been reported by Gerlsma and Stuur. EG stabilizes RNase A against thermal denaturation at low pH but unstabilizes or denatures the protein at high pH in the pH region studied. As show in Fig. 4, on the other hand, the T_d of chymotrypsinogen A is depressed by the addition of EG under all the conditions and the lowering of T_d appears to become more pronounced with increasing the pH and the corresponding T_d. That is, EG has a thermally unstabilizing effect on the protein in the pH 2 to 4 region. These results suggest that the EG-induced effect on the thermal stability of these proteins is dependent on the pH or temperature. However, it is unlikely that the EG effect depends directly on the pH, since the effect on the two proteins differs from each other at identical

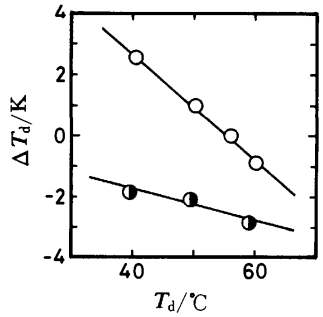

Fig. 5. Dependence of the variation of T_d induced by addition of 4 mol dm^{-3} EG, ΔT_d, of RNase A(○) and chymotrypsinogen A(◑) on the denaturation temperature.

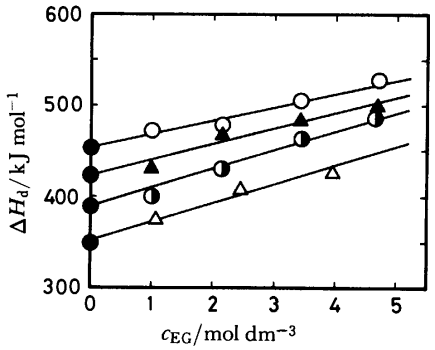

Fig. 6. Variation of the denaturation enthalpy of RNase A with the EG concentration at pH 2(△), 3(◑), 3.8(▲), and 5(○).

pH of 2 and 3 and the T_d of these proteins increases monotonously with increasing the pH in the acidic region. Therefore, the variation of T_d with the addition of EG of 4 mol dm^{-3}, ΔT_d, which is evaluated from a linear dependence of T_d on EG concentration, is plotted as a function of the corresponding temperature in Fig. 5. For both proteins, the ΔT_d appears to be a linear function of temperature, meaning that the EG-induced effect may be directly dependent on temperature.

The dependence of the denaturation enthalpy of RNase A on the EG concentration is shown in Fig. 6. Under all the conditions, ΔT_d increases almost linearly with increasing the EG concentration. Such behavior of ΔH_d was also observed for chymotrypsinogen A, though the degree of the change in ΔH_d with EG was slightly smaller for the protein than for RNase A. As shown in Table 1, the denaturation entropies at the denaturation temperature, $\Delta S_d(=\Delta H_d/T_d)$, of these proteins also increase monotonously with an increase in the concentration of EG. This means that the observed increase (or decrease) in T_d occurs because ΔH_d increases (or does not increase) as much as ΔS_d does upon the addition of EG.

The plot of ΔH_d as a function of ΔS_d gives a linear relationship, presented in Fig. 7, indicating that the EG-induced effect on the thermal stability of these proteins is closely related to the water structure around the protein molecule.[30] The compensation temperatures, which are defined as the slopes of the graph, are 375 and 364 K for RNase A and chymotrypsinogen A, respectively. Although these values are consider-

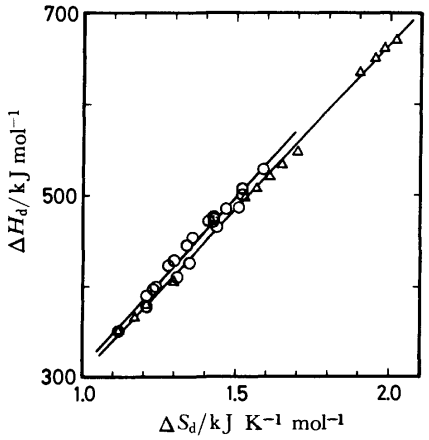

Fig. 7. Enthalpy-entropy compensation plots for the thermal denaturation of RNase A(○) and chymotrypsinogen A(△) in EG-water mixtures.

ably higher than the temperature range of 250 to 320 K observed for many processes, the value for RNase is in good agreement with the compensation temperature deduced from the results obtained for denaturants such as urea and guanidine hydrochloride.[31]

A more definite estimation of the effect of EG on the protein stability may be given by the comparison of the thermodynamic functions of denaturation, $\Delta G°$, $\Delta H°$, and $\Delta S°$, at identical temperatures. Assuming that the heat capacity change, ΔC_p^d, on denaturation is independent of temperature, standard thermodynamic parameters of denaturation at any temperature, T, can be calculated with T_d and ΔH_d by the equations:[32,33]

$$\Delta H° = \Delta H_d - \Delta C_p^d(T_d - T)$$
$$\Delta S° = \Delta H_d/T_d - \Delta C_p^d \ln (T_d/T)$$
$$\Delta G° = \Delta H° - T\Delta S°$$

Unfortunately, ΔC_p^d in each solvent composition can not be accurately determined in the present study. Thus the ΔC_p^d values of these proteins in mixed solvents were assumed to be identical with those in aqueous buffer, 4.57 kJ K^{-1} mol^{-1} for RNase A and 14.0 kJ K^{-1} mol^{-1} for chymotrypsinogen A, which were estimated from the linear temperature dependence of the ΔH_d in this experiment. This assumption will not cause significant error in standard thermodynamic parameters of denaturation when T is close to T_d, since ΔC_p^d does not seem to be largely affected by additions of EG. Therefore, these parameters were calculated at several temperatures in the transition region. Figure 8 represents the variation of $\Delta G°$, $\Delta H°$, and $\Delta S°$ calculated at 48 °C with the EG concentration at pH 3. It is evident that the $\Delta H°$ and $\Delta S°$ for both proteins are increasing functions of EG concentration, indicating that the enthalpy and entropy of transfer of denatured protein from water to aqueous EG are larger than those of native protein. On the other hand, although the variation induced by addition of EG is very small, the $\Delta G°$ for RNase increases obviously with increasing EG concentration, but that for chymotrypsinogen decreases. These findings suggest that the thermal stabilization of RNase by EG is dominantly produced by an enthalpic rather than an entropic effect. However, the unstabilization of chymotrypsinogen by EG may be attributed to the fact

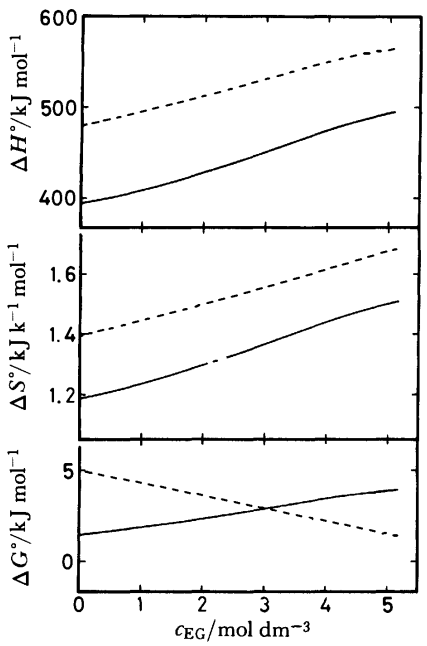

Fig. 8. Variation of the standard thermodynamic parameters of denaturation calculated at 48°C of RNase A (——) and chymotrypsinogen A (----) with the EG concentration.

that $\Delta H°$ does not increase as much as $\Delta S°$ does upon addition of EG. Therefore, the slight increase or decrease in $\Delta G°$ upon addition of EG is produced from the delicate balance between the increased $\Delta H°$ and $\Delta S°$, which may be affected by numerous factors such as temperature and the nature of the protein surface. These findings seem to offer direct evidence for regarding protein stabilization and denaturation (unstabilization) as a thermodynamically continuous phenomenon. The observed increase in $\Delta H°$ and $\Delta S°$ is similar to the observations by Brandts[23] that, at a given temperature, $\Delta H°$ and $\Delta S°$ are much larger for the denaturation of chymotrypsinogen in ethanol-water mixtures than in water. Such a trend of $\Delta H°$ has been also found for the thermal denaturation of RNase A in the same solvent system.[34]

The $\Delta G°$ values for RNase A and chymotrypsinogen A in water and aqueous EG are presented as a function of temperature in the transition region in Figs. 9 and 10, respectively. In the case of RNase, as can be seen from Fig. 9, the $\Delta G°$-temperature curves for these solutions cross at about 55 °C, corresponding roughly to the denaturation temperature of the protein at pH 3.8, which is almost independent of the pH. This means that, at temperatures lower than about 55 °C, EG is quite effective in increasing $\Delta G°$, that is, it stabilizes RNase against thermal denaturation while, at higher temperatures, it behaves as a rather unstabilizing (denaturing) agent for the protein. In the case of chymotrypsinogen, on the other hand, although the dotted line shown in Fig. 10 is the extrapolation of the curve, the crossing of the $\Delta G°$-temperature curves appears to occur at about 35 °C, which is considerably lower than that for RNase. The protein stabilization induced by polyhydric alcohols has been explained as a strengthening of the intramolecular hydrophobic

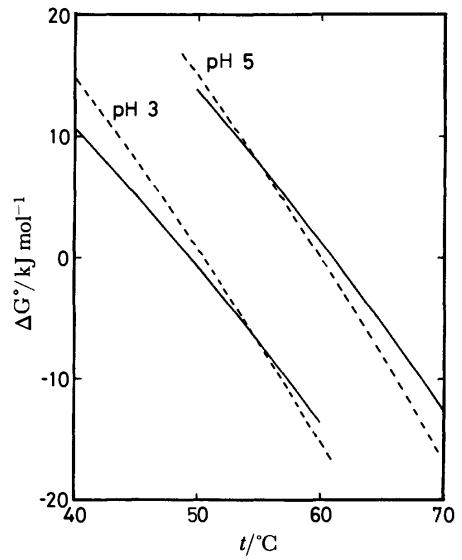

Fig. 9. Variation of $\Delta G°$ of RNase A in water (——) and aqueous EG (----) at pH 3 and 5 with temperature in the transition region.
EG concentrations are 4.64 mol dm^{-3} at pH 3 and 4.70 mol dm^{-3} at pH 5.

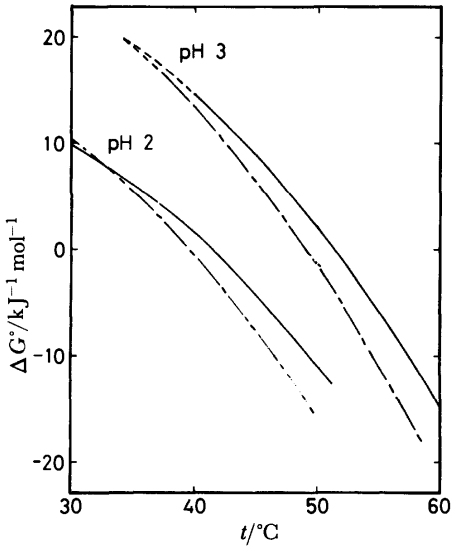

Fig. 10. Variation of $\Delta G°$ of chymotrypsinogen A in water (——) and aqueous EG (-—) at pH 2 and 3 with temperature in the transition region.
EG concentrations are 4.03 mol dm^{-3} at pH 2 and 4.70 mol dm^{-3} at pH 3. The dotted line shows the extrapolation of the curve.

interaction of the protein.[10-13] The conformational stability of proteins in aqueous medium is viewed, at present, as a result primarily of the pressure which water exerts on nonpolar residues, compressing them into the interior of the molecule. An enhancement of the hydrophobic effect in medium by addition of EG at low temperature would render more unfavorable the exposure to solvent of nonpolar groups buried in the interior of native protein. The pronounced relationship between temperature and the EG-induced effect on the thermal stability of these proteins may be explained on the basis of a solvent ordering effect, similar to that proposed by Brandts and Hunt[34] for the stabilizing effect of ethanol at low temperatures and low ethanol concentrations. According to their hypothesis, the mechanism is closely connected with the solvation which forms about exposed nonpolar groups at low temperature and with the disruption of the solvation structure which occurs as the temperature is increased. Ethanol or EG added may replace ordered water molecules around exposed hydrophobic groups, both solvent components becoming part of the solvation which surrounds the nonpolar side chains of the protein. In the case of ethanol, this structure is disrupted at low temperatures, permitting the formation of hydrophobic contacts between the nonpolar moiety of the alcohol and the nonpolar groups of the protein and leading to the denaturation of the protein. In the case of EG, however, such a solvation around the exposed nonpolar groups of a protein should remain intact up to relatively high temperature, at least near 55 °C for RNase and near 35 °C for chymotrypsinogen, since the hydrophobicity of EG is considerably smaller than that of ethanol. Furthermore, the interaction of the EG with the exposed nonpolar groups of proteins is not direct, as would be in the case of hydrophobic interactions, but it occurs indirectly through the strong interaction of EG molecule with the water of hydration around the nonpolar groups of the protein.

There is an important difference between RNase A and chymotrypsinogen A in the observed effect of EG on the thermal denaturation. These proteins differ greatly in the molecular parameters. The average hydrophobicity and polarity are 870 cal (1 cal=4.184 J) per residue and 1.73 for RNase A and 1040 cal per residue and 0.83 for chymotrypsinogen A.[35] RNase A is one of the most hydrophilic globular proteins and the content of nonpolar amino acid residues is very low, 49 residues per molecule. On the other hand, chymotrypsinogen A has high hydrophobicity and contains 112 nonpolar amino acids per molecule. Although it has been shown by Brandts and Hunt[34] that the fraction of the total number of residues which unfold during denaturation is smaller for chymotrypsinogen than for RNase, the number of newly exposed nonpolar groups following denaturation would be considerably larger in chymotrypsinogen than in RNase. Addition of EG seems to give rise to a decrease in the heat capacity of solvation of nonpolar groups.[34,36] Such a effect should be greater for chymotrypsinogen A than for RNase A. This may be partially responsible for the result that the observed decrease in $\Delta G°$ for chymotrypsinogen A upon addition of EG occurs because $\Delta H°$ does not increase as much as $\Delta S°$ does.

References

1) W. Kauzmann, *Adv. Protein Chem.*, **14**, 1 (1959).
2) P. H. Van Hipple and K.-Y. Wong, *J. Biol. Chem.*, **240**, 3909 (1965).
3) F. Franks and D. Eagland, *CRC Crit. Rev. Biochem.*, **1975**, 165.
4) J. C. Lee and S. N. Timasheff, *J. Biol. Chem.*, **256**, 7193 (1981).
5) M. J. Ruwart and C. H. Suelter, *J. Biol. Chem.*, **246** 5990 (1971).
6) M. L. Shelanski, F. Gaskin, and C. R. Cantor, *Proc.*

Natl. Acad. Sci. U. S. A., **70**, 765 (1973).
7) S. Y. Gerlsma, *Eur. J. Biochem.*, **14**, 150 (1970).
8) S. Y. Gerlsma and E. R. Stuur, *Int. J. Pept. Protein Res.*, **4**, 377 (1972).
9) J. F. Bock, D. Oakenfull, and M. B. Smith, *Biochemistry*, **18**, 5191 (1979).
10) K. Gekko, *J. Biochem. (Tokyo)*, **91**, 1197 (1982).
11) K. Gekko and S. N. Timasheff, *Biochemistry*, **20**, 4667, 4677 (1981).
12) K. Gekko and T. Morikawa, *J. Biochem. (Tokyo)*, **90**, 39 (1981).
13) K. Gekko, *J. Biochem. (Tokyo)*, **90**, 51, 1643 (1981).
14) H. Bull and K. Breese, *Biopolymers*, **17**, 21 (1978).
15) B. Lubas, M. Soltysk-Rasek, and I. Lesniewska, *Biochemistry*, **18**, 4943 (1979).
16) K. Satoh and K. Miyazawa, 19th Annual Meeting of the Biophys. Soc. Japan, Fukuoka, Oct. 1981, Abstr. p. 175.
17) Y. Fujita, Y. Iwasa, and Y. Noda, *Bull. Chem. Soc. Jpn.*, **55**, 1896 (1982).
18) R. L. Biltonen and E. Freire, *CRC Crit. Rev. Biochem.*, **1978**, 85.
19) P. L. Privalov, *Adv. Protein Chem.*, **33**, 167 (1979).
20) R. A. Scott and H. A. Scheraga, *J. Am. Chem. Soc.*, **85**, 3866 (1963).
21) J. F. Brandts and R. Lumry, *J. Phys. Chem.*, **67**, 1484 (1970).
22) L. C. Lee, K. Gekko, and S. N. Timasheff, *Methods Enzymol.*, **61**, 26 (1979).
23) J. F. Brandts, *J. Am. Chem. Soc.*, **86**, 4291 (1964).
24) T. Y. Tsong, R. P. Hearn, D. P. Wrathall, and J. M. Sturtevant, *Biochemistry*, **9**, 2666 (1970).
25) P. L. Privalov, E. I. Tiktopulo, and N. N. Khechinashvili, *Int. J. Pept. Protein Res.*, **5**, 22 (1973).
26) A. L. Jacobson and C. L. Turner, *Biochemistry*, **19**, 4534 (1980).
27) W. M. Jackson and J. F. Brandts, *Biochemistry*, **9**, 2294 (1970).
28) P. L. Privalov, N. N. Khechinashvili, and B. P. Atanasov, *Biopolymers*, **10**, 1865 (1971).
29) R. Biltonen, A. T. Schwartz, and I. Wadsö, *Biochemistry*, **10**, 3417 (1971).
30) R. Lumry and S. Rajender, *Biopolymers*, **9**, 1125 (1970).
31) V. Crescenzi and F. Delben, *Int. J. Protein Res.*, **3**, 57 (1971).
32) P. L. Privalov and N. N. Khechinashvili, *J. Mol. Biol.*, **86**, 665 (1974).
33) G. Velicelebi and J. M. Sturtevant, *Biochemistry*, **18**, 1180 (1979).
34) J. F. Brandts and L. Hunt, *J. Am. Chem. Soc.*, **89**, 4826 (1967).
35) C. C. Bigelow, *J. Theor. Biol.*, **16**, 187 (1967).
36) G. Dipaol and B. Belleau, *Can. J. Chem.*, **56**, 848 (1978).

Cycloadditions of Trifluoroacetonitrile Oxide with Olefins and Acetylenes

Kiyoshi TANAKA,* Hideyuki MASUDA, and Keiryo MITSUHASHI
Department of Industrial Chemistry, College of Technology, Seikei University, Musashino-shi, Tokyo 180
(Received January 24, 1984)

The regio- and stereoselectivity of the cycloadditions of trifluoroacetonitrile oxide (**1**) with olefins and acetylenes were described. The oxide **1**, generated *in situ* from trifluoroacetohydroximoyl bromide etherate in the presence of triethylamine, reacted with various monosubstituted olefins and acetylenes to give exclusively 5-substituted 3-trifluoromethyl-2-isoxazolines and -isoxazoles, respectively, whereas **1** cyclized with 1,2-disubstituted olefins and acetylenes to result in the formation of a mixture of two regioisomeric products. On the other hand, the cycloaddition of **1** with (*Z*)-β-methylstyrene afforded a mixture consisting of two regioisomeric isoxazolines retaining *Z*-configuration and one diastereoisomeric isoxazoline.

A number of heterocyclic compounds bearing a fluorine or trifluoromethyl group are known to be effective pharmaceutically and agrochemically,[1] but the introduction of such a fluorine group into heterocyclic rings has been limited.[2] As a part of research on applications of the fluorinated 1,3-dipolar compounds as building blocks of heterocycles with fluorine groups,[3] we remarked trifluoroacetonitrile oxide (**1**). Although only one report described the cycloadditions of the nitrile oxide **1**, liberated from trifluoroacetohydroximoyl chloride, the dipolarophiles employed were limited to the reactive ones such as acetylenic and enol ethers.[4] In the present paper, we wish to report that the oxide **1**, generated from trifluoroacetohydroximoyl bromide etherate (**2**), cyclizes with various olefins and acetylenes to give the corresponding 3-trifluoromethyl-2-isoxazolines and -isoxazoles,[5] and also to describe the regio- and stereoselectivity of the cycloadditions.

$$CF_3C \equiv N \rightarrow O$$

1

The bromide **2** was prepared by bromination of trifluoroacetaldehyde oxime[6] which was readily obtained from trifluoroacetaldehyde hydrate and hydroxylamine hydrochloride.

The reactions of **2** with monosubstituted olefins such as styrene, allyloxybenzene, allyl alcohol, and butoxyethylene proceeded smoothly in the presence of triethylamine at room temperature to afford exclusively 5-substituted 3-trifluoromethyl-2-isoxazolines **3** in good yields. Similarly, **2** was allowed to react with methyl acrylate, an olefin bearing electron-withdrawing group, to give only 5-methoxycarbonylisoxazoline in appreciable yield (Table 1). The structure of these 3-trifluoromethyl-2-isoxazolines was determined on the basis of the comparable chemical shifts of 5-methine and 4-methylene protons to those of 3-phenyl analogues reported in the literatures[7] and the existence of the H–F couplings between 4-methylene protons and trifluoromethyl group. Similarly, the oxide **1** readily underwent the cycloadditions with monosubstituted acetylenes. The reaction of **2** with phenylacetylene gave exclusively 5-phenyl-3-trifluoromethylisoxazole (**4a**) in excellent yield, where the alternative 1,3-addition product described in the reaction of benzonitrile oxide[8] was not detected at all. A similar reaction with 2-propyn-1-ol also gave **4b** in moderate yield and, however, that with methyl propiolate resulted in a tar-like matter. Dehydrogenation of **3a** with 2,3-dichloro-5,6-dicyano-*p*-benzoquinone (DDQ) was so sluggish that only 12% of **4a** was obtained (Scheme 1).

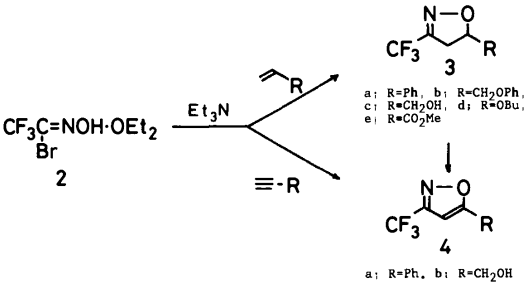

Scheme 1.

TABLE 1. PREPARATIONS OF ISOXAZOLINES **3** AND ISOXAZOLES **4**

3 or **4**	Yield[a] %	Bp(°C/mmHg)[Mp(°C)](lit)	IR $\tilde{\nu}$/cm^{-1} C=N	Formula	Calcd(Found)/% C	H	N
3a	84[b]	85—87/3.5	1628	$C_{10}H_8NOF_3$	55.82 (55.78)	3.75 (3.41)	6.51 (6.41)
3b	80	[48.5—49.5]	1620	$C_{11}H_{10}NO_2F_3$	53.88 (54.01)	4.11 (4.15)	5.71 (5.71)
3c	60	82—83/6	1635	$C_5H_6NO_2F_3$			8.28 (8.25)
3d	89	45—46/2(78—80/10)[c]	1625	—		—	
3e	82	76—77/6(64—66/3)[c]	1635	—		—	
4a	93	[44—45.5]	1610	$C_{10}H_6NOF_3$	56.35 (56.56)	2.84 (2.38)	6.57 (6.83)
4b	38	75—77/6	1603	$C_5H_4NO_2F_3$			8.38 (8.33)

a) Isolated yield. b) Besides **3a**, a trace of 1,1,1-trifluoro-4-phenyl-3-buten-2-one oxime was obtained. c) See ref. 4).

On the other hand, the cycloadditions of **1** with 1,2-disubstituted olefins under the similar conditions produced a mixture of regioisomeric products. The reaction with methyl crotonate gave a mixture of 4-methylisoxazoline **5a** and 5-methyl isomer **5a'** in 39% yield (**5a**/**5a'** ratio of 43/57). The cycloaddition with 1-methoxy-4-(1-propenyl)benzene proceeded more easily to give a mixture of **5b** and **5b'** in 87% yield (**5b**/**5b'** ratio of 93/7). Similarly, from the reaction with (*E*)-*β*-methylstyrene, 66% yield of a mixture of **5c** and **5c'** was obtained (**5c**/**5c'** ratio of 86/14). The cycloaddition with 1,2-disubstituted acetylene such as 1-phenyl-1-propyne, however, proceeded regioselectively to afford only **6** in 23% yield. The formation of its regioisomer was not observed at all. The structure of **6** is supported by the fact that dehydrogenation of **5c** with chromium trioxide gave **6** in 47% yield (Scheme 2).

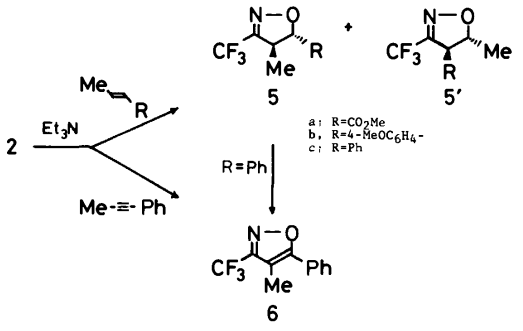

Scheme 2.

The stereoselectivity of the cycloaddition of **1** was next investigated. Since (*Z*)-stilbene and dimethyl maleate usually employed for such a purpose were both unreactive toward **1**, the reaction with (*Z*)-*β*-methylstyrene including 3% of its *E*-isomer was carried out, giving a mixture of two regioisomers with retention of *Z*-configuration, **7** and **7'**, and diastereoisomer of **7**, **5c**, in 30% yield (**7**/**7'**/**5c** ratio of 10/5/3). The stereochemical assignments are based on ^{1}H NMR spectra. The *Z*-configuration of **7** and **7'** is supported by both the more shielded methyl protons[9] and the bigger coupling constants between 4- and 5-methine protons[7b] in **7** and **7'** as compared to **5c** (Scheme 3). In the reaction mixture, 3% of (*E*)-*β*-methylstyrene was still present and, on further treatment of the reaction products with triethylamine, the ratio of **7**/**7'**/**5c** was found to be unchanged. These results indicate that **5c** may be directly led from (*Z*)-*β*-methylstyrene.

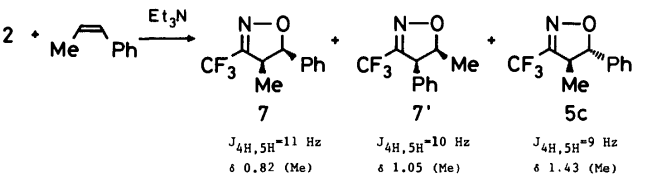

Scheme 3.

As a conclusion, the regioselectivity of the cycloadditions of **1** toward monosubstituted olefins and acetylenes, affording exclusively 5-substituted isoxazolines and isoxazoles, is similar to that of benzonitrile oxide,[7] whereas the tendency toward 1,2-disubstituted olefins is somewhat different. Summarized for comparison are the regioselective results of benzonitrile oxide,[7b,10] cyanogen *N*-oxide,[10] and benzenesulfonyl cyanide *N*-oxide[11] (Table 2). Trifluoromethyl group favors the formation of 4-methylisoxazolines **5**, compared with benzonitrile oxide, and its effect on the regioselectivity seems to be almost equal to that of cyano group. It also turns out that the regioselectivity depends on the configuration of the olefins used, namely, (*E*)-*β*-methylstyrene is more regioselective than (*Z*)-*β*-methylstyrene. It is also found that the cycloaddition proceeds with high stereoselectivity. However, the formation of the diastereoisomer **5c** in the case of (*Z*)-*β*-methylstyrene suggests that the partial inversion of the *Z*-configuration takes place during course of the cycloaddition, pointing out the possibility of the partial lack of the concerted process.

Experimental

All melting and boiling points are uncorrected. The IR spectra were recorded on a JASCO IRA-1 spectrometer. The ^{1}H and ^{19}F NMR spectra were measured with a JEOL JNM-PMX 60 spectrometer and a Hitachi R-24F spectrometer using an internal tetramethylsilane (TMS) and an external trifluoroacetic acid as a standard, respectively, the chemical shifts being given in *δ* ppm downfield. The MS spectra were obtained on a Finnigan 3300E GC-MS spectrometer operating at 120 eV.

Preparation of **2**. The previously reported procedures were modified for the preparations of trifluoroacetaldehyde hydrate and its oxime.[12] To a suspension of 7.6 g (0.20 mol) of lithium aluminium hydride in 500 ml of diethyl ether, dried over calcium chloride, was added dropwise a solution of 30.0 g (0.26 mol) of trifluoroacetic acid in 400 ml of diethyl ether holding the temperature below 5 °C. The mixture was stirred at 0 °C for an additional 1 h. To the mixture were added 18 ml of methanol, 16 ml of water, and 32 ml of concd

Table 2. Regioselectivity of nitrile oxides (R-C≡N→O)

R-C≡N→O R	Olefin or Acetylene	Ratio 4-Methyl product/5-Methyl product
CF_3-	(*E*)-CH_3CH=$CHCO_2Me$	43/57[a]
Ph-		34/66[b]
NC-		44.5/55.5[b]
PhO_2S-		62/38[c]
CF_3-	(*E*)-CH_3CH=CHC_6H_4OMe-4	93/7[a]
Ph-		78/22[d]
CF_3-	(*E*)-CH_3CH=CHPh	86/14[a]
CF_3-	CH_3C≡CPh	100/0

a) Determined by ^{19}F NMR and/or GLC analysis. b) See Ref. 9). c) See Ref. 10). d) See Ref. 7b).

sulfuric acid and then diethyl ether layer was separated. Water was added to the residual mixture and the mixture was extracted twice with diethyl ether. The combined ethereal extracts were washed with brine, dried over magnesium sulfate, and evaporated under reduced pressure to leave 33.9 g of crude trifluoroacetaldehyde hydrate.

To a mixture of 33.9 g of thus-obtained crude trifluoroacetaldehyde hydrate, 50 ml of methanol, 50 ml of water, 50 g of ice, and 20.3 g of hydroxylamine hydrochloride, was added dropwise 44 g of 50% aqueous sodium hydroxide. Then the temperature of the mixture was maintained below 35 °C. After stirring at room temperature for 10 h, the mixture was washed with diethyl ether, acidified to pH 6 with concd hydrochloric acid, and extracted twice with diethyl ether. The extracts were washed with water and brine, dried over magnesium sulfate, and distilled to give 28.3 g of trifluoroacetaldehyde oxime including small amount of diethyl ether (boiling range 78—79 °C).

Holding the temperature below 40 °C, a solution of 44.6 g of *N*-bromosuccinimide in 125 ml of *N,N*-dimethylformamide (DMF) was added dropwise to a solution of 28.3 g of trifluoroacetaldehyde oxime in 50 ml of DMF. After stirring at room temperature for 3 h, the mixture was poured into 400 ml of cold water and extracted with diethyl ether. The extracts were washed with water and brine, dried over magnesium sulfate, and distilled to afford 29.9 g of **2**; bp 115 °C (lit, bp 52—55 °C/72 mmHg (1 mmHg≈133.322 Pa))[13], 43% yield based on trifluoroacetic acid, ^{19}F NMR ($CDCl_3$) δ= 10.5 (s) and 10.3 (s), MS (*m/z*) 191 and 193 (M^+-Et_2O), 171 and 173 ($M^+-Et_2O\cdot HF$), and 111 (CF_3CNO^+).

Reactions of 2 with Monosubstituted Olefins. Triethylamine (4.89 g, 48.4 mmol) diluted with 20 ml of toluene was added to a solution of 6.45 g (24.2 mmol) of **2** and 7.55 g (72.6 mmol) of styrene in 50 ml of toluene over a period of 1 h and the mixture was stirred at room temperature for additional 10 h. After excess hexane ws added to the reaction mixture, the resulting salt (4.51 g) was collected on a filter. The filtrate was washed with water and brine, dried over magnesium sulfate, and evaporated to leave crude **3a** which was purified by distillation under reduced pressure to give 4.35 g (84%) of pure **3a**, ^{1}H NMR ($CDCl_3$) δ=3.07 (ddq, 1H), 3.57 (ddq, 1H), 5.76 (dd, 1H), and 7.30 (m, 5H).

Similarly, **3c**, **3d**, and **3e** were obtained and their ^{1}H NMR data are as follows; **3c**, ($CDCl_3$) δ=2.83 (br.s, 1H), 3.07 (m, 1H), 3.25 (m, 1H), 3.58 (dd, 1H), 3.90 (dd, 1H), and 4.93 (tdd, 1H), **3d**, (CCl_4) δ=0.95 (t, 3H), 1.15—1.80 (m, 4H), 2.85 (dm, 1H), 3.25 (dm, 1H), 3.30—4.05 (m, 2H), and 5.66 (dd, 1H), **3e**, (CCl_4) δ=3.33 (m, 1H), 3.50 (m, 1H), 3.77 (s, 3H), and 5.17 (dd, 1H).

The isoxazoline **3b** was also obtained from the reaction of **2** with 1.5 equiv of allyloxybenzene and the successive isolation by column chromatography (silica gel, hexane–ethyl acetate, 9:1). Thus-obtained **3b** was further recrystallized from hexane to give the white needles **3b**, ^{1}H NMR (CCl_4) δ=3.10 (m, 1H), 3.27 (m, 1H), 3.97 (d, 2H), 5.02 (tt, 1H), and 6.85—7.27 (m, 5H).

Reactions of 2 with Monosubstituted Acetylenes. In a similar manner, crude **4a** was obtained and purified by column chromatography (silica gel, hexane) followed by recrystallization from hexane, ^{1}H NMR (CCl_4) δ=6.67 (s, 1H) and 7.28—7.90 (m, 5H), whereas **4b** was purified by distillation under reduced pressure, ^{1}H NMR ($CDCl_3$) δ= 3.67 (br.s, 1H), 4.85 (s, 2H), and 6.56 (s, 1H).

Dehydrogenation of 3a to 4a. A solution of 1.00 g (4.65 mmol) of **3a** and 1.06 g (4.65 mmol) of DDQ in 10 ml of toluene was refluxed for 2 d. Diethyl ether was added to the reaction mixture and the resulting mixture was washed with water and brine, dried over magnesium sulfate, and evaporated under reduced pressure to leave oily matter which was submitted to short column chromatography (silica gel, hexane) to give 0.84 g of a mixture of **3a** and **4a** in the ratio of 86/14, according to ^{1}H NMR analysis. The isoxazole **4a** was separated by preparative GLC and its IR and ^{1}H NMR data are consistent with those obtained above.

Reactions of 2 with 1,2-Disubstituted Olefins. To a solution of 1.81 g (6.8 mmol) of **2** and 2.04 g (20.4 mmol) of methyl crotonate in 15 ml of toluene, was added dropwise a solution of 1.37 g (13.6 mmol) of triethylamine in 5 ml of toluene over a 75 min period and the mixture was stirred at room temperature for additional 15 h. The similar procedure described above gave 1.03 g of the white salt and the oily matter which was submitted to distillation (boiling range, 73—75 °C/5 mmHg) to produce 0.42 g (29%) of a mixture of **5a** and **5a'** in the ratio of 43/57 (^{19}F NMR analysis). The isoxazolines **5a** and **5a'** were isolated by preparative GLC, **5a** ^{1}H NMR (CCl_4) δ=1.43 (d, 3H), 3.70 (dq, 1H), 3.82 (s, 3H), and 4.67 (d, 1H), ^{19}F NMR (CCl_4) δ=14.3, **5a'**, ^{1}H NMR (CCl_4) δ=1.47 (d, 3H), 3.73 (dq, 1H), 3.78 (s, 3H), and 5.07 (dq, 1H), ^{19}F NMR (CCl_4) δ=14.7.

Found: N, 6.58%. Calcd for $C_7H_8NO_3F_3$: N, 6.63% (for a mixture of **5a** and **5a'**).

Similarly, a mixture of **5b** and **5b'** in the ratio of 93/7 was collected by distillation (boiling range. 115—119 °C/1 mmHg) and each isomer was isolated by preparative GLC, **5b**, ^{1}H NMR (CCl_4) δ=1.40 (d, J=7 Hz, 3H), 3.38 (dqm, 1H). 3.78 (s, 3H), 5.10 (d, J=9 Hz, 1H), and 6.7—7.2 (A_2X_2, 4H), IR (film) 1610 cm^{-1} (C≡N), **5b'**, ^{1}H NMR (CCl_4) δ=1.40 (d, J=7 Hz, 3H), 3.77 (s, 3H), 3.90 (dm, J=7 Hz, 1H), 4.67 (dq, 1H), 6.8—7.1 (A_2X_2, 4H), IR (film) 1610 cm^{-1} (C=N).

Found: N, 5.36%. Calcd for $C_{12}H_{12}NO_2F_3$: N, 5.40% (for a mixture of **5b** and **5b'**).

A mixture of **5c** and **5c'** in the ratio of 86/14 was also collected by distillation (boiling range, 87—92 °C/4 mmHg) in 66% yield, **5c**, ^{1}H NMR (CCl_4) δ=1.43 (d, J=7 Hz, 3H), 3.40 (dqm, 1H), 5.17 (d, J=9 Hz, 1H), and 7.3 (s, 5H), IR (film) 1620 cm^{-1} (C=N), **5c'**, ^{1}H NMR (CCl_4) δ=1.43 (d, J=7 Hz, 3H), 3.90 (dm, J=6 Hz, 1H), 4.67 (dq, 1H), and 6.9—7.3 (m, 5H), IR (film) 1610 cm^{-1} (C=N).

Found: N, 6.12%. Calcd for $C_{11}H_{10}NOF_3$: N, 6.11% (for a mixture of **5c** and **5c'**).

Reaction of 2 with 1-Phenyl-1-propyne. In a similar manner to the above, crude **6** was obtained and purified by column chromatography (silica gel, hexane) followed by recrystallization from hexane, mp, 69—69.5 °C, ^{1}H NMR ($CDCl_3$) δ=2.30 (s, 3H) and 7.4—7.8 (m, 5H), IR (KBr) 1615 cm^{-1} (C=N).

Found: C, 57.91; H, 3.45; N, 6.07%. Calcd for $C_{11}H_8NOF_3$: C, 58.16; H, 3.55; N, 6.17%.

Dehydrogenation of 5c to 6. A solution of 430 mg (1.88 mmol) of **5c**, 500 mg of chromium trioxide, and 3 drops of concd sulfuric acid in 10 ml of acetic acid was refluxed for 40 min and evaporated under reduced pressure. The resulting mixture was extracted with diethyl ether and extracts were washed with water and brine, dried over magnesium sulfate, and evaporated under reduced pressure to leave crude **6** which was purified by column chromatography (silica gel, hexane–ethyl acetate, 10:1) to give 200 mg (47%) of the white solid **6**, mp, 67.5—69.5 °C.

Reaction of 2 with (Z)-β-Methylstyrene. (*Z*)-β-Methylstyrene was obtained by hydrogenation with Lindlar catalyst according to the previously reported procedure.[14] The reaction of **2** with 1.3 equiv of (*Z*)-β-methylstyrene was carried out in a similar manner and a mixture of **7**, **7'**, and **5c** in the ratio of 10/5/3 (^{1}H NMR analysis) was collected in 30% yield by column chromatography (silica gel, hexane–ethyl acetate, 3:1). Each isomer was separated by preparative GLC, **7**, ^{1}H NMR (CCl_4) δ=0.82 (d, J=8 Hz, 3H), 3.60 (dqm, 1H), 5.73 (d, J=11 Hz, 1H), and 7.1—7.4 (m, 5H), IR (film)

1618 cm^{-1} (C=N), **7'**, ^1H NMR (CCl_4) δ=1.05 (d, J=6 Hz, 3H), 4.22 (d, J=10 Hz, 1H), 4.90 (dq, 1H), and 6.9—7.7 (m, 5H), IR (film) 1610 cm^{-1} (C=N). Spectral data of **5c** are consistent with those obtained above.

Found: N, 5.83%. Calcd for $C_{11}H_{10}NOF_3$: N, 6.11% (for a mixture of **7** and **7'**).

References

1) a) H. Kimoto and L.A. Cohen, *J. Org. Chem.*, **45**, 3831 (1980); b) R. Filler, "Advances in Fluorine Chemistry," Butterworths, London (1970), Vol. 6, p. 1; c) R. Filler, *Chemtech.*, **4**, 752 (1974).

2) a) Y. Kobayashi, I. Kumadaki, and T. Taguchi, *Yuki Gosei Kagaku Kyokai Shi*, **38**, 1119 (1980); b) R. D. Chambers and C. R. Sargent, "Polyfluoroheteroaromatic Compounds," in "Advances in Heterocyclic Chemistry," ed by A. R. Katritzky and A. J. Boulton, Academic Press, New York (1981), Vol. 28, p.1—71.

3) Part III on "Applications of the fluorinated 1,3-dipolar compounds as building blocks of the heterocycles with fluorine groups." Part II: K. Tanaka, H. Daikaku, and K. Mitsuhashi, *Chem. Lett.*, **1983**, 1463.

4) D. P. Del'tsova, E. S. Ananyan, and N. P. Gambaryan, *Izv. Akad. Nauk SSSR, Ser. Khim.*, **1971**, 362; *Chem. Abstr.*, **75**, 63699d (1971).

5) For the biological aspects of 3-perfluoroalkylisoxazoles, see a) J. B. Carr, H. G. Durham, and K. Hass, *J. Med. Chem.*, **20**, 934 (1977); b) V. N. Pathak and V. Grover, *Pharmazie*, **34**, 568 (1979); *Chem. Abstr.*, **92**, 181060n (1980).

6) K.-C. Liu, B. R. Shelton, and R. K. Howe, *J. Org. Chem.*, **45**, 3916 (1980).

7) a) R. Sustmann, R. Huisgen, and H. Huber, *Chem. Ber.*, **100**, 1802 (1967); b) K. Bast, M. Christl, R. Huisgen, W. Mack, and R. Sustmann, *ibid.*, **106**, 3258 (1973).

8) a) S. Morrocchi, A. Ricca, A. Zanarotti, G. Bianchi, R. Gandolfi, and P. Grünanger, *Tetrahedron Lett.*, **1969**, 3329; b) P. Beltrame, P. Sartirana, and C. Vintani, *J. Chem. Soc. (B)*, **1971**, 814; c) R. Huisgen, *J. Org. Chem.*, **41**, 403 (1976).

9) L. M. Jackman and S. Sternhell, "Applications of Nuclear Magnetic Resonance Spectroscopy in Organic Chemistry," Pergamon Press, Oxford (1969), Part 3, Chap. 3.

10) M. Christl and R. Huisgen, *Chem. Ber.*, **106**, 3345 (1973).

11) P. A. Wade and H. R. Hinney, *Tetrahedron Lett.*, **1979**, 139.

12) a) D. R. Husted and A. H. Ahlbrecht, *J. Am. Chem. Soc.*, **74**, 5422 (1952); b) L. W. Kissinger, W. E. McQuistion, M. Schwartz, and L. Goodman, *Tetrahedron*, **19**, 131, 137 (1963).

13) B. L. Dyatkin, A. A. Gevorkyan, and I. L. Knunyants, *Zh. Obshch. Khim.*, **36**, 1326 (1966); *Chem. Abstr.*, **65**, 16855h (1966).

14) H. Lindlar and R. Dubuis, "Organic Syntheses," Wiley, New York (1966), Vol. 46, pp. 89—92.

Preparation of 13-Substituted 8*H*-Dibenzo[*a*,*g*]quinolizin-8-ones by Intramolecular Wittig-Horner Reaction of Dialkyl 2-(*o*-Acylbenzoyl)-1,2-dihydro-1-isoquinolylphosphonates

Kin-ya AKIBA,† Yoshio NEGISHI, and Naoki INAMOTO*
Department of Chemistry, Faculty of Science, The University of Tokyo, Hongo, Tokyo 113
(Received January 27, 1984)

Dialkyl 2-(*o*-acylbenzoyl)-1,2-dihydro-1-isoquinolyl-phosphonates (**1**) were prepared by reactions of isoquinoline, *o*-acylbenzoyl chloride, and trialkyl phosphites. Treatment of **1** with lithium diisopropylamide gave 13-substituted 8*H*-dibenzo[*a*,*g*]quinolizin-8-ones by intramolecular Wittig-Horner reaction. Especially, 13-alkoxy and dimethylamino derivatives were obtained in good yields. A similar reaction of dimethyl 1-[*o*-(methoxycarbonyl)benzoyl]-1,2-dihydro-2-quinolylphosphonate was also described.

As a general method to introduce substituents into heteroaromatics, we recently reported preparation of a variety of heterocyclic phosphonates from the corresponding heteroaromatic cations and their use for carbonyl olefination to afford heterocycles containing *exo*-methylene groups.[1]

This method was extended to isoquinolinium salts, and it was found that dimethyl 2-isopropoxycarbonyl-1,2-dihydro-1-isoquinolylphosphonate, prepared from isoquinoline, isopropyl chloroformate, and trimethyl phosphite, afforded the corresponding 1-*exo*-methylene compounds by the Wittig-Horner reaction with various aldehydes, and the *exo*-methylene compounds thus obtained were readily converted to 1-substituted isoquinolines with hydrogen chloride.[2]

This paper describes on preparation of dialkyl 2-(*o*-acylbenzoyl)-1,2-dihydro-1-isoquinolylphosphonates (**1**) and their intramolecular Wittig-Horner reaction to afford 13-substituted 8*H*-dibenzo[*a*,*g*]quinolizin-8-ones (**2**).[3]

Results and Discussion

Synthesis of Dialkyl 2-(o-Acylbenzoyl)-1,2-dihydro-1-isoquinolylphosphonates (1). *o*-Aroylbenzoyl chlorides were used as acylating reagent of isoquinoline, but it is known that *o*-benzoylbenzoyl chloride (**3a**) exists as the tautomeric form, 3-chloro-3-phenylphthalide (**4a**)[4] which is unsuitable for the synthesis of **1a**.

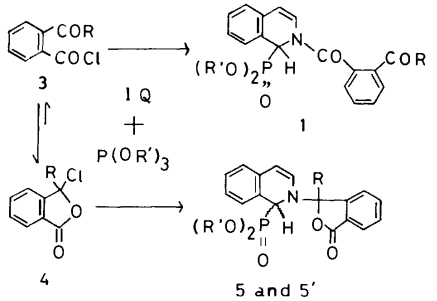

a: R = Ph, R′ = Me
b: R = *p*-MeC$_6$H$_4$, R′ = Me
c: R = MeO, R′ = Me
d: R = EtO, R′ = Me
c′: R = MeO, R′ = Et
d′: R = EtO, R′ = Et
e: R = Me$_2$N, R′ = Me
f: R = PhCH$_2$S, R′ = Me

Therefore, in order to increase the contribution of **3a** and to obtain **1a** as much as possible, a solution of isoquinoline (IQ) was added dropwise to a heated solution of **4a**, followed by addition of trimethyl phosphite. The results are shown in Table 1.

As seen in Table 1, the products were a mixture of the expected phosphonate (**1a**) and undesirable diastereomeric phosphonates (**5a** and **5′a**), 3-phenyl-3-(1-dimethoxyphosphinyl-1,2-dihydro-2-isoquinolyl)-phthalides, derived directly from **4a**.

It was found that the best yield of **1a** was obtained by use of a more dilute solution in propiononitrile as solvent. Under similar conditions **1b** was also prepared in good yield (see Table 1).

Although **5′b** could not be isolated in a pure state, the isomer which has higher melting point and larger J_{PCH} value was regarded as **5** and the other as **5′**.

On the other hand, since phthalic monoesters, monoamides, or monothioester gave only the corresponding chlorides **3c—f**, **1c—f** were prepared by usual method[5] in the absence of sodium iodide in 64—87% yields, except for **1f** (8.2% yield).

Dimethyl 1-[*o*-(methoxycarbonyl)benzoyl]-1,2-dihydro-2-quinolylphosphonate (**6**) was prepared by a similar method in 60% yield.

Intramolecular Wittig-Horner Reactions. Reactions of the phosphonates **1a**, **b** with lithium diisopropylamide (LDA) geve not only the expected 13-aryl-8*H*-dibenzo[*a*,*g*]quinolizin-8-ones (**2a**, **b**) but also phthalides (**7**) and a considerable amount of IQ.

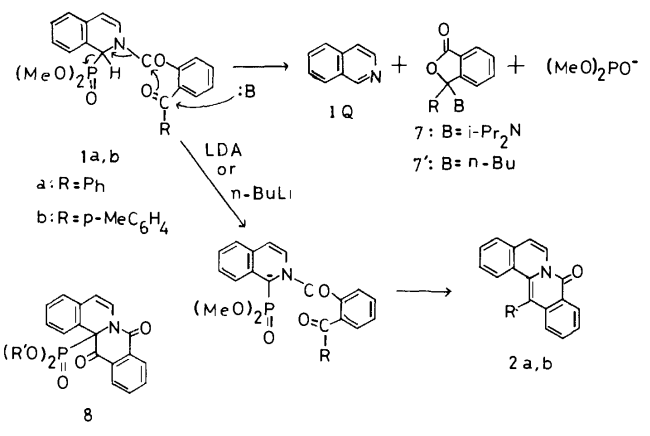

†Present address: Department of Chemistry, Faculty of Science, Hiroshima University, Higashisenda-machi, Hiroshima 730.

Table 1. Preparation of **1a** and **1b**

Solvent	Temp/°C	Concn/M[a]		Total yield/%	Ratio of 1:5:5'[b]
		4	IQ		
MeCN	82 (refl)	**a** 1.1	3.8	86	48:22:30
PhMe	111 (refl)	**a** 0.7	0.34	6.6	55:0:45
PhCN	120—130	**a** 0.3	0.36	20	80:5:15
EtCN	98 (refl)	**a** 0.3	0.33	81	76:9:15
EtCN	98 (refl)	**b** 0.6	1.48	65	42:23:35
EtCN	98 (refl)	**b** 0.15	0.24	93	68:16:16

a) 1 M=1 mol dm^{-3}. b) The ratios were determined from the peak areas of the following signals (each is doublet) in the NMR spectra of the mixtures using simultaneous equations: δ 3.56 and 3.66 for **1a**, 3.56 and 3.59 for **5a**, 3.50 for **5'a**, 3.54 and 3.66 for **1b**, 3.57 and 3.59 for **5b**, and 3.50 for **5'b**.

Table 2. Reaction products from **1** after quenching with methanol

1	Base	Yield/%		
		2	7 or 7'	IQ
1a	LDA	**2a** (31)	**7a** (7)	40
1a	*n*-BuLi	**2a** (9.4)	**7'a** (22)	53
1b	LDA	**2b** (4.5)	**7b** (6)	46
1c	LDA[a]	**2c** (76)		
1c'	LDA[a]	**2c** (66)		
1d	LDA	**2d** (67)		
1d'	LDA[a]	**2d** (75)		
1e	LDA	**2e** (67)		
1f	LDA	**2f** (3.0)		

a) Quenched with ethanol.

Formation of **7** and IQ is attributed to a nucleophilic attack of diisopropylamide anion toward the aroyl carbonyl group of **1a**, **b**. In fact, use of more nucleophilic butyllithium as base resulted in a low yield of **2** and a higher yield of **7'** (see Table 2).

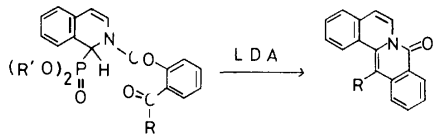

1c-f 2c-f

On the other hand, *o*-(alkoxycarbonyl)benzoyl phosphonates (**1c**, **d**, **c'**, **d'**) gave the corresponding **2c**, **d** in good yields (see Table 2), through the intramolecular Wittig-Horner reaction at the esteric carbonyl group. Formation of **2c**, **d** irrespective of kinds of the phosphonate esters or alcohols as quencher indicates no contribution of a β-keto phosphonate (**8**), which is formed by usual acylation of carbanion with ester. No formation of **8** is attributed to a relief of steric congestion and formation of an extended conjugate system in **2**.

There are a few reports on the intermolecular or intramolecular Wittig reaction at esteric carbonyl group of formate,[6] oxalate,[6] acetate,[7,8] benzoate,[8] oxomalonate (methylenemalonate),[9] and carbonate.[10]

Furthermore, *o*-(dimethylcarbamoyl)benzoyl phosphonate (**1e**) gave 13-dimethylamino derivative (**2e**) in 67% yield, through the intramolecular Wittig-Horner reaction at amidic carbonyl group. Recently, a similar intramolecular Wittig reaction at amidic carbonyl in *o*-(acylamino)benzylidenetriphenylphosphorane has been reported.[11]

Good yields of **2c—e** from **1c—e** are attributed to a prevention of side reactions by electron-donating effect of alkoxyl and dimethylamino groups.

In the case of **1f**, yield of **2f** was very poor (3%), probably because benzylthio group is a good leaving group as indicated by formation of benzyl methyl sulfide (42%), which is probably formed *via* reaction between two leaving groups, α-toluenethiolate and dimethyl phosphate anions.

The structures of **2** were determined by comparison of the spectral data with analogous compounds,[12-14] and by alkaline hydrolysis of **2a** to 1-[α-(*o*-carboxyphenyl)benzyl]isoquinoline (**9**).

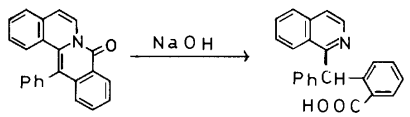

2a 9

A similar reaction of **6** with LDA gave 7-methoxy-12*H*-dibenzo[*b*,*f*]quinolizin-12-one (**10**) in 54% yield.

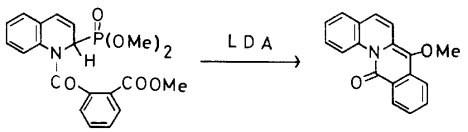

6 10

Experimental

All the melting points are uncorrected. IR spectra were measured with a Hitachi 260-30 spectrophotometer, ^{1}H NMR spectra with a Hitachi R-20B spectrometer using TMS as an internal standard and MS with a Hitachi RMU-6L mass spectrometer at 70 eV.

Synthesis of Dimethyl 2-(o-Benzoylbenzoyl)-1,2-dihydro-1-isoquinolylphosphonate (1a). A mixture of anhyd *o*-benzoylbenzoic acid[15] (1.04 g, 4.6 mmol) and $SOCl_2$ (0.87 ml, 12 mmol) was stirred at room temp until the reaction mixture became clear, and excess $SOCl_2$ was removed *in vacuo*. The residue (**4a**) in dry EtCN (10 ml) was refluxed under nitrogen. IQ (0.59 g, 4.6 mmol) in dry EtCN (13 ml) and then trimethyl phosphite (0.54 ml, 4.6 mmol) were added dropwise to the above refluxing soln, and the refluxing was continued for 1 h. After removal of the solvent, 4% aq $NaHCO_3$ (100 ml) was added to the residue and the mixture was extracted with CH_2Cl_2. The extract was washed with aq NaCl and dried ($MgSO_4$). Removal of the solvent gave a colorless mixture of **1a**, **5a**, and **5'a** (16:2:3; 1.64 g, 81% in total). Only **5a** was isolated by column chromatography (Al_2O_3, Et_2O). The residual mixture was separated by recrystallization. **1a**: Mp

157.1—157.9°C (from EtOAc-hexane); IR (KBr) 1670, 1620, and 1255 cm^{-1}; ^1H NMR ($CDCl_3$) δ=3.56, 3.66 (6H, 2d, J_{POCH}=10.2 Hz), 5.85 (1H, d, J=7.8 Hz), 6.07 (1H, d, J_{PCH}=18 Hz), 6.40 (1H, d, J=7.8 Hz), and 6.9—7.8 (13H, m); MS m/z (rel intensity) 447 (M^+; 0.3) and 209 (100). Found: C, 67.21; H, 4.96; N, 3.00%. Calcd for $C_{25}H_{22}NO_5P$: C, 67.11; H, 4.96; N, 3.13%. **5a**: Mp 185.2—185.7°C (from EtOAc); IR (KBr) 1765, 1630, and 1255 cm^{-1}. ^1H NMR ($CDCl_3$) δ=3.56, 3.59 (6H, 2d, J_{POCH}=10.5 Hz), 4.65 (1H, dd, J_{PCH}=19.2 Hz, J=1.5 Hz), 5.97 (1H, d, J=7.2 Hz), 6.09 (1H, dd, J=7.2 Hz, 1.5 Hz), and 6.7—8.1 (13H, m); MS m/z (rel intensity) 447 (M^+; 0.2) and 209 (100). Found: C, 67.26; H, 5.11; N, 3.05%. **5'a**: Mp 164.2—165.0°C (from EtOAc-hexane); IR (KBr) 1760, 1630, 1260, and 1250 cm^{-1}; ^1H NMR ($CDCl_3$) δ=3.50 (6H, d, J_{POCH}=10.2 Hz), 4.82 (1H, dd, J_{PCH}=16.8 Hz, J=1.5 Hz), 5.93 (1H, d, J=7.8 Hz), 6.07 (1H, dd, J=7.8 Hz, 1.5 Hz), and 6.9—8.0 (13H, m); MS m/z (rel intensity) 447 (M^+; 0.2) and 209 (100). Found: C, 67.40; H, 4.97; N, 3.00%.

Synthesis of Dimethyl 2-[o-(p-Toluoyl)benzoyl]-1,2-dihydro-1-isoquinolylphosphonate (1b). o-(*p*-Toluoyl)benzoic acid[16] was dried at 90°C overnight. A mixture of the anhyd acid (1.12 g, 4.7 mmol) and $SOCl_2$ (1.0 ml, 14 mmol) was treated similarly to that of **1a**. Then dry EtCN (30 ml), IQ (0.60 g, 4.7 mmol) in EtCN (15 ml), and trimethyl phosphite (0.55 ml, 4.7 mmol) were successively added. A similar treatment gave a colorless mixture of **1b**, **5b**, and **5'b** (9:2:2; 1.99 g, 93% in total). **5b** was isolated by column chromatography (Al_2O_3, Et_2O). **1b** was isolated by crystallization from the mixture of **1b** and **5'b**, the latter of which could not be isolated in pure state. **1b**: Mp 157.1—157.8°C (from EtOAc-hexane); IR (KBr) 1660, 1625, and 1260 cm^{-1}; ^1H NMR ($CDCl_3$) δ=2.32 (3H, s), 3.54, 3.66 (6H, 2d, J_{POCH}=10.5 Hz), 5.84 (1H, d, J=7.8 Hz), 6.05 (1H, d, J_{PCH}=18.6 Hz), 6.40 (1H, d, J=7.8 Hz), 7.0—7.3 (6H, m), and 7.45—7.7 (6H, m); MS m/z (rel intensity) 461 (M^+; 0.3) and 233 (100). Found: C, 67.46; H, 5.05; N, 3.14%. Calcd for $C_{26}H_{24}NO_5P$: C, 67.67; H, 5.24; N, 3.04%. **5b**: Mp 176.0—176.8°C (from EtOAc); IR (KBr) 1770, 1635, and 1260 cm^{-1}, ^1H NMR ($CDCl_3$) δ=2.33 (3H, s), 3.57, 3.59 (6H, 2d, J=10.5 Hz), 4.67 (1H, dd, J_{PCH}=19.8 Hz, J=0.9 Hz), 5.92 (1H, d, J=7.8 Hz), 6.11 (1H, dd, J=7.8 Hz, 0.9 Hz), 6.7—7.3 (6H, m), and 7.5—8.1 (6H, m); MS m/z (rel intensity) 461 (M^+; 0.2) and 223 (100). Found: C, 67.73; H, 5.26; N, 3.14%. **5'b**: ^1H NMR (partly) ($CDCl_3$) δ=3.50 (6H, d, J=10.5 Hz), 4.84 (1H, dd, J_{PCH}=16.2 Hz, J=0.9 Hz), 5.89 (1H, d, J=7.8 Hz), and 6.11 (1H, dd, J=7.8 Hz, 0.9 Hz).

Synthesis of Dimethyl 2-[o-(Methoxycarbonyl)benzoyl]-1,2-dihydro-1-isoquinolylphosphonate (1c). A mixture of methyl hydrogen phthalate[17] (1.78 g, 9.9 mmol) and $SOCl_2$ (5.0 ml, 69 mmol) was refluxed for 1 h. Excess $SOCl_2$ was evaporated and completely removed by repeating three times addition of dry benzene (2.5 ml each) and distillation. To the resulting chloride (**3c**) in an ice bath, MeCN (5 ml), IQ (1.28 g, 9.9 mmol) in MeCN (7 ml) and trimethyl phosphite (1.17 ml, 9.9 mmol) were added successively and the mixture was refluxed for 10 min. After removal of the solvent, 2% aq $NaHCO_3$ (50 ml) was added to the residue and the mixture was extracted with CH_2Cl_2. The extract was washed with aq NaCl and dried ($MgSO_4$). Removal of the solvent gave **1c** (3.3 g, 8.21 mmol) in 83% yield as colorless crystals, mp 154.1—154.6°C (from EtOAc); IR (neat) 1725, 1665, 1630, and 1260 cm^{-1}; ^1H NMR ($CDCl_3$) δ=3.59 (3H, s), 3.63, 3.75 (6H, 2d, J_{POCH} =10.5 Hz), 5.83 (1H, d, J=7.8 Hz), 6.15 (1H, d, J=7.8 Hz), 6.51 (1H, d, J_{PCH}=17.4 Hz), 7.0—7.8 (7H, m), and 8.0—8.3 (1H, m); MS m/z (rel intensity) 401 (M^+; 0.3) and 163 (100). Found: C, 59.99; H, 5.08; N, 3.59%. Calcd for $C_{20}H_{20}NO_6P$: C, 59.85; H, 5.02; N, 3.49%.

Synthesis of Diethyl 2-[o-(Methoxycarbonyl)benzoyl]-1,2-dihydro-1-isoquinolylphosphonate (1c'). This compd was prepared by a similar method to that of **1c** in 87% yield as colorless crystals, mp 91.9—92.6°C (from Et_2O-hexane); IR (KBr) 1720, 1660, 1620, and 1255 cm^{-1}; ^1H NMR ($CDCl_3$) δ=1.20, 1.25 (6H, 2t, J=6.6 Hz), 3.52 (3H, s), 3.7—4.5 (4H, m), 5.76 (1H, d, J=7.5 Hz), 6.12 (1H, d, J=7.5 Hz), 6.45 (1H, d, J_{PCH}=18.0 Hz), 6.9—7.7 (7H, m), and 7.95—8.15 (1H, m); MS m/z (rel intensity) 429 (M^+; 0.3) and 163 (100). Found: C, 61.41; H, 5.51; N, 3.26%. Calcd for $C_{22}H_{24}NO_6P$: C, 61.54; H, 5.63; N, 3.26%.

Synthesis of Dimethyl 2-[o-(Ethoxycarbonyl)benzoyl]-1,2-dihydro-1-isoquinolylphosphonate (1d). This compd was prepared by a similar method to that of **1c** in 80% yield as colorless crystals, mp 113.9—114.4°C (from Et_2O-hexane); IR (KBr) 1720, 1675, 1630, and 1270 cm^{-1}; ^1H NMR ($CDCl_3$) δ=1.02 (3H, t, J=6.9 Hz), 3.60, 3.73 (6H, 2d, J_{POCH}=10.8 Hz), 4.04, 4.07 (2H, 2q, J=6.9 Hz), 5.77 (1H, d, J=7.8 Hz), 6.13 (1H, d, J=7.8 Hz), 6.49 (1H, d, J_{PCH}=17.4 Hz), 6.9—7.7 (7H, m), and 8.0—8.15 (1H, m); MS m/z (rel intensity) 415 (M^+; 0.5), 177 (86), and 149 (100). Found: C, 60.68; H, 5.22; N, 3.46%. Calcd for $C_{21}H_{22}NO_6P$: C, 60.72; H, 5.34; N, 3.37%.

Synthesis of Diethyl 2-[o-(Ethoxycarbonyl)benzoyl]-1,2-dihydro-1-isoquinolylphosphonate (1d'). This compd was prepared by a similar method to that of **1c** in 64% yield as colorless crystals, mp 96.4—97.1°C (from EtOAc); IR (KBr) 1720, 1665, 1630, and 1260 cm^{-1}; ^1H NMR ($CDCl_3$) δ=1.00 (3H, t, J=6.6 Hz), 1.20, 1.26 (6H, t, J=6.6 Hz), 4.03 (2H, q, J=6.6 Hz), 3.6—4.5 (4H, m), 5.75 (1H, d, J=7.8 Hz), 6.14 (1H, d, J=7.8 Hz), 6.47 (1H, d, J_{PCH}=17.4 Hz), 6.9—7.8 (7H, m), and 8.0—8.15 (1H, m); MS m/z 443 (M^+; 0.5), 177 (100), and 149 (94). Found: C, 62.22; H, 6.00; N, 3.20%. Calcd for $C_{23}H_{26}NO_6P$: C, 62.30; H, 5.91; N, 3.16%.

Synthesis of Dimethyl 2-[o-(Dimethylcarbamoyl)benzoyl]-1,2-dihydro-1-isoquinolylphosphonate (1e). A mixture of *N,N*-dimethylphthalamic acid[18] (1.90 g, 9.8 mmol) and $SOCl_2$ (5.0 ml, 69 mmol) was refluxed for 1 h, and excess $SOCl_2$ was evaporated. After addition of dry benzene (5 ml) and evaporation, MeCN (10 ml) was added to the chloride (**3e**). IQ (1.28 g, 9.9 mmol) in MeCN (2 ml) was added to the refluxing suspension and after 10 min trimethyl phosphite (1.16 ml, 9.8 mmol) was added. The refluxing was continued for 10 min. After usual work-up, **1e** was obtained in 78% yield (3.2 g, 7.72 mmol) as colorless crystals, mp 131.7—132.5°C (from EtOAc-hexane (1:1)); IR (KBr) 1660, 1650, 1625, and 1260 cm^{-1}; ^1H NMR ($CDCl_3$) δ=2.92 (6H, br s), 3.55, 3.71 (6H, 2d, J_{POCH}=10.8 Hz), 5.84 (1H, d, J=7.8 Hz), 6.30 (1H, d, J_{PCH}=16.8 Hz), 6.47 (1H, d, J=7.8 Hz), and 7.0—7.6 (8H, m); MS m/z (rel intensity) 414 (M^+; 0.75) and 176 (100). Found: C, 60.64; H, 5.60; N, 6.83%. Calcd for $C_{21}H_{23}N_2O_5P$: C, 60.87; H, 5.59; N, 6.76%.

Synthesis of Dimethyl 2-[o-(Benzylthio)carbonylbenzoyl]-1,2-dihydro-1-isoquinolylphosphonate (1f). A mixture of *S*-benzyl o-carboxythiobenzoate[19] (3.72 g, 13.7 mmol) and $SOCl_2$ (7 ml) was refluxed for 1 h and excess $SOCl_2$ was removed *in vacuo*. To the residue was added dry benzene (3.5 ml) and the mixture was evaporated. This treatment was repeated twice. To the residue were added MeCN (10 ml), IQ (1.77 g, 13.7 mmol) in MeCN (5 ml), and trimethyl phosphite (1.62 ml, 13.7 mmol) successively. After refluxing for 10 min, MeCN was removed *in vacuo*, to the residue were added a small amount of ether and a trace of EtOAc, and ppt thus obtained (phthalic anhydride, 0.564 g) was filtered off. To the filtrate was added 3% aq $NaHCO_3$, and the mixture was extracted with CH_2Cl_2. The extract was washed with aq NaCl, dried ($MgSO_4$), and evaporated. The residue (5.12 g) was dissolved in CH_2Cl_2 (50 ml), successively washed with 2M aq HCl, 5% aq Na_2CO_3, and aq NaCl, dried ($MgSO_4$), and evaporated. The residue (2.83 g) was subjected to dry column chromatography (DCC; Al_2O_3, Et_2O) to afford **1f** (0.55 g, 1.12 mmol, 8.2%) as colorless crystals, mp 152—154°C (from EtOAc-hexane (1:1));

IR (KBr) 1660, 1620, and 1245 cm^{-1}; ^1H NMR ($CDCl_3$) δ= 3.55, 3.67 (6H, 2d, J_{POCH}=10.8 Hz), 4.05 (2H, s), 5.70 (1H, d, J=7.8 Hz), 6.10 (1H, d, J=7.8 Hz), 6.41 (1H, d, J_{PCH}=16.2 Hz), 6.9—7.7 (12H, m), and 7.8—8.3 (1H, m); MS *m/z* (rel intensity) 493 (M^+; 0.0008) and 91 (100). Found: C, 63.41; H, 4.74; N, 3.02%. Calcd for $C_{26}H_{24}NO_5PS$: C, 63.28; H, 4.90; N, 2.84%.

Synthesis of Dimethyl 1-[o-(Methoxycarbonyl)benzoyl]-1,2-dihydro-2-quinolylphosphonate (6). MeCN (2 ml) was added to acid chloride prepared from methyl hydrogen phthalate (1.81 g, 10.0 mmol) and $SOCl_2$ (5 ml) similarly to preparation of **1c**. To the above soln, quinoline (1.30 g, 10.1 mmol) in MeCN (7 ml), trimethyl phosphite (1.18 ml, 10.0 mmol), and NaI (2 g, 13 mmol) were successively added at 0°C with stirring, and the mixture was heated at 50°C with stirring for 10 min. After removal of the solvent, 2% aq $NaHCO_3$ (50 ml) was added to the residue, the mixture was extracted with CH_2Cl_2, the extract was washed with aq NaCl, dried ($MgSO_4$), and evaporated. The residue (3.05 g) was subjected to DCC (Al_2O_3, Et_2O) to give **6** (2.40 g, 5.98 mmol, 60% yield) as pale yellow oil; IR (neat) 1730, 1660, and 1300—1265 cm^{-1}; ^1H NMR ($CDCl_3$) δ=3.53, 3.75 (6H, 2d, J_{POCH}= 10.2 Hz), 3.83 (3H, s), and 5.8—8.2 (10H, m). Analytically pure sample could not be obtained because of a difficulty of purification. Therefore, crude material was used in the reaction.

Intramolecular Wittig-Horner Reaction. General Procedure Using LDA: The reaction was performed under nitrogen atmosphere. To phosphonate (**1**; 3.0 mmol) in tetrahydrofuran (THF) (20 ml) was added a LDA soln (3.5 mmol) in THF (5 ml) at −70°C. After stirred for 0.5 h, the temperature was gradually raised to room temp and kept at about 40°C for 0.5 h. After addition of methanol (3—6 ml), the solvent was removed and water (70 ml) was added to the residue. After usual work-up, the residue was separated or purified by column chromatography (SiO_2, Et_2O).

Reaction of 1a: **2a** (31%), IQ (41%), and **7a** (6%) were isolated. **2a**: Yellow crystals, mp 211.1—211.7°C (from CH_2Cl_2-Et_2O); IR (KBr) 1660 cm^{-1}; ^1H NMR ($CDCl_3$) δ=6.70 (1H, d, J= 8.1 Hz), 6.8—7.6 (12H, m), 8.6—8.7 (1H, m), and 8.67 (1H, d, J=8.1 Hz); MS *m/z* (rel intensity) 321 (M^+; 100). Found: C, 86.01; H, 4.69; N, 4.34%. Calcd for $C_{23}H_{15}NO$: C, 85.96; H, 4.70; N, 4.36%. **7a**: Colorless crystals, mp 126—128°C; IR (neat) 1750 cm^{-1}; ^1H NMR ($CDCl_3$) δ=1.03, 1.11 (12H, 2d, J=6.6 Hz), 3.27 (2H, sept, J=6.6 Hz), and 70—7.7 (9H, m). Found: *m/z* 309.1718. Calcd for $C_{20}H_{23}NO_2$: M, 309.1728.

The reaction of **1a** with *n*-BuLi gave IQ (53%) and a mixture of **2a** (isolated yield 9.4%) and **7'a** (could not be purified, 22% yield; IR (neat) 1760 cm^{-1}).

Reaction of 1b: A mixture of **2b** and an unidentified compd, IQ (46%), and **7b** (6%) (^1H NMR ($CDCl_3$) (partly) δ=1.02, 1.09 (12H, 2d, J=6.6 Hz), 2.21 (3H, s), 3.36 (2H, sept, J=6.6 Hz)) were obtained. Twice recrystallizations gave **2b** (4.5%) as yellow crystals, mp 215.2—215.9°C (from CH_2Cl_2-Et_2O); IR (KBr) 1660 cm^{-1}; ^1H NMR ($CDCl_3$) δ=2.50 (3H, s), 6.74 (1H, d, J=7.8 Hz), 6.9—7.7 (1H, m), 8.5—8.8 (1H, m), and 8.70 (1H, d, J=7.8 Hz); MS *m/z* (rel intensity) 335 (M^+; 100). Found: C, 85.66; H, 5.03; N, 4.21%. Calcd for $C_{24}H_{17}NO$: C, 85.95; H, 5.11; N, 4.18%.

Reaction of 1c: **2c** was obtained in 76% yield as yellow crystals, mp 143.8—144.7°C (from CH_2Cl_2-Et_2O); IR (KBr) 1650 cm^{-1}; ^1H NMR ($CDCl_3$) δ=3.83 (3H, s), 6.72 (1H, d,) J= 7.8 Hz), 7.3—8.2 (6H, m), 8.65 (1H, d, J=7.8 Hz), 8.55—8.80 (1H, dm, J=8 Hz), and 9.10—9.40 (1H, m); MS *m/z* (rel intensity) 275 (M^+; 19) and 260 (100). Found: C, 78.82; H, 4.48; N, 5.11%. Calcd for $C_{18}H_{13}NO_2$: C, 78.53; H, 4.76; N, 5.09%.

Reaction of **1c'** also gave **2c** in 66% yield.

Reaction of 1d: **2d** was obtained in 67% yield as yellow crystals, mp 181.7—182.3°C (from CH_2Cl_2-Et_2O); IR (KBr) 1650 cm^{-1}; ^1H NMR ($CDCl_3$) δ=1.50 (3H, t, J=6.9 Hz), 3.87 (2H, q, J=6.9 Hz), 6.63 (1H, d, J=7.8 Hz), 7.3—8.1 (6H, m), 8.55 (1H, d, J=7.8 Hz), 8.5—8.65 (1H, dm, J=8 Hz), and 9.0—9.3 (1H, m); MS *m/z* (rel intensity) 289 (M^+; 15) and 260 (100). Found: C, 78.58; H, 4.98; N, 4.82%. Calcd for $C_{19}H_{15}NO_2$: C, 78.87; H, 5.23; N, 4.84%.

Reaction of **1d'** also gave **2d** in 75% yield.

Reaction of 1e: **2e** was obtained in 67% yield as yellow crystals, mp 144.4—145.7°C (from CH_2Cl_2-Et_2O); IR (KBr) 1655 cm^{-1}; ^1H NMR ($CDCl_3$) δ=3.00 (6H, s), 6.67 (1H, d, J= 7.8 Hz), 7.35—7.65 (4H, m), 7.7—7.95 (2H, m), 8.60 (1H, d, J= 7.8 Hz), 8.55—8.75 (1H, dm, J=8 Hz), and 8.85—9.15 (1H, m); MS *m/z* (rel intensity) 288 (M^+; 100) and 273 (84). Found: C, 79.41; H, 5.29; N, 9.67%. Calcd for $C_{19}H_{16}N_2O$: C, 79.14; H, 5.59; N, 9.72%.

Reaction of 1f: The residue (234 mg) from reaction of **1f** (0.435 g, 0.882 mmol) was subjected to column chromatography (Al_2O_3, Et_2O-hexane (1:2)) to separate benzyl methyl sulfide (51 mg, 0.37 mmol, 42% yield) and crude **2f**. Pure **2f** was isolated by treatment with ether, 9.7 mg (0.026 mmol, 3.0%), yellow crystals, mp 115—118°C (from EtOAc-hexane); IR (KBr) 1660 cm^{-1}; ^1H NMR ($CDCl_3$) δ=3.68 (2H, s), 6.68 (1H, d, J= 7.8 Hz), 6.6—7.0 (4H, m), 7.2—7.7 (5H, m), 7.87 (1H, td, J=7.7 Hz, 1.7 Hz), 8.47 (1H, d, J=7.8 Hz), 8.61 (1H, d, J=10 Hz), 8.71 (1H, d, J=9.3 Hz), and 9.05—9.2 (1H, m); MS *m/z* (rel intensity) 367 (M^+; 0.9) and 276 (100). Found: C, 78.21; H, 4.92; N, 3.55%. Calcd for $C_{24}H_{17}NOS$: C, 78.45; H, 4.66; N, 3.81%.

Reaction of 6: **10** was obtained in 54% yield as yellow crystals (gradually decompose in soln), mp 299.5—301.2°C (decomp) (from CH_2Cl_2-Et_2O); IR (KBr) 1660 cm^{-1}; ^1H NMR ($CDCl_3$) δ=3.86 (3H, s), 6.94 (1H, s), 7.05—8.05 (7H, m), 8.6—8.8 (1H, m), and 9.35—9.65 (1H, m), MS *m/z* (rel intensity) 275 (M^+; 17), 260 (88), and 49 (100). Found: C, 78.73; H, 4.99; N, 5.34%. Calcd for $C_{18}H_{13}NO_2$: C, 78.53; H, 4.76; N, 5.09%.

Hydrolysis of 2a: A mixture of aq NaOH (20%; 2.4 ml) and **2a** (42.4 mg, 0.132 mmol) in EtOH (22 ml) was refluxed under nitrogen for 8 h. The reaction mixture was neutralized with dilute HCl and EtOH was evaporated. After addition of water (30 ml) to the residue, the mixture was extracted with CH_2Cl_2. The extract was dried ($MgSO_4$) and evaporated to give 1-[α-(*o*-carboxyphenyl)benzyl]isoquinoline (**9**) (37.1 mg, 83% yield), colorless crystals, mp 191—193°C (decomp) (from CH_2Cl_2-CCl_4); IR (KBr) 3100—2300 and 1705 cm^{-1}; ^1H NMR ($CDCl_3$) δ=6.9—7.4 (10H, m), 7.6—7.9 (1H, m), 8.3—8.45 (1H, m), and 8.35 (1H, d, J=5.7 Hz); MS *m/z* (rel intensity) 339 (M^+; 30), 321 (100), and 294 (66). Found: C, 81.43; H, 4.82; N, 4.21%. Calcd for $C_{23}H_{17}NO_2$: C, 81.40; H, 5.05; N, 4.13%.

References

1) K. Ishikawa, K. Akiba, and N. Inamoto, *Tetrahedron Lett.*, **1976**, 3695; K. Akiba, K. Ishikawa, and N. Inamoto, *Bull. Chem. Soc. Jpn.*, **51**, 2674, 2684 (1978).

2) K. Akiba, Y. Negishi, K. Kurumaya, N. Ueyama, and N. Inamoto, *Tetrahedron Lett.*, **22**, 4977 (1981), and unpublished work.

3) For preliminary report see: K. Akiba, Y. Negishi, and N. Inamoto, *Chem. Lett.*, **1982**, 349.

4) M. S. Newman and C. Courduvelis, *J. Am. Chem. Soc.*, **88**, 781 (1966), and references cited therein.

5) K. Akiba, Y. Negishi, and N. Inamoto, *Synthesis*, **1979**, 55.

6) M. Le Corre, *Bull. Soc. Chim. Fr.*, **1974**, 2005; V. Subramanyam, E. H. Silver, and A. H. Soloway, *J. Org. Chem.*, **41**, 1272 (1976).

7) W. G. Dauben and D. J. Hart, *Tetrahedron Lett.*, **1975**, 4353.

8) H. J. Bestmann and G. Schade, *Chem. Lett.*, **1983**, 997.
9) W. H. Ploder and D. F. Tavares, *Can. J. Chem.*, **48**, 2446 (1970).
10) H. Takeno and M. Hashimoto, *J. Chem. Soc., Chem. Commun.*, **1981**, 282.
11) M. Le Corre, A. Hercouet, and H. Le Baron, *J. Chem. Soc., Chem. Commun.*, **1981**, 14.
12) T. Kato and T. kitagawa, *Yakugaku Zasshi Jpn.*, **84**, 874 (1964).
13) D. W. Brown, S. F. Dyke, M. Sainsburg, and G. Hardy, *J. Chem. Soc. (C)*, **1971**, 3219.
14) D. E. Ames and O. Ribeiro, *J. Chem. Soc., Perkin Trans. 1*, **1976**, 1073.
15) K. W. F. Kohlrausch and R. Seka, *Ber.*, **77**, 469 (1944).
16) L. F. Fieser, *Org. Synth.*, Coll. Vol. 1, 517 (1932).
17) E. L. Eliel and A. W. Burgstahler, *J. Am. Chem. Soc.*, **71**, 2251 (1949).
18) R. L. Frank and F. E. Boettner, *J. Am. Chem. Soc.*, **67**, 1624 (1945).
19) S. Okumura, M. Masumura, and T. Horie, *Yuki Gosei Kagaku Kyokai shi*, **17**, 419 (1959).

Facile Synthesis of (2*R*,3*R*)-Phenylalanine-2,3-d_2 and NMR Study on Deuterated Gramicidin S[1]

Kenjiro TANIMURA, Tetsuo KATO,* Michinori WAKI, Sannamu LEE, Yasushi KODERA,† and Nobuo IZUMIYA

Laboratory of Biochemistry, Faculty of Science, Kyushu University 33, Higashi-ku, Fukuoka 812
†*Department of Chemistry, Faculty of Science, Fukuoka University, Jonan-ku, Fukuoka 814-01*

(Received January 30, 1984)

(2*R*,3*R*)-Phenylalanine-2,3-d_2 (D-Phe*) was synthesized through catalytic reduction of *cyclo*(-(*Z*)-2,3-dehydrophenylalanyl-D-alanyl-) under an atmosphere of $^2H_2$ and successive acid hydrolysis in the yield of 80% in high chiral induction. The D-Phe* thus obtained was used for synthesis of [D-Phe*$^{4,4'}$] gramicidin S (GS*). The ^{1}H NMR spectrum of GS* in DMSO-d_6 showed a sharp singlet at 2.98 ppm for the (3*S*)-proton of D-Phe* residue. It has been proposed that among rotamers of D-Phe aromatic side chain in GS the one with $\kappa_1=180°$ is predominant. The present observation provides sound evidence for assignments of D-Phe β-protons based on the proposal.

Selectively deuterated amino acid is important for studying conformations of biologically active peptides and proteins. Kirby and Michael[2] synthesized 3-deuterated aromatic amino acids by catalytic hydrogenation of *trans*-α-acylaminocinnamic acid-β-*d* derivatives and subsequent deacylation with acylase. Kainosho and Ajisaka[3] synthesized selectively deuterated L-amino acids by use of enzyme and studied conformations of the amino acids in aqueous solutions. Nagai and Kobayashi[4] used α-chymotrypsin instead of acylase and obtained both diastereomers, (2*S*,3*R*)-*N*-acetyl-L-phenylalanine-3-*d* and (2*R*,3*R*)-*N*-acetyl-D-phenylalanine-3-*d* ethyl ester in the yield of 6% each. The prefixes L and D are used here to clarify configuration at the α-center. These deuterated amino acids were used to the synthesis and conformational studies of [Met^5]enkephalin.[5,6] In every case, optical resolution was inevitable at the final stage in the amino acid synthesis, lowering the yields of deuterated products.

Izumiya *et al.*[7,8] recently developed a new method for synthesizing optically active amino acids, that is, catalytic hydrogenation of dipeptide anhydrides containing a dehydroamino acid residue and an L- or D-amino acid residue. They observed that the condensation of *cyclo*(-*N*-acetyl-glycyl-*N*-acetyl-L-alanyl-) with benzaldehyde exclusively yielded *cyclo*(-2,3-dehydrophenylalanyl-*N*-acetyl-L-alanyl-) of *Z* configuration. Deacetylation with hydrazine, catalytic hydrogenation in the presence of Pd black, and successive acid hydrolysis yielded L-phenylalanine in high chiral inductiction, 97.0%.[9]

This paper deals with the synthesis of (2*R*,3*R*)-phenylalanine-2,3-d_2 as an example of facile synthesis of the selectively deuterated and optically active aromatic amino acid. We also report the synthesis and ^{1}H NMR analysis of gramicidin S containing two residues of the deuterated D-phenylalanine.

Results and Discussion

Synthesis of (2R,3R)-Phenylalanine-2,3-d$_2$ (D-Phe).* (2*R*,3*R*)-Phenylalanine-2,3-d_2 was synthesized in a manner similar to that described for L-phenylalanine.[9] *cyclo*(-ΔPhe-D-Ala-) (**3**)[10] was catalytically reduced under an atmosphere of $^2H_2$ to give *cyclo*(-(2*R*,3*R*)-Phe-2,3-d_2-D-Ala-) (**4**) in an excellent yield. Chiral induction was estimated as 98.8% by HPLC. Compound **4** was hydrolyzed to give (2*R*,3*R*)-phenylalanine-2,3-d_2 (D-Phe*) (**5**); no L-isomer was detected by the modified Manning-Moore method.[11,12] Content of deuterium was estimated to be 90%±10% by use of ^{1}H NMR spectroscopy. As the chirality at α-center was so high, H–D exchange at the α-center should be, if any, negligible. Therefore, some 10% hydrogen observed in ^{1}H NMR spectrum was attributed to contamination in the course of deuteration. Stereochemistry of β-center was assigned to be *R* according to the literature[2] and results of previous experiments.[7-9] Kirby and Michael showed that hydrogenation of *trans*-α-acylaminocinnamic acid derivatives proceeded in *cis* configuration insensitive to variation of substituents and catalysts with at least 95% chirality.[2] In case of dehydrodipeptide anhydrides, rigid planar structure of the substrates favored highly chiral hydrogenation.[7-9] The ^{1}H NMR spectrum of D-Phe* (**5**) in TFA-*d* showed a singlet at δ=3.37 with an intensity of 1 H and another singlet at 3.58 with 0.1 H. The latter signal was attributed to βCH proton contaminated in deuteration. Exact chiral induction at the β-center was not determined.

Synthesis of [(2R,3R)-D-Phe-2,3-d$_2^{4,4'}$]gramicidin S (GS).* The deuterated D-phenylalanine thus obtained was used for the synthesis of gramicidin S (GS). ^{1}H NMR study on the synthetic deuterio-GS should give useful information on confirming the conformation of GS. Figure 1 shows the route for the synthesis. Boc-pentapeptide acid (**13**) was converted to the active ester, which was treated with TFA to remove the Boc group. The pentapeptide active ester thus obtained was subjected to cyclization in pyridine to give a mixture of desired [L-Orn(Z)$^{2,2'}$, D-Phe*$^{4,4'}$]gramicidin S (Z_2GS*) (**14**) and a by-product (cyclic monomer) which was removed by Sephadex LH-20 column chromatography. Compound **14** was hydrogenolyzed to give [D-Phe*$^{4,4'}$]-gramicidin S (GS*) (**15**). A part of **15** was used to prepare [L-Orn-(Boc)$^{2,2'}$, D-Phe*$^{4,4'}$]gramicidin S ((Boc)$_2$GS*) (**16**).

^{1}H NMR Study on Gramicidin S and Related Peptides. Figure 2 shows 90 MHz ^{1}H NMR spectra of **14** (a), Z_2GS (b), **15**·2HCl (c), and GS·2HCl (d). In Fig. 2 (a) and (c), each βCH signal in D-Phe* resonates as a sharp singlet. This indicates that highly stereoselective deuteration proceeded not only at α-center but also at β-center.

In regard to side chain conformation of GS, Dygert

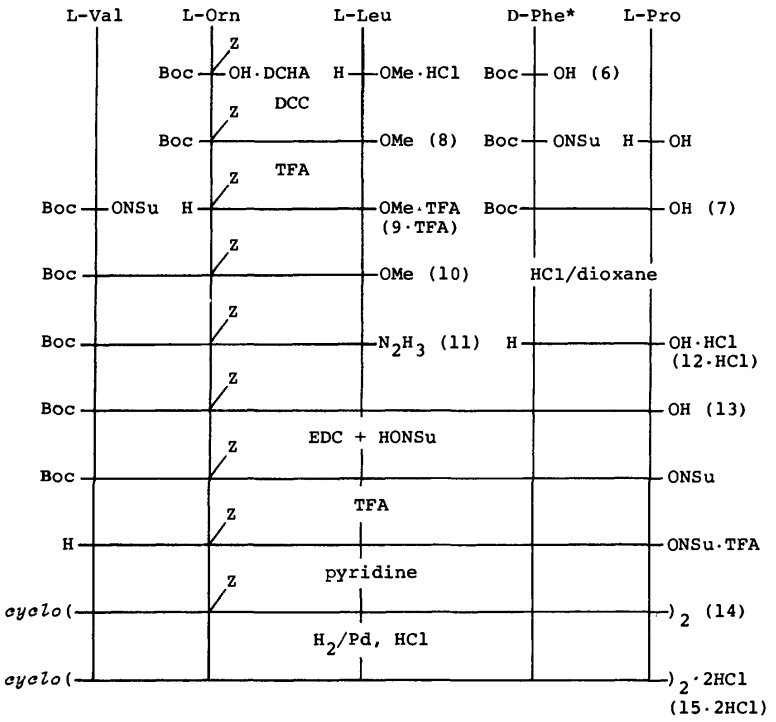

Fig. 1. Synthesis of deuterated gramicidin S.

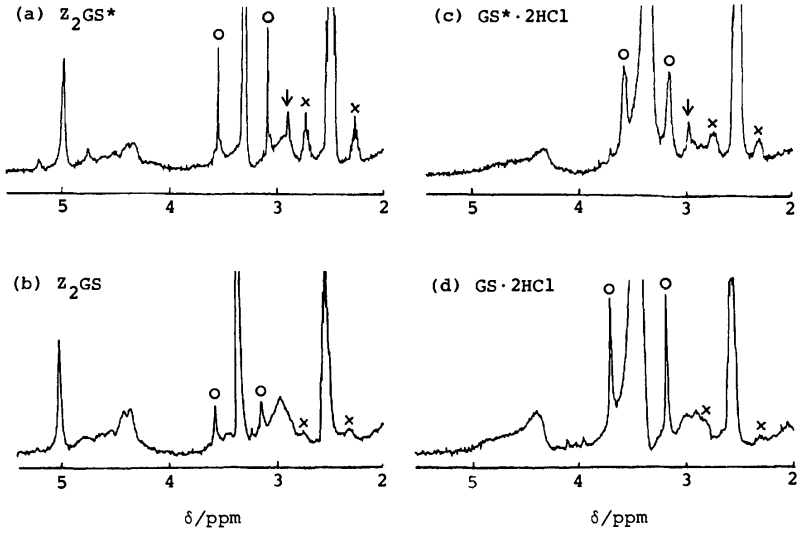

Fig. 2. 90 MHz ^{1}H NMR spectra of gramicidin S and related derivatives. Satelite of HDO (O); satelite of DMSO (X). Arrows in (a) and (c) indicate (3S)-proton signals.

et al.[13] proposed the D-Phe side chain conformation with $\kappa_1=180°$ to be most stable conformation as shown in Fig. 3. Rae and Scheraga[14] supported this proposal on the basis of ^{1}H NMR results. Assuming this D-Phe side chain conformation, Jones *et al.*[15] assigned the chemical shifts of D-Phe $H_{\beta 1}$ and $H_{\beta 2}$ protons in GS in CD_3OD solution as $\delta=3.04$ and 2.96, respectively. Krauss and Chan[16] also assigned them as $\delta=3.10$ and 2.96 in CD_3OD, and 2.97 and 2.88 in DMSO-d_6 solution. Figure 2 (c) shows that the (3S)-proton in GS* resonated at $\delta=2.98$ in DMSO-d_6 solution. As the protons named $H_{\beta 1}$ and $H_{\beta 2}$ correspond to *pro-S* and *pro-R*, respectively, this result agreed quite well with the assignments by Jones *et al.*[15] and by Krauss and

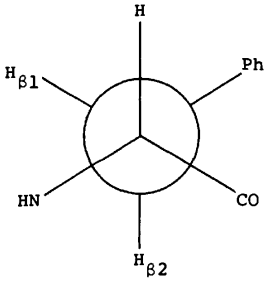

Fig. 3. Conformation for D-Phe side chain with $\kappa_1=180°$.

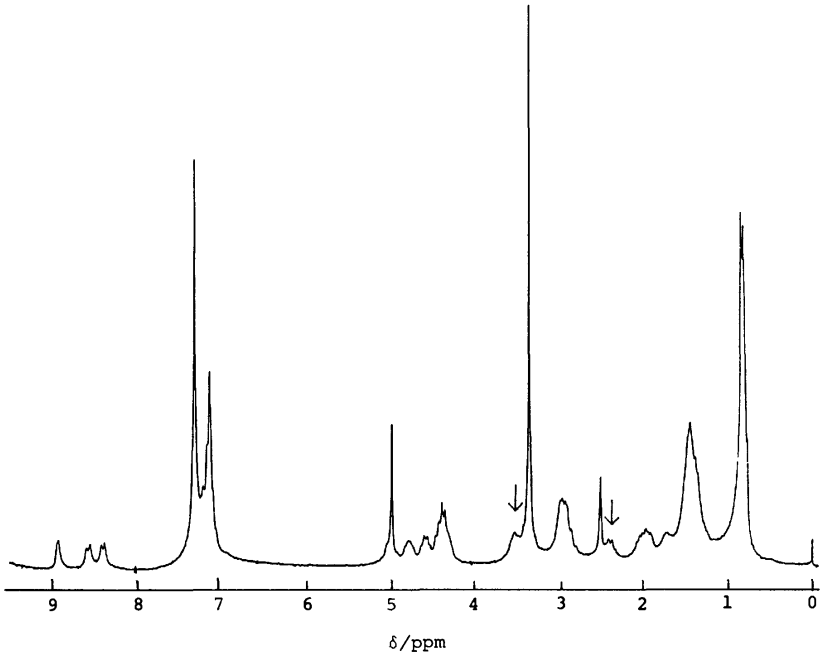

Fig. 4. 200 MHz ^{1}H NMR spectrum of bis(benzyloxycarbonyl)gramicidin S. Arrows indicate δCH_2-proton signals in L-Pro residues.

Chan.[16] Thus, our experimental results provided sound evidence for their assignments and the conformation of D-Phe side chain in GS with $\kappa_1=180°$.

Figures 2 (b) and (d) show that signals of L-Orn δ CH_2 and D-Phe βCH_2 overlap and appear as broad multiplets at about δ=2.9—3.0. The shape of the multiplets in (b) differs from that in (d), suggesting some chemical shift change between GS and Z_2GS. Similarly, the sharp singlet of D-Phe* (3S)-proton in Fig. 2 (a) resonates at δ=2.90 but the same singlet resonates at 2.98 in Fig. 2 (c). Benzyloxycarbonylation of GS* induced some 0.08 upfield shift of the (3S)-proton signal. Krauss and Chan[16] proposed the conformation of GS with intramolecular hydrogen bonds between L-Orn δNH and D-Phe C=O. If Z_2GS holds the same conformation, steric crowding around the D-Phe-L-Pro peptide bonds may be expected because bulky Z groups approach D-Phe side chains. However, 200 MHz ^{1}H NMR spectrum of Z_2GS (Fig. 4) showed that a δCH signal of L-Pro resonates at δ=2.40, indicating proximity of the D-Phe side chain to the pyrrolidine ring.[14] This means that the D-Phe side chain in Z_2GS maintains the orientation with $\kappa_1=180°$ in spite of possible steric crowding. The upfield shift of (3S)-proton of D-Phe* in Z_2GS* should be explained in terms of shielding effect due to the near-by Z group. Interestingly, the D-Phe* (3S)-proton in $(Boc)_2$GS* resonates at δ=2.93, showing minute difference between the aromatic and alkyl urethane groups in inducing chemical shift change of D-Phe (3S)-signal.

Experimental

All the melting points are uncorrected. TLC was carried out on silica gel G (Merck) with following solvent systems, the ratio in parentheses after each system being shown by volume: R_f^1, $CHCl_3$-MeOH (5:1); R_f^2, *n*-BuOH-AcOH-pyridine-water (4:1:1:2); R_f^3, $CHCl_3$-MeOH-AcOH (50:10:2). Optical rotations were measured on a Union high sensitivity polarimeter PM-71. HPLC was carried out on a Hitachi 635A liquid chromatograph and samples were detected at 210 nm absorption.

Synthesis of (2R,3R)-Phenylalanine-2,3-d_2. cyclo*(-ΔPhe-D-Ala-) (3)*: Z-Gly-D-Ala-OMe (**1**) was synthesized from Z-Gly-OH and H-D-Ala-OMe·HCl following the procedure for L-isomer;[8] yield of **1**, 86%; mp 91—93 °C; $[\alpha]_D^{23}$+20.6° (*c* 1, DMF). Reported values for L-isomer, mp 64—69 °C; $[\alpha]_D^{20}$ −21.0° (*c* 1, DMF).[8] Compound **1** in a mixture of MeOH and AcOH was hydrogenolyzed and then the filtrate was evaporated. The residue in *s*-BuOH which contains AcOH (0.1 M(1 M=1 mol dm^{-3})) was treated as described in the literature;[17] yield of *cyclo*(-Gly-D-Ala-) (**2**), 96%; mp 241—242 °C (dec); $[\alpha]_D^{21}$+21.4 (*c* 0.5, DMF). Reported values for L-isomer, mp 228—230 °C; $[\alpha]_D^{20}$−21.3° (*c* 1, DMF).[8] Possible polymorphism may explain high melting points of **1** and **2** compared to those of L-isomer. Compound **2** was converted to *cyclo*(-(*Z*)-ΔPhe-D-Ala-) (**3**) as described for L-isomer;[9] yield, 61%; mp 241—245 °C (dec); $[\alpha]_D^{21}$+18.0° (*c* 1, DMF). Reported values for L-isomer, mp 246—248 °C; $[\alpha]_D^{20}$−19.2° (*c* 1, DMF).

cyclo*(-(2R, 3R)-Phe-2, 3-*d_2*-D-Ala-) (4)*: Compound **3** (864 mg, 4 mmol) dissolved in DMF (150 ml) was deuterated in the presence of Pd black under an atmosphere of $^2H_2$ for 3 d at 0° and *ca.* 1 atm. Crystals precipitated in the course of reduction were crushed occasionally and dissolved in DMF with short-time heating. After filtration of Pd black, the solution was evaporated and the residue was collected with the aid of ether; yield, 845 mg (97%); R_f^1 0.82. The extent (98.8%) of chiral induction was determined by HPLC as described in the later section.

(2R,3R)-Phenylalaine-2,3-d_2 *(D-Phe*) (5)*: Compound **4** (437 mg, 2 mmol) was hydrolyzed in 6 M HCl (8 ml) at 110 °C for 4.5 h and the solution was evaporated. The residue was dissolved in water (100 ml) and the solution was treated for 90 min at room temperature with charcoal (9 g) which had been treated with 5% AcOH (120 ml) for 90 min.[18] After filtration, the charcoal was extracted with an aqueous solution (100 ml) containing 5% phenol and 20% AcOH, and

the extraction was repeated twice more. Combined extract was thoroughly washed with ether, diluted with water, and the solution was applied to a column of Dowex 50 (H^+ form) (0.9×8 cm). The column was washed with water, eluted with 1 M NH_4OH, and the eluate was evaporated. The residue (D-Phe*) was recrystallized from hot water-acetone; yield, 264 mg (80%); mp 240—243 °C; R_f^2 0.60. Optical purity was ascertained by the modified Manning-Moore procedure;[10,11] no L-phenylalanine was detected. Content of deuterium was estimated to be 90%±10% by the comparison of signal intensity of ^1H NMR spectra.

Separation of cyclo*(-Phe-Ala-) Diastereomers with HPLC.* The extent of chiral induction after deuteration of **3** was determined by the HPLC. Experimental conditions for separation of the diastereomers were as follows: Column, Li-Chrosorb RP-18 (4×150 mm); solvent, water-CH_3CN (8:1); flow rate, 1.2 ml/min; pressure, 180 kg/cm²; elution time, 7.5 min for *cyclo*(-L-Phe-D-Ala-) and 10.2 min for *cyclo*(-D-Phe-D-Ala-).

Synthesis of [(2R,3R)-Phe-2,3-$d_2^{4,4'}$]gramicidin S (GS).*

Boc-D-Phe-OH·DCHA (6·DCHA)*: Compound **5** was treated with $(Boc)_2O$[19] and the oily **6** was converted to crystalline DCHA salt; yield, 97%; mp 210—215 °C (dec); $[\alpha]_D^{26}$−26.9 (*c* 1, MeOH). Reported values for protio L-isomer, mp 210—212 °C; $[\alpha]_D^{27}$+29.2 (*c* 1, MeOH).[20]

Boc-D-Phe-L-Pro-OH (7)*: An oily Boc-D-Phe*-OH obtained from **6**·DCHA was converted to Boc-D-Phe*-ONSu by treatment with DCC and HONSu. This Boc-D-Phe*-ONSu was coupled with H-L-Pro-OH in the usual manner; yield, 74%; mp 167—170 °C; R_f^1 0.55. Reported value for protio **7**, R_f^1 0.54.[21]

Boc-L-Orn(Z)-L-Leu-OMe (8): To a chilled solution of Boc-L-Orn(Z)-OH·DCHA (3.83 g, 7 mmol) and H-L-Leu-OMe·HCl (1.27 g, 7 mmol) in CH_2Cl_2 (28 ml), was added DCC (1.44 g, 7 mmol), and the mixture was stirred at 0 °C overnight. After filtration, the solution was evaporated. The residue was dissolved in EtOAc, and the solution was washed with water, 10% citric acid, 4% $NaHCO_3$, and water, and dried (Na_2SO_4). After evaporation, the residue was crystallized by the addition of ether and petroleum ether; yield, 3.17 g (92%); mp 85—88 °C; $[\alpha]_D^{21}$−12.4 (*c* 1, DMF); R_f^1 0.79.

Found: C, 61.01; H, 8.04; N, 8.59%. Calcd for $C_{25}H_{39}O_7N_3$: C, 60.83; H, 7.96; N, 8.51%.

H-L-Orn(Z)-L-Leu-OMe·TFA (9·TFA): Compound **8** (2.96 g, 6 mmol) was treated with TFA (30 ml) at 0 °C for 20 min and the solution was evaporated. The oily residue was treated with ether and petroleum ether. Crystals were collected and washed with ether; yield, 2.49 g (83%); R_f^2 0.82. This was used to the next step without further purification.

Boc-L-Val-L-Orn(Z)-L-Leu-OMe (10): Into a solution of **9**·TFA (1.77 g, 3.5 mmol) in a mixture of tetrahydrofuran (7 ml) and NEt_3 (0.49 ml, 3.5 mmol), was added Boc-L-Val-ONSu (1.77 g, 3.5 mmol) at 0 °C. The mixture was stirred at room temperature overnight, evaporated, and diluted with EtOAc. The solution was treated as described for **8**; yield, 1.88 g (91%); mp 147—149 °C; $[\alpha]_D^{20}$−16.0° (*c* 1, DMF); R_f^1 0.71.

Found: C, 60.89; H, 8.25; N, 9.66%. Calcd for $C_{30}H_{48}O_8N_4$: C, 60.79; H, 8.16; N, 9.45%.

Boc-L-Val-L-Orn(Z)-L-Leu-N_2H_3 (11). Into a solution of **10** (1.78 g, 3 mmol) in DMF (6 ml), was added hydrazine hydrate (1.5 ml, 30 mmol). The mixture was left to stand at room temperature overnight. After the addition of water, precipitated crystals were collected, washed with water, and dried. Recrystallization from DMF-ether gave 1.40 g (79%); mp 199—200 °C; $[\alpha]_D^{20}$−15.2° (*c* 1, DMF); R_f^1 0.67.

Found: C, 58.66; H, 8.23; N, 14.37%. Calcd for $C_{29}H_{48}O_7N_6$: C, 58.76; H, 8.16; N, 14.18%.

H-D-Phe-L-Pro-OH·HCl (12·HCl)*: Compound **7** (176 mg, 0.48 mmol) was treated with 3.6 M HCl in dioxane (2.6 ml, 9.6 mmol) for 1 h and the solution was evaporated. The product was collected with the aid of ether; yield, 146 mg (100%); R_f^3 0.26. This was used to the next step without further purification.

Boc-L-Val-L-Orn(Z)-L-Leu-D-Phe-L-Pro-OH (13)*: Compound **11** (237 mg, 0.4 mmol) was changed to Boc-tripeptide azide with isopentyl nitrite following the literature.[22] The azide was coupled with **12**·HCl (146 mg, 0.48 mmol) in the usual manner; yield, 66 mg (20%); R_f^2 0.82. Reported value for protio **13**, R_f^2 0.82.[23]

cyclo*(-L-Val-L-Orn(Z)-L-Leu-D-Phe*-L-Pro-)₂ (Z_2GS*) (14)*: Into a chilled solution of **13** (105 mg, 0.11 mmol) in a mixture of DMF (0.5 ml) and CH_2Cl_2 (0.5 ml), were added HONSu (30 mg, 0.26 mmol) and EDC·HCl (50 mg, 0.26 mmol) at 0 °C. After being stirred at room temperature overnight, the solution was treated with cold water, and the precipitate (Boc-pentapeptide-ONSu) was collected. After drying, the precipitate was treated with TFA (1.3 ml) for 30 min and then evaporated. The residue (H-pentapeptide-ONSu·TFA) was dissolved in DMF (3 ml) and the solution was added dropwise into pyridine (40 ml) at room temperature. After 3 d, the mixture was evaporated and the residue was dissolved in MeOH. The solution was passed through Amberlyst 15 and A27 columns (1.8×3.5 cm each), washed with MeOH, and evaporated. Crude product (56 mg) was dissolved in MeOH and the solution was applied on a Sephadex LH-20 column (2×84 cm) and eluted with MeOH. Fractions containing **14** were evaporated; yield, 25.5 mg (28%); R_f^2 0.96. Reported value for protio Z_2GS, R_f^2 0.96.[24]

cyclo*(-L-Val-L-Orn-L-Leu-D-Phe*-L-Pro-)₂·2HCl (GS*·2HCl) (15·2HCl)*: A portion (5 mg) of **14** was dissolved in MeOH (4 ml) containing 40 µl of 0.3 M HCl in dioxane, the solution was hydrogenolyzed, and the filtrate was evaporated to give 4.0 mg of **15**·2HCl; R_f^1 0.74.

cyclo*(-L-Val-L-Orn(Boc)-L-Leu-D-Phe*-L-Pro-)₂ ($(Boc)_2GS$*) (16)*: A portion (3.0 mg) of **15**·2HCl was dissolved in a mixture of DMF (0.3 ml) and NEt_3 (2.0 µl) and treated with $(Boc)_2O$ (1.3 mg, 0.006 mmol) for 2 h. The mixture was evaporated and diluted with EtOAc. The solution was washed with water, dried, and evaporated to remain 2.8 mg of **16**; R_f^1 0.76.

^1H NMR spectroscopy. ^1H NMR spectra were recorded in DMSO-d_6 solution on a JEOL FX-90Q spectrometer or a JEOL FX-200 spectrometer at 29 °C. Tetramethylsilane was used as an internal reference; sample concentration, 10—30 mg/ml. The spectra obtained are shown in Figs. 2 and 4.

References

1) A part of this paper was briefly reported by K. Tanimura, T. Kato, M. Waki, and N. Izumiya, *Tetrahedron Lett.*, **24**, 3737 (1983).

2) G. W. Kirby and J. Michael, *J. Chem. Soc., Chem. Commun.*, **1971**, 187.

3) M. Kainosho and K. Ajisaka, *J. Am. Chem. Soc.*, **97**, 5630 (1975).

4) U. Nagai and J. Kobayashi, *Tetrahedron Lett.*, **1976**, 2873.

5) J. Kobayashi, U. Nagai, T. Higashijima, and T. Miyazawa, *Biochim. Biophys. Acta*, **577**, 195 (1979).

6) J. Kobayashi, T. Higashijima, U. Nagai, and T. Miyazawa, *Biochim. Biophys. Acta*, **621**, 190 (1980).

7) N. Izumiya, S. Lee, T. Kanmera, and H. Aoyagi, *J. Am. Chem. Soc.*, **99**, 8346 (1977).

8) T. Kanmera, S. Lee, H. Aoyagi, and N. Izumiya, *Int. J. Pept. Protein Res.*, **16**, 280 (1980).

9) Y. Hashimoto, H. Aoyagi, M. Waki, T. Kato, and N. Izumiya, *Int. J. Pept. Protein Res.*, **21**, 11 (1983).

10) Abbreviations according to IUPAC-IUB Commission, *Pure Appl. Chem.*,**40**, 217 (1974), are used throughout. Other abbreviations: DCC, dicyclohexylcarbodiimide; DCHA, dicyclohexylamine; DMF, *N*,*N*-dimethylformamide; DMSO, dimethyl sulfoxide; EDC·HCl, 1-ethyl-3-(3-dimethylaminopropyl)carbodiimide hydrochloride; HONSu, *N*-hydroxysuccinimide; HPLC, high performance liquid chromatography; ΔPhe, 2,3-dehydrophenylalanine; TFA, trifluoroacetic acid.
11) J. M. Manning and S. Moore, *J. Biol. Chem.*, **243**, 5591 (1968).
12) Y. Shimohigashi, S. Lee, and N. Izumiya, *Bull. Chem. Soc. Jpn.*, **49**, 3280 (1976).
13) M. Dygert, N. Gō, and H. A. Scheraga, *Macromolecules*, **8**, 750 (1975).
14) I. D. Rae and H. A. Scheraga, *Biochem. Biophys. Res. Commun.*, **81**, 481 (1978).
15) C. R. Jones, M. Kuo, and W. A. Gibbons, *J. Biol. Chem.*, **254**, 10307 (1979).
16) E. M. Krauss and S. I. Chan, *J. Am. Chem. Soc.*, **104**, 6953 (1982).
17) K. Suzuki, Y. Sasaki, N. Endo, and Y. Mihara, *Chem. Pharm. Bull.*, **29**, 233 (1981).
18) S. M. Partridge, *Biochem. J.*, **44**, 521 (1949).
19) L. Moroder, E. Hallett, E. Wünsch, O. Keller, and G. Wersin, *Hoppe-Seyler's Z. Physiol. Chem.*, **357**, 1651 (1976).
20) H. Otsuka and K. Inouye, *Bull. Chem. Soc. Jpn.*, **37**, 1465 (1964).
21) K. Sato, H. Abe, T. Kato, and N. Izumiya, *Bull. Chem. Soc. Jpn.*, **50**, 1999 (1977).
22) J. Honzl and J. Rudinger, *Collect. Czech. Chem. Commun.*, **26**, 2333 (1961).
23) M. Ohno, T. Kato, S. Makisumi, and N. Izumiya, *Bull. Chem. Soc. Jpn.*, **39**, 1738 (1966).
24) M. Waki and N. Izumiya, *Bull. Chem. Soc. Jpn.*, **40**, 1687 (1967).

 © 1984 The Chemical Society of Japan Bull. Chem. Soc. Jpn., 57, 2198—2202 (1984) [Vol. 57, No. 8

Preparation and Properties of AzaTCNQ⁻ Anion Salts and Mixed AzaTCNQ⁻/TCNQ⁻ Salts of *N*-Alkylpyridinium and Related Cations

Hirohisa TANAKA, Gen-etsu MATSUBAYASHI, and Toshio TANAKA*

Department of Applied Chemistry, Faculty of Engineering, Osaka University, Yamadaoka, Suita, Osaka 565

(Received January 31, 1984)

The [Cation]⁺ATCNQ⁻ type salts were prepared, where ATCNQ⁻ is (4-dicyanomethyl-1-pyridinio)-dicyanomethanide anion, so-called AzaTCNQ⁻ anion, and [Cation]⁺ are *N*-alkylpyridinium, 4-cyano-*N*-alkylpyridinium, (4-methyl-1-pyrazinio)dicyanomethanide, *N*-alkylquinolinium (alkyl=Me and Et), *N*-methylacridinium, and *N*-methylphenazinium. Electrical resistivities of these salts as compacted samples fall in the range 10^6—10^9 Ωcm at 25 °C. The mixed ATCNQ⁻/TCNQ⁻ salts (TCNQ⁻=7,7,8,8-tetracyano-*p*-quinodimethan radical anion) of *N*-alkylpyridinium and -quinolinium cations also were prepared; [Cation]⁺(ATCNQ⁻)$_{0.1}$(TCNQ⁻)$_{0.9}$ ([Cation]⁺=*N*-methylpyridinium, *N*-ethylpyridinium, and *N*-ethylquinolinium) and [*N*-methylquinolinium]⁺(ATCNQ⁻)$_{0.17}$(TCNQ⁻)$_{0.83}$ whose electrical resistivities (10^4—10^6 Ωcm at 25 °C) are somewhat smaller than those of the corresponding TCNQ⁻ salts. Stackings of ATCNQ⁻ and TCNQ⁻ anions are discussed on the basis of electronic reflectance and ESR spectra. The [Cation]⁺ATCNQ⁻ salts react with iodine in hexane to give [Cation]⁺ATCNQ⁻·I*x* ([Cation]⁺=*N*-methyl- and *N*-ethylpyridinium and -quinolinium; *x*=3.2—3.9). They exhibit electrical resistivities of 10^4—10^6 Ωcm at 25 °C, which are lower by the 10^2—10^3 order than the resistivities of the undoped [Cation]⁺ATCNQ⁻ salts.

Although the ATCNQ⁻ anion (**I**) (4-dicyanomethyl-

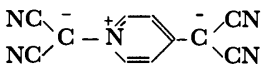

I

1-pyridinio)dicyanomethanide anion; so-called Aza-TCNQ⁻ anion) has a diamagnetic property with a $\bar{C}$–$\overset{+}{N}$ ylide bonding, the geometry is very similar to that of the TCNQ⁻ radical anion.[1,2] It would, therefore, be of interest to compare the properties of ATCNQ⁻ salts with those of the corresponding TCNQ⁻ radical anion salts. Thus, we reported previously the preparation and electrical resistivities of [Rh(RNC)$_4$]⁺ATCNQ⁻, and the corresponding mixed ATCNQ⁻/TCNQ⁻ and ATCNQ⁻/TCNQ⁻ /TCNQ salts (R=C_6H_5, 2,6-$Me_2C_6H_3$, and 2,4,6-$Me_3C_6H_2$) together with the crystal structure of [Rh(2,6-$Me_2C_6H_3NC)_4$]⁺ATCNQ⁻.[1] The present work was undertaken to elucidate the properties of the ATCNQ⁻ salts with organic cations having various reduction potentials.

This paper reports the preparation and electrical resistivities of several ATCNQ⁻ and mixed ATCNQ⁻/TCNQ⁻ salts with various organic cations (**1**—**9**) as well as salts obtained by the reaction of [Cation]⁺-ATCNQ⁻ salts with iodine. Interactions between the ATCNQ⁻ anion and the cations and between the ATCNQ⁻ anion and the TCNQ⁻ radical anion are discussed on the basis of electronic spectra and spin concentrations.

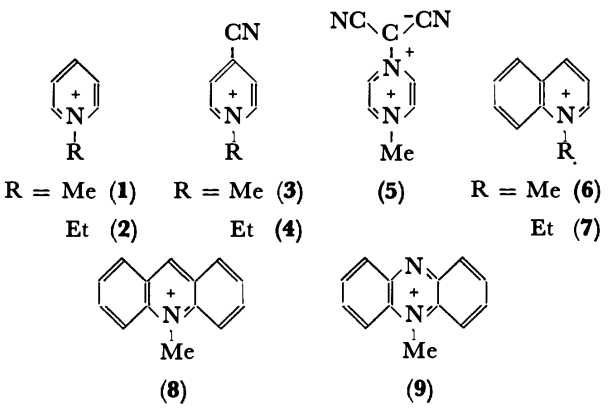

R = Me (**1**) Et (**2**) R = Me (**3**) Et (**4**) (**5**) R = Me (**6**) Et (**7**)

(**8**) (**9**)

Experimental

Materials. To a nitrobenzene (55 cm³) solution of (1-pyrazinio)dicyanomethanide[3] (0.55 g, 3.8 mmol) was added dimethyl sulfate (3.4 g, 27 mmol), and the mixture was stirred at room temperature for 4 d. The resulting precipitate was collected by filtration and recrystallized from methanol/benzene (1:1 v/v) to give orange needles of (4-methyl-1-pyrazinio)dicyanomethanide methyl sulfate in a 45% yield; mp 166—168 °C. Found: C, 39.82; H, 3.81; N, 20.13%. Calcd for $C_9H_{10}N_4O_4S$: C, 40.00; H, 3.73; N, 20.73%.

N-Ethylpyridinium bromide, *N*-methylpyridinium, *N*-alkylquinolinium, and 4-cyano-*N*-alkylpyridinium iodides (alkyl=Me and Et), and *N*-methylacridinium and *N*-methylphenazinium methyl sulfates were prepared by reactions of the corresponding base with an excess amount of alkyl halides or dimethyl sulfate according to the literature.[4] *N*-Alkylpyridinium and *N*-alkylquinolinium TCNQ⁻ salts (alkyl=Me and Et) were obtained by reactions of the corresponding pyridinium and quinolinium iodides with Li⁺TCNQ⁻ in methanol.[5] K⁺ATCNQ⁻ was prepared as described previously.[1]

Preparation of ATCNQ⁻ Salts. All the manipulations were carried out under nitrogen atmosphere. To a boiling aqueous (30 cm³) solution of K⁺ATCNQ⁻ (0.20 g, 0.82 mmol) was added *N*-methylpyridinium iodide (1.94 g, 8.8 mmol) in water (3 cm³). The mixture was allowed to stand in a refrigerator overnight to afford microcrystals of *N*-methylpyridinium ATCNQ⁻ salt (**1a**), which was collected by filtration and dried *in vacuo*, 52% yield. Similarly, the reactions of 4-cyano-*N*-methylpyridinium, 4-cyano-*N*-ethylpyridinium, *N*-methylquinolinium, and *N*-ethylquinolinium iodides with K⁺ATCNQ⁻ in water afforded the corresponding ATCNQ⁻ salts; **3a**, **4a**, **6a**, and **7a** in 52, 69, 40, and 48% yields, respectively. (4-Methyl-1-pyrazinio)dicyanomethanide, *N*-methylacridinium , and *N*-methylphenazinium-ATCNQ⁻ salts (**5a**, **8a**, and **9a**) were prepared in 46, 44, and 32% yields, respectively, by reactions of the corresponding pyrazinium dicyanomethylide, acridinium, and phenazinium methyl sulfates with K⁺ATCNQ⁻ in water.

An acetonitrile (300 cm³) solution containing K⁺ATCNQ⁻

(0.61 g, 2.5 mmol) and *N*-ethylpyridinium bromide (2.0 g, 11 mmol) was allowed to stand in a refrigerator overnight. A precipitate (KBr) was filtered off and the filtrate was evaporated to dryness under reduced pressure. The resulting solid was recrystallized from ethanol to afford needles of *N*-ethylpyridinium ATCNQ⁻ salt (**2a**) in a 46% yield.

Preparation of Mixed ATCNQ⁻/TCNQ⁻ Salts. An ethanol (40 cm³) solution containing **1a** (0.17 g, 0.55 mmol) and Li⁺TCNQ⁻ (0.12 g, 0.57 mmol) was allowed to stand in a refrigerator for one week to afford microcrystals of [*N*-methylpyridinium]⁺(ATCNQ⁻)$_{0.1}$ (TCNQ⁻)$_{0.9}$ (**1b**), which was collected by filtration and dried *in vacuo*, 58% yield. The mole ratio of ATCNQ⁻/TCNQ⁻ in the salt was determined from the electronic absorption spectrum in acetonitrile. Analogous reactions of **2a**, **6a**, and **7a** with Li⁺TCNQ⁻ in ethanol gave [*N*-ethylpyridinium]⁺(ATCNQ⁻)$_{0.1}$ (TCNQ⁻)$_{0.9}$ (**2b**), [*N*-methylquinolinium]⁺(ATCNQ⁻)$_{0.17}$ (TCNQ⁻)$_{0.83}$ (**6b**), and [*N*-ethylquinolinium]⁺(ATCNQ⁻)$_{0.1}$ (TCNQ⁻)$_{0.9}$ (**7b**) in 45, 28, and 73% yields, respectively.

Reactions of ATCNQ⁻ Salts with Iodine. Finely powdered **1a** (0.042 g, 0.14 mmol) was suspended in a hexane (25 cm³) solution of iodine (0.080 g, 0.28 mmol), and the mixture was stirred at room temperature under nitrogen atmosphere for 1 d. The resulting solid, [*N*-methylpyridinium]⁺ATCNQ⁻·$I_{3.2}$ (**1c**), was collected by filtration and dried *in vacuo*. Similar reactions of **2a**, **6a**, and **7a** with iodine in hexane gave the [Cation]⁺ATCNQ⁻·I_x salts (**2c**, **6c**, and **7c**; x=3.5 or 3.9).

Properties and analyses for the ATCNQ⁻ and the mixed ATCNQ⁻/TCNQ⁻ salts as well as the [Cation]⁺ATCNQ⁻·I_x salts are summarized in Table 1.

Physical Measurements. Electrical resistivities as compacted samples and electronic absorption spectra were measured as described previously.[6] Electronic reflectance spectra were recorded on a Hitachi 340 spectrophotometer equipped with a Hitachi NIR (near IR) or R-10A (UV and visible) integrating sphere unit. Cyclic voltammetric measurements were performed in acetonitrile using tetrabutylammonium perchlorate as a supporting electrolyte, as described elsewhere.[7] Spin concentrations of the ATCNQ⁻, the mixed ATCNQ⁻/TCNQ⁻, and the TCNQ⁻ salts as well as the ATCNQ⁻·I_x salts were determined at room temperature by comparing integrated signal intensities of the samples with that of 2,2-diphenyl-1-picrylhydrazyl (DPPH).

Results and Discussion

Electrical Properties. The temperature dependence of specific resistivities indicates that all the salts behave as typical semiconductors in the temperature range measured; 0—85 °C for [Cation]⁺ATCNQ⁻, 15—50 °C for the mixed ATCNQ⁻/TCNQ⁻ salts, and 0—20 °C for [Cation]⁺ATCNQ⁻·I_x(x=3.2—3.9).

Table 1. Properties and analyses of the ATCNQ⁻ salts

No.	Salt	Color[a]	Mp (dec.) θ_m/°C	Found (Calcd)[b] %C	%H	%N
1a	[C_5H_5N-Me]⁺ATCNQ⁻	brown (m)	234—237	67.50 (67.99)	4.01 (4.03)	28.02 (27.98)
2a	[C_5H_5N-Et]⁺ATCNQ⁻	light brown (n)	151—152	68.48 (68.78)	4.47 (4.49)	26.73 (26.73)
3a	[4-CN-C_5H_4N-Me]⁺ATCNQ⁻·0.5H_2O	purple (f)	167—170	64.77 (64.66)	3.54 (3.62)	29.47 (29.33)
4a	[4-CN-C_5H_4N-Et]⁺ATCNQ⁻	purple (m)	179—181	66.32 (67.25)	3.74 (3.86)	28.62 (28.89)
5a	[4-$C(CN)_2$-$C_4H_4N_2$-Me]⁺ATCNQ⁻	dark brown (m)	162	61.49 (62.46)	3.13 (3.03)	34.29 (34.50)
6a	[C_9H_7N-Me]⁺ATCNQ⁻	dark brown (m)	216—217	71.65 (71.99)	4.06 (4.03)	23.43 (23.99)
7a	[C_9H_7N-Et]⁺ATCNQ⁻	dark brown (m)	166—167	72.41 (72.51)	4.43 (4.43)	22.57 (23.06)
8a	[$C_{13}H_9N$-Me]⁺ATCNQ⁻	dark brown (m)	172—174	74.32 (74.99)	4.05 (4.03)	20.45 (20.99)
9a	[$C_{12}H_8N_2$-Me]⁺ATCNQ⁻	dark brown (m)	147—149	71.02 (71.82)	3.82 (3.77)	24.17 (24.42)
1b	[C_5H_5N-Me]⁺(ATCNQ⁻)$_{0.1}$-(TCNQ⁻)$_{0.9}$	black (m)	202—204	71.79 (72.02)	4.04 (4.05)	23.67 (23.93)
2b	[C_5H_5N-Et]⁺(ATCNQ⁻)$_{0.1}$-(TCNQ⁻)$_{0.9}$	black (m)	156—159	72.49 (72.63)	4.35 (4.04)	22.66 (23.67)
6b	[C_9H_7N-Me]⁺(ATCNQ⁻)$_{0.17}$-(TCNQ⁻)$_{0.83}$	purple (m)	208—210	74.30 (75.20)	3.83 (4.05)	20.66 (20.75)
7b	[C_9H_7N-Et]⁺(ATCNQ⁻)$_{0.1}$-(TCNQ⁻)$_{0.9}$	purple (m)	158—160	74.79 (75.85)	4.41 (4.45)	19.58 (19.70)
1c	[C_5H_5N-Me]⁺ATCNQ⁻·$I_{3.2}$	dark brown (p)	c	28.94 (28.90)	1.89 (1.71)	11.77 (11.90)
2c	[C_5H_5N-Et]⁺ATCNQ⁻·$I_{3.5}$	dark brown (p)	c	28.19 (28.50)	2.01 (1.86)	11.09 (11.08)
6c	[C_9H_7N-Me]⁺ATCNQ⁻·$I_{3.5}$	dark brown (p)	c	31.92 (31.74)	1.93 (1.76)	10.25 (10.58)
7c	[C_9H_7N-Et]⁺ATCNQ⁻·$I_{3.9}$	dark brown (p)	c	30.42 (30.75)	1.95 (1.88)	9.45 (9.78)

a) Crystal forms in parentheses; m: microcrystals, n: needles, f: flakes, p: powder. b) %I. **1c**: 57.62(57.46), **2c**: 58.34(58.56), **6c**: 55.57(55.92), **7c**: 57.47(57.59). c) Not measured.

Table 2. Specific resistivities as compacted samples (ρ) and activation energies (E_a) of the ATCNQ⁻- and related salts

Salt	$\rho_{25°C}$ / Ω cm	E_a / eV	Spin concentration / %
1a	3.1×10^{8}	1.1	0
2a	1.1×10^{6}	0.39	0
3a	5.2×10^{8}	0.72	0
4a	5.1×10^{8}	1.2	0
5a	4.1×10^{8}	0.66	0.30
6a	4.7×10^{9}	0.53	0
7a	7.7×10^{9}	0.77	0
8a	7.1×10^{8}	0.89	0.032
9a	2.3×10^{8}	0.92	7.5
1b	9.7×10^{4}	0.40	6.2
2b	4.2×10^{5}	0.44	6.2
6b	4.3×10^{6}	0.40	12
7b	1.4×10^{6}	0.36	5.2
1c	1.5×10^{5}	0.88	0.91
2c	9.1×10^{4}	0.47	0.85
6c	3.5×10^{6}	1.3	0.89
7c	1.2×10^{6}	1.8	0.50
$[C_5H_5N\text{-Me}]^+TCNQ^-$ (**1d**)	2.3×10^{5}	0.50	0.25
$[C_5H_5N\text{-Et}]^+TCNQ^-$ (**2d**)	7.5×10^{4}	0.50	0.11
$[C_9H_7N\text{-Me}]^+TCNQ^-$ (**6d**)	1.0×10^{7}	0.58	0.083
$[C_9H_7N\text{-Et}]^+TCNQ^-$ (**7d**)	1.4×10^{8}	0.69	0.43
A mixture of **1a**/**1d**[a]	5.6×10^{5}	b	b
2a/**2d**[a]	9.0×10^{5}	b	b
6a/**6d**[a]	1.1×10^{7}	b	b
7a/**7d**[a]	3.3×10^{8}	b	b

a) The mole ratios of **1a**/**1d**, **2a**/**2d**, **6a**/**6d**, and **7a**/**7d** are the same as those of **1b**, **2b**, **6b**, and **7b**. b) Not measured.

Specific resistivities at 25 °C ($\rho_{25°C}$) and the activation energies (E_a) calculated from the equation $\rho=\rho_0\exp(E_a/kT)$ are listed in Table 2, which involves also the $\rho_{25°C}$ and E_a values of the [Cation]⁺TCNQ⁻ salts and their mixtures with [Cation]⁺ATCNQ⁻, as well as spin concentrations of the salts obtained from ESR spectra. Salts of the [Cation]⁺ATCNQ⁻ type (**1a—9a**) exhibit fairly large $\rho_{25°C}$ values, which may be suggestive of an alternative ATCNQ⁻/[Cation]⁺ stack in the solid state.

The mixed ATCNQ⁻/TCNQ⁻ salts **1b**, **6b**, and **7b** except for **2b** display somewhat smaller $\rho_{25°C}$ and E_a values than the corresponding TCNQ⁻ salts in which the TCNQ⁻ radical anion assumes a columnar structure.[8] In addition, all the mixed salts are more conductive than the mixtures of the ATCNQ⁻ and TCNQ⁻ salts with the same ATCNQ⁻/TCNQ⁻ mole ratios as those in the respective mixed ATCNQ⁻/TCNQ⁻ salts. These results suggest the incorporation of the ATCNQ⁻ anion into the TCNQ⁻ radical anion column. Such an incorporation may bring about a disorder in the TCNQ⁻ column, which may be responsible for rather lower E_a Values of the mixed ATCNQ⁻/TCNQ⁻ salts than those of the TCNQ⁻ salts, as reported for $(TMTTF)_x(TMTSF)_{1-x}(TCNQ)$ (x= 0.005 and 0.03; TMTTF=tetramethyltetrathiafulvalene and TMTSF=tetramethyltetraselenafulvalene),[9] $(TTF)_x(TSF)_{1-x}(TCNQ)$ (x=0—1; TTF= tetrathiafulvalene and TSF=tetraselenafulvalene),[10] $(TMTSF)_2(ClO_4)_{0.95}(IO_4)_{0.05}$,[9] and $(TSF)(MTCNQ)_{0.1}(TCNQ)_{0.9}$(MTCNQ=methyltetracyanoquinodimethan).[11]

The temperature dependence of specific resistivities of the [Cation]⁺ATCNQ⁻·I_x salts is illustrated in Fig. 1. Although the plots of $\log\rho$ *vs.* $1/T$ give a linear relationship below 30 or 20 °C, they deviate from the straight lines above this temperature. The $\log\rho-1/T$ relations of **1c**, **6c**, and **7c**, however, had a reproducible nature in the range of 20—35 °C, while all the [Cation]⁺ATCNQ⁻·I_x salts decomposed above 35 °C.

Electronic Spectra and Magnetic Properties. Figure 2 shows the electronic reflectance spectra of K⁺-ATCNQ⁻ and **7a—7c**. The shoulder-like band around 23000 cm⁻¹ observed for K⁺ATCNQ⁻ (dotted line in Fig. 2), which corresponds to the absorption band at 22000 cm⁻¹ in acetonitrile, is due to the intramolecular charge transfer (CT) transition arising from the $\bar{C}$–$\overset{+}{N}$ ylide bond.[1] Salt **7a** also exhibits this band around 23000 cm⁻¹ (solid line in Fig. 2). Other several strong absorptions in the frequency region higher than 20000 cm⁻¹ observed for **7a** are ascribed to transitions within the ATCNQ⁻ anion or the cation. It should be noted that **7a** displays a band at 17500 cm⁻¹, which may be due to an electronic interaction between the ATCNQ⁻ anion and the cation, since both K⁺ATCNQ⁻ and *N*-ethylquinolinium perchlorate show no band in this region. Such a new band was observed also in the reflectance spectra of the other [Cation]⁺ATCNQ⁻ salts. The frequency of the band maxima (ν_{max}) newly appeared in the [Cation]⁺ATCNQ⁻ salts are listed in Table 3, together with cathode

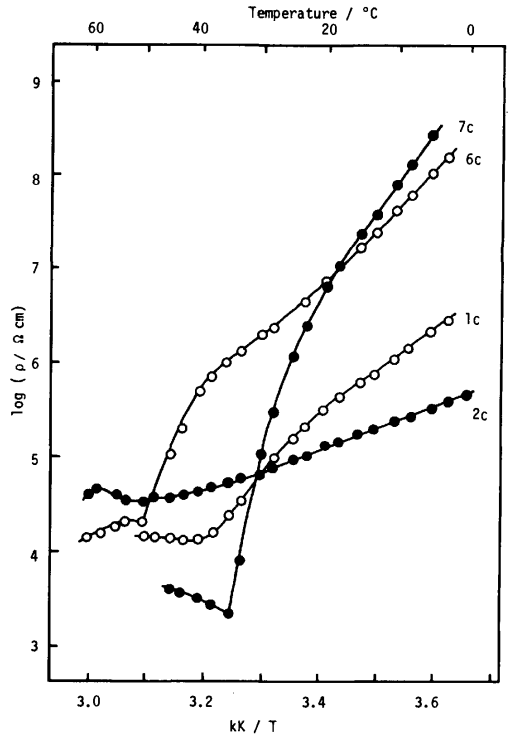

Fig. 1. Temperature dependence of the specific resistivities of the [Cation]⁺ATCNQ⁻·I_x salts.

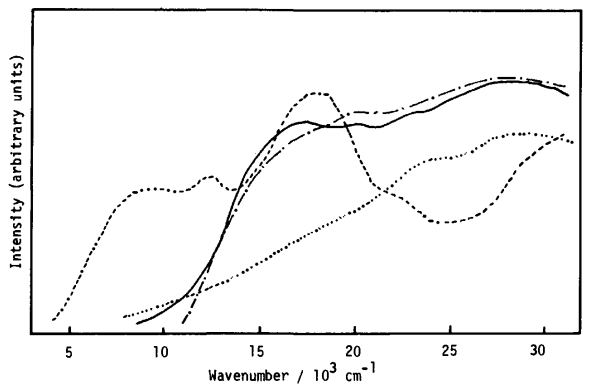

Fig. 2. Powder reflectance spectra of K⁺ATCNQ⁻ (·····), [C_9H_7N-Et]⁺ATCNQ⁻ (7a, ——), [C_9H_7N-Et]⁺(ATCNQ⁻)$_{0.1}$(TCNQ⁻)$_{0.9}$ (7b, ------), and [C_9H_7N-Et]⁺ATCNQ⁻·$I_{3.9}$ (7c, -·-·-).

peak potentials (E_{cp}) of the counter cations determined from cyclic voltammetry. There can be seen an approximate linear relation between ν_{max} and E_{cp} as shown in Fig. 3; ν_{max} decreases with the positive shift of E_{cp}, suggesting that the band is due to an intermolecular CT transition from the ATCNQ⁻ anion to the counter cations. The smaller difference between the anode peak potential of ATCNQ⁻ (0.54 V *vs.* SCE in acetonitrile)[1] and the E_{cp} value of a counter cation is expected to cause more effective CT. Although there has been observed no signal in the ESR spectra of **1a**—**4a**, **6a**, and **7a**, salts **5a**, **8a**, and **9a** displayed a weak ESR signal in the solid state, whose *g* values were essentially the same as that of DPPH (g=2.0037). Based on the signal intensities in comparing with that of DPPH, spin concentrations of **9a**, **5a**, and **8a** at room temperature were estimated 7.5, 0.3, and 0.032%, respectively,

TABLE 3. CT BAND MAXIMA (ν_{max}) OF THE ATCNQ⁻ SALTS AND CATHODE PEAK POTENTIALS (E_{cp}) OF THE COUNTER CATIONS

Salt	ν_{max} / cm⁻¹	E_{cp} / V *vs.* SCE
2a	21000	−1.36
1a	20500	−1.28
7a	17500	−0.92
6a	19500	−0.86
3a	19200	−0.76
4a	17900	−0.70
8a	15300	−0.41
5a	14700	−0.25
9a	10000	−0.11

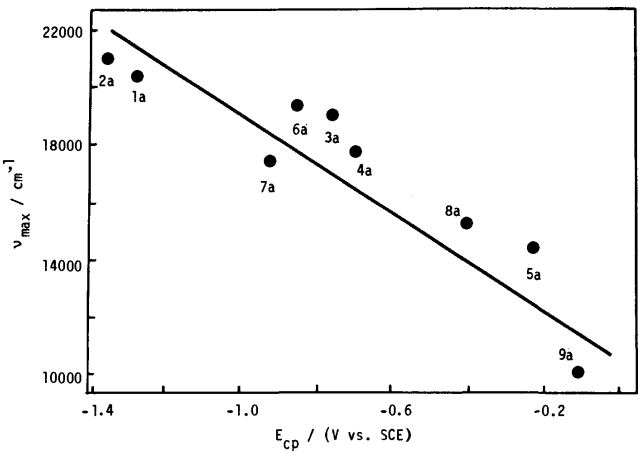

Fig. 3. Plots of CT band maxima (ν_{max}) of the ATCNQ⁻ salts *vs.* cathode peak potentials (E_{cp}) of the counter cations.

which indicates a radical formation caused by a stronger CT in these salts.

The reflectance spectrum of **7b** shows a band around 9500 cm⁻¹ (broken line in Fig. 2), which can be assigned to the CT transition between TCNQ⁻ radical anions as observed for simple salts such as Na⁺TCNQ⁻, Rb⁺TCNQ⁻ and [morpholinium]⁺TCNQ⁻.[8] In accordance with this, a strong band appears around 18000 cm⁻¹, which is the blueshifted LE_1 band characteristic of the dimeric interaction of the TCNQ⁻ radical anions. On the other hand, a weak band observed at 12000 cm⁻¹ is ascribed to the TCNQ⁻ radical anion monomer.[8] Salts **1b**, **2b**, and **6b** gave essentially the same spectra as **7b**. Thus, these mixed ATCNQ⁻/TCNQ⁻ salts are suggested to contain predominantly TCNQ⁻ radical anions with the dimeric interaction and small amounts of the ATCNQ⁻ anion seem to prevent the TCNQ⁻/TCNQ⁻ interaction, resulting in the formation of a part of monomeric TCNQ⁻. Although the TCNQ⁻ simple salts (**1d**, **2d**, **6d**, and **7d**) in which the TCNQ⁻ radical anion may have the dimeric interactionon[8] exhibited very weak signals, the mixed ATCNQ⁻/TCNQ⁻ salts displayed a sharp ESR signal (g=2.0037) with moderate intensities, resulting in much larger spin concentrations in the mixed ATCNQ⁻/TCNQ⁻ salts than in the TCNQ⁻ salts (Table 2). This is consistent with the assumption that the ATCNQ⁻ anions may prevent the dimeric

interaction between the $TCNQ^{-}$ radical anions in the mixed $ATCNQ^{-}/TCNQ^{-}$ salts.

The iodine-doped salts, **1c**, **2c**, **6c**, and **7c**, exhibited essentially the same IR absorption spectra as those of the undoped salts, **1a**, **2a**, **6a**, and **7a**, respectively, suggesting that the dopant has little effect on the skeletons of either cationic or anionic moieties. In the electronic reflectance spectra, however, the band due to the CT transition between $ATCNQ^{-}$ and the cation ($\approx 17000\,cm^{-1}$) is weakened (dot-dash line in Fig. 2). Thus, the introduction of iodine to the $ATCNQ^{-}$ salts seems to reduce the CT interaction between $ATCNQ^{-}$ and the cation. It is noted that the spin concentrations of **1c**, **2c**, **6c**, and **7c** obtained from ESR signal intensities are small (Table 2). Only a small portion of the $ATCNQ^{-}$ anion may, therefore, be oxidized by iodine; most of iodine as a dopant would remain as I_2 in the crystals. Small amounts of the oxidized $ATCNQ^{\cdot}$ radical may contribute to the conductivities of **1c**, **2c**, **6c**, and **7c**, which are 10^2—10^3 greater than those of **1a**, **2a**, **6a**, and **7a**, respectively.

References

1) G. Matsubayashi, H. Tanaka, T. Tanaka, and K. Nakatsu, *Inorg. Chim. Acta*, **63**, 217 (1982).
2) F. Wudl, "Chemistry and Physics of One-dimensional Metals," ed by H. J. Keller, NATO Adv. Study Inst., (1977), p. 249.
3) L. R. Melby, *Can. J. Chem.*, **43**, 1448 (1965).
4) L. R. Melby, R. J. Harder, W. R. Hertler, W. Mahler, R. E. Benson, and W. E. Mochel, *J. Am. Chem. Soc.*, **84**, 3374 (1962).
5) A. Rieche and P. Dietrich, *Chem. Ber.*, **96**, 3044 (1963).
6) S. Araki, H. Ishida, and T. Tanaka, *Bull. Chem. Soc. Jpn.*, **51**, 407 (1978).
7) G. Nagao, K. Tanaka, and T. Tanaka, *Inorg. Chim. Acta*, **42**, 43 (1980).
8) Y. Iida, *Bull. Chem. Soc. Jpn.*, **42**, 71 (1969); J. Tanaka, M. Tanaka, T. Kawai, T. Takabe, and O. Maki, *ibid*, **49**, 2358 (1976).
9) E. M. Engler, R. Green, R. Haen, Y. Tomkiewicz, K. Mortensen, and J. Berendzen, *Mol. Cryst. Liq. Cryst.*, **79**, 15 (1982).
10) E. M. Engler, B. A. Scott, S. Etemad, T. Penney, and V. V. Patel, *J. Am. Chem. Soc.*, **99**, 5909 (1977).
11) E. M. Engler, R. A. Craven, Y. Tomkiewicz, and B. A. Scott, *J. Chem. Soc., Chem. Commun.*, **1976**, 337.

 © 1984 The Chemical Society of Japan Bull. Chem. Soc. Jpn., 57, 2203—2210 (1984)

Synthetic Studies on Quinoxaline Antibiotics. II.[1] Synthesis of Triostin A[2]

Masaru SHIN,* Ken INOUYE, and Hideo OTSUKA
Shionogi Research Laboratories, Shionogi & Co., Ltd., Fukushima-ku, Osaka 553
(Received February 3, 1984)

Triostin A, a cyclic octadepsipeptide, was synthesized with Z-D-Ser[Boc-Ala-MeCys(Bzl)-MeVal]-OH and Z-D-Ser[H-Ala-MeCys(Bzl)-MeVal]-OTce as key intermediates.† The synthetic antibiotic was compared with natural triostin A in terms of chromatographic behaviors, NMR spectra, and antimicrobial activity to establish their identity. The NMR data on *S,S'*-dibenzyldihydrotriostin A showed that this intermediate lacking the disulfide linkage also existed as two conformers in chloroform. This observation excludes the possibility that the conformer equilibrium known to occur with triostin A is a consequence of the reversed chirality of the disulfide bond.

Triostin A[3] is a member of the triostin family of the quinoxaline antibiotics.[4] The triostins were isolated and structure-elucidated in these Laboratories.[3] The quinomycins[5] which constitute another family of quinoxaline antibiotics are represented by echinomycin[6] (or quinomycin A[5]). In contrast to the quinomycins which are produced by widely distributed streptomycetes, the triostins have ever been found only in a strain of *Streptomyces aureus*.[7] The quinoxaline antibiotics possess antibacterial[5] and cytotoxic[4,8] activities. They are known to bind DNA as bifunctional intercalating agents[9] and thereby inhibit RNA synthesis.[10] Triostin A is characterized by its cyclic octadepsipeptide structure with a cross-bridged disulfide linkage (Fig. 1).[3b,11] It contains an *N,N'*-dimethyl-L-cystine residue and two sets of D-serine, L-alanine, and *N*-methyl-L-valine residues. The 2-quinoxalinylcarbonyl (Qxc) moiety is attached to the amino group of the D-serine residues. Recent NMR studies have shown that triostin A exists as a mixture of two conformers in deuteriochloroform.[11,12] Kalman *et al.*[13] have postulated that occurrence of the two conformers is a consequence of the reversal of chirality of the disulfide bond, while Kyogoku *et al.*[14] attributed it to the *cis-trans* isomerization of the *N*-methyl peptide bonds. The former possibility has recently been ruled out because it was found that the *S,S'*-dibenzyl derivative of dihydrotriostin A (reduced form of triostin A) also had two conformers.[15]

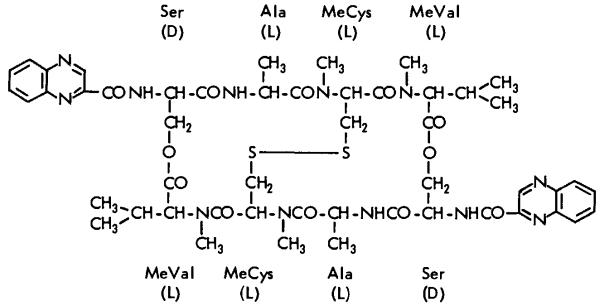

Fig. 1. Structure of Triostin A.

The synthesis of triostin A[16] and of some analogs[17,18] has been reported by Olsen *et al.* In a previous paper[1] we reported the synthesis of 2-quinoxalinylcarbonyl tetradepsipeptide derivatives of the types, Qxc-D-Ser(R^1-MeVal)-Ala-MeCys(Bzl)-OR^2 and Qxc-D-Ser[R^1-MeCys(Bzl)-MeVal]-Ala-OR^2 (R^1=Z, Bpoc, or H; R^2=Bu^t or H), but in the subsequent studies these derivatives proved to be poor intermediates for the synthesis of triostin A. The present paper describes our total synthesis of triostin A, performed with Z-D-Ser[Boc-Ala-MeCys(Bzl)-MeVal]-OH (**1**) and Z-D-Ser[H-Ala-MeCys(Bzl)-MeVal]-OTce (**2**) as key intermediates.

Figure 2 illustrates the procedure for the synthesis of the two tetradepsipeptide derivatives **1** and **2**. The starting material Z-D-Ser(Bu^t)-OH (**3**) was prepared as described for the corresponding L-isomer.[19] Com-

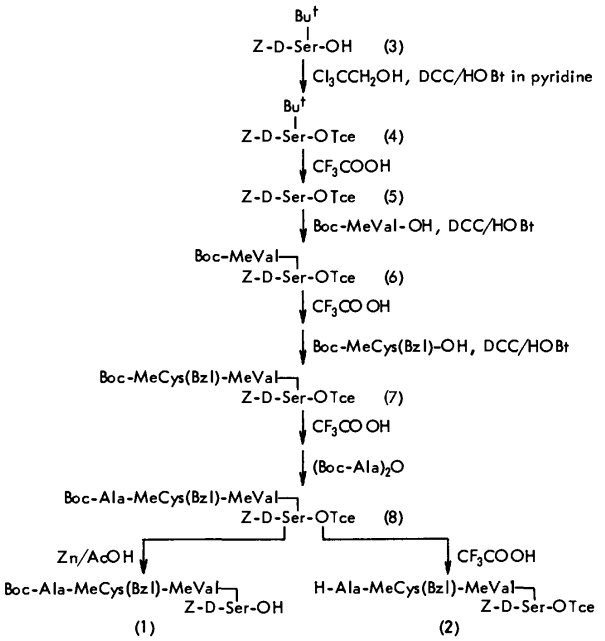

Fig. 2. Synthesis of tetradepsipeptide intermediates.

†Abbreviations used are those recommended by the IUPAC-IUB Commission on Biochemical Nomenclature [*Biochemistry*, **11**, 1726 (1972)] and include: MeCys, N-methyl-L-cysteine, MeVal; *N*-methyl-L-valine; Boc, *t*-butoxycarbonyl; Boc-SDP, *O-t*-butyl *S*-(4,6-dimethyl-2-pyrimidinyl) thiocarbonate; Bpoc, 1-(4-biphenylyl)-1-methylethoxycarbonyl; Qxc, 2-quinoxalinylcarbonyl; Z, benzyloxycarbonyl; Z(OMe), 4-methoxybenzyloxycarbonyl; Z(OMe)-SDP, *O-p*-methoxybenzyl *S*-(4,6-dimethyl-2-pyrimidinyl)thiocarbonate; Bu^t, *t*-butyl; Bzl, benzyl; Tce, 2,2,2-trichloroethyl; HOBt, 1-hydroxybenzotriazole; HONp, 4-nitrophenol; HOSu, *N*-hydroxysuccinimide; CDI, *N,N'*-carbonyldiimidazole; DCC, dicyclohexylcarbodiimide; DCU, *N,N'*-dicyclohexylurea; EDC, 1-ethyl-3-(3-dimethylaminopropyl)carbodiimide; DPPA, diphenylphosphorazidate; AcOH, acetic acid; TFA, trifluoroacetic acid; DCHA, dicyclohexylamine; DIEA, *N,N*-diisopropylethylamine; TEA, triethylamine; DMF, *N,N*-dimethylformamide; and THF, tetrahydrofuran.

pound **3** was esterified with 2,2,2-trichloroethanol (HOTce)[20] by the action of DCC in the presence of HOBt to give **4**. The yield of the Tce ester was as high as 97% when pyridine was used as a solvent. To remove the Bu^t group compound **4** was treated with TFA and the resulting Z-D-Ser-OTce (**5**) was coupled with Boc-MeVal-OH by the use of DCC-HOBt in pyridine[16] to give depsipeptide **6** in 60—70% yields. In the absence of HOBt the yield of **6** was 35% and the formation of *N*-acylurea was predominant (62%). Compound **6** was, after removal of the Boc group with TFA, coupled with Boc-MeCys(Bzl)-OH by the DCC-HOBt method[21] to give **7** in 70—80% yields. Compound **7** was also synthesized using Z(OMe)-MeVal-OH in place of Boc-MeVal-OH. Removal of the Boc group from **7** was followed by the incorporation of Boc-Ala to give **8**, in which the symmetrical anhydride $(Boc\text{-}Ala)_2O$ proved to be a good acylating agent, whereas the usual DCC-mediated coupling with Boc-Ala-OH failed to furnish the desired compound. When acylated with the mixed anhydride derived from Boc-Ala-OH and isobutyl chloroformate, Z-D-Ser[isobutoxycarbonyl-MeCys(Bzl)-MeVal]-OTce was the sole product (90%). The protected tetradepsipeptide (**8**) thus obtained in a 70% yield was treated with either Zn in 90% AcOH[22] to remove the Tce group or TFA to remove the Boc group, giving the key compounds **1** and **2**, respectively. The removal of the Tce group was complete within 3 h and compound **1** was obtained in a 90% yield. Further steps leading to the formation of triostin A are shown in Fig. 3.

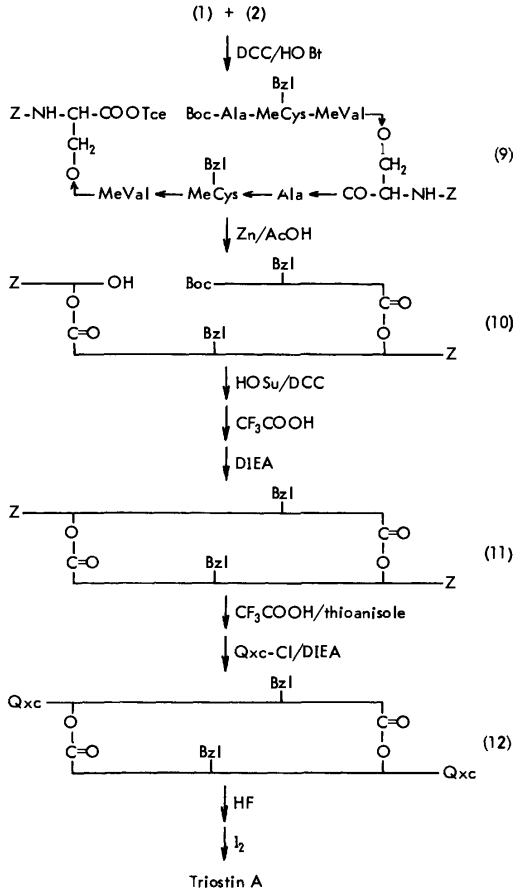

Fig. 3. Synthesis of triostin A.

The coupling of **1** and **2** with DCC-HOBt in THF afforded the linear octadepsipeptide (**9**) in 82—92% yields. Compound **9** was then treated with Zn in 90% AcOH to effect the complete removal of the Tce group giving **10** in yields higher than 90%. For the subsequent cyclization compound **10** was converted into the *N*-hydroxysuccinimide ester in the usual manner except for using HOSu and DCC in large excess and, after removal of the Boc group with TFA, the active ester was dissolved in a large volume of ethyl acetate. The cyclization was then initiated by the addition of DIEA under conditions of high dilution (0.2 mmol peptide/l). The progress of the reaction was monitored by high-performance liquid chromatography (HPLC) on a μ-Porasil column with 2-propanol-hexane (5:95) as solvent to show that the reaction was complete within 3 h. Cyclic octadepsipeptide **11** was isolated in pure form in 58% yield from **10** (mean for seven trials). The ^{1}H-NMR spectrum and the field desorption mass spectrum of **11** were consistent with the proposed structure. Conversion of **11** to *S,S'*-dibenzyl-dihydrotriostin A (**12**) was effected by selective removal of the Z group with TFA-thioanisole,[23] and the subsequent acylation with Qxc-Cl[24] or Qxc-ONp[1] in the presence of triethylamine. The yield of **12** was 28—37% as estimated by HPLC. The crude product was purified on silica-gel columns to give a pure preparation of **12** in an over-all yield of 13—22% from **11**. Compound **12** was treated with HF-anisole at 25 °C for 30 min to remove the benzyl groups, followed by treatment with iodine in methanol[25] to form the disulfide bond. The crude product was purified by silica-gel column chromatography and by recrystallization affording triostin A in a 20% yield from **12**. The synthetic antibiotic thus obtained was indistinguishable from natural triostin A in TLC and in HPLC (Fig. 5). The identity of natural and synthetic preparations was also confirmed by their superimposable 360 MHz ^{1}H-NMR spectra (Fig. 4). Synthetic triostin A was as active as natural triostin A when assayed for antimicrobial activity against *Bacillus subtilis* PCI-219. The minimum effective concentration was 0.5 μg/ml.

In 1978 Chakravarty and Olsen[16] briefly reported the first synthesis of triostin A, in which they used tetradepsipeptide fragments, Z-D-Ser[R-MeCys(Bam)-MeVal]-Ala-OH (I: R=Boc, II: R=H; Bam=benzamidomethyl), as intermediates to prepare their cyclic octadepsipeptide (III). Fragment couplings are usually susceptible to racemization at the *C*-terminal amino acid of the carboxyl component. In this case, therefore, racemization could occur at the Ala residue during the formation of a linear octadepsipeptide from I and II, and also in the subsequent cyclization leading to III. In fact, Olsen and collaborators[17] observed that a linear octadepsipeptide, an intermediate to des-*N*-tetramethyltriostin A, derived from Z-D-Ser[Boc-Cys(Acm)-Val]-Ala-OH and Z-D-Ser[H-Cys(Acm)-Val]-Ala-OTce (Acm=acetamidomethyl) by the EDC-HOBt method contained 6.4% of D-alanine. This means that 25.6% racemization had occurred to the Ala residue involved in the coupling reaction. This racemization was a problem in their synthesis of triostin A and analogs, although they suggested that the diaste-

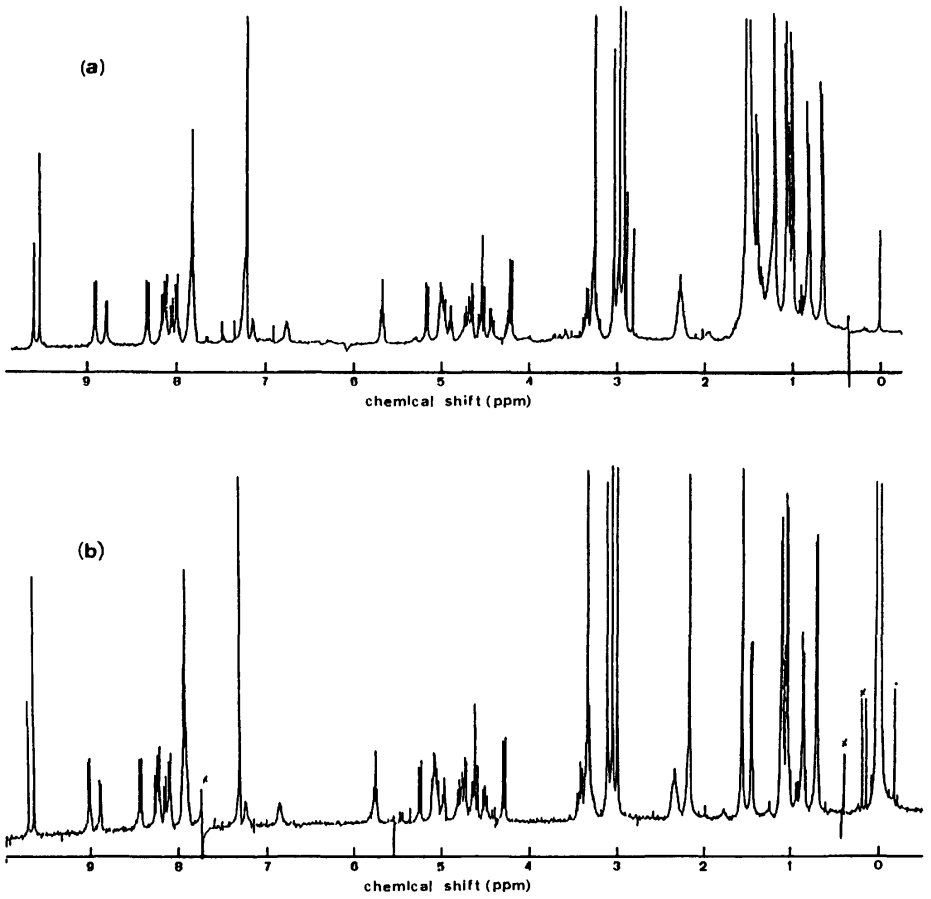

Fig. 4. 360 MHz ^{1}H-NMR spectra of (a) synthetic and (b) natural preparations of triostin A in $CDCl_3$.

reoisomeric impurity could largely be removed during purification. In our present synthesis of triostin A, the coupling of two tetradepsipeptides **1** and **2**, and the subsequent cyslization of the linear octadepsipeptide (**10**) were both performed by activation of the carboxyl function of the *O*-acylated Z-D-serine, Z-D-Ser(R)-OH (R=Boc-peptide group), to form a normal Ser-Ala bond, as shown in Fig. 2 and Fig. 3. This new approach should not only eliminate the danger of racemization, but also make the coupling reaction easier to proceed than what involves the *N*-methylamino acid.

Chakravarty and Olsen[16] stated that the removal of the Tce group from a depsipeptide of the type Z-D-Ser(R)-Ala-OTce (R=Boc-peptide) with zinc in acetic acid was incomplete (65%) in the case of tetradepsipeptide and it was practically impossible in the case of octadepsipeptide. In our synthesis (Fig. 2 and Fig. 3), on the other hand, the complete removal of the Tce group from a depsideptide of the type Z-D-Ser(R)-OTce (R=Boc-peptide) was readily achieved in both tetradepsipeptide **8** and octadepsipeptide **9** by the treatment with zinc in 90% acetic acid, suggesting that the Tce ester of the D-serine in **8** and **9** is exposed to the molecular surface, whereas the alanine ester in Olsen's intermediates is rather buried, especially in the case of the octadepsipeptide.

The cyclization of linear octadepsipeptide **10** was performed by the *N*-hydroxysuccinimide ester method as described above. Table 1 represents the results of the test experiment, in which the data show that the formation of cyclic peptide **11** from **10** is remarkably increased as the peptide concentration is decreased. This is naturally because the undesired formation of oligomers should be suppressed by lowering the concentration, while the intramolecular cyclization is independent of concentration. As is seen in Table 1, the yield of cyclic peptide **11** does not depend on the solvent used, we therefore employed ethyl acetate as solvent in the cyclization reaction of a preparative scale. Chakravarty and Olsen[16] synthesized a cyclic octadepsipeptide as intermediate to triostin A by one-step cyclization of the corresponding linear peptide with both *C*- and *N*-terminals unprotected, in which the yield of the cyclic peptide was 22% when the EDC-HOSu method and a peptide concentration of *ca.* 2.5 mmol/l were employed. In the case of cyclization leading to des-*N*-tetramethyltriostin A (nortriostin A) analogs,[17,18] however, higher yields up to 55% have been reported. In the present work we also tried this one-step method. Compound **10** was treated with TFA to remove the Boc group and the resulting material (2 mmol/l in THE or DMF) was treated with 5 or 10 equiv of DCC-HOBt, EDC-HOBt, or CDI at 25 °C, or with 5 equiv of DPPA[26] at 5 °C in the presence of DIEA (1 equiv). Among these the DPPA method gave the best result, producing cyclic peptide **11** in 24% yield as estimated by HPLC. The DCC-HOBt method pro-

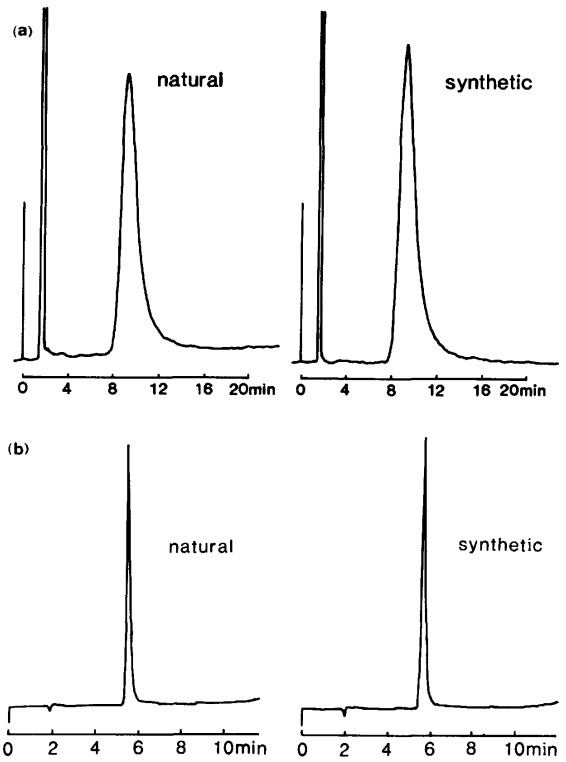

Fig. 5. HPLC profiles of synthetic and natural preparations of triostin A. (a) Column: m-Porasil, 30 cm×3.9 mm ID; solvent: 2-propanol-hexane (27.5:72.5); flow rate: 2 ml/min; detection: at 220 nm. (b) Column: Hypersil $3C_{18}$, 10 cm×6.0 mm ID; solvent: a linear gradient (20 min) of 50—90% CH_3CN in 0.1 M (1 M=1 mol dm^{-3}) triethylammonium acetate (pH 7.0); flow rate: 1 ml/min; detection: at 243 nm.

TABLE 1. CONCENTRATION DEPENDECY OF CYCLIZATION REACTION IN THE CONVERSION OF **10** TO **11**[a]

Concentration of peptide (mmol/l)	Solvent	Yield[b] (%)
20	EtOAc	13
2	EtOAc	39
0.2	EtOAc	56
20	DMF	12
2	DMF	42(31)[c]
0.2	DMF	58

a) The cyclization was carried out at 25 °C for 3 h and monitored by HPLC under the following conditions: column: μ-Porasil (Waters), 30 cm×3.9 mm ID; solvent: 2-propanol-hexane (5:95, v/v); flow rate: 2 ml/min; detection: at 220 nm and 243 nm. b) Overall yield of **11** from **10** (see Fig. 3). c) In the presence of HOBt (20 mmol/l).

duced **11** in 12, 19, and 14% yields when the peptide concentrations were 10, 2, and 0.4 mmol/l, respectively. These low yields may be ascribed to the peptide concentrations employed, which must have been lower than adequate for the activation of the linear peptide and, at the same time, too high to prevent the undesired intermolecular reaction of the activated peptide. In fact, the occurrence of a larger amount of by-products was observed in the one-step method than in the two-step cyclization by the active ester method.

The selective removal of the Z groups from **11** by the treatment with TFA-thioanisole was based on the "push-pull" mechanism described by Kiso *et al.*[23] Preliminary tests were performed with Z-Cys(Bzl)-OH, Z-MeCys(Bzl)-OH, Z-D-Ser[isobutoxycarbonyl-MeCys-(Bzl)-MeVal]-OTce, and Qxc-D-Ser(Z-MeVal)-Ala-MeCys(Bzl)-OH[1] as model compounds to show that in every case the Z group was completely removed in 4—6 h at 25 °C without appreciable cleavage of the *S*-benzyl group. The similar conditions (25 °C, 6 h) could be applied to compound **11** to give the N^{α}-free intermediate (*S,S'*-dibenzyldihydroapotriostin A) without any difficulties. The subsequent quinoxalylcarbonylation leading to **12** was carried out with 50—100% excess of Qxc-Cl and a minimum amount of TEA to minimize the O→N acyl shift at the D-Ser residue.

Compound **12** obtained above is the *S,S'*-dibenzyl derivative of dihydrotriostin A and lacks the disulfide bond. The ^{1}H-NMR data for **12** clearly show, however, that this compound still has two conformations in $CDCl_3$ as does triostin A itself. This evidence now excludes the possibility, postulated by Kalman *et al.*,[13] that the conformer isomerism of triostin A is resulted from the reversal of chirality of the disulfide bond.

Experimental

Thin-layer chromatography (TLC) was performed on silica-gel plates (precoated Kieselgel 60 F_{254}, Merck) with the following solvent systems (ratios by volume): A, chloroform-methanol (95:5); B, chloroform-methanol-acetic acid (95:5:3); C, benzene-ethyl acetate (90:10); D, benzene-ethyl acetate (70:30); E, benzene-ethyl acetate-acetic acid (70:30:3). Spots were revealed by UV, ninhydrin staining or by charring with sulfuric acid. For column chromatography, prepacked silica-gel columns (Lobar, size B or C, Merck) were mostly used. High-performance liquid chromatography (HPLC) was carried out on a Waters Associates Model 6000A solvent delivery system, equipped with a Waters U6K injector and a Japan Spectroscopic UVIDEC 100-II variable wavelength UV detector. Proton NMR spectra were recorded on a Varian T-60 NMR spectrometer operated at 60 MHz and/or a Bruker WM 360 wb NMR spectrometer at 360 MHz.

D-Serine was purchased from Fluka AG, Buchs, Switzerland, 2-methylquinoxaline from Aldrich Chemical Co., Inc., Milwaukee, WI, U.S.A., Boc-SDP and Z(OMe)-SDP from Protein Research Foundation, Osaka, diphenylphosphorazidate (DPPA) from Nakarai Chemicals, Ltd., Kyoto, and 2,2,2-trichloroethanol (TceOH) from Tokyo Kasei Kogyo Co., Ltd., Tokyo. *N*-Methyl-L-valine,[27] *N*-methyl-*S*-benzyl-L-cysteine,[28] quinoxaline-2-carboxylic acid (Qxc-OH),[6b] and 2-quinoxalinylcarbonyl chloride (Qxc-Cl)[24] were synthesized according to the literature. 4-Nitrophenyl quinoxaline-2-carboxylate (Qxc-ONp) was prepared as described previously.[1]

Z-D-Ser(Bu^t)-OH (3). This compound was prepared basically following the procedure described for the L-isomer;[19] mp 81—84 °C, $[\alpha]_D^{24}$ −18.5±0.6° (*c* 1.0, ethanol). Lit, for the L-isomer:[20] mp 83.5—85 °C, $[\alpha]_D^{23}$ +22.0° (*c* 1, ethanol). Found: C, 61.19; H, 7.19; N, 4.73%. Calcd for $C_{15}H_{21}NO_5$: C, 61.00; H, 7.17; N, 4.74%.

Z-D-Ser(Bu^t)-OTce (4). To a solution of **3** (14.8 g, 50 mmol), Tce-OH (8.22 g, 55 mmol), and HOBt (7.43 g, 55 mmol) in pyridine (100 ml) was added DCC (11.4 g,

55 mmol) and the mixture was stirred at 0—5 °C overnight. After removal of the separated DCU by filtration, the filtrate was evaporated *in vacuo*. The resulting material was dissolved in ethyl acetate and the solution was washed consecutively with ice-cold M hydrochloric acid, water, 5% sodium hydrogencarbonate, and water, dried over magnesium sulfate, and evaporated *in vacuo*. The residue (23 g) was subjected to chromatography on a column (6.0×28 cm) of silicagel (350 g, Kieselgel 60, Merck) with chloroform as solvent. The fractions containing the desired material, as monitored by TLC with benzene-ethyl acetate (90:10) as solvent, were collected and evaporated *in vacuo* to give a sirupy residue, which crystallized upon prolonged standing *in vacuo*; 20.8 g (97%), mp 67—70 °C, $[\alpha]_D^{25}$ +8.4±0.5° (*c* 1.0, methanol). TLC: homogeneous in system D. Found: C, 47.79; H, 5.23; N, 3.27; Cl, 24.90%. Calcd for $C_{17}H_{22}NO_5Cl_3$: C, 47.85; H, 5.20; N, 3.28; Cl, 24.92%.

Z-D-Ser-OTce (5). Compound **4** (4.27 g, 10 mmol) was treated with TFA (20 ml) at 25 °C for 30 min. After evaporation of the TFA *in vacuo* the residue was dissolved in ethyl acetate and the solution was washed with 5% sodium hydrogencarbonate and water, dried over magnesium sulfate, and evaporated *in vacuo*. The oily residue was subjected to a Lobar column (size C) with chloroform-methanol (95:5) as solvent. The chromatography was repeated twice and the fractions containing the desired compound as a single component were collected. Removal of the solvent *in vacuo* yielded **5** as a sirupy residue; 2.97 g (80%), $[\alpha]_D^{25}$ +14.9±0.5° (*c* 1.2, methanol). TLC: homogeneous in system A. Found: C, 42.31; H, 3.78; N, 3.75; Cl, 28.44%. Calcd for $C_{13}H_{14}NO_5Cl_3$: C, 42.13; H, 3.81; N, 3.78; Cl, 28.70%.

Boc-MeVal-OH Piperidine Salt. To a suspension of *N*-methyl-L-valine (9.18 g, 70 mmol) in water (40 ml) containing TEA (22.3 ml, 160 mmol) was added a solution of Boc-SDP (25.2 g, 105 mmol) in dioxane (40 ml) and the mixture was stirred at 25 °C overnight. After addition of ice-cold M sodium hydroxide (100 ml) and washing with ether, the aqueous solution was then acidified with ice-cold M hydrochloric acid. The product separated was taken into ethyl acetate and the organic solution was washed with water, dried over magnesium sulfate and evaporated *in vacuo*. The resulting oil was dissolved in ether and to this was added piperidine (5.02 g, 59 mmol). After evaporation of the ether the residue was crystallized from petroleum ether (16.4 g, 74%). Recrystallization from ethyl acetate-petroleum ether afforded a pure preparation of the desired compound; 13.0 g (59%), mp 97—99 °C, $[\alpha]_D^{25}$ −69.9±1.1° (*c* 1.0, methanol). Found: C, 60.24; H, 10.08; N, 8.52%. Calcd for $C_{11}H_{21}NO_4 \cdot C_5H_{11}N$: C, 60.73; H, 10.19; N, 8.85%.

The same compound was obtained in 54% yield with Boc-N_3 as acylating agent.[29]

Z(OMe)-MeVal-OH Piperidine Salt. *N*-Methyl-L-valine (2.62 g, 20 mmol) was acylated with Z(OMe)-SDP (7.61 g, 25 mmol) as in the corresponding Boc-derivative to give the desired compound; 3.98 g (52%), mp 92—93 °C, $[\alpha]_D^{22}$ −62.7±1.0° (*c* 1.0, methanol). Found: C, 63.36; H, 8.65; N, 7.20%. Calcd. for $C_{15}H_{21}NO_5 \cdot C_5H_{11}N$: C, 63.14; H, 8.48; N, 7.36%.

Boc-MeCys(Bzl)-OH DCHA Salt. *N*-Methyl-*S*-benzyl-L-cysteine (13.5 g, 60 mmol) was acylated with Boc-SDP in water-dioxane (1:2) in a manner similar to that described for Boc-MeVal-OH to give the desired compound as the DCHA salt (28.5 g). The crude product was purified by repeated recrystallization from ethyl acetate-petroleum ether; 24.6 g (81%), mp 104—105 °C, $[\alpha]_D^{24.5}$ −56.0±1.0° (*c* 1, methanol). Found: C, 66.27; H, 9.27; N, 5.39; S, 6.47%. Calcd for $C_{16}H_{23}NO_4S \cdot C_{12}H_{23}N$: C, 66.37; H, 9.15; N, 5.53; S, 6.33%.

Z-D-Ser(Boc-MeVal)-OTce (6). The piperidine salt of Boc-MeVal-OH (2.78 g, 8.8 mmol) was converted into the free acid by the treatment with Dowex 50W×8 (H^+ form) in 50% ethanol at 25 °C for 30 min. Boc-MeVal-OH obtained was dissolved in pyridine (25 ml) together with **5** (2.96 g, 8 mmol) and HOBt (1.19 g, 8.8 mmol), and to this was added a solution of DCC (1.82 g, 8.8 mmol) in pyridine (2 ml) at 0 °C. The mixture was stirred at 4 °C overnight, followed by evaporation *in vacuo*. The residue was dissolved in ethyl acetate and, after removal of precipitates by filtration, the solution was washed consecutively with ice-cold M hydrochloric acid, water, 5% sodium hydrogencarbonate and water, dried over magnesium sulfate and evaporated *in vacuo* to give an oil (5.1 g). The crude product was subjected to chromatography on a Lobar column (size C) with chloroform-methanol (99:1) as solvent. The fractions containing the desired material, as monitored by TLC with system C, were collected and evaporated *in vacuo*. The partially purified material was repeatedly chromatographed on Lobar columns with benzene-ethyl acetate systems as solvent to give **6** as an oil; 3.21 g (69%), $[\alpha]_D^{25}$ −28.3±0.5° (*c* 1.4, methanol). TLC: homogeneous in systems A and C. Found: C, 49.40; H, 5.82; N, 4.72; Cl, 18.19%. Calcd for $C_{24}H_{33}N_2O_8Cl_3$: C, 49.37; H, 5.70; N, 4.80; Cl, 18.22%.

Z-D-Ser[Z(OMe)-MeVal]-OTce (6a). Compound **6a** was synthesized as described for **6** except for the use of Z(OMe)-MeVal-OH in place of Boc-MeVal-OH; yield 74% (oil), $[\alpha]_D^{24}$ −24.1±0.6° (*c* 1.0, methanol). TLC: homogeneous in systems A and D. Found: C, 51.64; H, 5.19; N, 4.27; Cl, 16.16%. Calcd for $C_{28}H_{33}N_2O_9Cl_3$: C, 51.90; H, 5.13; N, 4.32; Cl, 16.42%.

Z-D-Ser[Boc-MeCys(Bzl)-MeVal]-OTce (7). *a) From 6.* Compound **6** (7.30 g, 12.5 mmol) was treated with TFA (30 ml) at 25 °C for 30 min, followed by evaporation *in vacuo*. The resulting oil was dissolved in ethyl acetate and the solution was washed with 5% sodium hydrogencarbonate, dried over magnesium sulfate, and evaporated *in vacuo*. The residue was dissolved in THF (25 ml) together with Boc-MeCys(Bzl)-OH, derived from the DCHA salt (6.97 g, 13.8 mmol) by the treatment with Dowex 50W×8 (H^+ form) in 50% ethanol, and HOBt (1.86 g, 13.8 mmol), and after addition of DCC (2.84 g, 13.8 mmol) the mixture was stirred at 4 °C overnight. The reaction mixture was then worked up in the usual manner to give a crude product (10.5 g) which was repeatedly chromatographed on a Lobar column (size C) with chloroform-methanol (95:5) and benzene-ethyl acetate (9:1) as solvent. The fractions containing the desired product as a single component were collected and evaporated *in vacuo* to give **7** as an oil; 7.47 g (76%), $[\alpha]_D^{27}$ −81.8±1.1° (*c* 1.1, methanol). TLC: homogeneous in systems A and D. Found: C, 52.95; H, 5.99; N, 5.22; S, 4.27; Cl, 13.33%. Calcd for $C_{35}H_{46}N_3O_9SCl_3$: C, 53.13; H, 5.86; N, 5.31; S, 4.05; Cl, 13.44%.

b) From 6a. Compound **7** was also synthesized from **6a** in basically the same manner as described in a); 74%(oil), $[\alpha]_D^{25.5}$ −81.1±1.1° (*c* 1.1, methanol). Found: C, 52.76; H, 5.86; N, 5.14; S, 4.41; Cl, 13.37%.

Z-D-Ser[Boc-Ala-MeCys(Bzl)-MeVal]-OTce (8). Boc-Ala-OH (1.70 g, 9 mmol) was treated with DCC (0.93 g, 4.5 mmol) in THF at 0—5 °C for 2 h. Removal of the separated DCU by filtration afforded a solution of $(Boc\text{-}Ala)_2O$. On the other hand, compound **7** (2.37 g, 3.0 mmol) was treated with TFA (12 ml) at 25 °C for 30 min, followed by evaporation *in vacuo*. The residue was, after being dried over potassium hydroxide pellets under reduced pressure, dissolved in THF and the solution was chilled at 0 °C. To this were then added DIEA (2.5 ml) and the solution of $(Boc\text{-}Ala)_2O$ obtained above. The mixture was stirred at 0—5 °C overnight and then worked up in the usual manner. The crude preparation of **8** was chromatographed on a Lobar column

(size C) with benzene–ethyl acetate (8:2) as solvent. The fractions containing the desired material were pooled and evaporated *in vacuo* to give **8** as amorphous solid; 2.00 g (77%), $[\alpha]_D^{25.5}$ −96.5±1.4° (*c* 1.0, methanol). TLC: homogeneous in systems A and D. Found: C, 52.81; H, 6.02; N, 6.35; S, 3.95; Cl, 12.55%. Calcd for $C_{38}H_{51}N_4O_{10}SCl_3$: C, 52.93; H, 5.96; N, 6.50; S, 3.72; Cl, 12.33%.

Unexpected Formation of Z-D-Ser[isobutoxycarbonyl-MeCys-(Bzl)-MeVal]-OTce. Boc-Ala-OH (0.23 g, 1.2 mmol) was dissolved in anhydrous THF (3 ml) and DIEA (0.21 ml, 1.2 mmol) was added. The solution was chilled to −10 °C and to this was added isobutyl chloroformate (0.16 ml, 1.2 mmol). The mixture was stirred for 1 min, after which there was added a solution of Z-D-Ser[H-MeCys(Bzl)-MeVal]-OTce TFA salt derived from **7** by the treatment with TFA as described in the prepation of **8**. The reaction mixture was stirred at 5 °C overnight and then worked up as usual. The crude product was chromatographed on a Lobar column (size B) with benzene–ethyl acetate (9:1) as solvent. The fractions containing the major product as a single component were collected, washed with water, and evaporated *in vacuo* to give an oily material; 0.71 g (90% as Z-D-Ser[isobutoxycarbonyl-MeCys(Bzl)-MeVal]-OTce), $[\alpha]_D^{25.5}$ −84.6±1.2° (*c* 1.0, methanol). TLC: homogeneous in systems A and D. Found: C, 52.83; H, 5.99; N, 5.20; S, 4.44; Cl, 13.34%. Calcd for $C_{35}H_{46}N_3O_9SCl_3$: C, 53.13; H, 5.86; N, 5.31; S, 4.05; Cl, 13.44%.

Z-D-Ser[Boc-Ala-MeCys(Bzl)-MeVal]-OH (1). Compound **8** (2.59 g, 3.0 mmol) was dissolved in 90% acetic acid (66 ml) and chilled in an ice-bath. To this was added zinc powder (9.8 g) and the mixture was stirred at 0 °C for 3 h. After the excess zinc had been filtered off, the filtrate was evaporated *in vacuo*. To the residue was added ethyl acetate and the mixture was washed with M hydrochloric acid and with water, dried over magnesium sulfate, and evaporated *in vacuo* to give a solid residue (1.6 g). The crude product was purified on a column of silica gel (110 g, Kieselgel H, Merck) with chloroform–methanol–acetic acid (99:1:1) as solvent to give compound **1** as amorphous solid; 1.97 g (90%), $[\alpha]_D^{25}$ −124.9±0.6° (*c* 1.0, methanol). TLC: homogeneous in systems B and E. Found: C, 59.16; H, 6.90; N, 7.67; S, 4.39%. Calcd for $C_{36}H_{50}N_4O_{10}S$: C, 59.42; H, 7.21; N, 7.68; S, 4.42%.

Z-D-Ser{Z-D-Ser[Boc-Ala-MeCys(Bzl)-MeVal]-Ala-MeCys-(Bzl)-MeVal}-OTce (9). Compound **8** (2.16 g, 2.5 mmol) was treated with TFA (25 ml) at 25 °C for 30 min, followed by evaporation *in vacuo*. The oily residue was dissolved in ethyl acetate and the solution was shaken with ice-cold 50% potassium carbonate, dried over magnesium sulfate and evaporated *in vacuo* to give Z-D-Ser[H-Ala-MeCys(Bzl)-MeVal]-OTce (**2**) as an oil. Compound **2** was dissolved in THF (50 ml) together with compound **1** (1.83 g, 2.5 mmol) and HOBt (0.51 g, 3.75 mmol) and to this solution was added DCC (0.77 g, 3.75 mmol) at 0 °C. The mixture was stirred at 5 °C overnight and then worked up in the usual manner. The crude product was chromatographed on a silica-gel column (Kieselgel 60, 5×16 cm) with chloroform–methanol (99:1) and then on a Lobar column (size C) with benzene–ethyl acetate (9:1) as solvent to give the linear octadepsipeptide (**9**) as amorphous solid; 3.21 g (87%), $[\alpha]_D^{25}$ −115.0±1.5° (*c* 1.0, methanol). TLC: homogeneous in systems A, B, D, and E. Found: C, 55.97; H, 6.25; N, 7.52; S, 4.65; Cl, 7.40%. Calcd for $C_{69}H_{91}N_8O_{17}S_2Cl_3$: C, 56.19; H, 6.22; N, 7.60; S, 4.35; Cl, 7.21%.

Z-D-Ser{Z-D-Ser[Boc-Ala-MeCys(Bzl)-MeVal]-Ala-MeCys-(Bzl)-MeVal}-OH (10). To a solution of **9** (3.54 g, 2.4 mmol) in 90% acetic acid (120 ml) was added zinc powder (7.85 g) at 0 °C and the mixture was stirred at 0 °C for 3 h. After removal of the excess zinc by filtration the solvent was evaporated *in vacuo*. The resulting oily residue was dissolved in ethyl acetate, washed with ice-cold M hydrochloric acid and water, dried over magnesium sulfate, and evaporated *in vacuo* to give a solid residue. This crude product was chromatographed on a silica-gel column (Kieselgel H, 6×20 cm) with chloroform–methanol–acetic acid (98:2:0.5) as solvent. The fractions containing the desired material were pooled, washed with water, dried over magnesium sulfate, and evaporated *in vacuo* to give **10** as amorphous solid; 3.03 g (94%), $[\alpha]_D^{25}$ −132.2±1.8° (*c* 1.0, methanol). TLC: homogeneous in systems B and E. Found: C, 59.88; H, 6.87; N, 8.11; S, 4.78%. Calcd for $C_{67}H_{90}N_8O_{17}S_2$: C, 59.89; H, 6.75; N, 8.34; S, 4.64%.

{Z-D-Ser[Z-D-Ser-Ala-MeCys(Bzl)-MeVal]-Ala-MeCys(Bzl)-MeVal}Dilactone, N,N′-Z$_2$-S,S′-Bzl$_2$-Dihydroapotriostin A (11). *a) By the Active Ester Method.* Compound **10** (0.269 g, 0.2 mmol) and HOSu (0.230 g, 2 mmol) were dissolved in THF (6 ml) and chilled in an ice-bath. To this was added DCC (0.413 g, 2 mmol) and the mixture was stirred at 0—5 °C for 3 h and at 25 °C for 2 h. The DCU which had formed was filtered off and the filtrate was evaporated *in vacuo* to give a residue which was then treated with TFA (10 ml) at 25 °C for 30 min, followed by evaporation *in vacuo*. The residue was, after being dried over sodium hydroxide pellets *in vacuo*, dissolved in ethyl acetate (1000 ml) and to this was added DIEA until the solution became neutral as checked with a piece of wetted pH indicator paper (Whatman). The reaction mixture was stirred at 25 °C for 3 h and, after concentration to a small volume, washed with M hydrochloric acid, water, and 5% sodium hydrogencarbonate, dried over magnesium sulfate, and evaporated *in vacuo*. The same cyclization reaction was carried out six times with 0.285 mmol each of compound **10** as starting material. The resulting crude product combined (4.4 g from 1.91 mmol of **10**) was chromatographed on a column (4×49 cm) of silica-gel (270 g, Kieselgel 60) with chloroform–methanol (98:2) as solvent. The fractions containing the desired material were combined and evaporated *in vacuo*. The residue was rechromatographed on a Lobar column (size C) with benzene–ethyl acetate (1:1) to give the title compound as amorphous solid; 1.36 g (58%), $[\alpha]_D^{23}$ −124.8±3.1° (*c* 0.5, methanol). NMR ($CDCl_3$, 360 MHz) δ=0.51 (d, 6H, MeVal γ- or γ′-CH_3), 0.71 (d, 6H, MeVal γ- or γ′-CH_3), 0.74 (d, 6H, Ala β-CH_3), 2.18 (m, 2H, MeVal β-CH), 2.47, 2.53 (m, 4H, MeCys β- and β′-CH_2), 2.82 (s, 6H, N-CH_3), 2.88 (s, 6H, N-CH_3), 3.42 (d, 2H, Bzl S-CH), 3.50 (d, 2H, MeVal α-CH), 3.67 (d, 2H, Bzl S-CH), 4.59 (m, 2H, Ser β-CH_2), 4.74 (m, 2H, Ala α-CH), 4.75 (m, 2H, Ser β-CH_2), 4.87 (m, 2H, Ser α-CH), 4.91 (d, 2H, Bzl O-CH_2), 5.40 (d, 2H, Bzl O-CH_2), 5.57 (m, 2H, MeCys α-CH), 7.2—7.4 (m, 20H, Bzl aromatic), 7.71 (d, 2H, Ala NH), and 8.22 (d, 2H, Ser NH). FD-MS: M^+ 1224. TLC: homogeneous in systems A and D. Found: C, 60.09; H, 6.57; N, 9.00; S, 4.85%. Calcd for $C_{62}H_{80}N_8O_{14}S_2$: C, 60.77; H, 6.58; N, 9.14; S, 5.23%.

b) By the DCC-HOBt Method. To a solution of **10** (0.336 g, 0.25 mmol) in dioxane (2.5 ml) was added 4 M hydrogen chloride in dioxane (10 ml) and the mixture was kept at 25 °C for 60 min, followed by evaporation *in vacuo*. The oily residue was dissolved in THF (125 ml) and to this were added HOBt (0.338 g, 2.5 mmol) and DIEA (0.09 ml, 0.5 mmol). After the subsequent addition of DCC (0.516 g, 2.5 mmol), the mixture was stirred at 25 °C for 44 h and then evaporated *in vacuo*. The residue was dissolved in ethyl acetate and the solution was filtered off and evaporated. The crude product was purified on a column (3.3×16 cm) of silica gel (50 g, Kieselgel H) with chloroform–methanol (95:5) as solvent. Rechromatography on a Lobar column (size B) in benzene–ethyl acetate (1:1) yielded **11** as amorphous solid; 0.064 g (21%), mp 100—102 °C, $[\alpha]_D^{25}$ −123.9±3.1° (*c* 0.5, methanol). Found: C, 60.73; H, 6.29; N, 8.84; S, 5.37%.

c) By the DPPA Method. Compound **10** (0.269 g, 0.2 mmol) was treated with hydrogen chloride in dioxane in the same manner as described above. The product was dissolved in DMF (100 ml) and chilled in ice. To this were then added DIEA (0.24 ml, 1.4 mmol) and DPPA (0.275 g, 1.0 mmol) and the mixture was stirred at 0 °C for 6 h. The crude product was purified on silica-gel columns in almost the same manner as described in b) to give purified **11** as amorphous solid; 0.053 g (22%), $[\alpha]_D^{22}$ −125.7±3.3° (*c* 0.5, methanol). Found: C, 60.28; H, 6.73; N, 8.66; S, 5.57%.

{Qxc-D-Ser[QxC-D-Ser-Ala-MeCys(Bzl)-MeVal]-Ala-MeCys-(Bzl)-MeVal}Dilactone, S,S'-Bzl$_2$-Dihydrotriostin A (12). Compound **11** (123 mg, 0.1 mmol) and thioanisole (1.2 ml) were dissolved in TFA (12 ml) and the mixture was kept at 25 °C for 6 h. Evaporation of the TFA *in vacuo* afforded an oily residue, which was dried over sodium hydroxide pellets *in vacuo*. The residue was then precipitated from ether-petroleum ether to give the TFA salt of *S,S'*-dibenzyldihydroapotriostin A as amorphous solid. TEA (0.028 ml, 0.2 mmol) was added to a stirred ice-cold solution of this solid in DMF (1 ml) and to this were then added Qxc-Cl (58 mg, 0.3 mmol) and TEA (0.056 ml, 0.4 mmol) simultaneously in three equal portions over 30 min. The reaction mixture was stirred at 0 °C for 6 h. The formation of **12** was 27, 30, 34, 36, and 37% at reaction time of 1, 2, 3, 4, and 6 h, respectively, as monitored by HPLC (Waters μ-Porasil, 3.9×300 mm; 2-propanol-hexane (27.5:72.5)). After dilution with ethyl acetate the mixture was successively washed with M hydrochloric acid, water, and 5% sodium hydrogencarbonate, dried over magnesium sulfate, and evaporated *in vacuo*. The residue was chromatographed on a column (1.7×22 cm) of silica-gel (20 g, Kieselgel H) with chloroform-methanol (99:1) and repeatedly rechromatographed on a Lobar column (size A) with ethyl acetate and with chloroform-methanol (99:1) as solvent. The resulting material was dissolved in ethyl acetate and the solution was washed with water, dried over magnesium sulfate and evaporated *in vacuo* to afford a pure preparation of **12**; 0.028 g (22%), $[\alpha]_D^{22.5}$ −152.6±1.9° (*c* 1.0, chloroform). NMR ($CDCl_3$, 360 MHz; I=conformer I, II=conformer II); δ=0.67 (d, 6H, MeVal γ- or γ'-CH_3, I), 0.78 (d, 6H, MeVal γ- or γ'-CH_3, I), 0.83 (d, 6H, MeVal γ- or γ'-CH_3, II), 1.09 (d, 6H, MeVal γ- or γ'-CH_3, II), 1.28 (d, 6H, Ala β-CH_3, I), 1.38 (d, 6H, Ala β-CH_3, II), 2.19 (m, 2H, MeVal β-CH, I), 2.36 (m, 2H, MeVal β-CH, II), 2.66, 2.67 (m, 4H, MeCys β- and β'-CH_2, I), 2.92, 2.99 (m, 4H, MeCys β- and β'-CH_2, II), 2.81, 2.89, 3.03, 3.12 (s, 12H, N-CH_3, I and II), 3.54, 3.80 (m, 8H, Bzl S-CH_2, I and II), 3.92 (m, 2H, MeVal α-CH, I), 4.38 (m, 2H, Ser β-CH_2, II), 4.41 (m, 2H, Ser β-CH_2, I), 4.59 (m, 2H, Ser β'-CH_2, II), 4.82 (m, 2H, Ala α-CH, II), 4.85 (m, 2H, Ser β'-CH_2, I), 5.02 (m, 2H, Ala α-CH, I), 5.13 (m, 2H, MeVal α-CH, II), 5.25 (m, 2H, Ser α-CH, I), 5.39 (m, 2H, MeCys α-CH, I), 7.07 (d, 2H, Ala NH, II), 7.2—7.4 (m, 10H, Bzl aromatic, I and II), 7.81, 7.89, 8.11, 8.22 (m, 8H, Qxc, I and II), 8.46 (d, 2H, Ala NH, I), 8.77 (d, 2H, Ser NH, II), 8.80 (d, 2H, Ser NH, I), 9.62 (s, 2H, Qxc 3-CH, I), and 9.67 (s, 2H, Qxc 3-CH, II). TLC: homogeneous in system A. Found: C, 59.43; H, 6.01; N, 12.82; S, 5.32%. Calcd for $C_{64}H_{76}N_{12}O_{12}S_2 \cdot H_2O$: C, 59.70; H, 6.11; N, 13.05; S, 4.98%.

Triostin A. Compound **12** (38.1 mg, 0.03 mmol) was treated with HF (6 ml) in the presence of anisole (0.3 ml) at 25 °C for 60 min. After the HF had been removed by evaporation, the residue was dissolved in methanol (30 ml) and the solution was neutralized with TEA. To this was added a solution of iodine (39 mg, 0.15 mmol) in methanol (2 ml) and the mixture was stirred at 25 °C for 2 h. The excess iodine was discharged with M sodium thiosulfate, in which the pH was kept neutral by the addition of 10% ascorbic acid. After removal of the solvent by evaporation *in vacuo*, the residue was purified on a silica-gel column (Kieselgel H, 1.7×23.5 cm) with chloroform-methanol (98:2) as solvent. The fractions containing the desired product were pooled and evaporated *in vacuo*. The resulting residue (9.8 mg) was crystallized from carbon tetrachloride-ethanol and recrystallized twice from dichloromethane-ethanol to afford pure triostin A; 7.0 mg (20%), mp 222—223 °C, $[\alpha]_D^{21.5}$ −151.9±19.8° (*c* 0.1, chloroform). The authentic sample of natural triostin A showed mp 220—223 °C. Lit. for natural triostin A:[3b,11] mp 245—248 °C dec, $[\alpha]_D^{23.5}$ −157±2° (*c* 0.97, chloroform). Lit, for synthetic triostin A:[16] mp 239—243 °C dec, $[\alpha]_D^{25}$ −154° (*c* 1.0, chlorofororm). λ_{max}^{MeOH} 243 nm (log ε 4.92), 317 nm (4.15), 325 nm (4.16). NMR: see Fig. 4. TLC: homogeneous in system A. HPLC: see Fig. 5. Found: C, 51.99; H, 5.89; N, 14.36; S, 6.05%. Calcd for $C_{50}H_{62}N_{12}O_{12}S_2 \cdot 3.5H_2O$: C, 52.21; H, 6.05; N, 14.61; S, 5.57%.

The authors express their sincere thanks to Professor Yoshimasa Kyogoku and Dr. Naoki Higuchi, Institute for Protein Research, Osaka University, for measurements and analysis of 360 MHz NMR spectra. Thanks are also due to Dr. Jun'ichi Shoji, Shionogi Research Laboratories, for generous gift of natural triostin A and for help with microbiological assays.

References

1) Part I: M. Shin, K. Inouye, and H. Otsuka, *Bull. Chem. Soc. Jpn.*, **51**, 1501 (1978).

2) This work was presented at the 18th Symposium on Peptide Chemistry, Nishinomiya, November 16, 1980. M. Shin, K. Inouye, H. Otsuka, N. Higuchi, and Y. Kyogoku, In: Peptide Chemistry 1980," ed by K. Okawa, Protein Research Foundation, Osaka (1981), p. 207.

3) a) Isolation: J. Shoji and K. Katagiri, *J. Antibiot.*, **A14**, 335 (1961). b) Structure: H. Otsuka and J. Shoji, *ibid.*, **A16**, 52 (1963); J. Shoji, K. Tori, and H. Otsuka, *J. Org. Chem.*, **30**, 2772 (1965); H. Otsuka and J. Shoji, *J. Antibiot.*, **A18**, 134 (1965); H. Otsuka and J. Shoji, *Tetrahedron*, **21**, 2931 (1965); **23**, 1535 (1967).

4) K. Katagiri, T. Yoshida, and K. Sato, "Antibiotics," ed by J. W. Corcoran and F. E. Hahn, Springer-Verlag, Heidelberg (1975), Vol. 3, p. 234 and references cited therein.

5) T. Yoshida and K. Katagiri, *J. Antibiot.*, **A14**, 330 (1961).

6) a) R. Corbaz, L. Ettlinger, E. Gäumann, W. Keller-Schierlein, F. Kradolfer, L. Neipp, V. Prelog, P. Reusser, and H. Zähner, *Helv. Chim. Acta*, **40**, 199 (1957); b) W. Keller-Schierlein and V. Prelog, *ibid.*, **40**, 205 (1957); c) W. Keller-Schierlein, M. Lj. Mihailović, and V. Prelog, *ibid.*, **42**, 305 (1959); d) D. G. Martin, S. A. Mizsak, C. Biles, J. C. Stewart, L. Baczynskyj, and P. A. Meulman, *J. Antibiot.*, **28**, 332 (1975); e) A. Dell, D. H. Williams, H. R. Morris, G. A. Smith, J. Feeney, and G. C. K. Roberts, *J. Am. Chem. Soc.*, **97**, 2497 (1975).

7) M. Kuroya, N. Ishida, K. Katagiri, J. Shoji, T. Yoshida, M. Mayama, K. Sato, S. Matsuura, Y. Niinomi, and O. Shiratori, *J. Antibiot.*, **A14**, 324 (1961).

8) S. Matsuura, *J. Antibiot.*, **A18**, 43 (1965).

9) a) M. J. Waring and L. P. G. Wakelin, *Nature*, **252**, 653 (1974); b) L. P. G. Wakelin and M. J. Waring, *Biochem. J.*, **157**, 721 (1976).

10) a) M. Waring and A. Markoff, *Mol. Pharmacol.*, **10**, 214 (1974); b) G. G. Gauge, Jr., N. P. Loshkareva, and I. B. Zbarsky, *Biochim. Biophys. Acta*, **166**, 752 (1968).

11) H. Otsuka, J. Shoji, K. Kawano, and Y. Kyogoku, *J. Antibiot.*, **29**, 107 (1976).

12) T. J. Blake, J. R. Kalman, and D. H. Williams, *Tetrahedron Lett.*, **1977**, 2621.
13) J. R. Kalman, T. J. Blake, D. H. Williams, J. Feeney, and G. C. K. Roberts, *J. Chem. Soc., Perkin 1*, **1979**, 1313.
14) K. Kawano, N. Higuchi, and Y. Kyogoku, In: "Peptide Chemistry 1976," Proceedings of the 14th Symposium on Peptide Chemistry, Hiroshima, 1976, ed by T. Nakajima, Protein Research Foundation (1977), p. 93.
15) a) Y. Kyogoku and N. Higuchi, *Biopolymers*, **20**, 1957 (1981); b) N. Higuchi, Y. Kyogoku, M. Shin, K. Inouye, and H. Otsuka, "Peptide Chemistry 1980," Proceedings of the 18th Symposium on Peptide Chemistry, Nishinomiya, 1980, ed by K. Okawa, Protein Research Foundation (1981), p. 95.
16) P. K. Chakravarty and R. K. Olsen, *Tetrahedron Lett.*, **1978**, 1613.
17) a) T. L. Ciardelli, P. K. Chakravarty, and R. K. Olsen, *J. Am. Chem. Soc.*, **100**, 7684 (1978); b) T. L. Ciardelli and R. K. Olsen, *ibid.*, **99**, 2806 (1977).
18) M. K. Dhaon and R. K. Olsen, *J. Org. Chem.*, **46**, 3436 (1981).
19) E. Schröder, *Justus Liebigs Ann. Chem.*, **670**, 127 (1963).
20) For the Tce ester see: R. B. Woodward, K. Heusler, J. Gosteli, P. Naegeli, W. Oppolzer, R. Ramage, S. Rangnathan, and H. Vorbrüggen, *J. Am. Chem. Soc.*, **88**, 852 (1966).
21) W. König and R. Geiger, *Chem. Ber.*, **103**, 788 (1970).
22) B. Marinier, Y. C. Kim, and J. M. Navarre, *Can. J. Chem.*, **51**, 208 (1973).
23) Y. Kiso, K. Ukawa, and T. Akita, *J. Chem. Soc., Chem. Commun.*, **1980**, 101.
24) H. C. Koppel, I. L. Honigberg, R. H. Springer, and C. C. Chen, *J. Org. Chem.*, **28**, 1119 (1963).
25) a) B. Kamber, *Helv. Chim. Acta*, **54**, 927 (1971); b) U. Ludescher and R. Schwyzer, *ibid.*, **55**, 2052 (1972).
26) T. Shioiri, K. Ninomiya, and S. Yamada, *J. Am. Chem. Soc.*, **94**, 6203 (1972); T. Shioiri and S. Yamada, *Chem. Pharm. Bull.*, **22**, 849, 855, 859 (1974).
27) P. Quitt, J. Hellerbach, and K. Vogler, *Helv. Chim. Acta*, **46**, 327 (1963).
28) D. Yamashiro, H. L. Aanning, L. A. Branda, W. D. Cash, V. V. S. Murti, and V. du Vigneaud, *J. Am. Chem. Soc.*, **90**, 4141 (1968).
29) S. Moore, R. P. Patel, E. Atherson, M. Kondo, J. Meienhofer, L. Blau, R. Bittman, and R. K. Johnson, *J. Med. Chem.*, **19**, 766 (1976).

Synthetic Studies on Quinoxaline Antibiotics. III.[1] Synthesis of Nortriostin A, a Triostin A Analog Lacking *N*-Methyl Groups on the Cystine and Valine Residues

Masaru SHIN,* Ken INOUYE, Naoki HIGUCHI,†,†† and Yoshimasa KYOGOKU†

Shionogi Research Laboratories, Shionogi & Co., Ltd., Fukushima-ku, Osaka 553

†*Institute for Protein Research, Osaka University, Yamadaoka, Suita, Osaka 565*

(Recieved February 3, 1984)

Nortriostin A, which is an analog of a cyclic octadepsipeptide antibiotic triostin A and contains one cystine and two valine residues substituted for the *N,N'*-dimethylcystine and *N*-methylvaline residues of the antibiotic, was synthesized with Z-D-Ser[Boc-Ala-Cys(MeBzl)-Val]-OH and Z-D-Ser[H-Ala-Cys(MeBzl)-Val]-OTce as key intermediates.††† The synthetic analog showed no antimicrobial activity at a concentration of 100 μg/ml and was found to exist as a single structure in solution as examined by ^{1}H-NMR spectroscopy. The latter observation suggests that the conformer equilibrium known to occur with triostin A is a consequence of the presence of *N*-methyl peptide bonds in the antibiotic molecule.

In the preceding paper we described the total synthesis of triostin A, a member of the triostin family of the quinoxaline antibiotics, with *S,S'*-dibenzyldihydrotriostin A as intermediate.[1] Triostin A is known to have two interconvertible conformations in solution and their occurrence has been explained by two possibilities: 1) the reversal of the chirality around the disulfide bond,[2] and 2) the *cis-trans* isomerization of the *N*-methyl peptide bonds.[3] The first possibility has recently been ruled out, because the presence of the two conformers was also shown with *S,S'*-dibenzyldihydrotriostin A which lacks the disulfide bond.[1,4] In the present work the des-*N*-tetramethyl analog of triostin A (we propose the name "nortriostin A" for des-N-tetramethyltriostin A.[5] For structure, see Fig. 1) was synthesized and its NMR pattern was compared with that of triostin A to elucidate the second possibility. The synthesis of nortriostin A was carried out in essentially the same manner as described for triostin A,[1] except that the *N*-methyl-L-cysteine and *N*-methyl-L-valine as starting materials were replaced by cysteine and valine, respectively, and the 4-methylbenzyl group[6] in place of the benzyl group was employed for the mercapto-group protection.

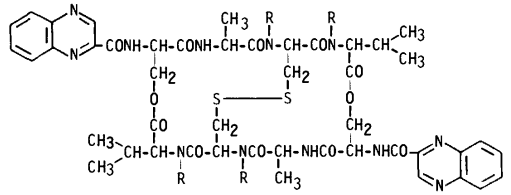

Triostin A: R=CH$_3$

Nortriostin A: R=H

Fig. 1. Triostin A and nortriostin A.

Z-D-Ser-OTce[1] was allowed to react in pyridine in the presence of HOBt with the symmetrical anhydride $(Boc\text{-}Val)_2O$, which had been prepared in advance from Boc-Val-OH by the action of DCC, to give a depsipeptide Z-D-Ser(Boc-Val)-OTce (**3**) in a 90% yield. Compound **3** could also be prepared by the direct coupling of Boc-Val-OH and Z-D-Ser-OTce with DCC in the presence of HOBt, but the yield was as low as 66%. Compound **3** was treated with TFA to remove the Boc group and then coupled with Boc-Cys(MeBzl)-OH (**2**) by the DCC-HOBt method[7] to give Z-D-Ser[Boc-Cys(MeBzl)-Val]-OTce (**4**) in 78% yield. Compound **4** was treated with TFA and the resulting product was coupled with the previously prepared

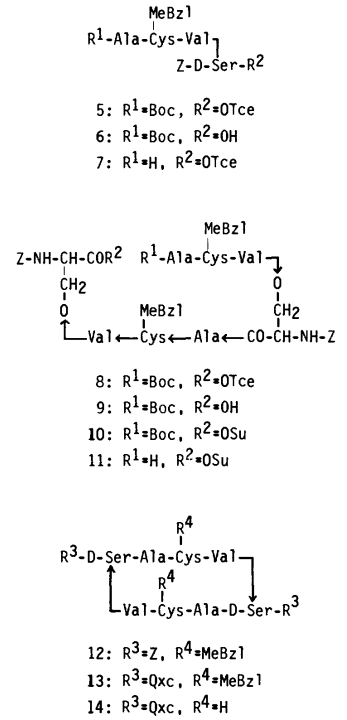

5: R^1=Boc, R^2=OTce
6: R^1=Boc, R^2=OH
7: R^1=H, R^2=OTce

8: R^1=Boc, R^2=OTce
9: R^1=Boc, R^2=OH
10: R^1=Boc, R^2=OSu
11: R^1=H, R^2=OSu

12: R^3=Z, R^4=MeBzl
13: R^3=Qxc, R^4=MeBzl
14: R^3=Qxc, R^4=H

Fig. 2. Intermediates involved in the synthesis of nortriostin A.

†† Present address: Suntory Research Center of Applied Microbiology, Shimamoto-cho, Mishima, Osaka 618.

††† Abbreviations used are those recommended by the IUPAC-IUB Commission on Biochemical Nomenclature (*Biochemistry*, **11**, 1726 (1972)) and include: MeCys, *N*-methyl-L-cysteine; MeVal, *N*-methyl-L-valine; Boc, *t*-butoxycarbonyl; Boc-SDP, *O-t*-butyl *S*-(4,6-dimethyl-2-pyrimidinyl) thiocarbonate; Qxc, 2-quinoxalylcarbonyl; Z, benzyloxycarbonyl; MeBzl, 4-methylbenzyl; Bzl, benzyl; Tce, 2,2,2-trichloroethyl; HOBt, 1-hydroxybenzotriazole; HOSu, *N*-hydroxysuccinimide; DCC, dicyclohexylcarbodiimide; DCU, *N,N'*-dicyclohexylurea; AcOH, acetic acid; TFA, trifluoroacetic acid; DIEA, *N,N*-diisopropylethylamine; TEA, triethylamine; DMF, *N,N*-dimethylformamide; and THF, tetrahydrofuran.

$(Boc\text{-}Ala)_2O$ in the presence of DIEA to produce tetradepsipeptide **5** (for structures of compounds **5**—**14**, see Fig. 2) in 66% yield.

One portion of the key intermediate **5** was treated with zinc in 90% acetic acid to remove the Tce ester giving **6** in a yield of 89%. Another portion of **5** was treated with TFA to remove the Boc group giving **7**. Compounds **6** and **7** were then coupled with DCC-HOBt to obtain the linear octadepsipeptide **8** in 72% yield. The treatment of **8** with zinc in 90% acetic acid at 0 °C for 3 h resulted in complete removal of the Tce ester giving **9** in 84% yield. Compound **9** was coupled to HOSu with DCC and the resulting active ester (**10**) was treated with TFA to give **11** as the TFA salt. For cyclization a DMF solution of **11** was diluted with ethyl acetate to a concentration of 0.2 mmol/l and neutralized with DIEA to initiate the reaction. The cyclic octadepsipeptide (**12**) was thus obtained in 48% yield. The ^{1}H-NMR spectrum and field desorption mass spectrum of **12** were consistent with the proposed structure.

The selective removal of the Z group from **12** by the TFA–thioanisole treatment[1,8] and the subsequent acylation with Qxc-Cl gave **13** as amorphous solid in 40% yield. The MeBzl groups on the Cys residues showed no sign of cleavage during the TFA–thioanisole treatment, but they were readily removed by the treatment with HF at 0 °C for 60 min in the presence of anisole to furnish dihydronortriostin A (**14**), which was, upon treatment with iodine in methanol[9] followed by silica-gel column chromatography and recrystallization, converted into nortriostin A (Fig. 1) in a yield of 40%.

Nortriostin A thus obtained was homogeneous in TLC in different solvent systems. The sufficient purity was also shown by HPLC on a μ-Porasil column in acetonitrile–2-propanol (95:5, v/v) and by reversed-phase HPLC on a Nucleosil $5C_{18}$ column in acetonitrile–10 mM (1M=1 mol dm^{-3}) phosphoric acid (50:50, v/v). The ^{1}H-NMR spectrum was consistent with the proposed structure when analyzed with reference to the spectra of natural[10] and synthetic[1] preparations of triostin A. As assayed for the inhibition of growth of *Bacillus subtilis* PCI-219, nortriostin A was found to be inactive even at a concentration of 100 μg/ml in contrast to triostin A, which was highly active at a level of 0.5 μg/ml.

The first synthesis of nortriostin A was described by Olsen and his associates in 1978,[5] in which they used the depsipeptide of the type Z-D-Ser(R^1)-Ala-OR^2 (R^1=Boc (or H)-Cys(Acm)-Val, R^2=H or Tce, Acm=acetamidomethyl) as intermediate. In this synthesis a problem was the occurrence of some racemization at the Ala residue involved in the fragment coupling and the subsequent cyclization reactions. In their recent report Olsen and his collaborators have synthesized nortriostin A from the depsipeptide of the type Z-D-Ser(R^1)-OR^2 (R^1=Boc (or H)-Ala-Cys(Acm)-Val, R^2=H or Bpa, Bpa=*p*-bromophenacyl).[11] Independently, we also used the latter type of intermediates in our synthesis of triostin A itself,[1] and in the present synthesis of nortriostin A as described above. In these syntheses the coupling of the two tetradepsipeptide intermediates and the subsequent cyclization were performed by activation of the carboxyl function of the Z-D-Ser-OH moiety. Therefore, little or no racemization was expected to occur at the Ser residue under ordinary coupling conditions. However, Olsen and his collaborators suggested the possibility of racemization of the D-Ser residues, based on the findings that the carbodiimide-mediated acylation of Z-D-Ser-OBpa with Boc-Val-OH in the presence of 4-(dimethylamino)pyridine and the acidolytic removal of the Boc group from Z-D-Ser[Boc-Ala-Cys(Acm)-Val]-OBpa followed by neutralization with sodium hydrogencarbonate were both accompanied by some formation of a dehydroalanine derivative Z-ΔAla-OBpa.[11] The Bpa ester was introduced in place of the Tce ester, which had been used in the form Z-D-Ser(R^1)-Ala-OTce in their previous synthesis of nortriostin A, because they were not able to prepare Z-D-Ser-OTce from Z-D-Ser-OH and HOTce by the DCC procedure. We also failed in this attempt but found that the esterification was readily achieved by using Z-D-Ser(Bu^t)-OH in place of Z-D-Ser-OH to give Z-D-Ser(Bu^t)-OTce, from which Z-D-Ser-OTce was derived by the TFA treatment.[1] Z-D-Ser-OTce was used as starting material in our synthesis of triostin A[1] and in the present synthesis of nortriostin A as described. Although the Tce group seems to be more favorable than the Bpa group because of the general trend that the former group is cleaved more readily than the latter under the reductive conditions, there is no available information as to whether the Tce group differs from the Bpa group regard to the effect on the dehydroalanine formation. At least we have no positive evidence for the formation of any dehydroalanine derivatives and for the occurrence of recemization.

The ^{1}H-NMR spectrum of nortriostin A was measured in deuteriochloroform to show that the hydrogens at position 3 of the two quinoxaline rings gave a single peak, indicating that nortriostin A, which differs from triostin A only by the absence of the *N*-methyl groups, exists as a single structure in solution. On the other hand, we have demonstrated that *S,S'*-dibenzyl-dihydrotriostin A, a derivative of triostin A which lacks the disulfide linkage but has the *N*-methyl peptide bonds, exists as two conformers.[1,4] These observations strongly support the view that the conformer equilibrium, which usually occurs with triostin A, is a consequence of the *cis-trans* isomerization of the *N*-methyl peptide bonds.[12]

Experimental

Thin-layer chromatography (TLC) was performed on silica-gel plates (precoated Kieselgel $60F_{254}$, Merck) with the following solvent systems (ratios by volume): A, chloroform–methanol (95:5); B, chloroform–methanol (90:10); C, chloroform–methanol–acetic acid (95:5:3); D, benzene–ethyl acetate (7:3). For detection the plates were subjected to ninhydrin staining or to sulfuric acid charring. Column chromatography was performed on prepacked columns (Lobar, size B or C, Merck) or home-made columns (Kieselgel 60, Merck). High-performance liquid chromatography (HPLC) was carried out on a Waters Associates Model 6000A solvent delivery system, equipped with a Waters U6K injector and a Japan Spectroscopic UVIDEC-100-II variable

wavelength UV detector. Proton NMR spectra were measured on a Bruker WM 360 wb NMR spectrometer operated at 360 MHz.

S-4-Methylbenzyl-cysteine (1). This compound was synthesized according to the literature;[6] mp 212—214 °C dec, $[\alpha]_D^{22}$ −4.1±1.4°, $[\alpha]_{365}^{22}$ +9.8±1.6° (*c* 0.3, M hydrochloric acid), $[\alpha]_D^{22}$ +23.7±0.9°, $[\alpha]_{365}^{22}$ +96.1±1.3° (*c* 1.0, M sodium hydroxide). Lit,[6] mp 209—211 °C dec.

Boc-Cys(MeBzl)-OH (2). To a solution of compound **1** (7.89 g, 35 mmol) and TEA (11 ml, 79 mmol) in dioxane-water (1:1, 40 ml) was added Boc-SDP (12.62 g, 53 mmol) and the mixture was stirred at 30 °C for 15 h. After addition of M sodium hydroxide (60 ml) at 0 °C the mixture was extracted twice with ether. The aqueous phase was then acidified with ice-cold M hydrochloric acid. The resulting oily precipitate was taken into ethyl acetate and the solution was washed with water, dried over magnesium sulfate and evaporated *in vacuo* to give an oil which was solidified by the addition of petroleum ether. Recrystallization from ethyl acetate-petroleum ether gave **2** as needles; 10.8 g (95%), mp 76—77 °C, $[\alpha]_D^{19}$−41.7±0.8 (*c* 1.0, acetic acid). Found: C, 58.89; H, 6.98; N, 4.25; S, 9.83%. Calcd for $C_{16}H_{23}NO_4S$: C, 59.05; H, 7.12; N, 4.30; S, 9.85%.

Z-D-Ser(Boc-Val)-OTce (3). *a) With (Boc-Val)$_2$O*: Boc-Val-OH (5.87 g, 27 mmol) was treated with DCC (5.57 g, 27 mmol) in pyridine at 0 °C for 60 min. To this was added a solution of Z-D-Ser-OTce (5.00 g, 13.5 mmol)[1] and HOBt (2.74 g, 20 mmol) in pyridine (10 ml) and the mixture was stirred at 5 °C for 20 h. The DCU which had formed was filtered off and the filtrate was evaporated *in vacuo* to give a residue, which was dissolved in ethyl acetate, and washed with ice-cold M hydrochloric acid, 5% sodium hydrogencarbonate and water. The solution was, after being dried over magnesium sulfate, evaporated *in vacuo* to give a crude preparation of **3** as an oil. The crude product was subjected to chromatography on a silica-gel column with chloroform-methanol (98:2) as solvent. The fractions containing the desired material were pooled and evaporated *in vacuo*. The residue was rechromatographed twice on a Lobar column (size B) with benzene-ethyl acetate (95:5) as solvent. Evaporation of the combined fractions containing the desired material as a single component gave a pure preparation of **3** as an oil; 7.46 g (97%), $[\alpha]_D^{21}$ +3.8±0.4° (*c* 1.0, methanol). TLC: homogeneous in systems A and D. Found: C, 48.77; H, 5.65; N, 4.85; Cl, 18.56%. Calcd for $C_{23}H_{31}N_2O_8Cl_3$: C, 48.48; H, 5.48; N, 4.92; Cl, 18.66%.

b) By the DCC-HOBt method. To an ice-cold solution of Boc-Val-OH (1.05 g, 4.8 mmol), Z-D-Ser-OTce (1.63 g, 4.4 mmol) and HOBt (0.65 g, 4.8 mmol) in pyridine (13 ml) was added DCC (1.00 g, 4.8 mmol) and the mixture was stirred at 5 °C overnight. The DCU which had formed was filtered off and the filtrate was evaporated *in vacuo*. The resulting oil was dissolved in ethyl acetate and this was washed with ice-cold M hydrochloric acid and 5% sodium hydrogencarbonate, dried over magnesium sulfate and evaporated *in vacuo*. The crude product thus obtained was purified on silica-gel columns as described above in a) to afford **3** as an oil; 1.65 g (66%), $[\alpha]_D^{23}$ +2.0±0.4° (*c* 1.0, methanol).

Z-D-Ser[Boc-Cys(MeBzl)-Val]-OTce (4). Compound **3** (6.84 g, 12 mmol) was treated with TFA (36 ml) at 25 °C for 40 min, followed by evaporation *in vacuo*. The resulting oil was dissolved in ethyl acetate and the solution was washed with 5% sodium hydrogencarbonate, dried over magnesium sulfate and evaporated *in vacuo*. The residue was dissolved in THF (70 ml) together with Boc-Cys(MeBzl)-OH (4.69 g, 14 mmol) and HOBt (1.95 g, 14 mmol). After addition of DCC (2.97 g, 14 mmol) at 0 °C, the mixture was stirred at the same temperature for 3 h and at 25 °C for 1 h. The reaction mixture was worked up in the usual manner to give a crude product which was repeatedly chromatographed on Lobar columns (size C) with chloroform-methanol (99:1) and benzene-ethyl acetate (8:2) as solvents to give **4** as amorphous solid; 7.31 g (78%) $[\alpha]_D^{22}$ −12.0±0.5° (*c* 1.0, methanol). TLC: homogeneous in systems A and D. Found: C, 52.38; H, 5.79; N, 5.19; S, 4.37; Cl, 13.13%. Calcd for $C_{34}H_{44}N_3O_9Cl_3S$: C, 52.55; H, 5.71; N, 5.41; S, 4.13; Cl, 13.69%.

Z-D-Ser[Boc-Ala-Cys(MeBzl)-Val]-OTce (5). Boc-Ala-OH (5.11 g, 27 mmol) was allowed to react with DCC (2.79 g, 13.5 mmol) in THF (30 ml) at 0 °C for 2 h. Removal of the separated DCU by filtration afforded a solution of (Boc-Ala)$_2$O. On the other hand, compound **4** (6.99 g, 9 mmol) was treated with TFA (27 ml) at 25 °C for 30 min, followed by evaporation *in vacuo*. The oily residue was, after being dried over sodium hydroxide pellets *in vacuo*, dissolved in THF (20 ml). The ice-cold solution was then combined with the (Boc-Ala)$_2$O obtained above and this was neutralized by the addition of DIEA. The mixture was then stirred at 5 °C overnight and worked up in the usual manner. The crude product was subjected to chromatography on a silica-gel column (Kieselgel 60, 6×33 cm) with chloroform-methanol (99:1) as solvent. The fractions containing the desired material were collected and evaporated *in vacuo*. Repeated rechromatography on a Lobar column (size C) with chloroform-methanol (99:1) and benzene-ethyl acetate (85:15 and 50:50) as solvents afforded a pure preparation of **5** as amorphous solid; 5.05 g (66%), $[\alpha]_D^{22}$ −25.1±0.7° (*c* 1.0, methanol). TLC: homogeneous in systems A, C, and D. Found: C, 52.46; H, 6.00; N, 6.80; S, 4.05; Cl, 11.82%. Calcd for $C_{37}H_{49}N_4O_{10}SCl_3$: C, 52.39; H, 5.82; N, 6.61; S, 3.78; Cl, 12.54%.

Z-D-Ser[Boc-Ala-Cys(MeBzl)-Val]-OH (6). Compound **5** (3.82 g, 4.5 mmol) in 90% acetic acid (135 ml) was treated with zinc powder 14.7 g) at 0 °C for 3 h. After the excess zinc had been filtered off, the filtrate was evaporated *in vacuo* and the residue dissolved in ethyl acetate was washed with ice-cold M hydrochloric acid and water, dried over magnesium sulfate and evaporated *in vacuo*. The resulting material was chromatographed on silica-gel columns (Kieselgel 60) with chloroform-methanol-acetic acid systems (95:5:0.5 and 98:2:1) as solvent to give a pure preparation of **6** as amorphous solid; 2.91 g (89%), $[\alpha]_D^{22}$−36.0±0.7° (*c* 1.0, methanol). TLC: homogeneous in system C. Found: C, 57.76; H, 6.79; N, 7.53; S, 4.53%. Calcd for $C_{35}H_{48}N_4O_{10}S\cdot 1/2H_2O$: C, 57.91; H, 6.80; N, 7.72; S, 4.42%.

Z-D-Ser{Z-D-Ser[Boc-Ala-Cys(MeBzl)-Val]-Ala-Cys(MeBzl)-Val}-OTce (8). Copound **5** (2.38 g, 2.8 mmol) was treated with TFA (28 ml) at 25 °C for 30 min, followed by evaporation *in vacuo*. The oily residue was dissolved in ethyl acetate and the solution was shaken with ice-cold 50% potassium carbonate, dried over magnesium sulfate and evaporated *in vacuo* to produce Z-D-Ser[H-Ala-Cys(MeBzl)-Val]-OTce (**7**) as an oil. This was then dissolved in THF (56 ml) together with compound **6** (2.03 g, 2.8 mmol) and HOBt (0.57 g, 4.2 mmol). The mixture was chilled in an ice-bath and, after addition of DCC (0.87 g, 4.2 mmol), stirred for 5 h at 0 °C and 1 h at 25 °C. The DCU which had formed was filtered off and the solvent was evaporated *in vacuo*. The solid residue was chromatographed on silica-gel columns (Kieselgel 60 and Kieselgel H) with chloroform-methanol (98:2) as solvent, followed by precipitation from methanol-ether to give a pure preparation of **8** as amorphous solid; 2.90 g (72%), mp 178—179 C°, $[\alpha]_D^{23}$ −41.4±0.8° (*c* 1.0, methanol). TLC: homogeneous in system B and in ethyl acetate. Found: C, 56.04; H, 6.11; N, 7.94; S, 4.68; Cl, 6.55%. Calcd for $C_{67}H_{87}N_8O_{17}S_2Cl_3$: C, 55.61; H, 6.06; N, 7.74; S, 4.43; Cl, 7.35%.

Z-D-Ser{Z-D-Ser[Boc-Ala-Cys(MeBzl)-Val]-Ala-Cys(MeBzl)-Val}-OH (9). Compound **8** (2.60 g, 1.8 mmol) was treated with zinc (5.88 g) in 90% acetic acid (280 ml) at 0 °C

for 3 h. After removal of the excess zinc by filtration the solvent was evaporated *in vacuo*. The residue was dissolved in chloroform–methanol (98:2) and the solution was washed with ice-cold M hydrochloric acid and water, dried over magnesium sulfate, and evaporated *in vacuo*. The crude product (2.34 g) was chromatographed on a silica-gel column (Kieselgel 60, 3.2×28 cm) with chloroform–methanol–acetic acid (98:2:0.5 and 95:5:0.5) as solvent to give **9** as glassy mass; 2.00 g (84%), mp 176—178 °C, $[\alpha]_D^{23}$ −62.7±1.0° (*c* 1.0, chloroform). Found: C, 58.98; H, 6.51; N, 8.31; S, 5.04%. Calcd for $C_{65}H_{86}N_8O_{17}S_2$: C, 59.34; H, 6.59; N, 8.52; S, 4.87%.

{Z-D-Ser[Z-D-Ser-Ala-Cys(MeBzl)-Val]-Ala-Cys(MeBzl)-Val}-Dilactone, N,N′-Z_2-S,S′-$MeBzl_2$-dihydroaponortriostin A (12). Compound **9** (0.132 g, 0.1 mmol) and HOSu (0.115 g, 1 mmol) were dissolved in DMF (1 ml). To this solution was added DCC (0.206 g, 1 mmol) at 0 °C and the mixture was stirred at 0 °C for 3 h and then at 25 °C for 2 h. The precipitates which formed upon addition of ether were filtered off and dried *in vacuo* to give the HOSu ester (**10**, Fig. 2). Compound **10** was treated with TFA (5 ml) at 25 °C for 30 min and the resulting **11** was precipitated by the addition of ether. These precipitates were dissolved in DMF (5 ml) and the solution was diluted with ethyl acetate (500 ml). To this was added DIEA until the solution became neutral and the mixture was stirred at 25 °C for 5 h. After removal of the solvent by evaporation *in vacuo*, the residue was dissolved in chloroform–methanol (98:2) and this was washed with M hydrochloric acid and 5% sodium hydrogencarbonate, dried over magnesium sulfate and evaporated *in vacuo*. The curde product was repeatedly chromatographed on a Lobar column (size A) with chloroform–methanol (98:2). The fractions containing the desired product as single component were pooled and evaporated *in vacuo* to afford **12** as amorphous solid; 58 mg (48%), mp 246—248 °C, $[\alpha]_D^{23}$ −76.3±1.2° (*c* 1.0, chloroform). NMR ($CDCl_3$, 360 MHz, 37 °C) δ=0.82 (d, 6H, Val γ- and γ′-CH_3), 0.84 (d, 6H, Val γ- and γ′-CH_3), 1.14 (d, 6H, Ala β-CH_3), 2.25 (m, 2H, Val β-CH), 2.28 (s, 6H, MeBzl-CH_3), 2.78 (m, 4H, Cys β- and β′-CH_2), 3.60 (s, 4H, MeBzl-CH_2), 4.23 (m, 2H, Ser β-CH_2), 4.27 (m, 2H, Ala α-CH), 4.44 (m, 2H, Ser α-CH), 4.56 (m, 2H, Ser β′-CH_2), 4.60 (m, 2H, Val α-CH), 4.63 (m, 2H, Cys α-CH), 5.12 (q, 4H, Bzl-CH_2), 6.28 (d, 2H, Ser NH), 6.30 (d, 2H, Cys NH), 6.96 (s, 2H, Ala NH), 7.11—7.33 (m, 18H, aromatic), and 7.87 (d, 2H, Val NH). Found: C, 59.80; H, 6.48; N, 9.14; S, 5.56%. Calcd for $C_{60}H_{76}N_8O_{14}S_2$: C, 60.18; H, 6.40; N, 9.36; S, 5.36%.

{Qxc-D-Ser[Qxc-D-Ser-Ala-Cys(MeBzl)-Val]-Ala-Cys(MeBzl)-Val}Dilactone, S,S′-$MeBzl_2$-dihydronortriostin A (13). Compound **12** (0.240 g, 0.2 mmol) and thioanisole (2.5 ml) were dissolved in TFA (25 ml) and the mixture was kept at 25 °C for 5 h, followed by evaporation *in vacuo*. The residue was triturated with ether to give amorphous precipitates, which were filtered off and dried *in vacuo* (0.28 g). These precipitates were dissolved in DMF (2 ml). To the stirred ice-cold solution were added 2-quinoxalinylcarbonyl chloride (Qxc-Cl, 0.077 g, 0.4 mmol) and TEA (0.14 ml, 1 mmol) and the reaction was allowed to proceed at 0 °C for 3 h and at 25 °C for 1 h. The solvent was evaporated *in vacuo*. The residue was dissolved in chloroform–methanol (98:2) and the solution was washed with M hydrochloric acid, dried over magnesium sulfate and evaporated *in vacuo*. The resulting material was chromatographed three times on silica-gel columns (Kieselgel H) with chloroform–methanol (98:2) to give **13** as amorphous solid; 102 mg (40%), mp 221—224 °C, $[\alpha]_D^{23.5}$ −113.8±3.8° (*c* 0.25, chloroform–methanol (98:2)). $\lambda_{max}^{CH_3CN}$ 242.5 nm (ε 77 300), 316 nm (ε 12 100), 325 nm (ε 11 900). NMR ($CDCl_3$, 360 MHz, 37 °C) δ=0.94 (m, 12H, Val γ- and γ′-CH_3), 1.41 (d, 6H, Ala β-CH_3), 2.26 (d, 6H, MeBzl CH_3), 2.37 (m, 2H, Val β-CH), 2.81 (m, 4H, Cys β- and β′-CH_2), 3.67 (m, 4H, MeBzl CH_2), 4.40 (m, 2H, Ala α-CH), 4.42 (m, 2H, Ser β′-CH_2), 4.62 (m, 2H, Ser β′-CH_2), 4.82 (m, 2H, Ser α-CH), 4.85 (m, 2H, Val α-CH), 5.20 (m, 2H, Cys α-CH), 6.56 (m, 2H, Cys NH), 7.01 (d, 2H, Ala NH), 7.12, 7.25 (m, 8H, aromatic), 7.87, 8.21 (m, 8H, Qxc), 8.12 (m, 2H, Val NH), 8.80 (d, 2H, Ser NH), and 9.63 (s, 2H, Qxc 3-CH), TLC: homogeneous in system B. Found: C, 58.04; H, 5.84; N, 12.99; S, 5.40%. Calcd for $C_{62}H_{72}N_{12}O_{12}S_2 \cdot 2H_2O$: C, 58.29; H, 5.68; N, 13.16; S, 5.02%.

Nortriostin A. Compound **13** (62 mg, 0.05 mmol) was treated with HF (10 ml) in the presence of anisole (0.5 ml) at 0 °C for 60 min. After removal of the HF by evaporation, the residue was dissolved in methanol (50 ml) and the solution was neutralized with TEA. To this was added a solution of iodine (66 mg, 0.25 mmol) in methanol and the mixture was stirred at 25 °C for 2 h. The excess iodine was discharged with 10% ascorbic acid and the solvent was removed by evaporation *in vacuo*. The residue was dissolved in chloroform–methanol (98:2) and the solution was washed with water, dried, and evaporated *in vacuo*. The resulting material was chromatographed two times on silica-gel columns (Kieselgel H) with chloroform–methanol (95:5). The fractions containing the desired product were collected and evaporated *in vacuo*. The residue was dissolved in chloroform–methanol (98:2, 1 ml) and to this was added ether (5 ml) to separate crystalline precipitates, which were filtered off, washed with ether, and dried *in vacuo* to give nortriostin A in pure state; 20 mg (39%), mp 213—215 °C, $[\alpha]_D^{20}$ −50.3±4.9° (*c* 0.1, chloroform). $\lambda_{max}^{CH_3CN}$ 242.5 nm (ε 89 600), 316 nm (ε 14 500), 326 nm (ε 14 200). NMR ($CDCl_3$ 360 MHz) δ=1.12 (d, 6H, Val γ- or γ′-CH_3), 1.16 (d, 6H, Val γ- or γ′-CH_3), 1.38 (d, 6H, Ala β-CH_3), 2.54 (m, 2H, Val β-CH), 2.93 (m, 4H, Cys β- and β′-CH_2), 4.45 (m, 2H, Ala α-CH), 4.65 (d, 2H, Ser β-CH_2), 4.84 (m, 2H, Val α-CH), 4.88 (m, 2H, Ser α-CH), 5.00 (d, 2H, Ser β′-CH_2), 5.68 (m, 2H, Cys α-CH), 6.30 (d, 2H, Ala NH), 6.54 (d, 2H, Cys NH), 7.92 (m, Qxc), 8.11 (d, Qxc), 8.25 (d, Qxc), 8.56 (d, 2H, Val NH), 8.79 (d, 2H, Ser NH), and 9.67 (s, 2H, Qxc 3-CH). Amino acid ratios in acid hydrolysate: Ser 0.92, Ala 1.06, Val 1.00, Cys not determined. Found: C, 50.40; H, 5.20; N, 15.15; S. 6.41%. Calcd for $C_{46}H_{54}N_{12}O_{12}S_2 \cdot 3.5H_2O$: C, 50.49; H, 5.62; N, 15.36; S, 5.86%.

References

1) Part II: M. Shin, K. Inouye, and H. Otsuka, *Bull. Chem. Soc. Jpn.*, **57**, 2203 (1984); M. Shin, K. Inouye, H. Otsuka, N. Higuchi, and Y. Kyogoku, "Peptide Chemistry 1980," Proceedings of the 18th Symposium on Peptide Chemistry, Nishinomiya, 1980, ed by K. Okawa, Protein Research Foundation (1981), p. 207.

2) J. R. Kalman, T. J. Blake, D. H. Williams, J. Feeney, and G. G. K. Roberts, *J. Chem Soc. Perkin 1*, **1979**, 1313.

3) K. Kawano, N. Higuchi, and Y. Kyogoku, "Peptide Chemistry 1976," Proceedings of the 14th Symposium on Peptide Chemistry, Hiroshima, 1976, ed by T. Nakajima, Protein Research Foundation (1977), p. 93.

4) Y. Kyogoku, N. Higuchi, M. Watanabe, and K. Kawano, *Biopolymers*, **20**, 1959 (1981).

5) T. L. Ciardelli, P. K. Chakravarty, and R. K. Olsen, *J. Am. Chem. Soc.*, **100**, 7684 (1978).

6) B. W. Erickson and R. B. Merrifield, *J. Am. Chem. Soc.*, **95**, 3750 (1973).

7) W. König and R. Geiger, *Chem. Ber.*, **103**, 788 (1970).

8) Y. Kiso, K. Ukawa, and T. Akita, *J. Chem. Soc. Chem. Commun*, **1980**, 101.

9) B. Kamber, *Helv. Chim. Acta*, **54**, 927 (1971); U. Ludescher and R. Schwyzer, *ibid.*, **55**, 2052 (1972).

10) H. Otsuka, J. Shoji, K. Kawano, and Y. Kyogoku, *J.*

Antibiot., **29**, 107 (1976).
11) M. K. Dhaon, J. H. Gardner, and R. K. Olsen, *Tetrahedron*, **38**, 57 (1982).
12) N. Higuchi, Y. Kyogoku, M. Shin, and K. Inouye, *Int. J. Peptide Protein Res.*, **21**, 541 (1983).

The Reactions of Nitrile Oxides with Methoxy *p*-Benzoquinones

Tohru HAYAKAWA, Koji ARAKI, and Shinsaku SHIRAISHI*
Institute of Industrial Science, The University of Tokyo, Roppongi, Minato-ku, Tokyo 106
(Received February 6, 1984)

The 1,3-dipolar cycloaddition reactions of nitrile oxides with methoxy *p*-benzoquinones are discussed in terms of FMO theory. The unusual reaction pattern of methoxy *p*-benzoquinones with nitrile oxides is interpreted by considering both antibonding secondary orbital interaction and SHOMO(quinone)-LUMO (nitrile oxide) interaction.

In the previous paper[1] we reported the site- and regio-selective reactions of nitrile oxides with substituted *p*-benzoquinones by means of the FMO theory, showing the correlation between the reaction modes and two types of FMO interactions. The quinones were shown to be classified into two groups; one is a group giving C=O adducts, the reactions of which are chiefly governed by HOMO (nitrile oxide)-LUMO (quinone) interaction, and the other is that giving C=C adducts, the reactions of wihch are chiefly governed by LUMO (nitrile oxide)-HOMO (quinone) interaction. The critical energy difference of the two interactions determining the reaction mode of the quinones was roughly estimated to be about 4 eV. Steric effect was a minor factor but could not be disregarded. However, the reaction of 2,6-dichlorobenzonitrile oxide with tetramethoxy-*p*-benzoquinone, which gives both C=O and C=C adducts, could not be clearly understood even by considering the steric effect. In order to rationalize the reaction pattern, we studied the reactions of nitrile oxides with other methoxy *p*-benzoquinones and the effect of methoxyl groups is discussed in terms of FMO theory. The unusual reaction pattern of methoxy quinones was shown to be interpreted by considering both the antibonding secondary orbital interaction and MO interaction involving SHOMO's of the quinones.

Results and Discussion

The results of the reactions of nitrile oxides with methoxy *p*-benzoquinones, such as 2-methoxy-*p*-benzoquinone (**2a**) and 2,6-dimethoxy-*p*-benzoquinone (**2b**) are shown in Scheme 1 together with the result of those with tetramethoxy-*p*-benzoquinone (**2c**). As nitrile oxides, 2,4,6-trimethylbenzonitrile oxide (**1a**) and 2,6-dichlorobenzonitrile oxide (**1b**) were used. The characterization data of the reaction pruducts are described in experimental section.

The reaction of **1b** with **2a** gave two regio isomeric C=C adducts, **3b** and **4b**, which were formed by addition onto the same reaction site, unsubstituted side, but in different orientation. This is a notable contrast to the reaction with 2-methyl-*p*-benzoquinone which gave two 1:1-C=C adducts formed by addition onto different reaction site (2,3- and 5,6-position) each other.[1] The formation ratio of the regio isomers **3b** and **4b** was about 3:2 from the results of ^{1}H NMR spectrum of the reaction product. The olefinic proton of **3b** resonates as a singlet at about 0.1 ppm lower field than

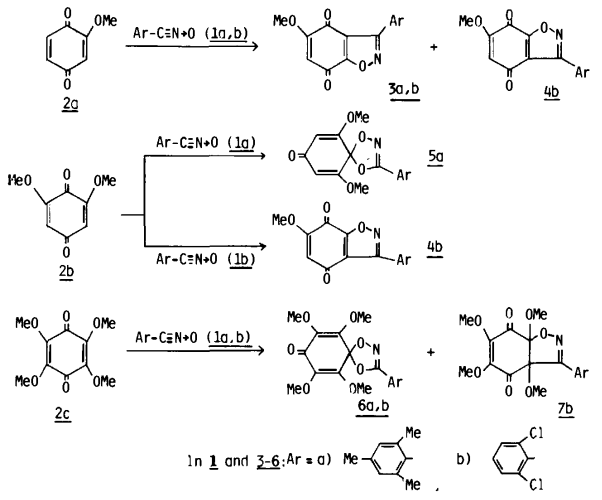

Scheme 1.

TABLE 1. ENERGY LEVELS AND COEFFICIENTS OF FMO OF METHOXY *p*-BENZOQUINONES

Quinone	FMO	ε(eV)	C_1	C_2	C_3	C_4	C_5	C_6	O_1	O_2	O_3	O_4	O_5	O_6
2a	LUMO	3.91	−0.33	−0.32	0.27	0.29	0.37	−0.35	0.51	0.16	—	−0.47	—	—
	HOMO	−7.49	0.10	−0.36	−0.55	0.15	−0.11	−0.13	0.29	0.48	—	0.40	—	—
	SHOMO	−8.92	−0.15	−0.12	−0.24	−0.13	0.52	0.52	−0.29	0.33	—	−0.22	—	—
2b	LUMO	4.25	−0.37	−0.33	0.28	0.28	0.28	−0.33	0.52	0.18	—	0.45	—	0.18
	HOMO	−6.86	0.07	−0.27	−0.36	0.22	−0.36	−0.27	0.27	0.30	—	0.53	—	0.30
	SHOMO	−7.65	0.00	−0.28	−0.48	0.00	0.48	0.28	0.00	0.41	—	0.00	—	−0.41
2c	LUMO	4.24	−0.36	−0.30	0.28	0.36	0.30	−0.28	0.48	0.16	−0.15	−0.48	−0.16	0.15
	HOMO	−6.08	0.05	−0.30	−0.32	0.05	−0.30	−0.32	0.32	0.33	0.34	0.32	0.33	0.34
	SHOMO	−6.15	−0.02	−0.34	−0.36	0.02	0.34	0.36	−0.03	0.39	0.36	0.03	−0.39	−0.36

a) The numbering of the atoms is following.

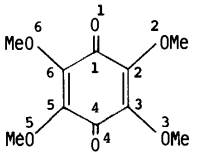

that of **4b**. The preparative separation of the two regio isomers was successfully effected by thin-layer chromatography. The reaction of **1a** with **2a** gave only one C=C adduct formed by addition onto 5,6-position in the orientation as shown in the Scheme 1.

The reaction of **2b** with **1a** has been known to give only C=O adduct,[2] while the reaction with **1b** gave exclusively the isoxazoloquinone **4b**, which was shown to be the same compound as the minor product in the reaction of **1b** with **2a**. In the reactions with **2c**, **1a** gave only C=O adduct, while **1b** gave both C=O and C=C adducts as reported before.[1,2] The difference in the modes of the reactions of **1a** and **1b** will be tried to be accounted in terms of FMO theory.

We list in Table 1 the energy values and FMO coefficients of methoxy *p*-benzoquinones calculated by *ab initio* method with STO-3G basis set[3] and in Table 2 those of nitrile oxides.[1] The geometry of quinone moiety of **2a** is that of *p*-benzoquinone[4] and that of substituent is standard one by Pople and Gordon.[5] The geometry of **2b** is that of X-ray result.[6] The substituent conformation was the most stable one by computation of the same manner described in the previous paper.[1]

The energy difference between LUMO (nitrile oxides)–HOMO (quinones) and HOMO (nitrile oxides)–LUMO (quinones) interaction is listed in Table 3. According to the energetical analysis described in the previous paper,[1] it may be predicted that the quinone **2b** will give a C=C adduct in either reaction of **1a** or **1b**. As mentioned above, however, the C=C adduct was obtained only in the reaction with **1b** and not with **1a** where C=O adduct was obtained. In addition, the high site-selectivity in the reactions is notable.

Considering the LUMO (nitrile oxide)–HOMO (quinone) interaction, one notes that the magnitude of the HOMO coefficients of the oxygen atoms of the methoxyl groups of methoxy *p*-benzoquinones is much larger than that of the carbon atoms of methyl groups of structurally similar methyl *p*-benzoquinones.[1] When nitrile oxides attack the methoxy-substituted C=C bond of the quinones, LUMO of nitrile oxides will experience an antibonding secondary orbital interaction with the oxygen orbital as shown in Fig 1. This antibonding secondary orbital interaction will decrease the net LUMO (nitrile oxide)-HOMO (quinone) overlapping to such an extent as the selectivity in the reactions may be significantly influenced. The importance of the antibonding secondary orbital interaction of methoxyl groups to the selectivity in the Diels-Alder reactions was pointed out by Tegmo-Larsson *et al.*[7] In this case, the interaction acts a role to reduce or diminish the primary orbital interaction. Gordon *et al.* rationalized the difference in the regio-selectivity between the 1,3-dipolar cycloaddition reactions of a nitrone with acrylonitrile and propiolonitrile by considering the secondary orbital interactions,[8] where the interaction acts to enhance or cooperate with the primary orbital interaction.

The quinone **2a** has two different C=C bonds. The carbon atoms of 2- and 3-positions have larger HOMO coefficients than those of 5- and 6-positions. Nevertheless the most efficient orbitals overlapping expected to be obtained in the interaction with the C=C of 2,3-position, no adduct added on the 2,3-position was obtained. This experimental result can not be rationalized by considering only the steric effect referred in the reaction with 2-methyl-*p*-benzoquinone,[1] but can be rationalized well by considering the secondary antibonding orbital interaction with the oxygen HOMO orbital of the methoxyl group.

In the reaction of **1a** with **2b**, HOMO (**1a**)-LUMO (**2b**) interaction becomes more important than the LUMO (**1a**)–HOMO (**2b**) interaction due to the antibonding secondary interactions as described above, and C=O addition occured exclusively. The kinetic data support this interpretation. The reaction rate of **2b** with **1a** is 10—100 times slower than those of other C=O addition reactions.[9] This is rationalized by the larger energy gap between HOMO (**1a**) and LUMO (**2b**). The addition across to the C=O bond of methoxy-substituted side is well understood by considering the larger LUMO coefficient magnitude of the carbon and oxygen atoms of the carbonyl.

The SHOMO's of methoxy-substituted quinones, especially those of **2b** and **2c**, lies close to that of HOMO, the energy difference being far less than 1 eV, while that of the other quinones being more than 1 eV. Therefore, in the reaction of **1b** with **2b**, LUMO (**1b**)–SHOMO (**2b**) interaction becomes more important and effects to increase net orbital overlapping, though SHOHO has also large coefficient on oxygen of methoxyl group. SHOMO does not act a role in favor of C=O addition because the coefficient on carbonyl group is zero.

The reaction with **2c** is also rationslized in terms of the same interactions mentioned above. Because of the antibonding secondary orbital intersction with

Table 2. Energy levels and coefficients of FMO of nitrile oxides

Nitrile oxide	FMO	ε(eV)	C_α[a]	C	N	O
1a	LUMO	5.58	0.50	0.27	−0.42	0.28
	HOMO	−6.12	−0.32	0.41	0.21	−0.69
1b	LUMO	4.43	0.55	0.22	−0.40	0.29
	HOMO	−6.89	−0.24	0.46	0.18	−0.73

a) This carbon connects with the dipole moiety.

Table 3. Energy difference between LUMO(nitrile oxides)-HOMO(quinones) and HOMO(nitrile oxides)-LUMO(quinones) interaction

	2a	**2b**	**2c**
1a	3.04	2.07	1.30
1b	1.12	0.15	−0.62

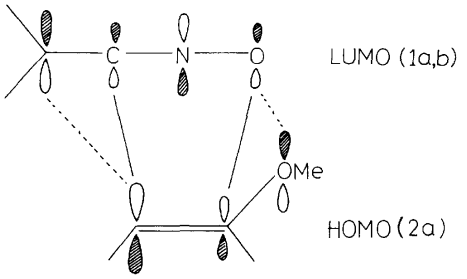

Fig. 1.

the oxygen atoms of methoxyl substituents acting to reduce the LUMO (**1a**)–HOMO (**2c**) overlapping, HOMO (**1a**)–LUMO (**2c**) interaction comes to be dominant to lead the C=O adduct formation in the reaction of **1a**. While in the reaction with **1b**, LUMO (**1b**)–SHOMO (**2c**) interaction favors C=C adduct formation due to the very small energy difference between SHOMO and HOMO of **2c** as shown in Table 1.

In the Diels-Alder reactions the role of the secondary orbtal interaction is widely recognized and applied, but in the 1,3-dipolar cycloaddition reactions not so much.[10] In this study it becomes clear that the antibonding secondary orbital interaction with oxygen atom of methoxyl substituent is the factor to control the site- and regio-selectivity in the cycloaddition reactions of nitrile oxides with methoxy *p*-benzoquinones. Moreover, it is shown that SHOMO becomes important in the interaction with the LUMO of the attacking reagent, when SHOMO lies close to HOMO.

Experimental

Melting points were measured using a micro-melting-point measuring apparatus (Yazawa Co., Ltd.) and are uncorrected. Column chromatography was conducted on silica gel (Wako gel C-200) with benzene as an eluent. IR spectra were recorded with a JASCO IRA-1 spectrophotometer. ^{1}H NMR spectra were measured in $CDCl_3$ with a JEOL JNM MH-100 spectrometer, and chemical shifts were reported in ppm from internal tetramethylsilane. Mass spectra were recorded with a Hitachi RMU-7L high resolution mass spectrometer.

Materials. 2,4,6-Trimethylbenzonitrile oxide (**1a**) and 2,6-dichlorobenzonitrile oxide (**1b**) were prepared by the method of Grundmann.[11] 2-Methoxy-*p*-benzoquinone (**2a**) was prepared by the method of Jeffreys.[12] 2,6-Dimethoxy-*p*-benzoquinone (**2b**) was prepared by the method of Will.[13]

*Reaction of 2,4,6-Trimethylbenzonitrile Oxide (1a) with 2-Methoxy-*p*-benzoquinone (2a).* A solution of 0.484 g (3 mmol) of **1a** and 0.829 g (6 mmol) of **2a** in 100 ml benzene was stirred for about 5 d at room temperature. Solvent was then evaporated under reduced pressure, and the residue was subjected to column chromatography. The first fraction gave 3-mesityl-5-methoxy-1,2-benzisoxazole-4,7-dione, **3a**, (0.62 g 69%), which was recrystallized from benzene–hexane. Mp 196—197 °C. IR (KBr) 1660 and 1690 cm^{-1} ($\nu_{C=O}$). ^{1}H NMR ($CDCl_3$) δ=2.09 (s, 6H, mesityl *o*-methyl), 2.36 (s, 3H, mesityl *p*-methyl), 3.89 (s, 3H, methoxyl methyl), 6.02 (s, 1H, olefinic), and 6.96 (s, 2H, aromatic)

Found: C, 68.78; H, 5.09; N, 4.88%. Calcd for $C_{17}H_{13}N_1O_4$: C, 68.68; H, 5.09; N, 4.71%.

*Reaction of 2,6-Dichlorobenzonitrile Oxide (1b) with 2-Methoxy-*p*-benzoquinone (2a).* The reaction was conducted and worked up in the same manner as the above. The second fraction gave a mixture of the regio-isomer, **3b** and **4b**, (0.41 g 44%). The NMR spectrum of the product revealed this to be a mixture of two C=C adducts. The signals at 6.05 and 5.94 due to the olefinic proton of the two adducts was in the ratio of 3:2. The product was separated by thin-layer chromatography with benzene–hexane 1:1 mixture as an eluent. 3-(2,6-Dichlorophenyl)-6-methoxy-1,2-benzisoxazole-4,7-dione, **4b**, was obtained from the first fraction zone, and recrystallized from benzene–hexane. Mp 190—193 °C. IR (KBr) 1660 and 1720 cm^{-1} ($\nu_{C=O}$). ^{1}H NMR ($CDCl_3$) δ=3.90 (s, 3H, methoxyl methyl), 5.94 (s, 1H, olefinic), and 7.43 (s, 3H, aromatic).

Found: C, 51.98; H, 2.14; N, 4.46%. Calcd for $C_{14}H_7N_1O_4Cl_2$: C, 51.88; H, 2.18; N, 4.32%.

The second fraction gave 3-(2,6-dichlorophenyl)-5-methoxy-1,2-benzisoxazole-4,7-dione, **3b**, which was recrystallized from benzene–hexane. Mp 181—182 °C. IR (KBr) 1670 and 1710 cm^{-1} ($\nu_{C=O}$). ^{1}H NMR ($CDCl_3$) δ=3.94 (s, 3H, methoxyl methyl), 6.05 (s, 1H, olefinic), and 7.47 (s, 3H, aromatic).

Found: C, 51.95; H. 2.10; N, 4.40%. Calcd for $C_{14}H_7N_1O_4Cl_2$: C, 51.88; H, 2.18; N, 4.32%.

*Reaction of 2,6-Dichlorobenzonitrile Oxide (1b) with 2,6-Dimethoxy-*p*-benzoquinone (2b).* A solutuion of 0.49 g (2.5 mmol) of **1b** and 0.42 g (2.5 mmol) of **2b** in 50 ml benzene was stirred for several days at room temperature and the solvent was evaporated under reduced pressure. The residue was worked up with column chromatography to give **4b**, (0.58 g 71%). The recrystallization was carried out from benzene–hexane.

References

1) T. Hayakawa, K. Araki, and S. Shiraishi, *Bull. Chem. Soc. Jpn.*, **57**, 1643 (1984).
2) S. Shiraishi, S. Ikeuchi, M. Seno, and T. Asahara, *Bull. Chem. Soc. Jpn.*, **51**, 921 (1978).
3) N. Kosugi, and H. Kuroda, *Chem. Phys. Lett.*, **74**, 490 (1980); N. Kosugi, Program GSCF2, Program Library, The Computer Center, The University of Tokyo (1981).
4) P. B. Rees, *Acta Crystallogr., Sect. B*, **26**, 1311 (1970).
5) J. A. Pople, and M. Gordon, *J. Am. Chem. Soc.*, **89**, 4253 (1967).
6) H. Schmalle, O. Jarchow, and B. M. Hausen, *Naturwissenschaften*, **64**, 534 (1977).
7) I. M. Tegmo-Larsson, M. D. Rozeboom, and K. N. Houk, *Tetrahedron Lett.*, **22**, 2043 (1981); I. M. Tegmo-Larsson, M. D. Rozeboom, N. G. Rondan, and K. N. Houk, *ibid.*, **22**, 2047 (1981).
8) M. D. Gordon, P. V. Alston, and A. R. Rossi, *J. Am. Chem. Soc.*, **100**, 5791 (1978).
9) S. Shiraishi, S. Ikeuchi, and M. Seno, *Nippon Kagaku Kaishi*, **1978**, 1127.
10) D. Ginsburg, *Tetrahedron*, **39**, 2095 (1983).
11) C. Grundmann, and R. Richter, *J. Org. Chem.*, **33**, 476 (1968).
12) J. A. D. Jeffreys *J. Chem. Soc.*, **1959**, 2153.
13) W. Will, *Ber.*, **21**, 602 (1888).

Restricted Rotation Involving the Tetrahedral Carbon. LV. Differential Effects of the *peri*-Substituents on the Rotational Barriers in 9-Ethyl-, 9-Allyl-, and 9-Benzyltriptycenes[1]

Gaku YAMAMOTO and Michinori ŌKI*

Department of Chemistry, Faculty of Science, The University of Tokyo, Bunkyo-ku, Tokyo 113

(Received February 14, 1984)

Energy barriers to rotation about the bridgehead-to-substituent bond in 9-ethyl-, 9-allyl-, and 9-benzyltriptycene derivatives with varying degrees of *peri*-substitution were studied by dynamic NMR and in one case by the classical kinetic method. In the singly *peri*-substituted series (1,4-dimethoxy derivatives) the barrier decreases in the order of 9-ethyl>9-allyl>9-benzyl. In the doubly *peri*-substituted series (1,8-dichloro derivatives) the barriers are alike irrespective of the 9-substituent, and in the triply *peri*-substituted series (1,4-dimethyl-8,13-dichloro derivatives) the barrier decreases in the order of 9-benzyl>9-allyl>9-ethyl. The reversal of the trend on the change in *peri*-substitution patterns may be explained on the basis of the change in the interaction between the *peri*- and 9-substituents in both the ground and the transition states.

Our recent ^{1}H NMR investigation on 9-benzyl-1,4-dimethoxytriptycene (**1c**) revealed that the free energy of activation, $\Delta G_c^{\ddagger}$, for the rotational isomerization (*ap*→±*sc*) was 11.9 kcal mol^{-1} (1 cal=4.184 J).[2] Meanwhile Nakanishi *et al.* reported the $\Delta G^{\ddagger}$ value of 13.8 kcal mol^{-1} for the same process in 9-ethyl-1,4-dimethoxytriptycene (**1a**) obtained by ^{13}C dynamic NMR study.[3] The higher barrier in the 9-ethyl derivative (**1a**) than in the 9-benzyl one (**1c**) made us to expect

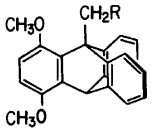

1

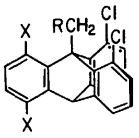

2 X=H
3 X=CH$_3$

a: R = CH$_3$
b: R = CH=CH$_2$
c: R = C$_6$H$_5$
d: R = 3,5-(CH$_3$)$_2$C$_6$H$_5$

that atropisomerism could be realized in a triply *peri*-substituted 9-ethyltriptycene such as **3a**, because the corresponding 9-(3,5-dimethylbenzyl) derivative (**3d**) had been shown to afford stable atropisomers with the free energy of activation for the *ap*→±*sc* isomerization of 25.3 kcal mol^{-1}.[4] To our surprise, **3a** showed a far lower barrier to rotation than expected, as will be discussed in this article. These findings urged us to study in some detail how the rotational barrier in 9-*prim*-alkyltriptycene derivatives might depend on the pattern of *peri*-substitution and the β-group in the 9-substituent. We chose ethyl, allyl, and benzyl groups as the 9-substituent, and 1-methoxy, 1,8-dichloro, and 1,8-dichloro-13-methyl as the representative of the single, double, and triple *peri*-substitution, respectively. Therefore we prepared compounds **2a**—**2c** and **3a**—**3c**, and studied the rotational barriers in these compounds.

Results

Syntheses. A Grignard reagent prepared from ethyl iodide, allyl bromide, or benzyl chloride was treated with 1,8-dichloroanthrone and the resulted alcohol was dehydrated to give 9-ethyl-, 9-allyl-, or 9-benzyl-1,8-dichloroanthracene (**4a**—**4c**). Reactions of benzyne and 3,6-dimethylbenzyne generated *in situ*

TABLE 1. ^{1}H HMR SPECTRAL DATA IN CDCl$_3$[a]

Compd	Rotamer	Population/%	CH$_2$	R	10-H	1-CH$_3$[b]	4-CH$_3$[b]
2a	±*sc*	100	3.24 dq, 4.36 dq (6.9, 15.0)	1.50 t (6.9)	5.19 s		
2b	±*sc*	100	4.10 m[c], *ca.* 5.3[d]	5.0—5.6 m (2H) 5.75—6.25 m (1H)	5.23 s		
2c	±*sc*	100	4.80 d, 5.98 d (18.0)		5.33 s		
3a	*ap*	57	4.03 q (6.8)	1.54 t (6.8)	5.44 s	2.32 s	2.67 s
	±*sc*	43	3.74 dq, 4.26 dq (6.8, 15.2)	1.44 t (6.8)	5.41 s	2.49 s	2.67 s
3b	*ap*	33	4.79 m	4.9—5.4 m (2H) 5.8—6.4 m (1H)	5.51 s	2.37 s	2.71 s
	±*sc*	67	4.52 dm, *ca.* 5.1[d]		5.49 s	2.51 s	2.71 s
3c	*ap*	29[e]	5.49 s		5.57 s	2.86 s	2.31 s
	±*sc*	71[e]	5.23 d, 5.78 d (19.2)		5.54 s	2.14 s	2.56 s

a) Obtained at *ca.* 35 °C except for **2a**, for which the data at −4 °C are given. Aromatic protons are not included. Chemical shifts are given in δ; s: singlet, d: doublet, t: triplet, q: quartet, m: multiplet, dq: double quartet, dm: double multiplet. In parentheses are coupling constants in Hz. b) In **3a** and **3b**, the signal pair with larger chemical shift differences are tentatively assigned to 1-CH$_3$. c) Apparent double doublet. d) Obscured by overlap with the vinyl protons. e) Obtained from the equilibrated mixture of atropisomers.

from the corresponding anthranilic acids with the anthracenes (**4a—4c**) gave the desired triptycene derivatives (**2a—2c** and **3a—3c**).[5] ^{1}H NMR spectral data of the triptycenes obtained are compiled in Table 1.

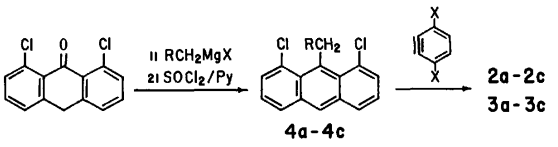

The analogy of compound **3d**[4] predicts that the *ap* atropisomer of **3c** would be stereoselectively formed under kinetically controlled conditions in the reaction of **4c** with 3,6-dimethylbenzyne, but actually a *ca.* 1:1 mixture of *ap*-**3c** and ±*sc*-**3c** was obtained probably due

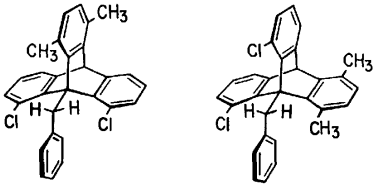

ap-**3c** ±*sc*-**3c**

to the high reaction temperature and the long reaction time. Column chromatography of the rotamer mixture of **3c** afforded a pure sample of ±*sc*-**3c** as this isomer was eluted faster than *ap*-**3c**. The *ap* isomer was concentrated up to 85%.

Classical Kinetic Measurements on 3c. The rotational barrier in **3c** seemed to be too high to be studied by dynamic NMR and was obtained by classical kinetics in the temperature range of 49—69 °C. An *ap*-enriched sample of **3c** in chloroform-*d* was placed in the NMR probe which had been preheated at a constant temperature and the change in the relative intensities of the 1- and/or 4-methyl proton signals was followed. The change was analyzed as a first-order reversible reaction and the rate constant for the *ap*→±*sc* isomerization was calculated. The rate constants thus obtained at four temperatures and the Eyring parameters therefrom are given in Table 2.

Dynamic NMR Studies on 2a—2c. ^{1}H NMR spectra of the 1,8-dichloro derivatives (**2a—2c**) at room temperature indicate that these compounds exist solely as ±*sc* rotamers and the +*sc* ⇌ −*sc* interconversion is slow on the NMR time scale. On raising the temperature, the signal due to the diastereotopic methylene protons broadened and coalesced into an isochronous

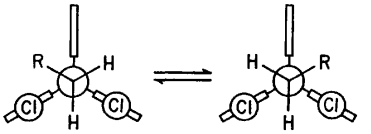

+*sc*-**2** −*sc*-**2**

signal. Rate constants at coalescence temperatures (T_c) were estimated by the use of Eq. 1,[6]

$$k_c = \frac{\pi}{\sqrt{2}}(\Delta\nu_{AB}^2 + 6J_{AB}^2)^{1/2} \quad (1)$$

where $\Delta\nu_{AB}$ is the chemical shift difference between the diastereotopic methylene protons and J_{AB} is the geminal coupling constant. The spectra at T_c for **2a** and **2c** were reproduced by theoretical calculations affording rate constants at T_c which are very similar to those from Eq. 1. This means that Eq. 1 can satis-

TABLE 2. KINETIC DATA OF **3c** IN $CDCl_3$

$$ap\text{-}\mathbf{3c} \underset{k_{-1}}{\overset{2k_1}{\rightleftharpoons}} \pm sc\text{-}\mathbf{3c}: K = 2k_1/k_{-1}$$

Temp	k_1	$\Delta G^{\ddagger}$	K
°C	$10^5\,s^{-1}$	kcal mol^{-1}	
69	44.9	25.3_5	2.3_2
62	21.4	25.3_1	2.2_9
54	8.5_8	25.2_9	2.2_4
49	4.6_7	25.2_8	2.2_4

$\Delta H^{\ddagger} = 24.1 \pm 0.8$ kcal mol^{-1}
$\Delta S^{\ddagger} = -3.6 \pm 2.3$ cal mol^{-1} K^{-1}

TABLE 3. DYNAMIC NMR DATA[a]

Compd	Obsd Protons	T_c °C	$\Delta\nu_c$[b] Hz	k_c s^{-1}	$\Delta G^{\ddagger}$[c,d] kcal mol^{-1}	K[e]	Solvent
1a[f]					14.6 (25 °C)	0.69 (−29 °C)	$CDCl_3$-CS_2-CD_3COCD_3
1b	2,3-H_2	−25	6.0	3.5	13.8	0.65	CD_2Cl_2
1c[g]					11.9 (−15 °C)	2.8 (−20 °C)	$CDCl_3$-CS_2
2a	CH_2	68	67.3 (15.0)	170	16.6		$CDCl_3$
2b	CH_2	78	72 (18)	188	17.0		$CDCl_3$
2c	CH_2	60	71.0 (18.0)	185	16.1		$CDCl_3$
3a	1-CH_3	94	10.3	6.9	20.2	0.75	C_6H_5Cl
	4-CH_3	76	3.1	1.4	20.3		
3b	1-CH_3	124	9.4	7.6	21.9	2.0	C_6H_5Cl
3c[h]					25.3 (54 °C)	2.2 (54 °C)	$CDCl_3$

a) Kinetic parameters refer to the *ap*→±*sc* process for **1a—1c** and **3a—3c** taking the degeneracy of ±*sc* rotamers into account and to the +*sc*⇌−*sc* process for **2a—2c**. b) In parentheses are the geminal coupling constants in Hz. c) Reliable to ±0.1 kcal mol^{-1} except for **2b**, for which the value is reliable to ±0.3 kcal mol^{-1}. d) Values at T_c unless otherwise noted. e) $K = [\pm sc]/[ap]$. f) Ref. 3. g) Ref. 2. h) Obtained by the classical kinetic method. See Table 2.

factorily predict k_c for $ABX_3 \rightleftharpoons BAX_3$ exchange as manifested in **2a** and this is probably because $\Delta\nu_{AB}$ is sufficiently large (67.3 Hz). In case of **2b**, the spectra were too complex to be theoretically simulated, but the coalsecence temperature was definitely identified. Success of Eq. 1 in predicting k_c for **2a** would justify the use of the equation also for **2b**, although allowance should be made for the inaccuracy of $\Delta\nu_{AB}$ and J_{AB} values because of the overlap of the signals. The kinetic data thus obtained for the $+sc \rightleftharpoons -sc$ process in **2a—2c** are given in Table 3.

Dynamic NMR Studies on 3a and 3b. ^{1}H NMR spectra of **3a** and **3b** indicated that both compounds

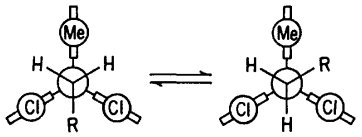

ap-**3** ±*sc*-**3**

exist as two rotamers, *ap* and ±*sc*. The relative populations of the rotamers were determined by integrating the 1- and/or 4-methyl signals and the rotamer assignment was made by carefully inspecting the methylene proton signals which appeared as complex multiplets because of the couplings with the methyl or the vinyl protons: the methylene protons are enantiotopic in *ap* and diastereotopic in ±*sc*. From the coalescence phenomena exhibited by the 1- and 4-methyl signals[7] the rate constants at T_c for the *ap*→±*sc* process in these compounds were obtained by the use of the graphical method according to Jaeschke *et al.*[8] and are shown in Table 3.

Dynamic NMR Study on 1b. Although our earlier study on the low temperature NMR of **1b** has shown that the ±*sc*/*ap* ratio at −32 °C is 0.7 in chloroform-*d*,[9] dynamic NMR measurements to obtain the rotational barrier had not been made. The methoxyl signals were not suitable as a DNMR probe not only because the chemical shift differences between the rotamers are very small but also because the signals overlap with the allylic methylene signals at low temperatures. The signal ascribed to the aromatic protons at 2- and 3-positions appears as a sharp singlet isolated from the other aromatic signals at room temperature in dichloromethane-d_2 which splits into two singlets at low temperatures. This indicates that the chemical shifts of the 2- and the 3-protons coincide with each other throughout the temperature range examined. Therefore this signal was used as a DNMR probe and the rate constant at T_c for the *ap*→±*sc* process was obtained by the graphical method.[8] The kinetic data obtained are also included in Table 3.

Discussion

The singly *peri*-substituted 9-allyl compound (**1b**) shows the energy barrier to the *ap*→±*sc* isomerization of 13.8kcal mol^{-1}, which ranks between the barrier in the 9-ethyl compound (**1a**) and the one in the 9-benzyl compound (**1c**) but is close to the value for **1a**. The energy barrier to the *ap*→±*sc* process in the triply *peri*-substituted 9-benzyl compound (**3c**) is very similar to that in **3d** reported before,[4] and this may be reasonable becuase the *m*-methyl groups should not significantly affect the barrier. It is rather unexpected that the rotational barrier found in the triply *peri*-substituted 9-ethyl compound (**3a**) is *ca.* 5 kcal mol^{-1} lower than that in the corresponding 9-benzyl compound (**3c**). The barrier in the 9-allyl derivative **3b** is somewhat higher than that in **3a** but still far lower than that in **3c**. This trend of the barrier heights, 9-benzyl>9-allyl>9-ethyl, is just the reverse of that found in the singly *peri*-substituted series (**1a—1c**). In the doubly *peri*-substituted series, *i.e.* the 1,8-dichloro compounds (**2a—2c**), the barriers to the $+sc \rightleftharpoons -sc$ interconversion are rather similar among the compounds.

As the energy barrier is the difference between the ground and the transition states, the energy situations in both states should be considered. In the ground state conformation of 9-benzyltriptycene derivatives, the phenyl group lies coplanar with the bridgehead-to-substituent bond, constituting a static gear system with a three-toothed and a two-toothed wheels as shown by **5** for 9-benzyltriptycene.[4b] Several of the

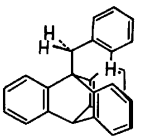

5

previous experimental results[4b] as well as molecular model considerations suggest the presence of a considerable steric interaction between the triptycene skeleton and the inner *o*-hydrogen of the phenyl group. Meanwhile, 9-allyl- and 9-ethyltriptycenes seem to suffer no such interactions judging from the probable ground state conformations **6** and **7**. We can therefore specu-

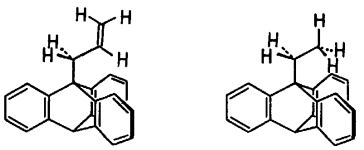

6 **7**

late that the ground state energy level is considerably higher in 9-benzyltriptycene than in 9-allyl or 9-ethyltriptycene. Introduction of *peri*-substituents would destabilize the ground state irrespective of the 9-substituent. The degree of destabilization in the

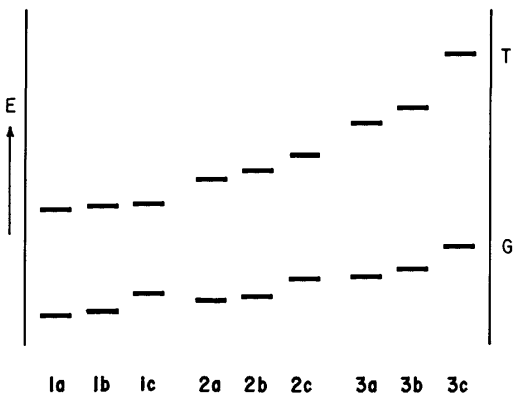

Fig. 1. Schematic energy diagram of the ground (G) and the transition (T) states. The energy scale is arbitrary.

ground state should be larger in 9-benzyl derivatives than in 9-allyl and 9-ethyl ones because of the intrinsic instability of 9-benzyltriptycene.

Although information on the transition states can not be obtained experimentally, some aspects of transition state energies may be discussed on the basis of the energy barriers obtained experimentally and the ground state energies discussed above: The energy diagram of the compounds may be shcematically drawn as shown in Fig. 1. From the diagram it is clearly seen that the destabilization in the transition state on going from the singly to the triply *peri*-substituted derivative is more effective in the 9-benzyl series than that in the 9-ethyl or the 9-allyl series.

These situations may be understood to some extent by the examination of the transition state conformations (**8** and **9**). Hereafter the behavior of the

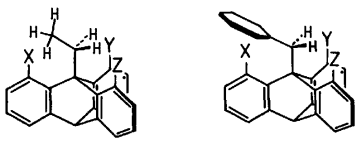

8

9

9-ethyl and the 9-benzyl compounds will be discussed; the 9-allyl compounds will behave like something between the two. Molecular model considerations reveal the difference in the probable transition state structure between the two series of compounds. In the 9-ethyl compounds (**8**), the methyl group interacts with the group X (H or Cl) at the edge, *i. e.* the methyl group does not reach the C–X bond axis with the methyl carbon ···X distance of 1.5 Å and the C–X···C angle of *ca.* 130° when X=H from the Dreiding model, while in the 9-benzyl compounds, the phenyl group extends over the group X, X being buried in the π-cloud of the benzene ring with X···benzene ring distance of 1.2 Å when X=H. In the actual molecules these distances should be larger because of the angular deformation.

In the singly *peri*-substituted compounds (X=Y=H, Z=OCH_3), the energy levels of **8** and **9** may be similar judging from the higher ground state energy level and the smaller energy barrier in **1c** than in **1a** (Fig. 1). In the doubly *peri*-substituted compounds (X=H, Y=Z=Cl) the two *peri*-chloro groups buttress the 9-substituent toward the *peri*-hydrogen both in the ground and the transition states. Destabilization due to the buttressing effect should naturally be larger in the transition state than in the ground state and the transition state **9** should be more strongly destabilized than **8** on the basis of the geometrical situations discussed above: the buttressing effect prevents angular deformations which relieve the steric strain caused by the β-group and X. This deduction is consistent with the larger increase of the energy barrier in the 9-benzyl series (**1c**→**2c**) than in the 9-ethyl series (**1a**→**2a**). In the triply *peri*-substituted compounds (X=Y=Cl, Z=CH_3), **9** should be far more strongly destabilized than **8**, because now a chloro group instead of a hydrogen interacts with the β-group of the 9-substituent and also the methylene group is buttressed by 8-chloro and 13-methyl groups.

Therefore, the order of the barrier heights in the singly *peri*-substituted compounds, 9-ethyl>9-allyl>9-benzyl, is mainly ascribed to the differences in the ground state energy. In the doubly *peri*-substituted compounds, the change in the transition state may parallel that in the ground state. In the triply *peri*-substituted compounds the difference in the transition state energy is most responsible for the order of the barrier heights.

Another intriguing feature is the rotameric equilibrium in the compounds examined. The equilibrium constant in **1b**, 0.65, is very similar to that in **1a**, suggesting that the main factor governing the both equilibria is the same, *i.e.* steric. The large preference for the $\pm sc$ rotamer in **1c** has been ascribed to an attractive interaction between the 1-methoxyl and the phenyl groups overwhelming the steric effect.[10] Almost exclusive existence of the $\pm sc$ rotamers in **2a**—**2c** can be understood on the basis of the steric effects. Among **3a**—**3c**, the 9-allyl (**3b**) and the 9-benzyl (**3c**) compounds behave similarly with each other and differently from the 9-ethyl compound (**3a**). The *ap* rotamers would be sterically favored on the basis of the generally accepted van der Waals radii of the *peri*-substituent (1.80 Å for Cl and 2.0 Å for methyl[11]), as manifested in **3a**. A hypothetical C–H···π interaction between the 1-methyl and the vinyl or the phenyl group might shift the equilibrium in favor of the $\pm sc$ rotamer in **3b** and **3c**.[12]

Experimental

Melting points are not corrected. ^{1}H NMR spectra at ambient temperature of *ca.* 35 °C were recorded on a Varian EM-390 (90 MHz) or a Hitachi R-20B (60 MHz) spectrometer in chloroform-*d* solutions with tetramethylsilane as the internal reference. Variable temperature ^{1}H NMR spectra were obtained on the R-20B spectrometer in 5—8% (w/v) solutions in dichloromethane-d_2 (**1b**), chloroform-*d* (**2a**—**2c** and **3c**), or chlorobenzene (**3a** and **3b**). Temperatures were calibrated using methanol and ethylene glycol samples.[13] Theoretical spectra were obtained on a Hitachi M-280H computer system at the Computer Center of the University of Tokyo using a modified verson of the DNMR program by Binsch.[14] Kinetic studies on **3c** were made following the procedure described before for **3d**.[4b]

1,8-Dichloro-9-ethylanthracene (4a). To an ethereal solution of the Grignard reagent prepared from 2.0 mL of ethyl iodide was added portionwise 2.63 g (10.0 mmol) of powdery 1,8-dichloroanthrone[15] and the mixture was stirred at room temperature for 1 h and treated with aqueous ammonium chloride to give 1,8-dichloro-9-ethyl-9,10-dihydro-9-anthrol [(^{1}H NMR ($CDCl_3$), δ=0.42 (3H, t, J=7.5 Hz), 2.75 (2H, q, J=7.5 Hz), 3.73 (1H, br s), 4.01 (2H, s), 6.9—7.5 (6H, m)]. The alcohol was treated with 4 mL of thionyl chloride and 7 mL of pyridine in 30 mL of ether under reflux for 15 min. The reaction mixture was washed with water, dried over magnesium sulfate, and concentrated. Column chromatography (alumina, hexane–dichloromethane) of the residue followed by recrystallization from tetrahydrofuran-hexane gave 1.64 g (60%) of **4a** as yellow granules, mp 101—102 °C. Found: C, 69.65; H, 4.12; Cl, 25.94%. Calcd for $C_{16}H_{12}Cl_2$: C, 69.84; H, 4.40; Cl, 25.76%. ^{1}H NMR ($CDCl_3$), δ=0.97 (3H, t, J=7.1 Hz), 4.18 (2H, q, J=7.1 Hz), 7.0—7.9 (6H, m), 8.12 (1H, s).

9-Allyl-1,8-dichloroanthracene (4b). Similarly as above, the reaction of 1,8-dichloroanthrone with the Grignard

reagent prepared from allyl bromide gave 9-allyl-1,8-dichloro-9,10-dihydro-9-anthrol [^{1}H NMR ($CDCl_3$), δ=3.51 (2H, br d), 3.92 (1H, br s), 3.98 (2H, s), 4.4—5.5 (3H, m), 7.0—7.5 (6H, m)], which was treated with thionyl chloride and pyridine to give 9-allyl-1,8-dichloroanthracene (**4b**) in 78% yield, mp 88—89 °C (from tetrahydrofuran-hexane). Found: C, 70.93; H, 4.10; Cl, 24.84%. Calcd for $C_{17}H_{12}Cl_2$: C, 71.10; H, 4.21; Cl, 24.69%. ^{1}H NMR ($CDCl_3$), δ=4.3—5.1 (2H, m), 5.4—6.2 (1H, m), 7.0—8.0 (6H, m).

General Procedure for the Synthesis of the Triptycenes. To a boiling solution of 1.5 mmol of an anthracene in 20 mL of 1,2-dimethoxyethane (DME) were added dropwise a solution of 2.5 mmol of an anthranilic acid in 10 mL of DME and a solution of 1.0 mL of isopentyl nitrite in 5 mL of DME, so that a considerable excess of isopentyl nitrite was always present in the reaction mixture. The mixture was heated under reflux for 1 h and concentrated. Column chromatography of the residue on alumina with hexane as the eluent followed by recrystallization from tetrahydrofuran-hexane gave the desired triptycene.

*1,8-Dichloro-9-ethyltriptycene (**2a**),* mp 231—232 °C, was prepared from **4a** and anthranilic acid in 53% yield. Found: C, 75.22; H, 4.29; Cl, 20.34%. Calcd for $C_{22}H_{16}Cl_2$: C, 75.22; H, 4.59; Cl, 20.19%.

*9-Allyl-1,8-dichlorotriptycene (**2b**),* mp 192—194 °C, was prepared from **4b** and anthranilic acid in 27% yield. Found: C, 76.18; H, 4.28; Cl, 19.61%. Calcd for $C_{23}H_{16}Cl_2$: C, 76.04; H, 4.44; Cl, 19.52%.

*8,13-Dichloro-9-ethyl-1,4-dimethyltriptycene (**3a**),* mp 251—252 °C, was prepared from **4a** and 3,6-dimethylanthranilic acid[16] in 78% yield. Found: C, 75.80; H, 5.10; Cl, 18.72%. Calcd for $C_{24}H_{20}Cl_2$: C, 75.99; H, 5.31; Cl, 18.69%.

*9-Allyl-8,13-dichloro-1,4-dimethyltriptycene (**3b**),* mp 233—235 °C, was prepared from **4b** and 3,6-dimethylanthranilic acid in 48% yield. Found: C, 76.75; H, 5.13; Cl, 18.21%. Calcd for $C_{25}H_{20}Cl_2$: C, 76.73; H, 5.15; Cl, 18.12%.

*9-Benzyl-8,13-dichloro-1,4-dimethyltriptycene (**3c**).* To a boiling solution of 9-benzyl-1,8-dichloroanthracene (**4c**)[4] and 1.5 mL of isopentyl nitrite in 30 mL of dichloromethane was added dropwise a solution of 1.15 g (6.9 mmol) of 3,6-dimethylanthranilic acid in 20 mL of tetrahydrofuran and the mixture was heated under reflux for 2 h. Column chromatography (alumina, hexane-dichloromethane) gave 890 mg (54%) of **3c** as *ca.* 1:1 mixture of the *ap* and ±*sc* rotamers. Earlier fractions of the column chromatography of the rotamer mixture on alumina with hexane as the eluent gave a pure sample of ±*sc*-**3c**, mp 208—210 °C. Found: C, 79.03; H, 5.00; Cl, 15.55%. Calcd for $C_{29}H_{22}Cl_2$: C, 78.91; H, 5.02; Cl, 16.06%. Later fractions of the chromatography gave a sample containing 85% at best of the *ap* rotamer.

References.

1) Part LIV: S. Murata, T. Mori, and M. Ōki, *Bull. Chem. Soc. Jpn.*, **57**, 1970 (1984).

2) M. Kono, H. Kihara, N. Nakamura, F. Suzuki, and M. Ōki, *Bull. Chem. Soc. Jpn.*, **52**, 1682 (1979).

3) H. Nakanishi and O. Yamamoto, *Bull. Chem. Soc. Jpn.*, **51**, 1777 (1981); The barrier value is recalculated taking the degeneracy of the ±*sc* rotamers into account.

4) a) G. Yamamoto and M. Ōki, *Angew. Chem., Int. Ed. Engl.*, **17**, 518 (1978); b) idem., *Bull. Chem. Soc. Jpn.*, **54**, 473 (1981).

5) Synthesis of **2c** is described in Ref. 4b.

6) M. Ōki, H. Iwamura, and N. Hayakawa, *Bull. Chem. Soc. Jpn.*, **37**, 1865 (1964); R. J. Kurland, M. B. Rubin, and W. B. Wise, *J. Chem. Phys.*, **40**, 2426 (1964).

7) The signals tentatively assigned to the 4-methyl group of the two rotamers are accidentally isochronous in chloroform-*d* (Table 1) but are anisochronous in chlorobenzene.

8) A. Jaeschke, G. Munsch, H. G. Schmid, H. Friebolin, and A. Mannschreck, *J. Mol. Spectrosc.*, **31**, 14 (1969).

9) G. Izumi, S. Hatakeyama, N. Nakamura, and M. Ōki, *Bull. Chem. Soc. Jpn.*, **54**, 258 (1981).

10) F. Suzuki and M. Ōki, *Bull. Chem. Soc. Jpn.*, **48**, 596 (1975).

11) L. Pauling, "The Nature of Chemical Bond," 3rd Ed., Cornell University Press, New York (1960), p 260.

12) S. Zushi, Y. Kodama, K. Nishihata, K. Umemura, M. Nishio, J. Uzawa, and M. Hirota, *Bull. Chem. Soc. Jpn.*, **53**, 3631 (1980) and references cited therein.

13) A. L. Van Geet, *Anal.Chem.*, **40**, 2227 (1968).

14) G. Binsch, *Top. Stereochem.*, **3**, 97 (1968).

15) E. de B. Barnett and M. A. Mathews, *J. Chem. Soc.*, **123**, 2549 (1923).

16) S. Gronowitz and G. Hansen, *Arkiv Kemi*, **27**, 145 (1967).

 © 1984 The Chemical Society of Japan Bull. Chem. Soc. Jpn., 57, 2224—2229 (1984) [Vol. 57, No. 8

Dynamic NMR as a Nondestructive Method for the Determination of Rates of Dissociation. V. Proton Affinities of *p*-Substituted *N,N*-Dibenzylanilines in Aprotic Solvents[1,2]

Michinori Ōki,* Manabu Ohira, Yasuhiro Yoshioka, Toshiari Morita, Hiroshi Kihara, and Nobuo Nakamura

Department of Chemistry, Faculty of Science, The University of Tokyo, Bunkyo-ku, Tokyo 113

(Received March 2, 1984)

Rates of proton exchange between *p*-substituted *N,N*-dibenzylanilinium ion and chloride ion in chloroform-*d* and acetonitrile-d_3 were determined by the dynamic NMR technique. Comparison of the kinetic proton affinity of the anilines in the aprotic solvents with the proton affinity of anilines in the gas phase and the basicity in water revealed that they could be linearly correlated. The feature of the kinetic data was a large positive entropy of activation which can be ascribed to the change from an ionic ground state to a covalent transition state. The entropy of activation was somewhat smaller in acetonitrile-d_3 than in chloroform-*d*. This was attributed to the change in the stage of the transition state for the exchange. A small amount of water which could not be removed easily from the aprotic solvents was proved not to harm the results.

Basicities of amines in water are well documented.[3] In recent years, proton affinity of amines in the gas phase was studied by the ion cyclotron resonance technique or high pressure mass spectrometry.[4] The results were treated thermodynamically to understand the basicity of amines in aqueous solutions by taking the solvation energy into consideration.[5] The correlation between the gas phase proton affinity and the basicity in water could be examined in detail due to the wealth of literatures on the latter. However, basicity data of amines in aprotic solvents are rather few. Therefore, the understanding of basicities in aprotic solvents requires experimental data which can be obtained by variety of methods.

The dynamic NMR technique had been playing some role in measuring the basicity of amines in various solvents. Grunwald, Lowenstein, and Meiboom pioneered in this area by showing that the methyl proton signal of methylamine in strongly acidic media was a quartet due to coupling with $-NH_3^+$ protons but it coalesced and became a singlet when the pH of the solution was raised.[6] Saunders and Yamada followed this work to study the rates of proton exchange and nitrogen inversion in *N,N*-dibenzylmethylamine.[7] This technique now becomes widely applicable and Delpuech and collaborators have studied the rates of inversion of various amines in acidic aqueous media.[8] They further elaborated the study in the area of acidic dimethyl sulfoxide solutions.[9] There exist some ambiguities in the exchange in aqueous solutions and strongly polar media: The acceptor of proton can be the free amine, the solvent, and the anion which is derived from the acid, though the free amine is assumed to be the acceptor in these cases. This may be one of the reasons for which the technique has a shortcoming.[10]

The rates of proton exchange of ammonium salts with bases in nonaqueous solutions have been reported in some instances other than dimethyl sulfoxide. Reynolds and Schaefer found that *N,N*-dibenzylmethylamine in trifluoroacetic acid did not show the disappearance of the coupling between NH^+ and CH.[11] This is reasonable because trifluoroacetic acid is a strong acid and trifluoroacetate anion exists as a very dilute solution. As is expected, Delpuech and Gay reported that the proton exchange takes place in a solution of *N*-methylpiperidine derivatives in formic acid.[12] Menger *et al.* determined the rates of proton exchange between *N,N*-dimethylcyclohexylammonium ion and pyridine in the presence of excess of the latter in chloroform-*d* by the dynamic NMR method.[13] Perrin and Wang reexamined the case.[14] Determination of the rates of proton transfer in trisubstituted methanes-triethylamine systems[15] may be considered another area of application of this technique.

We have demonstrated that topomerization by dissociation could be used for determination of the rates of dissociation. Thus dissociation of some organic halides was studied by this technique.[16] This technique is unique in the sense that the rates of dissociation can be determined in the absence of foreign materials, contrasting with the applications cited above which needed excess of either acids or proton accepting bases. Thus it will be possible to see "intrinsic" acidity of an ammonium ion in aprotic solvents by this method.

To observe topomerization by dissociation by dynamic NMR, the compound in question should fulfill the following requirements: 1) The presence of a pair of diastereotopic protons and 2) the site exchange on dissociation. We have found that *N,N*-dibenzylaniline hydrochloride satisfies the conditions and the rates of dissociation of the anilinium ion are suitable for the dynamic NMR study.[2] The principle of the topomerization processes may be written as in Scheme 1.

The benzylic protons are diastereotopic as far as the anilinium proton sticks to the nitrogen atom. When the proton dissociates, the amine inverts, and reprotonation takes place, the whole process corresponds to topomerization and exchange of the sites takes place. Since the free energy of activation for inversion of *N,N*-dibenzylmethylamine is 6.6 kcal/mol (1 cal= 4.184 J),[17] that for inversion of *N,N*-dibenzylaniline must be smaller than this value. Thus if the dynamic NMR technique affords the free energy of activation for the topomerization much higher than 6 kcal/mol, it will mean that we are looking at the proton exchange rates. It was indeed the case as will be discussed later. Then we obtain proton affinity of *N,N*-dibenzylaniline

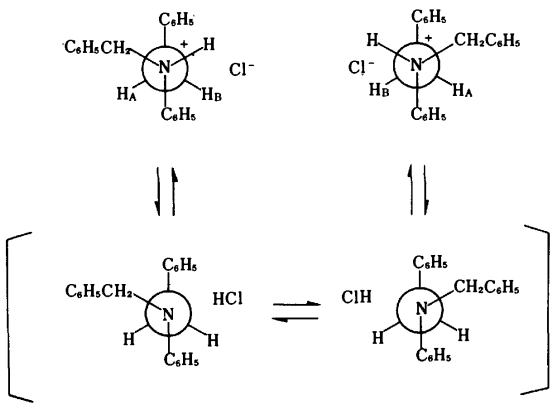

Scheme 1.

as free energy of activation or other kinetic parameters.

Being driven by the success in determining the kinetics, we extended the work to *p*-substituted *N,N*-dibenzylanilines to compare the proton affinity in aprotic solvents with that in the gas phase and the basicity in water. This paper describes the results and discusses the proton affinity of *p*-substituted *N,N*-dibenzylanilines in aprotic solvents together with some points which were important for obtaining reliable data.

Experimental

N,N-Dibenzylaniline is commercially available from Tokyo Kasei Co. and was used as received. It could be purified by recrystallization from ethanol, if necessary. ^{1}H NMR ($CDCl_3$) δ=4.57 (4H, s), 6.6—7.3 (15H, br s).

N,N-*Dibenzyl*-p-*methoxyaniline*. A mixture of 10.0 g (80 mmol) of *p*-methoxyaniline, 23 mL (200 mmol) of benzyl chloride and 20 g of potassium carbonate were heated at 100 °C for 5 h with stirring. The reaction mixture was poured into water and the organic compounds were extracted with ether. After evaporation of the solvent, the residue was recrystallized from ethanol to give 83.4% of the desired compound, mp 80.7 °C (lit,[18,19] mp 81—82 °C). ^{1}H NMR ($CDCl_3$) δ=3.71 (3H, s), 4.53 (4H, s), 6.70 (4H, s), 7.27 (10H, br s).

N,N-*Dibenzyl*-p-*nitroaniline*, mp 131.9 °C, was similarly prepared by heating *p*-nitroaniline and benzyl chloride at 150 °C for 7 d and was purified by recrystallization from hexane-dichloromethane. Found: C, 75.36; H, 5.72; N, 8.54%. Calcd for $C_{20}H_{18}N_2O_2$: C, 75.45; H, 5.69; N. 8.79%. ^{1}H NMR ($CDCl_3$) δ=4.76 (4H, s), 6.72 and 8.08 (4H, ABq, J= 9.6 Hz), 7.1—7.6 (10H, m).

N,N-*Dibenzyl*-p-*chloroaniline*, mp 104.5 °C, was prepared similarly. Found: C, 78.11; H, 5.80; N, 4.54; Cl, 11.55%. Calcd for $C_{20}H_{18}ClN$: C, 78.03; H, 5.89; N, 4.55; Cl, 11.51%. ^{1}H NMR ($CDCl_3$) δ=4.58 (4H, s), 6.60 and 7.03 (4H, ABq, J= 9.5 Hz), 7.1—7.4 (10H, br s).

N,N-*Dibenzyl*-p-*methylaniline*, mp 55.3 °C, was prepared from 2.1 g of *p*-methylaniline and 4.5 g of benzyl chloride in 20 mL of dioxane and 3 g of potassium carbonate by heating for 4 d. Found: C, 87.89; H, 7.08; N, 5.02%. Calcd for $C_{21}H_{21}N$: C, 87.76; H, 7.36; N, 4.87%. ^{1}H NMR ($CDCl_3$) δ= 2.20 (3H, s), 4.57 (4H, s), 6.63 and 6.93 (4H, ABq, J=10 Hz), 7.1—7.4 (10H, br s).

Hydrochlorides. The *N,N*-dibenzylanilines were dissolved in benzene and dry hydrogen chloride was introduced to the solution. The precipitate was collected (it was necessary for the methoxy compound to concentrate the solution) and recrystallized from either hexane-dichloromethane or hexane-tetrahydrofuran. They exhibited the following ^{1}H NMR spectra ($CDCl_3$) δ (only the *p*-substituent given). H, 4.77 (br s), 7.1—7.6 (15H, m); CH_3O, 3.67 (3H, s), 4.64 (4H, br s), 6.7—8.2 (14H, m); Cl, 4.66 (4H, s), 6.8—7.6 (14H, m); CH_3, 2.16 (3H, s), 4.65 (4H, s), 6.8—7.6 (14H, m).

N,N-Dibenzyl-*p*-nitroaniline hydrochloride lost hydrogen chloride on drying.

Dynamic NMR Measurement, Analysis, and Kinetic Parameters. Samples were dissolved in appropriate solvents to make up 30—70 mM solutions unless otherwise stated. ^{1}H NMR spectra were recorded on a JEOL FX-60 spectrometer which operated at 60 MHz. Data were accumulated 500—1000 times. Temperatures were directly read by a thermocouple. The total line shape analysis was performed with the use of a modified Binsch program.[20] The chemical shift differences and coupling constants of the AB protons were checked at several temperatures, where the exchange rate was negligibly small, and were found to be constant within the experimental error. The disappearance of coupling between the NH^+ and CH_2 protons were treated by assuming that J_{AX} and J_{BX} were inversely proportional to the rate constant. T_2 was estimated to be 0.1—0.2 s and treated as a variant, taking into account the line width of tetramethylsilane, together with the rate constant. The AB part of ABX (strictly speaking AA'BB'X) showed different line widths for the A and B protons, as are seen in Fig. 1, due to the different magnitude of couplings with the X proton. Typical values for the coupling constants (J_{AB}, J_{AX}, and J_{BX} and the chemical shift differences ($\Delta\nu_{AB}$) are compiled in Table 1. They differ to some extent by concentrations. The calculated and the observed spectra were compared by the visual fitting. The agreement between the two spectra was excellent.

The rate constant (s^{-1}) used for the calculation of activation parameters shown in Table 4 and 5 are as follows (*p*-substituent, solvent, and temperatures in °C in parentheses given).

p-CH_3O($CDCl_3$): 18.0 (8.1), 23.4 (10.3), 31.8 (12.5), 38.0 (14.7), 50.0 (16.9), 66.6 (19.1) 90.6 (21.3), 118 (23.5)

Table 1. Chemical shift differences ($\Delta\nu_{AB}$) and coupling constants (J_{AB}, J_{AX}, and J_{BX}) of *N,N*-dibenzylanilinium chlorides at low temperatures

p-Substituent	Solvent	$\Delta\nu_{AB}$/Hz	J_{AB}/Hz	J_{AX}/Hz	J_{BX}/Hz
CH_3O	$CDCl_3$	25.4	−12.6	3.7	7.8
	CD_3CN	22.0	−12.9	3.7	7.8
CH_3	$CDCl_3$	24.0	−13.1	3.2	7.0
	CD_3CN	22.7	−12.9	3.9	7.8
H	$CDCl_3$	25.9	−12.6	3.8	7.5
	CD_3CN	23.3	−12.8	3.7	8.1
Cl[a)]	$CDCl_3$	24.8	−12.9	3.4	7.1

a) The coupling constsnts of this entry are those of hydrobromide which were diverted to the hydrochloride because the latter compound showed evidence of exchange, though slow, at the lowest temperature attainable in this solvent.

p-$CH_3O(CD_3CN)$: 14.0(2.3), 19.0(4.9), 29.0(8.8), 41.9(11.9), 47.0(13.6), 57.0(14.9) 74.0(17.1)
p-$CH_3(CDCl_3)$: 12.0(−7.0), 17.0(−4.1), 20.0 (−3.5), 27.0(−1.1), 29.0(−0.6), 33.0(0.5), 48.0(3.1), 60.0(5.0), 84.0(7.9), 92.0(8.5), 122(11.0)
p-$CH_3(CD_3CN)$: 18.0(−5.2), 28.2(−2.0), 38.0 (0.6), 51.0(3.2), 62.0(4.9), 84.0 (7.5)
$H(CDCl_3)$: 13.4(−9.5), 25.0(−7.4), 35.4 (−5.1), 47.0(−2.9), 62.5(−0.7), 84.0(1.5), 110(3.7)
$H(CD_3CN)$: 32.0(−9.5), 54.0(−5.1), 93.0 (−0.7), 180(3.7)
p-$Cl(CDCl_3)$: 13.0(−27.8), 16.0(−25.8) 22.0 (−23.8), 29.0(−22.0), 41.0 (−19.6), 60.0(−17.9).

Results and Discussion

In Fig. 1 are shown temperature dependent spectra of the AB part of ABX signals of N,N-dibenzyl-p-methoxyaniline hydrochloride in chloroform-d together with the calculated. This was chosen because those of N,N-dibenzylaniline hydrochloride were given in a preliminary note.[2]

Although we observe the change in line shapes of the benzylic protons, the dynamic process needs proton acceptors. Since the solvents are not basic in the normal sense, we may neglect the possibility that solvent molecules act as proton acceptors. There are three possible acceptors: chloride ion, free amine, and water. Since water in the solvent was found not easily removable, we turned our attention to the effect of water. Two methodologies were used. First we observed the NH^+ proton signal at δ *ca.* 14 and followed the line shape at temperatures where the coalescence of the CH_2 proton signal took place. No change was observed. If water in the system were the proton acceptor, coalescence of the NH^+ signal with that of water would have been observed. Secondly, we examined the rates of topomerization in chloroform-d, which was carefully dried and to which water was intentionally added.

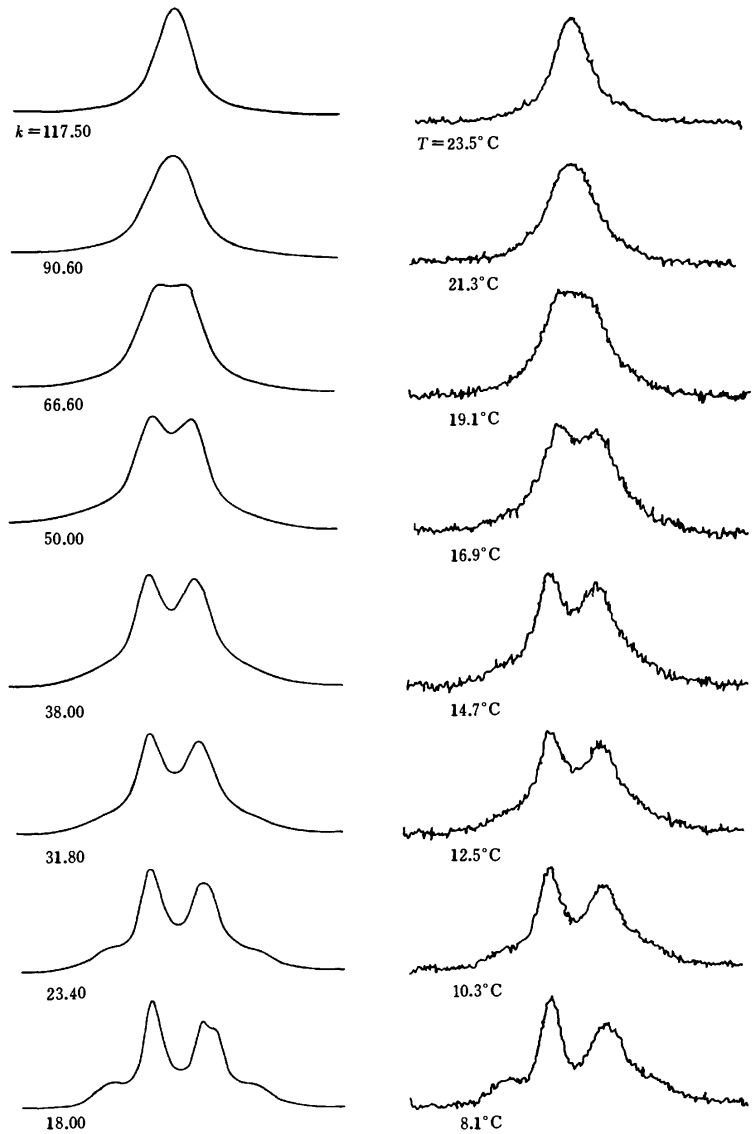

Fig. 1. Calculated and observed spectra of the AB part of ABX signals of N,N-dibenzyl-p-methoxyaniline hydrochloride in chloroform-d.

Table 2. Effect of water in the system on the kinetic parameters of proton-exchange in *N,N*-dibenzylanilinium chloride in chloroform-*d*

Run	1	2	3
Concentration of H_2O (mmol/L)	0.9	5.4	14.9
Correlation Coeff.	0.9991	0.9993	0.9926
$\Delta H^{\neq}$/kcal mol^{-1}	18.5±0.7	19.0±0.6	18.1±2.0
$\Delta S^{\neq}$/e. u.	18.0±2.6	19.7±2.4	16.5±7.4
$\Delta G^{\neq}_{273}$/kcal mol^{-1}	13.6	13.6	13.6

Table 3. Effect of concentration of substrate on kinetic parameters of proton exchange in *N,N*-dibenzylanilinium chloride in chloroform-*d*

Run	1	2	3
Concn/mmol L^{-1}	31.0	62.0	121.6
Correlation coeff.	1.0000	0.9993	0.9999
$\Delta H^{\neq}$/kcal mol^{-1}	20.9±0.0	19.6±0.6	20.3±0.0
$\Delta S^{\neq}$/e. u.	27.8±0.0	19.7±2.4	23.4±0.1
$\Delta G^{\neq}_{273}$/kcal mol^{-1}	13.3	13.6	14.0

Table 4. Substituent effect on kinetic parameters of proton exchange in *N,N*-dibenzylanilinium chloride in chloroform-*d*

p-Substituent	CH_3O	CH_3	H	Cl
T_c/°C	19.1	5.0	−0.7	−17.9
Correlation coeff.	0.998	0.999	0.999	0.995
$\Delta H^{\neq}$/kcal mol^{-1}	19.5±0.9	19.0±0.4	18.5±0.7	18.6±1.8
$\Delta S^{\neq}$/e. u.	16.6±3.1	17.9±1.4	18.0±2.6	22.8±7.5
$\Delta G^{\neq}_{273}$/ kcal mol^{-1}	15.0	14.1	13.6	12.4
k_{289}/s^{-1}	1.35×10^2	6.33×10^2	1.48×10^3	1.32×10^4

The results are compared in Table 2, where chloroform-*d* containing 5.4 mmol L^{-1} of water is the commercially available and is used as such. As are seen in Table 2, if water was intentionally added, the correlation coefficient in the Eyring plot became inferior and consequently the errors involved became large. Yet the free energy of activation is reproduced. We ran the similar determination of rates of dissociation in the methoxy compound with various concentrations of water. No effect of the water was observed. Therefore, as far as we use ordinary chloroform-*d*, the data are reliable. These results also rejects the possibility that water is the proton acceptor in the system.

If the free amine which exists in a minute amount in the system accepts proton, we should be able to observe the concentration effects. The data are collected at three concentrations and are summarized in Table 3. It may seem that the free energy of activation increases as the concentration increases. However, we do not believe that the tendency is significant because of the experimental errors which do not appear here. If free amine accepts proton, the rates of exchange of proton must increase as the concentration increases, contrary to the data shown in Table 3. Therefore, we conclude that the amine in the system, if any, is not the proton acceptor.

These two lines of evidence establish that the chloride ion in the system is the proton acceptor. From the concentration effect, we may conclude that the chloride ion, which exists as an ion pair with the anilinium ion, accepts proton in the process which is observed by the present technique.

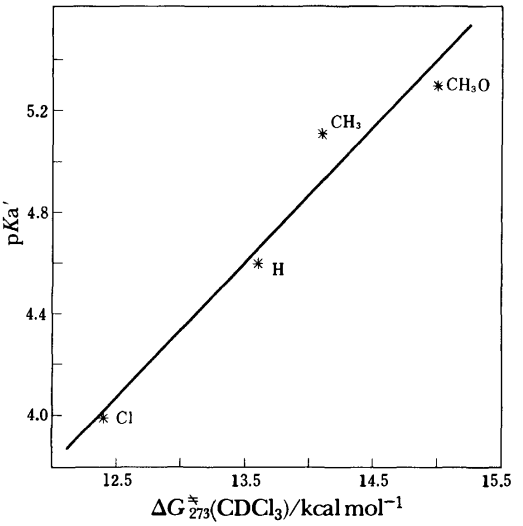

Fig. 2. Correlation between pK_a' values of *p*-substituted *N,N*-dimethylanilines and free energies of activation for the proton exchange of *p*-substituted *N,N*-dibenzylanilinium chlorides in chloroform-*d*.

Having established that the kinetic proton affinity of *N,N*-dibenzylaniline can be obtained by this technique, we turned our attention to the substituent effects. The study in this area will contribute to the genral understanding of acid-base properties of amines in aprotic solvents which are often important in organic chemistry. The results are compiled in Table 4. The results are in good agreement with the expectation from basicities in water: the *p*-methoxy compound is the strongest base and the chloro compound is the weakest of the four. It is unfortunate that the nitro compound failed to give stable hydrochloride but, if it could, the free energy of activation for the proton exchange of the compound must have been still smaller.

The feature of the data is a very large positive entropy of activation. Since the dissociation of a covalent compound into ionic species is known to be accompanied by a large negative entropy of activation,[21] the reaction studied here, from the ionic to the covalent, can be accompanied by positive entropy of activation. The freedom of motion of solvent molecules is cited to be responsible to the phenomena. The increase in entropy of activation seems to become large when we go from an electron-donating substituent to an electron-withdrawing one. If this trend is significant, that will mean that the transition state for the exchange is less covalent in the electron-rich compound than in the electron-poor one. That is the transition state is earlier in the former than in the latter. The enthalpy of activation varies little but there is a tendency that an electron-rich amine shows a large value.

It should be of interest to compare the proton affinity of the *N,N*-dibenzylanilines obtained here with those in water and in the gas phase. Hammett plot yielded a good linear relationship, the correlation coefficient being 0.979 and ρ being 3.59. Fig. 2 illustrates the relationship between the free energy of activation and the pK_a' values reported for *N,N*-dimethylanilines.[22] The correlation coefficient is 0.996. Since the proton

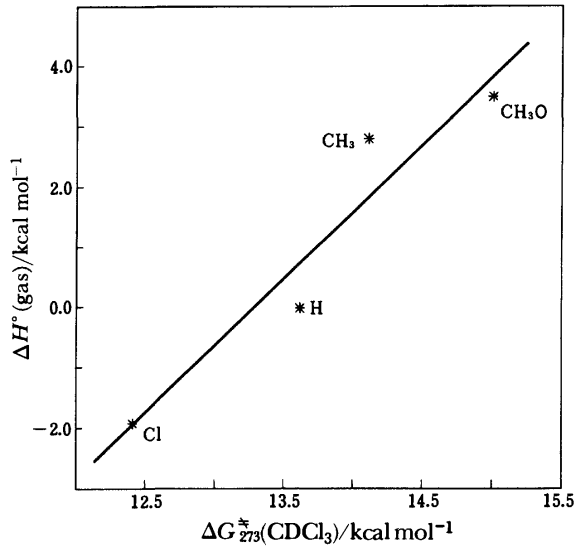

Fig. 3. Enthalpies of isodesmic process, $C_6H_5NH_3^+ + p\text{-}XC_6H_4NH_2 \rightleftharpoons C_6H_5NH_2 + p\text{-}XC_6H_4NH_3^+$ in the gas phase *vs.* free energies of activation for the proton exchange of *p*-substituted *N,N*-dibenzylanilinium chlorides in chloroform-*d*.

affinity of anilines in the gas phase is linearly correlated with the pK_a in water,[23] it will be no wonder to obtain a linear relationship between the proton affinity in the gas phase and that in the aprotic solvent. Figure 3 illustrates the result. The correlation coefficient is 0.958. Although it is known that the gas-phase proton affinity is quite different from the basicity in water when the structures of bases change,[4c] the proton affinity of substituted anilines in chloroform, at least, can be linearly correlated with the basicity in water and the proton affinity in the gas phase.

In order to get into further insight, we have tried to change the solvent. Acetone-d_6 was found to exchange proton with NH^+ and tetrahydrofuran was a poor solvent for the anilinium chloride. Acetonitrile-d_3 could afford data of 3 compounds, although the solubility of the chloro compound was too low to be practical in the measurement. The kinetic data are compiled in Table 5. The data have similar trends which are pointed out in the above sections on the behaviors in chloroform-*d* except some points discussed below.

Comparison of the data in acetonitrile-d_3 and those in chloroform-*d* reveals some interesting points. First of all, the solvent effect is not so dramatic as is expected from the change in dielectric constants. One might have expected that dissociation in acetonitrile should be slower than in chloroform because the ionic ground state is stabilized in the former. However, this similarity of the rates of dissociation in the two solvents is a mere coincidence at or near temperatures where coalescence of the signals takes place. When we divide the activation parameters into enthalpy of activation and entropy of activation, difference is clear. This may be one of the examples of enthalpy-entropy compensation effect.[24] Both enthalpy and entropy of activation with the chloroform solutions are larger than those with acetonitrile solutions. Possibly the transition state for the proton exchange in acetonitrile becomes earlier than that in chloroform because the ionic ground state is stabilized and the transition state is like the ground state in the former. The smaller entropy of activation in acetonitrile solutions than that in chloroform supports the idea. Thus we conclude that the transition state for the proton exchange in these aprotic solvents becomes early as the proton afinity of the base and the dielectric constant of the solvent increase. The rationale for the phenomena on the molecular basis undoubtedly includes the polar nature and/or hydrogen-bonding ability of the molecule but there may remain some others which are not clear at the moment.

Table 5. Substituent effect on kinetic parameters of proton exchange in *N,N*-dibenzylanilinium chloride in acetonitrile-d_3

p-Substituent	CH_3O	CH_3	H
T_c/°C	14.9	4.9	—
Correlation coeff.	0.999	0.999	0.999
ΔH^*/kcal mol^{-1}	17.0±0.6	17.4±0.5	17.2±0.8
ΔS^*/e. u.	8.6±2.3	12.3±1.9	13.7±2.8
ΔG^*_{273}/kcal mol^{-1}	14.7	14.0	13.4
k_{289}/s^{-1}	1.60×10^2	5.58×10^2	1.30×10^3

This work was supported by a Grant in Aid for Scientific Research of the Ministry of Education, Science and Culture, to which our thanks are due.

References

1) Part IV: M. Ōki and M. Ohira, *Chem. Lett.*, **1982**, 1267.
2) A preliminary note was published: M. Ōki, Y. Yoshioka, H. Kihara, and N. Nakamura, *Chem. Lett.*, **1980**, 1625.
3) For example, see D. D. Perrin, "Dissociation Constants of Organic Bases in Aqueous Solution", Butterworth, London (1965): Supplement, 1972.
4) a) M. S. B. Mansou, *J. Am. Chem. Soc.*, **87**, 2332 (1965); b) J. I. Brauman, J. M. Riveros, and L. K. Blair, *ibid.*, **93**, 3914 (1971); c) J. P. Briggs, R. Yamdagni, and P. Kebarle, *ibid.*, **94**, 5128 (1972).
5) F. M. Jones, III, and E. M. Arnett, *Progr. Phys. Org. Chem.*, **11**, 263 (1974): E. M. Arnett, F. M. Jones, III, M. Taagapera, W. G. Henderson, D. Holtz, J. L. Beauchamp, and R. W. Taft, *J. Am. Chem. Soc.*, **94**, 4724 (1972); R. W. Taft, J. F. Wolf, J. L. Beauchamp, G. Scorrano, and E. M. Arnett, *ibid.*, **100**, 1240 (1978).
6) E. Grunwald, A. Loewenstein, and S. Meiboom, *J. Chem. Phys.*, **27**, 630 (1957).
7) M. Saunders and F. Yamada, *J. Am. Chem. Soc.*, **85**, 1882 (1963).
8) a) J.-J. Delpuech and M.-M. Deschamps, *Nouv. J. Chim.*, **2**, 563 (1978); b) B. Bianchin, J. Chrisment, J.-J. Delpuech, M. N. Deschamps, D. Nicole, and G. Serratrice, *Protons Ions Involved Fast Dyn. Phenom., Proc. Int. Meet. Soc. Chim. Phys., 30th 1977*, 265: *CA*, **90**, 120775m (1979).
9) J.-J. Delpuech and B. Bianchin, *J. Am. Chem. Soc.*, **101**, 383 (1979). See also ref. 8b.
10) W. R. Morgan and D. E. Leyden, *J. Am. Chem. Soc.*, **92**, 4527 (1970).
11) W. F. Reynolds and T. Schaefer, *Can. J. Chem.*, **42**, 2119 (1964).
12) J.-J. Delpuech and C. Gay, *Tetrahedron Lett.*, **1966**, 2603.
13) F. M. Menger, T. D. Singh, and F. L. Bayer, *J. Am. Chem. Soc.*, **98**, 5011 (1976).

14) C. L. Perrin and W.-H. Wang, *J. Am. Chem. Soc.*, **104**, 2325 (1982).
15) V. K. Pogorelyi, T. B. Vishnyakova, and I. P. Gragerov, *Ter. Exsp. Khim.*, **18**, 590 (1982): *CA*, **98**, 34146r (1983).
16) M. Ōki, A. Shimizu, H. Kihara, and N. Nakamura, *Chem. Lett.*, **1980**, 607: A. Shimizu, Y. Sakamaki, K. Azuma, H. Kihara, N. Nakamura, and M. Ōki, *Bull. Chem. Soc. Jpn.*, **54**, 2774 (1981).
17) C. H. Bushweller, J. W. O'Neil, and H. S. Bilofsky, *Tetrahedron*, **28**, 2697 (1972).
18) F. Walls and J. Cabarello, *Bol. Inst. Quim. Univ. Nacl. Auton. Mex.*, **15**, 74 (1963): *CA*, **61**, 8215 (1964).
19) M. Sekiya, M. Tomie, and N. J. Leonard, *J. Org. Chem.*, **33**, 318 (1968).
20) G. Binsch, *Top. Stereochem.*, **3**, 97 (1968).
21) A. A. Frost and R. G. Pearson, "Kinetics and Mechanism," John-Wiley, New York (1953), p. 127.
22) Y. Ogata and I. Tabushi, *Bull. Chem. Soc. Jpn.*, **31**, 969 (1958).
23) K. D. Summerhays, S. K. Pollack, R. W. Taft, and W. J. Hehre, *J. Am. Chem. Soc.*, **99**, 4585 (1977).
24) J. E. Leffler, *J. Org. Chem.*, **20**, 1202 (1955).

Photoreduction of 2-Benzoylalkanoates

Michikazu YOSHIOKA,* Satoshi AOKI, Toshio SHIMIZU,† and Tadashi HASEGAWA*,†
Department of Chemistry, Saitama University, Shimo-okubo, Urawa, Saitama 338
†*Department of Chemistry, Tokyo Gakugei University, Nukuikitamachi, Koganeishi, Tokyo 184*
(Received February 21, 1984)

2-Benzoylalkanoates **1** undergo photoreduction with 2-propanol. The photoreduction products are classified into three types according to their origin: the homo-pinacol-type products **2**, **5**, **7**, and **8**, the mixed-pinacol-type product **3**, and the β-hydroxy ester **6**. The product distribution is affected by α-methyl substitution. The α-methyl substitution decreases the percentage of the homo-pinacol-type products and increases the percentage of the β-hydroxy ester.

Synthetic[1] and mechanistic[2] aspects of the photoreduction of aryl alkyl ketones have been extensively investigated, and work has also been done on the photoreduction of α-dicarbonyl compounds.[3] A number of α-substituted acetophenones form pinacols upon irradiation in 2-propanol or other suitable hydrogen-donating solvents.[4] However, little attention has been given to the photoreduction of β-dicarbonyl compounds. Singh and Kagan reported[5] that ethyl acetoacetate undergoes photoreduction with alcohols to give 4,5-dihydro-4-hydroxy-2(3*H*)-furanones *via* mixed pinacols. We report here that 2-benzoyl-alkanoates **1** undergo photoreduction with 2-propanol to give the homo- and the mixed-pinacol-type products, and the β-hydroxy ester, and that the course of the photoreduction is affected by α-methyl substituents.

Results and Discussion

Irradiation of ethyl benzoylacetate (**1a**) in 2-propanol with a high-pressure mercury lamp under nitrogen yielded *meso*- and *dl*-diethyl-3,4-dihydroxy-3,4-diphenyladipates (*meso*-**2a** and *dl*-**2a**) and 4,5-dihydro-4-hydroxy-5,5-dimethyl-4-phenyl-2(3*H*)-furanone (**3a**) in 34, 32, and 6% yields, respectively. The diastereomeric pinacols *meso*-**2a** and *dl*-**2a** could be isolated by silica-gel chromatography. These compounds *meso*-**2a**, *dl*-**2a**[6] and **3a**[7] were identified by comparison with authentic samples. The dihydro-2(3*H*)-furanone **3a** can best be explained as the *secondary* product derived from an initially formed mixed pinacol **4a**. No formation of the mixed pinacol is observed in acetophenone

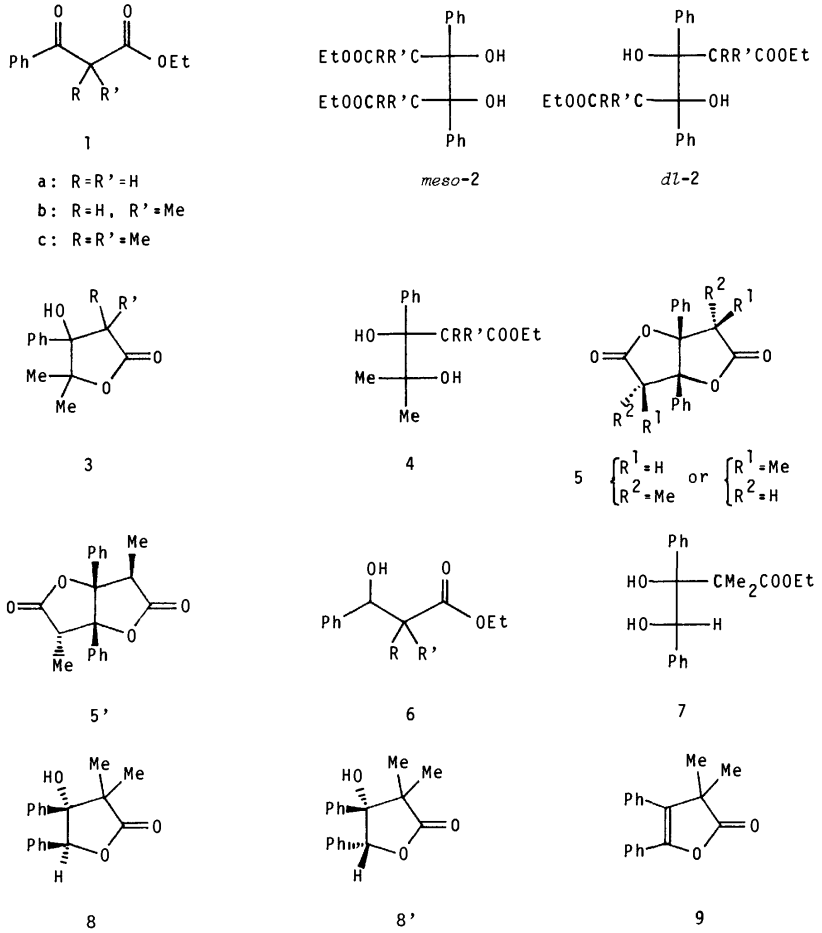

Fig. 1.

Table 1. Yields of the products in photolysis of **1a**, **1b**, and **1c**

Starting compound	Homo-pinacol-type product (Yield/%)								Mixed-pinacol-type product (Yield/%)	β-Hydroxy ester (Yield/%)
	meso-**2**	*dl*-**2**	**5**	**5′**	**7**	**8**	**8′**	Total	**3**	**6**
1a	34	32	—	—	—	—	—	66	6	—
1b	5	—	12	10	—	—	—	27	—	7
1c	—	—	—	—	7	11	1	19	14	27

photoreduction by 2-propanol.[2] Both the adipates and the dihydro-2(3*H*)-furanone formations were efficiently quenched by 1,3-pentadiene, and ethyl 2-naphthoylacetate, which is expected to have the lowest triplet with π,π^* configuration, gave no photoreduction products under the same conditions. Therefore, both the adipates and the dihydro-2(3*H*)-furanone arise from the n,π^* triplet state of the benzoylacetate **1a**.

Irradiation of ethyl 2-benzoylpropionate (**1b**) under the same conditions gave *meso*-diethyl-3,4-dihydroxy-2,5-dimethyl-3,4-diphenyladipate (**2b**), 4,8-dimethyl-1,5-diphenyl-2,6-dioxa-bicyclo[3.3.0]octane-3,7-diones (**5** and **5′**), and ethyl 3-hydroxy-2-methyl-3-phenylpropanoate (**6b**) in 5, 22 (**5**: 12, **5′**: 10), and 7% yields, respectively. The structure of **2b** was deduced from its spectroscopic and analytical data. The *meso*- and/or *dl*-isomers seem to be produced from photoreduction of the ester **1b**. However, the isolated photoproduct **2b** is deduced to be one of the isomers because the compound has a sharp melting point (184—185 °C) and shows a simple NMR spectrum. The pinacol **2b** is elucidated to have the *meso*-configuration because no dilactones were formed when the pinacol **2b** was heated at 240 °C for 30 min. The *dl*-**2a** lactonizes easily by heating, while *meso*-**2a** does not.[6] The *dl*-**2b** seems to cyclize to give dilactones **5** and **5′** under the experimental conditions. The geometry of the dilactones from *dl*-**2b** must be *cis* with respect to two phenyl groups. The stereoisomeric dilactones **5** and **5′** could be isolated by silica-gel chromatography. The IR spectra of **5** and **5′** showed the characteristic absorptions of a five-membered lactone at 1800 and 1790 cm^{-1}, respectively. The ^1H NMR signals of the two methyl groups in **5** appeared at δ 1.24 while those signals in **5′** were observed at δ 1.18 and 1.20. The methyl groups in **5** are equivalent and are either *cis* or *trans* to the neighboring phenyl group. On the other hand, one methyl group in **5′** might be *cis* to the neighboring phenyl group and the other might be *trans*. The ^{13}C NMR spectra also support the assignment of **5** and **5′**. The β-hydroxy ester **6b** was identified by direct comparison with an authentic sample.[8] This type of the product is found in acetophenone photoreduction with 2-propanol.[2] No products derived from a mixed pinacol were isolated; however, the possibility of their presence in small amounts cannot be eliminated.

Irradiation of ethyl 2-benzoyl-2-methylpropanoate (**1c**) under the same conditions gave 4,5-dihydro-4-hydroxy-3,3,5,5-tetramethyl-4-phenyl-2(3*H*)-furanone (**3c**), ethyl 3-hydroxy-2,2-dimethyl-3-phenylpropanoate (**6c**), ethyl 3,4-dihydroxy-2,2-dimethyl-3,4-diphenylbutanoate (**7**), and 4,5-dihydro-4-hydroxy-3,3-dimethyl-4,5-diphenyl-2(3*H*)-furanones (**8** and **8′**) in 14, 27, 7, and 12 (**8**: 11, **8′**: 1) % yields, respectively. The hydroxy ester **6c** was identified by comparison with an authentic sample.[9] The structural assignment of **3c** was based on its spectroscopic and analytical data. The IR spectrum of **3c** showed a γ-lactone carbonyl band at 1760 cm^{-1} and hydroxy bands at 3600 and 3400 cm^{-1}. The ^1H NMR spectrum showed four methyl singlets at δ 1.04, 1.20, 1.45, and 1.60. The lactone **3c** seems to be the *secondary* product derived from an initially formed mixed pinacol **4c**. In the photoreduction of isobutyrophenone or pivalophenone by 2-propanol, no mixed pinacols are found.[2] The structures of **7**, **8**, and **8′** were deduced from their spectroscopic and analytical data and further supported by the chemical evidence. The hydroxy lactone **8′** underwent dehydration to give 3,3-dimethyl-4,5-diphenyl-2(3*H*)-furanone (**9**) by heating in dioxane in the presence of *p*-toluenesulfonic acid, while the lactone **8** was recovered under the same conditions. Therefore, the hydroxyl group should be *trans* in **8′** and *cis* in **8** to the C_5-hydrogen atom. The dihydroxy ester **7** cyclized to give the lactone **8′** when the ester was heated at 250°C for 15 min. No isomeric lactone **8** could be detected. This fact suggests that the dihydroxy ester **7** has an *erythro*-geometry. The ester **7** seems to be produced from the homo-pinacol *meso*-**2c** and/or dl-**2c** *via* a phenyl ketone **10**, though these intermediates could not be isolated (Eq. 1). Elimination of ethyl 2-

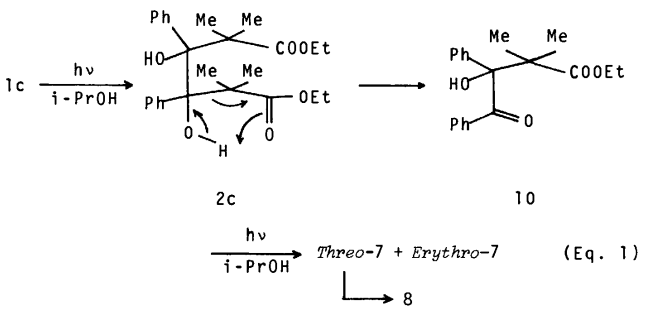

Scheme 1.

methylpropanoate from the pinacol **2c** probably occurs easily owing to the steric compression. Photoreduction of the ketone **10** will give the *erythro*-dihydroxy ester **7** and its *threo*-isomer. The IR absorption at 1690 cm^{-1} in the *erythro*-ester **7** suggests the presence of the intramolecular hydrogen bonding between the carbonyl group and the C_3-hydroxyl group. The hydrogen bonding is also expected in the *threo*-isomer. The rate of lactonization of these dihydroxy esters might be enhanced by the participation of the C_3-hydroxyl group because of the decrease in electron density at the carbonyl carbon atom. The *threo*-isomer is probably reactive enough to lactonize easily to give **8**. However, the *erythro*-isomer is stable under the experimental conditions. The stability of the *erythro*-isomer may be explained in terms of the lack of the participation of the C_3-hydroxyl group in the early stage of the transition

state,because of steric repulsive interaction between the C_4-phenyl and the C_3-hydroxyl group. The C_4-phenyl group must be eclipse to the C_3-hydroxyl group in the transition state.

Photoreduction products from 2-benzoylalkanoates **1a**, **1b**, and **1c** are classified into three types according to their origin: the homo-pinacol-type products **2**, **4**, **7**, **8**, and **8′**, the mixed-pinacol-type product **3**, and the β-hydroxy ester **6**. The total yield of the homo-pinacol-type products decreases upon α-methyl substitution, while that of the hydroxy ester increases upon the substitution. These results can be explained in terms of an increment of the steric hindrance in free radical combination.

Experimental

All melting points were uncorrected. The IR spectra were recorded on a JASCO IRA-2 spectrometer. The ^1H and ^{13}C NMR spectra were measured on a JEOL FX-90Q spectrometer using TMS as an internal standard. The mass spectra were obtained with a JEOL JMS-OlSG-2 spectrometer. Irradiations were carried out with an Ushio 450 W high-pressure mercury lamp or a Rikoh Kagaku 100 W high-pressure mercury lamp with a water-cooled Pyrex jacket.

Chemicals. Ethyl benzoylacetate (**1a**) from Tokyo Kasei Kogyo Co. was purified by distillation. Ethyl 2-benzoylpropanoate (**1b**),[9] ethyl 2-benzoyl-2-methylpropanoate (**1c**),[10] and ethyl 2-naphthoylacetate[11] were pepared according to the reported methods.

Photoreaction of 1a. A solution of **1a** (1.018 g, 5.30 mmol) in 2-propanol (60 cm^3) was irradiated for 30 h under nitrogen with a 450 W high-pressure mercury lamp. After removal of the solvent, the residue was chromatographed on silica gel. Elution with benzene–ethyl acetate (10:1) gave *meso*-**2a** (348 mg, 34%), *dl*-**2a** (330 mg, 32%), and **3a** (63 mg, 6%). The spectroscopic data of *meso*-**2a**, *dl*-**2a**, and **3a** were identical with those of the authentic samples.[6,7]

Photoreaction of 1b. A solution of **1b** (1.200 g, 5.83 mmol) in 2-propanol (120 cm^3) was irradiated for 3.5 h with a 100 W high-pressure mercury lamp. The usual work-up gave the unreacted ester **1b** (300 mg), *meso*-**2b** (46 mg, 5%), **5** (110 mg, 12%), **5′** (90 mg, 10%), and *threo/erythro* 1:1 mixture of **6b** (65 mg, 7%). The spectroscopic data of **6b** were identical with those of the authentic sample.[8] *meso*-**2b** mp 184—185 °C; IR ($CHCl_3$) 3500 and 1700 cm^{-1}; ^1H NMR ($CDCl_3$) δ= 0.59 (6H, d, J=7.0 Hz, CH_3), 0.78 (6H, t, J=7.2 Hz, CH_3), 3.55 (2H, q, J=7.0 Hz, CH), 3.56 (4H, q, J=7.2 Hz, CH_2), 3.86 (1H, s, OH), *ca.* 7.10—7.30 (6H, m, aromatic), and *ca.* 7.50—7.70 (4H, m, aromatic); ^{13}C NMR ($CDCl_3$) δ=1.36 (q, 4C), 46.8 (d, 2C), 60.2 (t, 2C), 79.7 (s, 2C), 127.1 (d, 8C), 128.3 (d, 2C), 144.8 (s, 2C), and 176.7 (s, 2C). Found: C, 69.28; H, 7.21%. Calcd for $C_{24}H_{30}O_6$: C, 69.54; H, 7.30%. **5** mp 191—192 °C; IR ($CHCl_3$) 1800 cm^{-1}; ^1H NMR ($CDCl_3$) δ=1.24 (6H, d, J=7.2 Hz, CH_3), 3.30 (2H, q, J=7.2 Hz, CH), *ca.* 6.65—7.00 (4H, m, aromatic), and *ca.* 7.00—7.40 (6H, m, aromatic); ^{13}C NMR ($CDCl_3$) δ=7.6 (q, 2C), 43.4 (d, 2C), 93.4 (s, 2C), 126.0 (d, 4C), 128.5 (d, 4C), 129.1 (d, 2C), 132.4 (s, 2C), and 174.5 (s, 2C); MS m/z 322 (M^+). Found: C, 74.35; H, 5.62%. Calcd for $C_{20}H_{18}O_4$: C, 74.51; H, 5.62%. **5′** mp 167—168 °C; IR ($CHCl_3$) 1790 cm^{-1}; ^1H NMR ($CDCl_3$) δ=1.18 (3H, d, J=8.4 Hz, CH_3), 1.20 (3H, d, J=7.2 Hz, CH_3), 3.11 (1H, q, J=8.4 Hz, CH), 3.17 (1H, q, J=8.4 Hz, CH), and *ca.* 6.60—7.40 (10H, m, aromatic); ^{13}C NMR ($CDCl_3$) δ=7.9 (q), 14.8 (q), 44.5 (d), 47.5 (d), 92.6 (s), 94.8 (s), 126.8 (d, 2C), 127.4 (d, 2C), 127.6 (d, 2C), 128.5 (d, 2C), 129.0 (d), 129.4 (d), 131.4 (s), 133.8 (s), 173.8 (s), and 176.2 (s). Found: C, 74.38; H, 5.62%. Calcd for $C_{20}H_{18}O_4$: C, 74.51; H, 5.62%.

Photoreaction of 1c. A solution of **1c** (4.000 g, 18.18 mmol) in 2-propanol (400 cm^3) was irradiated for 12 h with a 450 W high-pressure mercury lamp. The usual work-up gave the unreacted ester **1c** (2.164 g), **3c** (260 mg, 14%), **6c** (500 mg, 27%), **7** (125 mg, 7%), **8** (195 mg, 11%), and **8′** (20 mg, 1%). The spectroscopic data of **6c** was identical with those of the authentic sample.[9] **3c** mp 151—152 °C; IR ($CHCl_3$) 3600, 3400, and 1760 cm^{-1}; ^1H NMR ($CDCl_3$) δ=1.04 (3H, s, CH_3), 1.20 (3H, s, CH_3), 1.45 (3H, s, CH_3), 1.60 (3H, s, CH_3), 2.31 (1H, s, OH), and *ca.* 7.15—7.50 (5H, m, aromatic); ^{13}C NMR ($CDCl_3$) δ=23.5 (q), 23.9 (q), 26.0 (q), 27.0 (q), 48.6 (s), 83.7 (s), 88.3 (s), 126.6 (d, 2C), 127.6 (d, 2C), 127.8 (d), 140.5 (s), and 181.0 (s). Found: C, 71.53; H, 7.69%. Calcd for $C_{14}H_{18}O_3$: C, 71.77; H, 7.74%. **7** mp 106—107 °C; IR ($CHCl_3$) 3600, 3450, and 1690 cm^{-1}; ^1H NMR ($CDCl_3$) δ=0.94 (3H, s, CH_3), 1.05 (3H, t, J=7.0 Hz, CH_3), 1.32 (3H, s, CH_3), 2.76 (1H, d, J= 7.0 Hz, OH, D_2O exchangeable), *ca.* 3.10—3.70 (2H, m, CH_2), 5.32 (1H, d, J=7.0 Hz, CH), 5.64 (1H, s, OH, D_2O exchangeable), and *ca.* 7.20—7.80 (10H, m, aromatic); ^{13}C NMR ($CDCl_3$) δ=13.5 (q), 20.6 (q), 25.0 (q), 47.5 (s), 61.2 (t), 76.2 (d), 82.5 (s), 127.3 (d), 127.4 (d, 2C), 127.7 (d, 2C), 128.0 (d), 128.3 (d, 2C), 129.2 (d, 2C), 140.0 (s), 140.1 (s), and 178.2 (s). Found: C, 73.03; H, 7.25%. Calcd for $C_{20}H_{24}O_4$: C, 73.14; H, 7.37%. **8** mp 169—170 °C; IR ($CHCl_3$) 3550 and 1775 cm^{-1}; ^1H NMR ($CDCl_3$) δ=1.08 (3H, s, CH_3), 1.23 (3H, s, CH_3), 1.54 (1H, s, OH), 6.24 (1H, s, CH), and *ca.* 7.20—7.65 (10H, m, aromatic); ^{13}C NMR ($CDCl_3$) δ=16.2 (q), 22.8 (q), 49.7 (s), 81.8 (d), 83.3 (s), 126.8 (d, 3C), 128.3 (d, 3C), 128.6 (d, 2C), 128.8 (d, 2C), 133.0 (s), 137.3 (s), and 179.7 (s); MS m/z (rel intensity) 282 (M^+, 3), 148 (100), 133 (21), 105 (40), and 77 (19). Found: C, 76.51; H, 6.36%. Calcd for $C_{18}H_{18}O_3$: C, 76.57; H, 6.43%. **8′** mp 207—208 °C (lit,[12] 210—212 °C); IR ($CHCl_3$) 3450 and 1775 cm^{-1}; ^1H NMR ($CDCl_3$) δ=0.94 (3H, s, CH_3), 1.56 (3H, s, CH_3), 2.44 (1H, s, OH), 5.76 (1H, s, CH), and *ca.* 6.90—7.40 (10H, m, aromatic); ^{13}C NMR ($CDCl_3$) δ=19.6 (q), 21.9 (q), 48.9 (s), 84.7 (s), 85.1 (d), 125.4 (d, 2C), 125.6 (d, 2C), 127.5 (d, 2C), 127.8 (d, 2C), 127.9 (d, 2C), 134.7 (s), 138.3 (s), and 179.9 (s); MS m/z (rel intensity) 282 (M^+ 2), 148 (100), 134 (19), 105 (26), and 77 (10). Found: C, 76.53; H, 6.42%. Calcd for $C_{18}H_{18}O_3$: C, 76.57; H, 6.43%.

Dehydration of 8′. A solution of 23.0 mg of **8′** and 35 mg of *p*-toluenesulfonic acid in 11 cm^3 of dioxane was heated under reflux for 50 h. The solvent was evaporated, and the residue was extracted with ether. After the usual work-up, the reaction mixture was chromatographed on silica gel to give 18.8 mg (89%) of 3,3-dimethyl-4,5-diphenyl-2(3*H*)-furanone (**9**): mp 107—108 °C; IR ($CHCl_3$) 1800 cm^{-1}; ^1H-NMR ($CDCl_3$) δ=1.36 (6H, s, CH_3) and *ca.* 7.10—7.50 (10H, m, aromatic); ^{13}C NMR ($CDCl_3$) δ=23.4 (q, 2C), 48.1 (s), 123.9 (s), 126.9 (d, 3C), 128.2 (d, 3C), 128.8 (s), 129.0 (d, 2C), 129.7 (d, 2C), 132.6 (s), 145.4 (s), and 181.0 (s). Found: C, 81.88; H, 6.04%. Calcd for $C_{18}H_{16}O_2$: C, 81.79; H, 6.10%.

Thermolysis of 7. The dihydroxy ester **7** (8.8 mg) was sealed in a Pyrex tube, and heated at 250 °C for 15 min. The ^1H NMR analysis showed that the thermolysis mixture consists of ethanol, ethyl 2-methylpropanoate, benzoin, and dihydro-2(3*H*)-furanone **8′** in a 1:1:1:1 ratio.

References

1) A. Schönberg, "Preparative Organic Photochemistry," Springer-Verlag, New York (1968), pp. 198—213.

2) F. D. Lewis and J. G. Magyer, *J. Org. Chem.*, **37**, 2102 (1972) and the references cited therein.

3) E. S. Huyser and D. C. Neckers, *J. Org. Chem.*, **29**, 276 (1964).

4) S. G. Cohen, A. parola, and G. H. Parsons, Jr., *Chem. Rev.*, **73**, 141 (1973).

5) S. P. Singh and J. Kagan, *J. Chem. Soc., D*, **1969**, 1121.
6) E. Beschke, *Justus Liebigs Ann. Chem.*, **384**, 152 (1911).
7) A. Fabrycy and K. Koalowski, *Rocz. Chem.*, **41**, 251 (1967).
8) H. E. Zimmerman and J. English, Jr., *J. Am. Chem. Soc.*, **76**, 2291 (1954).
9) L. Birkhofer, A. Ritter, and H. Wieden, *Chem. Ber.*, **95**, 971 (1962).
10) P. L. Bayless and C. R. Hauser, *J. Am. Chem. Soc.*, **76**, 2306 (1954).
11) C. Weizman and E. B. Falkner, *J. Chem. Soc.*, **89**, 122 (1906).
12) R. B. Burpitt, K. C. Brannock, R. G. Nations, and J. C. Martin, *J. Org. Chem.*, **36**, 2222 (1971).

Optical Resolution of DL-Valine, DL-Leucine, and DL-Isoleucine by Formation of Adduct with L-Phenylalanine

Tadashi SHIRAIWA,* Akihiko IKAWA, Keiji SAKAGUCHI, and Hidemoto KUROKAWA
Faculty of Engineering, Kansai University, Yamate-cho, Suita-shi, Osaka 564
(Received March 7, 1984)

An alkaline solution containing L-phenylalanine (L-Phe) and one of DL-valine, DL-leucine, and DL-isoleucine is allowed to selectively form a precipitate composed of L-Phe and the aliphatic D-amino acid by adjusting the pH of initial solution to around 5.5 with hydrochloric acid. ^{1}H NMR spectra in deuterium oxide, elemental analyses, and infrared spectra of the precipitates indicate that they are adducts of the aliphatic D-amino acid and L-Phe in the molar ratio of 1:1. The free aliphatic D-amino acids with high optical purity (84—100%) may be recovered from the adducts in 49—63% yield. An attempt was made to obtain both the aliphatic D- and L-amino acids by using an aqueous solution containig the aliphatic DL-amino acid and L-Phe as an initial solution. The aliphatic L-amino acids obtained had optical purity of 47—85%.

A number of studies have been reported on optical resolution of DL-amino acids, and most of them have employed the preferential crystallization procedure.[1-8] Although the advantages of this procedure have been well recognized,[9,10] it should be noted that a racemate crystallizes as a conglomerate from a racemic solution and not as a racemic compound. Most of free DL-amino acids form racemic compounds and have no properties suitable for this procedure. Therefore, many of optical resolutions by this procedure have been carried out in the form of salts[3,6] or their derivatives such as *N*-acyl compounds.[1,2,4,5,7,8] Free optically active amino acids are recovered by hydrolysis of resolved derivatives, and the process may result in lowering of yield and partial racemization.

The diastereomeric procedure has also been employed for the optical resolution of DL-amino acids,[11-15] which does not require the racemate to be a conglomerate. However, since free DL-amino acids scarcely form salts with ordinary optically active organic acids or bases, their derivatives, such as *N*-acyl compounds and esters,[11-15] have been resolved by this procedure. Therefore, this procedure may have a disadvantage similar to that of the preferential crystallization procedure. In order to overcome this disadvantage, the free D- or L-amino acid should selectively form a salt or adduct with an optically active compound, and the free optically active amino acid should be easy to be recovered from the resolved salt or adduct.

Since it is possible to regard a DL-amino acids as an adduct composed of a pair of enantiomers, one enantiomer may form an adduct with an optically active amino acid. This paper describes an attempt to resolve aliphatic DL-amino acids, DL-valine (abbreviated as DL-Val), DL-leucine (DL-Leu), and DL-isoleucine (DL-Ile), *via* formation of adduct with L-phenylalanine (L-Phe). An alkaline solution containing the aliphatic DL-amino acid and L-Phe selectively gave a crystalline adduct of the aliphatic D-amino acid with L-Phe when the pH of the initial solution was adjusted to around 5.5 with hydrochloric acid. The free aliphatic D-amino acids were easy to be recovered from the adducts since active carbon is capable of adsorbing L-Phe and scarcely Val, Leu, or Ile.[16] The optical resolution of DL-Val, DL-Leu, and DL-Ile has been achieved with these ideas, and D-Val, D-Leu, and D-Ile with high optical purity (84—100%) were obtained in 49—63% yield. It was attemted to obtain the aliphatic D- and L-amino acids by using an aqueous solution as an initial solution, and the L-amino acids with optical purity of 47—85% were also obtained.

Experimental

Amino Acids. DL-Val and DL-Ile were purchased from Nakarai Chemicals, Ltd., and DL-Leu and L-Phe from Wako Pure Chemicals Ind. These amino acids were recrystallized from water. The specific rotation of the recrystallized L-Phe was $[\alpha]_D^{20}$ −4.5° (*c* 1.0, 5 mol dm^{-3} HCl) ($[\alpha]_D^{20}$ −4.5° (*c* 1.0, 5 mol dm^{-3} HCl)).[17]

Optical Resolution of DL-Valine. Procedure I: Equimolar amounts (0.01 mol) of L-Phe and DL-Val were dissolved in 20 cm^3 of 1 mol dm^{-3} aqueous sodium hydroxide and 10 cm^3 of water. The pH was adjusted to around 5.5 with 1 mol dm^{-3} hydrochloric acid. After adding 80 cm^3 ethanol, the solution was stirred for 90 min at room temperature. The precipitate (I-**1**) formed was collected by filtration. The filtrate was concentrated to 20 cm^3 under reduced pressure at around 40 °C, and the precipitate (I-**2**) deposited on cooling the solution at 0 °C for 45 min was filtered off.

Procedure II: A solution containing equimolar amounts (0.01 mol) of L-Phe and DL-Val in 150 cm^3 of water was concentrated to 40 cm^3 under reduced pressure at around 40 °C. The precipitate (II-**1**) formed was collected by filtration. After adding 20 cm^3 of ethanol to the filtrate, the solution was allowed to stand overnight at 0 °C. The precipitate (II-**2**) formed was collected by filtration. To the filtrate was added 160 cm^3 of ethanol and the solution was concentrated to 30 cm^3. The precipitate (II-**3**) deposited after cooling overnight at 0 °C was collected by filtration. The filtrate was evaporated to dryness under reduced pressure at around 40 °C, and the residue (II-**4**) was obtained.

Optical Resolution of DL-Leucine. Procedure I: Equimolar amounts (0.01 mol) of L-Phe and DL-Leu were dissolved in 20 cm^3 of 1 mol dm^{-3} aqueous sodium hydroxide and 40 cm^3 of water. The pH was adjusted to around 5.5 with 1 mol dm^{-3} hydrochloric acid. The solution was concentrated to 30 cm^3, and the precipitate (I-**1**) formed was collected by filtration. After adding 20 cm^3 of ethanol to the filtrate, the solution was concentrated to 20 cm^3. The precipitate (I-**2**) formed was filtered off.

Procedure II: Equimolar amounts (0.01 mol) of L-Phe and DL-Leu were added to 200 cm^3 of water and dissolved at around 60 °C. The solution was concentrated to 100 cm^3, and the precipitate (II-**1**) deposited after cooling overnight at 0 °C was collected by filtration. The filtrate was concentrated to 30 cm^3, and the precipitate (II-**2**) formed was collected by filtration. After adding 20 cm^3 of ethanol to the filtrate, the

solution was allowed to stand overnight at 0 °C, and the precipitate (II-3) formed was collected by filtration. The filtrate was evaporated to dryness under reduced pressure, and the residue (II-4) was obtained.

Optical Resolution of DL-*Isoleucine.* *Procedure I*: Equimolar amounts (0.01 mol) of L-Phe and DL-Ile were dissolved in 20 cm^3 of 1 mol dm^{-3} aqueous sodium hydroxide and 30 cm^3 of water. The pH was adjusted to around 5.5 with 1 mol dm^{-3} hydrochloric acid. The solution was concentrated to 20 cm^3, and the preciptitate (I-1) formed was collected by filtration. After adding 150 cm^3 of ethanol to the filtrate, the solution was stirred for 60 min at room temperature, and the precipitate (I-2) formed was filtered off.

Procedure II: A solution containing equimolar amounts (0.01 mol) of L-Phe and DL-Ile in 200 cm^3 of water was concentrated to 50 cm^3. The solution was allowed to stand overnight at 0 °C, and the precipitate (II-1) formed was collected by filtration. After adding 100 cm^3 of ethanol to the filtrate, the solution was stirred for 60 min at room temperature, and the precipitate (II-2) formed was collected by filtration. The filtrate was concentrated to 25 cm^3 and the solution was allowed to stand overnight at 0 °C. The precipitate (II-3) formed was collected by filtration. The filtrate was evaporated to dryness under reduced pressure, and the residue (II-4) was obtained.

Preparation of Free Aliphatic Amino Acids. The precipitates obtained in the above procedures were dissolved in a minimum amount of water. To the aqueous solution was added active carbon, and the mixture was shaken for 3 h at room temperature. The mixture was filtered, and the filtrate was evaporated to dryness under reduced pressure at around 40 °C. The ^1H NMR spectrum of the residue was measured without recrystallization, and it was confirmed that the residue was the free aliphatic amino acid and was free from L-Phe. The optical purities of the free aliphatic amino acids obtained were determined on the basis of the specific rotations of the corresponding L-amino acids.[17]

Preparation of Adducts. L-Phe (0.005 mol) and 0.01 mol of DL-Val, DL-Leu or DL-Ile were dissolved in 15 cm^3 of 1 mol dm^{-3} aqueous sodium hydroxide. Only to the alkaline solution containing L-Phe and DL-Leu was added 30 cm^3 of water. The pH of the alkaline solutions was adjusted to around 5.5 with 1 mol dm^{-3} hydrochloric acid at 0, 25, or 50 °C. From the solution containing L-Phe and DL-Leu, a precipitate appeared after a stirring for several minutes. From the solution containing L-Phe and DL-Val or DL-Ile, a precipitate was deposited by adding an appropriate amount of ethanol. After stirring for 5—120 min at the respective temperatures, the precipitates were filtered off and the ^1H NMR spectra were measured without recrystallization. The precipitates were treated with active carbon in a similar manner as above.

The adduct composed of L-Phe and D-Val with optical purity of 100%. Found: C, 59.34; H, 7.93; N, 9.95. Calcd for $C_{14}H_{22}N_2O_4$: C, 59.56; H, 7.85; N, 9.92. $[\alpha]_D^{20}$ −14.6 ° (*c* 0.50, 5 mol dm^{-3} HCl).

The adduct composed of L-Phe and D-Leu with optical purity of 100%. Found: C, 60.50; H, 8.19; N, 9.45. Calcd for $C_{15}H_{24}N_2O_4$: C, 60.79; H, 8.16; N, 9.45. $[\alpha]_D^{20}$ −9.5 ° (*c* 0.50, 5 mol dm^{-3} HCl).

The adduct composed of L-Phe and D-Ile with optical purity of 96.8%. Found: C, 60.49; H, 8.23; N, 9.44. Calcd for $C_{15}H_{24}N_2O_4$: C, 60.79; H, 8.16; N, 9.45. $[\alpha]_D^{20}$ −19.8 ° (*c* 0.50, 5 mol dm^{-3} HCl).

Measurements. Specific rotations were measured with a Union Giken high sensitivity PM-101 digital polarimeter in 5 mol dm^{-3} hydrochloric acid by using a 0.5 dm path length quartz cell. ^1H NMR spectra were recorded on a JEOL JNM-PMX 60 NMR spectrometer in deuterium oxide. Infrared spectra were obtained in the range 4000—400 cm^{-1} with a JASCO A-102 infrared spectrophotometer by the KBr disk method.

Results and Discussion

Formation of Adducts. The adducts of Val, Leu, and Ile with L-Phe were prepared under several conditions as given in Table 1. The adducts were determined by elemental analyses and ^1H NMR spectra in deuterium oxide and found to be composed of equimolar amounts of L-Phe and the aliphatic amino acid. Aqueous solutions of each adduct were treated with active carbon to remove L-Phe by adsorption.[16] The recovered free aliphatic amino acids were of D-configuration, and those obtained under the prescribed conditions had optical purity of about 100%. The results indicate that the alkaline solution containing the aliphatic DL-amino acid and L-Phe selectively give

Table 1. Results of preparation of adducts with L-phenylalanine

Aliphatic DL-amino acids[a]	Conditions			Yield of adduct	Free aliphatic amino acids		
	Temperature	Stirring time	Amount of added ethanol		Yield	Specific rotation[b]	Optical purity
	°C	min	cm^3	g	g(%[c])	°	%
DL-Val	0	5	10	0.385	0.154(26.3)	−28.8	100
	0	30	0	0.124	0.017(2.9)	−17.4	60.4
	0	30	50	0.951	0.367(62.6)	−21.6	75.1
	25	30	50	0.519	0.207(35.3)	−28.8	100
	50	120	150	0.352	0.139(23.7)	−28.8	100
DL-Leu	0	5	0	0.363	0.157(23.9)	−16.0	100
	0	30	0	0.779	0.324(49.4)	−9.6	60.2
	25	30	0	0.552	0.240(36.6)	−6.0	37.3
	50	120	0	0.332	0.142(21.6)	−4.8	30.1
DL-Ile	0	30	10	0.909	0.331(50.5)	−32.9	81.2
	25	5	30	0.351	0.125(19.1)	−39.2	96.8
	25	10	30	0.370	0.160(24.4)	−35.8	88.4
	25	30	30	0.524	0.222(33.8)	−35.7	88.1
	50	30	250	0.312	0.115(17.5)	−24.3	60.1

a) The amount of aliphatic DL-amino acids consumed by reaction was 0.01 mol and that of L-Phe was 0.005 mol. b) $[\alpha]_D^{20}$ (*c* 1.00, 5 mol dm^{-3} HCl). c) Yield(%)=(Yield(g)×100)/(1/2) (Reacted amount of DL-amino acid).

a crystalline adduct of the aliphatic D-amino acid with L-Phe.

Infrared Spectra. Infrared spectra of the adducts of the aliphatic D-amino acids with L-Phe were measured and were compared with those of the free DL- and L-amino acids. The spectral patterns are similar to those of the free DL-amino acids, different from those of the free L-amino acids. The bands due to groups COO^- and NH_3^+ were assigned as such since it is considered that the groups are most strongly influenced by formation of the adducts. The band at about 2950 cm^{-1} was assigned to the NH streching, the band at about 1625 cm^{-1} (shoulder) to the antisymmetric NH deformation, and the band at about 1500 cm^{-1} to the symmetric NH deformation. The antisymmetric CO band (ν_{CO}(as)) appears at about 1590 cm^{-1}, and the symmetric band at 1410 cm^{-1}. A most significant difference in the spectra is noticed between the ν_{CO}(as)'s of the adducts and L-Phe. The ν_{CO}(as) of L-Phe appears at 1558 cm^{-1}, whereas the spectra of the adducts have no bands in the range 1570—1530 cm^{-1}. The ν_{CO}(as)'s of the adducts are observed at wave number positions similarly to that of DL-Phe (1585 cm^{-1}). These results suggest that the interaction between the aliphatic D-amino acid and L-Phe in the adduct is analogous to that between a pair of the enantiomers in the DL-amino acid, and that these adducts are not mere mixtues of the aliphatic D-amino acid and L-Phe.

Optical Resolutions. The optical resolution of DL-Val, DL-Leu, and DL-Ile was achieved at room temperature by using two kinds of procedures (I and II). The results are given in Tables 2, 3, and 4. The precipitate numbers in these tables have been defined in the experimental section.

In procedure I, an alkaline solution containing equimolar amounts of L-Phe and the aliphatic DL-amino acid was used as an initial solution. The ^1H NMR spectra of precipitates **I-1** and **I-2** indicated that these precipitates are composed of equimolar amounts of L-Phe and the aliphatic amino acid. The Val, Leu, and Ile from the precipitates are of D-configuration, and the aliphatic D-amino acids with optical purity of 84—100% were obtained in 49—63% yield. After these precipitates were filtered off, sodium chloride was

TABLE 2. OPTICAL RESOLUTIONS OF DL-VALINE

Procedure	Precipitate		Free valine			
	No.	Yield / g	Yield / g(%[a])	Configuration	Specific rotation[b] / °	Optical purity / %
I	**I-1**	0.871	0.289(49.4)	D	−28.8	100
	I-2	0.689	0.125(21.3)	D	−5.5	19.1
II	**II-2**	1.029	0.300(51.2)	D	−28.3	98.3
	II-3	0.667	0.360(61.5)	L	+11.4	39.6
	II-4	0.349	0.204(34.8)	L	+24.6	85.4

a) Yield(%)=(Yield(g)×100)/0.586(g). b) $[\alpha]_D^{20}$ (*c* 1.00, 5 mol dm^{-3} HCl).

TABLE 3. OPTICAL RESOLUTIONS OF DL-LEUCINE

Procedure	Precipitate		Free leucine			
	No.	Yield / g	Yield / g(%[a])	Configuration	Specific rotation[b] / °	Optical purity / %
I	**I-1**	1.283	0.327(49.9)	D	−16.0	100
	I-2	0.375	0.065(9.9)	D	−16.0	100
II	**II-1**	0.378	0.149(22.7)	D	−16.0	100
	II-2	0.672	0.244(37.2)	D	−15.3	95.6
	II-3	0.199	0.045(6.9)	D	−10.7	66.9
	II-4	1.316	0.345(52.6)	L	+7.6	47.5

a) Yield(%)=(Yield(g)×100)/0.656(g). b) $[\alpha]_D^{20}$ (*c* 1.00, 5 mol dm^{-3} HCl).

TABLE 4. OPTICAL RESOLUTIONS OF DL-ISOLEUCINE

Procedure	Precipitate		Free isoleucine			
	No.	Yield / g	Yield / g(%[a])	Configuration	Specific rotation[b] / °	Optical purity / %
I	**I-1**	0.810	0.369(56.3)	D	−34.3	84.7
	I-2	0.220	0.046(7.0)	D	−36.2	89.6
II	**II-1**	0.757	0.230(35.1)	D	−33.1	81.7
	II-2	0.265	0.083(12.7)	D	−37.8	93.3
	II-3	0.899	0.244(37.2)	D	−4.7	11.6
	II-4	0.673	0.276(42.1)	L	+27.6	68.1

a) Yield(%)=(Yield(g)×100)/0.656(g). b) $[\alpha]_D^{20}$ (*c* 1.00, 5 mol dm^{-3} HCl).

also deposited with the mixture of the amino acids by further concentrating the filtrate or adding ethanol. Since it was tedious to remove sodium chloride, no attempt was made to obtain the aliphatic L-amino acids.

In procedure II, an aqueous solution containing only equimolar amounts of L-Phe and the aliphatic DL-amino acid was used as an initial solution, and it was attempted to obtain both the aliphatic D- and L-amino acids.

In the optical resolution of DL-Val by this procedure, the ^1H NMR spectrum and specific rotation indicated that precipitate II-**1** is L-Phe ($[\alpha]_D^{20}$ −4.4° (*c* 0.50, 5 mol dm^{-3} HCl)); L-Phe is allowed to crystallize first since the solubility of DL-Val is much higher than that of L-Phe. Precipitate II-**2** is composed of equimolar amounts of L-Phe and Val. The Val from this precipitate is of D-configuration, and was recovered in 51.2% yield with optical purity of 98.3%. Precipitates II-**3** and II-**4** are composed of Val and L-Phe in the molar ratio of around 1.8:1. L-Val was recovered from precipitate II-**4**, and was obtained in 34.8% yield, with optical purity of 85.4%.

In the optical resolution of DL-Leu by procedure II, precipitates II-**1** and II-**2** are composed of equimolar amounts of L-Phe and Leu. The D-Leu from these precipitates had over 95% optical purity, and was obtained in 60% total yield. L-Leu with optical purity of 47.5% was obtained from precipitate II-**4** in 52.6% yield. Precipitate II-**4** is composed of Leu and L-Phe in the molar ratio of 0.8:1.

In the optical resolution of DL-Ile by procedure II, precipitate II-**1** deposited from the initial solution is composed of Ile and L-Phe in the molar ratio of about 0.6:1, and precipitate II-**2** in 1:1. However, the D-Ile from these precipitates had high optical purity (81.7 and 93.3%), and the total yield was 47.8%. The molar amount of Ile contained in precipitates II-**3** and II-**4** was about 1.8 times that of L-Phe. The L-Ile from precipitate II-**4** had an optical purity of 68.1% and was obtained in 42.1% yield.

The above results indicate that it is possible to resolve DL-Val, DL-Leu, and DL-Ile *via* formation of adducts with L-Phe.

References

1) M. Shibazaki, Tokkyo Kokai, Sho 40-1576 (1965).
2) C. Fouquey and J. Jacques, *Bull. Soc. Chim. Fr.*, **1966**, 165.
3) S. Yamada, M. Yamamoto, and I. Chibata, *J. Org. Chem.*, **38**, 4408 (1973).
4) S. Yamada, M. Yamamoto, and I. Chibata, *J. Org. Chem.*, **40**, 3360 (1975).
5) C. Hongo, M. Shibazaki, S. Yamada, and I. Chibata, *J. Agric. Food Chem.*, **24**, 903 (1976).
6) T. Shiraiwa, Y. Ohmichi, K. Iwafuji, K. Fujimoto, and H. Kurokawa, *Nippon Kagaku Kaishi*, **1983**, 1070.
7) T. Shiraiwa, Y. Ohmichi, and H. Kurokawa, *Nippon Kagaku Kaishi*, **1983**, 1102.
8) T. Shiraiwa, S. Taniguchi, A. Ikawa, K. Iwafuji, and H. Kurokawa, *Nippon Kagaku Kaishi*, **1983**, 1189.
9) R. M. Secor, *Chem. Rev.*, **63**, 297 (1963).
10) A. Collet, M. J. Brienne, and J. Jacques, *Chem. Rev.*, **80**, 215 (1980).
11) J. P. Greenstein and M. Winitz, "Chemistry of the Amino Acids," John Wiley and Sons, Inc. (1960), Vol. 1, p. 715.
12) A. M. Krubiner, Ger. Offen. 1964422 (1970).
13) L. R. Hoffman, Brit. Pat. 1235810 (1970).
14) H. Nakamoto, M. Aburatani, and M. Inagaki, Ger. Offen. 2058516 (1971).
15) T. Shiraiwa, K. Umegaki, and H. Kurokawa, *Nippon Kagaku Kaishi*, **1983**, 1687.
16) S. M. Partridge, *Biochem. J.*, **44**, 521 (1949).
17) "Seikagaku Data Bukku," ed by the Japanese Biochemical Society, Tokyo Kagaku Dojin, Tokyo (1982), Vol. 1, p. 31.

Manufacturing Process of Sodium Hydroxide and Nitric Acid from Thermochemically Split Sodium Nitrate

Norio TAKEUCHI

Energy Chemistry Division, National Chemical Laboratory for Industry, Tsukuba Research Center, Yatabe, Ibaraki 305

(Received September 21, 1983)

For the manufacture of sodium hydroxide and nitric acid a new thermochemical process of splitting sodium nitrate has been proposed which consists of (i) splitting of sodium nitrate by iron(III) oxide, (ii) hydrolysis of sodium ferrate, and (iii) absorption of nitrogen dioxide into water. Key reactions (i) and (ii) have experimentally been verified. The overall heat requirement for the process is discussed on the basis of a material and heat flow-sheet of the process constructed.

Electricity has been rising in cost in many countries, particularly in Japan, since the first and second international rises in the price of crude oil. As a result, new energy-saving processes have been required for the manufacture of sodium hydroxide in place of the conventional electrolytic process of sodium chloride which consumes much electric energy.

There were two industrially practised processes of manufacturing sodium hydroxide except the conventional electrolytic process. Both of them used Na_2CO_3 as a raw material. As generally known, one of them was the oldest manufacturing process of NaOH that utilized a double decomposition reaction between Na_2CO_3 and $Ca(OH)_2$. Although this process was simple, it could only produce a dilute aqueous solution of NaOH with a poor conversion rate from carbonate to hydroxide. For instance, it produced a sodium hydroxide solution of 10—11 wt% with a conversion rate of about 90%. The other process was called the Löwig process.[1] This consisted of two reactions, one producing sodium ferrate through an interaction between Na_2CO_3 and Fe_2O_3 and the other being a hydrolysis of sodium ferrate to produce NaOH. The Löwig process had two merits: the first was that Fe_2O_3 used in the process could be reused without being consumed; the second was that a sodium hydroxide solution of about 30 wt% formed was industrially available. However, this process released CO_2 into the atmosphere. This is not preferable nowadays from a viewpoint of the prevention of global atmospheric pollution.

The process to be proposed in this study will neither release any gases into the atmosphere, nor produce any unnecessary by-products. The sodium hydroxide aqueous solution to be formed is industrially available in the respect of concentration, as with the Löwig process. In addition, the raw materials for this process are only $NaNO_3$ and H_2O. As generally known, $NaNO_3$ is contained in large quantity in Chile saltpeter which is an abundant natural resource in Chile and Peru.

The thermochemical splitting process of $NaNO_3$ proposed here is composed of the three chemical reactions

$$NaNO_3 + 1/2Fe_2O_3 \longrightarrow NaFeO_2 + NO_2 + 1/4O_2, \quad (1)$$

$$NaFeO_2 + 1/2H_2O \longrightarrow NaOH + 1/2Fe_2O_3, \quad (2)$$

$$NO_2 + 1/4O_2 + 1/2H_2O \longrightarrow HNO_3, \quad (3)$$

which sequence leads to the overall reaction

$$NaNO_3 + H_2O \longrightarrow NaOH + HNO_3. \quad (4)$$

Fe_2O_3 circulates between Reactions 1 and 2. Reaction 3 is the same as the absorption step of NO_2 into water in the current manufacturing process of nitric acid.

The object of the present work is divided into two: (1) Characterization and experimental verification of the reactions concerning the proposed process, and (2) construction of the material and heat flow-sheet to estimate the overall heat requirement for the manufacture of NaOH and HNO_3 by this thermochemical process.

Reaction Characteristics and Experimental Verification

Reaction 1. Thermal Analysis: Mixtures of $NaNO_3 + xFe_2O_3$ (x=0—1.0) were analyzed by DTA from 25 to 1000 °C in a stream of nitrogen at a heating rate of 300 °C/h. Every mixture used for the thermal analysis was 100 mg in a shape of powder. Powdered iron(III) oxide used was identified with hematite by X-ray diffraction pattern, and its particle size was 75—105 μm for 64 wt% and less than 46 μm for the rest. DTA curves were obtained by use of a differential thermal analyzer (Type TA3-L, Chyo Balance Corporation, Japan). Results are shown in Fig. 1. The endothermic peaks at 278 and 308 °C on every DTA curve in Fig. 1 correspond to the transition and fusion of $NaNO_3$.[2] Every curve shows a gradual endothermic peak over 400 °C which shifts to higher temperatures with increasing content of $NaNO_3$ in mixtures. The peaks for the mixtures at 600—700 °C indicate the end of reaction more clearly than the peak for pure $NaNO_3$. Both pure $NaNO_3$ and the mixtures, however, have similar patterns in their DTA curves. Therefore, it is estimated from

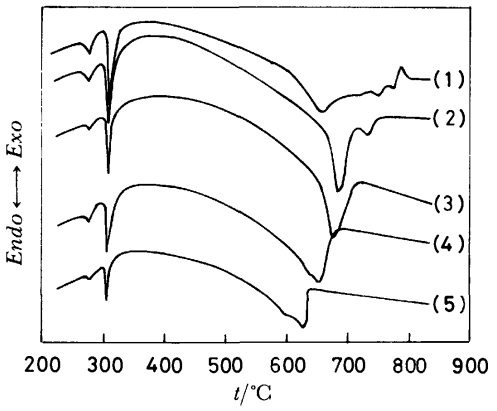

Fig. 1. DTA curves for mixtures of $NaNO_3$ and Fe_2O_3.
Heating rate: 5 °C/min, Atmosphere: N_2 50 ml/min.
$NaNO_3/Fe_2O_3$=(1): pure $NaNO_3$, (2): 2.5, (3): 2.0, (4): 1.5, (5): 1.0.

the thermal analysis that Reaction 1 is essentially a decomposition of $NaNO_3$ in conjunction with Fe_2O_3.

X-Ray Analysis: In order to grasp the outline of Reaction 1, an X-ray analysis was conducted with the solid phase. Mixed samples of $NaNO_3$ and Fe_2O_3 with various molar ratios ($NaNO_3/Fe_2O_3$=1.0, 1.5, 2.0, and 2.5) were heated in a platinum boat in an atmosphere of air at 950, 1000, and 1050 K. Each of solid residues was examined by X-ray analysis. X-Ray diffraction patterns were obtained by use of an X-ray diffractometer (Type Geigerflex RAD-III A, Rigaku Denki Corporation, Japan).

The solid residues obtained at 1050 K from every mixture showed only the X-ray pattern of $NaFeO_2$ except the unchanged Fe_2O_3. The solid residues obtained at 950 and 1000 K from the mixtures with molar ratios $NaNO_3/Fe_2O_3$=2.0 and 2.5 showed the X-ray patterns of both Na_3FeO_3 and $NaFeO_2$. $NaFeO_2$ may be regarded as the general component of the solid residues formed at 1050 K from the mixtures with molar ratios less than 2.0 of $NaNO_3/Fe_2O_3$, as far as the results of X-ray analysis is concerned.

Conversion Rate: Conversion rates from $NaNO_3$ to $NaFeO_2$ were determined at various reaction times. With the apparatus shown in Fig. 2, a mixture with a molar ratio $NaNO_3/Fe_2O_3$=2.0 in a platinum boat was heated in still or flowing air of 500 ml/min at 1 atm for a prescribed time. Then the solid residue in the platinum boat was hydrolyzed in boiling water to form NaOH. The amount in mole of the determined NaOH was regarded as equivalent to that of the $NaFeO_2$ formed by Reaction 1. The NaOH formed was determined by neutralization.

Results are shown in Figs. 3 and 4. As shown in Fig. 3, the reaction proceeds in still air at 1050 K faster than at 950 and 1000 K. In flowing air, however, as seen from Fig. 4, the reaction rate increased at 950 and 1000 K but was almost the same at 1050 K as in still air. This is because the total pressure of evolved vapor is more than 1 atm at 1050 K, whereas it is below 1 atm at 950 and 1000 K. The conversion rate does not reach 100% in either of the atmospheres of still and flowing airs at 1 atm. The maximum conversion rate is 95—96% in all the experimental conditions of this study.

In order to disclose the reason, amounts of evolved gas with Reaction 1 were determined.

Evolved Gas: About 2 g of a mixture ($NaNO_3/Fe_2O_3$=2.0 in molar ratio) in a platinum boat was heated for 30 min at 1050 K in an atmosphere of flowing O_2 and the evolved gas was allowed to be absorbed into 450 ml of 0.26 mol/l NaOH aqueous solution as shown in Fig. 2. The amount of the residual sodium hydroxide in the solution after the absorption of evolved gas was determined by neutralization. The solid residue in the platinum boat was hydrolyzed, and the NaOH formed was determined. According to the equilibrium constants[3] of the reaction $NO+1/2O_2 \rightleftarrows NO_2$, the species of nitrogen oxide in the evolved gas is NO at 1050 K but is NO_2 together with a large quantity of O_2 at room temperature where the gas is absorbed. Thus, the amount of absorbed NO_2 in coexistence with O_2 was compared with the initial amount of $NaNO_3$ for the determination of conversion rate on the basis of evolved NO_2. The result is shown in Fig. 5. As is clear from Fig. 5, the conversion rate on the basis of evolved NO_2 is almost 100% over the range 50—400 ml/min of oxygen flow, whereas that on the basis of formed NaOH is about 96% at the maximum. The drop in conversion rate at 500 ml/min of O_2 flow in Fig. 5 may be due to the fact that

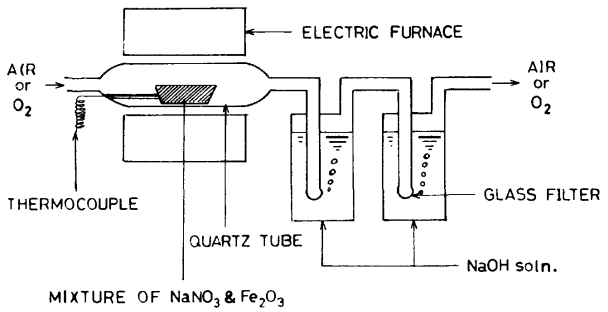

Fig. 2. Apparatus for reaction of splitting $NaNO_3$ with Fe_2O_3.

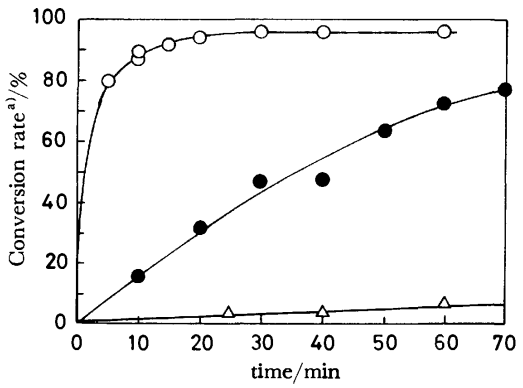

Fig. 3. Conversion rates of Reaction 1 at the various reaction times in still air.
○: 1050°K, ●: 1000°K, △: 950°K.
a) $\frac{\text{moles of formed NaOH}}{\text{moles of initial } NaNO_3} \times 100$

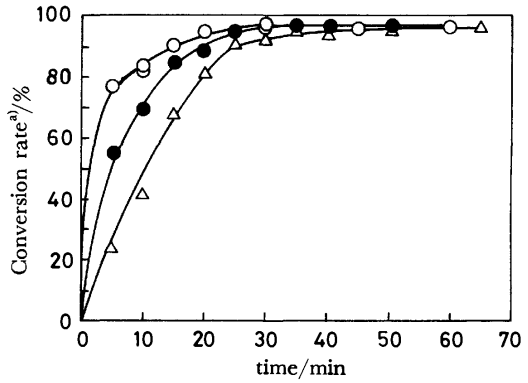

Fig. 4. Conversion rates of Reaction 1 at the various reaction times in flowing air of 500 ml/min. ○: 1050°K, ●: 1000°K, △: 950°K.
a) Defined in the same manner as in Fig. 3.

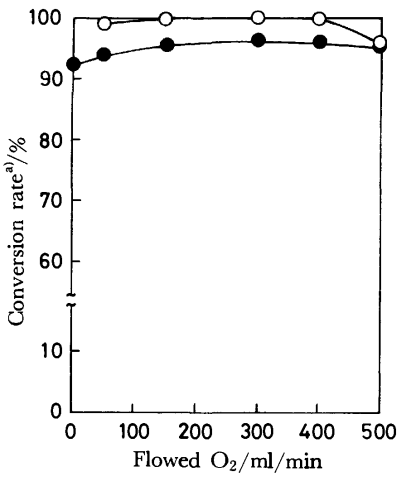

Fig. 5. Conversion rates of Reaction 1 on the bases of evolved NO_2(○), and of formed NaOH(●) at 1050°K under an atmospher of O_2.

NO_2 goes out of the absorbing solution with the flowing O_2 without being absorbed into the solution.

Reaction 2 (Hydrolysis of $NaFeO_2$). As already clarified by X-ray analysis, the general component of solid residue with Reaction 1 is $NaFeO_2$ at 1050 K at molar ratios less than 2.0 of $NaNO_3/Fe_2O_3$. Therefore, this study is focused on the hydrolysis of $NaFeO_2$ formed at 1050 K with Reaction 1.

Three samples of $NaFeO_2$ were hydrolyzed for the purpose of determining the maximum yield of NaOH from $NaFeO_2$. They were prepared at 1050 K in the respective molar ratios of $NaNO_3/Fe_2O_3$=1.0, 1.5, and 2.0.

Each sample of 1.3 g was added into a water of about 100 g and the suspended solution was boiled off down to half the volume with evaporation of water. After cooling, OH^- and CO_3^{2-} in the suspended solution were analyzed with an automatic titrator. As a result of this analysis, it was concluded that 95.4—96.4% of $NaFeO_2$ is converted to NaOH by hydrolysis with all the samples prepared from the mixtures with molar ratios $NaNO_3/Fe_2O_3$=1.0, 1.5, and 2.0, if 100% of the initial $NaNO_3$ is assumed to have been converted to $NaFeO_2$ in every preparation of the $NaFeO_2$ samples. In order to detect undecomposed $NaFeO_2$, an X-ray analysis was conducted on dry samples of solid residues after hydrolysis of $NaFeO_2$. However, any X-ray diffraction patterns assignable to sodium ferrate were not found; all the samples showed only the X-ray diffraction pattern of hematite.

For the purpose of investigating the mass balance of sodium with respect to Reactions 1 and 2, sodium was determined in three samples: (1) A solid residue from Reaction 1, (2) a solid residue after the hydrolysis of Reaction 2, and (3) solid sticks on the quartz tube wall and the SiO_2 powders around the platinum boat containing reactants for Reaction 1. The SiO_2 powders were used for catching vaporized $NaNO_3$, because $NaNO_3$ reacts with SiO_2.[2] The determination of sodium was conducted by flame emittion photometry after extraction of sodium ion into the aqueous solutions by decomposing the solids with hydrochloric acid, hydrofluoric acid, and perchloric acid. As a result, it was revealed that 95.4—96.4% of the sodium contained in the initial sodium nitrate forms $NaFeO_2$ which is easily hydrolyzed, and that 1.6—1.7% of the sodium coexists with Fe_2O_3 without forming NaOH after the hydrolysis of $NaFeO_2$. The residual percentage 1.9—3.0% of sodium is regarded as the $NaNO_3$ which vaporized without reacting with Fe_2O_3 during the heating step from room temperature to the reaction temperature. The vaporized $NaNO_3$ is probably caught during passage through the column packed with Fe_2O_3, because the sodium from vaporized $NaNO_3$ was detected in solid sticks on the quartz tube wall and the SiO_2 powders around the platinum boat. This vaporized $NaNO_3$ will, however, be regarded as lost in the later discussion of this paper, because it was not recovered in this study.

The hydrolysis rate of $NaFeO_2$ as a function of reaction time was also measured as shown in Fig. 6. A sample containing 0.2 g $NaFeO_2$ and 20 g water in a Teflon bottle was shaken and warmed in an oil bath at a constant controlled in temperature within ±0.1 °C. As seen from Fig. 6, features of hydrolysis rate with respect to reaction time are similar above 60 °C in that it takes as short as 30 min to reach the maximum hydrolysis rate. On the other hand, the hydrolysis of $NaFeO_2$ proceeds rather slowly below 50 °C. At any cases, the maximum hydrolysis rate is more than 98% in view of the already-stated fact that 1.9—3.0% of sodium in the initial $NaNO_3$ will not form $NaFeO_2$ in the step of preparation of the $NaFeO_2$ samples due to the vaporization of $NaNO_3$.

It is industrially important to clarify the achievable concentration of the sodium hydroxide aqueous solution obtainable by means of the hydrolysis of $NaFeO_2$. Figure 7 shows concentrations of sodium hydroxide aqueous solutions obtained with varied hydrolysis periods. In this experiment, the expected amount of water was added to each $NaFeO_2$ sample so that a sodium hydroxide solution of 50 wt% might be formed when the $NaFeO_2$ sample was perfectly hydrolyzed. The sodium hydroxide solutions were determined in concentration after they had been separated from iron(III) oxide by filtration with paper filters. As shown in Fig. 7, the concentration of sodium hydroxide solution reaches about 25 wt% at about 15 min from the start of hydrolysis, slowly increasing up to 28.5 wt% at 80 min from the start. Thus, these results suggests that the industrially achievable concentration of sodium hydroxide solution would be 25—28 wt%.

Reaction 3 (Production of HNO_3). The formation of nitric acid according to Eq. 3 is well known and quite similar to the absorption step of nitrogen dioxide into water in the current manufacturing process of nitric acid. This absorption step of nitrogen dioxide is successfully practical in many factories manufacturing nitric acid all over the world.

Thermodynamic Calculation

The enthalpy change (ΔH°_{298}), entropy change (ΔS°_{298}), and free energy change (ΔG°) for each of the reactions involved in the present process were calculated based on thermochemical data.[4,5] The results are shown in Table 1 and Fig. 8.

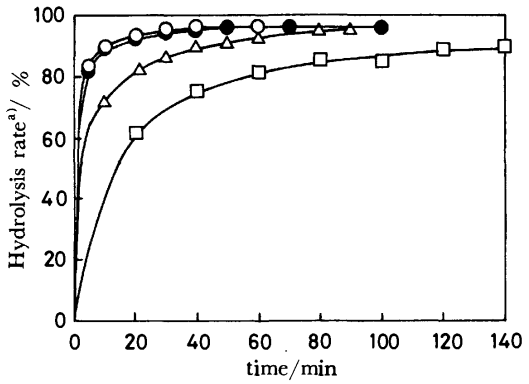

Fig. 6. Hydrolysis rates of $NaFeO_2$ with time at the various temperatures.
○: 70 °C, ●: 60 °C, △: 50 °C, □: 40 °C.

a) $\dfrac{\text{moles of formed NaOH}}{\text{moles of initial } NaFeO_2} \times 100$

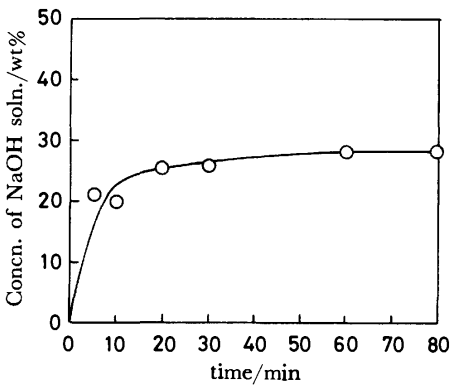

Fig. 7. Concentration of formed NaOH aqueous solution with hydrolysis time at 70 °C.
($NaFeO_2$ and H_2O were initially mixed so that about 50 wt% NaOH aqueous solution might be formed after 100% of $NaFeO_2$ was hydrolyzed)

Material and Heat Flow-sheet

An estimated material and heat flow-sheet for this process is shown in Fig. 9. In Fig. 9, R, E, and S refer to the reactor, heat exchanger, and separator, respectively. The other notations are as follows: the enthalpy change of reaction (ΔH°_T), the Gibbs free energy change (ΔG°_T), the heat input for heating the reactants ($Q_r=\Delta H^\circ_T-\Delta H^\circ_{298}$), and the heat output for cooling the products ($Q_P=\Delta H^\circ_T-\Delta H^\circ_{298}$).

The following assumptions were made for the construction of the flow-sheet:

$NaNO_3$ will be perfectly converted to $NaFeO_2$ with the stoichiometric ratio between $NaNO_3$ and Fe_2O_3. Q_P at E1 contains the reaction heat of $NO+1/2O_2\rightarrow NO_2$. The conversion rate for $NaFeO_2$ to NaOH will pessimistically be 95% at a molar ratio $H_2O/NaFeO_2=6.5$ for the formation of 27 wt% sodium hydroxide aqueous solution. ΔG°_{343} and ΔH°_{343} at R2 contain the free energy and enthalpy changes for the dissolution[6] of NaOH into H_2O. The conversion rate for NO_2 to HNO_3 will be 100% at 298 K. The concentration of nitric acid aqueous solution formed will be 64%. Therefore, the heat of dilution from 100 to 64 wt% of nitric acid solution is contained in ΔH°_{298} at R3. The heat unit in the flow-sheet is kcal.

Heat Requirement. The heat requirement (Q_{req}) for the process was calculated by using the equation[7-9] formulated on the basis of the flow-sheet in

Table 1. Enthalpy, entropy, and free energy changes (ΔH°_{298}, ΔS°_{298}, and ΔG°) for reaction 1—3[a]

Reaction	ΔH°_{298}/ kcal mol^{-1}[b]	ΔS°_{298}/ cal mol^{-1} K^{-1}[b]	ΔG°/ kcal mol^{-1}[b]
1	+51.4	+52.4	−1.9 at 1050 K
2	−9.1	+9.9	−19.2 at 343 K
3	−20.3	−42.0	−7.9 at 298 K
Total	+22.0	+20.3	

a) (1) $NaNO_3(s,l)+1/2Fe_2O_3(s)\rightarrow NaFeO_2(s)+NO_2(g)+1/4O_2(g)$. $NaNO_3$: liquid>579 K≧solid.
(2) $NaFeO_2(s)+1/2H_2O(l,g)\rightarrow NaOH\cdot 6aq+1/2Fe_2O_3(s)$.
(3) $NO_2(g)+1/4O_2(g)+1/2H_2O(l,g)\rightarrow HNO_3\cdot 2aq$
b) 1 cal=4.184 J.

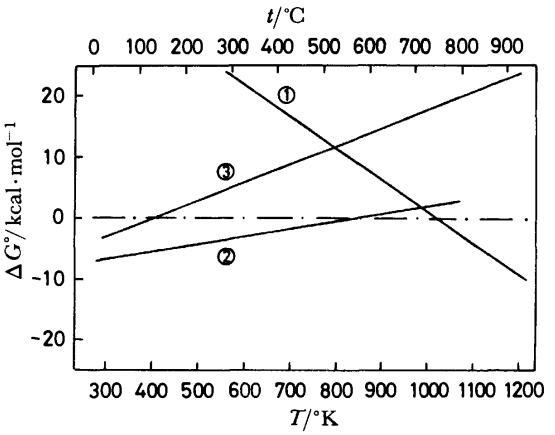

Fig. 8. Free energy change (ΔG°) *vs.* temperature plot for Reaction 1—3.
(1) $NaNO_3(s,l)+1/2Fe_2O_3\rightarrow NaFeO_2(s)+NO_2(g)+1/4O_2(g)$ $NaNO_3$: liquid>579°K≧solid
(2) $NaFeO_2(s)+1/2H_2O(l,g)\rightarrow NaOH\cdot 6aq+1/2Fe_2O_3(s)$ H_2O: gas>373°K≧liquid
3) $NO_2(g)+1/4O_2(g)+1/2H_2O(l,g)\rightarrow HNO_3\cdot 2aq$

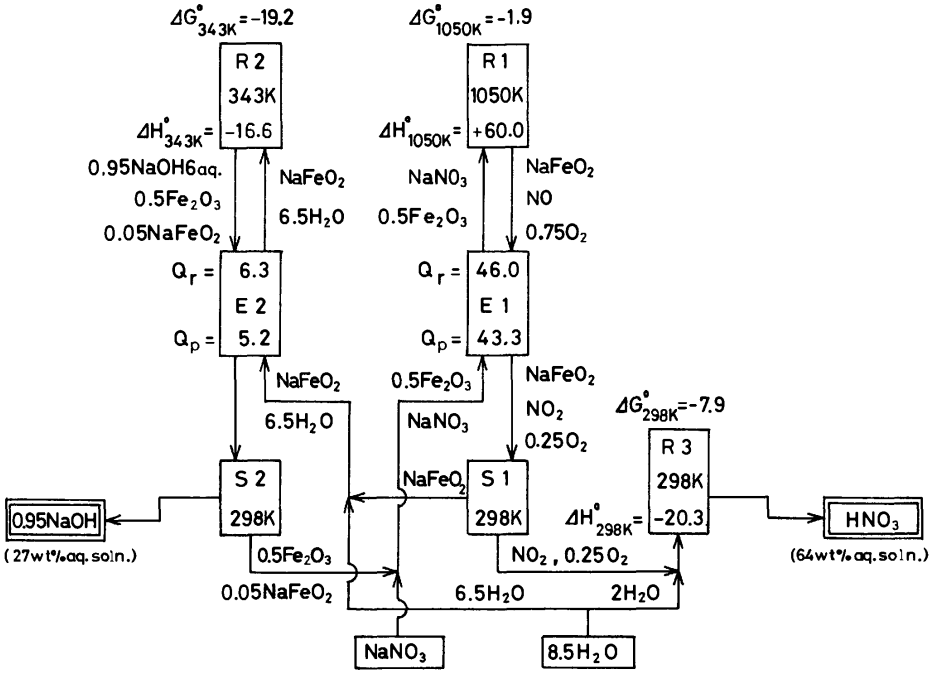

Fig. 9. Material and heat flow-sheet in a manufacturing process of NaOH and HNO_3 from thermochemically split $NaNO_3$.
R: reactor, E: heat exchanger, S: separator, Q_r: heat input for heating the reactants ($Q_r=\Delta H^\circ_T-\Delta H^\circ_{298K}$) Q_p: heat output for cooling the products ($Q_p=\Delta H^\circ_T-\Delta H^\circ_{298K}$)
(the heat unit in the flow-sheet is kcal)

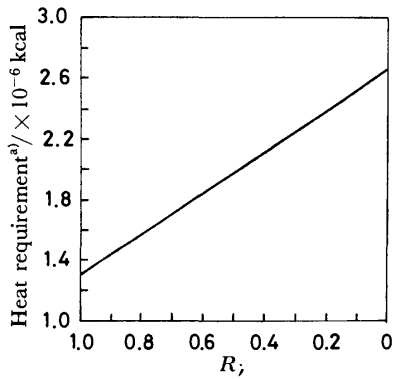

Fig. 10. Heat requirement of the thermochemical process of manufacturing NaOH and HNO_3 from $NaNO_3$.
a) Heat required in manufacturing 27 wt% NaOH aqueous solution containing NaOH of 1.000 ton, and 64 wt% HNO_3 aqueous solution containing HNO_3 of 1.658 ton.

$$Q_{req} = \sum(\Delta H_T^\circ + Q_r) - \sum Q_p \times R_i \quad (5)$$

Fig. 9, where R_i represents the ratio for the thermal regeneration. Figure 10 shows the change of the heat requirement with values of R_i. The heat requirement in Fig. 10 represents values applicable to a manufacture of 1.000 t of NaOH and 1.658 t of HNO_3. The energy required for the separation and transportation of materials in the process is neglected in the calculation of heat requirement.

The theoretical heat requirement for the manufacture of NaOH is calculated as 10.2 kcal/mol[10] the case of the electrolysis process of NaCl. Here, the heat of 10.2 kcal/mol does not include the heat required for the manufacture of accompanying Cl_2 with NaOH. If the fossil fuel equivalent to electrical energy is assumed to be three times the amount of the electrical energy delivered to the electrolysis process of NaCl, the theoretical heat requirement for the manufacture of NaOH is 0.765×10^6 kcal/*t*-NaOH. On the other hand, nitric acid is mostly manufactured *via* oxidation of ammonia. Ammonia is currently synthesized *via* the reaction between hydrogen from naphtha and nitrogen from air. The heat requirement for this synthesis is expected to be 4.03×10^6 kcal/*t*-NH_3.[11] The heat requirement for the manufacture of HNO_3 from NH_3 is assumed to be negligibly small in this discussion. Thus, the overall heat requirement for the manufacture of 1.658 t of HNO_3 is 1.80×10^6 kcal. As a result, the total heat requirement for the manufacture of 1.000 t of NaOH and 1.658 t of HNO_3 is estimated to be at least 2.56×10^6 kcal for the current manufacturing processes of NaOH and HNO_3. This value of heat requirement corresponds approximately to the case of thermal regeneration of as low as 5% in the process of this study, as is clear from Fig. 10. If thermal regeneration is practised to more than 5% in this thermochemical process, this process might be a more energy-saving process than the current manufacturing processes of NaOH and HNO_3.

Conclusion

1) A new thermochemical process for manufacture of NaOH and HNO_3 from $NaNO_3$ has successfully been devised which essentially comprises a combination of a splitting of $NaNO_3$ by Fe_2O_3 and a hydrolysis of $NaFeO_2$.

2) The feasibility of the two key reactions, (i) the splitting of $NaNO_3$ by Fe_2O_3 and (ii) the hydrolysis of $NaFeO_2$, has experimentally been verified. The conversion rate is 100% for reaction (i) at 1050 K and more than 98% for reaction (ii) at 343 K. Sufficiently high reaction rates are available for both the reactions.

3) A material and heat flow-sheet of the process has been constructed which is simple as shown in Fig. 9.

4) This proposed thermochemical process is expected to be more energy-saving than the current processes of manufacturing NaOH and HNO_3, if heat regeneration is practised to more than 5% in the process of this study.

Reference

1) *Chem. Trade J. & Chem. Eng.*, **61**, 322 (1917).
2) Y. Hoshino, T. Utsunomiya, T. Utsugi, and O. Abe, *Nippon Kagaku Kaishi*, **1980**, 690 (1980).
3) A. Richardson, *J. Chem. Soc. Trans.*, **51**, 397 (1887).
4) "Selected Values of Chemical Thermodynamic Properties," NBS TN270-8, U. S. Department of Commerce, (1981).
5) I. Barin and O. Knacke, "Thermochemical Properties of Inorganic Substances," Springer-Verlag, Berlin, Heidelberg, New York (1973).
6) R. Parsons, "Handbook of Electrochemical Constants," Butterworths Scientific Publication, London (1959).
7) J. E. Funk and R. M. Reinstrom, *Ind. Eng. Chem., Process Des. Dev.*, **5**, 336 (1966).
8) K. F. Knoche and J. E. Funk, *Ind. J. Hydrogen Energy*, **2**, 377 (1977).
9) M. Dokiya, H. Yokokawa, T. Kameyama, and K. Fukuda, *J. Electrochem. Soc. Japan*, **47**, 156 (1979).
10) M. Takahashi, *Soda and Chlorine*, **32**, 43 (1981).
11) M. Sittig, "Practical Techniques for Saving Energy in the Chemical, Petroleum and Metals Industries," Noyes Data Corporation, U. S. A. (1977).

 © 1984 The Chemical Society of Japan Bull. Chem. Soc. Jpn., 57, 2243—2246 (1984)

Conduction Band Formation through the Temporary Anion States in Organic Solids

Kenzo HIRAOKA* and Masaji NARA
Faculty of Engineering, Yamanashi University, Takeda-4, Kofu 400, Japan
(Received August 5, 1983)

The transmission of low-energy electrons (0—15 eV) through thin films of benzene, toluene, pyridine, aniline, styrene, and cyclohexene was studied. The electron transmission spectra of all the aromatic compounds studied are like each other in their forms. The energies of several prominent peaks in the electron transmission spectra are in good agreement with those of temporary anion states measured in the gas phase. It is suggested that vacant orbitals of free molecules form conduction bands in molecular crystals.

Recently our group[1-7] and Sanche *et al.*[8-10] reported a simple method for measuring the electronic levels of molecules condensed on a metal surface at low temperature. A sample film was bombarded by a beam of low-energy electrons, and the current transmitted through the film (I_t) was measured as a function of the incident electron energy (eV_i). The electron transmission spectra, recorded as dI_t/dV_i *vs.* eV_i, were found useful for the detection of optically forbidden electronic transitions[1] and the determination of energies of lowest conduction bands for many orgnic solids.[2-7]

The temporary anion states of organic compounds in the gas phase have been studied by electron transmission spectroscopy.[11-17] Jordan and Burrow observed the vertical temporary anion states at 1.15 and 4.85 eV for benzene, at 1.11 and 4.88 eV for toluene, and at 0.19, 0.90, 1.67, 3.37, and 4.72 eV for naphthalene.[11] In the electron transmission spectra of solids, peaks at ≈1.1 and ≈4.8 eV for benzene and toluene[2,4] and peaks at 1.6, 3.3 and 4.8 eV for naphthalene,[4] are observed. Peak energies of the transmission spectra are in agreement with the energies of temporary anion states measured by Jordan and Burrow. This suggests that peaks observed in the transmission spectra of these solids are originated from the temporary anion states.[4]

In our previous papers,[5,7] the peak positions in the transmission spectra for solid normal alkanes were connected with onset energies of conduction bands with high density of states. In this work, we give a further evidence that vacant orbitals of free molecules form conduction bands in organic insulators.

Experimental

The experimental procedure has been described elsewhere.[2] All samples were Tokyo Kasei extra pure products. The film thickness was controlled by the deposition time under the constant vapor pressure at 1.3×10^{-5} Pa.

Results

Transmission spectra for pyridine are shown in Fig. 1. The film thickness was changed from 2 to 16 langmuir (L).† The spectra for the 2 to 8 L films were almost identical. Comparing the transmission spectra of pyridine and monosubstituted benzenes with those of benzene, a marked similarity is observed, at least below 8 eV.

As described in our previous papers,[2,4] the electron energy calibration was made by comparing the transmission spectra with spectroscopic data obtained in the gas phase. Solid and gas phase data are in good agreement for benzene, toluene, pyridine, and naphthalene. Recently we measured the electron impact luminescence excitation spectra of a benzene thin film and verified that the assignment of peaks in the transmission spectrum of benzene was correct.[6]

Electronic excitation of molecules takes place in 10^{-15}—10^{-16} s. An excited molecule in the solid immediately polarizes surrounding molecules. The excitation energy in the solid is generally smaller than that in the gas phase by the difference of interaction energies for the ground and excited states *D*. Thus peak energies of the transmission spectra calibrated

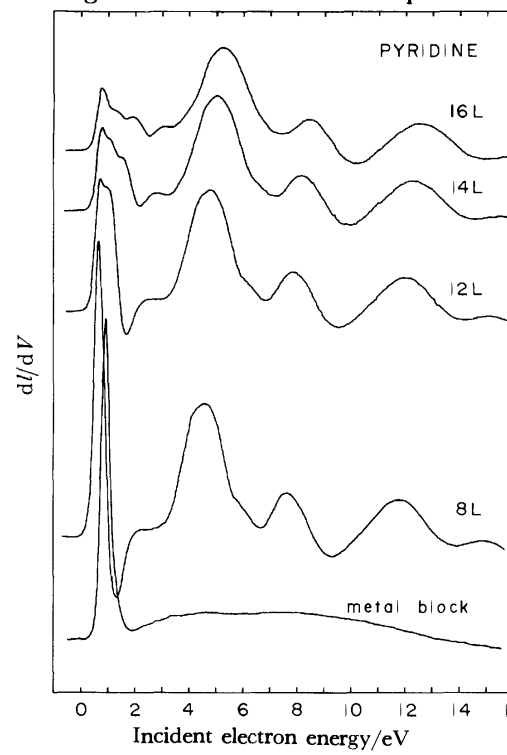

Fig. 1. The transmision spectra for pyridine. The electron energy scale was calibrated for the spectrum of an 8 L thick film. For films thicker than 8 L, all peaks including two new ones but the first peak uniformly shifted because of charging of the film. This shift was generally observed when the film was charged by electrons.

† The amount of the gas admitted in the vacuum chamber is expressed in langmuir units (1 L=1.33×10^{-4} Pa s).

by the gas-phase data would be overestimated by an amount of D. In molecular crystals the magnitude of D is known to be of the order of 1000 cm^{-1}.[35]

The peak energies of the transmission spectra for pyridine are in good agreement with those of the threshold electron-impact excitation spectrum measured in the gas phase by Van Veen and Plantenga[17] (see Table 1). The assignment of peaks above ≈7 eV is difficult because the ionization of molecules in the film obscures the spectra in this energy region.

When a pyridine film thicker than 8 L suffered charging, all peaks in the spectrum except the first one uniformly shifted and the first peak decreased with the appearance of two new peaks nearby as shown in Fig. 1. The peak energies of these two were determined to be 0.7 and 1.3 eV from the spectral shift. These levels correspond to the temporary anion states (shape resonances) of pyridine at 0.62 and 1.20 eV observed in the gas phase by Nenner and Schulz.[18] For another temporary anion state at 4.58 eV observed by them, a large peak was also observed near the value in the transmission spectra.

Table 1. The comparison of peak energies (eV) in transmission spectra with energy levels obtained with other spectroscopic methods and the estimated V_0 values

	Electron transmission (present work)	Energy level		V_0
Benzene	1.1	1.15[b]		−0.3(−0.1[j])
	2.0			
	2.8			
	4.0		3.9[c]	
	4.8	4.85[b]	4.80[c]	
	6.1		6.16[c]	
Toluene	1.1	1.1[b]		−0.3
	2.3			
	4.0		4.1[d]	
	4.8	4.88[b]		
	5.9		5.9[e]	
Pyridine	0.7[a]	0.62[b]		−0.9
	1.3[a]	1.20[b]		
	2.4			
	4.1		4.1[f]	
	4.8	4.58[b]	4.84[f]	
	6.3		6.32[f]	
Aniline		1.13[b]		−0.9
	1.8	1.85[b]		
	3.0		3.2[g]	
	5.2	5.07[b]		
Styrene	0.7[a]	0.25[b]		−0.9
	1.3	1.05[b]		
	2.3	2.48[b]		
	3.6			
	4.7	4.67[b]		
Naphthalene	0.8[a]	0.9[b]		−1.1(−1.4[j])
	1.6	1.67[b]		
	3.3	3.37[b]		
	4.8	4.72[b]		
	5.7		5.89[h]	
Cyclohexene	2.1	2.07[b]		0.4
	4.6		4.24[j]	

a) This peak was observed when a film was charged by electrons. b) Reference 11. c) Reference 19. d) Reference 20. e) Reference 21. f) Reference 17. g) Reference 22. h) Reference 23. i) Reference 24. j) Reference 25.

Figure 2 depicts the transmission spectra of cyclohexene, benzene, toluene, aniline, pyridine, and styrene. The spectrum of cyclohexene showed a decrease of the first peak and an appearance of a second peak with increasing sample deposition. This means that the lowest conduction band energy V_0 is positive for cyclohexene and negative for other aromatic compounds.[2,4] Because the second peak approximately corresponds to the lowest conduction band energy for a compound with positive V_0,[4] the second peak of the transmission spectrum of cyclohexene can be assigned to the zero of the energy of electrons in the solid. The electron energy scale for benzene, toluene, and pyridine was calibrated using spectroscopic data.[17,19–21] The energy scale for aniline and styrene was calibrated by comparing energies of peaks indicated in the transmission spectra with those of temporary anion states measured by Jordan and Burrow.[11] They are also compared with other spectroscopic data in Table 1 and Fig. 3.

By the calibration of electron-energy scale for the electron transmission spectra described above, the lowest conduction band energies V_0 can be estimated from the amounts of positive shifts of the transmission spectra.[4] The estimated V_0 values are listed in

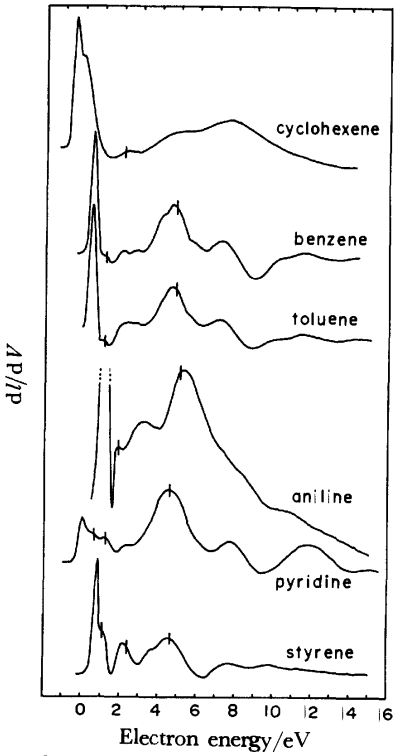

Fig. 2. The transmission spectra for cyclohexene, benzene, toluene, aniline, pyridine, and styrene. The film thickness is 16 L for pyridine and 10 L for the other compounds. The zero of the electron energy scale corresponds to the lowest conduction band energy except for pyridine. Positions of temporary anion states messured in the gas phase were indicated.[11]

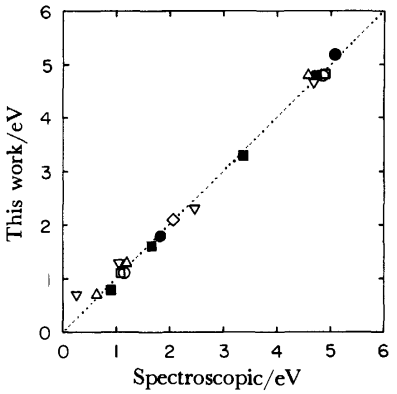

Fig. 3. The comparison of peak energies in the electron transmission spectra with temporary anion states measured in the gas phase.[11]. ○; benzene, □; toluene, △; pyridine, ●; aniline, ▽; styrene, ■; naphthalene, ◇; cyclohexene.

the last column of Table 1. The experimental error was estimated to be around ±0.3 eV. Riga *et al.*[25] compared the ESCA valence band spectra of solid polyacenes with gas phase UPS results, and obtained the V_0 values for solid benzene and naphthalene as -0.1 ± 0.2 and -1.4 ± 0.2 eV, respectively, which are fairly in good agreement with our values.

Discussion

Despite a good agreement of peak energies, there is a marked difference in their relative intensity between the transmission spectra and the threshold electron impact excitation spectra of aromatic compounds in the gas phase.[2-4,17] In the transmission spectra, peaks at about the same energies of temporary anion states are generally larger than those assigned for the exciton formation.[2,4,6,26-28] For example, excitonic peaks of pyridine observed at 4.1 ($^3A_1$) and 6.3 eV ($^1A_1$) are weaker than peaks at 0.7, 1.3, and 4.8 eV which are assigned to the temporary anion states. A large peak in the transmission spectra is due to sharp increase in the transmitted electron current at its energy. In our previous papers,[4-7] it was suggested that the transmission spectra reflect the profile of conduction bands and their peaks might correspond to the onsets of conduction bands with high density of states. Large peaks in the transmission spectra at the energies of temporary anion states suggest that the vacant orbitals of free molecules form unoccupied conduction bands when molecules are condensed.

Figure 4 shows the transmission spectra of benzene and styrene measured in the gas[11] and solid phases. The π_1^* and π_2^* states in the gas phase spectra have vibrational structures, unlike π_3^* and π_4^* states, their lifetimes ($\geq10^{-14}$ s) being longer than those of the latter (10^{-14}—10^{-15} s)[11]. It is notable that the short-lived temporary anion states (π_3^* and π_4^*) give the larger and broader peaks in the transmission spectra than long lived-states (π_1^* and π_2^*). This may be understood as follows. When an electron is taken in a resonant state of antibonding nature in a molecule, the nuclei will oscillate along a potential well with a large equilibrium internuclear distance. Thus, the molecule suffers vibrational excitation due to the resonance. The

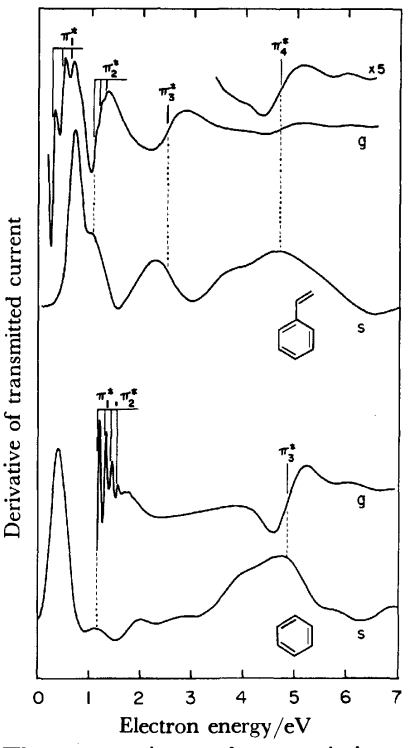

Fig. 4. The comparison of transmission spectra measured in the gas (g)[11] and solid (s) phases for benzene and styrene.

degree of excitation is a function of spatial displacement of the nuclei in the temporary anion, hence it depends upon a lifetime of the intermediate state. Through the formation of long-lived π_1^* and π_2^* states for solid benzene and toluene, a primary electron would have much chance to suffer inelastic scattering. On the contrary, short-lived π_3^* and π_4^* states are less involved in the vibrational excitation. Besides, an electron with an excess energy of a few eV may have a mean free path $l\leq37$ nm[29,30] in the solids. Under the circumstances, an electron generated by autoionization of a short-lived temporary anion may be delocalized in the initial phase and characterized by a wave vector k. In this case, an electron would propagate coherently in the solid and contribute to the increase of the transmitted electron current.

In principle, no level below the vacuum level is observed with the electron transmission experiment. For instance, the band originated from the π_1^* state of styrene cannot be detected in the transmission spectrum (Fig. 4). However, this band could be observed when the film suffered charging by electrons. Two new peaks were also observed for a charged pyridine film as described before. For compounds with negative V_0 values, one might examine some levels below the vacuum level by charging the films as much as $|V_0|$.

The energy of the lowest conduction band V_0 listed in Table 1 corresponds to the ground state energy of quasi-free electrons in the condensed phase. The theoretical model for the estimation of V_0 was given by Springett *et al.*[31] The second lowest conduction bands for benzene and toluene, for instance, are observed at 1.1 eV with respect to the lowest conduction band. These bands were generated from the lowest vacant molecular orbitals of free molecules as already

described.

For benzene, two peaks at 2.0 and 2.8 eV remain to be explained. In this energy region, unresolved peaks are also observed for toluene, aniline, octylbenzene,[4] biphenyl,[32] and pyridine. Because energies of these peaks are lower than the first excitonic levels, these peaks may also be due to the conduction bands. Since any kind of vacant molecular orbitals can contribute to the formation of conduction bands,[33] the origin of these bands could be the vacant molecular orbitals. Possible candidates for the formation of these bands are vacant C-C, C-H, and Rydberg orbitals. Although Jordan and Burrow could observe the transient anions associated with C-Cl* orbitals,[34] those associated with vacant C-C, C-H, and Rydberg orbitals have never been observed due to their very short lifetimes, and no comparison with the transmission spectra can be made at the present stage.

Stimulating discussions with Professor Yusei Maruyama of Institute for Molecular Science are gratefully acknowledged.

References

1) K. Hiraoka and W. H. Hamill, *J. Chem. Phys.*, **56**, 3185 (1972); **57**, 3870, 3881, 4058 (1972); **58**, 3686 (1973); **59**, 5749 (1973).
2) K. Hiraoka and M. Nara, *Bull. Chem. Soc. Jpn.*, **54**, 1589(1981).
3) K. Hiraoka and M. Nara, *Bull. Chem. Soc. Jpn.*, **54**, 3317 (1981).
4) K. Hiraoka, *J. Phys. Chem.*, **85**, 4008 (1981).
5) K. Hiraoka and M. Nara, *J. Phys. Chem.*, **86**, 442 (1982).
6) K. Hiraoka, M. Nara, and Y. Iijima, *J. Phys. Chem.*, **87**, 3959 (1983).
7) K. Hiraoka and M. Nara, *Chem. Phys. Lett.*, **94**, 589 (1983).
8) L. Sanche, *J. Chem. Phys.*, **71**, 4860 (1979).
9) G. Bader, L. Caron, and L. Sanche, *Solid State Comm.*, **38**, 849 (1981).
10) L. Sanche, G. Bader, and L. Caron, *J. Chem. Phys.*, **76**, 4016 (1982).
11) K. D. Jordan and P. D. Burrow, *Acc. Chem. Res.*, **11**, 341 (1978).
12) M. N. Pissnias, L. G. Christophorou, and J. G. Carter, *Chem. Phys. Lett.*, **13**, 433 (1972).
13) M. N. Pisanias, L. G. Christophorou, J. G. Carter, and D. L. McCorkle, *J. Chem. Phys.*, **58**, 2110 (1973).
14) L. G. Christophorou, D. L. McCorkle, and J. G. Carter, *J. Chem. Phys.*, **60**, 3779 (1974).
15) L. G. Christophorou, M. W. Grant and D. L. McCorkle, *Adv. Chem. Phys.*, **36**, 413 (1977).
16) J. R. Frazier, L. G. Christophorou, J. G. Carter, and H. C. Schweinler, *J. Chem. Phys.*, **69**, 3807 (1978).
17) E. H. Van Veen and F. L. Plantenga, *Chem. Phys. Lett.*, **30**, 28 (1975).
18) I. Nenner and G. J. Schulz, *J. Chem. Phys.*, **62**, 1747 (1975).
19) R. N. Compton, R. H. Huebner, P. W. Reinhardt, and L. G. Christophorou, *J. Chem. Phys.*, **48**, 901 (1968).
20) D. Lewis, P. B. Merkel, and W. H. Hamill, *J. Chem. Phys.*, **53**, 2750 (1970).
21) "DMS U. V. Atlas of Organic Compounds" Butterworths, London (1966).
22) D. S. McClure, *J. Chem. Phys.*, **17**, 905 (1949).
23) G. J. Verhaart, P. Brasem, and H. H. Brongersma, *Chem. Phys. Lett.*, **62**, 519 (1979).
24) R. P. Frueholz, W. M. Flicker, O. A. Mosher, and A. Kuppermann, *J. Chem. Phys.*, **70**, 1986 (1979).
25) J. Riga, J. J. Pireaux, R. Caudano, and J. J. Verbist, *Phys. Scr.*, **16**, 346 (1977).
26) O. H. Le Blanc, *J. Chem. Phys.*, **36**, 1082 (1962).
27) R. Silbey, J. Jortner, S. A. Rice, and M. T. Vala, *J. Chem. Phys.*, **42**, 733; **43**, 2925 (1965).
28) A. S. Davydov and E. F. Sheka, *Phys. Status Solidi*, **11**, 877 (1965).
29) S. Hino, N. Sato and H. Inokuchi, *Chem. Phys. Lett.*, **37**, 494 (1976).
30) S. Hino and H. Inokuchi, *J. Chem. Phys.*, **70**, 1142 (1979).
31) B. E. Springett, J. Jortner, and M. H. Cohen, *J. Chem. Phys.*, **48**, 2720 (1968).
32) K. Hiraoka and M. Nara, unpublished results.
33) R. M. Glaeser and R. S. Berry, *J. Chem. Phys.*, **44**, 3797 (1966).
34) P. D. Burrow, A. Modelli, N. S. Chiu, and K. D. Jordan, *J. Chem. Phys.*, **77**, 2699 (1982).
35) V. M. Agranovich and A. A. Zakhidov, *Chem. Phys. Lett.*, **68**, 86 (1979).

 © 1984 The Chemical Society of Japan Bull. Chem. Soc. Jpn., 57, 2247—2253 (1984)

Redox Behavior and Electrochromic Properties of Polypyrrole Films in Aqueous Solutions

Susumu KUWABATA, Hiroshi YONEYAMA,* and Hideo TAMURA

Department of Applied Chemisrty, Faculty of Engineering, Osaka University, Yamada-oka 2-1, Suita, Osaka 565

(Received September 29, 1983)

Polypyrrole films prepared by anodic polymerization of pyrrole on Pt or SnO_2-coated glass show redox behavior in aqueous electrolyte solutions containing a supporting electrolyte alone. Transfer of electrolyte anions into and from the film is involved in the redox reaction similarly with acetonitrile solutions already reported. Insertion of divalent anions into the film occurs in two steps but that of monovalent anions in one step, as judged from corresponding cyclic voltammograms. The change in film color which occurs in the redox reaction of the film was investigated in detail as a function of electrode potential and the charge consumed in the redox reaction. Polypyrrole is a promising material for electrochromic display devices.

Recently many reports have been published concerning electrochemical properties of electroconductive polymers. Among them, polypyrrole has been studied most extensively. Except for earlier reports by Weiss *et al.*,[1-3] most of electrochemical studies have been conducted on films prepared by anodic polymerization of pyrrole in an acetonitrile medium. According to Diaz *et al.*[4-9] polypyrrole-coated Pt electrodes show redox behavior in acetonitrile solutions: Insertion of anionic species into films and elimination of inserted anions from films occur in the oxidation and reduction of films, respectively; the oxidized film contains 0.25 mol of anions in 1 mol of pyrrole rings and exhibits high conductivity. Use was made of this property to stabilize unstable semiconductor electrodes such as *n*-Si and *n*-GaAs in aqueous solutions by coating electrode surface with thin polypyrrole films.[10-15]

Concerning electrochemical properties of polypyrrole films in aqueous solutions, redox behavior of several electroactive species such as $[Fe(CN)_6]^{3-/4-}$ and ferrocene/ferricenium has been investigated by use of Pt or Ta as the electrode substrate and it has been found that the polymer films serve as inert electrodes like Pt electrodes.[7,16-18] Their photoelectrochemical properties were also investigated in relation to the conduction mechanisms.[18] We have studied electrochemical properties of polypyrrole films in aqueous solutions containing a supporting electrolyte alone and found that the films exhibit redox behavior like those reported in acetonitrile solutions. In this paper electrochemical properties of polypyrrole films in aqueous solutions will be reported with particular reference to their redox behavior. Furthermore, it will be shown that the color of polypyrrole films changes with redox behavior. Preliminary results will also be presented on the application to electrochromic display devices which have been obtained with stable inorganic oxides such as WO_3[19-23] and organic materials such as phthalocyanines.[24] The color change of polymer-coated electrodes during the course of their polarization has been described with several polymers,[8,25,26] but no systematic study with focusing on the application to electrochromic display devices seems to have conducted.

Experimental

Preparation of Polypyrrole. Redox reactions of polypyrrole were investigated with its film prepared on a Pt substrate. For this purpose, a flat Pt plate was mounted on a Teflon electrode holder having an exposed electrode area of 1 cm^2. An anodic polymerization of pyrrole was carried out in an N_2 atmosphere in acetonitrile containing 0.1 mol dm^{-3} pyrrole and 0.3 mol dm^{-3} $LiClO_4$ at 0.3 mA cm^{-2} for 2 min. By this procedure polypyrrole of *ca.* 90 nm thickness was deposited on the Pt as determined with a multi-reflection interferometer (Mizojiri Kogaku, Model 2). The electrode prepared in this manner is denoted here by PPy/Pt. For the purpose of elemental analysis the film was prepared on a Pt electrode having a large area of *ca.* 20 cm^2 under the same conditions as described above except for the electrolysis time which was 20 min, and was teared away from the substrate. The film thickness in this case was *ca.* 220 nm.

Measurements of electrochromic properties of polypyrrole were carried out with a film prepared on a SnO_2-coated glass electrode. The SnO_2-coated glass electrode was prepared in this laboratory by pyrolysis of a spray mixture of 3 mol dm^{-3} $SnCl_4$, 0.15 mol dm^{-3} $SbCl_5$, and 1.5 mol dm^{-3} HCl,[27] and its area was 3.5 cm^2. An electrical lead wire was attached to its round rim with silver-epoxy by coating it first with epoxy resin and then with silicone rubber adhesive. The SnO_2-coated glass electrode prepared in this manner had an exposed area of *ca.* 3 cm^2, which was used as the substrate for the deposition of polypyrrole. The deposition was performed under the same conditions as in the case of PPy/Pt and the prepared electrode will be denoted here by PPy/OTE.

Electrochemical Measurements. Measurements were carried out in a Pyrex beaker type cell. A saturated calomel electrode (SCE) served as a reference electrode. Cyclic voltammograms were obtained by use of a potentiostat (Hokuto Denko HA-104), a function-generator (Hokuto Denko HB-104), and an X-Y recorder (Yokogawa Electric Inc. 3077). An electronic coulometer (Hokuto Denko HF-201) was used as required. For measurements of resistivity of polypyrrole films the four-probe method[28] was applied to a film sample which had been teared away from PPy/Pt by use of an adhesive tape.

Electron Probe X-Ray Microanalysis of Polypyrrole Films. A qualitative analysis of anions contained in polypyrrole films was performed to obtain direct information on the anion transfer into and from films which occur in the course of redox reaction of PPy/Pt electrodes. An energy dispersive electron probe X-ray microanalyzer (EPMA) (Horiba EMAX-1500E) connected to a scanning electron microscope (Hitachi S-450) served for this purpose.

Measurements of Electrochromic Properties. A PPy/OTE working electrode and a counter electrode (*ca.* 1 cm^2 Pt plate) were set in a quartz cell (20×10×40H mm). The cell was connected to a reference electrode (SCE) with a salt bridge and set in an UV-visible spectro-photometer (Shimadzu MPS-5000). The absorbance of polypyrrole films was measured *in situ* in the course of polarization measurements.

Results and Discussion

Redox Behavior of Polypyrrole in Aqueous Solutions. Cyclic voltammograms of PPy/Pt electrodes in 0.5 mol dm^{-3} KCl or 0.5 mol dm^{-3} Na_2SO_4 are shown in Fig. 1. Well-defined peaks are seen both in the anodic and cathodic potential scans. Peak currents increase linearly with increasing sweep rate from 20 to 100 mV s^{-1}, suggesting that these peaks are due to electrochemical reactions of the film itself.[29] In the KCl solution the anodic and cathodic peaks appear at −0.35 and −0.15 V, respectively, and the peak potentials are eventually invariant with sweep rate. On the other hand, two anodic peaks appear in the Na_2SO_4 solution, though the cathodic behavior is almost the same as in the KCl solution. The first peak like a shoulder appears at −0.44 V, whereas the more marked second peak shows a tendency to shift its potential towards the positive direction with increasing sweep rate.

Cyclic voltammograms were obtained in other kinds of electrolytes. The peak potential and current of the cyclic voltammograms obtained at the sweep rate of 50 mV s^{-1} are shown in Table 1. In the case of appearence of two anodic peaks, the peak potential and current at the lower potential are given with the subscript pa-1 and those at the higher potential with pa-2. When only one anodic peak appears the values are given in the column of pa-1. As recognized from this Table, monovalent anions give one anodic peak, while divalint anions give two peaks. The peak potential and current of cathodic waves are little influenced by the kind of electrolyte anions, whereas different situations can be seen in the anodic waves.

The $E_{pa\text{-}1}$ observed in divalent anions is more negative than $E_{pa\text{-}1}$ observed in monovalent anions, but $E_{pa\text{-}2}$ is more positive than the latter. Voltammograms obtained in individual solution were not remarkably varied in the temperature range 0—80° C. It is suggested from cyclic voltammograms obtained in the presence of divalent anions that the oxidation in this case occurs in two steps: In the first step, the surface of polypyrrole film may be oxidized weakly by attracting anions onto the polymer surface; in the following step, anions may be inserted into the film and an oxidation of the film occurs simultaneously. It is seen in Table 1 that $E_{pa\text{-}2}$ depends on the kind of anions; sulfate and hydrophosphate ions give nearly the same $E_{pa\text{-}2}$ except for Li_2SO_4, whereas WO_4^{2-} gives more anodic $E_{pa\text{-}2}$. The discrepancy in the values of $E_{pa\text{-}2}$ seems to be closely related to ionic radii of the anions[30] to be incorporated into the film. The ionic radii of hydrated HPO_4^{2-} and SO_4^{2-} are *ca.* 4 Å, while that of WO_4^{2-} is *ca.* 5 Å. If this difference is serious, it is then suggested that the larger the ionic radius of anions, the more anodic potentials are needed for the incorporation of anions into the film to take place. Experiments aiming at the verification of this hypothesis is in progress and will be reported in future. As to the monovalent anions given in Table 1, the ionic radii of Cl^-, Br^-, and I^- are *ca.* 3 Å and that of ClO_4^{2-} is 3.5 Å, which are smaller than those of the

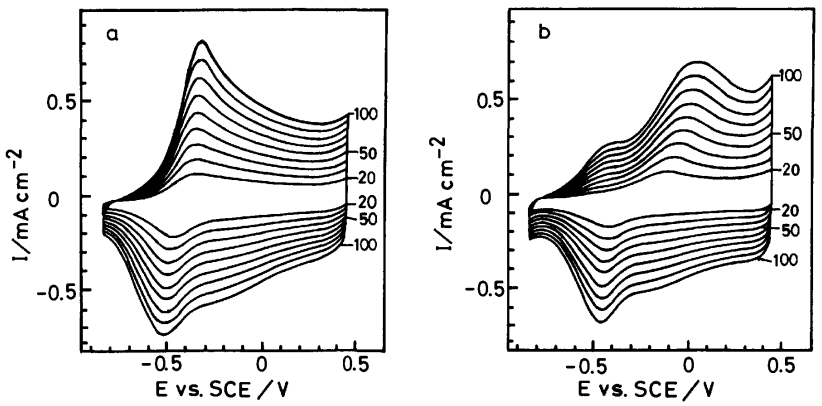

Fig. 1. Cyclic voltammograms of PPy/Pt electrodes at various sweep rates in an interval of dE/dt=10 mV s^{-1}. The number denotes the sweep rate in mV s^{-1}.
(a) in 0.5 mol dm^{-3} KCl (b) in 0.5 mol dm^{-3} Na_2SO_4

TABLE 1. PEAK POTENTIALS AND CURRENTS OF CYCLIC VOLTAMMOGRAMS OF PPy/Pt ELECTRODES OBTAINED AT dE/dt=50 mV s^{-1} IN A VARIETY OF ELECTROLYTES

Electrolyte[a]	E_{pa-1}/V	E_{pa-2}/V	E_{PC}/V	i_{pa-1}/mA	i_{pa-2}/mA	i_{PC}/mA
0.5 M KCl	−0.31		−0.47	0.36		−0.41
0.5 M KBr	−0.32		−0.46	0.34		−0.38
0.5 M KI	−0.29		−0.56	0.41		−0.36
0.5 M $LiClO_4$	−0.31		−0.48	0.39		−0.30
0.5 M Na_2SO_4	−0.44	0.04	−0.46	0.12	0.35	−0.34
0.5 M K_2SO_4	−0.45	0.02	−0.48	0.09	0.36	−0.35
0.5 M Li_2SO_4	−0.42	0.21	−0.44	0.07	0.38	−0.41
0.5 M Na_2HPO_4	−0.42	0.02	−0.36	0.13	0.41	−0.45
0.5 M Na_2WO_4	−0.42	0.45	−0.49	0.13	0.40	−0.43

a) 1 M=1 mol dm^{-3}.

divalent ions used, and the smaller size of monovalent anions may make the peak potential less positive than the $E_{pa\text{-}2}$ obtained for the divalent anions. In connection to this hypothesis, it seems important to notice that the onset potential of film oxidation is eventually the same between the monovalent and divalent ions.

Effects of the electrolyte concentration on cyclic voltammograms were investigated in KCl solutions. According to the results obtained, the peak potentials and currents were not appreciably varied with the concentration of electrolytes as long as it was higher than 10^{-3} mol dm^{-3}. In more dilute solutions, however, the voltammograms were deformed owing to IR drop in the electrolyte.[31]

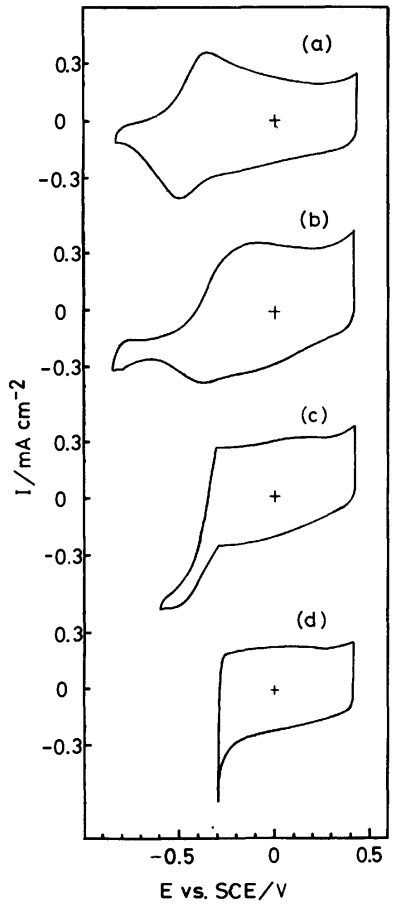

Fig. 2. Effects of solution pH on cyclic voltammograms of PPy/Pt electrodes in 1 mol dm^{-3} chloride solutions.
pH=(a) 5.5, (b) 2.0, (c) 1.5, (d) 0.6. dE/dt=50 mV s^{-1}.

Figure 2 shows effects of pH on the redox behavior of polypyrrole. The concentration of Cl^- anions was kept constant in this case. As noticed from Fig.2, the redox behavior appears in solutions having pH values higher than 2.0. In solutions of lower pH, hydrogen evolution becomes predominant, resulting in shadowing the redox behavior of polypyrrole itself.

It was reported in acetonitrile solutions[8] that the redox behavior is due to anion insertion into polypyrrole films and elimination of inserted anions from the film. In order to confirm whether or not this is true in aqueous solutions, anionic species in the film were analyzed by EPMA. The results are shown in Fig. 3. Figure 3-(a) is the spectrum of a PPy/Pt electrode prepared in the acetonitrile solution. A peak assignable to chlorine is seen, which gives the evidence that ClO_4^- is inserted into the film in the course of anodic polymerization. This electrode was kept in 0.5 mol dm^{-3} KI aqueous solution for 2 min at −0.85 V which is enough to cause the cathodic process of redox reaction, and then washed with water. Then the chlorine peak disappeared, as shown in Fig. 3-(b). When this sample was again kept for 2 min in the same solution at 0.45 V *vs.* SCE to cause the anodic process of redox reaction, peaks of iodine appeared as shown in Fig. 3-(c). Similar results of the occurrence of replacement of anionic species were obtained in other electrolytes such as KBr, Na_2SO_4, and Na_2HPO_4. Thus, it is evident that the redox reaction is accompanied with the anion transfer into and from the film.

Resistivity measurements and elemental analyses on polypyrrole films were carried out both for the original film prepared in the acetonitrile solution and for films polarized afterwards in 0.5 mol dm^{-3} KCl aqueous solution for 2 min at −0.85, 0, or 0.45 V *vs.* SCE.

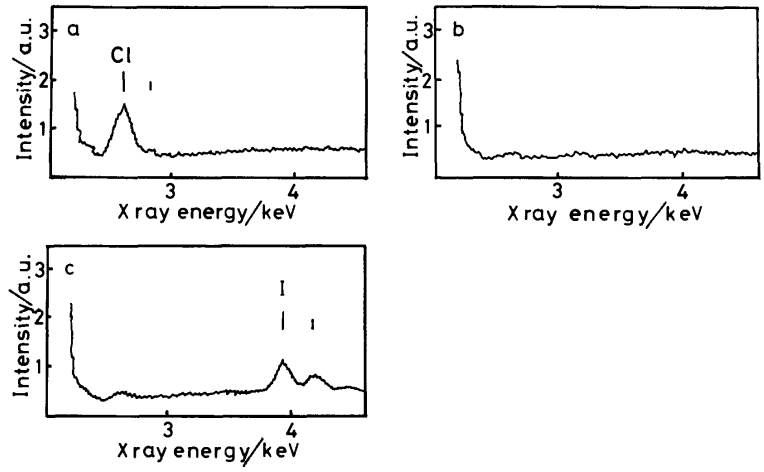

Fig. 3. EPMA spectra of PPy/Pt electrodes. (a) Original electrode prepared in 0.1 mol dm^{-3} $LiClO_4$/acetonitrile. (b) Reduced at −0.85 V *vs.* SCE in a 0.5 mol dm^{-3} KI aqueous solution for 2 min. (c) Successively oxidized at 0.45 V *vs.* SCE in the same solution for 2 min.

Prior to the measurements and analyses films were washed thoroughly with twice distilled water. The value of resistivity was found to be invariable for a few days in air. The observed results are shown in Table 2. In this table, the results of elemental analyses are given in relative molar ratio of each element to nitrogen. As expected, the original film has a low resistivity. When this film was polarized at −0.85 V in 0.5 mol dm^{-3} KCl aqueous solution, an elimination of a large part of the inserted ClO_4^- occurs and the resisitivity is enhanced. With an increase in anodic polarization, the incorporation of Cl^- anions into the film becomes appreciable as expected. Simultaneously, the resistivity becomes lowered. Judging from the results from the elemental analyses, the inserion of Cl^- is not completed at 0 V *vs.* SCE which is enough positive to the peak potential of voltammogram (see Fig. 1-(a)). It is noticed in the voltammogram that relatively large anodic currents flow in the potential region betweeen 0 and 0.45 V. At a glance, they seem to be attributable to capacitive currents,[9] but according to the results obtained that the content of Cl^- was increased by changing the polarization potential from 0 to 0.45 V *vs.*SCE, anodic oxidation of polypyrrole with insertion of anions still occurs in this potential region.

Another interesting point to be noticed is that the molar ratio of Cl^- was higher for the film polarized at 0.45 V in 0.5 mol dm^{-3} KCl than for the original film which contained the incorporated ClO_4^-. This result suggests that the charge involved in the redox process in 0.5 mol dm^{-3} KCl is higher than the excess charge retained in the film in the course of anodic polymerization of pyrrole. According to a literature,[8] 2.25 mol of electrons are involved in the electropolymerization of 1 mol of pyrrole, and 2 mol of electrons are consumed in the polymer chain formation. The extra amount of electrons is consumed in the ionization of film and the equivalent amount of anions is incorporated at that time. Judging from the results given in Table 2, our sample had an excess charge of 0.2 mol per mol of pyrrole when prepared in the acetonitrile solution, but more than 0.25 mol of electrons were found to be involved in the aqueous redox processes, as described below.

Table 2. Elemental analysis and resistivity of polypyrrole films polarized at different potentials in a 0.5 mol dm^{-3} KCl aqueous solution

E	Molar ratio to nitrogen				Resistivity
V *vs.* SCE	C	H	N	Cl	ohm cm
−0.85	4.06	3.33	1.00	0.03	3.9×10^{4}
0.00	4.03	3.28	1.00	0.15	1.2×10^{-2}
0.45	4.04	3.30	1.00	0.30	3.2×10^{-3}
Original	4.02	3.29	1.00	0.20	3.8×10^{-3}

According to the results with the original sample given in Table 2, 2.2 mol of electrons per mol of pyrrole are involved in the deposition of polypyrrole, whereas the results with the film polarized at 0.45 V suggest that 0.3 mol of eletrons can be used in the aqueous redox processes. The amount of charge consumed in the preparation of the PPy/Pt electrode was 36 mC cm^{-2}. When this sample was subjected to an anodic potential sweep from −0.8 to 0.4 V under the same conditions as chosen in the experiment shown in Fig. 1-(a), the charge of 4.8 mC cm^{-2} was consumed. Therefore, if such an assumption is made that 0.3 mol of electrons is involved in the aqueous redox processes, the charge capable of participating in the redox processes will be 36 mC cm$^{-2}\times0.3/2.2=4.9$ mC cm^{-2}, which is in fair agreement with the charge obtained in the course of anodic sweep.

These results undoubtedly support the validity of the reactions

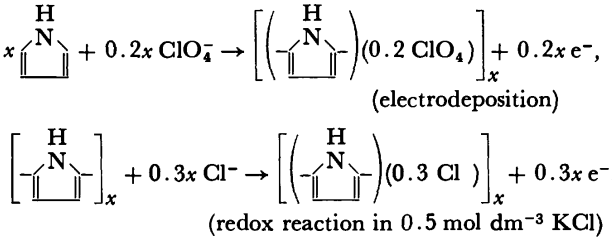

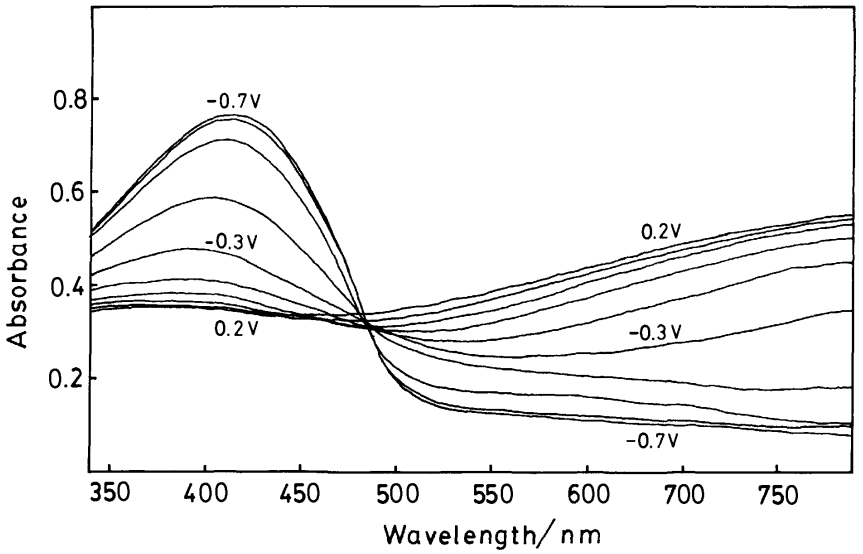

Fig. 4. Absorption spectra of a PPy/OTE electrode obtained *in situ* at different potentials in a 0.1 V interval in 0.5 mol dm^{-3} KCl.

Resistivity measurements were carried out for polypyrrole films prepared in the presence of other kinds of anions and almost the same values as shown in Table 2 were obtained. Judging from these results, electrical properties are primarily determined by charged conditions of polypyrrole which are controlled not by the kind but by the amount of incorporated anions.

Electrochromic Properties of Polypyrrole. It was reported[8,26] that the color of polypyrrole is variable with redox behavior in acetonitrile solutions. It was found that the same was true in aqueous solutions. The color change is reproducible and seems to be applicable to electrochromic display devices.

Visible absorption spectra of a PPy/OTE electrode, obtained under steady states at several different potentials, are shown in Fig. 4. Polymer films with incorporated Cl^- exhibit a brown-black color and show no appreciable absorption peaks. However, when the film is reduced, it turns yellow as recognized from an increase in absorption at wavelengths shorter than 500 nm. The absorption is thought to be assignable to the π-π^* transition of polypyrrole.[18] The coloring occurs noticeably at −0.1 V *vs.* SCE and is enhanced with an increase in cathodic potential up to −0.7 V, beyond which no appreciable increase in absorbance appears.

The change in the absorbance of polypyrrole films with electrolysis charge was pursued *in situ* in 0.5 mol dm^{-3} KCl. The films used were those prepared by anodic oxidation at 0.3 mA cm^{-2} for 2, 4, or 6 min in acetonitrile containing 0.1 mol dm^{-3} pyrrole and 0.3 mol dm^{-3} $LiClO_4$ and were initially reduced at −0.7 V in the solution for measurement. The absorbance of these films was then measured *in situ* during the course of anodic oxidation at 0.3 mA cm^{-2}. Results are given in Fig. 5-(a) as a function of the quantity of electricity consumed in the oxidation. The electrode potential values of the film in the initial and final stages (−0.7 and 0.4 V) and an intermediate stage (−0.2 V) are also given in the figure. In the final stage almost all the charges capable of being retained must have been accumulated in the film, as judged from the results given in Table 2. Fig. 5-(b) shows absorbances at these potetials as a function of the quantity of electricity consumed in the film preparation (Q_d) which is a measure of the film thickness. It is seen from this figure that the absorbance is proportional to the film thickness.

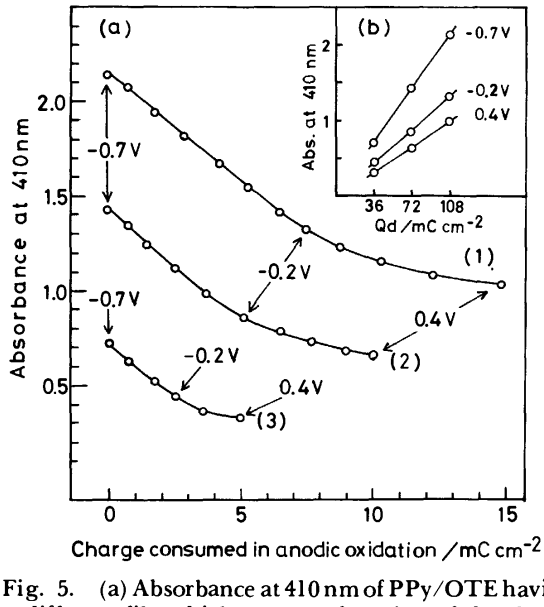

Fig. 5. (a) Absorbance at 410 nm of PPy/OTE having different film thickness as a function of the charge consumed in anodic oxidation at 0.3 mA cm^{-2} in 0.5 mol dm^{-3} KCl. (b) Absorbance at 410 nm of PPy/OTE at −0.7 V, −0.2 V, −0.4 V, in 0.5 mol dm^{-3} as a function of charge consumed for film preparation (Q_d).
The film preparation was carried out in acetonitrile containing 0.1 mol dm^{-3} pyrrole and 0.3 mol dm^{-3} $LiClO_4$ at 0.3 mA cm^{-2} for 2 min (Q=36 mC cm^{-2}) (1), for 4 min (Q_d=72 mC cm^{-2}) (2), and for 6 min (Q_d=108 mC cm^{-2}) (3).

According to Fig. 5-(a), for the films different in thickness linear relations with the same gradient are established between the absorbance and the charge consumed in the anodic oxidation of film in 0.5 mol dm^{-3} KCl as long as the electrode potential is more negative than −0.2 V. However, the rate of absorbance change becomes declined at potentials positive to −0.2 V. This behavior is in qualitatively agreement with the results shown in Fig. 4. The quantity of electricity consumed in the linear part is half the total charge capable of being stored, although with this amount of charge the absorbance at 410 nm changes by *ca.* 80% of the total change.

Relations for the linear part in Fig. 5-(a) are formulated as follows:

$$Abs = -0.119Q_c + 0.72 \text{ (for } Q_d = 36 \text{ mC cm}^{-2}), \quad (1)$$

$$Abs = -0.121Q_c + 1.44 \text{ (for } Q_d = 72 \text{ mC cm}^{-2}), \quad (2)$$

$$Abs = -0.120Q_c + 2.16 \text{ (for } Q_d = 108 \text{ mC cm}^{-2}), \quad (3)$$

where *Abs* denotes the absorbance at 410 nm and Q_c the charge consumed in the anodic oxidation. Since the absorbance is proportional to the quantity of electricity consumed in the film preparation, these equations may reduce to one equation

$$Abs = -0.12Q_c + 0.02Q_d. \quad (4)$$

Since the total amount of charge capable of being stored is $0.3/2.2 \times Q_d$ as stated above and half the charge is involved in the linear portion of the absorbance change (from −0.7 to −0.2 V), the upper limit of Q_c in the above equation is then $0.07Q_d$.

Cyclic voltammograms and absorbances at 410 nm of a PPy/OTE electrode are shown in Fig. 6 for the cases of 0.5 mol dm^{-3} KCl and 0.5 mol dm^{-3} Na_2SO_4. In the KCl solution the absorbance changes quite smoothly with variation in electrode potentials and the change in absorbance shows a hysteresis in the direction of potential sweep. A similar trend of change in absorbance appears also in the Na_2SO_4 solution. In both solutions the absorbance *vs.* potential relations show inflections at the potentials where the voltammograms show their peaks. Thus, two inflections are noticed in the voltammograms obtained on the anodic potential scan in 0.5 mol dm^{-3} Na_2SO_4. These results are closely related to the fact that the change in absorbance is brought about by the redox processes of polypyrrole.

Response behavior of absorbance to pulsed poten-

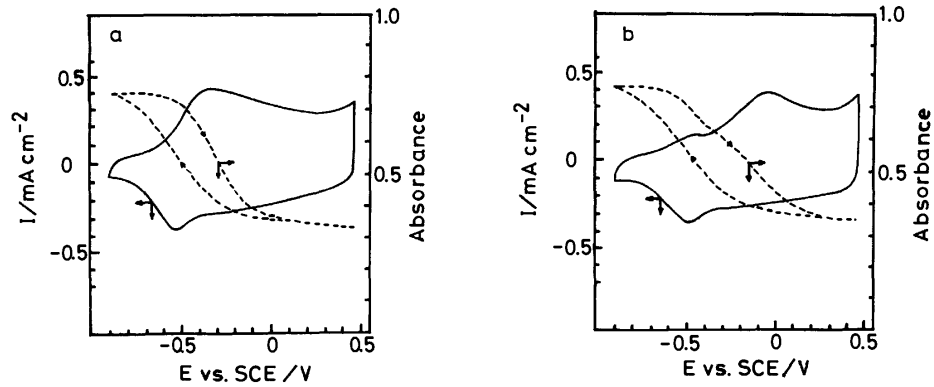

Fig. 6. Change in absorbance at 410 nm obtained *in situ* in the measurements of cyclic voltammograms. (a) in 0.5 mol dm^{-3} KCl (b) in 0.5 mol dm^{-3} Na_2SO_4. dE/dt=50 mV s^{-1}.

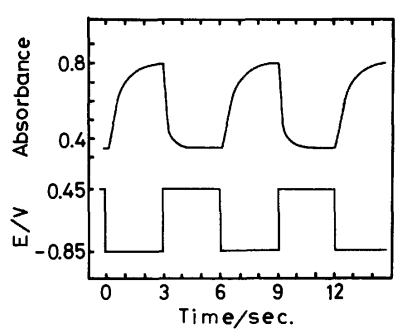

Fig. 7. Response behaviors of the absorbance change of the PPy/OTE electrode to repeated potential pulses of −0.85 V and 0.45 V *vs.* SCE in 0.5 mol dm^{-3} KCl. Absorbance was measured at 410 nm.

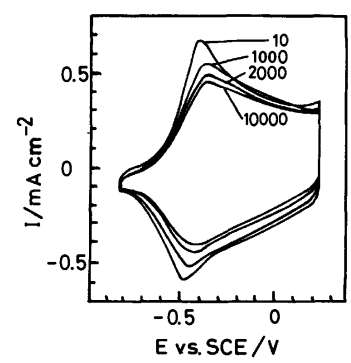

Fig. 8. Change in cyclic voltammograms of PPy/Pt electrode with the number of potential sweep cycles in 0.5 mol dm^{-3} KCl. The number in the figure denotes the cycle number. dE/dt=50 mV s^{-1}.

tials were investigated in 0.5 mol dm^{-3} KCl at 410 nm with a potential pulse of −0.85 or 0.45 V. Results are shown in Fig. 7. The response to the anodic pulse is faster than that to the cathodic one. The slowness of the cathodic response must be related to the fact that the polymer becomes resistive on application of −0.85 V. However, improvement of the response will be possible by appropriate choice of the film thickness, electrode area, and conductive substrate. Stability tests on the redox processes of polypyrrole were investigated in 0.5 mol dm^{-3} KCl with the PPy/Pt electrode. Results are shown in Fig. 8. The shape of voltammograms taken at the sweep rate of 100 mV s^{-1} becomes ill-defined with an increase in potential sweep cycles, but no appreciable change in film color is noticed to the naked eye during 10000 potential sweeps. These results suggest that polypyrrole is a promising candidate as a material for electrochromic display devices.

References

1) R. McNell, R. Siudak, J. H. Wardlaw, and D. E. Weiss, *Aust. J. Chem.*, **16**, 1056 (1963).
2) B. A. Bolto and D. E. Weiss, *Aust. J. Chem.*, **16**, 1076 (1963).
3) B. A. Bolto, R. Mcnell, and D. E. Weiss, *Aust. J. Chem.*, **16**, 1090 (1963).
4) A. F. Diaz and K. K. Kanazawa, *J. Chem. Soc., Chem. Commun.*, 635 (1979).
5) K. K. Kanazawa, A. F. Diaz, R. H. Geiss, W. D. Gill, J. F. Kwak, J. A. Logan, J. F. Rabolt, and, G. B. Street, *J. Chem. Soc., Chem. Commun.*, 854 (1979).
6) A. F. Diaz and J. I. Castillo, *J. Chem. Soc., Chem. Commun.*, 397 (1980).
7) A. F. Diaz, J. M. Vasquez Vallejo, and A. Martinez Duran, *IBM J. Res. Develop.*, **25**, 42 (1981).
8) A. F. Diaz, J. I. Castillo, J. A. Logan, and Wen-Young Lee, *J. Electroanal. Chem.*, **129**, 115 (1981).
9) A. F. Diaz, A. Martinez, and K. K. Kanazawa, *J. Electroanal. Chem.*, **130**, 181 (1981).
10) R. Noufi, D. Tench, and L. F. Warren, *J. Electrochem. Soc.*, **127**, 2310 (1980).
11) R. Noufi, A. J. Frank, and A. J. Nozik, *J. Am. Chem. Soc.*, **103**, 1849 (1981).
12) R. Noufi, D. Tench, and L. F. Warren, *J. Electrochem. Soc.*, **128**, 2596 (1981).
13) T. Skotheim and I. Lundström, *Appl. Phys. Lett.*, **40**, 281 (1982).
14) T. Skotheim, L. G. Petersson, O. Inganös, and I. Lundström, *J. Electrochem. Soc.*, **129**, 1737 (1982).
15) A. J. Frank and K. Honda, *J. Phys. Chem.*, **86**, 1933 (1982).
16) G. Cooper, R. Noufi, A. J. Frank, and A. J. Nozik, *Nature*, **295**, 578 (1982).
17) R. A. Bull, Fu-Ren. F. Fan, and A. J. Bard, *J. Electrochem. Soc.*, **129**, 1009 (1982).
18) T. Inoue and T. Yamase, *Bull. Chem. Soc. Jpn.*, **56**, 985 (1983).
19) S. K. Deb, *Appl. Opt. Suppl.*, **3**, 192 (1969).
20) M. Green and D. Richman, *Thin Solid Films*, **24**, 545 (1974).
21) H. N. Hersh, W. E. Kramer, and J. H. McGee, *Appl.*

Phys. Lett., **27**, 464 (1975).
22) S. K. Mohapatra, *J. Electrochem. Soc.*, **125**, 284 (1978).
23) R. J. Colton, A. M. Guzman, and J. W. Rabalais, *J. Appl. Phys.*, **49**, 409 (1978).
24) M. M. Nicholson, *J. Electrochem. Soc.*, **126**, 1490 (1979).
25) F. Garnier and G. Tourillon, *J. Electroanal. Chem.*, **148**, 299 (1983).
26) G. Tourillon and F. Garnier, *J. Phys. Chem.*, **87**, 2289 (1983).
27) B. Valdes, *Proc.* IRE, **42**, 420 (1954).
28) H. Kim and H. A. Laitinen, *J. Am. Chem. Soc.*, **58**, 23 (1975).
29) A. J. Bard and L. R. Faulkner, "Electrochemical Method," John Wiley and Sons, Inc., New York (1980), p. 522.
30) J. Kielland, *J. Am. Chem. Soc.*, **59**, 1675 (1937).
31) D. D. Macdonald, "Transient Techniques in Electrochemistry," Plenum Press, New York (1977), p. 195.

Basic Behaviors and Properties of the Electrodeposited Polyaniline

Akira KITANI,* Jinko IZUMI, Jun YANO, Yasuyuki HIROMOTO, and Kazuo SASAKI
Department of Applied Chemistry, Faculty of Engineering, Hiroshima University, Saijo-cho, Higashi-Hiroshima 724
(Received November 4, 1983)

Basic behaviors and properties of polyaniline(PA) deposited anodically on platinum electrodes have been studied on the following points. 1) Effect of the mode of electrolysis and supporting electrolytes in the film forming process. 2) Characteristics of charging-discharging processes. 3) Electric conductivity and elemental composition of PA. The different modes of electrolysis do not affect the characteristics of the PA electrode obtained. The growth rate of PA film is 2.7—2.8 times faster in sulfuric acid than in perchloric, nitric or hydrochloric acid. It is indicated that there are two types of doping; one is associated with the acid-base equilibrium between amino or imino group in the film and proton in the solution and the other is associated with the excess charge in the film produced by anodic oxidation. The electric conductivity of PA markedly decreases by the immersion in alkali solutions. The release of doped anion from PA by treating with an alkali solution is confirmed by the elemental analysis. The amount of anions occluded by the electrochemical doping process is determined to be 0.25—0.29 per monomer unit.

Polyaniline (PA) film as a typical electroconductive organic polymer has been first prepared by Diaz and Logan[1] by means of anodic oxidation of aniline in aqueous sulfuric acid. They used platinum as the anode electrode and the polymer film was deposited on it. Recently, Noufi and his coworkers[2] showed that the deposition of PA film is possible onto the surface of several semiconductor electrodes such as Cd-chalcogenides, Si, GaAs, and GaP. Since the latter materials are corrosive in aqueous media, the polymer coating will provide a new mean of the corrosion protection.

In contrast to polypyrrole[3], another representative conducting polymer, studies on polyaniline are very limited and, as far as we are aware, only two papers which are mentioned above have been published in the past. We thus attempted to study the basic characters of polyaniline in more detail.

Experimental

Electrode substrate used was a platinum wire having geometry of 1 mm in diameter and 10 mm in length ($S=ca.$ 0.3 cm^2). Only for the determination of doped anions released from the film, a platinum plate having surface area of *ca.* 8 cm^2 was used. Although two types of electrolysis, repeated potential cycling and controlled potential electrolysis, were employed in the film forming process, the most of measurements were made with PA electrode (PAE) prepared by potential cycling. The potential cycling was repeated usually 40 to 50 times in sulfuric acid solutions. Other details of electrochemical measurements are given at appropriate positions in the following description.

Electric conductivity of PA films was measured with the four-probe method described by van der Pauw.[4] Specimens used for the conductivity measurement were prepared by pressing the powdery product obtained by potentiostatic electrolysis.

All the potential values cited in this paper are those referred to a saturated calomel electrode. All experiments were carried out at room temperature.

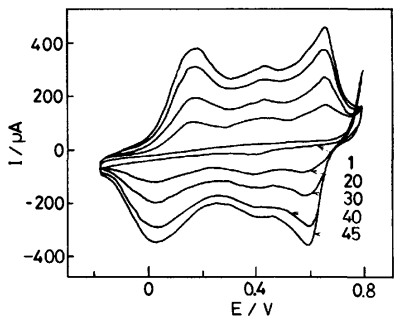

Fig. 1. Change of voltammograms in the preparation of polyaniline film by repeated potential cycling between −0.2 and 0.8 V. Numerical figure attached to each curve indicate number of potential cycle.
Solution: 0.1 M H_2SO_4+0.1 M aniline.
Sweep rate: 100 mV·s^{-1}.

Results and Discussion

1. Preparation of Polyaniline Film. Polyaniline film electrodes (PAE) were prepared in two different ways, repeated potential cycling and constant potential electrolysis. Figure 1 indicates the cyclic voltammogram observed with a platinum electrode immersed in 0.1 M H_2SO_4 containing 0.1 M aniline (1 M=1 mol dm^{-3}). The redox charge of polyaniline film continued to grow by the repetition of potential cycling. The cathodic charge in Fig. 1 increased linearly with the number of potential cycling. This indicates that the growth of polyaniline film is proportional to the number of potential cycling.

The possibility of preparing the film with constant potential electrolysis was next studied in 0.1 M H_2SO_4

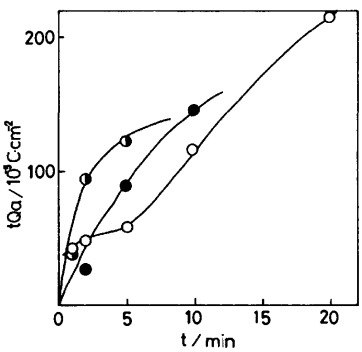

Fig. 2. Change in total anodic charge against the duration of constant potential electrolysis.
Electrode potential: 0.8 [●], 1.0 [○], 1.2 [◑] V.
Solution: 0.1 M H_2SO_4+0.1 M aniline.

containing 0.1 M aniline. The electrolyses were carried out at 0.8, 1.0, and 1.2 V, and the transient current was recorded for each measurement. After finishing the electrolysis, the electrode was subjected to the cathodic potential sweep to determine the charge associated with the redox reaction of the film itself, Qr.

The rate of aniline oxidation is a complicated function of the electrode potential. The total anodic charge, tQa, rapidly and monotonously approached to a saturation value at 0.8 and 1.2 V. Contrarily, at 1.0 V, the tQa-time curve made a step, where tQa almost ceased to increase, and again increased gradually. These are shown in Fig. 2.

Regardless of the electrode potential a tight thin film first appeared on the platinum surface and soon after that a powdery, non-adhesive structure which finally falls down from the electrode grew over the film surface. Inside of this massive structure, the thin film seems to grow progressively as far as tQa continues to increase. In fact, when Qr's were plotted against the time of anodic treatment, the curve forms were entirely similar to those shown in Fig. 2. The cyclic voltammograms exhibited by two PAE's prepared by the constant potential electrolysis and the potential cycling were almost the same and no practical difference was observed.

Although the constant potential electrolysis is complicated by the intervention of the powdery product, it is undoubted that a tight film of definite thickness is also obtained by this method. It should be also noted that by pressing the powdery product we can easily prepare a film or a pellet without spoiling electrode activity.

The effect of supporting electrolytes in the film forming process was studied. PAE was prepared by continuous potential cycling. The increase of doping charge per unit cycle, which is assumed as a measure of the rate of film growth, is listed in Table 1 to see the effect of electrolytes on the rate of film growth. It is indicated that the growth rate of PA film is extraneously faster in sulfuric acid. This may be partly attributed to the bivalency of sulfate anion.

The surface structure of PA film was observed by scanning electron microscopy. It was found that the film prepared in perchloric acid is rather smooth compared to that prepared in sulfuric acid.

2. Charging and Discharging Behavior. In the cyclic voltammograms of PAE in solutions containing no aniline, it is generally observed that the charge consumed in the anodic half cycle is exactly compensated in the succeeding cathodic half cycle. This was also the case, even though aniline was present in the solution, when PA film had already been grown enough after a number of potential cycling (Fig. 1). This indicates that, with a PAE having a thicker film, the film growth is slow enough and the charge consumed for it becomes negligible compared with the charge associated with the redox reaction of the film itself.

TABLE 1. EFFECT OF SUPPORTING ELECTROLYTES IN THE FILM PREPARATION PROCESS

Acid	No. of cycle	Doping charge	Doping charge/cycle
			mC cm^{-2}
0.1 M H_2SO_4	45	6.15	0.137
0.2 M $HClO_4$	80	3.85	0.0481
	135	6.33	0.0469
0.2 M HCl	135	6.30	0.0466
0.2 M HNO_3	200	10.2	0.0510

Potential cycling was repeated between −0.2 and 0.8 V at 0.1 V.s^{-1}.

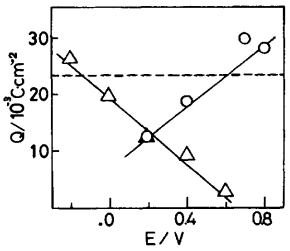

Fig. 3. Redox charge determined by potential step technique as a function of electrode potential.
○: determined from anodic going step from −0.2 V.
△: determined from cathodic going step from 0.8 V.
PAE used for this figure was prepared in 0.1 M H_2SO_4 and measurements were made in aniline free 0.1 H_2SO_4.

In order to see the nature of the charging and discharging reactions of the film more precisely, we employed the potential step technique. Figure 3 shows the results. Anodic charge in this figure was determined from the current decay at a given potential stepped up from the cathodic limiting potential (−0.2 V). Similarly, cathodic charge was determined by stepping down the potential from the anodic limiting potential (0.8 V). It is seen that both the anodic and cathodic charges are linear functions of the electrode potential showing that a PA film has a character of an electric condensor in the sense that the relation Q=CV holds.

Diaz and Logan[1] assumed that the charging-discharging processes of PA are the elimination-addition reactions of proton.

$$(C_6H_5N)_n = (C_6H_4N)_n + nH^+ + ne.$$

There is, however, another possibility of ingress and degress of anionic species in and out of the film as are known with polypyrrole.[3] We shall call this as the doping and undoping reactions.

$$(C_6H_4N)_n + pX^- = (C_6H_4N)_n^{p+}pX^- + pe.$$

In order to confirm the true mechanism, the cathodic dissolution of sulfate anions from the PA film was studied qualitatively. A PAE prepared in sulfuric acid was subjected to the cathodic reduction at −0.2 V in 0.1 M HCl containing $BaCl_2$. By this treatment it was observed that a white cloud grew at the film surface and spread gradually into the solution. The same subject was also studied by using benzenesulfonate as the doping anion. A PAE, which was made free from dopant by cathodic treatment, was oxidized at 0.8 V in 0.1 M benzenesulfonic acid. The PAE thus obtained was washed with water and then reduced at −0.2 V in sulfuric acid for 3 min. The dissolution of benzenesulfonate was confirmed by uv absorption spectra. It is indisputable that benzenesulfonate does dope into the film structue.

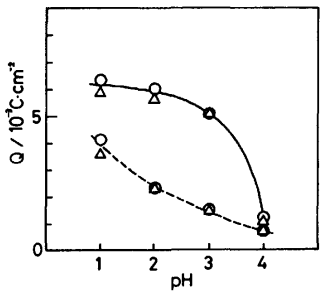

Fig. 4. Effect of the solution pH on the doping capacity.
Full line was obtained with PAE prepared in 0.1 M H_2SO_4 while broken line was obtained with PAE prepared in 0.2 M $HClO_4$.
△: anodic charge. ○: cathodic charge.

At present, it is not clear whether the charging-discharging process of PAE is of solely doping and undoping reactions. The possibility that the proton elimination mechanism is occurring simultaneously with the doping mechanism cannot be ruled out. Although the detailed mechanism is uncertain, it is undoubted that the doping mechanism is operating during the redox process of PAE. Another information concerning the amount of anions in the polymer structure was also obtained by the elemental analysis of PA, and will be discussed in the succeeding section.

3. Effect of the Solution pH. Figure 4 shows the effect of the solution pH on the doping charge of PAE. It is seen that the doping charge decreases with increasing pH and diminishes at about pH=4. Diaz and Logan[1] were aware of this fact and attributed to the difference of nucleophilicity of solvents without any further discussion. This behavior may be related to the acid-base equilibrium of amino or imino nitrogen in the film with proton in the solution. With the increase of the solution pH, the equilibrium will shift towards the deprotonation of amino or imino nitrogen. The deprotonated film seems to lose its electric conductivity. This is the reason why PAE is only active in acidic environments.

In fact, the electric conductivity of a film prepared in H_2SO_4 was decreased from 4.0 $\Omega^{-1}cm^{-1}$ (doped state) to 0.26 $\Omega^{-1}cm^{-1}$ (undoped state). When, however, the same film was immersed to an alkaline solution (0.1 M NaOH) the conductivity decreased to an unmeasurable value. The release of doped anion from powdery polyaniline by treating with an alkali solution was also confirmed by elemental analysis. Results will be described in detail in the succeeding section.

From the results described above, it can be concluded that there are two types of anions occluded in the film structure; one neutralizes protonic charges associated with the acid-base equilibrium (Type I) and the other

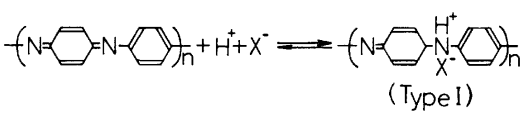

(Type I)

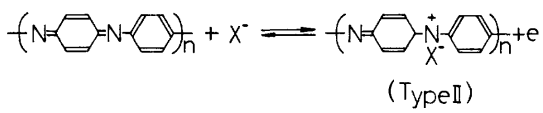

(Type II)

compensates the excess plus charges produced by anodic oxidation of film structure (doping process, Type II). The portioning of these two types of anions is an interesting problem to be studied in future studies.

4. Electric Conductivity. In aqueous solutions, PAE is electroactive only in acidic environments. In solutions of pH>4, no appreciable charge transfer reaction across the PAE/solution interface takes place. This was attributed to the loss of the electric conductivity of the film due to the deprotonation caused by the acid-base equilibrium. This sort of deactivation will occur only in the surface layer, so long as the time of contact with water is limited.

In order to confirm this view further, a PAE prepared in a sulfuric acid solution was transferred to an acetonitrile solution containing $NaClO_4$ as the supporting electrolyte to take voltammograms. Prior to transferring the electrode, the electrode was rinsed in an aqueous 0.1 M K_2SO_4 solution for 15 min and was washed with water and acetonitrile successively. Voltammograms shown in Fig. 5 were taken periodically as indicated in the figure caption. One can see that the electrode becomes inactive by the water treatment but recovers its activity gradually. Dashed curve in this figure stands for the electrode which has been washed merely with acetonitrile without rinsing in water. The recovery of the electrode activity may be related to the slow diffusion of protons from the inside of the film to its outer surface.

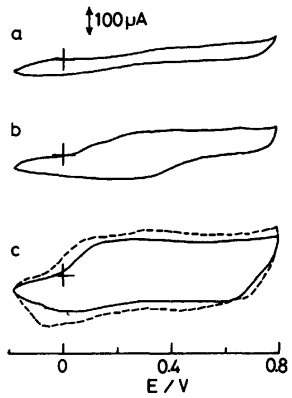

Fig. 5. Recovery of doping capacity during the immersion in acetonitrile.
PAE used was first rinsed in neutral K_2SO_4 solution for 15 min and was transferred into an acetonitrile solution.
a: just after the transfer, b: after 50 min, c: after 2 d.
Broken curve was taken by voiding the rinsing in K_2SO_4 solution.

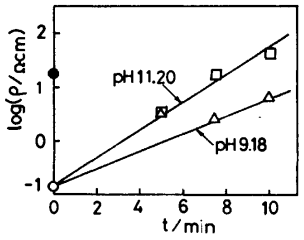

Fig. 6. Change of specific resistance of doped polyaniline with immersing time in alkaline solutions.
Full circle indicates undoped polyaniline.

Table 2. Elemental analysis of polyaniline powder prepared in perchloric acid

$C_6H_wN_x\ y$(dopant) $z(H_2O)$

Sample	W	X	Type I $y_I(HClO_4)$	Type II $y_{II}(ClO_4^-)$	Z
I(Oxidized form)	3.9_7	0.97	0.85*	0.29	2.35
II(Reduced form)	3.8_8	0.96	0.98	—	1.85
III(Deprotonated form)	4.7_7	0.98	—	0.29	0.16

* Caluculated from the total amount of dopants (y=1.14) and y_{II}.

The change of electric conductivity by the immersion in alkali solutions (pH=9.13 and 11.20) was measured with four probe method.[4] In this experiment PA powder prepared potentiostatically at 0.8 V in perchloric acid was pressed to form a pallet. Logarithum of specific resistance of doped polymer changed almost linearly with the immersion time as shown in Fig. 6. It is thus possible to control the conductivity of PA from conducting to semiconducting states by changing the immersion time and/or pH of the solution.

Full circle located on the ordinate stands for the resistivity of PA which was subjected to a prolonged cathodic undoping. It is worth noting that an appreciable conductivity is still retained by the reduced PA. This indicates that the electric conductivity of the PA film is largely determined by the amount of anions brought into the film by acid-base equilibrium.

5. Elemental Composition of PA. In the preceding section, we concluded that there are two types of dopants in the film; one is to neutralize protonic charges associated with acid-base equilibrium (Type I) and the other is to compensate the positive charges produced by anodic oxidation (Type II). In order to obtain informations concerning the amounts of Type I and Type II dopants the elemental analysis of PA was carried out.

Three kinds of different samples were prepared for this. The first sample was a massive PAE which was prepared by constant potential electrolysis at 0.8 V (Sample I, oxidized form). The same sample was further treated by cathodic reduction at 0 V (Sample II, reduced form). The third sample was basically the same as Sample I but was immersed in a 0.1 M NaOH solution for 2 h (Sample III, deprotonated sample). The amount of anions in Sample III should give the amount of Type II dopant. In all cases, the samples were scratched off from the electrode substrate and they were weighed and subjected to the elemental analysis. Results are summarized in Table 2, where w, x, y, and z are the numerals appearing in the assumed formula $C_6H_wN_x\cdot y$(Dopant)$\cdot z(H_2O)$, y_I and y_{II} discriminate the types of dopant.

The y_{II} value can also be determined by calculation if we know the initial weight of a given sample and the charge required for its cathodic reduction. The value thus determined was 0.25 which is in a good agreement with the value determined by elemental analysis, 0.29. The y_I value determined with Sample II should equal to x, if all of the nitrogen atoms of PA participate the acid-base equilibrium. The data confirms this expectation. The existence of water in PA should be correlated with the hydration of doping ions. A drastic change in z value appeared in Sample III may, perhaps, be an indication of that the hydration occurs predominantly to protons rather than anionic species.

The apparent formula of aniline moeity was determined to be C_6H_4N for both oxidized and reduced forms. By considering the amount of Type II doping is 0.25—0.29 per monomer unit, the overall polymerization reaction can be expressed as follows.

$$4n(C_6H_7N) \longrightarrow (C_6H_4N)_n^{+} + 12H^+ + 13e.$$

The hydrogen content of the deprotonated sample was somewhat larger than that of oxidized form. The reason is unknown now, but may be partly related to the partial hydrolysis catalyzed by base.

Qualitatively, similar results were obtained for the samples prepared in H_2SO_4. The total amount of dopants (assumed as SO_4^{2-}) was 1.13, 0.81, and 0.16 for oxidized, reduced, and deprotonated samples, respectively. Quantitative discussion is rather difficult because there is a possibility of existing as both monovalent and divalent anions, HSO_4^- and SO_4^{2-} being doped simultaneously.

This work was supportcd by Grant 57850257 supplied by the Ministry of Education, Science and Culture. The authors wish to express their thanks to Mr. Makoto Ogasawara for the measurement of elemental composition of PA.

References

1) A. f. Diaz and J. A. Logan, *J. Electroanal. Chem.*, **111**, 111 (1980).

2) R. Noufi, A. J. Nozik, J. White, and L. F. Warren, *J. Electrochem. Soc.*, **129**, 2261 (1982).

3) A. F. Diaz *et. al.*, *J. Chem. Soc., Chem. Commun.*, **1979**, 635, 854; **1980**, 397; *J. Electroanal. Chem.*, **108**, 377 (1980), **121**, 355 (1981), **129**, 115 (1981), **130**, 181 (1981); R. A. Bull, F. F. Fan, and A. J. Bard, *J. Electrochem. Soc.*, **129**, 1009 (1982); In regard to protection of semiconductor electrodes with polypyrrole, see T. Skotheim, L. G. Petersson, O. Inganas, and I. Lundstrom, *J. Electrochm. Soc.*, **129**, 1737 (1982).

4) L. J. van der Pauw, *Philips Res. Repts.*, **13**, 1 (1958).

Electronic Spectra of $(DBTTF)_3 \cdot SnBr_6$ Complex

Masashi TANAKA,* Kohji KAMIYA,† Jiro TANAKA,† and Shizuaki MURATA
Department of Chemistry, College of General Education, Nagoya University, Nagoya 464
†*Department of Chemistry, Faculty of Science, Nagoya University, Nagoya 464*
(Received February 17, 1984)

The polarized reflection spectra of $(DBTTF)_3 \cdot SnBr_6$ complex have been measured and the absorption spectra have been determined by the simulation of the observed reflection spectra. The 4000 cm^{-1} band polarized parallel to the stacking axis has been assigned to the charge resonance(CR) band. The theoretical analysis of the electronic structure of $(DBTTF)_3 \cdot SnBr_6$ complex has been made for the explanation of the energy and absorption intensity of the CR band.

Organic charge transfer radical salts of the electron donor TTF (tetrathiafulvalene) and the electron acceptor such as TCNQ (tetracyano-*p*-quinodimethane) display the high electrical conductivties.[1,2] These organic conductors show the special feature of their crystal structures. That is, electrons and holes are delocalized along segregated stacks of the cation donor and anion acceptor free radicals. Therefore, the presence of donor and acceptor stacks causes considerable complexities of solid state properties of organic conductors and there has been a considerable interest in the studies on their highly anisotropic electrical, optical, and magnetic properties. The optical properties of such pseudo-one-dimensional materials were analyzed by Hubbard Hamiltonian as was shown in our earlier paper on TCNQ complexes.[3] On the other hand, after the high conductivity was observed using a four-probe method in single crystals of TTF-TCNQ, many donors and acceptors were synthesized and the preparation of organic metal was intended. Dibenzotetrathiafulvalene (DBTTF) is one of them and the direct oxidation of DBTTF by halogens and metal halides were reported to yield complexes such as $(DBTTF)_2 \cdot I_3$,[4] $(DBTTF)_8 \cdot (SnCl_6)_3$,[5] and $(DBTTF)_3 \cdot SnBr_6$.[5]

In this paper, we report the polarized reflection spectra of $(DBTTF)_3 \cdot SnBr_6$ complex and the theoretical analysis of the new electronic structure found in the $(DBTTF)_3 \cdot SnBr_6$ system.

Experimental

DBTTF was prepared by Nakayama's method[6] and the crystal of $(DBTTF)_3 \cdot SnBr_6$ complex was prepared by the diffusion of DBTTF and $SnBr_4$ molecules in acetonitrile solution. Reflection spectra at the normal incidence were measured over a range of 4000—25000 cm^{-1} with a reflection microspectrophotometer made in our laboratory and all computations were carried out on a FACOM-M382 computer at the NAGOYA university computation center.

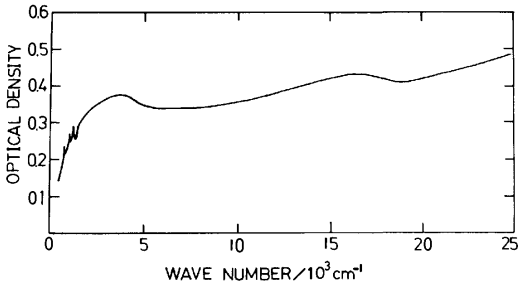

Fig. 1. Absorption spectrum of $DBTTF_3 \cdot SnBr_6$ complex in KBr disk.

Results and Discussion

The absorption spectrum of $(DBTTF)_3 \cdot SnBr_6$ complex in KBr disk is depicted in Fig. 1. The first band is located in the region of 4000 cm^{-1} and the threshold of this band overlaps with a few vibrational bands. The second band is observed at 15000 cm^{-1}.

$(DBTTF)_3 \cdot SnBr_6$ complex forms orthorhombic crystals of space group Pnn2 having two complexes in a unit cell. Projection onto the (100) plane is shown in Fig. 2.[7] The characteristic of the structure of the complex shows the stacking layer of the anion ($SnBr_6^-$) and the molecule DBTTF. Each layer elongates along the direction of the crystalline axis c, and the period along the layers consists of 1 and 3 units of $SnBr_6^-$ and DBTTF, respectively. For the molecule of DBTTF, the center of molecule is located along the direction of two-fold axis and the molecular plane is perpendicular to the stacking axis. Two of DBTTF molecules (molecules 1 and 2) overlaps each other completely, but one of them (molecule 3) has the configuration twisted for the other two molecules.

The polarized reflection spectra shown in Fig. 3 indicate that the 4000 cm^{-1} band observed in the c axis spectrum can be assigned to the band having the transition moment parallel to the intermolecular direction and the 15000 cm^{-1} band is due to the intramolecular transition of DBTTF cation radical.[8] Whole behavior of the observed reflection spectra is similar to that of $(DBTTF)_8 \cdot (SnCl_6)_3$ crystal except for the reflectivity value of 4000 cm^{-1} band ($R \simeq 80\%$).[9]

The reflectivity R can be expressed by the following

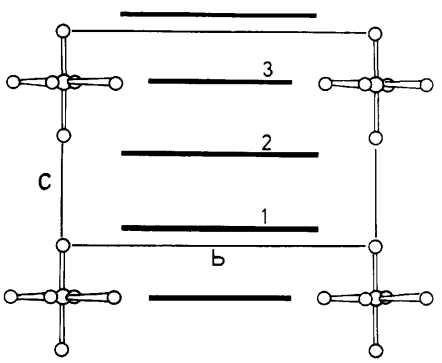

Fig. 2. Projection onto the (100) plane of the crystal of $DBTTF_3 \cdot SnBr_6$ complex.[7]

equations,[10]

$$R = \frac{1 + |\varepsilon| - \sqrt{2(|\varepsilon| + \varepsilon_1)}}{1 + |\varepsilon| + \sqrt{2(|\varepsilon| + \varepsilon_2)}}, \quad (1)$$

and

$$\varepsilon(\omega) = \varepsilon_1(\omega) + i\,\varepsilon_2(\omega) = \varepsilon_{core} + \sum_j \frac{\Omega_j^2}{\omega_j^2 - \omega^2 - i\,\omega\,\gamma_j}, \quad (2)$$

where $|\varepsilon| = \sqrt{\varepsilon_1(\omega)^2 + \varepsilon_2(\omega)^2}$. The parameters Ω_j, ω_j, and γ_j can be determined by the best fit of the calculated reflection values to the observed spectra. The obtained parameters are shown in Table 1 and the best fit curves are plotted in Fig. 3 for comparison with the experimental curves. The absorption coefficient $\alpha(\omega)$ based on these parameters can be obtained by the next equations.[11]

$$\alpha(\omega) = \frac{4\pi}{c\,n(\omega)}\omega\,\varepsilon_2(\omega), \quad (3)$$

and

$$n(\omega)^2 = \frac{1}{2}[\sqrt{\varepsilon_1(\omega)^2 + \varepsilon_2(\omega)^2} + \varepsilon_1(\omega)]. \quad (4)$$

The obtained absorption spectra are described in Fig. 4

Table 1. Dielectric parameters of the Lorentz fits of reflectivity data for $(DBTTF)_3 \cdot SnBr_6$

	//c spectrum	⊥c spectrum	
ε_{core}	2.94	3.10	
Ω_j/cm^{-1}	8700	9000	18500
ω_j/cm^{-1}	3800	15800	28000
γ_j/cm^{-1}	1910	4900	20000

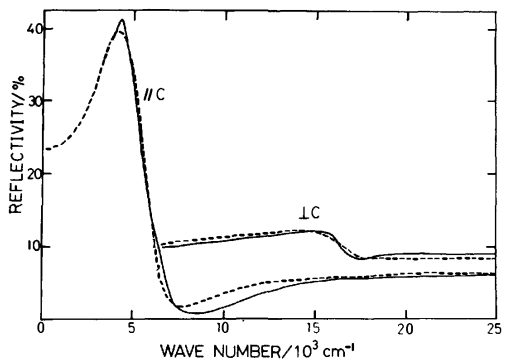

Fig. 3. Observed and calculated reflection spectra of the crystal of $DBTTF_3 \cdot SnBr_6$ complex (——: observed, ----: calculated).

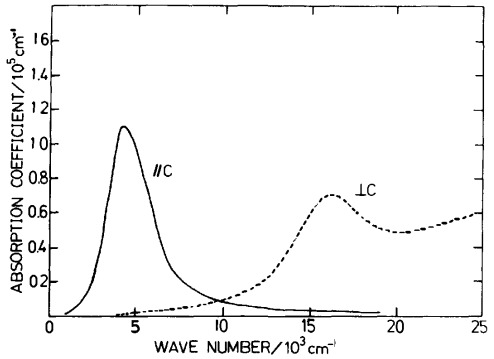

Fig. 4. Calculated absorption spectra of the crystal of $DBTTF_3 \cdot SnBr_6$ complex.

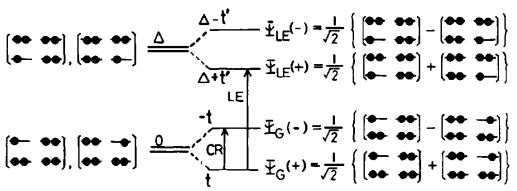

Fig. 5. Energy diagram of $DBTTF_3 \cdot SnBr_6$ complex.

and the oscillator strength f of the 4000 cm^{-1} band is estimated to be 0.3 by using the equation

$$f = \frac{m_e}{2\pi^2 N e^2}\int \omega \cdot \varepsilon_2(\omega)\,d\omega, \quad (5)$$

where N is the number density (2.49×10^{21} cm^{-3}) of $DBTTF \cdot SnBr_6$ complex in the crystal and m_e the electron mass. In order to explain the absorption intensity of the 4000 cm^{-1} band, $(DBTTF)_3 \cdot SnBr_6$ complex is proposed to have the electronic structure shown in Fig. 5. That is, the π-electron can transfer between the molecules 1 and 2 in the unit cell, although it can not move between the molecules 1 and 3, or 2 and 3. This model can be supported by the feature of the molecular overlap as is noted in the earlier paragraph. Accordingly, the DBTTF cation radical is either of the molecules 1 and 2.[7] Then, the ground configuration functions of $(DBTTF)_3 \cdot SnBr_6$ complex can be written as follows,

$$\Psi_{G,1} = a_{1,m}|HF>, \quad (6)$$

and

$$\Psi_{G,2} = a_{2,m}|HF>. \quad (7)$$

Here, $|HF>$ means the Hartree-Fock wavefunction of the neutral trimer $(DBTTF)_3$. $a_{1,m}$ and $a_{2,m}$ are the annihilation operators of the highest occupied molecular orbital ($\phi_{1,m}$ and $\phi_{2,m}$) of the molecules 1 and 2, respectively. On the other hand, the locally excited configurations of the cation radical can be expressed in the following equations,

$$\Psi_{LE,1} = a_{1,m-1}|HF>, \quad (8)$$

and

$$\Psi_{LE,2} = a_{2,m-1}|HF>, \quad (9)$$

where $a_{1,m-1}$ and $a_{2,m-1}$ are the annihilation operators of the next highest occupied orbitals ($\phi_{1,m-1}$ and $\phi_{2,m-1}$).

The wave functions and the energies of the ground state $\psi_G(+)$ and the lowest excited state $\psi_G(-)$ are given as the solution of the modified Hubbard Hamiltonian[3] in the next equations,

$$E_G(+) = t_{m,m},\ \Psi_G(+) = \frac{1}{\sqrt{2}}\{\Psi_{G,1} + \Psi_{G,2}\}, \quad (10)$$

$$E_G(-) = -t_{m,m},\ \Psi_G(-) = \frac{1}{\sqrt{2}}\{\Psi_{G,1} - \Psi_{G,2}\}, \quad (11)$$

where $t_{m,m}$ is the transfer integral between $\phi_{1,m}$ and $\phi_{2,m}$. The transition moment between $\psi_G(+)$ and $\psi_G(-)$ is given as follows,

$$<\Psi_G(+)|\mathbf{M}|\Psi_G(-)> = \frac{1}{2}\{<\phi_{1,m}|e\boldsymbol{r}|\phi_{1,m}> - <\phi_{2,m}|e\boldsymbol{r}|\phi_{2,m}>\} = \frac{e}{2}\boldsymbol{R}_{12}. \quad (12)$$

Here, $\boldsymbol{R}_{12}$ is the difference between the position vectors of the center of the molecules 1 and 2 and $\boldsymbol{R}_{12}$=3.58 A.[7] Then, the theoretical oscillator strength f^{theor} can be estimated as follows,

$$f^{theor} = 3 \times 1.085 \times 10^{11} E_{CR} |\boldsymbol{R}_{12}|^2/4 \simeq 0.4, \quad (13)$$

where $E_{CR}=2t_{m,m}$ is the transition energy in cm^{-1} ($\simeq$4000 cm^{-1}). The calculated value ($f^{theor}\simeq 0.4$) can be comparable with the observed one ($f\simeq 0.3$). Therefore, the 4000 cm^{-1} band can be called the charge resonance band (CR) corresponding to the transition from the state $\psi_G(+)$ to the state $\psi_G(-)$ as is depicted in Fig. 5. $(DBTTF)_3 \cdot SnBr_6$ complex is the first example of the one-dimensional complex having such electronic structure which is different from the dimer, alternant and island types shown in our earlier paper.[3]

References

1) J. Ferrais, D. O. Cowan, V. Walatka,Jr., and J. H. Perlstein, *J. Am. Chem. Soc.*, **95**, 948 (1973).
2) M. J. Cohen, L. B. Coleman, A. F. Garito, and A. J. Heeger, *Phys. Rev. B*, **10**, 1298 (1974).
3) J. Tanaka, M. Tanaka, T. Kawai, T. Takabe, and O. Maki, *Bull. Chem. Soc. Jpn.*, **49**, 2358 (1976).
4) M. Z. Aldoshina, R. N. Lubovskaya, and M. L. Khidekel, *Synthetic Metal*, **1**, 379 (1979/1980).
5) M. Z. Aldoshina, L. S. Verentennikova, R. N. Luboskaya, and M. L. Khidekel, *Izv. Akad. Nauk SSSR, Ser. Khim*, **1978**, 940.
6) J. Nakayama, K. Fujiwara, and M.Hoshino, *Bull. Chem. Soc. Jpn.*, **49**, 3567 (1976).
7) R. P. Shibaeva, L. P. Rozenberg, and P. M. Lobkobska, *Kristallografiya*, **20**, 943,(1975); **25**, 507 (1980).
8) C. Tanaka, J. Tanaka, K. Dietz, C. Katayama, and M. Tanaka, *Bull. Chem. Soc. Jpn.*, **56**, 405 (1983).
9) M. Tanaka, Y. Ando, and J. Tanaka, *Chem. Lett.*, **1983**, 1419.
10) A. A. Bright, A. F. Garito and A. J. Heeger, *Phys. Rev. B*, **30**, 1328 (1974).
11) F. Wooten, "Optical Properties of Solids," Academic Press, New York (1972).

 © 1984 The Chemical Society of Japan Bull. Chem. Soc. Jpn., 57, 2261—2265 (1984)

Intramolecular Interactions in the Ground and Excited States of 1,3-Bichromophoric Propanes in the Aqueous Cyclodextrin Solutions

Michiya ITOH* and Yoshihisa FUJIWARA
Faculty of Pharmaceutical Sciences, Kanazawa University, Takara-machi, Kanazawa 920
(Received March 12, 1984)

The enhanced fluorescence of several 1,3-bichromophoric propanes in aqueous cyclodextrin solutions has been investigated by the steady-state fluorescence spectra and fluorescence lifetimes. 1-(9,10-Dicyano-2-anthryl)-3-(1- and 2-naphthyl)propanes exhibit the intramolecular charge transfer complex fluorescence generated in the ground state in the presence of γ-cyclodextrin. Two bichromophoric propanes, 1,3-di-2-naphthylpropane and 1-(1-naphthyl)-3-(2-naphthyl)propane, in the aqueous β- and γ-cyclodextrin solutions show not only the intramolecular excimer but also the ground state complex fluorescences, though the ground state complex formation of dinaphthylpropane has never been observed in the homogeneous solution even at low temperature. The intramolecular interactions in the ground and excited states seem to be attributable to their intramolecularly geometrical restriction in the extraordinary nonpolar cavity of the cyclodextrins.

The photochemical and photoinduced interactions of organic molecules have been recently studied in the cyclodextrin inclusion systems. Ueno *et al.*[1] reported one host-two guest complex between γ-cyclodextrin (γ-CDx) and sodium 1-naphthylacetate exhibiting excimer fluorescence. The large cavity of γ-CDx is capable of including two molecules of 1-naphthylacetate which shows the characteristic excimer fluorescence, whereas the cavity of α- and β-CDx is too small to accomodate two guest molecules. Recently, Turro *et al.*[2] reported the enhanced intramolecular excimer formation of 1,3-bichromophoric propanes (BC) in the aqueous β- and γ-CDx solutions. They suggested that a stable CDx and BC complex is formed exhibiting excimer fluorescence in cases where the correspondence of the size and shape of the eclipsed conformation of BC system and the cavity of CDx is high and the ratio of excimer and monomer fluorescence intensities is much greater in these cases than in homogeneous solutions. In these so called excimer fluorescence, however, no information of the dynamic process of the excimer formation in the CDx cavity was presented; whether the fluorescence is attributable to the real excimer or to the excited state of the ground state complex in the CDx cavity is not obvious.

This paper presents the intramolecular ground state complex fluorescence of 1-(9,10-dicyano-2-anthryl)-3-(1- and 2-naphthyl) propanes (βα- and ββ-DCAN),[3] and the ground state complex fluorescence as well as the excimer of 1,3-dinaphthylpropanes in the aqueous CDx solutions. The ground state complex formation in the CDx cavity is prevailing to the intramolecular excimer in 1,3-di-2-naphthylpropane (ββ-DNP), while the excimer formation is significant in 1-(1-naphthyl)-3-(2-naphthyl)propane(βα-DNP)[4,5] The intramolecular ground state complex and excimer formations are discussed in terms of the dynamic process of the intramolecular interaction of BC moieties in the CDx cavity both in the ground and excited states.

Experimental

Cyclodextrins (Nakarai Chem.) were recystallized three times from water. The 1,3-bichromophoric compounds were prepared and purified by the methods reported in the previous papers.[3-5] Ion exchanged and distilled water was used. An aqueous CDx solutions of BC compounds were prepared by filtration through a micropore filter (Fuji Film Co. pore size 0.22 μm) after sonification for about 10 min. Absorption and fluorescence spectra were measured by a Hitachi 323 and MPF-4 spectrophotometers, respectively. Fluorescence decay curves were obtained by using the Ortec Single Photon Counting system with the PRA 510 nanosecond light pulser. The triple or double exponential decay was analyzed by the following equation,

$$I(t) = A_1 \exp(-t/\tau_1) + A_2 \exp(-t/\tau_2) + (1-A_1-A_2)\exp(-t/\tau_3), \quad (1)$$

where A_i and t_i are pre-exponential factor and fluorescence lifetime, respectively. The data analysis for the above equation was performed by a computer simulated deconvolution.[6] The criterion for the "best fit" was the minimum sum (Q) of the squares of the difference between observed (D_i) and calculated (D_i') data; an actual allowance was $Q<0.0001$. $Q=\sum_i^n (D_i-D_i')^2/n$, where n is the number of data, D_i and D_i' were normalized to 1.

Results and Discussion

The Ground State Complex Formation of DCAN in the Aqueous CDx Solution. Two 1,3-bichromophoric compounds, ββ- and βα-DCAN are completely insoluble in aqueous solution exhibiting no fluorescence. By adding γ-CDx in the aqueous solution, the

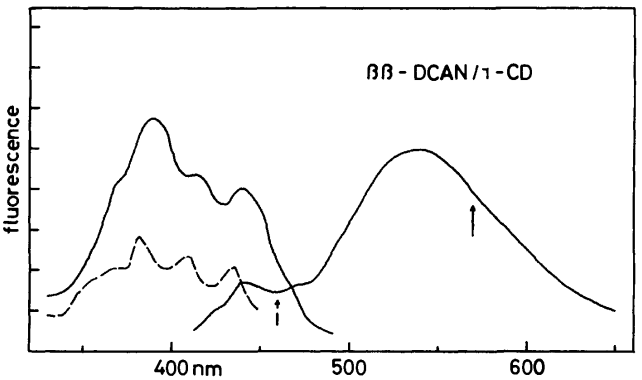

Fig. 1. Fluorescence (uncorrected, excited at 360 nm) and excitation spectra of the γ-CDx solution (10^{-2} mol dm^{-3}) of ββ-DCAN (1.8×10^{-7} mol dm^{-3}) at room temperature. The excitation spectra were monitored at 570 nm (——) and 460 nm (------).

fluorescence spectra were observed as shown in Fig. 1, where the solution was filtrated by micropore filter for removing microcrystals. However, no fluorescence was detected in the α- and β-CDx solutions. The fluorescence spectrum of this γ-CDx solution of ββ-DCAN exhibits a long wavelength fluorescence at 500—570 nm in addition to the 9,10-dicyanoanthryl moiety (DCA moiety) fluorescence at 430—500 nm at room temperature. The excitation spectrum of the former fluorescence is different from that of the latter and from the absorption spectrum of an ethanol solution of this compound. The excitation spectrum of the former long wavelength fluorescence is very similar to that of the ground state complex fluorescence observed in the 3-methylpentane (MP) solution at low temperature reported previously.[3] The MP solutions of ββ- and βα-DCAN show the ground state complex fluorescence at 500—570 nm at low temperature as well as the exciplex fluorescence at room temperature.[3] Further, the absorption spectra of the MP solution confirmed the ground state complex formation at low temperature. Therefore, the long wavelength fluorescence of the aqueous γ-CDx solution of ββ-DCAN may be ascribed not to the exciplex but to the ground state complex in the CDx cavity, though the ground state complex formation cannot be confirmed by the absorption spectra because of too weak absorption intensity. The similar ground state complex fluorescence was observed in the γ-CDx solution of βα-DCAN, whose fluorescence and excitation spectra are shown in Fig. 2. If the ≈550 nm fluorescence consists of the ground state complex and the exciplex fluorescence superimposed, the decay curve might be expressed by four or three components of exponential. However, the double exponential decay was observed throughout 450—580 nm region, though the ratio of the short lifetime component to the long was much larger at 430—530 nm than >530 nm. Therefore, the long wavelength and long lifetime fluorescence may be attributable mostly to the ground state complex mentioned above, even if a possibility of the small contribution of the exciplex fluorescence cannot entirely be removed at the present stage. The fluorescence lifetimes obtained in the aeration and deaeration are summarized in Table 1.

The fluorescence intensity ratio of the complex and DCA moiety is greater in ββ- than βα-DCAN. Further, the intensity ratio of the long lifetime component to the short one shows also a similar trend (Table 1). These facts suggest that the ground state complex formation is more significant in the former. The different fluorescence behavior between two compounds in γ-CDx solutions is well consistent with that of the enthalpy change of the complex formation in the MP solution at low temperature ($-\Delta H$=3.8 kcal mol^{-1} for ββ-DCAN and 2.6 kcal mol^{-1} for βα-DCAN, 1 kcal mol^{-1}=4.184 kJ mol^{-1}).[3] As mentioned above, these bichromophoric compounds form the ground state complex only in the nonpolar solvent such as MP at low temperature. Then, the experimental results obtained in the aqueous CDx solutions demonstrate that the inner cavity of CDx provide us with an extraordinary nonpolar and structurally restricted environment for the intramolecular interactions. The difference of the fluorescence behavior of the intramolecular ground state complex formation between ββ- and βα-DCAN may be attributable to the conformational difference of the complex formation in the CDx cavity as well as their inherent enthalpy change for the complex formation. The fluorescence lifetimes of the complex and the DCA moiety are almost invariant in the aeration and deaeration of the CDx solution, as summarized in Table 1. It seems that the excited state of the ground state complex in the CDx cavity are protected from the oxygen quenching as suggested by Turro *et al.*[2]

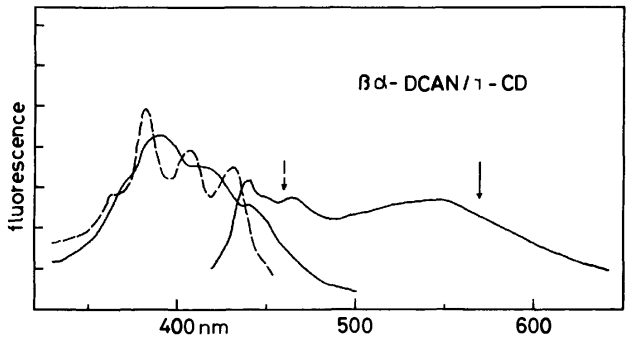

Fig. 2. Fluorescence (uncorrected, excited at 360 nm) and excitation spectra of the γ-CDx solution (10^{-2} mol dm^{-3}) of βα-DCAN (1.5×10^{-7} mol dm^{-3}). The excitation spectra were monitored at 570 nm (——) and at 460 nm (------).

Intramolecular Excimer and Ground State Complex Formations of DNP in the CDx Solutions. The aqueous β- and γ-CDx solutions of ββ-DNP show the long wavelength fluorescence in addition to the naphthyl moiety. The former fluorescence excitation spectra shown in Fig. 3 is in longer wavelength region than that of the naphthyl moiety and also the longest wavelength absorption band of DNP.[5] Therefore, it seems that the 400 nm fluorescence is ascribed to the intramolecular ground state complex of ββ-DNP in the CDx cavity. Further, the γ-CDx solution of ββ-DNP shows a similar fluorescence to that of β-CDx solution, as shown in Fig. 3(b). However, the excitation spectrum of this fluorescence shows only a faint red shift from that of the naphthyl moiety. The red shifted excitation spectrum seems to suggest that the ≈400 nm fluorescence consists of the superimposed spectra of the intramolecular excimer and ground state complex in the β-CDx solution. The fluorescence decay curves of 370—450 nm of ββ-DNP in the β- and γ-CDx solutions are shown in Figs. 4 and 5. The decay curve with-

Table 1. Fluorescence lifetimes (collected at ≈550 nm) of DCAN in γ-CDx solutions at room temperature (τ, ns)

	Aerated		Deaerated	
	τ_1	τ_2	τ_1	τ_2
ββ-DCAN	11 (82%)	43	14 (83%)	51
βα-DCAN	8 (90%)	37	10 (89%)	42

$I(t)=A\exp(-t/\tau_1)+(1-A)\exp(-t/\tau_2)$.
Data in bracket are fraction (A) of components.
Errors are approximately ±5%.

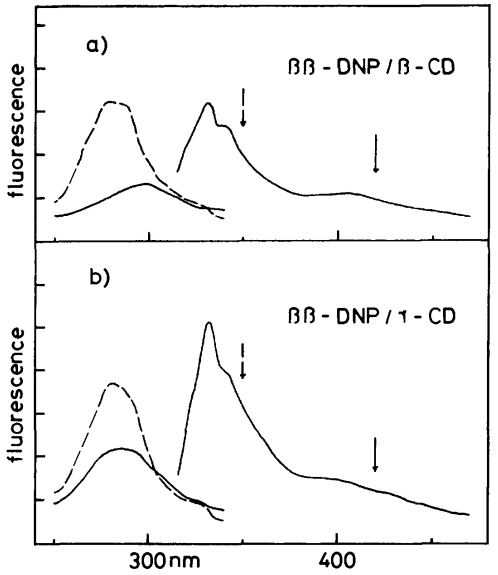

Fig. 3. Fluorescence (uncorrected, excited at 305 nm) and excitation spectra of the β- and γ-CDx solution (5×10^{-3} mol dm^{-3}) of $\beta\beta$-DNP (3.7×10^{-6} mol dm^{-3}) at room temperature. The excitation spectra were monitored at 420 nm (——) and at 350 nm (------).

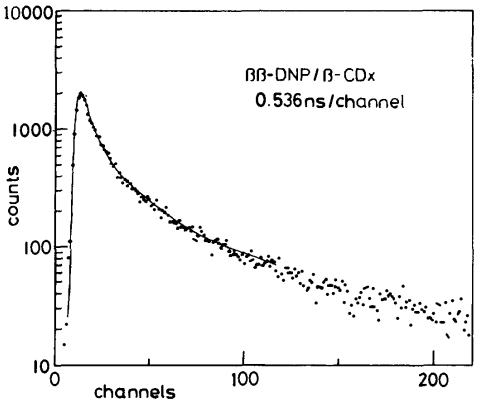

Fig. 4. Fluorescence decay curve of the long wavelength fluorescence (collected at 370—450 nm) of the β-CDx solution of $\beta\beta$-DNP (3.7×10^{-6} mol dm^{-3}) at room temperature. The curve shows the calculated decay based on the data shown in Table 2.

out fluorescence rise cannot be analyzed as a double exponential by any combination of parameters (τ_1, τ_2, A_1, and A_2 in Eq. 1), though decay curves look like a double exponential decay. The decay curves shown in Figs. 4 and 5 were analyzed as a triple exponential decay by the computer simulation, whose decay times are two short lifetimes and a long one as summarized in Table 2.

The aqueous β- and γ-CDx solutions of $\beta\alpha$-DNP exhibit remarkably enhanced fluorescence as shown in Fig. 6. A weak fluorescence ($\lambda_{max}\approx400$ nm) in β-CDx solution and a rather strong fluorescence (≈375 nm) in γ-CDx solution were observed in addition to the naphthyl moiety fluorescence. These fluorescence excitation spectra of both solutions shows rather similar to that of the naphthyl moiety fluorescence. Therefore, it seems that these fluorescence are mostly attributable to the intramolecular excimer of these compounds. The flurescence rise in the long wavelength fluores-

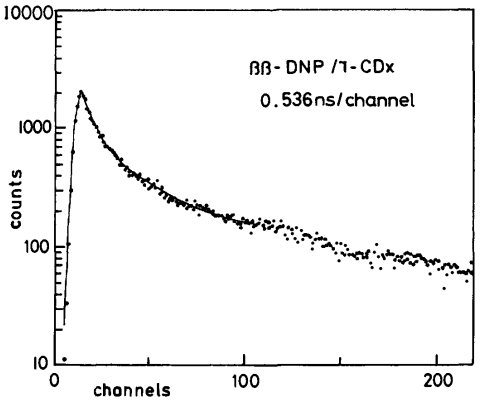

Fig. 5. Fluorescence decay of the long wavelength fluorescence (collected at 370—450 nm) of the γ-CDx solution of $\beta\beta$-DNP. The curve shows the calculated decay based on the data shown in Table 2.

Table 2. Fluorescence lifetimes (collected at 370—450 nm) of DNP in the CDx solutions at room temperature (τ ns)

DNP	CDx	Aerated τ_1	Aerated τ_2	Aerated τ_3	Deaerated τ_1	Deaerated τ_2	Deaerated τ_3
$\beta\beta$-DNP	β	1.5 (80%)	13.0 (18%)	46.2	1.9 (75%)	8.7 (20%)	48.2
	γ	1.4 (71%)	8.0 (22%)	56.3	1.8 (72%)	7.8 (20%)	56.0
$\beta\alpha$-DNP	β	1.8 (55%)	16.1 (6%)	53.6	2.0 (56%)	15.7 (2%)	53.7
	γ	1.6 (50%)	26.4 (18%)	107.3	1.6 (50%)	25.8 (19%)	93.8

$I(t)=A_1\exp(-t/\tau_1)+A_2\exp(-t/\tau_2)+(1-A_1-A_2)\exp(-t/\tau_3)$. Data in bracket are fraction of components. Errors are approximately ±5%.

cence decay curve of the β-CDx solution of $\beta\alpha$-DNP was observed in the excitation at 230 nm, though a small amount of the short decay component due to the naphthyl moiety sounds to be superimposed on the fluorescence rise. Upon excitation at 290 nm, however, no fluorescence rise was observed in this solution. Further, neither fluorescence in the excitation at 290 nm nor at 230 nm was detected in the γ-CDx solution of $\beta\alpha$-DNP. The lack of the fluorescence rise may be attributable to the involvement of the ground state complex fluorescence in the decay curve of the excimer. On the analogy of the ground state complex in $\beta\beta$-DNP, there may be a weak absorption band hidden by the absorption band due to the naphthyl moiety in this 290—330 nm region. The decay curves were analyzed also as a triple exponential decay without rise, as shown in Figs. 7 and 8, whose decay times are summarized in Table 2.

These results in the CDx solutions demonstrate that the intramolecular excimer and the ground state complex formations take place both in the β- and γ-CDx solutions of $\beta\alpha$- and $\beta\beta$-DNP, though the excimer formation is more significant in $\beta\alpha$-DNP than in $\beta\beta$-DNP. If the intramolecular excimer and ground state complex fluorescences can be observed in the almost same wavelength region (≈400 nm) and if the naphthyl moiety fluorescence may be overlapped in this re-

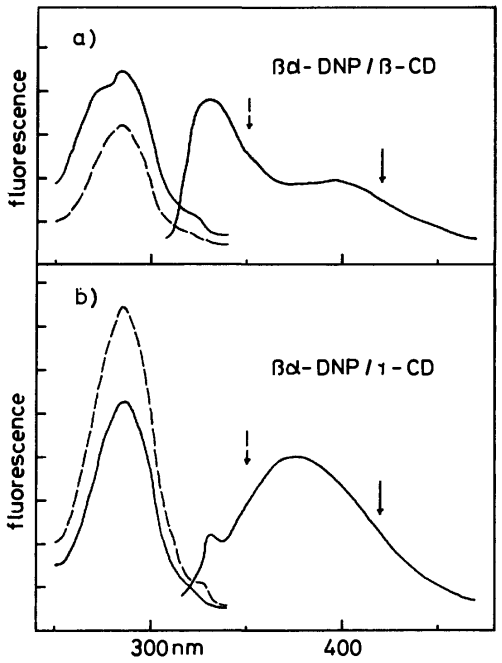

Fig. 6. Fluorescence (uncorrected, excited at 305 nm) and excitation spectra of the β- and γ-CDx (5×10^{-3} mol dm^{-3}) of $\beta\alpha$-DNP (3.7×10^{-6} mol dm^{-3}) at room temperature. The excitation spectra were monitored at 420 nm (——) and at 350 nm (------).

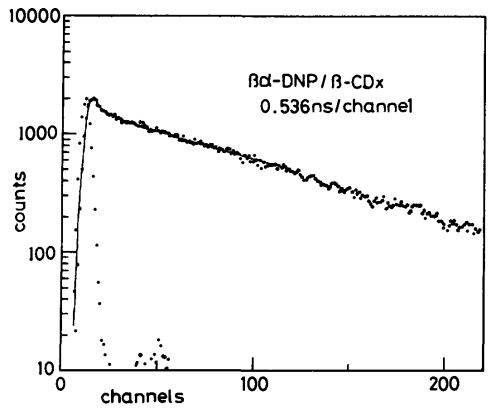

Fig. 7. Fluorescence decay of the long wavelength fluorescence (collected at 370—450 nm) of the β-CDx solution of $\beta\alpha$-DNP (3.7×10^{-6} mol dm^{-3}) at room temperature. The decay line is the calculated decay curve based on the data shown in Table 2.

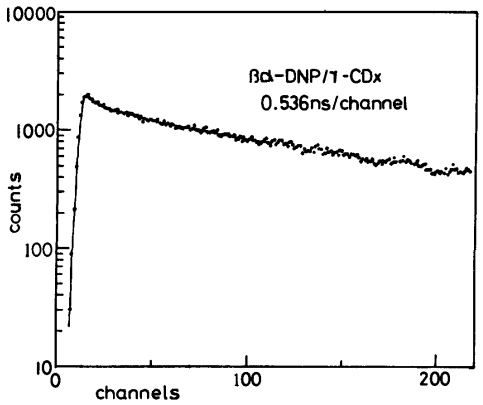

Fig. 8. Fluorescence decay of the long wavelength fluorescence (collected at 370—450 nm) of the γ-CDx solution of $\beta\alpha$-DNP (3.7×10^{-6} mol dm^{-3}). The line is the calculated decay curve based on the data shown in Table 2.

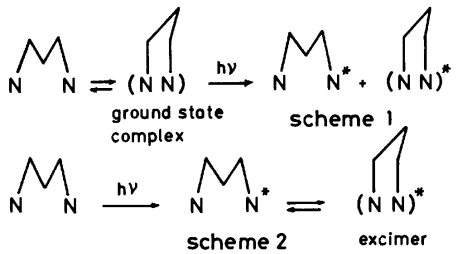

Fig. 9. Schematic reaction diagram of the intramolecular excimer and ground state complex formations (N=naphthyl moiety).

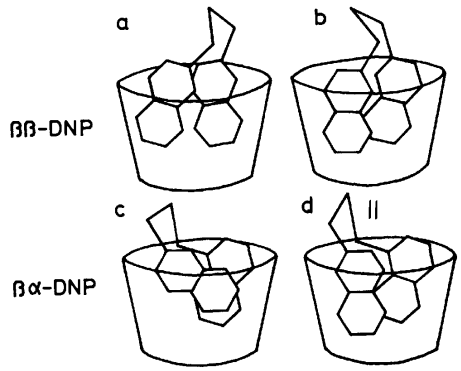

Fig. 10. Illustrated conformations of the ground state complex and/or excimer of $\beta\alpha$- and $\beta\beta$-DNP in the CDx cavity.

gion, four fluorescence decay components should be observed; two long time decay may be ascribed to the excimer and the ground state complex while two short ones to the naphthyl moiety fluorescence. However, the decay curve of the ≈400 nm fluorescence was analyzed approximately as three component decays, as mentioned above. If the excimer and ground state complex fluorescence spectra may show the approximately same fluorescence lifetime each other, the long lifetime decay due to the excimer and the ground state complex and two short lifetimes due to the naphthyl moiety may be observed. According to the well known reaction scheme as shown in Fig. 9, the shortest decay time (1—2 ns) of the naphthyl moiety fluorescence may be ascribed to the naphthyl moiety in the excited state equilibrium forming the excimer, while the decay time of 8—25 ns to that in the equilibrium with the ground state complex formation.

Turro *et al.*[2] reported the intramolecular excimer formation of $\alpha\alpha$-DNP in aqueous β- and γ-CDx solutions. The favor sturcture was proposed to be eclipsed and buried in the cavity of the CDx, where the long axes of naphthyl moieties are parallel each other. However, it is not obvious whether the structures of the fluorescent state of the ground state complex and the excimer are identical or different from each other. In the intermolecular electron donor acceptor systems, the identical fluorescent state of the exciplex and the ground state complex was evidenced as mentioned above.[7-9] However, no evidence for the identical fluorescent state of the excimer and the ground state complex has been reported, because there is no appro-

priate system exhibiting both excimer and ground state complex fluorescences . According to the geometrical allowance of the bichromophoric propanes in the CDx cavity, two each conformations of both $\beta\alpha$- and $\beta\beta$-DNP concerning with two naphthyl moieties may be considered, as shown in Fig. 10. The two closed conformers cannot be interchangeable in the small CDx cavity. If the excimer and ground state complex fluorescences may emit from an identical fluorescent state, both $\beta\alpha$- and $\beta\beta$-DNP may show similar excimer and ground state complex fluorescences, otherwise may show either the former or the latter fluorescence. However, $\beta\beta$-DNP is more favorable for the ground state complex, while $\beta\alpha$-DNP more favorable for the excimer mentioned above. Therefore, it is likely that the excimer is not identical with the fluorescent state of the ground state complex, though their fluorescence states cannot be assigned to the particular structure shown in Fig. 10.

References

1) A. Ueno, K. Takahashi, and T. Osa, *J. Chem. Soc., Chem. Commun.*, **1980**, 921.
2) N. J. Turro, T. Okubo, and G. C. Weed, *Photochem. Photobiol.*, **35**, 325 (1982).
3) M. Itoh, T. Mimura, H. Usui, and T. Okamoto, *J. Am. Chem. Soc.*, **95**, 4388 (1973).
4) E. A. Chandross and C. J. Dempster, *J. Am. Chem. Soc.*, **92**, 3586 (1970).
5) T. Mimura and M. Itoh, *J. Am. Chem. Soc.*, **98**, 1095 (1976).
6) P. R. Berington, "Data Deduction and Error Analysis of the Physical Sciences" McGraw Hill, New York, 1969.
7) M. Itoh and T. Mimura, *Chem. Phys. Lett.*, **24**, 551 (1974).
8) E. Gaweda and J. Prochorow, *Chem. Phys. Lett.*, **30**, 155 (1975).
9) M. Itoh, Y. Kumano, and T. Okamoto. *Bull. Chem. Soc. Jpn.*, **49**, 42 (1976).

The Complex Formation of Organomercury with 8-Quinolinol

Joji KUNIYA,* Kunishige NAITO, and Shinsuke TAKEI
Department of Industrial Chemistry, Faculty of Engineering, Ibaraki University, Nakanarusawa-cho, Hitachi 316
(Received May 13, 1983)

Organomercury(II)(RHg^+, R; ethyl, *n*-propyl, *n*-butyl) forms two kinds of water-soluble complexes, RHgq and RHg(q)$(OH)^-$, with 8-quinolinol(oxine Hq). These complex-formation reactions are studied by means of spectrophotometry, and the formation constants of these complexes, RHgOH, RHgOAc, and RHg(OH)$(OAc)^-$, in 4 %(v/v) ethanol at the ionic strength of 0.1 are determined. Reliable results are obtained for ethylmercury(II) and *n*-propylmercury(II) complexes.

There have been several reports and patents[1] on the reactions of alkyl- and arylmercury(II) (RHg^+) with 8-quinolinol (oxine Hq) in an aqueous solution, and in those reports the reaction product has been reported to be RHgq. However, complex-formation reactions have not yet been studied in detail.

In this study, complex-formation reactions of ethyl-, *n*-propyl-, and *n*-butyl-mercury(II) ($EtHg^+$, *n*-$PrHg^+$, *n*-$BuHg^+$) with 8-quinolinol in an aqueous solution have been investigated by means of spectrophotometry, and two kinds of water-soluble complexes, one of which is extractable into a nonpolar solvent such as benzene, have been found to be formed. Generally, 8-quinolinol forms water-insoluble complexes with all metals except alkali metals, therefore, the reactions of RHg^+ with 8-quinolinol are very interesting.

Experimental

1. Reagent. RHg^+ Solution: To a suspension of the desired amount of RHgBr synthesized by the Grignard reaction[2] in water 1.5 times the equivalent of Ag_2O freshly prepared from $AgNO_3$ was added, after which the solution was stirred for several days by use of a magnetic stirrer. After the complete precipitaton of the AgBr, the solution was made up to 0.1 M (1 M=1 mol dm^{-3}) in OH^- by the addition of solid NaOH and then left to stand overnight to ensure the quantitative precipitation of the dissolved Ag^+. Then after the filtration of the AgBr and the excess Ag_2O (to prevent the dissolution of Ag_2O the precipitate was not washed), the filtrate was neutralized with perchloric acid and diluted to about 5×10^{-2} M in RHg^+ with a pH of about 3. The standardization of the stock solution was done by the decomposition of RHg^+ on heating with nitric acid, followed by the gravimetric determination of Hg^{2+} as HgS. The stock solution was used after a 10-fold dilution with deionized water.

8-Quinolinol Solution: Guaranteed-reagent-grade 8-quinolinol was used as the ethanolic solution. This solution could not be used for over 3 d.

In this work, commercially available guaranteed-reagent-grade acetic acid, sodium acetate, and sodium perchlorate were used without further purification. The ethanol was purified by distillation as usual.

2. Aparatus. The absorption spectrum of a solution was measured with a Shimadzu MPS-50 recording spectrophotometer and a Hitachi 124 double-beam spectrophotometer. A Hitachi-Horiba F-5 pH meter was used for the pH measurement of a solution.

3. Experimental Procedure. To a 25.00-cm^3 measuring flask, desired amounts of RHg^+, acetic acid, sodium acetate, sodium perchlorate, and 8-quinolinol solutions were added, and then deionized water was added to bring the solution to the mark. The ionic strength of the solution was maintained at 0.1. Spectrophotometric and pH measurements were made on the solution after 1.5 h. Separately, the same measurements were made on the blank solution.

*Present address: Toshiba Silicone Co., Ltd., Nishishinmachi, Ota 373.

Results snd Discussion

By the addition of 8-quinolinol to an aqueous solution of $EtHg^+$, yellow coloration is obtained at a pH value above 5. The solution shows absorption maxima at 340 and 395 nm, and with an increase in the pH of the solution the absorbance at 340 nm decreases and that at 395 nm increases, as shown in Fig. 1. These spectra are different from that of the free 8-quinolinol solution in this pH range. Therefore, $EtHg^+$ is considered to form two kinds of complexes with 8-quinolinol, with the sbsorption maxima at 340 and 395 nm respectively. Both *n*-$PrHg^+$ and *n*-$BuHg^+$ with 8-quinolinol show the same coloration, and the wavelength at the absorption maximum is the same as that of $EtHg^+$ complexes. Hereafter, complexes with the absorption maxima at 340 and 395 nm will be denoted as Complexes **I** and **II** respectively.

In this study, 8-quinolinol is added as an ethanolic solution. Moreover, it is observed that the absorbance of each complex decreases with an increase in the concentration of ethanol, especially in the higher concentration range. Therefore, in this work the concentration of ethanol is fixed at 4% (v/v), and the effect of the concentration of ethanol on the complex formation is not studied.

The absorbance of complex solutions of RHg^+ with 8-quinolinol at 340 and 395 nm increases with stand-

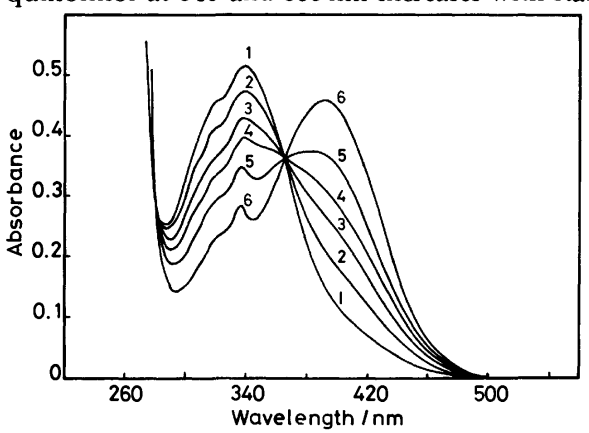

Fig. 1. pH Dependence of absorption spectrum of *n*-$PrHg^+$-8-quinolinol solution.
C_M°; 1.98×10^{-4} M, C_L°; 2.00×10^{-4} M.
pH: 1; 4.45, 2; 4.98, 3; 5.16, 4; 5.50, 5; 5.96, 6; 7.85.

ing and shows a constant value after standing for 1.5 h when RHg^+ is added in an excess to 8-quinolinol in a molar ratio, but the absorbance of the *n*-$BuHg^+$ complex solution decreases upon standing for over 5 h. Therefore, the measurement of the absorbance of complex solutions is made after they have stood for 1.5 h in a dark place.

The molar ratio of RHg^+ to 8-quinolinol in Complexes **I** and **II** is found by the continuous variation method to be 1 : 1 regardless of the kind of alkyl group.

At 340 and 395 nm, Complexes **I** and **II** and free 8-quinolinol show absroption. Therefore, the concentrations of Complexes **I** and **II** formed under the various conditions necessary to obtain the formation constants of these complexes are determined from the absorbance of the complex solution measured at 340 and 395 nm and the molar absorption coefficients of both complexes and 8-quinolinol at both wavelengths (the values for 8-quinolinol are the apparent ones at various pHs). The molar absorption coefficients of both complexes at 340 and 395 nm are determined as follows.

In Fig. 2 the absorbance of the $EtHg^+$–8-quinolinol solution at 340 nm is shown to be constant at pH values from 3.2 to 4.2, while that at 395 nm begins to increase at a pH of about 4.0. Moreover, the absorbance of the solution buffered with sodium acetate and acetic acid at 340 nm is lower than that of an unbuffered sodium perchlorate and perchloric acid solution. These findings show that 8-quinolinol forms Complex **I** with $EtHg^+$ quantitatively at pH values from 3.2 to 4.0 and that the acetate ion interferes with the formation of the complex. However, the interference from OAc^- is not observed when the concentration of OAc^- is lower than 5×10^{-3} M under the present conditions. From these results the molar absorption coefficients of Complex **I** at 340 and 395 nm are determined from the absorbance at these wavelengths when the molar ratio of $EtHg^+$ to 8-quinolinol is higher than 10 and when the pH values from 3.2 to 4.0 in the buffered solution in which the concentration of OAc^- is lower than 5×10^{-3} M. The molar absorption coefficients of the *n*-$PrHg^+$ and *n*-$BuHg^+$ Complex **I** at 340 and 395 nm are determined by similar procedures.

The absorbance of the RHg^+ Complex **II** at 340 and 395 nm are found to be constant in borate buffer solutions at pH values from 8 to 10, and the molar ratio of RHg^+ to 8-quinolinol is higher than 10. Therefore, the molar absorption coefficients of each complex at both wavelengths are determined from the absorbance measured under the conditions mentioned above.

In Table 1 the molar absorption coefficients of the RHg^+ Complexes **I** and **II** at the absorption maximum are tabulated. The variation in the value of the coefficient with the kind of alkyl group is small.

From the experimental results obtained above, the complex formation reactions may be analysed as follows.

The complex formation reactions of the **I** and **II** complexes can be written as follows:

$$RHg^+ + q^- + mY^{n-} = RHg(q)(Y)_m^{mn-}, \quad (1)$$

$$K = \frac{[RHg(q)(Y)_m^{mn-}]}{[RHg^+][q][Y^{n-}]^m}, \quad (2)$$

where Y^{n-} is an arbitrary anion in the solution which can combine with RHg^+ (hereafter, the charge of an ion will be omitted for the sake of simplicity). Moreover, the total concentration of RHg^+, C_M°, is shown as follows when the polynuclear complexes of RHg^+ are considered to be absent:

$$C_M^\circ = [RHg] + \sum [RHg(q)(Y)_m] + [RHgOH] + [RHg(OH)_2] + \cdots + [RHgA] + [RHg(A)_2] + \cdots + [RHg(OH)(A)] + \cdots. \quad (3)$$

Table 1. Molar absorption coefficients of RHg^+ complexes **I** and **II**

RHg^+	Molar absorption coefficients $cm^{-1}mol^{-1}dm^3$	
	Complex **I** (340 nm)	Complex **II** (395 nm)
$EtHg^+$	2700	2370
n-$PrHg^+$	2690	2320
n-$BuHg^+$	2730	2400

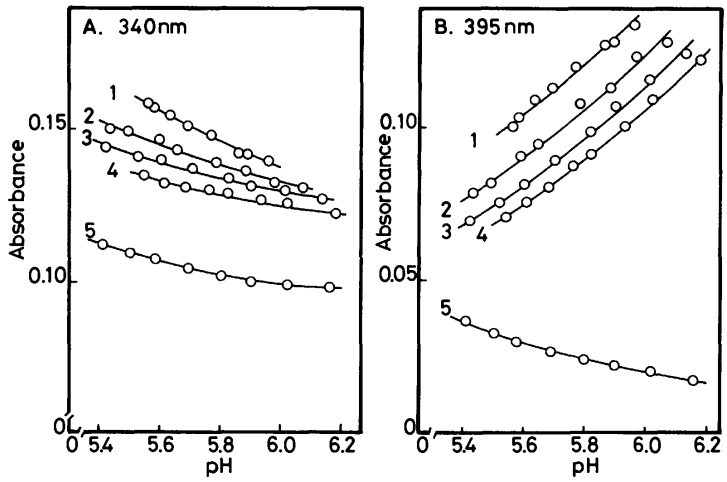

Fig. 2. pH Dependence of absorbance of $EtHg^+$–8-quinolinol complexes at 340 and 395 nm.
C_M°; 3.60×10^{-4} M, C_L°; 2.00×10^{-4} M.
[OAc]: 1; 2.00×10^{-3} M, 2; 6.00×10^{-3} M, 3; 1.00×10^{-2} M, 4; 1.40×10^{-2} M, 5; blank solution, [OAc]; 1.00×10^{-2} M.

Then:

$$C_M^\circ - \sum[RHg(q)(Y)_m] = C_M = [RHg](1+\beta_1[OH] + \beta_2[OH]^2 +\cdots+ \beta_1'[A] + \beta_2'[A]^2 +\cdots+ \beta_1''[OH][A] +\cdots = [RHg]\alpha, \quad (4)$$

where the β's are the formation constants of the respective complexes and where A represents the anions, except for OH^-, in the solution which can combine with RHg^+.

Similarly, the total concentration of 8-quinolinol, C_L°, can be written as follows:

$$C_L^\circ = \sum[RH(q)(Y)_m] + [H_2q] + [Hq] + [q]. \quad (5)$$

Then:

$$C_L^\circ - \sum[RHg(q)(Y)_m] = C_L = [q]\left(\frac{[H]^2}{k_1k_2} + \frac{[H]}{k_2} + 1\right) = [q]\gamma, \quad (6)$$

where k_1 and k_2 are the step-by-step acid-dissociation constants of 8-quinolinol; in this work, $pk_1=4.96$ and $pk_2=9.68$, values obtained under the present experimental conditions.

From (2), (4), and (6), (7), and (8) are introduced:

$$\frac{[RHg(q)(Y)_m]\alpha\gamma}{C_MC_L[Y]^m} = K'\frac{\alpha\gamma}{[Y]^m}, \quad (7)$$

$$K' = \frac{[RHg(q)(Y)_m]}{C_MC_L}.$$

$$\frac{[Y]^m}{K'\gamma} = \frac{\alpha}{K} = \frac{1}{K}(1+\beta_1[OH]+\beta_2[OH]^2+\cdots + \beta_1'[A] + \beta_2'[A]^2 +\cdots+ \beta_1''[OH][A] +\cdots$$

$$= \frac{1}{K}(1+\beta_1[OH]+\beta_2[OH]^2+\cdots) + \frac{1}{K}(\beta_1'+\beta_1''[OH]+\cdots)[A] + \frac{\beta_2'}{K}[A]^2 +\cdots. \quad (8)$$

In (7), C_M and C_L can be obtained from the total concentrations of RHg^+ and 8-quiolinol and the experimentally determined concentrations of Complexes **I** and **II** as shown in (4) and (6). Therefore, the value of K' for each complex can be determined experimentally. Moreover, the value of γ is calculated from the pH of the solution and from k_1 and k_2 as shown in (6).

In this study, the anions in the solution are OH^-, OAc^-, and ClO_4^-, and the complex formation of RHg^+ with ClO_4^- is not observed. Judging from the results in (4) and (8) it is necesssry to consider only OAc^- as A. Therefore, (8) indicates that the $[Y]^m/K'\gamma$ values which are obtained from the experimental results at a constant pH and at various concentrations of OAc^- are linear or quardratic against [OAc] when Y and m corresponding to (1) are utilized. Moreover, as the intercepts of straight lines or quadratic curves are functions of [OH], the K and β's are determined by plotting the values of the intercepts against [OH]. Similarly, the slopes of the straight lines or the coefficients of the [OAc] of the quadratic curves are functions of [OH]; therefore, the β' and β'' constants are determined by plotting the values of the slopes or coefficients of [OAc]. By these treatments, complex-formation reactions are studied.

In the treatments described above, polynuclear complexes of RHg^+ are neglected and the K' of each complex is assumed to be independent of the concentration of RHg^+. Under the conditions where pH= 5.4—6.2, $[OAc]=1.00\times10^{-2}$ M and $C_L^\circ=1.00\times10^{-4}$ M, the K' values of both Complexes, **I** and **II**, for $EtHg^+$ and n-$PrHg^+$ are found to be independent of C_M° when C_M° is 2.00×10^{-4} M or below. However, for the n-$BuHg^+$–8-quinolinol system it is necessary to maintain the total concentration of n-$BuHg^+$ at 1.3×10^{-4} M or below, even when $C_L^\circ=2.00\times10^{-4}$ M.

Figures 3 **A** and **B** show the variation in the K' values of $EtHg^+$ complexes with the pH under various concentrations of OAc^-. Both K' values decrease with

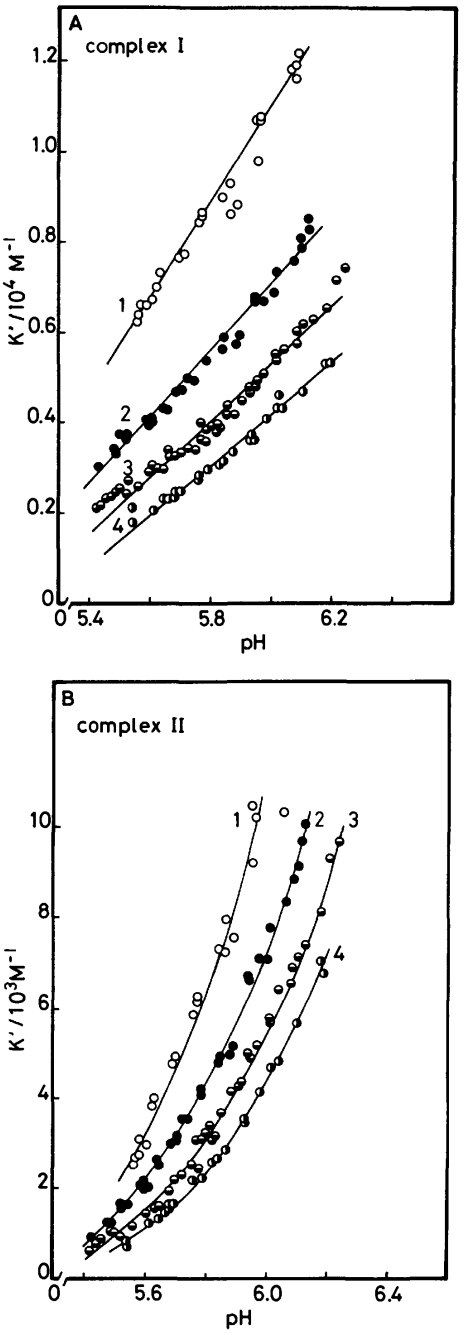

Fig. 3. pH Dependence of K' values of $EtHg^+$ complexes **I** and **II** under various concentrations of OAc^-.
[OAc]: 1; 2.00×10^{-3} M, 2; 6.00×10^{-3} M, 3; 1.00×10^{-2} M, 4; 1.40×10^{-2} M.

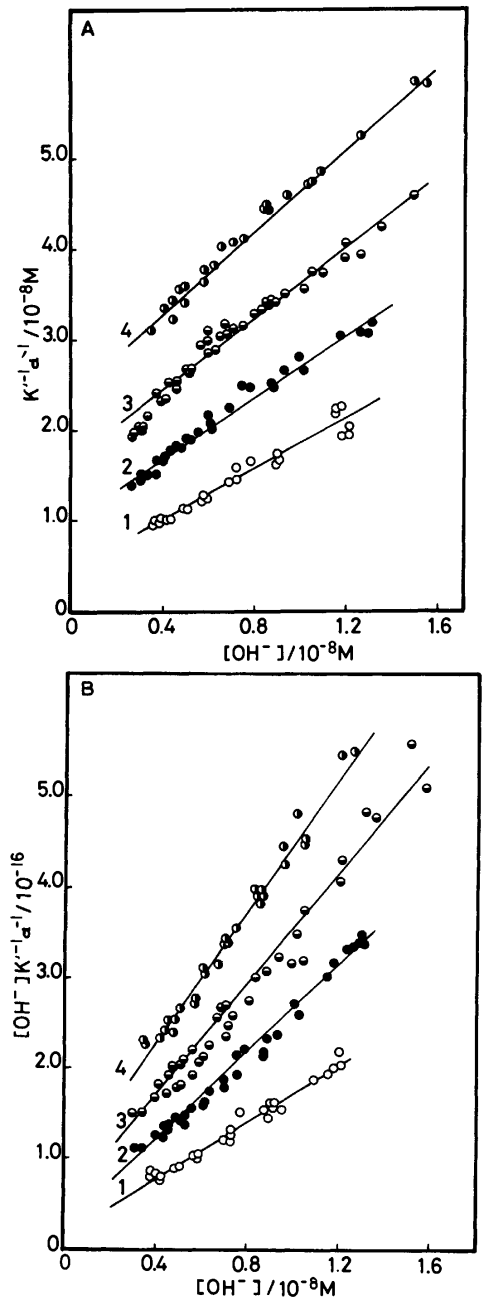

Fig. 4. **A**: Plot of $1/K'_a$ of $EtHg^+$ complex **I** against [OH].
B: Plot of $[OH]/K'_a$ of $EtHg^+$ complex **II** against [OH].
[OAc]: 1; 2.00×10^{-3}M, 2; 6.00×10^{-3}M, 3; 1.00×10^{-2}M, 4; 1.40×10^{-2}M.

an increase in the concentration of OAc^-; this result indicates that OAc^- interferes with the formation of complexes and that these complexes do not contain OAc^-. From this finding, OH^- is found to be Y in (1). In the following study, the K' values of each complex at various pHs are obtained by the treatment of the results shown in Fig. 3 as straight lines and quadratic curves and by interpolation. Then, from the results shown in Fig. 3, $[OH]^m/K'r$ is plotted against [OAc] by the use of the K' values of each complex and γ at various pHs; as shown in Figs. 4 **A** and **B**, straight lines are obtained for Complexes **I** and **II** when $m=0$ and 1 are utilized respectively. These results indicate that the Complexes of $EtHg^+$ **I** and **II** are EtHgq and EtHg(q)$(OH)^-$ respectively.

Moreover, the values of the intercept and slope of the straight lines shown in Figs. 4 **A** and **B** at various [OH] values are found to be linear against [OH]. The linear relations of the intercept and slope to [OH] indicate that $EtHg^+$ forms EtHgOH, EtHgOAc, and EtHg$(OH)(OAc)^-$ respectively. The formation constants of EtHgq, EtHg(q)$(OH)^-$, EtHgOH, EtHgOAc, and EtHg$(OH)(OAc)^-$ are determined from (8). Similar results are obtained for *n*-$PrHg^+$ and *n*-$BuHg^+$–8-quinolinol systems. The results obtained are tabulated in Table 2.

In Table 2, the formation constants of $EtHg^+$ and *n*-$PrHg^+$ complexes obtained separately by the method described above show a good agreement. Also the formation constant of EtHgOH, β_1, obtained in this work shows a good agreement with that previously reported by Waugh *et al.* These results indicate that the analytical method of complex-formation reactions presented here is reasonable and that the formation constants of $EtHg^+$ and *n*-$PrHg^+$ here estsblished are reliable. However, the formation constants of *n*-$BuHg^+$ with OH^- and OAc^- obtained separately show less agreement. Those results suggest that the formation of polynuclear complexes of *n*-$BuHg^+$ with OH^- affects the complex-formation reactions with 8-quinolinol. Therefore, in order to determine reliable formation constants of *n*-$BuHg^+$ complexes with 8-quinolinol, the OH^- and OAc^- setting of the experimental conditions is important to prevent polynuclear hydroxo complexes.

References

1) G. Faraglia, L. Poncucci, and R. Barieri, *Gazz. Chim. Ital.*, **93**, 1413 (1963); J. G. Wardeska, Ph. D. Dissertation,

Table 2. Formation constants of RHg^+ complexes

		$EtHg^+$	*n*-$PrHg^+$	*n*-$BuHg^+$
K_{RHgq}		$7.0\pm1.4\times10^{8}$	$5.2\pm1.0\times10^{8}$	$1.3\pm0.3\times10^{9}$
$K_{RHg(q)(OH)}$		$4.4\pm0.9\times10^{17}$	$7.5\pm1.5\times10^{16}$	$4.4\pm0.9\times10^{16}$
β_1	A*	$8.0\pm1.6\times10^{8}$	$8.0\pm1.6\times10^{8}$	$1.4\pm0.3\times10^{9}$
	B**	$5.5\pm1.4\times10^{9}$	$2.3\pm0.6\times10^{8}$	$4.1\pm1.0\times10^{8}$
β_1'	A*	$1.1\pm0.2\times10^{3}$	$6.7\pm1.3\times10^{2}$	$2.1\pm0.6\times10^{3}$
	B**	$2.0\pm0.3\times10^{3}$	$4.6\pm1.2\times10^{2}$	$7.1\pm2.0\times10^{1}$
β_1''	A*	$5.3\pm1.1\times10^{10}$	$6.7\pm1.3\times10^{9}$	$4.3\pm1.0\times10^{10}$
	B**	$8.3\pm2.1\times10^{11}$	$5.3\pm1.3\times10^{10}$	$9.3\pm2.5\times10^{10}$

A*: Obtained from the analysis of the formation reaction of Complex **I**. **B****: Obtained from the analysis of the formation reaction of Complex **II**. Previous work: β_1 of EtHgOH. 1.3×10^{9}. T. Waugh, H.F. Walton, and J.A.Laswick, *J.Phys.Chem.*, **59**, 395(1955).

Ohio Univ., **1967**. *Diss. Abstr.*, B28, 3211 (1968); A. Heymons, *Ger.*, 1114195 (1952); R. O. Weiss and S. J. Leaderer, U. S. Patent, 3130123 (1957), 2844508 (1958); T. Iida and E. Tomotori, Japan Patent, 6698, 6699 (1964).

2) M. M. Kreevoy and R. L. Hansen, *J. Am. Chem. Soc.*, **83**, 626 (1961).

 © 1984 The Chemical Society of Japan Bull. Chem. Soc. Jpn., 57, 2271—2275 (1984)

The Extraction of Organomercury with 8-Quinolinol into Benzene

Takao SUGIMOTO, Kunishige NAITO, and Shinsuke TAKEI*

Department of Industrial Chemistry, Faculty of Engineering, Ibaraki University, Nakanarusawa-cho, Hitachi 316

(Received May 13, 1983)

The extraction of organomercury(II)(RHg^+, R; ethyl, *n*-propyl, *n*-butyl, phenyl) with 8-quinolinol into benzene has been studied by means of spectrophotometry. This study confirmed that there was no co-extraction of electrically neutral species RHgOH by its investigation of the effect of the pH on the extraction of ethylmercury(II) chloride into benzene. Moreover, it was found that RHg^+ forms 1:1 complexes with both HPO_4^{2-} and PO_4^{3-}. The formation constants of these complexes and of hydroxo complexes have been determined.

Organomercury(II) (RHg^+) forms two kinds of water-soluble complexes with 8-quinolinol (oxine, Hq), and one of these can be extracted into an inert solvent such as benzene. The formation of water-soluble complexes of ethylmercury(II) ($EtHg^+$), *n*-propylmercury(II) (*n*-$PrHg^+$), and *n*-butylmercury(II) (*n*-$BuHg^+$) with 8-quinolinol has previously been reported.[1] In this work, the extraction of 8-quinolinates of $EtHg^+$, *n*-$PrHg^+$, *n*-$BuHg^+$, and phenylmercury(II) ($PhHg^+$) into benzene, together with the complex formation of $EtHg^+$ with Cl^- and its extraction into benzene and the complex formation of RHg^+ with OH^- and phosphate ions, has been investigated by means of spectrophotometry.

Experimental

1. Reagent and Apparatus. Organic Solvents. The benzene and carbon tetrachloride, reagent-grade, were purified by distillation.

Dithizone Solution in Carbon Tetrachloride: The purified dithizone solution in carbon tetrachloride was prepared by the usual method.[2]

RHg^+ Solution: All the RHg^+ solutions used were prepared and standardized by the method previously reported.[1]

All the other reagents used in this work were guaranteed-reagent-grade and were used without further purification.

A Shimadzu MPS-50 recording spectrophotometer and a Hitachi 124 double-beam spectrophotometer were used for the measurements of the absorption spectra and the absorbance of the solutions. A Hitachi-Horiba F-5 pH meter was used for the measurement of the pH of an aqueous solution.

2. Experimental Procedures. a. Extraction of EtHgCl into Benzene: The extraciton of $EtHg^+$ as dithizonate into carbon tetrachloride has been reported to be unaffected by the Cl^- and the pH under the experimental conditions applied in this work.[3] Then, after the extraction of EtHgCl from 10.00 cm^3 of an aqueous solution into 10.00 cm^3 of benzene, an aliquot amount of the aqueous solution was taken and $EtHg^+$ was extracted as dithizonate by the addition of a dithizone solution on the solution and shaking. Also, from the absorbance of dithizone in excess at 620 nm, the $EtHg^+$ was determined and the distribution ratio of $EtHg^+$ was obtained.

b. Extraction of RHg^+ 8-Quinolinate: Into a glass-stoppered test tube, desired amounts of NaH_2PO_4, Na_2HPO_4, and RHg^+ solutions were taken and deionized water was then added to make the solution up to 10.00 cm^3. To this solution 10.00 cm^3 of an 8-quinolinol solution in benzene was added, after which the solution was shaken for 30 min. After this solution had been separated into two layers, the absorbance of the organic solution at the absorption peak of the complex and the pH of the aqueous solution were measured.

Results and Discussion

The complex of RHg^+ with 8-quinolinol is extracted into benzene at a pH above about 5. In order to analyse the extraction reaction, it is necessary to ascertain whether or not the electrically neutral species RHgOH can be extracted into benzene. The extraction of methylmercury(II) and $PhHg^+$ halides from an acidic solution into nonpolar solvents has been studied;[4] then by the investigation of the effect of the pH of the extraction of EtHgCl, the extraction of EtHgOH was studied.

In Fig. 1, the distribution ratio of $EtHg^+$ increases with increase in the initial concentration of Cl^-; the

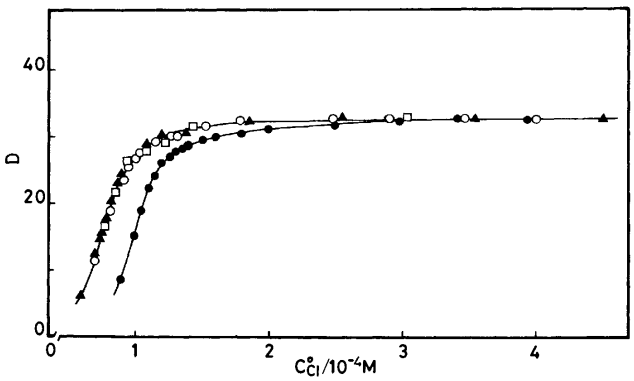

Fig. 1. Variation of distribution ratio of $EtHg^+$ with initial concentration of Cl^-.
●: pH; 1.0, C°_M; 1.07×10^{-4} M (1 M=1 mol dm^{-3}), ○: pH; 1.1, ▲: pH; 1.6, □: pH; 2.0, C°_M; 7.66×10^{-5} M.

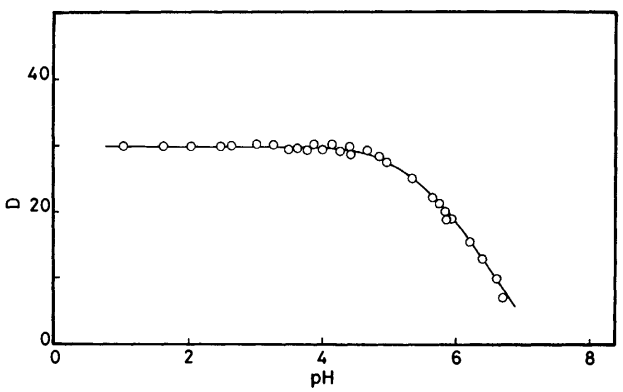

Fig. 2. Variation of distribution ratio of $EtHg^+$ with pH.
C°_M; 7.66×10^{-5} M, C°_{Cl}; 1.20×10^{-4} M.

higher distribution ratio is obtained when the initial concentration of RHg^+ is low. However, at higher concentrations of Cl^-, the same distibution ratio is obtained regardless of the intial concentration of $EtHg^+$.

Moreover, as is shown in Fig. 2, the distribution ratio of $EtHg^+$ decreases with the rise in the pH above 4.

These experimental results may be explained as follows. The distribution ratio D of $EtHg^+$ is written as follows;

$$D = \frac{[MCl]_o + [MOH]_o}{[M]+[MCl]+[MCl_2]+\cdots+[MOH]+[M(OH)_2]+\cdots} = \frac{p\beta_1[Cl] + p'\beta_1'[OH]}{1+\beta_1[Cl]+\beta_2[Cl]^2+\cdots+\beta_1'[OH]+\beta_2'[OH]^2+\cdots}, \quad (1)$$

where M represents $EtHg^+$, where β's are respective complex-formation constants, and where p and p' are the distribution constants of EtHgCl and EtHgOH respectively (the charges of the ions are omitted for the sake of simplicity).

In the experimental range shown in Fig. 1 the distribution ratio of $EtHg^+$ is independent of the pH; therefore, the formation of complexes with OH^- and the distribution of EtHgOH can be neglected, and (1) becomes;

$$\frac{1}{D} = \frac{1}{p} + \frac{1}{p\beta_1[Cl]} + \frac{\beta_2}{p\beta_1}[Cl] + \cdots. \quad (2)$$

From (2) it is found that the plot of $1/D$ against $1/[Cl]$ gives a straight line when the main species of the $EtHg^+$ complex with Cl^- is EtHgCl, whereas the plot of $1/D$ against [Cl] gives a straight line or a quadratic curve when $EtHg^+$ forms higher complexes such as $EtHgCl_2^-$ and $EtHgCl_3^{2-}$ with Cl^-.

Figure 3 shows that the plot of $1/D$ against $1/[Cl]$, in which [Cl] is the equilibrium concentration of Cl^- corrected to the distribution of Cl^- into benzene as EtHgCl, gives a straight line. On the other hand, the plot of $1/D$ against [Cl] gives a quadratic curve with negative coefficients. These results indicate that the main species formed in the aqueous layer in the experimental range is EtHgCl. From the reciprocal of the intercept and the slope of the straight line shown in Fig. 3 the distribution constant and the formation constant of EtHgCl are obtained as 33 ± 1 and $(2.7\pm0.5)\times10^5$ respectively. The formation constant of EtHgCl is almost the same as those of methylmercury(II) and

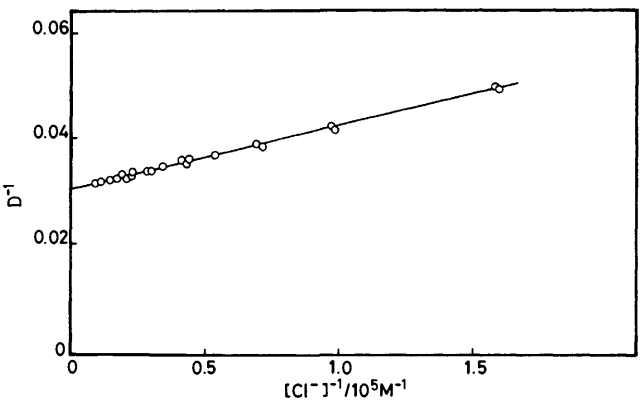

Fig. 3. Plot of 1/D of $EtHg^+$ against 1/[Cl].

PhHg$^+$ chlorides reported previously,[4] and no large variation with the R combined with Hg can be observed. The results shown in Fig. 2 seem to indicate that the distribution of EtHgOH in benzene is negligible. Then, from (1) the following relation is introduced;

$$\frac{1}{D} = \frac{1}{p} + \frac{1}{p\beta_1[Cl]} + \frac{\beta_1'[OH]}{p\beta_1[Cl]} + \frac{\beta_2'[OH]^2}{p\beta_1[Cl]} + \cdots. \quad (3)$$

By using the values of p and β_1 obtained above and the assumption that, in this experimental range, $EtHg^+$ forms a 1:1 complex only with OH^-, the value of β_1' is calculated from the experimental results shown in Fig. 2 and (3). By this treatment $\beta_1'=(1.7\pm0.1)\times10^9$ is obtained; this value shows fairly good agreement with that reported by Waugh *et al.*[5]

Therefore, it may be concluded that the distribution of EtHgOH in benzene is negligible and that, in this experiemntal range, $EtHg^+$ forms a 1:1 complex predominantly with OH^-. From these results, the extraction of the RHg^+ complex with 8-quinolinol into benzene is analysed on the assumption that the distribution of RHgOH in benzene is negligible, regardless of the R.

The absorption maxima of benzene solutions of the $EtHg^+$, *n*-$PrHg^+$, and *n*-$BuHg^+$ complexes and that of the $PhHg^+$ complex are observed at 378 nm and 375 nm respectively; therefore, the variation in the wavelength at the absorption peak with R is vary small. The absorption of free 8-quinolinol in benzene at the absorption maxima of the complexes is negligible.

The molar ratio of RHg^+ to 8-quinolinol in the complex is found by the continuous-variation method to be 1:1, regardless of the R.

At the peak wavelength, the absorbance of the extract of the RHg^+ complex from borate buffer solutions of pH values from 9.0 to 10.0 in the presence of an excess of 8-quinolinol shows constant value. Therefore, from the absorbance measured under the conditions shown above, the molar absorption coefficient of the complex solution at the peak wavelength is determined and the following results are obtained; $EtHg^+$ complex: 3.00×10^3; *n*-$PrHg^+$ complex: 3.04×10^3; *n*-

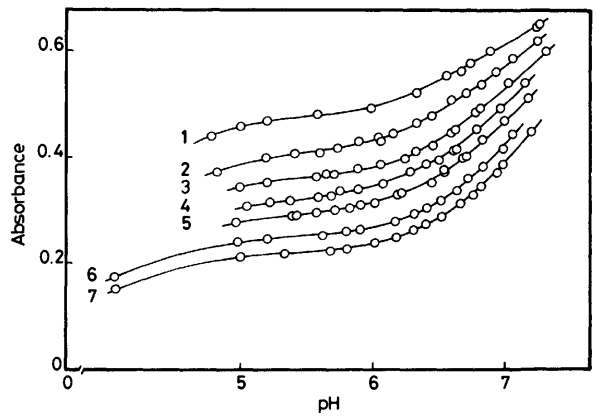

Fig. 4. Variation of the absorbance of $EtHg^+$–8-quinolinol complex in benzene with pH under various concentrations of phosphate.
C_M°; 2.55×10^{-4} M, C_L°; 4.00×10^{-3} M.
Total concentration of phosphate: 1; 0.02 M, 2; 0.03 M, 3; 0.04 M, 4; 0.05 M, 5; 0.06 M, 6; 0.08 M, 7; 0.10 M.

$BuHg^+$ complex: 3.03×10^3; $PhHg^+$ complex: 3.20×10^3. The variation in the molar absorption coefficient of the complexes with the R is very small except for the $PhHg^+$ complex, which shows a higher value.

Figure 4 shows the variation in the absorbance of the $EtHg^+$ complex extracts from phosphate buffer solutions in various concentrations with the pH. Similar results are obtained in other RHg^+ systems. In this work, the initial concentration of RHg^+ is made as high as possible in order to minimise the effect of the co-extraction of the RHg^+ complexes with, *e.g.*, the Cl^- contained as an impurity in the reagents used. However, in the present experimental range the distribution ratio of RHg^+ is independent of the initial concentration of RHg^+; therefore, the formation of polynuclear complexes of RHg^+ is considered to be negligible.

The experimental results shown in Fig. 4 may be analysed as follows.

The extraction of RHg^+ with 8-quinolinol can be written as;

$$RHg^+ + q^- = RHgq_{(o)}, \tag{4}$$

$$K_{ex} = \frac{[RHgq]_o}{[RHg][q]}. \tag{5}$$

As has been mentioned above, RHgOH is not distributed into benzene, and the distribution of complexes of RHg^+ with phosphate ions are found to be negligible, therefore, the distribution ratio D of RHg^+ can be written as;

$$D = \frac{[RHgq]_o}{C_M^\circ - [RHgq]_o}, \tag{6}$$

$$\begin{aligned} C_M^\circ - [RHgq]_o = C_M &= [RHg] + [RHgOH] \\ &+ [RHg(OH)_2] + \cdots + [RHgH_2PO_4] + \cdots \\ &+ [RHgHPO_4] + \cdots + [RHgPO_4] + \cdots \\ &+ [RHgq] + [RHg(q)(OH)] + \cdots \\ &= [RHg](1 + \beta_1'[OH] + \beta_2'[OH]^2 + \cdots \\ &+ K_1[H_2PO_4] + \cdots + K_1'[HPO_4] + \cdots \\ &+ K_1''[PO_4] + \cdots + K_f[q] + K_c[q][OH] + \cdots) \\ &= [RHg]\gamma, \end{aligned} \tag{7}$$

where C_M° is the initial concentration of RHg^+ in the aqueous solution and where the β's and K's are the formation constants of the respective complexes. From the measurement of the absorbance of the aqueous layer after extraction, $RHg(q)(OH)^-$ is found to be absent[1] and [RHgq] is considered to be negligible; therefore, in (7), the terms corresponding to [RHg(q)(OH)] and [RHgq] are omitted. The total concentration of 8-quinolinol, C_L°, can be written as follows;

$$\begin{aligned} C_L^\circ &= [H_2q] + [Hq] + [q] + [RHgq] \\ &+ [RHg(q)(OH)] + [Hq]_o + [RHgq]_o. \end{aligned}$$

As [RHgq] and [RHg(q)(OH)] can be neglected;

$$\begin{aligned} C_L^\circ - [RHgq]_o = C_L &= [H_2q] + [Hq] + [q] + [Hq]_o \\ &= [q]\left(\frac{[H]^2}{k_1k_2} + \frac{[H]}{k_2} + 1 + \frac{p''[H]}{k_2}\right) = [q]\,\alpha. \end{aligned} \tag{8}$$

From (5), (7), and (8), (9) is obtained;

$$K_{ex} = \frac{[RHgq]_o\,\alpha\gamma}{C_M C_L} = K_{ex}'\,\alpha\gamma \quad \frac{1}{K_{ex}'\alpha} = \frac{\gamma}{K_{ex}}. \tag{9}$$

In (9). K_{ex}' can be determined experimentally and the value of γ can be obtained from the step-by-step acid-dissociation constants of 8-quinolinol ($pk_1=5.13$, $pk_2=9.66$[6]), the distribution constant of 8-quinolinol between aqueous and benzene layers p'' ($p''=10^{2.44}$[7]), and the pH of the aqueous layer measured. From (7), the right-hand side of (9) becomes;

$$\begin{aligned} \frac{\gamma}{K_{ex}} &= \frac{1}{K_{ex}}(1 + \beta_1'[OH] + \beta_2'[CH]^2 + \cdots) \\ &+ \frac{1}{K_{ex}}(K_1[H_2PO_4] + K_1'[HPO_4] + K_1''[PO_4] + \cdots \\ &= \frac{1}{K_{ex}} f[OH] + \frac{[PO_4]}{K_{ex}}\left(\frac{K_1[H]^2}{k_2'k_3'} + \frac{K_1'[H]}{k_3'} + K_1'' + \cdots\right) \end{aligned} \tag{10}$$

$$= \frac{1}{K_{ex}} f[OH] + \frac{[HPO_4]}{k_{ex}}\left(\frac{K_1[H]}{k_2'} + K_1' + \frac{K_1''k_3'}{[H]} + \cdots\right), \tag{11}$$

where f[OH] represents the coefficient of $1/K_{ex}$ of the first term on the right-hand side and where k_2' and k_3' are the respective acid-dissociation constants of phosphoric acid ($pk_2'=6.71$, $pk_3'=11.8$[8]).

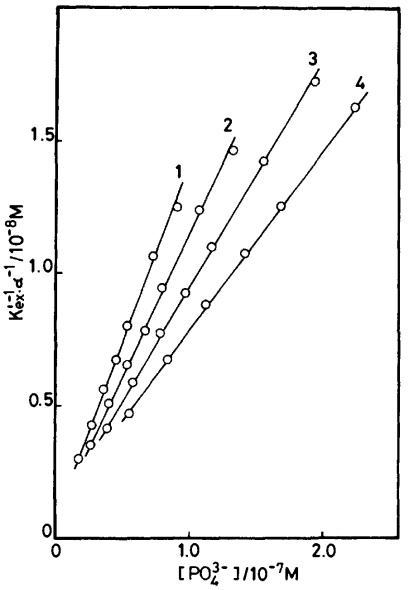

Fig. 5. Plot of $1/K_{ex}'$ a of $EtHg^+$–8-quinolinol complex against $[PO_4]$.

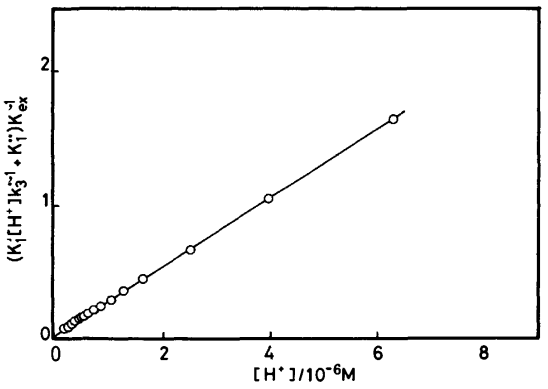

Fig. 6. Plot of Values of the slope of straight lines shown in Fig. 5 against [H].

TABLE 1. FORMATION CONSTANTS OF RHg^+ COMPLEXES

RHg^+	K_{ex}	β_1'	K_1'	K_1''
$EtHg^+$	$2.9\pm0.5\times10^{10}$	$1.7\pm0.3\times10^{9}$	$1.2\pm0.2\times10^{4}$	$2.8\pm0.7\times10^{8}$
n-$PrHg^+$	$1.4\pm0.5\times10^{11}$	$1.6\pm0.5\times10^{9}$	$1.4\pm0.3\times10^{4}$	$1.1\pm0.4\times10^{8}$
n-$BuHg^+$	$7.6\pm1.1\times10^{11}$	$1.1\pm0.1\times10^{9}$	$1.8\pm0.2\times10^{4}$	$2.7\pm0.6\times10^{8}$
$PhHg^+$	$2.0\pm0.7\times10^{13}$	$9.6\pm3.6\times10^{9}$	$1.8\pm0.4\times10^{5}$	$3.1\pm1.1\times10^{9}$

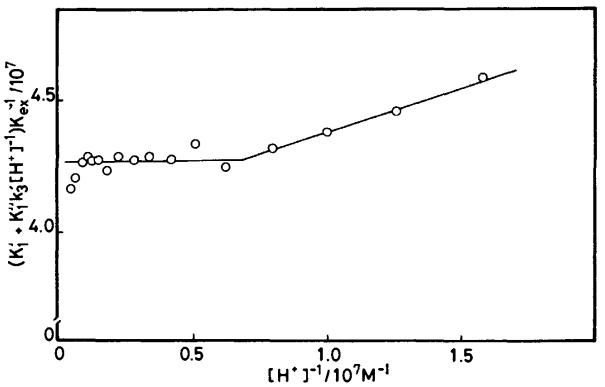

Fig. 7. Plot of values of the slope of straight lines obtained by plot of $1/K_{ex}'$ a of $EtHg^+$ complex *vs.* $[HPO_4]$ against $1/[H]$.

Equations (9), (10), and (11) indicate that $1/K_{ex}'\ \alpha$ at a constant pH is linear against $[PO_4]$ and $[HPO_4]$ and that the values of the intercept of both straight lines obtained at the same pH are equal. Moreover, intercepts of both straight lines are functions of [OH]; then, by plots of the value of the intercept against [OH], the hydroxo complexes of RHg^+ formed in the experimental range and the three constants K_{ex}, k_1' and k_2' are determined. On the other hand, the β values of the slopes of the straight lines obtained by the plot of $1/K_{ex}'\ \alpha$ against $[HPO_4]$ and $[PO_4]$ are functions of [H]; then, by plots of the values of the slope against [H] or $1/[H]$ complexes of RHg^+ with $H_2PO_4^-$, HPO_4^{2-}, and PO_4^{3-} and the formation constants of these complexes are determined on the bases of (10) and (11).

By these considerations, the experimental results shown in Fig. 4 are analysed. First, Fig. 5 shows the plot of $1/K_{ex}'\ \alpha$ of $EtHg^+$ against $[PO_4]$. A similar good linearity is obtained by the plot of $1/K_{ex}'\ \alpha$ against $[HPO_4]$, and the values of the intercept of both straight lines at the same [OH] show a good agreement with in a probable error of $\pm10\%$.

Moreover, the values of the intercept obtained from Fig. 5 are found to be linear against [OH]. This indicates that, in this experimental range, $EtHg^+$ forms a 1:1 complex with OH^- predominantly. In Table 1, the values of K_{ex} and β_1' obtained from this result on the basis of (10) are tabulated.

Figure 6 shows the plot of the value of the slope of the straight line shown in Fig. 5 against [H]. The good linearity indicates that there is no formation of a complex of $EtHg^+$ with $H_2PO_4^-$. The absence of the $EtHg^+$-$H_2PO_4^-$ complex is confirmed by the result that the values of the slopes of the straight lines obtained by a plot of $1/K_{ex}'\ \alpha$ against $[HPO_4]$ are linear against $1/[H]$ on the basis of (11), as shown in Fig. 7.

In Fig. 7, the slope of the straight line is zero below pH 6.8; therefore, below this pH the formation of $EtHgPO_4^{2-}$ is considered to be negligible. Figures 6 and 7 indicate that, in order to determine more precise values of the intercept and the slope of the straight line, the plot of $1/K_{ex}'\ \alpha$ against $[PO_4]$ is more suitable than that of $1/K_{ex}'\ \alpha$ against $[HPO_4]$. Therefore, in Table 1 the values of K_1' and K_1'' obtained by the treatment of the results shown in Fig. 6 by the least-squares method and by the use of the value of K_{ex} determined above are tabulated.

Similar results are obtained from the n-$PrHg^+$, n-$BuHg^+$, and $PhHg^+$ 8-quinolinate extraction systems. The results of the determinations are tabulated in Table 1. However, as shown in Fig. 8, plots corresponding to Fig. 6 in the $PhHg^+$ system give a curve; therefore, possibility of the formation of higher complexes of $PhHg^+$ with OH^- can not be neglected. It is found though, that the treatment of the whole curve as a quadratic curve does not give reasonable values of K_{ex}, β_1', and β_2'. Therefore, by the treatment of the region from a to b in Fig. 8 as a straight line, K_{ex} and β_2' are determined from the intercept and slope of this straight line.

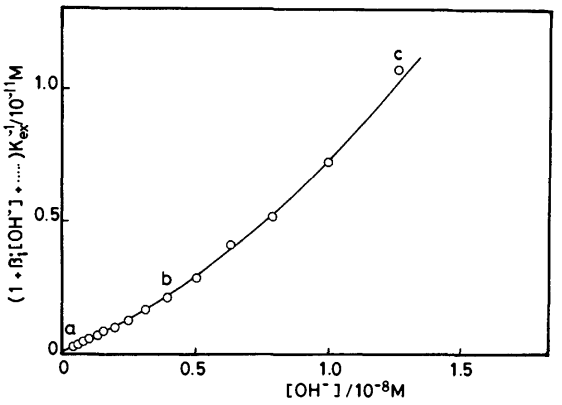

Fig. 8. Plot of values of the intercept of straight lines obtained by plot of $1/K_{ex}'$ a of $PhHg^+$ complex *vs.* $[PO_4]$ against [OH].

The formation of a 1:1 complex of methylmercury(II) with HPO_4^{2-} has been studied by Schwarzenbach *et al.*[9] and by Ingman *et al.*[10], but the formation of a complex of RHg^+ with PO_4^{3-} has not been reported previously. However, the formation constant of EtHgOH obtained here shows a good agreement with that reported previously[5] and that obtained by the study of the extraction of EtHgCl reported in this article. These results indicate that the method of analyzing a reaction presented here is reasonable. Therefore, it seems certain that RHg^+ forms complexes with both HPO_4^{2-} and PO_4^{3-}.

As has been mentioned above, $PhHg^+$ is considered to form higher complexes with OH^- in the present

experimental range, but those higher hydroxo-complex-formation reactions can not be studied in detail. However, the formation constant of PhHgOH obtained here agrees well with that obtained by Waugh *et al.*[5], 1.0×10^{10}. This indicates that $PhHg^+$ forms a 1 : 1 complex with OH^- predominantly in the region from *a* to *b*, that is at pH values from 4.8 to 5.8.

References

1) J. Kuniya, N. Naito, and S. Takei, *Bull. Chem. Soc. Jpn.*, **57**, 2266 (1984).
2) E. B. Sandell, "Colorimetric Determination of Traces Metals," 2nd ed., Interscience Publishers, New York (1950), p. 107.
3) V. L. Miller, D. Polley, and C. J. Gould, *Anal. Chem.*, **23**, 1286 (1951).
4) R. B. Simpson, *J. Am. Chem. Soc.*, **83**, 4711 (1961); O. Budevsky, F. Ingman, and D. H. Liem, *Acta Chem. Scand.*, **27**, 1277 (1973) ; J. Stray and K. Kratzer, *Radiochem. Radioanal. Lett.*, **28**, 53 (1977).
5) T. D. Waugh, H. F. Walton, and J. A. Laswick, *J. Phys. Chem.*, **59**, 395 (1955).
6) A. Albert and A. Hampton, *J. Chem. Soc.*, 505 (1954); D. Dyrssen, *Svenk. Kem. Tidskr.*, **66**, 234 (1954).
7) J. Mason and I. Lipschtz, *Talanta*, **18**, 1111 (1971).
8) G. Schwarzenbach and G. Geier, *Helv. Chem. Acta*, **46**, 906 (1963).
9) G. Schwarzenbach and M. Schellenberg, *Helv. Chim. Acta*, **48**, 28 (1950).
10) F. Ingman and D. H. Liem, *Acta Chem. Scand.*, **28**, 947 (1974).

A General Synthetic Approach of Spirovetivanes. The Synthesis of (±)-Solavetivone, (±)-Hinesol, and Related Compounds[1]

Akio MURAI,* Shingo SATO, and Tadashi MASAMUNE*
Department of Chemistry, Faculty of Science, Hokkaido University, Sapporo 060
(Received February 6, 1984)

The synthetic procedure leading to preparation of representative compounds, (±)-solavetivone and (±)-hinesol, of two classes of spirovetivanes, is described. The procedure involves Diels-Alder reaction of 4-substituted 5,6-dihydro-3,5-dimethylanisoles with methyl acrylate and π-cyclization of 4-(2-mesyloxyethyl)-4-prenyl-2-cyclohexen-1-one as key steps (Scheme 1).

Naturally occurring spirovetivanes are divided into two classes based on the relative configuration between the C-4–C-14 and C-5–C-6 bonds:[2,3] one class consists of a number of sesquiterpenes, represented by solavetivone and oxylubimin and isolated as stress compounds[4] from diseased potato tubers, possesses the *trans* configuration concerning the relevant bonds, while the other,[3,5] including hinesol, β-vetivone, and others isolated from vetiver oil, takes the *cis*-configuration. While considerable attention has been directed towards synthesis[3] of these sesquiterpenes owing to the characteristic skeleton, most of the works have been limited to the preparation of spirovetivanes belonging to the latter class. Only recently, Yamada,[6] Iwata,[7] and coworkers reported the synthesis of (±)-solavetivone, one of the simplest spirovetivanes of the former class. We have also searched a general procedure leading to the preparation of both classes of spirovetivanes and succeeded in the synthesis of (±)-solavetivone[8] (±)-(**1**), (±)-hinesol[5] (±)-(**2**), (±)-β-vetivone[5] (±)-(**3**), and close analogues. The result was published in a preliminary communication,[9] and its details are described in this paper.

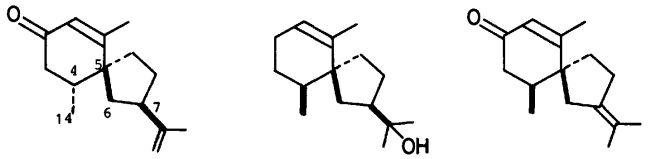

1 **2** **3**

Our synthetic plan involves two key steps as shown in Scheme 1: (i) Diels-Alder reaction of 4-substituted 3,5-dimethyl-5,6-dihydroanisoles (A) with methyl acrylate or its equivalents, giving cycloadducts (B), and (ii) π-cyclization[10] between the primary cationic carbon atom and prenyl double bond of the intermediates (D) derived from B *via* C. The *syn*- and *anti*-configurations of the C-8-methyl group in respect to the C-2–C-3 bond in B correspond to the *cis*- and *trans*-configurations between the C-5–C-6 and C-4–C-14-bonds in the spirovetivanes (E). If each of the *syn*- and *anti*-adducts is prepared stereoselectively under suitable conditions (step i), the respective classes of spirovetivanes would be synthesized effectively. On the other hand, there seem not to be any precedents for ring closure by the relevant π-cyclization (step ii). If the cyclization proceeds smoothly, examination of the Dreiding model indicates that the desirable spirovetivones (E) with the (4*SR*,7*SR*)-isopropyl moiety would be produced stereoselectively.

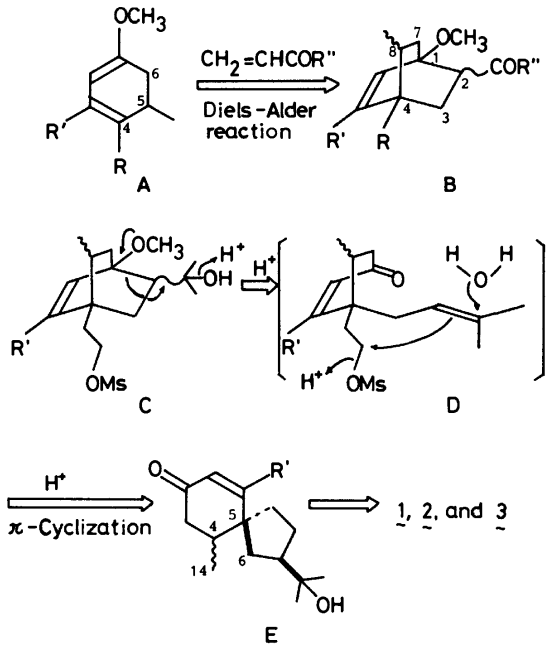

Scheme 1.

The starting diene (**4**), corresponding to A in Scheme 1, was prepared as follows. 3,5-Dimethylanisole was reacted with bromine in the presence of iron metal to give its 4-bromoanisole (**5**) (85%), which on reflux with magnesium turnings and allyl bromide in ether formed its Grignard reagent. Treatment of the reagent with allyl bromide afforded 4-allyldimethylanisole (**6**) (83% from **5**), which was converted by oxidation according to the Lemieux-Johnson procedure[10] followed by acetalization of the resulting aldehyde (**7**) into the corresponding acetal (**8**) (77% from **6**). The Birch reduction of **8** gave rise to the 3,6-dihydroanisole (**9**) (85%), which was isomerized by heating at 140 °C to yield the 5,6-dihydroanisole (**4**) (72% from **8**).

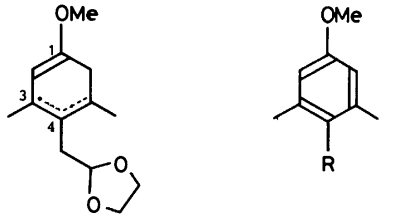

4 Δ^3, no Δ^4
9 Δ^4, no Δ^3

5 R=Br-
6 R=CH_2-CH=CH_2
7 R=CH_2CHO
8 R=CH_2CH<O, O>

Diels-Alder reactions of the dihydroanisoles were carried out under various conditions.[11] Treatment of the 1,4-diene (**9**) with methyl acrylate in the presence of dichloromaleic anhydride (DCMA)[12] and 2,6-di-*t*-butyl-*p*-cresol (BHT) at 85 °C for 14 d produced a mixture (77% based on the recovered **9**) of four stereoisomeric cycloadducts differing in the configuration at C-2 (2-*endo*- and 2-*exo*-$COOCH_3$) and C-8 (8-*syn*- and 8-*anti*-CH_3 to the C-2–C-3 bond). The product was a 6.6:1.0 mixture of the *endo* (**10**) and exo adducts (**11**), which were separated by chromatography. Each of the adducts (**10**) and (**11**) was estimated to be a 2.0:1.0 mixture of the *syn* and *anti* isomers. The configuration of **10** and **11** was assigned on the basis of the chemical shifts of the signals due to the C-2–H [δ 2.87 (dd, J=9.5 and 5 Hz) and 2.72 (ddd, J=10, 5, and 1 Hz, long-range coupling with 7-*anti*–H=1 Hz) for the *endo* and *exo* adducts]. The ratio of the *syn* and *anti* adducts was deduced from the relative intensity of the C-8–CH_3 [δ 1.04 (d, J=6 Hz, *endo*) and 0.96 (d, J=6 Hz, *exo*) for the *syn* adducts, and δ 0.87 (d, J=6 Hz, *endo*) and 0.75 (d, J=6 Hz, *exo*) for the *anti* adducts]. The cycloaddition, when carried out in ether at 20 °C and at 15000 atm (1 atm=101325 Pa) for 2 d, afforded a 3.2:1.0 (by NMR) mixture (65% based on the recovered **9**) of the *syn-endo* and *anti-endo* adducts (**10**) as the isolable products.[11] On the other hand, treatment of the 1,3-diene (**4**) with methyl acrylate at high temperature (190 °C) afforded a 0.9:1.0 (by NMR) mixture (75%) of the *syn* and *anti* adducts, each being a 2.0:1.0 mixture of the *endo* and *exo* isomers.[11] These results indicate that (i) in contrast to exclusive production of the *anti* adducts in the reactions with 4-unsubstituted[13] and 4-methyl dines,[14] introduction of ethyl and substituted ethyl groups into C-4 of the starting diene led to formation of the *syn* isomers, and (ii) ratios of the *syn*- isomers to the corresponding *anti*-isomers in the latter reactions increased with lowering temperature.

The *endo* adducts (**10**) (a 3.2:1.0 mixture of the *syn* and *anti* adducts) were transformed by a three-step process [(i) acid hydrolysis, (ii) hydride reduction, and (iii) treatment with methyllithium] into the corresponding bicyclooctene diols, which were separated easily to give the *syn-endo* (**12**) and *anti-endo* diols (**13**) in 60 and 15% yields, respectively [δ 1.06 (3H, d, J=7 Hz, 8-CH_3) for **12**, and δ 0.74 (3H, d, J=6 Hz) for **13**]. Likewise, the aforementioned 0.9:1.0 mixture of the *syn* and *anti* adducts were separated easily by chromatography into the *endo* (**10**) and *exo* adducts (**11**), which were treated in the same manner as mentioned above to give the corresponding diols. These diols were separated by chromatography to give the *syn-endo* (**12**), and *anti-endo* isomers (**13**) in 33 and 37% yields (from **10**), and the *syn-exo* (**14**) and *anti-exo* isomers (**15**) in 30 and 33% yield (from **11**), respectively [δ 0.98 (3H, d, J=7 Hz, 8-CH_3) for **14**, and δ 0.75 (3H, d, J=7 Hz) for **15**]. These bicyclooctenediols (**12**)—(**15**) were converted by treatment with methanesulfonyl chloride into the respective methanesulfonates (**12a**)—(**15a**).

Attempts to convert the *syn-endo* mesylate (**12a**) into the spirovetivanes (**16**) and (**17**) were examined

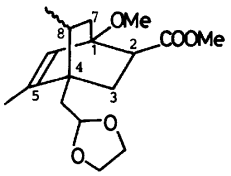

10 2-endo-COOMe
11 2-exo-COOMe

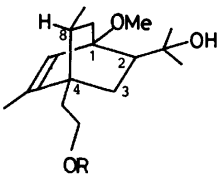

12 2-endo-$C(Me)_2OH$, R=H
12a 2-endo-$C(Me)_2OH$, R=Ms
14 2-exo-$C(Me)_2OH$, R=H
14a 2-exo-$C(Me)_2OH$, R=Ms

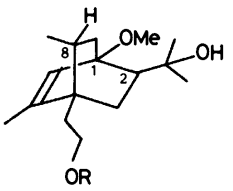

13 2-endo-$C(Me)_2OH$, R=H
13a 2-endo-$C(Me)_2OH$, R=Ms
15 2-exo-$C(Me)_2OH$, R=H
15a 2-exo-$C(Me)_2OH$, R=Ms

under various conditions: *e.g.*, tin(IV) chloride in dichloromethane at −78 °C, acetic acid at 110 °C, formic acid at 50 °C, and others. Finally, treatment of **12a** with oxalic acid (10 mol equiv) in 33% aqueous acetone at 85 °C for 4 h effected formation of the skeletone in question, giving two spirovetivanes (**16**), mp 38—41 °C, and (**17**), mp 121—123 °C, in 60 and 27% yields, respectively, in which the C-4–C-14 and C-5–C-6 bonds were oriented *cis* each other. Careful treatment of **12a** with formic acid at room temperature for 30 min gave prenylcyclohexenone (**18**), which on treatment under the same conditions as mentioned above gave **16** and **17** in 58 and 37% yields, respectively. The other *syn* adduct (**14a**) was also submitted to the same cyclization, giving **16** and **17** in 58 and 20% yields, respectively.

The π-cyclization must have taken place by attack of the prenyl double bond towards the primary cationic carbon atom formed by removal of the mesyloxyl group. It is noted that the isomer (**19**) differing from **16** in the C-7 configuration could not be detected by careful examination of IR and NMR spectra, and by GLC analysis. This high stereoselectivity for formation of the (4*SR*,7*SR*)-asymmetric center could be rationalized in terms of the relative stability of two conformers (**18A**) and (**18B**) with maximum overlap between the π-orbitals of the relevant primary cationic carbon atom and the prenyl double bond (Scheme 2). This seems to be the first example for such stereoselective ring closure.

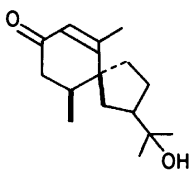

16 (7SR)-$C(Me)_2OH$
19 (7RS)-$C(Me)_2OH$

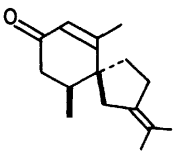

17

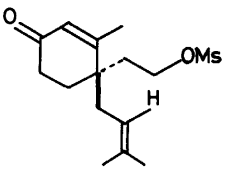

18

The spirovetivanes (**16**) and (**17**) were identified as authentic samples[5] of (±)-hinesolone and (±)-β-vetivone (**3**), respectively. The former could be trans-

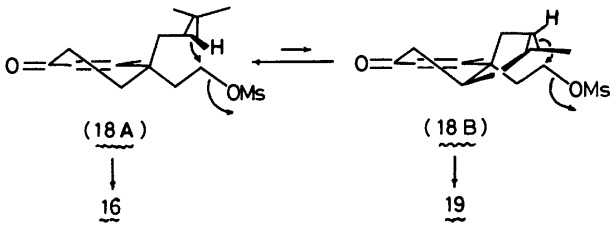

Scheme 2.

formed according to the procedures developed by Dauben and coworkers[5] into (±)-hinesol (**2**) and (±)-β-vetispirene. The present result constitutes a new synthetic pathway to the spirovetivanes isolated from vetiver oil.

The same treatment of the *anti-endo* mesylate (**13a**) in aqueous acetone produced two spirovetivanes (**20**), oil, and (**21**), mp 52—55 °C, with *trans*-oriented C-4–C-14 and C-5–C-6 bonds in 63 and 23% yields, respectively. Likewise, the *anti-exo* isomer (**15a**) afforded **20** and **21** in 69 and 26% yields, respectively. The latter (**21**) was identified as "10-epi-β-vetivone" by comparison of the spectral data with the reported ones.[15] Dehydration of **20** proceeded smoothly by heating with pyridine-modified alumina (Woelm, neutral) at 220 °C for 8 min[16] to give an isopropenyl compound, oil, in 60% yield, which formed its *syn*-, mp 107.5—109 °C, and *anti*-2,4-dinitrophenylhydrazones, mp 137—138 °C. It is emphasized that no isopropylidene derivative was detected in the dehydration product. The compound was identified as (±)-solavetivone by direct comparison with natural solavetivone (**1**) (MS, IR, NMR, and TLC). The present synthesis of (±)-solavetivone involves 12 steps with an overall yield of 3.2% from 3,5-dimethylanisole.

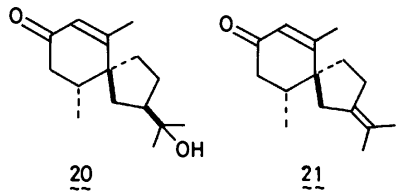

Experimental

All the melting and boiling points were uncorrected. The homogeneity of each compound was always checked by TLC over silica gel (Wakogel B-5F) with various solvent systems, and the spots were developed with cerium(IV) sulfate in dil sulfuric acid and/or concd sulfuric acid. The IR and NMR (100 MHz) spectra were measured in liquid state for oil and in chloroform for solid, and in [^{2}H]chloroform, respectively, unless otherwise stated. The abbreviations "s, d, t, m, and br," in the NMR spectra denote "singlet, doublet, triplet, multiplet and broad," respectively. Solvents and reagents were dried and distilled before use: diethyl ether and tetrahydrofuran (THF) (over sodium ketyl radical); benzene and carbon tetrachloride (CCl_4) (over phosphorus(V) oxide); triethylamine (over calcium hydride).

4-Bromo-3,5-dimethylanisole (5). To a solution of 3,5-dimethylanisole (82 g) in CCl_4 (600 ml) and iron powder (0.4 g) at −40—30 °C was added dropwise a solution of bromine (34 ml, 0.66 mol) in CCl_4 (200 ml) over a 3 h period. The solution was stirred for 2 h at the same temperature, and poured into 400 ml of ice and water, and extracted with dichloromethane, repeatedly. The combined organic solution was washed with 5% aqueous sodium hydrogencarbonate ($NaHCO_3$) and water, dried (Na_2SO_4), and concentrated *in vacuo* to leave an oil, which was distilled under reduced pressure to give **5** (110 g, 85%); bp 123—125 °C/15 Torr (1 Torr=133.322 Pa); MS, *m/z* 214 (M^+, base); IR, 1570, 1230, 1193, 1160, 1074, and 1015 cm^{-1}; NMR (CCl_4), δ 2.33 (6H, s), 3.69 (3H, s), and 6.53 (2H, s). Found: C, 50.56; H, 5.28%. Calcd for $C_9H_{11}OBr$: C, 50.26; H, 5.16%.

4-Allyl-3,5-dimethylanisole (6). To a solution of 2,6-dimethyl-4-methoxyphenylmagnesium bromide, prepared from **5** (35 g), magnesium turnings (4 g) and allyl bromide (1.2 ml) in ether (200 ml) under reflux with stirring for 18 h, was added a solution of allyl bromide (30 ml) in ether (60 ml) at room temperature under argon atmosphere. The solution was stirred under reflux for 16 h and then cooled to 0 °C. To the solution was added 2M† hydrochloric acid (50 ml) to dissolve the remaining magnesium metal. The resulting mixture was poured into saturated brine (200 ml) and extracted with ether, repeatedly. The organic layer was washed with 5% aq $NaHCO_3$ and saturated brine, dried and concentrated, and the resiude was distilled to give **6** (24.09 g): bp 112—130 °C/15 Torr; MS, *m/z* 176 (M^+, base); IR, 3080, 1640, 998, and 915 cm^{-1}; NMR (CCl_4), δ 2.21 (6H, s), 3.25 (2H, dt, *J*=5.5 and 1.8 Hz), 3.68 (3H, s), 4.69 (1H, ddt, *J*=17, 1.9, and 1.8 Hz), 4.82 (1H, ddt, *J*=10, 5.5, and 1.9 Hz), 5.82 (1H, ddt, *J*=17, 10, and 5.5 Hz), and 6.42 (2H, s). Found: C, 81.64; H, 9.06%. Calcd for $C_{12}H_{16}O$: C, 81.77; H, 9.15%.

4-(2,2-Ethylenedioxyethyl)-3,5-dimethylanisole (8). To a solution of **6** (20 g) in THF (400 ml) at room temperature was added a 0.16 M solution (4 ml) of osmium tetraoxide in THF, and the solution was stirred vigorously for 15 min. To the solution was added an aqueous solution (520 ml) containing sodium periodate (58 g) at 0 °C over a 3 h period. The resulting mixture was stirred at room temperature for 10 h, and precipitates formed were removed by filtration. The filtrate was concentrated *in vacuo* to remove THF and extracted with ethyl acetate, repeatedly. The acetate solution was washed with 5% aq sodium hydrogensulfite, water and saturated brine, dried and evaporated to leave 2,6-dimethyl-4-methoxyphenylacetaldehyde (**7**) (21.57 g); IR, 2840 and 1725 cm^{-1}; NMR (CCl_4), δ 2.23 (6H, s), 3.54 (2H, d, *J*=2 Hz), 3.72 (3H, s), 6.50 (2H, s), 9.45 (1H, t, *J*=2 Hz). This compound was used for the next reaction without further purification.

The aldehyde (**7**) (21.57 g), ethylene glycol (11 g) and *p*-toluenesulfonic acid monohydrate (2 g) were dissolved in benzene (400 ml), and the solution was stirred under reflux for 15 h, water being removed continuously by a Dean-Stark tube. The reaction mixture was cooled to room temperature, and poured into saturated brine (300 ml) and extracted with ethyl acetate (EtOAc), repeatedly. The organic layer was washed with 5% aq $NaHCO_3$ and saturated brine, dried, and then evaporated. The crude residue was crystallized from hexane (350 ml), filtered, and washed with hexane–ether (1:1) to give **8** (11.68 g). The filtrate was concentrated and separated by chromatography over alumina (300 g) with benzene to give a crystalline substance **8** (7.17 g), mp 79—81 °C (from ether); MS, *m/z* 222 (M^+); IR (Nujol), 1610, 1185, 1130, 1020, 930, 870, and 837 cm^{-1}; NMR (CCl_4), δ 2.27 (6H, s), 2.86 (2H, d, *J*=5 Hz), 3.66 (3H, s), 3.7 (4H, m), 4.82 (1H, t, *J*=5 Hz), and 6.40 (2H, s). Found: C, 79.14; H, 8.04%. Calcd for $C_{13}H_{18}O_3$: C, 70.24; H, 8.16%.

4-(2,2-Ethylenedioxyethyl)-3,5-dimethyl-3,6-dihydroanisole (9) and its 5,6-Dihydro Isomer (4). i) To a stirred mixture of **8** (7.55 g) in THF (400 ml) and liquid ammonia (700 ml), dried over potassium hydroxide pellets, was added small pieces of lithium (10 g) for 30 min. The mixture was stirred for 2 h

† 1 M=1 mol dm^{-3}.

and treated with absolute ethanol (100 ml) for 40 min. The resulting mixture, after removal of the ammonia followed by addition of ice-cooled water (500 ml), was concentrated, extracted with ether, dried, and evaporated to leave an oily residue, which on distillation gave **9** (6.475 g): bp 105—107°C/1 Torr; MS, *m/z* 224 (M^+); IR, 1701 and 1664 cm^{-1}; NMR, δ 1.08 (3H, d, J=7 Hz), 1.71 (3H, s), 3.51 (3H, s), 4.60 (1H, d, J=4 Hz), and 4.89 (1H, t, J=5 Hz).

ii) The reduction of **8** (10 g) was carrried out in the same manner as mentioned above except distillation. The crude 3,6-dihydroanisole (**9**) was heated at 140°C/29 Torr for 10 h and then distilled to give **4** (7.15 g): bp 152—160°C/13 Torr; UV (EtOH), 277 nm (ε 5000); MS, *m/z* 224 (M^+); IR, 1670, and 1645 cm^{-1}; NMR, δ 0.92 (3H, d, J=7 Hz), 1.79 (3H, s), 3.56 (3H, s), 4.77 (1H, t, J=1 Hz), and 4.88 (1H, t, J=5 Hz).

Diels-Alder Reaction. Method A; The Cycloadditon at 90°C and 1 atm: A mixture of **9** (13.32 g), DCMA (20 mg) and BHT (3 g) in methyl acrylate (80 ml) and benzene (40 ml) was heated at 90°C under argon at atmospheric pressure for 14 d. The red reaction mixture was distilled to remove excess of methyl acrylate and benzene. The syrupy residue was poured into 2M aqueous sodium hydroxide (NaOH) (300 ml), and extracted with ether (4×200 ml). The combined extracts were washed with saturated brine, dried, evaporated, and chromatographed over alumina (200 g) with benzene to give the crude starting diene (**9**, 23.6 g) and a mixture (11.79 g) of the adducts. The crude diene was distilled under reduced pressure to yield the pure starting diene (4.87 g). The crude mixture of the adducts was separated by chromatography over silica gel (400 g) with benzene and ethyl acetate (8:1) to give a mixture of the *exo*-adducts (1.20 g) and the endo-adducts (7.80 g) in 77% yield (based on the consumed starting diene): *endo* adducts (**10**); oil, MS, *m/z* 310 (M^+) and 224; IR, 1741, 1643, 1170, 1112, and 1100 cm^{-1}; NMR, δ 1.04 and 0.87 (2H, and 1H, each d, J=6 Hz), 1.87 and 1.80 (2H and 1H, each d, J=1 Hz), 2.87 (1H, dd, J=9.5 and 5 Hz), 3.32 and 3.64 (each 3H, s), 3.9 (4H, m), 4.93 and 4.98 (0.67 H and 0.33 H, each t, J=4 Hz), and 5.89 (1H, br s, W_H=7 Hz): *exo* adducts (**11**); oil, MS, *m/z* 310 (M^+) and 224; IR, 1738, 1642, 1194, 1130, and 1095 cm^{-1}; NMR, δ 0.96 (2H, d, J=6 Hz), 0.75 (1H, d, J=6 Hz), 1.81 and 1.75 (2H and 1H, each d, J=1 Hz), 2.72 (1H, ddd, J=10, 5, and 1 Hz), 3.35 and 3.66 (each 3H, s), 3.9 (4H, m), 4.93 and 4.89 (0.67 H and 0.33 H, each t, J=5 Hz), and 6.03 (1H, br s, W_H=6 Hz).

Method B; The Cycloaddition Under High Pressure: The Teflon tube (ϕ 8.1×35 mm) filled with the 1,4-diene (**4**) (452 mg), methyl acrylate (230 mg, freshly distilled), BHT (14 mg) and ether (0.5 ml) was kept in a high pressure apparatus, and the cycloaddition was performed at 15000 atm at room temperature for 2 d. The syrupy mixture was evaporated and the residue was separated by chromatography over alumina (19 g) with benzene to give the strating diene (131 mg) and the cycloadducts (190 mg, 65% based on the recovered diene), which was a 3.2:1.0 (by NMR) inseparable mixture (**10**) of the *syn-endo* and *anti-endo* adducts: oil; MS, *m/z* 310 (M^+) and 224 (retro Diels-Alder fragment); IR, 1741, 1643, 1170, 1112, and 1100 cm^{-1}; NMR, δ 1.04 (2.29 H, d, J=6 Hz), 0.87 (0.71 H, d, J=6 Hz), 1.87 (2.29 H, d, J=1 Hz), 1.80 (0.71 H, d, J=1 Hz), 2.87 (1H, dd, J=9.5 and 5 Hz), 3.32 and 3.64 (each 3H, s), 3.9 (4H, m), 4.93 (0.76 H, t, J=4 Hz), 4.98 (0.25 H, t, J=4 Hz), and 5.89 (1H, s).

Method C; The Cycloaddition at 190°C: A mixture of **9** (147 mg), DCMA (2 mg) and BHT (5 mg) in methyl acrylate (1.4 ml) was heated at 190°C for 4 d in a sealed tube. The reaction mixture was dissolved in ethyl acetate (50 ml) and evaporated to leave a tarry residue, which was purified by chromatography over silica gel (30 g) with ethyl acetate and benzene, giving a 0.9:1.0 (by NMR) mixture (**11**, 28 mg) of *syn-exo* and *anti-exo* adducts and a 0.9:1.0 mixture (**10**, 89 mg) of *syn-endo* and *anti-endo* adducts.

2-[2-(1-Hydroxy-1-methylethyl)-1-methoxy-5,8-dimethylbicyclo-[2.2.2]oct-5-en-4-yl]ethanols (12)—(15)[17] *and their Mesylates (12a)—(15a)*. i) A mixture of the *endo* adducts (**10**, 285 mg), prepared by method B, and 2M hydrochloric acid (6 ml) in ether (12 ml) was stirred at 40°C for 15 h. The aqueous layer was separated, saturated with sodium chloride and extracted with ethyl acetate (3×50 ml). The combined extracts were washed with 5% aqueous $NaHCO_3$ and saturated brine, dried and evaporated to give the corresponding bicyclooctene aldehyde (273 mg): oil, MS, *m/z* 266 (M^+); IR, 2730, 1738, 1728, 1650, 1370, 1200, 1179, and 1100 cm^{-1}; NMR (CCl_4), δ 1.16 (0.76H, d, J=6 Hz), 0.88 (0.24H, d, J=6 Hz), 1.81 (3H, s), 2.65 (1.52H, dd, J=8 and 2 Hz), 2.51 (0.48H, dd, J=8 and 1 Hz), 2.80 (1H, dd, J=9.5 and 5 Hz), 3.26 (3H, s), 3.58 (3H, s), 5.78 (0.76H, s), 5.83 (0.24H, s), 9.78 (0.76H, t, J=2 Hz), and 9.84 (0.24H, t, J=1 Hz). The aldehyde was used for the next reaction without further purification.

ii) To a solution of the aldehyde (170 mg) in methanol (5 ml) at 0°C was added sodium borohydride (100 mg). The mixture was stirred for 1 h, and evaporated to leave an oily residue, which was poured into saturated brine and extracted with ethyl acetate, repeatedly. The combined extracts were washed with 5% aqueous $NaHCO_3$ and saturated brine, dried, and evaporated to give an oil, which was purified by chromatography over silica gel (15 g) with benzene and ethyl acetate (3:1) to yield a 3.2:1.0 (by NMR) mixture of the *syn-endo* and *anti-endo* alcohols (223 mg): MS, *m/z* 268 (M^+), 182 and 151 (base): IR, 3460, 1730, 1460, 1192, 1170 1082 and 1030 cm^{-1}; NMR (CCl_4), δ 0.84 (0.7H, d, J=6 Hz), 1.00 (2.3H, d, J=6 Hz), 1.86 (2.3H, d, J=1 Hz), 1.81 (0.7H, d, J=1 Hz), 2.72 (1H, dd, J=10 and 6 Hz), 3.22 (3H, s), 3.59 (3H, s), 3.63 (1.52H, t, J=8 Hz), 3.62 (0.48H, t, J=8 Hz), 5.71 (0.76H, br s, W_H=7 Hz), and 5.72 (0.24H, br s, W_H=6 Hz).

iii) To a stirred solution of the *endo* alcohols (222 mg) in dry ether (25 ml) at room temperature was added 1.2 M methyllithium in ether (15 ml), prepared from methyl iodide (8.5 ml) and lithium (2.2 g) in ether (80 ml). After the solution was cooled at 0°C for 2 h, water (10 ml) was added carefully to the solution. The ether layer was separated, and the aqueous layer was extracted with ethyl acetate repeatedly. The combined ether and acetate extracts were washed with saturated brine, dried, and evaporated. The residue was purified by chromatography over silica gel (15 g) with benzene and ethyl acetate (3:2) to give two diols. The less polar one, which was identified as 8-*syn*-methyl-*endo* diol (**12**, 147 mg), exhibited the following physical properties: mp 101—103°C (from ether); MS, *m/z* 268 (M^+), 182, and 151 (base); IR (Nujol), 3450, 1648, 1470, 1092 and 1055 cm^{-1}; NMR, δ 0.98 (6H, s), 1.06 (3H, d, J=7 Hz), 1.81 (1H, d, J=1 Hz), 3.36 (3H, s), 3.67 (2H, t, J=8 Hz), and 5.89 (1H, br s, W_H=6 Hz). Found: C, 71.95; H, 10.33%. Calcd for $C_{16}H_{28}O_3$: C, 71.60; H, 10.52%. The more polar diol was identified as 8-*anti*-methyl-*endo* diol (**13**, 37 mg); MS, *m/z* 253 (M^+−15), 182, and 151 (base); IR, 3450, 1642, 1090, 1075 and 1040 cm^{-1}; NMR, δ 0.74 (3H, d, J=6 Hz), 0.92 (6H, s), 1.75 (3H, d, J=6 Hz), 1.88 (2H, t, J=8 Hz), 3.36 (3H, s), 3.73 (2H, t, J=8 Hz), and 5.91 (1H, br s, W_H=7 Hz). Found: *m/z* 253.1789. Calcd for $C_{15}H_{25}O_3$: M-CH_3, 253.1804.

iv) The *endo* (**10**, 7.64 g) and *exo* (**11**, 1.12 g) adducts, prepared by method A, were transformed according to the aforementioned three-step process [(i) 2M hydrochloric acid and ether (2:1), 40°C, 15 h, (ii) sodium borohydride in methanol, 0°C, 1 h, and (iii) methyllithium in ether, room temperature, 2 h] into the corresponding bicyclooctene diols, respectively. The *endo* diols were separated by chromatography to give **12** (3.559 g) and **13** (1.063 g), and the *exo* diols were likewise purified to yield *syn-exo* (**14**, 0.44 g) and *anti-exo* diols (**15**, 0.218 g). The latter compounds (**14**) and (**15**) showed the following spectra. **14**; MS, *m/z* 253 (M^+-15), 182, and 151 (base); IR, 3460, 1645, 1400, 1090 and

1043 cm^{-1}; NMR, δ 0.98 (3H, d, J=6 Hz), 1.10 and 1.26 (each 3H, s), 1.81 (3H, d, J=1 Hz), 3.33 (3H, s), 3.72 (2H, t, J=8 Hz), and 6.08 (1H, br s). Found: C, 72.03; H, 10.40%. Calcd for $C_{16}H_{28}O_3$: C, 71.60; H, 10.52%. **15**; MS, m/z 253 (M^+-15), 182, and 151 (base); IR, 3450, 1648, 1092, and 1050 cm^{-1}; NMR, δ 0.75 (3H, d, J=6 Hz), 1.02 and 1.24 (each 3H, s), 1.73 (3H, d, J=1 Hz), 3.32 (3H, s), 3.72 (2H, t, J=8 Hz), and 6.07 (1H, br s). Found: m/z 253.1819. Calcd for $C_{15}H_{25}O_3$: M-CH_3, 253.1804.

v) To a stirred solution of **12** (704 mg) in dry dichloromethane (140 ml) containing triethylamine (0.6 ml, 1.5 mol equiv) cooled at −78°C was added methanesulfonyl chloride (0.23 ml, 1.1 mol equiv) under nitrogen. The resulting mixture was stirred for 10 min, mixed with water (10 ml), and warmed to room temperature. The mixture was poured into 5% aqueous $NaHCO_3$ (10 ml) and extracted with ethyl acetate (4×30 ml). The combined extracts were washed with 5% aqueous $NaHCO_3$ and saturated brine, dried, and evaporated to give a crude *syn-endo* mesylate (**12a**) in quantitative yield (1.075 g): MS, m/z 346 (M^+), 260, 151, and 149 (base); IR, 3505, 1645, 1360, 1180, 1090, 980, and 950 cm^{-1}; NMR, δ 0.89 (6H, s), 1.08 (3H, d, J=6 Hz), 1.83 (3H, d, J=1 Hz), 2.93 and 3.39 (each 3H, s), 4.21 (2H, t, J=8 Hz), and 5.92 (1H, br s). The crude mesylate was used for the next reaction without further purification. Three other diols (**13**)—(**15**) were converted in the respective monomesylates (**13a**)—(**15a**) almost quantitatively. **13a**, oil, MS, m/z 346 (M^+), 260, 151, 149, and 136 (base); IR, 3500, 1645, 1355, 1185, 1093, 980, and 954 cm^{-1}; NMR, δ 0.78 (3H, d, J=6 Hz), 0.90 (6H, s), 1.77 (3H, d, J=1 Hz), 2.95 and 3.38 (each 3H, s), 4.24 (2H, t, J=8 Hz), and 5.94 (1H, br s): **14a**, oil, MS, m/z 346 (M^+), 260, 151, and 149 (base); IR, 3495, 1643, 1353, 1192, 1090, 976, and 948 cm^{-1}; NMR, δ 1.01 and 1.25 (each 3H, s), 1.04 (3H, d, J=7 Hz), 1.81 (3H, d, J=1 Hz), 2.92 and 3.32 (each 3H, s), 4.22 (2H, t, J=8 Hz), and 6.07 (1H, br s): **15a**, oil, MS, m/z 346 (M^+), 260, 151, 149, and 136 (base); IR, 3500, 2645, 1350, 1193, 1087, 985, and 953 cm^{-1}; NMR, δ 0.73 (3H, d, J=6 Hz), 1.08 and 1.32 (each 3H, s), 4.33 (2H, t, J=8 Hz), and 6.14 (2H, br s).

π-Cyclization Reactions. i) A mixture of **12a** (234 mg) in formic acid (99%, 14 ml) was stirred at room temperature for 30 min. The mixture was poured into ice-water (160 ml), neutralized by addition of solid sodium carbonate, and extracted with ether (4×100 ml). The organic layer was washed with 5% aq $NaHCO_3$ (2×50 ml), dried and evaporated to leave a crude prenylcyclohexenone mesylate (**18**, 220 mg): oil; IR, 1670, 1616, 1360 and 118 cm^{-1}; NMR, δ 1.06 (3H, d, J=6 Hz), 1.62 (3H, br s), 1.76 (3H, br s), 1.98 (3H, br s), 2.94 (3H, s), 4.06 (2H, t, J=8 Hz), 5.11 (1H, t, J=7 Hz), and 5.89 (1H, br s, W_H=6 Hz).

A solution of the crude **18** (142 mg) and oxalic acid dihydrate (150 mg, 10 mol equiv), water (6 ml) and acetone (3 ml) was stirred at 85°C for 4 h. The mixture was poured into 5% aqueous $NaHCO_3$ (40 ml), which was saturated with sodium chloride, and extracted with ethyl acetate (5×50 ml). The extracts were washed with 5% aq $NaHCO_3$ and saturated brine, dried, and evaporated. The residue was purified by chromatography over silica gel (5 g) with ethyl acetate and benzene to give two spirovetivanes (**16**, 41 mg) and (**17**, 23 mg), which were identified as (±)-hinesolone[5] and (±)-β-vetivone[5] (**3**) respectively. **16**, mp 121—123°C (from diisopropyl ether), and 116—120°C (from CCl_4) (lit,[5] 115—119°C); MS, m/z 218 (M^+-18, base); IR (CCl_4), 3640, 3475, 1665, and 1615 cm^{-1}; NMR (CCl_4), δ 1.01 (3H, d J=7 Hz), 1.24 (6H, s), 1.97 (3H, s), and 5.75 (1H, br s, W_H=6 Hz). Found: C, 76.15; H, 10.29%. Calcd for $C_{15}H_{24}O_2$: C, 76.22; H, 10.24%. **17** [(±)-β-vetivone], mp 38—41°C (from pentane), (lit,[7] 43.5—57°C); MS, m/z 218 (M^+, base); IR (CCl_4), 1680, 1618, 1383, 1350 and 1295 m^{-1}; NMR (CCl_4), δ 0.97 (3H, d, J=6 Hz), 1.62 and 1.64 (each 3H, br s), 1.87 (3H, s), and 5.65 (1H, br s, W_H=6 Hz). Found: C, 82.73; H, 10.11%. Calcd for $C_{15}H_{22}O$: C, 82.51; H, 10.16%.

ii) A mixture of **12a** (148 mg) in acetone (3 ml) and oxalic acid dihydrate (135 mg) in water (6 ml) was stirred at 85°C for 4 h. The reaction mixture was worked up as mentioned above to yield **16** (46 mg) and **17** (19 mg) in 60 and 27% yields, respectively.

iii) Treatment of **14a** (293 mg) with oxalic acid under the same manner as mentioned above [oxalic acid (720 mg) in water (14 ml) and acetone (7 ml), 85°C, 4 h] afforded **16** (117 mg) and **17** (54 mg) in 58 and 29% yields, respectively.

iv) A mixture of **13a** (697 mg) in acetone (12 ml) and oxalic acid dihydrate (1.58 g) in water (30 ml) was stirred at 85°C for 4.5 h. After being cooled, the mixture was concentrated to remove acetone, and extracted with ethyl acetate (4×100 ml). The combined extracts were washed with saturated brine, dried, evaporated, and purified by chromatography over silica gel (40 g) with benzene and ethyl acetate to give two spirovetivanes (**20**) and (**21**) in 63% (278 mg) and 23% (93 mg) yields, respectively, the latter (**21**) being identified as (±)-10-epi-β-vetivone.[15] **20**, oil; MS, m/z 218 (M^+-18, base); IR, 3480, 1668, 1615, 1383, and 946 cm^{-1}; NMR (CCl_4), δ 0.97 (3H, d, J=7 Hz), 1.18 and 1.95 (6H, and 3H, each s), and 5.65 (1H, br s). Found: C, 76.58; H, 10.13%. Calcd for $C_{15}H_{24}O_2$: C, 76.22; H, 10.24%. **21** [(±)-10-Epi-β-vetivone], mp 52—55°C (from pentane), (lit,[15] 53—54.5°C); MS, m/z 218 (M^+, base); IR (CCl_4), 1681, 1620, and 1386 cm^{-1}; NMR (CCl_4), δ 0.98 (3H, d, J=6 Hz), 1.61 and 1.62 (each 3H, s), and 5.66 (1H, br s). Found: C, 82.76; H, 10.05%. Calcd for $C_{15}H_{22}O$: C, 82.51; H, 10.16%.

v) The *anti-exo* mesylate (**15a**, 67 mg) was treated with oxalic acid (165 mg) in acetone (1.7 ml) and water (3.2 ml) at 85°C for 3 h to give two spirovetivanes (**20**) and (**21**) in 69 (26 mg) and 26% (9 mg) yields, respectively.

(±)-Solavetivone (1). In a glass tube, 11-hydroxysolavetivone (**20**, 50 mg) was finely mixed with pyridine-modified alumina[9] (0.2 g), prepared from neutral alumina (10 g, Woelm, activity grade I) and pyridine (0.2 ml) by stirring under reduced pressure (0.3 Torr) at room temperature for 6 h. The mixture was heated at 220°C (bath temperature) for 8 min under argon, cooled, and poured into ether (30 ml) and triethylamine (5 ml). The whole mixture was stirred for 2 h, and filtered through Celite, concentrated, and chromatographed over silica gel (3 g) with benzene to afford 26 mg (60%) of an isopropenyl compound, oil; MS, m/z 218 (M^+, base); IR, 3100, 1675, 1615, and 855 cm^{-1}; NMR, δ 1.00 (3H, d, J=7 Hz), 1.75 and 1.93 (each 3H, s), 4.74 (2H, s), and 5.74 (1H, s). Found: C, 82.67; H, 10.12%. Calcd for $C_{15}H_{22}O$: C, 82.51; H, 10.16%. The compound was identified as (±)-solavetivone (**1**) by direct comparison with natural solavetivone (MS, IR, NMR, and TLC).

To a solution of (±)-solavetivone (17 mg) in aq methanol (1 ml) at room temperature was added a solution (0.5 ml) of 2,4-dinitrophenylhydrazine (2,4-DNP), prepared from 2,4-DNP (1.0 g) in water (16 ml), 95% ethanol (18 ml), and concd sulfuric acid (3.7 ml). The mixture was stirred for 10 min, and filtrated to leave a red mass, which was dissolved in ether and filtrated. The ether filtrate was concentrated and purified by preparative TLC over silica gel with benzene followed by recrystallization from aqueous methanol to give two 2,4-dinitrophenylhydrazones (**1a**, 10 mg) and (**1b**, 5.5 mg). **1a**, mp 107.5—109°C; NMR, δ 0.99 (3H, d, J=6 Hz), 1.75 and 1.95 (each 3H, s), 4.73 (2H, s), and 6.02 (1H, s). Natural; mp 126°C, NMR, δ 0.99 (3H, d, J=6 Hz), 1.75 and 1.95 (each 3H, s), 4.73 (2H, s), and 6.04 (1H, s). **1b**, mp 137—138° C; NMR, δ 0.96 (3H, d, J=6 Hz), 1.76 and 2.03 (each 3H, s), 4.73 (2H, s), and 6.24 (1H, s). Natural; mp 137°C, NMR, δ 0.97 (3H, d, J=6 Hz), 1.76 and 2.03 (each 3H, s), 4.75 (2H, s), and 6.21 (1H, s).

References

1) Part XXXVI of "Studies on the phytoalexins," and Part XVI of "Synthetic Studies of Rishitin and Related Compounds". The following two communications are regarded as Parts XXXIV and XXXV and Parts XIV and XV of the respective series. a) A. Murai, S. Sato, and T. Masamune, *J. Chem. Soc., Chem. Commun.*, **1982**, 511; b) A. Murai, S. Sato, and T. Masamune, *J. Chem. Soc., Chem. Commun.*, **1982**, 513.

2) T. Masamune, A. Murai, and N. Katsui, *Kagaku to Seibutsu*, **16**, 648 (1978).

3) A. Murai, *J. Synth. Org. Chem. Jpn.*, **39**, 893 (1981).

4) For the recent reports, see: N. Katsui, Y. Takahashi, N. Sato, A. Murai, and T. Masamune, *Nippon Kagaku Kaishi*, 659 (1981), and references cited therein: R. C. Anderson, D. M. Gunn, J. M-Rust, P. M-Rust, and J. S. Roberts, *J. Chem. Soc., Chem. Commun.*, **1977**, 27; T. Fujimori, R. Kasuga, H. Kaneko, S. Sakamura, M. Noguchi, A. Furusaki, N. Hashiba, and T. Matsumoto, *ibid.*, **1978**, 563; D. T. Coxon, K. R. Price, J. B. Stothers, and A. Stoessl, *ibid.*, **1979**, 348.

5) W. G. Dauben and D. J. Hart, *J. Am. Chem. Soc.*, **99**, 7307 (1977), and references cited therein.

6) K. Yamada, S. Goto, H. Nagase, A. T. Christensen, *J. Chem. Soc., Chem. Commun.*, **1977**, 554.

7) C. Iwata, T. Fusaka, T. Fujiwara, K. Tomita, and M. Yamada, *J. Chem. Soc., Chem. Commun.*, **1981**, 463.

8) D. T. Coxon, K. R. Price, B. Howard, S. F. Osman, E. B. Kalan, and R. M. Zacharius, *Tetarhedron Lett.*, **1974**, 2921.

9) A. Murai, S. Sato, and T. Masamune, *Tetrahedron Lett.*, **22**, 1033, (1981).

10) R. Pappo, D. S. Allen, Jr., R. V. Lemieux, and W. S. Johnson, *J. Org. Chem.*, **21**, 478 (1956).

11) A. Murai, S. Sato, and T. Masamune, *Chem. Lett.*, **1981**, 429.

12) A. J. Birch and K. O. Dastur, *J. Chem. Soc., Perkin I*, **1973**, 165. For Preparation of DCMA, see, H. M. Relles, *J. Org. Chem.*, **37**, 3630 (1972).

13) K. P. Dastur, *J. Am. Chem. Soc.*, **96**, 2605 (1974).

14) A. Murai, H. Taketsuru, and T. Masamune, *Bull. Chem. Soc. Jpn.*, **53**, 1049 (1980).

15) W. R. Jackson and A. Zurgiyah, *J. Chem. Soc.*, **1965**, 5280.

16) E. von Rudloff, *Can. J. Chem.*, **39**, 1860 (1961).

17) These compounds should be designated as 2-[3-(1-hydroxy-1-methylethyl)-4-methoxy-6,7-dimethylbicyclo[2.2.2]-oct-5-enyl]ethanols according to the IUPAC numbering rule. However, in order to avoid confusion, we used the same numbering for all bicyclo[2.2.2]octane derivatives as that for B in Scheme 1 in this paper.

Efficient Synthesis of (±)-Solavetivone and (±)-[8,8-$^2H_2$]Solavetivone[1]

Akio MURAI,* Shingo SATO, and Tadashi MASAMUNE*
Department of Chemistry, Faculty of Science, Hokkaido University, Sapporo 060
(Received February 6, 1984)

An alternative and efficient synthesis of the title compounds is described. The synthesis involves cycloaddition of 2-methylene-4-methoxy-6-methyl-4-cyclohexenylacetonitrile with methyl vinyl ketone as a key step.

The title sesquiterpene, solavetivone[2] (**1**) is a representative member of the spirovetivane phytoalexins in the genus *Solanum* and has been considered to play an important role in the biosynthetic pathway[3] leading to formation of rishitin, one of the major phytoalexins in the family Solanaceae.[4] While attempts to elucidate this biosynthetic pathway have been made by several groups,[4] the requisite studies with labelled solavetivone have not been performed yet. In the preceding paper we described a general synthetic procedure leading to preparation of representative compounds, (±)-**1** and (±)-hinesol, of two classes of natural spirovetivanes.[1] However the overall yield (3.2%) of (±)-**1** was not always satisfactory for the present biosynthetic studies. This synthetic procedure involved cycloaddition of 4-substituted 3,5-dimethyldihydroanisoles with methyl acrylate, which controlled the relative configuration between the C-4–C-14 and C-5–C-6 bonds in spirovetivanes.[1,5] This stereochemical control in cycloaddition for preferential preparation of (±)-**1** has been improved by introducing a cyanomethyl group to C-4 of the relevant dihydroanisole. The group was less bulky than an ethyl group and converted into desirable functional groups. The result was recently published in preliminary communications,[6] and its details are described in the present paper.

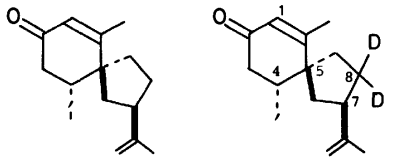

1 [8,8-$^2H_2$] **1**

The dihydroanisole (**2**) in question, equivalent to 4-methoxy-2,6-dimethyl-3-cyclohexenylacetonitrile, was prepared from readily available 3-methoxy-5-methyl-2-cyclohexenone[7] (**3**). Treatment of **3** with lithium diisopropylamide in tetrahydrofuran (THF) followed by addition of chloroacetonitrile in a 1:1 mixture of THF and hexamethylphosphoric triamide (HMPA) afforded 4-methoxy-6-methyl-2-oxo-3-cyclohexenylacetonitrile (**4**), which on the Wittig reaction with methylenetriphenylphosphorane in dimethyl sulfoxide (DMSO) was converted into **2** in 80% yield (from **3**).

The cycloaddition of **2** was carried out with methyl vinyl ketone in benzene in the presence of dichloromaleic anhydride (DCMA) and 2,6-di-*t*-butyl-*p*-cresol (BHT) under reflux for 3 d, when a mixture of four stereoisomeric cycloadducts differing in the configurations at C-2 and C-8 was obtained in 76% yield (based on the recovered **2**). The mixture was estimated by the NMR spectrum[1] to consist of a 2.7:1.0 mixture of the *endo* and *exo* adducts, each being a 3.5:1.0 mixture of the 8-*anti*- and 8-*syn*-methyl (in respect to the C-2–C-3 bond) isomers. Indeed, the mixture was separated by repeated chromatography over silica gel to give the *anti-endo* (**5**) [δ 0.79 (3H, d, J=6 Hz, 8-CH_3) and 3.02 (1H, dd, J=10 and 6 Hz, 2-H)], *anti-exo* (**6**) [δ 0.73 (3H, d, J=6 Hz) and 2.87 (1H, ddd, J=11, 6, and 1 Hz, long-range coupling between 2-*endo*-H and 7-*anti*-H=1 Hz)], *syn-endo* (**7**) [δ 1.06 (3H, d, J=6 Hz) and 2.99 (1H, dd, J=10 and 6 Hz)], and *syn-exo* adducts (**8**) [δ 1.14 (3H, d, J=6 Hz) and 2.87 (1H, ddd, J=11, 6, and 1 Hz)] in 43, 16, 12, and 4.5% yields, respectively. The result evidently indicated that the cycloaddition proceeded with predominant formation of the desirable *anti* isomers.

The *anti-endo* (**5**) and *anti-exo* adducts (**6**) were transformed by a three-step process [(i) treatment with methyllithium in ether, (ii) reduction with diisobutylaluminium hydride (DIBAH) in ether, and (iii) reduction with sodium borohydride ($NaBH_4$) in THF–water (2:1)] into the corresponding diols (**9**) and (**10**) in 96 and 75% yields, respectively. These diols were identified as the known intermediates[8] for synthesis of (±)-**1** and were smoothly converted into (±)-solavetivone by the procedure described into the preceding paper.[1] The present synthesis involved 9 steps and the overall yield was 16.6%.

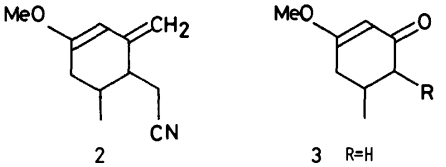

2 **3** R=H **4** R=CH_2CN

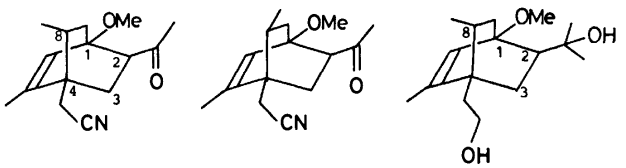

5 2-endo-Ac **6** 2-exo-Ac **7** 2-endo-Ac **8** 2-exo-Ac **9** 2-endo-$C(Me)_2OH$ **10** 2-exo-$C(Me)_2OH$

Preparation of the title deuterium-labelled (±)-solavetivone (±)-[8,8-$^2H_2$] (**1**) started with oxidation of the *anti-endo* bicyclooctene diol (**9**) with Jones reagent[9] into the corresponding acid (**11**) (88%). The acid (**11**) was transformed into the corresponding deuterated diol (**12**) according to the following procedure [(i) ethyl chloroformate and triethylamine in THF and (ii) reduction with sodium borodeuteride ($NaBD_4$, ^2H-content, over 98%) in water].[10] The resulting diol (**12**) exhibited the spectra practically identical with those of **9** with exception of the parent peaks

in the mass spectrum and the C-D stretching bands near 2200 cm^{-1} in the IR spectrum. The diol (**12**) was converted with methanesulfonyl chloride and triethylamine in dichloromethane into the monomesylate (**12a**), which was submitted to ring opening and ring closure (π-cyclization) under the reported conditions[1] [10 mol equiv oxalic acid in 33% aq acetone, 85°C, 4h], giving two spirovetivanes (**13**) and (**14**) in 58 and 13% yields (from **12**), respectively. The former underwent dehydration by heating with pyridine-modified alumina[11] to give its isopropenyl compound (±)-[8,8-$^2H_2$](**1**) in 64% yield. The deuterated compound revealed the spectra differing from those of (±)-solavetivone only in the following: MS, *m/z* 220 (M^+, 57%) and 218 (M^+−2, 0%) [8,8-$^2H_2$ content, *ca.* 100%]; IR, 2200 and 2100 cm^{-1}. This compound with two deuterium atoms at the inactive site (C-8) of (±)-solavetivone has been found to be effective for elucidation of the relevant biosynthetic pathway.[6b]

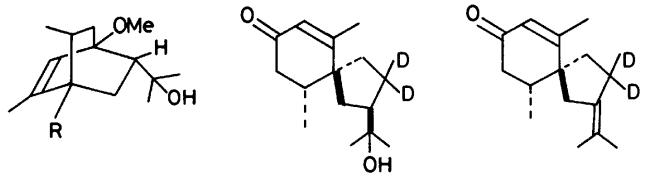

11 R=CH_2COOH
12 R=CH_2CD_2OH
12a R=CH_2CD_2OMs

13 **14**

Experimental

All the melting and boiling points were uncorrected. The homogeneity of each compound was always checked by TLC over silica gel (Wakogel B-5F) with various solvent systems, and the spots were developed with concd sulfuric acid. The IR and NMR (100 MHz) spectra were measured in liquid state for oil and in chloroform for solid, and in [^{2}H]chloroform, respectively, unless otherwise stated. The abbreviations "s, d, t, m, and br" in the NMR spectra denote "singlet, doublet, triplet, multiplet, and broad," respectively.

4-Methoxy-6-methyl-2-oxo-3-cyclohexenylacetonitrile (4). To a solution of lithium diisopropylamide, prepared from diisopropylamine (11.5 ml) and 1.5 M butyllithium in hexane (55 ml), in THF (75 ml) at −78°C was added 3-methoxy-5-methyl-2-cyclohexenone (**3**) (10.5 g) in THF (80 ml) under nitrogen over a 20 min period. After being stirred for 15 min, the mixture was added to a solution of HMPA (19.5 ml) and THF (20 ml), and the whole mixture was again stirred for 15 min. To the mixture was added chloroacetonitrile (7.5 ml), and the mixture was warmed gradually to room temperature over a 12 h period under stirring. The solution was poured into saturated brine (200 ml), and extracted with ethyl acetate (EtOAc). The combined extracts were washed with water (200 ml), dried, and concentrated to leave an oily residue, which was separated by chromatography over silica gel (120 g) with benzene and ethyl acetate. The material eluted was recrystallized from ether to give **4** (7.78 g, 58%, 94% based on the recovered starting material), mp 95—97°C; MS, *m/z* 179 (M^+); IR, 2225, 1650, 1610, 1390, 1235, 1168, 1006, and 840 cm^{-1}; NMR (CCl_4), δ 1.18 (2.5H, d, J=6 Hz), 0.96 (0.5H, d, J=6 Hz), 3.64 (3H, s), 5.30 (0.83H, s), and 5.22 (0.17H, s). Found: *m/z* 179.0956. Calcd for $C_{10}H_{13}NO_2$: M, 179.0946.

4-Methoxy-6-methyl-2-methylene-3-cyclohexenylacetonitrile (2). A solution of sodium methylsulfinylmethanide in DMSO was prepared by heating a mixture of sodium hydride (1.07 g as a 60% oil dispersion), washed with hexane, and DMSO (12 ml) at 75—80°C for 30 min under nitrogen. To this solution was added dropwise methyltriphenylphosphonium iodide (8.14 g) in DMSO (20 ml) at 10°C for 10 min, and the mixture was stirred at room temperature for 20 min. Compound **4** (3.00 g) in DMSO (15 ml) was added to this mixture at room temperature during 10 min. The whole suspension was stirred at room temperature for 14 h and then at 45°C for 7.5 h under stirring. The reaction mixture was cooled, poured into 5% aq sodium hydrogencarbonate ($NaHCO_3$, 100 ml) and extracted with ether (4×100 ml). The ether solution was washed with 5% aq $NaHCO_3$, dried, and evaporated to give a reddish syrup, which was separated by chromatography over alumina (180 g) with benzene to afford **2** [1.757 g, 71% based on the recovered starting material (0.505 g)], oil; MS, *m/z* 177 (M^+) and 162 (base); IR, 3080, 2220, 1646, 1608, 1220, 1167, 873 cm^{-1}; NMR (CCl_4), δ 0.99 (3H, d, J=6 Hz), 3.54 (3H, s), 4.72 (2H, s), and 5.17 (1H, s). Found: *m/z* 177.1158. Calcd for $C_{11}H_{15}NO$: M, 177.1153.

(2-Acetyl-1-methoxy-5,8-dimethylbicyclo[2.2.2]oct-5-en-4-yl)-acetonitrile (5)—(8).[12] Compound **2** (1.57 g) was refluxed with methyl vinyl ketone (20 ml), DCMA (10 mg) and BHT (0.1 g) in benzene (20 ml) for 3 d under argon atmosphere. The reaction mixture was concentrated *in vacuo*, and dissolved in ethyl acetate (300 ml). The solution was washed with 2M hydrochloric acid (HCl) (2×40 ml) and 5% aq $NaHCO_3$, dried, and evaporated. The residue was separated by careful chromatography over silica gel (200 g) with benzene and ethyl acetate to give three fractions (total 1.317 g, 60%; 76% based on the recovered starting material).

The first fraction (161 mg) eluted early was a 1:1 (by NMR) mixture of the *syn-exo* and *anti-exo* adducts, and was recrystallised from diisopropyl ether to afford the *syn-exo* adduct (**8**) (47 mg), and the filtrate concentrated gave the *anti-exo* adduct (**6**), (75 mg). The second fraction (296 mg) was a 2:1 (by NMR) mixture of the *anti-exo* and *anti-endo* adducts. The third fraction (850 mg) was a 3:1 (by NMR) mixture of the *anti-endo* and *syn-endo* adducts, and again purified by rechromatography over silica gel (30 g) with benzene-ether (10:1) to afford the *anti-endo* (**5**) (442 mg) and *syn-endo* adducts (**7**) (75 mg).

Each of the adducts exhibited the following physical properties: **8**, mp 103—109°C (from ether); MS, *m/z* 247 (M^+), 177, and 162 (base); IR, 2230, 1710, and 1095 cm^{-1}; NMR, δ 1.14 (3H, d, J=6 Hz), 1.91 (3H, d, J=1 Hz), 2.19 (3H, s), 2.40 (2H, s), 2.87 (1H, ddd, J=11, 6, and 1 Hz), 3.30 (3H, s), 6.07 (1H, br s, W_H=7 Hz). Found: *m/z* 247.1581. Calcd for $C_{15}H_{21}NO_2$: M, 247.1571. **6**, oil; MS, *m/z* 247 (M^+), 177, and 162 (base); IR, 2230, 1718, and 1100 cm^{-1}; NMR, δ 0.73 (3H, d, J=6 Hz), 1.82 (3H, d, J=1 Hz), 2.22 (3H, s), 2.48 and 2.67 (each 1H, d, J=16 Hz), 2.96 (1H, ddd, J=12, 5, and 1.5 Hz), 3.34 (3H, s), 6.12 (1H, br s, W_H=7 Hz). Found: *m/z* 247.1569. Calcd for $C_{15}H_{21}NO_2$: M, 247.1571. **5**, mp 64—67°C (from diisopropyl ether); MS, *m/z* 247 (M^+), 177, and 162 (base); IR, 2230, 1715, 1650, and 1095 cm^{-1}; NMR, δ 0.79 (3H, d, J=6 Hz), 1.78 (3H, d, J=1 Hz), 2.14 (3H, s), 2.63 (2H, s), 3.02 (1H, dd, J=10 and 6 Hz), 3.30 (3H, s), 5.88 (1H, br s, W_H=7 Hz). Found *m/z* 247.1571. Calcd for $C_{15}H_{21}NO_2$: M, 247.1571. **7**, mp 66—67°C (from diisopropyl ether); MS, *m/z* 247 (M^+), 177, and 162 (base); IR, 2225, 1715, 1645, and 1097 cm^{-1}; NMR, δ 1.06 (3H, d, J=6 Hz), 1.95 (3H, d, J=6 Hz), 2.13 (3H, s), 2.40, and 2.56 (each 1H, d, J=16 Hz), 2.99 (1H, dd, J=10 and 6 Hz), 3.30 (3H, s), and 5.82 (1H, br s, W_H=7 Hz). Found: *m/z* 247.1588. Calcd for $C_{15}H_{21}NO_2$: M, 247.1571.

2-[2-(1-Hydroxy-1-methylethyl)-1-methoxy-5,8-dimethylbiocyclo-[2.2.2]oct-5-en-4-yl]ethanols (9) and (10).[12] i) To a stirred solution of the *anti-endo* keto nitrile (**5**) (300 mg) in dry ether (16 ml) at −78°C was added a 1.0 M† methyllithium solution

† 1 M=1 mol dm^{-3}.

in ether (1.82 ml), prepared from methyl iodide (1.6 ml) and lithium (0.4 g) in ether (25 ml). The mixture was stirred for 1 h, poured into water (30 ml), and extracted with ethyl acetate (4×50 ml). The organic layer was washed with saturated brine, dried, and concentrated. The residue was separated by chromatography over silica gel (15 g) with benzene–ethyl acetate (5:1) to afford the starting ketone (59 mg) and hydroxy nitrile (258 mg), oil; MS, *m/z* 263 (M^+), 248, 245, and 177 (base); IR, 3520, 2225, and 1090 cm^{-1}; NMR, δ 0.88 (3H, d, J=6 Hz), 1.00 (6H, s), 1.78 (3H, d, J=1 Hz), 2.58 (2H, s), 3.37 (3H, s), and 6.03 (1H, br s, W_H=7 Hz).

To a stirred solution of the hydroxy nitrile (248 mg, 0.94 mmol) in ether (20 ml) at 0°C under nitrogen was added a 1.55 M solution of DIBAH in hexane (2.44 ml). The mixture was stirred at 0°C for 1 h, mixed with 2 M HCl (5 ml), and stirred for 15 min. The mixture was extracted with ethyl acetate and then worked up as usual to give hydroxy aldehyde (276 mg); IR, 3525 and 1722 cm^{-1}. The aldehyde was used for the next reaction without further purification.

To a mixture of the aldehyde (276 mg) in THF (10 ml) and water (5 ml) at 0°C was added $NaBH_4$ (50 mg) with stirring, and the mixture was stirred for 15 min and then nuetralized with 2 M HCl. The mixture was concentrated *in vacuo* to remove THF, poured into saturated brine, and extracted with ethyl acetate (3×60 ml). The combined extracts were washed with 2 M HCl, 5% aq $NaHCO_3$ and saturated brine, dried, and evaporated to leave an oily residue, which was separated by chromatography over silica gel (14 g) with benzene–ethyl acetate (3:2) to give the starting hydroxy nitrile (83 mg, 33%) and **9** (159 mg, 63%), the latter being identical with the *anti-endo* diol prepared in the previous paper.[1]

ii) The keto nitrile (**6**), (78 mg, 0.316 mmol) was transformed into hydroxy nitrile (64 mg, 77%) in the same manner as mentioned above, oil; MS, *m/z* 263 (M^+), 248, and 177 (base); IR, 3520, 2240, 1645, and 1072 cm^{-1}; NMR, δ 0.87 (3H, d, J=6 Hz), 1.11, and 1.34 (each 3H, s), 1.75 (3H, d, J=1 Hz), 2.56 (2H, s), 3.33 (3H, s) , and 6.17 (1H, br s, W_H=7 Hz).

To a solution of the hydroxy nitrile (63 mg, 0.24 mmol) in ether (6 ml) at 0°C under nitrogen was added a 1.5 M DIBAH solution in hexane (0.7 ml). The mixture was stirred for 2.5 h and worked up as usual to give crude aldehyde (63 mg).

The reduction of the aldehyde (63 mg) under the same conditions as mentioned above [$NaBH_4$ (10 mg) in THF (2.5 ml) and water (1 ml), 0°C, 15 min] afforded crude diol (66 mg), which was separated by chromatography over silica gel (4 g) with benzene–ethyl acetate (3:2) to afford an oily *anti-exo* diol (**10**), (50 mg, 78%). The *exo* diol (**10**) was identical with the *anti-exo* diol, prepared in the previous paper.[1]

(±)-[8.8-$^2H_2$]solavetivone (±)-[8.8-$^2H_2$] (1). i) To a solution of bicyclooctene diol (**9**) (1.67 g) in acetone (100 ml) at 0°C was added Jones reagent (10 ml), and the mixture was stirred for 2 h. When isopropyl alcohol (10 ml) was added to the mixture, green precipitates appeared and were removed by filtration through Celite. The filtrate was concentrated *in vacuo* to leave an oily residue, which was dissolved in ether (100 ml), and washed with 5% aq $NaHCO_3$ (3×30 ml), dried, and concentrated to give the starting diol (**9**) (233 mg). On the other hand, the aq $NaHCO_3$ solution was acidified to pH 2 with 2 M HCl and extracted with chloroform (3×100 ml). The chloroform extracts were dried and evaporated to afford crude acid (1.25 g), oil; IR, 3450, 1730, 1650, 1400, 1390, 1160, and 1090 cm^{-1}; NMR, δ 0.89 (3H, d, J=6 Hz), 1.01 and 1.74 (6H, and 3H, each s), 2.50 and 2.64 (each 1H, d, J=15 Hz), 3.34 and 5.93 (3H and 1H, each s). The acid was used for the next reaction without further purification.

ii) To a mixture of the acid (2.46 g) in THF (50 ml) and triethylamine (Et_3N) (1.5 ml, 1.2 mol equiv) at 0°C was added a solution of ethyl chloroformate (1.0 ml, 1.2 mol equiv) in THF (5 ml) over a 15 min period. The mixture was stirred for 4 h, and the precipitates were removed by filtration and washed with dry THF. The filtrate and THF washings were used for the next reaction.

iii) To a solution of $NaBD_4$ (0.87 g) (^2H content, over 98%) in water (20 ml) at 20°C was added the aforementioned, combined, THF solution over a 50 min period. The mixture was stirred for 5 h, neutralized with 2 M HCl, and concentrated. The residue was extracted with ethyl acetate (4×100 ml), washed with 10% aq sodium hydroxide, dried, evaporated, and separated by chromatography over silica gel (80 g) with benzene–ethyl acetate (1:1) to afford deuterated diol (**12**) (1.65 g), oil; MS, *m/z* 270 (M^+), 255, 184, and 151 (base); IR, 3475, 2190, 2098, 1648, 1400, 1385, 1098, and 1085 cm^{-1}; NMR, δ 0.74 (3H, d, J=6 Hz), 0.98 and 1.74 (6H and 3H, each s), 3.36 (3H, s), and 5.95 (1H, s).

iv) To a mixture of **12** (553 mg) and Et_3N (0.43 ml, 1.5 mol equiv) in dichloromethane (10 ml) at −78°C under nitrogen was added methanesulfonyl chloride (0.17 ml, 1.1 mol equiv) and the solution was stirred for 20 min. The mixture was poured into 5% aq $NaHCO_3$ (50 ml) and extracted with ether (4×70 ml). The ether solution was washed with 5% aq $NaHCO_3$ and saturated brine, dried, and evaporated *in vacuo* to give the corresponding mesylate (705 mg), which was immediatedly used for the next reaction.

v) A mixture of the mesylate (705 mg) and oxalic acid dihydrate (1.66 g) in water (33 ml) and acetone (12 ml) was heated at 85°C for 4 h under stirring. The mixture was neutralized with solid $NaHCO_3$, concentrated, and extracted with ethyl acetate (4×70 ml). The acetate solution was worked up as usual to leave an oily residue, which was separated by chromatography over silica gel (24 g) with benzene–ethyl acetate (3:1) to afford **13** (281 mg) and **14** (60 mg): **13**, oil; MS, *m/z* 238 (M^+), 220 (M^+−18, 28%), and 218 (0%); IR, 3450, 2200, 2100, 1670, 1615, and 1385 cm^{-1}; NMR, δ 0.96 (3H, d, J=7 Hz), 1.22 and 1.94 (6H and 3H, each s), 5.72 (1H, s).

A mixture of **13** (52 mg) and pyridine-modified alumina (0.2 g), prepared from alumina (Woelm, neutral, activity II-III, 10 g) and pyridine (0.2 ml) with stirring at room temperature at 1.6 Torr (1 Torr≈133.322 Pa) for 5 h, was heated in a glass tube at 220°C for 8 min under argon. The residue was dissolved in ether (40 ml) and Et_3N (5 ml), and stirred for 5 h under nitrogen. The mixture was concentrated and purified by chromatography over silica gel (3 g) with benzene–ethyl acetate (20:1) to afford (±)-[8.8-$^2H_2$]**1** (31 mg), oil; MS, *m/z* 220 (M^+, 57.1%), 218 (M^+−2, ~0%), 205 (12.7%), 192 (12.2%), 178 (44.2%), and 136 (base); IR, 3090, 2200, 2100, 1680, 1654, 1619, and 885 cm^{-1}; NMR, δ 1.00 (3H, d, J=7 Hz), 1.76 and 1.94 (each 3H, s), 4.73 (2H, s), and 5.75 (1H, s).

References

1) Part XXXVII of "Studies on the Phytoalexins," and Part XVII of "Synthetic Studies of Rishitin and Related Compounds." Parts XXXVI and XVI of the respective series, A. Murai, S. Sato, and T. Masamune, *Bull. Chem. Soc. Jpn.*, **57**, 2276 (1984).

2) D. T. Coxon, K. R. Price, B. Howard, S. F. Osman, E. B. Kalan, and R. M. Zacharius, *Tetrahedron Lett.*, **1974**, 2921; R. C. Anderson, D. M. Gunn, J. Murray-Rust, P. Murry-Rust, and J. S. Roberts, *J. Chem. Soc., Chem. Commun.*, **1977**, 27; N. Katsui, Y. Takahashi, N. Sato, A. Murai, and T. Masamune, *Nippon Kagaku Kaishi*, 659 (1981).

3) a) K. Sato, Y. Ishiguri, N. Doke, K. Tomiyama, F. Yagihashi, A. Murai, N. Katsui, and T. Masamune, *Phytochemistry*, **17**, 1901 (1978); b) E. B. Kalan and S. F. Osman, *Phytochemistry*, **15**, 775 (1976); E. B. Kalan, J. M. Patterson, and D. P. Schwarz, *Plant Physiology*, **57**, (supplement) Abstr., 473 (1976).

4) T. Masamune, A. Murai, and N. Katsui, *Kagaku no Ryoiki*, **36**, 673 (1982); A. Murai, *J. Synth. Org. Chem. Jpn.*, **39**, 893 (1981).

5) A. Murai, S. Sato, and T. Masamune, *Chem. Lett.*, **1981**, 429.

6) a) A. Murai, S. Sato, and T. Masamune, *J. Chem. Soc., Chem. Commun.*, **1981**, 904; b) A. Murai, S. Sato, A. Osada, N. Katsui, and T. Masamune, *J. Chem. Soc., Chem. Commun.*, **1982**, 32.

7) L. Cleaver, J. A. Croft, E. Ritchie, and W. C. Taylor, *Aust. J. Chem.*, **29**, 1989 (1976). Compound **3** was prepared by treatment of 5-methyl-1,3-cyclohexanedione with dimethyl sulfate and potassium carbonate in acetone under reflux (89%); *cf.*, R. N. Mirrington and G. I. Feutrill, *Org. Synth.*, **53**, 90 (1973).

8) These diols (**9**) and (**10**) corresponded to compounds **13** and **15** in Ref. 1.

9) A. Bowers, T. G. Halsall, E. R. H. Jones, and A. J. Lemin, *J. Chem. Soc.*, **1953**, 2548.

10) K. Ishizumi, K. Koga, and S. Yamada, *Chem. Pharm. Bull.* **16**, 492 (1968).

11) E. von Rudloff, *Can. J. Chem.*, **39**, 1860 (1961).

12) Compounds (**5**)—(**8**) should be designated as (3-acetyl-4-methoxy-6,7-dimethylbicyclo[2.2.2]oct-5-enyl)acetonitrile, and those (**9**) and (**10**) as 2-[3-(1-hydroxy-1-methylethyl)1-4-methoxy-6,7-dimethylbicyclo[2.2.2]oct-5-enyl]-ethanols, respectively, according to the IUPAC numbering rule. However, in this paper we used the same numbering for these bicyclo[2.2.2]octane derivatives as that for the corresponding compounds in the preceding paper.

Total Synthesis of (±)-Lubimin and (±)-Oxylubimin. I. Synthesis of (±)-15-Norsolavetivone and Related Compounds[1]

Akio MURAI,* Shingo SATO, and Tadashi MASAMUNE*
Department of Chemistry, Faculty of Science, Hokkaido University, Sapporo 060
(Received February 6, 1984)

The total synthesis of (±)-15-norsolavetivone, a key intermediate in the synthesis of oxygenated spirovetivane stress metabolites, is described.

The title compounds, lubimin[2] (**1**) and oxylubimin[2] (**2**), are representative members of a group of the spirovetivane sesquiterpenes, which are produced with rishitin[3] (**3**) by potato tubers infected with fungi and qualified as phytoalexins.[4,5] These stress metabolites are biosynthetic intermediates[6] in the major pathway from acetic acid to **3** *via* solavetivone (**4**) and are characterized structurally by the presence of five and six asymmetric centers in the spiro[4.5]decane system as well as the *trans*-disposed C-4–C-14 and C-5–C-6 bonds. Total synthesis of these highly oxygenated spirovetivane phytoalexins has recently been performed according to the synthetic plan shown in Scheme 1, which is divided into two parts: Synthesis of (±)-15-norsolavetivone (±)-(**5**) and related compounds (C in Scheme 1) as key intermediates, and their transformation into (±)-**1**, (±)-**2**, and related compounds such as (±)-10-epioxylubimin[7] (±)-(**6**). The result was published in two preliminary communications.[8] In the present paper the details of the synthesis of (±)-**5** are described.

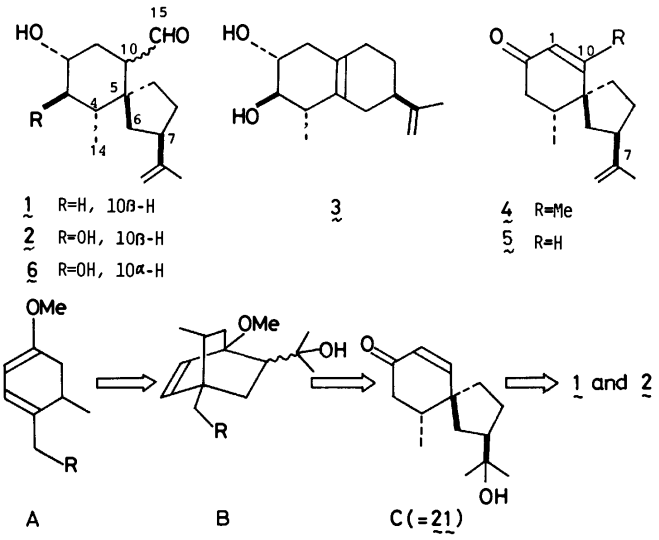

Scheme 1.

In the preceding paper[1] we reported efficient synthesis of (±)-**4**, which started with cycloaddition of 4-methoxy-6-methyl-2-methylene-3-cyclohexenylacetonitrile (**7**) with methyl vinyl ketone. The successful result led us consider that 4-methoxy-6-methyl-1,3-cyclohexadienylacetonitrile (**8**) would be one of the suitable starting materials for the present synthesis. The compound (**8**) was prepared as follows. Reduction of 4-methoxy-6-methyl-2-oxo-3-cyclohexenylacetonitrile[1] (**9**) with sodium hydrotrimethoxyborate[9] followed by acid treatment afforded 4-oxo-6-methyl-2-cyclohexenylacetonitrile (**10**) (70%), which on treatment with 2,2-dimethoxypropane and *p*-toluenesulfonic acid (TsOH) in *N*,*N*-dimethylformamide[10] (DMF) formed the aimed dihydroanisole (**8**) in 55% yield. Cycloaddition of **8** with methyl vinyl ketone at 150°C furnished a mixture of four stereoisomeric adducts, which was separated by chromatography to give the *endo* (**11**) and *exo* adducts (**12**) in 54 and 13% yields, respectively. The NMR spectra revealed that each of the adducts consisted of a 2.5:1.0 mixture of *anti* and *syn* isomers (see Experimental). These results indicated that the overall yield of the expected *anti*-bicyclooctene (B in Scheme 1) was only 18% from 3-methoxy-5-methyl-2-cyclohexenone,[1] a precursor of **9**. The low yield and low stereoselectivity in cycloaddition prompted us to search for another starting material.

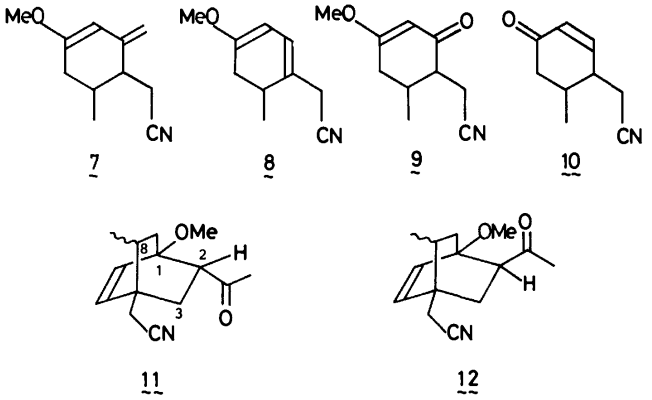

Our previous study[11] indicated that the cycloaddition of 4-substituted 3,5-dimethyldihydroanisoles with methyl acrylate varied, depending on the bulkiness of the 4-substituents. Thus 6-methoxy-4-methyl-2,3,4,5-tetrahydrobenzofuran (**13**) was selected as another suitable diene (A in Scheme 1) for the relevant cycloaddition. The compound (**13**) was prepared from commercially available orcinol dimethyl ether (**14**) as follows. Friedel-Crafts acylation of **14** with chloroacetyl chloride and aluminium chloride gave 2,3-dihydrobenzofuran-3-one (**15**), which on reduction with sodium borohydride ($NaBH_4$) in a mixture of tetrahydrofuran (THF) and methanol followed by hydrogenolysis over 10% palladium–charcoal in the same solvent mixture afforded 6-methoxy-4-methyl-2,3-dihydrobenzofuran (**16**) in 99% yield. The benzofuran (**16**), when submitted to the Birch reduction, was converted into its dihydro derivative (**17**), equivalent to the conjugate diene (**13**), in 81% yield.

The cycloaddition of **17** with methyl acrylate at 150°C in the presence of dichloromaleic anhydride (DCMA) proceeded as expected, giving only a 3:2 mixture of *syn*-8-methyl-6-*endo*-methoxycarbonyl- and *syn*-8-methyl-6-*exo*-methoxycarbonylbicyclo[2.2.2] oc-

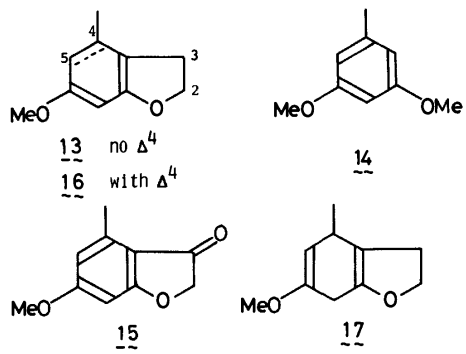

tene adducts (**18**) in 70% yields: *syn-endo* isomer, δ 0.83 (1.8H, s, 8-CH_3) and 4.91 (0.6H, s, 2-H); *syn-exo* isomer, δ 0.86 (1.2H, s) and 5.12 (0.4H, s). Hydrolysis of the mixture (**18**) with oxalic acid in aqueous methanol followed by acetylation furnished keto acetates (**19**) in 70% yield. Treatment of **19** with *p*-tolylsulfonylhydrazine and concd hydrochloric acid in THF under reflux gave its tosylhydrazones (~100%), which were converted under the Shapiro conditions[12] with excess of methylithium into *anti*-8-methylbicyclo[2.2.2]octene diols (**20**) in 71% yield.

Treatment of the diols (**20**), after monomesylation under the usual conditions, with oxalic acid (10 mol equiv) in a 1:5 heterogeneous mixture of water and methyl isobutyl ketone at 130°C for 8 h effected successive cleavage of the C-1–C-2 bond and ring closure[13] to give a mixture of three 15-norsolavetivanes with the *trans*-oriented C-4–C-14 and C-5–C-6 bonds, from which 11-hydroxy-15-norsolavetivane (**21**=C) with a (4*SR*, 7*SR*)-isopropyl moiety was isolated in 35% yield along with its (4*SR*, 7*RS*)-epimer (**22**) (25%) and a 7-isopropylidene derivative (**23**) (30%) by preparative HPLC over μ-Porasil. The relevant reactions, when carried out under the same conditions as those for solavetivones[13] (oxalic acid in a 2:1 homogeneous mixture of water and acetone) led to formation of **21**, **22**, and **23** in 16, 38, and 16% yields, respectively. These results strongly suggested that the bulkiness of the methyl group at C-10 controls conformations of the transition state in the ring closure[14] in question. The spirovetivane (**21**) underwent smooth dehydration on treatment with pyridine–modified alumina[16] to give (±)-15-norsolavetivone (±)-**5** in 68% yield. The synthesis of (±)-5 involved 11 steps and the overall yield was 5.7% from the orcinol (**14**).

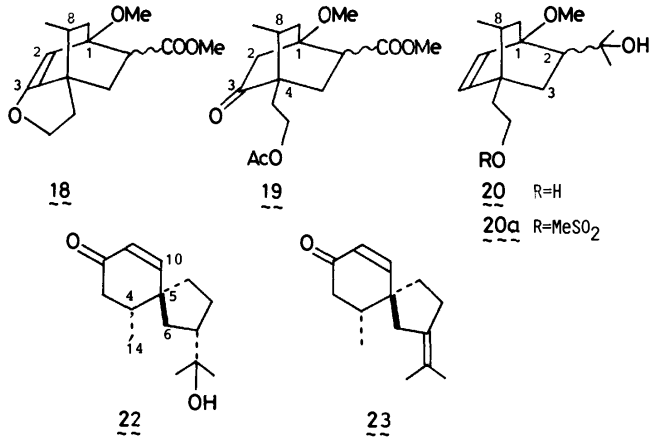

The relative configuration at C-7 in the 15-norspirovetivanes (**21**) and (**22**) was assigned tentatively on the basis of the following facts. Treatment of **21** with lithium diisopropylamide (LDA) in a mixture of THF and hexamethylphosphoric triamide (HMPA) and then with *t*-butyldimethylsilyl chloride in THF, followed by oxidation with perbenzoic acid in hexane,[15] furnished a mixture of the 3,4-diequatorial 3-silyl ether (**24**) and its 3-epimer (**25**), which were separated easily by chromatography in 51 and 25% yields, respectively: **24**, δ 3.89 (1H, d, J=11 Hz, 3-H), 5.78 and 6.80 (each 1H, d, J=10 Hz, 1- and 10-H); **25**, δ 4.40 (1H, d, J=4 Hz), 5.81 and 6.60 (each 1H, d, J=10 Hz). The same treatment of **22** afforded the corresponding 3,4-diequatorial 3-silyl ether (**26**) and its 3-epimer (**27**) in 50 and 26% yields, respectively: **26**, δ 3.90 (1H, d, J=11 Hz, 3-H), 5.72 and 6.67 (each 1H, J=10 Hz, 1- and 10-H); **27**, δ 4.41 (1H, d, J=11 Hz), 5.81 and 6.62 (each 1H, d, J=10 Hz). The observed difference in chemical shift (Δδ 0.13) of the proton at C-10 between **24** and **26** was explained well by the difference of the configuration at C-7; namely, the cyclohexane rings in **24** and **26** would take a half-chair conformation owing to the bulky 3-silyloxyl group (equatorial). Thus the hydroxyl group in the C-7 isopropyl moiety would be situated near the hydrogen atom at C-10 only in **24** and hence would deshield the proton in question. A definite assignment was provided by transformation of the 10-hydroxy-15-norspirovetivanes (**21**) and (**24**) into natural spirovetivanes.[16]

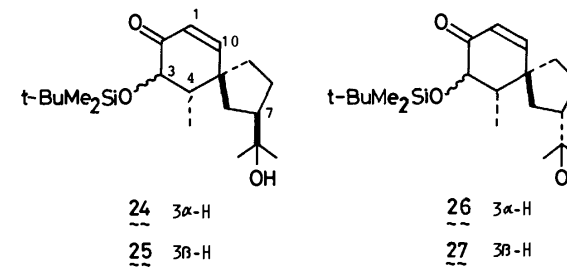

Experimental

All the melting and boiling points were uncorrected. The homogeneity of each compound was always checked by TLC over silica gel (Wakogel B-5F) with various solvent systems, and the spots were developed with concd sulfuric acid (H_2SO_4). The IR and NMR (100 MHz) spectra were measured in liquid state for oil and chloroform for solid, and in [^{2}H]-chloroform, respectively, unless otherwise stated. The preparative HPLC was carried out on Waters Associates Model 6000 A, and the column chromatography over silica gel (Kieselgel 60) or aluminium oxide (Aluminumoxide 90), respectively. The following solvents were dried and distilled before use: diethyl ether and THF (from sodium ketyl radical), benzene, carbon tetrachloride, carbon disulfide, and hexane (from phosphorus (V) oxide); triethylamine, DMF, 1,2-dimethoxyethane (DME), HMPA, and dimethyl sulfoxide (DMSO) (from calcium hydride), and ethanol (from magnesium).

4-Oxo-6-methyl-3-cyclohexenylacetonitrile (10). To a suspension of sodium hydride (3.4 g, 60% in oil) in refluxing THF (120 ml) was added freshly distilled methyl borate (7.31 ml, 64 mmol) under nitrogen over a 20 min period. The mixture was stirred for 30 min and cooled to room temperature. A solution of 4-methoxy-6-methyl-2-oxo-3-cyclo-

hexenylacetonitrile (**9**) (2.86 g, 16 mmol), prepared in the preceding paper,[1] in THF (20 ml) was added to the mixture, and stirred for an additional 24 h. To the reaction mixture at 0 °C was added 10% aq H_2SO_4 (20 ml). The whole mixture was stirred for 20 min, concentrated *in vacuo*, poured into 50 ml of saturated brine, and extracted with ethyl acetate (4×100 ml). The combined extracts were washed with 10% aq H_2SO_4 and saturated brine, dried, evaporated, and separated by chromatography over silica gel (120 g) with benzene to give **10** (1.463 g, 70% yield, based on the consumed **9**), oil; MS, *m/z* 149 (M^+); IR, 2220, 1685, and 1615 cm^{-1}; NMR, δ 1.17 (3H, d, J=6 Hz), 6.08 and 6.80 (each 1H, d, J=10 Hz). Found: 149.0844. Calcd for $C_9H_{11}NO$: M, 149.0841.

4-Methoxy-6-methyl-1,3-cyclohexadienylacetonitrile (8). A mixture of **10** (1.412 g), 2,2-dimethoxypropane (12 ml), *p*-TsOH (20 mg), methanol (0.2 ml) and DMF (12 ml) was refluxed under nitrogen for 19 h. The mixture was cooled, poured into aqueous sodium hydrogencarbonate ($NaHCO_3$) (30 ml), and extracted with ether (3×100 ml). The combined extracts were washed with 5% aq $NaHCO_3$, saturated brine, and dried over potassium carbonate and sodium sulfate. The extracts was concentrated and separated by chromatography over alumina (120 g) with benzene to give **8** [559 mg, 36% yield (55% yield, based on the recovered **10**)], oil; MS, *m/z* 163 (M^+), 148, and 108 (base): IR, 2225, 1670, 1610, and 1255 cm^{-1}; NMR, δ 1.04 (3H, d, J=6 Hz), 1.96 (1H, dd, J=16, 4 Hz), 2.3~2.8 (2H, m), 3.01 (2H, s), 3.54 (3H, s), 4.82 and 5.84 (each 1H, d, J=7 Hz). Found: *m/z* 163.0990. Calcd for $C_{10}H_{13}NO$: M, 163.0994.

Cycloaddition of 8. A mixture of **8** (160 mg) and 2,6-di-*t*-butyl-*p*-cresol (BHT) (5 mg) in methyl vinyl ketone (1 ml) was heated in a sealed tube at 150 °C for 2 d. The reaction mixture was cooled and evaporated to leave an oily residue, which was dissolved in ethyl acetate (50 ml). The mixture was washed with 2 M† hydrochloric acid (HCl) (2×20 ml), 5% aq $NaHCO_3$, saturated brine, dried, evaporated, and separated by chromatography over silica gel (20 g) with benzene–ethyl acetate to give a mixture of *anti*- and *syn-endo* adducts (**11**) (122 mg, 54%) and a mixture of the corresponding *exo*-adducts (**12**) (29 mg, 13%), each being a 2.5:1.0 mixture of *anti*- and *syn*-8-methylbicyclooctenes: **11**; MS, *m/z* 233 (M^+); IR, 2225, 1716, 1180, and 1110 cm^{-1}; NMR, δ 0.84 and 1.04 (2.14H and 0.86H, each d, J=6 Hz), 2.16 (3H, s), 2.62 and 2.48 (1.43H and 0.57, each s), 3.08 and 2.98 (0.72H and 0.28H, each dd, J=10 and 6 Hz), 3.32 (3H, s), 5.83 and 6.27 (each 0.72H, d, J=9 Hz), 6.18 and 6.24 (each 0.28H, d, J=9 Hz); **12**, oil; MS, *m/z* 233 (M^+); IR 2230, 1713, 1180, and 1108 cm^{-1}; NMR, δ 0.78 and 1.11 (2.14H and 0.86H, each d, J=6 Hz), 2.23 and 2.21 (2.14H and 0.86H, each s), 3.34 and 3.32 (2.14H and 0.86H, each s), 5.89 and 6.45 (each 0.72H, d, J=8 Hz), 6.17 and 6.45 (each 0.28H, d, J=8 Hz).

6-Methoxy-4-methyl-2,3-dihydrobenzofuran (16). To a solution of orcinol dimethyl ether (16.74 g, 0.11 mmol) in carbon disufide (110 ml) was added at 0 °C carefully powdered aluminium chloride (14.8 g, 0.11 mmol) with vigorous stirring and then at room temperature a solution of chloroacetyl chloride (9 ml, 0.11 mmol) in carbon disulfide (55 ml) over a 1 h period. The mixture was stirred under reflux for 7 h, distilled to remove the solvent, and cooled with an ice-water bath. To the residue were added chloroform (200 ml), ice-water (100 ml) and 2 M HCl, successively. The mixture was stirred for 40 min at 0 °C, when the residue was dissolved. The aqueous layer was separated and the chloroform extracts were washed with 2 M HCl (100 ml) and water (2×100 ml), dried, and concentrated to leave an oily residue, which crystallized on addition of diisopropyl ether (200 ml). Recrystallization from diisopropyl ether gave 6-methoxy-4-methyl-2,3-dihydrobenzofuran-3-one (**15**). (12.09 g, 62%), mp 123—124 °C; MS, *m/z* 178 (M^+, base); IR (Nujol), 1702, 1620, 1590, 1280, 1190, 1150, and 1080 cm^{-1}; NMR, δ 2.55 (3H, s), 3.85 (3H, s), 4.57 and 6.36 (each 2H, s). Found: C, 67.33%; H, 5.82%. Calcd for $C_{10}H_{10}O_3$: C, 67.40%; H, 5.66%. The filtrate was concentrated and purified by chromatography over silica gel (300 g) with benzene and ethyl acetate to give the starting orcinol dimethyl ether (0.52 g, 3%), **15** (2.25 g, 8.1%), and 3,5-dimethoxy-2-(chloroacetyl)toluene (2.05 g, 8.1%), mp 69—70.5 °C (from diisopropyl ether); MS, *m/z* 230 (M^++2), 228 (M^+), and 179 (base); IR (Nujol), 1701, 1605, 1575, 1330, 1155, and 1102 cm^{-1}; NMR, δ 2.27 and 3.80 (3H and 6H, each s), 4.49 (2H, s), 6.27 and 6.31 (each 1H, d, J=1 Hz). Found: C, 57.72; H, 5.71%. Calcd for $C_{11}H_{13}O_3Cl$: C, 57.77; H, 5.73%.

The chloroacetyl compound was transformed into **15** as follows. A mixture of the compound (13.3 g, 0.058 mmol) and powdered aluminium chloride (8.6 g) in carbon disulfide (150 ml) was heated under reflux for 22 h. After removal of the solvent and cooling at 0 °C, the residue was worked up as described above to give **15** (10.06 g, 97%).

ii) To a solution of **15** (12.09 g) in THF (250 ml) and methanol (150 ml) was added $NaBH_4$ (8 g) in four portions at 0 °C, and the mixture was stirred for an additional 1.5 h. To the reaction mixture was added acetone (100 ml), and the mixture was concentrated *in vacuo*. The residue was poured into a mixture of saturated brine (200 ml) and 5% aq $NaHCO_3$ (100 ml), and extracted with ethyl acetate (3×200 ml) and the combined extracts were washed with water (3×50 ml), dried, and evaporated to give a crystalline residue. Recrystallization from methanol afforded an analytical sample: mp 67—68 °C; MS, *m/z*, 180 (M^+) and 162 (base); IR (Nujol), 3240, 1623, 1603, 1200, and 1141 cm^{-1}; NMR, δ 2.35 and 3.74 (each 3H, s), 4.43 (1H, d, J=3 Hz), 4.45 (1H, d, J=5 Hz), 5.23 (1H, dd, J=5 and 3 Hz), 6.23 and 6.26 (each 1H, s). Found: C, 66.75; H, 6.70%. Calcd for $C_{10}H_{12}O_3$: C, 66.56; H, 6.71%. The crude residue was used for the next reaction without further purification.

A solution of the crude alcohol in THF (200 ml) and ethanol (200 ml) was treated with hydrogen over 4 g of 10% palladium on charcoal at room temperature under atmospheric pressure, until uptake of hydrogen ceased. The solution was filtered through Celite and concentrated under reduced pressure. The residue was recrystallized from methanol to give **16** (8.366 g), mp 54.5—56.5 °C; MS, *m/z* 164 (M^+, base); IR (Nujol), 1628, 1605, 1204, and 1140 cm^{-1}; NMR, δ 2.22 (3H, s), 3.05 (2H, t, J=8 Hz), 3.75 (3H, s), 4.57 (2H, t, J=8 Hz), and 6.23 (2H, s). Found: C, 73.34; H, 7.25%. Calcd for $C_{10}H_{12}O_2$: C, 73.14; H, 7.37%.

6-Methoxy-4-methyl-2,3,4,7-tetrahydrobenzofuran (17). To a mixture of **16** (15 g) in dry ether (700 ml) and liquid NH_3 (2 l) at −33 °C was added small pieces of lithium (28 g) over a 30 min period. The mixture was stirred for 2 h, and, after addition of 260 ml of ethanol over a 1 h period, was warmed to evaporate ammonia. The residue was mixed with water (1.4 l) at 0 °C, saturated with sodium chloride, and extracted with ether (5×300 ml). The combined ether extracts were washed with water (2×200 ml), dried, evaporated, and separated by chromatography over alumina (300 g) with benzene to leave **17** (12.3 g, 81%), oil; MS, *m/z* 166 (M^+) and 151 (base); IR, 1732, 1664, 1404, 1232, and 1164 cm^{-1}; NMR (CCl_4), δ 1.05 (3H, d, J=7 Hz), 3.50 (3H, s), 4.27 (2H, t, J=9 Hz), 4.47 (1H, d, J=4 Hz). Found: *m/z* 166.0982. Calcd for $C_{10}H_{14}O_2$: M, 166.0994.

2-(1-Methoxy-6-methoxycarbonyl-8-syn-methyl-3-oxobicyclo-[2.2.2]oct-4-yl)ethyl Acetate (19).[17] i) A mixture of **17** (50 g), methyl acrylate (120 ml), dichloromaleic anhydride (1 g), and BHT (2.5 g) was heated in an autoclave at 150 °C under argon atmosphere for 5 d. The mixture was dissolved in benzene

† 1 M=1 mol dm^{-3}.

(100 ml), concentrated, and separated by chromatography over alumina (2.4 kg) with benzene to afford a mixture of adducts (**18**) (52.90 g, 70%), oil; MS, *m/z* 252 (M^+), 221, 166, and 151 (base); IR, 1733, 1680, 1207, and 1172 cm^{-1}; NMR, δ 0.83 and 0.86 (1.8H and 1.2H, each d, J=6 Hz, 8-CH_3), 2.92 (1H, m, 6-H), 3.33 and 3.37 (1.8H and 1.2H, each s, 1-OCH_3), 4.91 and 5.12 (0.6H and 0.4H, each s, *endo*- and *exo*-2-H). The mixture of the adducts was used for the next reaction without further purification.

ii) A mixture of the adducts (**18**) (52.90 g), oxalic acid (300 g as dihydrate) in methanol (850 ml) and water (1.7 l) was stirred at room temperature for 2 h, and neutralized with solid sodium carbonate. The mixture was stirred for an additional 30 min, and concentrated *in vacuo*. The residue was saturated with sodium chloride, and extracted with ethyl acetate (4×500 ml). The combined acetate extracts were washed with saturated brine, dried, evaporated, and separated by chromatography over silica gel (2.0 kg) with benzene–ethyl acetate (3:2) to give keto alcohols (39.18 g). The mixture of *endo* and *exo* keto alcohols was used for the next reaction without further separation. However, an analytical sample of each alcohol was obtained by careful column chromatography. *exo*-Keto alcohol, oil; MS, *m/z* 270 (M^+), 184, 166, and 151 (base); IR, 3480, 1730, 1720, 1202, 1183, and 1116 cm^{-1}; NMR, δ 0.84 (3H, d, J=6 Hz), 3.06 (1H, ddd, J=10, 6, and 3 Hz), 3.28 (3H, s), 3.66 (2H, t, J=7 Hz), and 3.75 (3H, s). Found: C, 61.85; H, 8.25%. Calcd for $C_{14}H_{22}O_5$: C, 62.20; H, 8.20%. *endo*-Keto alcohol, oil; MS, *m/z* 270 (M^+), 184, 166, and 151 (base); IR, 3476, 1725, 1200, 1174, and 1113 cm^{-1}; NMR, δ 0.85 (3H, d, J=6 Hz), 2.92 (1H, dd, J=8 and 5 Hz), 3.25 (3H, s), 3.63 (2H, t, J=7 Hz), and 3.71 (3H, s). Found: C, 61.77; H, 8.26%. Clacd for $C_{14}H_{22}O_5$: C, 62.20; H, 8.20%.

iii) A mixture of the keto alcohols (30.2 g) in dry pyridine (300 ml) and acetic anhydride (120 ml) was stirred at 20°C under nitrogen for 23 h. The mixture was mixed with ethanol (100 ml) stirred for 30 min at 20°C, and concentrated at 50 °C *in vacuo* (15 Torr) (1 Torr=133.322 Pa). The residue was poured into ice-water (200 ml), and extracted with ethyl acetate (3×250 ml). The combined acetate extracts were washed with 2 M HCl (4×100 ml), dried, evaporated, and saparated by column chromatography over silica gel (200 g) with benzene–ethyl acetate (7:1) afforded **19** (30.54 g, 97% based on the recovered starting material), oil; MS, *m/z* 312 (M^+); IR, 1732, 1249, 1205, 1117, and 1115 cm^{-1}; NMR, δ 2.02 (3H, s), 3.25 and 3.24 (1.8H and 1.2H, each s), 3.70 and 3.73 (1.8H and 1.2H, each s), and 4.06 (2H, t, J=7 Hz).

*2-[2-(1-Hydroxy-1-methylethyl]-1-methoxy-8-*anti-*methylbicyclo-[2.2.2]oct-3-en-4-yl]ethanol (**20**)*[17] *and its monomesylate (**20a**).* i) A mixture of **19** (4.303 g, 0.014 mmol), *p*-tolylsulfonylhydrazine (2.73 g, 0.015 mmol) and concd HCl (0.5 ml) in THF (190 ml) was stirred under reflux for 20 h. The reaction mixture was cooled, concentrated *in vacuo*, and dried at 20°C for 10 h under reduced pressure (3 Torr), giving the crude hydrazone (7.30 g), amorphous: IR ($CHCl_3$), 3540, 3225, 1728, 1598, 1440, 1374, 1340, 1248, 1168, 1098, 1040, and 815 cm^{-1}.

To a solution of the crude tosyl hydrazone (7.30 g) in dry THF (600 ml) at 0°C under nitrogen was added a 1 M solution of methyllithium in ether (210 ml, 15 mol equiv), prepared from methyl iodide (160 ml) and lithium (40 g) in ether (250 ml), over a 1 h period. The mixture was heated at 35°C for 19 h, cooled, mixed carefully with water (100 ml) at 0°C, and concentrated to remove THF *in vacuo*. The residue was poured into saturated brine (400 ml), and extracted with ethyl acetate (4×200 ml). The combined extracts were washed with saturated brine (2×100 ml), dried, evaporated, and separated by chromatography over silica gel (250 g) with benzene–ethyl acetate (2:1) to yield **20** (2.479 g, 71% from **19**), oil; MS, *m/z* 254 (M^+), 239, and 236; IR, 3473, 1384, 1173, 1101, and 1050 cm^{-1}; NMR, δ 0.78 and 0.76 (1.8H and 1.2H, each d, J=7 Hz), 1.00 (3.6H, s), 1.10 and 1.34 (total 2.4H, each s), 3.39 and 3.37 (1.8H and 1.2H, each s), 3.75 (2H, t, J=7.5 Hz), 5.82 and 6.28 (each 0.6H, d, J=9 Hz), 5.74 and 6.44 (each 0.4H, d, J=9 Hz).

ii) To a solution of **20** (13.70 g, 0.054 mol), and triethylamine (12.8 ml, 1.7 mol equiv) in dichloromethane (270 ml) at −78°C under nitrogen was added methanesulfonyl chloride (4.7 ml, 1.1 mol equiv). The mixture was stirred for 15 min, mixed with 5% aq $NaHCO_3$ (20 ml), and warmed to room temperature. The mixture was again poured into 5% aq $NaHCO_3$ (200 ml), when the dichloromethane layer was separated. The aqueous layer was extracted with ethyl acetate (3×20 ml). The dichloromethane and acetate extracts were combined, washed with 5% aq $NaHCO_3$ (70 ml) and saturated brine (70 ml), dried, and concentrated to give crude monomesylates (**20a**), which were used for the next reaction.

*Norsolavetivanes (**21**), (**22**), and (**23**).* i) A mixture of **20a** (71 mg) and oxalic acid dihydrate (252 mg) in methyl isobutyl ketone (20 ml) and water (4 ml) was stirred at 130°C for 8 h. After being cooled and neutralized with solid sodium carbonate at 0°C, the mixture was poured into saturated brine and extracted with ethyl acetate (4×50 ml). The extracts were washed, dried, concentrated, and separated by chromatography over silica gel (6 g) with benzene–ethyl acetate (2:1) to give a mixture (18 mg, 60% based on the consumed starting material) of 15-nor-11-hydroxy-solavetivanes (**21**) and (**22**) and its isopropylidene analogue (**23**) (8.1 mg, 30%), oil; MS, *m/z* 204 (M^+); IR, 1685, 1362, and 1182 cm^{-1}; NMR, δ 0.99 (3H, d, J=7 Hz), 1.63 (6H, s), 5.85 and 6.71 (each 1H, d, J=10 Hz). Found: *m/z* 204.1550. Calcd for $C_{14}H_{20}O$: M, 204.1515. A mixture of **21** and **22** was separated by HPLC [Waters, μ-Porasil, eluted with hexane–ether (1:1) 5 ml/min] to give **21** (10.3 mg, 35%) and **22** (7.4 mg, 25%): **21**, R_t=28 min, oil; MS, *m/z* 222 (M^+); IR, 3495, 1678, 1383, 1362, 1178, and 944 cm^{-1}; NMR, δ 1.00 (3H, d, J=6 Hz), 1.21 (6H, s), 5.78 and 6.74 (each 1H, d, J=10 Hz). Found: *m/z* 222.1617. Calcd for $C_{14}H_{22}O_2$: M, 222.1620. **22**, R_t=23 min, oil; MS, *m/z* 222 (M^+); IR, 3490, 1680, 1614, 1387, 1140, and 940 cm^{-1}; NMR, δ 1.01 (3H, d, J=6 Hz), 1.22 (6H, s), 5.79 and 6.76 (each 1H, d, J=10 Hz). Found: *m/z* 222.1624. Calcd for $C_{14}H_{22}O_2$: M, 222.1620.

ii) A mixture of **20a** (106 mg) and oxalic acid dihydrate (282 mg) in acetone (3 ml) and water (6 ml) was stirred at 90°C for 8 h. The reaction mixture was worked up as described above to give a mixture (81 mg, 54%) of **21**, **22**, and **23** (21 mg, 16%). The mixture was separated by HPLC as described above to give **21** (24 mg, 16%) and **22** (57 mg, 38%).

*15-Norsolavetivone (**5**).* Compound **21** (165 mg) was mixed with pyridine-modified alumina (0.5 g), prepared from neutral alumina (Woelm, activity grade I) and pyridine withstirring under reduced pressure (0.3 Torr) at room temperature for 6 h. The mixture was heated in a glass tube at 220°C (bath temperature) for 8 min under argon, cooled, poured into ether (100 ml) and triethylamine (15 ml), and stirred for 3 h. The mixture was filtrated through Celite, concentrated, and separated by chromatography over silica gel (10 g) with benzene to afford **5** (75 mg, 68% yield based on the recovered starting material), oil; MS, *m/z* 204 (M^+) and 162; IR, 3090, 1687, 1650, and 890 $^{-1}$; NMR, δ 1.01 (3H, d, J=6 Hz), 1.73 (3H, s), 4.70 (2H, s), 5.78 and 6.70 (each 1H, d, J=10 Hz). Found: *m/z* 204.1499. Calcd for $C_{14}H_{20}O$: M, 204.1502.

*3-t-Butyldimethylsiloxy-11-hydroxy-2-oxo-15-nor-$\Delta^{1(10)}$-solavetivanes (**24**)—(**27**).* i) To a solution of LDA (1.5 mmol), prepared from diisopropylamine (0.21 ml, 1.51 mmol) in THF (5 ml) and 1.5 M butyllithium (1.5 mmol) in hexane (1 ml), was added **21** (134 mg, 0.6 mmol) in THF (3 ml) and

HMPA (0.26 ml) at −78°C under nitrogen, and the mixture was stirred for 30 min. A solution of *t*-butyldimethylchlorosilane (226 mg, 1.5 mmol) in THF (1 ml) was added to the mixture, and the whole mixture was warmed to room temperature and stirred for an additional 1 h. The mixture was shaken with ether (20 ml) and water (0.5 ml), dried, and concentrated to give an oily residue (426 mg). On the other hand, a solution of perbenzoic acid (96 mg, 0.72 mmol) in dry hexane was stirred at 0°C for 20 min. To this solution was added a solution of the oily residue (426 mg) in hexane (5 ml) at −15 °C. The mixture was warmed to room temperature, stirred for 1.5 h, poured into 30 ml of saturated brine, and extracted with ethyl acetate (4×50 ml). The combined extracts were washed with 5% aq $NaHCO_3$ (2×20 ml), dried, and evaporated to leave an oily residue, which was separated by chromatography over silica gel (10 g) with benzene–ethyl acetate (15:1) to afford **24** (91.5 mg) and **25** (45 mg) in 51 and 25% yields (based on the consumed starting material), respectively. **24**, oil; MS, *m/z* 337 (M^+-15); IR, 3620, 3450, 1698, 1615, 1257, 1145, 867, and 840 cm^{-1}; NMR, δ 1.08 (3H, d, J=7 Hz), 1.24 (6H, s), 3.89 (1H, d, J=11 Hz), 5.78 and 6.80 (each 1H, d, J=10 Hz). Found: C, 68.32; H, 10.13%. Calcd for $C_{20}H_{36}O_3Si$: C, 68.13; H, 10.29%. **25**, oil; MS, *m/z* 337 (M^+-15); IR, 3500, 1700, and 1260 cm^{-1}; NMR, δ 0.99 (3H, d, J=6 Hz), 1.23 (6H, s), 4.40 (1H, d, J=6 Hz), 5.81 and 6.60 (each 1H, d, J=10 Hz). Found: C, 68.45; H, 10.11%. Calcd for $C_{20}H_{36}O_3Si$: C, 68.13; H, 10.29%.

ii) Siloxylation of **21** (122 mg) was carried out under the same conditions as descrived above to give **26** (97 mg, 50%), and **27** (50 mg, 26%). **26**, oil; MS, *m/z* 337 (M^+-15); IR, 3625, 3470, 1700, 1620, 1150, 870, and 840 m^{-1}; NMR, δ 1.09 (3H, d, J=7 Hz), 1.22 (6H, s), 3.90 (1H, d, J=11 Hz), 5.72 and 6.67 (each 1H, d, J=10 Hz). Found: C, 68.41; H, 10.11%. Calcd for $C_{20}H_{36}O_3Si$: C, 68.13; H, 10.29%. **27**, oil; MS, *m/z* 337 (M^+-15), IR, 3495, 1700, 1260, 1150, 880, and 840 cm^{-1}; NMR, δ 0.94 (3H, d, J=6 Hz), 1.23 (6H, s), 4.41 (1H, d, J=4 Hz), 5.81 and 6.62 (each 1H, d, J=10 Hz). Found: C, 68.35; H, 10.15%. Calcd for $C_{20}H_{36}O_3Si$: C, 68.13; H, 10.29%.

References

1) Part XXXVIII of "Studies of the Phytoalexins" and Part XVIII of "Synthetic Studies of Rishitin and Related Compounds." Part XXXVII and XVII of the respective series, A. Murai, S. Sato, and T. Masamune, *Bull. Chem. Soc. Jpn.*, **57**, 2282 (1984).

2) N. Katsui, A. Matsunaga, H. Kitahara, F. Yagihashi, A. Murai, T. Masamune, and N. Sato, *Bull. Chem. Soc. Jpn.*, **50**, 1217 (1977), and references cited therein.

3) T. Masamune, A. Murai, M. Takasugi, A. Matsunaga, N. Katsui, N. Sato, and K. Tomiyama, *Bull. Chem. Soc. Jpn.*, **50**, 1201 (1977).

4) J. Kuć, W. W. Currier, and M. J. Shih, "Biochemical Aspects of Plant-Parasite Relationship," ed by J. Fried and D. R. Threlfall, Academic Press, New York (1976), p. 225; N. T. Keen and B. Bruegger, "Host Plant Resistance to Pests," ed by P. A. Hedin, American Chemical Society, Washington, D. C. (1977), p. 1; A. Stoessl, E. W. B. Ward, and J. B. Stothers, *ibid.*, p. 61.

5) T. Masamune, A. Murai, and N. Katsui, *Kagaku no Ryoiki*, **36**, 673 (1982), A. Murai, *J. Synth. Org. Chem. Jpn.*, **39**, 893 (1981).

6) K. Sato, Y. Ishiguri, N. Doke, K. Tomiyama, F. Yagihashi, A. Murai, N. Katsui, and T. Masamune, *Phytochemistry*, **17**, 1901 (1978); A. Murai, S. Sato, A. Osada, N. Katsui, and T. Masamune, *J. Chem. Soc., Chem. Commun.*, **1982**, 32.

7) N. Katsui, F. Yagihashi, A. Murai, and T. Masamune, *Chem. Lett.*, **1978**, 1205.

8) a) A. Murai, S. Sato, and T. Masamune, *J. Chem. Soc., Chem. Commun.*, **1982**, 512: b) A. Murai, S. Sato, and T. Masamune, *ibid.*, **1982**, 513.

9) W. R. Jackson and A. Zurgiyah, *J. Chem. Soc.*, **1965**, 5280.

10) M. J. Weiss, R. E. Schaub, G. R. Allen, Jr., J. F. Poletto, C. Pidacks, R. B. Conrow, and C. J. Coscia, *Tetrahedron*, **20**, 357 (1964).

11) A. Murai, S. Sato, and T. Masamune, *Chem. Lett.*, **1981**, 429.

12) R. H. Shapiro, Organic Reactions, **23**, 405 (1976).

13) A. Murai, S. Sato, and T. Masamune, *Tetrahedron Lett.*, **22**, 1044 (1981); A. Murai, S. Sato, and T. Masamune, *Bull. Chem. Soc. Jpn.*, **57**, 2276 (1984).

14) Ref. 13, Scheme 2.

15) G. M. Rubottom and J. M. Gruber, *J. Org. Chem.*, **43**, 1599 (1978).

16) Ref. 8 and A. Murai, S. Sato, and T. Masamune, *Bull. Chem. Soc. Jpn.*, **57**, 2291 (1984).

17) Compounds **19** and **20** should be designated as 2-(4-methoxy-5-methoxycarbonyl-7-*syn*-methyl-2-oxobicyclo-[2.2.2]octyl)ethyl acetate and 2-[3-(1-Hydroxy-4-methylethyl)-7-*anti*-methylbicyclo[2.2.2]oct-5-enyl]ethanol, respectively according to the IUPAC numbering rule. However, in this paper we used the same numbering for these compounds as that for 16 (C-1, carbon atom bearing the methoxyl group).

Total Synthesis of (±)-Lubimin and (±)-Oxylubimin. II. Transformation of (±)-15-Norsolavetivanes into (±)-Lubimin, (±)-Oxylubimin, and Related Compounds[1]

Akio MURAI,* Shingo SATO, and Tadashi MASAMUNE*
Department of Chemistry, Faculty of Science, Hokkaido University, Sapporo 060
(Received February 6, 1984)

The transformation of (±)-15-norsolavetivone and related compounds, into (±)-lubimin and (±)-oxylubimin, which constitutes the total synthesis of these highly oxygenated spirovetivane phytoalexins, is described.

In the preceding paper we reported the synthesis of (±)-15-norsolavetivone and its oxygenated derivatives from orcinol dimethyl ether. Transformation of these compounds into the title natural compounds has recently been completed, and the result was published in a preliminary communication.[2] In the present paper details of the transformation are described.

Conversion of (±)-15-norsolavetivone (**1**) into (±)-lubimin (**2**) was commenced with hydrocyanation by a modification of Nagata's conditions.[3] The reaction proceeded regio- and stereo-selectively, giving 10-cyano-15-norsolavetiv-11-en-2-one (**3**) as the sole isolable product in 81% yield. The NMR spectrum of **3** [δ 2.61 (2H, d, J=6 Hz, 1-H) and 3.10 (1H, t, J=6 Hz, 10-H)] indicated that the cyano ketone (**3**) is a mixture of rapidly equilibrating conformers, and hence the 10-cyano and 4-methyl groups are oriented *trans* each other. Reduction of **3** with the ammonia-borane complex in aqueous mixture[4] afforded a 2:1 mixture of 2-*equatorial*- (**4**) and 2-*axial*-hydroxy-10-*axial*-cyano-15-norsolavetivenes (**5**), which were easily separated by chromatography in 60 and 30% yields, respectively. In accordance with the assigned structures, the compounds (**4**) and (**5**) exhibited the following NMR spectra: **4**, δ 2.74 (1H, t, J=4 Hz, 10-H) and 3.97 (1H, br m, W_H=25 Hz, 2-H); **5**, δ 2.77 (1H, t, J=4 Hz) and 3.92 (1H, br m, W_H=12 Hz). These nitriles (**4**) and (**5**), when treated with diisobutylaluminium hydride in ether, were converted into the corresponding aldehydes (**6**) and (**7**) in 93 and 74% yields, respectively. The latter (**7**) was isolated as a 1:3 inseparable mixture of the hydroxy aldehyde and its acetal, as revealed by the IR and NMR spectra: IR, 3630, 3450, 2730, and 1719 cm^{-1}; NMR, δ 4.02 (0.25H, m, W_H=10 Hz, 2-H), 4.33 (0.75H, m, W_H= 16 Hz, 2-H), 5.18 (0.75H, br s, 15-H), and 9.73 (0.25H, br s, W_H=6 Hz, 15-H). These compounds (**6**) and (**7**) were identified as (±)-10-epilubimin[5] and (±)-2-epi-10-epilubimin[6] by direct comparison of the synthetic and natural samples (MS, IR, NMR, and TLC). After repeated epimerization[5] of **6** with base, (±)-lubimin (**2**) was isolated in an overall yield of 2.1% from orcinol dimethyl ether. Since lubimin (**2**) has been transformed into lubiminol[5b,7] (**8**) and isolubimin[5b,7,8] (**9**), 10-epilubimin (**6**) into 10-epilubiminol[5] (**10**) and 10-epiisolubimin[5,6,9] (**11**), and 2-epi-10-epi-lubimin (**7**) into 2-epi-10-epilubiminol[5b,6] (**12**), respectively, the present transformation implies the synthesis of these natural spirovetivane stress metabolites.

The synthesis of (±)-oxylubimin (**13**) was performed in the same manner as that of (±)-lubimin (**2**), starting with the 3-*t*-butyldimethylsilyl ether (**14**) of

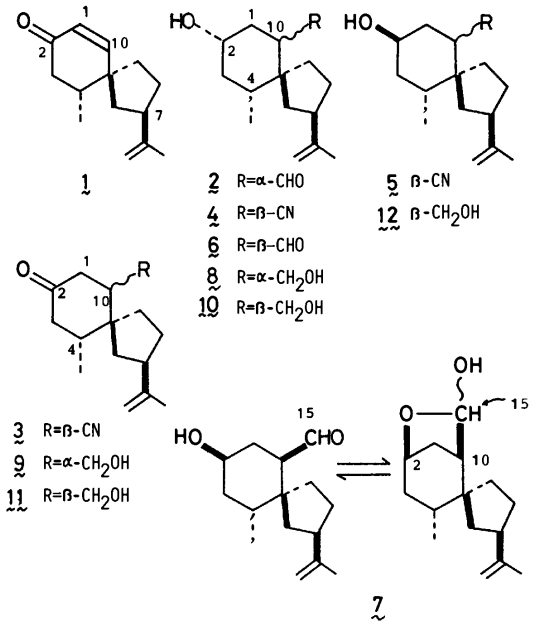

(3*SR*,4*RS*,7*SR*)-3,11-dihydroxy-15-norspirovetiv-1(10)-en-2-one, which had been prepared previously.[1,10] Hydrocyanation of **14** under the same conditions[3a] as that of 15-norsolavetivone (**1**) led only to regioselective formation of a mixture of the corresponding 10-*equatorial*- (**15**) and 10-*axial*-cyano-15 norsolavetivenes (**16**), which were separated easily by chromatogarphy in 44 and 32% yields, respectively. The NMR spectra of these compounds [**15**, δ 2.88 (1H, dd, J=12 and 4.5 Hz, 10-H) and 3.77 (1H, d, J=11 Hz, 3-H); **16**, δ 3.05 (1H, t, J=5 Hz) and 3.76 (1H, d, J=11 Hz)] supported the assigned configurations. Reduction of the cyano ketones (**15**) and (**16**) with the ammonia-borane complex[4] proceeded stereoselectively, in contrast with that of **3**, giving the corresponding 2-alcohols, which were converted into the respective 2,3-bis(*t*-butyldimethylsilyl) ethers (**17**) and (**18**) in 80 and 58% yields. The NMR spectra of these ethers [**17**, δ 2.58 (1H, dd, J=9 and 4 Hz, 10-H), 3.26 (1H, t, J=7 Hz, 3-H), and 3.50 (1H, m, W_H=20 Hz, 2-H); **18**, 3.10 (1H, dd, J=12 and 4 Hz), 3.52 (1H, t, J=4 Hz), and 3.72 (1H, m, W_H=12 Hz)] suggested that the A ring of **17** would probably take a deformed chair conformation with 2,3-diequatorial hydroxyl and 10-equatorial cyano groups, while **18** would adopt a slightly deformed one with 2,3-diaxial hydroxyl and 10-equatorial cyano groups owing to the bulkiness of the silyl groups. This assignment to the conformation was revealed clearly for the following compounds. Compounds **17** and **18**, when treated with

pyridine-modified alumina[10] at 220°C underwent dehydration to give the corresponding isopropenyl derivatives (**19**) and (**20**) in 74 and 75% yields, respectively. The NMR spectra [**19**, δ 2.48 (1H, dd, J=12 and 4 Hz, 10-H), 3.16 (1H, t, J=9 Hz, 3-H), and 3.44 (1H, m, W_H=20 Hz, 2-H); **20**, δ 3.05 (1H, dd, J=12 and 4 Hz), 3.50 (1H, t, J=4 Hz), and 3.69 (1H, m, W_H=14 Hz)] indicated that these compounds would be represented by conformations **19A** and **20A**. Removal of the silyl groups of **19** and **20** with hydrofluoric acid[12] afforded 10-*equatorial*- (**21**) and 10-*axial*-cyano-2,3-di-(*equatorial*-hydroxy)-15-norsolvetiv-11-enes (**22**) in 91 and 63% yields, respectively: **21**, δ 2.53 (1H, dd, J=12 and 4 Hz, 10-H), 2.97 (1H, t, J=11 Hz, 3-H), and 3.36 (1H, W_H=24 Hz); **22**, δ 2.66 (1H, t, J=4 Hz), 2.99 (1H, t, J=11 Hz), and 3.74 (1H, m, W_H=21 Hz). The compounds (**21**) and (**22**), when treated with diisobutylaluminium hydride in 1,2-dimethoxyethane, was converted into the corresponding aldehydes in 58 and 68% yields, which were identified as (±)-oxylubimin[12] (**13**) and (±)-10-epioxylubimin[12] (**23**), respectively, by direct comparison of the synthetic and natural samples. After repeated epimerization of **23**, the overall yield of (±)-oxylubimin amounted to 0.82% from orcinol dimethyl ether. The present result constitutes the first total synthesis of highly oxygenated spirovetivane phytoalexins.

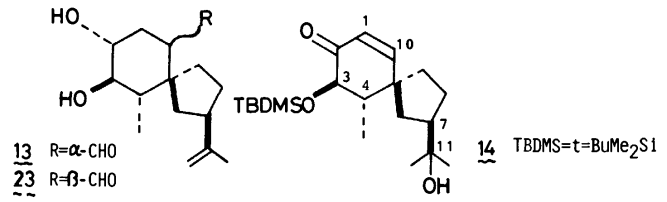

13 R=α-CHO
23 R=β-CHO

14 TBDMS=t-BuMe$_2$Si

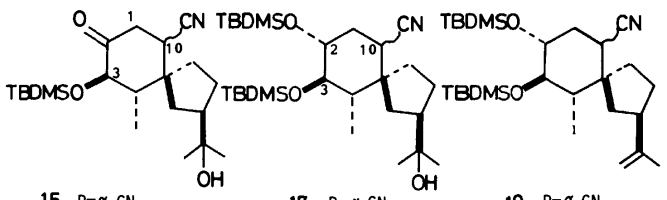

15 R=α-CN
16 R=β-CN

17 R=α-CN
18 R=β-CN

19 R=α-CN
20 R=β-CN

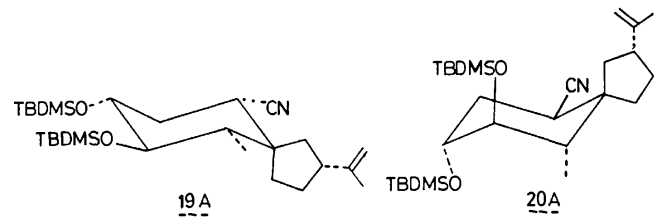

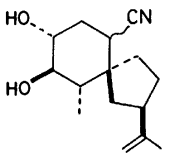

21 R=α-CN
22 R=β-CN

Experimental

A general procedure was described in the preceding paper.[1]

10-Cyano-15-norsolavetiv-11-en-2-one (3). To a solution of **1** (68 mg) in tetrahydrofuran (THF) (2 ml) at 0°C was added a solution of hydrogen cyanide (HCN) and triethylaluminium (Et_3Al), prepared from Et_3Al in hexane (15% w/w, Tokyo-Kasei) (1.5 ml) and 0.91 M† HCN in THF (1.2 ml) at 0°C for 5 min under stirring. The mixture was warmed to room temperature and stirred for 4 h. The mixture was mixed with 2 M hydrochloric acid (HCl) (2 ml) at 0°C and stirred for 20 min, and poured into saturated brine (30 ml), and extracted with ethyl acetate (4×40 ml). The acetate extracts were washed with 2 M aq sodium hydroxide (NaOH) (2×20 ml) and saturated brine, dried, evaporated, and separated by chromatography over silica gel (5 g) with benzene to afford **3** (58 mg), oil; MS, m/z 231 (M^+); IR, 3090, 2210, 1722, 1648, and 890 cm^{-1}; NMR, δ 0.99 (3H, d, J=6 Hz), 1.76 (3H, s), 2.61 (2H, d, J=6 Hz), 3.10 (1H, t, J=6 Hz), and 4.75 (2H, s). Found: m/z 231.1594. Calcd for $C_{15}H_{21}NO$: M, 231.1621.

10-Cyano-15-norsolavetiv-11-en-2-ols (4) and (5). To a mixture of **3** (30 mg) in methanol (3 ml) and water (1.5 ml) was added the ammonia-borane complex (5 mg). The mixture was stirred at 20°C for 2 h, poured into 2 M HCl (1 ml), and stirred for 20 min. The mixture was extracted with ethyl acetate (4×30 ml), dried, evaporated, and separated by chromatography over silica gel (3 g) with benzene–ethyl acetate (8:1) to give 2α-alcohol (**4**) (18 mg) and 2β-alcohol (**5**) (9 mg). **4**, oil; MS, m/z 233 (M^+); IR, 3460, 3096, 2215, 1650, and 890 cm^{-1}; NMR, δ 0.96 (3H, d, J=6 Hz), 1.71 (3H, s), 2.74 (1H, t, J=4 Hz), 3.97 (1H, br m, W_H=25 Hz), 4.66 (2H, s). Found: m/z 233.1755. Calcd for $C_{15}H_{23}NO$: M, 233.1776. **5**, oil; MS, m/z 233 (M^+); IR, 3460, 3090, 2215, 1648, and 888 cm^{-1}; NMR, δ 0.95 (3H, d, J=6 Hz), 1.71 (3H, s), 2.77 (1H, t, J=4 Hz), 3.92 (1H, br m, W_H=12 Hz), and 4.67 (2H, s). Found: m/z 233.1820. Calcd for $C_{15}H_{23}NO$: M, 233.1776.

(±)-2-Epi-10-epilubimin (7) and (±)-10-Epilubimin (6). To a solution of **5** (5 mg) in ether (4 ml) at 0°C was added 1.7 M diisobutylaluminium hydride in hexane (0.14 ml), and the mixture was stirred for 4 h at the temperature. The reaction was quenched by saturated brine, and extracted with ethyl acetate (4×200 ml). The extracts were washed with 2 M HCl and saturated brine, dried, evaporated and separated by chromatography to give **7** (3.7 mg), oil; MS, m/z 236 (M^+); IR, 3630, 3450, 3090, 2730, 1719, 1649, 1036, 1000, and 895 cm^{-1}; NMR (CCl_4), δ 0.87 (3H, d, J=6 Hz), 1.71 (3H, s), 4.02 (0.25H, m, W_H=10 Hz), 4.33 (0.75H, m, W_H=16 Hz), 4.63 (2H, s), 5.18 (0.75H, s), and 9.73 (0.25H, m, W_H=8 Hz). Found: m/z 236.1785. Calcd for $C_{15}H_{24}O_2$: M, 236.1777. Natural; NMR (CCl_4), δ 0.88 (3H, d, J=6 Hz), 1.72 (3H, s), 4.02 (0.25H, m, W_H=10 Hz), 4.32 (0.75H, br m, W_H=16 Hz), 4.64 (2H, s), 5.20 (0.75H, s), and 9.74 (0.25H, m, W_H=8 Hz).

Reduction of **4** (7 mg) was carried out under the same conditions as described above to give **6** (6.5 mg), oil; MS, m/z 236 (M^+), 218, and 205; IR, 3630, 3450, 3090, 1715, 1648, 1115, 1090, and 895 cm^{-1}; NMR, δ 0.95 (3H, d, J=7 Hz), 1.73 (3H, s), 3.72 (1H, m, W_H=24 Hz), 4.69 (2H, s), and 9.85 (1H, s). Found: m/z 236.1758. Calcd for $C_{15}H_{24}O_2$: M, 236.1777. Natural; NMR, δ 0.95 (3H, d, J=7 Hz), 1.73 (3H, s), 3.71 (1H, m, W_H=25 Hz), 4.69 (2H, s), and 9.85 (1H, s).

10-Cyano-3,10-dihydroxy-15-norsolavetiv-2-one 3-t-butyldimethylsilyl Ethers (15) and (16). To a solution of **14** (40 mg, 0.11 mmol) in THF (1 ml) at 0°C under nitrogen was added a solution of Et_3Al–HCN in THF, prepared from Et_3Al (0.55 mmol) in hexane (10% w/w) (0.55 ml) and 1.3 M

† 1 M=1 mol dm^{-3}.

HCN (0.33 mmol) in THF (0.25 ml) at 0°C for 5 min, and the mixture was stirred for 14 h at room temperature. The reaction mixture was poured into 2 M HCl (20 ml), and extracted with ethyl acetate (4×30 ml). The extracts were washed with 2 M aqueous NaOH (2×20 ml) and saturated brine (20 ml), dried, evaporated, and separated by chromatography over silica gel (4 g) with benzene–ethyl acetate (10:1) to give **15** (19 mg) and **16** (14 mg), respectively. **15**, mp 110—112°C (from hexane–diisopropyl ether) (1:1); MS, *m/z* 364 (M^+-15); IR, 3625, 3480, 2220, 1735, 1145, 865, and 840 cm^{-1}; NMR, δ 1.12 (3H, d, J=6 Hz), 1.23 (6H, s), 2.72 (1H, t, J=12 Hz), 2.75 (1H, dd, J=12 and 4.5 Hz), 2.88 (1H, dd, J=12 and 4.5 Hz), 3.77 (1H, d, J=11 Hz). Found: C, 66.57; H, 9.81; N, 3.91%. Calcd for $C_{21}H_{37}O_3NSi$: C, 66.44; H, 9.82; N, 3.69%. **16**, mp 132.5—133.5°C (from diisopropyl ether); MS, *m/z* 379 (M^+); IR, 3620, 3480, 2210, 1753, 1135, 860, and 840 cm^{-1}; NMR, δ 1.10 (3H, d, J=6 Hz), 1.23 (6H, s), 2.69 (2H, d, J=5 Hz), 3.05 (1H, t, J=5 Hz), and 3.76 (1H, d, J=11 Hz). Found: C, 66.16; H, 9.80; N, 3.84%. Calcd for $C_{21}H_{37}O_3NSi$: C, 66.44; H, 9.82; N, 3.69%.

(2SR,3SR,4RS,7SR,10RS)-10-Cyano-15-norsolavetivane-2,3,10-triol 2,3-Bis(t-butyldimethylsilyl) ether (17) and its 10-Epimer (18). i) A mixture of **15** (149 mg) and the ammonia–borone complex (14 mg) in methanol (6 ml) and water (3 ml) was stirred at room temperature for 2 h under nitrogen. To the mixture was added 2 M HCl (4 ml), and the whole mixture was concentrated *in vacuo*. The residue was extracted with ethyl acetate (4×30 ml), and the extracts were washed with 2 M HCl (1×20 ml) and saturated brine (20 ml), dried, and evaporated. The residue was separated by chromatography over silica gel (10 g) with benzene–ethyl acetate (2:1) to give triol (120 mg), mp 139—140°C (from hexane–ether, 1:1); MS, *m/z* 366 (M^+-15), and 348; IR, 3625, 3445, 2205, 1475, 1257, 1100, 1060, and 840 cm^{-1}; NMR, δ 1.00 (3H, d, J=6 Hz), 1.21 (6H, s), 2.53 (1H, dd, J=12 and 4 Hz), 3.01 (1H, t, J=11 Hz), and 3.34 (1H, br m, W_H=22 Hz).

A mixture of the triol (61 mg), *t*-butyldimethylchlorosilane (96 mg), and imidazole (86 mg) in *N,N*-dimethylformamide (0.6 ml) was heated at 50°C under argon for 48 h. The reaction mixture was poured into saturated brine (20 ml), and extracted with ethyl acetate (4×40 ml). The combined extracts were washed with saturated brine, dried, evaporated, and separated by chromatography over silica gel (8 g) with benzene–ethyl acetate (15:1) to give **17** (70 mg), mp 129—130°C (from diisopropyl ether); MS, *m/z* 480 (M^+-15); IR, 3630, 3460, 2215, 1120, and 840 cm^{-1}; NMR, δ 1.10 (3H, d, J=6 Hz), 1.20 (6H, s), 2.58 (1H, dd, J=9 and 4 Hz), 3.26 (1H, t, J=7 Hz), and 3.50 (1H, m, W_H=20 Hz). Found: C, 65.73; H, 10.63; N, 2.62%. Calcd for $C_{27}H_{35}O_3NSi_2$: C, 65.40; H, 10.77; N, 2.82%.

ii) Reduction of **16** (136 mg) under the same conditions as described above afforded the epimeric triol (101 mg), mp 181—182°C (from ethyl acetate); MS, *m/z* 366 (M^+-15); IR, 3630, 3460, 2210, 1480, 1265, 1100, and 842 cm^{-1}; NMR, δ 0.98 (3H, d, J=6 Hz), 1.19 (6H, s), 2.69 (1H, t, J=4 Hz), 3.04 (1H, t, J=11 Hz), and 3.72 (1H, m, W_H=22 Hz).

Silylation of the triol (70 mg) was carried out under the same conditions as described above to give **18** (71 mg), mp 85—87°C (from hexane); MS, *m/z* 480 (M^+-15); IR, 3620, 3500, 2220, 1090, 870, and 840 cm^{-1}; NMR, δ 1.02 (3H, d, J=7.5 Hz), 1.21 (6H, s), 3.10 (1H, dd, J=12 and 4 Hz), 3.52 (1H, t, J=4 Hz), and 3.72 (1H, m, W_H=12 Hz). Found C, 65.73; H, 10.46; N, 2.70%. Calcd for $C_{27}H_{53}O_3NSi_2$: C, 65.40; H, 10.77; N, 2.82%.

(2SR,3SR,4RS,7SR,10RS)-10-Cyano-15-norsolavetiv-11-ene-2,3-diol 2,3-Bis(t-butyldimethylsilyl) ether (19) and its 10-Epimer (20). i) A suspension of **17** (41 mg) and pyridine-modified alumina (0.25 g) in 1,3,5-triisopropylbenzene (0.3 ml) was heated at 220°C under argon for 30 min. The mixture was dissolved in ether (40 ml) and triethylamine (5 ml), stirred at room temperature under nitrogen for 5 h, and filtered through Celite. The filtrate was concentrated, and purified by chromatography over silica gel (7 g) with hexane–benzene (1:5) to give **19** (23.5 mg) (74% based on the consumed starting material), amorphous; MS, *m/z* 462 (M^+-15); IR, 3090, 2210, 1648, 1263, 1120, 890, and 840 cm^{-1}; NMR, δ 1.05 (3H, d, J=6 Hz), 1.72 (3H, s), 2.48 (1H, dd, J=12 and 4 Hz), 3.16 (1H, t, J=9 Hz), 3.44 (1H, m, W_H=20 Hz) and 4.68 (2H, s).

ii) Dehydration of **18** (57 mg) was carried out under the same conditions as described above to give **20** (32 mg) (75% based on the recovered starting material), amorphous; MS, *m/z* 477 (M^+); IR, 3085, 2215, 1650, 1270, 1095, 1015, 870, and 840 cm^{-1}; NMR, δ 1.01 (3H, d, J=6 Hz), 1.72 (3H, s), 3.05 (1H, dd, J=12 and 4 Hz), 3.50 (1H, t, J=4 Hz), 3.69 (1H, m, W_H=14 Hz), and 4.66 (1H, br s, W_H=7 Hz).

(2SR,3SR,4RS,7SR,10RS)-10-Cyano-15-norsolavetiv-11-ene-2,3-diol (21) and its 10-Epimer (22). i) A mixture of **19** (19 mg) and 46% hydrofluoric acid (0.35 ml) in THF (0.6 ml) and acetonitrile (0.3 ml) was stirred at room temperature for 6 h. Triethylamine (0.5 ml) was then added to the reaction mixture. The whole mixture was concentrated, and purified by chromatography over silica gel (2 g) with benzene–ethyl acetate (1:1) to give **21** (9 mg), mp 159—160°C (from ether); MS, *m/z* 249 (M^+); IR, 3600, 3450, 3080, 2215, 1646, and 895 cm^{-1}; NMR, δ 1.07 (3H, d, J=6 Hz), 1.74 (3H, s), 2.53 (1H, dd, J=12 and 4 Hz), 2.97 (1H, t, J=11 Hz), 3.36 (1H, m, W_H=24 Hz), and 4.72 (2H, s). Found: C, 72.51; H, 9.19; N, 5.50%. Calcd for $C_{15}H_{23}O_2N$: C, 72.25; H, 9.30; N, 5.61%.

ii) Desilylation of **20** (31 mg) was carried out under the same conditions as described above to give **21** (10 mg), mp 102—103°C (from ether); MS, *m/z* 249 (M^+); IR, 3600, 3450, 3090, 2220, 1650, and 895 cm^{-1}; NMR, δ 1.07 (3H, d, J=6 Hz), 1.72 (3H, s), 2.66 (1H, t, J=4 Hz), 2.99 (1H, t, J=11 Hz), 3.74 (1H, m, W_H=21 Hz), and 4.70 (2H, s). Found: C, 72.53; H, 9.20; N, 5.43%. Calcd for $C_{15}H_{23}O_2N$: C, 72.25; H, 9.30; N, 5.61%.

(±)-Oxylubimin (13). To a solution of **21** (8.5 mg) in 1,2-dimethoxyethane (1 ml) was added 1.7 M diisobutylaluminium hydride in hexane (0.4 ml) at room temperature. The mixture was stirred for 12 h, mixed with 2 M HCl (2 ml) at 0°C, poured into saturated brine (10 ml), and extracted with ethyl acetate (4×30 ml). The combined acetate extracts were washed with 5% aqueous sodium hydrogencarbonate (10 ml), and saturated brine, dried, concentrated, and separated by chromatography over silica gel (2 g) with benzene–ethyl acetate (2:1) to give **13** (5 mg), mp 79—81°C (from diisopropyl ether); MS, *m/z* 252 (M^+) and 234; IR, 3600, 3440, 3080, 2725, 1720, 1645, and 894 cm^{-1}; NMR, δ 1.05 (3H, d, J=6 Hz), 1.68 (3H, s), 3.00 (1H, t, J=9 Hz), 3.42 (1H, m, W_H=22 Hz), 4.65 (2H, s), and 10.00 (1H, d, J=2 Hz). Found: C, 71.54; H, 9.67%. Calcd for $C_{15}H_{24}O_3$: C, 71.39; H, 9.59%. Natural, mp 85—86°C (from diisopropyl ether); IR, 3600, 3440, 3080, 2727, 1720, 1646, and 894 cm^{-1}; NMR, δ 1.05 (3H, d, J=6 Hz), 1.69 (3H, s), 3.00 (1H, t, J=9 Hz), 3.43 (1H, m, W_H=23 Hz), 4.66 (2H, s), and 10.02 (1H, d, J=2 Hz).

(±)-10-Epioxylubimin (23). Reduction of **22** (9.5 mg) was carried out under the same conditions as described above to give **23** (6.5 mg), mp 121—123°C (from diisopropyl ether); MS, *m/z* 252 (M^+) and 234; IR, 3600, 3445, 3085, 2730, 1720, 1648, and 897 cm^{-1}; NMR, δ 1.05 (3H, d, J=6 Hz), 1.70 (3H, s), 3.03 (1H, t, J=9 Hz), 3.40 (1H, m, W_H=20 Hz), 4.66 (2H, s), and 10.04 (1H, s). Found: C, 71.27; H, 9.65%. Calcd for $C_{15}H_{24}O_3$: C, 71.39; H, 9.59%. Natural, mp 123—124°C (from diisopropyl ether); IR, 3600, 3445, 3085, 2730, 1719, 1647, and 895 cm^{-1}; NMR, δ 1.06 (3H, d, J=6 Hz), 1.71 (3H, s), 3.02 (1H, t, J=9 Hz), 3.41 (1H, m, W_H=20 Hz), 4.66 (2H, s), and 10.04 (1H, s).

References

1) Part XXXIX of "Studies of the Phytoalexins" and Part XIX of "Synthetic Studies of Rishitin and Related Compounds." Parts XXXVIII and XVIII of the respective series, A. Murai, S. Sato, and T. Masamune, *Bull. Chem. Soc. Jpn.*, **57**, 2286 (1984).

2) A. Murai, S. Sato, and T. Masamune, *J. Chem. Soc., Chem. Commun.*, **1982**, 513.

3) a) W. Nagata and N. Yoshioka, *Organic Reactions*, **25**, 255 (1977); b) Addition of 2-lithio-1,3-dithiane to **1** resulted in formation of a 1:1 mixture of 1,2- and 1,4-adducts; *cf.*, C. A. Brown and A. Yamauchi, *J. Chem. Soc., Chem. Commun.*, **1979**, 100; M. El-Bouz and L. Wartski, *Tetrahedron Lett.*, **21**, 2897 (1980).

4) G. C. Andrews and T. C. Crawford, *Tetrahedron Lett.*, **21**, 693 (1980).

5) a) N. Katsui, F. Yagihashi, A. Matsunaga, K. Orito, A. Murai, and T. Masamune, *Chem. Lett.*, **1977**, 723. b) N. Katsui, F. Yagihashi, A. Murai, and T. Masamune, *Bull. Chem. Soc. Jpn.*, **55**, 2424 (1982).

6) N. Katsui, Y. Takahashi, N. Sato, A. Murai, and T. Masamune, *Nippon Kagaku Kaishi*, **1981**, 659.

7) A. Stoessl, J. B. Brothers, and E. W. B. Ward, *Can. J. Chem.*, **56**, 645 (1978).

8) E. B. Kalan and S. F. Osman, *Phytochemistry*, **15**, 775 (1976).

9) N. Katsui, F. Yagihashi, A. Murai, and T. Masamune, *Chem. Lett.*, **1978**, 1205.

10) Compound **14** corresponds to "**24**" in the preceding paper.[1]

11) E. von Rudloff, *Can. J. Chem.*, **39**, 1860 (1961).

12) R. F. Newton, D. P. Reynolds, M. A. W. Finch, D. R. Kelly, and S. M. Roberts, *Tetrahedron Lett.*, **1979**, 3981, and references cited therein.

13) N. Katsui, A. Matsunaga, H. Kitahara, F. Yagihashi, A. Murai, T. Masamune, and N. Sato, *Bull. Chem. Soc. Jpn.*, **50**, 1201 (1977).

 © 1984 The Chemical Society of Japan Bull. Chem. Soc. Jpn., 57, 2295—2298 (1984)

Kinetics and Mechanism of Dissociation of (Acetylacetonato)[*N*-(*o*-carboxyphenyl)iminodiacetato]chromate(III) Ion in Acidic Media

Chinmay CHATTERJEE* and Aya Singh BALI

Chemistry Department, Indian Institute of Technology, Powai Bombay 400076, India

(Received Junuary 20, 1983)

Acid-catalyzed dissociation of (acetylacetonato) [*N*-(*o*-carboxyphenyl) iminodiacetato]chromate(III) ion has been studied kinetically in aqueous perchloric acid media over a temperature range (60—80 °C). Under these conditions the reaction occurs by two concurrent paths according to the following rate law: Rate= k_1[complex]+k_2[complex][H$^+$], where k_1 and k_2 are the appropriate rate constants for the spontaneous and acid-catalyzed pathways, respectively Analysis of the rate data corresponding to the rate constants k_1 and k_2 suggests solvent assisted dissociation of the complex and its conjugate acid for the two paths, respectively, and that the opening of the chelate ring is rate determining.

The amino carboxylate ligands have donor groups similar to the more common amino acid residues. Hence the ligand substitution at chromium(III) in amino carboxylate environments have considerable physiological significance. Ogino[1] and Sykes[2] have suggested that the addition of a free $-CH_2COOH$, $-CH_2COO^-$, or $-CH_2CH_2OH$ in an associative intramolecular step is responsible for the kinetic lability of [CrY(H_2O)]^n complexes towards the addition of unidentate X^- donor. Guardalabene *et al.*[3] reported similar pendant group assistance for the acid-catalyzed aquation of the 2,4-pentanedionato chelate ligand ($acac^-$) from [Cr(hedta) (acac)]$^-$ (hedta: hydrogenethylenediamine-*N,N,N',N'*-tetraacetate) whereas the acid-catalyzed aquation of [Cr(edda)(acac)] (edda: ethylenediamine *N,N*-diacetate) exhibited normal reactivity. In contrast to the extensive study of the acid-catalyzed dissociation of octahedral chromium(III) carboxylato chelates[4-7], limited data exist for the corresponding β-diketonato[3,8,9] complexes. It is well known[10] that metal acetylacetone ring possesses quasi-aromatic character which in turn reflects their exceptional stability and relative inertness. A mixed ligand octahedral complex of chromium(III) with carboxymethyl derivative of anthranilic acid (*N*-(*o*-carboxyphenyl)iminodiacetic acid, H_3 atda) as aromatic amino acid and acetylacetone has been described in the literature.[11] The kinetic studies of dissociation of the title complex appeared to be worthy of investigation for the following reasons:

(a) In order to examine the relative reactivity of aromatic amino acid and acetylacetone as coordinating ligand towards acid solution.

(b) Comparison of kinetic data of $acac^-$ release from Cr(tetradentateaminopolycarboxylate)$(acac)^-$ type complexes with and without pendant group.

Experimental

Materials and Reagents. Diaqua[*N*-(*o*-carboxyphenyl) iminodiacetato]chormium(III) trihydrate, Cr(atda) $(H_2O)_2\cdot 3H_2O$ and potassium (acetylacetonato)[*N*-(*o*-carboxyphenyl) iminodiacetato]chromate(III), K[Cr(atda)(acac)] were prepared following the method described in the literature.[11] The purity of the sample was checked by elemental analysis.

Found: C, 33.80; N, 3.52; H, 4.67%. Calcd for [Cr $(C_{11}H_8NO_6)(H_2O)_2]\cdot 3H_2O$: C, 33,67; N, 3,57; H. 4.59%. Found: C, 43.70; N, 3.12; H, 3.43%. Calcd for K $[Cr(C_{11}H_8NO_6)(C_5H_7O_2)]$: C, 43.64; N, 3.18; H, 3.41%. The positions and intensities of the d-d bands corresponding to $^4A_{2g}\rightarrow{}^4T_{2g}$ and $^4A_{2g}\rightarrow{}^4T_{1g}$ transitions in a pseudo-octahedral ligand field for both the complexes matched very well with the reported data.[11] Other chemicals used were of reagent grade purity or prepared in the pure state by suitable methods. Sodium perchlorate was used to adjust the ionic strength of the medium.

Kinetic Measurements. The aquation rates were monitored spectrophotometrically using a Varian Superscan 3 and a Toshniwal UV-visible spectrophotometer. Spectral examination of the experimental solutions revealed that under the conditions of acidity employed for the study the metal acetylacetone bond was found to undergo dissociation in preference to aromatic amino acid, atda, leading to diaqua product, [Cr(atda)$(H_2O)_2$]. The enhanced kinetic stability exhibited by aromatic amino acid can be ascribed to the effect of presence of more number of chelate rings in ligated amino acid in comparison to only one six membered (acetylacetonato) metal ring. The course of the aquation reaction in dilute perchloric acid (0.02—0.2 mol dm^{-3}) at an ionic strength 1.0 mol dm^{-3} was followed by observing the decrease in absorbance at 400 nm, where the absorbances of the reacting complex and the product differ appreciably. To follow the reaction a solution containing requisite quantities of perchloric acid and sodium perchlorate (for adjustment of ionic strength to 1.0 mol dm^{-3}) was thermostatted at the experimental temperature. After attainment of thermal equilibrium, the requisite quantity of the complex, K[Cr(atda)(acac)], was added and the solution was thoroughly mixed and diluted to a definite volume with water thermostatted at the experimental temperature. An aliquot was immediately withdrawn from this reaction mixture using a pipette jacketed with ice to quench the reaction and its absorbance was measured at 400 nm. This was repeated at subsequent time intervals. The experimental conditions were so chosen that pseudo-first order rate law was applicable and plots of log $(A_0-A_\infty)/(A_t-A_\infty)$ *versus* time (t) were linear for at least three to four half-lives and passing through the origin with $A_t=A_\infty$ at $10t_{1/2}$. The preliminary spectral observation of the reacting solutions after digesting for at least ten half-lives agreed well with spectra of the corresponding diaqua product, [Cr(atda)$(H_2O)_2$], indicating the absence of any complication due to reverse anation reaction of aqua complex.

Results and Discussions

Values of k_{obsd} (the first order rate constants) were determined at 50.0±0.1, 60.0±0.1, 70.0±0.1, and

TABLE 1. KINETIC PARAMETERS FOR AQUATION OF (ACETYLACETONATO)[*N*(*o*-CARBOXYPHENYL)-IMINODIACETATO]CHROMATE(III) ION (μ=1.0 mol dm^{-3})

Temp/°C	$k_1/10^{-5}$ s^{-1}	$k_2/10^{-4}$ mol^{-1} dm^3 s^{-1}
50.0±0.1	1.31±0.1	1.75±0.13
60.0±0.1	3.28±0.18	3.77±0.15
70.0±0.1	8.04±0.15	9.27±0.14
80.0±0.1	16.82±0.28	23.71±0.38
ΔH^*/kJ mol^{-1}	80.1±1.6	80.2± 4.1
ΔS^*/J K^{-1} mol^{-1}	−90.0±4.6	−71.6±11.3
(μ=0.1 mol dm^{-3})		
70.0±0.1	7.98±0.28	8.15±0.43

80.0±0.1 °C, for acid concentration 0.02—0.2 mol dm^{-3} at an ionic strength 1.0 mol dm^{-3} and have been found to vary with acid concentration in a manner which suggests that the dissociation of the title complex proceeds in accordance with the following rate law:

$$\text{Rate} = k_1[\text{complex}] + k_2[\text{complex}][H^+], \quad (1)$$

where k_1 stands for the first order rate constant for the uncatalyzed and k_2, second order rate constant describing the acid-catalyzed pathways, respectively. Using least squares method k_1 and k_2 values at different temperatures have been determined from the linear plot of k_{obsd} *versus* acid concentration (Fig. 1) and are listed in Table 1 along with the activation parameters ΔH^* and ΔS^* values evaluated using the Eyring equation. Sequence of changes consistent with the kinetic results are depicted below:

$$[Cr(atda)(acac)]^- + H_2O \xrightarrow[\text{slow}]{k_1} [Cr(atda)(-acac)(H_2O)]^-$$

$$[Cr(atda)(-acac)(H_2O)]^- \xrightarrow{+H_2O,\ \text{rapid}} [Cr(atda)(H_2O)_2] + acac^-$$

$$acac^- + H^+ \xrightarrow{\text{fast}} acacH$$

$$[Cr(atda)(acac)]^+ + H^+ \overset{K}{\rightleftharpoons} [Cr(atda)(acacH^+)]^- \quad \text{(conjugate acid)}$$

$$[Cr(atda)(acacH^+)]^- \xrightarrow[+H_2O]{k_2'} [Cr(atda)(-acacH)(H_2O)]$$

$$[Cr(atda)(-acacH)(H_2O)] \xrightarrow{+H_2O,\ \text{rapid}} [Cr(atda)(H_2O)_2] + acacH,$$

where -acac and -acacH stand for the ligand and its protonated form, respectively, functioning as monodentate ligand. The catalytic rate constant k_2 is related to k_2' and K by the relation

$$k_2 = \frac{Kk_2'}{1+K[H^+]}, \quad (2)$$

under the present experimental conditions $K[H^+] \ll 1$ as evident from the linearity of the plot of k_{obsd} *versus* $[H^+]$ even at highest perchloric acid concentration. Hence Eq. 2 reduces to $k_2 = K k_2'$. The activation parameters corresponding to k_2 thus involve both rate constants and equilibrium constants. Guardalabene *et al.*[3] studied the acid-catalyzed aquation of Hacac from [Cr(hedta)(acac)]$^-$ and [Cr(edda)(acac)] complexes. An accelerated rate of about 10^3 relative to [Cr(acac)$_3$] is observed for [Cr(hedta)(acac)]$^-$ complex whereas normal behaviour is found for [Cr(edda)(acac)] system. The pendant group effect for labilizing the release of acetylacetone has been proposed to account for the 10^3 enhancement. In both the cases rupture of Cr–O bond has been proposed to take place in the transition state similar to what has been suggested for the [Cr(acac)$_3$] system.[8] Since the present system under investigation does not possess any pendant carboxylato group, as a result no intramolecular assistance is observed. Similarity in reactivity of the present system with those of [Cr(acac)$_3$] and [Cr(edda)(acac)] thus substantiates the influence of pendant group in enhancement of rate.

The magnitude and sign of the activation parameters corresponding to uncatalyzed and acid-catalyzed paths in the present system is found to be comparable with those reported for [Cr(acac)$_3$]. It is thus logical to conclude that the reactions corresponding to rate constants k_1 and k_2 respectively in the present system proceed by mechanisms identical to those operative in the [Cr(acac)$_3$] system where acid independent step is suggested to involves a simple dissociation of [Cr (atda) (acac)]$^-$ complex, while the acid-catalyzed path involve a dissociation of the conjugate acid formed by protonation in a rapid pre-equilibrium step. Both rate-determining dissociations for uncatalyzed and acid-catalyzed paths in the present system thus involve a one-ended dissociation of a acetylacetonato chelate ring with the simultaneous entry of a molecule of water into the coordination sphere of chromium(III), followed by the rupture of a second Cr–O bond of the unidentate functioning acetylacetone ligand in a much faster process with a simultaneous entry of another molecule of water leading to [Cr(atda) (H$_2$O)$_2$] product. Structural,[12] spectral,[13] and chemical evidence[14] suggests that orbitals of π symmetry are involved in extensive electron delocalization and pseudoaromaticity, within the planar six-membered chelate ring of metal acetylacetonato complex. This special bonding is reflected in its relative kinetic inertness. Cleavage of one of the metal–acetylacetone bond of the chelate ring would destroy the π conjugation thus facilitating the rupture of the second metal–O bond as suggested in the above scheme. The magnitude of the rate constant corresponding to acid-catalyzed path, k_2', can be estimated in the following manner. Linearity of the plots in Fig. 1 indicates $1 \gg K[H^+]$ at $[H^+]=0.2$ mol dm^{-3}, leading to $K \ll 5$. Thus the value of k_2' is greater than 3.5×10^{-5} s^{-1} at 50.0 °C. In conformity with the proposed scheme, the rate constant corresponding to acid-catalyzed path is observed to be much higher than that of uncatalyzed process (Table 1). This can be ascribed to the fact that the acid-catalyzed path is suggested to involve the protonation of the chelated acetylacetone ligand thereby putting a formal positive charge on ligand oxygen atom .As

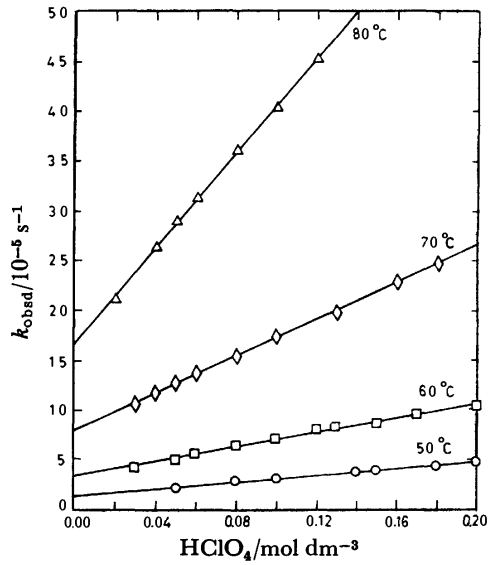

Fig. 1. Effect of acid concentration on k_{obsd} at different temperatures (Complex, 0.002 mol dm^{-3}; μ, 1.0 mol dm^{-3}).

a consequence of strong bonding between oxygen atom of the acetylacetone and H^+ ion in the protonated from of the complex (conjugate acid) further weakens the Cr–O bond and thus accounting for a greater lability for the fission of the bond as is indicated by the higher rate for the acid-catalyzed path. A similar trend has been observed in other acetylacetonato complexes of chromium(III).[4,8,9] Alternative pathways for acid catalysis may involve the association of the scavenging proton at the central carbon of the leaving Hacac giving rise to the following structure:

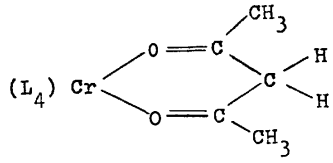

However, the above alternative scheme would leave keto groups as ligands which seems to be less probable.[15] In absence of conclusive evidence the alternative scheme cannot be excluded unambigously. The activation enthalpies corresponding to acid-catalyzed paths for [Cr(acac)$_3$], and [Cr (atda) (acac)]$^-$ are 20.2 kcal mol^{-1} and 19.2 kcal mol^{-1}, respectively. Comparable activation enthalpies clearly suggests that the total cost of bond adjustments is similar in two paths for Cr–O bond rupture. Similarity in activation parameters, ΔH^* and ΔS^* values (Table 1) for spontaneous and acid-catalyzed path seem to suggest that same type of mechanism is operative in the transition state for both the processes. As in the case of [Cr(acac)$_3$] system,[8] the entropy of activation corresponding to k_1 and k_2 in the present system has been found to be highly negative. The high negative ΔS^* values for k_1 and k_2 are compatible with processes in which participation of a molecule of water hydrogen bonded to ligand in the rate-determining step is important,[16] suggesting an assisted dissociative mechanism as depicted below, which also accounts for the low ΔH^* values:

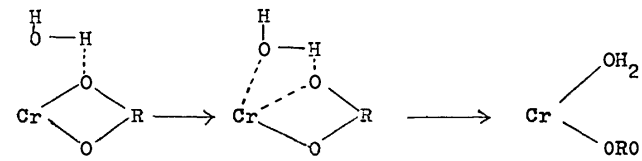

(Transition state)

where ORO stands for acac or acacH as the case may be. As in the case of [Cr(acac)$_3$] system, the entropy of activation, ΔS^* corresponding to uncatalyzed path for the present system is observed to be more negative than that of acid-catalyzed path. The relatively less negative value of ΔS^* for the H^+ dependent path is evidently due to the highly negative ΔS^* term for the dissociation of the chromium(III)–ligand bond being partly compensated by the positive ΔS^* term (also contributing to the overall ΔS^* for k_2) expected for the protonation pre-equilibrium, since this will lead to release of water molecules from the solvation spheres of aqueous H^+ ion. The effect of ionic strength on the rate of aquation has been studied and the values of k_1 and k_2 evaluated from a plot of k_{obsd} *vs.* [$HClO_4$] are presented in Table 1. Table 1 reveals that under otherwise identical conditions the uncatalyzed rate constant remained unaffected by the variation of ionic strength of the medium in accordance with the proposed mechanism. In contrast to the expected trend the value of k_2 is found to decrease slightly with decrease in ionic strength of the medium the reason of which is not clear at the present moment.

References

1) H. Ogino, T. Watanabe, and N. Tanaka, *Inorg. Chem.*, **14**, 2093 (1975).
2) Y. Sulfab, R. S. Taylor, and A. G. Sykes, *Inorg. Chem.*, **15**, 2388 (1976).
3) J. Guardalabene, S. Gulnac, N. Keder, and R. E. Shepherd, *Inorg. Chem.*, **18**, 22 (1979).
4) K. V. Krishnamurthy and G. M. Harris, *J. Phys. Chem.*, **64**, 346 (1960).
5) D. Banerjea and M. S. Mohan, *J. Inorg. Nucl. Chem.*, **27**, 1643 (1965).
6) D. Banerjea and C. Chatterjee, *J. Inorg. Nucl. Chem.*, **29**, 2387 (1967).
7) D. Banerjea and C. Chatterjee, *J. Inorg. Nucl. Chem.*, **30**, 3354 (1968).
8) D. Banerjea, *Z. Anorg. Allg. Chem.*, **359**, 305 (1968).
9) D. Banerjea and S. Sarkar, *J. Indian. Chem. Soc.*, **1**, **635** (1973).
10) J. P. Collman, *Adv. Chem. Ser.*, **37**, 78 (1963).
11) T. Tomita, E. Kyuno, and R. Tsuchiya, *Bull. Chem. Soc. Jpn.*, **42**, 947 (1969).
12) E. C. Lingafelter and R. L. Braun, *J. Am. Chem. Soc.*, **88**, 2951 (1966).
13) a) R. H. Holm and F. A. Cotton, *J. Am. Chem. Soc.*, **80**, 5658 (1958); b) D. W. Barnum, *J. Inorg. Nucl. Chem.*, **21**, 221 (1961); c) K. Nakamoto, P. L. McCarthy, A. Ruley, and A. E. Martell; *J. Am. Chem. Soc.*, **83**, 1066, 1272

(1961); d) C. K. Jorgensen, *Acta. Chem. Scand.*, **16**, 2406 (1962); e) R. E. Hester and R. A. Plane, *Inorg. Chem.*, **3**, 513 (1964); f) K. DeArmond and L. S. Forster, *Spectrochim. Acta*, **18**, 1393 (1963); g) D. R. Eaton, *J. Am. Chem. Soc.*, **87**, 3097 (1965); h) I. Hanazaki, F. Hanazaki, and S. Nagagura, *J. Chem. Phys.*, **50**, 276 (1969); i) A. M. Fatta and R. L. Lintvedt, *Inorg. Chem.*, **10**, 478 (1971).

14) J. P. Collman. R. A. Moss, H. Maltz, and C. C. Heindel, *J. Am. Chem. Soc.*, **83**, 531 (1961).

15) D. Meisel, K. H. Schmidt, and D. Meyerstein, *Inorg. Chem.*, **18**, 971 (1979).

16) R. E. Powell, *J. Phys. Chem.*, **58**, 528 (1954).

 © 1984 The Chemical Society of Japan Bull. Chem. Soc. Jpn., 57, 2299—2302 (1984)

A Study on Some Simple and Mixed Ligand *N,N*-Disubstituted Dithiocarbamates of Thallium(III)

G. Soundararajan and M. Subbaiyan*

Department of Analytical Chemistry, University of Madras, A. C. College Campus, Guindy, Madras 600025, Tamil 1 Nadu, India

(Received September 9, 1982)

Neutral tris (*N,N*-disubstituted dithiocarbamato) thallium (III) ((Tl(III)) has been prepared from acyclic dimethylamine, diethylamine, dipropylamine, dibutylamine, *N*-methylaniline, dibenzylamine, and from piperidine. Mixed ligand dithiocarbamates were found to form by ligand exchange reactions while mixing the simple, symmetric chelates in nonpolar solvents and got separated on preparative TLC layers of silica gel. These chelates were characterised by elemental analyses, IR, ^{1}H NMR, and electronic spectral studies.

Ligand exchange reaction and the formation of corresponding mixed ligand complexes have been reported by some authors for neutral *N,N*-disubstituted dithiocarbamates of some transition elements.[1-4] HPLC[1] and ^{1}H NMR[5] studies have shown that the rate of ligand exchange among the bis-chelates with square planar structure (with vacant axial positions) is faster than in tris-chelates with octahedral structure. The ligand exchange among neutral non-transition metal dithiocarbamates has so far not been studied in detail except the report of Stary and Ruzicka[6] about the formation of dithiocarbamate–dithizone mixed ligand complexes in solution for some Group V-a metalloids. It is also found that works dealing with tris(*N,N*-disubstituted dithiocarbamato)thallium(III) complexes are rare[7] than those of thallium(I) dithiocarbamates. Though Usatenko and Kucenko[8] speak of the relative instability of thallium(III) dithiocarbamates, solvent extraction studies[9] provide them with greater extraction and formation constants. Literature survey revealed that dimethyl and diethyl dithiocarbamates[10-13] of thallium(III) alone have been studied in some detail.

This work reports the preparation and characterisation of some simple symmetric tris (dithiocarbamate)s of thallium(III) from dipropylamine, dibutylamine, dibenzylamine, *N*-methylaniline, and piperidine. This also reports the formation of mixed ligand dithiocarbamates of thallium(III) from symmetric chelates in nonpolar solvents, their separation on preparative TLC layers and characterization.

Experimental

Sodium salts of the *N,N*-disubstituted dithiocarbamic acids were prepared from dimethylamine, diethylamine (BDH samples), dipropylamine (Fluka AG), dibutylamine (Merck-Schuchardt), *N*-methylaniline (BDH), dibenzylamine (KL), and from piperidine (Riedel) following the standard procedure.[7] At 0—5°C, amine, carbon disulfide (both in dioxane) and sodium hydroxide in minimum quantity of water were mixed in equimolar proportions with constant mechanical stirring. The sodium salts formed as white solids were separated by filtration and recrystallized from 2-propanol. Good yields were obtained in dioxane medium than in acetone (reported recently[14] while this work was in progress).

Thallium(III) tris (dithiocarbamate)s were prepared by mixing the metal ion (Tl(III) prepared from Tl(I) as reported[15]) and sodium salt of the ligand in aqueous solutions in 1:3 molar ratio. The yellowish orange solids precipitated were repeatedly washed with water, dried and recrystallized from chloroform.

Preparation of Mixed Ligand Complexes

20 mM (1M=1 mol dm^{-3}) of a thallium(III) dithiocarbamate (which is to be present in greater proportions) in 40 ml benzene was mixed with 10 mM (in 20 ml benzene) of another thallium(III) dithiocarbamate with different *N*-alkyl substituents and stirred well magnetically for 30 min at room temperature (29 °C). Mixed ligand chelates were formed in solution by the ligand exchange reaction among the symmetric chelates, and the following equilibrium was established.

$$2Tl(S_2CNR_2)_3 + Tl(S_2CNR_2')_3 \rightleftharpoons 3Tl(S_2CNR_2)_2(S_2CNR_2').$$

The resulting solution was concentrated under low pressure (0.1 Torr, 1 Torr≈133.322 Pa), spotted on preparative TLC plates (50 to 60 μl of solution per spot) and developed with xylene as the mobile phase. After development, the TLC layers corresponding to the mixed ligand complexes were scrapped off, extracted with minimum quantity of xylene or CCl_4 under inert atmosphere and the solvent was removed in a vacuum evaporator to get the shiny orange crystals of mixed ligand complexes.

Molecular weights were determined cryoscopically in benzene. Elemental analyses (C and H) were performed with a Perkin-Elmer (model 240 B) analyzer. Nitrogen was estimarted by micro Kjeldahl method and sulfur by gravimetry as $BaSO_4$. Electronic spectra were obtained with a Beckmann (Model 25)-UV-visible spectrophotometer in CCl_4. IR spectra were recorded with a Perkin-Elmer (model 199) spectrometer scanning the region 4000 to 200 cm^{-1} in KBr pellets. ^{1}H NMR spectra were recorded on a Varian 60 MHz instrument in CCl_4 ($CDCl_3$ in some cases) with TMS as the internal standard. Photodensitometric studies were made with Carl Zeiss, Jena (GDR) instrument and the spot areas were measured with an Angler Planimeter. Silica gel supplied by BDH were employed for preparing thin layers. All chemicals employed in this study were of analytical grade.

TABLE 1. ANALYTICAL DATA OF SOME SIMPLE AND MIXED LIGAND DITHIOCARBAMATES OF THALLIUM(III)

Complex	Found (Calcd) (%)				Mol wt	Mp-m/°C	Absorbance in 10^3 cm^{-1} in the visible region (log ε)
	C	H	N	S			
A	34.26 (34.39)	5.71 (5.79)	5.78 (5.73)	26.36 (26.23)	758 (733.3)	164	23.5 (3.36)
B	39.52 (39.67)	6.65 (6.66)	5.22 (5.14)	23.62 (23.53)	887 (817.5)	150	23.5 (3.41)
C	52.88 (52.90)	4.11 (4.14)	4.04 (4.11)	18.88 (18.82)	1044 (1021.6)	147	23.2 (3.43)
D	38.35 (38.37)	3.18 (3.22)	5.62 (5.59)	25.68 (25.61)	793 (751.2)	170 (decomp)	23.9 (3.32)
E	31.52 (31.55)	4.35 (4.41)	6.10 (6.13)	28.0 (28.10)	708 (685.2)	180 (decomp)	23.5 (3.30)
F	45.52 (45.58)	3.90 (3.94)	4.89 (4.83)	22.20 (22.13)	883 (869.4)	170 (decomp)	23.4 (3.38)
G	30.04 (30.15)	5.02 (5.06)	6.28 (6.21)	28.5 (28.4)	698 (677.2)	186	23.6 (3.31)
H	32.24 (32.36)	5.29 (5.43)	6.03 (5.96)	27.32 (27.27)	756 (705.3)	182 (decomp)	23.5 (3.32)
I	38.81 (38.83)	4.38 (4.43)	5.47 (5.43)	24.93 (24.87)	787 (773.3)	175 (decomp)	23.4 (3.31)

A: $Tl(S_2CN(n\text{-}C_3H_7)_2)_3$, B: $Tl(S_2CN(n\text{-}C_4H_9)_2)_3$, C: $Tl(S_2CN(CH_2C_6H_5)_2)_3$, D :$Tl(S_2CN(CH_3C_6H_5)_2)_3$, E: $Tl(S_2CN(C_5H_{10}))_3$, F: $Tl(S_2CN(CH_3)_2)\cdot(S_2CN(CH_2C_6H_5)_2)_2$, G: $Tl(S_2CN(C_2H_5)_2)_2\cdot(S_2CN(n\text{-}C_3H_7)_2)$, H: $Tl(S_2CN(C_2H_5)_2)_2\cdot(S_2CN(n\text{-}C_4H_9)_2)$, I: $Tl(S_2CN(C_2H_5)_2)_2\cdot(S_2CN(CH_2C_6H_5)_2)$.

Results and Discussion

Dithiocarbamates of thallium(III) ion derived from dipropylamine, dibutylamine, *N*-methylaniline, dibenzylamine, and piperidine are reported for the first time. The results of the elemental analyses presented in Table 1 are in accordance with their tris-chelate chemical compositions. In solid state, these chelates are stable indefinitely, if stored in dark. However in solutions of nonpolar solvents like benzene, chloroform, *etc.*, they decompose after a week. Molecular weight determination showed the presence of monomeric species in solution. Conductivity measurements in nitrobenzene showed their neutral, nonionic character.

On mixing the individual symmetric dithiocarbamates in nonpolar solvents, the unsymmetric mixed ligand complexes are formed and equilibrium is established.

$$2TlL_3 + TlL_3' \rightleftharpoons 3TlL_2L'$$

Photodensitometric studies at 420 nm of the resolved spots on thin layers (spotting known quantities of the stirred mixture)corresponded to about 60 to 65% conversion of symmetric chelates into ternary unsymmetric chelates. The log K values for the formation of these mixed ligand complexes (K=equilibrium constant=$([TlL_2L']^3/[TlL_3]^2[TlL_3'])$ arrived at from the equilibrium concentrations are around 1.36 to 1.45. (compound F=1.36, G=1.44, H=1.41, and I=1.38). The greater log K values observed relative to the statistical value of 0.83 show the stabilization of mixed ligand complexes by solvation or entropy effects. The total area of the spots of symmetric and unsymmetric chelates on the chromatogram is almost equal with the sum of the areas of two spots of the symmetric chelates, spotted separately. The mixed ligand chelates of Tl(III) are found not so labile as other transition metal chelates reported earlier[1-3,16] facilitating their separation on preparative TLC layers. However, the pale yellow streaks observed, with active, nonpolar solvents like chloroform, dichloro methane, *etc.*, as mobile phases indicate their partial disintegration into symmetric complexes. It is also found that with increase in

TABLE 2. THE hR_f VALUES OF SOME SIMPLE AND MIXED LIGAND DITHIOCARBAMATES OF THALLIUM(III)

Complex	Eluent		
	$CHCl_3$: C-C_6H_{12} (1 : 1)	$CHCl_3$: CCl_4 (1 : 1)	Xylene
I. Symmetric Simple Complexes			
$Tl(Me_2dtc)_3$	13.8	18.6	17.1
$Tl(Et_2dtc)_3$	29.7	40.6	33.3
$Tl(Pr_2dtc)_3$	57.7	67.4	56.6
$Tl(Bu_2dtc)_3$	82.5	95.9	91.4
$Tl((Pip)(dtc))_3$	28.8	35.4	23.8
$Tl(Bz_2dtc)_3$	67.4	81.6	80.0
II. Unsymmetric Mixed Ligand Complexes			
$Tl(Me_2dtc)_2Pr_2dtc$	28.2	44.8	37.8
$Tl(Me_2dtc)_2Bu_2dtc$	42.7	55.2	47.9
$Tl(Me_2dtc)(Bz_2dtc)_2$	30.3	54.1	49.5
$Tl(Et_2dtc)_2Pr_2dtc$	40.0	57.6	46.7
$Tl(Et_2dtc)_2Bu_2dtc$	51.4	67.0	60.8
$Tl(Et_2dtc)_2Bz_2dtc$	38.8	63.0	53.7
$Tl((Pip)(dtc))_2Pr_2dtc$	41.0	53.1	50.2
$Tl((Pip)(dtc))_2Bu_2dtc$	51.2	67.0	60.0
$Tl((Pip)(dtc))_2Bz_2dtc$	48.0	59.2	55.2

Layer thickness 0.25 mm. Activated at 100 °C for half an hour. Ascending development in closed chambers preequilibrated with eluent vapours for 1 h. Mobile phase movement upto 11 cm from the spotted region. C-C_6H_{12}=Cyclohexane

solvent phase polarity, the disintegration is accelerated, *i. e.*, in the order.

xylene<toluene<benzene<chloroform<dichloromethane.....

The formation of diagonally arranged spots on two dimensional TLC plates, as reported earlier,[1] with moderately polar mobile phases containing $CHCl_3$ or CH_2Cl_2 also support their instability in polar solvents.

Since Moriyasu and Hashimoto[2] showed that ligand exchange is dependent only on statistical factor, the nonpolar solvent molecules surrounding the neutral mixed ligand chelate molecules in solution may be presumed to prevent their collision among themselves, which lead to their disintegration. The hR_f values reported in Table 2 show that these mixed ligand chelates are intermediate in their migratory behaviour with respect to their parent chelates.

Electronic Spectra. All simple and mixed ligand dithiocarbamates show strong absorptions in the UV region around 38.5×10^3 cm^{-1} due to π–π^* transition.[17] Absorption maxima in the visible region around 23.5×10^3 cm^{-1} (log ε 3.3 to 3.4) for simple chelates (n–π^* transition) are considerably broadened for mixed ligand chelates (from 23.7 to 23.4×10^3 cm^{-1}, Figs. 1 and 2 and Table 1).

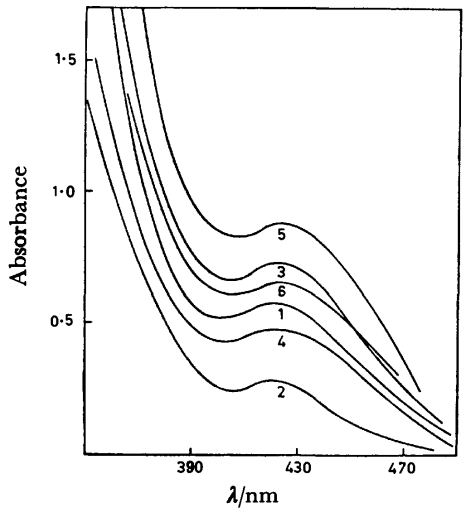

Fig. 1. Absorption spectra of symmetric simple dithiocarbamates of Thallium(III) in CCl_4.
1: $Tl(Me_2\,dtc)_3=2.5\times10^{-4}$ M, 2: $Tl(Et_2\,dtc)_3=1.4\times10^{-4}$ M, 3: $Tl(Pr_2\,dtc)_3=3.0\times10^{-4}$ M, 4: $Tl(Bu_2dtc)_3=1.8\times10^{-4}$ M, 5: $Tl(Bz_2\,dtc)_3=3.3\times10^{-4}$ M, 6: $Tl((Pip)(dtc))_3=3.3\times10^{-4}$ M.

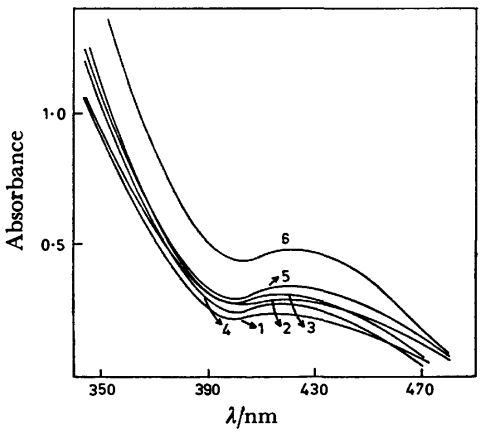

Fig. 2. Absorption spectra of some unsymmetric mixed ligand dithiocarbamates of Thallium (III) in CCl_4.
1: $Tl((Pip)(dtc))_2(Pr_2\,dtc)=1.2\times10^{-4}$ M, 2: $Tl((Pip)(dtc))_2(Bz_2dtc)=1.4\times10^{-4}$ M, 3: $Tl(Me_2\,dtc)_2(Pr_2\,dtc)=1.4\times10^{-4}$ M, 4: $Tl(Me_2\,dtc)_2(Bu_2\,dtc)=1.2\times10^{-4}$ M, 5: $Tl(Me_2\,dtc)(Bz_2\,dtc)_2=1.4\times10^{-4}$ M, 6: $Tl(Et_2\,dtc)_2(Pr_2\,dtc)=2.3\times10^{-4}$ M.

TABLE 3. ^{1}H NMR SPECTRAL DATA OF SOME SIMPLE AND MIXED LIGAND COMPLEXES OF THALLIUM(III) (IN CCl_4+TMS)

Complexe	A	B	C	D
$Tl(Me_2dtc)_3$	6.88(18 s)	—	—	—
$Tl(Et_2dtc)_3$	5.93(12 q)	8.47(18 t)	—	—
$Tl(Pr_2dtc)_3$	6.39(12 t)	8.14(12 m)	9.07(18 t)	—
$Tl(Bu_2dtc)_3$	6.46(12 t)	8.81(12 m)	8.92(12 m)	9.13(18 t)
$Tl(Bz_2dtc)_3$	4.74(12 s)	2.44(30 s-ϕ)	—	—
$Tl(Bu_2dtc)_2(Me_2dtc)$				
Me_2dtc	6.61(6 s)	—	—	—
	6.44(6 s)	—	—	—
Bz_2dtc	4.87(4 s)	2.74(20 s-ϕ)	—	—
	5.07(4 s)	—	—	—
$Tl(Et_2dtc)_2(Pr_2dtc)$				
Et_2dtc	5.87(8 s)	8.41(12 t)	—	—
Pr_2dtc	6.14(4 t)	8.00(4 m)	8.82(6 t)	—
$Tl(Et_2dtc)_2(Bu_2dtc)$				
Et_2dtc	6.28(8q)	8.54(12 t)	—	—
Bu_2dtc	6.34(4 t)	8.67(4 m)	8.81(4m)	9.09(6 t)
$Tl(Et_2dtc)_2(Bz_2dtc)$				
Et_2dtc	6.22(8q)	8.61(12 t)	—	—
Bz_2dtc	5.11(2 s)	2.83(10 s-ϕ)	—	—
	4.91(2 s)	—	—	—

s=singlet; t=triplet; q=quartet; m=multiplet.

Infrared Spectra. The characteristic absorption due to 'thioureide' bond (N=C) is observed in the region 1470 to 1490 cm^{-1}. The mixed ligand complexes show uniformly greater ν(C=N) infrared absorption frequencies corresponding to the increased flow of electron from N-atom to donor centres resulting in stronger M–S bond and more stable chelates. However, in general, for mixed ligand complexes, the dithiocarbamate group present in greater proportions determines their IR spectral characteristics. For simple chelates, the ν(C=N) frequencies are in the order diethyl->dipropyl->dibutyl->pentamethylene->dibenzyldithiocarbamates with respect to *N*-substituents.

The inductive effect of benzyl groups and the rigid heterocyclic ring structure of piperidino group[18] restrict the easy drift of electrons from N to C-atom resulting in decreased C=N bond order in their chelates. Though basic character increases from dimethylamine to dibutylamine, the increasing *N*-alkyl chain length (by mass effect) prevent[19] the electron flow from N to C-atom *via* hyperconjugation. The ν(C=S) frequencies are observed as single and strong peaks in the region 980 to 1005 cm^{-1} indicating the bidentate nature of dithiocarbamate moieties.[20] The increased ν(C=N bond order generally resulted in decreased ν(C=S) frequencies.

^1H NMR Spectra. Table 3 shows the ^1H NMR spectral data of some simple and mixed ligand dithiocarbamates of thallium(III). The α-proton signals are shifted significantly to new energy regions (mostly in downfield direction) in mixed ligand complexes in addition to the observation of new peaks for some mixed ligand chelates. The splitting of α-proton signals of methyl and benzyl groups in Tl (die. dtc)$_2$ (dibenz. dtc) (Table 3) and Tl (dime. dtc) (dibez. dtc)$_2$ observed may be due to complex stereochemical positioning of the two benzyl and methyl groups. In moderately polar $CDCl_3$+TMS solvent, the ^1H NMR signals of the mixed ligand chelates gradually get shifted to the regions as in parent chelates indicating their disintegration as discussed earlier. This observation as against that of Duffy[16] for iron(III) dithiocarbamates show the greater stability of thallium(III) mixed ligand chelates and also the importance of ^1H NMR spectra in the study of ligand exchange reactions as observed earlier.[4]

References

1) O. Liska, J. Lehotay, E. Brandsteterova, and G. Guiochon, *J. Chromatogr.*, **171**, 153 (1979); **172**, 379 (1979).
2) M. Moriyasu and Y. Hashimoto, *Bull. Chem. Soc. Jpn.*, **53**, 3590 (1980).
3) M. Moriyasu and Y. Hashimoto, *Chem. Lett.*, **1980**, 117.
4) R. Chant, A. R. Hendrickson, R. L. Martin, and N. M. Rohde, *Inorg. Chem.*, **14**, 1894 (1975).
5) E. Beinrohr and J. Garaj, *Collect. Czech. Chem. Commum.*, **45**, 1785 (1980).
6) J. Stary and J. Ruzicka, *Talanta*, **15**, 505 (1968); **14**, 909 (1967).
7) D. Coucouvanis, *Progr. Inorg. Chem.*, **11**, 271 (1971).
8) J. I. Usatenko and L. M. Kucenko, *Zh. Analit, Khim.*, **19**, 1315 (1964).
9) A. Wyttenbach and S. Bajo, *Anal. Chem.*, **47**, 2 (1975).
10) S. Akerstrom, *Ark. Kemi.*, **24**, 495 (1965).
11) F. A. Cotton, B. F. G. Johnson, and R. M. Wing, *Inorg. Chem.*, **4**, 502 (1965).
12) F. Bonati, S. Cemini, and R. Ugo, *J. Organomet. Chem.*, **9**, 395 (1967).
13) K. Hagiwara, H. Suzuki, and I. Muraki, *Bunseki Kagaku*, **10**, 607 (1961).
14) R. V. Moore, *Anal. Chem.*, **54**, 895 (1982).
15) G. Brauer, "Handbook of preparative Inorganic Chemistry". Academic Press, London (1963).
16) N. V. Duffy, W. G. Movious, and D. L. Uhrich, *Inorg. Chim. Acta*, **64**, L91 (1982).
17) M. J. Janssen, *Recl. Trav. Chim. Pays-Bas*, **79**, 1066 (1960).
18) C. Preti, G. Tosi, and P. Zannini, *J. Mol. Struct.*, **65**, 283 (1980).
19) D. Okatavec, E. Beinrohr, B. Siles, and J. Garaj, *Collect. Czech. Chem. Commun.*, **45**, 1495 (1980).
20) K. A. Jenssen, B. M. Dahl, P. H. Nielson, and G. Borch, *Acta Chem. Scand.*, **25**, 3709 (1974).

Mixed Chelates of Cadmium(II) with *N*-(2-Hydroxyethyl)ethylenediamine and Some Amino Acids

Chandra Pal Singh CHANDEL and Chand Mal GUPTA*
Department of Chemistry, University of Rajasthan, Jaipur-302004 India
(Received May 19, 1983)

An extended method of Schaap and McMasters[1] has been applied for the study of mixed-ligand complexes of Cadmium(II) with *N*-(2-hydroxyethyl) ethylenediamine (heda) and some amino acids polarographically at DME. The reduction of mixed-ligand complex at DME has been found to be reversible, and diffusion controlled at temp (30±0.5)°C and μ=1.0 M†† (KNO_3). The formation of MXY, MXY_2, and MX_2Y has been used to discuss the non-existence of MX_3 complexes, where X has been used for heda and Y for amino acids. The values of stability constants β_{01}, β_{02}, β_{03}, β_{11}, β_{12}, and β_{21} are 3.90, 6.80, 8.94, 8.85, 11.00, and 12.13 for Cd–heda–isoleucinate system, 4.30, 7.70, 9.80, 9.36, 11.75, and 12.42 for Cd–heda–glycinate system, 3.95, 6.81, 8.90, 8.35, 10.99, and 12.12 for Cd–heda–valinate system, 4.10, 7.10, 9.08, 9.02, 11.20, and 12.18 for Cd–heda–serinate system, 4.48, 8.02, 10.33, 9.55, 12.00, and 12.59 for Cd–heda–glutamate system, 4.24, 7.54, 9.54, 9.26, 11.62, and 12.33 for Cd–heda–alaninate system and 4.06, 7.06, 9.02, 9.00, 11.16, and 12.20 for Cd–heda–threoninate system respectively.

For the determination of mixed-ligand complexes where third complex does not exist in any one out of the simple systems studied, an extention has been made in the method of Schaap and McMasters.

In this communication the extended method of Schaap and McMasters has been used to discuss the mixed-ligand complex formation of cadmium(II) with *N*-(2-hydroxyethyl)ethylenediamine(heda) and isoleucinate, glycinate, valinate, serinate, glutamate, alaninate, and threoninate. The weeker ligand (amino acids) forms three complexes (MY, MY_2, and MY_3) while strong ligand (heda) does not form MX_3 complex.

A survey of literature reveals that the stability constants of the above type mixed-ligand complexes have not been evaluated to date, except our earlier studies.[3]

Theory

For a complexation reaction,

$$M + {}_iX + {}_jY \rightleftharpoons MX_iY_j.$$

Where i, j are stoichiometry numbers, X and Y are two different ligands and charges have been ignored for simplicity.

The overall stability constant β_{ij} for the above reaction is given by

$$\beta_{ij} = \frac{MX_iY_j}{M[X]^i[Y]^j}.$$

According to the method of Schaap and McMasters the formation function $F_{00}[X, Y]$ may be expressed by

$$\begin{aligned} F_{00}[X,Y] = {} & \{\beta_{00}+\beta_{01}[Y]+\beta_{02}[Y]^2+\beta_{03}[Y]^3\}[X]^0 \\ & + \{\beta_{10}+\beta_{11}[Y]+\beta_{12}[Y]^2\}[X] \\ & + \{\beta_{20}+\beta_{21}[Y]\}[X]^2 \\ & + \{\beta_{30}\}[X]^3, \end{aligned} \quad (1)$$

which may, for simplicity, be written as

$$F_{00}[X,Y] = A + B[X] + C[X]^2 + D[X]^3. \quad (2)$$

Where A, B, C, and D are constant for a given value of [Y], and have values as defined by equiv (1).

The plot of $F_{00}[X, Y]$ *vs.* [X] when extrapolated to [X]=0 on the $F_{00}[X, Y]$ axis, will give the value of the constant A which should essentially be equal to the value of $F_0[Y]$ for the simple M–Y system, as calculated by the method of DeFord and Hume. The constant B can be found similarly from the F_{10} [X, Y] function, defined as

$$\begin{aligned} F_{10}[X,Y] &= \frac{F_{00}[X,Y]-A}{[X]} \\ &= B + C[X] + D[X]^2, \end{aligned} \quad (3)$$

by obtaining the intercept from the plot of $F_{10}[X, Y]$ *vs.* [X]. Similarly, plots of $F_{20}[X, Y]$ and $F_{30}[X, Y]$ *vs.* [X] will give intercepts on $F_{20}[X, Y]$ and $F_{30}[X, Y]$ at [X]=0, as C and D respectively. The value of D should be equal (within experimental errors) to the overall stability constant of the MX_3 complex when calculated from the simple M–X system.

From the knowledge of values of B and C at two different concentrations of Y, the values of stability constants of mixed-ligand complexes MXY, MXY_2 and MX_2Y can be evaluated.

Experimental

Chemicals. *N*-(2-hydroxyethyl)ethylenediamine (heda) was obtained from Fluka A.G. (Switzerland) and serine from Merck and other amino acids from S.D.'s Chemical Co., while potassium nitrate was used as supporting electrolyte and gelatin as maxima suppressor.

Apparatus. Manual polarograph with capillary characteristics $m^{2/3}t^{1/6}=1.96\ mg^{2/3}s^{-1/2}$ in open circuit was used. Elico., Digital pH meter model Ll-120 was used to determine the pH of the solutions. The experimental technique was same as described earlier.[4]

Results

Binary Systems. The dissociation constants for *N*-(2-hydroxyethyl)ethylenediamine and amino acids were calculated by the method of Albert and Sergeant[5] which agreed well with literature.[6–8] (Table 1). The stepwise formation constants of the complexes of Cd(II) with amino acids were determined separately before

† Presented in XXII ICCC, Budapest (Hungary) 1982, Abstr. No. Th. p. 21, page 550.

†† 1 M=1 mol dm^{-3}.

TABLE 1. pK VALUES OF THE LIGANDS

Ligand	pK_2^H
Heda	9.80±0.01
Isoleucine	9.74±0.01
Glycine	9.62±0.02
Valine	9.50±0.02
Serine	9.10±0.02
Glutamic acid	9.40±0.02
Alanine	9.70±0.02
Threonine	9.12±0.02

TABLE 2. FORMATION CONSTANTS FOR BINARY COMPLEXES

Cadmium complex	Formation constants (log)	Cadmium complex	Formation constants (log)
Cd(heda)	5.39	Cd(serinate)	4.10
$Cd(heda)_2$	9.80	$Cd(serinate)_2$	7.10
Cd(isoleucinate)	3.90	$Cd(serinate)_3$	9.08
$Cd(isoleucinate)_2$	6.80	Cd(glutamate)	4.48
$Cd(isoleucinate)_3$	8.94	$Cd(glutamate)_2$	8.02
Cd(glucinate)	4.30	$Cd(glutamate)_3$	10.33
$Cd(glycinate)_2$	7.70	Cd(alaninate)	4.24
$Cd(glycinate)_3$	9.80	$Cd(alaninate)_2$	7.54
Cd(valinate)	3.95	$Cd(alaninate)_3$	9.54
$Cd(valinate)_2$	6.81	Cd(threoninate)	4.06
$Cd(valinate)_3$	8.90	$Cd(threoninate)_2$	7.06
		$Cd(threoninate)_3$	9.02

the study of the mixed-ligand system, by the method of DeFord and Hume.[2] The conditions used corresponded as closely as possible to those for the mixed systems *i.e.* ionic strength was 1.0 M (KNO_3) and temp. (303±1)K. The formation constants which are in good agreement with literature,[9–13] have been tabulated in Table 2.

Ternary Systems. The cadmium–heda–amino acid systems were studied by keeping the concentration of the weaker ligand (amino acids) constant at two different values while varying the concentration of heda in each case, the total cadmium concentration was kept at 5×10^{-4} M.

Free ligand concentration for each system has been calculated with the help of pH of the solution, pK values and amount of the ligand.

In all cases a single well-defined wave was obtained for which the plots of $-E_{de}$ *vs.* log $i/(i_d-i)$ gave a slope of (30±2) mV, indicating that the reduction is reversible and involves the transfer of two electrons. The reduction is diffusion controlled as evident by the direct proportionality of the limiting current to the square root of the effective height of mercury column.

By increasing the heda concentration, the half wave potential shifts towards more negative side and this shift is greater in the presence of the weaker ligands (amino acids) than in its absence. It signifies the formation of mixed-ligand complexes. The F_{10} function was evaluated by extending the method of Schaap and McMasters and A, B, and C were calculated by Leden's-graphical extrapolation method.[16] Stability constants

TABLE 3. STABILITY CONSTANTS OF MIXED-LIGAND COMPLEXES

System	log β_{11}	log β_{12}	log β_{21}
Cd-heda-isoleucinate	8.85	11.00	12.13
Cd-heda-glycinate	9.36	11.75	12.42
Cd-heda-valinate	8.85	10.99	12.12
Cd-heda-serinate	9.02	11.20	12.18
Cd-heda-glutamate	9.55	12.00	12.59
Cd-heda-alaninate	9.26	11.62	12.33
Cd-heda-threoninate	9.00	11.16	12.20

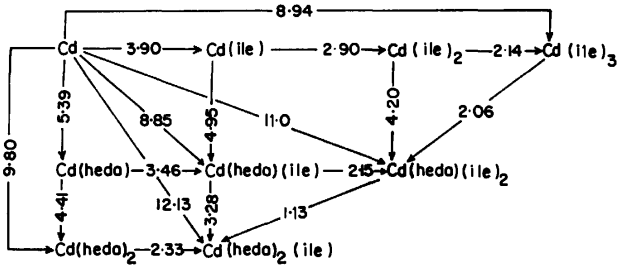

Scheme 1. Cadmium–heda–isoleucinate system.

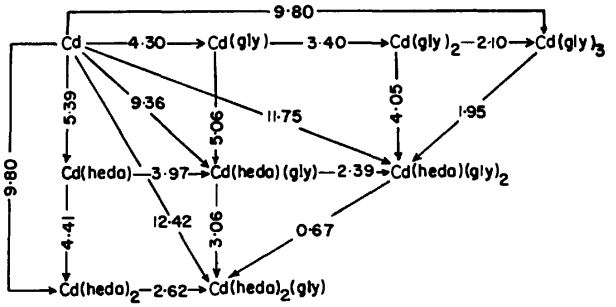

Scheme 2. Cadmium–heda–glycinate system.

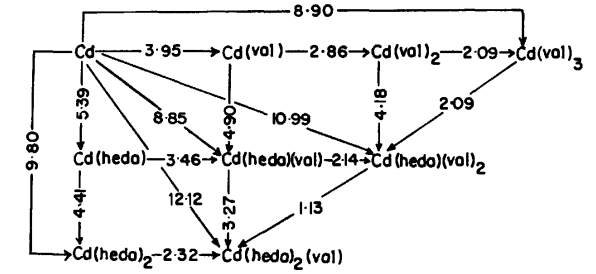

Scheme 3. Cadmium–heda–valinate system.

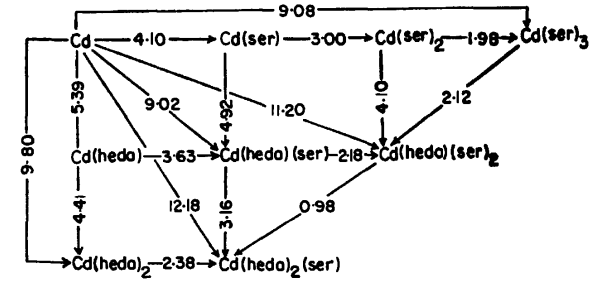

Scheme 4. Cadmium–heda–serinate system.

of mixed-ligand complexes have been presented in Table 3 and summarised in Schemes 1—7.

Discussion

The values of F_{20} for Cd–heda–isoleucinate are constant as 6.30×10^{10} and 2.80×10^{11} at 0.04 and 0.2 M of isoleucinate respectively (Tables 4 and 5). But these values differ appreciably with each other. Similar results have also been observed in Cd–heda–glycinate, Cd–heda–valinate, Cd–heda–serinate, Cd–heda–glutamate, Cd–heda–alaninate, and Cd–heda–threoninate. This proves the formation of maximum number of complexes, simple and mixed in each mixed-ligand system and these complexes contain more than one mixed-ligand species. It may be concluded that the formation of MXY, MXY_2 and MX_2Y mixed-ligand complexes is taking place in the solution.

With the help of Schemes 1—7 too, the formation of MXY, MXY_2, and MX_2Y may be explained. For the addition of heda to Cd(heda), Cd(ile), Cd(gly),

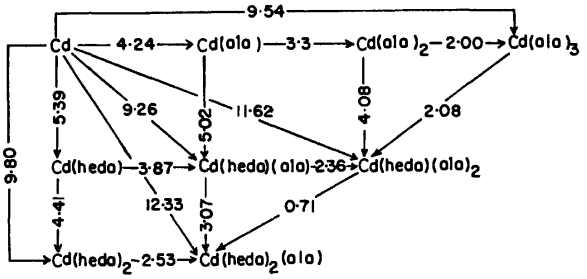

Scheme 6. Cadmium–heda–alaninate system.

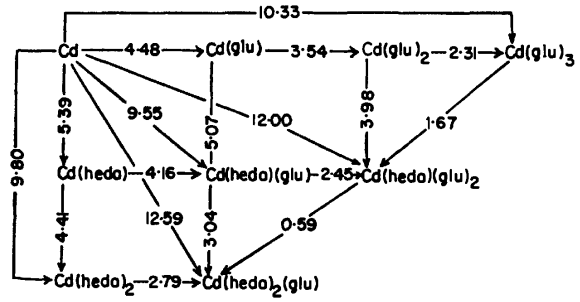

Scheme 5. Cadmium–heda–glutamate system.

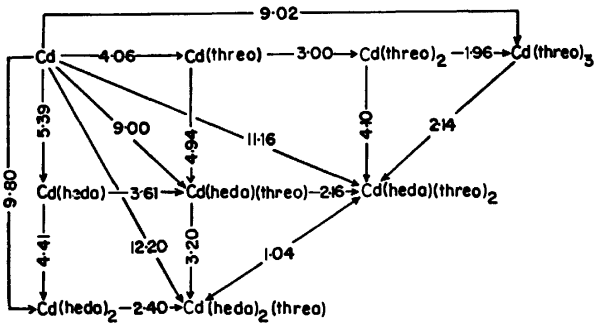

Scheme 7. Cadmium–heda–threoninate system.

Table 4. Data and results for cadmium–heda–isoleucinate system, (ile) = 0.04 M, $E_{1/2}$(M) = −0.580 V *vs.* SCE

$10^4\times$[X]/M	$\Delta E_{1/2}$/V	$\log\frac{I_M}{I_C}$	$F_{00}\times10^{-5}$	$F_{10}\times10^{-8}$	$F_{20}\times10^{-10}$	F_{00}(calcd)$\times10^{-5}$	ΔE/%*
0.52	0.145	0.0093	0.68	0.38	—	0.67	−1.47
2.68	0.152	0.0286	1.22	2.09	7.46	1.21	−0.82
8.14	0.162	0.0386	2.68	2.48	7.25	2.60	−2.99
24.22	0.177	0.0437	8.56	3.26	5.66	8.80	+2.80
46.10	0.189	0.0488	21.72	4.57	5.81	22.27	+2.53
102.46	0.207	0.0488	86.24	8.35	6.30	83.75	−2.89
148.36	0.215	0.0540	161.08	10.81	6.01	162.30	+0.76
218.30	0.224	0.0593	324.92	14.85	5.94	331.18	+1.93
290.69	0.231	0.0646	562.30	19.32	6.00	568.52	+1.11

$A=6.6\times10^4$ (calcd), $B=1.89\times10^8$, $C=(6.30\pm1.16)\times10^{10}$.

Table 5. Data and results for Cd–heda–isoleucinate system, (ile) = 0.2 M, $E_1/_2$(M) = −0.580 V *vs.* SCE

$10^4\times$[M]/M	$\Delta E_{1/2}$/V	$\log\frac{I_M}{IC}$	$F_{00}\times10^{-6}$	$F_{10}\times10^{-9}$	$F_{20}\times10^{-11}$	F_{00}(calcd)$\times10^{-6}$	ΔF/%*
10.24	0.211	0.0374	11.41	4.10	—	11.73	+2.80
34.72	0.221	0.0440	24.93	5.10	2.76	24.92	−0.04
66.18	0.229	0.0508	46.73	5.97	2.77	46.74	+0.02
152.46	0.243	0.0574	138.68	8.62	2.94	134.71	−2.86
198.66	0.247	0.0642	191.38	9.27	2.58	198.78	+3.87
274.40	0.254	0.0713	332.57	11.86	2.81	329.38	−0.96
344.26	0.259	0.0778	495.14	14.17	2.91	478.02	−3.46

$A=7.21\times10^6$ (calcd), $B=4.14\times10^9$, $C=(2.80\pm0.22)\times10^{11}$

* $\Delta F(\%)=\frac{100}{F_{00}(\text{exptl})}[F_{00}(\text{calcd})-F_{00}(\text{exptl})]$.

Cd(val), Cd(ser), Cd(glu), Cd(ala), and Cd(thr), the log values of stability constants are 4.41, 4.95, 5.06, 4.90, 4.92, 5.07, 5.02, and 4.94 respectively. These values indicate that it is easier for heda to add Cd (amino acids) than to Cd(heda) and also that the addition of heda is slightly favoured as the stability of the Cd(amino acids) decreases. The log K values for the addition of, isoleucinate- to Cd(ile) and Cd (heda) are 2.90 and 3.46, glycinate to Cd(gly) and Cd(heda) are 3.40 and 3.97, valinate to Cd(val) and Cd(heda) are 2.86 and 3.46, serinate to Cd(ser) and Cd(heda) are 3.00 and 3.63, glutamate to Cd(glu) and Cd(heda) are 3.54 and 4.16; alaninate to Cd(ala) and Cd(heda) are 3.30 and 3.87 and threoninate to Cd(thr) and Cd(heda) are 3.00 and 3.61, indicating that the mixed-ligand complexation is favoured.

The logarithms of stability constants for the addition of isoleucinate to $Cd(heda)_2$, Cd(heda) (ile), and $Cd(ile)_2$ are 2.33, 2.15, and 2.14 respectively and show that the mixed-ligand complex formation is preferred. The other systems follow suit.

The case of mixed-ligand complex formation by the addition of amino acids to $Cd(heda)_2$ and Cd(heda) (amino acids) may easily be confirmed on the basis of statistical considerations,[14] only when the values of stability constant of $Cd(heda)_3$ complex is known. In our experimental conditions such complex has not been identified but for the understanding view point such value may be evaluated by using equations 4—6 as proposed by Watters and Dewitt:[15]

$$\beta_{11} = 2 \times 3 \times \beta_{30}^{1/3} \times \beta_{03}^{1/3}, \quad (4)$$

$$\beta_{12} = 3 \times \beta_{30}^{1/3} \times \beta_{03}^{2/3}, \quad (5)$$

$$\beta_{21} = 3 \times \beta_{30}^{2/3} \times \beta_{03}^{1/3}. \quad (6)$$

These above equations are valid strictly when mixed-ligand complexation is characterised by the statistical factor. The values of stability-constants of $Cd(heda)_3$ complex so obtained from each system are given in Table 6.

Since all these β_{30} values are much higher than the stability constants of $Cd(heda)_2$, $Cd(heda)_3$ complex must exist at maximum heda concentration. This shows that the formation of $Cd(heda)_3$ complex is favoured by statistical factors whereas it does not exist in the simple system. The formation of $Cd(heda)_3$ may be opposed by some factors like the bulky nature of heda molecule.

By calculating the disproportionation constant K^D for the equilibria,

$$2Cd(heda)(\text{amino acids}) \rightleftharpoons Cd(\text{amino acids})_2 + Cd(heda)_2,$$

the tendency of the formation of 1:1:1 mixed ligand complex should be easily expressed. For statistical reasons the value of log K^D is −0.6 but the observed values are −1.10, −1.22, −1.11, −1.18, −1.28, −1.22, and −1.14 for Cd-heda-ile, Cd-heda-gly, Cd-heda-val., Cd-heda-ser., Cd-heda-glu., Cd-heda-ala and Cd-heda-thr, respectively. More negative values of log K^D for each equilibrium show that mixed-ligand complex formation is effected by some other factors.

TABLE 6. STABILITY CONSTANTS OF $Cd(heda)_3$ BY USING WATTERS AND DEWITTS EQUATIONS

System	Using equation 4	Using equation 5	Using equation 6
Cd-heda-isoleucinate	15.58	13.69	13.01
Cd-heda-glycinate	15.94	14.23	13.01
Cd-heda-valinate	15.31	13.75	12.99
Cd-heda-serinate	15.64	14.02	13.01
Cd-heda-glutamate	16.00	13.90	13.01
Cd-heda-alaninate	15.91	14.35	13.01
Cd-heda-threoninate	15.64	14.02	13.07

One of the authors (CPSC) is grateful to C.S.I.R., New Delhi for providing the fellowship and also thankful to Dr. N.P. Sachan, Chemistry Department, K.K. College, Etawah (U.P.) for his kind cooperation.

References

1) W. B. Schaap and D. L. McMasters, *J. Am. Chem. Soc.*, **83**, 4699 (1961).
2) D. D. DeFord and D. N. Hume, *J. Am. Chem. Soc.*, **73**, 5321 (1951).
3) N. P. Sachan, C. P. S. Chandel, and C. M. Gupta, *Chemica Scripta*, **20**, 111 (1982).
4) S. C. Khurana and C. M. Gupta, *Aust. J. Chem.*, **26**, 971 (1973).
5) A. Albert and E. P. Sergeant, "The Determination of Ionization Constants," Chapman & Hall, London (1971).
6) S. C. Khurana, J. K. Gupta and C. M. Gupta, *Electrochemi. Acta*, **18**, 59 (1973).
7) S. C. Khurana, *J. Inorg. Nucl. Chem.*, **34**, 2557 (1972).
8) R. L. Gustafson and A. E. Martell, *J. Am. Chem. Soc.*, **81**, 525 (1959).
9) S. K. Shah, Ph. D. Thesis University of Rajasthan, Jaipur, India (1980).
10) S. L. Jain, Jaikishan, and R. C. Kapoor, *Indian. J. Chem., Sect A* **18**, 133 (1979).
11) N. P. Sachan and C. M. Gupta, *Indian. J. Chem., Sect A* **18**, 82 (1979).
12) E. Botlare and O. Maruri, *Ann. Chem. (Rome)*, **66**, 663 (1976).
13) E. H. Hensen and J. Ruzicka, *Talanta*, **20**, 1105 (1973).
14) D. D. Perrin and V. S. Sharma, *J. Chem. Soc.*, **17**, 2060 (1969).
15) J. I. Watters and R. Dewitt, *J. Am. Chem. Soc.*, **82**, 1333 (1960).
16) L. Leden, *Z. Phys. Chem.*, **188**, 160 (1941).

The Reversibilities of the Adsorption and Desorption of Organic Compounds in Water

Kohei URANO,* Hisanao KANO, and Toshimasa TABATA
Department of Safety and Environmental Engineering, Yokohama National University, 156 Tokiwadai, Hodogaya-ku, Yokohama 240
(Received September 24, 1983)

Synopsis. The reversibilities of the adsorption and desorption of seventeen organic compounds in water on a granular activated carbon and a polystyrene adsorbent were examined by means of a batch-adsorption method. The adsorptions of many organic compounds were reversible, but the adsorptions of several phenolic compounds and aniline were irreversible for the activated carbon, because these compounds were adsorbed strongly on the surface of activated carbon by the π-electron combination. On the other hand, the adsorptions of all the organic compounds were reversible for the polystyrene adsorbent.

The applications of adsorption from solutions on solid adsorbents have been considerably developed and become very important in many fields,[1] such as in purification processes, water-treatment processes, and analytical methods. The reversibility of adsorption and desorption is an important characteristic of an adsorbate to consider in selecting the adsorbent and in determining the adsorption conditions in these applications. However, there have been few reports on the reversibilities of the adsorption and desorption[2] of organic compounds in water. In this report, therefore, the reversibilities of the adsorption and desorption of various organic compounds on an activated carbon or a polystyrene adsorbent are investigated.

Experimental

Seventeen organic compounds on a reagent grade were used as the adsorbates. A granular activated carbon and a polystyrene adsorbent whose properties are shown in Table 1 were used in this study.

The adsorption isotherms at 25°C were obtained by the same method as in the previous paper.[3] After measuring the equilibrium concentrations, the solutions of 50—90 cm^3 were removed from the flasks and equal amounts of pure water were added. The flasks were then again shake for 4 d at 25±0.5°C. After the equilibrium had been completely attained, the concentrations of the desorbed adsorbates were analyzed and the desorption isotherms were obtained. The reversibilities were examined by a comparison of the desorption isotherms with the adsorption isotherms. The concentrations of the adsorbates were determined from the ultraviolet absorbances and concentrations of the total organic carbon (TOC).

TABLE 1. PROPERTIES OF THE ADSORBENTS USED

Adsorbent	Name	Surface area	Pore volume/cm^3 g^{-1}	
		m^2 g^{-1}	Total	<20 nm
Activated carbon	Filtrasorb 400	1030	0.84	0.52
Polystyrene	XAD-4	640	1.48	1.07

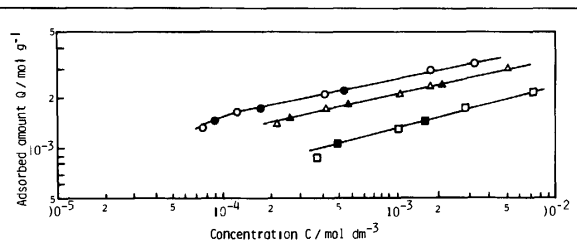

Fig. 1. Adsorption and desorption isotherms of fatty acids for activated carbon at 25°C.
(Open marks show adsorption, and black marks show desorption in Figs. 1—5)
○●: Pentanoic acid, △▲: hexanoic acid, □■: heptanoic acid.

Results and Discussion

Adsorption on Activated Carbon. The adsorption isotherms[3] and the desorption isotherms on the activated carbon are shown in Fig. 1—3 respectively as Freundlich expressions, the logarithmic relationships between the adsorbed amount Q (mol g^{-1}) and the equilibrium concentration C (mol dm^{-3}). The two isotherms agree with one another for many compounds, such as pentanoic acid, hexanoic acid, heptanoic acid, nitrobenzene, benzaldehyde, benzonitrile, benzoic acid, *m*-hydroxybenzoic acid, *m*-hydroxybenzaldehyde, benzenesulfonic acid, *p*-methylbenzenesulfonic acid, and *p*-ethylbenzenesulfonic acid. Therefore, the adsorptions and desorptions of these compounds are reversible. On the other hand, the desorption isotherms for phenol,

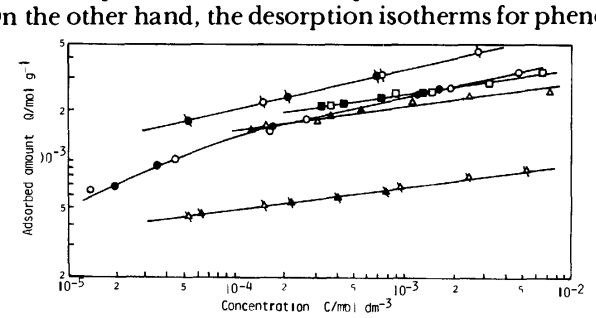

Fig. 2. Adsorption and desorption isotherms of substituted benzenes for activated carbon at 25°C.
○●: Benzoic acid, △▲: *m*-hydroxybenzoic acid, □■: *m*-hydroxybenzaldehyde, ◯●: nitrobenzene, △▲: *p*-methylbenzenesulfonic acid.

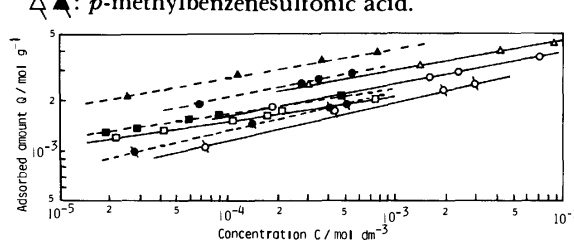

Fig. 3. Adsorption and desorption isotherms of several phenolic compounds and aniline for activated carbon at 25°C.
○●: Phenol, △▲: *m*-cresol, □■: *p*-nitorophenol, ◯●: aniline.

Table 2. Ratios of k for desorption to adsorption, k_{ds}/k_{ads}

Adsorbent	Phenol	*m*-Cresol	*p*-Nitrophenol	Aniline
Activated carbon	1.3	1.3	1.1	1.1
Polystyrene	1.0	—	1.0	1.0

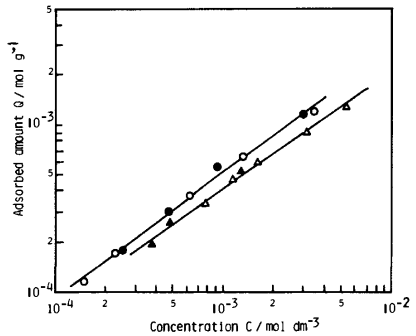

Fig. 4. Adsorption and desorption isotherms of benzoic acid and nitrobenzoic acid for polystyrene adsorbent at 25°C.
○●: Benzoic acid, △▲: *m*-nitrobenzoic acid.

m-cresol, *p*-nitrophenol, and aniline are higher and are parallel with their adsorption isotherms. Therefore, the adsorptions and the desorptions of these several phenolic compounds and aniline are irreversible. However, the values of n in the Freundlich equation, $Q=kC^{1/n}$, for the adsorption and the desorption isotherms are equal to one another. The ratios of the values of k for the desorption to the adsorption, k_{ds}/k_{ads}, show the levels of the irreversibility; they are summarized in Table 2. The ratios are large for phenol and *m*-cresol. Urano *et al.*[3] reported the energy distributions for the adsorptions of those compounds on the activated carbon and showed that the phenol and *m*-cresol adsorbed with especially high energies on the activated carbon. The adsorption energy for aniline was also slightly higher than those for the other aromatic compounds. These high adsorption energies show that those compounds combine strongly with the surface of activated carbons. It is known[2] that there are several electrophilic groups, such as the quinone group and the ketone group, on the surface of activated carbon. Since phenol, *m*-cresol, and aniline act as electron donors, these compounds may be adsorbed by the π-electron combination on the carbon surface. Urano *et al.*[3] reported that the amount of phenol adsorbed decreased with the oxidation of the activated carbon. This decrease may be due to the change in the electrophilic groups into non-electrophilic groups such as the carboxyl group with the oxidation. The reason for the reversible adsorptions of *m*-hydroxybenzoic acid and *m*-hydroxybenzaldehyde, which have a phenolic hydroxyl-group, may be that these compounds do not act as strong electron donors.

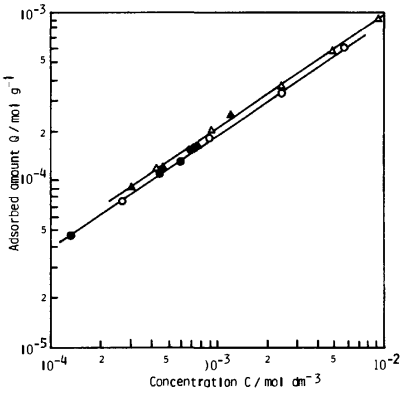

Fig. 5. Adsorption and desorption isotherms of phenol and aniline for polystyrene adsorbent at 25°C.
○●: Phenol, △▲: aniline.

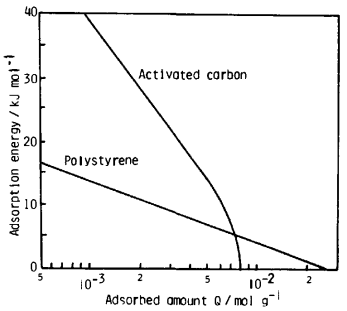

Fig. 6. Distributions of adsorption energy of phenol for activated carbon and polystyrene adsorbent at 25°C.

Adsorption on Polystyrene Adsorbent. The adsorption isotherms and the desorption isotherms on the polystyrene adsorbent are shown in Figs. 4 and 5 respectively. The adsorptions on the polystyrene adsorbent for all the organic compounds were reversible, because the polystyrene adsorbent has no active groups. The energy distribution for the adsorption of phenol on the polystyrene adsorbent was calculated by means of the following equation:[3] $Q=kC_s^{1/n}-E_{eq}/nRT$, where C_s is the saturated concentration, E_{eq} is the adsorption energy at Q, R is the gas constant, and T is the absolute temperature. It is obvious that the adsorption energy for the polystyrene adsorbent is much smaller than the energy for the activated carbon; this shows that the adsorption on the polystyrene adsorbent is completely physical.

References

1) K. Urano, *Industrial Water*, No. 232, 33 (1978).
2) J. S. Mattson and H. B. Mark, Jr., "Activated Carbon," Marcel Dekker, New York (1971).
3) K. Urano, Y. Koichi, and Y. Nakazawa, *J. Colloid Interface Sci.*, **81**, 477 (1981).

Pentane Isomerization Activity of Halogenated Rare Earth Intermetallics

Hayao IMAMURA,* Yuzo KATO, and Susumu TSUCHIYA
Department of Industrial Chemistry, Faculty of Engineering, Yamaguchi University, 2557 Tokiwadai, Ube 755
(Received November 19, 1983)

Synopsis. Binary halides formed by treating $ErAl_3$ with halogen elements were subjected to an characterization as skeletal isomerization catalysts for pentane. Halogenation of $ErAl_3$ in the presence of CH_2Cl_2 or CCl_4 gives rise to superacidic binary halides as a result of formation of V-center-type sites due to excess of halogen species.

There have been various studies published of catalytic properties of solid superacids.[1-5] Recently, we have found that in the presence of halogens X_2 (X_2= Cl_2, Br_2, and I_2), rare earth- or Th-group IIIB intermetallics are readily converted into binary halides which are characterized as superacids.[6] These halogenated intermetallic compounds are exceptionally active as skeletal isomerization catalysts for pentane under mild conditions. We believe that the extreme activity is due to superacidity, but their catalytic behavior markedly varies with preparative conditions for the binary halides. To obtain information about the isomerization activity of the binary halide catalysts formed by direct halogenation of rare earth intermetallics, the present study was undertaken.

In a standard procedure for preparing the catalyst, X_2 is added to finely ground intermetallics suspended in dichloromethane (CH_2Cl_2) solvent, and the mixture is stirred to obtain the binary halide in a slurry form in dry argon under anhydrous conditions.[6] Pentane is injected to initiate the isomerization. When 2 ml of pentane was added to an $ErAl_3$ (1 mmol)-I_2 (6 mmol) system in CH_2Cl_2, the activity at 0°C was evaluated from the pentane conversion in 30 min as 61% (Table 1). On the other hand, when the isomerization was conducted without CH_2Cl_2 solvent, the catalytic activity was significantly decreased for $ErAl_3$-Cl_2 and $ErAl_3$-I_2. As shown in Table 1, however, the activity was restored to some extent by addition of a small amount of CH_2Cl_2. These observations indicate that CH_2Cl_2 used as a solvent plays an important role in the development of superacidity in the present system. NMR and element analyses for $ErAl_3$-X_2 in the presence of CH_2Cl_2 revealed that metathetic halogen exchange takes place between the halogenated $ErAl_3$ and CH_2Cl_2 along with the formation of CH_2XCl. It is supposed that this promoting action of CH_2Cl_2 on the isomerization of pentane is ascribed in part to the halogen exchange. To check this, the isomerization reaction was examined by adding Cl_2 or Br_2 to $ErAl_3$-I_2, because changes in Gibbs energy at 25°C are favorable for the halogen exchange between metal iodides and Cl_2 (or Br_2). The reaction between the iodinated $ErAl_3$ and Cl_2 could be followed gravimetrically to find $ErAl_3I_{11.6}Cl_{0.4}$, which is actually active for the isomerization (Table 1).

TABLE 1. RESULTS OF THE ISOMERIZATION OF PENTANE

Catalyst	Solvent	Additive[a]	Conversion of pentane/%
$ErAl_3$-Cl_2	CH_2Cl_2	—	25[c]
	CCl_4	—	25[c]
	—[b]	—	1.8[d]
	—[b]	CH_2Cl_2	7.6[d]
$ErAl_3$-Br_2	CH_2Cl_2	—	58[c]
	—[b]	—	5.6[d]
$ErAl_3$-I_2	CH_2Cl_2	—	61[c]
	—[b]	—	none[d]
	—[b]	CH_2Cl_2	9.0[d]
	—[b]	CCl_4	6.3[d]
	—[b]	Cl_2	1.2[d]
	—[b]	Br_2	5.3[d]

a) CH_2Cl_2: 0.5 ml, CCl_4: 0.5 ml, Br_2: 3 mmol. b) Direct contact between $ErAl_3$ and X_2 was conducted *in situ* in pentane. c) The conversion (1 mmol $ErAl_3$-6 mmol X_2, solvent: 8 ml, pentane: 2 ml) was measured at 0°C and 30 min. d) The conversion (0.5 mmol $ErAl_3$-3 mmol X_2, pentane: 10 ml) was measured at 23°C and 6 h.

In addition, it can be presumed from Table 1 that the action of CH_2Cl_2 on $ErAl_3$-Cl_2 brings about another synergism for improving the catalytic activity, besides the halogen exchange. To understand this better, the chlorination of $ErAl_3$ was examined by using gravimetric techniques: after $ErAl_3$ was allowed to react at 23°C with the stoichiometric amount of chlorine required to chlorinate the Er and Al present in the alloy, CH_2Cl_2 (190 Torr) (1 Torr=133.322 Pa) was introduced into the system in place of chlorine gas. There was a further occurrence of the reaction between the chlorinated $ErAl_3$ and CH_2Cl_2 in which a large excess of chlorine species was taken up by the resulting binary halide. Carbon tetrachloride (CCl_4) behaved quite similarly to CH_2Cl_2. As shown in Table 1, for example, $ErAl_3$-I_2 exhibited an enhancement in activity to some extent when treated with CCl_4. For $ErAl_3$-Cl_2 in CCl_4 the active catalyst was such that the binary chloride formed contains chlorine species to an extent exceeding the stoichiometric amount by a factor of 1.3.

These results lead to speculations on the generation of active sites in terms of V-center-like effects which are induced by an excess of halogen. It is recognized that for alkali halides color centers formed in the crystal structure are often associated with catalytic activities.[7] ESR studies indicated that a strong ESR signal with a g value of 2.0059 and an overall width of *ca.* 60 G is formed at room temperature when CH_2Cl_2 or CCl_4 is added to the chlorinated $ErAl_3$. The siganl intensity remained unchanged over a period of 24 h. In view of

TABLE 2. RELATIVE INTENSITIES OF ESR SIGNALS MEASURED FOR VARIOUS CATALYST SYSTEMS

Catalyst system	Relative intensity of ESR signal
$ErAl_3$-Cl_2 in CH_2Cl_2	142
$ErAl_3$-Cl_2 in CCl_4	95
$AlCl_3$ in CH_2Cl_2 (or CCl_4)	3 (2)
$ErCl_3$ in CH_2Cl_2 (or CCl_4)	0.3 (0.5)
$ErCl_3$-$AlCl_3$(1:3) in CH_2Cl_2	1

the fact that the enhancing action of CH_2Cl_2 or CCl_4 on the isomerization activity was not noticeable for a 1:3 mixture of $ErCl_3$ and $AlCl_3$ or the individual compounds, a good correlation between the ESR signal intensity and the activity may be taken to have been observed for $ErAl_3$–Cl_2 in CH_2Cl_2 or CCl_4 (Table 2). Accordingly, it is concluded for the present system that CH_2Cl_2 or CCl_4-treated $ErAl_3$–X_2, possessing V-centers due to an excess of halogen species, shows superacidity.

Experimental

The rare earth intermetallic compound $ErAl_3$ used was obtained as a commercial product from Nippon Yttrium Co. Pentane was thoroughly dehydrated with sodium wires and subsequently distilled in dry argon. Dichloromethane and carbon tetrachloride were purified by distillation in the presence of phosphorus pentaoxide. The isomerization of pentane was investigated in the liquid phase over binary halides, which had been prepared *via* reaction of $ErAl_3$ with X_2 before each run. Special care was taken to exclude water and oxygen from the system. Further details regarding the procedure for the isomerization reaction have been described elsewhere.[6]

This research was supported by the Grant-in-Aid for Scientific Research from the Ministry of Education, Culture and Science. We are grateful to Mr. Toyoharu Saito, Tokyo Institute of Technology, for carrying out the elemental analyses.

References

1) G. A. Olah, K. Laali, and A. K. Mehrotra, *J. Org. Chem.*, **48**, 3360 (1983).

2) M. Hino, S. Kobayashi, and K. Arata, *J. Am. Chem. Soc.*, **101**, 6439 (1979).

3) H. Hattori, O. Takahashi, M. Takagi, and T. Tanabe, *J. Catal.*, **68**, 132 (1981).

4) Y. Ono, N. Kitajima, T. Nakajima, and T. Keii, "Proceedings of the 7th International Congress of Catalysis," ed by T. Seiyama and K. Tanabe, Kodansha Ltd., Tokyo (1980), p. 1006.

5) A. Krzywicki and M. Marczewski, *J. Chem. Soc., Faraday Trans. 1*, **76**, 1311 (1980).

6) H. Imamura and W. E. Wallace, *J. Catal.*, **64**, 238 (1980); H. Imamura, W. E. Wallace, and K. Soga, *ibid.*, **67**, 244 (1981); *Chem Lett.*, **1980**, 957.

7) E. H. Taylor, *Adv. Catal.*, **18**, 111 (1968).

Indexing of X-Ray Powder Diffraction Data for Potassium Hexafluorovanadate(III)

Koichiro KOYAMA,* Yasuhiko HASHIMOTO, Shinichiro OMORI, and Kazuo TERAWAKI
Department of Metallurgy and Materials Science, Himeji Institute of Technology, 2167 Shosha, Himeji 671-22
(Received December 8, 1983)

Synopsis. X-Ray powder diffraction data for K_3VF_6 are presented; the α form is monoclinic with a=1.2102(1), b=1.7456(2), c=1.2007(2) nm, β=92.58(1)° at 298 K; the β form is monoclinic with a=1.714(2), b=1.237(1), c=0.5479(2) nm, β=91.49(3)° at 453 K; the γ form is tetragonal with a=1.3708(5), c=0.8752(5) nm at 483 K; the low-temperature γ form, which contains a small amount of sodium ion, is tetragonal with a=1.3570(3), c=0.8671(2) nm at 298 K.

TABLE 1. X-RAY DIFFRACTION DATA FOR THE α FORM (Cu $K\alpha$ RADIATION)

No.	I/I_0	$2\theta_{obsd}$/°	d_{obsd} nm	d_{calcd} nm	hkl
1	1	16.893	0.5244	0.5241	031
2	81	17.839	0.4968	0.4974	220
3	24	20.323	0.4366	0.4368	040
4	5	21.213	0.4185	0.4180	032
5	1	22.200	0.4001	0.4000	23$\bar{1}$
6	1	22.635	0.3925	0.3923	231
7	2	23.495	0.3783	0.3785	31$\bar{1}$
8	1	25.137	0.3540	0.3542	240
9	1	25.689	0.3465	0.3464	321
10	4	26.534	0.3357	0.3357	31$\bar{2}$
11	7	26.895	0.3312	0.3316	330
12	2	27.581	0.3231	0.3227	33$\bar{1}$
13	34	28.888	0.3088	0.3086	24$\bar{2}$
14	100	29.533	0.3022	0.3020	052
15	2	30.284	0.2949	0.2949	33$\bar{2}$
16	2	30.594	0.2920	0.2919	251
17	2	31.205	0.2864	0.2864	411
18	2	32.387	0.2762	0.2762	16$\bar{1}$
19	2	34.044	0.2631	0.2632	053
20	2	34.581	0.2592	0.2588	15$\bar{3}$
21	21	36.121	0.2485	0.2487	440
22	11	36.636	0.2451	0.2454	44$\bar{1}$
23	10	37.533	0.2394	0.2394	50$\bar{1}$
24	9	38.276	0.2350	0.2352	501
25	2	38.677	0.2326	0.2329	36$\bar{1}$
26	5	39.051	0.2305	0.2305	07$\bar{2}$
27	7	39.629	0.2272	0.2272	43$\bar{3}$
28	8	39.894	0.2258	0.2257	172
29	6	40.374	0.2232	0.2233	451
30	53	41.322	0.2183	0.2184	080
31	2	42.749	0.2113	0.2114	45$\bar{2}$
32	27	43.201	0.2092	0.2090	31$\bar{5}$
33	1	44.491	0.2035	0.2031	503
34	2	44.952	0.2015	0.2014	27$\bar{3}$
35	18	45.606	0.1987	0.1987	53$\bar{3}$
36	2	46.219	0.1963	0.1963	434
37	2	46.462	0.1953	0.1953	28$\bar{2}$
38	3	46.897	0.1936	0.1935	282
39	2	47.763	0.1903	0.1903	54$\bar{3}$
40	3	48.058	0.1892	0.1891	19$\bar{1}$
41	1	48.674	0.1869	0.1870	63$\bar{1}$
42	2	49.346	0.1845	0.1845	27$\bar{4}$
43	2	49.798	0.1830	0.1830	53$\bar{4}$
44	25	51.598	0.17699	0.1769	603
45	11	52.798	0.17325	0.1732	642
46	2	53.530	0.17105	0.1710	60$\bar{4}$
47	7	54.642	0.16783	0.1678	27$\bar{5}$
48	3	54.847	0.16725	0.1673	42$\bar{6}$
49	4	55.434	0.16561	0.1657	12$\bar{7}$
50	4	56.947	0.16157	0.1616	73$\bar{2}$
51	1	58.236	0.15829	0.1583	662
52	6	59.850	0.15441	0.1545	75$\bar{1}$
53	1	60.630	0.15260	0.1526	2 11 $\bar{1}$
54	10	61.297	0.15110	0.1511	605
55	2	62.990	0.14744	0.1475	29$\bar{5}$
56	2	63.694	0.14598	0.1459	4 10 2
57	3	63.905	0.14555	0.1455	295
58	2	64.247	0.14486	0.1449	61$\bar{6}$
59	3	65.086	0.14319	0.1432	81$\bar{3}$
60	3	65.307	0.14276	0.1428	68$\bar{2}$
61	1	65.945	0.14153	0.1415	72$\bar{5}$
62	1	66.207	0.14104	0.1410	63$\bar{6}$
63	1	67.181	0.13923	0.1392	73$\bar{5}$
64	4	67.803	0.13810	0.1381	2 12 $\bar{2}$
65	3	68.142	0.13750	0.1375	68$\bar{3}$
66	2	70.449	0.13355	0.1336	18$\bar{7}$

Monoclinic; a=1.2102(1), b=1.7456(2), c=1.2007(2) nm, β=92.579(10)° at 289 K

The previous paper[1] has revealed that K_3VF_6 has four polymorphic forms and the transition points are 431, 473, and 491 K. When it contains a small amount of sodium ion, the γ and δ froms remain stable even at room temperature. This work was undertaken to present the X-ray powder diffraction data for the α, β, and γ forms, and to index their diffraction patterns.

Experimental

The potassium hexafluorovanadate(III) was prepared from V_2O_3 and KHF_2 of a special reagent grade in the manner reported previously.[1] The γ form which remains stable at room temperature—hereafter, designated the low-temperature γ form—was prepared using reagent-grade KHF_2. The X-ray diffraction pattern of the α form was taken with an X-ray diffractometer, Rigaku Denki Model SG-7, with

TABLE 2. X-RAY DIFFRACTION DATA FOR THE β FORM (Cu $K\alpha$ RADIATION)

No.	I/I_0	$2\theta_{obsd}$/°	d_{obsd} nm	d_{calcd} nm	hkl
1	31	17.677	0.5017	0.5015	220
2	10	20.330	0.4368	0.4370	21$\bar{1}$
3	21	20.766	0.4277	0.4281	211
4	1	26.516	0.3361	0.3363	32$\bar{1}$
5	3	26.627	0.3348	0.3344	330
6	28	28.904	0.3089	0.3092	23$\bar{1}$
7	100	29.240	0.3054	0.3059	231
8	15	35.789	0.2509	0.2508	440
9	6	37.082	0.2424	0.2424	341
10	4	37.692	0.2387	0.2389	222
11	6	39.601	0.2276	0.2274	32$\bar{2}$
12	11	39.743	0.2268	0.2268	13$\bar{2}$
13	10	39.951	0.2257	0.2256	132
14	4	40.311	0.2237	0.2239	15$\bar{1}$
15	72	41.301	0.2184	0.2185	42$\bar{2}$
16	15	42.220	0.2139	0.2140	422
17	6	45.279	0.2001	0.2000	52$\bar{2}$
18	28	51.406	0.17760	0.1777	21$\bar{3}$
19	7	51.946	0.17588	0.1759	213
20	3	52.366	0.17457	0 1747	12$\bar{3}$
21	10	54.555	0.16807	0.1681	64$\bar{2}$
22	6	59.832	0.15445	0.1544	523
23	7	60.472	0.15297	0.1530	46$\bar{2}$
24	13	60.582	0.15272	0.1525	34$\bar{3}$
25	1	63.841	0.14568	0.1457	63$\bar{3}$

Monoclinic; a=1.7136(19), b=1.2368(7), c=0.5479(2) nm, β=91.485(28)° at 453 K.

TABLE 3. X-RAY DIFFRACTION DATA FOR THE γ FORM (Cu $K\alpha$ RADIATION)

No.	I/I_0	$2\theta_{obsd}$ °	d_{obsd} nm	d_{calcd} nm	hkl
1	35	17.652	0.5024	0 5021	121
2	5	20.308	0.4373	0.4376	002
3	13	20.488	0.4335	0.4335	130
4	100	28.996	0.3079	0.3080	132
5	67	29.184	0.3060	0.3065	240
6	17	35.711	0.2512	0.2511	242
7	3	36.700	0.2447	0.2444	251
8	5	38.219	0.2353	0.2351	350
9	8	39.408	0.2285	0.2285	060
10	55	41.256	0.2186	0.2188	004
11	68	41.635	0.2167	0.2167	260
12	2	43.633	0.2073	0.2071	352
13	2	45.342	0.1998	0.1998	053
14	27	51.266	0.17806	0.1781	244
15	48	51.516	0.17725	0.1772	172
16	2	54.463	0.16834	0.1683	215
17	5	54.853	0.16723	0.1669	181
18	17	60.038	0.15397	0.1540	264
19	10	60.457	0.15300	0.1533	480

Tetragonal; a=1.3708(5), c=0.8752(5) nm at 483 K.

TABLE 4. X-RAY DIFFRACTION DATA FOR THE LOW-TEMPERATURE γ FORM (Cu K_α RADIATION)

No.	I/I_0	$2\theta_{obsd}$/°	d_{obsd} nm	d_{calcd} nm	hkl
1	37	17.842	0.4971	0.4972	121
2	8	20.487	0.4335	0.4336	002
3	10	20.691	0.4293	0.4291	130
4	100	29.276	0.3051	0.3050	132
5	67	29.458	0.3032	0.3034	240
6	2	31.615	0.2830	0.2827	103
7	3	34.595	0.2591	0.2590	051
8	17	36.105	0.2486	0.2486	242
9	2	36.884	0.2435	0.2436	033
10	5	37.104	0.2421	0.2420	251
11	5	38.664	0.2327	0.2327	350
12	2	39.263	0.2293	0.2292	233
13	2	39.683	0.2269	0.2268	152
14	2	39.793	0.2263	0.2262	060
15	35	41.632	0.2168	0.2168	004
16	45	42.062	0.2146	0.2146	260
17	3	44.121	0.2051	0.2051	352
18	2	45.161	0.2006	0.2005	062
19	2	45.811	0.1979	0.1979	053
20	2	46.900	0.1936	0.1935	134
21	2	47.830	0.1900	0.1899	253
22	15	51.778	0.17641	0.1764	244
23	25	52.048	0.17556	0.1755	172
24	2	53.727	0.17046	0.1709	543
25	2	55.027	0.16674	0.1668	215
26	5	55.546	0.16530	0.1652	181
27	2	58.075	0.15869	0.1586	354
28	10	60.664	0.15252	0.1525	264
29	5	61.071	0.15160	0.1517	480
30	2	63.603	0.14616	0.1461	055
31	2	63.923	0.14551	0.1455	183
32	2	64.103	0.14514	0.1451	291
33	2	68.461	0.13693	0.1370	316

Tetragonal; a=1.3570(3), c=0.8671(2) nm at 298 K.

Cu K_α radiation monochromated by pyrolytic graphite at a scanning speed of 0.0167°/s (1°/min) and a chart speed of 1.67×10^{-4} m/s (10 mm/min). The X-ray diffraction patterns of the β, γ and low-temperature γ forms were taken on the same diffractometer with a Ni-filtered Cu K_α radiation at the same scanning speed and the same chart speed as for the X-ray diffraction pattern of the α form. The diffraction angles were corrected by those of silicon added to the K_3VF_6 powder as an internal standard. Indexing of the diffraction patterns was made with the aid of the computer program, Program ITO, Version 9, originally developed by Visser[2] and improved by Johnson Jr. The lattice parameters were refined by a least-squares method. The wavelengths used were 0.154178 nm (Cu K_α) for $2\theta \leqq 51°$ and 0.154051 nm (Cu K_{α_1}) for $2\theta > 51°$ respectively.

Results

Tables 1—4 show the X-ray diffraction data for the α, β, γ and low-temperature γ forms, respectively. The α form is simple monoclinic with a=1.2102(1), b=1.7456(2), c=1.2007(2) nm, β=92.58(1)° at 298 K; the β form is simple monoclinic with a=1.714(2), b=1.237(1), c=0.5479(2) nm, β=91.49(3)° at 453 K; the γ form is body-centered tetragonal with a=1.3708(5), c=0.8752(5) nm at 483 K; the low-temperature γ form is body-centered tetragonal with a=1.3570(3), c=0.8671(2) nm at 298 K.

The authors wish to express their thanks to Professor Gerald G. Johnson Jr. of the Pennsylvania State University for sending the computer program, Program ITO, Version 9.

References

1) K. Koyama and Y. Hashimoto, *Bull. Chem. Soc. Jpn.*, **50**, 1333 (1977).
2) J. W. Visser, *J. Appl. Cryst.*, **2**, 89 (1969).

The Catalytic Properties of the Pd/Mica Model Catalyst

Yoshio TAKASU,* Kenji KASAHARA, and Yoshiharu MATSUDA
Department of Industrial Chemistry, Faculty of Engineering, Yamaguchi University, 2557 Tokiwadai, Ube 755
(Received December 16, 1983)

Synopsis. The apparent activation energy of an H_2–D_2 exchange reaction on a Pd/mica model catalyst system increased with the decrease in the particle size of palladium. The activity pattern as a function of the mean particle size was of a volcano-type, with a maximum at a particle size around 1.2 nm.

The effects of the metal-particle size on the catalytic properties of supported metal catalysts have not been clearly revealed. Most of the investigations which have aimed at revealing the size effects have been performed with catalysts prepared by the impregnation method. However, they have had the following difficulties: (1) the observation of small metal particles on supports (Al_2O_3, SiO_2 or active carbon) by TEM (transmission electron microscopy) is not easy; (2) the surface cleanness of metal particles on the support cannot be well guaranteed, and (3) the application of UPS (ultraviolet photoelectron spectroscopy) to reveal the valence-band structure of catalysts is substantially impossible.

The model-catalyst method will be able to overcome those concomitant problems. Many investigations with model catalysts have been performed using an UHV (ultra-high vacuum) system; however, scarcely no experiments which have examined both metal-particle size and catalytic-activity measurements have been made.[1–6]

In this study, palladium was evaporated onto a mica sheet in an UHV system, and its catalytic activity for an H_2–D_2 exchange reaction was measured *in situ*.

Experimrental

The features of the apparatus used for the preparation of the model catalysts and for the subsequent measurements of their catalytic activities have been described elsewhere.[7] The apparatus was capable of being evecuated to the pressure of 10^{-9} Torr (1 Torr=133.3 N m^{-2}). A cleaned mica-sheet support and a TEM mesh were set in the UHV chamber. The TEM sheet mesh was composed of fine mica powder fixed on evaporated carbon film which was held on a copper sheet mesh (#400). The mount of palladium evaporated was monitored by means of a quartz-thickness monitor (ANELVA EVM-32B). A transmission electron microscope (Japan Electron Optics, JEM-200-CX, bright field) was adopted for the observation of the palladium particles on the mica-sheet support.

Results and Discussion

Figure 1 shows some typical electron micrographs of the model catalyst, in which one can see palladium particles ranging in size from the observation limit of 0.6 nm to approximately 3 nm. The mean thickness $\bar{D}$ signifies the thickness of the palladium layer if the deposits were dense and did not form any island structure. The effective surface areas of these palladium catalysts were estimated by assuming all the palladium particles to be half-spheres.

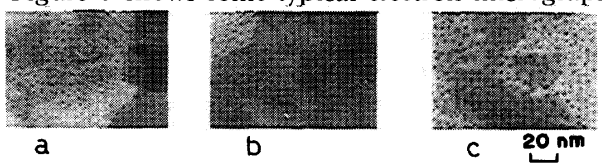

Fig. 1. Typical electron micrographs of Pd/mica model catalysts.
Mean thickness $\bar{D}$; a: 0.25 nm, b: 0.41 nm, c: 0.54 nm.

The H_2–D_2 exchange reaction on this Pd/mica model catalyst system obeyed a first-order reaction under the present experimental conditions. Figure 2 shows the specific activity towards the H_2–D_2 exchange reaction ($P_{H_2}=P_{D_2}=2.8\times10^{-2}$ Torr, 25°C) of this catalyst system as a function of the mean palladium-particle size. The activity pattern is of a "volcano" type, with a maximum at a particle size around $\bar{d}=1.2$ nm ($\bar{d}$ signifies the mean diameter of the palladium particles). Such an activity pattern has been found not only for the Pd/C and Pd/SiO_2 model catalyst systems in the H_2–D_2 exchange reaction reported elesewhere[7,8] but also for a Rh/SiO_2 powder catalyst system in benzene reduction.[9] Therefore, a hemispherical palladium particle with a diameter of 1.2 nm may be said to consist of about 30 atoms. Below $\bar{d}=1.2$ nm, the specific activity decreased rapidly with the decrease in $\bar{d}$. There-

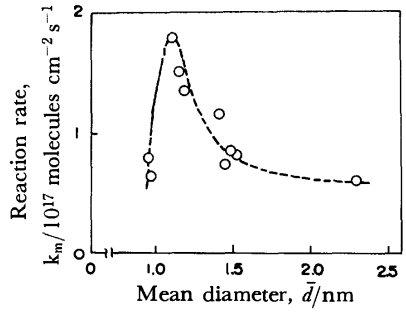

Fig. 2. Reaction rate for the H_2–D_2 exchange reaction, catalyzed by the Pd/mica catalyst, as a function of mean particle size $\bar{d}$.
Temperature: 25°C, pressure: $P_{H_2}=P_{D_2}=2.8\times10^{-2}$ Torr.

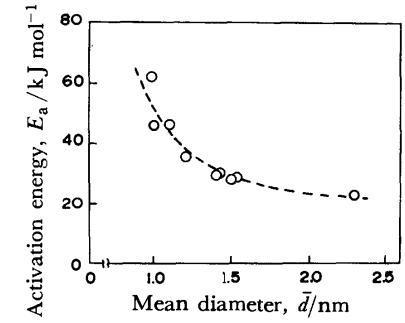

Fig. 3. Apparent activation energy for the H_2–D_2 exchange reaction, catalyzed by the Pd/mica model catalyst, as a function of mean palladium particle size $\bar{d}$.
Temperature range: 0—30°C.

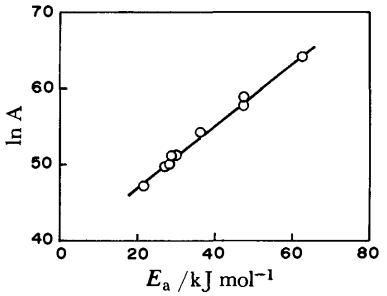

Fig. 4. Compensation effect for the H_2–D_2 exchange reaction, catalyzed by the Pd/mica model catalyst. The A means the preexponential factor in the Arrhenius equation.

fore, the contribution to the catalytic activity of the palladium particles below the observation limit of the electron microscopy (0.6 nm) must be extremely low.

Figure 3 shows the apparent activation energy of the reaction on this Pd/mica model catalyst system as a function of the mean particle size $\bar{d}$. It must be noted that the apparent activation energy gradually decreased with the increase in $\bar{d}$ from *ca.* 60 kJ mol^{-1} at $\bar{d}$ = 1.0 nm to *ca.* 20 kJ mol^{-1} at $\bar{d}$ = 2.4 nm. This tendency must not be directly affected by problems in determining the surface area of the catalyst. As with the specific activity, this tendency is analogous to the results of the Pd/C and Pd/SiO_2 model catalyst systems.[7,8] As shown in Fig. 4, a compensation effect between the apparent activation energy E_a and the preexponential factor A in the Arrenius equation exists for this H_2–D_2 reaction on the Pd/mica model catalyst system. This suggests that the reaction mechanism in this system is the same in all these palladium catalysts, while the activation energy differs.

As has been reported by many previous investigators, including us,[2,3,6] the valence band as well as the 3d levels of small particles of palladium shift to a higher binding energy from the bulk values with a decrease in the particle size. The shift of the valence band to a higher binding energy must be caused by either the intrinsic property of the very small metal particles or the support effect. The former effect has been proved by some investigators[6] on the basis of calculations; the latter effect is now under investigation by the present authors using various catalyst supports. In any event, the increase in the binding energy of the valence-band electrons in palladium particles with the decrease in the particle size must result in the decrease in the adsorption energy of hydrogen on the palladium particles. If this is the case, the increase in the apparent activation energy for the H_2–D_2 exchange reaction with the decrease in the particle size is likely to be caused by an increase in the activation energy for the dissociative adsorption of hydrogen. The rate-determining step of this H_2–D_2 exchange reaction has not been kinetically examined; however, we have pointed out that linear relationships exist between the catalytic activities of a hydrogen-recombination reaction or an H_2–D_2-exchange reaction and the amount of strongly adsorbed hydrogen (probably dissociative) on the cleaned first-transition metal wires as well as the cleaned Cu–Ni alloy plates.[10] On the other hand, the density of low-coordinated surface atoms rapidly increased with the decrease in the particle size.[11] If low-coodinated surface sites were more catalytically active than the higher-coordinated surface atoms, the catalytic activity would increase with the decrease in the particle size. However, the apparent activation energy increases with the decrease in the particle size, an activity maximum appeared at a certain particle size. In order to make a more decisive explanation, an *in-situ* investigation of adsorption and UPS studies using other supports are now being made.

We wish to thank Professor Z. Yoshii, Mr. M. Kimoto, and M. Nishimura of the Faculty of Medicine, Yamaguchi University, for their advice and help with the electron microscopy. This work was generously supported by the Watanabe Memorial Foundation, an RCA Research Grant, and the Kudo Science Foundation.

References

1) D. L. Doering, J. T. Dickinson, and H. Poppa, *J. Catal.*, **73**, 91, 104 (1982).
2) M. G. Mason, L. J. Gerenser, and S. T. Lee, *Phys. Rev. Lett.*, **39**, 288 (1977).
3) Y. Takasu, R. Unwin, B. Tesche, A. M. Bradshaw, and M. Grunze, *Surf. Sci.*, **77**, 219 (1978).
4) J. F. Hamilton and R. C. Baetzold, *Science*, **205**, 1213 (1979).
5) M. Arai, T. Ishikawa, and Y. Nishiyama, *J. Phys. Chem.*, **86**, 577 (1982).
6) M. G. Mason, *Phys. Rev. B*, **27**, 748 (1983).
7) Y. Takasu, K. Kasahara, Y. Matsuda, and I. Toyoshima, *Nippon Kagaku Kaishi*, **1984**, 1011.
8) Y. Takasu, T. Akimaru, K. Kasahara, Y. Matsuda, H. Miura, and I. Toyoshima, *J. Am. Chem. Soc.*, **104**, 5249 (1982).
9) W. F. Graydon and M. D. Langan, *J. Catal.*, **69**, 1890 (1981).
10) Y. Takasu and Y. Matsuda, *Electrochim. Acta*, **21**, 133 (1976).
11) J. R. Anderson, "Structure of Metallic Catalysts," Academic Press, London (1975).

Study of the Polymerization of Silicic Acid Adsorbed on Iron(III) Hydroxide by Trimethylsilylation-Gas Chromatography

Takushi YOKOYAMA,* Tsugio SHIMONO,† and Toshikazu TARUTANI
Department of Chemistry, Faculty of Science, Kyushu University 33, Hakozaki, Higashi-ku, Fukuoka 812
(Received December 21, 1983)

Synopsis. Polymerization of silicic acid adsorbed on iron (III) hydroxide from dilute monosilicic acid solutions in the concentration range 5—40 ppm (SiO_2) was studied over the pH range 6—12. Silicic acid species formed on the hydroxide were trimethylsilylated and trimethylsilyl derivatives were detected by gas chromatography. Monosilicic acid adsorbed polymerized, and dimer ($Si_2O_7^{6-}$), linear trimer ($Si_3O_{10}^{8-}$) and tetramer ($Si_4O_{13}^{10-}$), and cyclic tetramer ($Si_4O_{12}^{8-}$) were found as polymeric species.

Monosilicic acid adsorbed on or coprecipitated with iron (III) hydroxide rapidly polymerizes.[1,2] Polymerization of silicic acid adsorbed on iron (III) hydroxide has been studied by colorimetry and gel chromatography.[3] Although gel chromatography is useful to study the formation of relatively large polysilicic acids, no information is available on the formation of low-molecular-weight silicic acids such as dimer, trimer, *et al.* Lentz[4] described a chemical technique for the study of silicate structures based on trimethylsilylation of silicic acids. Trimethylsilyl (TMS) derivatives of silicic acids were isolated[5] and the method for the determination of TMS derivatives by gas chromatography was established.[6] The method proposed for the trimethylsilylation of the silicic acids assured that side reactions such as polymerization and depolymerization hardly proceed during the silylation and good reproducible results were obtained.[7] The change with time in the distribution of silicic acids in aqueous solutions was measured.[8]

In this work, the formation of low-molecular-weight silicic acid species in the early stage of polymerization of monosilicic acid adsorbed on iron (III) hydroxide was studied by trimethylsilylation-gas chromatography (TMS-GC).

Experimental

Samples and Reagents. All the reagents except hexamethyldisiloxane (HMDS; $(CH_3)_3Si\text{-}O\text{-}Si(CH_3)_3$) were of analytical reagent grade. HMDS was purified by distillation four times at 120 °C. A stock solution of monosilicic acid was prepared by dissolving silica gel (Mallinckrodt Chemical Works) in sodium hydroxide solution. A monosilicic acid solution of the desired concentration was prepared by diluting a stock solution before use. Iron(III) hydroxide was precipitated by adding sodium hydroxide solution to iron (III) chloride solution and then washed with distilled water. Iron (III) hydroxide was prepared immediately before each experiment.

Procedure. Monosilicic acid solution (0.5 dm^3) of an appropriate concentration was adjusted to the desired pH with hydrochloric acid and sodium hydroxide solution. Sodium chloride concentration was adjusted to 0.1 mol dm^{-3}. Iron (III) hydroxide (0.95×10^{-3} mol) was then introduced into the solution and the pH was readjusted. The suspension was stirred vigorously. The experiments were carried out in a thermostated bath at 25°C. After 30 min, the suspension was rapidly filtered. The concentration of monosilicic acid in the filtrate was determined by colorimetry. For the trimethylsilylation of silicic acid adsorbed on iron(III) hydroxide, the solid sample was added to a mixture of water (5 cm^3), concentrated hydrochloric acid (7.5 cm^3), 1-propanol (15 cm^3), HMDS (12 cm^3), which had been stirred for 1 h at 28°C. The mixture was then stirred for 1 h. The siloxane layer was separated from the aqueous layer and washed with water. The aqueous layer and the washed water were combined, and the water was vigorously shaken with 10 cm^3 of HMDS to extract the remaining TMS derivatives and the siloxane layer was separated and washed with water, then the two siloxane layers were combined. The siloxane layer was stirred for 4 h at room temperature in the presence of Amberlyst 15 cation-exchange regin (2 g). After filtration, the filtrate was evaporated to less than 10 cm^3 by distillation at 120—130°C, and adjusted to 10 cm^3 with isopropyl alcohol. TMS derivatives of silicic acid in the sample solution were analyzed by GC.[6]

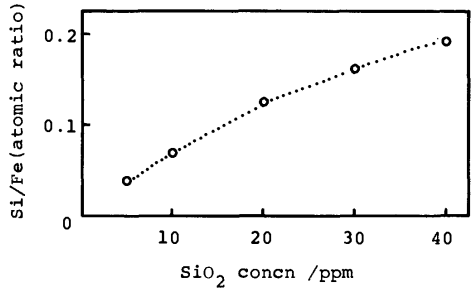

Fig. 1. Variation of Si/Fe ratio as a function of initial monosilicic acid concentration.
pH: 8.

Results and discussion

The effect of the initial concentration of monosilicic acid on the amount and polymerization of silicic acid adsorbed on iron (III) hydroxide was examined at pH 8. Figure 1 shows the variation of Si/Fe atomic ratio of monosilicic acid adsorbed to iron (III) hydroxide as a function of the initial concentration of monosilicic acid. The ratio is an indicator of the amount of silicic acid adsorbed on the hydroxide. The Si/Fe ratio increased with an increase in the initial concentration of monosilicic acid. The silicic acid adsorbed on iron (III) hydroxide was trimethylsilylated and the TMS derivatives were analyzed by GC. The results are shown in Fig. 2. Each silicic acid species is expressed in its anionic form. It was found to contain dimer ($Si_2O_7^{6-}$), linear trimer ($Si_3O_{10}^{8-}$) and tetramer ($Si_4O_{13}^{10-}$), and cyclic tetramer ($Si_4O_{12}^{8-}$) in addition to the monomer (SiO_4^{4-}). Figure 2 shows the variation of proportion of each silicic acid species as a function of the initial concentration of monosilicic acid. The proportion

† Present address: Resources and Environment protection Laboratory, Nippon Electric Co., Ltd., Takatsu-ku, Kawasaki 213.

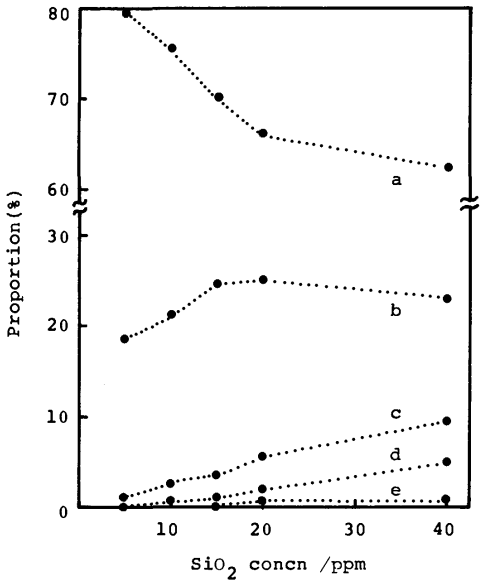

Fig. 2. Effect of initial monosilicic acid concentration on the proportion of various silicic acid species.
pH: 8.
a: SiO_4^{4-}, b: $Si_2O_7^{6-}$, c: $Si_3O_{10}^{8-}$, d: $Si_4O_{12}^{8-}$, e: $Si_4O_{13}^{10-}$.

was calculated by

$$\text{Proportion } (\%) = 100\ (p_i/\sum P_i)$$

where P_i is the peak intensity of the ith TMS derivative on the gas chromatogram. With increasing initial concentration of monosilicic acid, the proportion of monomer rapidly decreased and the proportion of the other silicic acid species increased. The results indicate that although monosilicic acid in solution at concentrations up to about 120 ppm at pH 8 does not polymerize, monosilicic acid adsorbed on iron(III) hydroxide easily polymerizes.

Adsorption of silicic acid by iron (III) hydroxide from 40 ppm (SiO_2) monosilicic acid solution and polymerization of adsorbed silicic acid was examined over the pH range 6—12. Figure 3 shows the variation of the Si/Fe ratio with pH. The maximum adsorption as a function of the pH occurred at around pH 9.5. Figure 4 shows the variation with pH of the proportion of silicic acid species. Although the linear tetramer was detected, it was not plotted in the figure because of its small amount. The polymerization of silicic acid adsorbed occurred at all the pH. It is noteworthy that monosilicic acid adsorbed on iron(III) hydroxide even in strongly alkaline solution (pH 12) polymerizes. Figure 4 suggests that the rate of polymerization of adsorbed silicic acid is most rapid at around pH 8 in the early stage of the adsorption of silicic acid, although the amount of adsorbed silicic acid is largest at around pH 9.5. In colorimetry, only monosilicic acid reacts with molybdic acid to form yellow molybdosilicic acid. As the polysilicic acid species shown in Fig. 4 depolymerize they are determined as monosilicic acid

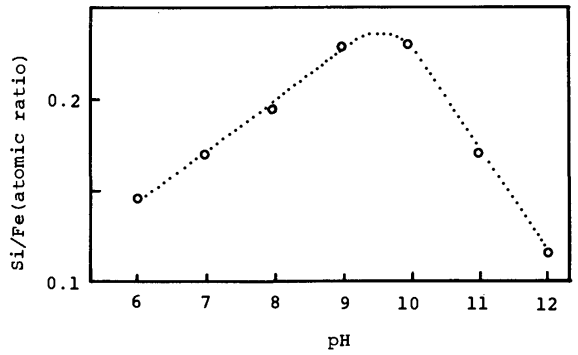

Fig. 3. Variation of Si/Fe ratio with pH.
Initial monosilicic acid concentration: 40 ppm (SiO_2).

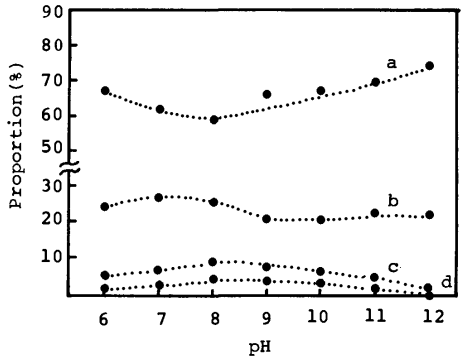

Fig. 4. Effect of pH on the proportion of various silicic acid species.
Initial monosilicic acid concentration: 40 ppm (SiO_2).
a: SiO_4^{4-}, b: $Si_2O_7^{6-}$, c: $Si_3O_{10}^{8-}$, d: $Si_4O_{12}^{8-}$.

by colorimetry,[8] but the formation of such species can not be detected by colorimetry. This work indicates that TMS-GC is useful to study the early stage of the polymerization of silicic acid adsorbed on the surface of a solid.

The present work was partially supported by a Grand-in-Aid for Scientific Research from the Ministry of Education, Science and Culture.

References

1) H. Harder and W. Flehmig, *Geochim. Cosmochim. Acta*, **34**, 295 (1970).
2) T. Tarutani and H. Kato, *Mem. Fac. Sci. Kyushu Univ., Ser. C*, **11**, 197 (1978).
3) T. Yokoyama, T. Nakazato, and T. Tarutani, *Bull. Chem. Soc. Jpn.*, **53**, 850 (1980).
4) C. W. Lentz, *Inorg. Chem.*, **3**, 574 (1964).
5) T. Shimono, H. Takagi, T. Isobe, and T. Tarutani, *J. Chromatogr.*, **197**, 59 (1980).
6) T. Shimono, T. Isobe, and T. Tarutani, *J. Chromatogr.*, **205**, 49 (1981).
7) T. Shimono, T. Isobe, and T. Tarutani, *Mem. Fac. Sci. Kyushu Univ., Ser. C*, **13**, 303 (1982).
8) T. Shimono, T. Isobe, and T. Tarutani, *J. Chromatogr.*, **258**, 73 (1983).

Oxygen Isotope Shifts in ^{17}O NMR Spectra of the Uranyl Ion

Woo-Sik JUNG, Yasuhisa IKEDA, Hiroshi TOMIYASU, and Hiroshi FUKUTOMI*
Research Labortory for Nuclear Reactors, Tokyo Institute of Technology, O-okayama, Meguro-ku, Tokyo 152
(Received January 13, 1984)

Synopsis. The ^{17}O NMR spectrum of uranyl oxygens enriched with ^{17}O gave three peaks. These peaks are assigned to the signals of three isotopomers, $[^{16}O{=}U{=}^{17}O]^{2+}$, $[^{17}O{=}U{=}^{17}O]^{2+}$, and $[^{18}O{=}U{=}^{17}O]^{2+}$. Chemical shifts for the signals of $[^{17}O{=}U{=}^{17}O]^{2+}$ and $[^{18}O{=}U{=}^{17}O]^{2+}$ were -0.054 ± 0.002 and -0.108 ± 0.002 ppm relative to $[^{16}O{=}U{=}^{17}O]^{2+}$, respectively.

The study of ^{17}O NMR spectra of oxygen in a dioxouranium(VI) ion, where hereafter uranyl oxygens will be used, was first reported by Rabideau.[1] He observed an asymmetric ^{17}O NMR signal with a shoulder on the high-field side for the uranyl oxygens in 6 M (1 M = 1 mol dm^{-3}) perchloric acid solution, and two peaks in 0.2 M perchloric acid solution. Rabideau suggested that these results may be due to the formation of polynuclear species of uranyl ions. However, the formation of polynuclear species is unlikely in highly acidic solutions.[2,3] He did not take account the difference in ^{17}O enrichment in the uranyl oxygens.

In order to examine Rabideau's results, we have observed the ^{17}O NMR spectra of the uranyl ion in solutions with different acid concentrations, and the effect of ^{17}O enrichment in the uranyl oxygens on the ^{17}O NMR spectrum.

Experimental

Uranyl perchlorate pentahydrate was prepared by dissolving $UO_3{\cdot}2H_2O$ in 60% perchloric acid (Wako Pure Chemical Ind. Ltd.). The $UO_3{\cdot}2H_2O$ was prepared by using the method of Ekstrom *et al.*[4] The uranyl perchlorate pentahydrate was recrystallized from distilled water five times, and the resulting crystals were dried *in vacuo*. The abundance of ^{17}O in enriched water used was 20.5 atom % (Merck, ^{16}O: 50.4, ^{18}O: 29.1 atom %) and 42.1 atom % (Merck, ^{16}O: 26.3, ^{18}O: 31.7 atom %). Uranyl oxygens were enriched by irradiation of uranyl perchlorate solution containing ^{17}O-enriched water with a 500-W high pressure mercury lamp.[5] Samples for the NMR measurements were prepared by adding D_2O (Merck) and perchloric acid to the enriched uranyl perchlorate solution, followed by introducing the sample solution into the NMR microcell (Wilmad). The microcell was inserted in 10 mm o.d. NMR tube (Wilmad) containing reference water. Measurements of the ^{17}O NMR spectra were carried out at 13.46 MHz on a JEOL JNM-FX 100 FT-NMR spectrometer. Typical spectral settings for the measurements of ^{17}O NMR spectra are as follows: 4K data points, 90° pulse angle corresponding to *ca.* 10 μs pulse width, 500 Hz spectral width, 1.95 ms recycle delay, and normally 5000 scans. Temperature was maintained at 293±1 K.

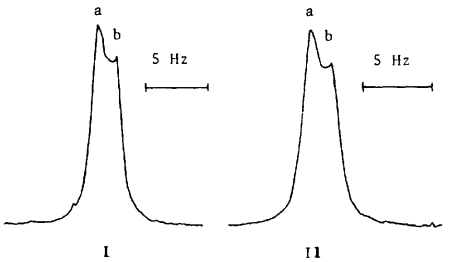

Fig. 1. ^{17}O NMR spectra of the uranyl oxygens at different acid concentrations. The uranyl oxygens were enriched by using $H_2{}^{17}O$ (20.5 atom %).
I: $[UO_2^{2+}]$=0.078 m, $[H^+]$=0.22 m, II: $[UO_2^{2+}]$=0.12 m, $[H^+]$=6.0 m.

Results and Discussion

The ^{17}O NMR spectra of the uranyl oxygens which were enriched by using $H_2{}^{17}O$ (20.5 atom %) were measured at different acid concentrations. The ^{17}O signal of uranyl oxygens was observed at *ca.* +1119 ppm[6] relative to water in 0.22 and 60 m (1 m=1 mol kg^{-1}) perchloric acid solutions. This result is in good agreement with those of earlier works.[1,7] Figure 1 shows the expanded ^{17}O signals of the uranyl oxygens, where no difference was observed in the lineshapes. The difference in chemical shifts between two peaks a and b was determined to be 0.107 ± 0.002 ppm.

The ^{17}O signal of the uranyl oxygens which were enriched by using $H_2{}^{17}O$ (42.1 atom %) was also measured in a 0.23 m perchloric acid solution, and the result is shown in Fig. 2. It is noted that the ^{17}O signal has three peaks p, q, and r, and peaks q and r are observed at -0.054 ± 0.002 and -0.108 ± 0.002 ppm from peak p, respectively. The difference in chemical shifts between two peaks a and b shown in Fig. 1 is the same as that between two peaks p and r shown in Fig. 2 within experimental errors. This result indicates that peak b corresponds to peak r.

From the results in Figs. 1 and 2, it is clear that the ^{17}O NMR lineshape of the uranyl oxygens does not depend on the acid concentration, but depends on the ^{17}O enrichment in the uranyl oxygens. This fact suggests that the change of lineshape is due to the difference in ratio of relative concentration of isotopomers of the uranyl ion, because the ratio changes with the ^{17}O enrichment in the uranyl oxygens.

As the uranyl ion has three isotopomers which are active for ^{17}O NMR, *i.e.*, $[^{16}O{=}U{=}^{17}O]^{2+}$, $[^{17}O{=}U{=}^{17}O]^{2+}$, and $[^{18}O{=}U{=}^{17}O]^{2+}$, three peaks in Fig. 2 may be assigned to these isotopomers. This deduction is supported

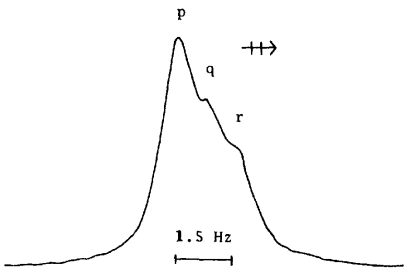

Fig. 2. ^{17}O NMR spectrum of the uranyl oxygens enriched by using $H_2{}^{17}O$ (42.1 atom %). $[UO_2^{2+}]$= 0.098 m and $[H^+]$=0.23 m.
Conditions of enrichment: each weight of $UO_2(ClO_4)_2{\cdot}5H_2O$ and $H_2{}^{17}O$ was 1.023 g and 0.3978 g, respectively.

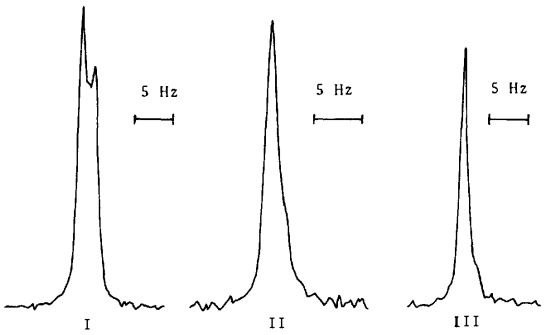

Fig. 3. Change in ^{17}O signals of the enriched uranyl oxygens by irradiation. The uranyl oxygens were enriched by using $H_2{}^{17}O$ (20.5 atom %). $[UO_2^{2+}]$= 0.065 m and $[H^+]$=3.8 m.
I: Before irradiation, II: after irradiation for 10 min, III: after irradiation for 15 min.

by the following results. Figure 3 shows the spectral change of ^{17}O signal of the uranyl oxygens by the irradiation of the enriched uranyl perchlorate solution with the mercury lamp. As is seen in Fig. 3, the intensity of the peak at high-field side decreases gradually with increasing the irradiation time. This phenomenon must be caused by oxygen exchange between the uranyl ion and bulk water, resulting in the variation of relative concentration ratio of three isotopomers. Hence, the peak at the lowest field in Fig. 3, which corresponds to peak a or p in Figs. 1 or 2, respectively, can be assigned to the signal of $[^{16}O{=}U{=}^{17}O]^{2+}$ isotopomer. The concentration of $[^{16}O{=}U{=}^{17}O]^{2+}$ is estimated to be at least ten times those of $[^{17}O{=}U{=}^{17}O]^{2+}$ and $[^{18}O{=}U{=}^{17}O]^{2+}$ at the exchange equilibrium after irradiation. Moreover, in view of the usual trend in the isotope effect on chemical shifts that the magnitude of the upfield shift is largest where the fractional change in mass upon substitution is largest,[8] peaks q and r in Fig. 2 may be assigned to the signals of $[^{17}O{=}U{=}^{17}O]^{2+}$ and $[^{18}O{=}U{=}^{17}O]^{2+}$, respectivery. As a result, peak b in Fig. 1 may be assigned to the signal of $[^{18}O{=}U{=}^{17}O]^{2+}$, since peak b corresponds to peak r as mentioned above. Although the ^{17}O signal of $[^{17}O{=}U{=}^{17}O]^{2+}$ was not able to be observed in Fig. 1, this result may arise from the fact that the relative concentration of $[^{17}O{=}U{=}^{17}O]^{2+}$ is low compared with those of $[^{16}O{=}U{=}^{17}O]^{2+}$ and $[^{18}O{=}U{=}^{17}O]^{2+}$.

From the conditions given in Fig. 2, we can calculate the probability for the occurrence of three isotopomers, assuming that oxygen isotopes are distributed statistically without the isotope effect in O=U=O bond. The ratio of probabilities is given as follows: $P_{16,17}$: $P_{17,17}$: $P_{18,17}$[9] = 0.282: 0.0676: 0.102. Therefore, the ratio of relative intensities of three isotopomers is estimated as follows: $I_{16,17}$: $I_{17,17}$: $I_{18,17}$[9] = 2.76: 1.32: 1.00. Assuming that the whole lineshape in Fig. 2 is formed by overlapping of three Lorentzian curves with the same linewidth, the best-fit calculated lineshape gives the ratio of relative intensities of three peaks p, q, and r as follows: I_p: I_q: I_r = 2.50: 1.00: 1.07. This ratio is in fair agreement with the calculated ratio of $I_{X,Y}$ from $P_{X,Y}$ values under the conditions given in Fig. 2.

It appears well established that the ^{17}O NMR spectra of uranyl oxygens have three peaks corresponding to three isotopomers of the uranyl ion, where the peak at the lowest field is assigned to the signal of $[^{16}O{=}U{=}^{17}O]^{2+}$ and the signals of $[^{17}O{=}U{=}^{17}O]^{2+}$ and $[^{18}O{=}U{=}^{17}O]^{2+}$ shift to the higher field by 0.054±0.002 and 0.108±0.002 ppm relative to $[^{16}O{=}U{=}^{17}O]^{2+}$. This result is the first finding with respect to the isotope shift through two equivalent bonds in ^{17}O NMR.

The authors with to express their thanks to Professor Gilbert Gordon of Miami University and Professor James H. Espenson of Iowa State University for helpful discussions and to Mr. Masao Nomura for the mass spectrometry of the oxygen isotopes. The present work was partially supported by a Grant-in-Aid for Scientific Research No. 57470035 from the Ministry of Education, Science and Culture.

References

1) S. W. Rabideau, *J. Phys. Chem.*, **71**, 2747 (1967).
2) C. F. Baes, Jr., and N. J. Meyer, *Inorg. Chem.*, **1**, 780 (1962).
3) R. M. Rush and J. S. Johnson, *J. Phys. Chem.*, **67**, 821 (1963).
4) A. Ekstrom, H. Loeh, C. H. Randall, L. Szego, and J. C. Taylor, *Inorg. Nucl. Chem. Lett.*, **14**, 301 (1978).
5) G. Gordon and H. Taube, *J. Inorg. Nucl. Chem.*, **16**, 272 (1961); K. Okuyama, Y. Ishikawa, Y. Kato, and H. Fukutomi, *Bull. Res. Lab. Nucl. Reactor*, **3**, 39 (1978).
6) IUPAC recommendations. *Pure Appl. Chem.*, **45**, 219 (1976).
7) L. G. Mashirov, D. V. Suglobov, and V. A. Scherbakov, *Radiokhimiya*, **17**, 881 (1975).
8) H. Batiz-Hernandez and R. A. Bernheim, *Prog. Nucl. Magn. Reson. Spectrosc.*, **3**, 63 (1967).
9) $P_{X,Y}$ and $I_{X,Y}$ refer to the probability for the occurrence and the relative intensity of $[^{X}O{=}U{=}^{Y}O]^{2+}$ isotopomer, respectively.

Stereochemistry of Halogen-Metal Exchange Reaction of Vinyl Halide with Grignard Reagent

Toshio SUGITA,* Yo-ichi SAKABE, Toshiaki SASAHARA, Mitsunori TSUKADA, and Katsuhiko ICHIKAWA
Department of Hydrocarbon Chemistry, Faculty of Engineering, Kyoto University, Sakyo-ku, Kyoto 606
(Received October 26, 1983)

Synopsis. Halogen-magnesium exchange was confirmed to proceed with stereospecific retention of configuration in the reaction of β-bromostyrene and butylmagnesium bromide.

Vinyl Grignard reagents were formed with retention of configuration from the corresponding vinyl halides. The stereospecificities of their formation reaction, however, were widely diversed. Yoshino and his co-workers reported that *cis*- and *trans*-styrylmagnesium bromides were formed in THF with 95 and 91% retention of configuration, respectively, but the stereospecificities were lowered to 69 and 59% in diethyl ether.[1] In the formation of aliphatically substituted vinyl Grignard reagents, various degrees of configurational retention, 60—90%, depending on the substituens, were observed.[2,3] To discuss these discrete experimental results, it is necessary to confirm the stereochemistry of the halogen-metal exchange of vinyl halides with Grignard reagents. Zakharkin and his co-workers have made extensive studies on the halogen-metal exchange reactions involving Grignard reagents with ordinary alkyl and aryl halides. They concluded that the mechanism of halogen-metal exchange reaction is the same for both organomagnesium and organolithium compounds.[4] This would imply that the halogen-magnesium exchange proceeds with retention of configuration. Although there are some reports which suggest that the halogen-magnesium exchange reaction proceeds with retention of configration,[5] the exact experimental results on the stereochemistry of exchange seem to be unavailable. In this paper, we wish to report that the halogen-magnesium exchange between β-bromostyrene (**1**) and butylmagnesium bromide (**2**) does proceed with stereospecific retention of configuration.

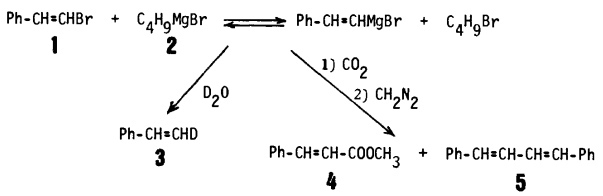

Scheme 1.

(*E*)-**1** was treated with **2** in 1,2-dimethoxyethane (DME) at ambient temperature for 2 h. The reaction mixture was then quenched by D_2O. The isomer ratios of the resulted styrene-β-d_1 (**3**) are summarized in Table 1. As a reference experiment, the same reaction was carried out using butyllithium instead of **2**, since halogen-lithium exchange was known to proceed with complete retention of configuration.[6] The isomer ratios of **3** resulting from the halogen-magnesium and halogen-lithium exchange reactions are almost the same value. These results suggest that the halogen-magnesium exchange proceeds with highly stereospecific retention of configuration, rather like the halogen-lithium exchange does.

It has already been pointed out that an unignorable amount of hydrocarbon is also produced during the formation of Grignard reagents.[5] If undeuterated styrene was produced prior to the D_2O treatment, it should be estimated as the (*Z*)-**3** in the present analytical method. Unfortunately, the exchange reaction of (*Z*)-**1** gave only 8% of styrene, which failed to be isolated purely enough for NMR analysis, and the isomer ratio could not be determined.

Carbonation of the resulting Grignard mixture was, therefore, examined in order to obtain unequivocal results. Yields and isomer ratios of the products resulting from the exchange and carbonation reactions are summarized in Table 1. As the carbonation of Grignard reagents proceeds with complete retention of configration,[2,7] the results of these experiments clearly demonstrate that the halogen-magnesium exchange proceeds with highly stereospecific retention of configuration. (*Z*)-**1** afforded methyl (*Z*)-cinnamate (**4**) with complete retention of configuration, but the exchange of (*E*)-**1** proceeded less stereospecifically. It should be noted that the degree of configurational retention of the vinylic Grignard reagents formation usually falls upon going from *cis*- to *trans*-isomer.

TABLE 1. HALOGEN-METAL EXCHANGE REACTION OF β-BROMOSTYRENE WITH BUTYLMAGNESIUM BROMIDE

1	**2**	Product yield/%				Recovered
(mmol)	(mmol)	**3** (*Z*/*E*)	**4** (*Z*/*E*)	**5** (*ZZ*/*EE*)	**6**[a]	**1**
Hydrolysis with D_2O						
E (10)	40	20 (21/79)			16	54
E (10)	40	22 (33/67)			21	33
Z (10)	30	8			13	67
E (10)	40[b]	32 (29/71)			—[c]	—[c]
Carbonation						
Z (21)	42		2.0 (97/3)	7.5 (84/16)	19	52
Z (28)	84		2.7 (100/0)	20.0 (62/38)	36	11
E (21)	42		1.6 (15/85)	29.5 (0/100)	—[c]	—[c]

a) 1-Phenyl-1-hexene. b) Butyllithium hexane solution instead of **2** was used. c) Not determined.

1,4-Diphenyl-1,3-butadiene (**5**) obtained from (*E*)-**1** was (*E,E*)-isomer alone, which certainly resulted from the halogen-magnesium exchange reaction followed by the coupling with the unreacted **1**. In contrast to the (*E*)-isomer, (*Z*)-**1** gave a mixture of (*Z,Z*)- and (*E,E*)-5, although the former predominated. The coupling reaction of Grignard reagents with vinyl halides appears not to be stereospecific, since the alkylations of 1-halo-1-alkenes with Grignard reagents gave mixtures of *cis*- and *trans*-alkenes.[8] In the present case, the coupling reaction of (*Z*)-**1** with (*Z*)-stytylmagnesium bromide, formed stereospecifically from (*Z*)-**1**, may afford (*E,Z*)-**5** as well as its (*Z,Z*)-isomer. The formation of (*E,Z*)-**5** could not, however, be confirmed in the present experiments. The (*E,Z*)-isomer might be isomerised to (*E,E*)-**5** during the reaction or in the isolation process due to its instability.[9]

In THF solution, the halogen-magnesium exchange could not be observed, though it was examined in various conditions.

Experimental

All melting points and boiling points are uncorrected. IR spectra were measured with a Hitachi EPI-G2 spectrometer. ^{1}H-NMR spectra were obtained with a JEOL PMX-60 spectrometer in $CDCl_3$ using TMS as the internal standard. GLC analyses were conducted by a Hitachi 163 gas chromatograph using a 2 m column packed with PEG-20M 20% on Chromosorb-W.

Materials. The solvents were freshly distilled over lithium aluminum hydride under argon before use. (*E*)-**1** was commercially available, and (*Z*)-**1** was synthesized by the reported method.[10] Each isomer was purified by recrystallization from pentane,[1] and was confirmed to be isomerically pure by its IR and ^{1}H-NMR spectra.

Halogen-Magnesium Exchange of β-Bromostyrene with Butylmagnesium Bromide and Hydrolysis with Deuterium Oxide. A solution of **2** was prepared as usual from butyl bromide (22.5 g, 0.164 mol) and magnesium (4.0 g, 0.165 mol) in 82 ml of THF. The solution was filtered through a sintered glass funnel in order to separate it from the remaining metal, and the Grignard reagent solution prepared was used for the subsequent reactions after it was standardized by the method of Watson and Eastham.[11] To a solution of (*E*)-**1** (2.0 g, 11 mmol) in 50 ml of DME, 30 ml of the solution of **2** (40 mmol) was added. The mixture was stirred at ambient temperature for 2 h. All these procedures were carried out under argon atmosphere. The reaction mixture was quenched with 2 ml of D_2O. The mixture was then treated with aqueous ammonium chloride, extracted with ether, and distilled using a Kugelrohr apparatus to give **3**, bp 55—65 °C/30 mmHg (oven temperature; 1 mmHg≈133.322 Pa). Yield of **3**, 20.3%, was determined by GLC. The isomer ratio of the resulting 3 was estimated as *E*:*Z*=79:21 by peak integrals of the doublets at δ 5.19 (*J*=9 Hz: *cis*-β-H of (*Z*)-**3**) and at 5.62 (*J*=18 Hz: *trans*-β-H of (*E*)-**3**).[1]

Carbonation of the Exchange Reaction Mixture. To a stirred solution of (*Z*)-**1** (3.48 g, 21 mmol) in 100 ml of DME, 30 ml of the solution of **2** (42 mmol) was added. The mixture was stirred at ambient temperature in dark under argon for 20 h. The reaction mixture was poured onto a slurry of freshly powdered Dry Ice and ether with vigorous stirring. The carbonated solution was poured into a mixture of ice and hydrochloric acid and the ether layer was separated. The aqueous layer was extracted with ether and the combined ether solutions were extracted with a saturated sodium hydrogencarbonate solution. The alkaline extracts were acidified and extracted with ether. To the ether extracts, an ether solution of diazomethane was added until the mixture turned slightly yellow. After removal of the solvent, the products were submitted to GLC analysis. The ether layer of the alkaline extract was washed with saturated sodium chloride and dried. After removal of the solvent, the residual products were analyzed by GLC. The yields of the products estimated by GLC were as follows: **4**, 2.0% (*Z*:*E*=97:3); methyl 3-phenylpropionate, 0.8%; styrene, 2.4%; unreacted (*Z*)-**1**, 52.2%; **5**, 7.5% (*ZZ*:*EE*=84:16); (*Z*)-1-phenyl-1-hexene (**6**), 19.4%. The products other than **5** were identified by the comparison of their GLC retention times, IR and/or ^{1}H-NMR spectra with those of authentic samples. **5** was isolated from the product mixture and identified by its spectral data. (*Z,Z*)-**5**: mp 62.5—63.5°C (lit,[8] mp 70.5°C); its IR spectrum was superimposable with the reported one.[11] (*E,E*)-**5**: mp 142—144°C; its IR and ^{1}H-NMR spectra were completely identical with Sadtler's standard spectra.

The authors, TS and MT, are grateful to Prof. Yoshinobu Takegami for his encouragement.

References

1) T. Yoshino, Y. Manabe, and Y. Kikuchi, *J. Am. Chem. Soc.*, **86**, 4670 (1964).
2) H. M. Walborsky and R. B. Banks, *Bull. Soc. Chim. Belg.*, **89**, 849 (1980).
3) B. Méchin and N. Naulet, *J. Organomet. Chem.*, **39**, 229 (1972); and references cited therein.
4) L. I. Zakharkin, O. Yu. Okhlobystin, and K. A. Bilevitch, *J. Organomet. Chem.*, **2**, 309 (1964).
5) H. M. Walborsky and M. S. Aronoff, *J. Organomet. Chem.*, **51**, 31 (1973).
6) D. Y. Curtin, E. W. Panek, B. L. Neff, H. Chu, and M. G. Panek, *J. Am. Chem. Soc.*, **97**, 3996 (1975).
7) H. M. Walborsky and A. E. Young, *J. Am. Chem. Soc.*, **86**, 3288 (1964).
8) M. Tamura and J. Kochi, *Synthesis*, **1971**, 303; R. J. P. Corriu and J. P. Masse, *J. Chem. Soc., Chem. Commun.*, **1972**, 144; K. Tamao, K. Sumitani, and M. Kumada, *J. Am. Chem. Soc.*, **94**, 4374 (1972).
9) J. H. Pinckard, B. Eille, and L. Zechmeister, *J. Am. Chem. Soc.*, **70**,1938 (1948).
10) S. J. Cristol and W. P. Norris, *J. Am. Chem. Soc.*, **75**, 2645 (1953).
11) S. C. Watson and J. F. Eastham, *J. Organomet. Chem.*, **9**, 165 (1967).
12) A. Butenandt, E. Hecker, and G. Zachau, *Chem. Ber.*, **88**, 1185 (1955).

A Radical-induced Extrusion Reaction of 2-(Benzylsulfonyl)tropones to 2- and 4-Benzyltropones

Hitoshi TAKESHITA,* Norihide MATSUO,† and Hiroaki MAMETSUKA
Reserch Institute of Industrial Science, 86, Kyushu University, Kasuga-koen, Kasuga, Fukuoka 816
†*Graduate School of Engineering Sciences, 39, Kyushu University, Kasuga-koen, Kasuga, Fukuoka 816*
(Received November 16, 1983)

Synopsis. Several 2-(benzylsulfonyl)tropones were thermolized to give 2- and 4-benzyltropones. The radical mechanism for the thermolysis was elucidated by a deuterium-labelling experiment.

Upon thermolysis, 2-(benzyloxy)tropones (**1**) can be transformed to the 3- (**2**) and 5-benzyltropolones (**3**) in good yields *via* a radical chain reaction.[1] This behavior in the thermal reaction was unexpected, so we have undertaken the study with some other derivatives; the findings obtained from the sulfonyl derivatives will be described here.

The substrates, 2-(benzylsulfonyl)tropones (**4**), with some amounts of 2-(benzylsulfinyl)tropones (**5**), were prepared by the *m*-chloroperbenzoic acid (MCPBA)-oxidation of the crresponding 2-(benzylthio)tropones (**6**).

These **6** were thermally unreactive up to 195°C, where **1** caused a rearrangement to **2** and **3**, but the corresponding sulfones, **4**, have caused a new type of thermally-induced elimination: by heating at 180°C to 225°C in tetralin, 2-(benzylsulfonyl)tropone (**4a**) yielded 2-benzyltropone (**7a**), 23%, a pale yellow oil,[2] and 4-benzyltropone (**8a**), 7.5%, a pale yellow oil. The structure of **8a** was determined by chemical correlation. After a brief treatment with hydrazine hydrate in ethanol, **8a** yielded a 3:2-mixture of 2-aminotropones. By preparative thin-layer chromatography (PTLC) on silica gel, the mixture furnished 2-amino-4-benzyltropone (**9**) and 2-amino-5-benzyltropolone (**10a**),[3] which was converted to the previously prepared 5-benzyltropolone (**3a**)[1] by alkaline hydrolysis.

Two other sulfones, *p*-methyl (**4b**) and *p*-bromo (**4c**) derivatives, gave similar products upon the thermolysis.

The results of the reaction in dimethyl sulfoxide (DMSO) were different. **4b** yielded *p*-toluic acid in 65%,[4] and the radical mechanism is likely to be operative. Indeed, the thermolysis of a 1:1-mixture of **4c** and deuterio-**4a** (**4a**-*d*), which consisted of d_3, d_2-, d_1, and d_0-derivatives (19:58:20:3), in dioxane revealed an extensive cross-over recombination of two components in the mass spectra (Table 1) of the thermolysates (**7a**, **7c**, **8a**, and **8c**), to leave no ambiguity for the intermolecular path.

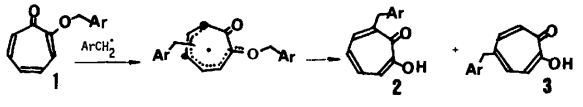

Scheme 1.

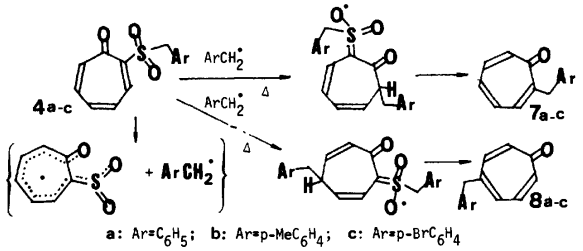

Scheme 2.

Consequently, the present reaction is another example of the radical substitution of benzyl group onto the tropone ring initiated by a homolysis of X–C bond of the C-2 position to form the delocalized species.

Experimental

Preparation of 2-(Benzylthio)tropone (6a). To an EtOH solution (3 cm³) of 2-mercaptotropone (200 mg) and NaOMe (100 mg), benzyl chloride (230 mg) was added and refluxed for 2 h on an oil bath. The mixture was evaporated, and the residue was chromatographed on a silica-gel column to give yellow needles, mp 98—99°C (**6a**). 237 mg (70%) [Found: C, 73.89; H, 5.38%. Calcd for $C_{14}H_{12}OS$: C, 73.65; H, 5.30%. δ[5]= 4.00 (2H, s) and 6.7—7.4 (10H, m). δ(C)=36.7, 127.5 (2C), 128.6 (2C), 128.9 (2C), 129.9, 132.6, 134.7 (2C), 136.1, 158.7, and 183.2. ν: 1615, 1555, 1460, 1385, 985, 915, 840, and 765 cm^{-1}].

2-(p-Methylbenzylthio)tropone (6b). This was prepared as colorless needles, mp 98—100.5°C [Found: C, 74.20; H, 5.79%. Calcd for $C_{15}H_{14}OS$: C, 74.35; H, 5.82%. δ=2.29 (3H, s), 3.98 (2H, s), and 6.7—7.3 (9H, m)], in 87% yield.

2-(p-Brmobenzylthio)tropone (6c). This was prepared as yellow needles, mp 133—135°C [Found: 54.46; H, 3.64%. Calcd for $C_{14}H_{11}OSBr$: C, 54.74; H, 3.61%. δ=4.02 (2H, s) and 6.8—7.5 (9H, m)], in 73% yield.

MCPBA-oxidatin of 6a. a): To a $CHCl_3$ solution (8 cm³) containing **6a** (455 mg, 2 mmol), MCPBA (740 mg, 3.4 mmol) dissolved in $CHCl_3$ (16 cm³) was added drop by drop for 4 h, and kept for an additional 24 h at 15—25°C. Then the separated crystals, MCBA, were filtered off, and the filtrate was washed with aqueous $NaHSO_3$, $NaHCO_3$, and NaCl, and dried on $MgSO_4$. Silica gel column chromatography of the organic solution afforded **4a**, 347 mg (67%), colorless needles, mp 113—114°C [Found; C, 64.83; H, 4.71%. Calcd for $C_{14}H_{12}O_3S$: C, 64.60; H, 4.65%. δ=4.90 (2H, s), 7.0—7.5 (9H, m), and 7.8—9.0 (1H, m). δ(C)=60.9, 127.6, 128.5 (2C), 128.7, 130.7 (2C), 131.5, 136.0, 139.5, 140.4, 143.7, 146.0, and 182.4. ν: 1635, 1585, 1305, 1270, 1215, 1145, 1125, and 780 cm^{-1}], and **5a**, 107 mg (22%), a colorless oil [Found: M$^+$, 244.0544. Calcd for $C_{14}H_{12}O_2S$: M$^+$, 244.0558. δ=3.95 (1H, d, J=12 Hz), 4.40 (1H, d, J=12 Hz), and 6.8—7.6 (10H, m). δ(C)=57.6, 128.0 (2C), 129.6, 130.3 (2C), 132.7, 135.5, 135.9, 137.3, 140.9, 155.9, and 183.6. ν: 1620, 1590, 1555, 1260, 1070, 1050, 875, 860, and 760 cm^{-1}].

TABLE 1. THE DEUTERIUM CONTENTS (%) IN THE PRODUCTS OF THE CROSS-OVER THERMOLYSIS OF **4a**-*d* AND **4c** DETERMINED BY MASS SPECTROMETRY

Products	d_0	d_1	d_2	d_3
7a	43.8	28.6	20.8	6.8
7c	48.9	35.8	10.4	4.9
8a	32.3	30.0	24.5	13.2
8c	35.4	26.7	22.8	15.0

b): Similarly, the oxidation of **6a** (115 mg, 0.5 mmol) in $CHCl_3$ (8 cm^3) with MCPBA (216 mg, 1.0 mmol) at 15—25°C for 24 h yielded 118 mg (91%) of **4a**.

2-(p-Methylbenzylsulfonyl)tropone (4b). This was prepared as colorless needles, mp 173—175°C [Found: C, 65.38; H, 5.12%. Calcd for $C_{15}H_{14}O_3S$: C, 65.67; H, 5.14%. δ= 2.26 (3H, s), 4.76 (2H, s), 6.8—7.3 (8H, m), and 7.83 (1H, dd, J=8, 2 Hz)], in 80% yield.

2-(p-Bromobenzylsulfonyl)tropone (4c). This was prepared as yellow needles, mp 135—137°C [Found: M^+, 337.9598 and 339.9590. Calcd for $C_{14}H_{11}O_3SBr$: M^+, 337.9612 and 339.9592. δ=4.77 (2H, s), 6.8—7.7 (8H, m), and 7.84 (1H, m)], in 99% yield.

Thermolysis of 4a. A tetralin solution (2 cm^3) of **4a** (136 mg) was heated at 215°C for 1.5 h on an oil bath under N_2 atmosphere. During the reaction, an intermittent evolution of SO_2 occurred. The mixture was then fractionated with a short silica-gel column and with PTLC to furnish **7a**, a colorless oil [Found: M^+, 196.0877. Calcd for $C_{14}H_{12}O$: M^+, 196.0888. δ=3.94 (2H, s), 6.8—7.3 (5H, m), and 7.21 (5H, s). δ(C)=40.5, 126.4, 128.5 (2C), 129.5 (2C), 132.6, 133.6, 135.4 (2C), 139.0, 140.6, 154.7, and 186.6], 24 mg (23%), which was identical with the sample prepared by the Nozoe's method,[2] and **8a**, a colorless oil [Found: M^+ 196.0889. δ=3.82 (2H, s) and 6.7—7.4 (10H, m). δ(C)=45.7, 126.9, 128.8 (2C), 128.9 (2C), 133.0, 136.2 (2C), 138.9, 140.3, 141.3, 148.2, and 187.6], 8 mg (7.5%).

The Reaction of 8a with Hydrazine Hydrate. An EtOH solution (10 cm^3) of **8a** (28 mg) was refluxed with 80% N_2H_4 hydrate (30 mg) for 2 h. Then, the mixture was fractionated with $CHCl_3$ and water, and the organic extract was purified by PTLC on silica gel to yield a yellow oil, **9**, 12 mg [Found: M^+, 211.0998. Calcd for $C_{14}H_{13}ON$: M^+, 211.0997. δ=3.88 (2H, s), 5.86 2H, m), 6.70 (1H, br. s), and 7.0—7.4 (8H, m)], and **10**, 9 mg [Found: M^+, 211.0998. δ=3.88 (2H, s), 5.82 (2H, br. s), 6.76 (1H, d, J=10 Hz), and 6.9—7.3 (8H, m)].

Hydrolysis of 10 to 3a. An EtOH solution (2 cm^3) of **10** (5 mg) and KOH (5 mg) was refluxed for 2 h. The mixture was then evaporated to dryness, acidified with dil HCl, and extracted with $CHCl_3$. Colorless needles, mp 119—120°C, 5 mg, thus obtained were identical in every respect to the previously prepared sample of **3a**.[1]

Thermolysis of 4b. A tetralin solution (5 cm^3) of **4b** (90 mg) was heated at 200°C for 1.7 h. The products isolated by PTLC were **7b**, a colorless oil, 19 mg (28%) [Found: M^+, 210.1047. Calcd for $C_{15}H_{14}O$: M^+ 210.1045. δ=2.30, 3.90 (2H, s), and 6.7—7.3 (9H, m)], and **8b**, a colorless oil, 5.5 mg (8%) [Found: M^+, 210.1043. δ=2.32 (3H, s), 3.78 (2H, s), and 6.7—7.4 (9H, m)].

Thermolysis of 4b in DMSO. A DMSO solution (0.3 cm^3) of **4b** (50 mg) was heated at 180°C for 1.5 h. The mixture was diluted with ether, and extracted with aqueous KOH to give 16 mg (65%) of colorless crystals, mp 178—179°C, which were identical with *p*-toluic acid.

Thermolysis of 4c. A tetralin solution (5 cm^3) of **4c** (170 mg) was heated at 225°C for 2 h. The products isolated by PTLC were **7c**, a colorless oil, 27 mg (20%) [Found: M^+, 274.0001 and 275.9958. Calcd for $C_{14}H_{11}OBr$: M^+, 273.9993 and 275.9973. δ=3.90 (2H, s) and 6.8—7.4 (9H, m)], and **8c**, a colorless oil, 1 mg (0.7%) [Found: M^+, 274.0009 and 275.9971. δ=3.78 (2H, s) and 6.7—7.5 (9H, m)].

Thermolysis of a 1:1-Mixture of 4a-d and 4c. A decalin solution (4 cm^3) of **4a**-*d* (123 mg) and **4c** (150 mg) was refluxed for 1.5 h on an oil bath under an N_2 stream. The mixture was then fractionated on a silica-gel column to give the thermolysates; their isotope distributions are given in Table 1.

References

1) H. Takeshita, H. Mametsuka, A. Chisaka, and N. Matsuo, *Chem. Lett.*, **1981**, 73.

2) T. Nozoe, T. Mukai, and I. Murata, *Proc. Jpn. Acad.*, **29**, 169 (1953).

3) In comparing the ^{13}C-NMR of these 2-aminobenzyltropones with the parent 2-aminotropone (**11**), the following chemical shift differences, $\Delta\delta$(C-*n*)=δ(11)−δ(9 or 10), were obtained; for **9**, $\Delta\delta$(C-3)=−2.2, $\Delta\delta$(C-4)=−20.2, $\Delta\delta$(C-5)= −1.4, and $\Delta\delta$(C-6)=−0.7, and for **10**, $\Delta\delta$(C-3)=1.8, $\Delta\delta$(C-4)= 0.1, $\Delta\delta$(C-5)=−13.5, and $\Delta\delta$(C-6)=−2.9.

4) H. Takeshita, H. Mametsuka, and N. Matsuo, *Bull. Chem. Soc. Jpn.*, **55**, 1137 (1982).

5) The NMR spectra were measured in $CDCl_3$ solutions, and the chemical shifts were expressed in δ scale from the internal Me_4Si.

Synthesis of 3-(Substituted Methyl)-2-phenyl-4*H*-1-benzothiopyran-4-ones

Hiroyuki NAKAZUMI,* Tamio UEYAMA, Hikaru SONODA, and Teijiro KITAO
Department of Applied Chemistry, College of Engineering, University of Osaka Prefecture, Sakai, Osaka 591
(Received November 17, 1983)

Synopsis. Reaction of 2-phenyl-4*H*-1-benzothiopyran-4-ones and related compounds with chloromethyl methyl ether and fuming sulfuric acid gave mainly 3-chloromethyl compound, whereas chloromethylation of methoxy-substituted thioflavones took place at another position or gave tris(chloromethyl) compound. 3-(Chloromethyl)thioflavone could be easily converted into various 3-(substituted methyl)-thioflavones which showed significant antimicrobial activity against *Trichophytons*.

We have attempted to prepare some 2-phenyl-4*H*-1-benzothiopyran-4-one (thioflavone) (**1**) which would be biologically and pharmacologically effective compounds.[1,2] We now examine the introduction of specific substituent groups (chloromethyl and acetoxymethyl) into the 3-position of **1**, because the introduction of these groups into the corresponding position of 1,4-naphthoquinones[3] and 4*H*-1-benzothiopyran-4-one 1,1-dioxides[4] is required for bioactivation. However, it is well known that no chloromethylation directly occurs at the 3-position of 4*H*-1-benzothiopyran-4-ones (thiochromones).[4] 3-(Chloromethyl)thioflavone **2a** may be a key compound, one which can be efficiently converted into other pharmacologically active compounds. Few reports are available on the preparation of the title compounds. In this paper, we report the direct chloromethylation of various thioflavones and related compounds.

A common chloromethylation of thiochromone 1,1-dioxides with formaldehyde and hydrogen chloride is well known; however, the thiochromone[4] and **1a** are not chloromethylated by the same method. Chloromethylation of **1a**[6] was accomplished by use of chloromethyl methyl ether and 60% fuming sulfuric acid, which were previously applied in the chloromethylation of benzyl chloride.[5] The chloromethyl derivative was determined to be 3-(chloromethyl)thioflavone **2a** on the basis of ^{1}H-NMR spectrum, in which

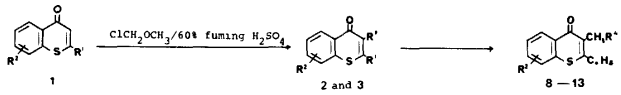

1 2 and 3 8—13

	R^1, R^2		R^1, R^2, R^3		R^2, R^4
1a	C_6H_5, H	**2a**	C_6H_5, H, CH_2Cl	**8**	H, NHC_6H_5
1b	CH_3, H	**2b**	CH_3, H, CH_2Cl	**9**	H, $N(CH_2CH_2)_2O$
1c	C_6H_5, 6-CH_3	**2c**	C_6H_5, 6-CH_3, CH_2Cl	**10**	H, $N(CH_2CH_2OH)_2$
1d	C_6H_5, 6-CH_3O	**2d**	C_6H_5, 6-CH_3O-5-CH_2Cl, H	**11**	H, OR
1e	4'-$CH_3OC_6H_4$, H	**2e**	3'5'-$(CH_2Cl)_2$-4'-$CH_3OC_6H_2$, H, CH_2Cl	**12**	H, $OCOCH_2CH_3$
1f	C_6H_5, 8-CO_2CH_3	**2f**	C_6H_5, 8-CO_2CH_3, CH_2Cl	**13**	6-CH_3, OCH_2CH_3
1g	4'-$NO_2C_6H_4$, H	**2g**	4'-$NO_2C_6H_4$, H, CH_2Cl		
1h	C_6H_5, 8-CH_3	**2h**	C_6H_5, 8-CH_3, CH_2Cl		
1i	4'-$CH_3C_6H_4$, H	**2i**	4'-CH_3-3'-$CH_2ClC_6H_3$, H, CH_2Cl		
		2j	4'-CH_3-3'-$CH_2OHC_6H_3$, H, CH_2Cl		
		3a	C_6H_5, H, CH_2OH		
		3b	CH_3, H, CH_2OH		
		3f	C_6H_5, 8-CO_2CH_3, CH_2OH		

Scheme 1.

a signal for a chloromethyl group appeared at δ 4.52 and a signal for a vinyl proton (δ 7.20) in the 3-position of **2a** disappeared. When the chloromethylation was carried out at 75°C, compound **3a** was isolated as the main product. 2-(Methyl)thiochromone **1b** and other thioflavones **1c—1i** were chloromethylated under the same conditions. In the case of 6-(methoxy)thioflavone **1d**, which possesses a powerful electron-donating group, chloromethylation did not take place at the 3-position, but at the 5-position. The ^{1}H-NMR signal for a chloromethyl group of product **2d** was shifted downfield to δ 5.58. On the other hand, a weak electron-donating methyl group at the same position led to 3-chloromethylated product **2c**. Methyl group and methoxycarbonyl group at the 8-position also led to 3-chloromethylated products **2h** and **2f**, respectively. Compound **3f** was isolated as a by-product. Chloromethylation of the thioflavone was also influenced by a substituent group in a phenyl group at the 2-position. Methoxyl and methyl substituent in the phenyl group led to tris(chloromethyl) compound **2e**, bis(chloromethyl) compound **2i**, and **2j**, respectively. The structure of compound **2j** was determined to be 3-(chloromethyl)-3'-(hydroxymethyl) derivative by means of its ^{1}H-NMR signal, which was shifted upfield to δ 2.44 for a OH proton of hydroxymethyl group, while the signal of the same group at the 3-position of compounds **3a**, **3b**, and **3f** appeared at δ 3.27—3.63. An electron-withdrawing nitro group at the 4'-position led to 3-chloromethyl compound **2g**. These results show that reaction of the thioflavone with chloromethyl methyl ether and fuming sulfuric acid generally gives only a 3-chloromethyated compound. The same chloromethylation of **1b**, flavone, and 2-methylchromone gave 3-chloromethyl derivatives **2b**, **4**, and **5** in 19—76% yields, respectively. New 3-(substituted methyl)thioflavones were easily prepared by reaction of **2a** with nucleophilic reagents, as shown in Scheme 1. For examples, reaction of **2a** with an excess of aniline, morpholine, bis(2-hydroxyethyl)amine, and sodium alkoxides[7] gave compounds **8—13**, respectively. The chlorine atom of a chloromethyl group of flavone derivative **4** was also converted into ethoxyl and acetoxyl group (compounds **6** and **7**) in good yields. The described method should be advantageous for direct transformation of thioflavones or flavone into their 3-(substituted methyl) derivatives.

An introduction of a chloromethyl group in the 3-position of **1a** resulted in significant antimicrobial activity against *Trichophytons* (MIC 0.195 μg/ml). 3-(Substituted methyl)thio-flavones **3a**, **9**, and **13** (MIC 0.00488—6.25 μg/ml), as well as 3-(alkoxymethyl)thioflavone **11**,[7] also exhibited activity against *Trichophytons*. On the other hand, the MIC of 3-(substituted methyl) flavones (MIC 1.56—25.0 μg/ml) became higher (*ca.* 10—200-fold) than that of the corresponding thioflavones.

Table 1. Physical Data of 3-(Chloromethyl)thioflavones (2) and 3-(Hydroxymethyl)thioflavones (3)

Compd	Yield[a] /%	Mp θ_m/°C	^{1}H-NMR (δ, in $CDCl_3$)	ν_{CO} /cm^{-1}	Mass, m/z (rel intensity)	Formula	Found (Calcd)(%) C	H	N
2a	76	130—132	4.52 (s,2H,CH_2) 7.46—7.61 (m,8H) 8.60 (m,1H,H-5)	1610	288 (M^++2,6) 286 (M^+,13) 251 (62) 250 (100)	$C_{16}H_{11}OSCl$	66.87 (67.01)	3.56 (3.87)	
2b	19	127—129	2.61 (s,3H,CH_3) 4.81 (s,2H,CH_2) 7.57—7.73 (m,3H) 8.64 (m,1H,H-5)	1610	226 (M^++2,20) 224 (M^+,50) 189 (97) 188 (51) 161 (100)	$C_{17}H_{13}OSCl$	58.77 (58.80)	3.83 (4.04)	
2c	59	154—157	2.50 (s,3H,CH_3) 4.43 (s,2H,CH_2) 7.43—7.58 (m,7H) 8.40 (s,1H,H-5)	1613	302 (M^++2,7) 300 (M^+,17) 265 (91) 264 (100)	$C_{17}H_{13}OSCl$	68.21 (67.88)	3.96 (4.36)	
2d	11	165—166	3.93 (s,3H,OCH_3) 5.58 (s,2H,CH_2) 7.22—7.66 (m,8H)	1605	318 (M^++2,16) 316 (M^+,37) 281 (36) 265 (76), 252 (100)	$C_{17}H_{13}O_2SCl$	64.13 (64.45)	3.98 (4.14)	
2e	8.0[b]	188—190	4.03 (s,3H,OCH_3) 4.51 (s,2H,CH_2) 4.72 (s,4H,CH_2) 7.65—7.71 (m,5H) 8.65 (m,1H,H-5)	1620	416 (M^++4,8) 414 (M^++2,21) 412 (M^+,20) 376 (80), 341 (73) 327 (97), 293 (100)	$C_{19}H_{15}O_2SCl_3$	54.99 (55.16)	3.42 (3.65)	
2f	77	146—148	4.02 (s,3H,OCH_3) 4.54 (s,2H,CH_2) 7.55—7.78 (m,6H) 8.54 (d,1H,J=8 Hz,H-5) 9.03 (d,1H,J=8 Hz,H-7)	1715 1608	346 (M^++2,5) 344 (M^+,12) 309 (71) 308 (100)	$C_{18}H_{13}O_3SCl$	62.54 (62.70)	3.73 (3.80)	
2g	50	220—222	4.46 (s,2H,CH_2) 7.20—7.88 (m,5H) 8.30—8.62 (m,3H)	1610	333 (M^++2,7) 331 (M^+,21) 296 (53) 295 (57), 250 (100)	$C_{16}H_{10}NO_3SCl$	57.68 (57.92)	2.68 (3.04)	3.87 (4.22)
2h	29	153—154	2.49 (s,3H,CH_3) 4.52 (s,2H,CH_2) 7.44—7.62 (m,7H) 8.52 (m,1H,H-5)	1615	302 (M^++2,17) 300 (M^+,43) 265 (75) 264 (100)	$C_{17}H_{13}OSCl$	67.58 (67.88)	4.16 (4.36)	
2i	14	164—167	2.48 (s,3H,CH_3) 4.50 (s,2H,CH_2) 4.66 (s,2H,CH_2) 7.35—7.71 (m,6H) 8.60 (m,1H,H-5)	1630	350 (M^++2,14) 348 (M^+,20) 313 (40) 312 (61), 311 (72) 276 (100)	$C_{18}H_{14}OSCl_2$	61.73 (61.90)	3.81 (4.04)	
2j	39	182—183	2.44 (s,1H,OH) 2.51 (s,3H,CH_3) 4.54 (s,2H,CH_2) 4.67 (s,2H,CH_2) 7.35—7.65 (m,6H) 8.59 (m,1H,H-5)	1605	332 (M^++2,10) 330 (M^+,23) 312 (42) 295 (17), 277 (71) 263 (94), 262 (100)	$C_{18}H_{15}O_2SCl$	65.73 (65.35)	4.56 (4.57)	
3a	38	175—177	3.60 (t,J=7 Hz,1H, OH) 4.47 (d,J=7 Hz,2H, CH_2) 7.30—7.58 (m,8H) 8.38 (m,1H,H-5)	1605	268 (M^+,26) 250 (100) 221 (39)	$C_{16}H_{12}O_2S$	71.94 (71.62)	4.22 (4.51)	
3b	9.0	147—149	2.52 (s,3H,CH_3) 3.63 (b,1H,OH) 4.75 (s,2H,CH_2) 7.58 (m,3H) 8.53 (m,1H,H-5)	1605	206 (M^+,100) 191 (54) 188 (78)	$C_{17}H_{10}O_2S$	63.94 (64.05)	4.62 (4.89)	
3f	6.3	149—150	3.27 (b,1H,OH) 3.95 (s,3H,CO_2 CH_3) 4.53 (s,2H,CH_2) 7.42—7.67 (m,6H) 8.40 (m,1H,H-5) 8.80 (dd,J=8 and 1.5 Hz,1H,H-7)	1710 1608	326 (M^+,21) 309 (23) 308 (100) 307 (33)	$C_{18}H_{14}O_4S$	65.88 (66.24)	4.22 (4.32)	

a) Yield based on the converted substrate (1a—1i). b) Isolated yield.

Experimental

All the melting points are uncorrected. ^{1}H-NMR spectra were taken on a JEOL JNM-MH-100 spectrometer with tetramethylsilane as an internal standard. IR spectra were recorded on a Shimazu IR-420 spectrometer using KBr pellets. Elemental analyses were recorded on a Yanaco CHN recorder MT-2. Mass spectra were recorded on a Hitachi RMU-6E mass spectrometer operating at 80 eV.

2-Phenyl-4H-1-benzothiopyran-4-ones and 2-Methyl-4H-1-benzothiopyran-4-one (1a—1i). Thioflavones and 2-methylthiochromone were generally prepared by Bossert's method.[6] The physical data of new derivative **1i** are as follows. **1i**; mp 120—121°C; 1608 cm^{-1} (C=O); ^{1}H-NMR ($CDCl_3$) δ=2.42 (s, 3H, CH_3), 7.20—7.36 (m,3H), 7.48—7.70 (m, 5H), and 8.57 (m, 1H, H-5); MS m/z (rel intensity) 252 (M^+, 100), 224 (96), and 223 (26). Anal. ($C_{16}H_{12}OS$) C, H.

General Procedure for Chloromethylation. Fuming sulfuric acid (60%; 14 ml) was added dropwise to a solution of approriate thioflavone **1** (35 mmol) in chloromethyl methyl ether (56 ml) with stirring. The reaction mixture was stirred at 60°C for 24 h, and then poured into cold water. The oily precipitate soon solidified, and the resulting solid was collected and washed with water. The crude product was chromatographed on silica gel, using benzene as an eluent, to give **2**. Recrystallization from benzene/hexane (10:1) gave a pure chloromethyl derivative **2**. The yields, mp's and spectral data of **2a—2j** and **3a, b, f** are summarized in Table 1.

Table 2. Physical Data of 3-(Substituted Methyl)thioflavones

Compd	Yield[a] /%	Mp θ_m/°C	^{1}H-NMR (δ, in $CDCl_3$)	ν_{CO} /cm^{-1}	Mass, m/z (rel intensity)	Formula	Found (Calcd)(%) C	H	N
8	46	116—118	4.18 (s,2H,CH_2) 6.21—7.05 (m,5H) 7.35—7.50 (m,8H) 8.43 (m,1H,H-5)	1610	343 (M^+,14) 252 (100)	$C_{22}H_{17}NOS$	76.58 (76.94)	4.57 (4.99)	3.99 (4.08)
9	65	164—166	2.25—2.41 (m,4H) 3.46—3.64 (m,6H) 7.35—7.57 (m,8H) 8.55 (m,1H,H-5)	1610	337 (M^+,15) 251 (100)	$C_{20}H_{19}NO_2S$	70.91 (71.19)	5.36 (5.68)	4.05 (4.15)
10	36	98—101	2.45 (t,J=6 Hz,4H, N-CH_2-), 3.25 (b, 2H,OH), 3.53 (t,J= 6 Hz,4H,-CH_2-O), 3.73 (s,2H,-CH_2 -N), 7.49—7.70 (m,8H), 8.65 (m, 1H,H-5)	1608	337 (17) 324 (20) 310 (23) 251 (100)	$C_{20}H_{23}NO_2S$	67.60 (67.58)	5.95 (5.96)	3.95 (3.94)
12	77	120—122	1.12 (t,J=7 Hz,3H, CH_2-$\underline{CH_3}$) 2.27 (q,J=7 Hz,2H, $\underline{CH_2}$-CH_3) 4.93 (s,2H,CH_2O) 7.37—7.53 (m,8H) 8.49 (m,1H,H-5)	1730 1615	—	$C_{19}H_{18}O_2S$	70.10 (70.35)	4.64 (4.97)	
13	66	99—101	1.15 (t,J=6 Hz,3H, CH_2-$\underline{CH_3}$), 2.49 (s, 3H, CH_3-6), 3.52 (q,J=6 Hz,2H, $\underline{CH_2}$-CH_3), 4.37 (s,2H,CH_2-O), 7.47—7.75 (m,7H) 8.47 (s,1H,H-5)	1618	—	$C_{19}H_{18}O_2S$	73.55 (73.52)	5.79 (5.85)	

a) Isolated yield

Compounds **4** and **5** were similarly prepared from flavone[8] and 2-methylchromone,[9] respectively. Compound **4**: yield 47%; mp 155—156°C (lit,[10] 156°C). Compound **5**: yield 76%; mp 103—104°C (lit,[10] 103—108°C).

3-(Substituted Methyl)-2-phenyl-4H-1-benzothiopyran-4-ones and 3-(Substituted Methyl)-2-phenyl-4H-1-benzopyran-4-ones (6—13). A mixture of compound **2a** and appropriate amine, sodium alkoxide or sodium propionate was heated at reflux for 2—5 h in dioxane, alcohol or propionic acid. The mixture was worked up as described above to give pure compounds **8—13**. The physical data of these compounds are listed in Table 2.

Compounds **6** and **7** were similarly prepared. 3-(Ethoxymethyl)flavone **6**: yield 75%; mp 102—114°C; 1640 cm^{-1} (C=O); ^{1}H-NMR ($CDCl_3$) δ=1.31 (t, J=7 Hz, 3H, -$CH_2\underline{CH_3}$), 3.73 (q, J=7 Hz, 2H, -$\underline{CH_2}CH_3$), 4.48 (s, 2H, -CH_2O), 7.52—7.84 (m, 6H), 7.99—8.13 (m, 2H), and 8.45 (d, J=7.5 Hz, 1H, H-5). Anal. ($C_{18}H_{16}O_3$) C, H. 3-(Acetoxymethyl)flavone **7**: yield 80%; mp 118—119°C (lit,[11] 115—118°C).

Determination of in Vitro Antimicrobial Activity. The minimal inhibitory concentrations (MIC) were determined by a standard two-fold serial dilution method using agar media for *Trichophyton rubrum, Trichophyton mentagrophytes,* and *Candida albicans.*

References

1) H. Nakazumi, T. Ueyama, T. Endo, and T. Kitao, *Bull. Chem. Soc. Jpn.*, **56**, 1251 (1983).

2) H. Nakazumi, T. Ueyama, and T. Kitao, *J. Heterocycl Chem.* **21**, 193 (1984).

3) A. J. Lin, B. J. Lillis, and A. C. Sartorelli, *J. Med. Chem.*, **18**, 917 (1975).

4) M. H. Holshouser, L. J. Loeffler, and I. H. Hall, *J. Med. Chem.*, **24**, 853 (1981).

5) H. Suzuki, *Bull. Chem. Soc. Jpn.*, **43**, 3299 (1970).

6) F. Bossert, *Justus Liebigs Ann. Chem.*, **680**, 40 (1964).

7) H. Nakazumi, T. Ueyama, and T. Kitao, *J. Med. Chem.*, to be published.

8) T. S. Wheeler, *Org. Synth.*, **32**, 72 (1952).

9) S. Binecki and E. Kesler, *Acta. Polon. Pharm.*, **13**, 503 (1965).

10) M. V. Shah and S. Sethna, *J. Indian Chem. Soc.*, **39**, 507 (1962).

11) H. Hofmann, G. Salbeck, and B. Meyer, *Ber.*, **103**, 2084 (1970).

Photochemical Reactions of Spiro[benzo[*b*]thiophene-2(3*H*), 1′-cyclopropan]-3-ones

Nobumasa KAMIGATA,* Koichi HAGIHARA, Satoshi HASHIMOTO, Hirokazu IIZUKA, and Michio KOBAYASHI
Department of Chemistry, Tokyo Metropolitan University, Fukazawa, Setagaya-ku, Tokyo 158
(Received November 26, 1983)

Synopsis. The photolysis of spiro[benzo[*b*]thiophene-2(3*H*),1′-cyclopropan]-3-one 1,1-dioxide (**1**) in benzene afforded 2-biphenylyl cyclopropyl ketone with extrusion of sulfur dioxide, whereas the irradiation of **1** in toluene or *p*-xylene formed photoreduced dimer and bibenzyl or 4,4′-dimethylbibenzyl, respectively. The photolysis of spiro-[benzo[*b*]thiophene-2(3*H*),1′-cyclopropan]-3-one in benzene afforded the valence isomer 2,3-dihydro[1]benzothieno[3,2-*b*]-furan.

In recent years, considerable attention has been focused on the photochemistry of five-membered heterocyclic ring systems.[1] We reported that the photochemical reactions of 2-aryl-1,2-benzisothiazol-3(2*H*)-ones in benzene give dibenzo[*b*,*f*][1,4]thiazepin-10(11*H*)-ones,[2] whereas the photolyses of 2-substituted 1,2-benzisothiazol-3(2*H*)-one 1,1-dioxides in benzene give *N*-substituted *o*-phenylbenzamides with extrusion of sulfur dioxide.[3] In our systematic investigations of photochemical reactions of benzisothiazoles and their analogues, we wish to report here the photochemical behavior of spiro[benzo[*b*]thiophene-2(3*H*),1′-cyclopropan]-3-one 1,1-dioxide (**1**) and spiro[benzo[*b*]-thiophene-2(3*H*),1′-cyclopropan]-3-one (**2**). These are expected to be photoreduced at the carbonyl group and to break their bonds at spiro carbon-sulfur atom or at the highly-strained three membered ring.

When a solution containing of **1** in benzene was irradiated under argon with light of wavelength >280 nm, an extremely clean conversion to a single photoproduct occurred. This product was deduced to be 2-biphenylyl cyclopropyl ketone (**3**) on the basis of its straightforward spectral properties (see experimental section). The reaction is quite similar to the photoreactions of 2-substituted 1,2-benzisothiazol-3(2*H*)-one 1,1-dioxides in benzene,[3] and hence the reaction could be accounted for by a homolytic process *via* radical intermediates **4**, **5**, and **6**, as shown in Scheme 1.

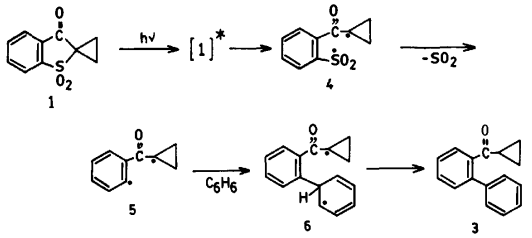

Scheme 1.

Meanwhile, when **1** was irradiated in toluene or *p*-xylene photoreduced dimer, 3,3″-bi[spiro[benzo[*b*]-thiophene-2(3*H*),1′-cyclopropane]]3,3″-diol 1,1,1″,1″-tetraoxide (**7**) was formed with bibenzyl or 4,4′-dimethylbibenzyl, respectively, in good yield. No detectable quantities of such photoreduced alcohol as spiro-[benzo[*b*]thiophene-2(3*H*),1′-cyclopropan]-3-ol 1,1-dioxide (**8**) could be observed in the reaction mixture. The photoreaction of **1** in these solvents suggests that **1** in the photoexcited state abstracts the hydrogen atom from the methyl group of toluene or *p*-xylene to give radical **9** and benzyl (or *p*-methylbenzyl) radical (**10**) faster than a homolytic cleavage to **4** occurs. The absence of the alcohol **8** suggests that radical **9** has no ability to abstract the hydrogen atom from the methyl group of toluene or *p*-xylene and survive until a coupling reaction occurs to give dimer **7** (Scheme 2).

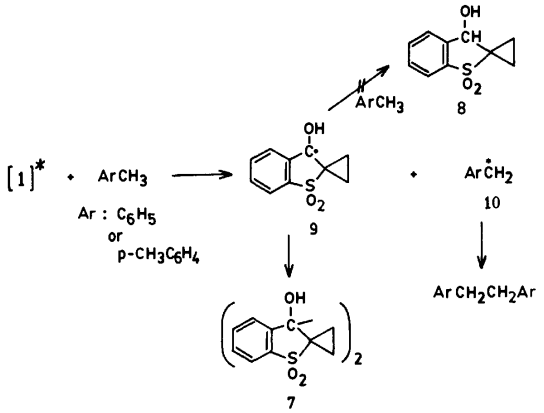

Scheme 2.

The photolysis of **1** was also carried out in 2-propanol and the photoreduced dimer **7** and pinacol were obtained. The reaction mechanism will be similar to the photolysis in toluene or *p*-xylene, involving the abstraction of the tertiary hydrogen from 2-propanol by **1** in the photoexcited state.

The photoreaction of **1** behaved in quite different manners in benzene, and in toluene, *p*-xylene, or 2-propanol. **1** in the photoexcited state abstracts a hydrogen when the solvents are hydrogen donating, whereas in benzene **1** cleaves the C–S bond homolytically, affording radical intermediates **4** and **5**. The photoreaction of 2-substituted 1,2-benzisothiazol-3(2*H*)-ones in benzene or 2-propanol, however, always included the extrusion of sulfur dioxide.[3] It is also noteworthy that **7** is the sole photoreduced product and no formation of any product like **8** is observed in the photolysis of **1**, in contrast to the reported photoreactions of phthalimides.[4]

The photoreaction of **2** in benzene afforded 2,3-dihydro[1]benzothieno[3,2-*b*]furan (**11**) as the only isolable product. The reaction mechanism will be accounted for by the homolytic reaction shown in Scheme 3.

In this case, the reaction seems to proceed *via* the homolytic cleavage of the strained cyclopropane ring affording radical **12** and the following ring construction to give **11**. The photolysis of **2** in toluene

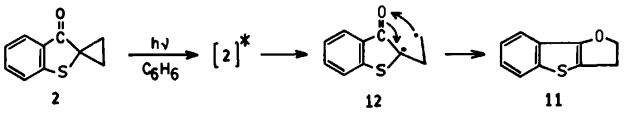

Scheme 3.

or *p*-xylene did not form any isolable product in spite of the starting material was consumed.

Experimental

Measurements. Melting points are uncorrected. IR and UV spectra were determined on a Hitachi EPI-G2 and a Hitachi 220A spectrophotometer. The proton magnetic spectra were recorded at 60 MHz by using a Hitachi R-20B spectrometer with TMS as an internal standard in $CDCl_3$. Mass spectra were determined with a JMS-DX300 high resolution mass spectrometer. Elemental analyses were carried out by using a Perkin-Elmer 240 elemental analyzer.

Materials. Spiro[benzo[*b*]thiophene-2(3*H*),1′-cyclopropan]-3-one (**2**) was prepared from *o*-mercaptobenzoic acid (15.4 g) and α-bromo-γ-butyrolactone (20.6 g) according to the method described in the literature:[5] yield 10.5 g (65%) as colorless prisms form hexane–dichloromethane, mp 69—70°C (lit, mp 70°C).[6] IR (KBr) 1680, 1590, 1450, 1320, 1080, 980, and 740 cm^{-1}; NMR ($CDCl_3$) δ 1.3—1.9 (4H, m) and 7.2—7.9 ppm (4H, m); UV (EtOH) 367 ($\varepsilon=2.67\times10^3$), 350 ($2.60\times10^3$), 267 ($5.50\times10^3$), 258 ($6.58\times10^3$), 237 ($3.36\times10^4$), and 208 nm ($1.29\times10^5$). Spiro[benzo[*b*]thiophene-2(3*H*),1′-cyclopropan]-3-one 1,1-dioxide (**1**) was prepared by the oxidation of **2** (5.2 g) with 13.7 g of perbenzoic acid in dichloromethane at 0°C: yield 5.6 g (91%) as colorless prisms from hexane–dichloromethane, mp 198—199°C (lit, mp 202°C).[6] IR (KBr) 1720, 1590, 1460, 1315, 1300, 1155, and 990 cm^{-1}; NMR ($CDCl_3$) δ 1.30—2.00 (4H, m) and 7.40—8.10 ppm (4H, m); UV (MeOH) 292 ($\varepsilon=6.55\times10^2$), 283 ($7.74\times10^2$), 246 ($9.64\times10^3$), and 210 nm ($3.35\times10^4$).

Photolysis of 1 in Benzene. A solution containing 200 mg of **1** in 220 cm^3 of benzene was irradiated under argon with a 450W medium-pressure mercury lamp (Hanovia) through a Corex filter sleeve for 8 h. Removal of the solvent under reduced pressure left a pale-yellow oil which was subjected to the chromatography on silica gel, using benzene as the eluent. 2-Biphenylyl cyclopropyl ketone (**3**) was isolated (130 mg, 86%)[7] with 58 mg of unreacted starting material **1**. The structure of **3** was assigned based on the following data: mp 81—82°C (from hexane); IR (KBr) 3020, 1670, 1595, 1450, 1435, 1280, 1040, and 990 cm^{-1}; NMR ($CDCl_3$) δ 0.50—0.72 (2H, m), 1.00—1.16 (2H, m), 1.64—1.88 (1H, m), 7.56 (5H, s), and 7.48—7.78 ppm (4H, m); Mass (20 eV) *m/z* 222 (M^+), 194, 165, 153, 69, and 41. Found: C, 86.39; H, 6.23%. Calcd for $C_{16}H_{14}O$: C, 86.45; H, 6.35%.

Photolysis of 1 in Toluene. A solution containing 200 mg of **1** in 220 cm^3 of toluene was irradiated under argon through a Pyrex filter sleeve for 18 h. After removal of the solvent, the photolysate was subjected to the chromatography on silica gel using a 2:1 hexane–ether mixture as the eluent to give bibenzyl (62 mg, 71%) and **7** (140 mg, 70%). The structure of bibenzyl was verified by comparison with an authentic sample, and that of **7** was identified on the basis of the following data: mp 276°C (decomp); IR (KBr) 3450, 3030, 1600, 1495, 1455, 1290, 1180, 1165, 1155, 1120, 1100, 1060, 1050, and 980 cm^{-1}; NMR (CD_3SOCD_3) δ 0.91—1.6 (4H, m), 6.8—8.2 ppm (4H, m); Mass *m/z* 418 (M^+), 362, 314, 209, 152, 136, 104, and 76. Found: *m/z* 209.02719. Calcd for $C_{10}H_9O_3S$: *m/z* 209.02719.

Photolysis of 1 in p-*Xylene.* A solution containing 200 mg of **1** in 220 cm^3 of *p*-xylene was irradiated under argon through a Pyrex filter sleeve for 18 h. After evaporation of the solvent, the photolysate was subjected to the chromatography on silica gel using a hexane–ether mixture as the eluent to give 4,4′-dimethylbibenzyl (78 mg, 77%) and **7** (150 mg, 75%). The structure of 4,4′-dimethylbibenzyl was verified by comparison with an authentic sample.

Photolysis of 1 in 2-Propanol. A solution containing 200 mg of **1** in 220 cm^3 of 2-propanol was irradiated under argon through a Pyrex filter sleeve for 16 h. After removal of the solvent, the photolysate was subjected to the chromatography on silica gel using a hexane–ether as the eluent to give pinacol (41 mg, 72%) and **7** (157 mg, 78%).

Photolysis of 2 in Benzene. A solution containing of 200 mg of **2** in 220 cm^3 of benzene was irradiated under argon through a Pyrex filter for 2 h. Removal of the solvent under reduced pressure left a dark oil which was purified by thick-layer (preparative thin layer) chromatography using a 1:1 mixture of dichloromethane–benzene as the eluent. **11** (9.7 mg, 9%)[7] was isolated with 93 mg of unreacted starting material. The structure of **11** was identified by comparison with an authentic sample.[8]

References

1) A. Padwa, "Rearrangements in Ground and Excited State," ed by P. de Mayo, Academic Press, New York (1980), Vol. 3, p. 501.

2) N. Kamigata, S. Hashimoto, S. Fujie, and M. Kobayashi, *J. Chem. Soc., Chem. Commun.*, **1983**, 765.

3) N. Kamigata, T. Saegusa, S. Fujie, and M. Kobayashi, *Chem. Lett.*, **1979**, 9.

4) Y. Kanaoka, *Acc. Chem. Res.*, **11**, 407 (1978); K. Maruyama, *Kagaku*, **34**, 740 (1978), and the references which are cited therein.

5) M. Kawada, Y. Kawano, H. Sugihara, S. Takei, and I. Imada, *Chem. Pharm. Bull.*, **29**, 1900 (1981); M. Kawada, and H. Sugihara, 45th National Meeting of the Chemical Society of Japan, April 1982, Abstr. II, p. 941.

6) M. Okitsu, H. Shimadzu, T. Kataoka, and M. Hori, *Heterocycles*, **6**, 1877 (1977).

7) The yield was based on the starting material consumed.

8) P. M. Weitraub and A. D. Sill, *J. Chem. Soc., Chem. Commun.*, **1975**, 784.

The Preparation of *N*-Protected Amino Alcohols and *N*-Protected Peptide Alcohol by Reduction of the Corresponding Esters with Sodium Borohydride. An Improved Procedure Involving a Slow Addition of a Small Amount of Methanol

Kenso SOAI,* Hidekazu OYAMADA, and Masako TAKASE

Department of Applied Chemistry, Faculty of Science, Science University of Tokyo, Kagurazaka, Shinjuku-ku, Tokyo 162

(Received December 19, 1983)

Synopsis. Esters of *N*-protected amino acids and an *N*-protected peptide were reduced selectively to the corresponding alcohols in high yields using lesser amounts of sodium borohydride than does the conventional method by the slow addition of methanol to the mixture of ester and $NaBH_4$ in *t*-butyl alcohol or tetrahydrofuran at 50°C.

N-Protected amino alcohols (**1**) and *N*-protected peptide alcohols (**2**) have received considerable recent attention. **1** can be utilized as intermediates in the preparation of amino aldehydes,[1] which are inhibitors of proteolytic enzymes[2] and are important synthetic intermediates.[3] On the other hand, **2** are intermediates of peptide aldehydes of which biological activity is different from the corresponding peptides.[4] **2** can also be used for the determination of carboxy (*C*-) terminals of peptides.[5]

In connection with the synthesis of **1** and/or **2**, following three types of the methods have been reported: (1) Reduction of carboxylic acid by a borane–tetrahydrofuran (THF) complex.[6] In principle, this method is not applicable to the synthsis of **2**, because the borane complex is known to reduce amide groups (peptide bonds).[7] (2) Reduction of activated ester, azide, acid anhydride *etc.*[8] The procedure needs the conversion of carboxylic acids to the appropriate activated compounds, which are often sensitive toward hydroxy or mercapto groups.[9] In the synthesis from methyl or ethyl esters, an hydrolysis step from ester to acid should be additionally required. (3) Reduction of common esters such as methyl or ethyl esters. We would like to point out that carboxy (*C*-) terminal groups are often protected as methyl or ethyl esters in peptide synthesis. Direct reduction of these esters is preferable to the type (2) reaction because the hydrolysis step of the esters is not required. Reduction of these esters by lithium aluminium hydride is accompanied by the reduction of the peptide bonds.[7] Reduction by sodium borohydride ($NaBH_4$) in water[10] or in 50% aqueous ethanol[11] has been reported. However, these methods require the use of a large excess of $NaBH_4$ (4—25 mol equiv) and relatively long reaction time (3 h—2 d). Moreover, the possibility of alkaline hydrolysis of the esters is present because the solvents contain water.

During our continuing study on the stereoselectivity[12a] and chemoselectivity[12b–e] of metal borohydride reductions, we have noticed that the role of MeOH is important.

In this paper, we wish to describe a convenient method for the repid and selective reduction of esters of *N*-protected amino acid and *N*-protected peptide with $NaBH_4$. The essential part of the procedure is the addition of a small amount of MeOH to the mixture of esters and $NaBH_4$.

TABLE 1. COMPARATIVE STUDY ON THE REDUCTION OF ETHYL ESTER OF *N*-(*t*-BUTOXYCARBONYL)-L-PHENYLALANINE (**3**) WITH SODIUM BOROHYDRIDE

Solvent	Molar ratio $\frac{NaBH_4}{3}$	Temp /°C	Time /min	Yield /% of **4**
50% aqueous EtOH[a]	2.0	50—55	30	61
Slow addition of MeOH to THF	2.0	50—55	30	88

a) See Ref. 11.

In the first place, we compared the effectiveness of the present procedure with the conventional method.[11] The results are shown in Table 1. Using the ethyl ester of *t*-butoxycarbonyl-L-phenylalanine [Boc-L-Phe(OEt), **3**] as a model compound, it was reduced with $NaBH_4$ (2 mol equiv) in THF by the addition of a small amount of MeOH at 50—55°C for 30 min. The yield of Boc-L-phenylalaninol (**4**) was 88%. On the other hand, reduction of **3** in 50% aqueous EtOH[11] under the same reaction conditions (amount of $NaBH_4$, reaction temperature, time) afforded only 61% of **3** in our hands. Therefore the present procedure would seem to be superior to the conventional method.

This procedure using a slow addition of MeOH was applied to the reduction of esters of other *N*-protected amino acids and peptide. As shown in Table 2, even a hindered peptide (2*S*, 2′*S*)-(*N*-benzyloxycarbonylprolyl)-proline methyl ester was found to be reduced selectively in 84% yield. *t*-Butyl alcohol instead of THF was also effective for the conversion of esters to the corresponding alcohols.

TABLE 2. SYNTHESIS OF *N*-PROTECTED AMINO ALCOHOL (**1**) AND PEPTIDE ALCOHOL (**2**)

Ester	Alcohol **1,2**	$\frac{NaBH_4}{ester}$	Solvent[a]	Yield /%[b]	Mp or Bp θ_m or θ_b °C	$[\alpha]_D^{20}$ (*c*, solvent)
Z-L-Phe-OEt		2.5	A	94	90—91 (90—92)[c]	−41.8°[c] (1.4, EtOH)
Boc-L-Phe-OEt (**3**)	**4**	2.0	B	88	94.5	−24.6°[d] (1.1, $CHCl_3$)
Z-L-Pro-OMe		2.5	A	89	150—151/ 0.005 mmHg	−39.5°[e] (1.7, $CHCl_3$)
Z-L-Pro-L-Pro-OMe (**5**)	**6**	2.4	A	84	114—114.5	−33.5° (1.0, $CHCl_3$)

a) A; *t*-BuOH:MeOH=5:1 (v/v). B; THF:MeOH=5:1 (v/v). b) Yields of the isolated products. c) Lit, $[\alpha]_D^{20}$ −41.5°(*c* 1.4, EtOH). A.Ito, *Chem. Pharm. Bull.*, **23**, 3081(1975). d) Lit, $[\alpha]_D^{23}$ −0.80° (*c* 1.1, $CHCl_3$). See Ref. 6. e) Lit, $[\alpha]_D$ −42.4°(*c* 1.0, $CHCl_3$). J.Cassel and A.Furst, *Helv. Chim. Acta*, **59**, 1917(1976).

As described above, esters of *N*-protected amino acids and peptides were reduced selectively to the corresponding alcohols in high yields with $NaBH_4$ in THF or *t*-BuOH by the addition of a small amount of MeOH. The present procedure requires a lesser amount of $NaBH_4$ and shorter reaction time than the conventional method.[11] Moreover it avoids the possibility of the hydrolysis of the esters during the reduction in an aqueous medium,[11] neither does it require alkaline earth metal salt additives.[13]

Experimental

All of the melting points were uncorrected. Tetrahydrofuran (THF) was distilled from lithium aluminium hydride prior to use. *t*-Butyl alcohol was purchased from Kanto Chemical Co., and was used without further purification. Reagent grade methanol was dried over molecular sieves (3 Å) and used without distillation.

General Procedure. MeOH (0.8 ml) was added dropwise over a period of 20 min to a mixture of ester of *N*-protected amino acid or peptide (1.0 mmol) and $NaBH_4$ (2.0—2.5 mmol) in *t*-BuOH or THF (4 ml) at 50—55 °C. The mixture was stirred for 10—25 min, then water (2.0 ml) was added to the reaction mixture. Most of the organic solvent was evaporated under reduced pressure. Brine (3 ml) was added, and the mixture was extracted with ether (5×8 ml). The extract was washed with brine (2×3 ml), dried over anhydrous sodium sulfate, then evaporated. The residue was purified by distillation or on silica gel TLC (ethyl acetate: MeOH=15:1 as developing solvent). The physical properties of the products are summarized in Table 2. Yields of the alcohols were 84—94%. Structures of known compounds were confirmed by NMR and IR spectra.

(*2S, 2'S*)-(N-*Benzyloxycabonylprolyl*)*prolinol* (**6**). Z-L-Pro-L-Pro-OMe (**5**)[14] was reduced according to the general procedure. **6** was obtained in 84% yield. Mp 114—114.5 °C. $[\alpha]_D^{20}$ −33.5° (*c* 1.0, chloroform). ^{1}H-NMR ($CDCl_3$): δ=1.2—2.4 (m, 8H), 3.0—4.7 (m, 9H), 5.1 (s, 2H), 7.25 (s, 5H); IR: 3520, 2960, 1700, 1650, 1440, 1365, 1180 cm^{-1}; MS: *m/z* 332 (M^+). Found: C, 65.09; H, 7.30; N, 8.45%. Calcd for $C_{18}H_{24}N_2O_4$: C, 65.04; H, 7.28; N, 8.43%.

References

1) a) C. F. Stanfield, J. E. Parker, and P. Kanellis, *J. Org. Chem.*, **46**, 4797 (1981); b) Y. Hamada and T. Shioiri, *Chem. Pharm. Bull.*, **30**, 1921 (1982); c) R. P. Sharma, M. G. Gore, and M. Akhtar, *J. Chem. Soc., Chem. Commun.*, **1979**, 875.

2) H. Umezawa, "Enzyme Inhibitors of Microbial Origin," Univ. of Tokyo Press, Tokyo, (1972).

3) E. Nakamura, *Tetrahdron Lett.*, **1981**, 663; M. Narita, M. Otsuka, S. Kobayashi, M. Ohno, Y. Umezawa, H. Morishima, S. Saito, T. Takita, and H. Umezawa, *ibid.*, **1982**, 525; H. Newmann, *J. Am. Chem. Soc.*, **95**, 4098 (1973).

4) For instance, [D-Ala^2, Leu^5-ol]enkephalin is known to be a long-lasting analog of enkephalin which is an opioid hormone. J. S. Morley, *Ann. Rev. Pharmacol. Toxicol.*, **20**, 81 (1980).

5) J. P. Greenstein and M. Winitz, "Chemistry of Amino Acids," John Wiley & Sons, New York, (1960).

6) C. F. Stanfield, J. E. Parker, and P. Kanellis, *J. Org. Chem.*, **46**, 4799 (1981).

7) For a review, see A. Hajós, "Complex Hydrides," Akademiai Kiado, Budapest, (1979).

8) J. Nikawa and T. Shiba, *Chem. Lett.*, **1979**, 981, and references cited therein.

9) N. Izumiya, M. Oono, T. Kato, and H. Aoyagi, "Peptide Gosei," Maruzen, Tokyo (1975), Chap. 5.

10) T. Hamada, M. Suzuki, and O. Yonemitsu, *Chem. Pharm. Bull.*, **20**, 994 (1972).

11) H. Seki, K. Koga, and S. Yamada, *Chem. Pharm. Bull.*, **15**, 1948 (1967).

12) a) K. Soai, K. Komiya, Y. Shigematsu, H. Hasegawa, and A. Ookawa, *J. Chem. Soc., Chem. Commun.*, **1982**, 1282; b) K. Soai, A. Ookawa, and H. Hayashi, *ibid.*, **1983**, 668; c) K. Soai, H. Oyamada, and A. Ookawa, *Synth. Commun.*, **12**, 463 (1982); d) K. Soai, A. Ookawa, H. Oyamada, and M. Takase, *Heterocycles*, **19**, 1371 (1982); e) K. Soai, H. Oyamada, M. Takase, and A. Ookawa, *Bull. Chem. Soc. Jpn.*, **57**, 1948 (1984).

13) In the presence of alkali earth metal salt, $NaBH_4$ is known to become $LiBH_4$ which is capable of reducing esters. H. C. Brown and B. C. S. Rao, *J. Am. Chem. Soc.*, **78**, 2582 (1956). See also Ref. 1b.

14) T. Mukaiyama, K. Soai, T. Sato, H. Shimizu, and K. Suzuki, *J. Am. Chem. Soc.*, **101**, 1455 (1979)

A Convenient Synthesis of 2-Acylmethyl-4,4-dimethyl-2-oxazolines. Useful Reagents for β-Keto Ester Synthesis

Yasuo TOHDA,* Toshihide KAWASHIMA, Masahiro ARIGA, Ryohei AKIYAMA, Hiroshi SHUDOH, and Yutaka MORI

Department of Chemistry, Osaka Kyoiku University, Minamikawahori, Tennoji-ku, Osaka 543

(Received December 19, 1983)

Synopsis. Acylation of 2,4,4-trimethyl-2-oxazoline with acid chlorides having no α-proton and triethylamine gave *C,N*-diacylated products. Hydrolysis of the products with potassium hydroxide gave the enols of 2-acylmethyl-oxazolines, which were selectively *C*-monoalkylated by alkyl halides.

β-Keto esters have been well known as useful starting materials for organic syntheses, and various synthetic methods of β-keto esters were developed.[1] Although 2-oxazoline is also known as the protecting group of carboxylic acids,[2] oxazoline derivatives of β-keto acids are scarcely known. Since 2-oxazoline group can be converted into a variety of functional groups more easily than esters,[3-6] the oxazoline derivatives of β-keto acids are expected to be more versatile starting materials than the corresponding β-keto esters. Here we report a convenient synthesis of this class of compounds by acylation of 2,4,4-trimethyl-2-oxazoline (**1**), which is easily obtained from acetic acid.[7]

Results and Discussion

When **1** was refluxed with two equivalents of benzoyl chloride in the presence of triethylamine in acetonitrile for 3 h, diacylated product **2a** was obtained in 97% yield. By the similar treatment of **1** with other acid chlorides having no α-proton, **1** was converted into the corresponding products **2b—2d** in good yields (Eq. 1). The acid chlorides having α-protons such as acetyl and isobutyryl chlorides did not give **2** due to decomposition of the reagents under the reaction conditions. IR spectra (Table 1) of **2a—2c** show carbonyl bands at 1675—1690 cm^{-1}, which indicate that they are amides (*C,N*-diacylated products) rather than esters (*C,O*-diacylated products). NMR spectra (Table 2) of **2a—2c** suggest that they are mixtures of two geometrical isomers in the solutions. The carbonyl band of **2d** is found at higher frequency, 1750 cm^{-1}. This can be attributed to poor conjugation between the oxazoline nitrogen and the bulky pivaloyl group.

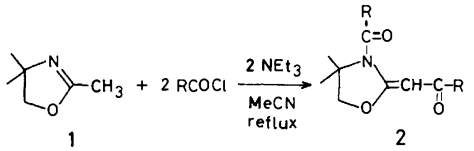

1 2 (1)

2a (R=C_6H_5) 97%, **2b** (R=$C_6H_4NO_2$-p) 99%,
2c (R=2-furyl) 82%, **2d** (R=t-C_4H_9) 90%.

The diacylated products, **2a—2c** were easily converted into unique enols (**3a—3c**) of 2-acylmethyl-2-oxazolines in good yields by treatment with excess methanolic potassium hydroxide at room temperature (Eq. 2). Hydrolysis of **2d** was carried out by refluxing with potassium hydroxide in ethanol for 30 h. The structure of **3** was determined based on the results of IR, NMR, and elemental analyses (Tables 1 and 2).

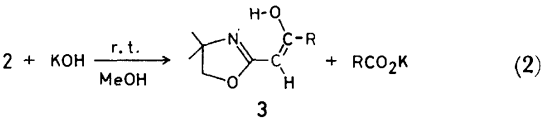

3 (2)

3a (R=C_6H_5) 93%, **3b** (R=$C_6H_4NO_2$-p) 95%,
3c (R=2-furyl) 88%,
3d (R=t-C_4H_9) 57% (under reflux in ethanol).

2-Ethyl-4,4-dimethyl-2-oxazoline was also benzoylated to **3e** (76%) by the similar treatment without isolation of intermediate **2e**. The treatment of 2-benzyl-4,4-dimethyl-2-oxazoline with benzoyl chloride and triethylamine gave **2f** (96%). Hydrolysis of **2f**

TABLE 1. IR SPECTRA AND ELEMENTAL ANALYSES OF THE OXAZOLINES

Compd	Mp θm /°C	IR spectra (Nujol) ν/cm⁻¹ ν(O-H)	ν(C=O)	ν(C=N or C=C)	Found/% C	H	N	Calcd/% C	H	N
2a	119-120	—	1675	1643	74.71	6.05	4.14	74.74	5.96	4.36
2b[a]	184-185.5	—	1680	1640	58.31	4.35	11.23	58.40	4.32	11.35
2c	148-149.5	—	1690	1640	63.39	5.01	4.58	63.78	5.02	4.65
2d	75-75.5	—	1750	1660	68.10	9.67	4.90	68.29	9.67	4.98
2f	149-152	—	1675	1640	78.75	5.83	3.53	78.57	5.83	3.52
3a	100.5-101	3220	—	1620	72.15	7.00	6.46	71.86	6.96	6.45
3b	163-164.5	3270	—	1620	59.68	5.36	10.74	59.53	5.38	10.68
3c	104-105	3220	—	1635	63.90	6.38	6.67	63.76	6.32	6.76
3d	94.5-95	3290	—	1635	66.86	9.79	7.04	66.97	9.71	7.10
3e	91-93	3240	—	1620	72.89	7.47	6.07	72.70	7.41	6.06
3f	185-186.5	3240	—	1625	78.07	6.65	4.76	77.79	6.53	4.77
3g	106-108.5	3180	—	1615	73.15	7.78	5.41	73.44	7.81	5.71
3h	156-158	3220	—	1635	77.87	6.88	4.45	78.15	6.89	4.56
3i	90-91	—	1690	1660	73.19	7.83	5.70	73.44	7.81	5.71

a) Containing a half molecule of acetonitrile.

TABLE 2. NMR SPECTRA OF THE OXAZOLINE

Compound	Isomer[a]	Chemical shifts (δ) in $CDCl_3$ Oxazoline ring protons $(CH_3)_2$	CH_2	α-Proton of 2-substituent	Other protons
2a	A[b]	1.28 (s, 6H)	3.89 (s)	6.37 (s)	7.2-7.8 (m, 10H).
	B	1.66 (s, 6H)	4.36 (s)	5.04 (s)	7.2-7.8 (m, 10H).
2b[c]	A	1.48 (s, 6H)	4.41 (s)	6.10 (s)	7.3-8.4 (m, 8H).
	B	1.59 (s, 6H)	4.51 (s)	4.96 (s)	7.3-8.4 (m, 8H).
2c	A	1.46 (s, 6H)	4.03 (s)	6.01 (s)	6.3-7.6 (m, 6H).
	B	1.60 (s, 6H)	4.30 (s)	5.14 (s)	6.3-7.6 (m, 6H).
2d	A[b]	1.26 (s, 6H)	3.86 (s)	5.78 (s)	1.13 (s, 9H), 1.31 (s, 9H).
2f	A[b]	1.23 (s, 6H)	3.88 (s)	—	7.1-7.7 (m, 13H), 8.0-8.2 (m, 2H).
3a	E[b]	1.42 (s, 6H)	4.12 (s)	5.55 (s)	7.3-7.5 (m, 3H), 7.7-7.9 (m, 2H).
3b	E[b]	1.48 (s, 6H)	4.23 (s)	5.55 (s)	7.98 (d, 2H, *J*=8.5 Hz), 8.24 (d, 2H, *J*=8.5 Hz), 10.5 (broad, 1H).
3c	E[b]	1.41 (s, 6H)	4.13 (s)	5.50 (s)	6.47 (dd, 1H, *J*=3.4 and 1.7 Hz), 6.97 (dd, 1H, *J*=3.4 and 0.8 Hz), 7.46 (dd, 1H, *J*=1.7 and 0.8 Hz).
3d[d]	E[b]	1.39 (s, 6H)	3.96 (s)	4.84 (s)	1.05 (s, 9H), 10.1 (broad, 1H).
3e	E[b]	1.41 (s, 6H)	4.13 (s)	—	1.80 (s, 3H), 7.3-7.6 (m, 5H), 10.4 (broad, 1H).
	K	1.19 (s, 3H) 1.22 (s, 3H)	3.85 (s)	4.35 (q, 1H *J*=6.6 Hz)	1.49 (d, 3H, *J*=6.6 Hz), 7.3-7.6 (m, 3H), 7.9-8.1 (m, 2H).
3f	E[b]	1.49 (s, 6H)	4.14 (s)	—	7.0-7.2 (m, 10H), 11 (broad, 1H).
3g	E	1.43 (s, 6H)	4.14 (s)	—	0.94 (t, 3H, *J*=7.3 Hz), 2.22 (q, 2H, *J*=7.3 Hz), 7.37 (s, 5H), 11.0 (s, 1H)
3h	E[b]	1.46 (s, 6H)	4.10 (s)	—	3.63 (s, 2H), 7.1-7.3 (m, 10H), 11.0 (s, 1H).
	K	1.05 (s, 3H) 1.35 (s, 3H)	3.79 (s)	4.63 (t, 1H, *J*=7.7 Hz)	3.34 (d, 2H, *J*=7.7 Hz), 7.0-7.6 (m, 8H), 7.9-8.2 (m, 2H).
3i	K[b]	1.29 (s, 6H)	3.80 (s)	—	1.60 (s, 6H), 7.2-7.5 (m, 3H), 7.9-8.1 (m, 2H).

a) A and B are geometrical isomers. E is an enol isomer and K is a keto isomer. b) Crystals of the compounds consist of only this isomer. c) Measured in DMSO-d_6. d) Measured in CCl_4.

by refluxing with triethylamine in methanol for 3 h gave **3f** in 75% yield. However, a similar treatment of 2-isopropyl-4,4-dimethyl-2-oxazoline with benzoyl chloride gave a ring opening product, 2-benzoylamino-1-isobutyryloxy-2-methylpropane in 67% yield, not *C*-acylated product. The results may be interpreted in terms of lower acidity of the α-proton of the isopropyl group and its higher steric hinderance. A six-membered analogue of **1**, 2,4,4,6-tetramethyl-5,6-dihydro-4*H*-1,3-oxazine was found to be less reactive to the acylating reagent.[8]

A plausible mechanism of the formation of **2** from **1** is as follows: The 2-methyl protons of **1** are activated by quaternarization of the ring nitrogen, and subsequent abstraction of the proton by triethylamine gives a nucleophilic ketene *N,O*-acetal intermediate. The lower reactivity of the dihydrooxazine may be attributed to the more crowded nitrogen. The intermediate is *C*-acylated, and the abstraction of the second α-proton gives less nucleophilic product **2**. When **1** was treated with an equimolar amount of benzoyl chloride and triethylamine, monoacylated product **3a** was not obtained at all, and the yield of **2a** was reduced to 20%. This fact is also consistent with the above mechanism.

On treatment of sodium salt of **3a** with three molar amounts of alkyl halides in DMF at room temperature, *C*-monoalkylated products (**3e**, **3g**, and **3h**) were selectively obtained in good yields (Eq. 3). Since hydroxyl bands, not carbonyl band, are observed at about 3200 cm^{-1} in the IR spectra of **3e—3h**, they are also enols in crystals. The NMR spectra show that they are in the keto-enol equilibria in solutions. Further methylation of **3e** by the similar treatment as above gave the *C,C*-dimethylated product, **3i**, in 78% yield. However, the reaction of **3a** with excess methyl iodide and sodium ethoxide in ethanol gave neither **3e** nor **3i**, but **3a** was recovered. This fact shows that the α-protons of the 2-acylmethyl group of **3** are not so activated as those of β-keto esters. Subsequently, selective monoalkylation can be more easily achieved for **3**.

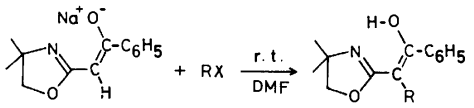

(3)

3e, **3g**, **3h**

3e (78%, RX=MeI),
3g (92%, RX=EtI; 55%, RX=EtBr),
3h (89%, RX=$C_6H_5CH_2Br$).

These results indicate that the oxazoline derivatives, **3**, of β-keto acids obtained by this method are versatile reagents for β-keto ester synthesis.

Experimental

All the melting points were uncorrected. NMR spectra were recorded on a Hitachi R-20B spectrometer. IR spectra were recorded on a Hitachi infrared spectrophotometer model 260-10. Physical properties of the oxazolines are summarized in Tables 1 and 2.

Benzoylation of 2,4,4-Trimethyl-2-oxazoline 1. Benzoyl chloride (28.4 g, 200 mmol) was added to a solution of **1** (11.3 g, 100 mmol) and triethylamine (25.3 g, 250 mmol) in acetonitrile (200 ml) at room temperature. The mixture was refluxed for 3 h, and the solvent was removed by a rotary evaporator. To the residue 100 ml of water was added and **2a** was extracted with chloroform. The organic layer was washed with 5% aqueous sodium carbonate and water, and dried over anhydrous sodium sulfate. Evaporation of the solvent yielded the crude product. Recrystallization from hexane–benzene (1:1) gave 31.1 g (97%) of pale yellow prisms (**2a**).

2-(β-Hydroxystyryl)-4,4-dimethyl-2-oxazoline (3a). To 100 ml of 1.5 M (1 M=1 mol dm^{-3}) methanolic potassium hydroxide 3.21 g (10 mmol) of **2a** was added at room temperature. After 6 h, precipitates were filtered off, and water was added to the filtrate. The mixture was extracted with chloroform and the organic layer was washed with water, and dried over anhydrous sodium sulfate. The solvent was removed by rotary evaporation and the residue was recrystallized from hexane–benzene (4:1) to give 2.02 g (93%) of colorless prisms (**3a**).

2-(β-Hydroxy-α-methylstyryl)-4,4-dimethyl-2-oxazoline (3e). To an equimolar amount of sodium ethoxide in ethanol 0.434 g (2 mmol) of **3a** was added and the solvent was removed by rotary evaporation. To the residue 0.85 g (6 mmol) of methyl iodide in 20 ml of DMF was added and the mixture was allowed to stand at room temperature for 5 h. The solvent was removed *in vacuo*, and 5% aqueous sodium carbonate was added to the residue. The mixture was extracted with chloroform. The extract was dried and the solvent was removed. The crude solid was recrystallized from hexane–benzene (4:1) to give 0.360 g (1.56 mmol) of colorless needles (**3e**).

2-(1-Benzoyl-1-methylethyl)-4,4-dimethyl-2-oxazoline (3i). Sodium salt of **3e** prepared from 0.462 g of **3e** and equimolar sodium ethoxide was treated with 0.85 g of methyl iodide in 20 ml of DMF at room temperature for 5 h. The usual workup yielded 0.426 g of colorless needles (**3i**) (87%).

References

1) A. P. Kozikowski and S. Goldstein, *J. Org. Chem.*, **48**, 1139 (1983); S. Y-K. Tam, R. S. Klein, F. G. de las Heras, and J. J. Fox, *ibid.*, **44**, 4854 (1979).

2) A. I. Meyers, D. L. Temple, D. Haidukewych, and E. D. Mihelich, *J. Org. Chem.*, **39**, 2787 (1974).

3) To esters and acids: A. I. Heyers and D. L. Temple, *J. Am. Chem. Soc.*, **92**, 6644 (1970).

4) To aldehydes: I. C. Nordin, *J. Heterocycl. Chem.*, **3**, 531 (1966).

5) To ketones: J. E. Dubois and C. Lion, *C. R. Acad. Sci., Ser. C*, **274**, 303 (1972).

6) To lactones: A. I. Meyers, E. D. Mihelich, and R. L. Nolen, *J. Org. Chem.*, **39**, 2783 (1974).

7) P. Allen and J. Ginos, *J. Org. Chem.*, **28**, 2759 (1963).

8) Reaction of 2,4,4,6-tetramethyl-5,6-dihydro-4*H*-1,3-oxazine with benzoyl chloride by the similar treatment yields the corresponding diacylated product (mp 166—167 °C) in 11% yield. Hydrolysis of the product to the corresponding enol (mp 81.5—83 °C) required refluxing with ethanolic potassium hydroxide for 5 h (yield 92%).

Convenient and Improved Synthesis of Tricarbonyl-(1,2-dihydropyridine)iron Complex

Ryohei YAMAGUCHI,* Yutaka NAKAZONO, and Mituyosi KAWANISI
Department of Industrial Chemistry, Faculty of Engineering, Kyoto University, Yoshida, Kyoto 606
(Received January 5, 1984)

Synopsis. (*N*-Alkoxycarbonyl-1,2-dihydropyridine)-tricarbonylirons are conveniently prepared in good yields by photo-irradiation in the presence of excess pentacarbonyliron without any solvent. ^{13}C NMR spectra of the complexes are also described.

Alhough chemistry and synthetic utility of tricarbonyl(1,3-cyclohexadiene)iron complexs have been extensively studied for past several years,[1,2] there have been few investigations on the *N*-heterocyclic analogues.[3] Alper first reported the synthesis of (*N*-alkoxycarbonyl-1,2-dihydropyridine)tricarbonyliron complexes by reaction of *N*-alkoxycarbonyl-1,2-dihydropyridines (**1**) with enneacarbonyldiiron.[3a] However, the yields were relatively low [42 and 34% for *N*-methoxycarbonyl- and *N*-ethoxycarbonyl-1,2-dihydropyridines (**2a** and **2b**), respectively] and, in addition, the reaction time was exceedingly long (40—60 h).

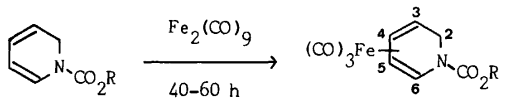

1a R=Me **2a** R=Me (Y=42%)
1b R=Et **2b** R=Et (Y=34%)

Scheme 1.

In connection with our recent study on synthesis and reaction of 1,2-dihydropyridines,[4,5] we are interested in the tricarbonyliron complex, because 1,2-dihydropyrodines have turned out to be valuable synthetic intermediates for alkaloids and other *N*-heterocycles[4] and therefore tricarbonyl(1,2-dihydropyridine)iron complexes may find inherent utility in these fields.

Results and Discussion

At first, we tried to prepare **2a** according to Alper's procedure. However, 50% conversion of the reaction could be achieved after 65 h and the yield was 23% (46% based on the conversion) in our hands. It is highly desirable to develop more convenient and improved procedure to prepare **2**. Then, we have tried photochemical reaction of **1** with pentacarbonyliron, since in some cases photochemical reactions of simple 1,3-dienes with pentacarbonyliron have been used for the preparation of tricarbonyl(1,3-diene)iron complexes.[6] Thus, we have found that photo-irradiation of **1** in the presence of cxcess pentacarbonyliron *without any solvent* affords **2** in good yield within reasonably short reaction time. The results are summarized in Table 1.

There are a few points which should be noted here. First, the reaction time is significantly diminished in comparison with the Alper's method which requires 40—60 h. Second, the yields are higher than those of the Alpers'. Third, as the amount of pentacarbonyliron increases, the yield becomes higher. Thus, **2a** could be obtained in up to 80% yield by 18 h irradiation in the prseence of 5 fold excess of pentacarbonyliron. The reaction was clean and 90—95% of unreacted pentacarbonyliron was recovered.

TABLE 1. PHOTOCHEMICAL REACTION OF **1** WITH PENTACARBONYLIRON

$$\mathbf{1} \xrightarrow[Fe(CO)_5]{h\nu} \mathbf{2}$$

R	**1** (mmol)	$Fe(CO)_5$ (mmol)	Time/h	Yield/%
Me	10	20	28	45
Me	10	30	16	75
Me	20	100	18	80
Et	10	30	18	55

The tricarbonyl(1,2-dihydropyridine)iron complex (**2a**) thus obtained gave the correct elemental analysis and was identical with the authentic sample prepared according to the Alper's procedure in spectroscopic comparison. However, we have observed 59—59.5° for the melting point of **2a**, whereas Alper described 42—44° for it. In order to obtain further evidence for the structure of **2a**, we have measured ^{13}C NMR spectrum of **2a**, which has not been reported yet. Only one absorption due to the terminal carhonyls appears at 210.6 ppm, indicating that the three carbonyls are equivalent to each other. Three signals due to the ester carbonyl, the methyl, and the methylene carbons appear in the ordinary regions (154.0, 52.8, and 44.9 ppm, respectively). On the other hand, four signals due to the olefinic carbons are considerably shifted to the up-fieldds (83.4, 75.6, 73.0, and 56.7 ppm, respectively), as is expected by the complexation with iron carbonyl.[7] The ^{13}C NMR of **2b** also showed the similar absorptions to that of **2a**, except for the ethyl carbons instead of the methyl carbon. These ^{13}C NMR spectra clearly indicate that the tricarbonyliron moiety is coordinated to the double bonds of the dihydropyridine but not to its nitrogen atom.[6]

Since enneacarbonyldiiron is prepared from pentacarbonyliron by photo-irradiation, the present procedure provides more convenient and efficient method for synthesis of tricarbonyl(1,2-dihydropyridine)iron complex than the reported one.[3a]

Experimental

All the temperature were uncorrected. The IR spectra were obtained on a Shimadzu IR-27 spectrometer. The MS spectra were taken by using a Hitachi RMS-4 mass spectrometer. The ^1H NMR spectra were obtained on a Varine EM-360 or EM-390 spectrometer and the ^{13}C NMR spectra were obtained on a Varian CFT-20 spectrometer, TMS being chosen as the internal standard.

N-Methoxycarbonyl- and N-Ethoxycarbonyl-1,2-dihydropyridines (1a and 1b). The 1,2-dihydropyridine derivatives were prepared by the reported method.[8]

*Tricarbonyl(N-methoxycarbonyl-1,2-dihydropyridine)iron (**2a**).* A mixture of **1a** (2.78 g, 20.0 mmol) and pentacarbonyliron (19.60 g, 100 mmol) in a Pyrex tube fitted with a small rubber balloon was irradiated with stirring by means of 220 W medium pressure mercury lamp at room temperature for 18 h. The excess pentacarbonyliron was removed under reduced pressure and recovered in a Dry Ice-acetone trap (14.00 g, 89%). The residue was chromatographed on silica gel. Elution by hexane followed by benzene gave **2a** (4.47 g, 80%), which crystallized on standing in a refrigerator. **2a**: mp 59.0—59.5°C. MS *m/z* (rel intensity): 279 (M^+, 1), 251 (M^+—28, 10), 223 (M^+—56, 11), 195 (M^+—84, 18), 79 (100). IR (CCl_4): 2040, 1945, 1715 cm^{-1}. ^1H NMR $\delta(CDCl_3)$: 5.33—5.67 (2H, m, H-4 and H-5), 4.90 (1H, br s, H-6), 3.68 (3H, s, $-OCH_3$), 3.10—3.43 (2H, m, H-2 and H-3), 2.93 (1H, d. d, J=15 and 3 Hz, H-2). ^{13}C NMR $\delta(CDCl_3)$: 210.6 (s, C=O), 154.0 (s, $-CO_2-$), 83.4 (d, C-6), 75.0 (d, C-4 or C-5), 73.0 (d, C-4 or C-5), 56.7 (d, C-3), 52.8 (q, $-OCH_3$), 44.9 (t, C-2).

*Tricarbonyl(N-ethoxycarbonyl-1, 2-dihydropyridine)iron (**2b**).* A mixure of **1b** (1.53 g, 10.0 mmol) and pentacarbonyliron (5.88 g, 30.0 mmol) was irradiated in the similar manner to the above for 18 h. The excess pentacarbonyliron was removed under reduced pressure and recovered in a Dry Ice-acetone trap (3.72 g, 95%). The residue was chromatographed on silica gel. Elution by hexane followed by benzene gave **2b** (1.61 g, 55%): MS *m/z* (rel intensity): 293 (M^+, 1), 265 (M^+—28, 2), 237 (M^+—56, 2), 209 (M^+—84, 3), 80 (100). IR (neat): 2030, 1970, 1715 cm^{-1}. ^1H NMR $\delta(CDCl_3)$: 5.33—5.68 (2H, m, H-4 and H-5), 4.90 (1H, br s, H-6), 4.15 (2H, q, J=7 Hz, $-OCH_2-$), 3.13—3.46 (2H, m, H-2 and H-3), 2.93 (1H, d. d, J=15 and 3 Hz, H-2), 1.27 (3H, t, J=7 Hz, $-CH_3$). ^{13}C NMR $\delta(CDCl_3)$: 210.5 (s, CO), 153.6 (s, $-CO_2-$), 83.2 (d, C-6), 75.7 (d, C-4 or C-5), 72.9 (d, C-4 or C-5), 61.8 (t, $-OCH_2-$), 56.8 (d, C-3), 44.8 (t, C-2), 14.6 (q, $-CH_3$).

References

1) Review; A. J. Pearson, *Acc. Chem. Res.*, **13**, 463 (1980).

2) M. F. Semmelhack and J. W. Herndon, *Organometallics*, **2**, 363 (1983), and references cited therein.

3) a) Preparation; H. Alper, *J. Organomet. Chem.*, **96**, 95 (1975); b) Dibromocardene insertion reaction into the complex; H. Alper and S. Amaratunga, *Tetrahedron Lett.*, **21**, 1589 (1980).

4) For pertinent reference of dihydropyridine chemistry; U. Eisner and J. Kuthan, *Chem. Rev.*, **72**, 1 (1972); D. M. Stout and A. I. Meyers, *ibid.*, **82**, 223 (1982).

5) R. Yamaguchi, Y. Nakazono, and M. Kawanisi, *Tetrahedron Lett.*, **24**, 1801 (1983).

6) R. B. King, "The Organic Chemistry of Iron," ed by E. A. K. v. Gustorf, F.-W. Grevels, and I. Fischler, Academic Press, New York (1978), Vol. 1, p. 525.

7) B. E. Mann and B. F. Taylor, "^{13}C NMR Data for Organometallic Compounds," Academic Press, New York (1981).

8) F. W. Fowler, *J. Org. Chem.*, **37**, 1321 (1972).

Preparation of Tetraalkyl 2,2′-Phthaloylbis[1,2-dihydro-1-isoquinolylphosphonate]s and their Reactions with Base

Kin-ya AKIBA,† Yoshio NEGISHI, and Naoki INAMOTO*
Department of Chemistry, Faculty of Science, The University of Tokyo, Hongo, Tokyo 113
(Received January 27, 1984)

Synopsis. The titled compounds were prepared and the reaction with lithium diisopropylamide followed by quenching with alcohol gave isoquinoline, 13-alkoxy-8*H*-dibenzo[*a*,*g*]quinolizin-8-ones, and dialkyl 2-(*o*-alkoxycarbonylbenzoyl)-1,2-dihydro-1-isoquinolylphosphonates.

We reported previously preparation of 13-substituted 8*H*-dibenzo [*a*,*g*]quinolizin-8-ones (**2**) by the intramolecular Wittig-Horner reaction of dialkyl 2-(*o*-acylbenzoyl)-1,2-dihydro-1-isoquinolylphosphonates (**3**).[1]

If the bis(phosphonate)s such as **1** are allowed to react with diketones under reaction conditions of the Wittig-Horner reaction, formation of the large-membered rings would be expected. Thus, a possibility of this type of reaction was examined.

Tetraalkyl 2,2′-Phthaloylbis [1,2-dihydro-1-isoquinolylphosphonate]s were prepared from isoquinoline (IQ), phthaloyl dichloride, and trialkyl phosphites in good yields as a diastereomeric mixtures of **1** and **1′**, where the isomers having lower melting points were regarded as **1**.

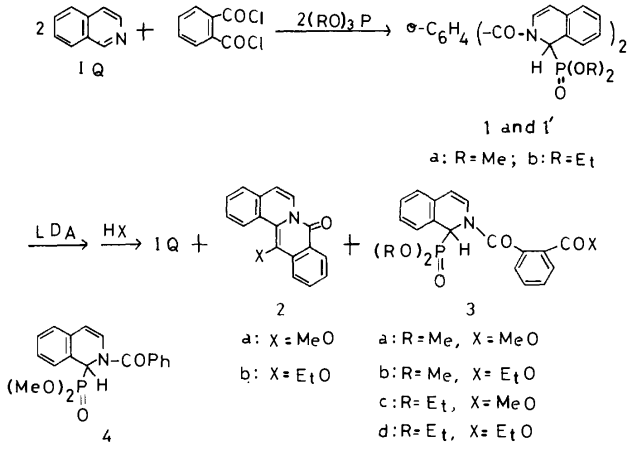

The reaction of a 1:1 mixture of **1a** and **1′a** with phthalaldehyde using two molar amounts of lithium diisopropylamide (LDA), followed by quenching with methanol, gave IQ (76%), **2a** (24%), and dimethyl 2-(*o*-methoxycarbonylbenzoyl)-1,2-dihydro-1-isoquinolylphosphonate (**3a**) (43%), indicating that phthalaldehyde did not take part in the reaction. Use of sodium methoxide (2 equiv) as a base gave mainly IQ and dimethyl phthalate.

In order to clarify the mechanism for the reaction, **1a** and **1b** were treated with LDA (1.3 equiv) at −70°C, then the reaction mixtures were quenched with alcohols, and allowed to stand at room temperature overnight. The results are summarized in Table 1, indicating that the 13-substituents in **2** are derived from the alcohols as quencher. However, the reaction of **1b** with LDA, followed by quenching with acetic acid, resulted in a quantitative recovery of a mixture of **1b** and **1′b** (5:8).

A similar reaction of dimethyl 2-benzoyl-1,2-dihydro-1-isoquinolylphosphonate (**4**)[2] as model with LDA, followed by quenching with methanol, gave a 1:1 mixture of IQ and methyl benzoate quantitatively.

From the above results, two mechanisms for formation of **2** and **3** are possible (see Scheme 1). Absence of a keto phosphonate (**5**) by quenching with acetic acid and the model experiment using **4** seem to support path A, though path B can not be ruled out completely.

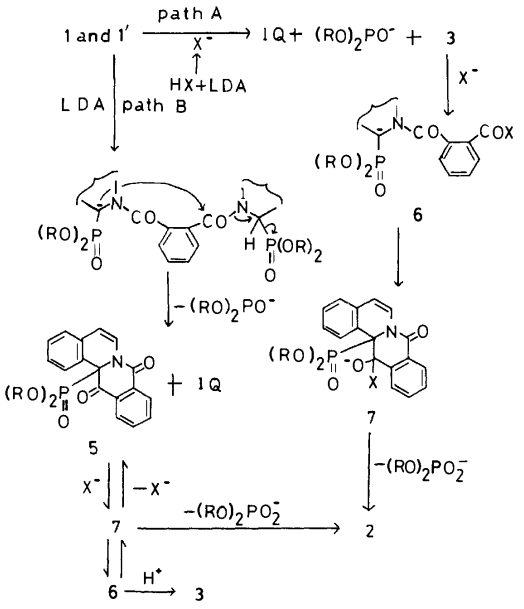

Scheme 1.

Experimental

Preparation of 1a. A mixture of phthaloyl dichloride (0.44 ml, 3.06 mmol) and IQ (0.79 g, 6.12 mmol) in MeCN (5 ml) was heated at 50—60°C for 10 min. To the above soln was added trimethyl phosphite (1.08 ml, 9.14 mmol) at 0°C and the mixture was refluxed for 10 min. After addition of aq $NaHCO_3$ (3%, 50 ml), the mixture was extracted with CH_2Cl_2. The extract was washed with aq NaCl and dried ($MgSO_4$). After removel of the solvent, the residue (2.2 g) was

Table 1. Reaction products from 1 and LDA (1.3 equiv)

1	R	X	Yield/% IQ	2	3
1a	Me	MeO	87	**2a** 18	**3a** 62
1a	Me	EtO	84	**2b** 43	**3b** trace
1b	Et	MeO[a]	84	**2a** 12	**3c** 56
1b	Et	EtO	74	**2b** 26	**3d** 55

a) Dimethyl phthalate was also produced in 4% yield.

† Present address: Department of Chemistry, Faculty of Science, Hiroshima University Higashisenda-machi, Hiroshima 730.

crystallized with ether to give a colorless mixture of **1a** and **1'a** (1.4:1; 1.55 g, 83%), which were separated by fractional recrystallization. **1a**: mp 208—209°C (from EtOAc-Et_2O); ^1H NMR ($CDCl_3$) δ=3.54, 3.59 (12H, 2d, J_{POCH}=10.8 Hz), 5.79 (2H, d, J=7.8 Hz), 6.25 (2H, d, J_{PCH}=17.7 Hz), 6.52 (2H, d, J=7.8 Hz), 6.8—7.0 (2H, m), 7.2—7.3 (6H, m), and 7.55 (4H, s); MS (70 eV) *m/z* (rel intensity) 608 (M^+; 0.5), 222 (48), and 93 (100). Found: C, 59.40; H, 4.95; N, 4.66%. Calcd for $C_{30}H_{30}N_2O_8P_2$: C, 59.21; H, 4.97; N, 4.60%. **1'a**: mp 224.9—225.8°C (from EtOAc-Et_2O); ^1H NMR ($CDCl_3$) δ=3.49, 3.67 (12H, 2d, J_{POCH}=10.8 Hz), 5.87 (2H, d, J=7.8 Hz), 6.09 (2H, d, J_{PCH}=17.7 Hz), 6.41 (2H, d, J=7.8 Hz), 7.0—7.2 (8H, m), and 7.55 (4H, s); MS (70 eV) *m/z* (rel intensity) 608 (M^+; 0.6), 222 (59), and 93 (100). Found: C, 59.48; H, 4.86; N, 4.70%.

Preparation of ***1b.*** Similarly to that of **1a**, phthaloyl dichloride (1.35 ml, 9.4 mmol), IQ (2.43 g, 18.8 mmol) in MeCN (13 ml), and triethyl phosphite (3.2 ml, 18.5 mmol) were allowed to react. On cooling the reaction mixture with ice, **1'b** precipitated (1.58 g, 25% yield). The filtrate was evaporated *in vacuo* and 3% aq $NaHCO_3$ (50 ml) was added to the residue and the mixture was extracted with CH_2Cl_2. The extract was washed with aq NaCl, dried ($MgSO_4$), and evaporated to give **1b** (4.00 g, 64% yield). **1b**: mp 168.2—169.2°C (from EtOAc-Et_2O); ^1H NMR ($CDCl_3$) δ=1.12 (6H, t, J=7.2 Hz), 1.15 (6H, t, J=7.2 Hz), 3.5—4.3 (8H, m), 5.72 (2H, d, J=7.8 Hz), 6.18 (2H, d, J_{PCH}=17.4 Hz), 6.47 (2H, d, J=7.8 Hz), 6.7—6.9 (2H, m), 7.0—7.3 (6H, m), and 7.51 (4H, m); MS (70 eV) *m/z* (rel intensity) 664 (M^+; 1.1), 398 (41), 250 (73), and 121 (100). Found: C, 61.29; H, 5.90; N, 4.19%. Calcd for $C_{34}H_{38}N_2O_8P_2$: C, 61.44; H, 5.76; N, 4.21%. **1'b**: mp 221.7—222.7°C (from EtOAc-Et_2O); ^1H NMR ($CDCl_3$) δ=1.09 (6H, t, J=6.9 Hz), 1.18 (6H, t, J=6.9 Hz), 3.5—4.3 (8H, m), 5.76 (2H, d, J=7.8 Hz), 5.95 (2H, d, J_{PCH}=16.8 Hz), 6.32 (2H, d, J=7.8 Hz), 6.8—7.2 (8H, m), and 7.56 (4H, s); MS (70 eV) *m/z* (rel intensity) 664 (M^+; 0.8), 398 (57), 250 (89), and 121 (100). Found: C, 61.14; H, 5.70; N, 4.26%.

Reaction of ***1a*** *and* ***1'a*** *in the Presence of Phthalaldehyde.* To a soln of LDA (2.38 mmol) in THF (50 ml) was added a mixture of **1a** and **1'a** (1:1) (604 mg, 0.99 mmol) at −50—−60°C and after 40 min phthalaldehyde (133 mg, 0.99 mmol) in THF (21.2 ml) was added dropwise at −65°C. After 0.5 h, the mixture was stirred at 40°C for 0.5 h and quenched with MeOH (2 ml). After filtration, the filtrate was evaporated and aq $NaHCO_3$ (2%, 50 ml) was added to the residue. The mixture was extracted with ether and then the aq layer was extracted with CH_2Cl_2. The combined extracts were washed with aq NaCl (50 ml), dried ($MgSO_4$), and evaporated. The residue (392 mg) was subjected to dry column chromatography (DCC) (SiO_2, Et_2O-hexane (1:1)) to give **2a**[1] (65 mg, 24%). IQ (97 mg, 76%), and **3a**[1] (171 mg, 43%).

Reaction of Bis(phosphonate)s (1) and LDA. General Method: To a soln of **1** (*ca.* 1 mmol) in THF (30 ml) was added at −70°C LDA (1.3 mmol) in THF (5 ml) under nitrogen atmosphere with stirring. After stirring for 0.5 h, alcohol (2 ml) was added at −70°C and the mixture was allowed to stand at room temp overnight. After removal of solvent *in vacuo*, 2% aq $NaHCO_3$ (50 ml) was added to the residue, the mixture was extracted with CH_2Cl_2, the extract was dried ($MgSO_4$), and evaporated to be subjected to DCC (SiO_2, Et_2O). The results were shown in Table 1. The products **2** and **3** were identified by the mps and spectral data.[1]

References

1) K. Akiba, Y. Negishi, and N. Inamoto, *Bull. Chem. Soc. Jpn.*, **57**, 2188 (1984).

2) K. Akiba, Y. Negishi, and N. Inamoto, *Synthesis*, **1979**, 55.

Ultrasounds in Synthetic Reactions. II. Convenient Methylenation of Carbonyl Compounds with Zinc-Diiodomethane[1]

Junzo YAMASHITA,* Yoshio INOUE, Takashi KONDO, and Harukichi HASHIMOTO
Department of Applied Chemistry, Faculty of Engineering, Tohoku University, Aramaki-Aoba, Sendai 980
(Received March 5, 1984)

Synopsis. Ultrasonic irradiation facilitates the methylenation of carbonyl compounds with zinc-diiodomethane reagent in tetrahydrofuran at room temperature.

The cyclopropanation of olefins with zinc-diiodomethane complex was first reported by Simmons and Smith,[2] and the methylenation of carbonyl compounds was also observed with this complex in the presence of an excess of zinc by Miyano, Hida, and Hashimoto of this laboratory.[3] The preparation of zinc-diiodomethane complex usually needs activated zinc-copper couple, which requires rather tedious procedure. Other methylenation procedures for aldehydes which use reagents involving Ti have been developed and given good yields, but they use highly air sensitive trimethylaluminium.[4,5] Dibromomethane-zinc-tetrachlorotitanium is a very good methylenation reagent for ketones but not for aldehydes.[5,6]

Ultrasounds have been successfully applied to accelerate a variety of organic reactions,[7] particularly those involving metals. We now wish to report that ultrasonic irradiation is also very useful for the methylenation reactions with zinc-iodomethane reagents: no chemical activation of commercial zinc powder is required, the reaction proceeds smoothly and rapidly at room temperature, and the yields are reproducible.

Experimental

Materials. Commercially available aldehydes and ketones were dried over Drierite and distilled under nitrogen atmosphere and stored for use. Tetrahydrofuran was distilled over sodium prior to use. Commercially available zinc powder was used as obtained. Commercially available diiodomethane was purified according to the known procedure.[3]

Analysis. Reaction products were identified by the retention volume on GLC and mass spectra (JEOL D300 mass spectrometer) compared with the authentic samples. The yields of products were determined by GLC. GLC was performed on a Hitachi 163 gas chromatograph (20 m glass capillary column coated with OV-17) or a Shimadzu GC 3AH gas chromatograph (Silicone DC-550 20 wt% on Diasolid M, squalane 20 wt% on Diasolid M, Silicone GE SE-52 20 wt% on Chromosorb W AW, or FFAP 10 wt% on Chromosorb W AW DMCS).

General Procedures for Methylenation Reactions. Methylenation of Benzaldehyde: To a 50 ml, 3-necked flask, which contained 1.57 g (24 mmol) of zinc powder previously dried at 100°C for 30 min under vacuum, were added 0.53 g (5 mmol) of benzaldehyde, 2.68 g (10 mmol) of diiodomethane, and 0.335 g (2.5 mmol) of durene (internal standard for GLC analysis) in 20 ml of THF, and irradiated for 20 min under nitrogen atmosphere in the water bath of an ultrasound laboratory cleaner (53 W, 41 kHz), which was maintained at room temperature. The yield of styrene was determined by GLC (FFAP 20 wt% on Chromosorb W AW DMCS at 120 °C).

Results and Discussion

The reactions of aldehydes or ketones with $Zn-CH_2I_2$ were carried out in THF at room temperature irradiated by ultrasound.

$$R_2C{=}O + CH_2I_2 \xrightarrow[\text{THF, room temp}]{\text{Zn, ultrasound}} R_2C{=}CH_2$$

The results were shown in Table 1. None or very small amount of olefins was detected when the similar reaction was carried out with ordinary magnetic stirrer instead of ultrasonic irradiation, though the longer reaction time afforded the corresponding olefin without the irradiation. The yield may be improved, for the reaction conditions are not optimum. Dibromomethane instead of diiodomethane can be used, but the longer reaction time is necessary (runs 7 and 8). Only low yields are obtained for ketones as indicated by runs 9 and 10, and this reaction is not recommended for ketones. The yields are comparable to those of previously reported procedures (40°C, 6 h in THF using activated zinc-copper couple), but the precise comparison is impossible, for the latter used 2 mol of carbonyl compounds to 1 mol of diiodomethane and the yields of olefins were based on diiodomethane.

In conclusion, the present method is a very convenient procedure for methylenation of aldehydes.

Table 1. Ultrasound-accelerated methylenation of carbonyl compounds with zinc-diiodomethane in THF at room temperature[a]

Run	Carbonyl compounds	Reaction time/min	Products	Yield %
1	Benzaldehyde	20	Styrene	70[b]
2	*p*-Methylbenzaldehyde	120	*p*-Methylstyrene	73
3	*p*-Methoxybenzaldehyde	90	*p*-Methoxystyrene	50
4	*p*-Chlorobenzaldehyde	15	*p*-Chlorostyrene	69[c]
5	1-Naphthaldehyde	120	1-Naphthylethene	54
6	Cinnamaldehyde	60	Phenylbutadiene	37
7	Heptanal	20	1-Octene	71
8	Heptanal[d]	300	1-Octene	58
9	Cyclohexanone	60	Methylenecyclohexane	18
10	Acetophenone	300	α-Methylstyrene	8

a) Reaction conditions; Zn 24 mmol, diiodomethane 10 mmol, substrate 5 mmol, THF 20 ml, room temperature. b) The yield increased to 82% when the reaction time was 60 min. c) Isolated yield was 57% (20 mmol scale). d) Dibromomethane was used instead of diiodomethane.

We would like to thank Dr. Sotaro Miyano of this laboratory for helpful discussions.

References

1) The previous report, Y. Inoue, J. Yamashita, and H. Hashimoto, *Synthesis* in press.

2) For a review, see H. E. Simmons, T. L. Cairns, S. A. Vladuchick, and C. M. Hoiness, *Org. React.*, **20**, 1 (1973).

3) S. Miyano, H. Hida, and H. Hashimoto, *Kogyo Kagaku Zasshi*, **69**, 2134 (1966); H. Hashimoto, M. Hida, and S. Miyano, *J. Organomet. Chem.*, **10**, 518 (1967); S. Miyano, M. Hida, and H. Hashimoto, *ibid.*, **12**, 263 (1968), and references cited therein.

4) F. N. Tebbe, G. W. Parshall, and G. S. Reddy, *J. Am. Chem. Soc.*, **100**, 3613 (1978).

5) K. Takai, Y. Hotta, K. Oshima, and H. Nozaki, *Tetrahedron Lett.*, **1978**, 2417.

6) L. Lombardo, *Tetrahedron Lett.*, **23**, 4293 (1982).

7) O. Repic and S. Vogt, *Tetrahedron Lett.*, **23**, 2729 (1982); B.-H. Han and P. Boudjouk, *Organometallics*, **2**, 269 (1983), and references cited therein.

Dielectric Relaxation of Some Aliphatic Ketones in Dilute Solution

Buta SINGH
Department of Physics, Punjabi University, Patiala, India.
(Received October 7, 1983)

Synopsis. Measurements of the relative permittivity at frequency of 10 GHz, and of the refractive index, have been made at 25 °C for (a) 2-haxanone, (b) 3-hexanone, (c) 3-Methyl-2-pentanone, (d) 3,3-dimethyl-2-butanone,(e) 2-heptanone, (f) heptanal, and (g) cyclohexanone, in dilute solutions of cyclohexane, decalin, and 1,4-dioxane, Dielectric relaxation times have been evaluated. It has been concluded that in the ketones and heptanal under study, dipole reorientation occurs mainly by an intramolecular relaxation process.

Crossley[1-3] has studied some ketones at a single concentration at different frequencies and has shown that dipole reorientation occurs primarily by the intramolecular rotation of the terminal acetyl group. The present work examines the dielectric absorption of five ketones together with heptanal and cyclohexanone in three nonpolar solvents, namely, cyclohexane, decalin, and 1,4-dioxane. Viscoelastic behaviour of these polar molecules is discussed in terms of intramolecular as well as overall molecular rotations. The possibility of solute-solvent interactions between the dioxane and these molecules is also discussed.

The polar materials as well as solvents used were of purest available grade and were distilled, whereever felt necessary, before use. The measured values of the refractive indices of polar materials and solvents were in agreement with the literature values where available.

Measurements of the relative permittivity ε' and dielectric loss factor ε'' at a frequency of 10 GHz were made by the 3-db technique using a Sanders VSWR Amplifier MKIII. Six samples at different concentrations in the range 0—0.03 weight fraction were studied for each material. The refractive index was measured using an Abbe refractometer.

Results

The values of a', a'', and a_D which are, respectively the slopes[4] of the plots of ε', ε'', and n_D^2 *versus* weight fraction of the solute, are given in Table 1. These slopes a', a'', and a_D were determined within 2, 4, and 5% respectively, by least square fitting using an appropriate program on a PDP8 digital computer. Values of a_∞, the slope of the plot of the relative permittivity at infinite frequencies, ε_∞, *versus* weight fraction of the solute, were calculated using the relation $a_\infty = 1.1\ a_D$. Dielectric relaxation time τ, has been evaluated using the relation[5,6]

$$\tau = \frac{a''}{\omega(a' - a_\infty)}.$$

Discussion

Values of τ are given in Table 2 and the same are compared with the literature values where availble.

TABLE 1. VALUES OF a', a'', a_D, AND a_∞ FOR MOLECULES AT 25 °C

Chemical	a'	a''	a_D	a_∞
	Solvent cyclohexane			
2-Hexanone	5.732	1.54	−0.146	−0.131
3-Hexanone	5.809	1.44	−0.160	−0.144
3-Methyl-2-pentanone	5.916	1.91	−0.162	−0.071
3,3-Dimethyl-2-butanone	6.138	1.11	−0.137	−0.123
2-Heptanone	5.268	1.44	−0.152	−0.137
Heptanal	3.951	0.96	−0.094	−0.085
Cyclohexanone	8.008	2.18	+0.109	+0.121
	Solvent decalin			
2-Hexanone	6.833	2.21	−0.281	−0.253
3-Hexanone	6.769	2.13	−0.289	−0.260
3-Methyl-2-pentanone	6.287	2.68	−0.275	−0.247
3,3-Dimethyl-2-butanone	6.836	1.74	−0.298	−0.268
2-Heptanone	5.658	2.22	−0.269	−0.242
Heptanal	4.119	1.30	−0.208	−0.187
Cyclohexanone	8.389	3.28	−0.134	−0.121
	Solvent 1,4-dioxane			
2-Hexanone	7.969	3.65	−0.091	−0.082
3-Hexanone	7.912	3.55	−0.079	−0.071
3-Methyl-2-pentanone	7.749	3.94	−0.136	−0.122
3,3-Dimethyl-2-butanone	8.189	3.02	−0.084	−0.076
2-Heptanone	6.634	3.34	−0.073	−0.066
Heptanal	4.814	2.11	−0.057	−0.051
Cyclohexanone	9.507	5.13	+0.102	+0.112

The measured values of τ for 2-hexanone in cyclohexane and decalin and for cyclohexanone in cyclohexane are found to compare well with the literature values. Values of τ are of the same order of magnitude as the relaxation time for acetyl group rotation in aromatic molecules[8-10] (≈7 p s) and for acetone[11,12] (3.2 p s) in dilute solution and are smaller than those acticipated for overall molecular rotation. This gives an indication that dipole reorientation in ketones occurs mainly by intramolecular rotation of the terminal acetyl group. The relaxation time for 2-hexanone is almost equal to that for 3-hexanone. This indicates that the location of the carbonyl group on the hydrocarbon chain has relatively little affect on the relaxation time for hexanones. Crossley,[1] too, has made the same conclusion from the studies on nonanones and decanones. The structure of ketones can be expressed as

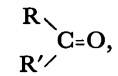

TABLE 2. VALUES OF τ, τ_{Lit}, τ_{Dec}/τ_c, AND τ_{Diox}/τ_c

Chemical	τ ps	τ_{Lit} ps	τ_{Dec} τ_c	τ_{Diox} τ_c
	Solvent cyclohexane			
2-Hexanone	4.1	4.0[1]	1.20	1.73
3-Hexanone	3.9	—	1.24	1.83
3-Methyl-2-pentanone	5.1	—	1.29	1.57
3,3-Dimethyl-2-butanone	2.8	3.2[3] (benzene)	1.38	2.06
2-Heptanone	4.2	—	1.40	1.85
Heptanal	3.8	—	1.28	1.82
Cyclohexanone	4.4	4.4[7]	1.37	1.97
	Solvent decalin			
2-Hexanone	4.9	5.2[2]		
3-Hexanone	4.8	—		
3-Methyl-2-pentanone	6.5	—		
3,3-Dimethyl-2-butanone	3.9	—		
2-Heptanone	6.0	—		
Heptanal	4.8	—		
Cyclohexanone	6.0	—		
	Solvent 1,4-dioxane			
2-Hexanone	7.2	—		
3-Hexanone	7.1	—		
3-Methyl-2-pentanone	7.9	—		
3,3-Dimethyl-2-butanone	5.8	—		
2-Heptanone	7.8	—		
Heptanal	6.9	—		
Cyclohexanone	8.7	—		

and the molecule may relax either by overall molecular reorientation or by twisting around the R–C and R'–C bonds. Second type of intramolecular relaxation process appears to make a large contribution to the absorption in the ketones under study. The dielectric relaxation behaviour of diphenyl ether and related compounds is also explained by the same type of relaxation process.

The relaxation time for 3,3-dimethyl-2-butanone in cyclohexane at 25 °C is 2.8 p s., which is comparable to that for acetone in benzene at 25 °C (=3.2 p s). In this molecule the *t*-butyl group R is compact in size and, therefore, dipole reorientation occurs by twisting around the R'–C bond only.

Values of τ for 2-heptanone is only slightly longer than that for 2-hexanone and the difference increases again with the increase in the viscosity of the solvent. Also, the ratio of the relaxation times in decalin to that in cyclohexane (τ_{Dec}/τ_c) for all the compounds in the present study is $\approx$1.3 (Table 2) which is rather smaller than the ratio of the viscosities of the solvents (η_{Dec}/η_c) which is $\approx$2.5. This indicates that the contribution of the overall molecular rotation to the relaxation process is quite small. The relative contribution to the value of τ by the intramolecular rotation and overall molecular rotation and with the increased viscosity of the solvent has been discussed in detail by Crossley.[3]

The relaxation time of heptanal has been found to be almost equal to that of 2-heptanone. Also, the value of τ_{Dec}/τ_c for heptanal is comparable to those for 2-hexanone and 3-hexanone. This shows that dipole reorientation in alkanals also takes place largely by intramolecular relaxation process. The value of τ for cyclohexanone is seen to be comparable to that for 2-hexanone and 2-heptanone in all the three solvents and the values of τ_{Dec}/τ_c and τ_{Diox}/τ_c, too, are almost the same. Cyclohexanone is known to be a rigid spherical molecule. Probably the dipole reorientation of the spherical cyclohexanone molecule involves roughly the same displacement of the surrounding molecules as in the case of the segment rotations of 2-hexanone or 3-methyl-2-pentanone. This is also confirmed from dielectric relaxation studies of ketones in a polystyrene matrix,[14] where dielectric dispersion for cyclohexanone has been found to occur in the same temperature region as for the low temperature dispersion (which has been attributed to the acetyl group rotation) for 2-hexanone and 2-heptanone.

The value of τ_{Diox}/τ_c for all the molecules under study (except for 3-methyl-2-pentanone) is$\sim$1.9 (Table 2) and is much larger than η_{Diox}/η_c (=1.33). Values of τ for these molecules in 1,4-dioxane are longer when compared with those in decalin though the viscosity of the latter is almost double than the former. It is known that the ketone molecule is a resonance hybrid in which the carbon atom of the carbonyl group assumes a positive character. This positive carbonyl carbon is liable to interact strongly with the lone-pair electrons of the oxygen atom in 1,4-dioxane resulting in large values of τ. Similar results have been reported for trihaloganated esters[15] and nitroalkanes.[6]

References

1) J. Crossley, *J. Chem. Phys.*, **56**, 2549 (1972).
2) J. Crossley, *Can. J. Chem.*, **51**, 2671 (1973).
3) J. Crossley, *Adv. Mol. Relax. Processes*, **6**, 39 (1974).
4) B. Singh and J. K. Vij, *Bull. Chem. Soc. Jpn.*, **48**, 2551 (1975).
5) J. K. Vij and K. K. Srivastava, *Trans. Faraday Soc.*, **66**, 1087 (1970).
6) B. Singh and J. K. Vij, *Adv. Mol. Relax Interaction Processes*, **22**, 177 (1982).
7) F. Dieringer, *Z. Phys.*, **145**, 184 (1956).
8) J. H. Calderwood and C. P. Smyth, *J. Am. Chem. Soc.*, **78**, 1295 (1956).
9) D. B. Farmer and S. Walker, *Tetrahadron*, **22**, 111 (1966).
10) F. K. Fong and C. P. Smyth, *J. Am. Chem. Soc.*, **85**, 548 (1963).
11) D. H. Whiffen and H. W. Thompson, *Trans. Faraday Soc.*, **41A**, 114 (1946).
12) F. J. Cripwell and B. B. M. Sutherland, *Trans. Faraday Soc.*, **42A**, 149 (1946).
13) F. K. Fong, *J. Chem. Phys.*, **40**, 132 (1964).
14) B. Singh, *J. Phys. Soc. Jpn.*, **50**, 2306 (1981).
15) H. D. Purohit, H. S. Sharma, and A. D. Vyas, *Bull. Chem. Soc. Jpn.*, **48**, 2785 (1975).

Kinetics of Copper(II) Incorporation in a Porphyrin Using Four Copper Salts

Nirmalendu DATTA-GUPTA*, Debasis MALAKAR, Sukla DATTA-GUPTA, and Richard GIBSON

Department of Natural Sciences, South Carolina State College Orangeburg, S. C. 29117 U.S.A.

(Received July 5, 1983)

Synopsis. Using excess of acetate, chloride, bromide, and sulfate salts, the kinetics of Cu(II) incorporation in *meso*-tetrakis (4-benzyloxyphenyl) porphyrin, in DMF solution, at different temperatures, have been done. The thermodynamic parameters have been calculated and a mechanism of Cu(II) insertion proposed.

The kinetics of copper(II) incorporation in porphyrins has been reported with nitrate,[1-3] perchlorate,[4,5] acetate,[6,7] sulfate,[8] and chloride[9] salts. Glacial acetic acid,[4,7] aqueous nitric acid,[1-3] acetic acid–water,[4] acetic acid–ethanol,[9] ethanol,[6] and 2.5% dodecyl sulfate[8] were some of the solvents used. No publication has yet appeared showing the effect of different anions attached to the copper(II) on the rate of metallation in a porphyrin under same conditions. We are reporting the kinetic data and a mechanism of copper(II) insertion in *meso*-tetrakis(4-benzyloxyphenyl)porphyrin (A) in DMF solution using the chloride, bromide, sulfate and acetate salts.

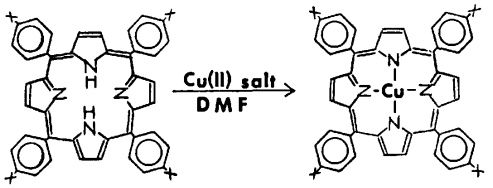

Starting with freshly distilled pyrrole and 4-(benzyloxy)benzaldehyde (Aldrich Chemical Company) and following the published procedure,[10] the porphyrin A, was prepared. Analytical sample of A was made by chromatography over silica gel with dichloromethane elution. A pure sample of the copper complex, B, was also made by the literature method.[11] Both A and B gave accurate elemental analysis.[12] Analytical grade copper salts and spectroscopic grade DMF (dried over Molecular Sieve 4A) were used.

The reaction rates were followed in 1.00 cm thermostatted cells (maintained to ±0.1 or better by a Neslab RTE-3 constant temperature circulator) and monitored with a Beckman Model 25 spectrophotometer. A typical kinetic study consisted of measuring the absorbances at 518 and 642 nm[13] over a period of time of a mixture of equal volume of 2.188×10^{-3} mol/dm^3 copper salt and 5.17×10^{-5} mol/dm^3 A at a pre-equilibrated temperature against 1.094×10^{-3} mol/dm^3 copper salt blank.[14] Standard procedure was used to calculate the concentrations of A and B.[15] In DMF solution the rate of copper(II) incorporation is known to be first order with respect to porphyrin as well as metal ion concentration.[9] Since the copper (II) ion concentration has been kept much higher, pseudo-first-order rate constants were obtained from the data of this study. A plot of time (minutes *vs.* In C_o/C_t, where C_o and C_t are molar concentrations of A at zero and t minutes respectively, yielded a straight line from which the first-order-rate constants (k) were calculated. (See Table 1)

Activation energy, E_a, was obtained from the slope of a plot $1/T$ (K^{-1}) *versus* log k. Thermodynamic parameters ΔG^*, ΔH^*, and ΔS^* were calculated using standard equations.[16] (see Table 2).

The relative rates of Cu(II) incorporation are found to be sulfate > bromide > chloride > acetate. The activation energy, E_a, and enthalpy of activation, ΔH^*, are highest with acetate and lowest with sulfate; the reverse relationship is observed with free energy of activation, ΔG^*. The entropy of activation decreases in the order, acetate > chloride > bromide sulfate. These data can be rationalized with an assumption that the Cu(II) insertion in DMF proceeds in two steps as follows:

$$\text{Step 1: } 4\text{BzO-TPP-H}_2 + \text{Cu(II)} \xrightarrow{k_1} 4\text{-B}_2\text{O-TPP-H}_2\cdot\text{Cu(II)(C)}^{17}$$

$$\text{Step 2: } 4\text{BzO-TPP-H}_2\cdot\text{Cu}^{+2} \xrightarrow{k_2} 4\text{BzO-TPP-Cu} + 2\text{H}^+$$

The first step is slow formation of an unstable complex C[17] and the second step rapidly forms the product B. The rate K_1 of the slower first step is dependent upon the nature of the anion attached to the Cu(II) or the nature of anion controls the availability of Cu(II). In the solid state copper(II) sulfate pentahydrate has four water molecules and an oxygen atom from each of two sulfate anions octahedrally arranged about the Cu(II) cation.[18] In DMF solution the water ligands may be easily removed, making the Cu(II) easily available to form C. Compared to copper(II) sulfate, the chloride and the bromide have polymeric chain structures formed by planar CuX_4 groups sharing opposite edges. The distances between the chlorine atoms in the chloride are shorter than the bromine atoms in the bromide.[19] It has been postulated that in DMF solution copper(II) chloride is present as

TABLE 1. THERMODYNAMIC PARAMETERS FOR COPPER PORPHYRIN FORMATION WITH DIFFERENT COPPER SALTS

	$CuSO_4\cdot5H_2O$	$CuBr_2$	$CuCl_2\cdot2H_2O$	$Cu(OAc)_2$
ΔG^*/kJ mol^{-1}	82.09	82.89	85.35	86.78
ΔH^*/kJ mol^{-1}	56.48	63.14	65.94	81.17
ΔS^*/J mol^{-1} K^{-1}	−87.53	−69.41	−64.06	−18.12
E_a/J	58, 915	65, 639	68, 450	83, 730

Table 2. Rate constants for copper porphyrin formation with different copper salts

Copper salt	Temp/°C	k/min^{-1}
$CuSO_4 \cdot 5H_2O$	9	0.0054
	16	0.0102
	23	0.0177
	30	0.0318
$CuBr_2$	23	0.0106
	30	0.0199
	37	0.0352
$CuCl_2 \cdot 2H_2O$	23	0.0065
	30	0.0125
	37	0.0226
$Cu(OAc)_2$	30	0.0076
	37	0.0146
	45	0.0363

[$CuCl^+ . CuCl_3^-$[9]]. If this is accepted, it is reasonable to think that copper(II) bromide in DMF solution should be present as $CuBr^+ \cdot CuBr_3^-$. The bromide species will be expected to form the complex C somewhat faster than the chloride species, because in the former the halogens are further apart from each other. Copper (II) acetate in the solid state has a dimeric structure which is expected to remain unchanged in DMF solution.[20] Therefore the Cu(II) from the dimeric acetate will be least favored, compared to sulfate, chloride and bromide, to form the complex C. The thermodynamic data (See Table 2) also suggest that the total gain in entropy due to solvation and subsequent distortion of the ordered structure of the copper salts is more than offset by the loss of entropy due to the formation of the complex C. This is most pronounced with the sulfate and least with acetate. The energy necessary to distort the geometry of the copper salts is greater than the energy released due to the formation of complex C. The difference between these two energies, *i.e.* ΔH^*, is maximum with acetate, and minimum with sulfate (see Table 2).

Two additional experiments have been performed to support the two-step mechanism proposed. The first experiment was to compare the Cu(II) incorporation in TPP-H_2[21] and TPP-D_2[21] in dry DMF solution using anhydrous copper(II) chloride at 23, 30, and 37 °C. The rates observed at these temperatures for both the compounds were identical,[22] supporting that the step 2 is not the rate limiting step.

The second experiment was to measure the Cu^{63}(II)[23] and Cu^{65}(II)[23] insertion in TPP-H_2 at 23, 30, and 37 °C in DMF. The ratio of the rate of Cu^{63}(II) to Cu^{65}(II) insertion found were 1.085(at 23 °C), 1.116 (at 30 °C), and 1.132(at 37 °C). This significant isotope effect supports the step 1 to be the rate limiting step. Our findings and conclusions are further supported by a recent report[24] on the kinetics of copper (II) incorporation into a series "picketfence" type porphyrins, dissolved in a mixture of toluene, 2-propanol, and water. It has been shown that (1) the slow step apparently involves an outersphere association (similar to our complex C) between a reactive intermediate of Cu(II) ion and the porphyrin followed by rapid metal incorporation and (2) the nature of reactive metal intermediate is responsible for the rapid metal incorporation.

Our research was supported by the NIH-MBRS Grant #RRO 8060.

References

1) E. B. Fleischer, E. I. Choi, P. Hambright, and A. Stone, *Inorg. Chem.*, **3**, 1284 (1964).
2) P. Hambright, *J. Inorg. Nucl. Chem.*, **32**, 2449 (1970).
3) P. Hambright and E. B. Fleischer, *Inorg. Chem.*, **9**, 1757 (1970).
4) E. I. Choi and E. B. Fleischer, *Inorg. Chem.*, **2**, 94 (1963).
5) H. W. Whitlock, R. Hanauer, M. Y. Oester, and B. K. Bower, *J. Am. Chem. Soc.*, **56**, 299 (1956).
6) B. D. Berezin and O. I. Koifman, *Russ. J. Phys. Chem.*, **46**, 24, (1972).
7) D. J. Kingham and D. A. Brisbin, *Inorg. Chem.*, **9**, 2034, (1970); D. A. Brisbin and D. A. Richards, *ibid*, **11**, 2849 (1972).
8) M. B. Lowe and J. W. Phillips, *Nature*, **194**, 1058 (1962).
9) O. Berezin and L. V. Klapova, *Russ. J. Phys. Chem.*, **45**, 1242 (1971).
10) N. Datta-Gupta and T. J. Bardos, *J. Heterocycl. Chem.*, **3**, 495 (1966).
11) A. D. Adler, F. R. Longo, F. Kampas, and J. B. Kim, *J. Inorg. Nucl. Chem.*, **32**, 2443 (1970).
12) Anal. Calcd for $C_{72}H_{54}O_4N_4$ (A): C, 83.24; H, 5.20; N, 5.39%. Found: C, 83.36; H, 5.33; N, 5.26%. Calcd for $C_{72}H_{52}O_4N_4Cu$ (B): C, 78.58; H, 4.73; N, 5.09%; Found: C, 78.64; H, 4.95; N, 5.07%.
13) Spectra in DMF, λ_{nm} ($\varepsilon \times 10^3$) for A: 421(470), 518 (14.3), 520(17.4), 542(5.5), 558(13.5), 600(5.1), 659(7.2). For B: 420(444), 518(4.2), 542(18.7), 584(4.4).
14) The copper salts in DMF solution have negligible absorbances at 518 and 542 nm.
15) H. H. Jeffe and M. Orchin, "Theory and Applications of Ultraviolet Spectroscopy," J. Wiley & Sons, New York 1962, Chap. 20.
16) A. J. Gordon and R. A. Ford, "The Chemist's Companion-A Handbook of Practical Data, Techniques and References," J. Wiley & Sons, New York, (1972), p. 136.
17) The complex, 4BzO-TPP-$H_2 \cdot$Cu(II), is like a "sitting-atop complex" (see "Porphyrins and Metalloporphyrins", First ed., ed by K. M. Smith, Elsevier, Amsterdam (1976), p. 248). It cannot be identified spectrally, perhaps because of its transient nature and its rapid conversion to the stable complex B.
18) R. B. Bishop and K. Jones, "Inorganic Chemistry-A Comprehensive Text," Interscience New York (1976), p. 732.
19) F. A. Cotton and G. Wilkinson, "Advanced Inorganic Chemistry-A Comprehensive Text," Interscience New York (1972), p. 912.
20) M. Kato, H. B. Jonassen, and J. C. Fanning, *Chem. Rev.*, **64**, 99 (1964).
21) TPP-H_2 is an abbreviation of *meso*-tetraphenylporphyrin. TPP-D_2 is TPP-H_2 in which the two protons on two nitrogens have been exchanged with deuterium. A pure sample of zinc complex of TPP-H_2 was reacted with CF_3COOD and the precipitate obtained was washed with D_2O. The product, TPP-D_2 dried over P_2O_5 at 100 °C showed no trace of N-H stretch near 300 cm^{-1}.
22) The rate constants are 0.0022 min^{-1} (at 23 °C), 0.0047 min^{-1} (at 30 °C), and 0.0091 (at 37 °C).
23) $Cu^{63}Cl_2 \cdot 2H_2O$ (99.89% Cu^{63}) and $Cu^{65}Cl_2 \cdot 2H_2O$ (99.69% Cu^{65}) were purchased from ICN Chemical and Radioisotope Division, Irvine, California.
24) G. M. Cole, D. W. Doll, and S. L. Holt, *J. Am. Chem. Soc.*, **105**, 4477 (1983).

The Synthesis of Polymeric Catalyst Using Ion Exchange Resin and Its Application for Esterification

Kyu-Ja WHANG,* Keun-Im LEE, and Yong-Keun LEE*,†

Department of Manufacturing Pharmacy, College of Pharmacy, Sookmyung Women's University, Seoul 140, Korea

† *Department of Chemistry, College of Science, Yonsei University, Seoul 120, Korea*

(Received August 26, 1983)

Synopsis. The copolymer complexes have been synthesized from cation and/or anion resin with metal catalyst such as aluminum chloride or iron(III) chloride. Electron microprobe X-ray analysis demonstrated that aluminum and iron were distributed uniformly in the copolymer complex. The catalytic activity for esterification of dibasic organic acids was discussed and showed that copolymer complex from porous type cation exchange resin was much better catalyst than that from gel type.

Polymers have been used broadly as a supporter[1] or as a catalyst[2,3] in various organic syntheses. Some of the advantages cited include substrate stabilization, reaction selectivity, increased yield and effective separation of the products. When used as a catalyst, they are usually polymer-metal complexes formed by linking polymers to metal catalyst such as $AlCl_3$ or $FeCl_3$. Such metal complexes are no longer volatile and far less hygroscopic.[4] Furthermore, the catalyst can be reused repeatedly, because the polymer-metal complexes are stable in the air,[5] and the products are more readily separable from the bulk.

Although these metal complexes have been used extensively in pharmaceutical industry for their improved catalytic effect, there have been some difficulties in material handling and even loss of polymer complexes when they were used in styrene–divinylbenzene matrix.[6] We have used ordinary ion exchange resins to form copolymers of $AlCl_3$ or $FeCl_3$ and found that they are much better catalysts in esterification of organic acids than either cation exchange resin itself or metal catalyst. The microstructures of both $AlCl_3$ and $FeCl_3$ copolymers have been analyzed using scanning electron microscope and electron microprobe X-ray analyzer.

Aluminum chloride copolymer complex (Ⓟ-$AlCl_3$) and iron(III) chloride copolymer complex (Ⓟ-$FeCl_3$) have been prepared from anhydrous $AlCl_3$ powder and anhydrous $FeCl_3$ powder with cation and/or anion exchange resin respectively following the method of Neckers.[7] The resins used in this experiment were gel and porous types with 30—50 mesh beads. The beads were the commercial cation and/or anion exchange resin beads (gel type : DIAION SK 1B and SA 10A, porous type : DIAION PK 212 and PA 312, Mitsubishi Chemical Ltd.); These beads were treated with $AlCl_3$ and/or $FeCl_3$ for periods of 30, 60, 90, 120, 150, and 180 min.

The aluminum and iron contents of the above complexes were analyzed with atomic absorption spectrophotometer. In general, the aluminum contents of Ⓟ-$AlCl_3$ synthesized from cation exchange resin of 30—50 mesh size (gel type : SK, porous type : PK) were greater than Ⓟ-$AlCl_3$ synthesized from anion exchange resin. As shown in Table 1, the aluminum content of the porous type resin complex was the highest when it was treated with $AlCl_3$ for 30—60 min.

TABLE 1. ALUMINUM AND IRON CONTENT IN COPOLYMER COMPLEX ACCORDING TO THE VARIOUS REACTION TIMES AND TYPE OF CATION EXCHANGE RESINS

Reaction time / min	Content/mg g^{-1}			
	Al/Ⓟ-$AlCl_3$		Fe/Ⓟ-$FeCl_3$	
	PK	SK	PK	SK
30	0.19	0.04	0.65	0.32
60	0.19	0.07	0.80	0.53
90	0.15	0.10	0.63	0.65
120	0.12	0.07	0.53	0.52
150	0.08	0.05	—	—
180	0.06	0.04	0.55	0.48

PK; DIAION PK 212, porous type. SK; DIAION SK 1B, gel type.

But the aluminum content of the gel type resin complex was highest when the resin was treated with $AlCl_3$ for 90 min. The iron content of the complex synthesized from gel type resin was also the highest when the resin was treated with $FeCl_3$ for 90 min, while that of the complex synthesized from porous type was the highest when the resin was treated with $FeCl_3$ for 60 min. In addition, it was observed that the content of iron of the complex was four to six times as much as that of the aluminum of the complex at their maximum activities.

To investigate the microstructure of copolymer complexes, these several beads were examined in detail using energy dispersive X-ray spectrometer, scanning electron micorscope and electron microprobe X-ray analyzer.

For the microscopic analysis, samples of copolymer complex were embeded in epoxy resin and then sectioned by microtome. In the micrographs of sectioned beads, the pores of SK Ⓟ-$AlCl_3$ and SK Ⓟ-$FeCl_3$ beads appeared smaller than those of SK Ⓟ bead. The difference between these beads were also observed with the porous types. Therefore, it is suggested that Al^{3+} and Fe^{3+} of the copolymer complexes may have replaced hydrogen ion in cation exchange resin. As shown in Fig. 1 we observed the singnal intensity of aluminum and iron respectively in the electron micropobe profiles of the copolymer complex of gel type bead. These singnal intensity were also observed with porous type bead. The present results demonstrated that aluminum and iron were distributed uniformly in the copolymer complex.

The esterifications of various dibasic acids with alcohols were carried out in order to examine the catalytic effect of copolymer complexes by the method described in our previous work.[6] The reactions of various aliphatic acids with alcohols using Ⓟ-$AlCl_3$ and Ⓟ-$FeCl_3$ as catalysts in mole ratio of 1 : 1 at 120 °C for 5 h are compared with the reaction using

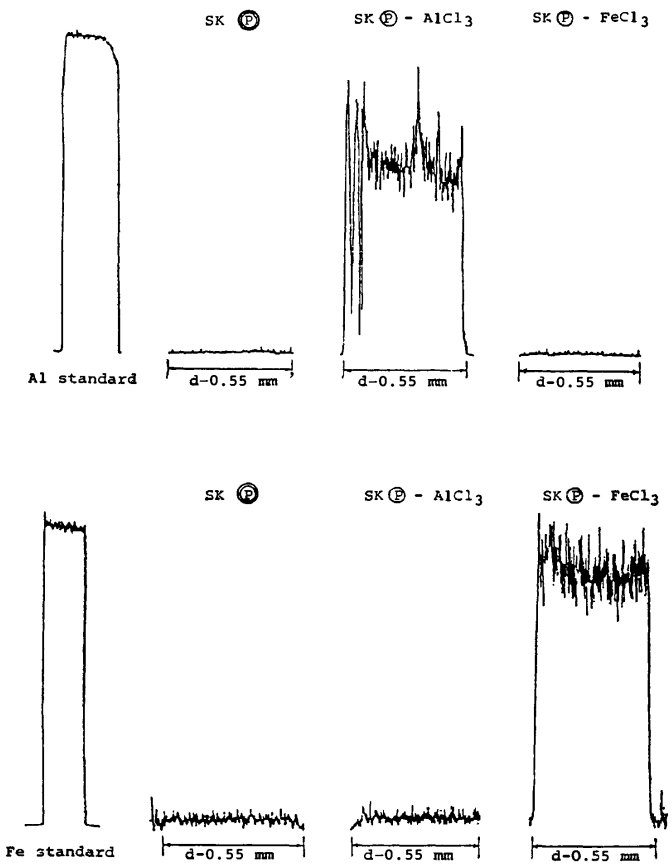

Fig. 1. Electron microprobe X-ray (Al-$K\alpha$ and Fe-$K\alpha$) profiles of a sectioned spherical bead of copolymer complex.
Treated with CS_2 only: SK Ⓟ.
Prepared from $AlCl_3$ for 90 min: SK Ⓟ-$AlCl_3$.
Prepared from $FeCl_3$ for 90 min: SK Ⓟ-$FeCl_3$.

TABLE 2. YIELD OF ESTERIFICATION OF THE VARIOUS ACIDS WITH ALCOHOLS

Acid	Alcohol	Mole ratio (acid : alcohol)	Yield/% PSVB-SO_3H PK	PSVB-SO_3H SK	Ⓟ-$AlCl_3$ PK	Ⓟ-$AlCl_3$ SK	Ⓟ-$FeCl_3$ PK	Ⓟ-$FeCl_3$ SK
Oxalic	Ethyl	1 : 1	31.66	25.43	83.10	67.26	70.44	56.25
Malonic	Ethyl	1 : 1	23.78	5.76	56.50	46.62	46.83	30.84
Succinic	Ethyl	1 : 1	20.49	3.49	49.14	32.45	34.37	24.75
Adipic	Ethyl	1 : 1	8.68	0.23	22.77	14.91	16.26	11.56
	Isopropyl	1 : 1	2.82	0	20.46	14.17	11.33	9.83
Maleic	Ethyl	1 : 1	6.95	4.11	25.51	19.45	19.68	15.29
Fumaric	Ethyl	1 : 1	1.19	0	20.34	14.37	12.86	8.22
Phthalic[a]	Ethyl	1 : 2	0	0	22.09	8.89	3.18	2.00
1,2-Cyclohexane dicarboxyric[a]	Ethyl	1 : 2	4.43	3.21	27.18	16.82	6.36	4.42

All reactions were carried out at 120 °C for 5 h using 0.5 g polymer catalyst respectively. a) Reaction time: 10 h. Ⓟ is cation exchange resin matrix.

cation exchange resin (PSVB-SO_3H) as shown in Table 2. The reactions of aromatic and alicyclic dibasic acids with alcohols in the mole ratio of 1 : 2 were also carried out for 10 h, and the result is included in Table 2. The yields of esterifications shown in Table 2 were determined by gas chromatography. Matsumoto[8] has demonstrated previously the catalytic activity of cation exchange resin. We now have observed that the Ⓟ-$AlCl_3$ and Ⓟ-$FeCl_3$ are better catalysts in esterification. Furthermore, the Ⓟ-$AlCl_3$ is a more effective catalyst than Ⓟ-$FeCl_3$. This agrees

TABLE 3. YIELD OF ESTERIFICATION OF MALONIC ACID WITH ETHYL ALCOHOL ACCORDING TO MOLE RATIO OF ACID AND ALCOHOL

Mole ratio (acid : alcohol)		Yield/% PSVB-SO_3H	Ⓟ-$AlCl_3$
1 : 1	Original	23.78	56.50
	Resynthesized	23.57	53.39
	Recycled	8.50	17.39
1 : 2	Original	16.98	48.72
	Resynthesized	16.26	45.00
	Recycled	4.29	13.34
1 : 4	Original	11.40	41.00
	Resynthesized	9.97	39.10
	Recycled	2.17	10.61

All reactions were carried out at 120 °C for 5 h using 0.5 g polymer catalyst respectively. Ⓟ is cation exchange resin matrix with porous type (PK).

with the fact that $AlCl_3$ is a better catalyst than $FeCl_3$.[9] In the case of esterification of saturated aliphatic dibasic acid with ethyl alcohol, the more methylene groups in the acid, the less yield is observed. This result shows that the electron-withdrawing group at the α-position of carboxylic acid enhances esterification. In the case of maleic acid, the reaction occured more quickly than its trans isomer fumaric acid. This has also been observed in the formation of maleic anhydride.[10] As shown in Table 2, the copolymer complexes are less effective catalysts in esterification of aromatic acid and alicyclic acids than aliphatic acid. Furthermore, the copolymer complex is very stable and not fragile, so can be reused. In Table 3, the catalytic effect of the resynthesized copolymer complex is the almost same as the original one whereas, in genaral, the recycled catalyst has less activity than the original one. Generally, copolymer complexes synthesized from porous type of cation exchange resin are better catalysts in the esterification than those synthesized from gel type resin. The catalytic activity is observed proportional to the aluminum and iron contents of copolymer complexes respectively.

References

1) R. B. Merrifield, *J. Am. Chem. Soc.*, **85**, 2149 (1963).
2) C. C. Leznoff and J. Y. Wong, *Can. J. Chem.*, **51**, 3756 (1973).
3) J. Y. Wong, C. Mannig, and C. C. Leznoff, *Angew. Chem., Int. Ed. Engl.*, **13**, 666 (1974).
4) N. M. Weinshenker, G. A. Crosby, and J. Y. Wong, *J. Org. Chem.*, **40**, 1966 (1975).
5) M. Capka, P. Svoboda, M. Cerny, and J. Hetfleje, *Tetrahedron Lett.*, **1971** 4787.
6) K. J. Whang and Y. K. Lee, *J. Kor. Chem. Soc.*, **22**, 184 (1978).
7) D. C. Neckers, D. A. Kooistra, and G. W. Green, *J. Am. Chem. Soc.*, **94**, 9284 (1972).
8) T. Matsumoto, *J. Pharm. Soc.*, **60**, 192 (1949).
9) O. C. Dermer, D. H. Wilson, F. M. Johnson, and V. H. Dermer, *J. Am. Chem. Soc.*, **63**, 2881 (1941).
10) S. H. Pine, J. B. Hendrickson, D. J. Cram, and G. S. Hammond, "Organic Chemistry," 4th ed, McGraw Hill, New York (1980), p. 93.

Single Step Synthesis of 4*H*-1,4-Benzothiazines

Radha Raman GUPTA,* Gopal Singh KALWANIA, and Rakesh KUMAR
Department of Chemistry, University of Rajasthan, Jaipur 302004, India
(Received October 15, 1983)

Synopsis. Single step synthesis of substituted 4*H*-1,4-benzothiazines is reported by the condensation and oxidative cyclization of substituted 2-aminobenzenethiol with β-dicarbonyl compounds in DMSO. The structures of the synthesized compounds have been confirmed by their elemental analyses and spectral studies.

4*H*-1,4-Benzothiazines resemble structurally with phenothiazines in having a fold along nitrogen sulfur axis and can be anticipated to possess biological activities like phenothiazines.[1-7] 4*H*-1,4-Benzothiazines have been prepared by the reaction of *o*-aminobenzenethiol with ethyl 2-chloroacetoacetate[8] or β-bromoketones/α,α-dimethoxy-β-bromoethane.[9] In these methods halogenated ethylacetoacetate and ketones are required, and therefore it is considered worthwhile to develop a convenient method for synthesis of 4*H*-1,4-benzothiazines involving the use of ethylacetoacetate or β-dicarbonyl compounds as such without converting them into halogenated form.

In the present communication a single step method is reported for the synthesis of hitherto unknown substituted 4*H*-1,4-benzothiazines which involve the condensation followed by oxidative cyclization of substituted 2-aminobenzenethiol with β-dicarbonyl compounds in DMSO (Scheme 1). We have used 3- and 5-substituted 2-aminobenzenethiols (1 : R=Me, Cl, MeO; R_1=Cl, Me) and β-dicarbonyl compounds such as ethylacetoacetate, dibenzoylmethane, benzoylacetone, and *p*-chlorobenzoylacetone. Two isomeric products of 4*H*- 1,4-benzothiazine may be formed theoretically, but compound (**1c**) predominates over the compound (**1d**) (identified by mass spectral studies).

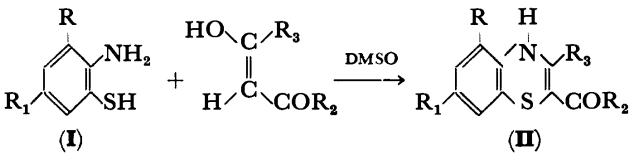

R=H, CH_3, OCH_3, Cl; R_1=CH_3, Cl, H
R_2=C_6H_5, CH_3, OC_2H_5, *p*-ClC_6H_4
R_3=CH_3, C_6H_5

Scheme 1.

The infrared spectra of all the benzothiazines invariably showed an NH absorption in the region of 3200—3390 cm^{-1} and carbonyl absorption in the region of 1570—1615 cm^{-1}. The weak absorption bands in the region of 1355—1485 cm^{-1} are attributed to C–CH_3 vibrations in substituted 4*H*-1,4-benzothiazines. The bands in the region of 1600—1510 cm^{-1} are attributed to C=C stretching vibrations. A broad signal in the region of τ 1.25—1.45 was observed in all the compounds arising due to an NH proton and the multiplets in the region of τ 2.2—3.6 are due to aromatic ring protons. A singlet peak centered at τ 6.2 arising due to an OCH_3 group in methoxy derivatives was also observed. All benzoyl 4*H*-1,4-benzothiazines showed peaks at m/z=M^+—105 (with high intensity), 105 ($CO^+C_6H_5$, base peak), and 77 ($C_6H_5^+$) by the loss of a benzoyl group, but did not show any peak corresponding to the M^+–$COCH_3$ or $COCH_3^+$ moiety, proving the structure of these benzothiazines to be **1c**. The 3,5-dimethyl-2-ethoxycarbonyl derivative gave peaks at m/z=M^+–C_2H_4, M^+–OC_2H_5, and M^+–C_2H_5.

TABLE 1. PHYSICAL DATA OF SUBSTITUTED 4*H*-1,4-BENZOTHIAZINES

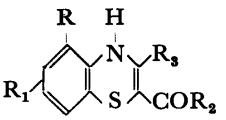

Compound				Mp θ_m/°C	Yield %	Molecular formula	Found %			Calcd %		
R	R_1	R_2	R_3				C	H	N	C	H	N
Cl	H	C_6H_5	CH_3	120	45	$C_{16}H_{12}NSOCl$	64.00	3.95	4.75	63.68	3.98	4.65
Cl	H	C_6H_4Cl	CH_3	127	60	$C_{16}H_{11}NSOCl_2$	57.20	3.30	4.25	57.14	3.28	4.17
CH_3	H	C_6H_4Cl	CH_3	205	55	$C_{17}H_{14}NSOCl$	64.82	4.45	4.48	64.65	4.44	4.44
OCH_3	H	C_6H_4Cl	CH_3	160	58	$C_{17}H_{14}NSO_2Cl$	61.70	4.30	4.25	61.53	4.22	4.22
OCH_3	H	C_6H_5	CH_3	142	40	$C_{17}H_{15}NSO_2$	68.75	5.10	4.75	68.68	5.05	4.71
CH_3	H	OC_2H_5	CH_3	162	69.5	$C_{13}H_{15}NSO_2$	62.15	6.05	5.60	62.65	6.02	5.62
CH_3	H	CH_3	CH_3	169	72.5	$C_{12}H_{13}NSO$	65.35	5.95	6.43	65.75	5.93	6.39
CH_3	H	C_6H_5	C_6H_5	105	66.0	$C_{22}H_{17}NSO$	76.50	4.98	4.13	76.96	4.95	4.08
CH_3	H	C_6H_5	CH_3	137	68.4	$C_{17}H_{15}NSO$	72.11	5.36	5.02	72.59	5.33	4.98
H	CH_3	C_6H_5	CH_3	208	71.8	$C_{17}H_{15}NSO$	73.02	5.34	5.01	72.59	5.33	4.98
H	Cl	C_6H_5	CH_3	247	72.5	$C_{16}H_{12}NSOCl$	63.49	3.97	4.68	63.68	3.98	4.64

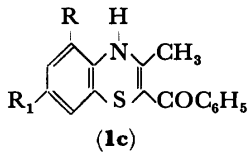

(**1c**)

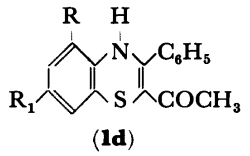

(**1d**)

Experimental

All the melting points are uncorrected. The purity of the synthesized compounds was tested on the elemental analysis and thin-layer chromatography of silica gel in various non-aqueous solvents. Infrared spectra of 4*H*-1,4-benzothiazines have been scanned in KBr on Perkin-Elmer 577 grating spectrophotometer and their NMR spectra were recorded on a Perkin-Elmer R12 B spectrometer using tetramethylsilane as an internal standard. The mass spectra were recorded on a JEOL, JMSD-300 mass spectrometer at 70 eV with 100 μA ionizing current.

*Preparation of Substituted 4*H*-1,4-Benzothiazines(II)*, The substituted 2-aminobenzenethiol[10-12] (1, 0.01 mol) was added to the stirred suspension of β-dicarbonyl compound (0.01 mol) (acetylacetone, ethylacetoacetate, dibenzoylmethane, benzoylacetone, or *p*-chlorobenzoylacetone) in DMSO (5 ml) and the resulting mixture was refluxed for 1 h. The mixture was cooled down to room temperature and a solid substance separated was filtered and crystallized from methanol. The physical data are given in Table 1.

References

1) M. Gordon, "Psychopharmacological Agents," Vol. II, "Medicinal Chemistry," Vol. 4-II, ed by M. Gordon Academic Press, New York (1967) pp. 119—132.
2) "A Survey of Antimalarial Drugs" ed by F. Y. Wiselogle J. W. Edwards Publ, Ann. Arbor. Mich. (1946) Vol. II, Part I, pp. 699—700.
3) H. Laborit and L. Leger, *Press Med.*, **38**, 492 (1950).
4) "The Merck Index of Chemical Drugs 7th edn" Merk & Com. Ind. Rahaw, N. J. 249 (1960).
5) Belg. Patent 869041: *Chem. Abstr.*, **91**, 27311 (1979).
6) B. B. O'Malley, R. Willhein, and P. F. Lusse Abstracts of Papers 138th Meeting of American Chemical Society, Sept. p. 66c (1960).
7) D. G. Friend and J. F. Lunnins, *J. Am. Med. Assoc.*, **153**, 480 (1953).
8) F. Duro, P. Condorelli, G. Ronsisvalle, *Ann. Chim.*, **63**, 45 (1973); *Chem. Abstr.*, **80**, 95856x (1974).
9) A. Y. Il'Chenko, *Ukr. Khim. Zh.*, **35**, 1185 (1969); *Chem. Abstr.*, **72**, 56667 (1970).
10) K. G. Ojha, S. K. Jain, and R. R. Gupta, *Synth. Commun.*, **12**, 457 (1979).
11) R. L. Mital and S. K. Jain, *J. Chem. Soc., C*, 2148 (1969).
12) J. L. Wood, "Organic Reactions," ed by R. Adams, Willey, New York (1959), Vol. III, p. 257.

 © 1984 The Chemical Society of Japan Bull. Chem. Soc. Jpn., 57, 2345—2351 (1984)

The Crystal and Molecular Structure of Quadrivalent Osmium Porphyrin; μ-Oxo-bis[methoxo(octaethylporphinato)osmium(IV)]

Hideki MASUDA,* Tooru TAGA, Kenji OSAKI, Hiroshi SUGIMOTO,† and Masayasu MORI†

Faculty of Pharmaceutical Sciences, Kyoto University, Shimoadachi-cho, Sakyo-ku, Kyoto 606

†*Faculty of Science, Osaka City University, Sugimoto, Sumiyoshi-ku, Osaka 558*

(Received July 11, 1983)

The crystal structure of the title complex has been determined by the X-ray method. The complex crystallizes in the monoclinic space group P2/c with a=24.171(9), b=14.037(3), c=24.401(9) Å, β=119.68(9)°, and Z=4. The structure was solved by the heavy-atom method and refined to R=0.094 for 3838 reflections. Two independent dimers exist with a crystallographically imposed two-fold axis in the unit cell. The two dimers are in an approximately orthogonal arrangement, and they take very similar conformations. The noticeable structural parameters are the average distances of 2.033(28) Å for Os^{IV}-N, 1.808(3) Å for Os^{IV}-O^{2-}, and 1.997(29) Å for Os^{IV}-OCH_3. The two porphinato cores bridged by a μ-oxo oxygen atom rotate around the approximately linear Os-O-Os bond (the average valence angle=178°) by 23(1)° from the eclipsed form. The porphine ring is planar within 0.10 Å, and deviation of the Os atom from the porphinato plane of the four nitrogen atoms is 0.06 Å. These results were compared, in the relation of the specific physicochemical properties in solution, with those of the corresponding Ru^{IV} complexes reported previously.

We have recently been studying the molecular and crystal structures of ruthenium(IV) porphyrins[1] as a model of quadrivalent iron porphyrins, which have received attention in relation to the structure of catalases, horseradish peroxidases, and cytochrome c peroxidases in the redox process.[2] In the recently established structures of the ruthenium(IV) porphyrins, the quadrivalent state of the metal ion was observed to be stabilized by the strong O^{2-} ligand in the axial direction, and such a structural aspect around the ruthenium(IV) ion gave a good assumption for the undetermined axial ligands around the iron(IV) ion in peroxidases. The quadrivalent osmium ion has the same number of outer-shell (d+s) electrons as the ruthenium(IV) ion, and it also forms iron(IV) porphyrin analogues. Several osmium(IV) porphyrin complexes have been obtained so far in similar reactions aimed at getting the ruthenium(IV) complexes;[1,3c] in those complexes the bivalent osmium porphyrins were oxidized to the quadrivalent state at the same time that the indole derivatives were oxidized by the molecular oxygen with the bivalent osmium porphyrins.[3] The physicochemical properties of the title complex in solution are very similar to those of the corresponding ruthenium(IV) complexes. The ^{1}H-NMR, absorption spectra, and cyclic voltammetry suggested that the osmium(IV) porphyrins formed a linear μ-oxo dimer structure as well as the ruthenium(IV) complexes. However, the osmium(IV) complex in an acid solution showed a slightly different behavior from the ruthenium(IV) complex. The μ-oxo oxygen atom had a high affinity for protons in the presence of a 1% acid such as CF_3COOH, HCl, and $HClO_4$.[3c] The cause of the high proton affinity might lie in the μ-oxo bridge structure of the osmium(IV) porphyrin dimer. A detailed comparison of the structure of the dimer with that of the ruthenium(IV) complex was of interest.

Experimental

Dark-violet plate-like crystals of the μ-oxo-bis[methoxo(octaethylporphinato)osmium(IV)] complex, $[Os^{IV}(oep)(OCH_3)]_2O$, obtained by the 2,3-dimethylindole treatment of $[Os^{II}(oep)(CO)(CH_3OH)]$ in dichloromethane,[3c] were subjected to X-ray experiments.

Crystal Data. $C_{74}H_{94}N_8O_3Os_2$, M=1522, monoclinic, space group P2/c, a=24.171(9), b=14.037(3), c=24.401(9) Å, β=119.68(9)°, U=7192(5) Å^3, Z=4, D_c=1.407 g cm^{-3}, D_m=1.40 g cm^{-3}, $F(000)$=3048, λ=0.71073 Å, μ(Mo $K\alpha$)=38.27 cm^{-1}.

The diffraction intensities were measured on a Rigaku AFC-5 diffractometer with graphite-monochromated Mo $K\alpha$ radiation. The intensity data of 4056 reflections in the $2\theta<50°$ range were collected in the ω–2θ scan mode with a scan rate of 5° min^{-1} and using a crystal with dimensions of 0.5×0.5×0.3 mm. During the course of the data collection, three reflections were monitored every 60 reflections. The intensity data were converted to the F_o data in the usual manner. Absorption correction was applied in the spherical approximation. The standard deviations $\sigma(F_o)$ were estimated by means of the counting statistics. A total of 3838 independent reflections with $F_o>3\sigma(F_o)$ were retained as observed, and used in solving and refining the structure.

The structure was solved by the heavy-atom method. The four osmium atoms were located by a sharpened Patterson synthesis. Although the systematic absences of $h0l$ for $l=2n+1$ led to two possible space groups, Pc and P2/c, the configuration was tentatively assumed to be the space group P2/c; the successive Fourier syntheses revealed the approximate structure. The block-diagonal least-squares refinement to examine the two possible space groups, P2/c and Pc, resulted in the rejection of the latter space group Pc, because it gave several abnormal bond distances and angles, and also gave non-positive temperature factors for some light atoms. Thus, a trial structure based on the space group P2/c was chosen for the further refinement. Several cycles of the block-diagonal least-squares refinement including the anisotropic thermal parameters were carried out with the weighting scheme of $w^{-1}=(\sigma^2(F_o)+(0.023F_o)^2)$. The atomic scattering factors[4a] and the anomalous dispersion terms[4b] were taken from the International Tables for X-Ray Crystallography, IV. The hydrogen atoms were included as a fixed contribution in the last cycle; their positions were assumed to be in accord with the idealized geometry (C-H=1.00 Å), and their temperature factors were assumed to be isotropic (B=8.00 Å^2). The final R value was 0.094. The final difference Fourier map showed no peak greater than 0.6 e/Å^3; most of the largest peaks were around the osmium atoms. All the computations

were performed on a FACOM M-200 computer at the Data Processing Center of Kyoto University by using the program system KPAX. The positional parameters of the non-hydrogen atoms are given in Table 1.[5]

Results and Discussion

The unit cell is comprised of four discrete μ-oxo dimers of $[Os^{IV}(oep)(OCH_3)]_2O$ (see Fig. 1). There are two independent dimers, A and B, which take an

Table 1. Fractional coordinates ($\times 10^4$) and isotropic thermal parameters, with estimated standard deviations in parentheses

Atom[a]	x	y	z	B_{eq}/Å^2 [b]	Atom[a]	x	y	z	B_{eq}/Å^2 [b]
Os(A)	569(1)	440(1)	2224(1)	5.39	C(31A)	−8(26)	−3445(40)	1480(21)	16.5
Os(B)	4402(1)	3807(1)	1673(1)	4.92	C(32A)	258(28)	−3687(40)	1071(29)	17.1
N(1A)	965(12)	1627(19)	2729(12)	5.43	C(33A)	1963(20)	−2687(29)	3803(22)	9.84
N(2A)	−21(11)	1280(20)	1462(11)	5.47	C(34A)	2399(21)	−3011(33)	3544(25)	11.4
N(3A)	204(14)	−690(19)	1695(15)	7.31	C(35A)	2496(26)	−760(31)	4680(26)	13.1
N(4A)	1177(11)	−336(17)	2948(13)	4.57	C(36A)	3123(27)	−600(47)	4646(30)	18.5
N(1B)	3797(13)	3074(20)	1806(14)	6.34	C(37A)	1119(25)	647(40)	1355(30)	15.7
N(2B)	4799(11)	2592(18)	1548(11)	4.33	C(1B)	3345(15)	3378(23)	1977(15)	4.89
N(3B)	5006(11)	4551(19)	1439(12)	5.12	C(2B)	2986(18)	2563(27)	2070(19)	7.78
N(4B)	3938(13)	5068(20)	1769(16)	7.43	C(3B)	3243(18)	1807(27)	1974(19)	7.43
O(1A)	0	411(20)	2500	5.73	C(4B)	3785(14)	2005(25)	1858(15)	5.25
O(1B)	5000	3801(25)	2500	7.48	C(5B)	4120(17)	1422(32)	1730(21)	8.90
O(2A)	1241(14)	437(20)	1964(12)	9.06	C(6B)	4603(18)	1653(28)	1577(17)	7.40
O(2B)	3723(11)	3853(19)	778(10)	6.90	C(7B)	4967(20)	1035(25)	1457(20)	7.64
C(1A)	1507(19)	1606(22)	3356(17)	6.17	C(8B)	5379(20)	1504(28)	1356(24)	9.56
C(2A)	1607(18)	2647(28)	3505(18)	7.10	C(9B)	5252(18)	2530(26)	1382(17)	7.13
C(3A)	1200(18)	3260(28)	3013(17)	7.18	C(10B)	5575(19)	3299(24)	1281(18)	6.63
C(4A)	790(15)	2505(31)	2509(17)	7.83	C(11B)	5450(14)	4223(21)	1307(14)	3.75
C(5A)	309(14)	2839(26)	1917(16)	5.35	C(12B)	5809(19)	5020(26)	1232(21)	8.55
C(6A)	−60(16)	2281(22)	1446(15)	5.42	C(13B)	5477(16)	5819(24)	1270(19)	6.11
C(7A)	−545(17)	2584(28)	803(18)	6.98	C(14B)	4998(19)	5596(26)	1438(18)	7.74
C(8A)	−852(19)	1788(29)	470(20)	8.66	C(15B)	4635(19)	6179(27)	1563(18)	7.21
C(9A)	−489(18)	995(28)	885(17)	7.29	C(16B)	4195(13)	5926(22)	1709(14)	4.46
C(10A)	−618(20)	4(32)	757(19)	10.0	C(17B)	3741(17)	6549(27)	1806(20)	7.72
C(11A)	−291(20)	−860(26)	1117(19)	8.08	C(18B)	3340(18)	6080(26)	1941(17)	7.24
C(12A)	−454(19)	−1813(31)	900(18)	8.79	C(19B)	3533(14)	5101(22)	1919(17)	4.94
C(13A)	8(15)	−2318(32)	1386(18)	9.28	C(20B)	3268(16)	4368(19)	2065(15)	4.87
C(14A)	307(17)	−1598(29)	1842(18)	8.26	C(21B)	2519(18)	2629(34)	2422(25)	11.5
C(15A)	805(16)	−1937(22)	2422(17)	5.63	C(22B)	1972(22)	2901(36)	1817(24)	11.8
C(16A)	1239(15)	−1266(28)	2999(15)	6.45	C(23B)	3080(20)	779(29)	1992(19)	8.12
C(17A)	1748(19)	−1680(27)	3580(18)	7.67	C(24B)	2629(25)	388(37)	1313(25)	12.9
C(18A)	1992(17)	−935(26)	3908(17)	6.43	C(25B)	5068(25)	−60(36)	1645(25)	12.5
C(19A)	1657(15)	−86(26)	3541(14)	5.84	C(26B)	4705(33)	−401(53)	1117(26)	19.7
C(20A)	1801(18)	853(22)	3725(17)	6.39	C(27B)	5992(26)	1171(34)	1284(21)	11.6
C(21A)	2143(17)	2965(25)	4199(17)	6.12	C(28B)	5740(27)	1136(43)	693(27)	15.8
C(22A)	2765(24)	2976(35)	4248(22)	11.8	C(29B)	6247(16)	4934(26)	1039(16)	5.91
C(23A)	1172(24)	4357(40)	3010(25)	13.2	C(30B)	5968(18)	4833(27)	332(19)	8.02
C(24A)	1510(31)	4725(37)	2702(27)	16.0	C(31B)	5754(18)	6878(31)	1355(19)	8.30
C(25A)	−736(22)	3612(30)	593(17)	9.23	C(32B)	5355(21)	7204(33)	716(24)	10.7
C(26A)	−325(28)	3993(26)	375(25)	12.4	C(33B)	3799(19)	7714(26)	1790(20)	8.31
C(27A)	−1385(21)	1689(30)	−198(19)	9.32	C(34B)	3436(22)	7988(35)	1089(27)	12.9
C(28A)	−1157(24)	1505(42)	−650(23)	15.2	C(35B)	2822(20)	6390(30)	2123(24)	10.1
C(29A)	−1002(25)	−2213(39)	265(22)	13.4	C(36B)	2209(21)	6232(37)	1573(23)	11.0
C(30A)	−686(26)	−2090(43)	−43(29)	17.3	C(37B)	3502(39)	3047(52)	361(29)	19.1

a) Symbols A and B in parentheses identify the atoms corresponding to the moieties (a) and (b) given in Fig. 2.
b) The equivalent isotropic temperature factors for non-hydrogen atoms were computed using the following expression: $B_{eq}=4/3(B_{11}a^2+B_{22}b^2+B_{33}c^2+2B_{12}ab\cos\gamma+2B_{13}ac\cos\beta+2B_{23}bc\cos\alpha)$. The B_{ij}'s are defined by: $\exp[-(h^2B_{11}+k^2B_{22}+l^2B_{33}+2hlB_{23}+2hlB_{13}+2hkB_{12})]$.

TABLE 2. BOND DISTANCES (l/Å) AND BOND ANGLES (ϕ/°), WITH ESTIMATED STANDARD DEVIATIONS IN PARENTHESES

(a) The coordination sphere of the osmium atom			
Os(A)-N(1A)	2.011(25)	Os(B)-N(1B)	1.942(35)
Os(A)-N(2A)	2.063(23)	Os(B)-N(2B)	2.052(27)
Os(A)-N(3A)	1.958(27)	Os(B)-N(3B)	2.091(32)
Os(A)-N(4A)	1.974(23)	Os(B)-N(4B)	2.169(33)
Os(A)-O(1A)	1.807(3)	Os(B)-O(1B)	1.809(3)
Os(A)-O(2A)	2.015(39)	Os(B)-O(2B)	1.979(19)
N(1A)-Os(A)-N(2A)	89.2(10)	N(1B)-Os(B)-N(2B)	91.8(12)
N(1A)-Os(A)-N(3A)	176.2(16)	N(1B)-Os(B)-N(3B)	174.4(11)
N(1A)-Os(A)-N(4A)	89.5(10)	N(1B)-Os(B)-N(4B)	95.2(12)
N(2A)-Os(A)-N(3A)	89.1(11)	N(2B)-Os(B)-N(3B)	86.2(11)
N(2A)-Os(A)-N(4A)	176.6(12)	N(2B)-Os(B)-N(4B)	177.2(7)
N(3A)-Os(A)-N(4A)	92.0(10)	N(3B)-Os(B)-N(4B)	95.2(12)
O(1A)-Os(A)-N(1A)	90.5(12)	O(1B)-Os(B)-N(1B)	93.6(9)
O(1A)-Os(A)-N(2A)	92.0(10)	O(1B)-Os(B)-N(2B)	89.3(10)
O(1A)-Os(A)-N(3A)	92.9(14)	O(1B)-Os(B)-N(3B)	91.5(8)
O(1A)-Os(A)-N(4A)	91.2(11)	O(1B)-Os(B)-N(4B)	93.1(12)
O(2A)-Os(A)-N(1A)	88.9(12)	O(2B)-Os(B)-N(1B)	85.4(11)
O(2A)-Os(A)-N(2A)	91.4(11)	O(2B)-Os(B)-N(2B)	93.2(10)
O(2A)-Os(A)-N(3A)	87.8(14)	O(2B)-Os(B)-N(3B)	89.5(10)
O(2A)-Os(A)-N(4A)	91.2(11)	O(2B)-Os(B)-N(4B)	84.4(11)
O(1A)-Os(A)-O(2A)	176.7(7)	O(1B)-Os(B)-O(2B)	177.3(11)
(b) The axial and equatorial ligands			
O(2A)-C(37A)	1.40(8)	O(2B)-C(37B)	1.44(7)
N(1A)-C(1A)	1.44(3)	N(1B)-C(1B)	1.42(5)
N(1A)-C(4A)	1.33(4)	N(1B)-C(4B)	1.51(4)
N(2A)-C(6A)	1.41(4)	N(2B)-C(6B)	1.41(4)
N(2A)-C(9A)	1.36(3)	N(2B)-C(9B)	1.35(6)
N(3A)-C(11A)	1.34(4)	N(3B)-C(11B)	1.35(5)
N(3A)-C(14A)	1.31(4)	N(3B)-C(14B)	1.47(4)
N(4A)-C(16A)	1.31(4)	N(4B)-C(16B)	1.40(4)
N(4A)-C(19A)	1.38(3)	N(4B)-C(19B)	1.20(6)
C(1A)-C(2A)	1.50(5)	C(1B)-C(2B)	1.52(5)
C(3A)-C(4A)	1.55(5)	C(3B)-C(4B)	1.50(6)
C(6A)-C(7A)	1.48(4)	C(6B)-C(7B)	1.37(6)
C(8A)-C(9A)	1.47(5)	C(8B)-C(9B)	1.48(5)
C(11A)-C(12A)	1.42(5)	C(11B)-C(12B)	1.48(5)
C(13A)-C(14A)	1.41(5)	C(13B)-C(14B)	1.44(7)
C(16A)-C(17A)	1.46(4)	C(16B)-C(17B)	1.51(5)
C(18A)-C(19A)	1.47(4)	C(18B)-C(19B)	1.46(5)
C(2A)-C(3A)	1.55(5)	C(2B)-C(3B)	1.31(6)
C(7A)-C(8A)	1.37(5)	C(7B)-C(8B)	1.32(7)
C(12A)-C(13A)	1.36(5)	C(12B)-C(13B)	1.41(5)
C(17A)-C(18A)	1.27(5)	C(17B)-C(18B)	1.34(6)
C(5A)-C(4A)	1.41(4)	C(5B)-C(4B)	1.29(6)
C(5A)-C(6A)	1.31(4)	C(5B)-C(6B)	1.43(7)
C(10A)-C(9A)	1.43(5)	C(10B)-C(9B)	1.42(6)
C(10A)-C(11A)	1.48(5)	C(10B)-C(11B)	1.34(4)
C(15A)-C(14A)	1.41(4)	C(15B)-C(14B)	1.34(6)
C(15A)-C(16A)	1.58(4)	C(15B)-C(16B)	1.33(6)
C(20A)-C(1A)	1.34(4)	C(20B)-C(1B)	1.43(4)
C(20A)-C(19A)	1.38(4)	C(20B)-C(19B)	1.35(5)
C(2A)-C(21A)	1.60(4)	C(2B)-C(21B)	1.73(8)
C(3A)-C(23A)	1.54(6)	C(3B)-C(23B)	1.50(5)
C(7A)-C(25A)	1.52(5)	C(7B)-C(25B)	1.59(6)
C(8A)-C(27A)	1.50(5)	C(8B)-C(27B)	1.64(8)

Table 2. (Continued)

C(12A)-C(29A)	1.56(5)	C(12B)-C(29B)	1.36(7)
C(13A)-C(31A)	1.60(7)	C(13B)-C(31B)	1.60(5)
C(17A)-C(33A)	1.51(5)	C(17B)-C(33B)	1.64(5)
C(18A)-C(35A)	1.68(6)	C(18B)-C(35B)	1.58(7)
C(21A)-C(22A)	1.45(7)	C(21B)-C(22B)	1.46(5)
C(23A)-C(24A)	1.45(9)	C(23B)-C(24B)	1.56(6)
C(25A)-C(26A)	1.44(9)	C(25B)-C(26B)	1.24(7)
C(27A)-C(28A)	1.48(8)	C(27B)-C(28B)	1.26(7)
C(29A)-C(30A)	1.32(9)	C(29B)-C(30B)	1.52(5)
C(31A)-C(32A)	1.47(9)	C(31B)-C(32B)	1.44(6)
C(33A)-C(34A)	1.54(8)	C(33B)-C(34B)	1.54(7)
C(35A)-C(36A)	1.57(9)	C(35B)-C(36B)	1.44(5)
Os(A)-O(1A)-Os(A)*	177.4(17)	Os(B)-O(1B)-Os(B)*	179.5(11)
Os(A)-O(2A)-C(37A)	124(2)	Os(B)-O(2B)-C(37B)	125(3)
Os(A)-N(1A)-C(1A)	123(2)	Os(B)-N(1B)-C(1B)	130(2)
Os(A)-N(1A)-C(4A)	124(2)	Os(B)-N(1B)-C(4B)	126(2)
Os(A)-N(2A)-C(6A)	127(1)	Os(B)-N(2B)-C(6B)	125(2)
Os(A)-N(2A)-C(9A)	128(2)	Os(B)-N(2B)-C(9B)	128(2)
Os(A)-N(3A)-C(11A)	135(2)	Os(B)-N(3B)-C(11B)	130(2)
Os(A)-N(3A)-C(14A)	130(2)	Os(B)-N(3B)-C(14B)	119(2)
Os(A)-N(4A)-C(16A)	129(1)	Os(B)-N(4B)-C(16B)	114(2)
Os(A)-N(4A)-C(19A)	132(2)	Os(B)-N(4B)-C(19B)	127(2)
C(1A)-N(1A)-C(4A)	113(2)	C(1B)-N(1B)-C(4B)	103(3)
C(6A)-N(2A)-C(9A)	105(2)	C(6B)-N(2B)-C(9B)	107(3)
C(11A)-N(3A)-C(14A)	94(2)	C(11B)-N(3B)-C(14B)	111(3)
C(16A)-N(4A)-C(19A)	99(2)	C(16B)-N(4B)-C(19B)	118(3)
N(1A)-C(1A)-C(2A)	101(2)	N(1B)-C(1B)-C(2B)	114(3)
N(1A)-C(4A)-C(3A)	111(2)	N(1B)-C(4B)-C(3B)	105(3)
N(2A)-C(6A)-C(7A)	109(2)	N(2B)-C(6B)-C(7B)	108(4)
N(2A)-C(9A)-C(8A)	114(3)	N(2B)-C(9B)-C(8B)	107(3)
N(3A)-C(11A)-C(12A)	110(3)	N(3B)-C(11B)-C(12B)	111(3)
N(3A)-C(14A)-C(13A)	122(3)	N(3B)-C(14B)-C(13B)	102(3)
N(4A)-C(16A)-C(17A)	119(2)	N(4B)-C(16B)-C(17B)	95(3)
N(4A)-C(19A)-C(18A)	111(2)	N(4B)-C(19B)-C(18B)	112(3)
C(1A)-C(2A)-C(3A)	115(3)	C(1B)-C(2B)-C(3B)	103(4)
C(2A)-C(3A)-C(4A)	99(3)	C(2B)-C(3B)-C(4B)	115(3)
C(6A)-C(7A)-C(8A)	108(3)	C(6B)-C(7B)-C(8B)	111(3)
C(7A)-C(8A)-C(9A)	104(2)	C(7B)-C(8B)-C(9B)	107(4)
C(11A)-C(12A)-C(13A)	102(3)	C(11B)-C(12B)-C(13B)	102(4)
C(12A)-C(13A)-C(14A)	101(3)	C(12B)-C(13B)-C(14B)	114(3)
C(16A)-C(17A)-C(18A)	101(3)	C(16B)-C(17B)-C(18B)	115(3)
C(17A)-C(18A)-C(19A)	110(2)	C(17B)-C(18B)-C(19B)	100(3)
N(1A)-C(1A)-C(20A)	129(2)	N(1B)-C(1B)-C(20B)	121(3)
N(1A)-C(4A)-C(5A)	131(3)	N(1B)-C(4B)-C(5B)	125(4)
N(2A)-C(6A)-C(5A)	124(2)	N(2B)-C(6B)-C(5B)	124(3)
N(2A)-C(9A)-C(10A)	120(3)	N(2B)-C(9B)-C(10B)	127(3)
N(3A)-C(11A)-C(10A)	115(3)	N(3B)-C(11B)-C(10B)	125(3)
N(3A)-C(14A)-C(15A)	124(3)	N(3B)-C(14B)-C(15B)	128(4)
N(4A)-C(16A)-C(15A)	121(2)	N(4B)-C(16B)-C(15B)	136(3)
N(4A)-C(19A)-C(20A)	122(2)	N(4B)-C(19B)-C(20B)	128(3)
C(20A)-C(1A)-C(2A)	130(2)	C(20B)-C(1B)-C(2B)	126(3)
C(3A)-C(4A)-C(5A)	118(3)	C(3B)-C(4B)-C(5B)	130(3)
C(5A)-C(6A)-C(7A)	127(3)	C(5B)-C(6B)-C(7B)	128(3)
C(8A)-C(9A)-C(10A)	127(3)	C(8B)-C(9B)-C(10B)	126(4)
C(10A)-C(11A)-C(12A)	126(3)	C(10B)-C(11B)-C(12B)	124(4)
C(13A)-C(14A)-C(15A)	114(3)	C(13B)-C(14B)-C(15B)	130(3)
C(15A)-C(16A)-C(17A)	120(3)	C(15B)-C(16B)-C(17B)	129(3)

TABLE 2. (Continued)

C(18A)-C(19A)-C(20A)	127(2)	C(18B)-C(19B)-C(20B)	120(4)
C(4A)-C(5A)-C(6A)	124(3)	C(4B)-C(5B)-C(6B)	128(4)
C(9A)-C(10A)-C(11A)	133(3)	C(9B)-C(10B)-C(11B)	125(4)
C(14A)-C(15A)-C(16A)	124(3)	C(14B)-C(15B)-C(16B)	127(3)
C(19A)-C(20A)-C(1A)	125(2)	C(19B)-C(20B)-C(1B)	126(4)
C(1A)-C(2A)-C(21A)	119(2)	C(1B)-C(2B)-C(21B)	127(3)
C(4A)-C(3A)-C(23A)	132(3)	C(4B)-C(3B)-C(23B)	117(3)
C(6A)-C(7A)-C(25A)	125(3)	C(6B)-C(7B)-C(25B)	125(5)
C(9A)-C(8A)-C(27A)	125(3)	C(9B)-C(8B)-C(27B)	120(4)
C(11A)-C(12A)-C(29A)	131(3)	C(11B)-C(12B)-C(29B)	125(3)
C(14A)-C(13A)-C(31A)	129(3)	C(14B)-C(13B)-C(31B)	121(3)
C(16A)-C(17A)-C(33A)	134(3)	C(16B)-C(17B)-C(33B)	120(3)
C(19A)-C(18A)-C(35A)	116(3)	C(19B)-C(18B)-C(35B)	126(3)
C(3A)-C(2A)-C(21A)	126(3)	C(3B)-C(2B)-C(21B)	128(4)
C(2A)-C(3A)-C(23A)	129(3)	C(2B)-C(3B)-C(23B)	128(4)
C(8A)-C(7A)-C(25A)	126(3)	C(8B)-C(7B)-C(25B)	121(4)
C(7A)-C(8A)-C(27A)	130(3)	C(7B)-C(8B)-C(27B)	133(3)
C(13A)-C(12A)-C(29A)	127(4)	C(13B)-C(12B)-C(29B)	131(4)
C(12A)-C(13A)-C(31A)	125(3)	C(12B)-C(13B)-C(31B)	122(3)
C(18A)-C(17A)-C(33A)	125(3)	C(18B)-C(17B)-C(33B)	125(4)
C(17A)-C(18A)-C(35A)	133(3)	C(17B)-C(18B)-C(35B)	135(3)
C(2A)-C(21A)-C(22A)	111(4)	C(2B)-C(21B)-C(22B)	90(4)
C(3A)-C(23A)-C(24A)	109(5)	C(3B)-C(23B)-C(24B)	111(3)
C(7A)-C(25A)-C(26A)	109(4)	C(7B)-C(25B)-C(26B)	98(4)
C(8A)-C(27A)-C(28A)	113(4)	C(8B)-C(27B)-C(28B)	101(4)
C(12A)-C(29A)-C(30A)	94(4)	C(12B)-C(29B)-C(30B)	115(3)
C(13A)-C(31A)-C(32A)	95(4)	C(13B)-C(31B)-C(32B)	98(3)
C(17A)-C(33A)-C(34A)	108(4)	C(17B)-C(33B)-C(34B)	106(3)
C(18A)-C(35A)-C(36A)	98(4)	C(18B)-C(35B)-C(36B)	107(4)

approximately orthogonal arrangement to each other. Each dimer has a two-fold axis through the μ-oxo oxygen atom, bisecting the line joining two osmium atoms in the dimer. Thus, the asymmetric unit consists of two [Os^{IV}(oep)(OCH_3)]-O- moieties. The two independent osmium porphinato moieties have similar conformations, as is illustrated in Figs. 2(a) and (b).

The numbering scheme for the carbon and nitrogen atoms in each [Os^{IV}(oep)(OCH_3)]-O- moiety is shown in Fig. 3. The bond distances and bond angles are listed in Table 2. The average bond distances and bond angles for chemically equivalent types of the bond in the osmium octaethylporphinato skeletons are also presented in Fig. 3. The average values agree with those of the corresponding bonds in the other metalloporphyrins,[6] within the limits of experimental error.

Figure 4 presents a perspective diagram of the environment of the osmium ion, with the average bond distances and bond angles. The porphine rings are planar within 0.10 Å, and the osmium ions are displaced by 0.06Å out of the plane defined by the four porphinato nitrogen atoms. The average Os-N distance, 2.033(28) Å,[7] is normal for the quadrivalent osmium ion, and it is comparable with the bivalent Os-N distance, 2.067(2) Å, reported in [Os^{II}(oep)(pyridine)(CO)].[8] The Os^{IV}-O^{2-} distances of 1.807(3) and 1.809(3) Å are comparable with the Ru^{IV}-O^{2-} distance of 1.793(2) Å in [Ru^{IV}(oep)Cl]$_2$O,[1b] with the chloride

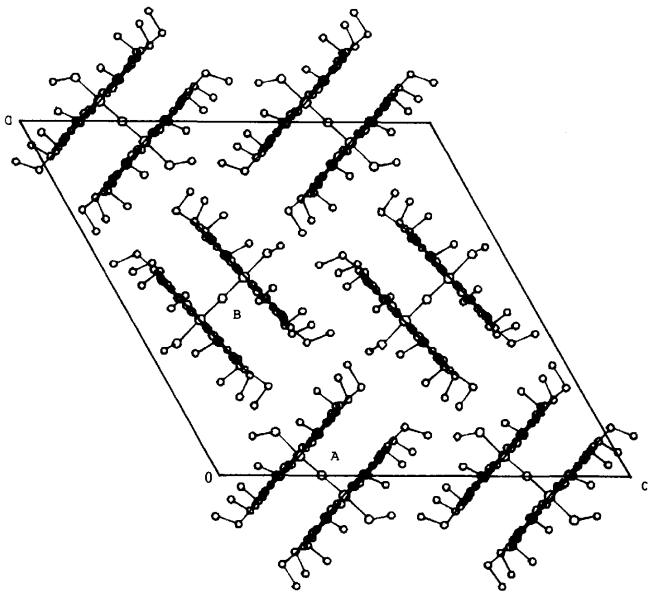

Fig. 1. Packing diagram of [Os^{IV}(oep)(OCH_3)]$_2$O crystal as viewed parallel to *b*.

atom as the external ligand, but it seems to deviate greatly from that of 1.847(13) Å in [Ru^{IV}(oep)(OH)]$_2$O.[1a] The average Os^{IV}-OCH_3 distance of 1.997(29) Å agrees with the 5% reduction of the sum of the ionic

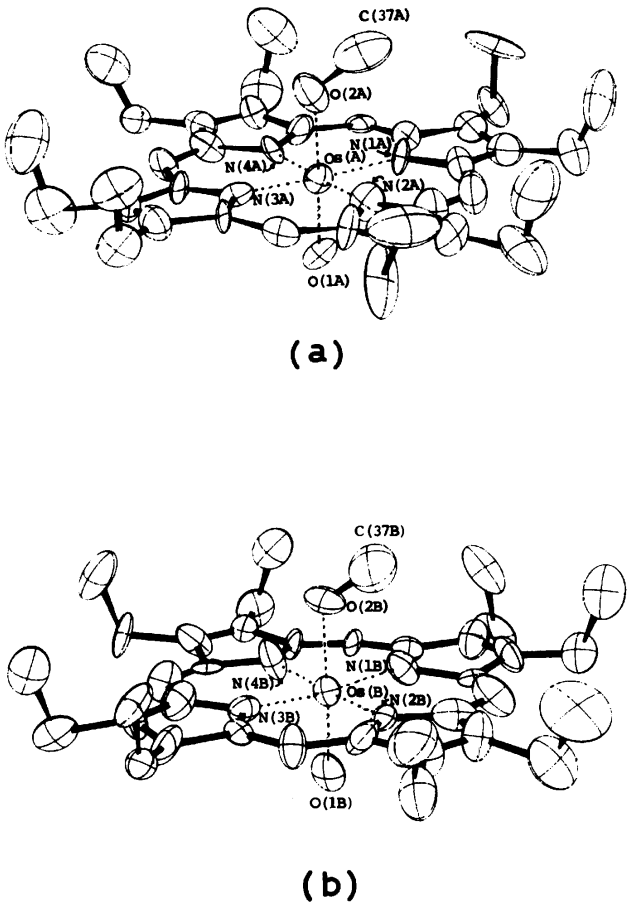

Fig. 2. Computer drawnings of the two independent osmium porphinato moieties, (a) and (b), showing 30 % probability thermal-vibration ellipsoids.

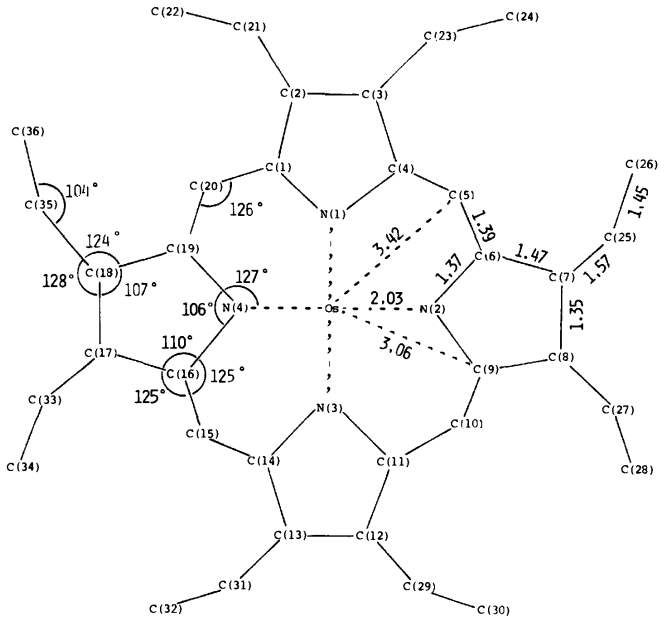

Fig. 3. Bond distances and bond angles averaged over the chemically equivalent bonds.

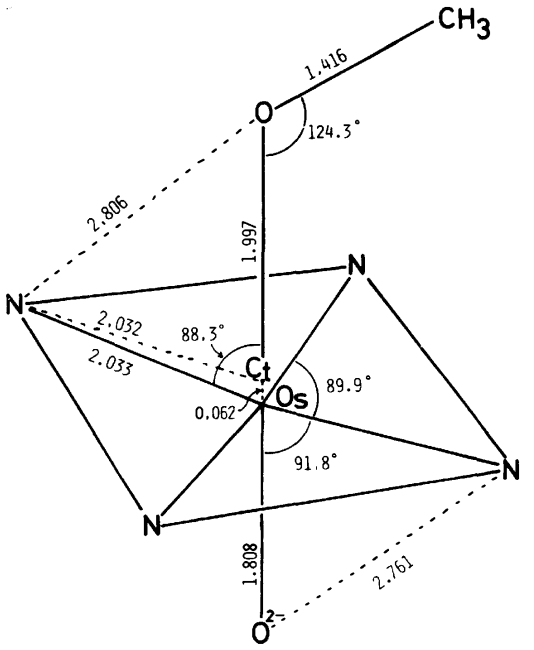

Fig. 4. Coordination sphere showing averaged bond distances and bond angles around the osmium(IV) atom in $[Os^{IV}(oep)(OCH_3)]_2O$. C_t represents the center of the porphinato skeleton.

radii,[11] 2.04 Å, due to the formation of the six-coordinate metal ion. The μ-oxo dimer consists of the two units of osmium porphyrins related by the two-fold symmetry through the O^{2-} atom. The Os–O–Os* bond has the valence angle of 178°. The two porphyrins are twisted with respect to each other so as to lie approximately midway between a staggered conformation and an eclipsed one, the N–Os–Os*–N* torsion angle being 23(1)°.[9] The average interplanar separation between the mean planes of the facing porphyrins is 3.7 Å; the closest interatomic distances are 3.60 Å for C(4A)–C(5A)* and 3.64 Å for C(11B)–C(20B)*. The binuclear porphyrin structure resembles those reported in $[Ru^{IV}(oep)(OH)]_2O$[1a] and $[Ru^{IV}(oep)Cl]_2O$,[1b] and, for the reason presented in the previous reports on the Ru^{IV} porphyrin dimers,[1] the structure is stabilized by the intramolecular π-π interactions between the face-to-face-contact porphyrins and by the $d\pi$-$p\pi$-$d\pi$ interaction in the Os^{IV}–O–Os^{IV}* bond. The diamagnetic property of this complex can also be well interpreted in terms of the π-π interactions in the Os^{IV}–O–Os^{IV}* bond system with the low-spin Os^{IV} atom.

As has been mentioned in the Introduction, the osmium-dimer complex in an acidic solution shows a high sensitivity for the protons, and the electron-donating ability of the μ-oxo bivalent anion (O^{2-}) in the Os^{IV}–O–Os^{IV} system is considerably stronger than that in the Ru^{IV}–O–Ru^{IV} system. This difference is reflected in the bond distances or bond angles around the μ-oxo oxygen. The observed Os^{IV}–O–Os^{IV} bond is almost as linear as the corresponding bonds in the ruthenium complexes,[1] in accordance with the statement of Tatsumi *et al.* that the μ-oxo dimers of d^n–d^n

($n<5$) electron systems prefer a linear M–O–M framework.[10] On the other hand, the Os^{IV}–O^{2-} distance is quite a bit smaller than the sum of the ionic radii;[11] it is also shorter than the Ru^{IV}–O^{2-} distance in $[Ru^{IV}(oep)(OH)]_2O$,[1a] although the Os^{IV}–O^{2-} distance is expected to be longer than the Ru^{IV}–O^{2-} distance from a comparison of the ionic radii of Os^{IV}(0.69 Å) and Ru^{IV}(0.65 Å) as observed in the $Os^{IV}O_2$ and $Ru^{IV}O_2$ crystals.[11,12] The short Os^{IV}–O^{2-} bond in the established structure may well account for the high sensitivity for the protons, because the shortening means a large distribution of electrons in the (Os^{IV}–O^2) π bonding orbital, and the electron-rich bonding orbital will be active for a proton.

The authors wish to thank professor Nobuo Morimoto and Dr. Katsutoshi Tomita, Faculty of Science, Kyoto University, for the use of the Rigaku AFC-5 diffracatometer.

References

1) a) H. Masuda, T. Taga, K. Osaki, H. Sugimoto, M. Mori, Z. Yoshida, and H. Ogoshi, *J. Am. Chem. Soc.*, **103**, 2199 (1981); b) H. Masuda, T. Taga, K. Osaki, H. Sugimoto, M. Mori, and H. Ogoshi, *Bull. Chem. Soc. Jpn.*, **55**,3887 (1982).

2) a) P. George, *Biochem. J.*, **55**, 220 (1953); b) A. S. Brill, *Compr. Biochem.*, **15**, 447 (1966); c) T. Iizuka, M. Kotani, and T. Yonetani, *Biochim. Biophys. Acta*, **167**, 257 (1968); d) T. H. Moss, A. Ehrenberg, and A. J. Bearden, *Biochemistry*, **8**, 4159 (1969); e) G. Lang, *Q. Rev. Biophys.*, **3**, 1 (1970).

3) a) Z. Yoshida, H. Sugimoto, and H. Ogoshi, "Biomimetic Chemistry," ed by D. H. Dolphin, C. Mckenna, Y. Murakami, and T. Tabushi, American Chemical Society, Washington D. C. (1980), Chap. 17; b) H. Sugimoto and M. Mori, *Chem. Lett.*, **1981**, 297; c) H. Sugimoto, T. Higashi, M. Mori, M. Nagano, Z. Yoshida, and H. Ogoshi, *Bull. Chem. Soc. Jpn.*, **55**, 882 (1982).

4) a) "International Tables for X-Ray Crystallography," ed by J. A. Ibers and W. C. Hamilton, Kynoch, Birmingham, England (1974), Vol. IV, p. 99; b) *ibid.*, p. 148.

5) The thermal parameters, fractional coordinates of the hydrogen atoms, and observed and calculated structure factors are deposited as Document No. 8431 at the office of the Editor of the Bulletin of the Chemical Society of Japan.

6) a) J. L. Hoard, "Porphyrins and Metalloporphyrins," ed by K. M. Smith, Elsevier, Amsterdam (1975), Chap. 8; b) J. L. Hoard, *Science (Washington, D. C.)* **174**, 1295 (1971); c) W. R. Scheidt, *Acc. Chem. Res.*, **10**, 339 (1977).

7) The value in parentheses is the esd for the averaged distance or angle. This notation is used throughout the paper.

8) J. W. Buchler, K. LamLay, and P. D. Smith, *J. Organomet. Chem.*, **110**, 109 (1976).

9) The atoms with and without an asterisk superscribed are associated with the upper and lower cores of the binuclear porphinato complex respectively.

10) K. Tatsumi and R. Hoffmann, *J. Am. Chem. Soc.*, **103**, 3328 (1981).

11) R. B. Heslop and P. L. Robinson, "Inorganic Chemistry," Elsevier: Maruzen, Amsterdam, and Tokyo, (1960).

12) a) C. E. Boman, *Acta Chem. Scand.*, **24**, 123 (1970); b) C. E. Boman, *ibid.*, **24**, 116 (1970).

Kinetic Studies of the Base Equilibrium of Secondary Amines on the Surface of Sodium Dodecyl Sulfate Micelle by Means of the Ultrasonic Absorption Method

Teruyo YAMASHITA, Minako SUMINO, Hiroshige YANO,* Shoji HARADA,† and Tatsuya YASUNAGA†

Daiichi College of Pharmaceutical Sciences, Tamagawa-cho 22-1, Minami-ku, Fukuoka 815

†*Department of Chemistry, Faculty of Science, Hiroshima University, Higashisenda-machi 1-1-89, Naka-ku, Hiroshima 730*

(Received October 29, 1983)

The ultrasonic relaxation absorption has been measured in aqueous solution of dipentylamine, dihexylamine, dioctylamine, *N*-methylphenethylamine, and *N*-ethylbenzylamine in the presence of the sodium dodecyl sulfate(SDS) micelle. The relaxation absorption has been ascribed to the base equilibrium of the amines on the surface of the micelle: $RR'NH_2^+ + OH^- \underset{k_b}{\overset{k_f}{\rightleftharpoons}} RR'NH + H_2O$. The rate constants $\gamma_\pm^2 k_f$, k_b, the apparent base dissociation constant K_b ($=k_b/\gamma_\pm^2 k_f$), and the volume change in the base equilibrium ΔV were obtained, where $\gamma_\pm$ is the mean activity coefficient for $RR'NH_2^+$ and OH^-. The dependence of the rate constants on K_b revealed that, in the detailed mechanism of the base equilibrium of the amines, $\underset{(I)}{RR'NH_2^+} + OH^- \underset{k_{21}}{\overset{k_{12}}{\rightleftharpoons}} \underset{(II)}{(RR'NH_2^+ \cdots OH^-)} \underset{k_{32}}{\overset{k_{23}}{\rightleftharpoons}} \underset{(III)}{RR'NH} + H_2O$, the rate-determining step is the proton-transfer process, (II) $\rightleftharpoons$ (III). The pK_b values of the secondary amines on the surface of the SDS micelle were 0.94—1.26 smaller than the corresponding values in the aqueous solution, and the micellar effect on pK_b was smaller than that of the primary amines. From the standpoint of the micellar effect, the structures of the amines solubilized in the micelle were discussed.

Detergent micelles have been of interest as a peculiar reaction field, and many investigations[1-3] have been carried out to reveal the controlling factors in the promotion or inhibition of various reactions on the surface of the micelle. However, only relatively slow reactions have been studied with the exception of our own previous studies[4,5] of the micellar effect on a rapid base equilibrium of primary amines by the use of the ultrasonic absorption method. In those previous works[4,5] (i) kinetic parameters were obtained for the base equilibrium of primary amines on the surface of the SDS micelle, (ii) linear relationships were observed between the logarithms of the rate constants and that of the base dissociation constant, and (iii) the rate-determining step was ascribed to the proton-transfer process in the ion pair. The purposes of the present work are to study kinetically the micellar effects on the base equilibrium of the secondary amines, to compare the results with those of the primary amines, and to study especially the effect of the *N*-alkyl or aryl groups on the electrostatic interactions between the amine cation and the anionic sulfate group of the micelle forming detergent.

Experimental

The dihexylamine purchased from Tokyo Kasei and *N*-ethylbenzylamine from Aldrich were purified by distillation. The dipentylamine from Katayama Kagaku, dioctylamine from Tokyo Kasei, *N*-methylphenethylamine from Aldrich, and SDS from BDH were used without further purification.

The ultrasonic absorption measurements were performed by the pulse technique over the frequency range of 5—105 MHz. The details of the apparatus were described elsewhere.[6] The velocity of the sound was measured by the sing-around method at 1.92 MHz. The density was measured by means of a pycnometer. The pH of the solution was measured by means of a Kyoto Electronics AT-117-type potentiometer. All the pH and ultrasonic measurements were carried out under a dry nitrogen gas atmosphere at 30 °C.

Results and Discussion

The ultrasonic relaxation absorption was observed for secondary amines of various basicities in a SDS micellar solution. All the absorptions were represented by a single relaxation equation;[7,8]

$$\alpha/f^2 = A/\{1+(f/f_r)^2\} + B, \quad (1)$$

where α is the absorption coefficient, f is the frequency, f_r is the relaxation frequency, and A and B are the relaxing and nonrelaxing absorptions respectively.

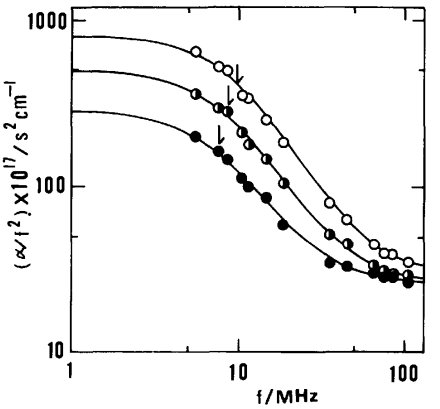

Fig. 1. Representative ultrasonic absorption spectra of the secondary amines (0.050 M†)–SDS (0.30 M) system at 30.0 °C. ○: Dipentylamine. ◑: *N*-Methylphenethylamine. ●: *N*-Ethylbenzylamine. The arrows indicate the relaxation frequency. († 1 M=1 mol dm^{-3})

Some representative absorption spectra are shown in Fig. 1. The absorption parameters obtained by fitting the data to Eq. 1 by means of a computer simulation are summarized in Table 1, along with the experimental conditions.

The ultrasonic behavior of the secondary amines in the SDS micellar solution was similar to that of the primary amines, which implies that the relaxation absorption can be assigned to the following reaction;

Table 1. Ultrasonic absorption parameters for various concentrations of secondary amines in the presence of SDS (0.30 M) at 30.0 °C

Σ[Amine] / M	pH	A / 10^{-17} s^2 cm^{-1}	B / 10^{-17} s^2 cm^{-1}	f_r / MHz	σ [a]
Dipentylamine					
0.015	11.83	339	26	5.6	0.60
0.020	11.89	337	28	6.3	0.55
0.025	11.91	472	30	6.9	0.51
0.030	11.97	532	30	7.3	0.48
0.036	12.01	588	27	8.5	0.45
0.043	12.06	638	30	8.9	0.43
0.050	12.11	785	29	9.7	0.40
Dihexylamine					
0.015	11.78	505	26	5.9	0.57
0.020	11.83	586	28	6.6	0.52
0.025	11.85	596	29	7.3	0.49
0.030	11.90	597	27	8.1	0.46
0.036	11.97	613	25	8.6	0.43
0.043	12.04	621	26	9.5	0.40
0.050	12.09	777	25	10.1	0.38
Dioctylamine					
0.015	11.70	358	30	6.4	0.52
0.020	11.76	382	31	7.2	0.48
0.025	11.83	429	33	8.1	0.44
0.030	11.88	441	29	8.6	0.41
0.036	11.95	453	29	9.6	0.39
0.043	12.00	522	25	10.3	0.36
0.050	12.07	558	26	11.2	0.34
N-Methylphenethylamine					
0.015	11.57	328	26	4.9	0.33
0.020	11.66	348	24	6.1	0.30
0.025	11.69	352	26	6.6	0.27
0.030	11.75	378	26	7.0	0.25
0.036	11.80	410	26	7.6	0.23
0.043	11.83	421	26	8.4	0.21
0.050	11.88	471	26	8.7	0.20
N-Ethylbenzylamine					
0.020	11.45	207	25	4.9	0.19
0.025	11.52	217	26	5.6	0.17
0.030	11.53	222	26	6.2	0.16
0.036	11.58	246	25	6.6	0.14
0.043	11.63	246	28	7.3	0.13
0.050	11.69	264	26	7.6	0.12

a) Degree of ionization.

$$RR'NH_2^+ + OH^- \underset{k_b}{\overset{k_f}{\rightleftharpoons}} RR'NH + H_2O, \quad (2)$$

where the hydrocarbon groups of an amine are solubilized in the core of the SDS micelle. The base dissociation constant, K_b^0, is given as;

$$K_b^0 = \frac{k_b}{k_f} = \frac{\gamma_\pm^2[RR'NH_2^+][OH^-]}{[RR'NH]} = \frac{\gamma_\pm^2\sigma^2 C_0}{1-\sigma}, \quad (3)$$

where σ is the degree of ionization, C_0 is the total concentration of the amine, and $\gamma_\pm$ is the mean activity coefficient. The relaxation frequency and the maximum relaxation absorption per wavelength, μ_{max}, for Reaction 2 are expressed by;[7,8]

$$2\pi f_r = \gamma_\pm^2 k_f([RR'NH_2^+] + [OH^-]) + k_b, \quad (4)$$

$$\mu_{max} = \frac{\rho u^2 \pi (\Delta V)^2}{2RT} \cdot \Gamma^{-1},$$

$$= \frac{\rho u^2 \pi (\Delta V)^2}{2RT} \cdot \frac{\sigma(1-\sigma)}{2-\sigma} \cdot C_0, \quad (5)$$

with;

$$\Gamma = [RR'NH_2^+]^{-1} + [OH^-]^{-1} + [RR'NH]^{-1}, \quad (6)$$

where ρ is the density of the solution, u is the velocity of sound, and ΔV is the volume change in the base equilibrium of the amine. Equation 4 can be rewritten as follows in terms of C_0 by using Eq. 3;

$$(2\pi f_r)^2 = 4\gamma_\pm^2 k_f k_b C_0 + k_b^2. \quad (7)$$

The experimental values of $(2\pi f_r)^2$ are plotted against C_0 in Fig. 2. The plots give a straight line, as predicted by Eq. 7; the result indicates that the relaxation absorption is due to Reaction 2. From the slope and the intercept of the straight line, the values of $\gamma_\pm^2 k_f$ and k_b respectively were obtained, and from their ratio, the apparent base dissociation constant, K_b ($=k_b/\gamma_\pm^2 k_f$), was obtained; all these parameters are listed in Table 2. The plots of μ_{max} against the Γ^{-1} calculated from the K_b obtained above and C_0 gave a straight line which goes through the point of origin of the coordinates, as shown

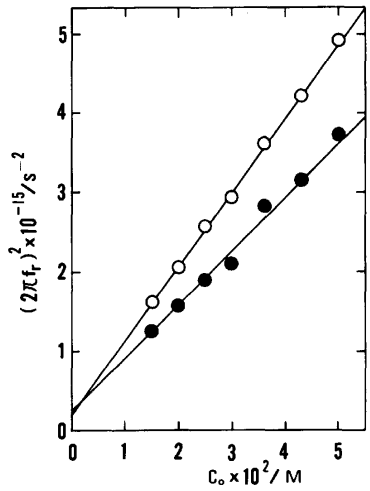

Fig. 2. Plots of $(2\pi f_r)^2$ *vs.* concentration of secondary amines in the presence of SDS (0.30 M) at 30.0 °C. ○: Dioctylamine. ●: Dipentylamine.

TABLE 2. KINETIC PARAMETERS FOR THE BASE EQUILIBRIUM OF SECONDARY AMINES ON THE SURFACE OF THE SDS MICELLE AT 30.0 °C

Amine	$\gamma_{\pm}^2 k_f$ / 10^8 M^{-1} s^{-1}	k_b / 10^7 s^{-1}	ΔV / cm^3 M^{-1}	pK_b[a]	pK_b[b]	$pK_{b(w)}$[c]
Dipentylamine	11.2	1.5	20.6	1.87	1.79	2.82
Dihexylamine	13.0	1.5	23.4	1.94	1.94	3.00
Dioctylamine	16.3	1.4	21.4	2.06	2.06	3.00
N-Methylphenethylamine	25.1	0.6	21.2	2.60	2.43	3.86
N-Ethylbenzylamine	37.2	0.3	18.6	3.07	2.89	4.32

a) The value of $pK_b = -\log(k_b/\gamma_{\pm}^2 k_f)$. b) The value evaluated from the values of C_0 and pH. c) Ref. 16.

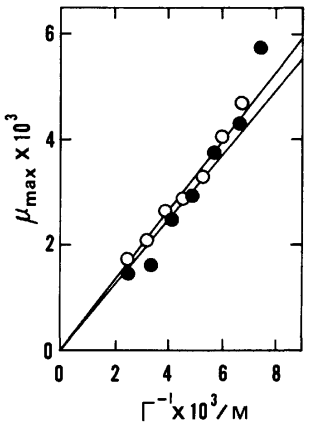

Fig. 3. Plots of μ_{max} *vs.* Γ^{-1} for the secondary amines in the presence of SDS (0.30 M) at 30.0 °C. ○: Dioctylamine. ●: Dipentylamine.

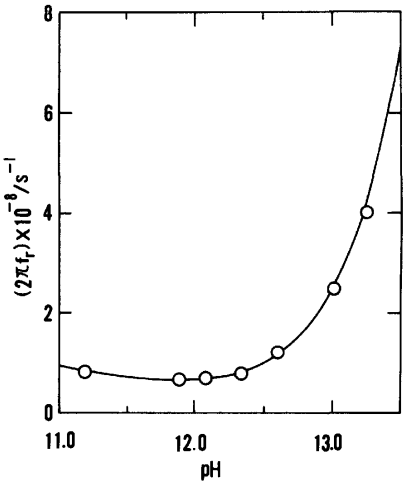

Fig. 4. pH dependence of the value of $2\pi f_r$ for the dioctylamine (0.050 M)–SDS (0.30 M) system at 30.0 °C. The solid line is the curve calculated by Eq. 4 with the values of $\gamma_{\pm}^2 k_f$, k_b, and K_b in Table 2. Circles are the experimental data.

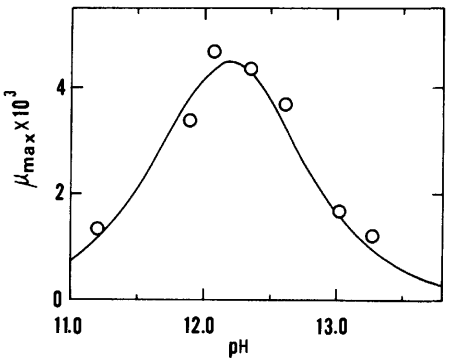

Fig. 5. pH dependence of μ_{max} for the dioctylamine (0.050 M)–SDS (0.30 M) system at 30.0 °C. The solid line is the curve calculated by Eq. 5 with the values of K_b and ΔV in Table 2. Circles are the experimental data.

in Fig. 3. A comparison with Eq. 5, also supports the idea that the relaxation absorption is due to Reaction 2. The value of ΔV was calculated from the slope of the straight line in Fig. 3.

The values of K_b can also be evaluated statically from the values of C_0 and pH in Table 1, together with the activity coefficient calculated by the use of the Davies equation;[9] they are listed in Table 2. As can be seen in the table, the value for each amine is in satisfactory agreement with that obtained above kinetically.

Further support of the assignment of the present relaxation absorption was given by the pH-dependences of the ultrasonic parameters. As a sample, the data for dioctylamine were obtained; the pH-dependences of f_r and μ_{max} are shown in Figs. 4 and 5 respectively. As can be seen in the figures, f_r and μ_{max} depend strongly on the pH, and the curves as calculated from Eqs. 3—6 by using the values of C_0, and the rate constants, K_b and ΔV obtained above express the experimental data satisfactorily. These results lead to the conclusion that the assignment of the absorption and the kinetic parameters obtained is reasonable.

The results demonstrate, among other things, the basicity dependence of the rate constants. As shown in Fig. 6, linear relationships were established for the plots of $\log \gamma_{\pm}^2 k_f$ *vs.* $\log K_b$ and $\log k_b$ *vs.* $\log K_b$. These relationships are expressed as;

$$\gamma_{\pm}^2 k_f = 10^{8.3} K_b^{-0.40} = 10^{8.3} (K_w/K_a)^{-0.40} = 10^{13.8} K_a^{0.40}, \quad (8)$$

$$k_b = 10^{8.3} K_b^{0.60}, \quad (9)$$

where K_w is the ionization constant of water and where K_a is the acid dissociation constant of an amine. These relationships are in contrast to those for the base equilibrium of amines in an aqueous solution,[10–14] where k_f is independent, while k_b is dependent on $K_b(w)$;

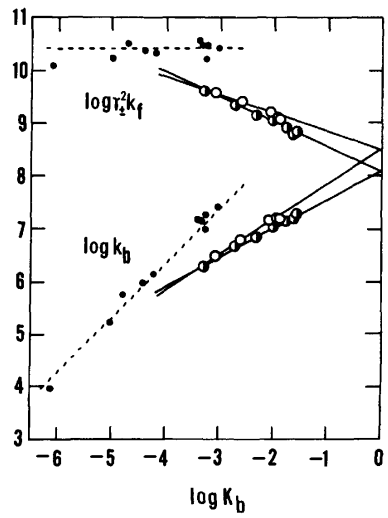

Fig. 6. Plots of the logarithms of the rate constants *vs.* $\log K_b$ for secondary amines (○) and primary amines[4,5] (◑) in the presence of SDS (0.30 M), and various amines in the absence of the micelle[11] (●).

$$k_{f(w)} = 10^{10.5}, \tag{10}$$

$$k_{b(w)} = 10^{10.5} K_{b(w)}, \tag{11}$$

where the subscript, (w), indicates the aqueous solution.

In general, the detailed mechanism of Reaction 2 has been described as;

$$\underset{\text{(I)}}{RR'NH_2^+} + OH^- \underset{k_{21}}{\overset{k_{12}}{\rightleftharpoons}} \underset{\text{(II)}}{(RR'NH_2^+\cdots OH^-)} \underset{k_{32}}{\overset{k_{23}}{\rightleftharpoons}} \underset{\text{(III)}}{RR'NH} + H_2O. \tag{12}$$

The (I)⇌(II) process is an ion pair formation and dissociation (diffusion process), and the rate constants, k_{12} and k_{21}, are dependent on the electric charge, the volume, and state of hydration, *etc.* of the ions; the proton-transfer still does not occur in the (I)⇌(II) process. Accordingly, k_{12} and k_{21} do not depend on the electron-donating (or-attracting) property of amines. On the other hand, the (II)⇌(III) process is a proton-transfer process in the ion pair, and the rate constants, k_{23} and k_{32}, are dependent mainly on the electron-donating (or-attracting) property of amines; that is k_{23} and k_{32} are dependent on K_b.

If (I)⇌(II) is the rate-determining step, the overall rate constants are expressed as;[10-14]

$$k_f = k_{12}, \tag{13}$$

$$k_b = k_{21} \cdot \frac{k_{32}}{k_{23}}. \tag{14}$$

These equations predict an independency of K_b from k_f and a linear dependency of K_b on k_b; these predictions are in good agreement with the results for the base equilibrium of amines in aqueous solutions, as seen in Eqs. 10 and 11 and in Fig. 6. However, the results of the present work, the K_b dependencies of k_f and k_b, *i.e.*, Eqs. 8 and 9, cannot be realized at all by means of Eqs. 13 and 14.

If (II)⇌(III) is the rate-determining step, on the other hand, k_f and k_b are given as follows;[5]

$$k_f = \frac{k_{12}}{k_{21}} \cdot k_{23}, \tag{15}$$

$$k_b = k_{32}. \tag{16}$$

Since (II)⇌(III) is a proton-transfer process in the ion pair, k_{23} will decrease and k_{32} will increase with an increase in K_b. Accordingly, Eqs. 15 and 16 provide a satisfactory interpretation of the K_b dependences of the rate constants in the base equilibrium of amines in a micellar solution. Then, the rate-determining step in Reaction 12 on the surface of a micelle is clarified to be the proton-transfer process in the ion pair, (II)⇌(III).

As can be seen in Eqs. 8 and 9, the kinetics of the base equilibrium of amines in the micellar system are in the form of the Brönsted catalysis law.[15] According to the Brönsted catalysis law, the right-hand side is composed of a constant and a term of a contribution of K_b, where the index (the Brönsted coefficient) expresses the degree of proton-transfer at the rate-determining step. The constant in Eqs. 8 and 9 corresponds to the rate constant of k_f (or k_b) when K_b=1; in other words, it reflects the magnitude of the activation energy of a reaction when the energy difference of the reactant and the product is zero. As can be seen in Eqs. 8—11, in the base equilibrium of amines on the surface of the SDS micelle, the value of the constant is more than two orders of magnitude smaller than that in the aqueous solution. This means that the former has a larger activation energy than the latter; the difference between them was found to be 3.0 kcal mol^{-1} by the use of the equation of $-RT$ ln $10^{8.3-10.5}$. The indices of the primary and the secondary amines in the micellar system were found to be about 0.5, which indicates that about half of the proton-transfer is performed at the rate-determining step. This fact supports the above-mentioned conclusion that the rate-determining step exists between (II) and (III) in Reaction 12.

As can be seen in Table 2, the pK_b values of the amines in an SDS micellar solution are much smaller than the corresponding values in an aqueous solution. This micellar effect on pK_b can be explained in terms of the cationic amino group being stabilized electrostatically by the surrounding anionic sulfate groups of the micelle and the dissociation of the amine being accelerated. Since the electrostatic interaction is proportional to the distance of the amino group and the anionic surface of the micelle, the difference in the pK_b values between the two solutions, ΔpK_b, will be used as a measure of the degree of penetration of an amine into the micelle. In fact, in a series of primary amines,[5] the largest of the ΔpK_b values, 1.77, was observed for octylamine, where a long alkyl chain causes the amine to be well solubilized in the micelle and causes the amino group to be close to the anionic surface of the micelle, while in the case of benzylamine, the hydrophobic group is small and the penetrates little into the micelle, and the micellar effect on pK_b is smaller, ΔpK_b=1.35. In the present study, the ΔpK_b values of the secondary amines (shown in Table 2) were smaller than those for

the primary amines, 1.35—1.77. Especially in the cases of the amines with two long alkyl groups, the ΔpK_b values were the smallest among those of the amines studied. From the standpoint of the micellar effect on pK_b, the secondary amines are not so deeply solubilized in the micelle as the primary amines because of the specific structures of the two hydrophobic groups. A similar picture can also be deduced from the kinetic results; as may be seen in Fig. 6, the K_b dependencies of k_f and k_b in the present work are a little closer to those in the aqueous solution than those for the primary amines in the SDS micellar solution. Therefore, the amino group of secondary amines might be located a little far from the anionic sulfate group of the micelle and closer to the bulk water, and the micellar effect on the base equilibrium seems to be a little smaller than that of primary amines.

In conclusion, the fundamental difference between the primary and secondary amines was not established in the reaction mechanism of the base equilibrium on the SDS micelle. However, small differences in the micellar effect on pK_b and in the K_b dependencies of the rate constants provided a picture of a little shorter penetration of the secondary amines into the SDS micelle than that of the primary amines.

The authors wish to thank the Computer Center of Kyushu University for its help in the calculation of the ultrasonic absorption parameters by means of the Facom M-200 Computer.

References

1) J. Fendler and E. Fendler, "Catalysis in Micellar and Macromolecular Systems," Academic Press, New York (1975).
2) "Micellization, Solubilization, and Microemulsions," ed by K. L. Mittal, Plenum Press, New York and London (1977), Vol. 2.
3) "Reaction Kinetics in Micelles," ed by E. H. Cordes, Plenum Press, New York and London (1973).
4) T. Yamashita, H. Yano, S. Harada, and T. Yasunaga, *J. Phys. Chem.*, **87**, 5482 (1983).
5) T. Yamashita, H. Yano, S. Harada, and T. Yasunaga, *J. Phys. Chem.*, **88**, 2671 (1984).
6) N. Tatsumoto, *J. Chem. Phys.*, **47**, 4561 (1967).
7) J. Stuehr and E. Yeager, "The Propagation of Ultrasonic Waves in Electrolytic Solutions," in "Physical Acoustics," ed by W. Mason, Academic Press, New York and London (1965), Vol. 2, Part B.
8) "Investigation of Rates and Mechanisms of Reactions," ed by G. Hammes, Part 2 in "Techniques of Chemistry," ed by A. Weissberger, John Wiley&Sons, New York (1974), Vil. 6.
9) C. W. Davies, "Ion Association," Butterworths, London (1962).
10) G. Maass, Ph. D. Thesis, Univ. of Göttingen (1962).
11) M. Eigen, G. Maass, and G. Schwarz, *Z. Phys. Chem.*, **74**, 319 (1971).
12) S. Nishikawa, T. Nakamoto, and T. Yasunaga, *Bull. Chem. Soc. Jpn.*, **46**, 324 (1973).
13) S. Nishikawa, T. Yasunaga, and N. Tatsumoto, *Bull. Chem. Soc. Jpn.*, **46**, 1657 (1973).
14) S. Nishikawa, T. Yasunaga, and K. Takahashi, *Bull. Chem. Soc. Jpn.*, **46**, 2992 (1973).
15) R. Breslow, "Organic Reaction Mechanisms," W. A. Benjamin, Inc., New York (1969).
16) Landolt-Börnstein, "Physikalische-Chemische Tabellen," Springer-Verlag, Berlin (1960).

 © 1984 The Chemical Society of Japan Bull. Chem. Soc. Jpn., 57, 2357—2360 (1984)

Kinetics of Solute-Solvent Interaction in Aqueous Solution of Butyl Carbitol by Ultrasonic Methods

Sadakatsu NISHIKAWA* and Masayuki SHIBATA
Department of Chemistry, Faculty of Science and Engineering, Saga University, Saga 840
(Received November 19, 1983)

Ultrasonic absorptions in the frequency range 4.5—220 MHz and sound velocities at 2.5 MHz were measured at 25 °C with aqueous solutions of Butyl Carbitol (diethylene glycol monobutyl ether) over the concentration range 0.497—3.00 mol dm^{-3}. Only a single relaxational process was observed and attributed to a perturbation of the equilibrium $AB \underset{k_{21}}{\overset{k_{12}}{\longleftrightarrow}} A+B$, where A is Butyl Carbitol as the solute and B is water as the solvent participating in the reaction. A data analysis has led to the estimates $k_{12}=3.4\times10^{7}$ s^{-1}, $k_{21}=2.0\times10^{8}$ dm^3 mol^{-1} s^{-1}, the standard volume change of reaction $\Delta V^\circ=0.32$ cm^3 mol^{-1}, and the standard enthalpy change $\Delta H^\circ=5.4$ kJ mol^{-1}. The effect of the hydrophobicity of solute molecules on the water structure is discussed by comparing the present results with previous ones for other aqueous nonelectrolyte solutions.

In a series of ultrasonic studies of aqueous solutions of nonelectrolytes,[1-8] we have found that different ultrasonic absorptions appear in the MHz frequency range depending upon the structure of solutes. They have been interpreted in terms of conventional relaxation theory. In order to analyze the relation between ultrasonic properties and structures of solute, a further accumulation of absorption results is desired for various nonelectrolytes over a wide frequency range and a concentration range. For this purpose, we have chosen Butyl Carbitol (diethylene glycol monobutyl ether) as a solute and have compared results obtained with those for other solutions. Another purpose of the present investigation is to elucidate why double relaxational processes have appeared in some solutions and a single process has in other solutions even when the structures of solutes are quite similar.

Experimental

Butyl Carbitol from Tokyo Kasei Co., Ltd. was distilled once under reduced pressure. No impurity was found by the gas-chromatographic method. Doubly distilled water was used as solvent. Concentrations of solutions were determined by weight.

Ultrasonic absorption coefficients were measured in the range 4.5—220 MHz by the pulse method.[9] Sound velocity was measured with an interferometer at 2.5 MHz. The temperature for measurements was 25 °C with a fluctuation within ±0.005 °C. The density of each solution was measured with a pycnometer, about 4.4 cm^3 in volume at various temperatures in order to determine thermal expansion coefficients. All ultrasonic, kinetic, and thermodynamic parameters were calculated with a microcomputer.

A complete set of ultrasonic absorption coefficients and velocities at various concentrations are available from one of the authors (S.N.) on request.

Results

No frequency dependence of α/f^2 is found in liquid Butyl Carbitol as is seen from Fig. 1, where α is the ultrasonic absorption coefficient and f is the frequency. A relaxational absorption is found at the concentrations above 0.701 mol dm^{-3}. With increasing concentration, the relaxational amplitude increases rapidly till 1.20 mol dm^{-3} and then decreases monotonously. The sound velocity in the solutions shows a maximum at around 0.804 mol dm^{-3}. Representative ultrasonic absorption spectra are shown in Fig. 1. In general, the sound absorption associated with a single relaxational process can be described by the equation

$$\alpha/f^2 = A/[1+(f/f_r)^2] + B, \quad (1)$$

where f_r is the relaxation frequency, A the relaxational amplitude, and B the background absorption. The absorptions over the concentration range 0.701—3.001 mol dm^{-3} are characteristic of a typical single relaxation. These ultrasonic parameters were determined so as to give the best fit of the experimental data to Eq. 1 by the nonlinear least mean square method. They are listed in Table 1 along with the results of the sound velocity, density, and thermal expansion coefficient as a function of analytical concentration, C_c. The values of α/f^2 calculated with the parameter thus evaluated are shown by the solid lines in Fig. 1.

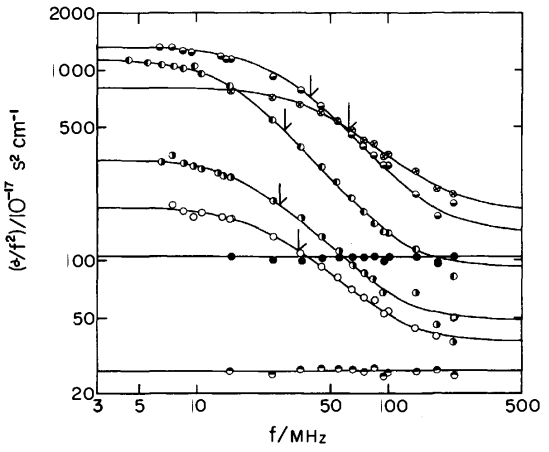

Fig. 1. Representative ultrasonic absorption spectra for aqueous solution of Butyl Carbitol at 25 °C. The arrows show the positions of the relaxation frequencies. The solid lines were calculated by means of Eq. (1). ◓: 0.497 mol dm^{-3}, ○: 0.750 mol dm^{-3}, ◑: 0.804 mol dm^{-3}, ◐: 0.990 mol dm^{-3}, ◒: 1.701 mol dm^{-3}, ⊗: 2.528 mol dm^{-3}, ●: pure Butyl Carbitol.

TABLE 1. ULTRASONIC AND THERMODYNAMIC PARAMETERS FOR AQUEOUS SOLUTIONS OF BUTYL CARBITOL AT 25 °C

C_e / mol dm^{-3}	f_r[a] / MHz	A[a] / 10^{-17} s^2 cm^{-1}	B[a] / 10^{-17} s^2 cm^{-1}	ρ / g cm^{-3}	c / m s^{-1}	θ / 10^{-4} deg^{-1}
0.701	47.0±0.9	77.9±0.8	30.0±2.0	0.9995	1568	3.9
0.726	46.5±0.9	99.4±1.1	29.0±2.5	0.9996	1568	3.5
0.750	33.9±0.7	151.2±1.1	38.0±1.7	0.9997	1569	3.8
0.804	27.2±1.2	293.3±3.1	47.6±3.1	0.9999	1572	4.1
0.900	26.7±0.8	604.6±3.7	57.7±2.2	0.9999	1572	4.1
0.990	21.7±1.1	1068±7	90.2±2.3	0.9999	1572	4.5
1.102	29.3±2.1	1152±24	79.4±5.7	1.0000	1568	4.6
1.200	30.1±2.1	1245±11	99.2±5.2	0.9997	1566	4.9
1.365	35.3±3.6	1252±25	110.9±9.6	0.9996	1562	5.1
1.701	39.1±4.6	1188±19	135.0±10.5	0.9982	1553	5.6
2.006	50.8±2.5	945.8±8.5	145.6±4.6	0.9971	1546	5.8
2.528	61.9±2.3	637.4±6.3	179.4±6.4	0.9950	1535	6.5
3.001	58.7±4.8	498.9±11.1	200.4±10.9	0.9915	1520	7.0

a) The errors in the ultrasonic parameters are the most probable ones.

As shown in Table 1, the relaxation frequency, which is related to the relaxation time τ, shows a curious concentration dependence, that is, the presence of a minimum. If the relaxation process results from usual reactions of the solutes, such a dependence may not be observed. The relaxational absorption seems to be a characteristic of the solution. Therefore, we consider a perturbation of equilibrium associated with the interaction between solute and solvent as the cause of the absorption. It is simply represented by the formula

$$\underset{C_1}{AB} \underset{k_{21}}{\overset{k_{12}}{\longleftrightarrow}} \underset{C_2}{A} + \underset{C_3}{B}, \qquad (2)$$

where A is Butyl Carbitol, AB complex, and B water which interacts with the solute. The C_i's indicate the equilibrium concentrations of each component. In order to analyze the absorption mechanism, it is assumed that water consists of two states, *i.e.*, the hydrogen-bonded and nonhydrogen-bonded waters, and that the transition rates for these two states are too fast to be observed in our frequency range.[10] It is also assumed that the nonhydrogen-bonded water may participate in the reaction. On these assumptions, the relation between relaxation frequency and analytical concentration is derived as,[3]

$$1/\tau = 2\pi f_r = k_{21}[(C_e - \beta C_w + K_{12})^2 + 4\beta C_w K_{12}]^{1/2} \qquad (3)$$

where β is the molar fraction of the nonhydrogen-bonded water, C_w the analytical concentration of water, and K_{12} is defined as $K_{12}=k_{12}/k_{21}$. The rate and thermodynamic parameters, k_{21}, β, and K_{12}, are assumed to be independent of the concentration in the limited range studied. These parameters were determined so as to give the best fit of the observed relaxation frequencies to Eq. 3 as follows: The values of f_r obtained experimentally show a minimum at around 1 mol dm^{-3} and this result provides the relation between β and K_{12}.[3] Initially, a value of β was assumed and K_{12} was calculated. Then, the rate constant k_{21} was determined so as to fit the experimental relaxation frequencies to Eq. 3 using the least mean square method. This procedure was repeated until the value of standard deviation (S.D.) reached a minimum. In this calculation, the smallest S.D. was obtained when C_e was 1.15 mol dm^{-3}. However, the result at 3.001 mol dm^{-3} was not used since it remarkably deviates from smoothed curve. The values of relaxation frequency calculated from the parameters evaluated are shown by the solid line in Fig. 2.

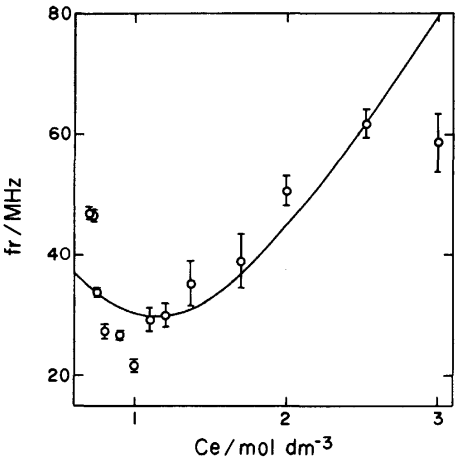

Fig. 2. Concentration dependence of the relaxation frequency for the aqueous solution of Butyl Carbitol at 25 °C. The solid line was calculated by means of Eq. (3) [S. D.=6.40 MHz].

Another parameter obtained from the measurements of the ultrasonic absorption and the velocity is a maximum excess absorption per wavelength, μ_m, which is expressed by the following equation on the assumption that the contribution of the relaxational specific heat is small:[3]

$$\mu_m = Af_r c/2 = \pi\rho c^2 \Gamma(\Delta V^\circ - \theta\Delta H^\circ/\rho C_p)^2/2RT \qquad (4)$$

where ρ is the density of solution, R the gas constant, T the absolute temperature, θ the thermal expansion coefficient, C_p the specific heat at constant pressure, ΔV° the standard volume change of the reaction, and

Table 2. Comparison of the rate and thermodynamic constants for aqueous solutions of some ethers at 25 °C

Solute	k_{12} / 10^7 s^{-1}	k_{21} / 10^8 dm^3 mol^{-1} s^{-1}	$\Delta H°$ / kJ mol^{-1}	$\Delta V°$ / cm^3 mol^{-1}	β	Ref.
Allyl Cellosolve	3.0±0.2	3.7±0.2	8.0±3.0	0.60±0.35	0.121	7
Propyl Cellosolve	9.6±1.3	1.3±0.2	5.4±2.5	0.30±0.15	0.100	4, 8
Isobutyl Cellosolve	5.5±0.7	2.5±0.3	8.8±0.4	0.38±0.03	0.0428	4
Butyl Cellosolve	4.2±0.7	1.7±0.3	13.0±0.4	0.67±0.06	0.0290	2, 4
Butyl Carbitol	3.4±0.6	2.0±0.4	5.4±0.1	0.32±0.01	0.0277	This work

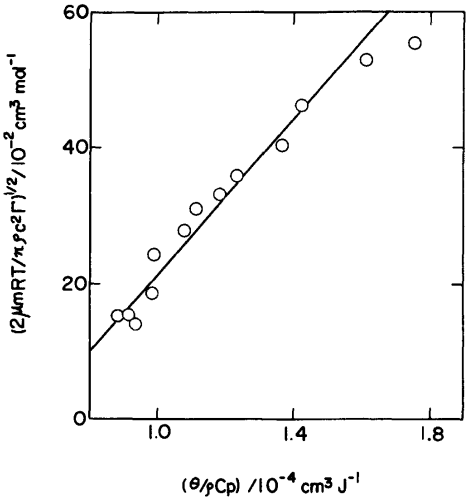

Fig. 3. The plots of $(2\mu_m RT/\pi\rho c^2\Gamma)^{1/2}$ *vs.* $\theta/\rho C_p$ for the aqueous solution of Butyl Carbitol.

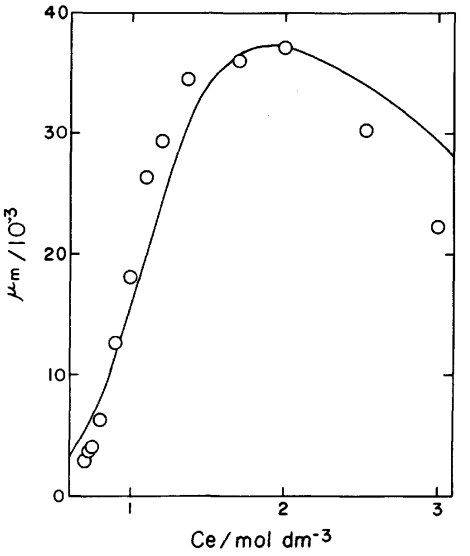

Fig. 4. Concentration dependence of the maximum excess absorption per wave length for the aqueous solution of Butyl Carbitol [S. D.=3.75×10^{-3}].

$\Delta H°$ the standard enthalpy change. The term Γ is derived for the reaction under consideration as $[1/C_1+1/C_2+1/C_3-1/(C_1+C_2+C_3)]^{-1}$. As reported in previous papers,[1,2] the concentration dependence of μ_m is controlled mainly by the term $\rho c^2\Gamma$. Precisely, however, term $\theta/\rho C_p$ depends on concentration. Therefore, we assume that the specific heat is given roughly by $C_p=2.28n_e+4.18(1-n_e)$(J deg^{-1} g^{-1}) in obtaining values of $\Delta V°$ and $\Delta H°$. Here, n_e is the molar fraction of Butyl Carbitol in the aqueous solution. The slope and intercept of $(2\mu_m RT/\pi\rho c^2\Gamma)^{1/2}$ *vs.* $\theta/\rho C_p$ plots shown in Fig. 3 provide with these values, as listed in Table 2. The concentration dependence of the density is well described by a cubic function of the analytical concentration of Butyl Carbitol as $\rho=0.99698+6.02505\times10^{-3}C_e-3.6627\times10^{-3}C_e^2+3.3096\times10^{-4}C_e^3$ (g cm^{-3}) [S. D.=2.5×10^{-4} (g cm^{-3})]; the sound velocity and thermal expansion coefficient are well expressed by the following polynomial equations: $c=1496.6+198.93C_e-179.32C_e^2+61.211C_e^3-7.5477C_e^4$ (m s^{-1}) [S.D.=2.3 (m s^{-1})] and $\theta=2.5295\times10^{-4}+2.1025\times10^{-4}C_e-2.0615\times10^{-5}C_e^2$ (deg^{-1}) [S.D.=1.1×10^{-5} (deg^{-1})]. The solid curve in Fig. 4 shows the values of μ_m which were calculated with the above thermodynamic parameters and Eq. 4.

Discussion

In order to interpret the observed relaxational process, several kinetical conditions have been applied: Firstly, even if the condition of water molecule is altered by addition of a solute, the association and dissociation processes between water molecules are too fast to be observed since their rates are estimated to be of the order of 10^{-12} s.[10] Secondly, any relaxation due to the internal rotation of solute may be ruled out because the concentration dependence of the observed relaxation frequency cannot be explained in terms of such a unimolecular reaction, and actually no relaxation phenomenon is found in pure Butyl Carbitol. Thirdly, the relaxation process due to the hydrogen bonding association of Butyl Carbitol molecules is probable. However, such a relaxation process is expected to be far beyond the MHz frequency range on the basis of estimates for various alcohols.[11,12] The high values of the background absorptions suggest the existence of such processes. Fourthly, although the association process of Butyl Carbitol molecules due to hydrophobic interaction is also conceivable, such phenomenon has been found for other ethers[1-4] with larger hydrophobic groups in lower frequency range than the observed frequency range. Finally, there is left only the relaxation process due to an interaction between ether and water molecules associated with hydrogen bonding, which has been shown to be capable of good interpretation of the experimental results in the preceding sec-

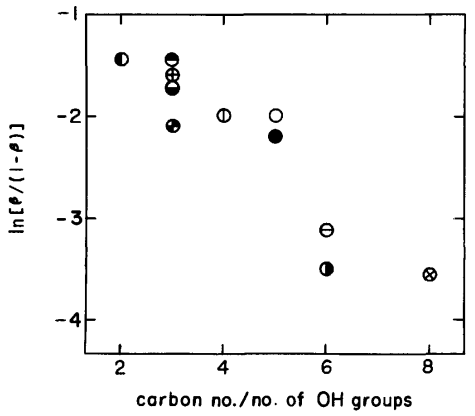

Fig. 5. Plots of the values of $\ln[\beta/(1-\beta)]$ *vs.* the carbon number per hydroxyl group for the aqueous solutions of a series of alcohols and ethers. ◐: 1,2-Butanediol, ◓: Allyl alcohol, ⊕: Isopropyl alcohol, ◒: Propyl alcohol, ◔: 1,6-Hexanediol, ⓘ: *t*-Butyl alcohol, ○: Allyl Cellosolve, ●: Propyl Cellosolve, ⊖: Isobutyl Cellosolve, ◑: Butyl Cellosolve, ⊗: Butyl Carbitol.

tion. According to our model, it is possible to estimate qualitatively the effect of Butyl Carbitol molecule on the water structure. The molar fraction β of nonhydrogen-bonded water in the aqueous solution which is calculated from Eq. 3 is listed in Table 2 along with those previously reported. The values may be taken to correspond exactly to the fraction of water capable of interacting with the solute or that of the less structured water molecules. The value for pure water is not less than 0.24.[13] On the other hand, those in the aqueous solutions are smaller than that of the water. This means that the addition of such nonelectrolytes into water causes water molecules to enter a more stabler state. This seems to be due to the hydrophobicity of the solute molecule. In order to examine its effect on the water structure we have plotted $\ln[\beta/(1-\beta)]$, which is related to the free energy change between the two states of water, against the carbon number per hydroxyl group for a series of alcohols and ethers, obtaining Fig. 5. With increasing carbon number per hydroxyl group, the value of $\ln[\beta/(1-\beta)]$ decreases, that is, the absolute value of the free energy change increases. This plot indicates that the ability to promote the water structure will increase with increasing hydrophobicity of the solute molecule.

It is interesting to note that a single relaxation process has been observed in the aqueous solution of Butyl Carbitol, whereas double relaxations are found in a solution of Butyl Cellosolve.[2] In the latter solution, one process is the same as that observed for Butyl Carbitol solution and the other, found around 7 MHz, has been attributed to a perturbation of equilibrium associated with an aggregation due to the hydrophobic interaction. The difference between the ultrasonic properties of these solutions may arise from the size of oxyethylene group, and the electrorepulsive force may affect the formation of the aggregate. This kind of difference has also been found in aqueous solutions of propyl alcohol[3] and Propyl Cellosolve.[8]

There is another interpretation for the absorption phenomenon in aqueous solutions of nonelectrolytes, which is based on the fluctuation model. Atkinson *et al.*[14-16] successfully analyzed observed absorptions in dioxiane, butylamine, and tetrahydrofuran solutions, which gave broad absorption spectra. They questioned the validity of such an approach as adopted in this report for reasons of unreliable complex formation, too slow rates for the hydrogen bonding, and inconsistent thermodynamic constants. However, as for the aqueous solution of Butyl Carbitol, a clear single relaxational absorption is observed, the simple 1-1 complex exists with equilibrium between the nonhydrogen-bonded water and single solute, the rate constant obtained corresponds to the overall process for the interaction in which the diffusion and rotation of reactants are also included, and the enthalpy change for the reaction seems reasonable because one reaction site is surrounded by many polar molecules.[17]

In conclusion, it has been elucidated from the present ultrasonic experiments for a series of alcohol and ether solutions that the ultrasonic absorption character will depend on the structure of solutes, that is, a single relaxational process occurs in solutions in which solutes have a relatively small hydrophobicity, whereas double relaxations appear with increasing hydrophobicity of solutes.

References

1) S. Nishikawa, M. Mashima, and T. Yasunaga, *Bull. Chem. Soc. Jpn.*, **49**, 1413 (1976).
2) S. Nishikawa, M. Tanaka, and M. Mashima, *J. Phys. Chem.*, **85**, 687 (1981).
3) S. Nishikawa, M. Mashima, and T. Yasunaga, *Bull. Chem. Soc. Jpn.*, **48**, 661 (1975).
4) S. Nishikawa and T. Uchida, *J. Soln. Chem.*, **12**, 771 (1983).
5) S. Nishikawa, *J. Chem. Soc., Faraday Trans. 1*, **79**, 2651 (1983).
6) S. Nishikawa and M. Mashima, *J. Chem. Soc., Faraday Trans. 1*, **78**, 1249 (1982).
7) S. Nishikawa and T. Yamaguchi, *Bull. Chem. Soc. Jpn.*, **56**, 1585 (1983).
8) S. Nishikawa, T. Yamashita, and M. Mashima, *Bull. Chem. Soc. Jpn.*, **55**, 1 (1982).
9) N. Tatsumoto, *J. Chem. Phys.*, **47**, 4561 (1967).
10) L. Hall, *Phys. Rev.*, **73**, 775 (1948).
11) W. Lempert, C. H. Wang, G. Fytas, and Th. Forfmuller, *J. Chem. Phys.*, **76**, 4872 (1982).
12) S. K. Kor, S. C. Deorani, B. K. Singh, R. Prasad, and U. S. Tandon, *Phys. Rev. A*, **4**, 1299 (1971).
13) C. M. Davis, Jr. and J. Jarzynski, *Adv. Mol. Relaxation Processes*, **1**, 155 (1967).
14) G. Atkinson, M. M. Emara, H. Endo, and B. L. Atkinson, *J. Phys. Chem.*, **84**, 259 (1980).
15) G. Atkinson, S. Rajagopalan, and B. L. Atkinson, *J. Chem. Phys.*, **72**, 3511 (1980).
16) G. Atkinson, S. Rajagopalan, and B. L. Atkinson, *J. Phys. Chem.*, **85**, 733 (1981).
17) M. Davis, "Hydrogen Bonding," ed by D. Hadzi, Pergamon Press, London (1956).

 © 1984 The Chemical Society of Japan Bull. Chem. Soc. Jpn., 57, 2361—2365 (1984)

Studies on the Phase Transition near the Melting Point in Acetylferrocene

Kumiko SATO,* Motomi KATADA, Hirotoshi SANO, and Michiko KONNO†
Department of Chemistry, Faculty of Science, Tokyo Metropolitan University, Fukasawa, Setagaya-ku, Tokyo 158
†*The Institute for Solid State Physics, The University of Tokyo, Roppongi-7, Minato-ku, Tokyo 106*
(Received December 5, 1983)

The entitled compound shows an anomalous temperature dependence of the mean-square amplitude of iron atoms derived from the Lamb-Mössbauer factor near the melting point. To clarify the anomaly, the crystal structure of this compound was determined at room temperature by X-ray diffraction. The crystal is monoclinic with space group $P2_1/c$, a=20.595(2), b=5.7909(4), c=18.840(2) Å, β=116.870(7)°, U=2004.4(3) Å^3, and Z=8. Weissenberg and oscillation photographs taken at a high temperature lead us to propose a model in which the acetylferrocene molecules rotate around the central iron atoms.

It is well-known that ferrocene undergoes an apparently second-order transition at 163.9 K from a disordered ($P2_1/a$) phase to an ordered ($F\bar{1}$, Z=16) phase.[1-3] In the low-temperature phase, the crystal consists of an ordered array of molecules, while it takes on a partial degree of rotational disorder structure above the transition point. Rotation of the cyclopentadienyl (C_p) rings has been observed in ^{1}H-NMR spectra, and ascribed to a cooperative jump-rotation, rather than a free rotation.[4]

Formylferrocene was reported by Daniel and Leadbetter to show a plastic crystal phase between 44 °C and the melting point.[5] The structure of the plastic crystal phase was assigned to a simple face-centered cubic lattice with a unit-cell parameter a=9.99 Å accompanied by an orientational disorder based on a diffuse scattering pattern.[5] Recently the structures of both the crystal and plastic phases have been determined to be orthorhombic by using single-crystal X-ray diffraction and the transition from the crystal to plastic phase has been attributed to translational molecular motions along the a axis, in accordance with the temperature dependence of the Mössbauer spectrum.[6]

1,1′,2,2′-Tetrachloroferrocene and 1,1′,2,2′,3,3′,4,4′-octachloroferrocene were also reported to exhibit a mesophase by Hedberg and Rosenberg.[7] The structure and the nature of the mesophase of 1,1′,2,2′-tetrachloroferrocene were studied using X-ray diffraction and Mössbauer spectroscopy.[8] 1,1′-Diethylferrocene was found to have a glassy state by thermal analysis, and the thermal vibration was studied by measuring the temperature dependence of the Lamb-Mössbauer factor for iron atoms.[9]

Although the critical phenomena before melting and phase transitions in ferrocene derivatives are of great interest, little is known concerning the structural features of the mesophases. It was preliminarily reported that some kind of transition occured a little below the melting points in acetyl and carboxylferrocenes.[10] In the present paper, the crystal structure of acetylferrocene was determined at room temperature by X-ray diffraction and the transitional process was investigated, based on the detailed data obtained from oscillation and Weissenberg photographs, Mössbauer spectroscopy and thermal analysis.

Experimental

Mössbauer Spectra. Acetylferrocene was prepared by the method described in Ref. 11, and purified by recrystallization and sublimation. The purity was confirmed by checking the melting point and by elemental analysis. No impurity was detected in IR, NMR, and Mössbauer spectra.

Mössbauer spectra were obtained using an Austine Science Associated Mössbauer spectrometer. Velocity calibration was carried out based on the room-temperature spectra of metallic iron. By fitting the resonance line-shape to a Lorentzian function, the Mössbauer parameters were extracted.

Low-temperature measurements were preformed using a CA thermocouple embedded in a copper sample holder in a cryostat. The precision of the temperature measurement was within approximately ±1° over a period of several hours. A high-temperature apparatus was constructed with a heater in a vaccum furnace. The samples were sealed to prevent sublimation. Temperature was checked by a CA thermocouple with precision of about ±0.1°.

Structure Determination and Refinement. Brown needle crystals of acetylferrocene were grown from a benzene-hexane solution. Although preliminary oscillation and Weissenberg photographs indicated an orthorhombic symmetry, this specimen was concluded to be a twin as described below. A single crystal of 0.30×0.25×0.35 mm was sealed in a Lindemann-glass capillary and the intensities were measured with Mo $K\alpha$ radiation monochromated by a graphite plate.

Crystal data are tabulated in Table 1. The positions of the Fe, C, and O atoms were deduced from the sharpened Patterson maps and successive Fourier syntheses. The posi-

Table 1. Crystal data at 24 °C

Acetylferrocene	M.W. 228.1
Monoclinic	
Space group	$P2_1/c$
a/Å	20.595(2)
b/Å	5.7909(4)
c/Å	18.840(2)
β/°	116.870(7)
U/Å^3	2004.4(3)
Z	8
D_c/g cm^{-3}	1.517
μ/cm^{-1}	1.54

tion of all the hydrogen atoms were deduced from difference synthesis. There are two crystallographically independent molecules I and II in a unit cell. After several cycles of refinement it turned out that the methyl groups of the two crystallographically independent molecules take two alternative sets of positions with an equal probability.

The block-diagonal least-squares program HBLS-4[12] was employed assuming anisotropic thermal parameters for the non-hydrogen atoms and isotropic thermal parameters for the hydrogen atoms. Two reflections, 210 and 102, were excluded in the refinement, since they suffered from secondary extinction. The atomic scattering factors were taken from International Tables for X-ray Crystallography (1974).[13] Unit weight was adopted for all the reflections. The R values reduced to 0.036 for 3194 independent reflections with $|F_o|>3\sigma(|F_c|)$ up to $2\theta=55°$. Final atomic parameters are given in Table 2.††

Acetylferrocene often crystallizes as a twin which pretends to have an orthorhombic unit cell as shown by dotted lines in Fig. 1, because c*sin (90-β*) is close to a*/2. There are two equivalent monoclinic components A and B described by solid and broken lines respectively, with a common b* axis; the rotation of the monoclinic component A around the c axis by 180° gives the component B.

Table 2. Positional parameters
($\times 10^5$ for FE and $\times 10^4$ for C and O)

	x	y	z	$B_{eq}\times 10$/Å^2
FE(1)	14365(2)	22916(9)	42569(3)	25(1)
C(1)	330(2)	1979(8)	3654(2)	39(1)
C(2)	661(2)	−191(7)	3736(2)	36(1)
C(3)	1126(2)	−77(8)	3367(2)	40(1)
C(4)	1082(3)	2137(9)	3061(2)	48(2)
C(5)	586(3)	3430(8)	3235(2)	48(1)
C(6)	1981(2)	5088(6)	4917(2)	32(1)
C(7)	2455(2)	3724(8)	4738(2)	37(1)
C(8)	2484(2)	1486(7)	5041(2)	35(1)
C(9)	2025(2)	1415(7)	5419(2)	31(1)
C(10)	1710(2)	3658(6)	5347(2)	27(1)
C(11)	1167(2)	4408(7)	5609(2)	35(1)
C(12)	828(3)	2603(9)	5896(3)	54(2)
O(1)	1011(2)	6422(5)	5594(2)	53(1)
FE(1′)	64602(2)	24021(9)	21803(3)	26(1)
C(1′)	6587(2)	−95(7)	1492(2)	36(1)
C(2′)	7197(2)	−61(7)	2251(2)	39(1)
C(3′)	7518(2)	2157(8)	2373(3)	44(1)
C(4′)	7103(2)	3494(7)	1675(3)	45(2)
C(5′)	6528(2)	2080(8)	1134(2)	38(1)
C(6′)	5543(2)	1531(7)	2274(2)	33(1)
C(7′)	6142(2)	1640(8)	3043(2)	38(1)
C(8′)	6434(2)	3903(9)	3159(2)	43(1)
C(9′)	6029(2)	5213(7)	2471(2)	36(1)
C(10′)	5468(2)	3776(6)	1914(2)	28(1)
C(11′)	4953(2)	4446(7)	1105(2)	34(1)
C(12′)	4464(2)	2610(9)	568(3)	51(2)
O(1′)	4920(2)	6423(6)	877(2)	52(1)

†† The complete, F_o-F_c data, atomic parameters of hydrogen atoms and bond distances are deposited as Document No. 8427 at the office of the Chemical Society of Japan.

Results and Discussion

Anomalous Mean-Square Amplitude of Iron Atom. Figure 2 shows the temperature dependence of the mean-square amplitude of the iron atoms estimated from the areal intensities of Mössbauer spectra of acetylferrocene.[10] The mean-square amplitude is proportional to the absolute temperature up to room temperature, indicating an harmonic intermolecular vibration. The value of the mean-square amplitude at room temperature by applying the high-temperature approximation[9] from 78 K to room temperature is 3.0×10^{-2} Å^2 for acetylferrocene, while the value based on the isotropic thermal factor in the X-ray diffraction study is 3.2×10^{-2} Å^2. A remarkable anomaly in the temperature dependence of the mean-square amplitude is found at temperatures a few degrees below the melt-

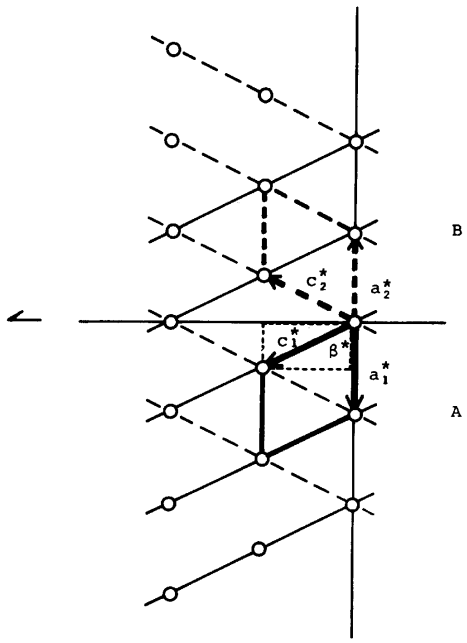

Fig. 1. Unit cell of the twinned crystal consisting of two equivalent monoclinic components looks like an orthorhombic unit cell shown by the dotted lines, because c*sin(90-β*) is close to a*.

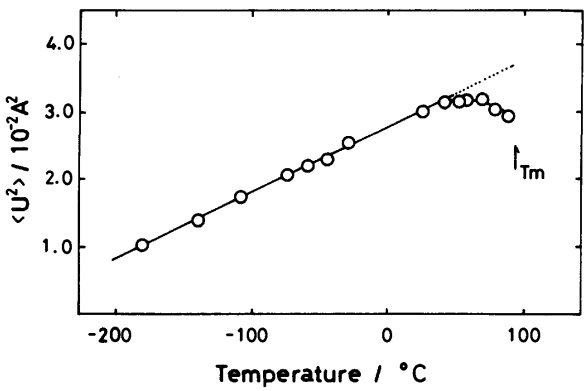

Fig. 2. Temperature dependence of the mean-square amplitude of the iron atoms in acetylferrocene.

ing point as shown in Fig. 2. The deviation from the dotted line suggests that the thermal motion cannot be explained by a simple harmonic oscillation model.

Crystal Structure. The C–C distances in the C_p rings are 1.392—1.442 Å; the Fe–C distances are 2.028—2.061 Å for the molecules I and II. These results agree with the values of the other ferrocene derivatives indicating no effect of the substituent on the Fe–C bondings.

Evidence for the reorientation in the substituent group and C_p ring of acetylferrocene has been deduced on the basis of the temperature dependence of the second moment of the ^{1}H-NMR lines.[4] The steep decrease of the line width and second moment between 50 and 210 K could be ascribed to the reorientation of the methyl groups about its triad axis and of th C_p rings about their five-fold axes of symmetry. The methyl group, unsubstituted C_p ring and substituted C_p ring, may initiate the reorientation in order of their moment of inertia with increasing temperature.

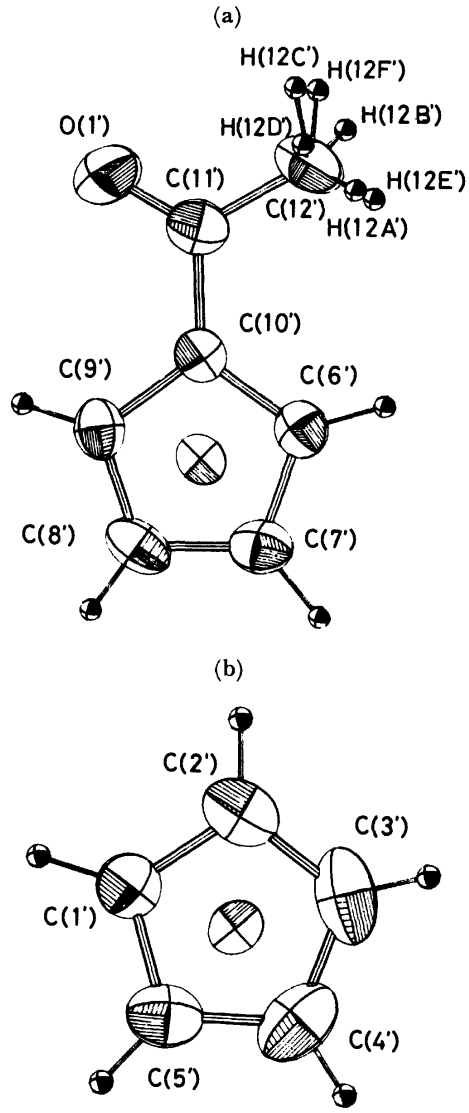

Fig. 3. Ellipsoids of the non-hydrogen atoms for molecule II are scaled at the 50 % probability. (a) substituted C_p ring and (b) unsubstituted C_p ring.

Figure 3 shows the vibrational ellipsoids of the C atoms in molecule II. A rigid-body analysis indicates that the principal libration axis of the C_p rings is nearly parallel to the five-fold molecular axis. The root-mean-square vibration amplitudes for the in-phase libration of the substituted C_p rings, 4.8° and 5.9°, are smaller than those of the unsubstituted C_p rings, 8.3° and 7.5° for molecules I and II, respectively, probably because steric hindrance of the acetyl groups reduces the thermal motion. On the other hand, the methyl hydrogen atoms in the acetyl groups take two alternative sets of positions with equal probability and the two orientations of the methyl groups are related by rotation of about 60° around the carbon–carbon bonds. The C and O atoms of the acetyl groups lie on approximately the planes of the aromatic rings owing to the existence of the complete conjugation between the acetyl groups and the C_p rings. The mean-square amplitudes of the C and O atoms in the direction perpendicular to the aromatic ring planes are about twice those estimated from the rigid-body motion, suggesting reorientation of the acetyl groups at high temperatures.

Figure 4 shows a projection of the structure along the b axis. There are two crystallographically independent molecules I and II in the unit cell. The eight iron atoms are located at *ca.* $y=1/4$ and $3/4$. A prominent feature of the crystal structure is the pairing of two molecules with respect to a center of symmetry, such as II and IV, and I and III, respectively. There is no intermolecular distance shorter than the sum of the van der Waals radii. The disordered hydrogen atoms of the methyl groups are illustrated by shaded circles.

Figure 5 shows the view of the structure perpendicular to the face (102). The C_p planes incline by about 20 degrees against the b axis in order to avoid contact with each other, and oxygen atoms are packed in the interior of the pairs. Intermolecular nearest distances are 2.29 Å between H(2)–H(12C) for the molecule I and 2.32 Å

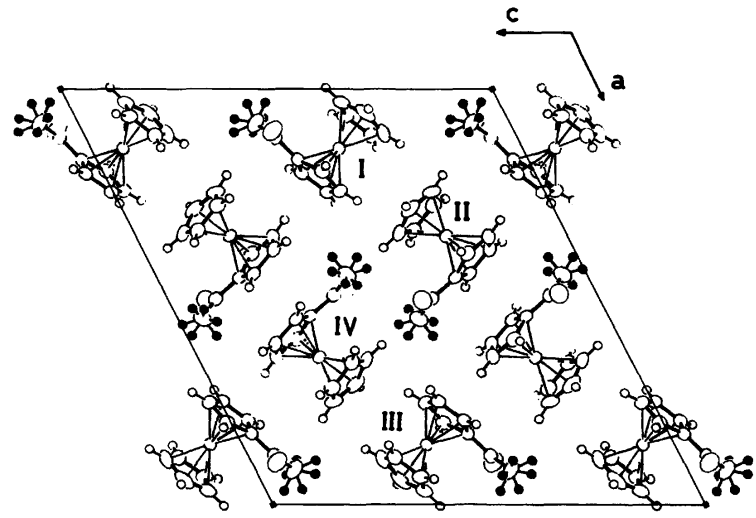

Fig. 4. Projection of the crystal structure of acetylferrocene along the b axis at room temperature. The disordered hydrogen atoms of acetyl groups are illustrated as shaded circles.

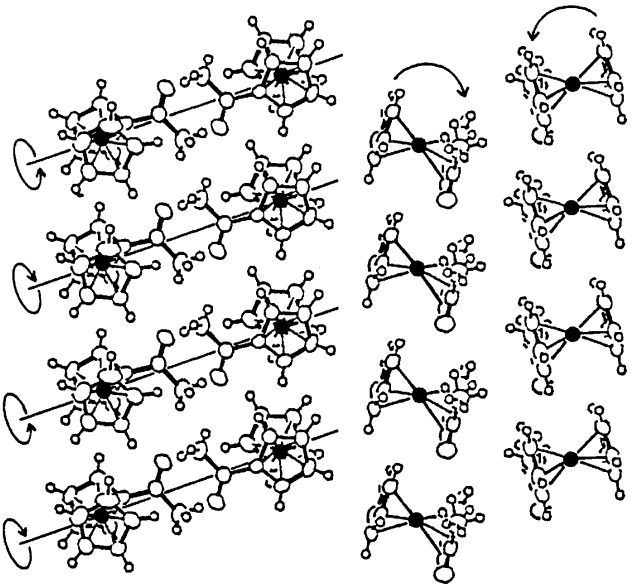

Fig. 5. View of the structure perpendicular to the face (102). The phase transition is associated with a co-operative phenomenon like in a series of rotating gears, that is, molecules reorient simultaneously around the iron-iron directions in the pairs.

between H(1′)–H(12C′) for the molecule II.

Rotational Phase Transition. Crystal specimens were heated in a stream of electrically heated air controlled with a precision of about ±0.25°. Both the Weissenberg and the oscillation photographs taken at temperatures up to the melting point (86 °C) showed that the diffraction pattern abruptly changed twice, at *ca.* 80 °C and 83 °C.

When the temperature was raised, the reflections split into two spots in the a*c* plane at *ca.* 80 °C. On increasing the temperature, the reflection intensities disappeared at *ca.* 83 °C except those corresponding to the 210, $\bar{1}12$, $\bar{3}02$, and 102 reflections in the original pattern. Those reflections are considered to be contributed largely by the iron atoms because they correspond to the planes containing the iron atoms at room temperature. Further, there appeared several additional satellite reflections along 3a*—2c* between 210 and $\bar{1}12$ as shown in Fig. 6. It was difficult to obtain the cell dimensions and the symmetry of the crystal owing to the deficiency of reflection data.

When the crystal specimen, heated once above *ca.* 83 °C, was cooled slowly back to room temperature, the Weissenberg photograph showed the same diffraction pattern as its original one or the two-fold rotated pattern. The latter photograph showed that the specimen remained as a single crystal but was rotated by 180° around the c axis with respect to the original orientation as shown in Fig. 7 by dotted lines. This indicates that the original structure, (A), shown by full lines, must be transformed into the rotated structure, (B), through a molecular motion at 83 °C. The interchange of the original structure with the resulting structure can

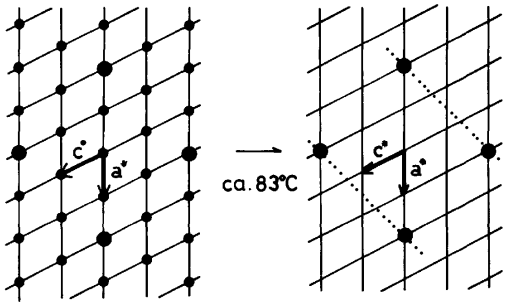

Fig. 6. Temperature dependence of Weissenberg photographs in the first layer.

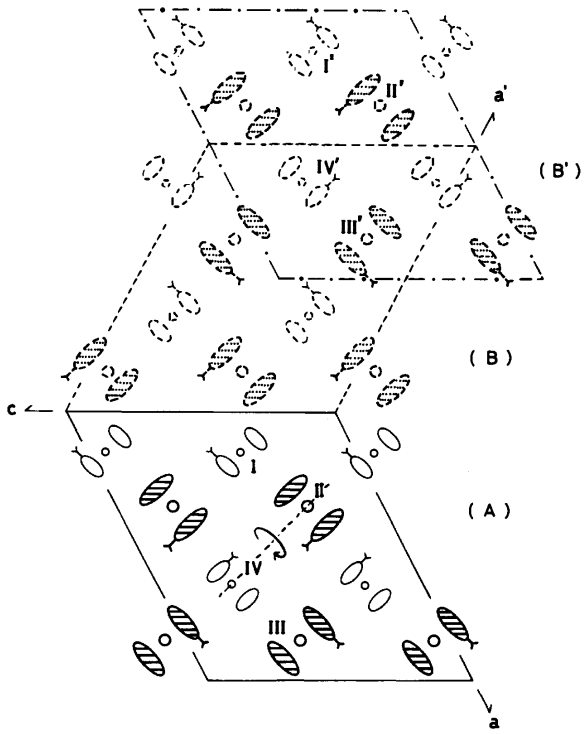

Fig. 7. Crystal structure of acetylferrocene at room temperature (A) before and (B) after heating to *ca.* 83 °C. The structure (B) shown by dotted lines is given by the rotation of the structure (A) shown by solid lines, around the c axis by 180 °, where the C_p rings are picturized with ellipses and the acetyl groups are Y-shaped symbols, and the molecular positions are expressed by different size of the ellipses and slant lines.

be interpreted in the same way as the twinning shown in Fig. 1, assuming a small potential barrier between the crystal components A and B.

These observations enable us to propose a plausible model for the phase transition at *ca.* 83 °C as follows. The structure (B′) shown by the chain lines in Fig. 7 is given by the rotation of the structure (A) around the c axis by 180° in the same way as described for the twinning of this compound. Because of the specific molecular arrangement, the crystal structure of the ferrocene

moieties in (B′) resembles that in (A) except for the position of acetyl groups; *i.e.*, molecules I, II, III, and IV correspond to molecules I′, II′, III′, and IV′, respectively. The structure (A) transforms to the structure (B′) by rotating the acetylferrocene molecules. This rotational interchange is considered to be effected by the simultaneous and cooperative rotation of pairs of adjacent molecules, such as II and IV, around the iron-iron direction in pairs as shown in Fig. 7. This model suggests that molecules jump rather than freely rotate between the two orientations, (A) and (B′), around the direction between the two adjacent iron atoms in the pairs of II and IV, and I and III, respectively, at *ca.* 83 °C. Each molecular reorientation may also be accompanied by a rotation of the acetyl group.

In the proposed model, the phase transition is assumed to be associated with a cooperative motion similar to that of a series of rotating gears as shown in Fig. 5. This model can also explain why there is no increase of the mean-square amplitude of the iron atoms with increasing temperature, as shown in Mössbauer spectra, since the central iron atoms would keep their positions in the transition state.

Mössbauer Spectra. Mössbauer spectra consist of a doublet with the isomer shift 0.40 to 0.42 mm s^{-1} and the quadrupole splitting 2.53 mm s^{-1} that reveals Fe(II) low-spin state. As shown in Fig. 8, there evidently occurs a progressive broadening above room temperature, although slight decrease of the line-width is expected in the high temperature region because of the decrease of the recoil-free fraction.

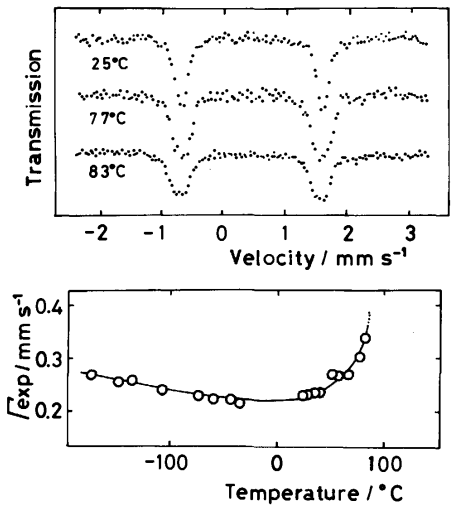

Fig. 8. Temperature dependence of the Mössbauer line-width for acetylferrocene.

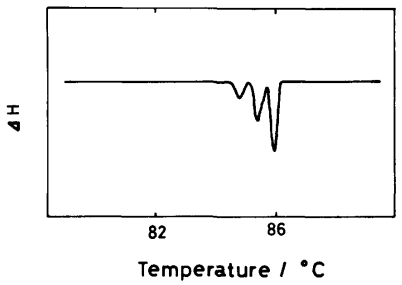

Fig. 9. Diferrential scanning calorimetric curve of acetylferrocene at heating rate 1 deg h^{-1}.

In addition to the fact of no increase of mean-square amplitude estimated by Mössbauer spectroscopy near the melting point, this behaviour may well be explained by assuming the relaxation effect of quadrupole split lines, caused by the fluctuation of the electric field gradient in the high temperature region. The process may be ascribed to a slow flipping between two equilibrium positions in the reorientational plane rather than to the rotational motion. The reorientational motion of acetylferrocene may be hindered by interaction with neighbouring molecules, for instance the steric hindrance of the acetyl groups.

Thermal Analysis. Figure 9 shows the results of Differential Scanning Calorimetry for acetylferrocene. Two endothermic peaks are observed below the melting point under an extremely slow heating rate, 1 deg h^{-1}. The peak closest to the peak of melting is ascribed to the molecular rotational phase transition, and the other peak to the rotation of acetyl groups, although further measurement are needed to justify more detailed discussion.

The authors wish to thank Prof. Yoshihiko Saito for his helpful discussions concerning the crystallographic aspects of this work and Dr. Tetsuzo Ito for creating an extended version of UNICS.

References

1) J. W. Edwards, G. L. Kington, and R. Mason, *Trans. Faraday Soc.*, **56**, 660 (1960).
2) P. Seiler and J. D. Dunitz, *Acta Crystallogr., Sect. B*, **35**, 1068 (1979).
3) F. Takusagawa and T. F. Koetzle, *Acta Crystallogr., Sect. B*, **35**, 1074 (1979).
4) L. N. Mulay and A. Attalla, *J. Am. Chem. Soc.*, **85**, 702 (1963); M. K. Makova, E. V. Lenova, Yu. S. Karimov, and N. S. Kochetkova, *J. Organomet. Chem.*, **55**, 185 (1973).
5) M. F. Daniel, A. J. Leadbetter, and R. M. Richardson, *J. Chem. Soc., Faraday Trans. 2*, **77**, 1851 (1981).
6) K. Sato, M. Iwai, H. Sano, and M. Konno, *Bull. Chem. Soc. Jpn.*, **57**, 634 (1984).
7) F. L. Hedberg and H. Rosenberg, *J. Am. Chem. Soc.*, **95**, 870 (1973); F. L. Hedberg and H. Rosenberg, *J. Thermal. Anal.*, **6**, 571 (1974).
8) K. Sato, M. Konno, and H. Sano, *Chem. Lett.*, **1984**, 17.
9) K. Sato, M. Katada, and H. Sano, *Chem. Lett.*, **1980**, 217.
10) K. Sato, M. Konno, and H. Sano, *Chem. Lett.*, **1982**, 817.
11) M. Rosenblum and R. B. Woodward, *J. Org. Chem.*, **80**, 5443 (1958).
12) T. Ashida (1976) UNICS. The Universal Crystallographic Computing System, The Crystallographic Society of Japan.
13) "International Tables for X-ray Crystallography," Kynoch Press, Birmingham (1974), Vol. IV.

New Transport Phenomenon. Enhanced Transport into a Membrane Due to the Presence of Polyelectrolyte

Mamoru NANGO,* Shozo OHTA, Masako MAEKAWA, Akira KATAYAMA,† and Nobuhiko KUROKI
Department of Applied Chemistry, College of Engineering, University of Osaka Prefecture, Sakai 591
(Received December 6, 1983)

The transport of chromophore into a membrane in the presence of polyelectrolyte is enhanced much as it is in the presence of simple salt. The presence of polyelectrolyte with different kinds of counterions seem to modify this observed enhancement. The differences in enhanced transport into the cellulose membrane in the presence of polyelectrolyte may suggest a new model for reinterpretation of the transport phenomenon in a biological system.

In previous publications,[1,2] it has been shown by Donnan membrane equilibrium theory that the adsorption of chromophore on cotton increases with addition of polyelectrolyte in the bulk solution. Thus, the chromophore is accumulated in the internal solution of cellulose due to the presence of polyelectrolyte which is not able to enter into the pores of the cellulose. One might expect, therefore, to find progressively enhanced transport of chromophore into a cellulose membrane with addition of polyelectrolyte. We here report the effect of polyelectrolytes and their counterions on transport of chromophore into a cellulose. There have been no reports of studies concerned with the transport of simple ions and chromophores into a membrane in the presence of polyelectrolyte. Enhanced transport of chromophores into a membrane because of the presence of polyelectrolyte is similar to such enhancement in the presence of simple salt. The dependence of such transport on different kinds of counterion suggest a new type of transport phenomenon that may provide useful information for a model for transport into the cell membrane of biological systems. Specifically, the uptake of chromophore into a cellulose membrane in the presence of polyelectrolyte with different kinds of counterion on the polymer chain, when compared with the sodium salt, has been sizably enhanced to provide the basis for the above statement.

Experimental

Materials. Chromophore(C.I. Direct Yellow 12, C.I. Direct Red 2 and, C.I. Direct Blue 15) was obtained and purified as described elesewhere.[2,3] Sodium alginate(NaAlg, MW: 10,000)(Kamogawa Kasei Co.), sodium polyacrylate(NaPA, MW: 37,000), sodium polymethacrylate(PMA, MW: 260,000), and sodium polystyrenesulfonate(NaPSS, MW: 69,000) (Polyscience Co.) were purified as described eleswhere[2] and converted to different kinds of counterion(NH_4^+, K^+, and Cs^+) with the corresponding hydroxide or carbonate, respectively. The conversion of counterion was above 90% by the analysis of Hitachi 50A atomic absorption spectrophotometer. In our experiment conditions, alginate(Alg) which does not interact with chromophore or cellulose,[2] was used as the biological polyelectrolyte. Commercial cotton and cellulose membrane(cellophane film) were soaked in boiled deionized distilled water for 1 and 3 h, respectively. Then, cotton was treated with methanol and cellulose membrane was washed with deionized distilled water. Carboxyl group contents of cotton and cellulose membrane determined by iodometry were 4.00 and 62.5 meq/dg, respectively.[2,3] T. Vickerstaff indicated that the water content of cellulose and cellulose membrane were 0.22 and 0.33 l/kg, respectively, consisting with the volume term of substrate(V) (see, Eq. 4) theoretically determined.[5] The degree of dissociation constant (α) of polyelectrolytes was measured by the method of selective ion sensitive electrodes of Orion Research 94-11.

Uptake and Transport of Chromophore to Cellulose. Uptake of chromophore for cotton and cellulose membrane was carried out at temperature of 90±0.5 °C for 6 h and 25±0.5 °C for 48 h, respectively.[2] The concentration of chromophore in solution ranged from 1.004×10^{-5} to 2.164×10^{-3} mol/l. The concentration of electrolyte and polyelectrolyte ranged from 1×10^{-2} to 10×10^{-2} mol/l. Accurately weighed uptaken samples were extracted with 25% aqueous pyridine. The concentration of chromophore extracted was determined using a Hitachi 124 spectrophotometer with 25% pyridine as reference. To prevent complications arising from cis-trans formation of C.I. Direct Yellow 12, bisazo derivative, the chromophore solution was illuminated for about 1 h just before measurement.[1,2] Transport of chromophore was measured in the apparatus of Amicon ultrafiltration cell as described elesewhere.[5] To obtain the interpolated degree of dissociation constant of polyelectrolyte, uptake of C.I. Direct Yellow 12 on cotton in the presence of polyelectrolytes containing the constant concentration of sodium chloride(0.01 M, 1 M=1 mol dm^{-3}) at 25 and 90 °C was done as described in the previous paper.[2] Interaction between polyelectrolytes and chromophore used in this system was neglegible as described with previous articles.[2,6]

Results and Discussions

Figure 1 compares the uptake of C.I. Direct Yellow 12 in a cellulose membrane in the presence of the sodium salt of galacturonic acid (a model for pyranose unit in sodium alginate) with that in the presence of sodium alginate. It is obvious that the adsorption isotherm in the presence of NaAlg differs from that in the presence of galacturonic acid. Thus, the effect of NaAlg on the uptake by the cellulose membrane differs from that of small molecule electrolytes such as galacturonic acid or an inorganic salt which are able to enter into the cellulose membrane.

Figure 2 illustrates the transport of C.I. Direct Yellow 12 into a cellulose membrane in the presence of NaAlg at 25 °C. As is apparent in Fig. 2, enhanced transport of chromophore into a cellulose membrane with addition

† Present address: Kyoto Women's University, Higashiyama-ku, Kyoto 605.

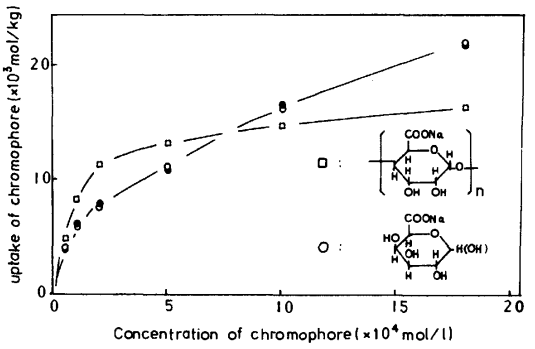

Fig. 1. Adsorption isotherm of C.I. Direct Yellow 12 into a cellulose membrane in the presence of either sodium alginate or the sodium salt of galacturonic acid at 25 °C.
□: sodium alginate (2×10^{-2} pyranose unit mol/l) ionization degree=0.4—0.5. ○: galacturonic acid sodium salt (1×10^{-2} mol/l). ●: sodium chloride (1×10^{-2} mol/l)

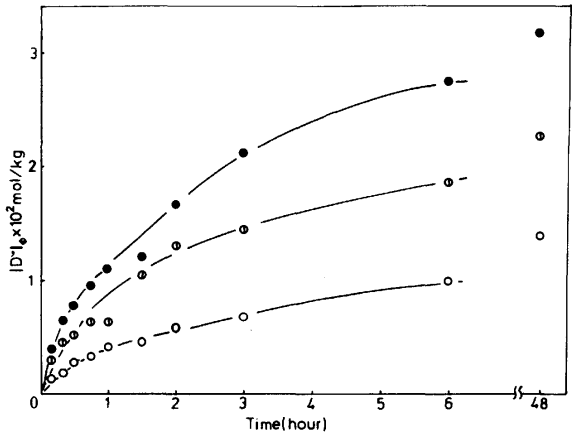

Fig. 2. Transport of C.I. Direct Yellow 12 into a cellulose membrane in the presence of sodium alginate at 25 °C.
○: 0.02 pyranose unit mol/l. ◑: 0.04 pyranose unit mol/l. ●: 0.06 pyranose unit mol/l.

of NaAlg was observed. Table 1 lists an example of transport of chromophore into a cellulose membrane. Transport increased progressively with addition of alginate, reaching a factor about 25 over that without NaAlg. This large enhancement may be due merely to the fact that a chromophore is accumulated inside the membrane film by a Donnan membrane-equilibrium effect.

Figure 3 illustrates the uptake of C.I. Direct Yellow 12 into a cellulose membrane in the presence of various polyelectrolytes at 90 °C. Table 1 lists an example of uptake of chromophore into a cellulose. As is apparent in Fig. 3 and in Table 1, the increase in the uptake of chromophore to cellulose for polyelectrolytes follows the order, NaAlg>NaPSS≳NaPMA≳NaPA, indicating the analogous order to the sequence of increase in the degree of dissociation constant for polyelectrolytes as described in Table 2. Figure 4 illustrates the adsorption isotherms of C.I. Direct Yellow 12 on cellulose

Table 1. Uptake of chromophore[a] into cellulose in the presence of polyelectrolyte at 25 and 90 °C

Polyelectrolyte × 10^2 unit mol/l		Uptake of chromophore (× 10^4 mol/kg cellulose)			
		90 °C		25 °C	
		cellulose membrane	cotton	cellulose membrane	cotton
NaAlg	(2)	42.5	24.2	133	55.7
	(4)	68.2		226	
	(6)			318	
	(10)	169			
NaPSS	(2)	25.7	20.8		47.5
	(4)		25.7		
NAPMA	(2)	20.8	15.3		42.4
NAPA	(2)	16.8	13.6		39.5
	(4)		21.5		
	(10)		39.4		
None		6.81	7.69	34.5	24.9

a) C.I. Direct Yellow (sodium salt) 1×10^{-3} mol/l. These results are consistent with the chromophore concentration used in this article($1—20\times10^{-4}$ mol/l).

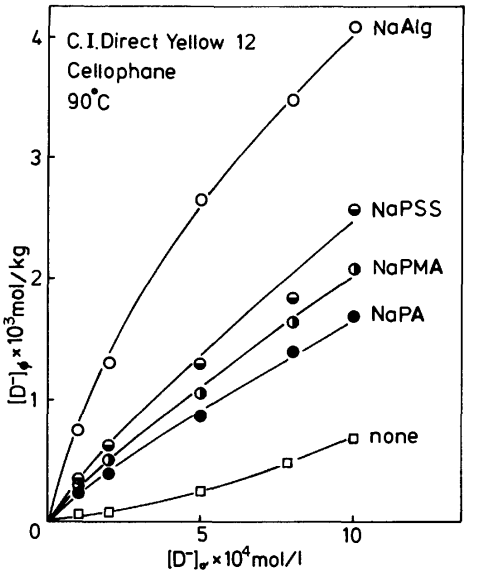

Fig. 3. Adsorption isotherm of C.I. Direct Yellow 12 into a cellulose membrane in aqueous solution of polyelectrolyte(0.02 unit mol/l) at 90 °C.
NaAlg: sodium alginate, NaPSS: sodium polystyrenesulfonate, NaPMA: sodium polymethacrylate, NaPA: sodium polyacrylate.

membrane in aqueous solutions of polyelectrolytes under conditions where sodium ion concentration is kept constant with corrected sodium ion concentration by using their measured value of dissociation constant for polyelectrolyte(see, α^* in Table 2). As is apparent in Fig. 4, the differences in the uptake of chromophore into cellulose membrane were largely reduced in comparison to those in Fig. 3. Thus, the differences in the uptake of chromophore into a cellulose membrane in aqueous solutions of various polyelectrolytes may be

TABLE 2. INTERPOLATED DEGREE OF DISSOCIATION CONSTANT (α) OF POLYELECTROLYTE

Polyelectrolyte	Dissociation constant			
	α at 25 °C	α at 90 °C	α^* at 25 °C	Ref(No.) at 25 °C
NaAlg	0.35± 0.05	0.40± 0.05	0.38± 0.02	0.50(2) 0.45(9) 0.33(10)
NaPSS	0.15± 0.05	0.20± 0.05	0.29± 0.02	0.35(11) 0.38(12) 0.40(6)
NaPA	0.15± 0.05	0.15± 0.05	0.23± 0.02	0.25(13) 0.28(14)
NaPMA			0.18± 0.02	

* Values measured by the method of selective ion sensitive electrode.

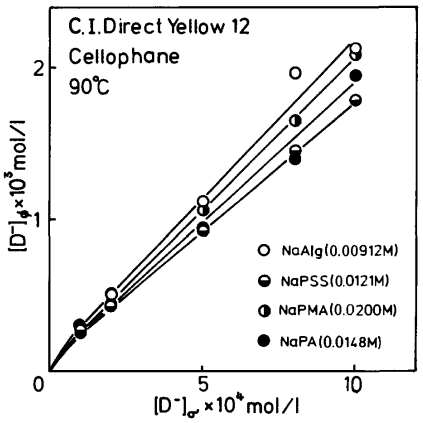

Fig. 4. Adsorption isotherm of C.I. Direct Yellow 12 into a cellulose membrane in aqueous solution of polyelectrolyte under condition of corrected sodium ion concentration (parenthesis) at 90 °C.

due to the fact that the differences in the degree of dissociation constant for polyelectrolytes has a crucial role on the differences in the uptake of chromophore into a cellulose membrane.

For the quantitative interpretation of the degree of dissociation constant of polyelectrolyte in the bulk solution on equilibrium uptake of chromophore, the following theoretical treatment was applied to the present results as described in the previous article.[2,5] As envisaged in the adsorption model on cellulose in Fig. 5, chromophore is assumed to be adsorbed in the internal solution of cellulose(i phase). Bulk phase(σ) is assumed to penetrate into the pore of cellulose membrane and this portion of it is designated as γ. It is assumed that polyanion($P_{\bar{n}}$) is present only in the σ phase. According to Donnan membrane-equilibrium between the two phase and maintaining electrical neutrality in each phase, the standard free energy ($-\Delta\mu^\circ$) can be calculated as described in the previous article.[2,7]

According to Donnan membrane-equilibrium between two phases, the ionic concentrations are related as follows;

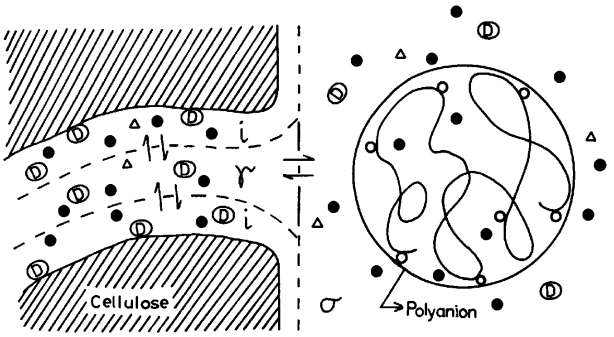

Fig. 5. Adsorption model on cellulose.
Alginate ion(polyion, $P_{\bar{n}}$) is present only in the bulk phase(σ). D, chromophore anion; ●, sodium ion (counterion of chromophore or polyelectrolyte); $P_{\bar{n}}$, alginate ion shown with pyranose unit mol; i, internal solution of cellulose; σ, bulk phase; γ, bulk phase assumed to penetrate into the pores of cellulose.

$$[Na^+]_\sigma^z[D^-]_\sigma = [Na^+]_\gamma^z[D^-]_\gamma = [Na^+]_i^z[D^-]_i \quad (1)$$

where z is the basicity of the dye(chromophore) anion and D^- is chromophore anion. For maintaining electrical neutrality in each phase,

$$\sigma \text{ phase: } [Na^+]_\sigma = z[D^-]_\sigma + \alpha[P^-]_\sigma + [Cl]_\sigma \quad (2)$$

where $\alpha[P^-]$ represents the concentration of polyanion shown with unit mol α represents the degree of ionization of polyelectrolyte to be calculated and $[Cl^-]$ represents the ionic concentration of chloride used as sodium chloride.

$$\gamma \text{ phase: } [Na^+]_\gamma = z[D^-]_\gamma + [Cl^-]_\gamma \quad (3)$$

$$i \text{ phase: } [Na^+]_i = \frac{z[D^-]_\phi}{V} + [Cl^-]_i \quad (4)$$

where V represents the volume term of i phase(cellulose membrane: 0.33 l kg^{-1}, cotton: 0.22 l kg^{-1})[5] and $[D^-]_\phi$ is the concentration of dye (chromophore) anion adsorbed into a cellulose membrane in mol kg^{-1} dry membrane.

Combination of Eqs. 1 and 3, $[Na^+]_i$ is obtained, where $[Na^+]_\phi = V[Na^+]_i$ and $[Na^+]_\phi$ is the concentration of sodium ion adsorbed in the cellulose membrane in mol kg^{-1} dry membrane.

The following equation was used to calculate the standard free energy of this uptake($\Delta\mu^\circ$).[5]

$$-\Delta\mu^\circ = RT \ln[Na^+]_\phi^z[D^-]_\phi / V^{z+1}[Na^+]_\gamma^z[D^-]_\gamma \quad (5)$$

$$= RT \ln[Na^+]_\phi^z[D^-]_\phi / V^{z+1}[Na^+]_\sigma^z[D^-]_\sigma \quad (6)$$

Thus, according to the computer simulation so that the standard free energy may has nearly constant value with various changes in the experimental conditions, the interpolated degree of dissociation constant(α) of polyelectrolyte can be obtained. Table 2 lists the interpolated degree of dissociation constant of polyelectrolyte with that measured by the method of sodium ion sensitive electrode. In addition, Table 3 lists an example of the standard free energy which has nearly constant value in these systems.

As is apparent in Table 2, the degree of dissociation constant corrected by computer simulation has fairly good agreement with that measured value by an ion

electrode, indicating that the differences in the degree of dissociation for polyelectrolytes with different kinds of ionizable groups induced the differences in the uptake of chromophore in aqueous solutions of various polyelectrolytes as described above in Fig. 1 and Table 1.

Further interesting trends of enhancement are seen in the transport of chromophore in the presence of polyelectrolytes with different kinds of counterions at 25° and 90 °C. Figure 6 illustrates the uptake of C.I. Direct Yellow 12 into a cellulose membrane in the presence of alginate with different kinds of counterions at 25 °C. Table 4 lists an example of the uptake of chromophores to cellulose in the presence of polyelectrolytes with different kinds of counterions at 25° and 90 °C. Thus, the uptake is substantially greater with the salt of potassium, cesium, and ammonium than the sodium salt. This enhanced uptake of chromophores may be due to the fact that the sodium salt of the chromophores is ion-exchanged with different kinds of counterion on the polymer chain in the bulk solution (σ) designated as in Fig. 5. The uptake by the cellulose of chromophore with different kinds of counterion in the absence of polyelectrolyte at both 25° and 90 °C is greater with the other counterion (K^+, Cs^+, and NH_4^+) than with Na^+ (Table 4).[8] Furthermore, the fact that the uptake of chromophore with different kinds of counterion in the presence of NH_4Alg at 90 °C is the same is consistent with the assumption of ion-exchange described above.

In addition, this different enhancement with different kinds of counterion in the uptake of chromophore may depend on the differences in the degree of dissociation constant of polyelectrolytes with different kinds of counterion as well as the differences in the uptake described in both Fig. 3 and Table 1.

In any event it is clear that the addition of polyelectrolytes leads to marked enhancement of uptake and ion transport into a cellulose membrane.

Ion transport into the cellulose membrane in the presence of polyelectrolytes provides an interesting model for transport in a biological system.

Table 3. Standard free energy change($-\Delta\mu^\circ$) of chromophore into a cellulose[a] in aqueous polyelectrolyte solutions containing a constant concentration of sodium chloride at 25 and 90 °C[b]

Polyelectrolyte ×10² mol/l	kcal mol⁻¹ 25 °C	90 °C
NaAlg (0)	4.32	3.29
(2)	4.29	3.11
(4)	4.32	3.22
(6)	4.36	3.63
NaPSS (0)	4.38	3.19
(2)	4.33	3.14
(4)	4.38	3.17
(6)	4.35	3.21
NaPA (0)	4.31	3.14
(2)	4.30	3.12
(4)	4.15	2.97
(6)	4.40	3.28

a) Cotton. b) Concentration of chromophore; 1×10^{-4} mol/l, concentration of sodium chloride; 1×10^{-2} mol/l. the dissociation constant of polyelectrolyte in this system is correspond to the value (α^*) as described in Table 2.

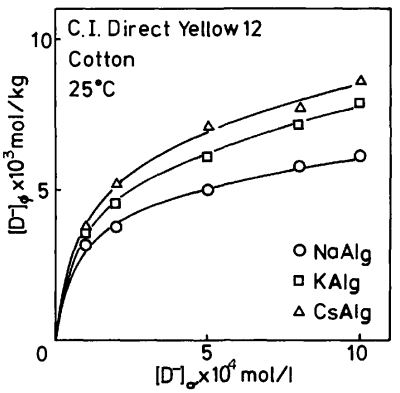

Fig. 6. Adsorption isotherm of C.I. Direct Yellow 12 on cotton in aqueous solution of alginate with different kinds of counterions(0.02 pyranose unit mol/l) at 25 °C.

Table 4. Uptake of chromophore into cellulose in the presence of alginic acid with different kinds of counterions at 25 and 90 °C

Polyelectrolyte[b]	Na^+	Uptake of chromophore/×10⁴ mol/kg cellulose[a] C.I. Direct Yellow 12 90 °C				25 °C			C.I. Direct Blue 15 90 °C	25 °C		C.I. Direct Red 2 90 °C
		NH_4^+	K^+	Cs^+	Na^+	NH_4^+	K^+	Cs^+	Na^+	Na^+	K^+	Na^+
NaAlg	43(24)				133(61)				(27)			41(84)
NH_4Alg	48(26)	48		49	172(67)				(26)			48
KAlg	(26)				164				(26)			
CsAlg	46(31)				181(77)				(30)			(95)
None	6.8(7.7)	9.7	9.0	9.0	35(25)	43	41	44	(5.5)	43	55	(30)

a) Parenthesis; values on cotton, concentration of chromophore used; 1×10^{-3} mol/l, these results are cosistent with the chromophore concentration used in this article($1—20\times10^{-4}$ mol/l). b) 0.02 pyranose unit mol.

M. N. wish to thank Prof. I. M. Klotz for comments on our manuscript. This research was supported by a grant from Asahi Glass Co. foundation.

References

1) M. Nango, M. Maekawa, A. Katayama, and N. Kuroki, *Sen-i Gakkaishi*, **35**, T-252 (1979).
2) M. Nango, M. Maekawa, A. Katayama, and N. Kuroki, *J. Appl. Polym. Sci.*, **25**, 2159 (1980).
3) M. Nango, E. Fukushima, M. Maekawa, A. Katayama, and N. Kuroki, *Sen-i Gakkaishi*, **36**, T-44 (1980).
4) M. Maekawa, M. Nango, A. Katayama, and N, Kuroki, *Sen-i Gakkaishi*, **35**, T-303 (1979).
5) T. Vickerstaff, "The Physical Chemistry of Dyeing," 2nd Ed., Oliver and Boyd, London (1954).
6) M. Maekawa, M. Hayashi, M. Nango, A. Katayama, and N. Kuroki, *Sen-i Gakkaishi*, **36**, T-184 (1981).
7) M. Nango, M. Maekawa, S. Tanihara, A. Katayama, and N. Kuroki, *Dyes and Pigments*, **2**, 49 (1981).
8) M. Nango, S. Ohta, Y. Shinmen, H. Kimura, and N. Kuroki, *Text. Res. J.*, in press.
9) T. Takahashi and K. Kimoto, *Bulletin of Tokyo University Industrial Institute*, **1**, No. 4 (1951).
10) A. Katchalsky, R. E. Cooper, J. Upadhyay, and A. Wasserman, *J. Chem. Soc.*, **1961**, 5198.
11) D. Dolar, J. Span, and S. Isokvic, *Biophys. Chem.*, **1**, 312 (1974).
12) M. Kowblansky and P. Ander, *J. Phys. Chem.*, **81**, 2024 (1977).
13) T. Okubo, Y. Nishizaki, and N. Ise, *J. Phys. Chem.*, **69**, 3690 (1965).
14) J. J. Huizenga, P. F. Grieger, and F. T. Wall, *J. Am. Chem. Soc.*, **72**, 2636 (1950).

 © 1984 The Chemical Society of Japan Bull. Chem. Soc. Jpn., 57, 2371—2375 (1984)

Liquid Crystal Formation in Binary Systems. X.[1] Potentially Smectogenic Behavior of Some *p*-Disubstituted Benzenes

Eiji CHINO, Yoshio MATSUNAGA,* and Mika SUZUKI
Department of Chemistry, Faculty of Science, Hokkaido University, Sapporo 060
(Received January 14, 1984)

Studies on binary systems with nematogenic *N*-(4-propoxybenzylidene)-4-hexylaniline revealed that 4-nitrophenyl alkanoates, alkyl 4-nitrobenzoates, *N*-(4-nitrophenyl)alkanamides, and *N*-alkyl-4-nitrobenzamides are potentially smectogenic. When the Schiff base is mixed separately with a homologous member from 4-nitrophenyl decanoate to tetradecanoate, a stable smectic A phase is induced and its maximum temperature is about 48 °C. The estimated latent transition points to this mesophase of these benzene derivatives are in the range from −25 to 10 °C. On the other hand, only metastable smectic A phases can be produced with hexyl to dodecyl 4-nitrobenzoates, the maximum temperatures being from 15 to 26 °C. While the metastable smectic B phase of the Schiff base is to some extent stabilized by the addition of the alkanoates, it is drastically depressed by the benzoates. The addition of *N*-(4-nitrophenyl)nonanamide to -dodecanamide produces a stable smectic A phase and also stabilizes the metastable smectic B phase. No smectic A phase is found in mixtures of the Schiff base with *N*-octyl- to *N*-dodecyl-4-nitrobenzamides, and the isotropic or nematic-smectic B transition point curves are almost horizontal indicating that these benzene derivatives have transitions to latent smectic B phases between 10 and 20 °C. Results obtained with some related compounds are also presented.

In one of the earlier papers of this series, we reported the induction of smectic phases by the addition of 4-alkoxynitrobenzenes to *N*-(4-propoxybenzylidene)-4-hexylaniline and the related compounds.[2] This Schiff base gives a nematic phase stable between 42 and 63 °C and a metastable smectic B phase below 21 °C. We concluded that the induction of smectic A phases in the above binary mixtures is indicative of the potentially smectogenic behavior of these *p*-disubstituted benzenes even though the upper limit of smectic temperature range is located at about −25 °C for 4-(dodecyloxy)nitrobenzene and lower for the other homologous members. With the hope of finding potentially smectogenic *p*-disubstituted benzenes with higher transition temperatures, we examined the phase diagrams of the binary systems composing of the above Schiff base and 4-nitrophenyl alkanoate (**1**), alkyl 4-nitrobenzoate (**2**), *N*-(4-nitrophenyl)alkanamide (**3**), and *N*-alkyl-4-nitrobenzamide (**4**) respectively. Esters are side chains widely shared by discogenic compounds, whereas amides were rarely studied but chosen for the present work because the $NHCOCH_3$ substituent, which can hydrogen-bond and has a strong dipole, is known to markedly enhance smectic thermal stabilities.[3]

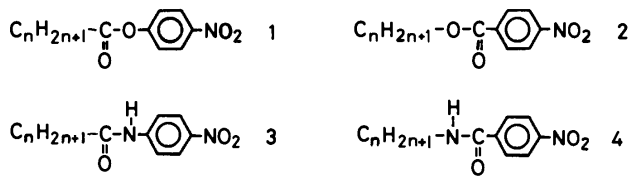

Experimental

Materials. Homologous series of 4-nitrophenyl alkanoates and *N*-(4-nitrophenyl)alkanamides were obtained by the acylation of 4-nitrophenol and 4-nitroaniline respectively. The products will be referred to as *n*COO, NO_2, and *n*CONH, NO_2 on the basis of the substituents where *n* is the number of carbon atoms in the alkyl group. The alkyl 4-nitrobenzoates and *N*-alkyl-4-nitrobenzamides were prepared by the reaction of 4-nitrobenzoyl chloride on alcohols and alkylamines respectively. They will be abbreviated as *n*OCO, NO_2, and *n*NHCO, NO_2. These disubstituted benzenes were purified by recrystallization, distillation under reduced pressure and/or column chromatography. Hereafter, *N*-(4-propoxybenzylidene)-4-hexylaniline will be denoted by (3O, 6) designating the alkoxyl and alkyl carbon numbers for the substituents.

Measurements. The calorimetric measurements and the identification of the mesophases were made as reported in our previous paper.[2]

Results and Discussion

4-Nitrophenyl Alkanoates (nCOO, NO_2). The homologous members from decanoate to tetradecanoate (*n*=9—13) were examined. Upon mixing with (3O, 6), they produce stable smectic A phases as exemplified by the phase diagrams of the binary systems with each of 10COO, NO_2, and 12COO, NO_2 (see Figs. 1a and b). The open and shaded circles indicate the transitions recorded during the processes of heating and cooling respectively.

The phase diagrams obtained with 9COO, NO_2, and 11COO, NO_2 resemble that given in Fig. 1a; namely, the coexistence of the isotropic and smectic phases occurs over a range of temperature. In contrast, no indication of the two-phase liquid system is found with 12COO, NO_2 or with 13COO, NO_2. The maximum temperature of the smectic A-isotropic transition point curve is not much affected by the alkyl chain length throughout the studied members, that is, 47—48 °C (see Curve a in Fig. 2). It is higher by about 10 °C than the melting points of the first two homologous members, is nearly the same as those of the next two, and is lower by about 10 °C than that of the last. The extrapolation of the transition point curve to 0 mol% of (3O, 6) yields more reliable latent transition temperature when the alkyl chain is shorter as the curve is observable over a wider composition range. Such a tendency is more or less shared by most of the homologous series studied in this paper. The estimated temperature varies from −25

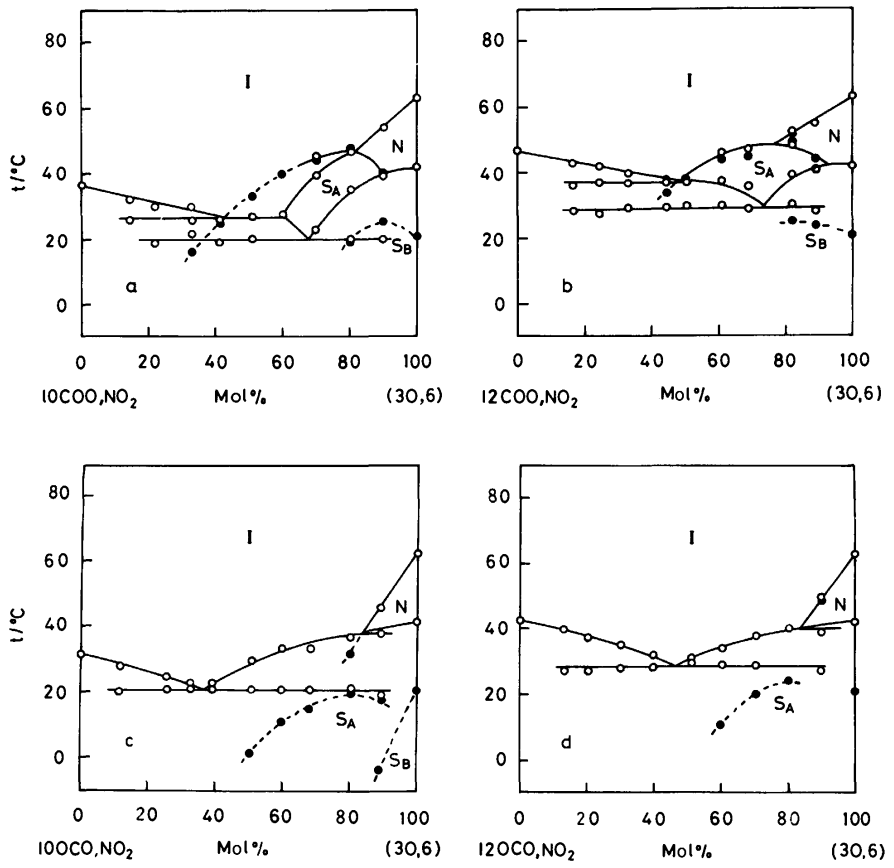

Fig. 1. Phase diagrams of (a) 10COO, NO_2–(3O, 6), (b) 12COO, NO_2–(3O, 6), (c) 10OCO, NO_2–(3O, 6), and (d) 12OCO, NO_2–(3O, 6) systems. The open and shaded circles are transitions observed in the processes of heating and cooling respectively.

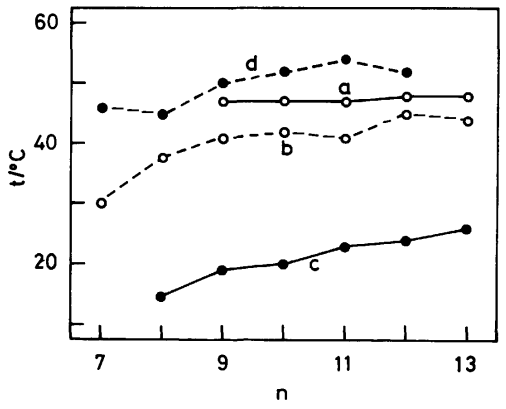

Fig. 2. Plots of the maximum temperatures of the induced smectic A phases against the length of the alkyl chain, *n*, for (a) *n*COO, NO_2–(3O, 6), (b) *n*COO, CN–(3O, 6), (c) *n*OCO, NO_2–(3O, 6), and (d) *n*CONH, NO_2–(3O, 6) systems.

to 10 °C. The values tend to be higher with the higher homologs. They are located below the melting points of *n*COO, NO_2 by 50 to 70 °C. If the isotropic melts were supercooled to such a large extent the appearance of smectic A phases of *n*COO, NO_2 could be achieved; therefore, these 4-nitrophenyl alkanoates may be considered as potential smectogens.

The monotropic smectic B phase of (3O, 6) is also stabilized by the addition of these benzene derivatives. The transition point curves are markedly convex upwards when *n* is even but not so when *n* is odd.

In order to supplement the above results, seven systems consisting of *n*COO, CN, and (3O, 6) were studied. The maximum temperatures of the smectic A-isotropic transition point curves are shown by Curve b in Fig. 2. They are slightly lower than those of the corresponding *n*COO, NO_2–(3O, 6) systems. The extrapolation of the transition point curve to 0 mol% of (3O, 6) also seems to yield lower temperatures; *e.g.*, −30 °C for 10COO, CN *vs.* −25 °C for 10COO, NO_2. As 4-cyanophenyl alkanoates have higher melting points than the 4-nitrophenyl compounds, the induced smectic A phases are metastable except for the cases *n*=9, 11, and 12. The stabilization of the smectic B phase of (3O, 6) observed with the 4-cyanophenyl esters is more remarkable than that with the 4-nitrophenyl esters. The observation made for the induced smectic A phase is consistent with the order of smectic terminal group efficiency for nitro and cyano groups given by Gray[3] but that made for the monotropic smectic B phase is in the reversed order.

Alkyl 4-Nitrobenzoates (nOCO, NO_2). The homologous series examined extends from the octyl to the tridecyl ester (*n*=8—13). When these 4-nitrobenzoates are added to (3O, 6), smectic A phases are induced in all the systems. However, they are entirely

metastable, the maximum of the isotropic-smectic A transition point curve lying in the range from 15 to 26 °C. Contrary to the alkanoates, the temperature raises with the increase of the alkyl chain length exhibiting a small but definite alternation (see Curve c in Fig. 2). The temperatures observed with 8OCO, NO_2, 9OCO, NO_2, and 11OCO, NO_2 are located above the eutectic points. For the sake of comparison with the effects of the isomeric compounds, the phase diagrams of the decyl and dodecyl ester-(3O, 6) systems are presented in Figs. 1c and d. These esters presumably have the potential to exhibit smectic A phases at temperatures as low as −65 to −40 °C. As is shown in Fig. 1c, the monotropic smectic B phase of the Schiff base shows a drastic depression on addition of 10OCO, NO_2. Furthermore, it must be noted that the slope of the nematic-isotropic transition point curve is much steeper than that observed with the 4-nitrophenyl alkanoates. Thus, the abillity to exhibit mesophases of the 4-nitrobenzoates is undoubtedly inferior to that of the above-mentioned isomerides.

It is worthwhile to note the alternation of the melting points of *n*COO, NO_2, and *n*OCO, NO_2. The former compounds melt at relatively higher temperatures when *n* is odd and the latter exhibit the opposite variation. Therefore, the melting point of *n*COO, NO_2 lies by 15 to 20 °C above that of the corresponding *n*OCO, NO_2 when *n* is odd. The difference is as small as 5 °C when *n* is even.

N-(4-Nitrophenyl)alkanamides (nCONH, NO_2). The replacement of the -O- group in the 4-nitrophenyl alkanoate with an -NH- group brings about a rise in the melting point by 30 to 40 °C depending upon *n*. When *n*=9 or more, the induced smectic A phase is enantiotropic in a certain range of composition and temperature in the binary system with (3O, 6). Even though the maximum temperatures of the transition point curves are in the range from 50 to 54 °C for these systems (see Curve d in Fig. 2), the smectic A phases are observable in the smaller ranges than those found for the *n*COO, NO_2-(3O, 6) systems. For example, the phase diagrams given in Figs. 3a and b may be compared with those in Figs. 1a and b. The observed smectic A-isotropic transition point curves are not long enough to estimate the temperatures for potential smectic A phases but suggest that they are not very different from those estimated for the 4-nitrophenyl alkanoates. As is illustrated in Fig. 3a, the monotropic smectic B phase of (3O, 6) is stabilized by the addition of 10CONH, NO_2.

In order to compare the role of a nitro group and a cyano group in the anilides on the smectogenic behavior, the system comprising 11CONH, CN, and (3O, 6) was included to the present work. The diagram is

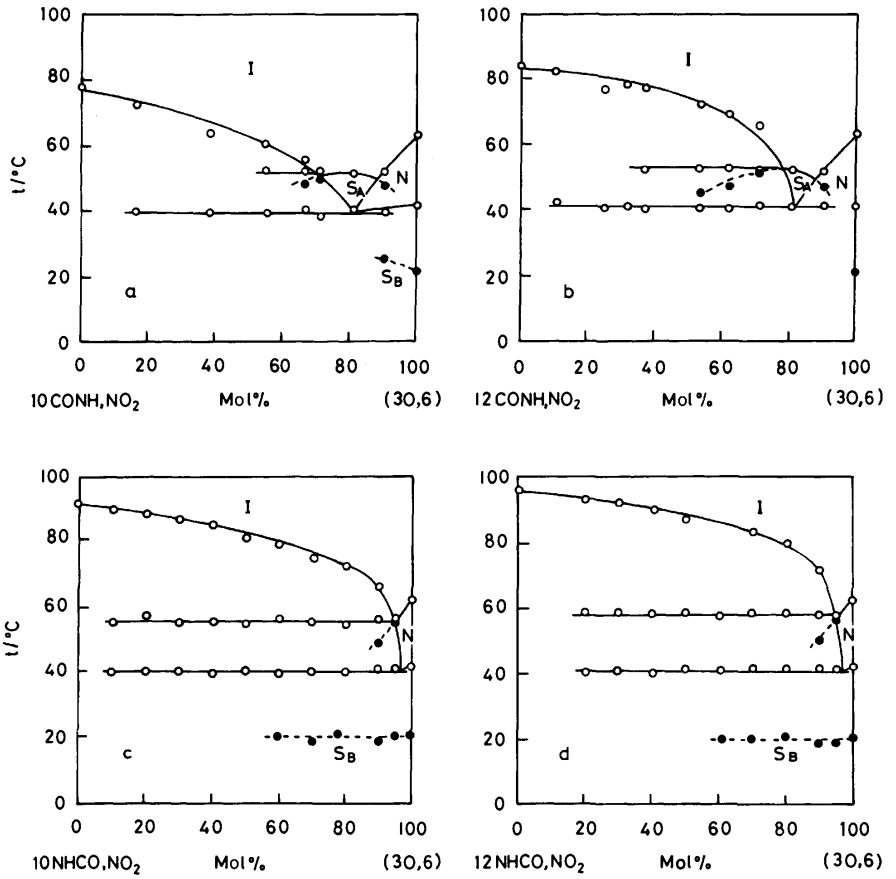

Fig. 3. Phase diagrams of (a) 10CONH, NO_2-(3O, 6), (b) 12CONH, NO_2-(3O, 6), (c) 10NHCO, NO_2-(3O, 6), and (d) 12NHCO, NO_2-(3O, 6) systems. As to the open and shaded circles, see the caption of Fig. 1.

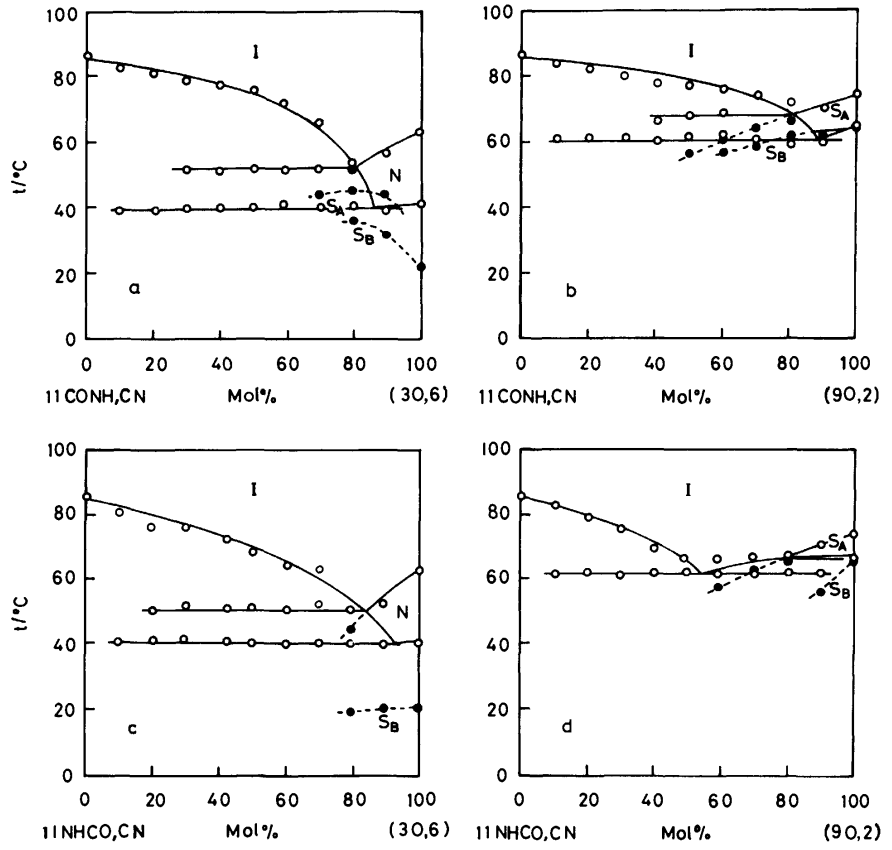

Fig. 4. Phase diagrams of (a) 11CONH, CN–(3O, 6), (b) 11CONH, CN–(9O, 2), (c) 11NHCO, CN–(3O, 6), and (d) 11NHCO, CN–(9O, 2) systems. As to the open and shaded circles, see the caption of Fig. 1.

given in Fig. 4a. A smectic A phase is induced but it is monotropic, the maximum temperature being 46 °C. This observation is in good accord with the tendency found by comparison between *n*COO, NO_2 and *n*COO, CN and also 4-alkoxynitrobenzenes and 4-alkoxybenzonitriles reported in a previous paper.[2] Moreover, it must be noted that the stabilization of the metastable smectic B phase by the cyanoanilide is much greater than that by the corresponding nitroanilide. The maximum temperature achieved by the former compound is 36 °C and that by the latter is 24 °C. This might imply that the 4-cyanoanilide has a potential smectic B phase at a relatively high temperature. This postulate is strongly supported by the phase diagram shown in Fig. 4b, where (3O, 6) is replaced by *N*-(4-nonyloxybenzylidene)-4-ethylaniline, (9O, 2), which exhibits stable smectic A and B phases. The diagram suggests that the latent smectic B phase of 11CONH, CN is located around 30 °C. This temperature is probably higher than that of the latent smectic A phase.

*N-Alkyl-4-nitrobenzamides (*n*NHCO, NO_2).* The melting points of the three compounds in this series (*n*=8, 10, and 12) are higher than those of the above isomerides as is seen from Figs. 3c and d. The effect of the change in molecular structure on the liquid crystal behavior is so remarkable that no smectic A phase is found in these mixtures. The monotropic smectic B phase is observable over a composition range as wide as 40 mol%. As the transition point curves are essentially horizontal, these 4-nitrobenzamides should have transition temperatures to latent smectic B phases between 10 and 20 °C. It may be noted that the nematic phase of the Schiff base is rapidly depressed by the presence of *n*NHCO, NO_2.

As is shown in Fig. 4c, the behavior of *N*-undecyl-4-cyanobenzamide is similar to those of the 4-nitrobenzamides described above except for the less drastic depression of the nematic phase and the limited observation of the nematic-smectic B transition point curve. The isotropic or nematic-smectic B transition point curves in Figs. 3c, 3d, and 4c are almost straight; therefore, the reason why no smectic A phase is induced by mixing with (3O, 6) may be ascribed to the absence of the thermal stability enhancement. The phase diagram prepared with (9O, 2) instead of (3O, 6) clearly demonstrates that the 4-cyanobenzamide has a transition point to a latent smectic A phase closely located to that to a latent smectic B phase (compare Fig. 4d with 4c). The observed short smectic A-smectic B transition point curve is concave upwards.

*N-(4-Nitrobenzylidene)alkylamines (*n*N=CH, NO_2).* Finally, we studied the effects of the addition of *N*-(4-nitrobenzylidene)alkylamines (*n*=9—13) as a series of the compounds involving a double bond linkage in the substituent. All the homologous members can induce smectic A phases exhibiting maximum temperatures from 40 to 41 °C. As is shown in Fig. 5, the com-

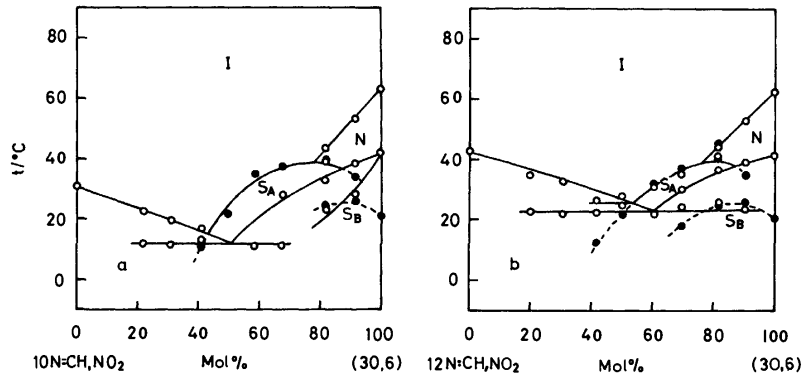

Fig. 5. Phase diagrams of (a) 10N=CH, NO_2–(3O, 6) and (b) 12N=CH, NO_2–(3O, 6) systems.
As to the open and shaded circles, see the caption of Fig. 1.

position range of the stable smectic A phase is fairly wide. The monotropic smectic B phase is appreciably stabilized. However, the latent smectic phases of these compounds are probably located at temperatures as low as −50 to −40 °C.

The above results emphasize that the particularly high transition temperatures to latent smectic phases can be achieved with the benzamides and anilides. As the suitability of the terminal substituent for liquid crystal formation may be at its most significant in simple systems we decided to extend our examination of thermal properties to a number of benzene derivatives carrying two or three of these terminal groups; namely, $C_nH_{2n+1}NHCO$ and $C_nH_{2n+1}CONH$. Some novel mesomorphic compounds have been discovered by this approach. Their properties will be the subject of the forthcoming papers.

The present work was partially supported by a Grant-in-Aid for Scientific Research No. 543001 from the Ministry of Education, Science and Culture.

References

1) Part IX, Y. Matsunaga and I. Suzuki, *Bull. Chem. Soc. Jpn.*, **57**, 1411 (1984).
2) E. Chino and Y. Matsunaga, *Bull. Chem. Soc. Jpn.*, **56**, 3230 (1983).
3) G. W. Gray, *Mol. Cryst.*, **1**, 333 (1966).

Electron Paramagnetic Resonance and Optical Detection of Magnetic Resonance Studies of the Lowest Excited Triplet States of Purine, Benzimidazole, and Indazole in Benzoic Acid Host Crystals

Masayo NODA,† Shin-ichi NAGAOKA,†† and Noboru HIROTA*
Department of Chemistry, Faculty of Science, Kyoto University, Kyoto 606
(Received February 2, 1984)

The triplet states ($^3\pi\pi^*$) of purine, benzimidazole, and indazole are investigated in benzoic acid crystals by electron paramagnetic resonance (EPR) and optical detection of magnetic resonance (ODMR) techniques. Well resolved phosphorescence spectra were obtained at 4.2 K. The T_1 states of purine and benzimidazole are located at 26409 and 26536 cm^{-1}, respectively. The zero field splittings (ZFS) are D=0.1042 cm^{-1}, $|E|$=0.0608 cm^{-1} for purine, and D=0.1123 cm^{-1}, $|E|$=0.0270 cm^{-1} for benzimidazole. The decay rate constants of the triplet sublevels are determined at 1.5 K and are compared with those of indole. From the angular dependence of the EPR signals, the probable orientations of purine and benzimidazole in benzoic acid hosts are determined. From the observed hyperfine splittings (hfs) spin distribution of the T_1 state of purine is estimated. (ρ_6= 0.20, ρ_8=0.27, and ρ_2=0.12). The effects of the nitrogen substitution in the pyrole ring of indole on the ZFS and spin distribution are discussed.

The lowest excited triplet (T_1) states of purine, benzimidazole and indazole have received considerable attention because of their possible importance in photobiological processes. Numerous spectroscopic,[1-9] EPR,[10-12] ODMR, and theoretical[13-15] investigations have been attempted before, but owing to poor solubility of these molecules in nonpolar solvents and difficulties in finding good host crystals, previous investigations have been limited severely. For example, neither well resolved phosphorescence spectra nor single crystal EPR spectra of the triplet states of these molecules have been reported.[16] Zero field ODMR[17-19] experiments have been made in rigid solution, but the sublevel schemes of the T_1 states as well as their decay properties are not completely understood. Details of the spin distributions in the T_1 states are also not known for these molecules.

In the course of investigations in this laboratory, we have found that benzoic acid (BAC) is a good host for polar molecules which are difficult to dissolve into the crystals of nonpolar molecules such as durene.[20] Therefore, we have attempted to investigate the properties of the T_1 states of purine, benzimidazole, indazole and indole in the mixed crystals of BAC by means of ODMR and EPR techniques in order to elucidate the properties of their T_1 states. Well-resolved phosphorescence spectra were obtained at 4.2 K, and the decay rate constants of the triplet sublevels as well as the zero field transition energies were determined at 1.5 K. Single crystal EPR experiments were also made to determine the sublevel schemes unambiguously and to obtain information about the spin distributions. Here we discuss the phosphorescence spectra, the zero field splittings (ZFS), the hyperfine splittings (hfs) and the sublevel decay properties of these molecules. Benzimidazole, indazole, and purine are also considered as nitrogen substituted indoles, respectively. In this work it was found that the triplet properties are strongly affected by the nitrogen substitution of indole. We discuss the variations in the decay and magnetic properties in this series of molecules.

Experimental

Sample Preparation. BAC (Wako) was purified by extensive zone refining. Purine (Sigma) was purified by recrystallization from toluene followed by vacuum sublimation. Benzimidazole (Aldrich) and indole (Aldrich) were purified by vacuum sublimation. Indazole (Tokyo kasei) was recrystallized twice from water and then sublimated in vacuum. Mixed crystals of BAC with desired guest molecules were grown by the standard Bridgman method. About one percent of the guest molecule was contained in the initial melt, but the actual concentration of the guest is considered to be very low. The molecular structures of the guest molecules and the numbering systems used here are given in Fig. 1.

Phosphorescence and ODMR Experiments. Phosphorescence spectra were obtained with the ODMR setups described elsewhere.[21] The ZFS and the decay rate constants were determined by the standard ODMR[22,23] and microwave induced delayed phosphorescence (MIDP)[24] experiments made at 1.5 K. Since the sublevel lifetimes are relatively long in the present systems, the effect of the spin lattice relaxation probably cannot be neglected entirely even at 1.5 K. The experimental errors in the determination of k_y are estimated to

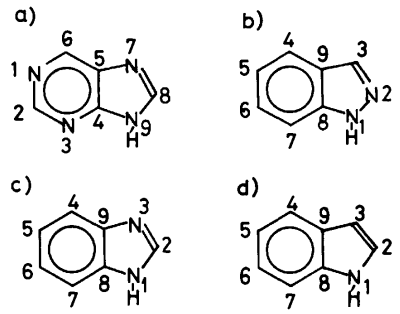

Fig. 1. Molecular structures and the numbering systems for a) purine, b) 1*H*-indazole, c) benzimidazole, d) indole.

Present address:
† Tokai Women's College, Kagamigahara, Gifu 504.
†† Division of Chemistry, Research Institute of Applied Electricity, Hokkaido University, Sapporo 060.

be ~10% and those of k_x and k_z are ~25%. Microwave modulated phosphorescence spectra were obtained by applying the microwave at the ODMR transition frequencies and detecting the changes in the phosphorescence intensities, while the monochromator was scanned.

EPR Measurements. EPR measurements were made at 4.2 K with a JEOL JES-FE3X spectrometer with a home-built liquid helium cryostat. The experimental procedures are essentially the same as those described previously.[20] The crystal was mounted on a wedge so that the applied field rotated within the molecular plane of BAC by rotating the sample holder. The method of mounting a crystal was described elsewhere.[16]

Results and Discussion

Phosphorescence Spectra. The phosphorescence spectra of purine, benzimidazole and indazole in BAC obtained at 4.2 K are all well resolved as shown in Fig. 2. Since these molecules are expected to be in well defined configurations by forming hydrogen bonds with BAC, highly resolved spectra are probably obtained.

The O-O band of benzimidazole is very strong and is located at 376.9 nm. The frequencies of the main vibrations appearing in the phosphorescence spectra are in good agreement with the ground state vibrational frequencies determined by IR and Raman studies as shown in Table 1. As discussed in detail in a separate paper,[16] indazole in BAC exists in two tautomeric forms, 1*H*-indazole and 2*H*-indazole. The strong O-O band of the 1*H*-indazole spectrum is located at 423.9 nm. The observed vibrational frequencies are given in Table 1 together with the IR data.

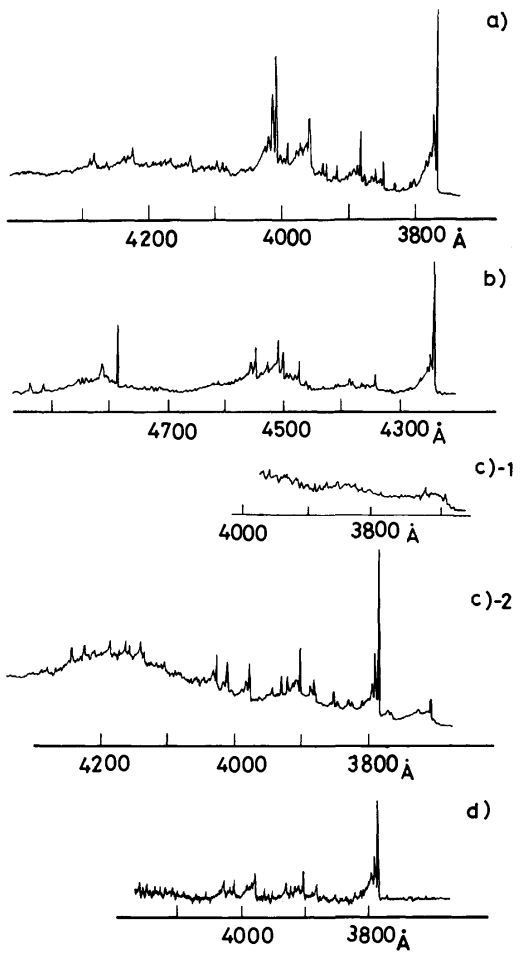

Fig. 2. Phosphorescence spectra in the mixed crystal of BAC at 4.2 K. a) benzimidazole, b) 1*H*-indazole, c)-1 benzoic acid X-trap, c)-2 purine, d) purine microwave modulated spectrum at 1.3 GHz.

The shortest wavelength band of the phosphorescence spectrum of purine in BAC appears at 368.85 nm, but the strongest band appears at 378.65 nm. The relative intensity of the former with respect to that of the latter depends on the sample preparation suggesting that the 368.85 nm band does not originate from purine. ODMR signals were observed at the bands with the wavelengths longer than 378.65 nm, but no ODMR signals were detected at the 368.85 nm band. The shorter wavelength portion of this spectrum resembles the corresponding portion of the phosphorescence spectrum of the BAC X-trap induced by anisole whose O-O band is located at 368.8 nm. (Fig. 2 c)-1) Therefore, it is concluded that the phosphorescence spectrum of purine in BAC in a superposition of the spectra coming from purine and the BAC X-trap. In order to eliminate the phosphorescence of the BAC X-trap and to obtain the genuine spectrum of purine, we have taken a microwave modulated phosphorescence spectrum. The spectrum obtained with the microwave modulation at 1.3 GHz is given in Fig. 2-d. It is seen that the spectrum has a very strong O-O band as those of benzimidazole and 1*H*-indazole. The main vibrational frequencies determined from the phosphorescence spectrum agree well with those determined from the IR and Raman spectra. (Table 1).

The strong O-O band observed here makes a striking contrast to the weak O-O bands found in the phosphorescence spectra taken in other environments, namely

Table 1. Main vibrational bands appearing in the phosphorescence spectra and the corresponding IR and Raman bands

	Purine		Indazole		Benzimidazole	
O-O	26409 cm^{-1}		23590 cm^{-1}		26536 cm^{-1}	
$\Delta\nu$ cm^{-1}	446		549		548	
	650	R 663			626	R 627
	780	R 795	775	IR 770	776	R 779
						IR 778
	909	IR 908			1010	R1006
						IR1004
	959	IR 963			1117	R1110
	1263	R1268	1224	IR1250	1274	R1274
						IR1274
	1480		1405	IR1380	1492	R1498
						IR1497
	1578	IR1565	1601	IR1605	1598	R1593
						IR1590

The Raman and IR frequencies for purine and indazole were determined in the present work. The values for benzimidazole were taken from Ref. 35.

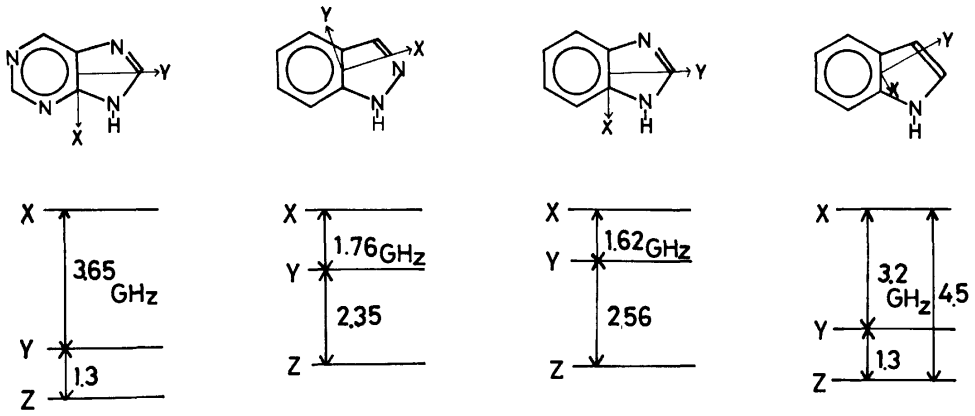

Fig. 3. Approximate direction of the principal axes of the ZFS and the sublevel schemes.

in a rare gas matrix,[8] powder,[7,9] and rigid solution.[2] The cause of this difference seems to be the following. While a well defined single site exists for purine in BAC, there are many sites with different O-O bands in other environments producing inhomogeneous broadenings of the spectra. In contrast to the sharp phosphorescence spectra of the above molecules, the spectrum of indole is very broad indicating the presence of prominent inhomogeneous broadening. The strong O-O bands and the relatively weak vibronic bands found for purine, benzimidazole, and indazole indicate that the structures of the T_1 states of these molecules are not much different from those of the ground states. The phosphorescence spectra of these three molecules are similar with the main vibronic bands at 0—780 cm^{-1}, 0—1270 cm^{-1}, and 0—1600 cm^{-1} (Table 1).

Sublevel Schemes and Zero Field Splittings. The ODMR signals were observed at 3.65 GHz and 1.30 GHz for purine, 2.56 GHz and 1.62 GHz for benzimidazole, 2.35 GHz and 1.76 GHz for 1 *H*-indazole and 4.5 GHz, 3.2 GHz, and 1.3 GHz for indole, respectively. These ODMR frequencies correspond to the transitions between the sublevels which are eigenstates of the following spin Hamiltonian;

$$\mathscr{H} = D\left(S_z^2 - \frac{1}{3}\mathbf{S}^2\right) + E(S_x^2 - S_y^2)$$

$$= -XS_x^2 - YS_y^2 - ZS_z^2, \qquad (1)$$

where $X=1/3D-E$, $Y=1/3D+E$ and $Z=-2/3D$.

Here we take the two in-plane spin axes as the X and Y axes. The Z axis is taken perpendicular to the molecular plane. The T_z sublevel is considered to be the bottom one as in the cases of other aromatic molecules. The top sublevel is taken as the X sublevel as shown in Fig. 3. We designate energies of the X, Y, and Z sublevels by T_x, T_y, and T_z, respectively.

The approximate directions of the X and Y axes were determined by the ratios of the radiative decay rate constants and the angular dependence of the EPR signals as discussed in the later sections. Whether $|T_y-T_z|>|T_x-T_y|$ or $|T_x-T_y|>|T_y-T_z|$ could not be determined from the ODMR experiments. In the former case $D>3|E|$ and in the latter $D<3|E|$. From the single crystal EPR experiments $D<3|E|$ was established previously in the case of indole, and this was also tentatively assumed for the other molecules because of the similarities of the molecular structures.[25] However, Svejda *et al.*[18] concluded $D>3|E|$ for benzimidazole from the analysis of the decay data of the ODMR signals in ethanol. It is, therefore, desirable to determine the zero field sublevel schemes unambiguously and we have examined the augular dependence of the EPR signals of benzimidazole, 1*H*-indazole and purine in BAC. The mixed crystals were mounted so that the applied field rotated in the X-Y planes, on the assumption that the guest molecules substitutionally replace the host molecules. The obtained angular dependence curves are shown in Fig. 4. Unfortunately the signals were rather weak and we were only able to observe parts of the angular dependence curves, but they are sufficient to determine whether $D>3|E|$ or $D<3|E|$. It is immediately clear from Fig. 4 that $D>3|E|$ in the case of benzimidazole and 1*H*-indazole, but $D<3|E|$ in purine. The curves obtained for benzimidazole and 1*H*-indazole are in good agreement with those predicted by solving the spin Hamiltonian

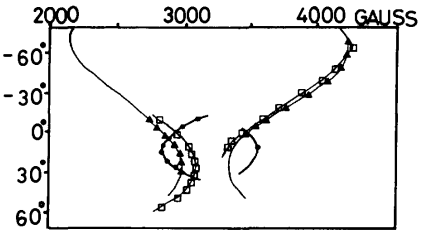

Fig. 4. Angular dependence of the EPR signals. ▲: Benzimidazole, □: 1*H*-indazole, ●: purine. The curves for benzimidazole and 1*H*-indazole are obtained by solving Eq. 2 with the ZFS determined by ODMR experiments. The curve for purine is drawn only for eye guide.

$$\mathscr{H} = \beta H \cdot g \cdot S + DS_z^2 + E(S_x^2 - S_y^2) \qquad (2)$$

with $g=2$ and the D and E values determined by the ODMR experiments. On the other hand, the agreement between the experimental and the predicted ones is poor for purine. This may be due to the deviation from the coplanarity of the guest and host molecules. The ZFS

determined in BAC are listed in Table 2 together with those determined in other hosts. The D and E values vary slightly depending on the host. $|E|$ of benzimidazole and 1H-indazole are smaller in BAC than in 1,4-dibromobenzene host (DBB), while $|E|$ of purine and indole are larger in BAC than in DBB. Though the ZFS are affected by the environment, the basic characteres of the T_1 states are considered to remain unchanged on going from one environment to the other.

Decay Properties. The relatively long lifetimes of all the molecules studied here indicate that the T_1 states are $\pi\pi^*$ in character. We have determined the total decay rate constants (k_i) and the relative radiative decay rate constants (k_i^r) of the triplet sublevels by the MIDP experiments (Table 2). In spite of the poor molecular symmetries the decay constants are remarkably sublevel dependent; k_y and k_y^r are by far the largest in each molecule. The observation that k_z is similar to k_x seems to indicate the effect of spin lattice relaxation. The sublevel decay rate constants of purine, benzimidazole, and indole in ethanol were previously estimated by Moller and Nishimura[17] from the decomposition of the decay curves obtained at 1.5 K into three components. The sublevel decay constants of benzimidazole was determined in a mixture of ethylene glycol-water (1 : 1) by Svejda, *et al.*[18] and those of indole was also determined in the neat crystal by Zuclich *et al.*[19] The values obtained in the present work are somewhat different from those reported previously.

Benzimidazole, indazole, and purine are considered to be nitrogen substituted indoles. The decay rare constants of these molecules are larger than those of indole and this is presumably due to the presence of low lying $^1n\pi^*$ and $^3n\pi^*$ states which are brought in by the nitrogen substitution. These states mix with the T_1 ($^3\pi\pi^*$) states and enhance both radiative and nonradiative decay rates. The increase in the radiative decay rate due to the $^1n\pi^*$ state is determined by the spin-orbit matrix element $\langle {}^1n\pi^*|\mathscr{H}_{so}|{}^3\pi\pi^*\rangle$, the energy separation between the $^1n\pi^*$ and $^3\pi\pi^*$ state, $E(^1n\pi^*)-E(^3\pi\pi^*)$ and the transition moment $\vec{M}(^1n\pi^*-S_o)$. The increase in the nonradiative decay rate constant is determined by the energy separations $E(^3n\pi^*)-E(S_o)$, and $E(^3n\pi^*)-E(^3\pi\pi^*)$ and the spin-orbit matrix elements $\langle {}^3n\pi^*|\mathscr{H}_{so}|S_o\rangle$ and $\langle {}^1n\pi^*|\mathscr{H}_{so}|{}^3\pi\pi^*\rangle$ as well as the matrix elements for vibronic couplings. In the present case spin-orbit matrix elements are mainly determined by the one center integral at the nitrogen atom.

When the one center integral at the nitrogen atom plays a dominant role in the relevant spin-orbit coupling matrix element for the increase in the radiative decay, the ratio of the increase in k_y^r (δk_y^r) to that in k_x^r (δk_x^r) is given by[26]

$$\delta k_y^r/\delta k_x^r = \cos^2\alpha/\sin^2\alpha \qquad (3)$$

where α is the angle between the X axis and the direction of the nitrogen lone pair orbital. A similar equation holds for the nonradiatiave decay. The data given in Table 2 show that the increases in the decay rates on going from indole to benzimidazole and 1H-indazole are mainly in k_y. Then the direction perpendicular to the lone pair orbital of the nitrogen atom must be close to the direction of the Y axes. This means that the Y axis of benzimidazole is along the direction of the long molecular axis as shown in Fig. 5, whereas that of 1H-indazole is along the short axis.

Because of the nitrogen substitution in the six-membered ring k_y of purine is larger than those of

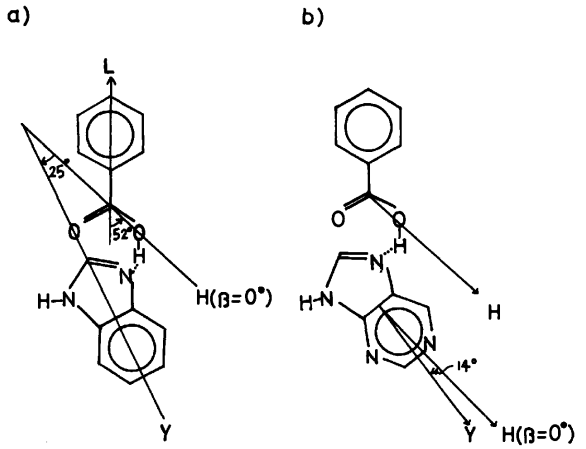

Fig. 5. The probable orientations of a) benzimidazole and b) purine in BAC. The dotted lines indicate hydrogen bonds.

Table 2. Zero field splitting parameters and the decay rate constants of sublevels

		Purine	Indazole	Benzimidazole	Indole
D cm^{-1}		0.1042 (0.1009)[a] (0.0990)[b]	0.1077 (0.1073)[a]	0.1123 (0.1178)[a] (0.1185)[b]	0.0967 (0.0978)[a]
$\|E\|$ cm^{-1}		0.0608 (0.0584)[a] (0.0647)[b]	0.0293 (0.0310)[a]	0.0270 (0.0362)[a] (0.0325)[b]	0.0533 (0.0453)[a]
k_i sec^{-1}	x	0.29	0.13	0.08	0.1
	y	2.1	0.85	0.57	0.3
	z	0.22	0.16	0.095	0.09
k_i^r	x	0.2	0.05	<0.1	<0.1
	y	1	1	1	1
	z	0.2	0.09	0.11	0.1

a) DBB, Ref. 25. ZFS are recalculated based on the sublevel scheme determined in this work. b) Ethylene glycol-water(1 : 1), Ref. 18.

Table 3. Energies of the $^3\pi\pi^*$, $^1n\pi^*$, and $^1\pi\pi^*$ states and the largest sublevel decay rate constants

	$E(^3\pi\pi^*)$ cm^{-1}	$E(^1n\pi^*)$ cm^{-1}	$E(^1\pi\pi^*)$ cm^{-1}	$E(^1n\pi^*)-E(^3\pi\pi^*)$ cm^{-1}	k_y sec^{-1}
Purine	26409	31408[e]		4499	2.1
Benzimidazole	26539	>35732[e]	36023[h]	>9193	0.57
Indazole	23590	>33272[e]	34473[i]	>9682	0.85
Indole	24135[a]		35233[j]		0.30
Quinoxaline	21639[b]	27070[f]	31950	5431	11.1[b]
Quinoline	21700[c]	29656[g]		7956	3.1[c]
Isoquinoline	21268[d]	30921[g]		9653	3.0[d]
Naphthalene					0.65[k]

a) Ref. 25. b) Ref. 36. c) and d) S. Yamauchi private communications. e) Ref. 7. f) Ref. 37. g) Ref. 38. h) Ref. 39. i) Ref. 40. j) Ref. 41. k) Ref. 42.

benzimidazole and indazole. The one center integrals at the nitrogen atoms 3 and 7 are considered to be important in determining the spin-orbit matrix elements because of a smaller spin density expected at the nitrogen atom 1. The Y axis of purine is also expected to be along the long axis of the molecule.

The increase of k_y on going from indole to benzimidazole, indazole, and purine are 0.27 sec^{-1}, 0.55 sec^{-1}, and 1.8 sec^{-1}, respectively. The difference between benzimidazole and indazole may be primarily due to the increased nonradiative decay rate constant of indazole because $E(T_1)-E(S_0)$ of indazole is smaller than that of benzimidazole by ~3000 cm^{-1}. The increase in the case of purine can be attributed to the increased spin-orbit matrix element due to the inclusion of two nitrogen atoms in the six-membered ring and smaller energy separations between the $^3\pi\pi^*$ state and the $^1n\pi^*$ and $^3n\pi^*$ states.

The observed increases in the decay rate constants by the nitrogen substitution in the indole skelton are, however, rather small when we compare them with the increases found for the nitrogen substitution in naphthalene. In Table 3 we compare the increases found for the present systems with those found for a series of molecules, quinoline, isoquinoline, and quinoxaline. As seen from the Table 2 the increases are about five times smaller for the present series.

The deuteration of purine reduces the decay rate constants, with $k_y[D]/k_y[H]=0.62$. This ratio is similar to that found for quinoxaline, $k_y[D]/k_y[H]=0.6$.[24c] The reduction of the decay rate constant is due to the decrease of the nonradiative decay rate constant. In the case of quinoxaline the ratio of the radiative and the nonradiative decay rate constants, $k^r:k^{nr}$ is estimated to be 5:7.[27] As in the case of quinoxaline the nonradiative decay is considered to occupy a significant part of the total decay in the case of purine. Then it is concluded that the increases in both radiative and nonradiative decay rate constants are much larger in the naphthalane series. Since energy denominators $E(^1n\pi^*)-E(^3\pi\pi^*)$ are similar for the both series, the differences in the spin-orbit matrix elements $\langle ^1n\pi^*|\mathscr{H}_{so}|^3\pi\pi^*\rangle$ and the transition moment $\mathbf{M}$ are likely to be responsible for the differences in the radiative decay rate constants. As to the nonradiative decay the increased Franck-Condon factor due to the smaller $E(T_1)-E(S_0)$ probably enhances the nonradiative decay in the naphthalene series.

Orientations of Guest Molecules and Hyperfine Interactions. We measured the angular dependence of the EPR signals from the point at which the cleavage plane is in the direction of the applied field. At this orientation the direction of the applied field is rotated by 52° from the direction of the long axis (L axis) of BAC as shown in Fig. 5. We measure the rotation angle (β) of the applied field from this point. The Y stationary point of benzimidazole is obtained at $\beta=25°$. In the same way the Y stationary point of purine is found at $\beta=14°$. As discussed in the last section the Y directions of benzimidazole and purine are along the long axes of the molecules. Then the approximate orientations of these molecules in the BAC host are given as shown in Fig. 5. These orientations are consistent with the hydrogen bonded structures.

Hfs of purine is obtained at its Y stationary point. (Fig. 6) This hfs comes from the protons because the in-plane nitrogen hyperfine coupling constants (hfcc) are expected to be small.[28] Using a Gaussian line shape for each hyperfine component, we simulate this spectrum with three coupling constants; 7.5, 4.2, and 3.2 G as shown in Fig. 6. We consider the hfs of the protons attached to the carbons 2, 6, and 8, since the spin density at N_9 is expected to be very small. When the applied field makes an angle θ with the direction perpendicular to the C-H direction, the hfcc of a proton in the $m_s=0\leftrightarrow m_s=1$ transition is given by

$$\Delta h(\beta) = [(\rho A_{\hat{x}\hat{x}}\cos^2\theta - \rho A_{\hat{y}\hat{y}}\sin^2\theta - g_n\beta_n H)^2 + \frac{\rho^2}{4}(A_{\hat{x}\hat{x}}-A_{\hat{y}\hat{y}})^2\sin^2 2\theta]^{1/2} - g_n\beta_n H. \quad (4)$$

Here $A_{\hat{x}\hat{x}}=-36.5$ G, $A_{\hat{y}\hat{y}}=-11.5$ G, and $A_{\hat{z}\hat{z}}=-23.5$ G[29,30] are the principal values of the hyperfine tensor of a proton attached to an aromatic carbon. (x and y are perpendicular and parallel to the C-H direction in the molecular plane, respectively. $\hat{z}$ is perpendicular to the molecular plane.) Since C_6-H is nearly perpendicular to the direction of the applied field at the Y stationary point, the largest hfcc 7.5 G is likely due to the proton at position 6. $\rho_6=0.20$ is immediately

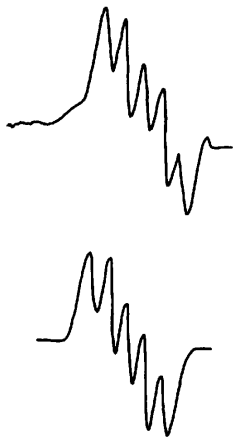

Fig. 6. Hyperfine structure in the EPR spectrum of purine in BAC. H//Y (β=0°). Upper: experimental, lower: simulated.

obtained from Eq. 4 with θ=0°. C_8–H is nearly parallel to the applied field and the hfcc is expected to be small. So we may consider the smallest hfcc 3.2 G is due to the proton at position 8. ρ_8=0.27 is obtained from Eq. 4 with θ=90°. The remaining hfcc 4.2 G is then assigned to the proton at position 2. ρ_2 is given to be 0.12 from Eq. 4 with θ=60°.

Magnetic Properties and the Nature of the Triplet States. One remarkable observation is that $|E|$ of benzimidazole and 1*H*-indazole are much smaller than that of $|E|$ of indole, despite the similarity of their structures. This indicates that the nitrogen substitution to the pyrrole ring of indole modifies the nature of the T_1 state drastically. In the previous work[25] it was shown that the ZFS and the nature of the T_1 state of indole are very similar to those of indene and benzofuran which are viewed as substituted benzenes with strongly mesomeric substituents. The large $|E|$ was attributed to a large delocalization of the unpaired electron into the -C=C- groups of the five-membered ring. On the other hand, much smaller $|E|$ values found for benzimidazole and 1 *H*-indazole indicate that the delocalization of the unpaired electron into the -C=N- groups is much less. The T_1 states of these molecules are approximately described by the excitation of an electron from the highest occupied molecular orbital (HOMO) to the lowest unoccupied molecular orbital (LUMO). The HOMO and LUMO of benzimidazole and 1*H*-indazole then must be very different from those of indole. The observed difference in the spin distributions also indicates this. It was suggested that in indole $\rho_4 \simeq \rho_8 \simeq 0.5\rho_6$, $\rho_3 < \rho_6$, and that ρ_5 and ρ_7 are small.[25] The analysis of the hfs in 1*H*-indazole indicates that ρ_4, ρ_7, and ρ_5 are large,[16] showing that the HOMO and LUMO of indole are strongly affected by the nitrogen substitution.

The ZFS and the spin distribution of purine are expected to be different from those of other in this series because of the presence of two nitrogen atoms in the six-membered ring. Here *D* is similar to those of others, but $|E|$ is very large, indicating larger spin densities in the -C=H- groups of the five-membered ring. The spin distribution in the triplet state is also very different from that of the purine anion. In the purine anion ρ_6 is very large (ρ_6=0.44),[31] but in the triplet state ρ_6 (0.20) is smaller than ρ_8 (0.27). ρ_8 in the anion is smaller than that in the triplet state. A simple π electron MO calculation indicates that the HOMO and the LUMO of purine are very different and that the spin distributions of the anion and the triplet state are very different. This expectation is born out experimentally. This difference in the spin distributions makes a marked contrast to the cases of many aromatic molecules in which the spin distributions in the triplet states are similar to those of anions.[30,32–34]

References

1) H. U. Schutt and H. Zimmerman, *Ber. Bunsenges. Phys. Chem.*, **67**, 54 (1963).
2) B. J. Cohen and L. Goodman, *J. Am. Chem. Soc.*, **87**, 5487 (1965).
3) C. Cailly and A. Boukhors, *C. R. Hebd. Seances Acad. Sci., Ser. C*, **264**, 480 (1967).
4) P. Loustauneau, *J. Chim. Phys. Phys-Chim. Biol.*, **68**, 1675 (1971).
5) B. S. Kirkiacharian, R. Santus, and C. Helen, *Photochem. Photobiol.*, **16**, 455 (1972).
6) J. W. Longworth, R. O. Rahn, and R. G. Shulman, *J. Chem. Phys.*, **45**, 2930 (1966).
7) M. J. Robey and I. G. Ross, *Photochem. Photobiol.*, **21**, 363 (1975).
8) J. J. Smith, *Spectrochimica Acta, Part A.*, **33**, 135 (1977).
9) Drobnik, J. and L. Augenstein, *Photochem. Photobiol.*, **5**, 13 (1966).
10) B. Smaller, *J. Chem. Phys.*, **37**, 1578 (1962).
11) C. Helen, R. Santus, and P. Douzou, *Photochem. Photobiol.*, **5**, 127 (1966).
12) J. Zuclich, *J. Chem. Phys.*, **52**, 3586 (1970).
13) A. Pullman and E. Kochanski, *Int. J. Quantum Chem.*, **15**, 251 (1967).
14) E. Kochanski and A. Pullman, *Int. J. Quantum Chem.*, **3**, 1055 (1969).
15) J. Zuclich, *J. Chem. Phys.*, **52**, 3592 (1971).
16) Parts of the results on 1*H*-indazole was reported in a recent related paper. M. Noda and N. Hirota, *J. Am. Chem. Soc.*, **105**, 6790 (1983).
17) G. Moller and A. M. Nishimura, *J, Phys. Chem.*, **81**, 147 (1977).
18) P. Svejda, R. R. Anderson, and A. H. Maki, *J. Am. Chem. Soc.*, **100**, 7131 (1978).
19) J. Zuclich, J. U. Schutz, and A. H. Maki, *Mol. Phys.*, **28**, 33 (1974).
20) S. Nagaoka and N. Hirota, *J. Chem. phys.*, **74**, 1637 (1981).
21) T. H. Cheng and N. Hirota, *J. Chem. Phys.*, **56**, 5019 (1972).
22) D. S. Tinti, M. A. El-Sayed, A. H. Maki, and C. B. Harris, *Chem. Phys. Lett.*, **3**, 343 (1969).
23) J. Schmidt and J. H. van der Waals, *Chem. Phys. Lett.*, **3**, 546 (1969).
24) a) J. Schmidt, W. S. Veeman, and J. H. van der Waals, *Chem. Phys. Lett.*, **4**, 341 (1969).
b) D. A. Antheunis, J. Schmidt, and J. H. van der Waals, *Chem. Phys. Lett.*, **6**, 355 (1970); c) *Mol. Phys.*, **22**, 1 (1971).

25) E. T. Harrigan and N. Hirota., *J. Am. Chem. Soc.*, **97**, 6647 (1975).
26) D. A. Antheunis, B. J. Botter, J. Schmidt, and J. H. van der Waals, *Mol. Phys.*, **29**, 49 (1975).
27) R. Li and E. C. Lim, *J. Chem. Phys.*, **57**, 605 (1972).
28) J. S. Vincent, *J. Chem, Phys.*, **52**, 3714 (1970).
29) Ph. J. Vergragt, J. A. Kooter, and J. H. van der Waals, *Mol. Phys.*, **33**, 1523 (1977).
30) N. Hirota, C. A. Hutchison, and P. Palmer, *J. Chem. Phys.*, **40**, 3717 (1964).
31) H. Ohya-Nichiguchi, Y. Shimizu, N. Hirota, and K. Watanabe, *Bull. Chem. Soc. Jpn.*, **53**, 1252 (1980).
32) N. Hirota, T. C. Wong, and E. T. Harrigan, *Mol. Phys.*, **29**, 903 (1975).
33) R. H. Clarke and C. A. Hutchison, *J. Chem. Phys.*, **54**, 2962 (1971).
34) R. P. Forsch, A. M. Ponte-Goncalves, and C. A. Hutchison, *J. Chem. Phys.*, **58**, 5209 (1973).
35) B. Borah and J. L. Wood, *Can. J. Chem.*, **54**, 2470 (1976).
36) McCleu, *J. Chem. Phys.*, **17**, 965 (1949).
37) R. W. Glass, L. C. Robertson, and J. A. Merrit, *J. Chem. Phys.*, **53**, 3857 (1970).
38) H. Moriyama, Y. Udagawa, and M. Iroh, Abstruct of the Symposium on Molecular and Electronic Structures, Hokkaido, 1977 P 452.
39) R. D. Gordon and R. F. Yang, *Can. J. Chem.*, **48**, 1722 (1979).
40) J. P. Byrne and I. G. Ross, *Aust. J. Chem.*, **24**, 1107 (1971).
41) J. M. Hollas, *Spectrochim. Acta*, **19**, 753 (1963).
42) M. Schwoerer and H. Sixl, *Chem. Phys. Lett.*, **2**, 14 (1968).

 © 1984 The Chemical Society of Japan Bull. Chem. Soc. Jpn., 57, 2383—2390 (1984)

Electrochemical Properties of Adriamycin Adsorbed on a Mercury Electrode Surface

Kenji KANO, Tomonori KONSE, Naomi NISHIMURA, and Tanekazu KUBOTA*
Gifu Pharmaceutical University, 6-1 Mitahora-higashi 5-chome, Gifu 502
(Received January 26, 1984)

The electrochemical behavior of adriamycin has been studied by means of cyclic d.c. and a.c. voltammetry with a hanging mercury drop electrode, quinizarin being used as a model compound. Both adriamycin and quinizarin are strongly adsorbed on the mercury electrode with their aromatic ring planes oriented parallel to the electrode surface, and give two sets of reduction waves. The first wave, due to the quinone moieties of the adsorbed adriamycin and quinizarin, has been explained on terms of a two-step one-electron surface redox reaction. The formal standard redox potentials, semiquinone formation constants, and charge transfer rate constants of the surface redox reaction of the quinone moieties have been determined. Although the reduced form of adriamycin is not very stable chemically, it is converted to a stable and electrochemically active form for a few minutes at pH 4.54. The second wave appearing at more negative potential would be due to a kinetic or catalytic process.

Adriamycin, a member of the anthracycline antibiotics, is a highly effective antineoplastic agent.[1] The antitumor properties of the anthracyclines correlate in many case with the ability to cause the intercalative inhibition of DNA temperate functions.[1,2] Some other mechanisms, such as the generation of free radical intermediates[3] and a bioreductive covalent attachment to DNA,[4] have been suggested. Serious disadvantages of this drug are the cardiotoxicity[5] and chromosomal damage,[6] which have been shown to be associated with the inhibition of mitochondrial electron transport to bring about the generation of hydrogen peroxide, superoxide anion, and hydroxyl radicals.[7] This behavior should be in intimate correlation with the redox properties of the drugs, which then have been the subject of intensive studies.[3,8-10]

Rao *et al.*[8] have investigated the electrochemical reduction behavior of daunomycin and adriamycin. They reported two sets of reduction waves. Since their experiments were carried out at quite a high concentration by using a hanging mercury electrode, the waves reported by them seem to be attributable to the redox systems of both the adsorbed and bulk species, and the analysis of the results has been semi-quantitative. The electrochemical behavior of adsorbed adriamycin has been also reported by Molinier-Jumel *et al.*[9] on the reduction at a mercury electrode, and by Baldwin *et al.*[10a] and Chaney and Baldwin[10b] on the oxidation at a carbon paste electrode. Their analyses of the electrochemical behavior of adsorbed adriamycin have, however, remained qualitative.

Recently Kakutani and Senda[11] have presented the theory of d.c. and a.c. voltammetry for a two-step surface redox reaction. This theory has been successfully applied to explain the electrochemical behavior of adsorbed flavin mononucleotide,[12] flavin adenine dinucleotide,[13] and glucose oxidase.[14] In this study, we have investigated the electrochemical behavior of adriamycin adsorbed on a hanging mercury drop electrode by means of cyclic d.c. and a.c. voltammetry, quinizarin being used as a model compound. The wave ascribed to the quinone moiety of the adsorbed adriamycin has been interpreted by applying the above theory of the two-step surface redox reaction. The thermodynamic and kinetic properties of the electrochemical redox reaction of the adsorbed adriamycin were able to be determined. We have also investigated the second wave, which appeared at a more negative potential than in the quinone wave. The results and discussions are presented in this paper.

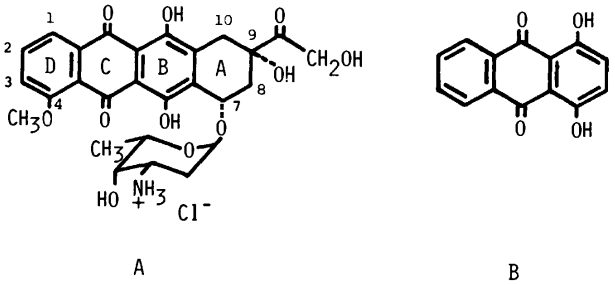

Fig. 1. Structure of adriamycin (A) and quinizarin (B).

Experimental

Chemicals. Adriamycin hydrochloride, obtained from Kyowa Hakko Kogyo Co., was used as received. The concentration of adriamycin in methanol solution was determined spectrophotometrically using $E^{1\%}_{1cm}$(495 nm)=223.[15] Quinizarin (1,4-dihydroxyanthraquinone), obtained from Ardrich Chemical Co., was purified by recrystallization from methanol. Its purity was checked by elemental analysis. Triply distilled water was used to prepare the electrolysis solution. Other chemicals were reagent grade quality.

Electrochemical Measurements. Cyclic d.c. voltammograms were recorded with a Yanagimoto P-1000 voltammetric analyzer, equipped with a Watanabe WX-4401 X-Y recorder. The a.c. voltammetric measurements were performed with a NF circuit LI-572B lock-in amplifier, equipped with the above potentiostat system. The NF circuit FG-121B function generator was used as an a.c. signal generator.

All the voltammetric measurements were made under potentiostatic conditions with a three-electrode system consisting of a Metrohm EA 290 hanging mercury drop working electrode (HMDE) with surface area 0.0187±0.0003 cm^2, a coiled platinum wire auxiliary electrode, and a Yanagimoto MR-P2 saturated calomel reference electrode (SCE). The buffer solutions of 0.2 mol dm^{-3} sodium acetate-acetic acid were used as the base solution for pH 2 to 6. The ionic strength of the base solutions was adjusted to 0.5 mol dm^{-3}

with potassium nitrate. A fresh mercury drop from the HMDE was exposed to the electrolysis solution for a given period of time, t_{exp}, at a constant d.c. potential, E_i. Then the d.c. voltage scan was started from E_i, with the scan rate v=100 mV s^{-1} for d.c. voltammetry and with v=10 mV s^{-1} for a.c. voltammetry, unless otherwise stated. In a.c. voltammetry, the amplitude of the superimposed a.c. voltage was adjusted to 10 mV peak to peak. The frequency and the amplitude of the a.c. signal were checked with a Iwatsu SS-5702 synchroscope. Electrochemical measurements were performed under nitrogen or argon atmosphere at 25.0±0.2 °C, unless otherwise noted.

Results

I. Electrochemical Behavior of Adriamycin. Figure 2 shows the cyclic d.c.voltammogram of 3.75×10^{-6} mol dm^{-3} adriamycin in a pH 4.54 acetate buffer, which was recorded after t_{exp}=3 min at E_i=−0.1 V. At such a low concentration, the current due to the redox reaction of diffusing adriamycin will be negligibly small compared with the current due to the surface redox reaction of adsorbed adriamycin. One-pair of the peak-shaped cathodic and anodic waves (I) and one irreversible cathodic wave (II) were observed at −0.45 V and −1.13 V, respectively. For the I waves, the peak potential of the anodic wave is negative by 10 mV compared with that of the cathodic one. We have studied in detail the electrochemical behavior of the I waves, which should be ascribed to the redox reaction of the quinone moiety of adriamycin adsorbed on the HMDE.

Cyclic D.c. Voltammetry of Wave I. Figure 3A shows the cyclic d.c. voltammogram of 1.46×10^{-6} mol dm^{-3} adriamycin at pH 4.54, which was recorded after t_{exp}=4 min at E_i=−0.2 V and with the switching potential, E_s=−0.7 V. A pair of cathodic and anodic waves are observed at −0.450 V. The shapes and heights of these two waves are practically identical except for the opposite current sign. The peak potential, $E_{p,I}$, and the half-peak width of the wave I, $\Delta E^{dc}_{p/2,I}$, are −0.450 V and 52 mV, respectively. Figure 3B shows the cyclic

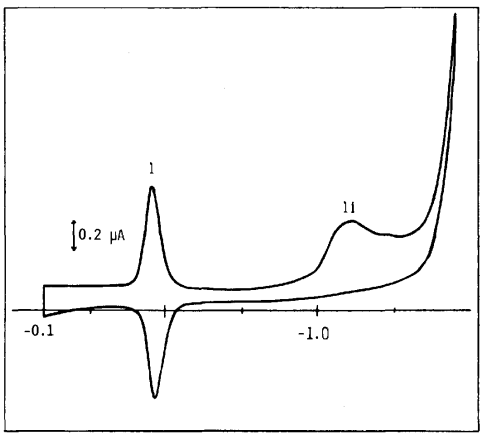

E/V *vs.* SCE

Fig. 2. Cyclic d.c. voltammogram of 3.75×10^{-6} mol dm^{-3} adriamycin in pH 4.54 acetate buffer. t_{exp}= 3 min at E_i=−0.1 V.

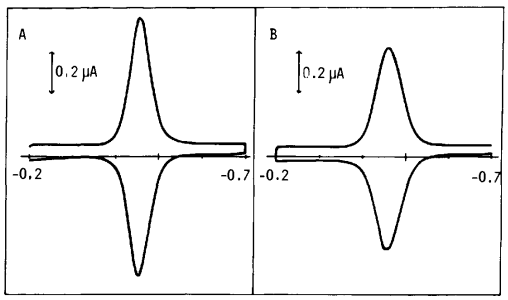

E/V *vs.* SCE

Fig. 3. Cyclic d.c. voltammograms of 1.46×10^{-6} mol dm^{-3} adriamycin in pH 4.54 acetate buffer. Voltage scan was started after t_{exp}=4 min from (A) E_i=−0.2 V and (B) E_i=−0.7 V.

voltammogram recorded with E_i=−0.7 V, where adriamycin is adsorbed in a reduced state. As in the case of Fig. 3A, a symmetrical pair of anodic and cathodic waves is observed. However, $E_{p,I}$ of the waves in Fig. 3B is more negative by 8 mV and $\Delta E^{dc}_{p/2,I}$ is larger by 18 mV compared with those of the waves in Fig. 3A.

We performed the multicyclic voltammetry in the potential range of −0.3 to −0.7 V, with t_{exp}=10 min at 7.98×10^{-7} mol dm^{-3} adriamycin. In the multicyclic voltammetry with E_i=−0.3 V and E_s=−0.7 V, $E_{p,I}$ shifts cathodic and the peak becomes broad and resharpened as the number of cycles is increased, and in about the 40th cycle the wave reaches a steady state, where $E_{p,I}$= −0.483 V and $\Delta E^{dc}_{p/2,I}$=65 mV. On the other hand, in the multicyclic voltammetry with E_i=−0.7 V and E_s= −0.3 V, $E_{p,I}$=−0.476 V, and $\Delta E^{dc}_{p/2,I}$=73 mV for the first scan, and $E_{p,I}$ shifts cathodic and the peak becomes sharp with the increasing number of cycles. In about the 20th cycle, the wave reaches a steady state; this coincides with the steady state wave obtained in the multicyclic voltammetry with E_i=−0.3 V. These results can be interpreted as follows. The parent compound is fundamentally d.c. reversible and the peak potential is −0.450 V as written above, but the reduced form is chemically not so stable and transferred into a chemically stable other form during the time in which adriamycin was in the reduced form. The chemically stable product is also electrochemically active and shows a d.c. reversible wave, whose peak potential is −0.483 V.

In the following, we have set the E_i at a more positive potential than the peak potential by at least 150 mV. Figure 4 shows the t_{exp} dependence of the cathodic peak height, $I_{p,Ic}$, obtained with E_i=−0.2 V. At lower concentrations of adriamycin, $I_{p,Ic}$ is proportional to $[(D/r)t_{exp}+2(D/\pi)^{1/2}t_{exp}^{1/2}]$, where D is the diffusion coefficient of adriamycin, estimated by the Ilkovic equation to be 7.53×10^{-6} cm^2 s^{-1}, and r is the radius of the HMDE (3.82×10^{-2} cm in this case). The slope of the plot is also proportional to the bulk concentration of adriamycin. These results indicate the diffusion-controlled adsorption of adriamycin at the spherical electrode surface, *i.e.* at the HMDE surface.[12,16,17] The wave heights reached to a certain limit, $I^{max}_{p,Ic}$, at the relatively high concentration of adriamycin and/or

prolonged exposure of the HMDE.

Table 1 summarizes the peak heights ($I_{p,Ic}$ and $I_{p,Ia}$), the peak potentials ($E^{dc}_{p,Ic}$ and $E^{dc}_{p,Ia}$), the half-peak widths ($\Delta E^{dc}_{p/2,Ic}$ and $\Delta E^{dc}_{p/2,Ia}$), and the integrated currents *i.e.* the electricities (Q_{Ic} and Q_{Ia}) of the cathodic and anodic waves with various v. The values of Q_{Ic} and Q_{Ia} were estimated from the area under the wave. Both $I_{p,Ic}$ and $I_{p,Ia}$ are proportional to v. The $I_{p,Ic}/I_{p,Ia}$ ratio is practically unity. $E^{dc}_{p,Ic}$ and $E^{dc}_{p,Ia}$, $\Delta E^{dc}_{p/2,Ic}$ and $\Delta E^{dc}_{p/2,Ia}$, and Q_{Ic} and Q_{Ia} coincide with each other and are independent of v. Further, $I_{p,Ic}$ and $I_{p,Ia}$ are proportional to Q_{Ic} and Q_{Ia}, respectively, as shown in Fig. 5. This means that the peak height at a given v is directly proportional to the amount of the adriamycin adsorbed on the electrode surface. These results indicate that the I wave can be ascribed to the reversible surface redox reaction under the limited conditions, where the effect of the following chemical reaction can be disregarded.

At lower pH than 6, the behavior of the cyclic d.c. voltammograms of adriamycin fundamentally resembles that of the voltammograms obtained at pH 4.54, except for the peak potential. The pH dependence of the peak potential is −60 mV per pH unit in the pH range of 2 to 6, which indicates two-electron two-proton redox reaction.

A.c. Voltammetry of Wave I. In the cyclic a.c. voltammetry of adriamycin adsorbed at E_i=−0.30 V and pH 4.54, the a.c. cathodic voltammogram is practically identical in height and shape with the anodic one. So, the a.c. voltammetric behavior has been studied only for the cathodic scan. Figure 6 shows the a.c. voltammograms recorded with a.c. frequency, f, of 100 Hz after

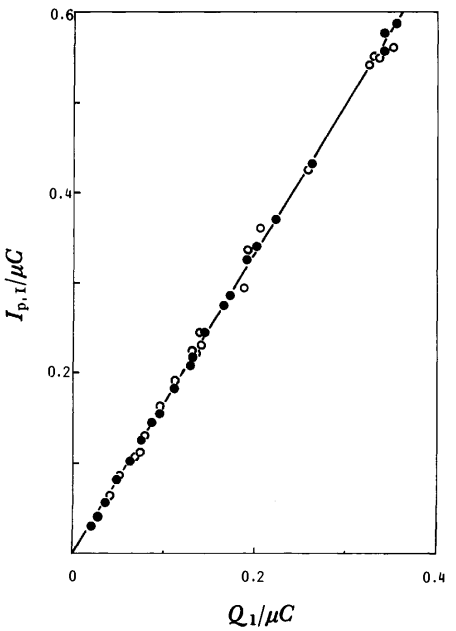

Fig. 5. Plot of the peak current against the electricity at pH 4.54. The closed and open circles correspond to the cathodic and anodic waves, respectively. E_i= −0.2 V.

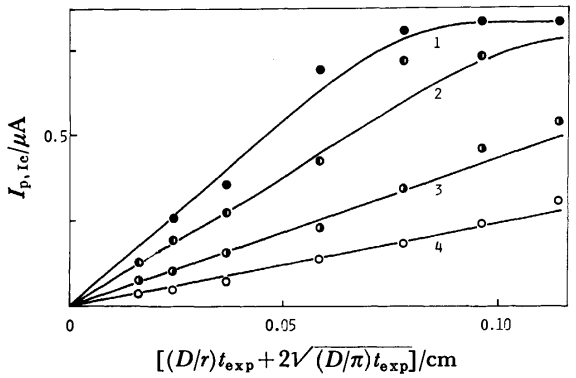

Fig. 4. Dependence of $I_{p,Ic}$ on t_{exp} at E_i=−0.2 V in pH 4.54 acetate buffer containing adriamycin at (1) 2.19×10^{-6} mol dm^{-3}, (2) 1.46×10^{-6} mol dm^{-3}, (3) 7.30×10^{-7} mol dm^{-3}, and (4) 3.65×10^{-7} mol dm^{-3}.

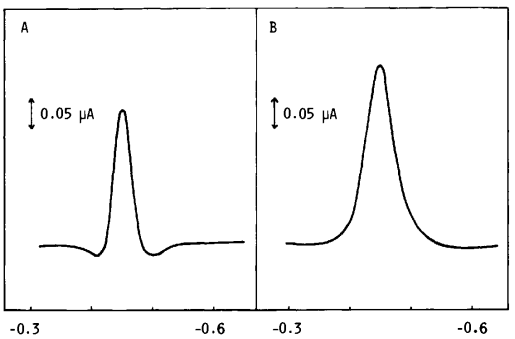

Fig. 6. A.c. voltammograms of 2.16×10^{-6} mol dm^{-3} adriamycin in pH 4.54 acetate buffer at 100 Hz. t_{exp} =2 min at E_i=−0.30 V. (A) Real component, (B) imaginary component.

TABLE 1. SCAN-RATE DEPENDENCE OF THE PEAK CURRENT, PEAK POTENTIAL, HALF-PEAK WIDTH, AND INTEGRATED CURRENT OF d.c. VOLTAMMOGRAM OF ADRIAMYCIN ADSORBED ON A MERCURY ELECTRODE AT pH 4.54[a)]

Scan rate	$I_{p,Ic}$	$I_{p,Ia}$	$E^{dc}_{p,Ic}$	$E^{dc}_{p,Ia}$	$\Delta E^{dc}_{p/2,Ic}$	$\Delta E^{dc}_{p/2,Ia}$	Q_{Ic}	Q_{Ia}
mV s^{-1}	μA		V *vs.* SCE		mV		μC	
20	0.086	0.085	−0.453	−0.454	52	52	0.211	0.213
50	0.188	0.186	−0.451	−0.451	52	52	0.211	0.212
100	0.348	0.347	−0.450	−0.452	52	52	0.212	0.210
200	0.649	0.648	−0.450	−0.453	52	52	0.209	0.210
500	1.705	1.700	−0.450	−0.451	53	53	0.211	0.211

a) $C_{adriamycin}$ = 1.46×10^{-6} mol dm^{-3}, t_{exp} = 2 min at E_i=−0.2 V.

TABLE 2. PEAK POTENTIAL AND HALF-PEAK WIDTH OF a.c. VOLTAMMOGRAM OF ADRIAMYCIN ADSORBED ON A MERCURY ELECTRODE AT pH 4.54[a)]

Frequency / Hz	E_p^{real}	E_p^{imag}	$\Delta E_{p/2}^{real}$/mV		$\Delta E_{p/2}^{imag}$/mV	
	V *vs.* SCE		Obsd	Calcd[b)]	Obsd	Calcd[b)]
100	−0.450	−0.450	37	42.0	50	52.4
200	−0.449	−0.453	40	42.4	53	53.2
300	−0.450	−0.448	41	43.1	55	54.5
400	−0.448	−0.450	45	44.0	57	56.2
500	−0.450	−0.450	45	45.1	60	58.2

a) $C_{adriamycin}=1.13\times10^{-6}$ mol dm^{-3}, $t_{exp}=3$ min at $E_i=-0.3$ V *vs.* SCE. b) Calculated by using $K=0.132$, $k_{sap}=8.80\times10^{3}$ s^{-1}, and $\theta=0.392$.

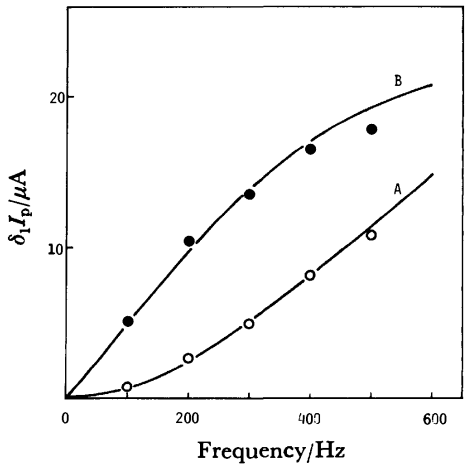

Fig. 7. Dependence of (A) $\delta_1 I_p^{real}$ and (B) $\delta_1 I_p^{imag}$ on a.c. frequency. A.c. voltammograms were recorded in pH 4.54 acetate buffer containing 1.13×10^{-6} mol dm^{-3} adriamycin after $t_{exp}=2$ min at $E_i=-0.30$ V. Solid lines represent theoretical curves[11)] calculated by using $K=0.132$, $k_{sap}=8.8\times10^{3}$ s^{-1}, and $\Gamma=4.04\times10^{-11}$ mol cm^{-2} ($\theta=0.392$).

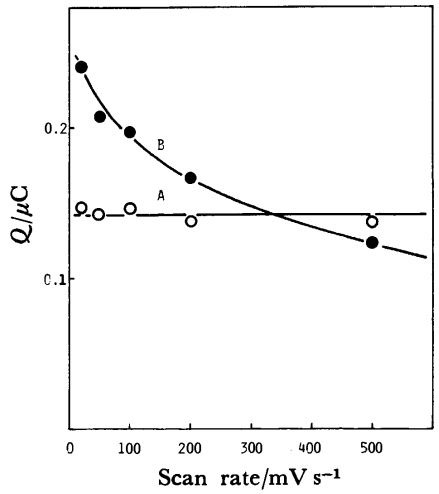

Fig. 8. Dependence of (A) Q_{Ic} and (B) Q_{II} on the scan rate in pH 4.54 acetate buffer containing 9.97×10^{-7} mol dm^{-3} adriamycin. D.c. voltammograms were recorded after $t_{exp}=3$ min at $E_i=-0.10$ V.

$t_{exp}=2$ min at $E_i=-0.3$ V in the pH 4.54 acetate buffer containing 2.16×10^{-6} mol dm^{-3} adriamycin. In all the a.c. voltammograms recorded in this study, the peak potentials of the real and the imaginary components, E_p^{real} and E_p^{imag}, are independent of the a.c. frequency between 100 and 500 Hz, and of the amount of the adsorbed adriamycin. They are also in accord with each other, and with the peak potentials of the corresponding d.c. voltammogram, as shown in Table 2. On the other hand, the peak currents, $\delta_1 I_p^{real}$ and $\delta_1 I_p^{imag}$, and the half-peak widths, $\Delta E_{p/2}^{real}$ and $\Delta E_{p/2}^{imag}$, of the real and imaginary components depend on f and on the amount of the adsorbed adriamycin, as shown in Fig. 7 and Table 2.

D.c. Voltammetry of Wave II. We have also studied the d.c. voltammetric behavior of the irreversible cathodic wave II, observed at −1.13 V with $v=100$ mV s^{-1} in a pH 4.54 acetate buffer. The peak potential of the wave II shifts cathodic by about 50 mV for the tenfold increase in the v range of 10 to 500 mV s^{-1}. The peak current of the II wave, $I_{p,II}$, grows parabolically with increasing v; here $I_{p,II}$ was obtained by subtracting the current of the base solution without adriamycin. Figure 8 shows the v dependence of the integrated current of the II wave, Q_{II}, as well as that of the cathodic wave I, Q_{Ic}, where the voltammograms were recorded with $E_i=-0.1$ V, and t_{exp} was set to be 3 min, which included the potential scanning time from E_i to the peak potential of wave II. Q_{II} decreases with increasing v. This coincides with the parabolic v dependence of $I_{p,II}$. The temperature coefficient of $I_{p,II}$ is 6.3% in the temperature range of 10 to 40 °C. These results indicate that wave II is kinetic or catalytic in character.

The current of wave II is reduced with addition of *N,N*-dimethylformamide (DMF). Curve 1 in Fig. 9 shows the dependence of $I_{p,II}$ on the amount of the added DMF. It disappears completely at the DMF concentrations beyond 20% (v/v).

II. Electrochemical Behavior of Quinizarin. Figure 10A shows the cyclic d.c. voltammogram of 3.98×10^{-6} mol dm^{-3} quinizarin in pH 4.54 acetate buffer. It was recorded after $t_{exp}=3$ min at $E_i=-0.1$ V. Just like the case of adriamycin, one pair of peak-shaped cathodic and anodic waves (I) and one irreversible cathodic wave (II) are recorded at −0.416 V and −1.095 V, respectively. However, the peak potentials of the cathodic and anodic waves I are in accord with each other, and the anodic peak current is about one-half

of the cathodic one. This I wave should be ascribed to the redox reaction of the quinone moiety of quinizarin adsorbed on the HMDE.

In the case of cyclic d.c. voltammetry starting with E_i=−0.2 V and setting the E_s in the potential range of −0.6 to −0.9 V, the shapes and heights of the cathodic and anodic waves become practically identical except for the opposite current sign (Fig. 10 B). $E_{p,I}$ and $\Delta E^{dc}_{p/2,I}$ of the wave are −0.416 and 53 mV, respectively, at pH 4.54. These values coincide well with those of the wave obtained with E_i=−0.7 V and E_s=−0.2 V. This kind of behavior of quinizarin is quite different from that of the aforementioned adriamycin, and shows that the reduced quinizarin is stable chemically, but partial desorption occurs at the more negative potential than −1.0 V. Detailed analysis of these waves in d.c. and a.c. voltammetry leads to the conclusion that the electrochemical behavior of wave I given by quinizarin is fundamentally the same as that of the d.c. reversible wave I given by adriamycin. The II wave decreases and disappears as more DMF is added, as shown in Fig. 9 (curve 2).

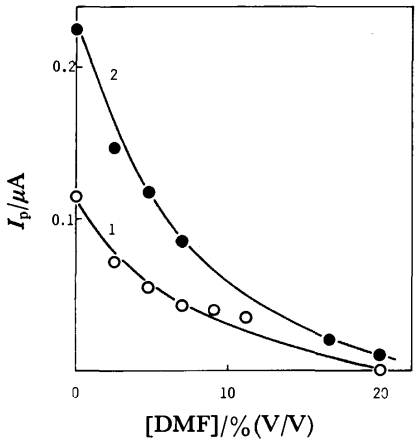

Fig. 9. Dependence of $I_{p,II}$ of (1) adriamycin and (2) quinizarin on the concentration of DMF. $C_{adriamycin}$ = 1.25×10^{-6} mol dm^{-3}, $C_{quinizarin}$ = 2.49×10^{-6} mol dm^{-3}, t_{exp}=3 min at E_i=−0.1 V.

Discussion

Adsorption of Adriamycin on Mercury Electrode Surface. The present study has revealed that adriamycin is strongly adsorbed on the HMDE surface and that the adsorption is controlled by diffusion. The peak current of the wave I is given by

$$I_p = kA\Gamma = kA[(D/r)t_{exp} + 2(D/\pi)^{1/2}t_{exp}^{1/2}]C, \quad (1)$$

where k is the proportional constant, A the electrode surface area, Γ the surface concentration of adriamycin per unit area, and C the bulk concentration of adriamycin. At large C and/or large t_{exp}, the maximum current, I_p^{max}, is obtained, so that the I_p^{max} is given by

$$I_p^{max} = kA\Gamma^{max}, \quad (2)$$

where Γ^{max} is the maximum Γ. By applying Eqs.(1) and (2) to such a plot as is shown in Fig.4, we estimated Γ^{max}=1.4×10^{-10} mol cm^{-2} at −0.2 V and at pH 4.54. The Γ and Γ^{max} values can also be estimated from the integrated current;

$$Q = nFA\Gamma \text{ and } Q^{max} = nFA\Gamma^{max}, \quad (3)$$

where n is the number of electrons transferred per molecule of adriamycin. For the I wave obtained with E_i=−0.20 V, this gives Γ^{max}=1.1×10^{-10} mol cm^{-2} at pH 4.54, by assuming n=2 (for the redox of quinone moiety). Further, when adriamycin is adsorbed at E_i=−0.65 V, where the reduced adriamycin is adsorbed, Γ^{max} is estimated to be 1.2×10^{-10} mol cm^{-2} by Eqs. (1) and (2), and 1.1×10^{-10} mol cm^{-2} by Eq. (3). The Γ^{max} values thus obtained by two different treatments agree well between the parent and reduced adriamycins, so that the adsorbed state of the reduced adriamycin is essentially the same as that of the parent adriamycin. Assuming that adriamycin is adsorbed on the electrode surface with its aromatic ring plane oriented parallel to the electrode surface and with its sugar moiety parpendicular to the electrode surface, a CPK molecular model[18] gives Γ^{max}=1.1×10^{-10} mol cm^{-2}.

The Γ^{max} value of 1.4×10^{-10} mol cm^{-2} was estimated for quinizarin by the two methods: One is the applica-

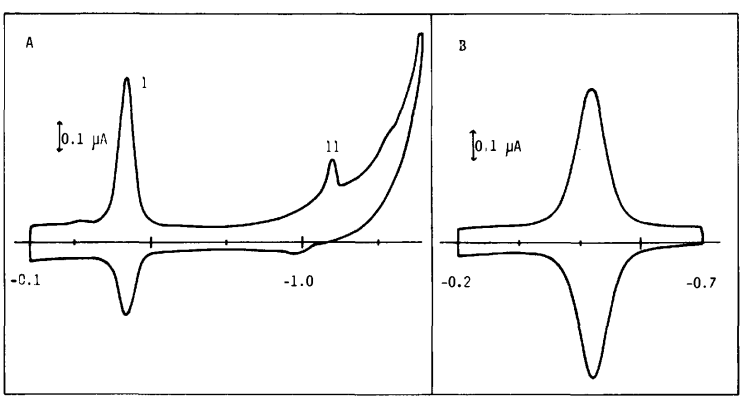

Fig. 10. Cyclic d.c. voltammograms of 3.98×10^{-6} mol dm^{-3} quinizarin in pH 4.54 acetate buffer. t_{exp}=3 min. (A) E_i=−0.1 V and E_s=−1.4 V, (B) E_i=−0.2 V and E_s=−0.7 V.

tion of Eq. (3), and the other is due to the CPK model method, where we assumed parallel orientation of its aromatic ring. The difference between Γ^{max} of adriamycin and quinizarin can be ascribed to the ring A in adriamycin, which is absent in quinizarin. In other words, the sugar moiety in the adsorbed adriamycin is directly surrounded by the solvent molecules. This conformation of the adsorbed adriamycin may be similar to that of the pyridine adduct of daunomycin in the crystal structure, in which strong hydrogen bonding is formed between the two axial oxygen groups at C_7 and C_9.[19]

Surface Redox Process of Quinone Moiety in Adsorbed Adriamycin. The I wave brought about by adriamycin adsorbed on the HMDE surface should be ascribed to the redox reaction of the quinone moiety. This wave is reversible under the conditions that the d.c. voltammogram is recorded with E_i=−0.2 V and E_s=−0.7 V. As was written in detail in the section "*Cyclic Votammetry of Wave I*" in the chapter "**Results**", the reduced form of adriamycin is not very stable, and is irreversibly transferred into other stable from, which is also capable of a reversible two-electron redox reaction. This chemical reaction would be considered as an irreversible elimination of the amino sugar moiety, giving rise to 7-deoxyadriamycinone, as stated by Rao *et al.*[8] This proposed process is supported by the fact that adriamycin is quantitatively converted into 7-deoxyaglycon by mild chemical reduction.[20] Furthermore, this reductive cleavage process is one important metabolic pathway.[21]

Let us now consider the d.c. reversible wave I produced by the parent adriamycin adsorbed at the more anodic potential side than the peak potential of wave I. The cyclic d.c. voltammetric behavior of wave I should be interpreted in terms of a two-step one-electron surface redox reaction:

$$\left.\begin{aligned} O_{ad} + e &\rightleftharpoons S_{ad} \\ S_{ad} + e &\rightleftharpoons R_{ad} \end{aligned}\right\}, \tag{4}$$

where O_{ad}, S_{ad}, and R_{ad} denote the oxidized (or parent), semiquinone and reduced from of the adsorbed adriamycin, respectively. The theory of the cyclic d.c. voltammogram and of the real and imaginary components of the a.c. current in the two-step surface redox reaction has been presented by Kakutani and Senda.[11] The theory predicts the following: If the two steps are d.c. reversible in the simplified case[22] and the semiquinone formation constant, K, is less than 16, the cathodic and anodic d.c. voltammograms may have a maximum at E'_o regardless of v and Γ. Here note that the E'_o corresponds to the standard surface redox potential of the couple O_{ad}/R_{ad}. Also, the half-peak widths, $\Delta E^{dc}_{p/2,Ic}$ and $\Delta E^{dc}_{p/2,Ia}$, will have the same value and are independent of v and Γ under the above conditions. Thus Eq. (5) is obtained:

$$\Delta E^{dc}_{p/2,Ic} = \Delta E^{dc}_{p/2,Ia} = (2RT/F)|\ln\zeta|, \tag{5}$$

where ζ is the solution of the equation, $\zeta^4-K\zeta^3+(K-4\sqrt{K}-6)\zeta^2-K\zeta+1=0$. The cathodic and anodic peak heights will be proportional to v and Γ, and are given by

$$\begin{aligned} I_{p,Ic} = I_{p,Ia} &= 2(F^2/RT)A\Gamma v/(2+\sqrt{K}) \\ &= (F/RT)Qv/(2+\sqrt{K}). \end{aligned} \tag{6}$$

Here K is defined by

$$\begin{aligned} K &= [S_{ad}]^2/[O_{ad}][R_{ad}] \\ &= \exp[(F/RT)(E'_{o1}-E'_{o2})], \end{aligned} \tag{7}$$

where E'_{o1} and E'_{o2} are the standard surface redox potentials of the couples O_{ad}/S_{ad} and S_{ad}/R_{ad}, respectively, and other symbols have their common meanings.

All experimental results obtained in this study agree well with these theoretical predictions (see Table 1 and Fig. 5), and E'_o=−0.450 V at pH 4.54. The K value at pH 4.54 has been determined to be 0.138±0.043 by Eq. (5) and 0.126±0.034 by Eq. (6). These agree well with each other.

The theory also leads to the following outcomes under the aforementioned conditions; E_p^{real} and E_p^{imag} will be independent of the a.c. frequency, f, and will coincide with E'_o. The ratio of $\delta_1 I_p^{real}$ to $\delta_1 I_p^{imag}$ at $E=E'_o$ is given by

$$(\delta_1 I_p^{real}/\delta_1 I_p^{imag})_{E=E'_o} = 2\pi f/k_{sap}(K)^{1/4} \tag{8}$$

where k_{sap} is the apparent rate constant of the first and the second charge transfer step. The present result is in line with the prediction discussed hitherto as shown in Table 2 and Fig. 11. The slope of the plot in Fig. 11 gives k_{sap} by applying the K value determined by d.c. voltammetry. The k_{sap} value has been estimated to be $8.8\times10^3\ s^{-1}$ at $\Gamma=4.04\times10^{-11}$ mol cm^{-2} ($\theta\equiv\Gamma/\Gamma^{max}$= 0.392), using K=0.132. According to the theoretical equations in the simplified case, we have calculated the half-peak widths and the peak currents of the real and imaginary components of a.c. voltammogram using the estimated values of K, k_{sap}, and Γ. Table 2 shows the experimental and theoretical values of $\Delta E_{p/2}^{real}$ and $\Delta E_{p/2}^{imag}$. Figure 7 shows the f dependence of the experimental values of a.c. peak current, where the solid lines represent the theoretical ones.

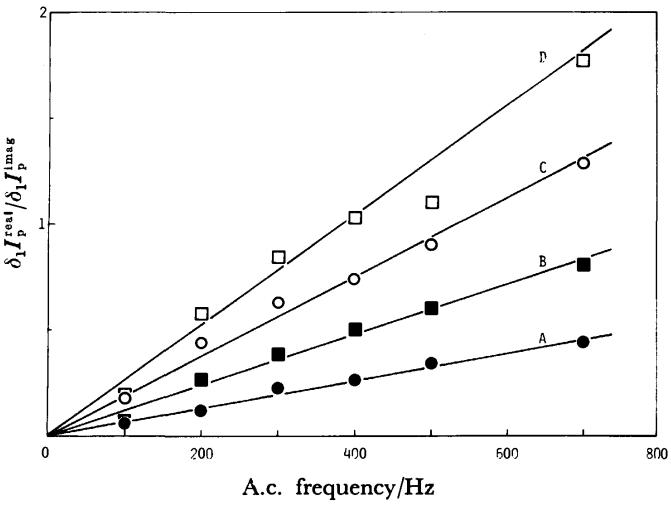

Fig. 11. Dependence of the a.c. peak current ratio, $\delta_1 I_p^{real}/\delta_1 I_p^{imag}$, on a.c. frequency at various total surface coverages of adriamycin in pH 4.54 acetate buffer. θ=(A) 0.19, (B) 0.39, (C) 0.65, and (D) 1.0.

Agreement between the experimental results and the theoretical predictions is good. The dependence of k_{sap} on the surface coverage, θ, is also given by Eq. (9)[11]

$$k_{sap} = k_{sap}(\theta \rightarrow 0)\exp(-a\theta), \quad (9)$$

where $k_{sap}(\theta \rightarrow 0)$ is the apparent rate constant at $\theta \rightarrow 0$, and a is the Frumkin's a-parameter of interaction between adsorbed molecules (a is positive for attraction and negative for repulsion). This situation is experimentally verified as shown in Fig. 12. From the slope of the plot in Fig. 12, we can estimate the a value. In conclusion, one can say that the cyclic d.c. and a.c. voltammetric behavior of the quinone moiety in the adriamycin adsorbed on the HMDE can be explained by the two-step surface redox mechanism. Now, the E'_{o1} and E'_{o2} values can be estimated by using the E'_o in Eq. (10) and the K in Eq. (7):

$$E'_o = (E'_{o1}+E'_{o2})/2. \quad (10)$$

Table 3 summarizes the above electrochemical data. We have also determined the electrochemical data of the quinone moiety of the adsorbed adriamycin at pH 2.49; these are listed in Table 3. In the range of pH lower than 6, E'_{o1} and E'_{o2} as well as E'_o shift linearly to negative with the slope of -60 mV/pH. This result indicates that each of two steps of the surface redox process involves one electron and one proton. Other electrochemical data obtained at pH 2.69 are practically identical with those obtained at pH 4.54. The electrochemical behavior of adsorbed adriamycin becomes complicated at elevated pH; this will be reported in a succeeding paper.

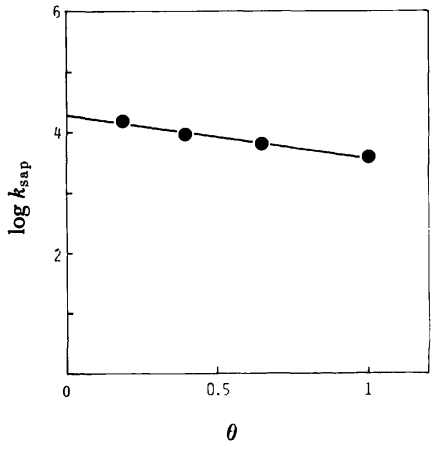

Fig. 12. Plot of log k_{sap} of adriamycin against θ at pH 4.54.

Similarly, the electrochemical behavior of the quinone moiety in the adsorbed quinizarin is explained by the above mechanism. The electrochemical data are summarized in Table 3. A decrease in $k_{sap}(\theta \rightarrow 0)$ and a-parameter is observed for quinizarin, compared with the values for adriamycin. The difference in E'_o between adriamycin and quinizarin is mainly ascribed to 4-methoxyl group of adriamycin. The K values of adriamycin and quinizarin are less than unity, indicating that the disproportionation of the adsorbed semiquinone form should be thermodynamically favorable.

Electrochemical Process in Wave II Produced by Adriamycin. The d.c. voltammetric behavior of the II wave indicates that the current has a kinetic or catalytic character. The II wave is also observed with quinizarin, but not with anthraquinone.[23] These facts suggest that the presence of two adjacent hydroquinone moieties in a molecule is essential for the appearance of the II wave. Note that the quinone moiety is reduced to the hydroquinone moiety at the potential where the II wave is observed. The process of wave II can thus be ascribed to the catalytic hydrogen evolution current catalyzed by two hydroxyl groups on adjacent benzene rings such as the oxonium compounds.[24] The fact that the II wave becomes small and disappears with the addition of DMF, an aprotic solvent, supports the proposed mechanism. Rao *et al.*[8] have ascribed this irreversible process to the reduction of the side-chain carbonyl group, on the basis of its similarily to the reduction processes of acetophenone and 1′-acetonaphtone. However, the side-chain carbonyl group of adriamycin is aliphatic and is not conjugated with the aromatic rings, differing very much from the carbonyl groups of acetophenone and 1′-acetonaphtone. In general, the reduction wave of aliphatic ketone can not be observed in the usual buffer solution.[25] Further, Rao *et al.*'s assignment can not explain the II wave produced by quinizarin, which is without the side-chain carbonyl group.

As a conclusion, the thermodynamic and kinetic information on the redox reaction of adriamycin adsorbed on a mercury electrode surface can be obtained by means of the cyclic d.c. and a.c. voltammetric study. This information would be useful in an elucidation of the action mechanism of adriamycin. The electrochemical behaviors of the adsorbed adriamycin in neutral and alkaline solutions and/or on a solid electrode will be published later.

The authors wish to express their sincere thanks to Professor Mitsugi Senda and Dr. Tadaaki Kakutani, Kyoto University, for their valuable discussions on this study.

Table 3. Electrochemical data of adriamycin and quinizarin adsorbed on a mercury electrode

Compound	pH	E'_o	E'_{o1}	E'_{o2}	K	$k_{sap}(\theta \rightarrow 0)$ / 10^4 s^{-1}	a
		V *vs.* SCE					
adriamycin	4.54	−0.450	−0.476	−0.424	0.132	1.98	1.66
adriamycin	2.69	−0.333	−0.357	−0.308	0.148	2.19	1.61
quinizarin	4.54	−0.418	−0.440	−0.396	0.178	0.73	0.94

References

1) A. Di Marco, F. Arcamore, and F. Zunino, "Antibiotics III-Mechanism of Action of Antimicrobial and Antitumor Agents," J. W. Corcoran and F. E. Hahn, eds., Springer, New York (1975), pp. 101—128.

2) S. Neidle, "Topics in Antibiotic Chemistry," ed by P. G. Sammes, John Wiley & Sons, New York (1978), Vol. 2, pp. 240—278.

3) N. R. Bachur, S. L. Gordon, and M. V. Gee, *Mol. Phrmacol.*, **13**, 901 (1977); L. W. Lown, S. K. Sim, K. C. Majumdar, and R. Y. Chang, *Biochem. Biophys. Res. Commun.*, **76**, 705 (1977); B. Kalynaraman, E. Perez-Reyers, and R. P. Mason, *Biochem. Biophys. Acta*, **630**, 119 (1980); S. Sato, M.Iwaizumi, K. Honda, and Y. Tamura, *Gann*, **68**, 603 (1977); J. W. Lown and H.-H. Chen, *Can. J. Chem.*, **59**, 3212 (1981).

4) B. K. Shinha and J. L. Gregory, *Biochem. Pharmacol.*, **30**, 2626 (1981); D. L. Kleyer and T. H. Koch, *J. Am. Chem. Soc.*, **105**, 5154 (1983).

5) E. A. Lefrak, J. Pitha, S. Rosenheim, and J. A. Gottlieb, *Cancer*, **32**, 302 (1973); J. P. Rinehart, R. P. Lewis, and S. P. Balcerzak, *Ann. Inter. Med.*, **81**, 475 (1974).

6) A. Di Marco, M. Gaetani, P. Orezzi, B. Scarpinato, R. Silvestrini, M. Soldati, T. Dasdia, and L. Valentini, *Nature*, **201**, 706 (1964).

7) T. Kishi, T. Watanabe, and K. Folkers, *Proc. Natl. Acad. Sci.*, **73**, 4653 (1976); Y. Iwamoto, I. L. Hansen, T. H. Porter, and K. Folkers, *Biochem. Biophys. Res. Commun.*, **58**, 633 (1974); T. Goodman and P. Hochstein, *Biochem. Biophys. Res. Commun.*, **77**, 797 (1977).

8) G. M. Rao, J. W. Lown, and J. A. Plambeck, *J. Electrochem. Soc.*, **125**, 534, 540 (1978).

9) C. Molinier-Jumel, B. Malfoy, J. A. Reynaud, and G. Aubel-Sadron, *Biochem. Biophys. Res. Commun.*, **84**, 441 (1978).

10) a) R. P. Baldwin, D. Packeff, and T. M. Woodcock, *Anal. Chem.*, **53**, 540 (1981); b) E. N. Chaney, Jr. and R. P. Baldwin, *Anal. Chem.*, **54**, 2556 (1982).

11) T. Kakutani and M. Senda, *Bull. Chem. Soc. Jpn.*, **53**, 1942 (1980).

12) T. Kakutani, K. Kano, S. Ando, and M. Senda, *Bull. Chem. Soc. Jpn.*, **54**, 884 (1981).

13) T. Kakutani, I. Katasho, and M. Senda, *Bull. Chem. Soc. Jpn.*, **56**, 1761 (1983).

14) T. Ikeda, S. Ando, and M. Senda, *Bull. Chem. Soc. Jpn.*, **54**, 2189 (1981).

15) F. Arcamone, G. Cassinelli, G. Franceschi, S. Penco, C. Pol, S. Redaelli, and A. Selva, "International Symposium on Adriamycin," S. K. Carter, A. Di Marco, M. Ghione, I. N. Krakoff, and G. Mathé eds., Springer Verlag, Berlin (1972), p. 16.

16) J. Koryta, *Collect. Czech. Chem. Commun.*, **18**, 206 (1953).

17) A. J. Bard and L. R. Faulkner, "Electrochemical Method-Fundamentals and Applications," John Wiley & Sons, New York (1980), p. 145.

18) R. A. Harie, "Molecules in Three Dimensions," Am. Soc. of Biol. Chem. Inc., Betheda, Meyland, U.S.A.

19) S. Neidle and G. Taylor, *Biochim. Biophys. Acta*, **479**, 450 (1977).

20) T. H. Smith, A. N. Fujiwara, D. W. Henry, and W. W. Lee, *J. Am. Chem. Soc.*, **98**, 1969 (1976).

21) V. P. Marshall, E. A. Reisender, L. M. Reineke, J. H. Johnson, and P. F. Wiley, *Biochemistry*, **15**, 4139 (1976); S. Takahashi and N. R. Bachur, *J. Pharmacol. Exptl. Ther.*, **195**, 41 (1975).

22) This is the case when $a_{ij}=a$ (i, j=O_{ad}, S_{ad}, and R_{ad}), $\alpha_n=\beta_n=0.5$ and $k_{sap}(n)=k_{sap}(n=1, 2)$, where a_{ij}, α_n, β_n, and $k_{sap}(n)$ are Frumkin's interaction parameter between the adsorbed molecules i and j, the cathodic and anodic transfer coefficients, and the apparent rate constant of the n-th charge tranfer step, respectively.

23) Unpublished result.

24) S. G. Mairanovskii, "Catalytic and Kinetic Waves in Polarography," B. M. Fabuss and P. Zuman, translators, Plenum Press, New York (1968), pp. 241—285.

25) I. Tachi, "Polarography," (in Japanese), Iwanami, Tokyo (1954), pp. 357—362.

 © 1984 The Chemical Society of Japan Bull. Chem. Soc. Jpn., 57, 2391—2395 (1984)

^{13}C-NMR Studies on Conformational Equilibria in Isopropyl Methyl Ether

Kenzabu TASAKI, Yuji SASANUMA,† Isao ANDO, and Akihiro ABE*
Department of Polymer Chemistry, Faculty of Engineering, Tokyo Institute of Technology, Ookayama, Meguro-ku, Tokyo 152
(Received February 8, 1984)

The energy difference between the two rotational isomers, *i.e.*, C_S and C_I, of isopropyl methyl ether has been elucidated from the observed vicinal ^{13}C-^{1}H coupling constant. The conventional Gutowsky method based on the simple rotational isomeric state model tends to give an underestimate, especially when the energy difference is large. A more elaborate treatment, which takes account of the overall profile of the torsional potential energy curve, has been attempted. Adoption of J_T=11.0—12.0 Hz for the trans coupling gave a value of 2.2± 0.2 kcal mol^{-1} for the energy difference $E_{C_S}-E_{C_I}$. This result is consistent with the range (2.4±0.6 kcal mol^{-1}) estimated by the matrix-isolation method as reported by Nakata *et al.*

In the structural studies of polymeric chains, we occasionally encounter a stereochemical arrangement which bears some resemblance to isopropyl methyl ether. Poly[oxy(1-methylethylene)][1] $\{CH_2CH(CH_3)O\}_n$ and poly(1-methoxyethylene)[2] $\{CH_2CH(OCH_3)\}_n$ are the typical examples. The energy difference between the two rotational isomers (*i.e.*, C_S and C_I) of isopropyl methyl ether is presumed to be large due to severe steric conflicts involved in the C_S form. Any accurate value of the energy difference ΔE ($=E_{C_S}-E_{C_I}$) has not been determined experimentally. The corresponding value of ΔE for 2-methylbutane, a hydrocarbon analogue of isopropyl methyl ether, has been known[3] to be 0.8 to 0.9 kcal mol^{-1}. Considering the fact that the C–O bond length is somewhat shorter than that of the C–C bond, ΔE for isopropyl methyl ether should be much larger than the value given above. Recently Nakata, Furukawa, Hamaguchi, and Tasumi[4] applied the matrix-isolation technique to this compound: A gaseous mixture with argon was blown agaist a cold surface of CsI plate which was kept at 20 K. The characteristic Raman bands were used for detection of the two rotational isomers trapped in the argon matrix. The energy difference ΔE estimated in this manner amounts to 2.4±0.6 kcal mol^{-1} over the temperature range 20—260 °C.

In this study, we have attempted to elucidate the same energy difference from the analysis of the ^{13}C-^{1}H vicinal coupling constant determined on $^{13}CH_3OC^1H(CH_3)_2$. The information thus acquired regarding the conformation of isopropyl methyl ether will be used in the configurational studies on poly[oxy(1-methylethylene)], which is the subject of forthcoming paper.[5]

Experimental

Isopropyl methyl ether was prepared by the Williamson synthesis from isopropyl alcohol and methyl iodide. Solvents used in the NMR measurements were commercially available and used without further purification.

Natural abundance proton-coupled ^{13}C-NMR spectra were obtained at 25 MHz by using a JEOL FX-100 spectrometer equipped with FT and gated decoupling systems. In the measurements, 300 transients were accumulated with a 90° rf pulse of 13.5 μs duration. The pulse repetition time was 9 s. The Fourier-transformed spectra contain 8192 data points for a 500 Hz spectral width, yielding a resolution of 0.06 Hz. The temperature were maintained within ±1.0 °C during the measurements. A 10-mm NMR sample tube was used.

† Present address: Toray Research Center, Sonoyama, Otsu 520.

Results

The spin system of the compound may be identified as A_3BX. The vicinal coupling constant $^3J_{CH}$ (identified as J_{BX}) can be easily obtained from the ^{13}C-NMR spectrum of the methoxyl carbon. The results are summarized in Table 1. Observed values of $^3J_{CH}$ increase nearly linearly with temperature. The temperature coefficients, $d \ln {}^3J_{CH}/dT$, estimated from these data are also included in the table. The coupling constant varies slightly with polarity of the medium as manifested by a change from 3.90 in cyclohexane-d_{12} (ε=2.023) to 3.79 in dimethyl-d_6 sulfoxide (ε=46.68), both values being determined at 20 °C. Measurements were also carried out on the neat liquid. The following analysis will be mostly performed with resort to the experimental data obtained in cyclohexane-d_{12}.

Elucidation of the Torsional Potential Energy Curve and Interpretation of Results

According to the conventional Gutowsky method,[6] $^3J_{CH}$ is given by

$$^3J_{CH} = J_T f_{C_S} + J_G(1-f_{C_S}). \quad (1)$$

TABLE 1. TEMPERATURE DEPENDENCE OF THE VICINAL COUPLING CONSTANT $^3J_{CH}$ FOR THE MOIETY ^{13}C-O-C-^{1}H IN ISOPROPYL METHYL ETHER

T/deg	$^3J_{CH}$/Hz		
	in cyclohexane-d_{12}	in dimethyl-d_6 sulfoxide	neat liquid
20	3.90	3.76	3.88
40	3.94	3.81	3.89
60		3.88	3.93
70	3.98	3.85	4.00
80	4.00		
90		3.93	4.00
$d \ln {}^3J_{CH}/dT \times 10^3$/K	0.41	0.63	0.47

Here f_{C_s} denotes fraction of the C_S conformer:

$$f_{C_s} = \exp(-\Delta E/RT)/[2+\exp(-\Delta E/RT)], \quad (2)$$

where R is the gas constant and T the temperature. The trans (J_T) and gauche couplings (J_G) are illustrated in Fig. 1. In this simple scheme, only the energy difference between the two preferred rotational isomeric states are considered. In principle, values of J_T, J_G, and ΔE can be determined by the least-squares method from the analysis of the observed temperature dependence of $^3J_{CH}$. The experimental data listed in Table 1 were however found to be reproducible by various combinations of J_T, J_G, and ΔE. Calculations were therefore carried out for given values of ΔE. The best-fit values of J_T and J_G derived from the analysis of the observed data in cyclohexane-d_{12} are plotted against ΔE (solid curves) in Fig. 2. While J_T increases markedly with ΔE, J_G stays nearly invariable over a wide range of ΔE. It should be noted here that the assumption of discrete rotational

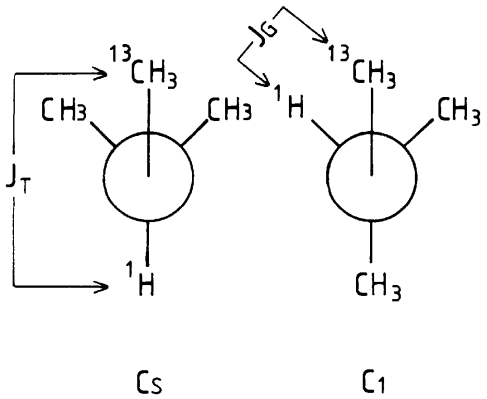

Fig. 1. Schematic representation of isomers and definition of the trans and gauche couplings.

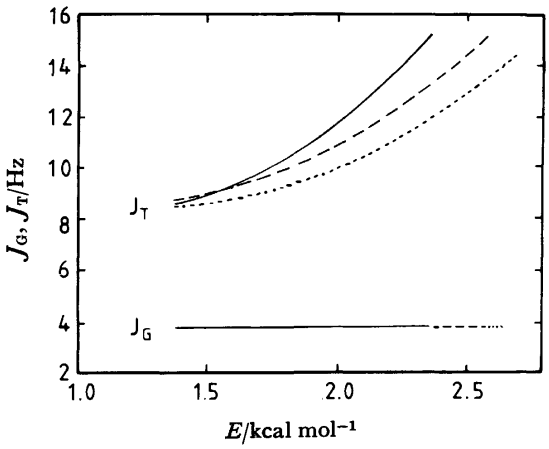

Fig. 2. Plot of best-fit values of J_T and J_G *vs.* ΔE. The results obtained according to the simple Gutowsky treatment (Eq. 1) are indicated by the solid curves. The $J(0)$ and $J(140°)$ values derived from the more elaborate scheme (Eq. 5) are used for the other curves. The height of the cis barrier ($\phi=180°$) is taken to be 1.2 and 1.8 kcal mol^{-1}, respectively, for the dotted and broken curves. The J_G *vs.* ΔE curves are all very similar and practically indistinguishable with each other: they are all represented by a solid curve.

isomeric states is, in principle, valid only when all the torsional potential energy minima are well-defined, and the energy differences among the minima are not too large.[7] Since one of the isomers (C_1) is far more stable than the other (C_S) in isopropyl methyl ether, the aforementioned criteria may not be valid in this system. In such a case, the average of $^3J_{CH}$ should be desirably determined over the entire profile of the torsional potential energy curve.

For this purpose, the potential energy curve for the internal rotation around the $(CH_3)_2CH\text{-}OCH_3$ bond was estimated by using the semiempirical energy expressions. Parameters adopted in these expressions for the three-fold torsional potentials and the 6-exp non-bonded interatomic interaction functions are identical with those used in our previous papers.[8,9] Bond lengths and bond angles used are as follows: l_{CC}=1.53 Å, l_{CO}=1.43 Å, and l_{CH}=1.10 Å; ∠CCC=∠CCH=∠OCH= 109.5°. The bond angle ∠COC was adjusted somewhat when the highly hindered C_S conformer was treated. The deformation energy for the bond angle was estimated by[9,10]

$$E(\theta) = D(\pi/180)^2(\theta-109.5)^2, \quad (3)$$

where θ is expressed in degrees, and D is set equal to 88 kcal mol^{-1}. As for the barriers situated on both sides of the C_S minimum, experimental results on *t*-butyl methyl ether $(CH_3)_3C\text{-}OCH_3$ are suggestive. The barrier to the internal rotation of this compound was reported to be 3.57 kcal mol^{-1} from IR studies in the gas phase.[11] Calculations were carried out so as to reproduce this value for the energy difference between the conformation at the top of the barrier ($\phi=\pm60°$) and that at the C_S minimum ($\phi=0$). Widening of the bond angle ∠COC was required besides adjustment of the rotation around the adjoining C–O and C–C bond. A set of values such as 116.4° and 113.0° for the bond angle ∠COC, respectively, at $\phi=\pm60°$ and 0 was found to give an energy difference as stated above. The value of ∠COC=113.0° is comparable with those observed for ether linkages carrying bulky substituents (*e.g.*, glycoside linkages in polysaccharides[12]). At the C_S minimum, the methoxyl group is situated syn to both of the terminal methyl groups. To alleviate steric conflicts between these groups, rotation angles about the adjoining C–C bonds were displaced by *ca.* 15° from the regularly staggered position. In the C_1 form, steric repulsions between the methoxyl and methyl groups can be largely reduced by the displacement ($\Delta\phi$) of the rotational minima from the regular position, *i.e.*, $\phi=\pm120°$. Locations and the energy of the C_1 minima were calculated by assuming a bond angle ∠COC= 111.5°, a similar value being adopted in the analysis of less hindered ethers.[8,9] The C_1 minima were thus estimated to occur at $\phi=\pm140°$. A displacement of $\Delta\phi=20°$ is in agreement with observations on compounds having a similar stereochemical arrangement.[13] The energy difference between the C_S and C_1 minima obtained in this manner is *ca.* 2 kcal mol^{-1}. On the same basis, the height of the barrier separating two C_1 minima was calculated to be *ca.* 1.2 kcal mol^{-1} as expressed relative to these minima. Results of these considerations are all

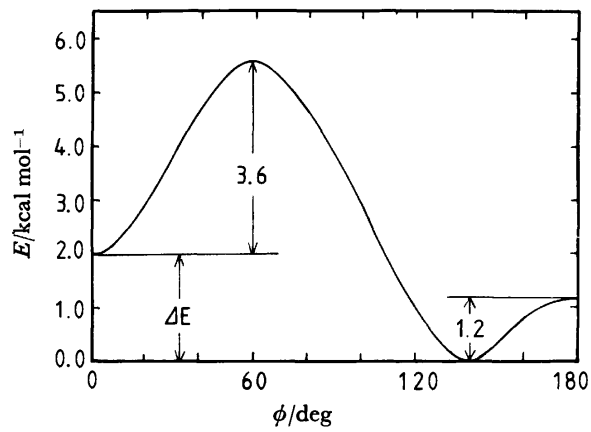

Fig. 3. Torsional potential energy curve for isopropyl methyl ether, CH_3-CH$(CH_3)_2$, estimated by using semiempirical energy calculations in consideration of experimental data on some relevant compounds. The slopes along the higher barrier are drawn by assuming trigonometric functions (see text). The value of ΔE, representing the energy difference between the two minima, will be treated as a variable in the present analysis. Numerical values are given in kcal mol^{-1}.

put together in Fig. 3, where the potential energy curve is shown as a function of ϕ. Since estimation of a reliable value of the energy is quite difficult for a highly strained conformation, trigonometric functions were assumed on both sides of the higher barrier at $\phi=\pm60°$. The slope of the curve drawn from the C_1 minimum ($\phi=\pm140°$) toward the lower barrier ($\phi=180°$) was estimated by the energy calculation.

Durig and Compton[14] deduced the profile of the potential energy curve for the internal rotation of ethyl methyl ether CH_3O-CH_2CH_3 by the analysis of vibrational spectra in the low frequency region. The potential energy barrier, associated with the conformation in which C–O eclipses C–H, resembles the barrier at $\phi=180°$ in isopropyl methyl ether. A value of 1.8 kcal mol^{-1} was estimated for the height of the barrier relative to the energy minimum in which CH_3O-CH_2CH_3 is gauche.[14] Effect arising from the choice of this value will be examined later.

The vicinal coupling constant for the moiety ^{13}C-O-C-^{1}H varies as a function of rotation angle ϕ defined for the C–O bond. The dihedral angle dependence of the coupling constant may be customarily represented by a conventional Karplus-type equation such as

$$J(\phi) = A\cos^2\phi + B\cos\phi + C. \quad (4)$$

In this expression, B is responsible for the difference between the trans and cis couplings, *i.e.*, $J(0)-J(180°)=2B$. The parameter C, which determines the $J(90°)$ value, is usually quite small. In the present treatment, we adopt a simplified expression in which C is set equal to zero. For given values of A and B, an average of the coupling constant $\langle J\rangle$ can be obtained according to the formula specified by the equation

$$\langle J\rangle = \int_0^{2\pi} J(\phi)\exp[-E(\phi)/RT]\mathrm{d}\phi \Big/ \int_0^{2\pi} \exp[-E(\phi)/RT]\mathrm{d}\phi. \quad (5)$$

Numerical computations were carried out for discrete ϕ values taken at 5° intervals. The whole process of calculations was iteratively repeated until experimental values of $^3J_{CH}$ were reproduced within the limit of uncertainty. With values of A and B so determined, $J(0)$ and $J(140°)$ were calculated for $\phi=0$ (the C_S minimum) and 140° (the C_1 minimum), respectively, from the Karplus relation (Eq. 4).

In order to elucidate a proper range of ΔE, the energy of the C_S minimum, $E(0)$, was tentatively raised or lowered in Fig. 3, the height of the barrier on both sides being kept constant (*i.e.*, $E(\pm60°)-E(0)=3.6$ kcal mol^{-1}). For each potential energy curve, a set of A and B, thus $J(0)$ and $J(140°)$, were determined. These results are indicated by the dotted curves in Fig. 2, where $J(0)$ and $J(140°)$ are adopted for J_T and J_G, respectively, and ΔE is taken to be the difference between the minimum energies for the C_S and C_1 forms. Values of J_T calculated according to the simple Gutowsky treatment based on the discrete isomeric state scheme (upper solid curve) are consistent with the results derived from the more elaborate analysis (upper dotted curve) only for very low values of ΔE (<1.5 kcal mol^{-1}). On the other hand, the J_G values are nearly unaffected by the procedure adopted in the analysis. Also shown by the broken curves in the figure are the results obtained on the basis of the torsional potential energy diagram in which the height of the barrier separating two C_1 minima is raised to 1.8 kcal mol^{-1} as suggested by Durig and Compton.[14] In this revised scheme, locations of the C_1 minima were kept unchanged at $\phi=\pm140°$, and the slope along the barrier was represented by a trigonometric function. An enhancement in the height of the torsional potential energy barrier causes some substantial upward shift in the J_T *vs.* ΔE curve (compare two curves indicated by the broken and dotted drawings). The corresponding J_G values are again indistinguishable with those derived from the other schemes.

Estimation of the Energy Difference ΔE

As is shown above, the Gutowsky analyses on the observed temperature dependence of the coupling constant $^3J_{CH}$ do not yield a unique solution for parameters J_T, J_G, and ΔE for the present compound. A reliable estimation of the J_T value is therefore required. Hamer *et al.*[15] and more recently Yamada *et al.*[16] have studied the dihedral angle dependence of the coupling constants $^3J_{CH}$ for various compounds containing the ^{13}C-O-C-^{1}H moiety. The former group deduced a value of $J(0)=6.0\pm0.5$ Hz for a variety of carbohydrate compounds, while the latter found $J(0)=6.8\pm0.7$ Hz from the analysis on cyclic compounds containing the acetal or ether linkages. These values are however apparently too low for the molecule under consideration. As is widely known, formation of a cyclic structure or introduction of electronegative substituents generally leads to a lower value of J_T.[17] For the present purpose, analyses on the observed coupling constants for the same moiety involved in some simple open-chain

methyl ethers should provide more reliable information. The coupling constants associated with the methoxyl hydrogen are reported for dimethyl ether (5.7 Hz), methyl *n*-propyl ether (5.2 Hz), and isopropyl methyl ether (5.0 Hz).[18] Since hydrogens on the terminal methyl group are all equivalent, they should be equally populated among three rotational states. Then, from the relation

$$^3J_{CH} = (1/3)(J_T+2J_G), \quad (6)$$

we estimate J_T=13.1, 11.6, and 11.0 Hz for the aforementioned compounds, respectively, by adopting a value of J_G=2.0 Hz, a standard value for an unstrained gauche coupling.[17] Adoption of an averaged value (12.0 Hz) for J_T in Fig. 2 yields ΔE=2.0, 2.2, and 2.4 kcal mol^{-1}, respectively, for the solid, broken, and dotted curves. Use of a lower value (11.0 Hz), which may also be a probable choice, gives ΔE=1.9, 2.0, and 2.2 kcal mol^{-1}, respectively. As is seen in Figure 2, the J_G value remains nearly invariable over a wide range of ΔE. A value of J_G=3.8±0.1 Hz is commonly applicable to all the models examined.

Plotted in Fig. 4 are the quantities $\langle J\rangle_T$ and $\langle J\rangle_G$ denoting respectively the averages of $J(\phi)$ over the range of ϕ associated with the Cs and C$_1$ minima: *i.e.*,

$$\langle J\rangle = z^{-1}\int_a^b J(\phi)\exp[-E(\phi)/RT]\mathrm{d}\phi, \quad (7)$$

and

$$z = \int_a^b \exp[-E(\phi)/RT]\mathrm{d}\phi, \quad (8)$$

where the interval (a,b) is taken to be (−60°, 60°) for $\langle J\rangle_T$ and (60°, 180°) for $\langle J\rangle_G$. Correspondingly, the abscissa of the figure represents the difference between the energies $\langle E_{C_s}\rangle$ and $\langle E_{C_1}\rangle$ averaged over the respective energy minimum:

$$\langle E\rangle = z^{-1}\int_a^b E(\phi)\exp[-E(\phi)/RT]\mathrm{d}\phi. \quad (9)$$

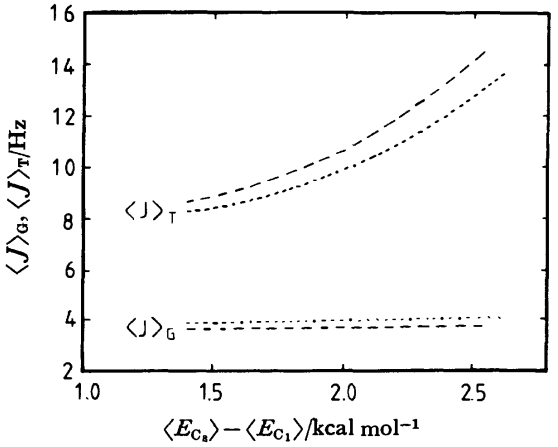

Fig. 4. The averages $\langle J\rangle_T$ and $\langle J\rangle_G$ plotted against $\langle E_{C_s}\rangle-\langle E_{C_1}\rangle$. The two curves differ with each other in the torsional potential energy curve used in the calculation. The dotted and broken curves are used to facilitate comparison with the corresponding plot in Fig. 2.

In these calculations, the integrations were again replaced by summations with discrete ϕ values taken at 5° intervals. The temperature was taken to be 20 °C. In principle, $\langle J\rangle_T$ and $\langle J\rangle_G$ evaluated in this manner should be more closely related to the parameters representing the trans and gauche couplings in the two-parameter expression. The curves drawn in Fig. 4 vary, however, very little from those given for $J(0)$ and $J(140°)$ in Fig. 2: For the ease of comparison, the broken and dotted drawings are used in common. These results arise from the fact that a small decrease in $\langle J\rangle_T$ from $J(0)$ is nearly exactly compensated by a concerted decrease in the energy term. In Fig. 4, two $\langle J\rangle_G$ curves are distinguishable with each other, but the difference is very small. Adoption of $\langle J\rangle_T$=11.0—12.0 Hz should therefore yield the same energy differences for $\langle E_{C_s}\rangle-\langle E_{C_1}\rangle$ as those (ΔE) derived above.

We finally conclude that the energy difference between the two conformers is in the range 2.2±0.2 kcal mol^{-1}. Values obtained from the simple Gutowsky treatment (1.9—2.0 kcal mol^{-1}) are a little too low. The present result is consistent with the range estimated by Nakata *et al.*[4] employing the matrix isolation technique.

Concluding Remarks

In the above treatment, the parameter C in the Karplus equation (Eq. 4) was taken to be zero. However, C is empirically known to be variable within the range ±1.0 Hz. Trial calculations indicate that use of a non-zero value for C causes only some minor modifications on the results: For the range of C given above, J_T and ΔE vary by an amount less than 0.3 Hz and 0.05 kcal mol^{-1}, respectively.

As is shown in Fig. 2, the discrepancy between the solid and either of the other two curves for J_T tends to be more enhanced as ΔE increases. At J_T=12.0 Hz, the difference amounts to 0.2 to 0.4 kcal mol^{-1} in the ΔE value. Assumption of discrete rotational isomeric states leads to a lower estimate of ΔE. In this regard, we should note some characteristic features of the torsional potential energy curve for this compound: 1) The energy difference between the Cs and C$_1$ minima is considerably high (>2 kcal mol^{-1}), 2) the height of the barrier separating the two C$_1$ minima is relatively low, and accordingly, 3) the shape of the potential well for the C$_1$ minimum is somewhat skewed. The effect arising from the latter factors is illustrated by the difference between the broken and dotted curves in Figs. 2 and 4.

Following the conventional rotational isomeric state treatment,[19] we may assign a statistical weight τ to the Cs form, the weight of unity being given to the C$_1$ state:

$$\tau = \tau_0\exp(-\Delta\langle E\rangle/RT) \quad (10)$$

where τ_0 reflects the shape of the energy minima, and $\Delta\langle E\rangle=\langle E_{C_s}\rangle-\langle E_{C_1}\rangle$. By definition, $\tau=z_{C_s}/z_{C_1}$. The partition functions z_{C_s} and z_{C_1} associated with the Cs and C$_1$ isomers, respectively, can be obtained by Eq. 8. We thus have

$$\tau = 0.88\exp(-2200/RT) \quad (11)$$

for the potential energy curve shown in Fig. 3: The temperature is taken to be 20 °C, and RT is expressed in kcal mol^{-1}. Use of the relation $f_{Cs}=\tau/(2+\tau)$ in place of Eq. 2 yields calculated values of $^3J_{CH}=3.88$ Hz and d ln $^3J_{CH}/dT=0.30\times10^{-3}$ K^{-1} for the temperature of 20 °C, values of J_T and J_G being set equal to 12.0 and 3.8 Hz, respectively. Experimental results obtained in cyclohexane-d_{12}. (*cf.* Table 1) are reasonably reproduced.

References

1) A. Abe, T. Hirano, and T. Tsuruta, *Macromolecules*, **12**, 1092 (1979).
2) A. Abe, *Macromolecules*, **10**, 34 (1977).
3) A. L. Verma, W. F. Murphy, and H. J. Bernstein, *J. Chem. Phys.*, **60**, 1540 (1974).
4) M. Nakata, Y. Furukawa, H. Hamaguchi, and M. Tasumi, 45th National Meeting of the Chemical Society of Japan, Tokyo, April 1982, Abstr. No. 4U15.
5) A. Abe, Y. Sasanuma, and I. Ando, to be published.
6) H. S. Gutowsky, G. C. Beldford, and P. E. McMahon, *J. Chem. Phys.*, **36**, 3353 (1962).
7) J. C. Schug, P. E. McMahon, and H. S. Gutowsky, *J. Chem. Phys.*, **33**, 843 (1960); V. M. S. Gil, *J. Magn. Reson.*, **43**, 28 (1981).
8) A. Abe and J. E. Mark, *J. Am. Chem. Soc.*, **98**, 6477 (1976).
9) K. Kato, K. Araki, and A. Abe, *Polym. J.*, **13**, 1055 (1981).
10) T. Shimanouchi, H. Matsuura, Y. Ogawa, and I. Harada, *J. Phys. Chem. Ref. Data*, **7**, 1323 (1978).
11) J. R. Durig, S. M. Craven, J. H. Mulligan, C. W. Hawley, and J. Bragin, *J. Chem. Phys.*, **58**, 1281 (1973).
12) M. Sundaralingam, *Biopolymers*, **6**, 189 (1968).
13) P. Corradini and I. W. Bassi, *J. Polym. Sci.*, **C16**, 3233 (1968); G. Natta, I. W. Bassi, and G. Allegra, *Makromol. Chem.*, **89**, 81 (1965).
14) J. R. Durig and D. A. C. Compton, *J. Chem. Phys.*, **69**, 4713 (1978).
15) G. K. Hamer, F. Balza, N. Cyr, and A. S. Perlin, *Can. J. Chem.*, **56**, 3109 (1978).
16) R. Yamada and I. Ando, *Polymer Preprints, Japan*, **32**, 835 (1983).
17) J. L. Marshall, "Carbon-Carbon and Carbon-Proton NMR Couplings," in "Methods in Stereochemical Analysis,", Vol 2, ed by A. P. Marchand, Verlag Chemie International, Florida (1983).
18) D. E. Dorman, D. Bauer, and J. D. Roberts, *J. Org. Cem.*, **40**, 3729 (1975).
19) P. J. Flory, "Statistical Mechanics of Chain Molecules," Interscience, New York (1969).

The Micellar Properties of 1-Dodecylpyridinium Chloride as Studied by the Ion-selective Electrodes

Tamaki MAEDA* and Iwao SATAKE
Department of Chemistry, Faculty of Science, Kagoshima University, Korimoto, Kagoshima 890
(Received February 23, 1984)

The surfactant ion and counterion activities of aqueous 1-dodecylpyridinium chloride with and without KCl were determined by using ion-selective electrodes. In the concentration range above the critical micelle concentration (cmc), the surfactant ion activity (a_+) was found to decrease gradually with increasing surfactant concentrations, while the reverse change was found for the counterion activity (a_-). As a result, the mean activity increased slightly but regularly with increasing concentrations. The concentration dependences of a_+ and a_- became progressively smaller as the salt concentration increased. An application of the charged phase separation model led to an apparent degree of counterion association to the micelle (β) of 0.70 regardless of the salt concentration. On the basis of these observations, the estimations were made for the concentration of monomeric surfactant ion (C_+) and the activity coefficients of counterion (γ_-) and surfactant ion (γ_+) above the cmc. The values of C_+ and γ_+ decreased appreciably, while that of γ_- increased with increasing concentrations. The value of β was also estimated from the concentration dependence of a_- and the validity of this method was discussed.

The ion-selective electrodes have widely been applied for the determination of counterion and surfactant ion activities in ionic surfactant solutions.[1-14] In most studies were used the sodium ion-sensitive glass electrodes,[2-5,7] as well as the anion-[1,6-9,14] and cation-[1,8-10,12,14] exchange membrane electrodes. In the presence of added salts, however, the liquid[11] and plastic[10,13] membrane electrodes have proved very useful because of their high selectivity for a surfactant ion over inorganic ions. It has been found that the counterion activity (a_+) in anionic surfactant solutions increases gradually with increasing surfactant concentrations through the break point at the critical micelle concentration (cmc).[1-5,7-10,12,14] According to the method advanced by Botré *et al.*,[1] an apparent degree (β) of counterion association to the micelle has been evaluated from the concentration dependence of a_+ above the cmc.[1-3,5,11] On the other hand, the surfactant ion activity (a_-) has been found to decrease monotonously with increasing surfactant concentrations above the cmc.[6-12,14] Sasaki *et al.*[7,8] and Koshinuma[9,14] have confirmed the validity of the charged phase separation model by demonstrating the constancy of $a_-a_+^{\beta}$. By ignoring the effect of micelles on the activity coefficients of monomeric ions, Sasaki *et al.*[7] and Cutler *et al.*[10] have calculated the intermicellar concentrations of counterion and surfactant ion above the cmc.

The ion-selective electrodes can also be applicable to cationic surfactant solutions, though their applications so far reported are confined mostly to anionic ones. In a previous paper,[15] we have reported that poly(vinyl chloride) membrane plasticized with bis (2-ethylhexyl) phthalate responds selectively to cationic surfactant ions, especially to 1-alkylpyridinium ion even in the presence of excess salts. The present paper is concerned with the potentiometric determination of counterion and surfactant ion activities in solution of 1-dodecylpyridinium chloride with and without added KCl.

Experimental

Materials. 1-Dodecylpyridinium chloride (DPC, Wako Pure Chemical Industry Co. Ltd.) was dissolved in hot ethanol and refluxed overnight with active carbon. After cooling the filtrate, the precipitate was purified further by repeated recrystallization from ethanol and by extraction with ether for 48 h. Potassium chloride of guaranteed grade and other chemicals of reagent grade were used without further purification.

Electromotive Force Measurements. The counterion and surfactant ion activities in DPC solutions were measured by using a chloride ion selective ceramic electrode, National IE-510103, and a poly (vinyl chloride) (PVC) membrane electrode, respectively. The following cells were constructed.

Chloride ion electrode | Sample solution (DPC, C; KCl, C_s) | 1 mol dm^{-3} NH_4NO_3 agar bridge | Reference electrode (Ag-AgCl)

Reference electrode (Ag-AgCl) | 1 mol dm^{-3} NH_4NO_3 agar bridge | Reference solution (DPC, 1×10^{-4} mol dm^{-3}) | PVC membrane | Sample solution (DPC, C; KCl, C_s) | 1 mol dm^{-3} NH_4NO_3 agar bridge | Reference electrode (Ag-AgCl)

The preparation of the PVC membrane electrode is described elsewhere.[15] The electromotive forces (EMF) of these cells were measured with an accuracy of ±0.1 mV by using a Yokogawa Universal Digital Meter Model 2502 connected to a voltage follower amplifier (input impedance≃$10^{13}\Omega$). Prior to the measurements with DPC solutions, the chloride ion electrode was calibrated with a sodium chloride solution of known activity.[16] This electrode was found to respond to the chloride ion down to 5×10^{-4} mol dm^{-3} with an ideal slope of 59.2 mV per decade change in chloride ion activity. In the case of PVC membrane electrode, the semilogarithmic plots of EMF *vs.* surfactant concentration gave a straight line with a slope of 59.1 mV in dilute concentration range below *ca.* 1×10^{-4} mol dm^{-3}. This fact suggests the Nernstian response of the PVC membrane electrode to the DPC ion.

All measurements were conducted at 25 °C. The PVC membrane was renewed after a series of experiments for a given salt concentration.

Results and Discussion

The electromotive forces (E) of the foregoing cells can be described as

$$E_+ = E_+^* - S\log(a_+/a_+^*), \quad (1)$$

$$E_- = E_-^* + S\log a_-, \quad (2)$$

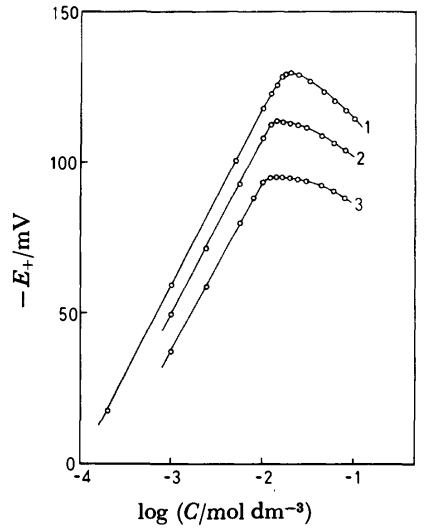

Fig. 1. The semilogarithmic plots of E_+ *vs.* C at 25 °C. 1; C_s=0, 2; C_s=0.01, 3; C_s=0.02 mol dm^{-3}. The curves 2 and 3 are displaced downward by 10 and 20 mV, respectively.

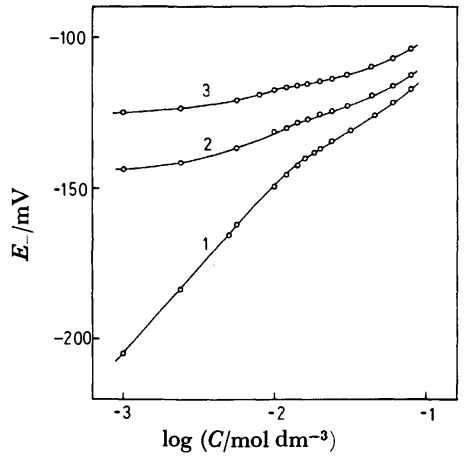

Fig. 2. The semilogarithmic plots of E_- *vs.* C at 25 °C. 1; C_s=0, 2; C_s=0.01, 3; C_s=0.02 mol dm^{-3}.

where E^a refers to the asymmetric potential of overall cell system, $E^\circ_\pm$ to the standard electrode potential, S to the Nernst slope (59.2 mV at 25 °C), and superscript r to the reference solution, respectively. In Figs. 1 and 2 are plotted E_+ and E_- against the logarithm of DPC concentration (C) in the presence and absence of KCl. The break point in these figures corresponds to the cmc (C_o) at a given salt concentration (C_s). In the concentration range above the cmc, the DPC ion activity (a_+) is seen to decrease monotonously with increasing surfactant concentrations, while the reverse is found for the chloride ion activity (a_-). As would be expected, these behaviors are similar to those of surfactant ion[6-12,14] and counter-ion[1-5,7-10,12,14] activities in anionic surfactant solutions. As can be seen from Figs. 1 and 2, the addition of KCl results in a succesive decrease in the slope of E_+ or E_- *vs.* log C plots above the cmc. Figure 3 shows the concentration dependence of $E_- - E_+$ which is a measure of the mean activity ($a_\pm$). It should be noted that

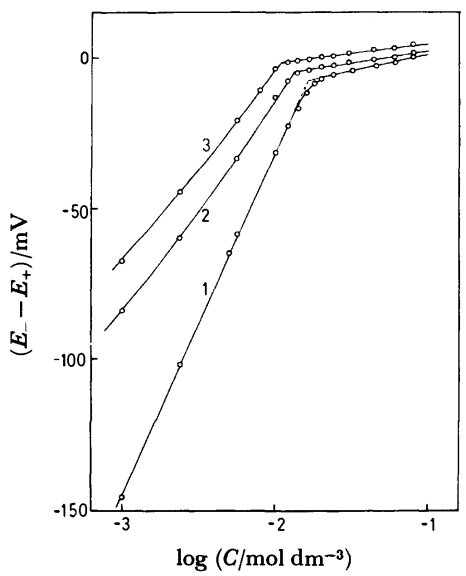

Fig. 3. The semilogarithmic plots of $E_- - E_+$ *vs.* C at 25 °C. 1; C_s=0, 2; C_s=0.01, 3; C_s=0.02 mol dm^{-3}.

the plot of $E_- - E_+$ *vs.* log C at higher surfactant concentrations than the cmc gives a straight line with a small but definite slope. Thus, we may write

$$\log(a_+a_-/a^\circ_+a^\circ_-) = [(E_- - E^\circ_-) - (E_+ - E^\circ_+)]/S = K_1\log(C/C_o), \quad (3)$$

where the superscript ° refers to the cmc. The values of K_1 and the cmc determined from the break points in Fig. 3 are summarized in Table 1. It can immediately be seen that an increase in salt concentration leads to a rapid decrease in K_1. In accord with the results obtained for anionic surfactant solutions,[7-10,12,14] these observations reveal that the mean activity of DPC above the cmc increases progressively with increasing surfactant concentrations unless an excess salt is added. For example in a salt free solution, the value of $a_\pm$ at 0.1 mol dm^{-3} is larger by a factor of 1.19 than that at the cmc.

In solutions of anionic surfactants such as sodium dodecyl sulfate (SDS)[7] and tetradecyl sulfate,[8] the charged phase separation model has been confirmed to hold over a wide concentration range above the cmc. According to this model, $a_+a^\beta_-$ should be constant at higher surfactant concentrations. It follows immediately from Eqs. 1 and 2 that

$$E_+/S = \beta(E_-/S) + \text{const.} \quad (4)$$

If β remains constant, therefore, the plot of E_+/S *vs.* E_-/S is anticipated to give a straight line with the slope of β. As is shown in Fig. 4, E_+/S depends in fact linearly on E_-/S in all cases studied, indicating that the charged phase separation model is also valid for DPC solution. It is worth noting that the value of β summarized in Table 1 is virtually independent of the added salt concentration.

In an attempt to estimate the intermicellar concentrations of surfactant ion and counterion in SDS solutions, Sasaki *et al.*[7] have assumed that the mean ionic molarities of these ions in a micellar solution and in a hypo-

Table 1. The potentiometric and micellar parameters of DPC solution at 25 °C

C_s/m mol dm^{-3}	C_o/m mol dm^{-3}	K_1	K_2/mV	K_3/mol^{-1} dm^3	β	β'
0	16.3	0.188	57.5	20.7	0.69	0.66
10	13.0	0.131	55.7	12.8	0.71	0.71
20	10.7	0.117	54.5	9.3	0.69	0.71

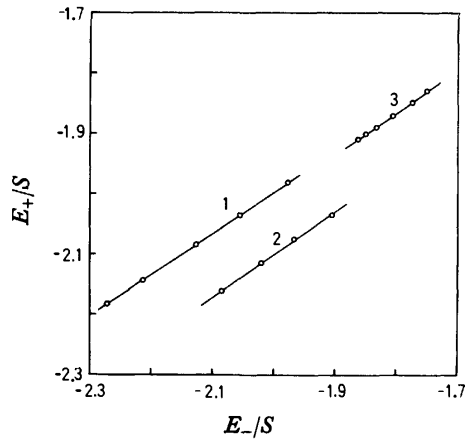

Fig. 4. Plots of E_+/S *vs.* E_-/S at 25 °C. 1; $C_s=0$, 2; $C_s=0.01$, 3; $C_s=0.02$ mol dm^{-3}. The curve 2 is displaced downward by 0.1.

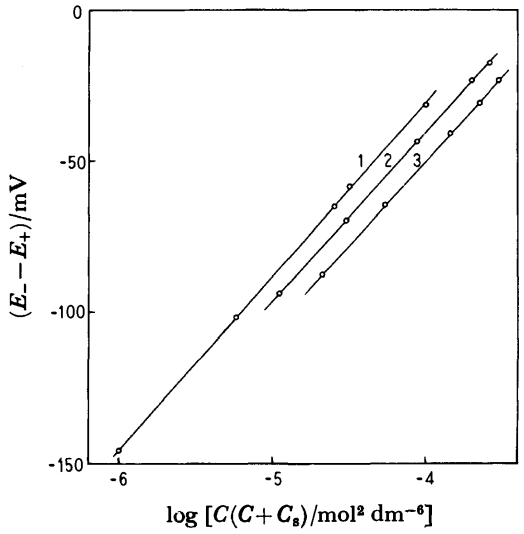

Fig. 5. Plots of $E_- - E_+$ *vs.* log$[C(C+C_s)]$ in the concentration range below the cmc at 25 °C. 1; $C_s=0$, 2; $C_s=0.01$, 3; $C_s=0.02$ mol dm^{-3}. The curves 2 and 3 are displaced downward by 10 and 20 mV, respectively.

thetical solution composing only of monomeric ions are identical with each other at a given mean activity. The same assumption was also made by Cutler *et al.*[10] in their potentiometric study of SDS solutions. Their calculation suggests that the intermicellar concentration of dodecyl sulfate ion is not constant but decreases regularly as the surfactant concentration increases.[7,10] Under the same assumption, we made the tentative estimations of the intermicellar concentration of 1-dodecylpyridinium ion (C_+) and ionic activity coefficients (γ_+, γ_-) in a bulk phase. Figure 5 shows the

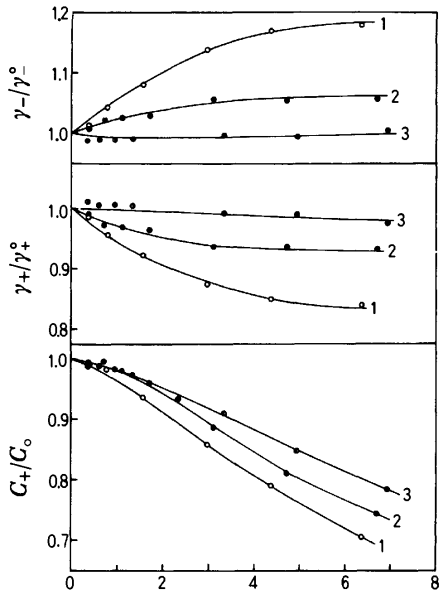

Fig. 6. The concentration dependences of C_+/C_0, $\gamma_+/\gamma_\pm^\circ$, and $\gamma_-/\gamma_\pm^\circ$ estimated from Eqs. 6, 7, and 8. 1; $C_s=0$, 2; $C_s=0.01$, 3; $C_s=0.02$ mol dm^{-3}.

change in $E_- - E_+$ with log$C_\pm^2$ in the concentration range below the cmc, where $C_\pm^2$ denotes $C(C+C_s)$. Regardless of the salt concentration, the plot is found to give a straight line, *i.e.*,

$$E_- - E_+ = \text{const.} + K_2 \log C_\pm^2. \quad (5)$$

The values of K_2 are included in Table 1. Since $C_\pm^2$ in the micellar solution is equal to $C_+[C_+ + C_s + (1-\beta)(C-C_+)]$, Eq. 5 may be rewritten as

$$(E_- - E_-^\circ) - (E_+ - E_+^\circ) = K_2 \log[C_+\{C_+ + C_s + (1-\beta)(C-C_+)\}/C_o(C_o+C_s)]. \quad (6)$$

Equation 6 allows us to estimate the change in C_+ with the surfactant concentration above the cmc. The knowledge of γ_+ and γ_- can then be obtained by substituting the following relations into Eqs. 1 and 2.

$$a_+ = \gamma_+ C_+, \quad (7)$$

$$a_- = \gamma_-[C_+ + C_s + (1-\beta)(C-C_+)]. \quad (8)$$

The values of $C_+/C_\pm^\circ$, $\gamma_+/\gamma_\pm^\circ$, and γ_-/γ_-° thus calculated are plotted in Fig. 6 as a function of $C-C_o$. An important feature of Fig. 6 is a gradual decrease in C_+ with the surfactant concentration though the deviation from C_o becomes progressively smaller as the salt concentration increases. A similar behavior has also been noted for SDS solution without added salt.[7,10] Another interesting feature of Fig. 6 is a marked de-

pendence of γ_+ and γ_- on the salt concentration. In the absence of added salt, an increase in surfactant concentration is accompanied by a decrease in the former while an anomalous increase in the latter. However, they tend eventually to level off. In the presence of 0.02 mol dm^{-3} KCl, neither γ_+ nor γ_- depends appreciably on the surfactant concentration. It is important to remember here that in the concentration range above the cmc, the total concentration of counterion in bulk phase, $C_+ + C_s + (1-\beta)(C-C_+)$, is always larger than that of coion, $C_+ + C_s$. Thus an increase in γ_-/γ_-° estimated above will be ascribed to an increase in the repulsive interaction between counterions in bulk phase compared to that at the cmc where the concentrations of counterion and coion are identical with each other.

An information about the degree of counterion association to the micelle can otherwise be obtained from the concentration dependence of counterion activity alone according to the method advanced by Botré *et al.*[1] In this treatment, it is usually assumed that the counterion activity coefficient and the concentration of monomeric surfactant ion remain constant even above the cmc.[1-3,5,11] On converting γ_- and C_+ in Eq. 8 to γ_-° and C_0 respectively and denoting β in this case by β', we have

$$\begin{aligned} a_-/a_-^\circ &= \exp[2.303(E_- - E_-^\circ)/S] \\ &= 1 + (1-\beta')(C-C_0)/(C_0+C_s) \\ &= 1 + K_3(C-C_0). \end{aligned} \tag{9}$$

In all cases studied, the plot of a_-/a_-° *vs.* $C-C_0$ gives a straight line with a slope of K_3. The values of K_3 and β' are summarized in Table 1. It can immediately be seen that the difference between β' thus estimated and β is negligibly small. We must keep in mind, however, that this agreement does not necessarily support the validity of the underlying assumption of Eq. 9, since the foregoing calculations show that both C_+ and γ_- depend appreciably on the surfactant concentration. In this connection, it is important to note that a similar relation to Eq. 9 can be derived under certain conditions even if C_+ and γ_- are dependent on the surfactant concentration. An expression of the counterion activity, Eq. 8, can formally be divided into two terms; $\gamma_-(C_+ + C_s)$ and $\gamma_-(1-\beta)(C-C_+)$. If each term is linearly dependent on the surfactant concentration, *i.e.*,

$$\gamma_-(C_+ + C_s) = \gamma_-^\circ(C_0 + C_s) + A\gamma_-^\circ(C-C_0) \tag{10}$$

and

$$\gamma_-(1-\beta)(C-C_+) = \gamma_-^\circ B(C-C_0), \tag{11}$$

we immediately have,

$$a_-/a_-^\circ = 1 + (A+B)(C-C_0)/(C_0+C_s). \tag{12}$$

This is exactly identical with Eq. 9 provided that the numerical value of $A+B$ is equal to $1-\beta'$. As is clearly shown in Fig. 7, indeed, the plots of the left hand sides of Eqs. 10 and 11 against the surfactant concentration give a straight line, respectively. In addition, the values of $A+B$ determined from Fig. 7 are in fair agreement with those of $1-\beta'$. Thus,the utility of Eq. 9 in determining the degree of counterion association to the micelle appears to rest on the fact that in micellar

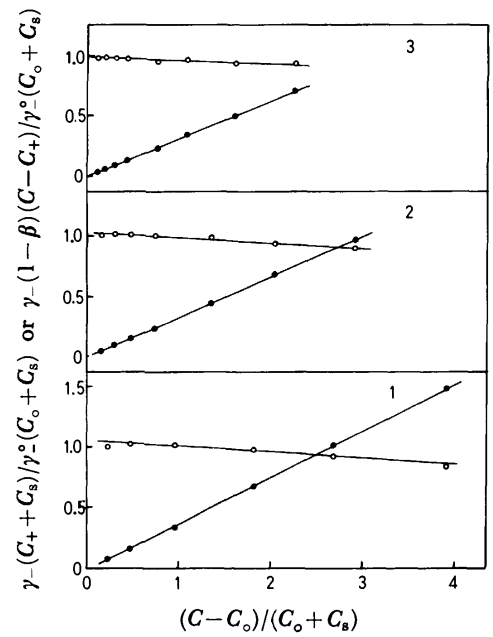

Fig. 7. The concentration dependences of the left hand sides of Eqs. 10 and 11. 1; $C_s=0$, 2; $C_s=0.01$, 3; $C_s=0.02$ mol dm^{-3}. ○; $\gamma_-(C_+ + C_s)/\gamma_-^\circ(C_0+C_s)$, ●; $\gamma_-(1-\beta)(C-C_+)/\gamma_-^\circ(C_0+C_s)$.

solution the counterion activity coefficient and the intermicellar concentration of the surfactant ion vary with the surfactant concentration so as to satisfy Eqs. 10 and 11.

The present work was partially supported by a Grant-in-Aid for Scientific Research No. 57540254 from the Ministry of Education, Science and Culture.

References

1) C. Botré, V. L. Crescenzi, and A. Mele, *J. Phys. Chem.*, **63**, 650 (1959).
2) L. Shedlovsky, C. W. Jakob, and M. B. Epstein, *J. Phys. Chem.*, **67**, 2075 (1963).
3) M. E. Feinstein and H. L. Rosano, *J. Colloid Interface Sci.*, **24**, 73 (1967).
4) P. Stenius and P. Ekwall, *Acta Chem. Scand.*, **21**, 1643 (1967).
5) I. Satake, T. Tahara, and R. Matuura, *Bull. Chem. Soc. Jpn.*, **42**, 319 (1969).
6) K. Kaibara, T. Nakahara, I. Satake, and R. Matuura, *Mem. Fac. Sci. Kyushu Univ. Ser. C.*, **7**, 1 (1970).
7) T. Sasaki, M. Hattori, J. Sasaki, and K. Nukina, *Bull. Chem. Soc. Jpn.*, **48**, 1397 (1975).
8) M. Koshinuma and T. Sasaki, *Bull. Chem. Soc. Jpn.*, **48**, 2755 (1975).
9) M. Koshinuma, *Bull. Chem. Soc. Jpn.*, **52**, 1790 (1979).
10) S. G. Cutler, P. Meares, and D. G. Hall, *J. Chem. Soc., Faraday Trans. 1*, **74**, 1758 (1978).
11) A. Yamauchi, T. Kunisaki, T. Minematsu, Y. Tomokiyo, T. Yamaguchi, and H. Kimizuka, *Bull. Chem. Soc. Jpn.*, **51**, 2791 (1978).
12) E. Vikingstad, *J. Colloid Interface Sci.*, **72**, 68 (1979).
13) J. E. Newbery, *J. Colloid Interface Sci.*, **74**, 483 (1980).
14) M. Koshinuma, *Bull. Chem. Soc. Jpn.*, **54**, 3128 (1981).
15) T. Maeda, M. Ikeda, M. Shibahara, T. Haruta, and I. Satake, *Bull. Chem. Soc. Jpn.*, **54**, 94 (1981).
16) J. Kielland, *J. Am. Chem. Soc.*, **59**, 1675 (1937).

 © 1984 The Chemical Society of Japan Bull. Chem. Soc. Jpn., 57, 2400—2403 (1984)

Analysis of Rotation-Vibration Bands of Sulfine, (CH_2SO), by FT-IR and Microwave Spectroscopy

Yoshinori KOGA,* Harutoshi TAKEO, Shigeo KONDO, Chi MATSUMURA, and Shinnosuke SAEKI
National Chemical Laboratory for Industry, Yatabe, Tsukuba, Ibaraki 305
(Received March 7, 1984)

The rotation-vibration bands of a transient molecule, sulfine, (methanethial S-oxide), have been observed by FT-IR and analyzed with the aid of microwave data, a part of which has been newly obtained in this study. The band center frequencies for ν_5 and ν_9 are determined to be 1175.75 cm^{-1} and 762.07 cm^{-1}, respectively. The good agreement between the observed and simulated band contours clarifies that the origin of these bands is sulfine.

The recent development of FT-IR spectroscopy has enabled us to observe high-resolution infrared spectra of less abundant species such as unstable molecules. If the observed rotation-vibration bands are analyzed to give reasonable values for the molecular constants, it will become evident that the spectrum is due to a particular unstable molecule. However, since many parameters are necessary for the analysis of infrared band envelopes, it is generally very difficult unless some of them have been determined previously from other sources. Since microwave spectroscopy gives the rotational and centrifugal distortion constants in the excited vibrational state as well as in the ground state, the joint study of FT-IR and microwave spectroscopy can be a powerful tool for the analysis of rotation-vibration bands. In the present study we applied this method to the analysis of the rotation-vibration bands of a transient molecule, sulfine.

The spectroscopic investigation of sulfine was first done by Block *et al.*[1] with microwave and infrared spectroscopy using flash vacuum pyrolysis of thiethane S-oxide or 1,3-dithiethane 1-oxide. The detailed analysis of the microwave spectrum of this molecule was carried out and reported by Penn and Olsen.[2] Later, the infrared spectrum of sulfine was studied by Powers *et al.*[3] using a matrix isolation method, and all the fundamental vibrations have been observed. However, only limited results on infrared spectra have been reported for gas phase sulfine.[1] They observed the two rotation-vibration bands at 1170 and 760 cm^{-1} which seemed to be due to sulfine, but they presented no support for their assignments of these bands to sulfine.

Since sulfine is produced by pyrolysis and has a fairly short lifetime, the spectra are naturally disturbed by the parent and decomposed materials. Therefore, it is very difficult to identify the spectrum unambiguously. In the present study, we observed the same two bands of sulfine in the gas phase as observed by Block *et al.* using FT-IR with relatively high resolution, and were able to identify them from the analysis of the band contours by the use of the rotational constants determined by microwave spectroscopy.

Experimental

Infrared Spectra. The infrared spectra were measured by the use of a Digilab model FTS-20C/D spectrophotometer. The optical system was modified as shown in Fig. 1. The collimated beam is taken out through the window attached to the side cover of the instrument. It is reflected by a flat mirror M_1 (80 mmϕ) and a spherical mirror M_2 (80 mmϕ and f=500 mm), and focused at the center of a gas cell. Then the image of the source is focused onto a detector by an off-axis ellipsoidal mirror M_3 (80 mmϕ, f_1=35 mm, and f_2=555 mm). The distance between the source and the detector is about 2.8 meters, and the separation between the mirrors M_2 and M_3 is about 1 meter. Thereby, a 700 mm sample cell with 40 mm diameter can be placed without disturbing the optical path. The detector, the mirrors, and the sample cell were set in the compartment covered with acrylic resin plates, and atmospheric water vapor was purged by dried air. A HgCdTe detector cooled with liquid nitrogen and a globar source were used in all measurements. The accuracy of the frequency of the FT-IR spectrometer was estimated to be better than 0.03 cm^{-1} from the comparison of the observed values for carbon monoxide with the data listed in Ref. 4.

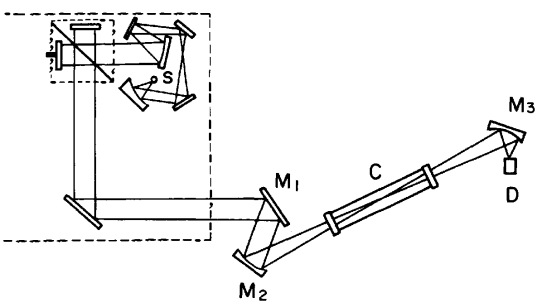

Fig. 1. Modified optical system.
S: glober, M_1: flat mirror, M_2: spherical mirror, M_3: off-axis ellipsoidal mirror, C: infrared cell, D: detector.

For the measurements of the sulfine spectrum, dimethyl sulfoxide was passed through a quartz tube heated up to 700 °C and the products of thermal decomposition were introduced into the cell and pumped through. The heated part of quartz was 20 cm long and 5 mm i.d. The pressure of dimethyl sulfoxide was carefully regulated by a needle valve and, thereby, a steady stream of the products was obtained in the flow-through system. The best sulfine spectrum was obtained at the $(CH_3)_2SO$ pressure of *ca.* 450 mTorr (1 Torr≈133.322 Pa) which was the maximum vapor pressure obtainable in the flow-through system at room temperature. The spectrum was measured at 0.1 cm^{-1} resolution using a 350 mm gas cell with 30 mm diameter and averaging over 512 scans. A triangular apodization function was used in the calculation of spectra.

In the observed spectra, C_2H_4 and SO_2 with medium intensity, along with CH_4 with strong intensity, were clearly identified. These molecules are known to be decomposition products of sulfine or dimethyl sulfoxide by the work of

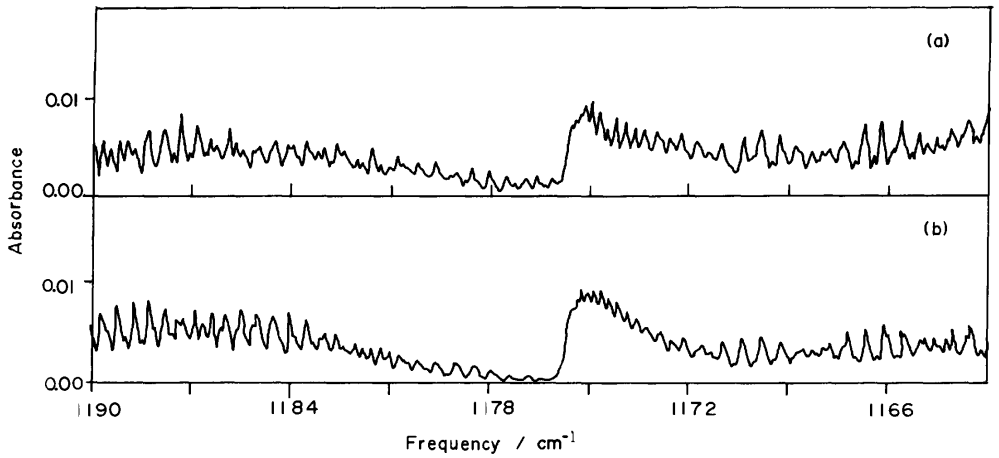

Fig. 2. Spectrum of ν_5 band of sulfine.
(a) Obsd. (b) Calcd.

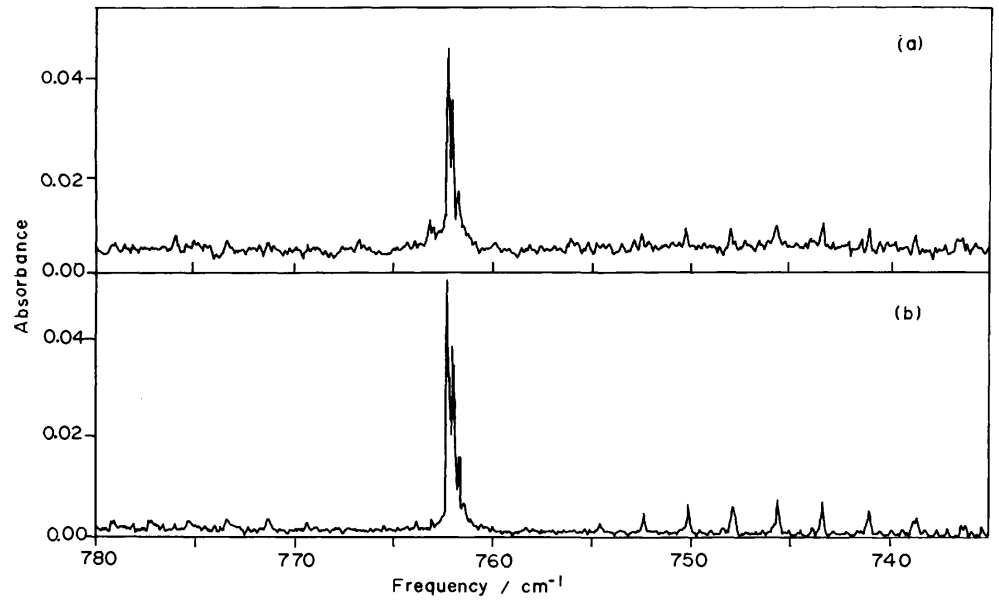

Fig. 3. Spectrum of ν_9 band of sulfine.
(a) Obsd. (b) Calcd.

Thyrion and Debecker[5] on the pyrolysis of $(CH_3)_2SO$. Besides the absorption bands due to these molecules, the rotation-vibration bands centered at 1175 cm^{-1} and 762 cm^{-1} were observed as shown in Figs. 2 and 3. These band positions agree with those reported by Block *et al.* The half-life of the molecular species giving these bands was about 25 min in the infrared cell, which was comparable with that in X-band copper waveguide cell reported by Penn and Olsen.[2] Although the lifetime of this molecule is much longer compared to the pumping speed, the strong infrared spectrum was obtained when the heated quartz tube was placed very near the inlet of the infrared cell. This suggests that this molecule tends to be lost in the narrow glass tube.

Microwave Spectra. The microwave spectrum was measured by a conventional Stark modulation spectrometer with a 3-meter X-band copper waveguide cell. The microwave sources are an HP-8672A frequency synthesizer and an HP-8690 microwave sweeper phase locked to the synthesizer. The sweeping was performed through an HP-IB system controlled by an HP-9835 desk-top computer.

The sample flow-through system was almost the same as used for the IR spectroscopy. However, the vapor pressure was optimum at about 20 mTorr. According to the results of the IR spectroscopy of matrix isolated sulfine,[3] the lowest fundamental vibration is ν_7 (394 cm^{-1}). The microwave spectrum in the excited ν_7 state was first searched for and several low-J transitions were easily identified from their characteristic Stark patterns. The spectral lines for the $2\nu_7$ state were also observed at the expected frequencies. Since the intensity of the ν_9 excited state spectrum was expected to be nearly the same as of $2\nu_7$, the assignment of the spectral lines was done by comparing them with corresponding $2\nu_7$, lines. All the observed transition frequencies and the rotational constants derived from them by least-squares fitting are listed in Table 1. Since the μ_b of sulfine is small, no b-type transitions for the vibrational satellites were observed and the A' rotational constants were not determined precisely.

Results and Discussion

The sulfine is a planar asymmetric top molecule with an asymmetry parameter $\kappa=-0.891$ and belongs to the

TABLE 1. OBSERVED MICROWAVE TRANSITIONS AND ROTATIONAL CONSTANTS OF SULFINE IN VARIOUS VIBRATIONAL STATES (MHz)

Transition	Ground[a]	ν_7		$2\nu_7$		ν_9	
	Obsd	Obsd	Δ[b]	Obsd	Δ	Obsd	Δ
1_{01}—0_{00}	17001.86	16988.85	0.13	16974.98	−0.04	16979.75	0.05
2_{02}—1_{01}	33928.87	33902.16	0.03	33874.96	0.01	33885.77	0.04
2_{12}—1_{11}	32216.49	32183.32	−0.01	32149.39	0.06	32201.41	0.02
2_{11}—1_{10}	35791.41	35771.52	−0.02	35750.70	−0.04	35717.42	0.01
3_{13}—2_{12}	48278.11	48228.82	−0.05	48178.01	−0.01	48256.90	−0.06
3_{12}—3_{13}	10723.27	10762.66	−0.01	10802.27	0.02	10546.13	−0.01
A	40404.500	40535(130)		40861(80)		39936(84)	
B	9394.837	9391.41(5)		9387.86(3)		9368.86(3)	
C	7607.120	7597.30(4)		7587.16(3)		7610.84(3)	

a) Obtained by R. E. Penn and R. J. Olsen. b) Δ=Obsd−Calcd.

C_s point group. Simulation spectra for the two bands observed in this work were obtained with the computer program written for calculating the rotation-vibration spectrum of the asymmetric top molecule. The details of the program have been described elsewhere.[6] After the line positions and intensities of the individual transitions were calculated the spectrum was simulated using a Lorentz type line shape function and a triangular slit function. A comparison of the two bands observed at 1175 and 762 cm^{-1} with the simulated ones leads to their unambiguous assignment to the CSO symmetric stretching mode (ν_5) and the CH_2 wagging mode (ν_9), respectively, of sulfine. The lower part of the ν_5 band was overlapped by the ν_1 band of SO_2 produced by pyrolysis. Nevertheless, PQR-structure of sulfine was readily distinguished from the mixed spectra. In principle, the ν_5 band is expected to be an a- and b-type hybrid band. However, the observed spectrum clearly shows that this band consists mainly of a-type band because of the weak line strength of the b-type band. In the course of simulation calculation, three excited state rotational constants (A'_5, B'_5, and C'_5) and the band center ν_5 were adjusted to fit the observed spectrum, keeping the ground state rotational and centrifugal distortion constants fixed at their microwave values,[2] and the excited state centrifugal distortion constants equal to the ground state values. In the analysis of the spectrum, 44 prominent peak positions in the absorption band were chosen to use in a least-squares fit for the determination of the molecular parameters. The molecular parameters derived are listed in Table 2, and the observed and calculated frequencies along with the assignments are given in Table 3. Each of the prominent peaks is assigned to the transition which makes the largest contribution to that particular peak. In Fig. 2 the observed and simulated spectra of ν_5 band are shown. The band center is determined as 1175.75 cm^{-1} which is slightly higher than the value of 1170 cm^{-1} reported by Block *et al.*,[1] while it is fairly different from the matrix value (1165 cm^{-1}).[3]

The ν_9 band should be a c-type band which corresponds to the perpendicular band in a prolate symmetric top and, therefore, a fairly strong Q-branch is expected at its center. In Fig. 3 the observed band is compared with the calculated spectrum. It is clearly seen that this band is of typical c-type and is compatible with the vibrational mode of the CH_2 wagging as has been estimated by Powers *et al.*[3] The prominent series of $^{r,p}Q$ branches were easily assigned from comparison with the calculated spectrum, whereas ^pP, ^pR, ^rP, and ^rR in many subbands were not resolved in the present measurements. Consequently, it was difficult to determine the three excited state rotational constants of this band only from the observed spectrum. Therefore, the measurement of the microwave spectrum in the excited ν_9 state was carried out. Since the A' rotational constant obtained by microwave spectroscopy had a large uncertainty as described previously, both the A' and band center were adjusted to fit the observed infrared spectrum, keeping all the other constants fixed at the microwave values. The determined molecular constants are listed in Table 2. Table 4 compares the observed and calculated values of the prominent peaks in the ν_9 band. The band center of ν_9 thus determined is 762.07 cm^{-1} which is close to the value of 760 cm^{-1} obtained by Block *et al.* and also near the matrix value (767 cm^{-1}).

In conclusion, the good agreement between the observed and calculated spectra of the ν_5 and ν_9 bands with the reasonable molecular parameters was obtained

TABLE 2. ROTATIONAL CONSTANTS AND BAND CENTERS OF ν_5 AND ν_9 (cm^{-1})

Ground state[a]	Band center	Excited state[b]
A''=1.3477493(10)	ν_5=1175.75(3)	A'=1.33686(41)
B''=0.31337495(23)		B'=0.31200(136)
C''=0.25374587(20)		C'=0.25314(148)
	ν_9=762.07(4)	A'=1.33684(119)
		B'=0.31251135(97)[c]
		C'=0.2538704(87)[c]

a) See Ref. 1. b) Standard deviations (3σ) are given in parentheses. c) These values were determined by MW measurement in this work.

Table 3. Observed and calculated wavenumbers of ν_5 band (cm^{-1})

Obsd	Δ[a]	J''	K_a''	K_c''	$-J'$	K_a'	K_c'	Obsd	Δ[a]	J''	K_a''	K_c''	$-J'$	K_a'	K_c'
1164.52	−0.02	21	0	21	20	0	20	1175.31	−0.01	6	6	0	6	5	1
1165.60	0.02	19	0	19	18	0	18	1175.48	0.03	5	5	0	5	4	1
1166.15	0.03	18	0	18	17	0	17	1177.42	0.01	2	0	2	3	0	3
1166.69	0.05	17	0	17	16	0	16	1177.96	0.00	3	0	3	4	0	4
1167.25	0.04	16	0	16	15	0	15	1178.50	0.00	4	0	4	5	0	5
1167.75	0.02	15	0	15	14	0	14	1179.04	0.01	5	2	4	6	4	3
1168.74	0.00	13	0	13	12	0	12	1179.28	0.00	5	1	4	6	1	5
1169.82	0.02	11	0	11	10	0	10	1179.59	0.03	6	0	6	7	0	7
1170.37	0.00	10	1	10	9	3	7	1180.13	0.00	7	2	6	8	4	5
1170.97	0.03	9	1	9	8	3	6	1180.55	0.02	8	0	8	9	0	9
1171.33	−0.03	8	0	8	7	0	7	1180.97	0.02	9	1	9	10	3	8
1171.69	−0.03	7	2	6	6	4	3	1181.21	−0.01	9	2	8	10	4	7
1172.17	−0.01	18	18	0	18	17	1	1181.51	0.02	10	0	10	11	0	11
1172.54	0.01	6	1	6	5	3	3	1181.94	−0.03	11	0	11	12	0	12
1172.90	−0.01	17	16	1	17	15	2	1182.54	0.07	12	0	12	13	0	13
1173.26	0.00	15	15	0	15	14	1	1182.78	0.03	12	2	11	13	4	10
1173.56	−0.01	14	14	0	14	13	1	1183.44	0.02	14	0	14	15	0	15
1173.86	−0.01	13	13	0	13	12	1	1183.93	−0.01	15	0	15	16	0	16
1174.12	−0.01	13	12	1	13	11	2	1184.41	−0.02	16	0	16	17	0	17
1174.39	0.00	11	11	0	11	10	1	1184.89	0.01	17	0	17	18	0	18
1174.60	−0.02	10	10	0	10	9	1	1185.37	0.01	18	0	18	19	0	19
1174.83	0.00	9	9	0	9	8	1	1185.85	0.00	19	0	19	20	0	20
1175.01	−0.01	8	8	0	8	7	1	1186.34	0.05	20	0	20	21	0	21
1175.19	0.01	7	7	0	7	6	1	1186.76	−0.04	21	0	21	22	0	22

a) Δ = Obsd − Calcd.

Table 4. Observed and calculated frequencies of ν_9 band peaks (cm^{-1})

Obsd	Obsd − Calcd	Assignment
775.29	0.00	$^rQ_6$
773.30	0.02	$^rQ_5$
771.12	−0.02	$^rQ_4$
769.31	0.01	$^rQ_3$
762.05	−0.02	$^rQ_0$
752.31	−0.01	$^pQ_5$
750.12	0.01	$^pQ_6$
747.85	0.00	$^pQ_7$
745.55	−0.02	$^pQ_8$
743.28	0.01	$^pQ_9$
740.92	−0.02	$^pQ_{10}$
738.56	−0.01	$^pQ_{11}$

by the joint analysis of FT-IR and microwave spectroscopy and it definitely confirmed that the origin of these bands is the sulfine molecule. In addition, the vibrational frequencies of ν_5 and ν_9 of sulfine were determined precisely.

References

1) E. Block, R. E. Penn, R. J. Olsen, and P. F. Sherwin, *J. Am. Chem. Soc.*, **98**, 1264 (1976).
2) R. E. Penn and R. J. Olsen, *J. Mol. Spectrosc.*, **61**, 21 (1976).
3) D. E. Powers, C. A. Arrington, W. C. Harris, E. Block, and V. F. Kalasinsky, *J. Phys. Chem.*, **83**, 1890 (1979).
4) A. R. H. Cole, "Tables of wavenumbers for the calibration of infrared spectrometers" Second edition, Pergamon Press, 1977.
5) F. C. Thyrion and G. Debecker, *Int. J. Chem. Kinet.*, **5**, 583 (1973).
6) T. Nakanaga, S. Kondo, Y. Koga, and S. Saeki, *J. Nat. Chem. Lab. Ind.*, **74**, 190 (1979).

The Thermal Properties of Liquid Crystalline Materials Incorporating Cyanothiophene and Cyanofuran

Shiro MIYAKE, Shigekazu KUSABAYASHI, and Shunsuke TAKENAKA*
Department of Applied Chemistry, Faculty of Engineering, Osaka University, Suita, Osaka 560
(Received March 10, 1984)

Some homologous series of cyanothiophene and cyanofuran compounds have been prepared. 4-Alkoxyphenyl 3-(5-bromo-2-thienyl)acrylate (**1**) and 4-alkoxyphenyl 3-(5-cyano-2-thienyl)acrylate (**2**), and 4-alkoxyphenyl 4-(5-bromo-2-furylcarbonyloxy)benzoate (**3**) and 4-alkoxyphenyl 4-(5-cyano-2-furylcarbonyloxy)benzoate (**4**) give rise to a nematic phase. For compound **4**, a smectic A phase which commences from the hexyloxy homolog has a bilayer (S_{A2}) arrangement of the molecules. The thermal stabilities of the mesophases are lower than those of the corresponding benzonitrile compounds. This arises from an increased molecular breadth around the terminal portion and the change of the dipole moment arising from the terminal cyano group bending with respect to the long molecular axis.

Liquid crystalline materials incorporating a cyanophenyl group as the terminal function are good nematogens for devices employing a twisted nematic mode. The molecules frequently give rise to very interesting phenomena such as an induced smectic A phase[1-3] or an enhancement of smectic A thermal stability[4,5] in some binary mixtures and reentrant phenomena.[6-8] In such cases, it is well known that a dipole moment arising from the terminal cyano group plays a very important role in determining the thermal behavior of the molecule.[8-10]

In this paper, we describe the preparation, and thermal and dielectric properties of cyanothiophene and cyanofuran compounds, **1**, **2**, **3**, and **4**, and some related compounds. In these series, the cyano group would occur at an angle with respect to the rotational axis of the entire molecule because of the thiophene and furan rings, and increase the molecular breadth.

Experimental

Method. The transition temperatures were determined by using a Nikon POH polarizing microscope fitted with a Mettler FP 52 heating stage and a control unit. The transition temperatures were also measured by using a Dainiseikosha SSC-560 differential scanning calorimeter. Indium (99.9%) was used as a calibration standard at a heating rate of 5 °C/min. The dielectric constants were measured by using an Andodenki TR-10 precision capacitance measurement system. The capacitor cell consisted of two indium coated glass electrodes separated by a 25 μm Mylar spacer. The cell temperature was controlled by means of a brass housing. The voltage applied was 0.4 V at 1 kHz. The alignment of molecules in the cell was achieved by applying a 1.0 T magnetic field. The capacitor cell was calibrated by highly purified benzene and acetonitrile.

Materials. 3-(5-Bromo-2-thienyl)acrylate was prepared by the reaction of 5-bromo-2-thiophenecarbaldehyde and malonic acid.[11] 3-(5-Bromo-2-thienyl) acryloyl chloride was reacted with 4-alkoxyphenols in dry benzene containing pyridine (5%), giving the homologous series of **1**. A similar reaction of 5-bromo-2-furancarbonyl chloride and 4-alkoxyphenyl 4-hydroxybenzoates[12] gave the homologous series of **3**.

4-Nonyloxyphenyl 4-(5-Cyano-2-furylcarbonyloxy)benzoate. A mixture of 4-nonyloxyphenyl 4-(5-bromo-2-furylcarbonyloxy)benzoate (3.4 g, 6.4 mmol) and copper(I) cyanide (0.86 g, 9.6 mmol) in anhydrous *N,N*-dimethylformamide (20 ml) was refluxed for 3 h.[13] After cooling, the dark brown solution was poured onto cold water (100 ml) containing ethylenediamine (8.0 g, 0.13 mol). The resulting solution was extracted with ether (50 ml×4 times). The purification was carried out by column chromatography on silica gel where a solvent mixture of pet. ether and ether (95:5) was used as an elution solvent, followed by recrystallization from absolute ethanol: 0.8 g, IR: ν_{CN}=2250 cm^{-1}. The homologous series of **2** and **4** were prepared similarly. The purity was checked by elemental analysis.

Results and Discussion

The transition temperatures for thiophene compounds **1** and **2** are summarized in Table 1. In the present study, three related compounds were prepared; 4-butylcyclohexyl 3-(5-cyano-2-thienyl)acrylate (T_{mp}=70.5 and $T_{N\cdot I}$=51.7 °C), 4-pentylcyclohexyl 3-(5-cyano-2-thienyl)acrylate (T_{mp}=85.7 and $T_{N\cdot I}$=70.2 °C), and 4-hexylphenyl 3-(5-cyano-2-thienyl)acrylate (T_{mp}=92.4 and $T_{N\cdot I}$=73.0 °C). For these compounds both melting points and nematic-isotropic transition temperatures are lower than those for series **2**.

The transition temperatures for the furan compounds **3** and **4** are summarized in Table 2. The nematic-isotropic transition temperatures reveal a familiar even-odd effect. The smectic properties for

TABLE 1. THE TRANSITION TEMPERATURES FOR SERIES **1** AND **2** (T/°C)

Compound	n	X	C	N		I
1	3	Br	.	89.9 —		
	4		.	89.5 —		
	5		.	79.2(.	57.3)	.
	6		.	77.3(.	66.8)	.
	7		.	76.4 .	63.7)	.
	8		.	76.4(.	70.7)	.
2	3	CN	.	115.0(.	105.8)	.
	4		.	115.4(.	96.6)	.
	5		.	99.2(.	92.2)	.
	6		.	85.9(.	97.3)	.
	7		.	95.7 .	95.8	.
	8		.	95.4 .	99.0	.

The values in the parentheses indicate the monotropic transitions.

Table 2. The transition temperatures for series **3** and **4** (T/°C)

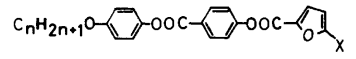

Compound	n	X	C	S_A	N	I
3	3	Br	.	129.1 —	. 132.6	.
	4		.	128.1 —	(. 124.1)	.
	5		.	115.5 —	. 120.6	.
	6		.	118.9 —	. 119.2	.
	7		.	121.3 —	. *1	.
	8		.	118.3 —	. 122.1	.
	9		.	122.1 —	. *1	.
	10		.	121.6 —	(. 113.4)	.
4	3	Br	.	147.2 —	. 157.3	.
	4		.	136.9 —	. 158.3	.
	5		.	142.5 —	. 153.5	.
	6		.	139.0(. 126.4)	. 125.6	.
	7		.	137.2(. 133.8)	. 147.4	.
	8		.	134.9 . 140.1	. 147.6	.
	9		.	134.3 . 143.1	. 144.1	.
	10		.	134.6 . 149.2	—	.

The values in the parentheses indicate the monotropic transitions. *1 Solidification proceeded.

series **4** commence from the hexyloxy homolog. In the present study, three related compounds were prepared; 4-butoxyphenyl 5-cyano-2-furancarboxylate (T_{mp}=104 °C) and 4-hexylphenyl 5-cyano-2-furancarboxylate (T_{mp}=95.5 °C), but none of them turned out to be mesogenic. 4-Hexylphenyl 4-(5-cyano-2-funylcarbonyloxy) benzoate gives rise to a nematic phase monotropically (T_{mp}=135 and T_{N-I}=129 °C). The assignment of the smectic phase for the heptyloxy homolog of series **4** was done by an examination of the isobaric diagrams shown in Fig. 1.

In the binary mixture of the heptyloxy homolog and 4-pentylphenyl 4-(4-octylbenzoyloxy)benzoate (Fig. 1a), the smectic A-nematic transition temperatures reveal a weak nonideal behavior in the range between 80 and 0 mol% of the heptyloxy homolog. However, both smectic phases are discontinuous in the range between 95 and 85 mol% of the heptyloxy homolog. A similar trend is observed in Fig. 1b. For the binary mixture of the heptyloxy homolog and 4-pentylphenyl 2-cyano-4-(4-octylbenzoyloxy)benzoate, an interesting fact is that the smectic A-nematic (isotropic) transitions show a linear correlation with additivity, whereas both smectic phases appear to be essentially immiscible. Here, it would be reasonable to assume that both nonpolar mesogens have a monolayer arrangement of the molecules in the smectic A phase. In Fig. 1c, the smectic phase of the heptyloxy homolog is also immiscible with the smectic A phase of *N*-[4-(4-octyloxybenzoyloxy)-benzylidene]-4-cyanoaniline where the molecules form a partially bilayer arrangement (S_{Ad}) in the smectic A phase.[14] For the binary phase diagram of the heptyloxy homolog and 4-pentylphenyl 4-(4-cyanobenzoyloxy)benzoate (5DB)[15] in Fig. 1d, on the other hand, both smectic phases are isomorphous, though the smectic-nematic transition temperatures show a nonideal behavior with additivity. 5DB has been known to form a bilayer arrangement (S_{A2}) of the molecules in the smectic A phase. These facts lead to the conclusion that the smectic phase of the heptyloxy homolog forms a smectic A modification with a bilayer arrangement of the molecules (S_{A2}). In Fig. 1a and 1b, the S_A-N transition temperatures show an ideal behavior in the range between 80 and 0 mol% of the heptyloxy homolog of series **4** and the apparent discontinuity in the range between 95 and 85 mol%. This indicates that the S_{A2} phase, although similar to the S_{A1} phase, is essentially different and immiscible with it and that the S_{A2} arrangement of the molecules is easily destroyed by a small amount of the nonpolar mesogens. In Fig. 1c, the rapid reduction of the S_A-N transition temperatures with increasing the composition of *N*-[4-(4-octyloxybenzoyloxy)benzylidene]-4-cyanoaniline indicates that the S_{A2} phase of the heptyloxy homolog of **4** has low affinity with the S_{Ad} phase.

From geometrical and electrical points of view, 3-(5-cyano-2-thienyl)acrylate and 5-cyano-2-furancarboxylate are very different from 3-cyanobenzoate. The geometries of cyanothiophene, cyanofuran, and benzonitrile are illustrated in Fig. 2. The cyano group in series **2** lies in the volume of a cylinder defined by rotation of the rest of the molecule about its longer molecular axis. The nematic-isotropic transition temperaturs for series **2** are lower by *ca.* 50 °C than those for the 4-alkoxyphenyl 4-cyanocinnamates,[16] whereas the cyano group does not increase the molecular breadth so much. Similarly, the nematic-isotropic transition temperatures for series **4** are lower by *ca.* 130 °C than those for the corresponding benzonitrile compounds.[15] The increased molecular breadth around the cyanofuran portion is one of the reasons for the low nematic stability. When the molecules form antiparallel correlations due to strong dipole-dipole

interaction, however, the bend of the terminal cyano group would be very unfavorable for the thermal stabilities of the mesophases, especially in the thermal stabillity of the nematic phase. The situation is shown in Fig. 3.

As a result, the bend of the cyano group would increase the breadth of the antiparallel dimer formed by the dipole-dipole interaction. The increased molecular breadth is assumed to be the other reason for the low nematic stabilities of series **2** and **4**. On the other hand, the axial separation of the molecules due to the bent geometry would reduce a repulsive interaction around the core portion. This, in turn, leads to an increase in relative thermal stability of the smectic A phase. Indeed, the ratios of the smectic A-nematic/nematic-isotropic transition temperatures for the series **4** lie in the range between 0.94 and ≈1. The values are very large compared with those for three ring compounds incorporating a cyano group at the terminal position,[17] indicating that for series **4** the thermal stabilities of the smectic A phase are relatively higher than those of the nematic phase.

From an electrical point of view, the cyano groups in series **2** and **4** are rather similar to the cyano group in 4-cyanobenzoate compounds, because a conjugation of the cyano group with the π electron system of the entire molecule generates greater polarity and polarisability, a general requisite of the mesophase stability. However, the bend of the cyano group strongly affects the dielectric behavior. The dielectric constants $\varepsilon_{/\!/}$ and $\varepsilon_{\perp}$ for the octyloxy homolog of series **2** are plotted against temperature in Fig. 4.

The dielectric anisotropy ($\Delta\varepsilon$) for the octyloxy homolog is *ca.* 1.8 at 90 °C, indicating that the anisotropy of the dipole moment arising from the cyano group is quite small. The anisotropy ($\Delta\varepsilon$) for the heptyloxy homolog of series **4** is *ca.* −3.0 at 139 °C. The negative value is expected from the theoretical calculation of the group dipole moments.[18] Therefore, the cyano groups in series **2** and **4** tend to

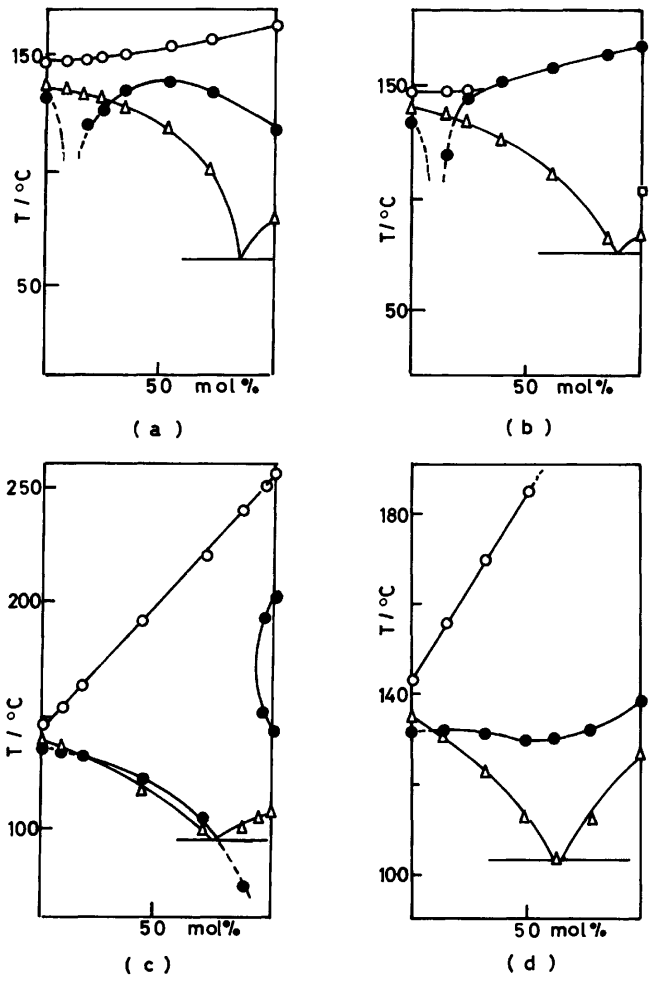

Fig. 1. The isobaric diagrams for the mixtures of (a) the heptyloxy homolog of **4** (on left) and 4-heptylphenyl 4-(4-octylbenzoyloxy)benzoate (on right), (b) the heptyloxy homolog of **4** (on left) and 4-heptylphenyl 4-(3-cyano-4-octylbenzoyloxy)benzoate (on right), (c) the heptyloxy homolog of **4** (on left) and *N*-[4-(4-octyloxybenzoyloxy)benzylidene]-4-cyanoaniline(on right), (d) the heptyloxy homolog of **4**(on left) and 4-pentylphenyl 4-(4-cyanobenzoyloxy)benzoate (on right). ○: nematic-isotropic, ●: smectic A-nematic (isotropic), and △: solid-mesophase transitions.

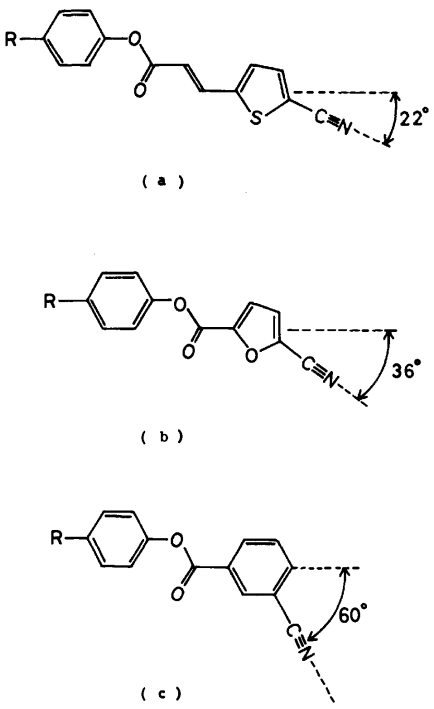

Fig. 2. The geometries of 3-(5-cyano-2-thienyl)acrylate (a), 5-cyano-2-furancarboxylate(b), and 3-cyanobenzoate(c).

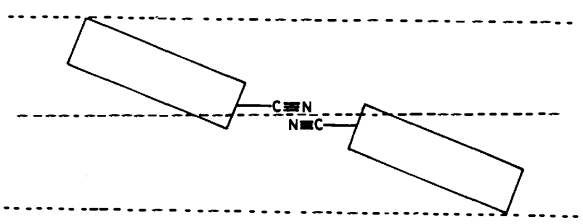

Fig. 3. A possible model for the antiparallel dimer for series **2** and **4**.

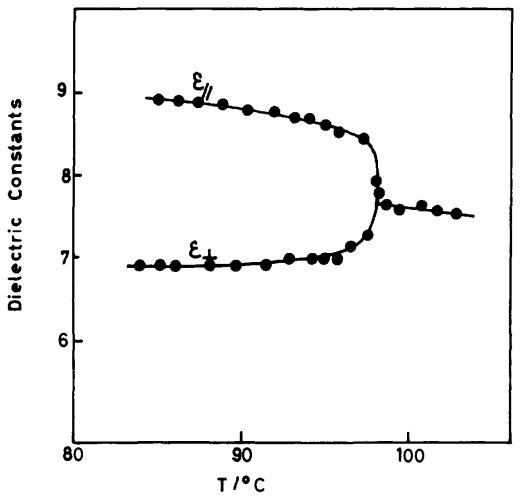

Fig. 4. Plot of the dielectric constants against temperature for the octyloxy homolog of series **2**.

increse the dipolarity perpendicular to the long molecular axis, as does the cyano group in 3-cyanobenzoate compounds.

Conclusion

The terminal cyano group has a very important role in determining the thermal and dielectric properties, and the bend of the cyano group with respect to the long molecular axis results in a decrease in the thermal stabilities of the mesophases and a reduction of the dielectric anisotropy. The formation of the bilayer smectic A phase (S_{A2}) for series **4** appears to be a rare case.

References

1) J. W. Park, C. S. Bak, and M. M. Labes, *J. Am. Chem. Soc.*, **97**, 4398 (1975).
2) C. S. Oh, *Mol. Cryst. Liq. Cryst.*, **42**, 1 (1977).
3) G. Heppke and E.-J. Ricter, *Z. Naturforsch.*, **33**, 185 (1978).
4) A. C. Griffin, R. F. Fisher, and S. J. Havens, *J. Am. Chem. Soc.*, **100**, 6329 (1978).
5) M. Domon and J. Billard, *J. Phys.*, **C3-40**, C3-413 (1979).
6) P. E. Cladis, R. K. Bogardus, and D. Aadsen, *Phys. Rev. A*, **18**, 2292 (1978).
7) W. Weissflog, G. Pelzl, and D. Demus, *Mol. Cryst. Liq. Cryst.*, **76**, 261 (1981).
8) N. H. Tinh, *Mol. Cryst. Liq. Cryst.*, **91**, 285 (1983).
9) A. M. Levelut and R. J. Tarento, *Phys. Rev. A*, **24**, 2180 (1981).
10) N. V. Madhusidana, B. S. Srikanta, and M. Subramanya, *Mol. Cryst. Liq. Cryst.*, **97**, 49 (1983).
11) G. W. Gray and B. Jones, *J. Chem. Soc.*, **1954**, 1467.
12) J. P. Van Meter and B. H. Klanderman, *Mol. Cryst. Liq. Cryst.*, **22**, 285 (1973).
13) J. C. Dubois and A. Beguin, *Mol. Cryst. Liq. Cryst.*, **47**, 193 (1978).
14) N. H. Tinh, A. Zann, J. C. Dubois, and J. Billard, *Mol. Cryst. Liq. Cryst.*, **56**, 323 (1980).
15) F. Hardouin, A. M. Levelut, and G. Sigaud, *J. Phys.*, **42**, 71 (1981).
16) F. B. Jones and J. J. Ratto, *J. Phys.*, **C1-36**, C1-413 (1975).
17) For example, see References 7 and 8.
18) R. T. Klingbiel, D. J. Genova, T. R. Criswell, and J. P. Van Meter, *J. Am. Chem. Soc.*, **96**, 7651 (1974).

The Microwave Spectrum of Acrylaldehyde Oxime

Manabu NIWASE, Kyoko KUBOTA, Kazuhiko YOSHIDA, Takeshi SAKAIZUMI, Masao ONDA, Osamu OHASHI,* and Ichiro YAMAGUCHI

Department of Chemistry, Faculty of Science and Technology, Sophia University, Chiyoda-ku, Tokyo 102

(Received March 21, 1984)

The microwave spectra of acrylaldehyde oxime and its deuterated derivative (CH_2=CH-CH=NOD) were observed in the frequency region from 8.5 to 35 GHz. The several a-type R-branch transitions in the ground vibrational state were identified and the following rotational constants in MHz were determined to be: A=34117±96, B=2363.007±0.011, and C=2210.616±0.011 for normal species and A=33950±103, B=2274.301±0.010, and C=2131.981±0.011 for deuterated species. The most plausible molecular structure to which the spectrum assigned is attributed has been deduced to be a *s-trans syn* geometrical conformer from the rotational constants experimentally determined. The dipole moment component μ_a in the ground vibrational state was determined to be 0.59 D from the Stark effects of J=2←1 transitions. The r_s coordinates of the OH hydrogen atom have been determined and the orientation of the OH bond in the molecule has been discussed.

Acrylaldehyde oxime has four possible geometrical isomers, as shown in Fig. 1, if this molecule is assumed to be planar. A theoretical study[1] has suggested that the most stable conformation of this molecule is a *s-trans E* form. Wolkowski *et al.*[2] has reported that the proton nuclear magnetic resonance spectrum of acrylaldehyde oxime showed only a *s-trans E* form to exist in a liquid state. However, the gas chromatogram and proton nuclear magnetic resonance spectrum of this molecule have indicated that this molecule has two geometrical isomers[3]: One of these isomers has an *E* form and the other one has a *Z* form. Each of these isomers has two possible rotational conformers with respect to the C-C single bond (See Fig. 1). Masuda *et al.*[3] could not conclude whether a (*Z*)-(acrylaldehyde oxime) molecule has a *s-trans Z* form or a *s-cis Z* form, or both, while the proton nuclear magnetic resonance spectrum of an (*E*)-(acrylaldehyde oxime) could be ascribed to a *s-trans E* form.

It is interesting to determine the molecular conformation of acrylaldehyde oxime, particularly of an anti isomer, in gas phase. We have observed the microwave spectra of acrylaldehyde oxime and its deuterated species and discussed its conformation and the orientation of the OH bond in this molecule.

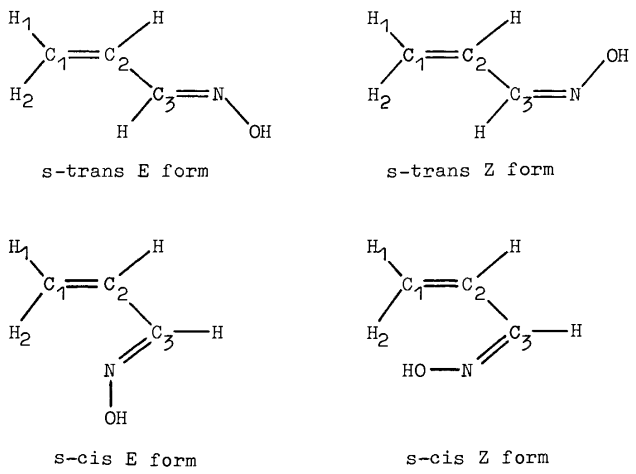

Fig. 1. Four possible geometrical isomers and the numbering of carbon and hydrogen atoms of acrylaldehyde oxime.

Experimental

Acrylaldehyde oxime was prepared and purified by Tuerck's[4] and Koral'nik's[5] methods. The deuterated species (CH_2=CH-CH=NOD) was prepared in the absorption cell itself as follows: First, the cell was flushed two or three times with D_2O vapour at room temperature. It was then pumped off for about half an hour. At the end of this time the sample of acrylaldehyde oxime was admitted into the cell. No attempt was made to separate the *E* and *Z* species; therefore, all measurements of the microwave spectrum were made with the equilibrium mixture of geometrical isomers in the absorption cell.

The microwave spectrometer used was of a conventional 100 kHz sinusoidal- and square-wave Stark modulation type with a phase sensitive detector. The spectrum was observed at 0—−10 °C or at room temperature, refreshing the sample about every half an hour.

Results and Discussion

Spectral Assignment and Conformation of Acrylaldehyde Oxime. There are four possible geometrical

Table 1. Structural parameters assumed for (*E*)-(acrylaldehyde oxime)

Bond length	r/Å	Bond angle	θ/°
C=C	1.345[a]	H_1-C=C	121.45[a]
C-C	1.470[a]	H_2-C=C	119.97[a]
C_1-H	1.086[a]	C_1=C_2-H	122.83[a]
C_2-H	1.084[a]	C=C-C	119.83[a]
C=N	1.276[b]	C-C=N(*syn*)	115.55[b]
N-O	1.408[b]	C-C=N(*anti*)	121.77[b]
O-H	0.956[b]	H-C=N(*syn*)	121.77[b]
C_3-H(*syn*)	1.085[b]	H-C=N(*anti*)	115.55[b]
C_3-H(*anti*)	1.086[b]	C=N-O	110.20[b]
		N-O-H	102.68[b]

The numbering of carbon and hydrogen atoms is given in Fig. 1.

a) Cherniak and Costain, *J. Chem. Phys.*, **45**, 101 (1966). See Ref. 6). b) Levine, *J. Chem. Phys.*, **38**, 2326 (1963). See Ref. 7).

isomers of acrylaldehyde oxime if this molecule is assumed to be planar. The assumed structural parameters[6,7] (Table 1) of this molecule showed that three geometrical isomers except for a *s-cis Z* conformer were nearly prolate symmetric rotors. Therefore, it was expected that the a-type R-branch transition lines would be relatively intense.

For normal species, the three $J=2\leftarrow1$ transitions with $K_{-1}=0$, 1 were first observed and identified by their characteristic Stark effects. The other a-type R-branch lines of $J=3\leftarrow2$ to $J=7\leftarrow6$ transitions with $K_{-1}=0$, 1 were then observed and assigned on the basis of the result from the $J=2\leftarrow1$ transitions. The correction terms, Δ_J, Δ_{JK}, of a first-order centrifugal distortion effect has been taken into account in order to explain the transition lines with high K_{-1} value.

For deuterated species, the observation and assignment of the spectrum were made in the same way as for normal species.

The results of the analyses of the spectra for both normal and deuterated species are in Tables 2 and 3. The small inertia defects ($\Delta I=I_c-I_a-I_b$) of -0.069 and -0.052 amu·Å^2 for normal and deuterated species confirm that this molecule is planar. The comparison between the observed rotational constants and the ones calculated from the molecular models (Table 4) has led to the conclusion that the spectrum assigned in this work is ascribed to an (*E*)-(*s-trans*-acrylaldehyde oxime).

r_s *Coordinates of the Hydroxyl Hydrogen Atom.* Since the acrylaldehyde oxime molecule to which the spectrum identified in this work is ascribed has a planar *s-trans E* form, there are two possible orienta-

Table 2. Observed transition frequencies (MHz) of acrylaldehyde oxime

Transition	Normal species		D species	
	Obsd	$\Delta\nu$[a]	Obsd	$\Delta\nu$[a]
$2_{02}-1_{01}$	9146.59	−0.10	8812.12	0.05
$2_{12}-1_{11}$	8994.73	−0.13	8670.51	0.23
$2_{11}-1_{10}$	9299.28	−0.37	8954.74	−0.15
$3_{03}-2_{02}$	13718.73	0.09	13217.04	0.13
$3_{13}-2_{12}$	13491.92	−0.02	13004.95	−0.12
$3_{12}-2_{11}$	13949.08	−0.03	13432.26	0.24
$3_{22}-2_{21}$	13721.04	0.07	13218.82	−0.10
$3_{21}-2_{20}$	13722.98	−0.18	13220.51	−0.33
$4_{04}-3_{03}$	18288.89	−0.05	17620.35	0.05
$4_{14}-3_{13}$	17988.44	−0.14	17339.51	0.00
$4_{13}-3_{12}$	18598.21	0.07	17908.84	0.05
$4_{23}-3_{22}$	18294.25	0.08	17624.77	−0.08
$4_{22}-3_{21}$	18299.54	−0.10	17629.65	0.02
$4_{32}-3_{31}$, $4_{31}-3_{30}$	18296.11*	0.20	17626.15*	−0.20
$5_{05}-4_{04}$	22857.03	0.01	22021.77	−0.01
$5_{15}-4_{14}$	22484.55	−0.11	21673.42	−0.07
$5_{14}-4_{13}$	23246.70	0.11	22385.07	0.01
$5_{24}-4_{23}$	22866.75	−0.22	22030.34	−0.10
$5_{23}-4_{22}$	22877.75	−0.17	22040.17	0.16
$5_{33}-4_{31}$	22870.76*	0.42	22033.32*	−0.03
$5_{32}-4_{31}$		0.42		−0.06
$5_{42}-4_{41}$, $5_{41}-4_{40}$	22870.16*	0.08		0.23
$6_{06}-5_{05}$	27422.38	0.05	26420.87	0.05
$6_{16}-5_{15}$	26980.16	0.12	26007.12	0.25
$6_{15}-5_{14}$	27894.30	−0.01	26860.66	−0.05
$6_{25}-5_{24}$	27439.20	−0.08	26435.80	0.18
$6_{24}-5_{23}$	27458.55	0.11	26452.28	−0.08
$6_{34}-5_{33}$	27445.05*	−0.02	26440.71*	0.07
$6_{33}-5_{32}$		−0.08		0.02
$6_{43}-5_{42}$, $6_{42}-5_{41}$	27444.32*	−0.10	26440.12*	0.10
$6_{52}-5_{51}$, $6_{51}-5_{50}$		−0.21		0.06
$7_{07}-6_{06}$	31984.31	−0.02	30816.98	−0.02
$7_{17}-6_{16}$	31474.65	0.09	30339.44	−0.07
$7_{16}-6_{15}$	32541.15	0.00	31335.46	−0.15
$7_{26}-6_{25}$	32010.97	−0.05	30840.38	0.08
$7_{25}-6_{24}$	32041.66	0.01	30867.04	−0.04
$7_{35}-6_{34}$	32020.20*	0.06	30848.37*	0.13
$7_{34}-6_{33}$		−0.10		0.00
$7_{44}-6_{43}$, $7_{43}-6_{42}$	32018.89*	−0.05		0.15
$7_{53}-6_{52}$, $7_{52}-6_{51}$		0.02	30847.28*	0.28
$7_{62}-6_{61}$, $7_{61}-6_{60}$	32019.40*	0.08		−0.03

a) Obsd−Calcd. The calculated transition frequencies were obtained from the rotational constants in Table 3.
* Not resolved.

Table 3. Observed rotational constants of acrylaldehyde oxime

	Normal species	D species
A/MHz	34117±96	33950±103
B/MHz	2363.007±0.011	2274.301±0.010
C/MHz	2210.616±0.011	2131.981±0.011
Δ_J/kHz	0.30±0.09	0.15±0.08
Δ_{JK}/kH$_z$	−5.89±0.25	−4.36±0.78
κ	−0.99045	−0.99105
ΔI[a]/amu·Å^2	−0.069	−0.052

a) $\Delta I=I_c-I_a-I_b$.

Table 4. Observed and calculated rotational constants (MHz) of acrylaldehyde oxime

Model	A	B	C	κ
	Normal species			
s-trans syn				
Model 1*	33902	2390.83	2233.33	−0.99005
Model 2*	31194	2449.22	2270.93	−0.96339
s-cis syn	19130	2989.54	2585.49	−0.95116
s-trans anti	16309	3232.61	2697.87	−0.92143
s-cis anti	9111	6040.54	3632.41	−0.12099
Obsd	34117	2363.007	2210.616	−0.99045
	D species			
s-trans syn				
Model 1*	33729	2297.94	2151.37	−0.99072
Model 2*	29335	2407.17	2224.62	−0.98653
Obsd	33950	2274.301	2131.981	−0.99105

* See Fig. 2 and text.

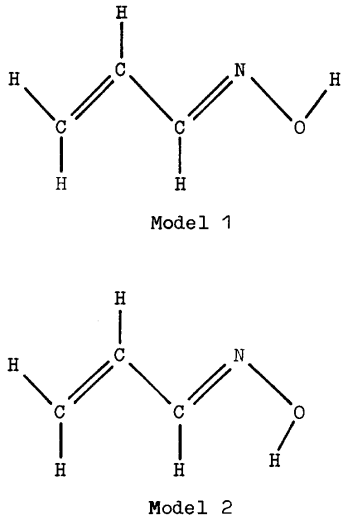

Fig. 2. Orientation of the OH bond in (*E*)-(acryladehyde oxime).

Table 5. r_s Coordinates of the OH hydrogen atom

Coordinate	Obsd	Calcd	
		Model 1	Model 2
$\|a\|$	2.901±0.005	2.902	1.826
$\|b\|$	0.29±0.06	0.29	1.16

c Coordinate was assumed to be zero.

tions of the hydroxyl group in this molecule: One of the two orientations of OH bond is the trans position with respect to the C=N double bond and another one is the cis position (Fig. 2).

Kraitchman's equation[8] gives the r_s coordinates of the hydroxyl hydrogen atom, using the rotational constants of both the normal and deuterated species in Table 3. The results obtained are given in the second column of Table 5. The third and fourth columns give the coordinates of the hydroxyl hydrogen atom calculated from Models 1 and 2 (Fig. 2). The observed r_s coordinates are in good agreement with the ones calculated from Model 1 in which the OH bond is at the trans position with respect to the C=N double bond. This result is consistent with the orientation of the OH bond in formaldehyde oxime[7] and acetaldehyde oxime.[9,10]

Dipole Moment. The dipole moment of this molecule was determined from measurements of the Stark effects of the 2_{12}←1_{11}, 2_{02}←1_{01}, and 2_{11}←1_{10} transitions. The electric field in the absorption cell was

Table 6. Stark coefficients (MHz cm^2 V^{-2}) and dipole moment (D) of acrylaldehyde oxime

Transition	$\|M\|$	$(\Delta\nu/E^2)$ 10^6		
		Obsd	Calcd-1	Calcd-2
2_{12}-1_{11}	1	14.76	14.35	14.32
2_{02}-1_{01}	0	−0.32	−0.32	−0.33
	1	0.26	0.28	0.30
2_{11}-1_{10}	0	0.26	0.24	0.23
	1	−13.62	−14.03	−13.99
$\|\mu_a\|$			0.594±0.009	0.593±0.030
$\|\mu_b\|$			0.7 ±2.9	0.8 ±6.5
$\|\mu_c\|$			0 (assumed)	0.4 ±4.9

calibrated by measuring the Stark shifts of the J=1←0 and J=2←1 transitions of OCS with the dipole moment of 0.715121 D.[11]

The Stark coefficients experimentally determined are given in the third column of Table 6. The fourth column of Table 6 shows the results (Calcd−1) obtained by the least-squares fit, assuming the value of μ_c=0 for this planar molecule. The results given in the fifth column of Table 6 (Calcd −2) were obtained by the least-squares fit, using all three components, μ_a, μ_b, and μ_c, as parameters. Both the Stark coefficients calculated by two assumptions are in good agreement with the ones experimentally obtained (See Table 6). Table 6 shows that the value of μ_a has been determined to be 0.59 D, while the values of μ_b and μ_c are indeterminable because of their large uncertainties.

References

1) Claude Leibovici, *Theor. Chim. Acta*, **10**, 311 (1968).
2) Z. W. Wolkowski, N. Thoai, and J. Wiemann, *Tetrahedron Lett.*, **1970**, 93.
3) S. Masuda, H. Kihara, and T. Ota, *Nippon Kagaku Kaishi*, **1974**, 608.
4) K. H. W. Tuerck and H. J. Lichtenstein, U. S. Patent 2417024 (1947); *Chem. Abstr.*, **41**, 3812h (1947).
5) N. G. Koral'nik, A. G. Erenshchenko, and B. E. Geller, *Zh. Prikl. Khim.*, **38**, 2858 (1965).
6) E. A. Cherniak and C. C. Costain, *J. Chem. Phys.*, **45**, 101 (1966).
7) I. N. Levine, *J. Chem. Phys.*, **38**, 2326 (1963).
8) J. Kraitchman, *A. J. Phys.*, **21**, 17 (1953).
9) O. Ohashi, R. Ishihara, K. Murakami, T. Sakaizumi, M. Onda, and I. Yamaguchi, *Bull. Chem. Soc. Jpn.*, **49**, 891 (1976).
10) O. Ohashi, H. Hara, K. Noji, T. Sakaizumi, M. Onda, and I. Yamaguchi, *Bull. Chem. Soc. Jpn.*, **50**, 834 (1977).
11) J. S. Muenter, *J. Chem. Phys.*, **48**, 4544 (1968).

 © 1984 The Chemical Society of Japan Bull. Chem. Soc. Jpn., 57, 2411—2416 (1984)

The Synthesis of Green Rust II(Fe^{III}_1-Fe^{II}_2) and Its Spontaneous Transformation into Fe_3O_4

Yutaka TAMAURA,* Takashi YOSHIDA,† and Takashi KATSURA
Department of Chemistry, Tokyo Institute of Technology, Ookayama, Meguro-ku, Tokyo 152
†*NEC Environment Engineering, Ltd., Miyamae-ku, Kawasaki 213*
(Received December 20, 1983)

Conditions for the synthesis of a pure green rust II with a definite chemical composition and its transformation reaction to Fe_3O_4 under a nitrogen atmosphere were studied. A pure green rust II with the composition of $(Fe^{3+})_1(Fe^{2+})_2(SO_4^{2-})(OH^-)_{5-2n}(O^{2-})_n$ was obtained by the air oxidation of an aqueous solution containing (0.05 mol dm^{-3}) Fe^{II} and (0.3 mol dm^{-3}) SO_4^{2-} ions at pH 6.8 and 25 °C. This iron composition differs from those estimated previously; therefore, the green rust II synthesized here is designated as green rust II(Fe^{III}_1-Fe^{II}_2). This green rust II is spontaneously transformed into Fe_3O_4 under a nitrogen atmosphere at 50—75 °C. It has been accepted that green rust II is transformed to Fe_3O_4 by oxidation. The above evidence suggests that the green rust II can be transformed into Fe_3O_4 not only by oxidation but also spontaneously without oxidants.

The atmospheric rusting of mild steel or low-alloy steel occurs when the steel surface comes into contact with atmospheric water. The Fe^{II} ion dissolved from the steel surface in the course of the rusting is oxidized by oxygen, and iron oxides and hydroxide oxides are formed. In the thin aqueous layer on the steel surface, the oxygen and water react with the iron or intermediates of the rusting process. Eventually, the steel surface is covered with oxides and hydroxide oxides(corrosion products). In the oxidation reaction of the Fe^{II} ion in the aqueous solution, the oxidation rate, the structure and composition of the initial and intermediate species, the pH, and the temperature determine what products are formed.[1-13] The influence of dissolved oxygen has been studied by Foroulis.[6] The significance of the oxidation rate of the dissolved Fe^{II} ion in the corossion of iron and steel in an aqueous solution was pointed out by Gilroy and Mayne.[7] The formation or transformation of iron oxides, hydroxide oxides, and green rusts in aqueous solutions have been studied by Kiyama,[2] Bernal *et al.*,[8] Misawa *et al.*,[1,4] and other workers.[9-13] The transformation reaction of γ-FeO(OH) to α-FeO(OH) has been studied by Schwertmann and Taylor,[9] Oosterhout,[10] and Inoue *et al.*[11] Recently, we have reported that γ-FeO(OH) is transformed to Fe_3O_4 by the adsorption of Fe^{II} ions.[12-13] Other intermediates in the corrosion process and in the oxidation of aqueous solutions containing Fe^{II} ions are greenish precipitates called "green rusts." They are formed by the air oxidation of a dissolved Fe^{II} ion in the presence of SO_4^{2-} or halogen ions, such as Cl^-, Br^-, and F^-, at neutral or slightly alkaline pH values, and are transformed to iron oxides or hydroxide oxides by further oxidation. A green rust I is formed in the presence of Cl^-, Br^-, and F^- ions, and a green rust II, in that of the SO_4^{2-} ion. Bernal *et al.*[8] reported on an X-ray crystallographic study of the green rusts. Misawa *et al.*[14,15] studied dissolved species, called "green complexes," of the Fe^{II} and Fe^{III} complexes.

This paper will describe a new reaction in which a green rust II is transformed to Fe_3O_4 without any oxidation reaction. At the beginning of this work, we undertook to prepare a green rust II with a definite chemical composition. However, the methods reported so far[2,8,14] were inadequate for the synthesis of such a green rust II. As a first report, this paper will describe the reaction conditions for the synthesis of the green rust II with a definite chemical composition, besides the new reaction. A detailed discussion of the relationship between the new reaction and the oxidation reaction of the green rust II will be presented in the subsequent paper.

Experimental

Chemicals. All the chemicals were of an analytical grade, and distilled water was used for the preparation of chemical solutions. The α- and β-FeO(OH) were perpared according to the methods of Kiyama[2] and of Kiyama and Takada[3] respectively. Fe_3O_4 and γ-FeO(OH) were synthesized by a method reported perviously.[13,16]

Apparatus. The reaction vessel used in previous papers was adopted.[16-18]

Chemical Analysis. The Fe^{II} and Fe_{total} contents were determined by means of the 2,2′-bipyridyl method[19] after dissolving the samples with a HCl solution (1:1). The Fe_{total} was determined after reducing Fe^{III} to Fe^{II} with hydroxylamine. The SO_4^{2-} content was determined using a X-ray fluorescence instrument (Toshiba X-ray Spectrometer Model AFV 777) from the intensity of sulpher in $BaSO_4$ precipitate collected on a glass fiber filter paper (Toyo Roshi GA 100 type).

Green Rust II Synthesis. A solution [0.7 dm^3, $FeSO_4 \cdot 7H_2O$ (10.0 g), Na_2SO_4 (25 g)] was oxidized with a mixed gas of air and nitrogen gas[air/N_2=1:1(atm), flow rate; 1.6 dm^3 min^{-1}] at pH 6.8±0.05 and 25 °C. During the oxidation, an alkaline solution (0.10 mol dm^{-3} NaOH) was added to maintain the reaction pH constant, and the volume of the alkaline solution consumed was read. When about 25 mol% of the Fe^{II} ion has been oxidized, nitrogen gas was passed through in place of the mixed gas; the reaction vessel was then cooled in a water bath chilled with ice. If the Fe^{II} ions are oxidized over 25 mol%, by-products such as α-FeO(OH) are produced. The greenish precipitate was collected by centrifugation under a nitrogen atmosphere, washed with a distilled water freed from oxygen (4 °C), and suspended in the distilled water (4 °C). The green rust II thus prepared is stable under a nitrogen atmosphere at a temperature below 4 °C.

For the measurement of the Fe^{II} and Fe^{III} contents of the

green rust II formed in the course of the synthesis, 0.005 dm^3 of the reaction suspension was transferred under a nitrogen atmosphere to a 0.05 dm^3 centrifuging tube chilled in ice water, and nitrogen gas was immediately flushed into the sample suspension to stop the reaction instantly. After 10 min, the sample was centrifuged under a nitrogen atmosphere at a low temperature (4 °C) at 3000 min^{-1} for 5 min. After the precipitate has been washed with cold distilled water freed from oxygen, the Fe^{II} and Fe^{III} contents were determined.

Electron Microscopy, IR Spectroscopy, and X-ray Diffractometry for the Green Rust II. A small portion of the reaction suspension was taken into a glass capillary tube whose inside was a vacuum; the capillary was then sealed and kept in cold water. The inside sample was mounted under a nitrogen atmosphere on a sample holder for electron microscopy. For the X-ray diffractometry, the precipitate obtained by centrifugation was mounted on a glass plate under a nitrogen atmosphere, and sealed with cellophane-tape to prevent oxidation. For the IR spectroscopy, the green-rust-II precipitate was washed with acetone freed from oxygen (4 °C), dried under a nitrogen atmosphere, and suspended in Nujol. The IR spectrum was taken by a Shimadzu IR spectrometer, Model IR 400, using a KBr cell under a nitrogen atmosphere.

Transformation Reaction of Green Rust II under a Nitrogen Atmosphere. The green-rust-II suspension (0.05 dm^3, 25 °C) was transferred into a 0.4-dm^3 portion of distilled water freed from oxygen. The temperature of the distilled water had been adjusted to get a given temperature after the mixing. The pH of the reaction suspension was adjusted by adding a NaOH solution during the reaction. After 4 h, the product was isolated by transferring 0.2 dm^3 of the reaction suspension to 0.1 dm^3 of an oxygen-free acetate buffer solution (pH 4.1, 0.05 mol dm^{-3}) to dissolve the Fe^{II} ions released during the transformation reaction. The product was collected by centrifugation under a nitrogen atmosphere, washed successively with oxygen-free water and acetone, and dried under a nitrogen atmosphere. The dried product was examined by means of X-ray diffractometry, electron microscopy, and IR spectroscopy. The chemical composition was determined after dissolving it with the HCl solution(1:1).

Results and Discussion

Conditions for Green Rust-II Synthesis. Curves A and A′ in Fig. 1 show the amounts of $Fe(OH)_2$ precipitate which were formed by adjusting the pH of the solutions containing Fe^{II} ions at high (Curve A; 0.3 mol dm^{-3}) and low (0.05 mol dm^{-3}) concentrations of SO_4^{2-} to those indicated in the figure at 25 °C. As may be seen here, most Fe^{II} ions dissolved at pH values below 6.8 at a high SO_4^{2-}-concentration. When a mixed gas of air and nitrogen gas was passed into the solution containing Fe^{II} ions at pH 6.8 and at a high SO_4^{2-}-concentration, the clear solution became turbid, and a greenish precipitate was formed by the oxidation of the Fe^{II} ions. Figure 2 shows the time variation of the Fe^{II} (Curve A) and Fe^{III} (Curve B) contents of the greenish precipitates formed in the course of air oxidation at pH 6.8. As can be seen here, the Fe^{II}/Fe^{III} mol ratio was maintained at nearly 2:1 during the reaction. This suggests that one mol of the Fe^{III} ions formed by oxidation combines with two mols of the Fe^{II} ions to form the greenish precipitate. The X-ray diffraction pattern of the greenish precipitate formed at an oxidation time of 40 min corresponded to that of the green rust II reported by Bernal *et al.*[8] In the IR spectrum, no bands of iron hydroxide oxides appeared, but a strong band of SO_4^{2-} (1100 cm^{-1}) and weak bands (720, 620 cm^{-1}) did appear. These results indicate the formation of the green rust II containing SO_4^{2-}. Figure 3 shows an electron micrograph of the product.

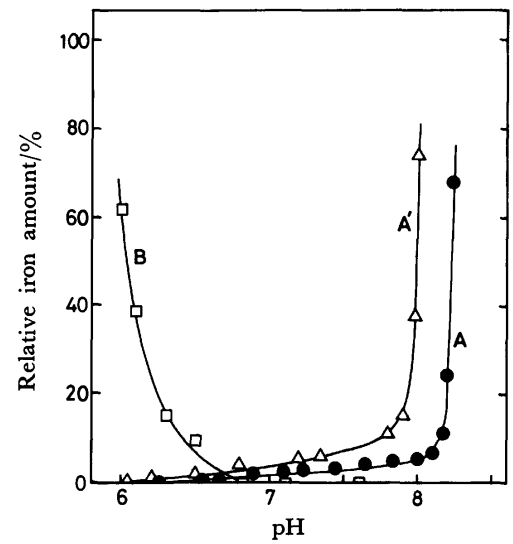

Fig. 1. The amount of $Fe(OH)_2$ precipitates which were formed by adjusting the pH of the solution containing Fe^{II} ion at high (Curve A; 0.3 mol dm^{-3}) and low (Curve A′; 0.05 mol dm^{-3}) concentrations of SO_4^{2-} to those indicated in the figure at 25 °C. The amount was estimated from the Fe^{II} in the precipitates which were formed by allowing the $Fe(OH)_2$ suspension to stand for 30 min after the addition of 0.1 mol dm^{-3} NaOH solution.
Curve B; relationship between the amount of the by-products and the reaction pH. The reaction suspension(0.05 dm^3) was taken and transferred to 0.1 dm^3 of the tartaric acid solution(10 w/v%, pH 6.0). After allowing to stand for 6 h, the amount of the total iron in the precipitate remained undissolved in the tartaric acid solution was determined.

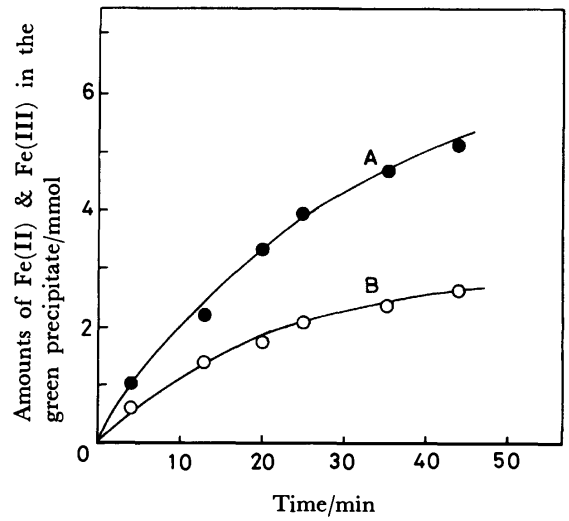

Fig. 2. The time variations of Fe^{II}(Curve A) and Fe^{III} (B) contents in the green rust II formed in the course of the synthesis.

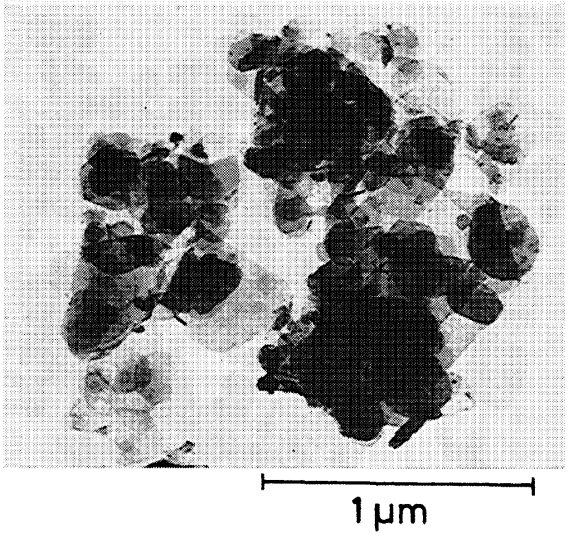

Fig. 3. Electron micrograph of the green rust II(Fe^{III}_1-Fe^{II}_2).

Table 1. Dissolution test of the green rust II, Fe_3O_4, and iron hydroxide oxides with a tartaric acid solution (10 w/v%, pH 6.0)

Iron oxides or hydroxide oxides added (7.2×10^{-4} mol; Fe_{total})	Amount of iron dissolved (mol; Fe_{total})
Green rust II	7.2×10^{-4}
Fe_3O_4	4.3×10^{-7}
α-FeOOH	2.9×10^{-7}
β-FeOOH	6.2×10^{-7}
γ-FeOOH	7.1×10^{-7}

After allowing the test suspensions to stand for 6 h under a nitrogen atmosphere, the concentration of the total iron in the supernatant was determined by the atomic-absorption method.

To ascertain the purity of the product, the green rust II obtained at pH 6.8 and at the high SO_4^{2-}-concentration was transferred to a tartaric acid solution (10 w/v%, pH 6.0), and the mixture was allowed to stand for 6 h. The green rust II dissolved completely (Table 1). However, as can be seen from the table, little of the α-, β-, and γ-FeO(OH) dissolved. This suggests that the green rust II contains no by-products such as hydroxide oxides, but is a pure green rust II. However, at pH values below 6.8 (at a high SO_4^{2-}-concentration), some by-products insoluble in the tartaric-acid solution were formed. The relationship between the amounts of the by-products and the reaction pH is given by Curve B in Fig. 1. In the IR spectrum of the by-products, key bands of α-FeO(OH) appeared strongly at 795 and 890 cm^{-1}, along with a very broad absorption over the range of 400—1000 cm^{-1}. The broad absorption could not be assigned, but it seems to be due to the Fe^{III} amorphous hydroxide oxides. Thus, the by-product can be said to be mainly composed of α-FeO(OH).

The results of the chemical analysis of the green rust II obtained at pH 6.8 and at a high SO_4^{2-}-concentration are given in Table 2, together with the OH^- amount consumed during the reaction. From the values in the table, the chemical formula can be estimated to be $(Fe^{3+})_1(Fe^{2+})_2(SO_4^{2-})(OH^-)_5$. Since Misawa *et al.*[4] suggested that green rusts contain hydroxo-bridges and oxo-bridges, the chemical formula can be generally represented by: $(Fe^{3+})_1(Fe^{2+})_2(SO_4^{2-})(OH^-)_{5-2n}(O^{2-})_n$, where n means the number of oxo-bridges. The iron composition of this green rust II is different from that estimated from the composition of the green complex II by Misawa *et al.*[15] The green rust II synthesized in the present study will hereafter be designated as green rust II(Fe^{III}_1-Fe^{II}_2).

Table 2. Results of the chemical analysis of the green rust II obtained after 30 min of air oxidation

Ions	mol	Ratio
Fe^{3+}	7.3×10^{-4}	1.0
Fe^{2+}	1.4×10^{-3}	1.9
SO_4^{2-}	6.1×10^{-4}	0.83
OH^-	3.4×10^{-3}	4.7

Equilibrium Consideration of the Formation of the Green Rust II. As may be seen in Curve B in Fig. 1, the amount of the by-product, which is mainly composed of α-FeO(OH) as has been mentioned above, increased with a decrease in the pH from 6.8 to 6.0. In the course of the reaction, Fe^{III} ions are formed by the oxidation of the Fe^{II} ions. In this pH range, the main species of the Fe^{III} ion formed by the oxidation is $Fe(OH)_2^+$, one of the hydrolysis species of the Fe^{3+} ion.[20] It is considered that α-FeO(OH) is formed by the polymerization of the $Fe(OH)_2^+$ ions. However, at pH values above 6.8, no such by-products are formed (Curve B in Fig. 1), and the green rust II is formed. This indicates that the $Fe(OH)_2^+$ ions preferentially combine with the Fe^{II} and SO_4^{2-} ions, and that they are transformed to the green rust II. Since the Fe^{2+} ion is more readily hydrolyzed into $FeOH^+$ at a higher pH in the pH range of 6—10,[20] The Fe^{II} ions which take part in the green-rust-II formation are considered to be $FeOH^+$ ions. Thus, the green rust-II formation will be written as:

$$Fe^{2+} + H_2O \rightleftharpoons FeOH^+ + H^+, \quad (1)$$

$$Fe(OH)_2^+ + 2FeOH^+ + SO_4^{2-} \rightleftharpoons (Fe^{3+})_1(Fe^{2+})_2(SO_4^{2-})(OH^-)_{5-2n}(O^{2-})_n + nH_2O. \quad (2)$$

The reversibility of Reaction (2) was also examined. When the pH of the green rust-II suspension containing a high SO_4^{2-}-concentration (0.3 mol dm^{-3}) was lowered to 5.5, the green rust II(Fe^{III}_1-Fe^{II}_2) was decomposed and a brownish precipitate was formed. In the IR spectrum of the precipitate, no key bands of iron hydroxide oxides appeared, but a very broad absorption appeared over the range of 400—1000 cm^{-1}, indicating that some amorphous precipitates of Fe^{III} were formed. Assuming that the reverse process of Reaction (2) takes place upon a lowering of the pH, it is considered that the $Fe(OH)_2^+$ ions released in the reverse process of Reaction (2) form the amorphous precipitates. How-

ever, the Fe^{II} ions released in the reverse process dissolve in the solution at pH 5.5, since their solubilities are fairly high at that pH. These considerations suggest that possibility that there exists the reverse process of Reaction (3). When the pH of the brownish suspension obtained above was raised to 8.0, a greenish precipitate was formed almost instantly. X-Ray diffractometry and chemical analysis showed that this greenish precipitate was the green rust II (Fe^{III}_1–Fe^{II}_2). Thus, the direct and reverse processes of Reaction (2) are considered to take place reversibly, and they seem to readily attain equilibrium. From Eqs. 1 and 2, the equilibrium constant for the formation of the green rust II is given by:

$$K = \frac{[H^+]^3}{[Fe(OH)_2^+][Fe^{2+}]^2[SO_4^{2-}]K_1^2K_w} \quad (3)$$

where K_1 and K_w are the hydrolysis constant of Fe^{2+} (Eq. 1) and the dissociation constant of water respectively. In the pH range of 6—7, $[Fe(OH)_2^+]$ is around 10^{-11}—10^{-12} mol dm^{-3}.[20] Equation 3 indicates that the lower values of the Fe^{2+}-concentration, the pH, and the SO_4^{2-}-concentration are unfavorable for the formation of the green rust II(Fe^{III}_1–Fe^{II}_2). When the Fe^{2+}-concentration is lowered as the oxidation reaction proceeds, Reaction (2) attains equilibrium, and the green rust II is no longer formed. The $Fe(OH)_2^+$ ions, which are formed by a further oxidation of the remaining Fe^{2+} ions, polymerize and form α-FeO(OH)(by-product). At a pH lower than 6.8, the formation of the by-product is initiated at an earlier stage of the oxidation reaction. This means that the amount of the by-products will increase with a decrease in the pH from 6.8, as is shown by Curve B in Fig. 1. When the reaction pH was further lowered to 5.5, no green rust II was formed, but only the by-products. In these experiments, the concentrations of Fe^{II} and SO_4^{2-} were 0.05 and 0.3 mol dm^{-3} respectively. For these values, the pH value of 5.5 is too small to form the green rust II in Eq. 3.

Spontaneous Transformation of the Green Rust II to Fe_3O_4 under a Nitrogen Atmosphere. When the green rust II(Fe^{III}_1–Fe^{II}_2)-suspension containing no oxidants was allowed to stand under a nitrogen atmosphere at 75 °C, the suspension spontaneously turns black, and the pH became around 7.8. Figure 4 shows the electron micrograph of the product; no particles of the green rust II are seen, but only the spherical or cubic particles characteristic of Fe_3O_4. The X-ray diffractometry, IR spectroscopy, and chemical analysis showed that the product is Fe_3O_4. In this reaction, no oxidants were used; therefore, the formation of Fe_3O_4 from the green rust II is given by:

$$2[(Fe^{3+})_1(Fe^{2+})_2(SO_4^{2-})(OH^-)_{5-2n}(O^{2-})_n] \longrightarrow$$
$$Fe_3O_4 + 3Fe^{2+} + 2SO_4^{2-} + 2(2-n)H_2O + 2OH^- \quad (4)$$

As can be seen from Eq. 4, three mols of Fe^{2+} ions and two mols of OH^- ions are released. One out of the three mols of Fe^{2+} ions will form $Fe(OH)_2$, and the remaining two be free. The pH after the mixing of the Fe^{2+} and OH^- ions at this ratio was around 7.6. This value agrees with that where the reaction pH is attained in the early stage of the reaction. At a pH around this pH value, some of the remaining Fe^{2+} ions are hydrolyzed,

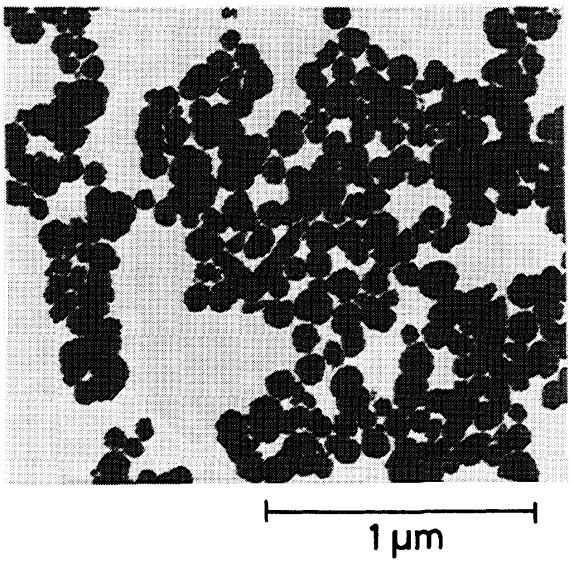

Fig. 4. Electron micrograph of the product which was obtained by allowing the green rust II(Fe^{III}_1–Fe^{II}_2)-suspension under a nitrogen atmosphere at 75 °C for 4 h. Concentrations of SO_4^{2-} and the green rust II; 0.018 mol dm^{-3} and 50 mmol dm^{-3}(Fe^{2+}), respectively.

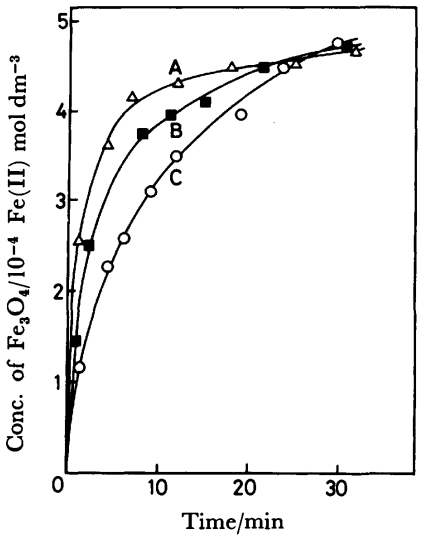

Fig. 5. The time variation of the Fe_3O_4-formation at various pH's(50 °C).
Curve A; pH 7.7, B; 9.8, and C; 10.6. Concentrations of SO_4^{2-} and the green rust II; 0.018 mol dm^{-3} and 50 mmol dm^{-3}(Fe^{2+}). The reaction suspension (0.05 dm^3) was taken and transferred to 0.1 dm^3 of the tartaric acid solution(10 w/v%, pH 6.0). After allowing to stand for 6 h, the amount of Fe^{II} in the precipitate remained undissolved in the tartaric acid solution was determined.

and the proton is released (Eq. 1). This is the cause of the gradual lowering of the pH in the transformation reaction.

Figure 5 shows the time variation in the Fe_3O_4-formation from the green rust II at various pH's(50 °C) under a nitrogen atmosphere. The reaction pH was maintained by adding an alkaline solution. As may be

Table 3. The rate of the spontaneous transformation of the green rust II into Fe_3O_4 at various temperatures under a nitrogen atmosphere

Temperature °C	Transformation rate to Fe_3O_4 (Fe^{2+} mol dm^{-3} min^{-1})
30	1.51×10^{-6}
50	6.38×10^{-5}
74	1.86×10^{-3}

The rate gradually became slow with time. The values in the table were evaluated from the tangent of the Fe_3O_4-formation curve at 0 time. Concentration of SO_4^{2-}: 0.018 mol dm^{-3}. Concentration of the green rust II: 50 mmol dm^{-3} (Fe^{2+}).

Table 4. The relationship between the concentration of the green rust II in the suspension and the rate of the spontaneous transformation of the green rust II into Fe_3O_4 under a nitrogen atmosphere at 50 °C

Green rust II conc. in the reaction suspension (Fe^{2+} mmol dm^{-3})	Transformation rate to Fe_3O_4 (Fe^{2+} mol dm^{-3} min^{-1})
4.9	7.07×10^{-6}
11	1.27×10^{-5}
25	3.36×10^{-5}

The rates were evaluated from the tangent of the Fe_3O_4-formation curve at 0 time. Concentration of SO_4^{2-}: 0.018 mol dm^{-3}.

seen here, the green rust II was transformed spontaneously to Fe_3O_4 without being oxidized, even at a pH above 7.8. However, the reaction pH affects the initial rates of the transformation reaction. The temperature and the SO_4^{2-}-concentration also affect the rate. The relationship between the initial rate and the temperature is given in Table 3. When the SO_4^{2-}-concentration became higher, the rate became slower, becoming extremely slow at 0.1 mol dm^{-3}.

The electron microscopy(Figs. 3 and 4) showed that plate particles of the green rust II are transformed to cubic or spherical particles of Fe_3O_4. This indicates that the transformation reaction proceeds through a dissolution-precipitation process. This process seems likely in view of the fact that no transformation occurred when the green rust II was dried under a nitrogen atmosphere after having been washed with a O_2-free acetone to remove as much water as possible. The transformation reaction is considered to involve the dissolution process of the green rust II. In this process, some dissolved species such as the green complex II[14] are released and transformed to Fe_3O_4 without being oxidized. If the transformation rate of the dissolved species is slower than the dissolution rate of the green rust II, the bulk solution is saturated with the dissolved species. In this case, the concentration of the dissolved species is kept constant, even though the number of particles of the green rust II in the suspension(green-rust-II concentration) is increased. This means that the rate of the Fe_3O_4-formation does not depend on the green-rust-II concentration. However, as is shown by Table 4, the rate of the Fe_3O_4-formation depends on the green-rust-II concentration. It is considered that the rate of the transformation of the dissolved species to Fe_3O_4 is fast, and that the dissolution of the green rust II is the rate-determining step of the reaction. At a higher concentration of the green rust II, the dissolution rate of the green rust II becomes faster as a result of the increase in the total surface area of the green-rust-II particles.

If the dissolved species is the green complex II with the composition of $[(Fe^{3+})(Fe^{2+})(OH^-)_x(O^{2-})_y]^{(5-2y-x)+}$,[14] the dissolution process of the green rust II is given by:

$$(Fe^{3+})_1(Fe^{2+})_2(SO_4^{2-})(OH^-)_{5-2n}(O^{2-})_n \rightleftharpoons [(Fe^{3+})(Fe^{2+})(OH^-)_{5-2n-m}(O^{2-})_n]^{m+} + Fe^{2+} + SO_4^{2-} + mOH^-, \quad (5)$$

where it is assumed that the oxo-bridges in the green rust II are transformed into the green complex II. The Fe_3O_4-formation from the green complex II may be written as:

$$2[(Fe^{3+})(Fe^{2+})(OH^-)_{5-2n-m}(O^{2-})_n]^{m+} + 2(m-1)OH^- \longrightarrow Fe_3O_4 + Fe^{2+} + 2(2-n)H_2O. \quad (6)$$

Equation 6 shows that the Fe_3O_4-formation reaction should depend largely on the reaction pH if Reaction (6) is the rate-determining step. However, as is shown by Fig. 5, the reaction rate did not increase with an increase in the reaction pH, but, rather, decreased. This suggests that the transformation step of the dissolved species to Fe_3O_4 is not the rate-determining step, as has been discussed above.

It has been accepted that green rust II is transformed to Fe_3O_4 by oxidation. However, the above evidence suggests that the green rust II can be transformed into Fe_3O_4 not only by oxidation, but also spontaneously without oxidation reaction.

References

1) T. Misawa, T. Kyuno, W. Suëtaka, and S. Shimodaira, *Corros. Sci.*, **11**, 35 (1971).
2) M. Kiyama, *Bull. Chem. Soc. Jpn.*, **47**, 1646 (1974).
3) M. Kiyama and T. Takada, *Bull. Chem. Soc. Jpn.*, **45**, 1923 (1972).
4) T. Misawa, K. Hashimoto, and S. Shimodaira, *Corros. Sci.*, **14**, 131 (1974).
5) S. Hamada and K. Kuma, *Bull. Chem. Soc. Jpn.*, **49**, 3695 (1976).
6) Z. A. Foroulis, *Corrosion*, **35**, 340 (1979).
7) D. G. Gilroy and J. E. O. Mayne, *Br. J. Corros.*, **1**, 107 (1965).
8) J. D. Bernal, D. R. Dasgupta, and A. L. Mackay, *Clay Min. Bull.*, **4**, 15 (1959).
9) U. Schwertmann and R. M. Taylor, *Clays and Clay Min.*, **20**, 159 (1972).
10) G. W. V. Oosterhout, *J. Inorg. Nucl. Chem.*, **29**, 1235 (1967).
11) K. Inoue, K. Ichimura, K. Kaneko, and T. Ishikawa, *Corros. Sci.*, **16**, 507 (1976).
12) Y. Tamaura, P. V. Buduan, and T. Katsura, *J. Chem. Soc., Dalton Trans.*, **1981**, 1807.
13) Y. Tamaura, K. Ito, and T. Katsura, *J. Chem. Soc., Dalton Trans.*, **1983**, 189.

14) T. Misawa, K. Hashimoto, and S. Shimodaira, *J. Inorg. Nucl. Chem.*, **35**, 4167 (1973).
15) T. Misawa, K. Hashimoto, W. Suëtaka, and S. Shimodaira, *J. Inorg. Nucl. Chem.*, **35**, 4159 (1973).
16) T. Katsura, Y. Tamaura, and G. S. Chyo, *Bull. Chem. Soc. Jpn.*, **52**, 96 (1979).
17) Y. Tamaura and T. Katsura, *J. Chem. Soc., Dalton Trans.*, **1980**, 825.
18) Y. Tamaura, S. Mechaimonchit, and T. Katsura, *J. Inorg. Nucl. Chem.*, **43**, 671 (1981).
19) I. Iwasaki, T. Katsura, T. Ozawa, M. Mashima, H. Haramura, and B. Iwasaki, *Bull. Volc. Soc. Jpn., Ser. 2*, **5**, 75 (1960).
20) C. F. Baes, Jr., and R. Mesmer, "The Hydrolysis of Cations," Wiley-Interscience Publications, New York (1976), p. 226.

 © 1984 The Chemical Society of Japan Bull. Chem. Soc. Jpn., 57, 2417—2421 (1984)

The Transformation of γ-FeO(OH) to Fe_3O_4 and Green Rust II in an Aqueous Solution

Yutaka TAMAURA,* Mervelina SATURNO, Kaoru YAMADA, and Takashi KATSURA
Department of Chemistry, Tokyo Institute of Technology, Ookayama, Meguro-ku, Tokyo 152
(Received February 17, 1984)

A mechanism of the transformation of γ-FeO(OH) to Fe_3O_4 and/or green rust II in an aqueous solution containing Fe^{II} ion in the presence or absence of the SO_4^{2-} ion at 298 K is described. γ-FeO(OH) is dissolved by two mols of Fe^{II} ions adsorbed on the surface of γ-FeO(OH), and a dissolved species (DS) is formed, which is then transformed to Fe_3O_4 or green rust II. The equilibrium of the formation of green rust II from γ-FeO(OH) is represented by:

$$K = [H^+]^2/(K_h^2[Fe^{2+}]^2[SO_4^{2-}]) \qquad K = 2.14 \times 10^8,$$

where K_h is the hydrolysis constant of Fe^{2+}. This equation shows that, for a given proton concentration(pH), higher concentrations of Fe^{2+} and SO_4^{2-} ions facilitate the formation of green rust II from γ-FeO(OH). When little green rust II is formed, the DS is transformed to Fe_3O_4.

The Fe^{II} ions dissolved from the steel surface in the course of the atmospheric rusting are oxidized by oxygen, and eventually the surface is covered with rusting products of iron oxides and hydroxide oxides. Studies of the formation of iron oxides and hydroxide oxides by the air oxidation of Fe^{II} ions in an aqueous solution give useful knowledge for an understanding of the atmospheric rusting of mild steel or low-alloy steel, as reported by Kiyama,[1] Bernal *et al.*,[2] and Misawa *et al.*[3] This oxidation reaction has also been studied in relation to the formation of ferrites in aqueous solutions; ferrites are formed by the air oxidation of an $Fe(OH)_2$ suspension containing other metal ions.[4-10] In these oxidation reactions, some intermediates are formed; greenish precipitates called "green rusts" are formed in the course of the oxidation reaction.[1-3] They are transformed to γ-FeO(OH) or Fe_3O_4 by further oxidation.

Recently we have ourselves reported that a green rust (green rust II) is spontaneously transformed into Fe_3O_4 without being oxidized[11] and that γ-FeO(OH) is transformed into Fe_3O_4 by Fe^{II} ions at pH 7—11 without any oxidation reaction.[12,13] Furthermore, ferrites are formed from a suspension containing γ-FeO(OH) and Fe^{II} and other metal ions without any oxidation reaction.[14,15] These findings suggest that there are two steps in the oxidation reaction where Fe_3O_4 or ferrites are formed: 1) The oxidation step of the Fe^{II} ion, where such intermediates as green rusts and γ-FeO(OH) are formed, and 2) the transformation step of the intermediates into Fe_3O_4 or ferrites without any oxidation reaction.

In the present paper, we have studied the transformation of γ-FeO(OH) into Fe_3O_4 and/or green rust II in the presence of Fe^{II} and SO_4^{2-} ions without any oxidation reaction. The reaction mechanism of the transformation will be discussed.

Experimental

Chemicals. All the chemicals were of an analytical grade, and distilled water was used for the preparation of the chemical solutions. The NaOH solution was prepared by dissolving NaOH in distilled water through which nitrogen gas had been passed to remove the dissolved oxygen. The γ-FeO(OH) was prepared according to the method described in a previous paper.[13]

Apparatus. The reaction vessel used in a previous paper was adopted.[13] The reaction vessel was immersed in a water bath, and the reaction temperature was kept at 298±0.5 K.

Procedures. Throughout the experiments, we tried to avoid leakage of oxygen into the reaction suspension. After passing nitrogen gas through a suspension of γ-FeO(OH) (0.7 dm^3, 0.002 kmol m^{-3}) of the desired pH (8.5 or 10.0), and $Fe(OH)_2$ suspension (0.02 dm^3, 0.40 kmol m^{-3}) of that pH was added. The suspension thus obtained will be referred to as "the reaction suspension." The reaction was initiated when the $Fe(OH)_2$ suspension was added. The reaction pH was maintained at 8.5 or 10.0±0.03 by adding a sulfuric-acid solution. The amount of released OH^- was estimated from the volume of the sulfuric-acid solution consumed. The time from the addition of the $Fe(OH)_2$ suspension is referred to as "the reaction time." In the course of the reaction, 0.005-dm^3 portions of the reaction suspension were taken out at constant time intervals using a syringe and transferred to a tartaric-acid solution (10 w/v%, pH 6.0, 0.04 dm^3). After allowing the suspension thus obtained to stand for 60 min, the suspension was centrifuged at 4000 r.p.m. The precipitate was washed with the tartaric-acid solution. The Fe_3O_4 formed and the γ-FeO(OH) left unreacted do not dissolve in the tartaric-acid solution, but the intermediate green rust II(GR-II) does. The precipitate thus obtained was dissolved in a 0.002-dm^3 HCl solution (1:1). The Fe^{II} and Fe_{total} in the solution were determined. The amount of Fe_3O_4 was evaluated from the Fe^{II} concentration by assuming the stoichiometric chemical composition of Fe_3O_4. The amount of γ-FeO(OH) left unreacted was evaluated from the difference between the amount of Fe^{III} in the precipitate and Fe_3O_4. The amount of the intermediate dissolved in the tartaric-acid solution was evaluated from the difference between the amount of Fe^{III} in the initial reaction suspension and the sum of the Fe^{III} in the Fe_3O_4 and γ-FeO(OH) found in the suspension. The intermediate dissolved in the tartaric-acid solution will henceforth be referred to as "the TA-soluble intermediate."

The sample for X-ray diffractometry was prepared as follows: The precipitate obtained through the centrifugation of the reaction suspension was mounted on a glass plate under a nitrogen atomosphere and sealed with cellophane tape to prevent oxidation. For the IR spectroscopy, the precipitate was washed with oxygen-free acetone to remove as much water as possible and then dried under a nitrogen atmosphere. The IR spectra of the dried product were obtained as Nujol mulls.

Chemical Analysis. The Fe^{II} and Fe_{total} concentrations were determined by the 2,2′-bipyridyl method.[16] The Fe_{total} concentration was determined after reducing the Fe^{III} to Fe^{II} with hydroxylamine.

Results and Discussion

Dissolved Species (DS) and the TA-soluble Intermediate. As reported previously,[13] when the Fe^{II} ion was added to the γ-FeO(OH) suspension (pH 8.5) in the absence of SO_4^{2-} (Curve A in Fig. 1), γ-FeO(OH) was transformed to Fe_3O_4 (Curve C). In this reaction, γ-FeO(OH) adsorbs the Fe^{II} ion, dissolves, and it transformed to Fe_3O_4.[13] The adsorption reaction is written as:

$$\gamma\text{-FeO(OH)}(s\text{-}) + FeOH^+ \rightleftharpoons \gamma\text{-FeO(OH)}(s\text{-}FeOH^+), \quad (1)$$
(ADInt)

where *s*- is the adsorption site of γ-FeO(OH) and where ADInt is the Fe^{2+}-adsorbed intermediate.[13,17] The dissolved species formed in the dissolution step will be composed of Fe^{II} and Fe^{III} ions. The dissolution step will be given by:

$$\text{ADInt} \longrightarrow (Fe^{2+})_x(Fe^{3+})_y \text{ complex}, \quad (2)$$
(DS)

where DS means the dissolved species.

As can be seen in Fig. 2, when the SO_4^{2-} ion was present in the reaction suspension, γ-FeO(OH) (Curve A) was not transformed to Fe_3O_4 (Curve C), but to a TA-soluble intermediate (Curve B); almost all of the γ-FeO(OH) was transformed to the TA-soluble intermediate in 60 min. The X-ray diffraction pattern of the TA-soluble intermediate precipitate formed within 60 min corresponded to that of green rust II. In the IR spectrum of the precipitate, strong bands due to SO_4^{2-} appeared at 1100 and 630 cm^{-1}. These results suggest that the DS formed in the dissolution step combines with the SO_4^{2-} ion and is transformed to green rust II (GR-II).

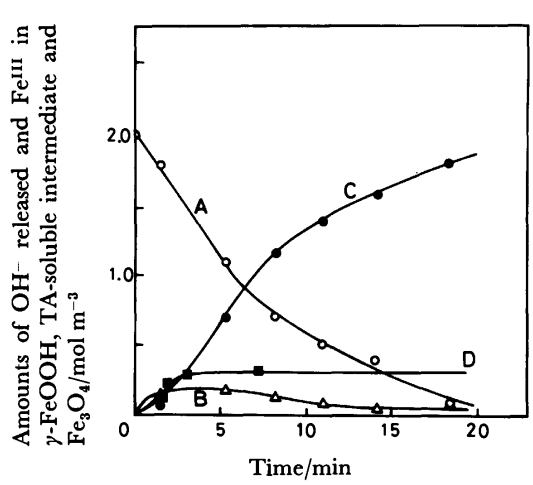

Fig. 1. The transformation of γ-FeOOH to Fe_3O_4 at pH 8.5. $Fe^{2+}/\gamma\text{-FeOOH}=3.60$, $SO_4^{2-}=0$ mol m^{-3}. Curve A; γ-FeOOH, B; TA-soluble intermediate, C; Fe_3O_4, D; OH^-.

Curves D in Figs. 1 and 2 show the release of OH^- during the formation of GR-II. These results suggest that no OH^- is released in the formation of Fe_3O_4, but only in that of GR-II. This OH^--releasing will be discussed later.

Here, we studied the effect of the Fe^{II} concentration on the formation of GR-II from γ-FeO(OH). The results are given in Figs. 3a and 3b, where the reaction pH and the concentrations of γ-FeO(OH) and SO_4^{2-} are the same as those of Fig. 2, but where the Fe^{II} concentrations in the reaction suspensions are lower than that of Fig. 2. As the Fe^{II} concentration in the reaction suspension decreased from 7.40 mol m^{-3} (Fig. 2) to 1.63 mol m^{-3} (Fig. 3b), the consumption of γ-FeO(OH) (Curve A) decreased. The relationship between the

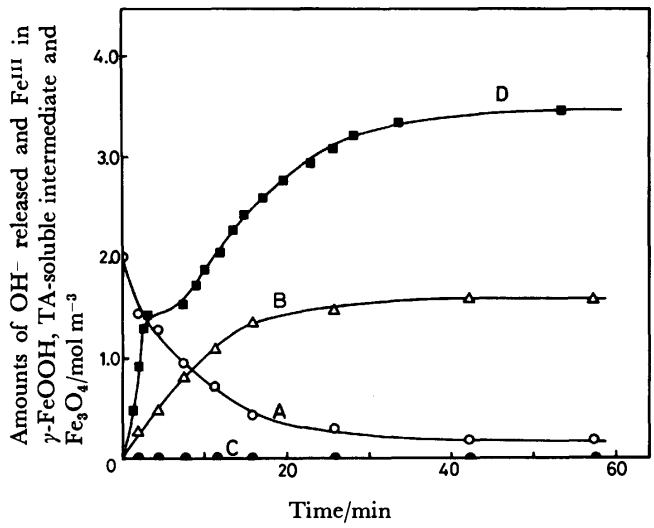

Fig. 2. The transformation of γ-FeOOH to green rust II at pH 8.5. $Fe^{2+}/\gamma\text{-FeOOH}=3.60$, $SO_4^{2-}=10.0$ mol m^{-3}. Curve A; γ-FeOOH, B; green rust II (TA-soluble intermediate), C; Fe_3O_4, D; OH^-.

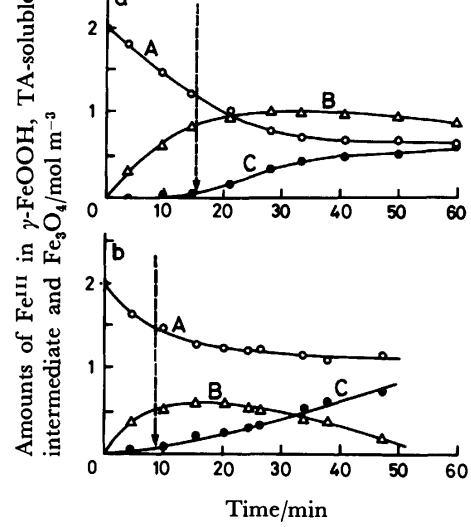

Fig. 3. Effect of Fe^{2+} concentration on the transformation of γ-FeOOH at pH 8.5 and at 10.0 mol m^{-3} of SO_4^{2-}. $Fe^{2+}/\gamma\text{-FeOOH}=1.50$(a), and 0.81(b). Curve A; γ-FeOOH, B; green rust II, C; Fe_3O_4.

Table 1. The effect of the Fe(II) concentration on the transformation of γ-FeOOH

Figure No.	$Fe^{2+}_{initial}$ (mol m^{-3})	γ-$FeOOH_{initial}$ (mol m^{-3})	$\frac{Fe^{2+}_{initial}}{\gamma\text{-}FeOOH_{initial}}$ (mol m^{-3})	γ-$FeOOH_{reacted}$ (mol m^{-3})	$\frac{Fe^{2+}_{initial}}{\gamma\text{-}FeOOH_{reacted}}$ (mol m^{-3})
2	7.40	2.06	3.60	1.92	3.70
3a	3.08	2.06	1.50	1.38	2.23
3b	1.67	2.06	0.81	0.68	2.46

amount of reacted γ-FeO(OH) and that of the Fe^{II} ions initially present in the reaction suspension is given in Table 1. The amount of Fe^{II} in the initial suspension is higher than the amount of γ-$FeO(OH)_{initial}$ in Figs. 2 and 3a, but lower than that in Fig. 3b (Column 4 in Table 1). The amount of γ-$FeO(OH)_{reacted}$ (Column 5) decreased as the initial amount of Fe^{II} decreased (Column 2). However, the mol ratios of $Fe^{2+}_{initial}/\gamma$-$FeO(OH)_{reacted}$ (Column 6) are approximately 2 at a $Fe^{2+}_{initial}/\gamma$-$FeO(OH)_{initial}$ ratio below 2 (column 4). This suggests that at least two mols of the Fe^{II} ions are needed to dissolve one mol of γ-FeO(OH). These results suggest that the dissolved species (DS) are composed of one Fe^{III} and two Fe^{II} ions.

Three Stages of γ-FeO(OH)-transformation Reaction. At lower Fe^{II} concentrations (Fe^{2+}/γ-$FeO(OH)_{initial}$ ratio below 2; Figs. 3a and 3b), the amount of GR-II increased, attaining its maximum as the reaction proceeded (Curve B). When the amount of GR-II became near the maximum in Figs. 3a and 3b (indicated by arrows), the Fe_3O_4 formation (Curve C) became prominent. The amount of Fe_3O_4 increased with time, accompanied by the consumption of γ-FeO(OH) (Curve A). However, as the reaction proceeded further (*cf.* Figs. 3a and 3b), the amount of GR-II decreased (slightly in Fig. 3a, but prominently in Fig. 3b). This decrease resulted in the Fe_3O_4-formation (Curve C) without any consumption of γ-FeO(OH), indicating that GR-II is transformed to Fe_3O_4.

Thus, at lower Fe^{II} concentrations (the $Fe^{2+}_{initial}/\gamma$-$FeO(OH)_{initial}$ ratio below 2), the DS is transformed to GR-II in the initial stage, and then to Fe_3O_4 in the second stage, where no further GR-II is formed. In the third stage, the transformation of GR-II to Fe_3O_4 mainly occurs.

On the other hand, at a high Fe^{II} concentration ($Fe^{2+}_{initial}/\gamma$-$FeO(OH)_{initial}$ ratio=3.60, Fig. 2), only the first-stage reaction is seen. In this case, an excess of Fe^{II} ions is present, since $Fe(OH)_2$ precipitates coexist throughout the reaction. This means that the suspension contains dissolved Fe^{II} ions, whose concentration is estimated to be about 10^{-4} kmol m^{-3} from the solubility product of $Fe(OH)_2$. On the other hand, in the case shown in Figs. 3a and 3b, since most of the Fe^{II} ions are consumed in the formation of GR-II, the concentration of the dissolved Fe^{II} ions seems to become lower than 10^{-4} kmol m^{-3} as the reaction proceeded. This lowering of the Fe^{II} concentration seems to cause the second-stage reaction. That is, in the second stage (Figs. 3a and 3b), the GR-II-formation reaction seems to attain an equilibrium as a result of the lowering of the concentration of the dissolved Fe^{II} ions.

Derivation of Empirical Formula of the Dissolved Species (DS). Since the Fe^{II} ion is adsorbed in the hydrolyzed form, $FeOH^+$, and since two mols of Fe^{II} ions seem to react with one mol of γ-FeO(OH), the adsorption step may be written as:

$$\gamma\text{-FeO(OH)}[(OH)_s(O)_s] + 2Fe(OH)_2 \rightleftharpoons \gamma\text{-FeO(OH)}[(OH)_sFeOH^+(O)_sFeOH^+] + 2OH^- \quad (3)$$
(ADInt*)

where the subscript s denotes the adsorption site. Here, it is assumed that one Fe^{II} ion is adsorbed on the OH group of γ-FeO(OH), and another, on the oxygen of the oxo-bridge of γ-FeO(OH). Since one OH^- ion takes part in the dissolution step,[13] the dissolution step may be given by:

$$ADInt^* + OH^- \longrightarrow DS. \quad (4)$$

In the absence of SO_4^{2-}, the γ-FeO(OH) is transformed to Fe_3O_4 (Fig. 1). In this reaction, it is considered that the DS is directly transformed to Fe_3O_4. Since the DS contains one Fe^{III} and two Fe^{II} ions, the Fe_3O_4-formation reaction from DS may be given by:

$$DS \longrightarrow 1/2Fe_3O_4 + 3/2Fe^{2+} + x/2OH^- + y/2H_2O. \quad (5)$$

The overall reaction obtained from Eqs. 3, 4, and 5 for the Fe_3O_4 formation from γ-FeO(OH) is written as:

$$\gamma\text{-FeO(OH)} + 2Fe(OH)_2 \longrightarrow 1/2Fe_3O_4 + 3/2Fe(OH)_2 + (x/2-2)OH^- + y/2H_2O. \quad (6)$$

or:

$$\gamma\text{-FeO(OH)} + 1/2Fe(OH)_2 \longrightarrow 1/2Fe_3O_4 + (x/2-2)OH^- + y/2H_2O \quad (6')$$

As stated previously, no OH^- is released during the Fe_3O_4 formation from γ-FeO(OH) (Curve D in Fig. 1). Therefore, $x=4$ in Eq. 6 or 6'. With $x=4$, we get $y=2$. With these x and y values, the DS composition is estimated from Eq. 5 to be $[(Fe^{2+})_2(Fe^{3+})(OH^-)_4(O^{2-})]^{1+}$.

Green Rust-II Formation Reaction from γ-FeO(OH). We know the following: The ratio of Fe^{II}/Fe^{III} in GR-II is 2;[11] the formation of one mol GR-II from one mol of γ-FeO(OH) and 2 mol of $Fe(OH)_2$ forms 2 mol of OH^- (Curves B and D in Fig. 2); the formation of GR-II from γ-FeO(OH) and $Fe(OH)_2$ requires the presence of SO_4^{2-} in the reaction suspension. In addition, GR-II is composed not of ions but of electroneutral precipitates. These findings lead to:

$$\gamma\text{-FeO(OH)} + 2Fe(OH)_2 + SO_4^{2-} \rightleftharpoons [(Fe^{2+})_2(Fe^{3+})_1O_n(OH)_{5-2n}]^{2+}\cdot SO_4^{2-} + 2OH^- + (n-1)H_2O. \quad (7)$$

If the GR-II is formed from DS in SO_4^{2-}-containing suspensions, then the reaction is given by:

$$[(Fe^{2+})_2(Fe^{3+})(OH^-)_4(O^{2-})]^+ + SO_4^{2-} \rightleftharpoons$$
(DS)
$$[(Fe^{2+})_2(Fe^{3+})_1O_n(OH^-)_{5-2n}]^{2+}\cdot SO_4^{2-}$$
(GR-II)
$$+ OH^- + (n-1)H_2O. \quad (8)$$

Equilibrium Consideration of the Green Rust-II Formation. A practical reaction for Eq. 7 is considered to be:

$$\gamma\text{-FeO(OH)} + 2FeOH^+ + SO_4^{2-} \rightleftharpoons$$
$$GR\text{-II} + (n-1)H_2O, \quad (9)$$

where it is assumed that a dissolved $FeOH^+$ ion is a reacting species for Reaction (7). Equation 9 means that $FeOH^+$ is adsorbed on γ-FeO(OH) and that GR-II is formed. The equilibrium constant, K, is given by:

$$K = 1/([FeOH^+]^2[SO_4^{2-}]) \quad (10)$$

or:

$$K = [H^+]^2/(K_h^2[Fe^{2+}]^2[SO_4^{2-}]), \quad (11)$$

where K_h is the hydrolysis constant of Fe^{2+}. Equation 11 tells that the concentrations of the dissolved Fe^{2+} and SO_4^{2-} ions and the proton (pH) affect the formation of GR-II from γ-FeO(OH). Here, we studied the effect of the SO_4^{2-} concentration. Figure 4 shows the results at a low SO_4^{2-} concentration (2.0 mol m^{-3}). As may be seen here, only the first-stage reaction (GR-II formation from γ-FeO(OH)) took place, as in the case of Fig. 2 (high SO_4^{2-} concentration; 10.0 mol m^{-3}). However, in the case of Fig. 4 (low SO_4^{2-} concentration; 2.0 mol m^{-3}), about one fourth of the γ-FeO(OH) remained unreacted, and the formation of GR-II seems to have ceased. This indicates that the formation of GR-II attained an equilibrium at a low SO_4^{2-} concentration. Since an excess of Fe^{II} ions was added, the $Fe(OH)_2$ precipitate coexisted with γ-FeO(OH) and GR-II, but the formation of GR-II did not proceed further because of a lack of dissolved SO_4^{2-}. The substitution of the solubility product of $Fe(OH)_2$ for $[Fe^{2+}]$ in Eq. 11 results in:

$$K = \left(\frac{K_w}{K_h K_{sol}}[OH^-]\right)^2[SO_4^{2-}]^{-1} \quad (12)$$

where K_w is the water-dissociation constant. The K value estimated from Eq. 12 is 2.14×10^8 for the values of $[OH^-]=10^{-5.5}$, $[SO_4^{2-}]=6.6\times10^{-4}$ kmol m^{-3}, $K_h=10^{-9.5}$,[18] and $K_{sol}=10^{-15.15}$.[18]

Table 2 summarizes the concentrations of the Fe^{II} ion calculated for various reaction conditions using Eq. 11 and the K value estimated above. The Fe^{II} concentrations evaluated at the points shown by arrows in Figs. 3a and 3b (Column 2 in Table 2) are lower than those estimated from the solubility product of $Fe(OH)_2$(Column 4). This supports the speculation that the lowering of the concentration of the dissolved Fe^{II} ion causes the cessation of the formation of GR-II from γ-FeO(OH). The Fe^{II} concentration calculated

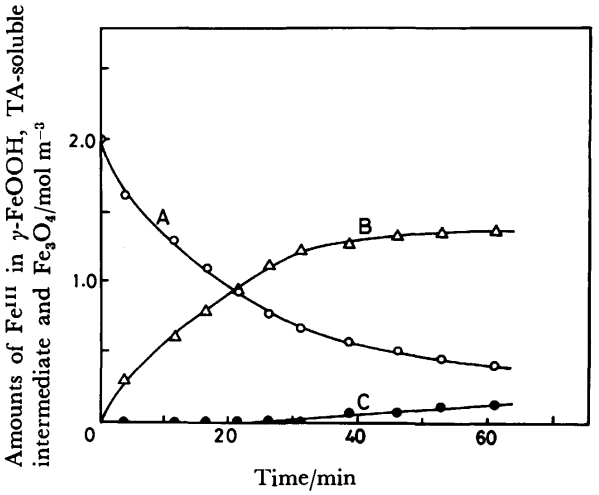

Fig. 4. Effect of SO^{2-} at a low concentration (2.0 mol m^{-3}) on the transformation of γ-FeOOH. pH 8.5, Fe^{2+}/γ-FeOOH=3.60. Curve A; γ-FeOOH, B; green rust II (TA-soluble intermediate), C; Fe_3O_4.

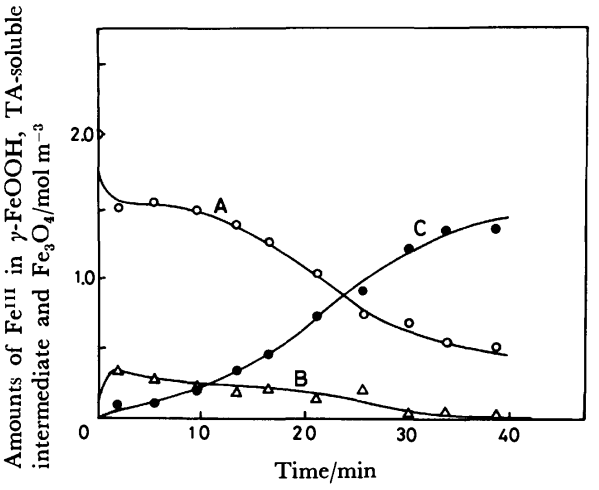

Fig. 5. The transformation of γ-FeOOH to Fe_3O_4 at pH 10.0. Fe^{2+}/γ-FeOOH=3.60, SO_4^{2-}=10.0 mol m^{-3} Curve A; γ-FeOOH, B; green rust II, C; Fe_3O_4.

TABLE 2. CONCENTRATIONS OF THE Fe(II) ION CALCULATED FOR VARIOUS REACTION CONDITIONS USING THE EQUATION $K=[H^+]^2/(K_h^2[Fe^{2+}]^2[SO_4^{2-}])$ AND $K=2.14\times10^8$

pH	Fe^{2+} Concentration Calcd (kmol m^{-3})	SO_4^{2-} Concentration (kmol m^{-3})	Fe^{2+} Concentration Evaluated from the Solubility Product of $Fe(OH)_2$ (kmol m^{-3})
8.5(Fig. 3a)	1.91×10^{-5}	9.13×10^{-3}	7.08×10^{-5}
8.5(Fig. 3b)	1.87×10^{-5}	9.48×10^{-3}	7.08×10^{-5}
10.0	5.75×10^{-7}	1.00×10^{-2} *	7.08×10^{-8}

* The Fe^{2+} concentration was calculated assuming this value, which is near those at pH 8.5.

at pH 10.0 and at a high SO_4^{2-} concentration (10.0 mol m^{-3}) is 5.75×10^{-7} kmol m^{-3}. On the other hand, the Fe^{II} concentration evaluated from the solubility product of $Fe(OH)_2$ at the same pH(10.0) is 7.08×10^{-8} kmol m^{-3}. This suggests that little GR-II is formed at the pH value of 10.0, even at a high SO_4^{2-} concentration. Figure 5 shows the results under those conditions (pH 10.0, SO_4^{2-}; 10.0 mol m^{-3}). As predicted above, the amount of GR-II was very small, and Fe_3O_4 was mainly formed (Curve C in Fig. 5). These results suggest that the DS is transformed to Fe_3O_4 when little GR-II is formed from the DS.

References

1) M. Kiyama, *Bull. Chem. Soc. Jpn.*, **47**, 1646 (1974).
2) J. D. Bernal, D. R. Dasgupta, and A. L. Mackay, *Clay Minerals Bull.*, **4**, 15 (1959).
3) T. Misawa, K. Hashimoto, and S. Shimodaira, *Corros. Sci.*, **14**, 131 (1974).
4) M. Kiyama, *Bull. Chem. Soc. Jpn.*, **51**, 134 (1978).
5) K. Kaneko and T. Katsura, *Bull. Chem. Soc. Jpn.*, **52**, 747 (1979).
6) T. Katsura, Y. Tamaura, and G. S. Chyo, *Bull. Chem. Soc. Jpn.*, **52**, 96 (1979).
7) Y. Tamaura, S. Mechaimonchit, and T. Katsura, *J. Inorg. Nucl. Chem.*, **43**, 671 (1981).
8) T. Kanzaki, J. Nakajima, Y. Tamaura, and T. Katsura, *Bull. Chem. Soc. Jpn.*, **54**, 135 (1981).
9) K. Kaneko, T. Takei, Y. Tamaura, T. Kanzaki, and T. Katsura, *Bull. Chem. Soc. Jpn.*, **52**, 1080 (1979).
10) Y. Tamaura and T. Katsura, *J. Chem. Soc., Dalton Trans.*, **1980**, 825.
11) Y. Tamaura, T. Yoshida, and T. Katsura, *Bull. Chem. Soc. Jpn.*, **57**, 2411 (1984).
12) Y. Tamaura, P. V. Buduan, and T. Katsura, *J. Chem. Soc., Dalton Trans.*, **1981**, 1807.
13) Y. Tamaura, K. Ito, and T. Katsura, *J. Chem. Soc., Dalton Trans.*, **1983**, 189.
14) K. Ito, Y. Tamaura, and T. Katsura, *J. Chem. Soc. Dalton Trans.*, **1983**, 987.
15) K. Ito, Y. Tamaura, and T. Katsura, *Bull. Chem. Soc. Jpn.*, submitted for publication.
16) I. Iwasaki, T. Katsura, T. Ozawa, M. Mashima, H. Hamamura, and B. Iwasaki, *Bull. Volc. Soc. Jpn., Ser. 2*, **5**, 75 (1960).
17) M. M. Benjamin and J. O. Leckie, *J. Colloid Interface Sci.*, **79**, 209 (1981).
18) C. F. Baes, Jr., and R. Mesmer, "The Hydrolysis of Cations," Wiley-Interscience Publications, New York (1976), p. 226.

The Base-Catalyzed Isomerization of the (Iminodiacetato)-(*N*-methyliminodiacetato)cobaltate(III) and Bis-(iminodiacetato)cobaltate(III) Ions

Hiroshi KAWAGUCHI,* Tomoharu AMA, and Takaji YASUI
Department of Chemistry, Faculty of Science, Kochi University, Akebono-cho, Kochi 780
(Received February 16, 1984)

The isomerization reaction among three geometrical isomers of $[Co(ida)(mida)]^-$ was studied in a basic aqueous solution. It has been found that the reaction scheme is *u-fac*⇌*mer*⇌*s-fac*. The rates of these isomerization paths have been determined as the functions of pH and temperature. The rate of the *u-fac*⇌*mer* change is considerably faster than that of the *mer*⇌*s-fac* change. The CD loss of the optically active *u-fac* isomer is caused by the isomerization process of *u-fac*⇌*mer*. The isomerization of the $[Co(ida)_2]^-$ system has also been measured, and the rate data analysed according to the same scheme as that used for the $[Co(ida)(mida)]^-$ system. It is suggested that the isomerizations of the $[Co(ida)(mida)]^-$ and $[Co(ida)_2]^-$ systems proceed through a conjugate-base intermediate.

Octahedral complexes containing two symmetrical terdentate ligands, such as dien, ida, and their analogs,[1] provide three possible geometrical isomers: *s-fac*, *u-fac*, and *mer* (Fig. 1). Legg and Cooke first isolated three geometrical isomers of $[Co(ida)(dien)]^+$.[2] Since then, all geometrical isomers possible in $[Co(dien)_2]^{3+}$ and $[Co(dien)(mdien)]^{3+}$ have been prepared by two groups, Keene *et al.*[3] and Kojima *et al.*[4] The series of the geometrical isomers of $[Co(ida)_2]^-$ became complete when the *mer* isomer was reported by Koine *et al.*[5] Recently, in our laboratory the *u-fac* isomers of $[Co(mida)_2]^-$ and $[Co(eida)_2]^-$, which had been considered not to form because of intramolecular repulsions, were prepared under acidic conditions,[6] and the crystal structure of *u-fac*-$K[Co(mida)_2]\cdot 1.5H_2O$ was determined by X-ray analysis.[7]

Although numerous data of the stereochemistry of the terdentate-ligand complexes have been reported,[8] few data on the rearrangement reactions (isomerization and racemization) of these complexes have been reported. Rearrangements in the octahedral complexes can occur by either of two path ways; the intramolecular pathway or the complete ligand-dissociation pathway. The major pathway of the intramolecular rearrangements involves twist and bond-rupture mechanisms, but the choice between twist and bond-rupture alternatives has seldom been unambiguous. It was hoped that the use of the terdentate-ligand complexes in mechanistic studies of rearrangement reactions might offer an opportunity of distinguishing between twist and bond-rupture alternatives, since the coupled chelate rings restrict the number of possible interconversions.

Searle *et al.* studied the isomerization of the $[Co(dien)(mdien)]^{3+}$ and $[Co(dien)_2]^{3+}$ complexes and proposed a mechanism occurring through a transient five-coordinate intermediate formed by bond-rupture.[9] The racemization rate of *mer*-$[Co(dien)_2]^{3+}$ was also measured.[10] This reaction process involves a change in the chiral disposition of two N-H bonds at the secondary nitrogen centers. Cooke has described the *u-fac*- and *s-fac*-$[Co(ida)_2]^-$ complexes as being isomerized to each other at a rate depending on the base concentration, and said that the equilibrium distribution of the isomers at room temperature was 28% *u-fac* and 72% *s-fac*.[11] Previously, we ourselves presented preliminary results concerning the reactivities of the $[Co(ida)_2]^-$, $[Co(ida)(mida)]^-$,[12] and $[Co(mida)_2]^-$ complexes.[6] In the present paper, we will describe a detailed study of the isomerization of the $[Co(ida)(mida)]^-$ and $[Co(ida)_2]^-$ systems.

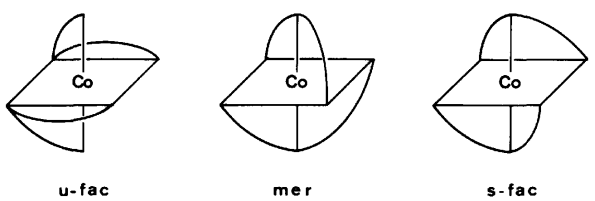

Fig. 1. Three geometrical isomers of the $[Co(L)_2]$ type complex, where L is a symmetrical terdentate ligand.

Experimental

Preparation of Complexes. The three geometrical isomers of $K[Co(ida)_2]$ and the *u-fac* and *s-fac* isomers of K-[Co(ida)(mida)] were prepared according to the method reported in our previous papers[6,12]: *s-fac*-$K[Co(ida)_2]\cdot 2H_2O$, *u-fac*-$K[Co(ida)_2]\cdot 2.5H_2O$, *mer*-$K[Co(ida)_2]\cdot H_2O$, *u-fac*-K-[Co(ida)(mida)]·$2H_2O$, and *s-fac*-$Na[Co(ida)(mida)]\cdot H_2O$.

mer-*K[Co(ida)(mida)]·0.5H₂O*: This complex was obtained by the isomerization of *u-fac*-$[Co(ida)(mida)]^-$ in a weak basic aqueous solution. Five grams of *u-fac*-K[Co-(ida)(mida)]·$2H_2O$ was dissolved in 250 cm^3 of water, after which the solution was adjusted to pH 8.4—8.5 with potassium hydroxide. An isomerization reaction was carried out at 30 °C for 40 min with constant stirring. The resulting solution was slightly acidified (pH 5—6) with acetic acid and evaporated quickly under reduced pressure at 30—35 °C until crystals of the unreacted *u-fac* isomer deposited. A large amount of methanol was added to them, and the *u-fac* isomer was filtered off. The filtrate was evaporated again, and the remaining *u-fac* isomer was removed. By repeating these procedures several times, the crude *mer* isomer was obtained. Recrystallization was carried out from a small amount of water by adding a mixture of methanol-acetone. The fine red crystals thus deposited were filtered and washed with acetone. Found: C, 28.18; H, 3,82; N, 7.27%. Calcd for K[Co(ida)(mida)]·$0.5H_2O$: C, 28.21; H, 3.42; N, 7.31%.

Optical Resolution. The *u-fac* isomers of $[Co(ida)_2]^-$

and [Co(ida)(mida)]$^-$ were resolved into optically active isomers by the methods described in our previous papers[6,12]: (+)$_{589}$-*u-fac*-K[Co(ida)(mida)]·1.5H$_2$O ($\Delta\varepsilon_{592}$=−2.52, $\Delta\varepsilon_{521}$=+2.86) and (+)$_{589}$-*u-fac*-K[Co(ida)$_2$]·H$_2$O ($\Delta\varepsilon_{588}$=−2.43, $\Delta\varepsilon_{509}$=+2.54).

Kinetic Studies. All the chemicals were of a reagent grade, and deionized water was degassed before use. The isomerization reactions were studied spectrophotochemically with the use of a Hitachi 557 spectrophotometer. The reaction vessel with jacket and the cell mounted in the cell holder of the spectrophotometer were thermostated at a constant temperature (±0.1 °C) with circulating water from a constant-temperature bath. During the experiments, the temperatures of the reaction vessel and cell were checked with a thermistor thermometer (Takara D221), and the pH of the reaction solution in the vessel by a Toa TSC-10A pH meter.

The reaction was started by stirring a buffer solution (2.0 cm^3) into the complex solution (18.0 cm^3) in the reaction vessel; *ca.* a 3-cm^3 quantity of this solution was then quickly transferred to the cell in order to record the spectral change in the suitable wave-length range at desired time-intervals. All solutions were prepared at the temperature where runs were to be made, and the following conditions were set: pH, 7.5—10.5 (Na_2HPO_4-KH_2PO_4 or Na_2CO_3-$NaHCO_3$ buffer); complex concentration, 2.8—3.0×10^{-3} mol dm^{-3}; ionic strength, 0.1 ($NaClO_4$); temperature, 25—35 °C. In the case of the isomerization between *mer* and *u-fac*, the wave-lengths chosen for kinetic study were 511 and 503 nm for the [Co(ida)(mida)]$^-$ and [Co(ida)$_2$]$^-$ systems respectively. For the isomerization from an equilibrium mixture of *u-fac* and *mer* to *s-fac*, these wave-lengths at the isosbestic points between *u-fac* and *mer* were chosen: 559 and 548 nm for the [Co(ida)(mida)]$^-$ and [Co(ida)$_2$]$^-$ systems respectively.

The rates of the loss of CD magnitude were measured by means of a JASCO J-22 spectrophotometer using the method and conditions described above.

The plots of $\ln(D_0-D_{eq})/(D_t-D_{eq})$ *vs.* the time and ln[CD magnitude] *vs.* the time gave straight lines over three times the half-lives. Analyses of the kinetic data were carried out on a NEC-8800 computer using the least-squares methods. In each of the rate analyses, the value of the standard error was within ±2% of the rate constant.

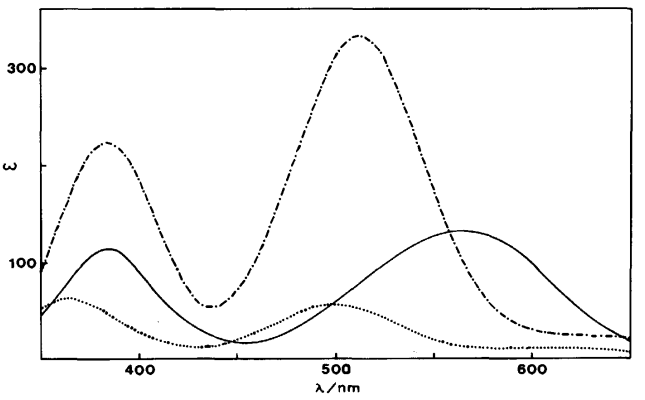

Fig. 2. Absorption spectra of three geometrical isomers of [Co(ida)(mida)]$^-$ in aqueous solution: *u-fac* (——), *mer* (—·—), and *s-fac* (·····).

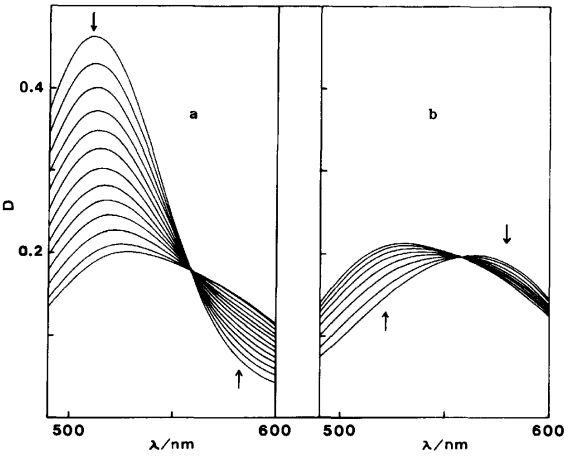

Fig. 3. The time-course changes of absorption spectra of *mer*- and *u-fac*-[Co(ida)(mida)]$^-$ in weak basic aqueous solutions at 30.0 °C. The record intervals are arbitrary: (a) *mer* (2.81×10^{-3} mol dm^{-3}), pH=8.02; (b) *u-fac* (2.98×10^{-3} mol dm^{-3}), pH=7.80.

Results and Discussion

mer-K[Co(ida)(mida)] Complex. The absorption spectrum of *mer*-[Co(ida)(mida)]$^-$, which was newly prepared, is shown in Fig. 2, together with those of the *u-fac* and *s-fac* isomers reported in a previous paper;[12] the numerical data are as follows. 1st band ($^1A_1\rightarrow{}^1T_1$), $\lambda_{sh}\simeq$625 nm ($\log\varepsilon\simeq$1.39) and λ_{max}=511 nm ($\log\varepsilon$=2.53); 2nd band ($^1A_1\leftrightarrow{}^1T_2$). λ_{max}=384 nm ($\log\varepsilon$=2.36); CT band, λ_{max}=226 nm ($\log\varepsilon$=4.29). The spectral behavior of *mer*-[Co(ida)(mida)]$^-$ is quite similar to that of *mer*-[Co(ida)$_2$]$^-$ and *mer*-[Co(mida)$_2$]$^-$. In these *mer* isomers, the 1st and 2nd absorption maxima shift to the lower-energy side in the order of [Co(ida)$_2$]$^-$<[Co(ida)(mida)]$^-$<[Co(mida)$_2$]$^-$, while the 1st and 2nd bands increase in intensity in the order of [Co(mida)$_2$]$^-$<[Co(ida)(mida)]$^-$<[Co(ida)$_2$]$^-$. These trends are in agreement with those observed in the *u-fac* isomers of [Co(ida)$_2$]$^-$, [Co(ida)(mida)]$^-$, and [Co(mida)$_2$]$^-$.[12]

As the *mer* isomers of [Co(ida)(mida)]$^-$ and [Co(ida)$_2$]$^-$ are not so stable in an aqueous solution (extremely unstable in a basic aqueous solution) and easily isomerize to the *u-fac* and/or *s-fac* isomers, the procedure of separating the *mer* isomer from the others should be carried out quickly at a low temperature. This is one of the reasons for the lower yields of *mer*-K[Co(ida)(mida)] and *mer*-K[Co(ida)$_2$]. These *mer* isomers have the dissymmetrical structure which arises from a chiral disposition of two noncoplanar ligands, but have not yet been resolved into optically active isomers. On the other hand, *mer*-[Co(mida)$_2$]$^-$ is quite stable, even in a weak basic aqueous solution, and has been resolved into optically active isomers.[5,13]

Isomerization Reactions of the [Co(ida)(mida)]$^-$ System. Figure 3 shows the spectral changes in *mer*- and *u-fac*-[Co(ida)(mida)]$^-$ in weak basic solutions. The *u-fac* isomer changed its spectrum with an isosbestic point at 559 nm, and it gave the final curve in Fig. 3-b after *ca.* 2 h. (We use the term "pseudo-equilibrium state" to describe this state.) However, after that time the intensity of the spectrum (at the pseudo-equilibrium state) began to decrease very slowly under the conditions of pH 7.80 at 30 °C. The prolonged reaction

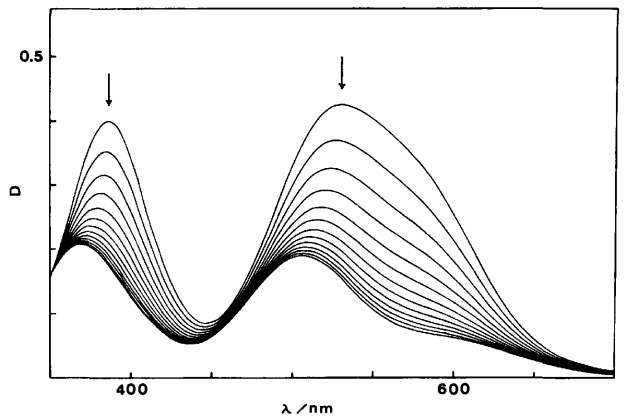

Fig. 4. The time-course change of absorption spectra of *u-fac*-[Co(ida)(mida)]$^-$ in basic aqueous solution (pH=10.10) at 30.0 °C. Record interval is 10 min.

gave the same spectral change as that shown in Fig. 4. The *mer* isomer also showed the spectral change with the passage of time in a weak basic solution, giving an isosbestic point at 559 nm (Fig. 3-a). The final curve in Fig. 3-a, recorded after *ca.* 1.5 h, is identical with that in Fig. 3-b. The subsequent spectral change was the same as that observed in the case of the *u-fac* isomer. The isosbestic point at 559 nm shown in Fig. 3 quite agrees with the point of intersection of the absorption curves of the *mer* and *u-fac* isomers in Fig. 2.

The spectral change in the second step, as shown in Fig. 4, occurred at a considerable rate in the higher-pH region (pH>10). The spectral pattern at the final equilibrium state is fairly close to that of the *s-fac* isomer. The same final spectral pattern was also observed for the final solution starting from the *s-fac* isomer. The resulting mixture at the final equilibrium state was chromatographed on a QAE-Sephadex column, but no other species except for the three geometrical isomers of [Co(ida)(mida)]$^-$ were detected. The *mer* isomer could not be clearly detected on the column chromatograph, because the *mer* isomer is present in a very small amount at the final equilibrium state and is not easily separated from the *s-fac* isomer on the QAE-Sephadex column.

With each spectral curve in Fig. 4, the intensities of absorption ($D(\lambda_x)$) at an arbitrary wave-length (λ_x) due to only *mer* and *u-fac* can be estimated using the following formulas.

$$D(\lambda_x) = D_{obsd}(\lambda_x) - \varepsilon_{s\text{-}fac}(\lambda_x)\cdot[s\text{-}fac]$$

$$D_{obsd}(559) = \varepsilon_{s\text{-}fac}(559)\cdot[s\text{-}fac] + \varepsilon_{u\text{-}fac}(559)\cdot[u\text{-}fac+mer]$$

$$[u\text{-}fac+mer]+[s\text{-}fac] = [\text{complex}]_0$$

where $[\text{complex}]_0$ is the initial concentration of the complex, where $D_{obsd}(\lambda_x)$ denotes the observed optical density at λ_x nm in Fig. 4, and where $\varepsilon(\lambda_x)$ is molar absorptivity at λ_x nm of the isomer shown as a subscript. The values of $D(\lambda_x)$ at various wave-lengths decrease in the same ratio to each other (Table 1). This suggests that the $[mer]/[u\text{-}fac]$ ratio can be regarded as constant during the isomerization reaction from the *u-fac-mer* mixture to the *s-fac* isomer except for the very first stage

Table 1. The intensities of absorption ($D(\lambda_x)$) at several wave-lengths (λ_x) attributably to only *mer*- and *u-fac*-[Co(ida)(mida)]$^-$, as calculated from the spectral data in Fig. 4

λ_x/nm	$D_t(\lambda_x)$ Time/min 10	30	60	$D_t(\lambda_x)/D_{60}(\lambda_x)$ Time/min 10	30	60
600	0.206	0.138	0.080	2.58	1.73	1
550	0.328	0.221	0.129	2.54	1.71	1
500	0.269	0.181	0.106	2.54	1.70	1
450	0.071	0.048	0.028	2.53	1.71	1
400	0.278	0.187	0.109	2.55	1.72	1

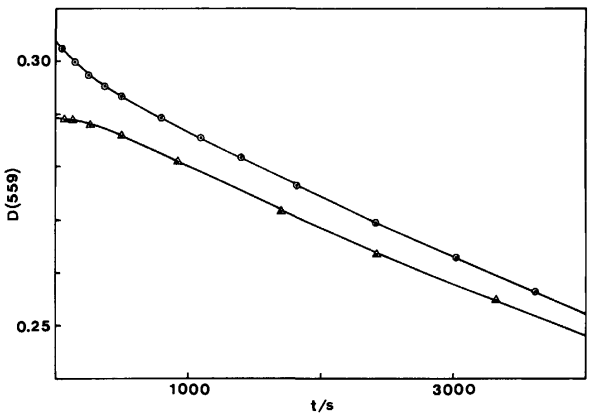

Fig. 5. The time-course changes of absorbance at 559 nm for *mer*- and *u-fac*-[Co(ida)(mida)]$^-$ in basic aqueous solutions: *mer* (—⊙—) 2.35×10^{-3} mol dm^{-3}, pH=9.09, 30.7 °C; *u-fac* (—△—△—) 2.30×10^{-3} mol dm^{-3}, pH=8.98, 30.4 °C.

of the reaction. Therefore, the reaction scheme of the isomerization reaction can be described as follows:

$$\begin{array}{ccc} & \overset{k_1'}{\rightleftharpoons} & \\ mer & & u\text{-}fac \\ & \underset{k_2'}{} & \\ & \underset{k_s'}{\downarrow}\ \uparrow\underset{k_{-s}'}{} & \\ & s\text{-}fac & \end{array} \qquad (1)$$

Thus, in order to study the isomerization of the [Co(ida)(mida)]$^-$ system, two independent experiments were carried out: The examinations of the *mer*⇌*u-fac* isomerization at pH 7.5—8.5 and of the (*mer*+*u-fac*)⇌*s-fac* isomerization at pH 9.5—10.5. The progress of the *mer*⇌*u-fac* isomerization was followed at 511 nm, and the D_t data for the analysis of kinetics were obtained during the isosbestic point at 559 nm was maintained. Each of the *mer* and *u-fac* isomers was used as a starting material under the same conditions, and the average value of D_{eq} (absorbance at the pseudo-equilibrium state) was used for the kinetic analysis.

The pseudo-first-order rate constants, k_s' and k_{-s}', can be determined from the intensity loss of absorption at 559 nm. However, it is ambiguous which isomer, *mer* or *u-fac*, in an equilibrium mixture isomerized to *s-fac*. Figure 5 shows the plots of absorbance at 559 nm

(D(559)) *vs.* the time using *mer* and *u-fac* as starting materials at pH 9 and 30 °C. In the run using *mer* as the starting material, the D(559) change in the very first stage of the reaction, where the equilibrium between *mer* and *u-fac* should not be achieved, is faster than that observed in the successive time-course. On the other hand, in the run using *u-fac* as the starting material, the initial D(559) change is slower than the subsequent change. These results support the idea that *s-fac* is produced from *mer*, and that Reaction Scheme (1) should be modified as follows:

$$\begin{array}{ccc} mer & \underset{k_2'}{\overset{k_1'}{\rightleftharpoons}} & u\text{-}fac \\ {\scriptstyle k_3'}\downarrow\uparrow{\scriptstyle k_4'} & & \\ s\text{-}fac & & \end{array} \qquad (2)$$

The relationships between the rate constants for Schemes (1) and (2) are $k_4'=k_{-s}'$ and $k_3'=(K+1)k_s'$, where K is equal to k_1'/k_2'. The pseudo-first-order and second-order rate constants for Scheme (2), k' and $k=k'/[OH^-]$, are listed in Table 2. The rate law for each isomerization path can be described as $R=k$[complex]-[OH$^-$], judging from the constancy of the k obtained in the runs with various pHs at a constant temperature (Table 2). The reaction rates for the (*mer*+*u-fac*)$\rightleftharpoons$*s-fac* change were independent of the sort of buffer (carbonate or phosphate buffer); however, an increase in the ionic strength from 0.1 to 1.0 increased the reaction rate (about 35%).

Isomerization Reactions of the [Co(ida)$_2$]$^-$ System. The *mer*-[Co(ida)$_2$]$^-$ complex showed spectral change in a weak basic solution (pH *ca.* 8.0) at 30 °C, giving an isosbestic point at 548 nm; this is consistent with the point of the intersection of the absorption curves of the *mer* and *u-fac* isomers. This implies that the spectral change is due to the *mer*→*u-fac* isomerization. After about 1.5 h, the spectra of the solution showed a nearly constant pattern (pseudo-equilibrium state), and the subsequent spectral change, which was attributed to the isomerization from a mixture of *u-fac* and *mer* to *s-fac*, was very slow under the conditions of pH *ca.* 8.0 and 30 °C. The spectral pattern at the pseudo-equilibrium state was almost identical with that of *u-fac*. Under the same conditions, the *u-fac* isomer showed a tendency of spectral change attributably to the isomerization to the *mer* isomer, but the change was very small. The equilibrium distribution of *u-fac* and *mer* is more favorable for *u-fac* than that in the case of the [Co(ida)(mida)]$^-$ complex.

In an aqueous solution buffered at pH *ca.* 10.0 at 30 °C, the isomerization from a mixture of *u-fac* and *mer* to *s-fac* occurred at a considerable speed, giving isosbestic points at about 474 and 445 nm, which are different from the points of intersection (481 and 443 nm) of the absorption curve of *u-fac* and that of *mer*. Judging from the observation of the isosbestic points, the [*mer*]:[*u-fac*] ratio can be regarded as constant in this process. The ratio ([*mer*]:[*u-fac*]=2.3:97.7) which was calculated using the molar absorptivities of three geometrical isomers at 474 nm was consistent with the ratio ([*mer*]:[*u-fac*]=1.8:98.2) calculated from the absorption data at the pseudo-equilibrium state, within the limits of experimental error.

The isomerizations of the [Co(ida)$_2$]$^-$ system were examined by the same method as that used in the case of the [Co(ida)(mida)]$^-$ system. Even though there was no obvious experimental fact supporting the idea that *s-fac* was produced from *mer*, it seems reasonable to assume that the isomerization scheme for the [Co(ida)$_2$]$^-$ system is the same as that for the [Co(ida)(mida)]$^-$ system. Thus, the data observed were analyzed according to

Table 2. The rate constants for the isomerization of the [Co(ida)(mida)]$^-$ and [Co(ida)$_2$]$^-$ systems in basic aqueous solutions

		[Co(ida)(mida)]$^-$			
T/°C	pH	$k_1'\times10^3$ / s^{-1}	$k_2'\times10^4$ / s^{-1}	$k_1\times10^{-2}$ / M^{-1} s^{-1}	$k_2\times10^{-2}$ / M^{-1} s^{-1}
24.8	8.03	0.282	0.735	2.66	0.693
27.2	8.03	0.403	1.08	3.17	0.850
30.0	7.47	0.193	0.537	4.46	1.24
30.0	8.02	0.647	1.80	4.21	1.17
30.0	8.27	1.19	3.32	4.37	1.21
30.0	8.45	1.81	5.03	4.37	1.21
32.5	8.04	1.07	3.01	5.58	1.57
34.4	8.06	1.48	4.14	6.45	1.80
T/°C	pH	$k_3'\times10^3$ / s^{-1}	$k_4'\times10^5$ / s^{-1}	$k_3\times10^{-1}$ / M^{-1} s^{-1}	$k_4\times10$ / M^{-1} s^{-1}
24.7	9.72	0.340	0.366	0.662	0.712
27.3	9.71	0.508	0.548	0.828	0.895
30.0	9.51	0.483	0.607	1.02	1.28
30.1	9.71	0.793	0.897	1.04	1.18
30.0	10.08	1.68	2.11	0.949	1.19
32.7	9.71	1.26	1.45	1.38	1.59
34.7	9.74	1.84	2.25	1.64	2.00

		[Co(ida)$_2$]$^-$			
T/°C	pH	$k_1'\times10^3$ / s^{-1}	$k_2'\times10^5$ / s^{-1}	$k_1\times10^{-2}$ / M^{-1} s^{-1}	k_2 / M^{-1} s^{-1}
25.2	8.03	0.221	0.398	2.05	3.65
27.6	8.03	0.352	0.634	2.66	4.79
30.3	7.86	0.382	0.689	3.50	6.31
30.2	8.32	1.05	1.89	3.37	6.07
32.8	8.14	1.07	1.93	4.35	7.83
34.5	8.15	1.48	2.67	5.21	9.38
T/°C	pH	$k_3'\times10^3$ / s^{-1}	$k_4'\times10^5$ / s^{-1}	$k_3\times10^{-1}$ / M^{-1} s^{-1}	$k_4\times10$ / M^{-1} s^{-1}
25.1	9.66	0.636	0.466	1.38	1.01
27.4	9.68	1.07	0.811	1.85	1.41
30.3	9.43	1.02	0.762	2.50	1.88
30.3	10.03	4.19	3.03	2.59	1.88
30.1	10.61	14.5	11.0	2.41	1.83
32.2	9.64	2.84	2.15	3.16	2.88
34.8	9.64	4.28	3.16	4.78	3.53

Each rate constant, k_n' ($n=1-4$), corresponds to that in Scheme (2). The 2nd-order rate constant, k_n, represents $k_n'/[OH^-]$.

Scheme (2). The kinetic parameters are listed in Table 2. As the reaction rates depend on the $[OH^-]$ concentrations with the first-order, the second-order rate constants can be calculated from $k=k'[OH^-]$ (Table 2).

The Loss of Optical Activities in the u-fac *Isomers.* The optically active *u-fac* isomers of the $[Co(ida)(mida)]^-$ and $[Co(ida)_2]^-$ complexes lost their CD strength with the passage of time in a basic aqueous solution. The rates of CD loss in these complexes depended on the $[OH^-]$ concentration with the first-order. Therefore, the rates are described by a rate law in this form: $-d[\text{CD strength}]/dt=k_{CD}[\text{complex}][OH^-]$. The rate parameters obtained are given in Table 3. In both the $[Co(ida)(mida)]^-$ and $[Co(ida)_2]^-$ complexes, the comparable values of k_{CD} with k_2 (rate constant for the *u-fac*→*mer* change) indicate that the loss of CD in the *u-fac* isomer is mainly caused by the isomerization process of *u-fac*→*mer*.

During the course of the *u-fac*→*mer* process for the systems of both $[Co(ida)(mida)]^-$ and $[Co(ida)_2]^-$, the CD spectra decreased in magnitude while keeping the spectral patterns of the optically active *u-fac* isomers used as starting materials. Thus, the isoextinct points of the CD change were observed on a base line. Such CD behavior implies that the *mer* isomer produced from optically active *u-fac* is racemate, but this does not exclude the possibility that *u-fac*→*mer* change might occur through a stereospecific pathway such as *Δ-u-fac*→*mer-δ*-NH,NCH$_3$ (or *Δ-u-fac*→*mer-λ*-NH,NCH$_3$). The dissymmetrical structure of the *mer*-$[Co(ida)(mida)]^-$ or *mer*-$[Co(ida)_2]^-$ complex is due to the chirality described by the stereochemical relationship between the N-H and N-CH$_3$ bonds (or two N-H bonds) of the nitrogen atoms in the two ligands. If the rate of the inversion at the N-center (of the coordinated ida) for the *mer* structure is fast enough compared with the rate of the *u-fac*→*mer* change, the result described above may be expected. (We use the term "inversion" to describe the configurational change about a secondary nitrogen center in *mer*-$[Co(ida)(mida)]^-$ or *mer*-$[Co(ida)_2]^-$ despite the absence of asymmetry.) For the *mer*-$[Co(dien)_2]^{3+}$, $[Co(NH_3)_4(Me\text{-}en)]^{3+}$, $[Co(NH_3)_4(sar)]^{2+}$, and $[Co(en)_2(sar)]^{2+}$ complexes, the rates of the inversion at the secondary nitrogen center have been measured. The observed processes were all described by a rate law of the same form: $R=k[\text{complex}][OH^-]$. The rate constants ($k$) were $2.4\times10^2\ M^{-1}s^{-1}$ for both $[Co(dien)_2]^{3+}$ [10] (at 35.0 °C) and $[Co(NH_3)_4(Me\text{-}en)]^{3+}$ [14] (at 34.3 °C), and $1.9\times10^4\ M^{-1}s^{-1}$ and $7.32\times10^4\ M^{-1}s^{-1}$ for $[Co(NH_3)_4(sar)]^{2+}$ [15] (at 30.0 °C) and $[Co(en)_2(sar)]^{2+}$ [16] (at 30.0 °C), respectively. Therefore, for the present *mer* complexes, which have not yet been optically resolved, the rates of inversion can be expected to be sufficiently faster than the rate of *u-fac*→*mer* isomerization.

Table 3. The rate constants for the CD loss of the optically active *u-fac* isomers of the $[Co(ida)(mida)]^-$ and $[Co(ida)_2]^-$ complexes in basic aqueous solutions at 30.0 °C

Complex	pH	k'_{CD} / s^{-1}	k_{CD} / $M^{-1}s^{-1}$
$[Co(ida)(mida)]^-$	8.11	1.90×10^{-4}	1.00×10^2
	9.46	4.55×10^{-3}	1.07×10^2
	10.05	1.60×10^{-2}	0.97×10^2
$[Co(ida)_2]^-$	8.15	1.89×10^{-5}	9.11
	9.76	7.61×10^{-4}	9.01
	10.05	1.53×10^{-3}	9.28

The second-order rate constant, k_{CD}, represents $k'_{CD}/[OH^-]$.

Mechanism of Isomerization Reactions. As shown in Table 2, the rate constants of the *u-fac*→*mer* change for $[Co(ida)_2]^-$ are much different from those for $[Co(ida)(mida)]^-$. The equilibrium distributions of the geometrical isomers in both the $[Co(ida)(mida)]^-$ and $[Co(ida)_2]^-$ systems are as follows (at 30 °C):

	u-fac(%)	*mer*(%)	*s-fac*(%)
$[Co(ida)(mida)]^-$	4.1	1.2	94.7
$[Co(ida)_2]^-$	29.0	0.5	70.5

These results indicate that the *u-fac* isomer in the $[Co(ida)(mida)]^-$ system is less stable than the *u-fac* isomer in the $[Co(ida)_2]^-$ system. This fact may be explained by means of the "steric effect" of the N-CH$_3$ group in the mida ligand. Through the examination of the molecular model for *u-fac*-$[Co(ida)(mida)]^-$, we can find the existence of steric repulsion between the N-CH$_3$ group of the mida ligand and the methylene group of the ida ligand. This is also supported by the ^{13}C-NMR data, in which the signals of the two α-carbons in the ida ring appear as more greatly separated doublet peaks in *u-fac*-$[Co(ida)(mida)]^-$ (Δ=2.21 ppm) than in *u-fac*-$[Co(ida)_2]^-$ (Δ=1.61 ppm).[12] The difference (Δ) in the chemical shift between the two acetate rings of an ida ligand is probably related to the difference in inter-ligand steric repulsion. The equilibrium distribution described above also shows that both the ida and mida ligands are liable to adopt the facial structure rather than the meridional one. The distribution value (29.0%) of *u-fac*-$[Co(ida)_2]^-$ is in fair agreement with that (28%) reported by Cooke.[11]

That no other species except for three geometrical isomers were detected in the isomerization reaction of the $[Co(ida)(mida)]^-$ system suggests that the ligand dissociation is not involved in the reaction; if such dissociation were involved, the reaction should provide disproportionation and/or hydrolysis products. Thus, the isomerization must involve only the intramolecular pathway. We can consider two possibilities for the intramolecular rearrangement: twist proceeding through the trigonal-prismatic transition state and bond-rupture forming a five-coordinate intermediate. (Rearrangement occurs in this intermediate and is followed by the recoordination of the $-COO^-$ group.) The *mer*⇌*s-fac* change in Scheme (2) can be sufficiently explained in terms of only the bond-rupture mechanism, whereas the *mer*⇌*u-fac* change may be described by the mechanisms of both bond-rupture and twist. The activation energies (E_a) for each process in Scheme (2) were obtained using the Arrhenius plots of the second-order rate constants in Table 2; the activation parameters calculated are given in Table 4. These

Table 4. The activation parameters for the base-catalyzed isomerization of the [Co(ida)(mida)]$^-$ and [Co(ida)$_2$]$^-$ complexes at 30 °C

	ΔH^* / kJ mol^{-1}	ΔS^* / J K^{-1} mol^{-1}
[Co(ida)(mida)]$^-$		
mer→*u-fac*	69.7±2.9	35.1± 9.7
u-fac→*mer*	75.0±3.2	42.0±10.7
mer→*s-fac*	69.5±2.0	4.0± 6.4
s-fac→*mer*	77.5±2.8	−6.9± 9.2
[Co(ida)$_2$]$^-$		
mer→*u-fac*	73.3±1.6	45.0± 5.4
u-fac→*mer*	73.3±1.7	11.6± 5.8
mer→*s-fac*	91.3±3.7	82.9±12.3
s-fac→*mer*	99.2±3.6	68.5±11.2

results do not offer any conclusive idea for determining the mechanism of the *mer*⇌*u-fac* change.

Cooke *et al.* have reported the base-catalyzed racemization of [Co(edta)]$^-$, which does not have protons on nitrogen atoms, and proposed a twist mechanism, the transient intermediate of which is a seven-coordinate species with the OH$^-$ group.[17] Also in the [Co(mida)$_2$]$^-$ system, which does not have protons on nitrogens, the *s-fac* and *mer* isomers were not isomerized; moreover, the optically active *mer* isomer was not racemized under the conditions of the present experiment. Therefore, for the present complexes with acidic secondary amine sites (ida), the base catalysis of the intramolecular isomerization pathway is more satisfactorily accounted for in terms of a rearrangement process which might proceed through the conjugate base species. The difference in activation energy between [Co(edta)]$^-$ (E_a=136.7 kJ mol^{-1}) and the present complexes may be connected with the difference in reaction mechanism between the two systems. Deprotonation seems to facilitate (1) some possibilities of nitrogen-to-cobalt pπ–dπ bonding (π stabilization) and (2) the adjustment of the bond angles at secondary amine sites which necessarily accompanies stereo change. All the experimental data for the present systems can be explained by the transient five-coordinated conjugate-base intermediate formed by bond-rupture, even though the possibility of twist mechanism should also be considered for the *u-fac*⇌*mer* change.

References

1) Abbreviations used: dien, diethylenetriamine; ida, iminodiacetate dianion; mdien, *N*,*N*-bis(2-aminoethyl)-methylamine; mida, *N*-methyliminodiacetate dianion; eida, *N*-ethyliminodiacetate dianion.

2) J. I. Legg and D. W. Cooke, *Inorg. Chem.*, **5**, 594 (1966).

3) F. R. Keene, G. H. Searle, Y. Yoshikawa, A. Imai, and K. Yamasaki, *J. Chem. Soc., Chem. Commun.*, **1970**, 784.

4) M. Kojima, M. Iwagaki, Y. Yoshikawa, and J. Fujita, *Bull. Chem. Soc. Jpn.*, **50**, 3216 (1977).

5) N. Koine, T. Tanigaki, J. Hidaka, and Y. Shimura, presented at the 28th Symposium on Coordination Chemistry, Matsuyama, Japan, October, 1978.

6) T. Ama, H. Kawaguchi, and T. Yasui, *Chem. Lett.*, **1981**, 323.

7) Y. Kushi, T. Ideno, T. Yasui, and H. Yoneda, *Bull. Chem. Soc. Jpn.*, **56**, 2845 (1983).

8) K. Okamoto, J. Hidaka, and Y. Shimura, *Bull. Chem. Soc. Jpn.*, **44**, 1601 (1971); *ibid.*, **48**, 2456 (1975); K. D. Gailey, K. Igi, and B. E. Douglas, *J. Coord. Chem.*, **5**, 171 (1976); Y. Yoshikawa, A. Kondo, and K. Yamasaki, *Inorg. Nucl. Chem. Lett.*, **12**, 351 (1976); K. Yamanari, J. Hidaka, and Y. Shimura, *Bull. Chem. Soc. Jpn.*, **50**, 2643 (1977); K. Okamoto, K. Wakayama, M. Ohmasa, and J. Hidaka, *Chem. Lett.*, **1981**, 453.

9) G. H. Searle, F. R. Keene, and S. T. Lincoln, *Inorg. Chem.*, **17**, 2362 (1978).

10) G. H. Searle and F. R. Keene, *Inorg. Chem.*, **11**, 1006 (1972).

11) D. W. Cooke, *Inorg. Chem.*, **5**, 1141 (1966).

12) T. Yasui, H. Kawaguchi, N. Koine, and T. Ama, *Bull. Chem. Soc. Jpn.*, **56**, 127 (1983).

13) N. Koine, T. Tanigaki, J. Hidaka, and Y. Shimura, *Chem. Lett.*, **1980**, 871.

14) D. A. Buckingham, L. G. Marzilli, and A. M. Sargeson, *J. Am. Chem. Soc.*, **89**, 825 (1967).

15) B. Halpern, A. M. Sargeson, and K. R. Turnbull, *J. Am. Chem. Soc.*, **88**, 4630 (1966).

16) M. Fujita, Y. Yoshikawa, and H. Yamatera, *Bull. Chem. Soc. Jpn.*, **50**, 3209 (1977).

17) D. W. Cooke, Y. A. Im, and D. H. Busch, *Inorg. Chem.*, **1**, 13 (1962).

Studies on the Inelastic Electron Tunneling Spectroscopy of *o*-Hydroxy-, *o*-Amino-, and *o*-Mercaptobenzoic Acid on Aluminium Oxide

Hideaki MONJUSHIRO,* Katsuo MURATA, and Shigero IKEDA
Department of Chemistry, Faculty of Science, Osaka University, Toyonaka, Osaka 560
(Received February 27, 1984)

Inelastic electron tunneling (IET) spectra were obtained for *o*-hydroxybenzoic acid (OHBA), *o*-aminobenzoic acid (OABA) and *o*-mercaptobenzoic acid (OMBA) adsorbed on aluminium oxide (AlO_x) grown on aluminium film and were analyzed by referring IR results. OHBA is adsorbed on AlO_x with both two functional groups, carboxyl and hydroxyl radicals. In the case of OABA, the adsorption occurs mainly with carboxyl group and the interaction between amino group and AlO_x is rather weak. Mercapto group of OMBA forms two kinds of hydrogen bonding, and a dissociated species on AlO_x. These results indicate that the surface of AlO_x used in this study is highly hydrated and hydroxyl groups on the oxide are reactive with the proton donating sites of the chemical species. IET spectra of *o*-fluoro- and *o*-chlorobenzoic acid were also observed for comparison.

Inelastic electron tunneling spectroscopy (IETS) is a kind of energy loss electron spectroscopy. The principle of IETS is based on the interaction between tunneling electrons and molecules on the interface of an insulating oxide layer and the metal. An excitation mode of a molecule is obtained as a function of energy of tunneling electrons. With respect to the molecular vibrations, both infrared and Raman active modes can be observed in IETS. The details of the principle, techniques and applications of IETS have been well reviewed by several authors.[1-3] Since this spectroscopy is very sensitive, vibrational spectra of molecules adsorbed on the insulating oxide layer with submonolayer coverage could be observed.[4] Therefore IETS is applicable to the state of arts analysis for trace amounts of chemical species. One should note in this case that chemical species containing various functional groups interact with the oxidized aluminium insulating surface, leading to the partial modification of the vibrational spectra of the active sites of a free molecule. And these studies are also helpful to understand the surface property such as acidity and basicity of aluminium oxide grown on aluminium metal.

This paper presents IETS studies on the molecules of bifunctional benzene derivatives: *o*-hydroxy-, *o*-amino-, and *o*-mercaptobenzoic acid on aluminium oxide grown on aluminium film. These compounds possess two different functional groups in single molecule. Comparative analysis on the difference of molecular vibrations between IETS and IR or Raman spectra was carried out to elucidate the adsorbed structure of the proposed compounds and to analyze the reactivity of the functional groups. The study was also attempted to understand the property of the aluminium oxide utilized for IETS measurement.

Experimental

Preparation of Tunneling Junction. Tunneling junctions of Al-Al oxide-Pb sandwich structure were prepared in a specially designed home-made vacuum chamber for this study as shown in Fig. 1. The chamber was evacuated with oil diffusion pump through liquid N_2 trap as low pressure as 2×10^{-5} Pa. It consists of two rooms, an evaporation room for the preparation of metal electrodes and a sample loading room where oxidation of aluminium electrode surface and sample loading are carried out. The entire process of junction preparation was accomplished in this chamber as follows. First, aluminium was evaporated onto a thoroughly cleaned glass slide under a pressure of 5×10^{-4} Pa or below. The oxidation of aluminium film was carried out by exposing it to oxygen gas saturated with water vapor for 5 min. And then 4 μl of sample solution was dropped on the oxide. During the loading procedure, the pressure of the evaporation room was maintained below 1×10^{-3} Pa. This enabled rapid performance of next evaporation process. Lead was evaporated finally to make film strips across the aluminium strip. Loaded junctions with a resistance of 40 to 1000 ohm at room temperature with 1 mm×1 mm junction area were available for measurements of IET spectra.

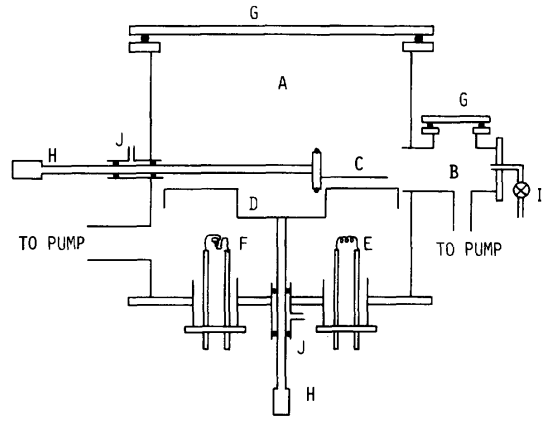

Fig. 1. Sample preparation chamber.
A: Evaporation room, B: sample loading room, C: substrate, D: mask, E : W spiral for Al evaporation, F : W basket for Pb evaporation, G: glass window, H: motion feedthrough, I : O_2 introducing cock, J: differential pumping.

Measurement of IET Spectra. IET spectra were measured by the device with circuit similar to that of Adler and Jackson[5] as shown in Fig. 2. The bias voltage (20 to 500 mV d.c.) across the junction was applied by low frequency function generator, and an a.c. modulation signal of 1.2 kHz was superimposed on the d.c. bias. The second harmonics of the modulation frequency, being proportional to d^2V/dI^2, was detected with a lock-in amplifier (NF model LI-574). Tunnel-

ing spectra were taken at liquid helium temperature 4.2 K, in a standard double glass liquid helium cryostat to obtain sufficient resolution.[1-3] Peak positions were read with digital voltmeter and the values were converted from millivolt to wavenumber with correlation of 1 mV=8.065 cm^{-1} and then a correction of $-7\ cm^{-1}$ was made to cancel out the superconducting energy gap of lead electrode. The observed line-width of the spectral peaks at half maximum was *ca.* 20 cm^{-1} with modulation voltage of 0.6 mV rms.

Chemicals. Chemicals used were obtained from Wako Pure Chemical Ind. or Nakarai Chemical Co. They were recrystallized before use. Acetone was used as solvent for sample loading.

Results and Discussion

IET Background Spectra. There appear invariably some peaks which contribute to insulating aluminium oxide and metal electrodes in IET spectra.[6] And there is a fear of observing additional peaks due to solvent molecule. In order to subtract these peaks, IET spectrum of the junction treated with acetone was compared with that obtained from the junction with sample solution. Figure 3 shows the IET spectrum obtained from the junction treated with acetone. The spectral feature is similar to that of unloaded junction and peaks due to adsorbed acetone are not present in the spectrum. Thus it is clear that acetone has no influence on the IET spectrum.

Although the surface property of aluminium oxide could be evaluated from the surface hydroxyl stretching frequency,[7] the observed hydroxyl stretching peak position in IET spectrum is thought to be shifted to lower wavenumber from substantial value due to image dipole effect of top lead electrode,[8,9] and the exact magnitude of the shift could not be estimated. However, the oxide used in this study is considered to be hydrated surface, because oxygen containing water vapor was employed to oxidize the aluminium surface at room temperature.[7]

IET Spectra of o-Substituted Benzoic Acids. The IET spectra of *o*-fluorobenzoic acid (OFBA), *o*-hydroxybenzoic acid (OHBA), and *o*-aminobenzoic acid (OABA) adsorbed on aluminium oxide are shown in Fig. 4. Figure 5 shows the IET spectra of *o*-chlorobenzoic acid (OCBA) and *o*-mercaptobenzoic acid (OMBA) adsorbed on aluminium oxide.

These spectra were obtained from junction loaded from 1 mg/cm^3 acetone solution. The observed spectral

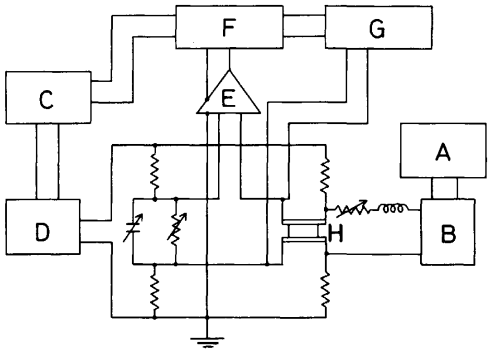

Fig. 2. Block diagram of IETS measurement circuit. A: Low frequency function generator, B : d.c. voltage supply, C: oscillator, D: attenuator, E: pre-amplifier, F: lock-in amplifier, G: X-Y recorder, H: tunnel junction.

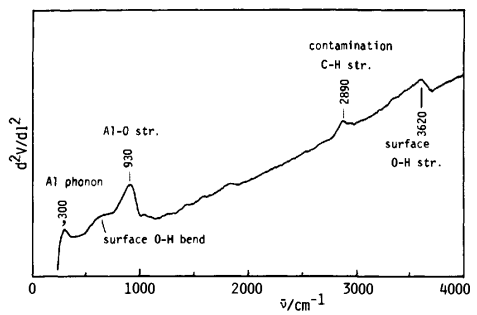

Fig. 3. IET background spectrum of Al–Al oxide–Pb junction.

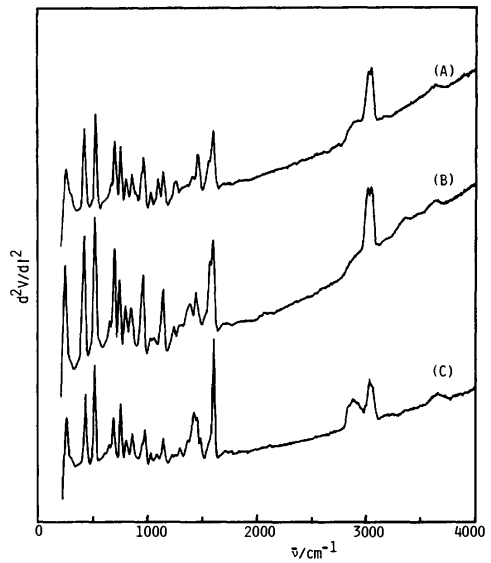

Fig. 4. IET spectra of (A): *o*-hydroxybenzoic acid, (B): *o*-aminobenzoic acid, and (C): *o*-fluorobenzoic acid adsorbed on aluminium oxide. Modulation voltage= 1.2 mV rms.

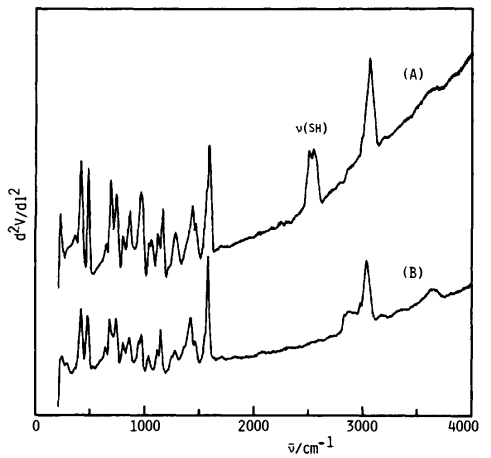

Fig. 5. IET spectra of (A): *o*-mercaptobenzoic acid and (B): *o*-chlorobenzoic acid adsorbed on aluminium oxide. Modulation voltage=1.2 mV rms.

range is from 230 to 4000 cm^{-1}. In these spectra each peak position is reproducible within experimental error of ±0.5 mV (±4 cm^{-1}). The observed values (peak positions and relative intensity) and their mode assignments are listed in Tables 1 and 2. The values of IR data (*o*-fluoro- and *o*-chlorobenzoate) are also listed for comparison. Each peak was assigned by referring to the IR and Raman spectra of *o*-disubstituted benzenes,[10,11] *o*-substituted benzoic acids and their alkali metal salts.[12]

Benzene Ring Modes: The vibrational modes of these compounds can be classified into two groups, namely the vibrational modes of benzene ring system and that of substituent groups. Since *o*-substituted benzoic acids are assigned to the C_s point group, the ring system would have 30 normal vibrations comprised of 21 a′ modes (in-plane modes) and 9 a″ modes (out of plane modes) and all modes are both IR and Raman active. Peaks observed in IET spectra of the proposed compounds could be easily identified with the corresponding normal vibrations of the related *o*-disubstituted benzene ring system. Of the expected four aromatic CH stretching modes, two or three peaks are found at a region of 3000 cm^{-1}, and the peak positions

Table 1. IET spectral data of *o*-fluoro-, *o*-hydroxy- and *o*-aminobenzoic acid on aluminium oxide

Symmetry class	Peak position[a]/cm^{-1}				Approximate description[b]
	o-F		*o*-OH	*o*-NH_2	
	IR[c]	IETS	IETS	IETS	
				3480 w-b	$\nu_a(NH_2)$
				3350 w-b	$\nu_s(NH_2)$
	3076 m	3058 m	3050 m	3062 s	ν(CH)
	3036 m	3034 m	3023 s	3022 s	
		3001 sh			
	1617 s	1612 vs	1606 s	1612 s	ν(CC) 8a
	1569 s		1575 m-b	1581 s-b	ν(CC) 8b
		1579 sh			
	1600 vs		1560 sh	1570 sh	ν_a(COO)
	1485 s	1491 w	1477 sh	1486 w	ν(CC) 19b
	1452 s	1458 m	1461 s	1458 m	ν(CC) 19a
	1410 vs	1430 m	1410 w-b	1405 w-b	ν_s(COO)
	1309 w	1301 w	1324 w-b	1316 w-b	Kekulé 14
a′	1264 w	1262 w	1258 w	1251 w	β(CH) 3
	1222 m	1225 w-b	1201 sh	1210 sh	X-sens.
	1163 w			1156 s	β(CH) 9a
		1149 m	1151 m-b		
	1144 w			1130 sh	X-sens.
	1099 m	1100 w	1099 w	1074 w	X-sens.
	1038 m	1033 w	1033 w	1037 w	β(CH) 18b
	861 s	868 w[d]	862 m[d]	860 m[d]	X-sens.
	811 m	808 w[d]	809 m[d]	813 m[d]	X-sens.
	660 m	652 w	671 w	666 w	X-sens.
	569 m	619 w	595 w	564 w	ρ(COO)
	544 w	522 vs[d]	536 vs[d]	531 vs[d]	X-sens.
	403 m	412 sh			X-sens.
	975 w	982 m	971 s	972 s	γ(CH) 5
	950 w	956 w	957 sh	955 sh	γ(CH) 17b
	(861)	868 w[d]	862 m[d]	860 m[d]	γ(CH) 10b
	800 s	808 w[d]	809 m[d]	813 m[d]	γ(COO)
a″	746 vs	758 s	761 s	755 m	γ(CH) 10a
	693 m	693 m	708 s	708 s	ϕ(CC) 4
	521 m	522 vs[d]	536 vs[d]	531 vs[d]	ϕ(CC) 16a
	443 m	437 s	429 vs	432 vs	ϕ(CC) 16b
		262 m	260 m-b	258 s-b	?
			895 w		?

a) Peak positions corrected as in the text, relative intensity also shown; s=strong, m=medium, w=weak, v=very, sh=shoulder, b=broad. b) Description of the modes based on Ref. 11; ν=stretching, ν_a=antisymmetric stretching, ν_s=symmetric stretching, β,ρ=in-plane deformation, γ,ϕ=out of plane deformation, X-sens.=associated with motion of substituent group. c) The IR data listed are of sodium *o*-fluorobenzoate, Ref. 12. d) Wavenumber used twice.

are down-shifted from IR data of the corresponding compounds, respectively. This is presumably due to the effect of top electrode of lead.[9] At the energy region below 1620 cm^{-1}, where the peak shift is negligible, 23 peaks are observed for OCBA, 22 for OMBA, 21 for OFBA and OABA and 20 for OHBA comparing to the expected 26 peaks for normal vibrational modes. Taking into account the coincidence of the wavenumber observed and the number of the peaks below IET spectral range, almost all modes of benzene ring system are observed in IET spectra. The close agreement of the frequency of ring modes between the IETS and IR data indicates that each benzene ring of these compounds has no strong interaction with aluminium oxide surface in chemisorbed structure. On the other hand, the vibrations of substituent functional groups observed in IET spectra show significant difference from those of parent molecules. This fact implies that substituent functional groups to be deformed by junction formation and interaction with aluminium oxide surface could be expected. The bond formation and interaction between the functional groups of sample molecules and aluminium oxide will be discussed below for each compounds.

Table 2. IET spectral data of o-chloro- and o-mercaptobenzoic acid on aluminium oxide

Symmetry class	Peak position[a]/cm^{-1}			Approximate description[b]
	o-Cl		o-SH	
	IR[c]	IETS	IETS	
a'			3079 sh	
	3075 m	3040 m	3038 vs	ν(CH)
	3050 m	2980 m	3009 sh	
			2540 m-b	ν(SH)
			2490[e]	
	1600 s	1592 vs	1587 vs	ν(CC) 8a
	1559 s			ν(CC) 8b
		1567 sh	1560 m-b	
	1589 vs			ν_a(COO)
	1472 s	1475 w	1466 w	ν(CC) 19b
	1431 s		1433 s-b	ν(CC) 19a
		1431 s-b		
	1400 vs		1400 sh	ν_s(COO)
	1313 w	1288 w	1287 w-b	Kekulé 14
	1260 w	1262 w	1270 w	β(CH) 3
	1162 w			X-sens.
		1158 m	1159 s	
	1152 w			β(CH) 9a
	1124 m	1125 w	1122 m	X-sens.
	1050 s		1066 m	X-sens.
		1047 w-b		
	1042 m		1041 w	β(CH) 18b
	842 s	858 sh	864 m[d]	X-sens.
	721 s	723 w	745 m[d]	X-sens.
	647 m	650 w	655 w	X-sens.
	552 m	529 w	612 w	ρ(COO)
	453 m	430 s[d]	427 vs[d]	X-sens.
a''	975 w	981 m	971 s	γ(CH) 5
	945 w	955 m	961 sh	γ(CH) 17b
	867 w	871 m	864 m[d]	γ(CH) 10b
	805 m	811 m	812 w	γ(COO)
	742 vs	751 s	745 m[d]	γ(CH) 10a
	693 m	690 s	695 s	ϕ(CC) 4
	490 w	486 s	494 vs	ϕ(CC) 16a
	408 w	430 s[d]	427 vs[d]	ϕ(CC) 16b
		367 w	364 w-b	?
		245 w-b	238 m-b	?
			911 vw	δ(CSH)

a) Peak positions corrected as in the text, relative intensity also shown; s=strong, m=medium, w=weak, v=very, sh=shoulder, b=broad. b) Description of the modes based on Ref. 11; ν=stretching, ν_a=antisymmetric stretching, ν_s=symmetric stretching, β,ρ,δ=in-plane deformation, γ,ϕ=out of plane deformation, X-sens.=associated with motion of substituent group. c) The IR data listed are of sodium o-chlorobenzoate, Ref. 12. d) Wavenumber used twice. e) Relative intensity of this peak shows sample to sample variation, see text.

o-Hydroxybenzoic Acid (OHBA): In the IET spectrum of OHBA chemisorbed on aluminium oxide, the most characteristic mode of carboxylic acid at *ca.* 1700 cm^{-1} corresponding to the C=O stretching vibration is absent. Instead, antisymmetric stretching mode of carboxylato group; ν_a(COO) is observed at 1560 cm^{-1} as a shoulder on the side of intense peak at 1575 cm^{-1} due to benzene ring skeletal stretching mode, and its symmetric stretching mode; ν_s(COO) appears at 1410 cm^{-1} as a broad peak. This indicates that OHBA is adsorbed on aluminium oxide as carboxylate similar to other carboxylic acids.[13,14]

Another characteristic feature of the IET spectrum of OHBA is that there appear no vibrational modes corresponding to hydroxyl group. Solid OHBA has its OH stretching band at 3240 cm^{-1} and in the case of alkali metal salts of OHBA, OH stretching band appears in the range of 2500 to 2900 cm^{-1} owing to the strong intramolecular hydrogen bonding with carboxylate ion.[15] In the IET spectrum, however, no peak due to OH stretching mode is observed in the 2500 to 3600 cm^{-1} region. In-plane bending mode of OH group expected to appear at *ca.* 1200 cm^{-1} is also missing in IET spectrum. A small shoulder at 1201 cm^{-1} in IET spectrum is assigned to substituent group sensitive mode of the ring system, because similar peaks are also observed in IET spectra of OFBA and OABA. These facts imply the formation of phenolate species on aluminium oxide surface in analogy to other phenols.[16] Then, two functional groups in the single molecule of OHBA might interact with aluminium oxide surface.

Two kinds of interaction mode would be presumed for the adsorption of OHBA on aluminium oxide surface. One would coordinate to a single aluminium atom with two active sites of a molecule to form a chelate ring, and the other is the coordination of each functional group to different aluminium atoms to form a bridge structure. If both functional groups coordinate to a single aluminium atom to form a surface chelate, the carboxylato group should have unidentate structure as shown in Fig. 6 (A). It is known that in

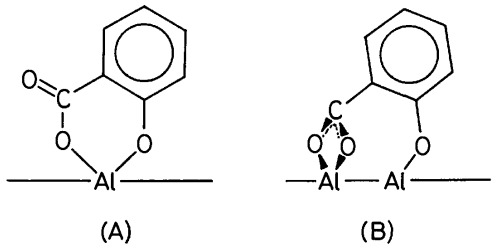

Fig. 6. Schematics of the chemisorption structure of *o*-hydroxybenzoic acid on aluminium oxide.
(A): Chelating structure, (B): bridging structure.

unidentate carboxylate, the wavenumber of ν(C=O) is higher than that of ν_a(COO$^-$) of free carboxylate ion and ν(C-O) is lower than that of ν_s(COO$^-$).[17] Peak positions for carboxylato stretching in IET spectrum of OHBA; ν_a(COO) at 1560 cm^{-1} and ν_s(COO) at 1410 cm^{-1} are in good agreement with IR data of *o*-hydroxybenzoate ion;[15,18,19] ν_a(COO$^-$) at 1546 cm^{-1} to 1593 cm^{-1} and ν_s(COO$^-$) at 1373 to 1410 cm^{-1}. Thus the carboxylato group of adsorbed OHBA is considered to be symmetrical structure like free ion and not unidentate structure. This suggests the adsorption of OHBA on aluminium oxide to form a bridge structure as shown in Fig. 6 (B).

o-Aminobenzoic Acid (OABA): Similar to the case of OHBA, in the IET spectrum of OABA, there observed no feature due to carboxyl group but carboxylato stretching modes appear at 1570 cm^{-1} and at 1405 cm^{-1}. Thus the adsorption of OABA with carboxyl group on aluminium oxide is evident to form surface carboxylate. Close similarity of those carboxylato stretching peak positions with those of OHBA indicates that surface carboxylate has symmetrical structure and chelation does not take place.

Most characteristic vibrational modes reflecting the nature of amino group is its stretching vibrations. In the case of OABA, free amino group gives symmetric and antisymmetric stretching modes in 3300 to 3500 cm^{-1} region,[20,21] amino group coordinated to metal ions such as Cu^{2+} exhibits two or three bands in 3100 to 3300 cm^{-1} region[22] and protonation of amino group would cause further down-shift of the bands. Figure 7 shows the expanded low-noise IET spectrum of OABA in the range of 2500 to 4000 cm^{-1}. Beside the peaks due to aromatic CH stretching modes at 3022 cm^{-1} and at 3062 cm^{-1} and surface OH stretching mode at *ca.* 3620 cm^{-1}, two broad and weak peaks are observed at 3350 cm^{-1} and 3480 cm^{-1}. These peaks could be assigned to symmetric and antisymmetric stretching modes of free amino group respectively. This fact implies that there are no strong interactions between amino group of OABA and aluminium oxide surface such as coordination to surface aluminium atom on the oxide or protonation by surface hydroxyl group observed for other amines by IETS.[23-25]

However, the both observed peaks corresponding to amino stretching vibrations are very broad (the linewidth at half maximum is at least 120 cm^{-1}). This suggests the existence of weak interaction between the amino group and the oxide surface. Formation of hydrogen bonding is most probable to explain the

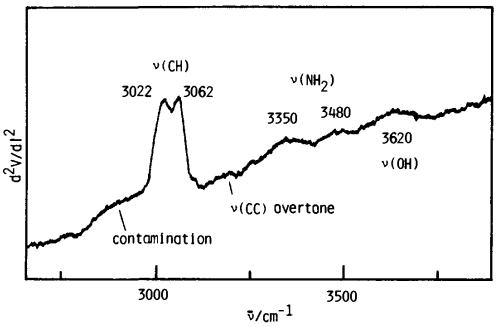

Fig. 7. Expanded IET spectrum of *o*-aminobenzoic acid adsorbed on aluminium oxide in the range of 2500 to 4000 cm^{-1}.

broadening of the amino stretching peaks. However, generally in IR spectra, hydrogen bonding causes the down-shift of corresponding stretching mode,[26] whereas IET spectrum shows no shift from free state frequency. This fact will not be explained by the simple hydrogen bonding assumption. Another modes of amino group expected to lie below 1650 cm^{-1} could not be assigned because of the complexity of the spectrum in this region. Thus further interpretations for the surface interactions between amino group and aluminium oxide surface is quite difficult in the present.

o-Mercaptobenzoic Acid (OMBA): In the IET spectrum of OMBA, there observed carboxylato stretching modes at *ca.* 1559 cm^{-1} and at 1400 cm^{-1}. Both peaks are considered to coincide with ring modes and accurate positions are not found from the spectrum. However, OMBA is considered to be adsorbed on aluminium oxide as carboxylate, because of missing of the carboxyl group vibrations. Although the IET spectrum of OMBA has been published by Hall and Hansma,[14] no data was given so far on the mercapto group frequency observed by IETS and no discussion has been done on the nature of mercapto group.

In IR spectroscopy, the free SH stretching modes of aromatic thiols generally appear near 2585 cm^{-1} and the steric and electronic effects have no influence on the SH stretching frequency.[27] In IET spectrum of OMBA, SH stretching modes appear at 2490 cm^{-1} and at 2540 cm^{-1}. The peak splitting indicates the presence of two kinds of species on the oxide. The down-shift of the peaks referred to IR data is to be due to either image dipole effect of top lead electrode[8,9] or hydrogen bonding of mercapto group. In the case of down-shift caused by top metal, the magnitude of the shift should be relate to the oscillating dipole moment strength of the mode. Whereas SH stretching mode of OMBA observed in IR spectrum is quite weak,[27] indicating a small oscillating dipole moment. Therefore the shift must be due not to the top metal effect, but to hydrogen bonding. And the both two SH stretching peaks in IET spectrum are broad on comparing with other peaks corresponding to the ring modes. This fact also supports the presence of hydrogen-bonded mercapto species on the oxide.

Hydrogen bonding of mercapto group of adsorbed OMBA could be classified into either of following three categories; (**I**) intermolecular hydrogen bonding, (**II**) intra-

molecular hydrogen bonding, and (**III**) hydrogen bonding with aluminium oxide surface. If the intermolecular hydrogen bonding(**I**) is presumed, the number of species(**I**) should be increase with increasing the surface concentration of OMBA. Consequently, the relative intensity of the peak corresponding to species(**I**) should increase. However, no correlation was found between the relative intensity of either peak at 2490 cm^{-1} or at 2540 cm^{-1} and the surface concentration of OMBA. Thus it is clear that species(**I**) is not present on the oxide.

OMBA in solid state or in solution is known to form intramolecular hydrogen bonding(**II**) between mercapto group and oxygen of carboxyl group. Mori *et al.* have studied the mercapto hydrogen bonding in solution by IR spectroscopy in detail.[27] They observed two bands in mercapto stretching wavenumber at 2558 cm^{-1} and at 2530 cm^{-1} in dilute carbon tetrachloride solution of OMBA, and assigned them to the mercapto species having hydrogen bonding with the ethoxyl and carbonyl oxygen atom, respectively. On the contrary, OMBA adsorbed on aluminium oxide forms carboxylate, and the two oxygen atoms of carboxylato group are considered to be equivalent character. Hence when the species(**II**) is formed on the oxide, only a single configuration must be allowed for OMBA and resulting in a single peak in IET spectrum. The peak position can be expected to appear at around the wavenumber between 2530 cm^{-1} and 2558 cm^{-1}. This assumption leads us to conclude the peak at 2540 cm^{-1} observed in IET spectrum to be due to the stretching mode of intramolecular hydrogen-bonding species(**II**).

The relative intensity of the peak at 2490 cm^{-1} varies by sample to sample. This variation indicates the high surface sensitivity of the interaction in nature. Thus the peak at 2490 cm^{-1} is considered to be due to mercapto group, which forms hydrogen bonding with oxide surface(**III**). Formation of hydrogen bonding between mercapto group and aluminium oxide surface has been already observed for methanethiol molecule by the use of IR spectroscopy.[28] The hydrogen-bonding species has its stretching mode at 2470 cm^{-1}. The peak position observed at 2490 cm^{-1} in IET spectrum of OMBA is close to this IR value. Therefore we assign the peak at 2490 cm^{-1} to be due to mercapto species(**III**).

In the course of the study on OMBA, we noticed that the intensity of the peak at 2490 cm^{-1} had a tendency to be stronger when the surface hydroxyl stretching peak appeared stronger in IET spectra. To make sure of this, water molecules were introduced into the complete junction by using infusion doping technique,[29] because the water infusion is expected to increase surface hydroxyl group on the oxide.

Figure 8 shows the expanded IET spectra of OMBA before(A) and after(B) infusion of water. By introducing water molecule into the junction, the peak at *ca.* 3620 cm^{-1} due to surface hydroxyl stretching mode and the peak at 2490 cm^{-1} due to mercapto species(**III**) are both intensified, although the intensities of other peaks remain unchanged. This result indicates that not only the number of surface hydroxyl group but that of mercapto group of struture(**III**) in the junction increase by water infusion. This phenomenon could be explained by assuming the presence of coordination species *via* sulfur atom to surface aluminium atom of the oxide before infusion of water. And this S-bonded species may react with water molecule introduced to form mercapto species(**III**). Consequently, there are three kinds of mercapto species on the aluminium oxide, namely intramolecular hydrogen-bonding species(**II**), species which forms hydrogen bonding with surface oxygen atom(**III**) and S-bonded species.

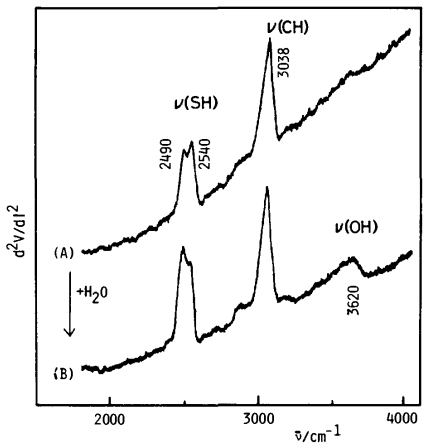

Fig. 8. Expanded IET spectrum of *o*-mercaptobenzoic acid (A): before and (B): after infusion of water.

Property of Aluminium Oxide Surface. The adsorbed feature of the proposed compounds may lead to a suggestion on the surface property of aluminium oxide grown on evaporated aluminium film. In IET spectra of *o*-substituted benzoic acids, it is found that the surface hydroxyl stretching intensity is less than that in back ground spectrum. This indicates the consumption of surface hydroxyl groups with the adsorption reaction of carboxyl group. A presumable reaction is that carboxyl group leaves proton and the proton reacts with surface hydroxyl group to form water. The water produced would be evacuated out during the junction preparation, since the vibrational modes of molecular water are absent in IET spectra. Similar surface reactions are considered to take place on the hydroxyl group of OHBA and partly on the mercapto group of OMBA with surface hydroxyl group.

As discussed above, OHBA is adsorbed on the oxide through both carboxyl and hydroxyl group to form bridge structure, and both functional groups are considered to react with surface hydroxyl groups. Therefore it is thought that there are many neighboring hydroxyl groups on the oxide used. In the case of OABA, amino group of ortho position does not coordinate to the oxidized aluminium despite the possible steric configuration. Then there must be few or no exposed aluminium ion (Lewis acid site)[30] around the carboxylate adsorption site on the oxide.

Consequently, we conclude that the surface of aluminium oxide grown by wet oxygen is highly hydrated and has many neighboring surface hydroxyl groups. The surface hydroxyl groups tend to react with Brønsted acids such as carboxyl group to form water, in other words, the oxide surface behaves as Brønsted base with respect to the proposed compounds.

Conclusion

The IETS of three kinds of *o*-substituted benzoic acid with functional groups, -OH, $-NH_2$, and -SH were studied. All compounds are adsorbed on aluminium oxide as benzoate. The second substituent functional groups show various types of interaction with the oxide surface.

The type of the adsorption reaction of these functional groups on the oxide of IET junction is specifically defined to be acid-base reaction. In this case, the oxide surface behaves as base (OH donor) and the functional groups behave as acid (H donor). The reactivity of the functional groups is the order of

$$-COOH,\ -OH > -SH \gg -NH_2.$$

The results show that the character of aluminium oxide surface utilized for IETS is quite different from that of γ-alumina, which is known to have acidic property.

On the other hand, these surface reactions affect negatively for the utilization of IETS to the identification of unknown chemical species. Further experiences to pile up more IETS data for various compounds are needed as well as the more precise analysis for the characterization of aluminium oxide of IET junction.

References

1) P. K. Hansma, *Phys. Rep.*, **30**, 145 (1977).
2) T. Wolfram (ed.), "Inelastic Electron Tunneling Spectroscopy" Springer Series in Solid-State Sciences, Vol. 4, Springer-Verlag (1978).
3) S. Ewert, *Appl. Phys. A.*, **26**, 63 (1981).
4) J. D. Langan and P. K. Hansma, *Surf. Sci.*, **52**, 211 (1975).
5) J. G. Adler and J. E. Jackson, *Rev. Sci. Instrum.*, **37**, 1049 (1966).
6) W. M. Bowser and W. H. Weinberg, *Surf. Sci.*, **64**, 377 (1977).
7) J. B. Peri, *J. Phys. Chem.*, **69**, 211 (1965).
8) J. R. Kirtley and P. K. Hansma, *Phys. Rev. B.*, **12**, 531 (1975).
9) J. R. Kirtley and P. K. Hansma, *Phys. Rev. B.*, **13**, 2910 (1976).
10) A. R. Katritzky and R. A. Jones, *J. Chem. Soc.*, **1959**, 3670.
11) J. H. S. Green, *Spectrochim. Acta, Part A.*, **26**, 1913 (1970).
12) J. H. S. Green, *Spectrochim. Acta Part A.*, **33**, 575 (1977).
13) C. S. Korman and R. V. Coleman, *Phys. Rev. B.*, **15**, 1877 (1977).
14) J. T. Hall and P. K. Hansma, *Surf. Sci.*, **76**, 61 (1978).
15) J. H. S. Green, W. Kynaston, and A. S. Lindsey, *Spectrochim. Acta*, **17**, 486 (1961).
16) I. W. N. McMorris, N. M. D. Brown, and D. G. Walmsley, *J. Chem. Phys.*, **66**, 3952 (1977).
17) K. Nakamoto, "Infrared and Raman spectra of inorganic and coordination compounds," Third ed, A Wiley-Interscience Publication, John Wiley and Sons. (1978) Part III.
18) B. J. Lindberg, *Acta Chem. Scand.*, **22**, 571 (1968).
19) G. E. Dunn and R. S. McDonald, *Can. J. Chem.*, **47**, 4577 (1969).
20) T. Inomata and T. Moriwaki, *Nippon Kagaku Zasshi*, **91**, 819 (1970).
21) A. Theoret, *Spectrochim. Acta, Part A.*, **27**, 11 (1971).
22) A. G. Hill and C. Curran, *J. Phys. Chem.*, **64**, 1519 (1960).
23) N. M. D. Brown, R. B. Floyd, W. J. Nelson, and D. G. Walmsley, *J. Chem. Soc., Faraday Trans. 1*, **76**, 2335 (1980).
24) S. D. Williams and K. W. Hipps, *J. Catal.*, **78**, 96 (1982).
25) N. M. D. Brown, R. J. Turner, and D. G. Walmsley, *J. Mol. Struct.*, **79**, 163 (1982).
26) S. N. Vinogradov and R. H. Linnell, "Hydrogen Bonding," Van Norstrand Reinhold Co. (1971), Chap. 3, pp. 47—64.
27) N. Mori, S. Kaido, K. Suzuki, M. Nakamura, and Y. Tsuzuki, *Bull. Chem. Soc. Jpn.*, **44**, 1858 (1971).
28) O. Saur, T. Chevreau, J. Lamotte, J. Travert, and J. C. Lavalley, *J. Chem. Soc., Faraday Trans. 1*, **77**, 427 (1981).
29) R. C. Jaklevic and M. R. Gaerttner, *Appl. Phys. Lett.*, **30**, 646 (1977).
30) K. Tanabe, "Solid Acids and Bases," Kodansha, Tokyo Academic Press, New York, (1970), Chap. 4.

 © 1984 The Chemical Society of Japan Bull. Chem. Soc. Jpn., 57, 2435—2439 (1984)

Synthesis and Cation-Complexing Ability of Oxo Crown Ethers Containing a Ferrocene Nucleus

Taeko IZUMI,* Takeshi TEZUKA, Sachiko YUSA, and Akira KASAHARA
Department of Applied Chemistry, Faculty of Engineering, Yamagata University, Yonezawa 992
(Received July 20, 1983)

Fifteen new oxo crown ethers having a ferrocene unit as an integral part of the ring member are reported. These oxo crown ethers were synthesized by the reaction of 1,1′-bis(chloroformyl)ferrocene with oligoethylene glycols or heterocyclic dialcohol compounds such as 2,6-bis(hydroxymethyl)pyridine by the high dilution method. Complexing ability of these compounds with alkali, alkaline earth, and transition metal cations was measured by the solvent extraction method.

Since Pedersen's pioneering work,[1] the synthesis of a great number of macrocyclic polyethers has been reported. Among them, several groups of workers[2] have described the preparation of a new type of crown ethers containing a ferrocene unit as a ring member, in which iron atom plays the role of a coordinating atom. In connection with crown ethers, attention has recently been paid to the oxo crown compounds, because some of them showed a different complexing tendency towards cations from normal crown ethers. In this report we describe the synthesis and study the complexing behavior of these ferrocenophanes with alkali, alkaline earth and transition metal picrates.

Results and Discussion

Synthesis. A large number of oxo crown compounds have been synthesized, and their properties were investigated by Bradshaw,[3-11] Vögtle,[12-14] and Kellogg.[15-18] Most of these compounds have been prepared through either the reaction between diacids and dihalides (ditosylates) of oligoethylene glycols (**1**), or the reaction between diacyl chlorides and oligoethylene glycols. Oepen and Vögtle[2a] reported that in the presence of pyridine the reaction between 1,1′-bis(chloroformyl)ferrocene (**2**) and **1** (n=1, 2, 3) in benzene led to the formation of oxo crown ethers (**3**) (n=1, 2, 3) in 29—36% yields, but no detailed spectral data were published (elemental analyses only), and 1,1′-ferrocenediyl dialcohol derivative (**4**) was not mentioned as the coproduct. They also did not refer to the formation of binuclear ferrocenophanes (**5**). In the present study, the syntheses of **3** and **5** were carried out without bases by the modification of Bradshaw's method.[9] For example, the reaction of **1** (n=1) with **2** in dry benzene led to the formation of 1,1′-bis(5-hydroxy-3-oxapentyloxycarbonyl)ferrocene (**4b**) as the main product, and 2,5,8-trioxa[9](1,1′)ferrocenophane-1,9-dione (**3b**) as the minor one. Furthermore, the reaction of **4b** with **2** afforded 2,5,8,22,25,28-hexaoxa[9.9](1,1′)-ferrocenophane-1,9,21,29-tetrone (**5b**). The results of the reactions are summarized in Tables 1 and 2.

The oxo crown ethers containing both a heteroatom such as N, O, or S and the ferrocene unit were synthesized in order to examine the influence of the electron donating heteroatoms on complexing ability of the cation. For example, the reaction of **2** with diols **6** such as 2,6-bis(hydroxymethyl)pyridine (**6a**) was carried out in the presence of the base and resulted in the formation of mononuclear ferrocenophane (**7**) and 1,1′-

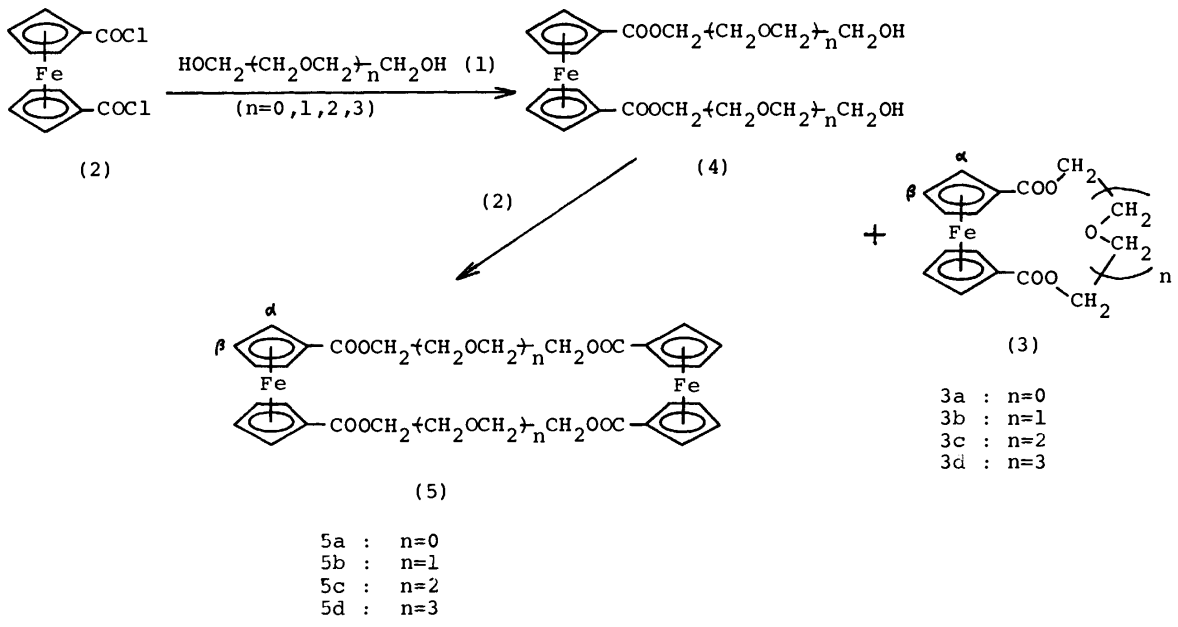

Fig. 1.

ferrocenediyl dialcohol derivative (**9**) (main product). Furthermore, the reaction of diol **9** with **2** led to the formation of **8**, but different results were obtained in the following two cases: 1,1′-Ferrocenediyl dialcohol (**9b**) was not obtained in the reaction of 2,5-bis(hydroxymethyl)furan (**6b**) with **2**, whereas, mononuclear ferrocenophane (**7b**) and binuclear ferrocenophane (**8b**) formed by the one-pot reaction. In addition, the reaction of 2,5-bis(hydroxymethyl)benzene (**6d**) with **2** gave mononuclear ferrocenophane (**7d**) and binuclear ferrocenophane (**8d**) together with 1,1′-ferrocenediyl dialcohol (**9d**). These results indicate that in most cases binuclear ferrocenophane is probably formed by the competitive reaction in the first reaction step, although the yield is extremely low ex-

Table 1. Reaction of 1,1′-bis(chloroformyl)ferrocene with oligoethylene glycol

Oligoethylene glycol	Product	Yield/%	Mp θ_m/°C (lit,)	Color
Ethyleoe glycol $n=0$	**3a**	28	187—188	red
	4a	51	oil	red
Diethylene glycol $n=1$	**3b**	26	134—135 (85)[2a]	red orange
	4b	59	oil	red
Triethylene glycol $n=2$	**3c**	23	129—130 (127)[2a]	orange
	4c	53	oil	red
Tetraethylene glycol $n=3$	**3d**	22	78—79 (60—62)[2a]	orange
	4d	55	oil	red

Table 2. Reaction of 1,1′-bis(chloroformyl)ferrocene with ferrocenyl dialcohol (**4a—d**)

Ferrocenyl dialcohol	Product	Yield/%	Mp θ_m/°C	Color
4a	**5a**	23	245—246	red orange
4b	**5b**	34	121—122	orange
4c	**5c**	36	106—107	yellow orange
4d	**5d**	35	oil	red

Table 3. Reaction of 1,1′-bis(chloroformyl)ferrocene with dialcohol (**6a—e**)

Dialcohol	Product	Yield/%	Mp θ_m/°C	Color
6a	**7a**	9	240—242 (decomp)	red
	9a	19	oil	red
6b	**7b**	1	145—146	orange
	8b	9	260—262 (decomp)	yellow
6c	**7c**	2	214—215	orange
	9c	49	123—124	orange
6d	**7d**	2	208—209	red
	8d	4	223—224	yellow
	9d	58	oil	red
6e	**7e**	2	134—135	orange
	9e	67	oil	red

Table 4. Reaction of 1,1′-bis(chloroformyl)ferrocene with ferrocenediyl dialcohol (**9a,c,d,e**)

Ferrocenediyl dialcohol	Product	Yield/%	Mp θ_m/°C	Color
9a	**8a**	5	231—232	yellow
9c	**8c**	5	245—246 (decomp)	yellow
9d	**8d**	39	223—224	yellow
9e	**8e**	5	214—215 (decomp)	yellow

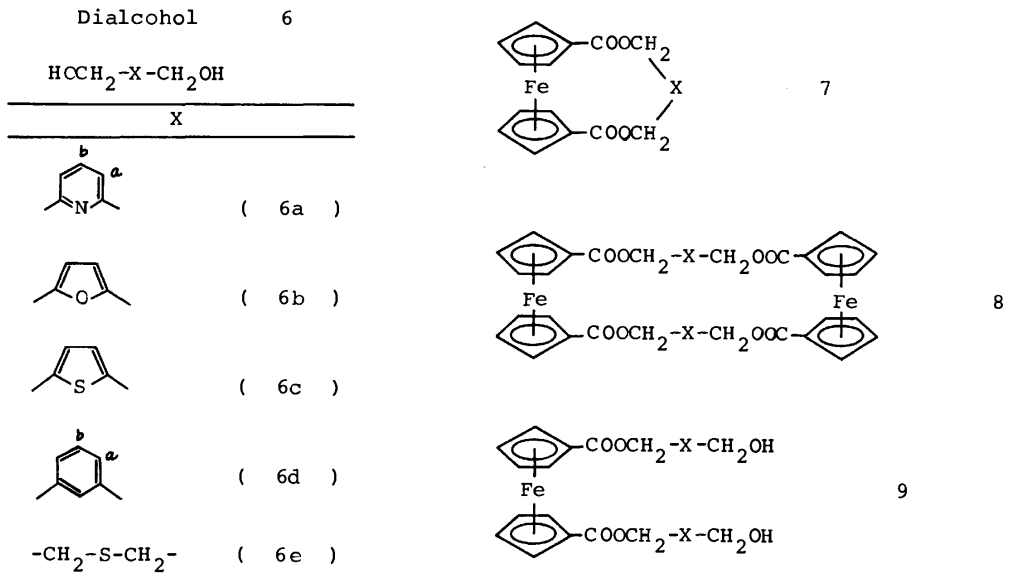

Fig. 2.

cept the above two cases. The results are summarized in Tables 3 and 4.

The structure of all ferrocenophanes thus prepared were determined on the basis of their IR, ^{1}H-NMR, and mass spectra and elemental analyses. The IR spectra of all the crown products showed the presence of an ester (1700—1720 cm^{-1}), a methylene (1460—1470 cm^{-1}), and a 1,1′-disubstituted ferrocene ring (815—840 cm^{-1}). In the ^{1}H-NMR spectra, the resonance for the α and β ring protons of the ferrocene nucleus appeared as the A_2B_2 pattern (triplet, J=4 Hz). In the ^{1}H-NMR spectra of ferrocenophane compounds, **7a—d** and **8a—d** possessing a heterocycle as a ring unit, the methylene protons are shifted to downfield by about 0.80—0.57 ppm as compared with those of **3a** and **5a**. This result was explained by the deshielding effect of the heteroaromatic (**7a—c** and **8a—c**) and aromatic rings (**7d** and **8d**).

Extraction Ability. The complexing ability of these ferrocenophanes toward alkali, alkaline earth, and transition metal cations was examined by Pedersen's extraction method.[19] The results are summarized in Table 5. As is known an increase in the number of the ester group leads to a drastic decrease of the electron donating ability of coordination sites,[20] and the presence of an ester group increases the selectivity toward alkali metal cations.[21] This tendency, however, was not observed clearly in the complexing ability of the ferrocenophanes as compared with that of polyoxaferrocenophanes.[2h,22] The ferrocenophanes (**3a—d** and **5a—d**) showed low complexing ability with alkali, alkaline earth, and transition metal cations without any difference in the extractability. Akabori *et al.*[2h,22] also reported a similar tendency in the extractability of alkali metal cations with polyoxa[*n*]ferrocenophanes prepared from 1,1′-dihydroxyferrocene and 1,1′-bis(hydroxymethyl)ferrocene. In ferrocenophanes **7e** and **8e**, it is anticipated that the incorporation of a sulfur atom (a soft atom) into the macrocycle has a strong influence on the complexing ability with transition metal ions (a soft atom) on the basis of the HSAB principle.[23] It should be emphasized that compound **8e** has a high complexing ability toward silver cation. Comparison of compound **7e** with **8e** suggests that complexing ability is influenced not only by the affinity of sulfur to a metal cation but also by the increase in the ring size. In order to know the influence of heteroatoms, extractability data of new ferrocenophanes (**7a—e** and **8a—e**) containing ferrocene and heterocyclic compound as a ring unit are listed in Table 5. These ferrocenophanes showed a poor extraction efficiency with alkali, alkaline earth, and transition metal cations, and only a small difference is found among their extractability. Compound **8a** is an exception and shows high preference toward silver ion. These results suggest that nitrogen atom has a higher affinity toward metal cations than sulfur atom (**7a** and **8a**). In Table 5, it is noteworthy that all ferrocenophanes are able to form stable complexes with silver, whereas ferrocene itself and many polyoxaferrocenophanes[2h,2j] prepared from 1,1′-dihydroxyferrocene were decomposed oxidatively by the complexed silver cation. Under acidic conditions ferrocenophanes **8a** and **8e** showed high complexing ability with mercury ion without decomposition of ferrocene nucleus. Poor complexing ability of all ferrocenophanes toward thallium ion as a transition metal cation is probably due to the nonfitness between the guest ion and the hole size of the host molecule.

Table 5. Extraction data (water-dichloromethane)[a]

Compound	Extracted/%					
	Na^+	K^+	Ba^{2+}	Tl^+	Ag^+	Hg^+ [b]
3a	2.7	1.3	2.0	0	2.9	—
3b	3.0	1.4	2.1	2.1	5.1	—
3c	3.0	1.5	2.8	2.6	6.9	—
3d	3.0	3.0	3.6	0.7	6.8	—
5a	2.4	2.6	3.6	1.4	3.3	24.3
5b	3.0	3.7	3.6	3.3	6.5	—
5c	3.7	4.4	4.3	0.2	6.9	—
5d	4.4	6.5	4.3	6.4	7.9	—
7a	10.1	11.4	5.7	2.1	14.3	—
8a	16.4	11.4	2.9	2.9	71.5	69.7
7b	0	0	0	0	0	—
8b	0.3	0	0	0	0	—
7c	2.4	2.6	3.6	1.4	3.3	—
8c	9.0	6.4	2.1	1.4	5.0	—
7d	0.7	2.0	0	0	2.1	—
8d	5.1	5.3	1.9	1.8	3.6	—
7e	4.3	5.4	0.4	1.4	2.6	—
8e	4.1	5.4	1.1	1.4	47.1	79.3

a) Equal volumes of water and dichloromethane are mixed, and the concentration of picric acid is 7.0×10^{-5} M(1M=1 mol dm^{-3}). Concentration of ferrocenophane: 7.0×10^{-4} M. Concentration of metal nitrate: 0.1 M. b) Concentration of $HgNO_3\cdot H_2O$: 0.1 M in 0.6 N HNO_3.

Experimental

Materials and Measurements. All melting points are uncorrected. 1,1′-Bis(chloroformyl)ferrocene (**2**),[24] 2,5-bis(hydroxymethyl)furan,[25] and 2,5-bis(hydroxymethyl)thiophene[26] were prepared as described in the literature. The other reagents employed were commercial materials or were prepared by the usual method. All inorganic compounds were of the reagent grade. The IR, ^{1}H-NMR, mass, and electronic spectra were recorded on Hitachi 260-10, Hitachi R-22 (CW), Hitachi R-90H (FT), Hitachi RMU-6M, and Hitachi 200-10 spectrometers, respectively.

Syntheses of 3a—d. General Procedure: Under nitrogen atmosphere a solution of **2** (8.1 g, 0.026 mol) in dry benzene (200 ml) was added dropwise over 20 h to a refluxing solution of oligoethylene glycols (n=0—3) (0.052 mol) in dry benzene (200 ml). An additional 48 h period of gentle refluxing followed. After the reaction mixture was cooled to room temperature and evaporated to dryness under reduced pressure, the residue was purified by silica-gel column chromatography. The first fraction eluted with benzene gave mononuclear ferrocenophanes **3a—d**, and the second fraction eluted with chloroform gave 1,1′-ferrocene dialcohols **4a—d**. These results are summarized in Table 1.

*2,5-Dioxa[6](1,1')ferrocenophane-1,6-dione (**3a**).* ^{1}H-NMR ($CDCl_3$) δ=4.46 (t, 4H, Fc-Hβ, J=4 Hz), 4.64 (s, 4H, -C$\underline{H}_2$C$\underline{H}_2$-), 4.48 (t, 4H, Fc-Hα, J=4 Hz). IR (KBr): 3100, 2900, 1710, 1470, 1280, 820 cm^{-1}. MS (70 ev): m/z 300 (M^+). λ_{max} (CH_3OH): 455 nm (ε 290). Found: C, 55.98; H, 4.10 %. Calcd for $C_{14}H_{12}FeO_4$: C, 56.03; H, 4.03%; M, 300.09.

*2,5,8-Trioxa[9](1,1')ferrocenophane-1,9-dione (**3b**).* ^{1}H-NMR ($CDCl_3$) δ=3.83 (m, 4H, -C$\underline{H}_2$O-), 4.38 (m, 4H, -COOC$\underline{H}_2$-), 4.46 (t, 4H, Fc-Hβ, J=4 Hz), 4.71 (t, 4H, Fc-Hα, J=4 Hz). IR (KBr): 3100, 2950, 1720, 1470, 1280, 825 cm^{-1}. MS (70 eV): m/z 344 (M^+). λ_{max} (CH_3OH): 450 nm (ε 281). Found: C, 55.72; H, 4.73%. Calcd for $C_{16}H_{16}FeO_5$: C, 55.84; H, 4.69 %; M, 344.15.

*2,5,8,11-Tetraoxa[12](1,1')ferrocenophane-1,12-dione (**3c**).* ^{1}H-NMR ($CDCl_3$) δ=3.76 (s, 4H, -OC$\underline{H}_2$C$\underline{H}_2$-), 3.90 (m, 4H, -COOC$\underline{H}_2$C$\underline{H}_2$O-), 4.40 (m, 4H, -COOC$\underline{H}_2$CH$_2$O-), 4.48 (t, 4H, Fc-Hβ, J=4 Hz), 4.75 (t, 4H, Fc-Hα, J=4 Hz). IR (KBr): 3100, 2950, 1720, 1470, 1280, 825 cm^{-1}. MS (70 eV): m/z 388 (M^+). λ_{max} (CH_3OH): 452 nm (ε 339). Found: C, 55.61; H, 5.10%. Calcd for $C_{18}H_{20}FeO_6$: C, 55.69; H, 5.19%; M, 388.20.

*2,5,8,11,14-Pentaoxa[15](1,1')ferrocenophane-1,15-dione (**3d**).* ^{1}H-NMR ($CDCl_3$) δ=3.69 (s, 8H, -OC$\underline{H}_2$C$\underline{H}_2$OC$\underline{H}_2$C$\underline{H}_2$O-), 3.79 (m, 4H, -COOCH$_2$C$\underline{H}_2$-), 4.39 (m, 4H, -COOC$\underline{H}_2$CH$_2$-), 4.39 (t, 4H, Fc-Hβ, J=4 Hz), 4.78 (t, 4H, Fc-Hα, J=4 Hz). IR (KBr): 3100, 2950, 1710, 1460, 1280, 825 cm^{-1}. MS (70 eV): m/z 432 (M^+). λ_{max} (CH_3OH): 452 nm (ε 355). Found: C, 55.62; H, 5.51%. Calcd for $C_{20}H_{24}FeO_7$: C, 55.57; H, 5.60%; M, 432.25.

*Syntheses of **5a—d**.* *General Procedure*: Under nitrogen atmosphere, **2** (3.1 g, 0.01 mol) diluted with 200 ml of dry benzene was added dropwise over 20 h to the solution of 1,1'-ferrocene dialcohols **4a—d** (0.01 mol) in 200 ml of dry benzene. Additional 48 h period of gentle refluxing followed. After the removal of the solvent under reduced pressure, the residue was purified by silica-gel column chromatography. The first fraction eluted with chloroform-acetone (10:1) gave binuclear ferrocenophanes **5a—d**. The second fraction eluted with chloroform-acetone (1:1) gave an oligomer as a reddish oil. These results are summarized in Table 2.

*2,5,19,22-Tetraoxa[6.6](1,1')ferrocenophane-1,9,21,29-tetrone (**5a**).* ^{1}H-NMR (FT) ($CDCl_3$) δ=4.46 (t, 8H, Fc-Hβ, J=3.96 Hz), 4.63 (s, 8H, -C$\underline{H}_2$C$\underline{H}_2$-), 4.89 (t, 8H, Fc-Hα, J=3.96 Hz). IR (KBr): 3100, 2950, 1720, 1460, 1270, 825 cm^{-1}. MS (70 eV): m/z 600 (M^+). λ_{max} (dioxane): 448 nm (ε 510). Found: C, 55.95; H, 4.11%. Calcd for $C_{28}H_{24}Fe_2O_8$: C, 56.03; H, 4.03%; M, 600.19.

*2,5,8,22,25,28,-Hexaoxa[9.9](1,1')ferrocenophane-1,9,21,29-tetraone (**5b**).* ^{1}H-NMR (FT) ($CDCl_3$) δ=3.83—3.94 (m, 8H, -CH$_2$C$\underline{H}_2$OC$\underline{H}_2$CH$_2$-), 4.41 (t, 8H, Fc-Hβ, J=3.95 Hz), 4.39—4.48 (m, 8H, -COOC$\underline{H}_2$-), 4.82 (t, 8H, Fc-Hα, J=3.95 Hz). IR (KBr): 3100, 2950, 1715, 1470, 1280, 815 cm^{-1}. MS (70 eV): m/z 688 (M^+). λ_{max} (dioxane): 448 nm (ε 580). Found: C, 55.78; H, 4.72%. Calcd for $C_{32}H_{32}Fe_2O_{10}$: C, 55.84; H, 4.69%; M, 688.29.

*2,5,8,11,25,28,31,34-Octaoxa[12.12](1,1')ferrocenophane-1,12,24,35-tetraone (**5c**).* ^{1}H-NMR ($CDCl_3$) δ=3.69 (s, 8H, -OC$\underline{H}_2$C$\underline{H}_2$O-), 3.76—3.81 (m, 8H, -COOCH$_2$C$\underline{H}_2$O-), 4.30—4.35 (m, 8H, -COOC$\underline{H}_2$CH$_2$O-), 4.38 (t, 8H, Fc-Hβ, J=4 Hz), 4.78 (t, 8H, Fc-Hα, J=4 Hz). IR (KBr): 3100, 2950, 1710, 1470, 1280, 820 cm^{-1}. MS (70 eV): m/z 776 (M^+). λ_{max} (dioxane): 449 nm (ε 532). Found: C, 55.61; H, 5.12%. Calcd for $C_{36}H_{40}Fe_2O_{12}$: C, 55.69; H, 5.19%; M, 776.40.

*2,5,8,11,14,28,31,34,37,40-Decaoxa[15.15](1,1')-ferrocenophane-1,15,27,41-tetrone (**5d**).* ^{1}H-NMR ($CDCl_3$) δ=3.62 (s, 16H, -OC$\underline{H}_2$C$\underline{H}_2$OC$\underline{H}_2$C$\underline{H}_2$O-), 3.71—3.76 (m, 8H, -COOCH$_2$-C$\underline{H}_2$O), 4.31—4.36 (m, 8H, -COOC$\underline{H}_2$CH$_2$O-), 4.37 (t, 8H, Fc-Hβ, J=4 Hz), 4.48 (t, 8H, Fc-Hα, J=4 Hz). IR (neat): 3100, 2950, 1710, 1465, 1280, 825 cm^{-1}. MS (70 eV): m/z 864 (M^+). λ_{max} (dioxane): 447 nm (ε 514). Found: C, 55.48; H. 5.66%. Calcd for $C_{40}H_{48}Fe_2O_{14}$: C, 55.57; H, 5.60%; M, 864.51.

*Syntheses of **7a—e**, **8b**, **d**, and **9a**, **c**, **d**, **e**.* A solution of **2** (5.9 g, 0.019 mol) in 200 ml of dry benzene was added dropwise to a solution of **6** (0.038 mol) and triethylamine (3.8 g, 0.038 mol) in acetonitrile (250 ml) for 20 h under nitrogen atmosphere. Additional 20 h period of gentle refluxing followed. After usual work-up, the products were separated by silica-gel column chromatography. The first fraction eluted with chloroform gave mononuclear ferrocenophanes **7a—e**. The second fraction eluted with chloroform-diethyl ether (9:1) gave **8b** or **8d** from **6b** and **6d**, respectively. The third fraction eluted with chloroform-methanol (9:1) gave ferrocene dialcohols **9a**, **c**, **d**, **e**. These results are summarized in Table 3.

*Syntheses of **8a**, **c**, **d**, **e**.* Under nitrogen atmosphere, reaction of **2** (9.6 g, 0.03 mol) with ferrocene dialcohols **9a**, **c**, **d**, **e** (0.03 mol) and triethylamine (3.0 g, 0.03 mol) in dry benzene (300 ml) gave compounds **8a**, **c**, **d**, **e**, respectively.

*2,11-Dioxa[3](2,6)pyridino[3](1,1')ferrocenophane-1,12-dione (**7a**).* ^{1}H-NMR ($CDCl_3$) δ=4.42 (t, 4H, Fc-Hβ, J=4 Hz), 4.92 (t, 4H, Fc-Hα, J=4 Hz), 5.36 (s, 4H, methylene), 7.06 (d, 2H, 2,6-disubstituted pyridine-H$_a$, J=8 Hz), 7.63 (d-d, 1H, 2,6-disubstituted pyridine-H$_b$, J=8 Hz). IR (KBr): 3100, 2950, 1710, 1600, 1460, 1280, 820 cm^{-1}. MS (70 eV): m/z 377 (M^+). λ_{max} (dioxane): 467 nm (ε 197). Found: C, 60.39; H, 3.92%. Calcd for $C_{19}H_{15}FeNO_4$: C, 60.50; H, 4.01%; M, 377.18.

*2,11,25,34,-Tetraoxa[3](2,6)pyridino[3](1,1')ferroceno-[3](2,6)-pyridino[3](1,1')ferrocenophane-1,12,24,35-tetrone (**8a**).* ^{1}H-NMR ($CDCl_3$) δ=4.39 (t, 8H, Fc-Hβ, J=4 Hz), 4.85 (t, 8H, Fc-Hα, J=4 Hz), 5.33 (s, 8H, methylene), 7.36 (d, 4H, 2,6-disubstituted pyridine-H$_a$, J=8 Hz), 7.70 (d-d, 2H, 2,6-disubstituted pyridine-H$_b$, J=8 Hz). IR (KBr): 3100, 2925, 1710, 1580, 1470 1280, 815 cm^{-1}. MS (70 eV): m/z 754 (M^+). λ_{max} (dioxane): 450 nm (ε 564). Found: C, 60.53, H, 3.94%. Calcd for $C_{38}H_{30}Fe_2N_2O_8$: C, 60.50; H, 4.01%; M, 754.36.

*2,10-Dioxa[3](2,5)furano[3](1,1')ferrocenophane-1,11-dione (**7b**).* ^{1}H-NMR ($CDCl_3$) δ=4.27 (t, 4H, Fc-Hβ, J=4 Hz), 4.71 (t, 4H, Fc-Hα, J=4 Hz), 5.21 (s, 4H, methylene), 6.49 (s, 2H, 2,5-disubstituted furan). IR (KBr): 3100, 2960, 1720, 1560, 1470, 1280, 840 cm^{-1}. MS (70 eV): m/z 366 (M^+). λ_{max} (dioxane): 450 nm (ε 329). Found: C, 59.11; H, 3.74%. Calcd for $C_{18}H_{14}FeO_5$: C, 59.05; H, 3.85%; M, 366.15.

*2,10,24,32-Tetraoxa[3](2,5)furano[3](1,1')ferroceno[3](2,5)furano-[3](1,1')ferrocenophane-1,11,23,33-tetrone (**8b**).* ^{1}H-NMR ($CDCl_3$) δ=4.16 (t, 8H, Fc-Hβ, J=4 Hz), 4.63 (t, 8H, Fc-Hα, J=4 Hz), 5.23 (t, 8H, methylene), 6.48 (t, 4H, 2,5-disubstituted furan). IR (KBr): 3100, 1720, 1560, 1280, 840, 770 cm^{-1}. MS (70 eV): m/z 732 (M^+). λ_{max} (dioxane): 450 nm (ε 630). Found: C, 59.12; H, 3.78%. Calcd for $C_{36}H_{28}Fe_2O_{10}$: C, 59.05; H, 3.85%; M, 732.31.

*2,10-Dioxa[3](2,5)thiopheno[3](1,1')ferrocenophane-1,11-dione (**7c**).* ^{1}H-NMR ($CDCl_3$) δ=4.39 (t, 4H, Fc-Hβ, J=4 Hz), 4.89 (t, 4H, Fc-Hα, J=4 Hz), 5.27 (s, 4H, methylene), 7.16 (s, 2H, 2,5-disubstituted thiophene). IR (KBr): 3100, 1700, 1280, 820, 770 cm^{-1}. MS (70 eV): m/z 382 (M^+). λ_{max} (dioxane): 450 nm (ε 205). Found: C, 56.47; H, 3.58%. Calcd for $C_{18}H_{14}FeO_4S$: C, 56.56; H, 3.69%; M, 382.21.

*2,10,24,32-Tetraoxa[3](2,5)thiopheno[3](1,1')ferrocenophane-1,11,23,33-tetrone (**8c**).* ^{1}H-NMR (FT) ($CDCl_3$) δ=4.07 (t, 8H, Fc-Hβ, J=3.95 Hz), 4.59 (t, 8H, Fc-Hα, J=3.95 Hz), 5.36 (s, 4H, methylene), 7.06 (s, 4H, 2,5-disubstituted thiophene). IR (KBr): 3100, 1700, 1280, 820, 770 cm^{-1}. MS (70 eV): m/z 764 (M^+). λ_{max} (dioxane): 450 nm (ε 690). Found: C, 56.64; H, 3.60%. Calcd for $C_{36}H_{28}Fe_2O_8S_2$: C, 56.56; H, 3.69%; M, 764.43.

2,11-Dioxa[3]methacyclo[3](1,1')ferrocenophane-1,12-dione (7d). ^{1}H-NMR ($CDCl_3$) δ=4.56 (t, 4H, Fc-H$_\beta$, J=4 Hz), 4.90 (t, 4H, Fc-H$_\alpha$, J=4 Hz), 5.44 (s, 4H, methylene), 7.10—7.45 (m, 4H, 1,3-disubstituted benzene). IR (KBr): 3100, 1720, 1500, 1290, 820, 780 cm^{-1}. MS (70 eV): 376 (M^+). λ_{max} (dioxane): 450 nm (ε 343). Found: C, 63.95; H, 4.34%. Calcd for $C_{20}H_{16}FeO_4$: C, 63.86; H, 4.29%; M, 376.19.

2,11,25,34-Tetraoxa[3]methacyclo[3](1,1')ferrocenophane-1,12,24,35-tetrone (8d). ^{1}H-NMR (FT) ($CDCl_3$) δ=4.29 (t, 8H, Fc-H$_\beta$, J=4.06 Hz), 4.77 (t, 8H, Fc-H$_\alpha$, J=4.06 Hz), 5.24 (s, 8H, methylene), 7.40 (d, 6H, 1,3-disubstituted benzene-H$_a$, J=1.3 Hz), 7.60 (br-s, 2H, 1,3-disubstituted benzene-H$_b$). IR (KBr): 3100, 1720, 1500, 1280, 840, 780 cm^{-1}. MS (70 eV): m/z 752 (M^+). λ_{max} (dioxane): 450 nm (ε 580). Found: C, 63.79; H, 4.23%. Calcd for $C_{40}H_{32}Fe_2O_8$: C, 63.86; H, 4.29%; M, 752.38.

2,8-Dioxa-5-thia[9](1,1')ferrocenophane-1,9-dione (7e). ^{1}H-NMR ($CDCl_3$) δ=3.00 (t, 4H, -COOCH$_2$C$\underline{H}_2$S-, J=10 Hz), 4.51 (t, 4H, Fc-H$_\beta$, J=4 Hz), 4.52 (t, 4H, -COOC$\underline{H}_2$-CH$_2$S-, J=10 Hz), 4.75 (t, 4H, Fc-H$_\alpha$, J=4 Hz). IR (KBr): 3100, 2950, 1710, 1460, 1275, 835 cm^{-1}. MS (70 eV): m/z 360 (M^+). λ_{max} (dioxane): 448 nm (ε 231). Found: C, 53.26; H, 4.43%. Calcd for $C_{16}H_{16}FeO_4S$: C, 53.35; H, 4.48%; M, 360.21.

2,8,22,28-Tetraoxa-5,25-dithia[9.9](1,1')ferrocenophane-1,9,21,29-tetrone (8e). ^{1}H-NMR (FT) ($CDCl_3$) δ=3.03 (t, 8H, -COOCH$_2$C$\underline{H}_2$S-, J=13.6 Hz), 4.46 (t, 8H, Fc-H$_\beta$, J=3.96 Hz), 4.48 (t, 8H, -COOC$\underline{H}_2$CH$_2$S-, J=13.6 Hz), 4.83 (t, 8H, Fc-H$_\alpha$, J=3.96 Hz). IR (KBr): 3100, 2950, 1720, 1465, 1280, 820 cm^{-1}. MS (70 eV): m/z 720 (M^+). λ_{max} (dioxane): 448 nm (ε 583). Found: C, 53.42; H, 4.53%. Calcd for $C_{32}H_{32}Fe_2O_8S_2$: C, 53.35; H, 4.48%; M, 720.42.

Solvent Extraction. Solvent extraction was carried out by the similar method as described by Pedersen.[19] The dichloromethane solution contained 7×10^{-4} M (1 M=1 mol dm^{-3}) of ferrocenophane, and 1×10^{-1} M of MNO_3 (M: metal cation). Equal volumes (10 ml) of the organic and the aqueous solutions were agitated thoroughly for 10 min at room temperature (20—23 °C). After setting the solution, upper aqueous layer was withdrawn, and its electronic spectrum was measured (picrate λ_{max}: 360 nm). A similar extraction was performed with pure dichloromethane. The concentration of the picrate was determined by using the calibration curve. The extractability was calculated by the following equation:

$$\text{Extractability} = \frac{C_0 - C}{C_0} \times 100$$

C_0: Initial concentration of the picrate.
C: Concentration of the picrate after extraction.

References

1) C. J. Pedersen, *J. Am. Chem. Soc.*, **89**, 7017 (1967).
2) a) G. Oepen and F. Vögtle, *Justus Liebigs Ann. Chem.*, **1979**, 1094; b) A. P. Bell and C. D. Hall, *J. Chem. Soc., Chem. Commun.*, **1980**, 162; c) A. Ratajczak and B. Czeck, *Polish J. Chem.*, **54**, 57 (1980); d) B. Czeck and A. Ratajczak, *ibid.*, **54**, 767 (1980); e) J. F. Biernat and T. Wilizawski, *Tetrahedron*, **36**, 2521 (1980); f) M. Sato, M. Kubo, S. Ebine, and S. Akabori, *Tetrahedron Lett.*, **1982**, 185; g) B. Czeck, A. Ratajczak, and K. Nagraba, *Monatsh. Chem.*, **113**, 965 (1982); h) S. Akabori, Y. Habata, Y. Sakamato, M. Sato, and S. Ebine, *Bull. Chem. Soc. Jpn.*, **56**, 537 (1983); j) S. Akabori, Y. Habata, M. Sato, and S. Ebine, *ibid.*, **56**, 1459 (1983).
3) G. E. Maas, J. S. Bradshaw, R. M. Izatt, and J. J. Christensen, *J. Org. Chem.*, **42**, 3937 (1977).
4) J. S. Bradshaw, C. T. Bishop, S. F. Nielsen, R. E. Asay, D. R. K. Masihdas, E. D. Flanders, L. D. Hansen, R. M. Izatt, and J. J. Christensen, *J. Chem. Soc., Perkin Trans. 1*, **1976**, 2505.
5) J. S. Bradshaw and S. T. Jolly, *J. Heterocycl. Chem.*, **16**, 1157 (1979).
6) M. D. Thompson, J. S. Bradshaw, S. F. Nielsen, C. T. Bishop, F. T. Cox, P. E. Fore, G. E. Maas, R. M. Izatt, and J. J. Christensen, *Tetrahedron Lett.*, **1977**, 3317.
7) J. S. Bradshaw, M. L. Campbell, L. A. Hassell, and J. K. Baxter, *J. Heterocycl. Chem.*, **16**, 721 (1979).
8) J. S. Bradshaw, L. D. Hansen, S. F. Nielsen, M. D. Thompson, R. A. Reeder, R. M. Izatt, and J. J. Christensen, *J. Chem. Soc., Chem. Commun.*, **1975**, 874.
9) J. S. Bradshaw and M. D. Thompson, *J. Org. Chem.*, **43**, 2456 (1978).
10) S. T. Jolly and J. S. Bradshaw, *J. Org. Chem.*, **45**, 3554 (1980).
11) J. S. Bradshaw, G. E. Maas, J. D. Lamb, R. M. Izatt, and J. J. Christensen, *J. Am. Chem. Soc.*, **102**, 467 (1980).
12) K. Frensch and F. Vögtle, *Tetrahedron Lett.*, **1977**, 2573.
13) K. Frensch, G. Oepen, and F. Vögtle, *Justus Liebigs Ann. Chem.*, **1979**, 858.
14) K. Frensch and F. Vögtle, *J. Org. Chem.*, **44**, 884 (1979).
15) T. J. V. Bergen and R. M. Kellogg, *J. Chem. Soc., Chem. Commun.*, **1976**, 964.
16) T. J. V. Bergen and R. M. Kellogg, *J. Am. Chem. Soc.*, **99**, 3882 (1977).
17) O. Piepers and R. M. Kellogg, *J. Chem. Soc., Chem. Commun.*, **1978**, 383.
18) R. M. Kellogg, T. J. Bergen, H. Doren, D. Hedstrand, J. Kooi, W. H. Kruizinga, and C. B. Troostwijk, *J. Org. Chem.*, **45**, 2854 (1980).
19) C. J. Pedersen, *Federation Proceeding*, **27**, 1305 (1968).
20) K. Matsushima, N. Kawamura, Y. Nakatsuji, and M. Okahara, *Bull. Chem. Soc. Jpn.*, **55**, 2181 (1982).
21) I. Tabushi, T. Nishiya, E. Kimura, K. Hattori, K. Odashima, K. Koga, and F. Toda, "Host-Guest no Kagaku", Kyoritsu Shuppan, 1979, p. 71.
22) S. Akabori, H. Fukuda, Y. Habata, M. Sato, and S. Ebine, *Chem. Lett.*, **1982**, 1393.
23) T. L. Ho, "Hard and Soft Acids and Bases Principles in Organic Chemistry", Academic Press, New York and London (1977), p. 162.
24) F. W. Knobloch and W. H. Rauscher, *J. Polym. Sci.*, **54**, 651 (1961).
25) J. W. Timko, S. S. Moore, D. M. Walba, P. C. Miberty, and D. J. Cram, *J. Am. Chem. Soc.*, **99**, 4207 (1977).
26) J. M. Griffing and L. F. Salisbury, *J. Am. Chem. Soc.*, **70**, 3417 (1941).

Ruthenium Catalyzed Reduction of Nitroarenes and Azaaromatic Compounds Using Formic Acid

Yoshihisa WATANABE,* Tetsuo OHTA, Yasushi TSUJI, Takao HIYOSHI, and Yasuo TSUJI
Department of Hydrocarbon Chemistry, Faculty of Engineering, Kyoto University, Sakyo-ku, Kyoto 606
(Received October 28, 1983)

Various nitroarenes having chloro, methyl, or methoxy substituents were reduced to the corresponding aminoarenes in high yields using formic acid in the presence of a catalytic amount of $RuCl_2(PPh_3)_3$. For example, 4-chloronitrobenzene was converted in 99% conversion with 98% selectivity at 125 °C for 5 h. 4-Nitroacetophenone was reduced chemoselectively to 1-(4-nitrophenyl)ethanol in 74% isolated yield under the same reaction conditions. Formic acid could also be employed as reductant for hydrogenation of heterocyclic compounds such as quinoline, indole, and quinoxaline in the presence of the ruthenium catalyst. 2-Methylquinoline was hydrogenated to 1,2,3,4-tetrahydro-2-methylquinoline in 93% conversion with 100% selectivity.

Reduction of nitroarenes is one of the most convenient methods of producing the aminoarenes which are the primary source for various aromatic nitrogen compounds. Molecular hydrogen or hydrogen chloride is generally employed as the hydrogen source in the reaction. However, applications of other hydrogen sources have been developed. As for the reduction of nitroarenes, water was combined with carbon monoxide as the hydrogen source in the water gas shift reaction (WGSR),[1] and amines,[2] alcohols,[3] and cyclohexene[4] were employed as hydrogen donors in transfer hydrogenation.

We have been using formic acid, which is easily derived from synthesis gas, in organic synthesis and have already reported its effectiveness for hydrogenation of carbonyl compounds.[5] In this paper, we describe the reduction of nitroarenes and azaaromatic compounds with formic acid in the presence of a homogeneous ruthenium catalyst.

Results and Discussion

Reduction of Nitroarenes. Nitroarenes were reduced to aminoarenes in high yields using formic acid in the presence of a catalytic amount of $RuCl_2(PPh_3)_3$ (Eq. 1, Table 1). Nitrobenzene was converted to aniline

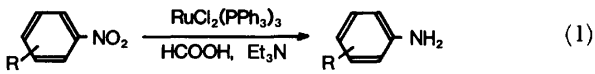

(1)

in 97% conversion with 97% selectivity. Methyl, methoxy, and chloro substituents at 2- or 4-position did not suppress the reaction. These observations were almost identical with the results reported by Knifton[6] who used molecular hydrogen as reductant in the presence of $RuCl_2(PPh_3)_3$. In the reduction of 4-nitroacetophenone by our system, 1-(4-nitrophenyl)ethanol was the major product, indicating that the reaction is chemoselective (Eq. 2). Knifton reported that 4-aminoacetophenone was mainly formed by molecular hydrogen in the presence of $RuCl_2(PPh_3)_3$ (A in Eq. 3)[7] and Heck also reported that 4-nitroacetophenone was reduced to 4-aminoacetophenone by use of triethylammonium formate in the presence of Pd/C (B in Eq. 3).[8] Furthermore, there have been few reports on the transition metal-catalyzed selective reduction of a carbonyl group in the presence of a nitro group. Tsuji *et al.*[9] have reported that $RuCl_2(PPh_3)_3$ catalyzed the selective reduction of benzaldehyde to benzyl alcohol in the presence of nitrobenzene by molecular hydrogen.

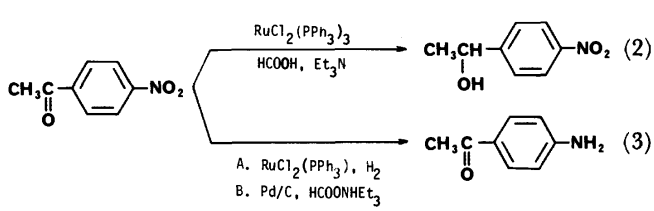

Table 1. Ruthenium-catalyzed reduction of several nitroarenes using formic acid[a]

Run	Nitroarene R=[b]	Product	Conv. of[c] nitroarene/%	Selectivity[d] to product/%
1	H	Aniline	97	97
2	2-Methyl	2-Methylaniline	99	96
3	2-Methoxy	2-Methoxyaniline	94	91
4	2-Chloro	2-Chloroaniline	100	94
5	4-Methyl	4-Methylaniline	86	96
6	4-Methoxy	4-Methoxyaniline	100	97
7	4-Chloro	4-Chloroaniline	99	98
8[e]	4-Acetyl	1-(4-Nitrophenyl)-ethanol		74[f]

a) The mixture of nitroarene (10 mmol), formic acid (33 mmol), Et_3N (35 mmol), ethanol (5 ml), and $RuCl_2(PPh_3)_3$ (0.05 mmol) was stirred at 125 °C for 5 h. b) See Eq. 1. c) Determined by GLC based on the amount of nitroarene used. d) Determined by GLC based on the conversion of nitroarene. e) Formic acid (20 mmol) was used, for 2.5 h. f) The figure in parenthesis is the isolated yield.

Figure 1 shows the pressure change during the reduction of nitrobenzene using formic acid in the presence of $RuCl_2(PPh_3)_3$. This result shows that only a little evolution of molecular hydrogen occurred in the early stage of the reaction.

This reaction proceeded without solvent with high selectivity but the use of solvent hastened the reaction. In Fig. 2, the reaction temperature *vs.* conversion of nitrobenzene is shown. The conversions were affected by the solvent employed. Over 90% conversion was attained at 125 °C in ethanol and at 180 °C in dioxane. Methanol, 2-propanol, and ethanol–benzene were also good solvents for this reaction (Table 2). Thus, alco-

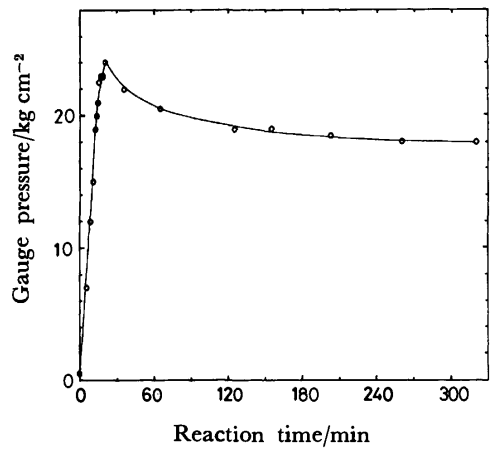

Fig. 1. Ruthenium-catalyzed Reduction of Nitrobenzene using Formic Acid. The pressure change during the reaction.
The mixture of nitrobenzene(10 mmol), formic acid (33 mmol), Et_3N (11.7 mmol), ethanol (5 ml), and $RuCl_2(PPh_3)_3$ (0.05 mmol) was heated at 125 °C in a 50 ml stainless steel autoclave.

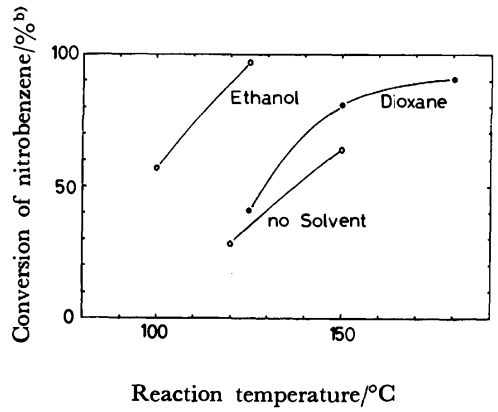

Fig. 2. Ruthenium-catalyzed Reduction of Nitrobenzene using Formic Acid.[a] Effect of Solvent.
a) The mixture of nitrobenzene(10 mmol), formic acid (33 mmol), Et_3N (35 mmol), $RuCl_2(PPh_3)_3$ (0.05 mmol) and solvent (5 ml) was heated for 5 h. b) Determined by GLC based on the amount of nitrobenzene used.

holic solvents gave good results. It is well known that alcohols are good hydrogen donor in the transfer hydrogenation. However, in the present reaction, removal of formic acid from ethanol solution gave aniline in only 2% yield. Therefore, the contribution of the transfer hydrogenation from ethanol was considered negligible in the reaction.

In the present reaction, a base was necessary for high conversion and good selectivity. Runs 14—17 indicate that the presence of triethylamine improved the conversion of nitrobenzene and the selectivity to aniline. *N*-Ethylaniline was obtained as a by-product.[10] The best result was realized in Run 17. Potassium hydroxide showed the same effect as triethylamine. However, good reproducibility was not obtained, since the reaction was heterogeneous.

Catalytic activities of several ruthenium compounds were examined, the results are listed in Table 4. $RuCl_2(PPh_3)_3$ was the most effective catalyst precursor and gave the best result. The highest turnover frequency was 350 (times/5 h) (Run 24). $RuH_2(PPh_3)_4$ and $RuHCl(PPh_3)_3$ also showed catalytic activities with triethylamine, but the conversions of nitrobenzene were

Table 2. Ruthenium-catalyzed reduction of nitrobenzene in various solvents[a]

Run	Solvent	Conversion of[b] nitrobenzene/%	Selectivity[c] to aniline/%
1	Ethanol	97	97
9	Dioxane	41	100
10	Methanol	87	91
11	2-Propanol	80	96
12[d]	Ethanol-benzene	92	100
13[e]	no solvent	28	93

a) The mixture of nitrobenzene (10 mmol), formic acid (33 mmol), Et_3N (35 mmol), $RuCl_2(PPh_3)_3$ (0.05 mmol), and solvent (5 ml) was stirred at 125 °C for 5 h. b) Determined by GLC based on the amount of nitrobenzene used. c) Determined by GLC based on the conversion of nitrobenzene. d) Ethanol (2.5 ml) and benzene (2.5 mmol) were used as solvents. e) Reaction temperature: 120 °C.

Table 3. Ruthenium-catalyzed reduction of nitrobenzene. Effect of the base[a]

Run	Base (mmol)	Reaction time/h	Conversion of[b] nitrobenzene/%	Selectivities[c]	
				Aniline	*N*-Ethylaniline
14		5	66	39	21
15	Et_3N (1.10)	5	76	57	16
16	Et_3N (10.0)	2.5	96	88	10
17	Et_3N (35.0)	2.5	96	95	4
18	Pyridine (10.0)	2.5	61	69	0
19	Et_2NH (10.0)	2.5	71	100	0
20	*n*-$BuNH_2$ (10.0)	2.5	41	98	0
21	TMED[d] (10.0)	2.5	48	85	0
22	KOH (10.0)	2.5	94	90	10

a) The mixture of nitrobenzene (10 mmol), formic acid (33 mmol), ethanol (5 ml), $RuCl_2(PPh_3)_3$ (0.05 mmol), and the base was stirred at 125 °C. b) Determined by GLC based on the amount of nitrobenzene used. c) Determined by GLC based on the conversion of nitrobenzene. d) TMED: *N*,*N*,*N*′,*N*′-Tetramethylethylenediamine.

low without the base (Runs 27 and 29). In order to investigate the role of chloro ligand on the catalyst precursor, $Et_3N \cdot HCl$ (0.1 mmol) was combined with $RuH_2(PPh_3)_4$ in the reduction of nitrobenzene (Run 30). However this resulted in only a slight improvement of the conversion and the selectivity.

There have been several ruthenium-catalyzed reduction of nitroarene. $RuCl_2(PPh_3)_3$ and $RuHCl(PPh_3)_3$ showed good catalytic activities with molecular hydrogen.[6] $Ru_3(CO)_{12}$,[1a,c] $Ru(acac)_3$,[1a] $[Ru(COD)py_4](BPh_4)_2$,[1b] and $H_4Ru_4(CO)_{12}$[1c] were employed as catalysts under water gas shift reaction conditions (with water and carbon monoxide pressure). $RuCl_3 \cdot 3H_2O$ catalyzed the transfer hydrogenation with indoline[2] and $Ru_3(CO)_{12}$ were used in the phase transfer reaction.[11] The present reduction system using formic acid shows the same results as (or better results than) the above catalytic systems under similar reaction conditions. Furthermore, in the procedure, an excess reductant is not necessary and 1.1 equiv formic acid is sufficient for obtaining high yields of the products. Formic acid is easy to handle as compared with molecular hydrogen and after the reaction formic acid was completely decomposed into carbon dioxide and hydrogen.

TABLE 4. RUTHENIUM-CATALYZED REDUCTION OF NITROBENZENE. CATALYTIC ACTIVITIES OF SEVERAL RUTHENIUM COMPOUNDS[a]

Run	Catalyst	Conversion of[b] nitrobenzene/%	Selectivity[c] to aniline/%
23		16	31
1	$RuCl_2(PPh_3)_3$	97	97
24[d]	$RuCl_2(PPh_3)_3$	49	70
25	$RuCl_3 \cdot nH_2O$	100	77
26	$RuHCl(PPh_3)_3$	71	94
27[e]	$RuHCl(PPh_3)_3$	27	82
28	$RuH_2(PPh_3)_4$	69	93
29[e]	$RuH_2(PPh_3)_4$	39	63
30[f]	$RuH_2(PPh_3)_4$	73	99

a) The mixture of nitrobenzene (10 mmol), formic acid (33 mmol), Et_3N (35 mmol), ethanol (5 ml), and a catalyst (0.05 mmol) was stirred at 125 °C for 5 h. b) Determined by GLC based on the amount of nitrobenzene used. c) Determined by GLC based on the conversion of nitrobenzene. d) Catalyst, 0.01 mmol. e) Without Et_3N. f) $Et_3N \cdot HCl$ (0.1 mmol) was added.

Reduction of Azaaromatic Compounds. Reductions of azaaromatic compounds by molecular hydrogen in the presence of the transition metal catalyst have been reported.[12] As for the ruthenium-catalyzed reaction, $RuCl_2(CO)_2(PPh_3)_2$ and $H_4Ru_4(CO)_{12}$[12d] catalyzed the reduction of quinoline derivatives. Ruthenium on carbon was used to the reduction of 2,3-benzopyrrole[12e] and the same catalyst was employed with hydrazine as the hydrogen source.[12c] Azaaromatic compounds were also reduced under WGSR conditions.[12d] The transfer hydrogenation is not applicable to azaaromatic compounds, since 1,2,3,4-tetrahydroquinoline, indoline, and their derivatives were very good hydrogen donors in the presence of transition metal catalysts.[13]

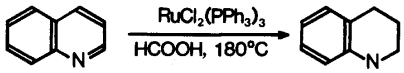

(4)

The formic acid-ruthenium catalyst was applied to the reduction of several azaaromatic compounds. The results are listed in Table 5. Formic acid was employed in stoichiometric amounts. In these reactions, different from the case of the nitroarenes, the addition of the base was not necessary for a high yield of the product. However, a higher reaction temperature was required for the high conversion (Runs 31 and 32). Thus, 1,2,3,4-tetrahydroquinoline was obtained in a reasonable yield by the reaction at 180 °C (Run 32). Prolonging the reaction time (18 h) increased the conversion. The hydrogenation occurred only at the azaaromatic ring. Other *N*-heterocyclic compounds were also hydrogenated at the *N*-heterocyclic rings (Runs 34—38). For indole derivatives, the conversions were rather low under the reaction conditions employed (Runs 36 and 37).

The highest catalytic activity was shown by

TABLE 5. RUTHENIUM-CATALYZED REDUCTION OF AZAAROMATIC COMPOUNDS USING FORMIC ACID[a]

Run	Substrate	Product	Conversion of[b] substrate/%	Selectivity[c] to product/%
31[d]	Quinoline	1,2,3,4-Tetrahydroquinoline	52	83
32	Quinoline	1,2,3,4-Tetrahydroquinoline	84	83
33[e]	Quinoline	1,2,3,4-Tetrahydroquinoline	95	80
34	2-Methylquinoline	1,2,3,4-Tetrahydro-2-methylquinoline	93	100
35	4-Methylquinoline	1,2,3,4-Tetrahydro-4-methylquinoline	85	99
36[f]	Indole	Indoline	53	83
37[f]	2-Methylindole	2-Methylindoline	50	80
38[f]	Quinoxaline	1,2,3,4-Tetrahydroquinoxaline	91	83
39	Isoquinoline		0	
40	Pyridine		0	

a) The mixture of a substrate (40 mmol), formic acid (80 mmol), and $RuCl_2(PPh_3)_3$ (0.1 mmol) was stirred at 180 °C for 6 h. b) Determined by GLC based on the amount of the substrate used. c) Determined by GLC based on the conversion of the substrate. d) Reaction temperature: 150 °C. e) Reaction time: 18 h. f) Benzene (20 ml) was used as solvent.

Table 6. Ruthenium-catalyzed reduction of quinoline. Catalytic activities of several ruthenium compounds[a)]

Run	Catalyst	Conversion of[b)] quinoline/%	Selectivity to[c)] 1,2,3,4-THQ/%
31	$RuCl_2(PPh_3)_3$	84	83
41	$RuCl_3 \cdot nH_2O + 3PPh_3$	83	82
42	$RuCl_3 \cdot nH_2O$	71	45
43	$Ru_3(CO)_{12}$	82	63
44	$RuH_2(PPh_3)_4$	12	50
45	$Ru(CO)_3(PPh_3)_2$	35	11

a) The mixture of quinoline (40 mmol), formic acid (80 mmol), and a catalyst (0.1 mmol) was stirred at 180 °C for 6 h. b) Determined by GLC based on the amount of quinoline used. c) Determined by GLC based on the conversion of quinoline. 1,2,3,4-THQ: 1,2,3,4-Tetrahydroquinoline.

$RuCl_2(PPh_3)_3$. An almost same equal activity was realized with $RuCl_3 \cdot nH_2O + 3PPh_3$ (Run 41). $Ru_3(CO)_{12}$ and $RuCl_3 \cdot nH_2O$ had some catalytic activities. However, $RuH_2(PPh_3)_4$ and $Ru(CO)_3(PPh_3)_2$ did not catalyze the reaction very much.

When the reaction was carried out with formic acid in the absence of the ruthenium catalyst, 1,2,3,4-tetrahydro-1-quinolinecarbaldehyde was isolated in only low yield (20%) (Eq. 5). This result suggests that the decomposition of formic acid is sluggish without the ruthenium catalyst.

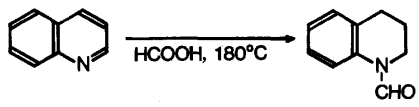

(5)

Other aromatic compounds were employed as substrates. However, pyrene, anthracene, phenanthrene, naphthalene, 2-methylnaphthalene, anisole, and benzene were almost inactive in the present hydrogenation by $RuCl_2(PPh_3)_3$-HCOOH system at 180 °C.

Experimental

All substrates, solvents and amines were obtained from commercial products and were freshly distilled *in vacuo* or recrystallized before use. Formic acid (99%), KOH, K_2CO_3, and $NH_4 \cdot HCl$ were used without further purification. The catalysts; $RuCl_2(PPh_3)_3$,[14] $RuHCl(PPh_3)_3$,[15] $RuH_2(PPh_3)_4$,[16] $Ru_3(CO)_{12}$,[16] and $Ru(CO)_3(PPh_3)_2$[18] were prepared by methods reported in the literature.

GLC analysis was performed on a Shimadzu GC-3BT apparatus. ^1H NMR spectra were obtained at 100 MHz with a JEOL JNM FX-100 pulsed Fourier Transform spectrometer or at 300 MHz with a Nicoled NTC-300 spectrometer equipped with a 1180E computer system. The JEOL JNM FX-100 pulsed Fourier Transform spectrometer was also used to measure the 25.05 MHz ^{13}C NMR spectra. The IR spectra were measured on a Hitachi model 215 grating spectrophotometer. Elemental analyses were performed at the Microanalytical Center of Kyoto University. The mass spectra were recorded on a JMS OlSG mass spectrometer.

Reduction of Nitroarenes. A nitroarene (10 mmol), formic acid (33 mmol), a ruthenium complex (0.05 mmol), Et_3N (35 mmol), and ethanol (5 ml) as an solvent were placed in a 50 ml stainless steel autoclave with a magnetic stirring bar. The air was replaced with argon. Then the autoclave was heated to 125 °C in 20 min and held at this temperature for 5 h. The reaction was terminated by rapid cooling. The reaction products were isolated by distillation or extraction with HCl aq (10%). The identification of the products were performed by comparing the spectral data(^{13}C, ^1H NMR and IR spectra) with those of authentic samples. The conversions of the substrate and the selectivities to the products were determined by GLC (3 mmϕ×3 m column packed with 10% Versamid 900 on Neopak 1A 60—80 mesh or 5% Apiezon Grease L on Neopak 1 A 60—80 mesh) by the internal standard methods.

1-(4-Nitrophenyl)ethanol: Isolated by medium-pressure column chromatography (silica gel, Merck No.9385, hexane-ethyl acetate as the eluent). IR (neat) 3360 (ν_{OH}), 1615 and 1350 (ν_{NO_2}), 1095 (ν_{COH}), and 870 cm^{-1} (ν_{CN}). ^1H NMR ($CDCl_3$) (100 MHz) δ=1.49 (d, 3H, CH_3), 3.75 (s, 1H, OH), 4.96 (q, 1H, CH), and 6.38—8.11 (m, 4H, phenyl ring). ^{13}C NMR ($CDCl_3$) δ=25.36 (q), 69.34 (d), 123.58 (d, 2C), 126.17 (d, 2C), 146.89 (s), and 153.47 (s).

Reduction of Azaaromatic Compounds. A 100 ml stainless steel autoclave with a magnetic stirrer bar was used in the reaction. A typical reaction with quinoline and formic acid will be described here to exemplify the general procedure adopted. A mixture of quinoline (40 mmol), formic acid (80 mmol), and $RuCl_2(PPh_3)_3$ (0.1 mmol) was stirred magnetically at 180 °C under an argon atmosphere for 6 h. In the reaction with indole, 2-methylindole, and quinoxaline, benzene (20 ml) was used as solvent.

Reaction products were isolated by distillation or column chromatography (silica gel). 1,2,3,4-Tetrahydroquinoline and indoline were identified by comparing the ^1H and ^{13}C NMR spectra with those of authentic samples. 1,2,3,4-Tetrahydro-2-methylquinoline,[19] 2,3-dihydro-2-methylindole,[20] and 1,2,3,4-tetrahydroquinoxaline[21] were identified by comparison of ^1H NMR and/or IR spectra with those of the literature. These products were further confirmed by their ^{13}C NMR spectra. 1,2,3,4-Tetrahydro-4-methylquinoline was determined by ^1H and ^{13}C NMR, IR, mass spectra, and elemental analysis. The analytical data are shown below.

1,2,3,4-Tetrahydro-2-methylquinoline: ^1H NMR (300 MHz) ($CDCl_3$) δ=1.15 (d, 3H, CH_3, J=6.3 Hz), 1.55 (d of d of d of d, 1H, axial proton on 3C, J_{gem}=12.7 Hz, J=11.3, 9.9, and 5.4 Hz), 1.87 (d of d of d of d, 1H, equatorial proton on 3C, J_{gem}=12.7 Hz, J=5.6, 3.6, and 3.3 Hz), 2.68 (d of d of d, 1H, equatorial proton on 4C, J_{gem}=16.4 Hz, J=5.4 and 3.6 Hz), 2.79 (d of d of d, 1H, axial proton on 4C, J_{gem}=16.4 Hz, J=11.3 and 5.6 Hz), 3.33 (q of d of d, 1H, proton on 2C (axial), J=9.9, 6.3, and 3.3 Hz), 3.55 (s, 1H, NH), 6.42 (d of d, 1H, J=7.2 and 0.9 Hz), 6.57 (t of d, 1H, J=7.2 and 0.9 Hz), 6.92 (d, 1H, J=7.2 Hz), and 6.93 (t, 1H, J=7.2 Hz). ^{13}C NMR ($CDCl_3$): δ=22.5 (q), 26.5 (t), 30.0 (t), 47.0 (d), 113.7 (d), 116.6 (d), 120.7 (s), 126.3 (d), 128.9 (d), and 144.3 (s).

2-Methylindoline: ^{13}C NMR ($CDCl_3$) δ=22.1 (q), 37.6 (t), 55.0 (d), 108.8 (d), 118.1 (d), 124.3 (d), 126.8 (d), 128.5 (s), and 150.6 (s).

1,2,3,4-Tetrahydroquinoxaline: ^{13}C NMR ($CDCl_3$) δ=41.2 (t), 114.5 (d), 118.4 (d), and 133.6 (s).

1,2,3,4-Tetrahydro-4-methylquinoline: ^1H NMR (300 MHz) ($CDCl_3$) δ=1.22 (d, 3H, CH_3, J=7.2 Hz), 1.58 (d of d of d of d, 1H, equatorial proton on 3C, J_{gem}=12.0 Hz, J=7.0, 7.0, and 3.6 Hz), 1.88 (d of d of d of d, 1H, axial proton on 3C, J_{gem}=12.0 Hz, J=8.4, 7.0, and 4.2 Hz), 2.83 (q of d, 1H, proton on 4C, J=7.2 and 7.2 Hz), 3.11 (d of d of d, 1H, equatorial proton on 2C, J_{gem}=11.5 Hz, J=7.0 and 4.2 Hz), 3.17 (d of d of d, 1H, axial proton on 2C, J_{gem}=11.5 Hz, J=8.4 and 3.6 Hz), 3.64 (s, NH), 6.34 (d, 1H, J=7.5 Hz), 6.58 (t, 1H, J=7.5 Hz), 6.91 (t, 1H, J=7.5 Hz), and 6.99 (d, 1H, J=7.5 Hz). ^{13}C NMR

($CDCl_3$) δ=22.6 (q), 29.8 (d), 30.2 (d), 38.9 (t), 114.0 (d), 116.7 (d), 126.3 (s), 126.6 (d), 128.2 (d), and 144.1 (s). IR (neat) 3390 cm^{-1} (ν_{NH}). MS (m/z) 147 (M^+) and 132 (M^+-CH_3). Calcd for $C_{10}H_{13}N$: C, 81.58; H, 8.90; N, 9.51%. Found: C, 82.07; H, 8.94; N, 9.72%.

Reaction of Quinoline with Formic Acid without Catalyst. Quinoline (40 mmol) and formic acid (80 mmol) were stirred magnetically in a 100 ml stainless steel autoclave at 180 °C for 6 h under an argon atmosphere. The reaction product was distilled and a colorless oil was obtained.

1,2,3,4-Tetrahydro-1-quinolinecarbaldehyde: Colorless oil, bp 94—98 °C/0.07 mmHg (1 mmHg≈133.322 Pa). ^1H NMR (100 MHz) ($CDCl_3$) δ=4.82 (quint, 2H), 2.71 (t, 2H), 3.71 (t, 2H), 7.07 (s, 4H), and 8.68 (s, 1H). ^{13}C NMR ($CDCl_3$) δ=22.1 (t), 27.1 (t), 40.1 (t), 116.8 (d), 124.2 (d), 126.9 (d), 128.5 (s), 129.5 (d), 137.1 (s), and 160.7 (d). IR (neat) 1670 cm^{-1} (ν_{CO}). MS (m/z) 161 (M^+), 132 (M^+-CHO). Calcd for $C_{10}H_{11}NO$: C, 74.51; H, 6.88; N, 8.69%. Found: C, 74.81; H, 6.91; N, 8.70%.

References

1) a) F. L'Eplattenier, P. Matlhys, and F. Calderazzo, *Inorg. Chem.*, **9**, 342 (1972); b) T. Okano, K. Fujiwara, H. Konishi, and J. Kiji, *Chem. Lett.*, **1981**, 1083; c) K. Cann, T. Cole, W. Slegeir, and R. Pettit, *J. Am. Chem. Soc.*, **100**, 3969 (1978); d) Y. Watanabe, Y. Tsuji, T. Ohsumi, and R. Takeuchi, *Tetrahedron Lett.*, **24**, 4121 (1983); e) A. F. M. Iqubal, *Tetrahedron Lett.*, **1971**, 3385; f) K. Kaneda, M. Hiraki, T. Imanaka, and S. Teranishi, *J. Mol. Catal.*, **12**, 385 (1981) and references cited therein.

2) H. Imai, T. Nishiguchi, and K. Fukuzumi, *Chem. Lett.*, **1976**, 655.

3) J. M. Landesberg, L. Katz, and C. Olsen, *J. Org. Chem.*, **37**, 930 (1972); K. F. Liou and C. H. Cheng, *ibid.*, **47**, 3018 (1982).

4) I. D. Entwistle, R. A. W. Johnstone, and T. J. Povall, *J. Chem. Soc., Perkin I*, **1975**, 1300. E. A. Braude, R. P. Linsted, and K. R. H. Wooldridge, *J. Chem. Soc.*, **1954**, 3586.

5) Y. Watanabe, T. Ohta, and Y. Tsuji, *Bull. Chem. Soc. Jpn.*, **55**, 2441 (1982).

6) J. F. Knifton, *J. Org. Chem.*, **41**, 1200 (1976).

7) J. F. Knifton, *Chem. Abstr.*, **81**, P 135689z, US Patent 3832401.

8) J. R. Weir, B. A. Patel, and R. F. Heck, *J. Org. Chem.*, **45**, 4926(1980). M. O. Terpko and R. F. Heck, *ibid.*, **45**, 4992 (1980).

9) J. Tsuji and H. Suzuki, *Chem. Lett.*, **1977**, 1085.

10) Y. Watanabe, Y. Tsuji, and Y. Ohsugi, *Tetrahedron Lett.*, **22**, 2667 (1981).

11) H. Alper and S. Amaratunga, *Tetrahedron Lett.*, **1980**, 2603.

12) a) M. Freifelder, "Catalytic hydrogenation in organic synthesis procedures and commentary" A Wiley-Interscience Publication, John Wiley & Sons, New York, N. Y., **1978**, p. 163; b) C. J. Love and F. J. McQuillin, *J. Chem. Soc., Perkin I*, **1973**, 2509; c) J. L. Miesel, G. O. P. O'Doherty, and J. M. Owen, *Chem. Abstr.*, 86, 29448p; d) R. H. Fish, A. D. Thormodsen, and G. A. Cremer, *J. Am. Chem. Soc.*, **104**, 5234 (1982); e) H. Dressler and M. E. Baum, *J. Org. Chem.*, **26**, 102 (1961).

13) T. Nishiguchi, K. Tachi, and K. Fukuzumi, *J. Org. Chem.*, **40**, 237 (1975).

14) P. S. Hallman, T. A. Stephenson, and G. Wilkinson, *Inorg. Synth.*, **12**, 237 (1970).

15) P. S. Hallman, B. R. McGarvey, and G. Wilkinson, *J. Chem. Soc.*, A, **1968**, 3142.

16) R. Young and G. Wilkinson, *Inorg. Synth.*, **17**, 75 (1977).

17) A. Mantovani and S. Cenini, *Inorg. Synth.*, **16**, 47 (1976).

18) N. Ahmad, J. J. Levison, S. D. Robinson, and M. F. Uttley, *Inorg. Synth.*, **15**, 48 (1974).

19) ^1H NMR: The Sadtler Standard NMR Spectra, 34, Spectral Number 21523M. IR: The Sadtler Standard Infrared Grating Spectra, 33, Spectral Number 32497.

20) ^1H NMR: The Sadtler Standard NMR Spectra, 28, Spectral Number 18133M. IR: The Sadtler Standard Infrared Grating Spectra, 49, Spectral Number 48152P.

21) ^1H NMR: The Sadtler Standard NMR Spectra, 28, Spectral Number 18420M. IR: The Sadtler Standard Grating Spectra, 13, Spectral Number 12806.

 © 1984 The Chemical Society of Japan Bull. Chem. Soc. Jpn., 57., 2445—2449 (1984)

Preferred Conformations of *cis*-4-Hydroxy-2-chromancarboxylates and Related Compounds. Molecular Force Field Interpretation

Minoru HIROTA,* Kazuhisa ABE, Masamichi SHIBATA, Hiroko SUEZAWA, Kaoru HANAYA,*,† Takashi MURAMATSU,† and Yusaku IKEGAMI††

Department of Applied Chemistry, Faculty of Engineering, Yokohama National University, Hodogaya-ku, Yokohama 240

†*Research Institute for Science Education, Miyagi University of Education, Aramaki, Aoba Sendai 980*

††*Chemical Research Institute of Non-Aqueous Solutions, Tohoku University, Katahira, Sendai 980*

(Received February 3, 1984)

In contrast to *cis*-4-hydroxy-2-tetralincarboxylates, *cis*-4-hydroxy-2-chromancarboxylates take diaxial conformation having 4-pseudoaxial-OH and 2-axial-COOR groups preferably. The preferred conformations of these compounds were rationalized by molecular force field (MM1/MMP1) calculations on the corresponding 2-tetralin- and 2-chromancarbaldehydes as model compounds.

In connection with a series of investigations concerning the stereochemistry of catalytic hydrogenations of 4-chromanones by one of the authors (K. H.), the configuration and conformations of 4-chromanols produced by the reduction has been investigated.[1-3] The cyclohexene-like half-chair conformation has been generally accepted for the ring conformation of 3,4-dihydro-2*H*-1-benzopyrans. However, Philbin and Wheeler[4] proposed a "sofa" conformation in which all but one of the endocyclic atoms are planar. They assumed that the barrier between the sofa and the half-chair conformations is significantly low in these compounds. Contrary to this conclusion, Bolger and co-workers[5] deduced from the vicinal coupling constants of the ring protons that the dihydropyran rings of 4-benzoyloxyflavans take half-chair conformations in solution.

Hanaya and co-workers[1,6-8] found a noteworthy difference in the cis-trans ratios of the alcohols produced by the catalytic hydrogenation of 3-substituted 1-tetralones (**1**) and 2-substituted 4-chromanones (**2**) from those produced by the aluminum isopropoxide reduction of the same ketones. Thus, the *cis*-tetralols

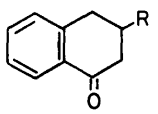

(**1**) R=CH_3, C_6H_5

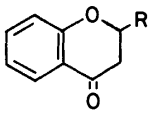

(**2**) R=CH_3, C_6H_5

(**3a**) and *cis*-chromanols (**4a**) were produced almost exclusively when the ketones (**1**) and (**2**) were hydrogenated over a Pd on charcoal or a Raney Ni catalyst, while the *trans*-alcohols (**3b**) predominated when the tetralones (**1**) were reduced by aluminum isopro-

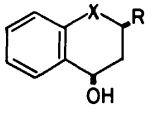

(**3a**) X=CH_2
(**4a**) Y=O

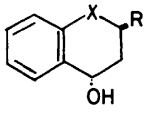

(**3b**) X=CH_2
(**4b**) X=O

R=CH_3, C_6H_5

poxide (the Meerwein-Ponndorf reduction). The catalytic hydrogenation of ethyl 1-tetralone-3-carboxylate gave similarly ethyl *cis*-4-hydroxy-2-tetralincarboxylate, which is revealed to be the less stable epimer by equilibration carried out in the presence of aluminium isopropoxide. The configurations and conformations of these alcohols were discussed on the basis of their infrared spectra in the OH stretching region.[3,9]

On the other hand, ^{1}H NMR vicinal coupling constants are also very powerful in assigning the conformations of different torsional angles about a single bond.[10] Conformations of some 4-substituted flavans were discussed by the complete analysis of their ^{1}H NMR spectra.[5] In this investigation, the conformations of alkyl 4-hydroxy-2-chromancarboxylates and related compounds deduced from the infrared and ^{1}H NMR spectroscopic evidence are shown to be reproduced by molecular force field calculations on 4-hydroxy-2-tetralin- and 4-hydroxy-2-chromancarboxaldehydes as the model compounds.

Experimental

Preparation of the materials by reducing the corresponding ketones has previously been reported.[7,11] ^{1}H NMR spectra were measured with a Hitachi R-20 and a JEOL C-60H spectrometers.

Molecular force field calculations were carried out at the computer center of the Institute for Molecular Science and at the computer center of the University of Tokyo by use of MM1/MMP1 program originally written by Allinger and co-workers[12] and modified by Osawa.

Results and Discussion

In order to determine the preferred conformations, ^{1}H NMR spectra of *cis*- and *trans*-4-hydroxy-2-tetralincarboxylates (**5a** and **5b**), *cis*-4-hydroxy-2-chromancarboxylate (**6a**), and their acetyl derivatives (**7a**, **7b**, and **8a**) were measured in chloroform-*d* at room temperature. In addition, the spectra of the alcohols in dimethyl-d_6 sulfoxide were also measured so as to assure the assignment of H on C(4) which is geminal to the hydroxyl group. The signal of H(4) was complicated by additional spin-spin interaction with hydroxyl proton in DMSO-d_6. The results of ^{1}H NMR measurement are summarized in Table 1.

Vicinal coupling constants have been shown to be

Table 1. Chemical shifts ($\delta_{H(4)}$) and vicinal spin-spin coupling constants ($J_{3,4}$) of ethyl *cis*-4-hydroxy-2-chromancarboxylate and related compounds in chloroform-*d* at room temperature

	$\delta_{H(4)}$/ppm	$J_{3,4}$/Hz[a]
Alcohols		
5a	5.28	5.9, 9.5 dd
5b	4.80	3.6 broad t
6a	4.81	5.0 t
3a[b]	5.21	6.0, 11.0 dd
3b[b]	5.13	3.0 t
Acetates		
7a	6.05	5.8, 8.0 dd
7b	6.09	3.4 t
8a	5.96	4.5 t

a) dd: doublet of doublets, t: triplet. b) The corresponding values of *cis*- and *trans*-3-phenyl-1-tetralols (**3a** and **3b**, respectively) are given for reference.

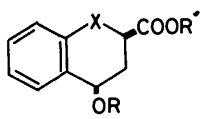

(**5a**) X=CH_2, R=H, R'=C_2H_5

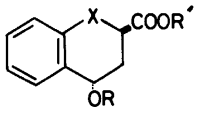

(**5b**) X=CH_2, R=H, R'=$CH(CH_3)_2$

(**6a**) X=O, R=H, R'=C_2H_5

(**6a**) X=O, R=H, R'=CH_3

(**7a**) X=CH_2, R=$COCH_3$, R'=C_2H_5

(**7b**) X=CH_2, R=$COCH_3$, R'=$CH(CH_3)_2$

(**8a**) X=O, R=$COCH_3$, R'=C_2H_5

very sensitive to the dihedral angle between the two mutually interacting ^1H nuclei. The dependency of vicinal coupling constant (J_{vic}) on dihedral angle (ϕ) was formulated by Karplus equation and similar equations[10,13,14] and proved to be useful in differentiating gauche ($\phi \approx 60°$) and anti ($\phi \approx 180°$) conformers about the C-C single bond. In the trans isomer (**5b**), the conformer carrying pseudoaxial(*a'*)-4-hydroxyl and equatorial(*e*)-2-alkoxycarbonyl groups is supposed to be predominant, since the alkoxycarbonyl group has a larger conformational free energy difference than the hydroxyl group (2.9 kJ mol^{-1} for OH and 4.6 kJ mol^{-1} for $COOCH_3$).[15] In this conformer, H(4) is pseudoequatorial and located gauche to both equatorial and axial protons on C(3)(*i. e.*, *e*-H(3) and *a*-H(3)). Vicinal coupling constants between axial and equatorial (J_{ae}) and equatorial and equatorial (J_{ee}) protons fall in the range between 2 and 3.5 Hz in the series of cyclohexane derivatives, which agrees with the observed coupling constants for **3b** and **5b**.

The cis isomers, on the other hand, are expected to take a 1,3-diequatorial (*i. e.*, equatorial-2-alkoxycarbonyl and pseudoequatorial-4-hydroxyl) conformation in the usual sense. As a consequence, a doublet of doublets is expected for H(4) due to axial-axial and axial-equatorial ^1H spin-spin interaction, since H(4) should occupy a pseudoaxial position in this conformer. In the case of *cis*-tetralin derivatives (**3a**, **5a**, and **7a**), the observed spectra are in line with the above assumption. However, the J_{vic} values of the *cis*-chroman derivatives (**6a** and **8a**) cannot adequately be interpreted by the 1,3-diequatorial conformation. In turn, slightly distorted 1,3-diaxial conformation (which has axial-2-ethoxycarbonyl and pseudoaxial-4-hydroxyl groups) or an equilibrium mixture of the diaxial and the diequatorial conformers is expected to prevail in these compounds. Thus, the triplets observed with **6a** and **8a** are explained by assuming the predominant 1,3-diaxial conformer having nearly identical J_{ae} and J_{ee} values. The coupling constants (5.0 and 4.5 Hz) seemed rather large for H(eq)-H(eq) and H(ax)-H(eq) spin-spin coupling and coexistence of a small amount of the 1,3-diequatorial conformer in a fast equilibrium with the diaxial one is expected. The coupling constant is not surprisingly large even when the 1,3-diaxial conformer alone is assumed to be present, since the J_{vic} value is calculated to be 4.1 Hz from the Lemieux's parametrization[14] of the Karplus equation assuming that the dihedral angle ϕ is 60°. Lemieux's parameters were derived empirically from the J_{vic} values of oxygen-containing six-membered rings such as 1,3-dioxane and sugars and might be suitable for the estimation of the J_{vic} values of the compounds in the chroman series.

In order to rationalize the conformational preference deduced from the observed NMR spectra, molecular force field calculations were carried out on *cis*- and *trans*-4-hydroxy-2-tetralincarbaldehydes (**9a** and **9b**, respectively) and 4-hydroxy-2-chromancarbaldehydes (**10a** and **10b**, respectively). Since the force field parameters for ester group is less trustworthy even in the revised version of MM1/MMP1 program, a model calculation replacing alkoxycarbonyl by formyl group

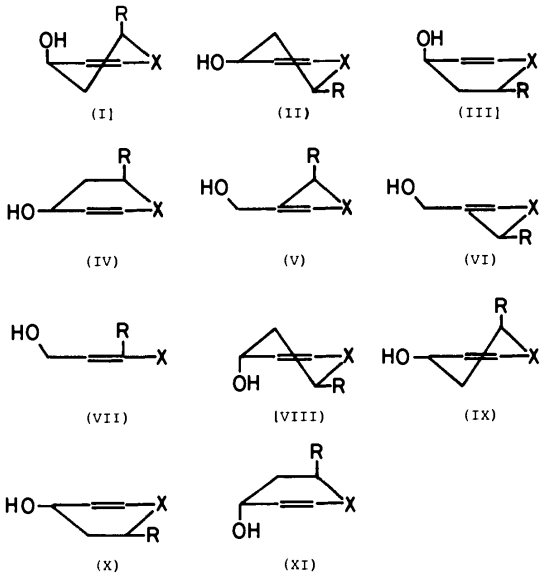

Fig. 1. Conformations selected for molecular force-field calculations. In the cases of **10a** and **10b** in Table 2 and **6a'** in Table 3, X refers to a divalent oxygen atom (O), while X is methylene group (CH_2) with the compounds **9a** and **9b** in Table 4. All coordinates were optimized whenever conformations are stable (*i. e.*, located at potential minima).

Table 2. Steric energies of *cis*- and *trans*-4-hydroxy-2-chromancarbaldehydes (**10a** and **10b**) obtained by MM calculation[a)]

	Conformations of **10a**							Conformations of **10b**			
	I	II	III	IV	V	VI	VII	VIII	IX	X	XI
E_c	3.35	3.10	3.85	3.22	3.77	3.43	3.77	3.18	3.39	3.31	3.60
E_b	9.46	10.04	12.22	13.22	7.15	8.28	26.90	9.33	9.67	14.06	11.38
E_{sb}	0.75	0.67	0.79	1.13	0.67	0.63	1.59	0.59	0.92	0.96	1.05
E_{vdw}*	43.05	40.67	48.41	44.69	44.60	43.05	52.05	42.76	42.34	44.77	48.28
E_{vdw}	−7.53	−8.58	−9.92	−9.33	−7.70	−8.49	−7.07	−9.12	−8.66	−9.08	−10.08
E_w	15.69	14.69	27.99	27.49	20.75	21.59	25.98	14.14	14.85	27.91	27.95
E_{tb}	−0.04	−0.04	−1.59	−1.67	−0.29	−0.33	−5.40	−0.08	−0.04	−1.63	−1.63
E_d	5.61	12.05	8.62	12.80	9.54	12.51	10.50	9.67	17.03	12.09	13.93
E	70.33	72.59	90.42	91.55	78.91	80.67	108.32	70.42	79.41	92.38	94.47
ΔE	0	2.26	20.09	21.22	8.58	10.34	37.99	0.09	9.08	22.05	24.14

a) All energies are given in kJ mol^{-1}.

was carried out in order to predict the preferred conformations of the esters **5a** and **6a**. As to *cis*-4-hydroxy-2-chromancarbaldehyde (**10a**), the steric energies were calculated on the seven conformationsin Fig. 1: I, half-chair carrying 4*a*′-OH and 2*a*-CHO; II, half-chair carrying 4*e*′-OH and 2*e*-CHO; III, half-boat carrying 4*a*′-OH and 2*e*-CHO; IV, half-boat carrying 4*e*′-OH and 2*a*-CHO; V, sofa carrying 2*a*-CHO; VI, sofa carrying 2*e*-CHO; and VII, planar conformations (illustrated in Fig. 1). Calculated steric energies (E)

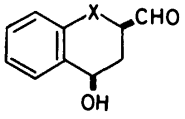

(**9a**) X=CH_2
(**10a**) X=O

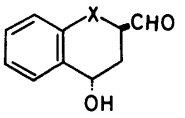

(**9b**) X=CH_2
(**10b**) X=O

and their components were given in Table 2, where E_c, E_b, E_{vdw}*, E_{vdw}, E_w, and E_d denote compression (stretching) energy, bending energy, van der Waals energy due to 1,4-interaction, van der Waals energy of other than 1,4-interaction, torsional energy, and dipole interaction energy terms, respectively. E_{sb} and E_{tb} are stretch-bend and torsion-bend cross terms. Similar calculations were carried out on the following four conformations of the trans isomer **10b**: VIII, half chair carrying 4*a*′-OH and 2*e*-CHO; IX, half-chair carrying 4*e*′-OH and 2*a*-CHO; X, half-boat carrying 4*e*′-OH and 2*e*-CHO; XI, half-boat carrying 4*a*′-OH and 2*a*-CHO (illustrated in Fig. 1).

When the total steric energies (E) are compared among the conformations, half-chair conformations are always more stable than other conformations assumed in the calculations. As expected, the half-chair conformation (VIII) carrying 4*a*′-OH and 2*e*-CHO groups is the most stable conformer of the trans isomer **10b**. Quite unexpectedly, the half-chair conformation (I) carrying 4*a*′-OH and 2*a*-CHO groups is estimated to be the most stable for the cis-chroman derivative **10a** by the calculation. The dihedral angles between H(4) and two H(3)'s are calculated to be 50.8° and 68.6°. The J_{vic} values for these dihedral angles from the modified Karplus equation[16] are 5.70 and 4.64 Hz, which reproduces the experimental results for **6a** and **8a** qualitatively. However, the steric energy difference between the most and the next stable conformations is relatively small. From the energy difference (2.26 kJ mol^{-1}), **10a** is expected to exist as a mixture of the two conformers I and II in 69% and 28% abundances, respectively, at room temperature (298 K) by assuming the Boltzmann distribution a priori. Under the conditions of fast equilibrium between the conformers, a similar doublet of doublets is expected as the first order spectrum for H(4).[17] In both cases the triplet-like band shape can be explained if the central two lines is assumed to overlap to each other by broadening.

The results of force field calculations on the two half-chair conformers corresponding to I and II of methyl *cis*-4-hydroxy-2-chromancarboxylate (**6a**′), another model compound for **6a**, are also given in Table 3. As mentioned above, the force field parameters for the ester group is less trustworthy. However, the conformation I is again the most stable. The conformer I becomes more stable relative to the conformer II in this calculation, suggesting higher abundance of the diaxial conformer I. This is also in line with the triplet signal observed.

In order to find out the reason for the stability of the conformer I, the energy terms in Table 2 were examined more carefully. The dipole interaction terms concerning OH, CHO, and ring oxygen are 6.44 kJ mol^{-1} more favorable for the conformer I than for the next stable conformer II. In contrast, van der Waals interaction energy disfavors conformer I considerably when compared with that of the conformer II. Conformations other than the two half-chairs are remarkably disfavored by the contribution of larger repulsive van der Waals and torsional energy terms. After all dipole interaction energy is the most important factor in determining the most stable conformation.

In order to discuss the difference in the conformational preference observed with *cis*-4-hydroxy-2-tetralincarboxylate **5a** and its 1-oxa anolog **6a**, the steric

TABLE 3. STERIC ENERGIES OF METHYL *cis*-4-HYDROXY-2-CHROMANCARBOXYLATE (**6a'**) OBTAINED BY MM CALCULATIONS[a)]

	Conformers of **6a'**						
	I	II	III	IV	V	VI	VII
E	92.55	101.67	118.45	115.31	98.58	106.94	137.07
ΔE	0	9.12	25.90	22.76	6.03	14.39	44.52

a) All energies are given in kJ mol^{-1}.

TABLE 4. STERIC ENERGIES OF *cis*- AND *trans*-4-HYDROXY-2-TETRALINCARBALDEHYDES (**9a** AND **9b**) OBTAINED BY MM CALCULATION[a)]

	Conformations of **9a**							Conformations of **9b**			
	I'	II'	III'	IV'	V'	VI'	VII'	VIII'	IX'	X'	XI'
E_c	3.05	2.64	3.51	3.14	3.39	2.89	3.22	2.94	2.92	2.95	3.56
E_b	5.73	6.23	7.28	9.12	6.11	6.44	24.52	5.27	6.44	10.01	7.71
E_{ab}	0.38	0.42	0.54	0.54	0.33	0.42	1.46	0.38	0.44	0.68	0.50
E_{vdw}*	42.55	36.69	44.02	40.75	40.88	37.53	49.41	40.56	38.10	40.62	44.53
E_{vdw}	−8.41	−8.12	−7.15	−7.61	−7.41	−7.91	−5.40	−8.56	−8.34	−7.32	−8.11
E_w	17.53	16.11	20.54	20.59	17.24	17.03	31.00	16.74	16.86	20.82	20.72
E_{tb}	−0.59	−0.59	−0.67	−0.67	−0.71	−0.75	−6.36	−0.49	−0.58	−0.85	−0.65
E_d	−3.72	1.67	−2.68	1.80	−2.63	1.38	0.46	2.74	3.62	3.24	−0.10
E	56.48	55.02	65.40	67.66	57.15	57.03	98.32	59.59	59.45	70.14	68.16
ΔE	1.46	0	10.38	12.64	2.13	2.01	43.30	4.57	4.43	15.12	13.14

a) All energies are given in KJ mol^{-1}.

energies for the seven conformations I'—VII' of the model compound **9a** (corresponding to the conformation I—VII, respectively, of **10a**) were calculated as given in Table 4. The most stable conformation of **5a** is estimated to be the half-chair conformation II' in which both 4-hydroxyl and 2-carbonyl groups are equatorial by calculation. The H(4*a'*)/H(3*e*) and H(4*a'*)/H(3*a*) dihedral angles of the conformer II' were calculated to be 50.0° and 166.3°, respectively, from which the spin-spin coupling constants ($J_{a'e}$ and $J_{a'a}$) are estimated to be 5.76 and 8.96 Hz, respectively. The results reproduce the observed coupling constants fairly well. Even in the case of **9a**, the conformation I' (carrying 4*a'*-OH and 2*a*-CHO groups) is considerably favored by the contribution of dipole interaction term. The stabilizing contribution is overcome by the increase in repulsive van der Waals interaction in **9a**. Apparent difference between the molecular structure of **10a** and **9a** is the presence of pseudoaxial hydrogen atom in **9a**, which is supposed to disfavor the axial conformation of formyl group. The sums of E_{vdw} terms between ring 1-CH_2 and 2-CHO groups (inclusive of 1,4-interaction terms) are nearly identical, however. Repulsion between the axial groups causes flattening of the cyclohexene ring, which, in turn, brings about large repulsive 1,4-interaction terms between the atoms in the ring.

The next stable (diaxial) conformer (I') of the aldehyde **9a** has a steric energy only 1.46 kJ mol^{-1} higher than the most stable (diequatorial) conformer (II'). This suggests the possibility for the coexistence of conformers other than II' to a considerable extent. Infrared spectrum of ethyl *cis*-4-hydroxy-2-tetralincarboxylate **5a** shows an absorption band assignable to axial hydroxyl group at 3621 cm^{-1}, which renders a support to the presence of 4*a'*-hydroxy-2*a*-alkoxycarbonyl conformer (I').[18)]

Similarly the model calculations on the trans aldehyde **9b** showed that the half-chair conformer (VIII') carrying 2*e*-formyl and 4*a'*-hydroxyl groups is the most stable, which is again in line with the triplet signal with relatively small J_{vic} values of H(4) for the *trans*-esters **5b** and **7b**.

The molecular force field calculations were carried out by HITAC M-200H computers of the Institute for Molecular Science and, in part, of the University of Tokyo to which the authors are grateful. The authors also thank Prof. Eiji Osawa, Hokkaido University, for his permission to use the MM1/MMP1 program.

References

1) K. Hanaya and K. Furuse, *Nippon Kagaku Zasshi*, **89**, 1002 (1968).
2) K. Hanaya, *Bull. Chem. Soc. Jpn.*, **43**, 442 (1970).
3) H. Iwamura and K. Hanaya, *Bull. Chem. Soc. Jpn.*, **43**, 3901 (1970).
4) E. M. Philbin and T. S. Wheeler, *Proc. Chem. Soc.*, **1958**, 167.
5) B. J. Bolger, A. Hirwe, K. G. Marathe, E. M. Philbin, and M. A. Vickars, *Tetrahehron*, **22**, 621 (1966).
6) K. Hanaya, *Nippon Kagaku Zasshi*, **87**, 995 (1966).
7) K. Hanaya, *Nippon Kagaku Zasshi*, **90**, 314 (1969).
8) S. Mitsui and A. Kasahara, *Nippon Kagaku Zasshi*, **89**, 1382 (1958).
9) K. Hanaya, S. Onodera, Y. Ikegami, H. Kudo, and K. Shimaya, *J. Chem. Soc., Perkin Trans. 2*, **1981**, 944.

10) For example, see: J. W. Emsley, J. Feeney, and L. H. Sutcliffe, "High Resolution Nuclear Magnetic Resonance Spectroscopy," Pergamon Press, Oxford (1965), p.166.
11) K. Hanaya, Y. Koga, A. Yamaguchi, H. Kudo, and Y. L. Chow, *Nouveau J. Chim.*, **6**, 149 (1982).
12) D. H. Wertz and N. L. Allinger, *Tetrahedron*, **30**, 1597 (1974); N. L. Allinger and Y. H. Yuh, MMI/MMPI program (1973), QCPE, #318.
13) M. Karplus, *J. Chem. Phys.*, **30**, 11 (1959).
14) The parameters of the Karplus equation (J_{vic}=Acos$^2\phi$+B) for oxygen-containing six-membered rings are also proposd by Lemieux and co-workers. R. U. Lemieux, J. D. Stevens, and R. R. Fraser, *Can. J. Chem.*, **40**, 1955 (1962).
15) E. L. Eliel, N. L. Allinger, S. J. Angyal, and G. A. Morrison, "Conformational Analysis," Interscience Publ., New York (1965), p.44.
16) In general, the Karplus type equations containing only quadratic term of cosϕ tend to underestimate the J_{vic} values when the dihedral angle ϕ is near 90°. Thus the following modified equation to estimate J_{vic} was proposed by M. Karplus (*J. Am. Chem. Soc.*, **85**, 2870 (1963)):

$$J_{vic}=4.22-0.5\cos\phi+4.5\cos^2\phi$$

from which the J_{vic} values were calculated to be 5.1 Hz assuming the dihedral angle to be 60°.
17) The ring reversal from I to II causes the change in dihedral angles from 68.6° to 167.0° for a pair of coupling protons and from 50.8° to 48.5° for the other pair. Thus the J_{vic} values were calculated to be 5.74 and 5.89 Hz, respectively, from the modified Karplus equation[16] as the averages weighted by the abundances of the conformers I and II from MM.
18) Infrared absorption spectra of **5a**, **5b**, and **6a** in the OH stretching region were determined as follows: **5a**, 3621 cm^{-1}(21) and 3599 cm^{-1}(52); **5b**, 3618 cm^{-1}(63); and **6a**, 3610 cm^{-1}(42) and 3596 cm^{-1}(31). Molar absorbances in 1 mol^{-1} cm^{-1} are given in parentheses. No other absorptions were observed in the OH stretching region even with the *cis*-compounds **5a** and **6a**, which excludes the possibility of strong intramolecular hydrogen bonding. See, K. Hanaya, T. Muramatsu, S. Onodera, Y. Ikegami, and M. Hirota, *Bull. Chem. Soc. Jpn.*, **57**, 1695 (1984).

The Acid-catalyzed Decomposition of Diazo Carbonyl Compounds. II. Synthesis of 2- or 5-Heteroatom-substituted Oxazoles

Toshikazu IBATA,* Tsuyoshi YAMASHITA, Makoto KASHIUCHI, Shyuji NAKANO, and Hiroyuki NAKAWA
Institute of Chemistry, College of General Education, Osaka University, Toyonaka, Osaka 560
(Received February 8, 1984)

The BF_3-catalyzed decomposition of *m*- and *p*-substituted α-diazoacetophenones in excess of methyl thiocyanate and ethyl thiocyanate gave the corresponding 2-methylthio-, and 2-ethylthio-5-aryloxazoles, respectively in good yields along with *s*-alkyl-*n*-aroylmethylthiocarbamates and α-ethoxyacetophenones. However, yields of 2-dimethylamino-5-aryloxazoles by the reaction of dimethylcyanamide with α-diazoacetophenones were poor. 5-Dimethylamino- or 5-alkoxy-4-aryl-2-methyloxazoles were prepared by the reaction of *N,N*-dimethyl-α-(*p*-nitrophenyl)diazoacetamide or alkyl aryldiazoacetates with nitriles. When ethyl phenyldiazoacetate or methyl *p*-chlorophenyldiazoacetate were used, ketazines of alkyl arylglyoxylates were obtained together with oxazoles.

Since the early proposal of Huisgen and his coworkers in 1961,[1] syntheses of oxazoles by the reaction of diazo carbonyl compounds with nitriles have extensively been studied.[2] The oxazole derivatives have recently been paid much attention for their pharmaceutical and biological activities.[3] In our previous paper of this series, we have reported the preparation of oxazoles by the BF_3-catalyzed reaction of α-diazo carbonyl compounds with nitriles.[4] In order to confirm the generality of the reaction, synthesis of 2- or 5-heteroatom-substituted oxazoles was studied.

Results and Discussion

Synthesis of 2-Heteroatom-substituted Oxazoles. Methyl thiocyanate was used as a nitrile component to introduce a methylthio group at the 2-position of oxazole ring. Decomposition of *p*-methoxy-α-diazoacetophenone was carried out in an excess of methyl thiocyanate in the presence of BF_3–etherate at 0 °C. Silica gel column chromatography of the reaction mixture after usual workup[3] gave a colorless crystalline product along with α-ethoxy-*p*-methoxyacetophenone[4] which was identified by the comparison of its IR and NMR spectra with the authentic sample prepared by the BF_3-catalyzed decomposition of the diazoacetophenone in ethanol.[5] Result of elemental analysis and spectral data indicated that the colorless product was 2-methylthio-5-(*p*-methoxyphenyl)oxazole (**3a**: Ar=*p*-$CH_3OC_6H_4$, X=SCH_3).

Similar treatment of *p*-chloro-α-diazoacetophenone yielded 2-methylthio-5-(*p*-chlorophenyl)oxazole (**3e**: Ar=*p*-ClC_6H_4, X=SCH_3) together with *S*-methyl (*p*-chlorophenacyl)thiocarbamate (**4e**: Ar=*p*-ClC_6H_4, X=SCH_3) and α-ethoxy-*p*-chloroacetophenone (**5e**)[5] as by-products. The thiocarbamate (**4e**) has two carbonyl absorption bands at 1685, 1640 cm^{-1}, and an NH absorption at 3325 cm^{-1} in its IR spectrum. The NMR spectrum shows a singlet SCH_3 signal at δ 2.38, a doublet CH_2 signal at δ 4.79 and a broad singlet of

Table 1. Yields and melting points of the BF_3-catalyzed reaction products of diazoacetophenones with alkyl thiocyanates, and dimethylcyanamide

Run	X	Ar	(3)		(4)	(5)
			Yield[a]/%	Mp θ_m/°C	Yield[a]/%	Yield[a]/%
a	SCH_3	*p*-$CH_3OC_6H_4$	79	82.0—82.2	—	6
b		*p*-$CH_3C_6H_4$	87	57.2—57.5	5	4
c		*m*-$CH_3C_6H_4$	87	oil	—	5
d		C_6H_5	78	57.0—58.0	3	5
e		*p*-ClC_6H_4	83	86.0—86.5	8	4
f		*m*-ClC_6H_4	91	61.0—61.5	—	4
g		*p*-BrC_6H_4	82	78.8—79.0	2	4
h		*p*-CNC_6H_4	85	139.0—140.0	—	3
i		*m*-CNC_6H_4	59	122.3—123.0	13	—
j		*p*-$NO_2C_6H_4$	73	148.8—150.0	10	2
k		*m*-$NO_2C_6H_4$	89	174.0—174.5	—	3
l	SC_2H_5	*p*-$CH_3OC_6H_4$	71	38.5—39.5	—	4
m		C_6H_5	66	oil	11	4
n		*p*-ClC_6H_4	65	48.8—49.0	9	5
o	$N(CH_3)_2$	*p*-$CH_3OC_6H_4$	33	101.0—103.0	b)	b)
p		C_6H_5	29	72.0—73.0	b)	b)
q		*p*-ClC_6H_4	5	96.0—98.0	b)	b)

a) Isolated yield by column chromatography. b) Not investigated.

NH at δ 6.50 besides aromatic proton signals.

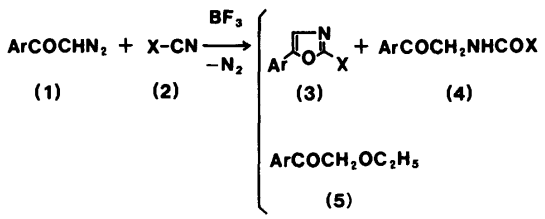

Other *m*- or *p*-substituted α-diazoacetophenones also gave corresponding oxazoles (**3**), thiocarbamates (**4**), and α-ethoxyacetophenones (**5**) in a similar reaction with methyl thiocyanate as is shown in Table 1. Proton NMR spectra of oxazoles (**3**) show signals of SCH_3 group in the region of δ 2.6—2.7, and that of *S*-methyl thiocarbamate (**4**) at δ 2.27—2.42. Decomposition of unsubstituted and substituted α-diazoacetophenones in the presence of ethyl thiocyanate also gave 2-ethylthio-5-aryloxazoles (3ı–ₙ: X=SC_2H_5). In these reactions, electron-attracting groups on the benzene ring of diazoacetophenones tend to increase the yields of the thiourethane derivatives. The reaction has been explained to be initiated by the attack of BF_3 on carbonyl oxygen of the diazo ketone affording diazonium betaine intermediate (**6**) which gave betaine (**7**) by attacking nitrile nitrogen under extrusion of nitrogen gas.[4] Cyclizaion of betaine (**7**) may produce oxazole (**3**). However, reaction of (**7**) with water contained in the reaction system may give thiocarbamate (**4**).[4] When aliphatic nitriles such as acetonitrile and propionitrile were used, no thiocarbamate (**4**) has been obtained unless considerable amount of water was added in the reaction system.[4]

Similarly 2-dimethylamino-5-aryloxazoles (**3**: X=N-$(CH_3)_2$) were obtained by the reaction of α-diazoacetophenones in excess of dimethylcyanamide (Table 1, run o—q). Low yields of the 2-dimethylaminooxazoles may

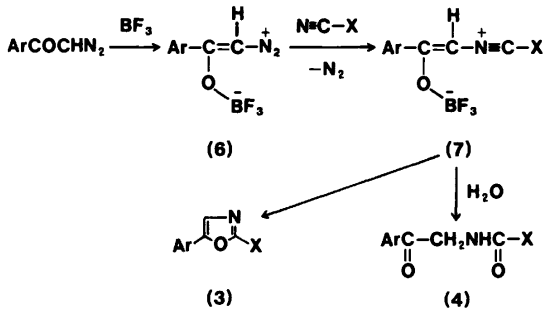

Scheme 1.

be attributed to the basicity of dimethylcyanamide which suppresses the catalytic activity of BF_3.

Synthesis of 5-Alkoxy-2-alkyloxazoles. Formation of 5-ethoxy-2-methyloxazole has been reported by the BF_3-catalyzed reaction of ethyl diazoacetate in acetonitrile.[4] Similar results were observed in the reactions of methyl *p*-nitrophenyldiazoacetate in acetonitrile and propionitrile to give corresponding 5-methoxy-4-(*p*-nitrophenyl)oxazoles (**9**) in high yields. However, ethyl phenyldiazoacetate and methyl *p*-chlorophenyldiazoacetate yielded ketazines of alkyl arylglyoxylates (**10**) together with the corresponding oxazoles.

The difference of the reactivity of these aryldiazoacetates is explained by the electronic effect of substituents on the phenyl ring. In the reaction of ethyl phenyldiazoacetate and methyl *p*-chlorophenyldiazoacetate, intermediate diazonium betaine (**12**) reacts either with nitrile or unreacted diazo compound competitively to give an oxazole or a ketazine respectively. However in the reaction of methyl *p*-nitrophenyldiazoacetate, electron-attracting nitro group decreased the nucleophilic reactivity of the diazo ketone toward the diazonium betaine (**12**), and consequently gave the oxazole (**9**) as a sole product by the attack on nitrile. The above mechanism is supported by the fact that the ratio of

Table 2. Yields of the reaction products of alkyl aryldiazoacetate with nitriles

Run	Aryldiazoacetate	Nitrile[a]	Reaction Temp/°C	Products[b]		
				Oxazole(**9**)	Ketazine(**10**)	Amide(**11**)
a	*p*-$NO_2C_6H_4$-C(=N_2)-$COOCH_3$	CH_3CN	50	75	—	5
b		C_2H_5CN	50	84	—	6
c		CH_3SCN	50	—	—	15
d	*p*-ClC_6H_4-C(=N_2)-$COOCH_3$	CH_3CN	0	33	32	—
		CH_3CN (2.0 ml)[c]	0	22	20	—
		(5.0 ml)[c]	0	53	28	—
		(10.0 ml)[c]	0	58	23	—
		(20.0 ml)[c]	0	68	16	—
		(0 ml)[d]	0	—	46	—
e	C_6H_5-C(=N_2)-$COOC_2H_5$	CH_3CN	10	27	49	—
f		C_2H_5CN	10	65	33	—

a) 10 ml of nitrile was used unless otherwise described. b) Isolated yield by column chromatography. c) 10 ml of benzene was used as a solvent, and aryldiazoacetate was added all at once. d) Reaction was carried out in absolute benzene.

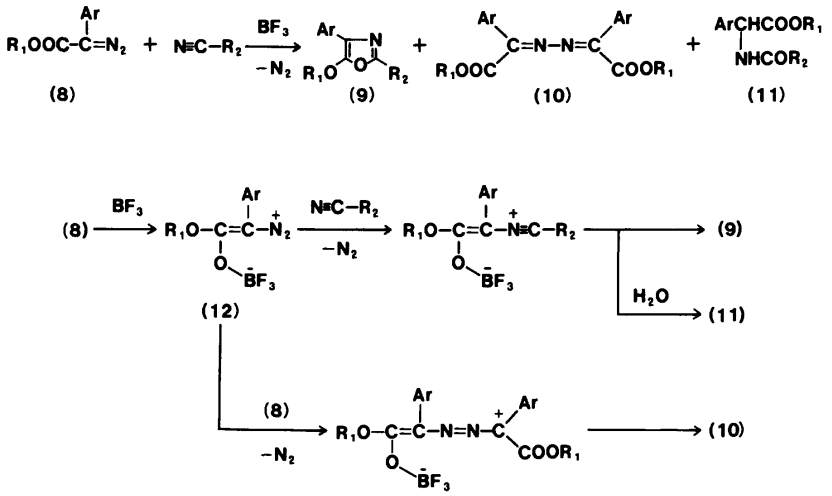

Scheme 2.

oxazole/ketazine changes depending upon the amount of acetonitrile used in the reaction of methyl *p*-chlorophenyldiazoacetate (Table 2). A similar decomposition of methyl *p*-chlorodiazoacetate in benzene without nitrile gave the ketazine (**10d**; 53%) and dimethyl bis(*p*-nitrophenyl)maleate (**13a**; 17%) and fumarate (**13b**; 26%) of which structures were determined tentatively on the basis of ester absorption of their IR spectra.

Propionitrile also showed a similar tendency to give an oxazole as a sole product in the reaction of methyl *p*-nitrophenyldiazoacetate. The BF_3-catalyzed decomposition of methyl *p*-nitrophenyldiazoacetate in methyl thiocyanate did not give the expected oxazole, 2-methylthio-5-methoxy-4-(*p*-nitrophenyl)oxazole, but gave methyl α-[(methylthio)carbonylamino]-*p*-nitrophenylacetate in 20% yield with intractable tarry product. This may be attributed to the unstability of the oxazole.

Similar treatment of *N,N*-dimethyl-α-(*p*-nitrophenyl)diazoacetamide (**14**) in excess of acetonitrile gave 5-dimethylamino-2-methyl-4-(*p*-nitrophenyl)oxazole (**15**) in 4% yield along with *N,N*-dimethyl-*p*-nitromandelamide (**16**; 39%) and *N,N*-dimethyl-α-(acetylamino)-*p*-nitrophenylacetamide (**17**; 26%).

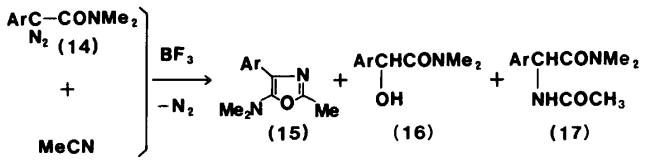

Ar = p-$NO_2C_6H_4$

The screening tests for the several biological activities of the oxazoles obtained in these reactions are now under investigation.

Experimental

Melting points were measured with Yanagimoto Melting Point Apparatus and described without correction. The IR spectra were recorded on Hitachi Infrared Spectrometer model 260-10. The ^1H NMR spectra were recorded in $CDCl_3$ solution at 90 MHz on a Varian Spectrophotometer model EM390 using TMS as an internal standard.

Materials. Diazoacetophenones were synthesized by the reaction of corresponding acid chlorides with excess of diazomethane in the presence of triethylamine according to Newman's method.[6] Methyl *p*-nitrophenyldiazoacetate, and *N,N*-dimethyl-*p*-nitrophenyldiazoacetamide were synthesized by the diazo group transfer reaction reported by Regitz.[7] *N,N*-Dimethyl-*p*-nitrophenyldiazoacetamide (**14**): mp 123.0—123.8 °C; IR (KBr) 2080 (diazo), 1635 (C=O of diazo amide), 1493, and 1325 cm^{-1} (NO_2); NMR ($CDCl_3$) δ=3.07 (s, NCH_3) and 7.40, 8.23 (ABq, *J*=9.3 Hz, Ar). Found: C, 51.36; H, 4.36; N, 23.73%. Calcd for $C_{10}H_{11}O_3N_4$: C, 51.28; H, 4.30; N, 23.92%.

Methyl *p*-chlorophenyldiazoacetate was prepared by the modified diazo group transfer reaction using KF-alumina as a base.[8] To a solution of 4.2 g (20 mmol) of methyl *p*-chlorophenylacetate and 4.3 g (20 mmol) of TsN_3 in acetonitrile 8.6 g of $KF-Al_2O_3$ was added and the mixture was stirred for 120 h at room temperature. Reaction mixture was filtered, and solid phase was washed with benzene. The filtrate was evaporated under reduced pressure and the residue was recrystallized from pentane solution. Methyl *p*-chlorophenyldiazoacetate: Orange crystals; mp 58.5—59.0 °C; yield 87%; IR (KBr) 2080 (diazo), 1690 cm^{-1} (ester C=O); NMR ($CDCl_3$) δ=3.82 (s, OCH_3), and 7.33, 7.35 (ABq, *J*=9.0 Hz, Ar). Found: C, 51.36; H, 3.33; N, 13.25%. Calcd for $C_9H_7O_2N_2Cl$: C, 51.32; H, 3.35; N, 13.30%.

Ethyl phenyldiazoacetate was prepared by the lead tetraacetate oxidation of ethyl phenylglyoxylate hydrazone.[9] Acetonitrile, propionitrile, methyl thiocyanate, ethyl thiocyanate, and dimethyl cyanamide were used after distillation of commercial reagents.

General Procedure of the BF_3-catalyzed Reaction of Diazoacetophenones with Methyl Thiocyanate or Ethyl Thiocyanate. Diazoacetophenone (3 mmol) was added in small portions to a solution of alkyl thiocyanate (10 ml) containing BF_3-etherate (0.5 ml) at 0 °C under magnetic stirring. The reaction proceeded with vigorous evolution of nitrogen and gave gray precipitate. After the N_2 evolution ceased, the reaction mixture was poured into cold water (50 ml) saturated with $NaHCO_3$. Organic products were extracted with ether (50 ml) twice. Combined ether layer was dried over anhydrous Na_2SO_4, solvent was evaporated and then excess thiocyanate was removed by distillation under reduced pressure. The residue was separated by column chromatography using silica gel/benzene. Products were assigned on the basis of NMR and IR spectra and elemental analyses (Tables 3 and 4).

Table 3. Spectral properties and analytical data of oxazoles (3)

Oxazole	Ar	X	IR (cm^{-1}) C=N	NMR (δ)			Anal[b]			Molecular formula
				C_4-H	S-CH_3 or S-C_2H_5	Others[a]	C	H	N	
3a	*p*-$CH_3OC_6H_4$	SCH_3	1485	7.14	2.67 (SCH_3)	3.81 (OCH_3)	59.63 (59.70)	4.94 (5.01)	6.48 (6.33)	$C_{11}H_{11}O_2NS$
3b	*p*-$CH_3C_6H_4$		1485	7.26	2.66 (SCH_3)	2.34 (CH_3)	64.11 (64.36)	5.42 (5.40)	6.88 (6.82)	$C_{11}H_{11}ONS$
3c	*m*-$CH_3C_6H_4$		1490	7.21	2.63 (SCH_3)	2.32 (CH_3)	c)			
3d	C_6H_5		1480	7.27	2.67 (SCH_3)		62.68 (62.80)	4.70 (4.74)	7.16 (7.32)	$C_{10}H_9ONS$
3e	*p*-ClC_6H_4		1482	7.25	2.67 (SCH_3)		53.10 (53.21)	3.55 (3.57)	6.42 (6.21)	$C_{10}H_8ONSCl$
3f	*m*-ClC_6H_4		1490	7.29	2.68 (SCH_3)		53.10 (53.21)	3.56 (3.57)	6.17 (6.21)	$C_{10}H_8ONSCl$
3g	*p*-BrC_6H_4		1480	7.28	2.67 (SCH_3)		44.45 (44.46)	2.96 (2.99)	5.20 (5.19)	$C_{10}H_8ONSBr$
3h	*p*-CNC_6H_4		1465	7.42	2.70 (SCH_3)		61.15 (61.09)	3.66 (3.73)	13.14 (12.96)	$C_{11}H_8ON_2S$
3i	*m*-CNC_6H_4		1482	7.38	2.70 (SCH_3)		61.36 (61.09)	3.66 (3.73)	12.94 (12.96)	$C_{11}H_8ON_2S$
3j	*p*-$NO_2C_6H_4$		1490	7.42	2.69 (SCH_3)		50.91 (50.84)	3.45 (3.41)	11.77 (11.86)	$C_{10}H_8O_3N_2S$
3k	*m*-$NO_2C_6H_4$		1480	7.42	2.71 (SCH_3)		50.84 (50.84)	3.38 (3.41)	11.80 (11.86)	$C_{10}H_8O_3N_2S$
3l	*p*-$CH_3OC_6H_4$	SC_2H_5	1505	7.17	1.48 (t, CH_3) 3.25 (q, SCH_2)	3.82 (OCH_3)	61.10 (61.25)	5.92 (5.57)	5.57 (5.95)	$C_{12}H_{13}O_2NS$
3m	C_6H_5		1480	7.29	1.43 (t, CH_3) 3.21 (q, SCH_2)		c)			
3n	*p*-ClC_6H_4		1480	7.20	1.46 (t, CH_3) 3.24 (q, SCH_2)		55.09 (55.11)	4.20 (4.20)	5.84 (5.84)	$C_{11}H_{10}ONSCl$
3o	*p*-$CH_3OC_6H_4$	$N(CH_3)_2$	1505	6.90		3.05 (NCH_3) 3.77 (OCH_3)	66.13 (66.03)	6.47 (6.47)	12.76 (12.84)	$C_{12}H_{14}O_2N_2$
3p	C_6H_5		1601	7.02		3.06 (NCH_3)	c)			
3q	*p*-ClC_6H_4		1485	7.16		3.11 (NCH_3)	c)			

a) The signals of aromatic protons are omitted, and signal pattern are singlet unless otherwise described. b) Calculated values are listed in the parentheses. c) Not isolated as pure crystals.

TABLE 4. MELTING POINTS, SPECTRAL PROPERTIES, AND ANALITICAL DATA OF THIOCARBAMATE (4)

Compd	Ar	X	Mp θ_m/°C	IR (cm^{-1})		NMR (δ)[a]			Anal (%)[b]		
				C=O	NH	SR	CH_2	NH[c]	C	H	N
4b	*p*-$CH_3C_6H_4$	SCH_3	d)			2.34	4.75(d) J=4.2	6.48	d)		
4d	C_6H_5		d)			2.36	4.80(d) J=4.4	6.58	d)		
4e	*p*-ClC_6H_4		165—166	1685 1640	3325	2.38	4.79(d) J=4.2	6.55	49.02 (49.28)	4.11 (4.14)	5.76 (5.75)
4g	*p*-BrC_6H_4		d)			2.27	4.66(d) J=4.4	6.43	d)		
4i	*m*-CNC_6H_4		143—144	1705 1635	3280	2.38	4.84(d) J=4.5	6.51	56.52 (56.39)	4.23 (4.30)	11.94 (11.96)
4j	*p*-$NO_2C_6H_4$		164—165	1695 1635	3325	2.42	4.88(d) J=4.4	6.44	47.02 (47.24)	4.02 (3.96)	11.23 (11.02)
4m	C_6H_5	SC_2H_5	120—122	1695 1640	3295	1.30(t) 2.98(q)	4.83(d) J=4.4	6.62	59.17 (59.17)	5.85 (5.87)	6.09 (6.27)
4n	*p*-ClC_6H_4		131—133	1690 1640	3320	1.31(t) 2.97(q)	4.80 J=4.2	6.53	52.64 (52.26)	4.88 (4.88)	5.10 (5.43)

a) The signals of aromatic protons are omitted, and signals are singlet unless otherwise listed. b) Calculated values are listed in parentheses. c) All NH signals are broad singlet. d) Pure thiocyanates were not obtained. e) Besides these signals singlet signal of methyl group is at δ=2.16.

General Procedure of the BF_3-catalyzed Decomposition of Alkyl Aryldiazoacetate in the Presence of Nitriles. A 3.0 mmol of alkyl aryldiazoacetate was added in small portions into 10 ml of nitrile containing 0.5 ml of BF_3-etherate at the temperature described in the Table 2. After vigorous evolution of N_2 gas ended, the reaction mixture was poured into 100 ml of ice water saturated with $NaHCO_3$. Organic products were extracted with ether (50 ml×2). Combined ether solution was dried over Na_2SO_4, ether was removed, and then the residue was chromatographed over silica gel.

Decomposition of Methyl p-*Nitrophenyldiazoacetate in Acetonitrile.* The reaction was carried out at 50 °C by the method described above. 5-Methoxy-2-methyl-4-(*p*-nitrophenyl)oxazole (**9a**): Yellow crystals; mp 121.0—122.0 °C; yield 75%; IR (KBr) 1495 cm^{-1} (C=N); NMR ($CDCl_3$) δ=2.43 (s, CH_3), 4.13 (s, OCH_3) 7.8—8.1 (m, Ar). Found: C, 56.56; H, 4.29; N, 11.90%. Calcd for $C_{11}H_{10}O_4H_2$: C, 56.41; H, 4.30; N, 11.96%. Methyl α-acetylamino-*p*-nitrophenylacetate (**11a**): Pale yellow crystals; mp 139.0—140.5 °C; yield 5%, IR (KBr) 3380 (NH), 1735 (ester C=O), 1650 (amide C=O), 1515, 1350 cm^{-1} (NO_2); NMR ($CDCl_3$) δ=2.04 (s, CH_3), 3.74 (s, OCH_3), 5.70 (d, J=7 Hz, NCH), and 7.5—8.2 (ABq, Ar). Found: C, 52.58; H, 4.72; N, 10.89%. Calcd for $C_{11}H_{12}O_5N_2$: C, 52.38; H, 4.80; N, 11.11%.

Decomposition of Methyl p-*Nitrophenyldiazoacetate in Propionitrile.* The reaction was carried out in a similar procedure described above. 2-Ethyl-5-methoxy-4-(*p*-nitrophenyl)oxazole (**9b**): Yellow crystals; mp 96.0—97.0 °C; yield 84%; NMR ($CDCl_3$) δ=1.36 (t, J=7.5 Hz, CH_3), 2.75 (q, J=7.5 Hz, CH_2), 4.13 (s, OCH_3), and 7.92, 8.23 (ABq, J=9.0 Hz, Ar). Found: C, 58.26; H, 4.87; N, 11.27%. Calcd for $C_{12}H_{12}O_4N_2$: C, 58.06; H, 4.87; N, 11.29%. Methyl α-propionylamino-*p*-nitrophenylacetate (**11b**): Pale yellow crystals; mp 144.0—145.0 °C; Yield 6%; IR (KBr) 3325 (NH), 1732 (ester C=O), 1650 (amide C=O), and 1512, 1355 cm^{-1} (NO_2); NMR ($CDCl_3$) δ=1.17 (t, J=7.5 Hz, CH_3), 2.31 (q, J=7.5 Hz, CH_2), 3.75 (s, OCH_3), 5.69 (d, J=6.6 Hz, NCH), 6.84 (br. d, NH), 7.56, 8.20 (ABq, J=9.0, Ar). Found: C, 54.15; H, 5.22; N, 10.50%. Calcd for $C_{12}H_{14}O_5N_2$: C, 54.13; H, 5.30; N, 10.52%.

Decomposition of Methyl p-*Nitrophenyldiazoacetate in Methyl Thiocyanate.* The reaction was performed in a similar procedure described above. Excess methyl thiocyanate was removed by distillation under reduced pressure before chromatography. Methyl α-[(methylthio)carbonylamino]-*p*-nitrophenylacetate (**11c**): Colorless crystals; mp 147.0—148.3 °C; yield 15%; IR (KBr) 3325 (NH), 1730 (ester C=O), 1645 (amide C=O), and 1505, 1340 cm^{-1} (NO_2); NMR ($CDCl_3$) δ=2.30 (s, SCH_3), 3.73 (s, OCH_3), 5.64 (d, J=7.0 Hz, NCH), 7.25 (br. d, NH), and 7.5—8.1 (ABq, Ar). Found: C, 46.68; H, 4.23; N, 9.74%. Calcd for $C_{11}H_{12}O_5N_2S$: C, 46.47; H, 4.26; N, 9.86%.

Decomposition of Methyl p-*Chlorophenyldiazoacetate in Acetonitrile.* The reaction carried out at 0 °C according to the procedure described above gave two products. 4-*p*-Chlorophenyl-5-methoxy-2-methyloxazole (**9d**): Colorless crystals; mp 76.2—76.8 °C; yield 54%; NMR ($CDCl_3$) δ=2.37 (s, CH_3), 3.99 (s, OCH_3), and 7.28, 7.68 (ABq, J=9.0 Hz, Ar). Found: C, 59.08; H, 4.53; N, 6.20%. Calcd for $C_{11}H_{10}O_2NCl$: C, 59.07; H, 4.51; N, 6.26%. Methyl *p*-chlorophenylglyoxylate azine (**10d**): Yellow crystals; mp 157.0—157.5 °C; yield 29%; IR (KBr) 1740 (ester C=O), 1612 cm^{-1} (C=N); NMR ($CDCl_3$) δ=3.99 (s, OCH_3) and 7.39, 7.72 (ABq, J=9.0 Hz, Ar). Found: C, 54.96; H, 3.57; N, 7.36%. Calcd for $C_{18}H_{14}O_4N_2Cl$; C, 54.98; H, 3.59; N, 7.13%.

Decomposition of Methyl p-*Chlorophenyldiazoacetate in Benzene.* Diazoacetate (3.0 mmol) was decomposed in absolute benzene containing 0.5 ml of BF_3-etherate. Chromatography of the reaction products after the usual procedure gave the ketazine (**10d**) in 53% yield along with two white crystalline products. Dimethyl bis(*p*-chlorophenyl)-maleate (**13a**): Colorless crystals; mp 153.0—154.0 °C; yield 17%; IR (KBr) 1725 cm^{-1} (ester C=O); NMR ($CDCl_3$) δ=3.54 (s, OCH_3) and 7.36 (s, Ar). Found: C, 59.33; H, 3.81%. Calcd for $C_{18}H_{14}O_4Cl_2$: C, 59.20; H, 3.86%. Dimethyl bis(*p*-chlorophenyl)fumarate (**13b**): Colorless crystals; mp 126.0—127.0 °C; yield 26%; IR (KBr) 1715 cm^{-1} (ester C=O); NMR ($CDCl_3$) δ=3.81 (s, OCH_3) and 7.02, 7.21 (ABq, J=8.5 Hz, Ar). Found: C, 59.07; H, 3.83%. Calcd for $C_{18}H_{14}O_4Cl_2$: C, 59.20; H, 3.86%.

Decomposition of Ethyl Phenyldiazoacetate in Acetonitrile. The reaction was carried out at 10 °C in excess of acetonitrile in the presence of BF_3-etherate. Two products were obtained. 5-Ethoxy-2-methyl-4-phenyloxazole (**9e**): Colorless oil; yield

27%; NMR ($CDCl_3$) δ=1.43 (t, CH_3), 2.03 (s, CH_3), 4.45 (q, CH_2), and 7.3—8.2 (m, Ph). Ethyl phenylglyoxylate azine (**10e**): Yellow crystals; mp 143.5—144.0 °C; yield 49%; IR (KBr) 1728 (ester C=O) and 1570 cm^{-1} (C=N); NMR ($CDCl_3$) δ=1.40 (t, CH_3), 4.47 (q, OCH_2), and 7.3—7.8 (m, Ph). Found: C, 68.12; H, 5.71; N, 7.93%. Calcd for $C_{20}H_{20}O_4N_2$: C, 68.17; H, 5.72; N, 7.95%.

Decomposition of Ethyl Phenyldiazoacetate in Propionitrile. The reaction at 10 °C gave corresponding oxazole along with the ketazine (**10e**; 35%). 5-Ethoxy-2-ethyl-4-phenyloxazole (**9f**): Colorless crystals; mp 22 °C; yield 65%; NMR (CDCl) δ=1.33 (t, CH_3), 1.42 (t, CH_3), 2.70 (q, CH_2), 4.27 (q, OCH_2), and 7.1—7.9 (m, Ph). Found: C, 71.86; H, 6.94; N, 6.51%. Calcd for $C_{13}H_{15}O_2N$: 71.86; H, 6.96; N, 6.45%

Decomposition of N,N-*Dimethyl*-p-*nitrophenyldiazoacetamide (14) in Acetonitrile.* The diazoacetamide (3 mmol) was decomposed by adding in small portions into 10 ml of acetonitrile containing 1.0 ml of BF_3-etherate at 0 °C. After the usual procedure described above, silica-gel column chromatography of the reaction mixture gave three products. 5-Dimethylamino-2-methyl-4-(*p*-nitrophenyl)oxazole (**15**): Yellow crystals; mp 103—104 °C; yield 4%; IR (KBr) 1510, 1345 cm^{-1} (NO_2); NMR ($CDCl_3$) δ=2.41 (s, CH_3), 2.82 (s, NCH_3), 7.9—8.2 (ABq, Ar). Found: C, 58.13; H, 5.28; N, 17.21%. Calcd for $C_{12}H_{13}O_3N_3$: C, 58.29; H, 5.30; N, 17.00%. *N,N*-Dimethyl-*p*-nitromandelamide (**16**): Colorless crystals; mp 189—190 °C; yield 39%; IR(KBr) 3280 (OH), 1640 (amide C=O), 1515, 1355 cm^{-1} (NO_2); NMR ($CDCl_3$) δ=2.79 (s, NCH_3), 3.02 (s, NCH_3), 4.75 (d, OH), 5.26 (d, CH), 7.4—8.3 (ABq, Ar). Found: C, 53.76; H, 5.37; N, 12.29%. Calcd for $C_{10}H_{12}O_4N_2$: C, 53.57; H, 5.39; N, 12.48%. α-Acetylamino-*N,N*-dimethyl-*p*-nitrophenylacetamide (**17**): Pale yellow crystals; mp 162—163 °C; yield 26%; IR (KBr) 3325 (NH), 1640 (amide C=O), 1490, 1350 cm^{-1} (NO_2); NMR ($CDCl_3$) δ= 2.01 (s, CH_3), 2.97 (s, NCH_3), 3.00 (s, NCH_3), 5.99 (d, CH), 7.63 (br. d, NH), and 7.5—8.2 (ABq, Ar). Found: C, 54.52; H, 5.72; N, 15.72%. Calcd for $C_{12}H_{15}O_4N_3$: C, 54.33; H, 5.70; N, 15.84%.

References

1) R. Huisgen, H. Koenig, G. Binsh, and H. J. Sturn, *Angew. Chem.*, **73**, 368 (1961).
2) I. J. Turchi and M. J. S. Dewar, *Chem. Rev.*, **75**, 389 (1975) and references cited therein.
3) B. H. Lipshutz and R. W. Hungate, *J. Org. Chem.*, **46**, 1410 (1981) and references cited therein.
4) T. Ibata and R. Sato, *Chem. Lett.*, **1978**, 1129; *Bull. Chem. Soc. Jpn.*, **52**, 3597 (1979).
5) M. Takebayashi, T. Ibata, H. Kohara, and Bu Hong Kim, *Bull. Chem. Soc. Jpn.*, **40**, 2392 (1967).
6) M. S. Newman and P. F. Beal III, *J. Am. Chem. Soc.*, **71**, 1506 (1949).
7) M. Regitz, *Chem. Ber.*, **98**, 1210 (1965).
8) J. Yamawaki, T. Ando, and T. Hanafusa, *Chem. Lett.*, **1981**, 1143.
9) E. Ciganek, *J. Org. Chem.*, **35**, 862 (1970).

 © 1984 The Chemical Society of Japan Bull. Chem. Soc. Jpn., 57, 2456—2462 (1984) [Vol. 57, No. 9

N-Hydroxy Amides. II[1]. *N*-Benzyloxy α-Amino Acid *N*-Hydroxysuccinimide Esters and Synthesis of a Hexapeptide Having an Alternating *N*-Hydroxy Amide-Amide Sequence

Kazuyuki SHIMIZU, Kazuyuki NAKAYAMA, and Masayasu AKIYAMA*
Department of Applied Chemistry for Resources, Tokyo University of Agriculture and Technology, Koganei, Tokyo 184
(Received February 25, 1984)

Acylation of a series of *N*-benzyloxy α-amino acid derivatives with *N*,*N*-phthaloyloglycine shows that the yield decreases with increasing bulkiness of the substituent even by the acyl chloride or mixed anhydride procedure, and that the use of an excess reagent or a double acylation technique is needed to attain a good yield. The low reactivity of the benzyloxyamino group enables us to utilize *N*-benzyloxy α-amino acid *N*-hydroxysuccinimide esters without *N*-protection in the acylation of the usual amino group. In an attempt to lengthen the chain of an *N*-hydroxy peptide, a hexapeptide anilide having an *N*-hydroxy-DL-alanylglycyl sequence was synthesized *via* *N*-benzyloxy peptides. The complex forming tendency of the hexapeptide with iron(III) is examined.

Considerable effort has been directed to the synthesis of peptides having *N*-hydroxy amide bonds in the chain.[1-4] In view of the unique biological activity of naturally occurring hydroxamic acids,[5-7] the synthetic *N*-hydroxy peptides are of interest as they may serve as models for intermediates in biogenetic transformation,[8] precursors of dehydropeptides[9] and ionophoric peptides[10] as well as physiologically active substances, such as hadacidin,[11] rhodotorulic acid and ferrichromes.[6] The biological activity of the natural hydroxamic acids centers on their unique ability to chelate iron(III) for cell-membrane transport.[6] Except for a few total syntheses of natural substances,[7,12] oligopeptides with two or more *N*-hydroxy amide groups in the chain have rarely been obtained.[13] There are few general procedures for introducing the *N*-hydroxy amide bond into a peptide sequence.[3,14] *N*-Benzylozy α-amino acids have been utilized under these circumstances.[15] Previously, we reported on the use of *N*-benzyloxy α-amino acid *N*-carboxy anhydrides (*N*-benzyloxy-NCAs) for a stepwise synthesis of an *N*-benzyloxy tetrapeptide.[16] Also it was reported that polymerization of these NCAs, followed by debenzylation, led to poly(*N*-hydroxy peptide)s.[1] In this paper we describe a procedure for obtaining sequential *N*-hydroxy peptides together with the related investigations, including an examination of iron(III) chelation.

Results and Discussion

By the use of benzyloxy-NCAs, introduction of an *N*-benzyloxy α-amino acid residue into a growing peptide having the usual amino terminus has become an easy process,[16] so that a key step in the synthesis of *N*-hydroxy peptides is subsequent acylation of the terminal benzyloxyamino group. Nucleophilic reactivity of the benzyloxyamino group decreases considerably due to the inductive effect of the oxygen and steric hindrance by the benzyloxy moiety. Kolasa and Chimiak commented briefly that acylation of the *N*-benzyloxy α-amino acids with a bulky side chain was difficult,[3] but the scope and limitations of the acylation reactions have not yet been fully investigated.

Careful examination of a coupling reaction between *N*,*N*-phthaloylglycine (Pht=GlyOH) and methyl *N*-benzyloxy-DL-alaninate (DL-H(PhCH$_2$O)AlaOMe) by using a few selected coupling methods[17] gave the following results (yield of the coupling after recrystallization); acyl chloride in DMF (69%), isobutyl chloroformate (65%), *N*-ethoxycarbonyl-2-ethoxy-1,2-dihydroquinoline (EEDQ) (46%), pivaloyl chloride (40%), 1,1-carbonyldiimidazole (CDI) (37%), *N*-hydroxysuccinimide (0%): Care was taken to allow a sufficient time for each coupling procedure. These results confirm that strong activation of the acyl group is necessary to attain practical yields. Using the acyl chloride or the mixed anhydride of *N*,*N*-phthaloylglycine, acylation of a series of methyl esters of *N*-benzyloxy α-amino acids and *N*-benzyloxy dipeptides (Scheme 1) was carried out as shown in Fig. 1. The dipeptide

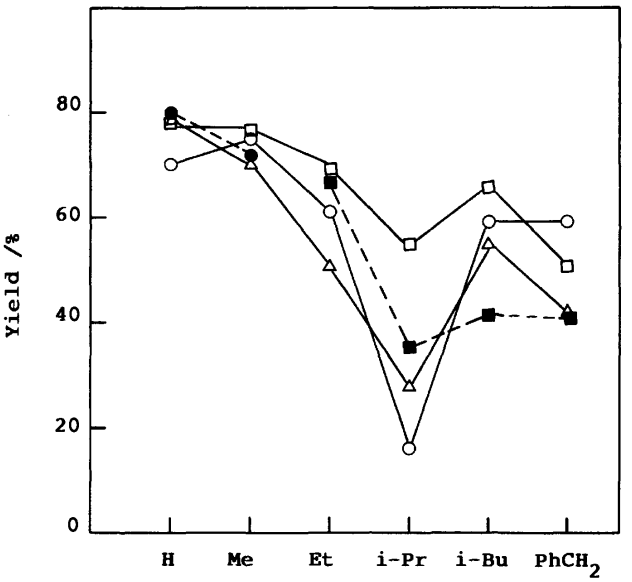

Fig. 1. Yield *vs.* α-substituent in the acylation of **1a—f** and **3a—f** with Pht=Gly-OH: —○— **1a—f** by acyl chloride under Schotten-Baumann conditions; —□— **1a—f** by acyl chloride in DMF; —△— **1a—f** by mixed anhydride with isobutyl chloroformate; —●— **3a—f** by acyl chloride under Schotten-Baumann conditions; —■— **3a—f** by acyl chloride in DMF. For a key, see Scheme 1.

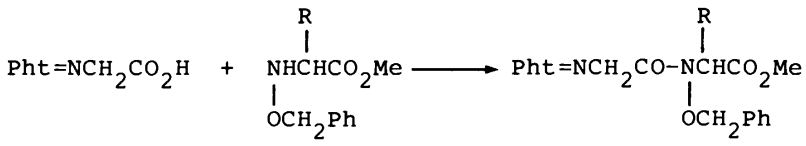

1a-f **2a-f**

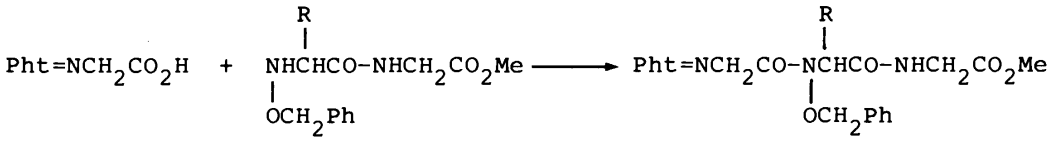

3a-f **4a-f**

a b c d e f

R = H, Me, Et, i-Pr, i-Bu, $PhCH_2$

Scheme 1.

Table 1. Products on acylation of *N*-benzyloxy amino acid derivatives

Product	Mp θ_m/°C	TLC[a] R_f^1	TLC[a] R_f^2	TLC[a] R_f^3	Found (Calcd)/% C	H	N
2a	117—118	0.85	0.81	0.62	61.96 (62.09	4.77 4.82	7.51 7.24)[b]
2b	136—137 (133—134)[c]	0.88	0.85	0.63			
2c	oil	0.88	0.85	0.63	64.08 (64.38	5.68 5.40	6.77 6.83)
2d	126—127	0.90	0.88	0.67	65.17 (65.08	5.64 5.70	6.59 6.60)
2e	oil	0.91	0.91	0.67	65.24 (65.08	6.21 5.99	6.53 6.33)[b]
2f	135—136	0.90	0.91	0.64	68.06 (67.98	5.05 5.03	5.88 5.87)[b]
4a	151—152	0.67	0.59	0.32	59.99 (60.13	4.82 4.82	9.55 9.56)
4b	132—133	0.79	0.66	0.52	60.50 (60.92	5.08 5.11	9.33 9.27)
4c	92— 94	0.84	0.69	0.57	61.67 (61.66	5.49 5.39	8.77 8.99)
4d	108—110	0.77	0.87	0.65	62.95 (62.36	6.06 5.65	8.38 8.73)
4e	136—137	0.88	0.74	0.66	62.83 (63.03	5.89 5.90	8.36 8.48)
4f	146—149	0.85	0.79	0.61	65.69 (65.77	5.14 5.14	8.09 7.94)

a) R_f^1, EtOAc; R_f^2, $CHCl_3$-MeOH-C_6H_6 (6:1:3); R_f^3, THF-hexane (1:1). b) $(1/4)H_2O$ is included in the calcd value. c) Ref. 3).

esters may serve as a model for growing *N*-benzloxy peptides. A decrease in the yield with increasing bulkiness of the α-substituents is clearly seen. This is ascribed to steric hindrance by the substituents. Only acyl chloride in DMF gave satisfactory results for most of the cases. The products in the acylation are summarized in Table 1. By a repetitive acylation or the use of excess reagents, these low yields may be improved (Table 2). This suggests a possibility of synthesizing longer peptides by the stepwise method.

The observation that the benzyloxyamino group did not react with the *N*-hydroxysuccinimide (HOSu) ester prompted us to utilize the benzyloxyamino acids in the

form of active esters without *N*-protection. Treatment of the *N*-benzyloxy α-amino acids with HOSu in the presence of DCC gave the corresponding active esters in good yields (Eq. 1). The esters were characterized as crystalline hydrochlorides except for that of *N*-benzyloxyglycine, which was converted into a more stable pentachlorophenyl ester (Table 3). These active esters reacted readily with methyl glycinate to afford the corresponding dipeptide methyl esters (Eq. 2 and Table 4), as did the *N*-benzyloxy-NCAs.[16]

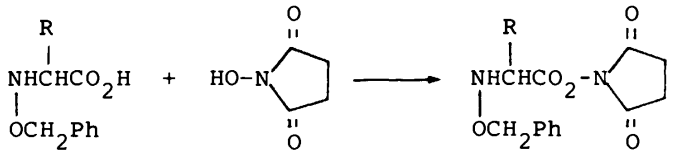

(1)

5a–f

a b c d e f

R = H, Me, Et, i-Pr, i-Bu, $PhCH_2$

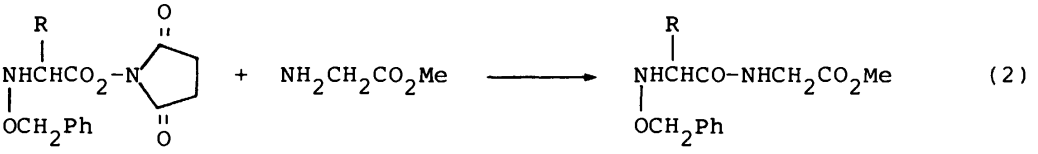

(2)

3a–f

Table 2. Excess reagents or a repetitive method on acylation

Run	Acyl Component (mmol)	Amino Component (mmol)	DMF ml	Temp °C	Time h	Yield %
1	Pht=Gly-Cl (2.8)	H-(BzlO)Phe-OMe (1.1)	10	−5	24	92
2	Pht=Gly-Cl (4.25)	H-(BzlO)Val-Gly-OMe (1.7)	25	−5	24	86
3	Pht=Gly-Cl (6.0)	H-(BzlO)Phe-Gly-OMe (2.5)	20	−5	24	91
4	Pht=Gly-OH[a] (10.0)	H-(BzlO)Phe-Gly-OMe (2.0)	30	−15	30	85
5	Pht=Gly-OH[a,b] (2.2)	H-(BzlO)Phe-Gly-OMe (2.0)	40	−15	30	68

a) Mixed anhydride procedure. b) Coupling was repeated 3 times under these conditions.

Table 3. *N*-benzyloxy dl-α-amino acid *N*-hydroxysuccinide esters (**5a—f**)

	Yield %	Mp θ_m/°C	TLC[a] R_f^1	TLC[a] R_f^4	Found (Calcd)[b]/(%) C	H	N
5a	98	113—114[c]	0.76	0.79	46.20 (49.61)	4.80 (4.80)	9.02 (8.90)
5a'[d]	79	92— 93			41.92 (41.95)	2.36 (2.35)	3.37 (3.26)
5b	94	134—136[c]	0.81	0.79	50.93 (51.15)	5.23 (5.21)	8.62 (8.52)
5c	85	129—130[c]	0.89	0.79	52.72 (52.56)	5.61 (5.59)	8.20 (8.17)
5d	87	139—140	0.84	0.96	54.07 (53.86)	6.05 (5.93)	7.77 (7.85)
5e	81	84— 85	0.87	0.96	60.85 (61.07)	6.65 (6.63)	8.42 (8.38)[e]
5f	88	135—136[c]	0.84	0.76	59.02 (59.34)	5.10 (5.23)	6.74 (6.92)

a) R_f^1, EtOAc; R_f^4, $CHCl_3$–MeOH (3:1). b) As the hydrochloride. c) With decomp. d) *N*-Benzyloxyglycine pentachlorophenyl ester. e) As the free base.

Removal of the protective group from *N*-benzyloxy peptides is also an important step for synthesis of *N*-hydroxy peptides. Using Pht=Gly-DL-(PhCH$_2$O)-Phe-Gly-OMe as a substrate, several debenzylation procedures were tested: These are HBr in AcOH, $(CF_3CO_2)_3B$ in CF_3CO_2H, and hydrogenation with Ni or a few types of Pd catalysts. The reaction was followed by HPLC. Hydrogenation with Pd catalysts[3,14] was found to be the most satisfactory.

In order to show the usefulness of the active esters and a facile peptide chain elongation, synthesis of a hexapeptide having an *N*-hydroxyalanylglycyl sequence was carried out. Thus, DL-H(PhCH$_2$O)Ala-OSu was coupled with glycinanilide to give a benzyloxy dipeptide anilide (**6**). A reaction cycle for lengthening the benzyloxy peptide chain was performed; *viz.* acylation of the terminal benzyloxyamino group with Boc-Gly-OH by the mixed anhydride method, followed by deprotection of the Boc-group and then subsequent coupling with H(PhCH$_2$O)Ala-OSu. The cycle was repeated and finally interrupted by coupling with Ac-(PhCH$_2$O)Ala-OSu. A critical step was acylation of the benzyloxyamino group by the mixed anhydride method. To secure a practical yield, a double acylation technique was performed for this step. The resulting acetyl hexapeptide (**10**) was debenzylated by catalytic hydrogenation to give an *N*-hydroxy hexapeptide (**11**). The outline of the synthesis is shown in Fig. 2 and the data for the intermediate peptides are summarized in Table 5.

This kind of alternating sequential peptides is of interest, since it has three *N*-hydroxy peptide units and presents possibilities of holding iron(III) intramolecularly and/or intermolecularly. Natural trihydroxamic acids such as desferrioxames form stable complexes

Table 4. Results of the reaction of **5a—f** with H-Gly-OMe

Product	Yield %	Mp (lit,[a] Mp) θ_m/°C		TLC R_f^1	TLC R_f^2
3a	70	122—125	(124—126)	0.56	0.48
3b	86	164—165	(165—166)	0.63	0.53
3c	73	170—171	(172—173)	0.74	0.43
3d	79	177—179	(183—184)	0.79	0.49
3e	86	137—138	(138—139)	0.91	0.61
3f	85	168—169	(168—169)	0.90	0.80

a) Ref. 16).

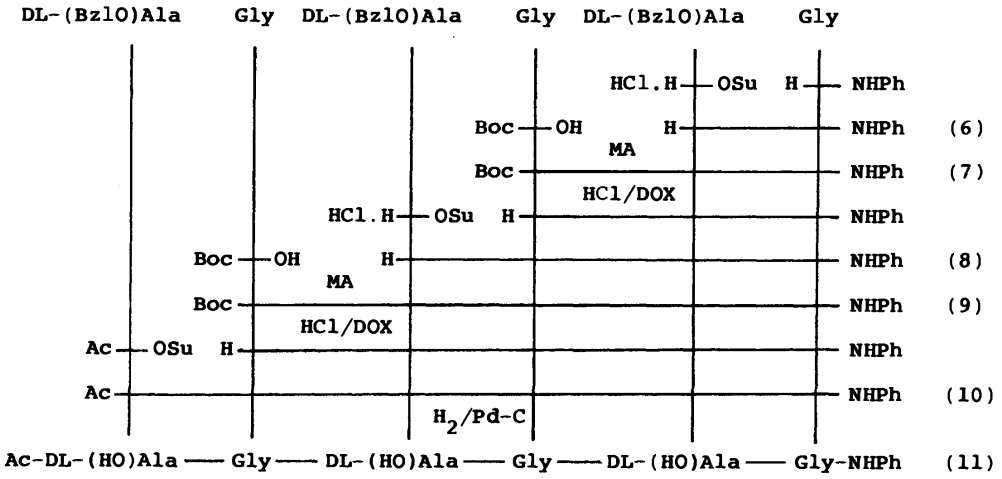

Fig. 2. Synthesis of an *N*-hydroxy hexapetide (**11**) *via* *N*-benzyloxy peptides (**6—10**): BzlO stands for PhCH$_2$O and DOX for dioxane. Acylation by the mixed anhydride procedure was repeated 3 times.

Table 5. Synthesis of *N*-hydroxy peptides (**6—11**)

Compound	Yield %	Mp θ_m/°C	TLC R_f^1	TLC R_f^2	TLC R_f^3	Found (Calcd)/% C	H	N
6	86	143—144	0.45	0.63	0.88	66.35 (66.03	6.79 6.47	12.89 12.84)
7	74	121—122	0.58	0.60	0.88	62.28 (61.96	6.84 6.66	11.71 11.56)
8	80	122—124	0.34	0.56	0.88	64.00 (64.16	6.21 6.28	12.59 12.47)
9	63	135—136	0.50	0.61	0.88	61.85 (61.82	6.47 6.45	11.58 11.69)
10	75	113—115	0.21	0.66	0.90	61.99 (61.69	6.15 6.19	11.31 11.45)
11	94	191—192 (decomp)			0.62	48.34 (48.67	5.86 5.86	16.96 17.28)

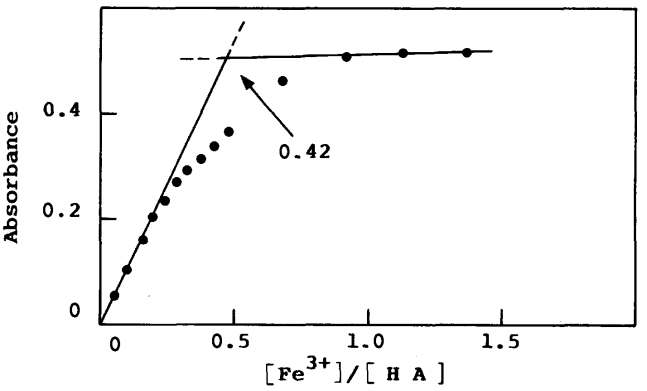

Fig. 3. Absorbance *vs.* the ratio of iron(III) to the hydroxamic acid (HA) units in 50 % aqueous DMF at pH=3 and 25 °C, ionic strength 0.1 (KNO_3). Absorbance at 463—487 nm.

with iron(III). On the other hand, little is known about the chelation tendency of synthetic *N*-hydroxy peptides.

The hexapeptide showed an intense violet color when mixed with $FeCl_3$ solution. The complex forming tendency was examined by determing the molar ratio of iron(III) to the *N*-hydroxy amide unit in 50% aq DMF solution.[1] The absorbance *vs.* the molar ratio plot (Fig. 3) reveals a curvature around an intersection of the two extrapolated straight lines. The intersection corresponds to the molar ratio of iron(III) to the *N*-hydroxy amide unit; the value being 0.33 for a 1:3 complex. A value of 0.42 was obtained for the present case, which is interpreted as a formation of an unstable complex rather than a stable 1:3 complex. This may be supported by a shift of λ_{max} to a longer wavelength (470 nm) coupled with a decrease in absorbance. It is known that a typical 1:3 complex, ferrioxamine B, shows its maximum at 420 nm while a 1:1 complex, which is usually observed for a monohydroxamic acid with iron(III) at low pH, has the maximum at 520 nm.[5] A 1:2 complex formation has been suggested for a polmyer system with λ_{max} at 466 nm[18] and also for an intermediate stage during transformation of a 1:3 complex to a 1:1 complex by an increasing acidity of the solution.[19-20] It appears that an alternating sequence of the *N*-hydroxy amide units is too dense to form a stable 1:3 complex either intramolecularly or intermolecularly.

Experimental

All the melting points are uncorrected. IR spectra were obtained with a JASCO model 403G spectrophotometer and ^1H NMR spectra were recorded on a JEOL FX200 spectrometer with TMS as internal standard. HPLC was carried out with a JASCO twincle apparatus by using a column packed with a Finepak SIL C_{18}. Microanalysis was performed in the Analytical Section, Institute of Physical and Chemical Research, Saitama. TLC was carried out by using Merck precoated silica gel 60 F_{254} plates: R_f^1, EtOAc; R_f^2, $CHCl_3$–MeOH–C_6H_6 (6:1:3); R_f^3, THF–hexane (1:1); R_f^4, $CHCl_3$–MeOH (3:1). The iron (III) complex molar ratio was determined as previously.[1] *N*-Benzyloxy-DL-amino acid methyl ester hydrochlorides ($PhCH_2ONHCH(R)CO_2Me \cdot HCl$) were obtained by treating the corresponding acid with HCL-saturated methanol: R, mp (lit,[21] mp); H, 125—126 °C (125—126 °C); Me, 130—131 °C (131—132 °C); Et. 114—116 °C (115—117 °C); *i*-Pr, 127—128 °C (127—130 °C); *i*-Bu, 115—117 °C (120—123 °C); $PhCH_2$, 119—120 °C (118—119 °C).

Coupling Methods. The following coupling procedures (a—f) were applied to the reaction of Pht=GlyOH with DL-$H(PhCH_2O)$AlaOMe; (a) acyl chloride in DMF, 3 h at −5 °C and 24 h at 25 °C; (b) mixed anhydride with $ClCO_2Bu^i$ in THF, 24 h at −15 °C and 48 h at 25 °C; (c) EEDQ in THF, 48 h at 30 °C; (d) mixed anhydride with pivaloyl chloride in THF, 48 h at 25 °C; (e) CDI in THF, 24 h at 0 °C and 24 h at 25 °C; (f) HOSu ester in THF, 72 h at 25 °C. In each case, a solution of an acyl active derivative of Pht=GlyOH was prepared either by simply dissolving the derivative or by adding an appropriate reagent to the solution of Pht=GlyOH (0.84 g, 4 mmol). To this solution was added $H(PhCH_2O)$Ala-OMe·HCl (0.982 g, 4 mmol) and Et_3N (0.404 g, 4 mmol, or 0.808 g in the case of acyl chloride). The resulting mixture was subjected to the above procedure (a—f). After evaporation of the solvent, the residue was extracted with AcOEt (100 mL) and the extract washed with 0.1 M (1 M=1 mol dm^{-3}) HCl, 5% $NaHCO_3$, and water, and then dried (Na_2SO_4). Evaporation of the solvent gave a crude product, which was recrystallized from AcOEt, mp 136—137 °C (lit,[3] mp 133—134 °C). Mp was depressed when the yield was less than 50%.

General Procedure for Acylation of N-Benzyloxy α-Amino Acid Derivatives. (A) Acyl Chloride under Schotten-Baumann Conditions: As a typical example, the preparation of Pht=Gly-DL-$(PhCH_2O)$Ala-Gly-OMe is described. To a mixture of DL-$H(PhCH_2O)$Ala-Gly-OMe·HCl (0.605 g, 2 mmol) in AcOEt (20 mL) and 5% $NaHCO_3$ (7 mL) was added Pht=Gly-Cl (0.447 g, 2 mmol) in AcOEt (20 mL) at 0—5 °C with vigorous stirring. The stirring was continued for 1 h at 5 °C and 48 h at room temperature, and AcOEt (60 mL) was added to extract the reaction products. The organic layer was washed with 0.1 M HCl, 5% Na_2CO_3, and water, and then dried over Na_2SO_4. Evaporation of the solvent gave the crude product; yield, 0.65 g (72%); mp 127—129 °C. The product was recrystallized from AcOEt–hexane to give a pure sample.

(B) Acyl Chloride in DMF: The preparation of Pht=Gly-DL-$(PhCH_2O)$Phe-Gly-OMe is given as an example. To a mixture of DL-$H(PhCH_2O)$Phe-Gly-OMe·HCl (1.13 g, 3 mmol) and Et_3N (0.61 g, 6 mmol) in DMF (30 mL) was added Pht=Gly-Cl (0.67 g, 3 mmol) in DMF (10 mL) at −10—−5 °C. After the mixture was stirred for 3 h at −5 °C and 48 h at room temperature, the solvent was removed under vacuum. The residue was dissolved in AcOEt (100 mL), and the organic layer was washed with 0.1 M HCl, 5% Na_2CO_3 and water, and dried over Na_2CO_3. Evaporation of the solvent gave a crude product, which was purified by column chromatography using Wakogel C-200; yield, 0.67 g (42%); mp 146—149 °C.

(C) Mixed Anhydride Procedure: The preparation of Pht=Gly-DL-$(PhCH_2O)$Abu-OMe is given as an example. A mixed anhydride was prepared from Pht=GlyOH (1.02 g, 5 mmol), Et_3N (0.505 g, 5 mmol) and isobutyl chloroformate (0.68 g, 5 mmol) in THF (30 mL) at −10 °C. To this was added DL-$H(PhCH_2O)$Abu-OMe·HCl (1.30 g, 5 mmol) and Et_3N (0.505 g, 5 mmol) in THF (10 mL) at −15 °C, and the mixture was stirred for 24 h at −20 °C and at 5 °C for 2 d. After evaporation of the solvent, the workup was carried out as above, to give an oily product.

N-Benzyloxy DL-*α-Amino Acid N-Hydroxysuccinimide Ester Hydrochlorides. General Procedure*: To a solution of *N*-benzyloxy α-amino acid (5 mmol) and *N*-hydroxysuccinimide (0.58 g, 5 mmol) in THF (10 mL) was added DCC (1.03 g, 5 mmol) in THF (10 mL) at 0 °C with stirring. The solution was kept for 1 h at 0 °C and for 20 h in the refri-

gerator. *N,N'*-Dicyclohexylurea (DCU) which separated was removed by filtration and the filtrate was evaporated to give a residue. It was diluted with AcOEt (20 mL) to give additional DCU. After separation of DCU, the filtrate was concentrated to give an oil or solid. This was treated with 1 M HCl in THF (20 mL) for 1 h at room temperature. Evaporation of the solvent gave the crude product. The product could be used for further coupling without purification. For an analytical sample, it was recrystallized from AcOEt-hexane.

Reactions of N-*Benzyloxy-α-amino Acid* N-*Hydroxysuccinimide Esters with H-Gly-OMe. General Procedure*: To a solution of H-Gly-OMe·HCl (0.25 g, 2 mmol) and Et_3N (0.202 g, 2 mmol) in $CHCl_3$ (10 mL), was added H($PhCH_2O$)-NHCHRCOOSu·HCl (2 mmol) and Et_3N (0.20 g, 2 mmol) in $CHCl_3$ (10 mL) at 0°C under stirring. The solution was kept for 2 h at 0°C and 1 d at room temperature. After evaporation of the solvent, the residue was diluted with AcOEt (50 mL), and the AcOEt solution was washed with 5% $NaHCO_3$ and water, and dried (Na_2SO_4). After the solvent was evaporated, the residue was treated with 2 M HCl in dioxane (3 mL) for 1 h at room temperature. Evaporation of the solvent gave the crude dipeptide hydrochloride, which was recrystallized from MeOH-ether.

*Pht=Gly-*DL*-(HO)Phe-Gly-OMe.* Pht=Gly-DL-($PhCH_2O$)Phe-Gly-OMe (2.65 g, 5 mmol), 10% Pd on carbon (0.030 g) and MeOH (10 mL) were placed in a hydrogenation apparatus. The mixture was shaken with H_2 under the atmospheric pressure for 24 h at 30 °C. The catalyst was filtered off, and the filtrate was evaporated to give the crude product. It was recrystallized from $CHCl_3$-hexane; yield, 1.93 g (88%); mp 183—184 °C (decomp). Found: C, 59.51; H, 4.76; N, 9.43. Calcd for $C_{22}H_{21}N_3O_7\cdot(1/4)H_2O$: C, 59.65; H, 4.66; N, 9.49%.

When the sample was mixed with a $FeCl_3$ solution, it gave an intense voilet color.

DL-*H($PhCH_2O$)Ala-Gly-NHPh (6).* To a solution of DL-H($PhCH_2O$)Ala-OSu·HCl (4.92 g, 15 mmol) and Et_3N (1.52 g, 15 mmol) in $CHCl_3$ (25 mL) was added H-Gly-NHPh·HCl (2.80 g, 15 mmol) in $CHCl_3$ (15 mL) containing Et_3N (1.52 g), and the mixture was stirred at room temperature. After 30 h, the mixture was washed with 5% $NaHCO_3$ and water, and dried (Na_2SO_4). Evaporation of the solvent gave the crude product, which was recrystallized from AcOEt-hexane; yield, 4.1 g (86%).

*Boc-Gly-*DL*-($PhCH_2O$)Ala-Gly-NHPh (7).* Boc-Gly-OH (0.29 g, 1.65 mmol) in THF (10 mL) containing Et_3N (0.167 g, 1.65 mmol) was converted into the mixed anhydride by adding isobutyl chloroformate (0.205 g, 1.5 mmol) in THF (5 mL) at −15 °C. To this mixture was added the dipeptide anilide (**6**) (0.491 g, 1.5 mmol) in DMF (10 mL), and the resulting mixture was stirred for 3 h at −15 °C and 12 h at 0 °C. After evaporation of the solvent, the residue was diluted with ethyl acetate (11 mL). The organic layer was washed with 5% $NaHCO_3$ and water, and dried over Na_2SO_4. Evaporation of the solvent gave the crude product (0.72 g). To ensure coupling, the crude product was subjected to the above acylation procedure two further times. The final product was chromatographed using Wakogel C-100 with EtOAc as eluant. The product obtained was 0.59 g (74% yield).

DL-*H($PhCH_2O$)Ala-Gly-*DL*-($PhCH_2O$)Ala-Gly-NHPh(8).* Boc-tripeptide anilide (**7**) (0.82 g, 1.69 mmol) was dissolved in dioxane (6 mL). To this was added 3.6 M HCl in dioxane (5 mL). The reaction mixture was stirred for 2 h at 5 °C and evaporated. The residue was triturated with ether and filtered. The product was recrystallized from MeOH-ether to give 0.60 g (85%) of the tripeptide anilide hydrochloride, mp 175—176 °C (decomp).

The tripeptide anilide hydrochloride (0.69 g, 1.65 mmol) and triethylamine (0.168 g, 1.65 mmol) were dissolved in $CHCl_3$ (15 mL). To the solution was added a solution containing H($PhCH_2O$)Ala-OSu (0.54 g, 1.65 mmol) and Et_3N (0.168 g, 1.65 mmol) in $CHCl_3$(10 mL) at 0 °C. The solution was stirred for 1 h at 0 °C and then for 24 h at room temperature. The $CHCl_3$ layer was washed with 5% $NaHCO_3$ and water, and dried (Na_2SO_4). Evaporation of the solvent gave a product (0.80 g), which was recrystallized from EtOAc-hexane; yield, 0.74 g (80%).

*Boc-Gly-*DL*-($PhCH_2O$)Ala-Gly-*DL*-($PhCH_2O$)Ala-Gly-NHPh (9).* Boc-GlyOH (0.193 g, 1.1 mmol) and Et_3N (0.113 g, 1.1 mmol) were placed in THF (10 mL) and cooled. To this was added $ClCO_2Bu^i$ (0.137 g, 1 mmol) in THF (5 mL) at −16°C. After 10 min, the tetrapeptide anilide (**8**) (0.56 g, 1 mmol) in DMF (10 mL) was added slowly to the mixed anhydride solution at −16 °C. The reaction mixture was stirred for 24 h at −16 °C, evaporated and diluted with EtOAc (40 mL). The organic layer was washed with 5% $NaHCO_3$ and water, and dried over Na_2SO_4. Evaporation of the solvent gave a residue. This residue was found to contain the starting tetrapeptide anilide; it was subjected two more times to a similar Boc-Gly mixed anhydride acylation. The crude residue thus obtained amounted to 0.84 g. It was purified by chromatography on a column of Wakogel C-100 with EtOAc as eluant by the flash technique; yield, 0.45 g (63%).

*Ac-*DL*-($PhCH_2O$)Ala-Gly-*DL*-($PhCH_2O$)Ala-Gly-*DL*-($PhCH_2O$)Ala-Gly-NHPh (10).* *Ac-*DL*-($PhCH_2O$)Ala-OSu*: To a solution of Ac-DL-($PhCH_2O$)Ala-OH (0.68 g, 2,9 mmol) and HOSu (0.33 g, 2.9 mmol) in THF (10 mL) was added DCC (0.59 g, 2.9 mmol) in THF (5 mL) at 0 °C. The solution was stirred for 1 h at 0 °C and kept in the refrigerator for 24 h. The crude product, which was obtained by the usual workup performed for a DCC reaction, was recrystallized from EtOAc-hexane; yield, 0.65 g (67%); mp 100—100.5 °C. Found: C, 57.11; H, 5.45; N, 8.35. Calcd for $C_{16}H_{18}N_2O_6$: C, 57.48; H, 5.43; N, 8.38 (%).

The pentapeptide anilide (**9**) (0.44 g, 0.61 mmol) was dissolved in dioxane (5 mL), to remove the Boc group. After the addition of 3.6 M HCl in dioxane (20 mL), the resulting solution was stirred for 2 h at room temperature and evaporated. The residue was triturated with ether, and the precipitate was filtered to give the pentapeptide anilide hydrochloride; yield, 0.346 g (86%).

The pentapeptide anilide hydrochloride (0.451 g, 0.52 mmol) and Et_3N (0.52 g, 0.52 mmol) were stirred in THF (10 mL) at 0 °C for 1 h. To this mixture was added Ac-DL-($PhCH_2O$)Ala-OSu (0.174 g, 0.52 mmol) in THF (10 mL). The reaction mixture was stirred for 48 h at 25 °C, evaporated and extracted with EtOAc (50 mL). The organic layer was washed successively with 5% $NaHCO_3$, 5% citric acid and water, and dried over Na_2SO_4. Evaporation of the solvent gave the crude product, 0.431 g (99%). The product was chromatographed on Wakogel C-200, to give a pure sample; yield, 0.325 g (75%).

*Ac-*DL*-(HO)Ala-Gly-*DL*-(HO)Ala-Gly-*DL*-(HO)Ala-Gly-NHPh (11).* The acetyl hexapeptide anilide (**10**) (0.240 g, 0.27 mmol), 10% Pd/C (0.040 g) and MeOH (20 mL) were placed in a hydrogenation apparatus, and the mixture shaken with H_2 for 72 h at 30 °C under atmospheric pressure. The catalyst was filtered off and the filtrate evaporated to give the product; yield, 0.154 g (95%). After recrystallization from MeOH, the product showed mp 191—192 °C (decomp). IR $\nu_{C=O}$, 1620—1680 cm^{-1} (-CONH- and -CON(OH)-); ^1H NMR (DMSO-d_6) δ=1.30 (9H, m, CH_3), 2.04 (3H, s, CH_3CO), 4.0 (6H, m, $-CH_2-$), 4.90 (3H, m, -CH-), 7.0—7.8 (8H, broad, -CONH- and $-C_6H_5$), 7.95 (1H, -HNPh), and 9.70 (3H, s, N-OH).

The sample gave a characteristic color when mixed with $FeCl_3$ solution.

We thank Messrs. Masayoshi Hasegawa, Masahisa Yoshimi, and Mizuhito Tani for performing some of the experiments.

References

1) Part I: K. Shimizu, M. Hasegawa, and M. Akiyama, *Bull. Chem. Soc. Jpn.*, **57**, 495 (1984).
2) J. D. M. Herscheid, R. J. F. Nivard, M. W. Tijhuis, H. P. H. Scholten, and H. C. J. Ottenheijm, *J. Org. Chem.*, **45**, 1880 (1980).
3) T. Kolasa and A. Chimiak, *Tetrahedron*, **33**, 3285 (1977).
4) N. Shinmon, M. P. Cava, and R. F. C. Brown, *J. Chem. Soc., Chem. Commun.*, **1980**, 1020.
5) J. B. Neilands, *Science*, **156**, 1443 (1967).
6) J. B. Neilands, "Inorganic Biochemistry," ed by G. Eichorn, Elsevier, New York (1973), p.167; T. Emery, *Adv. Enzymol. Relat. Areas Mol. Biol.*, **33**, 135 (1971); "Microbial Iron Metabolism," ed by J. B. Neilands, Academic Press, New York (1974), Chap. 5.
7) H. Maehr, *Pure Appl. Chem.*, **28**, 603 (1971).
8) U. Schmidt, J. Häusler, E. Ohler, and H. Poisel, *Fortschr. Chem. Org. Naturst.*, **37**, 251 (1979); H. C. J. Ottenheijm, R. Plate, J. H. Noordik, and J. D. M. Herscheid, *J. Org. Chem.*, **47**, 2147 (1982).
9) C. Shin, K. Nanjo, E. Ando, and J. Yoshimura, *Bull. Chem. Soc. Jpn.*, **47**, 3109 (1974).
10) Yu. A. Ovichinnikov and V. T. Ivanov, *Tetrahedron*, **31**, 2177 (1975).
11) E. A. Kaczka, C. O. Gitterman, E. L. Dulaney, and K. Folkers, *Biochemistry*, **1**, 340 (1962).
12) W. Keller-Schierlein and B. Maurer, *Helv. Chim. Acta*, **52**, 603 (1969); Y. Isowa, M. Ohmori, and H. Kurita, *Bull. Chem. Soc. Jpn.*, **47**, 215 (1974). See also: W. Wierenga, "The Total Synthesis of Natural Products," ed by J. Apsimmon, Wiley, New York (1981), Vol. 4, Chap. 3, p.274.
13) The compounds which have the *N*-hydroxy amide units in the main chain appaer to be only cyclic dipeptide derivatives.[14]
14) A. H. Cook and C. A. Slater, *J. Chem. Soc.*, **1956**, 4130; C. Shin, K. Nanjo, M. Kato, and J. Yoshimura, *Bull. Chem. Soc. Jpn.*, **48**, 2584 (1975); J. D. M. Hersheid, J. H. Colstee, and H. C. J. Ottenheijm, *J. Org. Chem.*, **46**, 3346 (1981).
15) T. Kolasa and A. Chimiak, *Tetrahedron*, **30**, 3591 (1974).
16) M. Akiyama, M. Hasegawa, H. Takeuchi, and K. Shimizu, *Tetrahedron Lett.*, **1979**, 2599.
17) M. Bodanszky, Y. S. Klausner, M. A. Ondetti, "Peptide Synthesis," 2nd. ed. Wiley, New York (1976).
18) A. Winston and E. T. Mazza, *J. Polym. Sci., Polym. Chem. Ed.*, **13**, 2019 (1975); A. Winston and Kirchner, *Macromolecules*, **11**, 597 (1978).
19) R. V. Christian, I. D. Leffler, and J. S. Dahler, *Anal. Chem.*, **26**, 1666 (1954).
20) G. Schwarzenbach and K. Schwarzenbach, *Helv. Chim. Acta*, **46**, 1390 (1963).
21) T. Kolasa, A. Chimiak, and A. Kitowska, *J. Pract. Chem.*, **317**, 252 (1975).

 © 1984 The Chemical Society of Japan Bull. Chem. Soc. Jpn., 57, 2463—2467 (1984)

Stereoelectronic and Homoconjugative Effect of Stereoselectivity. The Addition of Dichlorocarbene to 1,5-Dimethyl-6-methylenetricyclo[3.2.1.$0^{2,7}$]oct-3-en-8-one and Its Related Compounds

Makoto NITTA,* Shuji OKADA, and Masami KATO

Department of Chemistry, School of Science and Engineering, Waseda University, Shinjuku-ku, Tokyo 160

(Received February 25, 1984)

The reaction of dichlorocarbene with 1,5-dimethyl-6-methylenetricyclo[3.2.1.$0^{2,7}$]oct-3-en-8-one, its corresponding alcohol derivative, and 1,5,8-trimethyl-6-methylenetricyclo[3.2.1.$0^{2,7}$]oct-3-en-8-*endo*-ol occurs on the exocyclic double bond to give *exo* and *endo* adducts with preferential formation of the *exo* adduct. Dichlorocarbene addition to 1,3,5-trimethyl-6-methylenetricyclo[3.2.1.$0^{2,7}$]oct-3-en-8-one (**1d**) occurs on the endocyclic double bond from the *exo* side, while the reaction occurs on the exocyclic double bond from both the *exo* and *endo* sides in the case of the corresponding alcohol derivative. The stereoselectivity or site selectivity was discussed on the basis of the stereoelectronic and homoconjugative effects as well as the steric effect of the reaction. Several chemical transformations, along with the derivation of bis adducts of dichlorocarbene, were also studied for confirmation of the structure of mono adducts. 1,3-Dipolar cycloaddition of **1d** and its dichlorocarbene adduct with mesitonitrile oxide, giving the adducts on the exocyclic double bond, was also studied to suggest a possible causative factor to control the electrophilic addition in the indicated direction.

Recently the stereoselectivities and/or site selectivities of electrophilic reactions or cycloadditions of molecules containing proximal π-bonds have been investigated.[1] In a previous paper,[2] we have shown that the 1,3-dipolar cycloadditions of mesitonitrile oxide (MNO) or phenyl azide (PA) to 1,5-dimethyl-6-methylenetricyclo-[3.2.1.$0^{2,7}$]oct-3-en-8-one (**1a**), its alcohol derivative (**1b**), and 1,5,8-trimethyl-6-methylenetricyclo[3.2.1.$0^{2,7}$]oct-3en-8-*endo*-ol (**1c**) exhibit a remarkable stereoselectivity and site selectivity to give the products of **A**, **B**, and **C**. The stereoselectivity giving *exo* adduct **A** could be ascribed to the preferential MNO(LUMO)–**1a**,**b**(HOMO) interaction. When the *exo* attack on the exocyclic double bond is sterically hindered by the methyl group at 8-position of **1c**, the addition occurs on the endocyclic double bond to give **B**. In the dipolar cycloaddition of PA, PA(LUMO)–**1a**, **b**(HOMO) interaction giving the type **A** adduct could be prohibited by the large van der Waals nonbonded interaction of the phenyl group with the C_1–C_5 bridge of **1a**,**b**, thus the adduct **C** could be obtained.

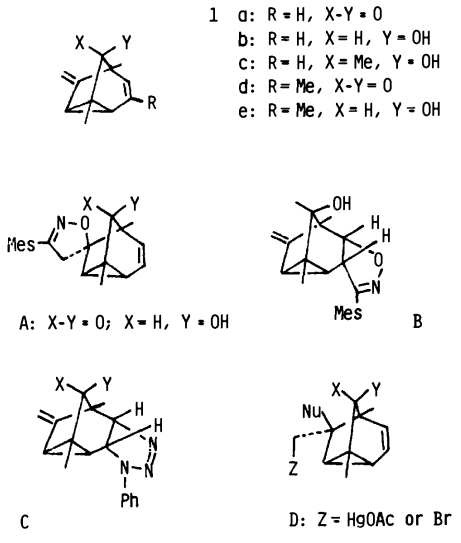

The prohibited *endo* attack of MNO and PA on the exocyclic double bond of **1a**,**b** or **1c** could be ascribed to the repulsive orbital interaction, which would be experienced with the endocyclic double bond. Similar stereoselection of electrophilic reactions such as solvomercuration, bromination and its related reaction on the exocyclic double bond of **1a**—**c** have been found to give the type D products.[3] In order to gain insight into the correlation for stereoselectivity of various electrophiles, the cheletropic reactions of dichlorocarbene with **1a**—**c** and its trimethyl analogue **1d**,**e** were investigated. In addition, 1,3-dipolar cycloadditions of **1d** and its dichlorocarbene adduct **2d** with MNO were also studied to find a plausible factor to control the stereoselectivity of 1,3-dipolar cycloaddition and dichlorocarbene addition.

Results and Discussion

The reaction of **1a**[4] with dichlorocarbene, generated by the usual phase transfer method,[5] occurred on the exocyclic double bond to give *exo* adduct **2a-ex** (48%) and *endo* adduct **2a-en** (31%) in a ratio of 3/2. A similar reaction of **1b**[6] with dichlorocarbene also afforded a mixture of two adducts, **2b-ex** (66%) and **2b-en** (16%), in a ratio of 4/1. The mixture was not separable. On oxidation with pyridinium chlorochromate, however, the mixture was converted to a mixture of **2a-ex** and **2a-en** (in a ratio of 4/1) in a 63% yield. Thus the correlation of **2a-ex** with **2b-ex** as well as **2a-en** with **2b-en** was clarified.

The structural proof for **2a-ex** and **2a-en** was based on the analytical and spectroscopic data. The stereochemical arrangement of the dichlorocarbene moiety of **2a-ex** and **2a-en** was deduced from the pseudo-contact NMR spectra obtained by using Eu(fod)$_3$. The relative downfield shifts of δ's are given in parentheses in the structural formulae.[7] The relatively large value of 1.14 for one of the methylene protons of the spirocyclopropane ring of **2a-ex**, as compared to the value of 1.01 for that of **2a-en**, could support the stereochemistry of the dichlo-

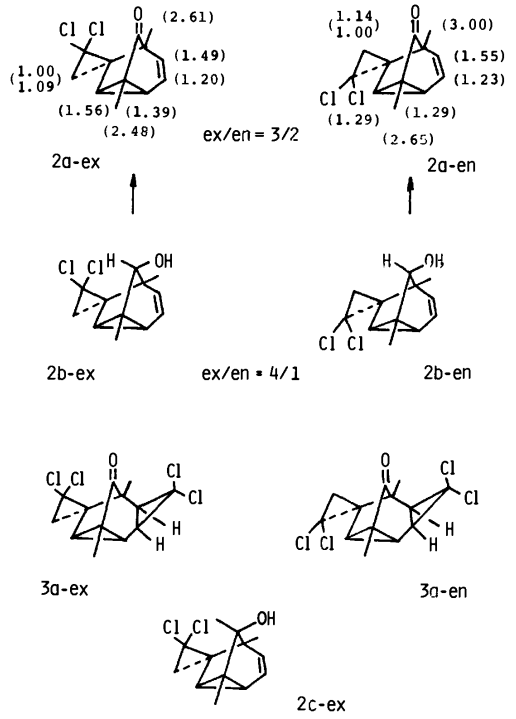

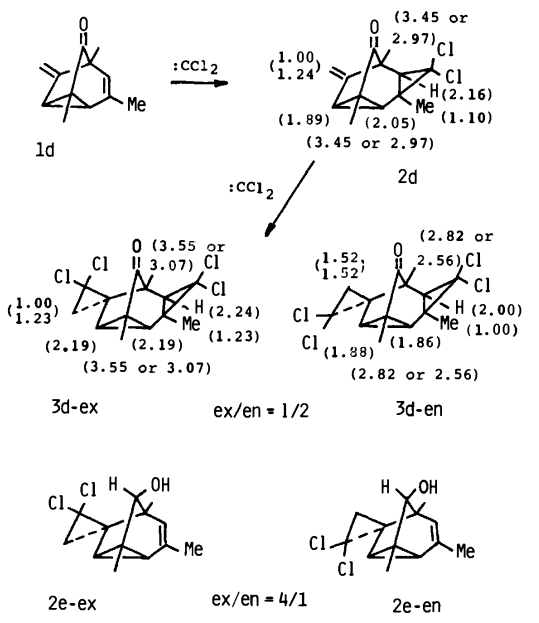

rocarbene moiety. Furthermore, in the reaction of **2a-ex** and **2a-en** with dichlorocarbene, the addition occured on the endocyclic double bond from the *exo* side giving **3a-ex** and **3a-en** respectively. The structures were deduced from the elemental analyses and the spectral data. Regarding the NMR spectra of **3a-ex** and **3a-en**, the noteworthy results include the chemical shifts of two hydrogens of dichlorocyclopropane moiety incorporated on the endocyclic double bond of **2a-ex** and **2a-en**. In the case of **3a-ex**, the key proton absorptions were seen at δ 2.37 and δ 2.50 (see Experimental). In the case of **3a-en**, however, the corresponding proton absorptions appeared at higher fields of δ 1.82 and δ 2.23. These trends are also observed for similar adducts, **2d-ex** and **2d-en** (*vide infra*). The *endo* orientation of chlorine ligand of spirocyclopropane moiety seems to cause a substantial change in long-range shielding. Assuming the *endo* attack of dichlorocarbene on the endocyclic double bond of **2a-ex** and **2a-en**, a chlorine atom comes very close to the spirocyclopropane carbon atom and the van der Waals nonbonded interaction would be very large. Consequently the *exo* attack giving **3a-ex** and **3a-ex** would be observed.

The reaction of **1c**,[8] which has a methyl group at 8-position, with dichlorocarbene afforded only **2c-ex**. This compound was also derived from the reaction of **2a-ex** with iodomethylmagnesium; thus the structure as well as the stereochemical arrangement of dichlorocyclopropane moiety could be assigned.

In contrast to the behavior of **1a**, reaction of the trimethyl analogue **1d**[4] with dichlorocarbene occurred on the endocyclic double bond from the *exo* side to give **2d**. In dichlorocarbene addition of cyclopropylethylenes, the rate enhancement caused by the methyl group has been observed.[9] The reaction of 2-cyclopropyl-1-propene proceeds 14 times faster than that of simple cyclopropylethylene itself. The methyl group at 3-position of **1d** could enhance the reactivity of the endocyclic double bond; thus only **2d** could be obtained. Furthermore the *exo* selectivity observed in the formation of **2d** may be ascribed to the steric effect of methyl group at 1- and 3-positions: the latter methyl group should come very close to the former one in the transition state.[10] The independent reaction of isolated **2d** with dichlorocarbene gave bis adducts, **3d-ex** and **3d-en** in a ratio of 1/2. The structural proof was based on elemental analyses and the spectroscopic data as well as on the pseudo-contact NMR spectra.[7]

Contrary to the reaction of **1d**, the reaction of the corresponding alcohol **1e**[6] with dichlorocarbene afforded a mixture of **2e-ex** and **2e-en** (in a ratio of 4/1) in a 60% yield. The *exo/endo* ratio is similar to that of the reaction of **1b**. The prohibited *exo* attack of dichlorocarbene on the endocyclic double bond (*cf.* the reaction of **1d**) could be explained by a steric effect of the chlorine ligand of the incorporating dichlorocarbene and OH group at 8-position. The mixture was not separable; however, the correct elemental analysis and mass spectral data were obtained. In the comparison of the NMR spectra of **2e-ex** and **2e-en**, particularly noteworthy are the chemical shifts of a hydrogen and a methyl group on the endocyclic double bond. In the case of **2e-ex**, the key proton absorptions were seen at δ 5.15 and δ 2.02, respectively (see Experimental). In the case of **2e-en**, however, these proton absorptions appeared at the higher fields of δ 4.79 and δ 1.92. This phenomenon is observed also for two protons on the endocyclic double bond in the pairs of NMR spectra of **2a-ex** (δ 6.20, 6.76) and **2a-en** (δ 5.08, 6.26). The difference of the stereochemical arrangement of chlorine atoms of the spirocyclopropane moiety may cause a substantial change in long-range shielding. Thus the structures of **2e-ex** and **2e-en** were deduced.

Regarding the stereoselection of the dichlorocarbene addition on the exocyclic double bond, *exo* adducts such as **2a,b,c-ex**, and **2e-ex**, were obtained preferentially as compared to the corresponding *endo* adducts. The

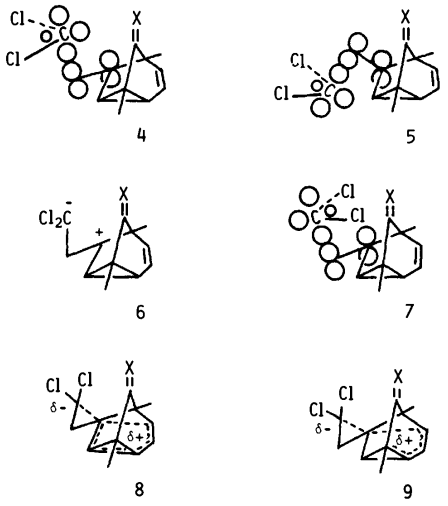

LUMO (p orbital) of the dichlorocarbene approaches the exocyclic double bond along the π axis closer to the least substituted carbon atom to form loose charge-transfer type complexes **4** and **5**, as illustrated. These could correspond closely in geometry to the valence structure **6**. The above approach was originally proposed on the basis of experimental data[12] and later on the basis of the theoretical calculations.[13] The approach of dichlorocarbene in the way illustrated as **7** could be unlikely because of a steric destabilization experienced with the chlorine ligand and the carbon skeleton in the present case. The complex **4** then collapses with rotation of the CCl_2 group to give an *exo* adduct, and **5** collapses to give an *endo* adduct.

Considering the *endo* approach **5** giving an *endo* adduct, interaction of the HOMO (carbene)with the appropriate occupied orbital of endocyclic double bond could cause a destabilizing effect in the transition state, as compared to that derived from **4** giving an *exo* adduct. Consequently an *exo* adduct could be favored over an *endo* adduct for **1a-c** and **1e**.

The additional explanation for the *exo* prevalence for **1a-c** and **1e** could be a homoconjugative stabilization of the transition state. Considering the developing-charge delocalization derived from **4** giving an *exo* adduct, an interaction of type **8** is bishomocyclopentadienyl cation, which is bishomoantiaromatic in nature and undoubtedly disfavored energetically.[14] However, interaction in the way of **9** removes the energetic disadvantage present in **8** and provides for intervention of a stabilized transition state.[15] This stabilizing effect seems to be reflected in the value of *exo/endo* ratio of products derived from **1b,d** (4/1) being larger than that from **1a** (3/2), the carbonyl group in which electrons from the cyclopropane ring could be released. The high stereoselectivity for **1c** giving **2c-ex** is still ambiguous.

In the reaction of **2d**, the product ratio of **3d-ex**/**3d-en** is 1/2, which is almost a reversed value of 3/2 for **2a-ex**/**2a-en**. The *endo* prevalence for the reaction of **2d** could be explained by a low degree of intervention of the dichlorocyclopropane into the stabilising effect on the developing cationic center illustrated as **9**. Furthermore the destabilizing effect arising from the interaction of HOMO(carbene) with an occupied orbital of endocyclic double bond for **1a-c**, and **1e** seems to be large, compared to that of **2d**, in which the double bond is replaced by the cyclopropane ring. This reduced repulsive interaction for **2d** also prefers **3d-en** over **3d-ex**.

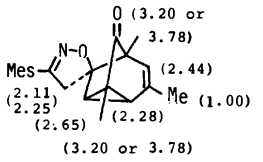

10

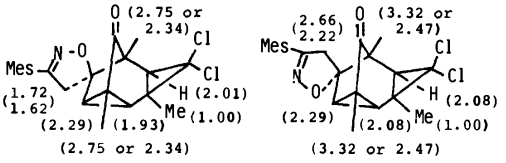

11-ex 11-en

The 1,3-dipolar cycloaddition of **1d** with MNO afforded only an *exo* adduct **10** as in the case of **1a**, **b**.[2] However, a similar reaction of **2d** with MNO gave two adducts, **11-ex** and **11-en**, in 71 and 6% yields. The structures of these adducts were deduced from the elemental analyses and from their spectroscopic data.[7] Thus the postulated repulsive interaction of MNO with the endocyclic double bond seems also to be larger than that of MNO with the cyclopropane bent bond.

Experimental

The melting points are uncorrected. The IR spectra were recorded on a Shimadzu IR-400 spectrometer. The mass spectral studies were conducted using a Hitachi RMU-60 spectrometer. All of the NMR spectra were recorded on a Hitachi R-25 or JEOL PS-100 spectrometer, using tetramethylsilane as the internal standard. The shift data were obtained by adding small increments of $Eu(fod)_3$ to the sample and then noting the extent to which each peak was shifted. The relative shift slopes were obtained by dividing each slope by the slope of the least shifted signal.

General Procedure for the Addition of Dichlorocarbene. To a stirred mixture of substrate, an adequate amount of chloroform, and triethylbenzylammonium chloride (TEBA), 50% (w/w) aqueous sodium hydroxide solution were added dropwise at 0 °C. In several cases, an adequate amount of dichloromethane was added to dilute the reaction mixture. After stirring for 1 h at 0 °C and 15 h at the ambient temperature, the resulting reaction mixture was poured into water and extracted with dichloromethane. After the removal of the dichloromethane, the resulting residue was purified as follows.

Reaction of 1a with Dichlorocarbene. The reaction was carried out using **1a** (1.0 g, 6.25 mmol), chloroform (1.49 g, 12.5 mmol) TEBA (30 mg), and sodium hydroxide solution (42 cm^3). The products were purified by column chromatography on Florisil using benzene as the eluent to give a mixture (1.75 g, 78%) of **2a-ex** (47%) and **2a-en** (31%) in a ratio of 3/2, which was determined by NMR spectroscopy. Repeated separation of the above mixture by TLC on silica gel using benzene-hexane (1/1) gave pure **2a-ex**. For **2a-ex**: mp 87—89 °C; IR CCl_4), 1742 cm^{-1}; NMR (CCl_4), δ=1.16 (3H, s), 1.41 (3H, s), 1.90 (2H, s), 2.17 (1H, d, J=7.5 Hz), 2.41 (1H, dxdxd, J=7.5, 5.0, 2.0 Hz), 6.20 (1H, dxd, J=7.2, 2.0 Hz), 6.76 (1H, dxd, J=7.2, 5.0 Hz); MS, m/z (rel intensity), 244 (M^+, 1),

242 (M^+, 2), 179 (100). The product **2a-en** was contaminated with **2a-ex** and the pure sample was not obtained; but the NMR spectrum was assigned as follows. For **2a-en**: NMR (CCl_4), δ=1.23 (3H, s) 1.45 (3H s), 1.54 (1H, d, J=7.5 Hz), 1.69 (1H, d, J=7.5 Hz), 1.87 (2H, m), 5.90 (1H, dxd, J=7.2, 2.0 Hz), 6.62 (1H, dxd, J=7.2, 5.0 Hz).

Reaction of 1b with Dichlorocarbene. The reaction was carried out using **1b** (500 mg, 3.1 mmol), chloroform (740 mg, 6.2 mmol), TEBA (30 mg), and sodium hydroxide solution (2.1 cm^{-3}). The products were purified by distillation to give 619 mg (82%) of a mixture of **2b-ex** (66%) and **2b-en** (16%). For **2b-ex**: NMR (CCl_4), δ=1.11 (3H, s), 1.31 (3H, s), 1.13—1.52 (2H, m), 1.55 (1H, d, J=7.2 Hz), 1.68 (1H, d, J=7.2 Hz), 3.33 (1H, s), 5.44 (1H, dxd, J=8.4, 1.7 Hz), 6.40 (1H, dxd, J=8.4, 5.4 Hz). For **2b-en**: NMR (CCl_4), δ=1.21 (3H, s), 1,39 (3H, s), 1.13—1.52 (4H, m), 3.65 (1H, s), 5.08 (1H d, J=8.2Hz) 6.26 (1H, d, J=8.2, 5.4 Hz).

Oxidtation of a Mixture of 2b-ex and 2b-en. To a stirred soltion of pyridinium chlorochromate (681 mg, 3.17 mmol) and anhydrous sodium acetate (58 mg, 0.7 mmol) in 30 cm^3 of anhydrous dichloromethane, a 4/1 mixture of **2b-ex** and **2b-en** (516 mg, 2.11 mmol) in 1 cm^3 of dichloromethane was added, followed by stirring for 10 h under a nitrogen stream. The reaction mixture was chromatographed on Florisil using dichloromethane as the eluent. The dichloromethane was evaporated and the resulting residue was distilled [bp 115—120 °C/792 Pa (bath temp)] to give a mixture (63%) of **2a-ex** and **2a-en** in a ratio of 4/1. The NMR spectrum of the mixture was identical with the authentic specimen, which was obtained from the reaction of **1a** with dichlorocarbene.

Reaction of 2a-ex with Dichlorocarbene. The reaction was carried out using **2a-ex** (150 mg, 0.62 mmol), chloroform (740 mg, 6.2 mmol), dichloromethane (0.5 cm^3), TEBA (20 mg), and sodium hydroxide solution (2.2 cm^3). The product was recrystallized from ethanol to give 144 mg (71%) of **3a-ex**: mp 149—151 °C; IR (CCl_4), 1742 cm^{-1}; NMR ($CDCl_3$), δ=1.18 (3H, s), 1.31 (3H, s), 1.52 (1H, d, J=8.3 Hz), 1.66 (1H, d, J=8.3 Hz), 1.91 (1H, d, J=6.7 Hz), 2.24 (1H, dxdxd, J=6.7, 3.3, 2.0 Hz), 2.37 (1H, dxd, J=11.1, 3.3 Hz), 2.50 (1H, dxd, J=11.1, 2.0 Hz); MS, m/z (rel intensity), 328 (M^+, 1), 326(M^+, 3), 322 (M^+, 2), 291 (100). Found: C, 47.76; H, 3.66%. Calcd for $C_{13}H_{12}OCl_4$: C, 47.89; H, 3.71%.

Reaction of the Mixture of 2a-ex and 2a-en with Dichlorocarbene. The reaction was carried out using a mixture of **2a-ex** and **2a-en** in a ratio of 3/2 (1.372 g, 5.65 mmol), chloroform (7.24 g, 60.5 mmol), TEBA (60 mg), and sodium hydroxide solution (10 cm^3). The products were separated by TLC on silica gel using benzene-hexane (1/1) to give **3a-ex** (632 mg, 34%), **3a-en** (452 mg, 25%), and a mixture of **2a-ex** and **2a-en** in a ratio of 5/2 (495 mg, 36%). For **3a-en**: mp 163—164 °C (from ethanol); IR (CCl_4), 1739 cm^{-1}; NMR ($CDCl_3$), δ=1.25 (3H, s), 1.31 (3H, s), 1.54 (1H, d, J=6.0 Hz), 1.63 (1H, d, J=6.0 Hz), 1.82 (1H, dxd, J=9.6, 2.6 Hz), 2.19 (1H, dxdxd, J=7.4, 2.6, 2.0 Hz), 2.23 (1H, dxd, J=9.6, 2.0 Hz), 2.24 (1H, d, J=7.4 Hz); MS, m/z (rel intensity), 332 (M^+, 80), 330 (M^+, 9), 328 (M^+, 9), 326 (M^+, 3), 324 (M^+, 3), 291 (100). Found: C, 47.95; H, 3.80%. Calcd for $C_{13}H_{12}OCl_2$: C, 47.89; H, 3.71%.

Reaction of 1c with Dichlorocarbene. The reaction was carried out using **1c** (300 mg, 1.7 mmol), chloroform (405 mg, 3.4 mmol), TEBA (20 mg), and sodium hydroxide solution (1.2 cm^3). The product was purified by distilation to give 315 mg (71%) of **2c-ex**: bp 118—122 °C/528 Pa (bath temp); NMR (CCl_4), δ=1.07 (3H, s), 1.09 (3H, s), 1.23 (3H, s), 1.26—1.65 (2H, m), 1.46—1.78 (2H, m), 5.52 (1H, dxd, J=8.5, 1.9 Hz), 6.42 (1H, dxd, J=8.5, 5.5 Hz); MS, m/z (rel intensity), 260 (M^+, 4), 258 (M^+, 5), 162 (100). Found: C, 59.76; H, 5.93%. Calcd for $C_{13}H_{16}OCl_2$: C, 60.25; H, 6.22%.

Independent Preparation of 2c-ex. To a stirred ethereal solution of iodomethylmagnesium, which was prepared from iodomethane (1.20 g, 8.5 mmol) and magnesium (48 mg, 1.98 mmol), a solution of **2a-ex** (120 mg, 0.49 mmol) in 5 cm^3 of ether was added dropwise over 20 min. After the addition was completed, the mixture was refluxed for 15 min. The reaction mixture was cooled and followed by addition of water and aqueous ammonium chloride. The mixture was extracted with ether and the extract was evaporated to give 106 mg (83%) of **2c-ex**: its spectral data were identical with the authenic specimen.

Reaction of 1d with Dichlorocarbene. The reaction was carried out using **1d** (507 mg, 2.91 mmol), chloroform (522 mg, 4.37 mmol), dichloromethane (1 cm^3), TEBA (30 mg), and sodium hydroxide solution (1.5 cm^3). The product was purified by TLC on silica gel using benzene as the eluent to give 664 mg (89%) of **2d**: mp 145—147 °C (from ethanol); IR (CCl_4), 1748 cm^{-1}; NMR ($CDCl_3$), δ=1.21 (3H, s), 1.24 (3H, s), 1.54 (3H, s), 1.33 (1H, d, J=2.8 Hz), 2.02 (1H, dxd, J=7.3, 2.8 Hz) 2.57 (1H, d, J=7.3 Hz), 4.73 (1H, s), 4.91 (1H, s); MS, m/z (rel intensity), 258 (M^+, 2), 256 (M^+, 3), 193 (100). Found: C, 60.48; H, 5.30%. Calcd for $C_{13}H_{17}OCl_2$: C, 60.72; H, 5.49%.

Reaction of 2d with Dichlorocarbene. The reaction was carried out using **2d** (257 mg, 1 mmol), chloroform (598 mg, 5 mmol), TEBA (20 mg), dichloromethane (1 cm^3), and sodium hydroxide solution (1.7 cm^3). The products were separated by TLC on silica gel using benzene as the eluent to give **3d-en** (160 mg, 47%) and **3d-ex** (78 mg, 22%). For **3d-ex**: mp 112—113 °C (from ethanol); IR (CCl_4), 1745 cm^{-1}; NMR (CCl_4), δ=1.10 (3H, s), 1.22 (3H, s), 1.72 (3H, s), 1.48 (1H, d, J=7.4 Hz), 1.59 (1H, d, J=7.4 Hz), 1.80 (1H, s), 1.85 (2H, broad s); MS, m/z (rel intensity), [M^+] is absent; 207 (100). Found: C, 49.45; H, 4.16%. Calcd for $C_{14}H_{14}OCl_2$: C, 49.45; H, 4.15%. For **3d-en**: mp 139—142 °C; IR (CCl_4), 1748 cm^{-1}; NMR (CCl_4), δ=1.15 (3H, s), 1.22 (3H, s), 1.53 (3H, s), 1.29 (1H, d, 8.6 Hz), 1.46 (1H, d, J=8.6 Hz), 2.21 (1H, d, J=6.8 Hz), 1.75 (1H, dxd, J=6.8, 2.4 Hz), 1.26 (1H, d, J=2.4 Hz); MS, m/z (rel intensity), [M^+] is absent; 207 (100). Found: C, 49.53; H, 3.90%. Calcd for $C_{14}H_{14}OCl_4$: C, 49.45; H, 4.15%.

Reaction of 1e with Dichlorocarbene. The reaction was carried out using **1e** (822 mg, 4.67 mmol), chloroform (837 mg, 7.0 mmol), dichloromethane (4 cm^3), TEBA (20 mg), and sodium hydroxide solution (2.3 cm^3). The purification by TLC on silica gel using benzene as the eluent gave a mixture (728 mg, 60%) of **2e-ex** (48%) and **2e-en** (12%). For a mixture of **2e-ex** and **2e-en**: MS, m/z (rel intensity), 260 (M^+, 3), 258 (M^+, 6), 106 (100). Found: C, 60.44; H, 6.43%. Calcd for $C_{13}H_{16}OCl_2$: C, 60.25; H, 6.22%. For **2e-ex**: NMR (CCl_4), δ=1.08 (3H, s), 1.33 (3H, s), 1.12—1.15 (2H, overlapping with methyl group), 1.55 (1H, d, J=7.0 Hz), 1.68 (1H, d, J=7.0 Hz), 2.02 (3H, d, J=1.4 Hz), 3.32 (1H, s), 5.15 (1H, broad s). For **2e-en**: NMR (CCl_4), δ=1.17 (3H, s), 1.41 (3H, s), 1.12—1.51 (4H, overlapping with methyl group), 1.92 (3H, d, J=1.4 Hz), 3.64 (1H, s), 4.79 (1H, broad s).

1,3-Dipolar Cycloaddition of 1d with Mesitonitrile Oxide. A solution of **1d** (174 mg, 1 mmol) and mesitonitrile oxide (161 mg, 1 mmol) in 3 cm^3 of anhydrous benzene was refluxed for 5 h. After the solvent removal *in vacuo*, the resulting residue was separated by TLC on silica gel using benzene-dichloromethane (1/1) as the eluent. The first band from the TLC plates contained 30 mg (17%) of **1d**. The second band from the TLC plates gave 271 mg (81%) of **4**: mp 123—124 °C; IR (CCl_4), 1742 cm^{-1}; NMR ($CDCl_3$), δ= 1.10 (3H, s), 1.32 (3H, s), 1.79 (3H, d, J=1.8 Hz), 1.89 (1H, dxd, J=7.5, 3.5 Hz), 2.23 (9H, broad s), 2.30 (1H, d, J=7.5 Hz), 2.94 (1H, d, J=18.5 Hz), 3.01 (1H, d, J=18.5 Hz), 5.11 (1H, dxd, J=3.5, 1.5 Hz), 6.84 (2H, s); MS, m/z (rel intensity), 335 (M^+, 19), 159 (100). Found: C, 78.58; H, 7.45; N, 3.89%. Calcd for $C_{22}H_{25}NO_2$: C,

78.77; H, 7.51; N, 4.17%.

1,3-Dipolar Cycloaddition of **2d** *with Mesitonitrile Oxide.* A solution of **2d** (257 mg, 1 mmol) and mesitonitrile oxide (161 mg, 1 mmol) in 3 cm^3 of anhydrous benzene was refluxed for 5 h. After the solvent was evaporated, the resulting residue was separated by TLC on silica gel using benzene as the eluent. The first band from the TLC plates contained 51 mg (20%) of **2d**. The second band from the TLC plates gave 27 mg (6%) of **11-en**: mp 148—149 °C; IR ($CHCl_3$), 1730 cm^{-1}; NMR ($CDCl_3$), δ=1.24 (3H, s), 1.28 (3H, s), 1.63 (1H, d, J=2.4 Hz), 1.73 (3H, s), 2.01 (1H, dxd, J=6.7, 2.4 Hz), 2.21 (6H, s), 2.24 (3H, s), 2.30 (1H, d, J=6.7 Hz), 2.89 (1H, d, J=18.4 Hz), 3.05 (1H, d, J=18.4 Hz), 6.85 (2H, s); MS, m/z (rel intensity), 421 (M^+, 1), 419 (M^+, 5), 417 (M^+, 6), 159 (100). Found: C, 65.85; H, 5.94; N, 3.55%. Calcd for $C_{23}H_{25}NO_2Cl_2$: C, 66.03; H, 6.02; N, 3.35%. The third band from the TLC plates gave 297 mg (71%) of **11-ex**: mp 186—187 °C; IR ($CHCl_3$), 1742 cm^{-1}; NMR ($CDCl_3$), δ=1.26 (3H, s), 1.29 (3H, s), 1.31 (1H, d, J=3.8 Hz), 1.58 (3H, s), 1.91 (1H, dxd, J=6.6, 3.8 Hz), 2.26 (9H, broad s), 2.35 (1H, d, J=6.6 Hz), 3.13 (1H, d, J=16.5 Hz), 3.18 (1H, d, J=16.5 Hz), 6.90 (2H, s); MS, m/z (rel intensity), 419 (M^+, 2), 417 (M^+, 3), 159 (100). Found: C, 66.09; H, 5.81; N, 3.41%. Calcd for $C_{23}H_{25}NO_2Cl_2$: C, 66.03; H, 6.02; N, 3.35%.

References

1) K. Okada and T. Mukai, *J. Am. Chem. Soc.*, **100**, 6509 (1978); L. A. Paquette, L. W. Hartel, R. Gleiter, and M. C. Bohm, *J. Am. Chem. Soc.*, **100**, 6510 (1978); L. A. Paquette and L. W. Hartel, *J. Am. Chem. Soc.*, **101**, 7620 (1979); L. A. Paquette, L. W. Hartel, R. Gleiter, M. C. Bohm, M. A. Beno, and G. G. Christoph, *J. Am. Chem. Soc.*, **101**, 7106 (1981); T. Sasaki, K. Hayakawa, and S. Nishida, *J. Am. Chem. Soc,*, **103**, 565 (1981); K. E. Green and L. A. Paquette, *J. Org. Chem.*, **48**, 1849 (1983).

2) M. Nitta, A. Omata, and S. Okada, *Bull. Chem. Soc. Jpn.*, in press.

3) M. Nitta, A. Omata, and H. Sugiyama, *Bull. Chem. Soc. Jpn.*, **55**, 569 (1982); Epoxidation reaction of **1a,d** also occurs on the exocyclic double bond from the *exo* side: M. Nitta, A. Omata, and H. Nakatani, *Bull. Chem. Soc. Jpn.*, **56**, 2009 (1983).

4) J. Zsindely and H. Schmid, *Helv. Chim. Acta*, **51**, 1510 (1968).

5) M. Makosza and M. Wawrzyniewicz *Tetrahedron Lett.*, **1969**, 4659 E. V. Dehmlow, *Angew. Chem. Int. Ed. Engl.*, **13**, 170 (1974); **16**, 493 (1977).

6) J. P-Katalinic, J. Zsindely, and H. Schmid, *Helv. Chim. Acta*, **57**, 223 (1974).

7) The numerical values presented in parentheses in the structural formulae in this paper are relative dowfield shifts of δ's obtained by using $Eu(fod)_3$.

8) G. M-Muller, P. Gilgen, J. Zsindely, and H. Schmid, *Helv. Chim. Acta*, **60**, 1758 (1977).

9) E. V. Dehmlow and A. Eulenberger, *Angew, Chem. Int. Ed. Engl.*, **17**, 674 (1978).

10) The cycloaddition of phenyl azide (PA) with **1a** gave an *endo* adduct of type **C**.[2] However, in the reaction of **1d** with PA, both *endo* and *exo* adducts were obtained in a ratio of 1/1. Thus the methyl group of 3-position of **1d** seems to affect the *endo-exo* selectivity, possibly using a steric reason.[11]

11) M. Nitta, S. Okada, and T. Kobayashi, unpublished results.

12) P. S. Skell and M. S. Chold, *J. Am. Chem Soc.*, **91**, 7131 (1969).

13) R. Hoffmann, D. W. Hayes, and P. S. Skell, *J. Phys. Chem.*, **76**, 664 (1972).

4) A. F. Diaz, M. Sakai, and S. Winstein, *J. Am. Chem. Soc.*, **92**, 7477 (1970); R. Breslow and J. M. Hoffman Jr., *J. Am. Chem. Soc.*, **94**, 2110 (1972).

15) H. Hart and M. Kuzuya, *J. Am. Chem. Soc.*, **98**, 1545 (1976).

The Chemistry of Substituted Norbornenes. Reactions of 5-Vinyl-2-norbornene and 5-Ethylidene-2-norbornene with Formic Acid

Yoshiharu INOUE,* Fumio TANIMOTO, and Hisao KITANO
Research Institute for Production Development, 15, Shimogamo Morimoto-cho, Sakyo-ku, Kyoto 606
(Received November 14, 1983)

Addition of formic acid to 5-vinyl-2-norbornene(**1**) and subsequent hydrolysis afford 6-vinyl-*exo*-2-norbornanol(**5**) and 5-vinyl-*exo*-2-norbornanol(**6**). Similarly, from 5-ethylidene-2-norbornene(**2**) are formed 6-ethylidene-*exo*-2-norbornanol(**14**), 5-ethylidene-*exo*-2-norbornanol(**15**), and 6-ethyltricyclo[2.2.1.$0^{2,6}$]heptan-3-ol(**16**). The hydroboration of **2** also leads to the formation of **14** and **15**. Thus, the vinyl- and ethylidene-*exo*-norbornanols, **5**, **6**, **14**, and **15**, and the corresponding *endo*-norbornanols, **9**, **10**, **21**, and **22**, have been synthesized. A structural analysis of these products by ^{13}C NMR revealed that under certain conditions, the ethylidene group of **2** exerts a great influence upon the reactivity of the norbornenyl ring double bond. Moreover, the fact that **16** derived from the addition of formic acid to **2** consists of both *exo*- and *endo*-hydroxy epimers is inconsistent with the previous observations that the *exo*-isomer is generally the sole product in related systems.

Much less work has been done on the chemical properties of both **1** and **2** which are commercially available norbornenes having an olefinic side chain. Especially, detailed investigations concerning the reactivity difference of the two different types of double bonds in **1** and **2** have not been made so far.

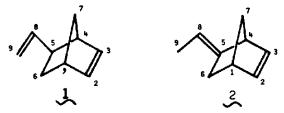

Recent studies of comparing the reactivity of the two double bonds in either **1** or **2** have clarified that the Diels-Alder reaction takes place more readily on the norbornenyl ring double bond in both **1** and **2**;[1] similarly, **2** undergoes addition of sulfur on the ring double bond,[2] whereas singlet oxygen,[3] peroxy acids,[4] and chlorosulfonyl isocyanate[5] add to **2** on the ethylidene group. On the other hand, the Prins reaction takes place on both double bonds in **2**,[6] and in addition, both **1** and **2** undergo hydroformylation on their both double bonds.[7] In any event, earlier studies as stated above have not clearly revealed the chemical behavior of both **1** and **2** from the standpoint of regio- and stereochemistry. In addition, the anticipation that the norbornanols having such an olefinic side chain could provide the intriguing reactive intermediate[4),8] has also encouraged us to initiate the current study.

The purpose of this work is to obtain a better understanding of what stereoelectronic influence is exerted on the reactivity of the norbornenyl ring double bond by participation of the unsaturated substituents, and to determine which one of the two double bonds in either **1** or **2** undergoes certain addition reactions preferentially.

Results and Discussion

In order to prepare vinylnorbornanols from **1** and to gain further information on reactivity difference between the two double bonds in **1**, we first studied addition of formic acid to **1**, leading to the formation of a mixture of 6-vinyl-*exo*-2-norbornyl formate(**3**) and 5-vinyl-*exo*-2-norbornyl formate(**4**) in a good yield.

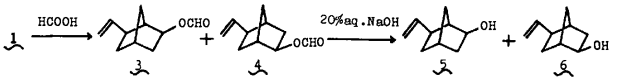

Here, products from the addition to the vinyl group and Wagner-Meerwein-type rearrangements *via* the bridged carbonium ion were not observed. A stereochemical assignment of the mixture of **3** and **4** was carried out by hydrolysis to a mixture of **5** and **6**, whose analysis by ^{13}C NMR showed that the hydroxyl group in both **5** and **6** exclusively occupied the *exo* position. It was also revealed that the ratio of **5** and **6** is *ca.* 1:1 by GC analysis. The result thus obtained is in accord with the earlier observation that the addition of formic acid to norbornene gives solely an *exo*-product[9], and also indicates that the vinyl group has no influence on the direction of the addition of formic acid to **1**.

Alternatively, application of the Jones oxidation to the mixture of **5** and **6** afforded a mixture of 6-vinyl-2-norbornanone(**7**) and 5-vinyl-2-norbornanone(**8**), which was subsequently reduced by $LiAlH_4$ to form a mixture of 6-vinyl-2-norbornanol(**9**) and 5-vinyl-2-norbornanol(**10**); the ^{13}C NMR spectrum of these products was in striking contrast to that of the mixture of **5** and **6** and revealed that the mixture of **9** and **10** had 78% *endo*- and 22% *exo*-hydroxyl group.

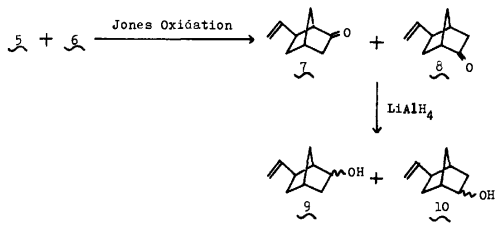

The direct preparation of the mixture of **7** and **8** by the oxidation of the mixture of **3** and **4** was successfully conducted according to the procedure described in the case of norbornyl formate.[9]

In order to achieve the synthesis of ethylidenenorbornanols from **2** and to examine the reactivity difference in the two double bonds in **2**, the addition of formic acid to **2** was carried out to give three prominent products, 6-ethylidene-*exo*-2-norbornyl formate(**11**), 5-ethylidene-*exo*-2-norbornyl formate(**12**), and 6-ethyltricyclo[2.2.1.

$0^{2,6}$]heptan-3-yl formate(**13**), in product ratio of 11+12/13=61:39.

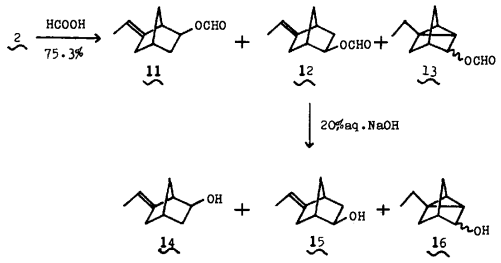

Although the three structural isomers, **11**, **12**, and **13**, can be distinguished readily by gas chromatography, isolation of pure compounds from the mixture by distillation was extremely difficult. In order to ascertain whether this reaction is stereospecific, the product mixture of **11**, **12**, and **13**, was hydrolyzed under alkaline conditions to yield a mixture of the corresponding alcohols, **14**, **15**, and **16**. The ^{13}C NMR spectrum of the alcohol mixture showed clearly that both **14** and **15** consist of 97% of the *exo* hydroxy epimer and that the ratio of **14** and **15** is 85:15. This particular positional orientation can be explained by preferential attack of H^+ upon C-2 of **2**, since C-2 (and, of course, C-8) has the richest electron density in the highest occupied frontier orbital of the homoconjugated diene system consisted of C-2, C-3, C-5, and C-8, and therefore, C-2 will be the site of attack by electrophile with its LUMO.[10]

For further study of stereochemical aspect of this reaction, an attempt was also made to prepare these compounds, **14** and **15**, by an alternative route. Thus, hydroboration-oxidation sequence was applied to **2** to provide a mixture of isomeric products, **14**, **15**, and 5-or 6-(1-hydroxyethyl)-2-norbornanol(**17**), together with *ca.* 1% of **16** unexpectedly formed.[11] Interestingly, ^{13}C NMR analysis of the mixture of **14** and **15** revealed that it consists of more than 91% of *exo*-isomer with the ratio of **14** and **15** being *ca.* 10:1. In the light of the fact that the hydroboration of norbornene gives 99.5% *exo*- and 0.5% *endo*-norbornanol,[12] we suggest that the lack of the *endo*-hydrogen at C-5 in **2** exerts a smaller steric effect on the addition of diborane to its norbornenyl ring double bond from the *endo* direction compared to norbornene, facilitating *endo* attack to increase the total amount of *endo*-products: this results in the diminished preference (~8.5%) for *exo* attack.

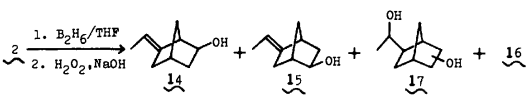

In the context of the structural investigation of the ethylidene-2-norbornanols, **14** and **15**, obtained from the two different types of methods illustrated above, preference of *exo* addition can be best explained by both the perturbation effect on the planarity of the π system[13] and the smaller steric hindrance.[11a]

Hydroboration of the mixture of **11**, **12**, and **13**, followed by distillation afforded **16**. The ^{13}C NMR spectrum of **16** revealed that it consists of 43% *exo*- and 57% *endo*-hydroxy epimers. This stereochemical outcome is surprising since most of addition reactions to norbornenyl ring double bonds proceed almost exclusively from the *exo* direction.[10,11b,11c,14] At this juncture, we propose the following mechanistic explanation; in the addition of formic acid to **2**, it is conceivable that protonation of **2** which occurs on C-8 having the richest electron density as stated above would give the carbonium ion intermediate(**18**),[15] whose molecular model suggests that the bond formation between C-2 and C-6 in **18** evidently renders the distance between C-2 and C-6 in **18** shorter than that between C-3 and C-5 in **2**.[13,16] Concurrently, the torsional strain in **18** thus generated puts C-3 and C-5 in **18** far away from each other, resulting in diminishing the steric interference induced by *endo*-hydrogen attached to C-5 toward a nucleophilic attack by formate anion at C-3 from the *endo* direction.

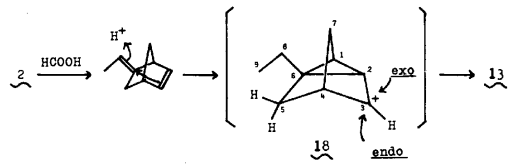

Alternative rationalization is that once the carbonium ion like **18** is formed, there is no need for considerations of electronic distribution governed by the molecular orbital theory, thereby giving no special preference for the direction of the addition.

Meanwhile, the mixture of **14** and **15** was oxidized by the Jones procedure to 6-ethylidene-2-norbornanone (**19**) and 5-ethylidene-2-norbornanone(**20**). Subsequent reduction with $LiAlH_4$ gave the corresponding norbornanols, **21** and **22**, whose ^{13}C NMR spectrum showed that the hydroxyl group occupied mainly the *endo* position.

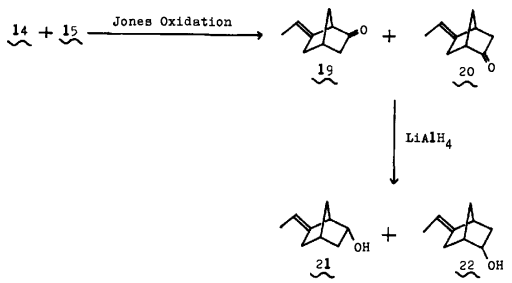

Experimental

Boiling points are uncorrected. GC analyses were carried out with a Hitachi Model 163 gas chromatograph, using either (A) a 90-m, 0.25-mm i.d. stainless-steel column coated with Silicone SE-30 at a flow rate of 1.2 ml/min., or (B) a 1-m, 5-mm i.d. stainless-steel column packed with 10% Silicone SE-30 on Chromosorb W at a flow rate of 30 ml/min. Percentages indicated for each component refer to computer-calculated peak areas without correction for response, and the retention time is given as (t_R) min. for each peak. ^1H NMR spectra were recorded with a Hitachi Model R-24B, using tetramethylsilane as internal reference. Proton decoupled ^{13}C NMR spectra were obtained on a JEOL FX 90Q with $CDCl_3$ as an internal lock; absorptions are reported relative to tetramethylsilane. The ratio of each component was determined by computer-calculated line intensities without correction for response. IR spectra were obtained with a Hitachi Model 160-10 infrared spectrophotometer. Elemental ana-

lyses were performed by the Laboratory for Organic Elemental Microanalysis, Faculty of Pharmaceutical Sciences, Kyoto University.

Materials. 5-Vinyl-2-norbornene, obtained from Aldrich Chemicals Corp., and 5-ethylidene-2-norbornene, obtained from Tokyo Chemicals Corp., were vacuum distilled before use. The 5-vinyl-2-norbornene employed consists of two stereoisomers,[17] *exo*-5-vinyl-2-norbornene and *endo*-5-vinyl-2-norbornene, and was determined on the basis of ^{1}H NMR spectra and GC (column A, 80 °C) analysis to be in the ratio *exo*/*endo* of 2/3. The 5-ethylidene-2-norbornene consists of *E*- and *Z*-isomers, and it was determined on the basis of ^{13}C NMR spectrum and GC (column A, 80 °C) analysis to be in the ratio *E*/*Z* of 77/23.[18]

6-Vinyl-exo-*2-norbornyl Formate(3) and 5-Vinyl*-exo-*2-norbornyl Formate(4).* Approximately 92.0 g (2.0 mol) of 98—100% formic acid was added to 60.0 g (0.5 mol) of 5-vinyl-2-norbornene(**1**), and the mixture was stirred at about 70 °C for 4 h. After removal of excess formic acid, the residue was distilled under reduced pressure to give 52.8 g (63.6% yield) of a mixture of **3** and **4**, bp 104—105 °C (22 mmHg, 1 mmHg≈133.322 Pa), n_D^{14} 1.4821. GC(column A, 140 °C) analysis of this compound indicated that the ratio of four components (t_R 19.3, 19.9, 20.4, and 21.0 min) was 3:27:35:35. IR (neat) ν_{max} 3090, 2920, 1720, 1640, 1170 cm^{-1}; ^{1}H NMR (CCl_4) δ=7.90(s,1H), 6.00—5.40(m,1H), 5.15—4.90(m, 2H), 4.80(s, 1H), 2.40—1.35(m, 9H). Found: C, 72.20; H, 8.36; O, 19.44%. Calcd for $C_{10}H_{14}O_2$: C, 72.29; H, 8.43; O, 19.28%.

6-Vinyl-exo-*2-norbornanol(5) and 5-Vinyl*-exo-*2-norbornanol (6).* To 30.0 g (0.18 mol) of the mixture of **3** and **4** was added 36.0 g (0.18 mol) of 20% NaOH solution and 25 ml of methanol, and then the mixture was refluxed for 2 h. After removal of methanol, the residual solution was saturated with NaCl and extracted with a mixture of ether and benzene. After the extract was dried over $MgSO_4$, the solvent was evaporated. The residue was vacuum distilled to afford 24.0 g (96.6% yield) of the mixture of **5** and **6**, bp 72—73 °C (1.5 mmHg), $n_D^{18.5}$ 1.5004, whose GC (column A, 140 °C) showed to consist of three components in the yields of 5 (t_R 14.9 min.), 45 (t_R 15.4 min.), and 51 (t_R 15.7 min)%, respectively. IR (neat) ν_{max} 3350, 3090, 2920, 1640, 1100 cm^{-1}; ^{1}H NMR ($CDCl_3$) δ=6.10—5.40 (m, 1H), 5.10—4.65 (m, 2H), 3.80—3.60 (s, 1H), 2.95—2.80 (s, 1H), 2.30—1.10 (m, 9H); ^{13}C NMR ($CDCl_3$, 4 lines as C-2 for the predominant isomers) (relative intensity) 74.2 (40.7), 74.0 (22.4), 73.9 (33.1), 69.2 (3.8) ppm. Found: C, 78.14; H, 10.20; O, 11.66%. Calcd for $C_9H_{14}O$: C, 78.26; H, 10.14; O, 11.59%.

6-Vinyl-2-norbornanone(7) and 5-Vinyl-2-norbornanone(8).
Method A: A sulfuric acid solution of chromium trioxide was prepared by dissolving 5.6 g (0.056 mol) of chromium trioxide in 8 ml of water, adding 8.6 g (0.088 mol) of concentrated sulfuric acid to the solution and then diluting the mixture with 16 ml of water. This solution was then added dropwise over a period of 30 min to a solution of 11.0 g (0.080 mol) of the mixture of **5** and **6** in 50 ml of acetone with stirring below 5 °C. The mixture was stirred at a temperature below 20 °C for 3 h and then mixed with $NaHSO_3$ solution to form two layers. The lower layer was extracted with petroleum ether, and the petroleum ether layer was then combined with the upper layer previously obtained. The combined layers were washed with saturated $NaHCO_3$ solution until they turned slightly basic and then with water and dried over $MgSO_4$. After the drying agent was removed by filtration, the solvent was distilled off. The residue was distilled under reduced pressure to afford 7.3 g (67.1% yield) of the mixture of **7** and **8**, bp 68—70 °C (7.0 mmHg), $n_D^{18.5}$ 1.4883, which gave a GC (column A, 150 °C) analysis consisting of two components in the yields of 54 (t_R 15.5 min) and 46 (t_R 16.0 min)%, respectively. IR (neat) ν_{max} 3090, 2950, 2870, 1740, 1630 cm^{-1}; ^{1}H NMR (CCl_4) δ=6.20—5.50 (m, 1H), 5.20—4.80 (m, 2H), 2.75—1.60 (m, 9H). Found: C, 79.30; H, 8.87; O, 11.83%. Calcd for $C_9H_{12}O$: C, 79.41; H, 8.82; O, 11.76%.

Method B: To a solution of 10.0 g (0.060 mol) of the mixture of **3** and **4** in 25 ml of acetone was added dropwise, with stirring, 31.0 ml of 8M (1M=1 mol dm^{-3}) chromic acid solution [this solution was prepared by dissolving 10.7 g (0.107 mol) of chromium trioxide in 20 ml of water, adding 8.9 ml (0.167 mol) of concentrated sulfuric acid to the solution and then diluting this solution with 40 ml of water] while the reaction mixture was maintained at temperatures in the range of 20 to 30 °C. After being stirred at room temperature overnight, the mixture was treated with $NaHSO_3$ until the dark-brown solution turned dark-green. Thus, the solution separated into two layers and the lower layer was extracted with petroleum ether. The extract was then treated as described in Method A; as the product was obtained 6.2 g (75.7% yield) of the mixture of **7** and **8**, bp 54—55 °C (1.2 mmHg), whose physical properties and spectroscopic data proved identical to those of the compound prepared by Method A.

6-Vinyl-endo-*2-norbornanol(9) and 5-Vinyl*-endo-*2-norbornanol(10).* To the ice-cooled suspension of 0.70 g (0.018 mol) of $LiAlH_4$ in 50 ml of dry tetrahydrofuran was added dropwise, with stirring, 5.0g (0.037 mol) of the mixture of **7** and **8**. After being stirred at room temperature for 3 h, the mixture was treated with ethyl acetate to destroy excess reducing agent and then with dilute sulfuric acid solution until the solution became slightly acidic. This solution was extracted with ether and then the extract was washed with saturated $NaHCO_3$ solution, with water, and dried over $MgSO_4$. After removal of the drying agent, the solvent was distilled off. The residue was distilled under reduced pressure to yield 4.7 g (92.0% yield) of the mixture of **9** and **10**, bp 80—81 °C (2.8 mmHg), $n_D^{18.5}$ 1.5004; the GC (column A, 140 °C) showed that the ratio of three peaks (t_R 15.5, 15.7, and 15.9 min) was 26:35:39; the IR and ^{1}H NMR data are identical to those of the mixture of **5** and **6**: ^{13}C NMR ($CDCl_3$, 7 lines as C-2 for the predominant isomers) (relative intensity) 74.3 (8.1), 74.2 (9.4), 74.0 (6.1), 72.6 (31.2), 72.1 (29.3), 71.8 (22.9), 65.6 (1.1) ppm. Found: C, 78.12; H, 10.30; O, 11.58%. Calcd for $C_9H_{14}O$: C, 78.26; H, 10.14; O, 11.59%.

6-Ethylidene-exo-*2-norbornyl Formate(11), 5-Ethylidene*-exo-*2-norbornyl Formate(12), and 6-Ethyltricyclo[2.2.1.0^{2,6}]heptan-3-yl Formate(13).* To 120.0 g (1.0 mol) of **2** was added 184.0 g (8.0 mol) of 98—100% formic acid, and the mixture was stirred at 80—90 °C for 5 h. After removal of excess formic acid, the residual liquid was distilled under reduced pressure to give 125.0 g (75.3% yield) of the mixture of **11**, **12**, and **13**, bp 58—62 °C (1.8—3.0 mmHg) [lit,[4] 69—71 °C (6 mmHg)], $n_D^{18.5}$ 1.4685, whose GC (column B, 80—130 °C) showed that the ratio of two peaks (t_R 5.6 and 6.6 min) was 39:61. IR (neat) ν_{max} 3090, 2930, 2870, 1720, 1660, 1170 cm^{-1}; ^{1}H NMR (CCl_4) δ=7.90 (s, 1H), 5.50—5.25 (m, 1H), 4.80 (s, 1H), 2.80—0.75 (m, 12H). Found: C, 72.35; H, 8.40; O, 19.25%. Calcd for $C_{10}H_{14}O_2$: C, 72.29; H, 8.43; O, 19.28%.

6-Ethylidene-exo-*2-norbornanol(14), 5-Ethylidene*-exo-*2-norbornanol(15), and 6-Ethyltricyclo[2.2.1.0^{2,6}]heptan-3-ol(16).*
A mixture of 20.0 g (0.120 mol) of the ester, **11**, **12**, and **13**, and 29.0 g of 20% NaOH solution was refluxed for 2 h and then extracted with a mixture of ether and benzene. The extract was rinsed with water and then dried over $MgSO_4$. After removal of the solvent, the residue was disitilled under reduced pressure to yield 15.3 g (92.4% yield) of a mixture of **14**, **15**, and **16**, bp 65—66 °C (1.0 mmHg) [lit,[4] 82—85 °C (6 mmHg)], $n_D^{18.5}$ 1.4911, which was proved by GC (column B, 80 °C) to consist of two components in the yields of 39 (t_R

4.6 min.) and 61(t_R 6.0 min)%, respectively: IR (neat) ν_{max} 3630, 3090, 2930, 2870, 1660, 1110 cm^{-1}; ^{1}H NMR (CCl_4) δ=5.50—5.05 (m, 1H), 3.85 (s, 1H), 2.95 (s, 1H), 2.45—0.70 (m, 11H); ^{13}C NMR ($CDCl_3$, 4 lines as C-2 for the predominant isomers) (relative intensity) 78.2 (14.5), 77.1 (24.5), 73.9 (50.0), 72.8 (11.0) ppm. Found: C, 78.31; H, 10.19; O, 11.50%. Calcd for $C_9H_{14}O$: C, 78.26; H, 10.14; O, 11.59%.

*6-Ethylidene-oxo-2-norbornanol(14), 5-Ethylidene-*exo*-2-norbornanol(15), and 5-or 6-(1-Hydroxyethyl)-2-norbornanol(17).* To a solution of 72.0 g (0.600 mol) of **2** in 250 ml of dry tetrahydrofuran was added 5.0 g (0.129 mol) of solid $NaBH_4$. To the ice-cooled solution was dropwise added 14.0 ml (0.111 mol) of boron trifluoride etherate over about 30 minutes, and then the mixture was stirred at 10—20 °C for about 2 h. To the reaction mixture was added 25.2 ml of water and 34.1 ml of 3M NaOH solution, and then 34.1 ml of 30% H_2O_2 solution was dropwise added. The resultant mixture was stirred at about 50 °C for 2 h and poured into 100 ml of a mixture of ether and benzene. The mixture was washed several times with small amounts of saturated NaCl solution. The separated organic layer was dried over $MgSO_4$, and the solvent was distilled off to afford residual materials which in turn were distilled under reduced pressure to give a colorless liquid, 23.7 g of a mixture of **14**, **15**, and **16** [yield based on boron trifluoride etherate: 52%; bp 60—61 °C (0.45 mmHg)]; $n_D^{18.5}$ 1.5060, as the first fraction, and the second fraction obtained a colorless, viscous liquid, 6.4 g of **17** [yield based on boron trifluoride etherae: 37%; bp 110—113 °C (0.5 mmHg)]; $n_D^{18.5}$ 1.5022. The GC (column A, 140 °C) analysis of the mixture of **14** and **15** indicated that the ratio of three peaks (t_R 13.7, 16.2, and 16.3 min) was 1:46:53; the data for the mixture of **14** and **15** are as follows: IR (neat) ν_{max} 3630, 3090, 2930, 2870, 1660, 1115 cm^{-1}; ^{1}H NMR (CCl_4) δ=5.65—5.15 (m, 1H), 3.85 (s, 1H), 3.00 (s, 1H), 2.55—0.70 (m, 11H); ^{13}C NMR ($CDCl_3$, 4 lines as C-2 for the predominant isomers)(relative intensity) 78.4(6.7), 77.1(5.7), 74.2(79.4), 73.1(8.20) ppm. Found: C, 78.05; H, 10.08; O, 11.87%. Calcd for $C_9H_{14}O$: C, 78.26; H, 10.14; O, 11.59%.

In turn, the GC (column B, 140 °C) analysis of **17** showed a single peak (t_R 3.0 min): IR (neat) ν_{max} 3625, 2920, 2870, 1110 cm^{-1}; ^{1}H NMR ($CDCl_3$) δ=4.80—4.50 (s, 1H), 4.35—3.80 (m, 1H) 3.75—3.25 (m, 1H), 2.50—0.75 (m, 13H). Found: C, 69.29; H, 10.18; O, 20.53%. Calcd for $C_9H_{16}O_2$: C, 69.23; H, 10.26; O, 20.51%.

6-Ethyltricyclo[2.2.1.0^{2,6}]heptan-3-ol(16). The mixture of **11**, **12**, and **13**, 25.0 g (0.151 mol), was dissolved in 100 ml of tetrahydrofuran and to the solution was added 3.23 g (0.042 mol) of solid $NaBH_4$. To the ice-cooled solution was dropwise added, with stirring, 14.2 ml (0.056 mol) of boron trifluoride etherate. After the mixture was stirred at room temperature for 1 h and at about 50 °C for 1 h, it was treated with 8.0 ml of water, 11.0 ml of 3M NaOH solution, and then slowly with 11.0 ml of 30% H_2O_2 solution, and the mixture was stirred at about 40 °C for 2 h. The mixture was extracted with ether and the ether extract was rinsed with water, and dried over $MgSO_4$. After removal of the ether, the residue (27.5 g) was dissolved in 50 ml of methanol and treated with 20 g of 10% NaOH solution. After the mixture was stirred under reflux for 2 h, methanol was removed by distillation and the residual oil was extracted with ether. After the ether layer was washed with water and dried over Na_2SO_4, the solvent was evaporated. The residue was distilled under reduced pressure to yield 6.5 g (31.2% yield) of **16**, bp 46 °C (0.06 mmHg); $n_D^{18.5}$ 1.4855. The GC (column A, 130 °C) analysis of **16** showed to consist of two components in the yields of 43(t_R 15.6 min.) and 57(t_R 16.1 min)%, respectively. IR (neat) ν_{max} 3630, 2925, 2870, 1115 cm^{-1}; ^{1}H NMR ($CDCl_3$) δ=4.05 (s, 1H), 3.80 (s, 1H), 2.00—0.75 (m, 12H); ^{13}C NMR ($CDCl_3$, 2 lines as C-2 for the predominant isomers) (relative intensity) 78.2(45.5), 77.1(54.5) ppm. Found: C, 78.41; H, 10.23; O, 11.36%. Calcd for $C_9H_{14}O$: C, 78.26; H, 10.14; O, 11.59%.

6-Ethylidene-2-norbornanone(19) and 5-Ethylidene-2-norbornanone(20). To an ice-cooled solution of 5.0 g (0.036 mol) of a mixture of **14** and **15**, obtained *via* hydroboration, in 30 ml of acetone was added dropwise, with stirring 20.0 ml of 8M chromium trioxide solution prepared according to Method B previously described in this section. The chromium trioxide solution was added at such a rate that the temperature did not rise above 30 °C. After being stirred at room temperature overnight, the mixture was worked up in the identical manner to that described in Method B. The product, a mixture of **19** and **20**, was obtained by vacuum distillation as a colorless liquid [yield, 68.0%; bp 49—50 °C (0.40 mmHg)]; $n_D^{18.5}$ 1.4930, whose GC (column A, 140 °C) indicated that the ratio of three components (t_R 16.0, 16.5, and 16.8 min) was 53:2:45; IR (neat) ν_{max} 3090, 2925, 2870, 1740, 1660 cm^{-1}; ^{1}H NMR (CCl_4) δ=5.50—5.20 (m, 1H), 2.85—0.75 (m, 11H). Found: C, 79.37; H, 8.88; O, 11.75%. Calcd for $C_9H_{12}O$: C, 79.41; H, 8.82; O, 11.76%.

*6-Ethylidene-*endo*-2-norbornanol(21) and 5-Ethylidene-*endo*-2-norbornanol(22).* To a stirred ice-cooled solution of 0.5 g (0.013 mol) of $LiAlH_4$ in 30 ml of tetrahydrofuran was added dropwise 3.6 g (0.026 mol) of a mixture of **19** and **20**. After the mixture was stirred at room temperature for 2 h, the reaction was quenched by slow addition of water, acidified with 10% sulfuric acid solution, and extracted with ether. The ether layer was washed with saturated $NaHCO_3$ solution, with water, and then dried over $MgSO_4$. After removal of the drying agent, the residual liquid was subjected to vacuum distillation.

The product, a mixture of **21** and **22**, was obtained as a colorless liquid [yield, 91.0%; bp 57—58 °C (0.20 mmHg)]; $n_D^{18.5}$ 1.5050, whose GC (column A, 140 °C) showed that it consists of three components in the yields of 11(t_R 15.0 min), 70(t_R 16.5 min.), and 19(t_R 16.8 min)%, respectively. IR (neat) ν_{max} 3630, 3090, 2920, 2875, 1660, 1110 cm^{-1}; ^{1}H NMR (CCl_4) δ=5.50—4.95(m, 1H), 3.80(s, 1H), 2.95(s, 1H), 2.50—0.75(m, 11H); ^{13}C NMR ($CDCl_3$, 4 lines as C-2 for the predominant isomers) (relative intensity) 78.5(6.5), 77.2(6.8), 74.0(12.5), 73.1(1.8), 71.9(60.6), 70.9(11.9) ppm. Found: C, 78.34; H, 10.09; O, 11.57%. Calcd for $C_9H_{14}O$: C, 78.26; H, 10.14; O, 11.59%.

Assignment of ^{13}C Chemical Shifts in Substituted Norbornanols

The previous studies[19] suggest that the ^{13}C proton-decoupled NMR spectrum for the substituted norbornanols described above mainly shows resonances at 75.0—65.0 ppm characteristic of C-2, α-carbon of a hydroxyl group and lead to the conclusion that the C-2 resonances of substituted 2-norbornanols are different in an *exo-endo* pair of isomers and γ-effect generates marked chemical-shift changes. On the basis of this empirical definition, the assignment of C-2 resonances was performed on vinylnorbornanols, **5**, **6**, **9**, and **10**, ethylidene norbornanols, **14**, **15**, **21**, and **22**, and ethyltricyclanol, **16**.

Firstly, as for 6-vinyl-2-norbornanol and 5-vinyl-2-norbornanol, the characteristic shift changes of the C-2 are best interpreted on the basis of the γ-effect. Thus, the *endo*-6-vinyl group is considered to cause a relatively marked upfield shift at C-2 due to steric interac-

tion between *endo*-6-vinyl group and either *endo*-hydrogen or *endo*-hydroxyl oxygen at C-2. In the case of *exo*-6-vinyl-2-norbornanol, C-2 should show a small upfield shift. By contrast, introduction of *endo*- and *exo*-vinyl group at C-5 is not expected to cause a significant shift change at C-2. Thus, the peaks at 74.2, 74.0, and 73.9 ppm for the mixture of **5** and **6** are reasonably identified as C-2 for *exo*-6-vinyl-*exo*-2-norbornanol, *endo*-5-vinyl-*exo*-2-norbornanol, and *exo*-5-vinyl-*exo*-2-norbornanol (but not differentiated respectively) and the absorption at 69.2 ppm can be assigned to C-2 for *endo*-6-vinyl-*exo*-2-norbornanol. Since there is no absorption between 73.0 and 72.0 ppm where the *endo*-hydroxy isomers should show C-2 resonances, we can conclude that no *endo*-hydroxy isomers can be detected in the mixture of **5** and **6**.

Turning to the ^{13}C NMR spectrum of the mixture of **9** and **10**, the peaks at 74.3, 74.2, and 74.0 ppm were identified as C-2 of *exo*-6-vinyl-*exo*-2-norbornanol, *endo*-5-vinyl-*exo*-2-norbornanol, and *exo*-5-vinyl-*exo*-2-norbornanol, although they are not differentiated respectively. Three lines at 72.6, 72.1, and 71.8 ppm should belong to C-2 of *endo*-5-vinyl-*endo*-2-norbornanol, *exo*-5-vinyl-*endo*-2-norbornanol, and *exo*-6-vinyl-*endo*-2-norbornanol (but not differentiated respectively) and the remaining peak at 65.6 ppm is identified as C-2 of *endo*-6-vinyl-*endo*-2-norbornanol, whereas the characteristic absorption for C-2 of *endo*-6-vinyl-*exo*-2-norbornanol is not observed in the chemical shift range predicted on the basis of the γ-effect.

By contrast with the influence of vinyl group, especially *endo*-vinyl group, upon the ^{13}C chemical shift at C-2 of the compounds above mentioned, the ethylidene group is considered to have very little influence on chemical shift from the well-known concept that the influence of the double bond upon the chemical shift is very weak when several bonds away.[20] Thus, the ^{13}C NMR spectra of both the mixture of **14** and **15**, obtained *via* hydroboration, and of **21** and **22** are demonstrated as follows: first in the case of the mixture of **14** and **15**, the peak at 74.2 ppm was assigned to C-2 of 6-ethylidene-*exo*-2-norbornanol and the line at 73.1 ppm could be assigned to C-2 of 5-ethylidene-*exo*-2-norbornanol. Interestingly, in this case, two absorptions at 78.4 and 77.1 ppm are observed, which apparently indicates the formation of **16** whose ^{13}C NMR spectrum will be discussed later in this section. Similarly, in the case of the mixture of **21** and **22**, two absorptions at 74.0 and 73.1 ppm are identified as C-2 of 6-ethylidene-*exo*-2-norbornanol and 5-ethylidene-*exo*-2-norbornanol, respectively. The remaining two main peaks at 71.9 and 70.9 ppm are assigned to C-2 of 6-ethylidene-*endo*-2-norbornanol and 5-ethylidene-*endo*-2-norbornanol, respectively.

Analogous effort to assign the C-2 resonances of the mixture of **14** and **15**, derived from the addition of formic acid to **2**, has been made. The two peaks at 78.2 and 77.1 ppm are identified as C-2 of the two epimers of **16**. Two lines at 73.9 and 72.8 ppm are assigned to C-2 of 6-ethylidene-*exo*-2-norbornanol and 5-ethylidene-*exo*-2-norbornanol, respectively.

The simplicity in the structure of **16**, including only two epimers, allows an unambiguous assignment of C-2. Thus, the peak at 78.2 ppm is identified as C-2 of *exo*-hydroxy epimer of **16**, and hence the remaining absorption at 77.1 ppm is assigned to C-2 of *endo*-hydroxy epimer of **16**.

We wish to thank Professor Teijiro Yonezawa of Kyoto University for helpful suggestions and valuable discussions. We are also grateful to Dr. Sakae Uemura of the Institute for Chemical Research, Kyoto University, and Dr. Hiroshi Fujimoto of Kyoto University for their valuable advice.

References

1) a) S. Tsuchida and M. Ogawa, *Sekiyu Gakkaishi*, **15**, 193 (1972); b) N. Nakai, S. Iwasa, Y. Ishii, and M. Ogawa, *Shikizai Kyokaishi*, **51**, 132 (1978); c) H. Kawachi and T. Akima, *Japan Kokai*, 72-31970 (1972).

2) T. C. Shields and A. N. Kurtz, *J. Am. Chem. Soc.*, **91**, 5415 (1969).

3) W. R. Adams and D. J. Trecker, *Tetrahedron*, **28**, 2361 (1972).

4) T. C. Shields, *Can. J. Chem.*, **49**, 1142 (1971).

5) E. J. Moriconi and C. C. Jalandoni, *J. Org. Chem.*, **35**, 2073 (1970).

6) V. I. Isagulyants, V. R. Melikyan, and V. V. Pokrovskaya *Dokl. Akad. Nauk Arm. SSR*, **55**, 179 (1972).

7) H. Fischer, F. Roehrscheid, L. Brinkman, and E. Reske, *Ger. Offen.*, 2163753 (1973).

8) a) Y. Inoue, F. Tanimoto, and H. Kitano, U.S. Patent 4331569 (1982); b) Y. Inoue, F. Tanimoto, and H. Kitano, U.S. Patent 4341665 (1982); c) G. C. Kitchens, U.S. Patent 3860635 (1975); d) M. A. Sprecker, U.S. Patent 4311861 (1982).

9) D. C. Kleinfelter and P. von R. Schleyer, *Org. Synth.*, **5**, 852 (1973).

10) I. Fleming, "Frontier Orbitals and Organic Chemical Reactions", John Wiley&Sons, New York, N. Y. (1976), 27.

11) a) H. C. Brown, W. J. Hammer, J. H. Kawakami, I. Rothberg, and D. L. Vander Jagt, *J. Am. Chem. Soc.*, **89**, 6381 (1967); b) H. C. Brown and G. Zweifel, *ibid.*, **83**, 2544 (1961); c) H. C. Brown and K. T. Liu, *ibid.*, **93**, 7335 (1971).

12) H. C. Brown and J. H. Kawakami, *J. Am. Chem. Soc.*, **92**, 1990 (1970).

13) G. Wipff and K. Morokuma, *Tetrahedron Lett.*, **1980**, 4445.

14) a) S. B. Soloway and S. J. Cristol, *J. Org. Chem.*, **25**, 327 (1960); b) L. Rand and R. J. Dolinski, *ibid.*, **31**, 4061 (1966); c) R. H. Perry, Jr., *ibid.*, **24**, 829 (1959); d) R. R. Sauers and P. E. Sonnet, *ibid.*, **29**, 754 (1964); e) W. E. Fichtman and M. Orchin, *ibid.*, **34**, 2790 (1969); f) S. J. Cristol and G. D. Brindell, *J. Am. Chem. Soc.*, **76**, 5699 (1954); g) D. I. Davies, L. T. Parfitt, C. K. Alden, and J. A. Claisse, *J. Chem. Soc., C*, **1969**, 1585; h) D. I. Davies and M. J. Parrott, *Tetrahedron Lett.*, **1972**, 2719; i) C. W. Jefford and W. Wojnarowski, *ibid.*, **1968**, 193.

15) For nortricyclonium ion or homoallylic cation, see a) J. D. Roberts and C. C. Lee, *J. Am. Chem. Soc.*, **73**, 5009 (1951); b) J. D. Roberts and W. Bennett, *ibid.*, **76**, 4623 (1954); c) J. D. Roberts, W. Bennett, and R. Armstrong, *ibid.*, **72**, 3329 (1950); d) J. D. Roberts, C. C. Lee, and W. H. Saunders, *ibid.*, **77**, 3034 (1955); e) S. Winstein, H. M. Walborsky, and K. Schreiber, *ibid.*, **72**, 5795 (1950); f) S. Winstein and M. Shatavsky, *Chem. and Ind.*, **1956**, 56.

16) E. Heilbronner and V. Schomaker, *Helv. Chim. Acta*, **35**, 1385 (1952).

17) T. Maeda, M. Muranaka, S. Hamanaka, and M. Ogawa, *Nippon Kagaku Kaishi*, **1974**, 1587.

18) This ratio was calculated by GC analysis on the assumption that the *E*-isomer has the lower boiling point than the *Z*-isomer.[19a] For more detail, see: R. G. Weiss and G. S. Hammond, *J. Am. Chem. Soc.*, **100**, 1172 (1978).

19) a) E. Lippmaa, T. Pehk, J. Paasivirta, N. Belikova, and A. Plate, *Org. Magn. Reson.*, **2**, 581 (1970); b) J. B. Grutzner, M. Jautelat, J. B. Dence, R. A. Smith, and J. D. Roberts, *J. Am. Chem. Soc.*, **92**, 7107 (1970).

20) E. Lippmaa, S. Rang, O. Eisen, and T. Pehk, *Eesti NSV Tead. Akad. Toim. Keemi Geol.*, **16**, 351 (1967).

A New Wittig Rearrangement of 2,2-Disubstituted 1,3-Dithianes

Hideyuki IKEHIRA* and Shigeo TANIMOTO*
Institute for Chemical Research, Kyoto University, Uji, Kyoto 611
(Received January 23, 1984)

Carbanions produced by deprotonation at the ring C-4 of 2,2-disubstituted 1,3-dithianes undergo a Wittig type rearrangement to give the anions of 2,2-disubstituted tetrahydrothiophene-3-thiols. After being trapped with several alkyl halides, these afford the corresponding 2,2-disubstituted 3-(alkylthio)tetrahydrothiophenes, which are difficult to prepare by other synthetic routes.

Recently, Wilson and his co-workers[1,2] studied the reaction of 1,3-dithiane with anionic bases in the gas phase. They observed that it undergoes deprotonation at C-5, in competition with that at C-2. However, the deprotonation at C-5 is recognized only for 1,3-dithiane in the gas phase. In a solution, the deprotonation usually occurs at C-2. For example, 1,3-dithiane and its 2-alkyl derivatives easily undergo deprotonation at the ring C-2 by butyllithium or lithium diisopropylamide (LDA), leading to the formation of 2-lithio-1,3-dithianes.[3] Many examples cited in the literature demonstrate the high nucleophilicity of the 2-lithio-1,3-dithianes as well as the utility of these reagents in synthetic organic chemistry.[3] On the other hand, 2-cyclohexylidene-1,3-dithiane is deprotonated at C-4 of the 1,3-dithiane ring by butyllithium in tetrahydrofuran.[4] The ring C-4 deprotonation has also been found by Hase and Lahtinen[5] in the reaction of several 2-alkyl-2-trimethylsilylmethyl-1,3-dithianes with butyllithium in the presence of hexamethylphosphoric triamide, but it competes with side chain deprotonation. In most cases, the carbanion produced by deprotonation at the ring C-2 or C-4 of 1,3-dithiane and its derivatives is stable and does not undergo further transformation under the carbanion-forming conditions. In the last-mentioned reaction proposed by Hase and Lahtinen,[5] however, the initially formed carbanion undergoes migration of trimethylsilyl group and succeeding formation of C-2 to C(α) double bond with suprafacial expulsion of S-3 as the thiolate anion under the carbanion-forming conditions. With this background, we expected that appropriate 2,2-disubstituted 1,3-dithianes should be deprotonated at C-4 by a strong base such as butyllithium or LDA. In this paper we wish to describe such a deprotonation by LDA and the behavior of the resulting anionic species, which would be made clear by trapping them by several alkyl halides.

Results and Discussion

We have studied the reactions of several 2,2-disubstituted 1,3-dithianes (**1**), such as 2,2-diaryl-1,3-dithianes (**1a**, **1b**, **1c**, and **1d**), 2-phenyl-2-trifluoromethyl-1,3-dithiane (**1e**), and 2-ethylthio-2-phenyl-1,3-dithiane (**1f**) with LDA in tetrahydrofuran in the presence or absence of *N*, *N*, *N'*, *N'*-tetramethylethylenediamine followed by adding an appropriate alkyl halide to the reaction mixture. These reactions resulted in the high-yield formation of the corresponding 2,2-disubstituted 3-(alkylthio)tetrahydrothiophenes (**4**) after the usual work-up procedure.

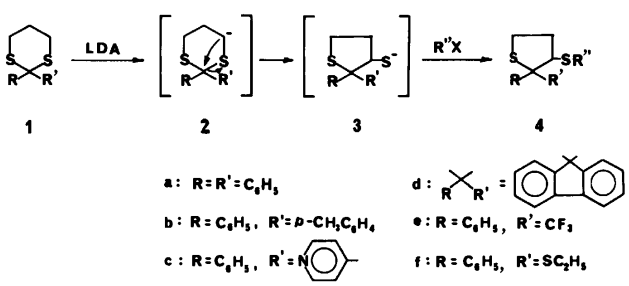

It is certain that the initial deprotonation occurred at the ring C-4 of **1**, because they possess no hydrogen at the ring C-2. Presumably, the initially formed anionic species (**2**) rearranges *via* 1,2-shift of the C-2 carrying two substituents from S-3 to C-4 as well as the simultaneous S-3 thiolate expulsion to give the anions (**3**) of 2,2-disubstituted tetrahydrothiophene-3-thiols. On trapping with alkyl halides, these afford **4**. This mechanistic interpretation reveals that the reaction is a Wittig type rearrangement involving migration of carbon from sulfur to an α-carbanion. Concerning such the rearrangement of sulfide and its homologues, to our best knowledge, only three reports have been published.[6-8] We chose 2,2-diphenyl-3-(methylthio)-tetrahydrothiophene **4a** [R''=CH_3] as a representative of the obtained products **4**. We studied its ^{1}H-NMR spectrum in $CDCl_3$ by decoupling experiments involving the protons on C-3, C-4, and C-5 of **4a** [R''=CH_3]. It is obvious from Fig. 1 that **4a** [R''=CH_3] involves the $-SCH_2CH_2CH<$ system, the methylthio, and two phenyl groups. Thus, the structure of **4a** [R''=CH_3] should be supported by the decoupled spectra, together with the ^{13}C-NMR and mass spectral data and analytical data.

This observation as well as the fact that the other products also exhibit spectral properties (^{1}H-NMR, ^{13}C-NMR, and mass spectra) and analytical data in good accordance with the assigned structures supports the reasonableness of the above mechanistic interpretation. Also, the occurrence of this conversion was recognized only when both the substituents at C-2 of **1** are electron-withdrawing groups, suggesting that the migrating carbon may be C-2 of the 1,3-dithiane ring. All attempts to submit 2-alkyl-2-aryl- and 2,2-dialkyl-1,3-dithianes such as 2-methyl-2-phenyl-, 2-ethyl-2-phenyl-, 2,2-dimethyl-, and 2,2-diethyl-1,3-dithiane to the same deprotonation-alkylation sequence failed and resulted in the recovery of the starting 1,3-dithianes. Thus, it may be claimed that the occurrence

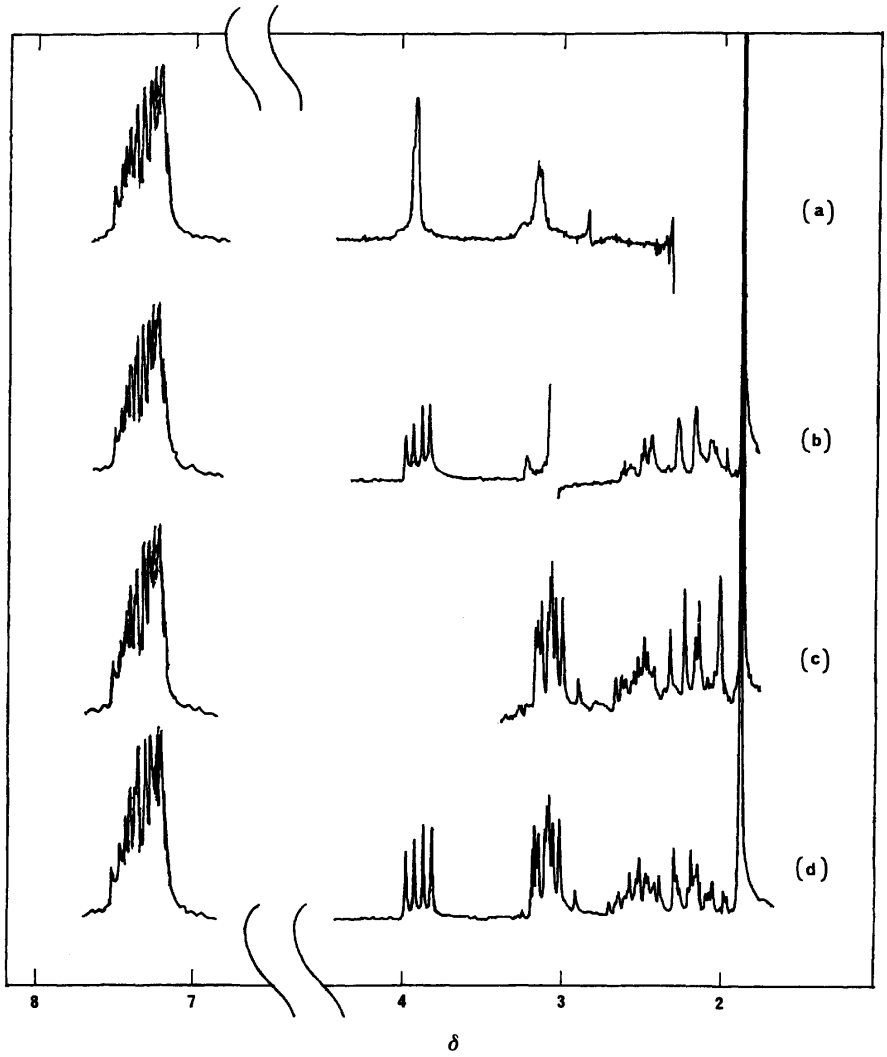

Fig. 1. The ^{1}H-NMR spectra of **4a**[R″=CH_3] in $CDCl_3$ where (a) the protons on C-4 are decoupled, (b) the protons on C-5 are decoupled, (c) the proton on C-3 is decoupled, and (d) none of the protons is decoupled.

Table 1. Formation of 2,2-disubstituted 3-(alkylthio)tetrahydrothiophenes (**4**) from 2,2-disubstituted 1,3-dithianes (**1**)

Starting 1,3-dithiane	Trapping agent (R″X)	Product[a)]	Yield/%	Mp θ_m/°C or [Bp θ_b/°C(Torr)†]
1a	CH_3I	**4a**[R″=CH_3]	94	75—76
1a	C_2H_5I	**4a**[R″=C_2H_5]	90	93—94
1a	$CH_3(CH_2)_3I$	**4a**[R″=$CH_3(CH_2)_3$]	93	[139(1.5)]
1a	$CH_3(CH_2)_3Br$	**4a**[R″=$CH_3(CH_2)_3$]	94	
1b	CH_3I	**4b**[R″=CH_3]	92	[119(5.5)]
1b	C_2H_5I	**4b**[R″=C_2H_5]	94	[135(1.2)]
1b	$CH_3(CH_2)_3I$	**4b**[R″=$CH_3(CH_2)_3$]	95	[149(1.1)]
1b	$CH_3(CH_2)_3Br$	**4b**[R″=$CH_3(CH_2)_3$]	76	
1c	CH_3I	**4c**[R″=CH_3]	58	133—134
1c	C_2H_5I	**4c**[R″=C_2H_5]	99	[128(2.5)]
1c	$CH_3(CH_2)_3I$	**4c**[R″=$CH_3(CH_2)_3$]	92	[136(4)]
1c	$CH_3(CH_2)_3Br$	**4c**[R″=$CH_3(CH_2)_3$]	61	
1d	CH_3I	**4d**[R″=CH_3]	90	139—140
1d	C_2H_5I	**4d**[R″=C_2H_5]	99	114—115
1d	$CH_3(CH_2)_3I$	**4d**[R″=$CH_3(CH_2)_3$]	97	—[b)]
1d	$CH_3(CH_2)_3Br$	**4d**[R″=$CH_3(CH_2)_3$]	44	

TABLE 1. Continued

Starting 1,3-dithiane	Trapping agent (R″X)	Product[a)]	Yield/%	Mp θ_m/°C or [Bp θ_b/°C(Torr)†]
1e	CH_3I	**4e**[R″=CH_3]	92	[132(3)]
1e	C_2H_5I	**4e**[R″=C_2H_5]	80	[133(2.5)]
1f	CH_3I	**4f**[R″=CH_3]	69	[133(3)]
1f	C_2H_5I	**4f**[R″=C_2H_5]	91	[150(3.5)]
1f	$CH_3(CH_2)_3I$	**4f**[R″=$CH_3(CH_2)_3$]	91	[162(3.5)]

a) The products **4c** were isolated by column chromatography(silica gel, 25% ethyl acetate/chloroform). The other products were also isolated by column chromatography(silica gel, 10% ethyl acetate/hexane). All products listed in this table were a mixture of diastereomers. They were also characterized by mass spectra in addition to ^{1}H-NMR, ^{13}C-NMR, and elemental analysis. b) Decomposes during distillation under reduced pressure.
† 1 Torr≈133.322 Pa.

TABLE 2. ^{1}H- AND ^{13}C-NMR SPECTRA OF **4a**, **4b**, AND **4c**

Compound	^{1}H-NMR (δ, $CDCl_3$)[a)]	^{13}C-NMR (δ, $CDCl_3$)[a)]
4a[R″=CH_3]	1.82(s, 3H), 2.2—2.6(m, 2H), 2.9—3.2(m, 2H), 3.8—4.0(m, 1H), 7.0—7.5(m, 10H)	15.09(q), 29.13(t), 34.46(t), 56.28(d), 68.09(s), 126.72(d), 127.01(d), 127.36(d), 128.12(d), 129.99(d), 143.21(s), 145.67(s)
4a[R″=C_2H_5]	1.15(t, 3H, J=7 Hz), 1.9—2.8(m, 4H), 2.9—3.2(m, 2H), 3.7—4.1(m, 1H), 7.0—7.5(m, 10H)	14.68(q), 26.27(t), 29.25(t), 35.51(t), 54.93(d), 68.09(s), 126.66(d), 126.95(d), 127.48(d), 128.06(d), 128.36(d), 129.29(d), 129.99(d), 143.33(s), 145.61(s)
4a[R″=$CH_3(CH_2)_3$]	0.6—1.1(m, 3H), 1.1—1.6(m, 4H), 2.0—2.8(m, 4H), 2.9—3.2(m, 2H), 3.7—4.1(m, 1H), 7.0—7.5(m, 10H)	13.63(q), 21.94(t), 29.08(t), 31.59(t), 31.94(t), 35.45(t), 55.23(d), 68.04(s), 126.54(d), 126.83(d), 127.42(d), 127.95(d), 129.93(d), 143.27(s), 145.56(s)
4b[R″=CH_3]	1.79(s, 1.5H), 1.85(s, 1.5H), 2.23(s, 3H), 2.1—2.5(m, 2H), 2.8—3.2(m, 2H), 3.6—4.0(m, 1H), 6.8—7.5(m, 9H)	14.92(q), 15.05(q), 20.89(q), 28.96(t), 34.34(t), 56.22(d), 56.34(d), 67.75(s), 67.86(s), 126.48(d), 126.83(d), 127.19(d), 127.30(d), 127.65(d), 127.95(d), 128.18(d), 128.71(d), 129.93(d), 136.02(s), 136.37(s), 140.29(s), 142.69(s), 143.27(s), 145.73(s)
4b[R″=C_2H_5]	1.15(t, 3H, J=7 Hz), 1.9—2.8(m, 4H), 2.28(s, 3H), 2.9—3.2(m, 2H), 3.7—4.1(m, 1H), 6.9—7.5(m, 9H)	14.68(q), 20.94(q), 26.21(t), 26.33(t), 29.13(t), 35.45(t), 54.93(d), 67.75(s), 67.86(s), 126.54(d), 126.83(d), 127.24(d), 127.36(d), 127.65(d), 127.95(d), 128.71(d), 129.93(d), 136.08(s), 136.43(s), 140.35(s), 142.63(s), 143.39(s), 145.67(s)
4b[R″=$CH_3(CH_2)_3$]	0.7—1.1(m, 3H), 1.1—1.7(m, 4H), 1.9—2.6(m, 4H), 2.27(s, 3H), 2.8—3.1(m, 2H), 3.5—3.9(m, 1H), 6.8—7.5(m, 9H)	13.57(q), 20.89(q), 22.06(t), 29.13(t), 29.43(t), 31.77(t), 32.12(t), 35.69(t), 55.75(d), 68.09(s), 68.21(s), 126.54(d), 126.89(d), 127.42(d), 127.54(d), 127.71(d), 127.95(d), 128.29(d), 128.71(d), 129.06(d), 129.23(d), 129.35(d), 130.05(d), 136.14(s), 136.43(s), 140.52(s), 142.81(s), 143.57(s), 145.85(s)
4c[R″=CH_3]	1.84(s, 1.5H), 1.90(s, 1.5H), 2.2—2.6(m, 2H), 2.9—3.2(m, 2H), 3.6—4.0(m, 1H), 7.0—7.4(m, 7H), 8.3—8.5(m, 2H),	14.98(q), 15.44(q), 29.13(t), 29.31(t), 34.28(t), 34.69(t), 55.87(d), 56.05(d), 67.22(s), 67.39(s), 122.39(d), 124.85(d), 127.30(d), 128.30(d), 129.82(d), 141.52(s), 144.09(s), 148.71(d), 149.71(d), 152.22(s), 154.51(s)
4c[R″=C_2H_5]	1.19(t, 3H, J=7 Hz), 2.1—2.6(m, 4H), 2.9—3.3(m, 2H), 3.7—4.1(m, 1H), 7.1—7.5(m, 7H), 8.4—8.6(m, 2H)	14.68(q), 26.33(t), 26.68(t), 29.19(t), 29.37(t), 35.57(t), 35.98(t), 54.99(d), 55.11(d), 67.45(s), 67.69(s), 122.50(d), 124.85(d), 127.24(d), 127.36(d), 127.48(d), 128.24(d), 129.88(d), 141.75(s), 144.15(s), 148.71(d), 149.65(d), 152.46(s), 154.56(s)
4c[R″=$CH_3(CH_2)_3$]	0.7—1.1(m, 3H), 1.1—1.8(m, 4H), 2.1—2.7(m, 4H), 2.9—3.2(m, 2H), 3.7—4.0(m, 1H), 7.1—7.5(m, 7H), 8.3—8.5(m, 2H)	13.57(q), 21.94(t), 29.19(t), 29.37(t), 31.65(t), 32.12(t), 32.53(t), 35.57(t), 35.92(t), 55.23(d), 55.40(d), 67.45(s), 67.69(s), 122.50(d), 124.85(d), 127.13(d), 127.24(d), 127.36(d), 127.48(d), 128.24(d), 129.88(d), 141.75(s), 144.15(s), 148.71(d), 149.65(d), 152.46(s), 154.56(s)

a) Measured at 25 °C.

Table 3. ^{1}H- and ^{13}C-NMR spectra of **4d**, **4e**, and **4f**

Compound	^{1}H-NMR (δ, $CDCl_3$)[a]	^{13}C-NMR (δ, $CDCl_3$)[a]
4d[R″=CH_3]	1.57(s, 3H), 2.4—2.8(m, 2H), 3.1—3.5(m, 2H), 3.5—3.9(m, 1H), 7.1—7.7(m, 8H)	15.97(q), 30.19(t), 37.27(t), 61.25(d), 66.05(s), 119.64(d), 123.73(d), 125.78(d), 127.30(d), 127.65(d), 128.12(d), 128.30(d), 139.88(s), 140.58(s), 148.13(s), 149.53(s)
4d[R″=C_2H_5]	0.83(t, 3H, J=7 Hz), 1.96(q, 2H, J=7 Hz), 2.5—2.9(m, 2H), 3.2—3.4(m, 2H), 3.5—3.9(m, 1H), 7.1—7.8(m, 8H)	14.74(q), 26.68(t), 30.19(t), 38.20(t), 59.26(d), 65.93(s), 119.64(d), 123.67(d), 125.61(d), 127.30(d), 127.59(d), 128.06(d), 128.24(d), 139.88(s), 140.69(s), 147.95(s), 149.65(s)
4d[R″=$CH_3(CH_2)_3$]	0.5—0.8(m, 3H), 0.8—1.3(m, 4H), 1.8—2.1(m, 2H), 2.5—2.9(m, 2H), 3.2—3.5(m, 2H), 3.5—3.9(m, 1H), 7.1—7.7(m, 8H)	13.46(q), 21.47(t), 30.19(t), 31.65(t), 32.35(t), 38.14(t), 59.38(d), 65.93(s), 119.58(d), 119.70(d), 123.67(d), 125.61(d), 127.30(d), 127.59(d), 128.06(d), 128.24(d), 139.94(s), 140.70(s), 147.95(s), 149.65(s)
4e[R″=CH_3]	1.80(s, 3H), 1.9—2.7(m, 2H), 1.7—3.2(m, 2H), 3.5—3.8(m, 1H), 7.0—7.3(m, 3H), 7.3—7.7(m, 2H)	15.44(q), 30.13(t), 36.15(t), 55.46(d), 121.80(s), 127.48(d), 128.06(d), 128.41(d), 130.05(d), 130.17(d), 133.09(s), 135.02(s)
4e[R″=C_2H_5]	1.11(t, 1.5H, J=7 Hz), 1.23(t, 1.5H, J=7 Hz), 2.35(q, 1H, J=7 Hz), 2.50(q, 1H, J=7 Hz), 2.2—2.7(m, 2H), 2.9—3.3(m, 2H), 3.7—3.9(m, 1H), 7.1—7.4(m, 3H), 7.4—7.7(m, 2H)	14.45(q), 26.33(t), 30.13(t), 37.21(t), 53.41(d), 121.86(s), 127.42(d), 128.00(d), 128.30(d), 128.47(d), 130.11(d), 135.26(s)
4f[R″=CH_3]	1.04(t, 3H, J=7 Hz), 1.0—1.7(m, 1H), 1.86(s, 3H), 2.47(q, 2H, J=7 Hz), 2.0—2.9(m, 2H), 2.9—3.7(m, 2H), 7.0—7.4(m, 3H), 7.5—7.8(m, 2H)	13.46(q), 15.50(q), 26.15(t), 29.25(t), 35.34(t), 61.54(d), 77.22(s), 127.36(d), 128.06(d), 128.36(d), 129.29(d), 140.70(s)
4f[R″=C_2H_5]	1.05(t, 3H, J=7 Hz), 1.10(t, 3H, J=7 Hz), 2.32(q, 4H, J=7 Hz), 2.0—3.8(m, 5H), 7.0—7.3(m, 3H), 7.5—7.8(m, 2H)	13.39(q), 14.68(q), 26.13(t), 29.18(t), 35.99(t), 59.24(d), 76.91(s), 127.22(d), 129.16(d), 140.67(s)
4f[R″=$CH_3(CH_2)_3$]	0.6—1.0(m, 3H), 1.05(t, 3H, J=7 Hz), 1.1—1.7(m, 4H), 2.38(q, 2H, J=7 Hz), 2.1—3.8(m, 7H), 7.0—7.4(m, 3H), 7.5—7.7(m, 2H)	13.39(q), 13.56(q), 21.84(t), 26.18(t), 29.24(t), 31.59(t), 31.99(t), 36.11(t), 59.65(d), 77.08(s), 127.28(d), 129.22(d), 140.73(s)

a) Measured at 25 °C.

Table 4. Analytical data of 2,2-disubstituted 3-(alkylthio)tetrahydrothiophenes (**4**)

Compound	Found/%			Calcd/%		
	C	H	N	C	H	N
4a[R″=CH_3]	71.03	6.26		71.28	6.33	
4a[R″=C_2H_5]	71.98	6.52		71.95	6.71	
4a[R″=$CH_3(CH_2)_3$]	73.04	7.25		73.11	7.36	
4b[R″=CH_3]	71.89	6.67		71.95	6.71	
4b[R″=C_2H_5]	72.54	7.05		72.56	7.05	
4b[R″=$CH_3(CH_2)_3$]	73.65	7.61		73.63	7.65	
4c[R″=CH_3]	66.80	5.89	4.82	66.85	5.96	4.87
4c[R″=C_2H_5]	67.66	6.25	4.53	67.73	6.35	4.65
4c[R″=$CH_3(CH_2)_3$]	69.22	6.95	4.10	69.25	7.04	4.25
4d[R″=CH_3]	71.74	5.59		71.78	5.67	
4d[R″=C_2H_5]	72.33	6.00		72.43	6.08	
4d[R″=$CH_3(CH_2)_3$]	73.59	6.72		73.57	6.79	
4e[R″=CH_3]	51.66	4.68		51.78	4.71	
4e[R″=C_2H_5]	53.31	4.95		53.40	5.17	
4f[R″=CH_3]	57.67	6.61		57.73	6.71	
4f[R″=C_2H_5]	59.05	7.05		59.10	7.09	
4f[R″=$CH_3(CH_2)_3$]	61.24	7.66		61.48	7.74	

of this conversion requires the presence of two electron-withdrawing groups at C-2 of the 1,3-dithiane ring. Although this method is applicable only to the above-mentioned 2,2-disubstituted 1,3-dithianes such as **1**, the mild conditions required and high yields of the objective **4**, as can be seen in Table 1, make this method valuable. Tables 2 and 3 give ^{1}H- and ^{13}C-NMR spectral data of **4a—c** and **4d—f**, respectively. The analytical data of **4** are listed in Table 4.

Experimental

All 2,2-disubstituted 1,3-dithianes (**1a**, **1b**, **1c**, **1d**, and **1e**) employed in this research were prepared by the $AlCl_3$-catalyzed reaction of the corresponding ketones with 1,3-propanedithiol. The compound **1f** was prepared from 2-lithio-2-phenyl-1,3-dithiane generated by the known method and diethyl disulfide in tetrahydrofuran at low temperature. Tetrahydrofuran and *N,N,N′,N′*-tetramethylethylenediamine were dried over lithium aluminium hydride and calcium hydride respectively, and then distilled prior to use. The other reagents were commercially available and were used without further purification.

Reactions Summarized in Table 1. To lithium diisopropylamide (LDA), prepared from diisopropylamine (0.35 g, 3.5 mmol) in tetrahydrofuran (7 ml) and 1.56 molar solution (2.12 ml, 3.3 mmol) of butyllithium in hexane, was added a solution of **1** (1.3 mmol) in tetrahydrofuran (4 ml) with stirring at −78 °C. Only when **1a** and **1b** were used as the dithiane component *N,N,N′,N′*-tetramethylethylenediamine (0.41 g, 3.5 mmol) was added[9] prior to the addition of **1**. The reaction mixture was allowed to warm to −15 °C and the stirring was continued for 1 h at the same temperature. The mixture was cooled again to −78 °C, and an appropriate alkyl halide (3.3 mmol) was added with stirring. The stirring was continued for 1 h at −10—−5 °C and for 24 more hours at room temperature. The reaction mixture was quenched with water (100 ml) and a saturated aqueous solution (20 ml) of ammonium chloride, and then extracted with diethyl ether (3×60 ml). The combined ethereal extracts were dried over anhydrous magnesium sulfate and concentrated *in vacuo* to give a pale yellow residue, which was subjected to column chromatography on silica gel. The eluents used for the column chromatography are indicated as the marginal notes of Table 1.

References

1) S. R. Wilson, P. Caldera, and M. A. Jester, *J. Org. Chem.*, **47**, 3319 (1982).
2) J. E. Bartmess, R. L. Hays, H. N. Khatri, R. N. Misra, and S. R. Wilson, *J. Am. Chem. Soc.*, **103**, 4746 (1981).
3) D. Seebach and E. J. Corey, *J. Org. Chem.*, **40**, 231 (1975).
4) D. Seebach and M. Kolb, *Justus Liebigs Ann. Chem.*, **1977**, 811.
5) T. A. Hase and L. Lahtinen, *Tetrahedron Lett.*, **22**, 3285 (1981).
6) J. F. Biellmann and J. L. Schmitt, *Tetrahedron Lett.*, **1973**, 4615.
7) T. Hayashi and H. Baba, *J. Am. Chem. Soc.*, **97**, 1608 (1975).
8) R. H. Mitchell, T. Otsubo, and V. Boekelheide, *Tetrahedron Lett.*, **1975**, 219.
9) When *N, N, N′, N′*-tetramethylethylenediamine was omitted in the runs using **1a** or **1b** as a starting substrate, the yields of **4a** or **4b** were greatly decreased.

 © 1984 The Chemical Society of Japan Bull. Chem. Soc. Jpn., 57, 2479—2483 (1984)

Selective Protection of Carbonyl Groups by Taking Advantage of a Combination of Solid Support and Girard's Reagent

Teiji CHIHARA, Erika WANIGUCHI,† Tamie WAKABAYASHI,† and Kazuo TAYA*,†

The Institute of Physical and Chemical Research, Wako, Saitama 351-01

†*Department of Chemistry, Tokyo Gakugei University, Koganei, Tokyo 184*

(Received February 21, 1984)

Some Girard's derivatives of 4-phenylbenzophenone were prepared in ethanol solution, in the presence of Amberlite IRC-50 as a catalyst. Supported samples of the derivatives were then prepared by addition of silica gel to the solution, followed by evaporation of the ethanol. The supported samples were reduced with lithium tri-*t*-butoxyhydroaluminate by being suspended in THF solution. Hydrolysis, followed by extraction of the product, yielded 4-acetyl-α-phenylbenzyl alcohol in an 80% selectivity. In the same way, 4-acetylbenzaldehyde yielded 1-(4-formylphenyl)ethanol in an 81% selectivity. Relatively unhindered carbonyl groups were preferentially protected. Utilization of Girard's reagents was successfully made as a protecting reagent and also as an extracting reagent of carbonyl compounds.

Many chemical reactions occur homogeneously, while various reactions occurring on solid surfaces are also known. Recently, solid adsorbents have been used as reaction media on which the reactions occur heterogeneously.[1] In almost all cases reagents were adsorbed on them, and some concepts for application of the adsorbents can be seen in the reports. In one concept, inorganic reagents such as potassium permanganate, sodium periodate, iron(III) nitrate, and iron(III) chloride were brought into an organic reaction system on solid adsorbents.[2-5] These inorganic reagents are insoluble in organic solvents, so they were adsorbed, forming monomolecular-like layers on the solid adsorbents. In addition, isolation of the products became easy by use of adsorbents, because inorganic by-products and tarry matter remain on the adsorbents.

We have reported the case in which a substrate was adsorbed.[6] Sodium hydrogensulfite adducts of carbonyl compounds are usually not soluble in organic solvents, but were stably adsorbed on silica gel and alumina in the absence of water. The adducts adsorbed on solid adsorbents could be brought into an organic reaction system. In this way, sodium hydrogensulfite was used for protection of the carbonyl groups in the organic reaction system.

From the same stand point the use of Girard's reagents for protection of carbonyl groups has been studied. Girard's reagents condense with carbonyl compounds to form water-soluble products. The carbonyl compounds are then recovered from the aqueous layer by hydrolysis or carbonyl exchange reaction.[7] While a semicarbazide hydrochloride is used to protect the carbonyl groups, Girard's reagent, a member of the substituted hydrazine group, has not been used to protect them because of the low solubilities of the derivatives in the usual organic solvents. We tried to use Girard's reagent for protection of the carbonyl groups by using it with adsorbents. As a representative of dicarbonyl compounds, 4-acetylbenzophenone (**1**) was chosen. It has two carbonyl groups. One of these, the benzoyl group, was reported not to react with Girard's reagent because of steric hindrance.[8] First, the derivative of **1** with Girard-T (**2**), α-(trimethylammonio) acetohydrazide chloride, was prepared. Then it was supported on silica gel and reduced with lithium tri-*t*-butoxyhydroaluminate (**3**). Analysis of the product showed that 4-acetyl-α-phenylbenzyl alcohol (**4**) was obtained in an 80% selectivity. Part of the results of this investigation was preliminary reported in an earlier paper,[9] and the details are given here.

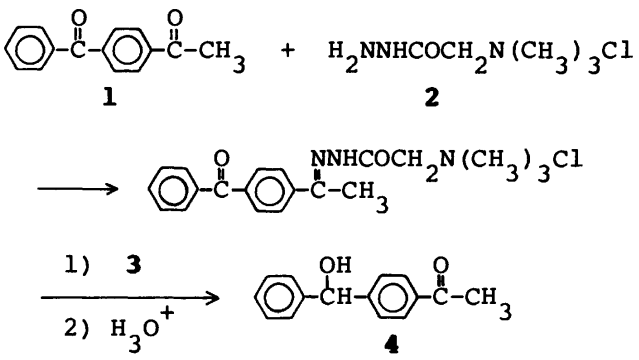

Results and Discussion

Selective Protection of the Acetyl Group of 4-Acetylbenzophenone (1). The effect of reaction time on the Girard's derivative formation was examined. Equal moles of **1** and **2** were allowed to react in the presence of Amberlite IRC-50 (**5**) as a catalyst to produce the derivative. After removal of the catalyst, silica gel was added to the solution, and the ethanol was evaporated. The derivative supported on silica gel was reduced with an excess of **3**. After hydrolysis the product was analyzed. The compositions of the products were plotted against the reaction time for the derivative formation in Fig. 1. This figure shows that the products of insufficient reaction time contained considerable amount of diol, 4-(1-hydroxyethyl)-α-phenylbenzyl alcohol (**6**). This is because considerable amount of **1** was left intact and was then reduced. Figure 1 also shows that the compositions of the products attained constant values after two hours. So the selectivity for **4** was about 80%. Two hours was sufficient to complete the formation of the derivative. In this way the reaction time was determin-

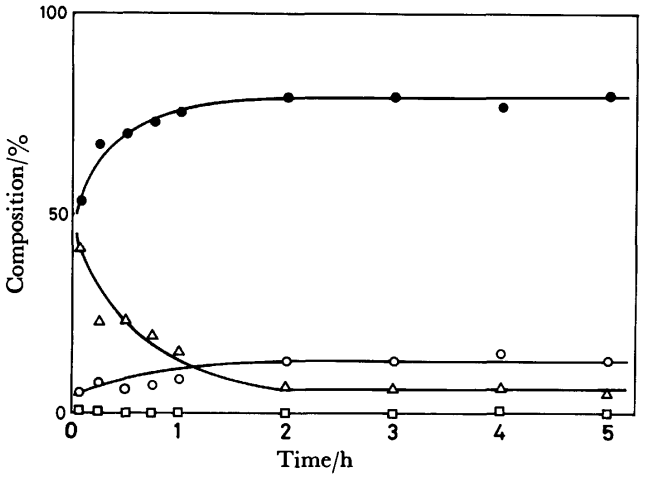

Fig. 1. Effect of reaction time for Girard-T derivative formation on selective protection of **1**.
Reaction temperature: 70 °C, **1** : **2**=1 : 1(mol/mol), **1**: silica gel=1 : 35(w/w), ○: **1**, ●: **4**, △: **6**, □: **11**.

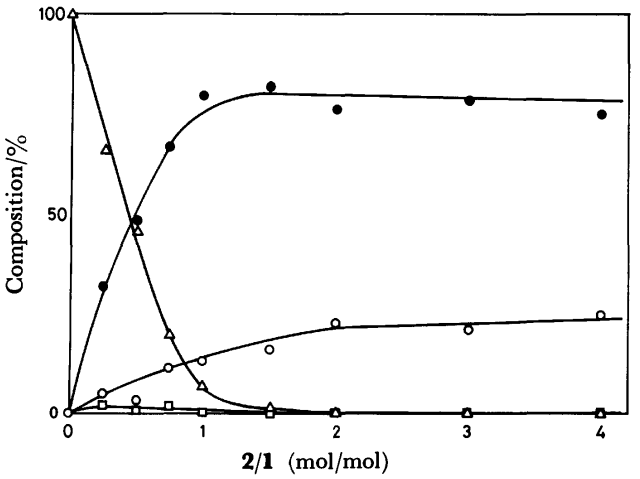

Fig. 2. Effect of amount of **2** on selective protection of **1**.
1: silica gel=1:35 (w/w), ○: **1**, ●: **4**, △: **6**, □: **11**.

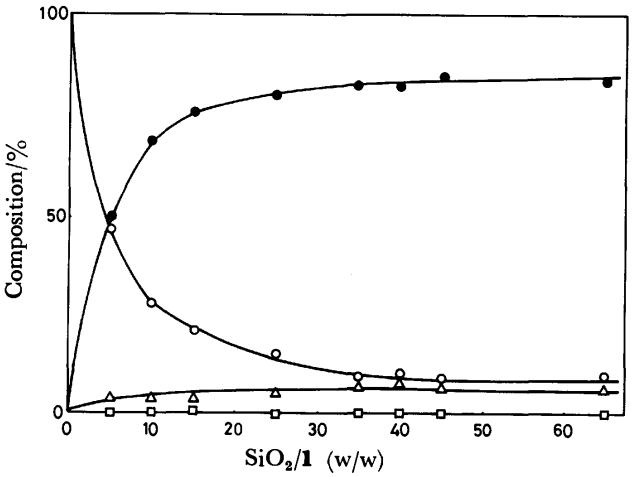

Fig. 3. Effect of amount of silica gel on selective protection of **1**.
1: **2**=1:1(mol/mol), ○: **1**, ●: **4**, △: **6**, □: **11**.

ed for each substrate or pair of substrates in competitive reaction at an appropriate reaction temperature. Milder reaction conditions were adopted unless a benzoyl group was contained. As Fig. 1 shows, the products contained about 13% of the starting material, **1**, unreduced, though equal mole of **2** and sufficient amount of **3** were used. Two cases are proposed for the explanation: (1) The benzoyl group of **1** was also protected by **2**. (2) Compound **1** or the derivative on the silica gel was covered with other molecules and prohibited from reacting with **3**.

The effect of the amount of Girard-T (**2**) on the selectivity was examined. The derivatives were prepared in varying ratios of **2** to 4-acetylbenzophenone (**1**), using **5** as a catalyst, and treated in the way described above. The compositions of the products were plotted against the amounts of **2** in Fig. 2. When more than equal moles of **2** to **1** was used, 4-acetyl-α-phenylbenzyl alcohol (**4**) was obtained in about 80% selectivity. An equal mole amount of **2** was sufficient for the selective protection of the acetyl group of **1**. The benzoyl group of **1** was not protected, for more than 75% of the benzoyl group was reduced in spite of the addition of **2** in excess.

The effect of the amount of silica gel was also examined. The derivatives were prepared from equal moles of **1** and **2** as described above. Then the adsorbed samples were prepared with varying amounts of silica gel and treated with the procedure described above. The compositions of the products are plotted against the amount of silica gel in Fig. 3. This figure shows that a significant amount of unreduced **1** was recovered when the amount of silica gel was little. The figure also shows that the amount of 4-acetyl-α-phenylbenzyl alcohol (**4**) increased with increasing amount of the silica gel up to 35 times that of **1**. Not less than 10 times silica gel is required for monolayer adsorption of the derivative: this comes from a rough estimate using simple molecular models.[10] Rough agreement was obtained amoung these values. In the reaction products, **1** was contained in more than 13% selectivity in spite of employing both lithium tri-*t*-butoxyhydroaluminate (**3**) and the silica gel in excess. The benzoyl group has been proven not to be protected with **2** from the preceding experiments. Then it is considered that partial multilayer adsorption on the silica gel prevented **1** or the derivative from contact with **3**. The ionic character of the derivative may facilitate the formation of the multi layer adsorption.

Girard-P (**7**), α-(1-pyridino) acetohydrazide chloride, and rarely Girard-D (**8**), α-(dimethylammonio) acetohydrazide chloride, are also used as the condensation reagents.[7] The effectiveness of these reagents was examined according to the manner described above. As presented in Table 1, **7** was a useful reagent for protection of the acetyl group of **1**, but **8** was not.

Acetic acid (**9**), as well as Amberlite IRC-50 (**5**), is known as a catalyst for the condensation of Girard's reagents with carbonyl compounds. The effect of **9** on the selective protection was examined. As can be seen from Table 1, **9** was not a suitable reagent for the selective protection, because a significant amount of

Table 1. Selective protection of **1** with girard's reagents

Girard's reagent[a]	Catalyst	Adsorbent	Product composition/%			
			1	**4**	**11**	**6**
2	**9**	SiO_2	41.4	51.8	0.6	6.2
2	**9**[b]	SiO_2	39.4	54.0	0.5	6.1
2	**5**	SiO_2	13.2	79.5	0.8	6.5
7	**5**	SiO_2	14.3	73.1	2.3	10.2
8	**5**	SiO_2	17.1	14.1	22.0	46.7
2	**5**	Celite	9.6	82.5	0.3	7.6
2	**5**	Al_2O_3	25.8	68.6	0.6	5.0

a) Equal moles of Girard's reagent and **1** were used. b) **9** was neutralized with sodium hydroxide.

Table 2. Selectivity for protection of carbonyl groups with **2**

Entry	Carbonyl compounds[a]		Recovery/%[b]		Conversion/%[c]		Selectivity for B[d]
	A	B	A	B	A	B	
1	4-phenylacetophenone	benzophenone	95	81	16.1	96.3	5.98
2	benzaldehyde	**17**	74	82	10.1	61.1	6.05
3	undecanal	2-undecanone	83	96	9.6	60.7	6.32
4	undecanal	3-undecanone	75	96	0.8	77.9	97.4
5	2-undecanone	3-undecanone	80	91	38.5	71.2	1.85
6	**15**	**16**	89	95	6.7	73.3	10.9

a) Equal moles of A, B, and **2** were used. b) Combined amount of unreduced substrate and product. c) Based on recovered products. d) (Conversion of B)/(Conversion of A).

4-acetylbenzophenone (**1**) was recovered without reduction. It is difficult to remove **9** completely from the adsorbed sample because of its relatively low vapor pressure and high polarity. The incomplete reduction of **1** could be attributed to the deposit of insoluble products produced by the reaction of **9** with tri-*t*-butoxyhydroaluminate (**3**) on the silica gel surface. A calculated amount of sodium hydroxide was added to neutralize **9** and to prevent the effect after condensation reaction. Then the adsorbed sample was prepared and reduced. As shown in Table 1, no improvement was observed. Consequently **9** was proven not to be a suitable catalyst for this purpose. In contrast to **9**, **5** brought about good selectivity. Moreover **5** could be easily removed from the reaction mixture by decantation. All the following experiments were undertaken by use of **5** as the catalyst.

Celite gave good selectivity, as Table 1 shows. Alumina was another effective adsorbent for the reaction, though the selectivity decreased a little. A similar result was obtained when silica-alumina (13% or 28% Al_2O_3) was used as adsorbent.

An attempt was made to utilize the Girard's reagent for protection of the carbonyl group in an aqueous solution without using solid support. Sodium borohydride (**10**) was used, for it can reduce carbonyl groups in aqueous solution. The derivative of **1** with **2** was prepared. Reduction of the derivative with **10** in the aqueous solution yielded 4-ethyl-α-phenylbenzyl alcohol preferentially and failed to yield **4**. Reductive cleavage occurred at the carbon-nitrogen double bond of the derivative.[11] Though this attempt was unsuccessful, another reducing agent can be utilized for this procedure.

It has been confirmed that the acetyl group of 4-acetylbenzophenone (**1**) had higher reactivity with **3** than the benzoyl group. When **3** was added to the THF solution of **1**, 4-(1-hydroxyethyl) benzophenone (**11**) was produced in a maximum 68% selectivity, while 4-acetyl-α-phenylbenzyl alcohol (**4**) was produced in a 19% maximum selectivity.

Protection Selectivity of Girard-T (2) for Carbonyl Groups. 4-Acetylbenzaldehyde (**12**) and 7-oxooctanal (**13**) were chosen as representatives of dicarbonyl compounds. The selective protection of the carbonyl groups with Girard-T (**2**) was examined by the method described above. When equal moles of **12** and **2** were allowed to react, 1-(4-formylphenyl) ethanol (**14**) was obtained in an 81.0% selectivity after reduction with **3**. When equal moles of **13** and **2** were allowed to react, 7-hydroxyoctanal was obtained in an 82.1% selectivity by the same procedure. In both cases the acetyl groups which existed together with the formyl groups were reduced preferentially. On the other hand, the acetyl group of 4-acetylbenzophenone (**1**) which existed together with the benzoyl group was not reduced. The treatment of **12** with twice the number of moles of **2** gave unreduced **12** in an 80.5% selectivity after reduction with **3**, which indicates that both carbonyl groups of **12** were protected with **2**. The protection of carbonyl groups depended both on the reactivity of the carbonyl groups and on the amount of **2** used.

The protection selectivity of **2** for other carbonyl groups was examined by a competitive reaction method combining two different kinds of carbonyl compounds. Table 2 presents the results. An acetyl group was selectively protected in the presence of a benzoyl group (entry 1), as can be expected from the result of **1**. Formyl

groups in the presence of acetyl groups (entries 2 and 3), the aldehyde in the presence of an ethyl ketone (entry 4), and the methyl ketone in the presence of the ethyl ketone (entry 5) of similar molecular structures were selectively protected. 4-Phenylcyclohexanone (**15**) in the presence of 2-methyl-4-phenylcyclohexanone (**16**) was also selectively protected (entry 6). Consequently, **2** responded sensitively to the differences of steric hindrance of the carbonyl groups, and hence **2** was effective as a reagent for selective protection of the unhindered carbonyl groups.

*Application of Girard-T (**2**) as a Protective as well as an Extractive Reagent.* An experiment was undertaken in which **2** acted as a protective reagent of a carbonyl group, in addition to acting as the usual extractive reagent. To 9.4 mmol of 4-acetylbenzaldehyde (**12**), 9.4 mmol of acetophenone (**17**) was added deliberately as an impurity. To a solution of the mixture, 9.4 mmol of **2** was added; this produced the derivative in the presence of **5**. The product was washed with water. The adsorbed sample of the derivative on silica gel was prepared from the aqueous solution. After reduction with **3** followed by hydrolysis, the products were extracted with benzene. The following compounds were identified by analysis: 1-(4-formylphenyl) ethanol (**14**) (85% wt), **12** (5.6% wt), **17** (1.7% wt) and 1-phenylethanol (**18**, 6.9% wt). In this stage, about 90% of the impure substances (**17** and **18**) were removed. After purification of this product by column chromatography, 6.6 mmol (69% yield) of **14** was obtained.

Conclusion

Girard's reagents were found to be effective reagents for protection of carbonyl groups in a nonaqueous reaction system when they were used with the solid supports. The solid support was used as a reaction media on which the reaction took place. Another example can be seen in our study of protecting carbonyl groups with sodium hydrogensulfite, in which the substrates were supported on the silica gel or alumina.[6] Other examples can be seen in many cases in which the reagents were supported.[1] A solid support will provide an effective reaction environment if suitable solvents which dissolve both the substrate and reagent are not available.

Experimental

Materials. 4-Acetylbenzophenone (**1**, mp 83—84 °C),[12] 4-acetylbenzaldehyde (**12**, bp 155 °C/15 mmHg, 1 mmHg=133.322 Pa),[13] 7-oxooctanal (**13**, bp 126 °C/16 mmHg),[14] 4-phenylacetophenone (**19**, mp 121—122 °C),[15] 4-phenylcyclohexanone (**15**, mp 78 °C),[16] and 2-methyl-4-phenylcyclohexanone (**16**, mp 139 °C)[17] were prepared by the reported methods. THF was dried over calcium hydride. Lithium tri-*t*-butoxyhydroaluminate (**3**) was prepared by the reported method.[18] Silica gel and alumina were Wakogel C-200 and activated alumina 200 mesh, respectively (Wako Pure Chemical Industries, Ltd.). Finely divided Celite 545 (Johns-Manville Sales Corp.) was used. Other materials were commercial products.

Methods. *Typical Reaction:* Equal moles of **1** (44.8 mg, 0.2 mmol) and Girard-T (**2**, 33.5 mg, 0.2 mmol) were added to ethanol (1.3 mmol) suspending Amberlite IRC-50 (**5**, 10 mg) and stirred for 2 h at 70 °C. After removal of **5** by decantation silica gel (1.6 g) was added and the ethanol was evaporated under reduced pressure (*ca.* 10 mmHg) at 60 °C. After the evaporation had apparently completed, the sample was evacuated for an additional 10 min. The recovery of **1** from this adsorbed sample was 98%, and hence only a small amount of **1** was lost in this evaporation procedure. The adsorbed sample thus obtained contained a trace amount of the ethanol, but was used for further reaction as such. To a solution of **3** (2 mmol) in THF (7 cm^3), the adsorbed sample was added and well mixed for 1 h; then the mixture was hydrolyzed with dilute hydrochloric acid or treated with formaldehyde.[19] The product was extracted with benzene and analyzed by GLC or HPLC. The reactant was recovered in a 98% yield, based on the adsorbed sample. Selectivity for the formation of 4-acetyl-α-phenylbenzyl alcohol (**4**) was 79.5%.

Competitive Reaction: Typically **19** (39.2 mg, 0.2 mmol), benzophenone (36.4 mg, 0.2 mmol), and **2** (33.5 mg, 0.2 mmol) were added to ethanol (1.3 cm^3) which included **5** (10 mg) in suspension. The mixture was stirred for 2 h at 80 °C to produce the derivatives. Hereafter the sample was treated by the procedures described above.

Analysis. Reaction products were identified with the authentic samples obtained commercially or synthesized independently. Product compositions were determined by GLC or HPLC. GLC analyses were carried out on Shimadzu gas chromatographs Model GC-7A and GC-4MPTF using columns packed with 10% polyethylene glycol 20000 on Chromosorb WAW, and columns packed with 10% Apiezon grease L on Chromosorb WAW. HPLC analyses were performed on a Waters liquid chromatograph consisting of a Model 6000A pump, a Model U6K injector, and a Model 440 absorbance detector equipped with a Radial-PAK C_{18} column and a Hitachi 635A liquid chromatograph equipped with a Waters Model 440 absorbance detector and a Radial-PAK C_{18} column. Forty percent methanol in water and 25% methanol in water with 1% triethylamine adjusted at pH 7.3 with phosphoric acid were used as the mobile phase. Recoveries of the substrate from the adsorbed samples were determined by the GLC analyses above described. For the substrates bearing aromatic nuclei, the data were confirmed by UV absorbance measurement using a Hitachi 124 Spectrophotometer. The results agreed with a difference of less than 2%.

References

1) A. McKillop and D. W. Young, *Synthesis*, **1979**, 401; G. H. Posner, *Angew. Chem., Int. Ed. Eng.*, **17**, 487 (1978).
2) S. L. Regen and C. Koteel, *J. Am. Chem. Soc.*, **94**, 4024 (1972).
3) K.-T. Liu and Y.-C. Tong, *J. Org. Chem.*, **43**, 2717 (1978).
4) A. Corneris, P.-Y. Herze, and P. Laszlo, *Tetrahedron Lett.*, **23**, 5035 (1982).
5) E. Kainan and Y. Mazur, *J. Org. Chem.*, **43**, 1020 (1978).
6) T. Chihara, T. Wakabayashi, and K. Taya, *Chem. Lett.*, **1981**, 1657.
7) A. Girard and G. Sandulesco, *Helv. Chim. Acta*, **19**, 1095 (1936); O. H. Wheeler, *J. Chem. Educ.*, **45**, 435 (1968).
8) O. H. Wheeler, *J. Chem. Educ.*, **45**, 435 (1968). Another paper reported that the benzoyl group reacted with **2** (L. F. Fieser and M. Fieser, "Reagents for Organic Synthesis," John Wiley, New York (1967), p.410.) Even if it is so, the benzoyl group seemed to be more difficult to react with **2** than the acetyl group.
9) T. Chihara, E. Waniguchi, T. Wakabayashi, and K. Taya, *Chem. Lett.*, **1983**, 1647.

10) The specific surface area of the silica gel was 350 m^2 per g by BET measurement. The Girard-T derivative of **1** was approximated to a rectangular plate of 200 nm×50 nm. The estimation was made by arranging this plate without gap or overlap on a plane, and repulsive or attractive interactions among the molecules were disregarded.

11) L. Caglioti and P. Grasselli, *Chem. Ind. (London)*, **1964**, 153.

12) R. P. Zelinski, B. W. Turnquest, and E. C. Martin, *J. Am. Chem. Soc.*, **73**, 5521 (1951); J. Cason, *J. Am. Chem. Soc.*, **68**, 2078 (1946).

13) L. Friedman and H. Shechter, *J. Org. Chem.*, **26**, 2522 (1961); P. Tinappe and E. Möltgen, *Arch. Pharm. (Weinheim, Ger.)* **309**, 766 (1976).

14) J. F. Oughton, U. S. Patent 3112330 (1963); *Chem. Abstr.*, **60**, 4011g (1964).

15) J. Luche and A. L. Gemal, *J. Am. Chem. Soc.*, **101**, 5848 (1979).

16) L. M. Long and H. R. Henze, *J. Am. Chem. Soc.*, **63**, 1939 (1941).

17) A. G. Cook, "Enamines," Marcel Dekker, New York (1969), p. 2 and p. 346.

18) H. C. Brown and R. F. McFarlin, *J. Am. Chem. Soc.*, **80**, 5372 (1958).

19) C. L. Teitelbaum, *J. Org. Chem.*, **23**, 646 (1958).

Structure Determination of Bitter Principles of *Ailanthus altissima*. Structures of Shinjulactones B, D, and E[1)]

Tetsuo FURUNO, Masami ISHIBASHI, Hirokazu NAORA, Tatsushi MURAE, Hiroshi HIROTA, Takahiko TSUYUKI, Takeyoshi TAKAHASHI,* Akiko ITAI,† and Yoichi IITAKA†

Department of Chemistry, Faculty of Science, The University of Tokyo, Hongo, Bunkyo-ku, Tokyo 113

†*Faculty of Pharmaceutical Sciences, The University of Tokyo, Hongo, Bunkyo-ku, Tokyo 113*

(Received March 7, 1984)

Bitter quassinoids, shinjulactones B, D, and E were isolated from *Ailanthus altissima* SWINGLE. Shinjulactone B is the first example of natural bitter principles with a 1,2-seco-1-nor-6(5→10)*abeo*-picrasane skeleton and shinjulactones D and E are a hexahydro derivative and a 6α-hydroxy derivative of ailanthone, respectively.

As a continuation of studies on bitter principles of Simaroubaceous plants,[2)] we have examined *Ailanthus altissima* SWINGLE and reported several new quassinoids.[1,3,4)] This paper describes the structure determination of shinjulactones B (**1**), D (**2**), and E (**3**) in detail.

Shinjulactone B (**1**) was isolated from both stem bark and root bark of the plant. The stem barks were extracted with hot water and the aqueous extract, after concentration, was continuously extracted with dichloromethane. The organic layer was evaporated to give a bitter residue, which was separated by silica-gel column chromatography. Gradient elution with methanol in chloroform gave shinjulactone B (**1**, *ca.* 0.001% yield) together with known quassinoids, amarolide 11-acetate,[5)] amarolide,[5)] shinjudilactone,[3)] and ailanthone (**4**).[4,6,7)] By the same procedure, shinjulactone B (**1**, *ca.* 0.004% yield) and shinjulactone D (**3**, *ca.* 0.001% yield) were isolated from the root bark together with known shinjulactone C,[3)] chaparrolide,[8)] and $\Delta^{13(18)}$-dehydroglaucarubolone,[9)] besides the known quassinoids mentioned above.

Shinjulactone B (**1**), mp 265.5—268 °C, was shown to have a norpicrasane skeleton, $C_{19}H_{22}O_7$, by high-resolution mass spectrum and elementary analysis. The IR spectrum showed the presence of hydroxyl(s) (3420 cm^{-1}), γ-lactone (1770 cm^{-1}), δ-lactone (1750 cm^{-1}), and a conjugated carbonyl (1680 cm^{-1}). The presence of a diosphenol grouping (**A**) was indicated by UV absorption maximum at 279 nm (ε 8100), which shifted to 330 nm on addition of alkali. These spectral data are similar to the observed values, 280 and 328 nm, for bruceantin in an ethanolic solution and an alkaline solution, respectively.[10)] The fact that shinjulactone B (**1**) possesses the diosphenol moiety in a ring other than A ring was inferred from the mass spectrum, in which a peak at *m/z* 151 (**B**) was not observed. This peak is characteristic of 3-hydroxy-2-oxo-3-picrasenes such as bruceantin and its congeners[10)] and 2-hydroxy-1-oxo-2-picrasenes.[10)] Instead of the peak at *m/z* 151, characteristic fragmentation peaks at *m/z* 265 $(M-C_5H_5O_2)^+$ and *m/z* 235 $(M-CH_2O-C_5H_5O_2)^+$ were observed; these peaks were not observed for normal quassinoids. The appearance of these peaks implies the presence of $C_5H_5O_2$ grouping susceptible of fragmentation on electron bombardment.

^1H and ^{13}C NMR spectra showed the presence of a tertiary methyl, a secondary methyl, a vinyl methyl, a hydroxymethyl (**C**), an olefinic proton (δ 5.95, dd), and a proton (δ 5.26) assignable to $C_{(7)}$-H on a δ-lactone terminus. On irradiation at δ 5.26, signals (δ 1.99, dd and δ 2.20, dd) due to $C_{(6)}$-H_2 changed into an AB quartet (J_{AB}=16 Hz). This observation indicates that the C-6 atom was connected with a carbon atom bearing no hydrogen atom, leading to a partial structure (**D**).

When the olefinic proton at δ 5.95 was irradiated, a doublet signal due to the vinyl methyl and a doublet

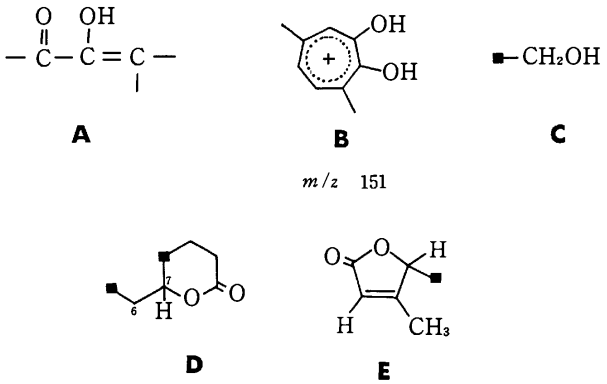

■ Carbon atom bearing no hydrogen atom

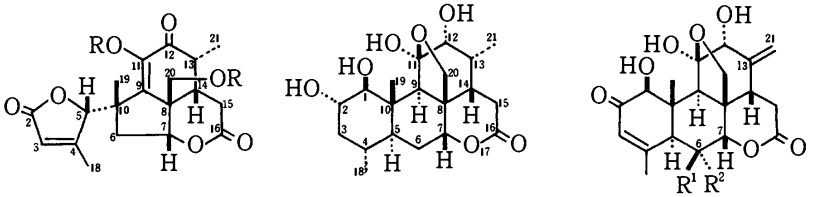

1 R=H
5 R=Ac

2

3 R^1=H R^2=OH
4 R^1=R^2=H

signal at δ 6.12 changed into singlets, respectively. On irradiation at the frequency of the vinyl methyl, an allylic coupling with J=2 Hz between the olefinic proton and the proton resonating at δ 6.12 was observed. Thus the partial structure (**E**) was proposed from these NMR measurement together with the IR absorption band due to the γ-lactone and with the $C_5H_5O_2$ moiety deduced from fragmentation of mass spectrum of **1**.

Although seven oxygen atoms of shinjulactone B (**1**) were thus characterized as shown in partial structures (**A**, **C**, **D**, and **E**), the whole structure for **1** with the norpicrasane skeleton could not be unambiguously constructed by connecting these partial structures.

Acetylation of **1** with acetic anhydride in pyridine gave a diacetate (**5**), mp 194—198 °C. Spectral information obtainable from **5** was of no use for the structure elucidation of shinjulactone B (**1**).

Unequivocal structure for shinjulactone B (**1**) was provided by X-ray diffraction analysis. A single crystal in orthorhombic space group $P2_12_12_1$ was obtained from methanol solution and the lattice parameters are a=12.594 (5), b=19.016 (8), and c=7.755 (3) Å. Four molecules of **1** and four water molecules are contained in the unit cell to give D_c=1.36 g cm^{-3}. Intensity data were collected on a Philips PW1100 automatic four-

Table 1. ^{1}H-NMR spectra of **1**, **2**, **3**, **5**, **7**, **8**, and **11** (δ (J/Hz))

	1	**2**	**3**	**5**	**7**	**8**	**11**
1-H		3.59 d (9)	4.54 s		4.70 d (9.5)	4.70 d (9.5)	5.28 s
2-H		*ca.* 4.05 br m			5.04 ddd (11, 9.5, 5)	*ca.* 5.0 m	
3-H	5.95 dd (2, 1)	*	6.18 m	5.96 m	1.25 m and *ca.* 2.1 m	*	6.10 m
4-H		*			1.63 m	*	
5-H	6.12 d (2)	*	*	5.63 br s	1.36 ddd (13, 11, 2.5)	*	3.53 d (11.5)
6-H	1.99 dd (16, 1)	*	4.62 dd (11.5, 3)	*	*ca.* 2.0 ddd (15, 2.5, 2.5)	*	5.25 dd (11.5, 3)
6-H′	2.20 dd (16, 6)	*		*	1.76 ddd (15, 13, 2.5)	*	
7-H	5.26 dd (6, 1)	4.43 br s	4.87 d (3)	4.98 d (5)	4.46 t (2.5)	4.44 t (2.5)	4.84 d (3)
9-H		2.95 s	*		3.41 s	3.17 s	3.22 s
12-H		3.97 br s	*		3.76 d (2.5)	5.03 d (*ca.* 2)	
13-H	3.30 m	*		*	*ca.* 2.15 m	*	
14-H	3.25 m	*	*	*	2.38 ddd (13, 6.5, 6)	*	*
15-H	2.92 dd (16, 13)	*	*	*	3.85 dd (19, 13)	*	*
15-H′	2.67 dd (16, 5)	*	*	*	2.74 dd (19, 6.5)	*	*
20-H	3.92 d (12)	3.73 d (8)	3.64 d (8)	4.41 d (12)	3.84 d (12.5)	3.86 d (13)	4.20 d (11.5)
20-H′	4.08 d (12)	4.14 d (8)	4.27 d (8)	4.73 d (12)	4.49 d (12.5)	4.51 d (13)	4.69 d (11.5)
4-CH_3	1.95 d (1)	0.83 d (6.5)	2.52 br s	1.93 d (1)	0.91 d (6.5)	0.91 d (6.5)	2.03 br s
10-CH_3	1.60 s	1.65 s	1.70 s	1.49 s	1.46 s	1.44 s	1.43 s
13-CH_3	1.05 d (7)	1.08 d (7)		1.11 d (7)	1.13 d (7)	0.97 d (6.5)	1.82 s
13=CH_2			5.13 br s 5.19 br s				
-OAc				2.13 s 2.31 s	1.94 s 1.98 s 2.07 s	1.82 s 1.96 s 2.08 s 2.20 s	2.07 s 2.14 s 2.17 s 2.22 s
Solv.	C_5D_5N	C_5D_5N	C_5D_5N	C_5D_5N	$CDCl_3$	$CDCl_3$	$CDCl_3$
MHz	400	270	90	100	400	90	400

* Not assigned.

circle diffractometer using monochromated Cu $K\alpha$ radiation. A total of 2096 independent structure factors with $F_o \geq 2.5\sigma(F_o)$ within $2\theta=156°$ were obtained by the $2\theta-\theta$ scanning mode. The structure was solved by the direct method using the MULTAN program. An E-map revealed the positions of all the non-hydrogen atoms, and the hydrogen atoms were located in a difference electron density map. The structure was refined by the block-diagonal least-squares calculations using

Table 2. Atomic positional parameters ($\times 10^4$) and isotropic temperature factors ($\times 10^2$) for non-hydrogen atoms of shinjulactone B (**1**) with estimated standard deviations in parentheses

Atom	x	y	z	B_{eq}[a]
O (1)	5917 (1)	8889 (1)	6721 (2)	346 (2)
O (2)	6255 (2)	8185 (1)	8968 (3)	640 (3)
O (3)	4881 (1)	10324 (1)	4402 (3)	370 (3)
O (4)	2743 (2)	10359 (1)	4543 (4)	546 (3)
O (5)	4077 (2)	7395 (1)	7845 (2)	511 (3)
O (6)	4802 (1)	7556 (1)	5335 (2)	445 (2)
O (7)	3164 (1)	7938 (1)	849 (2)	266 (2)
C (2)	6585 (2)	8502 (1)	7724 (3)	338 (3)
C (3)	7648 (2)	8567 (1)	7016 (4)	355 (4)
C (4)	7624 (2)	8955 (1)	5584 (4)	266 (3)
C (5)	6496 (2)	9191 (1)	5287 (3)	278 (3)
C (6)	5989 (2)	8150 (1)	3336 (3)	283 (3)
C (7)	4876 (2)	7864 (1)	3596 (3)	274 (2)
C (8)	4122 (2)	8476 (1)	3245 (3)	240 (2)
C (9)	4772 (2)	9121 (1)	3686 (3)	253 (2)
C (10)	5953 (2)	8964 (1)	3592 (3)	272 (2)
C (11)	4310 (2)	9735 (1)	4079 (3)	308 (3)
C (12)	3140 (2)	9788 (1)	4234 (3)	373 (3)
C (13)	2465 (2)	9135 (1)	3974 (4)	350 (3)
C (14)	3087 (2)	8452 (1)	4276 (3)	266 (3)
C (15)	3346 (2)	8335 (1)	6185 (3)	356 (3)
C (16)	4084 (2)	7733 (1)	6511 (3)	297 (3)
C (18)	8537 (2)	9147 (2)	4465 (5)	447 (4)
C (19)	6443 (2)	9364 (1)	2071 (3)	439 (4)
C (20)	3901 (2)	8479 (1)	1272 (3)	284 (3)
C (21)	1425 (2)	9168 (2)	4964 (6)	602 (5)

a) $B_{eq}=8\pi^2(u_1^2+u_2^2+u_3^2)/3$.

Table 3. Bond lengths of shinjulactone B (**1**) with estimated standard deviations in parentheses

Bond length		l/Å	Bond length		l/Å
Atom 1	Atom 2		Atom 1	Atom 2	
O (1)	C (2)	1.361 (3)	C (6)	C (10)	1.562 (3)
O (1)	C (5)	1.448 (3)	C (7)	C (8)	1.527 (3)
O (2)	C (2)	1.213 (3)	C (8)	C (9)	1.514 (3)
O (3)	C (11)	1.355 (3)	C (8)	C (14)	1.530 (3)
O (4)	C (12)	1.218 (3)	C (8)	C (20)	1.555 (3)
O (5)	C (16)	1.218 (3)	C (9)	C (10)	1.519 (3)
O (6)	C (7)	1.473 (3)	C (9)	C (11)	1.339 (3)
O (6)	C (16)	1.327 (3)	C (10)	C (19)	1.534 (3)
O (7)	C (20)	1.425 (3)	C (11)	C (12)	1.482 (3)
C (2)	C (3)	1.452 (4)	C (12)	C (13)	1.518 (3)
C (3)	C (4)	1.334 (4)	C (13)	C (14)	1.535 (3)
C (4)	C (5)	1.508 (3)	C (13)	C (21)	1.520 (4)
C (4)	C (18)	1.486 (4)	C (14)	C (15)	1.533 (3)
C (5)	C (10)	1.544 (3)	C (15)	C (16)	1.496 (3)
C (6)	C (7)	1.516 (3)			

Table 4. Bond angles of shinjulactone B (**1**) with estimated standard deviations in parentheses

Bond angle			ϕ/°
Atom 1	Atom 2	Atom 3	
C (2)	O (1)	C (5)	109.9 (2)
C (7)	O (6)	C (16)	124.9 (2)
C (3)	C (2)	O (1)	108.0 (2)
C (3)	C (2)	O (2)	131.3 (2)
O (1)	C (2)	C (2)	120.7 (2)
C (4)	C (3)	C (2)	109.9 (2)
C (5)	C (4)	C (3)	108.2 (2)
C (5)	C (4)	C (18)	124.6 (2)
C (3)	C (4)	C (18)	127.2 (2)
C (10)	C (5)	O (1)	108.6 (2)
C (10)	C (5)	C (4)	117.7 (2)
O (1)	C (5)	C (4)	103.9 (2)
C (7)	C (6)	C (10)	108.1 (2)
C (8)	C (7)	O (6)	115.3 (2)
C (8)	C (7)	C (6)	106.1 (2)
O (6)	C (7)	C (6)	108.9 (2)
C (9)	C (8)	C (7)	104.0 (2)
C (9)	C (8)	C (14)	111.5 (2)
C (9)	C (8)	C (20)	108.4 (2)
C (7)	C (8)	C (14)	114.4 (2)
C (7)	C (8)	C (20)	106.8 (2)
C (14)	C (8)	C (20)	111.2 (2)
C (10)	C (9)	C (8)	111.0 (2)
C (10)	C (9)	C (11)	127.5 (2)
C (8)	C (9)	C (11)	121.5 (2)
C (19)	C (10)	C (5)	109.7 (2)
C (19)	C (10)	C (6)	112.5 (2)
C (19)	C (10)	C (9)	109.5 (2)
C (5)	C (10)	C (6)	111.9 (2)
C (5)	C (10)	C (9)	109.7 (2)
C (6)	C (10)	C (9)	103.3 (2)
C (12)	C (11)	O (3)	117.2 (2)
C (12)	C (11)	C (9)	120.6 (2)
O (3)	C (11)	C (9)	122.1 (2)
C (13)	C (12)	O (4)	121.7 (2)
C (13)	C (12)	C (11)	119.3 (2)
O (4)	C (12)	C (11)	119.0 (2)
C (14)	C (13)	C (12)	112.8 (2)
C (14)	C (13)	C (21)	113.4 (2)
C (12)	C (13)	C (21)	112.4 (2)
C (15)	C (14)	C (8)	109.1 (2)
C (15)	C (14)	C (13)	112.3 (2)
C (8)	C (14)	C (13)	109.2 (2)
C (16)	C (15)	C (14)	114.0 (2)
O (7)	C (20)	C (8)	109.9 (2)
O (5)	C (16)	O (6)	117.1 (2)
O (5)	C (16)	C (15)	122.8 (2)
O (6)	C (16)	C (15)	120.1 (2)

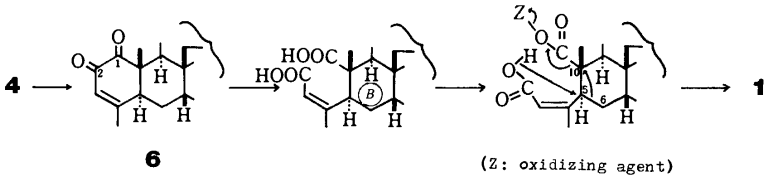

Scheme 1.

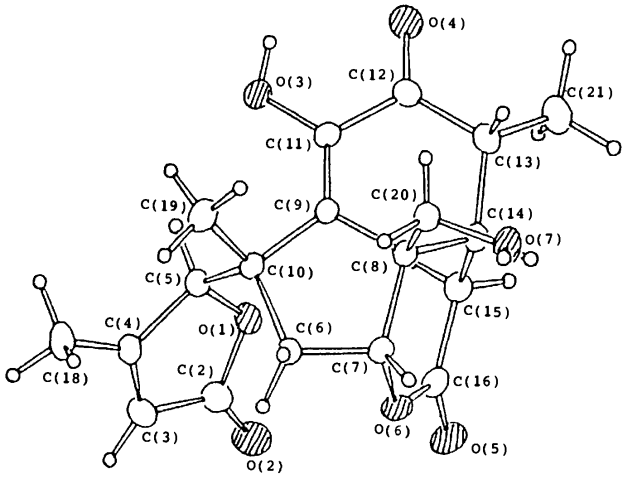

Fig. 1. Perspective view of shinjulactone B (1).[a)]
a) For clarity hydrogen atoms are represented by spheres of arbitrary radius.

anisotropic thermal parameters for non-hydrogen atoms and isotropic ones for hydrogen atoms. The final *R* factor was 0.039. The final atomic coordinates are listed in Table 2 and bond lengths and bond angles are listed in Tables 3 and 4.[11)]

Figure 1 is a computer-generated drawing of the molecule of **1**. The structure of shinjulactone B (**1**) is thus established as (5*R*,10*S*)-11,20-dihydroxy-12,16-dioxo-1,2-seco-1-nor-6(5→10)*abeo*-picrasa-3,9(11)-dien-2,5-olide. The novel 1,2-seco-1-nor-6(5→10)*abeo*-picrasane skeleton is likely derived biogenetically from ailanthone (**4**), a major picrasane-type bitter principle in *A. altissima*. Successive oxidation of an intermediate diketone (**6**) through bond-cleavage between $C_{(1)}$ and $C_{(2)}$ and decarboxylation accompanying with a contraction of the B ring and a formation of the α,β-unsaturated γ-lactone would afford shinjulactone B (**1**) (Scheme 1). Conversion of ailanthone (**4**) into shinjulactone B (**1**) is now in progress.

Shinjulactone D (**2**), mp 267—269 °C, was obtained together with shinjulactone B (**1**) and other known quassinoids from the aqueous extract of root bark of *A. altissima*. The molecular formula, $C_{20}H_{30}O_7$, was determined by high-resolution mass spectrum. The ^{1}H NMR spectrum was similar to that of ailanthone (**4**) except for a difference due to the absence of double bond, indicating the presence of hydroxyl(s), a δ-lactone, a tertiary methyl, two secondary methyls, and a hemiacetal group. In the mass spectrum of shinjulactone D (**2**), a fragment ion (**F**) was observed at *m/z* 268 ($C_{14}H_{20}O_5^{+\cdot}$) as a base peak. In comparison with the corresponding fragment ion at *m/z* 264 observed for ailanthone (**4**), the substitution pattern of the A ring was revealed. The UV spectrum showed no characteristic absorption maximum due to any ketone grouping. Therefore the presence of four hydroxyl groups containing a hemiacetal one was deduced. This is supported by acetylation of shinjulactone D (**2**) giving a triacetate (**7**) and tetraacetate (**8**).

The planer structure (**G**) is therefore proposed for shinjulactone D. The configuration of the hydroxyl groups at C-1, C-2, and C-12 of **2** was determined by measurement of ^{1}H and ^{13}C NMR spectra of **2**, **7**, and **8** and by proton magnetic double resonance (NMDR) measurement for **2**. In the ^{1}H NMR spectrum of **2**, signals due to three protons attached to hydroxyl-bearing carbons were observed at δ 3.59 (d, J=9 Hz), δ *ca.* 4.05 (br m), and δ 3.97 (br s), respectively. The doublet signal at δ 3.59 was assignable to H-1 and the NMDR measurement revealed the doublet signal coupled with the signal at δ 4.05 with a coupling constant, J=9 Hz, indicating a *trans*-diaxial-relationship for these protons. Thus the configurations of the vicinal hydroxyl groups were determined to be 1β-equatorial and 2α-equatorial, respectively.

The configuration of 12-H was established as follows. The doublet signals due to 12-H were observed at δ 3.76 for a triacetate (**7**) and δ 5.03 for a tetraacetate (**8**),

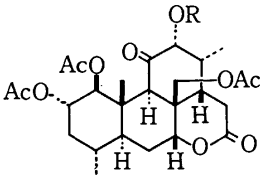

7 R=H
8 R=Ac

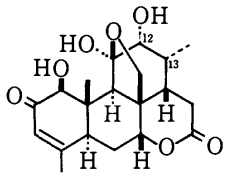

9

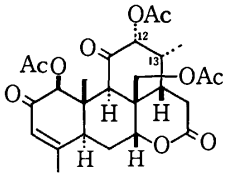

10

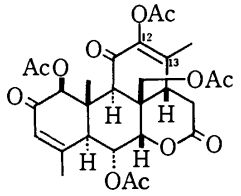

11

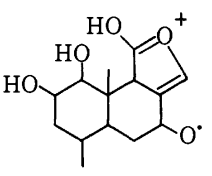

F

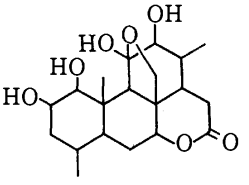

G

and their coupling constants were J=2.5 Hz and J=*ca.* 2 Hz, respectively. These values were almost the same as the coupling constant, J=3 Hz, observed for chaparrinone triacetate (**10**)[12] derived from chaparrinone (**9**). The observation implies that the configrations at C-12 and C-13 of shinjulactone D (**2**) are identical with those for chaparrinone (**9**) with 12β(equatorial)-H and 13β(axial)-H.

In conclusion, the structure of shinjulactone D (**2**) was established to be 11β,20-epoxy-1β,2α,11α,12α-tetrahydroxypicrasan-16-one and this compound corresponds to a perhydroailanthone derivative.

Shinjulactone E (**3**) was isolated from the stem bark of *A. altissima* collected in Hyogo Prefecture. Methanol extract was partitioned between carbon tetrachloride and water, and the aqueous layer was extracted with dichloromethane. From the organic layer, a fraction containing ailanthone as a main component was collected by silica-gel column chromatography. Minor components in the fraction were found to be chaparrinone (**9**), sitosteryl glucoside, and a new quassinoid. The new quassinoid, named shinjulactone E (**3**) was obtained by preparative TLC as amorphous solid in *ca.* 0.0001% yield. The molecular formula, $C_{20}H_{24}O_8$, was determined by high-resolution mass spectrum, indicating the presence of one more oxygen atom than that of ailanthone (**4**). The ^{1}H and ^{13}C NMR spectra showed the presence of a tertiary methyl, a vinyl methyl, an *exo*-methylene, an α,β-unsaturated carbonyl, and a lactone grouping; these observations suggest that shinjulactone E (**3**) would be a hydroxy derivative of ailanthone (**4**).

In the ^{1}H NMR spectrum of **3**, a lactone-terminus proton appeared at δ 4.87 as a doublet and a signal due to H-6 was observed at δ 4.61 as a double-doublet, resonating in lower field than that of ailanthone (**4**). Therefore the hydroxyl group was determined to be located at C-6.

On acetylation, shinjulactone E (**3**) gave a tetraacetate (**11**), mp 112—116 °C. In the ^{1}H NMR spectrum, two singlet signals due to vinyl methyls were observed at δ 1.82 and δ 2.03 together with signals due to a tertiary methyl and four acetyl groups. Seven methyl signals were observed in the ^{13}C NMR spectrum of **11**. The disappearance of the *exo*-methylene and the appearance of an additional vinyl methyl imply the occurrence of isomerization of the $C_{(13)}$–$C_{(21)}$ *exo*-double bond into an *endo*-double bond between $C_{(12)}$ and $C_{(13)}$ in the acetylation reaction to give an enol acetate.

On irradiation at δ 4.84 due to H-7, a double-doublet signal (J=11.5 and 3 Hz) at δ 5.25 due to H-6 of the tetraacetate (**11**) collapsed into a doublet, which was coupled with an α(axial)-H on C-5 with a coupling constant, $J_{5,6}$=11.5 Hz. On saturation at the frequency of H-6, the doublet signal due to H-7 changed into a singlet. Since the large coupling constant, $J_{5,6}$, suggests a *trans*-relationship between H-6 and H-5, the H-6 could be determined to be β(axial)-configuration. Therefore it is concluded that shinjulactone E (**3**) is formulated as 11β,20-epoxy-1β,6α,11α,12α-tetrahydroxypicrasa-3,13(21)-diene-2,16-dione (=6α-hydroxyailanthone) and the structure of the tetraacetate (**11**) is 1β,6α,12,20-tetraacetoxypicrasa-3,12-diene-2,11,16-trione.

Experimental[13]

Extraction and Isolation of Shinjulactones B (1) and D (2). The stem bark (11.2 kg), collected at the Botanical Gardens of Faculty of Science, the University of Tokyo in July 1979, was chipped and extracted with hot water (90 °C, 20 L) overnight. The extraction was repeated twice under the same conditions and the aqueous extracts were combined. Evaporation *in vacuo* gave a concentrated extract (*ca.* 13 L), which was divided into 8 portions and the each portion was continuously extracted with dichloromethane (1 L×2) overnight. All the extracts were combined and evaporated to give a residue (*ca.* 22 g). A part (14 g) of the residue, adsorbed on silica gel (35 g), was placed on a top of a silica-gel (700 g) column, and eluted with the following solvents in succession; $CHCl_3$ (1.4 L), 1%-MeOH in $CHCl_3$ (4.2 L), 2%-, 3%-, and 4%- (each 2.8 L), 5%- (4.2 L), 7%- (2.8 L), 10%-, and 30%-MeOH in $CHCl_3$ (each 1.4 L), and 85 fractions (each 280 mL) were collected. Elution with the 2%-MeOH in $CHCl_3$ gave amarolide 11-acetate (40 mg) and amarolide (650 mg), and elution with the 3%-MeOH in $CHCl_3$ shinjudilactone (50 mg) and ailanthone (1.3 g). Fractions 47—52 eluted with the 4%-MeOH in $CHCl_3$ gave crystals on standing, which were recrystallized from $CHCl_3$–MeOH to afford shinjulactone B (**1**; 110 mg).

The root bark (6.2 kg) was collected at the same botanical garden in August 1982. Extract with hot water was evaporated and continuously extracted with dichloromethane to give a residue (40 g), which was subjected to chromatographic separation of silica gel (2.6 kg). Amarolide 11-acetate (200 mg), amarolide (540 mg), shinjudilactone (1 g), and ailanthone (2.8 g) were eluted with 7—10%-MeOH in $CHCl_3$. Elution with 12%-MeOH in $CHCl_3$ afforded shinjulactone B (**1**; 240 mg) and 13%-MeOH in $CHCl_3$ gave shinjulactone C (130 mg) and chaparrolide (120 mg). Shinjulactone D (**2**; 50 mg) was obtained by elution with 14%-MeOH in $CHCl_3$ together with $\Delta^{13(18)}$-dehydroglaucarubolone (10 mg).

Extraction and Isolation of Shinjulactone E (3). The stem bark collected in Nishinomiya, Hyogo Prefecture, was extracted with hot methanol. The methanol extracts were concentrated and partitioned between carbon tetrachloride and water. The aqueous layer was separated and extracted with dichloromethane continuously. Organic layer was evaporated to give a residue, from which crude ailanthone was isolated by silica-gel chromatography. The crude ailanthone (10 g) was subjected to rechromatography on silica gel (300 g) eluting with 8%-MeOH in $CHCl_3$ and 30 fractions (each 75 mL) were collected. Chaparrinone (60 mg, from fr. 5), pure ailanthone (5 g, from frs. 7—10), and sitosteryl glucoside (1.5 g, from frs. 15—27) were obtained. Fractions 12—14 (82 mg) were combined and further separated by preparative TLC developed with 10%-MeOH in $CHCl_3$ and a fraction containing shinjulactone E (**3**) was obtained. Contaminated triterpenes in the fraction were separated off by crystallization from $CHCl_3$–MeOH to afford shinjulactone E (**3**; 23 mg) as amorphous solid.

Shinjulactone B (1). Prisms crystallized from $CHCl_3$–MeOH, mp 265.5—268 °C, $[\alpha]_D^{25}$ +167° (*c* 0.65, MeOH); IR (KBr) 3570, 3420, 1770, 1750, 1695, 1680, 1660, and 1635 cm^{-1}; UV (EtOH) 279 nm (ε 8100), which shifted to 330 nm on addition of alkali (pH *ca.* 11); ^{1}H NMR (Table 1); ^{13}C NMR (25.0 MHz, C_5D_5N) δ=12.3q, 16.3q, 23.8q, 28.3t, 37.4d, 39.7d, 40.4t, 48.8s, 51.6s, 64.3t, 85.2d, 87.1d, 120.4d, 138.5s, 145.1s, 167.7s, 168.8s, 171.5s, and 195.9s; MS *m/z* (%) 362 (M^+; 0.4), 344 (0.4), 332 (2.3), 265 (8.4), 235 (34), and 191 (100); Found: *m/z* 362.1395. Calcd for $C_{19}H_{22}O_7$: M 362.1365. Found: C, 60.81; H, 6.38%. Calcd for $C_{19}H_{22}O_7 \cdot 1/2H_2O$: C, 60.96; H, 6.19%.

11,20-Di-O-acetylshinjulactone B (5). A solution of

shinjulactone B (**1**; 9.3 mg) in acetic anhydride (2 mL) and pyridine (2 mL) was allowed to stand at room temperature for 2 d. The usual work-up gave a crude product, which was purified by preparative TLC developed with 8%-MeOH in $CHCl_3$ to afford diacetate (**5**; 9 mg), mp 194—198 °C (from acetone-hexane); IR (Nujol) 1770, 1750, 1720, 1685, 1660, 1640, and 1200 cm^{-1}; UV (EtOH) 240 nm (ε 8200); ^1H NMR (Table 1); ^{13}C NMR (25.0 MHz, C_5D_5N) δ=12.2q, 16.0q, 20.3q, 20.6q, 24.4q, 28.3t, 38.1d, 40.5d, 40.5t, 49.1s, 50.9s, 64.8t, 83.7d, 87.6d, 120.9d, 142.6s, 153.0s, 166.8s, 167.4s, 168.5s, 170.4s, 170.8s, and 192.0s; MS *m/z* (%) 446 (M^+; 8), 404 (40), 386 (30), 344 (45), 307 (70), 247 (90), and 177 (100); Found: *m/z* 446.1566. Calcd for $C_{23}H_{26}O_9$: M 446.1576.

Shinjulactone D (2). Mp 267—269°C (from acetone); $[\alpha]_D^{22}$ −44° (*c* 0.17, C_5H_5N); IR (KBr) 3400, 1730, 1215, and 1050 cm^{-1}; ^1H NMR (Table 1); ^{13}C NMR (67.80 MHz, C_5D_5N) δ=11.6q, 13.3q, 20.1q, 26.8t, 29.1d, 30.6t, 31.7d, 41.6s, 42.7s, 42.9d, 43.3t, 44.2d, 46.5d, 70.1d, 71.8t, 79.2d, 79.7d, 85.3d, 110.9s, and 169.9s; MS *m/z* (%) 382 (M^+; 8), 364 (3), 268 (100), and 250 (60); Found: *m/z* 382.1969. Calcd for $C_{20}H_{30}O_7$: M 382.1990.

1,2,20-Tri-O-acetylshinjulactone D (7). Shinjulactone D (**2**; 13.3 mg, crude) was acetylated with acetic anhydride (1 mL) in pyridine (2 mL) at room temperature for 20 h. The reaction product, after usual work-up, was purified by preparative TLC developed with 20%-acetone in benzene and crystallized from acetone-hexane to give a triacetate (**7**; 3.6 mg), mp 135—138 °C (sintered at 118—121 °C); IR (KBr) 3530, 2940, 1745, 1725 (sh), 1375, 1240, and 1040 cm^{-1}; ^1H NMR (Table 1); ^{13}C NMR (22.5 MHz, $CDCl_3$) δ=12.3, 13.5, 19.1, 20.7, 20.9, 21.5, 25.8, 27.2, 28.3, 35.4, 35.9, 39.0, 41.7, 43.0, 44.8, 48.2, 61.8, 70.8, 77.8, 82.3, 82.6, 170.2, 170.2, 170.4, 174.2, and 212.1; MS *m/z* (%) 508 (M^+; 13), 488 (25), 466 (8), 406 (25), 376 (42), 316 (50), and 55 (100); Found: *m/z* 508.2341. Calcd for $C_{26}H_{36}O_{10}$: M 508.2309.

1,2,12,20-Tetra-O-acetylshinjulactone D (8). Triacetate (**7**) was acetylated under the same conditions as above for 50 h to afford a tetraacetate (**8**) in almost quantitative yield, mp 129—132 °C (from acetone-hexane); IR (KBr) 1745, 1720 (sh), 1370, 1240, and 1040 cm^{-1}; ^1H NMR (Table 1); ^{13}C NMR (22.5 MHz, $CDCl_3$) δ=12.3, 13.0, 19.2, 20.7, 20.7, 20.9, 21.1, 25.6, 27.5, 27.8, 34.2, 35.9, 38.9, 41.7, 43.0, 44.3, 49.5, 61.8, 70.9, 78.1, 80.5, 80.6, 169.5, 169.6, 170.0, 170.2, 171.3, and 204.3; MS *m/z* (%) 550 (M^+; 6), 508 (20), 490 (18), 466 (25), 448 (100), 388 (65), and 328 (80); Found: *m/z* 550.2410. Calcd for $C_{28}H_{38}O_{11}$: M 550.2412.

Shinjulactone E (3). White amorphous solid, ^1H NMR (Table 1); ^{13}C NMR(22.5 MHz, C_5D_5N) δ=11.5, 26.8, 35.2, 43.7, 46.7, 48.2, 48.2, 48.5, 65.9, 71.7, 80.8, 82.0, 84.5, 110.6, 117.8, 128.1, 147.3, 165.3, 169.3, and 197.2; MS *m/z* (%) 392 (M^+; 10), 374 (50), 364 (45), 356 (20), and 314 (100); Found: *m/z* 392.1462. Calcd for $C_{20}H_{24}O_8$: M 392.1469.

1,6,12,20-Tetra-O-acetylshinjulactone E (11). Shinjulactone E (**3**; 22.6 mg, crude) was treated with acetic anhydride (0.5 mL) and pyridine (0.5 mL) in the presence of a catalytic amount of 4-(dimethylamino)pyridine at room temperature for 2.5 d. After usual work-up, purification by preparative TLC (developed with 1%-MeOH in $CHCl_3$) yielded a tetraacetate (**11**; 6.2 mg), mp 112—116 °C (from chloroform); IR (KBr) 1745, 1680, 1620, and 1235 cm^{-1}; UV (EtOH) 243 nm (ε 12000); ^1H NMR (Table 1); ^{13}C NMR (50 MHz, $CDCl_3$) δ=13.5q, 15.5q, 20.0q, 20.6q, 20.7q, 21.3q, 24.0q, 29.7t, 39.1d, 42.6s, 44.6d, 46.9s, 48.5d, 61.1t, 66.7d, 77.4d, 83.8d, 127.7s, 129.1d, 159.5s, 167.0s, 169.9s, 170.1s, 171.3s, 174.5s, 179.2s, 190.9s, and 191.7s; MS *m/z* (%) 560 (M^+; 10), 518 (65), 476 (80), 458 (50), 416 (85), 315 (90), 297 (80), and 43 (100); Found: *m/z* 560.1909. Calcd for $C_{28}H_{32}O_{12}$: M 560.1894.

The authors wish to thank Mr. Kazuhiro Matsushita of JEOL Co. Ltd. for measurement of NMR spectra.

References

1) Preliminary accounts of this report: T. Furuno, H. Naora, T. Murae, H. Hirota, T. Tsuyuki, T. Takahashi, A. Itai, Y. Iitaka, and K. Matsushita, *Chem. Lett.*, **1981**, 1797; M. Ishibashi, T. Furuno, T. Tsuyuki, T. Takahashi, and K. Matsushita, *Chem. Pharm. Bull.*, **31**, 2179 (1983).

2) T. Murae, A. Sugie, T. Tsuyuki, and T. Takahashi, *Chem. Pharm. Bull.*, **23**, 2188 (1975) and references cited therein.

3) M. Ishibashi, T. Tsuyuki, T. Murae, H. Hirota, T. Takahashi, A. Itai, and Y. Iitaka, *Bull. Chem. Soc. Jpn.*, **56**, 3683 (1983).

4) H. Naora, M. Ishibashi, T. Furuno, T. Tsuyuki, T. Murae, H. Hirota, T. Takahashi, A. Itai, and Y. Iitaka, *Bull. Chem. Soc. Jpn.*, **56**, 3694 (1983).

5) C. G. Casinovi, V. Bellavita, G. Grandolini, and P. Ceccherelli, *Tetrahedron Lett.*, **1965**, 2273; W Stöcklin, M. Stefanović, T. A. Geissman, and C. G. Casinovi, *ibid.*, **1970**, 2399.

6) J. Polonsky and J.-L. Fourrey, *Tetrahedron Lett.*, **1964**, 3983; A. Gaudemer, J.-L. Fourrey, and J. Polonsky, *Bull. Soc. Chim. Fr.*, **1967**, 1676.

7) C. G. Casinovi, P. Ceccherelli, G. Grandolini, and V. Bellavita, *Tetrahedron Lett.*, **1964**, 3991.

8) R. E. Mitchell, W. Stöcklin, M. Stefanović, and T. A. Geissman, *Phytochemistry*, **10**, 411 (1971).

9) J. Moron, J. Rondest, and J. Polonsky, *Experientia*, **22**, 511 (1966); S. M. Kupchan and J. A. Lacadie, *J. Org. Chem.*, **40**, 654 (1975).

10) S. M. Kupchan, R. W. Britton, J. A. Lacadie, M. F. Ziegler and C. W. Sigel, *J. Org. Chem.*, **40**, 648 (1975).

11) The complete F_o—F_c data, anisotropic thermal parameters for non-hydrogen atoms, atomic positional parameters and isotropic thermal parameters for hydrogen atoms, and bond lengths and bond angles containing hydrogen atoms are deposited as Document No. 8434 at the Office of the Editor of Bull. Chem. Soc. Jpn.

12) J. Polonsky and N. Bourguignon-Zylber, *Bull. Soc. Chim. Fr.*, **1965**, 2793.

13) General Procedures are the same described in the preceding papers.[3,4]

Acid-catalyzed Backbone Rearrangement of 5,6-Epoxyalnusanes and Preparation of Daturadiol[1)]

Motoo TORI, Masaki TAKAI, Yuzo MATSUMOTO, Yoshihiko MORIYAMA,† Takahiko TSUYUKI, Takeyoshi TAKAHASHI* Hiraku OHNISHI,†† Akiko ITAI,†† and Yoichi IITAKA††

Department of Chemistry, Faculty of Science, The University of Tokyo, Hongo, Bunkyo-ku, Tokyo 113
††*Faculty of Pharmaceutical Sciences, The University of Tokyo, Hongo, Bunkyo-ku, Tokyo 113*
†*Institute of Chemistry, Kyoto Prefectural University of Medicine, Taishogun, Kita-ku Kyoto 603*

(Received March 9, 1984)

Epoxidation of alnus-5-en-3β-yl acetate with *m*-chloroperbenzoic acid gave a 5β,6β-epoxide as a main product together with a 5α,6α-epoxide as a minor product. Treatment of the α-epoxide with $BF_3 \cdot OEt_2$ afforded a 1(10),5-diene and a mixture of 6α-hydroxy-12- and -18-ene derivatives. The 12-ene was converted into daturadiol (=olean-12-ene-3β,6β-diol).

On treatment with acid, oleanene-, lupene-, and baccharene-type triterpenes undergo backbone rearrangement generally in the opposite direction from the biogenesis and afford a number of migrated triterpenes derived from intermediate cations or their equivalent species corresponding to various biogenetic stages.

We have been investigating $BF_3 \cdot OEt_2$-catalyzed backbone rearrangement of 3β,4β-epoxyfriedelane,[2)] 3,4-epoxyshionanes,[3)] 3,4-epoxy-D:A-friedo-18β,19α*H*-lupanes,[4)] and 13,18-epoxybaccharan-3β-yl acetates,[5)] these epoxides possessing the epoxide ring on the terminal ring such as A or D ring. Epoxidation of alnus-5-en-3β-yl acetate (**1**) gives 5,6-epoxides, which on treatment with $BF_3 \cdot OEt_2$ would afford carbonium ions or their equivalents on B ring by cleavage of the epoxy ring. Now we examined behavior of the carbonium ions on B ring towards the backbone rearrangement. This paper describes the epoxidation of **1** and backbone rearrangement of epoxides catalyzed by $BF_3 \cdot OEt_2$. Conversion of dendropanoxide (**2**) into daturadiol (**3**) by utilizing these reactions is also described.

Acid treatment of dendropanoxide (**2**)[6)] gave a mixture of alnus-5-en-3β-ol (**4**) and alnus-5(10)-en-3β-ol (**5**),[7)] the former of which, after separation, was converted into its acetate (**1**). Sengupta *et al.*[8)] obtained an epoxide as the sole product by epoxidation of glut-5-en-3β-yl acetate (=alnus-5-en-3β-yl acetate (**1**)) with *m*-chloroperbenzoic acid (MCPBA) and assigned a 5α,6α-configuration to the epoxy-ring based on the steric consideration and ^1H NMR spectrum.

Epoxidation of **1** with MCPBA under the same conditions (in chloroform at 0 °C) as Sengupta's gave two epoxides. The major epoxide (**6**) was obtained in 77% yield and the minor one (**7**) in 16% yield, and the major epoxide (**6**) was found to be identical with the "Sengupta's epoxide." From the following observations, however, a question arose on the configuration of the epoxide ring which had been assigned by Sengupta. Two epoxides (**6** and **7**) were subjected to $BF_3 \cdot OEt_2$-catalyzed backbone rearrangement, respectively, and the mixtures of unsaturated hydroxy acetates were separated from the rearranged products (description on these reactions is given later). The mixture of hydroxy acetates obtained from the major epoxide (**6**) showed a broad singlet signal due to 6-H around δ 4.5 in the ^1H NMR, while that obtained from the minor epoxide (**7**) showed a broad signal due to 6-H around δ 4.0—4.1. Kocór *et al.*[9)] isolated a triterpene alcohol, daturadiol (**3**), from *Datura innoxia* MILL (Solanaceae) and reported that the monoacetate of daturadiol (**8**) (=6β-hydroxyolean-12-en-3β-yl acetate) showed a broad singlet due to 6α-H at δ 4.45 in the ^1H NMR spectrum. This implies that the broad singlet signal which appeared at *ca.* δ 4.5 is assignable to the 6α-H and, therefore, the hydroxyl group in the hydroxy acetates derived from the major epoxide (**6**) locates in β-orientation. These observations lead to the conclusion that the major epoxide (**6**), the "Sengupta's epoxide," should be a 5β,6β-epoxide and attack of the oxidizing reagent took

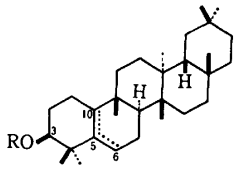

1 5-ene; R=Ac
4 5-ene; R=H
5 5(10)-ene; R=H
9 5-ene; R=PhCO
14 5(10)-ene; R=Ac

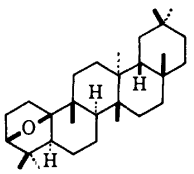

2

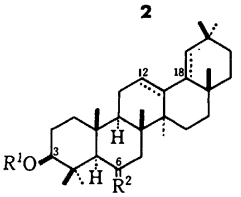

3 12-ene; R^1=H, R^2=β-OH,α-H
8 12-ene; R^1=Ac, R^2=β-OH,α-H
15 18-ene; R^1=Ac, R^2=α-OH,β-H
16 12-ene; R^1=Ac, R^2=α-OH,β-H
17 18-ene; R^1=Ac, R^2=O
18 12-ene; R^1=Ac, R^2=O
19 18-ene; R^1=H, R^2=O
20 12-ene; R^1=H, R^2=O
22 18-ene; R^1=Ac, R^2=β-OH,α-H

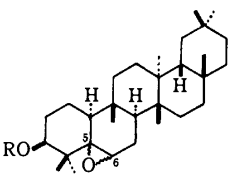

6 5β,6β-; R=Ac
7 5α,6α-; R=Ac
10 5β,6β-; R=H
11 5α,6α-; R=PhCO
12 5β,6β-; R=PhCO

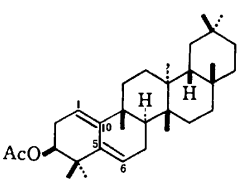

13

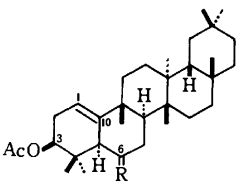

21 R=β-OH,α-H
23 R=O

place preferentially from β-face of the molecule in epoxidation of alnus-5-en-3β-yl acetate (**1**).

This conclusion was supported by the epoxidation reaction of alnus-5-en-3β-ol (**4**) and its benzoate (**9**) carried out under the same conditions as above. Epoxidation of alnus-5-en-3β-ol (**4**) gave a single epoxide (**10**). On acetylation, the epoxide (**10**) yielded an acetate, which was idential with the major epoxide (**6**). On the other hand, the benzoate (**9**) was epoxidized to give α- and β-epoxides (**11** and **12**) in a 1 : 1 ratio. Since the 3α-hydrogens of alnus-5-en-3β-ol (**4**), -3β-yl acetate (**1**), and -3β-yl benzoate (**9**) were observed as triplets at δ 3.48 (t-like, J=3 Hz), δ 4.66 (J=3 Hz), and δ 4.94 (J=3 Hz), respectively, in the ^{1}H NMR spectra, the substituents at C-3β are shown to exist in an axial-conformation.

Table 1. Atomic positional parameters (×10⁴) and isotropic thermal parameters (×10³) for non-hydrogen atoms of 5β,6β-epoxyalnusan-3β-yl acetate (**6**) with estimated standard deviations in parentheses

Atom	x	y	z	B_{eq}[a]
C (1)	−904(3)	5468(1)	5282(6)	390(5)
C (2)	−1666(3)	5182(1)	4202(6)	409(6)
C (3)	−1113(3)	4792(1)	3520(5)	351(5)
C (4)	−70(3)	4862(1)	2423(5)	331(5)
C (5)	598(2)	5198(1)	3370(5)	299(4)
C (6)	1737(3)	5223(1)	2947(6)	368(5)
C (7)	2327(32)	5625(12)	2939(68)	419( )
C (8)	1538(2)	5996(1)	3004(5)	296(4)
C (9)	718(3)	5946(1)	4621(5)	299(4)
C (10)	7(2)	5587(1)	3915(5)	285(4)
C (11)	18(3)	6336(1)	4650(6)	368(5)
C (12)	625(3)	6737(1)	4666(6)	369(5)
C (13)	1398(2)	6776(1)	2889(5)	292(4)
C (14)	2202(2)	6412(1)	2945(5)	298(4)
C (15)	2891(3)	6424(1)	1060(6)	386(5)
C (16)	3036(3)	6848(1)	103(6)	439(6)
C (17)	2975(3)	7224(1)	1492(6)	377(5)
C (18)	2036(3)	7187(1)	3008(5)	315(5)
C (19)	1293(3)	7562(1)	2903(6)	394(5)
C (20)	1860(3)	7980(1)	2965(6)	425(6)
C (21)	2726(3)	7997(1)	1379(7)	533(7)
C (22)	2812(3)	7602(1)	188(7)	489(6)
C (23)	524(3)	4453(1)	2290(7)	484(6)
C (24)	−334(3)	5002(1)	329(6)	458(6)
C (25)	1140(4)	5873(1)	6715(6)	457(6)
C (26)	699(3)	6768(1)	1011(5)	373(5)
C (27)	2947(3)	6441(1)	4725(6)	407(5)
C (28)	4063(3)	7268(1)	2498(7)	512(7)
C (29)	1007(4)	8308(1)	2563(9)	657(9)
C (30)	2320(4)	8055(1)	5004(8)	575(7)
C (31)	−1563(4)	4251(1)	5695(6)	485(6)
C (32)	−1163(5)	4003(1)	7396(8)	747(10)
O (1)	−870(2)	4548(1)	5265(4)	417(4)
O (2)	−2383(2)	4199(1)	4862(6)	692(6)
O (3)	1368(2)	5066(1)	4817(4)	416(4)

a) $B_{eq}=8\pi^2(u_1^2+u_2^2+u_3^2)/3$.

From these facts, the results obtained in these epoxidation reactions are explained reasonably as follows; in the epoxidation of alnus-5-en-3β-ol (**4**), the hydrogen-bond assisted an exclusive attack of the reagent from β-face of the molecule of **4**, while in the case of the benzoate (**9**), the attack from β-face was sterically hindered by the bulky benzoyloxyl group, resulting in a 1 : 1 ratio of the α- and β-epoxides (**11** and **12**), and in the case of the acetate (**1**), the reagent attacked preferentially from the β-side to give the β-epoxide (**6**) as the main product.

Thus the epoxide ring of the major epoxide (**6**) has been determined to exist in β-configuration. Unambiguous proof for the structure of the major epoxide (**6**) was given by single-crystal X-ray analysis. The crystals belong to orthorhombic space group $P2_12_12_1$, and the lattice parameters are a=12.618(4), b=32.776(9), and c=6.837(2) Å and D_c=1.14 g cm^{-3} with four molecules in a unit cell. Intensity data were measured on a Philips PW1100 automatic four-circle diffractometer using monochromated Cu $K\alpha$ radiation. A total of 2702, non-zero independent reflections with $3\leq\theta\leq$ 78 were obtained by $2\theta-\theta$ scanning mode. The structure was solved by the direct method using MULTAN program and was refined by the block-diagonal least-squares method. All hydrogen atoms were located on a difference electron density map. The final R-value was 0.047 assuming the anisotropic temperature factors for the non-hydrogen atoms and the isotropic ones for the hydrogen atoms. The final atomic coordinates are listed in Table 1 and bond lengths and bond angles are listed in Tables 2 and 3.[10] Figure 1 is a computer-generated perspective

Table 2. Bond lengths of 5β,6β-epoxyalnusan-3β-yl acetate (**6**) with estimated standard deviations in parentheses

Bond length		⟨l/Å⟩	Bond length		⟨l/Å⟩
Atom 1	Atom 2		Atom 1	Atom 2	
C (1)	-C (2)	1.533(5)	C (12)	-C (13)	1.542(5)
C (1)	-C (10)	1.532(5)	C (13)	-C (14)	1.568(4)
C (2)	-C (3)	1.528(5)	C (13)	-C (18)	1.571(4)
C (3)	-C (4)	1.532(5)	C (13)	-C (26)	1.559(5)
C (3)	-O (1)	1.470(4)	C (14)	-C (15)	1.555(5)
C (4)	-C (5)	1.530(4)	C (14)	-C (27)	1.541(5)
C (4)	-C (23)	1.540(5)	C (15)	-C (16)	1.549(5)
C (4)	-C (24)	1.540(5)	C (16)	-C (17)	1.556(5)
C (5)	-C (6)	1.468(4)	C (17)	-C (18)	1.578(5)
C (5)	-C (10)	1.524(4)	C (17)	-C (22)	1.542(5)
C (5)	-O (3)	1.452(4)	C (17)	-C (28)	1.543(5)
C (6)	-C (7)	1.513(40)	C (18)	-C (19)	1.546(4)
C (6)	-O (3)	1.456(5)	C (19)	-C (20)	1.548(5)
C (7)	-C (8)	1.537(40)	C (20)	-C (21)	1.540(6)
C (8)	-C (9)	1.562(5)	C (20)	-C (29)	1.545(6)
C (8)	-C (14)	1.570(4)	C (20)	-C (30)	1.530(7)
C (9)	-C (10)	1.559(4)	C (21)	-C (22)	1.533(6)
C (9)	-C (11)	1.553(4)	C (31)	-C (32)	1.507(7)
C (9)	-C (25)	1.546(5)	C (31)	-O (1)	1.341(5)
C (11)	-C (12)	1.539(4)	C (31)	-O (2)	1.194(6)

drawing of the molecule of the major epoxide, 5β, 6β-epoxyalnusan-3β-yl acetate (**6**).

5α,6α-Epoxyalnusan-3β-yl acetate (**7**) was treated with $BF_3 \cdot OEt_2$ in benzene to give a complex mixture, which was separated by column chromatography into two fractions. The less polar fraction (25%) was found to consist of mainly alnusa-1(10), 5-dien-3β-yl acetate (**13**) accompanied with a small amount of an unidentified product by GLC. The authentic sample of **13** was prepared by reaction of alnus-5(10)-en-3β-yl acetate (**14**) with selenium dioxide.[11]

The polar fraction (73%) was inferred to be a mixture of Δ^{18}- and Δ^{12}-hydroxy acetates (**15** and **16**) in a ratio of 1 : 1 by spectral inspection. Two signals at δ 4.85 (0.5H) and δ 5.17 (0.5H) in the ^{1}H NMR and two fragment ions at *m/z* 177 and *m/z* 218 in the mass spectrum[12] were indicative of the presence of Δ^{18}- and Δ^{12}-oleanene derivatives. Separation of the mixture was attempted by various chromatographic techniques, but all attempts failed. The mixture of hydroxy acetates (**15** and **16**) was converted into a mixture of keto acetates (**17** and **18**), which could not be separated at all. Then the mixture of **17** and **18** was subjected to alkaline hydrolysis to give a mixture of hydroxy ketones (**19** and **20**). Separation of the mixture was attained by HPLC to afford 3β-hydroxyolean-18-en-6-one (**19**; t_R=15.7 min) and -12-en-6-one (**20**; t_R=16.3 min). 3β-Hydroxyolean-18-en-6-one (**19**), mp 217.5—219 °C, showed a molecular ion at *m/z* 440.3659 ($C_{30}H_{48}O_2$) and a fragment ion at *m/z* 177.1623 ($C_{13}H_{21}$) which is characteristic of Δ^{18}-oleanene derivatives.[12] In the ^{1}H NMR spectrum, a singlet signal appeared at δ 4.88 assignable to 19-H. On the other hand, the other hydroxy ketone (**20**) with a longer retention time showed mp 243—245 °C

28 Table 3. Bond angles of 5β,6β-epoxyalnusan-3β-yl acetate (**6**) with estimated standard deviations in parentheses

Bond angle			φ/°	Bond angle			φ/°
Atom 1	Atom b	Atom 3		Atom 1	Atom 2	Atom 3	
C (2)	-C (1)	-C (10)	109.4(3)	C (14)	-C (13)	-C (18)	108.7(2)
C (3)	-C (2)	-C (1)	111.9(3)	C (14)	-C (13)	-C (26)	111.9(3)
C (4)	-C (3)	-C (2)	114.5(3)	C (12)	-C (13)	-C (18)	110.2(3)
C (4)	-C (3)	-O (1)	107.5(3)	C (12)	-C (13)	-C (26)	107.6(3)
C (2)	-C (3)	-O (1)	107.6(3)	C (18)	-C (13)	-C (26)	110.4(3)
C (5)	-C (4)	-C (3)	112.0(3)	C (15)	-C (14)	-C (8)	108.8(3)
C (5)	-C (4)	-C (23)	112.5(3)	C (15)	-C (14)	-C (13)	108.7(3)
C (5)	-C (4)	-C (24)	107.3(3)	C (15)	-C (14)	-C (27)	108.2(3)
C (3)	-C (4)	-C (23)	108.4(3)	C (8)	-C (14)	-C (13)	109.9(2)
C (3)	-C (4)	-C (24)	108.3(3)	C (8)	-C (14)	-C (27)	109.7(3)
C (23)	-C (4)	-C (24)	108.1(3)	C (13)	-C (14)	-C (27)	111.5(3)
C (6)	-C (5)	-C (4)	119.9(3)	C (16)	-C (15)	-C (14)	116.1(3)
C (6)	-C (5)	-C (10)	118.6(3)	C (17)	-C (16)	-C (15)	116.6(3)
C (6)	-C (5)	-O (3)	59.8(2)	C (18)	-C (17)	-C (16)	112.2(3)
C (4)	-C (5)	-C (10)	115.8(3)	C (18)	-C (17)	-C (22)	109.9(3)
C (4)	-C (5)	-O (3)	116.3(3)	C (18)	-C (17)	-C (28)	112.5(3)
C (10)	-C (5)	-O (3)	114.2(3)	C (16)	-C (17)	-C (22)	106.9(3)
C (7)	-C (6)	-C (5)	122.2(16)	C (16)	-C (17)	-C (28)	107.6(3)
C (7)	-C (6)	-O (3)	118.0(16)	C (22)	-C (17)	-C (28)	107.5(3)
C (5)	-C (6)	-O (3)	59.6(2)	C (19)	-C (18)	-C (13)	111.5(3)
C (8)	-C (7)	-C (6)	112.9(27)	C (19)	-C (18)	-C (17)	111.3(3)
C (9)	-C (8)	-C (7)	111.3(16)	C (13)	-C (18)	-C (17)	114.6(3)
C (9)	-C (8)	-C (14)	117.2(3)	C (20)	-C (19)	-C (18)	115.0(3)
C (7)	-C (8)	-C (14)	112.5(16)	C (21)	-C (20)	-C (19)	109.9(3)
C (10)	-C (9)	-C (8)	105.3(2)	C (21)	-C (20)	-C (29)	110.1(3)
C (10)	-C (9)	-C (11)	107.3(3)	C (21)	-C (20)	-C (30)	111.5(3)
C (10)	-C (9)	-C (25)	111.6(3)	C (19)	-C (20)	-C (29)	106.9(3)
C (8)	-C (9)	-C (11)	108.6(3)	C (19)	-C (20)	-C (30)	110.0(3)
C (8)	-C (9)	-C (25)	115.5(3)	C (29)	-C (20)	-C (30)	108.4(3)
C (11)	-C (9)	-C (25)	108.2(3)	C (22)	-C (21)	-C (20)	113.2(3)
C (1)	-C (10)	-C (5)	107.7(3)	C (17)	-C (22)	-C (21)	112.4(3)
C (1)	-C (10)	-C (9)	115.8(3)	C (32)	-C (31)	-O (1)	110.1(4)
C (5)	-C (10)	-C (9)	115.2(3)	C (32)	-C (31)	-O (2)	125.6(4)
C (12)	-C (11)	-C (9)	114.0(3)	O (1)	-C (31)	-O (2)	124.3(4)
C (13)	-C (12)	-C (11)	112.6(3)	C (3)	-O (1)	-C (31)	116.0(3)
C (14)	-C (13)	-C (12)	108.1(3)	C (5)	-O (3)	-C (6)	60.6(2)

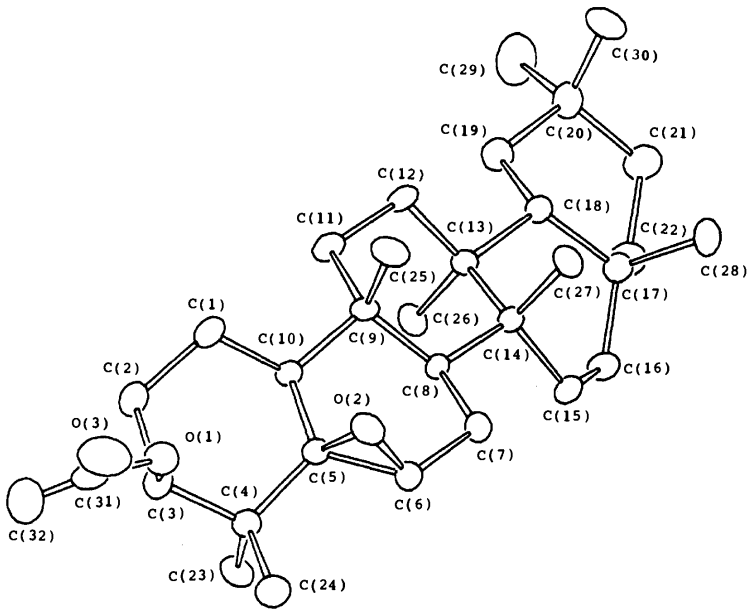

Fig. 1. Perspective view of 5β,6β-epoxyalnusan-3β-yl acetate(**6**).

(decomp), a triplet signal at δ 5.21 in the ^{1}H NMR, and a base peak at *m/z* 218.2027 ($C_{16}H_{26}$), these spectral data being compatible with 3β-hydroxyolean-12-en-6-one. Therefore the polar fraction obtained by the backbone rearrangement of the minor epoxide (**7**) was confirmed to be a mixture of 6α-hydroxyolean-18-en-3β-yl acetate (**15**) and -12-en-3β-yl acetate (**16**).

The hydroxy ketones (**19** and **20**), on acetylation, gave pure 6-oxoolean-18-en-3β-yl acetate (**17**) and -12-en-3β-yl acetate (**18**), respectively. The spectral data of the latter compound (**18**) were identical with those reported for a keto acetate derived from natural daturadiol (**3**).[9] The hydroxy ketone (**20**) was converted by lithium aluminium hydride-reduction into olean-12-ene-3β,6β-diol, spectra of which were completely identical with those of daturadiol (**3**).[9] On acetylation, the diol (**3**) gave a monoacetate (**8**), which is isomeric with the 6α-hydroxy acetate (**16**). The 6α-H of **8** appeared at δ 4.55 as a broad singlet signal in the ^{1}H NMR spectrum, from which the structural revision of "Sengupta's epoxide" had originated.

The major epoxide (**6**) was subjected to $BF_3 \cdot OEt_2$-catalyzed backbone rearrangement, followed by the usual work-up to give alnusa-1(10), 5-dien-3β-yl acetate (**13**; 3% yield) containing an unidentified diene-mixture, a hydroxy acetate (**21**; 74% yield), and a mixture (11% yield) of 6β-hydroxyolean-12-en-3β-yl acetate (**8**) and -18-en-3β-yl acetate (**22**). The new compound (**21**) showed a molecular ion peak at *m/z* 484.3934 ($C_{32}H_{52}O_3$), and the presence of a hydroxyl group, an acetoxyl group, and a trisubstituted double bond. The position of the double bond was determined by chemical conversion and ^{1}H NMR measurement. The hydroxy acetate (**21**) was dehydrated with phosphoryl chloride in pyridine to afford the diene (**13**). Oxidation of **21** with Jones reagent gave a keto acetate (**23**), whose ^{1}H NMR spectrum showed signals at δ 2.01(s, OAc), *ca.* 2.23(m, $C_{(2)}$–H_2; overlapping with $C_{(7)}$–H_2), 3.12 (br s, $C_{(5)}$–H), 4.82 (t, J=5 Hz, $C_{(3\alpha)}$–H), and 5.30(m, $C_{(1)}$–H). These spectral data suggest the presence of a 3β-acetoxy-1(10)-ene moiety, which was confirmed by a decoupling measurement of ^{1}H NMR spectrum. On irradiation around δ 2.23, the multiplet signal at δ 5.30 due to $C_{(1)}$–H changed into a doublet signal coupled with $C_{(5)}$–H (J=3 Hz) and the triplet signal at δ 4.82 due to $C_{(3\alpha)}$–H changed into a singlet. From these observations, the structure of hydroxy acetate (**21**) was determined to be 6β-hydroxyalnus-1(10)-en-3β-yl acetate.

These experiments clearly show that there was a remarkable difference in reaction behaviors between 5α,6α-epoxide (**7**) and 5β,6β-epoxide (**6**) towards the $BF_3 \cdot OEt_2$-catalyzed backbone rearrangement; the α-epoxide (**7**) gave mainly 18-ene and 12-ene derivatives (**15** and **16**; in 73% yield), while the β-epoxide (**6**) afforded 1(10)-ene and 1(10), 5-diene derivatives (**21** and **13**; in 77% yield) predominantly. One of the reasons why the backbone rearrangement of β-epoxide (**6**) did not proceed to C- and D-rings is likely to be ascribed to a steric factor. On attack of $BF_3 \cdot OEt_2$, the 5β,6β-epoxide ring would be cleaved to produce a carbonium ion on C-5, to which a migration of a hydride from C-10α would follow immediately to afford a cation at C-10. If a methyl group at C-9β migrates to the cationic center at C-10, a 1,3-diaxial steric hindrance would be brought about between the methyl group created on C-10β and a bulky BF_3-coordinated oxygen function in an axial-like configuration at C-6β. This steric hindrance might impede the backbone rearrangement of **6** towards C- and D-rings.

The conversion of dendropanoxide (**2**) into daturadiol (**3**) was thus accomplished *via* alnus-5-en-3β-yl acetate (**1**) and the 5α,6α-epoxide (**7**), which implies a formal total-synthesis of daturadiol (**3**), because a total synthesis of friedelin[13] and a conversion of friedelin into dendropanoxide (**2**)[14] have been carried out.

Experimental

General Procedures. Melting points were measured on a Mel-temp capillary melting point apparatus (Laboratory Devices) and are uncorrected. Infrared (IR) and ultraviolet absorption (UV) spectra were measured with a Hitachi 260-30 and a Hitachi 340 spectrometer, respectively. Mass (MS) spectra were run on a JEOL JMS-D300 mass spectrometer operating at 70 eV. Proton nuclear magnetic resonance (^{1}H NMR) spectra were taken in deuteriochloroform using a Varian EM 390 (90 MHz) or JEOL FX 90Q (90 MHz) spectrometer. Chemical shifts were expressed in δ downfield from tetramethylsilane as an internal standard and coupling constants in Hz. Gas-liquid chromatography (GLC) was carried out on a Shimadzu Gas Chromatograph GC-6A equipped with an FID (column: Dexsil 300GC, temperature: 270 °C, N_2: 70 mL/min). Analytical and preparative high performance liquid chromatography (HPLC) was carried out on a Waters Liquid Chromatograph ALC/GPC 202/401 at room temperature with an RI detector (column: μPORASIL 1/8″×1′, solvent: 20% ether-hexane, flow rate: 2.0 mL/min). Thin-layer chromatography (TLC) was carried out on Kieselgel 60 GF_{254} (E. Merck) and silica-gel column chromatography was done using Wakogel C-200 (Wako).

Epoxidation of Alnus-5-en-3β-yl Acetate (1). Alnus-5-en-3β-ol (**4**), prepared from dendropanoxide (**2**), was acetylated by the usual manner to give alnus-5-en-3β-yl acetate (**1**). The acetate (**1**; 290 mg) was dissolved in chloroform (12 mL) and treated with MCPBA (270 mg) at 0 °C. The usual work-up gave a residue (281 mg), which was separated by silica gel (60 g) column chromatography. Elution with benzene-ether (99:1) afforded 5α,6α-epoxide (**7**; 33 mg), mp 234—235 °C (from chloroform-acetone); IR (KBr) 1730, 1250, 1030, and 980 cm^{-1}; ^{1}H NMR δ=2.04 (3H, s) 3.23 (1H, t, J=2 Hz) and 4.88 (1H, dd, J=9 and 6 Hz); MS m/z (%) 484 (M^+; 5), 466 (10), 406 (70), 391 (37), 274 (62), 259 (68), 248 (40), 205 (89), 201 (48), 187 (72), 171 (72), and 95 (100), and 5β,6β-epoxide (**6**; 215 mg), mp 220.5—221 °C (from chloroform-acetone); IR (KBr) 1735 and 1255 cm^{-1}; ^{1}H NMR δ=2.08 (3H, s), 3.07 (1H, t, J=3 Hz), and 4.76 (1H, t, J=3 Hz); MS m/z (%) 484 (M^+; 2), 424 (7), 406 (20), 391 (11), 259 (16), 205 (38), 187 (24), and 95 (100).

Epoxidation of Alnus-5-en-3β-ol (4) and Alnus-5-en-3β-yl Benzoate (9). Alnus-5-en-3β-ol (**4**) and its benzoate (**9**) were epoxidized under the same conditions as above. The reaction product obtained from **4** was acetylated with acetic anhydride in pyridine to give 5β,6β-epoxyalnusan-3β-yl acetate (**6**) as the sole product.

The reaction product from **9** was shown to be a 1:1 mixture of 5α,6α-epoxide (**11**; ^{1}H NMR δ *ca.* 3.27, t-like; 6β-H) and 5β,6β-epoxide (**12**; ^{1}H NMR δ *ca.* 3.11, m; 6α-H) by TLC and ^{1}H NMR spectral measurement.

Backbone Rearrangement of 5α,6α-Epoxyalnusan-3β-yl Acetate (7). 5α,6α-Epoxyalnusan-3β-yl acetate (**7**; 33 mg) in benzene (6 mL) was treated with $BF_3 \cdot OEt_2$ (0.05 mL) at room temperature for 20 min. The reaction product, after addition of a saturated sodium hydrogencarbonate solution, was worked up as usual to give a residue, which was chromatographed on silica gel (8 g). Elution with benzene afforded a less polar product (8 mg; 25%) and a polar product (24 mg; 73%). The less polar product was shown to be identical with an authentic alnusa-1(10), 5-dien-3β-yl acetate (**13**; t_R=16.5 min) together with a small amount of unknown product (t_R=12.3 min) by GLC examination. The authentic sample of **13** was prepared by the dehydrogenation of alnus-5(10)-en-3β-yl acetate (**14**)[11] with selenium dioxide in boiling acetic acid. **13**: mp 207—208 °C (from chloroform-methanol); ^{1}H NMR δ=2.06 (3H, s), 4.71 (1H, dd, J=10 and 6 Hz), 5.21 (1H, m), and 5.67 (1H, t, J=4 Hz); MS m/z (%) 466 (M^+; 0.3), 406 (100), 391 (19), 274 (50), 259 (56), 205 (61), 171 (50), and 132 (65); UV (ethanol) λ_{max} (ε) 232 (14000), 238 (16000), and 245 nm (10000).

The polar product, a mixture of **15** and **16**, showed ^{1}H NMR δ=2.06 (3H, s), 4.04 (1H, m), 4.45 (1H, dd, J=9 and 6 Hz), 4.85 (0.5H, s), and 5.17 (0.5H, t, J=3 Hz); MS m/z 484 (M^+), 469, 466, 406, 391, 218 (base peak), 205, 204, 189, and 177.

Oxidation of the Mixture of Hydroxy Acetates (15 and 16). The mixture (25 mg) of **15** and **16**, dissolved in acetone (2 mL), was kept at 0 °C and oxidized with Jones reagent (0.05 mL) to give a mixture of 6-oxoolean-18-en-3β-yl acetate (**17**) and -12-en-3β-yl acetate (**18**); ^{1}H NMR δ=2.05 (3H, s), 4.41 (1H, dd, J=9 and 6 Hz), 4.90 (0.5H, s), and 5.21 (0.5H, t, J=3 Hz); MS m/z 482 (M^+), 467, 422, 407, 218 (base peak), 205, 189, and 177.

Alkaline Hydrolysis of the Mixture of Keto Acetates (17 and 18). The oxidation product (**17** and **18**), above obtained, was treated with 5% potassium hydroxide in methanol (3 mL) under a nitrogen atmosphere at room temperature for 15 h, and the usual work-up gave a mixture (18 mg) of hydroxy ketones (**19** and **20**). HPLC separation of the mixture gave a satisfactory result. 3β-Hydroxyolean-18-en-6-one (**19**; 9 mg), mp 217.5—219 °C (from chloroform-methanol), HPLC t_R=15.7 min, showed IR (film) 3450 and 1710 cm^{-1}; ^{1}H NMR δ=3.13 (1H, dd, J=9 and 6 Hz) and 4.88 (1H, s); MS m/z (%) 440 (M^+; 51), 425 (34), 205 (48), 204 (47), 189 (34), and 177 (100); high resolution MS m/z 440.3659 (Calcd for $C_{30}H_{48}O_2$: M, 440.3654) and m/z 177.1623 (Calcd for $C_{13}H_{21}$: 177.1643). 3β-Hydroxyolean-12-en-6-one (**20**; 9 mg), mp 243—245 °C (decomp) (from ether-hexane), HPLC t_R=16.3 min, showed IR (film) 3450 and 1705 cm^{-1}; ^{1}H NMR δ=3.16 (1H, dd, J=9 and 6 Hz) and 5.21 (1H, t, J=3 Hz); MS m/z (%) 440 (M^+; 20), 425 (7), 218 (100), 205 (22), 203 (26), and 189 (10); high resolution MS m/z 440.3613 (Calcd for $C_{30}H_{48}O_2$: M, 440.3653) and m/z 218.2027 (Calcd for $C_{16}H_{26}$: 218.2033).

Acetylation of 3β-Hydroxyolean-18-en-6-one (19) and -12-en-6-one (20). The Δ^{18}-hydroxy ketone (**19**; 8 mg) was acetylated with acetic anhydride in pyridine to give 6-oxoolean-18-en-3β-yl acetate (**17**; 7 mg), mp 220.5—222 °C (from ether-methanol); IR (film) 1730, 1710, and 1250 cm^{-1}; ^{1}H NMR δ=2.04 (3H, s), 4.40 (1H, dd, J=8 and 6 Hz), and 4.89 (1H, s); MS m/z (%) 482 (M^+; 77), 467 (54), 205 (84), 204 (66), 189 (59), and 177 (100); high resolution MS m/z 482.3741 (Calcd for $C_{32}H_{50}O_3$: M, 482.3758) and m/z 177.1634 (Calcd for $C_{13}H_{21}$: 177.1642).

The Δ^{12}-hydroxy ketone (**20**), on acetylation, gave 6-oxoolean-12-en-3β-yl acetate (**18**), mp 246—248 °C (from methanol); ^{1}H NMR δ=0.81, 0.89, 0.95, 0.98, and 1.00 (each 3H, s), 1.25 (6H, s), 1.30 (3H, s), 2.05 (3H, s), 4.42 (1H, t, J=7 Hz), and 5.23 (1H, t, J=3 Hz); MS m/z (%) 482 (M^+; 21), 467 (8), 218 (100), 205 (61), 203 (30), and 189 (22); high resolution MS m/z 482.3743 (Calcd for $C_{32}H_{50}O_3$: M, 482.3758) and m/z 218.1998 (Calcd for $C_{16}H_{26}$: 218.2033).

Reduction of 3β-Hydroxyolean-12-en-6-one (20). The hydroxy ketone (**20**; 9 mg) in tetrahydrofuran (1.5 mL) was treated with an excess of lithium aluminium hydride (20 mg) under reflux for 5 h and the reaction product was worked up as usual to give olean-12-ene-3β,6β-diol (**3**; 7 mg) as the sole product, mp 258—260 °C (chloroform-methanol), ^{1}H NMR δ=0.86 (3H, s), 0.90 (6H, s), 1.10, 1.13, 1.23, 1.30, and 1.35 (each 3H, s), 3.15 (1H, dd, J=8 and 6 Hz), 4.56 (1H, br s), and 5.24 (1H, t-like, J=3 Hz); MS m/z (%) 442 (M^+; 16), 218 (100), 205 (14), 203 (32), and 189 (13); high resolution MS m/z 442.3829 (Calcd for $C_{30}H_{50}O_2$: M, 442.3811) and m/z 218.2055 (Calcd for $C_{16}H_{26}$: 218.2035); these spectral data were found to be identical with those of daturadiol (**3**).[9]

Acetylation of Daturadiol (3). Daturadiol (**3**) was treated with acetic anhydride in pyridine to give daturadiol 3-monoacetate (**8**), ^{1}H NMR (FT) δ=0.84 (3H, s), 0.88 (6H, s), 0.95, 1.10, (each 3H, s), 1.26 (6H, s), 1.35 (3H, s), 2.06 (3H, s), 4.45 (1H, m), 4.55 (1H, br s), and 5.23 (1H, t, J=3 Hz); MS m/z (%) 484 (M^+; 13), 218 (100), 205 (22), 203 (24), and 189 (15).

Backbone Rearrangement of 5β,6β-Epoxyalnusan-3β-yl Acetate (6). 5β,6β-Epoxide (**6**; 168 mg) in benzene was treated with $BF_3 \cdot OEt_2$ at room temperature. After the usual work-up, the reaction product was subjected to separation by silica-gel column chromatography. Elution with benzene gave alnusa-1(10),5-dien-3β-yl acetate (**13**; 5 mg), 6β-hydroxyalnus-1(10)-en-3β-yl acetate (**21**; 125 mg), and a mixture (18 mg) of 6β-hydroxyolean-12-en-3β-yl acetate (**8**) and -18-en-3β-yl acetate (**22**). 6β-Hydroxyolean-1(10)-en-3β-yl acetate (**21**) showed mp 233—233.5 °C (from acetone–methanol); IR (KBr) 3570, 3400, 1720, and 1260 cm^{-1}; ^{1}H NMR δ =2.04 (3H, s), 4.26 (1H, br s), 5.21 (1H, dd, J=10 and 5 Hz), and 5.39 (1H, m); MS m/z 484 (M^+), 424 (base peak), 406, 391, 302, 274, 259, 205, 150, and 122; Found: m/z 484.3943. Calcd for $C_{32}H_{52}O_3$: M, 484.3917. The mixture of **8** and **22** showed IR (Nujol) 3550, 1710, 1270, and 1255 cm^{-1}; ^{1}H NMR δ=2.05 (3H, s), 4.46 (1H, m), 4.52 (1H, br s), 4.86 (0.7H, s), and 5.23 (0.3H, t-like J=3 Hz); MS m/z (%) 484 (M^+; 40), 469 (9), 391 (6), 218 (100), 205 (74), 204 (83), 189 (58), and 177 (48).

Derivatization of 6β-Hydroxyalnus-1(10)-en-3β-yl Acetate (21). Hydroxy acetate (**21**) was treated with phosphoryl chloride in pyridine to give the 1(10), 5-diene (**13**), which was shown to be identical with an authentic sample by GLC examination.

On oxidation with Jones reagent, the hydroxy acetate (**21**) afforded 6-oxoalnus-1(10)-en-3β-yl acetate (**23**), mp 199—201 °C (from benzene–methanol); ^{1}H NMR δ=2.01 (3H, s), 2.23 (m), 3.12 (1H, br s), 4.82 (1H, t, J=5 Hz) and 5.30 (1H, m); MS m/z (%) 482 (M^+; 11), 422 (62), 407 (100), 273 (14), 259 (5), 205 (9), and 149 (22); Found: m/z 482.3754. Calcd for $C_{32}H_{50}O_3$: M, 482.3759.

References

1) A preliminary account of this report: M. Tori, M. Takai, Y. Matsumoto, Y. Moriyama, T. Tsuyuki, T. Takahashi, A. Itai, and Y. Iitaka, *Chem. Lett.*, **1983**, 527.

2) M. Tori, T. Tsuyuki, and T. Takahashi, *Bull. Chem. Soc. Jpn.*, **50**, 3381 (1977).

3) S. Yamada, S. Yamada, K. Tachibana, Y. Moriyama, Y. Tanahashi, T. Tsuyuki, and T. Takahashi, *Bull. Chem. Soc. Jpn.*, **49**, 1134 (1976); K. Tachibana, M. Tori, Y. Moriyama, T. Tsuyuki, and T. Takahashi, *ibid.*, **50**, 1552 (1977).

4) Y. Yokoyama, Y. Moriyama, T. Tsuyuki, and T. Takahashi, *Bull. Chem. Soc. Jpn.*, **54**, 234 (1981).

5) K. Suemura, T. Irokawa, M. Tori, S. Ohta, Y. Moriyama, T. Tsuyuki, T. Takahashi, A. Itai, and Y. Iitaka, *Chem. Lett.*, **1982**, 1617.

6) Dendropanoxide (**2**) was obtained from leaves of *Gilibertia trifidus* Makino, which were collected at the Botanical Gardens, Faculty of Science, the University of Tokyo. The authors would like to thank Mr. Eiichi Ishii for collection of leaves of the plant.

7) H. R. Arthur and W. H. Hui, *J. Chem. Soc.*, **1961**, 551; J. H. Block and G. H. Constantine, Jr., *Phytochemistry*, **11**, 3279 (1972).

8) P. Sengupta, M. Sen, and S. Maiti, *J. Indian Chem. Soc.*, **57**, 1181 (1980).

9) M. Kocór, J. S. Pyrek, C. K. Atal, K. L. Bedi, and B. R. Sharma, *J. Org. Chem.*, **38**, 3685 (1973).

10) The complete F_o—F_c data, anisotropic thermal parameters for non-hydrogen atoms, atomic positional parameters and isotropic thermal parameters for hydrogen atoms, and bond lengths and bond angles containing hydrogen atoms are deposited as Document No.8435 at the Office of the Editor of Bull. Chem. Soc. Jpn.

11) A. C. Paton, F. S. Spring, and R. Stevenson, *J. Chem. Soc.*, **1958**, 2640.

12) H. Budzikiewicz, J. M. Wilson, and C. Djerassi, *J. Am. Chem. Soc.*, **85**, 3688 (1963).

13) R. E. Ireland and D. M. Walba, *Tetrahedron Lett.*, **1976**, 1071.

14) M. Tori, T. Torii, K. Tachibana, S. Yamada, T. Tsuyuki, and T. Takahashi, *Bull. Chem. Soc. Jpn.*, **50**, 469 (1977).

Constituents of Seeds of *Ailanthus altissima* SWINGLE. Isolation and Structures of Shinjuglycosides A, B, C, and D

Shin YOSHIMURA, Masami ISHIBASHI, Takahiko TSUYUKI, Takeyoshi TAKAHASHI,* and Kazuhiro MATSUSHITA†

Department of Chemistry, Faculty of Science, The University of Tokyo, Hongo, Bunkyo-ku, Tokyo 113

†*Application Center, Scientific Instrument Project, JEOL Co. Ltd., Nakagami, Akishima, Tokyo 196*

(Received May 2, 1984)

Four bitter quassinoid glycosides, shinjuglycosides A, B, C, and D were isolated from seeds of *Ailanthus altissima* SWINGLE and their structures were established to be 2-β-D-glucopyranosides of chaparrin, shinjulactone A, amarolide 11-acetate, and amarolide, respectively, from spectral data and enzymatic or acid-catalyzed hydrolysis.

Recently several quassinoid glycosides have been isolated from Simaroubaceous plants[1] and some of them have been shown to exhibit useful biological activities.[2] In our continuous studies of constituents of Simaroubaceous plants, we have investigated *Ailanthus altissima* SWINGLE (Japanese name: Shinju or Niwaurushi), and reported several new quassinoids isolated from the stem and root bark of the plant.[3,4] Now we examined bitter constituents in seeds of the plant. This paper describes isolation and structure determination of four new quassinoid glycosides named shinjuglycosides A, B, C, and D (**1**, **2**, **3**, and **4**). Although many quassinoids have been obtained from *A. altissima*, the isolation of their glycosides from the plant has not been reported yet.

Methanol extracts of seeds of *A. altissima* were defatted with hexane and partitioned between dichloromethane and water. The aqueous layer was subjected to separation by Dowex 1×2 anion exchange chromatography eluted with acetic acid in concentration of 0—2 M (1 M=1 mol dm^{-3}) linear gradient. A fraction eluted with about 0.2 M acetic acid was further purified by DEAE-Sephadex A-25 anion exchange chromatography (eluted with 0—0.5 M ammonium hydrogencarbonate linear gradient) and Sephadex G-10 gel filtration chromatography (eluted with water) to give a mixture of bitter substances. It was shown to consist of two com_ounds by ^{1}H NMR spectral measurement, but they could not be separated from each other by silicagel chromatography or reversed phase chromatography. However, they were separated by repetition of cellulose column chromatographies to give two new quassinoid glycosides, named shinjuglycoside A (**1**; *ca.* 0.015%) and shinjuglycoside B (**2**; *ca.* 0.03%).

The structure of shinjuglycoside A (**1**), mp 162—164 °C (decomp) was determined as follows. The molecular formula ($C_{26}H_{38}O_{12}$) was suggested by secondary ion mass spectrometry (SIMS) which showed the MH^+ peak at m/z 543. An abundant fragment ion at m/z 363 (MH^+-180) together with an ion at m/z 380 (M^+-162) observed in the EI mass spectrum indicated the presence of a hexose moiety. The structure of shinjuglycoside A (**1**) was inferred to be a β-D-glucoside of chaparrin (**5**)[5] from ^{1}H NMR spectrum. The sugar part was identified to be a D-glucose by the GLC examination after methanolysis and trimethylsilylation. Shinjuglycoside A (**1**) was hydrolyzed with β-glucosidase in 0.1 M acetate buffer (pH 5.0) at 37 °C for 2 weeks to afford chaparrin (**5**), which was identified by the comparison of mp, $[\alpha]_D$, IR, TLC, and ^{1}H NMR spectra with those of an authentic sample. The ^{13}C NMR spectrum of shinjuglycoside A (**1**) revealed that a signal due to C-2 of the aglycone part shifted to lower field by 9.8 ppm than that of chaparrin (**5**), indicating that the D-glucose must be attached at the C-2 position. In the ^{1}H NMR of **1**, an anomeric proton appeared at δ 5.22 as a doublet signal (J=7.6 Hz) and the coupling constants $J_{2',3'}$, $J_{3',4'}$, and $J_{4',5'}$ of the sugar part are all 8.9 Hz. Thus the structure of shinjuglycoside A (**1**) was determined to be 2-*O*-β-D-glucopyranosylchaparrin.[6]

When treated with acetic anhydride in pyridine at room temperature for 24 h, **1** gave a hexaacetyl deriva-

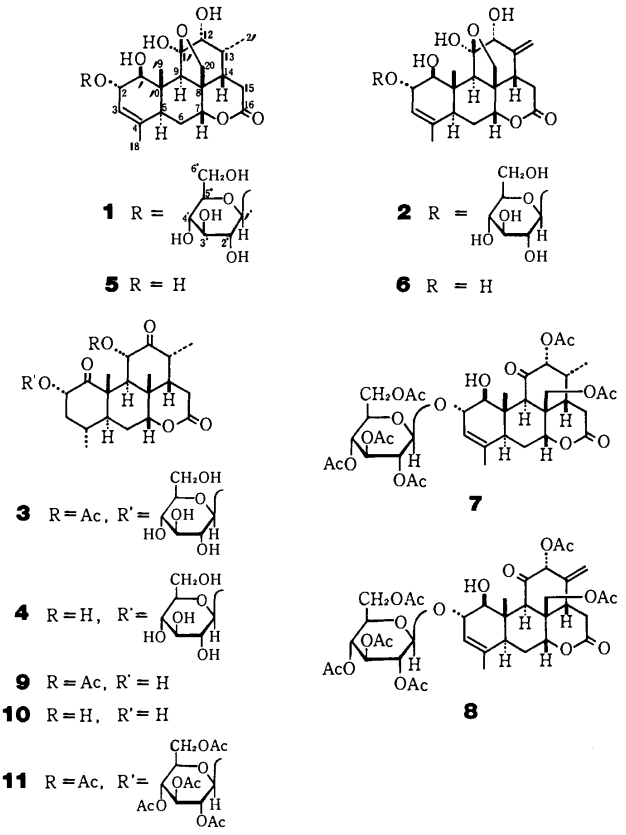

tive (**7**), mp 144—145 °C, which still showed the presence of hydroxyl(s) in the IR spectrum. SIMS of **7** showed an MH^+ ion at *m/z* 795 and a tetra-*O*-acetylhexose oxonium ion at *m/z* 331. In the ^1H NMR spectrum of **7**, six singlet signals due to the acetoxyl groups appeared at δ 2.02, 2.03, 2.04, 2.10, 2.17, and 2.18, and the signal of 12-H (δ 6.18, d, J=4.3 Hz) was observed at much lower field in comparison with that of **1** (δ 3.94, d, J=4.3 Hz). These findings indicate that **7** is 2′,3′,4′,6′,12,20-hexa-*O*-acetyl derivative of **1**.

The structure of shinjuglycoside B (**2**), mp 194—196 °C (decomp) was determined by the same chemical and spectral methods as those developed in **1**. Shinjuglycoside B (**2**) gave an MH^+ peak at *m/z* 541 in SIMS, indicating the molecular formula of $C_{26}H_{36}O_{12}$, and the presence of a hexose moiety was shown by fragment ions at *m/z* 378 (M^+ −162) in EI mass spectrum and at *m/z* 361 (MH^+ −180) in SIMS. Enzymatic hydrolysis of **2** gave shinjulactone A (**6**).[3] Glycosylation shift ($\Delta\delta$ 9.7) of the signal due to C-2 was observed in the ^{13}C NMR spectrum of **2**. The ^1H NMR spectrum of **2** showed an anomeric proton at δ 5.20 as a doublet signal (J=7.6 Hz) and the coupling constants of the sugar part are 8.6 Hz. Thus the structure of shinjuglycoside B (**2**) was determined to be 2-*O*-β-D-glucopyranosylshinjulactone A.

Under the same conditions as in the case of **1**, **2** also gave a hexaacetyl derivative (**8**), mp 145—148 °C. The structure of **8**, therefore, has been established to be 2′,3′,4′,6′,12,20-hexa-*O*-acetyl derivative of **2** from spectral data.

Bitter principles in the dichloromethane layer obtained by the partition (*vide supra*) were then investigated. The organic layer was separated by silica-gel column chromatography to afford four known quassinoids, amarolide,[7] chaparrinone,[8] ailanthone,[3] and chaparrin[5] in very low yields from less polar fractions. The fractions eluted with more than 20% methanol in chloroform were further subjected to separation by silica-gel column chromatography, silicic acid partition chromatography, and Sephadex G-10 gel filtration chromatography. Two new quassinoid glycosides named shinjuglycosides C (**3**) and D (**4**) were isolated in 0.005% and 0.002% yield, respectively.

Shinjuglycoside C (**3**), mp 180—185 °C, showed the presence of two secondary methyls, two tertiary

Table 1. ^1H-NMR spectra at 400 MHz of shinjuglycosides A and B (**1** and **2**)[a,b]

	1		**2**	
	δ	J	δ	J
1-H	4.00 d	7.6	4.07 d	7.9
2-H	4.57 m		4.57 m	
3-H	5.77 br s		5.80 br s	
5-H	2.55 br d	11.0	2.57 br d	12.8
6α-H	1.99 ddd	14.5, 2.7, 2.1	2.01 ddd	15, 2.5, 2.5
6β-H	1.83 ddd	14.5, 14.5, 2.7	1.85 ddd	15, 12.8, 2.5
7-H	4.46 t	2.7	4.57 t	2.5
9-H	3.00 s		3.21 s	
12-H	3.94 d	4.3	4.53 s	
13-H	2.42 m			
14-H	1.86 m		2.80 dd	13.6, 5.3
15α-H	3.22 dd	18.7, 14.0	3.55 dd	18.5, 13.6
15β-H	2.85 dd	18.7, 5.2	2.90 dd	18.5, 5.3
4-CH_3	1.45 br s		1.46 br s	
10-CH_3	1.58 s		1.56 s	
13-CH_3	1.10 d	7.3		
20-H	3.73 d	8.5	3.65 d	8.2
20-H′	4.15 d	8.5	4.13 d	8.2
21-H			5.20 d	1.5
21-H′			5.26 d	1.5
1′-H	5.22 d	7.6	5.20 d	7.6
2′-H	4.10 dd	7.6, 8.9	4.07 dd	7.6, 8.6
3′-H	4.23 t	8.9	4.21 t	8.6
4′-H	4.27 t	8.9	4.23 t	8.6
5′-H	3.99 m		3.97 m	
6′-H	4.41 dd	11.9, 5.2	4.39 dd	11.9, 5.2
6′-H′	4.58 dd	11.9, 2.4	4.53 dd	11.9, 2.4

a) δ and J are expressed in ppm and Hz, respectively. b) Measured in C_5D_5N.

Table 2. ^{13}C-NMR spectra of shinjuglycoside A (**1**), B (**2**), chaparrin (**5**) and shinjulactone A (**6**)[a,b]

Assignment No. of C	**1**	**5**	**2**	**6**[c]
1	83.9	83.8	83.9	83.6
2	82.6	72.8	82.4	72.7
3	123.8	127.0	123.8	127.1
4	136.0	134.9	135.9	134.8
5	41.5	41.9	41.5	41.9
6	25.9	26.2	25.8	26.2
7	78.9	79.2	78.9	79.2
8	46.2	46.3	45.6	45.8
9	42.7	42.9	47.9	48.0
10	41.7	41.8	41.9	41.9
11	110.6	110.7	110.4	110.5
12	79.6	79.7	80.6	80.7
13	30.5	31.8	147.7	148.0
14	44.3	44.6	44.6	44.9
15	31.7	30.6	35.3	35.4
16	170.4	170.5	169.5	169.6
18	21.1	21.2	21.1	21.2
19	10.5	10.7	10.5	10.6
20	71.8	71.8	72.6	72.7
21	13.2	13.3	118.2	118.0
1′	106.2		106.2	
2′	76.0		76.1	
3′	78.5		78.5	
4′	71.6		71.6	
5′	78.4		78.4	
6′	62.7		62.8	

a) Measured in C_5D_5N. b) Chemical shifts are expressed in δ-value. c) Chemical shifts and assignment described in Ref. 3 were found to be revised as shown in this table. Chemical shifts of the signals of C-5, C-10, and C-14 were assigned to be δ 49.6, 44.9, and 41.9, respectively, in Ref. 3.

TABLE 3. ^{1}H-NMR SPECTRA OF SHINJUGLYCOSIDE A HEXAACETATE (**5**) AND SHINJUGLYCOSIDE B HEXAACETATE (**6**)[a,b]

	5		**6**	
	δ	J	δ	J
1-H	4.44 d	8.0	4.42 d	8.0
2-H	4.10 m		4.06 dd	8.0, 4.6
3-H	5.75 br s		5.79 br s	
5-H	2.58[c]		2.64 br d	13.0
6α-H	d)		1.99 ddd	14.0, 2.4, 2.4
6β-H	1.79 ddd	15.0, 11.0, 2.5	1.81 ddd	14.0, 13.0, 2.4
7-H	4.49 t	2.5	4.58 t	2.4
9-H	3.02 s		3.27 s	
12-H	6.18 d	4.3	6.77 s	
13-H	2.58[c]			
14-H	d)		2.97 dd	13.8, 5.2
15α-H	2.97 dd	18.5, 14.0	3.30 dd	18.0, 13.8
15β-H	2.81 dd	18.5, 5.3	2.85 dd	18.0, 5.2
4-CH_3	1.46 br s		1.47 br s	
10-CH_3	1.30 s		1.31 s	
13-CH_3	0.80 d	7.3		
20-H	3.90 d	8.5	3.79 d	8.2
20-H′	4.24 d	8.5	4.24 d	8.2
21-H			5.35 s	
21-H′			5.45 s	
1′-H	5.34 d	7.9	5.36 d	7.6
2′-H	5.57 dd	7.9, 9.8	5.57 dd	7.6, 9.5
3′-H	5.53 t	9.8	5.54 t	9.5
4′-H	5.77 t	9.8	5.78 t	9.5
5′-H	4.10 m		4.11 ddd	9.5, 4.6, 2.4
6′-H	4.42 dd	12.2, 2.4	4.43 dd	12.2, 2.4
6′-H′	4.66 dd	12.2, 4.6	4.60 dd	12.2, 4.6
OAc	2.02, 2.03, 2.04, 2.10, 2.17, 2.18		2.02, 2.03, 2.04, 2.05, 2.18×2	

a) δ and J are expressed in ppm and Hz, respectively. b) Measured in C_5D_5N. c) Signals are overlapped. d) Signals are not assignable.

TABLE 4. ^{1}H-NMR SPECTRA OF SHINJUGLYCOSIDES C AND D (**3** AND **4**)[a,b]

	3		**4**	
	δ	J	δ	J
2-H	5.39 dd	11.3, 7.6	5.48 dd	11.3, 7.6
7-H	4.37 br s		4.30 t	3.7
9-H	3.40 d	13.4	3.09 d	12.8
11-H	5.62 d	13.4	4.67 d	12.8
13-H	3.13 quin	6.4	3.08 quin	6.4
15α-H	c)		2.28 dd	18.6, 12.5
15β-H	2.74 dd	18.6, 6.7	2.67 dd	18.6, 6.7
4-CH_3	0.97 d	6.7	1.00 d	6.7
8-CH_3	1.30 s[d]		1.45 s[d]	
10-CH_3	1.49 s[d]		1.50 s[d]	
13-CH_3	0.63 d	6.4	0.63 d	6.4
11-OAc	2.19 s			
1′-H	4.85 d	7.6	4.97 d	7.6
2′-H	4.10 dd	7.6, 8.6	4.09 dd	7.6, 8.9
3′-H	4.18 dd	8.6, 8.9	4.15 dd	8.9, 8.5
4′-H	4.23 dd	8.9, 8.9	4.24 dd	9.6, 8.5
5′-H	3.89 ddd	8.9, 5.5, 2.4	3.76 ddd	9.6, 5.2, 2.4
6′-H	4.38 dd	11.9, 5.5	4·35 dd	11.9, 5.2
6′-H′	4.58 dd	11.9, 2.4	4.50 dd	11.9, 2.4

a) δ and J are expressed in ppm and Hz, respectively. b) Measured in C_5D_5N. c) Signals are not assignable. d) The assignments of these signals may be reversed.

methyls, and one acetoxyl group in the 400 MHz ^{1}H NMR spectrum. Most of other protons including those attributed to a D-glucose residue were assigned (see Table 4). The molecular formula ($C_{28}H_{40}O_{12}$) was suggested by SIMS which showed the MH^+ peak at m/z 569, and an abundant fragment ion at m/z 407 ($MH^+ - 162$). The molecular formula was also supported by an intense peak observed at m/z 406 ($M^+ - 162$) in the EI mass spectrum. These spectral data suggest that shinjuglycoside C (**3**) consists of amarolide 11-acetate (**9**)[7] as an aglycone and β-D-glucopyranose as a sugar part. Acid hydrolysis of **3** with 1.5 M sulfuric acid–methanol (1:2) yielded D-glucose, and amarolide (**10**) concomitant with hydrolysis of 11-acetate moiety. The former was identified by GLC as its trimethylsilyl derivative, and the latter identified in comparison with an authentic sample by IR, ^{1}H NMR and TLC.

Shinjuglycoside D (**4**) was crystallized from methanol as colorless needles, mp 282—284 °C (decomp). The molecular formula ($C_{26}H_{38}O_{11}$) was given by SIMS which showed the $[M+Na]^+$ peak at m/z 549. The structure of **4** was suggested to be amarolide 2-β-D-glucopyranoside by the 400 MHz ^{1}H NMR spectrum (see Table 4). In the ^{13}C NMR, a glycosylation shift was observed between the signals due to C-2 of **4** and that of amarolide (**10**). Acid-hydrolysis of **4** yielded amarolide (**10**) and D-glucose, each of which was identified by the same method as described for **3**.

Acetylation of **3** and **4** afforded the same compound (**11**), mp 238 °C (from methanol–diethyl ether). In the IR spectrum of **11**, no hydroxyl was detected. In the mass spectrum (EI), the fragment ions were observed at m/z 676 ($M^+ - AcOH$) and at m/z 331 corresponding to a tetra-*O*-acetylhexose oxonium ion. In the ^{1}H NMR spectrum four methyl signals appeared at δ 0.92 (d, J=7.7, 13-CH_3), 1.05 (d, J=6.4, 4-CH_3), 1.29 (s, tertiary CH_3), and 1.54 (s, tertiary CH_3) together with five resonances due to the acetoxyl groups δ 2.01, 2.02, 2.07, 2.11, and 2.19.

Thus, the structure of **3** proves to be amarolide 11-acetate 2-β-D-glucopyranoside, and the structure of **4** to be amarolide 2-β-D-glucopyranoside.

Experimental

General Procedures. All melting points were measured on a Mel-temp capillary melting apparatus (Laboratory

devices) and uncorrected. Optical rotations were determined on a JASCO polarimeter DIP-181. Infrared (IR) spectra were measured on a Hitachi 260-30 spectrometer. Low and high resolution mass spectra (MS and HRMS, respectively) were run on a JEOL JMS-D300 mass spectrometer operating at 70 eV and secondary ion mass spectra (SIMS) on a Hitachi M-80 mass spectrometer. Proton nuclear magnetic resonance (^{1}H NMR) spectra (400 MHz) were taken using a JEOL JMN GX-400 spectrometer and carbon-13 nuclear magnetic resonance (^{13}C NMR) spectra (22.5 MHz) JEOL FX 90Q. Chemical shifts were expressed in ppm downfield from tetramethylsilane as an internal standard (δ value) and coupling constants in Hz. Thin-layer chromatography (TLC) was carried out on Kieselgel 60 GF_{254} coated in 0.25 mm or on TLC plates Kieselgel 60/Kieselgur F_{254} (E. Merck). Wakogel C-200 (Wako), Silicic acid AR (Mallincrodt), Dowex 1X2 (Dow Chemical), DEAE-Sephadex A-25, Sephadex G-10 (Pharmacia Fine Chemicals), or Cellulose microcrystalline (E. Merck) was used for column chromatography. Commercialized β-glucosidase available from Sigma Chemical Company was used.

Table 5. ^{13}C-NMR spectra of shinjuglycoside C(**3**), D(**4**), amarolide 11-acetate (**9**), and amarolide (**10**)[a,b]

Assignment No. of C	**3**	**9**	**4**	**10**
1	211.8	213.5	213.1	215.9
2	75.6	70.8	75.7	70.8
3	45.1	49.2	45.2	48.9
4	29.0	29.1	29.1	29.0
5	36.8	37.0	40.1	40.4
6	26.7	26.8	26.9	27.9
7	75.6	75.5	75.7	74.8
8	50.5	50.2	50.7	50.4
9	47.2	47.3	47.5	47.9
10	35.5	35.6	35.4	35.5
11	81.7	81.8	82.0	82.0
12	203.4	203.6	210.3	210.5
13	47.6	48.1	48.0	47.9
14	43.0	43.0	42.7	42.7
15	29.0	29.1	29.1	29.0
16	170.1	170.1	168.9	168.9
18	18.4	18.5	18.4	18.6
19	12.6	12.9	12.9	13.1
20	10.5	10.6	10.6	10.7
21	21.3	21.5	21.5	21.6
11-OAc	168.7	168.6		
	21.0	20.5		
1′	104.1		103.1	
2′	77.0		76.0	
3′	78.8		78.6	
4′	71.2		71.5	
5′	78.4		78.2	
6′	62.7		62.8	

a) Measured in C_5D_5N. b) Chemical shifts are expressed in δ-value.

Plant Materials. Seeds with pericarps of *Ailanthus altissima* Swingle were air-dried, and grinded to afford 3.7 kg of materials.

Extraction and Separation. Seeds (3.7 kg) was extracted with methanol (18 L×2) for 24 h. Extracts were concentrated, defatted with hexane, and partitioned between dichloromethane and water.

A half of the aqueous layer was concentrated to give brown tar (90 g), which was dissolved in distilled water (2 L). The aqueous solution was charged to Dowex 1×2 (OH^--form; 4.0×40 cm) and the resin was then washed with distilled water (2 L). The Dowex 1 column was then eluted with acetic acid (4 L) with 0—2 M linear gradient and 260 fractions (each 15 mL) were collected. Fractions 41—52 were combined and lyophilized to give a yellow powder (fraction A; 4.6 g).

A part of fraction A (3.6 g) was dissolved in a small amount of water and then charged to a column of DEAE-Sephadex A-25 (HCO_3^--form; 2.6×90 cm). Elution was performed with an aqueous ammonium hydrogencarbonate solution (4 L) with 0.01—0.5 M linear gradient and 400 fractions (each 10 mL) were collected. The fractions 113—157 were combined and lyophilized to give white powder (fraction B; 1.8 g). The fraction exhibited a bitter taste and was shown to be a complex mixture by TLC examination (Kieselgel 60/Kieselgur F_{254} developed with 2-propanol-conc. aqueous ammonia-water 6:1:1).

Fraction B was devided into three portions. Each portion was dissolved in a small amount of water and charged to a column of Sephadex G-10 (1.2×130 cm). Elution was performed with water, and 50 fractions (each 5 mL) were col-

Table 6. ^{1}H-NMR spectrum of 11-*O*-acetyl-2-*O*-(2′,3′,4′,6′-tetra-*O*-acetyl-β-D-glucopyranosyl)-amarolide (**11**)[a,b]

	δ	J		δ	J
2-H	4.90 dd	11.6, 7.6,	4-CH_3	1.05 d	7.7
5-H	1.48 ddd	14.9, 12.8, 3.4	13-CH_3	0.92 d	6.4
6β-H	1.80 ddd	14.9, 14.9, 1.8	8-CH_3	1.29 s[c]	
7-H	4.31 br s		10-CH_3	1.54 s[c]	
9-H	3.02 d	12.5	OAc	2.01, 2.02, 2.07, 2.11, 2.19	
11-H	5.28 d	11.5	1′-H	4.46 d	7.6
13-H	3.02 m		2′-H	5.02 dd	9.5, 7.6
14-H	2.38 ddd	12.5, 7.4, 4.6	3′-H	5.04 dd	9.5, 9.5
			4′-H	5.13 dd	9.8, 9.5
			5′-H	3.54 ddd	9.8, 4.9, 2.8
			6′-H	4.12 dd	12.2, 2.8
				4.21 dd	12.2, 4.9

a) δ and J are expressed in ppm and Hz, respectively. b) Measured in $CDCl_3$. c) The assignments of these signals may be reversed.

lected. The fractions 19—27, showing a bitter taste and two spots on TLC, were combined and lyophilized to give white powder (fraction C; 1.5 g).

Fraction C was applied to a Cellulose microcrystalline column (2.6×70 cm) and was eluted with acetone-water (9:1), and 50 fractions (each 15 mL) were collected. Fractions 22—27 were combined and evaporated to give shinjuglycoside A (**1**; 151 mg) and fractions 43—50 to give shinjuglycoside B (**2**; 119 mg). Fractions 28—42 (808 mg) were a mixture of shinjuglycosides A and B. A part of these fractions (578 mg) was separated by the same method to give **1** (50 mg), **2** (177 mg), and a mixture (350 mg) of **1** and **2**. This mixture was found to contain **1** and **2** in a ratio of *ca.* 1:2 by ^{1}H NMR spectral measurement.

A part (16.5 g) of the dichloromethane extract (*ca.* 60 g) obtained by the partition was separated by silica-gel column chromatography (C-200, 825 g; column A) eluted with 0, 1, 2, 3, 4, 5, 6, 7, 8, 9, 10 (each 1 L), 20, 40, 60% (each 2 L) methanol in chloroform, successively. Fractions of 500 mL each were collected. Fractions 25—32 (5.3 g) were combined and further separated by silica-gel column chromatography (C-200, 380 g; column B) eluted with the lower layer of a solvent mixture of chloroform-methanol-water (50:12:3). Fractions of 200 mL each were collected. Fractions 5—7 (1.4 g) of column B were subjected to separation by the silicic acid partition chromatography. Silicic acid (350 g) was mixed with water (235 mL) and packed in a column with chloroform (column C). Elution was performed with 0 (2 L), 3, 6, 9, 12, 15, 18, and 21% (each 1 L) ethanol in water-saturated chloroform. Fractions of 300 mL each were collected and monitored by TLC (ethyl acetate-methanol, 7:3). Fractions 8—13 (1.5 g) of column B were combined and also separated by silicic acid partition chromatography (silicic acid 400 g containing water 270 mL; column D). Elution was performed with the same solvent as that for column C and the effluent was collected in 200 mL-fractions.

Fractions 16—19 (175 mg) of column C were separated by column chromatography on Sephadex G-10 prepared by the same procedure as before to give shinjuglycoside C (140 mg). Fractions 27—30 (175 mg) of column D were separated to give shinjuglycoside D (80 mg) and a mixture (75 mg) of shinjuglycosides A and B by column chromatography on Sephadex G-10 prepared before.

Shinjuglycoside A (1). Amorphous solid, mp 162—164 °C (decomp); $[\alpha]_D^{21}$ +66.5° (*c* 3.79, MeOH); IR(KBr) 3400, 1720, and 1040 cm^{-1}; ^{1}H NMR (Table 1); ^{13}C NMR (Table 2); MS(SIMS) *m/z* 543 (MH^+) and 363; HRMS (EI) Found: *m/z* 380.1868. Calcd for $C_{20}H_{28}O_7$ ($M-C_6H_{10}O_5$): 380.1835.

Shinjuglycoside A Hexaacetate (7). Shinjuglycoside A (20 mg) was acetylated with pyridine (1 mL) and acetic anhydride (1 mL) for 50 h at room temperature. The usual work-up and silica-gel column chromatography afforded an amorphous solid (28 mg), mp 144—145 °C; IR (Nujol) 3550, 1750, 1240, and 1040 cm^{-1}; ^{1}H NMR (Table 3); MS (SIMS) *m/z* 795 (MH^+), 447, 405, 387, 345, 331, and 289; HRMS (EI) Found: *m/z* 674.2603. Calcd for $C_{34}H_{42}O_{14}$ ($M-C_4H_8O_4$): 674.2575.

Enzymatic Hydrolysis of 1. A mixture of **1** (64 mg) and β-glucosidase (20 mg) in 0.1 M acetate buffer (5 mL; pH 5.0) was allowed to stand for 2 weeks at 37 °C. The mixture was heated in boiling water for 10 min. After being cooled, the mixture was filtered and the filtlate was passed through a short column of Dowex 50 W (H^+). The effluent was evaporated to dryness *in vacuo*. The residue was purified by silica-gel column chromatography (C-200, 40 g, chloroform-methanol 7:3) to yield a crystalline chaparrin (18 mg).

Methanolysis of 1 and GLC Examination. A small amount of **1** in a tube was dried *in vacuo*, and 3% anhydrous HCl-MeOH (0.5 mL) was added. The tube was sealed and heated for 16 h at 80 °C. After being evaporated, the residue was trimethylsilylated by the usual method. Trimethylsilyl derivatives of methyl α-D-glucoside (t_R=6.2 min) and methyl β-D-glucoside (t_R=7.48 min) were deteacted by the GLC examination (GC-4BM, 1.5% OV-17, 1.0 m, 70 mL/min N_2, 156—245 °C, 4 °C/min).

Shinjuglycoside B (2). Amorphous solid, mp 194—196 °C; $[\alpha]_D^{20}$ +48.0° (*c* 2.77, MeOH); IR (KBr) 3400, 1720, and 1040 cm^{-1}; ^{1}H NMR (Table 1); ^{13}C NMR (Table 2); MS (SIMS) *m/z* 541 (MH^+) and 361; HRMS (EI) Found: *m/z* 378.1662. Calcd for $C_{20}H_{26}O_7$ ($M-C_6H_{10}O_5$): 378.1679.

Shinjuglycoside B Hexaacetate (8). Acetylation of **2** (35.3 mg) was carried out under the same conditions as described for **1** to give an amorphous solid (39.3 mg), mp 145—148 °C; IR (Nujol) 3550, 1740, 1220, and 1040 cm^{-1}; ^{1}H NMR (Table 3); MS (SIMS) *m/z* 793 (MH^+), 445, 403, 385, 343, 331, and 289; HRMS (EI) Found: *m/z* 672.2404. Calcd for $C_{34}H_{40}O_{14}$ ($M-C_4H_8O_4$): 672.2419.

Enzymatic Hydrolysis of 2. A mixture of shinjuglycoside B (126 mg) and β-glucosidase (50 mg) in 0.1 M acetate buffer (10 mL; pH 5.0) was treated by the same procedure as before. Shinjulactone A (**6**) was isolated and identified as the sole aglycone.

Methanolysis of **2** and GLC examination gave the same result as that obtained for **1**.

Shinjuglycoside C (3). Amorphous solid, mp 180—185 °C (decomp); $[\alpha]_D^{23}$ −37° (*c* 6.1, MeOH); IR (KBr) 3450, 1730, 1640, 1080, and 1040 cm^{-1}; ^{1}H NMR (Table 4); ^{13}C NMR (Table 5); MS (SIMS) *m/z* 569 (MH^+) and 407; HRMS (EI) Found: *m/z* 406.2005. Calcd for $C_{22}H_{30}O_7$ ($M-C_6H_{10}O_5$): 406.1992.

Acid Hydrolysis of 3. A solution of **3** (28 mg) in 1.5 M sulfuric acid-methanol (1:2, 10 mL) was refluxed for 7 h and then water (10 mL) was added. The mixture was concentrated *in vacuo* and extracted with dichloromethane three times. The combined dichloromethane layer was dried over anhydrous magnesium sulfate and evaporated to give a residue (7 mg), which was identified to be amarolide (**10**) by the comparison of IR, ^{1}H NMR and TLC with an authentic sample.

The aqueous layer obtained from the hydrolysis was passed through a short column of anion exchange resin (Amberlite IRA-400, OH^- form) and evaporated *in vacuo* to give a residue which was identified as D-glucose by GLC after trimethylsilylation.

Shinjuglycoside D (4). Colorless needles crystallized from methanol, mp 282—284 °C (decomp); $[\alpha]_D^{20}$ −42° (*c* 1.0, MeOH) IR (KBr) 3450, 1735, 1720, 1640, 1240, 1080, and 1040 cm^{-1}; ^{1}H NMR (Table 4); ^{13}C NMR (Table 5); MS (SIMS) *m/z* 549 ($[M+Na]^+$); HRMS (EI) Found: *m/z* 364.1908. Calcd for $C_{20}H_{28}O_6$ ($M-C_6H_{10}O_5$): 364.1886.

Acid Hydrolysis of 4. Hydrolysis of **4** with 1.5 M sulfuric acid-methanol (1:2) led to the isolation and identification of amarolide (**10**) and D-glucose.

11-O-Acetyl-2-O-(2′,3′,4′,6′-tetra-O-acetyl-β-D-glucopyranosyl)-amarolide (11) from 3 and 4. Shinjuglycoside C (17.8 mg) was acetylated with pyridine (1 mL) and acetic anhydride (1 mL) for 24 h at room temperature. The usual work-up and silica-gel column chromatography (C-200, 12g, ethyl acetate-dichloromethane 2:1) yielded, after crystallization from methanol-diethyl ether, a pentaacetate (**11**; 18 mg), as colorless needles, mp 238 °C; IR (Nujol) 1735, 1715, 1240, and 1040 cm^{-1}; ^{1}H NMR (Table 6); MS (EI) *m/z* (%) 676 (M^+−AcOH, 0.4), 616 (2), 556 (3), 543 (1), 514 (1), 501 (5), 483 (2), 454 (0.8), 441 (3), 390 (2), 375 (4), 348 (6), 331 (28), 271 (18), 169 (100), 109 (54), and 60 (64). HRMS (EI) Found: *m/z* 676.2741. Calcd for $C_{34}H_{44}O_{14}$ ($M-C_2H_4O_2$): 676.2732.

Under the same conditions, shinjuglycoside D was acetylated to give a crystalline residue. Recrystallization from

methanol–diethyl ether afforded **11** as colorless needles which was identified by mp, IR, ^{1}H NMR, MS, and TLC.

The authors wish to thank Dr. Teruhisa Noguchi of Suntory Biomedical Research for sample of *Ailanthus altissima*. The authors also thank Mr. Hideo Naoki of Suntory Bioorganic Research for the measurement of SIMS.

References

1) S. Bhatnagar, J. Polonsky, T. Prangé, and C. Pascard, *Tetrahedron Lett.*, **25**, 299 (1984); M. Okano, T. Fujita, N. Fukamiya, and T. Aratani, *Chem. Lett.*, **1984**, 221 and references cited therein.

2) I. H. Hall, Y. F. Liou, K. H. Lee, S. G. Chaney, and W. Willingham, Jr., *J. Pharm. Sci.*, **72**, 626 (1983); C. Moretti, J. Polonsky, M. Vuilhorgne, and T. Prangé, *Tetrahedron Lett.*, **23**, 647 (1982) and references cited therein.

3) H. Naora, M. Ishibashi, T. Furuno, T. Tsuyuki, T. Murae, H. Hirota, T. Takahashi, A. Itai, and Y. Iitaka, *Bull. Chem. Soc. Jpn.*, **56**, 3694 (1983).

4) M. Ishibashi, T. Tsuyuki, T. Murae, H. Hirota, T. Takahashi, A. Itai, and Y. Iitaka, *Bull. Chem. Soc. Jpn.*, **56**, 3683 (1983); T. Furuno, M. Ishibashi, H. Naora, T. Murae, H. Hirota, T. Tsuyuki, T. Takahashi, A. Itai, and Y. Iitaka, *Bull. Chem. Soc. Jpn.*, **57**, 2484 (1984).

5) T. A. Davidson, T. R. Hollands, P. De Mayo, and M. Nisbet, *Can. J. Chem.*, **43**, 2996 (1965).

6) J. J. M. Rowe, J. Hilton, and K. L. Rowe, *Chem. Rev.*, **70**, 1 (1970).

7) C. G. Casinovi, V. Bellavita, G. Grandolini, and P. Ceccherelli, *Tetrahedron Lett.*, **1965**, 2273; W. Stöcklin, M. Stefanović, T. A. Geissman, and C. G. Casinovi, *ibid.*, **1970**, 2399.

8) J. Polonsky and N. Bouguignon-Zylber, *Bull. Soc. Chim. Fr.*, **1965**, 2793; J. Polonsky, Z. Baskevitchi, H. E. Gottlieb, E. W. Hagaman, and E. Wenkert, *J. Org. Chem.*, **40**, 2499 (1975).

Hydrolysis of *N*-Salicylidene-2-methoxyethylamine. Intramolecular General Base Catalysis and Specific Effects of Boric Acid

Hiroaki NAGAMATSU, Tadashi OKUYAMA,* and Takayuki FUENO
Faculty of Engineering Science, Osaka University, Toyonaka, Osaka 560
(Received March 8, 1984)

Hydrolysis of *N*-salicylidene-2-methoxyethylamine is kinetically investigated at 30 °C. Intramolecular general base catalysis by the *o*-O^- substituent takes place in the neutral pH region. Nucleophilic catalysis by morpholine was also found to be operative. Added boric acid accelerates the hydrolysis above pH 5.5 while it decelerates the hydrolysis below pH 5.5. The hydrolysis rate as the function of the boric acid concentration follows a saturation curve in harmony with a reaction sequence involving a rapid equilibrium formation of a borate-substrate complex followed by its breakdown. The morpholine catalysis is inhibited by boric acid in accord with the slow reaction of morpholine with the complex. The water reaction of the complex is considered to involve a rearrangement of the complex and an intramolecular transfer of the boron-coordinated hydroxide ion to the iminium carbon.

Boric acid greatly accelerates the hydrolysis of *N*-salicylideneaniline.[1] We have found, however, that hydrolysis of a Schiff base derived from α-hydroxyisobutyrophenone is decelerated by boric acid in acidic solution although it is accelerated in alkaline solution.[2] These effects of boric acid on the hydrolysis of hydroxy Schiff base occur through a borate-substrate complex involving a boron–hydroxyl coordination. Possible mechanisms for this reaction were presented.[1,2]

Similar accelerative effects of boric acid were also found during hydrolyses of phenyl salicylate[3] and hydroxy thiocarboxylic *S*-esters.[4] It was concluded in the latter case that the catalysis takes place through a mechanism involving an intramolecular transfer of a boron-coordinated hydroxide ion within a borate-substrate complex.[4]

In the present investigation, hydrolysis of *N*-salicylidene-2-methoxyethylamine **1** is examined in the presence of boric acid as well as morpholine. Boric acid accelerates the hydrolysis above pH 5.5 while it decelerates the hydrolysis at lower pH. Nucleophilic catalysis of the hydrolysis by morpholine is retarded by added boric acid. A detailed mechanism of the borate action is presented.

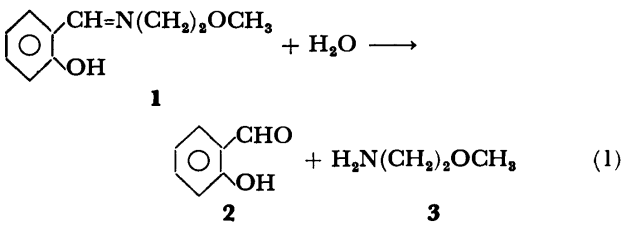

(1)

Results

Hydrolysis in the Absence of Boric Acid. Hydrolysis of Schiff base **1** was carried out at 30 °C in aqueous solution of the constant ionic strength of 0.10 maintained with KCl. The reaction was monitored by the decrease in the absorption of **1** at 275 nm. An isosbestic point was always observed at about 262 nm. The final spectra of the reaction mixtures agreed with the spectrum of salicylaldehyde **2** (λ_{max} 255 nm). The time-dependent absorbance changes obeyed the pseudo-first-order kinetics.

The hydrolysis rates were first measured without any added boric acid in usual buffer solutions of formate, acetate, and tertiary amines as well as HCl solutions in the pH range 2—12. Buffer effects were observed only below pH 6. Logarithms of the rate constants k_0 extrapolated to zero buffer concentration are plotted against pH in Fig. 1.

The pH-rate profile is quite similar to those observed for the hydrolysis of *N*-salicylideneisopropylamine[5,6] and *N*-salicylideneaniline[7] and may be interpreted in the same way (Scheme 1). The rate-determining step changes with pH from formation (pH>3) to decay (pH<3) of an α-amino alcohol intermediate. A rate increase above pH 8 must be due to the contribution from a zwitterionic from (**1**±) of **1**. The profile can be described by Eq. 2 according to Scheme 1: Equation 2 may be derived by applying the steady-state approximation to the α-amino alcohol intermediate **I**

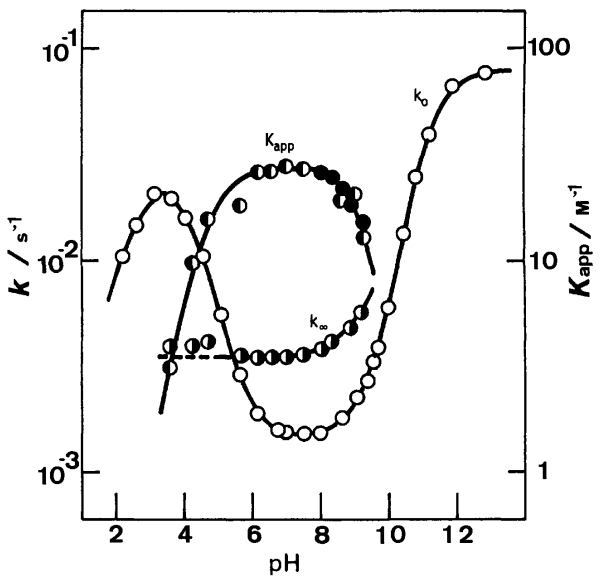

Fig. 1. pH dependences of hydrolysis rates and the equilibrium constant K_{app}. ○, k_0; ◑, k_∞; ◐, K_{app} obtained from the hydrolysis; ●, K_{app} obtained from the morpholine reaction. K_{app} refers to the right ordinate. For theoretical curves, see text.

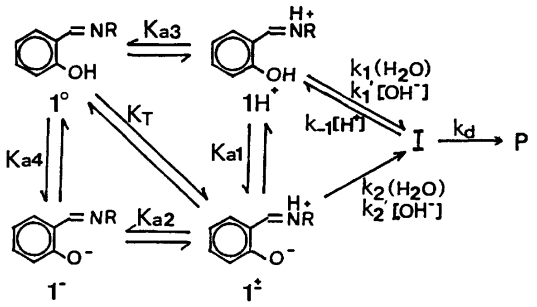

Scheme 1.

Table 1. Kinetic parameters for the hydrolysis of Schiff base **1** at 30 °C

k_1/s^{-1}	2.4×10^{-2}
k_2/s^{-1}	1.5×10^{-3}
$k_2'/M^{-1}\,s^{-1}$	3.7×10
$k_3/M^{-1}\,s^{-1}$	1.0×10^{3}
$k_4/M^{-1}\,s^{-1}$	1.6×10^{-1}
$k_M/M^{-1}\,s^{-1}$	2.7×10^{-2}
$(k_d/k_{-1})/M$	4.4×10^{-3}
K_{a1}/M (pK_{a1})	3.9×10^{-5} (4.4)
K_{a2}/M (pK_{a2})	7.0×10^{-12} (11.2)

in a usual way[5,6] with the correction for the additional equilibrium (K_T). Kinetic parameters (defined in Scheme 1) are summarized in Table 1.

$$k_0 = \frac{k_1[H^+]^2+(k_1'K_w+k_2K_{a1})[H^+]+k_2'K_{a1}K_w}{[H^+]^2+K_{a1}(1+1/K_T)[H^+]+K_{a1}K_{a2}}\cdot\frac{k_d/k_{-1}}{(k_d/k_{-1}+[H^+])} \quad (2)$$

The equilibrium constant K_T for the tautomerization $\mathbf{1}^{\circ}\rightleftharpoons\mathbf{1}^{\pm}$ is hard to determine, but it must be much greater than unity[9] in favor of zwitterion $\mathbf{1}^{\pm}$. The spectrum of **1** in aqueous solution at pH 4—11 has absorption maxima at 275 and 393 nm, which are characterstic of the iminium and phenolate functions, respectively.[8] The zwitterion $\mathbf{1}^{\pm}$ is stable owing to the contribution from the quinonoid resonance form.[9]

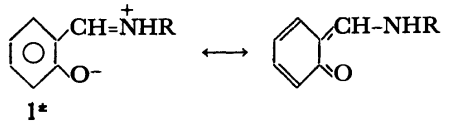

$\mathbf{1}^{\pm}$

Uncatalyzed (water-catalyzed) reactions observed in the neutral pH region (6.5<pH<8) can be attributed to the two kinetically indistinguishable reactions: The hydroxide reaction on the protonated substrate $\mathbf{1H}^+$ ($k_1'K_W/K_{a1}$) and the water reaction of $\mathbf{1}^{\pm}$ (k_2). If the former reaction were the main contributor to k_0, k_1' should have been $4\times10^6\ M^{-1}\,s^{-1}$,[10] which is too large (17-fold) as compared with a similar value for the hydrolysis of *N*-(*o*-methoxybenzylidene)-2-methoxyethylamine **4**.[11] The latter reaction must be the predominant reaction here and $k_2=1.5\times10^{-3}\ s^{-1}$, which is about 1/10 of k_1 and is not unreasonable in magnitude. Similar conclusions were reached before for other *N*-salicylidene amines.[6,7]

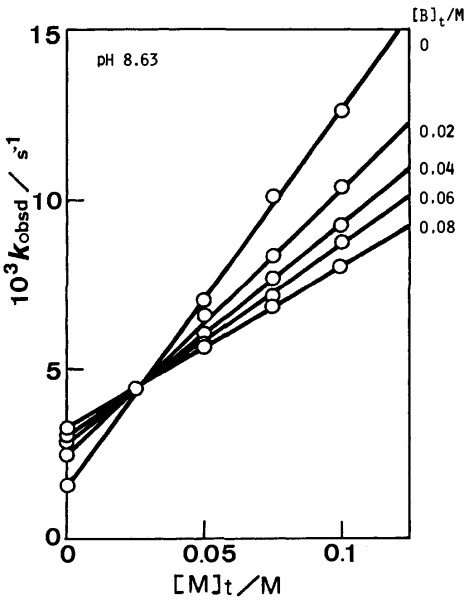

Fig. 2. Dependences of k_{obsd} on the concentration of morpholine $[M]_t$ at the concentrations of boric acid indicated.

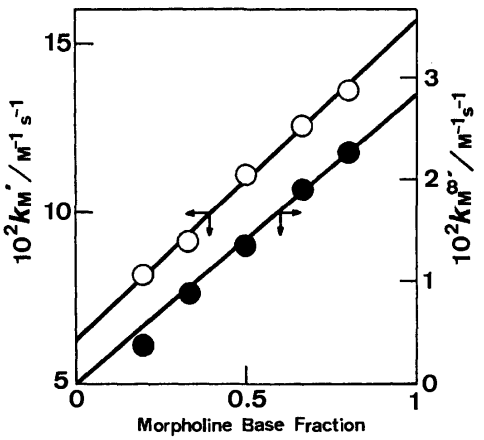

Fig. 3. Plots of k_M' (○) and $k_M^{\infty\prime}$ (●) against the base fraction of morpholine buffers.

The hydrolysis of **1** was remarkably accelerated by morpholine buffer at pH 8—9.3, although tertiary amines like 1,4-diazabicyclo[2.2.2]octane and *N*,*N*-dimethyl-2-hydroxyethylamine had no effects in this pH region. Furthermore, both UV spectra of the initial and final reaction solutions were respectively the same as those observed in other normal buffer solutions. Observed rate constants k_{obsd} increased linearly with total morpholine concentration $[M]_t$ (Eq. 3) as shown in Fig. 2.

$$k_{obsd} = k_0 + k_M'[M]_t \quad (3)$$

The observed catalytic constants k_M' are plotted against the base fraction of morpholine buffer in Fig. 3. The linear correlation gives the rate constants for base and conjugate acid dependences $k_M=0.16\ M^{-1}\,s^{-1}$ and $k_{MH}=0.063\ M^{-1}\,s^{-1}$.

$$k_M' = (k_{MH}[MH^+] + k_M[M])/[M]_t \quad (4)$$

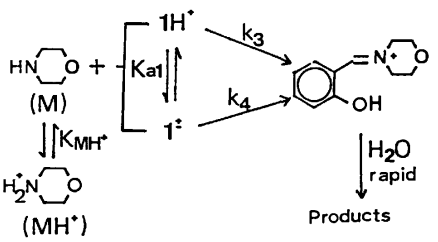

Scheme 2.

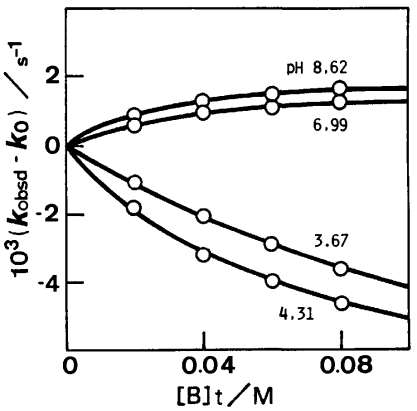

Fig. 4. Dependence of the hydrolysis rate of **1** on the boric acid concentration at pH indicated.

These accelerations must be due to the nucleophilic catalysis by morpholine. The reactive species of **1** in this nucleophilic reaction should be $\mathbf{1H^+}$ and $\mathbf{1^\pm}$, and the rate constants k_{MH} and k_M correspond to $k_3K_{MH^+}/K_{a1}$ and k_4 according to Scheme 2, respectively. Calculated values of k_3 and k_4 are given in Table 1.

Hydrolysis in the Presence of Boric Acid. When a small amount of boric acid was added to the reaction mixture, the hydrolysis was accelerated at high pH while it was decelerated at low pH. Although the spectrum of the initial solution of the substrate showed a new absorption band at 350 nm, that of the product solution was the same as that observed in the absence of boric acid. Induction periods were not observed in any kinetic runs.

Hydrolysis rates were measured with varying concentrations of boric acid at constant pH maintained with a second buffer (when necessary). The rate increased at pH>5.5 but decreased at pH<5.5 with total borate concentration $[B]_t$ as shown in Fig. 4. These changes follow a saturation curve described by Eq. 5, as observed for the hydrolysis of an α-hydroxy Schiff base.[2]

$$k_{obsd} = (k_0' + k_\infty K_{app}[B]_t)/(1 + K_{app}[B]_t) \quad (5)$$

Here, k_0' is the rate constant in the absence of boric acid and is usually equal to k_0 (negligible effects of the second buffer). The magnitude of k_∞ is greater at pH>5.5 but smaller at pH<5.5 than k_0. The curved rate dependence of Eq. 5 is consistent with a reaction sequence involving a rapid equilibrium formation of a borate-substrate complex followed by a slow breakdown of the complex to lead to the hydrolysis products.[2,12] K_{app} and k_∞ stand for the equilibrium constant for the complexation and the rate constant for the breakdown of the complex, respectively. They were evaluated from a least-squares treatment of the linear relation between k_{obsd} and $(k_{obsd}-k_0')/[B]_t$ in the same way as before.[2] The results are given in Table 2. In the pH range 4—6, where the hydrolysis is buffer-dependent, the "normal" buffer effects by boric acid must be taken into consideration. However, the general-base-catalytic acceleration by borate should be small enough to be neglected.[13] The second buffer used to maintain pH constant affects only the k_0' term but not the borate term.

Table 2. Kinetic parameters for the hydrolysis of **1** in the presence of boric acid at 30 °C

pH[a]	$10^3 k_\infty/s^{-1}$	K_{app}/M^{-1}
3.67[b]	4.0±1.5	3.4±1.0
4.31[c]	4.0±0.7	10.3±0.5
4.69[c]	4.2±1.0	15.4±0.8
5.66[d]	3.6±0.2	17.6±1.5
6.18[d]	3.5±0.1	25.8±0.6
6.52[d]	3.5±0.1	25.8±0.4
6.99[e]	3.5±0.2	28.1±0.8
7.50[e]	3.6±0.2	26.3±0.7
8.01[e]	3.8±0.2	23.9±1.0
8.33[f]	4.2±0.2	25.1±1.2
8.62[f]	4.5±0.1	18.4±1.0
8.94[f]	4.8±0.3	18.3±1.5
9.00[f]	5.6±0.2	20.2±2.0
9.19[f]	5.7±0.3	13.4±2.3
9.26[f]	4.9±0.2	12.9±1.3

a) pH (±0.03) were maintained with a buffer of 0.05 M. b) Formate. c) Acetate. d) 2-(*N*-Morpholino)-ethanesulfonate. e) *N*-Methylmorpholine. f) 1,4-Diazabicyclo[2.2.2]octane.

The effects of added boric acid were found also in the morpholine-catalyzed hydrolysis. When the pH and the morpholine concentration $[M]_t$ were kept constant, the rates increased at low $[M]_t$ and, in contrast, decreased at high $[M]_t$ with increasing $[B]_t$ (Fig. 5). At pH 8.6 and $[M]_t$=0.025 M, the observed rate was almost constant with varying $[B]_t$. In an opposite sense, at constant pH and $[B]_t$, the rates increased linearly with $[M]_t$ and lines (for various $[B]_t$) cross at a certain $[M]_t$ (*e.g.*, $[M]_t$=0.025 M at pH 8.6) as shown in Fig. 2. That is, in the presence of both boric acid ($[B]_t$=constant) and morpholine, k_{obsd} is described by Eq. 6.

$$k_{obsd} = k_0^B + k_M^B[M]_t \quad (6)$$

The slopes of the plots of Fig. 2, k_M^B, decreased with increasing $[B]_t$ as shown in Fig. 6. The curved dependences of $k_M^B[B]_t$ are described by Eq. 7 in the same way as Eq. 5.

$$k_M^B = (k_M + k_M^{\infty\prime}K_{app}[B]_t)/(1 + K_{app}[B]_t) \quad (7)$$

Kinetic parameters, $k_M^{\infty\prime}$ and K_{app}, obtained similarly are given in Table 3. Values of K_{app} obtained here agree well with those obtained in the absence of morpholine as shown with closed circles in Fig. 1.

The limiting rate constant $k_M^{\infty\prime}$ corresponds to that for the nucleophilic reaction of morpholine with the

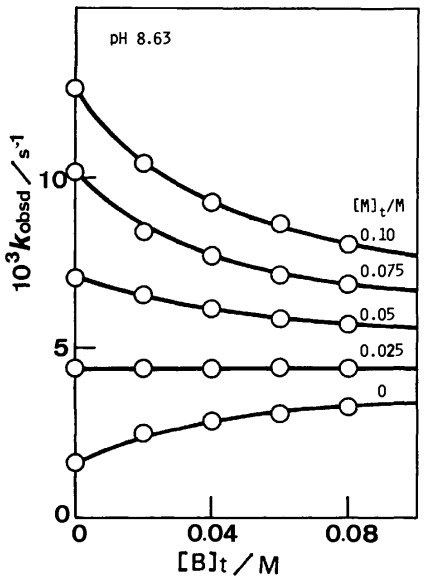

Fig. 5. Dependences of k_{obsd} on the concentration of boric acid at the concentrations of morpholine indicated.

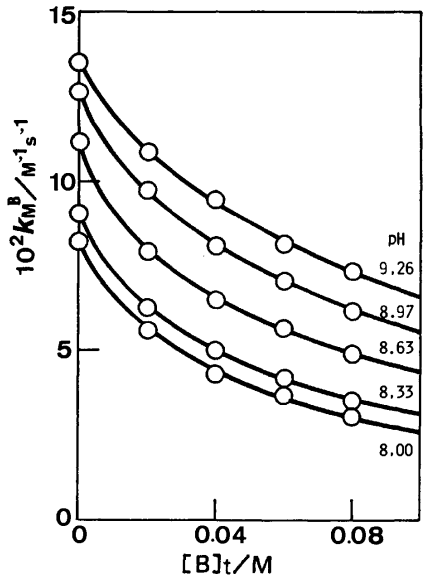

Fig. 6. Dependence of k_M^B on the boric acid concentration at pH indicated.

borate-substrate complex. The values of $k_M^{\infty\prime}$ are proportional to the base fraction of morpholine buffer as seen in Fig. 3, the slope being $k_M^{\infty}=2.7\times10^{-2}$ M^{-1} s^{-1}.

Discussion

Catalysis of Hydrolysis. Hydrolysis of Schiff base **1** derived from salicylaldehyde **2** is somewhat complicated because of tautomerization of the neutral substrate $\mathbf{1}^0 \rightleftharpoons \mathbf{1}^{\pm}$. This occurs because the zwitterion $\mathbf{1}^{\pm}$ is stabilized by resonance with the quinonoid form. The increase in hydrolysis rate at alkaline pH is ascribed to the reaction of $\mathbf{1}^{\pm}$ with hydroxide ion.

The predominant reaction in the neutral pH region is the water reaction of $\mathbf{1}^{\pm}$ but not the hydroxide reaction of $\mathbf{1H}^+$ as described above. The same conclusion was reached from the lack of salt effects[7] and the substituent effect[6] observed in the hydrolysis of *N*-salicylidene amines. Failure in the observation of buffer effects in this pH region seems to be incompatible with the water reaction, which should be catalyzed by general bases, but to conform with the hydroxide reaction. However, an intramolecular general base catalysis by the *o*-O^- group may make the external catalysis unnecessary.[14]

Table 3. Kinetic parameters obtained in the presence of both morpholine and boric acid

pH[a]	$10^2 k_M^{\infty\prime}$/M^{-1} s^{-1}	K_{app}/M^{-1}
8.00	0.33±0.15	25.0±1.9
8.33	0.82±0.08	24.7±3.1
8.63	1.3±0.3	22.7±3.1
8.97	1.9±0.2	18.9±2.8
9.26	2.2±0.2	14.8±2.2

a) ±0.03.

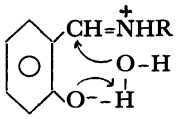

Such an intramolecular catalysis was once considered to occur during the hydrolysis of Schiff bases derived from salicylaldehyde[15] and 3-hydroxy-4-pyridinecarbaldehyde,[16] but it was later disregarded by comparisons of the reactivities of *o*- and *p*-hydroxy as well as methoxy derivatives of *N*-benzylideneisopropylamine.[5] However, the comparisons made by the latter authors do not seem to be adequate. First of all, they attributed the predominant reaction in the neutral pH region to the hydroxide reaction of the protonated substrate and the rate constants for the hydroxide reactions of hydroxy and methoxy substrates were compared. As mentioned above, the main reaction is the water reaction of the zwitterion in the case of salicylidene derivatives.

Comparisons of rate constants for various nucleophilic reactions at iminium functions are given in Table 4. Nucleophilic reactions of *o*-methoxybenzylidene derivative $\mathbf{4}^{11}$ are involved for the reference of the comparison. The rate constants are logarithmically plotted against pK_a of the conjugate acid of the nucleophiles in Fig. 7. Three points for $\mathbf{4H}^+$ fall on a straight line of slope (β) of 0.5. Two points (H_2O and morpholine) for $\mathbf{1H}^+$ fall also in the vicinity of the same line. Three points for zwitterion $\mathbf{1}^{\pm}$ can form a line of slope of about 0.35. However, the low sensitivity in relative nucleophilicity of less reactive substrate $\mathbf{1}^{\pm}$ (compared with $\mathbf{1H}^+$ or $\mathbf{4H}^+$) is not reasonable. These points may be rationalized as follows: Hypothetical nucleophilic reactivities of $\mathbf{1}^{\pm}$ would have formed a line of β=0.5 through a point for hydroxide ion but an intramolecular base-catalyzed acceleration of morpholine and water reactions by the *o*-O^- group resulted in the positive deviations of these points (10- and 300-fold for morpholine and water) from the hypothetical line. Such deviations

TABLE 4. RATE CONSTANTS FOR NUCLEOPHILIC REACTIONS OF VARIOUS IMINIUM SPECIES ($k_{Nuc}/M^{-1}s^{-1}$) AT 30 °C

Nucleophile (pK_a)	$1H^+$	$4H^+$ [a]	1	1B
H_2O (−1.7)	4.3×10^{-4}	8.8×10^{-4}	2.7×10^{-5}	6.3×10^{-5}
Morpholine (8.6)	1.0×10^{3}	3.2×10^{2}	1.6×10^{-1}	2.7×10^{-2}
OH^- (15.7)		2.3×10^{5}	3.7×10	1.1×10^{2}

a) Ref. 11.

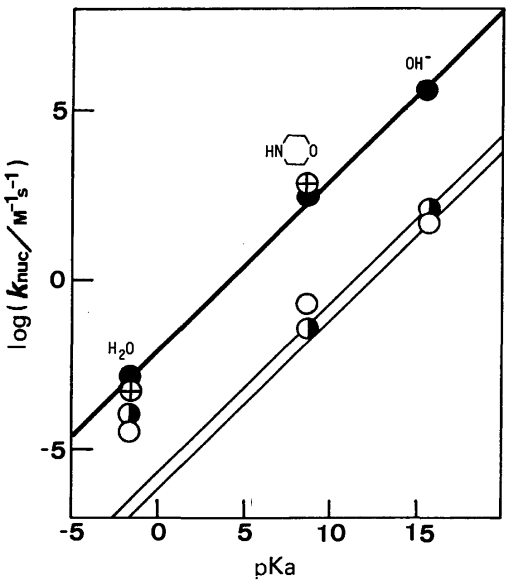

Fig. 7. Plot of $\log(k_{Nuc})$ against pK_a for various iminium species.
●, $4H^+$; ⊕, $1H^+$; ○, $1^\pm$; ◑, 1B.

of water reactions of the zwitterion of other *N*-salicylidene amines seemed to be observed as compared with benzylidene analogues.[5,7]

Nucleophilic catalysis of the Schiff base hydrolysis by morpholine is not unexpected since such catalysis of Schiff base formation is well known.[17] This catalysis must take place through transimination to form *N*-salicylidenemorpholinium ion, which is hydrolyzed rapidly (Eq. 8):

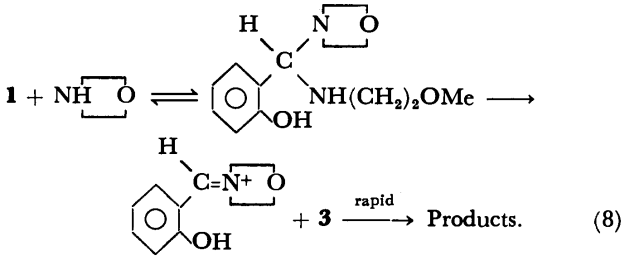

(8)

The rate-determining step of this reaction must be the initial nucleophilic reaction of morpholine with **1**. This is consistent with the observation that morpholine shows a nucleophilicity expected from the water and hydroxide reactions of $1H^+$ and $4H^+$ (Fig. 7), and is reasonable since a more basic amine is in general more readily released from a *gem*-diamine intermediate as observed during transiminations.[18] Transimination reactions are subject to buffer catalysis[18–20] and the morpholine reaction with $1^\pm$ may be facilitated by an internal catalysis by the salicylidene O^- group.

Effects of Boric Acid. The apparent equilibrium constants K_{app} for the complexation between **1** and boric acid show a bell-shaped change with pH as seen in Fig. 1. This change is described by Eq. 9, which is based on the assumption that the complex **1B** is formed from the neutral substrate 1^0 (the fraction is $(K_{a1}/K_T)[H^+]/\{[H^+]^2+K_{a1}(1+1/K_T)[H^+]+K_{a1}K_{a2}\}$) and boric acid (the fraction of acid form is $[H^+]/(K_{BH}+[H^+])$) with the equilibrium constant K_C (Eq. 10).

$$K_{app}=\frac{(K_CK_{a1}/K_T)[H^+]^2}{\{[H^+]^2+K_{a1}(1+1/K_T)[H^+]+K_{a1}K_{a2}\}(K_{BH}+[H^+])} \quad (9)$$

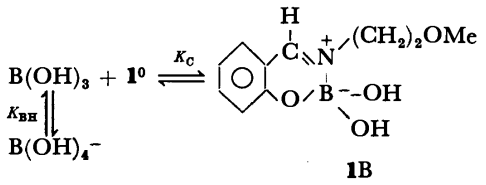

(10)

1B

A probable structure of **1B** must involve a tetra-coordinated boron. Chelate complexes formed from polyols and boric acid involve a tetra-coordinated boron center.[21,22] Complexes of a structure similar to **1B** were isolated as diacetates from the reaction of *N*-salicylidene amines with boric acid in acetic anhydride.[23]

A theoretical curve for the bell-shaped plot of Fig. 1 is calculated with parameters given in Table 1 and $K_C/K_T=27\ M^{-1}$ according to Eq. 9, where K_T is assumed to be much geater than unity ($1+1/K_T\simeq1$). If the K_T value is in the range of 10—60,[24] $K_C=300$—$1600\ M^{-1}$. The formation constant K_C is much greater than those observed for the complexation of 1,2-diols and boric acid,[21,25] but a similar value ($K_C=435\ M^{-1}$) was obtained for complexation between an α-hydroxy Schiff base and boric acid.[2]

The limiting rate constant k_∞ refers to the breakdown of complex **1B** to give hydrolysis products. The values of k_∞ are essentially constant below pH 7.5, but increase at higher pH (Fig. 1). This pH dependence of k_∞ is accommodated by the reactions of **1B** with water and hydroxide ion (Eq. 11): $k_5=3.5\times10^{-3}\ s^{-1}$ and $k_5'=1.1\times10^2\ M^{-1}s^{-1}$.

$$k_\infty=k_5+k_5'[OH^-] \quad (11)$$

A possible contribution from a cationic complex like $1B^+$ is unlikely,[26] since such a reaction was not found in the morpholine reaction. The rate constant k_M^∞ must be that for the nucleophilic reaction of morpholine with complex **1B**.

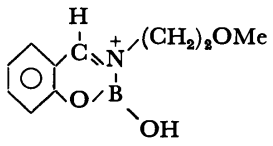

1B$^+$

Logarithms of the rate constants for the nucleophilic reactions on **1B** are plotted against pK_a for the corresponding nucleophiles with half-filled circles in Fig. 7. Points for hydroxide ion (k_5') and morpholine (k_M^∞) form a straight line of slope of 0.5, as found for the reaction with **4H**$^+$ and **1H**$^+$. However, the point for water (k_5) deviates upward by 2.5 log unit from the line. This 300-fold deviation of the k_5 point suggests that this reaction is not a simple water attack on the iminium carbon of **1B**. This water reaction is not catalyzed by a general base. Furthermore, the anomaly occurs only with water but not with morpholine. Boronic group of **1B** must participate in the reaction. A possible mechanism is presented in Scheme 3. This mechanism involves a rapid (but unfavorable) rearrangement of **1B** to an open zwitterionic complex, within which a rate-determining, intramolecular transfer of the hydroxide ion occurs from the boron to the iminium carbon. Similar reaction mechanisms have been presented for the boric acid-dependent hydrolyses of an α-hydroxy Schiff base[2] and hydroxy thiocarboxylic *S*-ester.[4]

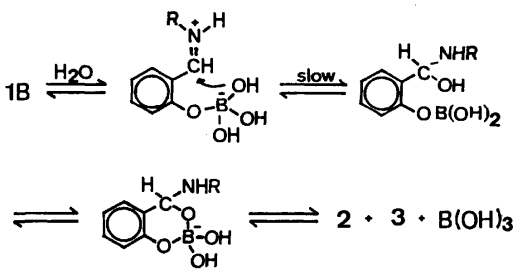

Scheme 3.

In conclusion, boric acid decelerates the hydrolysis of **1** in the low pH region where the reaction of **1H**$^+$ predominates, while it accelerates the hydrolysis at higher pH where **1**$^\pm$ is the reactive species. The reactivities of the iminium species are in the order: **1H**$^+$> **1B**>**1**$^\pm$. The water reaction of **1**$^\pm$ is catalyzed by the internal O$^-$ group in the *ortho* position.

Experimental

Materials. Salicylaldehyde (**2**) and 2-methoxyethylamine (**3**) were commercially obtained and distilled under nitrogen. Salicylidene-2-methoxyethylamine (**1**) was prepared from **2** and **3** by the reaction of the two components at 0 °C for 1 h. After taken up with ether and dried over $MgSO_4$, the products were distilled: bp 142 °C (7 mmHg (1 mmHg≈133.322 Pa)). Other chemicals were obtained as before.[2] Glass-distilled water was used throughout.

Kinetic Measuremens. All the aqueous solutions containing appropriate amounts of boric acid and other buffers were prepared at room temperature and adjusted to an ionic strength of 0.1 with KCl. A stock solution of the substrate **1** was obtained as an acetonitrile solution of about 10^{-3} M. Reactions were started by adding 30 μl of the substrate stock solution from a microsyringe into a 3-ml buffer solution equilibrated at 30±0.1 °C in a stoppered quartz cuvette inserted in a water-jacketed cell holder. The reaction was followed by the decrease in the absorption at 275 nm on a Shimadzu UV 200 or 140 spectrophotometer. Pseudo-first-order rate constants were calculated by a modified Guggenheim method.[27] Values of the pH of buffer and reaction solutions were determined by a Hitachi-Horiba F7 pH meter.

References

1) J. Hoffmann and V. Štěrba, *Collect. Czech. Chem. Commun.*, **37**, 2043 (1972).

2) H. Matsuda, H. Nagamatsu, T. Okuyama, and T. Fueno, *Bull. Chem. Soc. Jpn*, **57**, 500 (1984).

3) B. Capon and B. Ch. Ghosh, *J. Chem. Soc., B*, 472 (1966).

4) T. Okuyama, H. Nagamatsu, and T. Fueno, *J. Org. Chem.*, **46**, 1336 (1981).

5) W. Bruyneel, J. J. Charette, and E. de Hoffmann, *J. Am. Chem. Soc.*, **88**, 3808 (1966).

6) R. Herscovitch, J. J. Charette, and E. de Hoffmann, *J. Am. Chem. Soc.*, **96**, 4954 (1974).

7) J. J. Charette and E. de Hoffmann, *J. Org. Chem.*, **44**, 2256 (1979).

8) The protonated and neutral forms of *N*-(*o*-methoxybenzylidene)-2-methoxyethylamine (**4**) have λ_{max} at 276 and 249 nm, respectively. The anionic form of **2** has λ_{max} at 377 nm while the neutral **2** has λ_{max} at 324 nm.

9) R. Herscovitoh, J. J. Charette, and E. de Hoffmann, *J. Am. Chem. Soc.*, **95**, 5135 (1973).

10) 1 M=1 mol dm^{-3}.

11) H. Nagamatsu, M. Kitano, T. Okuyama, and T. Fueno, unpublished results.

12) a) Borate associates by itself at higher concentrations[12b] and this association could be responsible for the diminishing activity of boric acid. To avoid this effect [B]$_t$ was kept low enough. b) N. Ingri, G. Lagerstrom, M. Frydman, and L. G. Sillen, *Acta Chem. Scand.*, **11**, 1034 (1957); N. Ingri, *ibid.*, **16**, 439 (1962); **17**, 573, 581 (1963).

13) Rate constant for general base catalysis by acetate (pK_a=4.6) is 1.6×10^{-1} M^{-1} s^{-1}. If the Brønsted β is assumed to be 0.3, the catalytic constant for borate (pK_a=9.2) is calculated to be 3 M^{-1} s^{-1} and the contribution from borate ([B]$_t\leq$0.08 M) is estimated to be smaller than 10^{-4} s^{-1} at pH 6.

14) T. Okuyama, H. Shibuya, and T. Fueno, *J. Am. Chem. Soc.*, **104**, 730 (1982).

15) R. L. Reeves, *J. Org. Chem.*, **30**, 3129 (1965).

16) T. C. French, D. S. Auld, and T. C. Bruice, *Biochemistry*, **4**, 77 (1965).

17) E. H. Cordes and W. P. Jencks, *J. Am. Chem. Soc.*, **84**, 826 (1962).

18) K. Koehler, W. Sandstrom, and E. H. Cordes, *J. Am. Chem. Soc.*, **86**, 2413 (1964).

19) J. L. Hogg, D. A. Jencks, and W. P. Jencks, *J. Am. Chem. Soc.*, **99**, 4772 (1977).

20) H. Fischer, F. X. DeCandis, S. D. Ogden, and W. P. Jencks, *J. Am. Chem. Soc.*, **102**, 1340 (1980).

21) J. Böeseken, *Adv. Carbohyd. Chem.*, **4**, 189 (1949).

22) R. P. Oertel, *Inorg. Chem.*, **11**, 544 (1972).

23) S. M. Tripathi and J. P. Tandon, *J. Inorg. Nucl. Chem.*, **40**, 983 (1978).

24) H. Nagamatsu, T. Okuyama, and T. Fueno, *Bull. Chem. Soc. Jpn.*, **57**, 2508 (1984).

25) G. L. Roy, A. L. Laferriere, and J. O. Edwards, *J. Inorg. Nucl. Chem.*, **4**, 106 (1957).

26) An increasing tendency of k_∞ at low pH (<5) might be ascribed to the contribution from **1B**$^+$.

27) E. S. Swinbourne, *J. Chem. Soc.*, **1960**, 2371.

Effects of Boric Acid on the Rate and Equilibrium of Schiff Base Formation from Salicylaldehyde

Hiroaki NAGAMATSU, Tadashi OKUYAMA,* and Takayuki FUENO
Faculty of Engineering Science, Osaka University, Toyonaka, Osaka 560
(Received April 25, 1984)

Effects of boric acid on the formation of the Schiff base from salicylaldehyde and 2-methoxyethylamine (or glycinate) were examined in aqueous solution. From the formation constants in the absence and presence of boric acid, the equilibrium constants for the borate-Schiff base complexation were determined. The structure of the complex was deduced from the UV spectral analysis. Formation of the Schiff base was found to be accelerated by boric acid (pH 7—10). A mechanism for the reaction involving the complex is presented.

Hydrolysis of Schiff bases derived from an α-hydroxy ketone[1] and salicylaldehyde[2,3] is greatly influenced by added boric acid. Intermediacy of a borate-Schiff base complex was substantiated from kinetic investigations of the hydrolysis.[1,3] Since the Schiff base formation is reversible in aqueous solution and Schiff bases are stable in the presence of an excess amount of amine, the complexation could be examined in more detail under equilibrium conditions.

In the present investigation, the formation of the Schiff base (**1**) from salicylaldehyde (**2**) has been examined under such conditions both in the absence and presence of boric acid (Scheme 1). The Schiff base formation was accelerated by added boric acid. Complexation between boric acid and **1** was analyzed and the structure of the complex was deduced on the basis of the UV spectra. A mechanism for the reaction involving the borate-Schiff base complex is presented.

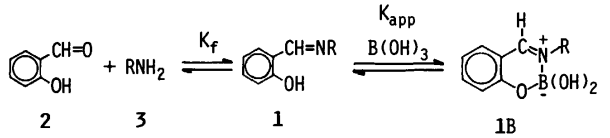

2 3 1 1B

a, R = $(CH_2)_2OCH_3$
b, R = $CH_2CO_2^-$

Scheme 1.

Results

Schiff Base Formation in the Absence of Boric Acid. All the reactions and UV-measurements were carried out at 30 °C in aqueous solution of an ionic strength of 0.10 maintained with KCl. UV spectral data of salicylaldehyde (**2**) and its derivatives are summarized in Table 1. Spectra of Schiff bases (**1**) at higher pH were recorded under equilibrium conditions in the presence of **2** and an excess amount of amines (**3**). Appropriate corrections were made for concomitant **2** by using the formation constant K_f obtained below. The spectra in HCl solutions were obtained as an initial spectrum immediately after mixing.

When a small amount of **2** is added into an aqueous solution containing a primary amine **3**, the absortion of Schiff base **1** develops at the expense of the absorption of **2**. On the contrary, addition of **1** into the amine solution causes the Schiff base bands to diminish with simultaneous appearance of the aldehyde bands. Both changes accompany two isosbestic points at about 260 and 345 nm at lower pH(<8) and at 260 and 375 nm at higher pH(>8.5). These spectral changes are no doubt results of the equilibrium between Schiff base **1** and aldehyde **2**. *o*-Methoxybenzaldehyde (**5**) and its Schiff bases (**4**) showed similar spectral changes. The UV measurements were made in the same way.

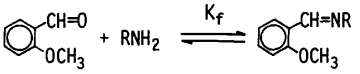

(1)

5 3 4

a, R = $(CH_2)_2OCH_3$
b, R = $CH_2CO_2^-$

The equilibrium constant K_f can be determined from these spectral changes as described in Experimental

Table 1. Maximum wavelengths of UV absorption of salicylidene derivatives[a]

No.[b]	X	Y	Condition	λ_{max}/nm ($10^4\,\varepsilon$)	
1a (**1aH**$^+$)	$N^+H(CH_2)_2OMe$	OH	1 M-HCl	275 (2.1)	348 (0.53)
1a (**1a**$^\pm$)	$N^+H(CH_2)_2OMe$	O^-	pH 8.9	275 (1.3)	393 (0.63)
1b (**1b**$^\pm$)	$N^+HCH_2CO_2^-$	O^-	pH 8.9	277 (1.4)	395 (0.67)
2 (**2**^{0})	O	OH	1 M-HCl	255 (1.2)	324 (0.34)
2 (**2**$^-$)	O	O^-	1 M-NaOH	264 (0.74)	377 (0.67)
4a (**4aH**$^+$)	$N^+H(CH_2)_2OMe$	OMe	1 M-HCl	276 (2.7)	347 (0.80)
4a (**4a**^{0})	$N(CH_2)_2OMe$	OMe	pH 8.9	249 (1.8)	305 (0.70)
4b (**4b**^{0})	$NCH_2CO_2^-$	OMe	pH 9.8	252 (1.8)	307 (0.74)
5	O	OMe	pH 8.9	255 (1.5)	322 (0.59)
1aB			pH 8.9	271 (1.5)	345 (0.41)
1bB			pH 8.9	273 (1.6)	345 (0.46)

a) *o*-$YC_6H_4CH{=}X$. b) A main form of the ionization states present is shown in parentheses.

Section. Results are summarized in Table 2.

Time-dependent changes of the absorbance gave pseudo-first-order rate constants k_{obsd}, which were not affected whether the reaction was started with **1** or **2**. The rate constant k_{obsd} linearly increased with the total amine concentration $[\mathbf{3}]_t$ (Fig. 1), but was independent of the buffer used to maintain pH constant. The observed rate constant k_{obsd} must be the sum of those for the forward and the reverse reactions (Eq. 2).

$$k_{obsd} = k_h + k_f[\mathbf{3}]_t \quad (2)$$

The intercept and the slope of the plot of k_{obsd} against $[\mathbf{3}]_t$ correspond to the rate constants for the hydrolysis (k_h) and formation (k_f) of Schiff base **1**, respectively. These rate constants obtained over pH 7—11 are summarized in Table 2. Both k_f and k_h obtained from the reaction of **2** (in the presence of **3a**) agree with those obtained from the reaction of **1a** within experimental errors. The values of k_h for the hydrolysis of **1a** are identical to those obtained previously in the absence of the amine.[3] The equilibrium constants $K_f(=k_f/k_h)$ calculated from the rate constants agree well with those

Table 2. Equilibrium and rate constants for the formation of schiff bases, **1a** and **1b**[a]

pH[b]	K_f/M^{-1} [c]	$10\,k_f/M^{-1}\,s^{-1}$ [d]	$10^3\,k_h/s^{-1}$ [d]	K_f/M^{-1} [e]
		1a		
7.00[f]	15.4±1.4(20)	0.312±0.011	1.57±0.01	
8.00[f]	113±2(100)	1.63±0.01(1.63±0.03)	1.58±0.01(1.55±0.03)	2
8.94[g]	202±2(200)	4.07±0.06(4.22±0.06)	2.02±0.08(1.93±0.07)	26
9.58[h]	142±3(130)	4.50±0.03(4.56±0.03)	3.50±0.05(3.50±0.03)	54
10.02[h]	82.6±1.3(87)	5.07±0.03(4.95±0.09)	5.80±0.03(5.86±0.10)	68
10.83[i]	22.7±0.6(27)	6.18±0.06	23.0±0.1	
11.40[i]				98
		1b		
7.50[f]	20.8±1.7(22)	0.451±0.006	2.08±0.01	
8.00[f]	39.3±0.9(38)	0.673±0.011	1.75±0.02	
8.94[g]	82.3±0.3(73)	1.51±0.03	2.06±0.05	
9.38[h]	75.8±2.1(74)	1.68±0.04	2.28±0.06	10
9.78[h]	57.0±1.2(56)	1.81±0.02	3.25±0.04	
10.02[h]				20
10.21[j]	35.0±0.8(37)	2.05±0.07	5.50±0.12	
10.83[i]	(13)	2.58±0.07	19.5±0.1	28
11.19[i]				30

a) In aqueous solutions of the ionic strength of 0.10 at 30 °C. Standard deviations are given. b) pH(±0.03) were maintained with buffers(f—j) of 0.05 M. c) Obtained spectrophotometrically. Values in parentheses are calculated from k_f and k_h. d) Obtained from the reaction of **2**. Values in parentheses were obtained from the reaction of **1**. e) K_f for **4** obtained spectrophotometrically. f) *N*-Methylmorpholine. g) 1,4-Diazabicyclo[2.2.2]-octane. h) 2-(Dimethylamino)ethanol. i) Triethylamine. j) Trimethylamine.

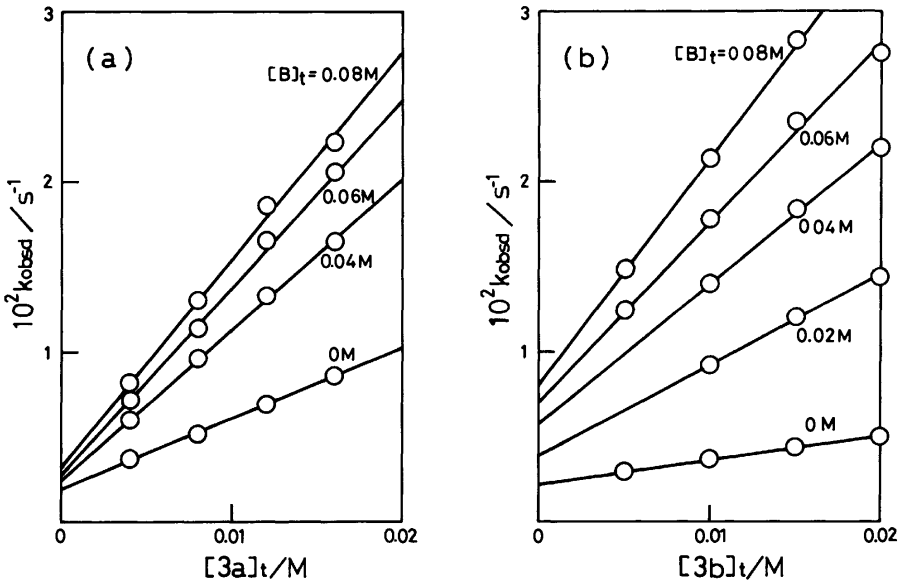

Fig. 1. Dependences of k_{obsd} on the amine concentrations for the formation of **1a** (a) and **1b** (b) from **2** at pH 8.94 and the boric acid concentrations indicated.

obtained spectrophotometrically, as summarized in Table 2.

Reactions in the Presence of Boric Acid. The UV spectra of **1** in the presence of boric acid were compared with those observed in its absence. On addition of boric acid, the absorbane at 393—395 nm of **1** diminished and a new absorption band appeared around 350 nm owing to the formation of a borate-Schiff base complex. The spectrum of aldehyde **2** was, however, not affected by the addition of boric acid; complexation between boric acid and **2** is negligible. The reactions involved are illustrated in Scheme 1. The apparent equilibrium constant K_f' for the Schiff base formation in the presence of boric acid can be spectrophotometrically determined in the same way as in the absence of boric acid. K_f' is defined by Eq. 3, where [**1B**] stands for the concentration of the complex **1B**. Since equilibrium constant K_{app} for the complexation is defined by Eq. 4,[3] the relation of Eq. 5 can bederived from Eqs. 3 and 4, where $[B]_t$ is total boric acid concentration.

$$K_f' = ([\mathbf{1}]+[\mathbf{1B}])/[\mathbf{2}][\mathbf{3}]_t, \quad (3)$$

$$K_{app} = [\mathbf{1B}]/[\mathbf{1}][B]_t, \quad (4)$$

$$K_f' = K_f + K_f K_{app}[B]_t. \quad (5)$$

The values of K_{app} were calculated as the ratio of the slope/intercept of the regression line of K_f' *vs.* $[B]_t$ (Fig. 2). Results are summarized in Table 3. The values of K_{app} for **1a** agree well with those obtained from the kinetic analysis of hydrolysis of **1a**.[3]

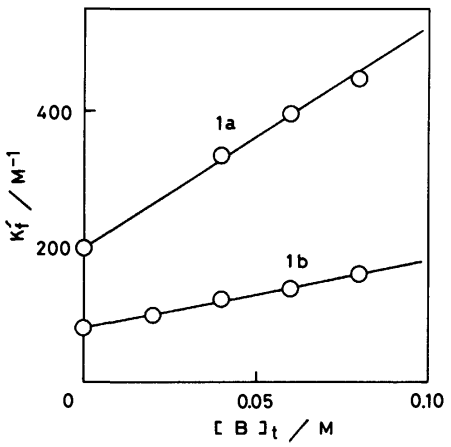

Fig. 2. Plots of K_f' against boric acid concentration at pH 8.94.

TABLE 3. EQUILIBRIUM AND RATE CONSTANTS FOR THE SCHIFF BASE FORMATION IN THE PRESENCE OF BORIC ACID[a]

pH[b]	K_{app}/M^{-1}	$k_f^B/M^{-1}s^{-1}$	$K_C/(K_T+1)/M^{-1}$
		1a	
7.02	27.4 ±0.7	1.36±0.03	27.6
8.02	24.7 ±0.8	9.09±0.12	26.3
8.94	16.3 ±0.4	11.7 ±0.2	25.3
9.58	5.68±0.19	4.16±0.09	19.3
		1b	
8.94	12.3 ±0.3	16.3 ±0.2	19.1
9.40	6.42 ±0.14	9.05±0.10	16.6

a) In aqueous solutions of the ionic strength of 0.10 at 30 °C. Standard deviations are given. b) ±0.03.

At a given ooncentration of boric acid $[B]_t$, the time-dependent absorbance changes followed the pseudo-first-order kinetics, and k_{obsd} increased linearly with the amine concentration $[\mathbf{3}]_t$ as observed in the absence of boric acid (Fig. 1).

$$k_{obsd} = k_h' + k_f'[\mathbf{3}]_t \quad (6)$$

The rate constant k_h' for the hydrolysis of **1a** agrees with that obtained in the absence of amine **3a**.[3] The rate

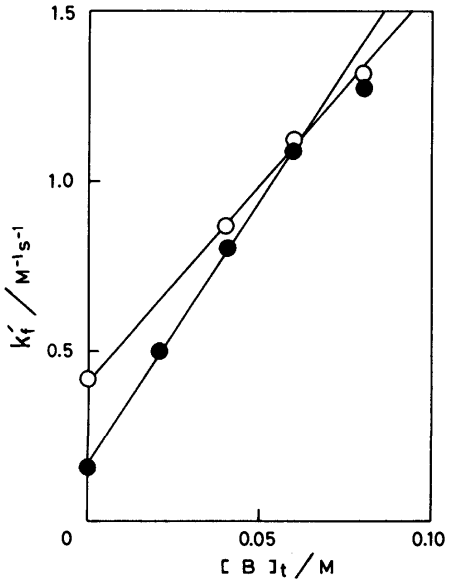

Fig. 3. Dependences of k_f' on boric acid concentration at pH 8.94 for the formation of **1a** (○) and **1b** (●).

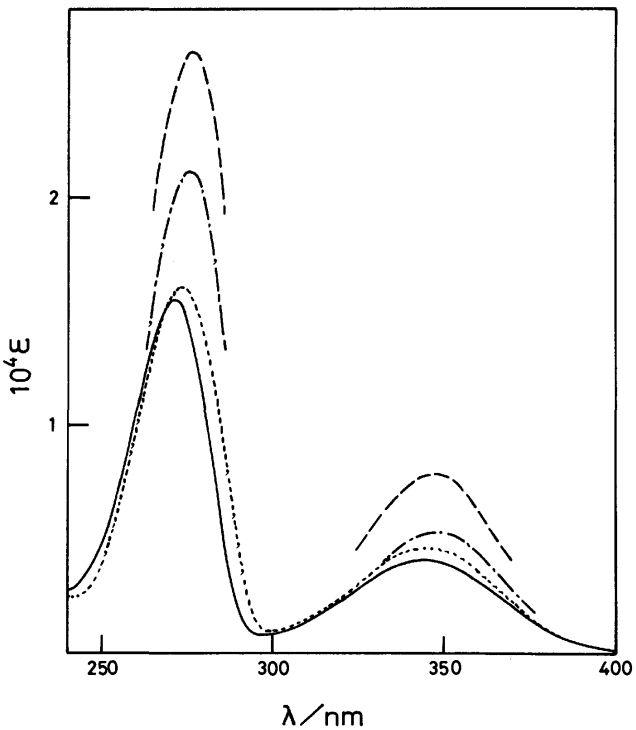

Fig. 4. UV spectra of borate complexes **1aB** (——) and **1bB** (·····) at pH 8.94. Spectra of **1aH**$^+$ (— — —) and **4aH**$^+$ (— —) are also shown.

constant k_f' for the formation of **1** increased linearly with $[B]_t$ (Fig. 3).

$$k_f' = k_f + k_f^B[B]_t \quad (7)$$

The intercepts of the plots of k_f' *vs.* $[B]_t$ are equal to the rate constants k_f obtained in the absence of boric acid ($[B]_t$=O). The third-order rate constants k_f^B are listed in Table 3.

Analysis of UV Spectra. The spectrum of Schiff base **1** in aqueous solution changes greatly by the addition of boric acid as mentioned above. In this aqueous solution, the complex **1B** must be present in an equilibrium concentration together with **1** and **2** as light-absorbing species (Scheme 1). Since we now know the equilibrium constants K_f and K_{app}, we can calculate the equilibrium fractions of **1**, **2**, and **1B**. The equilibrium fractions of **1aB**, **1a**, and **2** are, *e.g.*, 60, 37, and 3%, respectively, at pH 8.9, $[B]_t$=0.10 M,[4] and [3a]=0.625 M. The absorbances of **1aB** were thus calculated from the observed spectrum at every 5 nm over 240—400 nm using the extinction coefficients of **1** and **2** at each wavelength. The spectrum calculated in this way is shown in Fig. 4. The spectrum of **1bB** was also calculated in the same way. These spectra have two absorption maxima at 271(273) and 345 nm, which resemble closely those of the protonated Schiff bases **1aH**$^+$ and **4aH**$^+$ as may be seen in Fig. 4 (see also Table 1).

Discussion

UV Spectra. All the spectra of salicylaldehyde derivatives (*o*-YC_6H_4CH=X) listed in Table 1 have two absorption bands in the 250—275 and 305—395 nm regions. The iminium derivatives (X=N$^+$HR), as observed in HCl solutions, have a band at about 275 nm, while aldehyde (X=O) and the neutral imine (**4** in alkaline solution, X=NR) have a band around 255 nm. Although the spectra of **1** and **4** closely resemble each other in acid solutions, those observed in alkaline solutions are quite different. The spectra of **1** at pH 8.9 have a band typical of the iminium group (~276 nm) and largely red-shifted one (~394 nm). This feature of the spectrum of **1** conforms to the structure of the zwitterion **1**$^\pm$. The red-shift of the long-wavelength band (**1**$^\pm$ *vs.***2**$^-$) by the iminium function is generally observed; *e.g.*, **1H**$^+$ *vs.***2**^{0} and **4H**$^+$ *vs.***5**^{0}. The conclusion that the main species of *N*-salicylidene amine is the zwitterion **1**$^\pm$ in the neutral aqueous solution was previously reached from the comparisons of the spectra in aqueous and organic media.[5] This is also compatible with the kinetic results of the hydrolysis of **1a**.[3]

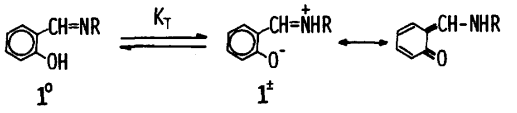

(8)

The tautomeric equilibrium (8) is largely shifted to the right-hand side owing to the stabilization by the quinonoid resonance.

The absorption spectrum of the borate complex **1B**, as shown in Fig. 4, has two bands in the vicinity of the wavelengths characteristic of the iminium and the neutral phenolic groups. This strongly suggests the structure of **1B** involving a positive nitrogen and a neutral (phenolic) oxygen as a result of boron coordination. A reasonable structure is given in Scheme 1. Similar complexes involving a tetracoordinated boron have in fact been isolated as diacetates from the reaction of *N*-salicylidene amines with boric acid in acetic anhydride.[6] Diphenylborinate adducts have recently been found to have a similar structure.[7] It is also well-known that *N*-salicylidene amines form stable chelate complexes with various metal ions.[8,9] The UV spectra of Zn(II) and Ni(II) complexes have the absorption bands in the vicinity of 270 nm and 350 nm.[10]

Schiff Base Formation. Formation of Schiff bases occurs through a nucleophilic attack of free amine base on the carbonyl group as illustrated in Scheme 2.[11,12]

The pH-equilibrium constant profile is bell-shaped (Fig. 5) and is represented by Eq. 9 where K_a and K_S are the acid dissociation constants of ammonium ion **3H**$^+$ and salicylaldehyde **2**^{0}, respectively (pK_S 8.3).

$$K_f = \frac{K_a(K_f^0[H^+] + K_f^- K_S)}{(K_a + [H^+])(K_S + [H^+])} \quad (9)$$

Constants K_f^0 and K_f^- refer to the equilibria involving the neutral (**2**^{0}) and anionic (**2**$^-$) aldehyde, respectively.

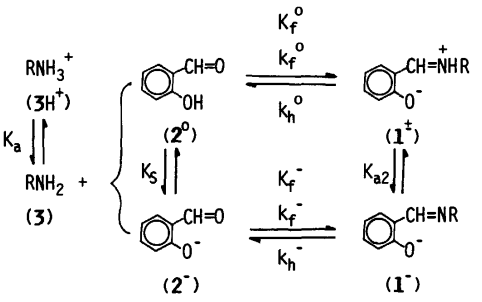

Scheme 2.

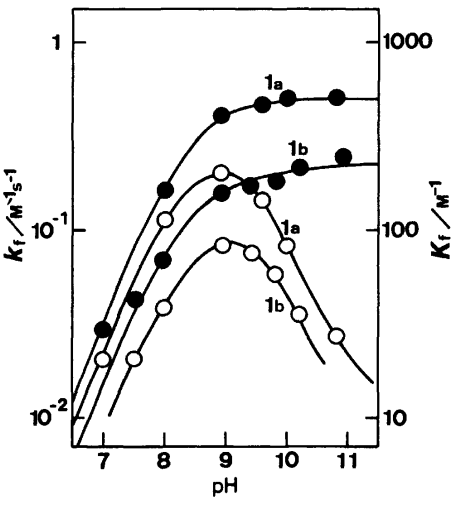

Fig. 5. pH profiles of rate constants k_f(●, left ordinate) and equilibrium constants K_f(○, right ordinate) for the formation of Schiff bases **1a** and **1b**.

The pH-rate profile also fits a similar equation (Eq. 10), although it appears to be different from the pH-K_f profile (Fig. 5).

$$k_f = \frac{K_a(k_f^0[H^+] + k_f^- K_S)}{(K_a + [H^+])(K_S + [H^+])} \quad (10)$$

The rate constant k_f^0 and k_f^- refer to the reactions of amine with $\mathbf{2}^0$ and $\mathbf{2}^-$, respectively. Theoretical curves calculated by Eqs. 9 and 10 with parameters given in Table 4 are shown in Fig. 5. The values of K_f^0 and K_f^- for **1a** satisfy the relationship $K_f^-/K_f^0 = K_{a2}/K_S$, which results from the equilibrium cycle in Scheme 2. Here, K_{a2} (7.0×10^{-12} M^{-1}) obtained during the hydrolysis kinetics[3] is used. The rate constants for the hydrolysis of **1a** can be calculated from previous results[3]: $k_h^0(k_2) = 1.5\times10^{-3}$ s^{-1} and $k_h^-(k_2'K_W/K_{a2}) = 7.8\times10^{-2}$ s^{-1}. The individual formation constants, $K_f^0(k_f^0/k_h^0) = 6.1\times10^3$ M^{-1} and $K_f^-(k_f^-/k_h^-) = 7.6$ M^{-1}, evaluated from these values agree well with those obtained spectrophotometrically. The formation constants for **1b** also agree with those reported.[9]

The equilibrium constants for the formation of Schiff base **4** corrected for the amine protonation are: **4a**, $K_f^0 = 100$ M^{-1} and **4b**, $K_f^0 = 31$ M^{-1}. These values are smaller than those (K_f^0) for *N*-salicylidene amines **1** by a factor of 10^2. The large values for **1** cannot simply be ascribed to a possible stabilization of **1** by an intramolecular hydrogen bonding. Stabilization of the Schiff base in a tautomeric form, $\mathbf{1}^{\pm}$, must be responsible for the facile formation of *N*-salicylidene amines. The zwitterionic form $\mathbf{1}^{\pm}$ is in fact a main species in neutral and weakly alkaline aqueous solutions as has been confirmed by UV spectroscopy.

The tautomeric oonstant K_T in aqueous solution is hard to estimate. If we assume that the formation constant $K_f^{0\prime}$ for the neutral Schiff base $\mathbf{1}^0$ (Scheme 3) is the same as that for the methoxy derivatives **4**, $K_T(=K_f^0/K_f^{0\prime})$ can be calculated as 60 and 116 for **1a** and **1b**, respectively.

Similar evaluation for *N*-salicylideneaniline gave $K_T = 6.3$.[13] For the derivatives from less basic amines, the zwitterionic form tends to be less important. These estimations for K_T would be an upper limit in their magnitudes, as the neutral form of salicylidene derivatives **1** be stabilized by an intramolecular hydrogen bonding.

The complexation was considered to involve the neutral Schiff base and boric acid (acid form) from the bell-shaped change of K_{app} with pH.[3] With the equilibrium constant K_C for the reaction (Eq. 11), K_{app} can be expressed as Eq. 12.

$$\begin{array}{ccc} \mathbf{1}^0 + B(OH)_3 & \overset{K_C}{\rightleftharpoons} & \mathbf{1B} \\ {\scriptstyle K_T}\uparrow\downarrow & & {\scriptstyle K_{BH}}\uparrow\downarrow \\ \mathbf{1}^{\pm} & & B(OH)_4^- \end{array} \quad (11)$$

$$K_{app} = K_C[H^+]/(K_{BH} + [H^+])(K_T + 1) \quad (12)$$

Values of $K_C/(K_T+1)$ were calculated with $K_{BH} = 6.3\times10^{-10}$ M^{-1} and are given in Table 3. Average values are: $K_C/(K_T+1) = 25$ and 18 M^{-1} for **1a** and **1b**, respectively. The value for **1a** agrees reasonably well with that obtained from the hydrolysis kinetics.[3] By using the above estimated values for K_T, the K_C values are 1500 and 2100 M^{-1} for **1a** and **1b**, respectively. The carboxylato group of **1b** does not appreciably participate in the complexation. The boron–carboxylato interaction, as considered for metal-ion complex,[9] is not important. The bicyclic structure must be strained owing to the short B–O (B–N) distances.

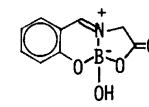

Boric acid accelerates the Schiff base formation and the catalytic constants k_f^B change with pH taking a maximum value at pH 9. Because of the nature of the reaction, the reactive species involved must be a free amine base and boric acid (acid form). The catalytic constants k_f^B were corrected for such protonation states according to Eq. 13.

$$k_f^{B\prime} = k_f^B(K_a + [H^+])(K_{BH} + [H^+])/K_a[H^+] \quad (13)$$

The corrected constants $k_f^{B\prime}$ are plotted against the fraction of the neutral salicylaldehyde $\mathbf{2}^0$ in Fig. 6. For either of the amines, the plots seem to fit a straight line through the origin. Thus, only the neutral aldehyde $\mathbf{2}^0$ is involved in this reaction but the ionized aldehyde $\mathbf{2}^-$ is not. To be strict, the transition state for the borate-catalyzed formation of the Schiff base **1** is neutral and consists of aldehyde, amine, and boric acid. The catalytic constants k_f^{B0} corrected for the neutral aldehyde are 560 and 1100 M^{-2} s^{-1} for **3a** and **3b**, respectively, from the slopes of the plots in Fig. 6. These values correspond to accelerations of about 60- and 190-fold at $[B]_t = 1$ M.

A probable reaction sequence of the boric acid-

TABLE 4. SUMMARY OF EQUILIBRIUM AND RATE CONSTANTS[a]

	1a	**1b**
pK_a[b]	9.58	9.78
K_f^0/M^{-1}	6.0×10^3	3.6×10^3
K_f^-/M^{-1}	7.8	3.8
k_f^0/M^{-1} s^{-1}	9.2	5.8
k_f^-/M^{-1} s^{-1}	0.61	0.24
$K_C/(K_T+1)$/M^{-1}	25	18
k_f^{Bo}/M^{-2} s^{-1}	560	1100

a) In aqueous solutions of the ionic strength of 0.10 at 30 °C. b) pK_a of $\mathbf{3}H^+$ obtained as the pH of the solution of $[\mathbf{3}H^+] = [\mathbf{3}]$.

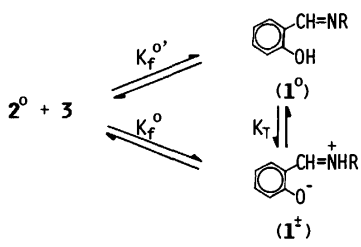

Scheme 3.

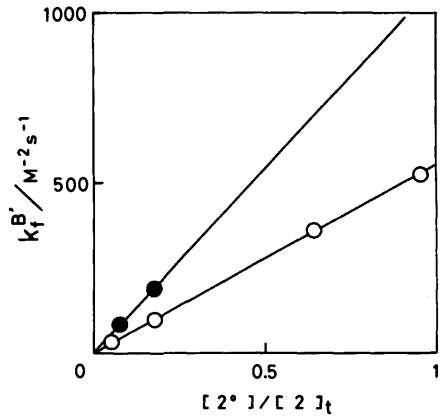

Fig. 6. Plots of $k_f^{B'}$ against the fraction of the neutral aldehyde 2^0 for the boric acid-catalyzed formation of **1a** (○) and **1b** (●).

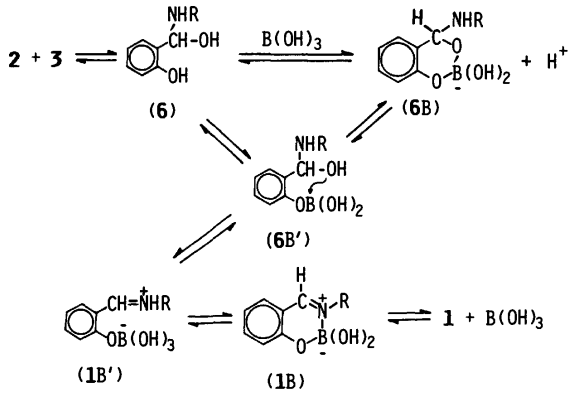

Scheme 4.

catalyzed Schiff base formation is given in Scheme 4. In alkaline pH region, formation of an α-amino alcohol intermediate (**6**) is rapid. **6** is a diol capable of forming a chelate complex (**6B**) with boric acid. However, the chelate complex cannot facilitate dehydration to lead to the Schiff base. The adduct (**6B'**) may exist in equilibrium at low concentration. Within this adduct, the hydroxyl group of the α-amino alcohol can readily transfer to the boron acceptor. The resulting zwitterion (**1B'**) rearranges to the stable borate-Schiff base complex (**1B**). This is precisely the microscopic reverse of the boric acid-assisted hydrolysis of the Schiff base.[3] Formation of a chelate complex (**6B''**) involving the amino-coordination to the boron is unlikely.

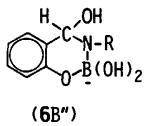

(6B")

Such complexes are not known in aqueous solution. The pH did not change when the two buffer solutions, each made from borate and 2-aminoethanol (or glycine) and adjusted at the same pH (≈9.2), were mixed (Eq. 14).

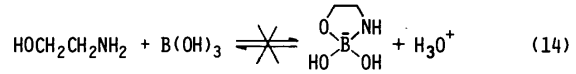

$$HOCH_2CH_2NH_2 + B(OH)_3 \rightleftharpoons + H_3O^+ \qquad (14)$$

In conclusion, the formation of *N*-salicylidene amines catalyzed by boric acid takes place through a mechanism given in Scheme 4.

Experimental

The UV measurements were carried out in a stoppered 10-mm quartz cuvette at a slitwidth of 1 nm on a Shimadzu UV 200 spectrophotometer. Some kinetic runs were also performed on a Shimadzu UV 140 spectrometer. The pH values of the buffer and reaction solutions were measured on a Hitachi-Horiba F7 pH meter.

Materials. Glycine **3b** and *o*-methoxybenzaldehyde **5** were commercially obtained. *N*-(*o*-Methoxybenzylidene)-2-methoxyethylamine **4a** was prepared in the same way as described previously for **1a**[3]: bp. 131 °C (4 mmHg).[14] All the other chemicals were obtained as before.[3]

Kinetic Measurement. All the aqueous solutions containing appropriate amounts of amine, boric acid, and buffers were prepared at room temperature and adjusted to the ionic strength of 0.10 with KCl. Reactions were started by adding 30 μl of a substrate soluion in acetonitrile from a microsyringe into 3 ml of a buffer solution equilibrated at 30±0.1 °C in a cuvette inserted in a water-jacketed cell holder. Pseudo-first-order rate constants were calculated usually by a modified Guggenheim method[15] from the time-dependent absorbance changes at 275 nm for **1**, and 335 nm at higher pH(>7) or 282 nm at lower pH(<7) for **4**. The infinite absorbances were compared occasionally between those observed and calculated.

Determination of the Formation Constant. The equilibrium constants were calculated from UV absorbance. Since amine **3** has no absorption above 220 nm, the relative concentration at equilibrium is expressed by the absorbance change: $[\mathbf{1(4)}]/[\mathbf{2(5)}]=(A_e-A_0)/(\varepsilon_1[\mathbf{2(5)}]_0-A_e)$ starting with **2(5)**, where A_0 and A_e are the absorbances at time zero and at equilibrium, and ε_1 and $[\mathbf{2}]_0$ stand for the extinction coefficient for **1** and

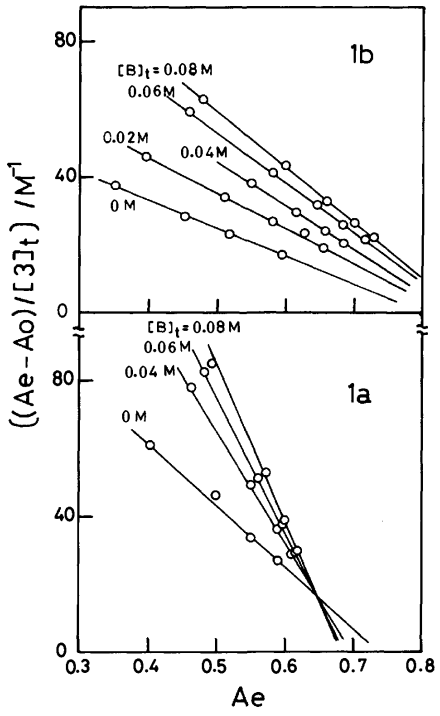

Fig. 7. Plots of $(A_e-A_o)/[3]_t$ against A_e at pH 8.94 and the boric acid concentrations indicated.

the initial concentration of **2**, respectively, or alternatively $[\mathbf{1}]/[\mathbf{2}]=(A_e-A_0)/(\varepsilon_2[1]_0-A_e)$ starting with **1** whose concentration is $[\mathbf{1}]_0$. Here ε_2 stands for the extinction coefficient for **2**. The values of $\varepsilon_1[\mathbf{2}]_0$ and $\varepsilon_2[\mathbf{1}]_0$ correspond to the limiting absorbances A_∞ at the infinite concentration of **3**. Thus the values of K_f ($=[\mathbf{1}]/[\mathbf{2}][\mathbf{3}]$) were determined from the slope of the plots of $(A_e-A_0)/[\mathbf{3}]_t$ against A_e according to Eq. 15 (Fig. 7).

$$(A_e-A_o)/[\mathbf{3}]_t = K_f(A_\infty-A_e) \quad (15)$$

References

1) H. Matsuda, H. Nagamatsu, T. Okuyama, and T. Fueno, *Bull. Chem. Soc. Jpn.*, **57**,500 (1984).

2) J. Hoffmann and V. Štěrba, *Collect. Czech. Chem. Commun.*, **37**, 2043 (1972).

3) H. Nagamatsu, T.Okuyama, and T. Fueno, *Bull. Chem. Soc. Jpn.*, **57**, 2502 (1984).

4) 1 M=1 mol dm^{-3}.

5) W. Bruyneel, J. J. Charette, and E. de Hoffmann, *J. Am. Chem. Soc.*, **88**, 3808 (1966).

6) S. M. Tripathi and J. P. Tandon, *J. Inorg. Nucl. Chem.*, **40**, 983 (1978).

7) E. Hohaus, *Monatsh. Chem.*, **111**, 863 (1980).

8) R. H. Holm, G. W. Everett, Jr., and A. Chakravorty, *Prog. Inorg. Chem.*, **7**, 83 (1966); L. Sacconi, *Coord. Chem. Rev.*, **1**, 126, 192 (1966).

9) D. L. Leussing, "Metal Ions in Biological Systems," H. Sigel ed., Marcel Dekker, New York (1976), vol. 5, chap. 1.

10) D. L. Leussing and K. S. Bai, *Anal. Chem.*, **4**, 575 (1968).

11) E. H. Cordes and W. P. Jencks, *J. Am. Chem. Soc.*, **84**, 826 (1962).

12) A. Williams and M. L. Bender, *J. Am. Chem. Soc.*, **88**, 2508 (1966).

13) J.J. Charette and E. de Hoffmann, *J. Org. Chem.*, **44**, 2256 (1979).

14) 1 mmHg≈133.322 Pa.

15) E. S. Swinbourne, *J. Chem. Soc.*, **1960**, 2371.

 © 1984 The Chemical Society of Japan Bull. Chem. Soc. Jpn., 57, 2515—2525 (1984)

A Stereocontrolled Total Synthesis of *C*-Nucleosides[1)]

Tsuneo SATO, Yoshihiro HAYAKAWA,† and Ryoji NOYORI*
Department of Chemistry, Nagoya University, Chikusa-ku, Nagoya 464
†*Chemical Instrument Center, Nagoya University, Chikusa-ku, Nagoya 464*
(Received March 10, 1984)

A stereocontrolled, general synthesis of chiral *C*-nucleosides has been achieved through a common lactonic *C*-β-glycoside intermediate which is readily obtainable from non-carbohydrate materials. Osmium tetraoxide-catalyzed *vic*-dihydroxylation of 8-oxabicyclo[3.2.1]oct-6-en-3-one gives, after acetonidation, (1*R**,5*S**,6*S**,7*R**)-6,7-isopropylidenedioxy-8-oxabicyclo[3.2.1]octan-3-one as a single stereoisomer. Baeyer-Villiger oxidation of the ketone affords the key intermediate, 2-(2,3-*O*-isopropylidene-β-ribofuranosyl)acetic acid lactone. The optically pure lactone having the natural D configuration is obtained through optical resolution of the seco acid by the Pirkle's method followed by relactonization. α-Aminomethylenation of the lactone with *t*-$C_4H_9OCH[N(CH_3)_2]_2$ yields 2-(2,3-*O*-isopropylidene-β-D-ribofuranosyl)-2-(dimethylaminomethylene)acetic acid lactone, which undergoes base-assisted condensation with urea followed by deprotection to furnish naturally occurring pseudouridine. Analogously, construction of heterocycles using thiourea and guanidine converts the aminomethylene lactone to unnatural pyrimidine *C*-nucleosides, 2-thiopseudouridine and pseudoisocytidine, respectively. Showdomycin in natural form can be prepared by two schemes. One approach consists of ozonolysis of the α-dimethylaminomethylene lactone, Wittig reaction using $(C_6H_5)_3PCHCONH_2$, and acid hydrolysis. The second entry makes use of 2-(2,3-*O*-isopropylidene-β-D-ribofuranosyl)acetic acid lactone as the intermediate, which is converted to 2-(2,3-*O*-isopropylidene-β-D-ribofuranosyl)-2-furfurylideneacetic acid lactone by the aldol reaction with furfural and dehydration. Methanolysis of the furfurylidene lactone and *t*-butyldimethylsilylation are followed by ozonolysis, Wittig condensation with $(C_6H_5)_3PCHCONH_2$, and hydrolysis to give the maleimide *C*-nucleoside. In addition, 6-azapseudouridine and 6-aza-2-thiopseudouridine are obtainable *via* intramolecular ring closures of the semicarbazone and thiosemicarbazone of methyl 2-(2,3-*O*-isopropylidene-β-D-ribofuranosyl)glyoxylate followed by deprotections, respectively. These overall transformations are accomplishable under complete stereochemical control.

C-Nucleosides are a class of compounds which possess a carbon–carbon linkage between the carbohydrate and heterocyclic moieties, and are distinguished from ordinary *N*-nucleosides in which an anomeric carbon (C-1′ position) of the sugar is linked to the aglycon by a carbon–nitrogen bond. Since the first isolation of pseudouridine (**1**) as a minor constituent in various transfer ribonucleic acids,[2)] a number of naturally occurring *C*-nucleosides have been isolated mainly from the culture filtrates of various *Streptomyces*.[3)] The *C*-nucleosides, based on their unique structural feature, have considerable stability to chemical hydrolysis and enzymatiac destruction and, as a consequence, most of them exhibit various biological properties of interest.[4–9)]

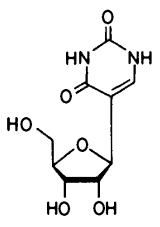

1

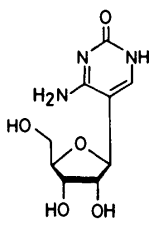

2

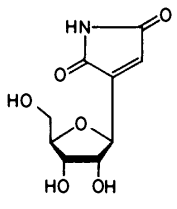

3

The biological importance has stimulated the exploration of synthetic routes leading to natural *C*-nucleosides as well as their artificial analogues. The synthetic processes fall into the following three main categories: (1) transformation of naturally occurring *C*-nucleosides, (2) elaboration of a nitrogen heterocycle onto a suitably modified carbohydrate, and (3) total synthesis starting from non-sugar precursors. Most of the existing approaches[10)] come under the first and second categories, which seem to lack effectiveness, however, because of difficulty in access of the starting materials and poor generality in the former case, and low stereoselectivity in the latter method. The third-category type of synthesis obviously allows maximum flexibility but development of any effective approaches of this type requires some new, efficient methodologies for creation of the four asymmetric centers in the ribose skeleton as well as a strategy for stereochemical control at the anomeric center so as to maintain the β-D-glycosyl structures.[11)] This paper discloses full accounts of our stereocontrolled, general entry to *C*-nucleosides starting from inexpensive non-carbohydrate substances. The highly chiral framework is created by simple operations *via* an intermediate having C_s symmetry; the ribose skeleton is made by the efficient [3+4] cyclocoupling between polybromo ketones and furans aided by low-valent transition metals[13)] and subsequent oxidative modification of the resulting oxa bicyclic structure.

Synthesis of Pyrimidine C-Nucleosides. This synthesis starts with the bicyclic enone **4**, which is readily obtainable by reductive cyclocoupling of α,α,α′,α′-tetrabromoacetone and furan promoted by $Fe_2(CO)_9$ in benzene[14)] or Zn/Ag couple in THF,[15)] followed by debromination with Zn/Cu couple in methanol. When **4** was treated with a slight excess of 70% solution of *t*-butyl hydroperoxide in *t*-butyl alcohol containing catalytic amounts of osmium tetraoxide and aqueous tetraethylammonium hydroxide at 0—25 °C[16)] and then with anhydrous $CuSO_4$ and *p*-toluenesulfonic acid in acetone, the oxygen functions were introduced to the double bond from the less hindered side[17)] with perfect stereoselectivity to give the acetonide **5** as a single, crys-

talline isomer in 68% yield. No stereoisomer was detected in the reaction mixture. The stereoselective conversion of **4** to **5** was also accomplished in 52% yield by the osmium tetraoxide-catalyzed reaction using 30% hydrogen peroxide as the oxidizing agent. The α stereochemistry of the acetonide was established on the basis of the ^{1}H NMR spectrum which exhibited a sharp singlet at δ 3.98 due to the equivalent H_6 and H_7 protons. A Dreiding model of this rigid tricyclic system indicated that the H-C(6)-C(5)-H (or H-C(7)-C(1)-H) dihedral angle is approximately 90°, consistent with the observed ~0 Hz spin-spin coupling constant; if the acetonide had alternative β orientation with the dihedral angle of 30—40°, a 5 to 6-Hz signal splitting would be anticipated.[18] Subsequent Baeyer-Villiger oxidation of **5**,[19] giving the key intermediate **6** of an adequate *C*-β-glycoside structure, was achieved in 81% yield (94% yield based on consumed **5**) in dichloromethane at room temperature by two equiv of trifluoroperacetic acid in the presence of buffer salts of Na_2HPO_4 and disodium dihydrogen ethylenediaminetetraacetate. The oxidation proceeded only slowly by use of *m*-chloroperbenzoic acid with a catalytic amount of 4,4'-thiobis(6-*t*-butyl-3-methylphenol), and the yield was reduced to 59%. The lactone formation was confirmed by the IR absorption at 1737 cm^{-1} (C=O). Thus the keystone intermediate having a highly chiral structure can be derived facilely starting from simple and symmetrical substances, acetone and furan. The optical resolution required for natural product synthesis was effected *via* the corresponding seco acid methyl ester **7**, obtained in 95% yield by methanolysis with sodium methoxide in methanol. We found that, in this case, the Pirkle's resolution procedure[20] was far superior to the traditional method involving salt formation.[1a] Heating of an equimolar mixture of racemic **7** and (*R*)-1-(1-naphthyl)ethyl isocyanate in toluene[20] followed by chromatographic separation produced the optically active, diastereomeric carbamates **8**, $[\alpha]_D^{15}$ −3.56° (*c* 0.337, $CHCl_3$), and **9**, $[\alpha]_D^{15}$ −1.25° (*c* 0.561, $CHCl_3$), in 43% and 46% yields, respectively. The desired seco acid methyl ester, D-**7**, was liberated from **8** in 80% yield by treatment with trichlorosilane and triethylamine in benzene.[20] The transformation of D-**7** to the optically pure lactone, D-**6**, mp 161—163 °C, $[\alpha]_D^{26}$ +84° (*c* 0.63, $CHCl_3$), was then achieved according to the known procedure.[21] This resolved lactone was identical in all respects with the authentic sample prepared from D-ribose.[22]

The synthetic sequence continues by introduction of formyl or its synthetic equivalent at position α to the lactone carbonyl. After many attempts without any respectable success, a Bredereck reagent was found to be among the most effective. Thus treatment of D-**6** with

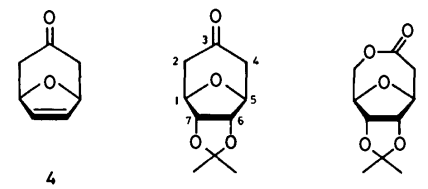

4 5 6

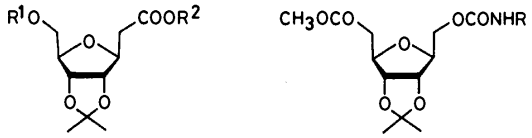

7, R^1 = H; R^2 = CH_3
8, R^1 = (*R*)-1-(1-naphthyl)-ethylaminocarbonyl; R^2 = CH_3
9, R = (*R*)-1-(1-naphthyl)ethyl

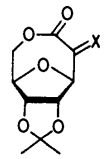

10, X = $CHN(CH_3)_2$
18, X = O
21, X = (*E*)-CHFur

t-$C_4H_9OCH[N(CH_3)_2]_2$[25] in DMF at 60 °C afforded the dimethylaminomethylene lactone, D-**10**, in 91% yield. The product showed the IR bands [1685 and 1680 cm^{-1} (C=O), and 1595 cm^{-1} (C=C)] and a UV absorption [296 nm (ε 13,500)] characteristic of α-dimethylaminomethylene lactone structure. The ^{1}H NMR spectrum displaying two sets of two singlets at δ 2.94 and 3.16 [$N(CH_3)_2$], and 6.69 and 7.34 (=CH) indicated that the product was a 1:2 mixture of the *E*- and *Z*-olefinic isomers. It should be noted that the hydroxy ester **7**, the seco form of **6**, is stereochemically quite labile under basic conditions and, hence, formylation or related operation by conventional standard procedures causes easy isomerization through the intramolecular retro-Michael reaction/recyclization sequence,[24,26] giving the more stable α epimer **11**. Use of the lactone **6** thus has the particular advantage in preservation of the "natural" stereochemical integrity at C-1'.[27]

The aminomethylene lactone, D-**10**, appeared to serve as a common intermediate for natural and unnatural pyrimidine *C*-nucleosides. For instance, when a mix-

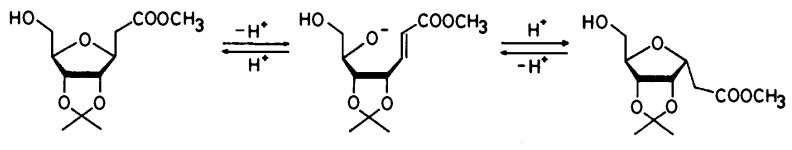

7 11

ture of D-**10** and urea was heated at reflux in 1 mol dm^{-1} ethanolic sodium ethoxide, there was obtained the uracil derivative, D-**12**,[29] mp 235—236 °C, $[\alpha]_D^{21}$ −18.1° (*c* 0.16, CH_3OH), in 60% yield. Removal of the isopropylidene group by exposure to 10% methanol solution of hydrogen chloride at 20 °C furnished pseudouridine (**1**), mp 243—244 °C, $[\alpha]_D^{21}$ −4.30° (*c* 0.47, H_2O), having spectral and physical properties identical with those of naturally occurring specimen. In addition, **1** is convertible to pseudocytidine (**2**),[29] a natural *C*-nucleoside, and 6-azapseudouridine (**13**),[30] an unnatural analogue, by the stereocontrolled, standard methods.

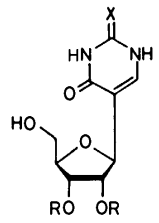

12, R–R = $C(CH_3)_2$; X = O
14, R–R = $C(CH_3)_2$; X = S
15, R = H; X = S

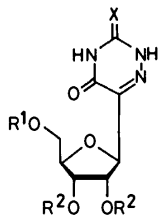

13, $R^1 = R^2$ = H; X = O
27, R^1 = $Si(CH_3)_2$-*t*-C_4H_9; R^2–R^2 = $C(CH_3)_2$; X = O
29, R^1 = $Si(CH_3)_2$-*t*-C_4H_9; R^2–R^2 = $C(CH_3)_2$; X = S
30, $R^1 = R^2$ = H; X = S

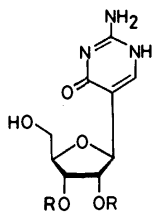

16, R–R = $C(CH_3)_2$
17, R = H

The lactone, D-**10**, underwent the sodium ethoxide-promoted condensation with thiourea in refluxing ethanol to produce the acetonide, D-**14**, $[\alpha]_D^{22}$ −8.0° (*c* 0.92, CH_3OH), in 81% yield. Subsequent deprotection with 10% solution of hydrogen chloride in methanol liberated 2-thiopseudouridine (**15**)[28] as a very hygroscopic solid in 90% yield.

Chemotherapeutically significant pseudoisocytidine (**17**)[28,31] could be also synthesized from D-**10** in a similar manner. Thus, construction of the heterocyclic nucleus using guanidine hydrochloride and sodium ethoxide in hot ethanol gave rise to D-**16**, mp 170—174 °C, $[\alpha]_D^{22}$ −50.8° (*c* 0.73, CH_3OH), in 81% yield, methanolysis of which catalyzed by hydrogen chloride afforded hyrochloride of D-**17**, [28,31] mp 212—215 °C, $[\alpha]_D^{22}$ +14.3° (*c* 0.49 H_2O), in 93% yield.

Noteworthy is that during these all heterocycle formation-deprotection sequences no epimerization occurred at the glycosidic position.

Synthesis of Showdomycin. We conceived that the lactone D-**6** or D-**10** may be useful for the synthesis of nucleosides other than pyrimidine ribo-*C*-nucleosides. The possibility of synthesis of showdomycin (**3**), a natural maleimide *C*-nucleoside,[32] was examined in two different ways. One approach used again D-**10** as the intermediate. When this lactone was exposed to ozone in ethyl acetate at −78 °C and then dimethyl sulfide at −78 °C to room temperature,[33] the labile keto lactone D-**18** was afforded, displaying a strong IR band due to the lactonic and keto carbonyls at 1732 cm^{-1} and no absorption for a conjugated olefin. This was subjected immediately to the Wittig reaction with $(C_6H_5)_3PCHCONH_2$[32a,34] in DMF to give D-**19**, mp 142—143 °C, $[\alpha]_D^{24}$ −2.31° (*c* 1.07, $CHCl_3$), in 30% yield. Removal of the isopropylidene block with aqueous trifluoroacetic acid completed the synthesis of showdomycin (**3**), mp 151—152 °C, $[\alpha]_D^{24}$ +48.7° (*c* 1.4 H_2O), which was identified by comparison with the natural product.

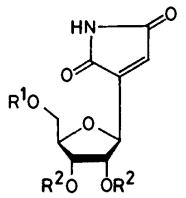

19, R^1 = H; R^2–R^2 = $C(CH_3)_2$
25, R^1 = $Si(CH_3)_2$-*t*-C_4H_9; R^2–R^2 = $C(CH_3)_2$

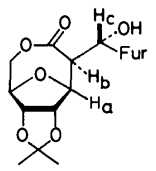

20

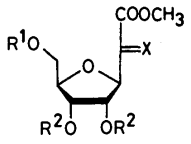

22, R^1 = H; R^2–R^2 = $C(CH_3)_2$; X = (*E*)-CHFur
23, R^1 = $Si(CH_3)_2$-*t*-C_4H_9; R^2–R^2 = $C(CH_3)_2$; X = (*E*)-CHFur
24, R^1 = $Si(CH_3)_2$-*t*-C_4H_9; R^2–R^2 = $C(CH_3)_2$; X = O
26, R^1 = $Si(CH_3)_2$-*t*-C_4H_9; R^2–R^2 = $C(CH_3)_2$; X = $NNHCONH_2$
28, R^1 = $Si(CH_3)_2$-*t*-C_4H_9; R^2–R^2 = $C(CH_3)_2$; X = $NNHCSNH_2$

Another entry to **3** utilizes aldol reaction of D-**6** and furfural assisted by lithium cyclohexylisopropylamide in THF at −78 °C, affording in 90% yield the adduct D-**20** (Fur=2-furyl), mp 139—141 °C, $[\alpha]_D^{21}$ +26° (*c* 2.63, $CHCl_3$). This was a single isomer and, on the basis of ^1H NMR, was revealed to have the *S* configuration at position α to the lactone carbonyl ($J_{Ha,Hb}$=5.0 Hz)[35] and the threo relationship[36] regarding the aldol moiety ($J_{Hb,Hc}$=9.0 Hz).[37] Dehydration of D-**20** was then effected by treatment with pivaloyl chloride in pyridine at 25 °C followed by heating in the same solvent at 90 °C, yielding D-**21**, mp 160—162 °C, $[\alpha]_D^{21}$ −143° (*c* 0.64, $CHCl_3$), quantitatively. The furfurylidene structure was proved by IR bands observed at 1715 (C=O) and 1627 cm^{-1} (C=C), and the ^1H NMR signal appearing as

a singlet at δ 7.24 (=CH). Ring-opening of the lactone with 0.05 mol dm^{-3} methanolic sodium methoxide at 0 °C, giving oily D-**22**, $[\alpha]_D^{21}$ +104° (*c* 2.90, $CHCl_3$), in 86% yield, followed by the silylation of the primary hydroxyl group with *t*-$C_4H_9(CH_3)_2SiCl$ and imidazole in DMF[38] gave quantitatively the methyl ester D-**23**, $[\alpha]_D^{21}$ −0.98° (*c* 0.44, $CHCl_3$), whose ^{1}H NMR data served to support its β-*C*-glycoside structure. The two isopropylidene-methyl singlets occurring at δ 1.25 and 1,56 with 0.31-ppm chemical shift difference is reminiscent of the spectral behavior of related isopropylidene ribonucleosides; the β anomers exhibit the chemical shift difference of >0.18 ppm, whereas the α anomers show the <0.10-ppm difference.[39] Ozonolysis of D-**23** in ethyl acetate at −78 °C followed by reductive workup with dimethyl sulfide yielded the unstable keto ester D-**24**, which without purification was subjected to the Wittig condensation with $(C_6H_5)_3PCHCONH_2$[32a,34] in chloroform to lead to D-**25**, $[\alpha]_D^{24}$ +2.1° (*c* 1.40, $CHCl_3$), in 29% yield (based on D-**23**). Subsequent trifluoroacetic acid-catalyzed hydrolysis produced showdomycin (**3**). Ozonolysis of the furfurylidene lactone, D-**21**, followed by the Wittig reaction also gave showdomycin acetonide, D-**19**, but only in 15% yield.

Such overall transformation have been achieved again without any epimerization at the anomeric center.

Synthesis of 1,2,4-Triazine C-Nucleosides. The keto ester D-**24** can be converted to certain 1,2,4-triazine *C*-nucleosides[40] in a stereospecific manner. For example, refluxing of a mixture of D-**24** and semicarbazide hydrochloride in aqueous methanol containing sodium acetate gave the semicarbazone D-**26**, $[\alpha]_D^{22}$ −1.6° (*c* 1.0, $CHCl_3$), in 30% yield (based on D-**23**) as a mixture of the syn and anti isomers. The isomeric ratio was assigned to be approximately 1:1 by the N–H ^{1}H NMR signals observed at δ 11.29 and 10.21,[41] respectively. Then the cyclization with 0.1 mol dm^{-3} ethanolic sodium ethoxide under reflux[42] furnished the 6-azauracil derivative, D-**27**, $[\alpha]_D^{25}$ −35.8° (*c* 8.90, $CHCl_3$), in 40% yield, hydrolysis of which gave 6-azapseudouridine (**13**),[30] mp 136—138 °C, $[\alpha]_D^{24}$ −23.4° (*c* 0.5, H_2O). In a similar fashion, treatment of D-**24** with thiosemicarbazide in refluxing methanol produced the thiosemicarbazone, D-**28**, $[\alpha]_D^{21}$ −0.71° (*c* 1.1, $CHCl_3$), in 25% yield (overall from D-**23**), which upon exposure to 0.1 mol dm^{-3} ethanolic sodium ethoxide at reflux temperature afforded D-**29**, $[\alpha]_D^{25}$ −1.4° (*c* 2.30, $CHCl_3$), in 56% yield. Deblocking of the protective groups with aqueous trifluoroacetic acid liberated 6-aza-2-thiopseudouridine (**30**),[30] mp 193—195 °C, $[\alpha]_D^{25}$ −3.5 °C(*c* 0.5, H_2O).

Conclusion. Our synthetic aim has thus in fact been realized. The salient feature of this total synthesis is use of the rigid bicyclic intermediates **4** and **6**. This allows strict stereochemical control throughout the overall transformation that consists of assembling the ribose moiety and elaboration of heterocyclic nuclei having the β configuration; the undesired stereomutation is precluded. In addition, the present route has practicability because of its directness and the ready availability of the starting materials. Of more importance is that this entry is capable of preparing various kinds of artificial *C*-nucleosides, particularly those with modified carbohydrate structures. Apparently this wide generality arises from the synthetic flexibility of the transition metal-mediated reductive cyclocoupling of appropriately substituted polybromo ketones and furan derivatives.[13,14] Analogues so far prepared by this method include various pyrimidine *C*-nucleosides containing 5′-alkylated,[43] 1′- or 4′-modified,[43a,44] 2′- or 3′-substituted,[43a,45] and 2′,3′-dialkylated ribose.[43a,46] Homo-*C*-nucleosides (homoshowdomycin,[47] homopyrazomycin,[47] and pyrimidine derivatives,[47a,48]) have been also synthesized.

We should add finally that successful examples were announced recently in preliminary disclosures for showdomycin synthesis *via* non-carbohydrate precursors, which laid on the Diels-Alder reaction between furan and an acrylic acid ester or an acetylenedicarboxylic acid derivative.[32e–g,49]

Experimental

General. Melting points uncorrected were obtained on a hot-stage apparatus. Elemental analyses were performed at the Faculty of Engineering of Nagoya University and the Fujisawa Pharmaceutical Co. Infrared (IR) spectra were recorded in a chloroform solution unless otherwise noted on a JASCO DS-402G or IRA-I spectrophotometer. Ultraviolet (UV)-visible light spectra in a stated solution were taken on a Hitachi 323 spectrophotometer. Proton nuclear magnetic resonance (^{1}H NMR) and proton decoupled ^{13}C NMR spectra were determined in a noted phase on Varian HA-100 and Varian CFT-20 instruments, respectively. Chemical shifts are given as parts per million (ppm) downfield from tetramethylsilane in δ units. In the ^{1}H NMR spectra, coupling constants are reported in hertz. Multiplicities are as follows: s; singlet, d; doublet, t; triplet, q; quartet, m; multiplet. Low-resolution mass spectra were measured on a Hitachi RMU-6C or JEOL D-100 instrument at an ionization potential of 70 eV and only a parent peak or prominent fragment peaks are described. Exact mass spectra were obtained at the Ono Pharmaceutical Co. or Institute for Molecular Science. Optical rotations were measured with a JASCO DIP-SL automatic polarimeter or a JASCO DIP-140 or 181 digital polarimeter. Analytical thin-layer chromatography (TLC) was done on a 5×2 cm of glass slide coated with 0.25-mm thickness of E. Merck Kieselgel 60 PF_{254}. For the preparative work, a 20×20 cm of glass plate coated with 1.0-mm thick layer of E. Merck Kieselgel 60 PF_{254} was employed. Use of E. Merck Kieselgel 60 (70—230 mesh) was made for column chromatography, unless otherwise state. High-performance liquid chromatography (HPLC) was achieved on a Waters 6000A instrument. All reactions in organic solutions were performed under an argon atmosphere. Concentration of solutions was carried out on a rotary evaporator under water aspirator pressures followed by a rotary oil vacuum pump. Organic solvents employed for the reactions were purified by standard procedures. *m*-Chloroperbenzoic acid was used after purification of commercially obtained material by the literature method.[53] Furfural was employed promptly after filtration through a short alumina column followed by distillation. A butyllithium–hexane solution required determination of the concentration by titration by the usual method.[54] *t*-Butoxybis(dimethylamino)methane was prepared according to the procedure of Bredereck.[25] Carbamoylmethylenetriphenylphosphorane made by the method of Trippett[34] was dried over P_2O_5 under 0.01 mmHg (1 mm Hg≈133.322 Pa) overnight before use.

(1R,5S*,6S*,7R*)-6,7-Isopropylidenedioxy-8-oxabicyclo[3.2.1]octan-3-one (5).* *A. By Oxidation with t-Butyl Hydroperoxide*: To a mixture of *t*-butyl alcohol solution (60 ml (1 ml=0.001 dm^3)) of 20% aq tetraethylammonium hydroxide (2.4 ml, 3.26 mmol) and 8-oxabicyclo[3.2.1]oct-6-en-3-one (**4**)[14,15] (3.72 g, 30 mmol) was added with vigorous stirring a 70% solution of *t*-butyl hydroperoxide in *t*-butyl alcohol (6.0 ml, 46.7 mmol) followed by a 0.02 mol dm^{-3} *t*-butyl alcohol solution of osmium tetraoxide (30 ml, 0.6 mmol) at 0 °C. The resulting yellow mixture was stirred at 0 °C for 30 min and at 20 °C for 5 h. The solution of *t*-butyl hydroperoxide (2.0 ml, 15.6 mmol), osmium tetraoxide (10 ml, 0.2 mmol), and aqueous tetraethylammonium hydroxide (1.0 ml, 1.4 mmol) were added renewedly and the reaction mixture was stirred again at 25 °C for 24 h. After quenching with 20% aq $Na_2S_2O_3$ solution (40 ml) at 0 °C, the mixture was stirred at 0 °C for 1 h. Viscous material obtained by evaporation was treated with acetone (100 ml) and the precipitates were removed by filtration through a Celite 545 pad. The filtrate was concentrated, giving an oil, which was dissolved in ethanol (50 ml) and then evaporated again. This dissolution-evaporation sequence was repeated twice more. A mixture of the resulting oil, anhydrous $CuSO_4$ (10 g, 62.7 mmol), and *p*-toluenesulfonic acid (100 mg) in acetone (100 ml) was stirred at 25 °C for 2 h. Removal of the insoluble material by filtration through a Celite 545 pad followed by concentration left an oily product, column chromatography of which with 1:1 ethyl acetate-hexane gave the acetonide **5** (4.05 g, 68%) as colorless crystals. Recrystallization from chloroform-hexane afforded an analytical sample, mp 119—121 °C: IR 1715 (C=O), 1378 and 1370 cm^{-1} (isopropylidene); ^1H NMR (benzene-d_6) δ=1.06 (s, isopropylidene CH_3), 1.47 (s, isopropylidene CH_3), 1.76 (d, J=16 Hz, $H_{2\beta}$ and $H_{4\beta}$), 2.08 (dd, J=6, 16 Hz, $H_{2\alpha}$ and $H_{4\alpha}$), 3.98 (s, H_6 and H_7), 4.23 (d, J=6 Hz, H_1 and H_5); mass spectrum m/z 198 (M^+). Anal. ($C_{10}H_{14}O_4$) C, H.

B. By Oxidation with Hydrogen Peroxide: Aqueous 30% hydrogen peroxide (100 ml, 863 mmol) was added at 0 °C over 2 h to a solution of **4** (11.6 g, 102 mmol), osmium tetraoxide (200 mg, 0.79 mmol), *t*-butyl alcohol (50 ml), and ether (50 ml) in acetone (500 ml). The reaction mixture was stirred at 20 °C for 13 h and then, after cooling to 0 °C, was quenched with $NaHSO_3$ (30 g). The resulting mixture was stirred at 20 °C for 3 h and evaporated until the volume was reduced to 50—100 ml. Extraction with ethyl acetate (200 ml×2, 100 ml) followed by concentration left an oil, which was mixed with anhydrous $CuSO_4$ (20 g, 125 mmol) and *p*-toluenesulfonic acid (50 mg) in acetone (200 ml), and stirred at 20 °C for 4 d. Removal of the insoluble solid by filtration followed by evaporation gave a viscous oil, whose column chromatography with a 1:3 to 2:1 ethyl acetate-hexane mixture as eluent afforded the colorless crystalline acetonide **5** (10.5 g, 52% yield), mp 119—121 °C.

(±)-2-(2,3-O-Isopropylidene-β-ribofuranosyl)acetic Acid Lactone (6). *A. With Trifluoroperacetic Acid*: A dichloromethane solution of trifluoroperacetic acid was prepared by mixing 90% hydrogen peroxide (9.62 ml, 255 mmol) and trifluoroacetic anhydride (43.3 ml, 305 mmol) in dichloromethane (200 ml) at 0 °C. This was added slowly with efficient stirring at 0 °C to a mixture of **5** (25.5 g, 127 mmol), Na_2HPO_4 (130 g, 915 mmol), and disodium dihydrogen ethylenediaminetetraacetate (2 g) in dichloromethane (200 ml), and the mixture was stirred at 25 °C for 12 h. After dilution with dichloromethane (200 ml) and addition of $Na_2S_2O_3 \cdot 5H_2O$ (40.5 g, 163 mmol) at 0 °C, the resulting mixture was further stirred at 25 °C for 5 h. Removal of insoluble material by filtration through a Celite 545 pad followed by evaporation produced a crude solid, which was subjected to column chromatography with a 1:1 to 3:1 ethyl acetate-hexane mixture, affording the unreacted ketone **5** (3.52 g, 14%) in the early fractions and the crystalline lactone **6** (22.1 g, 81% yield) in the late fractions. The yield of **6** based on consumed **5** was 94%. An analytical specimen of **6**, mp 146—147 °C (lit,[21] mp 140—141 °C), was collected by recrystallization from chloroform-hexane: IR 1737 cm^{-1} (C=O); ^1H NMR (benzene-d_6) δ=1.04 (s, 3 H, isopropylidne CH_3), 1.42 (s, isopropylidene CH_3), 2.16 (dd, J=3, 14 Hz, H_{2b}), 2.38 (dd, J=5.4, 14 Hz, H_{2a}), 3.10 (dd, J=3, 14 Hz, $H_{5'a}$), 3.51 (d, J=14 Hz, $H_{5'b}$), 3.96 (m, $H_{1'}$ and $H_{4'}$), 4.39 (d, J=6 Hz, $H_{2'}$), 4.58 (d, J=6 Hz, H_3); mass spectrum m/z 199 (M^+−15). Anal. ($C_{10}H_{14}O_5$) C, H.

B. With m-Chloroperbenzoic Acid: A 50-ml thick-glass tube charged with a magnetic stirring bar, **5** (2.0 g, 10 mmol), *m*-chloroperbenzoic acid (2.9 g, 16.8 mmol), sodium hydrogencarbonate (1.74 g, 20.7 mmol), and 4,4'-thiobis(6-*t*-butyl-3-methylphenol) (100 mg, 0.14 mmol) in chloroform (40 ml) was sealed and covered with an aluminum foil for shutting out the light. The ampule was immersed in a heating oil bath at 40—45 °C with stirring for 4 d. The resulting insoluble material was removed by filtration and washed with dichloromethane (20 ml). Concentration giving a yellow crystalline product followed by column chromatography with a 1:1 to 4:1 ether-hexane mixture afforded **6** (1.27 g, 59% yield) as colorless crystals, mp 146—147 °C after recrystallization. Unreacted **5** (810 mg, 41%) was recovered, hence the conversion yield was 99%.

(±)-Methyl 2-[(1S,2S*,3R*,4R*)-2,3-O-Isopropylidene-β-ribofuranosyl]acetate (7).* To a solution of the lactone **6** (200 mg, 1.00 mmol) in methanol (3 ml) was added dropwise 1 mol dm^{-3} methanolic sodium methoxide (1.20 ml) at room temperature over 5 min. Immediately after the addition was completed, the reaction mixture was quenched with 1 mol dm^{-3} solution of ammonium chloride in methanol (1.2 ml) and concentrated. The resulting residue was treated with water (5 ml) and extracted with dichloromethane (10 ml×3). The combined organic extracts were washed with brine and evaporated to give an oil, which was chromatographed on a silica-gel column (1:1 ethyl acetate-hexane) to afford **7** (233 mg, 95%) having the identical spectral data with those of the authentic sample alternatively prepared by the literature method.[24]

Methyl 5-O-(R)-1-(1-Naphthyl)ethylcarbamoyl-2-(2,3-O-isopropylidene-β-D-ribofuranosyl)acetate (8) and Methyl 5-O-(R)-1-(1-Naphthyl)ethylcarbamoyl-2-(2,3-O-bisopropylidene-β-L-ribofuranosyl)acetate (9). A mixture of **7** and (*R*)-1-(1-naphthyl)ethyl isocyanate in toluene (3 ml) was refluxed for 24 h under argon. Concentration of the resulting mixture gave a yellow oil, which was roughly purified by silica-gel column chromatography (35:65 ethyl acetate-hexane), yielding an oily mixture of the diastereomeric carbamates, **8** and **9**, (260 mg). This oil was subjected to preparative HPLC (10× 600 mm Hypersil-ODS, 40:60 H_2O-CH_3CN) to afford **8** [V_R 17.3 ml, 115 mg, 43% (86% theoretical yield)] and **9** [V_R 16.4 ml, 125 mg, 46% (92% theoretical yield)] as glassy syrups. **8**: $[\alpha]_D^{15}$ −3.56° (*c* 0.337, $CHCl_3$); IR 3440 (NH), 1730 cm^{-1} (C=O); ^1H NMR ($CDCl_3$) δ=1.23 (s, isopropylidene CH_3), 1.45 (s, isopropylidene CH_3), 1.56 (d, J=6.5 Hz, CHC$\underline{H}_3$), 2.5 (m, C$\underline{H}_2$COOCH$_3$), 3.56 (s, COOCH$_3$), 4.0 (m, $H_{1'}$, $H_{4'}$, and 2 $H_{5'}$), 4.4 (m, $H_{2'}$ and $H_{3'}$), 5.10 (d, J=6.5 Hz, NH), 5.50 (seven-line m, J=6.5 Hz, C$\underline{H}$NH), 7.1—8.1 (m, aromatic H). Found: m/z, 443.1936. Calcd for $C_{24}H_{29}NO_7$: 443.1942. **9**: $[\alpha]_D^{15}$ −1.25° (*c* 0.561, $CHCl_3$); IR 3440 (NH), 1730 cm^{-1} (C=O); ^1H NMR ($CDCl_3$) δ=1.22 (s, isopropylidene CH_3), 1.43 (s, isopropylidene CH_3), 1.53 (d, J=6.5 Hz, CHC$\underline{H}_3$), 2.47 (m, C$\underline{H}_2$COOCH$_3$), 3.50 (s, COOCH$_3$), 4.0 (m, $H_{1'}$, $H_{4'}$, and 2 $H_{5'}$), 4.4 (m, $H_{2'}$ and $H_{3'}$), 5.07 (br d, J=7 Hz, NH), 5.49 (m, C$\underline{H}$NH), 7.2—8.1 (m, aromatic H). Found: m/z, 443.1931. Calcd for $C_{24}H_{29}NO_7$: 443.1942.

Methyl 2-(2,3-O-Isopropylidene-β-D-ribofuranosyl)acetate (D-7). To a solution of **8** (83 mg, 0.19 mmol) and triethyl-

amine (46 mg, 0.45 mmol) in benzene (1.7 ml) was added trichlorosilane (31 mg, 0.23 mmol). The mixture was heated at reflux for 1 h under argon and quenched with water (3 ml). The organic layer was separated and the aqueous solution was extracted with dichloromethane (5 ml×3). The combined organic extracts were washed with brine (3 ml). Concentration gave an oil, which was subjected to column chromatography on silica gel (1:1 ethyl acetate–hexane) to give D-**7** (37 mg, 80%), $[\alpha]_D^{15}$ −6.28° (*c* 2.33, $CHCl_3$), identical in all respects with the authentic sample prepared according to the known procedure.[24]

2-(2,3-O-Isopropylidene-β-D-ribofuranosyl)-2-(dimethylaminomethylene)acetic Acid Lactone (D-10). A mixture of the lactone D-**6** (2.14 g, 10.0 mmol), *t*-butoxybis(dimethylamino)methane[25] (10 ml), and DMF (5 ml) was heated at 60 °C for 1 h. Evaporation of the resulting mixture *in vacuo* left an oily residue, which was chromatographed on a column packed with ammonia-treated silica gel. Elution with 1:1 ethyl acetate–hexane afforded a yellow syrup, D-**10** (2.45 g, 91% yield): IR 1685, 1680, 1595, 1420 cm^{-1}; UV λ_{max} (CH_3OH) 296 nm (ε 13500); mass spectrum *m/z* 269 (M^+). The ^1H NMR spectrum ($CDCl_3$) showed that the product consisted of *ca.* 2:1 mixture of *Z*- and *E*-olefinic isomers: δ=1.32 (s, isopropylidene CH_3), 1.51 (s, isopropylidene CH_3), 2.94 and 3.16 (two s's (1:2), $N(CH_3)_2$), 4.1—5.1 (m, $H_{1'}$, $H_{2'}$, $H_{3'}$, $H_{4'}$, and 2 $H_{5'}$), 6.69 and 7.34 (two s's (1:2), =CH). An analytical sample, mp 78—80 °C, was obtained by recrystallization from ether–hexane. Anal. ($C_{13}H_{19}NO_5$) C, H, N.

5-(2,3-O-Isopropylidene-β-D-ribofuranosyl)uracil (D-12). A mixture of D-**10** (4.12 g, 15.3 mmol), urea (4.59 g, 76.6 mmol), and 1 mol dm^{-3} solution of sodium ethoxide in ethanol (77 ml) was heated at reflux for 5 h under argon atmosphere. Evaporation of the reaction mixture left a residual syrup, which was dissolved in water (10 ml), and carefully neutralized by 6 mol dm^{-3} hydrochloric acid under monitoring with a pH test paper. An oil produced by concentration was diluted with ethanol (80 ml) and the insoluble material was removed by filtration. Evaporation followed by column chromatography using a 1:5 to 1:3 methanol–chloroform mixture as eluent gave the compound D-**12** (2.61 g, 60% yield), R_f 0.29 (1:5 methanol–chloroform) as slightly yellow crystals. Recrystallization from methanol–acetone–hexane produced the analytical sample, mp 235—236 °C (lit,[29] 233—234 °C), $[\alpha]_D^{21}$ −18.1° (*c* 0.16, CH_3OH): UV λ_{max} (CH_3OH) 263 nm (ε 5960), λ_{max} (0.1 mol dm^{-3} NaOH) 284 nm (ε 7110); ^1H NMR (dimethyl-d_6 sulfoxide) δ=1.27 (s, isopropylidene CH_3), 1.49 (s, isopropylidene CH_3), 3.53 (br s, 2 $H_{5'}$), 3.91 (br q, *J*=4.0 Hz, $H_{4'}$), 4.6—5.0 (m, $H_{1'}$, $H_{2'}$, $H_{3'}$, and OH), 7.55 (s, H_6), 10.93 (br s, NH), 11.14 (br s, NH); ^{13}C NMR (dimethyl-d_6 sulfoxide) δ= 25.45, 27.42, 61.74, 80.30, 81.55, 83.91, 84.33, 110.40, 112.81, 140.03, 151.05, 163.27. These physical and spectral data were superimposable on those of the authentic sample prepared by the method of literature.[29]

5-(β-D-Ribofuranosyl)uracil (Pseudouridine) (1). A mixture of solution of D-**12** (321 mg, 1.14 mmol) in methanol (5 ml) and 10% methanolic hydrogen chloride (5 ml) was stirred at 20 °C for 5 h. During this period there occurred pseudouridine (**1**) as colorless crystalline material, which was collected by filtration. A viscous residue left by concentration was dissolved in ethanol (5 ml) and evaporated. Repetition of this evaporation procedure followed by washing of the residue with ether (5 ml×3) gave additional **1**. Totally 259 mg (93%) of **1** was obtained. Recrystallization from methanol afforded an analytical sample, mp 243—244 °C (lit,[28] 221—222 °C), $[\alpha]_D^{21}$ −4.30° (*c*, 0.47, H_2O): UV λ_{max} (CH_3OH) 264 nm (ε 4750), λ_{max} (0.1 mol dm^{-3} HCl) 263 nm (ε 7560), λ_{max} (0.1 mol dm^{-3} NaOH) 285 nm (ε 7360); ^1H NMR (dimethyl-d_6 sulfoxide) δ=3.3—4.0 (m, $H_{2'}$, $H_{3'}$, $H_{4'}$, and 2 $H_{5'}$), 4.51 (d, *J*=4.0 Hz, $H_{1'}$), 4.54 (br s, 3 OH), 7.52 (d, *J*=6.0 Hz, H_6), 10.85 (d, *J*=6.0 Hz, H_1), 11.07 (br s, H_3); ^{13}C NMR (dimethyl-d_6 sulfoxide) δ=61.36, 70.62, 73.93, 78.88, 83.47, 111.05, 139.62, 150.98, 163.57. This compound showed the spectral and physical behavior identical with that of the naturally occurring specimen.

5-(2,3-O-Isopropylidene-β-D-ribofuranosyl)-2-thiouracil (D-14). A mixture of D-**10** (2.14 g, 7.96 mmol), thiourea (3.02 g, 39.8 mmol). and 1 mol dm^{-3} ethanolic sodium ethoxide (40 ml) was refluxed for 3 h under argon. Residue obtained by evaporation was dissolved in water (10 ml) and carefully neutralized with 6 mol dm^{-3} hydrochloric acid. Extraction with ethyl acetate (50 ml×5) and concentration of the combined organic layers afforded a yellow solid, which on column chromatography with a 1:30 to 1:5 methanol–chloroform mixture gave rise to D-**14** (1.93 g, 81% yield), R_f 0.65 (1:5 methanol–chloroform), as a slightly yellow foam, $[\alpha]_D^{22}$ −8.0° (*c*, 0.92, CH_3OH): UV λ_{max} (CH_3OH) 276 (ε 13930), 292 nm (12860), λ_{max} (0.1 mol dm^{-3} NaOH) 264 (ε 12920), 290 nm (10560); ^1H NMR (dimethyl-d_6 sulfoxide) δ=1.27 (s, isopropylidene CH_3), 1.49 (s, isopropylidene CH_3), 3.20 (br s, 2 $H_{5'}$), 3.91 (m, $H_{4'}$), 4.5—4.7 (m, $H_{1'}$, $H_{2'}$, and $H_{3'}$), 7.50 (s, H_6), 12.42 (br s, 2 NH); ^{13}C NMR (dimethyl-d_6 sulfoxide) δ=25.43, 27.36, 61.62, 79.94, 81.41, 84.02, 85.07, 112.84, 115.92, 139.11, 160.16, 175.39. Found: *m/z*, 300.07739. Calcd for $C_{12}H_{16}N_2O_5S$: 300.07798.

5-(β-D-Ribofuranosyl)-2-thiouracil (2-Thiopseudouridine) (D-15). A mixture of solution of D-**14** (763 mg, 2.56 mmol) in methanol (5 ml) and 10% solution of hydrogen chloride in methanol (7 ml) was stirred at 20 °C for 1 h and subsequently concentrated. The resulting residue was diluted with ethanol (7 ml) and evaporated. Dilution and evaporation sequence was repeated twice more to leave a colorless solid, which was washed with ether (7 ml×2). The solid was dried *in vacuo* producing 2-thiopseudouridine (D-**15**) (599 mg, 90% yield) as very hygroscopic, colorless crystals:[56] UV λ_{max} (CH_3OH) 275, 293 nm,[56] λ_{max} (0.1 mol dm^{-3} HCl) 274, 291 nm,[56] λ_{max} (0.1 mol dm^{-3} NaOH) 264, 284 nm;[56] ^1H NMR (dimethyl-d_6 sulfoxide) δ=3.5—4.1 (m, $H_{2'}$, $H_{3'}$, $H_{4'}$, and 2 $H_{5'}$), 4.59 (d, *J*=3.8 Hz, $H_{1'}$), 6.11 (br s, 3 OH), 7.60 (d, J=5.2 Hz, H_6), 12.28 (d, *J*=5.2 Hz, H_1), 12.37 (br s, H_3); ^{13}C NMR (dimethyl-d_6 sulfoxide) δ=62.26, 71.52, 74.76, 79.77, 84.37, 111.70, 140.58, 151.77, 164.44. The product was identical in all respects with an authentic sample of D-**15** synthesized according to the reported procedure.[28]

5-(2,3-O-Isopropylidene-β-D-ribofuranosyl)isocytosine (D-16). Guanidine hydrochloride (4.53 g, 45.5 mmol) was dissolved in 1 mol dm^{-3} solution of sodium ethoxide in ethanol (50 ml). This solution was added to D-**10** (2.45 g, 9.11 mmol) and heated at reflux for 3 h under argon. The reaction mixture was concentrated under reduced pressure and the resulting residue was dissolved in water (10 ml). After careful neutralization with 6 mol dm^{-3} hydrochloric acid by monitoring with a pH test paper, the aqueous solution was evaporated giving a viscous liquid, which was treated with ethanol (150 ml). Removal of the occurring precipitates by filtration followed by concentration gave rise to a colorless oil, which was chromatographed with a 1:30 to 1:5 methanol–chloroform mixture as eluent to produce D-**16** (2.09 g, 81% yield) as a colorless solid. Recrystallization from methanol gave an analytical specimen, mp 170—174 °C, $[\alpha]_D^{22}$ −50.8° (*c*. 0.73, CH_3OH); UV λ_{max} (CH_3OH) 226 (ε 5530), 290 nm (5390), λ_{max} (0.1 mol dm^{-3} NaOH) 233 (ε 12660), 277 nm (9860); ^1H NMR (dimethyl-d_6 sulfoxide) δ=1.27 (s, isopropylidene CH_3), 1.48 (s, isopylidene CH_3), 3.51 (br d, *J*=4.5 Hz, 2 $H_{5'}$), 3.93 (br q, *J*=3.8 Hz, $H_{4'}$), 4.5—4.9 (m, $H_{1'}$, $H_{2'}$, and $H_{3'}$), 6.97 (br s, NH_2), 7.63 (s, H_6); ^{13}C NMR (dimethyl-d_6 sulfoxide) δ=25.49, 27.52, 62.12, 81.77, 82.02, 83.57, 84.56, 112.27, 112.77, 152.81, 156.22, 163.25. Anal. ($C_{12}H_{17}N_3O_5$) C, H, N.

5-(β-D-Ribofuranosyl)isocytosine Hydrochloride (Pseudoisocytidine Hydrochloride) (Hydrochloride of D-17). To a suspension of D-**16** (1.24 g, 4.38 mmol) in methanol (10 ml) was added with efficient stirring 10% methanol solution (20 ml) of hydrogen chloride and the mixture was stirred at 20 °C for 1 h. The occurring colorless precipitates were collected by filtration. These crystals (1.14 g, 93% yield) were identified as pseudoisocytidine (D-**17**) hydrochloride by comparison of the spectral data and physical properties with the authentic sample, mp 212—215 °C (lit,[28] 215—216 °C), $[\alpha]_D^{22}$ +14.3° (*c* 0.49, H_2O): UV λ_{max} (CH_3OH) 225 (ε 9850), 290 nm (7000), λ_{max} (0.1 mol dm^{-3} NaOH) 233 (ε 9570), 277 nm (7270); ^1H NMR (dimethyl-d_6 sulfoxide) δ=3.4—4.0 (m, $H_{2'}$, $H_{3'}$, $H_{4'}$, and $H_{5'}$), 4.59 (d, *J*=2.7 Hz, $H_{1'}$), 7.83 (s, H_6), 8.53 (br s, NH_2).

2-(2,3-O-Isopropylidene-β-D-ribofuranosyl)maleimide (D-19) from D-10. To a solution of D-**10** (250 mg, 0.93 mmol) in ethyl acetate (20 ml) cooled at −78 °C was passed ozone for 10 min followed by nitrogen for 5 min. The resulting mixture was quenched by addition of dimethyl sulfide (1.0 ml, 846 mg, 13.6 mmol) and stirred at −78 °C for 1 h, at 0 °C for 3 h, and then at 20 °C for an additional 1 h. On removal of the solvent, there was left a yellow, oily material D-**18**; IR 1732 cm^{-1} (C=O), no olefinic absorption. This unstable compound was used for the subsequent reaction without further purification. To a solution of the crude product in DMF (3 ml) was added a solution of $(C_6H_5)_3PCHCONH_2$ (297 mg, 0.93 mmol) in DMF (3 ml) and the mixture was stirred at 20 °C for 1 h and at 50 °C for 2 h under argon. Evaporation under high vacuum afforded a residual oil, preparative TLC of which with ethyl acetate produced D-**19** (75.3 mg, 30% overall yield from D-**10**), mp 142—143 °C (ethyl acetate–hexane) (lit,[57] 140.5—141 °C), $[\alpha]_D^{24}$ −2.31° (*c* 1.07, $CHCl_3$). The product had identical spectral data and physical properties with those of the authentic sample prepared from natural showdomycin according to the known procedure.[57]

Preparation of Showdomycin Acetonide (D-19) from D-21. Ozone was passed through a solution of D-**21** (150 mg, 0.514 mmol) in ethyl acetate (20 ml) at −78 °C for *ca.* 10 min until the color of the solution became blue-violet. The excess ozone was removed by blowing nitrogen gas to the solution for 5 min. After quenching by addition of dimethyl sulfide (0.5 ml, 423 mg, 6.81 mmol), the mixture was stirred at −78 °C for 1 h, at 0 °C for 1 h, and at 25 °C for 1 h, and then concentrated. The resulting oil was dissolved in ethyl acetate (20 ml) and washed with brine (4 ml). The organic layer was dried over sodium sulfate and evaporated to yield a slightly yellow liquid. A mixture of this oil and $(C_6H_5)_3PCHCONH_2$ (180 mg, 0.565 mmol) in DMF (4 ml) was stirred at 25 °C for 1 h and then at 50 °C for 1 h under argon. Removal of the solvent *in vacuo* left a crude oil, whose preparative TLC with ethyl acetate produced the crystalline acetonide D-**19** (21 mg, 15% yield). Recrystallization from acetone–benzene afforded an analytical sample, mp 141—142 °C.

2-(β-D-Ribofuranosyl)maleimide (Showdomycin) (3). A mixture of D-**19** (100 mg, 0.37 mmol) and 80% aqueous trifluoroacetic acid (3 ml) was stirred at 20 °C for 10 min Evaporation *in vacuo* afforded a viscous residue, whose preparative TLC using 7:3 ethyl acetate–acetone gave rise to showdomycin (**3**) (77.9 mg, 92% yield). An analytical specimen displaying ^1H NMR and UV spectra and the optical rotation, $[\alpha]_D^{24}$ +48.7° (*c* 1.4, H_2O) (lit, +49.1°,[32f] +49.9°[57]), identical with the authentic natural product was obtained by recrystallization from acetone–benzene, mp 151—152 °C (lit, 152—153 °C,[32b] 153—154 °C,[6b] 154.5—156 °C,[32a] 160—161 °C[57]).

(2S)-2-(2,3-O-Isopropylidene-β-D-ribofuranosyl-2-[(S*)-(2-furyl)hydroxylmethyl]acetic Acid Lactone (D-20).* To a 0.3 mol dm^{-3} solution (10 ml) of lithium cyclohexylisopropylamide in THF–hexane was added at −78 °C a solution of D-**6** (500 mg, 2.3 mmol) in THF (10 ml) over 5 min with stirring. After 1.5 h, to this was added a solution of furfural (3.0 ml, 3.46 g, 36 mmol) in THF (5 ml) at −78 °C and stirring was continued for an additional 1 h. The reaction mixture was quenched with saturated aqueous oxalic acid solution (5 ml) and extracted with chloroform (100 ml, 50 ml, 30 ml). The combined organic extracts were washed with brine (10 ml), dried over sodium sulfate, and evaporated to yield a yellow crystalline product, which was subjected to column chromatography using successively a 1:1, 2:1, and 4:1 ether–hexane mixture, and finally with ether. The hydroxy lactone D-**20** (640 mg, 90% yield) was obtained as colorless crystals, mp 139—141 °C (from ethyl acetate–chloroform–hexane), $[\alpha]_D^{21}$ +26.0° (*c* 2.63, $CHCl_3$): IR 3200—3600 (OH), 1728 cm^{-1} (C=O); ^1H NMR ($CDCl_3$) δ=1.30 (s, isopropylidene CH_3), 1.46 (s, isopropylidene CH_3), 2.95 (d, *J*=7 Hz, OH), 3.48 (dd, *J*=5, 9 Hz, COCH), 3.97 (d, *J*=5 Hz, $H_{1'}$), 4.15 (dd, *J*=4.5, 14 Hz, $H_{5'a}$), 4.45 (dd, *J*=2.5, 4.5 Hz, $H_{4'}$), 4.55 (d, *J*=6 Hz, $H_{2'}$), 4.56 (dd, *J*=2.5, 14 Hz, $H_{5'b}$), 4.82 (d, *J*=6 Hz, $H_{3'}$), 5.25 (dd, *J*=7, 9 Hz, CHOH), 6.40 (m, furyl H_3 and H_4), 7.43 (m, furyl H_5); mass spectrum *m/z* 310 (M^+). Anal. ($C_{15}H_{18}O_7$) C, H.

2-(2,3-O-Isopropylidene-β-D-ribofuranosyl)-2-furfurylideneacetic Acid Lactone (D-21). To a cooled (0 °C) solution of D-**20** (300 mg, 0.76 mmol) in pyridine (5 ml) was added a solution of pivaloyl chloride (0.47 ml, 458 mg, 3.8 mmol) in pyridine (5 ml) over 2 min with efficient stirring under argon. After stirring at 0 °C for an additional 1 h and then at room temperature for 24 h, the reaction mixture was diluted with benzene (50 ml), washed with water (10 ml), and dried over sodium sulfate. Concentration under high vacuum (<0.01 mmHg) at room temperature for 30 min left a pale violet oil which was passed through a short silica-gel column using ether as eluent. Removal of the solvent of the filtrate gave a yellow oil, a solution of which in pyridine (15 ml) was heated at 80—90 °C for 13 h under argon. Dilution of the reaction mixture with benzene (50 ml), followed by concentration to dryness afforded a dark brown oil. The preparative TLC with 5:1 ether–hexane produced D-**21** (222 mg, 100% overall yield) as a gummy material, yielding an analytical sample by recrystallization from chloroform–hexane, mp 160—162 °C, $[\alpha]_D^{21}$ −143° (*c* 0.64, $CHCl_3$): IR 1715 (C=O), 1627 cm^{-1} (C=C), ^1H NMR ($CDCl_3$) δ=1.35 (s, isopropylidene CH_3), 1.58 (s, isopropylidene CH_3), 4.25 (m, 2 $H_{5'}$), 4.50 (m, $H_{4'}$), 4.70 (d, *J*=6 Hz, $H_{2'}$), 4.99 (d, *J*=6 Hz, $H_{3'}$), 5.74 (s, $H_{1'}$), 6.52 (dd, *J*=2, 4 Hz, furyl H_4), 6.78 (d, *J*=4 Hz, furyl H_3), 7.24 (s, COC=CH), 7.62 (d, *J*=2 Hz, furyl H_5); mass specturm *m/z* 292 (M^+). Anal. ($C_{15}H_{16}O_6$) C, H.

Methyl 2-(2,3-O-Isopropylidene-β-D-ribofuranosyl)-2-furfurylideneacetate (D-22). A solution of D-**21** (220 mg, 0.69 mmol) in methanol (7 ml) was mixed with a 90 mmol dm^{-3} methanolic sodium methoxide (10 ml) at 0 °C and stirred for 30 min. The resulting mixture was quenched by addition of an aqueous solution saturated with oxalic acid (5 ml) and extracted with chloroform (50 ml, 30 ml). The collected organic layers were washed with brine (10 ml) and dried over sodium sulfate. Evaporation *in vacuo* left an orange oil (210 mg), which was subjected to preparative TLC with 2:1 ethyl acetate–hexane, giving rise to D-**22** (190 mg, 86% yield) as a colorless liquid, $[\alpha]_D^{21}$ +104° (*c* 2.90, $CHCl_3$); IR 3620—3300 (OH), 1700 (C=O), 1635 cm^{-1} (C=C); ^1H NMR (benzene-d_6) δ=1.23 (s, isopropylidene CH_3), 1.58 (s, isopropylidene CH_3), 3.27 (s, OCH_3), 3.69 (dd, *J*=3, 12 Hz, $H_{5'a}$), 3.70 (br s, OH), 3.95 (dd, *J*=2, 12 Hz, $H_{5'b}$), 4.33 (m, $H_{4'}$), 5.13 (d, *J*=6 Hz, $H_{2'}$), 5.26 (d, *J*=6 Hz, $H_{3'}$), 5.95 (m, $H_{1'}$, and furyl H_4), 6.47 (d, *J*=3 Hz, furyl H_3), 6.93 (d, *J*=2 Hz, furyl H_5), 7.46 (s, COC=CH); mass spectrum *m/z* 324 (M^+). Anal. ($C_{16}H_{20}O_7$) C, H.

Methyl 2-[2,3-O-Isopropylidene-5-O-(t-butyldimethylsilyl)-β-D-ribofuranosyl]-2-furfurylideneacetate (D-23). A mixture

of D-**22** (190 mg, 0.59 mmol), *t*-butylchlorodimethylsilane (130 mg, 0.84 mmol), imidazole (120 mg, 1.8 mmol) in DMF (15 ml) was stirred at room temperature for 1 h. The reaction mixture was diluted with ether (50 ml) and washed with brine (10 ml). The organic layer was dried over sodium sulfate and concentrated to leave a yellow viscous oil. Preparative TLC with 1:1 ethyl acetate–hexane gave D-**23** (260 mg, 100% yield), $[\alpha]_D^{21}$ −0.98° (*c* 0.44, $CHCl_3$); IR 1710 (C=O), 1635 (C=C), 830 cm^{-1} (Si–O); ^1H NMR (benzene-d_6) δ=0.06 (s, $Si(CH_3)_2$), 0.98 (s, SiC_4H_9-*t*), 1.25 (s, isopropylidene CH_3), 1.56 (s, isopropylidene CH_3), 3.38 (s, OCH_3), 3.97 (d, *J*=6 Hz, $H_{5'a}$), 3.98 (d, *J*=5.5 Hz, $H_{5'b}$), 4.38 (q, *J*=6 Hz, $H_{4'}$), 5.02 (t, *J*=6 Hz, $H_{3'}$), 5.22 (dd, *J*=4, 6 Hz, $H_{2'}$), 5.90 (dd, *J*=2, 4 Hz, furyl H_4), 6.00 (d, *J*=4 Hz, $H_{1'}$), 6.41 (d, *J*=4 Hz, furyl H_3), 6.86 (d, *J*=2 Hz, furyl H_5), 7.44 (s, COC=CH); mass spectrum *m/z* 423 (M^+ −15). Anal. ($C_{22}H_{34}O_7Si$) C, H.

3-[2,3-O-Isopropylidene-5-O-(t-butyldimethylsilyl-β-D-ribofuranosyl]maleimide (D-25). Ozone was introduced into a solution of D-**23** (260 mg, 0.59 mmol) in dry ethyl acetate (30 ml) at −78 °C until the color of solution became blue-violet and then nitrogen gas was blown through this solution for 10 min at that temprature to remove an excess of ozone. After addition of dimethyl sulfide (1.0 ml, 846 mg, 13.6 mmol) at −78 °C, the reaction mixture was stirred at the same temperature for 1 h and for an additional 2 h under warming up to room temperature. Concentration gave a yellow crude product (430 mg), to which was added chloroform (30 ml) with vigorous shaking. Removal of the occurring precipitate by filtration through a Celite 545 pad, followed by evaporation of the filtrate left crude methyl 2-[2,3-*O*-isopropylidene-5-*O*-(*t*-butyldimethylsilyl)-β-D-ribofuranosyl]glyoxylate (D-**24**) as a yellow, viscous liquid; IR 1760 (shoulder, C=O), 1740 cm^{-1} (C=O); mass spectrum *m/z* 374 (M^+). This compound was so labile and attempted chromatography resulted in complete decomposition. Therefore this was employed in the next procedure without any purification.

A mixture of the crude D-**24** (obtained from 150 mg (0.40 mmol) of D-**32**) and $(C_6H_5)_3PCHCONH_2$ (270 mg, 0.80 mmol) in chloroform (20 ml) was stirred at room temperature. After 2 h, a solution of the phosphorane (130 mg, 0.39 mmol) in chloroform (5 ml) was added renewedly and stirring was continued for further 30 min. Concentration of the resulting mixture yielded an oily residue, which was subjected to preparative TLC with 2:1 ether–hexane, producing D-**25** (43 mg, 29% yield based on D-**23**), $[\alpha]_D^{24}$ +2.1° (*c* 1.40, $CHCl_3$); IR 3420 (NH), 1775 (C=O), 1726 (C=O), 1620 cm^{-1} (C=C); UV λ_{max} (CH_3OH) 221 nm (ε 13800); ^1H NMR ($CDCl_3$) δ=0.05 (s, $Si(CH_3)_2$), 0.85 (s, SiC_4H_9-*t*), 1.34 (s, isopropylidene CH_3) 1.59 (s, isopropylidene CH_3), 3.70 (br d, *J*=4.0 Hz, 2 $H_{5'}$), 4.20 (m, $H_{4'}$), 4.66 (m, $H_{2'}$ and $H_{3'}$), 4.82 (m, $H_{1'}$), 6.49 (t, *J*=2 Hz, H_3), 7.42 (br s, NH); mass spectrum *m/z* 368 (M^+ −15). Anal. ($C_{18}H_{29}NO_6Si$) C, H, N.

3-(β-D-Ribofuranosyl)maleimide (Showdomycin) (3). A mixture of D-**25** (130 mg, 0.339 mmol) and 80% aq trifluoroacetic acid (3 ml) was stirred at 25 °C for 10 min. Evaporation to dryness at room temperature under high vacuum (0.01 mmHg) left a white crystalline product. Column chromatography with 1:4 acetone–ethyl acetate gave showdomycin (**3**) 66 mg, 85% yield), mp 151—15 °C (acetone-benzene), which was consistent in all respects with the natural product.

Semicarbazone of Methyl 2-[2,3-O-Isopropylidene-5-O-(t-butyldimethylsilyl)-β-D-ribofuranosyl]glyoxylate (D-26). Into a cooled solution of D-**23** (720 mg, 1.70 mmol) in ethyl acetate (220 ml) at −78 °C was introduced ozone until the solution assumed blue-violet color. The solution was flushed with nitrogen gas in order to remove an excess of ozone for 10 min. The mixture was quenched with dimethyl sulfide (3.0 ml, 2.54 g, 4.08 mmol) at −78 °C and stirred at the same temperature for 1 h, at 0 °C for 1 h, and at room temperature for 1 h. Evaporation afforded a brown oil, which was dissolved in 66% aq methanol (45 ml) and to this were added semicarbazide hydrochloride (900 mg, 8.10 mmol) and sodium acetate (660 mg, 8.10 mmol). The mixture was stirred at 20 °C for 12 h and at 80 °C for 2 h, and then semicarbazide hydrochloride (600 mg, 5.40 mmol) and sodium acetate (440 mg, 5.40 mmol) were added renewedly. After stirring at 60 °C for 2 h, semicarbazide hydrochloride (300 mg, 2.70 mmol) and sodium acetate (220 mg, 2.70 mmol) in methanol (10 ml)–water (15 ml) were added again and the resulting mixture was maintained at 60 °C for an additional 2 h. An only residue obtained by concentration was treated with water (20 ml) and extracted with chloroform (150 ml, 100 ml, 50 ml). The combined organic extracts were washed with brine (20 ml) and dried over sodium sulfate. Removal of the solvent produced a viscous oil, preparative TLC of which using ethyl acetate gave D-**26** (220 mg, 30% yield from D-**23**) as an oil, $[\alpha]_D^{22}$ −1.6° (*c* 1.0, $CHCl_3$); IR 3520, 3400, 3300 (NH), 1703 (C=O), 1560 cm^{-1} (C=N); UV λ_{max} (CH_3OH) 265 nm (ε 8790); ^1H NMR ($CDCl_3$) δ=0.10 (s, $Si(CH_3)_2$), 0.89 (s, SiC_4H_9-*t*), 1.26 (s, isopropylidene CH_3), 1.29 and 1.37 (two s's, 1.5 H each, isopropylidene CH_3 of *E* or/and *Z* isomers), 3.70 (d, *J*=5 Hz, $H_{5'a}$), 3.87 (s, OCH_3), 3.6—4.0 (m, $H_{5'b}$), 4.1—5.2 (m, $H_{1'}$, $H_{2'}$, $H_{3'}$, and $H_{4'}$), 5.5—6.0 (br s, NH_2), 10.21 and 11.29 (two br s's, 0.5 H each NH of *E* or/and *Z* isomers). Anal. ($C_{18}H_{33}N_3O_7Si$) C, H, N.

6-[2,3-O-Isopropylidene-5-O-(t-butyldimethylsilyl-β-D-ribofuranosyl]-1,2,4-triazine-3,5(2H,4H)-dione (D-27). A mixture of the semicarbazone D-**26** (250 mg, 0.625 mmol) and a 0.1 mol dm^{-3} solution of sodium ethoxide in ethanol (12.5 ml, 1.25 mmol of sodium ethoxide) was refluxed for 3 h. A residual oil afforded by evaporation was dissolved in water (20 ml). The aqueous layer was acidified to pH 4 by careful addition of 0.5 mol dm^{-3} hydrochloric acid and extracted with ethyl acetate (50 ml×3). The collected organic extracts were washed with brine and dried over sodium sulfate. Removal of the solvent and the subsequent preparative TLC with 5:1 ether–chloroform produced D-**27** (100 mg, 40% yield) as an oil, $[\alpha]_D^{25}$ −35.8° (*c* 8.90, $CHCl_3$); IR 3500—3100 (NH), 1721 and 1698 cm^{-1} (C=O); UV λ_{max} (0.1 mol dm^{-3} HCl) 262 nm (ε 7420), λ_{max} (CH_3OH) 264 nm (ε 6920), λ_{max} (0.1 mol dm^{-3} NaOH) 258 (ε 5020), 293 nm (3230); ^1H NMR ($CDCl_3$) δ=0.04 (s, $Si(CH_3)_2$), 0.88 (s, SiC_4H_9-*t*), 1.37 (s, isopropylidene CH_3), 1.58 (s, isopropylidene CH_3), 3.77 (d, *J*=5 Hz, 2 $H_{5'}$), 4.20 (m, $H_{4'}$), 4.76 (dd, *J*=3, 6 Hz, $H_{2'}$), 5.0 (m, $H_{1'}$ and $H_{3'}$), 9.17 (br s, NH), 9.73 (br s, NH). Anal. ($C_{17}H_{29}N_3O_6Si$) C, H, N.

6-(β-D-Ribofuranosyl)-1,2,4-triazine-3,5(2H,4H)-dione (6-Azapseudouridine) (D-13). A mixture of D-**27** (158 mg, 0.406 mmol) and 80% aq trifluoroacetic acid (5 ml) was stirred at 25 °C for 10 min. The whole mixture was concentrated under reduced pressure to give a crystalline material. Recrystallization produced an analytical sample of D-**13** (65 mg, 63% yield) as colorless needles, mp 136—138 °C (lit,[30] 138—139 °C), $[\alpha]_D^{24}$ −23.4° (*c* 0.5, H_2O) [lit,[30] $[\alpha]_D^{25}$ −24.9° (*c* 0.5, H_2O)]; IR (KBr) 3400—3100 (NH and OH), 1720 and 1690 cm^{-1} (C=O); UV λ_{max} (CH_3OH) 264 nm (ε 6740); ^1H NMR (acetone-d_6) δ=3.0 (br s, OH), 3.54 (dd, *J*=3.3, 13.8 Hz, $H_{5'a}$), 3.74 (dd, *J*=2.7, 13.8 Hz, $H_{5'b}$), 3.97 (ddd, *J*=2.7, 3.3, 4.5 Hz, $H_{4'}$), 4.20 (dd, *J*=4.5, 5.3 Hz, $H_{2'}$), 4.45 (dd, *J*=5.3, 5.6 Hz, $H_{3'}$), 4.73 (d, *J*=5.6 Hz, $H_{1'}$), 11.70 (br s, 2 NH). These spectral and physical characters were identical with the reported ones.[30]

Thiosemicarbazone of Methyl 2-[2,3-O-Isopropylidene-5-O-(t-butyldimethylsilyl)-β-D-ribofuranosyl]glyoxylate (D-28). Through a solution of D-**23** (500 mg, 1.18 mmol) in ethyl acetate (150 ml) was blown ozone at −78 °C. When the solution took on blue color, introduction of ozone was stopped and nitrogen gas was blown into the solution at the same temperature for 5 min. The resulting colorless solution was

treated with dimethyl sulfide (2.0 ml, 1.69 g, 27.2 mmol) and then stirred at −78 °C for 1 h, at 0 °C for 1 h, and at room temperature for 1 h. Concentration gave a yellow oil, which was mixed with thiosemicarbazide (460 mg, 5.0 mmol) in methanol (25 ml) and refluxed for 12 h. After cooling, evaporation yielded a viscous oil, which was dissolved in chloroform (100 ml) and washed with water (15 ml). Concentration of the organic solution giving an orange oil, followed by preparative TLC with ether, afforded D-**28** (130 mg, 26% yield) as a colorless oil, $[\alpha]_D^{21}$ −0.71° (*c* 1.1, $CHCl_3$); IR 3520, 3380, 1731, 1715, 1582, 1465 cm^{-1}; UV λ_{max} (CH_3OH) 268 (ε 6760), 314 nm (5250); ^1H NMR ($CDCl_3$) δ=0.06 (s, $Si(CH_3)_2$), 0.87 (s, SiC_4H_9-*t*), 1.34 (br s, isopropylidene CH_3), 1.52 (br s, isopropylidene CH_3), 3.67 (s, OCH_3), 3.77 (m, 2 H5′), 4.2—4.8 (m, H1′, H2′, H3′, and H4′), 6.0—6.4 (br s, NH_2), 7.12 and 9.17 (two br s's, 0.5 H each, NH of *E* and/or *Z* isomers); mass spectrum *m/z* 447 (M^+). Anal. ($C_{18}H_{33}N_3O_6SSi$) C, H, N, S.

6-[2,3-O-Isopropylidene-5-O-(t-butyldimethylsilyl)-β-D-ribofuranosyl]-3-thioxo-2,3-dihydro-1,2,4-triazin-5(4H)-one (D-29). A mixture of D-**28** (200 mg, 0.45 mmol) and a 0.1 mol dm^{-3} solution of sodium ethoxide in ethanol (10 ml, 1.0 mmol of sodium ethoxide) was heated at reflux for 3 h and then evaporated to dryness. To a solution of the resulting dark brown liquid in water (10 ml) was added carefully 0.5 mol dm^{-3} hydrochloric acid until the pH of solution reached 4 and the aqueous layer was promptly extracted with ethyl acetate (40 ml×3). The combined organic extracts were dried over sodium sulfate and concentrated, affording a brown liquid. Preparative TLC with 1:1 ether–chloroform gave rise to D-**29** (104 mg, 56% yield) as an oil, $[\alpha]_D^{25}$ −1.4° (*c* 2.30, $CHCl_3$); IR 3500—3200 (NH), 1707 cm^{-1} (C=O); UV λ_{max} (0.1 mol dm^{-3} HCl) 213 (ε 7420), 269 nm (14100), λ_{max} (CH_3OH) 213 (ε 3720), 272 nm (12100), λ_{max} (0.1 mol dm^{-3} NaOH) 226 (ε 16200), 258 (11500), 313 nm (3230); ^1H NMR ($CDCl_3$) δ= 0.06 (s, $Si(CH_3)_2$), 0.88 (s, SiC_4H_9-*t*), 1.38 (s, isopropylidene CH_3), 1.59 (s, isopropylidene CH_3), 3.75 (d, *J*=5 Hz, 2 H5′), 4.17 (m, H4′), 4.77 (dd, *J*=3, 6 Hz, H3′), 5.0 (m, H1′ and H2′). Anal. ($C_{17}H_{29}N_3O_5SSi$) C, H, N, S.

6-(β-D-Ribofuranosyl)-3-thioxo-2,3-dihydro-1,2,4-triazin-5-(4H)-one (6-Azapseudouridine) (D-30). A mixture of D-**29** (100 mg, 0.247 mmol) and 80% aq trifluoroacetic acid (4 ml) was stirred at 25 °C for 20 min and then evaporated *in vacuo*. The resulting crude product was recrystallized from ethanol, affording an analytical specimen of D-**30** (47 mg, 70% yield) as colorless needles, mp 193—195 °C (lit,[30] 197—198 °C), $[\alpha]_D^{25}$ −3.5° (*c* 0.5, H_2O) [lit,[30] −3.7° (*c* 0.5, H_2O)]; IR (KBr) 3500—3100 (NH and OH), 1702 cm^{-1} (C=O); UV λ_{max} (0.1 mol dm^{-3} HCl) 215 (ε 10700), 269 nm (18600), λ_{max} (0.1 mol dm^{-3} NaOH) 259 (ε 13500), 313 nm (7580); ^1H NMR (acetone-d_6) δ=3.06 (br s, OH), 3.57 (dd, *J*=3.6, 12.7 Hz, H5′a), 3.83 (dd, *J*=2.5, 12.7 Hz, H5′b), 4.00 (ddd, *J*=2.5, 3.6, 4.2 Hz, H4′), 4.24 (dd, *J*=4.2, 5.7 Hz, H2′), 4.48 (dd, *J*=5.0, 5.7 Hz, H3′), 4.80 (d, *J*=5.0 Hz, H1′), 11.15 (br s, 2 NH).

Financial support by the Ministry of Education, Japanese Government, and generous gifts of D-ribose from Ajinomoto Co., pseudouridine from Kyowa Hakko Co., showdomycin from Shionogi Research Laboratory, and pseudoisocytidine hydrochloride from Dr. K. A. Watanabe of the Sloan-Kettering Institute for Cancer Research are acknowledged. We are also indebted to Mrs. R. Suzuki for her valuable contribution in some preliminary experiments.

References

1) *C*-Nucleoside Synthesis. 17. For part 16 see: T. Sato, H. Kobayashi, and R. Noyori, *Heterocycles*, **15**, 321 (1981). See also preliminary works of this paper: a) R. Noyori, T. Sato, and Y. Hayakawa, *J. Am. Chem. Soc.*, **100**, 2561 (1978); b) T. Sato, R. Ito, Y. Hayakawa, and R. Noyori, *Tetrahedron Lett.*, **1978**, 1829.

2) W. E. Cohn, *Biochim. Biophys. Acta*, **32**, 569 (1959); *J. Biol. Chem.*, **235**, 1488 (1960).

3) For reviews: R. W. Chambers, *Prog. Nucleic Acid Res. Mol. Biol.*, **5**, 349 (1966); E. Goldwasser and R. L. Heinrikson, *ibid.*, **5**, 399 (1966).

4) Oxazinomycin (minimycin) inhibits the growth of bacteria[5] and is active against transplantable tumors.[5] Showdomycin (**3**) shows antibacterial and antitumor behavior as well as inhibiting nucleic acid synthesis.[6] Pyrazomycin and pyrazomycin B inhibit virus multiplication.[7] Formycin has significant antiviral and antitumor activities, and supresses DNA, RNA, and protein synthesis.[8] Formycin B inhibits the pathogenic bacterium for rice plant decrease caused by *X. oryzae*[5a] and shows antiviral properties against influenza virus.[9] For the detail of biological activities of *C*-nucleosides, see the following reviews: R. J. Suhadolnik, "Nucleoside Antibiotics", Wiley-Interscience, New York, Chapters 9—11 (1970). P. Roy-Burman, "Analogues of Nucleic Acid Components," Springer-Verlag, New York (1970). S. Nakamura and H. Kondo, *Heterocycles*, **8**, 583 (1977).

5) a) S. Aizawa, T. Hidaka, N. Otake, H. Yonehara, K. Isono, N. Igarashi, and S. Suzuki, *Agr. Biol. Chem.*, **29**, 375 (1956); b) G. Koyama and H. Umezawa, *J. Antibiot.*, **18**, 175 (1965); c) T. Haneishi, T. Okazaki, T. Hata, C. Tamura, M. Nomura, A. Naito, I. Seki, and M. Arai, *ibid.*, **24**, 797 (1971); d) Y. Kusakabe, J. Nagatsu, M. Shibuya, O. Kawaguchi, C. Hirose, and S. Shirato, *ibid.*, **25**, 44 (1972).

6) a) S. Matsuura, O. Shiratori, and K. Katagiri, *J. Antibiot.*, **17A**, 234 (1964); b) H. Nishimura, M. Mayama, Y. Komatsu, H. Kato, N. Shimaoka, and Y. Tanaka, *ibid.*, **17A**, 148 (1964).

7) a) K. Gerzon, D. C. DeLong, and J. C. Cline, *Pure Appl. Chem.*, **28**, 489 (1971); b) F. Streightoff, J. A. Nelson, J. C. Cline, K. Gorzon, R. H. Williams, and D. C. DeLong, 9th Conference on Antimicrobial Agents and Chemotherapy, Washington D.C., 1969, American Chemical Society, Washington D.C., Abstr. No. 18; c) G. E. Gutowski, M. O. Chaney, N. D. Jones, R. L. Hamill, F. A. Davis, and R. D. Miller, *Biochem. Biophys. Res. Commun.*, **51**, 312 (1973).

8) M. Hori, E. Ito, T. Takida, G. Koyama, T. Takeuchi, and H. Umezawa. *J. Antibiot.*, **17A**, 96 (1964); M. Ishizuka, T. Sawa, S. Hori, H. Takayama, T. Takeuchi, and H. Umezawa, *ibid.*, **21A**, 1 (1968); H. Umezawa, T. Sawa, Y. Fukagawa, G. Koyama, M. Murase, M. Hamada, and T. Takeuchi, *ibid.*, **18A**, 178 (1965); R. H. Williams, K. Gerzon, M. Hoehen, and D. C. DeLong, 158th National Meeting of the American Chemical Society, New York, N.Y., 1969, American Chemical Society, Washington D.C., Abstract Micr. 38.

9) T. Kunimoto, T. Wakashiro, I. Okamura, T. Asajima, and M. Hori, *J. Antibiot.*, **21A**, 468 (1968); T. Takeuchi, J. Iwanaga, T. Aoyagi, M. Murase, T. Sawa, and H. Umezawa, *ibid.*, **20A**, 297 (1967).

10) For comprehensive reviews see: a) L. Goodman, "Basic Principles in Nucleic Acid Chemistry", ed by P. O. P. Tso, Academic Press, New York (1974), Vol. 1, p 93; b) G. D. Daves, Jr. and C. C. Cheng, *Prog. Med. Chem.*, **13**, 303 (1976); c) S. Hanessian and A. G. Pernet, *Adv. Carbohydr. Chem. Biochem.*, **33**, 111 (1976); d) S. D. Gero, J. Cleophax, D. Mercier, and A. Olesker, "Synthetic Methods for Carbohydrates", ed by H. S. El Khadem, American Chemical Society, Washington D.C. (1976), p 64; e) Y. Mizuno, O. Mitsunobu, and T. Hata, "Synthesis of Nucleosides and

Nucleotides (in Japanese)," Maruzen, Tokyo (1977), pp. 16—32; f) T. Sato and R. Noyori, *Kagaku* **33**, 74 (1978); g) K. Galankievicz, *Khim. Geterotsikl. Soedin.*, **1978**, 723; h) S. R. James, *J. Carbohydr. Nucl. Nucl.*, **6**, 417 (1979); i) H. Ogura and H. Takahashi, *Yuki Gosei Kagaku Kyokai Shi.*, **38**, 756 (1980); j) T. Sato and R. Noyori, *ibid.*, **38**, 862 (1980); k) T. Sato and R. Noyori, *ibid.*, **38**, 947 (1980); l) M. Ohno, "Anticancer Agents Based on Natural Product Models," ed by J. M. Cassady and J. D. Douros, Academic Press, New York (1980), pp 73—84; m) J. G. Buchanan, *Prog. Chem. Org. Natural Products*, **44**, 243 (1983).

11) Only two exceptions, pyrazomycin B[7c] and indochrome BIII,[12] have been known thus far.

12) H.-J. Knackmuss and J. Briaire, *Justus Liebigs Ann. Chem.*, **736**, 68 (1970); H.-J. Knackmuss, *Angew. Chem., Int. Ed. Engl.*, **12**, 139 (1973).

13) For reviews see: R. Noyori, *Acc. Chem. Res.*, **12**, 61 (1979); R. Noyori, *Ann. N. Y. Acad. Sci.*, **295**, 225 (1977); R. Noyori, *Kagaku Sosetsu*, **19**, 139 (1978); R. Noyori and Y. Hayakawa, *Org. React.*, **29**, 163 (1983).

14) H. Takaya, S. Makino, Y. Hayakawa, and R. Noyori, *J. Am. Chem. Soc.*, **100**, 1765 (1978).

15) T. Sato and R. Noyori, *Bull. Chem. Soc. Jpn.*, **51**, 2745 (1978).

16) K. B. Sharpless and K. Akashi, *J. Am. Chem. Soc.*, **98**, 1986 (1976). See also: V. VanRheenen, R. C. Kelly, and D. Y. Cha, *Tetrahedron Lett.*, **1976**, 1973; V. VanRheenen, D. Y. Cha, and W. M. Hartley, *Org. Synth.*, **58**, 43 (1978).

17) For the stereoselctive reaction of bicyclo[3.2.1]octan-3-one and related systems, see: A. H. Beckett, N. J. Harper, A. D. J. Balon, and T. H. E. Wattz, *Tetrahedron*, **6**, 319 (1959); Y. Hayakawa and R. Noyori, *Bull. Chem. Soc. Jpn.*, **47**, 2617 (1974); G. Büchi, H. Fliri, and R. Shapiro, *J. Org. Chem.*, **42**, 2192 (1977); Y. Hayakawa, Y. Baba, S. Makino, and R. Noyori, *J. Am. Chem. Soc.*, **100**, 1786 (1978), and references cited therein.

18) M. Karplus, *J. Chem. Phys.*, **30**, 11 (1959).

19) T. Sato, H. Kobayashi, and R. Noyori, *Bull. Chem. Soc. Jpn.*, **56**, 2661 (1983); T. Sato, H. Kobayashi, and R. Noyori, *Tetrahedron Lett.*, **21**, 2569 (1980); R. Noyori, H. Kobayashi, and T. Sato, *ibid.*, **21**, 2573 (1980).

20) W. H. Pirkle and M. S. Hoekstra, *J. Org. Chem.*, **39**, 3904 (1974).

21) a) W. J. Gensler, S. Chan, and D. B. Ball, *J. Am. Chem. Soc.*, **97**, 436 (1975); b) W. J. Gensler, S. Chan, and D. B. Ball, *J. Org. Chem.*, **46**, 3407 (1981).

22) The conversion was done according to the following sequence of known reactions: (1) acetonidation,[23] (2) Wittig condensation with methoxycarbonylmethylenetriphenylphosphorane,[24] (3) hydrolysis with sodium hydroxide,[21] and (4) lactonization.[21] For the recent work, see also: K. A. Cruickshank and C. B. Reese, *Synthesis*, **1983**, 199.

23) N. A. Hughes and P. R. H. Speakman, *Carbohydr. Res.*, **1**, 171 (1965).

24) H. Ohrui, G. H. Jones, J. G. Moffatt, M. L. Maddox, A. T. Christensen, and S. K. Byram, *J. Am. Chem. Soc.*, **97**, 4602 (1975).

25) H. Bredereck, G. Simchen, S. Rebsdat, W. Kantlehner, P. Horn, R. Wahl, H. Hoffmann, and P. Grieshaber, *Chem. Ber.*, **101**, 41 (1968).

26) H. Ohrui and S. Emoto, *J. Org. Chem.*, **42**, 1951 (1977).

27) Possibility of the *C*-nucleoside synthesis *via* the lactone **6** has been suggested previously.[21a] However, its direct formylation is quite difficult and, at least in our hand, no conditions were found which gave the formylated compound or the derivatives in satisfactory yield. The introduction of a C_1 unit, despite lack of stereochemical control, has been done with the ester **7** rather than the lectone **6**.[28]

28) C. K. Chu, K. A. Watanabe, and J. J. Fox, *J. Heterocycl. Chem.*, **12**, 817 (1975); C. K. Chu, I. Wempen, K. A. Watanabe, and J. J. Fox, *J. Org. Chem.*, **41**, 2793 (1976).

29) A. M. Michelson and W. E. Cohn, *Biochem.*, **1**, 490 (1962).

30) M. Bobek, J. Farkaš, and F. Šorm, *Collect. Czech. Chem. Commun.*, **34**, 1690 (1969); *Tetrahedron Lett.*, **1968**, 1543.

31) J. H. Burchenal, K. Ciovacco, K. Kalahar, T. O'Toole, R. Kiefner, M. D. Dowling, C. K. Chu, K. A. Watanabe, I. Wempen, and J. J. Fox, *Cancer Res.*, **36**, 1520 (1976).

32) Previous synthesis of showdomycin: a) G. Trummlitz and J. G. Moffatt, *J. Org. Chem.*, **38**, 1841 (1973); b) L. Kalvoda, J. Farkaš, and F. Šorm, *Tetrahedron Lett.*, **1970**, 2297; c) L. Kalvoda, *J. Carbohydr. Nucl. Nucl.*, **3**, 47 (1976); d) T. Inoue and I. Kuwajima, *J. Chem. Soc., Chem. Commun.*, **1980**, 251; e) A. P. Kozikowski and A. Ames, *J. Am. Chem. Soc.*, **103**, 3923 (1981); f) Y. Ito, T. Shibata, M. Arita, H. Sawai, and M. Ohno, *ibid.*, **103**, 6739 (1981); g) G. Just, T. J. Liak, M.-L. Lim, P. Potvin, and Y. S. Tsantrizos, *Can. J. Chem.*, **58**, 2024 (1980).

33) J. J. Pappas, W. P. Keaveney, E. Gancher, and M. Berger, *Tetrahedron Lett.*, **1966**, 4273.

34) S. Trippett and D. M. Walker, *J. Chem. Soc.*, **1959**, 3874.

35) In the alternative *R* stereoisomer, the coupling constant is expected to be close to 0 Hz. See: Y. Hayakawa, Y. Baba, S. Makino, and R. Noyori, *J. Am. Chem. Soc.*, **100**, 1786 (1978).

36) For the reasonable erythro/threo nomenclature see: footnote 8 in R. Noyori, I. Nishida, and J. Sakata, *J. Am. Chem. Soc.*, **103**, 2106 (1981), and footnote 32 in *idem, ibid.*, **105**, 1598 (1983).

37) H. O. House, D. S. Crumrine, A. Y. Teranishi, and H. D. Olmstead, *J. Am. Chem. Soc.*, **95**, 3310 (1973). R. A. Auerbach, D. S. Crumrine, D. L. Ellison, and H. O. House, *Org. Synth.*, **54**, 49 (1974).

38) E. J. Corey and A. Venkateswarlu, *J. Am. Chem. Soc.*, **94**, 6190 (1972).

39) J. L. Imbach, *Ann. N. Y. Acad. Sci.*, **255**, 177 (1975).

40) Such *C*-nucleosides have been prepared only by transformation of pseudouridine (**1**).[30]

41) G. Just and S. Kim, *Can. J. Chem.*, **55**, 427 (1977).

42) The cyclization was carried out according to the method cited in Ref 41.

43) a) T. Sato, M. Watanabe, H. Kobayashi, and R. Noyori, *Bull. Chem. Soc. Jpn.*, **56**, 2680 (1983); b) T. Sato, M. Watanabe, and R. Noyori, *Chem. Lett.*, **1978**, 1297; *Tetrahedron Lett.*, **1978**, 4403.

44) T. Sato, M. Watanabe, and R. Noyori, *Tetrahedron Lett.*, **1979**, 2897; *Heterocycles*, **14**, 761 (1980); T. Sato and R. Noyori, *Tetrahedron Lett.*, **21**, 2535 (1980).

45) T. Sato, H. Kobayashi, and R. Noyori, *Tetrahedron Lett.*, **21**, 1971 (1980); *Heterocycles*, **15**, 321 (1981).

46) T. Sato, M. Watanabe, and R. Noyori, *Chem. Lett.*, **1980**, 679.

47) a) T. Sato and R. Noyori, *Bull. Chem. Soc. Jpn.*, **56**, 2700 (1983); *ibid.*, **53**, 1195 (1980); b) T. Sato and R. Noyori, *Heterocycles*, **13**, 141 (1979).

48) T. Sato, K. Marunouchi, and R. Noyori, *Tetrahedron Lett.*, **1979**, 3669.

49) The Diels-Alder adducts also opened the preparation of a number of artificial *C*-nucleosides involving 2'-deoxyshowdomycin[50] and a bishomopyrazomycin analogue.[51] Use of cyclopentadiene in place of furan for the Diels-Alder reaction gave carboribosidic analogues.[52] Further, an approach to a 1,2,4-triazole homo-*C*-nucleoside was achieved through the key cycloaddition of furan and tetrachlorocyclopropene yielding 2,3,4,4-tetrachloro-8-oxabicyclo[3.2.1.]octa-2,6-diene.[21]

50) G. Just and M.-I. Lim, *Can. J. Chem.*, **55**, 2993 (1977).

51) G. Just, M. Ramjeesingh, and T. J. Liak, *Can. J. Chem.*, **54**, 2940 (1976). See also: G. Just and M. Ramjeesingh, *Tetrahedron Lett.*, **1975**, 985.

52) G. Just and B. Chalard-Faure, *Can. J. Chem.*, **54**, 861 (1976). G. Just and R. Ouellet, **54**, 2925 (1976); G. Just and S. Kim, *ibid.*, **54**, 2935 (1976); *ibid.*, **55**, 427 (1977).

53) N. N. Schwartz and J. H. Blumbergs, *J. Org. Chem.*, **29**, 1976 (1964).

54) S. C. Watson and J. F. Eastham, *J. Organomet. Chem.*, **9**, 165 (1967).

55) The 60-MHz ^{1}H NMR analysis of this lactone in benzene-d_6 was discussed independently by Gensler and his collaborators,[21b] who commented on our previously reported result[1a] and claimed that no splitting was detected due to the geminal spin-spin coupling between two protons α to the lactone carbonyl. In fact, however, the 100-MHz spectrum showed the clear AB splitting pattern with J=14 Hz for the geminal H_{1a} and H_{1b} hydrogens. In addition, there was observed the geminal coupling, J=14 Hz, between ribose-$H_{5'a}$ and -$H_{5'b}$ protons.

56) Optical rotation and molar extinction coefficient of UV absorptions have not been measured because of the extreme hygroscopicity.

57) Y. Nakagawa, H. Kano, Y. Tsukuda, and H. Koyama, *Tetrahedron Lett.*, **1967**, 4105.

Ozonization of Phenothiazine and Its Analogues

Masaki MATSUI,* Yoshihiko MIYAMOTO, Katsuyoshi SHIBATA, and Yoshimi TAKASE
Department of Industrial Chemistry, Faculty of Engineering, Gifu University, Yanagido, Gifu 501-11
(Received March 12, 1984)

When phenothiazine and phenoxazine were ozonized in dichloromethane, the cation radicals and the ozonate anion radical were detected, whereas, in the ozonization of phenoxathiin and thianthrene, these radicals were not observed. Formation of these radicals was more favorable as greater was the polarity of the solvent and lower was the oxidation potential of the substrate. Ozonization of phenothiazine and phenoxazine in polar solvents was explained by the electron-transfer mechanism accompanied by the electrophilic ozone attack, and that of phenoxathiin and thianthrene by the electrophilic ozone attack alone.

Reactions of ozone are classified into four types; (1) a 1,3-dipole represented by the Criegee ozonolysis mechanism,[1] (2) an electrophile in the ozonization of phosphines,[2] (3) a nucleophile as was reported by Olah *et al.*,[3] and (4) an electron acceptor which was reported in the ozonization of *p*-phenylenediamines[4] and amines.[5-7]

Ozonization of phenothiazine, phenoxathiin, thianthrene, and phenoxazine which possibly involves the electron-transfer was discussed.

Experimental

General. Ozone was generated by a Nihon Ozon 0-1-2 type ozonizor. Mass spectra were recorded with Hitachi M-52 and RMU-6M spectrometers. NMR, IR, and visible spectra were recorded on a Hitachi R-24 spectrometer, a Hitachi EPI-S2 spectrometer, and a Hitachi EPS-3T spectrometer, respectively. Gas and liquid chromatography was performed on a Shimadzu 4C-PF gas chromatograh and a Japan Spectroscopic Co. Familic 100N liquid chromatograph, respectively. Melting points were measured with a Yamato MP-21 melting point apparatus. Oxidation potential was measured with Niko NPGS-301 and NPS-2 apparatuses. Purity of the materials used was confirmed by gas and liquid chromatography.

Materials. Phenothiazine (**1a**) (Nakarai Chemicals, Ltd.) was recrystallized from ethanol; mp 185.4 °C (lit, 185.1 °C);[8] MS (20 eV) *m/z* (rel intensity) 199(M^+; 100), 198 (17), 167 (41), 166 (16), and 100 (10); ^{1}H NMR (DMSO-d_6) δ=6.5—7.1 (m, 8H) and 8.51 (s, 1H); IR (KBr disk) 3300 cm^{-1} (NH). Phenoxathiin (**1b**) was synthesized according to the literature;[9] mp 55.8 °C (lit, 56.5—57.5 °C);[9] MS (20 eV) *m/z* (rel intensity) 200 (M^+; 100), 171 (25), and 168 (30). Thianthrene (**1c**) (Tokyo Chemical Industry Co., Ltd.) was recrystallized from ethanol; mp 155.0 °C (lit, 155—157 °C);[10] MS (20 eV) *m/z* (rel intensity) 216 (M^+; 100), 184 (52), and 171 (12). Phenoxazine (**1d**) (Aldrich Chemical Co., Inc.) was used without further purification; mp 156.0 °C (lit, 154.5—156.0 °C);[11] MS (20 eV) *m/z* (rel intensity) 183 (M^+; 100), 154 (31), and 127 (8); IR (KBr disk) 3380 cm^{-1} (NH). Phenothiazine 5-oxide (**2a**) was synthesized according to the literature;[12] mp 252—254 °C (lit, 251—253 °C);[12] MS (70 eV) *m/z* (rel intensity) 215 (M^+; 56), 199 (31), 186 (92), 167 (100), and 153 (25); IR (KBr disk) 3170 (NH) and 1075 cm^{-1} (S=O). Phenoxathiin 10-oxide (**2b**) was synthesized by the oxidation of phenoxathiin with an equivalent molar amount of ozone, and recrystallized from ethanol; mp 152.4 °C (lit, 153—154 °C);[13] MS (20 eV) *m/z* (rel intensity) 216 (M^+; 62), 200 (100), 187 (59), and 168 (97); IR (KBr disk) 1035 cm^{-1} (S=O). Thianthrene 5-oxide (**2c**) was synthesized by the ozonization of thianthrene and recrystallized from ethanol; mp 141.8 °C (lit, 143.0—143.5 °C);[10] MS (20 eV) *m/z* (rel intensity) 232 (M^+; 20), 216 (22), 203 (15), 184 (100), 171 (12), and 152 (8); IR (KBr disk) 1075 cm^{-1} (S=O). 3*H*-Phenothiazin-3-one (**3a**) was synthesized according to the literature;[14] mp 164—166 °C (lit, 165—166 °C);[14] MS (20 eV) *m/z* (rel intensity) 213 (M^+; 37), 185 (100), and 141 (17); IR (KBr disk) 1630 cm^{-1} (C=O). 3*H*-Phenoxazin-3-one (**3d**) was synthesized by the ozonization of phenoxazine and purified by column chromatography (silica gel, dichloromethane); mp 213—215 °C (lit, 216—217 °C);[15] MS (20 eV) *m/z* (rel intensity) 197 (M^+; 100), 169 (94), 140 (19), and 114 (16); IR (KBr disk) 1615 cm^{-1} (C=O). 2-Chlorophenothiazine (**4a**) (Tokyo Chemical Industry Co., Ltd.) was employed without further purification; mp 193.0—194.5 °C (lit, 194—195 °C);[16] MS (20 eV) *m/z* (rel intensity) 235 (39), 233 (M^+; 100), 201 (22), and 198 (56); IR (KBr disk) 3300 cm^{-1} (NH). Thianthrene 5,10-dioxides (**5c** and **5'c**) were synthesized by the ozonization of thianthrene and purified by thin layer chromatography (silica gel, dichloromethane : hexane=5:1); *trans*-Thianthrene 5,10-dioxide (**5c**); mp 276—277 °C (lit, 284 °C);[17] MS (20 eV) *m/z* (rel intensity) 248 (M^+; 53), 232 (17), 216 (43), 200 (53), 184 (100), and 171 (33); IR (KBr disk) 1085 cm^{-1} (S=O). *cis*-Thianthrene 5,10-dioxide (**5'c**); mp 234.5—235.5 °C (lit, 249 °C);[17] MS (20 eV) *m/z* (rel intensity) 248 (M^+; 35), 232 (13), 216 (54), 200 (42), 184 (100), and 171 (46); IR (KBr disk) 1075 cm^{-1} (S=O).

Ozonization Reaction. Ozonization was carried out with an ozone-nitrogen mixture. The products were identified by comparing the retention time in the gas and liquid chromatography and mass spectra with those of authentic samples. The products were determined by GLC using a 2% Silicone OV-1 column, 3 mm×1 m, programmed from 80 to 240 °C at 10 °C min^{-1}. The conditions in LC were (1) SS-10 column, 0.5 mm×0.15 m, eluted with the mixed solution (dichloromethane : ethanol=25:1) and detection at 254 nm, and (2) SS-10 column, 0.5 mm×0.15 m, eluted with the mixed solution (dichloromethane : acetone=40:1) and detection at 254 nm.

Results and Discussion

The results of the ozonization reactions are shown in Table 1. Materials employed are shown in Fig. 1.

When phenothiazine (**1a**) was ozonized in dichloromethane, phenothiazine 5-oxide (**2a**), 3*H*-phenothiazin-3-one (**3a**), and 2-chlorophenothiazine (**4a**) were detected. Since the ozonization of phenothiazine 5-oxide gave 3*H*-phenothiazin-3-one (Run 9), it was concluded that phenothiazine reacted with one molar equivalent of ozone to give phenothiazine 5-oxide and 2-chlorophenothiazine, and further ozonization gave 3*H*-phenothiazin-3-one. Though the reactivity of phenothiazine with ozone increaed with the rise of the reaction temperature, the distribution of the products was scarcely affected (Runs 1,2,3, and 4). Since chlori-

Table 1. Results of the ozonization reaction[a)]

Run	Substrate	Solvent	Temp °C	Ozone (consumed) 10^{-4} mol	Conv %	Ozone[b)] (consumed) Substrate (reacted)	Yield[c)]/% 2	3	Others
1	**1a**	CH_2Cl_2	20	1.71	68	1.00	47	13	**4a** (6%)
2	**1a**	CH_2Cl_2	0	1.27	48	1.05	46	12	**4a** (Trace)
3	**1a**	CH_2Cl_2	−20	2.79	70	1.59	49	16	**4a** (2%)
4	**1a**	CH_2Cl_2	−78	3.57	62	2.29	51	11	**4a** (2%)
5	**1a**	$CHCl_3$	0	2.91	77	1.51	55	12	**4a** (8%)
6	**1a**	CCl_4	0	5.62	72	3.11	23	8	**4a** (11%)
7	**1a**	CH_3COOH	15	2.41	59	1.63	68	10	
8	**1a**	C_6H_{14}	0	0.23	55	1.05	25	3	
9	**2a**	CH_2Cl_2	0	0.15	64	0.99	—	14	
10	**1b**	CH_2Cl_2	0	17.88	67	1.07	97	—	
11	**1b**	CCl_4	0	17.81	72	0.99	90	—	
12	**1c**	CH_2Cl_2	0	5.35	72	0.80	92	—	
13	**1c**	CCl_4	0	7.27	78	1.01	88	—	**5c** (Trace)
14	**2c**	CH_2Cl_2	0	1.89	95	0.92	—	—	**5c** (81%), **5'c** (2%)
15	**1d**	CH_2Cl_2	0	7.73	92	1.03	—	5	Polymer

a) Ozonization was carried out with an ozone-nitrogen mixture on 0.251 mmol of phenothiazine (**1a**), 0.023 mmol of phenothiazine 5-oxide (**2a**), 2.50 mmol of phenoxathiin (**1b**), 0.926 mmol of thianthrene (**1c**), 0.216 mmol of thianthrene 5-oxide (**2c**), and 0.82 mmol of phenoxazine (**1d**) in 20 ml of solvent, respectively. b) Molar ratio. c) Yield was based on the substrate reacted with ozone.

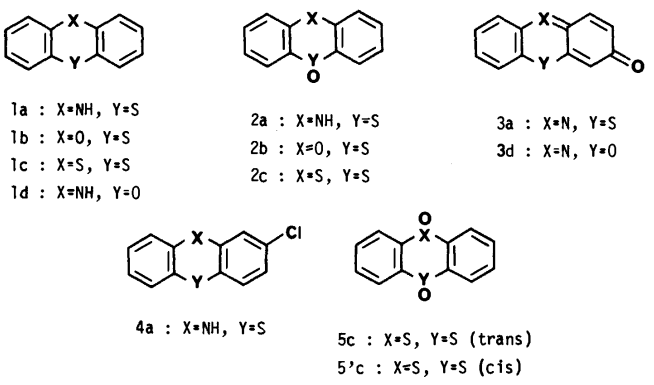

Fig. 1. Materials employed.

nated product **4a** was not formed, the yield of phenothiazine 5-oxide in acetic acid was greater than that in the chlorinated solvents (Runs 2,5, and 7). Since the yields of phenothiazine 5-oxide and 3*H*-phenothiazin-3-one in carbon tetrachloride and hexane were low compared with that in the other solvents (Runs 2,5,6,7, and 8), the electron-transfer mechanism during ozonization is suggested.

Phenoxathiin (**1b**) reacted with one molar equivalent of ozone to give phenoxathiin 10-oxide (**2b**) quantitatively. The reaction was scarcely affected by the polarity of the solvent (Runs 10 and 11).

When thianthrene (**1c**) was ozonized, thianthrene 5-oxide (**2c**), and a trace amount of *trans*-thianthrene 5,10-dioxide (**5c**) were detected. Ozonization of thianthrene 5-oxide gave *trans*-thianthrene 5,10-dioxide and *cis*-thianthrene 5,10-dioxide (**5'c**) in the ratio 97:3. The yield of thianthrene 5-oxide was scarcely affected by the solvent (Runs 12 and 13).

When phenoxazine (**1d**) was ozonized in dichloromethane, the reaction was complex and the product isolated was 3*H*-phenothiazin-3-one (**3d**), accompanied by unidentified polymers (Run 15).

When phenothiazine was ozonized in dichloromethane, the reaction mixture turned red in color. The visible absorption spectra during the reaction are shown in Fig. 2. The spectra showed the absorption maxima at 435 and 519 nm, which are close to those of the phenothiazine cation radical reported by Hason *et al.*,[18] and Brown *et al.*[19] The spectra have smaller peaks at 481 and 502 nm which are attributed to the uncharged radical.[20] Since an ozonate anion radical has been reported to undergo the hydrogen abstraction reaction,[21] cumene and triphenylmethane were added to the ozonized solution, and the mixture was allowed to stand for 0.5 h. The control experiment was also carried out. When cumene was ozonized, 2-phenyl-2-propanol was detected as was reported by Pryor *et al.*[22] However, since (1) the yield in the presence of phenothiazine (8%) was clearly greater than that in the absence of phenothiazine (trace), and (2) triphenylmethanol was not detected from the ozonized solution in the absence of phenothiazine, it was concluded that cumene and triphenylmethane reacted with the ozonate anion radicals to give 2-phenyl-2-propanol and triphenylmethanol, respectively. Since the reactivity of cumene with radicals is smaller than that of triphenylmethane,[23] yield of the ozonate anion radical with four molar equivalents of cumene gave only a trace amount of 2-phenyl-2-propanol. The result is shown in Table 2. As was expected, the ozonate anion radical was trapped in dichloromethane, chlorform, and acetic acid, in which the phenothiazine cation radical was detected (Runs 1,

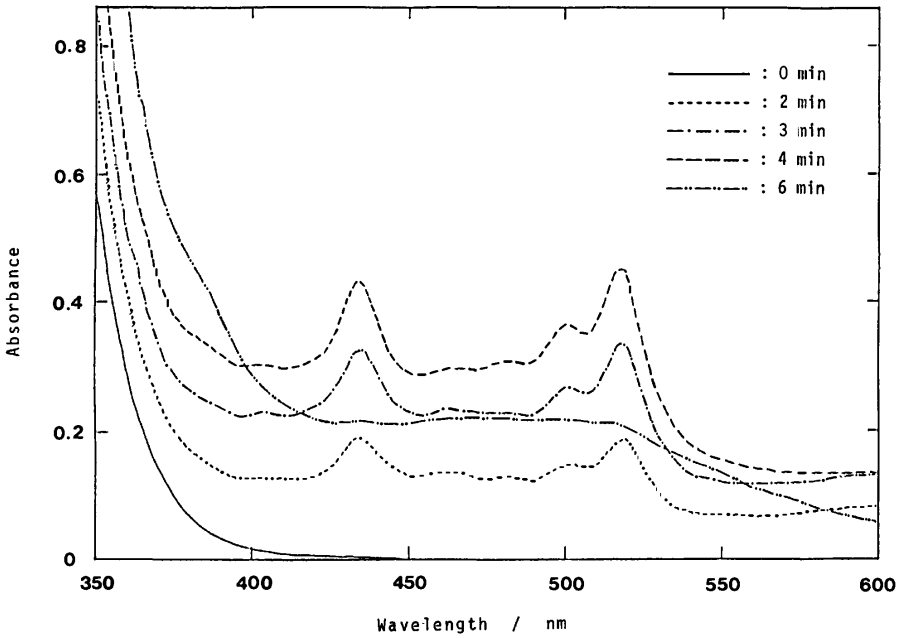

Fig. 2. Change in the visible spectrum of phenothiazine during ozonization.
Ozonization was carried out with an ozone–nitrogen mixture (ozone: 0.3 mmol, nitrogen: 50 cm^3 min^{-1}) on 0.251 mmol of phenothiazine in 50 ml of dichloromethane at 0 °C.

Table 2. Relation between the formation of a phenothiazine cation radical and the yield of the ozonate anion radical during the ozonization of phenothiazine[a)]

Run	Solvent	Formation[b)] of a cation radical	Yield[c)]/%	
			2-Phenyl-2-propanol	Triphenylmethanol
1	CH_2Cl_2	+	8	3
2	$CHCl_3$	+	7	3
3	CH_3COOH	+	7	2
4	CCl_4	−	0	0
5	C_6H_{14}[d)]	−	0	0

a) Ozonization was carried out with an ozone–nitrogen mixture (ozone: 1.0 mmol, nitrogen: 50 cm^3 min^{-1}) on 1 mmol of phenothiazine in 40 ml of solvent at 0 °C. To the ozonized solution, 140 and 4 molar equivalents of cumene and triphenylmethane were added, respectively. b) The cation radical was detected by the visible spectrum. c) Yield was based on the phenothiazine reacted. d) Ozonization was carried out with an ozone–nitrogen mixture (ozone: 0.3 mmol, nitrogen: 50 cm^3 min^{-1}) on 0.25 mmol of phenothiazine in 40 ml of solvent.

2, and 3). The greater the polarity of the solvent is, the easier is the formation of the ozonate anion radical. Such a tendency is similar to the solvent effect reported in the reaction of a superoxide ion.[24)]

Bailey *et al.* reported that *t*-butylamine cation radical produced in the ozonization underwent hydrogen abstraction reaction from 2,2,4-trimethylpentane to give 2,4,4-trimethyl-2-pentanol.[25)] However, since (1) an ozonate anion radical produced on magnesium oxide underwent hydrogen abstraction reaction,[21)] and (2) addition of cumene and triphenylmethane decreased the absorbance of phenothiazine cation radical, we have modified Bailey's mechanism, as shown in Eqs. (1)—(3),

$$O_3^{\cdot-} + RH \rightarrow R^{\cdot} + O_2 + OH^-, \quad (1)$$

$$R^{\cdot} + PTH^+ \rightarrow R^+ + RTH, \quad (2)$$

$$R^+ + OH^- \rightarrow ROH, \quad (3)$$

where RH is cumene and triphenylmethane, and PTH is phenothiazine.

Relations among oxidation potential ($E^{ox}_{1/2}$), formation of the cation radicals and yield of the ozonate anion radical in the ozonization of *N,N'*-diphenyl-*p*-phenylenediamine, phenothiazine, phenoxazine, phenoxathiin, and thianthrene are shown in Table 3. When *N,N'*-diphenyl-*p*-phenylenediamine, whose ozonization has been explained by the electron-transfer mechanism, was ozonized in dichloromethane, formation of the cation radical was observed, and the ozonate anion radical was also trapped (Run 1). In the ozonization of phenoxazine the solution turned red in color and visible spectrum showed the absorption maxima at 404 and 522 nm which are similar to that of the phenoxazine cation radical.[26)] The ozonate anion radical was also trapped in the yield of 6 and 2%, respectively (Run 3). Bailey *et al.* reported that ozonization of thianthrene in the presence of dilute sulfric acid gave the cation radical.[27)] When ozonization of phenoxathiin and thianthrene was carried out in dichloromethane, formation of the cation radicals and the ozonate anion radical were not observed (Runs 4 and 5). The result that the lower the oxidation potential is, the easier is the formation of the cation radical and the ozonate anion radical suggests that the electron-transfer process is the major path during the ozonization of phenothiazine and phenoxazine. On the other hand,

Table 3. Relations among the oxidation potential of the substrate, formation of the cation radicals, and the yield of an ozonate anion radical during ozonization[a)]

Run	Substrate	$E^{ox}_{1/2}$[b)]/V	Formation of the[c)] cation radical	Yield[d)]/%	
				2-Phenyl-2-propanol	Triphenylmethanol
1	*N,N'*-Diphenyl-*p*-phenylenediamine	0.35	+	19	4
2	Phenothiazine	0.59	+	8	3
3	Phenoxazine	0.60	+	6	2
4	Phenoxathiin	1.17	−	0	0
5	Thianthrene	1.21	−	0	0

a) Ozonization was carried out with an ozone-nitrogen mixture (ozone: 1.0 mmol, nitrogen: 50 $cm^3\ min^{-1}$) on 1.0 mmol of substrate in 40 ml of dichloromethane. To the ozonized solution, 140 and 4 molar equivalents of cumene and triphenylmethane were added, respectively. b) *vs.* SCE in acetonitrile. c) The cation radical was detected by the visible spectrum. d) Yield was based on the substrate reacted.

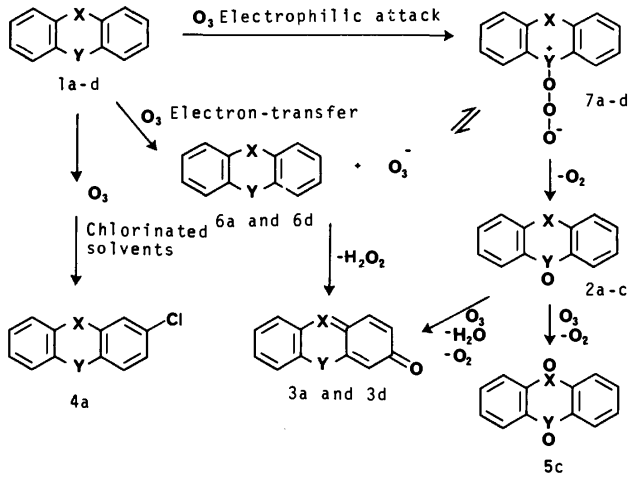

1a : X=NH, Y=S
1b : X=O, Y=S
1c : X=S, Y=S
1d : X=NH, Y=O

2a : X=NH, Y=S
2b : X=O, Y=S
2c : X=S, Y=S

3a : X=N, Y=S
3d : X=N, Y=O

4a : X=NH, Y=S

5c : X=S, Y=S (trans)

6a : X=NH, Y=S
6d : X=NH, Y=O

7a : X=NH, Y=S
7b : X=O, Y=S
7c : X=S, Y=S
7d : X=NH, Y=O

Scheme 1.

ozonization of phenoxathiin and thianthrene is explained by the electrophilic ozone attack.

The probable ozonization mechenism is shown in Scheme 1. When phenothiazine (**1a**) and phenoxazine (**1d**) are ozonized in the polar solvents, the cation radicals **6a** and **6d** are formed *via* the electron-transfer reaction. They are in equilibrium with the substrate-ozone adducts **7a** and **7d** in solution. Ozonization of phenothiazine (**1a**) in the chlorinated solvents gives 2-chlorophenothiazine (**4a**). Recombination of **6d** with the ozonate anion radical gives 3*H*-phenoxazin-3-one (**3d**). The substrate-ozone adducts **7a—d** were also formed *via* the electrophilic attack of ozone on the substrate and the adducts lose an oxygen molecule and give the S-oxides **2a—c**. Thianthrene 5-oxide (**2c**) is further ozonized to give thianthrene 5,10-dioxide (**5c**).

The authors thank Professor Teijiro Kitao of the University of Osaka Prefecture for useful discussion. The authors are grateful to Professor Yasusada Ueno and Associate Professor Hideki Minoura of Gifu University for the oxidation potential measurement.

References

1) R. Criegee and G. Wenner, *Ann. Chem.*, **564**, 9 (1949).
2) Q. E. Thompson, *J. Am. Chem. Soc.*, **83**, 845 (1961).
3) G. A. Olah, N. Yoneda, and D. P. Parker, *J. Am. Chem. Soc.*, **98**, 2251 (1976).
4) R. W. Layer, *Rubber Chem. Technol.*, **39**, 184 (1966).
5) P. S. Bailey and J. E. Keller, *J. Org. Chem.*, **33**, 2680 (1968).
6) P. S. Bailey, J. E. Keller, and T. P. Carter Jr., *J. Org. Chem.*, **35**, 2777 (1970).
7) P. S. Bailey, T. P. Carter Jr., and L. M. Southwick, *J. Org. Chem.*, **37**, 2999 (1972).
8) E. Knoevenagel, *J. Prakt. Chem.*, **89**, 2 (1914).
9) C. M. Suter and C. E. Maxwell, *Org. Synth.*, Coll. Vol. II, 485 (1950).
10) H. J. Shine and L. Piette, *J. Am. Chem. Soc.*, **84**, 4798 (1962).
11) M. P. Olmssted, *J. Org. Chem.*, **26**, 1901 (1961).
12) E. B. Barnett and S. Smiles, *J. Chem. Soc. London*, **95**, 1253 (1907).
13) H. J. Shine and R. J. Small, *J. Org. Chem.*, **30**, 2140 (1965).
14) R. Rummerer and S. Gassner, *Ber.*, **46**, 2324 (1913).
15) C. W. Bird and M. Latif, *Tetrahedron*, **36**, 529 (1980).
16) J. I. G. Cadogan, S. Kulik, C. Thomson, and M. J. Todd, *J. Chem. Soc. (C)*, **1970**, 2437.
17) A. Fava, P. B. Sogo, and M. Calvin, *J. Am. Chem. Soc.*, **79**, 1078 (1957).
18) P. Hanson and R. O. C. Norman, *J. Chem. Soc., Perkin Trans. 2*, **1973**, 264.
19) G. P. Brown, J. W. Cole Jr., and T. I. Crowell, *J. Org. Chem.*, **20**, 1772 (1955).
20) G. N. Lewis and J. Bigeleisen, *J. Am. Chem. Soc.*, **65**, 2419 (1943).
21) Y. Takita and J. H. Lunsford, *J. Phys. Chem.*, **83**, 683 (1979).
22) W. A. Pryor, N. Ohto, and D. F. Church, *J. Am. Chem. Soc.*, **105**, 3614 (1983).
23) G. A. Rossell, "Reactivity, Selectivity, and Polar Effects in Hydrogen Atom Transfer Reactions," in "Free Radicals," ed by J. K. Kochi, John Wiley, New York (1973), Vol. 1, Chap

7, pp. 275—331.
24) I. Saito, T. Matsuura, and K. Inoue, *J. Am. Chem. Soc.*, **103**, 188 (1981).
25) P. S. Bailey, "Ozonation in Organic Chemistry," Academic Press, Inc., New York (1982), Vol. 2, Chap. 7, pp. 155—224.
26) B. E. Hester and K. P. J. Williams, *J. Chem. Soc., Perkin Trans. 2*, **1981**, 852.
27) P. S. Bailey and A-I. Y. Khashab, *J. Org. Chem.*, **43**, 675 (1978).

 © 1984 The Chemical Society of Japan Bull. Chem. Soc. Jpn., 57, 2531—2534 (1984)

The Reaction of Primary Nitro Compounds with Dipolarophiles in the Presence of *p*-Toluenesulfonic Acid

Tomio SHIMIZU,* Yoshiyuki HAYASHI, and Kazuhiro TERAMURA
Department of Color Chemistry and Technology, Faculty of Industrial Arts, Kyoto Technical University, Matsugasaki, Sakyo-ku, Kyoto 606
(Received March 17, 1984)

3-Substituted 2-isoxazolines or isoxazoles were obtained from the reaction of primary nitro compounds [methyl nitroacetate, 2-nitro-1-phenylethanone, (nitromethyl)benzene, 1-nitropropane, and (phenylsulfonyl)-nitromethane] with dipolarophiles in refluxing mesitylene in the presence of a small amount of *p*-toluenesulfonic acid. The formation of these products can be explained in terms of 1,3-dipolar cycloaddition of nitrile oxide generated by a dehydration of the primary nitro compounds. On the other hand, 4,5-decamethylene-3-phenylsulfonyl-2-isoxazoline *N*-oxide was obtained from a similar reaction of (phenylsulfonyl)nitromethane with cyclododecene. The formation of the isoxazoline *N*-oxide can be explained on the basis of the intermediacy of 3,4-bis(phenylsulfonyl)furazan 2-oxide.

1,3-Dipolar cycloaddition reactions using nitrile oxides were one of versatile methods for the preparation of five-membered heterocycles. Many preparative methods of nitrile oxides have been known so far[1-7] (see Scheme 1) but each of these methods possesses at

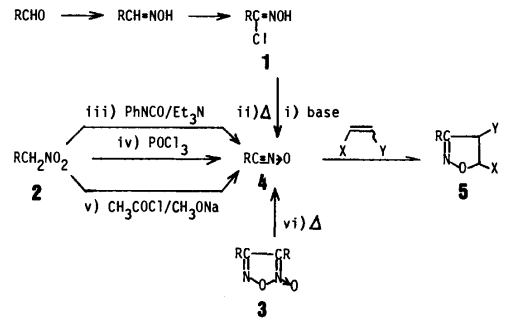

Scheme 1.

least one disadvantage; the method (i) is the most familiar one,[2] but several troublesome steps are necessary for the preparation of hydroximoyl chlorides (**1**), a precursor of nitrile oxides (**4**). On the other hand, one-step methods (iii—v)[4-6] using primary nitro compounds (**2**) which are more easily available than **1** appear to be an attractive one. However, an equimolar or an excess amount of reagents is required for the dehydration of **2**, and consequently, separation of the desired compounds from the reaction mixture is troublesome and considerable amounts of undesired by-products are formed in some cases. The present paper describes a new effective and simple method for the generation of nitrile oxides by the dehydration of **2** using a small amount of *p*-toluenesulfonic acid and the preparation of cycloadducts in the presence of dipolarophiles.

Results and Discussion

Removal of a proton from an aliphatic primary nitro compound gives a carbanion which can be alkylated (or acylated) at oxygen or carbon atom. *O*-Alkylation (or -acylation) gives nitronic esters (or anhydrides), which are generally unstable to heat and break down to a nitrile oxide, while *C*-alkylation (or acylation) gives by-products for the purpose of generation of a nitrile oxide. Acid catalyzed enolization and acid catalyzed dehydration of a hydroxyl group are well known. It is expected that a primary nitro compound would give a nitrile oxide in the presence of a trace of acid and it is shown to be the case.

The reactions between an equimolar mixture of several primary nitro compounds (**2a—e**) bearing various types of substituents and dipolarophiles were carried out in refluxing xylene or mesitylene for 6—20 h in the presence of a catalytic amount of *p*-toluenesulfonic acid. (see Eq. 1) 2-Isoxazolines (**5**) or isoxazoles (**6**) were

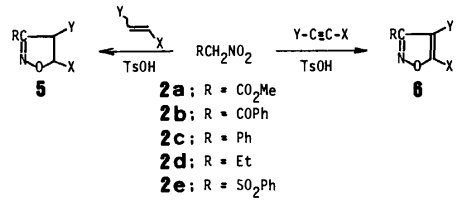

(1)

obtained from the reaction of **2a—e** with ethylenic or acetylenic dipolarophiles, respectively, in the yields shown in Table 1. The isolated yields in Table 1 are calculated on the reagents used. Unreacted primary nitro compounds could be recovered from the reaction mixture. The conversion of **2** to the products were over 80% in all cases shown in the Table. Though the reaction of **2a** with dipolarophiles proceeded slowly at the temperature of xylene refluxing, those of **2b—e** with dipolarophiles were too slow to be observed at this temperature. However, all of **2** reacted rapidly with dipolarophiles at the temperature of mesitylene refluxing. Formation of water was observed as the reaction proceeded. No remarkable improvement in the yields of the cycloadducts was observed after removing the water from the reaction system. On the other hand, 4,5-decamethylene-3-phenylsulfonyl-2-isoxazoline *N*-oxide (**7**) was the only isolable cycloadduct from the reaction mixture of **2e** and cyclododecene.

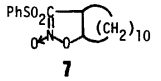

7

The structure of the cycloadducts (**5**, **6**, and **7**) was established on the basis of elemental analyses and spectral data (see Table 2). Physical properties of **5r**, **5s**, and

Table 1. Reactions of **2** and dipolarophiles in the presence of *p*-toluenesulfonic acid

Nitro Compound	Dipolarophile	Solvent	Product	Yield /%	Mp (Bp) /°C
2a	*N*-Phenylmaleimide	Xylene	**5a** [R=CO_2Me, X, Y=-CON(Ph)CO-]	70	223—225
2a	*N*-Butylmaleimide	Xylene	**5b** [R=CO_2Me, X, Y,=-CON(Bu)CO-]	36	Oil
2a	Diethyl fumarate	Xylene	**5c** (R=CO_2Me, X=Y=CO_2Et)	36	Oil
2a	Allylbenzene	Xylene	**5d** (R=CO_2Me, X=CH_2Ph, Y=H)	15	60—61
2a	1-Decene	Mesitylene	**5e** (R=CO_2Me, X=C_8H_{17}, Y=H)	18	44—45
2a	1-Tetradecene	Mesitylene	**5f** (R=CO_2Me, X=$C_{12}H_{25}$, Y=H)	25	66—68
2a	Allyl *p*-nitrophenyl ether	Mesitylene	**5g** (R=CO_2Me, X=$CH_2OC_6H_4NO_2$, Y=H)	22	87—88
2b	*N*-Phenylmaleimide	Mesitylene	**5h** [R=COPh, X, Y=-CON(Ph)CO-]	85	167—170
2b	Diethyl fumarate	Mesitylene	**5i** (R=COPh, X=Y=CO_2Et)	75	(180—187/ 0.8 mmHg)
2b	Allylbenzene	Mesitylene	**5j** (R=COPh, X=CH_2Ph, Y=H)	70	Oil
2b	Cyclododecene	Mesitylene	**5k** (R=COPh, X, Y=-$C_{10}H_{20}$-)	38	83—84
2b	1-Tetradecene	Mesitylene	**5m** (R=COPh, X=$C_{12}H_{25}$, Y=H)	53	Oil
2b	Allyl *p*-nitrophenyl ether	Mesitylene	**5n** (R=COPh, X=$CH_2OC_6H_4NO_2$, Y=H)	35	116—119
2b	DMAD[a]	Mesitylene	**6p** (R=COPh, X=Y=CO_2Me)	60	88—89 (160—172/ 5 mmHg)
2b	Phenylacetylene	Mesitylene	**6q** (R=COPh, X=Ph, Y=H)	46	79—80 (170—177/ 0.7 mmHg)
2c	*N*-Phenylmaleimide	Mesitylene	**5r** [R=Ph, X, Y=-CON(Ph)CO-]	54	170—172[b]
2c	Allylbenzene	Mesitylene	**5s** (R=Ph, X=CH_2Ph, Y=H)	29	64—65[c]
2c	1-Tetradecene	Mesitylene	**5t** (R=Ph, X=$C_{12}H_{25}$, Y=H)	45	72—73
2c	Allyl *p*-nitrophenyl ether	Mesitylene	**5u** (R=Ph, X=$CH_2OC_6H_4NO_2$, Y=H)	42	152—153
2d	*N*-Phenylmaleimide	Mesitylene	**5v** [R=Et, X, Y=-CON(Ph)CO-]	58	85—87
2d	*N*-Propylmaleimide	Mesitylene	**5w** [R=Et, X, Y=-CON(Pr)CO-]	35	(180—184/ 5 mmHg)
2d	DMAD[a]	Mesitylene	**6x** (R=Et, X=Y=CO_2Me)	15	(120—128/ 6 mmHg)
2e	Allylbenzene	Mesitylene	**5y** (R=SO_2Ph, X=CH_2Ph, Y=H)	39	114—115
2e	Allyl *p*-nitrophenyl ether	Mesitylene	**5z** (R=SO_2Ph, X=$CH_2OC_6H_4NO_2$, Y=H)	21	159—160
2e	Cyclododecene	Mesitylene	**7**	60	90—93[d]

a) DMAD; Dimethyl acetylenedicarboxylate. b) Lit,[8a] mp 174 °C. c) Lit,[8b] mp 72—73 °C. d) Lit,[9] mp 90—91 °C.

7 agreed well with those of known compounds.[8,9] The structure of oily cycloadducts (**5j** and **5m**) was further supported by conversion into crystalline hydrazones (**8**) by the reaction with *p*-nitrophenylhydrazine. (Eq. 2)

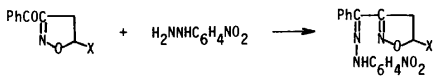

(2)

5j; X = CH_2Ph
5m; X = $C_{12}H_{25}$

8j; X = CH_2Ph
8m; X = $C_{12}H_{25}$

Though the formation of **5** and **6** may be ascribed to the results of a direct cycloaddition reaction of nitrile oxides (**4**), generated by the dehydration of **2**, with dipolarophiles, the isolation of **7** in a particular reaction may suggest an alternative reaction mechanism for these reactions. Recently, we reported that **7** was obtained from a nitrone-type cycloaddition reaction of 3,4-bis(phenylsulfonyl)furazan 2-oxide (furoxan) (**3e**) with cyclododecene.[9] Furthermore, furazan *N*-oxides (furoxan) bearing appropriate substituents are known to undergo dissociation into to moles of nitrile oxides

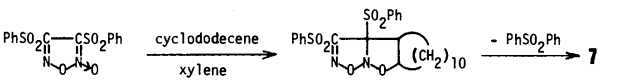

3e (3)

and give isoxazolines or isoxazoles by the following cycloaddition with dipolarophiles at the temperatures over 200 °C[7] (see route vi in Scheme 1). In view of these facts, it is necessary to examine the possibility of the intervention of furoxans in the reactions reported here. Although none of pure furoxans were isolated from the reaction mixture, we examined the reaction of furoxans (**3a—e**) with dipolarophiles in mesitylene at

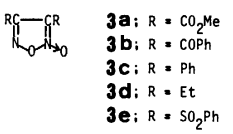

3a; R = CO_2Me
3b; R = COPh
3c; R = Ph
3d; R = Et
3e; R = SO_2Ph

the refluxing temperature. It was found that **3c** and **3d** were quite stable under the reaction conditions and were recovered quantitatively and that **3a** and **3b**

Table 2. NMR spectral data[a] of 5 and 6

Adduct	Chemical shift/δ
5a	3.87(s, 3H), 4.95(d, 1H, J=10 Hz), 5.82(d, 1H, J=10 Hz), 7.0—7.8(m, 5H)
5b	0.7—1.9(m, 7H), 3.5(t, 2H, J=7 Hz), 3.95(s, 3H), 4.75(d, 1H, J=10 Hz), 5.6(d, 1H, J=10 Hz)
5c	1.28(t, 3H, J=7 Hz), 1.32(t, 3H, J=7 Hz), 3.9(s, 3H), 4.25(q, 4H, J=7 Hz), 4.62(d, 1H, J=6.5 Hz), 5.35(d, 1H, J=6.5 Hz)
5d	2.6—3.45(m, 4H), 3.8(s, 3H), 4.7—5.3(m, 1H), 7.2(s, 5H)
5e	0.7—2.0(m, 17H), 2.8(dd, 1H, J=9 and 18 Hz), 3.28(dd, 1H, J=10 and 18 Hz), 3.87(s, 3H), 4.5—5.1(m, 1H)
5f	0.7—2.0(m, 25H), 2.77(dd, 1H, J=9 and 18 Hz), 3.27(dd, 1H, J=11 and 18 Hz), 3.87(s, 3H), 4.5—5.1(m, 1H)
5g	3.2—3.6(m, 2H), 3.9(s, 3H), 4.25(d, 2H, J=4.5 Hz), 5.0—5.5(m, 1H), 7.0(d, 2H, J=9 Hz), 8.2(d, 2H, J=9 Hz)
5h	5.2(d, 1H, J=10 Hz), 5.85(d, 1H, J=10 Hz), 7.2—7.9(m, 8H), 8.0—8.3(m, 2H)
5i	1.23(t, 3H, J=7 Hz), 1.35(t, 3H, J=7 Hz), 4.27(q, 2H, J=7 Hz), 4.33(q, 2H, J=7 Hz), 4.9(d, 1H, J=6.5 Hz), 5.4(d, 1H, J=6.5 Hz), 7.3—7.8(m, 3H), 8.1—8.4(m, 2H)
5j	2.6—3.6(m, 4H), 4.7—5.25(m, 1H), 7.2(s, 5H), 7.1—7.6(m, 3H), 7.9—8.2(m, 2H)
5k	0.8—2.2(m, 20H), 3.4—3.85(m, 1H), 4.6—5.0(m, 1H), 7.25—7.7(m, 3H), 8.0—8.35(m, 2H)
5m	0.7—2.1(m, 25H), 2.9(dd, 1H, J=9 and 17 Hz), 3.4(dd, 1H, J=11 and 17 Hz), 4.5—5.0(m, 1H), 7.2—7.7(m, 3H), 8.0—8.3(m, 2H)
5n	3.27(dd, 1H, J=9 and 18 Hz), 3.63(dd, 1H, J=10 and 18 Hz), 4.32(d, 2H, J=4.5 Hz), 5.25(ddt, 1H, J=4.5, 9, and 10 Hz), 7.1(d, 2H, J=9 Hz), 7.3—7.8(m, 3H), 8.17(d, 2H, J=9 Hz), 8.0—8.4(m, 2H)
6p	3.9(s, 3H), 4.03(s, 3H), 7.3—7.8(m, 3H), 8.0—8.3(m, 2H)
6q	7.05(s, 1H), 7.25—7.8(m, 6H), 7.8—8.0(m, 2H), 8.3—8.5(m, 2H)
5r	5.25(d, 1H, J=10 Hz), 5.75(d, 1H, J=10 Hz), 7.1—7.8(m, 8H), 7.8—8.2(m, 2H)
5s	2.6—3.55(m, 4H), 4.65—5.2(m, 1H), 7.25(s, 5H), 7.1—8.0(m, 5H)
5t	0.7—2.0(m, 25H), 2.9(dd, 1H, J=8 and 17 Hz), 3.4(dd, 1H, J=10 and 17 Hz), 4.4—5.0(m, 1H), 7.2—7.8(m, 5H)
5u	3.3(dd, 1H, J=8 and 17 Hz), 3.65(dd, 1H, J=10 and 17 Hz), 4.3(d, 2H, J=5 Hz), 4.8—5.4(m, 1H), 7.15(d, 2H, J=9 Hz), 7.3—7.9(m, 5H), 8.2(d, 2H, J=9 Hz)
5v	1.26(t, 3H, J=7 Hz), 2.3—2.9(m, 2H), 4.4(d, 1H, J=10 Hz), 5.4(d, 1H, J=10 Hz), 7.1—7.6(m, 5H)
5w	0.9(t, 3H, J=7 Hz), 1.25(t, 3H, J=7 Hz), 1.2—1.8(m, 2H), 2.2—2.7(m, 2H), 3.5(t, 2H, J=7 Hz), 4.35(d, 1H, J=10 Hz), 5.35(d, 1H, J=10 Hz)
6x	1.3(t, 3H, J=7 Hz), 2.9(q, 2H, J=7 Hz), 3.9(s, 3H), 4.0(s, 3H)
5y	2.7—3.6(m, 4H), 4.8—5.3(m, 1H), 7.2(s, 5H), 7.3—7.8(m, 3H), 7.8—8.1(m, 2H)
5z	3.2(dd, 1H, J=8 and 18 Hz), 3.6(dd, 1H, J=11 and 18 Hz), 4.0—4.5(m, 2H), 5.1—5.6(m, 1H), 6.9 (d, 2H, J=9 Hz), 7.7—8.4(m, 7H)

a) **5a**, **5h**, **5n**, **5r**, **5u**, and **5z** were dissolved in DMSO-d_6, the other substances were dissolved in $CDCl_3$.

underwent other types of cycloaddition reactions[9] and any trace of 3-methoxycarbonyl-2-isoxazolines or 3-benzoyl-2-isoxazolines could not be isolated from the reaction mixture. However, **5y**, **5z**, and **7** were obtained from the reaction of the furoxan **3e** with allylbenzene, allyl *p*-nitrophenyl ether, or cyclododecene, respectively, in yields similar to those from the reactions of the nitro compound **2e**. From these results, the most probable mechanism of the reaction of **2** with dipolarophiles in the presence of *p*-toluenesulfonic acid is as follows; acid-catalyst accelerates enolization of nitro compounds (**2**) into nitronic acid (**9**). Acid-catalyzed dehydration (or tosylation of the nitronic acid (**9**) followed by acid-catalyzed detosylation) gives nitrile oxides (**4**). The nitrile oxides undergo either a dimerization to furoxans (**3**) or a 1,3-dipolar cycloaddition with dipolarophiles depending on the nature of the substituents R. 1,3-Dipolar cycloadditions occur preferentially in the cases of R=CO_2Me, PhCO, Ph, and Et, and, on the other hand, a dimerization precedes the cycloaddition in the case of R=SO_2Ph. Bis-(phenylsulfonyl)furoxan (**3e**) was known to undergo two types of reactions (Eq. 3 or thermoreversion into the nitrile oxide) depending on the nature of dipolarophiles.[9]

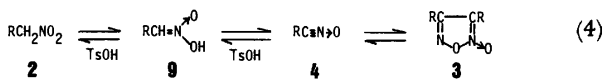

(4)

p-Toluenesulfonic acid was the best catalyst among the examined acids, CH_3CO_2H, CF_3CO_2H, and TsOH.

It is concluded that isoxazolines or isoxazoles can be easily obtained from primary nitro compounds in a moderate yield and the method is especially effective in the reaction with dipolarophiles which have a poor reactivity toward nitrile oxides at low temperature below 100°C because our method can apply at arbitrary high temperature.

Experimental

Measurements. All melting and boiling points are uncorrected. ^{1}H NMR spectra were measured on Varian T-60 A instrument with Me_4Si as an internal standard. All new crystalline products gave correct elemental analyses (±0.3% for C, H, and N).

Materials. Methyl nitroacetate,[10] 2-nitro-1-phenylethanone,[11] (nitromethyl) benzene,[12] (phenylsulfonyl)nitromethane,[13] bis(ethoxycarbonyl)furoxan,[14] dibenzoylfuroxan,[14] diphenylfuroxan,[15] diethylfuroxan,[4] and bis(phenylsulfonyl)furoxan[16] were prepared according to the method described in the literatures. 1-Nitropropane and *p*-toluenesulfonic acid monohydrate were commercially available and were used without further purification.

Reactions of Primary Nitro Compounds with Dipolarophiles. General Procedure. A mixture of an equimolar amount (20 mmol) of primary nitro compounds and dipolarophiles and a small amount of *p*-toluenesulfonic acid monohydrate (*ca.*~100 mg) was heated to reflux in mesitylene (50 ml) for 6 h. When xylene was used for the solvent instead of mesitylene, the mixture was refluxed for 20 h. In the case of the reaction with maleimides, a small amount (*ca.* 40 mg) of hydroquinone was also added. Evaporation of the solvent and other low-boiling products from the reaction mixture in a rotary evaporator gave the crude products. Crystalline crude products were recrystallized from appropriate solvents several times and some oily crude products were chromatographed (silica gel) with chloroform to give the crystalline products or pure oily products. The other oily crude products were purified by fractional distillation. Yields and melting (or boiling) points are shown in Table 1 and the NMR spectral data are shown in Table 2; 1 mmHg≈133.322 Pa.

*Reaction of 5-Benzyl (or -Dodecyl)-3-benzoyl-2-isoxazoline (**5j** or **5m**) with* p*-Nitrophenylhydrazine.* An ethanol solution (60 ml) of **5j** (or **5m**) (5 mmol) and *p*-nitrophenylhydrazine (5 mmol) was refluxed for 4 h. The subsequent evaporation of the solvent yielded a viscous oily material which solidified upon scratching with a glass rod. Recrystallization from ethanol gave yellow crystals (**8j** or **8m**). **8j**; 54% yield, mp 165—167 °C, NMR (DMSO-d_6) δ=2.8—3.6 (m, 4H), 4.7—5.2 (m, 1H). 7.2—7.5 (m, 12H), 8.15 (d, 2H, J=9 Hz), 11.5 (s, 1H, NH). Calcd for $C_{23}H_{20}N_4O_3$: C, 68.03; H, 5.19; N, 14.43%. Found: C, 67.95; H, 5.17; N, 14.50%. **8m**; 63% yield, mp 92.5—93 °C, NMR ($CDCl_3$) δ=0.7—2.0 (m, 25H), 2.75 (dd, 1H, J=9 and 16 Hz), 3.25 (dd, 1H, J=9 and 16 Hz) 4.3—5.0 (m, 1H), 7.23 (d, 2H, J=9 Hz), 7.43 (s, 5H), 8.15 (d, 2H, J=9 Hz), 12.0 (s, 1H, NH). Calcd for $C_{28}H_{38}N_4O_3$: H, 8.00; C, 70.26; N, 11.71%. Found: H, 8.10; C, 70.47; N, 11.80%.

*Reactions of Furoxans (**3a—e**) with Dipolarophiles.* The reaction was carried out according to the method previously reported[9] except for the use of mesitylene as the solvent. From the reaction of **3e** with allylbenzene, *p*-nitrophenyl allyl ether, or cyclododecene, **5y**, **5z**, and **7** were obtained in 35, 22, and 54% yield, respectively.

References

1) For reviews, see C. Grundmann and P. Grünanger, "The Nitrie Oxides," Springer-Verlag, New York (1971), pp. 31—61.

2) a) R. Sustmann, R. Huisgen, and H. Huber, *Chem. Ber.*, **100**, 1802 (1967); b) K. Bast, M. Christ, R. Huisgen, and W. Mack, *ibid.*, **106**, 3312 (1973).

3) a) L. Gajsler, R. M. Paton, J. H. Hall, and D. J. Harper, *J. Polym. Sci., Polym. Lett. Ed.*, **18**, 635 (1980); b) P. V. Finzi and M. Arbasino, *Ric. Sci., Rend., Sez. A*, **8**, 1484 (1965); M. Arbasino and P. Grünanger, *ibid.*, **7**, 561 (1964).

4) T. Mukaiyama and T. Hoshino, *J. Am. Chem. Soc.*, **82**, 5339 (1960)

5) G. B. Bachman and L. E. Strom, *J. Org. Chem.*, **28**, 1150 (1963).

6) K. Harada, E. Kaji, and S. Zen, *Chem. Pharm. Bull.*, **28**, 3296 (1980); **26**, 3254 (1978); *Nippon Kagaku Kaishi*, **1981**, 1195.

7) a) R. A. Whitney and E. S. Nicholas, *Tetrahedron Lett.*, **22**, 3371 (1981); b) W. R. Mitchell and R. M. Paton, *ibid.*, 2443 (1979) and references cited therein; c) J. Ackrell, M. Altaf-ur-Rahman, A. J. Boulton, and R. C. Brown, *J. Chem.. Soc., Perkin Trans. 1*, **1972**, 1587; d) A. J. Boulton and S. S. Mathur, *J. Org. Chem.*, **38**, 1054 (1973); e) A. Dondoni, G. Barbaro, A. Gattaglia, and P. Giorgianni, *ibid.*, **37**, 3196 (1972); f) For review, see A. Gasco and A. J. Boulton, *Adv. Heterocycl. Chem.*, **29**, 251 (1981).

8) a) W. I. Awad, S. Omran, and M. Sobhy, *J. Chem. U. A. R.*, **10**, 1 (1967); *Chem. Abstr.*, **68**, 114476u (1968); b) P. Grünanger, *Gazz. Chim. Ital.*, **84**, 359 (1954); *Chem. Abstr.*, **49**, 5436f (1955).

9) T. Shimizu, Y. Hayashi, T. Taniguchi, and K. Teramura, *Tetrahedron*, in press.

10) S. Zen, M. Koyama, and S. Kato, *Org. Synth.*, **55**, 77 (1976).

11) G. D. Parkes and E. H. Williams, *J. Chem. Soc.*, **1934**, 67.

12) A. P. Black and F. H. Babers, *Org. Synth.*, Coll. Vol. 2, 512 (1966).

13) P. A. Wade, H. R. Hinney, N. V. Amin, P. D. Vail, S. D. Morrow, S. A. Hardinger, and M. S. Saft, *J. Org. Chem.*, **46**, 765 (1981).

14) H. R. Snyder and N. E. Boyer, *J. Am. Chem. Soc.*, **77**, 4233 (1955).

15) Y. Yukawa and M. Sakai, *Nippon Kagaku Zasshi*, **87**, 79 (1966).

16) W. V. Farrar. *J. Chem. Soc.*, **1964**, 904.

 © 1984 The Chemical Society of Japan Bull. Chem. Soc. Jpn., 57, 2535—2537 (1984)

Branched-chain Sugars. XXXV. The Synthesis of L-Rubranitrose (2,3,6-trideoxy-3-*C*-methyl-4-*O*-methyl-3-nitro-L-*xylo*-hexopyranose)[1]

Juji YOSHIMURA,* Toshio YASUMORI, Tatsuya KONDO, and Ken-ichi SATO
Laboratory of Chemistry for Natural Products, Faculty of Science, Tokyo Institute of Technology, Nagatsuta, Midoriku, Yokohama 227
(Received April 16, 1984)

The title compound was stereoselectively synthesized from methyl 2,6-dideoxy-4-*O*-methyl-β-L-*threo*-hexopyranosid-3-ulose (**11**) through the successive conversions; cyanomesylation, reductive spiro aziridine formation, reductive ring-opening to the methyl-branched amino sugar, oxidation to the corresponding nitro sugar.

For rubranitrose, a component of the antibiotic rubradirin,[2] the structure was reprtred to be 2,3,6-trideoxy-3-*C*-methyl-4-*O*-methyl-3-nitro-L-*xylo*-hexopyranose (**1**) from X-ray analysis and the CD spectrum,[3] in which a positive Cotton effect was observed, opposite in sign to that of L-evernitrose (**2**).[4] However, Mallams *et al.*[5] pointed out that **1** should have D-configuration, from comparison of the CD spectrum and rotational value with D-kijanose (**3**), of which the configuration was assigned by the application of Hudson's Rules of Isorotation. In a previous communication,[6] we proved the correctness of the deduction of Mallams *et al.*, by the synthesis of **1** from D-glucose. This paper describes it in detail. In our synthesis, hexopyranosid-3-ulose was converted successively into the corresponding methyl-branched nitro sugar; *i.e.* cyanomesylation of the carbonyl group, reductive spiro aziridine formation by intramolecular S_N2 substitution, reductive ring-opening into methyl-branched amino sugar, and oxidation into the corresponding nitro sugar. The series of conversions was previously used for the synthesis of **2**[7] and its enantiomer.[8] Recently, Brimacombe *et al.*[9] communicated the synthesis of **1** and its enantiomer through the inversion of configuration of *C*-4 of methyl 3-trifluoroacetamido-2,3,6-trideoxy-3-*C*-methyl-α-L- and D-*ribo*-hexopyranoside (**4**), respectively.

Results and Discussion

For the synthesis of **1** through the aforementioned pathway, methyl 2,6-dideoxy-4-*O*-methyl-β-L-*threo*-hexopyranosid-3-ulose (**11**) was considered to be the most suitable key intermediate. Treatment of methyl 4,6-*O*-benzylidene-2-deoxy-α-D-*ribo*-hexopyranoside,[10] which was obtained from D-glucose through five-step conversions, with *N*-bromosuccinimide and barium carbonate in carbon tetrachloride gave unstable methyl 4-*O*-benzoyl-6-bromo-2,6-dideoxy-α-D-*ribo*-hexopyranoside (**5**) in 92% yield. It was found that *O*-methylation of **5** in *N*,*N*-dimethylformamide with methyl iodide and silver(I) oxide is nicely accomapnied with benzoyl migration to give the corresponding 3-*O*-benzoyl-4-*O*-methyl derivative (**6**) in 90% yield. Treatment of **6** in pyridine with silver(I) fluoride[11] gave a 3:2 mixture of the corresponding hex-5-enopyranoside (**8**) and 6-fluoro-6-deoxy derivative (**7**). The mixture could not be separated, and the presence of **7** was confirmed only by ^{19}F-NMR. Compound **8** was separated, after conversion into methyl 2,6-dideoxy-4-*O*-methyl-β-L-*lyxo*-hexopyranoside (**10**) *via* the corresponding 3-benzoate (**9**) in 49% yield. Oxidation of **10** with pyridinium chlorochromate gave the crystalline key intermediate (**11**) in 65% yield.

One-flask cyanomesylation of **11** by treatment overnight with hydrogen cyanide in dry pyridine, and then with methanesulfonyl chloride for 2 d at room temperature gave methyl 3-*C*-cyano-2,6-dideoxy-3-*O*-methylsulfonyl-4-*O*-methyl-β-L-*lyxo*-hexopyranoside (**12**) as crystals in 65% yield. In order to examine the stereoselectivity of cyanomesylation under the thermodynamic conditions,[12] cyanohydrine formation was

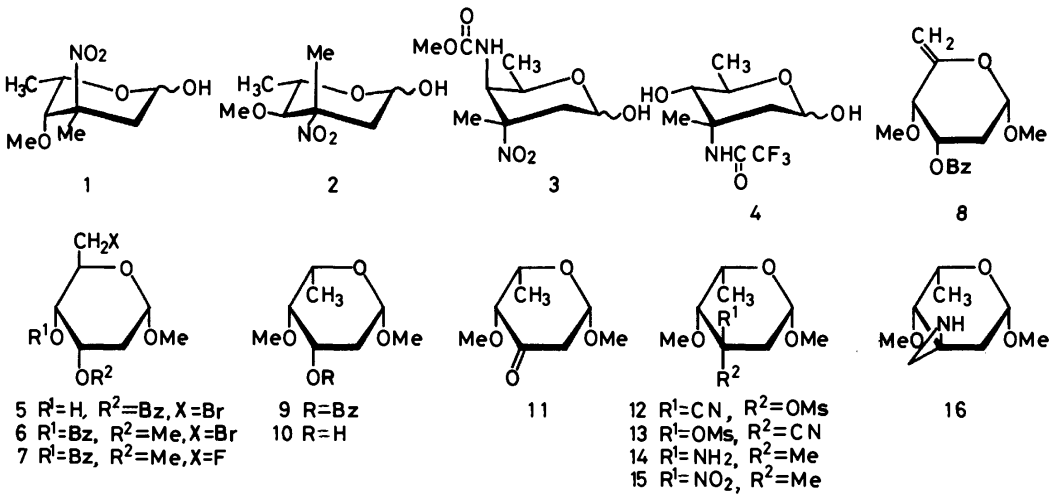

TABLE 1. ^{1}H AND ^{13}C-NMR DATA OF **1**

	Chemical shift (δ) and coupling constant (Hz) in ^{1}H-NMR							
	H-1 ($J_{1,2a}$)	H-2a ($J_{1,2e}$)	H-2e ($J_{2a,2e}$)	H-4 ($J_{4,5}$)	H-5 ($J_{5,6}$)	H-6	CMe	OMe
α-**1**	5.30 dd (2.5)	2.07 dd (3.5)	2.68 dd (14.5)	3.61 bs (1.0)	4.40 bq (6.5)	1.33 d	1.67 s	3.64 s
(Reported for α-D-**1**)	5.28 dd (2.5)	2.05 dd (3.5)	2.67 dd (14.5)	3.62 bs (<1)	4.40 bq (6.5)	1.33 d	1.67 s	3.62 s
	Chemical shift (ppm) of carbons in ^{13}C-NMR							
	C-1	*C*-2	*C*-3	*C*-4	*C*-5	*C*-6	*C*Me	OMe
α-**1**	92.51	37.17	63.45	79.65	69.84	16.79	25.84	62.69
β-**1**	90.58	34.46	62.96	79.43	69.84	16.36	25.14	62.58

carried out by treatment of **11** in dichloromethane with aqueous potassium cyanide and sodium hydrogencarbonate, followed by mesylation of the product in pyridine, to give a 1:4 mixture of **12** and its L-*xylo* isomer (**13**) in 83% yield. Reduction of **12** with lithium aluminium hydride gave the corresponding spiro aziridine (**16**) in 65% yield, which was converted into the methyl glycoside (**15**) of L-rubranitrose *via* the corresponding methyl-branched amino sugar (**14**) in 56% yield, by successive catalytic hydrogenolysis and oxidation with *m*-chloroperoxybenzoic acid. Hydrolysis of **15** in 0.05 M (1 M=1 mol dm^{-3}) sulfuric acid gave **1** {mp 147—148 °C, $[\alpha]_D$ −76° (*c* 0.48, ethanol, after 3 h); lit,[3] α-D-**1**: mp 150—153°, $[\alpha]_D$ +127°→ +86° (*c* 1.0, ethanol)} quantitatively. As shown in Table 1, ^{1}H-NMR parameters reveal the relative structure, and ^{13}C-NMR data indicate the presence of an equatorial *C*-methyl group.[13] Both the opposite sign of the optical rotational values and of the Cotton effect (the molar ellipticity at 285 nm of **1** in methanol was −1580; lit,[3] for β-acetate of the natural compound, +2500) between **1** and the natural product proved that the latter has the D-configuration.

Experimental

Melting points are uncorrected. Optical rotations were measured with a JASCO DIP-4 polarimeter in chloroform, and ^{1}H and ^{13}C-NMR were recorded in chloroform-*d* with JEOL PS-100 and JEOL FX-100 spectrometers, respectively, with tetramethylsilane as an internal standard, unless otherwise stated. Chemical shifts and coupling constants were recorded in δ and Hz units, respectively, and IR frequencies in cm^{-1}.

*Methyl 4-O-Benzoyl-6-bromo-2,6-dideoxy-α-D-*ribo*-hexopyranoside (5).* A suspension of methyl 4,6-*O*-benzylidene-2-deoxy-α-D-*ribo*-hexopyranoside (20 g, 75.2 mmol), *N*-bromosuccinimide (14.72 g, 82.7 mmol), and barium carbonate (80 g) in carbon tetrachloride (1.2 l) was refluxed for 2 h. The solution colored once red and then changed to colorless. The cooled reaction mixture was filtered, and the filtrate was evaporated to a half, poured into ice-water, then extracted with chloroform. The usual work-up of the extract, and purification of the product on a short column of silica gel gave **5** (22.7 g) as a sirup in 92.0% yield.

$[\alpha]_D$ +93.0° (*c* 1.0); NMR: δ=8.15—8.00 and 7.70—7.20 (m, 5H, Ph), 4.95 (dd, 1H, $J_{3,4}$=3.0, $J_{4,5}$=10.0, H-4), 4.95 (dd, 1H, $J_{1,2e}$=1.0, $J_{1,2a}$=3.6, H-1), 4.62—4.18 (m, 2H, H-3 and 5), 3.70—3.40 (m, 2H, H-6 and 6'), 3.50 (s, 3H, OMe), 2.22 (ddd, 1H, $J_{2e,3}$=3.6, H-2e), 2.04 (dt, 1H, $J_{2a,3}$=3.6, H-2a), and 1.75 (bs, 1H, OH).

Anal. ($C_{14}H_{17}O_5Br$) C, H, Br.

*Methyl 3-O-Benzoyl-6-bromo-2,6-dideoxy-4-O-methyl-α-D-*ribo*-hexopyranoside (6).* To a solution of **5** (13.8 g, 42.0 mmol) in *N*,*N*-dimethylformamide (50 ml) was added methyl iodide (17.9 g, 126 mmol) and silver(I) oxide (11.67 g, 50.4 mmol), and the mixture was stirred for 24 h at room temperature in the dark. After monitoring the disappearance of **5**, the mixture was filtered, and the filtrate was evaporated. The residual sirup was purified on a silica-gel column (benzene–aceonte 16:1) to give **6** (13.57 g) as a pale yellow sirup in 90.0% yield. $[\alpha]_D$+70.0° (*c* 1.9); NMR: δ=8.15—8.00 and 7.60—7.20 (m, 5H, Bz), 5.70 (dt, 1H, $J_{3,4}$=3.5, H-3), 4.83 (bd, $J_{1,2a}$=4.0, $J_{1,2e}$=1.0, H-1), 3.44 (dd, 1H, $J_{4,5}$=10.0, H-4), 4.24 (ddd, 1H, $J_{5,6}$=4.5, H-5), 3.90—3.60 (m, 2H, H-6 and 6'), 3.47 and 3.44 (each s, 6H, 2x OMe), 2.26 (ddd, 1H, $J_{2e,3}$=3.6, H-2e), and 1.98 (dt, 1H, $J_{2a,2e}$=15.5, $J_{2a,3}$=4.0, H-2a).

Anal. ($C_{15}H_{19}O_5Br$) C, H, Br.

Conversion of 6 into the Corresponding L-Sugar. A suspension of **6** (3.1 g, 8.64 mmol) and powdered silver(I) fluoride (3.1 g, 24.4 mmol) in dry pyridine (60 ml) was stirred for 40 h in the dark, then filtered. The filtrate was poured into ice-water, and extracted with chloroform. The extract was evaporated to give a yellow sirup, which was a 3:2 mixture of methyl 3-*O*-benzoyl-2,6-dideoxy-α-D-*erythro*-hex-5-enopyranoside (**8**) and methyl 3-*O*-benzoyl-2,6-dideoxy-6-fluoro-4-*O*-methyl-α-D-*ribo*-hexopyranoside (**7**). Because the mixture could not be separated, a solution of the mixture in methanol (36 ml) containing a few drops of acetic acid was hydrogenated in the presence of 10% palladium–carbon (383 mg) overnight, and then filtered. The filtrate was evaporated, and the dried residue was dissolved in 2M sodium hydroxide (30 ml). After stirring the solution at room temperature for 3 h, it was extracted with chloroform. Evaporation of the extract gave a yellow sirup which was fractionally crystallized from ethanol to give methyl 2,6-dideoxy-4-*O*-methyl-β-L-*lyxo*-hexopyranoside (**10**,739 mg) as white crystals in 48.6% overall yield. Mp 142.8—144 °C (ethanol); $[\alpha]_D$ +34.2° (*c* 1.0); NMR: 4.28 (dd, 1H, $J_{1,2a}$=10.0, $J_{1,2e}$=2.0, H-1), 3.90—3.30 (m, 2H, H-3 and 5), 3.64 and 3.51 (each s, 6H, 2×OMe), 3.16 (bd, 1H, $J_{3,4}$=3.6, $J_{4,5}$=<1, H-4), 2.00 (ddd, 1H, $J_{2e,3}$=5.0, $J_{2a,2e}$=12.0, H-2e), 1.67 (dt, 1H, $J_{2a,3}$= 10.0, H-2a), and 1.28 (d, 3H, H-6).

Anal. ($C_8H_{16}O_4$) C, H.

*Methyl 2,6-Dideoxy-4-O-methyl-β-L-*threo*-hexopyranosid-3-ulose (11).* A solution of **10** (500 mg, 2.84 mmol) and pyridinium chlorochromate (2.5 g, 11.6 mmol) in dichloromethane (12.5 ml) was stirred overnight at room temperature, and then evaporated roughly to dryness. The porduct was

purified directly on a silica-gel column (benzene–acetone 16:1) to give **11** (380 mg) as white crystals in 76.0% yield. Mp 38.8—40.4 °C (ethanol–hexane); $[\alpha]_D$ +92.0° (*c* 1.1); NMR: δ= 4.57 (dd, 1H, $J_{1,2a}$=8.0, $J_{1,2e}$=3.0, H-1), 3.74 (dq, 1H, $J_{4,5}$=3.0, $J_{5,6}$=6.4, H-5), 3.56 and 3.41 (each s, 6H, 2×OMe), 3.37 (m, 1H, H-4), 2.87 (dd, 1H, $J_{2a,2e}$=13.0, H-2a), 2.57 (ddd, 1H, $J_{2e,4}$= 1.0, H-2e), and 1.42 (d, 3H, H-6).

Anal. ($C_8H_{14}O_4$) C, H.

Cyanomesylation of 11. i) A solution of **11** (722 mg, 4.15 mmol) and hydrogen cyanide (170 mg, 6.19 mmol) in dry pyridine was kept at room temperature overnight, and then methanesulfonyl chloride (4.19 ml, 24.9 mmol) was added dropwise to it. The resulting solution was stirred for 2 d, diluted with chloroform, poured into ice–water, and then extracted with chloroform. The usual work-up of the extract, and purification of the product on a silica-gel column (benzene–acetone 8:1) gave methyl 3-*C*-cyano-2,6-dideoxy-3-*O*-methylsulfonyl-4-*O*-methyl-β-L-*lyxo*-hexopyranoside (**12**, 750 mg) as white plates in 64.8% yield. Mp 94.2—94.6 °C (ethanol); $[\alpha]_D$ −2.28° (*c* 1.0); NMR: δ=4.61 (dd, 1H, $J_{1,2a}$= 9.0, $J_{1,2e}$=3.0, H-1), 3.91 (dq, 1H, $J_{4,5}$=1.4, $J_{5,6}$=6.4, H-5), 3.25 (s, 3H, SMe), 3.67 (bs, 1H, H-4), 3.17 and 3.54 (each s, 6H, 2×OMe), 2.47 (ddd, 1H, $J_{2a,2e}$=12.4, $J_{2e,4}$=1.0, H-2e), 2.27 (dd, 1H, H-2a), and 1.37 (d, 3H, H-6).

Anal. ($C_{10}H_{17}O_6NS$) C, H, N, S.

ii) To a solution of **11** (210 mg, 1.2 mmol) in dichloromethane (2.8 ml) was added a solution of potassium cyanide (157 mg, 2.14 mmol) and sodium hydrogencarbonate (101 mg, 1.20 mmol) in water (1.5 ml) at 0 °C and the solution was stirred at room temperature overnight. The usual work-up of the solution gave a product, which was treated with methanesulfonyl chloride (553 mg, 4.83 mmol) to give a product, which was fractionally crystallized from ethanol to give crystals of L-*xylo* isomer (**13**) of **12**. The component in the filtrate was separated on a silica-gel column (benzene–acetone 8:1). Compound **13** and **12** were obtained in 68.3% (230 mg) and 13.7% (46 mg) yield, respectively.

13: mp 91.2—92 °C (ethanol); $[\alpha]_D$ +0.57 °C (*c* 1.5); NMR: δ=4.67 (dd, 1H, $J_{1,2a}$=9.0, $J_{1,2e}$=3.0, H-1), 4.03 (dq, 1H, $J_{4,5}$= 1.4, $J_{5,6}$=6.8, H-5), 3.76 and 3.54 (each s, 6H, 2×OMe), 3.33 (s, 3H, SMe), 3.57 (bs, 1H, H-4), 2.46 (ddd, 1H, $J_{2e,4}$=1.0, H-2e), 2.30 (dd, 1H, $J_{2a,2e}$=15.0, H-2a), 1.36 (d, 3H, H-6).

Anal. ($C_{10}H_{17}NO_6S$) C, H, N, S.

Spiro[aziridine-2,3'-(methyl 2,3,6-trideoxy-4-O-methyl-β*-*L*-xylo-hexopyranoside)] (16).* To a solution of **12** (200 mg, 0.717 mmol) in anhydrous ether (24 ml) was added lithium aluminium hydride (140 mg, 1.05 mmol), and the resulting suspension was refluxed for 2 h. The excess reagent was decomposed by addition of a small amount of water to the reaction mixture and filtered, and the precipitate was washed with ethanol. The filtrate and washings were combined and extracted with chloroform. Evaporation of the extract and purification of the product on a silica-gel column (ethanol) gave **16** (96.7 mg) as a sirup in 65.2% yield. $[\alpha]_D$ 0° (*c* 1.0); NMR: δ=4.60 (dd, 1H, $J_{1,2a}$=9.6, $J_{1,2e}$=2.5, H-1), 3.89 (dq, 1H, $J_{4,5}$=1.4, $J_{5,6}$=6.4, H-5), 3.54 (bs, 1H, H-4), 3.52 and 3.45 (each s, 6H, 2×OMe), 2.32 (dd, 1H, $J_{2a,2e}$= 13.5, H-2a), 2.35 (bs, 1H, NH), 1.90 and 1.83 (each s, 2H, NCH_2), 1.31 (d, 3H, H-6), and 1.05 (ddd 1H, $J_{2e,4}$=1.0, H-2e).

Anal. ($C_9H_{17}NO_3$) C, H, N.

Methyl 2,3,6-Trideoxy-3-C-methyl-4-O-methyl-3-nitro-β*-*L*-xylo-hexopyranoside (15).* A solution of **16** (187 mg, 1.0 mmol) in methanol (100 ml) was hydrogenolyzed under 120 atm hydrogen in the presence of Raney nickel (1.0 g) for 2 d, filtered, and then evaporated to give 3-amino-2,3,6-trideoxy-3-*C*-methyl-4-*O*-methyl-β-L-*xylo*-hexopyranoside (**14**) as a sirup, quantitatively. To a solution of the sirup in dichloromethane (3.0 ml) was added a solution of *m*-chloroperoxybenzoic acid (518 g, 3.0 mmol) in dichloromethane (3.0 ml) portionwise under refluxing, and the resulting solution was refluxed for 40 min, poured into 10% sodium sulfite solution, and then extracted with chloroform. The usual work-up of the extract, and purification of the product on a silica-gel column (benzene–acetone 6:1) gave **15** (123 mg) as a pale yellow sirup in 56.2% overall yield.

$[\alpha]_D$ −15.9° (*c* 0.8); NMR: δ=4.46 (dd, 1H, $J_{1,2a}$=9.6 $J_{1,2e}$= 2.2, H-1), 3.80—3.50 (m, 2H, H-4 and 5), 3.68 and 3.54 (each s, 6H, 2×OMe), 2.56 (ddd, 1H, $J_{2a,2e}$=14.6, $J_{2e,4}$=1.4, H-2e), 1.82 (dd, 1H, H-2a), 1.68 (s, 3H, CMe) and 1.36 (d, 3H, $J_{5,6}$= 6.0, H-6).

Anal. ($C_9H_{17}NO_5$) C, H, N.

L-Rubranitrose (1). A solution of **15** (56.7 mg, 0.26 mmol) in aq dioxane (1:1, 10.0 ml) of 0.05 M sulfuric acid was warmed at 90—95 °C for 2 h, neutralized with barium carbonate, and then filtered. The filtrate was evaporated, and the resulting sirup was purified on a silica-gel column (benzene–acetone 5:1) to give **1** (53.0 mg) as crystals in 98.0% yield. Physical properties of **1** were mentioned in Result and Discussion.

Anal. ($C_8H_{15}NO_5$) C, H, N.

References

1) Part XXXIV. J. Yoshimura, K. Hara, and M. Matsuzawa, *Bull. Chem. Soc. Jpn.*, **56**, 2189 (1983).

2) B. K. Bhuyan, S. P. Owen, and A. Dietz, *Antimicrob. Agents Chemother.*, **1965**, 91; C. E. Meyer, *ibid.*, **1965**, 97; F. Reusser, *Biochemistry*, **12**, 1136 (1973); H. Hoeksema, C. Chidester, S. A. Mizsak, and L. Bacznski, *J. Antibiot.*, **31**, 1067 (1978); A. P. Kozikowski, K. Sugiyama, and J. P. Springer, *Tetrahedron Lett.*, **1980**, 3257.

3) S. A. Mizsak, H. Hoeksema, and L. M. Pschigoda, *J. Antibiot.*, **32**, 771 (1979).

4) A. K. Ganguly, O. Z. Sarre, A. T. McPhall, and K. D. Onan, *J. Chem. Soc., Chem. Commun.*, **1977**, 313.

5) A. K. Mallams, M. S. Puar, and R. H. Rossman, *J. Am. Chem. Soc.*, **103**, 3938 (1981).

6) J. Yoshimura, T. Yasumori, T. Kondo, and K. Sato, *Carbohydr. Res.*, **106**, c1 (1982).

7) J. Yoshimura, M. Matsuzawa, K. Sato, and Y. Nagasawa, *Carbohydr. Res.*, **76**, 67 (1979).

8) J. Yoshimura, M. Matsuzawa, and M. Funabashi, *Bull. Chem. Soc. Jpn.*, **51**, 2064 (1978).

9) J. S. Brimacombe and K. M. M. Rahman, *Carbohydr. Res.*, **114**, c1 (1983).

10) A. Rosenthal and P. Catsoulacos, *Can. J. Chem.*, **46**, 2868 (1968).

11) T. M. Cheung, D. Horton, and W. Weckerle, *Carbohydr. Res.*, **58**, 139 (1977).

12) T. T. Thang, F. Winternitz, A. Lagranes, A. Olesker, and G. Lukacs, *Tetrahedron Lett.*, **21**, 4495 (1980); T. T. Thang and F. Winternitz, *J. Chem. Soc., Chem. Commun.*, **1979**, 153.

13) M. Miljković, M. Gligorijević, T. Sato, and D. Miljković, *J. Org. Chem.*, **39**, 1379 (1974); S. Omura, A. Nakagawa, A. Neszmelyi, S. D. Gero, A.-M. Sepulchre, F. Piriou, and G. Lukacs, *J. Am. Chem. Soc.*, **97**, 4001 (1975); K. Sato, K. Kubo, N. Hong, H. Kodama, and J. Yoshimura, *Bull. Chem. Soc. Jpn.* **55**, 938 (1982).

 © 1984 The Chemical Society of Japan Bull. Chem. Soc. Jpn., 57, 2538—2542 (1984) [Vol. 57, No. 9

Branched-chain Sugars. XXXVI. A New Synthesis of Methyl 4-*O*-Benzoyl-3-benzoylamino-2,3,6-trideoxy-3-*C*-methyl-α-L-*xylo*-hexopyranoside, a Derivative of the Branched-chain Amino Sugar of Antibiotic A35512B[1]

Toshio YASUMORI, Ken-ichi SATO, Hironobu HASHIMOTO, and Juji YOSHIMURA*
Laboratory of Chemistry for Natural Products, Faculty of Science, Tokyo Institute of Technology, Nagatsuta, Midoriku, Yokohama 227
(Received April 16, 1984)

The title compound was synthesized from methyl 4-*O*-benzyl-2,6-dideoxy-β-L-*threo*-hexopyranosid-3-ulose (**19**) through cyanomesylation, reductive spiro aziridine formation, and reductive ring-opening. When (2-methoxyethoxymethyl) group was used as the protecting group at *O*-4 of the above intermediate, it could not be removed at the final stage.

3-Amino-2,3,6-trideoxy-3-*C*-methyl-L-*xylo*-hexopyranose (**1**)[2] was found as a component of the new Gram-positive antibiotic, A35512B,[3] and characterized as the title compound (**2**).[2] In the preceding paper,[1] we have synthesized L-rubranitrose (**4**), having fundamentally the same configuration with **1**, from D-glucose. This paper describes a facile synthesis of **2** through a similar pathway. The first synthesis of **2** was accomplished from a non-carbohydrate diol obtained by fermentation of α-methylcinnamaldehyde with bakers' yeast.[4] In latter, *N*-acetyl derivative of **2** was obtained from its 4-epimeric derivative (**5**) by inversion,[5] which was derived from L-rhamnose.

Results and Discussion

In the synthesis of **4**, the coincidental migration of benzoyl group in methyl 6-bromo-2,6-dideoxy-4-*O*-benzoyl-α-D-*ribo*-hexopyranoside (**6**) with the introduction of methyl group on *O*-4, and the conversion of D-sugar to L-sugar were utilized. In the similar way, treatment of **6** with benzyl bromide and silver(I) oxide in *N*,*N*-dimethylformamide (DMF) in the dark gave the corresponding 3-*O*-benzoyl-4-*O*-benzyl derivative (**7**) in 92% yield. However, treatment of **7** in dry pyridine with silver(I) fluoride gave the 5-enopyranoside (**8**) and fluorine-substituted derivative of **7** in the ratio of 2:3, and catalytic hydrogenation of the unsaturated bond of **8** was undesirably accompanied with hydrogenolysis of 4-*O*-benzyl group to give methyl 3-*O*-benzoyl-2,6-dideoxy-β-L-*lyxo*-hexopyranoside (**9**) in 32% overall yield. Partial benzoylation of methyl 2,6-dideoxy-β-L-*lyxo*-hexopyranoside[6] gave also **9** in 85% yield, together with a small amount of the 4-benzoate (**10**) and 3,4-dibenzoate.

As was observed in the case of **6**, the benzoyl migration in equatorially oriented benzoyloxy group of **9** to the vicinal axial hydroxyl group took place very easily. Thus, the treatment of **9** with silver(I) fluoride in pyridine or with silver(I) oxide in DMF gave the corresponding 4-benzoate (**10**) quantitatively, and therefore, benzylation of **9** under the above conditions gave mainly the corresponding 4-*O*-benzoyl-3-*O*-benzyl derivative, which was confirmed by hydrogenolysis of the product into **10**. Similarly, reaction of **9** in dichloromethane with (2-methoxyethoxymethyl) chloride in the presence of *N*,*N*-diisopropylethylamine gave the corresponding 4-*O*-benzoyl-3-*O*-(2-methoxyethoxymethyl) (**11**) and 3-*O*-benzoyl-4-*O*-(2-methoxyethoxymethyl) (**12**) derivatives in the ratio of 1:1, and the mixture was *O*-debenzoylated into the corresponding 3-*O*-(2-methoxyethoxymethyl) (**13**) and 4-*O*-(2-methoxyethoxymethyl) (**14**) derivatives. These acyl migration are undesirable in the present synthesis.

Now, the reaction was accomplished under the conditions by the use of (2-methoxyethoxymethyl) triethylammonium chloride[7] to give **12** exclusively, which was then *O*-debenzoylated into **14** in 88% yield. Oxidation of **10** and **14** with pyridinium chlorochromate gave the corresponding pyranosid-3-uloses (**17** and **18**) in 91% and 98% yields, respectively. One-flask cyanomesylation of **17** and **18** under kinetic conditions[8] gave 4-*O*-benzoyl (**20**) and 4-*O*-(β-methoxyethoxymethyl) (**21**) derivatives of methyl 3-*C*-cyano-2,6-dideoxy-3-*O*-methylsulfonyl-β-L-*lyxo*-hexopyranoside in 35 and 73% yields, respectively. Reduction of **21** with lithium aluminium hydride gave the corresponding spiro aziridine (**23**) in 65% yield, which was then converted into methyl 3-benzoylamino-2,3,6-trideoxy-4-*O*-(2-methoxyethoxymethyl)-3-*C*-methyl-β-L-*xylo*-hexopyranoside

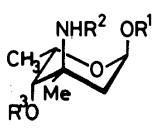

1 $R^1=R^2=R^3=H$
2 $R^1=Me, R^2=R^3=Bz$
3 $R^1=Me, R^2=Bz, R^3=H$

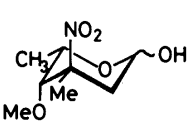

4

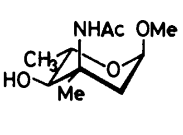

5

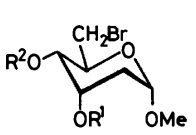

6 $R^1=H, R^2=Bz$
7 $R^1=Bz, R^2=Bn$

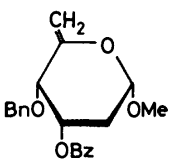

8

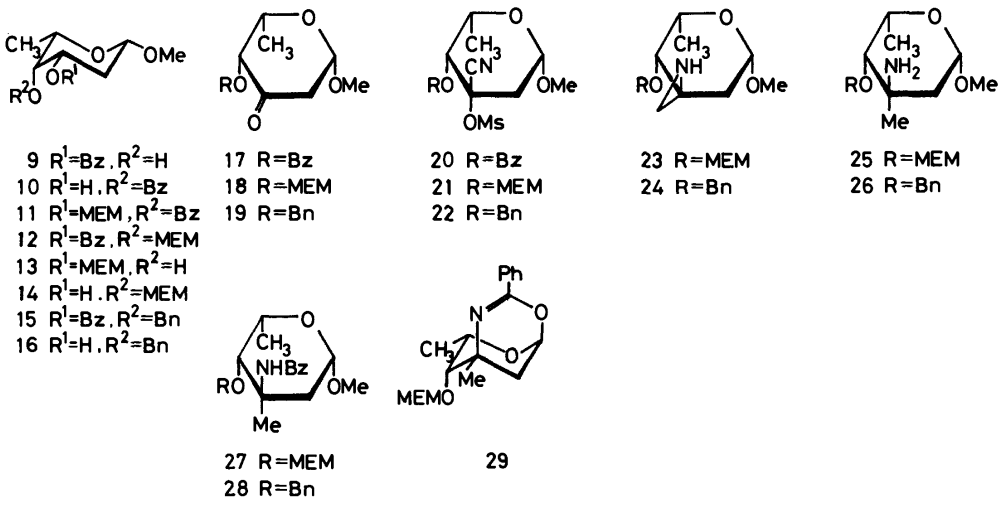

Table 1. ^{13}C-NMR chemical shifts (δ)[a] of **2**, **27**, and **28**

Carbons	**2**	**27**[b]	**28**
C-1	98.66	98.91	98.93
C-2	36.95	39.75	38.34
C-3	53.64	57.60	58.03
C-4	70.33	76.72	76.61
C-5	63.12	69.26	69.62
C-6	17.07	17.42	17.23
C-Me	22.76	23.45	23.35
O-Me	55.37	56.17	56.13
C=O	116.01	167.01	167.15
	165.58		

a) Data for benzene-carbons were omitted. b) (2-methoxyethoxymethyl) carbons from the terminal: 59.04, 68.48, 71.73, and 98.05 respectively.

(**27**) through hydrogenolysis into the corresponding methyl-branched amino sugar (**25**) followed by *N*-benzoylation. However, the 4-*O*-(2-methoxyethoxymethyl) group of **27** could not be removed. Treatment of **27** with 2-propanethiol and boron trifluoride etherate[9] gave unchanged **27**, and with zinc(II) chloride[7] in dichloromethane or with 1.5 M (1 M=1 mol dm^{-3}) methanolic hydrogen chloride[10] gave 8-(2-methoxyethoxymethoxy)-7-methyl-3-phenyl-4,6-dioxa-2-azabicyclo[3.3.1]non-2-ene (**29**) in 63 and 60% yields, respectively.

From the aforementioned result, benzyl group was chosen as the protecting group. Benzylation[11] of **9** with benzyl trichloroacetimidate and trifluoromethanesulfonic acid[12] was successfully proceeded to give the corresponding 4-*O*-benzyl derivative (**15**) in 62% yield, which was then debenzoylated to give **16**. Oxidation of **16** with pyridinium chlorochromate gave the corresponding pyranosid-3-ulose (**19**) in 84% yield. Cyanomesylation of **19** gave **22** in 65% yield, which was converted into the corresponding methyl-branched amino sugar (**26**) *via* the spiro aziridine derivative (**24**). Benzoylation of **26** in methanol gave the corresponding *N*-benzoyl derivative (**28**) quantitatively. Hydrogenolysis of **28** in methanol in the presence of palladium–carbon, followed by *O*-benzoylation of the product (**3**) in pyridine, was unexpectedly accompanied by anomerization to give **2** in 65% yield. This anomerization under neutral conditions was confirmed by repeated experiments. Physical constants of **2** thus obtained were identical with those reported for the sample obtained from antibiotic A35512B (see Experimental). In Table 1, ^{13}C-NMR data of **2**, **27**, and **28** were summarized. The results indicate the presence of an equatorially oriented methyl-group in these compounds,[13] and the substituent effects observed are rational to those have been reported.[14]

Experimental

Melting points are uncorrected. Optical rotations were measured with a JASCO DIP-4 polarimeter in chloroform, and ^{1}H and ^{13}C-NMR were recorded in chloroform-*d* with JEOL PS-100 and JEOL FX-90Q spectrometers, respectively, with tetramethylsilane as an internal standard, unless otherwise stated. Chemical shifts and coupling constants were recorded in δ (ppm) and Hz units, respectively, and IR frequencies in cm^{-1}.

*Methyl 3-O-Benzoyl-4-O-benzyl-6-bromo-2,6-dideoxy-α-*D*-ribo-hexopyranoside (7).* To a solution of methyl 4-*O*-benzoyl-6-bromo-2,6-dideoxy-α-D-*ribo*-hexopyranoside (1.61 g, 4.67 mmol) in *N*,*N*-dimethylformamide (10 ml) was added benzyl bromide (0.95 g, 5.61 mmol) and silver(I) oxide (1.32 g, 5.61 mmol), and the mixture was stirred in the dark for 24 h, filtered (after checking the consumption of the starting meterial with TLC), and the filtrate was evaporated. Purification of the residual sirup on a silica-gel column (benzene: acetone 16:1) gave **7** as a pale yellow sirup (1.87 g, 92.2%). $[\alpha]_D$ +65° (*c* 1.2); NMR: δ=8.27—7.96 and 7.86—7.04 (m, 10H, Bz and Ph), 5.79 (dt, 1H, $J_{3,4}$=3.0, H-3), 4.85 (dd, 1H, $J_{1,2a}$=4.0, $J_{1,2e}$=1.4, H-1), 4.79 and 4.47 (ABq, 2H, J_{gem}=11.0, CH_2Ph), 4.36 (m, 1H, H-5), 3.85—3.40 (m, 3H, H-4, 6, and 6′), 3.46 (s, 3H, OMe), 2.30 (ddd, 1H, $J_{2a,3}$=4.0, $J_{2a,2e}$=16.0, H-2a) and 2.00 (dt, 1H, H-2e).

Anal. ($C_{21}H_{23}O_4Br$) C, H, Br.

*Methyl 3-O-Benzoyl-2,6-dideoxy-β-*L*-lyxo-hexopyranoside (9).* i) A suspension of **7** (1.76 g, 4.2 mmol) and powdered dry silver(I) fluoride (1.55 g, 12.2 mmol) in dry pyridine (30 ml) was stirred for 40 h in the dark, poured into cold water, and then extracted with chloroform. The organic

layer was filtered, and evaporated. The residual yellow sirup contains 3-*O*-benzoyl-4-*O*-benzyl-2,6-dideoxy-α-D-*erythro*-hex-5-enopyranoside (**8**) and the substitution product; 6-fluoro-6-deoxy drivative in the ratio of 2:3. The mixture in methanol (20 ml) containing a few drops of acetic acid was hydrogenated in the presence of 10% palladium-carbon (200 mg) overnight. After monitering the disappearance of **8**, the usual work-up of the reaction mixture and purification of the product on a silica-gel column gave **9** (362 mg, 32.4%) as a yellow sirup. $[\alpha]_D$ −8.6° (*c* 1.4); NMR: δ=8.2—8.0 and 7.7—7.3 (m, 5H, Bz), 5.11 (ddd, 1H, $J_{2a,3}$=12.0, $J_{2e,3}$=6.0, H-3), 4.48 (dd, 1H, $J_{1,2a}$=8.6, $J_{1,2e}$=3.6, H-1), 3.83 (d, 1H, $J_{3,4}$=3.0, H-4), 3.65 (q, 1H, $J_{5,6}$=7.0, H-5), 3.53 (s, 3H, OMe), 2.20 (bs, 1H, OH), 2.17 (ddd, 1H, $J_{2a,2e}$=12.0, H-2e), 1.98 (dt, 1H, H-2a) and 1.35 (d, 3H, H-6).

Anal. ($C_{14}H_{18}O_5$) C, H.

ii) To a solution of methyl 2,6-dideoxy-β-L-*lyxo*-hexopyranoside[6] (4.93 g, 30.4 mmol) in dry pyridine (40 ml) was added benzoyl chloride (4.53 g, 32.2 mmol) dropwise at 0 °C, and the resulting solution was stirred overnight at room temperature. The usual work-up of the reaction mixture and purification of the product on a silica-gel column (benzene–acetone 8:1) gave **9** in 85.0% (6.88 g) yield. The residual part included 4-*O*-benzoyl (**10**) and 3,4-di-*O*-benzoyl derivatives.

*Methyl 4-O-Benzoyl-2,6-dideoxy-β-*L-lyxo-*hexopyranoside (**10**).* A suspension of **9** (130 mg, 0.488 mmol) and silver(I) oxide (2 g, 8.63 mmol) in DMF (20 ml) was stirred for 2 d at room temperature in the dark, and then filtered. The usual work-up of the filtrate gave **10** (130 mg) quantitatively. Mp. 122—124 °C (hexane–ethanol 1:1); $[\alpha]_D$ +30.3° (*c* 1.1). NMR: δ=8.3—8.0 and 7.7—7.3 (m, 5H, Bz), 5.26 (dd, 1H, $J_{3,4}$=4.0, $J_{4,5}$=1.0, H-4), 4.42 (dd, 1H, $J_{1,2a}$=9.5, $J_{1,2e}$=2.4, H-1), 4.03 (ddd, 1H, $J_{2a,3}$=12.2, $J_{2e,3}$=5.4, H-3), 3.72 (dq, $J_{5,6}$=6.7, H-5), 3.53 (s, 3H, OMe), 2.88 (bs, 1H, OH), 2.07 (ddd, 1H, $J_{2a,2e}$=12.0, H-2e), 1.84 (dt, 1H, H-2a) and 1.28 (d, 3H, H-6).

Anal. ($C_{14}H_{18}O_5$) C, H.

*(2-Methoxyethoxy) methylation of **9**.* i) A solution of **9** (172.5 mg, 0.648 mmol), (2-methoxyethoxymethyl) chloride (143 mg, 1.15 mmol), and *N*,*N*-diisopropylethylamine (167 mg, 1.29 mmol) in dichloromethane (10 ml) was stirred at room temperature overnight. The usual work-up of the reaction mixture gave a 1:1 mixture (226.8 mg) of methyl 4-*O*-benzoyl-2,6-dideoxy-3-*O*-(2-methoxyethoxymethyl)-β-L-*lyxo*-hexopyranoside (**11**) and its regioisomer (**12**) in 98.8% yield, which could not be separated in a pure state. Therefore, a solution of the mixture (226.8 mg) in methanol (10 ml) containing sodium (30 mg, 1.30 mmol) was stirred overnight at room temperature. The usual work-up of the reaction mixture gave a mixture (138.1 mg) of the corresponding 3-*O*-(2-methoxyethoxymethyl) (**13**) and 4-*O*-(2-methoxyethoxymethyl) (**14**) derivatives in 86.2% yield. Separation of the products on a silica-gel column (benzene–acetone 19:1) gave only a small amount of pure samples.

13: mp. 65—66 °C (hexane–ethanol 1:1); $[\alpha]_D$ −10.0° (*c* 0.9); NMR: δ=4.97 and 4.66 (ABq, 2H, J_{AB}=7.0, OCH_2O), 4.78 (dd, 1H, $J_{1,2a}$=3.0, $J_{1,2e}$=0.7, H-1), 4.12—3.72 (m, 3H, H-3, 4, and 5), 3.72—3.47 (m, 4H, OCH_2CH_2O), 3.40 (s, 3H, OMe), 3.33 (s, 3H, OMe in MEM), 1.92 (dd, 1H, $J_{2a,2e}$=9.0, H-2e), 1.82 (dd, 1H, H-2a), 1.32 (s, 1H, OH) and 1.23 (d, 3H, H-6).

Anal. ($C_{11}H_{22}O_6$) C, H.

14: mp 90—91 °C (hexane–ethanol 1:1); $[\alpha]_D$ −38.3° (*c* 1.1); NMR: δ=4.94 and 4.68 (ABq, 2H, J_{AB}=7.0, OCH_2O), 4.32 (dd, 1H, $J_{1,2a}$=9.6, $J_{1,2e}$=2.5, H-1), 3.91 (ddd, 1H, $J_{2a,3}$=9.6, $J_{2e,3}$=5.0, H-3), 3.56 (q, 1H, $J_{5,6}$=6.6, H-5), 3.54 (d, 1H, $J_{3,4}$=4.0, H-4), 3.47 (s, 3H, OMe), 3.76—3.48 (m, 4H, OCH_2CH_2O), 3.36 (s, 3H, OMe in MEM), 1.98 (ddd, 1H, $J_{2a,2e}$=12.0, H-2e), 1.67 (dt, 1H, H-2a), 1.92 (bs, 1H, OH), and 1.29 (d, 3H, H-6).

Anal. ($C_{11}H_{22}O_6$) C, H.

ii) A solution of **9** (162 mg, 0.608 mmol) and (2-methoxyethoxymethyl) trimethylammonium chloride (452 mg, 2.00 mmol) in acetonitrile (10 ml) was refluxed for 3h. The usual work-up of the mixture and purification of the product on a silica-gel column (benzene–acetone 19:1) gave sirupy **12** (215.6 mg) in quantitative yield. $[\alpha]_D$ +43.7° (*c* 1.5); NMR: δ=8.16—7.98 and 7.62—7.30 (m, 5H, Bz), 5.15 (ddd, 1H, $J_{2a,3}$=11.0, $J_{2e,3}$=6.0, H-3), 4.98 and 4.85 (ABq, J_{AB}=7.0, OCH_2O), 4.50 (dd, 1H, $J_{1,2a}$=8.0, $J_{1,2e}$=4.0, H-1), 3.91 (bd, $J_{3,4}$=3.0, H-4), 3.82 (q, 1H, $J_{5,6}$=6.6, H-5), 3.80—3.36 (m, 4H, OCH_2CH_2O), 3.52 (s, 3H, OMe), 3.28 (s, 3H, OMe in MEM), 2.16 (dt, 1H, $J_{2a,2e}$=11.0, H-2a), 2.03 (ddd, 1H, H-2e), and 1.37 (d, 3H, H-6).

Anal. ($C_{18}H_{26}O_7$) C, H.

O-Debenzoylation of thus obtained **12** (204 mg) with sodium methoxide by the aforementioned method gave **14** (126.1 mg) in 87.5% yield.

*Methyl 3-O-Benzoyl-4-O-benzyl-2,6-dideoxy-β-*L-lyxo-*hexopyranoside (**15**).* A solution of **9** (475 mg, 1.78 mmol) and benzyl trichloroacetimidate (1.35 g, 5.66 mmol) in cyclohexane (12 ml) and dichloromethane (6 ml) containing trifluoromethanesulfonic acid catalyst (0.72 ml of 0.435 M dichloromethane solution) was stirred for 3 d at room temperature. The usual work-up of the mixture and purification of the product on a silica-gel column (benzene–acetone 19:1) gave **15** (395 mg) as a sirup in 62.2% yield. $[\alpha]_D$ −2.4° (*c* 0.95); NMR: δ=8.16—7.96 and 7.68—7.20 (m, 10H, Bn and Bz), 5.18 (ddd, $J_{2a,3}$=11.5, $J_{2e,3}$=6.0, H-3), 4.82 and 4.62 (ABq, 2H, J_{AB}=12.0, CH_2Ph), 4.48 (dd, 1H, $J_{1,2a}$=8.4, $J_{1,2e}$=3.0, H-1), 3.68 (dd, 1H, $J_{3,4}$=3.0, H-4), 3.62 (dq, 1H, $J_{4,5}$=1.4, $J_{5,6}$=6.2, H-5), 3.53 (s, 3H, OMe), 2.26 (dt, 1H, $J_{2a,2e}$=11.5, H-2a), 2.07 (ddd, 1H, H-2e), and 1.29 (d, 3H, H-6).

Anal. ($C_{21}H_{24}O_5$) C, H.

*Methyl 4-O-Benzyl-2,6-dideoxy-β-*L-lyxo-*hexopyranoside(**16**).* A solution of **15** (350 mg, 0.982 mmol) in methanol (15 ml) containing sodium (40 mg, 1.74 mmol) was stirred overnight at room temperature. The usual work-up of the mixture and purification of the product on a silica-gel column (benzene–acetone 8:1) gave **16** (220 mg) in 88.7% yield. Mp. 63.5—64.0 °C (hexane–ethanol 1:1); $[\alpha]_D$ −9.5° (*c* 1.3); NMR: δ=7.52—7.20 (bs, 5H, Bn), 4.84 and 4.64 (ABq, 2H, J_{AB}=12.0, CH_2Ph), 4.49 (dd, 1H, $J_{1,2a}$=9.5, $J_{1,2e}$=2.6, H-1), 3.68 (ddd, $J_{2a,3}$=12.0, $J_{2e,3}$=5.4, H-3), 3.39 (dq, 1H, $J_{5,6}$=6.9, H-5), 3.48 (s, 3H, OMe), 3.42 (dd, $J_{3,4}$=3.0, $J_{4,5}$=1.4, H-4), 2.00 (bs, 1H, OH), 1.96 (ddd, 1H, $J_{2a,2e}$=9.6, H-2a), 1.68 (dt, 1H, H-2e), and 1.35 (d, 3H, H-6).

Anal. ($C_{14}H_{20}O_4$) C, H.

*Oxidation of **10**, **14**, and **16** into the Corresponding Pyranosid-3-uloses.* A suspension of **10** (435 mg, 1.63 mmol), pyridinium chlorochromate (PCC) (800 mg, 3.71 mmol) and a small amount of molecular sieves 3A in dichloromethane (15 ml) was stirred at room temperature overnight, and then filtered. The usual work-up of the filtrate, and purification of the product on a silica-gel column (benzene–acetone 8:1) gave methyl 4-*O*-benzyl-2,6-dideoxy-β-L-threohexopyranosid-3-ulose (**17**; 392 mg, 90.8%) as a sirup. $[\alpha]_D$ +20.0° (*c* 1.5); NMR: δ=8.2—8.0 and 7.7—7.3 (m, 5H, Bz), 5.35 (d, 1H, $J_{4,5}$=4.2, H-4), 4.87 (t, 1H, $J_{1,2a}$=$J_{1,2e}$=4.7, H-1), 4.24 (dq, $J_{5,6}$=6.8, H-5), 3.50 (s, 3H, OMe), 2.83 (d, 2H, H-2a and 2e) and 1.46 (d, 3H, H-6).

Anal. ($C_{14}H_{16}O_5$) C, H.

A similar oxidation of **14** (512 mg, 2.05 mmol) with PCC (912 mg, 4.23 mmol) gave the corresponding 3-ulose (**18**: 498 mg, 98.1%) as a sirup. $[\alpha]_D$ +27° (*c* 7.9); IR : 1740 cm^{-1} (C=O); NMR: δ=4.77 (s, 2H, OCH_2O), 4.63 (dd, 1H, $J_{1,2a}$=7.5, $J_{1,2e}$=3.4, H-1), 3.86 (bs, 1H, $J_{2e,4}$=1.4, H-4), 3.71 (q, $J_{5,6}$=6.2, H-5), 3.84—3.52 (m, 4H, OCH_2CH_2O), 3.53 (s, 3H, OMe), 3.39 (s, 3H, OMe in MEM), 2.90 (dd, 1H, $J_{2a,2e}$=

13.4, H-2a), 2.60 (ddd, 1H, H-2e), and 1.41 (d, 3H, H-6).

Anal. ($C_{11}H_{20}O_6$) C, H.

Oxidation of **16** (737 mg, 2.92 mmol) with PCC (1.50 g, 6.96 mmol) gave the product (**19**) (614 mg, 84.0%) as a sirup. $[\alpha]_D$ +40.4° (*c* 4.4); IR: 1740 cm^{-1} (C=O); NMR: δ=7.48—7.20 (m, 5H, Ph), 4.56 (dd, 1H, $J_{1,2a}$=8.0, $J_{1,2e}$=3.0; H-1), 4.68 and 4.36 (ABq, 2H, J_{AB}=12.0, CH_2Ph), 3.71 (dq, 1H, $J_{5,6}$=6.6, H-5), 3.51 (s, 3H, OMe), 3.46 (bd, 1H, $J_{4,5}$=2.0, H-4), 2.93 (dd, $J_{2a,2e}$=13.6, H-2a), 2.57 (ddd, 1H, $J_{2e,4}$=1.4, H-2e), and 1.37 (d, 3H, H-6).

Anal. ($C_{14}H_{18}O_4$) C, H.

Cyanomesylation of 17, 18, and 19. A solution of **17** (370 mg, 1.40 mmol) and hydrogen cyanide (50 mg, 1.85 mmol) in dry pyridine (8 ml) was stirred overnight at room temperature, and then methanesulfonyl chloride (964 mg, 8.42 mmol) was added to it. The reaction mixture was further stirred for 2 d at room temperature, poured into ice-water, and then extracted with chloroform. The usual work-up of the extract and purification of the product on a silica-gel column (benzene-acetone 19:1) gave methyl 4-*O*-benzoyl-3-*C*-cyano-2,6-dideoxy-3-*O*-methylsulfonyl-β-L-*lyxo*-hexopyranoside (**20**, 180 mg) as a sirup in 35% yield. NMR: δ=8.2—8.0 and 7.7—7.3 (m, 5H, Bz), 5.71 (s, 1H, H-4), 4.80 (dd, 1H, $J_{1,2a}$=9.3, $J_{1,2e}$=2.0, H-1), 4.22 (q, 1H, $J_{5,6}$=6.0, H-5), 3.61 (s, 3H, OMe), 3.20 (s, 3H, SMe), 2.84 (dt, 1H, $J_{2a,2e}$=12.5, $J_{2e,4}$=2.0, H-2e), 2.46 (dd, 1H, H-2a), and 1.33 (d, 3H, H-6).

Anal. ($C_{16}H_{19}O_7NS$) C, H, N.

Cyanomesylation of **18** (550 mg, 2.22 mmol) with hydrogen cyanide (200 mg, 7.40 mmol) and methanesulfonyl chloride (1382 mg, 12.06 mmol) in dry pyridine (10 ml) as above and purification of the product on a silica-gel column (benzen-acetone 14:1) gave the product (**21**, 570 mg) as a sirup in 72.8% yield. $[\alpha]_D$ +14.8° (*c* 1.3); NMR: δ=4.96 and 4.84 (ABq, 2H, J_{AB}=7.0, OCH_2O), 4.57 (dd, 1H, $J_{1,2a}$=9.2, $J_{1,2e}$=2.5, H-1), 3.95 (q, 1H, $J_{5,6}$=6.2, H-5), 3.92 (bs, 1H, H-4), 3.90—3.56 (m, 4H, OCH_2CH_2O), 3.54 (s, 3H, OMe), 3.39 (s, 3H, OMe in MEM) 3.25 (s, 3H, SMe), 2.67 (ddd, $J_{2a,2e}$=13.0, $J_{2e,4}$=1.0, H-2e), 2.31 (dd, 1H, H-2a), and 1.37 (d, 3H, H-6).

Anal. ($C_{13}H_{23}O_8NS$) C, H, N.

In a similar way, **19** (602 mg, 2.41 mmol) was cyanomesylated to give **22** (614 mg) as a sirup in 65.4% yield. $[\alpha]_D$ −4.95° (*c* 1.2); NMR: δ=7.6—7.2 (bs, 5H, Bn), 4.94 and 4.74 (ABq, 2H, J_{AB}=11.0, CH_2Ph), 4.59 (dd, 1H, $J_{1,2a}$=8.6, $J_{1,2e}$=3.0, H-1), 3.89 (q, 1H, $J_{5,6}$=6.4, H-5), 3.85 (s, 1H, H-4), 3.51 (s, 3H, OMe), 3.16 (s, 3H, SMe), 2.59 (dd, 1H, $J_{2a,2e}$= 12.4, H-2e), 2.40 (dd, 1H, H-2a), and 1.25 (d, 3H, H-6).

Anal. ($C_{16}H_{21}O_6NS$) C, H, N, S.

Spiro Aziridine Formation from 21 and 22. A suspension of **21** (447 mg, 1.26 mmol) and lithium aluminium hydride (72.0 mg, 1.90 mmol) in dry ether (55 ml) was refluxed for 2 h, and then a small amount of water was added to the reaction mixture. The mixture was filtered, and the ether solution was washed with water, dried, and evaporated. The residue was purified on a silica-gel column (ethyl acetate-ethanol 5:1) to give spiro [aziridine-2,3′-(methyl 2,3,6-trideoxy-4-*O*-(2-methoxyethoxymethyl)-β-L-*xylo*-hexopyranoside)] (**23**, 216 mg) as a sirup in 65.3% yield. $[\alpha]_D$ 0° (*c* 1.3); NMR: δ=4.88 and 4.66 (ABq, 2H, J_{AB}= 7.0, OCH_2O), 4.53 (dd, 1H, $J_{1,2a}$=9.6, $J_{1,2e}$=2.0, H-1), 3.85 (dq, 1H, $J_{5,6}$=7.0, $J_{4,5}$=1.4, H-5), 3.8—3.5 (m, 4H, OCH_2CH_2O), 3.68 (bs 1H, H-4), 3.49 (s, 3H, OMe), 3.37 (s, 3H, OMe in MEM), 2.75 (bs, 1H, NH), 2.31 (dd, 1H, $J_{2a,2e}$=13.8, H-2a), 1.07 (ddd, 1H, $J_{2e,4}$=1.3, H-2e), 1.95 and 1.75 (each s, 2H, CH_2N) and 1.29 (d, 3H, H-6).

Anal. ($C_{12}H_{23}O_5N$) C, H, N.

Similarly, **22** (460 mg, 1.29 mmol) was converted into the corresponding sirupy spiro aziridine (**24**, 210 mg) as above in 61.7% yield. $[\alpha]_D$ 0° (*c* 1.1); NMR: δ=7.5—7.2 (bs, 5H, Bn), 4.76 and 4.58 (ABq, 2H, J_{AB}=12.0, CH_2Ph), 4.60 (dd, 1H, $J_{1,2a}$=9.4, $J_{1,2e}$=2.4, H-1), 3.90 (dq, $J_{5,6}$=6.4, $J_{4,5}$=1.6, H-5), 3.53 (s, 3H, OMe), 2.55 (bs, 1H, H-4), 2.54 (bs, 1H, NH), 2.44 (dd, $J_{2a,2e}$=13.2, H-2a), 1.08 (ddd, 1H, $J_{2e,4}$=1.0, H-2e), 1.77 and 1.74 (each s, 2H, CH_2N) and 1.34 (d, 3H, H-6).

Anal. ($C_{15}H_{21}O_3N$) C, H, N.

4-O-(2-Methoxyethoxymethyl) (27) and 4-O-Benzyl (28) Derivatives of Methyl 3-Benzoylamino-2,3,6-trideoxy-3-C-methyl-β-L-xylo-hexopyranoside. A solution of **23** (180 mg, 0.689 mmol) in methanol (150 ml) was hydrogenolyzed in the presence of Raney nickel W-4 (2 ml) under 110 atm hydrogen at room temperature for 3 d and then filtered. The filtrate was evaporated, and the residue was benzoylated in pyridine (10 ml) with benzoyl chloride (226 mg, 1.61 mmol) in the usual manner to give sirupy **27** in 48.8% overall yield, after purification on a silica-gel column (benzene-acetone 8:1). $[\alpha]_D$ −18.8° (c 0.75); NMR: δ=7.76—7.56 and 7.48—7.30 (m, 5H, Bz), 5.85 (bs, 1H, NH), 4.92 and 4.82 (ABq, 2H, J_{AB}=6.5, OCH_2O), 4.58 (dd, 1H, $J_{1,2a}$=7.6, $J_{1,2e}$=4.7, H-1), 4.19 (bs, 1H, H-4), 3.93 (bq, 1H, $J_{5,6}$=6.4, H-5), 3.86—3.52 (m, 4H, OCH_2CH_2O), 3.51 (s, 3H, OMe), 3.40 (s, 3H, OMe in MEM), 1.70—2.00 (m, 2H, H-2e and 2a), 1.59 (s, 3H, CMe), and 1.30 (d, 3H, H-6).

Anal. ($C_{19}H_{29}O_6N$), C, H, N.

In a similar manner, **24** (190 mg, 0.722 mmol) was converted into **28** (193 mg) in 72.2% yield. Sirup; $[\alpha]_D$ −23.4° (*c* 1.6); NMR: 7.84—7.68 and 7.60—7.20 (m, 10H, Bn and Bz), 5.91 (bs, 1H, NH), 4.84 and 4.70 (ABq, 2H, J_{AB}=11.6, CH_2Ph), 4.60 (dd, 1H, $J_{1,2a}$=9.4, $J_{1,2e}$=3.0, H-1), 4.24 (bs, 1H, $J_{4,5}$=1.0, H-4), 3.95 (dq, $J_{5,6}$=6.4, H-5), 3.50 (s, 3H, OMe), 2.00 (dd, $J_{2a,2e}$=14.0, H-2a), 1.76 (ddd, 1H, $J_{2e,4}$=1.0, H-2e), 1.62 (s, 3H, CMe), and 1.32 (d, 3H, H-6).

Anal. ($C_{22}H_{27}O_4N$) C, H, N.

Attempted O-De (2-methoxyethoxy) methylation of 27. i) A solution of **27** (20 mg, 0.054 mmol) and zinc(II) bromide (64.5 mg, 0.286 mmol) in dichloromethane (2 ml) was stirred at room temperature overnight. The reaction mixture was washed with sodium hydrogencarbonate solution, and the usual work up, and purification of the product on a preparative TLC (benzene-acetone 14:1) gave 8-(2-methoxyethoxymethoxy)-7-methyl-3-phenyl-4,6-dioxa-2-azabicyclo[3.3.1]-non-2-ene (**29**) as a sirup in 63.3% (11.6 mg) yield. $[\alpha]_D$ −35° (*c* 1.3); NMR: δ=8.00—7.84 and 7.48—7.20 (m, 5H, Ph), 5.61 (t, 1H, $J_{1,2a}$=$J_{1,2e}$=2.0, H-1), 4.84 (s, 2H, OCH_2O), 3.90 (dq, 1H, $J_{5,6}$=6.7, $J_{4,5}$=1.8, H-5), 3.48 (bs, 1H, H-4), 3.84—3.44 (m, 4H, OCH_2CH_2O), 3.40 (s, 3H, OMe in MEM), 2.25 (dd, 1H, $J_{2a,2e}$=13.2, H-2a), 1.40 (s, 3H, CMe), 1.41 (dt, 1H, $J_{2e,4}$=1.4, H-2e), 1.20 (d, 3H, H-6).

Anal. ($C_{18}H_{25}O_5N$) C, H, N.

ii) Treatment of **27** (20 mg, 0.054 mmol) with 1.5 M hydrochloric acid in methanol (5.0 ml) for 15 min refluxing temperature gave also **29** (10.0 mg) in 59.6% yield.

Methyl 4-O-Benzoyl-3-benzoylamino-2,3,6-trideoxy-3-C-methyl-α-L-xylo-hexopyranoside (2). A solution of **28** (102 mg, 0.276 mmol) in methanol (20 ml) was hydrogenated overnight at room temperature in the presence of 10% palladium-carbon (100 mg), and then filtered. The filtrate was evaporated, and the dried residue was treated with benzoyl chloride (359 mg, 2.55 mmol) in pyridine (10 ml) at room temperature overnight. The usual work-up of the reaction mixture, and purification of the product on a silica-gel column (benzene-acetone 8:1) gave **2** (69.1 mg) in 65.3% yield.

Mp. 178—179°C (hexane-ethanol 1:1); $[\alpha]_D$ −191° (*c* 1.0, MeOH); MS: *m/z* 383 (M^+ for $C_{22}H_{25}O_5N$), 351 (M^+-CH_3OH); UV (EtOH): 231, 270, and 280 nm; CD: $\Delta\varepsilon$ 238.5=−11.3 (θ=−23.3 °M); NMR: δ=8.24—8.04, 7.90—7.80, and 7.64—7.35 (m, 10H, 2×Bz), 7.90 (bs, 1H, NH), 5.93 (bs, 1H, $J_{4,5}$=1.0, H-4), 5.00 (bd, 1H, $J_{1,2a}$=3.5, H-1), 4.33 (dq, $J_{5,6}$=6.5, H-5), 3.52

(s, 3H, OMe), 2.19 (dd, $J_{2a,2e}$=14.5, H-2a), 1.87 (bd, 1H, H-2e), 1.60 (s, 3H, CMe), and 1.15 (d, 1H, H-6). These data are identical with those of reported.[2]

Anal. ($C_{22}H_{25}O_5N$) C, H, N.

References

1) Part XXXV. J. Yoshimura, T. Yasumori, T. Kondo, and K. Sato, *Bull. Chem. Soc. Jpn.*, **57**, 2535 (1984).

2)M. Debono and R. M. Molly, *J. Org. Chem.*, **45**, 4685 (1980).

3) K. Michel, R. M. Shah, and R. L. Hamill, 17th Conference on Antimicrobial Agents and Chemotherapy, New York **1977**, Abstr.p. 41.

4) G. Fronza. C. Fuganti, P. Grasseli, and G. Pedrocchi-Frantoni, *Tetrahedron Lett.*, **22**, 5073 (1981).

5) J. S. Brimacombe, R. Hanna, and L. C. N. Tucker, *Carbohdr. Res.*, **105**, c1 (1982); *J. Chem. Soc. Perkin Trans 1*, **1983**, 2277.

6) T. M. Cheung, D. Horton, and Weckerle, *Carbohydr. Res.*, **74**, 93 (1979).

7) E. J. Corey, J.-L. Gras, and P. Ulrich, *Tetrahedron Lett.*, **1976**, 809.

8) J. Yoshimura, M. Matsuzawa, K. Sato, and Y. Nagasawa, *Carbohydr. Res.*, **76**, 67 (1979).

9) E. J. Corey, L. O. Weigel, A. R. Chamberlin, H. Cho, and D. H. Hua, *J. Am. Chem. Soc.*, **102**, 6613 (1980); K. Fuji, K. Ichikawa, M. Node, and E. Fujita, *J. Org. Chem.*, **44**, 1661 (1979).

10) J. Auerbach and S. M. Weinreb, *J. Chem. Soc., Chem. Commun.*, **1974**, 298.

11) T. Iversen and D. R. Bundle, *J. Chem. Soc., Chem. Commun.*, **1981**, 1240.

12) F. Cramer, K. Pawlzek, and H. J. Baldavf, *Chem. Ber.*, **91**, 1049 (1958).

13)S. Omura, A. Nakagawa, A. Neszmelyi, S. D. Gero, A.-M. Sepulchre, F. Piriou, and G. Lukacs, *J. Am. Chem. Soc.*, **97**, 4001 (1975); M. Miljković, M. Gligorijević, T. Sato, and D. Miljković, *J. Org. Chem.*, **39**, 1379 (1974).

14) T. T. Thang and F. Winternitz, *J. Chem. Soc., Chem. Commun.*, **1979**, 153; K. Sato, K. Kubo, N. Hong, H. Kodama, and J. Yoshimura, *Bull. Chem. Soc. Jpn.*, **55**, 938 (1982).

 © 1984 The Chemical Society of Japan Bull. Chem. Soc. Jpn., 57, 2543—2549 (1984)

Synthesis of a Heat-stable Enterotoxin (STh) Produced by a Human Strain SK-1 of Enterotoxigenic *Escherichia coli*

Haruo IKEMURA, Shoko YOSHIMURA, Saburo AIMOTO, Yasutsugu SHIMONISHI,* Saburo HARA,†
Tae TAKEDA,†† Yoshifumi TAKEDA,††† and Toshio MIWATANI††

Institute for Protein Research, Osaka University, Yamada-oka 3-2, Suita, Osaka 565
†Department of Chemistry, College of Science, Osaka University, Machikaneyama, Toyonaka, Osaka 560
††Research Institute for Microbial Diseases, Osaka University, Yamada-oka 3-1, Suita, Osaka 565

(Received April 19, 1984)

A peptide with the amino acid sequence proposed for a heat-stable enterotoxin (STh) produced by a human strain SK-1 of enterotoxigenic *Escherichia coli* was synthesized by a conventional method. Synthetic STh evoked fluid secretion in suckling mice at a dose of 0.8 ng, which is similar to the effective dose of native STh. The fluid secretion was completely inhibited by antisera raised against the native toxin. Furthermore, synthetic STh showed the same ^1H-NMR spectrum and heat-stability as native STh.

Recently, we[1-3] isolated and purified two heat-stable enterotoxins (named STh and STp) that were produced by enterotoxigenic *Escherichia coli* strain SK-1 and strain 18D, respectively, originated from human patients with diarrhea. We determined the sequences of the 19 and 18 amino acid residues of these enterotoxins to be as shown in Fig. 1. Lallier *et al.*[4,5] and Ronnberg *et al.*[6] also isolated ST's from the culture supernatants of enterotoxigenic *E. coli* strain F11(P155) of porcine origin and strain C57/26C2 of human origin and determined their amino acid sequences. These sequences were identical to that of STp determined by us.[3] Our investigations[1-3,7] and those of others[4-6,8] showed that the characteristic features of these heat-stable enterotoxins were as follows: 1) STh and STp have much structural similarity except in a few N-terminal residues. 2) One-third of the amino acid residues are half-cystine residues, which are located in identical positions in the two toxins and are joined intramolecularly by disulfide linkages. 3) The minimum effective doses of the two toxins are similar in suckling mouse assays. 4) The toxicities of STh and STp are both neutralized by both anti-STh and anti-STp antisera. These findings suggested that the common amino acid sequences of STh and STp are very important for expression of their ST toxicity. However, since it is difficult to isolate much toxin from the culture supernatants of bacteria, little is known about the biological and physicochemical properties or the structure-activity relationship of ST, except that it may be involved in the guanylate cyclase–cyclic GMP system.[9-12]

This study was carried out as part of a study on the molecular conformation-activity relationship of ST to confirm the primary structure proposed for STh and to develop a method for synthesizing the large amounts of STh necessary for biological studies. The following paper[13] deals with the synthesis of several shorter analogs of STh and the structure-activity relationship of STh.

Experimental

The general experimental and analytical methods used were described in the preceding paper.[14] YMC-packed column of ODS A-324 (10×300 mm) was obtained from Yamamura Chemical Laboratory Co. Ltd. (Kyoto). LiChrosorb RP-8 (5 μm particle size) was purchased from Merck Japan and packed into a column (8×300 mm) in our laboratory. Aminopeptidase M was obtained from Protein Research Foundation (Minoh, Osaka). Synthetic peptides were hydrolyzed in 4M (1 M=1 mol dm^{-3}) methanesulfonic acid or a mixture of 6 M HCl and propionic acid (v/v, 1/1) in evacuated sealed tubes at 110 °C for 24 h, and amino acids in the hydrolysates were analyzed in a Hitachi type-835 amino acid analyzer. Native STh was isolated from the culture supernatant of enterotoxigenic *E. coli* strain SK-1 and finally purified by high-performance liquid chromatography, as described previously.[2] The abbreviations used in this paper are those recommended by the IUPAC-IUB [*J. Biol. Chem.*, **247**, 977 (1972)]. Additional abbreviations are: MBzl, *p*-methylbenzyl; TFA, trifluoroacetic acid; DMF, *N,N*-dimethylformamide; TEA, triethylamine; DMSO, dimethyl sulfoxide.

Boc-Cys(MBzl)-Tyr-OBzl (Ia). Boc-Cys(MBzl)-OH·

	1 5 10 15	
Strain SK-1	Asn-Ser-Ser-Asn-Tyr-Cys-Cys-Glu-Leu-Cys-Cys-Asn-Pro-Ala-Cys-Thr-Gly-Cys-Tyr	Aimoto et al.[2]
Strain 18D	Asn-Thr-Phe-Tyr-Cys-Cys-Glu-Leu-Cys-Cys-Asn-Pro-Ala-Cys-Ala-Gly-Cys-Tyr	Takao et al.[3]
Strain 18D	Asn-Thr-Phe-Tyr-Cys-Cys-Glu-Leu-Cys-Cys-Tyr-Pro-Ala-Cys-Ala-Gly-Cys-Asn	Chan and Giannella[8]
Strain F11(P155)	Asn-Thr-Phe-Tyr-Cys-Cys-Glu-Leu-Cys-Cys-Asn-Pro-Ala-Cys-Ala-Gly-Cys-Tyr	Lazure et al.[4-5]
Strain C57/26C2	Asn-Thr-Phe-Tyr-Cys-Cys-Glu-Leu-Cys-Cys-Asn-Pro-Ala-Cys-Ala-Gly-Cys-Tyr	Ronnberg et al.[6]

Fig. 1. Amino acid sequences of heat-stable enterotoxins (ST) isolated from various strains of enterotoxigenic *E. coli*.

††† Present address: The Institute of Medical Science, The University of Tokyo, Shirokanedai 4-6-1, Minato-ku, Tokyo 108.

DCHA (48.1 g, 95.0 mmol) was dissolved with H-Tyr-OBzl·TosOH (54.7 g, 124 mmol) and TEA (4.00 ml) in $CHCl_3$ (1 l) and cooled below −10 °C. The solution was mixed with DCC (21.6 g, 104.5 mmol) and stirred at the same temperature for 1 h and then at room temperature overnight. The precipitate formed was filtered off and the filtrate was concentrated to a syrup under reduced pressure, dissolved in AcOEt and washed successively with 0.1 M HCl, 5% aq $NaHCO_3$, and water. The washed solution was dried over anhydrous Na_2SO_4 and concentrated under reduced pressure to a syrup, which was crystallized from AcOEt and hexane; wt 39.4 g (71.7%), mp 136—138 °C, $[\alpha]_D^{22}$ −28.1° (*c* 1.0, DMF).

Found: C, 66.83; H, 6.69; N, 4.89; S, 5.47%. Calcd for $C_{32}H_{38}O_6N_2S$: C, 66.41; H, 6.62; N, 4.84; S, 5.54%.

*Boc-Gly-Cys(MBzl)-Tyr-OBzl (**Ib**).* Compound **Ia** (39.4 g, 68.0 mmol) was dissolved in a mixture of CH_2Cl_2 (60 ml) and TFA (60 ml). The solution was stirred at room temperature for 40 min and concentrated to dryness under reduced pressure. The residue was repeatedly flushed with CH_2Cl_2 under reduced pressure to give a crystalline material, which was dissolved in DMF (500 ml). The solution was stirred with Boc-Gly-ONSu (21.3 g, 78.2 mmol) and *N*-methylmorpholine (15.0 ml) at 2—3 °C overnight. Then it was concentrated under reduced pressure to a syrup, which was dissolved in AcOEt and washed successively with 0.1 M HCl, 5% aq $NaHCO_3$ and water. The washed solution was dried over anhydrous Na_2SO_4 and then concentrated to a syrup under reduced pressure. The syrup was twice crystallized from AcOEt, ether and hexane; wt 37.4 g (86.5%), mp 79.5—81 °C, $[\alpha]_D^{22}$ −21.2° (*c* 1.0, DMF).

Found: C, 63.31; H, 6.58; N, 6.32; S, 5.13%. Calcd for $C_{34}H_{41}O_7N_3S \cdot 1/2H_2O$: C, 63.33; H, 6.57; N, 6.52; S, 4.97%.

*Boc-Cys(MBzl)-Thr-N_2H_3 (**Ic**).* Boc-Cys(MBzl)-OH·DCHA (52.8 g, 104 mmol) was dissolved with H-Thr-OEt·HCl (24.8 g, 135 mmol) and TEA (4.3 ml) in $CHCl_3$ (1 l). The solution was cooled below −10 °C, mixed with DCC (23.6 g, 114 mmol) and then stirred at the same temperature for 1 h and at room temperature overnight. The precipitate formed was filtered off and the filtrate was concentrated to a syrup under reduced pressure. The syrup was dissolved in AcOEt and washed successively with 0.1 M HCl, 5% aq $NaHCO_3$, and water. The washed solution was dried over anhydrous Na_2SO_4 and concentrated to a syrup under reduced pressure. The syrup was dissolved in EtOH (500 ml), mixed with 100% hydrazine hydrate (25.2 ml), and stirred at room temperature overnight. The gelatinous solid formed was collected with ether and reprecipitated twice from MeOH and ether; wt 37.5 g (81.9%), mp 125—127 °C, $[\alpha]_D^{22}$ −19.7° (*c* 1.0, DMF).

Found: C, 54.12; H, 7.54; N, 12.70; S, 7.15%. Calcd for $C_{20}H_{32}O_5N_4S$: C, 54.53; H, 7.32; N, 12.72; S, 7.28%.

Boc-Cys(MBzl)-Thr-Gly-Cys(MBzl)-Tyr-OBzl (1). Compound **Ib** (35.0 g, 55.0 mmol) was dissolved in TFA (100 ml) and stirred at room temperature for 1 h. The solution was concentrated to a solid under reduced pressure. Meanwhile, compound **Ic** (29.1 g, 66.0 mmol) was dissolved in DMF (150 ml) and cooled to −40—−50 °C. The solution was mixed with 4.39 M HCl in dioxane (45.1 ml) and isopentyl nitrite (9.7 ml) and stirred at −20 °C for 30 min. Then it was mixed with *N*-methylmorpholine (21.8 ml) and a solution of the above solid in DMF. The mixture was stirred at 0—2 °C overnight in a refrigerator and then concentrated to dryness under reduced pressure. The residue was dissolved in AcOEt and washed with 0.1 M HCl, 5% aq $NaHCO_3$, and water. The precipitate formed during the washing was collected and dissolved in hot EtOH and insoluble material was filtered off. The solution was concentrated under reduced pressure to a gelatinous solid, which was crystallized from EtOH; wt 38.3 g (73.7%), mp 157.5—159 °C, $[\alpha]_D^{18}$ −29.0° (*c* 1.0, DMF).

Found: C, 62.30; H, 6.72; N, 7.58; S, 6.86%. Calcd for $C_{49}H_{61}O_{10}N_5S_2$: C, 62.33; H, 6.51; N, 7.48; S, 6.79%.

*Z-Asn-Pro-Ala-OMe (**IIa**).* Z-Pro-Ala-OMe[15] (40.8 g, 122 mmol) was hydrogenated over 5% palladium-charcoal in the presence of HCl (1 equiv) in MeOH. The catalyst was filtered off and the filtrate was concentrated to dryness under reduced pressure. The residue was dissolved with Z-Asn-ONp (52.0 g, 134 mmol) and TEA (17.1 ml) in DMF (600 ml). The solution was stirred at room temperature overnight and then concentrated to a syrup under reduced pressure. The syrup was dissolved in AcOEt and washed successively with 0.1 M HCl, 5% aq $NaHCO_3$ and water. Crystals formed during the washing procedure were collected and recrystallized from a mixture of AcOEt, EtOH, and ether containing a trace amount of water; wt 39.5 g (72.2%), mp 115.5—118.5 °C, $[\alpha]_D^{22}$ −67.8° (*c* 1.0, DMF).

Found: C, 55.31; H, 6.29; N, 12.11%. Calcd for $C_{21}H_{28}O_7N_4 \cdot 1/2H_2O$: C, 55.13; H, 6.39; N, 12.25%.

*Boc-Cys(MBzl)-Cys(MBzl)-OMe (**IIb**).* Boc-Cys(MBzl)-OH·DCHA (114.0 g, 225 mmol) and H-Cys(MBzl)-OMe·HCl (62.1 g, 225 mmol) were dissolved in $CHCl_3$ (1.5 l) and cooled below −10 °C. The solution was stirred with DCC (51.1 g, 248 mmol) at the same temperature for 1 h and at room temperature overnight. The precipitate formed was filtered off and the filtrate was concentrated to an oil under reduced pressure. The oil was dissolved in AcOEt and insoluble material was filtered off. The filtrate was washed successively with 0.1 M HCl, 5% aq $NaHCO_3$, and water, and then dried over anhydrous Na_2SO_4. The dried solution was concentrated under reduced pressure to a syrup, which was crystallized from AcOEt and ether; wt 115.3 g (97.3%), mp 101—102.5 °C, $[\alpha]_D^{23}$ −52.3° (*c* 1.0, DMF).

Found: C, 61.62; H, 7.12; N, 4.94; S, 11.61%. Calcd for $C_{28}H_{38}O_5N_2S_2$: C, 61.51; H, 7.01; N, 5.12; S, 11.73%.

*Boc-Cys(MBzl)-Cys(MBzl)-N_2H_3 (**IIc**).* Compound **IIb** (115.1 g, 210 mmol) was dissolved in a mixture of DMF (200 ml) and MeOH (500 ml). Then 100% hydrazine hydrate (52.7 g) was added and the mixture was stirred at room temperature for 24 h. The precipitate formed was collected with ether; wt 109.2 g (94.9%), mp 149.5—150.5 °C, $[\alpha]_D^{23}$ −29.8° (*c* 1.0, DMF).

Found: C, 59.26; H, 7.06; N, 10.04; S, 11.60%. Calcd for $C_{27}H_{38}O_4N_4S_2$: C, 59.31; H, 7.01; N, 10.25; S, 11.73%.

*Boc-Cys(MBzl)-Cys(MBzl)-Asn-Pro-Ala-OMe (**IId**).* Compound **IIa** (39.5 g, 88.0 mmol) was hydrogenated over 5% palladium-charcoal in the presence of HCl (1 equiv) in MeOH (400 ml). The catalyst was filtered off and the filtrate was concentrated to a solid under reduced pressure. Meanwhile, compound **IIc** (48.1 g, 88.0 mmol) was dissolved in DMF (500 ml) and cooled below −20 °C. The solution was stirred with 4.39 M HCl in dioxane (60.1 ml) and isopentyl nitrite (13.0 ml) at the same temperature for 30 min. Then, the solution was mixed with the above solid and *N*-methylmorpholine (29.1 ml) and stirred at 4 °C for 3 d. The solution was concentrated under reduced pressure to a syrup, which was solidified in AcOEt. The solid was dissolved in $CHCl_3$, washed with water, and then dried over anhydrous Na_2SO_4. The dried solution was concentrated under reduced pressure to a syrup, which was crystallized from a mixture of $CHCl_3$, EtOH, and ether; wt 64.6 g (88.5%), mp 183 °C, $[\alpha]_D^{23}$ −65.0° (*c* 1.0, DMF).

Found: C, 57.89; H, 6.84; N, 9.98; S, 7.60%. Calcd for $C_{40}H_{56}O_9N_6S_2$: C, 57.95; H, 6.81; N, 10.14; S, 7.74%.

*Boc-Cys(MBzl)-Cys(MBzl)-Asn-Pro-Ala-N_2H_3 (**II**).* Compound **IId** (45.6 g, 55.0 mmol) was dissolved in DMF (500 ml). The solution was mixed with 100% hydrazine hydrate (55 ml) and stirred at room temperature overnight. The solution was concentrated under reduced pressure to a

syrup, which was triturated in ether. The solid formed was reprecipitated from hot EtOH and ether; wt 42.7 g (93.6%), mp 188.5—191 °C, $[\alpha]_D^{23}$ −54.6° (*c* 1.0, DMF).

Found: C, 55.56; H, 6.96; N, 13.23; S, 7.50%. Calcd for $C_{36}H_{56}O_8N_8S_2 \cdot H_2O$: C, 55.30; H, 6.90; N, 13.23; S, 7.59%.

Boc-Cys(MBzl)-Cys(MBzl)-Asn-Pro-Ala-Cys(MBzl)-Thr-Gly-Cys(MBzl)-Tyr-OBzl (III). Compound **I** (18.9 g, 20.0 mmol) was dissolved in TFA (40 ml) and stirred at room temperature for 40 min. The solution was concentrated to a solid under reduced pressure. Meanwhile, compound **II** (19.9 g, 24.0 mmol) was suspended in DMF (80 ml), cooled below −20 °C, and mixed with 4.39 M HCl in dioxane (16.4 ml) and isopentyl nitrite (3.4 ml). The suspension gradually became clear, and was stirred at −20 °C for 60 min. Then it was mixed with *N*-methylmorpholine (7.92 ml) and a solution of the above solid in DMF (80 ml). The mixture was stirred at 0—2 °C for 4 d and then concentrated to dryness under reduced pressure. The residue was washed with a mixture of AcOEt and water and then reprecipitated from hot EtOH and ether; wt 27.9 g (85.0%), mp 199 °C (dec), $[\alpha]_D^{18}$ −51.2° (*c* 1.0, DMSO).

Found: C, 60.15; H, 6.66; N, 9.33; S, 7.96%. Calcd for $C_{83}H_{105}O_{16}N_{11}S_4 \cdot H_2O$: C, 60.09; H, 6.50; N, 9.29; S, 7.73%.

Boc-Cys(MBzl)-Cys(MBzl)-Glu(OBu^t)-Leu-OEt (IVa). Z-Glu(OBu^t)-OH·DCHA (51.9 g, 100 mmol) was dissolved with H-Leu-OEt·HCl (23.5 g, 120 mmol) and TEA (2.80 ml) in $CHCl_3$ (1 l) and cooled below −10 °C. The solution was mixed with DCC (22.7 g, 110 mmol) and stirred at the same temperature for 1 h and then at room temperature overnight. The precipitate formed was filtered off and the filtrate was concentrated to an oil under reduced pressure. The oil was dissolved in AcOEt and washed successively with 0.1 M HCl, 5% aq $NaHCO_3$, and water. The washed solution was dried over anhydrous Na_2SO_4 and concentrated to a syrup under reduced pressure. The syrup was dissolved in MeOH (500 ml) and hydrogenated over 5% palladium-charcoal in the presence of HCl (1 equiv). The catalyst was filtered off and the filtrate was concentrated to a solid under reduced pressure. Meanwhile, compound **IIc** (49.2 g, 90.0 mmol) was dissolved in DMF (400 ml) and cooled below −20 °C. The solution was stirred with 4.39 M HCl in dioxane (60 ml) and isopentyl nitrite (13.3 ml) at the same temperature for 30 min and then mixed with *N*-methylmorpholine (29.0 ml) and the above solid. The mixture was stirred at 4 °C for 24 h in a refrigerator. The precipitate formed was filtered off and the filtrate was concentrated to a syrup under reduced pressure. The syrup was solidified in water and the solid was twice recrystallized from EtOH and water and from AcOEt and hexane; wt 64.1 g (82.9%), mp 149—152 °C, $[\alpha]_D^{23}$ −26.7° (*c* 1.2, DMF).

Found: C, 61.32; H, 7.87; N, 6.52; S, 7.29%. Calcd for $C_{44}H_{66}O_9N_4S_2$: C, 61.51; H, 7.74; N, 6.52; S, 7.47%.

Boc-Cys(MBzl)-Cys(MBzl)-Glu(OBu^t)-Leu-N_2H_3 (IV). Compound **IVa** (25.7 g, 30.0 mmol) was dissolved in MeOH (400 ml) and mixed with 100% hydrazine hydrate (30 ml). The solution was stirred at room temperature for 2 d and mixed with water. The resulting precipitate was collected by filtration and reprecipitated from EtOH and ether; wt 19.9 g (78.5%), mp 204 °C (dec), $[\alpha]_D^{23}$ −19.8° (*c* 1.0, DMF).

Found: C, 59.40; H, 7.69; N, 9.74; S, 7.53%. Calcd for $C_{42}H_{64}O_8N_6S_2$: C, 59.69; H, 7.63; N, 9.94; S, 7.59%.

Boc-Cys(MBzl)-Cys(MBzl)-Glu(OBu^t)-Leu-Cys(MBzl)-Cys-(MBzl)-Asn-Pro-Ala-Cys(MBzl)-Thr-Gly-Cys(MBzl)-Tyr-OBzl (V). Compound **III** (16.4 g, 10 mmol) was dissolved in TFA (35 ml) and stirred at room temperature for 80 min. The solution was concentrated to a solid under reduced pressure. Meanwhile, compound **IVa** (10.1 g, 12.0 mmol) was suspended in DMF (45 ml) and cooled below −20 °C. The suspension was mixed with 4.39 M HCl in dioxane (8.2 ml) and isopentyl nitrite (1.77 ml) and stirred at the same temperature for 60 min, when it gradually became clear. The resulting solution was mixed with *N*-methylmorpholine (4.0 ml) and a solution of the above solid in DMF (40 ml). The mixture was stirred at 0 °C for 4 d in a refrigerator and then concentrated to dryness under reduced pressure. The residue was collected with AcOEt, boiled in hot EtOH, cooled to room temperature, and filtered; wt 20.1 g (85.4%), mp 220 °C (dec), $[\alpha]_D^{18}$ −47.7° (*c* 1.0, DMSO).

Found: C, 60.95; H, 6.64; N, 8.75; S, 8.19%. Calcd for $C_{120}H_{157}O_{22}N_{15}S_6$: C, 61.23; H, 6.72; N, 8.92; S, 8.17%.

Z-Asn-Tyr-OEt (VIa). Z-Asn-OH (20.0 g, 75.0 mmol) was dissolved with H-Tyr-OEt·HCl (20.3 g, 82.5 mmol) and TEA (11.6 ml) in DMF (200 ml). The solution was cooled below −10 °C and mixed with HOBt (11.1 g, 82.5 mmol) and DCC (14.7 g, 71.3 mmol). The mixture was stirred at the same temperature for 1 h and at room temperature overnight. The precipitate formed was filtered off and the filtrate was concentrated to dryness under reduced pressure. The residue was washed successively with 0.1 M HCl and water and then reprecipitated from DMF and water; wt 31.6 g (96.9%), mp 170.5—172.5 °C, $[\alpha]_D^{20}$ +12.0° (*c* 1.0, DMSO).

Found: C, 60.45; H, 5.94; N, 9.05%. Calcd for $C_{23}H_{27}O_7N_3$: C, 60.39; H, 5.95; N, 9.19%.

Z-Ser-Asn-Tyr-OEt (VIb). Compound **VIa** (9.15 g, 20.0 mmol) was dissolved in MeOH (150 ml) and hydrogenated over 5% palladium-charcoal at atmospheric pressure in the presence of HCl (1 equiv). The catalyst was filtered off and the filtrate was concentrated to a solid under reduced pressure. Meanwhile, Z-Ser-N_2H_3 (5.60 g, 20.0 mmol) was dissolved in DMF (80 ml) and cooled below −20 °C. The solution was mixed with 4.39 M HCl in dioxane (13.7 ml) and isopentyl nitrite (2.95 ml) and stirred at the same temperature for 30 min. Then, the solution was mixed with *N*-methylmorpholine (6.60 ml) and the above solid, and stirred at 0—2 °C for 2 d. The precipitate formed was filtered off and the filtrate was concentrated to dryness under reduced pressure. The residue was crystallized from AcOEt and recrystallized from hot EtOH and AcOEt; wt 8.70 g (80.0%), mp 194—196 °C, $[\alpha]_D^{25}$ +6.2° (*c* 0.9, DMF).

Found: C, 57.22; H, 5.84; N, 10.21%. Calcd for $C_{26}H_{32}O_9N_4$: C, 57.35; H, 5.92; N, 10.29%.

Z-Asn-Ser-OMe (VIc). Z-Asn-OH (13.3 g, 50.0 mmol) was dissolved with H-Ser-OMe·HCl (8.60 g, 55.0 mmol) and *N*-methylmorpholine (6.05 ml) in DMF (150 ml). The solution was cooled below −10 °C and mixed with HOBt (7.4 g, 55 mmol) and DCC (9.8 g, 47.5 mmol). The mixture was stirred at the same temperature for 1 h and at room temperature overnight. The precipitate formed was filtered off and the filtrate was concentrated to crystalline material under reduced pressure. The material was recrystallized from AcOEt; wt 16.1 g (88.0%), mp 197—199 °C, $[\alpha]_D^{25}$ +8.4° (*c* 1.0, DMSO).

Found: C, 52.33; H, 5.68; N, 11.46%. Calcd for $C_{16}H_{21}O_7N_3$: C, 52.31; H, 5.76; N, 11.44%.

Z-Asn-Ser-N_2H_3 (VId). Compound **VIc** (16.0 g, 43.6 mmol) was dissolved in DMF (300 ml), mixed with 100% hydrazine hydrate (22.0 ml), and stirred at room temperature overnight. The crystalline material formed was boiled in hot EtOH and collected after cooling; wt 16.1 g (100%), mp 209 °C (dec), $[\alpha]_D^{23}$ −3.9° (*c* 1.0, DMSO).

Found: C, 47.76; H, 5.88; N, 18.97%. Calcd for $C_{15}H_{21}O_6N_5 \cdot 1/2H_2O$: C, 47.87 H, 5.89; N, 18.61%.

Z-Asn-Ser-Ser-Asn-Tyr-OEt (VIe). Compound **VIb** (8.70 g, 16.0 mmol) was hydrogenated over 5% palladium-charcoal in MeOH (100 ml). The catalyst was filtered off and the filtrate was concentrated to a solid under re-

duced pressure. Meanwhile, compound **VId** (6.50 g, 17.6 mmol) was suspended in DMF (100 ml) and cooled below −20 °C. The suspension was mixed with 4.39M HCl in dioxane (12.0 ml) and isopentyl nitrite (2.60 ml). The resulting solution was stirred at the same temperature for 30 min. The solution was mixed with *N*-methylmorpholine (5.80 ml) and the above solid. The mixture was stirred at 0 °C for 3 d and the precipitate formed was filtered off. The filtrate was concentrated under reduced pressure to a gelatinous solid, which was collected with AcOEt. Half the solid was boiled in hot EtOH and collected after cooling; wt 5.2 g (82.9%), mp 215 °C (dec), $[\alpha]_D^{23}$ +2.1° (*c* 1.0, DMSO).

Found: C, 52.05; H, 5.75; N, 12.81%. Calcd for $C_{33}H_{43}O_{13}N_7 \cdot 1/2H_2O$: C, 52.52; H, 5.88; N, 12.99%.

Z-Asn-Ser-Ser-Asn-Tyr-N_2H_3 (VI). Compound **VIe** (8.7 g, 8.0 mmol) was dissolved with 100% hydrazine hydrate (8.0 ml) in DMF (80 ml) and stirred at room temperature overnight. The resulting precipitate was collected with EtOH. The crystalline material was boiled in hot EtOH and filtered after cooling to room temperature; wt 5.0 g (93.9%), mp 207 °C (dec), $[\alpha]_D^{20}$ −9.2° (*c* 1.1, DMSO).

Found: C, 49.13; H, 5.88; N, 17.09%. Calcd for $C_{31}H_{41}O_{12}N_9 \cdot H_2O$: C, 49.66; H, 5.78; N, 16.81%.

Z-Asn-Ser-Ser-Asn-Tyr-Cys(MBzl)-Cys(MBzl)-Glu-Leu-Cys(MBzl)-Cys(MBzl)-Asn-Pro-Ala-Cys(MBzl)-Thr-Gly-Cys-(MBzl)-Tyr-OBzl (VII). Compound **V** (1.18 g, 0.5 mmol) was dissolved with anisole (0.2 ml) in TFA (10 ml) and stirred at room temperature for 2 h. The solution was concentrated under reduced pressure to a syrup. Meanwhile, compound **VI** (549 mg, 0.75 mmol) was dissolved in a mixture of DMF (5 ml) and DMSO (5 ml) and cooled below −10 °C. The solution was mixed with 4.39 M HCl in dioxane (0.51 ml) and isopentyl nitrite (0.11 ml) and stirred at −10 °C for 60 min. Then, the solution was mixed with *N*-methylmorpholine (1.0 ml) and a solution of the above syrup in DMF (5 ml). The mixture was stirred at 0 °C for 10 d, concentrated under reduced pressure, and then mixed with EtOH. The precipitate formed was collected, boiled in hot EtOH, and collected after cooling to room temperature; wt 1.13 g (78.0%), mp 214 °C (dec), $[\alpha]_D^{18}$ −40.0° (*c* 1.0, DMSO). Amino acid ratio in the acid hydrolysate: Asp, 2.93 (3); Thr, 0.97 (1); Ser, 1.61 (2); Glu, 1.03 (1); Pro, 0.98 (1); Gly, 1.00 (1); Ala, 1.04 (1); 1/2Cys, not determined; Leu, 1.05 (1); Tyr, 1.93 (2).

Found: C, 58.11; H, 6.40; N, 10.41; S, 6.76%. Calcd for $C_{142}H_{178}O_{32}N_{22}S_6 \cdot H_2O$: C, 58.50; H, 6.22; N, 10.57; S, 6.60%.

Deprotection, Air-oxidation and Purification of Toxic Peptides. Compound **VII** (290 mg, 100 μmol) was treated with anhydrous liquid hydrogen fluoride (10 ml) containing anisole (0.87 ml) at 0—2 °C for 60 min. The HF-reagent was removed under reduced pressure and the residue was dissolved in 99% formic acid (3.0 ml). The solution was washed three times with hexane and diluted with water to 5×10^{-5} M concentration of the peptide. The solution was adjusted to pH 8.0 by adding aqueous ammonia and kept at room temperature for 4 d with occasional stirring. Then it was adjusted to pH *ca.* 7.0 by adding glacial acetic acid and divided into two portions, which were each applied to a column (3×25 cm) of DEAE-Sephadex A-25 (acetate form). The adsorbed material was washed with water and eluted with 1500 ml of a linear gradient of 0 to 0.5 M AcOH. Fractions with toxicity were collected and lyophilized. The lyophilized material was purified on a reversed-phase column (Merck, LiChrosorb RP-8 5 μm, 8×300 mm) by HPLC with a linear gradient of 10% to 35% acetonitrile in 0.01 M ammonium acetate (pH 5.7). Fractions of eluate with toxicity were collected and lyophilized; wt 4.90 mg (4.8%).

Aminopeptidase M Digestion of ST_h. Native or synthetic ST_h (*ca.* 100 μg) was dissolved in 0.1 M Tris HCl buffer (100 μl) at pH 7.6 and digested with aminopeptidase M (5 μg) for 30 min at 40 °C. The reaction was stopped by addition of 1 M formic acid (100 μl). The solution was directly applied to a YMC-packed column ODS A-324 (10×300 mm) and the adsorbed material was eluted with a linear-gradient of 10—45% acetonitrile in 0.05% hexafluorobutyric acid (pH 2.51).

Biological Assay. ST activity was assayed in suckling mice of 2—4 d old, as described previously.[1]

Results and Discussion

Synthesis. First the protected linear peptide **VII** with the whole amino acid sequence of ST_h was prepared, as shown in the scheme in Fig. 2. Then the protecting groups of **VII** were removed by treatment with anhydrous liquid hydrogen fluoride.[16] The free linear peptide thus obtained was spontaneously air-

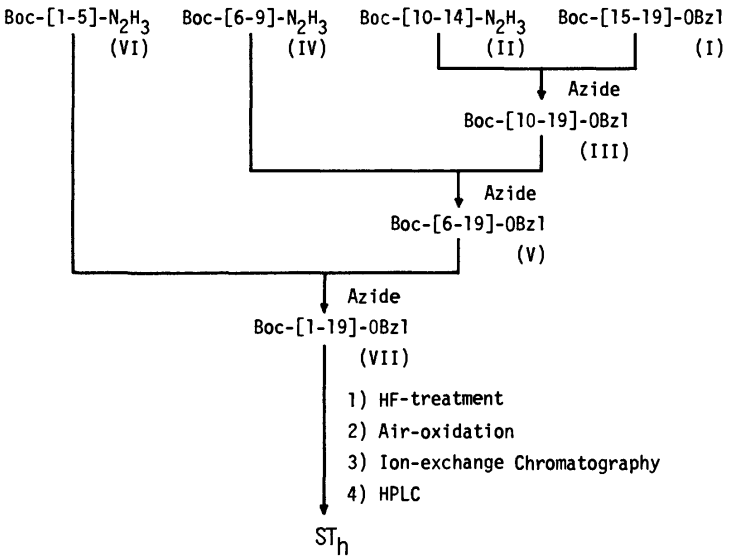

Fig. 2. Scheme for synthesis of ST_h.

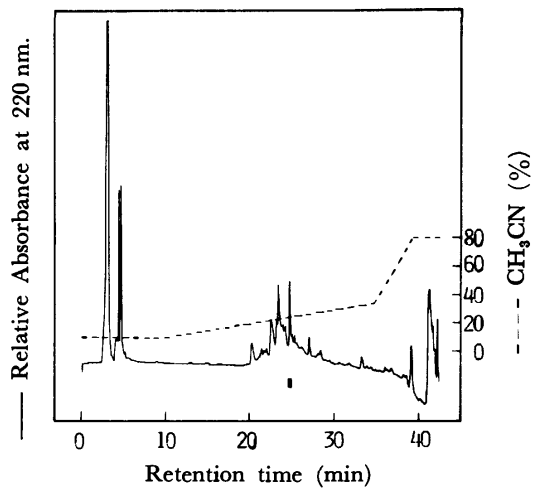

Fig. 3. HPLC profile on a LiChrosorb RP-8 column (5 μm, 4×250 mm) of HF-treated and air-oxidized solution of compound **VII**. The peak marked by a black bar showed toxicity.

oxidized in dilute solution (5×10^{-5}M) at pH 8.0 at room temperature. The air-oxidized solution was examined by high-performance liquid chromatography (HPLC) and results are shown in Fig. 3. Peak fractions were separated and toxicity of each was examined by the fluid accumulation test in suckling mice.[1] High toxicity was observed in the peak fraction shown by a black bar. This fraction was purified by ion-exchange chromatography followed by HPLC. The purified fraction had the same retention time on HPLC as native ST_h under two different conditions, as shown in Fig. 4. The yield of this fraction was 4.8% on the basis of the amount of the protected peptide **VII**. This yield was not surprisingly low, because there are 15 possible modes of formation of ST_h with three disulfide linkages from a linear peptide of ST_h and the environment for formation of disulfide linkages used in this work might be different from that in a biological system. The amino acid composition of synthetic ST_h agreed well with the theoretical one, as shown in Table 1.

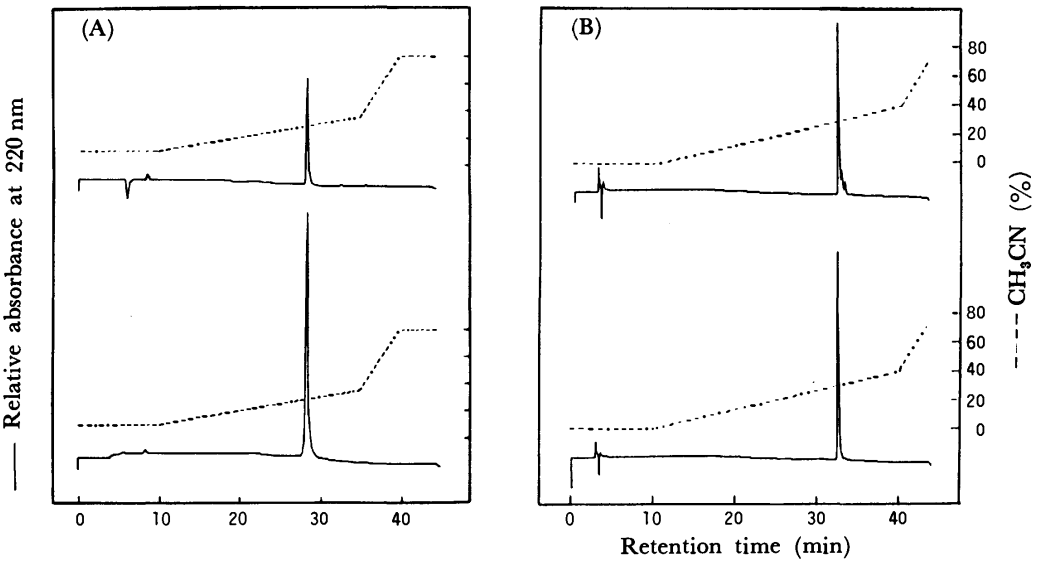

Fig. 4. HPLC profiles of native ST_h (upper) and synthetic ST_h (lower). (A) Column, LiChrosorb RP-8 (5 μm, 8×300 mm); starting solvent, 10% CH_3CN in 0.01 M $AcONH_4$ (pH 5.7). (B) Column, LiChrosorb RP-8 (5 μm, 4×250 mm); starting solvent, 10% CH_3CN in 0.05% TFA (pH 2.35).

Table 1. Amino acid compositions of synthetic and enzymatic-degraded peptides of ST_h[a]

	Synthetic			Native		
	ST_h	ST_h[3-19][b]	ST_h[4-19][b]	ST_h[c]	ST_h[3-19][d]	ST_h[4-19][d]
Asp	2.96(3)	1.98(2)	2.00(2)	2.96(3)	2.00(2)	2.01(2)
Thr	0.93(1)	0.95(1)	0.99(1)	0.96(1)	0.96(1)	1.00(1)
Ser	1.85(2)	0.97(1)	—	1.91(2)	0.97(1)	—
Glu	0.99(1)	1.01(1)	1.01(1)	1.16(1)	1.00(1)	1.04(1)
Pro	1.14(1)	1.14(1)	1.06(1)	1.26(1)	1.07(1)	1.11(1)
Gly	1.03(1)	1.05(1)	1.05(1)	1.21(1)	1.03(1)	1.04(1)
Ala	1.00(1)	1.00(1)	1.00(1)	1.00(1)	1.00(1)	1.00(1)
1/2Cys	5.56(6)	5.39(6)	5.50(6)	4.76(6)	5.34(6)	5.36(6)
Leu	1.03(1)	1.04(1)	1.04(1)	1.10(1)	1.05(1)	1.06(1)
Tyr	1.95(2)	2.00(2)	2.00(2)	1.92(2)	2.00(2)	1.99(2)

a) Values were calculated as mol/mol of Ala; numbers in parentheses indicate nearest integer values; b) Preparations from synthetic ST_h; c) Values cited from Ref. 2; d) Preparations from native ST_h.

Biological Activities. The toxicity of synthetic peptide ST_h was examined by the fluid accumulation test in suckling mice. The minimum effective dose of synthetic ST_h was 0.8 ng/100 μl, which was almost the same as that of native ST_h, as shown in Table 2. Furthermore, the toxicity of synthetic ST_h was neutralized not only by homologous anti-native ST_h antiserum but also by heterologous anti-native ST_p antiserum.[7]

Aminopeptidase M Digestion of Native and Synthetic ST_h. To obtain evidence that the synthetic ST_h had the same spacial structure as the native toxin, we treated synthetic and native ST_h with aminopeptidase M and compared the digests by HPLC, as shown in Fig. 5. The profile of the digest of synthetic ST_h was very similar to that of native ST_h. The peak fractions were separated and analyzed as described in the following paper.[13] The two major fractions were identified as ST_h[3-19] and ST_h[4-19], in which two and three N-terminal amino acid residues, respectively, of ST_h were removed. The minor peak fraction between undigested ST_h and ST_h[3-19] was identified as that of peptide ST_h[2-19] lacking the N-terminal Asn residue of ST_h. The same results were obtained on analysis of native ST_h, providing evidence that synthetic ST_h has the same structure as native ST_h.

Proton NMR Spectra. To confirm that synthetic peptide ST_h had the same tertiary structure as native ST_h, including the positions of disulfide linkages, we measured the 500 MHz ^{1}H-NMR spectra of synthetic and native ST_h. As shown in Fig. 6, the proton chemical shifts of synthetic ST_h were superim-

TABLE 2. BIOLOGICAL PROPERTIES OF SYNTHETIC ST_h

	Minimum effective dose (ng/100 μl)*	Neutralization by anti-native ST_h antiserum
Native ST_h	1.0	+
Synthetic ST_h	0.8	+

* Calculated from the recovery of amino acids in acid hydrolysates.

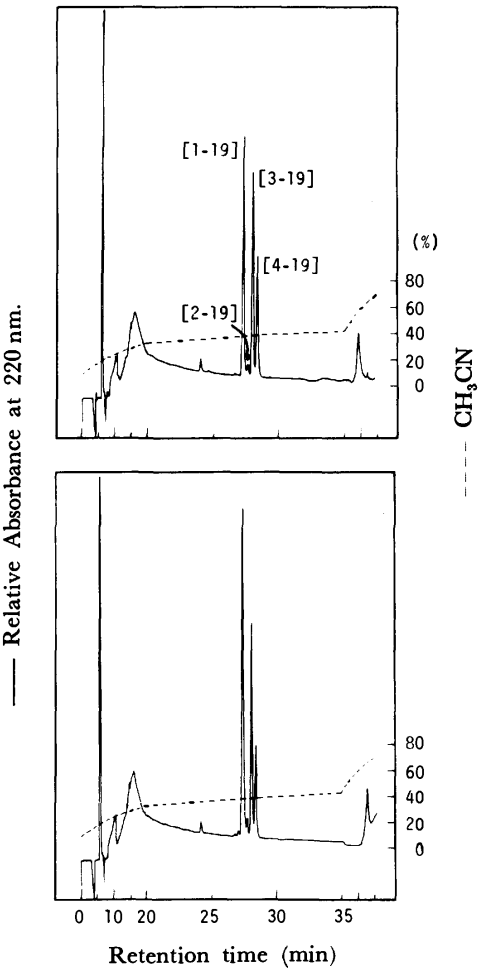

Fig. 5. HPLC profiles on a YMC ODS column (5 μm, 10×300 mm) of aminopeptidase M digests of native ST_h (upper) and synthetic ST_h (lower).

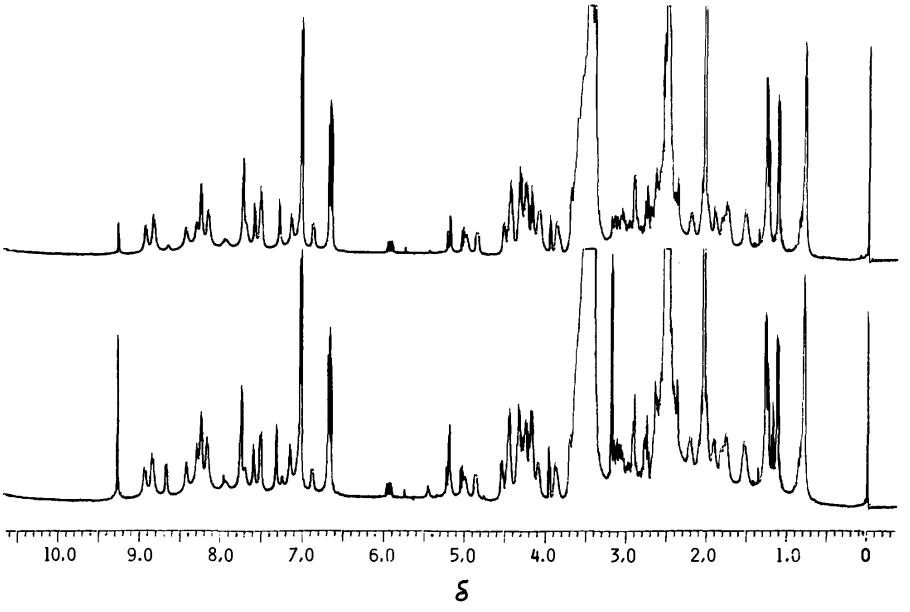

Fig. 6. 500 MHz ^{1}H-NMR spectra of synthetic ST_h (upper) and native ST_h (lower).

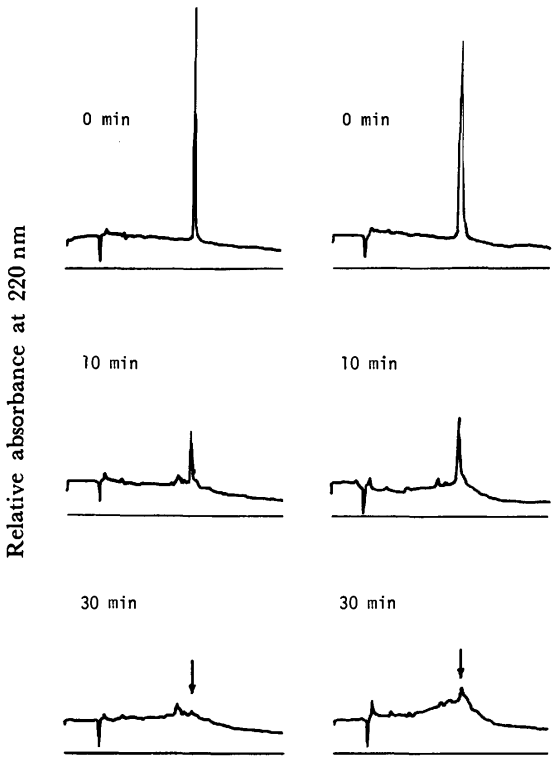

Fig. 7. HPLC profiles on a LiChrosorb RP-8 column (5 μm, 4×250 mm) of heat-treated native ST_h (left column) and synthetic ST_h (right column). The column was developed with a linear-gradient of 10 % to 35 % CH_3CN in 0.01 M $AcONH_4$ (pH 5.7) with increase of 1 %/min of CH_3CN at a flow rate of 0.5 ml/min.

posable on those of native ST_h, indicating that the synthetic peptide had the same three dimensional structure as native toxin.

Heat-stability We examined the heat-stability of synthetic ST_h by HPLC, as described previously.[17] Synthetic ST_h was confirmed to be stable on heating at 100 °C for 30 min like native ST_h, as illustrated in Fig. 7.

Thus, the synthetic ST_h obtained was found to be identical to native ST_h with respect to its physicochemical and biological properties, providing evidence that the amino acid sequence proposed for ST_h, a heat-stable enterotoxin of a human strain SK-1 of enterotoxigenic *Escherichia coli*, is correct. Furthermore, a method was developed for obtaining much toxin. The synthetic ST_h will be used for elucidating the biochemical and biological properties of ST and also for detecting ST-producing bacteria, which are very important epidemiologically.

This work was partly supported by a Grant-in-Aid for Scientific Research (No. 58122002) from the Ministry of Education, Science and Culture of Japan.

References

1) Y. Takeda, T. Takeda, T. Yano, K. Yamamoto, and T. Miwatani, *Infect. Immun.*, **25**, 978 (1979).
2) S. Aimoto, T. Takao, Y. Shimonishi, S. Hara, T. Takeda, Y. Takeda, and T. Miwatani, *Eur. J. Biochem.*, **129**, 257 (1982).
3) T. Takao, T. Hitouji, S. Aimoto, Y. Shimonishi, S. Hara, T. Takeda, Y. Takeda, and T. Miwatani, *FEBS Lett.*, **152**, 1 (1983).
4) R. Lallier, F. Bernard, M. Gendreau, C. Lazure, N. G. Seidah, M. Chretien, and S. St-Pierre, *Anal. Biochem.*, **127**, 267 (1982).
5) C. Lazure, N. G. Seidah, M. Chretien, R. Lallier, and S. St-Pierre, *Can. J. Biochem. Cell Biol.*, **61**, 287 (1983).
6) B. Ronnberg, T. Wadstrom, and H. Jornvall, *FEBS Lett.*, **155**, 183 (1983).
7) T. Takeda, Y. Takeda, S. Aimoto, T. Takao, H. Ikemura, Y. Shimonishi, and T. Miwatani, *FEMS Microbiol. Lett.*, **20**, 357 (1983).
8) S.-K. Chan and R. A. Giannella, *J. Biol. Chem.*, **256**, 7744 (1981).
9) M. Field, L. H. Graf, Jr., W. J. Laird, and P. L. Smith, *Proc. Natl. Acad. Sci., U.S.A*, **75**, 2800 (1978).
10) J. M. Hughes, F. Murad, B. Chang, and R. L. Guerrant, *Nature*, **271**, 755 (1978).
11) P. M. Newsome, M. N. Burgess, and N. A. Mullan, *Infect. Immun.*, **22**, 290 (1978).
12) R. A. Giannella and K. W. Drake, *Infect. Immun.*, **24**, 19 (1979).
13) H. Ikemura, H. Watanabe, S. Aimoto, Y. Shimonishi, S. Hara, T. Takeda, Y. Takeda, and T. Miwatani, *Bull. Chem. Soc. Jpn.*, **57**, 2550 (1984).
14) S. Yoshimura, M. Miki, H. Ikemura, S. Aimoto, Y. Shimonishi, T. Takeda, Y. Takeda, and T. Miwatani, *Bull. Chem. Soc. Jpn.*, **57**, 125 (1984).
15) E. Schroder, *Ann. Chem.*, **679**, 207 (1964).
16) S. Sakakibara, Y. Shimonishi, Y. Kishida, M. Okada, and H. Sugihara, *Bull. Chem. Soc. Jpn.*, **40**, 2164 (1967).
17) S. Aimoto, H. Watanabe, H. Ikemura, Y. Shimonishi, T. Takeda, Y. Takeda, and T. Miwatani, *Biochem. Biophys. Res. Commun.*, **112**, 320 (1983).

Heat-stable Enterotoxin (ST_h) of Human Enterotoxigenic *Escherichia coli* (Strain SK-1). Structure-activity Relationship

Haruo IKEMURA, Hiroyuki WATANABE, Saburo AIMOTO, Yasutsugu SHIMONISHI,* Saburo HARA,† Tae TAKEDA,†† Yoshifumi TAKEDA,††† and Toshio MIWATANI††

Institute for Protein Research, Osaka University, Yamada-oka 3-2, Suita, Osaka 565

†*Department of Chemistry, College of Science, Osaka University, Machikaneyama, Toyonaka, Osaka 560*

††*Research Institute for Microbial Diseases, Osaka University, Yamada-oka 3-1, Suita, Osaka 565*

(Received April 19, 1984)

For examination of the structure-activity relationship of ST_h, five shorter analogs of ST_h lacking one to five N-terminal amino acid residues of ST_h were synthesized. The synthetic peptides were confirmed to have the same intramolecular disulfide linkages as those in native ST_h. These peptides caused fluid accumulation in the intestine of suckling mice at almost the same molar levels as that of native ST_h. The toxicities of these peptides were also neutralized by antisera raised against native ST_h. These results indicated that the toxic and antigenic sites of ST_h are both located in the amino acid sequence between the Cys residue at the 5th position from the N-terminus and the C-terminal Tyr residue.

Heat-stable enterotoxins (named ST_h and ST_p) have been isolated from various strains of enterotoxigenic *Escherichia coli* and their amino acid sequences of 19 and 18 residues, respectively, have been determined[1-7] to be as shown in Fig. 1. These toxins are very similar in primary structure and have the same amino acid sequence from the Tyr residue near the N-terminus to the Tyr residue at the C-terminus, except at position 4 from the C-terminus. Six half-cystine residues are conserved in the same relative positions and are linked intramolecularly by disulfide bonds. These facts suggest that the common sequence is important for the toxicity and heat-stability of the toxins. However, it is difficult to obtain a large amount of the toxin from the culture supernatant of the bacteria, and so apart from these suggestion from the primary structures, little is known about the biological properties of the toxin, except that it seems to act on the guanylate cyclase-cyclic GMP system.[8-11] In the preceding paper,[12] we reported a method for chemical synthesis of ST_h in large quantity. This made it possible to investigate the biochemical and biological properties of the toxin and its analogs.

As part of an investigation of the structure-activity relationship of ST_h, in this work, we synthesized several shorter analogs of ST_h. We also found that a sequence lacking the five N-terminal amino acid residues of ST_h, which is identical to that of ST_p except for the 4th residue from the C-terminus, has the same biological properties as those of native ST_h.

Experimental

The general experimental and analytical methods used were described in the preceding paper.[12] The abbreviations used in this paper are those recommended by the IUPAC-IUB [*J. Biol. Chem.*, **247**, 977 (1972)]. Additional abbreviations are: MBzl, *p*-methylbenzyl; TFA, trifluoroacetic acid; DMF, *N,N*-dimethylformamide; TEA, triethylamine; DMSO, dimethyl sulfoxide.

*Z-Ser-Ser-OMe (**Ia**).* Z-Ser-N_2H_3 (12.7 g, 50.0 mmol) was dissolved in DMF (200 ml) and cooled below −20 °C. The solution was mixed with 4.39M HCl (1M=1 mol dm^{-3}) in dioxane (34.2 ml) and isopentyl nitrite (7.40 ml), stirred at the same temperature for 30 min, and then mixed with H-Ser-OMe·HCl (8.6 g, 55 mmol) and *N*-methylmorpholine (16.5 ml). The mixture was stirred at 3 °C for 24 h in a refrigerator. The precipitate formed was removed by filtration and the filtrate was concentrated to dryness under reduced pressure. The residue was triturated and recrystallized from AcOEt; wt 13.6 g (79.9%), mp 142—142.5 °C, $[\alpha]_D^{25}$ +10.1° (*c* 1.1, DMF).

Found: C, 52.94; H, 5.89; N, 8.28%. Calcd for $C_{15}H_{20}O_7N_2$: C, 52.94; H, 5.92; N, 8.23%.

*Z-Ser-Ser-N_2H_3 (**Ib**).* Compound **Ia** (5.1 g, 15 mmol) was dissolved with 100% hydrazine hydrate (7.50 ml) in MeOH. The solution was stirred at room temperature overnight, and the precipitate formed was collected and boiled in hot MeOH. The mixture was cooled and the precipitate was collected by filtration; wt 3.6 g (70.5%), mp 205 °C (dec), $[\alpha]_D^{25}$ +16.0° (*c* 0.9, DMF).

Found: C, 48.99; H, 5.90; N, 16.40%. Calcd for $C_{14}H_{20}O_6N_4$: C, 59.41; H, 5.92; N, 16.46%.

*Z-Ser-Ser-Asn-Tyr-OEt (**Ic**).* Z-Asn-Tyr-OEt[12] (5.95 g, 13.0 mmol) was dissolved in MeOH (100 ml) and hydrogenated over 5% palladium-charcoal at atmospheric pressure. The catalyst was filtered off and the filtrate was concentrated to a solid under reduced pressure. The solid was collected with ether. Meanwhile, compound **Ib** (3.40 g, 10.0 mmol) was dissolved in DMF (80 ml) and cooled below −20 °C. The solution was mixed with 4.39M HCl in

```
                1         5              10              15
                ·         ·              ·               ·
ST_h   Asn-Ser-Ser-Asn-Tyr-Cys-Cys-Glu-Leu-Cys-Cys-Asn-Pro-Ala-Cys-Thr-Gly-Cys-Tyr

ST_p        Asn-Thr-Phe-Tyr-Cys-Cys-Glu-Leu-Cys-Cys-Asn-Pro-Ala-Cys-Ala-Gly-Cys-Tyr
```

Fig. 1. Amino acid sequences of heat-stable enterotoxins (ST_h and ST_p) isolated from enterotoxigenic *Escherichia coli* strains SK-1 and 18D, respectively.

††† Present address: The Institute of Medical Science, The University of Tokyo, Shirokanedai 4-6-1, Minato-ku, Tokyo 108.

dioxane (8.2 ml) and isopentyl nitrite (1.77 ml) and then stirred at the same temperature for 20 min. The solution was mixed with *N*-methylmorpholine (3.96 ml) and the above solution of the solid in DMF (20 ml). The solution was stirred at 2—3 °C for 3 d and concentrated to dryness under reduced pressure. The residue was triturated in AcOEt and the resulting precipitate was twice reprecipitated from EtOH and AcOEt; wt 3.2 g (50.7%), mp 180.5—183 °C, $[\alpha]_D^{25}$ +7.1° (*c* 1.1, DMF).

Found: C, 53.31; H, 5.95; N, 10.72%. Calcd for $C_{29}H_{37}O_{11}N_5 \cdot H_2O$: C, 53.62; H, 6.05; N, 10.78%.

*Z-Ser-Ser-Asn-Tyr-N_2H_3 (**Id**).* Compound **Ic** (3.5 g, 5.5 mmol) was dissolved in DMF (30 ml) and mixed with 100% hydrazine hydrate (2.75 ml). The mixture was stirred at room temperature overnight and the precipitate formed was collected with EtOH. The precipitate was boiled in EtOH, cooled to room temperature, and filtered; wt 3.3 g (92.0%), mp 218 °C (dec), $[\alpha]_D^{25}$ −6.5° (*c* 1.0, DMSO).

Found: C, 51.56; H, 5.71; N, 15.82%. Calcd for $C_{27}H_{35}O_{10}N_7 \cdot 1/2H_2O$: C, 51.75; H, 5.79; N, 15.65%.

*Z-Ser-Ser-Asn-Tyr-Cys(MBzl)-Cys(MBzl)-Glu-Leu-Cys-(MBzl)-Cys(MBzl)-Asn-Pro-Ala-Cys(MBzl)-Thr-Gly-Cys-(MBzl)-Tyr-OBzl (**I**).* Compoud **V**[12] (1.18 g, 0.5 mmol) was dissolved with anisole (0.2 ml) in TFA (10 ml) at 0 °C and stirred at room temperature for 2 h. The solution was concentrated to a solid under reduced pressure. Meanwhile, compound **Id** (463 mg, 0.75 mmol) was suspended in DMF (5 ml) and cooled below −50 °C. The suspension was mixed with 6.72M HCl in dioxane (0.51 ml) and isopentyl nitrite (0.11 ml) and stirred at −20 °C for 30 min. The suspension became clear during this procedure, and was then mixed with *N*-methylmorpholine (1.0 ml) and a solution of the above solid in DMF. The mixture was stirred at 0 °C for 10 d and concentrated to dryness under reduced pressure. The residue was triturated in EtOH; wt 1.23 g (88.4%), mp 193 °C (dec), $[\alpha]_D^{20}$ −43.2° (*c* 1.0, DMSO). Amino acid ratio in the acid hydrolysate: Asp, 1.80 (2); Thr, 0.95 (1); Ser, 1.35 (2); Glu, 0.96 (1); Pro, 1.03 (1); Gly, 1.00 (1); Ala, 1.01 (1); 1/2Cys, not determined; Leu, 0.97 (1); Tyr, 1.68 (2).

Found: C, 57.87; H, 6.67; N, 9.66; S, 6.80%. Calcd for $C_{138}H_{172}O_{30}N_{20}S_6 \cdot 4H_2O$: C, 58.05; H, 6.35; N, 9.81; S, 6.74%.

*Z-Ser-Asn-Tyr-N_2H_3 (**IIa**).* Z-Ser-Asn-Tyr-OEt[12] (5.8 g, 10.7 mmol) was dissolved in DMF (30 ml) and mixed with 100% hydrazine hydrate (10.0 ml). The mixture was stirred at room temperature for 6 h and then concentrated to a solid under reduced pressure. The solid was recrystallized from DMF and EtOH; wt 5.8 g (100%), mp 241.5 °C (dec), $[\alpha]_D^{25}$ −11.5° (*c* 1.0, DMSO).

Found: C, 52.60; H, 5.72; N, 15.60%. Calcd for $C_{24}H_{30}O_8N_6 \cdot H_2O$: C, 52.55; H, 5.88; N, 15.32%.

*Z-Ser-Asn-Tyr-Cys(MBzl)-Cys(MBzl)-Glu-Leu-Cys(MBzl)-Cys(MBzl)-Asn-Pro-Ala-Cys(MBzl)-Thr-Gly-Cys(MBzl)-Tyr-OBzl (**II**).* Compound **V**[12] (1.18 g, 0.5 mmol) was dissolved with anisole (0.23 ml) in TFA (10 ml) at 0 °C and stirred at room temperature for 2 h. The solution was concentrated to a solid under reduced pressure. Meanwhile, compound **IIa** (318 mg, 0.6 mmol) was suspended in DMF (5 ml) and cooled below −50 °C. The suspension was mixed with 4.39M HCl in dioxane (0.41 ml) and isopentyl nitrite (0.09 ml) and stirred at −20 °C for 30 min. Then the resulting solution was mixed with *N*-methylmorpholine (1.0 ml) and a solution of the above solid in DMF (5 ml). The mixture was stirred at 0 °C for 2 d and concentrated to dryness under reduced pressure. The residue was triturated in 0.1 M HCl and collected. The material was boiled in hot EtOH and filtered after cooling to room temperature; wt 1.22 g (90.5%), mp 195 °C (dec), $[\alpha]_D^{16}$ −46.3° (c 1.0, DMSO). Amino acid ratio in the acid hydrolysate: Asp, 1.90 (2); Thr, 0.93 (1); Ser, 0.79 (1); Glu, 0.97 (1); Pro, 1.02 (1); Gly, 1.00 (1); Ala, 1.10 (1); 1/2Cys, not determined; Leu, 0.94 (1); Tyr, 1.81 (2).

Found: C, 58.82; H, 6.47; N, 9.52; S, 7.02%. Calcd for $C_{135}H_{167}O_{28}N_{19}S_6 \cdot 3H_2O$: C, 58.95; H, 6.34; N, 9.68; S, 7.00%.

*Z-Asn-Tyr-N_2H_3 (**IIIa**).* Z-Asn-Tyr-OEt[12] (4.57 g, 10.0 mmol) was dissolved in DMF (30 ml). The solution was mixed with 100% hydrazine hydrate (15 ml) and stirred at room temperature overnight. The gelatinous precipitate formed was collected with ether and reprecipitated from DMF and EtOH; wt 4.2 g (94.7%), mp 248 °C (dec), $[\alpha]_D^{20}$ −9.5° (*c* 0.5, DMSO).

Found: C, 54.91; H, 6.04; N, 15.58%. Calcd for $C_{21}H_{25}O_6N_5 \cdot H_2O$: C, 54.66; H, 5.90; N, 15.18%.

*Z-Asn-Tyr-Cys(MBzl)-Cys(MBzl)-Glu-Leu-Cys(MBzl)-Cys-(MBzl)-Asn-Pro-Ala-Cys(MBzl)-Thr-Gly-Cys(MBzl)-Tyr-OBzl (**III**).* Compound **V**[12] (1.18 g, 0.5 mmol) was dissolved with anisole (0.23 ml) in TFA (10 ml) at 0 °C and stirred at room temperature for 2 h. The solution was concentrated to a solid under reduced pressure. Meanwhile, compound **IIIa** (266 mg, 0.60 mmol) was dissolved in DMF (5 ml) and cooled below −50 °C. The solution was mixed with 4.39M HCl in dioxane (0.41 ml) and isopentyl nitrite (0.09 ml), stirred at −20 °C for 30 min and then mixed with *N*-methylmorpholine (1.0 ml) and a solution of the above solid in DMF (5 ml). The mixture was stirred at 0 °C for 3 d and then evaporated to a solid under reduced pressure. The solid was precipitated from DMF and EtOH; wt 1.16 g (88.9%), mp 203.5 °C (dec), $[\alpha]_D^{16}$ −46.9° (*c* 1.0, DMSO). Amino acid ratio in the acid hydrolysate: Asp, 1.92 (2); Thr, 0.92 (1); Glu, 0.98 (1); Pro, 1.00 (1); Gly, 1.00 (1); Ala, 1.03 (1); 1/2Cys, not determined; Leu, 0.99 (1); Tyr, 1.85 (2).

Found: C, 59.46; H, 6.56; N, 9.38; S, 7.36%. Calcd for $C_{132}H_{162}O_{26}N_{18}S_6 \cdot 3H_2O$: C, 59.53; H, 6.36; N, 9.47; S, 7.22%.

*Z-Tyr-Cys(MBzl)-Cys(MBzl)-Glu-Leu-OEt (**IVa**).* Boc-Cys(MBzl)-Cys(MBzl)-Glu(OBu^t)-Leu-OEt[12] (4.28 g, 5.0 mmol) was dissolved in CH_2Cl_2 (60 ml) and TFA (12.0 ml) was added to the solution. The solution was stirred at room temperature for 40 min and concentrated to a solid under reduced pressure. Meanwhile, Z-Tyr-N_2H_3 (1.98 g, 6.0 mmol) was dissolved in DMF (15.0 ml), cooled below −50 °C and mixed with 4.39M HCl in dioxane (4.1 ml) and isopentyl nitrite (0.88 ml). The solution was stirred at −20 °C for 30 min and then mixed with *N*-methylmorpholine (1.98 ml) and a solution of the above solid in DMF (10 ml). The mixture was stirred at 0—2 °C for 24 h and then concentrated to dryness under reduced pressure. The gelatinous residue was collected with AcOEt and reprecipitated from EtOH; wt 3.8 g (76.0%), mp 186.5—189.0 °C, $[\alpha]_D^{20}$ −14.3° (*c* 1.0, DMSO).

Found: C, 61.67; H, 6.48; N, 6.95; S, 6.27%. Calcd for $C_{52}H_{65}O_{11}N_5S_2 \cdot H_2O$: C, 61.33; H, 6.63; N, 6.88; S, 6.30%.

*Z-Tyr-Cys(MBzl)-Cys(MBzl)-Glu-Leu-N_2H_3 (**IVb**).* Compound **IVa** (3.8 g, 3.8 mmol) was dissolved in DMF (30 ml), mixed with 100% hydrazine hydrate (3.8 ml) and stirred at room temperature for 24 h. The precipitate formed was collected with EtOH, boiled in EtOH, cooled to room temperature and filtered; wt 3.0 g (80.0%), mp 212.5 °C (dec), $[\alpha]_D^{20}$ −14.7° (*c* 1.0, DMSO).

Found: C, 60.09; H, 6.69; N, 10.28 S, 6.51%. Calcd for $C_{50}H_{63}O_{10}N_7S_2 \cdot 1/2H_2O$: C, 60.34; H, 6.48; N, 9.85; S, 6.44%.

*Z-Tyr-Cys(MBzl)-Cys(MBzl)-Glu-Leu-Cys(MBzl)-Cys(MBzl)-Asn-Pro-Ala-Cys(MBzl)-Thr-Gly-Cys(MBzl)-Tyr-OBzl (**IV**).* Compound **V**[12] (1.64 g, 1.0 mmol) was dissolved with anisole (0.46 ml) in TFA (20 ml) at 0 °C and stirred at room temperature for 30 min. The solution was concentrated to a solid under reduced pressure. Meanwhile, compound **IVb** (1.18 g, 1.2 mmol) was dissolved in DMF (5 ml) and cooled below −50 °C. The solution was mixed with 4.39M HCl in dioxane (0.82 ml) and isopentyl nitrite (0.18 ml), stirred at −20 °C for 30 min, and was then mixed with TEA (1.2 ml)

and a solution of the above solid in DMF (7 ml). The mixture was stirred at 0 °C for 5 d and concentrated to dryness under reduced pressure. The residue was collected with EtOH, boiled in EtOH, and cooled to room temperature. The solid material was collected by filtration; wt 1.60 g (64.1%), mp 201.0 °C (dec), $[\alpha]_D^{16}$ −54.4° (*c* 1.0, DMSO). Amino acid ratio in the acid hydrolysate: Asp, 0.96 (1); Thr, 0.87 (1); Glu, 0.97 (1); Pro, 0.99 (1); Gly, 1.00 (1); Ala, 1.01 (1); 1/2Cys, not determined; Leu, 1.02 (1); Tyr, 2.09 (2).

Found: C, 60.93; H, 6.44; N, 8.88; S, 7.69%. Calcd for $C_{128}H_{156}O_{24}N_{10}S_6 \cdot 2H_2O$: C, 60.74; H, 6.37; N, 8.85; S, 7.60%.

Boc-Cys(MBzl)-Cys(MBzl)-Glu(OBu^t)-Leu-Cys(MBzl)-Cys(MBzl)-Asn-Pro-Ala-Cys(MBzl)-Thr-Gly-Cys(MBzl)-Tyr-OBzl (V). This compound was synthesized as described in the preceding paper.[12] Amino acid ratio in the acid hydrolysate: Asp, 0.95 (1); Thr, 0.89 (1); Glu, 0.96 (1); Pro, 0.93 (1); Gly, 1.00 (1); Ala, 1.03 (1); 1/2Cys, not determined; Leu, 0.99 (1); Tyr, 0.95 (1).

Deprotection, Air-oxidation and Purification of Toxic Peptides. Protected peptides **I**, **II**, **III**, **IV**, and **V** (100 μmol each) were treated with anhydrous liquid hydrogen fluoride (10 ml)[13] and spontaneously air-oxidized under similar conditions to those used for synthesis of ST_h. The air-oxidized materials were purified by ion-exchange chromatography on DEAE-Sephadex A-25 under the conditions described previously.[14] The peak fractions eluted were separated and assayed by the method described below. The toxic fractions were lyophilized and purified further by high-performance liquid chromatography (HPLC) under the conditions used for purification of ST_h, as described in the preceding paper.[12] The highly toxic fractions were isolated and lyophilized. The yields of purified peptides, ST_h[2-19], ST_h[3-19], ST_h[4-19], ST_h[5-19], and ST_h[6-19], were about 4.8, 5.8, 4.8, 5.3, and 27.4% on the basis of the amounts of the protected peptides **I**, **II**, **III**, **IV** and **V**, respectively.

Biological Assay. ST activity was assayed in suckling mice of 2—4 d old, as described previously.[1]

Aminopeptidase M Digestion of ST_h and its Analogs. Native and synthetic ST_h and synthetic analogs of ST_h (*ca.* 100 μg) were digested with aminopeptidase M (5 μg) in 0.1M Tris HCl buffer (100 μl) under the conditions described in the preceding paper.[12] The digested peptides were separated by HPLC as described in the preceding paper.[12]

Edman Degradation. A sample peptide (*ca.* 100μg) was allowed to react with phenyl isothiocyanate (40 μl) in 50% aq pyridine (0.3 ml) adjusted to pH 9.6 with *N*-methylmorpholine at 40 °C for 60 min. The reaction mixture was washed three times with benzene and then lyophilized. The lyophilized material was treated with a few drops of TFA at 40 °C for 20 min and dried under a stream of nitrogen. The residue was dissolved in 0.5M AcOH (0.2 ml) and washed with AcOEt. The aqueous layer was applied directly to a YMC-packed column ODS A-324 (10×300 mm) and the adsorbed material was eluted with a linear gradient of 10—40% acetonitrile in 0.05% TFA (pH 2.35) at a flow rate of 3 ml/min. The peak fractions were separated and lyophilized.

Heat-treatment. Synthetic peptides were each dissolved in 0.01M phosphate buffer (pH 7.2) at a concentration of 200 μg/ml. Sample solutions were sealed in capillary tubes and placed for given periods in an electric oven controlled at the required temperature. Then the tubes were rapidly cooled in an ice-bath and part of the solution (50 μl) was subjected to HPLC. HPLC was performed on a column of LiChrosorb RP-8 (4.6×250 mm). The column was developed with a linear qradient of 10—35% acetonitrile in 0.01M ammonium acetate (pH 5.7) with increase in acetonitrile of 1%/min at a flow rate of 0.5 ml/min.

Results and Discussion

Syntheses. First, protected linear peptides **I** to **V** lacking one to five N-terminal amino acid residues of ST_h, respectively, were synthesized, as shown in the

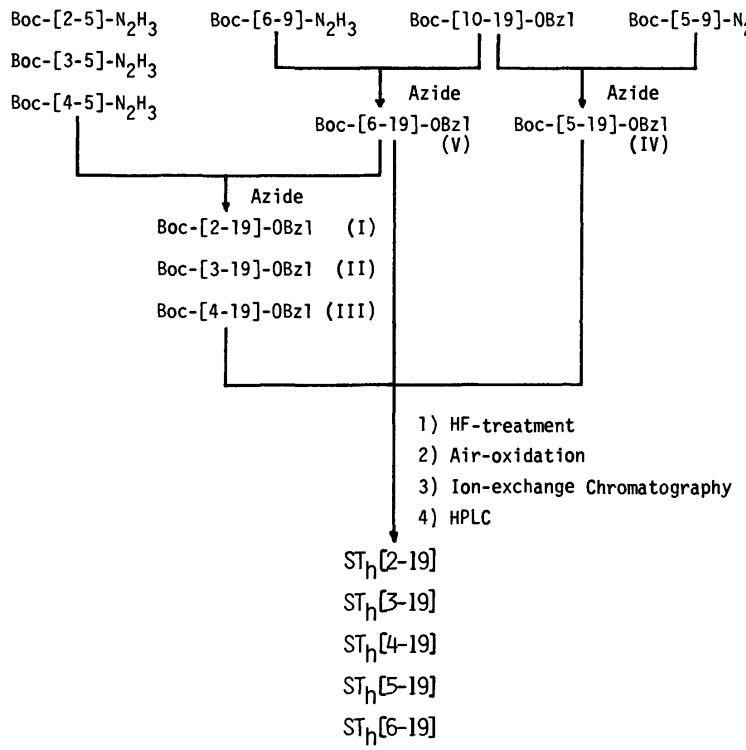

Fig. 2. Scheme for syntheses of shorter analogs of ST_h.

scheme in Fig. 2. Then these protected peptides **I** to **V** were treated with anhydrous liquid hydrogen fluoride[13] and spontaneously air-oxidized in dilute solution (5×10^{-5}M), as described for the synthesis of STh in the preceding paper.[12] The air-oxidized solutions of the deprotected peptides were subjected to HPLC, as shown in Fig. 3, and each fraction was separated and its toxicity was examined by the fluid accumulation test in suckling mice. The peak fractions shown by black bars had the highest toxicity. These fractions were purified by similar methods to those used for STh, as described in the preceding paper.[12] The fractions were confirmed to be pure by HPLC, as shown in Fig. 4, with a different buffer system as solvent from that used for the preparative purification. The amino acid compositions of the synthetic peptides are summarized in Table 1.

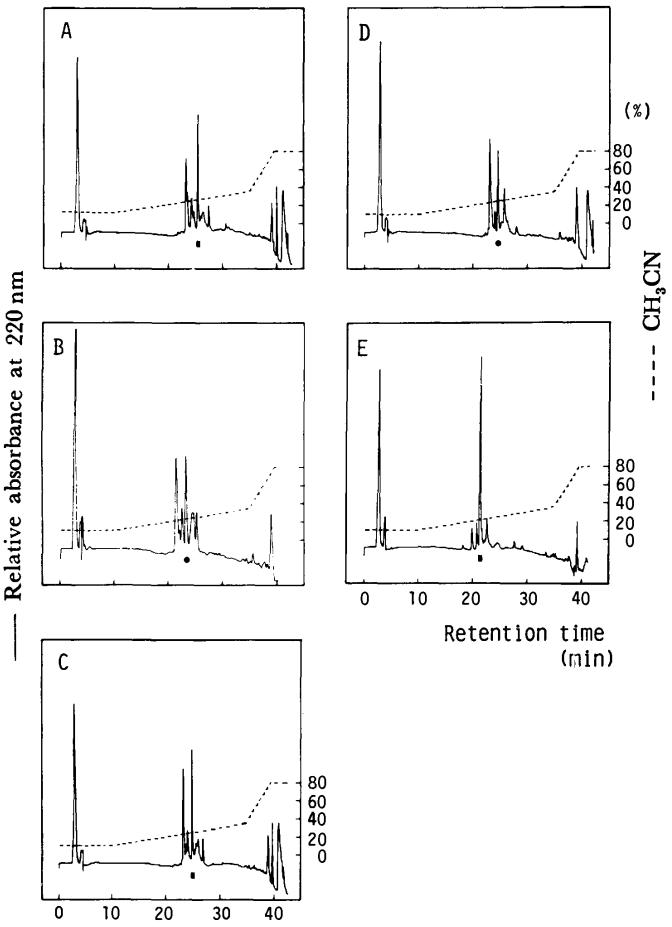

Fig. 3. HPLC profiles of deprotected and air-oxidized solutions of compounds **I**(A), **II**(B), **III**(C), **IV**(D), and **V**(E).
Column: LiChrosorb RP-8 (5 μm, 4×250 mm). The starting solvent was 10% CH_3CN in 0.01 M $AcONH_4$ (pH 5.7), and the flow rate was 1 ml/min.

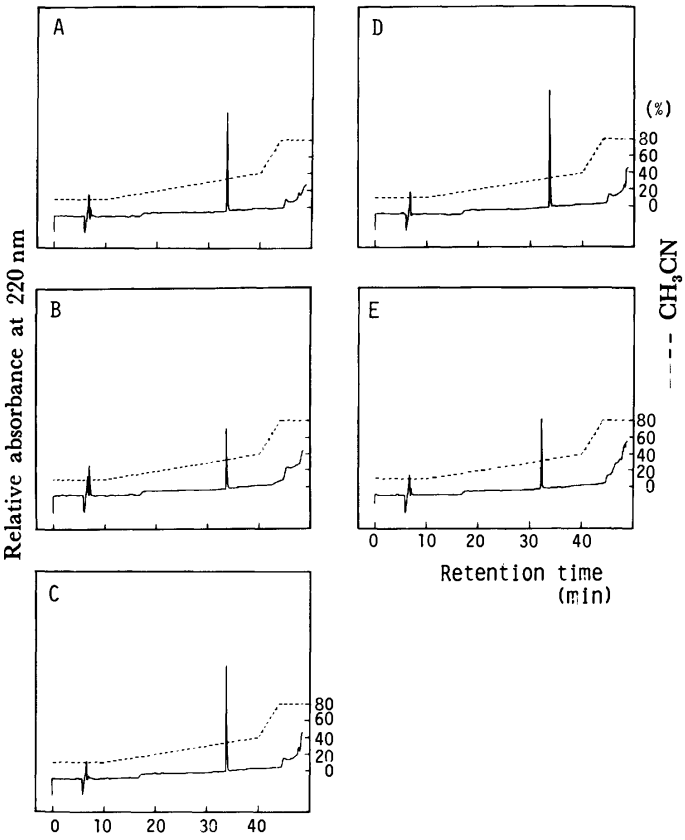

Fig. 4. HPLC profiles of synthetic STh[2-19] (A), STh[3-19] (B), STh[4-19] (C), STh[5-19] (D), and STh[6-19] (E) on a YMC-packed column ODS A-324 (5 μm, 10×300 mm). The starting solvent was 10 % CH_3CN in 0.05 % TFA (pH 2.35), and the flow rate was 2 ml/min.

Table 1. Amino acid compositions of shorter synthetic analogs of STh

	STh[2-19]	STh[3-19]	STh[4-19]	STh[5-19]	STh[6-19]
Asp	1.84(2)	2.02(2)	2.00(2)	1.07(1)	1.02(1)
Thr	0.92(1)	0.99(1)	1.00(1)	1.00(1)	1.01(1)
Ser	1.81(2)	0.96(1)	—	—	—
Glu	1.05(1)	1.02(1)	1.01(1)	1.02(1)	1.01(1)
Pro	0.99(1)	1.12(1)	1.10(1)	1.11(1)	0.99(1)
Gly	1.07(1)	1.03(1)	1.02(1)	1.04(1)	1.02(1)
Ala	1.00(1)	1.00(1)	1.00(1)	1.00(1)	1.00(1)
1/2Cys	4.82(6)	5.50(6)	5.47(6)	5.51(6)	5.39(6)
Leu	0.97(1)	1.03(1)	1.03(1)	1.03(1)	1.02(1)
Tyr	1.78(2)	1.98(2)	2.09(2)	1.98(2)	1.00(1)

Values were calculated as mol/mol of Ala; numbers in parentheses indicate nearest integer values.

High-performance Liquid Chromatography (HPLC) of ST_h Analogs. Shorter synthetic analogs of ST_h could be purified to homogeneity by HPLC under the conditions shown in Fig. 4. However, it was necessary to find conditions for elution of all or almost all the synthetic analogs of ST_h separately on HPLC, because all shorter synthetic analogs of ST_h except ST_h[6-19] had nearly the same retention times on HPLC under the conditions shown in Fig. 4. We tested several commercially available ODS columns and buffer solutions, and found that the following two procedures were satisfactory, although they did not separate all the ST_h analogs completely; i) A YMC-packed ODS column A-324 (10×300 mm) equilibrated with 0.05% heptafluorobutyric acid (pH 2.5) containing 10% CH_3CN and, after sample injection, developed with a gradient of 10% to 40% CH_3CN at a flow rate of

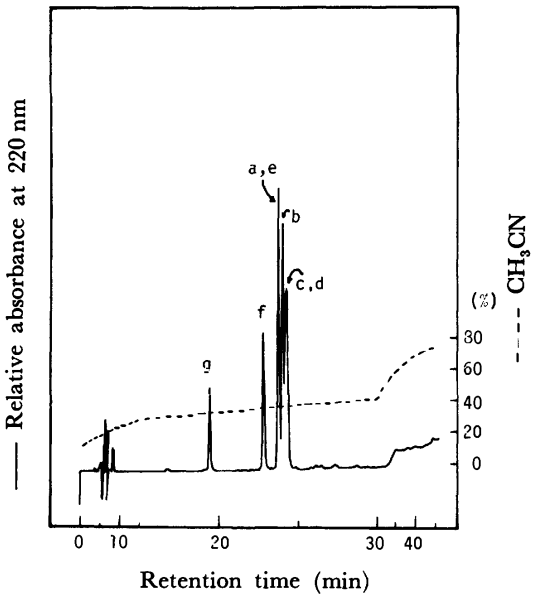

Fig. 5. HPLC profile of a mixture of synthetic ST_h [1-19] (a), ST_h[2-19] (b), ST_h[3-19] (c), ST_h [4-19] (d), ST_h[5-19] (e), and ST_h[6-19] (f) on a YMC-packed column ODS A-324 (5 μm, 10×300 mm). The starting solvent was 10% CH_3CN in 0.05% TFA (pH 2.35) and the flow rate was 3 ml/min. ST_h[6-18] (g) was added as an internal standard.

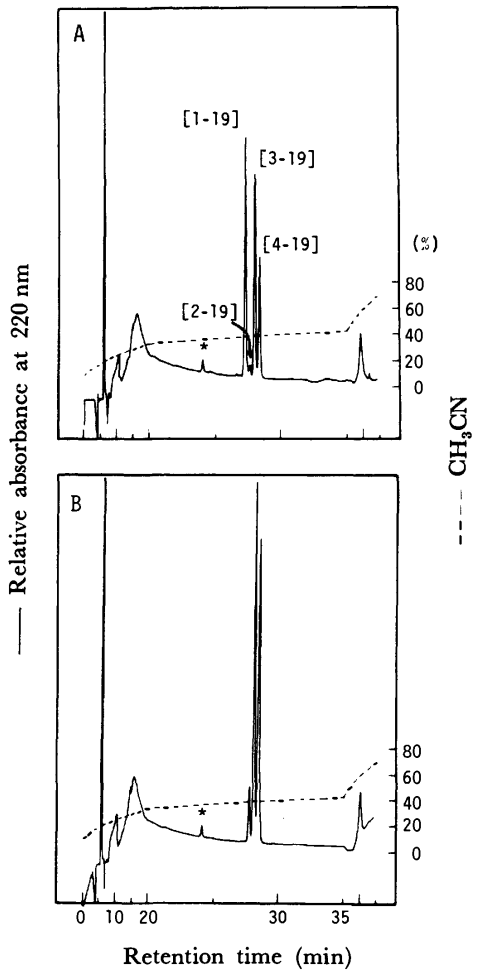

Fig. 6. HPLC profiles of digests of native ST_h (A) and synthetic ST_h[2-19] (B) with aminopeptidase M on a YMC-packed column ODS A-324 (5 μm, 10×300 mm). The starting solvent was 10% CH_3CN in 0.05 % heptafluorobutyric acid (pH 2.51) and the flow rate was 3 ml/min. ST_h[6-18] (peak denoted by*) was added to each digest as an internal standard.

TABLE 2. AMINO ACID COMPOSITIONS OF PEPTIDES OBTAINED BY ENZYMATIC AND EDMAN DEGRADATION OF NATIVE ST_h AND ITS SYNTHETIC ANALOGS

Starting peptide	Native ST_h		Synthetic ST_h[2-19]		Synthetic ST_h[4-19]	Synthetic ST_h[5-19]
Products	ST_h[3-19]	ST_h[4-19]	ST_h[3-19]	ST_h[4-19]	ST_h[5-19]	ST_h[6-19]
Asp	2.00(2)	2.01(2)	2.00(2)	1.98(2)	1.07(1)	1.08(1)
Thr	0.96(1)	1.00(1)	0.96(1)	1.00(1)	1.05(1)	1.03(1)
Ser	0.97(1)	—	0.96(1)	—	—	—
Glu	1.00(1)	1.04(1)	1.01(1)	1.00(1)	1.04(1)	1.02(1)
Pro	1.07(1)	1.11(1)	1.12(1)	1.02(1)	0.99(1)	1.11(1)
Gly	1.03(1)	1.04(1)	1.03(1)	1.04(1)	1.02(1)	1.00(1)
Ala	1.00(1)	1.00(1)	1.00(1)	1.00(1)	1.00(1)	1.00(1)
1/2Cys	5.34(6)	5.36(6)	5.48(6)	5.38(6)	5.58(6)	5.21(6)
Leu	1.05(1)	1.06(1)	1.05(1)	1.06(1)	1.05(1)	1.06(1)
Try	2.00(2)	1.99(2)	2.01(2)	2.00(2)	2.04(2)	1.00(1)

Values were calculated as mol/mol of Ala; numbers in parentheses indicate nearest integer values.

3 ml/min; ii) The same column developed under the same conditions as for i) but with 0.05% TFA instead of 0.05% heptafluorobutyric acid as the aqueous phase. The elution profile of a mixture of shorter synthetic analogs by the latter procedure is shown in Fig. 5. With this procedure, synthetic STh[1-19] and STh[3-19] could not be completely separated from STh[5-19] and STh[4-19], respectively.

Aminopeptidase M Digestion of Native STh and Identification of the Resulting Peptides with Synthetic Analogs. To confirm that shorter synthetic analogs of STh had intramolecular disulfide bonds at the same positions as those in native STh, we treated native STh with aminopeptidase M, isolated the resulting peptides and compared them with the synthetic analogs of STh by HPLC. The HPLC profile of the digest of native STh showed two major and one minor peak with a peak of undigested peptide, as illustrated in Fig. 6A. The materials in these fractions were separated and submitted to measurement of their molecular weights by fast atom bombardment mass spectrometry (data not shown) and amino acid analysis (Table 2). The two major fractions were identified as those of STh[3-19] and STh[4-19], which lacked two and three N-terminal amino acid residues, respectively, of STh. The minor peak fraction eluted between undigested STh and STh[3-19] was identified as that of a peptide STh[2-19] lacking the N-terminal Asn residue of STh, by comparison of its HPLC profile with that of native STh digested with aminopeptidase M (Fig. 6B). The shorter STh peptides lacking one to three amino acid residues (STh[2-19], STh[3-19], and STh[4-19]) thus prepared by digestion of native STh with aminopeptidase M were each mixed with an equal amount of the corresponding synthetic peptide and chromatographed on a reversed-phase column, as shown in Figs. 7A—7C. Each gave a single peak. Thus, synthetic STh[2-19], STh[3-19], and STh[4-19] were confirmed to have disulfide linkages in the same positions as those in native STh. The digestion of native STh with aminopeptidase M stopped with release of the three N-terminal amino acid residues and did not proceed further even when the ratio of the enzyme to STh was raised to 1/10 (w/w). Therefore, Edman degradation was carried out for further removal of the fourth and fifth amino acid residues of STh from the N-terminus, as described below.

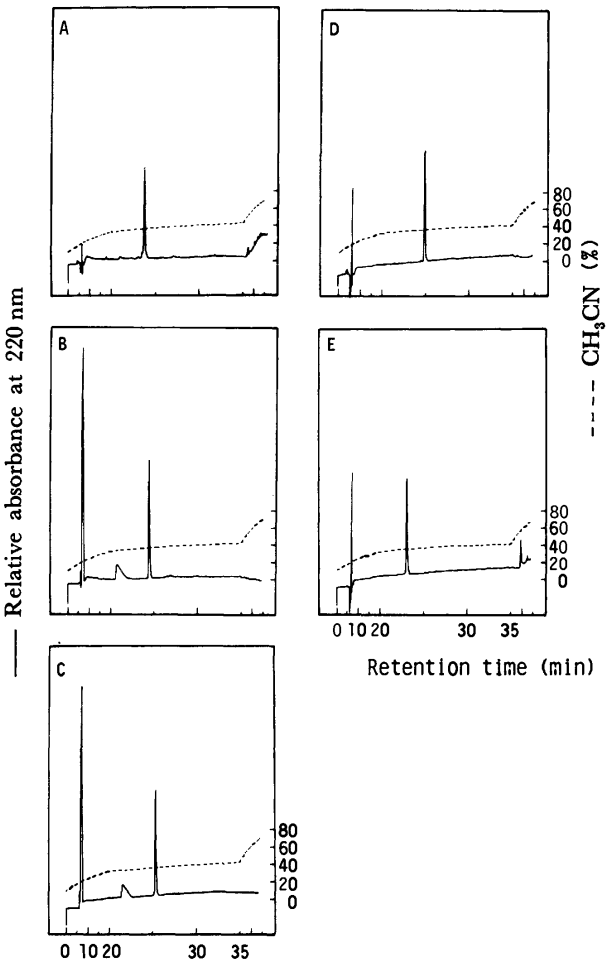

Fig. 7. HPLC profiles of mixtures of equal amounts of STh analogs on a YMC-packed column ODS A-324 (5 μm, 10×300 mm). The starting solvent was 10% CH_3CN in 0.05% TFA (pH 2.35), and the flow rate was 3 ml/min. (A) STh[2-19] enzymatically derived from native STh and synthetic STh[2-19]; (B) STh[3-19] enzymatically derived from native STh and synthetic STh[3-19]; (C) STh[4-19] enzymatically derived from native STh and synthetic STh[4-19]; (D) STh[5-19] prepared from synthetic STh[4-19] by Edman degradation and synthetic STh[5-19]; (E) STh[6-19] derived from synthetic STh[5-19] by Edman degradation and synthetic STh[6-19].

Edman Degradation and Comparison of the Degraded Peptides with Synthetic Peptides. Synthetic STh[4-19] was confirmed to have intramolecular disulfide linkages in the same positions as those in native STh, as described above. Then we subjected synthetic STh-[4-19] to Edman degradation[14] and obtained STh[5-19]. This shortened peptide of STh was purified by HPLC and its amino acid composition was analyzed (Table 2). A mixture of equal amounts of this peptide and synthetic STh[5-19] gave a single peak on HPLC, as shown in Fig. 7D, indicating that synthetic STh[5-19] was linked intramolecularly by disulfide bonds at the same positions as those in STh[4-19]. Then we degraded synthetic STh[5-19] by a similar method to that used for STh[4-19] and purified the degraded peptide by the same procedure as used for degraded STh[4-19]. The amino acid composition of the purified peptide is shown in Table 2. When this peptide was mixed with synthetic STh[6-19] and subjected to HPLC a single peak was obtained, as shown in Fig. 7E. Thus synthetic STh[6-19] had intramolecular disulfide linkages at the same positions as those in STh[5-19], and synthetic STh[5-19] and STh[6-19] were both intramolecularly linked by disulfide bonds in the same way as native STh.

Biological Activity. The toxicities of shorter synthetic analogs of STh were assayed as described previously.[1] The minimum effective doses of shorter synthetic analogs of STh were 1.0±0.4 ng, which were the same as that of native or synthetic STh within the limits of experimental error, as shown in Table 3.

These values were also almost the same as those for the corresponding peptides derived from native ST_h by digestion with aminopeptidase M or by Edman degradation. Furthermore, the toxicities of all the shorter synthetic analogs of ST_h were neutralized by anti-native ST_h antiserum. These results indicate that the active site of the toxicity of ST_h is located in the sequence between the Cys residue near the N-terminus and the C-terminal Tyr.

Heat-stability. Synthetic ST_h was found to have the same stability as that of native ST_h on boiling in phosphate buffer, as described in the preceding paper.[12] We examined the heat-stability of shorter synthetic analogs of ST_h by the method as described previously.[15] Synthetic ST_h[5-19] lacking four N-terminal amino acid residues of ST_h showed the same heat-stability as that of synthetic ST_h, as illustrated in Fig. 8. Furthermore, the toxicity of ST_h[5-19] was found to decrease with the duration of heat-treatment. Shorter synthetic analogs of ST_h lacking one to three the N-terminal amino acid residues of ST_h gave similar results (data not shown). On the other hand, synthetic ST_h[6-19] lacking five N-terminal amino acid residues of ST_h showed higher heat-stability than synthetic or native ST_h, as reported in a previous paper.[15] These results suggest that the sequence consisting of 13 amino acid residues from the Cys residue near the N-terminus to the C-terminal Tyr residue is essential for the heat-stability of the toxin. The enhanced structural stability of ST_h[6-19] may be due to decreased perturbation of the molecule on heating as a result of loss of the five N-terminal amino acid residues.

TABLE 3. BIOLOGICAL PROPERTIES OF SYNTHETIC ST_h ANALOGS

	Minimum effective dose (ng/100 μl)[a]	Neutralization by anti-native ST_h antiserum
Native ST_h	1.0 ng (0.5 pmol)[b]	+
Synthetic ST_h	0.8 ng (0.4 pmol)[b]	+
Synthetic ST_h[2-19]	0.8 ng (0.4 pmol)	+
Synthetic ST_h[3-19]	1.3 ng (0.7 pmol)	+
Synthetic ST_h[4-19]	1.1 ng (0.7 pmol)	+
Synthetic ST_h[5-19]	0.8 ng (0.5 pmol)	+
Synthetic ST_h[6-19]	0.6 ng (0.4 pmol)	+

a) Calculated from the recovery of amino acids in acid hydrolysates. b) Cited from Ref. 12.

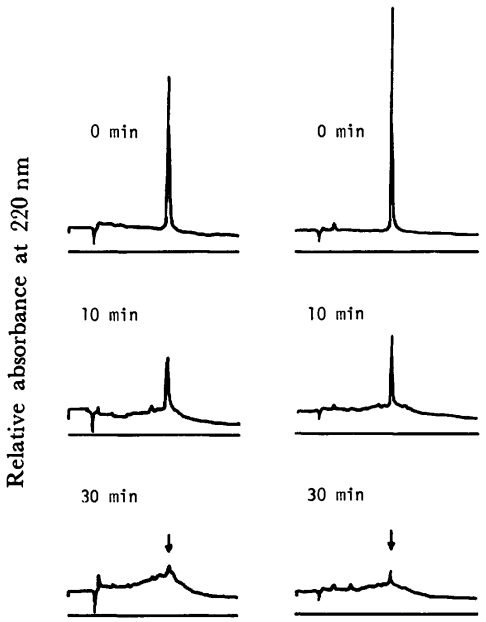

Fig. 8. HPLC profiles on a LiChrosorb RP-8 column (5 μm, 4×250 mm) of heat-treated synthetic ST_h(left column) and ST_h[5-19](right column).

This work was partly supported by a Grant-in-Aid for Scientific Research (No. 58122002) for the Ministry of Education, Science and Culture of Japan.

References

1) Y. Takeda, T. Takeda, T. Yano, K. Yamamoto, and T. Miwatani, *Infect. Immun.*, **25**, 978 (1979).
2) S. -K. Chan and R. A. Giannella, *J. Biol. Chem.*, **256**, 7744 (1981).
3) S. Aimoto, T. Takao, Y. Shimonishi, S. Hara, T. Takeda, Y. Takeda, and T. Miwatani, *Eur. J. Biochem.*, **129**, 257 (1982).
4) T. Takao, T. Hitouji, S. Aimoto, Y. Shimonishi, S. Hara, T. Takeda, Y. Takeda, and T. Miwatani, *FEBS Lett.*, **152**, 1 (1983).
5) R. Lallier, F. Bernard, M. Gendreau, C. Lazure, N. G. Seidah, M. Chretien, and S. St-Pierre, *Anal. Biochem.*, **127**, 267 (1982).
6) C. Lazure, N. G. Seidah, M. Chretien, R. Lallier, and S. St-Pierre, *Can. J. Biochem. Cell Biol.*, **61**, 287 (1983).
7) B. Ronnberg, T. Wadstrom, and H. Jornvall, *FEBS Lett.*, **155**, 183 (1983).
8) M. Field, L. H. Graf, Jr., W. J. Laird, and P. L. Smith, *Proc. Natl. Acad. Sci, U.S.A*, **75**, 2800 (1978).
9) J. M. Hughes, F Murad, B. Chang, and R. L. Guerrant, *Nature*, **271**, 755 (1978).
10) P. M. Newsome, M. N. Burgess, and N. A. Mullan, *Infect. Immun.*, **22**, 290 (1978).
11) R. A. Giannella and K. W. Drake, *Infect. Immun.*, **24**, 19 (1979).
12) H. Ikemura, S. Yoshimura, S. Aimoto, Y. Shimonishi, S. Hara, T. Takeda, Y. Takeda, and T. Miwatani, *Bull. Chem. Soc. Jpn.*, **57**, 2543 (1984).
13) S. Sakakibara, Y. Shimonishi, Y. Kishida, M. Okada, and H. Sugihara, *Bull. Chem. Soc. Jpn.*, **40**, 2164 (1967).
14) P. Edman and A. Henschen, "Protein Sequence Determination" ed by S. B. Needleman, Springer-Verlag, Berlin, Heidelberg, New York, (1975) p. 232.
15) S. Aimoto, H. Watanabe, H. Ikemura, Y. Shimonishi, T. Takeda, Y. Takeda, and T. Miwatani, *Biochem. Biophys. Res. Commun.*, **112**, 320 (1983).

 © 1984 The Chemical Society of Japan Bull. Chem. Soc. Jpn., 57, 2557—2564 (1984)

Hydrogenation and Hydrogenolysis. XVII.[1] The Selectivities of Platinum Group Metals in Catalytic Hydrogenation of 2-Naphthol and Tetrahydro-2-naphthols

Shigeo NISHIMURA,* Shin-ichi OHBUCHI, Kiyoshi IKENO, and Yasuhiro OKADA
Department of Applied Chemistry for Resources, Tokyo University of Agriculture and Technology, Koganei, Tokyo 184
(Received May 10, 1984)

Catalytic hydrogenation of 2-naphthol (NL) with the six platinum metals has been studied in *t*-BuOH at 80 °C and 4—5 MPa H_2 pressure. Selectivities for formation of 1,2,3,4- and 5,6,7,8-tetrahydro-2-naphthols (*ac*- and *ar*-TLs) have been determined by application of a kinetic equation. *ar*-TL was formed more predominantly than *ac*-TL over all the metals. The hydrogenation of *ac*- and *ar*-TLs has also been studied under the same conditions for comparison. The hydrogenation of NL and *ar*-TL was accompanied by extensive hydrogenolysis to give decalins over Os, Ir, and Pt, whereas the hydrogenolysis occurred only slightly over Ru, Rh, and Pd. In general the hydrogenolysis occurred to much lesser extents with *ac*-TL. The amounts of 2-decalone formed in hydrogenation of *ar*-TL have been determined by application of the kinetic equation. The 2-decalone was the *cis* isomer only except with Pd. For formation of the *cis* products at the ring juncture, hydrogenation of *ar*-TL was highly stereoselective with Ru, Rh, Os, and Ir, while hydrogenation of *ac*-TL was the most stereoselective with Os and Ir. The course of hydrogenolysis and the stereochemistry of hydrogenation are discussed from the comparative results on NL, *ar*-TL, and *ac*-TL.

The catalytic hydrogenation of aromatic compounds has been a subject of extensive studies not only as useful synthetic routes to alicyclic compounds but also from stereochemical and mechanistic viewpoints.[2] However, compared to a large number of studies on monocyclic aromatics, the catalytic hydrogenation of polycyclic aromatics has been investigated to rather limited extent.[3] One reason for this might be difficulties in the analysis of products that are often rather complicated. As the simplest polycyclic aromatics naphthalene and its derivatives have been hydrogenated with a variety of catalysts and conditions. Particular interests have been focused on the selectivity for formation of tetrahydro intermediates and the stereochemistry of hydrogenation in formation of decahydro derivatives.[2,3] The hydrogenation of naphthols has been interested as synthetic routes to 1,2,3,4- and 5,6,7,8-tetrahydronaphthols (abbreviated to *ac*- and *ar*-tetralols) that may be starting materials for further syntheses[4] or of therapeutic importance.[5,6] The selectivity for either *ac*- or *ar*-tetralol is known to be much influenced by the catalyst employed as well as by reaction conditions and additives.[2,7] The hydrogenation has also been studied for the stereochemistry of the resulting decahydronaphthols (abbreviated to decalols).[8—14] Among the platinum metals, platinum,[8—10] rhodium,[4,11] rhodium–platinum,[12] and ruthenium[13,14] have been used for complete hydrogenation to decalins and decalols, while palladium catalysts have been employed for selective transformation to the dihydro and tetrahydro derivatives.[6,7a,15] However, there appears to be few studies on the other platinum metals, and, to our knowledge, no comparative study on the six platinum metals with naphthols, although such a study has been reported by Weitkamp on the hydrogenation of naphthalene and its methyl derivatives.[3]

In this study the selectivities of the six platinum metals have been compared in the hydrogenation of 2-naphthol for formation of the two tetrahydro derivatives, *ac*- and *ar*-2-tetralols, for their trends towards hydrogenolysis, and for the stereochemistry in the formation of saturated compounds. The hydrogenation of *ac*- and *ar*-2-tetralols has also been studied under the same conditions for comparison.

Experimental

Materials. All the substrates hydrogenated are well documented compounds. Melting points are corrected. Their structures and purities were confirmed by NMR, IR, GC-MS, and GLC. 2-Naphthol (Wako Pure Chemical Industries) was purified by treating with Raney nickel in EtOH at 50—60 °C for 3 h to remove catalyst poisons. After removal of the catalyst, addition of water to the ethanol solution gave white crystals: mp 123 °C (lit,[16] mp 121—123 °C). *ac*- and *ar*-2-Tetralols were prepared from a mixture of them obtained by hydrogenation of 2-naphthol with Raney nickel in *i*-PrOH at 100 °C and 5—10 MPa. After removing the catalyst and solvent, the ethereal solution of the residue was extracted with 2% NaOH solution. Addition of hydrochloric acid to the extract gave crystals which were recrystallized from hexane: mp 61.5 °C (lit,[17] mp 61.5—62.5 °C). From the ethereal solution after removal of *ar*-2-tetralol, *ac*-2-tetralol was obtained by distillation at reduced pressure: bp 127 °C/6 mmHg (1 mmHg≈133.322 Pa); n_D^{25} 1.5620 (lit,[18] bp 120 °C/2 mmHg; n_D^{25} 1.5625). *trans*-Octahydro-2(1*H*)-naphthalenone (abbreviated to *trans*-2-decalone) was prepared by chromic acid oxidation of a trans-rich 2-decalol mixture obtained by isomerization of a 2-decalol mixture with Raney nickel at 160 °C and 0.2 MPa H_2. *cis*-Octahydro-2(1*H*)-naphthalenone (abbreviated to *cis*-2-decalone) was likewise obtained from a cis-rich mixture of 2-decalols. Both the *trans*- and *cis*-2-decalones were purified by a preparative GLC. *trans*-2-Decalone: n_D^{25} 1.4817 (lit,[19] n_D^{25} 1.4814); *cis*-2-decalone: n_D^{25} 1.4911 (lit,[19] n_D^{25} 1.4915). 3,4-Dihydro-2(1*H*)-naphthlenone (abbreviated to 2-tetralone) was obtained from Sigma Chemical Co. and used after distillation at reduced pressure: bp 93 °C/1 mmHg; n_D^{20} 1.5597 (lit,[20] bp 92—94 °C/1.8 mmHg; n_D^{20} 1.5594).

Catalysts. Unsupported metal catalysts were prepared by reducing the corresponding metal hydroxides (Ru, Rh, Ir) or oxides (Pt, Os) with hydrogen in water at atmospheric or elevated pressure.[21,22] Care was taken to remove

alkaline or acidic impurities with repeated reductions and washings. Pd-C catalyst (5% Pd) was obtained from Nippon Engelhard Co. and used throughout this study, since unsupported palladium was liable to deactivation during hydrogenation.

Solvent. *t*-Butyl alcohol (Wako Pure Chemical Industries) was distilled with addition of a small amount of sodium and stored in a refrigerator.

Hydrogenation. All hydrogenations were performed in a 40 ml stainless steel autoclave with a stirrer driven magnetically. The autoclave was immersed in an oil bath maintained at 80 °C during hydrogenation. The catalyst, the amount of which varied with metal, was pretreated with hydrogen at 80 °C and 5 MPa H_2 (15 min for Pd-C, 30 min for Rh, Ir, Os, and Pt, and 1 h for Ru). After the pretreatment the solvent was replaced by a new portion of *t*-butyl alcohol and then the substrate, dissolved in a small amount of the solvent, was added, the combined amount of the solvent being 16 ml. The mixture was hydrogenated at 80 °C and 4—5 MPa H_2 pressure.

Analysis of the Reaction Mixture. The reaction mixture was analyzed by GLC with 2-methoxynaphthalene as an internal standard. For the analysis of *cis*- and *trans*-decalins and tetralin, the reaction mixture was subjected directly to GLC, using a glass capillary column of OV-17 (0.3 mmϕ×30 m) at 70—130 °C programmed at 1 °C/min and with N_2 at 0.075 MPa. The retention times were 5.4 min (*trans*-decalin), 6.4 min (*cis*-decalin), 8.8 min (tetralin), and 33.9 min (2-methoxynaphthalene). For the analysis of four stereoisomeric 2-decalols, *ar*-2-tetralol, and 2-naphthol, the reaction mixture, after removal of the solvent, was trimethylsilylated and then subjected to GLC, using the same glass capillary column mentioned above under the same conditions. The retention times were 13.3 min (*trans,trans*-2-decalol (**1a**)), 16.9 min (*trans, cis*-2-decalol (**1b**)), 18.5 min (*cis,trans*-2-decalol (**1c**)), 19.3 min (*cis,cis*-2-decalol (**1d**)), 33.9 min (2-methoxynaphthalene), 35.5 min (*ar*-2-tetralol), and 38.8 min (2-naphthol). For the analysis of *ac*-2-tetralol, *trans*- and *cis*-2-decalones, and 2-tetralone, the trimethylsilylated products were subjected to GLC, using a DEGS column (3 mmϕ×3 m) at 170 °C and with N_2 at 0.09 MPa. The retention times were 13.2 min (*ac*-2-tetralol), 19.8 min (*trans*-2-decalone), 25.4 min (*cis*-2-decalone), 62.7 min (2-tetralone), and 65.3 min (2-methoxynaphthalene).

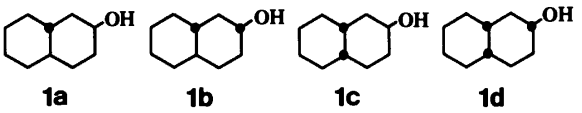

Results

Hydrogenation of 2-Naphthol to ar- *and* ac-*2-Tetralols.* Hydrogenation of 2-naphthol gives *ar*- and *ac*-2-tetralols as the intermediates leading to decalins and 2-decalols. In order to know the selectivities for the two tetralols, 2-naphthol was hydrogenated in *t*-butyl alcohol at 80 °C and 4—5 MPa of hydrogen pressure over the six platinum metals as catalysts. In

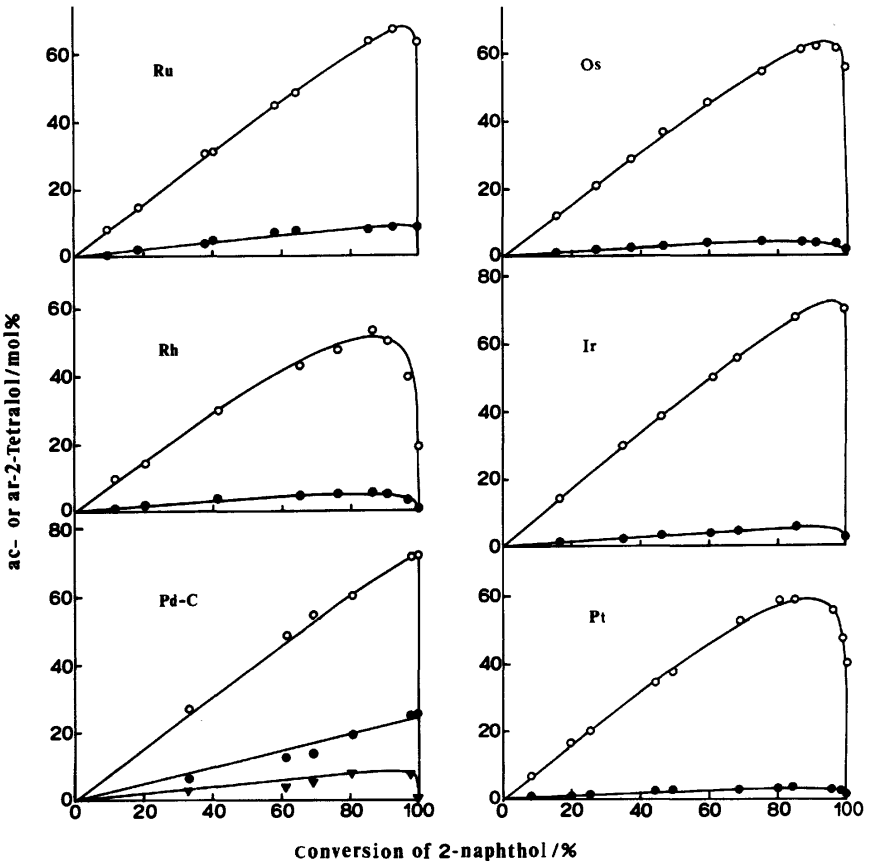

Fig. 1. Hydrogenation of 2-naphthol: formation of *ar*- and *ac*-2-tetralols. ○: *ar*-2-tetralol, ●: *ac*-2-tetralol (2-tetralone+*ac*-2-tetralol for Pd-C), ▼: 2-tetralone. The results show a set of separate experiments with varying conversions of 2-naphthol. The full lines show the theroretical curves given by Eq. 1. For the values of f and K, see Tables 1 and 8, respectively.

Fig. 1 are shown the variations in amount of the two tetralols during the course of hydrogenation as a function of 2-naphthol conversion. The selectivity for either *ar*- or *ac*-2-tetralol has been determined by application of Eq. 1 which is derived on the basis of the reaction pathways shown in Scheme 1.[23] C_{NL} and C_{TL} represent the concentrations of 2-naphthol and *ar*- or *ac*-2-tetralol, respectively, when the initial concentration of 2-naphthol is taken as unity. f is the fraction of 2-tetralol which leaves the catalyst surface and given by $k_1/(k_1+k_3)$ where k_1 and k_3 are the rate constants for the respective reaction pathways shown in Scheme 1. K is a constant which depends on the relative reactivity of 2-tetralol to 2-naphthol. The circles in Fig. 1 show the results of a set of experiments done separately for varying conversions of 2-naphthol. The full lines in Fig. 1 present the theoretical curves given by Eq. 1 when an appropriate set of values of f and K are selected to

$$C_{TL} = \frac{f}{K-1}(C_{NL} - C_{NL}^{K}) \quad (1)$$

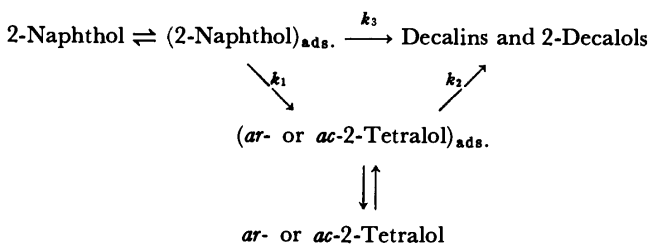

Scheme 1. Hydrogenation pathways of 2-naphthol.

represent best the variations in concentration of *ar*- or *ac*-2-tetralol throughout the course of the hydrogenation. With palladium 2-tetralone was formed together with the tetralols (see Fig. 1). Since 2-tetralone has been converted nearly quantitatively to *ac*-2-tetralol over palladium,[24] the sum of *ac*-2-tetralol and 2-tetralone is plotted in Fig. 1. The selectivities for the products other than the tetralols were obtained by extrapolating the varying selectivities with the conversion of 2-naphthol to the initiation of hydrogenation. The composition of the products at the initial stage of hydrogenation thus obtained by application of Eq. 1 and the extrapolation method is summarized in Table 1.

Hydrogenation of ar-*2-Tetralol.* Since *ar*-2-tetralol has been the predominant intermediate in the hydrogenation of 2-naphthol over all the catalyst metals investigated, the hydrogenation of *ar*-2-tetralol has also been studied in detail. Table 2 summarizes the composition of the products obtained on complete hydrogenation. Analysis of the reaction mixture during hydrogenation indicated that 2-decalone is formed as an intermediate, the amount of which depended on the catalyst metal used, as shown in Fig. 2. Hydrogenation with osmium, however, gave no detectable amount of 2-decalone. The selectivity for 2-decalone has been determined by application of Eq. 1 to the varying concentrations of the ketone with the conversion of *ar*-2-tetralol. The selectivity for iridium was evaluated by extrapolation method since the amounts of 2-decalone found were too small to apply Eq. 1. It is noteworthy

Table 1. Hydrogenation of 2-naphthol to *ar*- and *ac*-2-tetralols: selectivity for each product at initial stage[a]

Catalyst	Amount / mg	Selectivity/mol%[b]					
		DN	TN	DL	TO	*ac*-TL	*ar*-TL
Ru	4	0.7	0.5	10.5	0.0	10.6	77.7
Rh	4	0.7	0.6	11.9	0.0	8.6	78.2
Pd-C	150	0.0	0.0	0.1	8.5	15.4	76.0
Os	10	3.1	1.1	11.0	0.0	7.2	77.6
Ir	4	2.0	1.3	6.0	0.0	7.2	83.5
Pt	10	3.8	1.4	6.0	0.0	4.9	83.9

a) 2-Naphthol (600 mg) was hydrogenated in *t*-BuOH (16 ml) at 80 °C and 4—5 MPa H_2 pressure. b) DN: *cis*- and *trans*-decalins; TN: tetralin; DL: 2-decalols; TO: 2-tetralone; *ac*-TL: *ac*-2-tetralol; *ar*-TL: *ar*-2-tetralol.

Table 2. Hydrogenation of *ar*-2-tetralol: the composition of products at complete hydrogenation[a]

Catalyst	Amount / mg	Reac. time / h	Product composition/mol%[b]					
			t-DN	*c*-DN	*t,t*-DL	*t,c*-DL	*c,t*-DL	*c,c*-DL
Ru	6	2.5	0.1	0.5	0.4	0.6	28.2	70.2
Rh	4	1.1	0.1	1.0	0.9	2.9	17.4	77.7
Pd-C	300	12	0.1	0.1	9.5	21.8	10.5	58.0
Os	20	4.0	0.7	27.8	0.2	0.6	12.0	58.7
Ir	10	2.0	1.3	34.7	0.2	0.7	10.4	52.7
Pt	20	2.5	9.9	31.7	1.5	1.4	12.3	43.2

a) *ar*-2-Tetralol (617 mg) was hydrogenated in *t*-BuOH (16 ml) at 80 °C and 4—5 MPa H_2 pressure. b) For the notation of the compounds, see footnote b) in Table 1; *t* and *c* represent trans and cis.

that, except with palladium, the 2-decalone found was the cis isomer only and no trans isomer was observed. The amounts of 2-decalones thus determined are summarized in Table 3. Table 4 shows the results of the hydrogenation of *cis*-2-decalone with the six platinum metals and of *trans*-2-decalone with palladium catalyst.

Hydrogenation of ac-*2-Tetralol.* *ac*-2-Tetralol is another important intermediate of the hydrogenation of 2-naphthol, although it was found always in lesser amounts than *ar*-2-tetralol. In Table 5 is presented the composition of the products obtained at complete hydrogenation of *ac*-2-tetralol. Isomerization of *ac*-2-

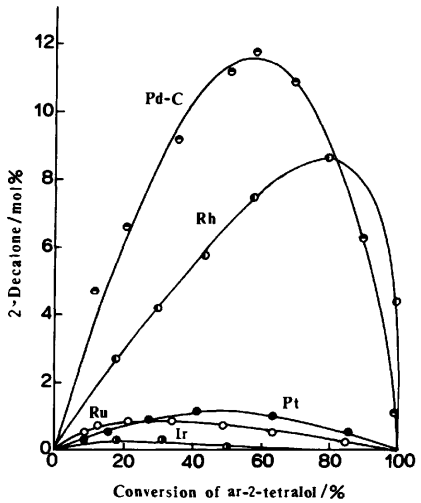

Fig. 2. Hydrogenation of *ar*-2-tetralol: formation of 2-decalone. The circles show a set of experiments with varying conversions of *ar*-2-tetralol. The full lines show the theoretical curves given by Eq. 1. For the values of f, see Table 3. The values of K are 7.2 for Ru, 0.37 for Rh, 1.33 for Pd-C, and 2.0 for Pt.

Table 3. Hydrogenation of *ar*-2-tetralol: amounts of 2-decalones as desorbed intermediates

Catalyst	2-Decalone/mol%	
	Trans	*Cis*
Ru	0.0	8.9
Rh	0.0	15.6
Pd-C	13.3	23.8
Os	0.0	0.0
Ir	0.0	3.5
Pt	0.0	4.4

Table 4. Hydrogenation of 2-decalones[a)]

Catalyst	2-Decalone	Product composition/mol%		
		c-DN	*c,t*-DL	*c,c*-DL
Ru	Cis	0.0	38.0	62.0
Rh	Cis	0.6	50.2	49.2
Pd-C	Cis	0.0	15.1	84.9
Os	Cis	0.1	33.8	66.1
Ir	Cis	0.1	39.9	60.0
Pt	Cis	4.1	22.2	73.7
		t-DN	*t,t*-DL	*t,c*-DL
Pd-C	Trans	0.0	19.8	80.2

a) 2-Decalone (630 mg) was hydrogenated in *t*-BuOH (16 ml) under the same conditions as for *ar*-2-tetralol (see Table 2).

Table 5. Hydrogenation of *ac*-2-tetralol: the composition of products at complete hydrogenation[a)]

Catalyst	Amount	Reac. time	Product composition/mol%[b)]					
	mg	h	*t*-DN	*c*-DN	*t,t*-DL	*t,c*-DL	*c,t*-DL	*c,c*-DL
Ru	6	2	0.1	0.4	2.7	9.2	34.9	52.7
Rh	4	2	0.3	1.3	3.1	9.5	28.1	57.7
Pd-C	400	24	0.8	0.8	18.0	30.2	22.3	27.9
Os	20	2	0.2	5.1	0.9	3.8	26.6	63.4
Ir	10	2	0.1	3.1	0.7	4.0	28.0	64.1
Pt	20	3	1.6	5.6	1.9	10.3	22.7	57.9

a) *ac*-2-Tetralol (617 mg) was hydrogenated in *t*-BuOH (16 ml) at 80 °C and 4—5 MPa H_2 pressure. b) For the notations of compounds, see footnote b) in Table 2.

Table 6. Hydrogenation of 2-naphthol to decalins and decalols[a)]

Catalyst	Amount	Reac. time	Product composition/mol%[b)]					
	mg	h	*t*-DN	*c*-DN	*t,t*-DL	*t,c*-DL	*c,t*-DL	*c,c*-DL
Ru	6	2	0.2	1.9	0.6	1.7	26.1	69.5
Rh	4	2	0.5	2.7	1.0	3.4	21.6	70.8
Pd-C	400	24	0.1	0.1	9.9	24.3	12.8	52.8
Os	20	4	1.0	34.0	0.2	0.8	11.0	53.0
Ir	10	2	1.2	31.8	0.2	1.0	12.0	53.8
Pt	20	3	8.3	28.6	2.1	2.3	14.2	44.5

a) 2-Naphthol (600 mg) was hydrogenated in *t*-BuOH (16 ml) at 80 °C and 4—5 MPa H_2 pressure. b) For the notations of compounds, see footnote b) in Table 2.

tetralol to *ar*-2-tetralol during hydrogenation was not found under the present conditions, although such an isomerization was observed by Weitkamp in the hydrogenation of methyltetrahydronaphthalenes.[3]

Hydrogenation of 2-Naphthol to Decalins and 2-Decalols. Table 6 summarizes the composition of the products obtained when 2-naphthol was hydrogenated completely to give decalins and 2-decalols.

Discussion

The Selectivity for Formation of ar- *and* ac-*2-Tetralols.* 2-Naphthol may be hydrogenated by way of either *ar*- or *ac*-2-tetralol as the intermediate leading to decalins and 2-decalols. The results in Table 1, however, indicate that, except over palladium, some 10—15% of 2-naphthol is hydrogenated apparently not through the tetralols and gives directly decalins and 2-decalols. Hydrogenation with palladium is an exception in that all naphthol is hydrogenated *via* either *ar*- or *ac*-2-naphthol and no other hydrogenation pathway was found on this metal. On the basis of the amounts of *ar*- and *ac*-2-tetralols determined, the selectivity ratios for hydrogenation of the unsubstituted ring (the benzene ring) to the substituted ring (the phenol ring) are shown in Table 7. The corresponding results on 2-methylnaphthalene obtained by Weitkamp[3] are also listed in the table for comparison. It is seen that the preferential hydrogenation of the unsubstituted ring is a common trend for both the compounds over all the catalysts. However, this trend is more pronounced in the hydrogenation of 2-naphthol than in 2-methylnaphthalene. Since the steric effect of the substituent against adsorption to catalyst is considered to be greater for the methyl group than for the hydroxyl group,[25] it would be difficult to explain the results by the steric effect of the substituent alone. Another explanation for the relative unreactivity of the phenol ring might be a great energy of resonance stabilization in the phenol ring that is estimated to be 22 kJ mol^{-1} greater than that in the benzene ring. A loss of the energy accompanying the activated adsorption would cause a difficulty in hydrogenation and this effect is considered to be greater in the phenol ring with a greater resonance energy.[2a] It is of interest that, in line with the results on methylnaphthalenes, the selectivity ratio is the smallest with palladium. As suggested by Weitkamp,[3] over palladium the product-controlling step may be different from those on the other metals, just as in the palladium-catalyzed hydrogenation of cycloolefins, where Siegel has proposed such a difference in product-controlling step between palladium and platinum.[27] The fact that with palladium no pathway other than the hydrogenations through the two tetralols was found indicates that an adsorption-desorption equilibrium has been established during hydrogenation with respect to 2-naphthol and the intermediate tetralols and gives a support for the suggestion made above. Such a complete establishment of adsorption-desorption equilibrium has also been observed in the palladium-catalyzed hydrogenation of isomeric cresols where the formation of methylcyclohexanones as intermediates has been shown to be quantitative.[28]

Table 7. Selectivity ratio for hydrogenation of the unsubstituted ring to the substituted ring

Catalyst	2-Naphthol	Catalyst	2-Methyl-naphthalene[a]
Ru	7.0	0.6% $Ru-Al_2O_3$	4.0
Rh	8.5	0.6% $Rh-Al_2O_3$	3.7
Pd-C	3.2	0.6% $Pd-Al_2O_3$	1.3
Os	9.3	5% Pd-C	3.0
Ir	9.8		
Pt	13.3		

a) Data based on the results in Fig. 11 by A. W. Weitkamp, *Adv. Catal.*, **18**, 1 (1968). 2-Methylnaphthalene was hydrogenated at 100 °C and *ca.* 7 MPa H_2 pressure.

The Rates of Hydrogenation of 2-Naphthol and 2-Tetralols. The relative rates of hydrogenation of *ar*- or *ac*-2-tetralol to 2-naphthol are given by the values of K in Eq. 1. The values were evaluated on the basis of the results shown in Fig. 1 and are summarized in Table 8. The rate constants in individual hydrogenation for 2-naphthol and *ar*-2-tetralol (k_{NL} and $k_{ar\text{-}TL}$) are also shown in Table 8. By assuming the relationship: K (*ar*-TL/NL)=($k_{ar\text{-}TL}/k_{NL}$)($b_{ar\text{-}TL}/b_{NL}$),[23] where K (*ar*-TL/NL) represents the relative reactivity of *ar*-2-tetralol to 2-naphthol and $b_{ar\text{-}TL}$ and b_{NL} are the adsorption coefficients for *ar*-2-tetralol and 2-naphthol, we can evaluate the relative ratio of the adsorption coefficients for *ar*-2-tetralol and 2-naphthol. These are also given in Table 8. The results in Table 8 clearly show that the low reactivities of *ar*-2-tetralol in the

Table 8. Rate data for the hydrogenation of 2-naphthol and 2-tetralols[a]

Catalyst	K(*ac*-TL/NL)	K(*ar*-TL/NL)	$10^3 k_{NL}$	$10^3 k_{ar\text{-}TL}$	$\frac{k_{ar\text{-}TL}}{k_{NL}}$	$\frac{b_{ar\text{-}TL}}{b_{NL}}$
			mol min^{-1} g $metal^{-1}$			
Ru	0.050	0.046	19.9	6.51	0.33	0.14
Rh	0.305	0.205	22.4	20.5	0.92	0.22
Pd-C	0	0.01	9.98	0.562	0.056	0.18
Os	0.33	0.074	4.32	2.50	0.58	0.13
Ir	0.12	0.046	9.65	6.31	0.65	0.07
Pt	0.24	0.16	3.66	2.88	0.79	0.20

a) K is the relative reactivity of *ac*- or *ar*-2-tetralol to 2-naphthol (see Eq. 1); k is a rate constant in individual hydrogenation; b represents the adsorption coefficient for 2-naphthol or *ar*-2-tetralol.

presence of 2-naphthol, as expressed by the small values of K (*ar*-TL/NL), result from a strong adsorption of 2-naphthol over *ar*-2-tetralol. Although the values of K for *ac*-2-tetralol are larger than those for *ar*-2-tetralol except over palladium, the situation would be similar for *ac*-2-tetralol as well. Hydrogenation with palladium is noteworthy in that the values of K are extremely small for both *ar*- and *ac*-2-tetralols, and in contrast to the other metals, the value of $k_{ar\text{-TL}}/k_{\text{NL}}$ is also very small (0.056). Thus it is concluded that in the palladium-catalyzed hydrogenation of 2-naphthol the difference in the rates between 2-naphthol and *ar*-2-tetralol plays a more important role than the difference in the strengths of adsorption for the selective formation of *ar*-2-tetralol. It will be possible that this situation affects the product controlling step over palladium to be different from those on the other metals, as suggested in the preceding discussion. On the other hand, with rhodium catalyst the rate constants in individual hydrogenation are almost of the same magnitude for 2-naphthol and *ar*-2-tetralol and the selectivity is mostly controlled by a difference in strength of adsorption between the two compounds.

The Ketones as Intermediates. It is well documented that cyclohexanones are formed as intermediates in the hydrogenation of phenols.[2] With Raney nickel[29] and palladium[28] the formation of the ketone intermediates has been shown to be quantitative in hydrogenation of phenol and cresols, respectively. With ruthenium and rhodium some 50—70% of methylcyclohexanones are formed in hydrogenation of cresols, while the detectable amounts of the ketones are very small over the 3rd row platinum metals (Os, Ir, Pt).[28,30] In the hydrogenation of 2-naphthol, the formation of 2-tetralone was observed over palladium to the extent of 8.5% as an intermediate to *ac*-2-tetralol (see Table 1). However, the ketone was not formed in detectable amounts over the other metals. It will be possible that the ketone is also formed over the metals other than palladium, but is hydrogenated without leaving the catalysts, because it is presumed that the benzene ring in 2-tetralone may contribute to a strong adsorption and/or a high reactivity of the ketone. On the other hand, the formation of 2-decalone was observed over the metals except osmium with *ar*-2-tetralol (Fig. 2). It should be noted that, except with palladium, the 2-decalone found was the cis isomer only (see Table 3). It seems that this is related to the high stereoselectivities of ruthenium and rhodium for formation of the cis products at the ring juncture, as will be discussed later. In general, the amounts of 2-decalone given in Table 3 are considerably smaller than those of methylcyclohexanones reported in the hydrogenation of cresols.[28,30] Probably the use of *t*-butyl alcohol as solvent has decreased the detectable amounts of 2-decalone since hydrogenation of *m*-cresol in *t*-butyl alcohol has also decreased the amounts of 3-methylcyclohexanone formed during hydrogenation, compared to the hydrogenation without solvent.[31]

Hydrogenolysis. The proportion of hydrogenolysis obtained in hydrogenation of 2-naphthol and *ac*- and *ar*-2-tetralols is summarized in Table 9. It is clearly seen from the results in Table 9 that the hydrogenolysis occurs far more extensively over the 3rd row platinum metals (Os, Ir, Pt) than over the 2nd row metals (Ru, Rh, Pd). This characteristics is much pronounced in the hydrogenation of *ar*-2-tetralol and 2-naphthol. A similar trend of the platinum metals have also been observed in the hydrogenation of cresols.[30] The degree of the hydrogenolysis, however, is much higher with 2-naphthol and *ar*-2-tetralol than with cresols. Such an extensive hydrogenolysis in a phenol ring has also been reported in the hydrogenation of 2,5-dimethylphenol with an iridium catalyst.[32] Hydrogenolysis occurs to much lesser extents with *ac*-2-tetralol which is a homobenzyl-type alcohol. The proportion of hydrogenolysis which occurs in the pathway not *via ac*- and *ar*-2-tetralols is unusually high with ruthenium and rhodium, compared to the results with *ar*-2-tetralol and 2-naphthol. It is presumed that unsaturated alcohols, rather than unsaturated ketones, are concerned as intermediates with the high degree of hydrogenolysis in the pathway leading to direct formation of decalins and 2-decalols. This consideration comes from the fact that hydrogenation of *ar*-2-tetralol gives only slight hydrogenolysis with ruthenium and rhodium, where formation of the intermediates leading to 2-decalone may be significant and the hydrogenation through this pathway may be accompanied by little hydrogenolysis.

Table 9. Proportion of hydrogenolysis in the hydrogenation of 2-naphthol and *ac*- and *ar*-2-tetralols

Catalyst	Proportion of hydrogenolysis/mol%				
	ac-TL	*ar*-TL	Pathway not via *ac*- and *ar*-TL	NL	
				Calcd	Obsd
Ru	0.5	0.6	10.3	1.7	2.1
Rh	1.6	1.1	9.8	2.2	2.1
Pd-C	1.6	0.2	—	0.5	0.2
Os	5.3	28.5	27.6	26.6	35.0
Ir	3.2	36.0	35.5	33.6	33.0
Pt	7.2	41.6	46.4	40.5	36.9

From the amounts of hydrogenolysis for *ar*- and *ac*-2-tetralols, and for the pathway not *via* the tetralols, together with the selectivities for the respective pathways, we can calculate the amounts of hydrogenolysis that would occur in the hydrogenation of 2-naphthol. In Table 9 the amounts of hydrogenolysis thus calculated are compared with those obtained in the complete hydrogenation of 2-naphthol (see Table 6). It is seen that agreements between the calculated and observed values are generally satisfactory. With osmium, however, a considerably greater amount of hydrogenolysis was obtained with 2-naphthol, although the reason for that is not certain.

Possible intermediates that may lead to the extensive hydrogenolysis over the 3rd row metals are not clear from the knowledge now available. Both allyl- and enol-type intermediates must be taken into consideration. It seems that the extensive hydrogenolysis is difficult to explain by the allyl-type intermediates alone, because, as presumed from the results on an allyl alcohol

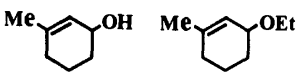

2 3

2 and its ethyl ether **3**,[1,30,33] allyl-type compounds are hydrogenolyzed not so extensively over the 3rd row metals as to be able to explain the present results. Rather, the high degree of hydrogenolysis over the 3rd row metals is a characteristics of an enol-type compounds towards hydrogenolysis as has been shown previously.[1,21] If this is the case, the intermediates leading to the extensive hydrogenolysis are presumed to be the adsorbed enols that are hydrogenated without being isomerized to the corresponding ketones, because 2-decalone, and possibly its precursors as well, should be hydrogenated with only slight hydrogenolysis even over the 3rd row metals, as shown in Table 4. The metals of low olefin isomerization activity such as the 3rd row metals may have a strong affinity for the olefinic bonds of the adsorbed enols and thus may activate the carbon–oxygen bond to be susceptible to hydrogenolysis, as has been discussed previously.[1,21]

The hydrogenolysis to give tetralin has also been observed at initial stages of the hydrogenation of 2-naphthol and *ar*-2-tetralol. The tetralin formation amounted to 7.2% with platinum in the hydrogenation of *ar*-2-tetralol. With the other metals, however, the amounts of tetralin detected were small and the route through tetralin will not be significant for the formation of decalins. The hydrogenolysis leading to tetralin is considered to occur through the half-hydrogenated states derived from *ar*-2-tetralol (an unsaturated enol), as shown in Scheme 2. This type of hydrogenolysis has previously been observed in the hydrogenation of *p*-ethoxytoluene in ethanol where toluene was formed to an extent of 8% over platinum.[33]

The Stereochemistry of Hydrogenation. In Table 10 are compared the amounts of the cis products at the ring juncture from hydrogenation of 2-naphthol and *ac*-and *ar*-2-tetralols. It is seen that, except with palladium and platinum, the selectivities for the cis products are very high for 2-naphthol and *ar*-2-tetralol. With *ac*-2-tetralol the selectivities decrease with ruthenium and rhodium to 88.0 and 87.1%, respectively. The high stereoselectivities of osmium and iridium are in accord with the results previously obtained with *o*-xylene and 1,2-dimethylcyclohexene.[34] However, the high stereoselectivities of ruthenium and rhodium as observed with 2-naphthol and *ar*-2-tetralol appear rather unusual, compared to the results on *ac*-2-tetralol as well as *o*-xylene and 1,2-dimethylcyclohexene.[2c] The unusually high selectivities of ruthenium and rhodium are probably related to the stereoselective formation of *cis*-2-decalone on the catalyst surface, because, as presumed from the results on cresols that the ketones are formed in the amounts of 50—70%, the hydrogenation through a ketone may be a significant pathway in hydrogenation of phenolic compounds over ruthenium and rhodium, although estimated amounts of 2-decalone were not so great (Table 3). The tendency of palladium to produce the trans products is in agreement with the results reported on aromatic hydrocarbons and related cycloolefins.[2c,3,27] A considerable amount of the trans isomer was also found in the 2-decalones formed from *ar*-2-tetralol over palladium. These results support the suggestion that the product controlling step over palladium differs from those on the other metals.

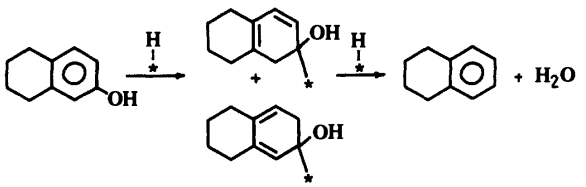

Scheme 2. Hydrogenolysis of *ar*-2-tetralol leading to the formation of tetralin.

TABLE 10. SELECTIVITY FOR THE CIS PRODUCTS AT RING JUNCTURE IN HYDROGENATION OF 2-NAPHTHOL AND *ac*- AND *ar*-2-TETRALOLS

Catalyst	Cis products/mol%		
	2-NL	*ac*-TL	*ar*-TL
Ru	97.5	88.0	98.9
Rh	95.1	87.1	96.1
Pd-C	65.7	51.0	68.6
Os	98.0	95.1	98.5
Ir	97.6	95.2	97.8
Pt	87.3	86.2	87.2

Table 11 shows the selectivities for formation of *cis*-2-decalols (cis,cis and cis,trans isomers) and *cis,cis*-2-decalol in the decalol mixture. It is seen that the high selectivities for *cis*-2-decalols from 2-naphthol and *ar*-2-tetralol considerably decrease for *cis,cis*-2-decalol. The decrease is particularly pronounced in the case of ruthenium (from 99.0% to 70.6% with *ar*-2-tetralol). These results suggest that a stepwise hydrogenation is occurring in the course to saturated products even over those metals that give high yields of the cis products at the ring juncture. It is noted that the yields of *cis*-2-decalols and *cis,cis*-2-decalol in hydrogenation of 2-naphthol and *ar*-2-tetralol are much higher with ruthenium (95.6 and 69.5% for 2-naphthol; 98.4 and 70.2% for *ar*-2-tetralol) and with rhodium (92.4 and 70.8% for 2-naphthol; 95.1 and 77.7% for *ar*-2-tetralol)

TABLE 11. STEREOCHEMISTRY OF THE FORMATION OF 2-DECALOLS IN HYDROGENATION OF 2-NAPHTHOL AND *ac*- AND *ar*-2-TETRALOLS

Catalyst	Cis isomers[a] and cis,cis isomer in 2-decalols /mol%					
	NL		*ac*-TL		*ar*-TL	
Ru	97.7	71.0	88.0	53.0	99.0	70.6
Rh	95.5	73.1	87.2	58.6	96.2	78.6
Pd-C	65.7	52.9	51.0	28.4	68.7	58.1
Os	98.5	81.5	95.0	66.9	98.9	82.1
Ir	98.2	80.3	95.1	66.2	98.6	82.3
Pt	93.0	70.5	86.9	62.4	95.0	74.0

a) *cis,cis*- and *cis,trans*-2-Decalols.

than with the 3rd row metals because of the occurrence of extensive hydrogenolysis with the latter metals. In accord with the results in the literature,[4,11,12] the highest yield of the cis,cis isomer was obtained in the hydrogenation of *ar*-2-tetralol with rhodium catalyst. The yield further increased to 85.4% in the hydrogenation at 30 °C and 10 MPa of hydrogen pressure. The selectivities for the cis,cis isomer is generally much lower with *ac*-2-tetralol, as would be expected, because *ac*-2-tetralol can be adsorbed to the catalyst to afford the cis,trans isomer as equally as to give the cis,cis isomer. It is noteworthy that in the hydrogenation of *ar*-tetralol the proportion of *cis,cis*-2-decalol in *cis*-2-decalols is the greatest with palladium (84.6%) and the value is very close to that obtained in the hydrogenation of *cis*-2-decalone (84.9%) (see Table 4). This is in line with the findings that the hydrogenation through a ketone may be the exclusive pathway in the palladium-catalyzed hydrogenation of phenols.[28] The reason for the high stereoselectivity of palladium in the formation of the cis,cis isomer from *cis*-2-decalone is not certain. Since the conformation of *cis*-2-decalone is accepted not to be fixed, the stereochemistry of hydrogenation of *cis*-2-decalone would be not simply interpreted, as discussed by Hückel and coworkers.[35]

References

1) Part XVI: S. Nishimura, K. Kagawa, and N. Sato, *Bull. Chem. Soc. Jpn.*, **51**, 3330 (1978).

2) For reviews, see a) H. A. Smith, "Catalysis," ed by P. H. Emmett, Vol. V, Reinhold Publishing Corp., New York (1957), p. 175; b) P. N. Rylander, "Catalytic Hydrogenation over Platinum Metals," Academic Press Inc., New York (1967); c) S. Nishimura, *J. Soc. Syn. Org. Chem. Jpn.*, **30**, 36 (1972).

3) A. W. Weitkamp, *Adv. Catal.*, **18**, 1 (1968).

4) A. I. Meyers, W. Beverung, and G. Garcia-Munoz, *J. Org. Chem.*, **29**, 3427 (1964).

5) B. C. McKusick, *J. Am. Chem. Soc.*, **70**, 2196 (1948).

6) G. Richter and G. R. Vegyezeti, Belg. Patent 826145 (1975).

7) a) G. Stork, *J. Am. Chem. Soc.*, **69**, 576 (1947); b) M. Kajitani, Y. Watanabe, Y. Iimura, and A. Sugimori, *Bull. Chem. Soc. Jpn.*, **48**, 2848 (1975) and references cited therein.

8) W. Hückel, R. Danneel, A. Gross, and H. Naab, *Justus Liebigs Ann. Chem.*, **502**, 99 (1933).

9) W. G. Dauben, E. Hoerger, and N. K. Freeman, *J. Am. Chem. Soc.*, **74**, 5206 (1952).

10) W. G. Dauben, R. C. Tweit, and C. Mannerskantz, *J. Am. Chem. Soc.*, **76**, 4420 (1954).

11) M. Freifelder and G. R. Stone, *J. Pharm. Sci.*, **53**, 1134 (1964).

12) S. Nishimura and H. Taguchi, *Bull. Chem. Soc. Jpn.*, **36**, 353 (1963).

13) A. C. Cope, R. J. Cotter, and G. G. Roller, *J. Am. Chem. Soc.*, **77**, 3594 (1955).

14) O. R. Rodig and L. C. Ellis, *J. Org. Chem.*, **26**, 2197 (1961).

15) L. J. Baskeyfield, J. D. Bell, J. Townend, and S. D. A. Pollock, U. S. Patent 4182916 (1980).

16) "Merck Index," 9th ed., ed by M. Windholz, Merck & Co., New Jersey (1967), p.830

17) G. Schroeter, Savonoe, H. Einbeck, H. Geller, and E. Riebensahn, *Justus Liebigs Ann. Chem.*, **426**, 120 (1922).

18) W. J. Svirbely, W. M. Eareckson, III, K. Matsuda, H. Pickard, I. S. Solet, and W. B. Tuemmler, *J. Am. Chem. Soc.*, **71**, 507 (1949).

19) E. E. Tamelen and W. C. Proost, *J. Am. Chem. Soc.*, **76**, 3632 (1954).

20) M. D. Soffer, M. P. Bellis, H. E. Gellerson, and R. A. Stewart, *Org. Syn.* Coll. Vol. 4, 903 (1963).

21) S. Nishimura, M. Katagiri, T. Watanabe, and M. Uramoto, *Bull. Chem. Soc. Jpn.*, **44**, 166 (1971).

22) S. Nishimura, M. Ishige, and M. Shiota, *Chem. Lett.*, **1977**, 535.

23) J. H. de Boer and R. J. A. M. Van der Borg, Actes Congr. Intern. Catal., 2e, Paris (1960), p. 919 (Editions Technip, Paris, 1961). See also S. Nishimura, M. Uramoto, and T. Watanabe, *Bull. Chem. Soc. Jpn.*, **45**, 216 (1972).

24) With other metals, hydrogenation to *cis*- and *trans*-2-decalones occurs simultaneously with the formation of *ac*-2-tetralol (S. Nishimura and S. Matsuzaki, unpublished observation).

25) J. Hine, "Structure Effects on Equilibria in Organic Chemistry," John Wiley & Sons, Inc., New York (1975), p. 103.

26) The standard enthalpy difference between phenol and cyclohexanol is 22.1 kJ mol^{-1} smaller than that between benzene and cyclohexane ("Kagaku Benran," Ed. Chem. Soc. Jpn., Vol. II, 2nd rev. ed., Maruzen, Tokyo (1975), p. 953).

27) S. Siegel, *Adv. Catal.*, **16**, 123 (1966).

28) Y. Takagi, S. Nishimura, and K. Hirota, *Bull. Chem. Soc. Jpn.*, **43**, 1846 (1970).

29) F. Coussemant and J. C. Jungers, *Bull. Soc. Chim. Belg.*, **59**, 295 (1950).

30) Y. Takagi, *Sci. Papers Ins. Phys. Chem. Res. (Tokyo)*, **64**, 39 (1970).

31) S. Nishimura and Shin-ichi Ohbuchi, unpublished observation.

32) P. N. Rylander and D. R. Steele, *Engelhard Ind. Tech. Bull.*, **6**, 41 (1965).

33) S. Nishimura, M. Uramoto, and T. Watanabe, *Bull. Chem. Soc. Jpn.*, **45**, 216 (1972).

34) S. Nishimura, F. Mochizuki, and K. Kobayakawa, *Bull. Chem Soc Jpn.*, **43**, 1919 (1970).

35) W. Hückel, M. Maier, E. Jordan, and W. Seeger, *Justus Liebigs Ann. Chem.*, **616**, 46 (1958).

 © 1984 The Chemical Society of Japan Bull. Chem. Soc. Jpn., 57, 2565—2568 (1984)

The Viscosity Coefficients of 18-Crown-6–Alkali Metal-ion Complexes

Fumio KAWAIZUMI,* Isao YAJIMA, Hiroyasu NOMURA, and Yutaka MIYAHARA
Department of Chemical Engineering, School of Engineering, Nagoya University, Chikusa-ku, Nagoya 464
(Received August 22, 1983)

The viscosities of LiCl, KCl, and CsCl have been measured in water and aqueous solutions containing 0.398 mol/dm^3 of 18-crown-6 (CR) at 25 °C. The *B*-coefficients of the alkali metal chlorides in water have been obtained using the theoretical values of the *A*-coefficients. The viscosity coefficients of 18-crown-6 itself have been determined in water and methanol. In systems containing crown ether, the viscosity increment due to the complex formed in solutions, $\Delta\eta_{[CR\text{-}M^+]Cl^-}$, has been evaluated by subtracting from the observed viscosity the increment attributed to non-coordinated crown ether and alkali metal chlorides in solutions. The two complex ions, [CR-K$^+$] and [CR-Cs$^+$], have nearly the same values of the *B*-coefficients, and these values are, in turn, approximately equal to that of 18-crown-6 in water. Measurements done on KCl in methanol containing 18-crown-6 have led to the finding that in methanol, 18-cown-6 and the [CR-K$^+$] ion take effectively the same *B*-value.

Macrocyclic polyether, crown ether, is known to form stable complexes with alkali or alkaline earth metal ions. The complex formation is characterized by the selectivity of certain crown ethers towards specific cations. A number of investigators[1–9] have endeavored to clarify the origin of the specificity observed in the interactions between crown ethers and metal ions in solutions. The metal ion is trapped in the central cavity of the crown ether by ion-dipole forces, and the ratio of the ionic radius of the cation to the dimension of the crown-ether cavity seems to be the most important factor governing the specificity of the complex formation, though an exception to the correlation of the cationic size with the hole size of crown ethers has been reported very recently.[8]

The effective volumes can presumably be expected to be different for the crown ether-cation complex and non-coordinated crown ether. When solute species flow in viscous media, the volume of solutes should affect the dragging resistance forces. Further, in spite of being a macroscopically measurable quantity, the viscosity of solutions has been found to give information on molecular interactions in solutions.

The purpose of this study is to determine the concentration dependence of the viscosity of solutions of three kinds of alkali chlorides (LiCl, KCl, and CsCl) in aqueous solutions containing 18-crown-6, and then to assess the contributions attributed to the crown ether-alkali metal-ion complexes. 18-Crown-6 has a very high solubility in water, which is an important factor in carrying out any viscometric study. The complex formation of an alkali metal ion with 18-crown-6 has been well confirmed for K$^+$ and Cs$^+$ ions in water, but this is not the case for Li$^+$. Therefore, as will be described in a later section, our experimental results for LiCl will be discussed from a standpoint different from that used for KCl and/or CsCl.

In order to compare the solvent effects, measurements have also been done for KCl in methanol and that containing 18-crown-6.

Experimental

Specimens and Solvents. The 18-crown-6 (abbreviated hereafter as CR) was purchased from the Nakarai Chemicals Co., Ltd. It was purified in a manner similar to the procedure proposed by Gokel and Cram;[10] about 50 g of CR were placed in an Erlenmeyer flask, into which 250 cm^3 of acetonitrile were then poured. The slurry was stirred and heated in a water bath held at 70 °C. A glass tube containing a drying agent was attached to the flask to prevent the penetration of humidity. The solution was then filtered. This process was repeated three times. After being stirred vigorously, the solution was allowed to cool to the ambient temperature. After the deposition of a fine white precipitate, the solution was kept in a refrigerator for 12 h. The precipitate was then collected by filtration. From the precipitate (CR-acetonitrile complex), acetonitrile was eliminated by heating at 35 °C under reduced pressure; then the product was kept in a vaccum for 48 h.

Guaranteed-grade chlorides were heated at 110—130 °C for more than 24 h; they were subsequently used without further purification.

Distilled and then deionized water was used as a solvent. The methanol was purified first by dehydrating it by means of a molecular sieve; then it was distilled by an ordinary procedure.

Apparatus and Measurements. In contrast to the case of the determination of the molecular weight of polymers, the use of an Ubbelohde viscometer of a conventional type is improper for the present purpose, since the degree of variation of the viscosity upon the addition of solutes with respect to the viscosity of pure solvent is relatively small. Therefore, an improved Ubbelohde viscometer with a sufficient efflux time at a low shear rate was designed and used. It has four successive bulbs, and the solution flows through a long capillary tube wound in a spiral form. The efflux times for water at 25 °C are 554, 887, and 1,377 s for the second, third, and fourth bulbs respectively. In addition, to determine the viscosity coefficient with a high degree of precision, measurements of the viscosity were carried out at approximately twenty different concentrations of salts in water as well as in aqueous solvents containing 18-crown-6 (the concentration of CR was 0.398 mol/dm^3), which have also served as solutions to determine the viscosity coefficients of non-coordinated 18-crown-6 in water. The concentration ranges of the salts investigated are much wider than in ordinary viscometric measurements.[11] On the other hand, in methanol, on account of the low solubility of KCl, experiments on KCl have been limited to concentrations far lower than in aqueous media (for KCl in methanol, up to *ca.* 0.03 mol/dm^3). The concentration of CR in methanol for KCl was 0.02085 mol/dm^3. Sample solutions were prepared by weight, and the concentrations of the solute were converted into volumetric concentration scales using the density data of solutions.

The densities were measured by means of a Digital Precision Density Meter, type DMA-02C, manufactured by the

Anton Paar Co., Ltd. The numerical values of density necessary were interpolated from the mathematical expression of the density-volumetric concentration relation obtained by the least-squares fitting of the experimental data.

All measurements were done at 25±0.05 °C.

Results and Discussion

Viscosity of LiCl, KCl, CsCl, and 18-Crown-6 in Water. The concentration dependence of the relative viscosity of dilute electrolyte solutions have been expressed in terms of the Jones-Dole equation:[12]

$$\eta_{rel} = 1 + Ac^{1/2} + Bc, \quad (1)$$

or:

$$\psi \equiv (\eta_{rel}-1)/c^{1/2} = A + Bc^{1/2}, \quad (2)$$

where c is the molarity. The B-coefficient has often been determined as a slope of the relation of Eq. 2 by plotting the data obtained in relatively dilute concentrations. However, our measurements, carried out up to rather high concentration ranges (for LiCl, to 0.65, and for KCl and CsCl, to 0.9—1 mol/dm^3), require a modified form of Eqs. 1 and 2:

$$\eta_{rel} = 1 + Ac^{1/2} + Bc + Dc^2, \quad (3)$$

or:

$$\psi = A + Bc^{1/2} + D(c^{1/2})^3. \quad (4)$$

The simultaneous determination of the parameters A, B, and D by means of simple least-squares fitting of the experimental data to the third-order equation of $c^{1/2}$ failed, for the analysis gave a negative value of A for the case of LiCl, a fact contradictory to the theory.[13,14] Therefore, the coefficients B and D have been determined in the following way: first, the A-coefficient was calculated according to the theory proposed by Falkenhagen.[13,14] Then, Eq. 4 was rearranged into the expression shown below:

$$(\eta_{rel}-1-Ac^{1/2})/c = B + Dc. \quad (5)$$

Using the calculated values of A-coefficients, the left-hand side of Eq. 5 was evaluated; meanwhile, the coefficients B and D have been obtained from the most suitable plot of the relation of Eq. 5. As an example, the case for CsCl is illustrated in Fig. 1. The unmerical values of the B- and D-coefficients thus obtained are summarized in Table 1, along with the values of the A-coefficient calculated and used. Our B-coefficients are in excellent agreement with the values given by Kaminsky[15] and Isono.[16] Differences exist, however, in the values of D. These differences seem to arise from the differences in the concentration ranges concerned in the measurements. Isono,[16] aiming to ascertain correlations between B- and D-coefficients, has carried out measurements in highly concentrated solutions (up to 3.5, 5.9, and 3.7 mol/dm^3 for KCl, CsCl, and LiCl respectively).

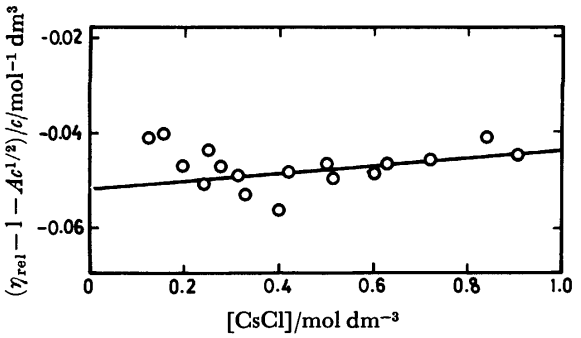

Fig. 1. Plot of $(\eta_{rel}-1-Ac^{1/2})/c$ against molar concentration c of CsCl in water at 25 °C.

The relative viscosities of aqueous solutions of 18-crown-6 measured in the concentrations less than 0.4 mol/dm^3 can be represented in terms of an equation similar to Eq. 3:

$$\eta_{rel} = 1 + B'c + D'c^2, \quad (6)$$

where the term corresponding to $Ac^{1/2}$ in Eq. 3 is dropped, for this term refers to interionic interaction and is unnecessary for non-electrolytic solute. The plot of $(\eta_{rel}-1)/c$ against c has led to the following values of the B'- and D'-coefficients:

$$B' = 0.846 \text{ dm}^3/\text{mol} \text{ and } D' = 0.559 \text{ (dm}^3/\text{mol)}^2.$$

Below, this B' value will be compared with the corresponding values of the [CR-M$^+$] ions.

Viscosity of LiCl, KCl, and CsCl in Aqueous Solutions Containing 18-Crown-6. The effects of an added solute on the relative viscosity should be expressed as:

$$\eta_{rel} = 1 + \Delta\eta_{solute}, \quad (7)$$

where $\Delta\eta_{solute}$ refers to the resultant variation in the relative viscosity of the solution due to the added solute. Aqueous solutions containing both 18-crown-6 and an electrolyte were prepared by introducing the electrolyte into the aqueous solutions containing 18-crown-6. First, the following relation has been considered as a starting equation for the data analysis:

$$\eta_{rel} = (1+\Delta\eta_{CR}) + \Delta\eta_{electrolyte}. \quad (8)$$

Mention should be made of the fact that the η_{rel} of the above equation is not related to the viscosity of the aqueous solutions containing 18-crown-6 to which the electrolyte is added, but to the viscosity of pure water.

Table 1. Viscosity coefficients of extended Jones-Dole equation for LiCl, KCl, and CsCl in water at 25 °C

	A[a]	B			D	
	[dm^3/mol]$^{1/2}$	[dm^3/mol]			[dm^3/mol]^2	
LiCl	0.0065	0.137	0.1425[b]	0.134[c]	0.0065	0.013[c]
KCl	0.0050	−0.0137	−0.0140[b]	−0.015[c]	0.0033	0.008[c]
CsCl	0.0049	−0.0517	−0.052[b]	−0.060[c]	0.0077	0.013[c]

a) Values calculated from theory. b) Values reported by M. Kaminsky.[15] c) Values reported by T. Isono.[16]

Equation 8 is equivalent to the assumption of a superposition of effects due to the crown ether and the electrolyte; in other words, there are no interactions between 18-crown-6 and electrolytic solutes in solutions. In actuality, however, such a crude assumption does not hold, and an attempt to represent experimental results in terms of Eq. 8 was unsuccessful for any kind of chloride investigated.

For KCl and CsCl, a complex formation with 18-crown-6 occurs.[1] We, therefore, have transformed Eq. (8) into the following form and analyzed the data related with KCl and CsCl:

$$\eta_{rel} = 1 + \Delta\eta_{CR} + \Delta\eta_{MCl} + \Delta\eta_{[CR-M^+]Cl^-}, \quad (9)$$

where $\Delta\eta_{[CR\cdot M^+]Cl^-}$ represents the variation in the solution viscosity due to the chloride of the crown ether-cation complex, $[CR\text{-}M^+]Cl^-$, formed in the solutions. Furthermore, considering the complex $[CR\text{-}M^+]Cl^-$ as an ordinary salt, we impose the following relation on $\Delta\eta_{[CR\cdot M^+]Cl^-}$:

$$\Delta\eta_{[CR\cdot M^+]Cl^-} = A(c_{[CR\cdot M^+]Cl^-})^{1/2} + Bc_{[CR\cdot M^+]Cl^-} \quad (10)$$

The actual contributions of $\Delta\eta_{CR}$, $\Delta\eta_{MCl}$, and $\Delta\eta_{[CR\cdot M^+]Cl^-}$ are dependent upon the amounts of the respective species present in the solutions. From the experimental concentrations and the stability constants, K, of the complex ions $[CR\text{-}M^+]$, the equilibrium concentrations of each solute species, $[M^+]$, $[CR]$, and $[CR\text{-}M^+]$, can be calculated. The stability constants of 18-crown-6-alkali metal ion complexes have been reported by Frensdorff[17] and by Izatt *et al.*[18] The values given by these authors are similar for the complex ion $[CR\text{-}K^+]$ ($\log K$=2.06[17] and 2.03[18]), while a certain difference exists for $[CR\text{-}Cs^+]$ ($\log K$=0.8[17] and 0.99[18]). We have used Frensdorff's values, which are concentration-equilibrium constants. After subtracting the amounts attributed to $\Delta\eta_{CR}$ and $\Delta\eta_{MCl}$, the resultant $\Delta\eta_{[CR\cdot M^+]Cl^-}$ has been found to be expressed in the form of the equation:

$$\frac{\Delta\eta_{[CR\cdot M^+]Cl^-}}{(c_{[CR\cdot M^+]Cl^-})^{1/2}} = A_{[CR\cdot M^+]Cl^-} + B_{[CR\cdot M^+]Cl^-}(c_{[CR\cdot M^+]Cl^-})^{1/2} \quad (11)$$

The results of the analysis of the data of CsCl carried out in this way are shown in Fig. 2. The straight line in Fig. 2 seems to support our approach. The final results of the $A_{[CR\cdot M^+]Cl^-}$ and $B_{[CR\cdot M^+]Cl^-}$ coefficients obtained, respectively, as the intercept and the slope of the relation of Eq. 11, are given in Table 2, which also includes the value of the B-coefficient of 18-crown-6.

As was mentioned in the last part of the introductory section of this paper, the stability constant of the complex ion $[CR\text{-}Li^+]$ has not been reported. Consequently, the analysis of our viscosity data for LiCl along the lines adopted for KCl and CsCl, namely, the analysis of the data using Eqs. 9 to 11, is impossible at present. However, as we have seen in the foregoing discussion, the simple additivity relation, as expressed in terms of Eq. 8, was unsuccessful in reproducing the experimental data for LiCl.

For the comparison of the B-coefficient of $[CR\text{-}M^+]Cl^-$ with that of 18-crown-6, the contribution from the

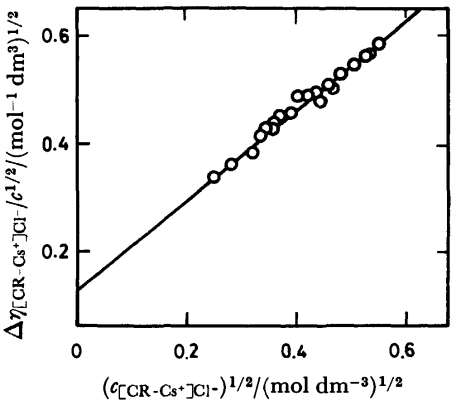

Fig. 2. Concentration dependence of $\Delta\eta_{[CR\text{-}Cs^+]Cl^-}/(c_{[CR\text{-}Cs^+]Cl^-})^{1/2}$ plotted against $(c_{[CR\text{-}Cs^+]Cl^-})^{1/2}$ for $[CR\text{-}Cs^+]Cl^-$ complex in water at 25 °C. The symbol c attached to the vertical axe means here $c_{[CR\text{-}Cs^+]Cl^-}$.

Table 2. Viscosity coefficients of 18-crown-6 and those assigned to 18-crown-6-alkali metal-ion complexes in aqueous solutions at 25 °C

	A $[dm^3/mol]^{1/2}$		B $[dm^3/mol]$
18-crown-6	—		0.846[b]
$[CR\text{-}K^+]Cl^-$	0.118	0.0082[a]	0.87
$[CR\text{-}Cs^+]Cl^-$	0.12		0.83

a) Theoretical value calculated using conductivity data reported in Ref. 9. b) B'-coefficient of Eq. 6.

Cl^- ion should be considered. Somewhat different values have been assigned to the values of the B-coefficient of the Cl^- ion on the basis of different criteria for the division: −0.007,[15] 0.014,[19] and −0.033.[20] In any case, the effect of the complex ion $[CR\text{-}M^+]$ is overwhelming. This fact enables us to compare the B values of Table 2. The complex ions $[CR\text{-}K^+]$ and $[CR\text{-}Cs^+]$ have similar values of the B-coefficients, and these values are near the B'-coefficient of the non-coordinated 18-crown-6 in water. Generally speaking, a direct comparison of the viscosity coefficient for an electrolyte with that for a nonelectrolyte is not free from disputation. This is because the concentration dependences of solution viscosities are expressed in different forms for electrolytes and nonelectrolytes. However, from the results given in Table 2, we can say that the dragging resistances of $[CR\text{-}K^+]$ and $[CR\text{-}Cs^+]$ complex ions are approximately the same as that of non-coordinated 18-crown-6 in water.

A theoretical evaluation of the A-coefficient is possible for the $[CR\text{-}K^+]Cl^-$ complex from the reported value of the limiting molar conductivity of the complex.[9] Our experimental A-coefficient of the $[CR\text{-}K^+]Cl^-$ complex is more larger than the theoretical one. A comparison of the experimental and theoretical A-coefficients for the $[CR\text{-}Cs^+]Cl^-$ complex is impossible because of the lack of conductivity data for this complex.

Viscosity Coefficients in Methanol Systems. As has already been mentioned in the Experimental section of this paper, viscosity measurements in methanol

Table 3. Viscosity coefficients of 18-crown-6, KCl, and [CR-K+]Cl complex in methanol at 25 °C

	A $[dm^3/mol]^{1/2}$	B $[dm^3/mol]$
18-crown-6	—	0.44[c]
KCl	0.024, 0.0173[a]	0.736, 0.7635[d]
$[CR\text{-}K^+]Cl^-$	0.039, 0.0208[b]	0.86

a) Theoretical value found in H. Falkenhagen, "Theorie der Electrolyte," S. Hirzel, Stuttgart (1971), Chap. 10. b) Theoretical value calculated using conductivity data reported by Y. Takeda.[9] c) B'-coefficient of Eq. 6. d) Value given by G. Jones and H. J. Fornwalt.[21]

systems have been carried out in relatively low concentration ranges. In such circumstances, the D- or D'-coefficient of Eq. 3 or Eq. 6 need not be taken into account. For KCl in methanol, the A- and B-coefficients have been determined simultaneously from the least-squares plotting of Eq. 2, without paying any attention to the theoretical values of A. On the contrary, the experimental data on 18-crown-6 in methanol and KCl in CR-methanol systems have been treated in a way analogous to that in the aqueous media described above. The numerical values of the viscosity coefficients in methanol systems obtained are shown in Table 3. Our B-coefficient for KCl in pure methanol is a little smaller than that in the literature,[21] while our experimental value of the A-coefficient is larger than the theoretical one. In our results, a small experimental B-coefficient is compensated for by a large experimental A-coefficient. The comparison of Tables 2 and 3 shows that the dragging resistance of 18-crown-6 is smaller in methanol than in water. For the discussion of B-coefficient of the complex ion $[CR\text{-}M^+]$, the contribution from the Cl^- ion, B_{Cl^-}, should be subtracted. The principle of the assignment of the B-coefficient of a salt into its constituent ionic B values has not been well established for the data in nonaqueous solvents. Criss and Mastroianni[22] evaluated the ionic B-coefficients in methanol on the assumption that $B_{K^+}=B_{Cl^-}$, as in water.[15] Following their results, we can obtain 0.48~0.49 dm^3/mol as the value of $B_{[CR\cdot K^+]}$. This value is approximately identical with that of non-coordinated 18-crown-6 in methanol. The results shown in Tables 2 and 3 lead to the conclusion that the hydrodynamic volume of the complex ion $[CR\text{-}K^+]$ remains effectively the same as that of the non-coordinated 18-crown-6, irrespective of the solvent media surrounding the complex ion. Further measurements will be required, however, to discuss whether or not the conclusion obtained in this work is applicable to other solvent systems.

The authors wish to express their thanks to Dr. Toshiaki Isono of the Institute of Physical and Chemical Research, who informed them of the numerical values of the viscosity coefficients of this study prior to publication.

References

1) G. W. Liesegang and E. M. Eyring, in "Synthetic Multidentate Macrocyclic Compounds," R. M. Izatt and J. J. Christensen, eds., Academic Press, New York (1978), Chap. 5.
2) H. Høiland, J. A. Ringseth, and E. Vikingstad, *J. Solution Chem.*, **7**, 515 (1978).
3) H. Høiland, J. A. Ringseth, and T. S. Brun, *J. Solution Chem.*, **8**, 779 (1979).
4) M. Shamsipur and A. I. Popov, *J. Am. Chem. Soc.*, **101**, 4051 (1979).
5) Y. Takeda, *Bull. Chem. Soc. Jpn.*, **52**, 2501 (1979).
6) Y. Takeda, H. Yano, M. Ishibashi, and H. Isozumi, *Bull. Chem. Soc. Jpn.*, **53**, 72 (1980).
7) Y. Takeda and H. Yano, *Bull. Chem. Soc. Jpn.*, **53**, 1720 (1980).
8) G. Michaux and J. Reisse, *J. Am. Chem, Soc.*, **104**, 6895 (1982).
9) Y. Takeda, *Bull. Chem. Soc. Jpn.*, **56**, 866 (1983).
10) G. W. Gokel and D. J. Cram, *J. Org. Chem.*, **39**, 2445 (1974).
11) For example, M. Kaminsky, *Z. Phys. Chem.* (Frankfurt am Main), **8**, 173 (1956).
12) G. Jones and M. Dole, *J. Am. Chem. Soc.*, **51**, 2950 (1929).
13) H. Falkenhagen, *Phys. Z.*, **32**, 745 (1931).
14) H. Falkenhagen and E. L. Vernon, *Phys. Z.*, **33**, 140 (1932).
15) M. Kaminsky, *Discuss. Faraday Soc.*, **24**, 171 (1957).
16) T. Isono (Inst. Phys. Chem. Res.), private communication.
17) H. K. Frensdorff, *J. Am. Chem. Soc.*, **93**, 600 (1971).
18) R. M. Izatt, R. E. Terry, B. L. Haymore, L. D. Hansen, N. K. Dalley, A. G. Avondet, and J. J. Christensen, *J. Am. Chem, Soc.*, **98**, 7620 (1976).
19) J. E. Desnoyers and G. Perron, *J. Solution Chem.*, **1**, 199 (1972).
20) A. Sacco, A. de Giglio, A. Dell'atti, and M. Petrella, *J. Chem. Soc., Faraday Trans. 1*, **77**, 2693 (1981).
21) G. Jones and H. J. Fornwalt, *J. Am. Chem. Soc.*, **57**, 2041 (1935).
22) C. M. Criss and M. J. Mastroianni, *J. Phys. Chem.*, **75**, 2532 (1971).

 © 1984 The Chemical Society of Japan Bull. Chem. Soc. Jpn., 57, 2569—2573 (1984)

The Structure of Liquid Alcohols by Neutron Diffraction. II. Molecular Structure of Ethyl Alcohol

Yukio TANAKA,† Norio OHTOMO,† and Kiyoshi ARAKAWA*

Research Institute of Applied Electricity, Hokkaido University, Sapporo 060

†*Faculty of Engineering, Hokkaido University, Sapporo 060*

(Received September 21, 1983)

The structure factor $S_m(Q)$ for liquid ethyl alcohol (C_2D_5OD) at room temperature was obtained by means of the time-of-flight (TOF) neutron diffraction method using electron LINAC. An analysis of the diffraction data was carried out and the molecular structure in liquid phase was determined as follows: the O-D, C-O, and C-C bond lengths are 0.960±0.010 Å, 1.410±0.010 Å and 1.510±0.010 Å, respectively.

In the preceding papers,[1-3] the structure of liquid water (D_2O) and the molecular conformation of liquid methyl alcohol (CD_3OD) were determined successfully by means of the LINAC-TOF neutron diffraction method. Then, as a part of a series of studies for hydrogen-bonded liquids, we have investigated the molecular structure of ethyl alcohol C_2D_5OD in liquid phase.

Several authors have performed studies of gaseous ethyl alcohol. Concerning molecular geometries, the coexistence of two molecular conformations has been reported, which are the hydroxyl trans form and the gauche one.[4-8] The O-H groups in liquid ethyl alcohol are known to be concerned with hydrogen bond.[9-11] But, due to the lack of experimental techniques, there is very scarce information of the molecular structure of ethyl alcohol in liquid phase, which is fundamental to the consideration on the hydrogen-bonded liquid structure. Because the molecular conformation of ethyl alcohol in liquid phase may be subjected to the effect of its comparatively large alkyl group as well as to that of hydrogen bonding, its geometry in liquid phase is very interesting in comparison with the cases of water[1,2] and methyl alcohol.[3]

These circumstances add special interest to the investigation of molecular conformations in liquid ethyl alcohol. The objective of the present work is not only to determine the molecular structure of ethyl alcohol C_2D_5OD in liquid phase but also to examine that of a series of hydrogen-bonded liquids, D_2O, CD_3OD, and C_2D_5OD. Then, we have carried out a LINAC-TOF neutron diffraction measurement on liquid ethyl alcohol and have made an analysis of the data to determine its molecular structure.

Experimental

The experiment was performed by means of the TOF neutron diffraction method using electron LINAC at Hokkaido University. Neutron scattering intensities were measured for liquid ethyl alcohol C_2D_5OD (purity of deuteration 99%, Commissariat à l' Energie Atomique (CEA), France) at room temperature at five different scattering angles: 2θ=30.0°, 40.0°, and 65.0° at 24.0±0.5 °C, 2θ=90.0° at 20.0±0.5 °C, and, 2θ=120.0 at 22.0±0.5 °C. A thin-walled cylindrical quartz vessel was used to contain the sample. Detailed experimental apparatus and procedures were reported elsewhere.[3,12] After all corrections (background, absorption, multiple scattering, inelastic scattering and incoherent scattering), absolute normalizations and Q-scale calibrations, we obtained structure factors $S_m(Q)$ for five different scattering angles as shown in Fig. 1. The coincidence of the values from different angles in each overlapping region of Q is quite well as seen in the figure, and, combining these data set, we obtained the final $S_m(Q)$ curve of wide Q range. The statistical error for values of the $S_m(Q)$ is smaller than 1.0%, and the resolving power $\Delta Q/Q$ less than a few % in the whole range of Q.

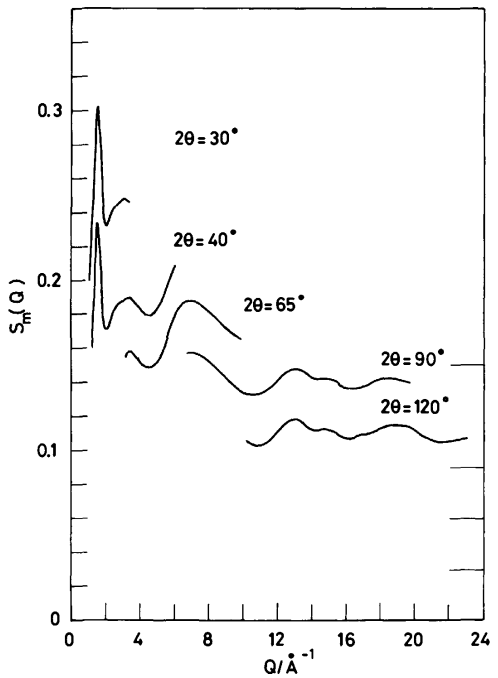

Fig. 1. Observed neutron structure factors $S_m(Q)$ for deutrated ethyl alcohol at various scattering angles.

Procedures of Analysis

Theoretical framework and procedures for determining the molecular structure from observed $S_m(Q)$ data have been stated previously,[3,13] and only a brief description is given here.

The intramolecular structure factor $f_1(Q)$, which is a dominant part of $S_m(Q)$ at higher Q, is written as,

$$f_1(Q) = \left(\sum_i b_i\right)^{-2} \sum_{ij} b_i b_j j_0(Qr_{ij}) \exp(-\gamma_{ij}Q^2), \quad (1)$$

where b_i is the coherent scattering length of i-th nucleus in the molecule, r_{ij} the distance between i-th and j-th nucleus, $2\gamma_{ij}$ the mean square variation to the distance r_{ij} and $j_0(x)=\sin x/x$ a zeroth order spherical Bessel function. $\sum$ is over all the nuclei in the molecule. With

respect to the mean square variation $2\gamma_{ij}$, we assume that $\gamma_{ij}=1/2D_{ij}^2r_{ij}$, where D_{ij} is estimated to be 0.03 Å$^{1/2}$ per Å for distances between carbon and oxygen atoms, 0.036 Å$^{1/2}$ for that between carbon atoms and 0.06 Å$^{1/2}$ for other distances in the molecule.[13]

The structure of ethyl alcohol molecule C_2D_5OD is shown in Fig. 2. The methyl group can rotate about the C-C axis in Fig. 2, and it is assumed that the three C-D bonds and the three DCD angles in the methyl group are all identical, respectively. It is also assumed that the deuterium atoms in the methylene group are located in plane symmetry about the CCO plane. The hydroxyl group can rotate about the C-O axis (Fig. 2). Then, we characterize the molecular structure by twelve structural parameters, *i.e.*, the bond lengths r_{OD}, r_{CO}, r_{CC}, r_{CD_M}, and r_{CD_N}, and, the angles COD, CCO, DCD_M, DCD_N, CCD_N, τ, and ϕ (Fig. 2). In order to determine these molecular parameters, $f_1(Q)$ were calculated for more than 15000 models by using Eq. 1 and the curves obtained were compared with the observed $S_m(Q)$ data in the higher Q region ($Q\gtrsim 6$ Å^{-1}).[3,13] The magnitudes of the parameters were varied in reference to the values given in Table 1.

Determination of the Molecular Structure

Observed Structure Factor Data. The structure factor data $S_m(Q)$ obtained for liquid ethyl alcohol C_2D_5OD is shown in Fig. 3. Comparing this $S_m(Q)$ data with those obtained for liquid water D_2O (Fig. 1 in Ref. 1 and Fig. 5 in Ref. 2), liquid methyl alcohol CD_3OD (Fig. 3 in Ref. 3) and liquid acetyl chloride CD_3COCl (Fig. 3 in Ref. 13) at room temperatures, we can point out several distinctive features as follows.

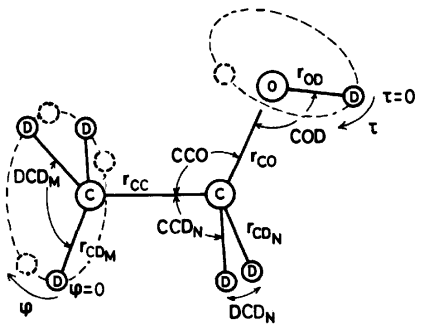

Fig. 2. The structure of deuterated ethyl alcohol (C_2D_5OD) molecule.

Table 1. Range of parameters

Parameter	Range	Interval of variation
r_{OD}/Å	0.930—1.010	0.010
r_{CO}/Å	1.380—1.445	0.005
r_{CC}/Å	1.480—1.540	0.010
r_{CD_M}/Å	1.070—1.100	0.005
r_{CD_N}/Å	1.070—1.100	0.005
COD/°	100.0—130.0	1.0
CCO/°	100.0—120.0	1.0
DCD_M/°	102.0—118.0	1.0
DCD_N/°	100.0—125.0	1.0
CCD_N/°	100.0—120.0	1.0
τ/°	0.0—360.0	5.0
ϕ/°	0.0—120.0	5.0
	free rotation	—

(1) With respect to the first peaks for the series of hydrogen-bonded systems, D_2O, CD_3OD, and C_2D_5OD, ratios of the heights to its $S_m(Q)$ values at $Q\to\infty$ decrease monotonously in the order of D_2O (≈2.0), CD_3OD (≈1.7), and C_2D_5OD (≈1.4). The same trend is seen for the peak positions (≈2.0 Å^{-1}, ≈1.8 Å^{-1}, and ≈1.5 Å^{-1} for D_2O, CD_3OD, and C_2D_5OD, respectively) as well as for their width as clearly seen.

(2) In the case of methyl alcohol CD_3OD, there is a doublet hump at *ca.* Q=4 Å^{-1}, and the similar but more subtle trend is observed for C_2D_5OD. On the other hand, for heavy water, there is a singlet hump at *ca.* Q=4 Å^{-1} of its $S_m(Q)$ curve. In the preceding paper of D_2O,[1,2] it is elucidated from the analysis of $S_m(Q)$ data that the hump is originated in the existence of the hydrogen-bonded liquid structure. Hydrogen-bonded structures are also expected in liquid CD_3OD and C_2D_5OD.[9-11] In addition to that, the calculated $f_1(Q)$ curves of these fluids have a peak at *ca.* Q=4 Å^{-1} (Ref. 3 for CD_3OD and Fig. 3 in this paper as seen in the next item), which is not seen in the case of water.[1,2] Then, these humps at *ca.* 4 Å^{-1} for CD_3OD and C_2D_5OD systems are due to the superposition of the two contributions: one of them is its intramolecular conformation and the other its intermolecular hydrogen-bonded structure.

(3) Concerning the second peaks at *ca.* Q=7 Å^{-1}, its intensity for CD_3OD and C_2D_5OD is distinctive, being in contrast to the broad second peak at *ca.* Q=8 Å^{-1} in the $S_m(Q)$ curve for D_2O. And, further, the position of each second peak is seen to shift to smaller Q side in the order of D_2O, CD_3OD, and C_2D_5OD (≈8.3 Å^{-1}, ≈7.1 Å^{-1}, and ≈6.8 Å^{-1}).

(4) Concerning the third peaks at *ca.* 13 Å^{-1}, the shoulder at *ca.* 14—15 Å^{-1} for C_2D_5OD is distinctive, being in contrast to the cases of D_2O and CD_3OD. It is noticeable that the nearly identical feature is seen in the data for liquid acetyl chloride.

(5) There are marked forth peaks at *ca.* Q=19 Å^{-1} of the data for CD_3OD and C_2D_5OD. These features are also seen in the case of liquid CD_3COCl.

Determination of Intramolecular Parameters for Liquid Ethyl Alcohol. By making the calculated $f_1(Q)$ curves fit with the observed $S_m(Q)$ data, we have determined the best structural parameters of liquid ethyl alcohol C_2D_5OD at room temperature as follows: r_{OD}=0.960±0.010 Å, r_{CO}=1.410±0.010 Å, r_{CC}=1.510±0.010 Å, r_{CD_M}=1.080±0.005 Å, r_{CD_N}=1.085±0.005 Å, COD=120.0±5.0°, CCO=105.0±1.0°, DCD_M=110.0±0.5DCD_N=112.0±3.0°, CCD_N=106.0±1.0°, and ϕ=12.0±5.0°.

Two structural models shown in Table 2, which differ only in the magnitudes of parameter τ determining the rotation angle of O-D bond, are found to give the best $f_1(Q)$ curves: τ=0.0°, the trans conformation and 160.0°, the gauche one. As seen in Fig. 3, the coincidence between the calculated $f_1(Q)$ curves for these models and the observed $S_m(Q)$ values is satisfactory

in the higher Q region ($Q \gtrsim 6$ Å^{-1}). The best structural parameters determined are tabulated in Table 3, together with those by other workers.[5,6,14]

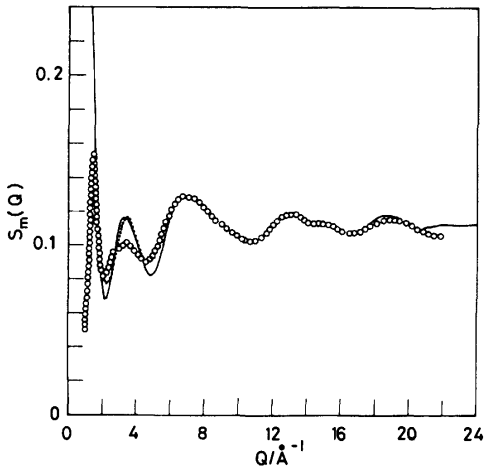

Fig. 3. Comparison between observed neutron structure factor $S_m(Q)$ and present $f_1(Q)$ curves calculated. ○: observed $S_m(Q)$, ——: calculated $f_1(Q)$ for the gauche conformation ($\tau=160.0°$, Table 2), ($\varepsilon=0.003327$), ·····: calculated $f_1(Q)$ for the trans conformation ($\tau=0.0°$, Table 2), ($\varepsilon=0.003328$).
ε is a measure for indicating the deviations of $f_1(Q)$ from the experimental data, and is expressed as,

$$\varepsilon=(\sum_i^N\{S_m(Q)_{obsd}-f_1(Q)_{calcd}\}^2)^{1/2}/\sum_i^N S_m(Q)_{obsd},$$

where N is the number of data points in the fitting range of Q, 6—18 Å^{-1}.

Structure of Molecules in Liquid State Compared with That in Gaseous One. By using microwave techniques, the geometrical parameters of ethyl alcohol molecules in gaseous phase were given by Sasada *et al.* for the trans and gauche conformations[5] and by Culot for the trans conformation[6] (Table 3). We have calculated the $f_1(Q)$ curves by using their parameters[5,6] and those are compared with the present $S_m(Q)$ curve in Fig. 4. Significant discrepancies between the present data and the $f_1(Q)$ curves calculated are seen on the whole range of Q. The disagreement at higher Q regions ($Q \gtrsim 6$ Å^{-1})[3,14] is ascribed to the variation of the intramolecular structure of molecules from gaseous to liquid states, as seen in Table 3.

One of the most interesting parameters of the molecule in liquid phase is the O-D distance, because a stretching of the bond length from gaseous to liquid phase gives a criterion for the strength of hydrogen bonds. As seen in Table 3, the present value of O-D distance obtained is 0.960±0.010 Å, and is nearly identical with that in gaseous state. It is distinguished from the cases of D_2O (0.98 Å)[1,2] and CD_3OD (0.99 Å),[3] and this trend suggests that the strength of hydrogen bonds for these fluid systems follows in the order of $C_2D_5OD \leq CD_3OD \leq D_2O$. The trend is also seen in the coordination numbers of these systems obtained by computer experiments.[11,15,16]

Concerning the C-O distance, we obtained the value of 1.410±0.010 Å. This is nearly identical with those obtained for gaseous dimethyl ether (1.410 Å)[17] and gaseous diethyl ether (1.408 Å),[18] and shorter than that obtained for gaseous ethyl alcohol by Culot (1.431 Å)[6]

Table 2. Geometrical parameters of best structural models determined by neutron diffraction method

r_{OD}/Å	r_{CO}/Å	r_{CC}/Å	r_{CD_M}/Å	r_{CD_N}/Å	COD/°	CCO/°	DCD_M/°	DCD_N/°	CCD_N/°	τ/°	ϕ/°	$\varepsilon\times10^3$
0.960	1.410	1.510	1.080	1.085	117.0	105.0	109.5	112.0	106.0	160.0	10.0	3.327
0.960	1.410	1.500	1.080	1.085	123.0	105.0	110.5	112.0	106.0	0.0	15.0	3.328

With respect to ε, see Fig. 3.

Table 3. Comparison of intramolecular parameters obtained for ehtyl alcohol molecule in the present study with those by other workers

	Present (liquid)	Montague *et al.*[a] (λ=0.5 Å liquid	Montague *et al.*[a] λ=0.7 Å)	Culot[b] (gas)	Sasada *et al.*[c] (gas)	Sasada *et al.*[c] (gas)
r_{OD}/Å	0.960±0.010	0.966±0.010	0.931±0.006	0.971	(0.9451)	(0.9451)
r_{CO}/Å	1.410±0.010	1.571±0.016	1.416±0.009	1.431	(1.4247)	(1.4273)
r_{CC}/Å	1.510±0.010	(1.5297)	(1.5297)	1.512	(1.5297)	(1.5297)
r_{CD_M}/Å	1.080±0.005	(1.0936)	(1.0936)	1.088—1.091[d]	(1.0936)	(1.0936)
r_{CD_N}/Å	1.085±0.005	(1.0936)	(1.0936)	1.098	(1.0936)	(1.0936)
COD/°	120.0°±5.0°	106.4°±1.7°	107.3°±1.2°	105.4°	108°32′±29′	108°32′±29′
CCO/°	105.0°±1.0°	111.1°±1.6°	113.3°±0.9°	107.8°	107°20′±14′	112°21′±30′
DCD_M/°	110.0°±0.5°	(108°38′)	(108°38′)	108.4—108.9°[d]	108°38′±42′	108°38′±42′
DCD_N/°	112.0°±3.0°	(109°30′)	(109°30′)	108.0°	109°05′±33′	109°05′±33′
CCD_N/°	106.0°±1.0°	(109°30′)	(109°30′)	110.7°	110°18′±42′	110°18′±42′
τ/°	{0.0° {160.0°±10.0°	—	—	0.0°	0.0°	126.0°±6.0°
ϕ/°	12.0°±5.0°	—	—	0.0°	0.0°	0.0°
Shape	trans/gauche	—	—	trans	trans	gauche

a) Neutron diffraction at reactor, Ref. 14. b) Microwave, Ref. 6. c) Microwave, Ref. 5. d) This author obtaines different values for each geometrical parameter. The values in parentheses were assumed.

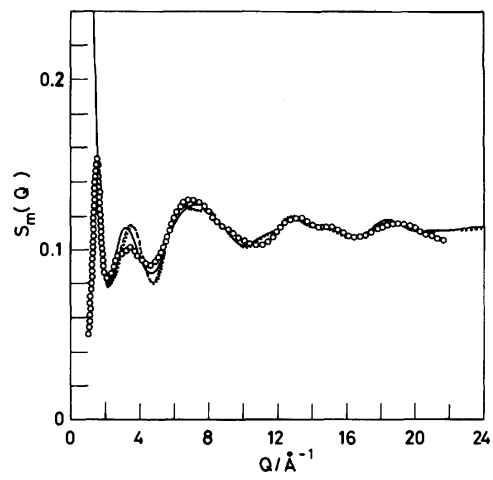

Fig. 4. Comparison between observed neutron structure factor $S_m(Q)$ and calculated $f_1(Q)$ curves for the models given by Sasada *et al.* and by Culot in gaseous phase.
○: observed $S_m(Q)$, ——: calculated $f_1(Q)$ for the gauche conformation by Sasada *et al.*[5] ($\tau=126.0°$, Table 3), ($\varepsilon=0.007080$), ----: calculated $f_1(Q)$ for the trans conformation by Sasada *et al.*[5] ($\tau=0.0°$, Table 3), ($\varepsilon=0.007084$), ·····: calculated $f_1(Q)$ for the trans conformation by Culot[6] ($\tau=0.0°$, Table 3), ($\varepsilon=0.006429$).
With respect to ε, see Fig. 3.

and that by Sasada *et al.* (1.4247 Å, assumed value).[5] The Montague's value of the C-O bond, 1.571 Å in liquid phase is too large, as mentioned in their article.[14] The C-C distance obtained is 1.510±0.010 Å, being in good agreement with that by Culot (1.512 Å) in gaseous phase.[6] With respect to the methyl group, a slight shortening of the C-D distance and a slight increase of the DCDM angles are observed in comparison with those in gaseous state, and the same trend is also observed in the case of methyl alcohol.[3] The methyl rotation angle obtained is 12.0±5.0° and is nearly identical with that for liquid methyl alcohol.[3] Concerning the models with freely-rotating methyl group, the $f_1(Q)$ calculated is found to disagree with the observed $S_m(Q)$ ($Q\gtrsim6$ Å^{-1}) in contrast to the case of CD_3OD.[3] With respect to the angular parameters in the ethylene group, DCDN and CCDN angles are 112.0±3.0° and 106.0±1.0°, respectively, and is different from those in gaseous phase, about 108.0—110.7° for both angular parameters (Table 3). The C-D bonds in the ethylene group are 1.085±0.005 Å, and are shorter than those in gaseous phase, 1.094—1.098 Å (Table 3). With respect to the hydroxyl rotation angle τ for the gauche ethyl alcohol molecule, the present value is 160.0±10.0° and larger than that in gaseous state, 126.0±6.0°.[5]

Trans and Gauche Conformations with Respect to the Hydroxyl Internal Rotation. As stated in the preceding item, two conformations concerning the rotation of the OD radical, trans and gauche forms, are expected to exist in gaseous phase. With respect to the energy difference between the two conformations, Radom *et al.* gave the value of 0.63 kcal/mol by *ab initio* calculations.[19] In a recent microwave study on ethyl alcohol, Kakar and Quade showed that the energy difference is only 41.2 cm^{-1} (=0.12 kcal/mol).[8] The number ratio of trans to gauche molecules in the vapour phase at room temperature was estimated to be 2:1 by Barnes and Hallam.[4]

Jönssen reported the coexistence of the two conformers in solid phase by means of the X-ray diffraction.[20] According to the results the number ratio of the two conformers becomes 1:1. On the other hand there is no information concerning the rotational isomers in liquid phase. Considering the interaction between molecules within liquid, we can expect that the energy difference between the conformers of the trans and gauche types in liquid phase is small, and that the two types coexist in liquid phase as well as in gaseous and solid phases. Due to the small energy difference, the main frame of molecules won't be affected strongly by the hydroxyl rotation angle. Then, the present results that the two geometrical models of trans and gauche types fit with the observed $S_m(Q)$ data (Table 2 and Fig. 3) suggest the coexistence of the two conformers in liquid ethyl alcohol. The $f_1(Q)$ curves calculated for these two models are undiscriminated with each other at higher Q region ($Q\gtrsim6$ Å^{-1}, Fig. 3), and show a slight difference at the lower ($Q<6$ Å^{-1}), where intermolecular contributions appear as well as intermolecular ones. And, the number ratio of the two conformers in liquids is not determined in the present study.

On the Intermolecular Contribution to the Total Structure Factor $S_m(Q)$— the Effect of Debye-Waller Factors for Intermolecular Atomic Pairs.

In the present series of studies of liquid alcohols,[3] we have determined intramolecular structures within liquids by making calculated structure factors fit with observed diffraction data in the higher Q region ($Q\gtrsim6$ Å^{-1}), as described above. The procedure of analysis has been applied by several workers[1-3,13,21,22] including us for determining molecular structures from neutron diffraction data of liquids. For its successful application, the following fact is presupposed as the one established empirically for those molecular fluids treated (D_2O, CD_3OD, C_2D_5OD, CD_3COCl, C_3O_2, *etc.*): the $S_m(Q)$ is practically identical with $f_1(Q)$ (Eq. (1)) in the higher Q region ($Q\gtrsim6$ Å^{-1}) as the result of comparatively rapid decay of the intermolecular terms with increasing Q. We consider, here, why the intermolecular contributions decay so rapidly with increasing Q in these liquids. The most deterministic factor of that behavior of intermolecular terms at the high Q region may be tentatively considered to be the Debye-Waller factor of atomic pair between two molecules, and we concentrate our present concern to this problem.

Concerning the Debye-Waller factors for intermolecular atomic distances, which is expressed as exp ($-\gamma_{ij}Q^2$) ($2\gamma_{ij}$: the mean-square amplitude for the variation of the distance), a few discussions will be given below. The mean-square amplitude for the variation of the distance between atoms i and j in molecles p and

q ($p \neq q$) can be expressed as,

$$2\gamma_{ij} = \langle \Delta r_{cip}^2 \rangle + \langle \Delta r_{cpq}^2 \rangle + \langle \Delta r_{cjq}^2 \rangle. \quad (2)$$

$\langle \Delta r_{cip}^2 \rangle$ is the mean-square amplitude for the variation of the distance between the center of molecule p and its i-th atom, and $\langle \Delta r_{cpq}^2 \rangle$ is that for the distance between the centers of the p-th and q-th molecules. In the expression described above, the thermal vibration of atoms within a molecule and the thermal Brownian motion of the molecule on the whole are safely considered to be independent with each other, and the simple sum formula consists. The term $\langle \Delta r_{cpq}^2 \rangle$ is expressed as,

$$\langle \Delta r_{cpq}^2 \rangle = \langle \Delta r_{cp}^2 \rangle + \langle \Delta r_{cq}^2 \rangle = 2\langle \Delta r_{cp}^2 \rangle, \quad (3)$$

where $\langle \Delta r_{cp}^2 \rangle$ is the term due to the Brownian motion of the center of the molecule p. Then,

$$\gamma_{ij} = \langle \Delta r_{cp}^2 \rangle + \frac{1}{2}(\langle \Delta r_{cip}^2 \rangle + \langle \Delta r_{cjq}^2 \rangle). \quad (4)$$

The term $\langle \Delta r_{cp}^2 \rangle$ can be determined approximately from the effective free volume v_f (the statistical average of fluctuational void space[23,24]) and the effective hard-sphere diameter of molecules. The magnitude of the effective hard-sphere diameter is estimated from the first peak region of the $S_m(Q)_{obsd}$ by using the Percus-Yevick equation, that is, by making the theoretial $S(Q)$ fit with the observed first peak of $S_m(Q)$.[25-28] At the same time, we can obtain the packing fraction ξ, and can estimate the magnitude of v_f by the use of the Percus-Yevick equation.[23-24] Thus, for CD_3OD and C_2D_5OD, the magnitude of $\langle \Delta r_{cp}^2 \rangle^{1/2}$ becomes nearly equal at room temperature: 0.12 Å (the magnitudes of ξ also become nearly equal for these two alcohols, 0.36). The γ_{ij} for the intermolecular D···D pair in CD_3OD and C_2D_5OD becomes $(0.12)^2 + \langle \Delta r_{cD}^2 \rangle$, and $\langle \Delta r_{cD}^2 \rangle \gtrsim (0.06)^2$. Thus, for the intermolecular D···D pair, the term $\exp(-\gamma_{ij}Q^2)$ is found to decay to e^{-1} at about $Q \sim 7$ Å^{-1}. As clearly seen in the above rough estimation, the γ_{ij} for the intermolecular atomic pair is dominated by the contribution from the thermal Brownian motion of molecules, and this is expected to be the dominant factor for the rapid decay of the intermolecular contribution to the $S_m(Q)$ at about 6—7 Å^{-1} (Fig. 5) in sharp contrast to the case of the intramolecular terms. This is considered to be the main support of the adequacy of determining the intramolecular parameters from the observed $S_m(Q)$ in the higher Q region ($Q \gtrsim 6$ Å^{-1}).

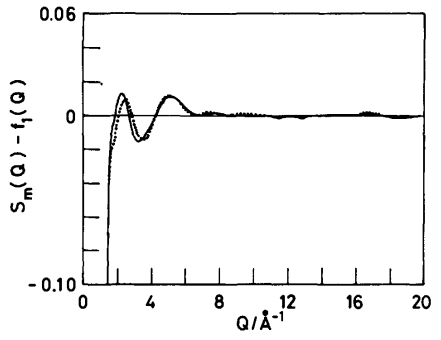

Fig. 5. Intermolecular contributions $S_m(Q)_{obsd} - f_1(Q)_{calcd}$ for the present two models.
——: intermolecular factor for the gauche conformation ($\tau = 160.0°$, Table 2), ·····: intermolecular factor for the trans conformation ($\tau = 0.0°$, Table 2).

Concluding Remarks

A neutron diffraction study of liquid ethyl alcohol (C_2D_5OD) by means of the LINAC-TOF method was performed and the structure of molecules within liquids was determined. The present result is primarilly due to the success in securing the structure factor data for wide Q range with sufficient accuracy. Then the result as well as the preceding one of CD_3OD[3] confirms the usefulness of the present LINAC-TOF neutron diffraction method to the structural study of polyatomic molecular fluids.

References

1) N. Ohtomo, K. Tokiwano, and K. Arakawa, *Bull. Chem. Soc. Jpn.*, **54**, 1802 (1981).
2) N. Ohtomo, K. Tokiwano, and K. Arakawa, *Bull. Chem. Soc. Jpn.*, **55**, 2788 (1982).
3) Y. Tanaka, N. Ohtomo, and K. Arakawa, *Bull. Chem. Soc. Jpn.*, **57**, 644 (1984).
4) A. J. Barnes and H. E. Hallam, *Trans. Faraday Soc.*, **66**, 1932 (1970).
5) Y. Sasada, M. Takano, and T. Satoh, *J. Mol. Spectrosc.*, **38**, 33 (1971).
6) J. P. Culot, Fourth Austin Symposium on Gas Phase Molecular Structure, Austin, Texas, 1972, Paper T8; through *J. Phys. Chem. Ref. Data*, **8**, 619 (1979).
7) J. R. During, W. E. Bucy, C. J. Wurrey, and L. A. Carreira, *J. Phys. Chem.*, **79**, 988 (1975).
8) R. K. Kakar and C. R. Quade, *J. Chem. Phys.*, **72**, 4300 (1980).
9) W. A. P. Luck, "Water", ed by F. Franks, Plenum, New York (1973) Vol. 2, Chap. 4.
10) A. N. Fletcher, *J. Phys. Chem.*, **76**, 2562 (1972).
11) W. L. Jorgensen, *J. Am. Chem. Soc.*, **103**, 345 (1981).
12) N. Ohtomo, Y. Tanaka, and K. Arakawa, *Bull. Faculty Eng. Hokkaido Univ.*, **109**, 43 (1982).
13) N. Ohtomo, and K. Arakawa, *Bull. Chem. Soc. Jpn.*, **53**, 1510 (1980).
14) D. G. Montague, I. P. Gibson, and J. C. Dore, *Mol. Phys.*, **47**, 1405 (1982).
15) R. H. Stillinger, *Science*, **209**, 451 (1980).
16) W. L. Jorgensen, *J. Am. Chem. Soc.*, **103**, 341 (1981).
17) U. Blukis, P. H. Kasai, and R. J. Myers, *J. Chem. Phys.*, **38**, 2753 (1963).
18) M. Hayashi and K. Kuwada, *Bull. Chem. Soc. Jpn.*, **47**, 3006 (1974); M. Hayashi, H. Imaishi, K. Ohno, and H. Murata, *ibid.*, **44**, 299 (1971).
19) L. Radom, W. J. Hehre, and J. A. Pople, *J. Am. Chem. Soc.*, **94**, 2371 (1972).
20) P.-G. Jönsson, *Acta Crystallogr., Sect. B*, **32**, 232 (1976).
21) R. Triolo and A. H. Narten, *J. Chem. Phys.*, **63**, 3624 (1975).
22) G. Walford, J. H. Clarke, and J. C. Dore, *Mol. Phys.*, **36**, 1581 (1978).
23) K. Arakawa and K. Kojima, *Bull. Chem. Soc. Jpn.*, **48**, 26 (1975).
24) K. Arakawa, K. Tokiwano, and K. Kojima, *Bull. Chem. Soc. Jpn.*, **50**, 65 (1977).
25) N. W. Ashcroft and J. Lekner, *Phys. Rev.*, **145**, 83 (1966).
26) N. W. Ashcroft and D. C. Langreth, *Phys. Rev.*, **156**, 685 (1967).
27) J. E. Enderby and D. M. North, *Phys. Chem. Liquids*, **1**, 1 (1968).
28) Y. Tanaka, N. Ohtomo, and K. Arakawa, *J. Phys. Soc. Jpn.*, **52**, 2093 (1983).

Sensitization of Polycrystalline $SrTiO_3$ Photoanodes by Lanthanum Doping

Byong-Tae CHANG,* Guy CAMPET,† Jean CLAVERIE,† and Paul HAGENMULLER†

Department of Chemistry, Faculty of Science, Korea University, Kodaira, Tokyo 187

†*Laboratoire de Chimie du Solide du C.N.R.S., Université de Bordeaux I, 351, cours de la Libération, 33405 Talence Cedex, France*

(Received January 30, 1984)

The behaviors of polycrystalline $La_xSr_{1-x}TiO_3$($x \leq 0.05$) electrodes in a photoelectrochemical cell for water decomposition have been investigated in aqueous NaOH electrolyte. The lanthanum substitution for strontium resulted in impressive visible photosensitization of the corresponding electrodes under anodic polarization. This visible photoresponse is based on the relatively deep subband gap states introduced into the forbidden band by lanthanum doping, in analogy with the polished undoped $SrTiO_3$ electrodes reported previously.

The practical realization of a photoelectrochemical system for the electrolysis of water will depend critically on the development of stable and efficient semiconductor electrodes. $SrTiO_3$ has received a great deal of attention as a semiconducting photoanode for the photodecomposition of water because it is chemically stable and requires no external biasing to generate H_2 and O_2.[1-12] However, it does not show visible light absorption due to its large band energy gap (3.2 ev). This is clearly insufficient for solar energy conversion applications. It is, therefore, very important to extend the $SrTiO_3$ spectral response in the visible region in realizing the efficient photodecomposition of water.

In our previous papers,[13,14] we have reported that mechanical polishing of undoped polycrystalline $SrTiO_3$ electrode surface results in an anomalous visible photoresponse extending to 600 nm with relatively negative onset potential of about −1V (*vs.* SCE, 1 M NaOH (1 M=1 mol dm^{-3})), and that the principal mechanism could be related to the introduction of subband states, $[Ti{:}3d(t_{2g})]_{sub}$ near the conduction band and $[O{:}2p]_{sub}$ near the valence band, by the mechanical polishing. These results suggests us the importance of controlling the formation of the subband states in the band gap by selected surface modifications or substitutions of Sr and/or Ti sites with appropriate dopants.

It is well-known that the reduced titnates such as n-TiO_2 and $SrTiO_3$ have a lot of defect energy levels in the forbidden band. The nature of these defects is largely dependent upon reduction temperature, oxygen activity, impurity additions, Sr/Ti ratio for $SrTiO_3$ and so on.[15-23] In general $SrTiO_3$ can be converted into n-type semiconductor by donor doping(*e.g.* niobium) and/or reduction in high vacuum or flowing hydrogen gas.[1,11,16,24] It is reasonable to think that lanthanum can be selected as a dopant of $SrTiO_3$ for three main reasons;

(i) stability in the trivalent state.

(ii) similarity of Sr^{2+} and La^{3+} ionic radii ($r_{Sr^{2+}}$= 0.140 nm, $r_{La^{3+}}$=0.132 nm) which insures a substitutional incorporation of lanthanum within the strontium sublattice.[25]

(iii) the compensation of extra charge resulting from partial $Sr^{2+} \rightarrow La^{3+}$ substitution may occur *via* electronic or lattice defects according to the reduction temperature and the oxygen partial pressure;[26,27]

$$Sr^{+2}_{1-x}La^{+3}_{x}Ti^{+4}O^{-2}_{3+x/2} \xrightarrow[\text{reduction}]{\text{Moderate}} Sr^{+2}_{1-x}La^{+3}_{x}Ti^{+4}_{1-y}Ti^{+3}_{y}O^{-2}_{3+x/2-y/2}, \quad (1)$$

$$\xrightarrow[\text{reduction}]{\text{Strong}} Sr^{+2}_{1-x}La^{+3}_{x}Ti^{+4}_{1-x}Ti^{+3}_{x}O^{-2}_{3}. \quad (2)$$

The presence of Ti^{+3} should confer n-character to $SrTiO_3$ and render the corresponding material performing as a photoanode, so La-doping can be expected to be a good method for controlling the formation of the subband states. Recently Odekirk and Blakemore have repored the enhancement of the photoactivity of lanthanum-doped, strongly reduced $SrTiO_3$ in microcrystalline ceramic form; La-doping ($x \leq 0.01$) provides an extention of the spectral response to longer wavelength and improves the quantum efficiency for all wavelengths.[28] Besides, Tsubomura *et al.* described briefly that lanthanum-doping showed week effect on the sensitization of $SrTiO_3$ photoanode at wavelengths longer than 400 nm.[29] The purpose of this paper is to study how lanthanum-doping changes the photoelectrochemical properties of polycrystalline $SrTiO_3$ electrodes and sensitizes it in more detail, in comparision with the mechanical polishing effects.

Experimental

The compounds synthesized in this work correspond to the compositions $Sr_{1-x}La_xTiO_{3+x/2}$ ($x \leq 0.05$). The polycrystalline samples have been prepared by heating the corresponding mixtures of $SrCO_3$, La_2O_3, and TiO_2 in air at 1350 °C for 16 h. The obtained powders were pelletized, sintered in air at 1400 °C for 16 h, and then reduced in flowing hydrogen gas at 1400 °C for 10—20 h to make them n-type. The conductivities of the samples after reduction were between 0.01—10 Ω^{-1} cm^{-1}.

Electrode preparation and electrochemical measurement procedures used to characterize the semiconductors have been described elsewhere.[13,14] 1 M NaOH solution was used as an electrolyte and all the potentials were referred to a saturated caromel electrode. To caluculate a quantum efficiency at each wavelength, the observed photocurrents were corrected for the spectral distribution of the light sourse(150W-Xe) and of the monochrometer. Impedance measurements have been performed a 10 kHz to get the flatband potential of the samples.

Results and Discussion

Figure 1 shows visible photocurrent (i_{vis})-potential curve of a La(0.5%)-doped sample (curve 1) under illumination of polychromatic visible light($\lambda \geq 400$ nm). For comparison, a similar curve of an polished undoped sample (curve 2) was also given in it. Dark currents were less than 10^{-6}A between -1.0 and 0.5 volts, and the visible photoreponses were very sharp. One can observed different behaviors of i_{vis}-potential curve for the above two; while the visible photocurrent of the polished undoped sample tends to be saturated as the potential becomes more positive, that of the lanthanum-doped sample increases almost linearly with a raising of the potential, at least below 1V. On the other hand, onset potential of i_{vis} for La-doped sample was found to be -0.8V, being more positive by 0.2V than that for the polished undoped sample. Such properties of the La-doped sample are very similar to those of Cr-doped $SrTiO_3$ photoanodes.[30]

As shown in Fig. 2, the effect of lanthanum-doping on the sensitization of $SrTiO_3$ becomes remarkable for [La]$\geq$0.5%. Too high concentration of the dopant ([La]$\geq$2%) leads to a decrease in the visible photocurrent as well as the full light photocurrent. Furthermore, mechanical polishing of the La-doped electrodes results in an enhancement of i_{vis} when [La]$\leq$1% as shown in curve 2.

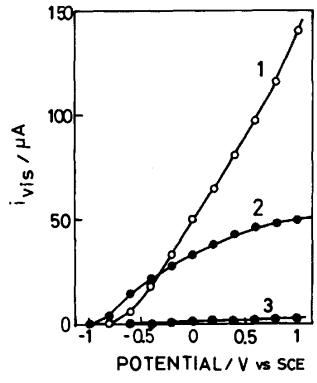

Fig. 1. Visible photocurrent-potential curves of La-(0.5 %)doped electrode(curve 1), the polished undoped electrode(curve 2), and the unpolished undoped electrode(curve 3) in 1 M NaOH ($\lambda \geq 400$ nm).

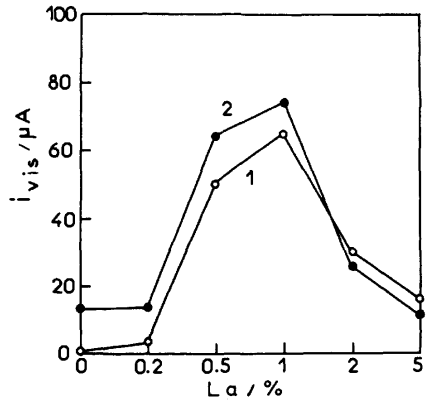

Fig. 2. Effect of the concentration of La-dopant on the sensitization of $SrTiO_3$ photoanode at 0 volt. curve 1; before polishing, 2; after polishing.

Mott-Schottky plots were constructed from capacitance *vs.* electrode potential measurements a 10 kHz and are shown in Fig. 3. The flatband potentials (V_{fb}), obtained from the intercepts of $1/C^2$ *vs.* potential, were found to be -1.35, -1.30, and -1.20 volts for [La]=0, 0.2 and 0.5%, respectively. This means that La-doping causes V_{fb} to shift to more positive direction. A striking feature of the Mott-Schottky plot is the break near -1V. This feature suggests us the existance of two kinds of donor levels, one very close to the conduction band and the other deep below it, as discussed on n-Fe_2O_3 electrodes.[31] According to Goodenough, counter-cation charge compensation of La^{+3} for Sr^{+2} introduces no anion vacancies to induce Ti^{+4} ion displacements, and the larger charge La^{+3} *vs.* Sr^{+2} ions stabilizes from the conduction band a shallow trap state which sharply reduces electron mobility, hindering electron-hole separation.[32] Typically it may be the case of heavily La^{+3}-doping; the full light photocurrent of La(0.5%)-doped sample at 0 volt was less than one tenth of the undoped sample. Lanthanum has a stronger affinity to oxygen than strontium because of its higher electron negativity. The covalent bond between titanium (mainly Ti^{+3}) and oxygen, neighboring La^{+3} on the opposite side, must be considerably weakened. Therefore, the formation of the above deep donor level could be associated with this lowering in the covalency between Ti^{+3} and O^{-2}. Analogous to the previously proposed mechanism of the sensitization of the polished undoped $SrTiO_3$,[14] it is reasonable to think that the appearance of the visible photoresponse by La-doping should result from the introduction of the deep subband gap states, $[Ti; 3d(t_{2g})]_{sub}$, accompanying the simultaneous introduction of the acceptor subband gap states, $[O; 2p]_{sub}$, above the valence band.

Figure 4 shows the effect of La-doping on wavelength dependences of the quantum efficiency(η) at 0 volt. It is obvious from comparison for curve 1 with curve 2 that La-doping results in a decrease of U.V. photocurrent, being inconsistent with Odekirk's results.[28] Thus the subband gap energy states introduced by La-doping act as intermediate centers for secondary recombination processes between the photogenerated conduction band

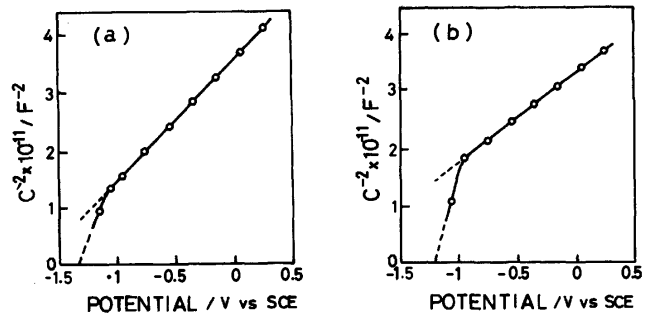

Fig. 3. Mott-Schottky plots at a frequency of 10 kHz for La-doped electrodes in 1 M NaOH.
(a) La(0.2 %), (b) La(0.5 %).

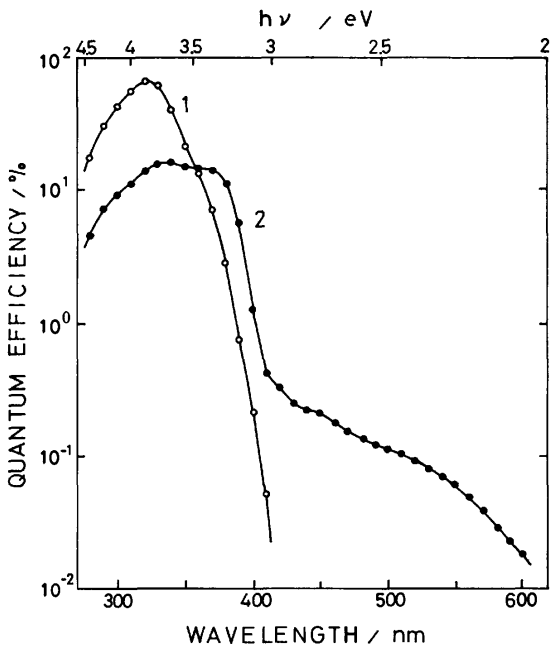

Fig. 4. Wavelength dependences of quantum efficiency of photocurrent for the undoped(curve 1) and La(1 %)doped(cuvre 2) electrodes at 0 volt in 1 M NaOH.

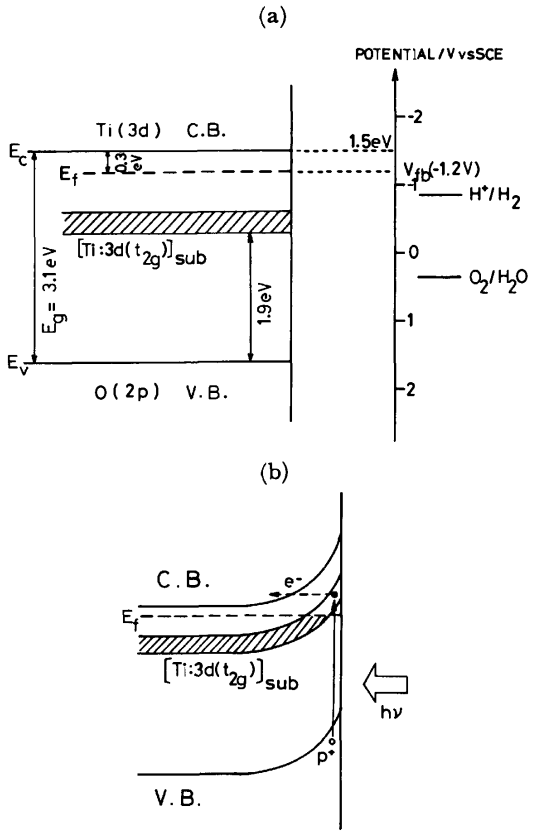

Fig. 5. Energy level diagram for La(0.5 %)-doped $SrTiO_3$ electrode at the flatband potential in 1 M NaOH (a) and a predominant mechanism giving rise to an anodic visible photoresponse (b).

electrons and valence band holes. At the same time, La-doping leads to a remarkable increase of the visible photoresponse down to 600 nm. Besides, one can see the appearance of shoulder near 370 nm in curve 2 for the La-doped sample. From $(\eta h\nu)^{1/2}$ *vs.* $h\nu$ plots by using Fig. 4, we can deduced a reduced value of E_g (3.10 eV) for the La(0.5%)-doped sample together with E_g=3.15 eV for the undoped sample. Furthermore, $(\eta h\nu)^{1/2}$ *vs.* $h\nu$ plots in the longer wavelengths can be extrapolated to E_g'=1.9 eV which probably corresponds to the energy gap between the top of the valence band and [Ti; $3d(t_{2g})]_{sub}$ or between the $[O; 2p]_{sub}$ and the bottom of the conduction band.

Based on the existence of the two subband gap energy states resulting from La-doping, two main mechanisms could be proposed to explain the production of the visible photocurrent. In mechanism I, the photocurrent is due to a direct electron excitation from the valence band to the empty [Ti; $3d(t_{2g})]_{sub}$ followed by a tunneling process of the excited electron to the conduction band. In mechanism II the electrons are photoexcited from the $[O; 2p]_{sub}$ to the conduction band by the visible light. The photogenerated holes must then tunnel into the valence band. Both processes I and II could take place simultaneously, especially under high anodic polarization.

Figure 5-(a) illustrates a schematic energy diagram at the flatband potential for the La(0.5%)-doped electrode in 1M NaOH solution when the mechanism I is assumed to be more predominant. From the observed value of V_{fb}=−1.20 volts and an assumption of $E_c-E_f\simeq$0.3 eV, the bottom of the conduction band, E_c, was set at −1.50 volts *vs.* SCE. The [Ti; $3d(t_{2g})]_{sub}$ states exist not only near the surface but also in the bulk of the electrode, differing from those in the polished undoped sample. As shown in Fig. 5-(b), anodic biasing is necessary for making the [Ti; $3d(t_{2g})]_{sub}$ states empty and for accelerating the tunneling process. The onset potential of the visible photocurrent must be much more positive than V_{fb}. As described above, the visible photocurrent of the polished undoped sample has a tendency to be saturated as the potential raises up. It appears to reflect the limited state density of the subband gap energy levels which decreases rapidly with the depth from the surface. On the other hand, in the La-doped sample the raising of anodic potential leads to a continuous increase in the empty state density by lowering E_f, and consequently results in the continuous increase of the visible photocurrent, at least below 1 volt.

Rerefences

1) T. Watanabe, A. Fujishima, and K. Honda, *Bull. Chem. Soc. Jpn.*, **49**, 355 (1976).

2) M. S. Wrighton, A. B. Ellis, P. T. Walczanski, P. L. Morse, M. B. Abrahamson, and D. S. Ginley, *J. Amer. Chem. Soc.*, **98**, 2774 (1976).

3) M. Okuda, K. Yoshida, and N. Tanaka, *J. Appl. Phys.*, **15**, 1599 (1976).

4) A. K. Ghosh and H. P. Maruska, *J. Electrochem. Soc.*, **124**, 1516 (1977).

5) M. H. Kung, H. S. Jarret, A. W. Sleight, and A. Ferretti, *J. Appl. Phys.*, **48**, 2463 (1977).

6) H. Yoneyama, M. Koizumi, and H. Tamura, *Bull. Chem. Soc. Jpn.*, **52**, 3449 (1979).

7) F. V. Kerchove, J. Vandermolen, W. P. Gomes, and F.

Cardon, Ber. Bunsenges. *Phys. Chem.*, **83**, 230 (1979).
8) F. P. Keffberg, K. Dwight, and A. Wold, *Solid State Commun.*, **30**, 443 (1979).
9) J. Vandermolen, W. P. Gomes, and F. Cardon, *J. Electrochem. Soc.*, **127**, 324 (1980).
10) J. F. Juliao, F. Decker, R. Brenzihofer, and M. Abramovich, *J. Electrochem. Soc.*, **127**, 2067 (1980).
11) J. B. Mavroides, J. A. Kafalas, and D. F. Kolesar, *Appl. Phys. Lett.*, **28**, 241 (1976).
12) M. A. Butler, M. Abramovich, F. Decker, and J, F. Juliao, *J Electrochem. Soc.*, **128**, 200 (1981).
13) B. Chang, G. Campet, J. Claverie, and P. Hagenmuller, *Solid State Commun.*, **43**, 335 (1982).
14) B. Chang, G, Campet, J. Claverie, P. Hagenmuller, and J. B. Goodenough, *J. Solid State Chem.*, **49**, 247 (1983).
15) A. K. Ghosh, F. G. Wakin, and R. R. Addiss, Jr., *Phys. Rev.*, **184**, 949 (1969).
16) E. Simanek, N. L. Huang Liu, and R. L. Wild, *J. Phys. Chem. Solids*, **33**, 951 (1972).
17) K. W. Blazey, R. Koch, and L. G. Bedorz, J. de Physique, Coll. C6, Suppl. No. 7, Tome 41, C6/511, 1980.
18) K. W. Blazey, R. Koch, and K. A. Müller, *Mat. Res. Bull.*, **16**, 1149 (1981).
19) U. Balachandran and N. G. Eror, *J. Solid State Chem.*, **39**, 351 (1981).
20) N.-H. Chan, R. K. Sharma, and D. M. Smyth, *J. Electrochem. Soc.*, **128**, 1762 (1981).
21) W. J. Lo and G. A. Somorjai, *Phys. Rev., B* **15**, 4942 (1978).
22) V. E. Henrich, G. Dresselhaus, and H. J. Zeiger, *Phys. Rev., B* **15**, 4908 (1978).
23) V. E. Henrich, G. Dresselhaus, and H. J. Zeiger, *J. Vac. Sci. Technol.*, **15**, 534 (1978).
24) H. P. R. Frederikse, W. R. Thurrer, and W. R. Hosler, *Phys. Rev.*, **134**, A442 (1964).
25) U. Balachandran and N. G. Eror, *Commun. Amer. Ceram. Soc., C* **64**, 75 (1981).
26) N. G. Eror and U. Balachadran, *J. Solid State Chem.*, **40**, 85 (1981).
27) B. Odekirk, U. Balachandran, N. G. Eror, and J. S. Blakemore, *Mat. Res. Bull.*, **17**, 199 (1982).
28) B. Odekirk and J. S. Blakemore, *J. Electrochem. Soc.*, **130**, 321 (1983).
29) M. Matsumoto, M. Hiramoto, and H. Tsubomura, *J. Electrochem. Soc.*, **130**, 326 (1983).
30) B. Chang, unpublished.
31) J. H. Kennedy and K. W. Frese, Jr., *J. Electrochem. Soc.*, **125**, 723 (1975).
32) G. Campet, M. P. Dare-Edwards, A. Hamnett, and J. B. Goodenough, *Nouv. J. Chimie*, **4**, 501 (1980).

The Reactions of Hydrogen and Deuterium Atoms with Four Ketenes

Hironobu UMEMOTO, Shigeru TSUNASHIMA,* Shin SATO,† Nobuaki WASHIDA,†† and Shiro HATAKEYAMA††
Department of Applied Physics, Tokyo Institute of Technology, Ookayama, Meguro-ku, Tokyo 152
†*Research Laboratory for Nuclear Reactors, Tokyo Institute of Technology, Ookayama, Meguro-ku, Tokyo 152*
††*Division of Atmospheric Environment, The National Institute for Environmental Studies, Tsukuba-gakuen, Ibaraki 305*
(Received March 3, 1984)

The rate constants of the reactions of hydrogen and deuterium atoms with four ketenes have been measured using a pulse radiolysis-resonance absorption technique. For hydrogen atoms, the temperature dependence was also examined in the range of 240—440 K. The rate constants were well expressed by these Arrhenius equations: k(H+ketene)=$3.9\times10^{6}\exp(-975/T)$; k(H+methylketene)=$7.4\times10^{6}\exp(-881/T)$; k(H+ethylketene)=$4.4\times10^{6}\exp(-728/T)$; k(H+dimethylketene)=$6.0\times10^{6}\exp(-773/T)$, in units of $m^3\,mol^{-1}\,s^{-1}$. No isotope effect between H and D atoms could be observed except for the gas-kinetic-collision frequency.

In the reaction of oxygen atoms with simple olefins, it was found that the rate constants increase with the increase in the number of substituted alkyl radicals: ethylene<propene≃1-butene<2-methylpropene≃*cis*- and *trans*-2-butene<2-methyl-2-butene<2,3-dimethyl-2-butene.[1] On the other hand, in the reactions of hydrogen atoms, the order is quite different: ethylene≃*cis*- and *trans*-2-butene≃2,3-dimethyl-2-butene<propene≃1-butene≃2-methyl-2-butene<2-methyl-propene.[2,3] The rate constants for deuterium atoms were found to be always $1/\sqrt{2}$ of those for hydrogen atoms, suggesting that this isotope effect is due to the difference in collision frequency.[3,4]

Recently, we measured the rate constants of the reactions of oxygen atoms with four ketenes: ketene and methyl-, ethyl-, and dimethylketenes, and found that the rate constants increase with the increase in the number of substituted alkyl radicals, the order is similar to that obtained with olefins: ketene<methylketene≃ethylketene<dimethylketene. It was also found that the reactions of the last three ketenes have negative activation energies.[5]

For a comprehensive understanding of this type of reaction, we have measured the Arrhenius parameters for the reactions of hydrogen atoms with these four ketenes, since no previous work has shown these parameters except for the reaction of hydrogen atoms with the simplest ketene.

Experimental

The details of the preparation of ketenes were described in a previous paper.[5] The method of the rate-constant measurement was similar to that described previously,[4,5] except that a wave memory (NF Circuit Design Block Co., WM-852) and an X-Y recorder (Riken Denshi Co., F-35) were used to record the decay of the hydrogen and deuterium atoms. Briefly, about 80 kPa of $H_2(D_2)$ gas containing a small amount of a ketene (1—10 Pa) was irradiated with an electron pulse generated by a Febetron 706 apparatus (Hewlett Packard Co.). After the pulse, the decay in the H(D) atoms was measured by the absorption of Lymann-α. As has been discussed previously,[2] the H(D)-atom concentration is less than 1/100 that of the ketene present in the reaction chamber. Therefore, the pseudo-first-order reaction rate can be determined from this decay curve. The temperature of the reaction vessel was controlled by winding it with a heating tape or by introducing N_2 gas from boiling liquid nitrogen to the surrounding copper tubing. The reactant temperature was measured with a copper-constantan thermocouple at the center in the reaction chamber prior to pulse-irradiation.

Results

The experimental results for hydrogen atoms are summarized in Fig. 1 in the form of Arrhenius plots. All the data are well characterized by Arrhenius equa-

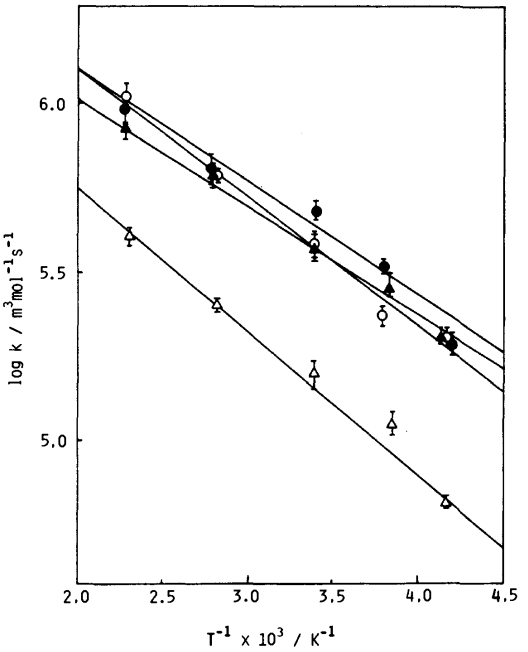

Fig. 1. Arrhenius plots for reactions H+CH_2CO (△), H+$CH_3(CH)CO$ (○), H+$C_2H_5(CH)CO$ (▲), and H+$(CH_3)_2CCO$ (●). The indicated error limits are 1σ diviations of the fit.

Table 1. Rate constants of H- or D-atom addition to ketenes at 295 K in units of $10^5\,m^3\,mol^{-1}\,s^{-1}$

	CH_2CO	$CH_3(CH)CO$	$C_2H_5(CH)CO$	$(CH_3)_2CCO$
H	1.6±0.2	3.8±0.3	3.7±0.4	4.8±0.3
D	1.2±0.1	2.8±0.2	2.5±0.3	4.1±0.2
k_D/k_H	0.76	0.75	0.68	0.85

Uncertainties are standard deviations.

Table 2. Arrhenius parameters for H+ketene reactions

Ketene	E_a/kJ mol^{-1}	A/10^6 m^3 mol^{-1} s^{-1}
CH_2CO	8.1±0.6	3.9±1.1
$CH_3(CH)CO$	7.3±0.8	7.4±2.4
$C_2H_5(CH)CO$	6.1±0.5	4.4±0.8
$(CH_3)_2CCO$	6.4±1.5	6.0±3.8

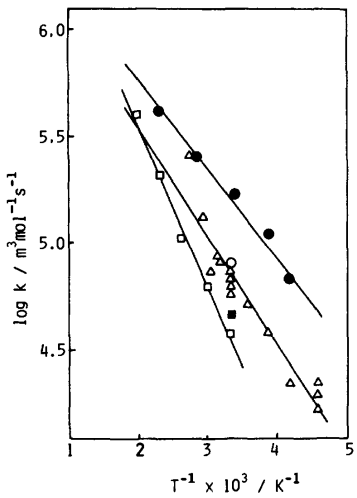

Fig. 2. Arrhenius plots for the reaction H+CH_2CO; △: Šlemr and Warneck; □,■: Michael *et al.*; ○: Carr *et al.*; ●: this work.

tions. The results at room temperature are also shown in Table 1. The Arrhenius parameters, as determined by the least-squares method, are listed in Table 2.

Discussion

There have been previous measurements of the temperature dependence of the reaction between hydrogen atoms and the simplest ketene.[6,7] Figure 2 compares their data with ours. Unfortunately, no two of the three measurements are in good agreement with each other. In this figure, two other measurements carried out at room temperature are also included.[7,8]

Šlemr and Warneck used a discharge-flow method combined with a mass-spectrometer.[6] Hydrogen atoms were generated by microwave discharge in a low-pressure helium-gas flow containing hydrogen. Ketene was introduced into the flow behind the discharge. The sampling of the gas mixture for mass-spectroscopic analysis was carried out *via* a pin hole located at the bottom of the cylindrical reactor. The rate constant was estimated by measuring the decrease as the concentration of ketene as a function of the distance of the reaction zone, in which atomic hydrogen was present in excess. The concentration of hydrogen atoms was measured in different runs by titration with nitrogen dioxide. The authors stated that a large error could be expected to occur in the estimation of the concentration of hydrogen atoms. If their measured concentration is twice as large, the rate constants they obtained will be in good agreement with ours. In the present experiments, however, the absolute concentration of hydrogen atoms is not necessary to estimate the rate constants.

Michael *et al.* used two techniques, flash photolysis-resonance fluorescence and discharge flow-resonance fluorescence.[7] The temperature dependence was measured only by the former method. In this measurement, hydrogen atoms were produced by the flash photolysis of a mixture of methane, ketene, and diluent argon at λ>105 nm or by the flash photolysis of a two-component mixture of ketene and argon at λ>165 nm. The time-resolved detection of hydrogen atoms was accomplished by observing scattered resonance fluorescence at 121.6 nm. According to their paper, they had difficulty in creating appropriate conditions under which the rate measurment could be carried out, because ketene strongly absorbs the resonance fluorescence from excited hydrogen atoms.

The present authors also found that the absorption coefficient of ketene at 121.6 nm is larger than those of the olefins, but no difficulties were found in measuring the decay of hydrogen atoms. The discrepancy between the results of the discharge-flow method and the present one may be explained by the difference in the total pressures. Since the present results were obtained in the presence of 80 kPa of hydrogen, the rate constants may be regarded as the high-pressure limits.[2] On the other hand, under low-pressure conditions, such as in the case of the discharge flow, the measured rate constants may not be the limits. This explanation, however, is not applicable to the results of Michael *et al.*, who could observe no total pressure dependence of the rate constants between 2.7 and 13.3 kPa.

In the reactions of oxygen atoms with ketenes, the rate constants increase with the increase in the number of substituted alkyl radicals; the result is similar to that obtained with olefins.[1,5] On the other hand, in the reactions of hydrogen atoms, ketenes and olefins have different tendencies in their reaction rates; in the case of olefins, both activation energies and preexponential factors decrease with the increase in the number of the substituted alkyl radicals, while no systematic change could be observed in the case of ketenes.[3,9,11] Especially, there are no large differences among the rate constants of methyl-, ethyl-, and dimethylketene. This suggests that the reaction paths may be different in the reactions of hydrogen atoms with olefins and ketenes.

An oxygen atom adds to the C=C double bond, and the intermediate complex is believed to be formed either with olefins or with ketenes, although the detailed structure is not known. Cvetanović suggested a π-complex-type structure for the intermediate complex in the reactions of oxygen atoms with olefins.[11] If a similar structure can be assumed for the complex in the reactions with ketenes, the effect of the substituted alkyl radicals may well be similar to those of both olefins and ketenes.

On the other hand, in the hydrogen-atom reactions with olefins, it is believed that the hydrogen atom adds to the C=C double bond at the C-atom with less substituted alkyl radicals. The *ab initio* calculation showed that the geometry at the saddle point in the reaction between the H-atom and propene is:[10]

$$H_3C\text{-}\underset{\vdots\,H}{CH}\text{-}CH_2.$$

In the investigation of the reaction mechanism of the reaction between hydrogen atoms and ketene, the following primary step has been proposed:[8]

$$H + CH_2CO \longrightarrow CH_3 + CO.$$

If this mechanism is also applicable to other ketenes,

$$H + \begin{matrix}R_1\\R_2\end{matrix}CCO \longrightarrow \begin{matrix}R_1\\R_2\end{matrix}CH + CO,$$

and the intermediate complex can be illustrated as follows:

$$\begin{matrix}R_1\\R_2\end{matrix}\!\!\diagdown\!\!\diagup C\text{-}C{=}O,\quad \vdots\,H$$

then the order of the rate constants of ketenes may not necessarily agree with those obtained in the reaction of hydrogen atoms with olefins. Bennett and Mile have found that ketene is unique in the reaction with atomic hydrogen at 77 K.[12] They employed a rotating cryostat in conjunction with electron-spin-resonance spectroscopy. When water was used as the matrix, acetyl and methyl radicals were detected. This suggests that the initial step of the reaction is the addition of H atoms to the methylene group of ketene to give the CH_3-C=O radical, followed by decomposition into CH_3 and CO. This mechanism was further confirmed by the experiments with D atoms. On the other hand, in a matrix of benzene, the addition of H atoms occurred at the central carbon atom to give the CH_2-CH=O radical, while in a matrix of adamantane, both CH_3-C=O and CH_2-CH=O radicals were observed. They emphasized that no such dependence of the site of addition on the nature of the matrix could be observed in the cases of other unsaturated compounds. Further experiments to identify the initial radical products from H atoms and ketene and alkyl substituted ketenes are highly desirable.

The isotope effect observed in the present experiments between H- and D-atom reactions can be explained by taking into account the difference in collision frequency, as has been discussed in the case of olefin reactions.[4]

References

1) K. Sugawara, Y. Ishikawa, and S. Sato, *Bull. Chem. Soc. Jpn.*, **53**, 1344 (1980).
2) Y. Ishikawa, M. Yamabe, A. Noda, and S. Sato, *Bull. Chem. Soc. Jpn.*, **51**, 2488 (1978).
3) T. Kyogoku, T. Watanabe, S. Tsunashima, and S. Sato, *Bull. Chem. Soc. Jpn.*, **56**, 19 (1983).
4) Y. Ishikawa and S. Sato, *Bull. Chem. Soc. Jpn.*, **52**, 984 (1979).
5) N. Washida, S. Hatakeyama, H. Takagi, T. Kyogoku, and S. Sato, *J. Chem. Phys.*, **78**, 4533 (1983).
6) F. Šlemr and P. Warneck, *Ber. Bunsen. Phys. Chem.*, **79**, 152 (1975).
7) J. V. Michael, D. F. Nava, W. A. Payne, and L. J. Stief, *J. Chem. Phys.*, **70**, 5222 (1979).
8) R. W. Carr, Jr., I. D. Gay, G. P. Glass, and H. Niki, *J. Chem. Phys.*, **49**, 846 (1968).
9) K. Sugawara, K. Okazaki, and S. Sato, *Bull. Chem. Soc. Jpn.*, **54**, 2872 (1981).
10) T. Watanabe, T. Kyogoku, S. Tsunashima, S. Sato, and S. Nagase, *Bull. Chem. Soc. Jpn.*, **55**, 3720 (1982).
11) R. J. Cvetanović, *Adv. Photochem.*, **1**, 115 (1963).
12) J. E. Bennett and B. Mile, *J. Chem. Soc. Faraday Trans. 1*, **69**, 1398 (1973).

 © 1984 The Chemical Society of Japan Bull. Chem. Soc. Jpn., 57, 2581—2583 (1984)

The Crystal and Molecular Structure of 3,4-Dimethyl-2,5-diphenyl-3,4-dihydro-3a-thia-1,3,4,6-tetraazapentalene

Fujiko Iwasaki* and Kin-ya Akiba†

Department of Materials Science, The University of Electro-Communications, Chofu-shi, Tokyo 182

†*Department of Chemistry, Faculty of Science, Hiroshima University, Hiroshima 730*

(Received March 5, 1984)

The crystal structure of 3,4-dimethyl-2,5-diphenyl-3,4-dihydro-3a-thia-1,3,4,6-tetraazapentalene has been determined by the X-ray method. The crystals are orthorhombic, space group Pbcn, a=14.533(4), b=9.285(3), c=11.305(2) Å, V=1525.4(6) Å^3, Z=4, D_x=1.343 Mg m^{-3}. The final R value is 0.060 for 1107 reflections. The molecule has an exact C_2 symmetry, with the central S-C bond coincident with the 2-fold axis of the crystal symmetry. The length of 1.904 Å of the two equivalent S-N bonds indicates that the molecule is a tetraaza analogue of the thiathiophthenes. The length of this S-N bond is 9% longer than the N-S single bond and significantly less than the sum of the van der Waals radii.

In the course of the 1,3-dipolar addition to 4,5-dihydro-1,2,4-thiadiazole a bond switch has taken place at the π-hypervalent sulfur atom,[1,2] An intermediate state of the reaction should be of a thiathiophthene type; in fact, a molecule of such a type has been found in the crystalline state.[3] An addition of *N*-methylbenzimidoyl chloride to 5-amino-1,2,3,4-thiatriazole gave 2-methyl-3-phenyl-5-imino-2,5-dihydro-1,2,4-thiadiazole hydrochloride. Further addition gave the molecule **I**.[4] For such symmetric substituents it is interesting to investigate whether the molecule of **I** has a symmetric or unsymmetric structure. An X-ray structure analysis was undertaken to elucidate the structure of **I**.

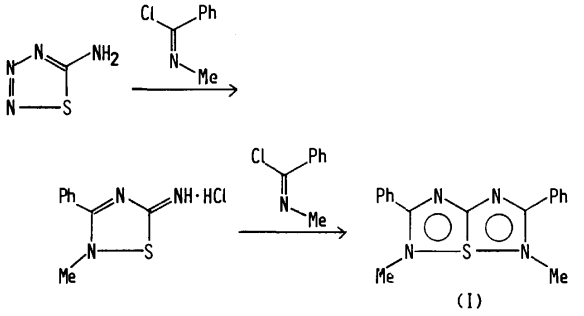

Scheme 1.

Experimental

Crystal Data: $C_{17}H_{16}N_4S$, Mw=308.40, Orthorhombic, Pbcn, a=14.533(4), b=9.285(3), c=11.305(2) Å, V=1525.4(6) Å^3, Z=4, D_x=1.343 Mgm^{-3}.

Colorless crystals were grown from benzene-hexane solution. Intensities were collected on a Rigaku automatic diffractometer with graphite-monochromated Mo $K\alpha$ radiation, using the crystal with approximate dimensions 0.15×0.25×0.35 mm. Reflections in the range $2\theta \leq 55°$ were measured by the ω–2θ scan technique with a scan width of 1.2°+0.5° tan θ and a scanning rate of 4° min^{-1} in 2θ. At both ends of the scan range 10 s background counts were taken for each reflection. 1107 Reflections had $|F_o| \geq 3\sigma(F_o)$ and were considered observed. No absorption corrections were applied.

The structure was solved by the direct method with the program MULTAN 78.[5] Non-hydrogen atoms were refined by the block-diagonal least-squares with anisotropic temperature factors to an R value of 0.09. A difference map showed the all hydrogen atoms. A possibility of a disordered structure was clearly eliminated by the examination of the D-map and anisotropic temperature factors. Further refinement with anisotropic temperature factors for non-hydrogen atoms and isotropic ones for H gave the final R value of 0.060. The quantity minimized was $\sum w(|F_o|-k^{-1}|F_c|)^2$. w=0.3 if $|F_o|<4.0$, w=1.0 if $4.0 \leq |F_o| \leq 16.0$ and $w=(16.0/|F_o|)^2$ if $|F_o|>16.0$. Atomic scattering factors were taken from "International Tables for X-ray Crystallography".[6] All computations were performed on a HITAC M180 Computer of the Data Processing Center of the University of Electro-Communications with the programs UNICS III,[7] MULTAN 78,[5] and ORTEP II.[8] The final atomic parameters are given in Table 1.[9]

Discussion

Figure 1 shows the atomic numbering of the crystal-chemical unit. Bond lengths and angles are listed in Table 2. The molecule has an exact C_2 symmetry, with

Table 1. Atomic coordinates (×10^4, for H ×10^3) and isotropic temperature factors

For non-H atoms $B=B_{eq}=4/3\sum_i\sum_j\beta_{ij}a_i\cdot a_j$.

Atom	x	y	z	B_{eq}/Å^2
S (6)	5000	4845 (1)	2500	2.8
C (3)	5000	2945 (6)	2500	2.5
N (1)	5787 (2)	4586 (4)	3830 (3)	2.9
C (2)	5854 (3)	3216 (4)	4117 (3)	2.7
N (3)	5433 (2)	2270 (3)	3383 (3)	2.7
C (11)	6157 (3)	5834 (5)	4454 (4)	3.4
C (21)	6288 (3)	2623 (5)	5200 (3)	2.9
C (22)	5859 (3)	1479 (5)	5760 (4)	3.4
C (23)	6215 (4)	899 (5)	6787 (4)	4.0
C (24)	7014 (4)	1435 (6)	7247 (4)	4.4
C (25)	7454 (4)	2561 (6)	6695 (4)	4.3
C (26)	7099 (3)	3159 (5)	5674 (4)	3.5
H (11)	676 (3)	601 (5)	420 (4)	3.2 (9)
H (12)	609 (3)	575 (5)	518 (4)	2.8 (9)
H (13)	580 (3)	669 (6)	420 (4)	4.2 (11)
H (22)	534 (4)	95 (7)	548 (5)	4.6 (12)
H (23)	589 (3)	22 (6)	718 (4)	3.8 (10)
H (24)	728 (4)	111 (6)	796 (5)	4.8 (12)
H (25)	796 (3)	293 (5)	694 (4)	3.1 (10)
H (26)	744 (4)	390 (7)	533 (5)	5.8 (14)

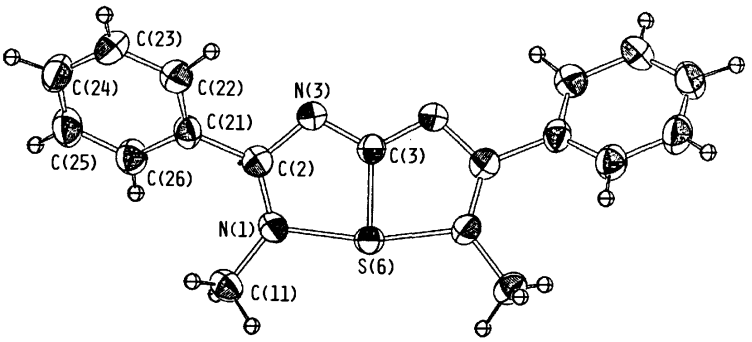

Fig. 1. Molecular structure with atomic numbering of the crystal-chemical unit. Twofold axis lies on the C(3)–S(6) bond. Each non-H atom is represented as a thermal ellipsoid with a 50% probability.

Table 2. Bond length and angle with their estimated standard deviations

Distance	l/Å	Distance	l/Å
S(6)-C(3)	1.764(5)	C(24)-C(25)	1.375(8)
S(6)-N(1)	1.904(4)	C(25)-C(26)	1.380(8)
N(1)-C(2)	1.316(5)	C(11)-H(11)	0.94(5)
C(2)-N(3)	1.354(5)	C(11)-H(12)	0.83(4)
C(3)-N(3)	1.336(6)	C(11)-H(13)	0.99(5)
N(1)-C(11)	1.460(6)	C(22)-H(22)	0.96(6)
C(2)-C(21)	1.483(6)	C(23)-H(23)	0.91(5)
C(21)-C(22)	1.385(6)	C(24)-H(24)	0.94(6)
C(21)-C(26)	1.388(6)	C(25)-H(25)	0.86(5)
C(22)-C(23)	1.380(7)	C(26)-H(26)	0.94(6)
C(23)-C(24)	1.367(8)		
Angle	ϕ/°	Angle	ϕ/°
C(3)S(6)N(1)	82.7(2)	C(21)C(26)C(25)	119.8(5)
N(1)S(6)N(1^{i})	165.5(2)	N(1)C(11)H(11)	110(3)
S(6)N(1)C(2)	111.2(3)	N(1)C(11)H(12)	111(3)
S(6)N(1)C(11)	120.2(3)	N(1)C(11)H(13)	108(3)
C(2)N(1)C(11)	128.4(4)	H(11)C(11)H(12)	115(4)
N(1)C(2)N(3)	116.3(4)	H(11)C(11)H(13)	105(4)
N(1)C(2)C(21)	126.4(4)	H(12)C(11)H(13)	108(4)
N(3)C(2)C(21)	117.2(4)	C(21)C(22)H(22)	127(4)
C(3)N(3)C(2)	111.5(4)	C(23)C(22)H(22)	112(4)
S(6)C(3)N(3)	117.9(4)	C(22)C(23)H(23)	119(3)
N(3)C(3)N(3^{i})	124.1(5)	C(24)C(23)H(23)	121(3)
C(2)C(21)C(22)	118.1(4)	C(23)C(24)H(24)	124(3)
C(2)C(21)C(26)	123.2(4)	C(25)C(24)H(24)	116(3)
C(22)C(21)C(26)	118.7(4)	C(24)C(25)H(25)	124(3)
C(21)C(22)C(23)	121.1(4)	C(26)C(25)H(25)	116(3)
C(22)C(23)C(24)	119.8(5)	C(21)C(26)H(26)	124(4)
C(23)C(24)C(25)	119.9(5)	C(25)C(26)H(26)	117(4)
C(24)C(25)C(26)	120.8(5)		

Superscript (i) $1-x$, y, $1/2-z$

the S(6)–C(3) bond coincident with the crystallographic 2-fold axis along the b axis. The S(6)–N(1) distance is 1.904 Å, 9% longer than the normal S–N single bond (1.74 Å).[10] Thus the molecule is found to be 3a-thia-1,3,4,6-tetraazapentalene, the tetraaza analogue of thiathiophthene (1,6,6a-trithiapentalene, **II**).[11] The corresponding lengths in **III**[3] are 1.983 and 1.833 Å, and in **IV**[12] 1.901 and 1.948 Å respectively. The average lengthening of the S–S bonds in the thiathiophthenes is

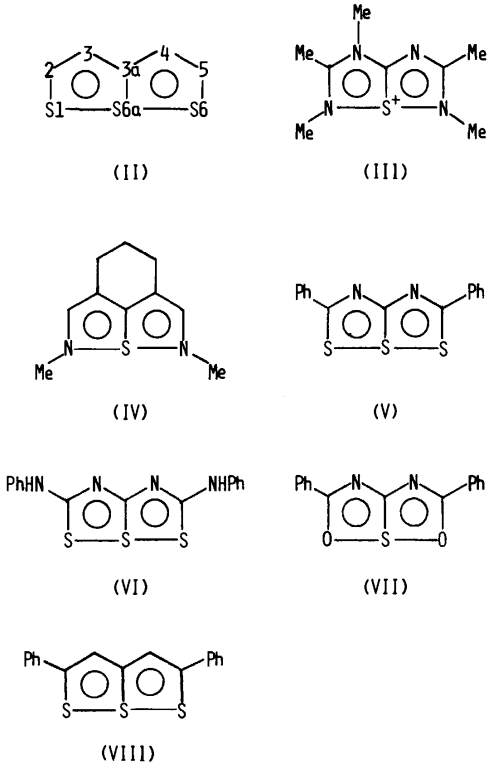

12%. The S–X (X=S, N, and O) bonds in the thiathiophthenes and in the related substances are weaker than other bonds in the molecule, and therefore are more affected by the substituents and/or by the crystalline field. The present molecule is the first example with the exactly equal S–N bonds among the N–S–N analogues of 1,6,6a-trithiapentalene. The CNDO/2 calculation based on the determined structure shows the net charges on the S and N atoms being +0.208 and −0.258 respectively. This suggests that there is an electrostatically attractive interaction between S and N. The existence of the molecule with the symmetrical N–S–N bond in the stable state is very interesting from the point of view of the 1,3-dipolar addition, where the bond-switch takes place at the π-hypervalent sulfur. Bürgi[13] pointed out that the correlation between the non-bonded and bonded S–S interactions of the thiathiophthenes corresponds to the reaction path of the linear exchange reac-

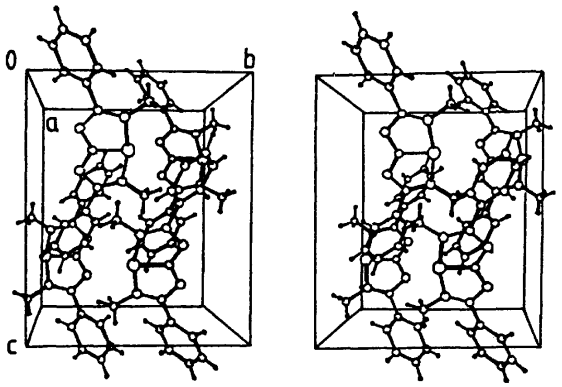

Fig. 2. Stereoscopic view of the crystal structure.

tion. The molecule of the symmetrical type should correspond to the intermediate model of the reaction such as 1,3-dipole additions.

Although the C(3)–S(6) length is longer than the corresponding ones in **III** (1.717 Å) and **IV** (1.742 Å), the longer values are also found in **V** (1.784 Å)[14] and in **VI** (1.789 Å).[15] The S(6a)–C(3a) lengths in the 1,6,6a-trithiapentalenes are remarkably constant within the range of 1.74—1.76 Å. The difference between the lengths of the S(6a)–C(3a) bonds in **I**, **V**, **VI**, and those of 1,6,6a-trithiapentalenes seems due to the presence of the two divalent N atoms in the rings of **I**, **V**, and **VI**. But for the dioxa derivative (**VII**) the short S–C bond (1.719 Å) was reported.[16] The length of the cyclic C(2)–N(3) bond is slightly longer than those in **V** (1.325 Å) and the length of the aromatic C–N bond in pyridine (1.340 Å), while the N(3)–C(3) distance is shorter than that of **V** (1.344 Å). In the 1,6,6a-trithiapentalenes the sum of the outer C(2)–C(3) and C(4)–C(5) lengths is always found to be smaller than the sum of the inner C(3a)–C(3) and C(3a)–C(4) lengths. This is the typical feature showing the resemblance between 1,6,6a-trithiapentalenes and naphthalene.[11] But in the case of 3,4-diaza derivatives such as **I**, **V**, **IV**, and **VII** no significant difference between the outer and inner N–C bonds is observed. The N(1)–C(2) bond is shorter than that of **IV** (1.388 Å) and the aromatic C–N bond. The C(2)–C(21) length is close to the average value of the corresponding C–C lengths in **V**. The N(1)–C(11) length is slightly shorter than the C–N single bond (1.47 Å). Such short C–N bonds are also found in **IV** (1.441 and 1.454 Å).

The equation for the least squares plane through the five membered ring is

$$-0.8152X+0.0375Y+0.5780Z=-4.163\ (\text{Å})$$

where X, Y, and Z in Å unit referred to the a, b, and c axes respectively. The deviations of S(6), N(1), C(2), N(3), C(3), C(11) and C(21) are 0.033, −0.039, 0.024, 0.012, −0.030, −0.028 and 0.198 Å respectively. The phenyl ring is planar with deviations within 0.007 Å. The dihedral angle between the planes of the central ring and the phenyl ring is 40.0°. The corresponding angles are 2.0 and 7.0° in **V**, 45.1 and 3.3° in **VIII**,[17] and nearly 0° in **VII**.

Figure 2 shows the stereoscopic view of the molecular packing. There are no significant intermolecular contacts shorter than the sum of the van der Waals radii.

References

1) K. Akiba, S. Arai, T. Tsuchiya, Y. Tamamoto, and F. Iwasaki, *Angew. Chem.*, **91**, 176 (1979); *ibid.*, (Int. ed. Engl.) **18**, 166 (1979).

2) K. Akiba, S. Arai, and F. Iwasaki, *Tetrahedron Lett.*, **1978**, 4117.

3) F. Iwasaki and K. Akiba, *Acta Crystallogr., Sect. B*, **37**, 180 (1981).

4) Y. Yamamoto and K. Akiba, *Heterocycles*, **13**, 297 (1979).

5) P. Main, S. E. Hull, L. Lessinger, G. Germain, J. P. Declercq, and M. M. Woolfson, MULTAN 78. A System of Computer Programs for the Automatic Solution of Crystal Structures from X-Ray Diffraction Data. Univs. of York and Louvain-la-Nerve, Belgium. (1978).

6) "International Tables for X-ray Crystallography," Birmingham, Kynoch Press (1974), Vol. IV.

7) T. Sakurai and K. Kobayashi, *Rikagaku Kenkyusho Hokoku*, **55**, 69 (1979).

8) C. K. Johnson, ORTEP II, Report ORNL-5138, Oak Ridge National Laboratory, Tennessee (1971).

9) The tables for the anisotropic temperature factors for non-hydrogen atoms and the F_o–F_c list are deposited as Document No. 8439 at the Office of the Chemical Society of Japan.

10) L. Pauling, "The Nature of Chemical Bond," 3rd ed. Cornell University Press, Ithaca (1960).

11) L. K. Hansen and A. Hordvik, *Acta Chem. Scand.*, **27**, 411 (1973).

12) A. Hordvik and K. Julshamn, *Acta Chem. Scand.*, **26**, 343 (1972).

13) H. B. Burgi, *Angew. Chem.* **87**, 461 (1975); *ibid.* (Int. ed. Engl.) **14**, 460 (1975).

14) A. Hordvik and L. M. Milje, *Acta Chem. Scand.*, **27**, 510 (1973).

15) A. Hordvik and P. Oftedal, *Acta Chem. Scand., Ser. A*, **35**, 663 (1981).

16) M. Dalseng, L. K. Hansen and A. Hordvik, *Acta Chem. Scand., Ser. A*, **35**, 645 (1981).

17) A. Hordvik, *Acta Chem. Scand.*, **25**, 1583 (1971).

Polarized Raman and Infrared Spectra of 2-Chloro- and 2-Bromopyrimidines

Sekiichiro NAKAMA,† Hiroko SHIMADA,* and Ryoichi SHIMADA††
Department of Chemistry, Faculty of Science, Fukuoka University, Nanakuma, Jonan-ku, Fukuoka 814
†*Department of Chemistry, Faculty of Liberal Arts, University of Yamaguchi, Yoshida, Yamaguchi 753*
††*Department of Chemistry, Faculty of Science, Kyushu University 33, Hakozaki, Higashi-ku, Fukuoka 812*
(Received March 7, 1984)

The polarized Raman and infrared spectra of 2-chloro- and 2-bromopyrimidines were studied. Assignments of the normal vibrations for these molecules were made on the basis of polarization behaviors of the Raman and infrared bands and also through the normal coordinate calculation.

The infrared spectrum of 2-chloropyrimidine was first observed by Short and Thompson[1] and Lafaix and Lebas.[2] Sarma[3] remeasured the infrared spectrum of this molecule and gave assignment for the in-plane vibrations based on the normal coordinate calculation. Allenstein *et al.*[4] studied the infrared and Raman spectra of 2-fluoro-, 2-chloro-, 2-bromo-, and 2-iodopyrimidines and gave assignments for the normal vibrations of these molecules. Their assignments were not made on the basis of enough experimental evidences and no reasonable vibrational analysis of the phosphorescence spectrum of 2-chloropyrimidine, which shows the characteristic vibrational structure due to the Cl atom, can be made using their assignments.

In this paper, the assignments for the normal vibrations of 2-chloro- and 2-bromopyrimidines are reexamined through measurements of polarization behaviors of the Raman and infrared spectra.

Experimental

Material. 2-Chloro- and 2-bromopyrimidines were synthesized from 2-aminopyrimidine by means of the diazo reaction. The crude products were recrystallized from isopentane and then purified by repeated vacuum distillations. The final purification was made by zone-refining of about 100 passages.

Optical Measurement. Polarization measurement of the Raman spectrum was made in molten and single crystal phases with a JEOL 400 T Laser Raman Spectrophotometer. The sample was excited with the 514.5 nm line from an Ar^+ ion laser. A well grown single crystal of 2-chloropyrimidine was obtained by the Bridgman method. Then a cubic sample of about 5 mm^3 was cut off, where the cleavage plane was selected as one of the planes of the cube and each edge of the cube was cut along the crystallographic axis with a polarization microscope. A block of single crystal of 2-bromopyrimidine could not be obtained because this molecule was decomposed by heating over many hours in the Bridgman furnace. Thus a single crystal of this molecule was grown in a capillary glass tube of about 70 mm in length and 3 mm in diameter having a sharp conical end by heating for about three hours in the Bridgman furnace. The method of measurement of the polarized Raman spectrum was exactly the same as that described previously.[5]

The infrared spectrum was observed in molten and single crystal phases with a Hitachi Infrared Spectrophotometer Model 345. The preparation of the single crystal sample and the method of measurement of the polarized infrared spectrum are exactly the same as those described previously.[6,7]

Normal Coordinate Calculation

A normal coordinate calculation was performed through the standard ***GF*** matrix method with a FACOM M-200 computer at the Computer Center of Kyushu University. The geometrical parameters of the 2-chloropyrimidine molecule were taken from the data determined by Furberg *et al.*[8] The molecular structure of 2-bromopyrimidine was assumed to be identical with that of 2-chloropyrimidine except for the C–Br bond, whose distance was assumed to be 0.185 nm. The ***F*** matrix elements for the in-plane vibrations were evaluated with the potential fields of an improved modification of the Urey-Bradley force field.[5,6,7] The potential field is given by

$$V = V_{UB} + \rho\{\Sigma(\Delta R,\Delta R)_o - \Sigma(\Delta R,\Delta R)_m + \Sigma(\Delta R,\Delta R)_p\} + \Sigma k^o(\Delta r,\Delta r) + \Sigma k^m(\Delta r,\Delta r) + \Sigma k^m(\Delta R,\Delta R) + \Sigma h^m(\Delta R,\Delta\alpha) + \Sigma h^m(\Delta R,\Delta\beta) + \Sigma f^o(\Delta\alpha,\Delta\alpha),$$

where the symbols such as V_{UB} are the same as those used in the previous papers.[5,6,7] The symbols given for the atoms and internal coordinates and the molecular axes are illustrated in Fig. 1. For the out-of-plane vibrations the valence force field and the ϕ type torsional coordinates were used. The notations of the force constants Q, q, P, p, and t are the same as those given by Whiffen.[9]

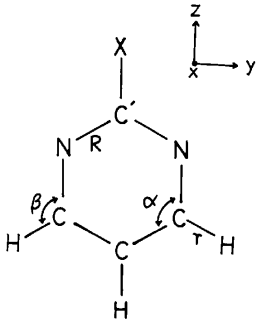

Fig. 1. Symbols given for the atoms and internal coordinates.

Results and Discussion

The force constants used for the in-plane and out-of-plane vibrations of 2-chloro- and 2-bromopyrimidines are listed in Tables 1 and 2, respectively. These values are consistent with the force constants given for pyrimidine.[10] The calculated frequencies and modes of the normal vibrations are given in Table 5.

Table 1. Force constants for in-plane vibrations

K_{C-N}	5.90	
K_{C-C}	4.65	
K_{C-H}	4.46	
K_{C-X}	2.07[a]	1.75[b]
H_{NCN}	0.75	
H_{NCC}	0.52	
H_{CNC}	0.40	
H_{CCC}	0.20	
H_{HCN}	0.19	
H_{XCN}	0.10[a]	0.08[b]
H_{HCC}	0.19	
$F_{C\cdots N\cdots C}$	0.52	
$F_{N\cdots C\cdots X}$	1.08[a]	0.92[b]
$F_{N\cdots C\cdots N}$	0.80	
$F_{N\cdots C\cdots C}$	0.51	
$F_{N\cdots C\cdots H}$	0.68	
$F_{C\cdots C\cdots C}$	0.80	
$F_{C\cdots C\cdots H}$	0.49	
ρ	0.26	
$k^{o}_{(H,H)}$	0.06	
$k^{m}_{(H,H)}$	−0.07	
$k^{m}_{(R,R)}$	−0.10	
$h^{m}_{(R,\alpha_H)}$	−0.05	
$h^{m}_{(R,\beta_X)}$	−0.06	
$h^{m}_{(R,\beta_H)}$	0.11	
$f^{o}_{(\alpha,\alpha)}$	0.08	

Force constants denoted by K, H, F, ρ, and k are given in J/dm² (=mdyn/Å) units, and those denoted by h and f are in pJ/dm rad (=mdyn/rad) and aJ/rad² (=mdyn Å/rad²) units, respectively. a) X is Cl atom. b) X is Br atom.

Table 2. Force constants for out-of-plane vibrations

$Q_{C'-N}$	0.17	
Q_{C-N}	0.18	
Q_{C-C}	0.20	
q^{o}	−0.06	
q^{m}	0.03	
P_X	0.36[a]	0.37[b]
P_H	0.34	
p^{o}	0.07	
$p^{m}_{H,X}$	−0.02	
$P^{m}_{H,H}$	−0.07	
p^{p}	0.02	
$t^{o}_{C'-N,X}$	−0.01	
$t^{o}_{C-N,H}$	−0.02	
$t^{o}_{C-C,H}$	−0.02	

Force constants are given in aJ/rad² (=mdyn Å/rad²) units. a) X is Cl atom. b) X is Br atom.

The polarized Raman and infrared spectra of 2-chloro- and 2-bromopyrimidines observed in single crystals are shown in Figs. 2, 3, 4, and 5, respectively. The infrared spectra measured with incident lights polarized parallel and perpendicular to the crystal growth direction, which was determined to be one of the crystallographic axes for both molecules, are referred to as // and ⊥ spectra and drawn with the solid and dotted lines, respectively. The polarized Raman spectrum of 2-chloropyrimidine single crystal was denoted by two characters such as uv. The first letter refers to the direction of polarization of the excitation light and the latter to that of the scattering light. Since the crystallographic analysis for the cleavage plane of 2-chloropyrimidine single crystal was not reported yet, the crystal growth direction was tentatively taken to the u axis and the direction perpendicular to it in the cleavage plane was taken to the v axis. The w axis was taken to the direction perpendicular to both the u and v axes. A single crystal of 2-bromopyrimidine grown in a capillary tube was held in a capillary cell system of JEOL Model RS-VTC41 in such a way that both the crystal growth direction and other one of the crystallographic axes make right angle to the excitation light beam polarized along the crystal growth direction. The scat-

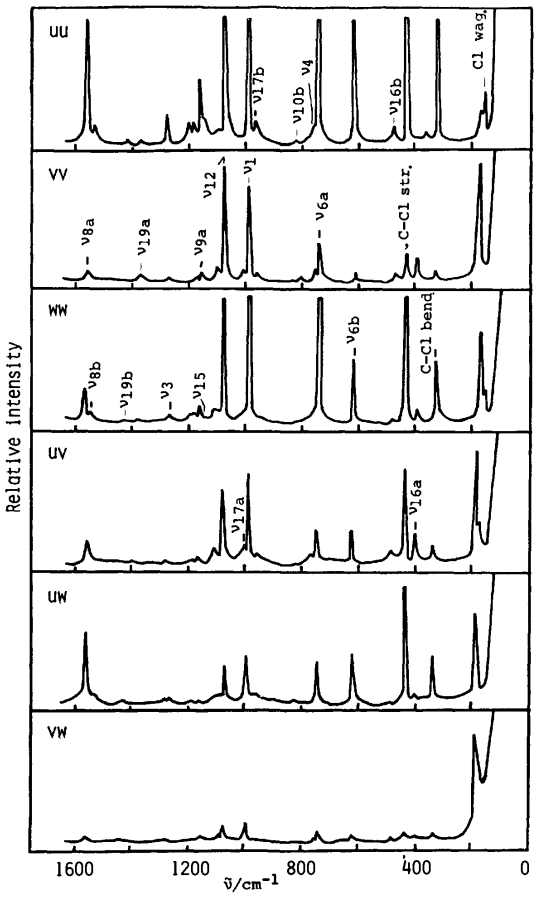

Fig. 2. Polarized Raman spectra of 2-chloropyrimidine single crystal.

tering light was observed from the direction perpendicular to the excitation light beam. The Raman spectra polarized parallel and perpendicular to the crystal growth direction are referred to as // and ⊥ spectra, respectively.

2-Chloropyrimidine. The non-totally symmetric Raman bands in the polarized single crystal Raman spectrum can be classified into three types based on their polarization behaviors as can be seen in Fig. 2. The relative intensity of each band belonging to the first type is strong in the uu spectrum and medium in the ww and uw spectra and weak in other spectra. The relative intensity of each second type band is weak in the uu, uv, and vv spectra and very weak in other spectra. The third type bands are observed with weak intensity in the uv and vv spectra and very weakly in other spectra. These three types of polarization behaviors are referred to as types A, B, and C, respectively.

The polarized infrared bands can be classified into three types I, II, and III based on their polarization behaviors as can be seen in Fig. 3. The bands belonging to the first type mainly constitute the // spectrum, that is, the bands are polarized nearly along the crystal growth direction. The intensity of each second type band in the // spectrum is nearly twice as strong as that in the ⊥ spectrum. The third type bands mainly constitute the ⊥ spectrum, that is, the bands are polarized exclusively perpendicular to the crystal growth direction.

Furberg *et al.*[8] analyzed the crystal structure of 2-chloropyrimidine and showed that the molecule crystallizes in the orthorhombic space group D_{2h}^{15}, where the molecular *x* axis orients nearly parallel to the crystal *b* axis and the *z* axis orients roughly parallel to the *c* axis although it leans somewhat toward the *a* axis. Therefore, the transition moments of the molecular vibrations belonging to the b_1 and a_1 symmetry species are expected to direct nearly along the crystal b and roughly along the *c* axes, respectively.

a_1 Species: Strongly polarized Raman bands observed at 437, 754, 990, 1078, 1163, 1380, 1561, 3010, and 3045 cm^{-1} in molten phase are straightforwardly assigned to the totally symmetric C–Cl stretching, ν_{6a}, ν_1, ν_{12}, ν_{9a}, ν_{19a}, ν_{8a}, ν_{13}, and ν_2 vibrations, respectively, on referring to the normal vibrations of pyrimidine[11–14] and other chlorinated pyrimidines,[6] and also based on the normal coordinate calculation. The corresponding single crystal infrared bands showed type I polarization behavior. This observation suggests that the crystal growth direction tends toward the crystal *c* axis.

b_2 Species: Infrared bands observed at 332, 626, 1154, 1277, 1384, 1425, 1540, and 3080 cm^{-1} in the single crystal spectrum showed type II polarization behavior and the corresponding single crystal Raman bands showed type A polarization behavior. These bands were assigned to the Cl bending, ν_{6b}, ν_{15}, ν_3, ν_{14}, ν_{19b}, ν_{8b}, and ν_{7b} vibrations, respectively, because higher frequencies of this band group are too much high to be assigned to the out-of-plane vibrations.

b_1 Species: Infrared bands observed at 477, 767, and 815 cm^{-1} in the single crystal spectrum showed type III polarization behavior and the corresponding crystal Raman bands showed type B polarization. These bands were assigned to the ν_{16b}, ν_4, and ν_{10b} vibrations, respectively. A Raman band observed at 960 cm^{-1} in single crystal showed type B polarization behavior and thus this band was assigned to the ν_{17b} vibration. A depolarized Raman band observed at 175 cm^{-1} in molten phase splits into two bands at 178 and 188 cm^{-1} in single crystal. The former band is clearly resolved in the uu, uv, and ww spectra while the latter is observed strongly in all spectra except for the uu. Therefore, the 178 cm^{-1} band was assigned to the Cl wagging vibration of b_1 species. The 188 cm^{-1} band may be ascribed to a lattice vibration.

a_2 Species: Raman bands observed at 405 and 1005 cm^{-1} showed type C polarization behavior in single crystal and no corresponding infrared bands could be observed. Therefore, these bands were assigned to the ν_{16a} and ν_{17a} vibrations, respectively.

The Raman bands observed at 330 and 437 cm^{-1} in molten phase, which were assigned to the Cl bending and C–Cl stretching vibrations, respectively, split into doublets separated by about 3 cm^{-1} in the Raman spec-

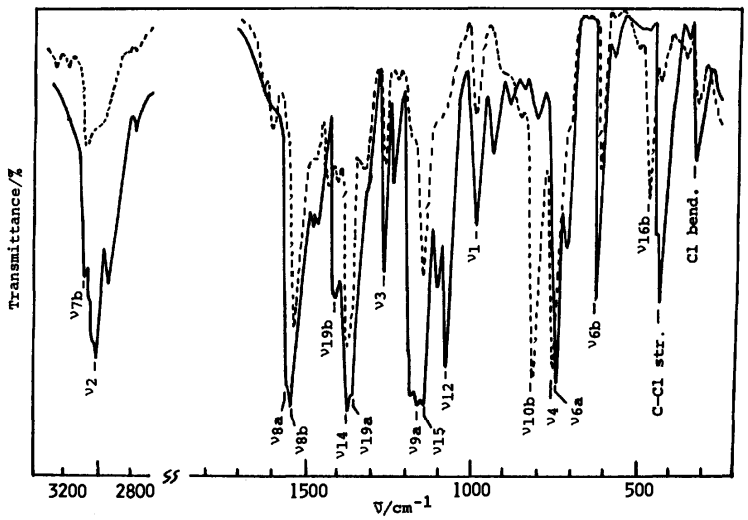

Fig. 3. Polarized infrared spectrum of 2-chloropyrimidine single crystal.

trum observed in solid phase under high resolution. The intensity ratio of the lower and higher frequency bands is about 1/3 for both bands. These splittings are ascribed to the isotopic shift, that is, the lower frequency band is due to the ^{37}Cl atom and the higher to the ^{35}Cl atom.

2-Bromopyrimidine. The depolarized Raman bands observed in molten phase show three different types of polarization behaviors in the single crystal Raman spectrum as can be seen in Fig. 4. The bands belonging to the first type can be observed clearly in the ⊥ spectrum. In the second type, the intensity of the // polarized band is slightly stronger than that of the ⊥ band. In the third type, the intensity of the ⊥ band is stronger than that of the // band. These three types of polarization behaviors are referred to as types A, B, and C, respectively. The polarized infrared bands of 2-bromopyrimidine were also classified into three types I, II, and III based on their polarization behaviors. In the first type, the intensities of the bands in the // and ⊥ spectra are nearly equal. In the second type, the intensity of the // band is stronger than that of the ⊥ band while in the third type, the intensity of the ⊥ band is much stronger than that of the // band.

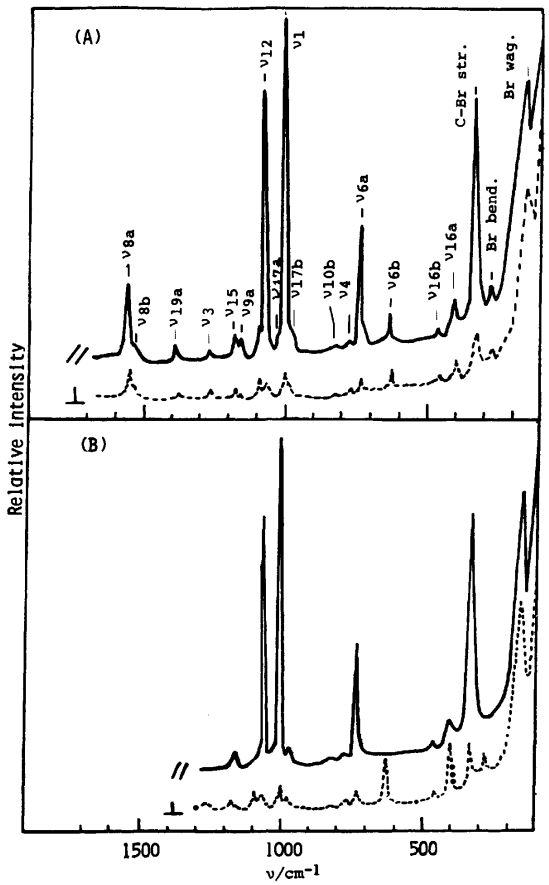

Fig. 4. Raman spectrum of 2-bromopyrimidine. (A): Depolarization behavior measured in moleten phase. (B): Polarization behavior measured in single crystal.

a_1 Species: Strongly polarized Raman bands observed at 330, 734, 998, 1074, 1157, 1381, 1559, 3013, and 3050 cm^{-1} in molten phase were straightforwardly assigned to the totally symmetric C–Br stretching, ν_{6a}, ν_1, ν_{12}, ν_{9a}, ν_{19a}, ν_{8a}, ν_{13}, and ν_2 vibrations, respectively on referring to the assignments given for pyrimidine and 2-chloropyrimidine, and also based on the calculation. The corresponding infrared bands showed type I polarization behavior in single crystal.

b_2 Species: Infrared bands observed at 276, 630, 1170, 1270, 1367, 1432, 1539, and 3080 cm^{-1} in single crystal showed type II polarization behavior and the corresponding Raman bands showed type A polarization behavior. These bands were assigned to the Br bending, ν_{6b}, ν_{15}, ν_3, ν_{14}, ν_{19b}, ν_{8b}, and ν_{7b} vibrations, respectively.

b_1 Species: Infrared bands observed at 465, 766, 826, and 960 cm^{-1} in single crystal showed type III polarization behavior and the corresponding Raman bands showed type B polarization. These bands were assigned to the ν_{16b}, ν_4, ν_{10b}, and ν_{17b} vibrations, respectively. A Raman band observed at 158 cm^{-1} showed type B polarization behavior and therefore this band was assigned to the Br wagging vibration of b_1 species.

a_2 Species: Raman bands observed at 400 and 1002 cm^{-1} showed type C polarization behavior and

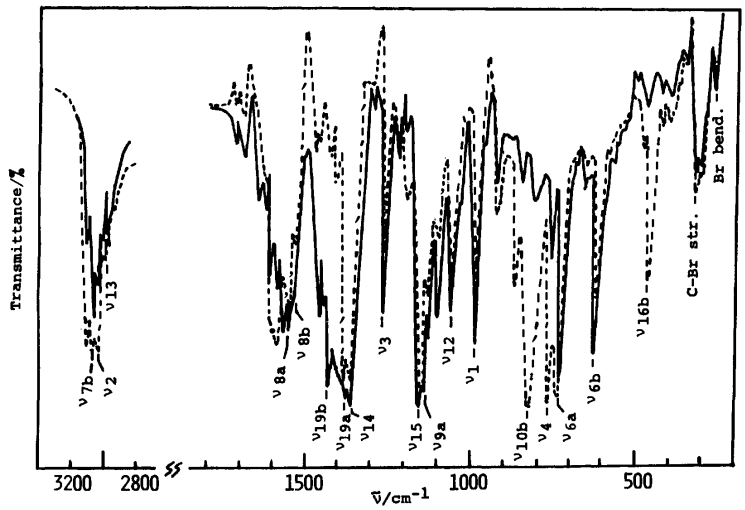

Fig. 5. Polarized infrared spectrum of 2-bromopyrimidine single crystal.

were assigned to the ν_{16a} and ν_{17a} vibrations, respectively. No corresponding infrared bands could be observed.

The isotopic splitting arising from the ^{79}Br and ^{81}Br atoms could not be observed because of small frequency differences due to the isotope. The single crystal infrared spectrum of 2-bromopyrimidine gave different polarization behavior from that of 2-chloropyrimidine. This may be due to different orientations of the two molecules in these single crystals. Detailed vibrational analyses of the Raman and infrared spectra of 2-chloro- and 2-bromopyrimidines are given in Tables 3 and 4, respectively. The normal vibrations are summarized in Table 5.

The assignments of the C–Cl stretching and ν_{6a} vibrations given by Sarma[3] are different from those given by Allenstein *et al.*[4] The normal coordinate calculation shows that the ν_{6a} vibration mixes with the C–X stretching vibration largely in 2-halopyrimidines, and this causes increase of the frequency of the ν_{6a} vibration and decrease of that of the C–X stretching vibration from their normal frequencies. Systematic vibrational analyses of the infrared and Raman spectra of 2-halopyrimidines given by Allenstein *et al.* support this mixing. These facts give the reasoning of assignments made by Allenstein *et al.* and us for the C–X stretching and ν_{6a} vibrations.

Sarma and Allenstein *et al.* assigned the 1169 cm^{-1} band of 2-chloropyrimidine to the ν_{15} vibration and 1158 cm^{-1} of 2-bromopyrimidine to the ν_3 vibration,

TABLE 3. VIBRATIONAL ANALYSIS OF THE RAMAN AND INFRARED SPECTRA OF 2-CHLOROPYRIMIDINE

Raman				Infrared			
$\tilde{\nu}/cm^{-1}$	Int.	Pol. Liq.	Pol. Cry.	$\tilde{\nu}/cm^{-1}$	Int.	Pol. Cry.	Assignment
178 188	m	dp	B				Cl wag.
327[a] 330	m	dp	A	332	m	II	Cl bend.
405	w	dp	C				ν_{16a}
434[a] 437	s	p		439	s	I	C–Cl str.
480	vw	dp	B	477	m	III	ν_{16b}
				580	w	II	ν_{16a}+Cl wag.
629	m	dp	A	626	s	II	ν_{6b}
				715	m	I	ν_{9a}−C–Cl str.
754	s	p		750	vs	I	ν_{6a}
770	vw	dp	B	767	vs	III	ν_4
807	vw	dp	B	815	vs	III	ν_{10b}
952	vw	p		950	m	I	ν_{6b}+Cl bend.
960	vw		B				ν_{17b}
990	vs	p		988	m	I	ν_1
1005	vw		C				ν_{17a}
1078	vs	p		1080	s	I	ν_{12}
1107	w	p		1102	m	I	ν_{8a}−C–Cl str.
				1154	vs	II	ν_{15}
1163	w	p		1163	vs	I	ν_{9a}
1195	w	p		1192	s	I	ν_{6a}+C–Cl str.
1264	vw	p		1250	m	I	$2\nu_{6b}$
1278	w	dp	A	1277	s	II	ν_3
1380	w	p		1378	vs	I	ν_{19a}
				1384	vs	II	ν_{14}
1425	vw	dp	A	1425	m	II	ν_{19b}
				1433	w	III	$2\nu_{6b}$+Cl wag.
				1468	w	I	ν_{15}+Cl bend.
1544	w	dp	A	1540	s	II	ν_{8b}
1561	m	p		1557	vs	I	ν_{8a}
3010	vw	p		3007	vw	I	ν_{13}
3045	s	p		3040	s	I	ν_2
3078	m	dp		3080	s	II	ν_{7b}
3087	m	p		3088	m	I	$2\nu_{8b}$
3120	m	p		3119	m	I	$2\nu_{8a}$

a) The lower and higher frequency bands are due to ^{37}Cl and ^{35}Cl atoms, respectively.

Table 4. Vibrational analysis of the raman and infrared spectra of 2-bromopyrimdine

Raman				Infrared			
$\tilde{\nu}$/cm^{-1}	Int.	Pol. Liq.	Pol. Cry.	$\tilde{\nu}$/cm^{-1}	Int.	Pol. Cry.	Assignment
158	m	dp	B				Br wag.
276	w	dp	A	276	w	II	Br bend.
330	vs	p		325	m	I	C-Br str.
400	w	dp	C				ν_{16a}
462	vw	dp	B	465	s	III	ν_{16b}
623	m	dp	A	630	vs	II	ν_{6b}
734	s	p		740	vs	I	ν_{6a}
765	vw	dp	B	766	vs	III	ν_4
820	vw	dp	B	826	vs	III	ν_{10b}
				875	m	III	ν_{6a}+Br wag.
				923	w	I	$2\nu_{16b}$
960	vw	dp	B	960	vw	III	ν_{17b}
998	vs	p		992	s	I	ν_1
1002	vw	dp	C				ν_{17a}
1074	vs	p		1073	m	I	ν_{12}
1090	w	dp	B				C-Br str.+ν_4
				1105	m	II	ν_{19a}−Br bend.
				1127	m	II	ν_{17a}+Br wag.
1157	w	p		1154	vs	I	ν_{9a}
1170	w	dp		1170	m	II	ν_{15}
				1200	w	III	$\nu_{6a}+\nu_{16b}$
1270	w	dp		1270	s	II	ν_3
				1367	vs	II	ν_{14}
1381	w	p		1378	vs	I	ν_{19a}
				1432	m	II	ν_{19b}
				1460	m	II	$2\nu_{8a}$
				1480	w	I	ν_{15}+C-Br str.
1530	vw	dp		1539	m	II	ν_{8b}
1559	s	p		1551	s	I	ν_{8a}
				1578	m	III	$\nu_{6a}+\nu_{10b}$
				1610	m	III	$\nu_{9a}+\nu_{16b}$
3013	vw	p		3016	w	I	ν_{13}
3050	m	p		3049	s	I	ν_2
3086	m	dp		3080	m	II	ν_{7b}
				3110	m	I	$2\nu_{8a}$

but these bands showed a_1 polarization behavior in the Raman and infrared spectra and hence these bands could not be assigned to the b_2 vibration. Frequencies of 1132 and 1165 cm^{-1} constitute the main progressions in the phosphorescence spectra of pyrimidine[15,16] and 2-chloropyrimidine,[15,17] respectively, and these frequencies are to be assigned to the ν_{9a} vibration. Hence the bands assigned to the ν_{15}, and ν_3 vibrations by Sarma and Allenstein *et al.* should be both assigned to the ν_{9a} vibrations of 2-chloro- and 2-bromopyrimidines.

Allenstein *et al.* assigned the 1270 and 1390 cm^{-1} bands of 2-chloropyrimidine and 1273 and 1385 cm^{-1} bands of 2-bromopyrimidine to the ν_{14} and ν_{19b} vibrations, respectively. These bands showed b_2 polarization behavior. On referring to the normal vibrations of pyrimidine, we assigned these bands to the ν_3 and ν_{14} vibrations, respectively. The normal coordinate calculation also supports these assignments.

Allenstein *et al.* observed a 760 cm^{-1} Raman band as a shoulder of the strong 754 cm^{-1} band and assigned it to the ν_{17a} vibration for 2-chloropyrimidine. We reexamined the observation of a Raman band showing a_2 polarization behavior around this region very carefully but no such a band could be observed. On the other hand, the polarized dark sublevel phosphorescence spectrum of pyrimidine indicates that a 1004 cm^{-1} band shows a_2 polarization behavior and thus this frequency should be assigned to the ν_{17a} vibration.[10] Therefore we assigned the 1005 cm^{-1} band showing a_2 polarization behavior in the Raman spectrum to the ν_{17a} vibration.

The normal coordinate calculation indicates that the ν_{16b} vibration mixes largely with the X wagging vibration. This mixing is supported by the observation that the frequencies of the ν_{16b} vibration for 2-chloro- and 2-bromopyrimidines increase from the frequency of 345 cm^{-1} for the ν_{16b} vibration of pyrimidine.

TABLE 5. NORMAL VIBRATIONS OF 2-CHLORO- AND 2-BROMOPYRIMIDINES

		2-Chloropyrimidine				2-Bromopyrimidine		
	Mode	Sarma[3]	Allenstein[4]	This work		Allenstein[4]	This work	
		$\bar{\nu}$/cm^{-1}	$\bar{\nu}$/cm^{-1}	Obsd $\bar{\nu}$/cm^{-1}	Calcd $\bar{\nu}$/cm^{-1}	$\bar{\nu}$/cm^{-1}	Obsd $\bar{\nu}$/cm^{-1}	Calcd $\bar{\nu}$/cm^{-1}
	C-X str.[a]	1144	434 441	437	442	329	330	334
	ν_2	3062	3080	3045	3055	3118	3050	3055
	ν_{13}	3033	3050	3010	3006	3044	3013	3006
	ν_{8a}	1559	1555	1561	1563	1558	1559	1164
a_1	ν_{19a}	1382	1370	1380	1389	1378	1381	1386
	ν_{9a}	754	1094	1163	1160	1105	1157	1152
	ν_{12}	1075	1078	1078	1072	1073	1074	1061
	ν_1	988	992	990	1004	989	998	998
	ν_{6a}	434	755	754	747	730 735	734	724
	ν_{7b}	3115	3055	3080	3082	3080	3080	3082
	ν_{8b}	1552	1564	1540	1542	1562	1539	1542
	ν_{19b}	1428 1435	1390	1425	1437	1385	1432	1438
b_2	ν_{14}		1270	1384	1372	1273	1367	1366
	ν_3	1202	1205	1277	1266	1158	1270	1264
	ν_{15}	1166	1169	1154	1158	1093	1170	1156
	X-bend		330	332	333	275	276	280
	ν_{6b}	626	629	626	622	624	630	622
a_2	ν_{17a}		760	1005	994		1002	994
	ν_{16a}		409	405	396	404	400	396
	ν_{17b}		855	960	951	838	960	952
	ν_{10b}		810	815	825	830	826	825
b_1	X wag.		194	178	165	160	158	155
	ν_4		772	767	762	762	766	764
	ν_{16b}		480	477	477	460	465	475

a) X is Cl or Br atom.

We believe that the assignments of the normal vibrations given for 2-chloro- and 2-bromopyrimidines are reliable and quite useful for the reasonable vibrational analysis of the phosphorescence spectrum of 2-chloropyrimidine, which will be reported soon.

References

1) L. N. Short and H. W. Thompson, *J. Chem. Soc.*, 1952, 168.
2) A. J. Lafaix and J. M. Lebas, *Spectrochim. Acta, Part A*, **26**, 1243 (1970).
3) Y. A. Sarma, *Spectrochim. Acta, Part A*, **30**, 1801 (1974).
4) E. Allenstein, P. Kiemle, J. Weidlein, and W. Podszun, *Spectrochim. Acta, Part A*, **33**, 189 (1977).
5) Y. Ishibashi, R. Shimada, and H. Shimada, *Bull. Chem. Soc. Jpn.*, **55**, 2765 (1982).
6) S. Kizuki, Y. Ishibashi, H. Shimada, and R. Shimada, *Mem. Fac. Sci. Kyushu Univ. Ser. C*, **13**, 7 (1981).
7) Y. Ishibashi, F. Arakawa, H. Shimada, and R. Shimada., *Bull. Chem. Soc. Jpn.*, **56**, 1327 (1983).
8) S. Furberg, J. Grøgaard, and B. Smedsrud, *Acta Chem. Scand., Ser. B.* **33**, 715 (1979).
9) D. H. Whiffen, *Philos. Trans. R. Soc. London, Ser. A*, **248**, 131 (1955).
10) M. Umemoto, T. Watanabe, and R. Shimada, Symposium on the Molecular Structure and Molecular Electronic Structure, Tokyo, October 1976, Abstr. No. 4B19; Y. Matsufuji, H. Shimada, and R. Shimada, ibid., Sendai, August 1983, Abstr. No. 1A08.
11) G. Sbrana, G. Adembri, and S. Califano, *Spectrochim. Acta*, **22**, 1831 (1966).
12) R. Foglizzo and A. Novak, *J. Chim. Phys.*, **64**, 1484 (1967).
13) F. Milani-Nejad and H. D. Stidham, *Spectrochim. Acta, Part A*, **31**, 1433 (1975).
14) L. Bokobza-sebagh and J. Zarembowitch, *Spectrochim. Acta, Part A*, **32**, 797 (1976).
15) N. Nishi, R. Shimada, and Y. Kanda, *Bull. Chem. Soc. Jpn.*, **43**, 41 (1970).
16) R. M. Hochstrasser and C. J. Marzzacco, *J. Mol. Spectrosc.*, **42**, 75 (1972).
17) S. Nakama, H. Shimada, R. Shimada, Y. Kanda, N. Nishi, and M. Kinoshita, Symposium on the Molecular Structure and Molecular Electronic Structure, Tokyo, October 1976, Abstr. No. 3B23.

 © 1984 The Chemical Society of Japan Bull. Chem. Soc. Jpn., 57, 2591—2595 (1984)

Intramolecular Orbital Interactions in 6,6′-Bi(1,4-dithiafulvenyl) Studied by Photoelectron Spectroscopy

Tsunetoshi KOBAYASHI,* Zen-ichi YOSHIDA,† Hiroshi AWAJI,†
Tokuzo KAWASE,† and Shigeo YONEDA†
The Institute of Physical and Chemical Research, Wako, Saitama 351
†*Department of Synthetic Chemistry, Kyoto University, Yoshida, Kyoto 606*
(Received March 15, 1984)

Photoelectron spectra of tetrathiafulvalene (TTF) and 6,6′-bi(1,4-dithiafulvenyl) (BDTF) were measured and compared with each other. The first photoelectron spectral band of BDTF is only slightly shifted relative to that of TTF, though the BDTF molecule is lengthened compared with the TTF molecule by two sp^2 carbon atoms. From the LCGO model orbital interaction analysis, this apparent anomaly is ascribed to the near cancellation of the effects of two main factors, the energy and the terminal atomic orbital coefficient differences between the central olefinic group π orbitals. Orbital interaction analysis as demonstrated in this work may be useful for molecular design, especially for orbital energy control.

In 1973 a charge transfer complex between tetrathiafulvalene (TTF) and tetracyano-*p*-quinodimethane was found to show high electrical conductivity.[1] This finding triggered off present-day active researches on organic metals. Especially several cation radical salts of tetramethyltetraselenafulvalene closely related to TTF was recently found to show superconductivity at low temperature.[2]

During the course of the study to develop good electron donors, 6,6′-bi(1,4-dithiafulvenyl) (BDTF, 2,2′-ethanediylidenebis[1,3-dithiole]) structurally closely related to TTF was recently synthesized.[3] In this paper the photoelectron (PE) spectra of TTF and BDTF are measured and compared with each other in order to get informations useful for molecular design.

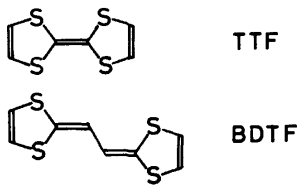

Fig. 1. Structural formulae of TTF and BDTF.

Experimental

Materials. Tetrathiafulvalene (TTF) purchased from the Aldrich Chemical Co. was recrystallized twice from hexane just before use. 6,6′-Bi(1,4-dithiafulvenyl) (BDTF) was synthesized as reported formerly[3] and purified by column chromatography (neutral alumina, benzene) and subsequent recrystallization from benzene.

Measurements. Vapor phase HeI PE spectra of TTF and BDTF were measured with the PE spectrometer described in Refs. 4 and 5. The sample inlet and target chamber systems were kept at 120 °C during the measurements. Xe gas was used as the internal reference standard for the calibrations of the energy scale.

Computational

Pariser-Parr-Pople (PPP) type SCF MO calculations of TTF and BDTF were carried out on a FACOM M-380 computer at the Institute of Physical and Chemical Research. The parameter set necessary in the calculations was taken from Ref. 6. The geometrical structural data for TTF were taken from Ref. 7. The bond angles and bond lengths of the central olefinic moiety of BDTF were assumed to be the same as those of *s-trans*-1,3-butadiene[8] and the dimensions of the two five-membered rings of BDTF were assumed to be the same as those in TTF.[7]

Results and Discussion

Photoelectron Spectral Band Assignments. The vapor phase HeI PE spectra of TTF and BDTF are shown in Fig. 2. The vertical ionization energies, E_{iv}, of TTF and BDTF obtained from the PE spectra are summarized in Table 1. The PE spectra of TTF were formerly reported,[9-11] but was remeasured this time for the sake of consistency. Our PE spectrum of TTF is consistent with those reported formerly.[9-11]

The first four PE spectral bands of TTF have already been assigned as $4b_{1u}\pi$, $3b_{3g}\pi$, $2a_u\pi$, and $2b_{2g}\pi$ from the top, respectively.[9b] Here in this paper the *z*-axes are taken perpendicular to the molecular planes for TTF and BDTF, and the *x*-axis is taken along the short molecular axis for TTF. The $2a_u$ and $2b_{2g}$ orbitals of TTF are completely localized on the two SCCS groups and are predicted degenerate within the simple zero-

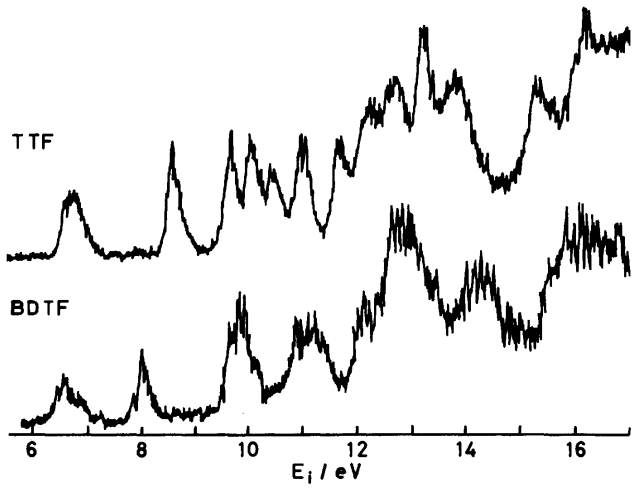

Fig. 2. Vapor phase HeI photoelectron spectra of TTF and BDTF.

TABLE 1. OBSERVED AND CALCULATED VERTICAL IONIZATION ENERGIES, E_{iv}, OF TTF AND BDTF WITH ORBITAL ASSIGNMENTS

Compd			E_{iv}/eV						
TTF	Obsd		6.72	8.56	9.71	10.04	10.50	11.0	
			$4b_{1u}$[a]	$3b_{3g}$[a]	$2a_u$[a]	$2b_{2g}$[a]	$3b_{1u}$[b]	$9b_{1g}$[b]	
	Calcd	PPP[c]	6.80	8.96	10.01	10.01	10.61		
			$4b_{1u}$	$3b_{3g}$	$2a_u$	$2b_{2g}$	$3b_{1u}$		
		LCGO[d]	6.72	8.49	9.88	9.88	10.51		
			$4b_{1u}$	$3b_{3g}$	$2a_u$	$2b_{2g}$	$3b_{1u}$		
BDTF	Obsd		6.61	8.02		9.70		10.82	11.3
			$6b_g$	$6a_u$	$5b_g$	$5a_u$	$4b_g$		
	Calcd	PPP[c]	6.87	8.63	10.11	10.12	10.20		11.35
			$6b_g$	$6a_u$	$5b_g$	$5a_u$	$4b_g$		$4a_u$
		LCGO[d]	6.77	7.93	9.86	9.88	9.88	11.02	
			$6b_g$	$6a_u$	$5b_g$	$5a_u$	$4b_g$	$4a_u$	

a) Ref. 9b. b) Ref. 11. c) The Pariser-Parr-Pople type calculation, see the text. d) The linear combination of group orbitals calculation, see the text.

differential overlap approximation, but in reality, are split slightly because of the long range through-space interactions with the $2a_u$ orbital above the $2b_{2g}$ orbital.[9b] As for the fifth and sixth bands of TTF, Gleiter *et al.*[9b] suggested that these bands should be ascribed to $9b_{1g}n$ and $3b_{1u}\pi$ bands, respectively, based on the MINDO/3 calculations. However, afterwards, Schweig *et al.*[11] assigned those bands as the $3b_{1u}$ and $9b_{1g}$ bands, respectively, from the comparison among the PE spectra of TTF, diselenadithiafulvalene, and tetraselenafulvalene.

For the PE spectral band assignments of BDTF, we use two types of computational methods. One is the linear combination of group orbitals (LCGO) method and the other one is the PPP type method. As the PPP type calculation with Fabian *et al.*'s parameter set[6] reproduces well the observed E_{iv}'s for the first five bands of TTF[9b] (see Table 1 also) on the assumption of the Koopmans theorem,[12] let us apply this method to the case of BDTF. The calculated results are given in Table 1.

The calculated ionization energies reproduce rather well the observed E_{iv}'s for the first three bands of BDTF. The calculation suggests that the observed third band corresponds to the three ionizations, and this is reasonable from the band intensity relative to those of the first two bands. The $5b_g$ and $5a_u$ orbitals of BDTF calculated by the PPP method correspond almost to the $2b_{2g}$ and $2a_u$ orbitals of TTF which are completely localized on the two SCCS groups. The $5b_g$ and $5a_u$ bands of BDTF, therefore, are expected to appear in the same energy region as the $2b_{2g}$ and $2a_u$ bands of TTF, that is, around 9.7—10.0 eV. This is consistent with the assignment suggested above for the 9.70 eV band of BDTF. It is uncertain from the PPP calculation if the fourth 10.82 eV band should be assigned as the $4a_u$ band.

Now we use the LCGO model to make the band assignments more definite. This model has been used by Gleiter *et al.*[9b] in the PE spectral band assignments of TTF formerly. In the LCGO model calculations the TTF molecule is regarded to be composed of three CC double bond groups and four sulfur atoms. The BDTF molecule is regarded to be composed of two CC double bond groups, four sulfur atoms, and a *trans*-butadiene-like group. The interactions among the π and π^* orbitals of the CC double bond groups and the n orbitals of the sulfur atoms are considered in the case of TTF. As for BDTF the contributions from the $1a_u\pi_1$, $1b_g\pi_2$, $2a_u\pi_3^*$, and $2b_g\pi_4^*$ orbitals of the central *trans*-butadiene type group are also taken into account.

At first we reestimate the parameter values necessary in the LCGO model calculations. The newly reevaluated basis group orbital energy values are summarized in Table 2. Of the values in Table 2 the occupied π orbital energies of the CC double bond groups and the *trans*-butadiene-like group were estimated by using the E_{iv} values of ethylene[13] and *trans*-butadiene[14] obtained by PE spectroscopy. The vacant π basis orbital energies of those component groups were estimated by using the electron affinities of ethylene[15] and *trans*-butadiene[16] obtained by electron transmission spectroscopy. The resonance integral values for the CS π bonds, β_{CS}, and the basis orbital energy values of the sulfur atoms, A_S, were readjusted as −1.90 eV and −9.57 eV, respectively, to reproduce the first, third, and fourth E_{iv} values of TTF. The β_{CS} and A_S values suggested by Gleiter *et al.*[9b] formerly were −1.80 eV and −9.4 eV, respectively, and these values are close to those readjusted here. The

TABLE 2. BASIS GROUP ORBITAL ENERGIES, A

Basis group orbital	A/eV[a]
Ethylene type group	
$(b_{1u})\pi_1$	−10.51
$(b_{3g})\pi_2^*$	1.78
trans-Butadiene type group	
$a_u\pi_1$	−11.46
$b_g\pi_2$	−9.03
$a_u\pi_3^*$	0.76
$b_g\pi_4^*$	2.8
Sulfur atom	
n	−9.57

a) For the evaluations of the A values, see the text.

calculated results for the first five bands of TTF with the new parameter set are given in Table 1, and the overall agreement between theory and experiment is satisfactory with the band ordering assigned formerly.[11]

Now let us apply the simple LCGO method with our new parameter set to BDTF in question. The calculated results are shown in Table 1. The calculated band ordering by the simple LCGO model is the same as that suggested by the PPP method. The predicted E_{iv} values for BDTF by the LCGO method are closer to the observed ones as for the first three bands than those by the PPP method. Now the first two bands are unambiguously assigned as the $6b_g$ and $6a_u$ bands, respectively, and the apparent third band is ascribed to the three bands, $5b_g$, $5a_u$, and $4b_g$ bands highly overlapping with one another. The assignment of the 10.82 eV band is left unsettled for further detailed examinations.

Orbital Interaction Analysis. It is quite natural to expect that the first E_{iv} of BDTF is far smaller than that of TTF because the BDTF molecule is extended longer than the TTF molecule just by almost the same length as in the case of *trans*-butadiene compared with ethylene, the first E_{iv} values of these compounds being 9.03 eV[14] and 10.51 eV,[13] respectively. In reality, however, the first band of BDTF is only slightly (by 0.11 eV) shifted to the lower energy side compared with that of TTF, while the second band of BDTF is reasonably shifted to the lower energy side by 0.54 eV compared with that of TTF. This small shift of the first band of BDTF relative to that of TTF is interesting because of its contradiction to natural expectation. Theoretically both LCGO and PPP type methods predict well the point that the first E_{iv} value of BDTF is very close to that of TTF. For the second bands of these molecules, the LCGO model predicts quantitatively the reasonably large E_{iv} difference, 0.5 eV, and the PPP method predicts semiquantitatively this tendency.

Now let us analyze the PE spectral band shifts of BDTF relative to TTF by the LCGO model. At first we examine the case of the first bands. The highest occupied molecular orbital (HOMO) of TTF is of b_{1u} symmetry and is regarded to be formed mainly by the interaction among the following occupied π group orbitals: One is the central ethylene type group π orbital, and other two ones are those formed by the in-phase (b_{1u}) type combinations of the occupied π orbitals of the two SCCS groups of the TTF molecule. On the other hand the HOMO of BDTF is of b_g symmetry and is regarded to be formed mainly by the interactions among the following orbitals: One is the b_g symmetry π_2 orbital of the *trans*-butadiene type group and other two ones are the orbitals formed by the out-of-phase combinations of the occupied π orbitals of the two SCCS groups. It is noticed that the $4b_g$ MO in the LCGO model of BDTF is completely localized on the two SCCS groups just as the $2b_{2g}$ MO of TTF and is not taken into account in the above consideration. The energies of those out-of-phase type group orbitals described above are almost equal to those of the corresponding in-phase type group orbitals. In addition to those the π_4^* orbital of the *trans*-butadiene type group is also expected to contribute to the b_g HOMO of BDTF from the symmetry reason.

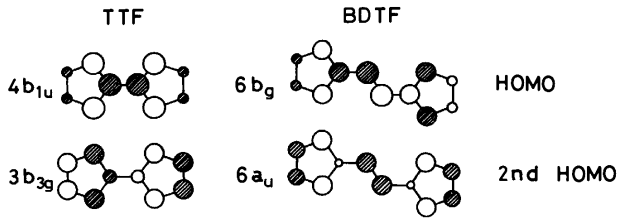

Fig. 3. Schematic representations of the first and second HOMO's of TTF and BDTF calculated by the PPP type method.

On the first stage we estimate the effect of the central olefinic group occupied π orbital energy change. In the case of TTF the central olefinic group π orbital energy is -10.51 eV, and the π_2 basis orbital energy of the *trans*-butadiene-like group is -9.03 eV. If we change the central olefinic group occupied π basis orbital energy from -10.51 eV to -9.03 eV, the effect of this change on the HOMO energy of TTF is evaluated to be -0.525 eV. Only 35% of the central olefinic group π orbital energy change is reflected on the HOMO energy change toward the destabilization.

In addition to the above effect, in the process of replacing the central ethylenic group of TTF by a *trans*-butadiene type group we must take into account the effect of the resonance integral change between the olefinic occupied π orbital and the group π orbital of the appropriate symmetry composed of the four sulfur atom 3p lone pair orbitals. The absolute values of the atomic orbital (AO) coefficients of the terminal carbon atoms of the central olefinic group HO-π-MO are 0.7071 in the case of the ethylene type group and 0.5727 in the case of the *trans*-butadiene type group. The latter values have been calculated by a modified CNDO method[17] for *trans*-butadiene. By using the latter values we can estimate the resonance integral value for the case of BDTF in question as -2.176 eV, that is, decrease in the absolute value by 0.5 eV from the corresponding one for TTF (-2.687 eV). By using this resonance integral value thus estimated we can estimate the additional HOMO energy change as -0.456 eV or stabilization of the HOMO by 0.456 eV. In this case the resonance integral value change influences almost directly on the HOMO energy change.

In order to estimate the effect of the π^* level on the HOMO energy, let us now introduce the π_4^* orbital of the *trans*-butadiene-like group into the above model with the appropriate symmetry. Thus, the effect is estimated to be 0.122 eV, or stabilization of the HOMO by 0.122 eV. From the above stepwise model calculations it is said that in replacing the central CC double bond in TTF by a longer *trans*-butadiene-like group, the central olefinic group HOMO energy change contributes considerably toward the stabilization of the HOMO by around 0.5 eV, while this effect is almost completely compensated by the decreases in the absolute values of the terminal AO coefficients of the central olefinic group HOMO. The HOMO stabilization effect of the π_4^* level of the central *trans*-butadiene-like group of BDTF is not so large (*ca.* 0.1 eV).

From the above model consideration it is concluded

that the anomalously small shift of the first band of BDTF compared with that of TTF can be explained by the almost perfect cancellation of the two main effects, the energy and the terminal AO coefficient changes of the central olefinic group π orbital.

Next let us compare the second E_{iv}'s of TTF and BDTF. The second E_{iv} of BDTF is smaller than that of TTF by *ca.* 0.5 eV, and this seems to be reasonable as stated before. Now we analyze the situation with the LCGO model. In the case of TTF the second HOMO is of b_{3g} symmetry and is contributed by the π^* orbital of the central ethylenic group toward stabilization. If we change only the energy of the central olefinic group vacant π basis orbital from 1.78 eV to 0.76 eV, the π_3^* basis orbital energy of the *trans*-butadiene type group, in TTF, the second HOMO stabilization by this change is only 0.04 eV and this effect is negligibly small.

Further let us change the absolute values of the terminal AO coefficients of the central olefinic group vacant π orbital from 0.7071 for the ethylene type group to 0.5595 for the *trans*-butadiene type π_3^* orbital. So the second HOMO of TTF is destabilized on this second step by 0.15 eV.

Introduction of the π_1 basis orbital of the *trans*-butadiene type group into this last model with the appropriate symmetry causes large destabilization of the second HOMO by 0.45 eV. From the above model calculations, it is concluded that the apparently reasonable decrease in the second E_{iv} energy of BDTF compared with that of TTF is ascribed mostly to the second HOMO destabilization caused by the contribution of the π_1 basis group orbital of the central *trans*-butadiene type group.

In the discussion so far we have been concerned with the apparent relative energy shifts of the first (second) bands of TTF and BDTF. However, from the standpoint of MO symmetry the HOMO and the second HOMO of TTF are to be correlated with the second HOMO and the HOMO of BDTF, respectively, that is, if we take the orbital symmetry into account, the original first band of TTF should be regarded to be shifted to the higher ionization energy side by 1.30 eV, while the second band of TTF is shifted to the lower ionization energy side by 1.95 eV, the ordering of the first and second bands being reversed, when the TTF molecule is stretched to BDTF.

Let us examine the HOMO energy shift of TTF in the above sence. The HOMO of TTF is of b_{1u} symmetry and contributed from the occupied group π orbital of the central CC double bond. In the LCGO model, if we change the basis orbital energy of this central CC double bond from -10.51 eV to -11.46 eV for the *trans*-butadiene type group π_1 orbital, the HOMO energy is only slightly stabilized by 0.24 eV. In this model if we change the terminal AO coefficients from 0.7071 for the ethylene π orbital to 0.4324 for the *trans*-butadiene π_1 orbital, the HOMO is additionally stabilized by 0.67 eV. In this model, if we introduce the π_3^* orbital of the *trans*-butadiene type group, the HOMO is further stabilized by 0.31 eV. The stabilization of the HOMO of TTF by the extension of TTF to BDTF is ascribed to the cumulative effect of the above three factors.

Next we discuss the second HOMO energy shift of TTF caused by the molecular lengthening to BDTF taking the orbital symmetries into account. The second HOMO of TTF is contributed from the π^* orbitals of the central olefinic group. If we change the π^* orbital energy of the central olefinic group in TTF from 1.78 eV for the ethylene type group to 2.8 eV for the *trans*-butadiene type group π_4^* orbital, the second HOMO of TTF is destabilized only by 0.03 eV. If we change in this model the absolute values of the terminal AO coefficients from 0.7071 for the ethylene π^* orbital to 0.4147 for the *trans*-butadiene π_4^* orbital, the second HOMO is further destabilized by 0.24 eV. If we introduce the π_2 basis orbital of the *trans*-butadiene type group into this model, the second HOMO is further considerably destabilized by 1.45 eV. The large destabilization of the second HOMO of TTF by the molecular lengthening to BDTF is mostly ascribed to the contribution of the π_2 orbital of the *trans*-butadiene type group.

Conclusion

Lengthening of a molecule toward its long molecular axis does not necessarily lead to the apparent efficient destabilization of the HOMO as seen in the case of TTF and BDTF treated in this paper. Anomalously small shift of the first PE spectral band of BDTF compared with that of TTF is ascribed to the near cancellation of the effects of two main factors, the energy and the terminal AO coefficient changes of the basis orbital of the central olefinic part. Orbital interaction analysis as demonstrated in this paper is expected to be useful for molecular design, especially for orbital energy control.

References

1) a) J. Ferraris, D. O. Cowan, V. Walatka, Jr., and J. H. Perlstein, *J. Am. Chem. Soc.*, **95**, 948 (1973); b) L. B. Coleman, M. J. Cohen, D. J. Sandman, F. G. Yamagishi, A. F. Garito, and A. J. Heeger, *Solid State Commun.*, **12**, 1125 (1973).

2) a) D. Jérome, A. Mazaud, M. Ribault, and K. Bechgaard, *J. Physique-Lett.*, **41**, L95 (1980); b) M. Ribault, G. Benedek, D. Jérome, and K. Bechgaard, *ibid.*, **41**, L397 (1980); c) K. Bechgaard, K. Carneiro, F. B. Rasmussen, M. Olsen, G. Rindorf, C. S. Jacobsen, H. J. Pedersen, and J. C. Scott, *J. Am. Chem. Soc.*, **103**, 2440 (1981) and references cited therein.

3) Z. Yoshida, T. Kawase, H. Awaji, I. Sugimoto, T. Sugimoto, and S. Yoneda, *Tetrahedron Lett.*, **24**, 3469 (1983).

4) T. Kobayashi, K. Yokota, and S. Nagakura, *J. Electron Spectrosc. Relat. Phenom.*, **2**, 449 (1973).

5) T. Kobayashi, T. Kubota, and K. Ezumi, *J. Am. Chem. Soc.*, **105**, 2172 (1983).

6) J. Fabian, A. Mehlhorn, and R. Zahradník, *J. Phys. Chem.*, **72**, 3975 (1968).

7) W. F. Cooper, N. C. Kenny, J. W. Edmonds, A. Nagel, F. Wudl, and P. Coppens, *J. Chem. Soc., Chem. Commun.*, **1971**, 889.

8) A. Almenningen, O. Bastiansen, and M. Trætteberg, *Acta Chem. Scand.*, **12**, 1221 (1958).

9) a) R. Gleiter, E. Schmidt, D. O. Cowan, and J. Ferraris, *J. Electron Spectrosc. Relat. Phenom.*, **2**, 207 (1973); b) R. Gleiter, M. Kobayashi, J. Spanget-Larsen, J. P. Ferraris, A. N. Bloch, K. Bechgaard, and D. O. Cowan, *Ber. Bunsenges. Phys. Chem.*, **79**, 1218 (1975).

10) A. J. Berlinsky, J. F. Carolan, and L. Weiler, *Can. J. Chem.*, **52**, 3373 (1974).

11) A. Schweig, N. Thon, and E. M. Engler, *J. Electron Spectrosc. Relat. Phenom.*, **12**, 335 (1977).
12) T. Koopmans, *Physica*, **1**, 104 (1934).
13) A. D. Baker, C. Baker, C. R. Brundle, and D. W. Turner, *Int. J. Mass Spectrom. Ion. Phys.*, **1**, 285 (1968).
14) M. Beez, G. Bieri, H. Bock, and E. Heilbronner, *Helv. Chim. Acta*, **56**, 1028 (1973).
15) N. S. Chiu, P. D. Burrow, and K. D. Jordan, *Chem. Phys. Lett.*, **68**, 121 (1979).
16) S. W. Staley, J. C. Giordan, and J. H. Moore, *J. Am. Chem. Soc.*, **103**, 3638 (1981).
17) T. Kobayashi, *J. Electron Spectrosc. Relat. Phenom.*, **9**, 381 (1976).

The Structure of the Cyclodextrin Complex. XVII. Crystal Structure of β-Cyclodextrin-Hexamethylenetetramine (1:1) Complex Hexahydrate

Kazuaki HARATA
Research Institute for Polymers and Textiles, 1-1-4 Yatabe-Higashi, Tsukuba, Ibaraki 305
(Received March 22, 1984)

The crystal structure of β-cyclodextrin-hexamethylenetetramine (1:1) complex hexahydrate was determined by the X-ray diffraction method. The crystal is monoclinic with the space group $P2_1$, $Z=2$, $a=15.285(3)$, $b=10.345(2)$, $c=20.118(2)$ Å, and $\beta=102.14(1)°$. The structure was solved by inspection of a Patterson map and the trial-and-error method combined with the rigid-body least-squares technique and refined by the block-diagonal least-squares method to the R-value of 0.056 for 4369 reflections ($\sin\theta/\lambda<0.55$). The β-cyclodextrin molecule is slightly distorted from the regular heptagonal structure. The orientation of two primary hydroxyl groups is statistically disordered. The secondary hydroxyl groups form intramolecular hydrogen bonds between adjacent glucose residues. The guest hexamethylenetetramine molecule, being located roughly at the center of the β-cyclodextrin ring, is in van der Waals contact with the interior surface of the host molecule. Two out of four nitrogen atoms of hexamethylenetetramine form N···H-O hydrogen bonds with water and adjacent β-cyclodextrin molecules. β-Cyclodextrin molecules are stacked along the crystallographic b axis, with which the plane through seven glycosidic oxygen atoms makes an angle of 46.7°, forming a "cage-type" packing. Water molecules occupy the intermolecular spaces between β-cyclodextrin molecules.

Cyclodextrins form inclusion complexes with a variety of guest molecules, of which shape and size are suitable to be accommodated within the cavity of the host macrocyclic ring.[1,2] Several β-cyclodextrin complexes with alcohol[3-5] and aromatic compounds[6-12] have been investigated by the X-ray method, and in these complexes the guest molecules have been found to be included within the host cavity. Compared with such linear or planar molecules, spherical molecules can be expected to be more favorably accommodated within the cylindrical cavity of β-cyclodextrin. Previously, we determined the crystal structure of the β-cyclodextrin-1,4-diazabicyclo[2.2.2]octane complex,[13] a complex with a spherically-shaped guest molecule. Hamilton and Sabesan have also reported the structure of the β-cyclodextrin complex with 1-adamantanecarboxylic acid[14] having a spherical adamantane moiety. In this paper, we present the crystal structure of β-cyclodextrin-hexamethylenetetramine complex in order to investigate how β-cyclodextrin includes the guest molecule with high symmetry ($\bar{4}3$ m).[15]

Experimental

β-Cyclodextrin and hexamethylenetetramine with *ca.* 1:1 molar ratio were dissolved in hot water. Colorless and prismatic crystals were obtained by standing the solution for a week at room temperature. Lattice parameters and diffraction intensities were measured on a Nicolet P3/F diffractometer with graphite-monochromated Cu $K\alpha$ radiation. The crystal was sealed in a quartz capillary with a drop of mother liquor to prevent from deterioration in air. The lattice parameters were refined by the least-squares method using 25 reflections in the 2θ range 35—40°. By using $\theta-2\theta$ scan mode, 4369 independent reflections with $|F_o|\geqq 3\sigma(F)$ were collected up to 115° in 2θ. No correction was made for absorption or extinction effect.

Crystal Data: $C_{42}H_{70}O_{35}\cdot C_6H_{12}N_4\cdot 6H_2O$, F.W.=1383.3, monoclinic, space group $P2_1$, $Z=2$, $a=15.285(3)$, $b=10.345(2)$, $c=20.118(2)$ Å, $\beta=102.14(1)°$, $V=3110.0(8)$ Å^3, $D_x=1.477$, $D_m=1.46$ g·cm^{-3}.

Determination and Refinement of the Structure

The orientation of the *pseudo* heptagonal axis of β-cyclodextrin was easily deduced by inspection of a Patterson map, and the translational parameters along the a and c axes were determined by the trial-and-error method. After the correction of the position and orientation of each glucose residue by the rigid-body least-squares method, atomic parameters were refined by the block-diagonal least-squares method. Successive Fourier and difference-Fourier syntheses revealed the positions of hexamethylenetetramine and water molecules. Occupancy factors of disordered hydroxyl groups were estimated from an electron-density map, but they were not refined. Further block-diagonal least-squares refinement of the structure, including 93 hydrogen atoms, achieved the R-value of 0.065. The quantity minimized was $\sum w(|F_o|-|F_c|)^2$ with $w=1.0$ for all the reflections. Atomic scattering factors were taken from the literature.[16] Final atomic coordinates and B_{eq} values are given in Table 1. Tables of observed and calculated structure factors, anisotropic temperature factors, atomic parameters of hydrogen atoms, bond distances, angles , and conformation angles of β-cyclodextrin, and the plane equation and atomic deviations from the plane of the seven glycosidic oxygen atoms are kept at The Chemical Society of Japan (Document No. 8440). The computation was carried out on a FACOM M-380 computer at the Center of Research Information Processing System, Agency of Industrial Science and Technology, Tsukuba.

Description and Discussion of the Structure

Outline of the Structure. A numbering scheme of the β-cyclodextrin-hexamethylenetetramine complex hexahydrate is shown in Fig. 1, and a stereo-view of the complex is given in Fig. 2. The β-cyclodextrin molecule is slightly distorted from the regular heptagonal symmetry. The guest hexamethylenetetramine

TABLE 1. ATOMIC COORDINATES AND B_{eq} VALUES

OC indicates the occupancy factor of disordered atoms.

	x	y	z	B_{eq}/Å^2	OC
C(1,G1)	6409(5)	3025(8)	1398(3)	2.87	
C(2,G1)	6555(5)	4494(8)	1459(4)	2.96	
C(3,G1)	5631(5)	5127(8)	1485(4)	3.14	
C(4,G1)	4945(5)	4721(8)	861(3)	2.79	
C(5,G1)	4876(5)	3233(8)	824(4)	3.00	
C(6,G1)	4293(6)	2835(11)	156(5)	5.75	
O(2,G1)	7218(3)	4801(6)	2049(3)	3.41	
O(3,G1)	5786(4)	6517(6)	1474(3)	4.45	
O(4,G1)	4096(3)	5232(5)	943(2)	2.50	
O(5,G1)	5760(3)	2717(5)	820(2)	2.98	
O(6,G1)	4095(4)	1461(8)	193(4)	7.23	
C(1,G2)	6866(5)	-233(8)	3465(3)	2.69	
C(2,G2)	7302(5)	1081(7)	3635(4)	2.77	
C(3,G2)	6794(4)	2085(7)	3156(3)	2.37	
C(4,G2)	6781(4)	1713(7)	2427(3)	2.20	
C(5,G2)	6407(5)	300(7)	2289(4)	2.76	
C(6,G2)	6530(5)	-242(8)	1605(3)	2.99	
O(2,G2)	7325(3)	1413(5)	4316(2)	3.04	
O(3,G2)	7235(3)	3332(5)	3263(2)	2.95	
O(4,G2)	6180(3)	2571(5)	1998(2)	2.44	
O(5,G2)	6868(3)	-576(5)	2790(2)	2.69	
O(6,G2)	7460(4)	-501(6)	1615(3)	3.52	
C(1,G3)	4220(5)	-2129(8)	4494(4)	3.62	
C(2,G3)	5053(6)	-1642(9)	4970(4)	3.75	
C(3,G3)	5520(5)	-654(8)	4606(4)	3.26	
C(4,G3)	5682(5)	-1210(8)	3952(4)	2.75	
C(5,G3)	4833(5)	-1770(8)	3506(4)	3.19	
C(6,G3)	4994(7)	-2589(11)	2921(4)	5.27	
O(2,G3)	4814(4)	-1128(7)	5557(3)	4.55	
O(3,G3)	6340(4)	-307(7)	5044(3)	4.21	
O(4,G3)	5978(3)	-177(5)	3578(2)	2.70	
O(5,G3)	4408(3)	-2646(5)	3903(3)	3.46	
O(6,G3)	5539(5)	-3693(9)	3169(5)	8.38	
C(1,G4)	926(5)	-365(8)	4377(4)	3.14	
C(2,G4)	1593(5)	-273(8)	5039(4)	3.02	
C(3,G4)	2558(5)	-204(8)	4937(3)	2.96	
C(4,G4)	2709(5)	-1305(8)	4485(4)	2.82	
C(5,G4)	2018(5)	-1314(8)	3824(4)	3.30	
C(6,G4)	2089(6)	-2465(10)	3364(4)	4.53	
O(2,G4)	1378(4)	815(6)	5414(3)	3.57	
O(3,G4)	3134(3)	-269(6)	5593(2)	3.46	
O(4,G4)	3588(3)	-1098(5)	4343(3)	3.00	
O(5,G4)	1148(3)	-1422(5)	3992(3)	3.15	
O(6,G4)	2012(7)	-3680(9)	3709(5)	9.57	0.80
O(6',G4)	1792(28)	-1985(50)	2650(23)	9.38	0.20
C(1,G5)	-760(5)	3423(7)	2819(3)	2.58	
C(2,G5)	-513(5)	3667(8)	3576(4)	2.89	
C(3,G5)	301(5)	2881(8)	3918(3)	2.82	
C(4,G5)	133(5)	1456(8)	3733(3)	2.57	
C(5,G5)	-124(5)	1279(7)	2968(4)	2.71	
C(6,G5)	-426(5)	-97(8)	2752(4)	3.44	
O(2,G5)	-327(4)	5024(5)	3709(3)	3.27	
O(3,G5)	454(4)	3073(6)	4632(2)	3.77	
O(4,G5)	958(3)	803(3)	4010(2)	2.84	
O(5,G5)	-904(3)	2088(5)	2693(2)	2.69	
O(6,G5)	-609(4)	-216(6)	2032(3)	3.78	
C(1,G6)	372(5)	6138(8)	909(4)	3.09	
C(2,G6)	29(5)	6839(7)	1478(4)	3.18	
C(3,G6)	173(5)	6003(7)	2106(4)	2.71	
C(4,G6)	-309(5)	4677(8)	1914(3)	2.65	
C(5,G6)	12(5)	4072(8)	1329(4)	3.19	
C(6,G6)	-586(6)	2917(10)	1045(4)	5.20	
O(2,G6)	519(4)	8045(5)	1610(3)	3.94	
O(3,G6)	-187(4)	6644(5)	2624(3)	3.20	
O(4,G6)	-51(3)	3892(5)	2509(2)	2.29	
O(5,G6)	-109(3)	4969(6)	759(2)	3.15	
O(6,G6)	-1565(8)	3342(14)	820(6)	5.94	0.55
O(6',G6)	-70(15)	2308(16)	559(8)	7.96	0.45
C(1,G7)	3662(5)	6138(8)	443(4)	2.84	
C(2,G7)	3393(5)	7318(8)	816(4)	3.13	
C(3,G7)	2683(5)	6943(8)	1197(4)	3.31	
C(4,G7)	1889(5)	6319(7)	714(3)	2.58	
C(5,G7)	2228(5)	5150(8)	366(3)	2.71	
C(6,G7)	1490(5)	4572(9)	-186(4)	3.82	
O(2,G7)	4182(4)	7793(6)	1260(3)	4.41	
O(3,G7)	2381(4)	8115(6)	1479(3)	4.59	
O(4,G7)	1294(3)	5905(5)	1137(2)	2.60	
O(5,G7)	2910(3)	5600(5)	19(2)	2.78	
O(6,G7)	1828(4)	3552(6)	-531(3)	4.22	
C(1,HT)	2808(8)	1224(13)	2585(6)	7.50	
C(2,HT)	4220(6)	2340(10)	2833(5)	4.59	
C(3,HT)	3059(7)	3079(13)	1952(5)	6.46	
C(4,HT)	3218(7)	2343(12)	3617(5)	5.87	
C(5,HT)	2062(7)	3108(17)	2713(7)	9.25	
C(6,HT)	3445(9)	4268(11)	2990(6)	7.20	
N(1,HT)	3496(5)	1954(9)	2284(4)	5.38	
N(2,HT)	2486(5)	1995(11)	3089(4)	6.65	
N(3,HT)	3897(5)	3114(8)	3348(4)	4.69	
N(4,HT)	2719(6)	3910(10)	2438(5)	7.47	
O(W1)	4182(7)	268(8)	1434(5)	9.48	
O(W2)	-1054(5)	833(9)	5070(4)	7.27	
O(W3)	2246(6)	956(10)	-166(6)	11.40	
O(W4)	1290(11)	204(18)	763(10)	21.86	
O(W5)	2571(5)	1725(7)	-3512(3)	5.76	
O(W6)	2014(4)	2223(6)	-2293(3)	4.10	

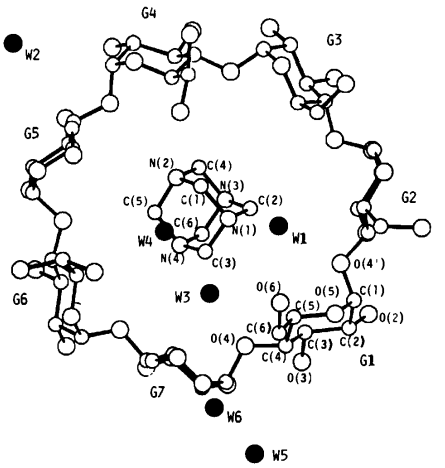

Fig. 1. Numbering scheme of the β-cyclodextrin–hexamethylenetetramine complex hexahydrate. Water molecules are shown by full circles.

molecule is located roughly at the center of the β-cyclodextrin ring, and is in van der Waals contact with the interior surface of the host molecule. β-

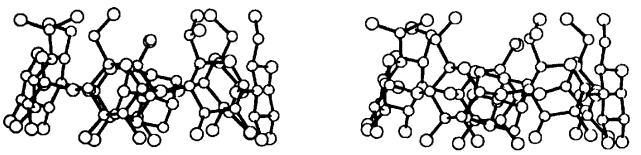

Fig. 2. Stereo-view of the β-cyclodextrin–hexamethylenetetramine complex.

Cyclodextrin molecules are stacked along the b axis, forming a "cage-type" packing. Water molecules occupy the intermolecular spaces between β-cyclodextrin molecules.

Conformation of β-Cyclodextrin. Average bond distances and angles for seven glucose residues (Fig. 3) are in good agreement with those of previously reported β-cyclodextrin complexes.[13] Two types of orientations are observed in the primary hydroxyl groups. The C(6)–O(6) bonds of the G1, G5, and G7 residues are in a *gauche-trans* conformation (to the C(5)–O(5) and C(5)–C(4) bonds, respectively), while the G2 and G3 residues have the C(6)–O(6) bonds with a *gauche-gauche* conformation. The orientation of the C(6)–O(6) bonds

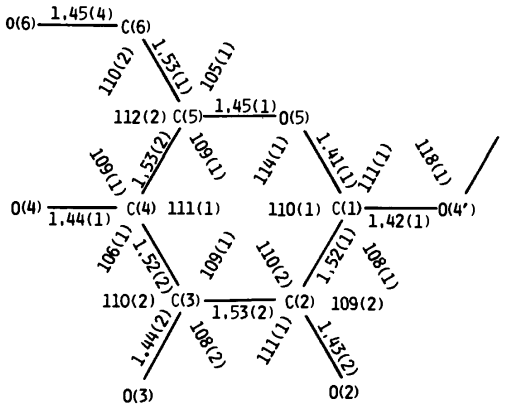

Fig. 3. Average bond distances and angles for seven glucose residues of β-cyclodextrin. Standard deviations in parentheses were estimated according to the equation:

$$\sigma = [\sum_{i=1}^{7} (x_i - \bar{x})^2/6]^{1/2}$$

where x_i refers to the bond distance or angle of the i-th residue and $\bar{x}$ is the average value.

in the G4 and G6 residues is statistically disordered, showing *gauche-trans* and *gauche-gauche* conformations.

The seven glycosidic oxygen atoms form a distorted heptagon. The radius of the heptagon, as shown in Table 2, is in the range 4.92—5.14 Å, and the O(4)···O(4′) distances between adjacent glucose residues being in the rage 4.31—4.45 Å. The average value of the radius is in good agreement with those found in the β-cyclodextrin complexes with 1,4-diazabicyclo[2.2.2]-octane (5.02 Å)[13] and 1-adamantanecarboxylic acid (5.03 and 5.08 Å).[14] The root-mean-square deviation, 0.077 Å, of O(4) atoms from the least-squares plane through the O(4) heptagon indicates the good planarity of the heptagon. As shown by the tilt-angles in Table 2, the G2, G5, and G7 residues are nearly perpendicular to the O(4) plane. The other residues incline by 14.7—17.3° with respect to the molecular axis of β-cyclodextrin, which is defined as the axis through the center of the O(4) heptagon and perpendicular to the heptagon. Distances between O(2) and O(3′) of the adjacent glucose residue are in the range 2.73—3.00 Å. These secondary hydroxyl groups are linked by the intramolecular hydrogen bonds; the O(2)-H···O(3) hydrogen bond is observed between the G1 and G2 residues, while the other hydrogen bonds are of the O(3)-H···O(2) type.

Structure of Hexamethylenetetramine. Hexamethylenetetramine has a high molecular symmetry ($\bar{4}3$ m) in the crystalline state.[15] In the cavity of β-cyclodextrin, the hexamethylenetetramine molecule shows no significant distortion from the $\bar{4}3$ m symmetry within the experimental error. The average values of C-N distance, N-C-N and C-N-C angles are 1.47(3) Å, 112(1)°, and 109(2)°, respectively. These values are in good agreement with those (1.464(4) Å, 113.3(9)°, and 107.5(5)°, respectively) found in the hexamethylenetetramine crystal at 298 K.[15]

Host-Guest Interaction. The hexamethylenetetramine molecule is roughly located at the center of the β-cyclodextrin cavity. The mirror plane through C(2,HT), C(5,HT), N(1,HT), and N(3,HT) is almost parallel to the molecular axis of β-cyclodextrin. The shortest intermolecular distance is 2.01 Å, which is found between hydrogen atoms of the C(5,HT)H_2 methylene group of the guest and the C(3,G5)H and C(5,G6)H methine groups of β-cyclodextrin. The shortest contact involving glycosidic oxygen atoms is 2.54 Å, which is found between O(4,G1) and a hydrogen atom of the C(3,HT)H_2 methylene group. The N(2) and N(4) nitrogen atoms of hexamethylenetetramine face to the interior surface of the β-cyclodextrin cavity, while the N(1) and N(3) atoms form N···H-O hydrogen bonds with the W2 water located at the primary hydroxyl side, and the O(2)-H hydroxyl group of the G3 residue in adjacent β-cyclodextrin at the secondary hydroxyl side, respectively. Therefore, the hexamethylenetetramine molecule is fixed within the β-cyclodextrin cavity by the hydrogen bonds and van der Waals force.

The position of hexamethylenetetramine in the β-cyclodextrin cavity is nearly the same as that of 1,4-

TABLE 2. GEOMETRICAL DATA FOR β-CYCLODEXTRIN

I. Radius of the O(4) heptagon

The radius is measured from the center of gravity of seven O(4) atoms to each O(4) atom.

Residue	Radius l/Å	Residue	Radius l/Å
G1	4.92	G5	5.05
G2	5.07	G6	5.07
G3	5.12	G7	5.14
G4	4.96	Average	5.05

II. O(4)···O(4) distance between adjacent glucose residues

Distance l/Å		Distance l/Å	
O(4, G1)···O(4, G2)	4.40	O(4. G4)···O(4, G5)	4.40
O(4, G1)···O(4, G7)	4.44	O(4, G5)···O(4, G6)	4.45
O(4, G2)···O(4, G3)	4.32	O(4, G6)···O(4, G7)	4.31
O(4, G3)···O(4, G4)	4.36	Average	4.38

III. Tilt-angle[a] and torsion-angle index[b]

Residue	Tilt-angle ϕ/°	Torsion-angle index ϕ/°
G1	17.3	123
G2	3.3	127
G3	16.8	120
G4	14.7	116
G5	5.3	120
G6	16.5	130
C7	6.0	119
Average	11.4	122

a) The tilt-angle is defined as an angle made by the O(4) plane and the plane through C(1), C(4), O(4), and O(4′) of each glucose residue. b) The torsion-angle index is defined as follows: $\phi = |\phi(C(1)\text{-}C(2))| + |\phi(C(2)\text{-}C(3))| - |\phi(C(3)\text{-}C(4))| - |\phi(C(4)\text{-}C(5))| + |\phi(C(5)\text{-}O(5))| + |\phi(O(5)\text{-}C(1))|$, where $\phi(C(1)\text{-}C(2))$ is the conformation angle of O(5)-C(1)-C(2)-C(3).

Table 3. Hydrogen-bond distances and angles

		Distance (l/Å)			Angle (φ/°)
		O-H	H···O	O···O	O-H···O
O(2,G1)-H·····O(3,G2)		0.85	2.03	2.87	170
O(2,G1)·····O(W6)	(f)			2.77	
O(3,G1)-H·····O(2,G7)		0.92	1.85	2.74	162
O(6,G1)···H(A)-O(W1)		0.94	1.83	2.76	170
O(6,G1)···H(B)-O(W3)		1.11	1.72	2.82	170
O(2,G2)·····H-O(3,G3)		0.93	1.99	2.92	180
O(2,G2)-H·····O(W2)	(a)	0.88	1.92	2.69	145
O(3,G2)-H·····O(3,G4)	(g)	1.14	1.78	2.87	158
O(6,G2)·····H-O(6,G5)	(a)	1.10	1.88	2.91	154
O(6,G2)·····H-O(6,G7)	(i)	1.04	2.00	2.81	133
O(6,G2)···H(B)-O(W6)	(i)	1.10	2.44	2.76	95
O(2,G3)·····H-O(3,G4)		0.96	1.78	2.73	170
O(2,G3)-H·····N(3,HT)	(j)	0.86	2.00	2.74	144
O(6,G3)·····O(W5)	(i)			2.86	
O(2,G4)·····H-O(3,G5)		0.96	2.09	3.00	158
O(2,G4)···H(B)-O(W5)	(c)	1.14	1.99	2.69	116
O(2,G4)·····H-O(2,G5)	(h)	1.05	1.72	2.75	166
O(3,G4)·····O(W5)	(c)			2.98	
O(6,G4)···H(A)-O(W2)	(h)	1.21	2.41	3.15	117
O(6',G4)·····O(2,G6)	(b)			2.54	
O(6',G4)·····H-O(3,G7)	(b)	1.21	1.75	2.69	130
O(2,G5)·····H-O(3,G6)		0.99	1.81	2.80	180
O(6,G5)·····H-O(2,G6)	(d)	0.79	2.05	2.75	148
O(2,G6)·····H-O(3,G7)		1.21	1.98	2.92	131
O(3,G6)···H(A)-O(W6)	(e)	0.69	2.29	2.80	132
O(6',G6)-H·····O(W4)		1.28	2.15	2.98	118
O(2,G7)-H·····O(W1)	(b)	1.12	2.23	2.58	95
O(3,G7)·····O(W4)	(b)			2.92	
O(6,G7)···H(A)-O(W3)		1.05	2.53	2.82	95
N(1,HT)···H(B)-O(W1)		1.13	1.93	2.80	131
O(W3)-H(A)·····O(W4)		1.05	2.47	2.72	92
O(W5)-H(A)·····O(W6)		1.15	1.68	2.81	166

Symmetry codes

None	x,	y,	z	e	-x,	1/2+y,	-z
a	1+x,	y,	z	f	1-x,	1/2+y,	-z
b	x,	1+y,	z	g	1-x,	1/2+y,	1-z
c	x,	y,	1+z	h	-x,	-1/2+y,	1-z
d	x,	-1+y,	z	i	1-x,	-1/2+y,	-z
				j	1-x,	-1/2+y,	1-z

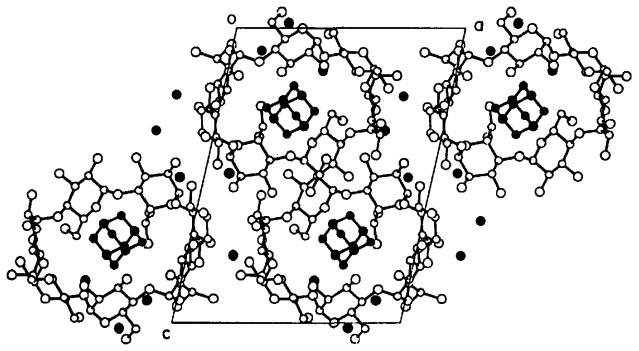

Fig. 4. Crystal structure viewed along the b axis.

diazabicyclo[2.2.2]octane,[13] but differs from that of the adamantane moiety of the 1-adamantane-carboxylic acid complex.[14] The adamantane moiety is found at the position near the primary or secondary hydroxyl side, and the carboxyl group forms hydrogen bonds with water molecules outside the cavity. Comparison of these structures suggests that the hydrogen-bond formation of the guest molecule is a more important factor to determine the host-guest geometry than van der Waals interaction.

Crystal Structure. The crystal structure is shown in Fig. 4 and 5. β-Cyclodextrin molecules are stacked along the b axis to form a "cage-type" structure similar to that found in the crystal of β-cyclodextrin.[17] The O(4) plane of β-cyclodextrin makes an angle of 46.7° with the b axis, as shown in Fig. 5. Both ends of the β-cyclodextrin cavity are blocked by adjacent β-cyclodextrin molecules. The spherical guest molecule is well accommodated within the "cage" of the β-cyclodextrin cavity. Water molecules are located in intermolecular spaces between β-cyclodextrin molecules, forming a hydrogen-bond network. W1, W3, and W4 are located near the primary hydroxyl side of the β-cyclodextrin ring, and are linked by the O(W1)-H···O(6, G1)···H-O(W3)-H···O(W4) hydrogen bonds (Table 3). W5 and W6 are also linked to each other by the O(W5)-H···O(W6) hydrogen bond, but the W2 water molecule is isolated, forming hydrogen bonds with β-cyclodextrin molecules.

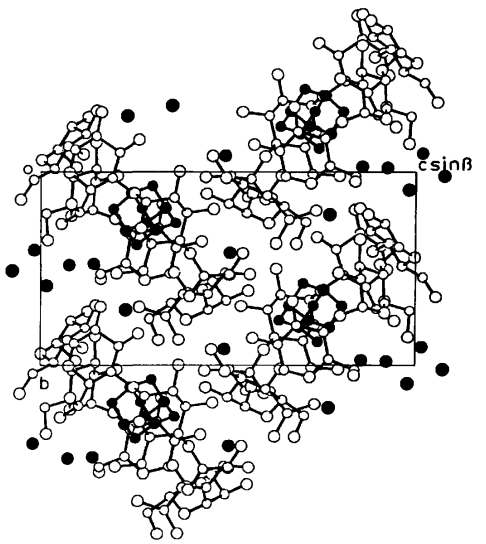

Fig. 5. Crystal structure viewed along the a axis.

References

1) M. L. Bender and M. Komiyama, "Cyclodextrin Chemistry," Springer-Verlag, Berlin (1978).
2) J. Szejtli, "Cyclodextrins and their Inclusion Complexes," Academiai Kiado, Budapest (1982).
3) K. H. Jogun and J. J. Stezowski, *Nature*, **278**, 667 (1979).
4) R. Tokuoka, M. Abe, T. Fujiwara, K. Tomita, and W. Saenger, *Chem. Lett.*, **1980**, 491.
5) K. Lindner and W. Saenger, *Carbohydr. Res.*, **107**, 7 (1982).
6) M. M. Harding, J. M. Maclennan, and R. M. Paton, *Nature*, **274**, 621 (1978).
7) J. J. Stezowski, K. H. Jogun, E. Eckle, and K. Bartels, *Nature*, **274**, 617 (1978).
8) R. Tokuoka, T. Fujiwara, and K. Tomita, *Acta Crystallogr., Sect. B*, **37**, 1158 (1981).
9) J. A. Hamilton and M. N. Sabesan, *Carbohydr. Res.*, **102**, 31 (1982).
10) M. B. Hursthouse, C. Z. Smith, M. Thornton-Pett, and J. H. P. Utley, *J. Chem. Soc., Chem. Commun.*, **1982**, 881.
11) K. Harata, K. Kawano, K. Fukunaga, and Y. Ohtani, *Chem. Pharm. Bull.*, **31**, 1428 (1983).
12) K. Uekama, F. Hirayama, T. Imai, M. Otagiri, and K. Harata, *Chem. Pharm. Bull.*, **31**, 3363 (1983).
13) K. Harata, *Bull. Chem. Soc. Jpn.*, **55**, 2315 (1982).
14) J. A. Hamilton and M. N. Sabesan, *Acta Crystallogr., Sect. B*, **38**, 3063 (1982).
15) L. N. Becka and D. W. J. Cruickshank, *Proc. R. Soc. London, Ser. A*, **273**, 435 (1963).
16) "International Tables for X-ray Crystallography," Vol. IV, Kynoch Press, Birmingham (1974).
17) K. Lindner and W. Saenger, *Carbohydr. Res.*, **99**, 103 (1982).

Tetrakis[3,5-bis(trifluoromethyl)phenyl]borate. Highly Lipophilic Stable Anionic Agent for Solvent-extraction of Cations

Hiroshi NISHIDA, Naoko TAKADA, Masaji YOSHIMURA,†
Takaaki SONODA, and Hiroshi KOBAYASHI*
Research Institute of Industrial Science, Kyushu University 86, Kasuga, Fukuoka 816
†*Department of Molecular Science and Technology, Graduate School of Engineering Sciences, Kyushu University 39, Kasuga, Fukuoka 816*
(Received March 9, 1984)

Tetrakis[3,5-bis(trifluoromethyl)phenyl]borate (TFPB) anion was highly lipophilic, practically insoluble in water, and durable against acid and oxidants. Partition equilibria of alkali TFPB between water and organic solvents and the stability in acid media are described and compared with the properties of the parent tetraphenylborate and of some fluorine-containing homologues.

Tetraphenylborate (TPB) (**1**) anion has a unique structure in which four phenyl groups are tetrahedrally bonded to the central boron atom of univalent negative charge.[1] The charged center is shielded by bulky lipophilic phenyl groups from the medium and no hydrophilic sites are present on the outside of the molecule. In this respect, the structure of TPB anion makes a strong contrast to those of ordinary organic anions such as conjugate bases of carboxylic and sulfonic acids, whose anionic oxygen atom is exposed into the surrounding medium and provides a strongly hydrophilic center. The relationship is just like that between a quarternary ammonium ion and less substituted ones, though the charge is opposite.

TPB anion forms hydrophobic ion pairs with various univalent cations, such as heavy alkali metals. By taking advantage of this property, TPB has been successfully applied as an ion-pairing agent to precipitation and solvent extraction of various organic and inorganic cations in aqueous solutions.[2]

One thing to be noticed is that TPB anion is chemically labile, especially in the presence of acids or oxidants.[3-8] This reagent must, therefore, be stored and used under strictly limited conditions. In the last two decades, several attempts have been made to overcome the drawback of chemical lability and at the same time to modify the physicochemical properties of TPB.[9-11]

Among them, tetrakis(*m*-trifluoromethylphenyl)borate (**2**) and the *p*-trifluoromethyl homologue (**3**) are worthy of attention. The strongly electron-withdrawing effect caused by the trifluoromethyl substituents would suppress the electrophilic attack by proton on to the phenyl-ring carbon ipso to the boron to increase the stability against acids.[5] And the hydrophobic fluorocarbon moieties would decrease the solubility of the ion pairs in an aqueous solution to promote the precipitate formation and the extraction into the organic solvent.[12]

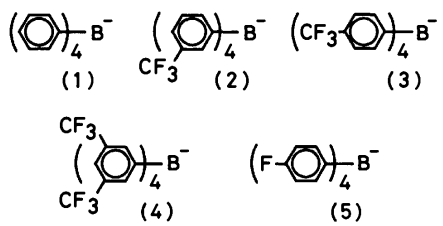

On the basis of these presumptions, the structure of tetrakis[3,5-bis(trifluoromethyl)phenyl]borate (TFPB) (**4**) was designed. Convenient preparations of the fluorinated TPB derivatives including TFPB and their properties were roughly reported.[13] This paper describes detailed examinations of the chemical stability and lipophilicity of TFPB. Preparation of TFPB according to the scheme of Fig. 1 is briefly described in the experimental section. The alkali metal salts of TFPB were practically insoluble in cold water, while being slightly soluble in hot water and readily dissolved in ethanol, ether, and acetone, and to a less extent in chloroform, dichloromethane, and toluene.

Results and Discussion

Chemical Stability. The increased chemical stability of TFPB (**4**) is noteworthy. The acid-catalyzed degradations of TPB (**1**), TFPB (**4**), and related fluorinated derivatives, (**2**) and (**3**), were kinetically followed. The decrease of the parent borate in aqueous methanol was monitored by HPLC and ^{19}F-NMR in the presence of a large excess of sulfuric acid. Respective pseudo-first-order kinetic plots gave good linear relationships. The rate constants in 63% aq methanol are compared in Table 1. Provided the reaction rate is regarded as a first-order dependence on the acid concentration,[3] the stability in acid media can be compared in terms of the relative half-life period. The comparison shows that

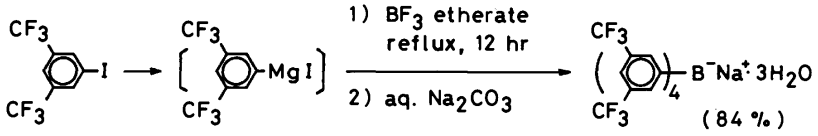

Fig. 1. Preparation scheme of TFPB.

Table 1. Comparisons of acid-catalyzed decomposition rates of tetraarylborates in aqueous methanol (methanol : water = 67 : 37)

Tetraaryl-borates	$\frac{[H^+]}{([H_2SO_4]\times 2)}$ / mol dm^{-3}	k_{obsd} / s^{-1}	$k_2=k_{obsd}/[H^+]$ / s^{-1} mol^{-1} dm^3	Relative half-life period
(1)	0.049	4.00×10^{-4}	8.00×10^{-3}	1
(2)	2.1	5.19×10^{-7}	2.47×10^{-7}	3.24×10^4
(3)	2.1	3.46×10^{-7}	1.65×10^{-7}	4.85×10^4
(4)	2.1	No decomp.	—	(Unmeasurable)
	8.2	No decomp.	—	

the trifluoromethylation on to the pendent phenyl rings increases the durability against acid to a striking extent. This extent was outstanding in TFPB; it showed no trace of decomposition after standing for one month in 4.1 mol dm^{-3} aq methanolic sulfuric acid at room temperature. The result was the same even when the sample was heated under reflux in 3.6 mol dm^{-3} methanolic sulfuric acid for 7 d.

If one assumes that electrophilic attacks by protons on to the phenyl-ring carbons ipso to the boron are correlated with the σ^+ value of trifluoromethyl groups,[5] the half-life period of TFPB can be estimated from an extrapolation of the log k_2–σ^+ plottings[14] of the upper three lines in Table 1, to be approximately 8000 d at 25 °C. This means that the reaction of TFPB takes 100 d to decompose 1% of the initial amount which might be an extent detectable by the present analytical method.

Under aerated conditions, oxidative degradation of TPB (**1**) and the trifluoromethylated derivatives (**2**), (**3**), and (**4**), were monitored by HPLC in a water–dichloromethane two-phase system. Decay curves are shown in Fig. 2. With the progress of oxidative degradation, two new peaks appeared in HPLC of the organic phase. These increased their peak areas as that of the parent borate peak decreased. One of the new peaks were assigned to the corresponding phenol and the other to the biphenyl. Although the stepwise degradation could not be differentiated, the *m*- and *p*-trifluoromethyl derivatives, (**2**) and (**3**), decomposed within 6 and 2.5 h, respectively, while TPB (**1**) took 10 h before the complete decomposition under our experimental conditions. The time when the borate peak disappeared corresponded to when those of the decomposition products ceased to increase. TFPB (**4**), on the other hand, indicated no trace of decomposition after being kept aerated for 21 h under the same conditions. If one takes account of the facts that TPB (**1**) was mostly partitioned into the aqueous phase, while the trifluromethylated derivatives, (**2**), (**3**), and (**4**), were partitioned into the dichloromethane phase during the air-oxidation in the present two-phase system, and that the solubility of oxygen in dichloromethane, though unavailable in the literature, might be estimated at about 10 times more than that in water based upon the data of homologous halomethanes at the same temperature,[15] it is obvious that the bis(trifluoromethyl)ation of the pendent phenyl groups enormously increased the durability of the TPB structure against the air-oxidation. TFPB was

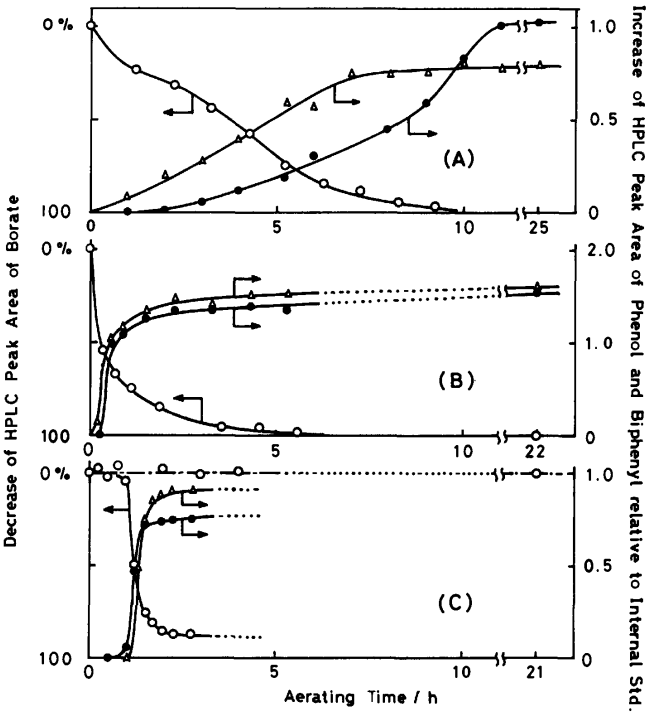

Fig. 2. Decay of the tetraarylborate (○) and occurrence of the corresponding phenol (△) and biphenyl (●) upon aeration.
(A): TPB (**1**), (B): *m*-trifluoromethyl deriv. (**2**), (C): *p*-trifluoromethyl deriv. (**3**) (——), and TFPB (**4**) (—·—).

also durable to a range of oxidants. It remained completely intact even after 22 h when its dichloromethane solution was stirred vigorously with 10% aqueous nitrous acid or 10% aqueous hypochlorite, and when treated with twice molar amounts of bromine in a chloroform solution at room temperature.[16]

Lipophilicity. Partition behaviors of the TFPB ion pairs with alkali metal ions were examined by HPLC in aqueous dichloromethane and aqueous toluene two-phase systems. The organic solvents might be regarded as the representatives of different polarities, and are frequently used as extractants.

Results are summarized in Tables 2 and 3, together with those of some related borates for comparisons.[13] The ion pairs were generally well extracted into a dichloromethane phase. One may readily notice that the saturated concentrations of alkali TFPB in the dichlo-

romethane phase are about 100 times higher than those of the others; these results indicated it to be highly lipophilic. Toluene was less efficient as an extractant of the ion pairs of such borates, as shown in Table 3. The borate was less soluble in this solvent, and so much remained in the aqueous phase.

Partitions between the two phases can be compared more clearly by their extraction coefficients, K_{ex}, which are given in Table 4. The values of TFPB salts are much higher than those of the others; especially the value of lithium salt was extremely increased. One may say that TFPB combined with toluene shows a somewhat different extraction behavior for alkali metal ions from the other homologues.

Unique behaviors of TFPB at the solvent extraction occurred not only in the partition equilibrium, but also in the phase-transfer rates, which were more than three times faster than that of tetrakis(*p*-fluorophenyl)borate (**5**), when compared by use of their lithium salts in both dichloromethane–water and toluene–water two-phase systems.[13]

As a conclusion, bis(trifluoromethyl)ation of the pendent phenyl rings of TPB was unexpectedly effective not only in the chemical stabilization of this ion-pairing agent, but also in the increase of solubility of its ion pairs in organic solvents and in the acceleration of the extraction rate. Also, the extraction coefficients varied depending upon the substituents on the pendent

TABLE 2. PARTITION OF ALKALI TETRAARYLBORATES BETWEEN AQUEOUS AND DICHLOROMETHANE PHASES

Tetraarylborates		Concn. of alkali tetraarylborate/mol dm^{-3}				
		Li	Na	K	Rb	Cs
(**1**)†	aq	$<10^{-6}$	$<10^{-6}$	$<10^{-6}$	$<10^{-6}$	$<10^{-6}$
	org	3.0×10^{-5}	1.0×10^{-5}	5.5×10^{-6}*	4.0×10^{-6}*	1×10^{-5}*
(**5**)†	aq	$<10^{-6}$	$<10^{-6}$	$<10^{-6}$	$<10^{-6}$	$<10^{-6}$
	org	3.9×10^{-5}	5.0×10^{-4}	2.6×10^{-4}	9.5×10^{-5}	1.7×10^{-4}
(**2**)†	aq	$<10^{-6}$	$<10^{-6}$	$<10^{-6}$	$<10^{-6}$	$<10^{-6}$
	org	3.0×10^{-5}	7.0×10^{-5}	7.0×10^{-5}	5.0×10^{-5}	3.1×10^{-5}
(**4**)	aq	5.6×10^{-7}	5.8×10^{-6}	5.8×10^{-7}*	2.0×10^{-7}*	1.7×10^{-7}*
	org	1.3×10^{-3}	3.4×10^{-3}	1.5×10^{-3}*	5.5×10^{-4}*	1.6×10^{-3}*

*, Occurrence of precipitates. †, Concentration in the aqueous phase was below the detection limit (10^{-6} mol dm^{-3}) of the spectrophotometric method.[17]

TABLE 3. PARTITION OF ALKALI TETRAARYLBORATES BETWEEN AQUEOUS AND TOLUENE PHASES

Tetraarylborates		Concn. of alkali tetraarylborate/mol dm^{-3}				
		Li	Na	K	Rb	Cs
(**1**)	aq	4.5×10^{-4}	4.3×10^{-4}	$<10^{-6}$*	1.0×10^{-6}*	$<10^{-6}$*
	org	1.4×10^{-5}	8.5×10^{-6}	5.0×10^{-6}*	5.5×10^{-5}*	1×10^{-5}*
(**5**)	aq	4.3×10^{-4}	4.3×10^{-5}	9.1×10^{-5}	5.2×10^{-5}*	$<10^{-6}$*
	org	1.5×10^{-5}	1.0×10^{-5}	9.5×10^{-6}	6.5×10^{-6}*	1×10^{-5}*
(**2**)	aq	7.2×10^{-6}	5.3×10^{-5}	8.7×10^{-6}*	6.2×10^{-6}	$<10^{-6}$*
	org	1.4×10^{-5}	1.6×10^{-5}	2.5×10^{-4}*	3.3×10^{-4}	3.5×10^{-4}*
(**4**)	aq	5.3×10^{-7}	5.7×10^{-7}	$\sim2\times10^{-8}$	$\sim2\times10^{-8}$	$\sim2\times10^{-8}$
	org	1.4×10^{-4}*	6.4×10^{-5}*	<DL*†	<DL*†	<DL*†

*, Occurrence of precipitates. †, Concentration in the organic phase was below the detection limit (DL) (1.6×10^{-7} mol dm^{-3}) of the present HPLC method.

TABLE 4. EXTRACTION COEFFICIENTS, K_{ex}, OF ALKALI TETRAARYLBORATES IN THE TWO-PHASE SYSTEMS, WHERE $K_{ex}=[MB]_{org}/[M^+]_{aq}[B^-]_{aq}$

Tetraaryl-borates	Two-phase system	Alkali ion				
		Li	Na	K	Rb	Cs
(**1**)	(A)	0.31	0.20	>50	550	—
(**5**)	(A)	0.35	23	1.0	1.3	—
(**2**)	(A)	0.19	3.0	2.9	5.3	—
(**4**)	(A)	2.5×10^{3}	1.3×10^{3}	—	—	—
	(B)	2.4×10^{4}	6.1×10^{3}	2.5×10^{4}	2.7×10^{5}	9.3×10^{4}

(A), Water–toluene system. (B), Water–dichloromethane system.

phenyl rings and the kinds of organic extractants. This result suggested the possibility of selective solvent-extraction for certain organic and inorganic cations by use of a proper organic extractant combined with an ion-pairing agent.

Further studies along this line are now being undertaken in this laboratory.

Experimental

^{1}H- and ^{19}F-NMR spectra were obtained on a JEOL FX-100 and Hitachi R-24B-F instruments in reference to the internal TMS and trifluoroacetic acid, respectively, unless otherwise described. HPLC charts were recorded on a Hitachi 380-30 liquid chromatograph combined with a spectrophotometric detector and a Shimadzu recording integrator C-R1A Chromatopac. A separating column 500 mm long was packed with Hitachi gel 3010. Methanol was an efficient eluant unless otherwise stated. Sodium tetraphenylborate (**1**) (Dotite Kalibor®) and sodium tetrakis(*p*-fluorophenyl)borate (**5**) (Dotite Cesibor®) were commercially available reagents. Sodium tetrakis(*m*-trifluoromethylphenyl)borate (**2**)[9] and the *p*-trifluoromethyl homologue (**3**)[9] were prepared in this laboratory.[13]

Preparation of Sodium Tetrakis[3,5-bis(trifluoromethyl)-phenyl]borate (4). An ethereal solution of boron trifluoride (365 mg, 2.52 mmol) was added dropwise over 40 min into an ethereal solution of 3,5-bis(trifluoromethyl)phenylmagnesium iodide, which was prepared from 1-iodo-3,5-bis(trifluoromethyl)benzene (4.78 g, 14.06 mmol), magnesium turnings (0.42 g, 17.1 mmol) and anhydrous ether (13 cm^3). The mixture was, after being refluxed for 12 h, poured portionwise into aqueous sodium carbonate (24.0 g in 100 cm^3 of water) with vigorous stirring. The precipitated magnesium carbonate was filtered off and washed with ether. The aqueous layer of the filtrate was separated from the ethereal one, saturated with sodium chloride, and extracted repeatedly with ether. All the ethereal extracts were combined with the initial ethereal layer, and evaporated under reduced pressure. The residual solid was succesively eluted from a silica-gel column with hexane, dichloromethane, and methanol. The borate was isolated in the form of hydrated sodium salt from the dichloromethane and methanol fractions. The yield was 2.0 g (84%). IR (KBr): 3500, 1350, 1280, and 1200—1100 cm^{-1}. ^{19}F-NMR (CH_3OH): 13.52 ppm (s). ^{1}H-NMR ($CDCl_3$–DMSO-d_6): 7.50—7.70 (m) and 2.95 (s).

Hot aqueous tetraethylammonium iodide was added to a saturated hot aqueous solution of the sodium TFPB to yield colorless precipitates, which were successively eluted from a silica-gel column with hexane, benzene, ether, and methanol. The solid residue, which was obtained from the ether and methanol fractions by evaporation, was washed with cold chloroform to give the tetraethylammonium salt, mp 181—182 °C. IR (KBr): 1350, 1280, and 1200—1100 cm^{-1}. λ_{max} (ε): 269 (4100) and 278 nm (3200). ^{1}H-NMR ($CDCl_3$–DMSO-d_6): 1.25 (tt, J=2 and 7 Hz, $-CH_3$, 12H), 2.75 (s, H_2O), 3.20 (q, J=7 Hz, $-CH_2-$, 8H), and 7.50—7.70 (m, aromatic, 12H). Found: C, 48.25; H, 3.23; N, 1.33%. Calcd for $C_{40}H_{32}NF_{24}B$; C, 48.36; H, 3.27; N, 1.09%.

Kinetics of Acid Decomposition of the Trifluoromethylated Derivatives. A methanol solution (0.3 cm^3) of the trifluoromethylated compound (**2**, **3**, or **4**) (*ca.* 20 mg) and the required amount of aqueous sulfuric acid were combined in an NMR tube at a lowered temperature and then kept at 25 °C in a thermostat. The intensity change in ^{19}F-NMR signals of the parent borate and those of the decomposition products were followed at specified intervals.

The signal of the *m*-trifluoromethyl compound (**2**) at 14.2 ppm diminished with the increments of those of the corresponding decomposition products at 13.8, 13.7, and 13.4 ppm. The signal of the *p*-trifluoromethyl compound (**3**) at 14.7 ppm and those of the decomposition products at 14.0, 13.6, and 13.4 ppm changed in a similar manner.

On the condition that the total peak area of ^{19}F-NMR signals were unchanged throughout the reaction, the logarithm of relative peak area of the parent compound was plotted against the reaction time to give a good linear relationship with a correlation coefficient (γ) more than 0.99 at least over one half-life period. The gradient of the correlation line gave a pseudo-first-order rate constant, k_{obs}. The apparent second-order rate constant, k_2, was derived according to the equation, $k_2=k_{obs}/[H^+]$, where $[H^+]$ means the acid concentration.

Kinetics of Acid Decomposition of TPB. An aqueous solution of TPB (6.82×10^{-2} mol dm^{-3}, 8.5 cm^3), aqueous sulfuric acid (0.123 mol dm^{-3}, 10.0 cm^3) and methanol (31.5 cm^3) were combined in a stoppered flask, and the resulting solution was kept at 25 °C in a thermostat. An aliquot (0.50 cm^3) was taken out of the solution at 10 min intervals and neutralized with aqueous sodium hydroxide (0.0815 mol dm^{-3}, 0.35 cm^3). A sample of 40 mm^3 from the aliquot was analyzed by HPLC at 266 nm. Since the chromatographic peak of TPB and those of the degraded borates were not well resolved, the rate constant of the acid decomposition of TPB was derived from the initial rate measured in the linear region (the 50-min period since the beginning) of the pseudo-first-order plotting to be 4.00×10^{-4} sec^{-1} with γ of 0.998.

Air-oxidation of TPB. A two-phase mixture of an aqueous solution of TPB (5.62×10^{-4} mol dm^{-3}, buffered at pH 6.0, 25 cm^3) and dichloromethane (25 cm^3) was aerated. Every hour, 40 mm^3 samples were taken out of the organic and aqueous phases and analyzed by HPLC. TPB and degraded borates were found in the aqueous phase to give an overlapped HPLC peak. The decay curve, consequently, depicted the descending overall area of the overlapped peaks. The resulting phenol and biphenyl were found in the organic phase. Both were assigned by the comparison of their retention time in HPLC and GLC with those of the authentic specimen.

Air-oxidation of the Trifluoromethylated Derivatives. A two-phase mixture of an aqueous solution (20 cm^3, buffured at pH 6.0) of the *m*-trifluoromethyl compound (**2**) (6.05×10^{-4} mol dm^{-3}) and a dichloromethane solution (20 cm^3) of 4,4′-difluorobiphenyl (2.43×10^{-4} mol dm^{-3} as an internal standard) was aerated. At specified intervals a sample (40 mm^3) from the aqueous phase and one (10 mm^3) from the organic phase were analyzed by HPLC. The HPLC peak of the parent borate (t_R=1.3 min) in the aqueous phase was closely overlapped with those of degraded borates, which were also completely decomposed within 6 h under the experimental conditions, thereafter no HPLC peaks were observed by a photometric detector at 270 nm. The relative increase of the decomposition products (t_R=2.5 and 5.3 min) in the organic phase were also followed against the internal standard (t_R=8.5 min).

Structures of the decomposition products were assigned with those obtained in a separate air-oxidation experiment by use of 0.80 mmol of the borate. The fraction of t_R=2.5 min was assigned tentatively to be *m*-trifluoromethylphenol by GC-MS (m/z=162 (M^+)) and ^{19}F-NMR measurement (a singlet at δ=98.89 ppm downfield from C_6F_6) and ^{1}H-NMR spectral comparison with that in the literature.[18] The fraction of t_R=5.3 min was an unsymmetric bis(trifluoromethyl)biphenyl by GC-MS (m/z=290 (M^+)) and ^{19}F-NMR data (two equal signals of δ=99.55 and 99.42 ppm downfield from C_6F_6).

Air-oxidation of TFPB (**4**) and the *p*-trifluoromethyl com-

pound (**3**) were carried out in a similar manner by use of an aqueous buffer (25 cm^3, pH 6) and a dichloromethane solution (25 cm^3) of the borate and 4,4'-difluorobiphenyl as an internal standard. The remaining parent borate and decomposition products from the *p*-trifluoromethyl compound were found in the organic phase and were determined in a similar manner against the internal standard.

Partition of Alkali TFPB in Organic Solvent-water Two-phase Systems. Typical Procedure. Dichloromethane-water System: A mixture of sodium TFPB (*ca.* 2×10^{-5} mol), alkali acetate (0.1 mol dm^{-3})-acetic acid buffer (pH 6.0, 250 cm^3) and dichloromethane (10.0 cm^3) was shaken until equilibrated (2 h) at 30 °C in a thermostat. Added amounts of lithium, sodium, potassium, rubidium, and cesium acetates were each large enough so that sodium ions from sodium TFPB were negligible.

The resulting mixture settled and separated into two layers. TFPB in the organic layer was determined by HPLC at 270 nm with 40 mm^3 of sample in reference to an internal standard (toluene). The eluant was methanol containing 10 v% of water. TFPB in the aqueous layer was extracted from a 200-cm^3 portion with 10 cm^3 of dichloromethane so that the solute was concentrated 20-fold over the fraction in the aqueous layer, to be determined by HPLC in a similar manner.

Toluene-water System: A mixture of the aqueous buffer (pH 6.0, 800 cm^3) containing the acetate of alkali ion to be examined, toluene (25.0 cm^3), and sodium TFPB (*ca.* 5×10^{-6} mol) was equilibrated at 30 °C by 16-h shaking.

TFPB in the toluene phase was determined by HPLC in reference to the internal standard (*o*-cresol). TFPB in the aqueous phase was preconcentrated by extraction and determined by a standard-addition method: The first aliquot (250 cm^3) from the aqueous layer was extracted with dichloromethane (7.0 cm^3) by 30-min shaking, the 2nd 250 cm^3 was done with the same solvent (7.0 cm^3) containing 1.21×10^{-7} mol of sodium TFPB, and the 3rd one was done in a similar manner by use of 2.42×10^{-7} mol of sodium TFPB. Each extract was analyzed for TFPB by HPLC with 40 mm^3 of sample. Extrapolation of the linear plotting of TFPB peak area against the standard increment of TFPB afforded the analysis of TFPB in the first aliquot.

This study was supported by the Grant-in-Aid for Scientific Research from the Ministry of Education, Science, and Culture (Project No. 56470056), and in part from the Asahi Glass Foundation for Industrial Technology, to whom the authors are grateful. Thanks are also due to Mr. Kazutaka Onitsuka for his experimental assistance in this work.

References

1) T. Davis and L. A. K. Staveley, *Trans. Faraday Soc.*, **53**, 19 (1957).
2) *e.g.* K. Ueno, M. Saito, and K. Tamaoki, *Bunseki Kagaku*, **17**, 1548 (1968); **18**, 81, 264 (1969).
3) J. N. Cooper and R. E Powell, *J. Am. Chem. Soc.*, **85**, 1590 (1963).
4) G. Wittig, G. Keicher, A. Ruckert, and P. Raff, *Ann.*, **563**, 110 (1949).
5) H. G. Kuivila and K. V. Nahabedian, *J. Am. Chem. Soc.*, **83**, 2159, 2164, 2167 (1961).
6) G. H. Geske, *J. Phys. Chem.*, **63**, 1062 (1959); **67**, 1743 (1962).
7) J. J. Eisch and R. J. Wilcsek, *J. Organomet. Chem.*, **71**, C-21 (1974).
8) J. L. R. Williams, J. C. Doty, P. J. Grisdale, R. Searle, T. H. Regan, G. P. Happ, and D. P. Maier, *J. Am. Chem. Soc.*, **89**, 5153 (1967).
9) J. T. Vandeberg, C. E. Moore, F. P. Cassaretto, and H. Posvic, *Anal. Chim. Acta*, **44**, 175 (1969).
10) M. Meisters, C. E. Moore, and F. P. Cassaretto, *Anal. Chim. Acta*, **44**, 287 (1969).
11) M. Meisters, J. T. Vandeberg, F. P. Cassaretto, H. Posvic, and C. E. Moore, *Anal. Chim. Acta*, **49**, 481 (1970).
12) R. A. Coburn and A. J. Solo, *J. Med. Chem.*, **19**, 748 (1976); M. E. Wolff and C. Hansch, *ibid.*, **17**, 898 (1974).
13) H. Kobayashi, T. Sonoda, K. Takuma, and Y. Inukai, *Rep. Asahi Glass Found. Ind. Technol.*, **42**, 137 (1983).
14) P. G. Gassman, F. Allison, and F. Fentiman, Jr., *Tetrahedron Lett.*, 1021 (**1970**).
15) "Solubilities of Inorganic and Metal-Organic Compounds," ed by W. F. Linke, American Chemical Society (1965), Vol. II, 4th Ed., pp. 1228, 1235.
16) *cf.* "New Applications of Organometallic Reagents in Organic Synthesis," ed by D. Seyferth, Elsevier Sci. Publish. Co., Amsterdam (1976), p. 101.
17) N. Takada, T. Sonoda, and H. Kobayashi, *Bunseki Kagaku*, **32**, E191 (1983).
18) C. J. Pouchert, "The Aldrich Library of NMR Spectra," Ed. II, Vol. 1, Aldrich Chemical Co., Inc., Milwaukee (1983).

 © 1984 The Chemical Society of Japan Bull. Chem. Soc. Jpn., 57, 2605—2611 (1984)

An X-Ray Diffraction Study on the Structures of Mono(glycinato)copper(II) and Tris(glycinato)-cuprate(II) Complexes in Aqueous Solution

Kazuhiko OZUTSUMI and Hitoshi OHTAKI*

Department of Electronic Chemistry, Tokyo Institute of Technology at Nagatsuta, 4259 Nagatsuta-cho, Midori-ku, Yokohama 227

(Received March 21, 1984)

The structures of mono(glycinato)copper(II) and tris(glycinato)cuprate(II) complexes in solution were determined by means of X-ray diffraction at 20 °C. The radial distribution curve obtained for solution A, in which comparable amounts of hexaaqua- and mono(glycinato)copper(II) complexes coexisted (the mole ratio $C_{gly}/C_{Cu}=0.700$, where C_i represents the total concentration of species i), showed that the mono(glycinato)copper(II) complex combined with four water molecules, two of which were at the distance of (1.98±0.01) Å at the equatorial position and the other two were of (2.27±0.01) Å at the axial one. The equatorial Cu–OH_2 bond length within the mono(glycinato)copper(II) was longer than that within the hexaaquacopper(II) ion (1.94 Å), whereas the axial Cu–OH_2 bond distance within the former complex was shorter than that within the latter (2.43 Å). Both lengths of the Cu–O and Cu–N bonds within the mono(glycinato)copper(II) ion were (1.99±0.02) Å. Thus the $[Cu(gly)(OH_2)_4]^+$ complex has an axially elongated octahedral structure. The X-ray scattering data of solution B with the C_{gly}/C_{Cu} mole ratio of 13.7, in which almost all Cu(II) ions formed the tris(glycinato)cuprate(II) complex were well explained in terms of a regular octahedral structure of the complex having the same Cu–O and Cu–N bond distances of (2.02±0.01) Å. The structure of the bis(glycinato)copper(II) complex was not determinable owing to its low solubility.

Many kinds of polyhedra appear in stereochemistry of copper(II) complexes, in which the coordination number of copper(II) ion is three, four, five or six. Of these a hexacoordinated copper(II) complex tends to have a distorted octahedral structure. A tetragonal distortion is frequently observed with the elongation of two bonds along the axis of the octahedron. Gažo *et al.*[1] collected crystal data for CuO_6, CuN_6, and CuN_4O_2 type complexes and discussed the correlation between equatorial and axial bond distances. The observation was that the equatorial and axial bond lengths correlated asymptotically with an increase of the interatomic distances within the equatorial plane, resulting in shortening the bond lengths along the axial direction.

Structures of copper(II) complexes have been extensively studied crystallographically. However, an axial bond distance in crystal may be significantly affected by an interaction between a ligand at the apex of a complex and counter ions around the complex ion, since an axial bond is essentially weak relative to an equatorial one. Thus, it seems to be desirable to investigate structures of copper(II) complexes without an effect of counter ions on copper(II)-ligand bonds along the axis.

Hexaaqua-,[2,3] some ammine-[4] and bis- and tris-(ethylenediamine)copper(II)[5] complexes in aqueous solution have been investigated so far by the X-ray diffraction method. All of the hexacoordinated complexes have an axially elongated octahedral structure. The equatorial bond distances are between 1.93 Å and 2.05 Å, whereas the axial bond lengths vary widely (2.3—2.9 Å). Recently the structures of tetraammine- and bis(ethylenediamine)copper(II) complexes in aqueous solution have been reported with a laboratory EXAFS apparatus.[6] Only four equatorial Cu–N bonds (≈2.03 Å) were detectable and the axial bond length was not determinable by the EXAFS measurement. The structure of a copper(II) chloride aqueous solution was studied by means of X-ray diffraction,[7] and it was reported that the equatorial sites of copper(II) ion were occupied by water molecules and chloride ions at 1.95 Å and 2.25 Å, respectively. However, the axial Cu–OH_2 and/or Cu–Cl bonds, which would appear at 2.2—2.3 Å for the former and at 2.8—3.0 Å for the latter, were not clearly observable because of overlapping of the peak owing to the axial bonds with that of the Cu–Cl (eq) bond within the complex and with the peak of the Cl–H_2O bond (≈3.1 Å) within the hydrated chloride ion. Distorted octahedral structures of copper(II)–chloro complexes were also found in methanol.[8]

Although there have been presented some structural data of copper(II) complexes in solution by the X-ray diffraction and EXAFS methods, no investigation has been carried out for structures of chelate complexes, except for ethylenediamine complexes, in solution. Therefore, in the present study we have attempted to determine the structures of glycinato copper(II) complexes in aqueous solution by the X-ray diffraction method.

In spite of a great importance of structural information of glycinato copper(II) complexes in the view point of coordination chemistry and biochemistry, the structure of only the bis(glycinato)copper(II) complex has been determined in crystal,[9] and structural data have been given for other complexes in neither solution nor the solid state. Therefore, we investigated the structures of the mono(glycinato)copper(II) and tris (glycinato)couprate(II) complexes in aqueous solution. The structure of the bis(glycinato)copper(II) complex in solution was not determinable by the present X-ray diffraction method due to its low solubility in water.

Experimental

Preparation and Analysis of Sample Solutions. All chemicals used were of reagent grade. Sample solutions were prepared by the similar way to that described in a previous

Table 1. The composition (mol dm^{-3}) and stoichiometric volume V per copper atom in solution A and per sodium atom in solutions B and C

	A	B	C
Cu	1.234	0.5842	—
Na	—	6.840	6.166
O	57.78	48.30	50.28
N	2.468	8.008	6.166
C	1.727	16.02	12.33
H	105.9	96.59	100.6
V/Å^3	1346	242.8	269.3
C_{gly}/C_{Cu}	0.700	13.7	—
density/g cm^{-3}	1.165	1.369	1.282
ρ_o/Å^{-3}	195.1	46.67	46.29

paper.[10] *Solution A*, in which the mono(glycinato)copper(II) complex was mainly formed, was prepared by dissolving powder of the bis(glycinato)copper(II) complex to a copper(II) nitrate solution. *Solution B* was prepared by mixing the bis(glycinato)copper(II) and sodium glycinate in water. Almost all copper(II) ions formed the tris(glycinato)cuprate(II) complex in this solution. *Solution C* was an aqueous sodium glycinate solution.

Bis(glycinato)copper(II) was prepared by mixing an aqueous copper(II) sulfate solution with a glycine solution which had been neutralized with $NaHCO_3$ and then recrystallized from water. Sodium glycinate was obtained by the same manner previously reported.[10] Copper(II) nitrate and copper(II) sulfate of reagent grade were recrystallized from water.

The total concentration of copper(II) ions (C_{Cu}) in the test solutions was electrogravimetrically determined as metallic copper. The total glycine concentration (C_{gly}) in the solutions was determined by the Kjeldahl method. Concentrations of nitrate ions in solution A and of sodium ions in solutions B and C were evaluated from the material balance of ions in the solutions. Densities of the sample solutions were measured by using a pycnometer. The composition of the solutions is given in Table 1.

Method of Measurement and Treatment of X-Ray Scattering Data. The apparatus used and method of measurements were described previously.[2,10,11] Mo $K\alpha$ radiation (λ= 0.7107 Å) was used and the scattered intensities were measured at discrete points of θ over the range 1°—70° (2θ is the scattering angle). Times required to accumulate 120000 counts were recorded at each point. The scattered intensities were scaled to the absolute ones after corrections for absorption, polarization and multiple scatterings of X-rays by a usual manner.[11]

The reduced intensities $i(s)$ were extracted from the scaled intensities $I(s)$ by subtracting independent coherent scatterings according to Eq. 1:

$$i(s) = I(s) - \sum_i n_i[\{f_i(s)+\Delta f_i'\}^2 + (\Delta f_i'')^2]. \quad (1)$$

The reduced intensities multiplied by s ($=4\pi\lambda^{-1}\sin\theta$) of the sample solutions are shown in Fig. 1. The radial distribution function $D(r)$ was calculated by the Fourier transform of the reduced intensities as follows:

$$D(r) = 4\pi r^2\rho_o + \frac{2r}{\pi}\int_0^{s_{max}} s\cdot i(s)\cdot M(s)\cdot\sin(rs)ds, \quad (2)$$

where ρ_o ($=\{\sum_i n_i\cdot f_i(0)\}^2/V$) is the average scattering density in the stoichiometric volume V of the solution, and s_{max} represents the maximum s-value attained in the measurement. The modification function $M(s)$ had the form given in Eq. 3,

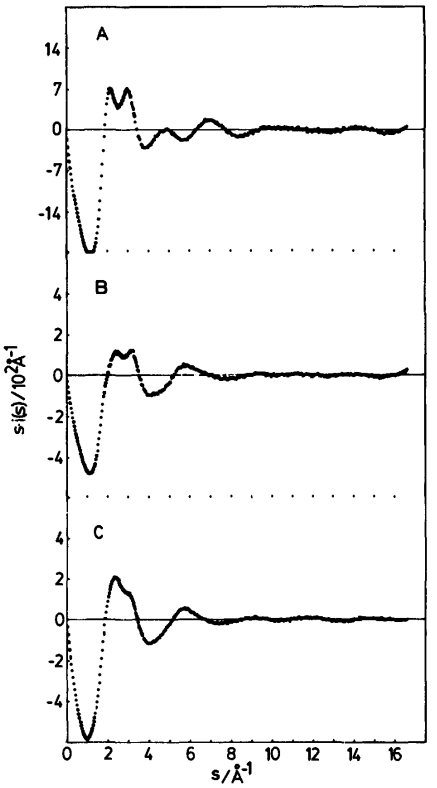

Fig. 1. The reduced intensities multiplied by s for solutions A, B, and C.

$$M(s) = \frac{[\sum_i n_i\cdot f_i(0)^2]}{[\sum_i n_i\cdot f_i(s)^2]}\cdot\exp(-k\cdot s^2). \quad (3)$$

The damping factor k was chosen as 0.01 Å^2 in the present case. In Eqs. 1—3 $f_i(0)$ and $f_i(s)$ denote the atomic scattering factors of atom i at s=0 and s, respectively. n_i is the number of atom i in the stoichiometric volume. $\Delta f_i'$ and $\Delta f_i''$ represent the real and imaginary parts of anomolous dispersion of atom i, respectively. The radial ($D(r)$) and differential radial ($D(r)-4\pi r^2\rho_o$) distribution curves of the test solutions are depicted in Figs. 2 and 3, respectively.

Calculations were performed by using by KURVLR[12] and NLPLSQ[13] programs with the computer at the Tokyo Institute of Technology and partly with the computer at the Institute for Molecular Science in Okazaki.

Results and Discussion

According to the formation constants of copper(II)-glycine complexes,[14] comparable amounts of the hexaaquacopper(II) and mono(glycinato)copper(II) complexes existed in solution A. The tris(glycinato)cuprate(II) complex is predominantly formed in solution B as a large excess of glycinate ions are contained. The coexistence of the bis(glycinato)copper(II) complex in both solutions needs not to be taken into consideration in the course of the analysis of the data, since the solubility of the bis(glycinato)copper(II) is low (about 0.025 mol dm^{-3}).

Structure of Mono(glycinato)copper(II) Complex. Figure 4 represents the radial distribution and differential radial distribution functions of solution A,

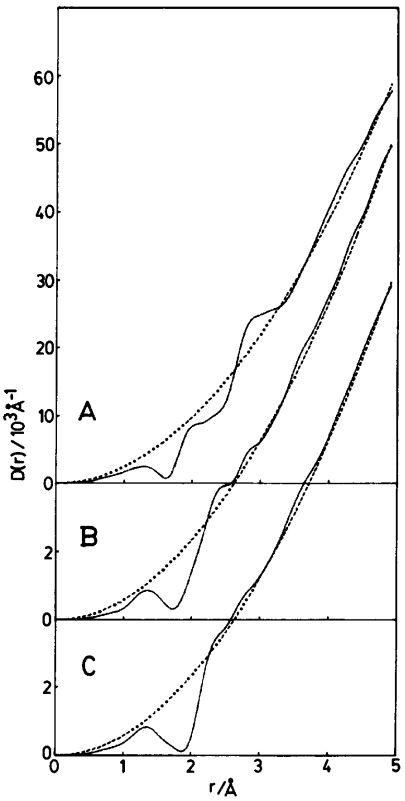

Fig. 2. The radial distribution curves, $D(r)$, for solutions A, B, and C. The curves of $4\pi r^2\rho_o$ are shown by dashed lines.

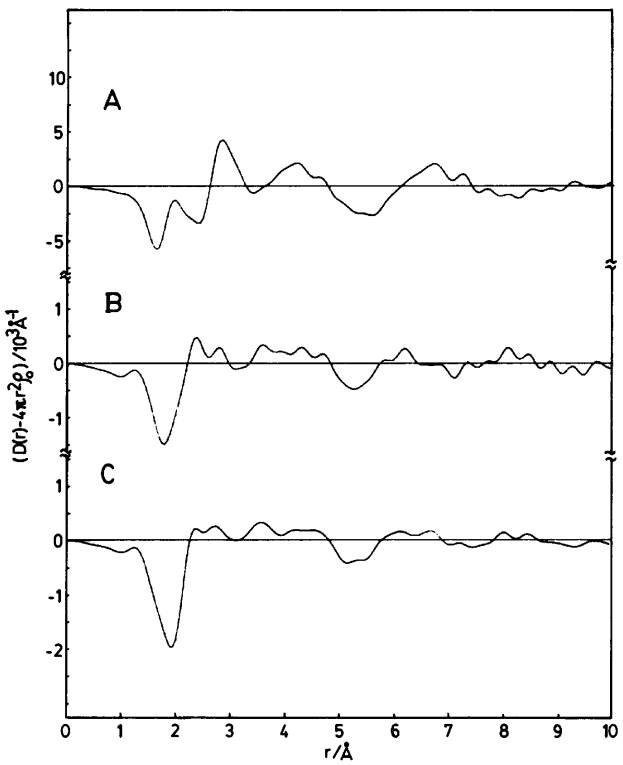

Fig. 3. The $(D(r)-4\pi r^2\rho_o)$ curves for solutions A, B, and C.

as well as the calculated peak shapes of each atom pair in the system which will be discussed in the later section. In the radial distribution curves (Figs. 4a and 4e) we see four peaks around 1.3, 2.0, 2.9, and 4.3 Å.

The small and broad peak appearing at 1.3 Å is due to the O-H bonds within water molecules, the N-O bonds within nitrate ions and N-H, C-H, C-C, C-N, and C...O bonds within glycinate ions. The second peak observed around 2.0 Å is attributable to the interactions of copper(II) ion with the ligand atoms in the first coordination shell. Nonbonding C···N, C···O, and O···O interactions within glycinate ions and O···O contacts within nitrate ions also contribute to the peak. The third peak at about 2.9 Å is ascribed to the nonbonding Cu···C interactions within the mono(glycinato)copper(II) ion, to the interactions between atoms within the ligands in the first coordination sphere of the complexes and to the O···O contacts of water mole-

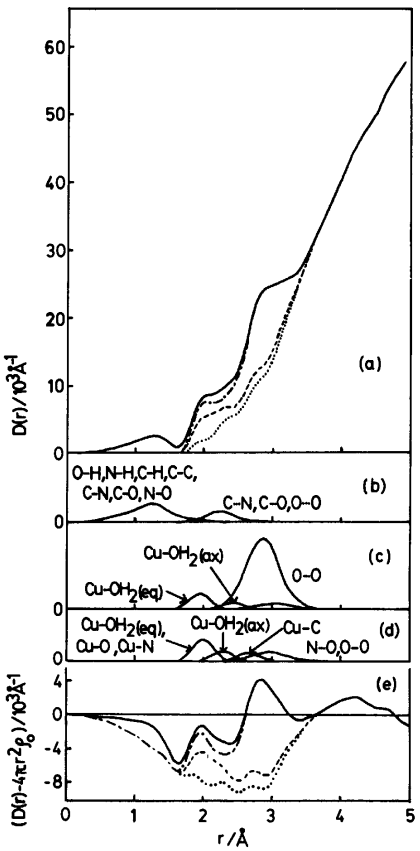

Fig. 4. (a) The radial distribution curve for solution A. (b) The theoretical peak shapes for O–H bonds within water molecule, intramolecular interactions within glycinate ion, and N–O and O···O pairs within nitrate ion. (c) The theoretical peaks for Cu–OH_2(eq), Cu–OH_2(ax), and O···O pairs within the hexaaquacopper-(II) complex and O···O contacts of water molecules in the bulk. (d) The theoretical peaks calculated for Cu–OH_2(eq), Cu–O, Cu–N, Cu–OH_2(ax), Cu···C, N···O, and O···O pairs within the mono-complex. (e) The corresponding $(D(r)-4\pi r^2\rho_o)$ curve to the $D(r)$ in (a). The chain, dashed, and dotted lines indicate the residual curves after subtraction of the theoretical peaks in (b), (c), and (d), respectively.

cules in the bulk. The fourth peak is composed of peaks owing to longer intramolecular interactions as well as intermolecular interactions between ions in the solution, which will not be taken into account in the present analysis.

In the first step of the analysis of the radial distribution curve, we subtracted the calculated peak shapes owing to the intramolecular interactions of water molecules, glycinate and nitrate ions. The parameter values used were the same as those described in the previous paper.[10] The residual curve thus obtained is shown in Fig. 4 by the chain line. The broad peak at about 2.0 Å suggested that the mono(glycinato)copper(II) as well as the hexaaquacopper(II) complexes had a distorted octahedral structure.

In order to estimate the structural parameters for the mono(glycinato)copper(II) complex, the concentration ratio of the $[Cu(OH_2)_6]^{2+}$ to $[Cu(gly)]^+$ ions in the solution must be evaluated. In the second step of the analysis, we assumed the concentration ratio of the hexaaquacopper(II) to mono(glycinato)copper(II) complexes to be 40:60 according to the stability constants reported in dilute solutions,[14] and the theoretical peaks owing to the intramolecular interactions of $[Cu(OH_2)_6]^{2+}$ and the O···O contacts in the bulk water were subtracted. In the course of the calculation, the structure parameters for the $[Cu(OH_2)_6]^{2+}$ ion and the bulk water were quoted from the works by Ohtaki and Maeda[2] and by Narten,[15] respectively. The analysis of the residual curve (···) indicated that the broad peak around 2.0 Å consisted of two peaks centered at 2.0 and 2.3 Å. The peak area corresponded to four Cu-O and Cu-N bonds for the former and two Cu-O bonds for the latter,[16] and hence the mono(glycinato)copper(II) complex has a form of a distorted octahedron with one glycinate ion and four water molecules. Thus, the glycinate ion and two of the water molecules coordinated to the Cu(II) ion at the equatorial positions and additional two water molecules bound at the axial ones. The distances of the nonbonding Cu···C pairs and the interactions between the ligand atoms in the first coordination shell were evaluated by employing the above structure model.

The least-squares calculations were carried out by using $s \cdot i(s)$ values in the high angle region ($s>5$ Å^{-1}) (Fig. 5). In order to avoid errors introduced by neglecting long-range interactions, the lower limit of the s-value was varied from 5 to 7 Å^{-1}. The intramolecular interactions of water molecules, glycinate and nitrate ions and of hexaaquacopper(II) complex and the O···O contacts in the bulk water were fixed at the literature values during the refinements. The calculations were performed by inserting bond distances roughly estimated from the analysis of the radial distribution curve as initial value. Various sets of the initial values were examined in the course of the least-squares calculations: in one case the length of the Cu-OH_2 (eq), Cu-O, and Cu-N bonds were assumed to be 2.00 Å, while the length of the Cu-OH_2 (ax) within the $[Cu(gly)(OH_2)_4]^+$ complex was 2.30 Å. Another assumption was made for the initial bond lengths inserted to be 1.94 Å for the Cu-OH_2 (eq) in the $[Cu(gly)(OH_2)_4]^+$, which was the same as that of the Cu-OH_2 (eq) within the hexa-

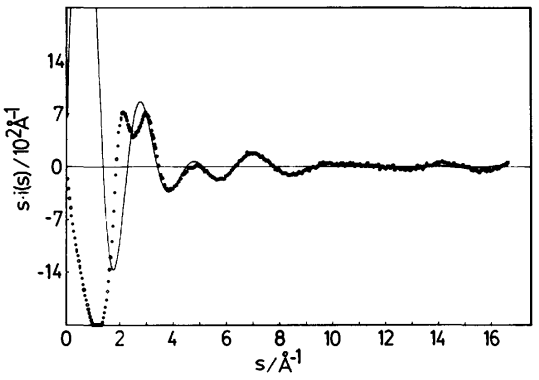

Fig. 5. The $s \cdot i(s)$ values for solution A. The observed curve is shown by circles and calculated one using parameter values listed in Table 2 by the solid line.

aquacopper(II) ion. Other bond lengths were assumed to be the same as those examined in the previous case.[10] Two additional assumptions were tested, in which the length of the Cu-OH_2 (eq) bond within $[Cu(gly)(OH_2)_4]^+$ was either 1.94 or 2.00 Å and the Cu-N and Cu-O bond distances were set to be a value between 1.95 to 2.05 Å. The different assumptions thus made, however, did not affect the result, and independent of the assumptions for the initial values inserted for the bond length within the $[Cu(gly)(OH_2)_4]^+$ complex, the values converged to those listed in Table 2.

In the course of the refinement described above, the concentration ratio of the hexaaquacopper(II) to mono(glycinato) copper(II) complexes was fixed at 40:60. At the next step of calculation, we changed the concentration ratio of the $[Cu(OH_2)_6]^{2+}$ to $[Cu(gly)(OH_2)_4]^+$ ions from 60:40 to 30:70 and performed the data refinement in the same way as described in the preceding section. The converged values coincided with those given in Table 2 within the standard deviations given in the previous calculations and were practically independent of the concentration ratio. The error square sum U,

$$U = \sum_{s_{min}}^{s_{max}} s^2(i(s)_{obsd} - i(s)_{calcd})^2 \quad (4)$$

for each set of the concentration ratios at different s-ranges examined are summarized in Table 3.

The minimum error square sum was obtained for the set in which the concentration ratio of the hexaaquacopper(II) to mono(glycinato)copper(II) complexes was 40:60, regardless of the s-ranges examined in the least-squares calculations.

From the result we concluded that the Cu-OH_2(eq), Cu-O and Cu-N bond lengths within the $[Cu(gly)(OH_2)_4]^+$ complex were approximately the same, and therefore, the complex has a distorted octahedral structure with a regular square plane. The concentration ratio of the $[Cu(OH_2)_6]^{2+}$ to $[Cu(gly)(OH_2)_4]^+$ complexes was 40:60 in the test solution.

Structure of Tris(glycinato)cuprate(II) Complex. The stability constant of the tris(glycinato)cuprate(II) complex has been reported to be small (log (K_3/mol^{-1} dm^3)$\simeq$0—1) and thus the solution in which the tris(glycinato)cuprate(II) complex is predominantly formed must contain a large excess of glycinate tions. In

TABLE 2. RESULTS OF THE LEAST-SQUARES REFINEMENT OF SOLUTION A.[a]
STANDARD DEVIATIONS ARE GIVEN IN PARENTHESES
r: bond distance (Å), b: temperature factor (Å^2).

Interaction	Parameter	$5<s/Å^{-1}<16$[c]	$6<s/Å^{-1}<16$	$7<s/Å^{-1}<16$
Cu-OH_2(eq)	r	1.98(1)	1.98(1)	1.97(1)
	b	0.0020(4)	0.0019(4)	0.0018(4)
Cu-O	r	1.99(2)	1.99(2)	1.99(2)
	b	0.0020(4)	0.0019(4)	0.0018(4)
Cu-N	r	1.99(2)	1.99(2)	1.99(2)
	b	0.0021(4)	0.0019(4)	0.0018(4)
Cu-OH_2(ax)	r	2.27(1)	2.27(1)	2.27(1)
	b	0.004[b]	0.004[b]	0.004[b]
N···O O···OH_2(eq) N···OH_2(eq) OH_2(eq)···OH_2(eq)	r	2.8[b]	2.8[b]	2.8[b]
	b	0.010[b]	0.010[b]	0.010[b]
O···OH_2(ax) N···OH_2(ax) OH_2(eq)···OH_2(ax)	r	3.0[b]	3.0[b]	3.0[b]
	b	0.010[b]	0.010[b]	0.010[b]
Cu···C	r	2.66(4)	2.69(4)	2.70(4)
	b	0.006[b]	0.006[b]	0.006[b]

a) The mole ratio of Cu^{2+} to $[Cu(gly)]^+$ complexes was assumed to be 40 : 60. b) The values were kept constant during the calculation. c) The calculated $s \cdot i(s)$ values shown in Fig. 5 were obtained by using the parameter values of this type.

TABLE 3. ERROR SQUARE SUMS (U) CALCULATED FOR THE BEST FIT VALUES OBTAINED BY THE LEAST-SQUARES REFINEMENT USING VARIOUS SETS OF s-RANGE AND MOLE FRACTION OF Cu^{2+} TO $[Cu(gly)]^+$

	mole fraction			
	$Cu^{2+}=0.3$	0.4	0.5	0.6
	$[Cu(gly)]^+=0.7$	0.6	0.5	0.4
s-range	$U\times10^{-4}$/Å^{-2}			
$5<s/Å^{-1}<16$	6.7	*6.4*	7.2	8.0
$6<s/Å^{-1}<16$	6.2	*6.1*	6.5	7.0
$7<s/Å^{-1}<16$	5.7	*5.6*	5.7	6.0

solution B in which the C_{Gly}/C_{Cu} mole ratio was 13.7, almost all of the Cu(II) ions were expected to be present as the $[Cu(gly)_3]^-$ complex. However, the concentration of Cu(II) ions was much lower than that of sodium and glycinate ions in the solution (see Table 1).

Since the large contribution of the hydrated sodium and free glycinate ions to the measured intensities hid the structural information of the tris(glycinato)-cuprate(II) complex in this solution, it was difficult to obtain the structural parameters for the tris(glycinato)-cuprate(II) complex with a reasonable accuracy with a direct analysis of the reduced intensities for solution B. Therefore, we tried to determine the structure of the tris(glycinato)cuprate(II) complex by subtracting the contribution of sodium and free glycinate ions from the X-ray scattering data for solution B by taking into account the scattered intensities of solution C (an aqueous sodium glycinate solution).

The radial distribution and differential radial distribution curves of solutions B and C depicted in Figs. 2 and 3 showed simlar patterns over the whole r range. A slight different shape, however, was observed around 2 Å, which was attributable to the interaction of copper(II) ion with donor atoms in its first coordination sphere. A direct comparison of the data for solutions B and C could be made because the ρ_o value (the average scattering density in a stoichiometric volume of a solution) of solution B was approximately the same as that of solution C (see Table 1).

The radial distribution functions of solutions B and C could be compared provided that the Fourier transform (Eq. 2) of their intensities would be carried out by using the same modification function. Since the modification functions were different for these solutions because of different atomic compositions of the solutions, the direct comparison of the radial distribution curves of solutions B and C offered only qualitative information about the structural difference of these solutions. Therefore, the structural data for the tris-(glycinato)cuprate(II) complex in solution B was extracted by subtracting the reduced intensities of solution C from those of solution B. The difference of the reduced intensities of the two solutions, $i(s)_{diff}$, which includes any structural difference between the two solutions, is shown in Fig. 6. Since the stoichiometric volume of the solutions was normalized to that containing one sodium atom, the contribution of hydrated sodium ions to the reduced intensities of the solutions was entirely eliminated from the $i(s)_{diff}$ curve. The difference in the concentrations of glycinate ions in the two solutions could remain to some extent in the $i(s)_{diff}$ curve, but the number of glycinate ions in the stoichiometric volumes of solutions B and C was 1.17 and 1.0, respectively, and thus the difference was very small.

The $i(s)_{diff}$ curve, therefore, contained only intensities owing to interactions between copper(II) ions and ligand atoms within the coordination sphere and the nonbonding Cu···C interactions. Intensity difference due to different numbers of water molecules in the stoichiometric volumes of solutions B and C (which were 4.72 and 6.15, respectively) might appear as a part of the $i(s)_{diff}$ curve.

The Fourier transform of the $i(s)_{diff}$ data gave only one peak centered at about 2.02 Å, which should be ascribed to the Cu-O and Cu-N interactions within the tris-(glycinato)cuprate(II) complex (see Fig. 7). A small hump appearing at the right wing of the peak was thought to be a spurious one, because the shape of the hump changed when the s_{max} value of the Fourier transform of the $i(s)_{diff}$ data was changed. Since the $i(s)_{diff}$ data had large uncertainties in the high angle region, the s_{max} value did not exceed 13 Å^{-1}.

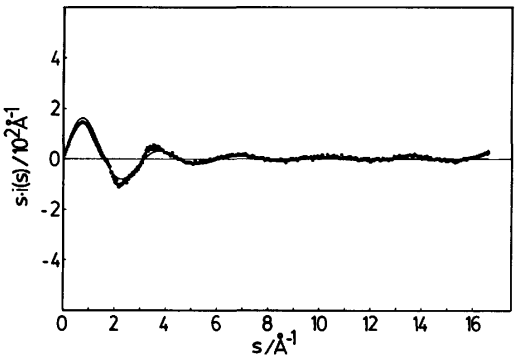

Fig. 6. The $s \cdot i(s)_{diff}$ curve (circles) obtained after subtracting reduced intensities of solution C from those of solution B. The solid line indicates the calculated values with the parameter values given in Table 4.

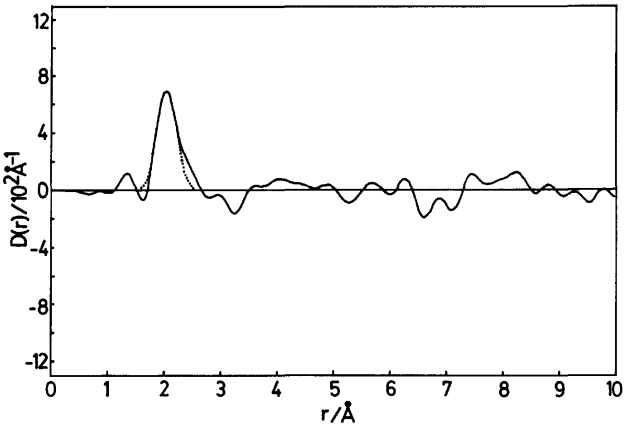

Fig. 7. The $D(r)$ curve obtained by the Fourier transform of the $s \cdot i(s)_{diff}$ values. Dotted line represents the theoretical peak shape for Cu-O and Cu-N bonds within the tris-complex.

Analysis of the peak shape (dotted line in Fig. 7) led to the Cu-O and Cu-N bond distances to be 2.02 Å and the temperature factors of the bonds to be 0.002 Å^2. The frequency factor of the sum of those of the Cu-O and Cu-N bonds was evaluated to be 6 from the area under the peak. The length of the nonbonding Cu···C interactions was estimated to be about 2.8 Å by using a suitable structure model of chelating glycinate ions within the tris(glycinato)cuprate(II) complex. However, no distinct peak corresponding to the Cu···C distance was observed in the curve in Fig. 7, probably the Cu···C peak having been cancelled by a part of the O···O peak due to the bulk water in solution C.

The structural parameters of the tris(glycinato)-cuprate(II) complex were determined by using a least-squares method for the $s \cdot i(s)_{diff}$ data over the range $s<13$ Å^{-1}. The lower limit of the s-values was changed from 0 to 2 Å^{-1}. In type-I refinement only two interactions, Cu-O and Cu-N, were taken into consideration. In type-II calculation contributions arising from intramolecular interactions within water molecules and glycinate ions were also taken into account, because the numbers of them in the stoichiometric volumes in solutions B and C were different. The frequency factors were kept constant to be 3 for both the Cu-O and Cu-N interactions in the course of the calculations. The results obtained by the two calculations were practically the same and were given in Table 4. When we inserted different lengths for the Cu-O and Cu-N bonds as initial values, they converged to indifferent values of the bond lengths through the least-squares calculations. Therefore, we concluded that the tris-(glycinato)cuprate(II) complex has a regular octahedral structure.

The lengths of Cu-OH_2(eq), Cu-O, Cu-N, and Cu-OH_2(ax) bonds within the $[Cu(OH_2)_6]^{2+}$,[2] $[Cu(gly)(OH_2)_4]^-$, and $[Cu(gly)_3]^-$ complexes in solution, together with those within the *cis*-$[Cu(gly)_2(OH_2)_2]$ in crystal, are tabulated in Table 5. In the *cis*-$[Cu(gly)_2(OH_2)_2]$ complex four sites in the square plane of the copper(II) ion were filled with two oxygen and two nitrogen atoms within the two glycinate ions coor-

Table 4. Least-squares refinements of the structural parameters for tris(glycinato)-cuprate(II) complex. Standard deviations are given in parentheses

Interaction	Parameter	I		II	
		$0<s/Å^{-1}<13$	$2<s/Å^{-1}<13$	$0<s/Å^{-1}<13$	$2<s/Å^{-1}<13$[a]
Cu-O	r/Å	2.01(1)	2.02(1)	2.01(1)	2.02(1)
	b/Å^2	0.0019(7)	0.0017(8)	0.0019(6)	0.0018(8)
Cu-N	r/Å	2.01(1)	2.02(1)	2.01(1)	2.02(1)
	b/Å^2	0.0021(6)	0.0020(7)	0.0021(6)	0.0020(6)

a) The calculated $s \cdot i(s)$ curve shown in Fig. 6 was drawn by using the parameter values given here.

TABLE 5. COPPER(II)-LIGAND BOND DISTANCES (r/Å) IN THE HYDRATED COPPER ION AND GLYCINATO-COPPER(II) COMPLEXES

Complex	Cu-OH_2(eq)	Cu-O	Cu-N	Cu-OH_2(ax)	Cu-O(ax)[c]
$[Cu(OH_2)_6]^{2+}$ [a]	1.94	—	—	2.43	—
$[Cu(gly)(OH_2)_4]^+$	1.98	1.99	1.99	2.27	—
cis-$[Cu(gly)_2(OH_2)]$[b]	—	1.946 1.957	1.984 2.021	2.404	2.742
$[Cu(gly)_3]^-$	—	2.02	2.02	—	—

a) Ref. 2. b) In crystal: Ref. 9. c) Carbonyl oxygen of a glycinate ion within an adjacent complex unit.

dinated and one apex of the distorted octahedron of the copper(II) ions was occupied by a water molecule. The oxygen atom at the other apex of the octahedron was a carbonyl oxygen of a glycinate ion combined with an adjacent copper(II) ion in the crystal.

The tris(glycinato)cuprate(II) complex has a regular octahedral structure, although the structure of the other copper(II)-glycinato complexes distorted. Regular octahedral structures of copper(II) complexes have been found for the $[Cu(en)_3]SO_4$,[17] $K_2Pb[Cu(NO_2)_6]$[18] and $[Cu(OMPA)_3](ClO_4)_2$[19] (OMPA refers to octamethylpyrophosphoramide) complexes in crystal. The indifferent bond length within a copper(II) complex was often explained in terms of the dynamic Jahn-Teller effect. However, we found that the regular octahedral $[Cu(en)_3]^{2+}$ complex in crystal had different Cu-N(eq) and Cu-N(ax) bond lengths in solution,[5] and thus the dynamic Jahn-Teller effect was not observed in the complex in solution. Since the dynamic Jahn-Teller effect can hardly be observed in principle in the structural analysis of complexes in solution by the X-ray diffraction method, the regular octahedral structure of the $[Cu(gly)_3]^-$ complex found in the present study is not an averaged structure of a dynamically distorted octahedron, but a relatively rigid regular one. The small temperature factors of the Cu-O and Cu-N bonds within the complex support this conclusion.

The work has been financially supported, in part, by the Grant-in-Aid for Scientific Research No. 57470054 from the Ministry of Education, Science and Culture. The financial aid by the Asahi Glass Foundation for Industrial Technology is also acknowledged. A part of computer calculations carried out in the present work has been performed at the Institute for Molecular Science in Okazaki.

References

1) J. Gažo, I. B. Bersuker, J. Garaj, M. Kabešová, J. Kohout, H. Langfelderová, M. Melník, M. Serátor, and F. Valach, *Coord. Chem. Rev.*, **19**, 253 (1976).
2) H. Ohtaki and M. Maeda, *Bull. Chem. Soc. Jpn.*, **47**, 2197 (1974).
3) M. Magini, *Inorg. Chem.*, **21**,1535 (1982).
4) T. Yamaguchi and H. Ohtaki, *Bull.Chem. Soc. Jpn.*, **52**, 415 (1979).
5) T. Fujita and H. Ohtaki, *Bull. Chem. Soc. Jpn.*, **56**, 3276 (1983).
6) M. Sano, T. Maruo, and H. Yamatera, *Bull. Chem. Soc. Jpn.*, **56**, 3287 (1983).
7) M. Magini, *J. Chem. Phys.*, **74**, 2523 (1981).
8) M. Ichihashi, H. Wakita, and I. Masuda, *Bull. Chem. Soc. Jpn.*, **56**, 3761 (1983).
9) H. C. Freeman, N. R. Snow, I. Nitta, and K. Tomita, *Acta Crystallogr.*, **17**, 1463 (1964).
10) K. Ozutsumi and H. Ohtaki, *Bull. Chem. Soc. Jpn.*, **56**, 3635 (1983).
11) H. Ohtaki, M. Maeda, and S. Ito, *Bull. Chem. Soc. Jpn.*, **47**, 2217 (1974); H. Ohtaki, T. Yamaguchi, and M. Maeda, *Bull. Chem. Soc. Jpn.*, **49**, 701 (1976).
12) G. Johansson and M. Sandström, *Chem. Scr.*, **4**, 195 (1973).
13) T. Yamaguchi, Doctor Thesis, Tokyo Institute of Technology, March (1978).
14) L. G. Sillén and A. E. Martell, "Stability Constants," Special Publication No. 17 (1964), The Chemical Society, London; A. E. Martell and R. M. Smith, "Critical Stability Constants," Plenum, New York (1974), Vol. 1.
15) A. H. Narten, *ORNL*-4578 (1970).
16) It is practically not possible to distinguish between Cu-O and Cu-N bonds by X-ray diffraction measurements. However, since we know that the complex formed in the present solution is the mono(glycinato)copper(II) complex and thus the oxygen and nitrogen donor atoms within the glycinate ion must occupy the two equatorial positions. Therefore, we assume that one of the four L's (L=O or N) must be N.
17) D. L. Cullen and E. C. Lingafelter, *Inorg. Chem.*, **9**, 1858 (1970).
18) D. L. Cullen and E. C. Lingafelter, *Inorg. Chem.*, **10**, 1264 (1971).
19) M. D. Joesten, M. S. Hussain, and P. G. Lenhert, *Inorg. Chem.*, **9**, 151 (1970).

Structure and Properties of Thallium(I) Formate Solutions

Kazuhiko OZUTSUMI, Hitoshi OHTAKI,* and Asao KUSUMEGI†
Department of Electronic Chemistry, Tokyo Institute of Technology at Nagatsuta, 4259, Nagatsuta-cho, Midori-ku, Yokohama 227
†*National Laboratory for High Energy Physics, Oho-machi, Tsukuba-gun, Ibaraki 305*
(Received April 28, 1984)

The structure of thallium(I) formate aggregates in concentrated aqueous thallium(I) formate solutions was investigated by the X-ray diffraction method at 25 °C for solutions A (10.77 mol dm^{-3}) and B (3.493 mol dm^{-3}). The former solution had the density of 3.189 g cm^{-3} and the C_{H_2O}/C_{Tl} mole ratio of 2.59, where C_i represents the total concentration of species i, and was an almost saturated solution at room temperature. From the analysis of the X-ray diffraction data of solution A, thallium(I) formate was found to be present as a tetramer $Tl_4(O_2CH)_4$. The nearest interatomic distances between thallium(I) and atoms within the formate ions in the tetramer were determined as Tl-O: 2.79(1) Å and Tl···C: 3.33(2) Å. The nonbonding Tl···Tl distances within the aggregate were estimated to be 3.92(1) Å, 4.34(1) Å, and 4.79(1) Å. The Tl-OH_2 bond length was also determined to be 3.22(3) Å, which was much larger than the distance expected from the sum of the ionic radius of thallium(I) ion (≈1.4 Å) and size of a water molecule (≈1.4 Å). A comparison of the radial distribution function of solution A with that of solution B, which had the C_{H_2O}/C_{Tl} mole ratio of 13.5, indicated that the aggregate decomposed by dilution. Raman spectra of four different thallium(I) formate aqueous solutions of 3.493 to 10.77 mol dm^{-3} were measured and the frequencies of the C-O and C=O stretchings of formate ions in the solutions were compared with those of free formate ion. Band shifts of the two frequencies observed for concentrated thallium(I) formate solutions indicated the existence of bridge-type formate ions coordinated to thallium(I) ions, and the result agreed with that observed by the X-ray diffraction analysis. Densities, refractive indices, viscosities and conductivities were measured for thallium(I) formate aqueous solutions with varying concentrations.

It has been well known that some thallium(I) carboxylates are extremely soluble in water. Densities of concentrated solutions become 2—4 g cm^{-3} and thus the solutions can be used as heavy liquids for gravity concentrations of ores. The solutions also have large absorptivity for high energy beams and good transparency for visible light. Therefore, applications of the solutions to transparent shields for radiation instead of lead glasses have been examined.[1-3] Mixtures of thallium(I) carboxylates and organic scintillators may provide useful detectors of radiation beams. In this connection it is interesting to investigate structures and properties of thallium(I) carboxylate solutions.

Another interest of the structural study of concentrated solutions of thallium(I) carboxylates is concerned with an investigation in which structures of crystal hydrates are compared with those of hydrate melts. It has often been reported that a part of the structure of a crystal hydrate still remains in a concentrated solution of the salt. X-Ray diffraction data of hydrate melts of $CaCl_2 \cdot 6H_2O$[4] and $Ca(NO_3)_2 \cdot 3.5H_2O$[5] have been interpreted in terms of a quasi-lattice structure of the corresponding crystal hydrates. Structures of concentrated solutions of magnesium, aluminium and indium(III) with monovalent anions have been studied by means of X-ray diffraction and the liquid structure has been approximated to a quasi-close-packing lattice structure of hydrated cations.[6,7] Enderby and his coworkers' studies[8-10] on the structure of nickel(II) chloride solutions by the neutron diffraction method have suggested a quasi-lattice arrangement of hydrated nickel(II) ions in the solutions.

In the present investigation we focus our attension on the structure of thallium(I) formate aggregates formed in solution and changes in physicochemical properties of thallium(I) formate solutions with the concentration of the solute.

The crystal structure of thallium(I) formate has recently been determined by Oddon *et al.*[11] and has been found that a formate ion bridges two thallium atoms as a bidentate ligand through the two oxygen atoms and infinite -HCOO-Tl-HCOO-Tl- chains are formed in crystal. A thallium(I) ion is surrounded with four oxygen atoms within formate ions, the Tl-O distances being 2.559, 2.565, 2.736, and 3.047 Å. The coordination polyhedron of the thallium(I) ion is trigonal bipyramidal with the thallium(I) ion at one apex of the equatorial triangle plane.

The X-ray diffraction method is employed in the present work for the structural determination of thallium(I) formate complexes in solution. Raman spectroscopic measurements are also carried out as a supplement to the X-ray structural analysis. Densities, refractive indices, viscosities and conductivities of thallium(I) formate solutions with varying concentrations are measured.

Experimental

Preparation and Analysis of Sample Solutions. Two kinds of test solutions (A and B) were prepared for X-ray diffraction measurements by dissolving thallium(I) formate of reagent grade in water. Solution A was an almost saturated solution of thallium(I) formate at room temperature, while solution B was about three times more dilute than solution A. Concentrations of thallium(I) ions in the solutions were determined by gravimetry as TlI. Concentrations of formate ions were estimated from the stoichiometry of thallium(I) formate. The composition of the sample solutions is listed in Table 1. Solutions used for measurements of Raman spectra, densities, refractive indices, viscosities and conductivities were prepared by diluting a stock solution of thallium(I) formate with water.

X-Ray Scattering Measurements. X-Ray scattering data were obtained at 25 °C with a JEOL $\theta-\theta$ type diffractometer equipped with a Philips Mo X-ray tube (λ=0.7107 Å).

Table 1. The composition (mol dm^{-3}) and stoichiometric volume V per thallium atom in the solutions

	A	B
Tl	10.77	3.493
O	49.47	54.11
C	10.77	3.493
H	66.63	97.73
V/Å^3	154.2	475.4
C_{H_2O}/C_{Tl}	2.59	13.5
density/g cm^{-3}	3.189	1.720

The method of measurements and data treatments were described elsewhere.[12,13] The measured scattering angle (2θ) ranged from 2° to 140°. Times requiring to accumulate 80000 counts were recorded at each angle of 2θ. All calculations were carried out by using programs KURVLR[14] and NLPLSQ.[15]

Raman Spectroscopic Measurements. Raman spectroscopic measurements were performed by using a JEOL JPG-400D spectrometer with the use of the 5145 Å excited line of Ar^+ laser.

Measurements of Physicochemical Properties. Densities of thallium(I) formate solutions were measured pycnometrically. Two pycnometers were used for the measurements and the results agreed each other within 0.05%. Measurements of viscosities of solutions were carried out by using an Ubbelohde-type viscometer and water was employed as the standard. The efflux time was measured with a stop watch. Conductivities of solutions were measured by a direct current method. A conductivity cell and electrical circuits used for the measurements were essentially the same as those designed in the literature.[16] A current-supplying electrode was a platinum electrode and a TOA-type HC-205 calomel electrode was employed to measure voltage drops. The reproducibility of the conductivity measurements was within 0.3%. The temperature was kept at (25.00±0.03) °C in all the physicochemical measurements. An Atago NAR-3 Abbe-type refractometer was employed to refractive index measurements of solutions with the use of the NaD line (5893 Å). The temperature for the refractive index measurements was regulated at (25.0±0.1) °C by circulating thermostated water through the refractometer.

Results and Discussion

The observed $s \cdot i(s)$ and $(D(r)-4\pi r^2(\rho_o)$ curves, where ρ_o denotes the average scattering density in the stoichiometric volume V per thallium atom, of the test solutions are shown in Figs. 1 and 2, respectively.

The structure of formate ion in crystal has been determined for various formates with monovalent cations. The intramolecular bond distances of a formate ion in the thallium(I) salt[11] do not appreciably differ from those in lithium,[17] sodium,[18] potassium[19] and ammonium formates.[20] Therefore, in the course of the analysis of the radial distribution functions of solutions A and B, the intramolecular bond lengths of formate ion were assumed to be the same as those in the

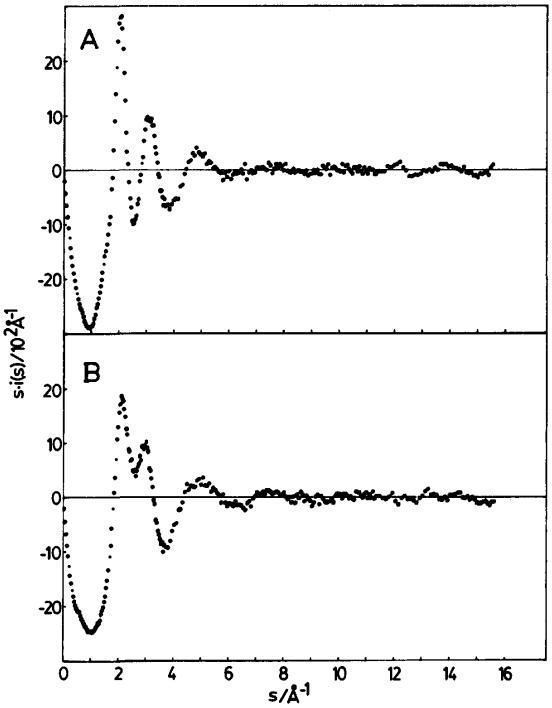

Fig. 1. The reduced intensities multiplied by s for solutions A and B.

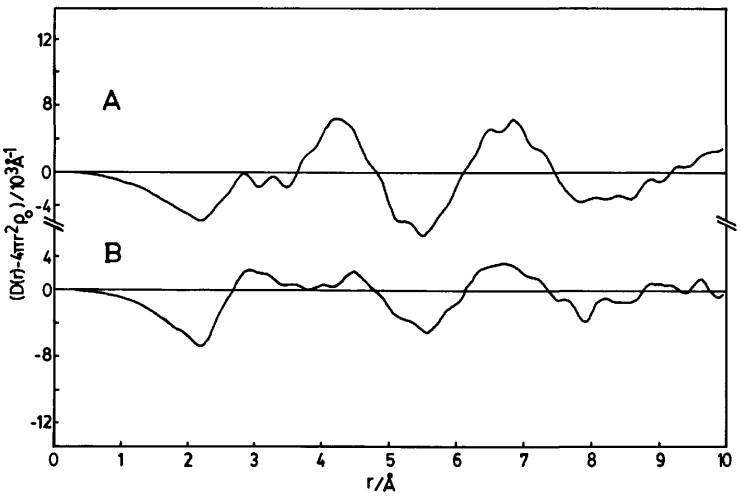

Fig. 2. The $(D(r)-4\pi r^2\rho_o)$ curves for solutions A and B.

thallium(I) formate crystal.[11] The temperature factors of atom-pairs within formate ion were taken from the electron diffraction data of the formic acid monomer in the gas phase.[21]

Structure of Thallium(I) Formate Aggregates in Solution A. The $s \cdot i(s)$ curve of solution A showed a sharper peak at 2.1 $Å^{-1}$ and a deeper minimum at 2.5 $Å^{-1}$ than the curve of solution B (see Fig. 1), and the radial distribution curve of solution A (Fig. 2) had a large and broad peak around 4.3 Å, which was not observed in the radial distribution curve of solution B.

The broad peak around 1.2 Å was composed of peaks owing to the O–H bonds within water molecules and the C–H and C⋯O bonds within formate ions. The second peak appearing at about 2.8 Å could be ascribed to the Tl–O bonds as was expected from the sum of their ionic radii. The hydrogen bonded O⋯O interactions within bulk water might contribute to the peak, but the contribution should be so small in such a concentrated thallium(I) formate solution that the O⋯O peak might be neglected in the course of the analysis of the radial distribution curve. The area of the peak gave the frequency factor of 3 for the Tl–O bond. If a thallium atom was combined with three formate ions, the nonbonding Tl⋯C distance should appear at about 3.2 Å. Therefore, the third peak observed at about 3.2 Å in Fig. 2 was attributed to be mainly due to the Tl⋯C distance within the thallium(I) formate aggregate.

The fourth peak around 4.3 Å was considered to be constructed by, at least, three peaks, because the broad peak had shoulders at both sides of the maximum. The large area of the peak could not well be explained in terms of the nonbonding Tl⋯O interactions and was only explainable by the existence of Tl⋯Tl interactions in the aggregate. By the trial-and-error method the peak could be divided into three peaks centered at 3.9, 4.4, and 4.8 Å, and the frequency factors of each peak corresponded to 0.5 (Tl⋯Tl) pairs, which indicated that each thallium(I) ion in the aggregate interacted with three thallium(I) ions with different distances (Fig. 3).

On the basis of the analysis of the radial distribution curve of solution A, calculated intensities and radial distribution curves drawn from model structures of various thallium(I) formate aggregates were compared with the experimental values. A dimer or a trimer structure was not acceptable because of their too small frequency factors for Tl⋯C and Tl⋯Tl interactions, and the area of the peak around 4.3 Å calculated by assuming a pentamer or a hexamer was too large compared with the peak area obtained by the experiment. The tetramer model depicted in Fig. 4 gave calculated intensities which satisfactorily agreed with observed ones over the s-range of 2—16 $Å^{-1}$ (see Fig. 5). The radial distribution curve drawn on the basis of the structural model thus proposed well explained the large peak found at 3.5—5 Å with two shoulders at the both side of the peak as seen in Fig. 3.

The least-squares method was applied to the $s \cdot i(s)$ curve for the refinement of the structural parameters of the tetramer by taking into account the formation of $Tl–OH_2$ bonds at each thallium(I) ion. The refinement was carried out over the range $s \geq 2.5$ $Å^{-1}$. All the

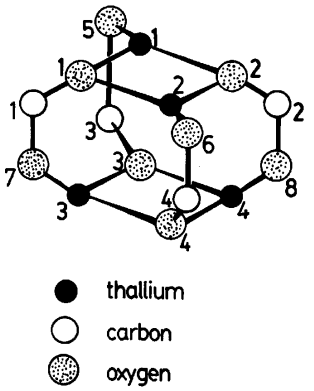

Fig. 4. The structure of $Tl_4(O_2CH)_4$ complex in solution.

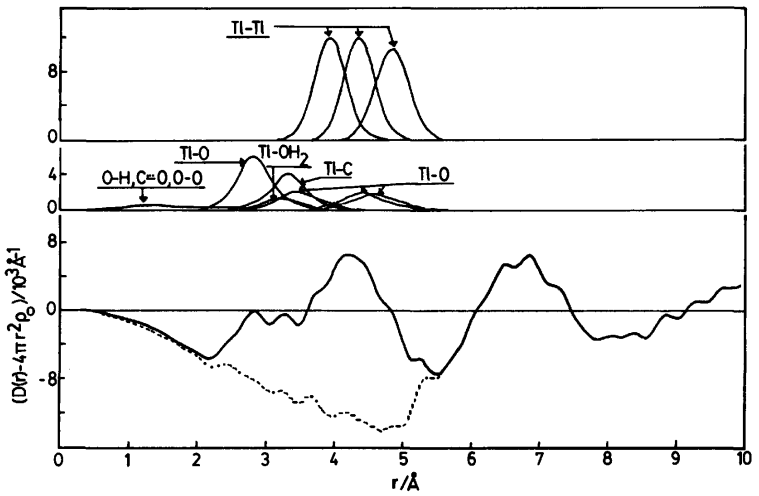

Fig. 3. The $(D(r)-4\pi r^2\rho_0)$ curve for solution A. The dashed line represents the residual curve after subtraction of the theoretical peaks calculated for the O–H bond within water molecule, C–H, C⋯O, and O⋯O pairs within formate ion and Tl–O, $Tl–OH_2$, Tl⋯C, Tl⋯O, and Tl⋯Tl interactions within $Tl_4(O_2CH)_4$.

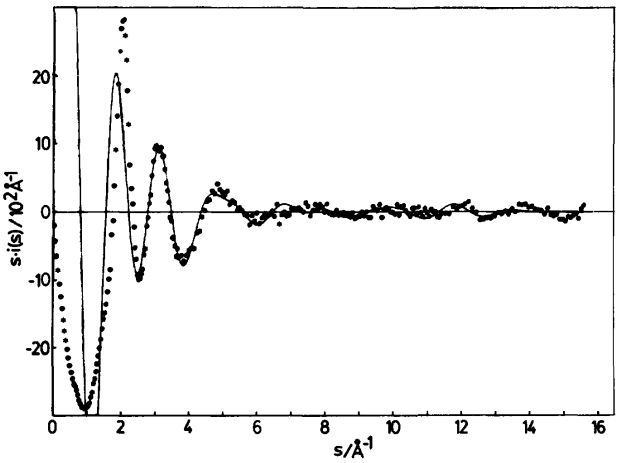

Fig. 5. The $s \cdot i(s)$ values for solution A. The observed curve is shown by circles and calculated one by the solid line.

interatomic distances and temperature factors were floated as independent variables. Frequency factors of atom-pairs within the model were fixed at values estimated from the model, except for the frequency factor for the Tl-OH_2 bonds. The agreement between calculated and experimental $s \cdot i(s)$ values was sufficient in the range $s \geq 2.5$ Å^{-1} (Fig. 5). The frequency factor for the Tl-OH_2 bond was estimated to be 0.7, which suggested that one water molecule combined with each thallium(I) ion in the tetramer, and therefore, the thallium(I) ion has the coordination number of 4. However, the Tl-OH_2 bond distance was much larger than the distance expected from the sum of the ionic radius of thallium(I) ion (≈1.4 Å) and the size of a water molecule (≈1.4 Å), the result suggesting a weak interaction between a thallium(I) ion and a water molecule.

In crystal of thallium(I) formate, the coordination number of the thallium(I) ion is four, and the thallium(I) ion is located at a corner of a triangle plane which is constructed with two oxygen and one thallium atoms, and other two oxygen atoms are situated above and below the plane. The model derived from the structure in the crystal did not give $s \cdot i(s)$ values which sufficiently fitted the experimental values.

The structural parameters finally obtained for the tetramer are listed in Table 2.

Structure of Solution B. The radial distribution curve of solution B did not give the large peak which had been observed in solution A, and therefore, the result showed that the thallium(I) formate tetramer did not exist as the predominant species in solution B and the aggregate decomposed by dilution. An asymmetrical peak at about 2.8 Å suggested the formation of bonds between thallium(I) and oxygen atoms in the solution, but the radial distribution curve was not explainable by assuming the formation of a simple 1:1 complex between thallium(I) and formate ions. In solution B there might be some complexes coexisting, but the radial distribution curve could not be analyzed without knowledge of formation constants for thallium(I) formate complexes, which had not been found in the literature. The conclusion which we can derive from the radial distribution curve is that the thallium(I) formate tetramer is not a predominant form in a relatively dilute solution, but can be the main species in a solution of extremely high concentration.

Raman Spectra. In Table 3 are summarized frequencies for vibrations found in Raman spectra of aqueous thallium(I) formate solutions of 3.493, 5.924, 8.528, and 10.77 mol dm^{-3}, as well as those observed in Raman and infrared spectra of thallium(I) formate crystal[11,22] and an aqueous potassium formate solution.[23]

Coordination types of carboxylato groups within complexes have been discussed on the basis of the change in the frequencies of the C-O ($\tilde{\nu}_2$) and C=O ($\tilde{\nu}_4$) stretching vibrations in the complexes by comparing with those in free carboxylate ions.[24] When a carboxylate ion coordinates to a metal ion as a unidentate ligand, $\tilde{\nu}$(C-O) and $\tilde{\nu}$(C=O) shift to lower and higher frequencies, respectively, than those in free ion. Thus the separation ($\Delta\tilde{\nu}$) between the two frequencies in the unidentate complexes becomes about 300—350 cm^{-1}, which is much larger than that in free ion (230—250 cm^{-1}). In the case of the formation of chelate complexes in which carboxylate ions coordinate to metal ions as a bidentate ligand, the $\tilde{\nu}$(C-O) band shifts toward the higher frequency side, while the $\tilde{\nu}$(C=O) band shifts toward the lower side, and

Table 2. Results of the least-squares refinements of solution A

Parameter values refined were bond distances(r), temperature factors(b), and frequency factors(n).

Interaction	$2.5 < s/$Å$^{-1} < 15.0$			$4.5 < s/$Å$^{-1} < 15.0$		
	r/Å	b/Å^2	n	r/Å	b/Å^2	n
Tl_1-O_1	2.81(1)	0.007(1)	3.0[a]	2.79(1)	0.008(1)	3.0[a]
Tl···C_1	3.31(2)	0.008(1)	3.0[a]	3.33(2)	0.009(1)	3.0[a]
Tl_1···O_8	3.43(4)	0.008(2)	1.0[a]	3.50(4)	0.009(2)	1.0[a]
Tl_1···Tl_2	3.92(1)	0.015(1)	0.5[a]	3.92(1)	0.014(1)	0.5[a]
Tl_1···Tl_3	4.35(1)	0.015(1)	0.5[a]	4.34(1)	0.015(1)	0.5[a]
Tl_1···O_3	4.39(7)	0.013(4)	1.0[a]	4.31(7)	0.009(4)	1.0[a]
Tl_1···O_7	4.53(8)	0.019(5)	1.0[a]	4.34(8)	0.010(5)	1.0[a]
Tl_1···Tl_4	4.83(1)	0.021(1)	0.5[a]	4.79(1)	0.021(1)	0.5[a]
Tl_1-OH_2	3.18(3)	0.011(4)	0.7(2)	3.22(3)	0.014(5)	0.8(2)

a) The values were kept constant during the calculation.

Table 3. Raman and infrared absorption frequencies (cm^{-1}) of formate ion[a]

	Thallium(I) Formate						Potassium Formate Solution[e]
	Solution/mol dm^{-3}				Crystal		
	3.493	5.924	8.528	10.77	(I)[c]	(II)[d]	
$\tilde{\nu}_1$	2828	2821	2815	2810	2786	2775	2803
$\tilde{\nu}_2$	1356	1350	1350	1347	1351, 1333	1342	1351
$\tilde{\nu}_3$	768	769	772	765	758	759	760
$\tilde{\nu}_4$	1573	1567	1564	1562	1590	1572, 1606	1585
$\tilde{\nu}_5$	1388	1379	1382	1379	1387, 1406	1357	1383
$\tilde{\nu}_6$	1070	1067	1064	1064	—	—	1069
$\Delta\tilde{\nu}$[b]	217	217	214	215		(248)	234

a) $\tilde{\nu}_1$: C-H stretching, $\tilde{\nu}_2$: Symmetric OCO stretching, $\tilde{\nu}_3$: Symmetric OCO deformation, $\tilde{\nu}_4$: Asymmetric OCO stretching, $\tilde{\nu}_5$: Asymmetric OCO deformation, $\tilde{\nu}_6$: Out-of-Plane deformation. b) $\Delta\tilde{\nu}$ represents the separation between $\tilde{\nu}_2$ and $\tilde{\nu}_4$. c) Ref. 24. d) Ref. 11. e) Ref. 25.

therefore, the $\Delta\tilde{\nu}$ value becomes smaller by 70—100 cm^{-1} than that of free carboxylate ions. In the bridge-type coordination, on the other hand, the values of the $\tilde{\nu}$(C-O) and $\tilde{\nu}$(C=O) frequencies do not appreciably differ from those in free carboxylate ions and thus the $\Delta\tilde{\nu}$ value remains in the region 200—250 cm^{-1}.

As seen from Table 3, the frequencies of the C-O and C=O stretchings for the thallium(I) formate complex in the solutions are about 1350 and 1570 cm^{-1}, respectively, and the $\Delta\tilde{\nu}$ value is 214—217 cm^{-1}. Therefore, we concluded that the formate ions within the complex existing in the solutions coordinate to thallium(I) ion with the bridge-type. The conclusion derived from the Raman spectra supports the result obtained in the X-ray diffraction measurement.

Physicochemical Properties of Thallium(I) Formate Solutions. Densities ρ and refractive indices n_D measured in thallium(I) formate solutions with varying concentrations are plotted against the concentration (Fig. 6). The plots gave almost straight lines over a wide range of concentration, and no clear indication was obtained for the complex formation between thallium(I) and formate ions beginning at a specific concentration of the solute.

In Fig. 7 are shown absolute viscosities η, specific viscosities η_{SP}, and kinematic viscosities ν of thallium(I) formate solutions as a function of the concentration of the solute. The absolute and specific viscosities monotonously increased with the concentration of thallium(I) formate. However, the kinematic viscosity of the solution first decreased and then increased with the concentration. The kinematic viscosity of thallium(I) formate solution was lower than that of water even in 9 mol dm^{-3} thallium(I) formate solution.

The specific conductivity κ of thallium(I) formate solutions had a broad maximum around 7 mol dm^{-3}, although the molar conductivity Λ of the solutions monotonouly decreased with the concentration (Fig. 8). The Walden products $\Lambda\eta$ of thallium(I) formate solutions are plotted against the concentration in Fig. 9. Walden products of lithium nitrate[25] and chlorate[26] solutions, in which the cation is highly hydrated and thus no contact ion-pair formation is expected, decreased and then increased after passing through a minimum at about 8 mol dm^{-3}. Silver nitrate, which was known to form the contact ion-pair in concentrated solutions,[27] had the Walden product which had a minimum at about 4 mol dm^{-3}.[28] The values of the

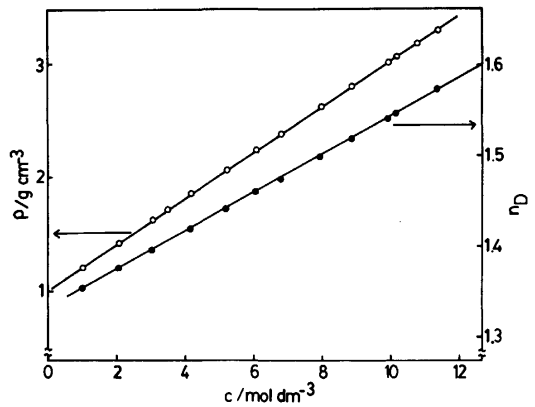

Fig. 6. Plots of density and refractive index *vs.* concentration.

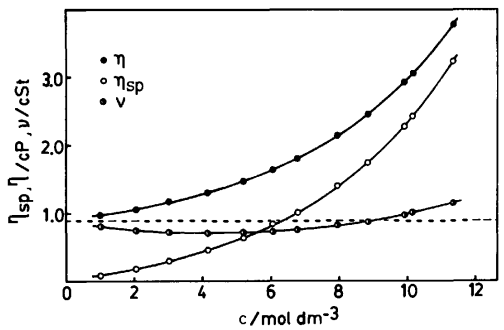

Fig. 7. Concentration dependence of viscosities. The dashed line indicates the value of water.

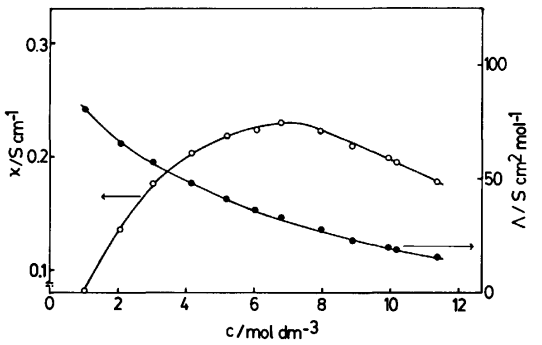

Fig. 8. Concentration dependence of conductivities.

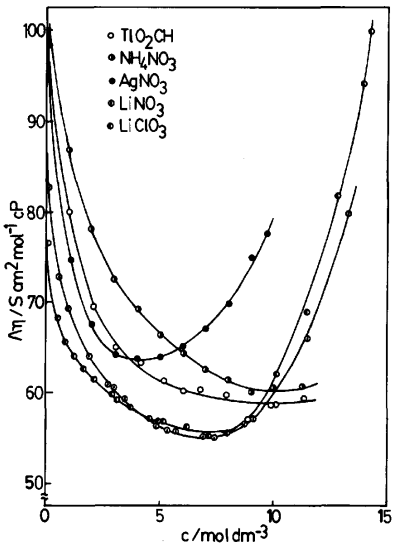

Fig. 9. Walden products of thalluim(I) formate, ammonium nitrate, silver nitrate, lithium nitrate, and lithium chlorate solutions.

Walden products of ammonium nitrate[28] and thallium(I) formate simply decreased with the concentration. It is still not clear what the minimum of the Walden product indicates, and no reliable theory has been proposed for explaining physicochemical properties in concentrated aqueous solutions. Therefore, it is not conclusive from the measurements of the physicochemical properties at which concentration thallium(I) formate begins to form the aggregates. Probably the aggregates gradually form with the increase in the concentration of the solute, and they may exist to some extent, besides mononucleic thallium(I) formate complex, even in a solution of relatively low concentration of the solute.

The work has been financially supported, in part, by the Grant-in-Aid for Scientific Research No. 57470054 from the Ministry of Education, Science and Culture. The financial aid by the Asahi Glass Foundation for Industrial Technology is also acknowledged. A part of the computer calculations carried out in the present work has been performed at the Institute for Molecular Science in Okazaki.

References

1) A. Kusumegi, K. Kondo, Y. Watase, Y. Yoshimura, and K. Miyake, *Nucl. Instrum. Methods*, **185**, 83 (1981).
2) A. Kusumegi, *Bull. Inst. Chem. Res., Kyoto Univ.*, **60**, 234 (1982).
3) A. Kusumegi, K. Kondo, Y. Watase, Y. Yoshimura, K. Miyake, Y. Hemmi, J. Haba, and K. Hara, *Nucl. Instrum. Methods*, **196**, 231 (1982).
4) G. Licheri, G. Piccaluga, and G. Pinna, *J. Am. Chem. Soc.*, **101**, 5438 (1979).
5) R. Caminiti, A. Musinu, G. Paschina, G. Piccaluga, and G. Pinna, *Z. Naturforsch., A*, **36**, 831 (1981).
6) M. A. Marques and M. I. D. B. Marques, *Proc. K. Ned. Akad. Wetensch. Ser. B*, **77**, 286 (1974).
7) M. I. D. B. Marques, M. I. Cabaço, M. A. S. Oliveira, and M. A. Marques, *Chem. Phys. Lett.*, **91**, 222 (1982).
8) R. A. Howe, W. S. Howells, and J. E. Enderby, *J. Phys. Chem.*, **7**, L111 (1974).
9) G. W. Neilson, R. A. Howe, and J. E. Enderby, *Chem. Phys. Lett.*, **33**, 284 (1975).
10) J. E. Enderby, *Proc. R. Soc. London, Ser. A*, **345**, 101 (1975).
11) Y. Oddon, A. Tranquard, and B. F. Mentzen, *Inorg. Chim. Acta*, **48**, 129 (1981).
12) H. Ohtaki, M. Maeda, and S. Ito, *Bull. Chem. Soc. Jpn.*, **47**, 2217 (1974).
13) H. Ohtaki, T. Yamaguchi, and M. Maeda, *Bull. Chem. Soc. Jpn.*, **49**, 701 (1976).
14) G. Johansson and M. Sandström, *Chem. Scr.*, **4**, 195 (1973).
15) T. Yamaguchi, Doctor Thesis, Tokyo Institute of Technology, March (1978).
16) L. A. King and F. R. Duke, *J. Electrochem. Soc.*, **111**, 712 (1964); F. R. Duke and L. Bissell, *ibid.*, **111**, 717 (1964).
17) A. Enders-Beumer and S. Harkema, *Acta Crystallogr., Sect. B*, **29**, 622 (1973).
18) W. H. Zachariasen, *J. Am. Chem. Soc.*, **62**, 1011 (1940); P. L. Markila, S. J. Rettig, and J. Trotter, *Acta Crystallogr., Sect. B*, **31**, 2927 (1975).
19) J. W. Bats and H. Fuess, *Acta Crystallogr, Sect. B*, **36**, 1940, (1980); B. F. Mentzen and Y. Oddon, *Inorg. Chim. Acta*, **43**, 237 (1980).
20) I. Nahringbauer, *Acta Crystallogr., Sect. B*, **24**, 565 (1968).
21) I. L. Karle and J. Karle, *J. Chem. Phys.*, **22**, 43 (1954).
22) J. D. Donaldson, J. F. Knifton, and S. D. Ross, *Spectrochim. Acta*, **20**, 847 (1964).
23) K. Ito and H. J. Bernstein, *Can. J. Chem.*, **34**, 170 (1956).
24) K. Nakamoto, "Infrared and Raman Spectra of Inorganic and Coordination Compounds," Wiley, New York (1978), p. 230; J. D. Donaldson, J. F. Knifton, and S. D. Ross, *Specrochim. Acta*, **21**, 1043 (1965).
25) A. N. Campbell, G. H. Debus, and E. M. Kartzmark, *Can. J. Chem.*, **33**, 1508 (1955).
26) A. N. Campbell and W. G. Paterson, *Can. J. Chem.*, **36**, 1004 (1958).
27) T. Yamaguchi, G. Johansson, B. Holmberg, M. Maeda, and H. Ohtaki, *Acta Chem. Scand.*, in press.
28) A. N. Campbell and E. M. Kartzmark, *Can. J. Chem.*, **33**, 887 (1955).

Extraction of Uranium(VI) by Emulsion Liquid Membrane Containing 5,8-Diethyl-7-hydroxy-6-dodecanone Oxime

Kenichi AKIBA,* Toshihiko TAKAHASHI, and Takuji KANNO
Research Institute of Mineral Dressing and Metallurgy, Tohoku University, Katahira-2, Sendai 980
(Received March 23, 1984)

Extraction of uranium(VI) by a liquid surfactant membrane has been studied. The stability of water-in-oil (w/o) emulsion dispersed in the continuous aqueous phase increased with an increase in surfactant concentrations and in the fraction of the organic phase in emulsion globules. Uranium(VI) in dilute acid solutions was extracted into (w/o) emulsions containing 5,8-diethyl-7-hydroxy-6-dodecanone oxime (LIX 63) as a mobile carrier and its concentration decreased according to $[U]_t=[U]_0 \exp(-k_{obsd}t)$. The apparent rate constants (k_{obsd}) increased with an increase in carrier concentrations and in external pH values, while they were slightly dependent on the stripping acid concentrations. Uranium was transported and concentrated into the internal aqueous droplets. The final concentration of uranium in the external aqueous phase dropped to about 10^{-3} of its initial value.

Separation of metal ions by liquid-liquid extraction can be achieved through the processes of extraction into the organic phase and stripping into the aqueous phase. Liquid membranes combining simultaneously both the extraction and the stripping processes have become of interest as a new technique of selective separation and concentration of metals from dilute aqueous solutions.[1,2] The extracting reagent plays a role as a mobile carrier in the membrane, and the metal ion can be concentrated by active transport against its concentration gradient across the liquid membrane.

Two types of liquid membranes, supported liquid membranes and emulsion liquid membranes, have been well known for separation of metal ions.[3,4] The effectiveness of liquid membrane method for the recovery of uranium from dilute solutions has been shown by means of supported liquid membranes containing various carriers,[5-7] and emulsion type liquid membranes of mixed carriers, bis(2-ethylhexyl) hydrogenphosphate and trioctylphosphine oxide, were also employed for uranium extraction from wet process phosphoric acid.[8] Emulsion liquid membranes consist of small droplets of the stripping aqueous phase stabilized by a surfactant and the extracting organic phase. They could give fast extraction owing to the large surface area of emulsion globules.

Previously, we revealed that a α-hydroxy ketone oxime, 5,8-diethyl-7-hydroxy-6-dodecanone oxime (LIX 63), is an excellent reagent for uranium extraction from weak acidic media[9] and also for a suitable ion carrier in the supported liquid membrane.[10] The present study deals with some of important factors affecting the stabilities of emulsions and the extraction of uranium(VI) by emulsion liquid membranes containing LIX 63 as a mobile carrier.

Experimental

Emulsion Liquid Membranes. The liquid membranes were composed of a nonionic surfactant, sorbitan monooleate (Span 80; Kao-Atlas) and 5,8-diethyl-7-hydroxy-6-dodecanone oxime (LIX 63; Henkel). The kerosene solutions of them were vigorously emulsified (20000 min^{-1} for 2 min) with stripping solutions of sulfuric acid (most commonly pH 1.5) by a high-speed homoginizer (Ultra-Disperser; Yamato Kagaku). No membrane strengthening agent such as liquid paraffin was added in the membrane solution, because there was little change in the stability of emulsion containing liquid paraffin up to 20 (w/v)%.

Emulsion Stability. The water-in-oil emulsion free from carriers was dispersed in ten times as much as the volume of water by stirring at 300 min^{-1}. To monitor the breaking of emulsions, stirring was stopped at time intervals so that the emulsion phase rose to the top of the beaker. After phase separation, samples of the aqueous phase were withdrawn and their pH values were measured with a pH meter (F-7ss; Horiba). When emulsions break down in the course of stirring, the internal stripping acid leaks out in the external aqueous phase. The emulsion breakdown was evaluated as percentage from the hydrogen ion concentrations as follows:

$$\varepsilon(\%) = \frac{([H^+]_{ext}-[H^+]_{ext,\,init.})V_{ext}}{[H^+]_{int}\times V_{int}} \times 100$$

where V refers to the volume and the subscripts ext and int represent the external and the internal aqueous phases, respectively.

Extraction of Uranium. The (w/o) emulsions containing LIX 63 were stirred with ten times as much as the volume of uranium solution (pH 3—4.5) containing ^{237}U as a tracer. The initial concentration of uranium was usually 10^{-5} mol dm^{-3}. After stirring at 300 min^{-1}, aliquots of the external aqueous solution were pipetted off for analysis at selected time intervals and their uranium concentrations were determined by measuring γ-radioactivities of ^{237}U with a NaI scintillation detector. The quantity of uranium moved into emulsion globules was evaluated from the difference between the concentrations in the external aqueous phase before and after stirring.

All experiments were carried out at 25 °C.

Results and Discussion

Emulsion Stability. When the (w/o) emulsion is dispersed by stirring in the continuous aqueous solution, the emulsion must be sufficiently stable in order to extract metal ions into the internal aqueous droplets. The emulsion breakdown will result in a lowering of extraction efficiency and loss of the extracted species. For the recovery of extracted metals, on the contrary, the emulsion must be readily broken by the use of demulsification techniques such as electrostatic means.[11]

The several factors governing the emulsion stability

have been examined in order to prepare the optimum emulsion liquid membranes suited for these conflicting requirements.

Figure 1 shows the effect of the surfactant concentration on the emulsion breakdown after stirring at 300 min^{-1}. The distilled water was stirred with emulsions consisting of equal volumes of the organic phase free from carriers and the sulfuric acid solution. The emulsion breakdown was less than 0.5% at Span 80 concentrations above 2 (w/v)%, indicating that the membrane was sufficiently stable, while the emulsion stability steeply decreased with a decrease in the surfactant concentrations less than 2%. No emulsion was formed at low Span 80 concentrations below 0.25% owing to a lack of the surfactant adsorbing the organic-aqueous interface. Though high concentrations of surfactant seem to be suitable for the stable emulsion, they would cause difficulties in demulsification. On the basis of the data, 2 (w/v)% of Span 80 was selected in the subsequent experiments.

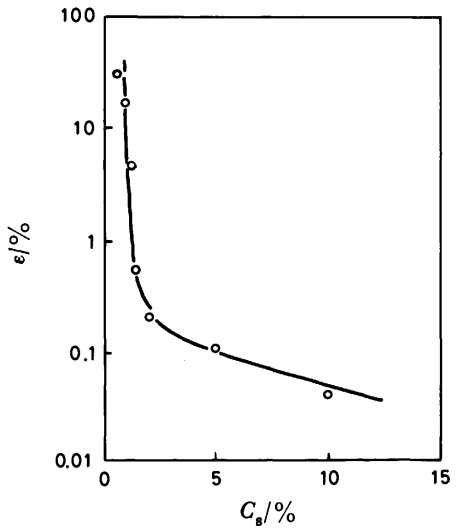

Fig. 1. Effect of Span 80 concentration on the emulsion breakdown after stirring at 300 min^{-1} for 40 min. V_{em}: 10 cm^3; V_{ext}: 100 cm^3.

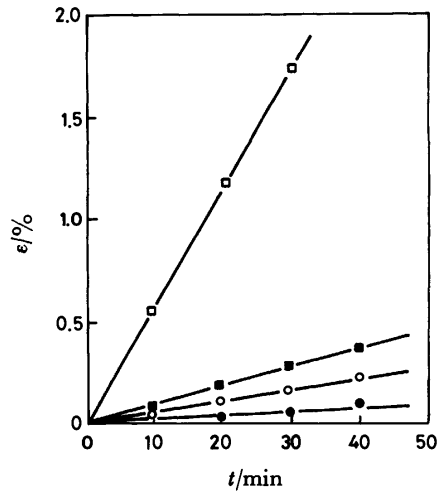

Fig. 2. Effect of stirring time on the emulsion breakdown. 2(w/v)% Span 80; V_{org}/V_{int}: □ 0.50, ■ 1.0, ○ 1.5, ● 2.0.

As shown in Fig. 2, the emulsion breakdown increased linearly with stirring time at 300 min^{-1}. This trend is marked with the emulsion of the low contents of the organic phase. The emulsion with the ratio (V_{org}/V_{int}) of 1 was found to be its optimum composition.

Equilibrium in Liquid-Liquid Extraction. Extraction equilibrium of uranium(VI) by LIX 63 (HR) can be expressed by,[9]

$$UO_2^{2+} + 2HR_{org} \overset{K_{ex}}{\rightleftharpoons} UO_2R_{2,org} + 2H^+. \quad (1)$$

The subscript org represents the organic phase, which corresponds to the membrane phase in the liquid membrane system. The extraction constants were obtained as $\log K_{ex}=-2.11$ and -3.32 for 0.1 mol dm^{-3} perchlorate and sulfate media, respectively. Based on these data, the hydrogen ion concentrations on both sides of the membrane can be adjusted so as to enhance the extraction in the external aqueous phase and the stripping in the internal aqueous phase. The overall processes promote the transport of the uranyl ion from the external to the internal aqueous phases through the liquid membrane and the transport of the hydrogen ion in the opposite direction.

Extraction by Emulsion Liquid Membrane. Effect of stirring on the extraction of uranium(VI) by the emulsion liquid membrane containing LIX 63 is shown in Fig. 3. The uranium solution at pH 4.2 was stirred with the emulsion having the volume ratio (V_{org}/V_{int}) of 1. The uranium concentrations in the external aqueous phase decreased with stirring time and then approached equilibrium. The rate of extraction increased with an increase in stirring speed, while the limiting value at equilibrium was approximately constant about 0.5% of the initial concentration irrespective of stirring speed under 500 min^{-1}, and little pH drop, *e.g.*, from 4.2 to 4.1, was observed at 500 min^{-1} for 1 h stirring. However, the external uranium concentration no longer decreased as above cases at higher speed of

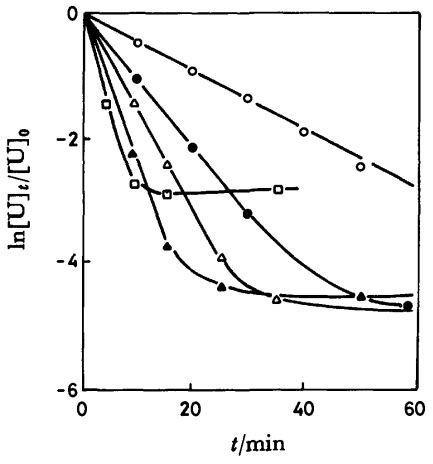

Fig. 3. Effect of stirring speed on the extraction of uranium(VI) by the emulsion liquid membrane. 5×10^{-3} mol dm^{-3} LIX 63; pH_{ext} 4.20; pH_{Int} 2.06; Stirring speed/min^{-1}: ○ 200, ● 300, △ 400, ▲ 500, □ 800.

stirring, and the pH drop became large, *e.g.*, from 4.2 to 3.7 at 800 min^{-1} for 40 min stirring. This anomalous behavior could be attributable to the high degree of emulsion breaking. Subsequent experiments were carried out at 300 min^{-1} where the emulsion breakdown during extraction was negligibly small.

Effect of Carrier Concentration. The rates of extraction were examined by varying carrier concentrations at 2 (w/v)% of Span 80 (Fig. 4). Plots of ln $[U]_t/[U]_0$ against time yielded a series of straight lines,

$$\ln\frac{[U]_t}{[U]_0} = -k_{obsd}t, \quad (2)$$

where $[U]_t$ and $[U]_0$ are the concentrations in the external aqueous phase at time t and initial one, respectively. The slope of the line gives the apparent rate constant, k_{obsd}. The plots of log (k_{obsd}/s^{-1}) *vs.* log ([LIX 63]/mol dm^{-3}) yielded the straight line with a slope of 0.61 (Fig. 5). Under these experimental conditions, about 99.5% of uranium in the external solution was extracted into the emulsion globules at equilibrium.

The high content of Span 80 resulted in a decrease in the extraction rate and further caused the extraction of small amounts of uranium by Span 80 alone. These findings together with the emulsion stability suggest that the optimum concentration of Span 80 lies in the 2% range. The uranium extraction by this 2% surfactant was negligibly small.

Effect of pH. It is important to maintain an appreciable pH gradient between the external and the internal aqueous phases, because this pH gradient provides an effective driving force of the active transport of uranium across the membrane.

Plots of log (k_{obsd}/s^{-1}) *vs.* pH_{ext} of the external aqueous phase gave the straight lines with slopes of about 1.3 at different concentrations of stripping acid (Fig. 6). As long as the internal acid concentrations were maintained high enough to strip uranium, the extraction rate increased with an increase in the external pH values.

The effect of stripping acid concentration on the extraction rate is illustrated in Fig. 7. Plots of log k_{obsd} *vs.* pH_{int} gave the linear lines with small negative slopes around −0.2 at different pH_{ext}. Varying the internal pH values over a fairly wide range has only a minor effect on the extraction rate.

From these findings, the extraction reaction into the membrane layers rather than the stripping reaction into

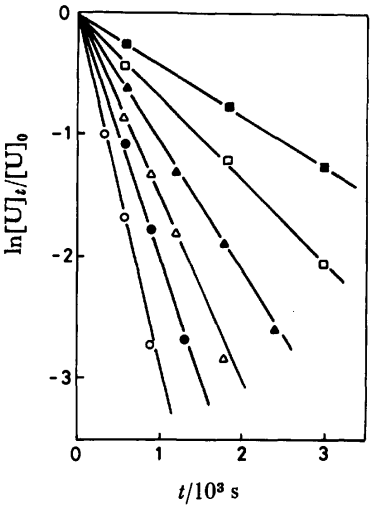

Fig. 4. Rate of uranium extraction by the emulsion liquid membrane. pH_{ext} 4.25; pH_{int} 2.48; [LIX 63]/mol dm^{-3}: ○ 2×10^{-2}, ● 10^{-2}, △ 5×10^{-3}, ▲ 2.5×10^{-3}, □ 1.25×10^{-3}, ■ 6.25×10^{-4}.

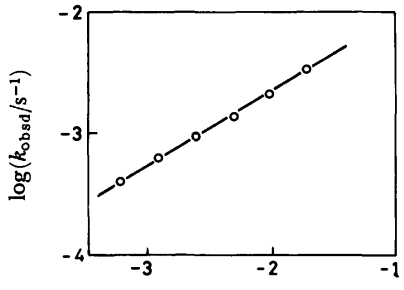

Fig. 5. Effect of the carrier concentration on the apparent rate constant.

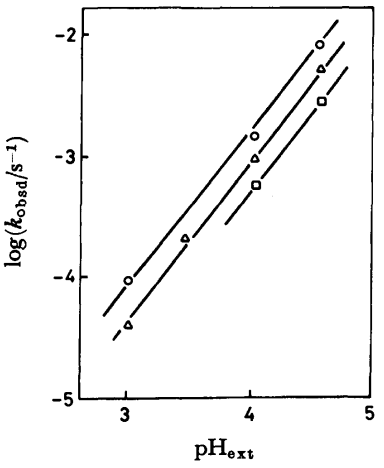

Fig. 6. Effect of pH of the external aqueous phase on the apparent rate constant. 5×10^{-3} mol dm^{-3} LIX 63; pH_{int}: ○ 0.93, △ 2.38, □ 3.52.

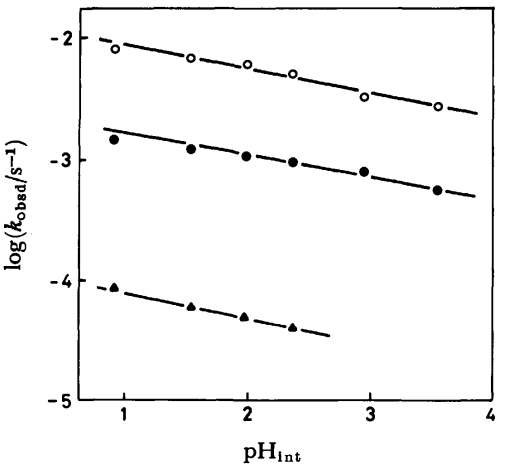

Fig. 7. Effect of pH of the internal aqueous phase on the apparent rate constant. 5×10^{-3} mol dm^{-3} LIX 63; pH_{ext}: ○ 4.58, ● 4.05, ▲ 3.03.

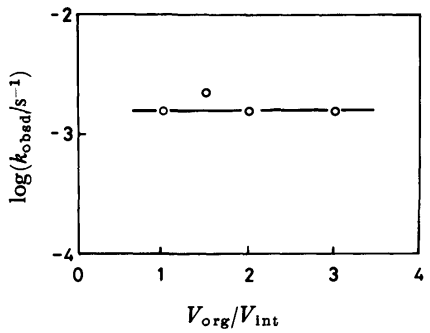

Fig. 8. Effect of the emulsion composition on the apparent rate constant. 5×10^{-3} mol dm^{-3} LIX 63; pH_{ext} 4.34; pH_{int} 1.98.

the internal aqueous phase probably contributes to the rate determining process. If the stripping reaction was the rate determining step, the content of the internal phase would also affect the extraction rate, but the k_{obsd} values at different compositions of emulsion, were nearly constant as seen in Fig. 8. This indicates that the stripping reaction is not of importance in the rate determining process.

The most significant factor for the carrier-mediated transport appears to control the external pH value maintaining the pH gradient against internal pH. The final concentration of external uranium was observed to decrease greatly under the large pH gradient; the uranium remaining in the external solution dropped to 10^{-3} of its initial concentration under the conditions of pH_{ext} 4.6 and pH_{int} 2.0.

Furthermore, wide variations in the initial uranium concentration ranging from 10^{-7} to 10^{-4} mol dm^{-3} gave no effect on the extraction efficiency and the extraction rate. The reagent LIX 63 in the membrane acts as an ion carrier from the outer to the inner solutions, rather than a metal storage phase in liquid-liquid extraction. Thus, uranium could be efficiently concentrated into small encapsulated droplets with the concentration factor of V_{ext}/V_{int} given by the volume ratio of the external to the internal aqueous phases.

References

1) N. N. Li, "Recent Development in Separation Science," CRC Press, Florida, (1981), Vol. VI.
2) J. Strzelbicki and W. Charewicz, *J. Inorg. Nucl. Chem.*, **40**, 1415 (1978).
3) K. H. Lee, D. F. Evans, and E. L. Cussler, *AIChE J.*, **24**, 860 (1978).
4) J. W. Frankenfeld, R. P. Cahn, and N. N. Li, *Sep. Sci. Technol.*, **16**, 385 (1981).
5) S. Sifniades, T. Largman, A. A. Tunick, and F. W. Koff, *Hydrometallurgy*, **7**, 201 (1981).
6) W. C. Babcock, R. W. Baker, D. J. Kelly, and E. D. LaChapell, Proc. Int. Solvent Extrn. Conf. (1980), Vol. II.
7) K. Akiba and T. Kanno, *Proc. Sym. Solvent Extraction*, **1983**, p. 63.
8) J. Bock and P. L. Valiant, Jr., *Ind. Eng. Chem., Fundam.*, **21**, 417 (1982).
9) K. Akiba and T. Kanno, *Solvent Extrn. Ion Exchange*, **1**, 729 (1983).
10) K. Akiba and T. Kanno, *Sep. Sci. Technol.*, **18**, 831 (1983).
11) H. Ino, N. Imaishi, M. Hozawa, and K. Fujinawa, *Kagaku Kogaku Ronbunshu*, **9**, 263 (1983).

 © 1984 The Chemical Society of Japan Bull. Chem. Soc. Jpn., 57, 2622—2627 (1984) [Vol. 57, No. 9

Enthalpies of Transfer of Single Ions and Metal Complexes from Water to an Aqueous Dioxane Solution

Shin-ichi ISHIGURO and Hitoshi OHTAKI*

Department of Electronic Chemistry, Tokyo Institute of Technology at Nagatsuta, 4259, Nagatsuta-cho, Midori-ku, Yokohama 227

(Received March 24, 1984)

Enthalpies of solution of some 1:1 and 2:1 electrolytes were determined in water and in a dioxane-water mixture (the dioxane content; 0.2 mole fraction or 55.0% w/w) by calorimetry at 25 °C. Enthalpies of transfer (ΔH_t°) of single ions from water to the dioxane-water mixture were obtained by employing the extrathermodynamic tetraphenylarsonium tetraphenylborate (TATB) assumption. Enthalpies of transfer of nickel(II) and copper(II) complexes with glycinate (gly^-) and ethylenediamine (en) were also evaluated for $[Ni(gly)_n]^{(2-n)+}$ (n=1—3), $[Ni(en)_n]^{2+}$ (n=1—3), and $[Cu(en)_n]^{2+}$ (n=1—2) by combining enthalpies of transfer of the relevant single metal ions and ligands with enthalpies of complex formation reactions $M+nL=ML_n$ ($M=Ni^{2+}$ or Cu^{2+} and $L=gly^-$ or en) in water and in the mixture. The enthalpies of transfer of the metal complexes examined here increased almost linearly with an increase in the number of the ligands within the complexes. The values of ΔH_t° of the ethylenediamine complexes of nickel(II) and copper(II) ions were all negative, as well as those of free Ni^{2+} and Cu^{2+} ions. On the other hand, the enthalpies of transfer of the noncharged $[Ni(gly)_2]$ and anionic $[Ni(gly)_3]^-$ complexes were positive, while that of the $[Ni(gly)]^+$ complex was still negative. The result suggested that hydration of the ligands coordinating to the central metal ions plays an essential role in the enthalpies of transfer of the metal complexes from water to the dioxane-water mixture.

In previous papers we reported formation constants or Gibbs energies, enthalpies and entropies of formation of ethylenediamine complexes of nickel(II)[1] and copper(II)[2] ions in water and in dioxane-water mixtures containing 0.1 and 0.2 mole fractions (35.2 and 55.0% w/w, respectively) of dioxane and discussed about solvent effects on the complex formation reactions.

Although it was pointed out that the Gibbs energies of transfer of metal ions from water to the dioxane-water mixtures were negative[3-5] and thus the metal ions should be more stable in the mixtures than in water, the formation of the ethylenediamine complexes of nickel(II) and copper(II) ions was more favorable in the dioxane-water mixtures than in water. This result indicated that the ethylenediamine complexes of nickel(II) and copper(II) ions should be more stabilized than the respective free metal ions on transferring the species from water to the dioxane-water mixtures, provided that the instabilization of the neutral ligand in the mixtures was not too significant compared with that in water.

NMR studies[6,7] suggested that metal ions were preferentially solvated with water in their primary coordination sphere over a wide range of composition of dioxane-water mixtures. Thus, we concluded[1-3] that the aqua and ethylenediamine complexes of nickel(II) and copper(II) ions were hydrated even in aqueous mixture of dioxane because of weaker donor property of dioxane (the donor number (DN)=14.8) than water (DN=18.0)[8] and the hydration of the metal ions and complexes was more enhanced in the mixtures than in water.

The above conclusion was supported by evidence from calorimetric measurements. Enthalpies of solution of some 1:1 electrolytes so far reported indicated that hydration of metal ions was strengthened in dioxane-water mixtures due, probably, to breaking of the hydrogen-bonded structure of water in the bulk solvents.[9,10] The enthalpies of transfer of the $[Ni(en)_n]^{2+}$ (n=1—3) complexes estimated were all negative, which showed that solvation of the complexes was enhanced in the dioxane-water mixtures.[1]

In order to expand our studies to other metal-ligand systems, we first undertook to determine enthalpies of transfer of single metal ions and ligands involved in the metal-ligand complexes from water to a dioxane-water mixture. The mixture of the dioxane content of 0.2 mole fraction (55.0% w/w) was chosen as the mixed solvent in the present study, because complex formation reactions of various metal ions were studied in this mixture in our laboratory. Moreover, various solvent properties of dioxane-water mixture show a significant variation with changing solvent composition in the water-rich region of about 0.2 mole fraction dioxane content.[11]

In the present work the extrathermodynamic tetraphenylarsonium tetraphenylborate assumption $\Delta H_t^\circ(Ph_4As^+)=\Delta H_t^\circ(BPh_4^-)$, was adopted[12] for dividing enthalpies of transfer of salts from water to the dioxane-water mixture into those of individual ions, where ΔH_t° denotes the enthalpy of transfer of a species from water to the 0.2 mole fraction dioxane-water mixture, which is given by the difference between enthalpies of solution of the species in the two solvents.

Enthalpies of transfer of Ni^{2+}, Cu^{2+}, and glycinate (gly^-) ions and ethylenediamine (en) from water to the 0.2 mole fraction dioxane-water mixture thus evaluated were combined with enthalpies of formation of the $[Ni(gly)_n]^{(2-n)+}$ (n=1—3), $[Ni(en)_n]^{2+}$ (n=1—3), and $[Cu(en)_n]^{2+}$ (n=1—2) complexes in the solvents and thus enthalpies of transfer of the metal complexes were obtained. The enthalpy of transfer of proton was calculated by using ΔH_t°'s of glycinate ion and glycine, and enthalpies of formation of glycine in water and in the dioxane-water mixture. Enthalpies of transfer of the Hen^+, H_2en^{2+}, and H_2gly^+ species from water to the

0.2 mole fraction dioxane-water mixture were also estimated.

Experimental

Reagents. All chemicals used were of reagent grade. *Nickel(II) and copper(II) chlorides* were prepared by dissolving respective metal oxides into hydrochloric acid of super special grade. The metal oxides had been prepared as described elsewhere.[1] The hexahydrates of nickel(II) and copper(II) chlorides were prepared by drying the solutions in a vacuum evaporator, and then dried at 150 °C in a vacuum oven to obtain the anhydrous salts. *Bis(glycinato)nickel(II) dihydrate crystals* were prepared by dissolving freshly precipitated nickel(II) carbonate to an aqueous glycine solution, and then recrystallized from water. The dihydrate salt was dried at 150 °C in a vacuum oven to obtain the anhydrous one. *Sodium glycinate* was prepared by mixing equimolar amounts of glycine and sodium hydroxide in methanol and recrystallized three times from methanol. Purity of the sodium glycinate thus prepared was more than 99.8%. *Glycine* was recrystallized three times from water. *Sodium perchlorate* was prepared and purified as described previously.[13] *Sodium tetraphenylborate, tetraethylammonium chloride, and tetraethyl ammonium perchlorate* used were recrystallized from acetone and then washed with ester. *Tetraphenylarsonium chloride and sodium chloride* were used without further purification and dried at 180 °C. All chemicals thus prepared and purified were stored in a vacuum desiccator over P_2O_5. *Dioxane and ethylenediamine* were dried by using metallic sodium and then distilled.

Calorimetric Measurements. Enthalpies of solution were measured in a room thermostated at (25.0±0.2) °C by using an MPS-11 calorimeter (Tokyo Riko, Tokyo). A teflon vessel was placed in an aluminium block controlled at (25.000±0.003) °C in an air-bath. All parts inserted in the vessel were made of teflon. A standard heater and a thermal sensor were sandwiched between the bottom of the vessel and the aluminium block. Powder of a sample salt was placed in a glass ampoule in a dry box over P_2O_5, and the ampoule was weighed and then sealed. An ampoule containing a given amount of a sample salt was immersed in a solvent of 50 cm^3 in the teflon vessel.

The measurement of heat of solution of a sample consisted of two stages I and II. A typical chart for a heat measurement of a sample salt is shown in Fig. 1.

A vessel equipped with an ampoule in a solvent was installed in an aluminium block. At the beginning of measurement, the vessel was thermally equilibrated with the aluminium block (temperature: θ_0). Then the vessel was heated with a standard heater for a given period of time from $t=0$ to $t=t_h$. Thus temperature of the vessel rose during the heating period then spontaneously fell and became to the initial temperature (θ_0) within a few hours (stage I). Then the ampoule was mechanically broken and the temperature increased or decreased depending on the exothermic or endothermic dissolution of a salt. In Fig. 1 an example for the endothermic dissolution of a salt (NaCl in this case) is depicted (stage II). The temperature change detected by using a thermal sensor was recorded in a JEC 6 electronic computer (JEOL, Tokyo) every second through a 10-bit AD converter. Measurements were performed with the aid of the on-line system for calorimetry developed in our laboratory.

Determination of Heat of Solution. Under nonadiabatic conditions, the change in temperature $\theta(t)$ of a vessel in which heat is evolved or absorbed by dissolution of a sample salt is followed by the equation 1:

$$C_p\{d\theta(t)/dt\} = q(t) - \lambda\{\theta(t)-\theta_0\}, \quad (1)$$

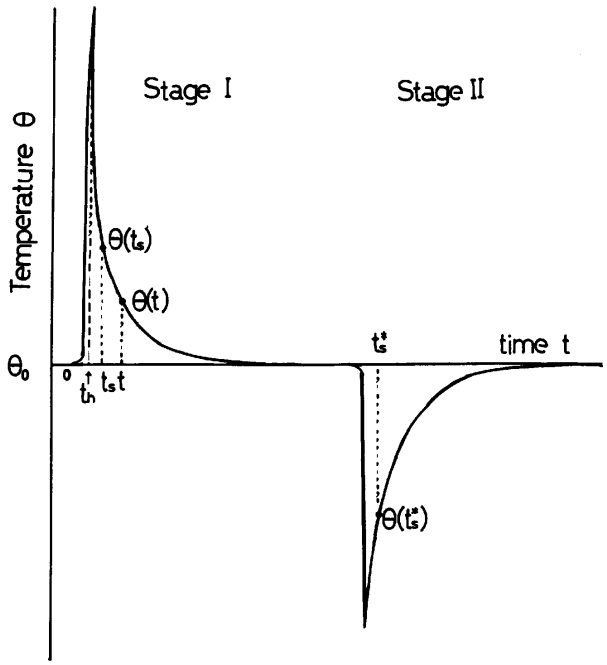

Fig. 1. A typical example for the calorimetric determination of heat of solution of a salt.

where C_p and λ stand for heat capacity and heat transfer coefficient of the vessel, respectively. $q(t)$ denotes heat evolved (or absorbed) per unit time at time t. Since $\theta(t)=\theta_0$ at $t=0$ and ∞, the total heat Q evolved (or absorbed) in the vessel is thus obtained by integrating measured temperatures from $t=0$ to $t=\infty$ as follows:

$$Q = \int_0^\infty q(t)dt = \lambda\int_0^\infty \{\theta(t)-\theta_0\}dt. \quad (2)$$

Therefore, in order to relate measured temperature changes to the total heat it is needed to know the values of C_p and λ. The values of C_p and λ were determined by heating the vessel with a standard heater at stage I in advance of dissolution of a salt at stage II.

At stage I, a standard heater was operated for a given period of time from $t=0$ to $t=t_h$ and a given amount of heat Q_{ev} was evolved. At $t>t_h$ where no more heat is evolved, temperature of the vessel spontaneously decreased. At a region of the spontaneous cooling of the vessel, a temperature at $t=t_s$, $\theta(t_s)$, ($t_s>t_h$) decreases according to Eq. 3:

$$\theta(t) - \theta_0 = \{\theta(t_s)-\theta_0\}\exp\{-\mu(t-t_s)\}, \quad (3)$$

where $\mu=\lambda/C_p$. The value of μ is obtained by plotting $\ln\{\theta(t)-\theta_0\}$ as a function of $(t-t_s)$, since $\ln\{\theta(t)-\theta_0\}=\ln\{\theta(t_s)-\theta_0\}-\mu(t-t_s)$.

The right hand side of Eq. 2 can be separated into two terms as follows:

$$\begin{aligned} Q_{ev} &= \lambda\left[\int_0^{t_s}\{\theta(t)-\theta_0\}dt + \int_{t_s}^\infty\{\theta(t)-\theta_0\}dt\right] \\ &= \lambda\left[\int_0^{t_s}\{\theta(t)-\theta_0\}dt \right. \\ &\quad \left. + \int_{t_s}^\infty\{\theta(t_s)-\theta_0\}\exp\{-\mu(t-t_s)\}dt\right]. \end{aligned} \quad (4)$$

At a given time t_s, $\theta(t_s)$ is a constant and thus the second term of Eq. 4 is given as $\{\theta(t_s)-\theta_0\}/\mu$.

Since Q_{ev} and μ are known and the first term of Eq. 4 is approximated by using the relation

$$\int_0^{t_s}\{\theta(t)-\theta_0\}dt = \sum_0^{t_s}\{\theta(t)-\theta_0\}\Delta t, \quad (5)$$

the constant λ and C_p are obtained as follows:

$$\lambda = Q_{ev}/[\sum_0^{t_s}\{\theta(t)-\theta_0\}\Delta t+\{\theta(t_s)-\theta\}/\mu], \quad (6)$$

$$C_p = \lambda/\mu. \quad (7)$$

In the course of the determination of μ, a certain time after 900 seconds beyond t_h (t_h=300 seconds) was taken as t_s and successive 70 points of $\theta(t)$ measured at every 30 seconds after t_s was subjected to the least-squares calculation for the ln-$\{\theta(t)-\theta_0\}$ plots *vs.* $(t-t_s)$. The value of Δt in Eq. 6 was one second, and all the t values employed in the course of the calculation of μ were used as t_s in the evaluation of λ by using Eq. 6. Thus the final λ value was obtained by averaging 70 λ's in each set of data with different t_s's.

Once we know the constants λ and C_p of the vessel, we can determine unknown heat evolved or absorbed by dissolution of a sample salt. An ampoule immersed in a solvent was mechanically broken and a salt in the ampoule dissolves exothermically or endothermically to yield a temperature change as is shown in Fig. 1, stage II, as an example (in the present example an endothermic dissolution process is given). The heat Q evolved or absorbed at dissolution of m moles of a salt is given, by using the constant λ and C_p obtained at stage I, as follows:

$$Q = \lambda[\sum_0^{t_s}\{\theta(t)-\theta_0\}\Delta t+(C_p/\lambda)\{\theta(t_s^*)-\theta_0\}]. \quad (8)$$

Q values were estimated at various t_s^* and the final Q value was determined by averaging the Q values estimated at various t_s^*. The uncertainty of the Q value was within ±0.5%. The enthalpy of solution of the salt (ΔH_s°) was thus given as $\Delta H_s^\circ = -Q/m$.

Results and Discussion

Enthalpies of Transfer of Single Ions. Enthalpies of solution of six salts were measured in water and in the 0.2 mole fraction dioxane-water mixture and the results are summarized in Table 1. Enthalpies of solution of the salts showed no appreciable dependence on the concentration except for NaCl and $(C_2H_5)_4NCl$ in the dioxane-water mixture. The values in Table 1 for NaCl and $(C_2H_5)_4NCl$ were obtained by extrapolating enthalpies of solution measured in the mixture with various concentrations of the salts to those at infinite dilution. The enthalpies of solution obtained in water for all the salts examined here agree with those in the literature within±1.2 kJ mol^{-1}.[14]

At infinite dilution all the salts in Table 1 were assumed to be fully dissociated both in water and in the dioxane-water mixture, and thus, the enthalpy of transfer of a salt i of 1:1 electrolyte (consisting of A^+ and B^-) from water to the mixture was represented as the sum of the enthalpies of transfer of each ionic component as follows:

$$\Delta H_t^\circ(A^+B^-) = \Delta H_t^\circ(A^+) + \Delta H_t^\circ(B^-). \quad (9)$$

Enthalpies of transfer of six single ions were thus evaluated from those of the salts in Table 1 by applying the extrathermodynamic TATB assumption $\Delta H_t^\circ(Ph_4As^+)=\Delta H_t^\circ(BPh_4^-)$ to the calculation and by minimizing the error-square sum $U=\sum\{\Delta H_{t,obsd}^\circ(i)-\Delta H_{t,calcd}^\circ(i)\}^2$.

Table 1. Enthalpies of solution (ΔH_s°) of some 1:1 electrolytes in water and in dioxane-water mixture (0.2 mole fraction of dioxane), and enthalpies of transfer (ΔH_t°) of the electrolytes from water to the mixture at 25 °C

Species	ΔH_s°(w) / kJ mol^{-1}	ΔH_s°(mix) / kJ mol^{-1}	ΔH_t° / kJ mol^{-1}
$NaBPh_4$	−20.0(−20.0)[a]	−39.4	−19.4
Ph_4AsCl	−10.2(−10.9)[a]	5.7	15.9
NaCl	4.4(3.8)[a]	0.2	−4.2
$NaClO_4$	15.0(13.8)[a]	−9.4	−24.4
$(C_2H_5)_4NClO_4$	32.2(31.0)[a]	23.2	−9.0
$(C_2H_5)_4NCl$	−12.4(−13.6)[a]	−1.4	−11.0

a) Values in parentheses are those quoted from Ref. 14.

Table 2. Enthalpies of transfer (ΔH_t°) of single ions from water to the dioxane-water (0.2 mole fraction of dioxane) at 25 °C.

Ion	ΔH_t°/kJ mol^{-1}
Ph_4As^+	0.4
BPh_4^-	0.4
Na^+	−19.8
Cl^-	15.5
$(C_2H_5)_4N^+$	−4.5
ClO_4^-	−4.6

The enthalpies of transfer of the single ions thus obtained are tabulated in Table 2. The enthalpies of transfer of all the salts in Table 1 were satisfactorily reproduced by those of the single ions in Table 2 within ±0.1 KJ mol^{-1}. The enthalpies of transfer of single ions in Table 2 are consistent with those calculated by interpolating the enthalpies of transfer from water to dioxane-water mixtures of different composition, which were obtained by employing the tetraphenylphosphonium tetraphenylborate assumption $\Delta H_t^\circ(Ph_4P^+)=\Delta H_t^\circ(BPh_4^-)$.[10]

Enthalpies of solution of $NiCl_2$, $CuCl_2$, sodium glycinate, glycine, and ethylenediamine were also measured in these solvents and the values are listed in Table 3. Sodium glycinate and ethylenediamine were dissolved in an alkaline solution to prevent protonation of the species. Glycine was dissolved in neutral solvents in which glycine form the zwitterion, Hgly. For all the species in Table 3, no appreciable change was found for the enthalpies of solution with the concentration of the salts over a range of 10^{-3} to 10^{-2} mol dm^{-3}. The enthalpy of solution of ethylenediamine obtained in water agreed well with the value reported by Nochols *et al.*[15]

It was also assumed that $NiCl_2$, $CuCl_2$, and sodium glycinate are completely dissociated in the solvents examined, and the enthalpies of transfer of nickel(II), copper(II) and glycinate ions from water to the dioxane-water mixture are thus estimated by subtracting the contribution of their counter ions which had been obtained in advance.

Table 3. Enthalpies of solution (ΔH_s°) of some compounds in water and in the dioxane-water mixture (0.2 mole fraction of dioxane), and their enthalpies of transfer (ΔH_t°) from water to the mixture at 25 °C

Species	ΔH_s°(w) / kJ mol^{-1}	ΔH_s°(mix) / kJ mol^{-1}	ΔH_t° / kJ mol^{-1}
$NiCl_2$	−79.9	−90.0	−10.1
$CuCl_2$	−56.3	−61.0	−4.7
Nagly[a]	−11.3	−2.4	8.9
Hgly	15.0	16.2	1.2
en[b]	−34.5(−32.0)	−34.8	−0.3

a) Dissolved in solutions containing 0.01 mol dm^{-3} NaOH. b) Dissolved in solutions containing 0.1 mol dm^{-3} LiOH and 3 mol dm^{-3} $LiClO_4$. The value in parentheses was obtained in the same alkaline solution without $LiClO_4$.

Enthalpies of Transfer of Proton, Protonated Glycine and Protonated Ethylenediamine. Glycinate ion (gly^-) reacts with proton to form the zwitterionic glycine (Hgly or $NH_3^+CH_2COO^-$) in solution. The enthalpy of the reaction, $H^+ + gly^- = Hgly$, was −57.9 and −62.7 kJ mol^{-1} in water (ΔH°_{Hgly}(w)) and in the dioxane-water mixture (ΔH°_{Hgly}(mix)), respectively.[16] The difference between the enthalpies of formation of Hgly in these solvents is related to the enthalpies of transfer of the species participating in the formation reaction as follows:

$$\Delta H^\circ_{Hgly}(mix) - \Delta H^\circ_{Hgly}(w) = \Delta H_t^\circ(Hgly) - \Delta H_t^\circ(H^+) - \Delta H_t^\circ(gly^-). \quad (10)$$

Since the ΔH_t° values of gly^- and Hgly were already determined as described in the previous section, the enthalpy of transfer of proton $\Delta H_t^\circ(H^+)$ from water to the mixture could be evaluated. By knowing ΔH_t°(en) and $\Delta H_t^\circ(H^+)$ thus obtained and the enthalpies of formation of Hen^+ in the two solvents,[1] the enthalpy of transfer of Hen^+ could also be estimated.

By the same procedure as described above the enthalpies of transfer of H_2gly^+ and H_2en^{2+} from water to the 0.2 mole fraction dioxane-water mixture were calculated, since the enthalpies of formation of these species in both solvents were known:

$$\Delta H_t^\circ(H_2L^{(q+2)+}) = \Delta H_t^\circ(HL^{(q+1)+}) + \Delta H_t^\circ(H^+) + \Delta H^\circ_{H_2L}(mix) - \Delta H^\circ_{H_2L}(w), \quad (11)$$

where L denotes gly ($q=-1$) or en ($q=0$), and $\Delta H^\circ_{H_2L}$(s) stands for the enthalpy of the second stepwise formation reaction, $H^+ + HL^{(q+1)+} = H_2L^{(q+2)+}$, in solvents. The value of $\Delta H^\circ_{H_2L}$ for glycine was determined to be −5.5 and −10.3 kJ mol^{-1} in water and in the dioxane-water mixture, respectively.[16] The values for ethylenediamine were reported previously.[1] The enthalpies of transfer of glycinate ion and ethylenediamine and their protonated species, as well as the value for proton, from water to the dioxane-water mixture thus evaluated are summarized in Table 4.

The enthalpy of transfer of proton was −22.7 kJ mol^{-1}, which was close to that of sodium ion (−19.8 kJ mol^{-1}).

Table 4. Enthalpies of transfer (ΔH_t°) of single species from water to the 0.2 mole fraction dioxane-water mixture at 25 °C

Species	ΔH_t° / kJ mol^{-1}	Species	ΔH_t° / kJ mol^{-1}
H^+	−22.7	$[Ni(gly)]^+$	−12.7
Ni^{2+}	−41.1	$[Ni(gly)_2]$	12.3
Cu^{2+}	−35.7	$[Ni(gly)_3]^-$	39.8
gly^-	28.7	$[Ni(en)]^{2+}$	−38.9
en	−0.3	$[Ni(en)_2]^{2+}$	−35.2
Hgly[a]	1.2	$[Ni(en)_3]^{2+}$	−30.2
H_2gly^+	−26.3	$[Cu(en)]^{2+}$	−35.0
Hen^+	−20.0	$[Cu(en)_2]^{2+}$	−33.1
H_2en^{2+}	−41.7		

a) Zwitterion, $NH_3^+CH_2COO^-$.

The ΔH_t° value of ethylenediamine was practically zero. The ΔH_t° values of Hen^+ and H_2en^{2+} were −20.0 and −41.7 kJ mol^{-1}, respectively, the latter value being almost double of the former. These results suggest that the enthalpies of transfer of the protonated ethylenediamine species are mostly influenced by the change in the enthalpies of solvation of charged ammonio groups within the species.

The enthalpy of transfer of protonated glycine H_2gly^+, which has a charged ammonio group and a noncharged carboxyl group, was −26.3 kJ mol^{-1}, the value being slightly more negative than that of Hen^+. Glycinate ion involving an anionic carboxylato group and a neutral amino group gave a positive ΔH_t° value (28.7 kJ mol^{-1}).

The enthalpy of transfer of zwitterionic glycine was small (1.2 kJ mol^{-1}), which might be compared with that of ethylenediamine (−0.3 kJ mol^{-1}). In fact, the enthalpy of hydration of glycine zwitterion in water was estimated to be −243 kJ mol^{-1},[17] which was considerably negative compared with those of noncharged molecules such as methylamine (−45.2 kJ mol^{-1}) and neutral acetic acid (−52.7 kJ mol^{-1}), although the value for the glycine zwitterion was less negative than those of H_2gly^+ (−365.4 kJ mol^{-1}) and gly^- (−379.5 kJ mol^{-1}).[17] The result suggests that the glycine zwitterion is strongly hydrated in water through both the ammonio and carboxylato groups. Two plausible interpretations for the small enthalpy of transfer of glycine from water to the dioxane-water mixture may be given: 1) hydration of a zwitterion is restricted to the vicinity of charged groups and is not appreciably changed when a part of water of the solvent is replaced with dioxane, 2) a large, negative enthalpy of transfer of an ammonio group is cancelled by a large, positive enthalpy of transfer of a carboxylato group within a zwitterionic glycine. Since the entropy of transfer of glycine between the two solvents is estimated to be −21 JK^{-1} mol^{-1},[16] which is rather largely negative, the latter interpretation is more acceptable.

Neutral Bis(glycinato)nickel(II) Complex. Enthalpy of transfer of the neutral bis(glycinato)nickel(II) complex can be determined without the extrathermody-

namic assumption. However, the solubility of the complex was too low in both water and the dioxane-water mixture to directly measure the heat of solution of the complex with a sufficient accuracy. Therefore, the complex salt was dissolved in each of the solvents containing sodium or lithium glycinate in which the neutral species was expected to be fully converted to the tris(glycinato)nickel(II) complex, and thus, the measured enthalpy at dissolution of the bis(glycinato)nickel(II) complex in the solvents was given as the sum of the enthalpy of solution (ΔH_{s1}°) of the complex and the enthalpy (ΔH_{3}°) of the reaction, $Ni(gly)_2+gly^-=Ni(gly)_3^-$, in the solvents. Since the latter was already known,[16] the former value was determinable.

The enthalpy of solution (ΔH_{s2}°) of the dihydrate salt $[Ni(gly)_2(H_2O)_2]$ was also determined by the same procedure as mentioned above in the two solvents. In a given solvent used, as is shown in Fig. 2, enthalpies of solution of the bis(glycinato)nickel(II) (ΔH_{s1}°) and diaquabis(glycinato)nickel(II) (ΔH_{s2}°) complexes are related to the enthalpy of reaction 12, ΔH_{h}°:

$$Ni(gly)_2(c) + 2H_2O(s) = Ni(gly)_2(H_2O)_2(c), \quad (12)$$

where (c) and (s) denote the crystalline and solution states, respectively. The enthalpy values of ΔH_{s1}°, ΔH_{s2}°, and ΔH_{h}° thus obtained in water and in 0.2 mole fraction dioxane-water mixture are summarized in Table 5, together with the values of ΔH_{3}° in the solvents.

The difference between the enthalpies of reaction 12 in water ($\Delta H_{h}^{\circ}(w)$) and in the 0.2 mole fraction dioxane-water mixture ($\Delta H_{h}^{\circ}(mix)$) is attributed to the enthalpy of transfer of two moles of water from water to the dioxane-water mixture:

$$\Delta H_{h}^{\circ}(w) - \Delta H_{h}^{\circ}(mix) = 2\Delta H_{t}^{\circ}(H_2O). \quad (13)$$

The values of ΔH_{h}° were −60.0 and −58.8 kJ mol^{-1} in water and in the dioxane-water mixture, respectively,

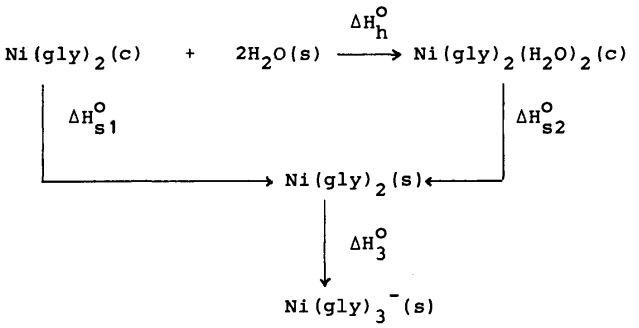

Fig. 2. Relationship between ΔH_{s1}°, ΔH_{s2}°, ΔH_{h}°, and ΔH_{3}°.

and thus, the $\Delta H_{t}^{\circ}(H_2O)$ value was estimated to be −0.6 kJ mol^{-1}. This result is consistent with the fact that the heat of mixing of water with dioxane is only slightly exothermic in a composition of water-rich.[18] The relatively small $\Delta H_{t}^{\circ}(H_2O)$ value suggested that the interaction energy between water molecues or between water and dioxane molecules in the dioxane-water mixture was not appreciably different from that between water molecules in water.

Since the interaction energies between solvent molecules in the two solvents are thus concluded to be similar, the difference in the enthalpies of transfer of ions and complexes in the two solvents should be ascribed to the different solvation energies of the species in the solvents.

Enthalpies of Transfer of Metal Complexes. By a similar way of evaluation of enthalpies of transfer of protonated glycine and ethylenediamine as described in the previous section, the enthalpies of transfer of glycinato and ethylenediamine complexes of nickel(II) ions and ethylenediamine complexes of copper(II) ions were determined. The enthalpies of formation of a complex ML_n (charge is omitted) pertaining to the reaction, $M+nL=ML_n$, in water ($\Delta H_{\beta n}^{\circ}(w)$) and in the 0.2 mole fraction dioxane-water mixture ($\Delta H_{\beta n}^{\circ}(mix)$) are related to the enthalpies of transfer of the free metal ion M, ligand L and the complex ML_n as follows:

$$\Delta H_{\beta n}^{\circ}(mix) - \Delta H_{\beta n}^{\circ}(w) = \Delta H_{t}^{\circ}(ML_n) - \Delta H_{t}^{\circ}(M) - n\Delta H_{t}^{\circ}(L). \quad (14)$$

The enthalpies of formation of the (glycinato)nickel(II) complexes[16] and ethylenediamine complexes of nickel(II) and copper(II) ions[1,2] have been measured in both solvents. Since the enthalpies of transfer of free nickel(II), copper(II), and glycinate ions and ethylenediamine have been determined in the previous sections, the enthalpies of transfer of the relevant metal complexes can be evaluated by using Eq. 14. The ΔH_{f}° value for the $[Ni(gly)_2]$ complex thus evaluated was in accord with that obtained by the difference $\Delta H_{s1}^{\circ}(mix)-\Delta H_{s1}^{\circ}(w)$ in enthalpies of solution of the anhydrous bis(glycinato)nickel(II) complex salt in water and in the dioxane-water mixture. Enthalpies of transfer of the metal complexes thus obtained are summarized in Table 4, together with the enthalpies of transfer of the free metal ions and ligands.

It has been known that metal ions are preferentially solvated by water molecules in the first coordination sphere in dioxane-water mixtures of water-rich,[6,7] and thus the difference in the enthalpies of solvation of ions, as well as complexes whose first coordination shells are

Table 5. Enthalpies of solution, ΔH_{s}°/kJ mol^{-1}, of anhydrous (ΔH_{s1}°) and dihydrate (ΔH_{s2}°) salts of bis(glycinato)nickel(II) complexes in water and in 0.2 mole fraction dioxane-water mixture and related enthalpies (definition of which is given in Fig. 2) at 25 °C

	$\Delta H_{s1}^{\circ}+\Delta H_{3}^{\circ}$	$\Delta H_{s2}^{\circ}+\Delta H_{3}^{\circ}$	ΔH_{3}° a)	ΔH_{s1}°	ΔH_{s2}°	ΔH_{h}°
water	−66.0	−6.0	−35.5	−30.5	29.5	−60.0
mixture	−55.4	3.4	−36.7	−18.7	40.1	−58.8
ΔH_{t}°(w→mix)	10.6	9.4	−1.2	11.8	10.6	1.2

a) Ref. 16.

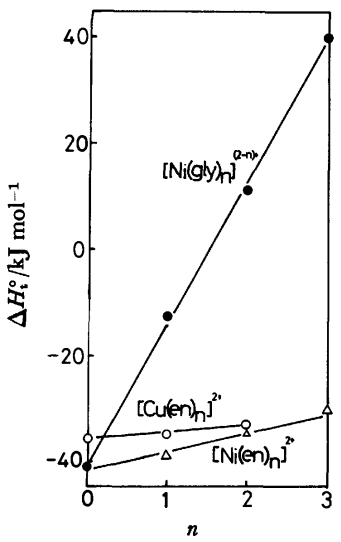

Fig. 3. Enthalpies of transfer of the (glycinato)nickel (II), (ethylenediamine)nickel(II) and (ethylenediamine)copper(II) complexes plotted against n, the number of ligands within the complexes.

filled with ligands, in water and the dioxane–water mixture should be caused by the change in solvation in the second and further solvation shells.

Plots of the ΔH_t° values of the $[Ni(gly)_n]^{(2-n)+}$, $[Ni(en)_n]^{2+}$, and $[Cu(en)_n]^{2+}$ complexes against n are shown in Fig. 3. They linearly increased with n for all the complexes, although the changes in ΔH_t° of the latter two were rather insensitive to n.

The ethylenediamine complexes of nickel(II) and copper(II) ions gave relatively large negative values of ΔH_t°. Since the first coordination shell of the metal ions within the complexes were occupied by ethylenediamine and/or water molecules, the result showed that solvation of the second coordination shell of the species was enhanced in the mixture than in water, although the enhancement may be less pronounced in a complex with a larger number of ethylenediamine coordinated to the metal ion.

In the case of the glycinato complexes of nickel(II) ions in which the charge of the complexes change from +2 (for Ni^{2+}) to −1 (for $[Ni(gly)_3]^-$), the ΔH_t° values of the complexes much more steeply increased with n than those of $[Ni(en)_n]^{2+}$ and $[Cu(en)_n]^{2+}$ did, the charge of these complexes being independent of n. Although the ΔH_t° value of the $[Ni(gly)]^+$ complex was still negative, the value was much less negative than the values of H^+ and Na^+. The ΔH_t° values for $[Ni(gly)_2]$ and $[Ni(gly)_3]^-$ were positive, the latter being much larger than that of glycinate ion. The result indicated that the solvation structure of the second coordination shell of the $[Ni(gly)_2]$ and $[Ni(gly)_3]^-$ complexes was partly destroyd in the dioxane–water mixture compared with that in water.

The linear relationship between ΔH_t° and n for the $[Ni(gly)_n]^{(2-n)+}$ complexes suggests that solvation of glycinate ions coordinated to the central nickel(II) ion is most responsible for the stabilization of the solvation structure of the second coordination shell of the complexes. In the $[Ni(gly)_n]^{(2-n)+}$ complexes, one of oxygen atoms within each carboxylato group of glycinate ions combines with the central metal ions, while the other oxygen atom of the carboxylato group faces to solvent molecules in the second coordination shell to interact each other. Since free glycinate ion has a positive value of ΔH_t°, the interaction between the latter glycinato-oxygen atom and solvent molecules in the second coordination shell may have a contribution to the ΔH_t° values of the complexes to make them more positive. The linear change in the ΔH_t° of the $[Ni(gly)_n]^{(2-n)+}$ complexes with n suggests that the interaction between the glycinato-oxygen atom and solvent molecules in the second coordination shell may proportionally change with the number of the oxygen atoms. The same trend can be seen for the ΔH_t° values of $[Ni(en)_n]^{2+}$ and $[Cu(en)_n]^{2+}$, although the change in the ΔH_t° values with n is much less pronounced compared with those of $[Ni(gly)_n]^{(2-n)+}$, probably due to the invariable charge of the former complexes and a relatively small ΔH_t° value of ethylenediamine.

The work has partially been supported by the Grant-in-Aid for Scientific Research No. 57470054 from the Ministry of Education, Science and Culture and by the Asahi Glass Foundation for Industrial Technology.

References

1) S. Ishiguro, Y. Oka, and H. Ohtaki, *Bull. Chem. Soc. Jpn.*, **56**, 2426(1983).
2) S. Ishiguro, Y. Oka, and H. Ohtaki, *Bull. Chem. Soc. Jpn*,. **57**, 391 (1984).
3) T. Kawai, S. Ishiguro, and H. Ohtaki, *Bull. Chem. Soc. Jpn.*, **53**, 2221 (1980).
4) H.Matsui and H. Ohtaki, *Bull. Chem. Soc. Jpn.*, **50**, 1472 (1977).
5) C. F. Wells, *J. Chem, Soc., Faraday Trans. 1*, **1978**, 1569.
6) L. S. Frankel, T. R. Stengle, and C. H. Langford, *Can. J. Chem.*, **46**, 3183 (1968).
7) A. Fratiello and D. C. Douglass, *J. Chem. Phys.*, **39**, 2017 (1963).
8) V. Gutmann, "The Donor-Acceptor Approach to Molecular Interactions", Prenum, New York and London (1978).
9) D. Feakins and C. T. Allan, *J. Chem. Soc., Faraday Trans. 1*, **1976**, 314.
10) N. Bhatnagar, *Can. J. Chem.*, **54**, 3487 (1976).
11) E. S. Amis and J. F. Hinton, "Solvent Effects on Chemical Phenomena", Academic Press, New York and London (1973).
12) B. G. Cox and A. J. Parker, *J. Am. Chem. Soc.*, **95**, 402 (1973).
13) H. Ohtaki, *Denki Kagaku*, **44**, 151 (1976).
14) B. G. Cox, G. R. Hedwig, A. J. Parker, and D. R. Watts, *Aust. J. Chem.*, **27**, 477 (1974).
15) N. Nochols, R. Sköld, C. Spink, and I. Wadsö, *J. Chem. Thermodynamics*, **8**, 993 (1976).
16) S. Ishiguro, T. Pithprecha and H. Ohtaki, to be published.
17) M. J. Locke and R. J. Sullivian, *J. Am. Chem. Soc.*, **105**, 4226 (1983).
18) J. R. Goates and R. J. Sullivian, *J. Phys. Chem*, **62**, 188 (1958).

Crystal Structures and Characterization of Cobalt(II), Manganese(II), and Zinc(II) Complexes of 2-[Bis-(2-benzimidazolylmethyl)amino]ethanol

Kazuhiro TAKAHASHI, Yuzo NISHIDA, and Sigeo KIDA*
Department of Chemistry, Faculty of Science, Kyushu University 33, Hakozaki, Higashi-ku, Fukuoka 812
(Received March 26, 1984)

Cobalt(II), manganese(II), and zinc(II) complexes with the tripodal ligand, 2-[Bis(2-benzimidazolylmethyl)-amino]ethanol, bbt, were prepared and characterized by infrared and electronic spectra, magnetism, and conductivities. Their crystal structures were determined by X-ray diffraction method. Crystal data: [Co(bbt)(NCS)$_2$] (**1**), space group $P2_12_12_1$(orthorhombic), a=12.881(1), b=17.970(2), c=9.076(1) Å; [Mn(bbt)(NCS)$_2$](**2**), space group $P2_12_12_1$(orthorhombic), a=18.179(2), b=13.073(2), c=9.097(2) Å; [Zn(bbt)(NCS)$_2$](**3**), space group $P2_1/a$(monoclinic), a=15.421(4), b=14.803(4), c=10.589(3) Å, β=115.81(2)°. The final R values are 0.044 (**1**), 0.054 (**2**), and 0.079 (**3**), for non-hydrogen atoms. The coordination geometries of **1** and **2** can be described as a distorted octahedron. In **3**, the alcoholic oxygen of bbt is not in coordination, hence the zinc ion is five-coordinated forming a highly distorted trigonal bipyramid. In all the complexes, thiocyanate ions coordinate in *cis* form with the nitrogen atoms. The magnetic measurements revealed that **1** and **2** are high spin complexes.

In some metalloenzymes, imidazole nitrogen of histidine moiety coordinates to a metal ion in the active sites.[1] The X-ray crystallographic study of the zinc enzyme, carboxypeptidase A,[2] have revealed the active site structure where two imidazoles are bound to the zinc(II) ion. The metal-substituted carboxypeptidase A showed remarkable changes from the native enzyme in the peptidase and esterase activities.[3] One of the origins of the changes was ascribed to the structural rearrangement of the active site due to the change in coordination occured on the metal ion. Thus, it is interesting to examine for a series of metal complexes how the coordination structure changes depending on metal ions.

In a preceding paper,[4] we reported the crystal structures of [Cu(bbt)X]$ClO_4 \cdot CH_3OH$(X is Cl or Br), whose coordination geometry is a square pyramid. The ligand, bbt, is a benzimidazole-containing ligand with a 3NlO mixed donor set,[5] as shown in Fig. 1, and has a substantial flexibility in coordination structure.

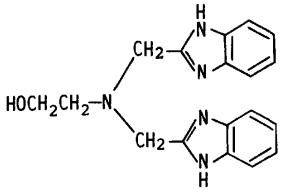

Fig. 1. Chemical structure of bbt.

In this study, we prepared the Co(II), Mn(II), and Zn(II) complexes with the general formula, [M^{II}(bbt)$(NCS)_2$], and determined their crystal structures by X-ray diffraction method in order to investigate the metal-dependent feature of coordination structure. Furher characterizations were carried out by infrared and electronic spectra, magnetism, and conductivities. A part of this work was reported as preliminary form.[6]

Experimental

Preparations. The ligand, bbt, was prepared as described previously.[5] [Co(bbt)(NCS)$_2$](**1**), [Mn(bbt)(NCS)$_2$](**2**), and [Zn(bbt)(NCS)$_2$](**3**) were prepared by the following method. A methanol solution (10 ml) of respective metal(II) nitrate hexahydrate (2 mmol) and a hot methanol solution (30 ml) of bbt·H_2O (2 mmol) were mixed. To this solution was added a methanol solution(10 ml) of NH_4NCS (5 mmol). The resulting solution was allowed to stand for several days, the crystals of **1**, **2**, and **3** were obtained as violet irregular prisms, pale pink prisms, and colorless columnar crystals, respectively. They were filtered and dried *in vacuo* on P_2O_5 for 2 d. **1** Found: C, 48.31; H, 3.86; N, 19.32%. Calcd for $C_{20}H_{19}N_7OS_2Co$: C, 48.39; H, 3.86; N, 19.75%. **2** Found: C, 48.83; H, 3.93; N, 19.87%. Calcd for $C_{20}H_{19}N_7OS_2Mn$: C, 48.78; H, 3.89; N, 19.91%. **3** Found: C, 47.81; H, 3.78; N, 19.19%. Calcd for $C_{20}H_{19}N_7OS_2Zn$: C, 47.77; H, 3.81; N, 19.50%.

Measurements. Infrared spectra were recorded by a Hitachi-Perkin Elmer Grating Infrared Spectrophotometer Model 225. Magnetic susceptibilities were measured by the Faraday method. Conductivities of solutions were measured at 25±1 °C, using a Yanaco Conductivity Outfit MY-8. Absorption spectra were recorded by the use of a Shimadzu UV-240 spectrophotometer for 200—850 nm and a Shimadzu MPS-5000 spectrophotometer for 650—1400 nm. Absorption spectra on nujol mull were obtained by the latter instrument for 250-1400 nm.

X-Ray Crystallographic Analyses. Reflection data of the complexes were measured on a Rigaku-Denki Automatic Four-circle Diffractometer AFC-5, using graphite monochromated Mo $K\alpha$ radiation (λ=0.71069 Å) at 294±1 K. Lattice constants were determined from least-squares fit of 25 strong reflections for **1**($18<2\theta<31°$), 20 reflections for **2**($21<2\theta<39°$), and **3**($18<2\theta<33°$). Intensity data were collected by the $\omega-2\theta$ scan technique in the range of $2.5<2\theta<50°$ with a scan rate of 6°/min for **1**, and 8°/min for **2** and **3**. For weak reflections, the intensity measurement was repeated up to three times depending on their intensities. Three standard reflections were monitored after every 97 reflections, and their intensities of each complex showed good stability during the data collection. The intensity data were corrected for Lorentz and polarization effects, but not for absorption. Independent reflections with $|F_o|>3\sigma(|F_o|)$ were considered as "observed" and used in the structure analyses.

The structure of each complex was solved by the heavy atom and successive Fourier and difference-Fourier methods, and refined by the block-diagonal least-squares procedures. The final refinements were performed using anisotropic ther-

TABLE 1. CRYSTALLOGRAPHIC AND EXPERIMENTAL DATA FOR THE COMPLEXES **1**, **2**, AND **3**

Complex	**1**	**2**	**3**
Space group	$P2_12_12_1$ (orthorhombic)	$P2_12_12_1$ (orthorhombic)	$P2_1/a$ (monoclinic)
a/Å	12.881(1)	18.179(2)	15.421(4)
b/Å	17.970(2)	13.073(2)	14.803(4)
c/Å	9.076(1)	9.097(2)	10.589(3)
β/°			115.81(2)
V/Å^3	2100.8(4)	2161.9(7)	2176(1)
Z	4	4	4
D_c/g cm^{-3}	1.57	1.43	1.54
D_m/g cm^{-3} a)	1.57	1.49	1.56
μ(Mo $K\alpha$)/cm^{-1}	10.7	8.1	13.7
Crystal size/mm^3	0.3×0.4×0.5	0.3×0.3×0.6	0.4×0.4×0.5
No. of unique reflections ($\|F_o\|>3\sigma(\|F_o\|)$)	2007	2583	2462
R_1 c)	0.044	0.054	0.079
R_2 d)	0.051	0.060	0.087
Largest peak/eÅ^{-3} b)	0.50	0.42	0.74

a) Measured by n-C_6H_{14}/$BrCH_2CH_2Br$ floatation. b) Largest peak in the final difference-Fourier map. c) $R_1=\Sigma\|\|F_o\|-|F_c\|\|/\Sigma|F_o|$. d) $R_2=[\Sigma(|F_o|-|F_c|)^2/\Sigma|F_o|^2]^{1/2}$.

TABLE 2. ATOMIC POSITIONAL(×10^4) AND THERMAL PARAMETERS WITH THEIR ESTIMATED STANDARD DEVIATIONS IN PARENTHESES

[Co(bbt)(NCS)$_2$] (**1**)

Atom	x	y	z	B_{eq}/Å^2
Co	1262(1)	1712.6(4)	−746(1)	1.9
N(A)	−86(5)	1843(4)	−1995(7)	3.2
C(A)	−934(5)	1912(4)	−2362(7)	2.5
S(A)	−2138(1)	2024(1)	−2930(2)	3.2
N(B)	543(5)	1887(3)	1226(6)	3.0
C(B)	404(5)	1752(4)	2460(8)	2.9
S(B)	190(2)	1571(1)	4196(2)	4.1
N(1)	1812(4)	2747(3)	−1445(6)	2.4
N(2)	2533(5)	3429(3)	−3238(6)	3.0
C(1)	2355(5)	2734(4)	−2693(8)	2.6
C(2)	1620(5)	3506(4)	−1161(7)	2.3
C(3)	1086(5)	3842(4)	9(8)	2.7
C(4)	967(6)	4605(4)	−50(9)	3.4
C(5)	1360(7)	5032(4)	−1234(9)	3.8
C(6)	1938(6)	4704(4)	−2366(9)	3.6
C(7)	2053(5)	3937(4)	−2295(8)	2.8
N(3)	1101(4)	565(3)	−1039(6)	2.4
N(4)	1480(5)	−484(3)	−2267(7)	2.9
C(8)	1634(5)	267(4)	−2115(8)	2.7
C(9)	515(5)	−14(4)	−451(8)	2.5
C(10)	−237(6)	−18(4)	685(9)	2.9
C(11)	−715(6)	−678(4)	1021(8)	2.9
C(12)	−455(6)	−1348(4)	274(9)	3.4
C(13)	301(6)	−1355(4)	−866(9)	3.1
C(14)	754(5)	−676(4)	−1188(8)	2.7
N(5)	2551(5)	1408(3)	−2396(6)	2.7
C(15)	2692(6)	2040(4)	−3440(8)	3.2
C(16)	2253(6)	721(4)	−3196(8)	2.9
C(17)	3509(6)	1249(5)	−1502(9)	3.4
C(18)	3599(5)	1777(5)	−191(8)	3.4
O	2684(3)	1634(3)	707(5)	2.6

[Mn(bbt)(NCS)$_2$] (**2**)

Atom	x	y	z	B_{eq}/Å^2
Mn	797.6(4)	1391(1)	1830(1)	2.2
N(A)	666(4)	2784(5)	623(7)	4.0
C(A)	594(3)	3605(5)	187(7)	3.1
S(A)	465(1)	4761(1)	−444(2)	3.7
N(B)	642(4)	2002(5)	3950(6)	4.1
C(B)	788(4)	2145(5)	5184(8)	3.3
S(B)	974(1)	2367(2)	6887(2)	4.6
N(1)	1978(3)	1432(4)	1452(5)	2.9
N(2)	3005(3)	1008(4)	230(6)	3.2
C(1)	2264(4)	879(5)	361(7)	3.0
C(2)	2556(3)	2000(5)	2015(7)	2.8
C(3)	2565(4)	2734(5)	3133(8)	3.2
C(4)	3233(4)	3194(5)	3474(8)	3.5
C(5)	3886(4)	2911(6)	2722(9)	3.8
C(6)	3886(4)	2169(5)	1601(8)	3.4
C(7)	3208(4)	1735(5)	1271(7)	3.0
N(3)	−224(3)	720(4)	1017(6)	2.7
N(4)	−864(3)	−70(4)	−745(6)	3.4
C(8)	−183(4)	155(5)	−204(7)	3.0
C(9)	−977(3)	880(5)	1267(6)	2.5
C(10)	−1317(3)	1419(5)	2399(7)	3.0
C(11)	−2081(4)	1495(6)	2321(8)	3.8
C(12)	−2487(4)	1045(7)	1169(9)	4.3
C(13)	−2157(4)	481(6)	71(9)	4.2
C(14)	−1378(4)	405(5)	163(7)	3.2
N(5)	1129(3)	−45(4)	110(6)	2.9
C(15)	1809(4)	247(6)	−675(7)	3.3
C(16)	510(4)	−194(6)	−897(7)	3.8
C(17)	1281(5)	−969(5)	1043(8)	3.8
C(18)	746(5)	−1039(5)	2315(7)	3.6
O	887(2)	−151(3)	3248(5)	3.0

Table 2. Continued

[Zn(bbt)(NCS)$_2$] (**3**)

Atom	x	y	z	B_{eq}/Å^2
Zn	2859(1)	4483(1)	1273(1)	4.1
N(A)	2983(6)	3339(5)	2418(9)	5.5
C(A)	3300(7)	2821(6)	3290(10)	4.2
S(A)	3781(2)	2101(2)	4542(3)	5.2
N(B)	2706(7)	4059(6)	−557(8)	5.9
C(B)	2710(7)	3808(7)	−1554(10)	4.6
S(B)	2708(3)	3391(3)	−2971(3)	7.5
N(1)	4188(5)	4953(5)	2479(7)	3.5
N(2)	5231(5)	6007(5)	3696(7)	3.6
C(1)	4329(7)	5827(6)	2730(8)	3.4
C(2)	5054(6)	4521(6)	3309(8)	3.2
C(3)	5336(7)	3617(6)	3410(9)	3.9
C(4)	6280(7)	3407(7)	4297(10)	4.4
C(5)	6961(7)	4092(7)	5087(10)	4.7
C(6)	6689(7)	4988(7)	4988(10)	4.5
C(7)	5725(6)	5185(6)	4071(8)	3.5
N(3)	1735(6)	5138(5)	1307(7)	3.9
N(4)	770(5)	6321(5)	1042(8)	4.1
C(8)	1474(6)	5972(6)	804(9)	3.8
C(9)	1103(6)	4923(6)	1894(9)	3.8
C(10)	1012(7)	4141(7)	2586(10)	4.7
C(11)	334(8)	4157(8)	3124(11)	5.4
C(12)	−262(8)	4918(8)	2986(11)	5.6
C(13)	−182(7)	5687(7)	2286(11)	5.1
C(14)	496(6)	5669(6)	1741(10)	4.2
N(5)	2967(6)	6183(5)	565(7)	4.1
C(15)	3573(7)	6519(6)	2008(8)	3.6
C(16)	1950(7)	6482(7)	51(10)	4.0
C(17)	3337(8)	6438(9)	−478(11)	5.8
C(18)	4351(10)	6209(9)	−119(12)	6.7
O	4995(6)	6890(5)	790(9)	6.5

mal parameters for non-hydrogen atoms. The final shifts in the atomic parameters were less than 53(**1**), 19(**2**), and 51%(**3**) of their estimated standard deviations. Final difference-Fourier map of each complex showed no significant electron density of non-hydrogen atom(>1 e Å^{-3}). The crystallographic data, some of the experimental details, and the R values of the complexes are given in Table 1.

All calculations were carried out on a FACOM M-200 computer at the Computer Center of Kyushu University by the use of local version[7] of the UNICS-II[8] and ORTEP programs.[9] The atomic scattering factors were adopted from the International Tables for X-ray Crystallography.[10] Lists of their structure factors and anisotropic thermal parameters have been deposited at the office of the Chemical Society of Japan as a Document No.8441.

The final positional and isotropic thermal parameters of **1**, **2**, and **3** are given in Table 2.

Results and Discussion

Molecular Structures. The ORTEP drawings of **1**, **2**, and **3** are shown in Figs. 2, 3, and 4, respectively. The atomic numberings are labelled in the same manner for all the complexes. Selected bond distances and angles of their coordination spheres are given in Table 3.

Table 3. Selected interatomic distances and angles of the coordination spheres of **1**, **2**, and **3** with their estimated standard deviations in parentheses

Complex	**1**	**2**	**3**
Distances(l/Å)			
M-N(A)	2.086(6)	2.140(6)	2.045(9)
M-N(B)	2.040(6)	2.107(6)	1.951(10)
M-N(1)	2.089(6)	2.175(5)	2.008(7)
M-N(3)	2.089(5)	2.183(5)	2.090(9)
M-N(5)	2.302(6)	2.517(5)	2.652(8)
M-O	2.262(4)	2.400(4)	—
N(A)-C(A)	1.148(9)	1.152(9)	1.133(13)
C(A)-S(A)	1.647(7)	1.633(7)	1.607(10)
N(B)-C(B)	1.160(9)	1.168(9)	1.119(16)
C(B)-S(B)	1.633(8)	1.612(7)	1.624(12)
Angles(ϕ/°)			
N(A)-M-N(B)	94.7(2)	97.6(2)	105.1(4)
N(A)-M-N(1)	91.0(2)	90.5(2)	96.0(3)
N(A)-M-N(3)	87.6(2)	94.2(2)	104.4(4)
N(A)-M-N(5)	105.9(2)	110.1(2)	162.4(3)
N(A)-M-O	176.2(2)	177.1(2)	—
N(B)-M-N(1)	106.5(2)	105.5(2)	113.1(4)
N(B)-M-N(3)	102.6(2)	110.4(2)	116.4(3)
N(B)-M-N(5)	159.2(2)	152.1(2)	91.3(3)
N(B)-M-O	82.3(2)	80.5(2)	—
N(1)-M-N(3)	150.9(2)	142.8(2)	118.1(3)
N(1)-M-N(5)	76.7(2)	71.6(2)	71.2(3)
N(1)-M-O	87.6(2)	92.2(2)	—
N(3)-M-N(5)	75.8(2)	72.2(2)	72.9(3)
N(3)-M-O	95.3(2)	84.4(2)	—
N(5)-M-O	77.3(2)	72.0(2)	—
M-N(A)-C(A)	163.9(6)	169.3(6)	160.1(8)
N(A)-C(A)-S(A)	178.4(4)	178.2(6)	178.2(9)
M-N(B)-C(B)	152.3(6)	155.5(6)	173.4(9)
N(B)-C(B)-S(B)	178.9(7)	178.5(7)	176.6(10)

As shown in Fig. 2, coordination geometry of **1** is described as a distorted octahedron with the principal axis through N(A), Co, and O. The equatorial plane consists of N(1), N(3), N(5), and N(B). The molecular structure of **2** is similar to that of **1** in general aspect. Each coordination bond length of **2** is slightly longer than the corresponding bond length of **1**. The deviations of the equatorial atoms from the least-squares plane (see Table 4) are smaller for **1** than those for **2**. The bond length differences between **1** and **2** are similar to those between the Co(II) and Mn(II) complexes of [M^{II}(2,2′-bipyridine)$_2$(NCS)$_2$].[11]

The ligand arrangements of **1** and **2** are similar to that of the already reported [Cu(bbt)X]ClO$_4$·CH$_3$OH (X is Cl or Br).[4] In these complexes, the three donor nitrogens(N(1), N(3), N(5)) of bbt occupy three vertexes of the basal plane of a square pyramid and the alcoholic oxygen(O) the apical position. The two benzimidazolyl planes[12] are nearly parallel (dihedral angle of the two planes: 19.5° for **1**; 16.7° for **2**; 4.7° for [Cu(bbt)X]ClO$_4$·CH$_3$OH(X is Cl or Br)).

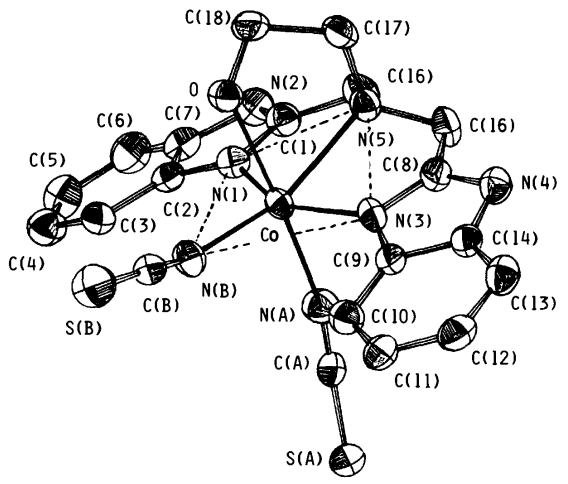

Fig. 2. ORTEP drawing of [Co(bbt)(NCS)$_2$](**1**) (thermal ellipsoids are drawn at 50% probability level).

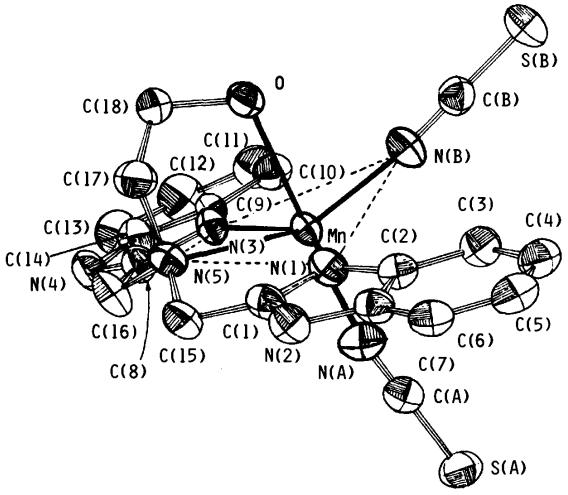

Fig. 3. ORTEP drawing of [Mn(bbt)(NCS)$_2$](**2**) (thermal ellipsoids are drawn at 50 % probability level).

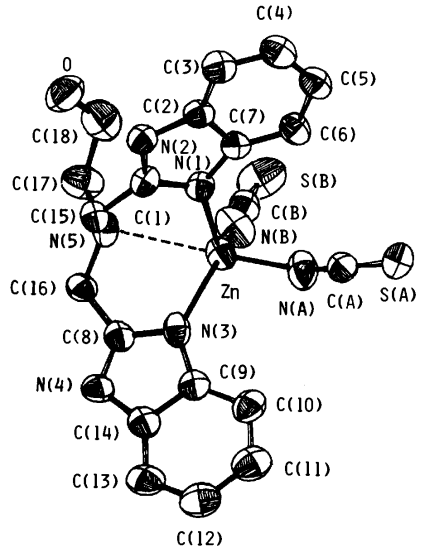

Fig. 4. ORTEP drawing of [Zn(bbt)(NCS)$_2$](**3**) (thermal ellipsoids are drawn at 50 % probability level).

The metal-dependent nature of bbt appears in the Zn(II) complex, **3**. As shown in Fig. 4, the alcoholic oxygen does not coordinate to Zn(II) ion. The coordination number of Zn(II) is five, and the geometry can be regarded as a highly distorted trigonal bipyramid with one weak coordination bond, Zn-N(5)(2.652(7) Å). The dihedral angle of the two benzimidazolyl planes(67.1°) is larger than those of **1**, **2**, and [Cu(bbt)X]ClO_4·CH_3OH(X is Cl or Br).

In all the present complexes, the two thiocyanate ions coordinate in *cis* form with their nitrogen atom. Each M-NCS bond is almost linear, the deviations of the M-N-C angles from 180° being in the range 6—28°.

Intermolecular Distances. Significant intermolecular distances less than 3.51 Å are listed in Table 5. The distances, N(4)-O in **1** and **3**, and N(2)-O in **2** are less than 3 Å, implying the presence of hydrogen bonds. The distances S(A)-O in **1** and **2**, and S(B)-O and S(A)-N(2) in **3** also suggest the presence of weak hydrogen bonds since their distances are less than or nearly equal to the sum of van der Waals radii of sulfur atom (1.8 Å) and oxygen(1.5 Å) or nitrogen atom(1.55 Å).[13]

In **1** and **2**, there seems to exist a contact between

Table 4. Equations of least-squares planes of the equatorial atoms of **1** and **2**, and deviations of the atoms in their coordination spheres

Complex	Equation of least-squares plane[a] [Deviations of atoms from the plane/Å]
1	Plane through N(1), N(3), N(5), and N(B) $0.7771x-0.1214y+0.6176z=0.6308$ [N(1) −0.226, N(3) −0.235, N(5) 0.273, N(B) 0.188, N(A) −2.237, O 2.096, Co −0.160]
2	$0.1210x-0.7897y+0.6015z=0.0266$ [N(1) −0.275, N(3) −0.263, N(5) 0.329, N(B) 0.209, N(A) −2.414, O 2.102, Mn −0.286]

a) The equation is expressed as $Ax+By+Cz=D$, where x,y,z are in Å units referred to the crystallographic axes.

Table 5. Selected contact distances(<3.51 Å) of the complexes

Complex	Contact (i) – (ii)	Distance(l/Å)	Symmetry code of atom (ii)
1	N(4)-O	2.968(7)	$1/2-x, -y, z-1/2$
	S(A)-O	3.154(5)	$x-1/2, 1/2-y, -z$
	C(A)-S(B)	3.497(7)	$x, y, z-1$
	N(A)-S(B)	3.509(7)	$x, y, z-1$
2	N(2)-O	2.925(7)	$1/2-x, -y, z-1/2$
	S(A)-O	3.170(5)	$-x, 1/2+y, 1/2-z$
	C(A)-S(B)	3.480(7)	$x, y, z-1$
	N(A)-S(B)	3.487(7)	$x, y, z-1$
3	N(4)-O	2.876(11)	$x-1/2, 3/2-y, z$
	S(B)-O	3.307(8)	$1-x, 1-y, -z$
	S(A)-N(2)	3.341(8)	$1-x, 1-y, 1-z$

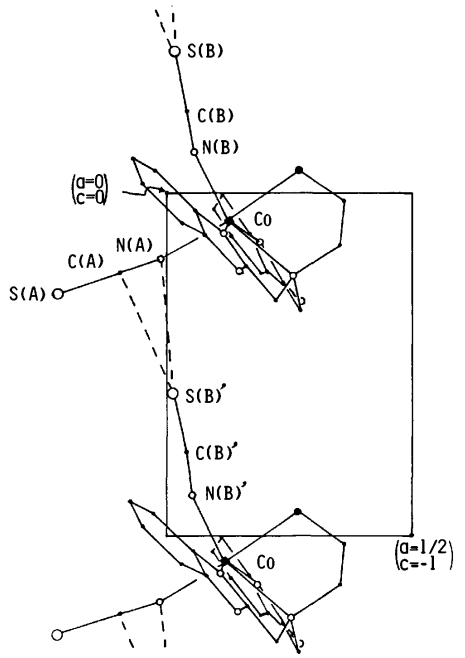

Fig. 5. Perspective view of the C≡N and S contact in the crystal **1**.

Table 6. Electronic spectral, conductance, and magnetic data

Complex	$\tilde{\nu}_{max}/10^3$ cm^{-1} a) Solution	Mull	Λ_m Ω^{-1} mol^{-1} cm^2	μ_{eff}/B.M. (295 K)
1	17.7[206]	19.4	82b)	4.76
	13.0[≈16]	13.0sh		
2			75c)	5.99
3			80b)	

a) Band maxima in visible region; sh indicates a shoulder; molar extinction coefficient ε(mol^{-1} cm^2) is in brackets. b) Solvent methanol at 1×10^{-3} mol dm^{-3} (25 °C). c) Solvent DMF at 1×10^{-3} mol dm^{-3}(25 °C).

thiocyanate C≡N and S of adjacent complex entities, as shown in Fig. 5. In the case of **3**, no such contact was observed.

Characterization of the Complexes. The infrared spectra of **1**, **2**, and **3** in KBr disks are similar to each other in 400—4000 cm^{-1} region. Each spectrum showed two sharp peaks due to the N-coordinated thiocyanate ions,[14] *i.e.*, at 2108 and 2070 cm^{-1} for **1**, 2097 and 2063 cm^{-1} for **2**, and 2093 and 2070 cm^{-1} for **3**. The splitting of the ν(CN) band is compatible with the *cis*-coordination of the two thiocyanate ions which was verified by X-ray analyses.

Electronic spectra, conductance, and magnetic data are listed in Table 6. The effective magnetic moments of **1** and **2** indicate that both are high spin complexes.[15] The electronic spectra of **1** in methanol and nujol mull are shown in Fig. 6. Both spectra show two broad bands in the visible region (*cf.* Table 6), which are assignable to the $^4T_{1g}(F)\rightarrow{}^4T_{1g}(P)$ and $^4T_{1g}\rightarrow{}^4A_{2g}$ transitions on the assumption of octahedral symmetry.[16] The high intensity and broadening of these bands are implying a considerable distortion from the regular octahedron. The molar conductance value of **1** in methanol indicates a 1:1 electrolyte,[17] suggesting that one of the thiocyanate ions is replaced by a methanol molecule. This is compatible with the observed spectral differences in band position and shape between two phases. The conductivity measurements also showed that **2** and **3** are 1:1 electrolytes in the solutions.[17] No bands due to d-d transitions were observed for **2** and **3** in either nujol or solution.

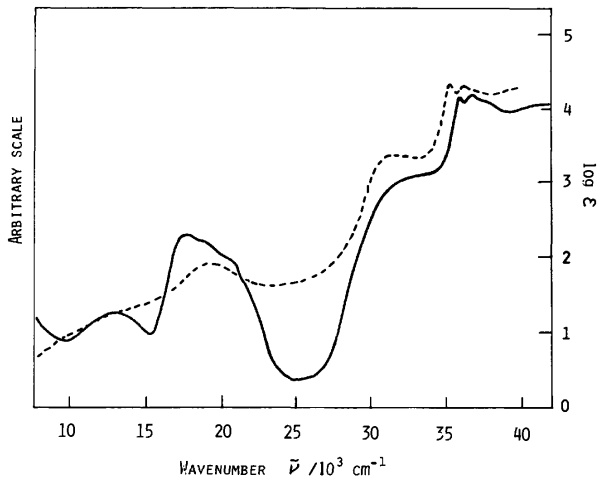

Fig. 6. Electronic spectra of **1**.
——: MeOH solution, ----: Nujol mull.

The authors wish to express their appreciation to Professor Hisashi Ōkawa for his helpful discussions.

References

1) F. A. Cotton, and G. Wilkinson, "Advanced Inorganic Chemistry," 4th ed, John Wiley & Sons, New York (1980), pp. 1310—1345; J. A. Ibers, and R. H. Holm, *Science*, **209**, 223 (1980).
2) W. N. Lipscomb, *Chem. Soc. Rev.*, **1**, 319 (1972); D. C. Rees, M. Lewis, R. B. Honzatko, W. N. Lipscomb, and K. D. Hardman, *Proc. Natl. Acad. Sci. U.S.A.*, **78**, 3408 (1981).
3) B. L. Vallee, J. A. Pupley, T. L. Coombs, and H. Neurath, *J. Am. Chem. Soc.*, **80**, 4750 (1958); J. E. Coleman, and B. L. Vallee, *J. Biol. Chem.*, **235**, 390 (1960); M. W. Makinen, L. C. Kuo, J. J. Dymonsky, and S. Jaffer, *ibid.*, **235**, 390 (1979).
4) Y. Nishida, K. Takahashi, and S. Kida, *Mem, Fac. Sci., Kyushu Univ., Ser. C*, **13**(1), 27 (1981).
5) K. Takahashi, E. Ogawa, N. Oishi, Y. Nishida, and S. Kida, *Inorg. Chim. Acta*, **66**, 97 (1982).
6) K. Takahashi, Y. Nishida, and S. Kida, *Inorg. Chim. Acta*, **77**, L185 (1983).
7) S. Kawano, *Rep. Comp. Cent. Kyushu Univ.*, **13**, 39 (1980).
8) "Universal Crystallographic Computer Program System," ed by T. Sakurai, The Crystallographic Society of Japan, Tokyo (1967).
9) C. K. Johnson, Report No. 3794, Oak Ridge National Laboratory, Oak Ridge, Tennessee (1965).
10) "International Tables for X-ray Crystallography," Kynoch Press, Birmingham (1974), Vol. IV, pp. 71—80.
11) M. V. Veidis, B. W. Dockum, F. F. Charron Jr, and W. M. Reiff, *Inorg. Chim. Acta*, **53**, L197 (1981).

12) The deviations of the benzimidazolyl atoms from their least-squares planes fall in the range of ±0.04 Å for all the complexes.
13) J. E. Huheey, "Inorganic Chemistry," 2nd ed, Harper & Row, New York (1978), pp. 230—232.
14) K. Nakamoto, "Infrared and Raman Spectra of Inorganic and Coordination Compounds," 3rd ed, John Wiley & Sons, New York (1977), pp. 270—274.
15) A. Earnshaw, "Introduction to Magnetochemistry," Academic Press, London (1968), Chap. 3.
16) D. Sutton, "Electronic Spectra of Transition Metal Complexes," McGraw-Hill, New York (1968), Chap. 5.
17) W. L. Geary, *Cood. Chem. Rev.*, **7**, 81 (1971).

 © 1984 The Chemical Society of Japan Bull. Chem. Soc. Jpn., 57, 2634—2640 (1984) [Vol. 57, No. 9

X-Ray Structural Study on Molecular Stereochemistries of Six-coordinate Zn(II) Complexes of *trans*-ZnX_2N_4 Type. Out-of-plane Displacement of Zn(II) from a Plane Formed by In-plane Four Nitrogens

Tasuku Ito,* Masako Kato, and Haruko Ito
Department of Applied Molecular Science, Institute for Molecular Science, Okazaki National Research Institutes, Okazaki 444
(Received March 30, 1984)

Molecular structures of *trans*-bis(isothiocyanato)(1,4,8,11-tetraazacyclotetradecane and 1,4,8,12-tetraazacyclopentadecane)zinc(II) complexes, $[Zn(NCS)_2(C_{10}H_{24}N_4)]$ (**1**) and $[Zn(NCS)_2(C_{11}H_{26}N_4)]$ (**2**), have been determined by X-ray analyses. Crystal data are: for **1**, orthorhombic, space group $P2_1nb$, a=14.502(2), b=18.163(2), c=6.552(1) Å, V=1718.0(4) Å^3, Z=4; for **2**, monoclinic, space group $P2_1/a$, a=14.453(2), b=14.436(1), c=9.213(1) Å, β=104.82(1)°, V=1858.3(4) Å^3, Z=4. Coordination geometries about Zn(II) in **1** and **2** are of the pseudo-octahedral type with two NCS groups at the trans positions, but the Zn(II) ion in each compound deviates from a plane defined by the four nitrogens of the macrocyclic ligand by 0.179 Å on the average in **1** and 0.193 Å in **2**. Structural features of **1** and **2** suggest, complemented with data reported previously for out-of-plane Zn(II) structures, that potential surface regarding the out-of-plane displacement is very flat. The Zn–NCS distance has been found to decrease as an in-plane Zn–N length (or cavity size of the ligand) increases. The observed negative correlation is substantially stronger than those for Ni(II) and Co(III) complexes and discloses the softness of a Zn(II) ion.

This paper is one of a series of investigations on metal ion characteristics viewed from the correlation between axial and in-plane coordination bond lengths of tetragonal six-coordinate complexes. The aim and method of the studies have been described elsewhere along with a historical review.[1] In order to visualize metal ion characteristics from this point of view, we have carried out *ab initio* MO calculations and X-ray analyses for a series of complexes which have the same or very similar coordination environments. In the theoretical approach, we have discussed the metal ion characteristics on the basis of potential energy surfaces of *trans*-$[MCl_2(NH_3)_4]$ ($M=Co^{3+}$, Fe^{2+}, Ni^{2+}, and Zn^{2+}) along the axial and in-plane coordination bonds.[1] In the experimental approach, we have determined the structures of a series of complexes of *trans*-MX_2N_4 type ($M=Ni^{2+}$, Zn^{2+}, and Co^{3+}). Tetraazacycloalkanes with different ring sizes, 1,4,8,11-tetraazacyclotetradecane ([14]aneN$_4$), 1,4,8,12-tetraazacyclopentadecane ([15]aneN$_4$), and 1,5,9,13-tetraazacyclohexadecane ([16]aneN$_4$), were used as in-plane ligands, so as

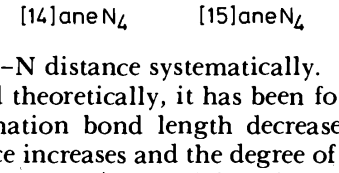

[14]aneN$_4$ [15]aneN$_4$

to vary an M–N distance systematically. Both experimentally and theoretically, it has been found that the axial coordination bond length decreases as the in-plane distance increases and the degree of the negative correlation is strongly metal ion dependent (Zn^{2+}> Ni^{2+}>Co^{3+}). A summary of the studies[1] and structural details of the Ni(II) complexes[2] have been described elsewhere.

The present paper reports structural details of the compounds, $[Zn(NCS)_2([14]aneN_4)]$ (**1**) and $[Zn(NCS)_2([15]aneN_4)]$ (**2**). We have tried to synthesize *trans*-dichloro- and *trans*-bis(isothiocyanato)zinc(II) complexes with the tetraazacycloalkanes. We succeeded in the isolation of single crystals suitable for X-ray work only for **1** and **2**. Other combinations of in-plane and axial ligands did not afford single crystals of the desired six-coordinate Zn(II) complexes, but gave mostly five-coordinate complexes.

As will be discussed later, the most characteristic feature in molecular stereochemistries of **1** and **2** is the out-of-plane displacement of Zn from the plane formed by four nitrogens of the in-plane ligand (hereafter abbreviated as the N_4 plane). It is well characterized that Zn(II) complexes with porphine or its analogs, $[Zn(H_2O)(tpp)]$ (tpp=5,10,15,20-tetraphenylporphine),[3a] [(Zn(py)(tpyp)] (tpyp=5,10,15,20-tetra(4-pyridyl)porphine),[3b] and Zn(hexylamine)(pc) (pc=phthalocyanine)[3c], are five-coordinate complex with the square pyramidal geometry. It had been suspected that the Zn(II) atom is too large to fit into the cavities of the porphinato or phthalocyanato ligands, though examples of the in-plane structure were recently found for [Zn(pc)][4] and $[Zn(tpp)]\cdot(toluene)_2$.[5] The results of X-ray analyses of **1** and **2** have shown that the cavity sizes of the present macrocyclic ligands are somewhat larger than those of the porphinato or phthalocyanato complexes. Therefore, it seems that whether Zn(II) in six-coordinate complexes of the *trans*-ZnX_2N_4 type takes an out-of-plane position or an in-plane position is not solely determined by the relative sizes of a hole of a macrocyclic ligand and a Zn(II) ion.

Experimental

Materials. The tetraazacycloalkanes, [14]aneN$_4$ and [15]aneN$_4$, were purchased from Strem Chemical Inc.

Preparation of [Zn(NCS)$_2$([14]aneN$_4$)] (1). $ZnCl_2$ was allowed to react with an equimolar amount of [14]aneN$_4$ in

H_2O at 50 °C for 1 h. To the filtered solution was added two equivalents of KSCN at room temperature. Immediate complexation occurred to yield a white precipitate. The product was dissolved in $CHCl_3$ and the filtered solution was evaporated to dryness. The residue was recrystallized from nitromethane. Anal. Calcd for $[Zn(NCS)_2([14]aneN_4)]=ZnS_2C_{12}H_{24}N_6$: C, 37.74; H, 6.34; N, 22.01%. Found: C, 37.65; H, 6.42; N, 21.94%. IR (Nujol mull): 3210(NH), 2025(CN) cm^{-1}.

Preparation of [Zn(NCS)$_2$([15]aneN$_4$)] (2). This compound was synthesized in a similar way using [15]aneN$_4$ in place of [14]aneN$_4$. The crude product was recrystallized from acetonitrile. Anal. Calcd for $[Zn(NCS)_2([15]aneN_4)]=ZnS_2N_6C_{13}H_{26}$: C, 39.44; H, 6.62; N, 21.23%. Found: C, 39.70; H, 6.71; N, 21.50%. IR (Nujol mull): 3180(NH), 2050(CN) cm^{-1}.

Measurements. IR spectra were recorded on a HITACHI 295 spectrophotometer.

Collection and Reduction of X-ray Diffraction Data. Diffraction data were obtained on a Rigaku AFC-5 four-circle diffractometer with use of graphite-monochromatized Mo $K\alpha$ radiation. The intensity data were corrected for Lorentz-polarization effects. Absorption corrections were applied with a numerical integration procedure with a Gaussian grid (6×6×6). The procedures used for data collection were standard and have been described previously.[6] Pertinent crystallographic data for the compounds are summarized in Table 1.

Solution and Refinement of the Structures. Both the structures were solved and refined by standard Patterson, Fourier, and block-diagonal least-squares techniques. The atomic scattering factors for non-hydrogen atoms were taken from Ref. 7 and those for hydrogen from Stewart, Davidson, and Simpson.[8] The effects of anomalous dispersion for non-hydrogen atoms were corrected in structure factor calculations. The weights (w) were taken as $w=[\sigma_c^2+(0.015|F_o|^2)]^{-1}$. Non-hydrogen and hydrogen atoms were refined anisotropically and isotropically, respectively.

Calculations of the refinements for both the compounds converged nicely. However, we noticed in the structure of compound **1** thus obtained that a thermal ellipsoid of the Zn atom is extraordinarily elongated along the normal to the N_4 plane of the [14]aneN$_4$ ligand. The Zn atom in **1** was found to take an out-of-plane position and thus the two axial coordination bond distances differed substantially from each other. Even the shorter axial coordination bond length [Zn–N(5)=2.247(6) Å] was somewhat longer than normal Zn(II)–NCS bond lengths.[9] Then we collected intensity data for another crystal of **1** grown from a chloroform–methanol mixture and solved the structure. The resultant structural features were essentially the same. The situation seemed to be similar to that reported in the erroneous structure analysis

Table 1. Crystallographic parameters

	1	**2**
Formula	$ZnS_2N_6C_{12}H_{24}$	$ZnS_2N_6C_{13}H_{26}$
Fw	381.86	395.90
Crystal system	orthorhombic	monoclinic
Space group	$P2_1nb$	$P2_1/a$
a/Å	14.502(2)	14.453(2)
b/Å	18.163(2)	14.436(1)
c/Å	6.522(1)	9.213(1)
β/deg	—	104.823(9)
V/Å^3	1718.0(4)	1858.3(4)
Z	4	4
D_x/g cm^{-3}	1.476	1.415
D_m/g cm^{-3}	1.472	1.419
μ/mm^{-1}	1.17	1.58
2θ limits/deg	2—65	2—60
Unique data[a]	1598	2533
R	0.042	0.052
R_w	0.045	0.062

a) $|F_o|>3\sigma(|F_o|)$.

Table 2. Atomic parameters for $[Zn(NCS)_2([14]aneN_4)]$ (**1**)[a]

Atom	x	y	z
Zn[b]	0	1231(4)	273(18)
Zn'[c]	-184(9)	1244(7)	-111(18)
S(1)	2956(6)	904(2)	2903(4)
S(2)	-3088(6)	1526(2)	-2511(4)
N(1)	-551(7)	159(3)	143(10)
N(2)	-1030(8)	1440(4)	2421(10)
N(3)	422(7)	2324(3)	-55(9)
N(4)	875(8)	1052(4)	-2318(11)
N(5)	1031(8)	998(6)	2586(10)
N(6)	-1186(8)	1488(5)	-2579(10)
C(1)	-1073(9)	76(5)	2040(15)
C(2)	-1633(8)	787(6)	2390(13)
C(3)	-1484(9)	2165(6)	2365(12)
C(4)	-807(9)	2807(5)	2271(13)
C(5)	-307(7)	2897(4)	276(14)
C(6)	910(9)	2361(5)	-2046(14)
C(7)	1497(9)	1708(6)	-2357(13)
C(8)	1365(9)	337(5)	-2257(14)
C(9)	681(10)	-294(6)	-2182(15)
C(10)	133(9)	-415(3)	-178(13)
C(11)	1863(9)	956(5)	2696(11)
C(12)	-1950(11)	1511(6)	-2568(12)

a) Parameters are multiplied by 10^4. b) Occupancy factor=0.64. c) Occupancy factor=0.36.

Table 3. Atomic parameters for $[Zn(NCS)_2([15]aneN_4)]$ (**2**)[a]

Atom	x	y	z
Zn	2387(1)	825(1)	2414(1)
S(1)	3995(1)	2738(1)	6470(2)
S(2)	1353(1)	-1371(1)	-1508(2)
N(1)	2295(4)	1649(4)	393(5)
N(2)	3428(4)	65(4)	1596(7)
N(3)	2395(4)	-159(3)	4133(5)
N(4)	1137(3)	1533(3)	2615(6)
N(5)	3369(3)	1699(4)	3843(5)
N(6)	1248(5)	-327(4)	957(7)
C(1)	2760(8)	1133(6)	-686(8)
C(2)	3782(6)	680(6)	486(12)
C(3)	4175(6)	-412(6)	2693(10)
C(4)	3743(7)	-1052(6)	3572(11)
C(5)	3334(6)	-627(5)	4749(9)
C(6)	2046(6)	201(6)	5394(7)
C(7)	1065(6)	639(6)	4875(9)
C(8)	1037(5)	1600(6)	4135(8)
C(9)	1117(6)	2480(6)	2067(9)
C(10)	882(7)	2519(7)	516(15)
C(11)	1309(6)	1895(6)	-402(10)
C(12)	3627(4)	2133(4)	4911(6)
C(13)	1298(4)	-773(4)	-71(6)

a) Parameters are multiplied by 10^4.

on an aqua(tetraphenylporphinato)zinc(II) complex, [Zn(H_2O)(tpp)],[10] the structure of which was later redetermined by taking disorder in the Zn atom location into consideration.[3a] Then the structure of **1** was solved in a similar way with the Zn atom in two disordered positions.[11] The Zn atom was located at two positions, equidistantly above (Zn) and below (Zn') the N_4 plane. Full-matrix least squares calculations were carried out under the restricted condition that the sum of occupancy factors (P) of Zn and Zn' equals one. Final P_{Zn} and $P_{Zn'}$ values were 0.64 and 0.36. In the converged structure, geometries of [Zn(NCS)$_2$([14]aneN$_4$)] and [Zn'(NCS)$_2$([14]aneN$_4$)] are related approximately to each other by inversion at the center of the N_4 basal plane (Ct).

For **1**, all the hydrogen atoms were located by the difference syntheses and their positional and isotropic thermal parameters were refined. However, for **2**, 19 hydrogens out of 26 were found and included in the calculations.

The final R indices are listed in Table 1. Positional parameters for non-hydrogen atoms are given in Tables 2 and 3.[12] All the calculations were carried out on the HITAC M-200H computer at the Computer Center of the Institute for Molecular Science with the Universal Crystallographic Computation Program System UNICS III.[13]

Description of the Structure

Figure 1 shows perspective views of the complexes **1** and **2**. As shown in Fig. 1, the geometry about the Zn in each compound is of the pseudo octahedral type with NCS^- groups at the trans positions. Table 4 lists relevant bond lengths and angles. Deviations of atoms included in the first coordination sphere from the N_4 best plane are given in Table 5. Figure 2 represents perspective diagrams of the coordination environments of the Zn atoms in **1** and **2**.

[Zn(NCS)$_2$([14]aneN$_4$)] (1). The structure of this compound was solved assuming that the Zn atom is disordered above and below the N_4 plane. The Zn and Zn' atoms are displaced by 0.177(3) and 0.184(4) Å from the N_4 plane toward the N(5) and N(6) atoms of the NCS^- ligands, respectively. The overall stereochemistry of the macrocyclic ligand is essentially the same as that found for Ni(II),[2] Zn(II),[15,16] Pd(II),[16] Pd(IV),[16] and Ag(II)[16] complexes with [14]aneN$_4$. The alternating six- and five-membered chelate rings are in the stable chair and gauche conformations, respectively. Intermolecular hydrogen-bonds operate between sulfur atoms and secondary amine groups of the neighbouring complexes.[17] If the complex with the ring conformations assumes a structure with high symmetry such as C_{2h} or C_i, the occupancy factors of the Zn and Zn' atoms should be 0.5 each. However, intramolecular and packing interactions including the hydrogen

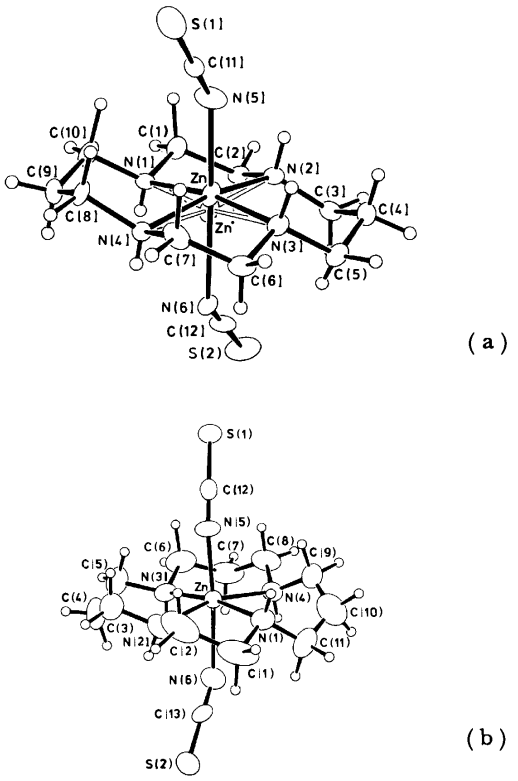

Fig. 1. Molecular structures: (a) [Zn(NCS)$_2$([14]aneN$_4$)] (**1**), the disordered Zn atom with a minor occupancy factor is shown with open bonds; (b) [Zn(NCS)$_2$([15]aneN$_4$)] (**2**), seven hydrogens are located at the calculated positions (see text).

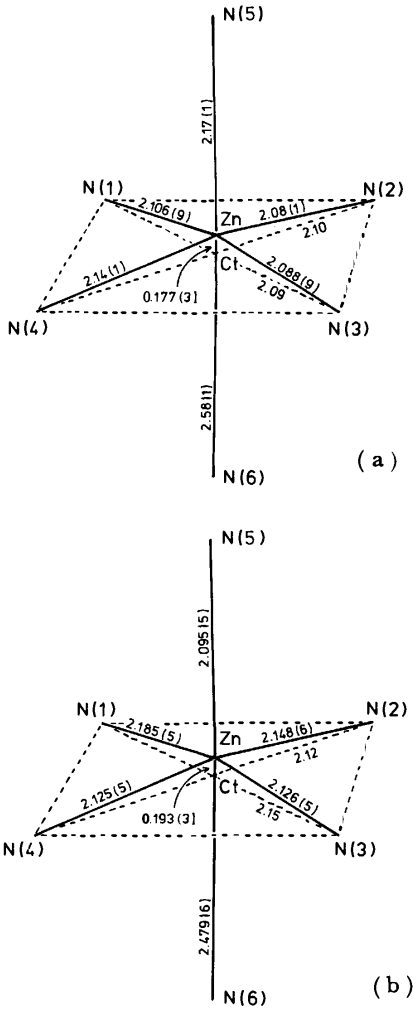

Fig. 2. Coordination geometries about the Zn atoms: (a) [Zn(NCS)$_2$([14]aneN$_4$)] (**1**), the geometry about the Zn atom with a major occupancy factor is shown; (b) [Zn(NCS)$_2$([15]aneN$_4$)] (**2**). Ct represents a center of donor atoms of the macrocyclic ligand.

TABLE 4. RELEVANT BOND DISTANCES (Å) AND ANGLES (DEG) FOR $[Zn(NCS)_2([14]aneN_4)]$ AND $[Zn(NCS)_2([15]aneN_4)]$

$[Zn(NCS)_2([14]aneN_4)]$ (**1**)

Zn	-N(1)	2.106(9)		Zn'	-N(3)	2.151(14)	
Zn	-N(2)	2.083(13)		Zn'	-N(4)	2.133(16)	
Zn	-N(3)	2.088(9)		Zn'	-N(5)	2.529(16)	
Zn	-N(4)	2.138(13)		Zn'	-N(6)	2.214(15)	
Zn	-N(5)	2.166(13)		S(1)	-C(11)	1.594(16)	
Zn	-N(6)	2.576(13)		S(2)	-C(12)	1.651(18)	
Zn'	-N(1)	2.046(14)		N(5)	-C(11)	1.211(18)	
Zn'	-N(2)	2.089(15)		N(6)	-C(12)	1.108(20)	
N(1)	-Zn -N(2)	85.6(4)		N(1)	-Zn' -N(2)	87.0(6)	
N(1)	-Zn -N(3)	170.3(3)		N(1)	-Zn' -N(3)	169.4(7)	
N(1)	-Zn -N(4)	93.0(5)		N(1)	-Zn' -N(4)	94.9(6)	
N(1)	-Zn -N(5)	96.2(5)		N(1)	-Zn' -N(5)	87.4(5)	
N(1)	-Zn -N(6)	83.4(4)		N(1)	-Zn' -N(6)	94.7(6)	
N(2)	-Zn -N(3)	96.1(4)		N(2)	-Zn' -N(3)	94.1(6)	
N(2)	-Zn -N(4)	170.1(6)		N(2)	-Zn' -N(4)	169.9(8)	
N(2)	-Zn -N(5)	93.6(6)		N(2)	-Zn' -N(5)	83.7(5)	
N(2)	-Zn -N(6)	88.5(4)		N(2)	-Zn' -N(6)	98.9(6)	
N(3)	-Zn -N(4)	83.7(4)		N(3)	-Zn' -N(4)	82.3(5)	
N(3)	-Zn -N(5)	93.2(4)		N(3)	-Zn' -N(5)	82.2(5)	
N(3)	-Zn -N(6)	87.1(4)		N(3)	-Zn' -N(6)	95.6(6)	
N(4)	-Zn -N(5)	96.4(4)		N(4)	-Zn' -N(5)	86.5(6)	
N(4)	-Zn -N(6)	81.5(5)		N(4)	-Zn' -N(6)	90.8(6)	
N(5)	-Zn -N(6)	177.9(6)		N(5)	-Zn' -N(6)	176.8(7)	
Zn	-N(5) -C(11)	137.8(9)		S(1)	-C(11) -N(5)	178.5(13)	
Zn	-N(6) -C(12)	132.0(10)		S(2)	-C(12) -N(6)	178.5(15)	

$[Zn(NCS)_2([15]aneN_4)]$ (**2**)

Zn	-N(1)	2.185(5)		S(1)	-C(12)	1.648(6)	
Zn	-N(2)	2.148(6)		S(2)	-C(13)	1.599(6)	
Zn	-N(3)	2.126(5)		N(5)	-C(12)	1.145(7)	
Zn	-N(4)	2.125(5)		N(6)	-C(13)	1.163(9)	
Zn	-N(5)	2.095(5)					
Zn	-N(6)	2.479(6)					
N(1)	-Zn -N(2)	82.8(2)		N(3)	-Zn -N(5)	93.5(2)	
N(1)	-Zn -N(3)	170.6(2)		N(3)	-Zn -N(6)	80.3(2)	
N(1)	-Zn -N(4)	86.8(2)		N(4)	-Zn -N(5)	96.3(2)	
N(1)	-Zn -N(5)	95.2(2)		N(4)	-Zn -N(6)	84.7(2)	
N(1)	-Zn -N(6)	91.0(2)		N(5)	-Zn -N(6)	173.8(2)	
N(2)	-Zn -N(3)	92.8(2)		Zn	-N(5) -C(12)	152.7(5)	
N(2)	-Zn -N(4)	164.5(2)		Zn	-N(6) -C(13)	129.9(6)	
N(2)	-Zn -N(5)	96.0(2)		S(1)	-C(12) -N(5)	178.8(5)	
N(2)	-Zn -N(6)	84.0(2)		S(2)	-C(13) -N(6)	178.8(6)	
N(3)	-Zn -N(4)	95.7(2)					

TABLE 5. DEVIATIONS (Å) OF ATOMS FROM A PLANE DEFINED BY FOUR IN-PLANE NITROGENS OF THE MACROCYCLIC LIGAND

	1	**2**
N(1)[a]	0.006(7)	0.032(7)
N(2)[a]	−0.006(7)	−0.040(8)
N(3)[a]	0.006(7)	0.028(7)
N(4)[a]	−0.006(6)	−0.027(7)
N(5)	2.341(7)	2.288(6)
N(6)	−2.392(6)	−2.276(8)
Zn	0.177(3)	0.193(3)
Zn'	−0.184(4)	—

a) Atoms used in the calculation of the best plane.

bonds lower more or less the symmetry of the skeletal structure of the macrocyclic ligand to cause the difference in the occupancy factors.

$[Zn(NCS)_2([15]aneN_4)]$ (2). Three six-membered and one five-membered chelate rings adopt a chair-chair-skew-gauche conformational sequence. The ring conformation of this type has been found for $[Ni(NCS)_2([15]aneN_4)]$.[2] But the [15]aneN$_4$ ligand in $[NiCl_2([15]aneN_4)]$[2] and $[\{Zn([15]aneN_4)\}_3(O_2COCH_3)_2](ClO_4)_4$,[15] and that in $[CoCl_2([15]aneN_4)](ClO_4)$ (green form)[18] have been reported to take chair-skew-chair-gauche and skew-skew-skew-gauche conformations, respectively.

The Zn atom in this compound also takes an out-of-plane position and is displaced by 0.193(3) Å from the N$_4$ best plane toward the N(5) atom. The Zn-N(6)

distance lengthens to 2.479(6) Å, while the Zn–N(5) distance of 2.095(5) Å is within the normal range. Sulfur atoms are again involved in intermolecular hydrogen-bonds with secondary amine groups of the neighbouring complexes.[17]

It has been reported that, in metal complexes with the [15]aneN$_4$ ligand in the chair-chair-skew-gauche conformation, notable structural distortions arise at the periphery of the N(1) atom, which links a gauche five-membered and a skew six-membered chelate ring.[2] Typical distortions in such compounds are lengthening of an M–N(1) bond and deviation of the N(1) atom from the N$_4$ best plane. But, in compound **2**, such strains are relieved to some extent by the displacement of the Zn atom from the N$_4$ plane. This is evidenced by comparison of bond distances and angles associated with the N(1) atom of the present compound and those for [Ni(NCS)$_2$([15]aneN$_4$)].[2]

Discussion

There are two distinct features in the coordination geometries of compounds **1** and **2**: (i) the Zn atom is displaced *ca.* 0.2 Å from the mean plane formed by the four nitrogens of the macrocyclic ligand; (ii) there is a negative correlation between in-plane and axial coordination bond lengths. The out-of-plane displacement of the Zn causes, in each compound, rather large inequalities in two axial coordination bond lengths. The differences amount to 0.38 Å on the average for both **1** and **2**. The distances between the Zn atoms and the weakly bonded NCS$^-$ groups [Zn–N(6)=2.58(1) Å and Zn′–N(5)=2.53(1) Å for **1**, and Zn–N(6)=2.479(6) Å for **2**] appear to be rather long as coordination bond distances. However, the Zn atoms in these compounds should be described as six-coordinate, since deviations of Zn(II) from basal plane reported for the five-coordinate Zn(II) complexes with the square-pyramidal geometry are much larger. It is interesting to note that, in each compound, the nitrogens of the weakly bonded and the strongly bonded NCS$^-$ groups are nearly equidistant from the mean N$_4$ plane: for **1**, Ct–N(5)=2.35, Ct–N(6)=2.40 Å; for **2**, Ct–N(5)=2.29, Ct–N(6)=2.29 Å (see Fig. 2).

The hole sizes found for the present tetraazacycloalkane complexes (Ct–N distance) are 2.10 Å for **1** and 2.13 Å for **2**, and are larger than those of the Zn(II) porphinato or phthalocyanato complexes (1.98—2.07 Å). In spite of this, the Zn atoms in the present compounds take out-of-plane positions. Table 6 collates bond lengths and angles within the [M([14]aneN$_4$)] moieties of various metal complexes containing the [14]aneN$_4$ ligand. In all the compounds, the [14]aneN$_4$ ligand adopts the same overall stereochemistry with the most stable chelate ring conformations. The values in Table 6 are averaged assuming C_{2h} symmetry for the [M([14]aneN$_4$)] moiety. The compounds are listed in increasing order of the Ct–N distance. Some important facts are noted in Table 6 relative to the observed out-of-plane structures. Except for Zn(II) complexes, all the compounds in Table 6 take the in-plane structures. Interestingly, the largest cation, Ag(II), the ionic radius of which is much larger than a Zn(II) ion, sits precisely in the N$_4$ plane [Ag–N=2.158(2) Å].[19] Furthermore, half of Zn(II) atoms in the crystal structure of [Zn(O_2C-OCH_3)([14]aneN$_4$)](ClO_4) take the in-plane position.[15] These observations suggest that simple argument, such that Zn(II) is too large to be accomodated into the cavity in a planar fashion to result in the out-of-plane structure,[3a] must be changed. In Table 6, various bond lengths and angles increase or decrease smoothly, or remain unchanged on going from shorter to longer Ct–N structures, in general. However, it can be seen that some structural parameters such as bond angles of N–M–N(6*) and C–C–C (see footnotes of Table 6 for notations) deviate from the trend in the out-of-plane Zn structures and return to the original tendency in the Ag(II) complex. There is no doubt that cumulative bond length and angle strain is relieved by taking the out-of-plane structure in the Zn(II) complexes. It is also certain from Table 6 that sizes of Ag(II) and Zn(II) ions are larger than a natural cavity size of the [14]aneN$_4$ ligand. In the case of the Ag(II) complex, much larger electronic strain would be introduced if the Ag(II) took an out-of-plane position.

A Zn(II) ion has an electronic configuration of $(3d)^{10}$ and thus no ligand field stabilization due to 3d electrons takes place for a Zn(II) complex. *Ab initio* MO calculations for *trans*-[$ZnCl_2(NH_3)_4$] show that the potential surface along the direction of the out-of-plane displacement of Zn is very flat.[20] It is likely that very similar situations exist for the Zn(II) complexes with the out-of-plane structures. Since the potential surface along the direction in an isolated complex is very flat, it would be affected easily in its crystalline state by the potential from surrounding ions and packing forces. Subtle intra- or intermolecular forces including the intermolecular hydrogen bonds seem to be responsible for the out-of-plane structures. Conversely, it follows that a Zn(II) ion might take the in-plane position if the situation were otherwise. In fact, such examples have been found for [Zn(O_2COCH_3)([14]aneN$_4$)](ClO_4), and [{Zn([15]aneN$_4$)}$_3$(O_2COCH_3)$_2$](ClO_4)$_4$.[15] The out-of plane structures found for the present Zn(II) complexes are associated not only with the relative size between Zn(II) and the cavity but also with the flatness of the potential surface along the normal to the N$_4$ plane.

The $^{13}C\{^1H\}$ NMR spectrum of compound **1** in $CDCl_3$ shows only four signals, which are assignd to C–$\underline{C}H_2$–C (δ, 28.6), two N–$\underline{C}H_2$ carbons (δ, 47.9 and 49.4), and N$\underline{C}$S (δ, 133.9). The observed spectral pattern indicates that compound **1** has C_{2h} symmetry in solution. Such symmetry can be expected when the Zn atom sits precisely in the N$_4$ plane and the [14]aneN$_4$ ligand takes a chair-gauche-chair-gauche conformation, or when the Zn atom moves up and down passing through the N$_4$ hole at a faster rate than an NMR time scale. We failed to answer this question.[21] As for compound **2** in solution, whether the Zn takes the in-plane position or the out-of-plane position was not clear from the NMR study, because **2** has no symmetry element even if Zn were in the in-plane position.

On going from the fourteen-membered to the fifteen membered rings, average in-plane Zn–N or Ct–N distances increased by *ca.* 0.04 Å. The amount of the increase is slightly smaller than those in the Ni–N dis-

Table 6. Mean bond lengths (Å) and angles (deg) of metal complexes with 1,4,8,11-tetraazacyclotetradecane(L)[a,b,c]

	Ni^{II} (low spin)	Ni^{III} (low spin)	Pd^{II}	Pd^{II}-Pd^{IV}	Pd^{IV}	Ni^{II} (high spin)		Zn^{II} (in-plane)	Zn^{II} (out-of-plane)		Ag^{II}
Compound	[NiL]-$(PF_6)_2$[d]	[$NiCl_2L$]-(ClO_4)[e]	[PdL]-$(ClO_4)_2$[f]	PdClL-$(ClO_4)_2$[f,g]	$PdCl_2L$-$(NO_3)_2$[f]	$NiCl_2L$[h,i]	$Ni(NCS)_2$-L[i]	ZnL$(O_2CO$-$CH_3)(ClO_4)$[j]	$Zn(NCS)_2$-L[k]	ZnL$(O_2CO$-$CH_3)(ClO_4)$[j]	[AgL]-$(ClO_4)_2$[l]
M-N	1.945(8)	1.970(7)	2.051(4)	2.054(13)	2.062(3)	2.067(1)	2.074(7)	2.100(16)	2.105(31)	2.117(68)	2.158(4)
N-C(5*)	1.480(8)	1.489(13)	1.465(45)	1.478(11)	1.488(3)	1.477(6)	1.477(6)	1.470(6)	1.480(17)	1.473(9)	1.472(3)
N-C(6*)	1.489(12)	1.489(3)	1.460(10)	1.488(20)	1.484(1)	1.483(2)	1.477(4)	1.481(6)	1.480(26)	1.469(12)	1.486(1)
C-C(5*)	1.505(6)	1.493(2)	1.510(18)	1.491(13)	1.514(2)	1.514(3)	1.510(12)	1.514(6)	1.520(10)	1.501(7)	1.531(4)
C-C(6*)	1.508(13)	1.503(6)	1.560(1)	1.517(8)	1.516(3)	1.527(6)	1.516(7)	1.521(1)	1.521(10)	1.510(7)	1.518(3)
N-M-N(5*)	86.7(1)	86.2(4)	83.1(3)	84.4(3)	84.7(1)	85.3(1)	85.3(2)	84.8(1)	84.8(25)	83.4(2)	84.0(1)
N-M-N(6*)	93.3(1)	93.8(8)	96.9(3)	95.6(3)	95.3(1)	94.7(1)	94.7(2)	95.2(1)	94.4(21)	90.9(2)	96.0(1)
M-N-C(5*)	108.4(1)	107.8(11)	108.1(20)	107.6(13)	106.7(0)	106.3(1)	105.7(4)	105.4(8)	106.7(5)	106.0(47)	104.5(3)
M-N-C(6*)	119.6(8)	119.2(2)	115.6(1)	115.8(1)	115.8(0)	116.3(1)	116.2(6)	115.1(1)	115.1(3)	114.0(60)	111.5(3)
N-C-C(5*)	106.8(1)	107.1(11)	106.3(18)	109.4(10)	107.2(7)	109.3(7)	109.0(1)	109.4(8)	109.2(3)	110.0(5)	109.7(1)
N-C-C(6*)	112.2(8)	111.7(7)	112.9(14)	112.1(5)	112.0(3)	111.9(1)	112.3(2)	112.1(1)	111.8(1)	113.5(7)	112.6(3)
C-C-C	112.3(3)	113.6(6)	116.5(9)	117.7(7)	115.1(2)	115.8(1)	116.5(5)	117.1(4)	115.8(1)	115.4(4)	117.5(2)
C-N-C	110.1(1)	111.8(8)		113.1(3)	114.2(2)	113.7(5)	114.6(5)	115.0(7)	114.9(2)	114.3(1)	115.1(5)

a) Values are averaged assuming that each compound has C_{2h} symmetry. b) Abbreviations: 5*, five-membered ring; 6*, six-membered ring. c) Crystal radii (Å) are 0.70 (low spin Ni^{3+}), 0.78 (Pd^{2+}), 0.76 (Pd^{4+}), 0.84 (high spin Ni^{2+}), and 0.89 (Zn^{2+}) (R. D. Shannon, C. T. Prewitt, *Acta Crystallogr., Sect. B*, **25**, 925 (1969)). Ionic radius of Ag^{2+} is 1.01 Å ("Kagaku Benran," Maruzen, Tokyo (1975)). d) Ref. 14. e) T. Ito, M. Sugimoto, K. Toriumi, H. Ito, *Chem. Lett.*, **1981**, 1477. f) M. Yamashita, H. Ito, K. Toriumi, T. Ito, *Inorg. Chem.*, **22**, 1566 (1983). g) A mixed valence complex, $[Pd^{II}L][Pd^{IV}Cl_2L](ClO_4)_4$. h) B. Bosnich, R. Mason, P. T. Pauling, G. B. Robertson, M. L. Tobe, *Chem. Commun.*, **1965**, 97. i) Ref. 2. j) Ref. 15. k) The present study. l) $P\bar{1}$ form. T. Ito, H. Ito, K. Toriumi, *Chem. Lett.*, **1961**, 1101.

tances (0.05—0.06 Å) for one ring member added similarly in Ni(II) complexes with the same tetraazacycloalkanes.[2] The increases are not as large as expected from calculations of strain energy minimizations for free ligand molecules (0.10—0.15 Å).[22] The shorter axial coordination bond length (Zn–N(5)) in **1** is longer than the corresponding distance (Zn–N(5)) in **2**. The longer one (Zn–N(6)) in **1** is also longer than the corresponding distance (Zn–N(6)) in **2**. That is, the axial coordination bond length decreases as the in-plane distance increases. The same relationship also holds when the mean distance of Zn–N(5) and Zn–N(6) or an average Ct–NCS^- distance is taken as the "axial bond length".

It is most reasonable to consider the observed correlation to be a result of the electronically controlled cis effect, since the crystal structures of **1** and **2** show no significant steric effects that would cause the correlation. The degree of the correlation found for the Zn complexes is substantially stronger than those reported for a series of similar Ni(II) and Co(III) complexes.[1]

We have previously discussed the electronic origin that gives rise to the correlations between intramolecular coordination bond lengths from the viewpoint of the potential energy surface.[1] A section of the potential surface along the in-plane and axial coordination bond axes is an ellipse which is elongated in the M–X directon and has a tilt with respect to the coordination bond axes. Such features of the potential surface are primarily responsible for the experimentally observed correlations. Furthermore, the shape of the potential surface, *i.e.*, the degree of the correlation is closely related to softness or hardness in the HSAB concept[23] for metal ions.[1] The present result indicates that a Zn(II) ion is much softer than a Ni(II) ion, though Pearson classifies both of these ions into borderline between soft and hard metal ions.[23]

In structures containing the thiocyanate ion bonded to a metal atom through nitrogen, a wide range of metal-isothiocyanate bond angles have been obtained, though the majority of examples fall in the range 150—180°.[24] It has also been suggested that inter- and intra-molecular forces affect this angle though such effects are often difficult to prove.[24] The angles found for the present complexes are somewhat smaller than the normal values. The values for **1** range from 132.0(10)° to 137.8(9)°. For **2**, one of the angles [Zn–N(6)–C(13)] narrows down to 129.9(6)°, which is comparable to the smallest value so far reported, 129°, for bis(isothiocyanato)- bis(*N,N'*-dimethylethylenediamine)-copper(II).[24]

References

1) T. Ito, M. Kato, and H. Ito, *Bull. Chem. Soc. Jpn.*, **57**, 1556 (1984).

2) T. Ito, M. Kato, and H. Ito, *Bull. Chem. Soc. Jpn.*, **57**, 2641 (1984).

3) a) M. D. Glick, G. H. Cohen, and J. L. Hoard, *J. Am. Chem. Soc.*, **89**, 1966 (1967); b) D. M. Collins and J. L. Hoard, *ibid.*, **92**, 3761 (1970); c) T. Kobayashi, T. Ashida, N. Uyeda, E. Suito, and M. Kakudo, *Bull. Chem. Soc. Jpn.*, **44**, 2095 (1971).

4) W. R. Scheidt, M. E. Kastner, and K. Hatano, *Inorg. Chem.*, **17**, 706 (1978).

5) W. R. Scheidt and W. Dow, *J. Am. Chem. Soc.*, **99**, 1101 (1977).

6) M. Sugimoto, J. Fujita, K. Toriumi, H. Ito, and T. Ito, *Inorg. Chem.*, **22**, 955 (1983).

7) "International Tables for X-ray Crystallography," Kynoch Press, Birmingham (1974), Vol. IV.

8) R. F. Stewart, E. R. Davidson, and W. T. Simpson, *J. Chem. Phys.*, **42**, 3175 (1965).

9) A Zn(II)–NCS bond length in [Zn(NCS)(tren)](SCN) has been reported to be 2.03 Å [P. C. Jain, E. C. Lingafeltrer, and P. Paoletli, *J. Am. Chem. Soc.*, **90**, 519 (1968)].

10) E. B. Fleischer, C. K. Miller, and L. E. Webb, *J. Am. Chem. Soc.*, **86**, 2342 (1964).

11) A difference Fourier map calculated without the Zn atom contribution showed only a broad peak elongated perpendicularly to the N_4 plane at a distance of 0.097(3) Å from it.

12) Hydrogen atomic coordinates, thermal parameters of non-hydrogen atoms, lists of observed and calculated structure factors, and tables of full bond lengths and angles are kept in the Office of the Chemical Society of Japan (Document No. 8442).

13) T. Sakurai and K. Kobayashi, *Rikagaku Kenkyusho Hokoku*, **55**, 69 (1979).

14) H. Ito and T. Ito, unpublished study.

15) M. Kato and T. Ito, submitted for publication.

16) See Table 6.

17) The hydrogen-bond parameters are as follows.

$[Zn(NCS)_2([14]aneN_4]$ (**1**)		$[Zn(NCS)_2([15]aneN_4)]$ (**2**)	
S(1)···N(1)^{i}	3.52(1) Å	S(1)···N(3)^{i}	3.604(5) Å
S(2)···N(3)^{ii}	3.42(1)	S(2)···N(4)^{ii}	3.487(5)
		S(2)···N(1)^{iii}	3.467(5)

Key to symmetry operations

(i)	$0.5+x$	$-y$	$-z$	(i)	$0.5-x$	$0.5+y$	$1-z$
(ii)	$0.5+x$	$0.5-y$	$0.5+z$	(ii)	$-x$	$-y$	$-z$
				(iii)	$0.5-x$	$-0.5+y$	z

18) H. Ito, M. Kato, and T. Ito, unpublished study.

19) T. Ito, H. Ito, and K. Toriumi, *Chem. Lett.*, **1981**, 1104.

20) The calculations were carried out by using a double ζ quality basis set for metal 3d orbitals and minimal basis set for the others as in Ref. 1. Details will be reported elsewhere.

21) The spectral pattern was essentially the same in a more polar solvent such as CD_3OD, where the out-of-plane structure may be more stabilized. And the spectrum remained unchanged when the temperature was lowered down to −87.5 °C in CD_2Cl_2.

22) L. Y. Martin, L. J. DeHayes, L. J. Zompa, and D. H. Busch, *J. Am. Chem. Soc.*, **96**, 4046 (1974).

23) R. G. Pearson, *J. Chem. Educ.*, **45**, 581, 643 (1968).

24) M. B. B. Drew, and A. H. B. Othman, *Acta Crystallogr., Sect., B*, **31**, 613 (1975), and references cited therein.

 © 1984 The Chemical Society of Japan Bull. Chem. Soc. Jpn., 57, 2641—2649 (1984)

The Structures of *trans*-Dichloro- and *trans*-Bis(isothiocyanato)nickel(II) Complexes with 1,4,8,11-Tetraazacyclotetradecane, 1,4,8,12-Tetraazacyclopentadecane, and 1,5,9,13-Tetraazacyclohexadecane. The Negative Correlation between the Axial and In-plane Coordination Bond Lengths in Tetragonal Ni(II) Complexes of the *trans*-NiX_2N_4 Type

Tasuku Ito,* Masako Kato, and Haruko Ito
Department of Applied Molecular Science, Institute for Molecular Science, Okazaki National Research Institutes, Okazaki 444
(Received February 9, 1984)

The molecular structures of the six titled compounds, which contain 14-membered, 15-membered, or 16-membered tetraazamacrocyclic ligands, have been determined by single crystal X-ray analyses. On going from smaller to larger rings, the average in-plane Ni–N distance increased by 0.05—0.06 Å for each ring member added. For a series of complexes with given axial ligands (X), the mean axial coordination bond length (Ni–X) was found to decrease as the average in-plane distance (Ni–N) increased. The degree of the negative correlation was stronger for complexes with weaker axial ligands (Cl^-) than for those having stronger axial ligands (NCS^-). Similar negative interrelationships between the Ni–X and Ni–N distances have been found for complexes which have the same in-plane macrocyclic ligand, but different axial ligands. The molecular stereochemistries of the complexes have been discussed. For all the complexes with the 1,4,8,12-tetraazacyclopentadecane ligand, a structural disorder of the same type has been found: gauche five-membered and skew six-membered chelate rings are randomly interchanged in the crystal. This arises mainly from the similarity of the bite angles of the five- and six-membered chelate rings in the gauche and the skew conformations respectively.

This paper is one of a series of investigations of metal-ion characteristics viewed from the correlation between the axial and in-plane coordination bond lengths in tetragonal six-coordinate complexes of the *trans*-MX_2N_4 type ($M=Ni^{2+}$, Zn^{2+}, and Co^{3+}). The aim and method of the studies have been described in a previous paper along with a historical review.[1] In this series of investigations, we have carried out *ab initio* MO calculations and X-ray analyses for a series of complexes which have the same or very similar coordination environments. Both experimentally and theoretically, it has been found that the axial M-X distance decreases as the in-plane M–N distance increases. The degree of the negative correlation is strongly metal ion dependent and varies in the order: $Zn^{2+}>Ni^{2+}>Co^{3+}$. A summary of the studies[1] and the structures of the Zn complexes[2] have been described elsewhere. The present paper reports the structural details and the correlation observed for the titled Ni(II) complexes: [$NiCl_2$([14]aneN$_4$)] (**1**), [$NiCl_2$([15]aneN$_4$)] (**2**), [$NiCl_2$([16]aneN$_4$)] (**3**), [Ni(NCS)$_2$([14]aneN$_4$)] (**4**), [Ni(NCS)$_2$([15]aneN$_4$)] (**5**), and [Ni(NCS)$_2$([16]aneN$_4$)] (**6**).

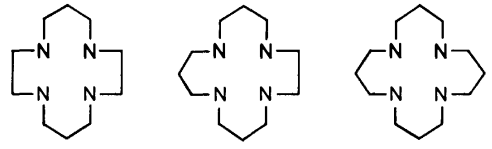

[14]aneN$_4$ [15]aneN$_4$ [16]aneN$_4$

As in-plane ligands, the tetraazacycloalkanes shown above were employed. On going from smaller to larger rings, the average M–N bond lengths can be varied systematically.[3,4] As axial ligands (X), we chose Cl^- and NCS^-, which have a relatively weak and a strong ligand field strength respectively, so that it was possible to investigate the effect of the ligand field strength on the correlation.

The structure of **1** was reported previously by Bosnich *et al.*[5] We have now redetermined the structure, aiming at an improvement in the accuracy of the structure analysis, and also because the atomic parameters for this compound have not been reported.

In this study, we have also measured the far-infrared spectra of a series of complexes of this type in order to see if the electronic interaction between the in-plane and axial ligands is manifested in the stretching vibrations of the coordination bonds.

Experimental

Materials. All the compounds **1**—**6** were prepared according to the reported synthetic procedures.[3] Blue violet column crystals of **2**, violet block crystals of **5**, and blue block crystals of **6** were grown slowly from a methanol solution. Pink prismatic crystals of **1**, green polyhedral crystals of **3**, and red violet plates of **4** were obtained by recrystallization from a methanol–chloroform mixed solvent, nitromethane, and acetonitrile, respectively.

Measurement. The far-infrared spectra were recorded as nujol mull on polyethylene film with a Nicolet FT-IR 7199A spectrometer.

Collection and Reduction of X-ray Diffraction Data. The diffraction data were obtained on a Rigaku AFC-5 four-circle diffractometer by the use of graphite-monochromatized Mo $K\alpha$ radiation. The lattice parameters were obtained from the least-squares fit of 40—50 2θ values with $26°<2\theta<30°$. The $\theta-2\theta$ scan mode was used at a scan rate of 3° min^{-1} to record the intensities. The intensities of three standard reflections were monitored for each crystal at 100-

Table 1. Crystallographic parameters

Compound	1	2	3	4	5	6
Formula	$NiCl_2N_4C_{10}H_{24}$	$NiCl_2N_4C_{11}H_{26}$	$NiCl_2N_4C_{12}H_{28}$	$NiS_2N_6C_{12}H_{24}$	$NiS_2N_6C_{13}H_{26}$	$NiS_2N_6C_{14}H_{28}$
Fw	329.93	343.96	357.98	357.19	389.22	403.24
Crystal system	monoclinic	monoclinic	triclinic	triclinic	monoclinic	monoclinic
Space group	$P2_1/n$	$P2_1/a$	$P\bar{1}$	$P\bar{1}$	$P2_1/a$	$P2_1/a$
a/Å	13.607(1)	14.504(1)	10.169(2)	14.172(1)	14.653(3)	14.822(3)
b/Å	8.3685(9)	8.3019(8)	11.530(2)	15.201(1)	14.386(2)	14.522(2)
c/Å	6.6207(8)	6.6771(6)	9.639(1)	8.394(1)	9.151(2)	14.522(3)
α/deg	90	90	65.17(1)	79.80(1)	90	90
β/deg	103.585(8)	100.24(1)	115.57(1)	102.94(1)	105.92(2)	106.00(1)
γ/deg	90	90	120.76(1)	90.17(1)	90	90
V/Å^3	732.8(1)	791.2(1)	846.5(3)	1733.3(3)	1854.9(6)	1909.0(5)
Z	2	2	2	4	4	4
D_x/g cm^{-3}	1.495	1.444	1.404	1.438	1.394	1.403
D_m/g cm^{-3}	1.495	1.448	1.415	1.437	1.391	1.407
μ/mm^{-1}	1.667	1.547	1.450	1.350	1.265	1.231
2θ limits/deg	2—60	2—65	2—60	2—60	2—60	2—60
Unique data[a]	5374	1980	2801	5374	2236	2801
R	0.027	0.059	0.032	0.033	0.055	0.039
R_w	0.036	0.076	0.046	0.038	0.076	0.039

a) ($|F_o|>3\sigma(|F_o|)$)

reflection intervals. The fluctuations of their F_o values were within experimental error. The intensity data were corrected for the Lorentz-polarization effects and for the absorption. The pertinent crystallographic data for the compounds are summarized in Table 1.

Solution and Refinement of the Structures. All the structures were solved and refined by standard Patterson, Fourier, and block-diagonal least-squares techniques. The atomic scattering factors for non-hydrogen atoms were taken from Ref. 6, and those for hydrogen, from Stewart, Davidson, and Simpson.[7] The effect of anomalous dispersion for non-hydrogen atoms was corrected in the structure factor calculations. The weight (w) was taken as $w=[\sigma_c^2+(0.015|F_o|)^2]^{-1}$, where σ_c denotes a standard deviation of F_o as calculated from the counting statistics.

In the cases of Compounds **2** and **5**, each of which has the [15]aneN$_4$ ligand with a six-membered chelate ring and a five-membered chelate ring in the skew and gauche conformations respectively, significant disorder was found in the crystal structure. The disorder occurs in such a way that the gauche five-membered chelate ring and the skew six-membered chelate ring are randomly interchanged in the crystal. The general structural features found for the moiety are depicted in Fig. 1. For the disordered chelate rings, Fourier maps showed relatively sharp peaks for nitrogens, but very broad peaks for carbon atoms. The central carbon (C_b) was generally not found clearly in a Fourier map, and so it was located by a difference synthesis. The carbon atom adjacent to the nitrogen (C_a or C_c) appeared as a broad single peak, but was not observed as two peaks corresponding to the five- and six-membered chelate rings. Therefore, the structures were refined assuming occupancy factors of 1.0 for C_a and C_c, and 0.5 for C_b.

Except for Compounds **2** and **5** which involve disorder, the difference syntheses permitted the location of all the hydrogen atoms, and their positional and isotropic thermal parameters were refined. The final R indices are listed in Table 1, while the positional parameters for non-hydrogen atoms are given in Table 2.[8]

All the calculations were carried out on the HITAC M-200H computer at the Computer Center of the Institute for Molecular Science using the Universal Crystallographic Computation Program System UNICS III.[9]

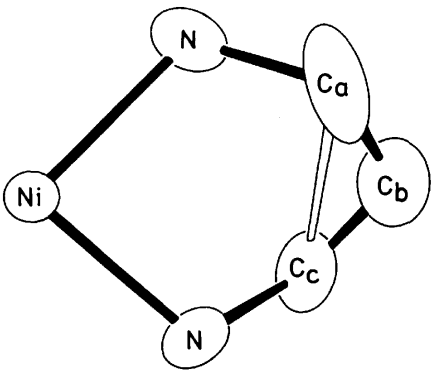

Fig. 1. Disorder of the gauche five-membered and skew six-membered chelate rings in [15]aneN$_4$ complexes.

Description of the Structures

Figure 2 shows the perspective views of Complexes **1**—**6**. As shown in Fig. 2, the geometries about Ni in all the compounds are of the *trans*-NiX_2N_4 type. The coordination bond distances and angles are given in Table 3. Table 4 lists the deviations of the atoms in a first coordination sphere from a NiN_4 best plane formed with Ni and the in-plane four nitrogens for Complexes **3**, **5**, and **6**. The data for **1**, **2**, and **4** are not given, since in these compounds the Ni atom lies at a center of symmetry.

trans-[NiCl$_2$([14]aneN$_4$)] (1). The total stereochemistry is the same as that reported previously.[5] The accuracy of the bond lengths and angles is raised approximately one order of magnitude, as evidenced by

their esd values. The alternating two six- and two five-membered chelate rings are in the stable chair and gauche conformations, respectively.

trans-*[NiCl₂([15]aneN₄)]* (**2**). The structure of this compound was solved under the crystallographic requirement that the Ni atom lies at a center of symmetry, even though the entire molecule cannot have such a symmetry element. This is because of the structural disorder described in the previous section. As is shown in Fig. 2(b), the three six-membered and one five-membered chelate rings are in a chair–skew–chair–gauche conformational sequence.

Table 2. Atomic coordinates and their standard deviations

Atom	x	y	z
$[NiCl_2([14]aneN_4)]$ (1)[a]			
Ni	0	0	0
Cl	7629(3)	16244(5)	31674(6)
N(1)	13211(10)	-13193(17)	6691(21)
N(2)	7095(10)	13642(16)	-18392(19)
C(1)	18934(14)	-8404(24)	-8794(29)
C(2)	17896(13)	9445(24)	-12353(27)
C(3)	5227(14)	31122(21)	-18496(27)
C(4)	-6021(15)	35000(22)	-24576(30)
C(5)	-12048(14)	30698(21)	-8507(28)
$[NiCl_2([15]aneN_4)]$ (2)[b]			
Ni	0	0	0
Cl	797(1)	1500(1)	-2413(1)
N(1)	-706(2)	-1350(4)	-2478(4)
N(2)	-1165(3)	1599(5)	-512(5)
C(1)	-1724(4)	-1030(8)	-2813(6)
C(2)	-1800(4)	1092(10)	-2823(8)
C(3)	-1079(5)	3212(8)	-60(8)
C(4)	-579(5)	3401(7)	2086(9)
C(5)	478(5)	3076(6)	2392(7)
C(6)	2144(9)	-116(16)	3526(16)
$[NiCl_2([16]aneN_4)]$ (3)[a]			
Ni	13077(4)	25507(3)	18912(7)
Cl(1)	2724(8)	-902(6)	28217(9)
Cl(2)	26146(8)	50780(6)	10687(11)
N(1)	14128(27)	26683(23)	40998(13)
N(2)	35887(24)	23578(22)	28833(15)
N(3)	9671(30)	24151(23)	-3981(17)
N(4)	-11650(25)	23875(22)	10233(19)
C(1)	30206(39)	32448(39)	51664(21)
C(2)	39953(41)	24328(44)	55832(23)
C(3)	47440(36)	28527(41)	43002(25)
C(4)	45024(38)	27838(40)	17768(27)
C(5)	35394(45)	22569(42)	2900(29)
C(6)	24183(47)	29401(38)	-8690(31)
C(7)	-792(50)	31203(36)	-16593(33)
C(8)	-18183(48)	22739(39)	-17352(35)
C(9)	-21717(38)	15496(35)	-1367(37)
C(10)	-18658(35)	17629(33)	23760(39)
C(11)	-12313(41)	27088(35)	34032(41)
C(12)	5604(41)	35037(32)	38202(43)
$[Ni(NCS)_2([14]aneN_4)]$ (4)[a]			
Ni(1)	0	0	0
S(1)	20054(6)	19516(6)	-30031(9)
N(11)	11599(16)	249(15)	19868(11)
N(12)	7960(16)	-10087(13)	-5057(13)
N(13)	6881(16)	9782(14)	-14560(15)
C(11)	17393(22)	-8047(22)	21568(17)
C(12)	17867(21)	-9580(19)	4660(19)
C(13)	7225(25)	-10392(22)	-22785(21)
C(14)	-3137(27)	-10476(23)	-32436(23)
C(15)	-9162(25)	-1946(24)	-35262(25)
C(16)	12341(18)	13854(15)	-20901(27)
Ni(2)	0	50000	0
S(2)	19578(6)	67676(5)	-33479(31)
N(21)	-8647(15)	61578(13)	-7459(33)
N(22)	6671(15)	55724(13)	20144(35)
N(23)	10354(16)	55869(15)	-13113(37)
C(21)	-3772(21)	68034(17)	2621(39)
C(22)	95(22)	63235(18)	20254(41)
C(23)	9585(21)	49521(18)	36173(43)
C(24)	16169(21)	41953(20)	35244(45)
C(25)	11471(20)	34948(18)	25421(47)
C(26)	14204(17)	60810(16)	-21442(49)
Ni(3)	50000	0	0
S(3)	29223(5)	16029(5)	23623(53)
N(31)	55613(14)	12721(13)	-1864(55)
N(32)	41450(14)	4712(13)	-23555(57)
N(33)	38945(15)	4244(14)	10366(59)
C(31)	51279(20)	-18320(16)	15966(61)
C(32)	45857(21)	13050(17)	-29852(63)
C(33)	39815(20)	-1825(18)	-35026(65)
C(34)	35461(20)	-10326(18)	-27792(67)
C(35)	42003(20)	-16602(16)	-13445(69)
C(36)	34837(17)	9118(15)	15737(71)
Ni(4)	50000	50000	0
S(4)	71684(5)	32421(5)	-21026(75)
N(41)	42765(14)	39038(13)	9345(77)
N(42)	38727(14)	51301(13)	-20945(79)
N(43)	58169(15)	41442(13)	-9647(81)
C(41)	32924(19)	39822(17)	-1577(83)
C(42)	33592(19)	42890(17)	-19562(85)
C(43)	41418(21)	54018(18)	-37076(87)
C(44)	46790(22)	62677(19)	-37881(89)
C(45)	57068(21)	62138(18)	-27215(91)
C(46)	63902(17)	37741(14)	-14113(93)
$[Ni(NCS)_2([15]aneN_4)]$ (5)[b]			
Ni	2387(1)	763(1)	2414(1)
S(1)	1260(2)	-1380(2)	-1547(2)
S(2)	4058(2)	2734(2)	6489(2)
N(1)	1192(4)	1499(4)	2635(6)
N(2)	2409(5)	-172(4)	4203(6)
N(3)	3576(5)	76(5)	1910(10)
N(4)	2338(5)	1642(4)	511(7)
N(5)	1521(5)	-204(4)	952(7)
N(6)	3293(4)	1655(4)	3885(7)
C(1)	1100(6)	1582(6)	4216(10)
C(2)	1123(7)	635(8)	4973(11)
C(3)	2091(7)	172(7)	5479(9)
C(4)	3340(8)	-636(7)	4843(11)
C(5)	3705(9)	-1031(8)	3594(15)
C(6)	4166(11)	-400(10)	2896(15)
C(7)	3965(8)	618(12)	817(14)
C(8)	3609(14)	987(11)	-319(20)
C(9)	2694(9)	1262(8)	-732(10)
C(10)	1335(8)	1974(9)	-214(14)
C(11)	925(14)	2531(12)	493(21)
C(12)	1181(7)	2456(6)	1997(11)
C(13)	1408(4)	-701(5)	-71(8)
C(14)	3607(5)	2106(5)	4948(8)
$[Ni(NCS)_2([16]aneN_4)]$ (6)[a]			
Ni	23499(3)	7171(3)	22249(7)
S(1)	12844(7)	-15384(7)	-14539(9)
S(2)	40274(8)	26506(7)	62474(11)
N(1)	35235(19)	513(19)	16597(13)
N(2)	23532(20)	-2442(20)	40182(15)
N(3)	12003(18)	15062(19)	25784(17)
N(4)	22061(18)	15497(18)	1502(19)
N(5)	14515(20)	-2497(20)	8504(21)
N(6)	32624(19)	15730(19)	36962(23
C(1)	41773(27)	-4823(28)	28802(25)
C(2)	36748(32)	-11814(30)	35710(27)
C(3)	32161(31)	-7785(31)	46972(29)
C(4)	19904(29)	761(28)	52728(31)
C(5)	10556(28)	5621(31)	47529(33)
C(6)	11001(25)	15206(28)	41293(35)
C(7)	12217(26)	24721(25)	20548(37)
C(8)	8968(28)	25745(28)	3523(39)
C(9)	12084(25)	18127(26)	-5116(41)
C(10)	25439(26)	10788(26)	-10204(43)
C(11)	35950(28)	9459(29)	-6124(45)
C(12)	40535(23)	7309(26)	10199(47)
C(13)	13665(21)	-7977(23)	-885(49)
C(14)	35837(21)	20231(22)	47489(51)

(continued)

a) Parameters are multiplied by 10^5. b) Parameters are multiplied by 10^4.

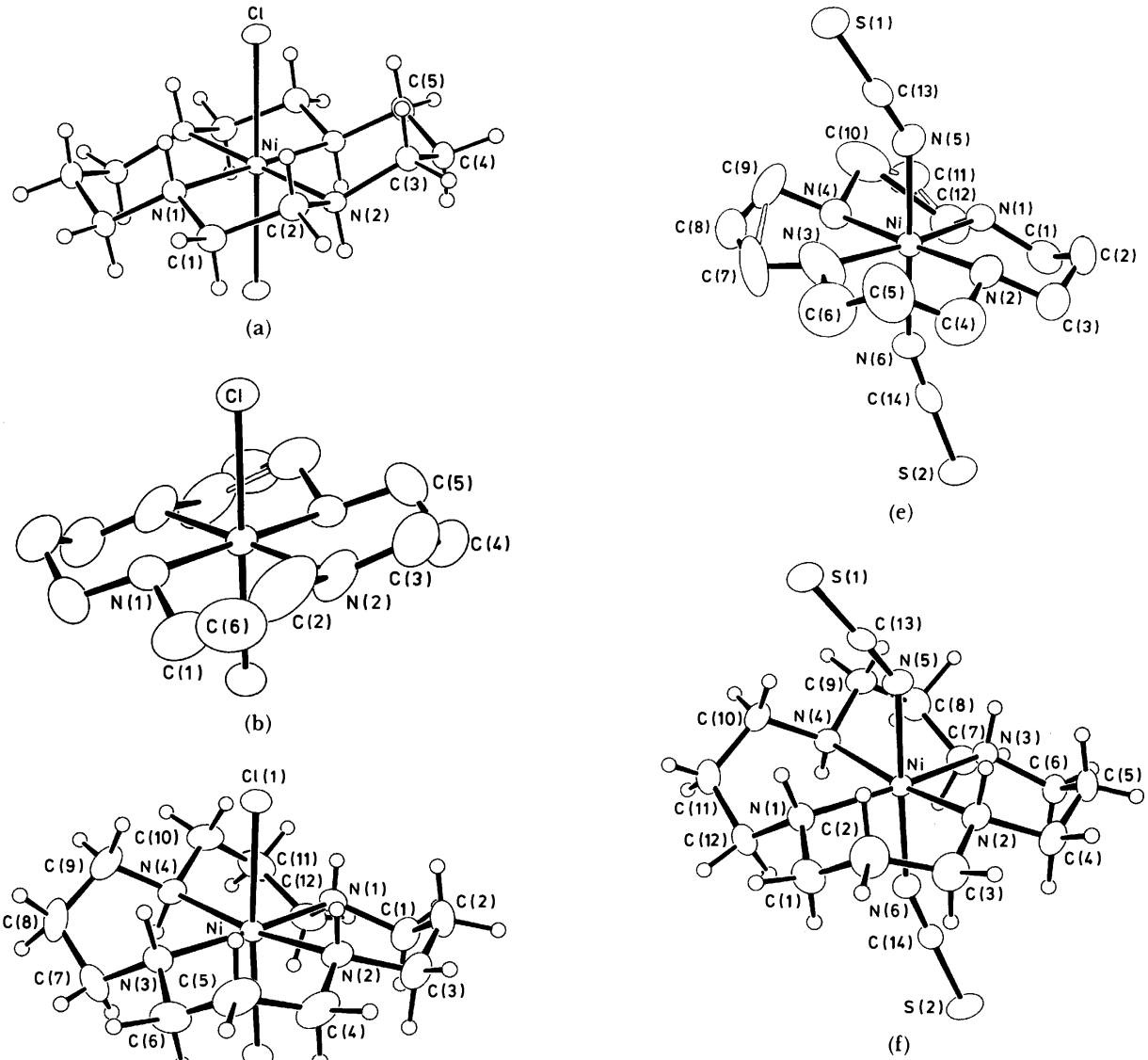

Fig. 2. Perspective views of the structures: (a) $[NiCl_2([14]aneN_4)]$(**1**); (b) $[NiCl_2([15]aneN_4)]$ (**2**); (c) $[NiCl_2([16]aneN_4)]$ (**3**); (d) $[Ni(NCS)_2([14]aneN_4)]$ (**4**); (e) $[Ni(NCS)_2([15]aneN_4)]$ (**5**); (f) $[Ni(NCS)_2$-$([16]aneN_4)]$ (**6**). In (b) and (e), which involve disorder, one linkage of the macrocyclic skeleton is shown with solid bonds, and the alternative with open bonds. The drawing (d) corresponds to the complex (b) in Fig. 4.

trans-[NiCl₂([16]aneN₄)] (3). The entire molecule constitutes a crystallographically asymmetric unit and thus has no rigorous symmetry. However, as Fig. 3 shows, there is an approximate symmetry plane, which lies perpendicular to the coordination plane of the [16]aneN$_4$ ligand, passing through Ni, N(2), and N(4) atoms. The four six-membered chelate rings adopt a chair-chair-skew-skew conformational sequence. The coordination bond lengths and angles show that the coordination geometry deviates appreciably from D_{4h} symmetry (Table 3). The Ni–N(4) distance [2.211(3) Å] is by far the longest among the Ni–N bonds, and the two Ni–Cl distances differ by 0.107 Å.

trans-[Ni(NCS)$_2$([14]aneN$_4$)] (4) There are four crystallographically independent [Ni(NCS)$_2$([14]-aneN$_4$)] complexes, in each of which Ni resides at a center of symmetry. The total stereochemistries of the [14]aneN$_4$ ligands in these complexes are essentially the same and are very similar to that found for **1**. The coordination bond lengths are slightly different in the four complexes. The in-plane Ni–N distances range from 2.064(2) to 2.082(2) Å, while the corresponding axial Ni–N (NCS) distances vary from 2.130 (2) to 2.075(6) Å. Though the ranges of the in-plane or axial bond lengths are very limited, a negative correlation is noted between them (*vide infra*).

Of particular interest is the wide variety of orientation modes of the NCS$^-$ groups (Fig. 4). The tilts of the Ni–N (NCS) bonds from the normal to the NiN$_4$ best planes range from 1.3° to 1.9°. The Ni–N–C and N–C–S angles within the NCS$^-$ groups range from 156.2(2) to

TABLE 3. BOND LENGTHS (l/Å) AND ANGLES (ϕ/°)

[NiCl$_2$([14]aneN$_4$)] (1)

Ni	-Cl	2.5101(4)	Cl	-Ni	-N(1)	86.68(4)
Ni	-N(1)	2.067(1)	Cl	-Ni	-N(2)	91.97(4)
Ni	-N(2)	2.066(1)	N(1)	-Ni	-N(2)	85.3(1)

[NiCl([15]aneN$_4$)] (2)

Ni	-Cl	2.497(1)	Cl	-Ni	-N(1)	88.5(1)
Ni	-N(1)	2.104(3)	Cl	-Ni	-N(2)	91.8(1)
Ni	-N(2)	2.124(4)	N(1)	-Ni	-N(2)	87.2(1)

[NiCl([16]aneN$_4$)] (3)

Ni	-Cl(1)	2.535(1)	Cl(1)	-Ni	-N(4)	89.5(1)
Ni	-Cl(2)	2.428(1)	Cl(2)	-Ni	-N(1)	0.3(1)
Ni	-N(1)	2.143(2)	Cl(2)	-Ni	-N(2)	91.5(1)
Ni	-N(2)	2.186(3)	Cl(2)	-Ni	-N(3)	90.5(1)
Ni	-N(3)	2.142(2)	Cl(2)	-Ni	-N(4)	97.4(1)
Ni	-N(4)	2.211(3)	N(1)	-Ni	-N(2)	92.6(1)
Cl(1)	-Ni -Cl(2)	172.93(4)	N(1)	-Ni	-N(3)	174.4(1)
Cl(1)	-Ni -N(1)	91.3(1)	N(1)	-Ni	-N(4)	87.1(1)
Cl(1)	-Ni -N(2)	81.5(1)	N(2)	-Ni	-N(3)	92.9(1)
Cl(1)	-Ni -N(3)	88.6(1)	N(2)	-Ni	-N(4)	171.1(1)
			N(3)	-Ni	-N(4)	87.3(1)

[NI(NCS)$_2$([14]aneN$_4$)] (4)

Ni(1)	-N(11)	2.069(2)	N(11)	-Ni(1)	-N(12)	85.0(1)
Ni(1)	-N(12)	2.064(2)	N(11)	-Ni(1)	-N(13)	88.3(1)
Ni(1)	-N(13)	2.130(2)	N(12)	-Ni(1)	-N(13)	90.5(1)
Ni(2)	-N(21)	2.066(2)	N(21)	-Ni(2)	-N(22)	85.5(1)
Ni(2)	-N(22)	2.076(3)	N(21)	-Ni(2)	-N(23)	91.1(1)
Ni(2)	-N(23)	2.128(3)	N(22)	-Ni(2)	-N(23)	89.1(1)
Ni(3)	-N(31)	2.082(2)	N(31)	-Ni(3)	-N(32)	85.4(1)
Ni(3)	-N(32)	2.079(5)	N(31)	-Ni(3)	-N(33)	90.7(1)
Ni(3)	-N(33)	2.108(5)	N(32)	-Ni(3)	-N(33)	89.1(1)
Ni(4)	-N(41)	2.081(4)	N(41)	-Ni(4)	-N(42)	85.4(2)
Ni(4)	-N(42)	2.075(6)	N(41)	-Ni(4)	-N(43)	89.8(2)
Ni(4)	-N(43)	2.119(6)	N(42)	-Ni(4)	-N(43)	91.9(3)

[NI(NCS)$_2$([15]aneN$_4$)] (5)

Ni	-N(1)	2.102(6)	N(1)	-Ni	-N(6)	91.6(2)
Ni	-N(2)	2.122(6)	N(2)	-Ni	-N(3)	91.8(3)
Ni	-N(3)	2.161(9)	N(2)	-Ni	-N(4)	176.6(2)
Ni	-N(4)	2.137(6)	N(2)	-Ni	-N(5)	87.1(2)
Ni	-N(5)	2.099(6)	N(2)	-Ni	-N(6)	91.2(2)
Ni	-N(6)	2.059(5)	N(3)	-Ni	-N(4)	86.9(3)
N(1)	-Ni -N(2)	94.7(3)	N(3)	-Ni	-N(5)	86.7(3)
N(1)	-Ni -N(3)	173.0(3)	N(3)	-Ni	-N(6)	90.7(3)
N(1)	-Ni -N(4)	86.4(3)	N(4)	-Ni	-N(5)	89.6(2)
N(1)	-Ni -N(5)	91.2(2)	N(4)	-Ni	-N(6)	92.0(2)
			N(5)	-Ni	-N(6)	176.8(2)

[Ni(NCS)$_2$([16]aneN$_4$)] (6)

Ni	-N(1)	2.175(3)	N(1)	-Ni	-N(6)	90.2(1)
Ni	-N(2)	2.164(2)	N(2)	-Ni	-N(3)	93.6(1)
Ni	-N(3)	2.152(3)	N(2)	-Ni	-N(4)	171.2(1)
Ni	-N(4)	2.224(2)	N(2)	-Ni	-N(5)	84.1(1)
Ni	-N(5)	2.103(3)	N(2)	-Ni	-N(6)	91.3(1)
Ni	-N(6)	2.051(2)	N(3)	-Ni	-N(4)	87.1(1)
N(1)	-Ni -N(2)	93.6(1)	N(3)	-Ni	-N(5)	92.9(1)
N(1)	-Ni -N(3)	172.8(1)	N(3)	-Ni	-N(6)	89.0(1)
N(1)	-Ni -N(4)	85.9(1)	N(4)	-Ni	-N(6)	87.1(1)
N(1)	-Ni -N(5)	88.5(1)	N(4)	-Ni	-N(6)	97.4(1)
			N(5)	-Ni	-N(6)	175.2(1)

168.2(2)° and from 177.8(5) to 179.2(2)°, respectively. All the NCS^- groups are involved in intermolecular hydrogen-bonds between the sulfur atoms and the secondary amine groups of the neighboring complexes,[10] forming a linear chain along the a-axis. The orientations of the NCS^- groups are mainly determined by these hydrogen-bonds.

trans-[Ni(NCS)$_2$([15]aneN$_4$)] (5) In this compound, the three six-membered rings and one five-membered ring are in a chair–chair–skew-gauche conformational sequence. Although the total stereochemistry of the [15]aneN$_4$ ligand differs from that in **2**, a similar structural disorder was observed for the gauche five-membered and the skew six-membered chelate rings (Fig. 2(e)). The combination of the chiral configurations of the four nitrogen donors are the same

Table 4. Deviations (d/Å) of nickel and donor atoms from a NiN_4 plane defined by nickel and four in-plane nitrogens for complexes **3**, **5**, and **6**

3		**5**		**6**	
Ni	0.072	Ni	0.040	Ni	0.058
N(1)	0.063	N(1)	0.002	N(1)	0.081
N(2)	−0.096	N(2)	−0.020	N(2)	−0.106
N(3)	0.063	N(3)	−0.001	N(3)	0.081
N(4)	−0.101	N(4)	−0.019	N(4)	−0.113
Cl(1)	−2.456	N(5)	−2.057	N(5)	−2.043
Cl(2)	2.497	N(6)	2.099	N(6)	2.105

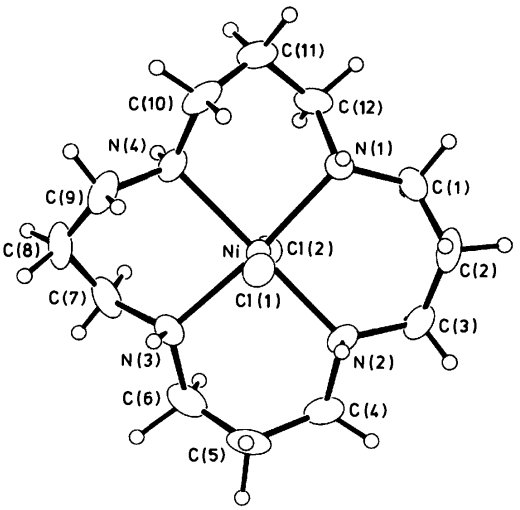

Fig. 3. Structure of [NiCl$_2$([16]aneN$_4$)] (**3**) as viewed along the normal to the NiN$_4$ plane.

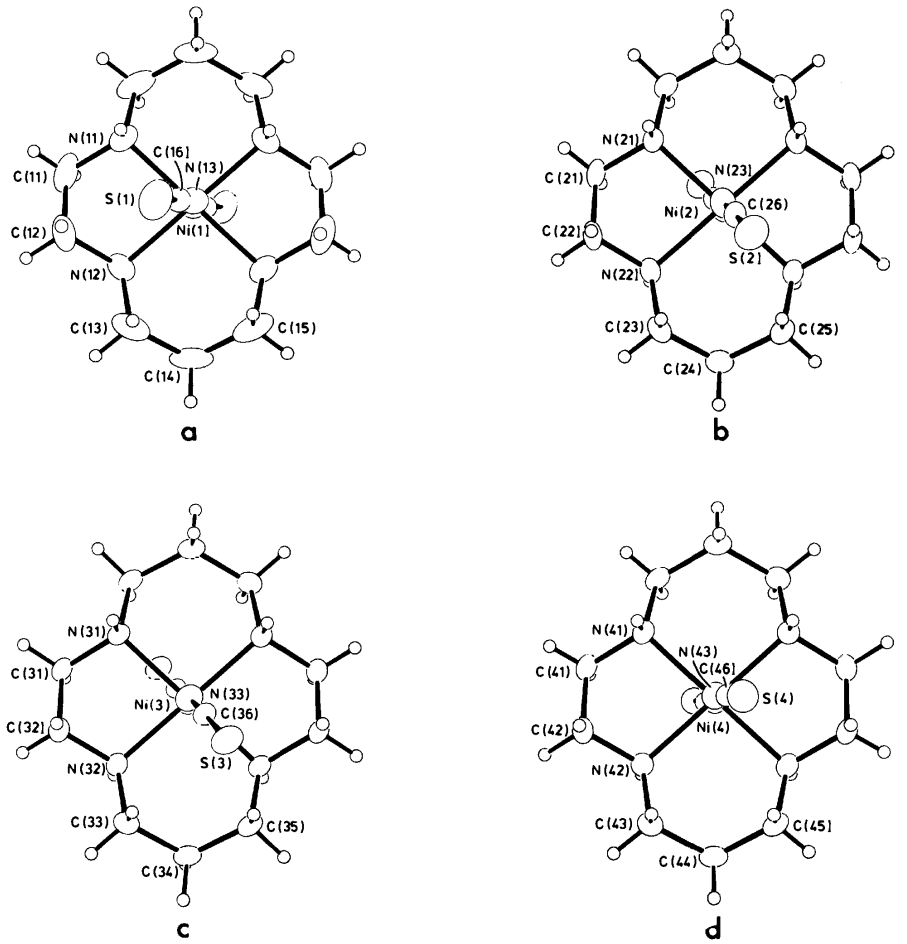

Fig. 4. Dispositions of NCS^- ligands in four crystallographically independent [Ni(NCS)$_2$([14]aneN$_4$)] complexes (**4**).

as those in **3**. The structural distortions characteristic of the nitrogen configurations will be discussed later.

trans-*[Ni(NCS)$_2$([16]aneN$_4$)] (**6**)* Four six-membered chelate rings adopt chair–chair–skew–skew conformations, as in the *trans*-dichloro analogue **3**. The nitrogen configurations are the same as those in **3** and **5**. The distortions arising from the nitrogen configuration will be discussed in a subsequent section. The orientation of the NCS^- ligands is, again, caused by intermolecular hydrogen-bonds between the sulfur atoms and the amine nitrogens of the neighboring complexes.[10]

Discussion

Stereochemistries of Coordinated Macrocyclic Ligands. It has been known that the cyclic nature of the tetraazacycloalkane ligand gives rise to isomerism as a result of the difference in the combination of the chiralities of the four coordinated secondary amine nitrogens.[11] In all the present complexes having the [14]aneN$_4$ ligand, the macrocyclic ligands adopt the same nitrogen configurations, and thereby have the same overall skeletal structure. Alternating two six- and two five-membered chelate rings are in the chair and gauche conformations, respectively. This ring conformation has been known to be the most strain free among the five possible isomers when the [14]aneN$_4$ ligand is coordinated in a planar fashion.[11] The same stereochemistry of the [14]aneN$_4$ ligand has been found in the crystal structures of [Ni([14]aneN$_4$)](PF$_6$)$_2$,[12a] [Ni([14]aneN$_4$)I]I,[12b] [NiCl$_2$([14]aneN$_4$)](ClO$_4$),[13] [Pd([14]aneN$_4$)](ClO$_4$)$_2$,[14] [PdCl$_2$([14]aneN$_4$)](NO$_3$)$_2$,[14] [Pd([14]aneN$_4$)][PdCl$_2$([14]aneN$_4$)](ClO$_4$)$_4$,[14] [Zn(O$_2$CCH$_3$)([14]aneN$_4$)](ClO$_4$),[15] and [Ag([14]aneN$_4$)](ClO$_4$)$_2$ (P$\bar{1}$-form)[16].

Busch and his associates separated two configurational isomers each for *trans*-[CoCl$_2$([15]aneN$_4$)]$^+$ and *trans*-[CoCl$_2$([16]aneN$_4$)]$^+$ and discussed the stereochemical stabilities of the isomers and other possible configurational isomers on the basis of strain energy calculations, the ^{13}C NMR spectra, and the chemical properties.[4] The overall stereochemistry of the macrocyclic skeleton found for **5** is the same as that reported for the most stable brown isomer of [CoCl$_2$([15]aneN$_4$)]$^+$ (Isomer I in their notation). However, the overall structure of **2** is the type of neither the Isomer I nor the Isomer II of [CoCl$_2$([15]aneN$_4$)]$^+$. The latter was found to be a skew-skew-skew-gauche form.[4,17] The calculations of strain-energy minimization for *trans*-[CoCl$_2$([15]aneN$_4$)]$^+$ show that the conformational structure of **2** is the second least strained among six possible configurational isomers.[4] We did not obtain in the synthetic and X-ray studies any indication of the presence of isomers for the trans-dichloro Ni(II) complex of [15]aneN$_4$. The skeletal structures of [16]aneN$_4$ found in **3** and **6** are the same as that reported for the green isomer of [CoCl$_2$([16]aneN$_4$)]$^+$ (Isomer II).[4]

It is known that the cyclic nature of tetraaza macrocyclic ligands in a planar coordination introduces strain in the metal-donor atom distance, the chelate (bite) angle subtended at the central metal atom, and so on.[11] Such strain is generally relieved by relaxing the coplanarity of the metal-donor atom set. Except for **1**, **2**, and **4**, in which Ni atoms reside at the inversion center, all the structures show a distortion of the NiN$_4$ set toward the tetrahedral character (Table 4).

The combinations of the nitrogen configurations in complexes **3**, **5**, and **6** are all of the same type : three NH protons are above, and the remaining one below, the NiN$_4$ plane. The former ones are bound to three nitrogens, N(1), N(2), and N(3), which are involved in two adjacent six-membered chelate rings in the chair form, while the latter is bound to N(4), which links two skew rings or a skew and a gauche ring. The following structural distortions are commonly noted in these compounds and are likely to be characteristic of the skeletal structure arising from the configuration : inequality in the in-plane Ni–N distances, inequality in the two axial bond lengths, distortion of the in-plane donor atom set of a tetrahedral character, and a fairly large deviation of the Ni atom from the mean NiN$_4$ plane. Among the complexes, the distortion of the in-plane donor atom set toward the tetrahedral character becomes larger in this order: **6**>**3**>**5**. This is ascribed to the suitability of size between the hole of the macrocycle and the high-spin octahedral Ni^{2+}: (i) the 16-membered macrocycle is less fit for Ni^{2+} than the 15-membered one, and (ii) the cavity size of the [16]aneN$_4$ ligand in **6** enlarges as compared with that of **3**, because of the cis effect (see below).

When the cavity size is larger than the natural or the best fit size for Ni^{2+}, the deviations of carbon atoms adjacent to donor nitrogens from the mean plane of the chelate ring generally become larger. As a result, in Complexes **3** and **6**, which have [16]aneN$_4$, C(9) and C(10) atoms are disposed so close to one of the axial coordination sites as to exert a steric effect, and the resulting steric hindrance causes the lengthening of the axial bond [Ni–Cl(1) in **3** and Ni–N(5) in **6**].

Correlation between Axial and In-plane Coordination Bond Lengths. As expected, the in-plane Ni–N distance increases with an increase in the number of ring members of the macrocyclic ligand. This increase in the Ni–N distance amounts to 0.05—0.06 Å for each ring member added. The increase is not, however, as large as expected from calculations of the strain energy minimization for free ligand molecules (0.10—0.15 Å).[18] The observed correlations between the average Ni–N and Ni–X distances are shown in Fig. 5. The data reported previously for the same types of complexes with similar tetraazamacrocyclic or diamine ligands are also included: *trans*-[NiCl$_2$(N$_4$7)],[20] *trans*-[NiCl$_2$(N$_4$9)],[20] *trans*-[Ni(NCS)$_2$(NH$_3$)$_4$],[21] and *trans*-[Ni(NCS)$_2$(en)$_2$].[22] As is seen in Fig. 5, there exists a negative correlation for each series of complexes with given axial ligands: the axial coordination bond length decreases as the in-plane distance increases. Similar observations have also been reported for some other systems.[23–25] The results in Fig. 5 were obtained assuming that each metal-donor atom set (*trans*-NiX$_2$N$_4$) has D$_{4h}$ symmetry. Although some Ni–X and Ni–N distances in Fig. 5 show quite a large standard deviation because of distortion from the D$_{4h}$ symmetry, there is no doubt that the negative

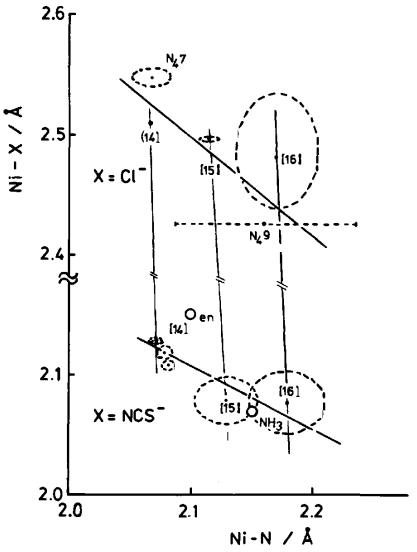

Fig. 5. Correlation between axial and in-plane coordination bond lengths in Ni(II) complexes of the *trans*-NiX_2N_4 type. Size of a dashed ellipse or line illustrate an esd obtained upon averaging chemically or crystallographically nonequivalent distances,[19] while that of a full-line figure within the dashed one shows an arithmetic mean of esd's for individual metal-ligand distances. Ligand abbreviations: [14]=[14]aneN$_4$, [15]=[15]aneN$_4$, [16]=[16]aneN$_4$, en=ethylenediamine, and N$_4$7 and N$_4$9 see Ref. 20. For NH_3 and en complexes, no esd values were reported.

interrelationship holds. The data points for Complexes **3** and **6** deviate from the smoothed lines in Fig. 5. In these complexes, there exists an obvious steric effect that causes a lengthening of the M-X bond, as described previously. Unless the steric constraint were present, the mean M-X bond distances in these complexes would be somewhat shorter and the data points would approach the smoothed lines.

It is interesting to note that the data for the four crystallographically inequivalent molecules of *trans*-[Ni(NCS)$_2$([14]aneN$_4$)] show a clear trend for the negative correlation within a very limited range of metal-ligand distances (see Fig. 5).

When the $NiCl_2N_4$ and $Ni(NCS)_2N_4$ systems are compared, the slope for the chloro complexes is steeper than that for the isothiocyanato complexes. This indicates that the weaker the axial ligand field is, the stronger the correlation. The effect of the ligand field strength of the axial ligand upon the correlation has been explained theoretically on the basis of the features of the potential energy surface.[1]

From the data given in Fig. 5, it is possible to see changes in the M-N distances of complexes with the same in-plane ligand upon alterations in the axial ligand. Although the number of data for such comparisons are very limited and the changes in the M-N distances are very small, the thin lines in Fig. 5 likely show the presence of a negative dependence of the in-plane Ni-N lengths on the axial Ni-X bond distances.

Coordination geometries found for Ni(II) complexes with 1,4,7,10-tetraazacyclotetradecane (N$_4$7) may provide further evidence for the occurrence of such an electronic interaction between the axial and in-plane ligands. Interestingly, the structural analyses reveal that coordination geometries of $[NiCl_2(N_47)]$[25] and $[Ni(NCS)_2(N_47)]$[26] are of the trans-type and of the cis-type with the macrocycle folded, respectively. It is most reasonable to consider the observed cis and trans stereochemistries to be a result of the electronically controlled cis effect. If strong axial ligands such as NCS^- are to coordinate at the axial positions, the Ni-N (in-plane) distance must be elongated. However, it is impossible with this macrocycle, since the hole size of this particular macrocycle is equal to or slightly smaller than necessary to accommodate a high-spin octahedral Ni^{2+}.[27]

Busch and his coworkers observed a very similar phenomenon in a ligand field electronic spectral study of a series of the same type of Ni(II) complexes.[3] They found that the ligand field strength of an axial ligand (Dq^z) decreases as the in-plane ligand field strength (Dq^{xy}) increases, and they termed this the "*electronic cis effect*". The correlation found in the electronic spectral study and that observed in the present study seem to have the same electronic origin.

We have previously discussed the electronic origin that brings about the correlations in Fig. 5 from the standpoint of the potential energy surface.[1] A section of the potential surface along the in-plane and axial coordination bond axes is an ellipse which has a tilt with respect to the coordination bond axes. When the ligand field strength of the axial ligand is weaker than the in-plane ligand field, the ellipse is elongated in the Ni-X direction. Such features of the potential surface are primarily responsible for the observed correlation of the coordination bond lengths.[1] It has also been shown that the slope of the line showing the interrelationship in Fig. 5 discloses the degree of softness[28] of a Ni(II) ion semiquantitatively.[1]

Figure 6 shows plots of the Ni-Cl stretching frequencies [ν(Ni-Cl)] *vs.* the Ni-Cl and Ni-N bond distances. Band assignments to the Ni-Cl stretching vibrations were made by a comparison of the spectra of *trans*-dichloro, *trans*-dibromo, and *trans*-bis(isothiocyanato) complexes with a series of macrocyclic ligands. It was impossible from only such simple comparisons to assign bands due to Ni-N stretching vibrations. As a result, we failed to figure a plot of ν(Ni-Cl) *vs.* ν(Ni-N), but the following discussion is possible on the basis of the IR data in Fig. 6. Under rigorous D_{4h} symmetry, a single band due to the antisymmetric Ni-Cl stretching vibration (ν_a) is expected to appear. When the complex has lower symmetry, two bands due to antisymmetric and symmetric vibrations (ν_a and ν_s) will appear. Single bands were observed at 198 cm^{-1} for **1**, at 223 cm^{-1} (very broad) for **2**, at 225 cm^{-1} for $[NiCl_2(N_49)]$, and at 187 cm^{-1} for $[NiCl_2(N_47)]$. On the other hand, Compound **3** showed two clearly separated sharp bands at 216 (ν_a) and 178 cm^{-1} (ν_s). This result corresponds to the relatively large difference in the two Ni-Cl distances in **3**. As shown in Fig. 6(a), the antisymmetric band ν_a(Ni-Cl) shifts to higher frequencies as the Ni-Cl distance decreases. When the ν_a(Ni-Cl) band posi-

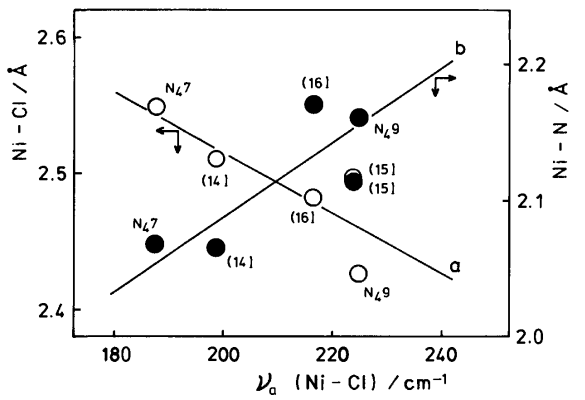

Fig. 6. Plots of antisymmetric Ni–Cl stretching frequencies (ν_a(Ni–Cl))/cm^{-1}) *vs.* mean Ni–Cl distances (a) and *vs.* average Ni–N distances (b). See the caption of Fig. 5 for the ligand abbreviations.

tions are plotted against the Ni–N distance, a reversed relationship is obtained (Fig. 6(b)). This result suggests, though indirectly, that the electronic cis effect is manifested in the far infrared spectra due to coordination bond stretching vibrations.

Structural Disorder Characteristic of [15]aneN$_4$ Complexes. We have thus far determined five structures of metal complexes containing the [15]aneN$_4$ ligand : the present two complexes, **2** and **5**, *trans*-[CoCl$_2$([15]aneN$_4$)](ClO$_4$) (green form),[17] [Zn(NCS)$_2$([15]aneN$_4$)],[2] and [{Zn([15]aneN$_4$)}$_3$(O$_2$COCH$_3$)$_2$](ClO$_4$)$_4$.[29] All the compounds have a gauche five-membered and a skew six-membered chelate ring in a pair. We found the same type of disorder common to all these structures. The general features are shown in Fig. 1. Because of this disorder, the bond distances of C$_a$–C$_b$ and C$_b$–C$_c$ appear somewhat shorter, whereas the C$_a$–C$_c$ distance is longer, than the normal value. It is worth noting that, in spite of the presence of the significant disorder, the positional parameters of the nitrogens involved in the disordered chelate rings were refined to have reasonably small esd values. This indicates that the nitrogens for the five- and six-membered rings are at nearly the same position in the crystal structure; therefore, the bite angles of the gauche five- and skew six-membered chelate rings must be very similar. In fact, the bite angles found for the skew six-membered rings which are not involved in the disorder (87.3(1)° and 87.1(1)° for **3**, and 87.1(1)° and 85.9(1)° for **6**) are close to the normal value of the gauche chelate rings (~86°).[11] Concomitantly, the bite angles found for the disordered ring average 87.2(1)° for **2** and 86.7(3)° for **5**. The disorder in the crystals of the [15]aneN$_4$ complexes is considered to arise mainly from such a situation.

References

1) T. Ito, M. Kato, and H. Ito, *Bull. Chem. Soc. Jpn.*, **57**, 1556 (1984).
2) T. Ito, M. Kato, and H. Ito, *Bull. Chem. Soc. Jpn.*, **57**, 2634 (1984).
3) L. Y. Martin, C. R. Sperati, and D. H. Busch, *J. Am. Chem. Soc.*, **99**, 2968 (1977).
4) Y. Hung, L. Y. Martin, S. C. Jackels, A. M. Tait, and D. H. Busch, *J. Am. Chem. Soc.*, **99**, 4029 (1977).
5) B. Bosnich, R. Mason, P. T. Pauling, G. B. Robertson, and M. L. Tobe, *J. Chem. Soc., Chem. Commun.*, **1965**, 97.
6) "International Tables for X-ray Crystallography," Kynoch Press, Birminghum, England (1974), Vol. IV.
7) R. F. Stewart, E. R. Davidson, and W. T. Simpson, *J. Chem. Phys.*, **42**, 3175 (1965).
8) Tables of the anisotropic thermal parameters, hydrogen positional parameters, and lists of the observed and calculated structure factors are kept in the office of the Chemical Society of Japan (Document No. 8432).
9) T. Sakurai and K. Kobayashi, *Rikagaku Kenkyusho Hokoku*, **55**, 69 (1979).
10) The hydrogen-bond parameters are as follows:

[Ni(NCS)$_2$([14]aneN$_4$)] (**4**)		[Ni(NCS)$_2$([16]aneN$_4$)] (**6**)	
S(1)···N(32)^{i}	3.664(2) Å	S(1)···N(3)^{i}	3.541(3) Å
S(2)···N(42)^{i}	3.536(2)	S(1)···N(4)^{ii}	3.561(3)
S(3)···N(11)^{i}	3.460(2)	S(2)···N(2)^{iii}	3.649(3)
S(4)···N(22)^{ii}	3.546(2)		

Key to symmetry operations:

(i)	x	y	z	(i)	$-x$	$-y$	$-z$
(ii)	$1-x$	$1-y$	$-z$	(ii)	$0.5-x$	$-0.5-y$	$-z$
				(iii)	$0.5-x$	$0.5+y$	$1-z$

11) N. F. Curtis, "Coordination Chemistry of Macrocyclic Compounds," ed by G. A. Melson, Plenum, New York (1979), Chap. 4.
12) a) H. Ito and T. Ito, unpublished study; b) L. Prasad and A. McAuley, *Acta Crystallogr. Sect. C*, **39**, 1175 (1983).
13) T. Ito, M. Sugimoto, K. Toriumi, and H. Ito, *Chem. Lett.*, **1981**, 1477.
14) M. Yamashita, H. Ito, K. Toriumi, and T. Ito, *Inorg. Chem.*, **22**, 1566 (1983).
15) M. Kato and T. Ito, *Inorg. Chem.*, submitted for publication.
16) T. Ito, H. Ito, and K. Toriumi, *Chem. Lett.*, **1981**, 1101.
17) H. Ito, M. Kato, and T. Ito, unpublished results.
18) L. Y. Martin, L. J. DeHayes, L. J. Zompa, and D. H. Busch, *J. Am. Chem. Soc.*, **96**, 4046 (1974).
19) An esd for the mean valus of more than three chemically or crystallographically nonequivalent bond lengths is taken to be $[\sum \Delta_i^2/(n-1)]^{1/2}$, where Δ_i is the deviation of the ith value in a set of n such values from the arithmetic mean of the n values. In the case of n=2, it is taken to be the largest of three values: The esd for one parameter (q_1), the esd for the other (q_2), or $|q_1-q_2|/2$.
20) N$_4$7=1,4,7,10-tetraazacyclotetradecane, N$_4$9=1,4,7,10-tetraazacyclohexadecane. M. Sugimoto, J. Fujita, H. Ito, K. Toriumi, and T. Ito, *Inorg. Chem.*, **22**, 955 (1983).
21) M. A. Poraj-Kosic, E. K. Jukhno, A. C. Anciskina, and L. M. Dikareva, *Kristallografiya*, **2**, 371 (1957); Struc. Rep. 21, 407.
22) B. W. Brown and E. L. Ligafelter, *Acta Crystallogr.*, **16**, 753 (1963).
23) B. J. Hathaway and A. A. G. Tomlinson, *Coord. Chem. Rev.*, **5**, 1 (1970).
24) J. Gǎzo, R. Bǒca, E. Jóna, M. Kabešová, Ľ. Macášková, and J. Šima, *Coord. Chem. Rev.*, **43**, 87 (1982), and the references cited therein.
25) M. Sugimoto, J. Fujita, H. Ito, K. Toriumi, and T. Ito, *Inorg. Chem.*, **22**, 955 (1983).
26) M. Sugimoto, H. Ito, K. Toriumi, and T. Ito, *Acta Crystallogr., Sect. B*, **38**, 2453 (1982).
27) M. Sugimoto, M. Nonoyama, T. Ito, and J. Fujita, *Inorg. Chem.*, **22**, 950 (1983).
28) R. G. Pearson, *J. Chem. Educ.*, **45**, 581, 643 (1968).
29) M. Kato and T. Ito, 33rd Meeting on Coordination Chemistry, Osaka, Oct. 1983; Abstr., p. 468.

 © 1984 The Chemical Society of Japan Bull. Chem. Soc. Jpn., 57, 2650—2656 (1984) [Vol. 57, No. 9

Cobalt(III) Complexes with $[N_{6-n}X_n]$ type Ligands. IV.[1] The Preparation and Properties of Tetraammine(salicylideneaminato)cobalt(III) and Diamminebis(salicylideneaminato)cobalt(III) Complexes

Yoshihisa YAMAMOTO* and Eiko TOYOTA
Faculty of Pharmaceutical Sciences, Higashi Nippon Gakuen University, Ishikari-Tobetsu, Hokkaido 061-02
(Received Febuary 14, 1984)

Tetraammine(salicylideneaminato)cobalt(III) complexes, $\left[Co\left(\begin{smallmatrix}HN{=}HC\\ \\ O\end{smallmatrix}\right)(NH_3)_4\right]X_2\cdot nH_2O$ (X: Cl, NO_3, ClO_4, and picrate) and diamminebis(salicylideneaminato)cobalt(III) complexes, $\left[Co\left(\begin{smallmatrix}HN{=}HC\\ \\ O\end{smallmatrix}\right)_2(NH_3)_2\right]X\cdot nH_2O$ (X: Cl, NO_3, ClO_4, and picrate), have been isolated from a reaction mixture of $CoCl_2\cdot 6H_2O$, 25% aqueous ammonia, 30% H_2O_2 and salicylaldehyde, and characterized. In the latter complexes, the three isomers of green, orange and brown color have been isolated by column chromatography on alumina and their configurations have been established by their NMR spectra, *i.e.*, the configuration of the green complex is in the *trans-trans-trans* positions for two ammine ligands, and two phenoxyl groups and two CH=NH groups of the coordinated salicylideneaminato ligands, respectively, while those of the orange and brown complexes are in the *trans-cis-cis* and *cis-cis-trans* positions, respectively.

Previously, we have been concerned with the preparation, properties and isomers of the mixed ligand complexes of the $[CoN_{6-n}O_n]$ type, *e·g*, salicylato(amine)cobalt(III) complexes,[2-7] $[Co(sal\text{-}R)L]X\cdot nH_2O$, and amine(8-quinolinolato)cobalt(III) complexes,[8-12] $[Co(oxine\text{-}R)_lL]X_m\cdot nH_2O$, (L: NH_3, en, bpy, trien, 2,3,2-tet, 3,2,3-tet, and 3,3,3-tet; R: H, Me; *l*: 1 or 2; *m*: 1 or 2). The *cis*-β_1 and β_2 isomers of salicylato(quadridentate amine)cobalt(III) complexes have been isolated and the ^1H and ^{13}C chemical shifts of their amine protons, methylene protons and methylene carbons have been assigned. In addition, the configurations of the coordinated two (2-methyl-)8-quinolinolato ligands in ethylenediaminebis(2-methyl-8-quinolinolato)cobalt(III) complexes[8] and diamminebis(8-quinolinolato)cobalt(III) complexes[10,11] have been reported. The former of these complexes has a *cis-trans* configuration for the two oxygen and two nitrogen atoms, and the latter has a *trans-cis* configuration for the two oxygen and two nitrogen atoms.

Many investigations of bis- or tris(*N*-substituted salicylideneaminato)metal complexes have been reported especially concerning the preparation,[13-28] geometrical isomerism,[28-30] IR spectra,[14-16] absorption spectra,[14-23] NMR spectra,[14,29] and magnetic susceptibilities.[15-19,24,25] However the isolation and stereochemistry of the mixed ligand metal complexes with salicylideneaminato ligand and the derivatives in an octahedral configuration have not previously been described except for dichlorobis(*N*-substituted salicylideneaminato) metal,

$$\left[M\left(\begin{smallmatrix}R\\ |\\ N{=}HC\\ \\ O\end{smallmatrix}\right)_2Cl_2\right]$$

(M: Ti,[31] Mo,[32] Sn,[33] and Th[34]), and tetraammine(salicylideneaminato)cobalt(III) complexes,

$$\left[Co\left(\begin{smallmatrix}HN{=}HC\\ \\ O\end{smallmatrix}\right)(NH_3)_4\right]Cl_2\cdot H_2O.$$[35]

In the stereochemistry of

$$\left[M\left(\begin{smallmatrix}R\\ |\\ N{=}HC\\ \\ O\end{smallmatrix}\right)_2Cl_2\right],$$

the configuration of the coordinated *N*-substituted salicylideneaminato ligands is *trans-trans* for the two phenoxyl and two CH=NR groups. However, other isomers with *cis-trans* configurations and *cis-cis* configurations for the two phenoxyl and two CH=NR groups of the coordinated salicylideneaminato ligand and the *N*-substituted derivatives have not yet been reported. The present paper deals with the preparation and properties of the mixed ligand complexes with salicylideneaminato and ammine ligands of tetraammine(salicylideneaminato)cobalt(III) complexes,

$$\left[Co\left(\begin{smallmatrix}HN{=}HC\\ \\ O\end{smallmatrix}\right)(NH_3)_4\right]X_2\cdot nH_2O$$

and diamminebis(salicylideneaminato)cobalt(III) complexes,

$$\left[Co\left(\begin{smallmatrix}HN{=}HC\\ \\ O\end{smallmatrix}\right)_2(NH_3)_2\right]X\cdot nH_2O$$

(X: Cl, NO_3, ClO_4, pic), and deals with the assignment of the configuration of the latter complexes.

Results and Discussion

The abbreviations of the ammine(salicylideneaminato)cobalt(III) complexes studied in this research are listed in Table 1. Russet tetraammine(salicylideneaminato)cobalt(III) chloride hydrate,

TABLE 1. THE ABBREVIATIONS OF THE AMMINE(SALICYLIDENEAMINATO)COBALT(III) COMPLEXES

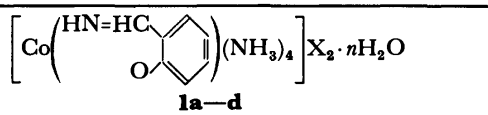

1a—d

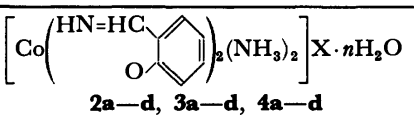

2a—d, 3a—d, 4a—d

	1a	**1b**	**1c**	**1d**	**2a**	**2b**	**2c**	**2d**	**3a**	**3b**	**3c**	**3d**	**4a**	**4b**	**4c**	**4d**
X	Cl	NO_3	ClO_4	pic	Cl	NO_3	ClO_4	pic	Cl	NO_3	ClO_4	pic	Cl	NO_3	ClO_4	pic
n	1	0	0	0	1	1	0	0	1	2	0	0		1	0	0
Form					*trans—trans—trans*				*trans—cis——cis*				*cis—cis——trans*			
					NH_3—O—CH=NH				NH_3—O—CH=NH				NH_3—O—CH=NH			

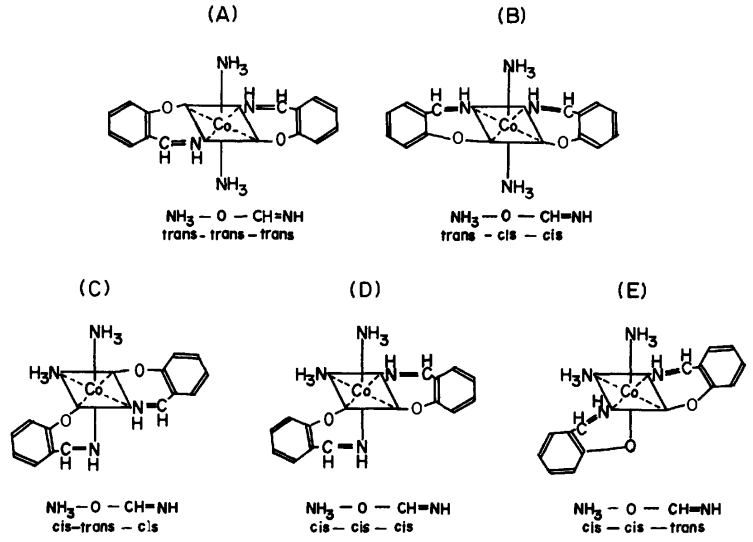

Fig. 1. The configurations of 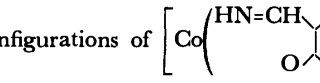 .

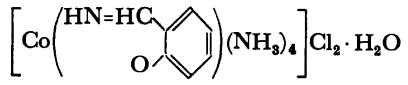

(**1a**), and green and orange diamminebis(salicylideneaminato)cobalt(III) chloride hydrate,

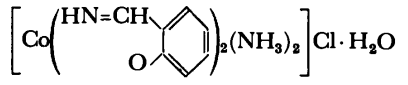

(green: **2a**; orange: **3a**), have been isolated by column chromatography on alumina from a reaction mixture of $CoCl_2 \cdot 6H_2O$, 25% aqueous ammonia, 30% H_2O_2 and salicylaldehyde. Brown diamminebis(salicylideneaminato)cobalt(III) nitrate hydrate (**4b**) has been isolated by chromatography on alumina from a reaction mixture of **2a** and silver nitrate, while the corresponding chloride (**4a**) could not be isolated on the solid state (*cf.* Experimental section). The corresponding nitrates (**1b**, **2b**, **3b**), perchlorates (**1c**, **2c**, **3c**, **4c**) and picrates (**1d**, **2d**, **3d**, **4d**) have been prepared from a reaction mixture of **1a**, **2a**, **3a**, or **4b** and silver nitrate, sodium perchlorate, or picric acid, respectively. The diamminebis(salicylideneaminato)cobalt(III) complex has five possible isomers of A, B, C, D, and E as is shown in Fig. 1. The configurations of isomers A, B, C, and E have C_2 symmetry, while isomer D has C_1 symmetry.

The electric conductivities of **1a—c** in aqueous solutions were 190—220 S cm^2 equiv^{-1} and those of **2a—c**, **3a—c** and **4b—c** were 100—110 S cm^2 equiv^{-1} as is shown in the experimental section. In the IR spectra, bands due to the C=N streching vibrations[14-16,31,33,34] and rocking deformation vibrations[36-38] of all complexes were observed at 1625 cm^{-1} and in the 810—830 cm^{-1} regions, respectively (*cf.* Experimental section). These complexes are diamagnetic complexes of low spin type from their magnetic susceptibilities. In the absorption spectra of **1a—c**, **2a—c**, **3a—c**, and **4b—c** in methanol, the absorption bands at about 380 nm are assigned to the charge transfer band[10,11] and those at about 540 nm or 610 nm are the first absorption bands as shown in Table 2. The ε values at about 380 nm of **2a—c**, **3a—c**, and **4b—c** are larger than those of **1a—c** as shown in Table 2.

The ^{1}H NMR spectra of all complexes were measured in DMSO-d_6 and the ^{13}C NMR spectra of **1a**, **2a**, **3a**, and **4b** were measured in D_2O and 14% ammonia-D_2O solution as shown in Fig. 2. The ^{1}H and ^{13}C NMR spectra of **2a—d**, **3a—d**, and **4b—d** are consistent with C_2 symmetry.[8,11,39,40] In the ^{1}H NMR spectra, the signals at 2.6—4.1 ppm of these complexes are assigned to the protons of the coordinated ammine ligands. The multiplet signals at 6.4—7.3 ppm are assigned to the ring protons of the coordinated salicylideneaminato ligand (abbreviation: the

TABLE 2. ^{1}H NMR SPECTRA AND ABSORPTION BANDS OF **1a—d**, **2a—d**, **3a—d**, AND **4a—d** COMPLEXES

No	NH_3 δ				δ					Absorption bands in methanol λ/nm (ε)		
	$N(1)H_3$	$N(4)H_3$	$N(2)H_3$	$N(3)H_3$ $[N(1)H_3+N(2)H_3]$	ring protons	CH=N	$^3J_{HCNH}$ Hz	C=NH	Picrate δ			
1a	3.26(s 6H)	3.46(s 3H)	4.07(s 3H)		6.43—7.30(m 4H)	8.00(d 1H)	10.5	11.08(d 1H)[1]		378(2750)	475 sh(185)	550(110)
1b	3.07(s 6H)	2.89(s 3H)	3.81(s 3H)		6.47—7.32(m 4H)	8.03(d 1H)	10.5	10.48(d 1H)[1]		378(2820)	475 sh(185)	550(110)
1c	3.03(s 6H)	2.78(s 3H)	3.76(s 3H)		6.48—7.33(m 4H)	8.03(d 1H)	10.5	10.48(d 1H)[1]		378(2880)	475 sh(185)	550(110)
1d	3.09(s 6H)	2.85(s 3H)	3.82(s 3H)		6.51—7.37(m 4H)	8.08(d 1H)	10.5	10.57(d 1H)	8.55(s 4H)[1]			
2a				[2.60(s 6H)]	6.44—7.36(m 8H)	8.27(d 2H)	11.2	11.16(d 2H)[1]		383(4850)		610(85)
2b				[2.59(s 6H)]	6.43—7.34(m 8H)	8.27(d 2H)	11.2	11.17(d 2H)[1]		385(4760)		605(85)
2c				[2.58(s 6H)]	6.43—7.34(m 8H)	8.25(d 2H)	11.2	11.15(d 2H)[1]		385(4640)		610(85)
2d				[2.60(s 6H)]	6.45—7.36(m 8H)	8.29(d 2H)	11.2	11.17(d 2H)	8.54(s 2H)[1]			
3a				[2.68(s 6H)]	6.43—7.37(m 8H)	7.87(d 2H)	10.5	10.59(d 2H)[1]		384(5070)	480 sh(415)	538(200)
3b				[2.72(s 6H)]	6.45—7.37(m 8H)	7.90(d 2H)	10.5	9.98(d 2H)[1]		384(4850)	480 sh(420)	538(200)
3c				[2.73(s 6H)]	6.43—7.33(m 8H)	7.88(d 2H)	10.5	9.99(d 2H)[1]		383(5140)	480 sh(400)	538(200)
3d				[2.73(s 6H)]	6.46—7.37(m 8H)	7.92(d 2H)	10.5	10.02(d 2H)	8.52(s 2H)[1]			
4a[a]				[3.51(s)]	6.44—7.27(m)	7.75(d)	10.5	10.27(d)[1]				
4b				[3.49(s 6H)]	6.42—7.26(m 8H)	7.72(d 2H)	10.5	10.26(d 2H)[1]		380(4650)		530(280)
4c				[3.47(s 6H)]	6.44—7.29(m 8H)	7.74(d 2H)	10.5	10.27(d 2H)[1]		380(4500)		530(280)
4d				[3.48(s 6H)]	6.44—7.28(m 8H)	7.74(d 2H)	10.5	10.27(d 2H)	8.50(s 2H)[1]			

Solvent and standard: 1) DMSO-d_6, internal TMS ($\delta=0$). a): Experimental section.

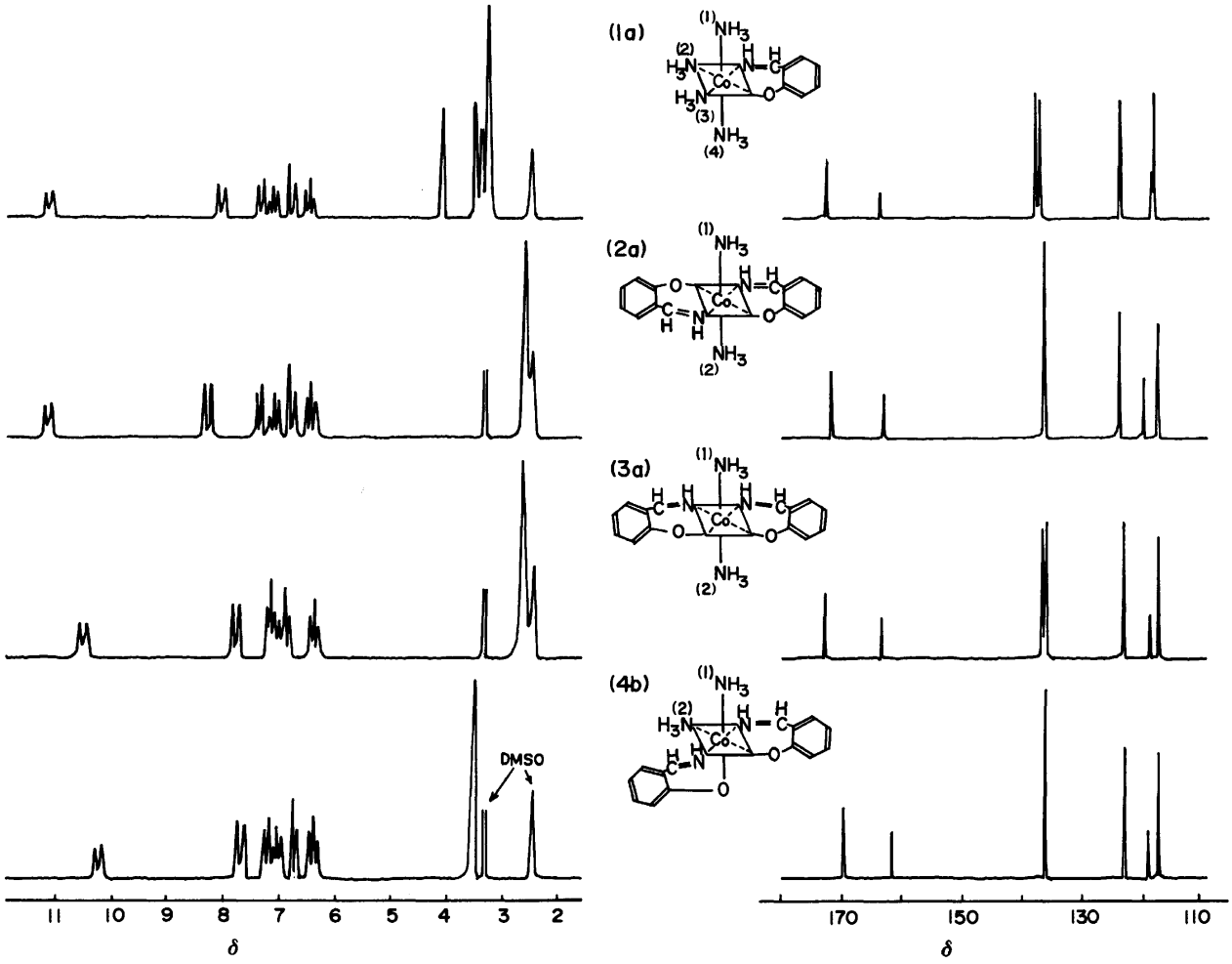

Fig. 2. The ^1H and ^{13}C NMR spectra of **1a**, **2a**, **3a**, and **4b** complexes.

1a: $\left[Co\left(HN{=}HC\text{-}C_6H_3(O)\text{-}O\right)(NH_3)_4\right]Cl_2\cdot H_2O$, **2a**: *trans-trans-trans*-$\left[Co\left(HN{=}HC\text{-}C_6H_3(O)\text{-}O\right)_2(NH_3)_2\right]Cl\cdot H_2O$,

3a: *trans-cis-cis*-$\left[Co\left(HN{=}HC\text{-}C_6H_3(O)\text{-}O\right)_2(NH_3)_2\right]Cl\cdot H_2O$, **4b**: *cis-cis-trans*-$\left[Co\left(HN{=}HC\text{-}C_6H_3(O)\text{-}O\right)_2(NH_3)_2\right]NO_3\cdot H_2O$.

chelate ligand). The doublet signal at about 8 ppm can be assigned to the CH=N proton.[29,33,34] The doublet signal at 10—11 ppm can be assigned to the C=NH proton of the chelate ligand. Their coupling constants (J_{HCNH}) are 10.5 or 11.2 Hz as shown in Table 2. The ^1H NMR spectrum of **1a** showed three singlet signals in the intensity ratios of 2:1:1 for the coordinated ammine ligands. The signal at 3.26 ppm (6H) is assigned to the protons of the two ammine ligands of N(1)H_3 and N(4)H_3 in the positions *cis* to the coordinated chelate ligand, because the two ammine ligands should be equivalent.[11] The singlets at 3.46 ppm (3H) and at 4.07 ppm (3H) are assigned to the protons of the ammine ligands of N(2)H_3 and N(3)H_3 in the position trans[6,11,41] of the phenoxyl and CH=NH group of the coordinated chelate ligand, respectively. The signals of the ammine protons and the C=NH proton of **1a** are at a lower field than those of **1b—d**.

The signal at 3.49 ppm of **4b** is similar to that (3.46 ppm, 3H) of N(2)H_3 of **1a**, and thus the signal of **4b** can be assigned to the ammine protons in the *trans* positions of the phenoxyl groups of the coordinated chelate ligands. Thus, the configuration of complexes **4a—d** can be assigned to isomer E, in *cis-cis-trans* positions as shown in Fig. 1. On the other hand, the chemical shifts of the coordinated ammine ligands of **2a** and **3a** are very different from that of the coordinated ammine ligands of **4b**, and are close to that of N(1)H_3 and N(4)H_3 in the *trans* positions of **1a**. Accordingly the ammine proton signals of **2a** and **3a** can be assigned to those in the *trans* position to each other. A clear distinction between complexes **2a** and **3a** was found in the CH=NH proton signals of their ^1H NMR spectra as shown in Fig. 2. The CH=NH proton signals of **2a** are at a lower field than those of **3a**. Thus, the configuration of the two CH=NH groups of the coordinated chelate ligands of **2a** is *trans*[6,10,41] because the nitrogen atom of CH=NH group is less electronegative than the oxygen atom of the phenoxyl

group. In addition, the chemical shift (8.27 ppm) of the CH=N proton signal of **2a** is similar to that[34] (8.5 ppm) of the CH=N proton signal of dichlorobis-(*N*-phenyl salicylideneaminato)thorium complex,

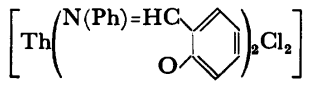

(**5**). This is *trans-trans-trans* for the two chloro ligands, the two phenoxyl groups and the two CH=N(Ph) groups of the coordinated chelate ligands, respectively. Accordingly the configuration of **2a** has been assigned to isomer A, which is *trans-trans-trans* and that of **3a** has been assigned to isomer B which is *trans-cis-cis* as shown in Fig. 1.

The ^{13}C NMR spectra of **1a**, **2a**, 3a, and **4b** showed seven signals for the chelated ligand as shown in Fig. 2. Their chemical shifts were assigned on the basis of the results of those of salicylaldehyde[42] and tetraammine(salicylato)cobalt(III) chloride hydrate.[6] The ^{13}C NMR results, color, decomposition temperature of the complexes are collected in the experimental section.

Experimental

Measurements. The NMR spectra were recorded with an FX-60 apparatus (JEOL) for ^{13}C NMR and with an R-40 apparatus (Hitachi) for ^{1}H NMR. The IR spectra were recorded as potassium bromide disks with an IR-27G apparatus (Shimadzu). The visible absorption spectra were recorded with a Shimadzu MPS-5000 recording spectrophotometer. The electric conductivities of the aqueous solutions were determined by the use of a conductometric meter CM-30 (Shimadzu) at room temperature. The magnetic susceptibilities were measured by the Faraday method using a magnetic balance (Shimadzu) at room temperature.

Preparation of Complexes. Tetraammine(salicylideneaminato)cobalt(III) Chloride Hydrate (1a), Diamminebis(salicylideneaminato)cobalt(III) Chloride Hydrate (2a and 3a) and Hexaamminecobalt(III) Chloride (6): A 25% aqueous ammonia (40 cm^3) was added to an aqueous solution (20 cm^3) of $CoCl_2 \cdot 6H_2O$ (10.0 g, 42.0 mmol), and about 5 cm^3 of 30% H_2O_2 solution was added slowly to the solution at 0 °C. The color of the solution changed from brown to red. A methanol solution (50 cm^3) of salicylaldehyde (5.13 g, 42.0 mmol) was added dropwise to the solution during 2 h at 50 °C. The solution was stirred for 1 d at 50 °C, concentrated with a rotary evaporator at 50 °C, and dried over silica gel. Complexes **1a**, **2a**, and **3a** were extracted with 200 cm^3 of dry methanol from the dried reaction mixture. The methanol solution was concentrated to about 50 cm^3 with a rotary evaporator at 50 °C, the complex **1a** precipitated was filtered and recrystallized twice from water-ethanol. The separation of complexes **2a** and **3a** from the filtrate was achieved by column chromatography on alumina. On elution with methanol, the effluent of the first green band (complex **2a**) was collected, concentrated and recrystallized from 10% aqueous ammonia twice. The effluent of the second orange band (complex **3a**) was collected, concentrated and recrystallized twice from water. The russet band of complex **1a** in the filtrate moved only slightly on alumina. Complex **6** which remained was not soluble in dry methanol. Complex **2a** isomerizes to **4a** at 20 °C in DMSO, methanol and water, but the isomerization is very slow in 10% aqueous ammonia at 20 °C. Yields: 3.6 g (25.5%) for **1a**; 2.8 g (17.2%) for **2a**; 0.65 g (4.0%) for **3a**; 3.59 g (32%) for **6**. Found **1a**: C, 25.26; H, 6.34; N, 20.66; Cl, 21.57%. **2a**: C, 43.98; H, 5.17; N, 14.16; Cl, 9.77%. **3a**: C, 43.55; H, 5.66; N, 14.12; Cl, 9.57%. Calcd for **1a**: $CoC_7H_{20}N_5O_2Cl_2$ (MW 336.11) C, 25.01; H, 6.00; N, 20.84; Cl, 21.10%. **2a** and **3a**: $CoC_{14}H_{20}N_4O_3Cl$ (MW 386.73) C, 43.48; H, 5.21; N, 14.49; Cl, 9.17%. Color **1a**: russet; **2a**: green; **3a**: orange. Dp: 161—163 °C for **1a**; 195—197 °C for **2a**; 163—165 °C for **3a**. Λ=220 for **1a**, 104 for **2a**, and 102 S cm^2 equiv^{-1} for **3a** in water. IR spectra: 1625 cm^{-1} (C=N), 810 cm^{-1} ($\rho_r(NH_3)_r$) for **1a** and **2a**: 1625 cm^{-1} (C=N), 825 cm^{-1} ($\rho_r(NH_3)_r$) for **3a**. ^{13}C NMR spectra: δ 117.9(c-1)*, 163.2(c-2), 117.5(c-3), 137.0(c-4), 123.1(c-5), 136.3 (c-6), 173.0(c-7) in D_2O. **2a**: δ 119.3(c-1), 163.5(c-2), 117.1 (c-3), 136.2(c-4), 123.4(c-5), 136.2(c-6), 172.6(c-7) in 14% ammonia-D_2O. **3a**: δ 118.6(c-1), 163.0(c-2), 117.0(c-3), 137.0 (c-4), 123.1(c-5), 136.2(c-6), 174.2(c-7) in D_2O.

Brown Diamminebis(salicylideneaminato)cobalt(III) Chloride (4a): Complex **4a** was identified by the isomerization of **2a** in DMSO, methanol and water. A brown band of **4a** and a green band of **2a** are separated by column chromatography on alumina from a methanol solution of **2a**. From a brown solution, complex **2a** was obtained, complex **4a** could not be obtained in the solid state. The ^{1}H NMR spectrum of **4a** was observed in DMSO solution of **2a** at room temperature.

Tetraammine(salicylideneaminato)cobalt(III) Nitrate (1b): An aqueous solution of silver nitrate (4.04 g, 23.8 mmol) was added to an aqueous solution of **1a** (4.0 g, 11.9 mmol), the mixture was stirred, and the precipitated silver chloride was filtered. The filtrate was concentrated and recrystallized from water twice. Yield: 3.6 g (81.5%). Found: C, 22.24; H, 4.74; N, 26.09%. Calcd for $CoC_7H_{18}N_7O_7$ (MW 371.20) C, 22.65; H, 4.89; N, 26.41%. Color: reddish brown. Dp: 147—148 °C. Λ=215 S cm^2 equiv^{-1} in water. IR spectrum: 1625 cm^{-1} (C=N), 810 cm^{-1} ($\rho_r(NH_3)_r$).

Tetraammine(salicylideneaminato)cobalt(III) Perchlorate (1c): An aqueous solution of sodium perchlorate (2.2 g, 18.0 mmol) was added to an aqueous solution of **1a** (3.0 g, 8.9 mmol), the mixture was stirred for 1 h at 40 °C, and was concentrated with a rotary evaporator and dried. Complex **1c** was extracted with 15 cm^3 of acetone from the dried reaction mixture. The acetone solution was concentrated and recrystallized from water twice. Yield: 3.0 g (75.6%). Found: C, 19.04; H, 4.50; N, 15.78; Cl, 16.13%. Calcd for $CoC_7H_{18}N_5O_9Cl_2$ (MW 446.09) C, 18.85; H, 4.07; N, 15.70; Cl, 15.89%. Color: reddish brown. Dp: 212—215 °C. Λ=191 S cm^2 equiv^{-1} in water. IR spectrum: 1625 cm^{-1} (C=N), 810 cm^{-1} ($\rho_r(NH_3)_r$).

Tetraammine(salicylideneaminato)cobalt(III) Picrate (1d): An aqueous solution of **1a** (0.5 g, 1.49 mmol) was added to an aqueous solution of picric acid (0.68 g, 2.97 mmol), the mixture was stirred. The complex **1d** was precipitated, filtered, washed with water and dried. Yield: 0.18 g (77.3%). Found: C, 32.67; H, 3.06; N, 21.73%. Calcd for $CoC_{19}H_{22}N_{11}O_{15}$ (MW 703.39) C, 32.44; H, 3.15; N, 21.90%. Color: yellowish brown. Dp: 185—187 °C. IR spectrum: 1625 cm^{-1} (C=N), 810 cm^{-1} ($\rho_r(NH_3)_r$).

trans-trans-trans *and* cis-cis-trans-*Diamminebis(salicylideneaminato)cobalt(III) Nitrate Hydrate (2b and 4b)*: An aqueous solution of silver nitrate (1.1 g, 6.48 mmol) was added to a methanol-water (1:1) solution of **2a** (2.5 g, 6.46 mmol), the mixture was stirred, and the precipitated silver chloride was filtered. The filtrate was concentrated and the complexes **2b** and **4b** were separated by column chromatography on alumina. On elution with methanol, the effluent of the first green band (**2b**) was collected and concentrated and recrystallized from methanol-ether twice. The effluent of the second brown band (**4b**) was collected, concentrated and recrystallized from methanol-ether twice. Yields: 0.85 g

*: position: Table 2.

(31.8%) for **2b** and 0.96 g (36.0%) for **4b**. Found **2b**: C, 40.94; H, 4.56; N, 17.25%. **4b**: C, 40.24; H, 4.49; N, 17.10%. Calcd for $CoC_{14}H_{20}N_5O_6$ (MW 413.28) C, 40.69; H, 4.88; N, 16.95%. Color **2b**: greenish brown; **4b**: brown. Dp: 186—188 °C for **2b**; 183—185 °C for **4b**. Λ=108 for **2b**, 105 S cm^2 equiv^{-1} for **4b** in water. IR spectra: 1625 cm^{-1} (C=N), 820 cm^{-1} (ρ_r-$(NH_3)_r$) for **2b**; 1625 cm^{-1} (C=N), 830 cm^{-1} ($\rho_r(NH_3)_r$) for **4b**. ^{13}C NMR spectrum **4b**: δ 119.0(c-1), 162.8(c-2), 117.2 (c-3), 136.2(c-4), 122.7(c-5), 136.2(c-6), 170.8(c-7) in D_2O.

trans-cis-cis-*Diamminebis(salicylideneaminato)cobalt(III) Nitrate Dihydrate (3b)*: This complex was prepared from the reaction mixture of silver nitrate (0.22 g, 1.30 mmol) and **3a** (0.5 g, 1.29 mmol). The mixture was stirred, and the silver chloride precipitate filtered. The filtrate was concentrated on a rotary evaporator. A small amount of silver complex in the filtrate was excluded by column chromatography on alumina. Complex **3b** was recrystallized from methanol-ether twice. Yield: 0.37 g (66.5%). Found: C, 38.77; H, 5.30; N, 16.55%. Calcd for $CoC_{14}H_{22}N_5O_7$ (NW 431.30) C, 38.99; H, 5.14; N, 16.24%. Color: orange. Dp: 180-182 °C. Λ=107 S cm^2 equiv^{-1} in water. IR spectrum: 1625 cm^{-1} (C=N), 830 cm^{-1} ($\rho_r(NH_3)_r$).

trans-trans-trans *and* trans-cis-cis-*Diamminebis(salicylideneaminato)cobalt(III) Perchlorate (2c and 3c)*: An aqueous solution of sodium perchlorate (0.16 g, 1.31 mmol) was added to a methanol-water (1:1) solution of **2a** or **3a** (0.5 g, 1.29 mmol), and the precipitated complex **2c** or **3c** was filtered, and washed with ethanol-ether. Yields: 0.53 g (94.9%) for **2c**, 0.51 g (91.4%) for **3c**. Found **2c**: C, 38.90; H, 4.17; N, 12.76; Cl, 8.65%. **3c**: C, 38.61; H, 4.22; N, 12.43; Cl, 7.90%. Calcd for $CoC_{14}H_{18}N_4O_6Cl$ (MW 432.71) C, 38.86; H, 4.19; N, 12.95; Cl, 8.19%. Color **2c**: green; **3c**: orange. Dp: 225—226 °C for **2c**; 225—227 °C for **3c**. Λ=112 for **2c**, 106 S cm^2 equiv^{-1} for **3c** in water. IR spectra: 1625 cm^{-1} (C=N), 810 cm^{-1} ($\rho_r(NH_3)_r$) for **2c**; 1625 cm^{-1} (C=N), 830 cm^{-1} ($\rho_r(NH_3)_r$) for **3c**.

cis-cis-trans-*Diamminebis(salicylideneaminato)cobalt(III) Perchlorate (4c)*: This complex was prepared from the reaction mixture of sodium perchlorate (0.1 g, 0.82 mmol) and **4b** (0.34 g, 0.82 mmol) according to the method of **1c**, and recrystallized from methanol-ether. Yield: 0.15 g (42.3%). Found: C, 38.73; H, 4.16; N, 12.76; Cl, 8.76%. Calcd for $CoC_{14}H_{18}N_4O_6Cl$ (MW 432.71) C, 38.86; H, 4.19; N, 12.95; Cl, 8.19%. Color: brown. Dp: 197—199 °C. Λ=103 S cm^2 equiv^{-1} in water. IR spectrum: 1625 cm^{-1} (C=N), 830 cm^{-1} ($\rho_r(NH_3)_r$).

trans-trans-trans, trans-cis-cis *and* cis-cis-trans-*Diamminebis(salicylideneaminato)cobalt(III) Picrate (2d, 3d, and 4d)*: These complexes were prepared from the reaction mixture of picraic acid (0.3 g, 1.31 mmol) and **2a** or **3a** (0.5 g, 1.29 mmol) or **4b** (0.54 g, 1.31 mmol) according to the method of **1d** Yields: 0.69 g (95.3%) for **2d**, 0.63 g (87.0%) for **3d**, 0.57 g (77.6%) for **4d**. Found **2d**: C, 42.10; H, 4.08; N, 17.15%. **3d**: C, 42.39; H, 3.81; N, 17.11%. **4d**: C, 42.51; H, 3.55; N, 17.11%. Calcd for $CoC_{20}H_{20}N_7O_9$ (MW 561.36) C, 42.79; H, 3.59; N, 17.47%. Color **2d** and **3d**: yellowish brown, **4d**: orange. Dp: 184—185 °C or **2d**, 193—194 °C for **3d**, 171—172 °C for **4d**. IR spectra: 1625 cm^{-1} (C=N), 820 cm^{-1} ($\rho_r(NH_3)_r$) for **2d**, 1625 cm^{-1} (C=N), 830 cm^{-1} ($\rho_r(NH_3)_r$) for **3d**; 1625 cm^{-1} (C=N), 825 cm^{-1} ($\rho_r(NH_3)_r$) for **4d**.

Solubility: Complexes **1a—c** are readily soluble in water and DMSO, and soluble in methanol and DMF, though insoluble in the other common organic solvents. Complex **1c** is soluble in acetone. Complex **1d** is soluble in DMSO, DMF and acetone, and somewhat soluble in methanol, and insoluble in water. Complexes **2a—d**, **3a—d**, and **4b—d** are soluble in DMSO. Complexes **2c—d**, **3c—d**, and **4c—d** are soluble in acetone. Complexes **2a—b**, **3a**, and **4b** are soluble in water, though **2c**, **3b—c**, and **4c** are slightly soluble, and **2d**, **3d**, and **4d** are insoluble in water. Complexes **2a—c**, **3b—c**, and **4b—c** are soluble in methanol, though **2d** and **3a** are somewhat soluble in methanol.

References

1) Part III: Ref. 8.
2) Y. Yamamoto, H. Kudo, and E. Toyota, *Bull. Chem. Soc. Jpn.*, **56**, 1051 (1983).
3) Y. Yamamoto, E. Toyota, and N. Mitsudera, *Bull. Chem. Soc. Jpn.*, **53**, 3517 (1980).
4) Y. Yamamoto and E. Toyota, *Bull. Chem. Soc. Jpn.*, **52**, 2540 (1979).
5) Y. Yamamoto and E. Toyota, *Chem. Pharm. Bull.*, **26**, 2275 (1978).
6) Y. Yamamoto, *Bull. Chem. Soc. Jpn.*, **51**, 2894 (1978).
7) Y. Yamamoto, M. Mori, H. Yoneda, S. Misumi, and K. Ito, *Bull. Chem. Soc. Jpn.*, **42**, 984 (1969).
8) Y. Yamamoto and E. Toyota, *Bull. Chem. Soc. Jpn.*, **57**, 47 (1984).
9) Y. Yamamoto, E. Toyota, and Y. Yamamoto, *Bull. Chem. Soc. Jpn.*, **56**, 2721 (1983).
10) Y. Yamamoto, R. Kataoka, S. Imahara, and T. Amano, *Bull. Chem. Soc. Jpn.*, **54**, 2972 (1981).
11) Y. Yamamoto, *Chem. Lett.*, **1980**, 1555.
12) Y. Yamamoto and E. Toyota, *Chem. Pharm. Bull.*, **28**, 3153 (1980).
13) J. Endo, *Nippon Kagaku Kaishi.*, **65**, 428 (1944).
14) H. Kuma and S. Yamada, *Bull. Chem. Soc. Jpn.*, **49**,2115 (1976).
15) M. M. Patel and R. P. Patel, *J. Indian Chem. Soc.*, **51**, 770 (1974).
16) S. Yamada, *Coord. Chem. Rev.*, **1**, 415 (1966).
17) S. Yamada, K. Yamanouchi, W. Mori, and M. Kishita, *Bull. Chem. Soc. Jpn.*, **49**, 2111 (1976).
18) K. Yamanouchi and S. Yamada, *Inorg. Chim. Acta.*, **12**, 109 (1975).
19) L. Sacconi, M. Ciampolini, F. Maggio, and F. P. Cavasino, *J. Am. Chem. Soc.*, **84**, 3246 (1962).
20) K. Yamanouchi and S. Yamada, *Bull Chem. Soc. Jpn.*, **49**, 163 (1976).
21) H. Nishikawa and S. Yamada, *Bull. Chem. Soc. Jpn.*, **37**, 1154 (1964).
22) H. Nishikawa, S. Yamada, and R. Tsuchida, *Z. Naturforsch.*, **17b**, 78 (1962).
23) H. Nishikawa, S. Yamada, and R. Tsuchida, *Z. Anorg. Allgem. Chem.*, **316**, 278 (1962).
24) L. Sacconi and M. Ciampolini, *J. Chem. Soc.*, **1964**, 276.
25) B. O. West, *J. Chem. Soc.*, **1962**, 1374.
26) S. Yamada, E. Ohno, and K. Yamanouchi, *Bull. Chem. Soc. Jpn.*, **41**, 535 (1968).
27) S. Yamada and H. Nishikawa, *Bull. Chem. Soc. Jpn.*, **36**, 755 (1963).
28) B. O. West, *J. Chem. Soc.*, **1960**, 4944.
29) A. Chakravorty and R. H. Holm, *Inorg. Chem.*, **3**, 1521 (1964).
30) M. Ciampolini, F. Maggio, and F. P. Cavasino, *Inorg. Chem.*, **3**, 1188 (1964).
31) N. S. Biradar and V. H. Kulkarni, *J. Inorg. Nucl. Chem.*, **33**, 3847 (1971).
32) A. V. D. Bergen, K. S. Murray, and B. O. West, *Aust. J. Chem.*, **25**, 705 (1972).
33) N. S. Biradar and V. H. Kulkarni, *J. Inorg. Nucl. Chem.*, **33**, 2451 (1971).
34) N. S. Biradar and V. H. Kulkarni, *Z. Anorg. Allg. Chem.*, **387**, 275 (1972).
35) Y. Yamamoto and E. Toyota, *Chem. Pharm. Bull.*, **30**, 2262 (1982).

36) K. Nakamoto, "Infrared Spectra of Inorganic and Coordination Compounds, "Wiley-Interscience, New York (1970) p.150.
37) J. K. Wilmshurst, *Can. J. Chem.*, **38**, 467 (1960).
38) G. F. Svatos, D. M. Sweeny, S. Mizushima, C. Curran, and J. V. Quagliano, *J. Am. Chem. Soc.*, **79**, 3313 (1957).
39) S. Utsuno, A. Hayashi, S. Kondo, and M. Utsumi, *Chem. Lett.*, **1979**, 351.
40) S. Utsuno and M. Sekizaki, *Inorg. Nucl. Chem. Lett.*, **15**, 259 (1979).
41) W. L. Jolly, A. D. Jarris, and T. S. Briggs, *Inorg. Chem.*, **4**, 1064 (1965).
42) L. F. Johnson and W. C. Jankowski, "Carbon-13 NMR Spectra, A Collection of Assigned, Coded, and Indexed Spectra," Wiley-Interscience, New York (1972), No. 231, 293.

© 1984 The Chemical Society of Japan

NOTES

Bull. Chem. Soc. Jpn. 57, 2657—2658 (1984)

Intramolecular Photocycloaddition of Noncyclic Polyether Compounds Containing α,ω-Dicinnamates End Groups and Uptake of Alkali Metal Thiocyanates with Them[1)]

Kazuhisa HIRATANI* and Sei-ichi AIBA

Industrial Products Research Institute, Higashi 1-chome, Yatabe-machi, Tsukuba-gun, Ibaraki 305

(Received December 26, 1983)

Synopsis. Noncyclic polyethers containing two cinnamoyl end groups have been prepared, they were cyclized by photosensitized intramolecular addition. The uptake of alkali metal (sodium and potassium) thiocyanates with these compounds and their ability to extract has been investigated before and after the cyclization.

Intramolecular photocycloaddition in α,ω-dicinnamates to construct macrocycles has been studied by several groups,[2)] but there are few applications of them to prepare cyclic polyethers which exhibit, for example, the extracting ability for cations.[3)] Conversion of the noncyclic polyethers to the cyclic ones will bring about a change of the ability in the cation-uptake. In this paper we wish to report the photo-induced intramolecular cyclization of noncyclic oligoethylene glycol derivatives containing cinnamoyl group at both ends of the molecule and the ability of uptake for alkali thiocyanate with them.

Results and Discussion

As shown in Scheme 1, three noncyclic polyether compounds having two cinnamoyl end groups were prepared by the reaction of an oligoethylene glycol with two mole equivalents of cinnamoyl chloride in the presence of triethylamine. By this procedure, tetraethylene glycol dicinnamate (**1**), 1,2-bis[2-[2-(cinnamoyl)ethoxy]ethoxy]benzene (**2**), and 1,2-bis[2-[2-[2-(cinnamoyl)ethoxy]ethoxy]ethoxy]benzene (**3**) were obtained. 1,2-Bis[2-(2-acetoxyethoxy)ethoxy]benzene (**4**) was also prepared to allow comparison of the abilities of uptake. In Table 1, the analytical data are summarized.

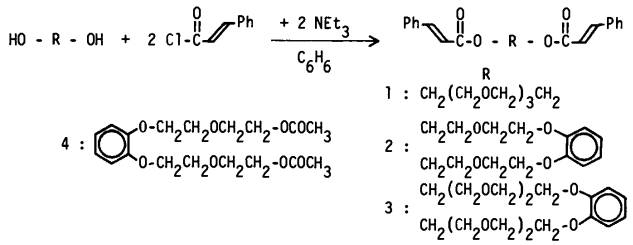

Scheme 1. Preparation of polyethers with two cinnamoyl end groups.

Intramolecular photocycloaddition of biscinnamates (**1**)—(**3**) was carried out by high dilution technique in acetone using a 400-W high pressure mercury lump under bubbling of gaseous nitrogen in the presence of a catalytic amount of benzophenone as a sensitizer (Scheme 2): **5**; yield 27%, NMR ($CDCl_3$) δ=3.4—4.7 (12H, m, cyclobutane ring+oligo(oxyethylene)), 3.67 (8H, s, oligo(oxyethylene)), 7.33 (10H, s, C_6H_5) ppm; and **6**; yield 21%, NMR ($CDCl_3$) δ=3.0—4.5 (24H, m, cyclobutane ring+oligo(oxyethylene)), 6.89 (4H, s, *o*-phenylene), and 7.32 (10H, s, C_6H_5) ppm. But an attempt to prepare the corresponding cycloadduct from **2** was unsuccessful. In the IR spectra, the absorption band based on cinnamoyl C=C double bond (at 1635 cm^{-1} for **1** and **3**) disappeared completely after the photoirradiation. In the proton NMR, the signal

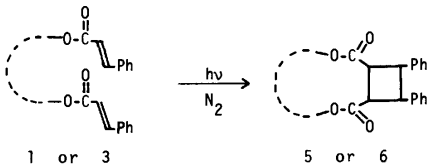

Scheme 2. Intramolecular photocycloaddition of polyethers with cinnamoyl groups.

Table 1. Analytical data of noncyclic polyethers

Polyether	Yield %	Elemental analysis	H,%	C,%	NMR spectrum(δ ppm from TMS in $CDCl_3$) -CH=CH-	C_6H_5	$-OCH_2CH_2O-$	*o*-C_6H_4	CH_3
1	65	Found	6.40	68.26	6.48(d) 7.70(d) (10 Hz)	7.41	3.70(s) 3.77(t) 4.35(t)	—	—
		Calcd	6.65	68.71					
2	73	Found	6.19	69.70	6.47(d) 7.65(d) (10 Hz)	7.42	3.8—4.6 (m)	6.93(s)	—
		Calcd	6.27	70.32					
3	62	Found	6.60	67.95	6.50(d) 7.80(d) (10 Hz)	7.43	3.73(s) 3.6—4.5 (m)	6.92(s)	—
		Calcd	6.67	68.12					
4	58	Found	7.02	57.59	—	—	3.84(m) 4.17(m)	6.93(s)	2.07(s)
		Calcd	7.08	58.37					

Table 2. Solubilization of thiocyanate salts into CH_2Cl_2

Polyether	Amount of solubilized thiocyanates (mol of MSCN/mole of polyether)[a]	
	NaSCN	KSCN
1	0.12	≈0
2	0.22	≈0
3	0.48	0.53
4	0.21	≈0
5	0.21	0.03
6	0.45	0.34

a) The values were calculated from elemental analysis.

of the olefin proton of **1** disappeared in **5** and the signal for the cyclobutane ring protons appeared at around 4 ppm. The stereochemistry at the point of closure could not be elucidated from the cyclobutane protons since these were obscured by other oxyethylene protons. But it is presumed that such macrocyclic ring-closure in solution phase may be δ-addition(anti, head to head) according to the literature.[2b] In addition, the mass spectroscopic data confirmed that the molecular weights of **5** and **6** are exactly the same as those of **1** and **3**, respectively.

Thus, the ability of uptake for sodium and potassium thiocyanates with these compounds was examined. After we mixed the polyether and powdered alkali thiocyanate in dichloromethane at room temperature, we determined the amount of alkali thiocyanates solubilized into the solvent by elemental analysis (see Experimental). The results are shown in Table 2. The 17-membered ring compound (**5**) can uptake NaSCN two times better than **1**, whereas both **1** and **5** can uptake very little KSCN. Noncyclic polyether (**3**), which has a longer oxyethylene moiety compared with **1**, exhibits better uptake for K^+ salt than that for Na^+ salt. On the other hand, the 26-membered ring compound (**6**) can solubilize Na^+ salt a little more than K^+ salt.

Contrary to our expectation, the difference in the selectivity and ability of uptake between cyclic and noncyclic compounds was not so large. It could be considered that the cyclobutane structure bearing two ester groups largely distorts the cyclic polyether structure and therefore their ability of uptake can not be improved distinctly compared with that of noncyclic ones. Furthermore, it has been reported that the metal ion complexing properties of crown ethers containing ester groups are generally different from the corresponding ones which are formed from ethylene glycol units.[4] Our failure may be attributed to the introduction of both cyclobutane ring and two ester groups into a macrocyclic system.

In the extraction of alkali salts by noncyclic polyethers, (**1**)—(**4**), the longer the oxyethylene chain is, the better the ability of uptake is. It means that in this case the structure of end groups of these noncyclic polyethers has little effect on their ability of uptake.

Experimental

The 2-(2-chloroethoxy)ethanol and 2-[2-(2-chloroethoxy)-ethoxy]ethanol were commercially available (Aldrich Chem. Co.) and were used without further purification. The NMR and IR spectra were recorded on a Varian EM-360 (60 MHz) using TMS as the internal standard and on a JASCO IRA-1 infrared spectrometers, respectively. The mass spectrum was measured with a Hitachi M-52 mass spectrometer.

General Procedure for the Preparation of Noncyclic Polyethers. 1,2-Bis[2-(2-hydroxyethoxy)ethoxy]benzene and 1,2-bis[2-[2-(2-hydroxyethoxy)ethoxy]ethoxy]benzene were prepared by the reaction of catechol with 2 mole equivalents of 2-(2-chloroethoxy)ethanol and 2-[2-(2-chloroethoxy)ethoxy]ethanol, respectively, in the presence of powdered potassium carbonate in DMF. Then, to the benzene of the mixture of 1 mole equivalent of the oligoethylene glycol and 2 mole equivalents of triethylamine was added dropwise 2 mole equivalents of cinnamoyl chloride at room temperature. After the solution was stirred for 12 h at room temperature, the solution was washed with water and dried with magnesium sulfate. After removal of benzene by evaporation, the residue was submitted to column chromatography(chloroform) on silica gel.

General Procedure of Irradiation. Irradiations on a preparative scale were performed with Pyrex-filtered light from a 400-W high pressure mercury lamp (Riko) under bubbling of gaseous nitrogen in an immersion apparatus.

Preparation of 5. An acetone (250 ml) solution of 1.3 g of **1** and 0.01 g of benzophenone was irradiated in the Pyrex cell described above at 40 °C for 7 h. After solvent was removed, the remaining reaction products were isolated by column chromatography on alumina. The first elution with chloroform gave a colorless oily product, **5**, which was identified with IR, NMR, and mass spectroscopic method and elementary analysis. The other product were also oily and seemed to be intermolecular adducts(oligomeric products) because of their high viscosity. Further identification was not done.

In a similar manner, a cyclic product, **6**, was isolated.

Extraction Procedure. In a typical experiment, to the solution (0.1 g of the polyether prepared in 5 ml of dichloromethane) 0.5 g of alkali thiocyanate powder was added, and then the mixture was stirred for 12 h at room temperature. The insoluble salt was filtered off and the solvent was evaporated from the filtrate. The amounts of alkali thiocyanate solubilized into dichloromethane was determined by elementary analysis. The results are summarized in Table 2. Under these conditions, thiocyanate salts in the absence of the polyether did not dissolve in dichloromethane at all.

References

1) Part VIII on "Synthesis and Properties of Noncyclic Polyether Compounds." Presented at the 42nd National Meeting of the Chemical Society of Japan, Sendai, September 1980, Abstr., No. 1I04.

2) a) M. Freedman, Y. Mohadger, J. Rennert, S. Soloway, and I. Waltcher, *Org. Prep. Proc.*, **1**, 267 (1969); J. Rennert, *Photogr. Sci. Eng.*, **15**, 60 (1971); J. Rennert, S. Soloway, I. Waltcher, and B. Leons, *J. Amer. Chem. Soc.*, **94**, 7242 (1972); b) J. A. Ors and K. Srinivasan, *J. Amer. Chem. Soc.*, **100**, 315 (1978); *J. Chem. Soc., Chem. Commun.*, **1978**, 400.

3) G. W. Gokel and S. H. Korzeniowski, "Macrocyclic Polyether Syntheses," Springer-Verlag, Berlin Heidelberg New York (1982), p 225.

4) J. S. Bradshaw, G. E. Maas, R. M. Izatt, and J. J. Christensen, *Chem. Rev.*, **79**, 37 (1979).

Zeta Potentials of Metal Oxides in Aqueous Solution of Water-soluble Titanate Coupling Agents

Kunio ESUMI* and Kenjiro MEGURO

Department of Applied Chemistry and Institute of Colloid and Interface Science, Science University of Tokyo, Kagurazaka, Shinjuku-ku, Tokyo 162

(Received January 13, 1984)

Synopsis. The zeta potentials of γ-Fe_3O_4 and TiO_2 were measured as a function of the amount of water-soluble titanate coupling agents added in aqueous solution. Compared with untreated samples, the zeta potential of γ-Fe_3O_4 increased negatively with an increase of the amount of water-soluble titanate coupling agents, while that of TiO_2 changed little. Furthermore, after a washing process, it was confirmed by ESCA measurement that a certain amount of water-soluble titanate coupling agent still remained on the surface of the γ-Fe_3O_4.

Silane and titanate coupling agents for modifying many fillers have been employed[1-3] to improve the bonding between reinforcements and polymer matrices. When coupling treatments are applied to a dispersion system containing porous material in solution, electrokinetic measurement[4] is a useful method to detect changes in the surface properties. Esumi *et al.*[5,6] studied the change in the zeta potential of metal oxides coated with coupling agents and they found that the zero point of the charge of the metal oxides coated with (3-aminopropyl)triethoxysilane and tris[2-(2-aminoethylamino)ethoxy]isopropoxytitanium(IV) is shifted to a higher value.

It is known that chelated titanate coupling agents can be made water-soluble *via* a quaternization technique which converts water-insoluble chelated titanates to water-soluble, ionic quadrivalent nitrogen salt complexes. Such water-soluble titanate coupling agents seem very interesting materials because they can be applied to aqueous dispersion system.

In this work the influence of water-soluble titanate coupling agents on the surface properties of γ-Fe_3O_4 and TiO_2 was investigated by measuring their zeta potential and ESCA spectra.

Experimental

Materials. The titanate coupling agents used in this study were bis{*O'*,*O'*-dioctyl pyrophosphato(1-)}(1-oxoethylenedioxy)titanium(KR-238S) and bis{*O'*,*O'*-dioctyl pyrophosphato(1-)}(ethylenedioxy)titanium(KR-138S), kindly supplied by Ajinomoto Co. As metal oxides, γ-Fe_3O_4 and TiO_2 (rutile) were obtained from BASF and Teikoku Kako, respectively. The specific surface areas of γ-Fe_3O_4 and TiO_2 determined by nitrogen adsorption at its liquid temperature were 6.1 and 49 m^2/g. The zero point of charge for sample was 7.5 for γ-Fe_3O_4, 4.2 for TiO_2.

Procedure. Quaternization of titanate coupling agents was made by the addition of triethylamine(TEA) into the coupling agents. The mixing ratios were 1:1 bg weight for KR-138S-TEA and 1:0.5 for KR-238S-TEA. The water-soluble titanate coupling agent obtained was then added to deionized water and the metal oxide added to the solution, dispersed in an ultrasonic cleaning bath.

Measurements of the zeta potential for the dispersed system were conducted using a Pen Kem Laser 500 Zeta Potential. The pH of the suspension was measured with a Corning pH meter.

ESCA spectra of γ-Fe_3O_4 treated with water-soluble titanate coupling agents were obtained using a Kokusaidenki VK-5B photoelectron spectrometer equipped with an aluminium $K\alpha$ X-ray source.

Results and Discussion

Figure 1 shows the zeta potentials of γ-Fe_3O_4 and the pH values of the suspensions as a function of the amount of water-soluble titanate coupling agents added. The zeta potential value of γ-Fe_3O_4 increased negatively with increase of the amount of KR-238S-TEA added and reached about −40 mV, while the pH of the suspension was in the range between 7—7.8. Since

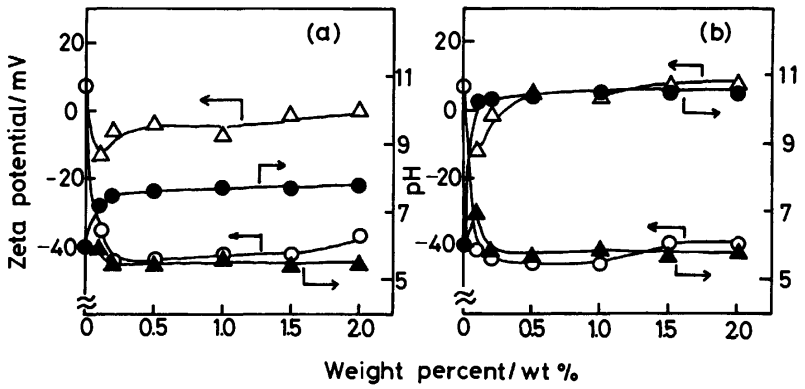

Fig. 1. Zeta potential of γ-Fe_3O_4 and the pH value of the suspension as a function of amount added of water-soluble titanate coupling agents: (a) KR-238S-TEA, (b) KR-138S-TEA; (○,●) immediate measurement, (△,▲) measurement after washing process.

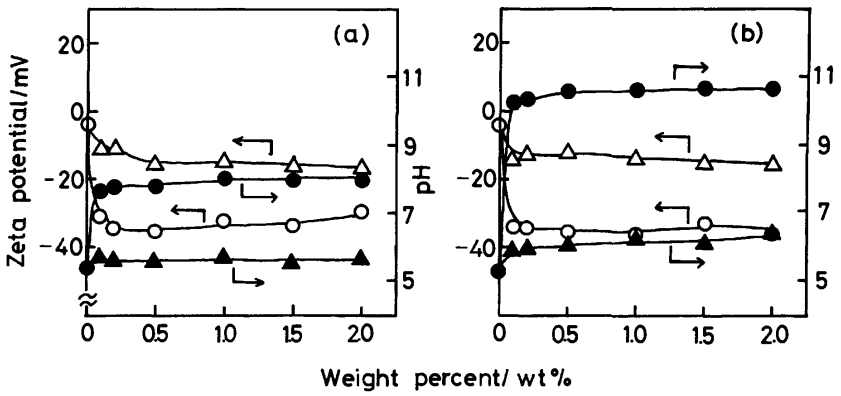

Fig. 2. Zeta potential of TiO_2 and the pH value of the suspension as a function of amount added of water-soluble titanate coupling agents: (a) KR-238S-TEA, (b) KR-138S-TEA, (○,●) immediate measurement, (△,▲) measurement after washing process.

the zero point of the charge (ZPC) for untreated γ-Fe_3O_4 was about 7.5, it seems that the complexes of KR-238S-TEA are adsorbed on the surface of γ-Fe_3O_4, resulting in a negative zeta potential. The change in the zeta potential of γ-Fe_3O_4 by addition of KR-138S-TEA was analogous to that for KR-238S-TEA. Further, from the measurement of the ESCA spectra for the samples treated with KR-238S-TEA and KR-138S-TEA, a Ti 2P photopeak due to water-soluble titanate coupling agents was detected. This result indicates that these water-soluble titanate coupling agents are adsorbed on γ-Fe_3O_4.

The attachment strength of the water-soluble titanate coupling agents was estimated by measuring the zeta potential of γ-Fe_3O_4 treated after a washing process. The γ-Fe_3O_4 particles in the presence of the water-soluble titanate coupling agent were collected and washed five times with a 10 ml of deionized water, then dispersed in deionized water. After such a washing process, the zeta potential of γ-Fe_3O_4 for KR-238S-TEA showed a negative value, while the sample for KR-138S-TEA provided a positive zeta potential with a value of +12 mV which is almost the same as for the untreated sample at pH=5.5. These results suggest that after washing, for KR-238S-TEA some titanate molecules still remain on the surface of γ-Fe_3O_4, but not for KR-138S-TEA. To confirm that some titanate molecules exist on the surface of γ-Fe_3O_4 after the washing process, ESCA spectra were measured. It was observed that the Ti 2P photopeak for KR-238S-TEA was detected, but not for KR-138S-TEA. Thus, it is found that the attachment of KR-238S-TEA on the surface of γ-Fe_3O_4 is much stronger than that of KR-138S-TEA.

Figure 2 gives the zeta potential of TiO_2 and the pH of the suspension for addition of various amounts of water-soluble titanate coupling agents. In both KR-138S-TEA and KR-238S-TEA, the zeta potential values by addition of the water-soluble titanate coupling agents were close to those of the untreated samples, indicating that adsorption of these titanate coupling agents scarcely occurs on TiO_2 or may occur by ion exchange. Also, after the washing process, the zeta potential of TiO_2 was −20 mV which is almost identical to that of the untreated sample at about pH=6. Thus, the zeta potential of TiO_2 by addition of various amounts of water-soluble titanate coupling agents and after the washing process changed little compared with that of an untreated sample.

References

1) P. W. Erickson and E. P. Plueddemann, "Composite Materials," Academic Press, New York (1974), Vol. 6, Chap. 6, P. 1.
2) M. R. Rosen, *J. Coat. Technol.* **50**, 70 (1978).
3) C. H. Chiang, N. I. Liu, and J. L. Koenig, *J. Colloid Interface Sci.*, **86**, 26 (1982).
4) W. H. Koh, *J. Colloid Interface Sci.*, **71**, 613 (1979).
5) K. Esumi and K. Meguro, *Bull. Chem. Soc. Jpn.*, **56**, 331 (1983).
6) K. Esumi and K. Meguro, *Bull. Chem. Soc. Jpn.*, **56**, 935 (1983).

The Thermal Decomposition of CF_3I in Ar

Ko SAITO,* Yuji YONEDA, Hiroyuki TAHARA,
Sadao KIDOGUCHI, and Ichiro MURAKAMI
Department of Chemistry, Faculty of Science, Hiroshima University, Higashisenda-machi, Naka-ku, Hiroshima 730
(Received February 24, 1984)

Synopsis. The thermal decomposition of CF_3I behind reflected shock waves was studied by means of the UV absorption over the temperature range of 935—1235 K and in the density range of 6.3×10^{-6}—3.8×10^{-5} mol cm^{-3}. The decomposition rate was in the fall-off region, and the main process was the C-I bond fission. The rate constants corresponding to the limiting high- and low-pressure regions were determined to be;

$$k_\infty = 10^{14.67}\exp(-27200/T)\ \mathrm{s}^{-1}$$

and;

$$k_0/[\mathrm{Ar}] = 10^{14.71}\exp(-15000/T)\ \mathrm{cm}^3\ \mathrm{mol}^{-1}\ \mathrm{s}^{-1}.$$

In connection with the other halogenated methanes, the thermal unimolecular rate constant of the CF_3I decomposition is interesting from such points of view as the contribution of the internal vibrational modes to the bond rupture and the energy transfer in collisions between the reactant and the heat bath. In the past, the high-pressure rate constant for the primary process, $CF_3I \rightarrow CF_3+I$, was determined by Danidov *et al.*[1] in the temperature range between 608—723 K. Skorobogatov[2] evaluated an Arrhenius expression for the rate constant over the temperature range between 400—1400 K on the basis of the equilibrium constant and the rate data for the reverse reaction. In their study of the kinetics of the CF_3 radical, Modica and Sillers[3] used a low-pressure rate constant evaluated from the classical collision theory, not from experiments.

The main purpose of the present study is to determine the high- and low-pressure rate constants for the primary reaction in order to ascertain the unimolecular behavior in Ar.

Experimental

A 9.4-cm-i.d. shock tube was used for this experiment. The optical system to follow the UV absorption was essentially the same as in previous works;[4,5] that is, a deuterium lamp, a 25-cm monochromator, a photomultiplier, and a digital memory were the basic line-up of the time-resolved absorption system. The disappearance rate of the shock-heated CF_3I was measured by observing the absorption at 290 nm with FWHM=1.65 nm. The absorption coefficient (base e) was determined to be $(1.8\pm0.5)\times10^5$ cm^2 mol^{-1} over the temperature range of 900—1250 K.

CF_3I (PCR Research Chemicals) was used after trap-to-trap distillations. Mixtures (0.67—2.0 mol% CF_3I in Ar) were prepared in 25-l cylindrical glass reservoirs and then allowed to stand for more than 12h before use.

Results and Discussion

Figure 1 shows some typical absorption records at different temperatures. The apparent first-order rate constant, k_a, was determined by means of this definition: $k_a=-\mathrm{d}(\ln[CF_3I])/\mathrm{d}t$. The k_a's observed varied with the total density, suggesting that the decomposition was in the fall-off region. Table 1 lists the Arrhenius parameters for k_a determined at three different total densities.

In order to evaluate the high- and low-pressure rate constants, k_∞ and $k_0/[\mathrm{Ar}]$, the fall-off data were extrapolated to high and low pressures along with the fall-off curves, which were themselves calculated by the reduced form of the Kassel theory.[6] This was performed in the usual manner described in a previous paper.[7] By fitting the fall-off curves to the data points, the two Arrehnius expressions for the limiting pressures were evaluated as;

$$k_\infty = 10^{14.67}\exp(-27200/T)\ \mathrm{s}^{-1}$$

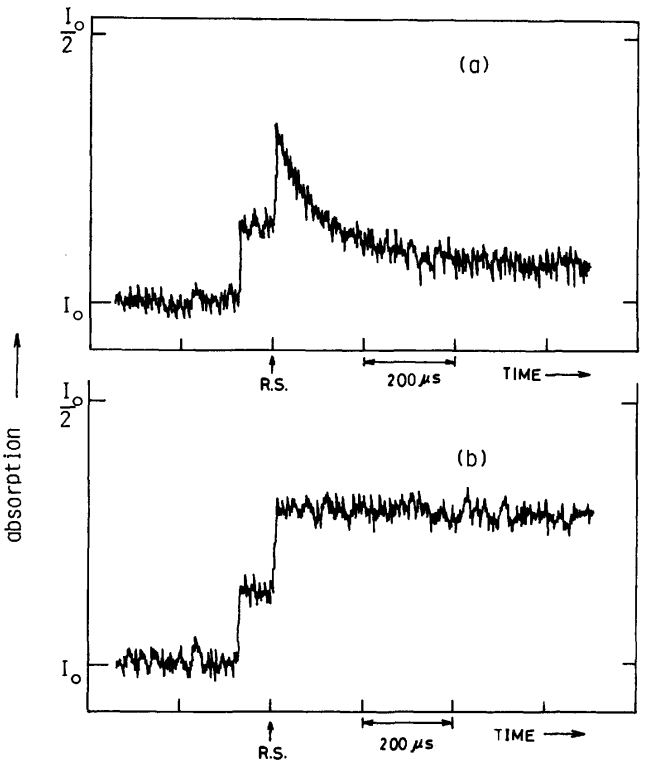

Fig. 1. Typical absorption records at 290 nm. a: [M] $=2.20\times10^{-5}$ mol cm^{-3}, Temp=1200 K, 1.0 mol% CF_3I in Ar; b: [M] $=2.05\times10^{-5}$ mol cm^{-3}, Temp= 930 K, 1.0 mol% CF_3I in Ar.

TABLE 1. ARRHENIUS PARAMETERS FOR k_a

Total density / mol cm^{-3}	A / cm^3 mol^{-1} s^{-1}	E_a / kJ mol^{-1}
6.3×10^{-6}	5.8×10^8	130
1.0×10^{-5}	1.6×10^9	134
$(3.5\pm0.3)\times10^{-5}$	9.6×10^9	146

and;

$$k_0/[\mathrm{Ar}] = 10^{14.71}\exp(-15000/T)\ \mathrm{cm^3\ mol^{-1}\ s^{-1}},$$

with an error limit of about 50% in the temperature range of 950—1235 K.

The initial decay of CF_3I diluted in Ar is considered to proceed *via* the following reactions;

$$(1)\quad CF_3I\ (+Ar) \longrightarrow CF_3 + I\ (+Ar),$$

$$(2)\quad CF_3I + I \longrightarrow CF_3 + I_2,$$

$$(3)\quad CF_3I + CF_3 \longrightarrow CF_2I + CF_4,$$

$$(4)\quad CF_3I + CF_3 \longrightarrow C_2F_6 + I.$$

The effects of Reactions (2)—(4) on the decay rate were examined by using a series of reactions with appropriate rate constants. As a result, the participation of these secondary reactions was found to be negligibly small at the early stage, where the decay rates were measured. Thus, it was ascertained that the evaluated values for k_∞ and $k_0/[\mathrm{Ar}]$ corresponded to Reaction (1).

The Arrhenius parameters for k_∞ obtained in the present work are comparable to the values estimated by Skorobogatov,[2] $k_\infty = 10^{14}\exp(-26500/T)\ \mathrm{s^{-1}}$. The present rate constant exceeds this by a factor of 2.6 at 1000 K; it is thus in good agreement. However, the value obtained by Danidov *et al*,[1] $k_\infty = 10^{15.40}\exp(-23750/T)\ \mathrm{s^{-1}}$, exceeds the present value by about two orders at 1000 K. For the low-pressure-rate constant, on the other hand, there are no experimental data to be compared. An estimation by Modica and Sillers[3] using the classical collision theory is too low (less than two orders) compared with the present results. The cause of this large discrepancy is perhaps the high bond-dissociation energy (240.1 kJ $\mathrm{mol^{-1}}$) used in their calculation.

The weak collision parameters were calculated by the use of a relation between observed and strong collision rate constants,[8] as has been performed for some similar molecules.[5,7] Table 2 lists the calculated results for the collision efficiency, β_c, and the average energy transferred per collision, $\langle\Delta E\rangle$, together with the data for CH_3I.[5]

It is of interest to compare the rate data between CF_3I and CH_3I in the same temperature range, because the molecular constants of these molecules differ substantially from each other, although the dissociation energies of the C-I bonds are very close. We can see from Table 2 there is no serious difference in the weak collision parameters between the two systems. However, the dissociation of CH_3I in Ar was in the low-pressure region; this was in contrast to that of CF_3I under the same conditions.[5] The fall-off pressures at 1100 K were estimated to be 130 and 2270 atm for CF_3I and CH_3I respectively.[9] This apparently low fall-off pressure of the CF_3I decomposition seems to show that this molecule acts as if its internal degrees of freedom were larger than that of CH_3I. In fact, the effective numbers of the internal freedom, S_{eff}, are 5.76 and 3.06 for CF_3I and CH_3I respectively, where $S_{eff} = -T^{-1}[d\ln Q_{vib}/d(1/T)]$.[6] The fall-off pressure of the CF_3I decomposition is rather close to that of the CF_3CN decomposition in Ar at the same temperature.[10]

Table 2. Comparison of weak collision parameters between CF_3I and CH_3I

System	T/K	β_c	$-\langle\Delta E\rangle$/J $\mathrm{mol^{-1}}$
CF_3I-Ar[a]	1100	0.032	490
	1200	0.021	347
CH_3I-Ar[d]	1100	0.028	393
	1200	0.021	326

a) Input data for the calculation of the strong collision-rate constants: threshold energy, $E_0 = 223$ kJ $\mathrm{mol^{-1}}$; Lennard-Jones collision diameters,[b] $\sigma(CF_3I) = 5.05$ Å, $\sigma(\mathrm{Ar}) = 3.54$ Å; Lennard-Jones well depths,[b] $\varepsilon(CF_3I)/k = 300$ K, $\varepsilon(\mathrm{Ar})/k = 119$ K; vibrational frequencies of CF_3I,[c] 1074, 1185(2), 742, 539(2), 284, 260(2) $\mathrm{cm^{-1}}$. b) R. C. Reid, J. M. Prausnitz, and T. K. Sherwood, "The Properties of Gases and Liquids," 3rd ed., McGraw-Hill, N. Y. (1977). c) JANAF Thermochemical Tables, 2nd ed., Natl. Bur. Stand. (1971). d) Ref. 5.

References

1) O. B. Danidov, V. V. Edagin, V. Yu. Zadesskii, and I. L. Yanev, *Kinet. Katal.*, **16**, 302 (1975).

2) G. A. Skorobogatov, *Kinet. Katal.*, **23**, 18 (1982).

3) A. P. Modica and S. J. Sillers, *J. Chem. Phys.*, **48**, 3283 (1968).

4) K. Saito, T. Yokubo, T. Fuse, H. Tahara, O. Kondo, T. Higashihara, and I. Murakami, *Bull. Chem. Soc. Jpn.*, **52**, 3507 (1979).

5) K. Saito, H. Tahara, O. Kondo, T. Yokubo, T. Higashihara, and I. Murakami, *Bull. Chem. Soc. Jpn.*, **53**, 1335 (1980).

6) J. Troe and H. G. Wagner, *Ber. Bunsenges. Phys. Chem.*, **71**, 937 (1967). The Kassel parameters for the reaction considered are: $S_k = 6.52$, 6.76, and 6.98, and $B_k = 21$, 20, and 18 at 1000, 1100, and 1200 K respectively.

7) O. Kondo, K. Saito, and I. Murakami, *Bull. Chem. Soc. Jpn.*, **53**, 2133 (1980).

8) J. Troe, *J. Chem. Phys.*, **66**, 4745, 4758 (1977).

9) This value was evaluated from the fall-off curves calculated for the decomposition of CH_3I.

10) The data are cited K. Okada, O. Kajimoto, and T. Fueno, *Bull. Chem. Soc. Jpn.*, **51**, 4434 (1978).

Hydrates of Organic Compound IX. Enclathration of Methyl and Ethyl Alcohols within the Water Lattice of Tetrahydrofuran Clathrate Hydrate

Hiroshi MATSUI† and Haruo NAKAYAMA*
†*The Radio Isotope Center and Department of Chemistry*
Faculty of Engineering, Yokohama National University,
Tokiwadai, Hodogaya-ku, Yokohama 240
(Received February 24, 1984)

Synopsis. The amount of methyl or ethyl alcohol existing in a hydrate solid deposited from ternary mixtures of methyl (or ethyl) alcohol-tetrahydrofuran-water has been determined using ^{14}C-labeled alcohols. It was found that these alcohols could be enclathrated within the water lattice of tetrahydrofuran clathrate hydrate.

In a previous paper[1] a phase-diagrammatic method for examining the ability of an alcohol to form a clathrate-like hydrate in the presence of a reference substance, ethylene oxide or tetrahydrofuran, has been proposed and it has been concluded that both methyl and ethyl alcohols can be enclathrated within the water lattice of tetrahydrofuran(THF) hydrate (Type II). However, this method may lead to a wrong conclusion in some cases, especially when (1) a peak position in a phase diagram is obscured because of the flatness of the peak and (2) the peak position does not apparently shift owing to a complicated change of activity coefficients of the components concerned with their concentrations.[2] In fact, some other measurements have concluded that methyl alcohol cannot be enclathrated within the water lattice of such hydrates as ethylene oxide and THF.[2]

The purpose of this paper is, therefore, to carry out a direct measurement of the amount of either methyl or ethyl alcohol present in the solid carefully formed from a ternary mixture of the alcohol-THF-water by using radioactive alcohols.

Experimental

Procedure and Measurements. A mixture (about 10 g) containing given amount of either methyl or ethyl alcohol (^{14}C-labeled, 0.1—0.3 μCi), tetrahydrofuran(THF), and water was prepared. The mixture was inserted into one portion of a forked glass vessel, and cooled until the solid phase appeared. It was then gradually warmed until only a small amount of the solid remained undissolved. Then the mixture was kept standing for more than 12 h at an appropriate temperature mentioned below in order to grow the solid as slowly as possible.

A known amount (0.5—3 g) of the solid sample, which was separated from its supernatant solution by filtration, was dissolved in a given amount of scintillator, Insta-gel (Packard Instrument Co., Inc.). The radio activity of the sample was measured using the TRI-CARB 460C Automatic Liquid Scintillation System (Packard Instrument Co., Inc.).

Determination of the Experimental Conditions. In Fig. 1, the solid-liquid phase diagrams[1] for the ethyl alcohol-THF-water systems are shown, in which the dissolution temperature is plotted against the sum of the mole fractions, $X=X_{THF}+X_{alc}$, where X_{THF}, and X_{alc} are the mole

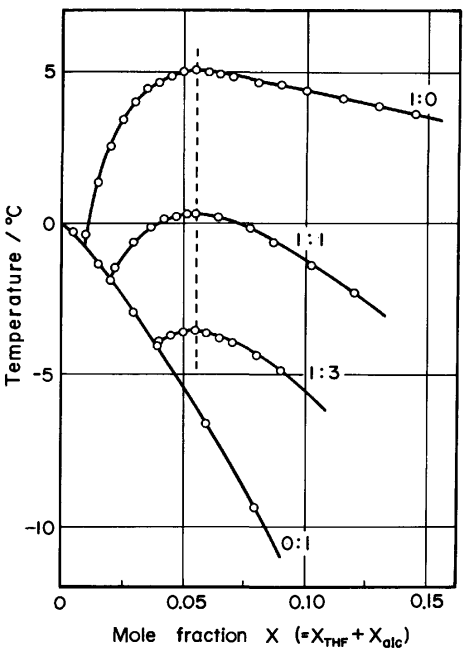

Fig. 1. The solid-liquid phase diagrams for THF–ethyl alcohol–water systems. Explanations are given in the text.

fractions of THF and ethyl alcohol, respectively. Each curve corresponds to the system in which the ratio $X_{THF}:X_{alc}$ is kept constant. The curve marked 1:0 is for the THF-water binary system and the congruent melting point at 5.1 °C and X=0.056 indicates the formation of the clathrate hydrate of THF (Type II). Similarly the curve marked 0:1 is for the ethyl alcohol-water binary system. This curve indicates no formation of a clathrate hydrate in the temperature range examined in agreement with several other experiments.[3-5] However, the other two curves (marked with 1:1 and 1:3) in Fig. 1 give no information about the composition of the solid phase since, in these ternary systems, the abscissa of Fig. 1 does not indicate a solid phase composition even at a peak position.[1] A direct determination of the composition of the solid phase is the object of this study as mentioned above. Preliminary experiments showed that, (1) for the systems containing ethyl alcohol with $X_{THF}+X_{alc}$=0.056 and $X_{THF}:X_{alc}$=1:1—1:3, solid phases formed at temperatures higher than −10 °C were morphologically different from those formed below −10 °C and the latter were identified with ice, and (2) the solid formed from the mixture containing much ethyl alcohol than $X_{THF}:X_{alc}$=1:4 was found to be ice. Systems containing methyl alcohol also showed similar behavior except that the limit of the ratio $X_{THF}:X_{alc}$ was 1:6 instead of 1:4. From these facts, appropriate experimental conditions were determined as follows: temperature=−6 °C, the molar ratio $X_{THF}:X_{alc}$=1:1—1:3 for ethyl alcohol and

1:0.5—1:4 for methyl alcohol. The mole fraction X was kept constant at 0.056 in all cases.

Results and Discussion

Estimation of the Amount of the Liquid Phase Adhering to the Solid Phase. In order to know the composition of the solid phase exactly, we must first estimate the weight fraction, y, of the liquid phase coexisting with the wet solid sample separated from a supernatant solution. Since, if alcohol can form a mixed clathrate hydrate with THF expressed by a formula $(\text{alcohol})_x(\text{THF})_{1-x}\cdot 17H_2O$, x should decrease with increasing temperature, as exemplified by other systems,[6] we tentatively assumed that x was equal to zero for the solid formed at a temperature as high as possible. Based upon this assumption the value of y was estimated to be 0.46 for the systems containing ethyl alcohol from the radioactivity measurements for the solid formed from the mixtures of $X_{THF}:X_{alc}=1:1$ at −2.5 °C and −3.7 °C, and 0.35 for the systems containing methyl alcohol from the data corresponding to $X_{THF}:X_{alc}=1:0.5$ at −0.5 °C. We further assumed that the same y values could be used in analyzing the experimental results since (1) the appearance of the solid phase (formed at −6 °C) was closely the same as when values above y were estimated, and (2) the temperature dependence of y was proved to be negligible.

Enclathration of Alcohols within the Water Lattice of the Clathrate Hydrate of THF. Using the y values evaluated above, the observed x's in an assumed formula $(\text{alcohol})_x(\text{THF})_{1-x}\cdot 17H_2O$ are summarized in Table 1. Each value is an average of 5—10 measurements.

Table 1 shows that x's for the systems containing ethyl alcohol are relatively small, around 0.05, and almost constant irrespective of the molar ratio $X_{THF}:X_{alc}$, indicating that ethyl alcohol can be enclathrated within the lattice of the THF clathrate hydrate from the following reasons: (1) if ethyl alcohol cannot form a mixed clathrate hydrate with THF, x should likewise be zero as assumed in the estimation of y; and (2) a solid-liquid phase diagram of the system which forms a mixed clathrate hydrate requires that x should be constant at a given temperature regardless of the composition of the system,[6] in fair agreement with the above experimental results.

Table 1. The observed x values in the assumed formula $(\text{alcohol})_x(\text{THF})_{1-x}\cdot 17H_2O$ for the solid formed at −6 °C in ternary mixtures of alcohol–THF–water with $X_{THF}+X_{alc}=0.056$

Alcohol	X_{THF} : X_{alc}	x
Ethyl alcohol	1 : 2	0.055
	1 : 3	0.044
Methyl alcohol	1 : 2	0.024
	1 : 3	0.16
	1 : 4	0.29

It can also be concluded that methyl alcohol is included within the THF clathrate hydrate lattice since the x values in Table 1 are larger than zero. However, in contrast to the systems containing ethyl alcohol, x increases with increasing methyl alcohol content. Although a precise explanation for this phenomenon cannot be given because of the lack of any other information, one possibility would be that methyl alcohol can also be accommodated within such vacant water cages as 12-hedron or 14-hedron as well as 16-hedron as its concentration increases. This phenomenon will be, in a sense, a typical one for an inclusion compound as exemplified by the fact that, in a gas hydrate, the degree of occupancy of a guest molecule increases with increasing its partial pressure.

References

1) H. Nakayama and M. Hashimoto, *Bull. Chem. Soc. Jpn.*, **53**, 2427 (1980).
2) D. W. Davidson, S. R. Gough, J. A. Ripmeester, and H. Nakayama, *Can. J. Chem.*, **59**, 2587 (1981).
3) A. D. Potts and D. W. Davidson, *J. Phys. Chem.*, **69**, 996 (1965).
4) P. Boutron and A. Kaufmann, *J. Chem. Phys.*, **68**, 5032 (1978).
5) J. B. Ott, J. R. Goates, and B. A. Waite, *J. Chem. Thermodyn.* **11**, 739 (1979).
6) H. Nakayama, M. Asano, Y. Nakajima, and K. Hanno, *Nippon Kagaku Kaishi*, **1983**, 269.

Primary Structure and Molecular Evolution of Protein. Internal Homology and Intramolecular Evolutionary Tree of Calmodulin

Yôichi IIDA

Department of Chemistry, Faculty of Science, Hokkaido University, Sapporo 060

(Received March 7, 1984)

Synopsis. One notable feature of the primary structure of calmodulin is its internal homology. It can be subdivided into four domains having a similar amino acid sequence. In the present paper, an intramolecular evolutionary tree was constructed with the four domains. The origin and evolution of calmodulin was discussed on the basis of these results.

Origin and evolution of protein is one of the most important problems in biology and biochemistry. Evolutionary trees of typical proteins, such as cytochrome c and globins, have been constructed with a number of biological species.[1] In previous papers,[2,3] we studied molecular evolution of calmodulin (CaM), one of the calcium-binding proteins. It has four calcium-binding sites, and interacts reversibly with Ca^{2+} to form a calmodulin-Ca^{2+} complex.[4] CaM plays an important role in regulating other enzymatic reactions or cellular processes. The complete amino acid sequence of bovine brain CaM was first determined by Watterson *et al.*[5] and by Kasai *et al.*[6] It contains 148 amino acids and has a trimethylated lysin at position 115.

One notable feature of CaM is that it is widely distributed throughout eukaryotes and that the primary structure of CaM is highly conservative against evolution.[2] Another interesting feature is that the primary structure of CaM has internal homology, that is, it can be subdivided into four domains having a similar amino acid sequence. This is shown, for example, in Fig. 1 with bovine brain CaM, where the first domain (residues 8 to 40), the second (residues 44 to 76), the third (residues 81 to 113) and the fourth (residues 117 to 148) are aligned for purposes of comparison. The amino acids which do not belong to the four domains are residues 1 to 7, 41 to 43, 77 to 80 and 114 to 116. These are the linking sequences between the domains. In the following, we only discuss the amino acids belonging to the four domains. In the previous paper,[3] we found by visual inspection that the amino acid sequence homology is greatest when the first domain is aligned with the third, and the second domain with the fourth . In order to explain this fact, a two-step intragenic duplication model (refer to Fig. 4 of Ref. 3) was proposed to the primary amino acid sequence of CaM. In this model, it is assumed that an ancestral one-domain quarter-calmodulin (AQ) underwent an elongation by the first intragenic duplication, which resulted in an ancestral two-domain half-calmodulin (AH). In the period from the birth of AH to the next intragenic duplication (stage 1 in Fig. 4 of Ref. 3), AH underwent evolutionary changes and some replacements of amino acids occurred in it. At the end of stage 1, the second intragenic duplication took place, resulting in an ancestral four-domain calmodulin (AC). In the period from the birth of AC to the present time (stage 2 in Fig. 4 of Ref. 3), AC underwent further evolution and some replacements of amino acids took place.

```
                 8
Domain (1)  -Gln-Ile-Ala-Glu-Phe-Lys-Glu-Ala-Phe-Ser-Leu-Phe-
                44
Domain (2)  -Thr-Glu-Ala-Glu-Leu-Gln-Asp-Met-Ile-Asn-Glu-Val-
                81
Domain (3)  -Ser-Glu-Glu-Glu-Ile-Arg-Glu-Ala-Phe-Arg-Val-Phe-
               117
Domain (4)  -Thr-Asp-Glu-Glu-Val-Asp-Glu-Met-Ile-Arg-Glu-Ala-

                20
(1)  Asp-Lys-Asp-Gly-Asp-Gly-Thr-Ile-Thr-Thr-Lys-Glu-
                56
(2)  Asp-Ala-Asp-Gly-Asp-Gly-Thr-Ile-Asp-Phe-Pro-Glu-
                93
(3)  Asp-Lys-Asp-Gly-Asp-Gly-Tyr-Ile-Ser-Ala-Ala-Glu-
               129
(4)  Asp-Ile-Asp-Gly-Asp-Gly-Gln-Val-Asn-Tyr-Glu-Glu-

                32
(1)  Leu-Gly-Thr-Val-Met-Arg-Ser-Leu-Gly-
                68
(2)  Phe-Leu-Thr-Met-Met-Ala-Arg-Lys-Met-
               105
(3)  Leu-Arg-His-Val-Met-Thr-Asn-Leu-Gly-
               141
(4)  Phe-Val-Gln-Met-Met-Thr-Ala-Lys
```

Fig. 1. Comparison and homology of the amino acid sequences of the four domains in bovine brain calmodulin. The first domain (residues 8 to 40), the second (residues 44 to 76), the third (residues 81 to 113) and the fourth (residues 117 to 148) are aligned for purposes of comparison.

Clearly, this model is based on the finding that relations between the first and third domains and between the second and fourth domains are closest. However, these two relations do not necessarily support the above two-step intragenic duplication model. In order to support this model definitely, we should construct intramolecular phylogenetic tree of the four domains. If such a tree is once constructed, we can clearly show how the four domains are related with one another.

There have been known two approaches to construct such an evolutionary tree;[1] one is common ancestor method and the other, matrix method. If the evolutionary rate of protein is slow enough, the two methods reach the same conclusion. In the present paper, we construct intramolecular evolutionary tree of the four domains of bovine brain CaM by the use of the common ancenstor method. "Maximum parsimony method" is used for this purpose. It is generally known that codons of m RNA are translated into amino acids of protein. Any codon is composed of a series of three nucleotides and is expressed by "the genetic code". Therefore, the observed difference of amino acid residues of CaM between the domains (see Fig. 1) is attributable to the difference of nucleotides between the corresponding codons. Referring to the

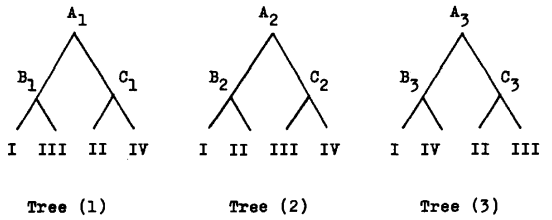

Fig. 2. Three possible intramolecular evolutionary trees (1), (2), and (3) for the four domains of bovine brain calmodulin. The first domain, the second, the third and the fourth are indicated by I, II, III, and IV, respectively. See Fig. 1 for the amino acid sequences of those domains. In each tree, we assume amino acid sequences of common ancestral domains (A_i), (B_i), and (C_i), (i=1, 2 or 3), so that the total number of nucleotide substitutions within the tree can be minimized (the maximum parsimony method). For further details, see the text.

genetic code, we assume that the difference of amino acids is given by the least number of nucleotide substitutions of the codons. In order to examine the above intragenic duplication model, we assume three evolutionary trees, as shown in Fig. 2. The tree (1) represents the evolutionary change, where the first and third domains were diverged from the common ancestral domain (B_1), while the second and fourth domains, from the common ancestor (C_1). The common ancestors (B_1) and (C_1) had been diverged from the common ancestral domain (A_1). Clearly, the tree (1) represents faithfully the evolutionary change of the above-mentioned intragenic duplication model. That is, the common ancestor (A_1) corresponds to the former or latter half of AH, since at the birth of AH it was formed by duplication of AQ. In a similar way, the common ancestor (B_1) corresponds to the first or third domain of AC, while the common ancestor (C_1), to the second or fourth domain of AC (see Fig. 4 of Ref. 3).

In addition to the tree (1), we further consider two possible evolutionary trees (2) and (3). The tree (2) assumes that the first and second domains were diverged from the common ancestral domain (B_2), while the third and fourth domains, from the common ancestor (C_2). These two common ancestors had been diverged from the common ancestral domain (A_2). In this tree, the relations between the first and second domains and between the third and fourth domains are closest. In a similar way, the tree (3) assumes that the first and fourth domains came from the common ancestral domain (B_3), while the second and third domains, from the common ancestor (C_3). Both (B_3) and (C_3) had come from the common ancestral domain (A_3). In order to determine which tree is most probable, we use the maximum parsimony method. In each tree, we assume amino acid sequences of common ancestral domains (A_i), (B_i), and (C_i), (i=1, 2 or 3), so that the total number of nucleotide substitutions within the tree can be minimized. In order to do this, we note a lack of one amino acid of the fourth domain at position 149 (see Fig. 1). The corresponding amino acid residues of the first, second and third domains are Gly at position 40, Met at position 76 and Gly at position 113, respectively. These three amino acid residues are excluded from our counting, because we cannot compare the amino acid residues in all four domains. Taking into account the remaining amino acid residues in the four domains, we calculated the minimum number of nucleotide substitutions of the trees (1), (2), and (3) as 65, 72, and 72, respectively. Therefore, the maximum parsimony method rejects the evolutionary trees (2) and (3) and suggests that the evolutionary tree (1) is most probable. This conclusion confirms that the homologies between the first and third domains and between the second and fourth domains are greatest, and supports strongly our previous two-step intragenic duplication model for the primary amino acid sequence of CaM.

References

1) See, for example, M. O. Dayhoff, "Atlas of Protein Sequence and Structure," National Biomedical Research Foundation, Washington, D. C. (1972), Vol. 5.
2) Y. Iida, *Bull. Chem. Soc. Jpn.*, **55**, 2683 (1982).
3) Y. Iida, *J. Mol. Biology*, **159**, 167 (1982).
4) N. Y. Cheung, *Science*, **207**, 19 (1980).
5) D. M. Watterson, F. Sharief, and T. C. Vanaman, *J. Biol. Chem.*, **255**, 962 (1980).
6) H. Kasai, Y. Kato, T. Isobe, H. Kawasaki, and T. Okuyama, *Biomed. Res.*, **1**, 248 (1980).

cDNA Sequences and Molecular Evolution of Calmodulin Genes of Chicken and Eel

Yôichi IIDA
Department of Chemistry, Faculty of Science, Hokkaido University, Sapporo 060
(Received April 18, 1984)

Synopsis. c DNA sequences of calmodulin genes taken from chicken and eel were compared to investigate the molecular evolution of its protein. One notable feature of the amino acid coding region of the gene is that the second positions of codons are more conservative than the first positions, while the third positions are highly diverged to exhibit almost saturation. This kind of behaviour is reminiscent of that of the histone gene.

Origin and evolution of protein is one of the most important problems in biology and biochemistry. Recently, primary nucleotide sequences have been determined with a number of genes which code for proteins. Studies on molecular evolution of proteins in terms of such DNA sequences are very interesting. Calmodulin (CaM) is one of the calcium-binding proteins.[1-3] It has four calcium-binding sites, and interacts reversibly with Ca^{2+} to form a calmodulin-Ca^{2+} complex. It contains 148 amino acids and has a trimethylated lysine at position 115. One notable feature of CaM is that it is widely distributed throughout eukaryotes and that the primary amino acid sequence is highly conservative against evolution. In previous papers,[4,5] we examined the origin and evolution of CaMs in terms of their primary amino acid sequences. So for, their amino acid sequences have been determined with a number of representative species.[1-5] However, little information was known with the m RNAs that code for CaM. Recently, Lagacé *et al.* and Putkey *et al.* isolated m RNAs of CaM from the electroplax of electric eel (Electrophorus electricus) and from chicken brain, respectively,[6,7] and their c DNAs (DNA complementary to m RNA) have been cloned and sequenced. Therefore, it is very interesting to compare the DNA sequences between both biological species. We pay attention to how the highly conservative amino acid sequence of CaM is related to the coding region of c DNA.

Figure 1 shows the amino acid coding regions of the nucleotide sequences of CaM c DNAs for chicken and eel. The numbers indicate amino acid positions. The initiation (ATG) and termination (TGA) codons are common to the two species. If we exclude these two codons, the coding region of the c DNA is composed of 148 codons. For the two species, the corresponding codons are aligned and compared in Fig. 1. Those nucleotides which are different between the two species are indicated by asterisk (*). The other nucleotides are found to be identical between the two. As is expected from the highly conservative amino acid sequences of CaM, the primary nucleotide sequences in the amino acid-coding regions of the respective c DNA are highly homologous, with an overall homology of 79%. Particularly, the first and second positions (replacement sites) of codons show markedly higher degree of homology than does the overall homology. In contrast to these, the third positions (silent sites) of codons are very much diverged.

In order to treat these situations more quantitatively, we consider one-parameter and two-parameter models for evaluating the degree of nucleotide changes proposed by Kimura *et al.*[8] In estimating the evolutionary distances between homologous sequences in terms of the number of nucleotide substitutions, corrections for multiple and revertant changes at homologous sites are important. The total number of nucleotide substitutions per site, K, which separate two sequences and therefore involve two branches each with time length T, is expressed by $K=2Tk$, where k is the total rate of substitutions per site per year. In the one-parameter model where probability of every nucleotide substitution is assumed to be common, K is given by[8]

$$K = -\frac{3}{4}\ln\left(1-\frac{4\lambda}{3}\right), \tag{1}$$

where λ is the fraction of sites for which two sequences differ from each other. From the data of Fig. 1 of the chicken and eel CaM genes, the λ value for the first positions of codons was calculated as 7/148=0.0473, while the values for the second and third positions, as 1/148=0.00676 and 84/148=0.568, respectively. As can be seen from the highly conservative amino acid sequences of CaM, the magnitudes of λ for the replacement sites are extremely small, while that for the silent site is found to be larger than 1/2. If nucleotide substitutions occur randomly, the λ value will show a saturated value of 3/4=0.75. In view of this, the value for the third position appears to approach such a saturated value. Using Eq. 1, the K values for the first, second and third positions of codons were calculated as 0.049 (±0.019), 0.0068 (±0.0068) and 1.06 (±0.17), respectively, where the figures in parentheses show standard error.[8]

In the two-parameter model, the probabilities of transition type nucleotide substitutions and transversion type substitutions are discriminated. The transitions are substitutions of purines by purines (A↔G), and pyrimidines by pyrimidines (T↔C), while the transversions are substitutions in which a purine is replaced by a pyrimidine, or a pyrimidine is replaced by a purine (A or G↔T or C). In this model, the K value is expressed by[9]

$$K = -\frac{1}{2}\ln\{(1-2P-Q)\sqrt{1-2Q}\}. \tag{2}$$

Here, P and Q are given by the fraction of sites for which two sequences differ from each other with respect to transition type and transversion type substitutions, respectively. In the chicken and eel CaM genes, P and Q for the first positions of codons were calculated as 4/148=0.0270 and 3/148=0.0203, respectively. These values lead to K=0.049 (±0.019) for the first positions, where the figure in parentheses shows stan-

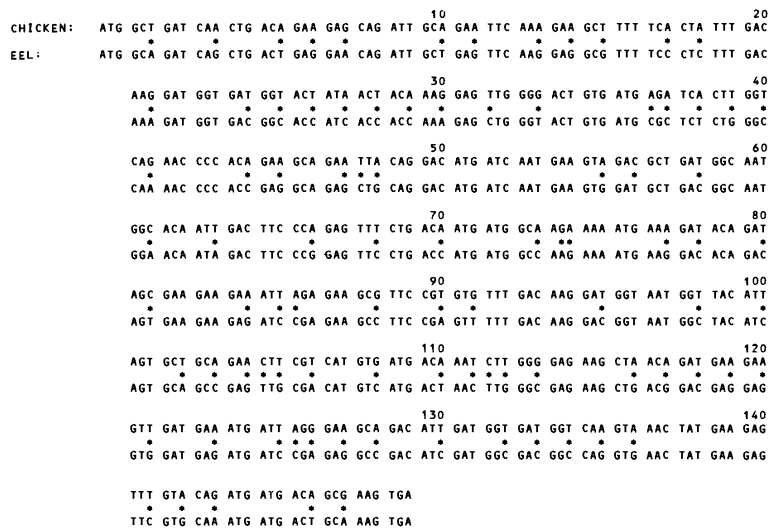

Fig. 1. Comparison and homology of the amino acid coding regions of the c DNA sequences taken from chicken and electric eel (Electrophorus electricus).[6,7] The initiation (ATG) and termination (TGA) codons are common between the two species. The numbers indicate amino acid positions. Those nucleotides which are different between the two species are shown by asterisk (*).

dard error.[9] Similarly, for the second positions, $P=1/148=0.00676$, $Q=0.00000$ and $K=0.0068$ (± 0.0068), and for the third positions, $P=53/148=0.358$, $Q=31/148=0.209$ and $K=1.44$ (± 0.49). In all three positions, P is greater than $(1/2)Q$, indicating that the transitions have occurred more frequently than have the transversions. In this respect, the two-parameter model is more realistic than the one-parameter model, and the following discussion will be made with the two-parameter model.

The most notable feature of the CaM genes is that the K value of the third positions (K_3) is much greater than those of the first (K_1) and second (K_2) positions. This means that the pressure by natural selection has been strongly applied to amino acid sequences of CaM, while the third positions of codons are almost neutral against evolution; most of the third positions are synonymous with respect to changes of amino acid residues. It is also found that the magnitude of K_2 is less than that of K_1. The order of $K_2<K_1<K_3$ holds generally with various protein genes, such as β-globin gene.[10]

Using the equation of $K=2Tk$, we estimate the values of k, the rate of nucleotide substitutions per site per year. We assume that the common ancestor of eel and chicken CaMs diverged $T=3.5\times10^8$ years ago (the time of divergence into osteichthyes and amphibians).[11] Then, the values of k for the first, second and third positions of codons of CaM are calculated as $k_1=0.070\times10^{-9}$, $k_2=0.0097\times10^{-9}$ and $k_3=2.1\times10^{-9}$, respectively. These results may be compared with histone H4 which is known to be the most highly conservative protein against evolution. The rate of amino acid substitutions per site per year of histone H4 is known as $k_{aa}=0.006\times10^{-9}$.[12] The value of k_2 of CaM is of comparable order with that of k_{aa}, while the value of k_1 of CaM is about ten times larger than that of k_{aa}. Therefore, although the first positions of codons of CaM are less conservative than those of histone H4, the conservative properties of these two proteins are comparable with each other. In contrast to these, the rate of $k_3=2.1\times10^{-9}$ of the third positions of CaM is as high as 2.3×10^{-9} of fibrinopeptide or $(3.7\pm1.4)\times10^{-9}$ of the third nucleotide positions of histone H4 gene.[12] The latter two values are known as the highest rate of nucleotide substitutions. It is remarkable that, in CaM gene, synonymous mutant substitutions have occurred with the highest rate, while the amino acid substitutions have occurred with as low rate as that of histone H4.

References

1) W. Y. Cheung, *Science*, **207**, 19 (1980).
2) T. Takagi, T. Nemoto, K. Konishi, M. Yazawa, and K. Yagi, *Biochem. Biophys. Res. Commun.*, **96**, 377 (1980).
3) M. Yazawa, K. Yagi, H. Toda, K. Kondo, K. Narita, R. Yamazaki, K. Sobue, S. Kakiuchi, S. Nagano and Y. Nozawa, *Biochem. Biophys. Res. Commun.*, **99**, 1051 (1981).
4) Y. Iida, *Bull. Chem. Soc. Jpn.*, **55**, 2683 (1982).
5) Y. Iida, *J. Mol. Biology*, **159**, 167 (1982).
6) L. Lagacé, T. Chandra, S. L. C. Woo and A. R. Means, *J. Biol. Chem.*, **258**, 1684 (1983).
7) J. A. Putkey, K. F. Ts'ui, T. Tanaka, L. Lagacé, J. P. Stein, E. C. Lai and A. R. Means, *J. Biol. Chem.*, **258**, 11864 (1983).
8) M. Kimura and T. Ohta, *J. Mol. Evol.*, **2**, 87 (1972).
9) M. Kimura, *J. Mol. Evol.*, **16**, 111 (1980).
10) "Molecular Evolution, Protein Polymorphism and The Neutral Theory," ed by M. Kimura, Springer-Verlag, Berlin, Heidelberg, New York, p. 31 (1982).
11) A. S. Romer, "Vertebrate Paleontology," Third Edition, The University of Chicago Press, Chicago and London (1966).
12) M. Kimura, *Nature*, **267**, 275 (1977).

Preparation of Sodium Bis(L-aspartato)rhodate(III)

Masatoshi WATABE,* Kenji FURIHATA, and Yoshio ODAKA
General Education Department, Kogakuin University Nakano-cho, Hachioji-shi, Tokyo 192
(Received November 11, 1983)

Synopsis Bis(L-aspartato) rhodate(III) complex was prepared and separated into three isomers, and their absorption, CD curves and ^{1}H NMR spectra are presented. The geometrical configurations of three isomers are assigned mainly on the basis of the spectral analogy between this complex and the $[Co(L\text{-}asp)_2]^-$ complex.

Numerous studies of cobalt(III) complexes containing amino carboxylate ion have been reported,[1-3] but only a few rhodium(III) complexes with amino carboxylate ion have been studied.[4] As both cobalt(III) and rhodium(III) have the same low spin d^6 electronic configuration, the spectral features of the rhodium(III) complexes should resemble those of the cobalt(III) complexes having the same ligands. Smith and Sawyer[4] have reported on the preparation and the characterization by ^{1}H-NMR spectra of rhodium(III) complexes having iminodiacetate ion (=ida) and *N*-methyliminodiacetate ion (=mida), in which UV and ^{1}H-NMR spectra of these complexes resemble those of the cobalt(III) complexes having the same ligand. The present paper deals with the preparation and the assignment of Bis(L-aspartato) rhodate(III).

Experimental

To a hot solution (20 cm^3) containing 2g of $Rh(NO_3)_3$ (0.007 mol) 4 mol dm^{-3} KOH solution was added untill the pH of the solution reached 7. The precipitate was centrifuged and suspended in 80 cm^3 of water containing 1.84 g of aspartic acid (0.0138 mol) in a pyrex tube and heated at 120—130 °C for five hours. After cooling, the tube was opened carefully and a small quantity of metallic rhodium removed by filtration. This solution was loaded on a QEA-Sephadex A-25 anion exchanger column (50×300 mm). After the elution of the cation and non charged complexes with water, the column was eluted with 0.1 mol dm^{-3} NaCl solution. Five bands descended and showed yellow or yellow brown color (R1, R2, R3, R4, and R5; those are named in the order of elution). The bands R1, R2, and R3 were the desired isomers as established below. The separation of R2 and R3 was not good. The complexes corrsponding to bands R4 and R5 did not possess one minus charge because these bands gradually spread with 0.1 mol dm^{-3} NaCl solution. Each eluate was concentrateed by using a rotary evaporator at room temperature. Calcd for $Na[Rh(L\text{-}asp)_2]\ 2H_2O$ C, 21.80; H, 4.12; N, 6.36%. Found (R1): C, 21.75; H, 4.01; N, 6.55%. Found (R2): C, 21.86; H, 4.36; N, 6.37. Found (R3): C, 22.00; H, 4.05; N, 6.45%.

Spectral Measurements. Visible absorption and circular dichroism spectra were measured with JASCO-UV505 and JASCO-J20 spectrometers in aqueous solution. ^{1}H NMR spectra were measured with a Varian FT-80A spectrometer in D_2O solution with TSP (sodium 3-(trimethylsilyl) propionate) as an internal standard.

Results and Discussion

Figure 1 shows the possible isomers of $[Rh(L\text{-}asp)_2]^-$. These complexes are composed of one

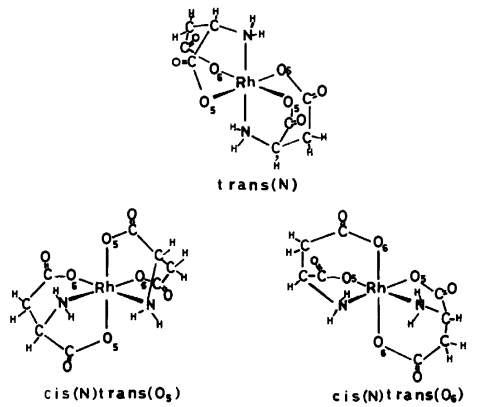

Fig. 1. The three possible isomers of $[Rh(L\text{-}asp)_2]^-$.

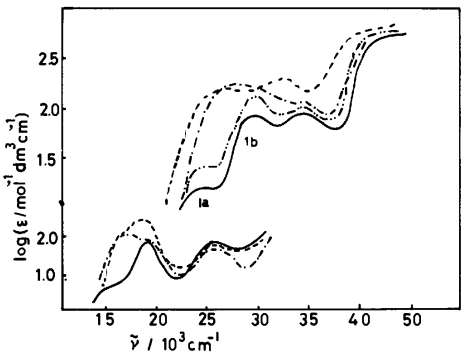

Fig. 2. Visible absorption spectra of $[Rh(L\text{-}asp)_2]^-$· (upper) R1 ——, R2 ----, R3 —·—, *trans*(N)-$[Rh(ida)_2]^-$, —··—, and $[Co(L\text{-}asp)_2]^-$· (lower) F ——, S ---- and T —·—.

trans(N) and two *cis*(N) isomers. The two *cis*(N) isomers are designated *cis*(N) *trans*(O_5) and *cis*(N) *trans*(O_6) as in the case of bis(L-aspartato) cobaltate(III) complexes.[5] Figure 2. shows the UV spectra of $[Rh(L\text{-}asp)_2]^-$ along with those of $[Co(L\text{-}asp)_2]^-$ and *trans*(N)-$[Rh(ida)_2]^-$. The lowest energy band of the R1 isomer split into well-separated components (24300 and 29400 cm^{-1}) and the splitting pattern in the first and the second absorption band regions agree with those of *trans*(N)-$[Rh(ida)_2]^-$. The isomer R1, therefore, is assigned as the *trans*(N) isomer (Fig. 1). It should be noted that the peak maximum of this isomer in the second absorption band region lies *ca.* 8000 cm^{-1} higher than that of the F isomer of $[Co(L\text{-}asp)_2]^-$[1] while the peak maximum of 1b (29400 cm^{-1}) in the first absorption band region lies *ca.* 10000 cm^{-1} higher than that of the F isomer of $[Co(L\text{-}asp)_2]^-$ (Table 1). This larger shift of the first absorption band causes the smaller seperation between the peak maxima of the first and the second absorption band than the corresponding separation for *trans*(N)-$[Co(L\text{-}asp)_2]^-$. This relation also prevails between *trans*(N)-$[Rh(ida)_2]^-$ and *trans*(N)-$[Co(ida)_2]^-$.

TABLE 1. AB AND CD DATA FOR $[Rh(L\text{-}asp)_2]^-$ AND ITS RELATED COMPLEXES

	First absorption				Second absorption			
	AB		CD		AB		CD	
	$\bar{\nu}_{max}$*	log ε*	$\bar{\nu}_{max}$	$\Delta\varepsilon$*	$\bar{\nu}_{max}$	log ε	$\bar{\nu}_{max}$	$\Delta\varepsilon$
trans(N)-$[Rh(L\text{-}asp)_2]^-$	24.30	1.22	24.40	0.53	34.50	1.93	33.90	0.36
	29.40	1.93	29.85	1.08				
cis(N)*trans*(O_5)-$[Rh(L\text{-}asp)_2]^-$	25.80	2.06	24.40	−0.18	33.20	2.23	33.20	0.16
cis(N)*trans*(O_6)-$[Rh(L\text{-}asp)_2]^-$	27.03	2.24	27.03	1.12	34.48	2.07	33.90	−0.16
	29.40	2.25	31.25	−0.47				
trans(N)-$[Co(L\text{-}asp)_2]^-$	15.87	1.16	16.50	0.35	26.46	1.89	25.10	0.42
	19.53	1.90	19.40	1.42			28.40	−0.10
cis(N)*trans*(O_5)-$[Co(L\text{-}asp)_2]^-$	16.70	1.89	17.90	−1.36	26.18	1.87	26.00	0.62
cis(N)*trans*(O_6)-$[Co(L\text{-}asp)_2]^-$	17.24	2.09	17.30	3.71	26.40	1.80	25.00	−0.54
trans(N)-$[Rh(ida)_2]^-$	25.00	1.45			35.20	2.02		
	30.45	2.12						
cis(N)-$[Rh(ida)_2]^-$	27.16	2.43			33.8	2.37		

* $\bar{\nu}/10^3$ cm^{-1}, ε/mol^{-1} dm^3 cm^{-1}.

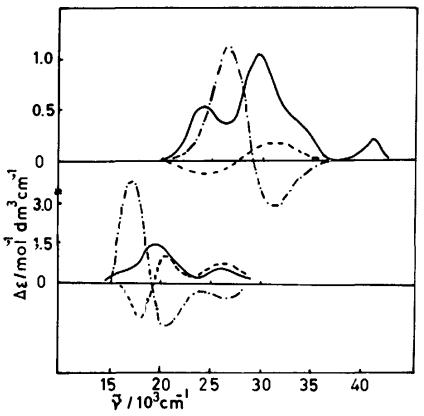

Fig. 3. CD spectra of $[Rh(L\text{-}asp)_2]^-$ (upper); R1 ——, R2 ----, and R3 —·—, and $[Co(L\text{-}asp)_2]^-$ (lower); F ——, S ----, and T —·—.

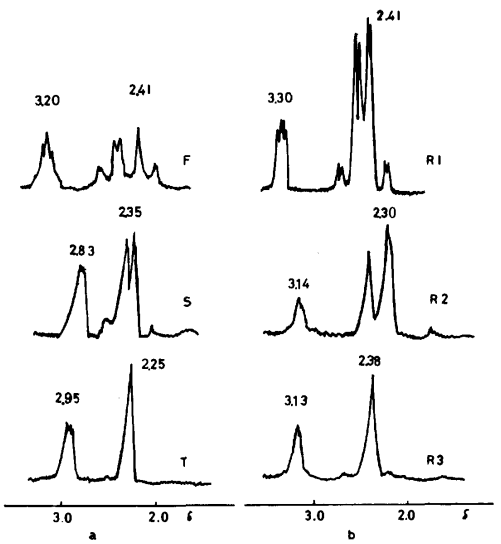

Fig. 4. ^{1}H-NMR spectra of $[Co(L\text{-}asp)_2]^-$ (left side); F, S, and T and $[Rh(L\text{-}asp)_2]^-$ (right side); R1, R2, and R3. ppm from TSP.

The three CD spectra are shown in Fig. 3 along with those of $[Co(L\text{-}asp)_2]^-$. From the crystal-structural analysis,[2] the geometry of the T isomer has been determined as a *cis*(N) *trans*(O_6) configuration. These three CD spectra of the $[Rh(L\text{-}asp)_2]^-$ complexes closely resemble those of $[Co(L\text{-}asp)_2]^-$ except that the peak maxima shift to higher energies. We assigned the R2 and the R3 isomers as *cis*(N) *trans*(O_5) and *cis*(N) *trans*(O_6).

^{1}H NMR spectra of the $[Rh(L\text{-}asp)_2]^-$ complex are shown in Fig. 4 along with those of the $[Co(L\text{-}asp)_2]^-$. The resemblance of the ^{1}H NMR spectra (80 MHz) between $[Rh(L\text{-}asp)_2]^-$ and $[Co(L\text{-}asp)_2]^-$ is notable. We have reported that when X is an oxygen atom in the moiety -CH-NH_2-Co-X (X is trans to NH_2), the methine proton signals appear at a slightly higher magnetic field than is the case where X is a nitrogen atom.[3] This trend holds for most cobalt(III) complexes. The chemical shifts of the methine proton of $[Rh(L\text{-}asp)_2]^-$ are 3.30 ppm for R1, 3.14 ppm for R2 and 3.13 ppm for R3. These values suggest that the chemical shift trend holds good in the rhodium(III) complex. However the two *cis*(N) isomers can not be distinguished only from this terend of the ^{1}H NMR data. On the basis of the elemental analysis data and the resemblance of the spectra between the $[Rh(L\text{-}asp)_2]^-$ and the $[Co(L\text{-}asp)_2]^-$ complexes, we assigned the isomers R1,R2, and R3 as *trans*(N), *cis*(N) *trans*(O_5), and *cis*(N) *trans*(O_6).

Reference

1) S. Yamada, J. Hidaka, and B. E. Douglas, *Inorg. Chem.*, **10**, 2187 (1971).

2) I. Oonishi, S. Sato, and Y. Saito, *Acta Cryst allogr Sect. B.*, **31**, 1318 (1975).

3) M. Watabe, K. Onuki, and S. Yoshikawa, *Bull. Chem. Soc. Jpn.*, **48**, 687 (1975).

4) B. B. Smith and D. T. Sawyer, *Inorg. Chem.*, **7**, 922 (1968).

5) The three isomers of $[Co(L\text{-}asp)_2]^-$ were named F, S, and T isomers in the order of elution and were assigned as *trans*(N), *cis*(N) *trans*(O_5), and *cis*(N) *trans*(O_6), respectively.

The Preparation of Pyridinium μ-Oxo-bis[nitrilotriacetatodioxomolybdate(VI)] and Pyridinium Di-μ-oxo-bis[nitrilotriacetatooxomolybdate(V)] Monohydrate and the X-ray Structure of the Molybdenum(VI) Complex

Keiji MATSUMOTO,* Yoshiaki MARUTANI, and Shun-ichiro OOI
Department of Chemistry, Faculty of Science, Osaka City University, Sumiyoshi-ku, Osaka 558
(Received December 7, 1983)

Synopsis. Nitrilotriacetato complexes of Mo^{VI} and Mo^{V} were prepared and the X-ray structure of the former complex is described. On the basis of the UV-visible and IR spectra and elemental analyses, the latter complex is formulated as $(pyH)_2[Mo_2O_4(ntaH)_2]\cdot H_2O$.

As a part of studies on the structure of molybdenum complexes,[1-3] we describe here the preparation of nitrilotriacetato complexes of Mo^{VI} and Mo^{V}, and the X-ray structure of the molybdenum(VI) complex.

Experimental

Preparation of $(pyH)_2[Mo_2O_5(ntaH)_2]$ (1). Pyridine(py) was added to nitrilotriacetic acid($ntaH_3$) (2 m mol) in 20 ml of water and the solution was adjusted to pH 7—8. To this solution was added 2 m mol of MoO_3 and the suspension was warmed on a water bath with stirring for 0.5 h at 60 °C. During the reaction pyridine was added in order to keep pH 7—8. The resulting solution was filtered, evaporated to 4 ml, and methanol (5 ml) and acetone (8 ml) added. Colorless crystals were obtained after standing a couple of days. Yield, 270 mg. Found: C, 32.50; H, 3.36; N, 6.87%. Calcd for $(pyH)_2[Mo_2O_5(ntaH)_2]$; C, 32.60; H, 3.24; N, 6.92%.

Preparation of $(pyH)_2[Mo_2O_4(ntaH)_2]\cdot H_2O$ (2). $(pyH)_2[MoOCl_5]$ (2 m mol) and $ntaH_3$ (2 m mol) were added to 20 ml of water. The solution was warmed at 60 °C with stirring for 0.5 h and was adjusted to pH 7—8 with pyridine. The solution was filtered, evaporated to 7 ml, and methanol (5 ml) and acetone (5 ml) were added. Brown crystals were obtained after standing for 24 h. Yield, 520 mg. Found: C, 32.47; H, 3.58; N, 6.83%. Calcd for $(pyH)_2[Mo_2O_4(ntaH)_2]\cdot H_2O$: C, 32.52; H, 3.48; N, 6.90%.

Crystal Data of 1: $C_{22}H_{26}O_{17}N_4Mo_2$, F. W.=810.4, triclinic, space group $P\bar{1}$, a=17.244(8) Å, b=12.161(4) Å, c=7.558(2) Å, α=104.99(3)°, β=83.36(3)°, γ=74.88(3)°, Z=2, D_m=1.84 g cm^{-3}, D_c=1.86 g cm^{-3}, μ(Mo $K\alpha$)=9.42 cm^{-1}, λ(Mo $K\alpha$)=0.7107 Å, U=1449.3(8) Å^3.

The intensities were measured on a Philips PW1100 diffractometer. Crystal size: 0.23×0.32×0.39 mm^3; scan speed: 0.033° s^{-1}; scan range: 1.0°; backgroung measurement at each side of the scan range: half of the scan time; maximum 2θ value: 50°; number of reflections with $F_o^2 \geq 3\sigma(F_o^2)$: 4338.

The refinement of the structure was performed by the block-diagonal least-squares method. The function minimized was $\sum w(F_o-|F_c|)^2$, where $w=1/\sigma^2(F_o)$ was used. The R value was 0.031 ($R_w=[\sum w\Delta F^2/\sum wF_o^2]^{1/2}$=0.047). In the final cycles of the refinement hydrogen atoms were included but their parameters were not refined. Hydrogen atoms defined by the geometry of the complex were located at calculated positions and those bonded to OA5 and OB5 atoms were found in the difference Fourier map. All the parameter shifts were less than 0.3σ. The maximum peak in the final difference Fourier map was 0.6 eÅ^{-3}. The atomic scattering factors, with corrections for anomalous scattering of Mo were taken from Ref. 4. The F_o-F_c Tables, anisotropic temperature factors, and coordinates of hydrogen atoms are preserved by the Chemical Society of Japan (Document No. 8429). The atomic coordinates are listed in Table 1. Computations were performed on a FACOM 230-60 computer at Osaka City University and on an ACOS 900 computer at the Crystallographic Research Center. Institute for Protein Research, Osaka University. The programs in the UNICS were used.[5]

The absorption spectrum was recorded on a Hitachi 330 spectrophotometer and infrared spectra were obtained in KBr disks with a JASCO IRA-1 spectrophotometer.

Results and Discussion

Figure 1 gives a perspective view of the complex in **1**. The complex has an approximate two fold axis. The complex consists of two octahedra sharing a single non-linear oxo bridge (MoA-OB-MoB=167.0(2)°). The two terminal oxo ligands on each Mo are mutually cis and cis to the bridging oxo. The $Mo(O_t)_2$ (O_t=terminal oxo) groups lie on the same side of the complex. The distorted octahedral coordination of each Mo is formed by two terminal and one bridging oxo (O_b), and two carboxylato oxygen atoms and one amino nitrogen atom of ntaH. One carboxylate group in ntaH is free from the coordination. The Mo-O_t distances (1.683(3)—1.700(3) Å) are comparable to those in cis dioxo complexes (Table 2).[6] The average Mo-O_b distance is 1.876(6) Å. The two Mo-O distances to the ntaH ligand in each Mo at 2.072(2) (trans to O_b) and 2.151(6) Å (trans to O_t) indicate that O_t has a larger trans bond weakening effect. The Mo-N bond (trans to O_t) is longer than

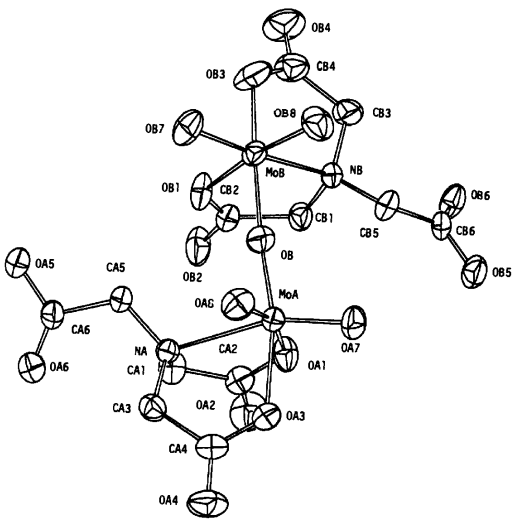

Fig. 1. A perspective view of $[Mo_2O_5(ntaH)_2]^{2-}$.

Table 1. Atomic coordinates and temperature factors for $(pyH)_2[Mo_2O_5(ntaH)_2]$ with their estimated standard deviations in parentheses

Atom	x	y	z	U_{eq}/Å^2 a)
MoA	0.15255(2)	0.14765(3)	0.27443(5)	0.0282
NA	0.2809(2)	0.1925(3)	0.2724(4)	0.028
OA1	0.1769(2)	0.1962(3)	0.0249(4)	0.045
OA2	0.2424(2)	0.2854(3)	−0.1333(5)	0.064
OA3	0.1245(2)	0.3315(3)	0.3773(4)	0.039
OA4	0.1566(2)	0.4916(3)	0.5219(5)	0.052
OA5	0.4847(2)	0.0136(3)	0.2843(5)	0.051
OA6	0.4395(2)	0.2092(3)	0.3293(5)	0.055
OA7	0.0535(2)	0.1628(3)	0.2559(5)	0.049
OA8	0.1607(2)	0.1304(3)	0.4876(4)	0.045
CA1	0.3058(3)	0.2108(4)	0.0898(6)	0.039
CA2	0.2371(3)	0.2356(4)	−0.0146(5)	0.033
CA3	0.2608(3)	0.3045(4)	0.4286(6)	0.035
CA4	0.1754(3)	0.3840(3)	0.4447(5)	0.034
CA5	0.3441(3)	0.0938(4)	0.3021(6)	0.039
CA6	0.4276(3)	0.1132(4)	0.3062(6)	0.037
OB	0.2101(2)	−0.0080(2)	0.1252(4)	0.041
MoB	0.74578(2)	0.17435(3)	−0.01603(5)	0.0289
NB	0.7966(2)	0.1441(3)	0.2594(4)	0.028
OB1	0.6568(2)	0.1219(3)	0.1407(4)	0.046
OB2	0.6241(2)	0.0358(3)	0.3516(5)	0.056
OB3	0.6896(2)	0.3313(3)	0.2001(4)	0.048
OB4	0.6657(3)	0.4391(3)	0.4944(5)	0.055
OB5	0.9948(2)	−0.0506(3)	0.2614(4)	0.042
OB6	0.9097(2)	0.0968(3)	0.5021(4)	0.042
OB7	0.6828(2)	0.2200(3)	−0.1573(4)	0.049
OB8	0.8289(2)	0.2174(3)	−0.0644(5)	0.055
CB1	0.7503(3)	0.0764(4)	0.3395(6)	0.038
CB2	0.6708(2)	0.0787(4)	0.2745(5)	0.032
CB3	0.7813(3)	0.2654(4)	0.3901(6)	0.040
CB4	0.7063(3)	0.3526(4)	0.3690(6)	0.043
CB5	0.8847(3)	0.0762(4)	0.1926(6)	0.036
CB6	0.9307(2)	0.0418(4)	0.3378(6)	0.033
NC	−0.0206(3)	0.6729(4)	0.0289(6)	0.062
CC1	0.0474(3)	0.6120(5)	−0.0954(7)	0.057
CC2	0.1146(3)	0.5577(4)	−0.0426(8)	0.058
CC3	0.1133(3)	0.5679(5)	0.1429(8)	0.066
CC4	0.0420(4)	0.6329(5)	0.2698(7)	0.070
CC5	−0.0232(4)	0.6843(5)	0.2084(8)	0.058
ND	0.5988(3)	0.5329(4)	0.1277(8)	0.087
CD1	0.5555(5)	0.6302(6)	0.2660(9)	0.096
CD2	0.5043(3)	0.7168(5)	0.0440(8)	0.059
CD3	0.5052(4)	0.7275(5)	0.2187(9)	0.080
CD4	0.5485(4)	0.6107(5)	−0.0969(8)	0.079
CD5	0.5975(4)	0.5210(5)	−0.0494(9)	0.069

a) $U_{eq}=(U_{11}+U_{22}+U_{33})/3$.

Table 2. Interatomic distances and bond angles with their estimated standard deviations in parentheses

Bond length(l/Å)		Bond angle(ϕ/°)	
MoA-OB	1.870(3)	MoA-OB-MoB	167.0(2)
MoA-OA1	2.145(3)	OB-MoA-OA7	104.7(2)
MoA-OA3	2.071(3)	OB-MoA-OA8	99.2(2)
MoA-OA7	1.695(3)	OA7-MoA-OA8	106.4(2)
MoA-OA8	1.695(3)	OA1-MoA-NA	73.6(1)
MoA-NA	2.413(3)	OA3-MoA-NA	73.0(1)
MoB-OB	1.881(3)	OB-MoB-OB7	104.8(2)
MoB-OB1	2.156(3)	OB-MoB-OB8	100.3(2)
MoB-OB3	2.075(4)	OB7-MoB-OB8	105.3(2)
MoB-OB7	1.700(3)	OB1-MoB-NB	72.6(1)
MoB-OB8	1.683(3)	OB3-MoB-NB	73.4(1)
MoB-NB	2.426(3)		
Possible hydrogen bond(l/Å) a)			
NC(I)···OA1	2.883(6)		
ND···OB3	2.766(7)		
OA5···OB2	2.581(5)		
OB5···OB6(II)	2.634(4)		

a) Roman numerals refer to the following equivalent positions: (I) $-x$, $1-y$, $-z$; (II) $2-x$, $-y$, $1-z$.

the Mo–O bond (trans to O_t).

The IR spectrum of **2** gives the stretching vibrations of the Mo=O groups at 920 and 945 cm^{-1} and that of the Mo_2O_2 group at 783 cm^{-1}.[7] The IR spectra of the symmetric and assymmetric stretching vibrations of the carboxylato groups are similar in **1** and **2**. The UV-visible spectrum of **2** in pH 4 sodium acetate/acetic acid buffer solution gives two absorption peaks at 380 nm (shoulder, ε=162 l mol^{-1}cm^{-1}) and 297 nm (ε=5080 l mol^{-1} cm^{-1}). The spectrum is similar to that of $[Mo_2O_4(edta)]^{2-}$.[8] On the basis of the UV-visible and IR spectra and elemental analyses we formulate **2** as pyridinium di-μ-oxo-bis[nitrilotriacetatooxomolybdate(V)] monohydrate, $(pyH)_2[Mo_2O_4(ntaH)_2]\cdot H_2O$.

We wish to thank Dr. Takashi Shibahara for the sample of $(pyH)_2[MoOCl_5]$ and Mr. Junichi Gohda for elemental analyses.

References

1) T. Shibahara, H. Kuroya, K. Matsumoto, and S. Ooi, *Inorg. Chim. Acta*, **54**, L75 (1981).
2) T. Shibahara, S. Ooi, and H. Kuroya, *Bull. Chem. Soc. Jpn.*, **55**, 3742 (1982).
3) T. Shibahara, H. Kuroya, K. Matsumoto, and S Ooi, *Bull. Chem. Soc. Jpn.*, **56**, 2945 (1983).
4) "International Tables for X-Ray Crystallography," Kynoch Press, Birmingham (1974), Vol. IV, pp. 71, 148.
5) "The Universal Crystallographic Computation Program System," The Crystallographic Society of Japan, Tokyo (1969).
6) B. Spivack and Z. Dori, *Coord. Chem. Rev.*, **17**, 99 (1975); E. I. Stiefel, *Prog. Inorg. Chem.*, **22**, 1 (1977).
7) A. Kay and P. C. H. Mitchell, *J. Chem. Soc., A*, **1970**, 2421.
8) Y. Sasaki and A. G. Sykes, *J. Chem. Soc., Dalton Trans.*, **1974**, 1468.

Formation Process of Aluminium Nitride by the Vapor-phase Reaction of Aluminium Trichloride with Ammonia

Yuzo SAEKI,* Suh Ho PARK, Akimasa YAJIMA, and Masayo AKIYAMA
Research Laboratory of Resources Utilization, Tokyo Institute of Technology, 4259, Nagatsuta-cho, Midori-ku, Yokohama 227
(Received March 21, 1984)

Synopsis. The reaction products of gaseous $AlCl_3$ with ammonia were $AlCl_3 \cdot 3NH_3$ at 200—500 °C, AlN, $AlCl_3 \cdot 3NH_3$, NH_4Cl at 550—900 °C, and AlN, NH_4Cl at 1000 °C. AlN is considered to be formed by the reaction of gaseous $AlCl_3 \cdot 3NH_3$, formed by the reaction of gaseous $AlCl_3$ with ammonia, with ammonia above *ca.* 550 °C.

The properties of aluminium nitride (AlN) suggest that AlN has potential applications in electronic devices for high-temperature operations. AlN has become of interest as a piezoelectric film material. Concerning the deposition of AlN from aluminium trichloride ($AlCl_3$) by the vapor-phase reaction, Chu *et al.*[1] have reported the epitaxial growth of AlN by the reaction of gaseous $AlCl_3$ with ammonia. Bauer *et al.*[2] have studied the dependence of the AlN deposition rate on the conditions of the vapor-phase reaction of $AlCl_3$ with ammonia and the properties of the AlN films formed. Arnold *et al.*[3] have examined the yields of AlN films by the vapor-phase reaction of $AlCl_3$ with ammonia under various reaction conditions and estimated that the decomposition of $AlCl_3$–NH_3 adduct, formed in the reaction process, significantly contributes for the formation of AlN. However, the formation process of AlN by the vapor-phase reaction of $AlCl_3$ with ammonia has not been revealed. In this paper, the reaction products of gaseous $AlCl_3$ with ammonia at 200—1000 °C were examined. Also, the possible reactions which were considered to occur during the reaction process were examined. From these results, the formation process of AlN by the vapor-phase reaction of $AlCl_3$ with ammonia is discussed.

Experimental

The $AlCl_3$ used was prepared by the reaction of pure aluminium (Al 99.99%) with chlorine at 400 °C.[4] The chemical analysis gave Al, 20.2; Cl, 79.8% (calcd for $AlCl_3$: Al, 20.24; Cl, 79.76%). The ammonia was dried by passing it over sodium hydroxide granules and barium oxide powders.

Experimental apparatus and procedures for examining the reaction products of gaseous $AlCl_3$ with ammonia are the same as those described in the previous paper.[5] Gaseous $AlCl_3$ was formed by heating solid $AlCl_3$ (10 g) at 165 °C and was carried by a stream of argon (50 cm^3/min) into the reaction zone. The mean flow-rate of gaseous $AlCl_3$ was 6.0 cm^3 Al_2Cl_6(g)/min. Ammonia was simultaneously introduced at a flow-rate of 100 cm^3/min into the reaction zone through a separate tube. The reaction was allowed to proceed for 2 h.

The aluminium, chlorine and ammonia contents of the $AlCl_3$–NH_3 adduct formed were determined by chelatometric titration,[6] gravimetric method as AgCl, and the Kjeldahl method, respectively, after dissolving the sample in 3M-nitric acid. Thermogravimetry (TG) of the $AlCl_3$–NH_3 adduct was performed by using a thermal balance with a quartz helix (the sensitivity: approximately 113 mm/g). The sample (0.2 g) was heated at a rate of 2.5 °C/min and the flow-rate of ammonia or argon was maintained at 50 cm^3/min.

Results and Discussion

The products formed by heating gaseous $AlCl_3$ in an ammonia stream at various temperatures were examined by both X-ray analysis[7,8] and chemical analysis.

The products formed at 200—500 °C showed the same X-ray diffraction pattern, which was clearly different from those of known aluminium compounds. From the chemical analysis of the products at 200—500 °C, the ratios of Al:Cl:NH_3 of the products were calculated to be 1:3.00:3.06—3.35. As will be described later, it was found that the products absorbed ammonia. From these results, the removal of the ammonia absorbed by heating the product in an argon stream was examined by using the thermal balance. The result showed that the ammonia absorbed into the products was removed by heating the products in an argon stream at 150 °C for 3 h. A typical chemical analysis of the products formed at 200—500 °C after the removal of the ammonia absorbed gave Al, 14.6; Cl, 57.6; NH_3, 27.6%. The ratio of Al:Cl:NH_3 was calculated to be 1:3.00:3.00. From the results, it was considered that the products formed at 200—500 °C had a composition of $AlCl_3 \cdot 3NH_3$ (calcd for $AlCl_3 \cdot 3NH_3$: Al, 14.63; Cl, 57.67; NH_3, 27.70%).

The reaction products of gaseous $AlCl_3$ with ammonia at various temperatures above 200 °C are summarized in Table 1. Unreacted $AlCl_3$ was not observed throughout the temperature range of this work.

To elucidate the reaction process of gaseous $AlCl_3$ with ammonia, the behavior of the $AlCl_3 \cdot 3NH_3$, which had been formed during the reaction process, on heating in an ammonia stream was examined.

Table 1. Reaction products of gaseous $AlCl_3$ with ammonia at various temperatures

Temp/°C	Products	
	In the reaction zone	Outside the reaction zone
200—300	$AlCl_3 \cdot 3NH_3$	$AlCl_3 \cdot 3NH_3$
350—500	—	$AlCl_3 \cdot 3NH_3$
550—650	AlN (6—28)	$AlCl_3 \cdot 3NH_3$; NH_4Cl
700—900	AlN (42—82)	AlN, $AlCl_3 \cdot 3NH_3$; NH_4Cl
1000	AlN (86)	AlN; NH_4Cl

Note: the values in parentheses are mole percentages of gaseous $AlCl_3$ converted to AlN.

Table 2. Reaction products of gaseous $AlCl_3 \cdot 3NH_3$ with ammonia at various temperatures

Temp/°C	Products	
	In the reaction zone	Outside the reaction zone
500	—	$AlCl_3 \cdot 3NH_3$
550—650	AlN (6—33)	$AlCl_3 \cdot 3NH_3$; NH_4Cl
700—800	AlN (58—82)	AlN, $AlCl_3 \cdot 3NH_3$; NH_4Cl
900	AlN (85)	AlN; NH_4Cl

Note: the values in parentheses are mole percentages of gaseous $AlCl_3 \cdot 3NH_3$ converted to AlN.

The result of TG of $AlCl_3 \cdot 3NH_3$ in an ammonia stream showed that $AlCl_3 \cdot 3NH_3$ gradually absorbed ammonia at room temperature. The weight gain due to the absorption of ammonia reached a constant value after about 5 h. By heating the sample after the absorption, it lost weight gradually above about 60 °C, and the weight decreased markedly above about 230 °C. The weight loss reached 100% above about 370 °C. Vaporization of $AlCl_3 \cdot 3NH_3$ was observed during the weight loss above 230 °C. To obtain more detailed information on the behavior of $AlCl_3 \cdot 3NH_3$ on heating in an ammonia stream, $AlCl_3 \cdot 3NH_3$ (1.0 g) in a quartz boat was placed in a straight reaction tube. Ammonia was introduced into the reaction tube at a flow-rate of 100 cm^3/min. The sample part was then placed in the centre of an electric furnace maintained at a specified temperature for 1 h. The products obtained inside and outside the boat were examined. The results indicated that $AlCl_3 \cdot 3NH_3$ vaporized in an ammonia stream and that the percentage of the vaporized $AlCl_3 \cdot 3NH_3$ was 0% at 200 °C, <1% at 230 °C, 1% at 250 °C, 9% at 280 °C, 48% at 300 °C, and 100% at 320 and 350°C.

The reaction of gaseous $AlCl_3 \cdot 3NH_3$ with ammonia was then examined under similar experimental conditions for examining the reaction products of gaseous $AlCl_3$ with ammonia, described before. Gaseous $AlCl_3 \cdot 3NH_3$ was formed by heating solid $AlCl_3 \cdot 3NH_3$ in a stream of ammonia (50 cm^3/min) at 330 °C and was introduced into the reaction zone. The mean flow-rate of $AlCl_3 \cdot 3NH_3$ was 9.0 cm^3/min. The reaction products of gaseous $AlCl_3 \cdot 3NH_3$ with ammonia at various temperatures are shown in Table 2.

The results showed that the reaction of gaseous $AlCl_3 \cdot 3NH_3$ with ammonia occurred above about 550 °C to form AlN and NH_4Cl.

From the above-mentioned experimental results, the formation process of AlN by the vapor-phase reaction of $AlCl_3$ with ammonia can be represented as follows: The reaction of gaseous $AlCl_3$ with ammonia to form $AlCl_3 \cdot 3NH_3$ occurs first. Above about 550 °C, the gaseous $AlCl_3 \cdot 3NH_3$ reacts with ammonia to form AlN.

References

1) T. L. Chu, D. W. Ing, and A. J. Noreika, *Solid-State Electron.*, **10**, 1023 (1967).
2) J. Bauer, L. Biste, and D. Bolze, *Phys. Status Solidi A*, **39**, 173 (1977).
3) H. Arnold, L. Biste, and Th. Kaufmann, *Krist. Tech.*, **13**, 929 (1978).
4) Y. Shoji, K. Tatsumi, R. Matsuzaki, and Y. Saeki, *Bull. Chem. Soc. Jpn.*, **53**, 269 (1980).
5) A. Yajima, Y. Segawa, R. Matsuzaki, and Y. Saeki, *Bull. Chem. Soc. Jpn.*, **56**, 2638 (1983).
6) H. Flaschka and H. Abdine, *Z. Anal. Chem.*, **152**, 77 (1956).
7) JCPDS, Powder Diffraction File 25-1133.
8) ASTM, Powder Diffraction File 7-7.

Conversion of Alcohols into Haloalkanes in Tertiary Phosphine/Methyl Halide/4-Methyl-1,2,4-triazolidine-3,5-dione (MTAD) System

Tatsuo OSHIKAWA* and Mitsuji YAMASHITA

Department of Applied Chemistry, Faculty of Engineering, Shizuoka Usniversity, Hamamatsu 432

(Received November 28, 1983)

Synopsis. Alcohols were succesfully converted to the corresponding alkyl halides using the betaine provided by tertiary phosphine/4-methyl-1,2,4-triazolidine-3,5-dione (MTAD) system. Stereospecific reaction involving inversion of configuration on the carbon atom (S_N2 reaction) was clarified.

In a series of studies on 4-methyl-1,2,4-triazolidine-3,5-dione (MTAD), reaction of diene and ene components were examined. These are known to act as a dienophile or enophile[1] towards MTAD.[2] The previous studies on MTAD were mainly limited to the addition reaction.

This report describes the transformation of alcohols **2** such as benzyl alcohol (**2a**), cyclohexanol (**2b**), (−)-menthol (**2c**), (−)-borneol (**2d**), and (−)-2-octanol (**2e**) to the haloalkanes **5** using tertiary phosphine and MTAD system. Stereospecific conversion of alcohols into haloalkanes with inversion of configuration by using the conventional method with well known reagents such as dihalophosphine[3,4] afforded the inverted products. However, conversion of alcohols into haloalkanes using a betaine formed from reaction of triphenylphosphine with MTAD has not previously been reported. Reaction of triphenylphosphine with diethyl azodicarboxylate is known to form a betaine-like intermediate **1**.[5]

Results and Discussion

In the present reaction, the yields of **5** were extremely high and they did not depend on the choice of the tertiary phosphine used *i.e.*, triphenylphosphine or tributylphosphine (Table 1). The reaction can be explained by assuming the successive formation of a betaine **1** and an alkoxyphosphonium salt **3**. Methyl halide methylate intermediates **3** liberate a halide anion which, in turn, attacks the carbon atom of the alkoxide group in the Arbzov type intermediate, *i.e.*, alkoxyphosphonium salt **4**.[6,7] By using this procedure, alcohols **2c** and **2e** were successfully converted into the corresponding halides with inversion of configuration (S_N2 type reaction)[6] at the carbon atom (Table 2).

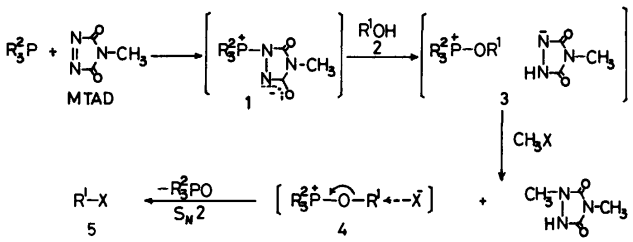

Attempted reaction of compound **2b** with methyltriphenylphosphonium bromide to promote the dissociation of the halogen in the presence of an equimolar amount of MTAD was unsuccessful. These results show that the tertiary phosphine/methyl halide/MTAD system does not proceed *via* a formation of methyltriphenylphosphonium halide, that the system is effective for halogenation of alcohols in the yield and stereospecificity, and that the intermediate of first formed key betaine **1** as well as the last Arbzov type one

TABLE 1. CONVERSION OF ALCOHOLS **2** INTO HALOALKANES **5** (TERTIARY PHOSPHINE/METHYL HALIDE/MTAD SYSTEM)

Alcohol **2a—e** R^1OH	R^2_3P	CH_3X	Product **5a—e**[a] R^1X	Purity/% G.L.C.	Yield /%	IR (cm^{-1})	Bp (°C)/mmHg, (mp °C) Found	reported
Benzyl alcohol	Ph	I	Benzyl halide[b]	100	92	1200, 645	101—102/15	102/15[11]
(**2a**)	Ph	Br	(**5a**)	100	91	1158, 680	81—82/18	80—81/16[8]
	n-Bu	I		100	89	1200, 645		
	n-Bu	Br		100	87	1158, 680		
Cyclohexanol	Ph	I	Cyclohexyl halide[b]	95	74	1170, 650	68—69/10	72/15[11]
(**2b**)	Ph	Br	(**5b**)	95	71	1160, 680	58—60/15	163—165[12]
	n-Bu	Br		95	75	1170, 650		
(−)-Menthol	Ph	I	Neomenthyl halide[b]	100	88	1170, 650	120—121/15	122—123/17[8]
(**2c**)	Ph	Br	(**5c**)	100	88	1165, 645	103—104/15	91/7[13]
	n-Bu	Br		100	88	1165, 645		
(−)-Borneol	Ph	Br	(+)-Bornyl bromide[c]	—	75	1180, 685	(129—131)	(133)
(**2d**)	*n*-Bu	Br	(**5d**)	—	76	1180, 685		
(−)-2-Octanol	Ph	I	(+)-2-Iodooctane	81	65	1180, 680	101—102/18	42/0.5[4]
(**2e**)			(**5e**)					

a) Satisfactory ^1H NMR spectra have been obtained for all haloalkanes **5**. b) Haloalkanes **5a**, **5b**, and were identified by G.L.C. being compared with authentic samples. c) Haloalkane **5d** was isolated by chromatography on silica gel.

Table 2. Haloalkanes **5c—e** from opticaly active alcohols **2c—e** (Tertiary phosphine/methyl halide/MTAD system)

Haloalkane[a] (**5c—e**)	Temp °C	$[\alpha]_D$ Found	$[\alpha]_D$ Reported
Neomenthyl iodide (**5c**)	17.0	+39.6° (c=1.01, EtOH)	+41.2° [8]
Neomenthyl bromide (**5c**)	13.5	−7.26° (c=1.01, EtOH)	−10.45° [8]
(+)-Bornyl bromide (**5d**)	15.0	−2.39° (c=1.01, EtOH)	+21.2° [9]
(+)-2-Iodooctane (**5e**)	17.0	+23.8° (c=1.02, EtOH)	+19.53° [4]

a) Optical rotations of the alcohols **2c**, **2d**, and **2e** were −49°, −37.7°, and −9.9°, respectively.

Table 3. Conversion of alcohols **2** into haloalkanes **5** (Ph_3P/CH_3I/DEADC[a] system)

R^1OH	Product	Purity/% (G.L.C)	Yield[b]/%	$[\alpha]_D$
2a	Benzyl iodide	98	90	—
2b	Cyclohexyl iodide	78	61	—
2c	Neomenthyl iodide	100	92	+39.4 (c=1.02, EtOH)
2e	(+)-2-Iodooctane	96	92	+23.5 (c=1.02, EtOH)

a) DEADC=Diethyl azodicarboxylate (EtO-C(=O)-N=N-C(=O)-OEt). b) Isolated yield by distillation.

play an important role in the stereospecific halogenation. Comparison of the yield and stereospecificity of the present method with that using the triphenylphosphine/diethyl azodicarboxylate/methyl iodide system[5] in conversion of alcohols **2** into iodoalkanes **5** (Table 3) shows that this method is an exellent alternative for preparation of haloalkanes. No large difference in the purity of haloalkanes was recognized in the tow methods.

This new procedure has some advantages in preparing haloalkanes, *i.e.*, mild reaction conditions, high product yield, and facile work up to remove tertiary phosphine oxide and 2,4-dimethyl-1,2,4-triazolidine-3,5-dione.

Identification of the products **5** was established by comparison with authentic samples by IR and ^1H NMR spectra, optical rotation, and/or retention time of G. L. C.

Experimental

Measurements. Melting points were measured on a Yanagimoto Seisakusho micro melting point apparatus. ^1H NMR spectra were recorded on a Hitachi R-24 (60 MHz) spectrometer with TMS as an internal standard, IR spectra on a JASCO A-3 infrared spectrophotometer, G. L. C. on a Yanagimoto Gas Chromatograph GCG-550T, and optical rotations were determined with JASCO DIP-4 digital and Atago Polax photometers.

Preparation of Neomenthyl Iodide (5c); Typical Procedure: A solution of MTAD (2.4 g, 21 mmol) in tetrahydrofuran (20 ml) was added to a tetrahydrofuran (30 ml) solution of (−)-menthol (**2c**) (3.0 g, 19 mmol) and triphenylphosphine (5.5 g, 21 mmol) at a temperature of 0 °C. After 10—15 min, methyl iodide (2.7 g, 19 mmol) in tetrahydrofuran (5 ml) was added to the solution (excess methyl halide caused the yield of haloalkanes to be decreased). The mixture was stirred for 6 h at room temperature, then, the solvent was evaporated under reduced pressure. The product was taken up into ether, the insoluble material filtered off and washed with ether to removed triphenylphosphine oxide and 2,4-dimethyl-1,2,4-triazolidine-3,5-dione.

The filtrate was evaporated under reduced pressure, and the residue separated by thin-layer chromatography (silica gel, 1:1 ether/benzene) or distilled under reduced pressure (bp 120—121 °C/15 mmHg, 1 mmHg=133.322 Pa) to give pure neomenthyl iodide (**5c**) in 88% yield, ^1H NMR ($CDCl_3$), δ=0.86 (d, J=7.1 Hz, 3H, CH_3), 0.96 (d, J=7.1 Hz, 6H, $CH(C\underline{H}_3)_2$), 0.63—2.43 (m, 9H, $C\underline{H}(CH_3)_2$ and ring protons other than CHI), and 4.63 (m, 1H, CHI); IR ν_{max}^{neat}, 1170 cm^{-1} (C-I); $[\alpha]_D^{17.0}$ +39.6° (c=1.01, C_2H_5OH) (lit,[8] neomenthyl iodide $[\alpha]_D$ +41.2°); G. L. C. retention time 2 min (column: Versamide 20%, 900 on Neopack 1A, 60/80 mesh; carrier gas; H_2 (1 Kg/cm^2); column temperature: 141 °C; column length: 2 m).

The authers wish to express their thanks to Professor M. Suzuki's laboratory of Shizuoka University for providing facility for measurement of the optical rotation.

References

1) W. Adam and O. De. Lucchi, *Angew. Chem., Int. Ed. Engl.*, **19**, 762 (1980).
2) R. C. Cookson and S. S. Gupe, *Org. Synth.*, **51** 121 (1971).
3) L. Hiner, H. Oediger, and H. Hoffman, *Ann.*, **626**, 26 (1959).
4) D. G. Coe, S. R. Landauer, and H. N. Rydon, *J. Chem. Soc.*, **1954**, 2281.
5) O. Mitsunobu, *Synthesis.*, **1981**, 1, and references cited therein.
6) H. Loibarer and E. Zbiral, *Helv. Chim. Acta.*, **59**, 2100 (1976).
7) H. Kung and P. Schmidt, *Tetrahedron Lett.*, **1979**, 2123.
8) T. Kurssanow, *Chem. Zentr.*, 1923, **III**, 1074.
9) O. Wallach and E. Conrady, *Ann.*, **252**, 156 (1889); H. Heikman, P. Baeckstrom, and K. Torssel, *Acta. Chem. Scand.*, **22**, 2034 (1968).
10) R. H. Pickard and J. Kenyon, *J. Chem. Soc.*, **99**, 69 (1911).
11) M. Lauwers, B. Reginer, M. V. Eenoo, J. N. Denis, and A. Krief, *Tetrahedron Lett.*, **1979**, 1801.
12) G. A. Wiley, R. L. Hershkowitz, B. M. Rein, and B. C. Chung, *J. Am. Chem. Soc.*, **86**, 964 (1964).
13) M. Yamashita, Y. Soeda, N. Suzuki, M. Yamada, K. Tsunekawa, T. Oshikawa, and S. Inokawa, *Bull. Chem. Soc. Jpn.*, **56**, 1871 (1983).

Preparation of 5-Substituted-2-pyrrolin-4-ones from *N*-(4-Oxo-2-pyrrolin-5-yl)sulfoximines

Hiroshi YOSHIDA,* Shoichi BANDO, Shosuke NAKAJIMA,
Tsuyoshi OGATA, and Kiyoshi MATSUMOTO†
Department of Applied Chemistry, Faculty of Engineering, Shizuoka University, Hamamatsu 432
†*College of Liberal Arts and Sciences, Kyoto University, Kyoto 606*
(Received December 13, 1983)

Synopsis. In trifluoroacetic acid, immonium cations were generated from *S,S*-dimethylsulfoximines in which the pyrrolinone ring was substituted. Nucleophiles such as alcohols, thiocyanic acid, thiols, or acetylacetone reacted with the immonium salts to yield 5-substituted 2-pyrrolin-4-ones.

In previous papers[1,2] we have reported the reaction of diphenylcyclopropenone with compounds in which C=N groups such as imidate, amidine, imidothioate, or *N*-imidoyl sulfoximine were substituted, giving pyrrolinone derivative as the major product:

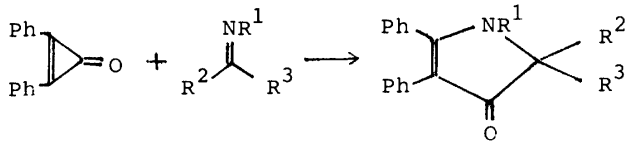

R^1,R^2=Alkyl, Aryl: R^3=RO, R_2N, RS, $Me_2\overset{\oplus}{S}(O)\overset{\ominus}{N}$

In the continuation of our studies on the chemical and physical properties of imines and ylides, we have been much interested in the chemical nature of the pyrrolinone-substituted sulfoximines (**1a—d**) which posess high thermostability.

Table 1. The reaction of the pyrrolinone-substituted sulfoximines **1a—d** with nucleophiles

Reactants		Product	
Sulfoximide	XH		Yield/%
1a	EtOH	**2a**(X=EtO)	94
	HOH	**2a**(X=OH)	89
	t-BuSH	**2a**(X=*t*-BuS)	71
1b	EtOH	**2b**(X=EtO)	80
	Ac_2CH_2	**2b**(X=Ac_2CH)	85
1c	HSCN	**2c**(X=NCS)	84
	Ac_2CH_2	**2c**(X=Ac_2CH)	77
	MeOH	**2c**(X=MeO)	88
	EtOH	**2c**(X=EtO)	93
	i-PrOH	**2c**(X=*i*-PrO)	81
	HOH	**2c**(X=OH)	96
	PhSH	**2c**(X=PhS)	74
	4-ClC_6H_4SH	**2c**(X=4-ClC_6H_4S)	65
	EtSH	**2c**(X=EtS)	58
	t-BuSH	**2c**(X=*t*-BuS)	64
1d	EtOH	**2d**(X=EtO)	90

Table 2. Physical properties of pyrrolinones **2a—d**

2	Mp θ_m/°C	^{1}H-NMR (δ in $CDCl_3$)[a]	M+	Anal Found (Calcd) (%)		
				C	H	N
2a(X=OH)	151—152	2.83(3H, s, Me)	341	80.65 (80.92)	5.60 (5.61)	3.89 (4.10)
2a(X=*t*-BuS)	205—207	1.46(9H, s, *t*-Bu), 3.08(3H, s, MeN)	413	78.84 (78.41)	6.36 (6.58)	3.45 (3.39)
2b(X=Ac_2CH)	145—146	0.80(3H, t, J=7 Hz, $C\underline{H}_3CH_2$), 2.24(3H, s, Ac), 2.27(3H, s, Ac), 3.19(2H, dq, J=4 and 7 Hz, CH_2), 5.29(1H, s, CHCO)	437	79.12 (79.61)	6.26 (6.22)	3.24 (3.20)
2c(NCS)	174—176	2.16(3H, s, Me)	458	78.37 (78.58)	4.73 (4.84)	5.93 (6.11)
2c(Me_2NCSNH)	148—150	2.13(3H, s, $\underline{Me}C_6H_4$), 3.03(6H, s, Me_2N)	503	76.28 (76.31)	5.63 (5.80)	8.07 (8.34)
2c(Ac_2CH)	214—215	1.98(3H, s, Ac), 2.10(3H, s, Ac), 2.13(3H, s, $\underline{Me}C_6H_4$) 4.70(1H, s, CHCO)	499	81.87 (81.74)	5.73 (5.85)	2.86 (2.80)
2c(*i*-PrO)	185—188	1.15(3H, d, J=7 Hz, $\underline{Me}$CH), 1.42(3H, d, J=7 Hz, $\underline{Me}$CH), 2.13(3H, s, $\underline{Me}C_6H_4$), 3.9—4.5(1H, m, CHCO)	459	83.25 (83.63)	6.33 (6.36)	2.81 (3.05)
2c(OH)	202—206	2.14(3H, s, Me)	417	83.50 (83.43)	5.42 (5.55)	2.89 (3.35)
2c(PhS)	164	2.18(3H, s, Me)	509	82.14 (82.48)	5.16 (5.34)	2.93 (2.75)
2c(4-ClC_6H_4S)	185—190	2.16(3H, s, Me)	543	77.06 (77.26)	4.66 (4.82)	2.72 (2.57)
2c(*t*-BuS)	170—172	1.48(9H, s, *t*-Bu), 2.13(3H, s, Me)	489	81.16 (80.94)	6.48 (6.39)	2.77 (2.86)

a) Aryl ring protons were observed at δ 6.4—8.1.

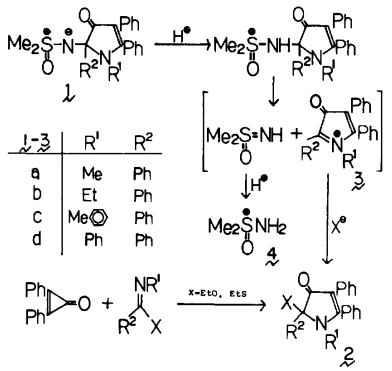

Scheme 1.

Table 3. ^{1}H-NMR spectra of the terminal group R^1 of the parent sulfoximines **1a—c** and the corresponding cations **3a—c**

	δ in $CDCl_3$[a]
1a	2.80(s, MeN)
3a	3.07(bs, MeN)[b]
1b	0.61(t, CH_3), 3.34(dq, CH_2N)
3b	0.98(t, CH_3), 3.3—3.9(bm, CH_2N)[b]
1c	2.09(s, $\underline{Me}C_6H_4$)
3c	2.20(s, $\underline{Me}C_6H_4$)[b]

a) Phenyl ring protons appeared at δ 6.4—8.0 as multiplets. b) Trifluoroacetic acid (10% v/v) was added.

The sulfoximines **1a—d** were stable in ethanolic sodium hydroxide. In acidic ethanol (hydrochloric or trifluoroacetic acid). However, **1a—d** decomposed easily within one day to **2a—d** (X=EtO) in good yields. In trifluoroacetic acid **1a—d** gave dark brown solutions within 5 min. Treatment of these with nucleophiles such as alcohols, thiols, thiocyanic acid, or acetylacetone yielded 2-pyrrolin-4-one derivatives **2a—d** (X) as listed in Table 1, while, treatment of the acid solution of **1a** with primary or secondary amine gave no amino-substituted products, with only resinous mass being formed. The products **2a** (X=EtO), **2b** (X=EtO), **2c** (X=EtO, EtS), and **2d** (X=EtO) were identical to the compounds obtained from the reaction of diphenylcyclopropenone with the corresponding imidates or imidothioate. The structure of the other compounds listed in Table 1 was elucidated on the basis of their ^{1}H-NMR, MS, and elemental analyses (Table 2).

The structure of the product obtained by the reaction with thiocyanic acid was found to be not thiocyanate but isothiocyanate, since **2c** (X=NCS) reacted with dimethylamine to yield **2c** (X=Me_2NCSNH) in a good yield.

A plausible mechanism for the formation of **2a—d** was shown in Scheme 1. The initial step involves the protonation of the imino nitrogen of **1a—d** followed by the elimination of sulfoximine to give iminium cations **3a—d**. The eliminated sulfoximine yielded S-aminosulfoxonium salt in trifluoroacetic acid.[3] The formation of the cations has been supported as follows. The color of the solution of **1a—d** in $CDCl_3$ changed from yellow to dark brown immediately on addition of trifluoroacetic acid. ^{1}H-NMR spectra of the brown solutions showed the signals of the substituents of **3a—c** shifted to lower field compared with those of the parent sulfoximines **1a—c** (Table 3) together with aminodimethylsulfoxonium ion **4** (δ=3.49). The down field shift of the alkylsubstituents of carbonium ions has been well documented.[4] The cations **3a—d** in trifluoroacetic acid were stable at room temperature for a day when they were kept from the atmospheric moisture. Addition of a nucleophile to the solutions, the color of which turned yellow within a minute, gave 5-substituted pyrrolinones **2a—d(X)**; none of the starting **1a—d** was recovered.

Experimental

General. Melting points are uncorrected. ^{1}H-NMR spectra were recorded on a Hitachi-Perkin Elmer R-24 (60 MHz) spectrometer using TMS as an internal standard, and mass spectra on a Hitachi RMU-7M mass spectrometer.

*Preparation of Pyrrolinone-substituted Sulfoximines **1a—d**.* Sulfoximines **1a—d** were prepared according to the previously reported method.[1]

*The Reaction of the Sulfoximines **1a—d** with Nucleophiles.* In a stoppered flask, sulfoximine **1** (1 mmol) in trifluoroacetic acid (3 cm^3) was stirred for 5 min to give a dark brown solution. To the solution was added a nucleophile [alcohol, sodium thiocyanate, acetylacetone (3 mmol) or thiol (1 mmol)]. We stirred the mixture until the color of the solution changed to yellow. To the mixture, water (15 cm^3) was added and the product was extracted with chloroform. The extract was dried over sodium sulfate and evaporated under reduced pressure. The crude product was either recrystallized from an appropriate solvent or purified by chromatography over silica gel. The results are collected in Table 1 and physical properties of new compounds are shown in Table 2.

References

1) H. Yoshida, S. Sogame, Y. Takishita, and T. Ogata, *Bull. Chem. Soc. Jpn.*, **56**, 2438 (1983).

2) H. Yoshida, S. Sogame, S. Bando, S. Nakajima, T. Ogata, and K. Matsumoto, *Bull. Chem. Soc. Jpn.*, **56**, 3849 (1983).

3) The authors are indebted to the referees for the discussion.

4) a) G. Frankel and D. G. Farnum, "Carbonium Ions" vol I, ed by G. A. Olah and P. v. R. Schleyer, Interscience Publishers, New York (1968), p. 237; b) L. M. Jackmann and S. Sternhill, "Application of Nuclear Magnetic Resonance Spectroscopy in Organic Chemistry," 2nd ed, Pergamon Press, Oxford (1969), P. 249.

Aryliminodimagnesium Reagents. VII. The Moderate Electron-donating Ability Estimated by Oxidation Peak Potentials

Masao Ōkubo,* Toshiki Tsutsumi, Akio Ichimura,† and Toyokichi Kitagawa†

Department of Chemistry, Faculty of Science and Engineering, Saga University, Honjō-machi, Saga 840

†*Department of Chemistry, Faculty of Science, Osaka City University, Sumiyoshi-ku, Osaka 558*

(Received December 16, 1983)

Synopsis. Oxidation peak potentials of *p*-$RC_6H_4N(MgBr)_2$ and *p*-RC_6H_4MgBr (R=CH_3O, CH_3, F) were determined by cyclic voltammetry with a platinum disk electrode in tetrahydrofuran. The potentials obtained proved to be a semiquantitative measure of electron-donating abilities of organomagnesium reagents.

It was proposed very recently that aryliminodimagnesium reagent ($ArN(MgBr)_2$, aryl-IDMg) was less reactive—less "electron-donating"—than arylmagnesium reagent (ArMgBr): The proposal remained entirely qualitative because it was based on comparison of the distribution of major and minor products formed in the reactions with carbonyl and nitro compounds.[1] Even the clearly different behavior of azobenzene toward $ArN(MgBr)_2$ and ArMgBr (Scheme 1)[2] suggests

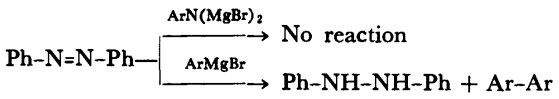

Scheme 1.

strongly but still qualitatively that the latter reagent is much more electron-donating than the former, and determination of oxidation potentials as a quantitative measure of electron-donating abilities is needed. The electrochemical reduction of a wide variety of electron-accepting organic compounds were studied extensively: The correlation of reduction potentials with Hammett's substituent constants were reviewed.[3] The study of electrochemical oxidation potentials of carbanions[4,5] and amide anions[6] as well as their correlation with substituent constants[7] are now in progress. In the field of electrochemistry of organomagnesium reagents, an important result was provided by the measurement of anodic overvoltages of some alkyl Grignard reagent at constant current density.[8] In this paper, the result of a voltammetric study for estimating semiquantitatively the oxidation potentials of *p*-$RC_6H_4N(MgBr)_2$ and *p*-RC_6H_4MgBr (R=CH_3O, CH_3, F) will be described.

Procedures. Cyclic voltammograms were recorded on a Yanaco P-1000 Voltammetric Analyzer having electrolysis cell equipped with three electrodes: working electrode (Pt-disk), reference electrode (Ag-wire), and counter electrode (Pt-wire). Tetrahydrofuran, which has been used as the reaction solvent, was used also for electrolysis: Tetrabutylammonium perchlorate (TBAP, 0.2M) was used as the supporting electrolyte. The concentration of organomagnesium reagents was 1.0—2.0×10^{-3}M (1 M=1 mol dm^{-3}), and all the measurements were carried out under nitrogen atmosphere. Contamination of the surface of working electrode was unavoidable, and the surface was polished by use of alumina powder prior to the individual measurements.

The typical voltammogram with a scan rate of 50 mV/s is shown in Fig. 1. Two oxidation peaks were observed in every case, the first peak(I) being assigned to the initial oxidation of the magnesium reagent and the second peak(II) to the further oxidation of the initially formed radical species. Even when the faster scan rate(500 mV/s) was applied, a very small reduction peak was observed only in two cases: The electrode process is almost completely irreversible and the redox potential was not determined by this method. For comparison of the values of oxidation peak potentials[9] with each other, the observed potentials of I were normalized by use of the redox potential of ferrocenium/ferrocene couple added as internal standard: 0.400 V *vs.* NHE.[10]

ArN(MgBr)₂ and ArMgBr. The normalized oxidation peak potentials of individual reagents were plot-

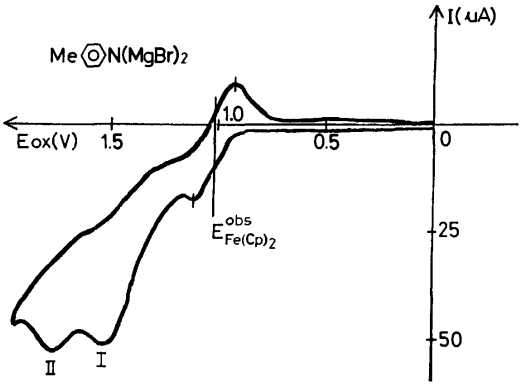

Fig. 1. Cyclic voltammogram of *p*-methylphenyl-IDMg reagent using Ag-wire as reference electrode.

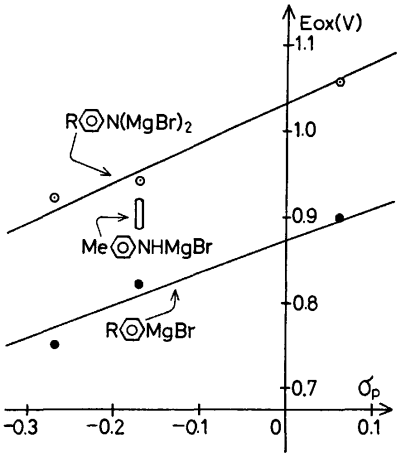

Fig. 2. Plot of oxidation peak potentials *vs.* substituent constants σ_p. The values of potentials are normalized using the redox potential of ferrocenium/ferrocene couple as internal standard.

ted against substituent constants (σ_p, Fig. 2): The difference between the potentials of two kinds of reagent was 120—170 mV. The higher oxidation peak potentials of IDMg in comparison with those of ArMgBr support the previous suggestion of the lower electron-donating ability of the former reagent than that of the latter.[1,2,11] The substituent effect on the oxidation peak potentials ($CH_3O<CH_3<F$) of the respective kinds of reagent is in accord with the effect on the electron-donating ability suggested previously.[2] The reaction constants(ρ) were not determined since the potentials obtained are not the redox potentials but the oxidation peak potentials which, however, proved to be at least a semiquantitative measure of electron-donating abilities of organomagnesium reagents.

ArNHMgBr and ArN(MgBr)$_2$. The oxidation peak potentials of *p*-CH_3-substituted PhNHMgBr, PhN(MgBr)$_2$, and PhMgBr were also compared (Fig. 2). The potential of the anilinomagnesium reagent was difficult to be determined precisely, however, the medium potential compared with those of ArMgBr and IDMg was established.

The higher ability of ArNHMgBr than that of ArN(MgBr)$_2$ as electron donors is suggested from the result of an experiment, which, however, is performed in an unadvisable manner. When the IDMg reagent[12] containing a small amount (*ca.* 5%) of anilinomagnesium species was allowed to react with a nitroarene, a large amount of unidentifiable dark brown materials was formed with a heavy loss of the expected azoxyarene:[13] The result is due to the preferential electron-transfer from the anilinomagnesium species, the process being followed by decomposition and/or polymerization of nitroarene anion radical.[14] The reactivity of different types of magnesium reagents, *i.e.*, ArMgBr, ArSMgBr, ArNHMgBr, ArN(MgBr)$_2$, and ArOMgBr, in the replacement reaction of β-methoxy α,β-enones is discussed elsewhere.[15]

The lower electron-donating ability of ArN(MgBr)$_2$ than that of ArNHMgBr is ascribable to the presence of two positive Mg atoms attached to the anionic nitrogen atom.

References

1) M. Ōkubo, M. Yoshida, K. Horinouchi, H. Nishida, and Y. Fukuyama, *Bull. Chem. Soc. Jpn.*, **56**, 1196 (1983).
2) M. Ōkubo, T. Takahashi, and K. Koga, *Bull. Chem. Soc. Jpn.*, **56**, 199 (1983).
3) P. Zuman, "Substituent Effects in Organic Polarography," Plenum Press, New York (1967).
4) E. Buncel and T. Durst, Ed., "Comprehensive Carbanion Chemistry," Chapt. 5 (by R. D. Guthrie), Elsevier, Amsterdam (1980).
5) J. K. Kochi, "Organometallic Mechanisms and Catalysis," Academic Press, New York (1978), p.512.
6) S. Bank, A. Schepartz, P. Giammatteo, and J. Zubieta, *J. Org. Chem.*, **48**, 3458 (1983).
7) R. Bauer and H. Wendt, *Angew. Chem., Int. Ed. Engl.*, **17**, 202 (1978).
8) T. Holm, *Acta Chem. Scand., Ser. B*, **28**, 809 (1974).
9) D. H. Evans, K. M. O' Connell, R. A. Petersen, and M. J. Kelly, *J. Chem. Educ.*, **60**, 290 (1983).
10) R. R. Gange, C. A. Koval, and G. C. Lisensky, *Inorg. Chem.*, **19**, 2854 (1980).
11) M. Ōkubo and Y. Uematsu, *Bull. Chem. Soc. Jpn.*, **55**, 1121 (1982).
12) M. Ōkubo and S. Ueda, *Bull. Chem. Soc. Jpn.*, **53**, 281 (1980).
13) M. Ōkubo and K. Koga, *Bull. Chem. Soc. Jpn.*, **56**, 203 (1983).
14) G. A. Russell, E. G. Janzen, and E. T. Strom, *J. Am. Chem. Soc.*, **86**, 1807 (1964).
15) M. Ōkubo, M. Yoshida, and H. Yanase, *Bull. Chem. Soc. Jpn.*, submitted.

Temperature and Isotope Effects in the Reactions of Phenylcarbene with Acetone

Hideo TOMIOKA,* Yasuji OZAKI, Hiroyuki NAKAMURA, and Yasuji IZAWA
Department of Industrial Chemistry, Faculty of Engineering, Mie University, Tsu, Mie 514
(Received January 5, 1984)

Synopsis. Phenylcarbene generated in acetone solution gives oxirane, vinyl ether and 1,3-dioxolane presumably *via* initial attack of the singlet state on the lone pair electrons of carbonyl oxygen leading to a carbonyl ylide, whereas a C-H insertion product arising from the triplet markedly increases in matrix environments.

In the past few years several research groups have studied the chemistry of carbenes in rigid matrices at low temperature.[1-4] In the case of carbenes with triplet ground states there are profound differences between the chemistry observed in fluid solution at ambient temperature and that obtaining in a matrix at −196 °C. For example, arylcarbene generated in olefinic solution at ambient temperature gives cyclopropanes almost exclusively which are mostly derived from the singlet state, whereas arylcarbene generated in olefinic matrices at −196 °C result in a dramatic increase in C-H insertion products at the expense of the cyclopropanes.[2] It has been proposed[1-4] that these C-H insertion products are formed *via* an abstraction-recombination of the triplet carbene on the basis of extensive spectroscopic and chemical evidence for the presence of the ground-state triplet carbene in the low temperature matrix photolysis of most aryldiazomethanes at −196 °C. Similar dependence of the product distribution upon the temperature at which the arylcarbene is generated has been observed in its reactions with alcohol,[1a] ether,[1f] amine,[1f] and halide,[1e] and pertinent information as to the relationship between the multiplicity and reaction pattern of the carbene is available from these studies.

In this work we have extended the matrix study of carbene reactions by investigating the mechanism of its reaction with ketone. In contrast to the intensive study lavished upon the reaction of carbenes with carbon-carbon double bonds,[5] only scant information is available concerning the reactions with the carbon-oxygen double bond. Interest in this reaction has intensified and a number of papers have appeared on the subject in the last few years.[6]

Results and Discussion

A solution of phenyldiazomethane (**1**) in degassed acetone was irradiated in a Pyrex tube at different temperatures. GLC analysis of the product mixture revealed the presence of oxirane (**2**), vinyl ether (**3**), 1,3-dioxolane (**4**) and 4-phenyl-2-butanone (**5**), along with toluene, bibenzyl, *cis*- and *trans*-stilbenes, and aldehyde azine as indicated in equation (1). The product distributions at different temperatures were determined by GLC analysis as summarized in Table 1. It is evident from the Table that the product distributions are highly dependent on the temperature at which the irradiation was carried out. Photolysis of **1** in acetone at 0 °C, for example, gave **4** as the main product along with **2** and **3**. When the photolysis was carried out below −150 °C, however, **5** became the main reaction product at the expense of 1,3-dioxolane.

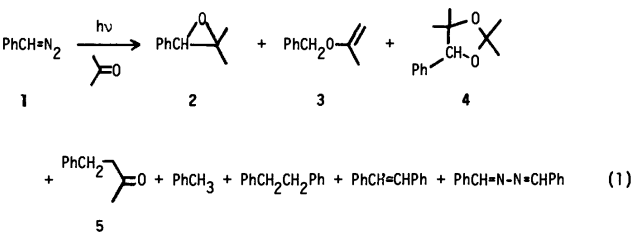

(1)

The phenomena are similar to those observed[1-4] in the reaction of phenylcarbene with other substrates, *e.g.*, alcohol,[1a] and can be explained as follows. Phenylcarbene (**6**) is expected to react with acetone in its singlet state to form carbonyl ylide (**7**) as a result of electrophilic attack on the nonbonding electrons of the carbonyl oxygen, since it is well known[5] that most singlet carbenes can react as Lewis acids by sharing a pair of nonbonding electrons. The formation of a carbonyl ylide by reaction of carbene with acetone has been demonstrated recently by Wong, Griller, and Scaiano.[7] They generated singlet fluorenylidene, which was identified spectrophotometrically, and followed its capture by acetone to from a carbonyl ylide. The carbonyl ylide (**7**) thus formed collapses *via* three competing reaction pathways:[8] (a) ring-closure to give oxirane (**2**), (b) intramolecular proton shift to yield vinyl ether (**3**), and (c) reaction with a second acetone molecule leading to dioxolane (**4**). A sharp decrease in the yield of **4** in the solid phase reaction is then expected on the basis of the above scheme since mobility of a molecule in a matrix is limited and the intermolecular pathway becomes unfavorable.

Table 1. Product distribution as a function of temperature in photolysis of **1** in acetone-H_6 (D_6)

T/°C	Yield/%[a]			
	2	**3**	**4**	**5**
0[b]	4.6 (5.9)	10.8(5.7)	20.9(41.6)	0(0)
−78[b]	4.5 (2.2)	6.9(3.6)	16.2(33.5)	0(0)
−110[c]	10.5 (2.3)	8.2(4.7)	12.3(31.2)	<1(0)
−150[c]	6.0 (2.6)	9.8(3.8)	5.5 (0.7)	20.0(4.7)
−196[c]	1.9(11.4)	1.8(4.3)	1.3 (1.3)	21.1(0.7)

a) Determined by GC. Yields in parentheses are for irradiations in acetone-d_6. Other products detected in each experimental condition were toluene, bibenzyl, stilbenes and aldehyde azine. b) Liquid phase. c) Solid phase.

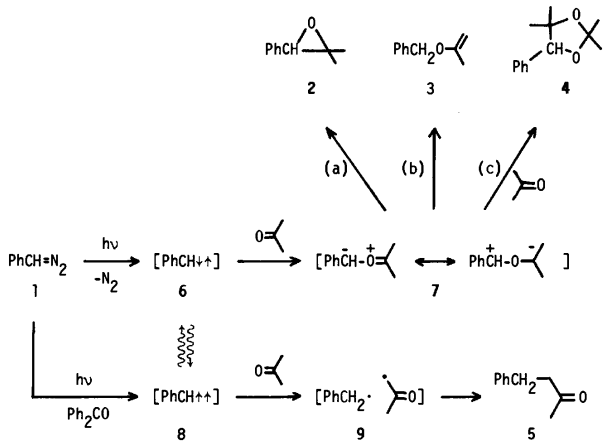

4-Phenyl-2-butanone on the other hand, should presumably arise from insertion of phenylcarbene into the C–H bonds of acetone. Since this compound is only formed in a matrix environment, we propose that the triplet state is responsible for its formation. Thus, triplet phenylcarbene (**8**) generated in the matrix abstracts hydrogen from the host acetone to give the radical pair (**9**), which recombines with high efficiency to afford **5** due to the limited diffusibility of the radical pair.

The reason why triplet reactivity appears at low temperature has been a key question. A reasonable explanation has been advanced recently by Senthilnathan and Platz.[3] Their kinetic analysis of the decay of triplet arylcarbenes in a rigid matrix has demonstrated that a predominant decay path of triplet carbene is by hydrogen atom tunneling. The availability of this tunneling pathway at low temperature leads to the hydrogen abstraction products. One of the characteristic phenomena of the tunneling reaction is a large kinetic isotope effect. For example, Wong and Williams[9] have observed that k_H/k_D is larger than 1.3×10^3 for intermolecular hydrogen atom abstraction by $CH_3\cdot$ from a CH_3NC matrix at −150 °C. Measured isotope effects with triplet arylcarbenes are much more modest. Thus, k_H/k_D is 23 for hydrogen atom abstraction by diphenylcarbene from toluene at −196 °C.[3a] The kinetic results are consistent with the isotope effects on the product distribution. For example, product analyses of the reaction of phenylcarbene in deuterated alcoholic matrices at −196 °C revealed that a substantial isotope effect was observed for C–H (D) insertion while the isotope effect on O–H (D) insertion was small.[1h,3c] With these precedents in mind we irradiated **1** in acetone-d_6 at various temperatures. The results summarized in the Table clearly indicate that there is a substantial isotope effect in the C–H insertion process at −196 °C; the yield of 4-phenyl-2-butanone is reduced by almost a factor of 20 in acetone-d_6. In the light of the lack of an isotope effect on the O–H (D) insertion process of singlet phenylcarbene compared with a substantial isotope effect in C–H insertion in deuterated alcoholic matrices at −196 °C, the considerable isotope effect on C-H insertion leading to **5** supports the view that **5** arises from a triplet carbene, presumably *via* hydrogen atom tunneling followed by recombination of the resulting radical pairs (**9**).

Experimental

Materials. Phenyldiazomethane **1** was prepared immediately before use as described in the literature. Acetone-d_6 was purchased from E. Merck and used without purification. Authentic samples of the phenylcarbene adducts with acetone (**2**—**5**) were prepared as follows. Oxirane **2** was obtained by the oxidation of 2-methyl-1-phenyl-1-propene with *m*-chloroperbenzoic acid. Vinyl ether **3** was prepared by the reaction of benzyl alcohol with propylene in the presence of iodine and mercuric oxide followed by treatment of the resulting 2-benzyloxypropyl iodide with ethanolic KOH. 1,3-Dioxolane **4** was isolated from the reaction mixture by column chromatography on silica-gel. Satisfactory spectroscopic and mass spectral data have been obtained on all compounds.

Product Analyses. All irradiations for product analyses were conducted with use of a water-cooled Halos 300-W high-pressure mercury lamp. In a typical procedure, 0.005 mmol of **1** was added to 2.0 cm^3 of acetone in Pyrex tubes. The sample was then degassed by three freeze-thaw cycles, and the sample tube sealed under vacuum. The tube was suspended in a transparent Pyrex Dewar flask filled with coolant and irradiated until all **1** was destroyed.[1c] The product identification and yields were conveniently determined by GC (Silicone OV-17 on Diasolid L) and GC-MS (Shimadzu GC-MS 1000 spectrometer) techniques.

References

1) a) H. Tomioka and Y. Izawa, *J. Am. Chem. Soc.*, **99**, 6128 (1977); b) H. Tomioka, *ibid.*, **101**, 256 (1979); c) H. Tomioka, G. W. Griffin, and K. Nishiyama, *ibid.*, **101**, 6009 (1979); d) H. Tomioka, H. Ueda, S. Kondo, and Y. Izawa, *ibid.*, **102**, 7817 (1980); e) H. Tomioka, S. Suzuki, and Y. Izawa, *Chem. Lett.*, **1980**, 293; f) H. Tomioka, S. Suzuki, and Y. Izawa, *Bull. Chem. Soc. Jpn.*, **55**, 492 (1982); g) H. Tomioka, S. Suzuki, and Y. Izawa, *J. Am. Chem. Soc.*, **104**, 3156 (1982); h) H. Tomioka, Y. Ozaki, and Y. Izawa, *Bull. Chem. Soc. Jpn.*, **56**, 1239 (1983).

2) a) R. A. Moss and U.-H. Dolling, *J. Am. Chem, Soc.*, **93**, 954 (1971); b) R. A. Moss and M. A. Joyce, *ibid.*, **99**, 1262 (1977); c) R. A. Moss and J. K. Huselton, *ibid.*, **100**, 1314 (1978); d) R. A. Moss and M. A. Joyce, *ibid.*, **100**, 4475 (1978).

3) a) V. P. Senthilnathan and M. S. Platz, *J. Am. Chem. Soc.*, **102**, 7637 (1980); b) **103**, 5503 (1981); c) M. S. Platz, V. P. Senthilnathan, B. B. Wright, and C. W. McCurdy, Jr., *ibid.*, **104**, 6494 (1982); d) J. Zayas and M. S. Platz, *Tetrahedron Lett.*, **24**, 3689 (1983).

4) C.-T. Lin and P. P. Gasper, *Tetrahedron Lett.*, **21**, 3553 (1980).

5) For reviews, see (a) W. Kirmse, "Carbene Chemistry," 2nd ed, Academic Press, New York, N. Y. (1971); b) "Carbenes," ed by R. A. Moss and M. Jones, Jr., Wiley, New York (1974), Vol. 1.

6) See for example, M. Békhazi and J. Warkentin, *J. Am. Chem. Soc.*, **105**, 1289 (1983), and references cited therein.

7) P. C. Wong, D. Griller, and J. C. Scaiano, *J. Am. Chem. Soc.*, **104**, 6631 (1982).

8) J. N. Bradley and A. Ledwith, *J. Chem. Soc.*, 3480 (**1963**).

9) J.-T. Wong and F. Williams, *J. Am. Chem. Soc.*, **94**, 2930 (1972).

Oxidation of 2,6-Bis(hydroxymethyl)phenols to 2-Hydroxyisophthalaldehydes by MnO_2

Shozo TANIGUCHI

Department of Industrial Chemistry, Ibaraki Technical College, Nakanefukayatsu, Katsuta, Ibaraki 312

(Received January 20, 1984)

Synopsis. A facile and direct preparative method of 2-hydroxyisophthalaldehydes from 2,6-bis(hydroxymethyl) phenols using activated manganese(IV) oxide is described. The aldehydes are obtained in good yields.

2-Hydroxyisophthalaldehyde derivatives (**2**) are useful compounds for the investigation of binuclear metal complexes,[1-4] and macrocyclic binuclear metal complexes.[5,6] Since binuclear copper(II) complexes have been prepared from Schiff bases of **2a** by Robson[1a] and Okawa[2a], the investigatons have been directed toward the study of their molecular structures,[5,6b] affinity[3b,6c] for carbon monoxide and ethylene, intermolecular electron transfer process,[6a] and redox behavior.[4,6] All of these investigations adopted the Ullmann's method[7] for the preparation of **2**, but the reaction is achieved through the following three-steps: conversion of 2,6-bis(hydroxymethyl)-4-methylphenol (**1a**) to the tosylated diol, its oxidation to the tosylated diformyl compound by sodium dichromate, and final formation of **2a** by treatment in sulfuric acid. This method is cumbersome and the yield of the compound is low. Once the aldehydes are synthesized, the route to the final ligand compounds is fairly straightfoward. Therefore, a facile and direct preparation of the aldehydes is an important factor for the synthesis of the binuclear metal complexes.

Recently, the reaction of **1b** with vanadyltriisopropylate was found to afford 3,3′-[oxybis(methylene)] bis[5-*t*-butyl-2-hydroxybenzaldehyde] (**3**) as the major product and **2b** as the by-product.[8] Since manganese(IV) oxide prepared by heating a manganese(II) salt such as carbonate or oxalate at 220—280 °C, is known to oxidize salicyl alcohol to salicylaldehyde in good yield,[9] the activated MnO_2 can be used for oxidation of **1** to **2**. In this paper, the author reports the results of the present procedure, and the desired products were obtained in 67—70% yields in a sufficiently pure state for most purposes.

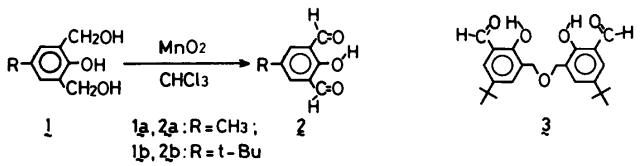

1 **1a**, **2a**: R=CH3; **1b**, **2b**: R=t-Bu **2**

3

Experimental

All melting points are uncorrected. The IR spectra were recorded on a Hitachi EPI-G3 spectrometer in KBr disks. The ^1H NMR spectra and mass spectra were recorded on a Hitachi R-24B spectrometer with TMS as the internal standard in $CDCl_3$ solution, and a Hitachi M-70 mass spectrometer, respectively.

Reagents. Compounds **1** were prepared by a modification of the literature method.[7] Activated manganese(IV) oxide[10] was prepared by heating manganese(II) carbonate at 250 °C for 5 h.

General Procedure. Compound **1** (10 g) was added to manganese(IV) oxide (80 g) suspended in 300 ml of $CHCl_3$ in a 500 ml Erlenmeyer flask, and the mixture was stirred by a magnetic stirrer at room temperature. The phenol which was slightly soluble in the solvent dissolved within about 3 h. After 2 d, the solution was filtered. The solid was washed twice thoroughly with 200 ml each of $CHCl_3$, and the washings were added to the original filtrate.[11] The combined solution was evaporated to yield a pale yellow solid (6.5—6.9 g). The yields and analytical data of the products are described below.

2a: 67% yield, mp 130 °C (lit, mp 133.5 °C,[7] mp 129—130 °C[4]); IR (cm^{-1}) 2880 (formyl CH), 1682 (formyl C=O), 1668 (formyl C=O associated with OH), 1216 (phenolic C-O); ^1H NMR δ=2.83 (3H, s, methyl), 7.73 (2H, s, aromatic), 10.15 (2H, s, CHO), 11.35 (1H, s, OH); MS *m/z* 164 (M^+).

2b: 70% yield, mp 105 °C; IR (cm^{-1}) 2880 (formyl CH), 1692 (formyl C=O), 1662 (formyl C=O associated with OH), 1224 (phenolic C-O); ^1H NMR δ=1.24 (9H, s, methyl), 7.83 (2H, s, aromatic), 10.17 (2H, s, CHO), 11.28 (1H, s, OH); MS *m/z* 206 (M^+); Calcd for $C_{12}H_{14}O_3$: C, 69.89; H, 6.84. Found: C, 69.79; H, 6.84.

References

1) a) R. Robson, *Inorg. Nucl. Chem. Lett.*, **6**, 125 (1970); b) I. E. Dickson and R. Robson, *Inorg. Chem.*, **13**, 1301 (1974); c) B. F. Hoskins, R. Robson, and G. A. Williams, *Inorg. Chim. Acta.*, **16**, 121 (1976) and references cited therein.

2) a) H. Okawa, *Bull. Chem. Soc. Jpn.*, **43**, 3019 (1970); b) H. Okawa and S. Kida, *ibid.*, **44**, 1172 (1971); c) H. Okawa, S. Kida, Y. Muto, and T. Tokii, *ibid.*, **45**, 2480 (1972); d) T. Ichinose, H. Okawa, and S. Kida, *ibid.*, **47**, 3045 (1972) and references cited therein.

3) a) J. J. Grzybowsky, P. H. Merrell, and F. L. Urbach, *Inorg. Chem.*, **17**, 3078 (1978); b) J. J. Grzybowsky and F. L. Urbach, *ibid.*, **19**, 2604 (1980).

4) R. S. Drago, M. J. Desmond, B. B. Corden, and K. A. Miller, *J. Am. Chem. Soc.*, **105**, 2287 (1983).

5) C. L. Spiro, S. L. Lambert, T. J. Smith, E. N. Duesler, R. R. Gagné, and D. N. Hendrickson, *Inorg. Chem.*, **20**, 1229 (1981).

6) a) R. R. Gagné, C. A. Koval, T. J. Smith, and M. C. Cimolino, *J. Am. Chem. Soc.*, **101**, 4571 (1979); b) R. R. Gagné, R. P. Kreh, and J. A. Dodge, *ibid.*, **101**, 6917 (1979); c) R. R. Gagné, C. L. Spiro, T. J. Smith, C. A. Hamann, W. R. Thies, and A. K. Shiemke, *ibid.*, **103**, 4073 (1981).

7) F. Ullmann and K. Brittner, *Chem. Ber.*, **42**, 2539 (1909).

8) S. Taniguchi, Abstr. of the 33rd Symposium of Thermosetting Plastics, Tokyo, October, 27, 1983, p.37.

9) M. Harfenist, A. Bavley, and W. A. Lazier, *J. Org. Chem*, **19**, 1608 (1954).

10) Compounds **2** were obtained in low yields by heating with commercial manganese(IV) oxide at 250 °C for 5 h.

11) After filtration the remaining solid consisting mainly of manganese(IV) oxide was dried and treated in aq NaOH solution. The color of the solution changed to fluorescent greenish-yellow. By acidifying the solution, a small amount of compounds **2** was generally obtained.

Characteristic Transport Properties of Diaza-crown Ethers for Primary and Secondary Ammonium Cations

Hiroshi TSUKUBE

Department of Chemistry, College of Liberal Arts and Science, Okayama University, Okayama 700

(Received February 13, 1984)

Synopsis. Simple lipophilic diaza-crown ethers show unique transport properties for primary and secondary ammonium salts, which are markedly different from those observed with common crown ether systems.

An important advantage of aza-crown ethers over oxa-crown ethers is the presence of soft nitrogen donor atoms which can offer characteristic complexing and transporting abilities.[1] Recently, pyrido-crown ethers and their analogues have received much attention as specific ligand and/or carrier for primary ammonium cations and some metal ions.[2] Here we report that simple diaza-crown ethers show new and unique cation transport properties, especially for a series of amino acid ester salts. They were demonstrated to transport both primary and secondary ammonium cations with high efficiency and unique selectivity, which were not attained in the oxa-crown ether systems.

Three kinds of lipophilic diaza-crown ethers having 15- to 21-membered rings, **1**—**3**, were employed as cation carriers (Fig.). They were easily prepared from benzyl chloride and corresponding diaza-crown ethers (see Experimental), and have limited solubilities in water. In the liquid membrane system employed,[3] the crown ether carrier dissolved in the chloroform membrane phase mediates the transport of guest cation and co-transported anion from the source aqueous phase through the membrane phase into the receiving aqueous phase by complexing and solubilizing guest salt into the membrane phase.

The diaza-crown ethers **1**—**3** showed high transport abilities for various ammonium cations of amino acid esters, while they offered low transport rates for K^+ and other metal ions (Table). It is of particular importance that they transport "secondary" ammonium cation of proline ester with efficiency comparable to those observed for primary ammonium cations. Although many kinds of oxa-crown ethers are known to transport primary ammonium cations effectively like the carrier **4**, such an effective transport of secondary ammonium cation has not been achieved in these oxa-crown ether systems. Since the employed diaza-crown ethers have various cavity sizes (diameter: *ca.* 2.0—4.0 Å), our results strongly suggest that nitrogen donor atoms in the macrocycles play an important role in complexation and transportation of ammonium cations. Probably, guest ammonium cation would be tightly attached by "two" hydrogen bonds to two diametrical nitrogen donor atoms in the diaza-crown ether. Similar complex structures have been proposed in the diazametacyclophane and related systems.[4]

Table also indicates that diaza-crown ethers **1**—**3** have largely different transport selectivities from those observed in the oxa-crown ether **4** system. When the crown ether **4** was employed, hydrophobic primary ammonium salts such as phenylalanine and tryptophan esters were much more effectively transported than the hydrophilic glycine and alanine esters. On the other hand, diaza-crown ethers **1**—**3** offered high transport rates for a variety of ammonium salts including glycine, alanine, and proline esters. Recently we demonstrated that lipophilic macrocyclic polyamine-type carriers showed parallel transport trend for a series of amino acid esters.[5] Hence, introduction of the nitrogen donor atoms into the macrocycles would offer not only

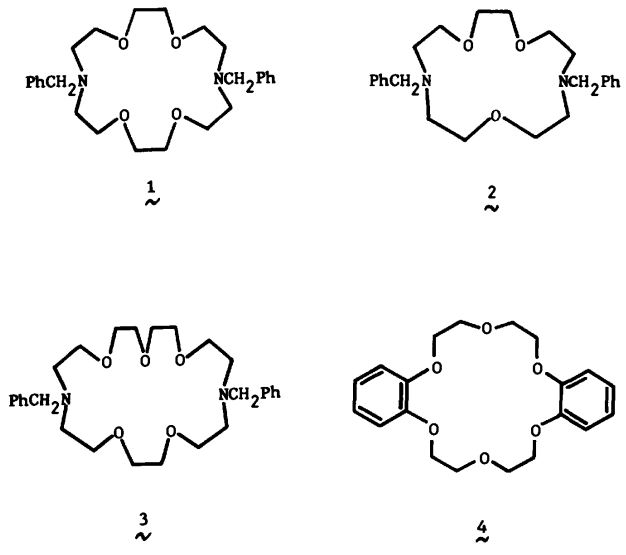

Fig. Macrocyclic carriers examined.

TABLE. CATION TRANSPORT PROPERTIES OF DIAZA-CROWN ETHER CARRIERS

Guest	Additive	Transport rate ×10⁶ mol/h			
		1	**2**	**3**	**4**
NaCl	$NaClO_4$	0.5	0.5	0.7	0.2
KCl	$NaClO_4$	0.8	0.4	0.4	5.6
NH_4Cl	$NaClO_4$	2.5	0.9	1.0	0.4
PheOEt·HCl	None	1.2	0.2	0.8	0
	$NaNO_3$	3.3	1.6	3.9	1.2
	NaSCN	6.3	8.6	8.1	9.6
	$NaClO_4$	3.8	4.3	6.8	11.9
TrpOEt·HCl	$NaClO_4$	6.0	5.7	5.4	13.2
LeuOEt·HCl	$NaClO_4$	5.6	6.2	7.2	12.3
AlaOEt·HCl	$NaClO_4$	8.2	6.6	7.2	1.4
GlyOEt·HCl	$NaClO_4$	8.7	8.7	9.3	1.0
ProOMe·HCl	$NaClO_4$	5.3	6.7	6.6	0.2

Transport conditions: Source aqueous phase; guest salt, 0.5 mmol. Additive, 1.0 mmol/H_2O, 5 ml. Membrane; carrier, 0.0372 mmol/$CHCl_3$, 12 ml. Receiving aqueous phase; H_2O, 5 ml.

high efficiency but also unique selectivity in the transport process.

The nature of co-transported anion has a pronounced effect on the cation-transport rate. As frequently reported in the crown ether-type carrier systems,[6] ClO_4^-, SCN^-, and other hydrophobic anions were required to promote this cation-transport process. Since we confirmed that diaza-crown ethers having 15- to 21-membered ring sizes showed potential transport properties for ammonium salts, they may provide wide applications in the cation-transport and in the related biomimetic systems.

Experimental

Materials. Diaza-crown ethers **1**—**3** were prepared in a two-phase reaction system (chloroform/water). Typically, a chloroform solution (15 ml) of benzyl chloride (3.48 g) was added dropwise to an aqueous solution (15 ml) of "Kryptofix 22" (Merck Japan, 3.00 g) and NaOH (2.00 g). After vigorous stirring at room temperature overnight, the organic layer was washed with aqueous HCl solution and water, and dried over Na_2SO_4. The solvent was removed, and recrystallization from ether gave colorless crystals **1**: Mp 82 °C (lit, 80 °C).[1b] Yield, 80%. IR (Nujol) 1602, 1498, 1125, 755, and 705 cm^{-1}. ^1H NMR (60 MHz, $CDCl_3$) δ=2.83 (8H, t, $NC\underline{H}_2CH_2$), 3.50—3.73 (20H, m, $OC\underline{H}_2CH_2$, $NC\underline{H}_2C_6H_5$), 7.23—7.40 (10H, m, $CH_2C_6\underline{H}_5$).

The carriers **2** and **3** were similarly prepared and purified by column chromatography on alumina (elute, $CHCl_3$). **2**: yellowish oil, 65%. IR (neat) 1600, 1495, 1450, 1125, 735, and 700 cm^{-1}. ^1H NMR ($CDCl_3$) δ=2.67—2.95 (8H, t+t, $NC\underline{H}_2CH_2$), 3.52—3.73 (16H, m, $OC\underline{H}_2CH_2$, $NC\underline{H}_2C_6H_5$), 7,17—7.45 (10H, m, $CH_2C_6\underline{H}_5$). **3**: yellowish oil, 58%. IR (neat) 1600, 1495, 1455, 1100, 740, and 700 cm^{-1}. ^1H NMR ($CDCl_3$) δ=2.83 (8H, t, $NC\underline{H}_2CH_2$), 3.53—3.77 (24H, m, $OC\underline{H}_2CH_2$, $NC\underline{H}_2C_6H_5$), 7.20—7.47 (10H, m, $CH_2C_6\underline{H}_5$). Satisfactory elemental analyses were obtained for these carriers.

Phenylalanine ethyl ester, leucine ethyl ester, alanine ethyl ester, and glycine ethyl ester were obtained from Nakarai Chem. Ltd., and other employed esters were purchased from Tokyo Chem. Ind. Ltd.

Transport Procedure. The transport experiments were carried out at room temperature in a U-tube glass cell (2.0 cm, i.d.) as reported before.[3] The carrier in chloroform (12 ml) was placed in the base of the U-tube, and two aqueous phases (5 ml, each) were placed in the arms of the U-tube, floating on the chloroform phase. The membrane phase was stirred with a magnetic stirrer. The transport rates were calculated from the initial rates of appearance of co-transported anion, ClO_4^-, into the receiving aqueous phase, which were determined by means of ion-selective electrode (Orion Model 93-81). Phenylalanine and tryptophan esters were also monitored spectroscopically. Reproducibility was confirmed as ±15% or better.

This research was supported in part by a Grant-in-Aid for Scientific Research No.58740230 from the Ministry of Education, Science, and Culture, Japan.

References

1) H. K. Frensdorff, *J. Am. Chem. Soc.*, **93**, 600 (1971); N. Wester and F. Vögtle, *J. Chem. Res.*(S), 400 (1978); J. M. Lehn and P. Vierling, *Tetrahedron Lett.*, **21**, 1323 (1980); K. Matsushima, H. Kobayashi, Y. Nakatsuji, and M. Okahara, *Chem. Lett.*, **1983**, 701; H. Tsukube, *J. Chem. Soc., Chem. Commun.*, **1984**, 315.

2) M. Newcomb, J. M. Timko, D. M. Walba, and D. J. Cram, *J. Am. Chem. Soc.*, **99**, 6392 (1977); B. Tümmler, G. Maass, E. Weber, W. Wehner, and F. Vögtle, *ibid.*, **99**, 4683 (1977); J. S. Bradshaw, G. E. Maas, J. D. Lamb, R. M. Izatt, and J. J. Christensen, *ibid.*, **102**, 467 (1980); S. Shinkai, T. Minami, T. Kouno, T. Kusano, and O. Manabe, *Chem. Lett.*, **1982**, 499; H. Tsukube, *Bull. Chem. Soc. Jpn.*, **55**, 3882 (1982).

3) K. Maruyama, H. Tsukube, and T. Araki, *J. Am. Chem. Soc.*, **104**, 5197 (1982).

4) J. C. Metcalfe and J. F. Stoddart, *J. Am. Chem. Soc.*, **99**, 8317 (1977).

5) H. Tsukube, *J. Chem. Soc., Chem. Commun.*, **1983**, 970.

6) J. D. Lamb, J. J. Christensen, S. R. Izatt, K. Bedke, M. S. Astin, and R. M. Izatt, *J. Am. Chem. Soc.*, **102**, 3399 (1980); H. Tsukube, *Bull. Chem. Soc. Jpn.*, **56**, 1883 (1983).

Studies on Lactams. VII.[1] Conformation of D-Glucono-1,5-lactam

Haruo OGURA, Kimio FURUHATA, Hiroaki TAKAYANAGI,*
Nobuyasu TSUZUNO, and Yoichi IITAKA†
School of Pharmaceutical Sciences, Kitasato University Shirokane, Minato-ku, Tokyo 108
†*Faculty of Pharmaceutical Sciences, The University of Tokyo, Hongo, Bunkyo-ku, Tokyo 113*
(Received February 18, 1984)

Synopsis. The structure of D-glucono-lactam (5-amino-5-deoxy-D-glucono-lactam) has been established by means of X-ray crystal structure analysis. The stereochemistry of D-glucono-lactam in crystal was determined to be a half-chair conformation.

In earlier papers,[2] we reported on the lactam rule in relation to the sign of the n-π^* carbonyl Cotton effect for the stereochemistry of the lactam ring. There are, however, difficulties to decide the ring conformation of six-membered lactams from the sign of the n-π^* Cotton effect, because the ring chiralities of δ-lactams are known to take both half-chair and half-boat conformations.[3,4] In this paper, we report the conformation of D-glucono-lactam in crystal determined by X-ray analysis.

Experimental

The crystals are colorless prisms. A specimen of D-glucono-lactam with the dimensions of 0.30×0.25×0.25 mm was used for the intensity measurements. The density was measured by the flotation method in a mixture of petroleum ether and carbon tetrachloride. The cell constants were determined by the least-squares procedure from the 2θ values of 24 reflections measured on a diffractometer using monochromated Cu $K\alpha$ radiation. Three dimensional intensity data were collected on a Rigaku automatic four-circle diffractometer with graphite monochromated Cu $K\alpha$ radiation. Background was counted for 10s at both sides of each peaks. Three standard reflections were measured every 50 reflections during the course of collection. A total of 1120 of independent reflections were collected. Reflections having an intensity exceeding the corresponding standard deviations by a factor of five were treated as observed. 912 reflections with $2\theta<140°$ were retained and corrected for Lorentz and polarization factors but not for absorption factor.

Crystal Data. $C_6H_{11}O_5N$, MW 177.16, mp 207 (dec), $[\alpha]_D$ −42° (c=1, water), crystal system orthorhombic, space group $P2_12_12_1$ a=11.721(1) Å, b=13.471(2), c=4.926(1), V=777.8(1) Å^3, Z=4, $F(000)$=376, D_c=1.514 g·cm^{-3}, D_o=1.51.

Determination and Refinement of the Structure. The crystal structure was solved by the multi-solution method (MULTAN),[5] using 108 normalized structure factors with $E\geqq1.3$. Origin and enantiomorph fixings were carried out automatically by the program. Two of the eight possible solutions gave high combined figures of merit and the E map from one of these showed sensible positions and bond relations for all the non-hydrogen atoms. Refinement of the positional parameters of the twenty atoms was carried out by the block-diagonal matrix least-squares method, in which the other non-hydrogen atoms were assumed to be carbon atoms, the quantity minimized being $\sum w(|F_o|-|F_c|)^2$ with w=1.0 for all the reflections used. Five cycles of calculation gave an R-value of 0.17. The oxygen and nitrogen atoms were deduced from chemical considerations, the bond lengths and the unusually low values of the parameters due to assuming those atoms as carbon. Further refinement carried out with anisotropic thermal parameters gave an R-value of 0.07.

All the hydrogen atoms of the molecule were found from difference maps, and they were refined with isotropic thermal parameters. Five cycles of the refinement by the block-diagonal least-squares method gave the final R value of 0.043 for 912 reflections. The final atomic parameters and the atomic scattering factors for C, O, N were given by Cromer and Mann.[6] The final atomic parameters are given in Table 1. Anisotropic thermal parameters of non-hydrogen atoms and complete F_o-F_c data are deposited as Document No.8430 at the Office of the Editor of the Bull. Chem. Soc. Jpn.

Results and Discussion

The bond lengths and angles are given in Tables 2 and 3. No abnormal lengths and angles were found in the structure. The molecular framework with numbering of the atoms is shown in Fig. 1. From this perspective view of the molecule, the conformation of the compound clearly takes the half-chair form. As shown in Table 4, the torsional angle of C(2)-C(1)-N-C(5) is −4.8°, which means that atoms C(2), C(1), N, and C(5)

Table 1. Atomic coordinates (×10^4) and their standard deviations in parentheses and equivalent isotropic temperature factors

Atom	x	y	z	a) B_{eq}/Å^2
C (1)	9509 (3)	6911 (3)	11129 (9)	1.9
C (2)	8391 (3)	6406 (3)	10253 (9)	1.3
C (3)	7920 (3)	6817 (3)	7636 (9)	1.4
C (4)	7875 (3)	7941 (3)	7781 (9)	1.6
C (5)	9073 (3)	8369 (3)	8135 (9)	1.4
C (6)	8997 (3)	9448 (3)	8980 (11)	1.4
O (1)	10155 (2)	6484 (2)	12715 (8)	2.3
O (2)	8523 (2)	5365 (2)	10173 (7)	2.0
O (3)	6790 (2)	6475 (2)	7192 (7)	1.5
O (4)	7417 (2)	8355 (2)	5384 (7)	2.4
O (5)	10131 (2)	9850 (2)	9137 (7)	1.2
N (1)	9726 (3)	7808 (2)	10147 (8)	1.5
H (C2)	777 (4)	650 (3)	1177 (9)	1.0
H (C3)	841 (3)	662 (3)	599 (9)	1.0
H (C4)	731 (3)	811 (3)	948 (9)	0.9
H (C5)	948 (3)	832 (3)	629 (8)	0.7
H (C6)	855 (4)	978 (4)	736 (12)	1.4
H′ (C6)	865 (4)	951 (3)	1074 (10)	1.1
H (O2)	859 (4)	526 (3)	859 (11)	1.2
H (O3)	668 (4)	590 (4)	611 (11)	1.3
H (O4)	661 (5)	832 (5)	532 (16)	2.4
H (O5)	1012 (4)	1041 (3)	1031 (10)	1.1
H (N)	1041 (4)	808 (3)	1086 (10)	1.1

a) W. C. Hamilton, *Acta Crystallogr.*, **12**, 609 (1959).

Table 2. Bond lengths (l/Å) and their standard deviations in parentheses

C(1)-C(2)	1.538(6)	C(2)-H(C2)	1.04(3)
C(2)-C(3)	1.508(6)	C(3)-H(C3)	1.03(2)
C(3)-C(4)	1.517(7)	C(4)-H(C4)	1.09(4)
C(4)-C(5)	1.528(6)	C(5)-H(C5)	1.03(3)
C(5)-C(6)	1.515(6)	C(6)-H(C6)	1.05(3)
C(5)-N	1.463(8)	C(6)-H'(C6)	0.97(3)
N -C(1)	1.326(8)	O(2)-H(O2)	0.94(4)
C(1)-O(1)	1.231(7)	O(3)-H(O3)	0.95(3)
C(2)-O(2)	1.411(2)	O(4)-H(O4)	0.95(2)
C(3)-O(3)	1.419(6)	O(5)-H(O5)	0.95(3)
C(4)-O(4)	1.412(2)	N -H(N)	0.95(3)
C(6)-O(5)	1.436(5)		

Table 3. Bond angles (ϕ/°) and their standard deviations in parentheses

C(2)-C(1)-O(1)	119.7(4)	C(5)-C(4)-C(3)	110.5(3)
C(2)-C(1)-N	117.6(4)	C(5)-C(4)-O(4)	107.2(3)
O(1)-C(1)-N	122.6(4)	C(3)-C(4)-O(4)	111.6(3)
C(3)-C(2)-C(1)	112.9(3)	C(6)-C(5)-C(4)	109.8(3)
C(3)-C(2)-O(2)	112.4(3)	C(6)-C(5)-N	109.3(3)
C(1)-C(2)-O(2)	110.7(3)	C(4)-C(5)-N	111.3(3)
C(4)-C(3)-C(2)	109.8(3)	O(5)-C(6)-C(5)	108.8(4)
C(4)-C(3)-O(3)	107.4(3)	C(1)-N-C(5)	128.1(4)
C(2)-C(3)-O(3)	110.7(3)		

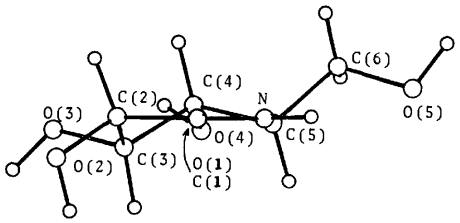

Fig. 1. A perspective view of the D-glucono-1,5-lactam molecule and the atomic numbering.

Table 4. Some torsional angles (ϕ/°)

C(2)-C(1)-N-C(5)	−4.8
C(1)-C(2)-C(3)-C(4)	−50.0
C(4)-C(5)-N-C(1)	16.2
C(3)-C(2)-C(1)-N	21.7
C(3)-C(4)-C(5)-C(6)	−166.1
C(3)-C(4)-C(5)-N	−43.8
C(2)-C(1)-N-H(N)	177.1
O(1)-C(1)-N-H(N)	−1.9

are placed on the same plane. Torsional angles C(1)-N-C(5)-C(4) and N-C(1)-C(2)-C(3) are 16.2° and 21.7° respectively. Vertical distances of C(3) and C(4) from the plane (C(2)-C(1)-N-C(5)) are 0.44 and 0.30 Å respectively. The vicinal coupling constant between the hydrogen atoms attached to C(2) and C(3), C(3), and C(4), C(4), and C(5) should be all *ca.* 10 Hz, because the dihedral angles H(2)-C(2)-C(3)-H(3), H(3)-C(3)-C(4)-H(4), and H(4)-C(4)-C(5)-H(5) are 169.0°, 176.9°, and 166.9° respectively. The observed coupling constants (in $CDCl_3$) $J_{2,3}$, $J_{3,4}$, and $J_{4,5}$ of the

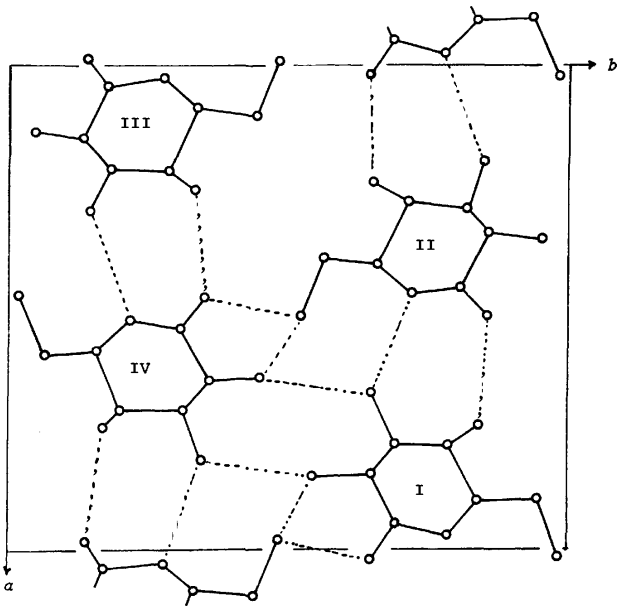

Fig. 2. Projection of the Crystal Structure along c Axis.

Table 5. Bond lengths and bond angles of intermolecular hydrogen bond

	Length(l/Å)	Angle(ϕ/°)
N-H···O(3)	2.92	178
O(1)···H-O(4)	2.82	165
O(2)-H···O(5)	2.73	171
O(5)-H···O(1)	2.71	171
O(3)-H···O(2)	2.70	160

compound are all 9.5 Hz, which indicate that the conformation of D-glucono-lactam has the same half-chair conformation both in crystal and in solution. The crystal structure of the compound projected along the c axis is shown in Fig. 2. Hydrogen bonds are shown by broken lines. The hydrogen bonding distances and angles are listed in Table 5.

The authors with to thank Dr. S. Inouye, Meiji Seika, Ltd., for supplying D-glucono-lactam.

The present work was supported by a Grant-in-Aid for Scientific Research No.58570883 from the Ministry of Education, Science, and Culture of Japan.

References

1) Part VI, H. Ogura, K. Furuhata, and K. Furuhata, *Chem. Pharm. Bull., (Tokyo)*, **23**, 2474 (1975).

2) H. Ogura, H. Takayanagi, and K. Furuhata, *Chem Lett.*, **1973**, 387; H. Takayanagi, K. Kubo, and K. Furuhata, *J. Am. Chem. Soc.*, **95**, 8056 (1973); H. Ogura, H. Takayanagi, and K. Furuhata, *J. Chem. Soc., Perkin Trans. 1*, **1976**, 665.

3) H. Wolf, *Tetrahedron Lett.*, **1965**, 1075; **1966**, 5151.

4) H. Meguro, T. Konno, and K. Tuzimura, *Tetragedron Lett.*, **1975**, 1309.

5) G. Germain, P. Main, and M. M. Woolfson, *Acta Crystallogr., Sect. A*, **27**, 368 (1971).

6) D. J. Cromer and J. B. Mann, *Acta Crystallogr., Sect. A*, **24**, 321 (1968).

A Novel Route to *N*-Phenyl-*C*-(trifluoromethyl)nitrilimine from 3-Phenyl-5-trifluoromethyl-2,3-dihydro-1,3,4,2-oxadiazaphosphole

Kiyoshi TANAKA,* Toh-ru IGARASHI, Seiji MAENO, and Keiryo MITSUHASHI
Department of Industrial Chemistry, Seikei University Musashino-shi, Tokyo 180
(Received February 28, 1984)

Synopsis. Thermolysis of 3-phenyl-5-trifluoromethyl-2,2,2-tris-(*p*-tolyloxy)-2,3-dihydro-1,3,4,2-oxadiazaphosphole in the presence of various olefins gave the 1,3-dipolar cycloadducts of *N*-phenyl-*C*-(trifluoromethyl)nitrilimine *in situ* formed. The similar decomposition in aniline afforded *N*-phenyltrifluoroacetamide phenylhydrazone.

Pentacovalent phosphorus compounds (phosphoranes) have high potential as synthetic reagents[1] but only a little information is available.[2] A cyclic oxyphosphorane is known to decompose with the formation of phosphine oxide and a polar intermediate (**1**) which cyclizes inter- or intramolecularly as shown below. Such a reaction mode could be utilized as a general method for the synthesis of heterocyclic compounds:[3] for example, Burger and his co-workers have been exploring the reactions of benzonitrile bis(trifluoromethyl)ylide generated from 5,5,5-trialkoxy-2-phenyl-4,4-bis(trifluoromethyl)-4,5-dihydro-1,3,5-oxazaphosphole.[4] We have previously described the preparation of 3-phenyl-5-trifluoromethyl-2,2,2-tris(*p*-tolyloxy)-2,3-dihydro-1,3,4,2-oxadiazaphosphole (**2**) and its possibile use as a precursor of *N*-phenyl-*C*-(trifluoromethyl)nitrilimine (**3**).[5]

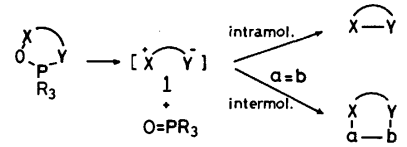

In the present paper, we wish to report that thermolysis of the phosphole **2** in the presence of various olefins or nucleophiles like aniline affords the corresponding 1,3-dipolar cycloadducts or 1,3-adducts, respectively, of the nitrilimine **3** formed *in situ*. Such results must indicate the phosphole **2** to be the novel effective source of the nitrilimine **3**.[6]

The thermal decomposition of **2** in the presence of excess styrene was carried out at 140 °C for 24 h to give 1,5-diphenyl-3-trifluoromethyl-2-pyrazoline (**5a**) in 73% yield along with 65% of tris(*p*-tolyl) phosphate (**4**). A similar cleavage did not take place at 110 °C, the greater part of **2** being recovered unchanged. In the presence of methyl acrylate and methacrylate, thermolysis of **2** provided the corresponding pyrazolines **5b** and **5c** in 98 and 73% yields, respectively. On the other hand, in the case of methyl crotonate, the formation of both the pyrazoline **5d** and its regioisomer **5'd** in the ratio of 80/20 was found. The structure of these pyrazolines was determined by their elemental analyses and spectral data or by comparison with our authentic samples. The regioselectivity of these cycloadditions of **3** derived from **2** was analogous to that from *N*-phenyltrifluoroacetohydrazonoyl chloride which, for example, with methyl crotonate, gives a 90/10 mixture

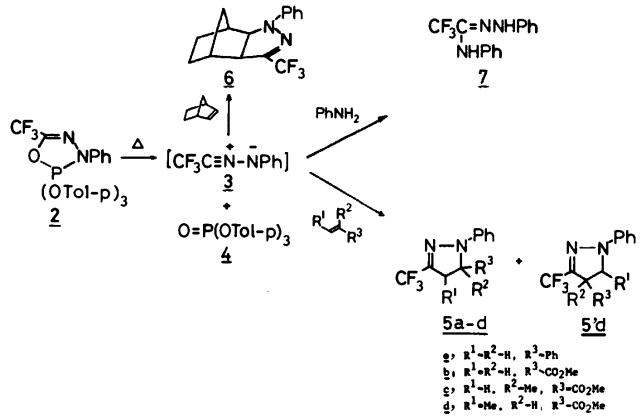

of **5d** and **5'd**.[7]

Cycloaddition was also found to occur when **2** was decomposed in the strained olefin like norbornene, where the syn-adduct **6** was exclusively obtained in 48% yield. The exo-configuration of **6** is supported by the absence of coupling between the bridgehead protons and the corresponding vicinal pyrazoline protons in ^{1}H NMR.[8] Similarly, on the cleavage of **2** in aniline, the 1,3-addition product, *N*-phenyltrifluoroacetamide phenylhydrazone (**7**), was produced in 61% yield.

The present alternative route to **3** has the advantage that the thermal decomposition of **2** is carried out at a relatively low temperature and under neutral conditions.[9]

Experimental

All melting and boiling points are uncorrected. The IR spectra were recorded on a JASCO IRA-1 spectrometer. The ^{1}H and ^{31}P NMR spectra were measured with JEOL JNM-PMX 60 and FX 90Q spectrometers using tetramethylsilane and 85% phosphoric acid as internal and external standards, respectively; the chemical shifts are given in δppm downfield. The MS spectra were obtained with a Finnigan 4023 GC-MS DS spectrometer.

Preparation of **2**. Phosphorus pentachloride 5.20 g (24.9 mmol) was added to a stirred suspension of 4.74 g (23.2 mmol) of *N*-phenyltrifluoroacetohydrazide in 40 ml of toluene. The mixture was stirred at room temperature for an additional 2 h with evolution of hydrogen chloride. The solvent was evaporated under reduced pressure to leave oily matter which was distilled to give 7.33 g (93%) of 2,2,2-trichloro-3-phenyl-5-trifluoromethyl-2,3-dihydro-1,3,4,2-oxadiazaphosphole, bp 124—126 °C/12 mmHg (1 mmHg= 133.322Pa), IR(film) 1650 cm^{-1} (C=N), ^{1}H NMR ($CDCl_3$) δ=7.3 (br. s). A mixture of 2.00 g (5.9 mmol) of trichlorophosphole thus obtained and 3.19 g (17.7 mmol) of *O*-trimethylsilyl-*p*-cresol in 20 ml of toluene was refluxed for 4.5 h. The solvent was removed to leave a residue which was recrystallized from hexane to give the colorless crystals **2**, 1.78 g (54%), mp 96—97 °C, IR (KBr) 1648 cm^{-1} (C=N),

^{1}H NMR (CCl_4) δ=2.3 (s, 9H), 6.8 (A_2X_2, 12H), and 7.4 (br. s, 5H), ^{31}P NMR ($CDCl_3$) δ=−69.0, MS (CI, *m/z*) 583 ($M+C_2H_5$)$^+$ and 555 $(M+H)^+$.

Found: C, 62.82; H, 4.62; N, 4.78. Calcd for $C_{29}H_{26}F_3N_2O_4P$: C, 62.82; H, 4.73; N, 5.05.

Thermolysis of **2** *in Styrene.* A mixture of 0.55 g (1.0 mmol) of **2** and 0.52 g (5.0 mmol) of styrene in 20 ml of xylene was refluxed for 24 h and the solvent was removed. The resulting oily matter was placed on a column (silica gel) and eluted with hexane–chloroform (1:1) to give 0.21 g (72%) of **5a** and 0.24 g (65%) of **4**. The pyrazoline **5a** was further purified by recrystallization from hexane. **5a**; mp 87.5—88.5 °C, IR (KBr) 1610 cm^{-1} (C=N), ^{1}H NMR (CCl_4) δ=2.88 (ddq, *J*=8, 18, 2 Hz, 1H), 3.60 (ddq, *J*=12, 18, 2 Hz, 1H), 5.25 (dd, *J*=8, 12 Hz, 1H), and 6.5—7.5 (m, 10H).

Found: C, 66.25; H, 4.52; N, 9.75. Calcd for $C_{16}H_{13}F_3N_2$: C, 66.20; H, 4.51; N, 9.65.

In a similar manner, **6** was isolated in 47% yield. **6**; mp 78.5—79.5 °C (recrystallized from methanol), IR (KBr) 1595 cm^{-1} (C=N and Ph), ^{1}H NMR ($CDCl_3$) δ=1.1—1.7 (m, 6H), 2.5—2.8 (m, 2H), 3.33 (dm, *J*=10 Hz, 1H), 4.20 (d, *J*=10 Hz, 1H), and 6.8—7.4 (m, 5H).

Found: C, 64.44; H, 5.34; N, 10.03. Calcd for $C_{15}H_{15}F_3N_2$: C, 64.28; H, 5.39; N, 9.99.

Thermolysis of **2** *in Methyl Crotonate.* A mixture of 1.50 g (2.7 mmol) of 2 and 3.0 ml of methyl crotonate in a sealed tube was stirred at 140—145 °C for 24 h. The product ratio was determined by GLC analysis of the reaction mixture; **5d**/**5'd** ratio of 80/20. After excess methyl crotonate was removed, 0.73 g (94%) of a mixture of **5d** and **5'd** was obtained by column chromatography (silica gel, hexane–chloroform, 3:2). Each pyrazoline was isolated by preparative GLC. **5d**; IR (film) 1750 cm^{-1} (C=O), ^{1}H NMR (CCl_4) δ=1.43 (d, *J*=7 Hz, 3H), 3.51 (dqm, *J*=7, 7 Hz, 1H), 3.70 (s, 3H), 4.35 (d, *J*=7 Hz, 1H), and 6.7—7.4 (m, 5H). **5'd**; IR (film) 1750 cm^{-1} (C=O), ^{1}H NMR (CCl_4) δ=1.37 (d, *J*=7 Hz, 3H), 3.63 (dm, 1H), 3.72 (s, 3H), 4.77 (dq, *J*=7, 7 Hz, 1H), and 6.6—7.3 (m, 5H).

Found: C, 54.43; H, 4.57; N, 9.75 (for a mixture of **5d** and **5'd**). Calcd for $C_{13}H_{13}F_3N_2O_2$: C, 54.55; H, 4.58; N, 9.79.

Similarly, **5b** and **5c** were isolated in 98 and 73% yields, respectively. **5b**; mp 58—60 °C (lit,[7] 60—61.5 °C), IR (KBr) 1745 (C=O) and 1620 cm^{-1} (C=N), ^{1}H NMR ($CDCl_3$) δ=2.8—3.5 (m, 2H), 3.71 (s, 3H), 4.87 (dd, *J*=11, 9 Hz, 1H), and 6.8—7.4 (m, 5H). **5c**; colorless oil, IR (film) 1745 cm^{-1} (C=O), ^{1}H NMR (CCl_4) δ=1.59 (s, 3H), 3.00 (dm, *J*=17 Hz 1H), 3.53 (dm, *J*=17 Hz, 1H), 3.73 (s, 3H), and 6.7—7.4 (m, 5H).

Found: C, 54.40; H, 4.57; N, 9.73. Calcd for $C_{13}H_{13}F_3N_2O_2$: C, 54.55; H, 4.58; N, 9.79.

Thermolysis of **2** *in Aniline.* A mixture of 1.50 g (2.7 mmol) of **2** and 5.04 g (54.2 mmol) of aniline in 30 ml of xylene was refluxed for 15 h and the solvent was removed. To the residual oil was added diethyl ether and the mixture was washed twice with water, dried over magnesium sulfate, and evaporated. The resulting oily matter was submitted to column chromatography (silica gel, hexane–chloroform, 1:1) to give 0.46 g (61%) of **7** which was further purified by recrystallization. **7**; mp 66.5—67.5 °C (hexane), IR (KBr) 3360 cm^{-1} (NH), ^{1}H NMR ($CDCl_3$) δ=5.5 (br. s, 1H) and 6.8—7.4 (m, 11H).

Found: C, 60.07: H, 4.28; N, 15.10. Calcd for $C_{14}H_{12}F_3N_3$: C, 60.21; H, 4.33; N, 15.05.

References

1) D. Hellwinkel, "Penta- and Hexaorganophosphorus Compounds," in "Organic Phosphorus Compounds," ed by G. M. Kosolapoff and L. Maier, Wiley Interscience, New York (1972), Vol. 3, Chap. 5B; J. Emsley and D. Hall, "The Chemistry of Phosphorus," Harper and Row, New York (1976), Chap. 6.

2) T. Kubota, S. Miyashita, T. Kitazume, and N. Ishikawa, *J. Org. Chem.*, **45**, 5052 (1980).

3) F. Ramirez and C. D. Telefus, *J. Org. Chem.*, **34**, 376 (1969); G. Gaudiano, R. Mondelli, P. P. Ponti, C. Ticozzi, and A. Umani-Ronchi, *J. Org. Chem.*, **33**, 4431 (1968); H. J. Bestmann and R. Kunstmann, *Chem. Ber.*, **102**, 1816 (1969); T. Mukaiyama and T. Kumamoto, *Bull. Chem Soc. Jpn.*, **39**, 879 (1966).

4) K. Burger, J. Fehn, and E. Moll, *Chem. Ber.*, **104**, 1826 (1971); K. Burger, W. D. Roth, K. Einhellig, and L. Hatzelman, *ibid.*, **108**, 2737 (1975).

5) K. Tanaka, T. Igarashi, and K. Mitsuhashi, *Chem. Lett.*, **1983**, 507.

6) Part IV on "Applications of the fluorinated 1,3-dipolar compounds as building blocks of the heterocycles with fluorine groups." Part III: K. Tanaka, H. Masuda, and K. Mitsuhashi, *Bull. Chem. Soc. Jpn.*, **57**, 2184 (1984).

7) K. Tanaka, S. Maeno, and K. Mitsuhashi, *Chem. Lett.*, **1982**, 543.

8) R. Huisgen, H. Knupfer, R. Sustmann, G. Wallbillich, and V. Weberndörfer, *Chem. Ber.*, **100**, 1580 (1967).

9) For example, thermolysis of 2,5-diphenyltetrazole was carried out at 150 °C; R. Huisgen, M. Seidel, J. Sauer, J. W. McFarland, and G. Wallbillich, *J. Org. Chem.*, **24**, 892 (1959).

A Convenient Procedure for Iodination of Electron-rich Aromatic Compounds using Iodine-Copper(II) Acetate

C. Akira HORIUCHI* and J. Yasuo SATOH
Department of Chemistry, Rikkyo (St. Paul's) University, Nishi-Ikebukuro, Toshima-ku, Tokyo 171
(Received March 28, 1984)

Synopsis. The iodination of some electron-rich aromatic compounds, namely, three polymethylbenzenes, aniline, phenol, anisole, and phenetole, using iodine-copper(II) acetate in acetic acid, afforded the corresponding iodo compound in high yield.

Much work has been reported on the bromination and chlorination of aromatic compounds. However, since it is known that iodination is usually difficult accomplish due to the reducing effect of the hydrogen iodide produced, the iodination of aromatic compounds has been carried out in the presence of an oxidizing reagent such as nitric acid, iodic acid, sulfur trioxide, or hydrogen peroxide.[1] Many procedures are available for the iodination of activated aryl compounds by iodine-thallium(I) acetate,[2] iodine-mercury(II) acetate,[3] iodine-silver(I) acetate,[4] iodine-ammonium hexanitratocerate(IV),[5] and alkali metal iodide-ammonium hexanitratocerate(IV).[5] Moreover, Bird and Surridge recently reported[6] that the iodination of aromatic compounds with iodine and copper(II) halide gave the aryl iodides. Still more recently, it was reported the iodination of the less reactive substrates with iodine-aluminum(III) and copper(II) chloride[7] gave the corresponding aryl halide.

We have been investigating a novel iodination using iodine-copper(II) acetate; and as a first step in this research project, we reported earlier the α-iodination of ketones,[8] and the regioselective iodination of estradiol, estriol, and estrone.[9] In the work described in these reports, we demonstrated that iodine-copper(II) acetate in acetic acid is a useful reagent for the syntheses of some iodo compounds.

In the present paper, we report the iodination of some activated aryl compounds, namely, three polymethylbenzenes, aniline, phenol, anisole, and phenetole.

The reactions of the polymethylbenzenes, mesitylene (**1**), durene (**2**), and pentamethylbenzene (**3**) with iodine and copper(II) acetate in acetic acid under refluxing for 5—9 h yielded in all cases the iodo compound (**8**—**10**) (70—89%). All products were characterized by comparisons of their NMR and IR spectra and their melting points with those of authentic samples. Similarly, the reaction of aniline (**4**) afforded 4-iodoaniline (**11**) in a good yield. In the cases of anisole (**5**) and phenetole (**6**), *para*-substituted products (**12** and **13**) were obtained. This result is in agreement with the fact that the iodination of anisole using thallium(I) acetate[2] or copper(II) chloride[6] occurs at the *para*-position. The method used in the present work gave a better yield than Cambie's one. In the case of phenol (**7**), it was found that *ortho*-attacked products, namely, 2-iodo- (**15**) (64%) and 2,6-diiodo-phenol (**14**) (11%), and 4-iodo derivative (**16**) (5%) were obtained. This agrees with the result of the iodination using thallium(I) acetate or silver(I) acetate; and both of these results are also supported by our earlier finding that the iodination using the iodine-copper(II) acetate of the 3-hydroxy-estrogen derivative occurred at the *ortho*-position,[9] while the reaction of 3-methoxyestrogen derivative resulted in the recovery of the starting material. Thus, it was found that the iodine and copper(II) acetate used in these reactions were efficient and selective iodinating agents for electron-rich aromatic compounds.

Experimental

All the melting points are uncorrected. The IR and NMR spectra were measured using a Hitachi model 215 grating infrared spectrometer and a nuclear magnetic resonance spectrometer, Hitachi-Perkin Elmer R-20A, in carbon tetrachloride with TMS as an internal standard.

General Procedure. A mixture of a substrate (1.1×10^{-2} M), iodine (1.0 mol. equiv), and copper(II) acetate (1.0 mol. equiv) in acetic acid (50 ml) was stirred under refluxing for 6—9 h. The precipitated copper(I) iodide was removed by filtration, and the filtrate was poured into water and extracted with ether. The ethereal solution was washed with sodium hydrogencarbonate solution and with water, then

TABLE 1. PRODUCTS AND ISOLATED YIELDS (%) IN THE IODINATION OF ELECTRON-RICH AROMATIC COMPOUNDS (**1**—**7**)

Materials	Time/h	Products	Isolated yield/%	Mp θ_m/°C	Lit. Mp θ_m/°C
Mesitylene (**1**)	5	Iodomesitylene (**8**)	80	30—31	32—34[10]
Durene (**2**)	6	Iododurene (**9**)	89	79—80	80—81[11]
Pentamethylbenzene (**3**)	9	Iodopentamethylbenzene (**10**)	70	139—140	141—142[11]
Aniline (**4**)	2	4-Iodoaniline (**11**)	90	61—62	59—62[2]
Anisole (**5**)	10	4-Iodoanisole (**12**)	69	48—49	48—50.5[2]
Phenetole (**6**)	10	4-Iodophenetole (**13**)	80	29—30	29[12]
Phenol (**7**)	4	2,6-Diiodophenol (**14**)	11	66—67	65.5—67.5[2]
		2-Iodophenol (**15**)	64	43—44	42—43[2]
		4-Iodophenol (**16**)	5	92—93	92—94[10]

dried with anhydrous sodium sulfate. After removal of the desiccant, evaporation of the solvent left a solid, which was recrystallized from hexane to give the corresponding aryl iodide.

Iodination of Phenol (**7**). A mixture of phenol (**7**) (1.021 g), iodine (2.753 g), and copper(II) acetate (2.167 g) in acetic acid was treated according to the general procedure. After the usual work-up, the resultant oil was chromatographed on silica gel (50 g). Elution with hexane (50 ml) and benzene (70 ml) gave plates of **14** (420 mg) from hexane, mp 66—67 °C. The next fraction, eluted by the same solvent (70 ml), on crystallization from hexane gave plates of **15** (1.529 g), mp 43—44 °C, while the last fraction, eluted with the same solvent (30 ml), on crystallization from hexane gave plates of **16** (115 mg), mp 92—93 °C.

References

1) H. Suzuki, "Shinjikken-Kagaku Kohza," ed by T. Tachibana, Maruzen & Co., Tokyo (1977), Vol. 14, Part I, pp 418—425.

2) R. C. Cambie, P. S. Rutledge, T. S. Palmer, and P. D. Woodgate, *J. Chem. Soc., Perkin Trans. 1*, **1976**, 1161.

3) M. Stefanovic, Lj. Krstic, and S. Mladenovic, *Tetrahedron Lett.*, **1971**, 3311.

4) W. G. Dauben and H. Tilles, *J. Am. Chem. Soc.*, **72**, 3185 (1950); D. Popa, E. Schwenk, and E. Klinsberg, *ibid.*, **72**, 2623 (1950).

5) T. Sugiyama, *Bull. Chem. Soc. Jpn.*, **54**, 2847 (1981).

6) C. W. Baird, Jr. and J. H. Surrindge, *J. Org. Chem.*, **35**, 3436 (1970).

7) T. Sugita, M. Idei, Y. Ishibashi, and Y. Takegami, *Chem. Lett.*, **1982**, 1481.

8) C. A. Horiuchi and J. Y. Satoh, *Synthesis*, **1981**, 312.

9) C. A. Horiuchi and J. Y. Satoh, *J. Chem. Soc., Chem. Commun.*, **1982**, 671.

10) H. Suzuki and R. Goto, *Nippon Kagaku Zasshi*, **84**, 284 (1963).

11) H. Suzuki, T. Sugiyama, and R. Goto, *Bull. Chem. Soc. Jpn.*, **37**, 1858 (1964).

12) B. Prager, P. Jacobson, P. Schmidt, and D. Stern, "Beilsteins Handbuch der Organischen Chemie," Springer-Verlag, Berlin (1923), Vol. 6, p.208.

The Reaction of Diethyl Acyl Phosphites with α,β-Unsaturated Carbonyl Compounds

Yoshiki OKAMOTO* and Toshio AZUHATA
The Institute of Scientific and Industrial Research, Osaka University, Mihogaoka 8-1, Ibaragi, Osaka 567
(Received April 9, 1984)

Synopsis. Diethyl acetyl and diethyl benzoyl phosphites reacted with propenal and 3-buten-2-one to give 1,4-addition products respectively. While the reaction of diethyl acetyl phosphite with 2-butenal and 2-methyl- and 3-phenylpropenals gave 1,2-addition products exclusively.

Trialkyl phosphites are known to react sluggishly with aldehyde. The reaction requires rather drastic conditions or much long reaction time and give several addition compounds such as 1:1, 1:2 or 1:3 in relatively low yield.[1] Dialkyl trimethylsilyl phosphite reacts smoothly with aldehyde and ketone to produce [α-(trimethylsiloxy) alkyl] phosphonate.[2] In the case of the reaction with α,β-unsaturated carbonyl compounds, the adducts resulting from 1,2 and 1,4 modes of addition have been obtained.[2] Diethyl acetyl phosphite (**1a**) reacted in diethyl ether exothermically with chloroacetaldehyde to give diethyl (1-acetoxy-2-chloroethyl)-phosphonate (56—95%).[3] Chloral, benzaldehyde, and 3-methylbutanal reacted also in same manner. The unchlorinated aldehyde required higher temperature.[4]

In this report, the reaction of diethyl acyl phosphite (**1**) with α,β-unsaturated carbonyl compounds is reported.

The reaction of diethyl acyl phosphite (**1**) with propenal (**2a**) proceeded exothermically at room temperature, while the reaction with α- or β-substituted α,β-unsaturated aldehyde (**2**) required heating to the refluxing temperature of benzene for several hours.

Propenal (**2a**) reacted with diethyl acetyl phosphite (**1a**) to give a mixture of 1,4-addition product (**3a**) and several unidentified products. In the case of the reaction of **2a** with diethyl benzoyl phosphite (**1b**), only 1,4-addition product (**3b**) was isolated in 69% yield. Diethyl 2,2-dimethylpropionyl phosphite (**1c**) did not reacted with **2a**. 3-Buten-2-one (**2b**) reacted also smoothly with **1a** and **1b** to afford only 1,4-addition products (**3c** and **3d**) respectively. On the other hand, when α- or β-substituted α,β-unsaturated aldehyde (**2c**, **2d**, and **2e**) was allowed to react with **1a**, only 1,2-addition products (**4a**, **4b**, and **4c**) were obtained exclusively. But 4-methyl-3-penten-2-one did not react with **1a**. Diethyl benzoyl phosphite (**1b**) did not react with these substituted aldehydes (**2c**, **2d**, and **2e**). Such a restricted limitation of the reaction may be caused by the high sensitivity of the dialkyl acyl phosphite (**1**) to steric hindrance. ^{1}H-NMR spectroscopy and GLC analysis of these products showed them to be in pure states, but assignment of olefin geometries could not be done.

1a: R^1=Me
1b: R^1=Ph
1c: R^1=Me_3C

2a: R^2=R^3=R^4=H
2b: R^2=R^3=H, R^4=Me
2c: R^2=Me, R^3=R^4=H
2d: R^2=R^4=H, R^3=Me
2e: R^2=Ph, R^3=R^4=H

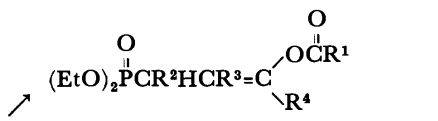

3a: R^1=Me, R^2=R^3=R^4=H
3b: R^1=Ph, R^2=R^3=R^4=H
3c: R^1=Me, R^2=R^3=H, R^4=Me
3d: R^1=Ph, R^2=R^3=H, R^4=Me

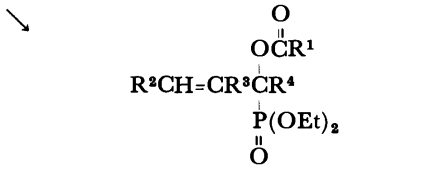

4a: R^1=Me, R^2=Me, R^3=R^4=H
4b: R^1=Me, R^2=R^4=H, R^3=Me
4c: R^1=Me, R^2=Ph, R^3=R^4=H

Experimental

Dialkyl acyl phosphites were prepared from diethyl phosphorochloridite and sodium carboxylates.[5] Benzene was distilled under nitrogen from calcium hydride. Aldehydes and ketones were freshly distilled. All reactions were carried out under an atmosphere of nitrogen with the rigid exclusion of moisture from reagent and glasswares. ^{1}H NMR spectra were recorded on a JNM FX-100 spectrometer. Analytical gas chromatography were performed on a Shimadzu GC-7A gas chromatograph using a 2 m glass column of 2% OV-17 on a 60-80 mesh DMCS Chromosorb W support.

General Procedure. To a flask equipped with a reflux condenser, a magnetic stirrer, and an addition funnel were added 10 ml of benzene and 20 mmol of carbonyl compound. While the mixture was stirred at room temperature, 20 mmol of dialkyl acyl phosphite was added dropwise. After completion of addition, the solution was refluxed for 3 h. Distillation at atmospheric pressure removed the solvent. Susequent vacuum distillation afforded the product. The purity was checked by GLC analysis and ^{1}H NMR spectroscopy. The results are summarized in Table 1.

Table 1. Yields and physical properties of products (**3** and **4**)

Compd No.	Yield %	Bp °C/Pa	Formula	Found(Calcd)(%) C	H	P	^{1}H NMR, δ, in $CDCl_3$
3a	23	132—134/133	$C_9H_{17}O_5P$	45.15 (45.77	7.32 7.25	13.45 13.11)	1.32(6H, t, J_{HH}=7.1 Hz, CH_3), 2.71(2H, ddd, J_{HP}=22.0 Hz, J_{HH}=7.8 Hz, J_{HH}=1.4 Hz, PCH_2), 2.17(3H, s, $COCH_3$), 4.11(4H, quintet, J_{HH}=J_{HP}=7.1 Hz, OCH_2), 4.95(1H, ddt, J_{HP}=6.3 Hz, J_{HH}=7.8 Hz, J_{HH}=4.7 Hz, -CH=), 7.18(1H, ddt, J_{HP}=6.9 Hz, J_{HH}= 4.7 Hz, 1.4 Hz, =CHO)
3b	56	140—145/13	$C_{14}H_{19}O_5P$	56.23 (56.38	6.47 6.42	10.42 10.38)	1.30(6H, t, J_{HH}=7.1 Hz, CH_3), 2.87(2H, ddd, J_{HP}=23 Hz, J_{HH}=7.9 Hz, J_{HH}=1.5 Hz, PCH_2) 4.14(4H, quintet, J_{HP}=J_{HH}=7.1 Hz, OCH_2), 5.11(1H, ddt, J_{HP}=6.6 Hz, J_{HH}= 7.9 Hz, J_{HH}=4.8 Hz, -CH=), 5.30—5.42(1H, m, =CHO), 7.4—8.2(5H, m, arom)
3c	68	135—140/93	$C_{10}H_{19}O_5P$	47.87 (48.00	7.69 7.65	12.47 12.38)	1.32(6H, t, J_{HH}=7.1 Hz, CH_3), 1.94(3H, dd, J_{HP}=5.1 Hz, J_{HH}=1.2 Hz, $=CCH_3$), 2.50(2H, dd, J_{HP}=21.7 Hz, J_{HH}=7.6 Hz, CH_2P), 2.16 (3H, s, $COCH_3$), 4.10(4H, quintet, J_{HP}= J_{HH}=7.1 Hz, OCH_2), 5.06(1H, dtq, J_{HP}=6.5 Hz, J_{HH}=7.6 Hz, J_{HH}=1.2 Hz, -CH=)
3d	56	160—164/26	$C_{15}H_{21}O_5P$	57.29 (57.69	6.77 6.78	10.15 9.92)	1.31(6H, t, J_{HH}=7.1 Hz, CH_3), 2.07(3H, dd, J_{HP}=4.9 Hz, J_{HH}=1.0 Hz, $=CCH_3$), 2.59(2H, dd, J_{HP}=21.5 Hz, J_{HH}=7.6 Hz, CH_2P), 4.10 (4H, quintet, J_{HP}=J_{HH}=7.1 Hz, OCH_2), 5.20 (1H, J_{HP}=7.6 Hz, J_{HH}=6.0 Hz, J_{HH}=1.0 Hz, CH=), 7.3—8.2(5H, m, arom)
4e	49	126—129/66	$C_{10}H_{19}O_5P$	48.24 (48.00	7.76 7.65	12.55 12.38)	1.33(6H, t, J_{HH}=7.0 Hz, CH_3), 1.84(3H, dd, J_{HH}=1.6 Hz, J_{HH}=3.0 Hz, $=CCH_3$) 2.03(3H, s, $COCH_3$), 3.98(4H, quintet, J_{HP}=J_{HH}=7.0 Hz, OCH_2), 4.15—4.35(1H, m, OCH), 5.13— 5.30(1H, m, HC=), 5.40—5.50(1H, m, HC=)
4f	48	123—125/66	$C_{10}H_{19}O_5P$	48.26 (48.00	7.50 7.65	12.51 12.38)	1.33(6H, t, J_{HH}=7.0 Hz, CH_3), 1.75(3H, dd, J_{HH}=7.0 Hz, J_{HH}=1.3 Hz, $=CHCH_3$), 2.13 (3H, s, $COCH_3$), 4.07(4H, quintet, J_{HP}= J_{HH}=7.0 Hz, OCH_2), 4.38—4.40(1H, m, CHO), 5.59—5.64(1H, m, HC=), 5.85—5.90 (1H, m, HC=)
4g	65	160—163/39	$C_{15}H_{21}O_5P$	57.78 (57.69	6.71 6.78	9.86 9.92)	1.33(6H, t, J=6.9 Hz, CH_3), 2.17(3H, s, $COCH_3$), 4.18(4H, quintet, J_{PH}=J_{HH}=6.9 Hz, OCH_2), 5.84(1H, ddd, J_{HP}=15.0 Hz, J_{HH}=7.4 Hz, J_{HH}=1.0 Hz, HCO), 6.02(1H, ddd, J_{HP}=7.3 Hz, J_{HH}=16.0 Hz, J_{HH}=5.3 Hz, HC=), 6.78(1H, ddd, J_{HP}=4.8 Hz, J_{HH}= 16.0 Hz, J_{HH}=1.0 Hz, HC=), 7.2—7.5(5H, m, arom)

References

1) F. Ramirez, "Organo-Phosphorus Compounds, special lectures presented at the Symposium on Organo-Phosohorus Compounds held in Heidelberg, Germany, 1964," Butterworths, London (1964), p. 337.

2) M. Sekine, I. Yamamoto, A. Hashizume, and T. Hata, *Chem. Lett.*, **1977**, 485; D. A. Evans, K. M. Hurst, and J. M. Takacs, *J. Am. Chem. Soc.*, **100**, 3467 (1978).

3) A. N. Pudovik, T. K. Gazizov, Y. Y. Samitov, and T. V. Zykova, *Zh. Obshch. Khim.*, **37**, 706 (1967).

4) L. V. Nesterov, R. A. Sabirova, and N. E. Krepysheva, *Zh. Obshch. Khim.* **39**, 1943 (1969).

5) K. Sasse, "Methoden der Organischen Chemie, Organische Phosphorverbindungen Teil 2," ed by E. Müller, Georg Thieme Verlag, Stuttgart (1964), p. 113.

 © 1984 The Chemical Society of Japan Bull. Chem. Soc. Jpn., 57, 2695—2699 (1984)

Preliminary Work on Orientation of Nematic Liquid-Crystalline Molecule by Electronic Spectra

Michio KOBAYASHI, Toshiyuki KASAHARA,† Keihachiro NAKAJIMA††
Kazunori MARUYAMA, and Yoshie TANIZAKI*
Department of Materials Science and Technology, Technological University of Nagaoka, Nagaoka 949-54
(Received December 23, 1983)

Absorption spectra of a nematic liquid-crystalline molecule (4-butyl-4′-ethoxyazobenzene) were measured in sandwich-type cells with very thin gaps which ranged from 0.2 to 1.0 μm when the cells were empty. The intensity ratio of the first (354 nm) to second (240 nm) band in the liquid state (86 °C) decreases as the state changes into liquid-crystalline (LC) states (70 and 48 °C). According to results of dichroism analysis and MO calculation, the 354 nm and 240 nm bands are due to π-π^* transitions polarized along the molecular long and short axes, respectively (with an angle of about 66°to each other). This finding coupled with an assumption that the molecular orientation of the liquid state is isotropic, allows a qualitative discussion on the orientation of molecule in the LC state, leading to a conclusion that the molecular long axis against the cell surface takes two kinds of orientation with respective tendencies to be parallel in the interface region and perpendicular in the bulk region.

Descriptions[1] have been given for a problem concerning the orientation of liquid-crystalline (LC) molecules, *i.e.*, the problem of the orientational order parameter.[2] Many approaches to this problem seem to be limited to optical phenomena associated with the refractive index or, indirectly, to dichroic and anisotropic magnetic properties of guest dye molecules, which are induced by orientation of host LC molecules. No direct approaches by means of analyzing anisotropic absorption spectra of oriented LC molecules from the viewpoint of electronic structure, have been attempted except few cases,[3,4] where linear dichroisms of LC molecules oriented by rubbing were measured but no interpretation of spectra was given.[4]

Since the electronic transition moment of a molecule has to be correlated closely with the molecular structure if the absolute transition direction of LC molecule itself is known or determined beforehand, knowledge of the molecular orientation of LC state should be obtained *via* analysis of anisotropic electronic spectra. Thus, for instance, the relative intensity of two absorption bands of a molecule in the isotropic (liquid) state, whose transition moment vectors cross each other, must change depending on its orientation in the LC state.

With a view to investigating the molecular orientation in the LC state from the viewpoint of molecular structure, we conducted an experiment as the first step to make sure the above consideration. As a result, we observed the fact that the relative intensity of the first and second bands of an LC molecule which is considered to take the nematic phase[5] changes with transition from the liquid (isotropic) to LC state. The present communication will report the cause for anisotropic absorption spectra and results obtained through qualitative discussion on the state of molecular orientation induced by that cause.

Experimental

Commercially available 4-butyl-4′-ethoxyazobenzen (BEAB) was purified by repeated recrystallization from aqueous ethanol. Polarized absorption spectrum of BEAB in a stretched poly(vinyl alcohol) (PVA) film was measured with a Shimadzu UV-360 spectrophotometer equipped with a rotatable Rochon-type polarizer. The polarization of electronic absorption bands of BEAB was determined by the stretched PVA film method.[6,7]

The sandwich-type cell used comprised two polished quartz glass plates of 3×23×23 mm size. We did not apply intentionally to the glass plates any surface treatments such as rubbing or coating. The two glass plates were held tight with adhesive except the cell entrance of appropriate size through which melted BEAB was introduced. The gaps of the empty cells were estimated to be in the range 0.2—1.0 μm from interference spectra recorded on the UV-360. In a vacuum vessel, the sample was melted and was introduced into the cell through the entrance by being sucked up under atmospheric pressure.

The cell was set in a cell holder which was specially designed to fit the sample compartment of UV-360. The temperature in the cell holder could be controlled within about ±1 °C with a handmade temperature controller. In the liquid-crystalline (nematic) state, however, all sample cells prepared as above exhibited a slight positive dichroism such that the direction of sucking up provides an optical axis, though the liquid (isotropic) state did not show any dichroism. The dichroism reappeared whenever the sample cell was cooled to the LC state after it had been heated to the isotropic state.

Results

The absorption spectrum of BEAB in ethanol indicates that the absorbance of the first band (A_1) is larger than that of the second (A_2) (see Table 1). The intensity ratio $R_{12}=A_1/A_2$ is about 1.71, which is considered as the value when BEAB is free from the molecular interaction.

Figure 1 shows the polarized absorption spectra of BEAB in a stretched PVA film, where $A_\parallel$ and $A_\perp$ are the absorbances for the polarized lights whose electric vectors are parallel to and perpendicular to the stretching direction of the film, respectively. R_d is the ratio of the absorbances (optical densities), $R_d=A_\parallel/A_\perp$.

It is known that a long molecule in a polymer film under uniaxial stretching inclines its long axis preferentially to the stretching direction of film. Thus it

† Present address: Fuji Xerox Co., Ltd., Takematsu, Ashigara 250-01.

†† Present address: Ôji Paper Co., Ltd., Ôji-cho, Kasugai 486.

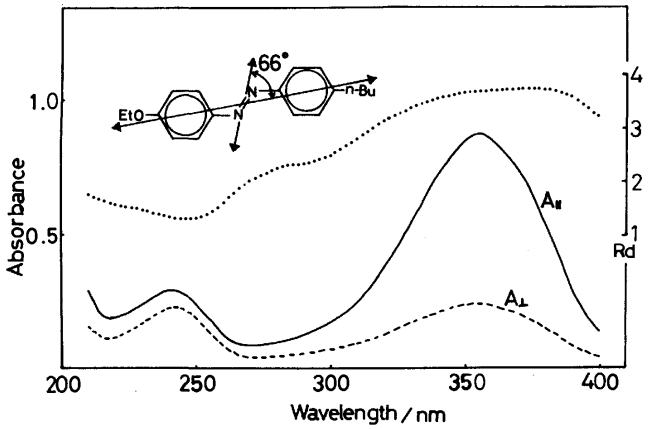

Fig. 1. Polarized absorption spectra of BEAB in a stretched PVA film. R_s=3.86 is the stretch ratio of the film (Ref. 6). The angle between the transition moments of the first (354 nm) and second (240 nm) bands is obtained from the values of R_d and R_s by the dichroism analysis (Ref. 7).

TABLE 1. EXPERIMENTAL AND CALCULATED RESULTS FOR THE ABSORPTION SPECTRUM OF BEAB

Band	λ_{max} /nm[a,d]	$\varepsilon[f]$[a,d]	Polarization[b]	Angle[c,d]
1	345[362]	21400[1.24]	17.5° (log axis)	66°[76°]
2	237[235]	13100[0.33]	48.5° (short axis)	

a) Observed in ethanol. ε is the extinction coefficient and f is the oscillator strength. b) The angle of the transition moment to the orientation axis of molecule (Ref. 7). c) The angle between the two transition moments as determined by the dichroism analysis (Ref. 7). d) [ ]: Results calculated by the semiempirical MO (PPP) method.

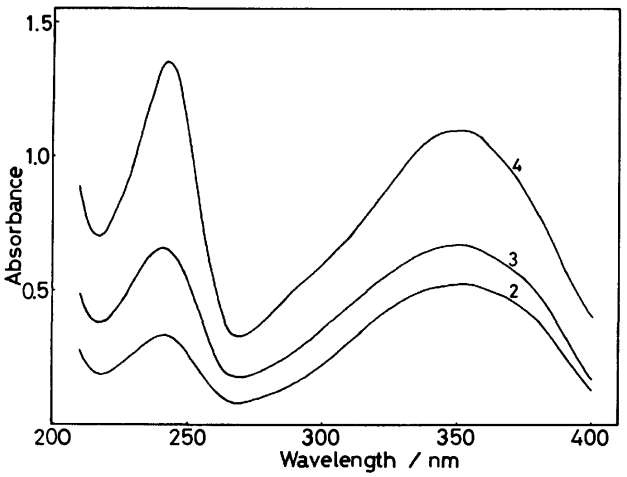

Fig. 2. Absorption spectra of BEAB in the LC state at the lower temperature (48 °C). The number indicated along the curve is the measurement number in Table 2.

follows that the R_d value for a long axis-polarized band is high, whereas for a short axis-polarized band is low. According to Fig. 1, the R_d value is high for the first band (354 nm) and is low for the second (240 nm), implying that the first and second bands are polarized along the long and short molecular axes, respectively. The transition moments corresponding to the two bands cross each other, as shown in Fig. 1, with an angle of about 66° as determined from the R_d values by the dichroism analysis.[7]

In Table 1, the observed results for the absorption spectra of BEAB are compared with the results calculated by the semiempirical MO (PPP) method.[8] The calculated results reproduce the observed ones fairly well.

Absorption spectra of BEAB in sandwich-type cells with various gaps have been measured with natural light for the liquid state (at 86 °C) and for the LC states at higher (70 °C) and lower (48 °C) temperatures. The spectra at the lower temperature are shown in Fig. 2 as an example. Spectra observed with different cells having different gaps, *i.e.*, different optical path lengths in the range 0.2—1.0 μm, indicate that the absorption intensity for the isotropic state is directly proportional to the path length, whereas for the LC state, as is evident from Fig. 2, the relative intensity of A_1 and A_2 changes with path length (compare the R_{12} values in Table 2).

Discussion

The intensity ratios R_{12} ($=A_1/A_2$) for different path lengths estimated for the isotropic state are almost constant as given by $R_{12}=1.69\pm0.04$ (see R_{12} of Liq. (86 °C) in Table 2), which can be compared with $R_{12}^0=1.71$ for the free BEAB molecule. The former is nearly equal to the latter. Let us assume, therefore, that the molecular structure of BEAB in the isotropic state is similar to that in ethanol solution, and that the angle between the transition moments of A_1 and A_2 of the molecule itself is kept constant even in the LC state.

The fact that the R_{12} values for the isotropic state are almost constant irrespective of the cell gap, refers to two useful facts: First, Lambert's law is regarded as being realized. Therefore, the absorbance can be substituted for the optical path length of cell of which the absolute value is difficult to be determined, in such a concrete way that different cell gaps for the LC state can be graduated by referring to the absorbances for the corresponding cells in the isotropic state. Second, the R_{12} value of 1.69 is considered as the value of isotropic distribution of the BEAB molecules. The extent of anisotropy of the LC state, therefore, can be determined from the deviation of R_{12} from $R_{12}=1.69$.

The absorption spectrum of BEAB changes as follows: As the condition goes from the isotropic to LC state at the higher temperature and then to the lower temperature, the absorbance of the first band decreases considerably, while the second band increases slightly. This means that the dimension of the projection of the molecular long axis onto the plane of cell becomes smaller with the change from the liquid to LC state. In other words, the BEAB molecule tends to incline its long axis to the direction of light propagation, *i.e.*, to the direction perpendicular to the plane of the cell.

Now, let us examine the relation between R_{12} of LC state and the cell gap. The data of R_{12} are summarized in Table 2, where, in place of cell gaps, the absorbances

TABLE 2. ABSORPTION DATA FOR NATURAL LIGHT OF BEAB IN VARIOUS CELL GAPS

Cell No.	Meas. No.	Cell gap[a] (Abs.)	Intensity ratio R_{12} Liq.(86°C)	LC(70°C)	LC(48°C)
I[b]	1	0.40	1.69	1.75	1.67
	2	0.51	1.68	1.68	1.58
II	3	0.96	1.67	1.24	1.02
III[b]	4	1.93	1.71	1.07	0.808
	5	2.37	1.73	1.01	0.765
IV	6	2.92	1.68	0.987	0.723

a) The absorbance (Abs.) of the first band in the isotropic state is used instead of cell gap. b) The data of the two measurements of cell Nos. I and III are those obtained for different spots of the same cells.

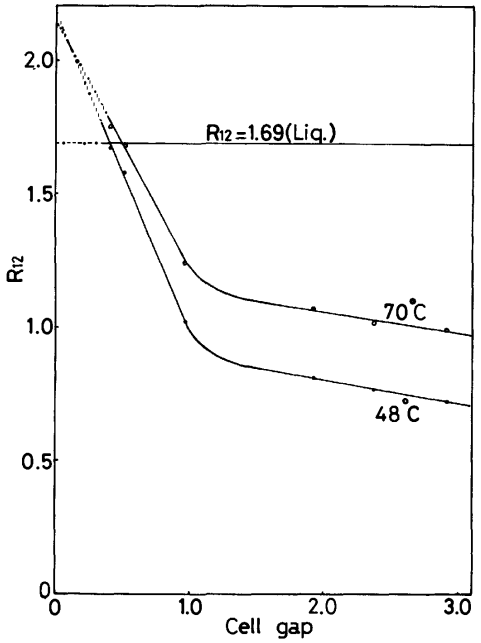

Fig. 3. The R_{12}-cell gap relations for BEAB in the isotropic state (86°C) and in the LC states at higher (70°C) and lower (48°C) temperatures. R_{12} is the absorbance ratio of the first and second bands. The cell gap is graduated by the absorbance for the first band in the isotropic state.

of the first band measured in the liquid state are used. From the data in Table 2, the relationship between R_{12} and cell gap (in absorbance scale) is obtained as shown in Fig. 3. According to the figure, the R_{12} values for the LC state are smaller than 1.69 for the liquid state except for very small cell gaps.

Figure 3 shows that the R_{12} value decreases steeply in the range of smaller cell gaps and slowly in that of larger cell gaps. Figure 3 shows also that the two slopes of R_{12} at the lower (48°C) and the higher temperature (70°C) are nearly equal to each other in the range of cell gaps larger than 1.0, and moreover that the difference of R_{12} in this range is larger than that in the smaller range of cell gaps.

The above-mentioned facts about the behavior of R_{12} indicate that the thinner the cell gap, the greater the emphasis of the characteristic of R_{12} in the interface region and that the thicker the greater that of R_{12} in the bulk region. In order to discuss the above characteristics, we have considered that the molecular orientation in a cell can be divided into two kinds of orientation states with respective characteristics in the interface and bulk regions.

Taking into account that the two interfaces are common to all cells, the difference between the thick and thin cells is attributable to the part of bulk. For this reason, we can get absorption spectra for the bulk itself from difference spectra for various cell thicknesses. In this way, difference spectra have been obtained for the LC state at the higher and lower temperatures. The difference spectra at the lower temperature are shown in Fig. 4 as an example. As is evident from this figure, all of the difference spectra in the respective temperatures are quite similar in shape to one another. This indicates that the oriented state in the bulk region is kept constant independently of the thickness. Moreover, the relative intensity of the first band is apparently larger for the higher temperature than for the lower. This implies that the inclination of the molecular long axis is prevented and is caused to shift to an isotropic state by elevation of temperature. Incidentally, though not observed apparently in the difference spectra at the higher temperature, a new band appears

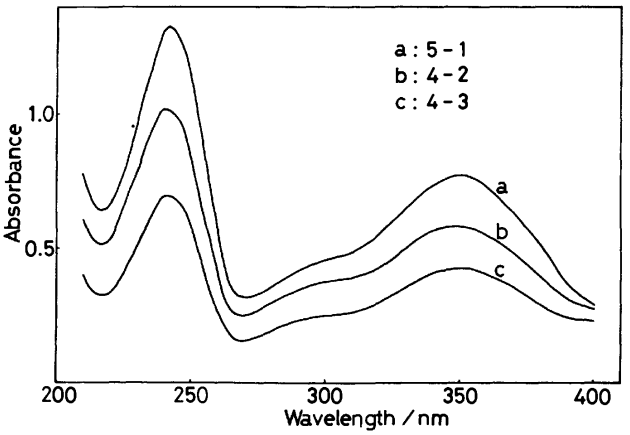

Fig. 4. The difference spectra of BEAB in the LC state at the lower temperature (48°C). The numbers given for a, b, and c are the measurement numbers (Table 2) used for subtruction.

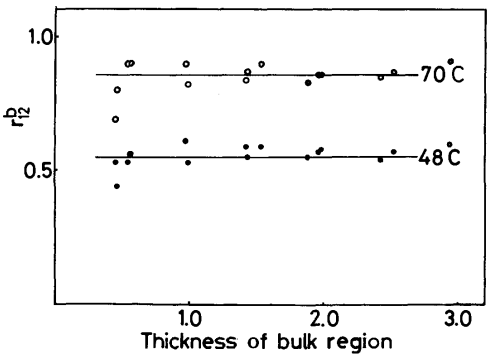

Fig. 5. The relation of r_{12}^b and thickness of bulk region in the LC state. The r_{12}^b value is the ratio of the first and second bands of difference spectrum. The thickness is graduated by absorbance of the first band in the isotropic state.

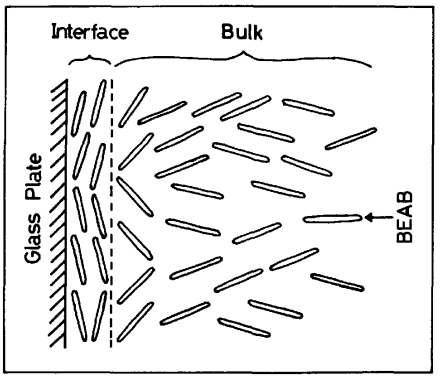

Fig. 6. A model for the molecular orientation of BEAB in the LC state in a thin glass cell.

at around 290 nm in Fig. 4, but at present its cause remains unexplained.

Defining r_{12}^{b} for difference spectra in the same sense as R_{12} and plotting r_{12}^{b} against the thickness of bulk, we obtain Fig. 5. For each temperature, r_{12}^{b} is regarded as nearly constant, the average values being about 0.6 (48 °C) and 0.9 (70 °C). These values are smaller than those corresponding to R_{12} (Fig. 3), which suggests that the intensity ratio (r_{12}^{f}) of the first and second bands for the interface region is larger than $R_{12}=1.69$. In fact, the R_{12} value larger than 1.69 is observed for the thinnest cell in the LC state (see Table 2 and Fig. 3).

If this is true, it is concluded that the LC state consists of two kinds of orientation states such that the molecular long axis inclines to the direction parallel to the cell plane in the interface region or perpendicular to the cell plane in the bulk region. Figure 6 shows schematically a model for the orientation of BEAB molecules in the cell. This model gives explanations for the findings already pointed out in Fig. 3 as follows: According to the model in Fig. 6, the following expression for R_{12} is obtained:

$$R_{12}=\frac{A_1}{A_2}=\frac{\varepsilon_1^{f}p^{f}+\varepsilon_1^{b}p^{b}}{\varepsilon_2^{f}p^{f}+\varepsilon_2^{b}p^{b}},$$

where ε and p are the molecular extinction coefficient and path length (cell gap), respectively, the superscripts f and b indicate the interface and bulk regions, respectively, and the subscripts 1 and 2 stand for the first and second bands, respectively. In the above expression, only p^{b} is a variable, which increases with increasing cell gap. R_{12} is, therefore, a hyperbolic function of p^{b}. $R_{12}\simeq\varepsilon_1^{b}/\varepsilon_2^{b}=r_{12}^{b}$ for $p^{b}\gg p^{f}$, and $R_{12}=\varepsilon_1^{f}/\varepsilon_2^{f}=r_{12}^{f}$ for $p^{b}=0$. Since $r_{12}^{b}<r_{12}^{f}$, the first derivative of R_{12} with respect to p^{b} is negative. Thus, the R_{12} value decreases along the hyperbolic curve with increasing cell gap (p^{b}), *i.e.*, the R_{12} value decreases steeply in the range of smaller cell gaps and gradually in that of larger cell gaps, which tendency is responsible for approximately two straight lines of different slopes to have been observed as shown in Fig. 3. When the temperature (T) is raised in the LC state, the molecular orientations in the interface and bulk regions approach each other through thermal motion, resulting in the same orientation ($r_{12}^{f}=r_{12}^{b}=1.69$) in the isotropic state. In other words, if $T<T'$, $r_{12}^{f}(T)>r_{12}^{f}(T')>1.69$ and $r_{12}^{b}(T)<r_{12}^{b}(T')<1.69$. The model predicts, therefore, that the two curves for the higher and lower temperatures in Fig. 3 must cross each other, which seems indeed to have been realized as the dotted lines at the small cell gaps. Strictly speaking, the model does not, however, explain the finding that the slopes of the two lines for 70 and 48 °C in Fig. 3 are nearly equal for larger cell gaps, because the model claims that the slopes of the two hyperbolic curves for different temperatures are the same only when they are both zero (horizontal). Therefore, the model in Fig. 6 is applicable fairly well to smaller cell gaps, but finds some difficulty in being applied to larger cell gaps.

To tell the truth, we expected at first that the orientation state in LC is only one kind. But actually, as shown in Fig. 6, it has become clear that the two kinds of orientation states exist in a cell. The orientation state in the bulk region, in this case, is thought to be the orientation in the LC state itself. (The reason why the molecules in the bulk region are arranged altogether perpendicularly to the cell plane is not clear.) If so, what makes the orientation in the interface induced? As pointed out in the Experimental section, the dichroism always reappears in the LC state even after it has disappeared in the isotropic state. This means that the orientation in the interface does not originate from the so-called flow alignment.[9] Therefore, the motive force for the orientation in the interface must remain on the cell wall. As the motive force concerned, a kind of rubbing effect in the interface region is considered which is generated by the friction when the melted sample is sucked up into the cell.

Knowledge of the rubbing effect on the cell wall *via* the fluid just mentioned may be obtained, provided that an absorption spectrum for the interface region has been determined and then, from analysis of the spectrum, details of the molecular arrangement relative to the cell wall have been clarified.

In principle, an absorption spectrum may be determined for the interface region as well as for the bulk region and accordingly the molecular orientations in both the regions may be analyzed in a three dimensional space. However, in this preliminary work, we could not do so because of the involvement of considerably large experimental errors as manifested in Fig. 5. But qualitatively, the above-mentioned conclusions concerning the orientation of BEAB molecules in the cell can be derived.

We wish to thank Professor Shunsuke Kobayashi, Department of Electronic Eng., Tokyo University of Agriculture and Technology, for his helpful suggestion about the experimental technique for cell preparation. The present work was partially supported by a Grant-in-Aid (to Y. T.) from Nippon Seiki Co., Ltd., Nagaoka, Niigata, to which we wish to express our thanks.

References

1) H. Kelker and R. Hatz, "Handbook of Liquid Crystals," Verlag Chemie, Weinheim (1980), Chaps. 3, 6, and 10; S. Chandrasekhar and N. V. Madhusudana, *Appl. Spectrosc. Rev.*, **6**, 189 (1972); M. J. Stephen and J. P. Straley, *Rev. Mod. Phys.*, **46**, 617 (1974); M. Sukigara, *Hyomen*, **16**, 189 (1978);

P. G. de Gennes, "The Physics of Liquid Crystals," Clarendon Press, Oxford (1975), Chap. 2; "Introduction to Liquid Crystals," ed by E. B. Priestley, P. J. Wojtowicz, snd P. Sheng, Plenum Press, New York (1975), Chaps. 3 and 6; "Liquid Crystals and Ordered Fluids," ed by J. F. Johnson and R. S. Porter, Plenum Press, New York (1974), Vol. 2, pp. 85, 125.

2) W. Maier and A. Saupe, *Z. Naturforsch.*, **13a**, 564 (1958); **14a**, 882 (1959); **15a**, 287 (1960); **16a**, 816 (1961).

3) W. Maier and A. Saupe, *Z. Phys. Chem. N. F.*, **6**, 327 (1956); A. Saupe, *Z. Naturforsch.*, **18a**, 336 (1963); A. Saupe, *Mol. Cryst. Liq. Cryst.*, **16**, 87 (1972).

4) M. Mizuno, T. Shinoda, H. Mada, and S. Kobayashi, *Mol. Cryst. Liq. Cryst.*, **41**, 155 (1978); **56**, 111 (1979).

5) R. Steinstrasser and L. Pohl, *Z. Naturforsch.*, **26b**, 577 (1971).

6) T. Hoshi and Y. Tanizaki, *Z. Phys. Chem. N. F.*, **71**, 230 (1970); T. Hoshi, H. Yamamoto, T. Miyauchi, S. Mori, M. Kobayashi, and Y. Tanizaki, *Ber. Bunsenges. Phys. Chem.*, **86**, 330 (1982).

7) Y. Tanizaki, *Bull. Chem. Soc. Jpn.*, **32**, 75 (1959); **38**, 1798 (1965).

8) R. Pariser and R. G. Parr, *J. Chem. Phys.*, **21**, 466, 767 (1953); J. A. Pople, *Trans. Faraday Soc.*, **49**, 1375 (1953); J. A. Pople, *Proc. Phys. Soc. (London)*, **A68**, 81 (1955); M. Mataga and K. Nishimoto, *Z. Phys. Chem. N. F.*, **13**, 140 (1957).

9) R. S. Porter, E. M. Barall, II, and J. F. Johnson, *J. Chem. Phys.*, **45**, 1452 (1966); W. Helfrich, *J. Chem. Phys.*, **50**, 100 (1969); R. Chang, *Mater. Res. Bull.*, **7**, 267 (1972).

Internal Heavy Atom Effects on the Exciplex Fluorescence: Anthracene-*N,N*-Dimethylaniline System

Sanyo HAMAI
Department of Physics, Miyazaki Medical College, Kiyotake, Miyazaki 889-16
(Received February 6, 1984)

Intrinsic fluorescence yields of exciplexes, ϕ_f^0, have been determined for halogenated systems of anthracene (A)-*N,N*-dimethylaniline (DMA) in cyclohexane. By the substitution of a chlorine atom for a hydrogen atom in either A or DMA, ϕ_f^0 is reduced to about 1/5, whereas by the bromine substitution it is reduced to about 1/80. When more than one halogen atom of the same kind are substituted in the A-DMA exciplex, the first substitution causes more prominent reduction in ϕ_f^0 than the subsequent substitution does. Although there is a remarkable irregularity in the fluorescence quantum yields of halogenated anthracenes which were used as the electron acceptors in the exciplexes, ϕ_f^0 varies regularly according to the kind and the number of the halogen substitutions. The internal heavy atom effect on ϕ_f^0 is explained by the enhancement of the intersystem crossing rate to the triplet state.

It has been well established that heavy atoms such as halogens affect many relaxation processes in excited molecules.[1] The fluorescence yields of benzene[2], naphthalene,[3,4] and phenanthrene[5] are reduced by the substitution of a halogen atom, demonstrating the internal heavy atom effect. On the other hand, fluorescence yields of halogen-substituted anthracenes are known not to exhibit such normal heavy atom effects. The fluorescence yields of anthracene, 9,10-dichloroanthracene, 9-bromoanthracene, and 9,10-dibromoanthracene have been reported to be 0.36 (in cyclohexane),[6] 0.55 (in cyclohexane),[6] 0.018 (in 2,2-dimethylbutane/pentane (8:3)),[7] and 0.094 (in cyclohexane).[8] The anomalous photophysical properties including "inverse heavy atom quenching" of halogenated anthracenes are explained by the small energy gap between the first excited singlet state (S_1) and the second excited triplet state (T_2) through which the nonradiative crossing occurs, and by the energy level inversion caused by the substitution between these two states.[9-11] In anthracene derivatives, which of the S_1 and T_2 states is higher than the other is governed critically by the kind(s) and position(s) of the substituent group(s).

Only a few studies have been made on the fluorescence of the halogen-substituted exciplex systems. For the exciplexes of benzo[*ghi*]perylene and dibenzo[*def*, *mno*]chrysene with *p*-chloro-*N,N*-dimethylaniline, Watkins has reported the reduction in the fluorescence yields of these exciplexes.[12,13] No exciplex fluorescence has been observed for the systems of some 9- or 9,10-substituted anthracene-bromobenzene derivatives.[14] In the case of the intramolecular charge-transfer states of 6-(arylamino)-2-naphthalenesulfonate derivatives, the fluorescence yields have been found not to be influenced by the halogen substitution.[15]

The aim of this work is to investigate systematically how the halogen substitution on the individual component constituting the exciplex affects the fluorescence yield of the exciplex. Anthracene-*N,N*-dimethylaniline, which is a typical exciplex,[16] was chosen as an unsubstituted parent exciplex.

Experimental

Anthracene (A) was obtained from Wako, 1-chloroanthracene (CA) from Aldrich, 9,10-dichloroanthracene (DCA) from Tokyo Kasei, 9-bromoanthracene (BA) from Aldrich, and 9,10-dibromoanthracene (DBA) from Tokyo Kasei. Anthracene and its halogen derivatives were purified by column chromatography. *N,N*-Dimethylaniline (DMA) purchased from Tokyo Kasei was distilled under reduced pressure. *p*-Chloro-*N,N*-dimethylaniline (CDMA) was synthesized from *N,N*-dimethyl-*p*-phenylenediamine by the Sandmeyer reaction,[17] and recrystallized twice from ethanol. *p*-Bromo-*N,N*-dimethylaniline (BDMA) obtained from Fluka AG was recrystallized twice from cyclohexane. Cyclohexane, used as the solvent, was percolated through a silica-gel column.

Absorption spectra were measured with a Hitachi 124 spectrophotometer, and fluorescence spectra were recorded on a Shimadzu RF-501 spectrofluorophotometer equipped with a cooled EMI 9789 QA photomultiplier. Fluorescence was viewed at right angles to the direction of excitation. Fluorescence spectra were corrected for the spectral response of the detection system. The correction factor was obtained by the previously described method[18] employing a Rhodamine B quantum counter (below 600 nm) and a standard solution method[19] using 4-(dimethylamino)-4'-nitrostilbene (above 600 nm). Measurements were made on cyclohexane solutions of a fixed concentration of anthracene (2×10^{-5} mol dm^{-3}) or halogenated anthracene (1×10^{-5} mol dm^{-3}) and the varying concentrations of DMA derivatives. Samples for fluorescence measurements were nitrogen bubbled. 9.10-Diphenylanthracene in deaerated cyclohexane was used as a standard (ϕ_f= 0.90) for the fluorescence yield determinations.[20] All the measurements were made at 25±0.1 °C.

Results and Discussion

For every combination of the electron donor (DMA or its derivative) and the electron acceptor (A or its derivative) used in this work, the exciplex fluorescence was observed. As is usually the case the exciplex fluorescence is structureless and red-shifted from the monomer fluorescence of A or its derivative.[21] The positions of the fluorescence maxima of the exciplexes involving the same acceptor have been found to be independent of the kind of the donor to within ≈5 nm. In addition, the energy differences between the acceptor and its exciplex fluorescence have been found to be nearly constant, irrespective of the kind of acceptor. These results suggest that the geometrical structure and the potential energy curve of the halogen-substituted exciplex are similar to those of the unsubstituted

exciplex A-DMA. The exciplex formation can be described by the following scheme:[22]

$$M^* + Q \underset{k_2}{\overset{k_1}{\rightleftharpoons}} (MQ)^*$$

$$M + h\nu_f \quad M \quad M + Q + h\nu_f' \quad M + Q$$

Here M* is anthracene (or its halogen derivative) in the excited singlet state, Q is DMA (or its halogen derivative), and (MQ)* is the exciplex formed between M* and Q. k_1, k_2, k_f, k_n, k_f', and k_n' are the rate constants for exciplex formation, exciplex dissociation, radiative transition of M*, nonradiative transition of M*, radiative transition of (MQ)*, and nonradiative transition of (MQ)*, respectively.

Under photostationary conditions, the relation between the intrinsic fluorescence yield of the exciplex, ϕ_f^0 $(=k_f'/(k_f'+k_n'))$, and the fluorescence yield of the exciplex, ϕ_f, at a given donor concentration [Q] is expressed by

$$\frac{1}{\phi_f} = \frac{1}{\phi_f^0} + \frac{(k_f+k_n)(k_2+k_f'+k_n')}{k_1 k_f'} \frac{1}{[Q]}.$$

The intrinsic fluorescence yield ϕ_f^0 can be evaluated from a plot of $1/\phi_f$ *vs.* $1/[Q]$. As typical examples, plots for A-DMA, A-CDMA, and A-BDMA are displayed in Fig. 1. From the intercepts of the straight lines as shown in Fig. 1, the intrinsic fluorescence yields ϕ_f^0 for all

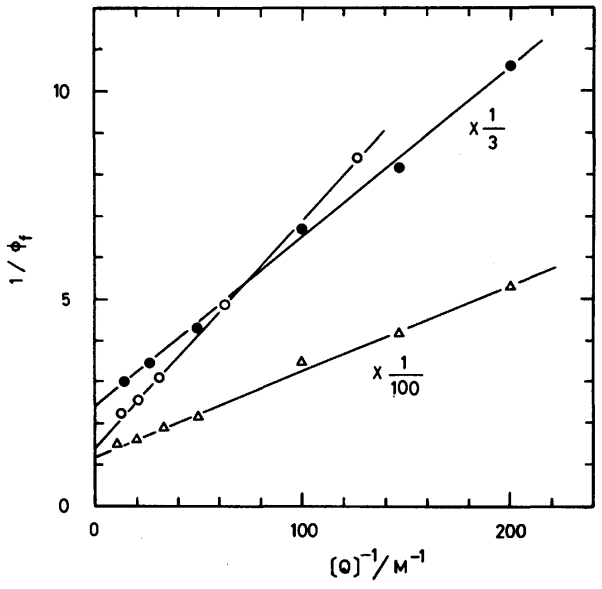

Fig. 1. Plots of $1/\phi_f$ *vs.* $1/[Q]$.
○: A-DMA, ●: A-CDMA, △: A-BDMA.

TABLE 1. INTRINSIC FLUORESCENCE YIELDS OF EXCIPLEXES (ϕ_f^0) AND FLUORESCENCE YIELDS OF THEIR COMPONENT ACCEPTORS (ϕ_f(monomer)) IN CYCLOHEXANE

	ϕ_f(monomer)	ϕ_f^0		
		DMA	CDMA	BDMA
A	0.32	0.72	0.14	0.0083
CA	0.11	0.14	0.071	0.0053
DCA	0.60	0.087	0.080	0.0056
BA	0.013	0.0086	0.0075	0.0041
DBA	0.13	0.0047	0.0049	0.0038

the combinations of the donor and acceptor have been determined. They are listed in Table 1.[23] Also included in Table 1 are the fluorescence yields, ϕ_f(monomer), of anthracene and of its halogen derivatives.

It can be seen from Table 1 that the value of ϕ_f^0 in every row drops in going from left to right (with the increase in the atomic number of the heavy atom in the electron donor). The only exception for this trend is ϕ_f^0 of DBA-CDMA, which is the same as that of DBA-DMA within experimental uncertainties. The substitution of the chlorine atom in A-DMA decreases ϕ_f^0 to about 1/5, whereas the bromine substitution decreases ϕ_f^0 to about 1/80. Such regularity in ϕ_f^0 is further confirmed by looking at ϕ_f^0 in the columns of Table 1 (the exciplexes consisting of the same electron donor). As in the case of the rows (the exciplexes consisting of the same electron acceptor), ϕ_f^0 decreases in going from top to bottom. Table 1 also shows that the values of ϕ_f^0 do not depend on whether the halogen atom is substituted in the donor or acceptor component (*e.g.*, for the case of A-CDMA and CA-DMA *etc.*). When two halogen atoms of the same kind are introduced in the exciplex, ϕ_f^0 is further reduced by the second substitution of the halogen atom. However, the effect of the second substitution on ϕ_f^0 is much less than that of the first one.

The ratio of the exciplex fluorescence yield of the monosubstituted exciplex to that of the unsubstituted exciplex, R, is 0.19 for the chlorine-atom substitution (both for CA-DMA and A-CDMA), whereas R is 0.012 for the bromine-atom substitution (both for BA-DMA and A-BDMA). The ratio of the fluorescence yield of the halogenated aromatic monomer to that of the unsubstituted parent monomer has been reported to be 0.081 for chlorobenzene and <0.002 for bromobenzene at room temperature.[2] Moreover, these ratios have been found to be 0.080 and 0.017 for 1-chloronaphthalene and 1-bromonaphthalene, respectively.[4] Thus, both for chlorine and bromine substitution, the values of R for the A-DMA exciplex system are comparable with the reported values for benzene and naphthalene monomers, except for bromobenzene. It appears, therefore, that the internal heavy atom effect on the exciplex fluorescence is caused by a similar mechanism to that in the case of the aromatic monomer fluorescence, that is, by a normal heavy atom effect enhancing the rate of the intersystem crossing to the triplet state as the deactivation process.

The first excited singlet state of anthracene is lowered by 4200 cm^{-1} by virtue of the exciplex formation with DMA.[16] For the halogen-substituted exciplexes, almost the same stabilization energy is expected from their similar spectroscopic characteristics. On the other hand, laser photolysis studies on the systems of A-DMA and A-*N*,*N*-diethylaniline have revealed that the triplet state produced from the singlet exciplex is the triplet state of not the exciplex but of anthracene itself.[24,25] Although the energy level of the triplet exciplex is unknown, this fact indicates that the triplet state of the exciplex, to which the singlet exciplex decays, is dissociative.

On the basis of these facts, the result that ϕ_f^0 is regularly and stepwisely reduced by the halogen

substitution in the A–DMA exciplex system may be explained as follows. In contrast to halogenated anthracene, no inversion of the energy level between the first excited singlet state and the second triplet state occurs in the halogenated exciplexes of the A–DMA systems. Therefore, the intersystem crossing rate to the triplet state, which immediately dissociates to the triplet state of the halogenated anthracene, is accelerated by the substitution of halogen.

With respect to the heavy atom effect for the triplet exciplex, detailed studies of Steiner and Winter were performed by flash spectroscopy.[26,27] They have determined the radical yields and rate constants in the quenching reaction of thionine triplet with the series of monohalogen substituted anilines.[26] The radical yield decreases with increasing the spin-orbit coupling constant of the halogen substituent. This result is explained in terms of the internal heavy atom effect on the $T \rightarrow S_0$ intersystem crossing rate in the triplet exciplex.[26,27] The internal heavy atom effects in the singlet exciplexes of the A–DMA systems found in this study are thus qualitatively similar to those observed for the triplet exciplexes.

The author wishes to thank Professor Fumio Hirayama for his valuable discussion.

References

1) S. P. McGlynn, R. Sunseri, and N. Christodouleas, *J. Chem. Phys.*, **37**, 1818 (1962); S. Siegel and H. S. Judeikis, *J. Chem. Phys.*, **42**, 3060 (1965); G. G. Giachino and D. R. Kearns, *J. Chem. Phys.*, **52**, 2964 (1970); H. Singh and J. D. Laposa, *Chem. Phys. Lett.*, **36**, 639 (1975); J. C. Miller, J. S. Meek, and S. J. Strickler, *J. Am. Chem. Soc.*, **99**, 8175 (1977).

2) A. Harriman and B. W. Rockett, *J. Chem. Soc., Perkin Trans. 2*, **1974**, 217.

3) V. L. Ermolaev and K. K. Svitashev, *Opt. Spectrosc.*, **7**, 399 (1959).

4) R. S. Davidson, R. Bonneau, J. Joussot-Dubien, and K. R. Trethewey, *Chem. Phys. Lett.*, **74**, 318 (1980).

5) F. Masetti, U. Mazzucato, and G. Galiazzo, *J. Lumin.*, **4**, 8 (1971).

6) I. B. Berlman, "Handbook of Fluorescence Spectra of Aromatic Molecules," 2nd ed, Academic Press, New York (1971).

7) H. Dreeskamp, E. Koch, and M. Zander, *Chem. Phys. Lett.*, **31**, 251 (1975).

8) R. P. Detoma and D. O. Cowan, *J. Am. Chem. Soc.*, **97**, 3291 (1975).

9) H. Dreeskamp and J. Pabst, *Chem. Phys. Lett.*, **61**, 262 (1979).

10) Kam-Chu Wu and W. R. Ware, *J. Am. Chem. Soc.*, **101**, 5906 (1979).

11) E. C. Lim, J. D. Laposa, and J. M. H. Yu, *J. Mol. Spectrosc.*, **19**, 412 (1966); R. G. Bennett and P. J. McCartin, *J. Chem. Phys.*, **44**, 1969 (1966).

12) A. R. Watkins, *Chem. Phys. Lett.*, **43**, 299 (1976).

13) A. R. Watkins, *J. Phys. Chem.*, **83**, 1892 (1979).

14) D. Schulte-Frohlinde and H. Hermann, *Ber. Bunsenges. Phys. Chem.*, **81**, 562 (1977).

15) E. M. Kosower and H. Dodiuk, *J. Phys. Chem.*, **82**, 2012 (1978).

16) Man-Him Hui and W. R. Ware, *J. Am. Chem. Soc.*, **98**, 4718 (1976).

17) A. Pinner, *Ber.*, **20**, 149 (1887).

18) S. Hamai and F. Hirayama, *J. Chem. Phys.*, **71**, 2934 (1979).

19) E. Lippert, W. Nagele, I. Seibold-Blankenstein, U. Staiger, and W. Voss, *Z. Anal. Chem.*, **170**, 1 (1959).

20) S. Hamai and F. Hirayama, *J. Phys. Chem.*, **87**, 83 (1983).

21) For the exciplexes involving A, DCA, and DBA as an acceptor, the fluorescence maxima are 475, 530, and 550 nm, respectively.

22) A. E. W. Knight and B. K. Selinger, *Chem. Phys. Lett.*, **10**, 43 (1971).

23) Our value of ϕ_f^0 for the A–DMA exciplex (0.72) is somewhat lower than the value of 0.81 ± 0.03 calculated from its rate constants for the elementary processes obtained by Hui and Ware (Ref. 16).

24) E. J. Land, J. T. Richards, and J. K. Thomas, *J. Phys. Chem.*, **76**, 3805 (1972).

25) T. Nishimura, N. Nakashima, and N. Mataga, *Chem. Phys. Lett.*, **46**, 334 (1977).

26) U. Steiner and G. Winter, *Chem. Phys. Lett.*, **55**, 364 (1978).

27) G. Winter and U. Steiner, *Ber. Bunsenges. Phys. Chem.*, **84**, 1203 (1980).

 © 1984 The Chemical Society of Japan Bull. Chem. Soc. Jpn., 57, 2703—2711 (1984)

Reversing-Pulse Electric Birefringence of Poly(γ-methyl L-glutamate) in Hexafluoro-2-propanol

Kazuyoshi UEDA
Faculty of Science, Hiroshima University, Higashisenda-machi, Naka-ku, Hiroshima 730
(Received March 8, 1984)

Reversing-pulse electric birefringence (RPEB) signals of poly(γ-methyl L-glutamate) (PMLG) were measured, for the first time, in hexafluoro-2-propanol at 25 °C and at 535 nm. Quantitative analyses were carried out on the steady-state birefringence and the field-free decay time ($<\tau>_{EB}$) in the wide field strength region and also on the rise, reverse, and decay portions in the low field strength region by taking into account the continuous molecular length distribution of a fractionated PMLG sample. The weight-average length (l_w), permanent dipole moment (μ_w), polarizability anisotropy ($\Delta\alpha_w$), and the degree of polydispersity (l_w/l_n) were evaluated by two procedures: one from the analysis of the reverse-transient portion and the other from the field-free decay portion of RPEB signals. These two sets of the parameters should be identical with each other, if the electrooptical and hydrodynamic properties of PMLG do not change during the field-on and field-off processes. However, the length of the PMLG helix is shorter by about 18% in the presence of an electric field than that in the absence of the field. In order to explain this discrepancy, a new concept of reversible conformational transition under the external electric field is introduced.

Poly(γ-methyl L-glutamate) (PMLG) in solution has been studied by the methods of spectroscopy, circular dichroism, linear dichroism,[1-3] in order to resolve an important optical problem, that is, the strong-coupling exciton theory of the helical polypeptide.[4-6] For this purpose the PMLG molecule has been regarded as a suitable model, because it has no strongly absorbing chromophore in the side chain in the far ultraviolet region and exists as a helix in some organic solvents. In order to clarify the optical properties, the exact solution conformation of PMLG must be confirmed. However, few reports have appeared on this subject.[7,8] Although the electric birefringence (EB) is very useful for such studies,[9-11] only one study was reported, in which the Kerr constant of PMLG was measured in a mixed organic solvent.[7]

In this work, the reversing-pulse electric birefringence (RPEB) of PMLG in hexafluoro-2-propanol (HF2P) has been measured to determine the hydrodynamic and electrooptical properties in detail. Recently, some analytical procedures have been developed for the experimental data of polydisperse systems which were obtained by the rectangular pulse EB[12-16] and electric dichroism[17] methods. These enable one to estimate the weight-average molecular length and the breadth of the distribution from the decay signals. As compared with those methods, the RPEB method has a special feature that the parameters, which characterize the molecular weight distribution, can be determined independently from the two portions of a transient signal; one from the field-free decay and the other from the field-on reverse portion.[18,19] Therefore, the two sets of the molecular parameters obtained respectively in the presence and the absence of an external electric field may be compared. The results indicate that the transient processes in these two portions differ from each other.

The purposes of this work are (1) to evaluate quantitatively the discrepancy between the reverse and the decay processes involved in the RPEB signals of PMLG in HF2P by taking into account the molecular length distribution, (2) to clarify the electrooptical properties and solution conformation, and (3) to ascertain the effect of the applied electric field. The results are discussed by assuming some possible causes, such as molecular association, flexibility, partial destruction of helix, and electric field-induced conformational transition. By simulating the rise, reverse, and decay processes of the RPEB signal, a possible conformational change under the electric field is proposed on the basis of the change of the molecular length of the PMLG helix.

Experimental

Materials and Viscometric Characterization. Poly(γ-methyl L-glutamate), (PMLG), was purchased from Pilot Chemicals, Inc. (Watertown, Mass., USA). It was prepared by polymerizing the corresponding *N*-carboxyanhydride with sodium methoxide in dioxane. The specific viscosity, η_{sp}/c, [c=0.2% in dichloroacetic acid (DCA)] was 3.40, as supplied by the manufacturer. This sample was dissolved in chloroform and the solution was filtered to remove insoluble lumps. The PMLG sample in the clear solution was fractionated into five fractions with ethanol as precipitant by the successive precipitation method.[11] The third fraction was used in the present work. 1,1,1,3,3,3-Hexafluoro-2-propanol (HF2P) for spectroscopy (Merck) was used without further purification. Reagent-grade DCA (Tokyo Kasei Kogyo Co.) was shaken with P_2O_5 and then kept overnight in the dark. The supernatant was distilled under reduced pressure at 6 mmHg (1 mmHg=133.3 Pa) in a nitrogen gas atmosphere.[20] PMLG was dissolved in HF2P and in DCA after drying under reduced pressure at 78.3 °C for 10 h. The viscosity of all samples was measured in a Ubbelohde-type dilution viscometer at 25 °C. The intrinsic viscosity of PMLG in DCA, $[\eta]_{DCA}$, was 267 cm³/g in the concentration range 1.0—11.0 mM (1 mM=10^{-3} mol dm^{-3}). The concentration of PMLG was expressed in terms of monomer units throughout this work. From the value of $[\eta]_{DCA}$, the weight-average molecular weight (M_w) was estimated to be 13.5×10^4 (the degree of polymerization, DP_w, is 943) by using the relationship between $[\eta]_{DCA}$ and M_w which was obtained by Okamoto and Sakamoto.[7] The intrinsic viscosity of PMLG in HF2P, $[\eta]_{HF2P}$, was found to be 931 cm³/g in the concentration range 1.7—10.6 mM). The viscosity of HF2P was also obtained to be 1.595 cP (1 cP=10^{-3} Pa s).

RPEB Measurements. All RPEB signals were measured at 25 °C and at 535 nm on an apparatus which was designed

and constructed in this laboratory.[18,21] The data acquisition and processing were achieved with a system consisting of a two channel transient wave memory (Riken Denshi Model TCH-4000(s), whose maximum sampling time is 50 ns/word, 8 bit, 4 kw) and of a microcomputer (Oki Denki IF-800 Model 10).[22] The signals were accumulated in arbitrary numbers, averaged, and then stored on a floppy disk. A quarter-wave plate was inserted in the optical path. The electric birefringence, Δn, was expressed as $\Delta n=\lambda\delta/2\pi d$, where δ is the phase retardation, λ is the wavelength *in vacuo*, and d is the optical path length of a Kerr cell, which was made of Kel-F.[23] The electrode gaps are 0.207 cm (d=1.0 cm) and 0.33 cm (d=2.0 cm), respectively. The Kerr constant of HF2P, B_{HF2P}, was found to be positive and 5.6×10^{-13} cm V^{-2}. This value is very small compared with the Kerr constant of PMLG solution, but cannot be ignored for a dilute PMLG solution ($c\leq0.49$ mM); hence, the phase retardation, δ_{HF2P} ($=2\pi dBE^2$), was subtracted from the δ values observed for dilute solutions.

Analysis of Data. For a polydisperse polymer solution, in which rigid rodlike solutes show a continuous distribution of molecular weights, *i. e.*, lengths, the steady-state electric birefringence at an arbitrary electric field strength E is expressed with the weight-average orientation function, $\langle\Phi\rangle_w$, as[15,24]

$$\Delta n(\infty)=\frac{2\pi\bar{C}_v}{n}(g_3-g_1)\langle\Phi(\beta(l),\gamma(l))\rangle_w, \quad (1)$$

where n is the refractive index of the solution, $\bar{C}_v$ is the volume fraction of the solute, and (g_3-g_1) is the optical anisotropy factor. $\beta(l)=\mu(l)E/kT$ and $\gamma(l)=\Delta\alpha(l)E^2/kT$, where $\mu(l)$ is the permanent dipole moment and $\Delta\alpha(l)$ is the polarizability anisotropy of the molecule with length l.

In the low electric field region where the Kerr law holds, the reverse portion of a normalized RPEB signal is expressed as[18,25]

$$\frac{\Delta n(t)}{\Delta n(\infty)}=\frac{\int_a^b\Delta n(\infty,l)\left\{1-\frac{3\beta(l)^2}{\beta(l)^2+2\gamma(l)}(e^{-2\theta_{11}(l)t}-e^{-6\theta_{11}(l)t})\right\}dl}{\int_a^b\Delta n(\infty,l)dl}, \quad (2)$$

where θ_{11} is the rotary diffusion coefficient of the cylindrical molecule with a diameter of $2b$. In this work, θ_{11} is calculated by using Broersma's equation.[26] $\Delta n(\infty,l)=(2\pi\bar{C}_v/15n)\times(g_3-g_1)\,\phi(l)\,[\beta(l)^2+2\gamma(l)]$, where $\phi(l)$ is the fraction of solute molecules with length l. $\phi(l)$ is proportional to $lf_n(l)$, where $f_n(l)$ is the probability density function, which is defined on the basis of the number of solute molecules.[13,15] The length distribution of PMLG molecules in a soluion is assumed to be logarithmic-normal (the Lansing-Kraemer distribution).[27] Then, $f_n(l)$ was given by[28]

$$f_n(l)=\frac{1}{\omega l\sqrt{\pi}}\exp\left[-\frac{1}{\omega^2}\left(\ln\frac{l}{l_L}\right)^2\right], \quad (3)$$

where ω and l_L are parameters with which the weight-average molecular length, l_w, may be defined as $l_w=l_L(l_w/l_n)^{3/2}$ and the degree of polydispersity, expressed in terms of the ratio of weight- to number-average lengths, l_w/l_n, as $l_w/l_n=\exp(\omega^2/2)$. Similarly, the rise portion of the same RPEB signal is given as[29]

$$\frac{\Delta n(t)}{\Delta n(\infty)}=1-\frac{\int_a^b\Delta n(\infty,l)\left\{\frac{3\beta(l)^2e^{-2\theta_{11}(l)t}-[\beta(l)^2-4\gamma(l)]e^{-6\theta_{11}(l)t}}{2[\beta(l)^2+2\gamma(l)]}\right\}dl}{\int_a^b\Delta n(\infty,l)dl}. \quad (4)$$

The decay portion is written as

$$\frac{\Delta n(t)}{\Delta n(0)}=\frac{\int_a^b\Delta n(0,l)e^{-6\theta_{11}(l)t}dl}{\int_a^b\Delta n(0,l)dl}, \quad (5)$$

where $\Delta n(0,l)\equiv\Delta n(\infty,l)$. In all calculations, the upper and lower integral limits a and b were set as 50 and 6450 Å instead of (0, ∞).

The intrinsic viscosity for thin rods can also be calculated by taking into account the polydispersity of molecular lengths. By using Simha's equation,[30] it can be expressed as follows:

$$\frac{\langle[\eta]\rangle}{\bar{v}}=\frac{\int_a^b lf_n(l)\left\{\left(\frac{l}{2b}\right)^2\left[\frac{1}{15(\ln l-\ln b-1.8)}+\frac{1}{5(\ln l-\ln b-0.8)}\right]+\frac{14}{15}\right\}dl}{\int_a^b lf_n(l)dl}, \quad (6)$$

where $\bar{v}$ is the average partial specific volume of solutes and $\langle[\eta]\rangle$ is the weight-average intrinsic viscosity.[29,31] Once the $f_n(l)$ is determined from Eq. 3 with the parameters l_w and l_w/l_n which are obtained from the reverse-transient analysis by assuming an appropriate value of b, $\langle[\eta]\rangle$ can be calculated from Eq. 6. By comparing the calculated $\langle[\eta]\rangle$ with the experimentally obtained $[\eta]$, the selection can be made for the most probable value of b that reproduces both the observed $[\eta]$ and the reverse-transient signal from several likely values of b by an iteration procedure.[29]

Results and Discussion

Steady-state Birefringence of PMLG. Figure 1 shows a typical RPEB signal of PMLG in HF2P with an applied pulse field. In this case, twenty signals were accumulated and then averaged to improve the signal-to-noise ratio. After an electric pulse is applied, the signal rises, reaches a steady-state, then decays to the baseline after the pulse is terminated. The sign of the signal is positive. Similarly to the previous cases of poly(α-L-glutamic acid), (PGA),[18] and poly(γ-benzyl L-glutamate), (PBLG),[29] the RPEB signal of PMLG

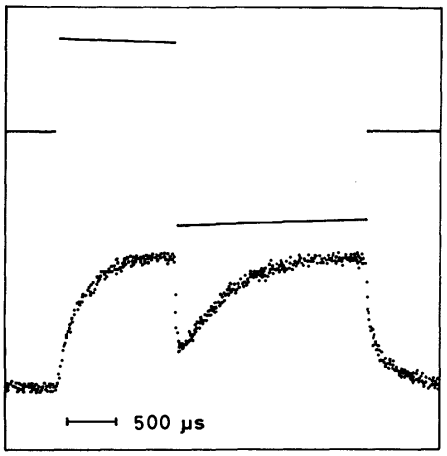

Fig. 1. A typical RPEB signal of PMLG in HF2P and an applied electric pulse field. The signal was digitized with a transient wave memory and averaged twenty-fold in real time with a microcomputer. The sampling time is 1 μs/word. The concentration: 7.82 mM. The field strength: 3.39 kV/cm.

shows a large dip in the reverse portion. This result immediately indicates that the permanent dipole moment contributes to the electric field orientation of PMLG.[25] Figure 2 shows the dependence of the steady-state phase retardation δ on field strength. Values of δ tend to saturate at higher fields, but are proportional to the square of field strength in the low field region ($E<3.5$ kV/cm), that is, the Kerr law holds (insert).

The Kerr constant, B, is defined as

$$B = \frac{1}{\lambda}\left[\frac{\Delta n}{E^2}\right]_{E\to 0} = \frac{1}{2\pi d}\left[\frac{\delta}{E^2}\right]_{E\to 0}. \quad (7)$$

Figure 3 shows plots of δ/E^2 against the square of electric field strength. Values of δ/E^2 are nearly constant below 3.5 kV/cm. By extrapolating these values to zero field strength, the Kerr constant was calculated. The specific Kerr constant, B/c, is given in Table 1, and also shown in Fig. 4(a). The values of B/c are independent of the concentration of PMLG. The intrinsic Kerr constant, $(B/c)_{c\to 0}$, was found to be 6.2×10^{-7} cm^4 g^{-1} V^{-2}. This value is rather small: about one half of the intrinsic Kerr constant obtained for PBLG[19] and about one-third for PGA[18] of almost the same molecular size.

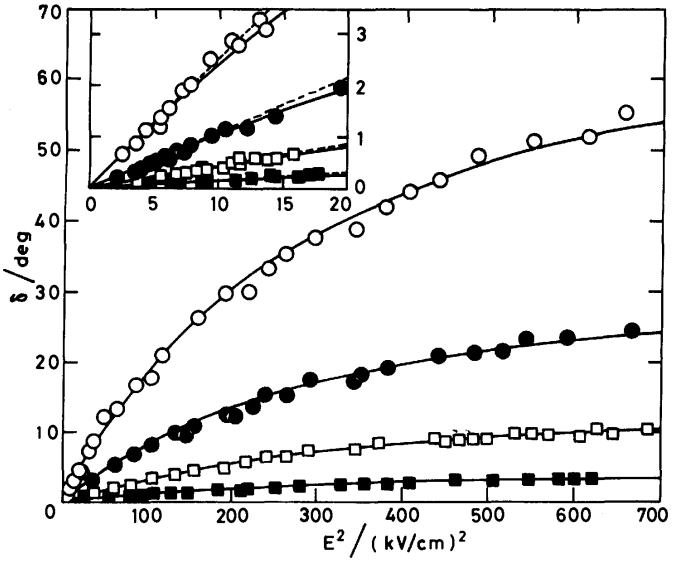

Fig. 2. The field-strength dependence of the steady-state electric birefringence, δ, of PMLG in HF2P. Insert: the low field strength region. The concentrations of PMLG are 7.82 mM (○), 3.52 mM (●), 1.41 mM (□), and 0.49 mM (■). The solid lines represent the theoretical curves with parameters in Table 2. The dotted lines represent the Kerr law.

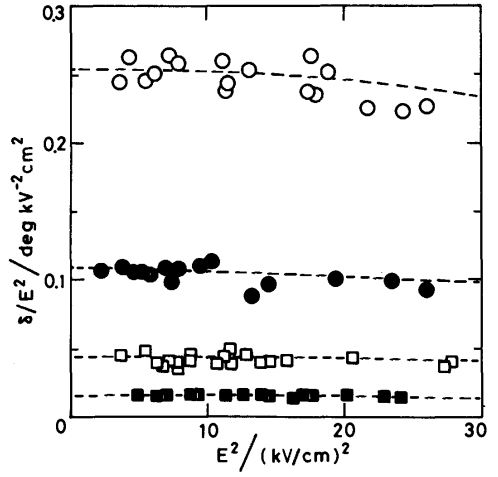

Fig. 3. The phase retardation per square of field strength, δ/E^2, in the low field strength region. Symbols are the same as in Fig. 2.

In order to investigate the aggregation of PMLG helices, values of δ at four electric field strengths were measured in detail over a wide range of concentrations. For example, the values of δ/c were still almost constant at a fifty-fold dilution (0.15 mM), as plotted in Fig. 4(b). Since they would change with molecular association,[32-34] no intermolecular association of PMLG seems to occur below 8 mM. This conclusion is also confirmed in the later section, where the relation between the molecular weight and molecular length is discussed.

Reverse-transient Process of PMLG. The minimum in the reverse portion of an RPEB signal can be specified by t_m, the time required for the signal to reach the minimum after the pulse reversal, and Δ_m, the height from the baseline at t_m. Both t_m and Δ_m are

Table 1. Specific Kerr constant B/c, reverse-transient minimum position, $(t_m)_{E\to 0}$ and $(\Delta_m)_{E\to 0}$, and weight-average relaxation time, $\langle\tau\rangle_w$, of PMLG in HF2P at various concentrations c.

c	B/c	$(t_m)_{E\to 0}$	$(\Delta_m)_{E\to 0}$	$\langle\tau\rangle_w$
mM	10^{-7}cm^{4}g^{-1}V^{-2}	μs		μs
7.82	6.3	80.0	0.33	94.5
3.52	6.1	69.0	0.38	81.0
1.41	6.2	64.5	0.38	70.0
0.49	6.4	56.0	0.36	63.0

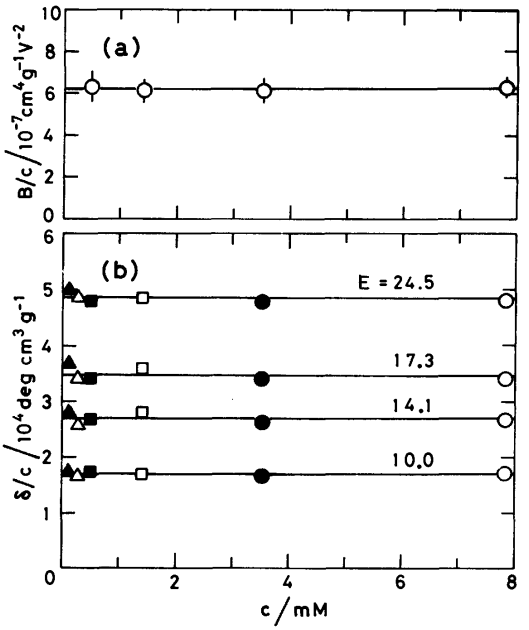

Fig. 4. (a) The dependence of the specific Kerr constant, B/c, on concentration and (b) the dependence of δ/c on concentration at four selected field strengths. The field strength, E, in kV/cm. In (b) the symbols are the same as in Fig. 2; moreover, two lower concentrations, 0.3 mM (△), 0.15 mM (▲), are also added.

plotted against the square of field strength in Fig. 5. The limiting values at zero field strength, $(t_m)_{E\to 0}$ and $(\Delta_m)_{E\to 0}$, are given in Table 1. From these values, the reverse portion of the RPEB signal can be analyzed with the aid of Eq. 2 to determine the values of l_w, l_w/l_n, and $(\beta_w)^2/2\gamma_w$. (This procedure was shown in detail in Figs. 7 and 8 in Ref. 18.) The theoretical orientation function $\langle\Phi\rangle_w$ can then be calculated with those parameters [l_w, l_w/l_n, $(\beta_w)^2/2\gamma_w$] which are given in Table 2. By comparing $\langle\Phi\rangle_w$ with experimentally obtained δ values in a wide range of field strengths, on a double logarithmic plot, the values of μ_w, $\Delta\alpha_w$, and the optical anisotropy factor (g_3-g_1) can be obtained separately (the matching procedure).[11,35] These values are also given in Table 2. The best-fitted theoretical curve of δ was calculated by using these values with the aid of Eq. 1, and is shown in Fig. 2 by a solid line at each concentration of PMLG. The curves agree well with experimental points in all cases over the entire field strength region.

By using a weight-average degree of polymerization of 943, the permanent dipole moment per residue was calculated to be 2.2—2.4 D (1 D=3.336×10^{-30} C m). Such values are about half of the known values of the polypeptide main chain residue moment (4.8—5.0 D/res).[36] In fact, previously obtained values are 5.3 D/res for PGA and 3.5—4.0 D/res for PBLG.[18,19] This may be due to the side chain conformation of PMLG, which differs from that of PGA and PBLG, that is, the side chain of PMLG may be oriented so as to cancel the main chain moment more effectively. Wada[36] has discussed some possible conformations of the side chain of polypeptides and the values of dipole moments associated with these conformations. He pointed out that a side chain moment of about 2.5 D/res, at maximum, may direct in opposition to the permanent dipole moment of the main chain. Thus, the small value of the permanent dipole moment of PMLG in HF2P, as revealed in the present work, can be explained by the side chain conformation.

Decay Process of PMLG. The decay portion of a RPEB signal is related to the rotational relaxation time of a solute molecule. From the decay curve, the electric birefringence-average relaxation time, $\langle\tau\rangle_{EB}$, may be obtained by the area method.[37] Figure 6 shows plots of $\langle\tau\rangle_{EB}$ for PMLG solutions at four concentrations against the square of the steady-state field strength applied prior to the decay. A slight dependence of $\langle\tau\rangle_{EB}$ on concentration was observed, probably because of the solute-solute interaction of PMLG molecules. Values of $\langle\tau\rangle_{EB}$ also depend on field strength, indicating that this PMLG sample is polydisperse

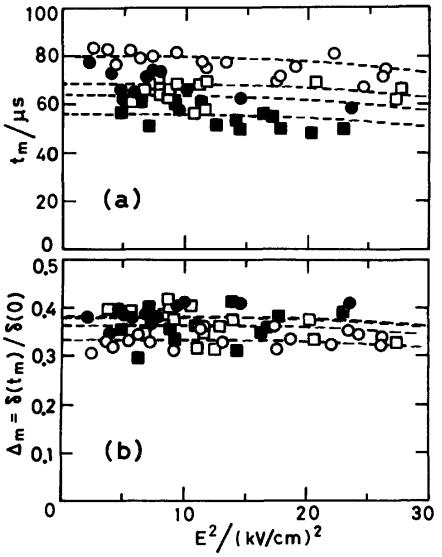

Fig. 5. The field strength dependence of the minimum position in the reverse-transient signal of PMLG in HF2P. (a) The time required for the signal to reach the minimum, t_m, and (b) the normalized phase retardation at t_m, $\Delta_m=\delta(t_m)/\delta(0)$. Symbols are the same as in Fig. 2. The limiting values of $(t_m)_{E\to 0}$ and $(\Delta_m)_{E\to 0}$ are given in Table 1.

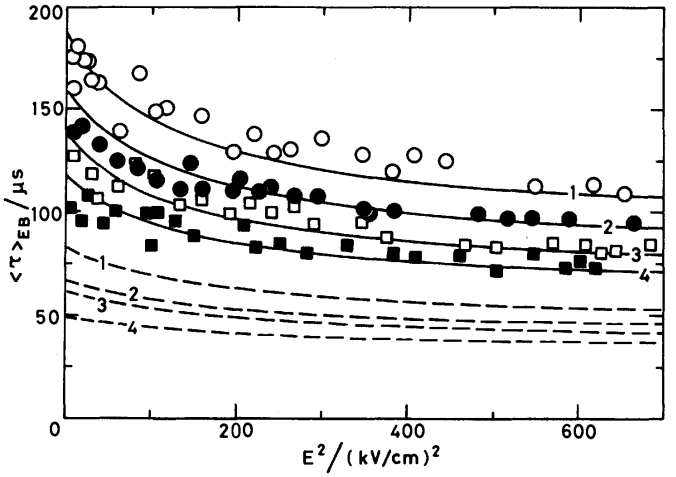

Fig. 6. The electric birefringence-average relaxation time, $\langle\tau\rangle_{EB}$, versus the square of the field strength before the start of decay. Symbols are the same as in Fig. 2. The solid lines were calculated with the decay parameters, while the dashed lines were calculated with the reverse-transient parameters. Numerals indicate the concentrations: (1) 7.82 mM, (2) 3.52 mM, (3) 1.41 mM, and (4) 0.49 mM.

TABLE 2. ELECTROOPTICAL AND HYDRODYNAMIC PROPERTIES OF PMLG IN HF2P, OBTAINED FROM THE ANALYSIS OF THE REVERSE PORTIONS OF RPEB SIGNALS

c / mM	l_w / Å	l_w/l_n	$(\beta_w)^2/2\gamma_w$	μ_w / 10^3D[a]	$\Delta\alpha_w$ / 10^{-17}cm^3[b]	$(g_3-g_1)\times10^3$
7.82	1300	1.12	2.9	2.25	4.2	2.6
3.52	1260	1.10	2.0	2.12	5.5	2.4
1.41	1230	1.10	2.0	2.06	5.1	2.7
0.49	1190	1.08	2.0	2.06	5.1	2.6

a) 1D=3.336×10^{-30} C m. b) 1 cm^3=1.113×10^{-16} F m^2

with respect to molecular length.[17]

The field strength dependence of $\langle\tau\rangle_{EB}$ can be expressed by the following equation, which takes into account the molecular length distribution:[17]

$$\langle\tau\rangle_{EB} = \frac{\int_a^b \tau(l)\Phi(\beta(l), \gamma(l))lf_n(l)dl}{\int_a^b \Phi(\beta(l), \gamma(l))lf_n(l)dl}. \quad (8)$$

With the aid of Eq. 8, the parameters (l_w, l_w/l_n) can be obtained from decay signals quite independently without relying on the result of the reverse-transient signals given in the preceding section. At infinitely high fields, Φ approaches unity, and the $\langle\tau\rangle_{EB}$ becomes the weight-average relaxation time $\langle\tau\rangle_w$,[17] which does not depend on the electric parameters $\beta(l)$ and $\gamma(l)$, but only on the parameters (l_w, l_w/l_n). The theoretical relationships between $\langle\tau\rangle_w$ and the parameters (l_w, l_w/l_n) were calculated from Eq. 4 in Ref. 17. The results are shown in Fig. 7, where the dashed lines are experimental values of $\langle\tau\rangle_w$. These were obtained by extrapolating observed values of $\langle\tau\rangle_{EB}$,

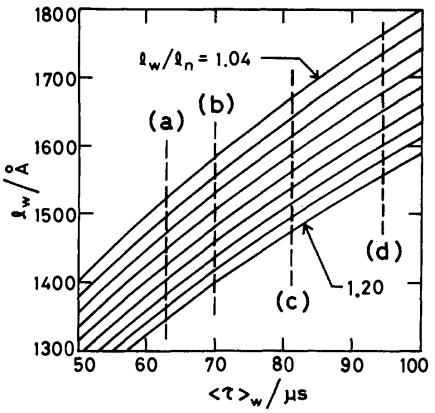

Fig. 7. Theoretical relationship between the weight-average relaxation time, $\langle\tau\rangle_w$, and the weight-average length, l_w, with the degree of polydispersity, l_w/l_n, as parameter. Values of l_w/l_n range between 1.04 and 1.20 at intervals of 0.02. The logarithmic-normal distribution was used. The relaxation time $\tau(l)$ was calculated by using Broersma's equation with a diameter 2b of 10.5 Å. Dashed lines indicate the experimental values of $\langle\tau\rangle_w$, for concentrations of (a) 0.49 mM, (b) 1.41 mM, (c) 3.52 mM, and (d) 7.82 mM.

which were plotted either against E^{-1} or against E^{-2}, to infinitely high field strength.[17] Several sets of paired values (l_w, l_w/l_n) can be obtained from the intersections between the theoretical curves and each dashed line. With each pair (l_w, l_w/l_n) thus evaluated, the theoretical curves of Δn *vs.* E^2 and of $\langle\tau\rangle_{EB}$ *vs.* E^2 can be computed from Eqs. 1 and 8 at various values of [$(\beta_w)^2/2\gamma_w$, β_w] as parameters. By matching these theoretical curves with experimentally observed plots of δ *vs.* E^2 (Fig. 2) and of $\langle\tau\rangle_{EB}$ *vs.* E^2 (Fig. 6), the best set of values can be searched for [l_w, l_w/l_n, $(\beta_w)^2/2\gamma_w$, β_w] by the trial-and-error method (this procedure is referred to as "procedure I"), and then μ_w, $\Delta\alpha_w$, and (g_3-g_1) may be separately evaluated. These values are all given in Table 3. The solid curves in Fig. 6 represent the theoretical $\langle\tau\rangle_{EB}$ *vs.* E^2 curves, which were calculated from Eq. 8. They are all in good agreement with experimental values, thus indicating that the parameters [l_w, l_w/l_n, $(\beta_w)^2/2\gamma_w$, β_w] were evaluated correctly.

Similarly to the above, the $\langle\tau\rangle_{EB}$ *vs.* E^2 curves can also be calculated by using the parameters obtained from the reverse-transient signals (Table 2). These theoretical curves are shown in Fig. 6 by dashed curves, but surprisingly they differ from the observed points of $\langle\tau\rangle_{EB}$ far beyond experimental errors. This unexpected result indicates that the reverse process for an RPEB signal is different from the decay. Some possible explanations will be considered in the following sections.

Simulation of RPEB Signal. With the two sets of parameters [l_w, l_w/l_n, $(\beta_w)^2/2\gamma_w$], one from the reverse-transient process and the other from the decay process, the theoretical curves of the rise, reverse, and decay portions of RPEB signals of PMLG at various concentrations were calculated from Eqs. 2, 4, and 5, in order to justify the correctness of the estimated parameters. The RPEB signal at 3.52 mM was calculated as an example and is shown in Fig. 8. The rise (Fig. 8(a)) and reverse (Fig. 8(b)) portions of the observed data (dots) under an applied external field are well reproduced by the curve (solid line) calculated with the reverse-transient parameters [l_w=1260 Å, l_w/l_n=1.10, $(\beta_w)^2/2\gamma_w$=2.0], but definitely deviate from the curve (dash-dot line) calculated with the decay parameters [l_w=1530 Å, l_w/l_n=1.15, $(\beta_w)^2/2\gamma_w$=3.0]. On the other hand, the observed decay data (Fig. 8(c)) transfer, upon removal of the pulse field, from the theoretical curve with the reverse-transient parameters

Table 3. Electrooptical and hydrodynamic properties of PMLG in HF2P, obtained from the analysis of the decay portions of RPEB signals

c / mM	l_w[a] / Å	l_w/l_n	$(\beta_w)^2/2\gamma_w$	μ_w / 10^3D	$\Delta\alpha_w$ / 10^{-17}cm^3	$(g_3-g_1)\times10^3$
7.82	1610	1.15	3.0	2.23	3.7	2.7
	1650	(1.12)[b]				
3.52	1530	1.15	3.0	2.14	3.7	2.8
	1590	(1.10)[b]				
1.41	1450	1.15	3.0	2.18	3.9	2.8
	1510	(1.10)[b]				
0.49	1410	1.14	3.0	2.18	3.9	2.8
	1470	(1.08)[b]				

a) The lengths l_w in the upper row were obtained by "procedure I" and those in the lower row by "procedure II". b) Values in parentheses are obtained from the reverse-transient portions (Table 2).

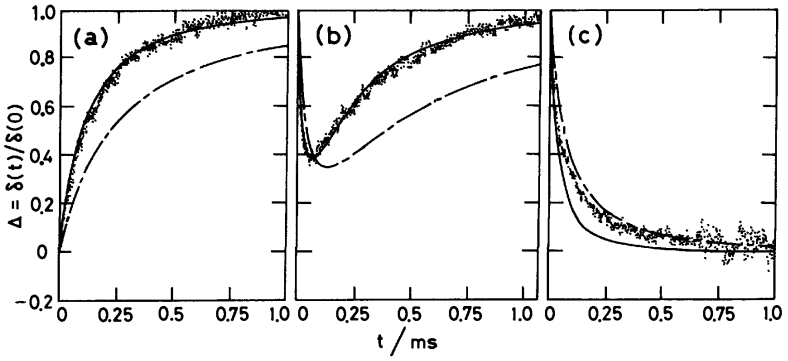

Fig. 8. Comparison of the rise (a), reverse (b), and decay (c) portions of a normalized RPEB signal of PMLG at 3.52 mM with theoretical curves. The observed data were average of 150 signals taken below 3.5 kV/cm in the Kerr law region. The solid curves represent the simulated RPEB signal which was calculated with the reverse-transient parameters (l_w=1260 Å, l_w/l_n=1.10, $(\beta_w)^2/2\gamma_w$=2.0), while the dash-dot-dashed curves represent the signal calculated with the decay parameters (l_w=1530 Å, l_w/l_n=1.15, $(\beta_w)^2/2\gamma_w$=3.0). The logarithmic-normal distribution (2b=10.5 Å) was assumed.

to the one with the decay parameters in the time course between 20—200 μs. The same results have been obtained for many RPEB signals at other concentrations and field strengths. Any RPEB signal of PMLG in HF2P must therefore contain two processes with different sets of molecular parameters during the application and removal of an external electric field.

Since the steady-state and the reverse-transient are observed under the presence of an electric field, a combination of these data should give consistent results. On the other hand, the decay parameters obtained with the steady-state data by "procedure I" should only be apparent. It is now clear, therefore, that the decay portion of the RPEB signal must be analyzed without recourse to the steady-state value. By assuming that the PMLG molecules change identically regardless of their lengths under an electric field, the degree of polydispersity l_w/l_n may be considered to be constant in the presence and absence of the field. Then, with the value of l_w/l_n in Table 2, which was obtained from the reverse portion, the weight-average molecular length l_w can be determined from $<\tau>_w$ (this is referred to as "procedure II"), as was shown in Fig. 7. The values of l_w thus obtained are given in the second row at each concentration in Table 3. The difference in l_w estimated from two procedures (I and II) is no more than 60 Å or 4%, being comparable with experimental errors. Therefore, the difference in the molecular lengths obtained from the reverse (Table 2) and the decay (Table 3) should be attributed to the direct effect of an applied electric field and not to the analytical procedures.

The reverse-transient portion is a process under the influence of an applied field (Fig. 8(b)): an observed value of t_m at the minimum position is 69 μs, while the one calculated with the reverse-transient parameters is also 69 μs, clearly differing from the one calculated with the decay parameters, 136 μs. It has been shown that t_m does not depend on the electric properties, such as $(\beta_w)^2/2\gamma_w$ and μ_w, but depends only on l_w and l_w/l_n, even if a sample is polydisperse.[18] Therefore, the discrepancy resulting from the application and removal of a pulse field can clearly be attributed to the difference in molecular lengths of PMLG helices. Four possible explanations for this discrepancy may be considered. (1) The PMLG helices are flexible enough to be bent under an electric field. (2) They associate to form molecular aggregates in HF2P which transform from one type to another, when the electric pulse is applied. (3) In HF2P they are partly broken to have, *e.g.*, a coiled tail by the electric field. (4) They are subjected to field-induced conformational transition.

In the case of (1), the slightly bending PMLG helices in solution may be stretched under an electric field. The RPEB signal would rise fast at the initial stage, then slow down due to a rotational relaxation of straightened longer molecules. This idea is not supported by the experimental signals in the rise portion. Conversely, the originally straight PMLG helices may be bent momentarily due to an abrupt rotation caused by the applied field. Here, they must return to the original form, when the RPEB signal reaches the steady-state. They should then behave like a straight rod in the subsequent decay process, but the actual decay curve contains a transfer (Fig. 8(c)). Moreover, we have studied the RPEB of a PBLG sample with an average molecular length of 2450 Å.[19,29] This PBLG helix may be fairly flexible, considering the persistence length of PBLG (about 1200 Å);[38,39] yet the $<\tau>_{EB}$ *vs.* E^2 curve was well reproduced by the parameters which were obtained from the reverse portion. The difference between reverse-transient and decay processes can not be attributed to the flexibility of PMLG molecules.

The second case (2) may be ruled out immediately because intermolecular association does not occur in this solution, as shown in Fig. 4. This notion is additionally supported by the degree of polymerization obtained from the intrinsic viscosity in DCA (DP=943). If the conformation of PMLG is the α-helix,[40,41] the length should be about 1400 Å (1.5 Å×943), which agrees well with the value of l_w, as obtained from the analysis of the decay portion of RPEB signals (Table 3).

Therefore, the PMLG helices undoubtedly remain molecularly dispersed at low concentration. The third case (3) may be excluded on the basis that, if a PMLG helix is partially broken by the electric field, the helix should be steadily unwound with an increase in field strengths. In such a case, the field strength dependence of the steady-state value could no longer be simulated by a single set of parameters [l_w, l_w/l_n, $(\beta_w)^2/2\gamma_w$, β_w] in Table 2, which would change continuously and considerably by the destruction of helices with increasing field strength. Figure 2 shows clearly that this is contrary to the experimental results. The last case (4) remains as the most probable and more precise discussions will be given in the following sections.

Intrinsic Viscosity and Molecular Conformation. Once taken under the same conditions, both the intrinsic viscosity and the RPEB data in HF2P may be combined to obtain the hydrodynamical diameter of a PMLG molecule in the following way.[29] Since the intrinsic viscosity was determined in the absence of electric field, the parameters (l_w, l_w/l_n) evaluated from the decay signal must be used. These values were first calculated for three diameters (10, 10.5, and 11 Å) by "procedure II"; hence, three sets of (l_w, l_w/l_n). Three intrinsic viscosity values, $<[\eta]>$, at each concentration were calculated with the aid of Eq. 6 for the three parameter sets. The results are shown with open symbols in Fig. 9(a). A value of 0.763 was used for the partial specific volume of PMLG.[7,8] By comparing the values of $<[\eta]>$ extrapolated to zero concentration with the observed value of $[\eta]_{HF2P}$, a diameter of 10.5 Å was selected for 2*b*. For comparison, the values of $<[\eta]>$ were also calculated by using the parameters (l_w, l_w/l_n) evaluated from the decay signal by "procedure I," and are plotted with closed symbols in Fig. 9(a). The result clearly indicates that the diameter is not affected by two analytical methods, and that the value of 10.5 Å is adequate for the diameter of a PMLG helix. It must be stated that, for all analyses in the preceding sections, the value of 10.5 Å was used as the best hydrodynamic diameter of PMLG.

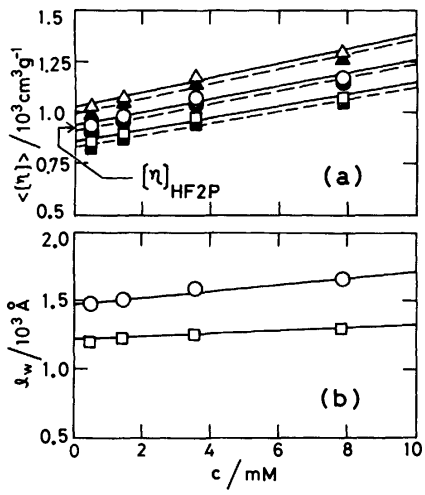

Fig. 9. (a) The dependence of the calculated intrinsic viscosities, $<[\eta]>$, and (b) the dependence of the length l_w on concentration of PMLG in HF2P. The diameters are 2b=10 Å (△, ▲), 10.5 Å (○, ●), and 11 Å (□, ■). The theoretical values were calculated from the parameters of "procedure I" (open symbols and solid lines), and of "procedure II" (closed symbols and dashed lines). Arrow indicates the observed $[\eta]_{HF2P}$. The values of l_w (○) were obtained from the decay portion (lower rows in Table 3) and (□) from the reverse portion (Table 2).

Molecular Length of PMLG. Figure 9(b) shows two plots of the weight-average molecular length l_w against concentration; one from the reverse-transient (squares) and the other from the decay (circles). Being dependent on concentration, probably due to solute-solute interaction, values of l_w should be extrapolated to zero concentration, in order to obtain the molecular length free from such interaction. The limiting values are: $(l_w)_{R,c\to0}$=1210 Å from the reverse-transient process and $(l_w)_{D,c\to0}$=1470 Å from the decay process. Thus, the length of PMLG helix is shorter by about 18% under an electric field than that in the absence of the field. From the degree of polymerization of this PMLG sample, the length per residue is determined to be 1.56 Å/res from $(l_w)_{D,c\to0}$ and is 1.29 Å/res from $(l_w)_{R,c\to0}$. It should be pointed out that these values nearly correspond to the α-helix (1.5 Å/res)[40,41] and the ω-helix (1.3 Å/res),[42-44] respectively.

A Possible Model of Conformational Transition. Finally, a plausible mechanism of the conformational transition induced by the electric field will be discussed on the basis of reversible helix-to-helix alteration. A helical segment is illustrated on the left-hand side in Fig. 10, where an α-helix structure is used as a model. A peptide residue of the main chain is inclined at 64.5° relative to the helix axis, and the length per residue, $h_D \equiv (l_w)_{D,c\to0}/DP_w$, is taken to be 1.56 Å. The plane of the peptide unit is assumed to be parallel to the axis. Although the direction of the permanent dipole moment has not been fully established as yet, it is generally assumed to make an angle of 56.2° relative to the

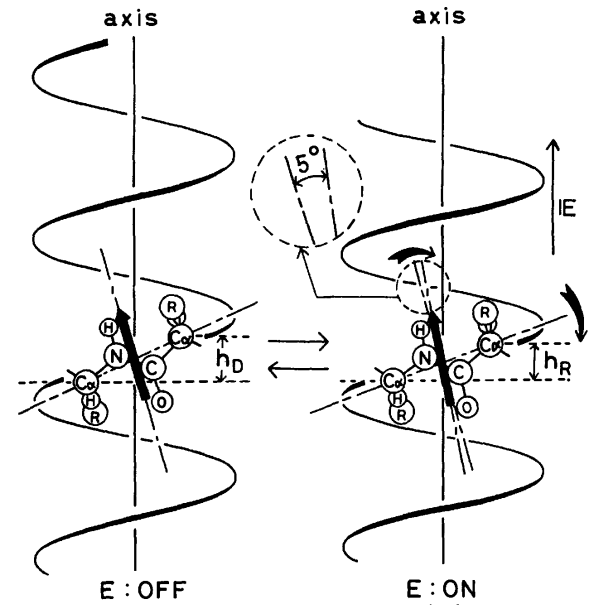

Fig. 10. A possible mechanism for electric field-induced conformational transition of PMLG in HF2P. (a) Electric field is off, and (b) electric field is on. See text for details.

C–N bond.[36,45] A probable direction is indicated with an arrow.

When an electric pulse field is applied, the dipole moment in each peptide group would be oriented toward the helix axis because of the interaction between the field strength and the dipole moment. As a result, the axial translation per residue may be shortened, as shown on the right-hand side of Fig. 10. The PMLG helix would be distorted in such a way that a shorter helix appears. In order to lower the axial translation by about 18% ($h_R \equiv (l_w)_{R,c\to 0}/DP_w = 1.29$ Å), the direction of the permanent dipole moment would have to be rotated clockwise around the normal to the helix axis by no more than 5 degrees, as indicated on the right-hand side of Fig. 10. It is reasonable to believe that this conformational transition occurs in the low field strength region (the lowest field strength in this study is about 1 kV/cm), for the change of the moment direction could possibly be less than 5° being associated with no drastic alteration of the helix backbone or hydrogen-bond breaking. The change in axial translation per residue from 1.56 Å to 1.29 Å is in the same order as that of the α- to ω-helices. Both helices belong to the same intramolecular hydrogen-bond-forming class and their stability is energetically comparable.[43,46] The PMLG helix in HF2P probably transforms from an α-helix to an ω-helix in the presence of an electric field. Matsumoto *et al.*[47] measured the electric birefringence of poly(α-L-glutamic acid) in a dimethyl sulfoxide–methanol mixtures. They discussed the possibility that the PGA helix (presumably the α-helix) is induced to be the ω-helix by solvent composition.

In the present work, the electric field-induced conformational transition of PMLG in HF2P was discovered in the course of an extensive analysis of RPEB signals. The usefulness of the RPEB method is evident in investigating the molecular properties of polypeptides in solutions subjected to electric fields.

Conclusion

By analyzing the reverse and decay portions of the RPEB signal of PMLG independently, two sets of the same molecular parameters (l_w, l_w/l_n, μ_w, $\Delta\alpha_w$) were obtained. The length l_w from the reverse portion differs from the decay portion, the former being shorter about 18% than the latter. The dipole moment per residue of PMLG (2.2—2.4D) is only about one half that of PGA or PBLG.[18,19] The side chain moment of PMLG must considerably cancel the contribution from the main chain moment. A plausible mechanism was proposed to explain the reversible shortening of the helical length upon application of an external electric field. With due considerations of the parameters evaluated in this work, it was concluded that the PMLG molecule probably forms an α-helix in the absence of an electric field, but transforms to another helix, possibly an ω-helix, by the electric field.

The author wishes to thank Associate Professor Kiwamu Yamaoka for his continuous support and encouragement in the course of this study. The author also wishes to thank Mr. Shinobu Yamamoto for his skilled assistance in computer programming.

References

1) W. B. Gratzer, G. M. Holzwarth, and P. Doty, *Proc. Natl. Acad. Sci. USA*, **47**, 1785 (1961).
2) G. Holzwarth and P. Doty, *J. Am. Chem. Soc.*, **87**, 218 (1965).
3) R. Mandel and G. Holzwarth, *J. Chem. Phys.*, **57**, 3469 (1972).
4) W. Moffitt, *Proc. Natl. Acad. Sci. USA*, **42**, 736 (1956).
5) W. Moffitt, *J. Chem. Phys.*, **25**, 467 (1956).
6) W. Moffitt, D. D. Fitts, and J. G. Kirkwood, *Proc. Natl. Acad. Sci. USA*, **43**, 723 (1957).
7) Y. Okamoto and R. Sakamoto, *Nippon Kagaku Zasshi*, **90**, 669 (1969).
8) Y. Ishimuro, S. Yamaguchi, F. Hamada, and A. Nakajima, *Biopolymers*, **20**, 2499 (1981).
9) "Molecular Electro-Optics, Part 2," ed by C. T. O'Konski, Marcel Dekker, New York (1978).
10) K. Yoshioka and H. Watanabe, "Pyhsical Principles and Techniques of Protein Chemistry, Part A," ed by S. J. Leach, Academic Press, New York (1969), Chap. 7.
11) K. Yamaoka, Ph. D. Dissertation, University of California, Berkeley, CA, 1964.
12) M. Matsumoto, H. Watanabe, and K. Yoshioka, *Biopolymers*, **6**, 929 (1968).
13) S. Kobayasi, *Biopolymers*, **6**, 1491 (1968).
14) M. Matsumoto, H. Watanabe, and K. Yoshioka, *Kolloid Z. Z. Polym.*, **250**, 298 (1972).
15) M. Matsumoto, H. Watanabe, and K. Yoshioka, *Biopolymers*, **9**, 1307 (1970).
16) J. Schweitzer and B. R. Jennings, *Biopolymers*, **11**, 1077 (1972).
17) K. Yamaoka and K. Fukudome, *Bull. Chem. Soc. Jpn.*, **56**, 60 (1983).
18) K. Yamaoka and K. Ueda, *J. Phys. Chem.*, **86**, 406 (1982).
19) K. Ueda, M. Mimura, and K. Yamaoka, *Biopolymers*, in press.
20) H. Watanabe, *Nippon Kagaku Zasshi*, **85**, 603 (1964).
21) K. Yamaoka, T. Ichibakase, K. Ueda, and K. Matsuda, *J. Am. Chem. Soc.*, **102**, 5109 (1980).
22) K. Yamaoka, S. Yamamoto, and K. Ueda, *Polymer Preprints, Japan*, **32**, 689 (1983).
23) K. Yamaoka and E. Charney, *Macromolecules*, **6**, 66 (1973).
24) C. T. O'Konski, K. Yoshioka, and W. H. Orttung, *J. Phys. Chem.*, **63**, 1558 (1959).
25) I. Tinoco, Jr. and K. Yamaoka, *J. Phys. Chem.*, **63**, 423 (1959).
26) S. Broersma, *J. Chem. Phys.*, **32**, 1626 (1960).
27) The type of distribution function is not too critical when a well fractionated sample is utilized. See also Ref. 19.
28) W. D. Lansing and E. O. Kraemer, *J. Am. Chem. Soc.*, **57**, 1369 (1935).
29) K. Ueda, M. Nomura, and K. Yamaoka, *Biopolymers*, **22**, 2077 (1983).
30) H. L. Frisch and R. Simha, "Rheology, Vol. 1," ed by F. R. Eirich, Academic Press, New York (1956), Chap. 14.
31) C. Wolff, A. Silberberg, Z. Priel, and M. N. Layec-Raphalen, *Polymer*, **20**, 281 (1979).
32) H. Watanabe, *Nippon Kagaku Zasshi*, **86**, 179 (1965).
33) J. C. Powers, Jr. and W. L. Peticolas, *Biopolymers*, **9**, 195 (1970).
34) W. Pyżuk and T. Krupkowski, *Makromol. Chem.*, **178**, 817 (1977).
35) K. Yamaoka and K. Matsuda, *Macromolecules*, **14**, 595 (1981).

36) A. Wada, *Adv. Biophys.*, **9**, 1 (1976).
37) K. Yoshioka and H. Watanabe, *Nippon Kagaku Zasshi*, **84**, 626 (1963).
38) V. N. Tsvetkov, I. N. Shtennikova, V. S. Skazka, and E. I. Rjumtsev, *J. Polym. Sci., Part C*, **16**, 3205 (1968).
39) S. Itou, N. Nishioka, T. Norisuye, and A. Teramoto, *Macromolecules*, **14**, 904 (1981).
40) L. Pauling, R. B. Corey, and H. R. Branson, *Proc. Natl. Acad. Sci. USA*, **37**, 205 (1951).
41) L. Pauling and R. B. Corey, *Proc. Natl. Acad. Sci. USA*, **37**, 235 (1951).
42) W. L. Bragg, J. C. Kendrew, and M. F. Perutz, *Proc. Roy. Soc.*, **A203**, 321 (1950).
43) E. M. Bradbury, L. Brown, A. R. Downie, A. Elliott, W. E. Hanby, and T. R. R. McDonald, *Nature*, **183**, 1736 (1959).
44) E. M. Bradbury, L. Brown, A. R. Downie, A. Elliott, R. D. B. Fraser, and W. E. Hanby, *J. Mol. Biol.*, **5**, 230 (1962).
45) D. A. Brant, W. G. Miller, and P. J. Flory, *J. Mol. Biol.*, **23**, 47 (1967).
46) R. E. Dickerson and I. Geis, "The Structure and Action of Proteins," Harper and Row, New York (1969), Chap. 2.
47) M. Matsumoto, H. Watanabe, and K. Yoshioka, *Biopolymers*, **12**, 1729 (1973).

Stopped-flow Kinetic Studies of Cu^{2+} Ion Binding to Bovine Serum Albumin

Naohisa KURE, Hitoshi NAKATSUJI, Takayuki SANO, and Tatsuya YASUNAGA*
Faculty of Science, Hiroshima University, Higashisenda-machi, Naka-ku, Hiroshima 730
(Received March 17, 1984)

The interaction of Cu^{2+} ion with bovine serum albumin (BSA) was studied statically by equilibrium dialysis and ultraviolet spectrophotometric titration techniques, and kinetically by the stopped-flow method with transmittance detection at 255 nm. The static measurements showed the presence of one primary binding site and a number of weaker binding sites at pH 5.2. Stopped-flow measurements were undertaken in the pH region of 4—6.4 where a single reaction process was observed on the order of several seconds following the rapid absorbance change within the dead-time of the apparatus. This single reaction process was attributed to reaction of Cu^{2+} ion with the primary BSA site. The analyses of pH and concentration dependences of both the relaxation time and absorbance change confirmed the presence of two types of bound Cu^{2+} species to the primary binding site. One type formed during the dead-time of the apparatus is postulated as a square-planar complex formed between Cu^{2+} and the three N-terminal peptides of BSA. This reaction occurs with Cu^{2+} being exchanged for hydrogen ions on the N-terminal peptides. The second type of bound Cu^{2+}, observed by stopped-flow method is thought to result from a bimolecular binding of Cu^{2+} ion a deprotonated imidazolyl group in the third position of the histidyl residue; the value of the molar extinction coefficient for this species, determined kinetically, suggests a further coordination of the β-carboxyl group to the bound Cu^{2+}.

Various studies on the binding of Cu^{2+} ions to bovine serum albumin (BSA),[1-3] the 1—24 N-terminal peptide unit of BSA,[4-6] and the 1—4 N-terminal peptide unit of BSA[5] have confirmed the presence of at least two types of bound species in neutral and low pH regions. A chelated complex, predominant above pH 6, between Cu^{2+} ion and the three N-terminal peptides (Asp-Thr-His-) of BSA shows a square-planar configuration made by coordinations by α-amino, imidazolyl, and two peptide nitrogen atoms to the central Cu^{2+} ion.[3,4] Another type of species has been identified in the low pH range below 5.5. Iyer *et al.*[7] have reported the presence of two types of complexes between Cu^{2+} and N-terminal site of a synthetic peptide of human serum albumin (HSA) and have pointed out the necessity of kinetic studies for elucidation of the mechanism in forming of these complexes.

In the present study, the binding nature of Cu^{2+} ion to BSA was investigated both statically by equilibrium dialysis and ultraviolet (UV) spectrophotometric titration techniques and kinetically by stopped-flow measurements in the pH range where the two types of bound Cu^{2+} species coexist. A plausible mechanism of Cu^{2+} binding to the peptide sites is proposed; the molecular structure of the complexes is also discussed.

Experimental

Materials. Bovine serum albumin (prepared from Fraction V and essentially fatty acid-free) was purchased from Sigma Chem. Co. and used without further purification. The concentration of BSA was determined spectrophotometrically.[8] Solutions of Cu^{2+} ion were made by direct weighing of $CuSO_4$ anhydrous. The pH values of the solutions were adjusted by H_2SO_4 and/or KOH. No pH buffers were added. All measurements were made in 1 mM† solutions of K_2SO_4. Analytical grade reagents were used throughout.

Equilibrium Dialysis. The extent of binding was measured by the equilibrium dialysis technique at pH 5.2 with a dialysis cell (Sanko Plastics Co. type 5044-05) having ten separate chambers. After 72 to 84 hours of dialysis at 25±1 °C, concentrations of Cu^{2+} in the dialysed solutions were determined with a Perkin-Elmer Model 5000 atomic absorption spectrophotometer. The detection limit of this method for Cu^{2+} concentration was 1.5×10^{-7} M. The pH values of the dialysed solutions were 5.2±0.08.

Spectrophotometry. The difference spectra of BSA solutions in the presence and absence of Cu^{2+} ions were measured in the ultraviolet region using a Union Giken SM 401 spectrophotometer at 25±0.2 °C.

Stopped-flow Experiments. The kinetic measurements were carried out using a Union Giken Stopped-flow spectrophotometer RA 401. The dead-time of this apparatus is 5 ms. For the case of very small amplitudes, an accurate relaxation time was obtained by signal averaging 2—10 measurements using the averaging capabilities of the wave memory apparatus. All kinetic measurements were made at 25±0.2 °C.

Results and Discussion

Binding Parameters. Klotz and Curne[9] reported that at most there are sixteen sites on BSA for binding Cu^{2+} ions at pH 4.83, but data obtained in their study were limited to high binding conditions, *i.e.*, at a binding ratio, r, (moles of bound Cu^{2+}/moles of protein) >1.5. Naik *et al.*[10] determined the binding isotherm of Cu^{2+} with BSA at low binding conditions with the Cu^{2+} titration technique using a Cu^{2+} ion-specific electrode. However, in our investigations using the Cu^{2+} ion-specific electrode, we found that BSA ions significantly lower the voltage of the Cu^{2+} ion-specific electrode which results in serious errors in the binding data. Consequently, the binding data were obtained at low binding conditions using an equilibrium dialysis technique, measuring Cu^{2+} in dialysed solutions with atomic absorption.

Figure 1 illustrates a Scatchard plot of the binding of Cu^{2+} ion to BSA at pH 5.2±0.08. The shape of the isotherm reveals the existence of at least two classes of binding sites. The analysis of this plot, using the maximum number of Cu^{2+} sites per BSA molecule of 16,[9] yields the binding parameters: n_p=0.8—1.3, K_p=(5.5—8.8)$\times10^5$ M^{-1}, n_s=14.7—15.2, K_s=(5.4—5.8)×

† 1 M=1 mol dm^{-3}.

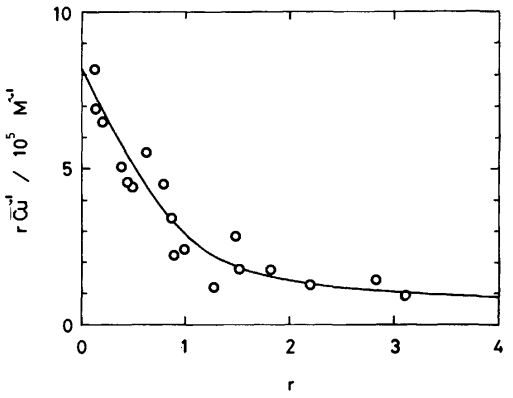

Fig. 1. Scatchard plot of the binding of Cu^{2+} ion to BSA in 1 mM K_2SO_4 solution at pH 5.2±0.08 and 25±1 °C. The circle represents the observed data, and the solid line shows the theoretical curve calculated using n_p=1, K_p=7.2×10^5 M^{-1}, n_s=15 and K_s= 5.6×10^3 M^{-1}.

10^3 M^{-1} where the n and K are the number of binding sites and the binding constants, respectively; the subscripts p and s refer to the primary and secondary binding sites, respectively. As can be seen in Fig. 1, the observed data fall on the theoretical curve calculated using these values. These results are consistent with the assignment of one primary binding site and fifteen secondary ones to the BSA molecule under the present pH conditions.

Ultraviolet Spectrophotometric Titration. The Cu^{2+}–BSA complex exhibits a strong ultraviolet (UV) absorption maximum around 250 mn in addition to two maxima at 525 nm and 650—700 nm in the visible region.[3,4] The absorption band around 250 nm, characteristic of Cu^{2+} complexes with amino acids[11,12] and peptides,[12–17] has been assigned to a charge transfer transition from amino, carboxylato, imidazolyl groups and ionized peptide nitrogen to Cu^{2+} ions. The absorbance increased linearly for this charge transfer absorption band up to a metal to protein ratio (M/P) of about unity at pH 5.2±0.02 as shown in Fig. 2(a). Since the absorbance of free Cu^{2+} ion is negligibly small at the present wavelength, the observed change in absorbance (ΔA^{255}) may be written as

$$\Delta A^{255}/\text{cm} = (\varepsilon^{255}_{c,app} - \varepsilon^{255}_{BSA}) \cdot \bar{C}, \quad (1)$$

where and ε^{255}_{BSA}, $\varepsilon^{255}_{c,app}$ and $\bar{C}$ denote the molar extinction coefficient of BSA, the apparent molar extinction coefficient of Cu^{2+}-BSA complex and its equilibrium concentration, respectively; the superscript 255 refers to the wavelength. The variation of $\varepsilon^{255}_{c,app}-\varepsilon^{255}_{BSA}$, which is given by calculating $\Delta A^{255}/\bar{C}$ using the binding parameters obtained above, was represented as a function of binding ratio r in Fig. 2 (b). Reasonable constancy of $\varepsilon^{255}_{c,app}-\varepsilon^{255}_{BSA}$ up to an r value of unity further confirms the presence of one primary binding site. The molar extinction coefficient $\varepsilon^{255}_{c,app}$ of the complex formed on the primary site was estimated to be 24500 M^{-1} cm^{-1} by using a value of 21400 M^{-1} cm^{-1} for ε^{255}_{BSA}.

Experimental Results in Stopped-flow Measurements. In order to elucidate the dynamic mechanism of the complex formation on the primary site, stopped-flow measurements were undertaken at a fixed and small

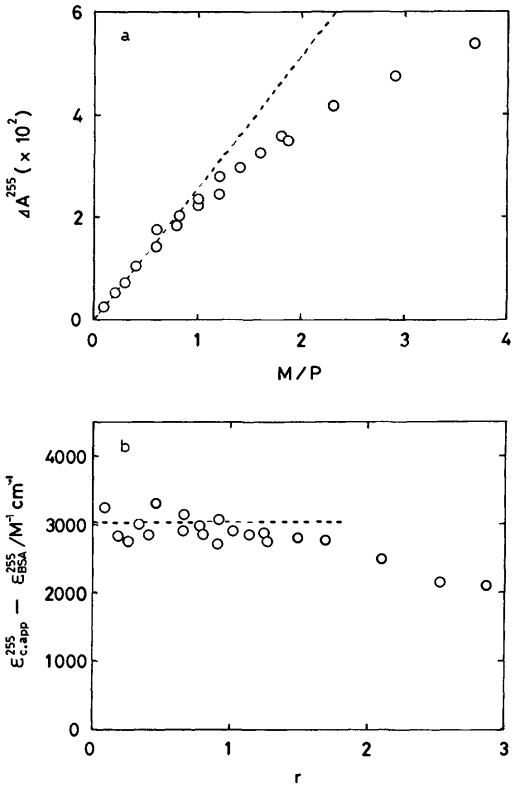

Fig. 2. (a) M/P dependence of the absorbance change (per 1 cm path-length) at 255 nm measured by titrating BSA (1.0×10^{-5} M) solutions with various amounts of Cu^{2+} ions, at pH 5.2±0.02 and 25± 0.2 °C. (b) A plot of $\varepsilon^{255}_{c,app}-\varepsilon^{255}_{BSA}$ *vs.* binding ratio r.

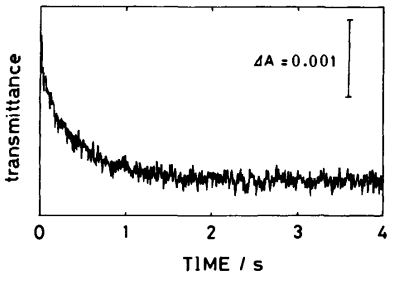

Fig. 3. A typical oscillographic trace of the stopped-flow experiment of the reaction between Cu^{2+} ion (2.0×10^{-6} M) and BSA (1.0×10^{-5} M) monitored by the change in the transmittance intensity (increasing upward) at 255 nm, pH 4.6 and 25±0.2 °C in 1 mM K_2SO_4 solution. The magnitude of the absorbance change is indicated by the bar in the upper right-hand corner.

M/P ratio of 0.2. The reaction between Cu^{2+} ion and BSA was followed by monitoring the change in transmittance at 255 nm. As shown in Fig. 3, a definite decrease in transmittance intensity was observed within several seconds at every pH value and concentration examined. Other reactions were not discernible within the time resolution of the apparatus (5 ms—100 s). The spectra of the solutions after mixing were quite stable over a period of two days.

The relaxation time of the reaction was determined by the semilogarithmic plot of the reaction curve near the equilibrium point. The variation of the reciprocal relaxation time (τ^{-1}) with pH, and with concentration

at pH 4.6 and 5.2 are represented in Figs. 4, 5, and 6, respectively.

The absorbance change (ΔA_{SF}^{255}) estimated from the reaction trace observed by the stopped-flow measurements, the total absorbance change (ΔA_{total}^{255}) due to reaction measured statically with a spectrophotometer at 255 nm, and the difference between ΔA_{total}^{255} and ΔA_{SF}^{255}, which corresponds to the absorbance change (ΔA_{DT}^{255}) within the dead-time of the stopped-flow apparatus are represented in Fig. 7 as a function of pH.

pH Dependence of Absorbance Changes. As can be seen in Fig. 7, the changes in the magnitude of ΔA_{SF}^{255} and ΔA_{total}^{255} as a function of pH reveal the presence of at least one rapid reaction process within the dead-time of the apparatus in addition to the one actually observed (see, *e.g.*, the change in ΔA_{DT}^{255}). The pH dependence of ΔA_{DT}^{255} implies that this rapid reaction involves the exchange of Cu^{2+} ions with hydrogen ions bound to BSA and that the complex formed from this process predominates above pH 6. These observed properties are characteristic of chelation complex formation between Cu^{2+} and the N-terminal three peptides (Asp-Thr-His-) of BSA, as has been reported in various studies on the binding of Cu^{2+} ions to BSA[3,4] and the model peptides of BSA.[4-6] Accordingly, the absorbance change within the dead-time is attributed to the formation of the chelation complex. On the other hand, ΔA_{SF}^{255} shows a quite different pH dependence, exhibiting a maximum around pH 4.8. This reveals that the reaction observed by the stopped-flow measurements results in a different kind of bound species from the chelated one. The bound species may correspond to the type of complex observed at low pH region in visible spectroscopic studies by others.[3,4]

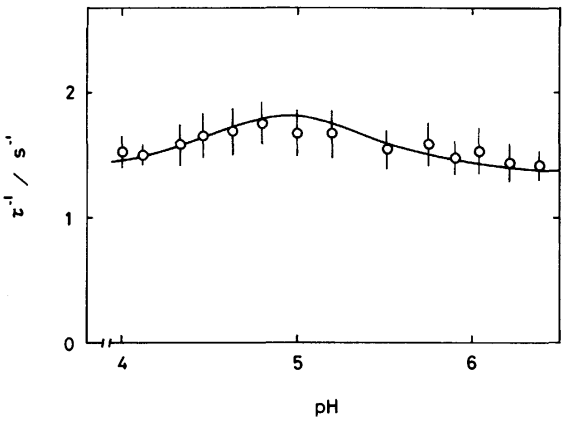

Fig. 4. The pH dependence of τ^{-1} at the fixed concentrations of Cu^{2+} ion (2.0×10^{-6} M) and BSA (1.0×10^{-5} M).

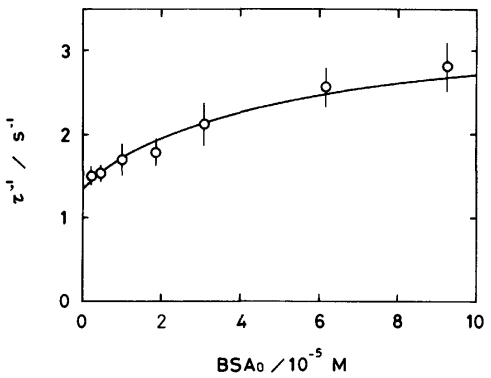

Fig. 5. The variation of τ^{-1} with the total concentration of BSA (BSA_0) at a fixed M/P of 0.2 and pH 4.6.

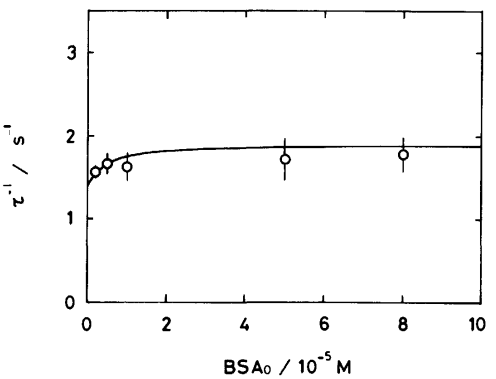

Fig. 6. The variation of τ^{-1} with the total concentration of BSA (BSA_0) at a fixed M/P of 0.2 and pH 5.2.

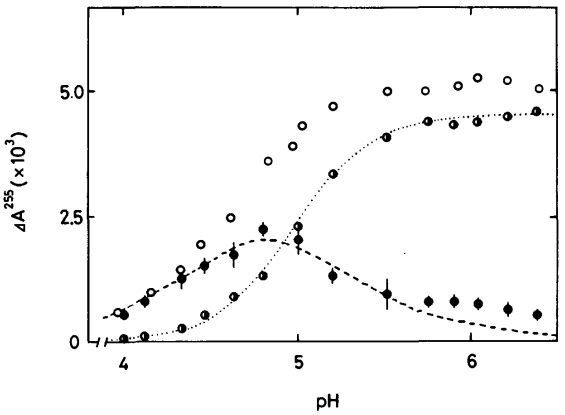

Fig. 7. The pH dependence of absorbance changes at 255 nm due to the reaction between Cu^{2+} (2.0×10^{-6} M) and BSA (1.0×10^{-5} M): ○, the total absorbance change (ΔA_{total}^{255}) measured spectrophotometrically; ●, the absorbance change (ΔA_{SF}^{255}) observed by stopped-flow method; ◑, the absorbance change within the dead-time of the stopped-flow apparatus (ΔA_{DT}^{255}) determined from $\Delta A_{total}^{255} - \Delta A_{SF}^{255}$ at each pH value.

Rapid Reaction within Dead-time of Apparatus. A reaction scheme of the chelation complex, formed rapidly within the dead-time of the apparatus, was examined on the basis of the pH dependence of ΔA_{DT}^{255}. In the neutral pH region, the three N-terminal peptides (Asp-Thr-His-) have three titratable hydrogen ions from the β-carboxyl and α-amino groups in the first terminal aspartly residue and from the imidazolyl group in the third possition of histidly residue. The pK_a values of these function groups, obtained from a titration study of the N-terminal 1—4 peptide of BSA by Bradshow *et al.*,[6] were 3.4, 7.7, and 6.7, respectively. As judged from these values, only the two deprotonation equilibria of the β-carboxyl and imidazolyl groups are important under the present pH range of 4—6.4. Therefore, the three N-terminal peptides of BSA may be represented by the following equilibria,

$$S_1 \overset{K_{\beta c}}{\underset{H}{\rightleftharpoons}} S_2 \overset{K_{im}}{\underset{H}{\rightleftharpoons}} S_3 \qquad \text{(I)}$$

H, $K_{\beta c}$, and K_{im} are the hydrogen ion and the deprotonation constants of β-carboxyl and imidazolyl groups, respectively; the S_i (i=1, 2, and 3) refer to the possible protonation and/or deprotonation states of the titratable groups on the three N-terminal peptides, defined as

S_1: Asp(protonated β-carboxyl)-Thr-His(protonated imidazolyl);

S_2: Asp(deprotonated β-carboxyl)-Thr-His(protonated imidazolyl);

S_3: Asp(deprotonated β-carboxyl)-Thr-His(deprotonated imidazolyl),

where α-amino group in the terminal aspartyl residue is protonated in every states. Since it is common for a transition metal ion to bind to a ligand in the protonated state by exchanging itself with a hydrogen ion,[18-20] every S_1, S_2, and S_3 are assumed to be available in the binding of Cu^{2+} ion. Under this assumption, by considering the competition of Cu^{2+} ion with the variously available hydrogen ions, the following reaction scheme was examined:

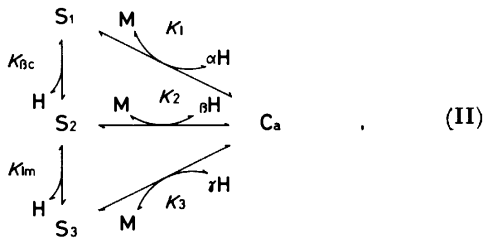

(II)

where M, C_a, and K_i (i= 1, 2, and 3) denote the free Cu^{2+} ion, the chelated complex and the binding constant of each step, respectively; and where α, β, and γ are the number of hydrogen ions released from each binding reaction step, respectively. The cyclic nature of the reaction requires

$$K_1 = K_{\beta c}K_2 = K_{\beta c}K_{1m}K_3, \qquad (2)$$

$$\alpha = \beta + 1 = \gamma + 2. \qquad (3)$$

By use of the molar extinction coefficient ($\varepsilon^{255}_{C_a}$) of C_a and that of BSA, the equation of a net absorbance change resulting from the formation of C_a is given by

$$\Delta A^{255}_{DT}/\text{cm} = (\varepsilon^{255}_{C_a} - \varepsilon^{255}_{BSA})\cdot \bar{C}_{a,r}, \qquad (4)$$

with

$$\bar{C}_{a,r} = \frac{1}{2A}\{A(M_0+S_0) + B - \sqrt{A^2(M_0-S_0)+2AB(M_0+S_0)+B^2}\}, \qquad (5)$$

$$A = K_1/\bar{H}_r^3, \qquad (6)$$

$$B = 1 + K_{\beta c}/\bar{H}_r + K_{\beta c}K_{1m}/\bar{H}_r^2, \qquad (7)$$

where a bar with a subscript r and a subscript 0 refer to the equilibrium concentration after the rapid equilibria and the total concentration of each species, respectively. In the present analyses, the values of 4×10^{-4} M for $K_{\beta c}$ and 2×10^{-7} for K_{im} reported by Bradshow *et al.*,[6] were adopted. The equilibrium hydrogen ion concentration was approximated by the final concentration of hydrogen ion since the pH changes in solution after mixing were within ±0.03 of the initial pH. The observed ΔA^{255}_{DT}, plotted *vs.* $\bar{C}_{a,r}$ calculated for various values of α and K_1, is shown in Fig. 8. As can be seen in the figure, an excellent linear correlation passing through the origin was found for α=3 demonstrating the plausibility of reaction Scheme II. The values of K_1, K_2, and K_3 obtained using α=3 are listed in Table 1. From the slope of the straight line in Fig. 8, the value of $\varepsilon^{255}_{C_a}$ was estimated to be 23700 $M^{-1}cm^{-1}$. As can be seen in Fig. 7, the data of ΔA^{255}_{DT} fall on the theoretical curve (dotted line) calculated from Eqs. 4—7 using this value.

Reaction Process Observed by Stopped-flow Method. Since the reaction was observed under the conditions where complex formation at the primary site predominates, the following three types of reactions at the N-terminal site were considered: (a) Reactions succeeding the rapid formation of the chelation complex, (b) intermediate reactions occurring during the formation of chelation complex, and (c) reactions

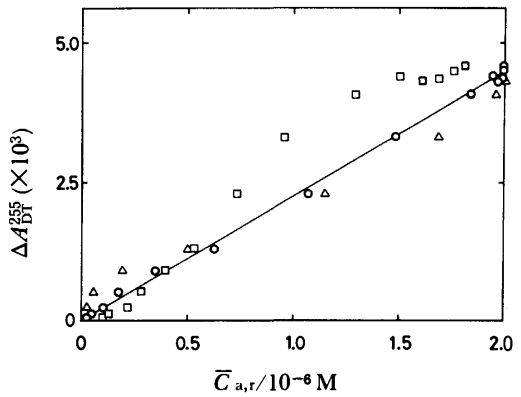

Fig. 8. Plots of ΔA^{255}_{DT} *vs.* $\bar{C}_{a,r}$ calculated for various values of α and K_1: □, α=2 and $K_1=2.4\times10^{-4}$ M; ○, α=3 and $K_1=4.8\times10^{-9}M^2$; △, α=4 and $K_1=5.6\times10^{-14}M^3$.

TABLE 1. EQUILIBRIUM AND RATE CONSTANTS FOR BINDING OF Cu^{2+} ION TO BSA AT 25 °C AND MOLAR EXTINCTION COEFFICIENTS OF COMPLEXES AT 255 nm

K_p[a]	K_1	K_2	K_3	K_b	k_b	k_{-b}	K_{app}[b]
$10^5\,M^{-1}$	$10^{-9}\,M^2$	10^{-5} M		$10^6\,M^{-1}$	$10^6\,M^{-1}s^{-1}$	s^{-1}	$10^5\,M^{-1}$
7.2±1.6	4.8±0.8	1.2±0.2	60±10	3.9±0.8	5.2±1.3	1.3±0.1	4.1±0.7

$\varepsilon^{255}_{c,app}$[a]	$\varepsilon^{255}_{C_a}$	$\varepsilon^{255}_{C_b}$	$\varepsilon^{255}_{c,app}$[b]
$M^{-1}cm^{-1}$	$M^{-1}cm^{-1}$	$M^{-1}cm^{-1}$	$M^{-1}cm^{-1}$
24500	23700	26200	24400

a) Statically obtained for the primary binding site at pH 5.2. b) Calculated from Eqs. 12 and 13 for pH 5.2 using equilibrium constants and molar extinction coefficients obtained kinetically.

essentially independent of the formation of the chelation complex. Among these, reactions in group (a) expected only at higher pH, were eliminated from consideration. Furthermore, since the present reaction takes place after the establishment of the chelation complex, reaction in group (b) could also be excluded. Therefore, only reactions in group (c) needed further investigation. As can be seen in Figs. 5 and 6, the difference in the concentration dependences of τ^{-1} obtained at different pH values implies the contribution of a specific protonation/deprotonation state of the N-terminal peptides to the present reaction, and the increase of τ^{-1} at pH 4.6 with increasing concentration suggests a bimolecular reaction. In addition, the approximate constancy in τ^{-1} obtained at various pH values as shown in Fig. 4 implies that hydrogen ions do not participate directly in the present reaction. These observations suggest a simple binding reaction of Cu^{2+} ion with the N-terminal peptides at a given pH-dependent state. Thus, bimolecular binding mechanisms between Cu^{2+} ion and the N-terminal site in each of three different states, designated with S_1, S_2, and S_3, were examined in detail. Among these, binding reactions with S_1 and S_2 were discounted due to poor agreement between the data and theoretical τ^{-1} calculated at the corresponding pH and concentration conditions. Subsequently, the binding reaction between Cu^{2+} ion and S_3 was examined. By combining the rapid equilibria (Scheme II) with the binding reaction, the mechanism is rewritten as

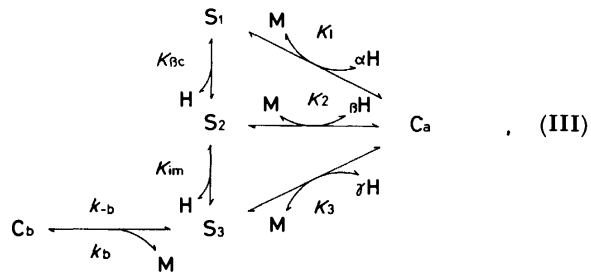

(III)

(present reaction) (rapid equilibria)

with

$$K_b = k_b/k_{-b}, \tag{8}$$

where k_b, k_{-b}, and K_b are the forward and backward rate constants and the equilibrium constant, respectively. Under the conditions of constant hydrogen ion concentration, the equation of τ^{-1} for the present reaction is given by

$$\tau^{-1} = k_{-b}\left[K_b\frac{\bar{S}_3(F-K_3\bar{M}/\bar{H})}{F(1+K_3\bar{S}_3/\bar{H})}+\frac{\bar{M}}{F}+1\right], \tag{9}$$

with

$$F = (1+\bar{H}/K_{\beta c})(\bar{H}+K_3\bar{S}_3)/K_{1m}+K_3(\bar{M}+\bar{S}_3)/\bar{H}+1, \tag{10}$$

where the overbar refers to the equilibrium concentration of each reacting species. The concentration term in the bracket in Eq. 9 was calculated for various values of K_b. A plot of τ^{-1} measured at various pH values and concentrations *vs.* the concentration term obtained for $K_b=3.9\times10^6\,M^{-1}$ gave a good correlation passing through the origin. From the slope of this line, the value of k_{-b} was determined to be $1.3\,s^{-1}$ and that of k_b calculated to be $5.2\times10^6\,M^{-1}s^{-1}$. Theoretical

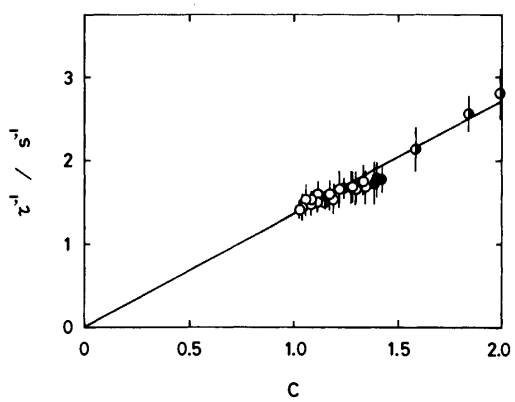

Fig. 9. A plot of τ^{-1} obtained at each pH value and concentration *vs.* the concentration term in Eq. 9, designated by C in this figure and calculated for $K_b=3.9\times10^6\,M^{-1}$.

curves of τ^{-1} obtained for these values are drawn in Figs. 4, 5, and 6, respectively. Good agreement between the theoretical curves and the data as shown in the figures confirms the plausibility of reaction mechanism III.

The absorbance change ΔA^{255}_{SF}, accompanying the present reaction is related linearly to the equilibrium concentration of the complexes as follows:

$$\Delta A^{255}_{SF}/cm = (\varepsilon^{255}_{C_a}-\varepsilon^{255}_{BSA})(\bar{C}_a-\bar{C}_{a,r}) + (\varepsilon^{255}_{C_b}-\varepsilon^{255}_{BSA})\bar{C}_b, \tag{11}$$

where $\varepsilon^{255}_{C_b}$ denotes the molar extinction coefficient of the complex C_b. As shown in Fig. 7, the variation of ΔA^{255}_{SF} with pH (drawn with the dashed line), calculated from Eq. 9 by use of the K_b value obtained above, for $\varepsilon^{255}_{C_b}=26200\,M^{-1}cm^{-1}$ gives good fit with data at each pH value. This fact further supports the validity of mechanism III.

The equilibrium and rate constants and the molar extinction coefficients (at 255 nm) of the complexes determined in the present analyses are summarized in Table 1. Using these values, the apparent association constant K_{app}, defined as $(\bar{C}_a+\bar{C}_b)/(\bar{S}_1+\bar{S}_2+\bar{S}_3)\cdot\bar{M}$, and the apparent molar extinction coefficient $\varepsilon^{255}_{c,app}$, can be calculated from the following relations:

$$K_{app} = \frac{K_1/\bar{H}+K_{\beta c}K_{1m}K_b/\bar{H}^2}{1+K_{\beta c}/\bar{H}+K_{\beta c}K_{1m}/\bar{H}^2}, \tag{12}$$

and

$$\varepsilon^{255}_{c,app} = \frac{\varepsilon^{255}_{C_a}\bar{C}_a+\varepsilon^{255}_{C_b}\bar{C}_b}{\bar{C}_a+\bar{C}_b}. \tag{13}$$

The values calculated for pH 5.2 are also listed in Table 1 together with those of K_p and $\varepsilon^{255}_{c,app}$ obtained from the equilibrium dialysis and UV spectrophotometric titration studies performed at pH 5.2, for the primary complex on BSA. The agreement between the values obtained kinetically and statically strongly support mechanism III as well as the assumptions adopted.

The presence of a Cu^{2+}–BSA complex at low pH, appearing below pH 5.5 and exhibiting a broad maximum around 650—700 nm, was confirmed by Breslow,[3] and Peters and Blumenstock.[4] However, the specific binding site on BSA of this complex has not yet been clarified. The present static and kinetic studies reveal that the low pH complex, detected directly by stopped-flow method, is formed in competition with

the chelation complex on the N-terminal site of BSA. This consists with the results of the potentiometric titration study[7] of the binding between Cu^{2+} and a derivative of the native-sequence tripeptide (Asp-Ala-His-NHMe)[21] of the N-terminal site of human serum albumin (HSA). Some useful information regarding the structure of the low pH complex can be derived from the present kinetic results. As shown in Scheme III, the selective formation of the low pH complex in the specific state, S_3, reveals the coordination of a deprotonated nitrogen atom of imidazolyl group with the Cu^{2+} ion. Furthermore, the absence of the proton release in this process supports further the suggestion, by Breslow based on the visible spectroscopy,[3] that the coordination of peptide nitrogen atoms may not be involved in the structure of low pH complex. In addition, the larger value in the molar extinction coefficient of the low pH complex ($\varepsilon_{C_b}^{255}=26200$) compared to that of chelated one ($\varepsilon_{C_a}^{255}=23700$) suggests a charge transfer from the oxygen atom rather than nitrogen atom; hence, the low pH complex likely involves the β-carboxylato group of the terminal aspartyl residue. From these observations, the most likely configuration for the low pH complex is a *di*-coordinated structure involving a nitrogen atom of imidazolyl group and an oxygen atom of β-carboxylato group. The rate-determining step for the coordination of the small ligands to Cu^{2+} ion has been assigned to the metal-water exchange process (10^7—10^9 $M^{-1}s^{-1}$).[22-26] However, the value of 5.2×10^6 $M^{-1}s^{-1}$ for the second-order formation rate constant k_b is small compared to those values. This implies a higher activation energy is involved in the formation process of the low pH Cu^{2+}-BSA complex. One possible explanation is that a conformational change is the rate-determining process which is required to allow the β-carboxylato group to coordinate to the bound Cu^{2+}.

On the other hand, the chelation complex is formed faster than the time resolution of the present stopped-flow apparatus. As shown by Scheme III and the pK_a values of each N-terminal site group, at most two hydrogen ions are expelled by the formation of the chelation complex in the range of pH 5—6. In contrast with the present result, the square-planar structure of the chelation complex, originally proposed by Peters and Blumenstock[4] and further supported by Shearer *et al.*,[5] requires four released hydrogen ions in the corresponding pH region. This inconsistency in the number of released hydrogen ions may imply that only two hydrogen ions of the four possible compete with Cu^{2+} ion in the formation of the chelation complex. Further elucidation requires application of a rapid relaxation technique to the present system.

References

1) I. M. Kolthoff and B. R. Willeford, *J. Am. Chem. Soc.*, **80**, 5673 (1958).
2) T. Peters, Jr., *Biochim. Biophys. Acta*, **39**, 546 (1960).
3) E. Breslow, *J. Biol. Chem.*, **239**, 3252 (1964).
4) T. Peters and F. A. Blumenstock, *J. Biol. Chem.*, **242**, 1574 (1967).
5) W. T. Shearer, R. A. Bradshow, and F. R. N. Gurd, *J. Biol. Chem.*, **242**, 5451 (1967).
6) R. A. Bradshow, W. T. Shearer, and F. R. N. Gurd, *J. Biol. Chem.*, **243**, 3817 (1968).
7) K. S. Iyer, S. Lau, S. H. Laurie, and B. Sarker, *Biochem. J.*, **169**, 61 (1978).
8) E. J. Cohn, W. L. Hubhes, and J. H. Weare, *J. Am. Chem. Soc.*, **69**, 1753 (1947).
9) I. M. Klotz and H. G. Curme, *J. Am. Chem. Soc.*, **70**, 939 (1946).
10) D. V. Naik, C. F. Jewell, and S. G. Schulman, *J. Pharm. Sci.*, **64**, 1243 (1975).
11) D. W. Urry and H. Eyring, *J. Am. Chem. Soc.*, **86**, 4574 (1964).
12) J. M. Tsangaris, J. W. Chang, and R. B. Martin, *J. Am. Chem. Soc.*, **91**, 726 (1969).
13) H. Takesada, H. Yamagaki, and A. Wada, *Biopolymers*, **4**, 713 (1966).
14) S. Yamashoji, H. Yoshida, and G. Kajimoto, *Yukagaku*, **25**, 128 (1976).
15) K. Yamaoka and T. Masujima, *Bull. Chem. Soc. Jpn.*, **52**, 1286 (1979).
16) J. C. Leyte, L. H. Zuiderweg, and M. von Reisen, *J. Phys. Chem.*, **72**, 1127 (1968).
17) T. Nozawa and N. Hatano, *Makromol. Chem.*, **141**, 21 (1971).
18) F. P. Cavasino, *J. Phys. Chem.*, **69**, 4380 (1965).
19) K. Tamura, S. Harada, M. Hiraishi, and T. Yasunaga, *Bull. Chem. Soc. Jpn.*, **51**, 2928 (1978).
20) K. Tamura, S. Harada, Y. Funaki, and T. Yasunaga, *Bull. Chem. Soc. Jpn.*, **55**, 813 (1983).
21) L-Aspartyl-L-alanyl-L-histidine *N*-methylamide.
22) A. Tanaka, H. Ogawa, and M. Kamada, *Bull. Chem. Soc. Jpn.*, **36**, 530 (1963).
23) M. Eigen, *Pure Appl. Chem.*, **6**, 97 (1963).
24) T. J. Swift and R. E. Connick, *J. Chem. Phys.*, **37**, 307 (1962).
25) R. G. Wilkins, *J. Chem. Soc.*, **1957**, 4520; **1962**, 4475.
26) M. Eigen and R. G. Wilkins, *Advan. Chem. Ser.*, **49**, 55 (1964).

The X-Ray Fluorescence Spectroscopy of Inorganic Solids. VII. The Fe $K\beta_{1,3}$ Energy Shifts in Oxide Glasses

Michiko YOSHIOKA, Takashi MAEKAWA,* and Toshio YOKOKAWA
Department of Chemistry, Faculty of Science, Hokkaido University, Sapporo 060
(Received January 27, 1984)

The Fe $K\beta_{1,3}$ energy shifts in the binary sodium borate, silicate, and phosphate glasses containing small amounts of the iron ion were examined. The Fe $K\beta_{1,3}$ energy decreases with an increase in the sodium oxide content in the borate and silicate glasses. The data are in accordance with those of previous studies that the coordination number of the Fe(III) ion is four in the borate and silicate glasses and six in the phosphate glasses. The structure of the coordination sphere around the Fe(III) ion in the borate glasses was also discussed.

Many studies have been reported about the chemical state of the transition metal ions in oxide glasses and melts. Especially, the optical and magnetic studies have provided much information about the valency state and the coordination number of these ions in the various host glasses.[1] Recently the coordination number of the Fe(III) ion in the binary glasses was estimated by means of Mössbauer spectroscopy; thus, it can be said the coordination number of the Fe(III) ion is six in Na_2O–P_2O_5 glasses and nearly four in Na_2O–SiO_2 and K_2O–B_2O_3 glasses.[2-4] The X-ray energy of the constituents of the oxide glasses varies slightly depending on their chemical surroundings (coordination number, bond polarity, and so on), as the previous studies of Al, Si, K have revealed.[5-7] In the present work, a two-crystal spectrometer was used for the measurement of the X-ray energy of the iron ion in the binary sodium borate, silicate, and phosphate glasses. The results were discussed in terms of the effective positive charge and the coordination number of the Fe(III) ion in these glasses.

Experimental

Apparatus. The iron fluorescence spectra were obtained by means of a two-crystal spectrometer as has been described in a previous paper.[8] The analyzing crystals were Ge ($2d$=0.6533 nm). The chromium X-ray tube (50 kV, 30 mA) was used for the primary excitation. The energy shifts were obtained by the "standard spectra method" developed in our laboratory.[9] The reference material was α-Fe_2O_3. The measurements were repeated at least ten times, and the limit of error was estimated, assuming the t-distribution, with a 95% certainty.

Samples. The glassy samples were prepared by melting weighed quantities of SiO_2, $NaH_2PO_4 \cdot 2H_2O$, H_3BO_3, and Na_2CO_3 of a guaranteed reagent grade in a platinum crucible for 10—12 h at around 1000 °C (at around 1200 °C for silicates). The iron ion was added in the form of Fe_2O_3 or sometimes $Fe(COO)_2$. No appreciable difference was observed between the chosen starting materials.

Valency Change by X-ray Irradiation. High-energy irradiation generates the various defect centers in the glasses. When the transition metal ions are present in the glasses, they may react with defect centers to change their valency state. Bishay and Makar reported that a part of the Fe(II) ions change to Fe(III) ions when γ-ray irradiation in $CaO \cdot P_2O_5$ glass.[10] However, no differences were observed in the energy shifts of the same sample with different durations of the irradiation time. This means that the degree of the valency change is negligibly small under the present experimental conditions.

Results and Discussion

The $K\beta_{1,3}$ energy shifts in the binary glasses are summarized in Table 1 and are plotted in Fig. 1. The energy shifts depend on the composition and on the

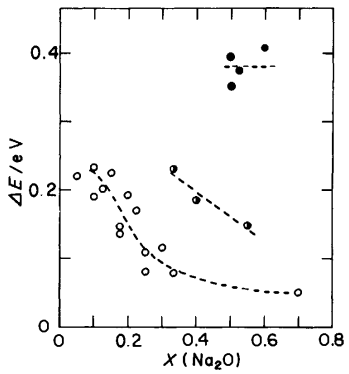

Fig. 1. $K\beta_{1,3}$ energy shift of iron ion in binary glasses.
○ Na_2O–B_2O_3; ◑ Na_2O–SiO_2; ● Na_2O–P_2O_5.
The reference material is α-Fe_2O_3.

TABLE 1. Fe $K\beta_{1,3}$ ENERGY SHIFTS FOR BINARY GLASSES
$\Delta E = E(\text{Sample}) - E(\alpha\text{-}Fe_2O_3)$

x	ΔE/eV
$xNa_2O \cdot (1-x)B_2O_3$+0.3 mol% Fe_2O_3	
0.05	0.221±0.027
0.10	0.189±0.057
	0.232±0.026
0.125	0.201±0.073
0.15	0.225±0.015
0.175	0.135±0.043
	0.146±0.068
0.20	0.193±0.025
0.225	0.170±0.038
0.25	0.080±0.024
	0.108±0.073
0.30	0.115±0.054
0.333	0.078±0.035
0.70	0.049±0.058
$xNa_2O \cdot (1-x)SiO_2$+1.0 mol% Fe_2O_3	
0.333	0.230±0.033
0.40	0.184±0.019
0.55	0.148±0.020
$xNa_2O \cdot (1-x)P_2O_5$+1.0 mol% Fe_2O_3	
0.50	0.351±0.043
	0.395±0.040
0.525	0.375±0.031
0.60	0.409±0.040

kind of glass in which the iron ion was doped. In each system, the characteristic behavior is as follows.

i) Fe ion in sodium borate glasses: The Fe $K\beta_{1,3}$ energy gets smaller with an increase in the sodium oxide content, and the energy drops abruptly at the particular mole fraction of the sodium oxide.

ii) Fe ion in sodium silicate glasses: The Fe $K\beta_{1,3}$ energy also decreases with an increase in the sodium oxide content. However, there seems to be no such sharp change in the shift with the composition as is seen in the sodium borate glasses.

iii) Fe ion in sodium phosphate glasses: The energy shifts are more positive than those in the above two systems. The composition dependence of the energy shifts could not be detected because of the narrow composition range covered in this work.

In the preliminary experiments, the X-ray energy shifts of Fe $K\beta_{1,3}$ in various crystalline iron compounds were measured. The results were in quantitative agreement with that of the previous author[11] and so will not be presented here. However, the data suggest that the energy depends primarily on the effective positive charge on the Fe atom rather than on its formal charge, and that it changes with the coordination number. Thus, CN^-, S^{2-}, O^{2-}, and SO_4^{2-} as the counter anion in compounds gives rise to a negative shift of Fe $K\beta_{1,3}$ in that descending order nearly irrespective of the formal charge of the Fe atom. When O^{2-} is the common counter ion (*i.e.*, Fe_2O_3, FeO, FeO(OH), Fe_3O_4), the structure of the coordination polyhedron affects the shift. On the other hand, iron is substantially in the trivalent state in the glasses examined in the present study.[12] Therefore, the data of the energy shift will be discussed from the viewpoint of the effects of the bulk basicity of host glasses and of the coordination number upon the iron(III) ion.

In our laboratory, the basicities of oxide melts have been measured in terms of the thermodynamic activity of Na_2O in Na_2O–P_2O_5, –B_2O_3, –SiO_2, and other binary systems. P_2O_5 was found to be a quite acidic oxide. The Na_2O activity in borate melts changes drastically (by an order of 10^4) at around 20 mol% Na_2O.[13] These observations are in good agreement with the present results. Thus, the Fe(III) ion is the most positively charged in phosphate glasses, and becomes firmly coordinated with oxygen atoms with an increase in the basicity.

Kurkjian and Sigety concluded that the Fe(III) ion is tetrahedrally coordinated in silicate and octahedrally coordinated in phosphate glasses.[2] Park and Chen, from their EXAFS measurements, showed that the Fe(III) ion coordinates six oxygens in sodium disilicate glass.[14] Morinaga *et al.* also found the same Fe(III) ion in the acidic range of the system.[3] Nishida and Takashima showed that the Fe(III) ion coordinated with four oxygen atoms is predominant in potassium borate glasses.[4] These results, taken together, enable us to conclude that the Fe(III) ion coordinates six oxygen atoms in such an acidic range as in phosphate glass and four oxygens in a less acidic range. The boundary seems to be somewhere around a $K\beta_{1,3}$ energy of 0.25 eV referred to that of α-Fe_2O_3. Koster and Rieck's work[15] on the Fe $K\beta_{1,3}$ energy shift in crystalline compounds in relation to the coordination number are in qualititative agreement with the present results for the glassy materials, although the absolute values differ between the two systems.

B_2O_3 is more acidic than SiO_2 as long as the Na_2O activity is compared at the same composition on a molar basis. Considering the number of atoms of B and Si in one mole of the oxide, however, the order of their acidity becomes nearly the same. This partly accounts for the sequential difference between the basicity, (silicate>borate>phosphate), and the Fe $K\beta_{1,3}$ shifts (borate>silicate>phosphate).

It is worthwhile to consider further the energy shift as a function of the composition in the borate glasses. In the low concentration range of the alkali metal oxide, the borate network consists mainly of a tetrahedral unit, accompanied by the alkali ions as charge compensators, in addition to the trigonal unit without the non-bridging oxygen ions. The further addition of the alkali oxide produces in the network a non-bridging oxygen ($-BO^-$). In the latter composition range, the Fe(III) ion can coordinate with the $-BO^-$ end group and make a coordination sphere with four bridging oxygens and one sodium ion ($[FeO_4]Na$). In the former range, however, some discussion is needed. The Fe(III) ion in this range is forced to accommodate itself to poor O^{2-} or O^- circumstances. Thus, the Fe(III) ions dissolve in the borate network without joining the sodium ions. Lacy proposed a tricluster model about the structure of the aluminium ions, a model in which the aluminium ion coordinates the bridging oxygen in the acidic glasses.[16] From the similarity in the atomic dimensions between the Al(III) and Fe(III) ions, one possible explanation of the structure of the coordination sphere around the Fe(III) ion can be made by means of the above picture. On the other hand, Kawazoe *et al.* introduced a π-electron concept to aid in understanding the borate anomaly.[17] In the low alkali content glasses, the p_π electrons of the oxygens delocalize among the network composed of the trigonal unit (for example, the boroxol ring). The appearance of a tetrahedral unit in the network (tetraborate, diborate, and so on) reduces the degree of resonance and causes an abrupt change in the basicity. Thus, either a tricluster type or an interstitial dissolution among boroxol groups may explain the existence of the Fe(III) ion in the network of the low alkali content glasses. The abrupt change in the $K\beta_{1,3}$ energy at 20 mol% Na_2O may correspond to the structural change in the coordination sphere around the Fe(III) ion in conjunction with the large structural change in the glass matrices.

References

1) J. Wong and C. A. Angell, "Glass Structure by Spectroscopy," Marcel Dekker, New York (1976).

2) C. R. Kurkjian and E. A. Sigety, *Phys. Chem. Glasses*, **9**, 73 (1968).

3) K. Morinaga, Y. Suginohara, and T. Yanagase, *Nippon Kinzoku Gakkai Shi*, **40**, 480 (1976).

4) T. Nishida and Y. Takashima, *J. Non-Cryst. Solids*, **37**, 37 (1980).

5) T. Maekawa, N. Kikuchi, S. Sumita, and T. Yokokawa, *Bull. Chem. Soc. Jpn.*, **51**, 780 (1978).

6) T. Maekawa and T. Yokokawa, *Spectrochim. Acta, Part B*, **37**, 713 (1982).
7) S. Sumita, T. Maekawa, and T. Yokokawa, *Adv. X-Ray Chem. Analysis Japan*, **13**, 1 (1981).
8) T. Maekawa, N. Kikuchi, N. Fukuda, and T. Yokokawa, *Bull. Chem. Soc. Jpn.*, **51**, 777 (1978).
9) N. Kikuchi, T. Maekawa, and T. Yokokawa, *Bull. Chem. Soc. Jpn.*, **52**, 1260 (1979).
10) A. Bishay and L. Makar, *J. Am. Ceram. Soc.*, **52**, 606 (1969).
11) K. I. Narbutt, *Phys. Chem. Minerals*, **5**, 285 (1980).
12) T. Yokokawa, *Can. Metall. Quart.*, **20**, 21 (1981).
13) H. Itoh, A. Sasahira, T. Maekawa, and T. Yokokawa, *J. Chem. Soc., Faraday Trans. 1*, **80**, 473 (1984).
14) J. W. Park and H. Chen, *Phys. Chem. Glasses*, **23**, 107 (1982).
15) A. S. Koster and G. D. Rieck, *J. Phys. Chem. Solids*, **31**, 2505 (1970).
16) E. D. Lacy, *Phys. Chem. Glasses*, **4**, 234 (1963).
17) H. Kawazoe, H. Hosono, and T. Kanazawa, *J. Non-Cryst. Solids*, **29**, 159 (1978).

 © 1984 The Chemical Society of Japan Bull. Chem. Soc. Jpn., 57, 2721—2724 (1984)

Molybdenum Peroxo Complex. Structure and Thermal Behavior

Koichi SEGAWA,* Katsumi OOGA, and Yasuhiko KURUSU
Department of Chemistry, Faculty of Science and Technology, Sophia University, 7-1 Kioicho, Chiyoda-ku, Tokyo 102
(Received February 23, 1984)

The molybdenum peroxide (Mo-y) prepared by oxidation of molybdenum metal with hydrogen peroxide has been studied to determine its structure and thermal behavior. Temperature programmed decomposition has been used to study the thermal stability of Mo-y. Two distinct peaks, I and II, of decomposition processes are discernible in Mo-y. Peak I corresponds to the elimination of water of crystallization and peak II to the decomposition of a peroxide ion of Mo-y. IR and UV examinations support the results of the thermal analysis. The IR band at 931 cm^{-1} and the UV band at 381 nm show the same thermal behavior. Both bands are attributable to the peroxide ion of Mo-y. Spectroscopic studies show that Mo-y has the tetrahedral coordination derived from the single molybdenum complex, which has double bond oxygens attached to Mo atom and has a symmetric type of peroxide ion with one water of crystallization.

Molybdenum peroxide is obtained by oxidation of molybdenum metal powder or molybdenum trioxide with hydrogen peroxide; it has one more oxygen than molybdenum oxide and shows other distinctive features. This molybdenum peroxide (yellow crystallites, abbrreviated as Mo-y) exhibits catalytic activities or acts as an oxygen carrier for a wide variety of organic reactions. For example, Mo-y is active for catalytic dehydration and stoichiometric oxidation of various alcohols and for catalytic epoxidation of various olefinic compounds with *t*-butyl hydroperoxide.[1,2] According to the results derived from these reactions, Mo-y shows dual-function properties: acid properties and oxidation properties as an oxygen carrier.

In the present paper, we describe a neat conclusion about the structure of Mo-y reached by comparing spectral data and thermal behavior.

Experimental

Preparation of Molybdenum Peroxide (Mo-y). The preparation procedure of Mo-y for the work reported here was described in detail previously.[3] In brief, 6.3 g of molybdenum metal powder (Mo: 99.9%, Wako Chemical Co.) was reacted with ice-cooled 50 cm^3 of hydrogen peroxide (30%, Mitsubishi Gas Chemical Co. Ltd.). The solution was maintained below 310 K for 1 h and was allowed to stand for several days at room temperature. A yellow precipitate formed from the solution. The precipitate was collected by filtration and dried under vacuum at room temperature.

Thermal Analysis. Both thermal gravimetrical analysis (TGA) and temperature programmed decomposition (TPDE) experiments were performed under vacuum conditions. About 100 mg of a sample was charged in a quartz basket attached to a standard vacuum system (1×10^{-4} Pa). A McBain type of quartz spiral spring was hung down to the sample basket. The weight change during the TGA experiment was determined by the change in length of the quartz spring (sensitivity: 0.02 mm mg^{-1}), which was equipped with a displacement meter (type 2U, Shinko Electronic Co.).

For TPDE examination, the pressure change of the decomposed gas of the sample was monitored by a vacuum gauge which recorded automatically. Both experiments were operated simultaneously.

Infrared Spectroscopy. A vacuum tight IR cell having KBr windows was designed to fit an infrared spectrometer (260-50, Hitachi Co.) and to be attachable to a vacuum system. Samples (3—5 mg) were dispersed on a thin silicone plate (1×2 cm). The cell was arranged such that a sample plate could be lowered into slots between the optical windows for the spectroscopic examination and withdrawn upward by a magnet into a heated portion (self-contained furnace) for various treatments described below.

UV-Diffuse Reflectance Spectroscopy. A photomultiplexer (R446U, Shimadzu Co.) was attached in the sample cavity of a spectrometer (UV-240, Shimadzu Co.). Each sample of Mo-y (about 50 mg), after a specified heat treatment, was charged into a cell which was covered by a quartz glass plate. $BaSO_4$ was used as a reference.

X-Ray Powder Diffractometry. X-Ray powder diffraction patterns were obtained by a RAD-2A (Rigaku Electronic Co.) diffractometer. The sample of X-ray analysis were the same samples as used for the UV measurements mentioned above.

Results and Discussion

Thermal Analysis. A Mo-y sample which had been previously dried under vacuum at room temperature was evacuated at 323 K for 2 h in the system. A small amount of physically adsorbed water was desorbed during this treatment. TGA and TPDE were carried out from 323 K up to 600 K, and the temperature was raised at various constant rates (4—10 K min^{-1}). Figure 1 shows the TGA curve which was obtained under vacuum conditions. The weight de-

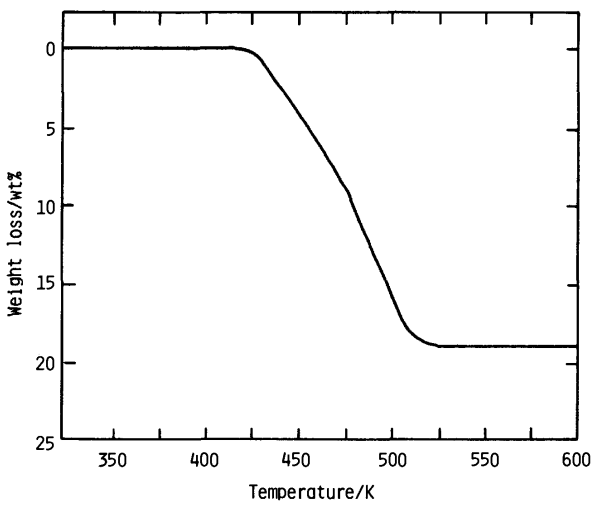

Fig. 1. TGA curve of Mo-y. Heating rate: 5 K min^{-1}.

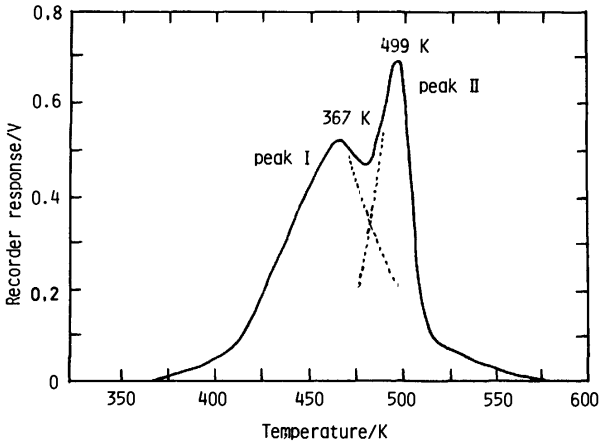

Fig. 2. TPDE spectrum of Mo-y. Heating rate: 5 K min^{-1}.

crease started about 420 K and completed at around 530 K. A well-reproduced weight decrease was observed, based on the weight of the starting Mo-y: it amounted to 19.1±0.1 wt%. The TGA curve represents a one-stage decomposition of Mo-y. However, the curve at around 470 K (10—13 wt% decrease) shows a slight *S* shape.

It is clear that the TPDE spectrum in Fig. 2 represents a two-stage decomposition of Mo-y. When the contributions of these peaks are estimated, the area ratio of peak I at 367 K to peak II at 499 K is about 2 to 1. This result suggests that the thermal decomposition of Mo-y has two kinds of decomposition species. Theoretical derivations[4] give Eq. (1) for the TPDE experiments:

$$\frac{\mathrm{d}\ln(T_m^2/\beta)}{\mathrm{d}\ln(1/T_m)} = \frac{E_d}{R} \qquad (1)$$

where T_m is the temperature which corresponds to the maximum rate of decomposition for a sample, β is the heating rate, and E_d is the activation energy for the decomposition. Figure 3 shows the Arrhenius plots for the decomposition of Mo-y; these were derived from Eq. (1) at various heating rates (4—10 K min^{-1}). The slopes for peaks I and II in Fig. 3 yield activation energies of 41.6 kJ mol^{-1} and 106.0 kJ mol^{-1}, respectively. A result for peak I shows elimination of some relatively weaker chemical species, which could be related to the water molecules generated from Mo-y. On the other hand, the activation energies for peak II represent the decomposition of Mo-y; this peak has rather higher thermal stabilities than peak I. Thus peak II must be correlated to the decomposition of peroxide ion of Mo-y.

Infrared Spectroscopy. Figure 4 (A) shows the IR spectrum of Mo-y evacuated at room temperature in the vacuum cell. After 1 h, the vacuum conditions inside the cell reached 1×10^{-4} Pa. The OH asymmetrical and symmetrical stretching frequencies were observed at 3517 cm^{-1} and 3450 cm^{-1}, together with OH bending vibration of water molecules at 1615 cm^{-1}, respectivery. It can be seen that water molecules of Mo-y are rather easily replaced by D_2O molecules at room temperature (P_{D_2O}=0.7 kPa). OD stretching bands in spectrum (B) were observed at 2620 cm^{-1} and 2540 cm^{-1}, while the bending modes for HDO and D_2O were also observed

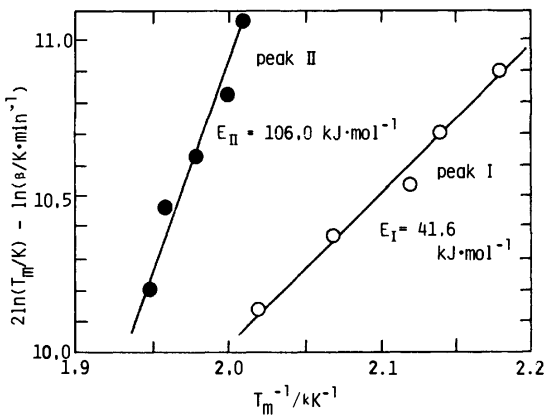

Fig. 3. Arrhenius plots for decomposition of Mo-y. T_m: Temperature of the maximum rate of decomposition for peaks I and II, β: heating rate (K min^{-1}).

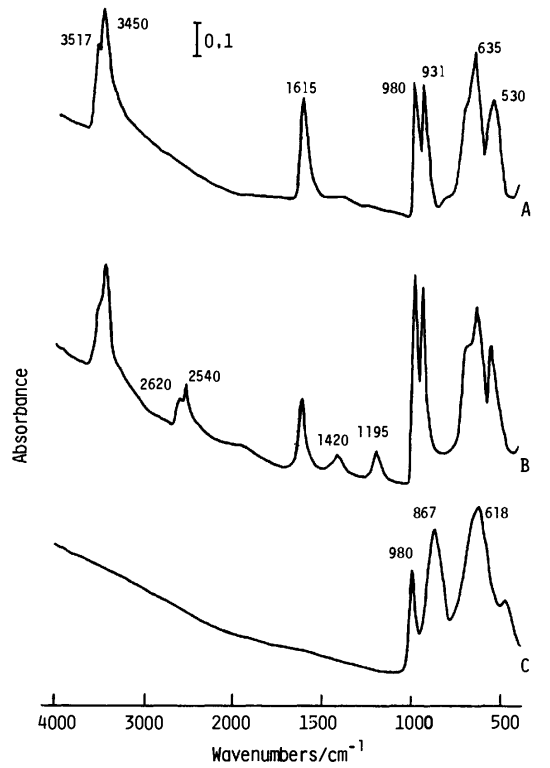

Fig. 4. IR spectra of Mo-y after various treatments. A: Evacuated at room temperature for 2 h, B: exchanged with gaseous D_2O at room temperature, C: evacuated at 673 K.

at 1420 cm^{-1} and 1195 cm^{-1}. The IR sample was evacuated at various temperatures, which were chosen from the characteristics of the results of TGA and TPDE experiments. The relationship between the normalized integrated intensities of OH stretching and bending bands at various evacuation temperatures gives a straight line going through the origin, as shown in Fig. 5. These results suggest that the water molecule is attached to the molybdenum peroxide molecule with a hydrogen bond. There is no evidence of Mo–OH bonding because the stretching frequencies are relatively lower (3517 and 3450 cm^{-1}) than that of water molecules at 3652 cm^{-1}.[5]

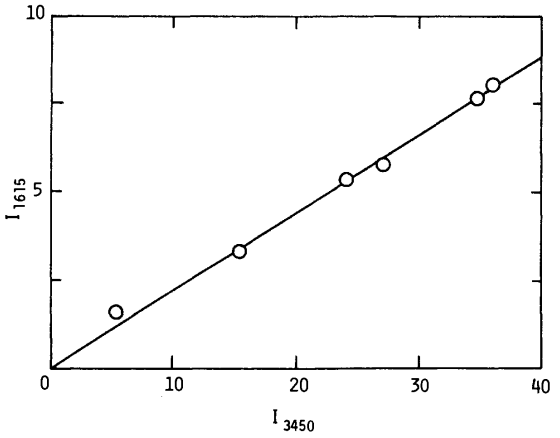

Fig. 5. Integrated intensities of OH stretching and bending vibrations of Mo-y for various evacuation temperatures.

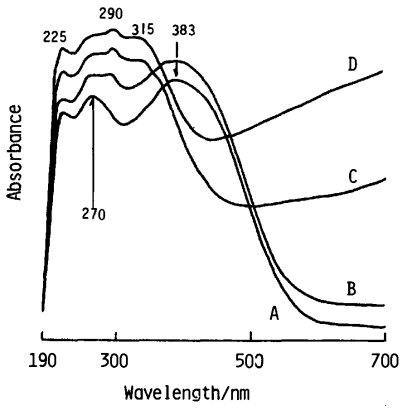

Fig. 6. UV-diffuse reflectance spectra of Mo-y after various treatments. A: Evacuated at room temperature, B: evacuated at 423 K, C: evacuated at 503 K, D: evacuated at 583 K.

At the lattice vibration region of oxides, spectrum (A) shows the stretching vibration of Mo=O,[6] which gives a band at 980 cm^{-1}; this band was also observed in spectrum (C), for the sample evacuated at 673 K. Asymmetric and symmetric stretching of Mo-O were observed at 635 cm^{-1} and 530 cm^{-1}, respectively. No bands of bridging oxygen for Mo-O-Mo[7] were obserbed in spectrum (A). However, after evacuation at 673 K, spectrum (C) shows the bands of Mo-O-Mo at 867 cm^{-1} and 618 cm^{-1}. Furthermore, the band at 931 cm^{-1} in spectrum (A) also disappeared in spectrum (C); this band could be attributed to the O-O stretching vibration of the peroxy structure of Mo-y. In general, the O-O vibration of superoxide ion (O_2^-) and peroxide ion (O_2^{2-}) appears at *ca.* 1140 cm^{-1} and *ca.* 800 cm^{-1}, respectively.[8] However, the O-O stretching frequencies of the symmetric type of peoxide ion appear lower between 932 cm^{-1} to 742 cm^{-1};[9] their location seems to depend on the electronegativities of each transition metal. Mimoun *et al.*[10] ascribed the band of vanadium peroxo complex ranging from 940 cm^{-1} to 935 cm^{-1} to the O-O stretching vibration. As was stated previously, the O-O stretching can be observed in a broad region. But the assignment of the O-O stretching of Mo-y is supported by the results of the thermal

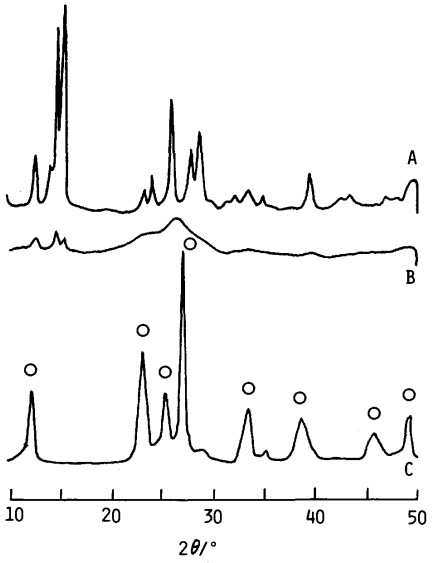

Fig. 7. XRD patterns of Mo-y evacuated at various temperatures. A: Room temperature, B: 473 K, C: 623 K.

analysis. According to the TPDE spectrum in Fig. 2, the thermal decomposition corresponding to peak II seems to coincide with the properties of the band at 931 cm^{-1}, which can be attributed to the decomposition of the peroxide ion of Mo-y.

UV-Diffuse Reflectance Spectroscopy. The UV-diffuse reflectance spectra of Mo-y after various treatments are shown in Fig. 6. Spectrum (A) showed a $2t_2$ to $3t_2$ transition at 225 nm and a t_1 to $3t_2$ adsorption at 270 nm; these are associated with the charge transfer bands of a $Mo^{6+}=O^{2-}$ for the tetrahedral coordination derived from the single molybdenum complex.[11] The additional band at 383 nm in spectra (A) and (B) disappeared after evacuation at temperatures 505 K to 583 K in spectra (C) and (D). The spectra (C) and (D) are quite similar to the authentic spectrum of molybdenum trioxide. These are not characteristic of the tetrahedral coordination: in comparison with spectrum (A), both (C) and (D) have an additional band (290 nm or 315 nm) which corresponds to the octahedral coordination of Mo^{6+}.[12]

X-Ray Diffractometry. Figure 7 shows the XRD patterns of Mo-y. (A) is freshly prepared Mo-y; this was the same sample as used for the UV examinations. The finely crystallized particles of Mo-y became amorphous after evacuation at 473 K; this pattern is shown in (B). (C) shows the sample after evacuation at 623 K. Almost all the lines obtained here in (C) are superimposed on the lines of authentic crystallites of molybdenum trioxide which is marked as open circle. The results shows the rearrangements of the lattice structure of Mo-y from tetrahedral to another that might be octahedral in configuration.

The results of the TGA and TPDE measurements suggest that the 19.1 wt% weight decrease is equivalent to the loss of one molecule of water of crystallization and half a molecule of oxygen gas from Mo-y, as shown in Eq.(2):

$$[MoO_4 \cdot H_2O] \xrightarrow{\Delta} MoO_3 + H_2O + 1/2O_2. \quad (2)$$

The elimination of water of crystallization occurred

at a somewhat lower temperature (peak I in Fig. 2) than that of peroxide ion (peak II) of Mo-y. Spectroscopic investigations show that Mo-y consists of the tetrahedral coordination derived from a single molybdenum complex, which has double bond oxygens attached to the Mo atom and has a symmetric type of peroxide ion with one water of crystallization. The idealized structure of Mo-y can be shown as Scheme 1.

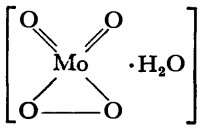

Scheme 1.

Vanadium (V) peroxo complexes which homolytically cleave to give V^{4+}–OO· species are different from the known molybdenum or tungsten peroxo complexes which heterolytically cleave to M^{+}–O–O^{-} species.[10] The O–O vibration of Mo-y appears at higher wave number region. This result is similar to that of vanadium peroxo complexes reported by Mimoun *et al.*,[10] and it may be ascribable to Mo-y having a different reactivity from other peroxo complexes which react heterolytically.

References

1) a)Y. Kurusu, R. Kaya, and N. Ishii, *Nippon Kagaku Kaishi*, **1978**, 1262; b) Y. Kurusu, Y. Matsumura, and N. Ishii, *ibid.*, **1979**, 383.
2) Y. Kurusu, Y. Masuyama, and T. Nishio, "Proc. of the 4th Int. Conf. on the Chem. and Uses of Mo," (1982) p. 241.
3) Y. Kurusu, *Bull. Chem. Soc. Jpn.*, **54**, 293 (1981).
4) S. J. Gentry, N. W. Hurst, and A. Jones, *J. Chem. Soc., Faraday Trans. 1*, **1979**, 1688.
5) S. E. Horsley, D. V. Nowell, and D. T. Stewart, *Spectrochimica Acta*, **30A**, 535 (1974).
6) N. Mizuno, K. Katsumura, Y. Yoneda, and M. Misono, *J. Catal.*, **83**, 384 (1983).
7) K. Eguchi, Y. Toyozawa, N. Yamazoe, and T. Seiyama, *J. Catal.*, **83**, 32 (1983).
8) K. Nakamoto, "Infrared and Raman Spectra of Inorganic and Coordination Compounds," 3rd ed, Wiley, New York (1978) p. 297.
9) J. E. Lyons, "Aspects of Homogeneous Catalysis," ed. by R. Ugo, D. Reidel, Dordrecht-Holland (1977) Vol. 3, p. 10.
10) H. Mimoun, L. Saussine, E. Daire, M. Postel, J. Fischer, and R. Weiss, *J. Am. Chem. Soc.*, **105**, 3101 (1983).
11) Y. Iwasawa, Y. Sato, and H. Kuroda, *J. Catal.*, **82**, 289 (1983).
12) N. Giordano, A. Castellan, J. C. J. Bart, A. Vashi, and F. Campadlli, *J. Catal.*, **37**, 204 (1975).

 © 1984 The Chemical Society of Japan Bull. Chem. Soc. Jpn., 57, 2725—2729 (1984)

Syntheses, and Crystal and Molecular Structures of Tris(benzamide)-bis(*O,O'*-diisopropyl dithiophosphato)lanthanoid(III) *O,O'*-Diisopropyl Dithiophosphate (M=Gd, Tb, Dy, Er, and Yb)

Kiyofumi NAGAI,* Reiko NAKAMURA, Mamoru SHIMOI, and Akira OUCHI
Department of Chemistry, College of Arts and Sciences, The University of Tokyo, Komaba 3-8-1, Meguro-ku, Tokyo 153
(Received March 9, 1984)

Five isomorphous lanthanoid(III) complexes were synthesized, and the structure of the terbium (**1**) and erbium (**2**) complexes were determined by the use of the single-crystal X-ray diffraction method. Crystals of **1** and **2** are monoclinic, with the space group $P2_1/n$, and the cell constants are: (**1**) a=25.076(8), b=15.446(3), c=14.579(8) Å, β=100.77(4)°; (**2**) a=25.036(20), b=15.228(4), c=14.805(19) Å, β=99.50(12)°. The structures were solved by the heavy-atom method and refined by the block-diagonal least-squares method. The final R values of **1** and **2** are 0.061 and 0.055 respectively. They consist of discrete complex cations and dithiophosphate anions. The central metal atom of the cationic complex is hepta-coordinated, and it is in a pentagonal bipyramidal geometry, where four sulfur atoms of two dithiophosphate ions and one oxygen atom of a benzamide ligand take the equatorial positions, while two benzamide oxygen atoms are in the axial positions.

Although lanthanoid elements are "hard" acid according to the HSAB theory,[1] their complexes of *O,O'*-dialkyl dithiophosphate (R_2dtp),[2-4] *N,N*-dialkyldithiocarbamates,[5] and dialkyl dithiophosphinates[6] have already been reported. Pinkerton obtained two kinds of *O,O'*-diethyl dithiophosphate-triphenylphosphine oxide lanthanoid(III) mixed complexes, $[M(Et_2dtp)_3\{(C_6H_5)_3PO\}_2]$ (where M=La—Pr, and Et=C_2H_5) and $[M(Et_2dtp)_2\{(C_6H_5)_3PO\}_3](Et_2dtp)$ (where M=Nd—Lu), and established their structures by means of the X-ray diffraction technique.[3] The present authors previously tried to obtain such types of mixed complexes of the *O,O'*-diisopropyl dithiophosphate, using *N,N*-dimethylacetamide (dma) as the additional ligand, but only $[M(iPr_2dtp)_3(dma)_2]$[where M=La or Nd; iPr=$(CH_3)_2CH$}-type complexes of light lanthanoids were obtained, as was reported in a previous paper.[7] Furthermore, we obtained a series of mixed complexes of the heavy lanthanoid elements with the formula $[M(iPr_2dtp)_2(bza)_3](iPr_2dtp)$ (where M=Gd, Tb, Dy, Er, and Yb; bza=benzamide). The present paper reports on the structures of the terbium(III) (**1**) and erbium(III) (**2**) complexes as determined by the X-ray diffraction technique.

Experimental

Preparation of $[Er(iPr_2dtp)_2(bza)_3](iPr_2dtp)$, and the Tb, Dy, and Yb Complexes. Erbium (III) chloride hexahydrate ($ErCl_3\cdot6H_2O$)(0.61 g, 1.6 mmol) and sodium *O,O'*-diisopropyl dithiophosphate (2.0 g, 8.6 mmol) were dissolved in 25 cm³ of 2-propanol, and the solution was refluxed for 20 min at about 80 °C. After the residue had then been filtered off, 0.57 g (4.7 mmol) of benzamide was added to the filtrate and the mixture was allowed to stand for 5 min at about 65 °C to terminate the reaction. The solution was then evaporated to dryness using the vacuum rotary evaporator at about 65 °C. The residue was dissolved in 5 cm³ of 2-propanol, the insoluble matter was filtered off, and the filtrate was left in a silica-gel desiccator for several days. The crystalline product was then filtered off, washed with diisopropyl ether, and dried in a vacuum desiccator at the ambient temperature. The yield was about 0.83 g (0.71 mmol, 45%). The Tb, Dy, and Yb complexes were obtained in almost the same way.

Preparation of $[Gd(iPr_2dtp)_2(bza)_3](iPr_2dtp)$. The added benzamide should be more than three times the metal salt in mole units. After the 2-propanol solution of the crude product has been concentrated by a vacuum rotary evaporator, it was left in diisopropyl ether vapor at the ambient temperature for several days. The $[Gd(iPr_2dtp)_2(bza)_3](iPr_2dtp)$ complex was thus precipitated. The yield of the complex was 0.80 g (0.69 mmol, 31%) from 0.83 g of $GdCl_3\cdot6H_2O$ (2.2 mmol).

$[Gd(iPr_2dtp)_3(bza)_2]$ was obtained if the added benzamide was less than 2.1 times the starting metal salt in mole units.

All the complexes thus obtained are stable in air for several months. The elemental analyses and their magnetic moments, as measured by means of a Gouy balance at the ambient temperature, are shown in Table 1.

TABLE 1. ANALYSES, YIELDS OF THE SYNTHESES, AND MAGNETIC MOMENTS OF THE COMPLEXES, $[Ln\{[(CH_3)_2CHO]_2PS_2\}_2(H_2NCOC_6H_5)_3][\{((CH_3)_2CHO)_2PS_2\}]$

Ln		Ln(%)	C(%)	H(%)	N(%)	Yield/%	μ_{eff}/BM[a]
Gd	Found	13.56	40.22	5.47	3.60	31	7.7_1
	Calcd	13.55	40.36	5.47	3.64		
Tb	Found	13.50	40.18	5.46	3.58	41	10.0_1
	Calcd	13.67	40.30	5.46	3.63		
Dy	Found	13.92	40.06	5.49	3.52	56	10.8_7
	Calcd	13.94	40.19	5.45	3.60		
Er	Found	14.61	39.92	5.48	3.47	45	9.5_8
	Calcd	14.29	40.00	5.43	3.59		
Yb	Found	14.74	39.31	5.28	3.56	67	4.3_9
	Calcd	14.71	39.83	5.40	3.57		

a) 1 BM=9.274078(36)×10^{-24} J T^{-1}.

TABLE 2. FINAL ATOMIC COORDINATES ($\times 10^5$ for M and 10^4 for the other atoms) AND EQUIVALENT ISOTROPIC TEMPERATURE FACTORS (B_{eq}/Å^2) OF NON-HYDROGEN ATOMS, WITH ESTIMATED STANDARD DEVIATIONS IN PARENTHESES

	M=Tb				M=Er			
Atom	x	y	z	B_{eq}/Å^2 [a]	x	y	z	B_{eq}/Å^2 [a]
M	66953(2)	30631(2)	46182(3)	4.7	66847(2)	29933(3)	46826(4)	4.1
S(1)	6135(2)	1933(2)	3267(3)	9.3	6128(2)	1845(2)	3400(3)	7.9
S(2)	6762(1)	3689(2)	2829(2)	7.3	6801(1)	3573(2)	2938(2)	5.8
P(1)	6357(1)	2646(2)	2286(2)	7.9	6383(2)	2532(2)	2424(3)	6.3
S(3)	7368(1)	4560(2)	4783(2)	5.1	7372(1)	4470(2)	4815(2)	4.5
S(4)	7029(1)	3495(2)	6541(2)	5.8	6999(1)	3433(2)	6541(2)	5.5
P(2)	7486(1)	4423(2)	6160(2)	5.0	7471(1)	4357(2)	6169(2)	4.5
S(5)	9221(1)	2466(2)	1114(2)	7.3	9177(1)	2454(2)	1080(3)	6.9
S(6)	9192(1)	1428(2)	3131(3)	8.9	9120(2)	1391(2)	3048(3)	8.8
P(3)	9289(1)	2509(2)	2477(2)	7.2	9202(1)	2495(2)	2400(3)	6.8
O(100)	7439(2)	2250(4)	4677(5)	7.4	7402(3)	2146(5)	4764(5)	6.2
O(200)	5954(2)	3914(3)	4569(4)	5.2	5960(3)	3861(4)	4607(5)	4.8
O(300)	6267(2)	2052(3)	5407(5)	5.7	6267(3)	2010(5)	5477(5)	5.7
C(101)	7841(4)	1833(5)	4517(7)	6.0	7813(4)	1766(7)	4569(8)	5.9
C(102)	7947(4)	957(6)	4923(7)	6.3	7967(5)	914(8)	4988(9)	6.8
C(103)	7647(4)	667(7)	5537(9)	8.4	7679(6)	567(8)	5593(10)	7.9
C(104)	7739(5)	−133(8)	5943(10)	9.8	7811(7)	−221(10)	6021(10)	9.4
C(105)	8120(6)	−633(8)	5757(11)	11.4	8215(8)	−673(12)	5869(14)	13.9
C(106)	8393(8)	−390(11)	5092(17)	22.1	8509(12)	−340(17)	5289(23)	31.9
C(107)	8327(7)	415(9)	4693(14)	17.9	8392(10)	461(15)	4844(21)	27.2
N(1)	8170(3)	2191(5)	4009(7)	7.3	8091(4)	2133(7)	3986(7)	7.9
C(201)	5735(3)	4597(5)	4202(6)	4.9	5749(4)	4554(7)	4209(7)	4.4
C(202)	5133(3)	4619(5)	3863(6)	5.1	5152(4)	4592(7)	3897(7)	4.2
C(203)	4845(3)	3900(6)	4017(8)	6.2	4848(4)	3872(8)	4042(9)	5.9
C(204)	4274(4)	3892(7)	3724(9)	7.8	4293(4)	3862(8)	3760(11)	7.6
C(205)	4022(4)	4602(7)	3259(9)	7.6	4055(4)	4592(8)	3320(10)	6.8
C(206)	4319(4)	5303(7)	3101(9)	7.7	4365(5)	5297(8)	3158(10)	7.3
C(207)	4876(3)	5328(6)	3393(8)	6.6	4914(4)	5310(7)	3430(9)	6.0
N(2)	6028(3)	5279(4)	4102(7)	6.8	6065(3)	5241(5)	4131(7)	5.9
C(301)	5870(3)	1840(5)	5719(7)	5.0	5841(4)	1811(7)	5766(7)	4.7
C(302)	5745(3)	919(5)	5831(6)	4.6	5712(4)	861(6)	5880(7)	4.3
C(303)	5343(4)	647(6)	6293(7)	6.2	5295(5)	613(7)	6315(8)	6.0
C(304)	5230(4)	−206(7)	6377(9)	7.8	5184(5)	−270(8)	6396(9)	7.5
C(305)	5515(4)	−812(7)	5985(9)	8.4	5465(6)	−882(8)	6033(10)	7.9
C(306)	5914(5)	−562(7)	5532(10)	9.0	5893(6)	−628(8)	5613(11)	8.1
C(307)	6036(4)	322(6)	5452(7)	6.3	6025(5)	247(7)	5541(9)	6.0
N(3)	5542(3)	2458(5)	5939(6)	6.9	5514(4)	2446(6)	5957(7)	6.7
O(1)	5865(3)	2894(5)	1512(5)	7.9	5914(3)	2794(5)	1636(5)	6.7
C(11)	5410(5)	3424(9)	1709(8)	9.3	5462(5)	3363(10)	1829(9)	7.7
C(12)	4903(5)	2864(12)	1557(12)	14.0	4938(6)	2834(14)	1649(14)	13.0
C(13)	5337(6)	4214(9)	1091(12)	11.8	5439(8)	4180(11)	1216(13)	11.3
O(2)	6676(3)	2126(6)	1621(7)	11.3	6719(4)	1918(6)	1871(7)	9.4
C(21)	7240(6)	2048(8)	1700(11)	11.4	7176(9)	2080(12)	1536(15)	16.6
C(22)	7381(8)	1093(10)	2073(16)	16.4	7554(7)	1472(23)	1586(27)	32.0
C(23)	7462(8)	2207(15)	932(13)	17.8	6971(24)	2096(27)	570(23)	44.8
O(3)	7377(2)	5282(4)	6672(4)	6.0	7359(3)	5242(5)	6655(5)	5.5
C(31)	7655(4)	6098(6)	6514(8)	6.8	7660(5)	6052(8)	6506(9)	6.5
C(32)	7205(5)	6787(7)	6320(10)	9.1	7222(6)	6763(8)	6300(11)	8.2
C(33)	8104(5)	6264(8)	7365(9)	9.0	8102(6)	6208(10)	7353(10)	8.8
O(4)	8114(2)	4290(4)	6557(5)	6.2	8092(3)	4214(5)	6575(5)	5.8
C(41)	8441(4)	3632(7)	6189(8)	7.4	8433(5)	3560(9)	6212(10)	7.4
C(42)	8554(5)	2898(9)	6891(12)	11.3	8548(6)	2819(10)	6898(13)	10.6
C(43)	8942(4)	4105(10)	6015(10)	11.1	8929(6)	4049(12)	6016(13)	12.1
O(5)	8867(3)	3185(4)	2778(6)	9.1	8761(4)	3147(5)	2685(7)	8.7
O(51)	8819(6)	4078(7)	2423(10)	10.9	8709(7)	4071(8)	2373(11)	9.4
C(52)	8292(6)	4180(9)	1772(13)	12.6	8215(7)	4168(11)	1636(14)	12.2
C(53)	8900(8)	4670(8)	3327(12)	13.8	8711(11)	4616(10)	3234(14)	15.9
O(6)	9882(3)	2912(4)	2838(6)	8.7	9775(4)	2952(6)	2781(6)	7.9
C(61)	10194(6)	2856(9)	3802(10)	10.3	10069(7)	2906(12)	3722(10)	10.7
C(62)	10379(8)	3770(12)	4074(15)	16.9	10267(10)	3844(15)	4013(17)	17.0
C(63)	10642(7)	2230(13)	3768(13)	15.5	10519(8)	2284(16)	3750(16)	16.5

a) The equivalent isotropic temperature factors for non-hydrogen atoms were computed using the following expression: $B_{eq}=4/3(B_{11}a^2+B_{22}b^2+B_{33}c^2+B_{13}ac\cos\beta)$. The B_{ij}'s are defined by: $\exp[-(h^2B_{11}+k^2B_{22}+l^2B_{33}+2klB_{23}+2hlB_{13}+2hkB_{12})]$.

Single-crystal X-ray Analysis. **1** and **2** are isomorphous and monoclinic, the space group being $P2_1/n$. Their crystallographic data are as follows:

1. $TbC_{39}H_{63}N_3O_9P_3S_6$, F. W.=1162.3, a=25.076(8), b=15.446(3), c=14.579(8) Å, β=100.77(4)°, U=5547(3) Å^3, D_m=1.41(3), D_x=1.39 Mg m^{-3}, μ(Mo$K\alpha$)=1.67 mm^{-1}, Z=4.

2. $ErC_{39}H_{63}N_3O_9P_3S_6$, F. W.=1170.4, a=25.036(20), b=15.228(4), c=14.805(19) Å, β=99.50(12)°, U=5567(8) Å^3, D_m=1.41(3), D_x=1.39 Mg m^{-3}, μ(Mo$K\alpha$)=1.94 mm^{-1}, Z=4.

The crystals of **1** and **2** used for the structure determination were about 0.3×0.3×0.4 mm^3 in size. All their edges were ground off, but they were not shaped into spheres.

The reflections in the range of $3°<2\theta<50°$ were collected on a Rigaku AFC-6A automated four-circle diffractometer, with graphite monochromated Mo$K\alpha$ radiation (the scan speed and scan width for **1** and **2** were 2° min^{-1} and 1.40+0.5tanθ°, and 4° min^{-1} and 1.50+0.5tanθ°, respectively), the ω-scan technique being employed. The intensities were corrected for Lorentz and polarization factors, but no correction was made for absorption and extinction. Among the 10196 and 10222 independent reflections collected for **1** and **2**, 6538 and 5220 with $|F_o|>3\sigma(|F_o|)$ were respectively used for the structure determination.

Structure Determination. The structure of **2** was solved by the heavy-atom method. The positional and thermal parameters were refined by the block-diagonal least-squares method. Although all the non-hydrogen atoms were found, we could not determine the positions of any hydrogen atoms from the Fourier map.[8] At the first stage of the refinement of **1**, the positional and thermal parameters of **2** were tentatively applied; they were then refined by the block-diagonal least-squares method in the same way as that of **2**.

The final R values obtained for **1** and **2** are 0.061 and 0.055 respectively,[9] applying the anisotropic temperature factors for non-hydrogen atoms. In each calculation, twenty-one hydrogen atoms obtained by the calculation[8] were included, with their positional and thermal parameters fixed and assuming B_{iso}=10.0.

There is a large void near a isopropyl group (C(22), C(23)) and a phenyl group (C(106), C(107)), and the thermal parameters of these four atoms are abnormally large, although no significant peaks remained in the difference Fourier synthesis map.

All the calculations were carried out on a HITAC M-200H computer at the Computer Center of the University of Tokyo, using the local version of the UNICS program.[10] The atomic-scattering factors were taken from Ref. 11.

Other Measurements. The visible absorption spectra were measured with a Hitachi 124 spectrophotometer. The X-ray powder patterns of these complexes were obtained by the use of Model DX-GO-F JEOL, using Cu$K\alpha$ radiation in the range from 4° to 40° in 2θ.

Results and Discussion

The final atomic parameters of **1** and **2** are listed in Table 2, while the bond lengths and angles and short intermolecular distances are tabulated in Table 3.[12] The perspective drawing of **1** around the central

TABLE 3. SELECTED BOND LENGTHS AND BOND ANGLES OF THE Tb AND Er COMPLEXES, $[M\{[(CH_3)_2CHO]_2PS_2\}_2(H_2NCOC_6H_5)_3][(CH_3)_2CHO]_2PS_2$ (where M=Tb, Er), WITH ESTIMATED STANDARD DEVIATIONS IN PARENTHESES

Bond length	l/Å		Bond length	l/Å	
	M=Tb	M=Er		M=Tb	M=Er
M-S(1)	2.806(4)	2.781(5)	M-S(2)	2.816(4)	2.790(6)
M-S(3)	2.845(2)	2.818(3)	M-S(4)	2.850(4)	2.814(6)
M-O(100)	2.236(6)	2.198(7)	M-O(200)	2.267(5)	2.232(7)
M-O(300)	2.296(7)	2.264(9)	S(1)-P(1)	1.967(6)	1.973(7)
S(2)-P(1)	1.988(4)	1.981(5)	P(1)-O(1)	1.556(8)	1.564(10)
P(1)-O(2)	1.586(12)	1.575(12)	S(3)-P(2)	1.985(5)	1.986(6)
S(4)-P(2)	1.978(4)	1.973(5)	P(2)-O(3)	1.572(7)	1.575(9)
P(2)-O(4)	1.587(6)	1.586(8)	S(5)-P(3)	1.964(6)	1.946(8)
S(6)-P(3)	1.961(4)	1.964(6)	P(3)-O(5)	1.605(8)	1.593(10)
P(3)-O(6)	1.605(8)	1.610(9)	O(100)-C(101)	1.255(12)	1.255(15)
O(200)-C(201)	1.261(10)	1.279(13)	O(300)-C(301)	1.252(12)	1.251(14)
S(6)···N(1)	3.290(10)	3.319(14)	N(3)···S(5^{i})	3.371(9)	3.386(11)
S(5)···N(2^{ii})	3.439(7)	3.429(9)			
Bond angle	**ϕ/°**		**Bond angle**	**ϕ/°**	
	M=Tb	M=Er		M=Tb	M=Er
S(1)-M-S(2)	70.85(11)	71.57(13)	S(1)-M-S(3)	140.93(9)	141.31(11)
S(1)-M-S(4)	148.50(10)	147.67(12)	S(1)-M-O(100)	88.98(18)	88.9(2)
S(1)-M-O(200)	92.18(15)	91.53(19)	S(1)-M-O(300)	73.47(19)	73.5(2)
S(3)-M-S(4)	70.50(8)	70.91(11)	O(100)-M-O(200)	179.7(2)	179.7(2)
O(100)-M-O(300)	92.8(2)	91.5(3)	M-S(1)-P(1)	88.36(17)	88.89(19)
M-S(2)-P(1)	88.65(16)	88.46(17)	S(1)-P(1)-S(2)	111.0(2)	110.9(2)
S(1)-P(1)-O(1)	111.8(3)	112.7(4)	S(2)-P(1)-O(2)	112.1(4)	112.4(4)
M-S(3)-P(2)	88.45(14)	88.52(17)	M-S(4)-P(2)	88.44(15)	88.91(18)
S(3)-P(2)-S(4)	112.10(17)	111.2(2)	S(3)-P(2)-O(3)	112.6(3)	112.6(3)
S(4)-P(2)-O(4)	113.1(2)	113.0(3)	S(5)-P(3)-S(6)	117.9(2)	118.4(2)
S(5)-P(3)-O(5)	111.2(3)	112.2(4)	S(6)-P(3)-O(6)	111.2(3)	111.0(4)
M-O(100)-C(101)	167.1(6)	162.1(7)	M-O(200)-C(201)	141.9(5)	141.4(7)
M-O(300)-C(301)	147.2(6)	146.3(7)	O(100)-C(101)-N(1)	119.7(8)	119.8(11)

Keys to the symmetric opertions: i: $-0.5+x$, $0.5-y$, $0.5+z$; ii: $1.5-x$, $-0.5+y$, $0.5-z$.

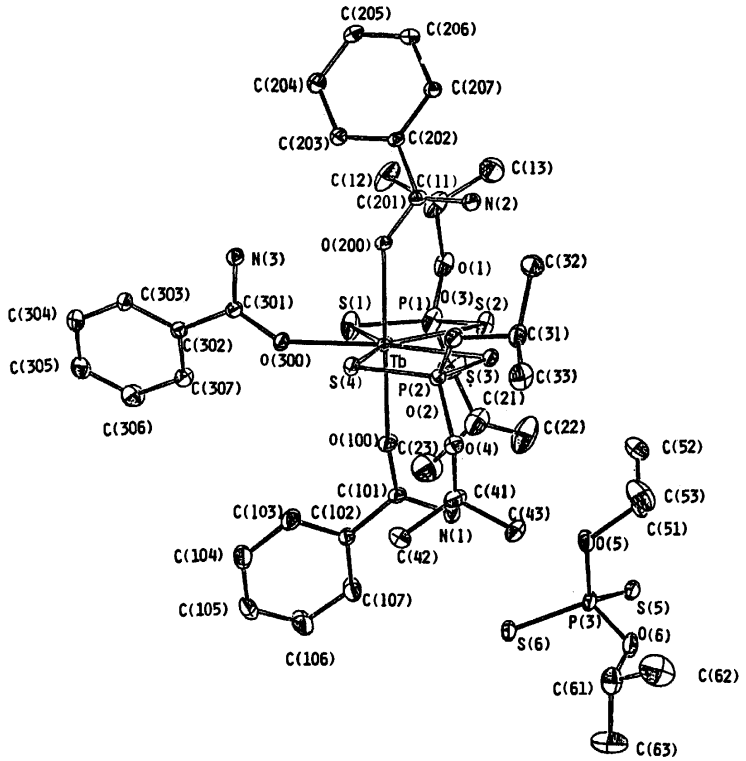

Fig. 1. A perspective drawing of the terbium(III) complex with the numbering scheme.

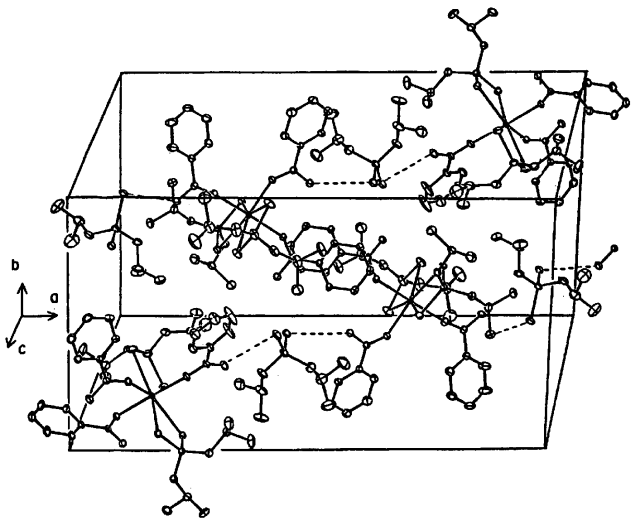

Fig. 2. Crystal packing diagram of the terbium(III) complex.

metal atom, together with the numbering scheme, is shown in Fig. 1, and the crystal packing diagram, in Fig. 2. The general features of **2** are the same as those of **1**, and the numbering scheme of **2** is the same as that of **1**. The metal atoms in the crystals have no mutual magnetic interaction with each other, judging from the magnetic-moment data shown in Table 1. The complex molecule is mono-cationic, and its electric charge is balanced by the $(iPr_2dtp)^-$ anion existing separately. Some interatomic distances, such as S(6)···N(1), N(3)···S(5^{i}), S(5)···N(2^{ii}) (where the keys to the symmetry operations are: i: $-0.5+x$, $0.5-y$, $0.5+z$; ii: $1.5-x$, $-0.5+y$, $0.5-z$), are shorter than 3.5 Å; they may be hydrogen bonds, since the S···H–N hydrogen bond has been reported to be about 3.42 Å in length between S and N.[13]

The central metal atom of the complex is heptacoordinated and is in a pentagonal-bipyramidal geometry, where four sulfur atoms of two iPr_2dtp ligands and one oxygen atom of a bza ligand take the equatorial position, while two bza oxygen atoms from the two ends of the axis. The positional deviations of the coordinated sulfur and oxygen atoms, as well as of the central metal atom, from the average pentagon plane are: **1**. 0.095 Å at the maximum (0.055 Å in the average); **2**. 0.070 Å at the maximum (0.041 Å in average).

As is shown in Table 3, the bond lengths of the M–S pair of each coordinated ligand are approximately the same; however, M–S(1) and M–S(2) are significantly shorter than M–S(3) and M–S(4). The difference in the average M–S bond lengths of Complexes **1** and **2** is 0.029 Å, which is comparable with the difference in their ionic radii, Tb=1.040 and Er=1.004 Å.[14]

The bond lengths of the P–S pair of each ligand are approximately the same, too. Therefore, it is likely that the P=S double bonds of the ligands in both complexes are delocalized. Each Er–O bond length is shorter than that of the corresponding Tb–O by about 0.035 Å; this is also approximately the same as the difference in the ionic radii. The metal–oxygen bond length of the equatorial ligand (Er of Tb–O(300)) is slightly longer than those of the axial ligands in each complex, probably because of the steric effect of the vicinal sulfur atoms on the plane. The other bond lengths, as well as the bond angles of **2** are in good agreement with the corresponding values of **1**. The unit-cell volume of **2** is

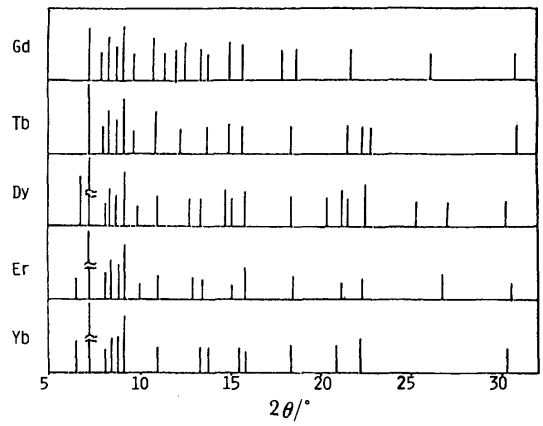

Fig. 3. X-Ray powder patterns of the five lanthanoid(III) complexes.

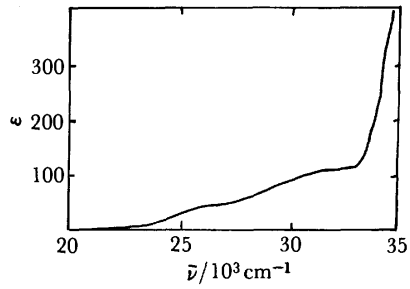

Fig. 4. Absorption spectra of the Yb(III) complex in an acetonitrile solution. (1.88 mmol dm^{-3})

larger than that of **1**, although the unit-cell volume of the series of isomorphous lanthanoid(III) complexes commonly decreases when the metal atomic number increases.[15–18]

The X-ray powder patterns of the gadolinium(III), terbium(III), dysprosium(III), erbium(III), and ytterbium(III) complexes, which have the same chemical formula, judging from the results of elemental analysis, are shown in Fig. 3. They can likely be divided into two groups on the base of their features; Gd(III) and Tb(III) make one group, and the others, another one. This is why we have analysed the two isomorphous structures of **1** and **2**.

In some lanthanoid complexes, extraordinary charge-transfer bands in the near-ultraviolet region have been reported.[2,5,19] The absorption spectra of the Yb complex in an acetonitrile solution are shown in Fig. 4. Although the solid is colorless, the solution is yellow in color, and a charge-transfer band is found at about 33000 cm^{-1}.

The authors wish to thank the Shin-Etsu Chemical Co., Ltd., for presenting the highly pure lanthanoid oxides. This work is partially supported by a Grant-in-Aid for Scientific Research (No. 57430011) from the Ministry of Education, Science, and Culture.

References

1) R. G. Pearson, *J. Chem. Educ.*, **45**, 581, 643 (1968).
2) A. A. Pinkerton, Y. Meserri, and C. Rieder, *J. Chem. Soc., Dalton Trans.*, **1978**, 85.
3) A. A. Pinkerton and D. Schwarzenbach, *J. Chem. Soc., Dalton Trans.*, **1976**, 2464, 2466.
4) A. A. Pinkerton and D. Schwarzenbach, *J. Chem. Soc., Dalton Trans.*, **1981**, 1470.
5) M. Cianpolini, N. Nardi, P. Colamario, and P. Orioli, *J. Chem. Soc., Dalton Trans.*, **1977**, 379.
6) A. A. Pinkerton and D Schwarzenbach, *J. Chem. Soc., Dalton Trans.*, **1980**, 1300.
7) K. Nagai, Y. Sato, S. Kondo, and A. Ouchi, *Bull. Chem. Soc. Jpn.*, **56**, 2605 (1983).
8) The positions of some phenyl- and isopropyl-methine-hydrogen atoms were obtained by calculation on the assumption of C-H=1.0 Å.
9) $R=\sum||F_o|-|F_c||/\sum|F_o|$
10) "The Universal Crystallographic Computation Program System (UNICS)," ed, by T. Sakurai, Crystallographic Society of Japan, Tokyo (1967).
11) "International Tables for X-Ray Crystallography," Kynoch Press, Birmingham (1974), Vol IV, pp. 72, 150: Vol. III, p. 166.
12) The position of some hydrogen atoms, the final thermal parameters, and the final F_o–F_c tables, and some supplemental bond lengths and angle data are deposited as Document No. 8436 at the office of the Editor of the Bull. Chem. Soc. Jpn.
13) L. N. Kuleshova and P. M. Zorkii, *Acta Crystallogr., Sect. B*, **37**, 1363 (1981).
14) R. D. Shannon, *Acta Crystallogr., Sect. A*, **32**, 751 (1976).
15) J. W. Moore, M. D. Glick, and W. A. Baker, Jr., *J. Am. Chem. Soc.*, **94**, 1858 (1972).
16) Y. Koizumi, H. Sawase, Y. Suzuki, T. Takeuchi, M. Shimoi, and A. Ouchi, *Bull. Chem. Soc. Jpn.*, **57**, 1809 (1984).
17) M. C. Favas, D. L. Kepert, B. W. Skelton, and A. H. White, *J. Chem. Soc., Dalton Trans.*, **1980**, 454.
18) J. W. Bates, R. Kalus, and H. Fuess, *Acta Crystallogr., Sect. B*, **35**, 1225 (1979).
19) J. L. Nugent, R. D. Baybarz, J. L. Burnett, and J. L. Ryan, *J. Phys. Chem.*, **77**, 1528 (1973).

The Bridging Tridentate-type Carboxylato Ligand in Isomorphous Guanidinium Di(μ-acetato)bis(triacetatoaqualanthanoidates(III)), $[(NH_2)_3C]_2[M_2(CH_3CO_2)_8(H_2O)_2]$, (M=La, Ce, Pr, Nd, and Sm)

Hiroshi SAWASE,† Yukio KOIZUMI,† Yasuo SUZUKI,† Mamoru SHIMOI, and Akira OUCHI*
Department of Chemistry, College of Arts and Sciences, The University of Tokyo, Komaba 3-8-1, Meguro-ku, Tokyo 153
†*Department of Industrial Chemistry, Faculty of Engineering, Meiji University, Higashi-Mita, Tama-ku, Kawasaki-shi, Kanagawa 214*
(Received April 9, 1984)

The M–O bond lengths and some bond angles of the acetato ligands in the title compounds were compared with each other using their structural data as obtained by the single-crystal X-ray diffraction method. With the increase in the atomic number of the central metal atom, the length of the weakest M–O bond in the bridge increases, even though all the other M–O bonds are shortened. This fact can be explained as follows: as the number of ligating oxygen atoms around the central metal atom is almost at a maximum in these complexes, the sharing space of the tenth coordinating atom on the coordination sphere decreases when the radius of the central metal atom is shortened as a result of the lanthanoid contraction effect.

It has already been reported by some authors that the light and heavy lanthanoid complexes of the same ligand are often in different geometries around the central metal atom, where the coordination number of the former is higher than that of the latter.[1,2,3] Therefore, it is expected that, even in a series of isomorphous lanthanoid complexes, some bond lengths change systematically in the order of the atomic number of the central metal. For example, if the number of the coordinating atoms around the central metal atom is large, some ligating atom can be expected to leave farther from the center when the atomic number of the metal increases and its space on the coordination sphere decreases; however, no investigations of such a phenomenon yet been reported. Exact data about the problem are hard to obtain by the comparison of the structural data of only a few discrete members of the isomorphous complexes, especially those measured by different authors.

On the other hand, the structure of the carboxylato complexes is an interesting theme of research because of their complicated structures. As has been shown by Catterick, the ligands are in many types of coordination modes in the complexes.[4] They are classified as follows (some types of bonding are shown schematically in Fig. 1; the numbering scheme in the figure is also used in Table 4 and in its explanations); i) One metal atom is coordinated to one of the carboxyl oxygen atoms. ii) One metal atom is coordinated to each of the carboxyl oxygen atoms, thus forming four-membered chelate ring. iii) Two metal atoms are coordinated to each oxygen atom of a carboxyl group, bridged by the ligand. In this paper, the *Z*, *E* expression is used to show their conformation; if the other carboxyl oxygen and ligating metal atoms are bonded on the same side of a C–O bond of a carboxyl group, it is named *Z*, and if they are on different sides, it is shown by *E*. Therefore, the bridges are classified into these three groups; a) *Z*, *E*, b) *E*, *E*, and c) *Z*, *Z*, conformations, which correspond with the *syn-anti*, *anti-anti* and *syn-syn* classifications of Catterick respectively.[4] iv) One oxygen atom (O(1)) of a carboxylato chelate around a metal atom (M) is also bonded to another metal atom (M′), and, as a whole, the ligand acts as a tridentate. There are many examples of this iv type bridges in lanthanoid carboxylates.[5,6,7,9–18] Moreover, such bridging has also been reported in some manganese[19] and copper complexes,[20,21] as well as in calcium acetate.[22] In many cases, bridges of this type are deformed, and usually the O(1)–M bond is longer than O(2)–M or O(1)–M′; sometimes it is the longest M–O bond in the complex. Therefore, this bond may be removed first when the area of the coordination sphere decreases.

The change in some bond lengths and bond angles of the bridging carboxylato ligands can be expected to be affected not only by the change in the radius of the central metal atom, but also by the mutual steric interactions of the ligands. Therefore, in order to study the effect of the size of the central metal atom

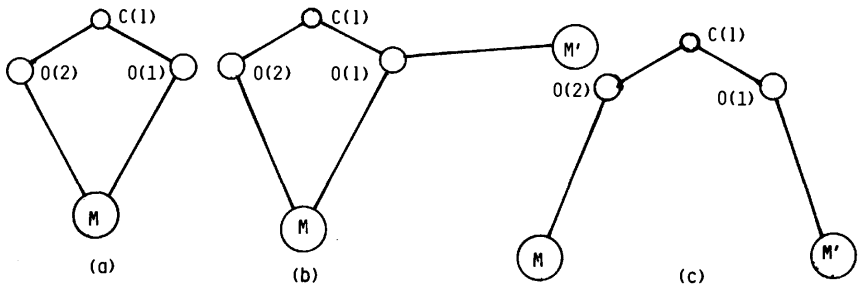

Fig. 1. Schematic presentation of ligands: a) chelating (type ii); b) tridentate type bridging (type iv); c) (*Z*,*Z*) type bridging (type iiic) carboxylate ligand.

on the coordination mode, avoiding the other steric influences, we have made a comparative structural study of the bridging acetato ligand, using the series of isomorphous complexes indicated in the title. Although Porai-Koshits has reported the structure of the cerium complex,[23] the data were not refined enough (R=0.177). Therefore, we have reinvestigated its structure, too.

Experimental

Synthesis of Guanidinium Di(μ-acetato)bis(triacetatoaqualanthanoidates(III)). The complexes in the title, where the metal is La, Ce, Pr, Nd, or Sm, were obtained by means of Canneri's method.[24] The crude product thus obtained was dissolved into water containing a little guanidinium acetate and then recrystallized by being left standing in a sillca-gel desiccator for several days. Although this synthetic method was also used in an attempt to obtain the same type of complexes of heavier lanthanoids, these attempts were not successful even when a large excess of guanidinium acetate was added; in these cases, only the guanidinium acetate and lanthanoid acetate (in their hydrated form) were precipitated separately. Anal. ($M_2C_{18}H_{40}O_{18}N_6$) M, C, H, N. (where M= La, Ce, Pr, Nd, or Sm).

Single-crystal X-ray Analysis. Crystals with dimensions of 0.3×0.3×0.4 mm³ of the lanthanum(III), cerium(III), and praseodymium(III), 0.4×0.4×0.3 mm³ of neodymium(III), and 0.3×0.3×0.3 mm³ of the samarium(III) complexes, were used for the measurement. All edges were ground off, but they were not shaped into spheres. They are isomorphous, and monoclinlc, with the space group $P2_1/n$; Z=2 for the formula $[(NH_2)_3C]_2[M_2(CH_3CO_2)_8(H_2O)_2]$. Other crystallographic data, some experimental conditions, and the final R values obtained by applying the anisotropic temperature factors,[25] are tabulated in Table 1.

The reflections were collected on a Rigaku AFC-6A automated four-circle diffractometer with graphite monochromated Mo $K\alpha$ radiation (0.7107 Å), at the scan speed 4° min⁻¹, by means of the θ-2θ scan technique. From the measured independent reflections, those with $(|F_o|)>3\sigma(|F_o|)$ were selected and were used for the calculations. The intensities were corrected for Lorentz and polarization factors, but no correction was made for absorption and extinction. All the calculations were carried out on a HITAC M-200H computer of the Computer Center of the University of Tokyo, using a local version of the UNICS program.[26] The atomic-scattering factors were taken from the table.[27]

Structure Determination. The structure of the lanthanum(III) complex was solved by the heavy-atom method. The positions of the central metal and some oxygen atoms were deduced from three-dimensional Patterson map, while all the other non-hydrogen atoms were found successively by repeated Fourier syntheses and by the block-diagonal least-squares method.

The structure of the other tetraacetato complexes were solved by assuming that their atomic coordinates were almost the same as those of the isomorphous lanthanum(III) complex. Therefore, at the first step, the final parameters for the lanthanum(III) complex were tentatively applied to them, and then they were refined as usual.

Results and Discussion

The final atomic parameters and their equivalent isotropic temperature factors are shown in Table 2, while some interatomic distances as well as bond angles are tabulated in Table 3. The perspective drawing of the complex around the central lanthanum atom, with the numbering scheme used in Tables 2 and 3, is shown in Fig. 2,[28] and the schematic bonding mode of the lanthanum(III) complex around a metal atom in Fig. 3.

The complex is in a dimer form. Each central-metal atom of the title complexes is deca-coordinated, being coordinated to ten oxygen atoms, and is in a distorted *cis*-bicapped cube (tetradecahedron) geometry including the weak M-O bonding from the bridging ligand. Each metal atom has three chelating acetato ligands, and each is bridged to the next metal atom by two "tridentate" acetato ligands.

In the titled complexes, as shown in Table 3, all the C-O bond lengths, as well as the O(n1)-C(n1)-O(n2) bond angles (where n=1, 2, 3, or 4), are not much different from each other, and they are almost the same as those of the other lanthanoid carboxylates.[5,6,11,12,15,18] All the M-O bond lengths of the same metal complex are about the same except for the long M-O(41), and the corresponding bond length of M-O(nn') (where n=1, 2, 3, or 4; n'=1 or 2) decreases depending on the order of the atomic number of the respective central metal, while that of M-O(41) increases in the same order.

Table 4 shows the selected bond lengths and bond angles of the coordinated carboxyl groups in the title complex as well as in some related lanthanoid carbox-

Table 1. Crystallographic data of the $[(NH_2)_3C]_2[M_2(CH_3CO_2)_8(H_2O)_2]$ complexes

M=	La	Ce	Pr	Nd	Sm
a(l/Å)	18.398(8)	18.373(4)	18.364(9)	18.370(7)	18.409(4)
b(l/Å)	8.524(2)	8.495(3)	8.458(3)	8.432(3)	8.405(2)
c(l/Å)	11.003(5)	10.960(2)	10.931(5)	10.911(3)	10.830(3)
β(ϕ/°)	106.60(4)	106.60(2)	106.65(3)	106.76(2)	106.92(1)
U(v/Å³)	1653.7(12)	1637.3(8)	1626.6(12)	1618.3(10)	1603.2(7)
D_m(d/Mg m⁻³)	1.81(3)	1.83(3)	1.85(3)	1.89(3)	1.92(3)
D_x(d/Mg m⁻³)	1.82	1.84	1.86	1.88	1.92
μ(Mo $K\alpha$)(n/mm⁻¹)	2.62	2.85	3.04	3.28	3.76
F.W.	906.36	908.80	910.36	917.02	929.24
Number of reflections measured.	2068	2491	2471	2768	2589
Reflections used for the calculation	1801	2119	2150	2380	2198
Measured range (ϕ/°)	3—42	3—46	3—46	3—48	3—47
R	0.030	0.032	0.037	0.033	0.030

Table 2. Final atomic coordinates ($\times 10^4$) with estimated standard deviations in parentheses, and their equivalent isotropic temperature factors (B_{eq}/Å^2)

1) Guanidinium di(μ-acetato)bis(triacetatoaqualanthanate(III))

Atom	x	y	z	B_{eq}/Å^2 [a)]
La	5762.7(2)	3396.2(4)	4240.1(4)	1.8
O(W)	4440(3)	2190(5)	3912(5)	3.0
O(11)	6840(3)	4929(5)	3547(5)	3.2
O(12)	6420(3)	5965(5)	5043(4)	2.9
O(21)	5996(3)	820(5)	5623(5)	2.8
O(22)	6965(3)	2392(5)	5866(4)	2.5
O(31)	5343(3)	2038(7)	1991(5)	4.1
O(32)	6452(3)	1391(6)	3230(5)	3.6
O(41)	4615(3)	5761(5)	3821(4)	2.8
O(42)	5224(3)	5388(6)	2414(4)	3.3
N(1)	8063(3)	1073(7)	3900(6)	2.8
N(2)	9362(3)	1311(7)	4812(6)	2.9
N(3)	8536(4)	2219(7)	5901(6)	3.4
C(1)	8640(4)	1534(8)	4856(7)	2.7
C(11)	6809(4)	6058(9)	4262(7)	2.6
C(12)	7225(5)	7571(10)	4183(9)	5.1
C(21)	6680(4)	1146(8)	6135(7)	2.2
C(22)	7174(4)	35(9)	7117(8)	4.0
C(31)	5950(4)	1264(8)	2196(7)	2.8
C(32)	6060(5)	162(11)	1193(8)	5.0
C(41)	4726(4)	6079(8)	2771(7)	2.6
C(42)	4233(6)	7254(12)	1908(9)	6.1

2) Guanidinium di(μ-acetato)bis(triacetatoaquacerate(III))

Atom	x	y	z	B_{eq}/Å^2 [a)]
Ce	5763.2(2)	3389.5(4)	4238.7(3)	1.7
O(W)	4445(3)	2196(6)	3896(5)	2.8
O(11)	6833(3)	4908(6)	3549(4)	3.1
O(12)	6413(3)	5949(6)	5042(4)	2.9
O(21)	5987(3)	823(6)	5604(4)	2.7
O(22)	6955(3)	2402(5)	5864(4)	2.4
O(31)	5343(3)	2051(7)	1991(5)	3.9
O(32)	6443(3)	1384(6)	3239(5)	3.3
O(41)	4607(3)	5781(6)	3828(4)	2.7
O(42)	5222(3)	5374(6)	2435(4)	3.0
N(1)	8060(3)	1067(8)	3906(6)	2.9
N(2)	9351(3)	1288(7)	4803(6)	2.8
N(3)	8531(3)	2211(8)	5895(6)	3.1
C(1)	8641(4)	1522(8)	4858(7)	2.3
C(11)	6804(4)	6041(8)	4259(7)	2.4
C(12)	7231(5)	7552(11)	4195(9)	4.8
C(21)	6671(4)	1143(8)	6132(6)	2.2
C(22)	7161(4)	33(10)	7111(8)	3.8
C(31)	5943(4)	1262(8)	2191(7)	2.5
C(32)	6062(5)	159(11)	1194(8)	4.8
C(41)	4725(4)	6084(8)	2780(6)	2.2
C(42)	4237(6)	7252(12)	1898(9)	5.6

3) Guanidinium di(μ-acetato)bis(triacetatoaquapraseodymate(III))

Atom	x	y	z	B_{eq}/Å^2 [a)]
Pr	5764.2(2)	3381.0(5)	4238.3(4)	1.6
O(W)	4451(3)	2212(6)	3892(5)	2.6
O(11)	6830(3)	4872(7)	3547(5)	2.8
O(12)	6409(3)	5926(7)	5037(5)	2.7
O(21)	5977(3)	816(7)	5593(5)	2.7
O(22)	6949(3)	2405(6)	5856(5)	2.2
O(31)	5342(4)	2045(8)	1991(6)	4.0
O(32)	6441(3)	1373(7)	3251(6)	3.2
O(41)	4602(3)	5789(7)	3840(5)	2.7
O(42)	5222(3)	5358(7)	2451(3)	3.0
N(1)	8054(4)	1055(9)	3898(7)	2.9

N(2)	9346(4)	1269(8)	4796(6)	2.7
N(3)	8526(4)	2210(9)	5894(6)	2.9
C(1)	8641(4)	1506(9)	4856(7)	2.2
C(11)	6800(5)	6018(10)	4249(8)	2.6
C(12)	7228(6)	7522(12)	4193(11)	4.9
C(21)	6663(4)	1144(9)	6124(7)	2.1
C(22)	7158(5)	31(12)	7110(9)	3.7
C(31)	5944(4)	1256(9)	2194(8)	2.4
C(32)	6060(6)	155(12)	1197(9)	4.4
C(41)	4721(4)	6093(10)	2785(7)	2.0
C(42)	4235(7)	7283(14)	1902(10)	5.5

4) Guanidinium di(μ-acetato)bis(triacetatoaquaneodymate(III))

Atom	x	y	z	B_{eq}/Å^{2} [a]
Nd	5766.3(2)	3369.3(4)	4237.5(3)	1.6
O(W)	4462(3)	2228(6)	3894(5)	2.5
O(11)	6821(3)	4862(6)	3536(5)	2.8
O(12)	6401(3)	5913(6)	5036(4)	2.5
O(21)	5974(3)	808(6)	5587(5)	2.5
O(22)	6944(3)	2397(6)	5852(4)	2.2
O(31)	5341(3)	2059(7)	1984(5)	4.0
O(32)	6436(3)	1367(6)	3251(5)	3.2
O(41)	4596(3)	5815(6)	3849(4)	2.7
O(42)	5215(3)	5343(6)	2467(5)	2.9
N(1)	8051(3)	1038(8)	3893(6)	2.8
N(2)	9343(3)	1251(7)	4790(6)	2.6
N(3)	8528(4)	2194(8)	5894(6)	2.9
C(1)	8637(4)	1493(8)	4853(7)	2.1
C(11)	6792(4)	6005(9)	4251(7)	2.3
C(12)	7226(5)	7512(11)	4200(9)	4.5
C(21)	6660(4)	1136(8)	6125(7)	2.1
C(22)	7152(5)	16(10)	7112(8)	3.5
C(31)	5940(4)	1249(9)	2197(7)	2.4
C(32)	6059(5)	149(12)	1189(8)	4.5
C(41)	4722(4)	6097(9)	2800(6)	2.1
C(42)	4253(6)	7290(13)	1908(9)	5.3

5) Guanidinium di(μ-acetato)bis(triacetatoaquasamarate(III))

Atom	x	y	z	B_{eq}/Å^{2} [a]
Sm	5782.7(2)	3311.8(4)	4231.7(3)	1.8
O(W)	4474(3)	2257(6)	3866(5)	2.5
O(11)	6801(3)	4823(6)	3520(5)	2.9
O(12)	6390(3)	5856(6)	5045(5)	2.8
O(21)	5974(3)	750(6)	5555(5)	2.7
O(22)	6946(3)	2338(6)	5841(5)	2.4
O(31)	5351(3)	2076(7)	1945(6)	4.2
O(32)	6430(3)	1337(7)	3239(5)	3.3
O(41)	4566(3)	5914(7)	3883(5)	3.3
O(42)	5189(3)	5277(6)	2537(5)	3.0
N(1)	8037(3)	967(8)	3888(6)	2.9
N(2)	9328(3)	1199(8)	4760(6)	2.8
N(3)	8532(4)	2123(8)	5898(6)	3.0
C(1)	8634(4)	1432(8)	4845(7)	2.2
C(11)	6777(4)	5959(9)	4247(7)	2.4
C(12)	7204(6)	7484(11)	4210(10)	4.7
C(21)	6659(4)	1080(9)	6109(7)	2.3
C(22)	7142(5)	−27(10)	7122(8)	3.5
C(31)	5940(4)	1249(9)	2153(7)	2.4
C(32)	6075(5)	157(11)	1136(8)	4.4
C(41)	4712(4)	6113(9)	2844(7)	2.3
C(42)	4282(6)	7343(13)	1907(9)	5.7

a) The equivalent isotropic temperature factors were computed using the following expression: $B_{eq}=4/3(B_{11}a^2+B_{22}b^2+B_{33}c^2+B_{13}ac\cos\beta)$. The B_{ij}'s are defined by: $\exp[-(h^2B_{11}+k^2B_{22}+l^2B_{33}+2klB_{23}+2hlB_{13}+2hkB_{12})]$.

Table 3. Bond lengths and bond angle of the complexes $[(NH_2)_3C]_2[M_2(CH_3CO_2)_8(H_2O)_2]$, with their estimated standard deviations (in parentheses)

Bond lengths M	La(l/Å)	Ce(l/Å)	Pr(l/Å)	Nd(l/Å)	Sm(l/Å)
M-O(11)	2.661(6)	2.634(6)	2.615(7)	2.605(6)	2.562(7)
M-O(12)	2.535(5)	2.512(5)	2.491(6)	2.477(5)	2.455(5)
M-O(21)	2.636(6)	2.607(6)	2.593(7)	2.579(6)	2.553(6)
M-O(22)	2.563(5)	2.539(5)	2.517(6)	2.501(5)	2.474(5)
M-O(31)	2.640(8)	2.621(9)	2.612(10)	2.602(9)	2.588(9)
M-O(32)	2.563(7)	2.539(7)	2.522(8)	2.507(7)	2.465(7)
M-O(41)	2.860(5)	2.880(5)	2.891(6)	2.919(5)	3.074(6)
M-O(42)	2.601(6)	2.571(6)	2.547(7)	2.529(7)	2.475(7)
M-O(41′)	2.529(8)	2.505(8)	2.483(9)	2.465(8)	2.401(9)
M-O(W)	2.570(5)	2.552(5)	2.533(6)	2.509(5)	2.488(5)
C(11)-O(11)	1.255(12)	1.248(11)	1.248(13)	1.251(12)	1.246(12)
C(11)-O(12)	1.268(14)	1.270(14)	1.272(16)	1.269(14)	1.274(14)
C(21)-O(21)	1.253(8)	1.254(8)	1.258(9)	1.258(8)	1.260(8)
C(21)-O(22)	1.258(9)	1.259(9)	1.260(11)	1.257(10)	1.253(10)
C(31)-O(31)	1.261(9)	1.256(9)	1.256(10)	1.258(10)	1.251(10)
C(31)-O(32)	1.248(11)	1.254(11)	1.255(13)	1.249(12)	1.259(12)
C(41)-O(41)	1.259(14)	1.254(14)	1.260(16)	1.254(14)	1.242(15)
C(41)-O(42)	1.244(11)	1.240(11)	1.249(12)	1.243(11)	1.244(11)
M···M^{i}	4.564(2)	4.563(1)	4.564(2)	4.577(1)	4.682(1)
Bond lengths M	**La(ϕ/°)**	**Ce(ϕ/°)**	**Pr(ϕ/°)**	**Nd(ϕ/°)**	**Sm(ϕ/°)**
O(11)-M-O(12)	49.88(17)	50.22(18)	50.57(20)	50.95(18)	51.64(19)
O(21)-M-O(22)	49.68(16)	50.07(17)	50.64(20)	50.83(18)	51.40(18)
O(31)-M-O(32)	49.4(2)	49.7(2)	49.9(2)	50.1(2)	50.6(2)
O(41)-M-O(42)	46.73(17)	46.53(17)	46.53(20)	46.28(18)	44.39(19)
O(41)-M-O(41′)	64.4(2)	64.3(2)	64.0(2)	63.8(2)	63.0(2)
O(W)-M-O(31)	71.4(2)	71.2(2)	71.2(2)	71.5(2)	72.0(2)
O(12)-M-O(21)	122.39(16)	122.39(16)	122.98(20)	123.17(18)	124.01(19)
O(21)-M-O(32)	71.1(2)	70.8(2)	70.7(2)	70.8(2)	70.9(2)
O(31)-M-O(42)	67.5(2)	67.4(2)	67.5(2)	67.2(2)	67.2(2)
M-O(41)-M^{i}	115.61(15)	115.67(16)	116.0(2)	116.20(17)	117.0(2)
O(11)-C(11)-O(12)	120.8(7)	120.6(7)	120.1(8)	120.6(7)	120.4(7)
O(21)-C(21)-O(22)	120.9(6)	120.2(7)	120.5(8)	120.3(7)	120.4(7)
O(31)-C(31)-O(32)	120.3(9)	119.5(9)	119.5(10)	119.5(9)	118.9(9)
O(41)-C(41)-O(42)	121.0(7)	121.0(7)	120.1(8)	120.7(8)	121.5(8)

Key to the symmetric operations: i: 1.0−x, 1.0−y, 1.0−z.

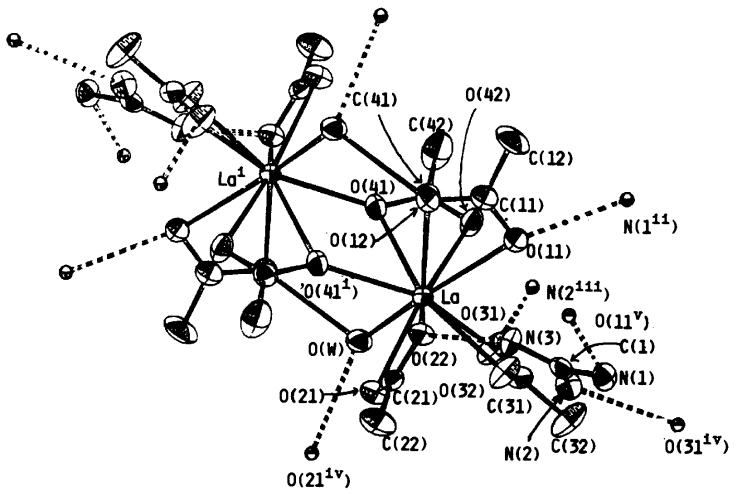

Fig. 2. A perspective drawing of $[(NH_2)_3C]_2[La_2(CH_3CO_2)_8(H_2O)_2]$ with the numbering scheme. Key to the symmetric operations: i, 1.0−x, 1.0−y, 1.0−z; ii, 1.5−x, 0.5+y, 0.5−z;, iii, −0.5+x, 0.5−y, −0.5+z; iv, 0.5+x, 0.5−y, 0.5+z; v, 1.5−x, −0.5+y, 0.5−z.

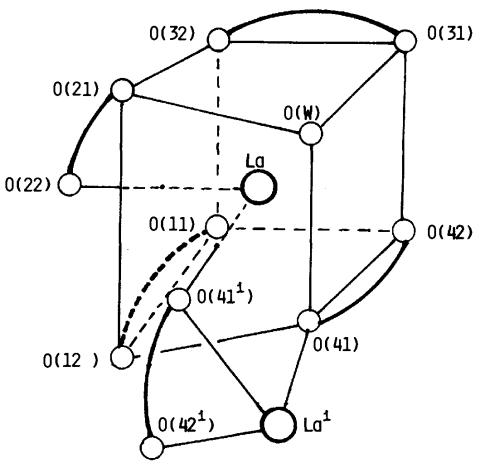

Fig. 3. Schematic presentation of the *cis*-bicapped cube geometry around a La(III) atom.

TABLE 4. THE INTERATOMIC DISTANCES AND BOND ANGLES OF SOME CARBOXYLATE LIGANDS

Type[a]	Complex[b]	Central metal	Average M-O[c]	Elongation of M-O(1)[d]	M-O(2) -C(1)	M-O(1) -C(1)	M'-O(1) -C(1)	Ref.[e]
ch	1	Gd	2.468		93.9	92.8		5
ch	2	Ho	2.437		94.7	92.4		6
ch	3	Er	2.416		92.2	93.7		f
Z,E	4	Ho	2.341	62.5	140.3	61.8	145.2	8
Z,E	5	Er	2.336	63.8	142.2	60.4	146.4	8
E,E	4	Ho	2.388	89.9	130.3	18.8	133.7	8
E,E	5	Er	2.379	90.2	129.5	20.6	132.1	8
Z,Z	6	Pr	2.436	61.9	140.7	59.1	140.7	9
Z,Z	7	Ho	2.308	69.3	143.4	59.2	144.3	10
Z,Z	8	Sm	2.375	61.7	138.2	61.1	142.8	11
tri	18	Ca	2.475	−6.2	92.6	93.4	151.3	22
tri	1	Gd	2.439	5.4	97.8	92.9	151.7	5
tri	2	Ho	2.391	7.1	98.2	91.8	152.5	6
tri	3	Er	2.367	8.2	99.2	92.3	151.9	f
tri	9	Ce	2.591	−1.4	96.3	94.0	148.5	12
tri	10	Ce	2.497	7.6	99.7	89.3	168.6	13
tri	10	Ce	2.521	6.0	98.3	91.3	155.7	13
int	11	Nd	2.483	14.5	104.3	87.5	157.9	14
int	12	La	2.525	15.6	104.9	85.9	159.5	11
int	13	Pr	2.443	18.5	104.3	81.0	159.4	15
int	14	La	2.587	18.8	107.9	87.5	155.4	14
int	6	Pr	2.467	28.3	111.4	79.7	174.6	9
int	11	La	2.549	44.2	123.4	71.4	169.1	14
int	14	Nd	2.411	45.1	124.8	73.1	170.0	14
int	15	Er	2.292	58.2	136.0	70.3	157.9	16
int	7	Ho	2.306	53.5	128.6	68.4	164.6	9
int	16	Eu	2.391	63.1	140.3	62.5	152.6	17
int	17	Dy	2.260	66.3	138.8	60.8	163.3	18
	GL	La	2.563	11.6	102.6	89.7	150.3	
	GC	Ce	2.538	13.5	103.9	88.5	151.2	
	GP	Pr	2.515	15.0	105.2	88.2	151.2	
	GN	Nd	2.497	16.9	106.2	86.8	152.4	
	GS	Sm	2.438	26.1	111.9	82.3	156.3	

a) ch: chelate, tri: tridentate-type bridge, *E,E*, *E,Z*, and *Z,Z*: each type of bridge, int: intermediate of tri- and *Z,Z*-type bridges. b) The complexes including the respective ligands. 1,$[Gd_2(CH_3CO_2)_6(H_2O)_4]\cdot 4H_2O$; 2, $[Ho_2(CH_3CO_2)_6(H_2O)_4]\cdot 4H_2O$; 3, $[Er_2(CH_3CO_2)_6(H_2O)_4]\cdot 4H_2O$; 4, $[Ho(HCO_2)_3(H_2O)_2]_n$; 5, $[Er(HCO_2)_3(H_2O)_2]_n$; 6, $[Pr(CF_3CO_2)_3(H_2O)_3]_n$; 7, $[Ho(HL)_3(H_2O)_2]_n[Cr(NCS)_6]_n\cdot 2H_2O$ (HL=nicotic acid); 8, $[SmL_6(H_2O)_4]$; 9, $[Ce(CH_3CO_2)_3(H_2O)]_n$; 10, $[CeL'_3(H_2O)]_n$ (HL'=*m*-hydroxybenzoic acid); 11, $[LaL'_3(H_2O)_2]_n(HL')_n\cdot 2nH_2O$; 12, $[La_2L_6(H_2O)_4]$; 13, $[Pr_2L_6(H_2O)_4]$; 14, $[NdL'_3(H_2O)_2]_n(HL')_n\cdot 2nH_2O$; 15, $[ErL''_3(H_2O)_2]_n$(HL''=isonicotic acid); 16, $[EuL''_2(H_2O)_4]_n(NO_3)_n$; 17, $[Dy_2L'''_6(H_2O)_4]$ (HL'''=*p*-aminobenzoic acid); 18, $[Ca(CH_3CO_2)_2(H_2O)]_n$; GL—GS, $[(NH_2)_3C]_2[M_2(CH_3CO_2)_8(H_2O)_2]$, where M of GL=La, GC=Ce, GP=Pr, GN=Nd, and GS=Sm. c) Average of the bond lengths of M-O(2) and M'-O(1). d) Each value (*d*)was obtained from the respective interatomic distance, l_1, l_2 or l_3, by means of the following equations: $d=\{(l_3-l_m)/l_m\}\times 100$ and $l_m=(l_1+l_2)/2$, where l_1=M-O(2), l=M'-O(1), and l_3=M-O(1). e) References. f) Although the structural data of this complex has already been reported by Porai-Koshits.[7] These data are new ones obtained by the present authors.[28]

ylates. The numbering scheme of the atoms used in the table as well as in its explanation presented below is shown in Fig. 1.

Typical examples of some bond lengths and bond angles of the four membered chelate ring of the lanthanoid carboxylates are shown in Table 4 as the "ch" group. In many cases, the two M-O-C bond angles are not the same; they are about 90 and 95° respectively, where the M-O, which is about 3% longer than the other one, has the larger M-O-C angle. Usually the planarity of the chelate ring is good, although there are some exceptions.

As shown in Table 4, the bridging ligands in lanthanoid formates (Complexes 4 and 5 in Table 4) have forms a little different from those of the other carboxylates. A special *Z,E*-type bridge is found in them, where the M-O(2)-C(1) (*Z*-side) and M'-O(1)-C(1) (*E*-side) bond angles are about 140 and 145° respectively, and where both the M and M' atoms are almost on the carboxyl COO plane. The interatomic distance, M···O(1), from the *Z*-side metal to the *E*-side oxygen atom is about 3.8 Å, about 63% longer than the average of M-O(2) and M'-O(1), while the M···M' distance is about 6.0 Å. Typical *E,E*-type bridges are found in the same formates. They are about symmetric, and the M-O(2)-C(1) and M'-O(2)-C(1) bond

angles as well as the interatomic distances, M···O(1) and M′···O(2), are about the same; 129—132° and 4.51—4.53 Å respectively. The M···M′ distance is about 6.7 Å.

Typical examples of *Z,Z*-type bridge are shown as the *Z,Z* group in Table 4. As is shown in the table, this type of bridging is about symmetric in terms of bond lengths and bond angles: M–O(2) and M′–O(1); M···O(1) and M′···O(2); M–O(2)–C(1) and M′–O(1)–C(1), and M–O(1)–C(1) and M′–O(2)–C(1) are almost the same. However, in their real forms, M and M′ atoms are not strictly on the C(1), O(1), O(2) plane. The M···M′ distance is about 4.2···4.5 Å. As the M···O(1) distance is about 62% longer than the average of M–O(2) and M′–O(1), an effective bonding between them is not probable.

An idealized figure of the tridentate-type bridge, deduced from those of calcium acetate[22] and others, is shown in Fig. 1b; the ligand forms a chelate around the M atom, while another metal atom, M′, approaches the O(1) atom from the direction of the extension of O(2)···O(1); the M–O(2) and M′–O(1) bond lengths, as well as that of M–O(1) are not very different from each other; both of the metal atoms are almost on the carboxyl C(1), O(1), O(2) plane, and the expected C(1)–O(1)–M′ angle is about 150° (*E*-side). However, in many of the "tri"-type ligands shown in Table 4, M–O(2)–C(1) and M–O(1)–C(1) are each about 93—99°, the former commonly larger than the latter. The M–O(1) bond length is longer than M–O(2) or M′–O(1) by several per cent, the latter two being approximately the same, although M′–O(2) is much longer (more than 4 Å).

In the cases of more deformed tridentate-type bridges, they are classified separately in Table 4 as the "int"-group. They range from the one resembling a tridentate bridge to the one having almost the structure of the *Z,Z*-type bridge. In the "tri"-type bridge, the M′ atom is on the *E*-side, and in the *Z,Z*-type one, on the *Z*-side, although the C(1)–O(1)–M′ angle is about the same in both cases (140—150°). In the series of "int"-group members, the angle seems not to change in definite way, for the shift of the M′-atom position from the C(1), O(1), O(2) plane is irregular in them. On the other hand, the elongation of the M–O(1) length compared with the mean of the M–O(2) and M′–O(1) lengths increasing from 15 to 66%, the C(1)–O(2)–M bond angle increasing from 110 to 140°, and the C(1)–O(1)–M bond angle decreasing from 86 to 60°, they change in about the same order, while the position of the M′ atom moves from the *E* side to *Z* side, at least at the early stage of the series; their values of the typical tridentate- and the *Z,Z*-type bridges are 0 and 63%, 97 and 140°, and 92 and 60° respectively. Of course, there are some irregularities in some examples, especially when the positional deviations of the M and M′ atoms from the carboxyl C(1), O(1), O(2) plane are large. In the cases of the last four members of the "int"-group series, the elongation of the M–O(1) length is very large, almost the same as that of the *Z,Z*-type bridges, and no interaction between them can be expected; however, its symmetry in shape is not so good as in the *Z,Z*-type bridges.

The corresponding data from the ligands in the titled complexes are shown in the GL—GS column in Table 4. The bond lengths and bond angles of these complexes resemble those of the "int"-group ones. The deviations of their bond lengths and bond angles from the typical tridentate-type bridge are in the order of the increase on the atomic number of the central metal. Therefore, the bridge in the lanthanum complex has the most resemblance, and that of the samarium, the least similarity, to the tridentate bridge. However, even in the samarium complex, the elongation percentage of M–O(1) is about 26%, and the M–O(2)–C(1) and M–O(1)–C(1) angles are 111.9 and 82.3° respectively; these values correspond with those of some early members in the "int"-group series shown in the table. Therefore, the M–O(1) bonding of the titled complexes is expected to be effective, although such bond may be weaker than those of the typical tridentate ones and the bonds are weakened in the order of the atomic number of the central metal. As the geometrical environments of the bridge, except for the size of the central metal atom, are about the same in all these isomorphous complexes, this change in the M–O(1) length can be expected to be concerned mainly with the contraction of the central-metal atomic radius.

Although this is only one example, the authors have recognized that, in a series of lanthanoid complexes where the coordination number of the central metal atom is large, the weakest bonding is continuously weakened depending on the decrease in the coordination sphere; this fact can also be expressed by saying that the coordination number of the central metal atom of such complexes decreases continuously depending on the increase in the atomic number of the central metal.

The authors wish to thank The Shin-Etsu Chemical Co., Ltd., for aiding this study by presenting us with the highly pure lanthanoid oxides. The helpful discussions about this research with Mr. Kiyofumi Nagai and Miss Reiko Nakamura are also gratefully acknowledged. The present work was partially supported by a Grant-in-Aid for Scientific Research (No. 57430011) from the Ministry of Education, Science and Culture.

References

1) A. A. Pinkerton and D. Schwarzenbach, *J. Chem. Soc., Dalton Trans.*, **1976**, 2466.
2) T. Moeller, "The Lanthanides" in "Comprehensive Inorganic Chemistry," ed by J. C. Bailar, Jr., *et al.*, Pergamon Press, New York (1973), Vol. 4, p. 94.
3) S. Kondo, M. Shimoi, A. Ouchi, and T. Takeuchi, *Bull. Chem. Soc. Jpn.*, **55**, 2840 (1982).
4) J. Catterick and P. Thornton, "Advances in Inorganic Chemistry and Radiochemistry," Acad. Press., New York (1977), Vol. 20, p. 291.
5) M. C. Favas, D. L. Kepert, B. W. Skelton, and H. White, *J. Chem. Soc., Dalton Trans.*, **1980**, 454.
6) J. W. Bats, R. Kalus, and H. Fuess, *Acta Crystallogr., Sect. B*, **35**, 1225 (1979).
7) L. A. Aslanov, I. K. Abdul'minev, M. A. Porai-Koshits, and V. I. Ivanov, *Dokl. Akad. Nauk. SSSR*, **205**, 343 (1972).
8) H. R. Wenk, *Z. Krystallogr.*, **154**, 137 (1981).

9) S. P. Bone, D. B. Sowerby, and R. D. Verma, *J. Chem. Soc., Dalton Trans.*, **1978**, 1544.
10) J. Kay, J. W. Moore, and M. D. Glick, *Inorg. Chem.*, **11**, 2818 (1972).
11) J. W. Moore, M. D. Glick, and W. A. Baker, Jr., *J. Am. Chem. Soc.*, **94**, 1858 (1972).
12) G. Sadikov, G. A. Kukina, and M. A. Porai-Koshits, *Zh. Strukt. Khim.*, **8**, 551 (1967).
13) Y. Koizumi, H. Sawase, Y. Suzuki, M. Shimoi, and A. Ouchi, *Bull. Chem. Soc. Jpn.*,**57**, 1677 (1984).
14) Y. Koizumi, H. Sawase, Y. Suzuki, T. Takeuchi, M. Shimoi, and A. Ouchi, *Bull. Chem. Soc. Jpn.*, **57**, 1809 (1984).
15) L. A. Aslanov, I. K. Abdul'minev, and M. A. Porai-Koshits, *Zh. Strukt. Khim.*, **13**, 468 (1972).
16) I. K. Abdul'minev, L. A. Aslanov, M. A. Porai-Koshits, and R. A. Chupakhina, *Zh. Strukt. Khim.*, **14**, 383 (1973).
17) L. A. Aslanov, I. D. Kiekbaev, I. K. Abdul'minev, and M. A. Porai-Koshits, *Kristallographia*, **19**, 170 (1974).
18) M. S. Khiyalov, I. R. Amiraslanov, Kh. S. Mamedov, and E. M. Novsumov, *Koord. Khim.*, **7**, 445 (1981).
19) F. F. Bertant, T. Q. Duc, P. Burlet, P. Burlet, M. Thomas, and J. M. Moreau, *Acta Crystallogr., Sect B*, **30**, 2234 (1974).
20) M. Bukowska-Strzyzewska, *Acta Crystallogr.*, **19**, 357 (1965).
21) G. A. Barclay and C. H. L. Kennard, *J. Chem. Soc.*, **1961**, 3289.
22) E. A. Klop, A. Schouten, P. van der Sluis, and A. L. Spek, *Acta Crystallogr., Sect. C*, **40**, 51 (1984).
23) G. G. Sadikov, G. A. Kukina, and M. A. Porai-Koshits, *Zh. Strukt. Khim.*, **12**, 859 (1971).
24) C. Canneri, *Gazz. Chim. Ital.*, **55**, 33, 36 (1925).
25) $R=\sum||F_o|-|F_c||/\sum|F_o|$
26) "The Universal Crystallographic Computation Program System (UNICS)," ed by T. Sakurai, Crystallographic Society of Japan, Tokyo (1967).
27) "International Tables for X-Ray Crystallography," Kynoch Press, Birmingham (1974), Vols. III and IV.
28) The final thermal parameters and the final F_o-F_c tables of the titled complexes and of $[Er_2(CH_3CO_2)_6(H_2O)_4]\cdot 4H_2O$, the perspective drawing, the crystallographic data, and the final coordinates of the Er(III) complex are deposited as Document No. 8437 at the office of the Editor of the *Bull. Chem. Soc. Jpn.*

Ion Exchange from a Nonaqueous Solution. Zinc (II) Bromide and Iodide in Ethylene Glycol

Tetsu KUMAGAI
Himeji Institute of Technology, Shosha, Himeji, Hyogo 671-22
(Received March 14, 1984)

The distribution behavior of the zinc ion in sodium bromide and iodide solutions between the cation-exchange resin for forced-flow liquid chromatography and the absolute or aqueous ethylene-glycol phase was investigated radiometrically. From the experimental data, consecutive complex formation constants for zinc bromide and iodide in the glycol have been calculated by the nonlinear least-squares method. The results are as follows: in absolute glycol $\beta_1^{Br}=2.60$ and $\beta_2^{Br}=3.91$ for zinc bromide, $\beta_1^{I}=2.36$ and $\beta_2^{I}=3.04$ for zinc iodide; in 5 wt% aqueous glycol $\beta_1^{Br}=2.30$, $\beta_2^{Br}=3.32$, and in 10 wt% aqueous glycol, $\beta_1^{Br}=1.87$, $\beta_2^{Br}=2.78$, respectively.

There have been many investigations of the complex formation of metal ions in a pure or aqueous organic solvent, especially using such electrochemical methods as the emf, electric conductivity, and ion-selective electrode techniques. However only a little work seems to have been done on complex formation in a nonaqueous solution using a distribution method between the two phases, for example, the solvent-extraction and ion-exchange techniques. Previously, the solvent-extraction method between the polar organic and nonpolar organic phases has been studied in order to gain knowledge that the metal-ion equilibrium in a nonaqueous system.[1-6] However there are not many polar solvents immiscible with the nonpolar solvents. In contrast to the solvent extraction, the ion-exchange method seems to be hopeful because some of the exchange resins for the forced-flow liquid chromatography can resist many of the organic solvents and so the distribution equilibrium can be easily reached between the resin and the metal ions.

In previous papers,[7,8] the present author and his co-workers have reported data on the formation constants of zinc chloride in pure and aqueous ethylene glycol, and in aqueous methanol, obtained using the ion-exchange method. The aim of the present work is to extend our research to bromide and iodide complexes of zinc in pure and aqueous ethylene glycol using the ion-exchange method.

Experimental

Materials and Apparatus. Zinc-65 was supplied as the chloride in hydrochloric acid by New England Nuclear, Boston, Mass., U. S. A. The radioactive tracer was converted into perchlorate by the addition of perchloric acid, followed by repeated evaporation. It was dissolved with ethylene glycol. Reagent-grade ethylene glycol was dried on zeolite and distilled under reduced pressure.

The cation-exchange resin, Hitachi custom ion-exchange resin 2611, for the liquid chromatograph was washed with 1 mol dm^{-3} hydrochloric acid and converted into the Na^+ form by the use of a 0.2 mol dm^{-3} sodium-chloride solution. After having been washed with pure water and dried in a vacuum, the resin was stored over phosphorus pentaoxide in a desiccator. The stock zinc solution was prepared by dissolving dry zinc oxide with perchloric acid, evaporating to near dryness, and diluting it with ethylene glycol.

The procedure of ion-exchange was essentially the same as that described in a previous paper.[8] Sixteen milliliters of an ethylene-glycol solution of sodium halide containing sodium perchlorate, zinc perchlorate (1×10^{-6} mol dm^{-3}) with radioactivities, and perchloric acid (1×10^{-5} mol dm^{-3}) were stirred together with portions (10—50 mg) of the dry resin, in a 30-cm^3 centrifugal tube equipped with a grass stopper by using a magnetic stirrer for 12 h in a thermostat at 25°C. After the equilibrium had been attained, the solution and the resin phase were separated by centrifugation. Two milliliters of the solution phase were pipetted out, and the γ-activities were counted with a well-type scintillation counter, Metro Electronics Model PBW-6.

Results and Discussion

The distribution of zinc in present system was practically independent of the range of zinc perchlorate (5×10^{-7}—1×10^{-4} mol dm^{-3}). Therefore in subsequent studies, 1×10^{-6} mol dm^{-3} of zinc perchlorate in an ethylene-glycol solution was used.

Even stirring for 30 min was found to be enough for the attainment of the distribution equilibrium. In the present studies, however stirring for 12 h was adopted, because ethylene glycol has a somewhat high viscosity and the resin was a little difficult to disperse in the glycolic solution. The influence of the cation-exchange resin on the distribution of zinc was examined with regard to resin amounts of 1.25, 2.5, and 5.0 g dm^{-3}, while keeping the other variables constant. As is to be expected from Eq. 10, a linear relationship between log D^* and the resin amount was observed, with a slope of about 1, in various bromide concentrations (Fig. 1).

The equilibria in the ethylene glycol phase are expressed as follows:

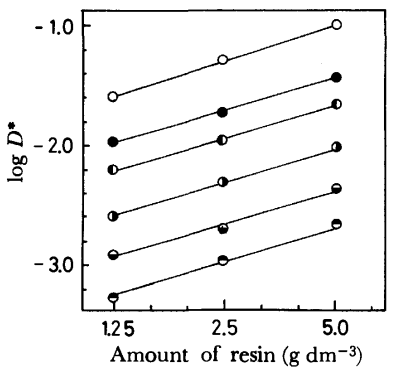

Fig. 1. Influence of resin amount in sodium bromide system (pure ethylene glycol).
Concentration of sodium bromide; ○: 0.03 mol dm^{-3}, ●: 0.05 mol dm^{-3}, ◐: 0.07 mol dm^{-3}, ◑: 0.10 mol dm^{-3}, ◒: 0.15 mol dm^{-3}, ◓: 0.20 mol dm^{-3},

$$Zn^{2+} + 2X^- = ZnX_2 \quad (\beta_n^X), \quad (1)$$

$$Zn^{2+} + 2Y^- = ZnY_2 \quad (\beta_n^Y), \quad (2)$$

$$ZnX^+ + Y^- = ZnXY \quad (K_m^Y), \quad (3)$$

$$ZnY^+ + X^- = ZnXY \quad (K_m^X), \quad (4)$$

$$Zn^{2+} + Na_2R = ZnR + 2Na^+ \quad (\beta_n^R), \quad (5)$$

$$ZnX^+ + Na_2R = ZnXNaR + Na^+ \quad (K_m^{RX}), \quad (6)$$

$$ZnY^+ + Na_2R = ZnYNaR + Na^+ \quad (K_m^{RY}). \quad (7)$$

Here, X^- denotes the halide ion, Y^- shows ClO_4^-, and R stands for the two functional groups in the resin.

The total concentration of zinc in the resin phase, $(C_{Zn})_R$, is defined as follows:

$$(C_{Zn})_R = m_{ZnR} + m_{ZnXNaR} + m_{ZnYNaR}. \quad (8)$$

Here m stands for the weight molarity.

The total zinc concentration in the glycol phase at equilibrium, $(C_{Zn})_E$, is given by:

$$(C_{Zn})_E = C_{Zn} + C_{ZnX} + C_{ZnX_2} + C_{ZnY} + C_{ZnY_2} + C_{ZnXY}$$
$$= (m_{Zn} + m_{ZnX} + m_{ZnX_2} + m_{ZnY} + m_{ZnY_2} + m_{ZnXY})/\rho. \quad (9)$$

Here ρ is the density of the glycolic solution.

The distribution coefficient, D, is defined as:

$$D = (C_{Zn})_R/(C_{Zn})_E. \quad (10)$$

Equations 8—10 are rewritten using Eqs. 1—7 as follows:

$$(C_{Zn})_R = \left(\frac{\gamma_{Zn}\cdot\gamma_{Na_2R}\cdot m_{Zn}}{\gamma_{ZnR}\cdot\gamma_{Na}^2\cdot m_{Na}^2}\cdot\beta_2^R + \frac{\gamma_{Zn}\cdot\gamma_X\cdot\gamma_{Na_2R}\cdot m_{Zn}\cdot m_X}{\gamma_{Na}\cdot\gamma_{ZnXNaR}\cdot m_{Na}}\cdot K_m^{RX}\cdot\beta_1^X + \frac{\gamma_{Zn}\cdot\gamma_Y\cdot\gamma_{Na_2R}\cdot m_{Zn}\cdot m_Y}{\gamma_{Na}\cdot\gamma_{ZnYNaR}\cdot m_{Na}}\cdot K_m^{RY}\cdot\beta_1^Y\right)\cdot m_{Na_2R}, \quad (8')$$

$$(C_{Zn})_R = \left(\gamma_{Zn}\cdot m_{Zn} + \frac{\gamma_{Zn}\cdot\gamma_X\cdot m_{Zn}\cdot m_X}{\gamma_{ZnX}}\cdot\beta_1^X + \frac{\gamma_{Zn}\cdot\gamma_X\cdot m_{Zn}^2\cdot m_X^2}{\gamma_{ZnX_2}}\cdot\beta_2^X + \frac{\gamma_{Zn}\cdot\gamma_Y\cdot m_{Zn}\cdot m_Y}{\gamma_{ZnY}}\cdot\beta_1^Y + \frac{\gamma_{Zn}\cdot\gamma_Y^2\cdot m_{Zn}\cdot m_Y^2}{\gamma_{ZnY_2}}\cdot\beta_2^Y + \frac{\gamma_{Zn}\cdot\gamma_X\cdot\gamma_Y\cdot m_{Zn}\cdot m_X\cdot m_Y}{\gamma_{ZnXY}}\cdot\beta_1^X\cdot K_m^Y\right)\Big/\rho, \quad (9')$$

$$D = m_{Na_2R}\cdot\rho\cdot\left(\frac{\beta_2^R}{\gamma_{Na}^2\cdot m_{Na}^2} + \frac{\gamma_X\cdot m_X}{\gamma_{Na}\cdot m_{Na}}\cdot K_m^{RX}\cdot\beta_1^X + \frac{\gamma_Y\cdot m_Y}{\gamma_{Na}\cdot m_{Na}}\cdot K_m^{RY}\cdot\beta_1^Y\right)\Big/(1 + \sum\gamma_X^n\cdot m_X^n\cdot\beta_n^X/\gamma_{ZnX_n} + \sum\gamma_Y^n\cdot m_Y^n\cdot\beta_n^Y/\gamma_{ZnY_n} + \gamma_X\cdot\gamma_Y\cdot m_X\cdot m_Y\cdot\beta_1^X\cdot K_m^Y/\gamma_{ZnXY}). \quad (10')$$

Here, γ stands for the activity coefficient of each ion, γ_{Na_2R}, γ_{ZnR}, γ_{ZnXR}, and γ_{ZnYR} can be regarded as 1, and $\gamma_{ZnX}=\gamma_{ZnY}$, $\gamma_{ZnX_2}=\gamma_{ZnY_2}=\gamma_{ZnXY}$. γ_X, γ_Y, γ_{Zn}, and γ_{Na} are calculated, on the basis of Debye-Hückel's theory, as;

$$\ln\gamma_X = \ln\gamma_\pm^{1/2} = -\left(\frac{A|Z^+Z^-|I^{1/2}}{1+BdI^{1/2}}\right)^{1/2}, \quad (11)$$

$$A = 8.1622\times\frac{\rho}{\varepsilon^{3/2}}\times10^2 \quad B = 2.9127\times\left(\frac{\rho}{\varepsilon}\right) \text{ at } 25\,^\circ\text{C}. \quad (12)$$

Here, d denotes the parameter of the ionic radius (Å unit), I represents the ionic strength; m_{Na_2R} is expressed as g resin (Na-form)/dm^3 ethylene glycol, and ε is the dielectric constant of ethylene glycol. The dielectric constant of 5% aqueous ethylene glycol was obtained by the interpolation of the constants of 100, 90, and 80% ethylene glycol.[9] In the Zn^{2+}–X–Y system, the sum of m_X and m_Y was kept constant, and sodium halide and sodium perchlorate are assumed to dissociate perfectly into ions in the glycolic solution. Therefore, the $m_{Na}=m_X+m_Y$ holds good. Hence, Eq. 10′ can be transformed as a function of the halide-ion weigth molarity, m_X. As it is assumed that β_2^R is much greater than β_1^R, β_1^R can be disregarded.

In the zinc halide system, Eq. 10′ can be converted into the following fractional functions:

$$D^* = \frac{P_{(1)}+P_{(2)}L^2}{1+P_{(3)}L+P_{(4)}L^2}. \quad (13)$$

Here, $L=\gamma_X\cdot m_X$, $D^*=D\cdot\gamma_{Na}^2\cdot m_{Na}^2/\rho$, $P_{(1)}=\beta_2^R\cdot m_{Na_2R}$, $P_{(2)}=\beta_1^X\cdot K_m^{RX}\cdot m_{Na_2R}$, $P_{(3)}=\beta_1^X/\gamma_{ZnX}$ and $P_{(4)}=\beta_2^R$.

In the zinc halide perchlorate system, Eq. 10′ can be reduced to:

$$D^* = \frac{(P_{(1)}+P_{(2)}m_X+P_{(3)}m_Y)}{1+P_{(4)}m_X+P_{(5)}m_X^2+P_{(6)}m_Y+P_{(7)}m_Y^2+P_{(8)}m_X\cdot m_Y}. \quad (14)$$

Here $D^*=D\cdot\gamma_{Na}^2\cdot m_{Na}^2/\rho$, $P_{(1)}=m_{Na_2R}\cdot\beta_2^R$, $P_{(2)}=m_{Na_2R}\cdot\beta_1^X\cdot K_m^{RY}\cdot\gamma_X\cdot\gamma_{Na}\cdot m_X\cdot m_{Na}$, $P_{(3)}=m_{Na_2R}\cdot\beta_1^Y\cdot K_m^{RY}\cdot\gamma_{Na}\cdot\gamma_Y\cdot m_{Na}\cdot m_Y$, $P_{(4)}=\gamma_X\cdot\beta_1^X/\gamma_{ZnX}$, $P_{(5)}=\gamma_X^2\cdot\beta_2^X$, $P_{(6)}=\gamma_Y\cdot\beta_1^Y/\gamma_{ZnY}$, $P_{(7)}=\gamma_Y^2\cdot\beta_2^Y$, and $P_{(8)}=\gamma_X\cdot\gamma_Y\cdot m_X\cdot m_Y\cdot\beta_1^X\cdot K_m^Y$.

Each activity coefficient, γ, was calculated from Eqs. 11 and 12 as a function of the ionic strength. These coefficients have a constant ionic strength.

To obtain the parameters, $P_{(i)}$, of Eqs. 13 and 14, we used the computer program of the nonlinear least-squares method, a modified Gauss-Newton method; the valuses obtained by this procedure were then tested by the aid of the curve-fitting method using computer graphics.

The dependence of log D^* on the bromide activity calculated using Eq. 11 in pure and aqueous ethylene glycol is shown in Figs. 2—4. The figures show that the distribution of zinc decreases precipitiously in the lower activity range of bromide and gradually in the higher range. The stability constants obtained by using the program described above are listed in Table 1.

Figure 5 indicates the dependence of the zinc distribution on the iodide activity in pure ethylene glycol in 1.25, 2.5, and 3.75 g resin per 1 dm^3 glycol. Though the zinc distribution decreases abruptly with the increase in the iodide activity, much as in the case of the bromide system, the magnitude of the decrease in the iodide system is somewhat less than that in the bromide one. This means that zinc-iodide complexes are less stable than the corresponding bromide complexes. This results are listed in Table 1. The blending of water for pure ethylene glycol leads to considerably large errors in the calculations of the stability constants of zinc iodide because of a lowering of the stability.

The variation in the zinc distribution in the presence of both bromide and perchlorate ions was examined in order to make the ionic strength in the glycol solution constant. The distribution coefficient of zinc is plotted

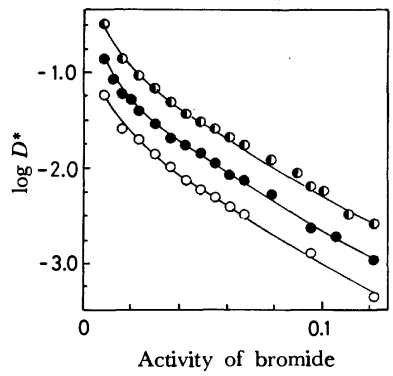

Fig. 2. Distribution coefficients of zinc bromide system in the pure glycolic solution.
amount of resin; O: 1.25 g dm^{-3}, ●: 2.50 g dm^{-3}, ◐: 5.00 g dm^{-3}.

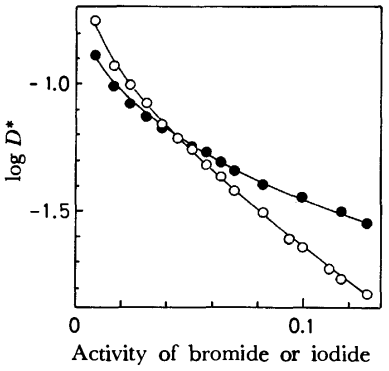

Fig. 3. Distribution of zinc bromide and zinc iodide system in the 5% aqueous glycolic solution.
O: NaBr, resin 1.36 g dm^{-3}, ●: NaI, resin 0.91 g dm^{-3}.

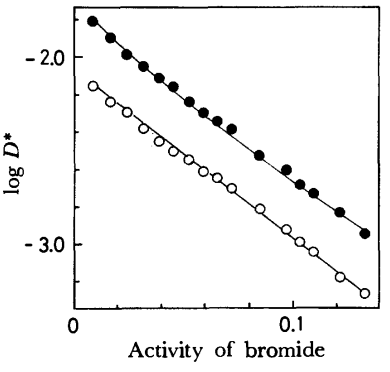

Fig. 4. Distribution coefficients of zinc bromide in the 10% aqueous ethylene glycol.
amount of resin; O: 1.0 g dm^{-3}, ●: 2.0 g dm^{-3}.

in Fig. 6 as a function of the concentration of bromide and perchlorate ions. As there exist 8 parameters in Eq. 14 in the present system, it is very difficult to obtain exact values. Only the value of K_m can be calculated; it is listed in Table 1. Similally, in the zinc iodide-perchlorate system, exact results were not obtained.

The decreasing order of stability of zinc halide complexes in ethylene glycol is as follows; Cl>Br>I≃ ClO_4. Also the stability constants in ethylene glycol are somewhat smaller than those in methanol.

References

1) M. Matsui, T. Aoki, O. Inoue, and T. Shigematsu, *Bull. Inst. Chem. Res. Kyoto Univ.*, **52**, 652 (1974).
2) M. Matsui, T. Aoki, H. Enomoto, and T. Shigematsu, *Anal. Lett.*, **8** (4), 247 (1975).
3) M. Matsui, H. Doe, T. Hirade, and T. Shigematsu, *Anal. Lett.*, **12** (A13), 1385 (1979).
4) H. Doe, M. Matsui, and T. Shigematsu, *Bull. Inst. Chem. Res. Kyoto Univ.*, **57**, 343 (1979).
5) H. Doe, M. Matsui, and T. Shigematsu, *Bull. Inst. Chem. Res. Kyoto Univ.*, **58**, 133 (1980).
6) T. Aoki, *Bull. Inst. Chem. Res. Kyoto Univ.*, **59**, 191 (1981).
7) S. Iwasaki, M. Sugiyama, M. Matsui, and T. Kumagai, *Bull. Inst. Chem. Res. Kyoto Univ.*, **61**, 340 (1983).
8) T. Kumagai, *Bull. Chem. Soc. Jpn.*, **57**, 1348 (1984).
9) T. F. Humbel and J. P. Scherrer, *Helv. Phys. Acta*, **26**, 17 (1953).

TABLE 1. STABILITY CONSTANTS OF ZINC BROMIDE AND ZINC IODIDE

log β	β_1^X	β_2^X	K_m^X
X=Br, pure E.G.	2.60±0.06	3.91±0.06	—
X=Br, 5% aqueous E.G.	2.30±0.06	3.32±0.06	—
X=Br, 10% aqueous E.G.	1.87±0.07	2.78±0.07	—
X=I, pure E.G.	2.36±0.06	3.04±0.06	—
Ionic strength 0.1, 0.2	—	—	0.3±0.1

E.G.=Ethylene glycol.

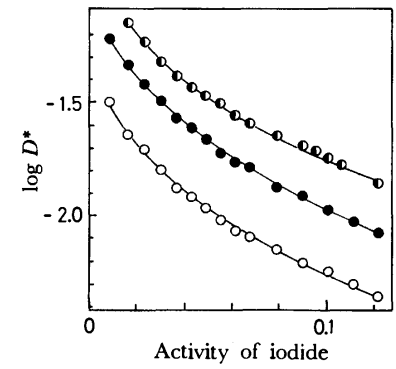

Fig. 5. Distribution coefficients variation *vs.* activity of iodide in the pure glycolic solution.
amount of resin; O: 1.25 g dm^{-3}, ●: 2.50 g dm^{-3}, ◐: 3.75 g dm^{-3}.

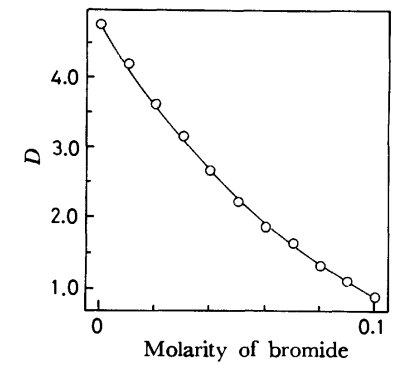

Fig. 6. Distribution coefficients variation *vs.* molarity of sodium bromide in the pure ethylene glycol at constant ionic strength (0.1).
Amount of resin 2.50 g dm^{-3}, (NaBr)+($NaClO_4$)=0.1.

 © 1984 The Chemical Society of Japan Bull. Chem. Soc. Jpn., 57, 2741—2747 (1984)

Preparation of Ni- or Pt-Containing Cyclic Esters by Oxidative Addition of Cyclic Carboxylic Anhydrides and Their Properties

Kenji SANO, Takakazu YAMAMOTO,* and Akio YAMAMOTO

Research Laboratory of Resources Utilization, Tokyo Institute of Technology, 4259 Nagatsuta, Midori-ku, Yokohama 227

(Received March 21, 1984)

Metal containing cyclic ester complexes, $L\overline{NiCHR^1CHR^2COO}$ (L=1,2-bis(diphenylphosphino)ethane (dpe) or 2,2′-bipyridine (bpy); R^1, R^2=H or CH_3) and $L_n\overline{PtCOCH_2CH_2COO}$ (L=tricyclohexylphosphine (PCy_3) or dpe; n=1 or 2), have been prepared by oxidative addition of cyclic carboxylic anhydrides to zero-valent metal complexes. These complexes have been characterized by elemental analysis and spectroscopies (IR as well as ^{1}H-, ^{13}C{^{1}H}-, and ^{31}P{^{1}H}-NMR) and chemical reactivities. Rate of the oxidative addition of succinic anhydride to Ni(bpy)(cod) (cod=1,5-cyclooctadiene) is expressed by a second order rate equation, $R=k$[Ni(bpy)(cod)][succinic anhydride], and temperature dependence of k gives the activation energy of 68 kJ mol^{-1}. The reaction of methylsuccinic anhydride with $Ni(cod)_2$ in the presence of tertiary phosphine or bpy affords two isomers, $L_n\overline{NiCH_2CH(CH_3)COO}$ and $L_n\overline{NiCH(CH_3)CH_2COO}$, corresponding to two modes of C–O bond cleavage in methylsuccinic anhydride promoted by Ni; dependence of the ratio between the two isomers on the kind of ligand added and reaction conditions has been examined.

Metallacycles are regarded as key intermediates in numerous metal-catalyzed reactions.[1] Especially, much attention has been paid to the role of the metallacycles in metathesis[2] and cycloaddition[3] of olefins and isolation of several metallacycles consisting of transition metal and hydrocarbons has been reported. However, there have been only few reports concerning with the metallacycles containing functional groups, which have potential value in synthetic chemistry. Our research group has reported preparation of metal-containing cyclic amide and ester type complexes by the reaction of zero-valent metal complexes with unsaturated amides and acids.[4,5a]

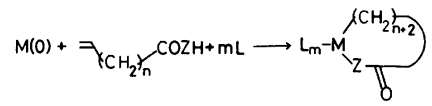

(1)

n=1,0 M=Ni, Pd; Z=NH, O
m=1, 2

Other research groups also, independently from our work described above, reported preparation of similar metallacycles through two different synthetic routes: (i) Cycloaddition of olefin or acetylene with carbon dioxide or isocyanate (Eq. 2)[6] and (ii) oxidative addition of cyclic carboxylic anhydrides.[7]

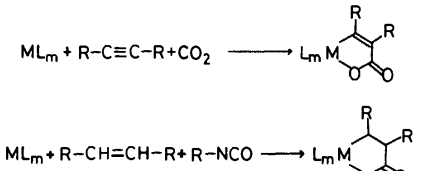

(2a)

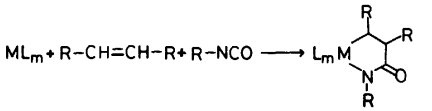

(2b)

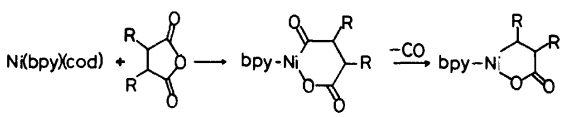

(3)

bpy: 2,2′-bipyridine, cod: 1,5-cyclooctadiene

However, as for the latter preparative method (Eq. 3) characterization of the complexes obtained is based only on their rough elemental analysis and IR spectra, and more unequivocal characterization of the complexes by other instrumental analysis and chemical reactivities is required.

In order to develop the chemistry of the transition metal-containing cyclic ester type complexes and to establish the mechanism of the oxidative addition of cyclic carboxylic anhydrides to transition metal complexes, we have expanded this oxidative addition reaction by using other transition metal complexes as well as other cyclic carboxylic anhydrides and characterized the isolated complexes by elemental analysis, spectroscopy (IR and NMR), and chemical reactivities. Upon confirmation of the structures of these complexes, we examined kinetics of oxidative addition of cyclic carboxylic anhydrides to the Ni(0) complexes.

Oxidative addition of acyclic carboxylic anhydrides to Ni(0) and Pd(0) complexes has been already reported from our research group,[5c] and some of the data described in this paper have been reported in communication form.[5b]

Results and Discussion

Oxidative Addition of Cyclic Carboxylic Anhydride to Zero-valent Nickel Complexes. Succinic Anhydride: The reaction of Ni(0) with succinic anhydride in the presence of appropriate ligands such as bpy and PCy_3 gives five membered nickel-containing cyclic esters, **2**.

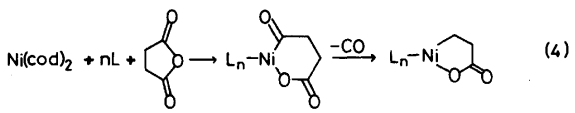

(4)

1 **2**

1a: bpy 2a: bpy

1b: PR_3 2b: PR_3

Complex **2** is considered to be formed through oxidative addition of succinic anhydride to Ni giving six-membered 2-oxo-nickel-containing cyclic ester **1** first followed by its decarbonylation. Carbon monoxide thus released is trapped by Ni(0) complexes to afford $Ni(CO)_2L_n$, (see Experimental); therefore stoichiometry of the formation of **2** seems to be expressed by the following equation,

$$3Ni(cod)_2 + (2n+n')L + \text{succinic anhydride} \longrightarrow \mathbf{2}\,\mathbf{2} + Ni(CO)_2L_{n'} \quad (5)$$

Uhlig and his coworkers reported the isolation of **1**a,[7b] however our attempts to isolate the intermediate complex **1**a have not been successful. High sensitivity to air and/or low solubility of **2** prevented its full characterization, and thus **2** has been converted into a stable and soluble dpe complex by ligand exchange reaction,

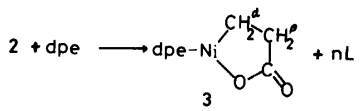

(6)

dpe : 1,2 -bis(diphenylphosphino)ethane

Use of dpe-d_4, $Ph_2PCD_2CD_2PPh_2$, affords **3**-d_4. In our previous work we observed that Ni-containing cyclic ester type complexes having dpe ligand have high stability and solubility in solvents,[4] and dpe has much higher coordinating ability than bpy and monodentate phosphine toward divalent organonickel complexes.[8] Attempts to prepare **3** directly according to Eq. 4 was not successful presumably due to formation of inert $Ni(dpe)_2$.

Table 1 summarizes the analytical data, yields, and color of **3** and related complexes. Figure 1 shows the ^{1}H-NMR spectrum of **3**. Its NMR data, together with those of other related complexes are summarized in Table 2. The coupling patterns of H^α and H^β have been analyzed by homodecouplings. Magnitudes of the

Table 1. Analytical data of Nickel and Platinum-containing cyclic esters

Complex	Analysis[a] C	H	Ni	Color	Mp θ_m/°C	Yield/%[c]
3	66.0 (65.8)	5.3 (5.3)		yellow	300(decomp.)	33
4[b]			19.5 (19.5)	red	155—180 (decomp.)	60
5	66.7 (66.2)	5.7 (5.5)		yellow	175—180 (decomp.)	43
8	65.7 (66.2)	5.9 (5.5)		yellow	260(mp) 265(decomp.)	57
9	46.3 (45.9)	6.7 (6.4)		white	170—175	34
10	56.1 (56.2)	8.2 (8.7)		white	170—175 (decomp.)	37
11	52.0 (51.9)	4.5 (4.4)		yellow	132—135 (decomp.)	45

a) Calculated value in parentheses. b) Microanalysis was not feasible due to its high sensitivity to air. c) Mol of isolated complex per mol of the starting metal complex.

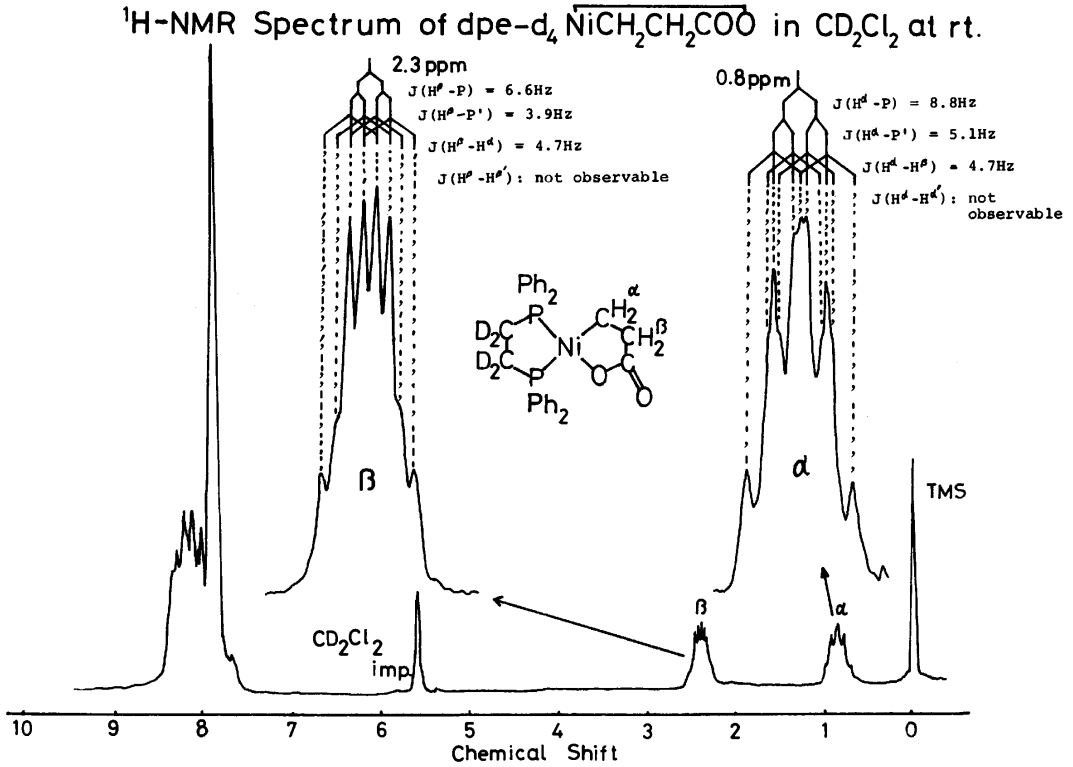

Fig. 1. ^{1}H-NMR spectrum of **3**-d_4 in CD_2Cl_2.

TABLE 2. IR AND NMR DATA OF NICKEL AND PLATINUM-CONTAINING CYCLIC ESTERS

Complex	IR[a]	^{1}H-NMR (δ)/ppm[b]		^{13}C{^{1}H}-NMR/ppm[b]	^{31}P{^{1}H}-NMR
	$\nu_{(C=O)}$/cm^{-1}	Condition			ppm[c]
3	1635 vs	d	0.8 (2H, ddt, 8.8Hz, 5.1Hz, 4.7Hz, CH_2^{α}), 2.3 (2H, ddt, 6.6Hz, 3.9Hz, 4.7Hz, CH_2^{β}), 7.5—7.9 (20H, m, Ph)	18.6 (dd, 60.1Hz, 23.5Hz, CH_2), 22.6 (dd, 29.3Hz, 11.7 Hz, CH_2 of dpe), 28.4 (dd, 30.8Hz, 22.0Hz, CH_2 of dpe, 37.9 (s, CH_2), 129—133 (m, Ph), 190.8 (d, 6.1Hz, $\underline{C}O$)	41.2(s) 64.9(s)
4	1620 vs 1360 s	d	0.8 (2H, br, CH_2^{α}), 1.3 (2H, br CH_2^{β}), 2.2 (2H, br, CH_2^{γ}), 7.8—9.0 (8H, m, bpy)		
		e	1.2 (2H, br, CH_2^{α}), 1.6 (2H, br, CH_2^{β}), 2.6 (2H, br, CH_2^{γ})		
5	1640 vs	d	0.4—0.9 (1H, m, CH_2), 1.0 (3H, d, 6.8Hz, CH_3), 2.0—2.6 (1H, m, CH_2), 2.3—2.6 (1H, br, CH), 7.2—7.6 (20H, m, Ph)	21.7 (dd, 10.3Hz, 2.9Hz, $\underline{C}H_3$), 25.1 (dd, 29.3Hz, 11.7Hz, $\underline{C}H_2$ of dpe), 29.3 (dd, 58.6Hz, 21.98 Hz, $\underline{C}H_2$), 30.0 (dd, 29.3 Hz, 20.5Hz, $\underline{C}H_2$ of dpe), 42.5 (s, $\underline{C}H$), 129—133 (m, Ph), 191.2 (s, $\underline{C}O$),	40.9 (d, 1.95Hz), 65.1 (d, 1.95Hz),
8	1640 vs	d	0.52 (3H, t, 7Hz, CH_3) 1.4 (1H, m, CH), 1.7 (1H, ddd, 16Hz, 13Hz, 6Hz, CH_2), 2.9 (1H, dd, 16Hz, 6Hz, CH_2), 7.2—7.6 (20H, m, Ph)	19.3 (d, 3.5Hz, $\underline{C}H_3$), 22.3 (dd, 27.8Hz, 4.7Hz, $\underline{C}H_2$ of dpe), 27.4 (dd, 18.7 Hz, 56.4Hz, $\underline{C}H$), 34.2 (dd, 27.6Hz, 17.3Hz, $\underline{C}H_2$ of dpe) 46.5(d, 2.3Hz, $\underline{C}H_2$), 127.6—131.2 (m, Ph), 201.0 (d, 5.0Hz, $\underline{C}O$)	63.5 (d, 9.8Hz), 42.1 (d, 9.8Hz),
9	1560 vs 1650 m				
10	1610 vs 1640 sh				
11	1630 vs	d	2.2 (2H, td, 6.1Hz, 2.4Hz, CH_2^{α}), 2.9 (2H, t, 6.1Hz, CH_2^{β}), 7.5—7.9 (20H, m, Ph)	36.0—42.7 (m, CH_2 of dpe), 46.6 (t, 8.5Hz, $\underline{C}H_2^{\alpha}$), 50.95 (d, 36.6Hz, $\underline{C}H_2^{\beta}$), 127.1—134.0 (m, Ph), 205.6 (d, 3.7Hz, $\underline{C}OO$), 204.3 (s, $\underline{C}O$)	38.3 (d, 4.4Hz, with satellites J(Pt—P)= 1430.2Hz), 43.5 (d, 4.4Hz, with satellites J(Pt—P)= 3510.9Hz)

a) Measured in KBr disk, vs=very strong, s=strong, sh=shoulder, b) From internal TMS, s=singlet, d=doublet, t=triplet, m=multiplet, br=broad. c) From external PPh_3 (downfield positive). d) In CD_2Cl_2 at room temperature. e) In pyridine-d_5 at room temperature.

coupling constants between protons as well as proton and ^{31}P are reasonable for the metallacyclic structure shown above. Figure 1 shows magnetic equivalence of the two H^{α}'s and H^{β}'s due to planarity of Ni-containing 5-membered ring or rapid steric interconversion of 5-membered ring. Figure 2 shows the ^{13}C{^{1}H}-NMR spectrum of **3**. The signals of the CH_2 carbons of dpe ligand are assigned unequivocally by comparing the ^{13}C{^{1}H}-NMR spectrum of **3** with that of **3**-d_4. The other signals are assigned on the basis of their chemical shifts and magnitudes of the ^{13}C-^{31}P coupling constants. The appearance of the H^{α} and $\underline{C}H_2^{\alpha}$ signals at considerably high magnetic fields in the ^{1}H- and ^{13}C{^{1}H}-NMR spectra, respectively, indicates the presence of the CH_2 group directly bonded to nickel. IR spectrum of the complex **3** shows a strong $\nu_{(C=O)}$ band at 1640 cm^{-1}.

The reaction of complex **3** with CO gives succinic anhydride and nickel carbonyl complex. The result not only supports the structure shown above but also

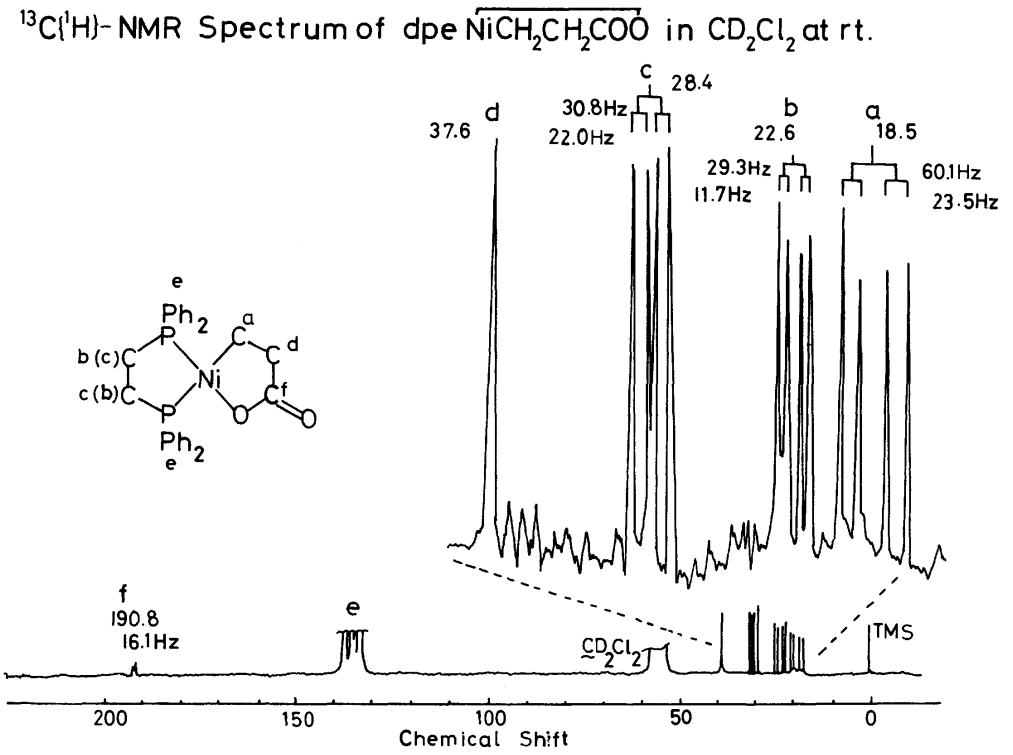

Fig. 2. $^{13}C\{^1H\}$-NMR spectrum of **3** in CD_2Cl_2.

reveals reversibility of the decarbonylation reaction and the oxidative addition.

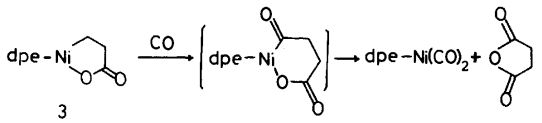

(7)

Results of reaction of metal-containing cyclic complexes with CO are summarized in Table 3.

Glutaric Anhydride: Reaction of glutaric anhydride with Ni(bpy)(cod) in THF gives a new six-membered ring complex, **4**.

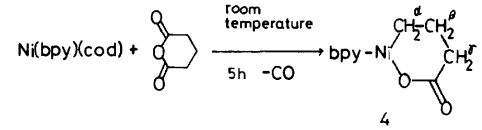

(8)

CO released is trapped as $Ni(bpy)(CO)_2$ similarly to the case of reaction with succinic anhydride. Complex **4** is very air sensitive but has a moderate solubility in organic solvents. ^1H-NMR spectrum of **4** shows three groups of signals of the methylene groups of **4** with the same intensity at 0.8, 1.3, and 2.2 ppm in CD_2Cl_2. The NMR signals are somewhat broadened possibly by a paramagnetic character of **4**, contamination with paramagnetic decomposition product(s) of **4** or rapid conformational change of the six-membered ring of **4**. Reaction of **4** with CO affords glutaric anhydride in 29% yield. On treatment with maleic anhydride in CH_2Cl_2 **4** gives a β-elimination product, 3-butenoic acid, in quantitative yield. These observations support the above six-membered structure of **4**.

Thermal decomposition of complex **4** in solid state or in a CH_2Ph_2 solution above 160 °C releases CO_2 and propylene in 20—30% yield, demonstrating occurrence

TABLE 3. REACTION OF METAL-CONTAINING CYCLIC ESTERS WITH CO

Complex	Products (% yield per the complex)
3	Succinic anhydride (55) $dpeNi(CO)_2$[a]
4	Glutaric anhydride (29) $bpyNi(CO)_2$[a]
8	Methylsuccinic anhydride (96) $dpeNi(CO)_2$[a]
9	Succinic anhydride (13) Pt-(CO) complex[a]
11	No reaction

a) Identified by IR.

of the following bond cleavage in six-membered ring or ring contracted five-membered ring.

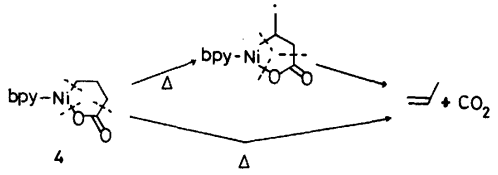

(9)

Addition of dpe to the solution of complex **4** gives a five-membered complex **5** in a high yield, demonstrating that complex **4'** has been completely isomerized to the five membered complex **5** under the experimental conditions.[5a]

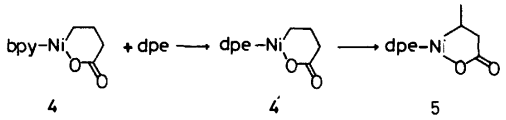

(10)

Factors controlling the ring contraction will be reported elsewhere.

Methylsuccinic Anhydride: Oxidative addition of methylsuccinic anhydride to Ni(bpy)(cod) gives two isomeric complexes, **6** and **7**, corresponding to two modes (A or B) of the oxidative addition.

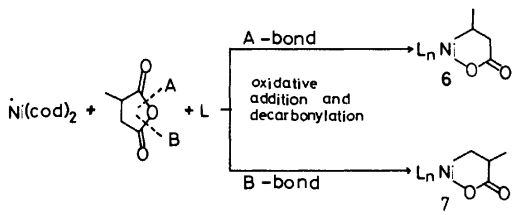

(11)

The ratio of **6** to **7** was determined by measuring intensity of $^{31}P\{^1H\}$-NMR signals of complexes **5** and **8** after ligand exchange reaction with dpe. The **6**/**7** ratio varies depending on the ligand employed and the reaction temperature. The results are given in Table 4.

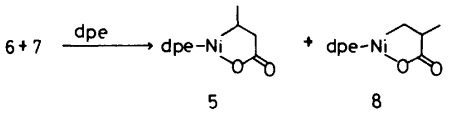

(12)

Complex **8** was independently prepared according to the following reaction.

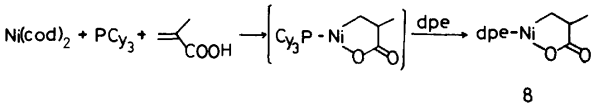

(13)

PCy_3 : tricyclohexylphosphine

The new complex **8** is characterized by elemental analysis, IR- and NMR (^1H-, $^{13}C\{^1H\}$-, and $^{31}P\{^1H\}$-) spectroscopy, and chemical reactivities. Coupling patterns observed in ^1H- and $^{31}P\{^1H\}$-NMR spectra are similar to those observed in ^1H- and $^{31}P\{^1H\}$-NMR spectra of the previously reported nickel-containing cyclic amides complex (dpe-$\overline{NiCH_2CH(CH_3)CONH}$) prepared from methacrylamide.[4] The NMR data are included in Table 2. Reaction of complex **8** with CO gives methylsuccinic anhydride in a quantitative yield as shown in Table 3. Table 4 summarizes effect of ligand added and reaction conditions on the distribution of products, **6** and **7**, which are formed by cleavage of A- and B-bonds, respectively. Examination of Table 4 clearly indicates that the oxidative addition involving the B-bond cleavage proceeds preferentially to the oxidative addition with the A-bond cleavage. This seems to be attributable to steric influence of the methyl substituent rather than electronic influence of the methyl substituent. When bpy or 4,4′-dimethyl-2,2′-bipyridine is used as ligand, the ratio of **7** against **6** increases with lowering of the reaction temperature, indicating that activation energy for the oxidative addition of the B-bond is smaller than that of the A-Bond.

Kinetics of the Oxidative Addition: Oxidative addition of succinic anhydride to Ni(bpy)(cod) is followed by observing change of visible spectrum which shows clear isosbestic points. The reaction obeys first order kinetics concerning the concentration of Ni(bpy)(cod) as shown in Fig. 3.

$$-\frac{d[Ni(bpy)(cod)]}{dt} = k'[Ni(bpy)(cod)]. \quad (14)$$

The dependence of the pseudo-first-order rate constant k' on the concentration of succinic anhydride is shown in Fig. 4, which demonstrates that k' is proportional

Table 4. Effect of additive ligand on the regioserectivity of C–O bond cleavage of methylsuccinic anhydride

Ligand(L)	L/Ni	Temp/°C	6(%)	7(%)
bpy	1	30	45	55
bpy	1	20	44	56
bpy	1	10	36	64
bpy	1	0	28	72
Me_2bpy[a]	1	20	29	71
Me_2bpy[a]	1	10	24	76
Me_2bpy[a]	1	0	25	75
PCy_3	1	20	36	64
PCy_3	1	10	42	58
PCy_3	1	0	44	56
PEt_3	4	20	25	75
PEt_3	4	10	27	73
PEt_3	4	0	18	82
$P(n\text{-}Bu)_3$	4	10	21	79
PEt_2Ph	2	10	28	72

a) 4, 4′-dimethyl-2,2′-bipyridine.

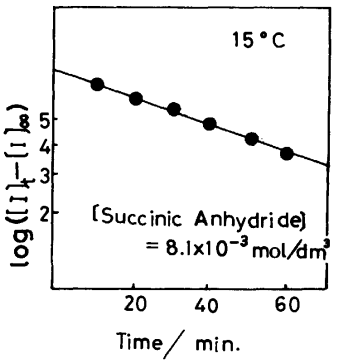

Fig. 3. First-order plot for the reaction of Ni(bpy)-(cod) with succinic anhydride.

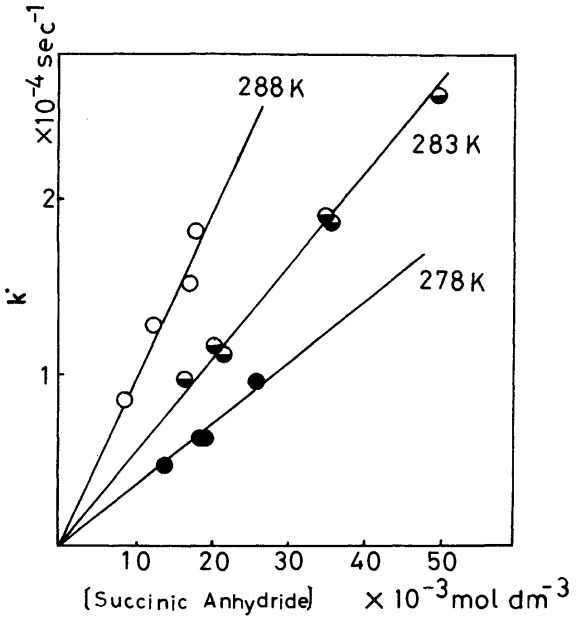

Fig. 4. Dependence of k' on concentration of succinic anhydride.

to [succinic anhydride]. Thus, the rate of reaction is expressed by second-order rate equation,

$$-\frac{d[Ni(bpy)(cod)]}{dt} = k[Ni(bpy)(cod)][\text{succinic anhydride}]. \quad (15)$$

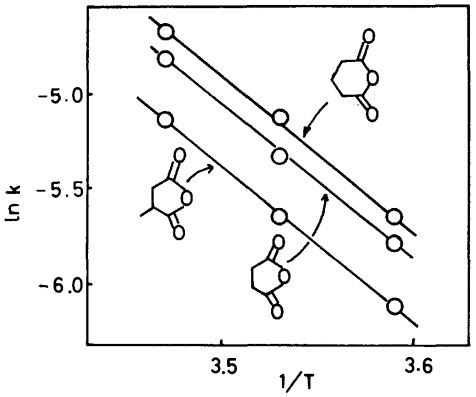

Fig. 5. Arrhenius plot of the rate constant.

Similar second-order rate equations are also obtained for other cyclic carboxylic anhydrides. From the Arrhenius plot of k against $1/T$, the activation energy for the oxidative addition of cyclic carboxylic anhydride to Ni(bpy)(cod) is estimated as shown in Table 5. The $\Delta H^{\ddagger}$ values obtained for the present oxidative addition of cyclic carboxylic anhydrides are considerably smaller than the $\Delta H^{\ddagger}$ value (88 kJ mol^{-1})[8] obtained for the oxidative addition of phenyl propionate to Ni(0) complex, indicating that the oxidative addition of cyclic carboxylic anhydride to Ni(0) is an energetically easier process than the oxidative addition of ester to Ni(0).

Oxidative Addition to Zero-valent Platinum. A reaction of $Pt(cod)_2$ with a mixture of PCy_3 (1 mol/$Pt(cod)_2$) and succinicanhydride (1 mol/$Pt(cod)_2$) in THF at room temperature affords a white insoluble complex, which is considered to have the following platinum-containing cyclic structure as judged from its IR spectrum and analytical data (Table 1). When 2 mol of PCy_3 per mol of $Pt(cod)_2$ is added, the reaction affords a similar platinum cyclic complex **10** having two PCy_3 ligands.

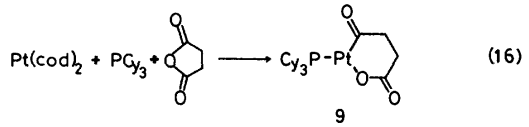

(16)

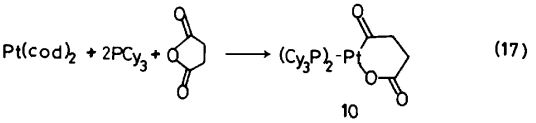

(17)

Low solubility of these complexes presumably due to its polymeric structure prevented analyzing their structures by NMR spectroscopy. However, a ligand exchange reaction with dpe in CS_2 gives a soluble dpe-coordinated complex **11**.

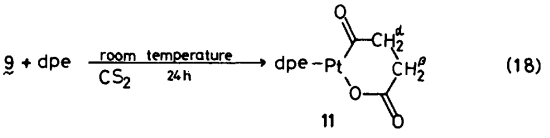

(18)

By using dpe-d_4, **11**-d_4 is prepared.

IR spectrum of complex **9** shows two strong bands at 1650 cm^{-1} and 1560 cm^{-1} assignable to $\nu_{(C=O)}$ of the acyl group and $\nu_{(C=O)}$ of the carboxylato group. These two peaks overlap in IR spectra of **10** and **11**. NMR data of **11** are included in Table 2, and consistent with the above structure. Appearance of the peak of the acyl carbon at 240.3 ppm in $^{13}C\{^1H\}$-NMR spectrum as well as the appearance of all H and $\underline{C}H_2$ signals at relatively low magnetic fields in the ^1H- and $^{13}C\{^1H\}$-NMR spectra, respectively, indicates that the decarbonylation has not taken place, in contrast to the analogous nickel complex **1** which undergoes the ready decarbonylation. Reaction of **11** with Br_2 affords the reductive elimination product, succinic anhydride, in 27% yield.

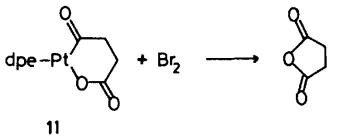

(19)

These observations support the non-decarbonylated 2-oxo-platinum-containing cyclic structure shown above.

When other ligands (bpy, PPh_3, $P(CH_2Ph)_3$, $PMePh_2$, dpe) are added to the mixture of $Pt(cod)_2$ and succinic anhydride, oxidative addition did not take place even at elevated temperatures. Blake and his coworkers[7] reported oxidative addition of perfluorinated succinic anhydride to $Pt(PPh_3)_2(C_2H_4)$.

In contrast to the Ni(0) and Pt(0) complexes, Pd(0) complexes ($Pd(PCy_3)_2$ and bis(1,5-diphenyl-1,4-pentadien-3-one) palladium (0))[9] did not show any apparent change on interaction with the cyclic carboxylic anhydrides at room temperature. A coordinatively unsaturated Rh(I) complex, $RhCl(PPh_3)_3$, showed no apparent change on the interaction with the cyclic carboxylic anhydrides, either.

TABLE 5. ACTIVATION PARAMETERS FOR OXIDATIVE ADDITION OF CYCLIC CARBOXYLIC ANHYDRIDES TO ZERO-VALENT NICKEL [a]

Substrate	$\Delta E_a^{\ddagger}$	$\Delta S_{283}^{\ddagger}$	$\Delta H_{283}^{\ddagger}$	$\Delta G_{283}^{\ddagger}$
	kJ mol^{-1}	J deg^{-1} mol^{-1}	kJ mol^{-1}	kJ mol^{-1}
Succinic anhydride	67.7	−48.5	65.2	79.0
Methyl-succinic anhydride	69.4	−45.1	66.9	71.9
Glutaric anhydride	67.7	−46.8	65.2	78.6

a) Ni(bpy)(cod).

Experimental

General, Materials, Analysis, and Spectroscopic Measurement. Reactions were carried out under N_2 or Ar as reported in papers from our research group.[4] $Pt(cod)_2$ was prepared according to the literature.[11] Commercially available $Ni(cod)_2$ was recrystallized from hot toluene. Microanalysis of C and H was performed by Mr. Saito of our laboratory with Yanagimoto CHN Autocorder MT-2. Ni content of **4** was determined by titration method.[12] IR spectra were recorded on a Hitachi Model 295 spectrometer, ^1H-NMR spectra on a JEOL Model JNM-PS-100 spectrometer, and ^{13}C- and ^{31}P-NMR spectra on JEOL Model JNM-PFT-PS-100 Fourier transform spectrometer. GLC analysis of organic products was performed with Shimadzu GC-3BT gas chromatograph.

Preparation of Complexes. **2**: Complex **2a** was pre-

pared according to literature.[7] From the reaction system we obtained $Ni(CO)_2(bpy)$ (confirmed by IR[13]) besides **2a**. Other complexes of type **2** were prepared analogously by using monodentate tertiary phosphines, but isolation of the complexes was not feasible and the crude complexes were used in further reaction with dpe (see text).

3: A THF (10 cm^3) solution containing 340 mg (1.2 mmol) of $Ni(cod)_2$, 190 mg (1.2 mmol) of bpy, and 120 mg (1.2 mmol) of succinic anhydride was stirred for 3 h at 25 °C to obtain a red precipitate from the homogeneous solution. The precipitate was separated by filtration and washed with hexane repeatedly, and then dissolved in CH_2Cl_2 (10 cm^3) containing 490 mg (1.2 mmol) of dpe at room temperature. The solution was filtered, and the filtrate was dried under reduced pressure. The residual solid was washed with THF repeatedly and dried under vacuum to obtain yellow **3**. yield=221 mg (33%).

4: A THF solution (40 cm^3) containing 3.0 g (11 mmol) of $Ni(cod)_2$, 1.7 g (11 mmol) of bpy, and 1.3 g (11 mmol) of glutaric anhydride was stirred for 6 h at 25 °C to obtain a red precipitate. The complex was filtered, washed with hexane repeatedly and dried to yield 2.0 g (60%) of a red complex **4**.

5: A CH_2Cl_2 solution (40 cm^3) containing 53 mg (0.18 mmol) of complex **4** and 70 mg (0.18 mmol) of dpe was stirred at room temperature. After change of color from red to yellow, the solution was filtered. The filtrate was dried under reduced pressure to obtain a yellow solid, which was washed with Et_2O repeatedly and dried to yield 41 mg (43%) of **5**.

8: A THF solution (5 cm^3) containing 510 mg (1.9 mmol) of $Ni(cod)_2$ and 520 mg (1.9 mmol) of PCy_3 and 0.16 cm^3 (1.9 mmol) of methacrylic acid was stirred for 24 h at 0 °C. Then, 740 mg (1.9 mmol) of dpe was added to the solution to obtain a yellow precipitate, which was separated by filtration, washed with THF and hexane repeatedly, and dried under vacuum to yield 580 mg (57%) of **8**.

9 and **10**: A THF (4 cm^3) solution containing 170 mg (0.4 mmol) of $Pt(cod)_2$ and 41 mg (0.4 mmol) of PCy_3 was stirred for 1 h at room temperature to obtain a white precipitate, which was separated by filtration, washed with hexane repeatedly, and dried under vacuum to obtain 81 mg (31%) of **9**. Complex **10** was prepared analogously using 2 mol of PCy_3 per mol of $Pt(cod)_2$ (yield=37%).

11: A CS_2 (10 cm^3) solution containing 440 mg (0.80 mmol) of **9** and 320 mg (0.80 mmol) of dpe was stirred for 24 h. CS_2 was removed by evaporation and the residue was washed with benzene repeatedly. Extraction with acetone (10 cm^3), and removing acetone by evaporation gave a white solid from which **11** was extracted by CH_2Cl_2. This extract was dried to obtain a white residue which was washed with hexane and dried to yield 245 mg (46%) of **11**.

Reaction of Methylsuccinic Anhydride: A Schlenk tube containing a THF solution of $Ni(cod)_2$ (0.1 mol/cm^3) and methylsuccinic anhydride (0.1 mmol/cm^3) was placed in a thermostated water bath. Ligand (see text) was added to the solution to start the reaction. After 1 h, dpe was added to the solution and solvent was removed under reduced pressure. The residue was washed with hexane to remove dpe-$Ni(CO)_2$ and free ligands.

Reaction of the Complex with CO: A 20 cm^3-Schlenk tube containing a CH_2Cl_2 (3—4 cm^3) solution of the complex (0.1—0.2 g) was evacuated and 1 atm of CO was introduced. The products were analyzed by GLC, GC-mass, and IR.

Kinetics: Dry THF was introduced into a quartz Schlenk tube connected to a UV cell by trap to trap distillation. 1,5-Cyclooctadiene was added to stabilize Ni(bpy)(cod). Then, THF solutions containing cyclic carboxylic anhydride and Ni(bpy)(cod) were added to the reaction vessel, and the change of visible spectrum with time was measured.

References

1) A. Stockis and R. Hoffmann, *J. Am. Chem. Soc.*, **102**, 2952 (1980) and references cited therein.

2) R. H. Grubbs, *Prog. Inorg. Chem.*, **24**, 1 (1978); R. L. Banks *Chem. Tech.* 494 (1979); T. J. Leigh, *Chem. Soc. Rev.*, **4**, 155 (1975); N. Calderon, J. P. Lawrence, and E. A. Ostead, *Adv. Organometal. Chem.*, **17**, 449 (1979); H. Yamazaki and Y. Wakatsuki, *Kagakusosetsu*, **32**, 161, (1981).

3) Y. Inoue, Y. Sasaki, and H. Hashimoto, *Bull. Chem. Soc. Jpn.*, **51**, 2375 (1978); *Chem. Lett.*, **1979**, 855; *ibid.*, **1978**, 633; *Bull. Chem. Soc. Jpn.*, **53**, 3329 (1980); H. Alper and F. Urso, *J. Am. Chem. Soc.*, **105**, 6737 (1983).

4) T. Yamamoto, K. Igarashi, J. Ishizu, and A. Yamamoto, *J. Chem. Soc., Chem. Commun.*, **1979**, 554; T. Yamamoto, K. Igarashi, S. Komiya, and A. Yamamoto, *J. Am. Chem. Soc.*, **102**, 7448 (1980).

5) a) K. Sano, T. Yamamoto, and A. Yamamoto, *Chem. Lett.*, **1982**, 695; b) *ibid.*, **1983**, 115; c) S. Komiya, A. Yamamoto, and T. Yamamoto, *ibid.*, **1981**, 193.

6) H. Hoberg, and D. Schaefer, *J. Organomet. Chem.*, **236**, C28 (1982); D. Walther, E. Dinjus, J. Sieler, J. Kaser, O. Lindvist, and L. Anderson, *ibid.*, **240** 289, (1982); H. Hoberg, D. Schaefer, and Burkhart, *ibid.*, **228**, C21 (1982); H. Hoberg, and B. W. Oster, *ibid.*, **234**, C35 (1982).

7) V. E. Uhlig, G. Fenske, und B. Nestler, *Z. Anorg. Allg. Chem.* **465**, 141—146 (1980). Oxidative addition of fluorine-activated cyclic carboxylic anhydride (perfluorinated succinic anhydride) to transition metal complexes giving metallacycles has been also reported; D. M. Blake, S. Sields, and L. Wyman, *Inorg. Chem.*, **13**, 1959 (1974).

8) T. Yamamoto, J. Ishizu, T. Kohara, S, Komiya, and A. Yamamoto *J. Am. Chem. Soc.*, **102**, 3758 (1980); T. Kohara, T. Yamamoto, and A. Yamamoto, *J. Organometal. Chem.*, **192**, 265 (1980).

9) a) R. van der Linde and R. O. de Jongh, *J, Chem. Soc., Chem. Commun.*, **1971**, 563; b) W. Kuran and A. Musco, *Inorg. Chim. Acta.* **12**, 187 (1975); c) S. Otsuka, T. Yoshida, M. Matsumoto, and K. Nakatsu, *J. Am. Chem. Soc.*, **98**, 5950 (1976).

10) T. Ukai, H. Kawazura, and Y. Ishii, *J. Organometal. Chem.*, **65**, 253, (1974); K. Itoh, F. Ueda, K. Hirai, and Y. Ishii, *Chem. Lett.*, **1977**, 877.

11) G. E. Herberich, and B. Hessner, *Z. Naturforsch.*, **34b**, 638 (1979).

12) T. Michino, M. Nakagawa, and H. Wada, *Nippon Kagaku Zasshi.*, **82**, 590 (1961).

13) T. Yamamoto, T. Kohara, and A. Yamamoto, *Bull, Chem. Soc. Jpn.*, **54**, 2161 (1981).

Liquid-Liquid Distribution Study of the Dissociation of Perchloric, Nitric, and Picric Acids in Polar Organic Solvents

Tatsuya SEKINE,* Tohru YOSHIKATA, and Takashi SAITOU
Department of Chemistry, Science University of Tokyo, Kagurazaka, Shinjuku-ku, Tokyo 162
(Received March 28, 1984)

The liquid-liquid distribution equilibria of perchioric, nitric, and picric acids between water and 4-methyl-2-pentanone or 4-methyl-2-pentanol have been determined at 298 K by measuring the concentrations of the anions in the two phases by spectrophotometry. The distribution ratio always increased on increase of the acid concentration; this was explained in terms of an increase in the degree of association of the acids in the organic phase. It was concluded from the analysis of the distribution data that the dissociation constant of perchloric acid was the highest and the value of picric acid was higher than that of nitric acid in 4-methyl-2-pentanone. The dissociation constant of picric acid was also higher in 4-methyl-2-pentanol than that of nitric acid; it was similar to that of perchloric acid. The differences of the dissociation constants were larger in 4-methyl-2-pentanone than in 4-methyl-2-pentanol.

In a previous study of solvent extraction of several mineral acids into 4-methyl-2-pentanone (MIBK), it was found that the shape of the extraction curve as a function of the acid concentration was appreciably different for different acids.[1] Several factors in the liquid-liquid system could be responsible for this and the difference in the dissociation of the acid in the organic phase might be one of the reasons. In order to learn further details of this problem, the liquid-liquid distribution ratio of perchloric, nitric, and picric acids between water and 4-methyl-2-pentanone or 4-methyl-2-pentanol has been measured as a function of the acid concentration and the extraction constant. The dissociation constant in the organic solvents were also calculated for these acids.

Experimental

The solvents and the acids were of reagent grade. The solvents were washed first with 0.5 mol dm^{-3} perchloric acid and then twice with water. They were then washed twice with 0.5 mol dm^{-3} sodium hydroxide solution and water. The solvent was finally washed several times with water. The concentrations of the stock solutions of the acids were determined by titration with standard sodium hydroxide solution. A 6 cm^3 portion of an aqueous acid solution and the same volume of the solvent were placed in a stoppered glass tube (capacity 20 cm^3). The two phases were vigorously agitated by a mechanical shaker for 15 min and centrifuged. A portion was pipetted from each phase and each was transferred separately into another tube.

The distribution ratio of picric acid was determined as follows. A 5 cm^3 portion of an aqueous 0.01 mol dm^{-3} solution of tetrabutylammonium chloride was added to the tube containing the equilibrated organic phase and the two phases were agitated for about 5 min in order to exchange the proton of the extracted picric acid with the tetrabutylammonium ion and thus all the picrate in the organic phase was in the anionic form whose optical density was higher than that of the acid form. Since the acid concentration in the aqueous phase was always lower than 1×10^{-4} mol dm^{-3} (its pK_a is 0.3[2]), this acid should be completely in the dissociated form. The amount of picrate was determined from the optical absorption of the organic phase thus obtained at 364 nm ($\varepsilon=1.50\times10^4$ in 4-methyl-2-pentanol) or 375 nm ($\varepsilon=1.80\times10^4$ in 4-methyl-2-pentanone). The amount of picrate ions in the equilibrated aqueous phase was also determined from the absorption at 355 nm ($\varepsilon=1.45\times10^4$ in aqueous solutions).

The distribution ratio of perchloric and nitric acid was determined as follows. A 5 cm^3 portion of water was added to the tube containing the equilibrated organic phase. The two phases were agitated in order to back-extract the acid and then centrifuged. A 4 cm^3 portion of the aqueous phase was transferred to another tube and a 1 cm^3 portion of 1×10^{-3} mol dm^{-3} solution of Crystal Violet and a 5 cm^3 portion of chlorobenzene were added. The two phases were vigorously agitated for 5 min and centrifuged. When the acid concentration was high, the amount extracted was large. In such a case, the washed solution was diluted with water before the dye and the solvent were added and a 4 cm^3 portion of the resulted solution was treated in the same manner as above. The optical absorption of the organic phase was measured at 596 nm. The apparent molar absorption coefficient after this treatment was 1.06×10^5 for perchloric acid and 3.35×10^4 for nitric acid. When the distribution ratio was low, the acid in the aqueous phase at equilibrium was calculated from the amount initially present in the aqueous phase and that extracted into the organic phase. In other cases, the aqueous phase was treated in the manner described above in order to determine the acid concentration. When the acid concentration was higher than 0.1 mol dm^{-3}, however, titration with a standard barium hydroxide was also employed for the determination of the acid in both phases. The water content in the organic phase was determined by a Karl-Fischer titration.

Statistical

In the present paper any species in the organic phase is denoted by a subscript "org" and that in the aqueous phase by lack of any subscript. Solvent extraction of an acid which dissociates in the aqueous phase may be written as;

$$H^+ + A^- \rightleftharpoons HA_{(org)}$$

$$K_{ex} = \{HA\}_{org}\{H^+\}^{-1}\{A^-\}^{-1}$$

$$= (\gamma_{HA}^{org})(\gamma_{\pm HA})^{-2}[HA]_{org}[H^+]^{-1}[A^-]^{-1}, \quad (1)$$

where $(\gamma_{\pm HA})$ is the mean activity coefficient of the acid in the aqueous phase and (γ_{HA}^{org}) is the activity coefficient of the acid in the associated form in the organic phase. When the extracted acid also dissociates in the organic phase, the equilibrium may be written as;

$$HA_{(org)} \rightleftharpoons H^+_{(org)} + A^-_{(org)}$$

$$K_{a(org)} = \{H^+\}_{org}\{A^-\}_{org}^{-1}\{HA\}_{org}^{-1}$$

$$= (\gamma_{\pm HA}^{org})^2(\gamma_{HA}^{org})^{-1}[H^+]_{org}[A^-]_{org}[HA]_{org}^{-1}, \quad (2)$$

where $(\gamma^{org}_{\pm HA})$ is the mean activity coefficient of the acid in the dissociated form in the organic phase. The distribution ratio of the acid in the absence of any other acids and salts of A^- may be written as;

$$D = [HA]_{org,\,total}/[HA]_{total}$$
$$= ([HA]_{org}+[H^+]_{org})/([HA]+[H^+])$$
$$= ([HA]_{org}+[A^-]_{org})/([HA]+[A^-]) \quad (3)$$
$$= (K_{ex}(\gamma_{\pm HA})^2(\gamma^{org}_{HA})^{-1}[A^-]^2 + \sqrt{K_{a(org)}K_{ex}}(\gamma_{\pm HA})(\gamma^{org}_{\pm HA})^{-1}[A^-])/([HA]+[A^-]). \quad (4)$$

When the acid dissociation in the aqueous phase is complete, the distribution ratio may be given as;

$$D = (\gamma_{\pm HA})^2(\gamma^{org}_{HA})^{-1}K_{ex}[A^-] + (\gamma_{\pm HA})(\gamma^{org}_{\pm HA})^{-1}\sqrt{K_{ex}K_{a(org)}}. \quad (5)$$

The values of $(\gamma_{\pm HA})$ were taken from the literature.[3] When the material concentration in the organic phase is low, both of the activity coefficients (γ^{org}_{HA}) and $(\gamma^{org}_{\pm HA})$ can be taken as unity, Eq. 5 can then be rewritten as;

$$D = (\gamma_{\pm HA})^2K_{ex}[H^+] + (\gamma_{\pm HA})K_{ex}K_{a(org)}. \quad (6)$$

From the values of D determined against $[H^+]$, the values of K_{ex} and $K_{a(org)}$ may be calculated on the basis of Eq. 6 by a successive approximation method using a least squares computer program.

Results and Discussion

Figures 1 and 2 give the log D *vs.* log $[H^+]$ plots of the acids. By the least squares calculation of these data, the extraction constant in Eq. 2 and the acid dissociation constant in the organic phase in Eq. 3 were obtained as listed in Table 1. The solid curves in Figs. 1 and 2 were calculated by Eq. 6 using the values of these constants.

As seen from Table 1, extraction constants of perchloric and nitric acid into 4-methyl-2-pentanol are higher than into 4-methyl-2-pentanone but that of picric acid is one order higher into the ketone. The increase in the slope of the plot on increasing the acid concentration can be explained in terms of the higher degree of association of the acid at higher concentration in the organic phase as seen from Eq. 5.

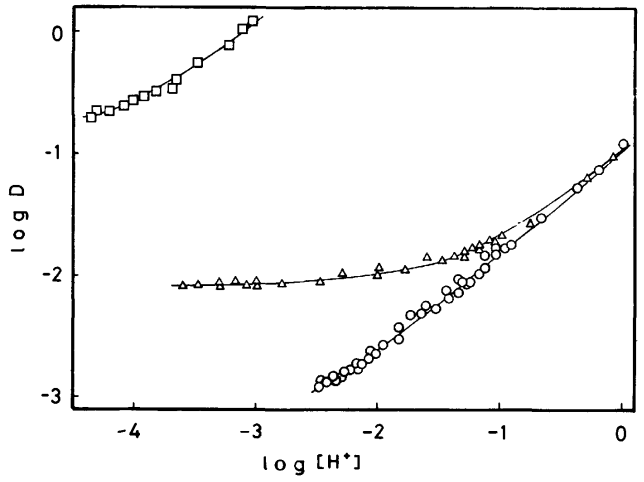

Fig. 1. The distribution ratio of acids as a function of their concentration in the equilibrated aqueous phase when solvent is 4-methyl-2-pentanone. Acids: perchloric acid (△), nitric acid (○), and picric acid (□). The solid curves were calculated by Eq. 6 using the value in Table 1.

In aqueous solutions, the acid strengths are in the order of perchloric acid>nitric acid>picric acid. The two mineral acids dissociate completely in their aqueous solutions. Picric acid is not a weak acid and its dissociation in aqueous solution is nearly complete over the concentration range of the present study. However, all of the acids are weak in these two organic solvents. Perchloric acid is always the strongest in both of the solvents but picric acid in 4-methyl-2-pentanol is as strong as perchloric acid. The difference in the strength of the acid is greater in 4-methyl-2-pentanone than in 4-methyl-2-pentanol and perchloric acid is weaker in the alcohol than in the ketone but the other two acids show an opposite tendency.

Several properties, such as the dielectric constant, solvation of the proton and anion, and interactions among the solvent molecules should affect the dissociation of the acid in these solvents. Furthermore, the solvents are saturated with water. It was found that the water content determined by Karl-Fischer titration was nearly constant except when the acid concentration in the aqueous phase was higher than 0.1 mol dm^{-3}. Above this an increase of water content was observed but the calculated values of K_{ex} and $K_{a(org)}$ were not affected whether or not the data obtained in this higher acid concentration range were included in the calculation.

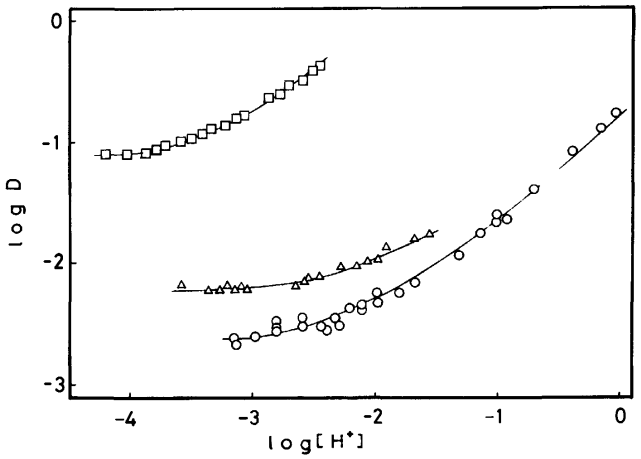

Fig. 2. The distribution ratio of acids as a function of their concentration in the equilibrated aqueous phase when solvent is 4-methyl-2-pentanol. Acids: perchloric acid (△), nitric acid (○), and picric acid (□). The solid curves were calculated by Eq. 6 using the value in Table 1.

Table 1. Extraction constant (Eq. 1) and acid dissociation constant (Eq. 2) in organic solvents

	4-methyl-2-pentanone		4-methyl-2-pentanol	
	$pK_{a(org)}$	$\log K_{ex}$	$pK_{a(org)}$	$\log K_{ex}$
Perchloric acid	3.5	−0.6	4.3	−0.2
Nitric acid	6	−0.6	4.8	−0.4
Picric acid	4.7	3.1	4.4	2.1

The association of strong acids in organic solvents have been extensively studied by conductimetry and potentiometry (for example Ref. 2 and Refs. 4 to 7 and also the references cited therein). Another approach to this problem is spectrophotometry which is however, applicable only when the optical absorption changes on acid dissociation as for picric acid.[5-6] The previous papers[5-7] observe that the strong acids which dissociated completely or nearly completely in aqueous solutions dissociated only partially in polar organic solvents. Furthermore the order of the dissociation in the solvents could be different from that in aqueous solutions and it could also be different in different organic solvents. For example, it was pointed out that the dissociation of picric acid was higher in dimethyl sulfoxide than of perchloric acid. This was explained in terms of the solvation of the former being stronger than that of the latter.[2]

In the present study, the solvents were saturated with water whereas in most of these previous studies, the solvents had been distillated and the water content should be much below saturation level. However, the tendency of the acid dissociation found in the present study is similar to that found previously. It can be pointed out that although the water content was different at different acid concentrations, a set of values of the two equilibrium constants could explain the results reasonably over a wide range of acid concentration.

There have been few quantitative studies of acid dissociation in organic solvents by liquid-liquid distribution methods. The present results indicate that this method is favorable for because even though the determination is done spectrophotometrically it can also be applied to those acids which have no strong optical absorption. If a dye of high molar extinction is used, it is possible to determine the equilibrium even when the acid concentration is low. However, it should also be noted that control of the water content in the solvent is not possible and several coexisting anions may interfere with the determination. Furthermore, the solvent should be water-immiscible and the anion should at least to some extent be extractable with a cationic dye.

The authors are very grateful for Dr. Satoshi Kusakabe for his valuable discussions during this study.

References

1) T. Sekine, T. Fukushima, and Y. Hasegawa, *Bull. Chem. Soc. Jpn.*, **43**, 2638 (1970).
2) I. M. Kolthoff and P. J. Elving, ed., "Treatise on Analytical Chemistry," 2nd ed., Part I, Vol. 2 (1979).
3) B. E. Conway, "Electrochemical Data," Elsevier Publishing Company, Amsterdam (1952).
4) D. B. Bruss and G. E. A. Wyld, *Anal. Chem.*, **29**, 232 (1957).
5) L. Marple and J. S. Fritz, *Anal. Chem.*, **35**, 1223 (1963).
6) M. K. Chantooni, Jr. and I. M. Kolthoff, *J. Phys. Chem.*, **82**, 994 (1978).
7) M. K. Chantooni, Jr. and I. M. Kolthoff, *Anal. Chem.*, **51**, 133 (1979).

Preparation and Characterization of [S-(2-Aminoethyl)-L-homocysteinato]-cobalt(III) Complexes with Bidentate Ligands

Masutaro SUZUKI, Osamu ARISATO, Ken-ichi OKAMOTO,* Hisahiko EINAGA,† and Jinsai HIDAKA
Department of Chemistry, University of Tsukuba, Sakura, Ibaraki 305
†*Institute of Materials Science, University of Tsukuba, Sakura, Ibaraki 305*
(Received April 4, 1984)

Three kinds of cobalt(III) complexes with S-(2-aminoethyl)-L-homocysteinate (L-aehc) and a bidentate ligand (glycinate, oxalate, and ethylenediamine) were prepared and chromatographically separated into the quasi-enantiomeric isomers: *Δ*L-*trans(O)·mer(N)-R(S)*, *Δ*L-*cis(O)·mer(N)-R(S)*, *Λ*L-*cis(O)·mer(N)-S(S)*, and *Λ*L-*cis(O)·fac(N)-S(S)* for the glycinato complex, *Δ*L-*trans(N)-R(S)* and *Λ*L-*cis(N)-S(S)* for the oxalato one, and *Δ*L-*R(S)* and *Λ*L-*S(S)* for the ethylenediamine one. These isomers were characterized from their electronic absorption, CD, and ^{13}C NMR spectra. The conformations of the six-membered N-S chelate ring in the L-aehc, of the chair for *Δ*L-*R(S)* and of the chair or skew-boat for *Λ*L-*S(S)*, were suggested on the basis of the ^{13}C NMR spectra. The CD spectra of the isomers are discussed in relation to their geometrical and absolute configurations.

CD spectra of the cobalt(III) complexes with a thioether-type terdentate ligand such as L-methioninate, S-methyl-L-cysteinate and their derivatives have been investigated in relation to the stereochemical properties of the coordinated sulfur donor atom.[1-8] In these works, however, the chiral sulfur atom, *R(S)* or *S(S)*[9] configuration, has been suggested to be configurationally labile.[6,10] S-(2-Aminoethyl)-L-homocysteinate (L-aehc) functions as a quadridentate ligand to a cobalt(III) ion and forms two five-membered (N-S and N-O) chelate rings and a six-membered (N-S) one (Fig. 1). Accordingly, the L-aehc cobalt(III) complex gives a fixed chiral sulfur atom as well as the cobalt(III) complexes with (2-aminoethylthio)acetate[11] or (2*R*)-2-(carboxymethylthio) propionate.[12] The L-aehc ligand can take two kinds of coordination modes which are mutually quasi-enantiomeric, as shown in Fig. 1. The sulfur donor atom in (a) or (c) of Fig. 1 takes only *S(S)* configuration, while two configurations, *R(S)* and *S(S)*, are possible for the sulfur donor atom in (b) or (d), depending on the possible conformations, chair and skew-boat, of the six-membered N-S ring. Of the four isomers for [Co(L-aehc)(gly)]$^+$, two isomers were determined to be the *Δ*L-*trans(O)·mer(N)-R(S)* and *Δ*L-*cis(O)·mer(N)-R(S)* ones by the X-ray crystal structure analysis.[13-15]

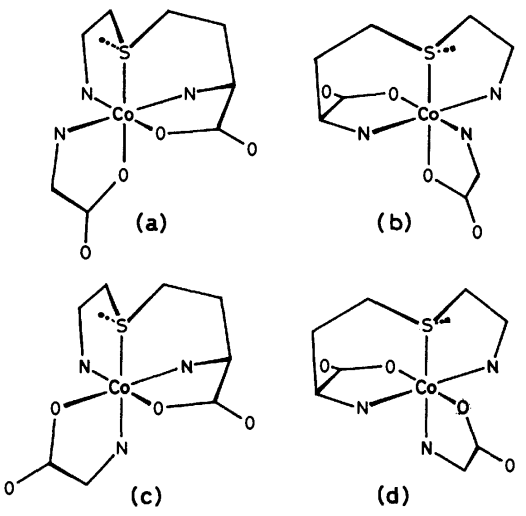

Fig. 1. Possible isomers of [Co(L-aehc)(gly)]$^+$: (a) *Δ*L-*cis(O)·mer(N)-S(S)*, (b) *Δ*L-*cis(O)·mer(N)-R(S)*, (c) *Λ*L-*cis(O)·fac(N)-S(S)*, and (d) *Δ*L-*trans(O)·mer(N)-R(S)*. *Δ*L-*cis(O)·mer(N)-S(S)* and *Δ*L-*trans(O)·mer(N)-S(S)* are omitted.

In this work, the [Co(L-aehc)(bidentate)]-type complexes were prepared and chromatographically separated into their possible isomers, namely, four isomers for the glycinato complex, two for the oxalato one, and two for the ethylenediamine one. The [Co(L-aehc)$(NH_3)_2]^{2+}$ and [Co(L-met)$(NH_3)_3]^{2+}$ complexes were also prepared in order to compare the CD spectra with the isomers of [Co(L-aehc)(en)]$^{2+}$. The coordination modes of L-aehc, *Λ*L-*S(S)*, *Δ*L-*R(S)*, and *Δ*L-*S(S)*, were suggested from comparisons of the CD and ^{13}C NMR spectra of the *Δ*L-*trans(O)·mer(N)-R(S)*- and *Δ*L-*cis(O)·mer(N)-R(S)*-[Co(L-aehc)(gly)]$^+$ isomers with those of the remaining isomers of the gly complex and of the isomers of the ox and en complexes.

Experimental

Preparation of Ligand. S-(2-Aminoethyl)-L-homocysteine was prepared by a procedure similar to that used for the preparation of S-(carboxymethyl)-L-homocysteine,[16] using 2-bromoethanamine hydrobromide instead of chloroacetic acid. The reaction mixture was neutralized with a 1 mol dm^{-3} aqueous solution of sodium hydroxide and the deposited sodium chloride was filtered off. The filtrate was poured onto a column of Dowex 50W-X8 (H^+ form, 5 cm×40 cm). After unreacted L-methionine had been swept with a 0.2 mol dm^{-3} sodium citrate buffer solution (pH 4.25), the desired product was eluted with a 1.0 mol dm^{-3} aqueous ammonia. The eluate was concentrated with a rotary evaporator until it became sirupy. It was neutralized with concd hydrobromic acid and to the solution was added a large amount of acetone. The crystals were collected by filtration and then washed well with acetone. Found: C, 27.59; H, 5.89; N, 10.53%. Calcd for L-Haehc·HBr=$C_6H_{14}N_2O_2S$·HBr: C, 27.57; H, 5.83; N, 10.80%.

Preparation and Separation of Complexes. 1) (S-(2-Aminoethyl)-L-homocysteinato)(glycinato)cobalt(III) Perchlorate: [Co(L-*aehc*)(*gly*)]ClO_4. A solution containing 4.0 g of L-Haehc·HBr and 2.0 g of glycine in 40 cm^3 of water was adjusted to pH 7 with a 1 mol dm^{-3} aqueous solution of sodium hydroxide. To this solution was added a solution containing 4.8 g of $CoCl_2·6H_2O$ in 40 cm^3 of water, 0.5 g of activated charcoal, and 8.0 g of PbO_2. The mixture was stirred at *ca.* 65 °C for 15 min and then filtered. The filtrate was poured onto a column of Dowex 50W-X8 (200—400 mesh, Na^+ form, 3 cm×40 cm). After the column had been swept with water, the adsorbed band was eluted with a 0.1 mol dm^{-3} aqueous

solution of NaCl. Four colored bands; red-violet (A-1), violet (A-2), red-violet (A-3), and red (A-4), were eluted in this order. It was found from the absorption and CD spectral measurements that A-1, A-2, A-3, and A-4 eluates contained *Δ*L-*trans(O)*·*mer(N)*, *Δ*L-*cis(O)*·*mer(N)*, *Δ*L-*cis(O)*·*mer(N)*, and *Λ*L-*cis(O)*·*fac(N)* isomers, respectively. Each eluate was concentrated to a small volume with a rotary evaporator below 25 °C and the deposited NaCl was filtered off. The filtrate was passed through a column of Sephadex G-10 (3.5 cm×100 cm) by elution with water. By use of an anion-exchange column (QAE-Sephadex A-25, ClO_4^- form, 3 cm×20 cm), the chloride salt in the eluate was converted into the perchlorate one. The eluate was concentrated to a small volume again. After adding a small amount of ethanol, the solution was kept in a refrigerator for several days. The crystals which appeared were collected by filtration and recrystallized from water by addition of ethanol. Found for A-1: C, 23.44; H, 4.14; N, 10.13%. Found for A-4: C, 23.36; H, 4.16; N, 10.13%. Calcd for [Co(L-aehc)(gly)]ClO_4= $CoC_8H_{17}N_3O_8SCl$: C, 23.45; H, 4.18; N, 10.25%. Found for A-2: C, 23.30; H, 4.57; N, 9.83%. Found for A-3: C, 22.48; H, 4.41; N, 9.80%. Calcd for [Co(L-aehc)(gly)]$ClO_4\cdot H_2O$: C, 22.46; H, 4.49; N, 9.82%.

2) (S-(2-Aminoethyl)-L-homocysteinato)(oxalato)cobalt(III): [Co(L-aehc)(ox)]. This complex was prepared by the same procedure as in *1)*, using oxalic acid dihydrate instead of glycine. The reaction mixture was filtered and the filtrate was passed through columns of Dowex 1-X8 (Cl^- form, 4 cm×25 cm) and Dowex 50W-X8 (Na^+ form, 4 cm×25 cm) in order to remove charged compounds. The concentrated eluate was poured onto a column of QAE-Sephadex A-25 (Cl^- form, 3.0 cm×150 cm) and eluted with water. The adsorbed band was separated into two bands, dark-violet (B-1) and purple (B-2), in this order. It was found from the absorption and CD spectral measurements that B-1 and B-2 eluates contained *Δ*L-*trans(N)* and *Λ*L-*cis(N)* isomers, respectively. Each eluate was concentrated to a small volume with a rotary evaporator below 25 °C and kept in a refrigerator overnight. The complex which precipitated was collected by filtration, then washed with ethanol and ether. B-1 isomer was obtained as violet needle crystals and B-2 isomer as light purple powder. Found for B-1: C, 29.42; H, 4.02; N, 8.60%. Found for B-2: C, 29.27; H, 3.98; N, 8.57%. Calcd for [Co(L-aehc)-(ox)]=$CoC_8H_{13}N_2O_6S$: C, 29.63; H, 4.04; N, 8.64%.

3) (S-(2-Aminoethyl)-L-homocysteinato)(ethylenediamine)cobalt-(III) Perchlorate: [Co(L-aehc)(en)]$(ClO_4)_2$. A solution containing 2.0 g of L-Haehc·HBr in 40 cm^3 of water was adjusted to pH 7 with a 1 mol dm^{-3} aqueous solution of sodium hydroxide. To this solution were added 2.0 g of *trans*-[$CoCl_2(en)_2$]Cl[17] and 0.5 g of activated charcoal. The resulting mixture was stirred at *ca.* 75 °C for 15 min. The color of the solution changed from green to violet and finally to orange-red. The mixture was filtered and the filtrate was poured onto a column of Dowex 50W-X8 (200—400 mesh, Na^+ form, 3.5 cm×30 cm). After the column had been swept with water, the adsorbed band was eluted with a 0.5 mol dm^{-3} aqueous solution of NaCl. Four colored bands: a red-violet, another red-violet, orange-red (C-1), and orange (C-2), were eluted in this order. It was found from the absorption and CD spectral measurements that C-1 and C-2 eluates contained the desired isomers, but the earlier two red-violet eluates contained a by-product; the absorption spectra of the two eluates did not show any sulfur-to-metal charge transfer band in the region of 30—35×10^3 cm^{-1}.[1-4,6-8,10-12] Each of the C-1 and C-2 eluates was concentrated to a small volume with a rotary evaporator below 25 °C. The solution was passed through columns of Sephadex G-10 (3.5 cm×100 cm) and QAE-Sephadex A-25 (ClO_4^- form, 3 cm×20 cm), by elution with water as in *1)*. To the eluate concentrated again was added a small amount of methanol; this mixture was kept in a refrigerator for several days. The complex which precipitated was collected by filtration, then washed with methanol and ether. C-1 isomer was obtained as orange-red needle crystals and C-2 isomer as orange-red powder. Found for C-1: C, 18.91; H, 4.55; N, 10.88%. Calcd for [Co(L-aehc)(en)]$(ClO_4)_2\cdot H_2O$=$CoC_8H_{21}N_4O_{10}SCl_2\cdot H_2O$: C, 18.72; H, 4.53; N, 10.92%. Found for C-2: C, 18.89; H, 4.12; N, 11.12%. Calcd for [Co-(L-aehc)(en)]$(ClO_4)_2\cdot 0.5H_2O$: C, 19.05; H, 4.20; N, 11.11%.

4) (S-(2-Aminoethyl)-L-homocysteinato)diamminecobalt(III) Chloride: [Co(L-aehc)$(NH_3)_2$]Cl_2. To a solution containing 2.0 g of L-Haehc·HBr in 200 cm^3 of water was added 3.5 g of *cis*-K[$Co(CO_3)_2(NH_3)_2$]·H_2O.[18] To this solution was gradually added 3 mol dm^{-3} hydrochloric acid with stirring at *ca.* 45 °C until the evolution of carbon dioxide ceased. The color of the solution changed from blue-violet to dark red. The mixture was filtered and the filtrate was poured onto a column of SP-Sephadex C-25 (Na^+ form, 3 cm×90 cm). After the column had been swept with water and 0.02 mol dm^{-3} acetic acid (pH 4.5), the adsorbed band was eluted with a 0.2 mol dm^{-3} aqueous solution of NaCl. Only the red band was eluted; it was concentrated to a small volume with a rotary evaporator below 20 °C. The solution was passed through a column of Sephadex G-10 (4 cm×45 cm) and then poured onto a column of SP-Sephadex C-25 (Na^+ form, 3 cm×90 cm) again. The adsorbed band was eluted by the same conditions as described above. Four colored bands: red, red-violet, red (D-1), and another red (D-2), were eluted in this order. It was found from the comparison with the absorption and CD spectra of [Co(L-aehc)(en)]$^{2+}$ isomers that D-1 and D-2 eluates contained the desired isomers. Since the yield was very poor, the desired isomers could not be isolated. The concentration of the complex cation in each eluate was evaluated by the plasma emission spectral analysis.

5) Triammine(L-methioninato)cobalt(III) Perchlorate: [Co-(L-met)$(NH_3)_3$]$(ClO_4)_2$. A solution containing 4.8 g of ammonium chloride and 7.2 cm^3 of 25% aqueous ammonia in 40 cm^3 of water were added to a solution containing 4.0 g of L-methionine in 12 cm^3 of water. To this solution was added a solution containing 1.7 g of $Co(CH_3COO)_2\cdot 4H_2O$ in 40 cm^3 of water and 10 g of PbO_2. The molar ratio, Co^{2+}: L-methionine: NH_3: NH_4^+, was 1:1:3:3.5. This solution was stirred at *ca.* 60 °C for 18 min, cooled to room temperature, and then filtered. The filtrate was poured onto a column of SP-Sephadex C-25 (Na^+ form, 4 cm×120 cm). After the column had been swept with water and then with a 0.03 mol dm^{-3} aqueous solution of NaCl, the adsorbed band was eluted with a 0.18 mol dm^{-3} aqueous solution of NaCl. Three colored bands: pink, orange-pink, and orange, were eluted in this order. It was found from the absorption and CD spectral measurements that the second eluate contained the desired complex. The second eluate was concentrated to a small volume with a rotary evaporator and the deposited NaCl was filtered off. The filtrate was passed through a column of QAE-Sephadex A-25 (ClO_4^- form, 3 cm×20 cm) by elution with water. The eluate was concentrated to a small volume. The crystals which appeared were collected by filtration, then washed with ethanol and ether. Found: C, 12.25; H, 4.05; N, 11.89%. Calcd for [Co(L-met)$(NH_3)_3$]$(ClO_4)_2\cdot 0.5H_2O$=CoC_5H_{19}-$N_4O_{10}SCl_2\cdot 0.5H_2O$: C, 12.88; H, 4.32; N, 12.02%.

Measurements. The electronic absorption spectra were recorded with a JASCO UVIDEC-1 spectrophotometer and the CD spectra with a JASCO J-20 spectropolarimeter. The concentration of D-1 or D-2 isomer for [Co(L-aehc)$(NH_3)_2$]$^{2+}$ was measured with a Jarrell-Ash model 96—975 plasma Atom Comp. The ^1H and ^{13}C NMR spectra were recorded on a JEOL JNM-FX-100 NMR spectrometer at the probe temperature in D_2O or 70% $DClO_4$ solvent. Sodium 2,2-dimethyl-2-silapentane-5-sulfonate (DSS) was used as an internal

reference.

Results and Discussion

Structural Assignment. Two pairs of quasi-enantiomeric geometrical isomers, *Λ*L-*cis(O)·mer(N)* and *Δ*L-*cis(O)·mer(N)*, and *Λ*L-*cis(O)·fac(N)* and *Δ*L-*trans(O)·mer(N)*, are expected for [Co(L-aehc)(gly)]$^+$, regardless of the chiral sulfur atom, *R*(*S*) or *S*(*S*), in L-aehc (Fig. 1).[15] In the first absorption band region, A-1

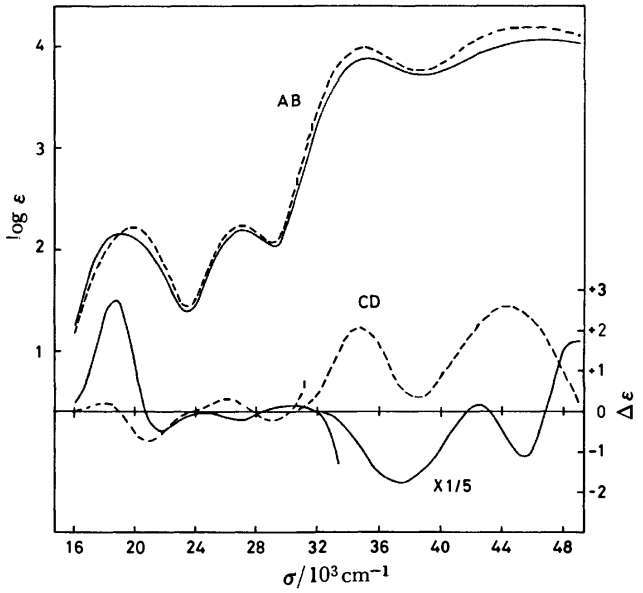

Fig. 2. Absorption and CD spectra of [Co(L-aehc)(gly)]$^+$: *Λ*L-*cis(O)·mer(N)* (——) and *Δ*L-*cis(O)·mer(N)* (------).

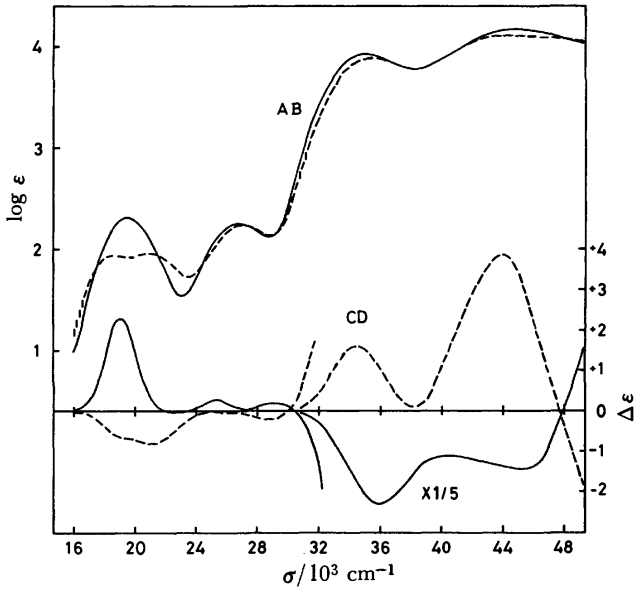

Fig. 3. Absorption and CD spectra of [Co(L-aehc)(gly)]$^+$: *Λ*L-*cis(O)·fac(N)* (——) and *Δ*L-*trans(O)·mer(N)* (------).

TABLE 1. ABSORPTION AND CD SPECTRAL DATA OF [Co(L-aehc)(L)] (L=gly, ox, en, and $(NH_3)_2$), AND [Co(L-met)$(NH_3)_3]^{2+}$

Complex	Absorption $\sigma/10^3\,cm^{-1}$ ($\varepsilon/mol^{-1}\,dm^3\,cm^{-1}$)	CD $\sigma/10^3\,cm^{-1}$ ($\Delta\varepsilon/mol^{-1}\,dm^3\,cm^{-1}$)
*Λ*L-*trans(O)·mer(N)*-[Co(L-aehc)(gly)]$^+$	18.52 (1.93)	19.23 (−0.66)
	21.14 (1.96)	21.20 (−0.81)
	27.03 (2.24)	28.57 (−0.21)
	35.34 (3.88)	34.56 (+7.83)
	44.64 (4.11)	44.21 (+18.8)
*Λ*L-*cis(O)·mer(N)*-[Co(L-aehc)(gly)]$^+$	18.94 (2.16)	18.67 (+2.75)
	27.03 (2.23)	21.74 (−0.51)
	36.36 (3.89)	26.89 (−0.21)
	46.95 (4.08)	30.12 (+0.14)
		37.60 (−0.75)
		42.55 (+0.79)
		45.45 (−5.56)
*Λ*L-*cis(O)·mer(N)*-[Co(L-aehc)(gly)]$^+$	18.90 (2.22)	17.80 (+0.19)
	27.03 (2.23)	20.83 (−0.77)
	34.97 (3.99)	25.97 (+0.28)
	45.45 (4.19)	28.96 (−0.22)
		34.60 (+10.1)
		44.44 (+13.0)
*Λ*L-*cis(O)·fac(N)*-[Co(L-aehc)(gly)]$^+$	19.53 (2.32)	19.05 (+2.35)
	26.81 (2.26)	22.58 (−0.02)
	36.36 (3.92)	25.32 (+0.31)
	44.64 (4.18)	28.90 (+0.23)
		35.59 (−11.5)
		45.05 (−7.09)
*Λ*L-*trans(N)*-[Co(L-aehc)(ox)]	19.53 (2.10)	16.61 (+0.17)
	26.25 (2.27)	19.69 (−0.87)
	34.72 (3.92)	25.45 (+0.11)
	42.92 (4.11)	28.01 (−0.42)
		34.13 (+11.3)
		38.17 (−2.39)
		45.05 (+15.3)

Table 1. Continued

Complex	Absorption $\sigma/10^3\,cm^{-1}$ ($\varepsilon/mol^{-1}\,dm^3\,cm^{-1}$)	CD $\sigma/10^3\,cm^{-1}$ ($\Delta\varepsilon/mol^{-1}\,dm^3\,cm^{-1}$)
Λ_L-*cis(N)*-[Co(L-aehc)(ox)]	18.73 (2.20)	18.15 (+1.86)
	26.18 (2.19)	20.79 (−0.27)
	34.60 (3.88)	23.98 (+0.03)
	43.67 (4.09)	26.25 (−0.12)
		28.57 (+0.03)
		36.76 (−5.24)
		42.92 (+6.16)
		46.95 (−4.33)
Λ_L-[Co(L-aehc)(en)]$^{2+}$	20.58 (2.10)	19.96 (−1.04)
	27.93 (2.23)	28.41 (−0.39)
	35.56 (3.96)	35.09 (+6.07)
	46.30 (4.18)	43.29 (+15.4)
Λ_L-[Co(L-aehc)(en)]$^{2+}$	19.92 (2.21)	19.16 (+3.30)
	27.78 (2.28)	22.08 (−0.91)
	35.56 (3.89)	26.45 (+0.12)
	44.64 (4.09)	29.32 (+0.42)
		31.85 (+0.48)
		36.90 (−12.7)
		44.44 (−5.68)
Λ_L-[Co(L-aehc)$(NH_3)_2$]$^{2+}$	19.92 (2.29)	20.20 (−1.43)
	27.78 (2.4 sh[a])	25.32 (+0.14)
	34.84 (3.95)	28.41 (−0.55)
	46.73 (4.11)	33.56 (+9.87)
		42.55 (+10.4)
Λ_L-[Co(L-aehc)$(NH_3)_2$]$^{2+}$	19.88 (2.34)	18.90 (+1.73)
	27.78 (2.46 sh)	21.51 (−0.48)
	34.97 (3.96)	25.19 (+0.12)
	45.66 (4.36)	27.25 (−0.08)
		28.99 (+0.05)
		35.71 (−6.58)
		46.30 (−4.17)
[Co(L-met)$(NH_3)_3$]$^{2+}$	20.00 (2.03)	20.00 (+0.50)
	27.03 (2.2 sh)	27.47 (−0.16)
	34.36 (3.94)	30.58 (+0.06)
	47.62 (4.22)	35.84 (−5.64)
		46.30 (+6.87)

a) sh denotes a shoulder.

isomer of [Co(L-aehc)(gly)]$^+$ exhibits well separated two absorption components, A-2 and A-3 isomers exhibit a broad band, and A-4 isomer exhibits a sharp band (Figs. 2 and 3, and Table 1). These splittings of the first absorption bands agree well with the splitting patterns which can be expected from the semiempirical calculation[19] on the basis of the ligand field strength, N>S>O.[1-4,6-8,10-13] Of these isomers, A-1 and A-3 isomers were determined to be Λ_L-*trans(O)·mer(N)*[13] and Λ_L-*cis(O)·mer(N)*,[14] respectively, by the X-ray crystal structure analysis and then A-2 isomer was assigned to Λ_L-*cis(O)·mer(N)* from a comparison of the absorption and CD spectra with those of A-3 one.[14] Thus A-4 isomer is Λ_L-*cis(O)·fac(N)*. For the [Co(L-aehc)(ox)] complex, the isomers are regulated to a pair of quasi-enantiomeric isomers, Λ_L-*trans(N)* and Λ_L-*cis(N)* (Fig. 1). In the first absorption band region, B-1 isomer of [Co(L-aehc)(ox)] exhibits a band with an explicit shoulder on the lower energy side and B-2 isomer exhibits a sharp band (Fig. 4 and Table 1). These spectral patterns suggest that B-1 isomer is Λ_L-*trans(N)* and B-2 one Λ_L-*cis(N)*. Similarly, the two isomers, Λ_L and Λ_L, are possible for the ethylenediamine complex, [Co(L-aehc)(en)]$^{2+}$. In this case, however, it is

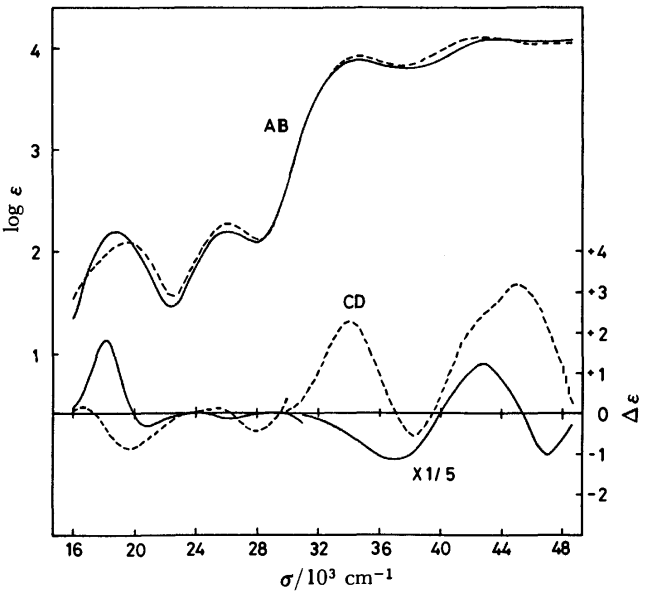

Fig. 4. Absorption and CD spectra of [Co(L-aehc)(ox)]: Λ_L-*cis(N)* (——) and Λ_L-*trans(N)* (------).

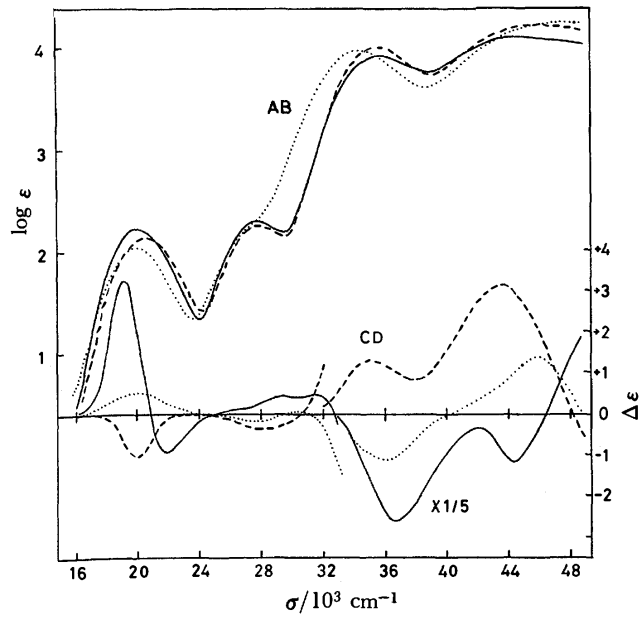

Fig. 5. Absorption and CD spectra of [Co(L-aehc)(en)]$^{2+}$: Λ_L (——) and Δ_L (------), and [Co(L-met)$(NH_3)_3$]$^{2+}$ (……).

difficult to assign the structure of the two isomers on the basis of their first absorption bands (Fig. 5), so their ^{13}C NMR spectra were measured.

The ^{13}C NMR spectra of the six isomers of the gly and ox complexes can be classified into two groups according to the distribution of the chemical shifts due to the β-methylene carbon atom of L-aehc (Fig. 6). One group, the Δ_L isomers, exhibits the resonance line in the range of 40—43 ppm (A-1, A-3, and B-1 isomers), while the other, the Λ_L isomers, exhibits the line in the range of 34—37 ppm (A-2, A-4, and B-2 isomers). The same trend was observed for the ^{13}C NMR spectra of the two isomers of [Co(L-aehc)(en)]$^{2+}$, namely, the resonance line for the β-methylene carbon atom of C-1 isomer (34.51 ppm) appears at a higher field than that of C-2 one (40.25 ppm) (Fig. 6). Stereomodel examination reveals that the interligand interaction between the six-membered N-S chelate ring containing the β-methylene and the five-membered N-S chelate ring of L-aehc is more remarkable for the Λ_L isomer than for the Δ_L one. Taking the classification based on the ^{13}C NMR spectral behavior of the β-methylene carbon and the steric effects of the chemical shift of carbon[19,20] into consideration, the C-1 isomer of [Co(L-aehc)(en)]$^{2+}$ is tentatively assigned to Λ_L and the C-2 isomer to Δ_L. This assignment is consistent with that from their CD spectra (*vide infra*).

According to the model constructions, the coordinated sulfur atom of the Λ_L isomer is limited to *S*(*S*) configuration, whereas that of the Δ_L isomer is able to take *R*(*S*) and *S*(*S*) configurations which depend on the conformation of the six-membered N-S chelate ring in L-aehc, namely, the *R*(*S*) coordination takes with a chair-formed N-S chelate ring and the *S*(*S*) coordination with a skew-boat one. In fact, Δ_L-*trans(O)*·*mer(N)*-[Co(L-aehc)(gly)]$^+$ (A-1) has the *R*(*S*) configuration and the six-membered N-S chelate ring in the chair form,[13] and the Δ_L-*cis(O)*·*mer(N)* isomer

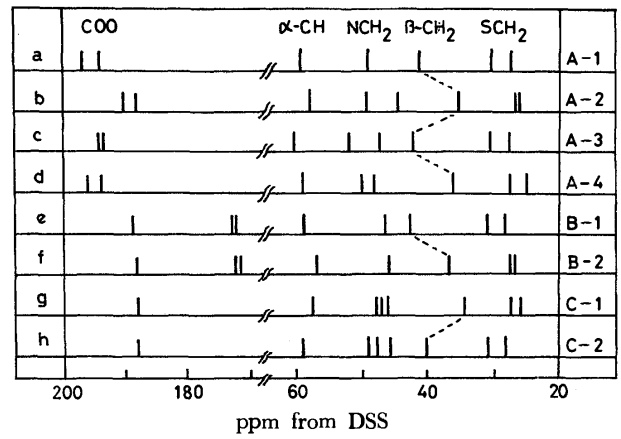

Fig. 6. The distribution of ^{13}C NMR chemical shifts of [Co(L-aehc)(L)].
a—d: L=gly; e and f: L=ox; g and h; L=en.

(A-3) also has *R*(*S*) with the chair-formed N-S chelate ring.[14] These two glycinato isomers show similar ^{13}C NMR spectral behavior on the carbon atoms of L-aehc to those of the Δ_L-*trans(N)*-[Co(L-aehc)(ox)] and Δ_L-[Co(L-aehc)(en)]$^{2+}$ ones (Fig. 6). The distribution of the chemical shifts for each carbon atom of L-aehc seems to be related with the interligand interaction between the six-membered N-S chelate ring and the five-membered N-S chelate ring, as in the case of the chemical shift for the β-methylene carbon mentioned above. Thus it is suggested that the six-membered N-S chelate ring for the ox and en complexes takes a chair conformation (simultaneously *R*(*S*) configuration) in the Δ_L isomers.

Two isomers, Δ_L and Λ_L, are possible for [Co(L-aehc)$(NH_3)_2$]$^{2+}$ as well as the ethylenediamine complex. The absorption spectra of D-1 and D-2 isomers of the diammine complex are quite similar to those of the [Co(L-aehc)(en)]$^{2+}$ and [Co(L-met)$(NH_3)_3$]$^{2+}$ complexes over the whole region (Figs. 5 and 7). Furthermore, the CD spectral patterns of D-1 and D-2 isomers also agree well with those of [Co(L-aehc)(en)]$^{2+}$ isomers (*vide infra*).

CD Spectra. The CD spectra of the L-aehc complexes are shown in Figs. 2—5 and 7, and their data are summarized in Table 1. Three pairs of quasi-enantiomeric geometrical isomers for the gly and ox complexes exhibit approximately enantiomeric CD patterns, respectively, though some deviations are observed in the first absorption band region (Figs. 2—4). This enantiomeric CD spectral relationship can be applied for the assignment of the two isomers of [Co(L-aehc)(en)]$^{2+}$, namely, Λ_L for C-1 isomer and Δ_L for C-2 one (Fig. 5). This assignment agrees with that based on their ^{13}C NMR spectra mentioned above. Similarly, D-1 and D-2 isomers of [Co(L-aehc)$(NH_3)_2$]$^{2+}$ correspond to Δ_L- and Λ_L-[Co(L-aehc)(en)]$^{2+}$, respectively, as shown in Fig. 7. Here, it should be noted that Δ_L-[Co(L-aehc)$(NH_3)_2$]$^{2+}$ (D-1) isomerized gradually to Λ_L one (D-2) in aqueous solution, while Λ_L isomer did not. This trend in isomerization agrees with the suggestion from the stereomodel examination that L-aehc prefers Λ_L coordination to Δ_L one, because of more strained *R*(*S*) caused by the Δ_L coordination of L-aehc. Further study is being undertaken to investigate the isomerization

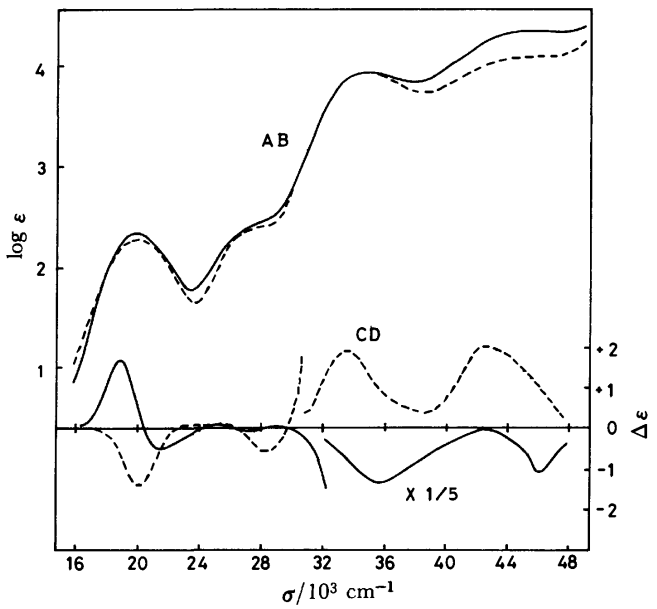

Fig. 7. Absorption and CD spectra of [Co(L-aehc)-$(NH_3)_2]^{2+}$: Δ_L (——) and Δ_L (------).

in detail.

In order to estimate the CD contribution due to the L-methionine moiety of L-aehc, the triammine(L-methioninato)cobalt(III) complex, $[Co(L\text{-met})(NH_3)_3]^{2+}$, was prepared. The ^1H NMR spectrum of the triammine complex exhibits a peak (2.34 ppm) with a shoulder at lower field due to the *S*-methyl protons, suggesting the coexistence of *R*(*S*) and *S*(*S*) isomers. This result suggests that the CD spectrum of $[Co(L\text{-met})(NH_3)_3]^{2+}$ is mainly due to *S*(*C*) of the L-met (Fig. 5). In contrast to the triammine complex, $[Co(L\text{-aehc})(NH_3)_2]^{2+}$ and $[Co(L\text{-aehc})(en)]^{2+}$ have two additional CD contributions besides that due to *S*(*C*) of L-aehc, namely, one from the configurational chirality due to the skew pair of chelate rings of L-aehc and the other the chirality due to the sulfur donor atom, though the two contributions can not be separated. As shown in Fig. 5, the CD curves of $[Co(L\text{-aehc})(en)]^{2+}$ isomers in the region of $24—48\times10^3\,cm^{-1}$ are almost enantiomeric, taking into account that the CD curve of $[Co(L\text{-met})(NH_3)_3]^{2+}$ is subtracted from that of Δ_L- or Λ_L-$[Co(L\text{-aehc})(en)]^{2+}$, while their CD patterns in the first absorption band region deviate significantly from the enantiomeric relation. The same situation holds for each of the quasi-enantiomeric pairs of the other L-aehc complexes (Figs. 2—4). The Λ_L isomers of all the L-aehc complexes exhibit a similar CD pattern ((+) and (−) from lower energy) in the first absorption band region, regardless of the geometrical configurations with respect to the coordinated atoms, while the patterns of Δ_L isomers depend remarkably on their geometrical configurations. These CD spectral behaviors of Δ_L and Λ_L isomers in the first absorption band region are also observed for the CD spectra of the *S*-(carboxymethyl)-L-homocysteinato and *S*-(2-carboxyethyl)-L-homocysteinato complexes.[22] These deviations in the first absorption band region seem to be attributed to the difference of configurational chiralities due to the coordinated L-aehc, Δ_L-*R*(*S*) and Λ_L-*S*(*S*), rather than the chiral sulfur atom, taking account of the fact that the CD patterns of *R*(*S*)- and *S*(*S*)-[Co(*R*-cmtp or *R*-cetp)$(NH_3)_3]^+$, which are mainly contributed to the chirality due to the sulfur donor atom, are almost enantiomeric in the first absorption band region (where *R*-cmtp and *R*-cetp denote (2*R*)-2-(carboxymethylthio)propionate and (2*R*)-2-(2-carboxyethylthio)propionate).[12]

References

1) J. Hidaka, S. Yamada, and Y. Shimura, *Chem. Lett.*, **1974**, 1487.
2) K. Yamanari, J. Hidaka, and Y. Shimura, *Bull. Chem. Soc. Jpn.*, **50**, 2451 (1977).
3) T. Isago, K. Igi, and J. Hidaka, *Bull. Chem. Soc. Jpn.*, **52**, 407 (1979).
4) K. Okamoto, K. Wakayama, H. Einaga, S. Yamada, and J. Hidaka, *Bull. Chem. Soc. Jpn.*, **56**, 165 (1983).
5) R. J. Magee, W. Mazurek, M. J. O'Conner, and A. T. Philip, *Aust. J. Chem.*, **27**, 1629 (1974).
6) K. Okamoto, T. Isago, M. Ohmasa, and J. Hidaka, *Bull. Chem. Soc. Jpn.*, **55**, 1077 (1982).
7) T. Konno, K. Okamoto, and J. Hidaka, *Bull. Chem. Soc. Jpn.*, **56**, 2631 (1983).
8) K. Okamoto, H. Maki, and J. Hidaka, *Bull. Chem. Soc. Jpn.*, **57**, 595 (1984).
9) The symbols, *R*(*S*), *S*(*S*), and *S*(*C*), denote the absolute configurations of the chiral sulfur donor atom and the carbon atom, respectively.
10) W. G. Jackson and A. M. Sargeson, *Inorg. Chem.*, **17**, 2165 (1978).
11) K. Yamanari, J. Hidaka, and Y. Shimura, *Bull. Chem. Soc. Jpn.*, **50**, 2299, 2643 (1977).
12) M. Suzuki, K. Okamoto, H. Einaga, and J. Hidaka, *Bull. Chem. Soc. Jpn.*, **55**, 3929 (1982).
13) K. Okamoto, M. Suzuki, H. Einaga, and J. Hidaka, *Bull. Chem. Soc. Jpn.*, **56**, 3505 (1983).
14) K. Okamoto, M. Suzuki, and J. Hidaka, *Chem. Lett.*, **1983**, 401.
15) The symbols, Δ_L and Λ_L, are designed on the basis of the configurational chirality due to the skew pair of the chelate rings of the L-aehc (Fig. 1). In former papers,[13,14] Δ and Λ correspond to Δ_L and Λ_L, respectively.
16) M. D. Armstrong and J. D. Lewis, *J. Org. Chem.*, **16**, 749 (1951).
17) J. C. Bailar, Jr., *Inorg. Synth.*, **2**, 222 (1946).
18) M. Shibata, *Nippon Kagaku Zasshi*, **87**, 771 (1966).
19) H. Yamatera, *Bull. Chem. Soc. Jpn.*, **31**, 95 (1958).
20) C. A. Chang and B. E. Douglas, *J. Coord. Chem.*, **9**, 93 (1979).
21) D. M. Grant and B. V. Cheney, *J. Am. Chem. Soc.*, **89**, 5315 (1967).
22) The present authors, to be published.

 © 1984 The Chemical Society of Japan Bull. Chem. Soc. Jpn., 57, 2757—2760 (1984)

Development of a Laboratory EXAFS System and Its Application to Aqueous Nickel(II) Ammine Solutions

Mitsuru SANO,* Tetsuya MARUO,† and Hideo YAMATERA†

Laboratory of Inorganic Chemistry, College of General Education, Nagoya University, Nagoya 464

†*Department of Chemistry, Faculty of Science, Nagoya University, Nagoya 464*

(Recieved May 1, 1984)

A laboratory EXAFS system with a curved crystal has been developed. This apparatus consists of a usual X-ray tube, a spectrometer with a Johan-type curved crystal, and two proportional counters detecting the X-rays. The resolution and performance tests have been carried out and excellent spectra have been obtained for NiO. With this system, aqueous solutions of ammine and ethylenediamine nickel(II) salts have been studied. The spectra were analyzed by the curve-fitting method by reference to the spectra of appropriate crystals containing the corresponding complexes. The values obtained for the Ni–N distances are 2.12±0.01 Å. These values are very close to those of the corresponding complexes in crystals.

The extended X-ray absorption fine structure (EXAFS) technique for the study of the molecular structure has made a rapid development and has been applied to a variety of problems.[1] Synchrotron orbital radiation (SOR) is evidently of great value in EXAFS spectroscopy; however, the use of an SOR facility is inevitably accompanied by various restrictions as to place and time.

In previous papers, we reported EXAFS studies of aqueous cyanocuprate(I)[2] and copper(II) ammine[3] solutions with a laboratory system equipped with a position-sensitive photodiode array. The system has advantages of high efficiency in the data collection and of little dependence on the X-ray flux fluctuation with time. This detector has an excellent position resolution (28μ/channel) which may be applied for SOR facilities[4] and for a small angle scattering apparatus[5] as a highly efficient X-ray detector. However, continuous X-rays generated by the tube contain many characteristic lines from the target as well as contaminants. When the photodiodes detect all the X-rays without energy resolution, the voltage applied to the anode of the X-ray tube is restricted in order to avoid the contamination of the higher-order reflections; then the brightness of the continuous X-rays is kept at low. Thus the application of our system with a photodiode array is limited to particular kinds of chemical elements.

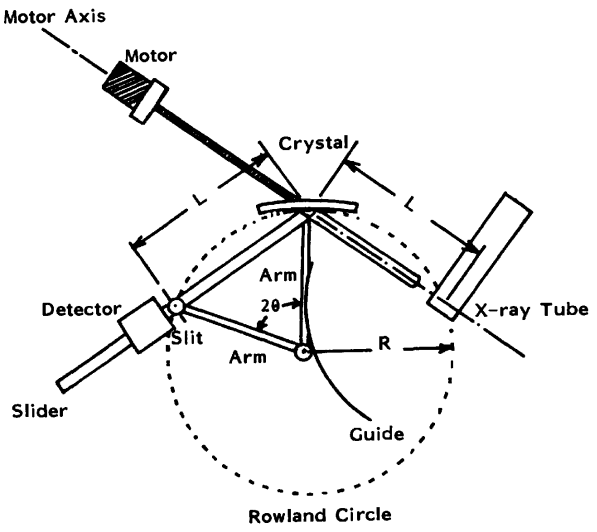

Fig. 1. Schematic diagram of the X-ray monochromator with a Johan-type curved crystal.

In order to extend the EXAFS study of solution systems, we have developed a new laboratory EXAFS system with a Johan-type curved crystal. We have carried out its performance test and then applied the method to the structural study of aqueous solutions of ammine and ethylenediamine nickel(II) salts.

Ammine complexes of metal ions are the most fundamental and important species in coordination chemistry. Fujita and Ohtaki[6] studied the structure of the aqueous ethylenediamine nickel(II) solutions by the X-ray diffraction technique. They reported Ni–N distances of 2.10 Å for the bis-complex and 2.20 Å for the tris-complex. X-ray studies of the solid tris-ethylenediamine complex salts[7–10] gave about 2.1 Å for the Ni–N bond distances; the results on solutions are not consistent with those on crystals. Our EXAFS results will be given below.

System Configuration

The laboratory EXAFS system consists of three parts; a usual X-ray generator, a spectrometer with a curved crystal, and an X-ray detector system. The X-ray spectrometers with a bent crystal have been reported by Knapp *et al.*,[11] Williams,[12] Thulke *et al.*,[13] and Tohji *et al.*[14] The present system is basically of the same configuration as theirs, but has two features, the spectrometer with a Johan crystal and one stepping motor and the counter system with energy resolution activity.

A. X-ray Source. The X-rays are generated by a Rigaku 2kW X-ray generator equipped with a Philips fine focus X-ray tube with a Mo anode. The X-rays are emitted from a vertical square (8-mm high) on the anode. Its effective width at a take-off angle of 6° is about 0.04 mm.

B. Spectrometer. The basic geometrical arrangement for the EXAFS spectrometer is schematically shown in Fig. 1. The essential features of this instrument are the same as the Applied Research Laboratories design.[15] The anode of the X-ray generator, the LiF crystal ($2d$=4.027 Å) and the receiving slit are held on a Rowland circle. The guide, arms, and wires (not shown in Fig. 1) were provided to effect the following movements as a function of θ:

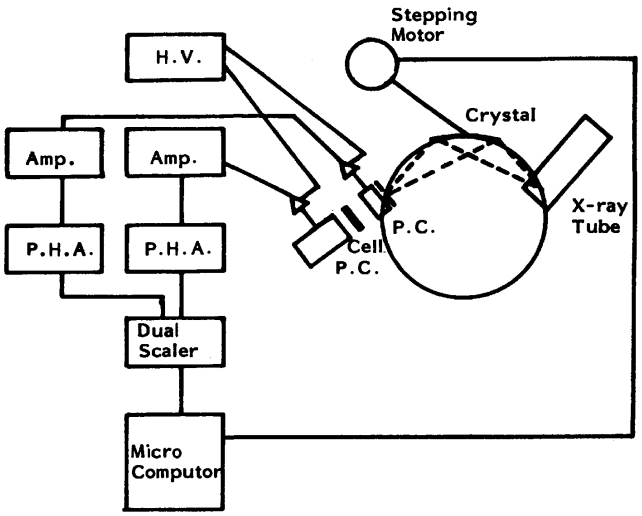

Fig. 2. Schematic diagram of the laboratory EXAFS system.

(1) The crystal moves on the motor-axis in a straight line away from the source aperture, thereby increasing the crystal-source distance, L, in accordance with $L=2R\sin\theta$. (2) The detector moves keeping the relation $r=2R\sin 2\theta$, where r is the distance between the source and the detector. (3) The detector slit is always directed toward the center of the crystal. Above conditions have been accomplished by one stepping motor. As the Rowland geometry is satisfied, the radiation with $n\lambda=2d\sin\theta$ is Bragg-diffracted from the LiF crystal and subsequently focused at the receiving slit on the Rowland circle. The focusing by the Johan crystal is less satisfactory than that by the crystal of the Johansson type. However, the monochromator can be more easily adjusted.

C. Detection System. The block diagram of the detection system is shown in Fig. 2. Monochromatized X-ray coming through the receiving slit passes first through a proportional counter which monitors the intensity of the radiation incident on the sample(I_0). The intensity of the X-ray which is transmitted by the sample is then measured by the second proportional counter. The photon received by each counter is converted to an electric pulse, which is amplified, pulse-hight-analyzed and counted. Both signals from the first and the second proportional counters are counted until the number of signals detected by the first (I_0) counter reaches the preset-number of the dual scaler. After reading-out, the spectrometer is set to the next Bragg angle, and both counters are started again. The spectra are stored on a magnetic disk of a microcomputer (SORD M223-Mark V) which also controls the stepping motor. A high voltage supply (1.6 kV) operates the two proportional counters (90% Ar–10% CH_4 gas flow at 1 atm).

Performance

The resolution of an X-ray spectrometer based on the Johan crystal optics is lower than that based on the Johansson's. The experimental resolution was obtained from the measured intensity profile of the characteristic emission lines of the impurity copper

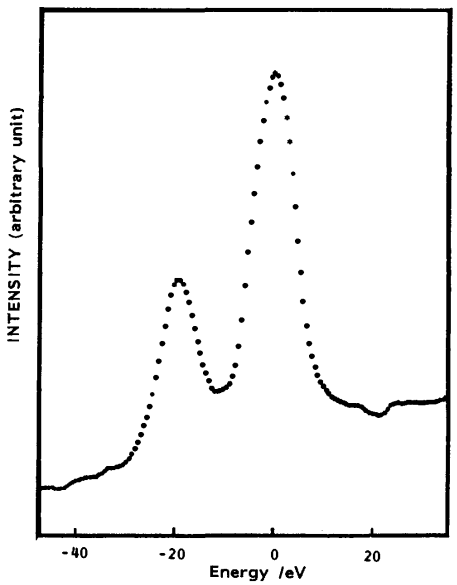

Fig. 3. Cu $K\alpha$ doublet obtained with a LiF(220) Johan-type crystal.

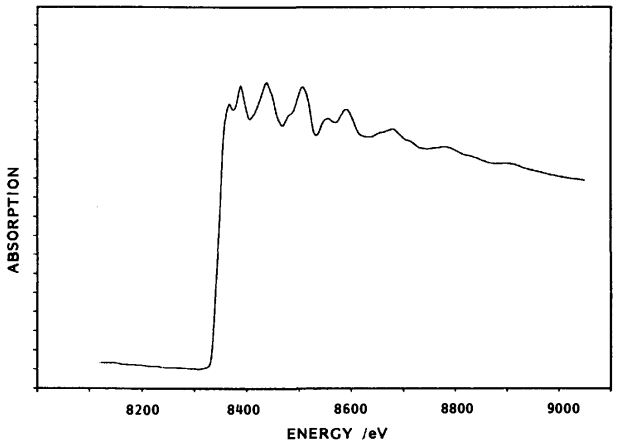

Fig. 4. X-ray absorption spectrum of 5-μm thick Ni foil.

contained in the anode of the X-ray tube. Figure 3 shows the $K\alpha$ doublet of Cu. A resolution satisfactory for measuring EXAFS was obtained when the receiving slit was set to 0.1 mm. In these conditions, the X-ray source operating at 16 kV and 5 mA gave an X-ray flux of 5×10^4 cps.

Since metal foil shows a pronounced EXAFS and is easily available, it has widely been used as a standard sample in EXAFS measurements. Figure 4 shows the absorption spectrum of Ni foil obtained from a run of 4-h measurement at 16 kV and 5 mA. The feature is almost identical with that obtained with SOR.

As an example of the results obtained for substances of chemical interest, the subtracted EXAFS oscillation $\chi(k)$ and the Fourier transform of $k^3\chi(k)$ of NiO powder are shown in Fig. 5(a) and (b). EXAFS up to 14 $Å^{-1}$ in the k range above the edge is clearly seen. The Fourier transform indicates the existence of some atoms, all in accordance with the known crystal structure when the phase shift is taken into account.

It is often quoted that characteristic lines from contaminated anode materials seriously impair the

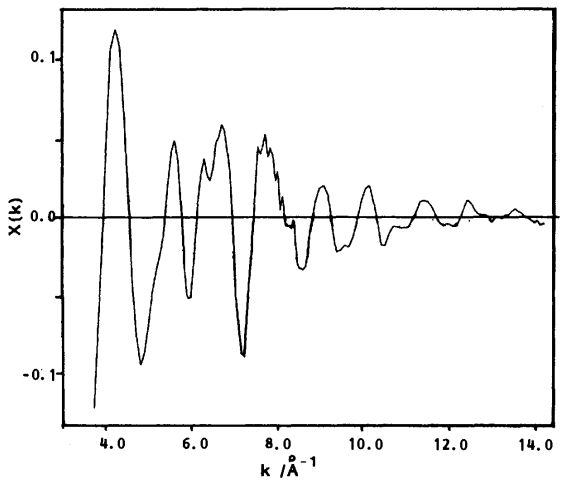

Fig. 5a. EXAFS spectrum of NiO.

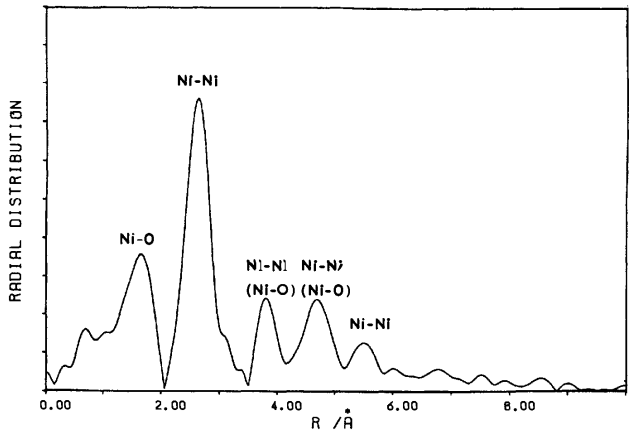

Fig. 5b. Fourier transformation of Fig. 5a.

quality of EXAFS spectra. For example, the L_α and L_η lines of W from the filament overlap the absoption spectrum of Ni. However, this difficulty can be avoided with a proper electronic circuits employed here. Measurements on two examples evidenced that the present system can give spectra good enough for a practical EXAFS analysis.

It is worth to discuss the advantage of the use of the proportional counter system over an ion-chamber system for the X-ray flux of our laboratory apparatus. The leak current of the ion chamber may be of the order of 10^{-16} A, which corresponds to *ca.* 10^3 photons. When the X-ray flux is high, for example 10^{10} photons/s, as in SOR, this leak current causes no trouble. But it is serious matter in a laboratory spectrometer operating with 10^6—10^5 photons/s. Although the photon counting systems with proportional (and scintillation) counters need the correction for the dead time in a higher X-ray flux, a proportional counter with a proper electronic circuit is preferred in this case.

Experimental

Aqueous solutions of ammine and ethylenediamine nickel(II) salts were prepared by dissolving $Ni(NO_3)_26H_2O$ in aqueous solutions of ammonia and ethylenediamine. The concentrations were determined by standard methods; Ni (0.300 M (1 M=1 mol dm^{-3})) and NH_3 (6.58 M) for ammine solution and Ni (0.292 M) and en (1.05 M) for ethylenediamine solution. The known stability constants show that the main species contained in these solutions are $[Ni(NH_3)_6]^{2+}$ for the ammine and $[Ni(en)_3]^{2+}$ for the ethylenediamine solutions. A plastic cell contained a small volume of the sample solution between windows spaced 1.0 mm apart. The solid sample was well grounded and deposited on to a piece of scotch-tape.

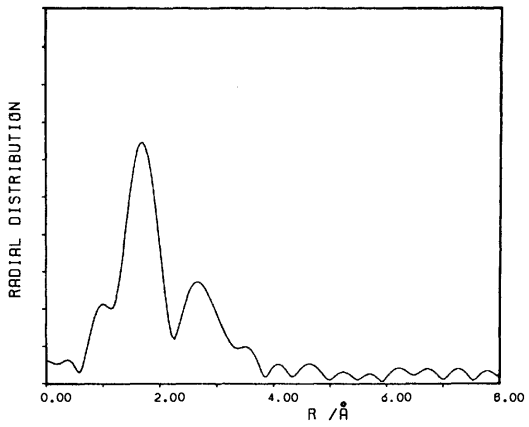

Fig. 6. Fourier transformation of the EXAFS spectrum of aqueous $[Ni(en)_3]^{2+}$ solution.

Data Analysis

The EXAFS spectra have been analyzed by following the standard procedure. The absorption background before the edge has been substracted from the experimental absorption spectrum, and the resulting spectrum $\mu(k)$ was normalized by using the atomic absorption coefficient $\mu_0(k)$, in order to give the χ(k) fine structure defined by $\chi(k)=[\mu(k)-\mu_0(k)]/\mu_0(k)$. The photoelectron wave vector is given by $k=[(E-E_0)2m/\hbar^2]^{1/2}$, where E is the photon energy and E_0, some reference energy which may not coincide with the energy of the absorption edge.

Result for the Solutions of the Ammine and Ethylenediamine Complexes

Figure 6 shows the results of Fourier transformation from the k space to the r space for aqueous $[Ni(en)_3]^{2+}$ solution. The radial distribution curve shows two peaks, of which the main one should correspond to the N atoms of the coordinated ethylenediamine ligands and the smaller one may be due to the C atoms of the ligands.

The curve-fitting analysis was performed according to the method of Cramer *et al.*[16] using the following formula.

$$k^2\chi(k) = c_0Nr^{-2}\exp(-c_1k^2)k^{-c_2}\sin[a_0+(a_1+2r)k+a_2k^2],$$

N and r represent the coordination number and the interatomic distance, respectively, and c_0—c_2 are the parameters for the amplitude functions and a_0—a_2 the phase shift parameters. To determine the parameter values, we first examined the spectra of the cryslalline $[Ni(en)_3]SO_4$ and $[Ni(en)_3](NO_3)_2$ of which the structures are known ($r_{Ni\text{-}N}$=2.124 Å for sulfate,[7] $r_{Ni\text{-}N}$= 2.120 Å for nitrate,[8] and N=6 for both complexes).

TABLE 1. CROSS-CHECK OF THE RESULTS OF LEAST-SQUARES FITS TO EXAFS DATA FOR CRYSTALLINE $[Ni(en)_3](NO_3)_2$ AND $[Ni(en)_3]SO_4$

	Coordination number	Ni–N distance/Å
$[Ni(en)_3](NO_3)_2$	5.7±0.8(6.0)	2.11±0.01(2.120)[a]
$[Ni(en)_2]SO_4$	6.2±0.8(6.0)	2.13±0.01(2.124)[b]

a) Obtained with parameters derived from the EXAFS of $[Ni(en)_3]SO_4$. (The values in parentheses are the results of an X-ray diffraction study.[8]) b) Obtained with parameters derived from the EXAFS of $[Ni(en)_3](NO_3)_2$. (The values in parentheses are the results of an X-ray diffraction study.[7])

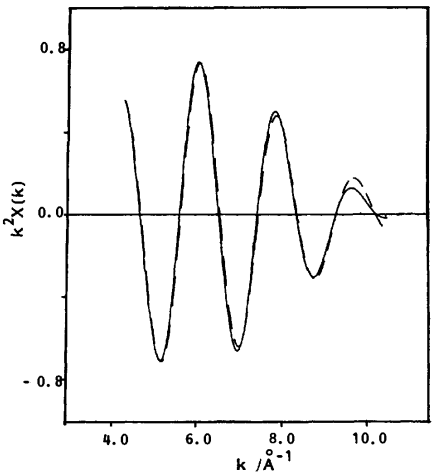

Fig. 7. First-shell fit for determining the structure of $[Ni(en)_3]^{2+}$ in solution by use of a set of parameters derived from the spectrum of solid $[Ni(en)_3]SO_4$. The solid line is the filtered EXAFS spectrum and dashed line is the least-squares fit.

With the fixed N and r, we obtained two sets of six parameters by curve-fitting the Fourier-filtered spectra for the isolated Ni–N interaction. For checking the accuracy of the results from analyses with these parameters, the least-squares fit to the filtered spectrum of each compound was carried out with the set of parameters obtained above for the other compound. The values obtained for N and r are shown in Table 1, which demonstrates that the analysis adopted here gives a reliable structural information.

Then we determined the N and r values for the ammine and the ethylenediamine complexes of nickel(II) in aqueous solutions with both sets of parameters. The Fourier-filtered and the least-squares fit curves are shwon in Fig. 7 for a solution of ethylenediamine nickel(II) nitrate; a set of parameters obtained from the spectrum of solid $[Ni(en)_3](NO_3)_2$ was used in the analysis. The numerical results are summarized in Table 2. Analyses with two different sets of parameters gave results in good agreement with each other. The measured coordination numbers are about six and the measured Ni–N distances are about 2.12 Å for both complexes in solutions. The values for the ethylenediamine complex are close to those for the same complex in the crystals, but are significantly different from that obtained by Fujita *et al.*[6] from their diffraction study on a solution. This inconsistency needs further investigation. Generally speaking, the EXAFS method as applied to solutions has the advantage that it detects only the interatomic interactions in which the nickel atom (or any other atom concerned) is involved, whereas the X-ray diffraction method gives a diffraction pattern which is the superposition of various diffractions by different pairs of atoms at different distances.

TABLE 2. RESULTS OF THE CURVE FITTING ANALYSIS OF THE EXAFS SPECTRA OF AQUEOUS $[Ni(NH_3)_6]^{2+}$ AND $[Ni(en)_3]^{2+}$ SOLUTIONS

	Set of parameters	Coordination number	Ni–N distance/Å
$[Ni(NH_3)_6]^{2+}$	A	6.0±0.8	2.13±0.01
	B	5.7±0.8	2.12±0.01
$[Ni(en)_3]^{2+}$	A	6.1±0.8	2.13±0.01
	B	5.8±0.8	2.12±0.01

A: Parameters derived from the spectrum of solid $[Ni(en)_3](NO_3)_2$. B: Parameters derived from the spectrum of solid $[Ni(en)_3]SO_4$.

The authors (especially M. S.) would like to thank Prof. K. Taniguchi of Osaka Electrocommunication University for his encouraging suggestions and useful discussions.

Reference

1) B. K. Teo and D. C. Joy, "EXAFS spectroscopy, techniques, and applications," Plenum press, New York, (1981).
2) M. Sano, T. Maruo, and H. Yamatera, *Chem. Phys. Lett.*, **101**, 211 (1983).
3) M. Sano, T. Maruo, and H. Yamatera, *Bull. Chem. Soc. Jpn.*, **56**, 3287 (1983).
4) T. Matsushita, to be published.
5) M. Sano, unpublished work.
6) T. Fujita and H. Ohtaki, *Bull. Chem. Soc. Japan*, **55**, 455 (1982).
7) M. Ul-Hague, C. N. Caughlan, and K. Emerson, *Inorg. Chem.*, **9**, 2421 (1971).
8) L. N. Swink and M. Atoji, *Acta Crystallogr.*, **13**, 639 (1960).
9) R. E. Cramer, W. Van Doorne, and J. T. Huneke, *Inorg. Chem.*, **15**, 529 (1976).
10) R. E. Cramer and J. T. Huneke, *Inorg. Chem.*, **17**, 365 (1978).
11) G. S. Knapp, Haydn Chen, and T. E. Klippert, *Rev. Sci. Instrum.*, **49**, 1658 (1978).
12) A. Williams, *Rev. Sci. Instrum.*, **54**, 193 (1983).
13) W. Thulke, R. Haensel, and P. Rabe, *Rev. Sci. Instrum.*, **54**, 277 (1983).
14) K. Tohji, Y. Udagawa, T. Kawasaki, and K. Masuda, *Rev. Sci. Instrum.*, **54**, 1482 (1983).
15) E. P. Bertin, "Principles and practice of X-Ray Spectrometric Analysis," 2nd ed, Plenum Press, New York, (1970).
16) S. P. Cramer, K. O. Hodgson, E. I. Stiefel, and N. E. Newton, *J. Am. Chem. Soc.*, **100**, 2748 (1978).

 © 1984 The Chemical Society of Japan Bull. Chem. Soc. Jpn., 57, 2761—2767 (1984)

Formose Reactions. XXI. A Selective Formation of Dihydroxyacetone in the Formose Reaction in *N,N*-Dimethylformamide

Yoshihiro SHIGEMASA,* Yoshihiro SASAKI, Nasuo UEDA, and Ruka NAKASHIMA
Department of Industrial Chemistry, Faculty of Engineering, Tottori University, Tottori 680
(Received November 11, 1983)

Dihydroxyacetone (DHA) was obtained in good yield from the selective formose reaction which was conducted with 2-(dimethylamino)ethanol and vitamin B_1 in *N,N*-dimethylformamide (DMF). The major products were isolated from the formose and identified as dihydroxyacetone and 2-(1,2-dihydroxyethyl)-5-(2-hydroxyethyl)-4-methylthiazole by spectral data. Vitamin B_1 suppressed the vaporization of formaldehyde from the reaction solution. Irrespective of the 2-(dimethylamino)ethanol concentration (above 0.1 M (1M=1 mol dm^{-3})), the maximum yield of DHA was 80—90 glc% at 1.0 M formaldehyde concentration, when the formaldehyde consumption was above 90%. Above 3.0 M formaldehyde concentration, selective formation of DHA (above 80 glc%) was obtained at the early stage of the reaction. The scheme for the formation of DHA in the formose reaction in the presence of vitamin B_1 was also proposed.

Dihydroxyacetone, a fermentation product of glycerol,[1] has been used as a building block for pharmaceuticals, dyes, foodgrade emulsifiers, plasticizers, fungicides, and alkyd-type resins. It is, furthermore, noted as a key intermediate in a novel pathway for formaldehyde fixation in methanol-utilizing yeasts.[2] Several methods of preparation of DHA by chemical means were studied.[3] It is also formed in the formose reaction catalyzed by aq-alc $Ca(OH)_2$.[4] Recently, Inoue *et al.*[5] reported that dihydroxyacetone was obtained in a good yield (80%) when the formose reaction was carried out in dioxane in the presence of 3-ethylbenzothiazolium bromide and triethylamine at 100 °C. The formose reaction[6] catalyzed by triethylamine and a derivative of thiazole in DMF solution at 100 °C was found to give no branched sugars such as glucose, galactose, xylose, and glyceraldehyde dimer. Furthermore at the early stage of the reaction glyceraldehyde dimer was the major products. It is important that three carbon carbohydrates such as dihydroxyacetone and glyceraldehyde are obtained in high selectivity.

We have studied the effects of various reaction conditions on the product distribution, such as catalysts, the concentration of formaldehyde and catalyst, the reaction temperature, the kind of solvent and so on. In our studies,[7-12] it has been found that some formose reactions in H_2O or methanol give selectively 2-(hydroxymethyl)glycerol (2-HG), 3-(hydroxymethyl)pentitol (3-HP), 2,4-bis(hydroxymethyl)pentitol (2,4-BHP), pentaerythritol (PE), 2,4-bis(hydroxymethyl)-3-pentulose (2,4-BH-3-P), 3-(hydroxymethyl)pentofuranose (3-HPF), or 3,3-bis(hydroxymethyl)-3-deoxy-tetrono-1,4-lactone (3,3-BH-3-DT-1,4-L), and these products have been isolated in a pure form. All of these products are branched sugars and sugar alcohols. It is interesting to study the formose reaction, using dipolar aprotic solvents such as DMF and dimethyl sulfoxide (DMSO) instead of protic solvents such as H_2O and methanol. We have searched for the catalysts which give the simple product-distribution in the gas chromatogram of trimethylsilyl derivatives, using DMF and DMSO as a solvent and have already reported that dihydroxyacetone (DHA) is formed selectively in the presence of 2-(dimethylamino)ethanol and vitamin B_1.[13] The role of vitamin B_1 was also observed: in the absence of vitamin B_1, formaldehyde vaporized and a self-condensation of

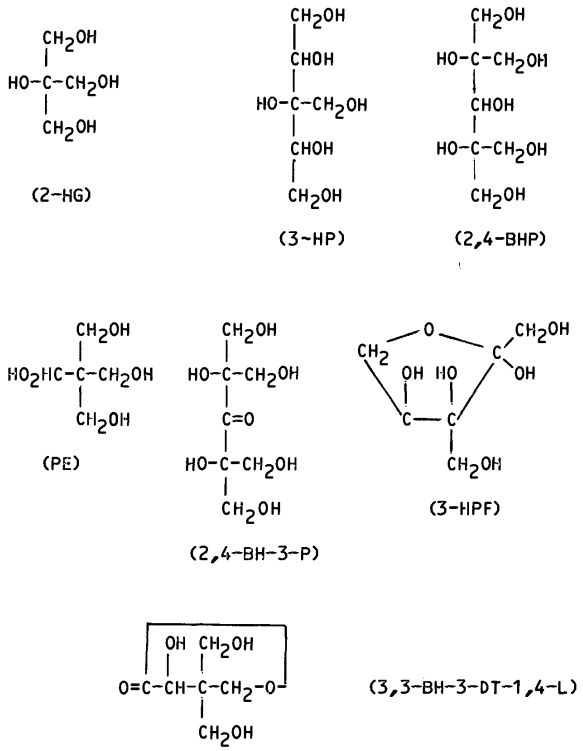

vaporized formaldehyde to paraformaldehyde took place very readily under the given reaction conditions; in the presence of vitamin B_1, however, such reactions were sufficiently suppressed for the formose reaction in DMF to occur smoothly. A product derived from vitamin B_1 was also isolated and assigned to be 2-(1,2-dihydroxyethyl)-5-(2-hydroxyethyl)-4-methylthiazole (**I**) on the basis of spectroscopic data.

The purpose of this paper is to report the effects of various inorganic and organic catalysts on the formose reaction in DMF and to reveal the effects of vitamin B_1, the reaction temperature, and the concentration of 2-(dimethylamino)ethanol and formaldehyde on the formation of DHA and (**I**).

Experimental

Materials. Two types of paraformaldehyde were used. Paraformaldehyde produced by Merck Co. (95%) had a smaller particle size and gave a faster HCHO consumption

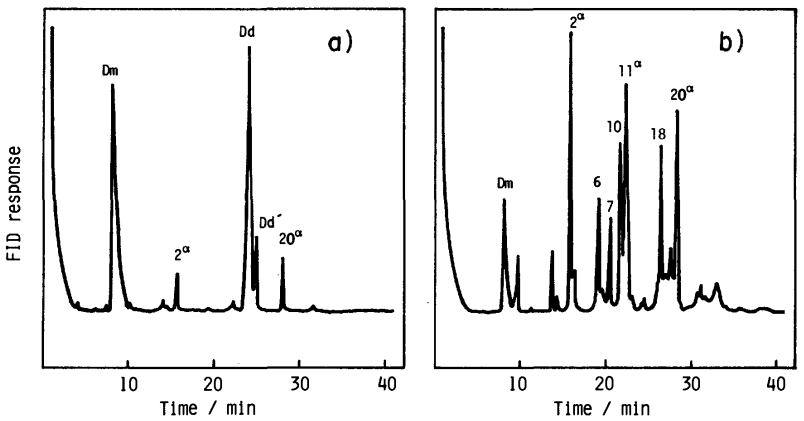

Fig. 1. The glc patterns of trimethylsilylated products from: (a) the selective formose reaction for 180 min starting from [HCHO]= 1.1 M, [2-(Dimethylamino)ethanol]=0.11 M, [Vitamin B_1-HCl]= 0.028 M and DMF=180 ml at 60°C, and (b) non-selective formose reaction for 5 min starting from [HCHO]=1.1 M, [$Ca(OH)_2$]=0.11 M, [Vitamin B_1-HCl]=0.028 M and DMF=180 ml at 100°C.

than that of Mitsubishi Gas Chem. (86%), but the differences in the product-distribution and the formose yield between the two were small. All the inorganic and organic bases used as catalysts were of analytical grade. DMF was purified in the usual way.[14]

Procedure. A representative example of the reaction is as follows. A five-necked flask (200 ml), which contained 180 ml of DMF, was preequilibrated at 60°C in a thermostat under nitrogen; the reaction was then initiated, followed by the addition of 2-(dimethylamino)ethanol (1.8 g, 0.11 M), paraformaldehyde (Merck Co., 6.3 g, 1.1 M), and vitamin B_1-HCl (1.7 g, 0.028 M) in this order. At suitable intervals, 5 ml aliquots were withdrawn into a 10 ml flask, and the reaction was quenched immediately by acidification with 9M HCl. The aliquots were analyzed for formaldehyde following the method of Bricker *et al.*,[15] except that the optical density was measured at 579 nm. Then, the reaction mixture was concentrated under reduced pressure (25—30°C/2 mmHg†) to yield a brownish syrup (6.5 g). The product yield and distribution were determined as the pertrimethylsilylated products by gas-liquid chromatography. The yield (mg/ml) was measured by the internal standard (pentaerythritol) method. The glc pattern (Fig. 1a) clearly indicates the selective formation (90%) of the product corresponding to the peaks Dm, Dd, and Dd', the retention times of which are the same as those of pertrimethylsilylated dihydroxyacetone. Furthermore, the glc analysis of peracetylated products indicated one major peak in the same manner as that of authentic DHA.

Separation and Identification of Products. The product corresponding to glc peaks Dm, Dd, and Dd' was isolated as follows: The formose syrup (6.5 g) obtained by the above reaction was acetylated with acetic anhydride in pyridine, and the reaction mixture was extracted with chloroform, the extract was concentrated to 4 ml and re-extracted with 400 ml of water. Then, the water layer was concentrated to 25 ml and 4 g of active carbon was added to the concentrated solution. Acetylated dihydroxyacetone (2.5 g, hydroscopic) was obtained as a yellow crystalline form by eluting the active carbon with methanol, followed by concentrating the methanol solution. ^{1}H NMR ($CDCl_3$) δ=2.15 (6H, s, 2×O-$COCH_3$) and 4.8 (4H, s, 2×C-CH_2). The molecular ion was observed at *m/z* 174 in the electron impact mass spectrum. IR (KBr) 1745 (C=O), 1418, 1373, 1239 (OAc), and 1052 cm^{-1}. The IR spectrum was in agreement with that of an authentic sample of acetylated dihydroxyacetone.

Deacetylation of the peracetylated products with barium hydroxide gave the original product, and the trimethylsilyl derivative showed exactly the same glc behaviour as that for the directly trimethylsilylated product. The product corresponding to peaks Dm, Dd, and Dd', therefore, was assigned as a mixture of dihydroxyacetone monomer and its diastereomeric dimers (**II**).

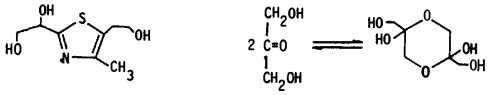

(I) (II)

The product (**I**) (40 mg, colorless syrup) corresponding to the glc peak 20$^\alpha$ was also isolated by chromatography on an active carbon column with water and methanol as eluent, followed by purification of the acetyl derivative of 20$^\alpha$ with thin-layer chromatography (benzene/EtOAc=1/1). IR (KBr) 1750 (C=0), 1640 (C=N-C), 1370, 1240 (OAc), and 1050 cm^{-1}. ^{1}H NMR ($CDCl_3$) δ=2.07 (6H, s, 2×O-CO-CH_3), 2.16 (3H, s, O-CO-CH_3), 2.36 (3H, s, C-CH_3), 3.06, 4.23 (each 2H, t, -CH_2), 4.47 and 4.64 (each 1H, dd, J_{AX}=7.08 Hz, J_{BX}=3.62 Hz, **H**-A, B), and 6.24 (1H, dd, J_{AX}=7.08 Hz, J_{BX}=3.62 Hz, **H**-X). ^{13}C NMR ($CDCl_3$) δ=170.7 (s, **C**OCH_3), 170.4 (s, **C**OCH_3), 169.7 (s, **C**OCH_3), 161.6 (s, C-2), 149.6 (s, C-4), 128.2 (s, C-5), 70.6 (d, C-2'), 64.6 (s, C-2''), 63.9 (t, C-5''), 25.9 (t, C-5'), 20.9 (q, **C**OCH_3), 20.7 (q, **C**OCH_3), and 14.9 (q, CH_3). The chemical ionization mass spectra using *i*-C_4H_{10}, NH_3, or ND_3 as a reagent gas[16] showed a quasi-molecular ion at *m/z* 330 (MH^+), 347 ($M \cdot NH_4^+$), or 351 ($M \cdot ND_4^+$), respectively, which precisely indicated a molecular weight of 329. These results suggested that the acetate of the product (**I**) had no active hydrogen in the molecule. Deacetylation of the acetate with barium hydroxide gave product (**I**) as a colorless syrup. IR (KBr) 3350 (br., OH), 1630 (C=N-C), 1550, 1440, 1320, 1190, and 1050 cm^{-1}. ^{1}H NMR(CD_3OD) δ=2.29 (3H, s, C-CH_3), 2.90 and 3.69 (each 2H, t, -CH_2-), 3.74 (2H, d, -CH_2OH), and 3.83 (^{1}H, t, >CHOH). ^{13}C NMR (CD_3OD) δ=171.8 (s, C-2), 148.9 (s, C-4), 129.8 (s, C-5), 73.5 (d, C-2') 67.4 (t, C-2''), 63.1 (t, C-5''), 30.5 (t, C-5'), and 14.7 (q, CH_3). The chemical ionization mass spectra using *i*-C_4H_{10}, NH_3, or ND_3 as a reagent gas showed a quasi-molecular ion at *m/z* 204 (MH^+), 221 ($M \cdot NH_4^+$), or 228 ($d_3M \cdot ND_4^+$), respectively, which precisely indicated a molecular weight of 203 and the presence of three active hydrogens in the molecule. These results led us to assign 20$^\alpha$ to be 2-(1,2-dihydroxyethyl)-5-(2-hydroxyethyl)-

† 1 mmHg≈133.322 Pa.

4-methylthiazole as the product derived from vitamin B_1.

Results and Discussion

Formose Reactions in DMF in the Presence of Inorganic and Organic Bases. The formose reactions were carried out with various inorganic bases (Table 1). In the case of LiOH and $Pb(CH_3COO)_2 \cdot Pb(OH)_2$, formaldehyde was consumed smoothly, but after 2 h of reaction time, NaOH, $Mg(OH)_2$, $Ba(OH)_2$, and $Pb_2O(OH)_2$ gave little formose. LiOH, $Ca(OH)_2$, and $Sr(OH)_2$ were found to give the product of GP-11 selectively which had the same retention time as 3,3-BH-3-DT-1,4-L.[7] Under these reaction conditions, the formose yield was low and considerable paraformaldehyde adhered to the upper part of the reaction flask as described previously.[13]

The results of the formose reactions catalyzed by various inorganic bases and organic bases in the presence of vitamin B_1 are summarized in Tables 2 and 3, respectively. In Table 2, product (**I**) corresponding to glc peak 20$^{\alpha}$ which was derived from vitamin B_1 was

Table 1. Formose reactions catalyzed by various inorganic bases[a]

Base	Time	HCHOconsumption	Main products/glc%[b]						Total yield[f]
	min	%	2	10	11	18	19	26	mg·ml^{-1}
$LiOH \cdot H_2O$	10	90	8.4		37.2	10.9	9.4		
			(0.06)	e)	(0.26)	(0.07)	(0.06)	e)	0.69
NaOH	180	c),d)	e)	e)	e)	e)	e)	e)	
KOH	120	67[d]	e)	e)	12.5	13.5	8.0	10.0	
					(0.27)	(0.30)	(0.17)	(0.22)	2.18
$Mg(OH)_2$	180	c),d)	e)	e)	e)	e)	e)	e)	
$Ca(OH)_2$	180	48[d]	e)	e)	25.8	e)	e)	e)	
					(0.10)				0.39
$Sr(OH)_2 \cdot 8H_2O$	180	48[d]	e)	e)	41.9	e)	e)	e)	
					(0.30)				0.71
$Ba(OH)_2 \cdot 8H_2O$	120	c),d)	e)	e)	e)	e)	e)	e)	
$Pb(CH_3COO)_2 \cdot Pb(OH)_2$	6	90	11.1	17.8	10.3	7.0	e)	e)	
			(0.41)	(0.65)	(0.38)	(0.26)			3.66
$Pb_2O(OH)_2$	180	39[d]	e)	e)	e)	e)	e)	e)	

a) DMF=180 ml, [HCHO]=1.1 M, [Base]=0.11 M, Temp=100 °C, pH: not adjusted, Stirring rate=240 min^{-1}. b) Parentheses indicate yield(mg/ml) measured by the internal standard(pentaerythritol) method. c) Solid paraformaldehyde remained in the reaction solution. d) A lot of paraformaldehyde adhered to the flask. e) GLC was below 1%. f) Total yield(mg/ml) is the summation of yield of each product measured by the internal standard(pentaerythritol) method.

Table 2. Formose reactions catalyzed by various inorganic bases in the presence of vitamin B_1[a]

Base	Time	HCHOconsumption[b]	Main products/glc%[c]							Total yield[h]
	min	%	DHA	1$^{\beta}$	2$^{\alpha}$	10	11$^{\alpha}$	18	20$^{\alpha}$	mg·ml^{-1}
$LiOH \cdot H_2O$	8	93	54.1	e)	14.2	e)	5.4	e)	7.4	
			(6.37)		(1.68)		(0.64)		(0.87)	11.77
	10	77[d]	42.1	e)	25.3	e)	7.7	e)	e)	
KOH			(2.97)		(1.78)		(0.54)			7.05
	15	89	10.5	e)	22.4	8.3	15.1	13.3	7.4	
			(1.45)		(3.10)	(1.15)	(2.09)	(1.84)	(1.02)	13.82
$Ca(OH)_2$	3	97	9.3	e)	19.6	7.9	13.7	6.0	10.7	
			(1.44)		(3.02)	(1.22)	(2.11)	(0.93)	(1.65)	15.45
$Sr(OH)_2 \cdot 8H_2O$	5	98	6.3	e)	6.4	9.6	11.2	8.9	11.7	
			(0.87)		(0.88)	(1.33)	(1.55)	(1.23)	(1.62)	13.87
NaOH	120	34[d),g]	e)	22.6	e)	e)	e)	e)	14.4	
				(0.29)					(0.18)	1.29
$Ba(OH)_2 \cdot 8H_2O$	30	98	30.7	e)	16.8	e)	9.5	5.5	10.0	
			(4.96)		(2.70)		(1.54)	(0.88)	(1.61)	16.13
$Mg(OH)_2$	120	97	e)	e)	14.0	6.5	10.7	9.6	21.4	
					(1.84)	(0.85)	(1.41)	(1.26)	(2.81)	13.13
$Pb_2O(OH)_2$	60	90	e)	e)	24.6	14.0	10.3	e)	13.0	
					(2.84)	(1.61)	(1.19)		(1.50)	11.51
f)	120			46.7						
				(0.22)						0.41

a) DMF=180 ml, [HCHO]=1.1 M, [Base]=0.11 M, [Vitamin B_1-HCl]=0.028 M, Temp=100 °C, pH: not adjusted, Stirring rate=240 min^{-1}. b) The amount of paraformaldehyde adhering to the flask was small. c) Parentheses indicate yield(mg/ml) measured by internal standard(pentaerythritol) method. d) Solid paraformaldehyde remained in the reaction solution. e) GLC was below 1%. f) Paraformaldehyde and base were not added. g) A lot of paraformaldehyde adhered to the flask. h) Total yield(mg/ml) is the summation of yield of each product measured by the internal standard(pentaerythritol) method.

TABLE 3. FORMOSE REACTIONS CATALYZED BY VARIOUS ORGANIC BASES IN THE PRESENCE OF VITAMIN B_1[a]

Base	Time	HCHOconsumption[b]	Main products/glc%[c]					Total yield[g]
	min	%	DHA	1^{β}	2^{α}	20^{α}	24^{α}	mg·ml^{-1}
dimethylamine (abt. 40% in water)	120	26[d]	f)	6.6 (0.04)	f)	f)	f)	0.55
morpholine	120	52[e]	f)	13.0 (0.13)	f)	f)	f)	0.97
N,N-dimethyl-aniline	120	40[e]	f)	17.1 (0.40)	f)	6.6 (0.15)	10.9 (0.25)	2.32
β-picoline	120	22[d),e]	f)	13.7 (0.21)	f)	14.0 (0.21)	f)	1.51
N-methyl-morpholine	120	38[d),e]	44.1 (1.93)	f)	f)	34.1 (1.49)	10.7 (0.47)	4.38
triethanolamine	60	75	f)	f)	f)	11.6 (1.49)	f)	2.09
trimethylamine (30% in water)	60	93	75.2 (10.49)	f)	6.2 (0.87)	9.7 (1.35)	f)	13.95
2-(dimethyl-amino)ethanol	30	91	82.0 (11.79)	f)	f)	8.5 (1.22)	f)	14.35
triethylamine	30	91	81.7 (8.64)	f)	5.1 (0.54)	8.0 (0.84)	f)	10.58
N-methyl-piperidine	30	93	81.4 (10.16)	f)	5.6 (0.70)	7.3 (0.92)	f)	12.49

a) DMF=180 ml, [HCHO]=1.1 M, [Base]=0.11 M, [Vitamin B_1-HCl]=0.028 M, Stirring rate=240 min^{-1}., pH: not adjusted, Temp=100°C. b) The amount of paraformaldehyde adhering to the flask was small. c) Parentheses indicate yield(mg/ml) measured by the internal standard(pentaerythritol) method. d) A lot of paraformaldehyde adhered to the flask. e) Solid paraformaldehyde remained in the reaction solution. f) GLC was below 1%. g) Total yield(mg/ml) is the summation of the yield of each product measured by the internal standard(pentaerythritol) method.

formed. LiOH, KOH, and $Ba(OH)_2$ were found to give DHA selectively. Compared with the cases in the absence of vitamin B_1, formaldehyde was consumed smoothly, the yield of formose increased, and the amount of formaldehyde adhering to the reaction vessel was small. In the absence of base, the formose reaction did not proceed and the added formaldehyde was recovered entirely over 120 min. Hence, it can be concluded that by itself vitamin B_1 has no catalytic action for the formose reaction in DMF. As shown in Table 3, (**I**) was also formed except in the case of dimethylamine and morpholine. Dimethylamine, morpholine, *N,N*-dimethylaniline, and β-picoline were found to give gas chromatogram peak number 1^{β} (GP-1^{β}) as a major product which was formed easily when vitamin B_1 was heated in DMF; 2-(dimethylamino)ethanol, trimethylamine, *N*-methylpiperidine, and triethylamine were found to give the good yield of DHA.

Effects of Vitamin B_1. As described above, the formose reactions in the presence of vitamin B_1 gave smoother formaldehyde consumption, better yield of formose, and less formaldehyde adhering to the reaction vessel. The solubility of formaldehyde in DMF at 60 or 100°C was measured in the presence or absence of vitamin B_1 with the results shown in Fig. 2. The amount of dissolved formaldehyde in DMF and the solution rate increased with an increase in temperature. At 60°C, formaldehyde scarcely vaporized and remained in the solution, but at 100°C, the vaporization of formaldehyde proceeded smoothly and the formaldehyde concentration in the solution decreased rapidly. In the presence of vitamin B_1, however, the vaporization of formaldehyde was suppressed. Furthermore, solid paraformaldehyde remained in the solution.

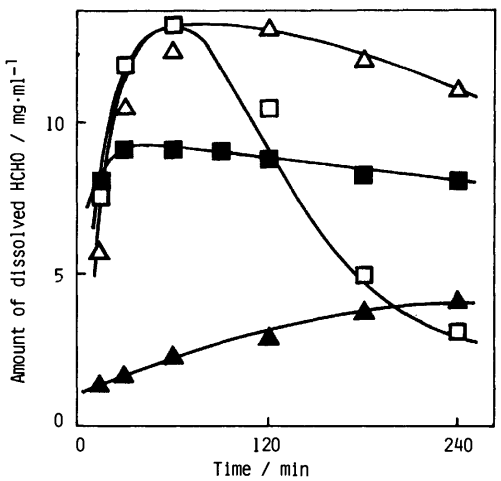

Fig. 2. Solubility of HCHO in DMF.
DMF=180 ml, [HCHO]=1.1 M, Stirring rate=240 min^{-1}. □, Temp=100°C; ▲, Temp=60°C; ■, Temp=100°C; up to 15 min and 60°C after 15 min; △, Temp=100°C; [Vitamin B_1-HCl]=0.028 M.

In all cases studied, the total amount of adhering, dissolved, and residual formaldehyde at 240 min was nearly equal to the amount of formaldehyde added. These results suggest that the interaction between vitamin B_1 and formaldehyde yields the Lapworth intermediate (**III**)[6,17] which is well known as "active aldehyde" in the transketolase reaction.[18]

Figure 3 shows the relationship between the vitamin B_1 concentration and the yield of DHA in the presence of 2-(dimethylamino)ethanol at 100°C. As the reaction proceeded, the yield of DHA increased and reached a constant value. The yield of DHA increased with increasing vitamin B_1 concentration up to a concentration

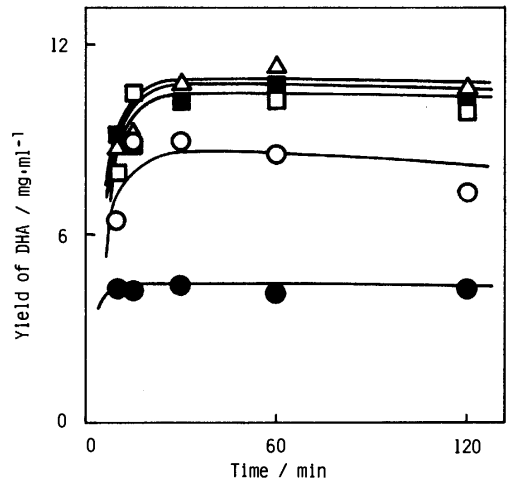

Fig. 3. Effect of vitamin B_1 concentration on the yield of DHA.
DMF=180 ml, [2-(Dimethylamino)ethanol]=0.11 M, [HCHO]=1.1 M, Stirring rate=240 min^{-1}, Temp=100°C.
[Vitamin B_1-HCl] (M): ●, 0.007; ○, 0.014; □, 0.028; ■, 0.042; △, 0.056.

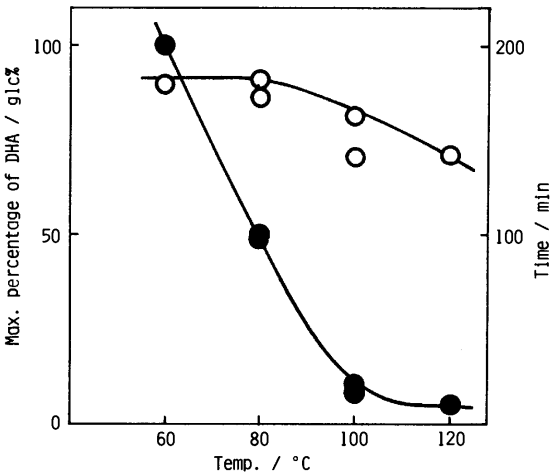

Fig. 4. Effect of temperature on the reaction time when DHA shows maximum percentage in glc and the value of its maximum percentage.
DMF=180 ml, [2-(Dimethylamino)ethanol]=0.11 M, [HCHO]=1.1 M, [Vitamin B_1-HCl]=0.028 M, Stirring rate=240 min^{-1}.
○, Max. percentage of DHA (glc%); ●, The time(min) when DHA showed max. percentage.

of 0.028 M. In the absence of vitamin B_1, 4.4 g of paraformaldehyde adhered to the upper part of the reaction vessel after 120 min of reaction time, when the formaldehyde consumption was 11% and DHA no longer formed. GP-2$^{\alpha}$ formed in *ca.* 20 glc% yield at 0.007 M of vitamin B_1 and, with an increase in vitamin B_1 concentration, decreased to less than 1 glc% at 0.028 M. The yield of product (**I**), furthermore, increased with increasing concentration of vitamin B_1.

Effects of the Reaction Temperature. The influence of the reaction temperature on the formose reaction was studied. This included the yield of DHA, the product distribution, the formaldehyde consumption *etc.* The results are shown in Fig. 4. By raising the reaction temperature, the formaldehyde consumption

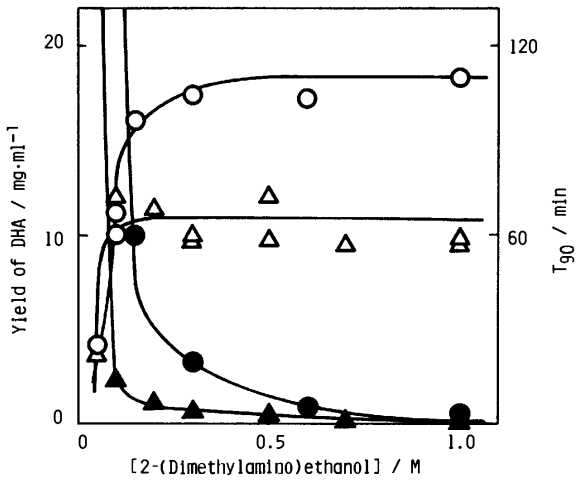

Fig. 5. Effect of the concentration of 2-(dimethylamino)ethanol on the yield of DHA and T_{90}.
DMF=180 ml, [Vitamin B_1-HCl]=0.028 M, Temp.=100°C, Stirring rate=240 min^{-1}. Yield of DHA, [HCHO] (M): △, 1.1; ○, 3.0. T_{90}, [HCHO] (M): ▲, 1.1; ●, 3.0.

rate increased, the yield of DHA decreased, and the side-products (**I**) and GP-2$^{\alpha}$ formed appreciably. The time at which DHA showed maximum percentage in the gas chromatogram decreased rapidly with an increase in the reaction temperature and at that time the formaldehyde consumption was above 90%. Irrespective of the reaction temperature, the amount of DHA hardly changed after reaching the maximum value. It can therefore be presumed from these results that even at the high reaction temperature of 100 or 120°C, DHA is stable under these reaction conditions.

Effects of the 2-(Dimethylamino)ethanol Concentration. Figure 5 shows the relationship between the yield of DHA, the formaldehyde consumption, and the 2-(dimethylamino)ethanol concentration. With an increase in the 2-(dimethylamino)ethanol concentration, the yield of DHA and the decreasing rates of the total sugar and DHA increased, however, above 0.1 and 0.15 M of the base concentration at the formaldehyde concentration of 1.0 and 3.0 M, respectively, the maximum yield of DHA had a constant value regardless of the base concentration. The maximum total sugar yield were 10—13 and 30—35 mg/ml, respectively. The maximum percentage of DHA, furthermore, was 80—90 and 60—80 glc% at 1.0 and 3.0 M of the formaldehyde concentration, when the formaldehyde consumption was above 90 and 60—80%, respectively. At a formaldehyde concentration of 3.0 M the formation of other products which might be derived from DHA reduced the selectively for DHA formation. The time (T_{90}) when the formaldehyde consumption reached 90% shortened with increasing base concentration. This suggests that 2-(dimethylamino)-ethanol not only catalyzes the formose reaction, but also decomposes the products formed. It is also considered that DHA is the principal in the formose reaction. Product (**I**) was detected only below 0.1 M of the base concentration at 1.0 M of the formaldehyde concentration, however, at 3.0 M of formaldehyde, the yield of product (**I**) was 1—2 mg/ml, regardless of the base concentration.

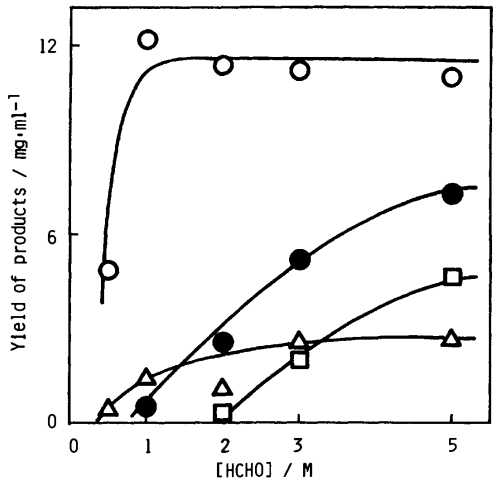

Fig. 6. Effect of HCHO concentration on the yield of products.
DMF=180 ml, [2-(Dimethylamino)ethanol]=0.11 M, [Vitamin B_1-HCl]=0.028 M, Stirring rate=240 min^{-1}, Temp=100°C.
○, DHA; ●, 2$^{\alpha}$; □, 10; △, 20$^{\alpha}$.

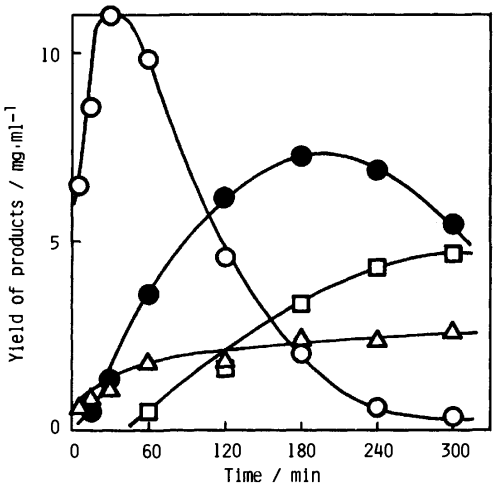

Fig. 7. Time-courses of the yield of products.
DMF=180 ml, [HCHO]=5.0 M, [2-(Dimethylamino)-ethanol]=0.11 M, [Vitamin B_1-HCl]=0.028 M, Stirring rate=240 min^{-1}, Temp=100°C.
○, DHA; ●, 2$^{\alpha}$; □, 10; △, 20$^{\alpha}$.

Effects of the Formaldehyde Concentration on the Product Distribution. The relationship between the formaldehyde concentration and the product distribution is shown in Fig. 6. Irrespective of the formaldehyde concentration (above 1.0 M), the maximum amounts of DHA and product (**I**) showed constant values of *ca.* 12 and 2 mg/ml, respectively. However, by raising the formaldehyde concentration, the yields of GP-2$^{\alpha}$ and GP-10 increased; the isolation and structure elucidation of these products are now under investigation. The proportion of DHA in the total products decreased. Above 3.0 M formaldehyde concentration, the selective formation of DHA (above 80 glc%) occurs during the early stage of the reaction. Concerning the formation of glyceraldehyde, the same phenomenon was observed by J. Castells *et al.*[6]: Paraformaldehyde (1.33 mol) was added, with continuous stirring, to a solution of triethylamine (186 mmol) and 3-benzyl-5-(2-hydroxyethyl)-4-methylthiazolium chloride (185 mmol) in DMF (250 ml) at 100°C. The amount of DHA formed, furthermore, decreased rapidly with in increase in the formaldehyde concentration. Figure 7 shows the typical time-courses of the products. In these experiments, the formaldehyde consumption at 300 min was 85%. GP-2$^{\alpha}$ and GP-10 increased instead of DHA decreasing. These results suggest that DHA is a precursor of GP-2$^{\alpha}$ and GP-10 and play an important role in the formose reaction.

Scheme for DHA Formation. J. Castells *et al.*[6] suggested the following scheme concerning the formation of glycolaldehyde, glyceraldehyde, and DHA in the formose reaction carried out under the similar reaction conditions to ours. In the scheme they made two assumptions: (1) The Lapworth intermediate (**III**) did not attack ketone carbonyl groups. This assumption was based on the fact that no branched-chain products were isolated in any benzoin condensation.; (2) The Lapworth intermediate (**III**) did not react, or reacted slowly, with aldohexoses, due to the predominance of hemiacetal forms (masked aldehyde carbonyl groups).

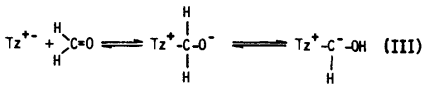

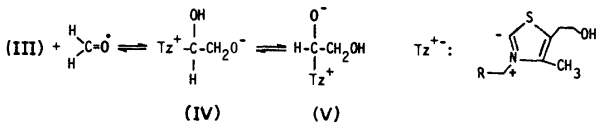

In penetrating studies on benzoin and acetoin formation in the presence of thiamine and other thiazolium compounds pursued by Breslow and others,[18,19] the hydrogen atoms at position 2 of the thiazolium ring was found to exchange rapidly in a deuterated solvent. The product (**I**), furthermore, was detected in the products of the formose reaction in the presence of vitamin B_1. These results suggest the presence of the intermediate (**IV**) which would give the intermediate (**V**). Then, the two following paths may be considered: Further addition of formaldehyde and formation of DHA (Path 1); formation of glycolaldehyde and glyceraldehyde (Path 2).

Path 1

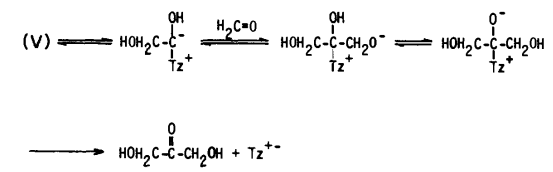

Path 2

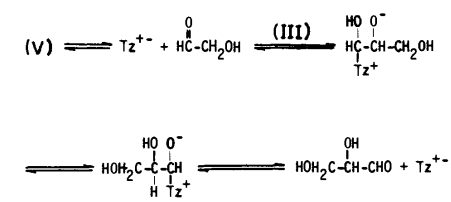

The formation of glycolaldehyde and glyceraldehyde as minor products and of dihydroxyacetone (DHA) as a major product suggests that Path 1 would be predominant under the reaction conditions investigated in this report. The above formulation of the reaction mechanism, however, can not explain why Path 1 proceeds in preference to Path 2, and how the substituent group on the nitrogen atom of the thiazolium ring affects the formation of DHA.

Conclusions. From these observations, one can draw the following conclusions. First, vitamin B_1 has no catalytic action for the formose reaction in DMF by itself, but gives more smooth formaldehyde consumption, better yield of formose, and the formation of 2-(1,2-dihydroxyethyl)-5-(2-hydroxyethyl)-4-methylthiazole and some complexes with formaldehyde. Second, by raising the reaction temperature, the side-reactions also proceed easily, however, even at such high reaction temperatures as 100 or 120°C, DHA is stable under these reaction conditions. Third, DHA is the principal intermediate in the formose reaction and is decomposed by the excess of base.

Finally, the present investigation provides the following guide-lines for obtaining high DHA yield in batch-reaction systems. Further addition of formaldehyde to DHA and the decomposition of DHA must be minimized. This may be done at low formaldehyde concentrations, at relatively low reaction temperature (60°C), and at high [base]/[HCHO] ratios with low base concentrations, or by stopping the reaction at an early stage in the case of high formaldehyde concentrations.

References

1) Wallestein Co., U. S. Patent 2948658 (1960); K. Gomeric and J. Suput, *Mikrobiologija*, **6**, 77 (1969).

2) N. Kato, T. Higuchi, C. Sakazawa, T. Nishizawa, Y. Tani, and H. Yamada, *Biochim. et Biophys. Acta.*, **715**, 143 (1982).

3) T. Ando, S. Shioi, and M. Nakazawa, *Bull. Chem. Soc. Jpn.*, **45**, 2611 (1972); H. P. den Otter, *Rec. Trav. Chim. Pays-Bas*, **56**, 474 (1937); BASF, *Ger. Offen*, 2558525 (1977).

4) O. E. Lavanevskii and A. A. Morozov, U.S.S.R. Patent 498281; *Chem. Abstr.*, **84**, 89620g.

5) T. Matsumoto, M. Yamamoto, and S. Inoue, 46th Spring Meeting of Chem. Soc. Jpn., Kyoto, April 1983 Abstr. No. 3H29; T. Matsumoto and S. Inoue, *J. Chem. Soc., Chem. Commun.*, **1983**, 171.

6) J. Castells, F. Geijo, and F. Lopez-Calahorra, *Tetrahedron Lett.*, **21**, 4517 (1980).

7) Y. Shigemasa, K. Oogaki, N. Ueda, R. Nakashima, K. Harada, N. Takeda, M. Suzuki, and S. Saito, *J. Carbohydr. Chem.*, **1**, 325 (1983).

8) Y. Shigemasa, O. Nagae, C. Sakazawa, R. Nakashima, and T. Matsuura, *J. Am. Chem. Soc.*, **100**, 1309 (1978).

9) Y. Shigemasa, Y. Matsuda, C. Sakazawa, and T. Matsuura, *Bull. Chem. Soc. Jpn.*, **50**, 222 (1977).

10) Y. Shigemasa, S. Akagi, R. Nakashima, and S. Saito, *Carbohydr. Res.*, **80**, C1 (1980).

11) Y. Shigemasa, T. Hamada, M. Hirabayashi, E. Waki, R. Nakashima, K. Harada, N. Takeda, and M. Suzuki, *Chem. Lett.*, **1981**, 899.

12) Y. Shigemasa, M. Kawahara, C. Sakazawa, R. Nakashima, and T. Matsuura, *J. Catal.*, **62**, 107 (1980).

13) Y. Shigemasa, H. Matsumoto, Y. Sasaki, N. Ueda, R. Nakashima, K. Harada, N. Takeda, M. Suzuki, and S. Saito, *J. Carbohydr. Chem.*, **2**, 343 (1983); Y. Shigemasa, Y. Sasaki, N. Ueda, and R. Nakashima, 46th Spring Meeting of Chem. Soc. Jpn., Kyoto, April 1983, Abstr. No. 3H25.

14) T. Tachibana, Ed., "Shin Jikken Kagaku Kohza," Maruzen, Tokyo (1975), Vol. 1, p. 457.

15) C. E. Bricker and H. R. Johnson, *Ind. Eng. Chem.*, **17**, 400 (1945).

16) M. Suzuki, K. Harada, N. Takeda, and A. Tatematsu, *Biochemical Mass Spectrometry*, **81**, 332 (1981).

17) A. Lapworth, *J. Chem. Soc.*, **85**, 1206 (1904).

18) L. O. Krampitz, G. Greull, D. B. S. Miller, J. B. Bicking, H. R. Skeggs, and J. M. Sprague, *J. Am. Chem. Soc.*, **80**, 3719 (1958).

19) R. Breslow, *J. Am. Chem. Soc.*, **79**, 1762 (1957); **80**, 3719 (1958).

Regio- and Stereocontrolled Synthesis of Allenic and Acetylenic Derivatives. Organotitanium and Boron Reagents

Kyoji FURUTA, Masaharu ISHIGURO, Ryuichi HARUTA, Nobuo IKEDA, and Hisashi YAMAMOTO*
Department of Applied Chemistry, Nagoya University, Chikusa, Nagoya 464
(Received December 26, 1983)

The propargyltitanium reagents derived from 1-alkylpropyne condensed with aldehydes to give α-allenyl alcohol regioselectively, while the allenyltitanium reagents generated from 1-alkyl-1-butyne derivatives gave *threo*-β-acetylenic alcohols with high regio- and stereoselectivities. The course of the reaction was determined by the substitution pattern of starting alkynes. The similar reactions of metallated 1,3-bis(trialkylsilyl)propyne or (trialkylsilyl)acetonitrile with aldehydes were also investigated.

The importance of the propargylic anions in synthetic chemistry emerged from the recognitions of their utility for the extension of the carbon chain and facility in the interconversion of the functionality.[1] Their applicability in organic synthesis, however, has been limited because of the difficulties in controlling the regio- and stereoselectivities of the reaction. As it is often pointed out, the propargylic anion may be in equilibrium with allenic anion.[2] Thus, in the condensation with carbonyl compounds, two products, acetylenic and allenic alcohols, can be formed. Furthermore, each product may consist of two stereoisomers, *i. e.*, *erythro* and *threo* isomers.[3] Under the ordinary reaction conditions, therefore, these four isomers should be produced. Thus, to achieve the selective reaction, it is necessary to solve the regiochemical (allenic and acetylenic) and stereochemical (*erythro* and *threo*) problems at the same time. The similar ambiguity should be observed in the reaction of allylic anions.[4]

In general, the structure and reactivities of the ambident anion are highly dependent on the nature of the countercations and solvents.[5] In our continuative studies on the organometallic reagents, we found the propargylic titanium reagents partially solved the aforementioned problems. We also investigated the reaction of nitrile anion,[6] which had an analogous structure with propargylic anion, and observed that the boron as a countercation gave the best result in this particular case.

We report here a regio- and stereocontrolled synthesis of allenic and acetylenic alcohols using propargyltitanium reagents. The application of the methodology for the synthesis of enynes and α,β-unsaturated nitriles were also described herein.[7]

Results and Discussion

Synthesis of Allenic and Acetylenic Alcohols. The lithio propargylic derivatives, which were easily generated from substituted propyne derivatives and *t*-butyllithium, were subject to condensation with aldehydes as such or after the exchange of the lithium ion by subsequent treatment with appropriate metal salts (Scheme 1).

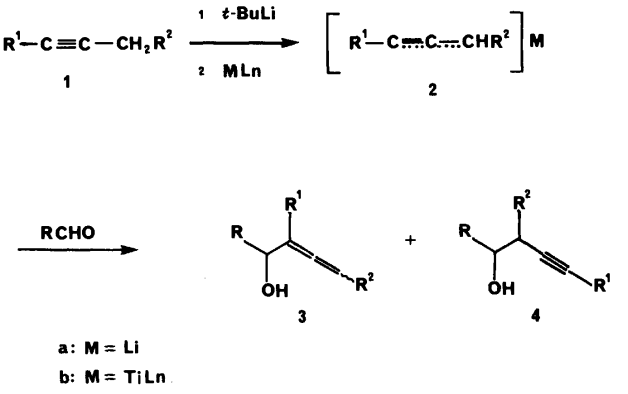

Scheme 1.

The lithio reagent **2a** (R^1=Me, R^2=H) derived from 2-butyne reacted with cyclohexanecarbaldehyde in tetrahydrofuran (THF) solvent to give a mixture of α-allenic and β-acetylenic alcohol **3** and **4**, respectively, in the ratio of 42:58. On the other hand, the titanium derivative **2b** (R^1=Me, R^2=H) gave the α-allenic alcohol **3** without contamination of any β-acetylenic alcohol **4**. The slight alteration in product distribution was observed by changing the solvent from THF to ether. The effects caused by changing the metal cation and solvent were studied in detail and the results are summarized in Table 1.

TABLE 1. THE REGIOSELECTIVITY OF THE REACTION OF METALLATED 2-BUTYNE WITH CYCLOHEXANECARBALDEHYDE[a]

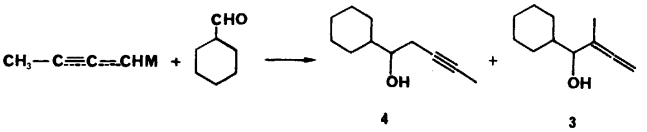

4 3

Entry	Metal[b]	Solvent	4	3[c]
1	*t*-BuLi	Ether	34	66
2	*t*-BuLi	THF	58	42
3	$Ti(OPr^i)_4$	Ether	3	97
4	$Ti(OPr^i)_4$	THF	1	99
5	$B(OPr^i)_3$	Ether	69	31
6	$B(OPr^i)_3$	THF	75	25
7	Et_2AlCl	THF	10	90
8	$Et_2AlCl+H_2O$	THF	7	93
9	MgI_2	THF	19	81
10	$ZnBr_2$	Ether	9	91
11	$ZnBr_2$	THF	17	83
12	$SnCl_2$	THF	7	93

a) The reactions were carried out on 2 mmol scale. The crude products were directly subject to GLC analysis. b) One equivalent of MLn was used for the metal exchange except for entries 7 and 8. Entry 7: Et_2AlCl, 2 equiv; Entry 8: $Et_2AlCl+H_2O$ (2:1), 2 equiv. c) Isomer ratio was determined by GLC analysis.

TABLE 2. THE REGIOSELECTIVITY OF THE REACTION OF TITANIUM REAGENTS WITH ALDEHYDES

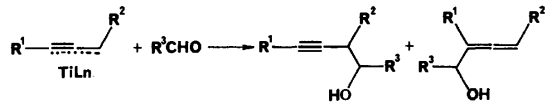

Entry	R^1	R^2	R^3	4/3[a,b] Ratio	Yield of 4+3/%
1	$Si(CH_3)_3$	H	Cyclohexyl	1:99 (58:42)[c]	93
2	$Si(CH_3)_3$	H	Phenyl	1:99 (65:35)	87
3	CH_3	H	Cyclohexyl	1:99 (53:47)	90
4	CH_3	H	Phenyl	1:99 (49:51)	80
5	$Si(CH_3)_3$	CH_3	Cyclohexyl	>99: 1	69
6	$Si(CH_3)_3$	CH_3	Phenyl	>99: 1	79
7	CH_3CH_2	CH_3	Cyclohexyl	>99: 1 (84:16)	42
8	Phenyl	CH_3	Cyclohexyl	94: 6 (93: 7)	89
9	Phenyl	CH_3	Phenyl	>99: 1 (98: 2)	92

a) Determined by GLC analysis. b) Values in parenthesis refer to ratios of **4**/**3** obtained in the reactions with lithium reagents. c) 56:44 using Mg ion; 75:25 using Zn ion.

The regioselectivity is heavily dependent on the kind of metal ion. Thus, the titanium reagent showed the highest regioselectivity (entry 4) in a variety of metal ions investigated.[8] In most cases, THF was a superior solvent to ether.

Since the unusual selectivities of the titanium reagents became apparent from the above results, their reactivities were examined in detail. The results were summarized in Table 2.

The titanium reagent generated from 1-substituted propyne (**2b**, R^1=alkyl or trialkylsilyl, R^2=H) condensed with an aldehyde to give the α-allenic alcohol **3** exclusively, similar to that observed in the reaction of 2-butyne (entries 1—4). However, a dramatic alteration in the product distribution occurred when the reactions of the homologous titanium reagents derived from 1,3-disubstituted propyne (**2b**, R^1=alkyl or trialkylsilyl, R^2=Me) were conducted with the same aldehydes. Thus, none of the corresponding α-allenic alcohols were detected, and instead the β-acetylenic alcohols **4** were obtained (entries 5—9). The high regioselectivity appears to be general for a range of acetylenes and aldehydes. Although the corresponding lithio derivatives generally gave the less selective results, in the case of 1,3-disubstituted propyne, even the lithio derivatives showed moderate to fairly high selectivities (entries 7—9).

From the above results, the characteristic features of the reaction may be summarized as follows. The substitution pattern of the starting alkynes plays a dominant role in determining the regioselectivity of the reaction: The alkynes having a substituent on propargylic carbon (**1**, $R^2 \neq H$) produced β-acetylenic alcohols exclusively, while allenic alcohols were obtained from the alkynes not substituted at propargylic carbon (**1**, R^2=H).

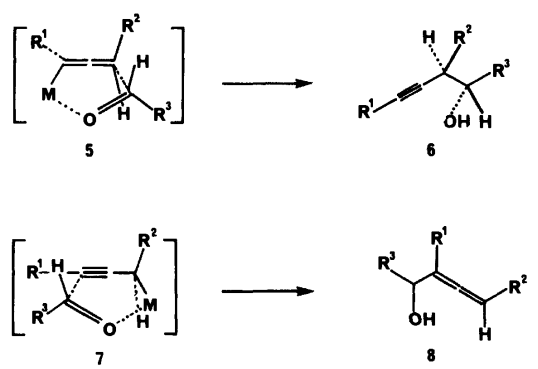

Fig. 1. S_Ei' process.

It is currently assumed that the addition of the allenic and acetylenic organometallics to the carbonyl takes place through an allylic rearrangement of the organometallic by a chelate transition state depicted in Fig. 1.[9]

That is to say, an allenic organometallic produced the β-acetylenic alcohol, while the α-allenic alcohol was derived from an acetylenic reagent. On the basis of these mechanistic considerations, the highly regioselective reaction of the titanium reagents could be explainable as follows. The titanation of the propargylic anion took place with extremely high regioselectivity to produce either allenic or acetylenic titanium derivatives depending on the substitution pattern of the original alkynes. Indeed, the IR spectrum of the titanium reagent in THF derived from 1-(trimethylsilyl)-1-butyne showed a strong absorption at 1898 cm^{-1} characteristic for allenic structure,[10] while that of the reagent derived from 1-(trimethylsilyl)propyne revealed only acetylenic absorption at 2092 cm^{-1},[10] in accord with the above speculation. In contrast to the highly selective formation of either allenic or acetylenic structure with titanium reagent, other metal cations, Li^+, MgX^+, *etc.*, furnished a mixture of the allenic and the acetylenic reagent in a variable ratio depending on the metal cations used. Siteselectivity was assumed to be determind primarily by steric requirements, and the steric repulsion between R^2 and metal centre (Fig. 2) provided conclusive factor of selectivity.

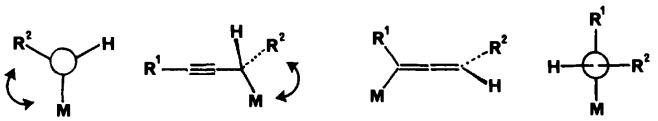

Fig. 2. Steric repulsion.

While the general trend of the regioselectivity of the titanium reagents has become apparent, it was of considerable interest to us to determine whether the tita-

Table 3. Stereoselectivity[a)]

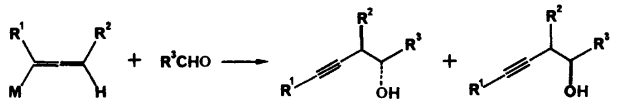

9 10

Entry	R^1	R^2	R^3	Metal[b)]	9/10[c)]Ratio	Yield of 9+10/%
1	Me_3Si	Me	Cyclohexyl	Li	62:38	48
2	Me_3Si	Me	Cyclohexyl	Mg	65:35	42
3	Me_3Si	Me	Cyclohexyl	Ti	89:11 (93:7)[d)]	69(71)[d)]
4	Me_3Si	Me	Phenyl	Ti	30:70	79
5	Phenyl	Me	Cyclohexyl	Li	80:20	67
6	Phenyl	Me	Cyclohexyl	Ti	>99: 1	89
7	Et	Me	Cyclohexyl	Ti	91: 9 (93:7)[d)]	42(35)[d)]
8	Me_3Si	OTHP	Cyclohexyl	Zn	71:29	51[e)]
9	Me_3Si	OTHP	Cyclohexyl	Ti	90:10	67[e)]
10	Me_3Si	OTHP	n-C_5H_{11}	Ti	88:12	65[e)]
11	Me	OTHP	Cyclohexyl	Li	81:19	44[e)]
12	Me	OTHP	Cyclohexyl	Zn	88:12	48[e)]
13	Me	OTHP	Cyclohexyl	Ti	94: 6	81[e)]
14	Me	OTHP	n-C_5H_{11}	Ti	95: 5	76[e)]
15	Me	$OCMe_2OMe$	n-C_5H_{11}	Ti	93: 7	57[e)]
16	Me	OTHF	Cyclohexyl	Ti	95: 5	59[e)]
17	Me	OTHF	n-C_5H_{11}	Ti	95: 5	68[e)]

a) Unless specified, reactions were carried out at −78 °C for 1 h(entries 1—7) or at −78 °C for 0.5 h and 20 °C for 0.5 h (entries 8—17). b) Ti, $Ti(OPr^i)_n$; Mg, MgI; Zn, ZnBr. c) Determined by GLC analysis. Ratios of diacetates for entries 8—17. d) The reaction was carried out at −100°C for 1 h. e) Yields refer to the corresponding diols produced by acid hydrolysis(TsOH in methanol) of the protecting groups.

nium reagents would exhibit an extraordinary diastereoselection for the β-acetylenic alcohol synthesis. Accordingly, we have carefully examined the diastereomeric ratios of the β-acetylenic alcohols (Table 3).

As summarized in Table 3, diastereomeric ratio is influenced significantly by the nature of the counter cation. Thus, the lithium, magnesium, and zinc reagents afforded the mixture of *erythro* and *threo* alcohols with low to moderate stereoselectivities. The enhanced selectivity was now observed with titanium reagents. The titanium reagents afforded predominantly the *threo*-β-acetylenic alcohols (entries 3, 6, and 7) and *erythro*-α,β-acetylenic diols[11] (entries 9—17) with synthetically useful levels of stereoselectivities. The alkoxyl group served as a bulky substituents and did not give a special influence on the regio- and stereoselectivities of the reaction. Such stereoregulation may be understandable simply by considering the same chelate type transition state (Fig. 3).

The titanium reagent which was present as the allenic form with a tight metal-carbon bond, forms the two six-membered ring chelate transition states, T_1 and T_2, according to the direction of the carbonyl approach. As is apparent from the Fig. 3, the steric repulsion between R and R_2 controls the course of the carbonyl approach to the reaction centre. Therefore, the transition state T_1 is more favorable than T_2 and the predominant production of the *threo* adduct *via* T_1 was observed.

Examination of the other data in Table 3 reveals several other trends: (1) Most remarkable is the reaction with benzaldehyde exhibiting an opposite stereoselection,[12] that is, *erythro*-β-acetylenic alcohol was obtained albeit in a lower level of selectivity(entry 4); (2) a trimethylsilyl group at R^1 of the reagents gave

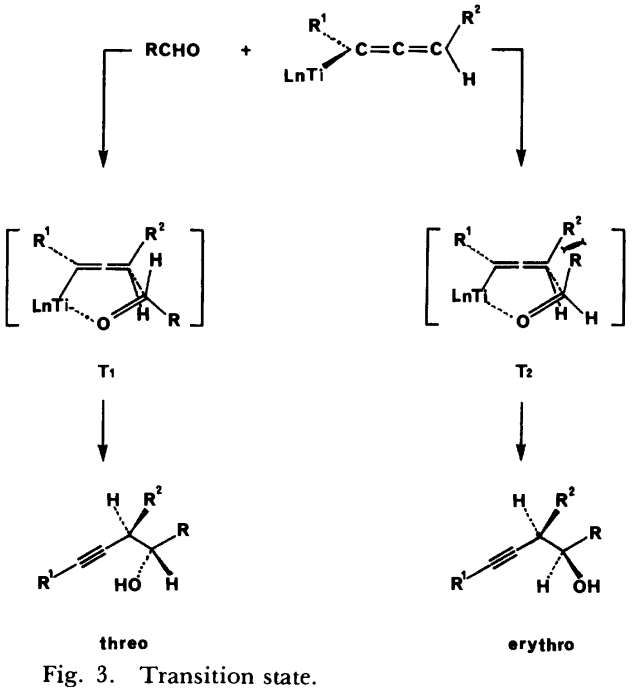

Fig. 3. Transition state.

slightly lower selectivities for the reaction (entries 9 and 10); (3) a lower reaction temperature leads to higher selectivities (entries 3 and 7). The reverse change in stereoselectivity observed in the reaction with benzaldehyde can not be fully explicable at present, but a similar anomaly has been observed elsewhere.[13]

It should be noted that the condensations of the titanium reagent with ketones were unsuccessful, and starting ketones were recovered. Similar chemoselectivities for the titanium reagents were reported.[8]

Synthesis of Enyne and α,β-Unsaturated Nitrile. The regio- and stereoselective behaviours of the propargyltitanium reagents in carbonyl addition have now become apparent in detail. Thus the additional applications of the similar reagents were examined for synthetic purposes.

We[1h] have already reported an efficient silicon-mediated (*Z*)-enyne synthesis using metallated 1,3-bis(trialkylsilyl)propyne as exemplified in Eq. 1.[11,14]

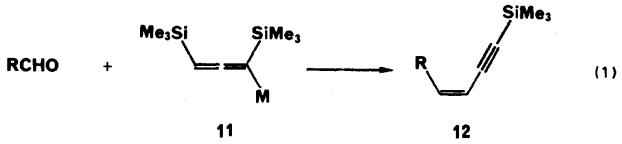

11 12 (1)

It was demonstrated that the alkyl groups on silicon provide powerful steric screening effect which plays an important role for the stereochemical course of the reaction. It was also pointed out that the tightness of the bond with counterion has a similar potential as a control element in stereochemistry: In order to maximize the stereoselectivity of the reaction, "a tight chelate transition state" should be achieved. For example, a magnesium chelate may be tighter than that for lithium, thus maximizing the steric effect. Unfortunately, however, the elimination step of Peterson olefination seems to proceed smoothly when lithium, sodium or potassium derivatives are used, the magnesium derivatives being comparatively slow to undergo elimination.[15] Taking these requirements and aforementioned results into account, we have tested the titanium reagents for the enyne synthesis.

1,3-Bis(trialkylsilyl)propyne[16] was treated with *t*-butyllithium and then with titanium tetraisopropoxide. The condensation with aldehydes was then conducted (Table 4). As seen from the Table 4, (*Z*)-enynes were obtained exclusively except for the reaction with benzaldehyde. The anomalous behaviour of benzaldehyde was described previously.[13]

Since the syn elimination mechanism of the β-oxide trialkylsilyl derivatives in Peterson reaction has been accepted,[17] the stereoselectivity of the reaction should be determined by the direction of the initial attack of carbanion to carbonyl.[18] For the diastereoselective addition of the titanium reagents, the similar explanation employed previously may be given again (Fig. 3): With this substituted pattern, the allenic (not acetylenic) titanium reagent was predominantly produced. Therefore, in Fig. 3, one might anticipate that the transition state T_2 might be destabilized relative to T_1 due to the R↔R^2 (R^2=R_3Si) steric repulsion. As a result, (*Z*)-enyne was produced selectively *via* transition

Table 4. Enyne synthesis[a]

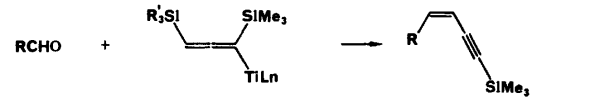

Entry	R_3'	R	Z:E[b]	Yield(Z+E)[c]/%
1	Me_3	Cyclohexyl	17:1	87
2	*t*-BuMe$_2$	Cyclohexyl	20:1	73
3	Me_3	Phenyl	1:8	88
4	*t*-BuMe$_2$	Phenyl	1:1	60
5	*t*-BuMe$_2$	Pentyl	>50:1	70

a) All reactions were performed as described in the text. b) Olefin ratio was determined by GLC. c) Values reported are isolated yields.

Table 5. Synthesis of α, β-unsaturated nitriles

Entry	Aldehyde[a]	Reagent	Metal	Condition[b]	Yield[c]/%	Z/E[d]
1	*c*-$C_6H_{11}CHO$	Me_3SiCH_2CN	Li	A	82	7:1
2			Ti	A	94	11:1
3			B	A	90	12:1
4			B	B	90	16:1
5			B	C	78	23:1
6		Ph_3SiCH_2CN	Mg	D	80	9:1[1h]
7			B	B	90	11:1
8		*t*-$BuMe_2SiCH_2CN$	Mg	D	76	6:1[1h]
9			B	B	85	15:1
10	$C_5H_{11}CHO$	Me_3SiCH_2CN	B	A[e]	72	7:1
11			B	B	68	9:1
12			B	C	52	13:1
13		Ph_3SiCH_2CN	Mg	D	63	5:1[1h]
14			B	B	72	7:1
15	C_5H_9CHO	Me_3SiCH_2CN	Li	B	46	5:1
16			B	B	81	8:1
17			B	C	66	6:1
18		Ph_3SiCH_2CN	Li	A[f]	60	2:1
19			B	B	84	6:1
20		*t*-$BuMe_2SiCH_2CN$	B	B	84	8:1
21	C_6H_5CHO	Me_3SiCH_2CN	Li	A[e]	86	3:1
22			B	A[e]	90	3:1
23			B	C	71	2:1

a) *c*-$C_6H_{11}CHO$: Cyclohexanecarbaldehyde; $C_5H_{11}CHO$: Hexanal; C_5H_9CHO: 2-Hexenal; C_6H_5CHO: Benzaldehyde. b) A: −78 °C, 1 h; 25 °C, 30 min; B: −78 °C, 1 h; C: −78 °C, 30 min; HMPA was added after the addidion of the aldehyde to the anions. D: −78 °C, 5 min; 50 °C, 1 h. c) Values reported are for isolated product. d) *Z*/*E* ratio was determined by GLC. e) 25 °C, 1 h. f) 25 °C, 2 h.

state T_1.

Next we called our attention to the nitrile anion which has analogous structure to the propargyl anion except that it has no substituents at a terminal nitrogen atom. Thus we investigated the reaction of α-silyl-substituted acetonitrile anion which condensed with aldehyde to give α,β-unsaturated nitriles through addition-elimination sequences.[19] Judging from the similarity of the reaction system to the α-silylated propyne, a (*Z*)-olefin may result from this reaction. The α,β-unsaturated nitrile is a useful synthetic intermediate since it is easily converted to the synthetically useful α,β-unsaturated carbonyl compound.[20]

The metallated derivatives of (trialkylsilyl)acetonitrile[21] was condensed with various aldehydes and the results were summarized in Table 5.

Surprisingly, the reaction of simple lithio reagent with aldehyde produced the *Z*-isomer with moderate stereoselectivity (entry 1).[22] The titanium reagents showed a little improvements, but the boron reagents are much superior.[23] In contrast to the previous observations of propargyl anions, the stereochemical course of the reaction showed little dependence on the steric screening effect of the silyl group, but the effects of the reaction temperature and the solvent were crucial. Thus the longer reaction period at room temperature tends to decrease the stereoselectivity of the reaction (entries 3 and 4). Since the presence of excess base (LDA) also decreases the selectivity, secondary isomerization of the produced olefin may be caused by the base particularly at higher temperature.[24] Consequently the quenching of the reaction at low temperature is essential to accomplish the selective reaction.[25]

It should be notable that the addition of HMPA to the reaction mixture remarkably raised the proportion of *Z*-isomer (entry 5). The role of HMPA is not clear, but the rate of the desilylation is clearly accelerated by the addition of HMPA. The lack of the selectivity in the condensation with benzaldehyde was observed as previously, which may be due to the intervention of a competing electron-transfer pathway, or an acyclic transition state.[13]

The regioisomer, ketenimine, which corresponded to the allenyl alcohol for the reaction of propargylic anion, was not detected in a series of this reaction.[26] Since the transition state for this reaction could be regarded as similar to that of propargyl anion, the *Z*-selectivity could be readily understandable. For nitrile anion, however, the site of metallation could be recognized as occurred predominantly at nitrogen atom for all metals studied.[27] This is presumably due to the steric requirement along with the strong affinity of metal-nitrogen bond.

Experimental

General. ^{1}H NMR spectra were taken on a JNM-PMX 60 spectrometer. The chemical shifts are reported in parts per million relative to TMS. The infrared spectra were recorded on a Hitachi 260-10 spectrometer in CCl_4 solution unless otherwise stated. The isomeric ratio of the products was determined by gas-liquid chromatography (GLC) using a Hitachi Model 163 and 164 instruments equipped with a flame ionization detector using nitrogen as carrier gas. For TLC analysis throughout this work, Merck precoated TLC plates (silica gel 60 GF_{254}, 0.25 mm, or silica gel 60 HF_{254} silanized, 0.25 mm) were used. The products were purified by preparative column chromatography on silica gel E. Merck Art. 9385, or silanized silica gel E. Merck Art. 7719. Microanalyses were accomplished at the Institute of Applied Organic Chemistry, Faculty of Engineering, Nagoya University. Unless otherwise specified, all reactions were carried out under an atmosphere of dry argon. In experiments requiring dry solvents, ether and tetrahydrofuran (THF) were distilled from sodium-benzophenone. Benzene, hexane, and toluene were dried over sodium metal. Dichloromethane was dried over 4A Molecular Sieve. Pyridine and triethylamine were stored over potassium hydroxide pellets. Hexamethylphosphoric triamide (HMPA) was used after distillation from CaH_2. Other commercially supplied materials were used as received.

Preparation of 1-(Trimethylsilyl)propyne.[16] To a solution of propyne (20 g, 0.50 mol) in ether (600 ml) was added butyllithium in hexane (1.6 mol dm^{-3} solution, 312 ml, 0.50 mol) at −78 °C under argon. After stirring for 1 h at the same temperature, chlorotrimethylsilane (63 ml, 0.50 mol) was added to this solution. The resulting mixture was stirred at 25 °C for 12 h and then poured into 2 mol dm^{-3} hydrochloric acid. The organic layer was separated and the aqueous layer was extracted with ether. The combined extracts were dried and evaporated. The residue was distilled under atmospheric pressure to give 1-(trimethylsilyl)propyne (34 g, 60%). Bp 94—98 °C; ^{1}H NMR (CCl_4) δ=0.15 (s, 9H), 1.93 (s, 3H).

Preparation of 1-Trimethylsilyl-1-butyne.[28] To a solution of 1-butyne (15 g, 0.28 mol) in ether (500 ml) was added butyllithium in hexane (1.6 mol dm^{-3} solution, 160 ml, 0.26 mol) at −78 °C under argon. After stirring for 1 h at the same temperature, chlorotrimethylsilane (33 ml, 0.26 mol) was added to the reaction mixture. The mixture was stirred at 25 °C for 12 h and then poured into 2 mol dm^{-3} hydrochloric acid. The organic layer was separated and the aqueous layer was extracted with ether. The combined extracts were dried and evaporated. The residue was distilled under atmospheric pressure to give 1-trimethylsilyl-1-butyne (23 g, 70%). Bp 115—116 °C; ^{1}H NMR (CCl_4) δ=0.13 (s, 9H), 1.16 (t, *J*=7 Hz, 3H), 2.21 (q, *J*=7 Hz, 2H).

Preparation of 3-(Tetrahydro-2-pyranyloxy)-1-trimethylsilyl propyne. To a solution of 2-propyn-1-ol (11 g, 0.20 mol) and 3,4-dihydro-2*H*-pyran (22 ml, 0.24 mol) in ether (300 ml) was added *p*-toluenesulfonic acid monohydrate (4 g, 21 mmol) at 0 °C. The mixture was stirred for 0.5 h at 0 °C and 1 h at 25 °C. Then, the reaction mixture was poured into water and the product was extracted with ether. The ether layer was washed with brine, dried over sodium sulfate, and evaporated. Chromatography of the residual crude oil on a silica-gel column (2:1, hexane-ether) afforded 3-(tetrahydro-2-pyranyloxy)propyne (24 g, 86%). ^{1}H NMR (CCl_4) δ=1.3—2.0 (m, 6H), 2.40 (t, *J*=2.5 Hz, 1H), 3.3—4.0 (m, 2H), 4.23 (d, *J*=2.5 Hz, 2H), 4.80 (m, 1H); IR (neat) 3300 cm^{-1}.

To a solution of 3-(tetrahydro-2-pyranyloxy)propyne (5.6 g, 40 mmol) in ether (100 ml) was added butyllithium in hexane (1.6 mol dm^{-3} solution, 25 ml, 40 mmol) at −78 °C. After stirring for 1 h at −78 °C, chlorotrimethylsilane (5.0 ml, 40 mmol) was added to this mixture. The resulting mixture was stirred at 25 °C for 12 h and then poured into 2 mol dm^{-3} hydrochloric acid and extracted with ether. The combined extracts were dried and evaporated. Chromatography of the crude product on a silica-gel column (15:1 hexane-ether) afforded 3-(tetrahydro-2-pyranyloxy)-1-(trimethylsilyl)propyne (6.9 g, 81%). ^{1}H NMR (CCl_4) δ=0.13 (s, 9H), 1.1—2.0 (m, 6H), 3.4—3.9 (m, 2H), 4.03 (s, 2H), 4.63 (t, *J*=2 Hz, 1H); IR (neat) 2190 cm^{-1}. Found: C, 62.38; H, 9.22%. Calcd for $C_{11}H_{20}O_2Si$: C, 62.21; H, 9.49%.

Preparation of 1-(Tetrahydro-2-pyranyloxy)-2-butyne.[29] To a solution of 2-butyn-1-ol (5 ml, 66 mmol) and 3,4-dihydro-2*H*-pyran (9.0 ml, 99 mmol) in ether (130 ml) was added *p*-toluenesulfonic acid monohydrate (1.9 g, 10 mmol) at 0 °C. After stirring for 0.5 h at 0 °C and then 1 h at 25 °C, the reaction mixture was poured into water and extracted with ether. The ether layer was washed with brine, dried, and evaporated. Chromatography of the residual oil on a silica-gel column (10:1 hexane–ether) afforded 1-(tetrahydro-2-pyranyloxy)-2-butyne (10 g, 98%). R_f=0.7 (10:1 hexane–ether); ^{1}H NMR (CCl_4) δ=1.3—1.9 (m, 6H), 1.75 (t, J=2.5 Hz, 3H), 3.2—3.8 (m, 2H), 4.0 (q, J=2.5 Hz, 2H), 4.65 (m, 1H); IR (neat) 2250 cm^{-1}.

Preparation of 1-(1-Methoxy-1-methylethoxy)-2-butyne. To a solution of 2-butyn-1-ol (2.0 ml, 26 mmol) and 2-methoxypropene (3.6 g, 50 mmol) in dichloromethane (30 ml) was added *p*-toluenesulfonic acid monohydrate (0.75 g, 3.9 mmol) at 0 °C. The resulting mixture was stirred at 0 °C for 20 min and treated with triethylamine (1.4 ml, 10 mmol) at 0 °C. The mixture was poured into water and the product was extracted with ether. The organic layer was dried and concentrated. Chromatography of the resulting oil on a silica-gel column (4:1 hexane–ether) afforded 1-(1-methoxy-1-methylethoxy)-2-butyne (2.77 g, 75%). R_f=0.8 (4:1 hexane–ether); ^{1}H NMR (CCl_4) δ=1.33 (s, 6H), 1.83 (t, J=2.5 Hz, 3H), 3.20 (s, 3H), 4.05 (q, J=2.5 Hz, 2H); IR (neat) 2250 cm^{-1}.

Preparation of 1-(Tetrahydro-2-furyloxy)-2-butyne. To a solution of 2-butyn-1-ol (2.0 ml, 26 mmol) and 2,3-dihydrofuran (2.8 g, 40 mmol) in ether (30 ml) was added *p*-toluenesulfonic acid monohydrate (0.75 g, 3.9 mmol) at 0 °C. After stirring for 0.5 h at 0 °C and 1 h at 25 °C, the mixture was poured into water and the product was extracted with ether. The organic layer was dried and concentrated. Chromatography of the crude product on a silica-gel column (10:1 hexane–ether) afforded 1-(tetrahydro-2-furyloxy)-2-butyne (2.8 g, 77%). ^{1}H NMR (CCl_4) δ=1.83 (m, 7H), 3.7—4.0 (m, 2H), 4.15 (m, 2H), 5.27 (m, 1H); IR (neat) 2230 cm^{-1}.

Metallation of Acetylenic Compounds. To a solution of acetylenic compounds (2.0 mmol) dissolved in dry THF (5 ml) was added *t*-butyllithium in pentane (1.8 mol dm^{-3} solution, 1.11 ml, 2.0 mmol) at −78 °C with stirring, and the resulted slightly yellow solution was stirred at 0 °C for 1 h leading to complete lithiation. Corresponding titanium derivatives were prepared by adding titanium tetraisopropoxide (0.60 ml, 2.0 mmol) to a solution of the lithio salt obtained as above at −78 °C. The boron derivatives were similarly prepared with use of one equivalent of boron triisopropoxide. Magnesium, zinc, and tin(II) derivatives were generated by adding one equivalent of magnesium iodide,[30] zinc bromide, or tin(II) chloride, respectively. For the preparation of aluminium reagents, two equivalents of diethylaluminium chloride (hexane solution) were used.

IR Analysis of Metallated Alkyne Derivatives. The lithio derivative of a 1-(trimethylsilyl)propyne solution in THF obtained as above was transferred into IR cell under nitrogen, and the spectrum was measured. IR 1880 cm^{-1} (m, allenic), 2020 cm^{-1} (m, acetylenic). The IR spectra of the other metallated reagents: Titanated 1-(trimethylsilyl)propyne: 2092 cm^{-1}. Titanated 1-trimethylsilyl-1-butyne: 1898 cm^{-1}.

*Reaction of **2b** with Cyclohexanecarbaldehyde.* To a cooled solution (−78 °C) of **2b** (2.0 mmol) in THF was added freshly distilled cyclohexanecarbaldehyde (0.22 ml, 1.8 mmol) over a period of 5 min at −78 °C, and the mixture was stirred at −78 °C for 1 h. The resulting mixture was poured into ice-cooled 1 mol dm^{-3} hydrochloric acid, and the product was extracted with ether repeatedly. The combined ethereal layer was dried and concentrated *in vacuo*. The crude product was purified by silica-gel column chromatography (1:2 ether–heaxne) to give 1-cyclohexyl-3-pentyn-1-ol and 1-cyclohexyl-2-methyl-2,3-butadien-1-ol (269 mg, 90% total yield). GLC analysis of the product revealed the ratio of 1:99.

1-Cyclohexyl-3-pentyn-1-ol: R_f=0.35 (2:1 hexane–ether); ^{1}H NMR (CCl_4) δ=0.7—2.0 (m, 11H), 1.78 (t, J=2.4 Hz, 3H), 2.25 (m, 2H), 3.30 (m, 1H), 4.62 (br s, 1H); IR 2275 cm^{-1}.

1-Cyclohexyl-2-methyl-2,3-butadien-1-ol: R_f=0.43 (2:1 ether–hexane); ^{1}H NMR (CCl_4) δ=0.72—2.22 (m, 11H), 1.62 (t, J=3 Hz, 3H), 2.02 (s, 1H), 3.67 (br d, 1H), 4,63 (m, 2H); IR 1970 cm^{-1}. Found: C, 79.31; H, 10.73%. Calcd for $C_{11}H_{18}O$: C, 79.46; H, 10.91%.

1-Cyclohexyl-4-trimethylsilyl-3-butyn-1-ol:[1g] ^{1}H NMR (CCl_4) δ=0.14 (s. 9H), 0.92—2.0 (m, 12H), 2.32 (d, J=5.4 Hz, 2H), 3.37 (br s, 1H); IR 2180 cm^{-1}.

1-Cyclohexyl-2-trimethylsilyl-2,3-butadien-1-ol:[1g] ^{1}H NMR (CCl_4) δ=0.12 (s, 9H), 0.86—2.03 (m, 12H), 3.81 (br s, 1H), 4.38 (d, J=2 Hz, 2H); IR 1930 cm^{-1}. Found: C, 69.49; H, 10.60%; Calcd for $C_{13}H_{24}OSi$: C, 69.58; H, 10.78%.

1-Phenyl-4-trimethylsilyl-3-butyn-1-ol:[1f,g] ^{1}H NMR (CCl_4) δ=0.08 (s, 9H), 2.47 (d, J=6.2 Hz, 2H), 3.23 (br d, J=3 Hz, 1H), 4.60 (dt, J=3 and 6.2 Hz, 1H), 7.17 (s, 5H); IR 2180 cm^{-1}.

1-Phenyl-2-trimethylsilyl-2,3-butadien-1-ol:[1f,g] ^{1}H NMR (CCl_4) δ=0.02 (s, 9H), 3.33 (br s, 1H), 4.45 (d, J=3 Hz, 2H), 5.17 (t, J=3 Hz, 1H), 7.19 (s, 5H); IR 1930 cm^{-1}; MS m/z: 218 (M^+).

1-Phenyl-3-pentyn-1-ol:[1f] ^{1}H NMR (CCl_4) δ=1.70(t, J=2.5 Hz, 3H), 2.42 (dq, J=2.5 and 6 Hz, 2H), 2.77 (br s, 1H), 4.60 (t, J=6 Hz, 1H), 7.18 (s, 5H).

2-Methyl-1-phenyl-2,3-butadien-1-ol:[1f,31] ^{1}H NMR (CCl_4) δ= 1.47 (t, J=3 Hz, 3H), 3.04 (br s, 1H), 4.68 (m, 2H), 4.98 (br s, 1H), 7.16 (s, 5H); IR 1960 cm^{-1}; MS m/z: 160 (M^+).

1,4-Diphenyl-2-methyl-3-butyn-1-ol (Mixture of erythro *and* threo *Isomers)*: ^{1}H NMR (CCl_4) δ=1.06 and 1.14 (2d, J=7 Hz each, 3H), 2.85 (quintet, J=7 Hz, 1H), 3.08 (br s, 1H), 4.45 (m, 1H), 7.17 (m, 10H); IR 2250 cm^{-1}. Found: C, 86.16; H, 7.07%; Calcd for $C_{17}H_{16}O$: C, 86.41; H, 6.82%.

erythro-*1-Cyclohexyl-2-methyl-4-trimethylsilyl-3-butyn-1-ol*:[32] ^{1}H NMR (CCl_4) δ=0.13 (s, 9H), 0.78—2.03 (m, 12H), 1.13 (d, J=6.5 Hz, 3H), 2.52 (quintet, J=6.5 Hz, 1H), 3.20 (t, J=5 Hz, 1H); IR 2170 cm^{-1}.

threo-*1-Cyclohexyl-2-methyl-4-trimethylsilyl-3-butyn-1-ol*:[32] ^{1}H NMR (CCl_4) δ=0.15 (s, 9H), 0.87—2.08 (m, 12H), 1.18 (d, J= 7 Hz, 3H), 2.60 (dq, J=2 and 7 Hz, 1H), 2.95 (m, 1H); IR 2160 cm^{-1}. Found: C, 70.70; H, 10.81%; Calcd for $C_{14}H_{26}OSi$: C, 70.52; H, 10.99%.

erythro-*2-Methyl-1-phenyl-4-trimethylsilyl-3-butyn-1-ol*:[33] ^{1}H NMR (CCl_4) δ=0.07 (s, 9H), 1.07 (d, J=7 Hz, 3H), 2.28 (br s, 1H), 2.67 (quintet, J=7 Hz, 1H), 4.51 (d, J=6.2 Hz, 1H), 7.21 (s, 5H); IR 2180 cm^{-1}.

threo-*2-Methyl-1-phenyl-4-trimethylsilyl-3-butyn-1-ol*:[33] ^{1}H NMR (CCl_4) δ=0.14 (s, 9H), 1.05 (d, J=7 Hz, 3H), 2.35 (br s, 1H), 2.68 (quintet, J=7 Hz, 1H), 4.38 (d, J=7 Hz, 1H), 7.23 (s, 5H); IR 2180 cm^{-1}. Found: C, 72.48; H, 8.95%. Calcd for $C_{14}H_{20}OSi$: C, 72.36; H, 8.67%.

threo-*1-Cyclohexyl-2-methyl-3-hexyn-1-ol*:[32] ^{1}H NMR (CCl_4) δ=0.57—2.20 (m, 13H), 1.10 (t, J=7 Hz, 3H), 1.13 (d, J=6.8 Hz, 3H), 2.57 (m, 1H), 2.92 (m, 1H), 3.22 (br s, 1H).

erythro-*1-Cyclohexyl-2-methyl-3-hexyn-1-ol*:[32] ^{1}H NMR (CCl_4) δ=0.87—2.37 (m, 14H), 1.11 (d, J=7 Hz, 3H), 1.13 (t, J=7.5 Hz, 3H), 2.49 (m, 1H), 3.17 (m, 1H).

erythro-*1-Cyclohexyl-2-methyl-4-phenyl-3-butyn-1-ol*:[32] ^{1}H NMR (CCl_4) δ=0.69—2.35 (m, 12H), 1.24 (d, J=6.4 Hz, 3H), 2.74 (quintet, J=6.4 Hz, 1H), 3.32 (t, J=6.4 Hz, 1H), 7.22 (br s, 5H); IR 2250 cm^{-1}.

threo-*1-Cyclohexyl-2-methyl-4-phenyl-3-butyn-1-ol*:[32] ^{1}H NMR (CCl_4) δ=0.67—2.34 (m, 12H), 1.27 (d, J=6.8 Hz, 3H), 2.80 (dq, J=4 and 6.8 Hz, 1H), 3.03 (br s, 1H), 7.20 (m, 5H); IR 2240 cm^{-1}. Found: C, 84.16; H, 9.23%. Calcd for $C_{17}H_{22}O$: C, 84.25; H, 9.15%.

Reaction of Metallated Alkoxyalkyne Reagents with Aldehydes. The following procedure is representative for these type

of reagents (entries 8—17 in Table 3). *t*-Butyllithium in pentane (1.8 mol dm^{-3} solution, 0.83 ml, 1.5 mmol) was added dropwise to a solution of 1-(tetrahydro-2-pyranyloxy)-2-butyne (231 mg, 1.5 mmol) in dry THF (4 ml) with stirring under argon at −78 °C. After 40 min at −78 °C, titanium tetraisopropoxide (0.45 ml, 1.5 mmol) was added dropwise to the resulting orange solution of the anion, and the slightly darkened solution was stirred there for 10 min. Freshly distilled hexanal (0.155 ml, 1.3 mmol) was added over a period of 5 min at −78 °C, and the mixture was stirred at −78 °C for 30 min and then at 20 °C for 30 min. The reaction mixture was poured into ice-cooled 1 mol dm^{-3} hydrochloric acid, and the product was extracted with ether repeatedly. The combined ethereal layer was concentrated *in vacuo* to give a crude hydroxy ether, which was dissolved in dry methanol (5 ml) at 0 °C. *p*-Toluenesulfonic acid monohydrate (5 mg) was added, and the mixture was stirred at 20 °C for 30 min. After the consumption of all tetrahydropyranyl ether by TLC assay, the reaction was terminated by the addition of excess sodium hydrogencarbonate (10 mg). The suspension was concentrated *in vacuo*, and the slurry was directly subjected to column chromatography on silica gel (2:1 ether–hexane) to afford 2-decyne-4,5-diol (168 mg, 76%). The diol was acetylated by Ac_2O–pyridine, and the GLC analysis of the diacetate revealed the isomeric ratio of 95:5 (*erythro*:*threo*).[34]

2-Decyn-4,5-diol: ^{1}H NMR (CCl_4) δ=0.5—1.67 (m, 11H), 1.87 (d, J=3 Hz, 3H), 2.97 (br s, 2H), 3.63 (m, 1H), 4.28 (dq, J=3 and 3 Hz, 1H); IR 3400, 2260 cm^{-1}. Found: C, 70.32; H, 10.68%. Calcd for $C_{10}H_{18}O_2$: C, 70.55; H, 10.65%.

1-Cyclohexyl-4-trimethylsilyl-3-butyn-1,2-diol:[35] ^{1}H NMR (CCl_4) δ=0.16 (s, 9H), 0.75—2.17 (m, 11H), 2.78 (br s, 2H), 3.17 (dd, J=4 and 6 Hz, 1H), 4.22 (d, J=4 Hz, 1H); IR 3400, 2200 cm^{-1}.

1-Trimethylsilyl-1-nonyn-3,4-diol:[35] ^{1}H NMR (CCl_4) δ=0.16 (s, 9H), 0.66—1.58 (m, 11H), 2.14 (br m, 1H), 2.69 (m, 1H), 3.48 (m, 1H), 4.13 (m, 1H); IR 3400, 2230cm^{-1}.

1-Cyclohexyl-3-pentyn-1,2-diol: ^{1}H NMR (CCl_4) δ=0.67—2.33 (m, 11H), 1.88 (d, J=2 Hz, 3H), 2.83 (br s, 2H), 3.32 (dd, J=3 and 7 Hz, 1H), 4.41 (dq, J=3 and 4 Hz, 1H); IR (neat) 3400, 2280 cm^{-1}. Found: C, 72.34; H, 10.10%. Calcd for $C_{11}H_{18}O_2$: C, 72.49; H, 9.95%.

Preparation of 1,3-Bis(trimethylsilyl)propyne.[16] To a solution of 1-(trimethylsilyl)propyne (13.5 g, 120 mmol) in ether (200 ml) were added *N,N,N′,N′*-tetramethylethylenediamine (21.1 ml, 140 mmol) and butyllithium in hexane (1.6 mol dm^{-3} solution, 87.5 ml, 140 mmol) at −5 °C under argon. After stirring for 30 min, chlorotrimethylsilane (17 ml, 134 mmol) was added and the mixture was stirred at 25 °C for 12 h. The resulting mixture was poured into ice-cooled water and the product was extracted with ether. The combined extracts were dried and evaporated. The residue was distilled under reduced pressure to give 1,3-bis(trimethylsilyl)propyne (16.6 g 75%). Bp 75—76 °C (34 mmHg†): ^{1}H NMR ($CDCl_3$) δ=0.17 and 0.24 (2s, 9H each), 1.61 (s, 2H).[16]

Preparation of 3-(t-Butyldimethylsilyl)-1-(trimethylsilyl)propyne. To a solution of 1-(trimethylsilyl)propyne (22.4 g, 200 mmol) in ether (300 ml) was added *t*-butyllithium[36] in pentane (1.8 mol dm^{-3} solution, 111 ml, 200 mmol) at −5 °C. After stirring for 30 min, *t*-butyldimethylsilyl chloride (30.1 g, 200 mmol) was added and the mixture was stirred for 12 h. The resulting mixture was poured into ice-cooled water and the product was extracted with ether. The combined extracts were dried and concentrated. The residue was distilled under reduced pressure to give 3-(*t*-butyldimethylsilyl)-1-(trimethylsilyl)propyne (24.4 g, 54%). Bp 106—107 °C (31 mmHg); ^{1}H NMR ($CDCl_3$) δ=0.14 and 0.19 (2s, 15H), 0.98 (s, 9H), 1.63 (s, 2H); MS *m/z*: 226 (M^+).

† 1 mmHg≈133.322 Pa.

Reaction of Metallated 1,3-Bis(trialkylsilyl)propyne with Aldehydes.[37] The following experimental procedure is representative. To a solution of 1,3-bis(trimethylsilyl)propyne (368 mg, 2.0 mmol), in THF (4 ml) was added *t*-butyllithium in pentane (1.8 mol dm^{-3} solution, 1.1 ml, 2.0 mmol) at −78 °C. After 1 h at −78 °C, titanium tetraisopropoxide (0.60 ml, 2.0 mmol) was added to the mixture and the solution was stirred for 10 min at −78 °C. Cyclohexanecarbaldehyde (0.22 ml, 1.8 mmol) was added to the solution and the resulting mixture was stirred at −78 °C for 30 min and then at 25 °C for 1 h. The reaction mixture was poured into 1 mol dm^{-3} hydrochloric acid, and the product was extracted with ether repeatedly. The combined ethereal layer was concentrated *in vacuo* to give a crude oil, which was subjected to column chromatography on silica gel (hexane) to afford 4-cyclohexyl-1-trimethylsilyl-3-buten-1-yne (323 mg, 87%). GLC analysis of the product revealed the isomeric ratio of 17:1 (*Z*:*E*).[38]

(Z)-4-Cyclohexyl-1-trimethylsilyl-3-buten-1-yne:[37] ^{1}H NMR (CCl_4) δ=0.17 (s, 9H), 0.77—1.95 (m, 10H), 2.57 (br m, 1H), 5.27 (d, J=11 Hz, 1H), 5.72 (dd, J=8.5 and 11 Hz, 1H); IR 2150, 1450, 1255, 1015, 700 cm^{-1}.

(E)-4-Cyclohexyl-1-trimethylsilyl-3-buten-1-yne:[37] ^{1}H NMR (CCl_4) δ=0.13 (s, 9H), 5.28 (d, J=16 Hz, 1H), 6.02 (dd, J=7 and 16 Hz, 1H), 0.65—2.0 (m, 11H); IR 2150, 1450, 1250, 960 cm^{-1}.

(Z)-1-Trimethylsilyl-3-nonen-1 yne:[39] ^{1}H NMR (CCl_4) δ=0.17 (s, 9H), 0.8—1.5 (m, 9H), 2.27 (m, 2H), 5.33 (d, J=11 Hz, 1H), 5.80 (dt, J=7 and 11 Hz, 1H); IR 2150, 1250, 1050, 700 cm^{-1}.

(E)-1-Trimethylsilyl-3-nonen-1-yne:[39] ^{1}H NMR(CCl_4) δ=0.13 (s, 9H), 0.76—1.58 (m, 9H), 2.10 (m, 2H), 5.32 (d, J=16 Hz, 1H), 6.08 (dt, J=7 and 16 Hz, 1H); IR 2150, 1260, 1095, 960 cm^{-1}.

(Z)-4-Phenyl-1-trimethylsilyl-3-buten-1-yne:[37] ^{1}H NMR(CCl_4) δ=0.22 (s, 9H), 5.56 (d, J=11 Hz, 1H), 6.53 (d, J=11 Hz, 1H), 7.18 (m, 3H), 7.72 (m, 2H).

(E)-4-Phenyl-1-trimethylsilyl-3-buten-1-yne:[37] ^{1}H NMR (CCl_4) δ=0.20 (s, 9H), 6.05 (d, J=16 Hz, 1H), 6.93 (d, J=16 Hz, 1H), 7.27 (s, 5H).

Preparation of (Trimethylsilyl)acetonitrile.[19b] To a mixture of chlorotrimethylsilane (36 g, 0.33 mol) and activated granular zinc (38 g, 0.58 mol), in THF–benzene (1:1, 400 ml) was added a solution of chloroacetonitrile (22 g, 0.29 mol) in benzene (20 ml). The resulting mixture was heated under reflux for 30 h and then poured into a buffer solution (AcONa–AcOH, 300 ml). The organic layer was separated and the aqueous layer was extracted with benzene. The combined extracts were dried and concentrated. The residue was distilled under reduced pressure to give (trimethylsilyl)acetonitrile (13.5 g, 41%). Bp 65 °C (20 mmHg); ^{1}H NMR (CCl_4) δ=0.23 (s, 9H), 1.53 (s, 2H); IR (neat) 2215 cm^{-1}. This compound was also prepared from bromoacetonitrile in the similar manner.[19b]

Preparation of (Triphenylsilyl)acetonitrile. To a solution of acetonitrile (4.1 g, 0.10 mol) in THF (200 ml) was added butyllithium in hexane (1.6 mol dm^{-3}, 62.5 ml, 0.10 mol) at −78 °C. After stirring for 20 min, chlorotriphenylsilane (29.5 g, 0.10 mol) in THF (50 ml) was added at −78 °C and the mixture was stirred at −78 °C for 30 min and then 25 °C for 5 h. The resulting mixture was poured into water and the product was extracted with ether. The combined extracts were dried and concentrated to give a crude product. Recrystallization from acetone–methanol gave colourless crystals of (triphenylsilyl)acetonitrile (16.7 g, 56%). Mp 135.5—136 °C (acetone); ^{1}H NMR ($CDCl_3$) δ=2.30 (s, 2H), 7.45 (br s, 15H); IR 2250 cm ; MS *m/z*: 299 (M^+).

Preparation of (t-Butyldimethylsilyl)acetonitrile. To a solution of acetonitrile (4.1 g, 0.10 mol) in THF (200 ml) was added butyllithium in hexane (1.6 mol dm^{-3}, 62.5 ml, 0.10 mol) at −78 °C. After stirring for 20 min, *t*-butyldimethylsilyl chloride (15.1 g, 0.10 mol) in THF (50 ml) was

added at −78 °C and the mixture was stirred at −78 °C for 30 min and 25 °C for 5 h. The resulting mixture was poured into water and the product was extracted with ether. The combined extracts were dried and concentrated. The residue was distilled under reduced pressure to give (*t*-butyldimethylsilyl) acetonitrile (7.75 g, 50%). Bp 102 °C (30 mmHg); ^{1}H NMR ($CDCl_3$) δ=0.19 (s, 6H), 0.95 (s, 9H), 1.54 (s, 2H); IR 2250 cm^{-1}; Mp 71—72 °C; MS *m/z*: 155 (M^+).

Reaction of Metallated (Trialkylsilyl)acetonitrile with Aldehydes.[19b] The following experimental procedure provides details of the typical preparation of (*Z*)-unsaturated nitriles: To a solution of (trimethylsilyl)acetonitrile (113 mg, 1.0 mmol) in THF (2 ml) was added dropwise butyllithium in hexane (1.6 mol dm^{-3} solution, 0.63 ml, 1.0 mmol) at −78 °C. After 10 min, boron triisopropoxide (0.231 ml, 1.0 mmol) was added at −78 °C and the solution was stirred there for an additional 10 min. Cyclohexanecarbaldehyde (0.121 ml, 1.0 mmol) in THF (0.5 ml) was added slowly and after 2 min, dry HMPA (0.4 ml) was added to the reaction mixture and stirring was continued for 1 h. Addition of water to the mixture at −78 °C, then the product was extracted with ether. The combined organic layer was dried and concentrated. Chromatography of the crude product on silica-gel column (1:6 ether-hexane) gave 3-cyclohexylacrylonitrile (105 mg, 78%). GLC analysis of the product revealed 23:1 (*Z*)-isomer.[38]

(Z)-3-Cyclohexylacrylonitrile (Contains ca. 4% of the (E)-Isomer):[19c] R_f=0.46 (1:6 ether-hexane); ^{1}H NMR (CCl_4) δ= 0.72—3.0 (m, 11H), 5.15 (d, *J*=11 Hz, 1H), 6.23 (dd, *J*=10 and 11 Hz, 1H); IR 2910, 2840, 2210, 1625, 740 cm^{-1}. Found: C, 80.08; H, 9.73; N, 10.18%. Calcd for $C_9H_{13}N$: C, 79.95; H, 9.69; N, 10.36%.

(Z)-2-Octenenitrile (Contains ca. 7% of the (E)-Isomer):[19c] R_f=0.44 (1:5 ether-hexane); ^{1}H NMR (CCl_4) δ=0.63—2.0 (m, 9H), 2.0—2.67 (m, 2H), 5.22 (d, *J*=11 Hz, 1H), 6.37 (dt, *J*=7 and 11 Hz, 1H); IR 2960, 2940, 2860, 2230, 1630, 740 cm^{-1}; Found: C, 78.17; H, 10.56; N, 10.92%. Calcd for $C_8H_{13}N$: C, 78.00; H, 10.63; N, 11.37%.

(2Z,4E)-2,4-Octadienenitrile (Contains ca. 11% of the (E,E)-Isomer):[40] R_f=0.35 (1:5 ether-hexane); ^{1}H NMR (CCl_4) δ=0.94 (t, *J*=7 Hz, 3H), 1.17—1.83 (m, 2H), 1.92—2.5 (m, 2H), 5.00 (d, *J*=10 Hz, (*Z*)-isomer), 5.20 (d, *J*=15 Hz, (*E*)-isomer), 5.83—7.0 (m, 3H); IR 2975, 2940, 2875, 2225, 1645, 740 cm^{-1}.

(Z)-3-Phenylacrylonitrile (Contains ca. 25% of the (E)-Isomer):[19b,c] R_f=0.31 (1:5 ether-hexane); ^{1}H NMR (CCl_4) δ= 5.33 (d, *J*=12 Hz, (*Z*)-isomer), 5.76 (d, *J*=17 Hz, (*E*)-isomer), 7.00 (d, *J*=12 Hz, 1H), 7.33 and 7.72 (m, 5H); IR 3050, 3030, 2220, 1615, 970, 775, 750, 685 cm^{-1}.

We thank the Asahi Glass Foundation for financial support of this work.

References

1) Recent reviews: a) "The Chemistry of the Carbon-Carbon Triple Bond," ed by S, Patai, Wiley, New York (1978); b) "The Chemistry of Ketenes, Allenes, and Related Compounds," ed by S. Patai, Wiley, New York (1980); c) L. Brandsma and H. D. Verkruijsse, "Synthesis of Acetylenes, Allenes and Cumulenes," Elsevier, Amsterdam (1981); d) "The Chemistry of the Allenes," ed by S. R. Landor, Academic Press, London (1982), Vol. 1—3; Recent efforts: e) G. Eyring, B. Curry, A. Brock, and J. Lugtenburg, *J. Am. Chem. Soc.*, **102**, 5392 (1980); f) T. Mukaiyama and T. Harada, *Chem. Lett.*, **1981**, 621; g) R. G. Daniels and L. A. Paquette, *Tetrahedron Lett.*, **22**, 1579 (1981); h) Y. Yamakado, M. Ishiguro, N. Ikeda, and H. Yamamoto, *J. Am. Chem. Soc.*, **103**, 5568 (1981); i) E. J. Corey and C. Rücken, *Tetrahedron Lett.*, **23**, 719 (1982); j) N. R. Pearson, G. Hahn, G. Zweifel, *J. Org. Chem.*, **47**, 3364 (1982); k) R. Haruta, M. Ishiguro, N. Ikeda, and H. Yamamoto, *J. Am. Chem. Soc.*, **104**, 7667 (1982).

2) For example, see pp. 343—379 of Ref. 1a.

3) For a definition of "*erythro-threo*," see R. Noyori, I. Nishida, and J. Sakata, *J. Am. Chem. Soc.*, **103**, 2106 (1981).

4) For recent reviews: J.-F. Biellmann, *Org. React.*, **27**, 1 (1982); Y. Yamamoto, Y. Naruta, "Yuki Kinzoku Kagaku," Maruzen, Tokyo (1983); R. W. Hoffmann, *Angew. Chem., Int. Ed. Engl.*, **21**, 555 (1982).

5) S. A. Shevelev, *Russ. Chem. Rev. (Engl. Transl.)*, **39**, 844 (1970); L. M. Jackman and B. C. Lange, *Tetrahedron*, **33**, 2737 (1977); D. Seebach and K.-H. Geiss, "New Applications of Organometallic Reagents in Organic Chemistry," Elsevier, Amsterdam (1976), p. 22; see also, P. W. K. Lau and T. H. Chan, *Tetrahedron Lett.*, **1978**, 2383.

6) D. S. Watt, *Tetrahedron Lett.*, **1974**, 707 and references are cited therein.

7) For preliminary accounts of the present work, see: a) M. Ishiguro, N. Ikeda, and H. Yamamoto, *J. Org. Chem.*, **47**, 2225 (1982); **48**, 142 (1983); b) R. Haruta, M. Ishiguro, K. Furuta, A. Mori, N. Ikeda, and H. Yamamoto, *Chem. Lett.*, **1982**, 1093.

8) For recent reviews: M. T. Reetz, "Topics in Current Chemistry," Springer, Berlin (1982), pp. 1—54; B. Weidmann and D. Seebach, *Angew. Chem., Int. Ed. Engl.*, **22**, 31 (1983); D. Seebach, B. Weidmann, and L. Widler, "Modern Synthetic Methods 1983," ed by R. Scheffold, Wiley, New York and Salle/Sauerländer, Aarau (1983), pp. 217—353.

9) a) M. Saniere-Karila, M. L. Capmau, and W. Chodkiewicz, *Bull. Soc. Chim. Fr.*, **1973**, 3371; b) E. Favre and M. Gaudemar, *J. Organomet. Chem.*, **92**, 17 (1975).

10) See pp. 367—368 of Ref. 1b.

11) For a similar approach to prepare *erythro* diols, see: F. Mercier, N. Le Goff, and R. Epsztein, *C. R. Acad. Sci., Ser. C*, **279**, 525 (1974); *J. Organomet. Chem.* **108**, 165 (1976).

12) We thank Professor Y. Yamamoto for bringing the error of our preliminary report, see Ref. 7a.

13) The lack of stereoselectivity of the condensation of α-silyl anions with aromatic aldehydes was observed previously, see Ref. 1h and 1i. An electron transfer pathway or an acyclic transition state may be proposed for these anomalous results of aromatic aldehydes, see: E. C. Ashby and A. B. Goel, *J. Am. Chem. Soc.*, **103**, 4983 (1981); S. Murata, M. Suzuki, and R. Noyori, *ibid.*, **102**, 3248 (1980).

14) For recent reviews of Peterson olefination, see: a) T.-H. Chan, *Acc. Chem. Res.*, **10**, 442 (1977); b) A. W. P. Jarvie, *Organomet. Chem. Rev., Sect A*, **6**, 153 (1970).

15) I. Fleming, "Comprehensive Organic Chemistry," ed by D. N. Jones, Pergamon Press, Oxford (1979), Vol. 3, pp. 640—644.

16) Prepared from 1-(trimethylsilyl)propyne, see: E. J. Corey and H. A. Kirst, *Tetrahedron Lett.*, **1968**, 5041. For another preparation of this compound, see: F. Jaffe, *J. Organomet. Chem.*, **23**, 53 1970); M. Laguerre, J. Dunogues, and R. Calas, *ibid.*, **145**, C34 (1978).

17) P. E. Hudrlik, D. Peterson, and R. J. Rona, *J. Org. Chem.*, **40**, 2263 (1975).

18) V. Rautenstrauch, *Helv. Chim. Acta*, **57**, 496 (1974); F. Mercier, R. Epsztein, and S. Holand, *Bull. Soc. Chim. Fr.*, **1972**, 690.

19) a) I. Ojima, M. Kumagai, and Y. Nagai, *Tetrahedron Lett.*, **1974**, 4005; b) I. Matsuda, S. Murata, and Y. Ishii, *J. Chem. Soc., Perkin Trans. 1*, **1978**, 26; c) Y. Sato and Y. Niinomi, *J. Chem. Soc., Chem. Commun.*, **1982**, 56; d) H. Okada, I. Matsuda, and Y. Izumi, *Chem. Lett.*, **1983**, 97. See also, D. N. Brattesani and C. H. Heathcock, *Tetrahedron Lett.*, **1974**, 2279; D. Danion and R. Carrie, *Tetrahedron*, **28**, 4223 (1972).

20) For a general review, see: "The Chemistry of the Cyano Group," ed by S. Patai, Wiley, New York (1970); A. J. Fatiadi, "Preparation and Synthetic Applications of Cyano Com-

pounds," in press.

21) (Trimethylsilyl)acetonitrile was reported to undergo clean metallation with lithium diisopropylamide at low temperature (Ref. 19). Butyllithium was found to be equally effective for the above transformation.

22) The similar reactions of lithio propionitrile or phenylacetonitrile with aldehydes gave β-hydroxy nitrile in modest stereoselectivities.

23) The reactions of corresponding magnesium derivatives were previously reported, see Ref. 1h.

24) Addition of excess base (LDA) to the reaction mixture after treatment with the aldehyde resulted in a lower selectivity.

25) Slightly higher temperature was necessary in the case of magnesio reagents.

26) G. Tennant, "Comprehensive Organic Chemistry," ed by I. O. Sutherland, Pergamon Press, Oxford (1979), Vol. 2, p. 545.

27) G. Stork, L. D. Cama, and D. R. Coulson, *J. Am. Chem. Soc.*, **96**, 5268 (1974); G. Stork and J. F. Cohen, *ibid.*, **96**, 5270 (1974); J. B. Moffat, *J. Chem. Soc., Chem. Commun.*, **1980**, 1108.

28) C. C. Shen and C. Ainsworth, *Tetrahedron Lett.*, **1979**, 87.

29) L. Gouin, M. C. Faroux, O. Riobe, *Bull. Soc. Chim. Fr.*, **1966**, 2320.

30) Freshly prepared from magnesium and iodine in ether.

31) J. Pornet, B. Randrianoelina, and L. Miginiac, *J. Organomet. Chem.*, **174**, 15 (1979).

32) The stereochemical assignment of the acetylenic alcohols was based on the NMR analyses and GLC behaviour in comparison with the authentic sample prepared independently. *threo*-1-Cyclohexyl-2-methyl-4-trimethylsilyl-3-butyn-1-ol was prepared as follows. Wittig reaction of cyclohexanecarbaldehyde with triphenylphosphonium ethylide gave (*Z*)-1-cyclohexylpropene as a major product.[41] Oxidation of the olefin with *m*-CPBA followed by ring opening with diethyl(trimethylsilylethynyl)aluminium[42] afforded the mixture of *threo*-1-cyclohexyl-2-methyl-4-trimethylsilyl-3-butyn-1-ol and 3-cyclohexyl-5-trimethylsilyl-4-pentyn-2-ol (regioisomer). GLC behaviour of the former product was in complete coincidence with the major product of the reaction of titanium reagents. *erythro*-1-Cyclohexyl-2-methyl-4-trimethylsilyl-3-butyn-1-ol was prepared as follows.

Treatment of the (*E*)-1-cyclohexylpropene, which was prepared by the established procedure[43] from the reaction of cyclohexanecarbaldehyde and triphenylphosphonium ethylide, with *m*-CPBA followed by ring opening with the above aluminium reagent gave the *erythro*-1- cyclohexyl-2-methyl-4-trimethylsilyl-3-butyn-1-ol and its regioisomer, 3-cyclohexyl-5-trimethylsilyl-4-pentyn-2-ol. Both isomers of 1-cyclohexyl-2-methyl-4-phenyl-3-butyn-1-ol and 1-cyclohexyl-2-methyl-3-hexyn-1-ol were prepared in a similar manner.

33) The stereochemistry of this compound was determined by the NMR analysis after the conversion to the corresponding aldol product:[44] Treatment of this acetylenic alcohol with mercury(II) sulfate and sulfuric acid gave 4-hydroxy-3-methyl-4-phenyl-2-butanone. ^{1}H NMR spectrum of this product (CCl_4) revealed absorptions at 4.5 (d, J= 8 Hz, weak) and 4.9 ppm (d, J=4 Hz, strong) arising from the benzyl protons. The smaller coupling constant may be expected to belong to *erythro*-isomer.[45]

34) The stereochemistry of this compound was determined as follows. Epoxidation of 1-hexen-3-ol with *t*-BuOOH-VO(acac)$_2$ followed by ring opening with lithium dibutylcuprate-(I) reagent (excess) gave the *erythro*-4,5-decanediol.[46] The NMR analysis and GLC behaviour were identical with the hydrogenation product from entries 14, 15, and 17.

35) The stereochemical assignment of this compound was based on the NMR analysis and GLC behaviour in comparison with the authentic sample prepared independently. Treatment of (*Z*)-4-cyclohexyl-1-trimethylsilyl-3-buten-1-yne, which was prepared by the reported procedure,[1h] with osmium tetraoxide[47] gave *erythro*-1-cyclohexyl-4-trimethylsilyl-3-butyn-1,2-diol. The acetylated product (acetic anhydride-pyridine) of this diol was identical with the major isomer from entries 8 and 9. *erythro*-1-Trimethylsilyl-1-nonyn-3,4-diol was prepared in a similar manner.

36) The butyllithium-*N*,*N*,*N*′,*N*′-tetramethylethylenediamine method may cause the rearrangement of acetylenic bond.

37) E. J. Corey and R. A. Ruden, *Tetrahedron Lett.*, **1973**, 1495.

38) The *Z*-isomer was characterized by an infrared absorption at ≈700 cm^{-1} and coupling constant between the vicinal olefinic hydrogens of ≈11 Hz observed in the ^{1}H NMR spectrum. On the other hand, the *E*-isomer was characterized by an infrared absorption at 960—970 cm^{-1} and a coupling constant of ≈16 Hz.

39) H. Kleijn, H. Westmize, K. Kruithof, and P. Vermeer, *Recl. Trav. Chim. Pays-Bas*, **98**, 27 (1979).

40) K. Utimoto, N. Sakai, H. Nozaki, *J. Am. Chem. Soc.*, **96**, 5601 (1974).

41) I. Gosney and A. G. Rowley, "Organophosphorus Reagents in Organic Synthesis," ed by J. I. G. Cadogon, Academic Press, New York (1979), pp. 17—153; M. Schlosser, *Top. Stereochem.*, **5**, 1 (1970).

42) T. Mole and E. A. Jeffery, "Organoaluminium Compounds," Elsevier, Amsterdam (1972).

43) M. Schlosser and K. F. Christmann, *Liebigs Ann., Chem.* **708**, 1 (1967).

44) D. A. McCrae and L. Dolby, *J. Org. Chem.*, **42**, 1607 (1977).

45) C. H. Heathcock, C. T. Buse, W. A. Kleschick, M. C. Pirrung, J. E. Sohn, and J. Lampe, *J. Org. Chem.*, **45**, 1066 (1980).

46) A. Yasuda, S. Tanaka, H. Yamamoto, and H. Nozaki, *Bull. Chem. Soc. Jpn.*, **52**, 1701 (1979).

47) Review: M. Schröder, *Chem. Rev.*, **80**, 187 (1980).

Stereocontrolled Synthesis of (±)-Asperlin and Related Stereoisomers Using Organotitanium Reagent

Hiroaki HIRAOKA, Kyoji FURUTA, Nobuo IKEDA, and Hisashi YAMAMOTO*
Department of Applied Chemistry, Nagoya University, Chikusa, Nagoya 464
(Received December 26, 1983)

The naturally occurring antibiotics asperlin and related fungal metabolites containing a 5,6-dihydro-2-pyrone moiety have been synthesized stereoselectively. The propargyltitanium reagent derived from 1-trimethylsilyl-3-(tetrahydropyranyloxy)propyne condensed with crotonaldehyde affords the corresponding *erythro* alcohol as the major product, which is converted to (±)-asperlin and the related three stereoisomers in seven steps.

The recent discovery of the regio- and stereoselective synthesis of β-acetylenic alcohols[1] using titanium reagents[2] has substantially simplified the task of stereoselective construction of 3-alkene-1,2-diols and the related structures. We now report the use of this process as a key step in a simple, stereoselective synthesis of (±)-asperlin and related fungal metabolites containing a 5,6-dihydro-2-pyrone moiety, isolated from growing cultures of *Aspergillus nidulans*.[3]

The acetylenic tetrahydropyranyl ether **1** was prepared from propargyl alcohol by reaction with 3,4-dihydro-2*H*-pyran in ether containing a catalytic amount of *p*-toluenesulfonic acid (94%), and then with butyllithium–chlorotrimethylsilane in ether at ambient temperature for 1 h (98%). Successive treatment of acetylene **1** at −78°C with *t*-butyllithium, titanium tetraisopropoxide, and finally crotonaldehyde effected smooth, stereoselective alkylation to the alcohol **2** in 75% yield (*erythro*: *threo*=95:5). The similar high degree of stereoselectivity has been found previously when the carbon α to acetylene is functionalized, for example, the tetrahydropyranyl ether of propargyl alcohol.[1,2] Exposure of the resulting trimethylsilylacetylene to potassium fluoride in methanol at room temperature for an overnight produced **3** in 90% yield.

The construction of the structure of δ-lactone was carried out by three steps. The acetylene **3** was converted to the dilithio derivative by reaction with butyllithium in dry tetrahydrofuran and then allowed to react with excess paraformaldehyde at room temperature. The resulting propargylic alcohol **4** was reduced with hydrogen using Pd–$CaCO_3$ as catalyst in benzene to afford the (*Z*)-allylic alcohol **5** (81%). Oxidation with activated manganese dioxide in dichloromethane gave the δ-lactone **6** directly.[4]

Tetrahydropyranyl group in **6** was cleaved using *p*-toluenesulfonic acid in methanol at room temperature for 30 min to afford the corresponding alcohol **7** (88%). Acetylation of **7** with acetic anhydride–pyridine produced the acetate **8** which was treated with *m*-chloroperbenzoic acid in dichloromethane at room temperature to give *erythro*-5,6-dihydro-5-acetoxy-6-(*trans*-1,2-epoxypropyl)-2*H*-pyran-2-one (**9**) in 83% yield. Chromatographic separation of **9A** and **9B**, using silica gel and ether–hexane (1:1) as the eluent, gave the pure **9A** and **9B** (3:5).[3f,5]

The *threo*-isomer **11** was obtained by Mitsunobu reaction.[6] Thus, the alcohol **7** was treated with diethyl azodicarboxylate and triphenylphosphine in acetic acid and tetrahydrofuran at room temperature for 30 min to give the isomerically pure 5β-acetate **10**.[3f] Exposure of **10** to *m*-chloroperbenzoic acid in dichloromethane at room temperature yielded after chromatography on silica gel (±)-asperlin and its stereoisomer (47% from **7**). The less polar epoxide **11A** was shown to be spectroscopically identical with naturally derived asperlin.[3]

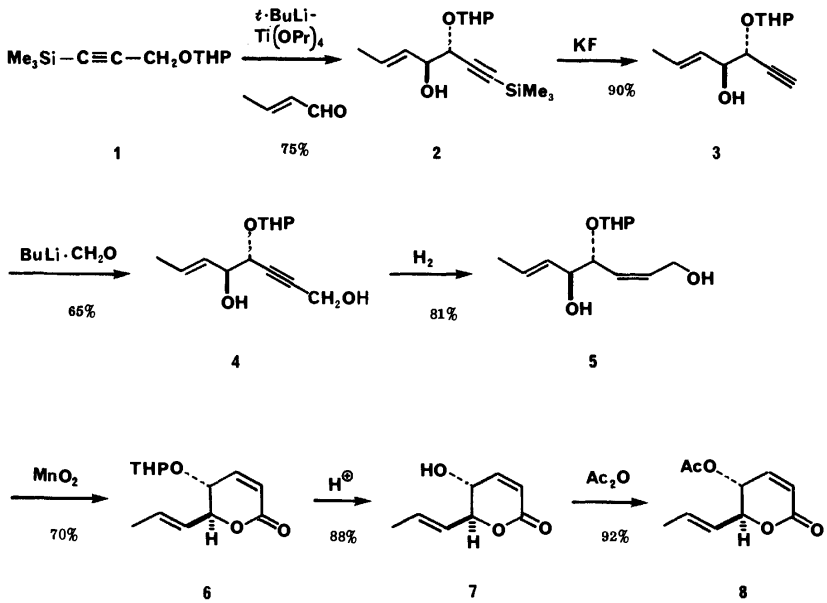

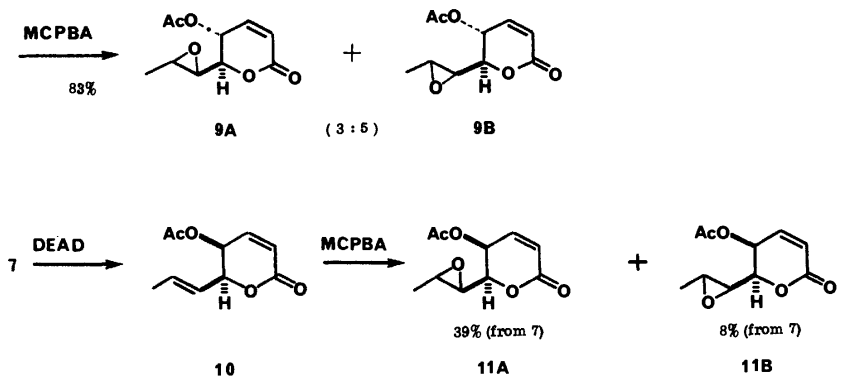

TABLE 1. INHIBITORY EFFECTS OF (±)-ASPERLIN AND STEREOISOMERS ON THE GROWTH OF KB-CELLS *in vitro*

Compound	IC_{50}(μg/ml)
9A	>10
9B	6.1
11A((±)-Asperlin)	6.2
11B	7.2

Preliminary inhibitory test of **9A**, **9B**, **11A**, and **11B** on the growth of KB-cells *in vitro* was shown in Table 1.[7]

Experimental

General. ^{1}H NMR spectra were taken on a JNM-PMX 60 spectrometer. The chemical shifts are reported as parts per million relative to TMS as the internal standard. The infrared spectra were recorded on a Hitachi 260—10 spectrometer in CCl_4 solution unless otherwise stated. The isomeric ratio of the products was determined by gas-liquid phase chromatography (GLC) using Hitachi Model 163 and 164 instruments equipped with a flame ionization detector using nitrogen as carrier gas. For TLC analysis throughout this work, Merck precoated TLC plates (silica gel 60 GF_{254}, 0.25 mm, or silica gel 60 HF_{254} silanized, 0.25 mm) were used. The products were purified by preparative column chromatography on silica gel E. Merck Art. 9385, or silanized silica gel E. Merck Art. 7719. Microanalyses were accomplished at the Institute of Applied Organic Chemistry, Faculty of Engineering, Nagoya University. Unless otherwise specified, all reactions were carried out under an atmosphere of dry argon. In experiments requiring dry solvents, ether and tetrahydrofuran (THF) were distilled from sodium-benzophenone. Benzene was dried over sodium metal. Dichloromethane was dried over **4A** molecular sieves. Pyridine was stored over potassium hydroxide pellets. Other commercially supplied materials were used as received.

3-(Tetrahydro-2-pyranyloxy)-1-(trimethylsilyl)propyne (1). To a mixture of propargyl alcohol (5.82 ml, 100 mmol) and 3,4-dihydro-2*H*-pyran(11.0 ml, 120 mmol) in dry ether (100 ml) was added a catalytic amount of *p*-toluenesulfonic acid (0.2 g) at 0 °C. After the mixture was stirred for 30 min at room temperature, the solution was poured into aqueous sodium hydrogencarbonate and the product was extracted with ether. The combined extracts were washed with water, dried over magnesium sulfate, and concentrated *in vacuo*. Purification of the residue by chromatography on silica gel using ether-hexane (1:12) as eluent to give the propargyl ether as a colorless oil (13.2 g, 94%). A solution of the resulting acetylene (12.6 g, 90 mmol) in dry ether (100 ml) was treated with butyllithium in hexane (1.6 mol dm^{-3} solution, 61.8 ml, 98.9 mmol) dropwise at 0 °C. After the resulting white suspension was stirred for 30 min at 0 °C, chlorotrimethylsilane (12.6 ml, 98.9 mmol) was added at 0 °C. After being stirred for 1 h, the solution was poured into diluted hydrochloric acid and the product was extracted with ether repeatedly. The combined ether layers were washed with water, dried over magnesium sulfate and concentrated *in vacuo*. Purification of the residue by chromatography on silica gel using ether-hexane (1:30) as eluent to afford the ether **1** as a colorless liquid (18.9 g, 99%). ^{1}H NMR (CCl_4) δ=0.17 (s, 9H, Me_3Si), 1.63 (m, 6H, CH_2), 3.21—3.88 (m, 2H, C(6')H_2), 4.10 (s, 2H, ≡C-CH_2), 4.69 (m, 1H, C(2')H); IR 2970, 2205, 1260, 1135, 1040, 860 cm^{-1}; Found: C, 62.38; H, 9.22%. Calcd for $C_{11}H_{20}O_2Si$: C, 62.21, H, 9.49%. TLC analysis showed a single spot (R_f=0.61; 1:2, ether-hexane).

(5E)-erythro-*3-(Tetrahydro-2-pyranyloxy)-1-trimethylsilyl-5-hepten-1-yn-4-ol (2).* To a solution of the acetylene **1** (3.18 g, 15 mmol) in dry tetrahydrofuran (15 ml) at −78 °C was added *t*-butyllithium in pentane (1.96 mol dm^{-3} solution, 7.65 ml, 15.0 mmol) dropwise over 5 min. The resulting red solution was stirred for 1 h at −78 °C and treated with titanium tetraisopropoxide (4.47 ml, 15.0 mmol). After stirring 10 min at −78 °C, the orange solution was treated with crotonaldehyde (1.14 ml, 14.0 mmol), and was then stirred 10 min at −78 °C, allowed to reach room temperature over 1 h. The yellow solution was diluted with ether and washed with diluted hydrochloric acid. The dried (magnesium sulfate) ether layers were concentrated and the residue was subjected to chromatography on silica gel using ether-hexane (1:7) as eluent to give the alcohol **2** as a colorless oil (2.96 g, 75%). ^{1}H NMR (CCl_4) δ=0.15 (s, 9H, Me_3Si), 1.4—2.0 (m, 9H), 2.6 (s, 1H, OH), 3.27—4.30 (m, 4H), 4.78 (m, 1H), 5.33—5.77 (m, 2H, CH=CH); IR 3600, 3450, 2960, 2880, 2200, 1685, 1260, 1025, 850 cm^{-1}; Found: C, 63.59; H, 9.41%. Calcd for $C_{15}H_{26}O_3Si$: C, 63.78; H, 9.28%. TLC analysis showed a single spot (R_f=0.30; 1:2, ether-hexane). GLC analysis of the hydrolized diol showed that the product was 95% pure *erythro* isomer and contained 5% of *threo* isomer.

(5E)-erythro-*3-(Tetrahydro-2-pyranyloxy)-5-hepten-1-yn-4-ol (3).* A mixture of **2** (2.91 g, 10.3 mmol), potassium fluoride (2.99 g, 51.5 mmol), and methanol (20 ml) was stirred overnight at ambient temperature, then diluted with ether, washed with water, dried (magnesium sulfate), and concentrated to a light yellow oil which was subjected to chromatography on silica gel using ether-hexane (2:5) as eluent to give the acetylene **3** as an oil (1.95 g, 90%). ^{1}H NMR (CCl_4) δ=1.7 (m, 9H), 2.33 (t, J=2 Hz, 1H, ≡CH), 2.62 (m, 1H), 3.27—4.40 (m, 4H), 4.87 (m, 1H), 5.52—5.77 (m, 2H, CH=CH); IR 3600, 3450, 3320, 2950, 1685, 1130, 1030, 970 cm^{-1}; Found: C, 68.51; H, 8.69%. Calcd for $C_{12}H_{18}O_3$: C, 68.54; H, 8.63%. TLC analysis showed a single spot (R_f=0.32; 1:2, ether-hexane).

(6E)-erythro-*4-(Tetrahydro-2-pyranyloxy)-6-octen-2-yn-1,5-diol (4).* A solution of the acetylene **3** (8.60 g, 41.0 mmol) in dry tetrahydrofuran (90 ml) at 0 °C was treated with

butyllithium in hexane (1.60 mol dm^{-3} solution, 51.2 ml, 82.0 mmol). The pale yellow solution was stirred 1 h at 0 °C and treated with paraformaldehyde (6.14 g, 205 mmol). After stirring 10 min at 0 °C and 30 min at room temperature, the mixture was poured into diluted hydrochloric acid and the product was extracted with ether. The combined extracts were washed with water, dried (magnesium sulfate), and concentrated. Purification of the residue by chromatography on silica gel using ethyl acetate–hexane (1:1) as eluent to furnish the alcohol **4** as a colorless liquid (6.36 g, 65%). ^{1}H NMR (CCl_4) δ=1.7 (m, 9H), 3.61 (m, 4H), 4.12 (m, 2H), 4.20 (br s, 2H, CH_2OH), 4.90 (m, 1H), 5.47—5.77 (m, 2H, CH=CH); IR 3410, 2970, 1260, 1130, 1030, 870 cm^{-1}; Found: C, 64.77; H, 8.53%. Calcd for $C_{13}H_{20}O_4$: C, 64.98; H, 8.39%. TLC analysis showed a single spot (R_f=0.28; ether).

(2Z,6E)-erythro-4-(Tetrahydro-2-pyranyloxy)-2,6-octadien-1,5-diol (5). A mixture of the alcohol **4** (4.94 g, 20.6 mmol), Lindlar catalyst (5 g) and quinoline (0.655 ml) in benzene (80 ml) was stirred 12 h at room temperature under hydrogen (1 atm). The mixture was filtered, and the filter cake was washed with ether repeatedly. The filtrates were combined and concentrated *in vacuo*. The residue was subjected to chromatography on silica gel using ethyl acetate–hexane (2:3) as eluent to yield the (*Z*)-allylic alcohol **5** as a colorless oil (4.05 g, 81%). ^{1}H NMR (CCl_4) δ=1.7 (br s, 6H), 1.73 (d, *J*=6 Hz, 3H, CH_3), 3.50 (m, 2H), 3.83—4.47 (m, 6H), 4.60 (m, 1H), 5.13—6.13 (m, 4H, olefinic protons); IR 3410, 2955, 1250, 865 cm^{-1}; Found: C, 64.73; H, 8.87%. Calcd for $C_{13}H_{22}O_4$: C, 64.43; H, 9.15%; R_f=0.23 (ether).

5,6-Dihydro-6-[(E)-1-propenyl]-5-(Tetrahydro-2-pyranyloxy) 2H-pyran-2-one (6). Activated manganese (IV) oxide (25.7 g, 296 mmol) was added portionwise to a stirred solution of the diol **5** (3.89 g, 16.1 mmol) in dichloromethane (120 ml) at room temperature. After stirring 12 h at room temperature, the reaction mixture was filtered, and the filter cake was washed well with ether. The solvent was removed *in vacuo*, leaving a pale yellow oil which was submitted to chromatography on silica gel using ethyl acetate–hexane (1:5) as eluent to afford the lactone **6** as a colorless liquid (2.67 g, 70%). ^{1}H NMR (CCl_4) δ=1.63 (br m, 6H), 1.76 (d, *J*=7 Hz, 3H, =CCH_3), 3.27—4.33 (m, 4H), 4.77 (m, 1H), 5.57—6.10 (m, 3H), 6.73 (dd, *J*=9 and 3 Hz, C(4)H); IR 2955, 1740, 1125, 1030 cm^{-1}; Found: C, 65.33; H, 7.77%. Calcd for $C_{13}H_{18}O_4$: C, 65.53; H, 7.61%. TLC analysis showed a single spot (R_f=0.64; ether).

5,6-Dihydro-5-hydroxy-6-[(E)-1-propenyl]-2H-pyran-2-one (7). The lactone **6** (1.72 g, 7.20 mmol) was dissolved in dry methanol (20 ml) and treated with a catalytic amount of *p*-toluenesulfonic acid (150 mg) at room temperature. After stirring 30 min at room temperature, the reaction mixture was poured into aqueous sodium hydrogencarbonate and the product was extracted with ethyl acetate three times. The combined organic layers were washed with water, dried over magnesium sulfate, and concentrated. The residue was submitted to chromatography on silica gel using ether–hexane (3:1) as eluent to give the alcohol **7** as a colorless liquid (978 mg, 88%). ^{1}H NMR ($CDCl_3$) δ=1.75 (d, *J*=6 Hz, 3H, CH_3), 3.1 (s, 1H, OH), 4.03—4.82 (m, 2H), 5.43—6.07 (m, 3H), 6.83 (dd, *J*=2 and 10 Hz); IR 3410, 2960, 2930, 2860, 1720, 1260, 1080, 1020 cm^{-1}; Found: C, 62.06; H, 6.74%. Calcd for $C_8H_{10}O_3$: C, 62.32; H, 6.54%. TLC analysis showed a single spot (R_f=0.46; ether).

5,6-Dihydro-5-acetoxy-6-[(E)-1-propenyl]-2H-pyran-2-one (8). A mixture of the alcohol **7** (154 mg, 1.00 mmol), pyridine (1 ml) and acetic anhydride (1 ml) was allowed to stand at room temperature for 1 h. The resulting solution was poured into aqueous sodium hydrogencarbonate and the product was extracted with ethyl acetate repeatedly. The combined organic layers were washed with brine and dried over magnesium sulfate. Concentration yielded the acetate **8** as an oil (181 mg, 92%). ^{1}H NMR (CCl_4) δ=1.73 (d, *J*=6 Hz, 3H, CH_3), 2.05 (s, 3H, Ac), 4.77 (t, *J*=6 Hz, 1H, C(6)H), 5.23 (m, 1H, C(5)H), 5.4—5.9 (m, 2H, propenyl), 6.03 (br d, *J*=10 Hz, 1H, C(3)H), 6.68 (dd, *J*=4 and 10 Hz); IR 1745, 1375, 1225, 1025 cm^{-1}. TLC analysis showed a single spot (R_f=0.62; ether). This product was used for the next reaction without further purification.

(±)-Asperlin (11A) and Related Stereoisomers (9A, 9B, and 11B). The crude acetate **8** (165 mg, 0.842 mmol) was dissolved in dichloromethane (3 ml) at 0 °C and the solution was treated with *m*-chloroperbenzoic acid (415 mg, 1.68 mmol). After stirring overnight at ambient temperature, the mixture was poured into aqueous sodium sulfite and the product was extracted with ethyl acetate several times. The combined organic layers were washed with water, dried over magnesium sulfate and concentrated *in vacuo*. The residue was subjected on silica-gel chromatography using ether–hexane (1:1) as eluent to afford two isomeric epoxides **9A** (less polar fraction, 57 mg, 32%) and **9B** (more polar fraction, 91 mg, 51%).

9A: ^{1}H NMR (CCl_4) δ=1.33 (d, *J*=5 Hz, 3H, CH_3), 2.07 (s, 3H, Ac), 2.63—3.13 (m, 2H, epoxide), 4.07 (t, *J*=6 Hz, 1H, C(6)H), 5.35 (t, *J*=4 Hz, 1H, C(5)H), 6.03 (d, *J*=10 Hz, 1H, C(3)H), 6.77 (dd, *J*=4 and 10 Hz, 1H, C(4)H); IR 3000, 2940, 1750, 1375, 1230 cm^{-1}; Found: C, 56.88; H, 5.86%. Calcd for $C_{10}H_{12}O_5$: C, 56.60; H, 5.70%. TLC analysis showed a single spot (R_f=0.60; ether).

9B: ^{1}H NMR (CCl_4) δ=1.30 (d, *J*=5 Hz, 3H, CH_3), 2.10 (s, 3H, Ac), 2.73—3.15 (m, 2H), 4.47 (t, *J*=4 Hz, 1H, C(6)H), 5.37 (t, *J*=4 Hz, 1H, C(5)H), 6.00 (d, *J*=10 Hz, 1H, C(3)H), 6.67 (dd, *J*=4 and 10 Hz, 1H, C(4)H); IR 2990, 2950, 1750, 1380, 1230, 1120, 1030 cm^{-1}; Found: C, 56.47; H, 5.83%. Calcd for $C_{10}H_{12}O_5$: C, 56.60; H, 5.70%. TLC analysis showed a single spot (R_f=0.46; ether).

A solution of the alcohol **7** (0.33 g, 2.14 mmol), triphenylphosphine (2.81 g, 10.7 mmol), and acetic acid (0.613 ml, 10.7 mmol) in dry tetrahydrofuran (10 ml) was combined with a solution of diethyl azodicarboxylate (1.68 ml, 10.7 mmol) in tetrahydrofuran (4.3 ml) at room temperature. After 30 min, the reaction mixture was poured into aqueous sodium hydrogencarbonate and the product was extracted with ethyl acetate several times. The combined extracts was washed with water, dried over magnesium sulfate, and concentrated *in vacuo*. The residual oil was subjected to simple short-path chromatography (ether–hexane, 2:1) and the crude product was used for the next reaction without further purification.

The oxidation was carried out in an analogous manner from the above acetate to produce the two isomeric epoxides **11A** (less polar fraction, 177 mg, 39% from the alcohol **7**) and **11B** (more polar fraction, 37 mg, 8% from the alcohol **7**).

(±)-Asperlin (11A):[3] ^{1}H NMR ($CDCl_3$) δ=1.37 (d, *J*=5 Hz, 3H, CH_3), 2.13 (s, 3H, Ac), 2.90—3.28 (m, 2H, epoxide), 4.17 (dd, *J*=3 and 7 Hz, 1H, C(6)H), 5.32 (dd, *J*=3 and 6 Hz, 1H, C(5)H), 6.17 (d, *J*=10 Hz, 1H, C(3)H), 7.03 (dd, *J*=6 and 10 Hz, 1H, C(4)H); IR 3000, 2960, 1750, 1380, 1230, 1040, 760 cm^{-1}; Found: C, 56.76; H, 6.04%. Calcd for $C_{10}H_{12}O_5$: C, 56.60; H, 5.70%. TLC analysis showed a single spot (R_f=0.51; ether).

11B: ^{1}H NMR (CCl_4) δ=1.32 (d, *J*=5 Hz, 3H, CH_3), 2.12 (s, 3H, Ac), 2.75—3.15 (m, 2H, epoxide), 4.28 (t, *J*=4 Hz, 1H, C(6)H), 5.47 (dt, *J*=4 and 6 Hz, 1H, C(5)H), 6.07 (d, *J*=10 Hz, C(3)H), 6.73 (dd, *J*=6 and 10 Hz, 1H, C(4)H); IR 2990, 2950, 1750, 1380, 1230, 1050 cm^{-1}; Found: C, 56.77; H, 6.20%. Calcd for $C_{10}H_{12}O_5$: C, 56.60; H, 5.70%. TLC analysis showed a single spot (R_f= 0.37; ether).

We acknowledge Professor T. Nishiguchi for helpful discussions.

References

1) M. Ishiguro, N. Ikeda, and H. Yamamoto, *J. Org. Chem.*, **47**, 2225 (1982); **48**, 142 (1983); K. Furuta, M. Ishiguro, R. Haruta, N. Ikeda, and H. Yamamoto, *Bull. Chem. Soc. Jpn.*, **57**, 2768 (1984).

2) For recent reviews of the synthetic reactions using organotitanium reagents, see: M. T. Reetz, in "Topics in Current Chemistry," Springer, Berlin (1982), pp. 1—54; B. Weidmann and D. Seebach, *Angew. Chem. Int. Ed. Engl.*, **22**, 31 (1983); D. Seebach, B. Weidmann, and L. Widler, in "Modern Synthetic Methods 1983," ed by R. Scheffold, Wiley, New York and Salle/Sauerländer, Aarau (1983), pp. 217—353.

3) a) A. D. Argoudelis and J. F. Zieserl, *Tetrahedron Lett.*, **1966**, 1969; b) R. H. Evans, Jr., G. A. Ellestad, and M. P. Kunstmann, *Tetrahedron Lett.*, **1969**, 1791; c) W. Rosenbrook, Jr. and R. E. Carney, *Tetrahedron Lett.*, **1970**, 1867; d) M. Tanabe, T. Hamasaki, D. Thomas, and L. Johnson, *J. Am. Chem. Soc.*, **93**, 273 (1971); e) S. Lesage and A. S. Perlin, *Can. J. Chem.*, **56**, 2889 (1978); f) Jiu, Kraychy, Mizuba, U. S. Patent, 3909362 (1975).

4) J. S. Pizey, "Synthetic Reagents," Wiley, New York (1974), Vol. 2, p. 164.

5) By analogy to the TLC behavior of natural asperlin and its isomer, the less polar isomer has tentatively been assigned to **9A**.

6) O. Mitsunobu, *Synthesis*, **1981**, 1.

7) We thank Ono Pharamaceutical Company, Inc. for the biological tests.

 © 1984 The Chemical Society of Japan Bull. Chem. Soc. Jpn., 57, 2781—2790 (1984)

Selective Condensation of [3-(Alkylthio)allyl]titanium Reagent with Carbonyl Compounds

Kyoji FURUTA, Yoshihiko IKEDA, Noriyuki MEGURIYA, Nobuo IKEDA, and Hisashi YAMAMOTO*
Department of Applied Chemistry, Nagoya University, Chikusa, Nagoya 464
(Received December 26, 1983)

[3-(Ethylthio)allyl]titanium reagent generated easily from allyl ethyl sulfides condensed with aldehydes to give *erythro*-β-hydroxy sulfides in highly regio- and stereoselective manner. In contrast, crotyl ethyl sulfide reacted with aldehydes affording δ-hydroxy vinyl sulfide exclusively. The substitution pattern of the starting sulfide can have a pronounced effect on the selectivity in this condensation reaction. *erythro*-β-Hydroxy sulfide obtained was transformed stereoselectively to the *trans*-vinyloxirane or 1,3-alkadiene.

The role of the sulfur function in synthetic chemistry has become increasingly extensive.[1] In particular, the α-carbanion stabilized by sulfur contributed to the many important developments in sulfur utilizing synthetic chemistry.[2] Especially noteworthy is a large body of data relating to the reaction of sulfur-stabilized allylic carbanions.[2] The alkylthioallyl anion generated easily by treating the alkyl allyl sulfide with strong base can react with a variety of electrophiles to give synthetically useful intermediates. Efficient and useful methods for the extension of carbon chain by means of such reagents have recently been described.[3] Unsaturated β-hydroxy sulfide, which can be obtained in the reaction of alkylthioallyl anion with carbonyl compounds, has a potential utility as it can be easily converted to the alkenyloxiranes or 1,3-alkadienes. If it can be possible to obtain this olefinic β-hydroxy sulfide regio- and stereoselectively, the general route to stereochemically pure alkenyloxiranes or 1,3-alkadienes may be established. Previous investigators have attempted to optimize the stereoselectivity of the reaction. Consequently, the available methods afford only one substitution type of pure olefinic β-hydroxy sulfides after a rather tedious sequence in high yields.[2,3]

The major problem encountered in the reaction of allylic carbanions with carbonyl compounds is the one concerning the regio- (α/γ) and stereoselectivities (*erythro/threo*) of the reaction. Generally, it has been thought that the reactivity and the structure of the metallated carbanions are highly dependent on the countercation and solvents.[4] For example, it has been often observed that the lithio derivatives have shown little selectivity in some reactions, but the use of some other metals gave excellent results in the same reactions. In our continuous studies on the reaction of anionic species, we have confirmed the important role of metal countercation in the reaction. Among others, the organotitanium reagents have shown unusual results over a wide range of reactions.[5] This particular reactivity of the titanium reagents has not been fully understood,but it might be suggested that the rather tight nature of carbon–titanium bond and susceptibility to the steric demand are the origin of the selectivity. From this point of view, it may be meaningful to examine the ability of the [3-(alkylthio)allyl]titanium reagents for the selective reaction.

This paper deals with the reaction between a wide variety of [3-(alkylthio)allyl]titanium reagents and carbonyl compounds as a promising versatile synthetic method. Application of this methodology to the stereoselective syntheses of alkenyloxiranes and 1,3-alkadienes were also described.[6]

Results and Discussion

Regio- and Stereoselectivity. Easily prepared [3-(alkylthio)allyl]titanium reagent of type **1** from alkyl lithioallyl sulfide and titanium tetraisopropoxide was subjected to the reaction with carbonyl compounds. The major results of our findings are illustrated in Table 1. Several trends emerge from these data. First,

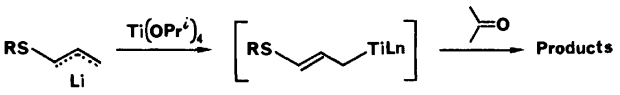

1

the substitution pattern of the starting sulfide can have a pronounced effect on α/γ ratio in the final condensation products. With unsubstituted allyl sulfides (R^1=R^2=R^3=R^4=H, entries 1—10), α-adducts were produced selectively with most of the aldehydes studied (the α % was about 95—99%). Even the aromatic aldehydes and ketones gave α-adduct with high regioselectivities.[7] On the other hand, a dramatic change in product distribution occurs when the condensation with aldehyde was carried out by using γ-substituted allyl sulfides (R^3 and/or R^4=Me, entries, 15, 16, and 19). In these cases, excellent γ-selectivity was observed. α- or β-Mono- and α,β-disubstituted allyl sulfides (R^1 and/or R^2=Me) were, however, showed a very high α-selectivities again. Furthermore, it is highly interesting that α,γ-disubstituted allyl sulfide (R^1=R^3=Me) gave the α-adduct almost exclusively (entry 18).

The second important trend that may be seen from the data in Table 1 is the exceedingly high *erythro* selectivity of the reaction. For example, [3-(phenylthio)allyl]titanium reagent generated from allyl phenyl sulfide reacted with cyclohexanecarbaldehyde at α-position to give *erythro*-β-hydroxy sulfide exclusively (entry 1). For the reaction with aromatic aldehyde and α,β-unsaturated aldehyde, the *erythro* selectivity was relatively low (entries 4, 5, and 10) compared with other saturated systems. This anomalous trend of unsaturated system was often observed in other similar type of reactions,[7] and may be due to an acyclic transition state or other electronic factors.[8] One electron transfer mechanism in the reaction of aromatic carbonyl compounds with some carbanion species was confirmed experimentally by Ashby.[8a] If such was

TABLE 1. REGIO- AND STEREOSELECTIVITIES[a]

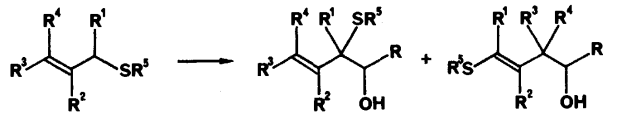

Entry	Sulfide					Carbonyl compd[b]	Product,[c] Yield/%	
	R^1	R^2	R^3	R^4	R^5		α-Adduct (*erythro/threo*)[d]	γ-Adduct
1	H	H	H	H	Ph	A	99(>30:1)	<1
2	H	H	H	H	Et	A	99(>30:1)	<1
3	H	H	H	H	Et	B	87(>30:1)	5
4	H	H	H	H	Et	C	93(9:1)	3
5	H	H	H	H	Et	D	94(6:1)	2
6	H	H	H	H	Et	E	90[e]	7
7	H	H	H	H	Et	F	95(>30:1)	5
8	H	H	H	H	*t*-Bu	A	93(>30:1)	2
9	H	H	H	H	*t*-Bu	B	90(>30:1)	<1
10	H	H	H	H	*t*-Bu	D	99(9:1)	<1
11	CH_3	H	H	H	Ph	A	99(>30:1)	<1
12	CH_3	H	H	H	Et	A	70(>30:1)	<1
13	H	CH_3	H	H	Ph	A	96(>30:1)	4
14	H	CH_3	H	H	Et	A	98(>30:1)	2
15	H	H	CH_3	H	Ph	A	2	98
16	H	H	CH_3	H	Et	A	<1	93
17	CH_3	CH_3	H	H	Ph	A	83(>30:1)[f]	<1
18	CH_3	H	CH_3	H	Ph	A	85(>30:1)[f]	4
19	H	H	CH_3	CH_3	Ph	A	<1	99

a) All reactions were performed on a 2—3 mmol scale with the same experimental procedure as described in the text. b) Freshly distilled prior to use. A: Cyclohexanecarbaldehyde; B: Hexanal; C: 2-Hexenal; D: Benzaldehyde; E: 4-*t*-Butylcyclohexanone; F: Acetophenone. c) Isolated pure product. d) Unless otherwise specified, stereochemical assignments were based on conversion to the corresponding oxiranes. *erythro/threo* Ratio was determined by GLC analyses of the α adduct and/or the corresponding oxirane. e) The major product (97%) was found to be the structure having an axial hydroxyl group. f) Structure determination was not unambiguous but was based on (1) extrapolation from the other examples and (2) the characteristic features of NMR spectrum which were almost identical with those of entry 11 and different from those of the *threo* isomer.

the case, it was surprising that aromatic ketone revealed an exceedingly high *erythro* selectivity (entry 7).

It should be noted that the *erythro* stereoselectivity was not affected by the α and/or β branching of the starting sulfides. In addition, these regio- and stereoselectivities were not affected by the difference in another groups (R^5) on the sulfides. The corresponding [3-(alkylthio)allyl]lithium or other similar organometallic species are totally unsatisfactory reagents[3] for such rigorously regio- and stereoselective transformations. For example, [1-methyl-1-(phenylthio)allyl]lithium (see entry 11 of Table 1) gave 33% yield of the α-adduct (*erythro/threo*=61:39) and 62% yield of the γ-adduct. Analogously, [2-methyl-1-(phenylthio)allyl]lithium (see entry 13 of Table 1) produced 26% yield of the α-adduct (*erythro/threo*=52:48) and 73% yield of the γ-adduct.

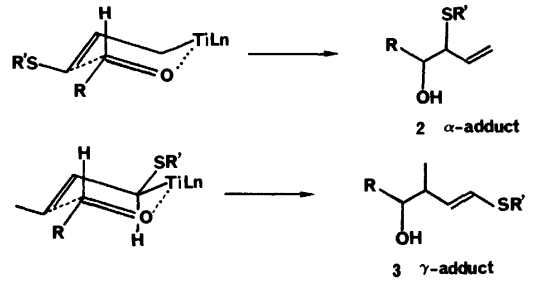

2 α-adduct

3 γ-adduct

The possible explanation of these observation is as follows. It is generally assumed that the addition of the allylic organometallics to the carbonyl takes place through an allylic rearrangement of the organometallics by a chelate transition state (Fig. 1).[9] From this point of view, the structural feature of organometallic species may considerably influence on the regioselectivity of the reaction. Thus, the metal site in the organometallic reagents may be the cotrolling factor of the regioselectivity. It is very useful to know the structure of the organometallic reagents for the estimation of the course of the reactions, but it is, of course, not an easy task. In this case, our efforts to confirm the structure (metal site) of the anionic species by a physical technics gave, hitherto, unsuccessful results. Consequently, the only method for an understanding of the selectivity of this reaction is to examine the product distributions. If one can accept the assumption of the allylic rearrangement mechanism, the alkylthioallyl anion which has a countercation at the γ-position should give the α-adduct, and in contrast, that with cation at α-position to sulfur affords γ-adduct (see Fig. 1). In conclusion, the metal site of the alkylthioallyl anion can be rationalized as follows; (1) for unsubstituted allyl sulfide (entries 1—10), titanium moiety is attached at γ-position to sulfur; (2) γ-substituted allyl sulfide (entries 15, 16, and 19) has, in contrast, the titanium

metal at its α-position; (3) α- or β-mono- and α,β-disubstituted allyl sulfides are metallated at γ-position again; (4) α,γ-disubstituted allyl sulfide (entry 18) is metallated at γ-position with remarkably high selectivity. Thus, the metallation (titanation) of the alkyl allyl sulfide is very sensitive to the substitution pattern of the starting allyl sulfide. If these trends are owing to the steric factor between the titanium metal and geminal substituent, the complete selectivity for the crotyl sulfide metallation is very surprising.

Next noticeable results is the high *erythro* selectivity of the reaction. The predominant formation of *erythro*-β-hydroxy sulfide (α-adduct) was explicable by considering the transition state structure for an allylic rearrangement mechanism stated above (see Fig. 1). As shown in Fig. 1, a six-membered ring transition state in which both R'S and R groups are equatorial is more favorable, and *erythro* product is thus formed. Apparently, it should be expected that the large substituents at α-position of the allyl sulfide reduce the stereoselectivity as a result of the disordering of the sulfide stereochemistry in the transition state (axial-equatorial).

The Synthesis of Alkenyl Oxiranes and Dienes. As the general trends of the reaction of [3-(alkylthio)allyl]-titanium reagents with carbonyl compounds became clear, our attention turned to the synthetic applications of this reaction. Thus, the well-known procedure to desulfurize β-hydroxy sulfides *via* sulfonium salt formation followed by base-catalyzed cyclization[10] converts this reaction into a new stereoselective entry to alkenyloxirane synthesis.[11]

A few examples of this transformation were summarized in Table 2.

Table 2. Stereoselective synthesis of alkenyloxiranes[a]

Entry	Hydroxy Sulfide	Oxirane	*cis*:*trans*[b]	Yield/%	^{1}H NMR δ[i]
1	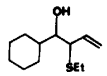	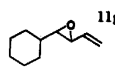 11g)	c)	96	2.95 (dd, *J*=2, 5.5 Hz, 1H), 2.43 (br, 1H)[j]
2	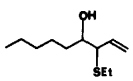	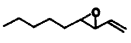	96:4	86	2.88 (dd, *J*=2, 5.5 Hz, 1H), 2.61 (br, 1H)[k]
3	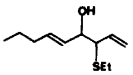	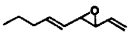	88:12[d]	97	3.2 (d, *J*=6.2 Hz, 2H)[l]
4	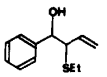	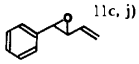 11c, j)	86:14	94	3.15 (dd, *J*=2, 6 Hz, 1H), 3.55 (d, *J*=2 Hz, 1H)[m]
5	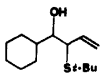	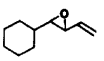	c)	83	
6	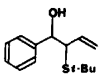	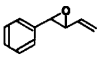	90:10	62	
7	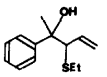	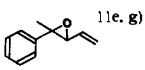 11e, g)	98:2[e]	95	3.25 (d, *J*=5.5 Hz, 1H), 1.63 (s, 3H, Me)
8	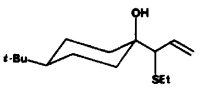	11b, h)	f)	93	3.04 (d, *J*=5.5 Hz, 1H)
9	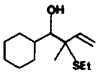	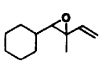	c), g)	82[h]	1.33 (s, 3H, Me), 2.17 (br, 1H)
10	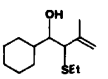	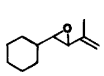	93:7[d]	94	2.98 (d, *J*=2 Hz, 1H), 2.5 (br, 1H)[n]

a) All reaction were performed on a 0.5 mmol scale. b) Unless otherwise specified, stereochemical assignments were based on the NMR analyses of the oxiranes. *cis*/*trans* Ratio was determined by GLC and/or NMR analyses. c) Not determined. Two isomers were not separated on GLC, but pure *trans* isomer was confirmed by NMR analysis. d) Determined by NMR analysis. e) This product was transformed to the saturated oxirane, and spectrally identified by comparison with an authentic specimen prepared independently. f) The stereochemical assignment was based on the method of Trost. The equatorial/axial ratio was 96:4 (GLC). The major isomer was the one depicted in Table. g) Stereochemical assignment was based on NMR analysis of the saturated oxirane derived from the corresponding saturated hydroxy sulfide. The saturated oxirane was >95% pure *trans* by GLC analysis (trace amount of *cis* isomer was detected). h) It should be noted that the usual reaction conditions gave none of the desired product in this case (see text). The same reaction proceeds but in very low yield with use of the corresponding phenylthio derivatives. i) Measured in $CDCl_3$. j) *cis*-Isomer: ^{1}H NMR δ=3.20 (dd, *J*=5, 6 Hz, 1H), 2.58 (br, 1H). k) *cis*-Isomer: ^{1}H δ=3.19 (dd, *J*=5, 6 Hz, 1H). l) *cis*-Isomer: ^{1}H NMR δ=3.47 (m, 2H). m) *cis*-Isomer: ^{1}H NMR δ=4.03 (d, *J*=4 Hz, 1H). n) *cis*-Isomer: ^{1}H NMR δ=3.18 (d, *J*=4 Hz, 1H).

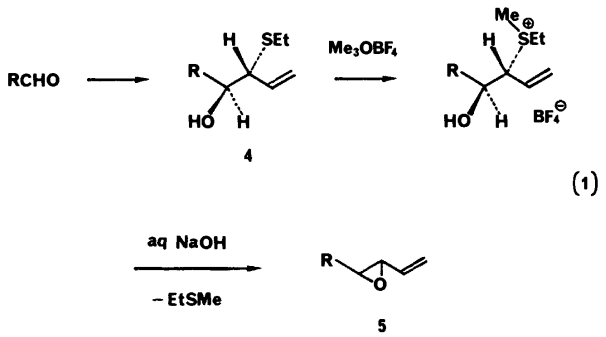

This desulfurization reaction is known to proceed *via* anti attack of oxide ion to sulfonium carbon in complete stereospecific manner. Thus, the *erythro*-β-hydroxy sulfides should be converted to *trans*-oxiranes. Actually, *trans*-oxirane was obtained as a major isomer and the isomer ratios (*trans/cis*) were parallel to those of the β-hydroxy sulfide (*erythro/threo*).

It should be noted that the efficiency of this transformation highly depends on steric factors, especially on the size of alkyl substituents on sulfur atom. Thus, the phenylthio and *t*-butylthio derivatives resulted in lower yield of oxirane than the corresponding ethylthio compound (see entries 1 and 5, 4 and 6 in Table 2). The same reaction in entry 10 but with the use of the phenylthio derivatives proceeds with fairly low yield.

The significant feature of this method can be seen for the preparation of trisubstituted oxiranes, for which there exists no stereoselective methodology (entries 7—9). Thus, two types of trisubstituted oxiranes can be prepared stereoselectively by this method in compliance with the appropriate choice of the starting materials (Eqs. 2 and 3).

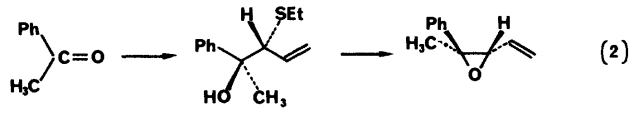

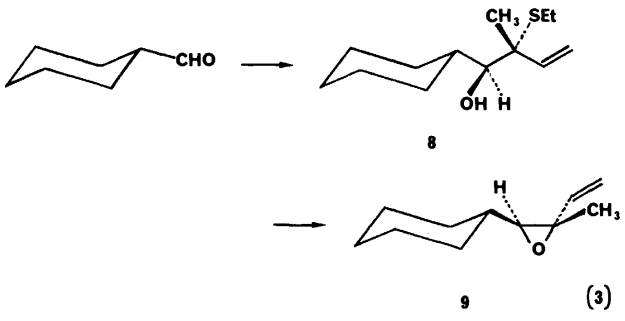

Another type of stereoselection is also observed in entry 8 of Table 2. It was known that the diphenylsulfonium allylide reacted with 4-*t*-butylcyclohexanone to give two isomeric vinyloxiranes **10** and **11** in a ratio of 1:4.[11b] In comparison with this data, it can be stated that the equatorial attack selectivity of the [3-(alkylthio)ally]titanium reagent is exceedingly high (96%).

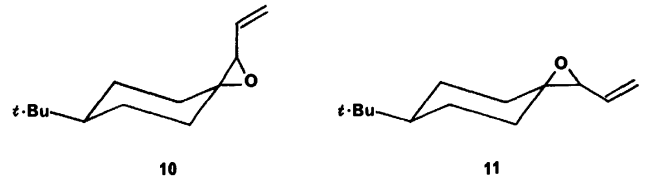

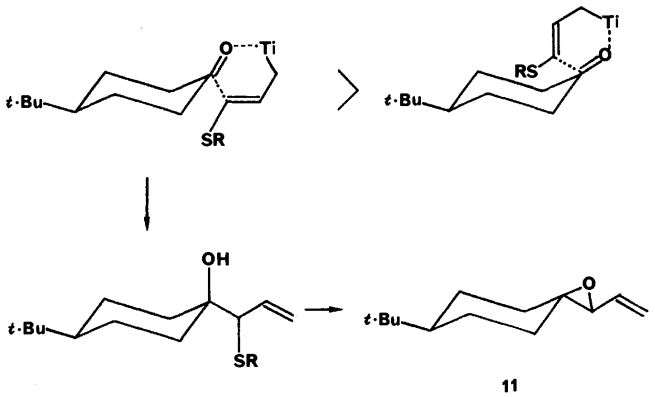

11

We next chose to examine the related reaction system in which the alkyl substituent was replaced by the silyl group. As mentioned in the preceeding section, the α-substituent of the starting allyl sulfides induce the α regioselectivity of the product and may give the significant influence on the *erythro* selectivity of the reaction. The silyl substituent in place of alkyl group may be expected to function in the same way. The silyl group when positioned at α to sulfur has the potential of Peterson elimination[12] following α-selective addition to carbonyl compounds so as to produce 2-(alkylthio)-1,3-alkadiene, an intriguing structure as a Diels-Alder component. Thus the metallation of **12**,[3g,13] metal exchange with titanium tetraisopropoxide as usual manner, and condensation with cyclohexanecarbaldehyde followed by elimination of Me_3SiO^- afforded the (*E*)-sulfide **13** (*E*/*Z*=10:1).[14]

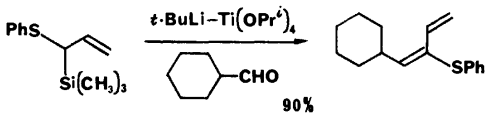

12 13

The formation of the elimination product is indicative of the α-selective addition of this reagent to carbonyl. As the syn elimination of the Me_3SiO^- in Peterson reaction gains general acceptance,[12] the product (*E*)-dienyl sulfide **13** must result from the α-*erythro*-selective carbonyl addition of the reagent. Although the other possible explanation is the α-*threo*-selective carbonyl addition followed by anti elimination, the α-*erythro*-selective reaction mechanism seems to be more likely since the similar syn elimination of Me_3SiO^- using titanium tetraisopropoxide was observed previously[15] and since allyltrimethylsilane on treatment with *t*-BuLi-Ti(OPr^i)$_4$ followed by cyclohexanecarbaldehyde gave the (*Z*)-diene selectively.[16]

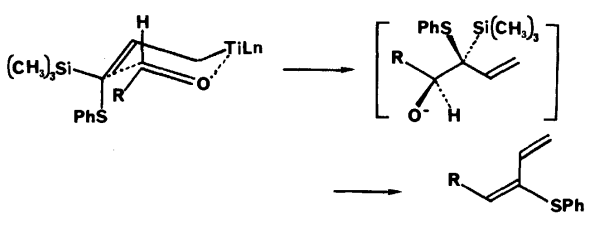

13

It should be noted that the reverse positioning (equatorial→axial) of the sulfur group in transition state is essential for the *erythro* selective addition of this reagent (Fig. 2). The direction of two substituents, phenylthio and trimethylsilyl group, in transition state may be determined by the thermodynamic requirement (relative stability between the possible transition states). Thus, the large trimethylsilyl group should have the equatorial position.

Further interesting results were obtained from the direct dehydration from the sulfide **14** (entry 1 of Table 1). Sequential treatment of the *erythro*-β-hydroxy sulfide **14** in THF first with butyllithium, then methanesulfonyl chloride and finally two equivalents of *t*-butyllithium produced the (*Z*)-sulfide **15** stereospectifically. This reaction is highly stereospecific. Thus,

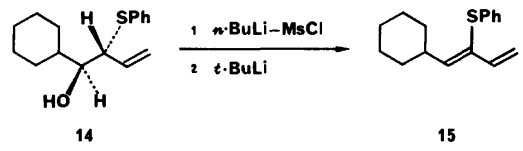

14 **15**

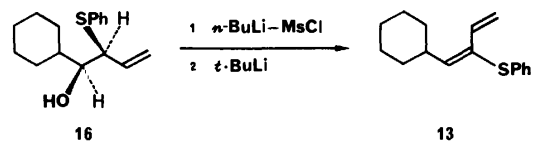

16 **13**

the corresponding *threo* isomer **16**, obtained from the [3-(phenylthio)allyl]lithium and aldehyde followed by chromatographic separation, gave the (*E*)-isomer **13** exclusively under the same reaction conditions. Thus the remarkable syn elimination of MsOH should be concluded. The mechanistic details of this reaction will be published elsewhere.

For the confirmation of the stereochemistry of the dienes, the sulfides **13** and **15** were converted to the corresponding sulfoxides through $NaIO_4$ oxidation. The large downfield shift (ΔH_1 shift=6.38 ppm) of the resonances of HC=CS(O)Ph of the product derived from **13** in the presence of Eu(fod)$_3$ (0.4 equiv) is expected from its *E* configuration. On the other hand, the (*Z*)-isomer revealed a small downfield shift (1.29 ppm) under the same conditions. The model experiment of (*E*)- and (*Z*)-2-cyclohexylvinyl phenyl sulfoxides gave a supporting result for this characteristic shift of absorption spectra (Table 3).

Table 3. ^{1}H NMR Parameters of vinyl sulfoxides[a]

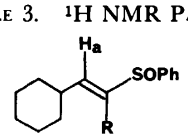

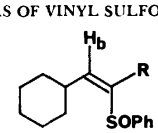

R	δH_a	δH_b	δH_c[b]	ΔH[c]
H	6.42		11.02	4.60
CH=CH$_2$	6.22		12.60	6.38
H		~5.8	7.13	~1.3
CH=CH$_2$		5.98	7.27	1.29

a) Chemical shifts are reported in parts per million downfield from the internal TMS reference. b) δH_E shows the chemical shift of H_a or H_b in the presence of 0.4 equiv of Eu(fod)$_3$. c) $\Delta H=\delta H_E-\delta H_a$ (or δH_b).

Exposure of these sulfides **13** and **15** to methylation conditions with MeMgI under Ni catalyst[17] led to dienes **17** and **18**, respectively with rigorous stereospecificities.

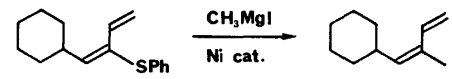

13 **17**

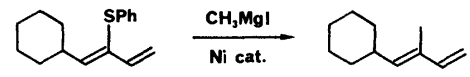

15 **18**

Experimental

General. ^{1}H NMR spectra were taken on a JNM-PMX 60 spectrometer. The chemical shifts are reported as parts per million relative to TMS as the internal standard. The infrared spectra were recorded on a Hitachi 260-10 spectrometer in CCl_4 solution unless otherwise stated. The isomeric ratio of the products was determined by gas-liquid phase chromatography (GLC) using a Hitachi Model 163 and 164 instruments equipped with a flame ionization detector using nitrogen as carrier gas. For TLC analysis throughout this work, Merck precoated TLC plates (silica gel 60 GF_{254}, 0.25 mm, or silica gel 60 HF_{254} silanized, 0.25 mm) were used. The products were purified by preparative column chromatography on silica gel E. Merck Art. 9385, or silanized silica gel E. Merck Art. 7719. Microanalyses were accomplished at the Institute of Applied Organic Chemistry, Faculty of Engineering, Nagoya University. Unless otherwise specified, all reactions were carried out under an atmosphere of dry argon. In experiments requiring dry solvents, ether and tetrahydrofuran (THF) were distilled from sodium-benzophenone. Benzene, hexane, and toluene were dried over sodium metal. Dichloromethane was dried over 4A molecular sieves. Other commercially supplied materials were used as received.

Preparation of Allyl Sulfides. Method A:[18] To a mixture of thiol (0.15 mol) and sodium methoxide (0.17 mol) in methanol (200 ml) was added allyl bromide (0.15 mol) at 0 °C, and the mixture was stirred at 0 °C for 1 h and 25 °C overnight. The resulting mixture was poured into 2 mol dm^{-3} sodium hydroxide and the product was extracted with ether. The organic layer was washed with brine, dried, and freed of solvent. Distillation of the residue gave desired allyl sulfide. Method B: To a solution of alkyl allyl sulfide (48 mmol) dissolved in THF (50 ml) was added *t*-butyllithium in pentane (48 mmol) dropwise at −78 °C, and the resulted solution was stirred for 10 min at the same temperature and 30 min at 0 °C leading to complete lithiation. Then, the mixture was cooled to −78 °C again and methyl iodide (60 mmol) was added to this solution. After stirring for 10 min at −78 °C and 10 min at 0 °C, and further 20 min at 25 °C, the resulting mixture was poured into 2 mol dm^{-3} hydrochloric acid. The product was extracted with ether, and the combined organic layer was dried and freed of solvent. Distillation of the residue gave desired allyl sulfide.

Preparation of Phenyl 1-(Trimethylsilyl)allyl Sulfide.[19] To a solution of allyl phenyl sulfide (15 g, 100 mmol) in THF

TABLE 4. PREPARATION OF ALLYL SULFIDES[a]

Sulfides	Method[b]	Yield(%)	Bp(°C)/mmHg	^{1}H NMR δ[c]
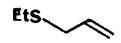	A	72	110—115/760	1.20(t, 7Hz, 3H), 2.41(q, 7Hz, 2H), 3.06(d, 6.5Hz, 2H), 4.8—5.3(m, 2H), 5.75(ddt, 6.5, 9, and 18Hz, 1H).[3b,19a]
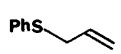	A	84	110—111/23	3.43(d, 6.5Hz, 2H), 4.98(dd, 1 and 10Hz, 1H), 5.02(dd, 1 and 18Hz, 1H), 5.83(ddt, 6.5, 10, and 18Hz, 1H).[18]
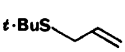	A	66[d]	58—60/37	1.30(s, 9H), 3.11(d, 7Hz, 2H), 4.80—5.27(m, 2H), 5.80(ddt, 7, 9.5, and 17Hz, 1H).[20]
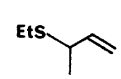	B	70	124—125/760	1.19(t, 7Hz, 3H), 1.28(d, 7Hz, 3H), 2.36(q, 7Hz, 2H), 3.23(dt, 7 and 7Hz, 1H), 4.87(dd, 1 and 16Hz, 1H), 4.92(dd, 1 and 10Hz, 1H), 5.33—5.92(m, 1H).[19c]
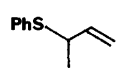	B	79	e)	1.35(d, 7Hz, 3H), 3.68(dt, 7 and 7Hz, 1H), 4.87(dd, 1 and 16Hz, 1H), 4.88(dd, 1 and 10Hz, 1H), 5.4—6.07(m, 1H), 7.20(m, 5H).[18]
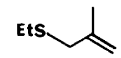	A	83	36—37/19	1.18(t, 7Hz, 3H), 1.78(s, 3H), 2.34(q, 7Hz, 2H), 3.0(s, 2H), 4.72(s, 2H).[19b]
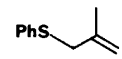	A	89	113—115/18	1.83(s, 3H), 3.42(s, 2H), 4.74(s, 2H), 7.17(m, 5H).[2a,21]
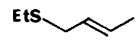	A	87[f]	42—47/19	1.19(t, 7Hz, 3H), 1.70(m, 3H), 2.38(q, 7Hz, 2H), 2.99(m, 2H), 5.42(m, 2H).[19b]
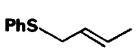	A	96[g]	119—122/20	1.64(d, 3.5Hz, 3H), 3.41(m, 2H), 5.46(m, 2H), 7.14(s, 5H).[18,21]
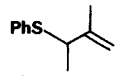	B	78	118—122/19	1.38(d, 7Hz, 3H), 1.82(s, 3H), 3.68(q, 7Hz, 1H), 4.62(s, 2H), 7.18(m, 5H).[22]
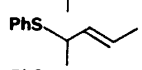	B	72[h]	130—132/26	1.32(d, 7Hz, 3H), 1.58(d, 5Hz, 3H), 3.59(dt, 7 and 7Hz, 1H), 5.31(m, 2H), 7.17(m, 5H).[21]
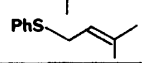	A	90	133—139/23	1.56(s, 3H), 1.69(s, 3H), 3.42(d, 7.5Hz, 2H), 5.24(t, 7.5Hz, 1H), 4.16(m, 5H).[23]

a) The reactions were performed on 50—250 mmol scale. b) Method A: Thiol-sodium methoxide-allyl bromide; Method B: Allyl sulfide-*t*-butyllithium-methyl iodide. c) ^{1}H NMR spectrum were measured in CCl_4 solution. d) This product was contaminated with *ca.* 15% of diallyl sulfide, which could not be separated. The mixture was used for the reaction. e) Purified by silica-gel column chromatography (hexane, R_f=0.24). A small amount of the regioismer, 1-butenyl phenyl sulfide, was also produced as a side product, but it could be separated out by column chromatography (hexane, R_f=0.35). f) This contains *ca.* 8% of the *Z*-isomer. g) This contains *ca.* 4% of the *Z*-isomer and 5% of the regioisomer, 1-methylallyl phenyl sulfide. They could be separated out by repeated fractional distillation. h) This contains *ca.* 10% of *Z*-isomer.

(200 ml) was added *t*-butyllithium in pentane (2.0 mol dm^{-3} solution, 50 ml, 100 mmol) at −78 °C. The solution was stirred at 0 °C for 30 min, and then cooled to −78 °C again. Titanium tetraisopropoxide[24] (32.7 ml, 110 mmol) was added to the mixture and the resulting solution was stirred for 10 min at the same temperature. To this solution was added chlorotrimethylsilane (12.7 ml, 100 mmol) at −78 °C, and stirring was continued for 10 min at −78 °C and 1 h at 0 °C. The reaction mixture was poured into 2 mol dm^{-3} hydrochloric acid and the product was extracted with ether. The combined organic layer was dried and concentrated.[25] Fractional distillation of the residue gave phenyl 1-(trimethylsilyl)-allyl sulfide (14.6 g, 66%). Bp 73—74 °C (0.9 mmHg†); ^{1}H NMR (CCl_4) δ=0.13 (s, 9H), 3.12 (d, *J*=8.5 Hz, 1H), 4.86 (dd, *J*=1 and 8.5 Hz, 1H), 4.88 (dd, *J*=1 and 17 Hz, 1H), 5.72 (dt, *J*=8.5 and 17 Hz, 1H).

Reaction of [3-(Alkylthio)allyl]titanium Reagents with Carbonyl Compounds. The following experimental procedure provides details of typical reaction conditions. To a solution of allyl phenyl sulfide (0.36 g, 2.4 mmol) in THF (8 ml) was added butyllithium[26] in hexane (1.6 mol dm^{-3} solution, 1.5 ml, 2.4 mmol) dropwise at −78 °C, and the orange mixture was stirred at 0 °C for 30 min. Titanium tetraisopropoxide (0.71 ml, 2.4 mmol) was added to the solution at −78 °C, and the resulting solution was stirred for 10 min. Cyclohexanecarbaldehyde (0.24 ml, 2.0 mmol) was added over a period of 5 min at −78 °C, and the mixture was stirred at −78 °C for 10 min and then at 0 °C for 1 h. Then the mixture was poured into 2 mol dm^{-3} hydrochrolic acid and the product was extracted with ether. The organic layer was dried and concentrated. Chromatography of the residue on silica-gel column[27] (4:1 hexane-ether) gave *erythro*-1-cyclohexyl-2-phenylthio-3-buten-1-ol (0.52 g, 99%).[28] GLC analysis of the product revealed the isomeric ratio of >30:1 (*erythro*: *threo*). Stereochemical assignments of the sulfide-carbonyl adducts were based on conversion to the corresponding oxiranes.

erythro-*1-Cyclohexyl-2-phenylthio-3-buten-1-ol*: R_f=0.30 (4:1 hexane-ether); ^{1}H NMR (CCl_4) δ=0.55—2.3 (m, 11H), 2.17 (d, *J*=3 Hz, 1H), 3.30 (m, 1H), 3.73 (dd, *J*=4 and 8.5 Hz, 1H), 4.96 (dd, *J*=2 and 16.5 Hz, 1H), 5.04 (dd, *J*=2 and 10 Hz, 1H), 5.83 (ddd, *J*=8.5, 10, and 16.5 Hz, 1H), 7.2 (m, 5H); IR 3550, 3090, 2930, 2860, 1645, 1450 cm^{-1}; Found: C, 73.20; H, 8.47%. Calcd for $C_{16}H_{22}OS$: C, 73.23; H, 8.45%.

erythro-*1-Cyclohexyl-2-ethylthio-3-buten-1-ol*: R_f=0.38 (2:1 hexane-ether); ^{1}H NMR (CCl_4) δ=1.22 (t, *J*=7 Hz, 3H), 0.83—2.17 (m, 12H), 2.42 (q, *J*=7 Hz, 2H), 3.33 (m, 2H), 5.00 (dd, *J*=2 and 18 Hz, 1H), 5.10 (dd, *J*=2 and 8 Hz, 1H), 5.42—6.08 (m, 1H); IR 3550, 3090, 2920, 2850, 1640, 1450 cm^{-1}; Found: C, 66.95; H, 10.30%. Calcd for $C_{12}H_{22}OS$: C, 67.23; H, 10.35%.

erythro-*3-Ethylthio-1-nonen-4-ol*: R_f=0.31 (2:1 hexane-ether); ^{1}H NMR (CCl_4) δ=0.73—1.73 (m, 14H), 1.85 (m, 1H), 2.41 (q, *J*=7 Hz, 2H), 3.15 (dd, *J*=4.2 and 8 Hz, 1H), 3.50 (m, 1H), 4.98 (dd, *J*=2 and 16 Hz, 1H), 5.05 (dd, *J*=2 and 9 Hz, 1H), 5.37—

† 1 mmHg≈133.322 Pa.

6.00 (m, 1H); IR 3500, 3090, 2950, 2860, 1635, 1450 cm^{-1}; Found: C, 65.60; H, 10.73%. Calcd for $C_{11}H_{22}OS$: C, 65.29; H, 10.96%.

erythro-*3-Ethylthio-1,5-nonadien-4-ol*: R_f=0.30 (2:1 hexane-ether); ^{1}H NMR (CCl_4) δ=0.71—1.79 (m, 8H), 1.80—2.21 (m, 3H), 2.42 (q, J=7 Hz, 2H), 3.18 (dd, J=5 and 8.5 Hz, 1H), 3.99 (m, 1H), 4.99 (dd, J=2 and 17 Hz, 1H), 5.05 (dd, J=2 and 9 Hz, 1H), 5.36—5.96 (m, 3H); IR 3500, 3070, 2950, 2860, 1635, 1450 cm^{-1}; MS m/z: 200 (M^+).

erythro-*2-Ethylthio-1-phenyl-3-buten-1-ol*: R_f=0.38 (2:1 hexane-ether); ^{1}H NMR (CCl_4) δ=1.19 (t, J=7 Hz, 3H), 2.18—2.67 (m, 3H), 3.38 (dd, J=5 and 9 Hz, 1H), 4.58—5.17 (m, 3H), 5.33—6.00 (m, 1H); IR 3460, 3070, 2970, 2930, 1640, 1450 cm^{-1}; Found: C, 69.49; H, 7.63%. Calcd for $C_{12}H_{16}OS$: C, 69.18; H, 7.74%.

4-t-Butyl-1-[1-(ethylthio)allyl]cyclohexanol: R_f=0.45 (2:1 hexane-ether); ^{1}H NMR (CCl_4) δ=0.85 (s, 9H), 1.03—1.82 (m, 12H), 1.87 (br s, 1H), 2.43 (q, J=7 Hz, 2H), 2.98 (d, J=10 Hz, 1H), 4.95 (dd, J=3 and 18 Hz, 1H), 5.02 (dd, J=3 and 9 Hz, 1H), 5.38—5.97 (m, 1H); IR 3520, 2950, 1630, 1440 cm^{-1}; MS m/z: 256 (M^+).

erythro-*3-Ethylthio-2-phenyl-4-penten-2-ol*: R_f=0.33 (4:1 hexane-ether); ^{1}H NMR (CCl_4) δ=1.17 (t, J=7 Hz, 3H), 1.60 (s, 3H), 2.34 (q, J=7 Hz, 2H), 2.70 (s, 1H), 3.35 (d, J=10 Hz, 1H), 4.87 (dd, J=2 and 18 Hz, 1H), 4.95 (dd, J=2 and 9.5 Hz, 1H), 5.68 (ddd, J=9.5, 10, and 18 Hz, 1H), 7.23 (m, 5H); IR 3500, 3060, 2980, 2880, 1640, 1450 cm^{-1}; MS m/z: 222 (M^+).

erythro-*1-Cyclohexyl-2-(t-butylthio)-3-buten-1-ol*: ^{1}H NMR (CCl_4) δ=0.7—2.12 (m, 12H), 1.32 (s, 9H), 3.03—3.37 (m, 1H), 3.43 (dd, J=4 and 9 Hz, 1H), 4.87—5.28 (m, 2H), 5.87 (ddd, J=9, 9, and 18 Hz, 1H); IR 3400, 2930, 1635, 1450 cm^{-1}; MS m/z: 242 (M^+).

erythro-*1-Phenyl-2-(t-butylthio)-3-buten-1-ol*: ^{1}H NMR (CCl_4) δ=1.28 (s, 9H), 2.52 (m, 1H), 3.46 (dd, J=4.5 and 8.5 Hz, 1H), 4.53—5.12 (m, 3H), 5.65 (ddd, J=8.5, 8.5, and 17 Hz, 1H), 7.10 (s, 5H); IR 3400, 3070, 2970, 1640, 1450 cm^{-1}; MS m/z: 236 (M^+).

erythro-*3-(t-Butylthio)-1-nonen-4-ol*: ^{1}H NMR (CCl_4) δ=0.7—1.62 (m, 11H), 1.32 (s, 9H), 2.42 (br d, J=7 Hz, 1H), 3.35 (dd, J=4 and 8 Hz, 1H), 3.53 (m, 1H), 5.05 (dd, J=2 and 10 Hz, 1H), 5.17 (dd, J=2 and 17 Hz, 1H), 5.90 (ddd, J=8, 10, and 17 Hz, 1H); IR 3530, 3090, 2960, 2860, 1640, 1460 cm^{-1}; MS m/z: 230 (M^+).

erythro-*1-Cyclohexyl-2-methyl-2-phenylthio-3-buten-1-ol*: R_f=0.39 (4:1 hexane-ether); ^{1}H NMR (CCl_4) δ=1.29 (s, 3H), 0.66—1.99 (m, 11H), 2.52 (br s, 1H), 3.25 (br s, 1H), 4.83 (dd, J=1 and 17 Hz, 1H), 5.01 (dd, J=1 and 11 Hz, 1H), 6.21 (dd, J=11 and 17 Hz, 1H), 7.26 (m, 5H); IR 3620, 3090, 2930, 2850, 1640, 1450 cm^{-1}; Found: C, 74.12; H, 8.81%. Calcd for $C_{17}H_{24}OS$: C, 73.86; H, 8.75%.

erythro-*1-Cyclohexyl-2-ethylthio-2-methyl-3-buten-1-ol*: R_f=0.33 (4:1 hexane-ether); ^{1}H NMR (CCl_4) δ=1.18 (t, J=7 Hz, 3H), 1.39 (s, 3H), 0.8—1.97 (m, 11H), 2.13—2.57 (m, 3H), 3.23 (br d, J=4.5 Hz, 1H), 4.97 (dd, J=2 and 17 Hz, 1H), 5.07 (dd, J=2 and 10 Hz, 1H), 6.08 (dd, J=10 and 17 Hz, 1H); IR 3480, 3080, 2920, 2850, 1635, 1450 cm^{-1}; Found: C, 68.11; H, 10.60%. Calcd for $C_{13}H_{24}OS$: C, 68.37; H, 10.59%.

erythro-*1-Cyclohexyl-3-methyl-2-phenylthio-3-buten-1-ol*: R_f=0.23 (8:1 hexane-ether); ^{1}H NMR (CCl_4) δ=0.87—2.2 (m, 12H), 1.82 (s, 3H), 3.2—3.53 (m, 1H), 3.62 (d, J=7 Hz, 1H), 4.75 (m, 2H), 7.17 (m, 5H); IR 3600, 3090, 2940, 2860, 1650, 1600, 1450 cm^{-1}; Found: C, 73.95; H, 8.78%. Calcd for $C_{17}H_{24}OS$: C, 73.86; H, 8.75%.

erythro-*1-Cyclohexyl-2-ethylthio-3-methyl-3-buten-1-ol*: R_f=0.35 (8:1 hexane-ethyl acetate); ^{1}H NMR (CCl_4) δ=1.20 (t, J=7 Hz, 3H), 1.80 (s, 3H), 1.0—2.0 (m, 12H), 2.33 (q, J=7 Hz, 2H), 3.27 (br s, 2H), 4.83 (m, 2H); IR 3500, 3080, 2940, 2860, 1650, 1450 cm^{-1}; Found: C, 68.47; H, 10.67%. Calcd for $C_{13}H_{24}OS$: C, 68.37; H, 10.59%.

1-Cyclohexyl-2-methyl-4-phenylthio-3-buten-1-ol: R_f=0.20 (8:1 hexane-ether); ^{1}H NMR (CCl_4) δ=1.06 (d, J=7 Hz, 3H), 0.67—2.0 (m, 12H), 2.45 (m, 1H), 3.03 (br s, 1H), 5.63—6.33 (m, 2H), 7.18 (br s, 5H); IR 3500, 3080, 2930, 2850, 1590, 1450 cm^{-1}; Found: C, 73.91; H, 8.76%. Calcd for $C_{17}H_{24}OS$: C, 73.86; H, 8.75%.

1-Cyclohexyl-4-ethylthio-2-methyl-3-buten-1-ol: R_f=0.22 (8:1 hexane-ethyl acetate); ^{1}H NMR (CCl_4) δ=1.07 (t, J=7 Hz, 3H), 1.34 (d, J=7 Hz, 3H), 0.83—2.11 (m, 12H), 2.44 (m, 1H), 2.63 (q, J=7 Hz, 2H), 3.00 (m, 1H), 5.38 (dd, J=8 and 15 Hz, 1H), 5.92 (d, J=15 Hz, 1H); IR 3550, 2920, 2840, 1440, 980, 970 cm^{-1}; Found: C, 68.54; H, 10.65%. Calcd for $C_{13}H_{24}OS$: C, 68.37; H, 10.59%.

erythro-*1-Cyclohexyl-2,3-dimethyl-2-phenylthio-3-buten-1-ol*: R_f=0.36 (4:1 hexane-ether); ^{1}H NMR (CCl_4) δ=1.25 (s, 3H), 0.75—2.0 (m, 11H), 2.03 (s, 3H), 2.12 (s, 1H), 3.41 (br m, 1H), 4.80 (br s, 1H), 4.90 (br s, 1H), 7.25 (m, 5H); IR 3600, 3500, 3080, 2920, 2850, 1635, 1450 cm^{-1}; Found: C, 74.45; H, 9.06%. Calcd for $C_{18}H_{26}OS$: C, 74.43; H, 9.02%.

erythro-*1-Cyclohexyl-2-methyl-2-phenylthio-3-penten-1-ol*: R_f=0.39 (4:1 hexane-ether); ^{1}H NMR (CCl_4) δ=1.28, (s, 3H), 1.65 (d, J=6 Hz, 3H), 0.75—1.83 (m, 11H), 2.52 (d, J=2 Hz, 1H), 3.17 (d, J=2 Hz, 1H), 5.23 (dq, J=6 and 16 Hz, 1H), 5.83 (d, J=16 Hz, 1H), 7.27 (m, 5H); IR 3540, 3080, 2930, 2850, 1450, 975 cm^{-1}; Found: C, 74.23; H, 8.98%. Calcd for $C_{18}H_{26}OS$: C, 74.43; H, 9.02%.

1-Cyclohexyl-2,2-dimethyl-4-phenylthio-3-buten-1-ol: R_f=0.25 (4:1 hexane-ether); ^{1}H NMR (CCl_4) δ=1.08 (s, 6H), 0.86—1.94 (m, 12H), 3.01 (s, 1H), 5.97 (s, 2H), 7.14 (s, 5H); IR 3650, 3080, 2930, 2850, 1590, 1480, 1450, 1100, 970 cm^{-1}; Found: C, 74.63; H, 9.07%. Calcd for $C_{18}H_{26}OS$: C, 74.43; H, 9.02%.

Synthesis of Vinyloxiranes.[10] *The following experimental procedure is typical for the conversion of β-hydroxy sulfides to oxiranes*: To a suspension of trimethyloxonium tetrafluoroborate (0.54 mmol) in dichloromethane (2 ml) was added β-hydroxy sulfide (0.50 mmol) dissolved in dichloromethane (2 ml) at 0 °C, and the mixture was stirred at 0—25 °C until all the sulfide had been consumed (TLC assay). Then, 0.5 mol dm^{-3} sodium hydroxide solution (5 ml) was added to the mixture at 0 °C, and the resulting two phases mixture was efficiently stirred for 1—12 h at 25 °C. The reaction mixture was poured into water and the product was extracted with ether. The combined organic layer was dried and concentrated. Chromatography of the residual oil on silica-gel column (20:1 hexane-ether) gave the pure vinyloxirane.[29] 4-Cyclohexyl-3,4-epoxy-3-methyl-1-butene (entry 9 in Table 2) could not be prepared by this typical procedure, but was efficiently formed by treating the sulfonium salt obtained as above with butyllithium (1 equiv) at −78 °C.

The *trans*-oxirane was generally characterized by a coupling constant between the vicinal oxirane hydrogenes of ≈2 Hz[11] observed in the ^{1}H NMR spectrum. On the other hand, the *cis*-oxirane was characterized by a coupling constant of ≈4 Hz.[11]

The stereochemistry of 3,4-epoxy-4-phenyl-1-pentene was determined as follows. To a solution of propyltriphenylphosphonium bromide (1.55 g, 4 mmol) in THF (10 ml) was added butyllithium in hexane (1.6 mol dm^{-3}, 2.5 ml, 4 mmol) at 0 °C, and the mixture was stirred for 30 min at the same temperature. Acetophenone (0.47 ml, 4 mmol) dissolved in THF (1 ml) was added to the solution and the resulting mixture was stirred for 2 h at 0 °C and 0.5 h at 25 °C. Then, the reaction mixture was poured into water and the product was extracted with ether. The combined organic layer was dried and evaporated. Chromatography of the residual oil on silica-gel column (hexane) gave 2-phenyl-2-pentene (530 mg, 91%). NMR analysis of this product revealed an isomeric ratio of *ca.* 7:3 (*Z*:*E*).[30] ^{1}H NMR (CCl_4) δ=0.57—1.41 (m), 1.98 (s, 3H), 1.67—2.44 (m, 2H), 5.31 (br t, J=6.5 Hz, *Z*-isomer), 5.61 (br

t, J=7 Hz, *E*-isomer), 7.04 (m, 5H). To a solution of *m*-chloroperbenzoic acid (271 mg, 1.1 mmol) in dichloromethane (4 ml) was added 2-phenyl-2-pentene (150 mg, 1.0 mmol) dissolved in dichloromethane (2 ml) at 0 °C. The mixture was stirred for 1 h at 0 °C, and then poured into aqueous sodium sulfite solution. The product was extracted with ether and washed with aqueous sodium hydrogencarbonate. The combined organic layer was dried and concentrated. Chromatography of the residue on silica-gel column gave the isomeric mixture of 2,3-epoxy-2-phenylpentane (156 mg, 96%). GLC analysis of this product revealed the isomeric ratio of 28:72 (*trans*:*cis*). ^{1}H NMR CCl_4 δ=0.67—1.35 (m, 5H), 1.56 (s, 3H), 2.58 (t, J=6 Hz, *trans* isomer), 2.80 (t, J=5.8 Hz, *cis* isomer), 7.13 (s, 5H). NMR spectrum and GLC behaviour of the major isomer of this product was in complete agreement with the product derived from the sulfide-carbonyl adduct by the following sequence: (1) Reduction of double bond by H_2NNH_2–H_2O_2–$CuSO_4$ in aquous ethanol at 0—25 °C (60%); (2) Epoxidation by the general method described in text (90%).

3-Ethylthio-2-phenyl-2-pentanol: ^{1}H NMR (CCl_4) δ=0.77—1.43 (m, 8H), 1.58 (s, 3H), 2.1—2.77 (m, 4H), 7.22 (m, 5H).

trans-*2,3-Epoxy-2-phenylpentane*: ^{1}H NMR (CCl_4) δ=0.83—1.33 (m, 5H), 1.56 (s, 3H), 2.58 (t, J=6 Hz, 1H), 7.12 (s, 5H); MS m/z: 162 (M^+).

The stereochemistry of 4-cyclohexyl-3,4-epoxy-3-methyl-1-butene was determined as follows. To a solution of propyltriphenylphosphonium bromide (1.93 g, 5.0 mmol) in THF (15 ml) was added butyllithium in hexane (1.6 mol dm^{-3} solution, 3.13 ml, 5.0 mmol) at 0 °C, and the mixture was stirred for 1 h at the same temperature. Methyl iodide (0.31 ml, 5.0 mmol) was added to the mixture and the solution was stirred for 1 h at 0 °C. To the resulting dark brown solution was added butyllithium in hexane (3.13 ml, 5.0 mmol) at 0 °C. After stirring for 1 h, cyclohexanecarbaldehyde (0.61 ml, 5.0 mmol) was added to the solution at 0 °C and stirring was continued for 1 h. The reaction mixture was poured into water and the product was extracted with ether. The combined organic layer was dried and concentrated. Chromatography of the residual oil on silica-gel column (pentane) gave 1-cyclohexyl-2-methyl-1-butene (0.52 g, 69%). GLC analysis of this product revealed an isomeric ratio of *ca.* 1.3:1 (*E*:*Z*). ^{1}H NMR ($CDCl_3$) δ=1.00 (t, J=7 Hz), 1.60 (d, J=1.5 Hz, *E*-isomer), 1.67 (d, J=1.8 Hz, *Z*-isomer), 0.67—2.33 (m), 4.95 (br d, J=8 Hz, 1H). To a solution of *m*-chloroperbenzoic acid (271 mg, 1.1 mmol) in dichloromethane (4 ml) was added 1-cyclohexyl-2-methyl-1-butene (152 mg, 1.0 mmol) dissolved in dichloromethane (2 ml) at 0 °C. The mixture was stirred for 1 h at 0 °C, and then poured into aqueous sodium sulfite solution. The product was extracted with ether and washed with aqueous sodium hydrogencarbonate. The combined organic layer was dried and concentrated. Chromatography of the residue on silica-gel column gave the isomeric mixture of 1-cyclohexyl-1,2-epoxy-2-methylbutane (162 mg, 96%). ^{1}H NMR ($CDCl_3$) δ=1.27 (s, *trans*-isomer), 1.29 (s, *cis*-isomer), 0.67—2.11 (m), 2.41 (br, 1H). GLC analysis of this product showed an isomeric ratio of *ca.* 1.4:1 (*trans*:*cis*).[31] The major isomer (*trans*) was spectrally and chromatographically in complete agreement with the product derived from the sulfide-carbonyl adduct by the following sequence: (1) Reduction of the double bond by H_2NNH_2–H_2O_2–$CuSO_4$ in aqueous ethanol at 0—25 °C (44%); (2) Epoxidation by usual manner (89%).

1-Cyclohexyl-2-ethylthio-2-methyl-1-butanol: ^{1}H NMR ($CDCl_3$) δ=1.08 (t, J=7 Hz), 1.24 (s, 3H), 0.67—2.02 (m), 2.32 (m, 1H), 2.43 (q, J=7 Hz, 2H), 3.09 (br d, J=4 Hz, 1H).

1-Cyclohexyl-1,2-epoxy-2-methylbutane: ^{1}H NMR (CCl_4) δ=1.17 (s, 3H),[32] 0.67—2.08 (m, 16H), 2.18 (br, 1H); ($CDCl_3$) δ=1.26 (s, 3H), 0.67—2.08 (m, 16H), 2.39 (br, 1H); MS m/z: 168 (M^+). GLC analysis of this product showed a >95% purity of *trans* isomer.

Reaction of Metallated 4 with Cyclohexanecarbaldehyde. To a solution of phenyl 1-(trimethylsilyl)allyl sulfide (445 mg, 2.0 mmol) in THF (5 ml) was added *t*-butyllithium in pentane (2.0 mol dm^{-3} solution, 1.0 ml, 2.0 mmol) at −78 °C, and the mixture was stirred at 0 °C for 1 h. Titanium tetraisopropoxide (0.65 ml, 2.2 mmol) was added to the solution at −78 °C, and the resulting mixture was stirred for 10 min. Cyclohexanecarbaldehyde (0.24 ml, 2.0 mmol) was added at −78 °C and the solution was stirred for 10 min at −78 °C and 1 h at 0 °C, and further 1 h at 25 °C. Then the mixture was poured into 2 mol dm^{-3} hydrochloric acid and the product was extracted with ether. The organic layer was dried and concentrated. Chromatography of the residue on silanized silica-gel column (hexane) gave (*E*)-1-cyclohexyl-2-phenylthio-1,3-butadiene (440 mg, 90%). GLC analysis of the product revealed the *E*/*Z* ratio of 10:1. R_f=0.59 (hexane, silanized silica gel); ^{1}H NMR (CCl_4) δ=0.41—1.91 (m, 10 H), 2.57 (br, 1H), 5.11 (ddd, J=1, 1, and 10.4 Hz, 1H), 5.61 (dd, J=1 and 17 Hz, 1H), 5.99 (br d, J=9.6 Hz, 1H), 6.64 (dd, J=10.4 and 17 Hz, 1H), 7.03 (br s, 5H); IR 3080, 3020, 2940, 2870, 1633, 1590, 1485, 1460, 1450, 1040, 986, 928, 910 cm^{-1}; MS m/z: 244 (M^+).

Dehydration of 1-Cyclohexyl-2-phenylthio-3-buten-1-ol. To a solution of *erythro*-1-cyclohexyl-2-phenylthio-3-buten-1-ol (525 mg, 2.0 mmol) in THF (8 ml) was added butyllithium in hexane (1.6 mol dm^{-3} solution, 1.25 ml, 2.0 mmol) at 0 °C. Methanesulfonyl chloride (0.155 ml, 2.0 mmol) was added to the mixture and stirring was continued for 1 h at 0 °C. Then, the resulting mixture was cooled to −78 °C and treated with *t*-butyllithium in pentane (2.0 mol dm^{-3} solution, 2.0 ml, 4.0 mmol). After stirring for 2 h at 0 °C, the mixture was poured into ice-cooled 2 mol dm^{-3} hydrochloric acid and the product was extracted with ether. The organic layer was dried and concentrated to give oily product. Chromatography of the crude product on silica-gel column (hexane) gave(*Z*)-1-cyclohexyl-2-phenylthio-1,3-butadiene (318 mg, 65%). R_f=0.31 (hexane); ^{1}H NMR (CCl_4) δ=0.72—1.97 (m, 10H), 2.82 (br m, 1H), 4.94 (dd, J=1 and 10 Hz, 1H), 5.42 (dd, J=1 and 16.4 Hz, 1H), 6.01 (d, J=9 Hz, 1H), 6.28 (dd, J=10 and 16.4 Hz, 1H); IR 3080, 3020, 2940, 2870, 1635, 1595, 1482, 1455, 1450, 1035, 990, 918, 908 cm^{-1}; MS m/z: 244 (M^+).

The corresponding *E*-isomer was prepared by this method from the *threo*-1-cyclohexyl-2-phenylthio-3-buten-1-ol. The NMR spectrum and GLC behaviour of this compound were complete agreement with the product from the reaction of metallated **4** with aldehyde.

NMR Analysis of Vinyl Sulfoxides. (*E*)- and (*Z*)-1-cyclohexyl-2-phenylsulfinyl-1,3-butadiene were prepared by the oxidation of the corresponding sulfides with sodium periodate (excess, in MeOH–H_2O, 2:1).

(E)-1-Cyclohexyl-2-phenylsulfinyl-1,3-butadiene: ^{1}H NMR (CCl_4) δ=0.9—2.07 (m, 10H), 2.42 (br m, 1H), 5.17 (dd, J=1.5 and 11 Hz, 1H), 5.36 (dd, J=1.5 and 17.5 Hz, 1H), 6.22 (d, J=9.5 Hz, 1H), 6.25 (dd, J=11 and 17.5 Hz, 1H), 7.34 (m, 5H).

(Z)-1-cyclohexyl-2-phenylsulfinyl-1,3-butadiene: ^{1}H NMR (CCl_4) δ=0.82—2.08 (m, 10H), 3.07 (br m, 1H), 4.99 (dd, J=2 and 10.4 Hz, 1H), 5.37 (dd, J=2 and 18 Hz, 1H), 5.98 (d, J=10 Hz, 1H), 6.14 (dd, J=10.4 and 18 Hz, 1H), 7.41 (br s, 5H).

(*E*)- and (*Z*)-2-cyclohexylvinyl phenyl sulfoxide were prepared by the following sequence: (1) Condensation of cyclohexanecarbaldehyde with phenyl lithio(trimethylsilyl)-methyl sulfide (1 equiv) in THF; (2) Separation of (*E*) and (*Z*)-2-cyclohexylvinyl phenyl sulfide by silica-gel column chromatography (hexane); (3) Oxidation with sodium periodate (5 equiv, in MeOH–H_2O, 2:1).

(E)-2-Cyclohexylvinyl Phenyl Sulfoxide: ^{1}H NMR (CCl_4) δ=0.78—2.36 (m, 11H), 6.00 (d, J=15.5 Hz, 1H), 6.42 (dd, J=5.5 and 15.5 Hz, 1H), 7.41 (m, 5H).

(Z)-2-Cyclohexylvinyl Phenyl Sulfoxide: ^{1}H NMR (CCl_4) δ= 0.72—2.13 (m, 10H), 2.97 (br, 1H), 5.8 (m, 2H), 7.43 (m, 5H).

NMR spectra of the mixture of vinyl sulfoxides (0.50 mmol) and shift reagent, tris(6,6,7,7,8,8,8-heptafluoro-2,2-dimethyl-3,5-octanedionato)europium (0.20 mmol), in carbon tetrachloride (0.70 ml) were taken (see Table 3).

Synthesis of 1-Cyclohexyl-2-methyl-1,3-butadiene. To a mixture of 1-cyclohexyl-2-phenylthio-1,3-butadiene (244 mg, 1.0 mmol) and [$NiCl_2(PPh_3)_2$] (65 mg, 0.1 mmol) in benzene (10 ml) was added methylmagnesium iodide in ether (5.0 mmol) which was prepared from magnesium (300 mg, 12 mmol) and methyl iodide (0.25 ml, 4 mmol) in ether (10 ml). After the removal of ether from the reaction system, the mixture was heated for 2 h under reflux. The resulting mixture was poured into 2 mol dm^{-3} hydrochloric acid and the product was extracted with ether. The organic layer was washed with 1 mol dm^{-3} sodium hydroxide, and then brine. The combined organic layer was dried and concentrated. Chromatography of the residue on silica-gel column (hexane) gave 1-cyclohexyl-2-methyl-1,3-butadiene. *(E)*-1-Cyclohexyl-2-methyl-1,3-butadiene: 70% yield; R_f=0.6 (hexane); ^{1}H NMR (CCl_4) δ=1.71 (d, J=1.5 Hz, 3H), 0.64—1.98 (m, 10H), 2.29 (br m, 1H), 4.72—5.39 (m, 3H), 6.24 (dd, J=10.8 and 17.6 Hz, 1H); IR 2920, 1780, 1640, 1610, 1440, 990, 890 cm^{-1}; MS m/z: 150 (M^+).

(Z)-1-Cyclohexyl-2-methyl-1,3-butadiene: 78% yield; R_f=0.58 (hexane); ^{1}H NMR (CCl_4) δ=1.76 (s, 3H), 0.6—2.02 (m, 10H) 2.33 (br m, 1H), 4.76—5.37 (m, 3H), 6.65 (dd, J=10.4 and 17.6 Hz, 1H); IR 2920, 1800, 1645, 1595, 1440, 990, 900 cm^{-1}; MS m/z: 150 (M^+).

References

1) General review, for example: B. M. Trost and L. S. Melvin, Jr., "Sulfur Ylides," Academic Press, New York (1975).

2) For a general reviews, see: a) D. A. Evans and G. C. Andrews, *Acc. Chem. Res.*, **7**, 147 (1974); b) B-T. Gröbel and D. Seebach, *Synthesis*, **1977**, 357; c) S. Warren, *Acc. Chem. Res.*, **11**, 401 (1978); d) H. J. Reich, *ibid.*, **12**, 22 (1979); e) E. Negishi, "Organometallics in Organic Synthesis," Wiley, New York (1980), Vol. 1; f) J. F. Biellman and J. B. Ducey, *Org. React.* **27**, 1 (1982).

3) a) T. Hayashi, N. Fujita, T. Oishi, and T. Takeshima, *Tetrahedron Lett.*, **21**, 303 (1980); b) R. W. Hoffmann and B. Kemper, *Tetrahedron Lett.*, **21**, 4883 (1980); c) Y. Yamamoto, H. Yatagai, and K. Maruyama, *J. Org. Chem.*, **45**, 195 (1980); d) M. R. Bin, R. K Haynes, T. L. Houston, and W. R. Jackson, *Tetrahedron Lett.*, **21**, 573 (1980); e) Y. Yamamoto, Y. Saito, and K. Maruyama, *Tetrahedron Lett.*, **23**, 4959 (1982); f) H. Baba, T. Hayashi, and T. Oishi *Chem. Pharm. Bull.*, **30**, 3852 (1982); g) K. S. Kyler, M. A. Netzel. S. Arseniyadis, and D. S. Watt, *J. Org. Chem.*, **48**, 383 (1983).

4) S. A. Shevekev, *Russ. Chem. Rev. (Engl. Transl.)*, **39**, 844 (1970); L. M. Jackman and B. C. Lange, *Tetrahedron*, **33**, 2737 (1977); P. W. K. Lau and T. H. Chan, *Tetrahedron Lett.*, **1978**, 2383; see also, D. Seebach and K.-H. Geiss, "New Application of Organometallic Reagents in Organic Chemistry," Elsevier, Amsterdam (1976), p. 22.

5) M. Ishiguro, N. Ikeda, and H. Yamamoto, *J. Org. Chem.*, **47**, 2227 (1982); K. Furuta, M. Ishiguro, R. Haruta, N. Ikeda, and H. Yamamoto, *Bull. Chem. Soc. Jpn.*, **57**, 2777 (1984). For some recent synthetic methods using organotitanium reagents, see: M. T. Reetz, in "Topics in Current Chemistry," Springer, Berlin (1982), pp. 1—54; B. Weidmann and D. Seebach, *Angew. Chem., Int. Ed. Engl.*, **22**, 31 (1983); D. Seebach, B. Weidmann, and L. Widler, in "Modern Synthetic Methods 1983," ed by R. Scheffold, Wiley, New York and Salle/Sauerländer, Aarau (1983), pp. 217—353.

6) For preliminary accounts of the present work, see: Y. Ikeda, K. Furuta, N. Meguriya, N. Ikeda, and H. Yamamoto, *J. Am. Chem. Soc.*, **104**, 7663 (1982), **105**, 3745 (1983).

7) The anomalous behaviour of benzaldehyde has been observed elsewhere; see Ref. 5.

8) a) E. C. Ashby and A. B. Goel, *J. Am. Chem. Soc.*, **103**, 4983 (1981); b) S. Murata, M. Suzuki, and R. Noyori, *J. Am. Chem. Soc.*, **102**, 3248 (1980).

9) M. Saniere-Karila, M. L. Capmau, and W. Chodkiewicz, *Bull. Soc. Chim. Fr.*, **1973**, 3371; E. Favre and M. Gaudemar, *J. Organomet. Chem.*, **92**, 17 (1975).

10) J. R. Shanklin, C. R. Johnson, J. Ollinger, and R. M. Coates, *J. Am. Chem. Soc.*, **95**, 3429 (1973); S. Kano, T. Yokomatsu, and S, Shibuya, *J. Chem. Soc., Chem. Commun.*, **1978**, 785.

11) Recent efforts for the preparation of disubstituted oxiranes: a) G. G. Lyle and L. K. Keefer, *J. Org. Chem.*, **31**, 3921 (1966); b) R. W. La Rochelle, B. M. Trost, and L. Krepski, *J. Org. Chem.*, **36**, 1126 (1971); c) J.-C. Paladini and J. Chuche, *Bull. Soc. Chim. Fr.*, **1974**, 187; d) D. Van Ende and A. Krief, *Tetrahedron Lett.*, **1976**, 457; e) D. Seebach, K.-H. Geiss, and M. Pohmakotr, *Angew. Chem. Int. Ed. Engl.*, **15**, 437 (1976); f) M. Yamaguchi and T. Mukaiyama, *Chem. Lett.*, **1979**, 1279; g) M. Ochiai and E. Fujita, *Tetrahedron Lett.*, **21**, 4369 (1980); h) W. C. Still and V. J. Novack, *J. Am. Chem. Soc.*, **103**, 1283 (1981); i) M. Yamaguchi and T. Mukaiyama, *Chem. Lett.*, **1982**, 237; j) J. Auge and S. David, *Tetrahedron Lett.*, **24**, 4009 (1983); k) J. B. Ousset, C. Mioskowski, and G. Solladie, *Tetrahedron Lett.*, **24**, 4419 (1983).

12) For a general review, see: T.-H. Chan, *Acc. Chem. Res.*, **10**, 442 (1977); see also: A. W. P. Jarvie, *Organomet. Chem. Rev. Sect. A*, **6**, 153 (1970); For stereoselective olefination using Peterson reaction, see: Y. Yamakado, M. Ishiguro, N. Ikeda, and H. Yamamoto, *J. Am. Chem. Soc.*, **103**, 5568 (1981).

13) K. Hiroi and L.-M. Chen, *J. Chem. Soc., Chem. Commun.*, **1981**, 377; K. S. Kyler and D. S. Watt, *J. Am. Chem. Soc.*, **105**, 619 (1983).

14) The *E*-isomer was slowly isomerized to the *Z*-isomer at 25 °C.

15) R. Haruta, M. Ishiguro, K. Furuta, A. Mori, N. Ikeda, and H. Yamamoto, *Chem. Lett.*, **1982**, 1093.

16) Our unpublished results. See also: F. Sato, Y. Suzuki, and M. Sato, *Tetrahedron Lett.*, **23**, 4589 (1982); M. T. Reetz and B. Wenderoth, *ibid.*, **23**, 5259 (1982).

17) H. Okamura, M. Miura, and H. Takei, *Tetrahedron Lett.*, **1979**, 43; E. Wenkert, T. W. Ferreira, and E. L. Michelotti, *J. Chem. Soc., Chem. Commun.*, **1979**, 637.

18) C. D. Hurd and H. Greengard, *J. Am. Chem. Soc.*, **52**, 3356 (1930); A. C. Cope, D. E. Morrison, and L. Field, *J. Am. Chem. Soc.*, **72**, 59 (1950); W. E. Parham, and S. H. Groen, *J. Org. Chem.*, **30**, 728 (1965); H. Kwart and E. R. Evans, *J. Org. Chem.*, **31**, 413 (1966).

19) a) L. Brandsma, *Rec. Trav. Chim. Pays-Bas*, **89**, 593 (1970); b) W. Ando, S. Kondo, K. Nakayama, K. Ichibori, H. Kohoda, H. Yamato, I. Imai, S. Nakaido, and T. Migita, *J. Am. Chem. Soc.*, **94**, 3870 (1972); c) T. Kubota, S. Miyashita, T. Kitazume, and N. Ishikawa, *J. Org. Chem.*, **45**, 5052 (1980).

20) D. S. Tarbell and W. E. Lovett, *J. Am. Chem. Soc.*, **78**, 2259 (1956); C. C. Price and W. H. Snyder, *J. Org. Chem.*, **27**, 4639 (1962).

21) J. F. Biellmann, J. B. Ducep, and J. Vicens, *Tetrahedron*, **32**, 1801 (1976).

22) P. Brownbridge and S. Warren, *J. Chem. Soc., Chem. Commun.*, **1975**, 820; *J. Chem. Soc., Perkin Trans. 1*, **1977**, 1131.

23) P. M. Atlani, J. F. Biellmann, S. Dube, and J. J. Vicens, *Tetrahedron Lett.*, **1974**, 2665, see also 2f.

24) Lithio reagent gave a mixture of regioisomers, which were difficult to separate.

25) This compounds may undergo thioallylic rearrangement

to give phenyl 3-(trimethylsilyl)allyl sulfide. Addition of 2,6-di-*t*-butyl-4-methylphenol can effectively prevent the rearrangement.

26) Deprotonation of allyl phenyl sulfide could be accomplished with butyllithium without any difficulties. In contrast, *s*- or *t*-butyllithium was required for alkyl allyl sulfide. *t*-Butyllithium recommended for the generation of 1-alkylallyl phenyl sulfide anion.

27) For prevention of thioallylic rearrangement of the produced phenyl sulfides, small amount of hydroquinone or 2,6-di-*t*-butyl-4-methylphenol was added during the workup and chromatographic operations.

28) Trace amount of regioisomer, 1-cyclohexyl-4-phenylthio-3-buten-1-ol, was also formed. This was isolated by column chromatography (R_f=0.15, 4:1 hexane–ether).

29) This reaction is highly stereospecific. Thus, the corresponding *cis*-isomers were prepared under the same reaction conditions from the *threo*-β-hydroxy sulfides, which were obtained from the reaction of [3-(alkylthio)allyl]lithium reagents followed by separation by column chromatography.

30) I. Gosney and A. G. Rowley, in "Organophosphorus Reagents in Organic Synthesis," ed by J. I. G. Cadogan, Academic Press, New York (1979), pp. 17—153.

31) The latter peak (long retention time) was assigned to the *trans*-isomer (carbowax, N_2 carrier).

32) The corresponding *cis*-isomer has an absorption at 1.19 ppm. See: W. S. Johnson, T.-T. Li, D. J. Faulkner, and S. F. Cammpell, *J. Am. Chem. Soc.*, **90**, 6225 (1968).

33) Financial support from the Ministry of Education, Japanese Government (Grant-in-aid 57550543) is acknowledged.

 © 1984 The Chemical Society of Japan Bull. Chem. Soc. Jpn., 57, 2791—2796 (1984)

Ab Initio Self-consistent Field MO Calculations of Ethanethiol and Ethanol

Masaru OHSAKU,* Takehiro ICHIISHI, Akira IMAMURA, and Michiro HAYASHI
Department of Chemistry, Faculty of Science, Hiroshima University, Higashisenda-machi, Naka-ku, Hiroshima 730
(Received February 23, 1984)

Ab initio self-consistent field MO calculations were performed on EtSH and EtOH, and the optimized geometries were obtained by the use of the STO-3G and STO-3G* basis sets. It was found that *ab initio* MO calculations reproduced the observed geometries of these molecules sufficiently well. The variation in the observed bond angle, α(CCX) (X=S and O), from the *trans* to the *gauche* rotamers, which was observed by means of microwave spectroscopy, was very reasonably reproduced from the results of these calculations. The total energy calculated gives a reasonable explanation of the stability between the rotational isomers.

Ethanethiol is well known as one of the simplest molecules to exhibit *trans-gauche* isomerism around the CC–SH bond. Ethanol is its oxygen analog. However, up to the present time, there have appeared no reports which have successfully determined independently the molecular structures of the *trans* and *gauche* forms of ethanol; this has been because of the very large spectral splitting due to the internal rotation of the OH group. A very large number of experimental works in the geometrical mode have been published during the last decade: For EtSH, *e.g.*, by microwave[1–4] and far-IR[5,6] spectroscopies, and for EtOH, by microwave studies.[7,8] Among these publications, the main interests of spectroscopists have been on the experimental result that the bond angle α(CCS) of EtSH widens sharply from the *trans* form (T-form) to the *gauche* form (G-form).[3,4] The same trend is also seen in the structurally analogous molecules, *e.g.*, ethyl methyl sulfide.[9,10] A part of these experimental results has already been explained by *ab initio* calculations.[11] Theoretical works on the basis of the LCAO SCF molecular orbital calculations had also been performed with various methods; that is, semiempirical calculations on EtSH[12–14] and *ab initio* calculations on EtOH[15,16] and related molecules[17–19] have been carried out. However, as far as we know, no *ab initio* conformational study of ethanethiol has been published; although an *ab initio* calculation was performed on MeSH very early in the *ab initio* age.[20] Some other thiols have also been treated by semiempirical and *ab initio* MO procedures.[13,21]

In the present article, the geometry of EtSH was optimized by means of the *ab initio* energy-gradient method, and the difference in α(CCS) between *trans* and *gauche* forms was explained in terms of the through-space interaction. Similar calculations were performed on EtOH for comparison.

Method of Calculations

Calculations were performed by the use of the Gaussian 80 program package.[22] Geometry optimization was made by the gradient method,[23] which is included in the Gaussian 80 package. The basis sets used were STO-3G and STO-3G*. The 3-21G basis was also partly used for EtSH, and the 4-31G* basis, was for EtOH.

First, in order to confirm the observed geometrical parameters of EtSH, a full geometrical optimization was performed by the use of the STO-3G and STO-3G* basis sets.

For further analysis, in order to save computer cpu time, only the α(CCS) angle was then optimized, while the other geometries were transferred from the observed *trans* ones and were fixed during the optimization;[2] that is, in the calculations for the T- and G- forms, the geometry of the observed *trans* form was commonly used.

Nonbonded atomic interactions which correspond to the through-space interaction were then quantitatively analyzed by means of the following procedure. The SCF equation can be expressed as in Eq. (1);[24]

$$FC = SCE. \tag{1}$$

Elements of Fock matrix and overlap integrals were written as in Eqs. (2) and (3) respectively:

$$F_{rs} = I_{rs} + \sum_{t=1}^{m}\sum_{u=1}^{m} P_{tu}[(rs|tu) - (1/2)(rt|su)] \tag{2}$$

$$S_{rs} = \int x_r(1)x_s(1)d\tau, \tag{3}$$

where I_{rs}, P_{tu}, and $(rs|tu)$ or $(rt|su)$ indicate the one-electron integral, the density matrix, and the two-electron integral respectively. When the Fock matrix elements, F_{rs}, and the overlap integral, S_{rs}, between certain atomic orbitals, *e.g.*, r and s, are set equal to zero, the SCF equation, in which the interaction between those pairs is not taken into account, can be obtained as in Eq. (4);

$$F'C' = S'C'E'. \tag{4}$$

When all of the interactions between the AOs which belong to, *e.g.*, the A atom and those belonging to the B atom are cut off, the interaction between the A and B atoms can be considered to be dropped. The difference in the total energy obtained between Eqs. (1) and (4) shows the interaction energy between the certain atomic pair, A and B, in question. Using these equations, the interaction energy between nonbonded atoms (the through-space interaction) can be obtained quantitatively. For this purpose, a part of the Gaussian 80 program package was modified, and during these calculations the geometry was fixed. It should be mentioned that a more sophisticated procedure of analysis might be possible by using the localized orbitals as the basis sets in Eq. (2). The programming for this purpose is not so easy. In the present paper, there-

fore, the rough procedure presented above was employed for the analysis as a first approximation.

Results and Discussion

Ethanethiol. The optimized geometries are shown in Tables 1-a and -b.

There is an excellent agreement between the theoretically calculated and the observed geometries, and it can be seen that there is no remarkable difference between the geometries obtained by the STO-3G and STO-3G* basis sets. However, the STO-3G* basis set, which has a polarization function on the sulfur atom, gives a geometry different from that obtained by the use of STO-3G. As for the bond lengths, the r(C–H) and r(C–C) values do not depend greatly on the difference in the basis set. However, r(C–S) and r(S–H) vary with the change of the set. That is, the STO-3G basis set gives

Table 1-a. STO-3G and STO-3G* optimized structural parameters[a] of EtSH for the *trans* conformation, compared with the microwave-spectroscopy data

Group	Parameters[b]	Experiment		Theory	
		Set A[c]	Set B[d,e]	STO-3G*	STO-3G
CH_3C	r(CH_s)	1.095	1.093	1.086	1.086
	r(CH_a)	1.092		1.086	1.086
	α(CCH_s)	109.67	109.70	110.28	110.26
	α(CCH_a)	110.58		110.86	110.90
	α(H_sCH_a)	108.88	(109.23)	108.24	108.27
	α(H_aCH_a)	108.12		108.34	108.34
CCH_2S	r(CH)	1.090	1.088	1.091	1.089
	r(CC)	1.529	1.530	1.546	1.541
	α(CCS)	108.57	(108.55)	110.24	110.76
	α(HCH)	108.90	(107.23)	107.09	107.11
	α(HCC)	110.23	109.57	108.78	108.99
	α(HCS)	109.43	110.92	110.92	110.35
CSH	r(SH)	1.322	1.328	1.320	1.331
	r(SC)	1.820	1.829	1.790	1.806
	α(HSC)	96.22	95.23	94.95	95.26

a) Bond lengths are in A; angles, in degrees. b) See also Fig. 1. c) From Ref. 2. d) From Ref. 4. e)Figures in parentheses are those derived from the proposed parameters.

Table 1-b. STO-3G and STO-3G* optimized structural parameters[a] of EtSH for the *Gauche* conformation, compared with the microwave-spectroscopy data

Group	Parameters[b]	Experiment		Theory	
		Set A[c]	Set B[d,e]	STO-3G*	STO-3G
CH_3C	r(CH_s)			1.087	1.087
	r(CH_a^1)	1.091	1.093	1.086	1.086
	r(CH_a^2)			1.085	1.086
	α(CCH_s)	110.50		109.54	109.41
	α(CCH_a^1)	110.62	109.70	111.20	110.14
	α(CCH_a^2)			110.23	109.83
	α($H_sCH_a^1$)	109.03		107.87	108.06
	α($H_sCH_a^2$)		(109.23)	108.90	108.74
	α($H_a^1CH_a^2$)	106.92		111.64	110.44
CCH_2S	r(CH^1)	1.089	1.088	1.090	1.087
	r(CH^2)			1.091	1.088
	r(CC)	1.528	1.530	1.548	1.545
	α(CCS)	113.62	(113.27)	113.49	113.30
	α(H^1CH^2)	106.58	(107.32)	109.04	109.39
	α(H^1CC)	110.70	109.57	109.87	109.88
	α(H^2CC)	111.32		109.31	109.31
	α(H^1CS)	104.88	(106.12)	104.72	106.33
	α(H^2CS)	109.27	(110.80)	110.48	108.67
CSH	r(SH)	1.336	1.328	1.320	1.330
	r(SC)	1.814	1.829	1.792	1.808
	α(HSC)	96	95.23	94.98	95.36
Dihedral angle	τ(CCSH)	61.75	(60)	62.80	61.87

a) Bond lengths are in A; angles, in degrees. b) See also Fig. 1 c) From Ref. 3. d) From Ref. 4. e) Figures in parentheses are those derived from the proposed parameters.

longer bond lengths of r(C–S) and r(S–H) than those of the STO-3G*. A similar tendency was found in ethyl methyl sulfide;[11] *i.e.*, the bond length, r(C–S), calculated by the use of the STO-3G* set is *ca.* 0.015 A shorter than that obtained by the use of the STO-3G set. With these bond angles, we cannot see any clear differences between the geometries calculated by the STO-3G and STO-3G* sets except for the ones including the sulfur atom. The STO-3G basis reproduced poorly the α(CCS) of the protonated species $EtSH_2^+$. It is well known that the d-functions on the sulfur atom are also necessary to produce a proper geometry in the ionized sulfur compounds.[25] Therefore, most of the calculations to be discussed hereafter were those based on the STO-3G*.

We then optimized the α(CCS) angle of EtSH using the observed geometrical parameters[2] in order to save computer cpu time and simplify the problem. The geometry of the *gauche* form was transferred from the *trans* form except for the dihedral angle about the CC–SH bond; 60° was used for this angle. The results of the optimization are 109.10° and 113.50°, obtained by means of the STO-3G* basis set for the *trans* and *gauche* forms respectively. There is a very good agreement with the experimental values:

108°34′ (*trans*) and 113°37′ (*gauche*),[2,3]

108°33′ (*trans*) and 113°16′ (*gauche*).[4]

With ethyl methyl sulfide, the same tendency of the α(CCS) angle has previously been found in experimentation between the *trans* and *gauche* forms[9,10] and this has been reproduced by calculations.[11] The difference in the total energy ($E_{trans}-E_{gauche}$) between the *trans* and *gauche* forms obtained is 369 cal/mol, (1 cal=4.184 J) a value obtained by using the STO-3G* basis set under the optimized α(CCS), while that observed is 406±43 cal/mol.[4] Between the observed and calculated values, an excellent agreement is obtained.

In order to analyze the effect of the lone pairs on the sulfur atom or of some other interactions on the variation of the α(CCS) angle, some model calculations were performed on the $EtSH_2^+$ species, in which a proton is attached to a lone pair orbital of the sulfur atom in the EtSH molecule. Here, in the case of the *trans* form, there is only one possibile way to attach a proton onto one of the lone pair orbitals, as one can easily understand from Fig. 1. However in the case of the *gauche* form, there are two possibilities, as is shown in Fig. 2, and these two forms can be distinguished from each other. These two forms are named *gauche*-1 and *gauche*-2 in the present article. By calculating the total energies for these structures, we can estimate the effect of the lone pair orbitals on the sulfur atom or of some other interactions which govern the geometry.

In order to evaluate the result for $EtSH_2^+$, a negative ionic species, EtS^-, was also calculated. The calculated bond populations between methyl carbon and thiol hydrogen are listed in Table 2, together with the optimized α(CCS) values for EtSH, $EtSH_2^+$, and EtS^-. By examining the variation in the bond population between the $C_1\cdots H$(SH) shown in this table, the population was found to change little from the EtSH to the $EtSH_2^+$ species in the case of the *trans* form. The value of the *gauche*-1 form varies considerably from the EtSH to the $EtSH_2^+$ species, but it varies little in

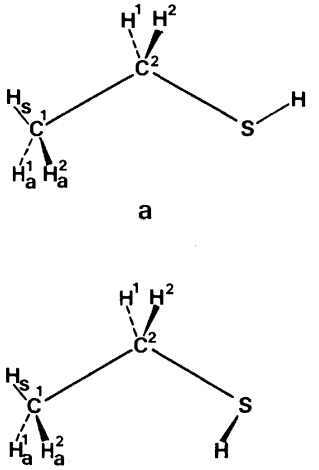

Fig. 1. Schematic structure and atom numberings for the *trans* and *gauche* isomers of EtSH. In the case of EtOH, S atom is substituted by O atom.
a) *Trans* form, b) *Gauche* form.

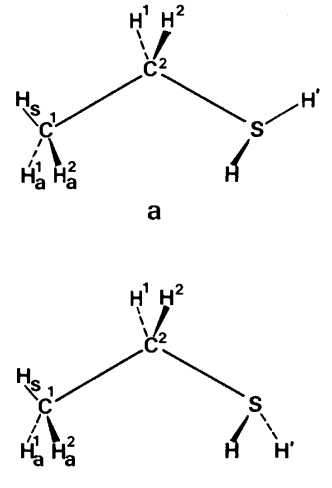

Fig. 2. Two possibilities of a proton addition onto a lone-pair orbital on a sulfur atom. Newly added proton is indicated as H′. In the case of EtOH, S atom is substituted by O atom.
a) *Gauche*-1 form, b) *Gauche*-2 form.

TABLE 2. BOND POPULATION AND α(CCS) OF EtSH, $EtSH_2^+$, AND EtS^- (STO-3G*)

I) Bond population C^1(Me)···H(SH)

	EtSH	$EtSH_2^+$	EtS^-
Trans	0.000600	0.000591	
Gauche-1[a]	−0.001343	−0.000186	
Gauche-2	−0.001343	−0.001137	

II) α(CCS)[b]

	EtSH	$EtSH_2^+$	EtS^-
Trans	109.10	105.65	111.24
Gauche-1[a]	113.50	104.26	111.24
Gauche-2	113.50	113.53	111.24

a) See also Fig. 2. b) Unit: degree

Table 3. Total energy and energy difference of EtSH with or without interaction between certain bonds(STO-3G*)[a]

Cut	*Trans*(a)[c]	*Trans*(b)[c]	*Gauche*(b)	*Gauche*(a)
Normal	−295880.659	−295880.025	−295881.028	−295880.336
$C^1\cdots H$[b]	−295875.670	−295875.516	−295907.161	−295916.480
	−4.989	−4.509	26.133	36.144
$H_a^2\cdots H$	−295880.680	−295880.077	−295886.736	−295891.125
	0.021	0.052	5.708	10.789

a) Unit: kcal/mol b) See also Fig. 1. c) In (a), the α(CCS) angle used was 109.10°, and in (b), that used was 113.50°.

Table 4. Structural parameters[a] of EtOH used for computations

Group	Parameters[b]	Values[c]
CH_3C	r(CH_s)	1.088
	r(CH_a)	1.091
	α(CCH_s)	110.5
	α(CCH_a)	110.1
	α(H_sCH_a)	108.8
	α(H_aCH_a)	108.4
CCH_2O	r(CH)	1.098
	r(CC)	1.512
	α(CCO)	Optimized
	α(HCH)	108.0
	α(HCC)	110.7
COH	r(OH)	0.971
	r(OC)	1.431
	α(HOC)	105.4

a) Bond lengths are in A; angles, in degrees. b) Notations used are the same as those used for the sulfur analog. c) From Ref. 8.

Table 5. Bond population and α(CCO) of EtOH, $EtOH_2^+$ and EtO^- (STO-3G)

I) Bond population C^1(Me)···H(OH)

	EtOH	$EtOH_2^+$	EtO^-
Trans	0.002796	0.001915	
Gauche-1[a]	−0.002963	−0.001214	
Gauche-2	−0.002963	−0.001017	

II) α(CCO)[b]

	EtOH	$EtOH_2^+$	EtO^-
Trans	108.52	111.59	111.03
Gauche-1[a]	113.42	110.19	111.03
Gauche-2	113.42	115.78	111.03

a) See also Fig. 2. b) Unit: degree

the case of the *gauche*-2. Here in this table, the positive figure indicates the attractive interaction, while the negative one, the repulsive one. In the case of the *gauche*-1 form, whose geometrical situation after protonation is very analogous to the *trans* form of $EtSH_2^+$, the quantity of the variation is the largest of all. In the case of the T-form, the interaction between the nonbonded pair $C_1\cdots H$(SH) is attractive. On the other hand, in the case of the G-form, the interaction between them is repulsive. As a result, it can be understood, that in the case of the *gauche*-1 form, the repulsive interaction could be weakened by the addition of a proton to the sulfur atom. This is reflected in the variation in the α(CCS) angle, 113.50° → 104.27°, as will be discussed in the following section.

Let us now discuss the variation in the α(CCS) bond angle. The α(CCS) angle of the T-form narrows about four degrees from the EtSH to the $EtSH_2^+$ species. That of the *gauche*-1, though, decreases dramatically upon the proton addition and stays around nearly the same value as the *trans* form. However, in the case of the *gauche*-2 form, it does not vary any more on the variation from the EtSH to the $EtSH_2^+$ species. This implies that one of the lone pair orbitals, the one which lies on the C–C–S plane, plays an important role in governing the α(CCS) angle of the EtSH. This is one of the most important findings of the present article. It is also very interesting that the angle α(CCS) of the EtS^- species becomes nearly the average value of the *trans* and *gauche* forms.

In order to analyze the interaction between the nonbonded atomic pairs, we have carried out SCF calculations by cutting off the Fock matrix elements, F_{rs}, and, at the same time, the overlap integrals, S_{rs}, between certain atomic pairs according to the procedure described above. The calculations were performed with two geometrical sets, the optimized ones at the T- and G-forms. The pairs contributing greatly to governing the energy are summarized in Table 3.

By cutting off the interactions between the $C_1\cdots H$(SH) pair, the *trans* form raises the energy, while the *gauche* form lowers it. The positive value of the energy difference shows that the cut interaction in question is repulsive, while negative value is attactive.

Here, two types of interactions were taken into consideration: a) $C_1\cdots H$(SH) and b) $H_a^2\cdots H$(SH), because in these pairs the difference in the bond population between the *trans* and *gauche* forms is the largest of all.

From Table 3, it is found, for the *trans* form, that the total energy including the $C_1\cdots H$ interaction is lower than that without this interaction; that is, the $C_1\cdots H$ interaction stabilizes the molecule in the *trans* form. Upon a variation in α(CCS), the interaction energy is larger in the case of a smaller α(CCS) angle. This implies that a smaller α(CCS) angle is more favorable than a larger one in the *trans* case. On the other hand, in the case of the *gauche* form, the state without this interaction is more stable than the state with it. When this interaction is included, the repulsive force becomes smaller in a wider α(CCS) angle than in a narrower angle. As a result, the *gauche* form has a wider angle of α(CCS) than that of the T-form.

With the $H_a^2\cdots H$ interaction, in the case of the *trans* form, the magnitude of the interaction energy is rela-

Table 6. Total energy and energy diffrence of EtOH with or without interaction between certain bonds (STO-3G)[a]

Cut	*Trans*(a)[c]	*Trans*(b)[c]	*Gauche*(b)	*Gauche*(a)
Normal	−95464.947	−95463.916	−95464.712	−95463.750
$C^1 \cdots H$[b]	−95448.521	−95448.853	−95530.287	−95550.590
	−16.426	−15.063	65.575	86.840
$H_a^2 \cdots H$	−95465.243	−95464.300	−95470.786	−95475.864
	0.296	0.384	6.074	12.114

a) Unit: kcal/mol b) See also Fig. 1. c) In (a), the α(CCO) angle used was 108.52°, and in (b), that used was 113.42°.

tively small, and it does not depend greatly on the α(CCS) angle. However, in the case of the *gauche* form, it seems that a wider α(CCS) is more favorable.

The calculated results indicate a reasonable explanation of the observed geometry. As a result, it can be concluded that, in addition to the lone pair orbital, such nonbonded interactions as those between $C_1 \cdots$ H(SH) and between $H_a^2 \cdots$H(SH) are also responsible for the determination of the α(CCS) angle. This is another interesting finding of the present work.

Ethanol. In order to confirm the result obtained for EtSH, the present analysis was extended to test the oxygen analog, EtOH. With this molecule, the geometry optimization by using the 4-21G set had already been performed by Schäfer *et al.*[15,16] Therefore in the present article, the α(CCO) angle alone was optimized for the analysis. The geometry used for the calculation is summarized in Table 4. Geometrical parameters were commonly both used for the *trans* and *gauche* forms except for the dihedral angle τ(CC–OH), whose value, 60.0°, was used for the G-form. The STO-3G set was used for the computations, while the 4-31G* set was partly used for the sake of comparison. The total energy of the T-form obtained is smaller than that of the G-form: $E_{gauche} - E_{trans} = ca.$ 0.2 kcal/mol. This agrees well with the previous calculations.[15,16] The bond population and α(CCO) are shown in Table 5. The angle of α(CCO) obtained for the *gauche* form is wider by *ca.* 5 degrees than that for the *trans* form, although the geometrical parameters for the *gauche* form has not yet been experimentally determined. The bond population decreases in the *trans* form from EtOH to $EtOH_2^+$, while it increases in the *gauche*-1 and *gauche*-2 forms. In the case of EtSH, the population of the *trans* form varies very slightly. However, in the case of EtOH, it changes remarkably. The tendency of the population in the G-form of EtOH is also different from that of EtSH. That is, in the case of EtSH, the populations of *gauche*-1 and *gauche*-2 are considerably different from each other. However, in EtOH, the bond populations of the *gauche*-1 and *gauche*-2 forms show nearly the same trend.

Now let us discuss the variation in the α(CCO) angle. The angle of the *trans* form widens by *ca.* three degrees from the parent to the protonated species. An inverse tendency has already been seen in the sulfur analog. In the case of the G-form, the angle decreases in the *gauche*-1 and increases in the *gauche*-2 for $EtOH_2^+$, in comparison with EtOH. The same tendency was also seen in EtSH. In EtO^-, the angle of α(CCO) obtained is nearly the average of those of the *trans* and *gauche* forms.

Table 7. Dipole moment (Debye)

I) EtSH

	Obsd		Calcd		
			STO-3G*	STO-3G	3-21G
Trans	1.56[a]	1.58[c]	0.472	1.016	2.043
Gauche	1.77[b]	1.61[c]	0.472	1.038	2.150

a) From Ref. 2. b) From Ref. 3. c) From Ref. 4.

II) EtOH

	Obsd	Calcd	
		STO-3G	4-31G*
Trans	1.441[d]	1.442	1.857
Gauche		1.533	1.955

d) From Ref. 27.

The change in the total energy by cutting off a certain Fock element and the overlap integral is given in Table 6. The tendency obtained on EtOH is, in general, analogous to that of EtSH. An examination of the absolute value shows that the interaction energy between $H_a^2 \cdots$H(OH) in EtOH is nearly the same as in EtSH. However, in the case of $C_1 \cdots$H(OH), the variations in the interaction energy in EtOH are much larger than those in EtSH. This means that the interaction between C_1 and H(OH) in EtOH is much stronger than the corresponding one in EtSH. This type of interaction may stabilize the *trans* form more, and may destabilize the *gauche* form more in EtOH than in EtSH.

Dipole Moments. It is very difficult to obtain an agreement between the experimental and calculated values in the dipole moments. We have summarized in Table 7 the observed and calculated dipole moments of EtSH. An examination of the observed moments[2–4] shows that the value of the *gauche* form is a bit larger than the *trans* one. From the estimation of the dielectric constant, however, a rather smaller value (1.39 Debye) was proposed.[26] The tendency between the *gauche* and *trans* forms is also seen in the calculations by using the STO-3G and 3-21G basis sets. The absolute values did not, however, perfectly reproduce the observed values when any of these basis sets was used. The STO-3G* basis set reproduces a fairly smaller value than those of the observed. On the other hand, the 3-21G reproduces values a bit larger. The value of the STO-3G lies between those calculated by STO-3G* and 3-21G.

The dipole moment of EtOH has been reported,[27] and the present STO-3G basis set reproduces the observed values well.

Conclusions

The relative conformational stability of EtSH and EtOH was very well reproduced by *ab initio* MO calculations. The interesting changes in α(CCX) (X=S or O) with the variation in the rotational isomers could also be explained by the present analysis. That is, the main factors governing the α(CCX) angle (X=S or O) are: (a) one of the lone pair orbitals on the sulfur or oxygen atom, (b) the interaction between the non-bonded $C_1 \cdots H(XH)$ (X=S or O), and (c) that between $H_a^2 \cdots H(XH)$ (X=S or O).

We are very grateful to the Computer Center of the Institute for Molecular Science and the Information Processing Center of Hiroshima University for their generous permission to use their HITAC M-200H systems.

References

1) M. Hayashi, H. Imaishi, K. Ohno, and H. Murata, *Bull. Chem. Soc. Jpn.*, **44**, 872 (1971).
2) M. Hayashi, H. Imaishi, and K. Kuwada, *Bull. Chem. Soc. Jpn.*, **47**, 2382 (1974).
3) J. Nakagawa, K. Kuwada, and M. Hayashi, *Bull. Chem. Soc. Jpn.*, **49**, 3420 (1976).
4) R. E. Schmidt and C. R. Quade, *J. Chem. Phys.*, **62**, 3864 (1975).
5) A. S. Manocha, W. G. Fateley, and T. Shimanouchi, *J. Phys. Chem.*, **77**, 1977 (1973).
6) F. Inagaki, I. Harada, and T. Shimanouchi, *J. Mol. Spectrosc.*, **46**, 381 (1973).
7) Y. Sasada, M. Takano, and T. Satoh, *J. Mol. Spectrosc.*, **38**, 33 (1971).
8) J. P. Culot, *Austin Symp. Gas Phase Mol. Struct.*, (1972), T8.
9) M. Hayashi, M. Adachi, and J. Nakagawa, *J. Mol. Spectrosc.*, **86**, 129 (1981).
10) M. Adachi, J. Nakagawa, and M. Hayashi, *J. Mol. Spectrosc.*, **91**, 381 (1982).
11) J. L. Brédas, M. Dufey, J. G. Fripiat, and J. M. Andre, *Mol. Phys.*, **49**, 1451 (1983).
12) M. J. S. Dewar, D. H. Lo, and C. A. Ramsden, *J. Am. Chem. Soc.*, **97**, 1311 (1975).
13) M. Ohsaku, N. Bingo, W. Sugikawa, and H. Murata, *Bull. Chem. Soc. Jpn.*, **52**, 355 (1979).
14) M. J. S. Dewer and M. L. McKee, *J. Comput. Chem.*, **4**, 84 (1983).
15) L. Schäfer, C. van Alsenoy, and J. N. Scarsdale, *J. Mol. Struct. (Theochem)*, **86**, 349 (1982).
16) C. van Alsenoy, J. N. Scarsdale, J. O. Williams, and L. Schäfer, *J. Mol. Struct. (Theochem)*, **86**, 365 (1982).
17) P. Bowers and L. Schäfer, *J. Mol. Struct.*, **69**, 233 (1980).
18) J. O. Williams, J. N. Scarsdale, L. Schäfer, and H. J. Geise, *J. Mol. Struct. (Theochem)*, **76**, 11 (1981).
19) L. Schäfer, C. van Alsenoy, J. O. Williams, and H. J. Geise, *J. Mol. Struct. (Theochem)*, **76**, 349 (1981).
20) J. B. Collins, P. v. R. Schleyer, J. S. Binkley, and J. A. Pople, *J. Chem. Phys.*, **64**, 5142 (1976).
21) M. Ohsaku and H. Murata, *J. Mol. Struct. (Theochem)*, **85**, 125 (1981).
22) J. A. Pople, J. S. Binkley, R. A. Whiteside, R. Krishnan, R. Seeger, D. J. Defrees, H. B. Schlegel, S. Topiol, and L. R. Kahn, *Quant. Chem. Prog. Exch.*, **13**, 406 (1981).
23) H. B. Schlegel, *J. Comput. Chem.*, **3**, 214 (1982).
24) C. C. J. Roothaan, *Rev. Mod. Phys.*, **23**, 69 (1951).
25) S. Wölfe, L. A. LaJohn, F. Bernardi, A. Mangini, and G. Tonachini, *Tetrahedron Lett.*, **24**, 3789 (1983).
26) E. C. E. Hunter and J. R. Partington, *J. Chem. Soc.*, **1931**, 2062; **1932**, 2812.
27) M. Takano, Y. Sasada, and T. Satoh, *J. Mol. Spectrosc.*, **26**, 157 (1968).

 © 1984 The Chemical Society of Japan Bull. Chem. Soc. Jpn., 57, 2797—2801 (1984)

Dissolution States of Normal Alkane Derivatives with a Polar Group in Water

Nobuo NISHINO, Satoshi MORIMOTO,† and Masao NAKAMURA*

Department of Chemistry, Faculty of Science, Tokai University, 1117 Kitakaname, Hiratsuka 259-12

†*Research Institute for Polymers and Textiles, 1-1-4 Yatabe-Higashi, Tsukuba 305*

(Received March 26, 1984)

This paper proposes a method by means of which the heat of solution at an infinite dilution of an organic compound in water, directly measured by means of calorimetry at a given temperature, is extended over a wide range of temperatures by the use of a phase diagram with water. The heat of solution at an infinite dilution in water over a temperature range from 290 to 350 K, which is estimated by this method for some alkanols and alkanoic acids, increases with a rise in the temperature and has a transition temperature from the exothermic region to the endothermic region which is close to the minimum dissolution temperature in the solubility curve in water for each substance. The increase in the heat of solution might be due to the breakdown of the iceberg formed around the alkyl group. The difference between the partial molar heat capacity at an infinite dilution and the molar heat capacity at the pure state, $\Delta_s c_p^{\circ}$, has its maximum at a certain temperature. The higher homolog shows a sharper curve with a lower maximum temperature. The curve of $\Delta_s c_p^{\circ}$ *vs.* the temperature for 2- or 3-alkanol corresponds to that for the lower 1-alkanol. These facts reveal that a polar group, such as OH and COOH, would preferentially break the weaker structure of the iceberg within its breaking sphere, which structure should break down at a lower temperature.

In previous papers,[1,2] the present authors have constructed phase diagrams for binary systems of water and normal alkane derivatives, such as alkanols, alkylamines, and alkanoic acids, in which each aqueous-phase line commonly has a minimum point at a temperature, but in which the corresponding organic-phase line is monotonical. Such phenomena suggest that the state of the aqueous phase changes with the temperature, while those of the organic phases do not change so much. It is now believed that an ice-like structure of water, referred to as an "iceberg," is formed around a dissolved nonpolar alkyl group, but gradually breaks down with a rise in the temperature.[3] If this is true, the partial molar enthalpy of such a solute in water should increase with a rise in the temperature. The change in the partial molar enthalpy of a solute with the temperature must be reflected by the change in the heat of solution, since the heat of evaporation is almost independent of the temperature for such substances.[1] It has been shown that the heat of solution at an infinite dilution, $\Delta_s h_2^{\circ}$ can be evaluated correctly from the phase diagram and the activity coefficient of the organic substance in its own phase, γ_2^{or}, according to the following equation, when the solubility of the organic substance in water is so small that the aqueous phase may be regarded as an ideal dilute solution:[2]

$$\Delta_s h_2^{\circ} = R\left[\frac{\partial \ln (x_2^{or}\gamma_2^{or}/x_2^{aq})}{\partial T^{-1}}\right]_{p.sat}, \qquad (1)$$

where x_2^{or} and x_2^{aq} are the mole fractions of an organic substance in organic and aqueous phases at mutual saturation respectively; T, the absolute temperature, p, the pressure, and R, the gas constant, and where "sat" designates mutual saturation. Unfortunately, γ_2^{or} is available for only a few substances in the literature.[4,5]

The following approach, however, can be used instead of measurements of γ_2^{or} to evaluate $\Delta_s h_2^{\circ}$ over a wide range of temperatures. When mutual saturation is maintained under a constant pressure, the differential of ln γ_2^{or} with respect to the reciprocal of the absolute temperature, T^{-1}, can be expressed by:

$$\left[\frac{\partial \ln \gamma_2^{or}}{\partial T^{-1}}\right]_{p.sat} = \left[\frac{\partial \ln \gamma_2^{or}}{\partial \ln x_2^{or}}\right]_{T,p}\left[\frac{\partial \ln x_2^{or}}{\partial T^{-1}}\right]_{p.sat} + \left[\frac{\partial \ln \gamma_2^{or}}{\partial T^{-1}}\right]_{p,x_2^{or}}, \qquad (2)$$

because γ_2^{or} is, in general, a function of T, p, and x_2^{or}. The partial pressures of 1-propanol over its mixtures with water at several temperatures are available in the literature;[4] the literature shows that the estimated activity coefficients of 1-propanol are not so dependent on the temperature as on the composition, as is shown in Fig. 1. If $[\partial \ln \gamma_2^{or}/\partial T^{-1}]_{p,x_2^{or}}$, therefore, is assumed to be negligible in comparison with the first term, Eq. 2 is reduced to:

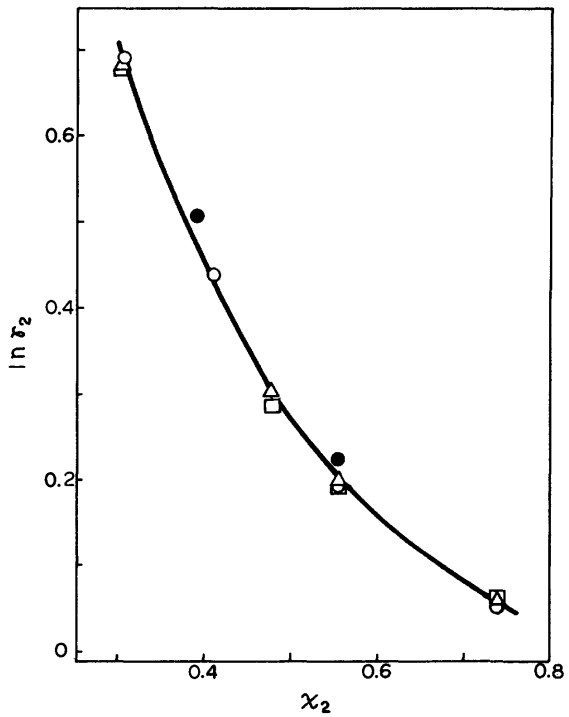

Fig. 1. Plots of the activity coefficient of 1-propanol in the mixture with water *vs.* the mole fraction of 1-propanol calculated from the vapor pressures.[4]
●: 303.50 K, ○: 323.07 K, △: 339.09 K, □: 353.95 K.

$$\left[\frac{\partial \ln \gamma_2^{or}}{\partial T^{-1}}\right]_{p,sat} = \left[\frac{\partial \ln \gamma_2^{or}}{\partial \ln x_2^{or}}\right]_{T,p}\left[\frac{\partial \ln x_2^{or}}{\partial T^{-1}}\right]_{p,sat}. \quad (3)$$

The substitution of Eq. 3 into Eq. 1 gives:

$$\Delta_s h_2^{\circ} = R\left[\frac{\partial \ln \gamma_2^{or}}{\partial \ln x_2^{or}}\right]_{T,p}\left[\frac{\partial \ln x_2^{or}}{\partial T^{-1}}\right]_{p,sat} + R\left[\frac{\partial \ln (x_2^{or}/x_2^{aq})}{\partial T^{-1}}\right]_{p,sat}. \quad (4)$$

If $\Delta_s h_2^{\circ}$ is actually determined at a certain temperature besides the phase diagram, then $[\partial \ln \gamma_2^{or}/\partial \ln x_2^{or}]_{T,p}$ at that temperature can be obtained by the aid of Eq. 4. The values for $\Delta_s h_2^{\circ}$ at other temperatures may now be estimated, if $[\partial \ln \gamma_2^{or}/\partial \ln x_2^{or}]_{T,p}$ is assumed to be independent of the temperature. The solubility of water in an organic phase, $(1-x_2^{or})$, does not change very markedly between 290 and 350 K.[2] The heats of solution at an infinite dilution, $\Delta_s h_2^{\circ}$, have been measured calorimetrically at 298 or 303 K for several compounds.[6-12] The purpose of the present paper is to determine the dependence of $\Delta_s h_2^{\circ}$ on the temperature as exactly as possible, in order to elucidate the dissolution states of normal alkane derivatives with a polar group in water over a wide range of temperatures, including the change in the iceberg formed around the alkyl groups.

Experimental

The alkanols and alkanoice acids used were the same as those described in a previous paper.[1] They were used after having been dried over calcium hydride and were above 99.9% in purity, as verified by gas chromatography using a Shimadzu GC-4CM PF apparatus.

Measurements were made of the heats of mixing various amounts of a solute with a constant amount of water, 5.55 mol, at 298 K by using a 8721-1 solution calorimeter of the precision calorimetry system (LKB Produkter AB), according to a procedure described elsewhere.[13]

Results and Discussion

Temperature Dependence of the Heat of Solution at an Infinite Dilution. Figure 2 shows that the heats of mixing, ΔH, of normal alkane derivatives with water, measured at 298 K, are proportional to the number of moles of the normal alkane derivative added, n_2, while the amount of water is always constant, 5.55 mol. This means that the solutions are dilute enough to be regarded as ideal dilute solutions; therefore, the slope of each straight line is equal to the heat of solution at an infinite dilution, $\Delta_s h_2^{\circ}$ for each substance.[14] The values for $\Delta_s h_2^{\circ}$ obtained are summarized in Table 1, together with the values from the literature.[7,11] The value of -8.24 ± 0.08 kJ mol^{-1} for 1-pentanol can be compared with that of -8.08 ± 0.42 kJ mol^{-1} measured by Aveyard and Mitchell,[7] which is closer than those obtained by other authors.[6,8,9] The values of $[\partial \ln \gamma_2^{or}/\partial \ln x_2^{or}]_{T,p}$ are also listed in Table 1; they were estimated from the $\Delta_s h_2^{\circ}$ values in Table 1 and the phase diagrams with water,[2] according to Eq. 4. The value for 1-butanol, -1.09, is comparable to that of -1.01 estimated from

Table 1. Heats of solution at infinite dilution and $[\partial \ln \gamma_2^{or}/\partial \ln x_2^{or}]_{T,p}$ of normal alkane derivatives in water at 298 K

Substance	$\Delta_s h_2^{\circ}$ / kJ mol^{-1}	$\left[\frac{\partial \ln \gamma_2^{or}}{\partial \ln x_2^{or}}\right]_{T,p}$
1-Butanol	-9.00 ± 0.42[a]	-1.09
1-Pentanol	-8.24 ± 0.08	-1.30
1-Hexanol	-5.77 ± 0.42[a]	-1.31
2-Pentanol	-11.82 ± 0.08	-0.65
2-Hexanol	-10.81 ± 0.05	-0.55
2-Heptanol	-9.62 ± 0.14	-1.04
3-Pentanol	-12.80 ± 0.08[b]	-0.79
3-Hexanol	-12.59 ± 0.46[b]	-1.75
Pentanoic acid	-0.50 ± 0.21[a]	-0.72
Hexanoic acid	0.92 ± 0.42[a]	-0.74

a) Ref. 7. b) Ref. 11.

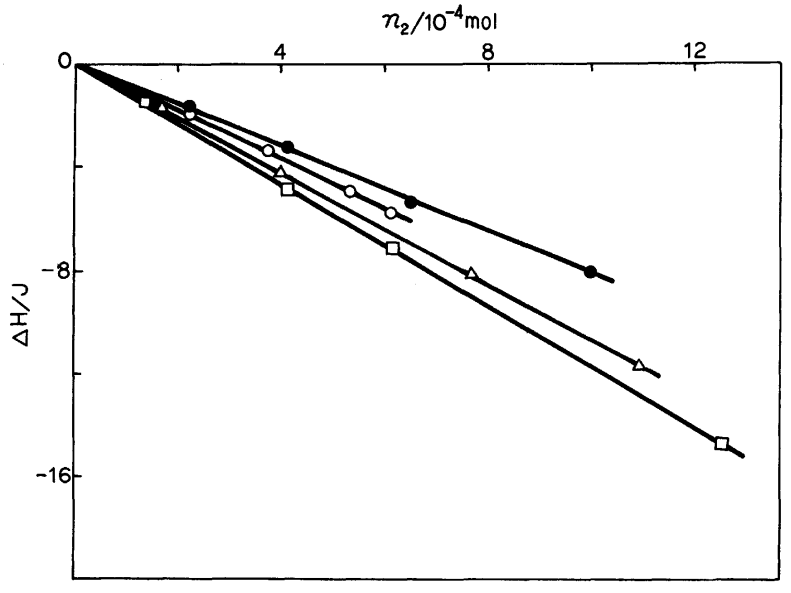

Fig. 2. Heat of mixing of n_2 mol of normal alkane derivatives with 5.55 mol of water at 298 K.
●: 1-Pentanol, □: 2-pentanol, △: 2-hexanol, ○: 2-heptanol.

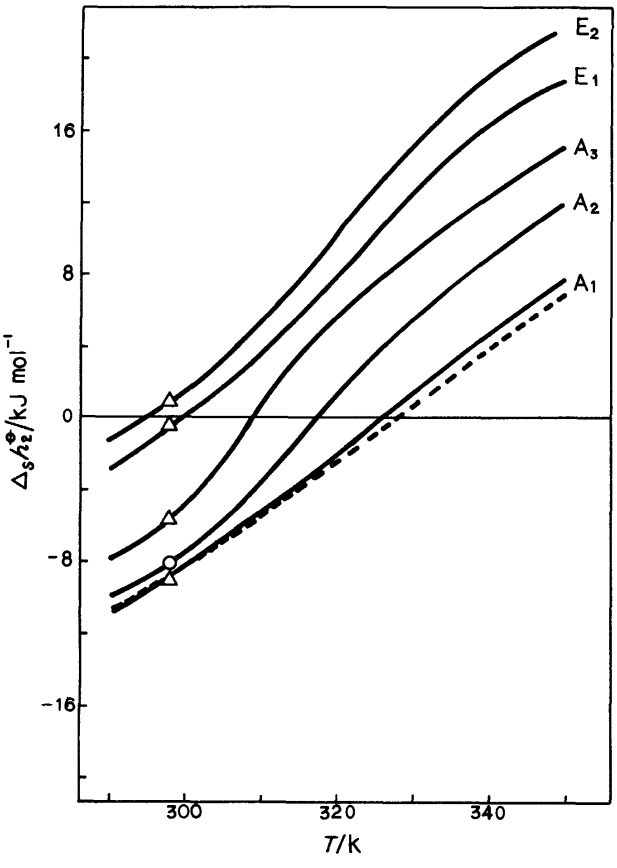

Fig. 3. Heat of solution at an infinite dilution *vs.* temperature for 1-alkanols and alkanoic acids.
A_1: 1-Butanol, A_2: 1-pentanol, A_3: 1-hexanol, E_1: pentanoic acid, E_2: hexanoic acid.
O and Δ are directly measured by calorimetry (O: obtained here, Δ: from the literature.) Dotted line is obtained by substituting γ_2^{or} of 1-butanol[5] into Eq. 4.

the partial vapor pressures at 298 K.[5] The heats of solution at an infinite dilution, $\Delta_s h_2^\circ$ at other temperatures were estimated from the value of $[\partial \ln \gamma_2^{or}/\partial \ln x_2^{or}]_{T,p}$ in Table 1 and the phase diagram,[2] again by the aid of Eq. 4, assuming $[\partial \ln \gamma_2^{or}/\partial \ln x_2^{or}]_{T,p}$ to be constant over the range of temperatures in which the phase diagram was measured. The values of $\Delta_s h_2^\circ$ thus obtained are plotted against the temperature in Figs. 3 and 4, in which O and Δ are directly measured by means of calorimetry. Butler *et al.* have obtained the activity coefficient of 1-butanol, γ_2^{or}, over a wide range of compositions with water at 298 K by the determination of the partial vapor pressure.[5] The values of $\Delta_s h_2^\circ$ obtained from γ_2^{or} and the phase diagram by the use of Eq. 4, superimposed as a dotted line in Fig. 3, are substantially coincident with the line, A_1, estimated by the present method over the whole range of temperatures.

The heat of solution at an infinite dilution, $\Delta_s h_2^\circ$ increases with a rise in the temperature, from negative to positive, for each substance. Thus, there is a transition temperature, T_t, from the exothermic region to the endothermic region, *i.e.*, the temperature at which $\Delta_s h_2^\circ = 0$. The transition temperature, T_t, is close to the minimum dissolution temperature, T_m, on the solubility curve of the substance in water,[1] within the difference between 0.5 and 6.3 K.

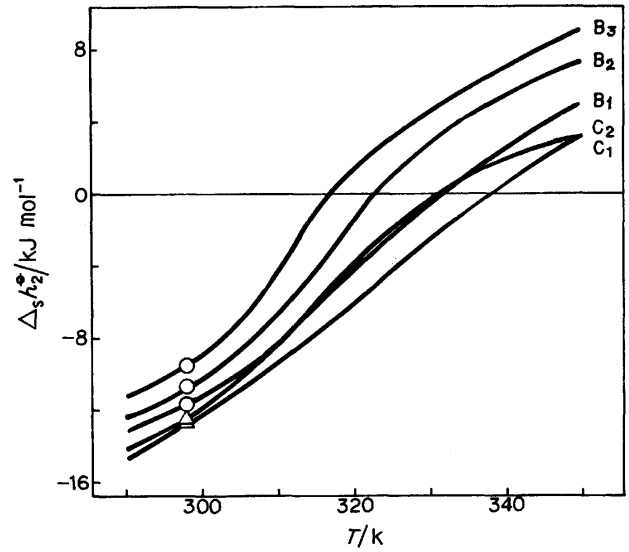

Fig. 4. Heat of solution at an infinite dilution *vs.* temperature for 2- and 3-alkanols in water.
B_1: 2-Pentanol, B_2: 2-hexanol, B_3: 2-heptanol, C_1: 3-pentanol, C_2: hexanol, O and Δ are directly measured by calorimetry. (O: obtained here, Δ: from the literature)

The Breakdown of the Iceberg with the Temperature. The increase in the heat of solution at an infinite dilution, $\Delta_s h_2^\circ$, with the temperature, as shown in Figs. 3 and 4, may be attributed mainly to the increase in the partial molar enthalpy of the solute at an infinite dilution in the aqueous solution, since the heat of evaporation is almost independent of the temperature.[1] When an organic molecule with a hydrophobic group, such as an alkyl group, is introduced in water, the water molecules in the vicinity of the dissolved hydrophobic group form a so-called iceberg, which gradually breaks down with the subsequent rise in the temperature.[3] Such phenomena should make the partial molar enthalpy of the solute higher with the temperature.

The tangent of the curve in Figs. 3 and 4 is equal to the difference between the partial molar heat capacity of the solute at an infinite dilution and its molar heat capacity at the pure state, $\Delta_s c_{p2}^\circ$. The relations between $\Delta_s c_{p2}^\circ$ and the temperature are shown in Figs. 5, 6, 7, and 8 for each homologous series; all the curves are characterized as having a maximum at a certain temperature, T_x. The curves reveal that most of the water molecules in the iceberg break down around T_x and reinforce the concept that the iceberg structure disappears at a higher temperature.[15,16] The higher homolog shows a sharper curve with a lower T_x in any series. The curve for 2- or 3-alkanol in Figs. 6 and 7 corresponds to that for the lower 1-alkanol in Fig. 5. These facts suggest that there are structures different in strength in an iceberg around an alkyl group; the weaker one breaks down at the lower temperature, and a polar group, such as OH or COOH, acts as a breaker against the iceberg,[17] preferentially the weaker structure, which should break down at the lower temperature. If a polar group is assumed to have a certain breaking sphere, the number of water molecules in an iceberg within the sphere would be more for 2- or 3-alkanol than for 1-alkanol. Thus, it may

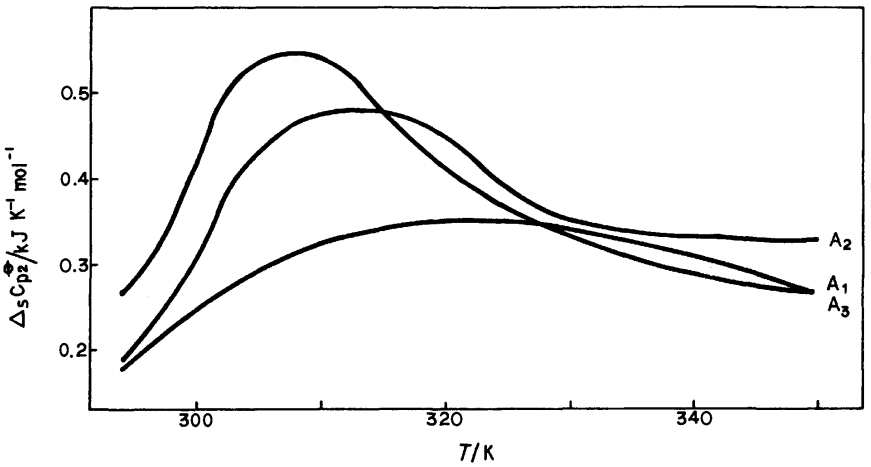

Fig. 5. The difference between the partial molar heat capacity at an infinite dilution in water and the molar heat capacity at the pure state for 1-alkanols.
A_1: 1-Butanol, A_2: 1-pentanol, A_3: 1-hexanol.

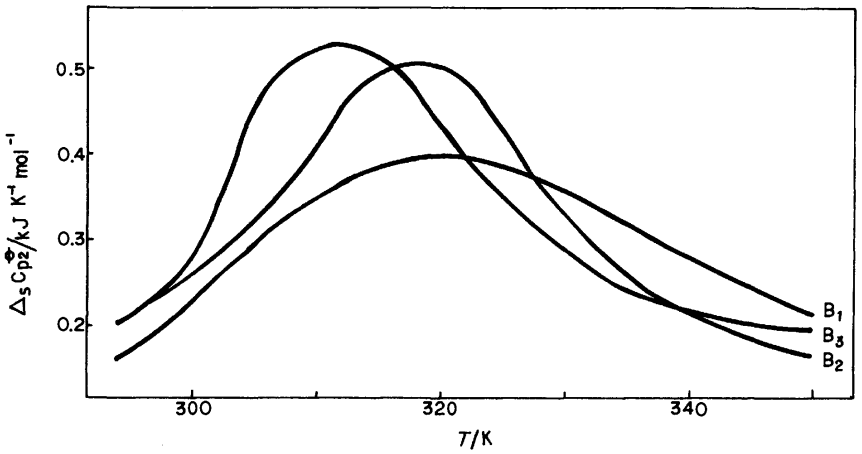

Fig. 6. The difference between the partial molar heat capacity at an infinite dilution in water and the molar heat capacity at the pure state for 2-alkanols. B_1: 2-Pentanol, B_2: 2-hexanol, B_3: 1-heptanol.

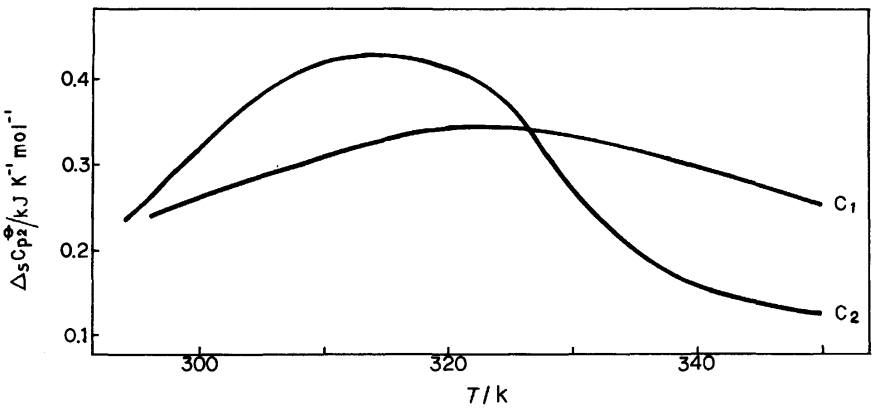

Fig. 7. The difference between the partial molar heat capacity at an infinite dilution in water and the molar heat capacity at the pure state for 3-alkanols.
C_1: 3-Pentanol, C_2: 1-hexanol.

be concluded that a polar group breaks the weaker structure of the iceberg within its breaking sphere. In addition, the COOH group must be a stronger breaker than the OH group, because the curves for alkanoic acids in Fig. 8 are broader curves, with higher T_x values, than the corresponding curves for 1-alkanols in Fig. 5.

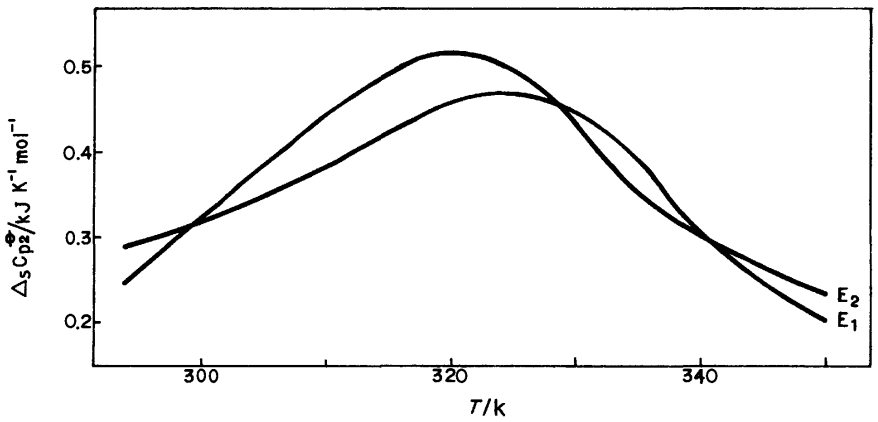

Fig. 8. The difference between the partial molar heat capacity at an infinite dilution in water and the molar heat capacity at the pure state for alkanoic acids.
E_1: Pentanoic acid, E_2: hexanoic acid.

The authors wish to express their thanks to Professor G. L. Bertrand, University of Missouri-Rolla, for many valuable discussions.

References

1) N. Nishino and M. Nakamura, *Bull. Chem. Soc. Jpn.*, **51**, 1617 (1978).
2) N. Nishino and M. Nakamura, *Bull. Chem. Soc. Jpn.*, **54**, 545 (1981).
3) H. S. Frank and M. W. Evans, *J. Chem. Phys.*, **13**, 507 (1945).
4) M. Vrewsky, *Z. Phys. Chem.*, **81**, 1 (1912).
5) J. A. V. Butler, D. W. Thomson, and W. H. Maclennan, *J. Chem. Soc.*, **1933**, 674.
6) R. Aveyard and A. S. C. Lawrence, *Trans. Faraday Soc.*, **60**, 2265 (1964).
7) R. Aveyard and R. W. Mitchell, *Trans. Faraday Soc.*, **64**, 1757 (1968).
8) E. M. Arnett, W. B. Kover, and J. V. Carter, *J. Am. Chem. Soc.*, **91**, 4028 (1969).
9) C. V. Krishnan and R. L. Friedman, *J. Phys. Chem.*, **73**, 1572 (1969).
10) D. J. T. Hill and L. R. White, *Aust. J. Chem.*, **27**, 1905 (1974).
11) S. Cabani, G. Conti, V. Mollica, and L. Lepori, *J. Chem. Soc., Faraday Trans. 1*, **71**, 1943 (1975).
12) J. Konicek and I. Wadsö, *Acta Chem. Scand.*, **25**, 1541 (1971).
13) S. Morimoto, *Bull. Chem. Soc. Jpn.*, **52**, 2250 (1979).
14) T. Miura and M. Nakamura, *Bull. Chem. Soc. Jpn.*, **50**, 2528 (1977).
15) P.-A. Leduc, J.-L. Forter, and J. E. Desnoyers, J. Phys. Chem., **78**, 1217 (1974).
16) K. Shinoda, *J. Phys. Chem.*, **81**, 1300 (1977).
17) D. B. Dahlberg, *J. Phys. Chem.*, **76**, 2045 (1972).

 © 1984 The Chemical Society of Japan Bull. Chem. Soc. Jpn., 57, 2802—2808 (1984) [Vol. 57, No. 10

^{1}H NMR and Differential Scanning Calorimetry Studies on Molecular Motions and Phase Transitions in Butylammonium Bromide

Shin-ichi FUKADA, Ryuichi IKEDA, and Daiyu NAKAMURA*
Department of Chemistry, Faculty of Science, Nagoya University, Chikusa, Nagoya 464
(Received March 29, 1984)

The temperature dependences of the ^{1}H NMR spin-lattice relaxation time and of the second moment of ^{1}H NMR absorptions in the temperature ranges of 90—400 K and 77—456 K, respectively, were studied for butylammonium bromide and its *N*-deuterated analog. There are three known crystalline phases in butylammonium bromide as a result of two phase transitions which are confirmed by the present differential thermal analysis (DTA) experiments. The transition temperatures determined in this study are 200 and 249 K for butylammonium bromide. In the low temperature phase of this salt, CH_3 groups perform the C_3 reorientation with a relatively low activation energy of 11.0 kJ mol^{-1}. The asymmetric T_1 curves observed suggest the existence of some kind of disorder in the crystal structure of this phase. In the intermediate phase, the C_3 reorientation of NH_3^+ groups and the 180° flip motion of butylammonium chains are activated with the activation energies of 23 and 14 kJ mol^{-1}, respectively. The present NMR results for the high temperature phase indicate the occurrence of the conformational melting of the cation chains. The mechanism of the phase transitions is discussed.

It is known that alkylammonium halides involving rather short carbon chains up to C_{10} usually form tetragonal crystals at room temperature.[1-4] In the series of these crystals, the long axis of the carbon chain is located along the crystallographic fourfold axis. Therefore, the presence of dynamical disorder is expected in the arrangement of alkylammonium chains about their long axes.[4] With decreasing temperature, the motion of linear alkylammonium chains should become slow and finally be frozen. This suggests that the tetragonal crystals of these compounds lose their fourfold axis at lower temperatures and are transformed into less symmetric ones. In fact, many of the higher members of the series undergo solid-state phase transitions around or below room temperature,[5] and propyl- and pentylammonium chloride are known to form less symmetric monoclinic crystals at low temperatures.[6,7] Accordingly, it is thought that the molecular motions of alkylammonium chains play an important role in the mechanism of these phase transitions.

Tsau and Gilson[8] studied the wide-line ^{1}H NMR of various alkylammonium chlorides from C_3 to C_{10}, and discussed mainly on the molecular motions of the cations in solid. Recently, the motion of cations in methylammonium halides[9-11] and propylammonium chloride[12] was studied in more detail by use of pulsed and wide-line ^{1}H NMR techniques.

The present investigation of butylammonium bromide by ^{1}H NMR, differential scanning calorimetry (DSC), and differential thermal analysis (DTA) has been undertaken in order to obtain detailed information on the molecular motion of butylammonium cations in solid and also on the mechanism of the successive phase transitions taking place below room temperature.[5]

Experimental

Butylammonium bromide (baBr) was prepared by neutralizing an ethanol solution of butylamine with hydrobromic acid. Colorless crystals separated were purified by recrystallization which was performed twice from a nearly saturated solution of the salt dissolved in a mixed solvent of ethanol and diethyl ether by cooling it very gradually. Vacuum sublimation at *ca.* 80 °C was also employed as another purification method. A partially deuterated analog $C_4H_9ND_3Br$, which is hereafter abbreviated as baBr-d_3, was obtained from the normal salt by repeated recrystallization from heavy water. The deuterated analog thus prepared was finally recrystallized from deuterated ethanol (C_2H_5OD) solution by slowly evaporating the solvent. Since the purified samples were highly hygroscopic, they were carefully dried in vacuum desiccators and sealed in aluminium sample holders for DSC or glass ampouls for NMR and DTA measurements.

The second moment (M_2) of ^{1}H NMR absorptions recorded at 40 MHz were determined at various temperatures between 77 and 456 K by means of a JEOL JNM-MW-40S wide-line NMR spectrometer. The measurements of ^{1}H spin-lattice relaxation time T_1 at the resonance frequency of 20 MHz were carried out by use of a homemade spectrometer[13] and those at 12.6 and 32 MHz were made by another pulsed spectrometer constructed using a transmitter and a receiver from MATEC, Inc.[14] A conventional 180°-τ-90° pulse sequence was used to determine T_1.

A Parkin-Elmer DSC-1B differential scanning calorimeter was employed to determine enthalpy changes at the solid-solid phase transitions and at the melting of the samples. The temperature of the samples was scanned at a rate of 5 K min^{-1}. The values of the transition enthalpies observed at lower temperatures were calibrated against that of succinonitrile observed at 233 K. The melting of indium was also used as a calibration standard for the melting enthalpy. A homemade DTA apparatus was used to determine the phase transition and the melting temperatures.

Results

DTA curves recorded for baBr are shown in Fig. 1. When the sample was cooled from room temperature, two exothermic anomalies appeared at 246 and 195 (±1) K. When it was warmed from *ca.* 80 K, three endothermic ones were observed at 200, 249, and 478 (±1) K. The last one was due to the melting of the sample. The two solid-solid phase transitions showed thermal hysteresis. The samples purified by the two different methods described in the experimental section yielded DTA curves analogous to each other giving the same transition temperatures, T_{tr} as well as the same melting point. Accordingly, it is concluded that baBr undergoes two first-order solid-solid phase transitions at 200 and 249 K. The temperatures of the former transition (200 K) and of the melting agree well with those determined by Tsau and Gilson[5] in their DSC study (198 and 479 K), while the transition temperature

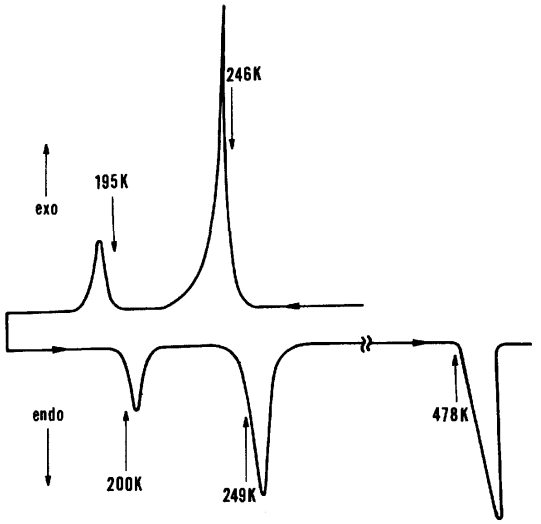

Fig. 1. DTA curves of baBr.

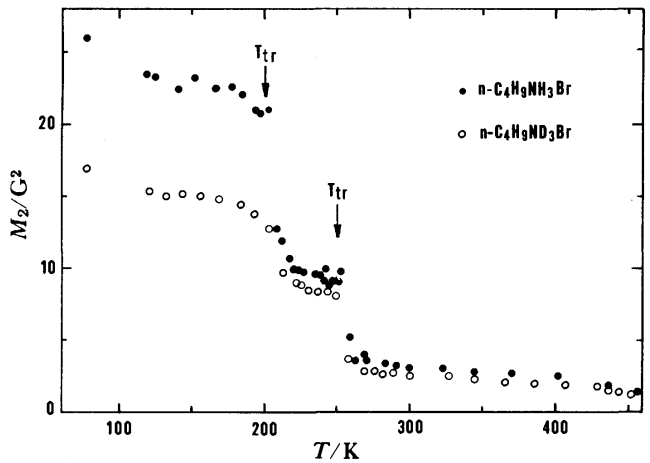

Fig. 2. Temperature dependences of the second moment M_2 of ^{1}H NMR absorptions.

of 249 K is considerably lower than that of 257 K reported by the same authors. For baBr-d_3, two heat anomalies showing quite similar DTA curves to those of baBr were observed at 198 and 249 ($\pm$1) K on heating.

The enthalpy changes (ΔH_{tr}) of the phase transitions determined by the DSC measurements of baBr on heating were 1.5$_3$ and 5.7$_4$ kJ mol^{-1} for the phase transitions at 200 and 249 K, respectively, and 8.3$_0$ kJ mol^{-1} for the melting at 478 K. These transition enthalpies in the present study are much larger than the corresponding ones (0.93 and 5.18 kJ mol^{-1} for the low and high transition temperatures, respectively) reported by Tsau and Gilson.[5]

The temperature dependence of M_2 values observed for baBr and baBr-d_3 is indicated in Fig. 2. These values were obtained with increasing the temperature of the sample. From *ca.* 100 K to *ca.* 170 K, baBr yielded an almost constant M_2 value of 23 G^2. In a rather narrow temperature range of 180—200 K, the M_2 value decreased gradually, whereas it decreased discontinuously to 13 G^2 at *ca.* 200 K. This temperature agrees well with the lowest T_{tr} determined by DTA. With increasing temperature above 200 K, the M_2 value gradually decreased until it became 9 G^2 at 250 K.

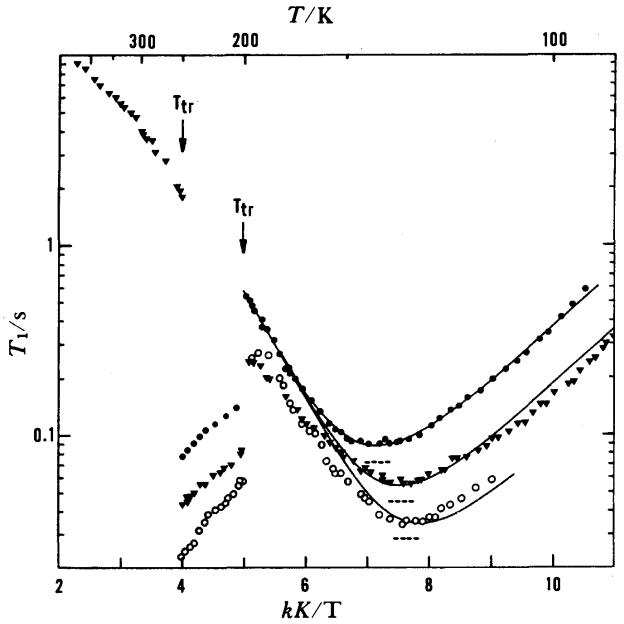

Fig. 3. Temperature dependences of the proton T_1 at 32 (●), 20 (▼), and 12.6 (○) MHz observed for baBr. The solid lines show the theoretical curves fitted by the method of least-squares. The broken lines show the T_1 minima predicted by the BPP theory.

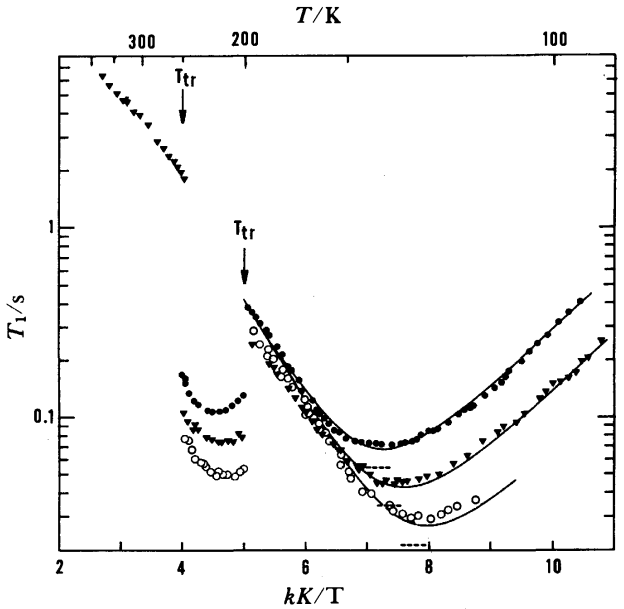

Fig. 4. Temperature dependences of the proton T_1 at 32 (●), 20 (▼), and 12.6 (○) MHz for baBr-d_3. The solid lines show the theoretical curves fitted by the method of least-squares. The broken lines show the T_1 minima predicted by the BPP theory.

Immediately above this temperature, the M_2 value dropped again discontinuously to 4 G^2 in agreement with the occurrence of the phase transition at 249 K. Between 260 and 320 K, the almost constant M_2 value of 3 G^2 was observed. With increasing temperature further, M_2 gradually decreased to *ca.* 1.5 G^2 at *ca.* 460 K. The partially deuterated analog yielded a temperature dependence curve of M_2 similar to that of baBr although the M_2 value of the latter was expectedly larger than that of the former at the same temperature.

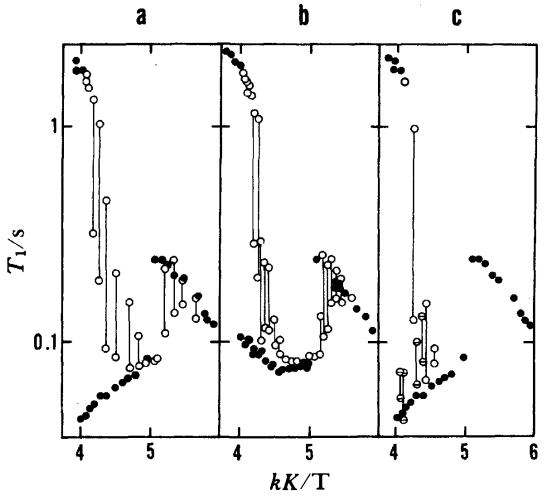

Fig. 5. Proton T_1 values (at 20 MHz) determined for baBr (a, c) and baBr-d_3 (b). Dots indicate the T_1 data obtained with increasing temperature, while open circles are those observed with decreasing temperature. The T_1 interval determined at a given temperature on the cooling run is shown by a vertical line connecting two open circles indicating the longest and shortest T_1 values. The symbols (⊖) indicate the T_1 values obtained with increasing temperature for the sample which had been cooled down to 215 K in advance.

The T_1 values measured at 12.6, 20, and 32 MHz are plotted in Figs. 3 and 4 for baBr and baBr-d_3, respectively. These values were determined at various temperatures between 90 and 400 K. The measurements were made with increasing the temperature of the sample. Each salt yielded a T_1 curve having discontinuities at 200 and 249 K in agreement with the T_{tr}'s determined by DTA. With decreasing temperature, on the other hand, the temperature dependence curve of T_1, which was different from that obtained on the heating run, was observed below each T_{tr} for both salts. In a rather narrow temperature range below each T_{tr}, nonexponential decay of ^{1}H magnetization could be observed for both salts, even though the sample temperature was kept constant for more than half an hour. In these ranges of temperature the longest and shortest T_1 could be approximately determined from the magnetization recovery curve. The results are indicated in Figs. 5a and 5b for the measurements at 20 MHz. It should be noted, here, that the T_1 interval between the longest and shortest values determined at a given temperature varies to some extent at every cooling run of the T_1 measurements.

In the above temperature ranges, another type of anomalous behavior of T_1 was observed. When the sample cooled somewhat below each T_{tr} in advance was warmed, the T_1 values did not reversibly follow those obtained on the cooling run, but decreased roughly along those of the heating run as shown in Fig. 5c. This anomalous behavior is understandable by considering that crystal domains of lower temperature phases newly produced through each phase transition develop gradually with decreasing temperature. Namely, the sample in these temperature ranges is thought to be a mixture of at least two different crystalline phases, the mixing ratio of which is changed with decreasing temperature. The above explanation is compatible with the DTA results that each heat anomaly is accompanied by a long tail only on the low temperature side of the cooling run.

In the low temperature phase, both baBr and baBr-d_3 showed a broad T_1 minimum on the T_1 curve observed at each resonance frequency.

In the intermediate phase, the T_1 value of baBr decreased steadly with increasing temperature to the higher T_{tr}, whereas each of three T_1 curves observed for baBr-d_3 with increasing temperature yielded a shallow minimum. At the T_{tr}, the T_1 values of baBr increased suddenly by about two orders of magnitude. A similar T_1 jump was also observed for baBr-d_3.

In the high temperature phase, long T_1 values were obtained for both salts and they increased monotonously with increasing temperature. No frequency dependence of T_1 was observed in this phase for both baBr and baBr-d_3.

Discussion

The theoretical values of M_2 for four motional states of the cation in solid baBr can be calculated by use of the Van Vleck formula.[15] The results are given in Table 1 along with the total M_2 values of baBr-d_3 calculated in the same way.

In the calculation, all bond angles in the cation were assumed to be tetrahedral and the C-H, N-H, C-C, and C-N bond distances were taken as 1.096, 1.045, 1.540, and 1.470 Å respectively, in accordance with Tsau and Gilson.[8] A trans-zigzag conformation was also assumed for the cation chain.

According to Hendricks,[1] baBr forms tetragonal crys-

TABLE 1. CALCULATED SECOND MOMENTS (M_2/G^2) OF BUTYLAMMONIUM ION IN BUTYLAMMONIUM BROMIDE

Contribution	Rigid lattice	CH_3 rot.	$(CH_3+NH_3^+)$rot.	$(CH_3+NH_3^+)$rot. +Chain 180° flip	$(CH_3+NH_3^+$ +Cation) rot.
Intra CH_3	5.4	1.4	1.4	0.45	0.34
NH_3^+	7.3	7.3	1.8	0.61	0.45
CH_2	5.4	5.4	5.4	5.44	1.36
Other Intra-Ionic	3.8	3.2	2.5	1.44	0.63
Inter Ionic	~5.0	~4.0	~3.2	~2.0	~1.5
Total					
baBr	26.9	21.3	14.3	9.9	4.3
baBr-d_3	(21.2)	(14.2)	(14.2)	(9.6)	(3.6)

tals at room temperature with $a=5.02$ Å, $c=15.23$ Å, and $Z=2$. In the crystal, the cations are packed together between the layers consisting of bromide ions and form a thick layer perpendicular to the c-axis, where the axes of the cationic chains are situated parallel to the c-axis. As to the accurate arrangement of the cations in the layer, no information is available up to date. This is probably because there is a good possibility for the cations in the layer to take highly disordered orientation about their chain axes even at room temperature. Therefore, we estimated the interionic contribution to M_2 by assuming the probable arrangement of the cations in the unit cell as depicted in Fig. 6. The reduction factors of M_2 arising from the averaging of the magnetic dipolar interactions through the molecular motions were evaluated with reference to the methods described in the literature.[16-18]

The ^{1}H spin-lattice relaxation study also furnishes valuable information concerning the molecular motion of the cation. If magnetic dipolar relaxation is governed by the molecular motion such as the reorientation of CH_3 or NH_3^+ groups in a ba$^+$ cation, T_1 can be written as,[19]

$$T_1^{-1} = Cf(\tau) = C\{\tau/(1+\omega^2\tau^2) + 4\tau/(1+4\omega^2\tau^2)\}. \quad (1)$$

Here, C, τ, and ω denote the motional constant, the correlation time of the motion responsible for the relaxation in question, and the angular resonance frequency, respectively. Assuming an Arrhenius-type relation between τ and the activation energy, E_a of the motional process, one obtains

$$\tau = \tau_\infty \exp(E_a/RT), \quad (2)$$

where τ_∞ is the correlation time at the limit of infinite temperature.

Low-Temperature Phase. Below 170 K, the nearly constant M_2 values of 23 and 15 ($\pm$2) G^2 were obtained for baBr and baBr-d_3, respectively. These values agree fairly well with those calculated under the assumption of the motional model that only the CH_3 group of the cation reorients about its C_3 axis. This means that the CH_3 groups of the cations in this phase reorient more frequently than 10^5 Hz.

The analysis of T_1 gives an analogous conclusion. The broad T_1 minimum($T_{1\,min}$) observed for each salt is attributable to the C_3 reorientation of the CH_3 groups because of its short minimum value. This indicates that the correlation time of the CH_3 reorientation is *ca.* 10^{-9} s even at about 130 K in agreement with the foregoing discussion of the second moment.

It is noteworthy that the T_1 data observed for both compounds are unexplainable by the BPP theory (Eq. (1)) in the following three respects. First, the $T_{1\,min}$ values observed for baBr which are 90, 56, and 34 ms at the resonance frequencies of 32, 20, and 12.6 MHz, respectively, and also those for baBr-d_3 which are 72, 45, and 19 ms in the same order of the resonance frequencies are all considerably longer than the theoretical values estimated from Eq. (1). For example, the calculated $T_{1\,min}$'s at 32 MHz are 72 and 54 ms for baBr and baBr-d_3, respectively, if an isolated CH_3 group with the H···H distance of 1.79 Å is assumed. Secondly, the observed T_1 curves are all highly asymmetric. Namely, the slopes of the T_1 curve on the low and high temperature sides of each minimum are considerably different from each other. Finally, the frequency dependence of T_1 values on the low temperature side of the minimum disagrees with the relationship ($T_1 \propto \omega^2$) derived from Eq. 1.

Conner[20] showed that shallow and asymmetric T_1 curves similar to those of the present compounds can be explained by introducing continuously distributed correlation times into Eq. 1. We assume a Cole-Davidson type distribution of τ given by [21]

$$\left.\begin{aligned} g(\tau) &= \frac{\sin\beta\pi}{\pi}\left(\frac{\tau}{\tau_0-\tau}\right)^\beta & \tau \leqq \tau_0 \\ &= 0 & \tau > \tau_0 \end{aligned}\right\}, \quad (3)$$

where β represents a width of the distribution and τ_0 is a limit of τ. The value of $\beta(0<\beta\leqq 1)$ is a measure of the relative weight of the shorter correlation times than τ_0 and in the limit of $\beta=1$, a single correlation time as used in the BPP theory is obtained. Using Eq. 3, T_1 becomes

$$T_1^{-1} = C\left[\frac{\tau_0 \sin(\beta \tan^{-1}\omega\tau_0)}{\omega\tau_0(1+\omega^2\tau_0^2)^{\beta/2}} + \frac{2\tau_0 \sin(\beta \tan^{-1} 2\omega\tau_0)}{\omega\tau_0(1+4\omega^2\tau^2)^{\beta/2}}\right]. \quad (4)$$

The theoretical T_1 curves expressed by Eqs. 2—4 were fitted to the values observed at 32 MHz for baBr and baBr-d_3 by use of a least mean squares method. The fitted curves (at 32 MHz) are shown in Figs. 3 and 4. The values of the unknown parameters determined from this fitting calculation are given in Table 2. By use of these values of the parameters, the theoretical T_1 curves at 20 and 12.6 MHz are also calculated and exhibited in Figs. 3 and 4. The observed T_1 values agree well with the corresponding calculated curves. The obtained motional constants (see Table 2) also agree well with the values calculated using the geometry of the CH_3 group employed in the calculation of M_2. The values of E_a thus obtained are very close to the average value of E_a for the end CH_3 groups in various kinds of crystalline paraffines,[22] which is *ca.* 11 kJ mol^{-1}, and also to the potential barrier to the internal rotation of the CH_3 group in gaseous $CH_3CH_2CH_2F$ (12.4 kJ mol^{-1}).[23] This indicates that the crystal field hindering the CH_3 rotation is quite small in the low temperature phase of the present compounds.

From the β values obtained, we can expect the existence of some kind of disorder in the low temperature phase. As a possible reason for the existence of

Table 2. Activation energies (E_a), motional constants (C), parameters representing width of τ distribution (β), and pre-exponential factor (τ_∞) obtained from observed T_1 curves at 32 MHz for the CH_3 reorientations in baBr and baBr-d_3

Compound	E_a/kJ mol^{-1}	$C\times10^{-9}$/s^{-2}*	β	$\tau_\infty\times10^{13}$/s
baBr	11.0	2.2(1.95)	0.51	4.2
baBr-d_3	10.0	2.6(2.60)	0.60	7.6

*The values in parentheses are theoretical ones obtained by use of the BPP equation without distribution of τ.

this disorder, we can presume the following. The disordered structure of the crystal existing in the higher temperature phases, for which we will discuss below may be partly supercooled down to the low temperature phase. To obtain information about this disorder, we measured T_1 of the samples which had been annealed in the following manner; the samples were first cooled gradually from the room temperature phase to the intermediate one and kept at *ca.* 200 K for from several hours to two weeks. After that, they were again cooled slowly to the low temperature phase and, then, one sample was kept at *ca.* 180 K for several hours, and the other was at 77 K for half a day. The observed values of T_1 for the two samples agreed with each other. The values coincide also with those of the normally cooled samples within experimental errors. Accordingly, this disordered structure of the low temperature phase seems to have a very long relaxation time.

At various temperatures between *ca.* 160 and 200 K, the T_1 values of baBr observed at 12.6 and 20 MHz disagree with those at 32 MHz, whereas no such marked disagreement can be observed for baBr-d_3 in the same temperature range. To obtain information about this disagreement, we measured the frequency dependence of T_1 values between 10 and 32 MHz at a fixed temperature of 189 K which is immediately below the low T_{tr}, and obtained a broad T_1 minimum of 19 ms at 18 ± 4 MHz. Since the T_1 of the quadrupolar bromine nuclei in baBr crystals can be expected to decrease near the T_{tr}, the broad T_1 minimum of baBr is considered as resulting from Zeeman-quadrupolar cross relaxation between protons and bromine nuclei,[24] both of which interact through N-H···Br type hydrogen bonds. The above disagreement of the T_1 values may be also explained by the same relaxation mechanism. Although no NQR frequency data are available for baBr, the value of *ca.* 18 MHz seems to be reasonable as an NQR frequency of bromine in baBr crystals because similar frequencies (12—18 MHz) have been reported for analogous alkylammonium bromides.[25]

Intermediate Phase. The shallow T_1 minimum observed for baBr-d_3 clearly indicates the existence of a new relaxation process in the intermediate phase. On the other hand, the sharp decrease of T_1 with increasing temperature obtained for baBr can be attributed to another more effective relaxation process. The shallow T_1 minimum which is also expected to exist in baBr can be thought to be masked by the sharp decrease of T_1 in the case of baBr.

When the T_1 curve of baBr-d_3 was subtracted from that of baBr after a correction for the difference of the number of protons in these two compounds was made, the resultant $\log T_1$ of baBr showed an almost linear decrease against T^{-1} in the nearly whole temperature range of this phase. Although no minimum was observed on the corrected T_1 curve, this linear T_1 decrease can be assigned to the C_3 reorientation of the NH_3^+ groups because this T_1 decrease disappears by *N*-deuteration. From the linear portion of the corrected T_1 curve of baBr, the activation energy for the NH_3^+ reorientation was evaluated as 23 kJ mol^{-1}. It is interesting to note that this E_a value is considerably larger than that for the CH_3 reorientation evaluated above. This means that the NH_3^+ groups are tightly fixed on the layer formed by bromide anions through weak hydrogen bonding, although the CH_3 groups are situated in a weak crystal field produced by the surrounding alkyl chains.

Other alkylammonium bromides having similar crystal structures to that of baBr, such as methylammonium bromide[10] and propylammonium bromide,[26] have fairly close E_a values for the reorientations of the NH_3^+ and CH_3 groups. For propylammonium chloride, strong interactions between the NH_3^+ groups and the Cl^- ions are expected. However, the reorientations of the CH_3 and NH_3^+ groups give rise to their T_1 minima at nearly the same temperature and have the activation energies of 10.0 and 15.5 kJ mol^{-1}, respectively.[12]

From the analysis of the second moment, a conclusion similar to that derived above for the intermediate phase of baBr-d_3 can be obtained. When baBr-d_3 having no NH_3^+ groups was warmed, a marked decrease in M_2 was observed around the low T_{tr}. This clearly indicates that some new motional processes other than the NH_3^+ reorientation are responsible for the reduction of M_2.

Although the M_2 values of baBr and baBr-d_3 obtained for this phase decrease rather sharply at first with increasing temperature, they yield almost the constant values of 9.5 and 8.5 (±1) G^2, respectively, at the higher temperatures. Referring to the calculated values of M_2 listed in Table 1, these plateau values observed are too small to be attributed to the motional state of the cations performing only the CH_3 and NH_3^+ reorientations. Furthermore, these values are too large, if one assigns them to the motional model in which the cation rotates as a whole about its long axis while it keeps the rigid conformation of the chain with the end CH_3 and NH_3^+ groups rotating. Therefore, some new motional modes other than the above ones should be adopted in the interpretation of the M_2 values obtained in this phase.

As a possible relaxation process, we take up the 180° flip motion (C_2 reorientation) of the cation about its long axis. This motion is acceptable for the cations shown in Fig. 6, because each NH_3^+ group can form the same type hydrogen bonds with the surrounding Br^- ions even after the 180° flipping. Although the crystal structure of the intermediate phase is necessarily different from that of the high temperature phase, local atomic arrangements around the NH_3^+ groups are expected to be similar for both phases.

As another analogous motional process, the 90° flip motion of the cation about its long axis can be proposed. This type of motion was found to exist in $(n\text{-}C_3H_7NH_3)_2CdCl_4$[27] and $(n\text{-}C_{10}H_{21}NH_3)_2CdCl_4$.[28] The calculated values of M_2 for this motional model, however, are 6.8 and 5.8 G^2 for baBr and baBr-d_3, respectively, these values are too small as compared with the experimental ones. The model of the 180° flip process of the cation together with the independent reorientations of the CH_3 and NH_3^+ groups yielded the M_2 values given in Table 1. These are in good agreement with the observed plateau values of *ca.* 9.5

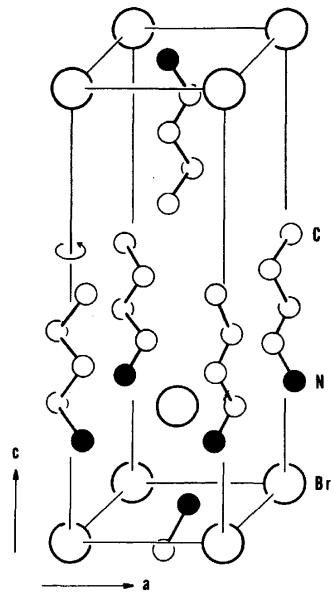

Fig. 6. Predicted crystal structure of baBr at room temperature. The orientations of the cation chains are statistically distributed along the *c* axis.

and 8.5 G^2 for baBr and baBr-d_3, respectively. Accordingly, it can be concluded that there exists the 180° flip motion of butylammonium chains activated in the intermediate phase of baBr. The E_a value for this motion roughly estimated from the T_1 curves of baBr-d_3 is listed in Table 3.

The entropy change, ΔS_{tr} ($=\Delta H_{tr}/T_{tr}$) at the phase transition of 200 K was determined as 7.6 J mol^{-1} K^{-1} from the present DSC experiments. If we assume that the observed ΔS_{tr} is due only to the orientational freedom obtained by butylammonium ions during the transition, this entropy change can be expressed by $R\ln\Omega$ where R and Ω are the gas constant and the number of the orientations permissible to the cation above T_{tr}, respectively. By use of the observed ΔS_{tr}, we obtain Ω=2.5, which is reasonably explained by our model of the 180° flip process.

Reorientations of the ethyl or the propyl group of the cation, *i.e.*, dynamic *trans-gauche* isomerization can be taken as a new motional process alternative to the 180° flip. Although this isomerization is found to exist in the crystalline paraffine ($C_{19}H_{40}$) by ^{1}H NMR studies,[22] the concentration of the gauche conformation is low (less than 1%). From ^{2}H NMR measurements, a similar result is obtained even for the high temperature rotator phase of the paraffine.[29] Accordingly, it is expected that the gauche isomers generated in this phase of baBr or baBr-d_3 are few and give only a minor contribution to the reduction of M_2 and also to the relaxation time.

High-Temperature Phase. At the high T_{tr}, each salt of baBr and baBr-d_3 showed a sudden change of M_2. Above the T_{tr}, the M_2 value of the high temperature phase decreased gradually with increasing temperature, suggesting that some motional process governing the M_2 is gradually growing. The M_2 values observed for baBr and baBr-d_3, respectively, at 300 K are 3.2 and 2.3 (±0.5) G^2, and at 435 K, 1.9 and 1.7 (±0.2) G^2. These M_2 values of baBr and baBr-d_3, respectively, are smaller than those of 4.3 and 3.6 G^2 calculated on the basis of a

Table 3. Activation energies (E_a) derived for the motion of baBr and baBr-d_3 from spin-lattice relaxation times

Phase Compound	E_a/kJ mol^{-1}	mode
Low temp phase		
baBr	11.0±1	CH_3 reorient.
baBr-d_3	10.0±1	CH_3 reorient.
Intermed. phase		
baBr	23±2	NH_3^+ reorient.
baBr-d_3	14±2	chain 180° flip
High temp phase		
baBr	10.0±0.5(250—300 K)	Whole cationic rotation
	5.8±0.5(310—430 K)	Whole cationic rotation
baBr-d_3	8.2±0.5(250—280 K)	Whole cationic rotation
	6.7±0.5(290—400 K)	Whole cationic rotation

motional model where the cation having its rotating CH_3 and NH_3^+ groups rotates as a whole about its chain axis. This result indicates the existence of some motional processes other than the chain rotation. One of the motions that we can expect to take place in the high temperature phase is the rotation of the cations accompanied by the conformational disorder of the alkyl chain. The observed gradual decrease of M_2 suggests that crystal domains where the cations perform such a motion grow gradually in the crystal with increasing temperature.

The presence of the ba$^+$ cations having such a high degree of movability in the crystal can be proved from the large entropy change (23 J mol^{-1} K^{-1}) observed at the transition to the high temperature phase. This is much larger than that of fusion (17 J mol^{-1} K^{-1}) and is comparable to those reported for various crystals at their transition to a plastic phase.[30] On the other hand, the melting entropy observed is fairly small even though the cation has many allowable conformations in the alkyl chain. Even compounds with no conformational freedom of ions such as NaSCN, KSCN, and KN_3 have the melting entropies of 30—40 J mol^{-1} K^{-1}.[31] These results support our explanation of the second moments and, therefore, it can be concluded that the conformational melting of the cation chains occurs in the high temperature phase.

With increasing temperature, the T_1 value of both salts showed a remarkable increase at the high T_{tr}. This means that the motional time constant of the cations decrease so much at the T_{tr}. In other words, the cations in this phase can move quite freely as compared with those of the intermediate phase. With increasing temperature furthermore the T_1 value increased fairly steeply, although a somewhat nonlinear relation was observed between $\log T_1$ and T^{-1}. The E_a values of baBr determined from the slopes of the T_1 curves are 10.0 and 5.8 kJ mol^{-1} at *ca.* 280 and 380 K, respectively, while those of baBr-d_3 are 8.2 and 6.7 kJ mol^{-1} at the respective temperatures as above. These results suggest that the random chain rotation of the cations mainly contributes to the ^{1}H relaxation at lower temperature in this phase, while contribution from other relaxation process, the dynamic *trans-gauche* isomerization for example, gradually increases with increasing temperature.

Conclusion

From the present study of NMR the low temperature phase can be considered to have a disordered structure, probably of static nature, about the environment of the CH_3 groups. The only motion detected by NMR in this phase was the C_3 reorientation of the CH_3 groups. In the intermediate phase, the 180° flip motion of the cation about its long axis as well as the C_3 reorientation of the NH_3^+ groups are expected to take place. From these motional processes, the intermediate phase is characterized to be a dynamically disordered phase about the orientation of the cations. Above the high temperature transition, the cations obtain much more motional freedom than those in the intermediate phase. The conformational disorder of the cations is considered to develop in the crystals with increasing temperature.

When baBr was cooled through the high T_{tr}, marked nonexponential behavior of T_1 indicating the coexistence of at least two crystalline phases was observed in a fairly wide temperature range. This can be explained by considering that the random axial orientation of the ba^+ chains in the high temperature phase is partially frozen below the T_{tr} and the disordered chains are gradually settled in the stable arrangement with decreasing temperature.

Tsau and Gilson[8] studied the wide-line NMR of butylammonium chloride which is known to show two phase transitions, and assigned the decrease of M_2 at the low T_{tr} to the reorientation of butyl chains with rotating CH_3 and rigid NH_3^+ groups. However, the present study reveals that the NH_3^+ groups of baBr reorient very rapidly even in the intermediate phase. This may be due to the N-H···Br type hydrogen bonds which are weaker than those of the N-H···Cl type.

The authors are particularly indebed to Mr. K. Kawase and Dr. K. Toriyama in the Government Industrial Research Institute of Nagoya for carrying out DSC experiments.

This work was partially supported by a Grand-in-Aid for Scientific Research No. 57470012 from the Ministry of Education, Japan.

References

1) S. B. Hendricks, *Z. Kristallogr.*, **68**, 189 (1928).
2) S. B. Hendricks, *Z. Kristallogr.*, **67**, 465 (1928).
3) R. W. G. Wyckoff, "Crystal Structures," 2nd ed. Interscience Publishers, New York, (1966), Vol. 5, Chap. XIVA.
4) M. V. King and W. N. Lipscomb, *Acta Crystallogr.*, **3**, 222 (1950).
5) J. Tsau and D. F. R. Gilson, *J. Phys. Chem.*,**72**, 4082 (1968).
6) M. V. King and W. N. Lipscomb, *Acta Crystallogr.*,**3**, 227 (1950).
7) J. C. Southard, R. T. Milner, and S. B. Hendricks, *J. Chem. Phys.*,**1**, 95 (1933).
8) J. Tsau and D. F. R. Gilson, *Can. J. Chem.*,**51**, 1990 (1973).
9) S. Albert and J. A. Ripmeester, J. Chem. Phys., **58**, 541 (1973).
10) H. Ishida, R. Ikeda, and D. Nakamura, *Phys. Status Solidi A*, **60**, K115 (1980); *J. Phys. Chem.*,**86**, 1003 (1982).
11) H. Ishida, R. Ikeda, and D. Nakamura, *Phys. Status Solidi A*, **70**, K151 (1982).
12) S. Albert and J. A. Ripmeester, *J. Chem. Phys.*,**69**, 3967 (1978).
13) L. S. Prabhumirashi, R. Ikeda, and D. Nakamura, *Ber. Bunsenges. Phys. Chem.*,**85**, 1142 (1981).
14) S. Gima, Y. Furukawa, R. Ikeda, and D. Nakamura, *J. Mol. Struct.*,**111**, 189 (1983).
15) J. H. Van Vleck, *Phys. Rev.*,**74**, 1168 (1948).
16) E. R. Andrew, *J. Chem. Phys.*,**18**, 607 (1950).
17) G. W. Smith, *J. Chem. Phys.*,**42**, 4229 (1965).
18) M. J. R. Hoch, *J. Chem. Phys.*,**65**, 2522 (1976).
19) N. Bloembergen, E. M. Purcell, and R. V. Pound, *Phys. Rev.*, **73**, 679 (1948).
20) T. M. Conner, *Trans. Faraday Soc.*,**60**, 1574 (1964).
21) D. W. Davidson and R. H. Cole, *J. Chem. Phys.*,**19**, 1484 (1951).
22) M. Stohrer and F. Noack, *J. Chem. Phys.*,**67**, 3729 (1977).
23) E. Hirota, *J. Chem. Phys.*,**37**, 283 (1962).
24) D. E. Woessner and H. S. Gutowsky, *J. Chem. Phys.*, **29**, 804 (1958).
25) J. J. R. Fraústo da Silva and L. F. Vilas Boas, *Rev. Port. Quim.*,**14**, 115 (1972).
26) Data of our preliminary measurements.
27) G. Chapuis, *Acta Cryst.*, **B34**, 1506 (1978).
28) R. Kind, S. Plesko, H. Arend, R. Blinc, B. Zeks, J. Seliger, B. Lozar, J. Slak, A. Levstik, C. Filipic, V. Zagar, G. Lahajnar, F. Milia, and G. Chapuis, *J. Chem. Phys.*,**71**, 2118 (1979).
29) M. G. Taylor, E. C. Kelusky, I. C. P. Smith, H. L. Casal, and D. G. Cameron, *J. Chem. Phys.*, **78**, 5108 (1983).
30) N. G. Parsonage and L. A. K. Staveley, "Disorder in Crystals," Clarendon Press, Oxford, (1978), Chap. 10.
31) G. J. Janz, "Molten Salts Handbook," Academic Press, N. Y., (1967).

 © 1984 The Chemical Society of Japan Bull. Chem. Soc. Jpn., 57, 2809—2815 (1984)

Electrodic Properties and Surface Characteristics of Ni-V Alloys for Water Electrolysis Cathode Materials

Ken-ichi MACHIDA, Michio ENYO,* Keisuke OGURO,† and Masanori NAKANE†

Research Institute for Catalysis, Hokkaido University, Sapporo 060

†*Government Industrial Research Institute, Midorigaoka, Ikeda-shi, Osaka 563*

(Received May 21, 1984)

Hydrogen evolution reaction on a series of hydrogen absorbing Ni-V alloys, *viz.* Ni_2V, NiV, and NiV_3, before and after pretreatments with aq HF was studied in 1 M NaOH (1 M=1 mol dm^{-3}) at 288—333 K by a galvanostatic overpotential transient technique. Results are related with the surface characteristics revealed by XPS techniques. It is concluded that the Ni in the Ni-V alloys is mainly responsible for their electrochemical properties and that the reaction proceeds *via* the Volmer-Tafel reaction route with mixed rate-determining characteristics: The activation heats are 7.7, 6.8, and 6.8 kcal mol^{-1} (1 cal=4.184 J) for two elementary steps, Volmer and Tafel, and the overall reaction, respectively. The electrocatalytic activity of the Ni-V alloys, particularly NiV_3, is drastically enhanced through the treatment with aq HF, and this is in parallel with the formation of porous Ni layers on their surface, namely the increase of the effective surface area. Potentiality of the alloys for water electrolysis cathode materials is indicated by a higher electrocatalytic activities of the Ni-V alloys over ordinary Raney nickel electrodes. Hydrogen absorbability of the alloys was also investigated: NiV_3 stored hydrogen up to [H]/[M]=$\leq$0.3 after a cathodic polarization at about −400 mV hydrogen overpotential, but that in Ni_2V or NiV was far smaller.

Overpotential is one of the major factors which decrease efficiency of electrochemical processes and, accordingly, the electrode is often made to possess a large surface area.[1] We have reported recently that a series of amorphous Ni-Ti and Ni-Zr alloys after a brief treatment with aq HF attain a high electrocatalytic activity for the hydrogen electrode reaction (HER). Surface characterizations including XPS observations indicated that this is due to formation of a porous layer rich in nickel on their surface during the acid treatment, similar to usual Raney nickel electrodes.[2]

The Raney nickel materials are usually prepared from Ni-Al or Ni-Zn alloys by leaching Al or Zn out with alkaline solutions. Further, we have shown in a previous paper[3] that essentially the same electrocatalytic activity is obtained by the use of aq HF as the developer instead of aq NaOH. Since V is rapidly soluble in aq HF as compared with Ni, similar to Ti or Zr, we may apply it in developing a series of Ni-V alloys.

Various elements including those of Va group such as V are known to form hydrides,[4] and thus noted as hydrogen storage materials, similar to a series of alloys containing rare earth elements.[5] The element V itself has a high hydrogen absorbability and forms nonstoichiometric hydrides up to [H]/[V]=2.0 at ambient pressure and temperature.[6] Further, effects of Ti, Cr, Fe, and Co as alloying elements on the hydrogen solubility of V-based alloys have been reported by Eguchi and Morozumi[7] or Lynch *et al.*[8]

In the Ni-V system, there are four types of intermetallic compounds (Ni_3V, Ni_2V, NiV, and NiV_3) which crystallize with tetragonal (I4/mmm),[9a] orthorhombic (Immm),[9b] tetragonal ($P4_2/mmm$),[9c] and cubic ($Pm3n$)[9d] systems, respectively. However, no systematic study has so far been reported on their hydrogen storage property.

The HER on many electrocatalytically active metals in aqueous solutions consists of two elementary steps, *viz.* the discharge of proton (in acidic solutions) or water (in alkaline solutions), the Volmer step, and the recombination of hydrogen adatoms H(a), the Tafel step.

Volmer step:

$$H^+B + e \rightleftharpoons H(a) + B \quad (B=H_2O, OH^-), \qquad (1)$$

Tafel step:

$$2H(a) \rightleftharpoons H_2. \qquad (2)$$

Use of thin foils of hydrogen permeating metals or alloys as hydrogen electrodes has a particular advantage in the mechanistic studies: The kinetics of the individual elementary steps of the HER can be obtained by analyzing transient rise and decay characteristics of the overpotential. The overpotential components shared by the constituent steps can individually be evaluated because of a large difference in the relaxation time constant between the Volmer step, which is very fast, and the Tafel step, which is extremely slow because of slow rate of variation in the activity of H(a) on the electrode surface.[10] The same technique may be applied to the Ni-V alloys to derive kinetics of the individual elementary steps and determine the mechanism of the HER.

Experimental

Preparation of Electrodes. The alloy ingots (about 5 g) with compositions of Ni_2V, NiV, and NiV_3 were synthesized from Ni (99.9%) and V (99.9%) by arc-melting as described elsewhere.[11] Their weight loss during the fabrication was negligible, or the composition of the product was essentially equal to the starting one. The alloys obtained were annealed at 1300 K for 10—15 h *in vacuo* (*ca.* 5×10^{-4} Pa), spark-cut into slices (0.5—1.0 mm in thickness), and then the surface was polished with emery papers (no. 170—200). Powder X-ray diffraction patterns of Ni_2V and NiV agreed with those in the literatures,[9b,c] but not for NiV_3 [the powder data (d_{obsd}/Å and I/I_0) observed within $(\sin\theta)/\lambda<0.50$ Å^{-1} were as follows: 2.33, 60; 2.19, 60; 2.13, 55; 2.08, 45; 2.02. 100; 1.99, 85; 1.94, 45]. The acid treatment of a series of Ni-V alloys was made with 1 M HF solution at room temperature, the period being 10 h for Ni_2V or NiV and 10—30 min for NiV_3, respectively.

Electrochemical Measurements. The electrodic properties of the Ni-V alloys were investigated in 1 M NaOH at

288—333 K according to the technique described previously.[2] The electrolytic solution was prepared from special grade NaOH (Merck Japan, Ltd.) with water obtained from a Millipore pure water system. A platinized Pt was used for a hydrogen reference electrode. Roughness factor (*RF*) of the test electrode was evaluated from double layer capacitance data assuming *a* value of 18 $\mu F\,cm^{-2}$ (true), usually observed on Hg electrode.

XPS Measurements. Surface analysis of the Ni–V alloys was performed using an ESCA apparatus (VG-III) with Al $K\alpha$ X-ray radiation. The binding energy values recorded were calibrated using the $4f_{7/2}$ signal (83.8 eV) from a gold plate which was employed as an internal standard. Surface sputtering by Ar^+ ion bombardment was carried out under the condition of 1—2 keV and 4—10 $\mu A\,cm^{-2}$. The depth D_s sputtered by the bombardment was estimated from the following equations,[12]

$$D_s = \frac{N_{Ar} \cdot Y \cdot M}{N_A \cdot \rho} \times 10^8\ \text{Å}, \quad (3)$$

$$N_{Ar} = \frac{I \cdot T}{1.6 \times 10^{-9}}, \quad (4)$$

where N_{Ar} is the Ar^+ ion flux density in ions per second, Y is the sputtering yield, M is the atomic weight, N_A is Avogadro's number, ρ is the density of the alloys, I is the ion current density in amperes and T is the duration of the bombardment in seconds. The Y value was deduced by averaging the sputtering yields for each pure component of the alloy, which were in turn evaluated by interpolation of the values determined by Kanaya *et al.*[12] at given Ar^+ ion energy values (1.0, 1.5, and 2.0 keV). An average atomic weight corresponding to the alloy composition was used for M.

Results and Discussion

Electrochemical Properties. The electrocatalytic activity of the nontreated (as-obtained) Ni_2V and NiV alloys for the HER was relatively high, so that the reversible HER potential was realized soon after introduction of the electrode into the electrochemical cell. The electrode of NiV_3, without the pretreatment which was performed later, did not give the potential because of its very low activity.

On metal and alloy electrodes which have high solubility as well as mobility of hydrogen in the bulk, a plateau region should appear on the short time (several seconds) galvanostatic overpotential rise and decay transient curves before the attainment of the steady-state polarization or equilibrium potential, respectively.[2,13] Such overpotential plateaus were indeed seen clearly on both the nontreated Ni_2V and NiV alloy electrodes. Typical rise and decay transient curves observed on the NiV alloy electrode are shown in Fig. 1. As discussed previously,[10] we can estimate two overpotential components, η_1 and η_2', for the step of discharge of water and the step of recombination of hydrogen adatoms, respectively.

Tafel plots of η_1 on the nontreated Ni_2V and NiV alloy electrodes both in the cathodic and anodic regions are shown in Fig. 2. The approximate symmetry of these curves about the abscissa and the slope (about 120 mV/decade) of the linear portions of the "Tafel lines" indicate that η_1 should represent the component overpotential for a one-electron transfer reaction, namely, the Volmer step. The symmetry factor (for the cathodic unidirectional current) is 0.5—0.6 near the reversible potential, as same as that observed earlier on $LaNi_5$ and Ni–Ti alloy electrodes.[2,13c] Likewise,

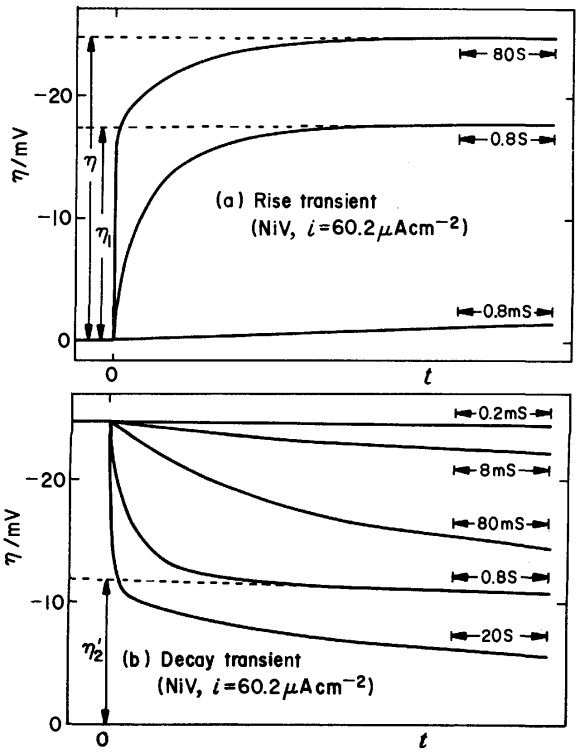

Fig. 1. Typical galvanostatic overpotential (a) rise and (b) decay transients with various time scales on a nontreated NiV alloy electrode. 1 M NaOH, 303 K. $-i$=60.2 $\mu A\,cm^{-2}$ (apparent).

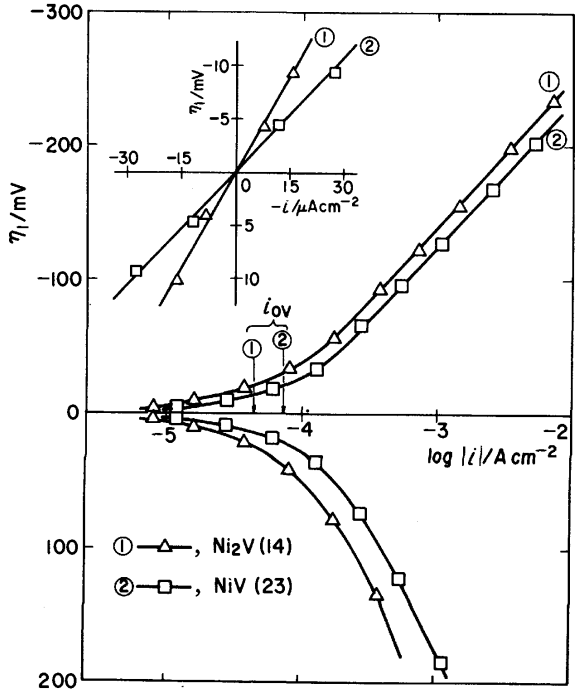

Fig. 2. Cathodic and anodic polarization behaviours of the rapidly rising overpotential component η_1 on both nontreated Ni_2V and NiV alloy electrodes. The arrows on the abscissa indicate i_{ov} as evaluated from the linear plots (the inset figure) of η_1 *vs.* i near the reversible potential. The numerals in the parentheses indicate the *RF* values. 1 M NaOH, 303 K.

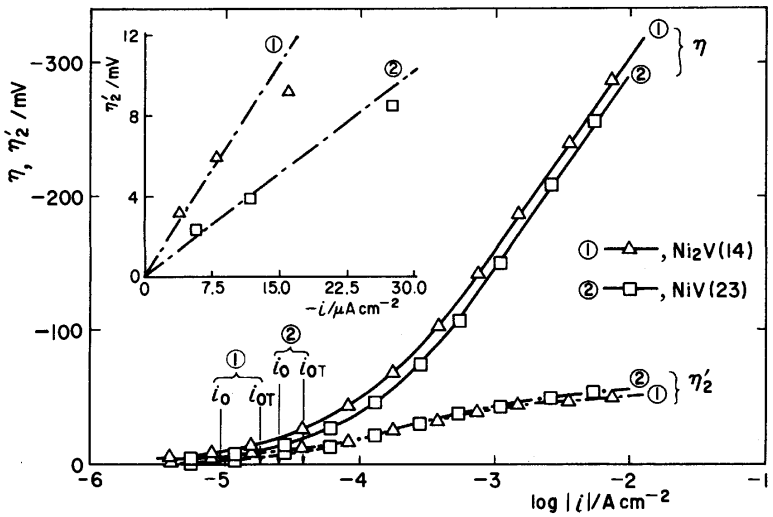

Fig. 3. Cathodic polarization behaviours of the total overpotential η and the slowly decaying overpotential component η_2' on both nontreated Ni_2V and NiV alloy electrodes. The arrows on the abscissa indicate i_o and i_{oT} obtained at low overpotentials (the inset figure). The numerals in the parentheses indicate the *RF* values. 1 M NaOH, 303 K.

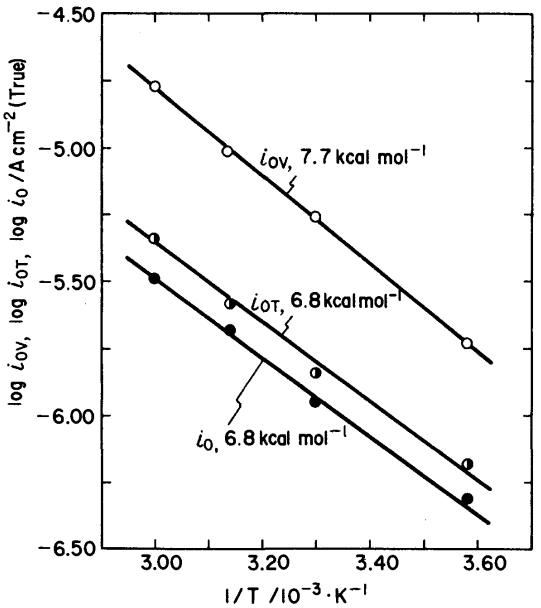

Fig. 4. Arrhenius plots of the exchange current densities for the Volmer and Tafel elementary steps and the overall reaction on the nontreated NiV alloy electrode with *RF*=29. The numerals give their corresponding activation heats. 1 M NaOH.

the approximate linearity of the cathodic η_2' *vs.* log i behaviours with the slope of about 30 mV/decade, as shown in Fig. 3, indicates that η_2' should be attributed to the Tafel step, as same as the case of the Pd electrode reported previolusly.[13a]

The exchange current densities of the Volmer and Tafel elementary steps, i_{oV} and i_{oT}, were obtained from the polarization resistance at low overpotentials (see the inset figures in Figs. 2 and 3) in a similar manner as the cases of other hydrogen absorbing electrodes.[13c] These values are both around the same order of magnitude, 10^{-4} A cm^{-2} (apparent) and hence, the reaction is of the mixed rate-determining type. The characteristics are similar to those of ordinary Ni electrodes. The exchange current density, i_o, of the overall reaction is readily evaluated by the relationship, $1/i_o=1/i_{oV}+1/i_{oT}$. In Figs. 2 and 3, the values of i_{oV}, i_{oT}, and i_o are respectively indicated by arrows on the abscissa.

The activation heats of the reaction steps are determined from the temperature dependences of the exchange current densities. Typical Arrhenius plots obtained on the NiV alloy electrode (*RF*=29) are shown in Fig. 4. The activation heats observed are 7.7, 6.8, and 6.8 kcal mol^{-1} for the Volmer and Tafel elementary steps and the overall reaction, respectively. These values practically agree with those determined on some Ni-based alloy electrodes, of which the reaction is also catalyzed by the nickel in the alloy matrix.[2,13c] It is noted that the heat values as well as rate data of the Tafel step and the overall reaction are close to each other. This means that the overall reaction around the reversible hydrogen electrode potential must be more intimately controlled by the Tafel step than by the Volmer step. On the other hand, the slope of the linear portion of the Tafel lines at high cathodic overpotentials is around 120 mV/decade and this is attributable to the one-electron transfer step. Necessity of variation of the overall kinetics as such in the case of the mixed rate-determining reaction has been discussed elsewhere.[10]

It is seen that the electrocatalytic activity of the specimens of the Ni-V alloys, particularly NiV_3, is drastically improved by the treatment with aq HF, along with increase in the *RF* values. Another tendency observed is that the higher the Ni content in the alloy matrix is, the higher the *RF* values attained are. Presumably, the specimen containing a larger amount of V is attacked more readily by aq HF than those of lower V content, and thus gives rise to the surface more effectively roughened.

Typical galvanostatic rise and decay behaviours on the HF-treated NiV_3 electrode are given in Fig. 5. These are similar to those of the nontreated specimens, but

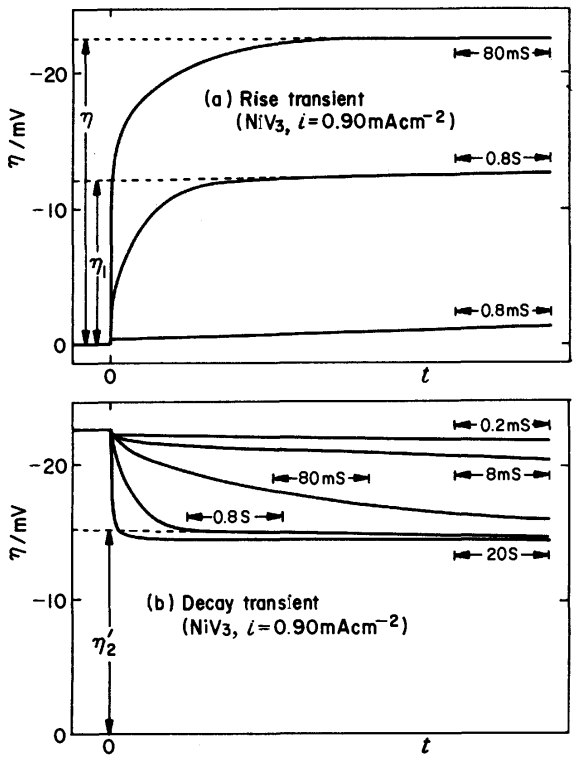

Fig. 5. Typical galvanostatic overpotential (a) rise and (b) decay transients with various time scales on a HF-treated NiV_3 alloy electrode. 1 M NaOH, 303 K. i=0.90 mA cm^{-2}.

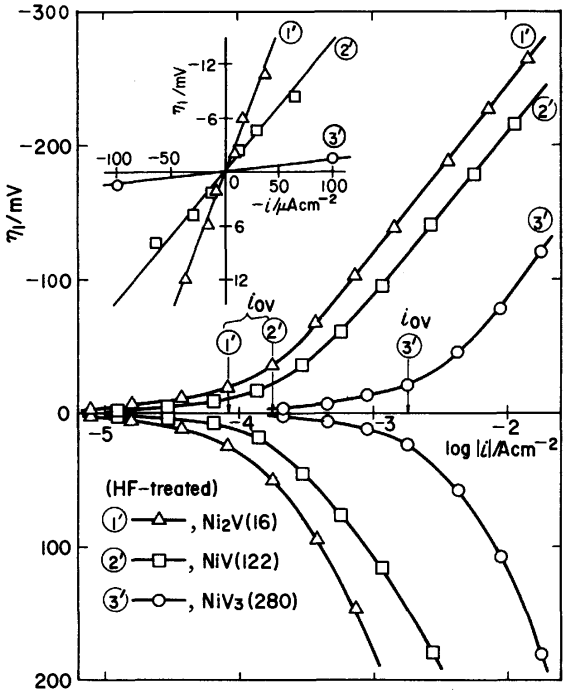

Fig. 6. Cathodic and anodic polarization behaviours of the rapidly rising overpotential component η_1 on a series of HF-treated Ni-V alloy electrodes. The arrows on the abscissa indicate i_{oV} as evaluated from the linear plots (the inset figure) of η_1 *vs.* i near the reversible potential. The numerals in the parentheses indicate the *RF* values. 1 M NaOH, 303 K.

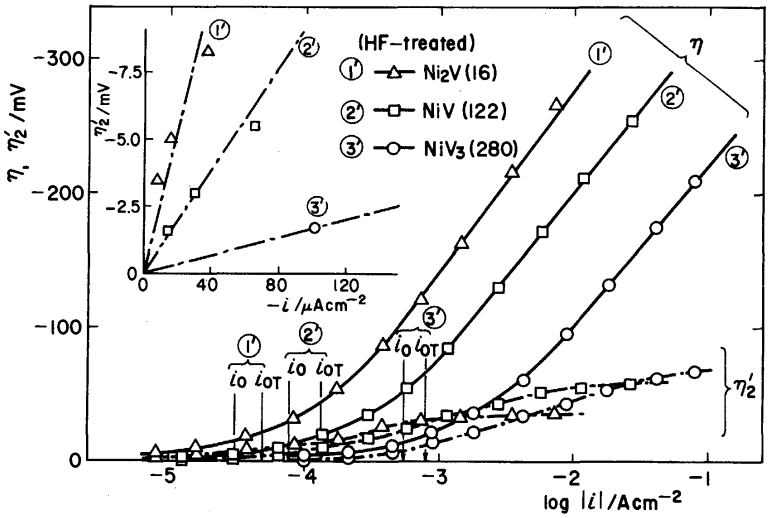

Fig. 7. Cathodic polarization behaviours of the total overpotential η and the slowly decaying overpotential component η'_2 on a series of HF-treated Ni-V alloy electrodes. The arrows on the abscissa indicate i_{oT} obtained at low overpotentials (the inset figure) and i_o evaluated by the relation of $1/i_o=1/i_{oV}+1/i_{oT}$. The numerals in the parentheses indicate the *RF* values. 1 M NaOH, 303 K.

the ratio η'_2/η of the HF-treated NiV_3 specimens is somewhat larger than those of the nontreated or HF-treated Ni_2V and NiV electrodes. This might indicate, on NiV_3, that the rate of diffusion in the solution phase begings to play a role in controlling the overall rate because these electrodes are highly active.

The polarization behaviours with respect to η_1, η'_2, and η on a series of HF-treated Ni-V alloys are given in Figs. 6 and 7. These characteristics are altogether essentially the same with those observed above on the nontreated electrodes.

The numerals in the parentheses in Figs. 6 and 7 represent the *RF* values of the electrodes. It is seen that the exchange current densities of the Volmer and Tafel steps, i_{oV} and i_{oT}, are almost in parallel with the *RF* values. Thus, the NiV_3 alloy electrodes which have *RF*

values of several hundreds give the i_{oV} and i_{oT} values around 10^{-3} A cm^{-2} (apparent). Yet, as the limiting current of the H_2 diffusion in solution is of the same order of magnitude with this value, the value of i_{oT} is likely to be somewhat under-estimated from the real value.

The exchange current density (i_o) of the overall reaction, evaluated by the relation $1/i_o=1/i_{oV}+1/i_{oT}$, is naturally also enhanced by the increase of the roughness. The electrocatalytic activity of the HF-treated alloys, particularly NiV_3, is as high as that of smooth of electrodes ($i_o=\leq 10^{-3}$ A cm^{-2}) on apparent surface area basis.

The HF-treated NiV_3 alloys could store hydrogen up to [H]/[M]$=\leq 0.3$ by cathodic polarization for 10—20 h at $\eta=\leq -400$ mV. (The amount absorbed in the Ni_2V and NiV specimens was negligible even after polarization for several days.) The condition with respect to hydrogen pressure P_{H_2}, to which the cathode is effectively exposed, can be obtained from the over-potential component η_2', as discussed in previous work,[14] as

$$-\eta_2' = \frac{RT}{2F} \ln P_{H_2} \qquad (5)$$

In Fig. 8, the relation between η_2' (or log P_{H_2}) and [H]/[M] ratios observed on the HF-treated NiV_3 alloy electrode (RF=530) is shown: The [H]/[M] ratios are evaluated by collecting the H_2 gas liberated from the alloy after termination of the polarization current. Also shown in this figure are typical absorption isotherms of Cr–V alloys (and not data for the Ni–V alloys, which are not available) reported by Lynch *et al.*[8] It is generally seen that the hydrogen absorbability of the V-based alloys containing Cr, Fe, or Co[7,8] is lowered with increase of the content of the added element (see Fig. 8).

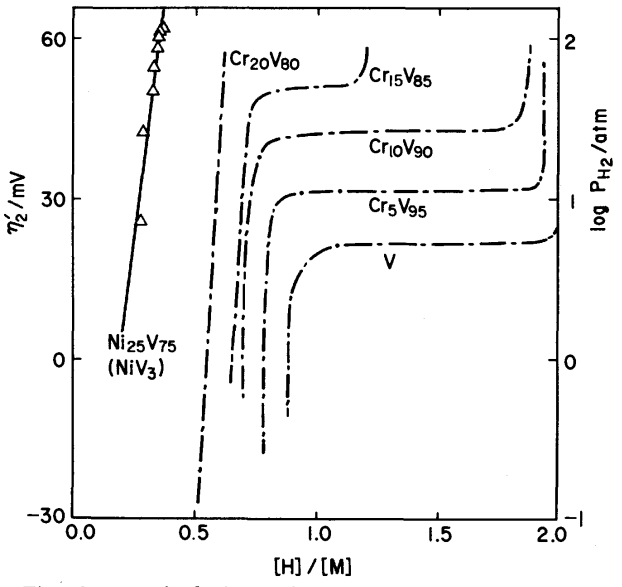

Fig. 8. Typical absorption isotherms (η_2' or log P_{H_2} *vs.* [H]/[M]) obtained on the NiV_3 alloy electrode with RF=530 after a cathodic polarization at η= 50—400 mV at 303 K for 10—20 h. The absorption isotherms of Cr–V alloys at 313 K reported by Lynch *et al.*[7] are shown for comparison.

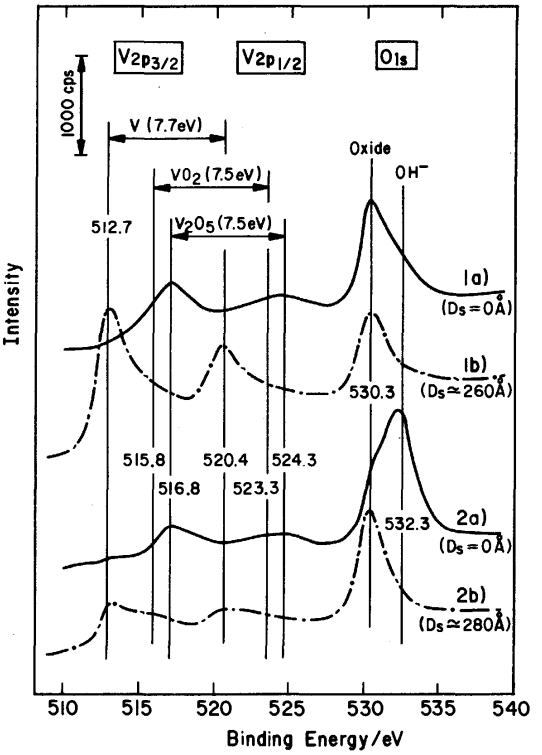

Fig. 9. XPS patterns of the V_{2p} and O_{1s} electrons on the NiV_3 alloys before (solid-lines) and after (broken-lines) Ar^+ ion bombardments up to D_s=250—300 Å, respectively. Spectra: 1a) and 1b), nontreated specimens; 2a) and 2b), HF-treated specimens.

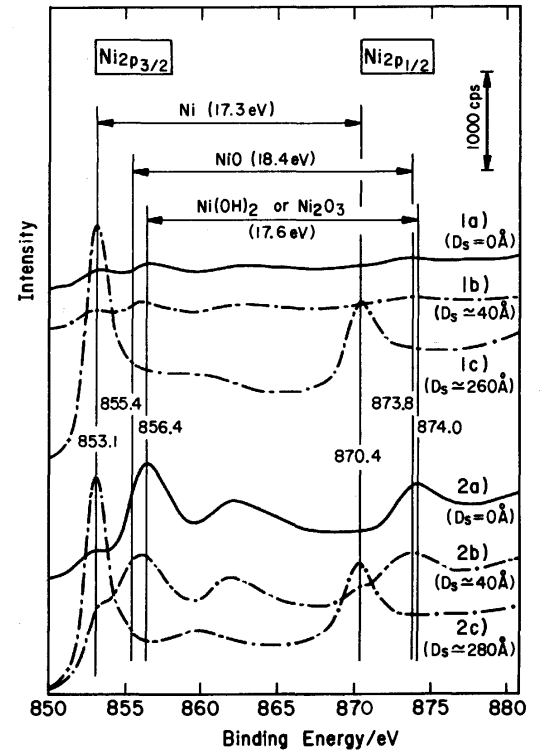

Fig. 10. XPS patterns of the Ni_{2p} electrons on the NiV_3 alloys before (solid-lines) and after (broken-lines) Ar^+ ion bombardments up to D_s=40—300 Å, respectively. Spectra: 1a), 1b), and 1c), nontreated specimens; 2a), 2b), and 2c), HF-treated specimens.

The same tendency might be expected with the Ni–V alloys, namely the larger the amount of Ni was, the smaller the amount of the stored hydrogen would be. Thus, in Fig. 8, the position of the isotherms of the NiV_3 alloy ($Ni_{25}V_{75}$) which appear at left-hand side of the line for $Cr_{20}V_{80}$ seems reasonable. The Ni–V alloys containing still smaller concentration of Ni may have a possibility as cathode materials if those of higher hydrogen absorbability are desired.

Surface Characterization. A series of XPS patterns of the Ni–V alloys have been observed before and after the treatment with aq HF. On the nontreated specimens, the signals from V are very strong compared with those from Ni. However, the spectrum intensity of Ni is drastically increased on the HF-treated Ni–V alloys, particularly NiV_3, while that of V is decreased. Typical X-ray photoelectron spectra derived from the V_{2p}, O_{1s}, and Ni_{2p} electrons on the NiV_3 alloys are given in Figs. 9 and 10, together with assignments given according to XPS data listed in a handbook.[15] (Practically the same spectra have been observed on other Ni–V alloys, *viz.* Ni_2V and NiV.)

The $V_{2p3/2}$ or $V_{2p1/2}$ signals on the nontreated and HF-treated Ni–V alloys consists mainly of two spectrum bands; The peak positions are *ca.* 515.8 and 516.8 eV for $V_{2p3/2}$ and *ca.* 523.3 and 524.3 eV for $V_{2p1/2}$, respectively. The V_{2p} spectra around 515.8 and 523.3 eV are assigned to the vanadium of VO_2 while the signals at the other peak positions are attributable to the V_{2p} electrons of V_2O_5. Signals of the metallic V become observable only after the Ar^+ ion bombardments up to the D_s of 100—200 Å. Therefore, most of the vanadium on the alloy surface exists as oxides which are probably electrocatalytically inert. This would explain the low activity of the nontreated NiV_3 alloys towards the HER.

The O_{1s} spectra on the Ni–V alloys have peaks at 530.3 and 532.3 eV, which are assigned to the oxygens of anhydrous oxides (V_2O_5, NiO, *etc*) and hydroxides (hydroxyl groups), respectively, but the latter spectrum band is significantly decreased after the Ar^+ ion bombardments ($D_s = \leq 50$ Å). This observation indicates that the hydroxides exist only near the surface.

The signals of Ni_{2p} electrons on the nonbombarded specimens appear at *ca.* 853.1, 855.4, and 856.4 eV for $Ni_{2p3/2}$ (and at *ca.* 870.4, 873.8, and 874.0 eV for $Ni_{2p1/2}$). Among them, the nickels of metal and NiO are responsible for two $Ni_{2p3/2}$ spectra (853.1 and 855.4 eV), but the remaining spectrum band is not precisely assigned to that of $Ni(OH)_2$ which is expected to exist near the surface according to the observations of the O_{1s} signal from hydroxyl groups: The same spectra have been observed on the specimens of which the hydroxyl groups are completely removed by the Ar^+ ion bombardments (see spectra 1b) and 2b) in Fig. 10). Perhaps, the Ni_{2p} spectrum bands at 856.4 and 874.0 eV may be due to the nickels of $Ni(OH)_2$ or Ni_2O_3. Signals from NiF_2 which have been observed previously on the HF-treated Ni–Al alloys[3] were not detected on a series of the HF-treated Ni–V alloys preparaed in this work.

The surface concentration ratios $C^S_{Ni/V}$ of the component metals on the nontreated and HF-treated Ni–V alloys are estimated from the integral peak intensity I of Ni_{2p} and $V_{2p3/2}$ using the following equation:

$$C^S_{Ni/V} = \frac{I_{Ni}/S_{Ni}}{I_V/S_V}, \quad (6)$$

where S is the atomic sensitivity factor for X-ray. In this work, $S_{Ni}=5.4$ and $S_V=1.4$ listed in the literature[15] are employed.

The relationships between $C^S_{Ni/V}$ and the nominal bulk compositions, $C^B_{Ni/V}$, of the Ni–V alloys before and after the acid treatments are shown in Fig. 11(a). For all the nontreated specimens, the surface Ni concentration is lower than the bulk one (below the broken-line), or the surface is enriched in V. On the other hand, the $C^S_{Ni/V}$ value of the Ni–V alloys containing a large amount of V, particular NiV_3, is significantly increased by the acid treatment. This means that the vanadium near the surface of the V-rich alloys is effectively dissolved out with aq HF and a Ni-rich layer is formed.

In Fig. 11(b), the in-depth profiles of the $C^S_{Ni/V}$ of the nontreated and HF-treated NiV_3 alloys are given. It is clearly seen that the $C^S_{Ni/V}$ value of the HF-treated specimen differs considerably from that of the nontreated one. The electrochemical capacitance data also indicate that the layer is very porous, and hence it may be considered as a kind of Raney nickel material. Consequently, the high electrocatalytic activity of the HF-treated NiV_3 alloy is concluded to be brought about by the porous Ni-rich layer formed on the surface, after leaching V out with aq HF.

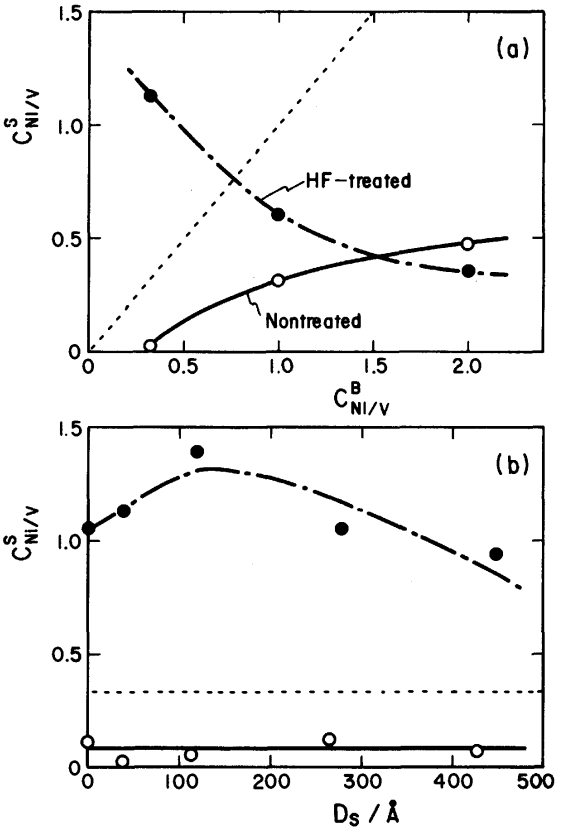

Fig. 11. (a) Relationship between the surface and bulk atomic ratios ($C^S_{Ni/V}$ and $C^B_{Ni/V}$) in a series of Ni–V alloys before and after the acid treatment. The broken line represents the case that $C^S_{Ni/V}$ equals $C^B_{Ni/V}$. (b) In-depth profiles of the surface atomic ratios $C^S_{Ni/V}$ for NiV_3 alloys before and after the acid treatment. The broken line indicates $C^S_{Ni/V}$.

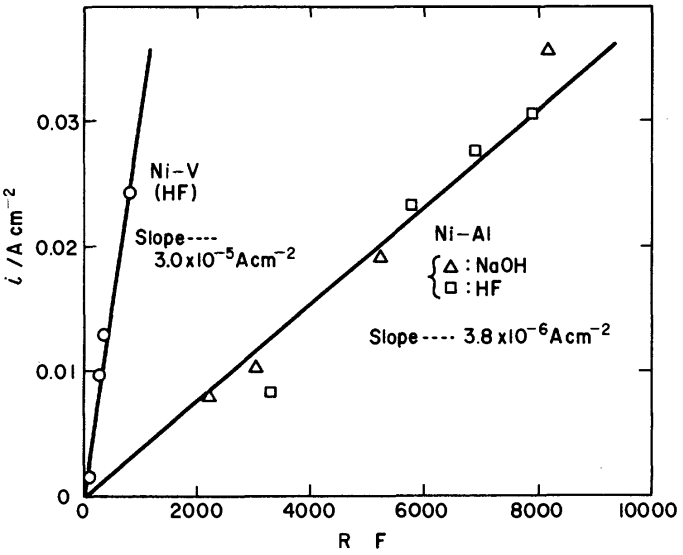

Fig. 12. Relationships between the current density (at η=−100 mV) and *RF* values on the HF-treated Ni-V alloy electrodes (○), together with those[3] on the Raney nickel electrodes treated with aq NaOH (△) and HF (□).

Synergistic Effect. It is noteworthy that a synergistic effect between Ni and V is suggested in the electrocatalytic activity on true unit surface area basis. In Fig. 12, the relation between the current density at η arbitrarily chosen at −100 mV and *RF* values on the HF-treated Ni-V alloys is shown, together with that on ordinary Raney nickel electrodes.[3] The current density on the Ni-V alloys as well as Raney nickel alloys increases linearly with the *RF* values but the slopes are clearly different. The slope (which gives the average current density per true unit surface area) is about 3.0×10^{-5} A cm^{-2} on the Ni-V alloy electrodes and this is about one order of magnitude higher than that of ordinary Raney nickel electrodes (3.8×10^{-6} A cm^{-2}). As reported elsewhere,[3] the difference in the electrocatalytic activity caused by the use of different developer, *viz.* aq NaOH or aq HF, is practically negligible. The difference in the slopes, therefore, indicates existence of a synergistic effect between Ni and V.

Conclusion

The HER on a series of the Ni-V alloy electrodes, *viz.* Ni_2V, NiV, and NiV_3, in 1 M NaOH is mainly catalyzed by nickel on the surface. The reaction proceeds *via* the Volmer-Tafel route with mixed rate-determining characteristics. The electrocatalytic activity as well as the *RF* values is drastically improved after the treatments with aq HF. On the NiV_3 alloy, in particular, the electrocatalytic activity attained is very high, being comparable with that of smooth Pt electrodes. A synergistic effect of about one order of magnitude is indicated. In view of this effect as well as their ability to produce porous Ni layers, the Ni-V alloys can be a potential candidate as a cathode material for water electrolysis.

The present work is partly supported by Grants-in-Aid for Scientific Research No. 58750629 from the Ministry of Education. Science, and Culture.

References

1) A. G. Pschenichinikov, *Int. J. Hydrogen Energy*, **7**, 51 (1982).
2) K. Machida, M. Enyo, I. Toyoshima, K. Miyahara, K. Kai, and K. Suzuki, *Bull. Chem. Soc. Jpn.*, **56**, 3393 (1983).
3) K. Machida and M. Enyo. *J. Res. Inst. Catal. Hokkaido Univ.*, in press.
4) W. M. Mueller, J. P. Blackledge, and G. G. Libowitz, "Metal Hydrides," Academic Press, New York (1968), pp. 2—7.
5) "Hydrides for Energy Storage," ed by A. F. Andresen and A. J. Maeland, Pergamon Press, New York (1978).
6) J. J. Reilly and R. H. Wiswall, *Inorg. Chem.*, **9**, 1678 (1970).
7) T. Eguchi and S. Morozumi, *Nippon Kinzokugakkai-shi*, **38**, 1025 (1974).
8) J. F. Lynch, J. J. Reilly, and F. Millot, *J. Phys. Chem. Solids.*, **39**, 883 (1978).
9) The file of X-ray powder diffraction standards by the American Society for Testing and Materials. Inorganic compounds: a), 13-523; b), 17-715; c), 7-397; d), 19-854.
10) M. Enyo, "The Comprehensive Treatise of Electrochemistry," ed by B. E. Conway *et al.* Plenum, New York (1983), Vol. 7, pp. 241-300.
11) Y. Osumi, A. Kato, H. Suzuki, M. Nakane, and Y. Miyake, *J. Less-Common Met.*, **66**, 67 (1979).
12) K. Kanaya, K. Hojou, K. Koga, and K. Toki, *Jpn. J. Appl. Phys.*, **12**, 1297 (1973).
13) a) M. Enyo and T. Maoka, *J. Electroanal. Chem.*, **108**, 277 (1980); b) M. Enyo, T. Yamazaki, K. Kai, and K. Suzuki, *Electrochim. Acta*, **28**, 1573 (1983); c) K. Machida, M. Enyo, G. Adachi, and J. Shiokawa, *Electrochim. Acta*, **29**, 807 (1984).
14) a) T. Maoka and M. Enyo, *Electrochim. Acta*, **26**, 607 (1981); b) T. Maoka and M. Enyo, *Electrochim. Acta*, **26**, 615 (1981).
15) C. D. Wagner, W. M. Riggs, L. E. Davis, J. F. Moulder, and G. E. Muilenberg, "Handbook of X-Ray Photoelectron Spectroscopy," Perkin-Elmer Co., Physical Electronics Div. (1979).

 © 1984 The Chemical Society of Japan Bull. Chem. Soc. Jpn., 57, 2816—2819 (1984) [Vol. 57, No. 10

The Influence of Culture Conditions on the Fibrillation of Cellulose Gel Produced by *Acetobacter xylinum*

Akira KAI

Department of Industrial Chemistry, Faculty of Technology, Tokyo Metropolitan University, Fukazawa, Setagaya-ku, Tokyo 158

(Received February 27, 1984)

The influence of the culture conditions, such as the temperature of incubation and the pH of the culture medium, on the fibrillation of cellulose gels produced by *Acetobacter xylinum* was studied by means of electron microscopy. The incubation temperature did not show any influence on the fibrillation of cellulose gels as long as it was in the range between 10 to 28 °C. However, in the incubation at 5 °C the fibrillation occurred very slowly. When incubation was carried out at 5 °C, the fibril produced by the 5 °C incubation maintained an amorphous state for about 3 h, and the microscopic fibrils appeared in the fibril only after incubation for 12 h. However, the width of the microscopic fibril was not influenced by the temperature of incubation. The pH of the medium influenced the linear growth rate of a fibril. The rate increased with an increase in the pH, reached the maximum at pH 6.8, and decreased at higher pHs. The fibrillation occurred more rapidly at a constant temperature as the linear growth rate was lowered, but the width of a microscopic fibril was not influenced by the pH of the medium, just as it was not influenced by the temperature.

The fibril just after production by *Acetobacter xylinum* (*A. xylinum*) seems to be in a homogeneous, amorphous state.[1,2] However, When the amorphous fibril is extruded from the cell, it becomes clearer that its cellulose chains are already arranged as sheets of monomolecular layers corresponding to the ($1\bar{1}0$) plane of Cellulose I.[3,4] In the amorphous fibril regarded as an assembly of the cellulose sheets, microscopic fibrils with almost the same width (about 40 Å) were always developed in the course of time.[5,6] It is interesting to study whether the width of a microscopic fibril is dependent on the culture conditions, that is, the crystallization conditions, or whether it is dependent on the fact that, when cellulose is extruded from the synthesizing sites in the envelope of a bacterial cell,as reported by Brown *et al.*[7] and Zaar,[8] the precursors of microscopic fibrils are already included in it.

In this paper the influence of the culture conditions, such as the incubation temperature and the pH of the medium, on the fibrillation of cellulose gels produced by *A. xylinum* was studied by means of electron microscopy.

Experimental

Culture of Cells and Preparation of the Samples for Electron Microscopy. The methods described previously[3] were employed.

Preparation of Cellulose-free Cell Suspension: An amount of 10 ml of an *A. xylinum*-preserved culture medium (IFO 13693) was added to 100 ml of an complex medium, and the mixture was incubated at 28 °C for 72 h. An amount of 10 ml of the liquid phase of the starter culture was added to 100 ml of the fresh complex medium, and the mixture was incubated at 28 °C for 48 h. The cells collected from the incubated medium according to the method of previous papers[1,3] were suspended in 60 ml of a buffer solution with a pH value of 6.8.

Samples for the Study of the Influence of the Temperature of Incubation: A 4-ml quantity of a 0.2 wt% glucose medium with 2 wt% sodium tungstophosphate (pH 6.8) was added to 36 ml of a cell suspension. A drop of the culture medium was immediately placed on a sheet mesh covered with a collodion membrane and incubated in a 100% RH atmosphere at a given temperature for a given time. After the fibrils thus produced had been allowed to settle on the sheet mesh by removing the medium, they were dried over P_2O_5 for more than 24 h at room temperature and then observed through an electron microscope.

Samples for the Study of the Influence of the pH of a Medium: After the cell suspension and the 0.2 wt% glucose medium with 2 wt% sodium tungstophosphate had been adjusted to a given pH with 1 M† HCl or NaOHaq respectively, a 4-ml quantity of the glucose medium was added to 36 ml of the cell suspension. A drop of the culture medium was placed on a sheet mesh and incubated in a 100% RH atmosphere at 28 °C for a given time. After this incubation, samples for electron microscopy were prepared as has been described above.

Measurement of the Linear Growth Rate of a Fibril. The linear growth rate of a fibril under a given pH was obtained from the relation between the time of incubation and the mean length of ten fibrils after glucose incubation. The linear growth rate was constant within the range of the measureable length of a fibril.

For electron microscopy, all the preparations were examined with a JEOL JEM-100U electron microscope operating at 80 kV.

Results and Discussion

Brown *et al.*[9] suggested that the rate of crystallization

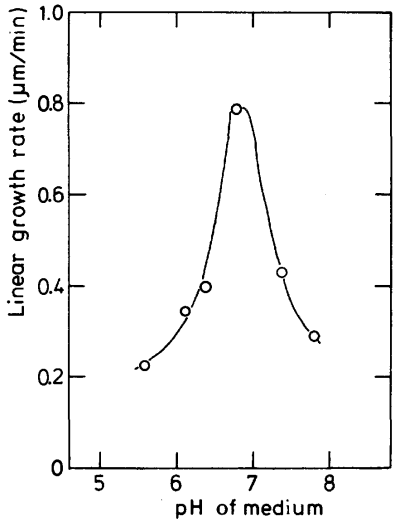

Fig. 1. Influence of the pH of medium on the linear growth rate of a fibril. The temperature of incubation; 15 °C.

† 1 M=1 mol dm^{-3}.

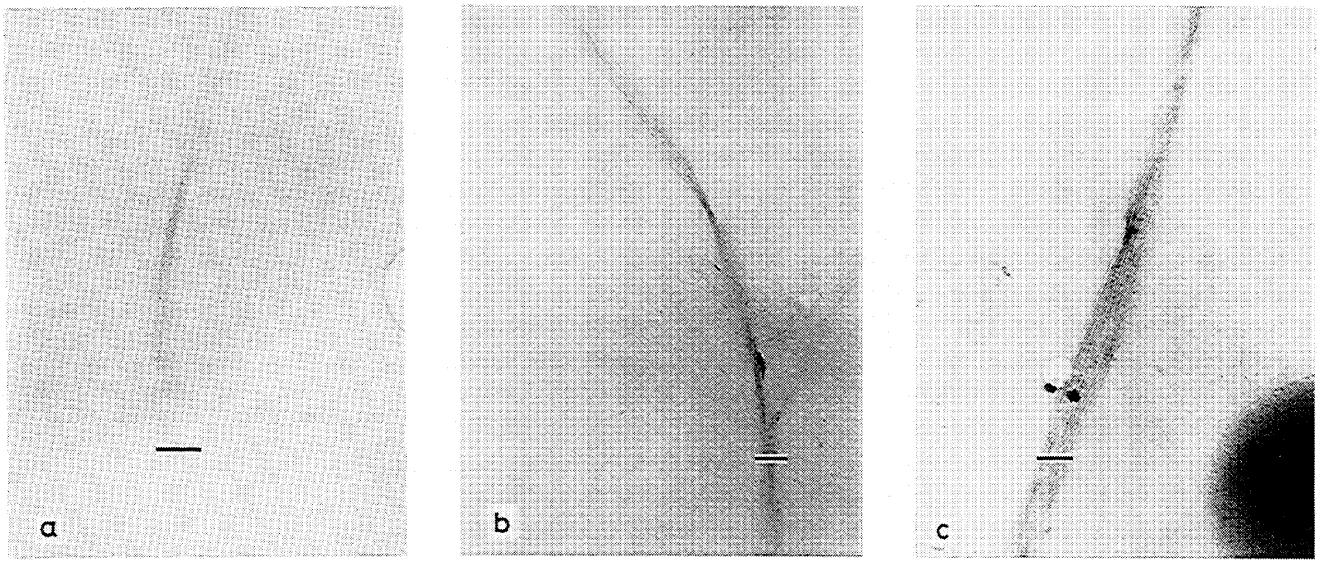

Fig. 2. Electron micrographs of the fibrils from the 5 °C incubation (pH 6.8) for a given time. Time of incubation; a: 3 h, b: 6 h, c: 12 h. Scale bar=0.1 μm

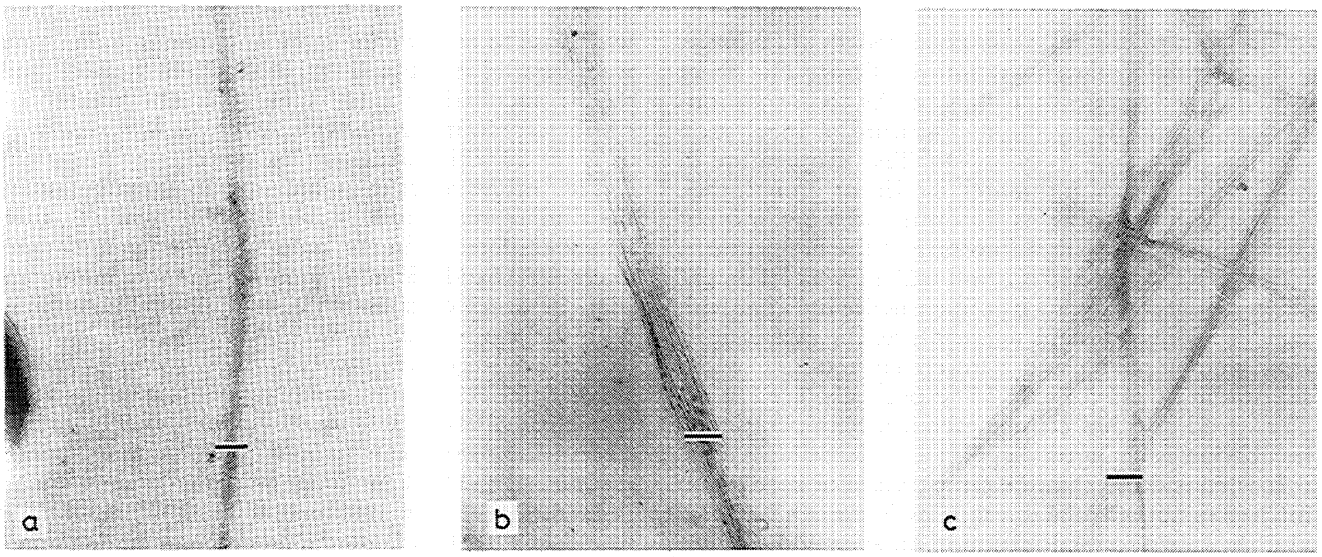

Fig. 3. Electron micrographs of the fibrils from the 10 °C incubation (pH 6.8) for a given time. Time of incubation; a: 3 h, b and c: 6 h. Scale bar=0.1 μm

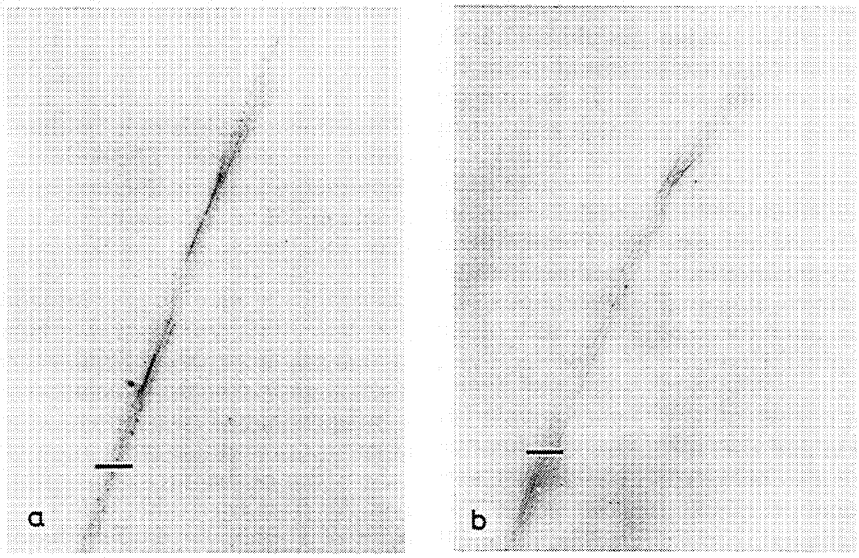

Fig. 4. Electron micrographs of the fibrils from the incubated medium of pH 5.5 at 28 °C for a given time. Time of incubation; a: 1 h, b: 3 h. Scale bar= 0.1 μm

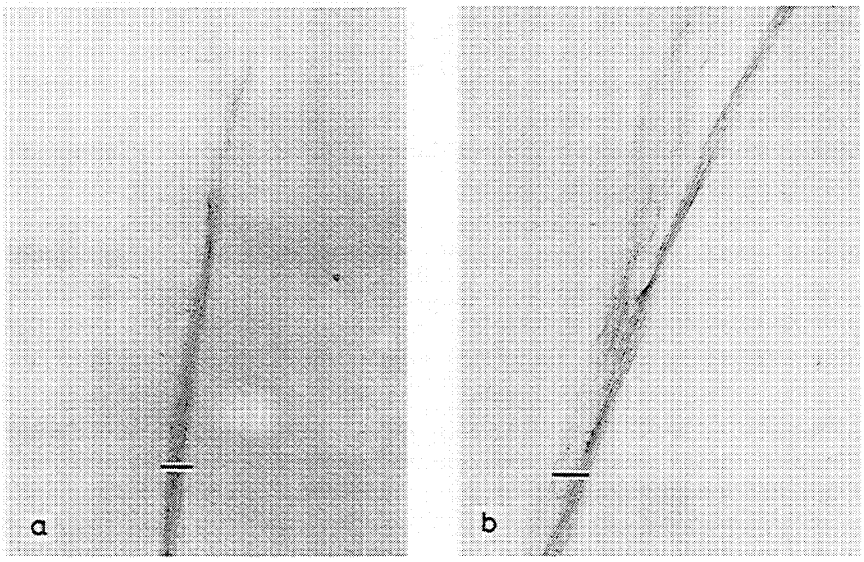

Fig. 5. Electron micrographs of the fibrils from the incubated medium of pH 7.7 at 28°C for a given time. Time of incubation; a: 1 h, b: 3 h. Scale bar= 0.1 μm

of the amorphous cellulose produced by *A. xylinum* influences the linear growth rate of a fibril. The linear growth rate is basically influenced by the conditions of culture, mostly by the temperature of incubation and the pH of the medium.[3,6] The temperature of incubation greatly influences the linear growth rate. The growth rate is at its maximum (2.6 μm/min) at 28°C and lowers with a lowering of the temperature: 1.3 at 20°C, 0.39 at 10°C, and 0.27 at 5°C. The pH of the medium also much influences the linear growth rate. Under a constant temperature, the rate is at its maximum at pH 6.8 and is lowered to about 1/4 of the maximum at pH 5.5 and 7.7 respectively (see Fig. 1). This trend does not change even if the temperature of incubation is changed.

It is considered that the temperature of incubation influences not only the linear growth rate of a fibril but also the rate of crystallization of an amorphous fibril. The fibril made by the incubation under the most suitable culture conditions (28°C, pH 6.8) maintained an amorphous state for about 30 min after production. The uneven staining behavior of the fibrils could be observed about 1 h later, striations were found to run parallel to the long axis of the fibril about 3 h later, and microscopic fibrils were developed about 5 h after.[6] The microscopic fibril was already in a crystalline state.[10] The resistance to alkali of a fibril with uneven staining behavior showed Cellulose I crystalline.[10]

The fibrils made by incubation at 5°C could be stained homogeneously with sodium tungstophosphate over a long period (Fig. 2a). An uneven staining behavior of the fibril was found only after the 6-h incubation (Fig. 2b), and the microscopic fibrils were found in the fibril from the 12-h incubation (Fig. 2c). It became clear that the linear growth rate of a fibril became lower under the 5°C incubation and that the fibrillation of an amorphous cellulose also occurred more slowly than under the 28°C incubation.

Although the linear growth rate of a fibril is close to that of the 5°C incubation under the 10°C incubation, the rate of the fibrillation of an amorphous cellulose was close to that of the 28°C incubation. Striations were parallel to the long axis of a fibril in the fibril from the 3-h incubation at 10°C (Fig. 3a). The microscopic fibrils were found in the fibril from the 6-h incubation as is the 28°C incubation (Fig. 3b, c).

The influence of the temperature of incubation on the fibrillation is remarkable at 5°C. However, there was no difference in the influence at temperatures between 10°C and 28°C. Moreover, it is very interesting that the width of a microscopic fibril does not change with the temperature of incubation.

The linear growth rate could be lowered by changing the pH of the medium from pH 6.8, however, the rate of fibrillation was increased accordingly. In the case of the medium with a pH of 5.5, striations were distinctly found in the fibril from the 1-h incubation (Fig. 4a), and the microscopic fibrils were already found in the fibril from the 3-h incubation (Fig. 4b).

In the case of pH 7.7, the linear growth rate is near to that in the case of pH 5.5. Striations were also clearly found in the fibril from the 1-h incubated medium with a pH of 7.7 (Fig. 5a). The microscopic fibrils were found in the fibril from the 3-h incubation (Fig. 5b).

It became clear that the fibrillation became faster with a lowering of the linear growth rate by changing the pH at a constant temperature. The width of a microscopic fibril, however, was not influenced by the pH as it was in the case of the temperature.

The temperature of incubation and the pH of the medium influence the rate of fibrillation of an amorphous cellulose fibril, but they do not influence the width of a microscopic fibril developed in it later. These facts suggest that an amorphous fibril, when extruded from the cell, consists of the precursors of microscopic fibrils independent of each other. If an amorphous fibril after production is a mere assembly of cellulose sheets, the width of the microscopic fibril thus developed may differ from each other. However, the fact that the width of a microscopic fibril hardly changes suggests that the precursors of microscopic fibrils have structures which are able to join with each

other at its surface, but which can not gather to form a crystalline. The structure of the precursor of a microscopic fibril must be hereafter examined in more detail.

The relation between the crystallization of an amorphous fibril and its linear growth rate suggested by Brown *et al.*[9] could not found in this study. This problem must, therefore, be also studied hereafter in more detail.

References

1) A. Kai, J. Kogusuri, and Y. Kobayashi, *Nippon Kagaku Kaishi*, **1982**, 148.
2) C. H. Haigler, R. M. Brown, and M. Benziman, *Science*, **210**, 903 (1980).
3) A. Kai, *Bull. Chem. Soc. Jpn.*, **57**, 836 (1984).
4) A. Kai, *Makromol. Chem. Rapid Commun.*, **5**, 307 (1984).
5) A. Kai, J. Kogusuri, and Y. Kobayashi, *Nippon Kagaku Kaishi*, **1982**, 536.
6) A. Kai, J. Kogusuri, and Y. Kobayashi, *Nippon Kagaku Kaishi*, **1982**, 1934.
7) R. M. Brown, J. H. Willison, and C. L. Richardson, *Proc. Natl. Acad. Sci. USA*, **73**, 4565 (1976).
8) K. Zaar, *Cytobiologie*, **16**, 1 (1977).
9) M. Benziman, C. H. Haigler, R. M. Brown, A. R. White, and K. L. Copper, *Proc. Natl. Acad. Sci. USA*, **77**, 6678 (1980).
10) A. Kai and T. Koseki, *Bull. Chem. Soc. Jpn.*, **57**, 1437 (1984).

Cadmium(II)-, Magnesium(II)-, and Zinc(II)-bearing Ferrites Formed from γ-FeOOH at Various Reaction pH's

Kazuo Ito,*,† Yutaka Tamaura, and Takashi Katsura
Department of Chemistry, Tokyo Institute of Technology Ookayama, Meguro-ku, Tokyo 152
(Received November 21, 1983)

The reaction of γ-FeOOH with the metal (Cd(II), Mg(II), or Zn(II)) and Fe(II) ions in solution gave the metal ion-bearing ferrites without oxidation. The ferrites obtained were the stoichiometric Mg(II)- and Zn(II)-bearing ferrites [$Mg_{0.27}Fe_{2.73}O_{4.00}$ (pH 10.6), $Zn_{0.38}Fe_{2.61}O_{4.00}$ (pH 10.5)] at pH 7.5—11.4, and the nonstoichiometric Cd(II)-bearing ferrites [$Cd_{0.19}Fe_{2.68}O_{4.00}$ (pH 10.2)] at pH 7.5—10.5 (25 °C). The Cd(II)- and Mg(II)-ion content in the ferrites increases with an increase in the reaction pH, but the Zn(II)-ion content is almost constant at pH 7.5—10.5. This pH dependence of the metal-ion content in the ferrites agrees with that of the fractional adsorption of these metals on γ-FeOOH. This suggests that only the adsorbed metal ions are incorporated into the ferrites. The pH dependence of these metal-ion contents in the air-oxidation reaction is also similar to that in the transformation reaction from γ-FeOOH. This transformation reaction seems to be one process in the air-oxidation reaction.

The formation of metal ion-bearing ferrites in solution by the air-oxidation of a $Fe(OH)_2$ suspension in the presence of other metal ions at temperatures above 60 °C has previously been studied.[1-11] The reaction pH affects the amount of metal ions incorporated into the ferrites.[5-7] Recently, we found that γ-FeOOH is transformed to Fe_3O_4 in the presence of the Fe(II) ion.[12,13] This transformation reaction is triggered by the adsorption of the Fe(II) ion on γ-FeOOH.[13] In the presence of Fe(II) and Zn(II) ions, γ-FeOOH is transformed to Zn(II)-bearing ferrites.[14] We proposed that the Zn(II) ions were adsorbed on γ-FeOOH and subsequently incorporated to form the Zn(II)-bearing ferrites.[14,15] It seems likely that any ferrite would be formed from γ-FeOOH in the presence of Fe(II) and other metal ions. In the present experiment, we have investigated the formation of Cd(II)-, Mg(II)-, and Zn(II)-bearing ferrites from γ-FeOOH at various reaction pH's; we will also discuss briefly the pH effect of the metal-ion contents in the ferrites, in relation to the adsorption of the metals on γ-FeOOH.

Experimental

Chemicals. All the chemicals used in the present work were of an analytical grade, and the chemical solutions were prepared by the use of distilled water. The NaOH solution was prepared by the use of distilled water through which nitrogen gas had been passed to remove any dissolved oxygen. The γ-FeOOH was prepared according to a method described previously.[13]

Apparatus. The reaction vessel which had been used in a previous paper was adopted.[1]

Procedure. After adding a M(II) (M=Cd, Mg, or Zn)-ion solution (0.02 dm^3, 0.27 mol/dm^3, pH 3.0) to the γ-FeOOH suspension (0.75 dm^3, pH 4.0), nitrogen gas was passed through for 2 h to remove any dissolved oxygen and carbon dioxide. $FeCl_2$ solution (0.02 dm^3, 0.54 mol/dm^3. pH 3.0) was then added to the suspension, and the pH was raised to the desired value. When the pH became the desired value (7.5—11.4), the reaction was initiated and the reaction pH became lower. The reaction pH was kept constant by adding an alkaline solution. During the reaction, nitrogen gas was passed through the suspension to prevent any oxidation reaction. After the reaction has continued for 60 h (25 °C), the reaction suspension was centrifuged at 4000 rpm under a nitrogen atmosphere. The precipitate was then washed with an acetate buffer solution (pH 4.1, 0.05 mol/dm^3) to isolate the products by dissolving the unreacted Fe(II) and M(II) ions. The precipitate was washed further with distilled water and then with acetone to remove the water as completely as possible. The washing water and acetone had been deaerated by passing nitrogen gas through to prevent oxidation. Finally, the precipitate was dried under a nitrogen atmosphere (room temperature). The products thus obtained were examined by means of X-ray diffractometry, IR spectroscopy, and Mössbauer spectroscopy.

Metal-ion Adsorption on γ-FeOOH. Into a 1.0-dm^3 polyethylene beaker, 0.8 dm^3 of a γ-FeOOH suspension containing the M(II) ion (iron of γ-FeOOH: 10 mmol, M(II)-ion concentration: 5×10^{-5} mol/dm^3, NaCl concentration: 6×10^{-5} mol/dm^3) was transferred. The suspension temperature was maintained at 25±0.2 °C, and nitrogen gas was passed through the suspension to remove the carbon dioxide and to stir the suspension. When the suspension pH became constant after adding an alkaline solution, 0.01 dm^3 of the suspension was taken out by means of a syringe and immediately filtered using a Millipore filter (pore size; 220 nm). The M(II)-ion concentration in the filtrate was measured by means of an atomic-absorption method (Varian Techtron, AA 875 type).

Chemical Analysis. The Fe(II) and Fe_{total} concentrations were determined by the 2,2'-bipyridyl method.[16] When the Fe_{total} was determined, the Fe(III) ion was reduced to the Fe(II) ion with hydroxylamine.

Results and Discussion

X-Ray Diffraction Patterns, IR and Mössbauer Spectra, Chemical Compositions and Lattice Constants. In the present study, the mole ratio among the Fe(II) ion, the M(II) ion (M=Cd, Mg, or Zn), and γ-FeOOH (as Fe) in the initial suspension was fixed at 1:2:2. This reaction was initiated by adding the Fe(II) ion. However, the reaction rate was extremely slow at pH values below 7, and no reaction at all occurred at pH values below 6.5. Therefore, in the present paper, no data will be given for pH values below 6. As has been reported previously,[13] the Fe(II) ion is adsorbed on γ-FeOOH at pH values above around 6.8, and the γ-FeOOH is transformed to Fe_3O_4 by the adsorption of the Fe(II) ion on γ-FeOOH. These results suggest that

†Present address: Toshiba Corporation, R & D Center, 1 Komukai, Saiwai-ku, Kawasaki 210

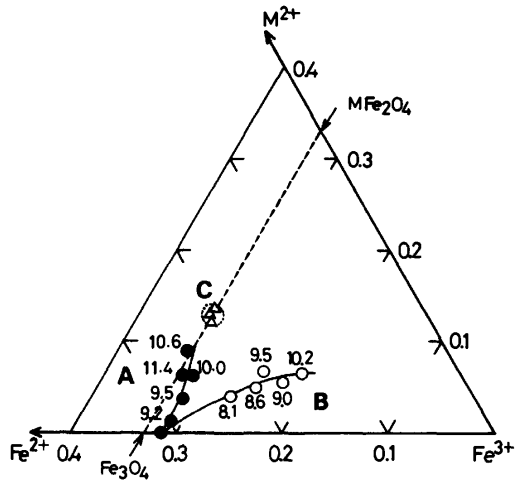

Fig. 1. Ternary diagram showing the chemical compositions of Mg(II)-bearing ferrites(A), Cd(II)-bearing ferrites(B), and Zn(II)-bearing ferrites(C). The values given at the points indicate the reaction pH. M^{2+} means the metal ions of Mg(II), Cd(II), or Zn(II).

the reaction in the present work also proseeds by means of the adsorption of the Fe(II) ion on γ-FeOOH. In the X-ray diffraction patterns of the products, only the peaks of the spinel-type compound appeared. In the IR spectra, no bands of γ-FeOOH or other iron (III) oxides were observed, but bands of ferrites were observed. These results indicate that the γ-FeOOH was completely transformed to ferrites. All the lines of the Mössbauer spectra were assigned to ferrites, as will be described below.

Figure 1 shows the chemical compositions of the ferrites formed at various reaction pH's. The values given at the points for Curves A and B are the reaction pH values. The small region denoted by C represents the chemical compositions of the Zn(II)-bearing ferrites. The Zn(II) ion contents in the ferrites remain nearly constant at various reaction pH values, and their compositions are included in the small region. The straight line (broken line) connecting Fe_3O_4 and MFe_2O_4 corresponds to the stoichiometric chemical compositions of M(II)-bearing ferrites ($M_{1-x}Fe_{2+x}O_4$). As can be seen from Fig. 1, the chemical compositions of the Zn(II)- and Mg(II)-bearing ferrites (A and C) are nearly stoichiometric, but those of the Cd(II)-bearing ferrites (B) deviate fairly much from stoichiometry [$Cd_{0.19}Fe_{2.68}O_{4.00}$ (pH 10.2)]. The deviation increases with an increase in the Cd(II)-ion content in the ferrite. This suggests that vacant sites of the Cd(II)-bearing ferrites increase with an increase in the Cd(II) content in the ferrites. The nonstoichiometric Cd(II)-bearing ferrites were also formed in the air-oxidation reaction,[6] so the Cd(II)-bearing ferrites seem to be oxidized easily. These may cause the nonstoichiometry of the Cd(II)-bearing ferrites. The relationship between the M(II)-ion content in the ferrites and the reaction pH will be described later.

Figure 2 gives the room-temperature Mössbauer spectra of the M(II)-bearing ferrites with the highest M(II)-ion content. Spectrum a corresponds to the Fe_3O_4 formed from γ-FeOOH. The spectra of the Fe_3O_4 and

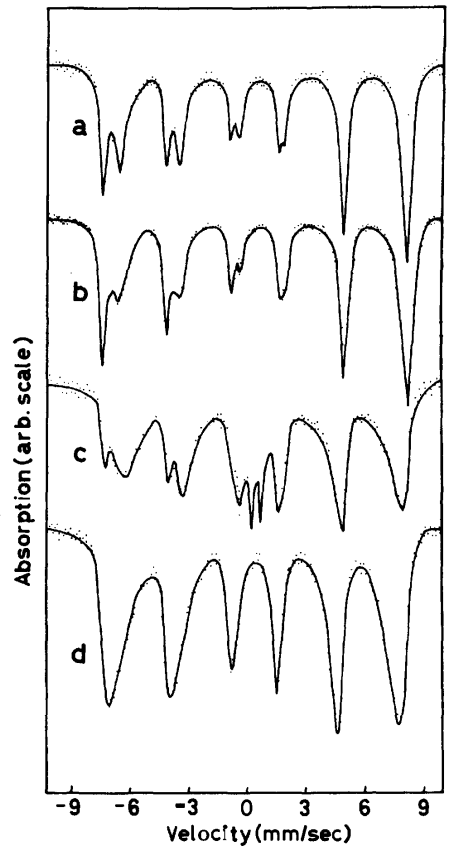

Fig. 2. Room temperature Mössbauer spectra of magnetite formed from γ-FeOOH(a), Mg(II)-bearing ferrite (b), Zn(II)-bearing ferrite (c), and Cd(II)-bearing ferrite (d). The chemical compositions of the ferrites are $Fe_{2.93}O_{4.00}$ (a), $Mg_{0.27}Fe_{2.73}O_{4.00}$ (b), $Zn_{0.38}Fe_{2.61}O_{4.00}$ (c), and $Cd_{0.19}Fe_{2.68}O_{4.00}$ (d) respectively.

the Mg(II)-bearing ferrites show two distinct hyperfine patterns; one is due to the tetrahedral Fe(III) ions (A site), and the other, to the octahedral Fe(III) and Fe(II) ions (B site). The line intensities at the B site for the Mg(II)-bearing ferrites are lower than those for the Fe_3O_4. This indicates that the Mg(II) ion is incorporated into the B site of the ferrites. The spectrum of the Zn(II)-bearing ferrite (Spectrum c) shows two broadened Zeeman patterns and a quadrupole doublet. Dobson *et al.*[17] reported that the Zn(II)-bearing ferrite ($Zn_{0.6}Fe_{2.4}O_{4.0}$) formed by a solid-state reaction had a similar pattern in its spectrum. The Zn(II)-bearing ferrites from γ-FeOOH seem to have the same ionic distribution as those produced by the soild-state reaction. The spectra of the Cd(II)-bearing ferrites (Spectrum d) show six broadened absorption lines. This broadening may come from the nonstoichiometry and/or the Cd(II)-ion incorporation into the spinel structure.

The lattice constant of the Zn(II)-bearing ferrite with the highest Zn(II) content in Fig. 1 ($Zn_{0.38}Fe_{2.61}O_{4.00}$) was 0.8416 nm. This higher value of the lattice constant than that of Fe_3O_4 (0.8397 nm)[18] confirms the incorporation of the Zn(II) ion into the lattice point by replacing the Fe(II) ion in Fe_3O_4 with the Zn(II) ion. The lattice constant of the Mg(II)-bearing ferrite with the highest Mg(II)-ion content in Fig. 1 ($Mg_{0.27}Fe_{2.73}O_{4.00}$)

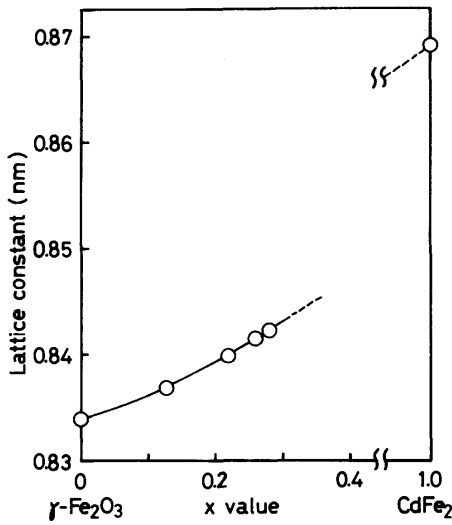

Fig. 3. The relationship between the lattice constants and the x values of the completely oxidized Cd(II)-bearing ferrites. The x values represent the mole ratio of $CdFe_2O_4$ to ($CdFe_2O_4$+γ-Fe_2O_3).

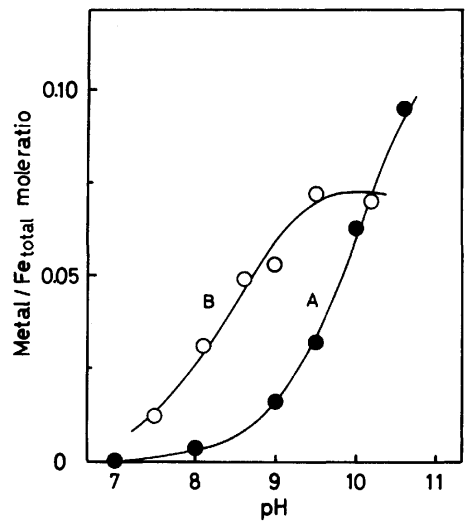

Fig. 4. pH dependence on the metal ion contents incorporated into Mg(II)-bearing ferrites (A) and Cd(II)-bearing ferrites (B).

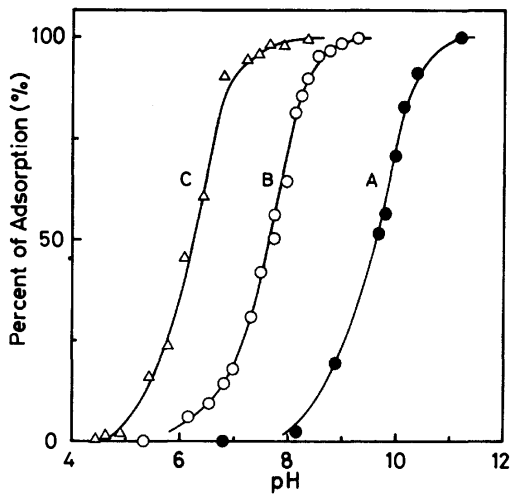

Fig. 5. Fractional adsorption of Mg(II) (A), Cd(II) (B), and Zn(II) (C) on γ-FeOOH as a function of pH.

was 0.8388 nm, slightly lower than that of Fe_3O_4. The lattice constant of $MgFe_2O_4$ (0.8387 nm)[19] is near to that of Fe_3O_4; therefore, the lattice constant probably is not so greatly changed by replacing the Fe(II) ion in Fe_3O_4 with the Mg(II) ion. The Cd(II)-bearing ferrites were nonstoichiometric; they formed a solid solution among Fe_3O_4, γ-Fe_2O_3, and $CdFe_2O_4$, so the lattice constant is determined by means of these three components. To simplify the analysis of the lattice constants, the component number of the nonstoichiometric Cd(II)-bearing ferrites in Fig. 1 was reduced to two (a solid solution between γ-Fe_2O_3 and $CdFe_2O_4$) by oxidizing the ferrites. The Cd(II)-bearing ferrites are readily oxidized at 150 °C for 2 d, since their particle size is small (100—200 nm). Figure 3 shows the relationship between the lattice constant and the mole fraction x of the $CdFe_2O_4$ component in the solid solution between γ-Fe_2O_4 and $CdFe_2O_4$. The lattice constant of γ-Fe_2O_3 and $CdFe_2O_4$ were determined by Schrader and Büttner[20] and by Roberts and Merwin[21] respectively. The lattice constants of the oxidized Cd(II)-bearing ferrites fall between those of γ-Fe_2O_3 and $CdFe_2O_4$. This confirms the incorporation of the Cd(II) ion into the lattice structure of the ferrites.

pH Effect of M(II)-ion Contents in Ferrites. Figure 4 shows the relationship between the Mg(II) and Cd(II) ion contents in the ferrites, and the reaction pH. As may be seen in Fig. 4, the Mg(II) (Curve A)- and Cd(II) (Curve B)-ion contents increase with an increase in the reaction pH. The Zn(II)-ion content remained almost constant, as has been mentioned above. Next, we compared this result (Fig. 4) with the adsorption of M(II) on γ-FeOOH at various pHs. Figure 5 shows the relationship between the fractional adsorption of M(II) and the solution pH. Curves A, B, and C are fractional adsorptions of Mg(II), Cd(II), and Zn(II) respectively. All of them increase from near nil to near 100% with an increase in the pH. The pH regions of the pH-adsorption edges (the sharp rise of the curves) for Zn(II), Cd(II), and Mg(II) increase in this order. Over the pH values from pH 7 to 11, where the ferrites are formed from γ-FeOOH, this adsorption behavior is quite similar to the incorporation profiles against the pH. The pH regions of the pH-adsorption edges fit those of the pH-incorporation edges for the Cd(II) and Mg(II) ions (Fig. 4). Measures, the adsorbed amount and the incorporated amount of Zn(II) both remain constant in this pH region. This strongly suggests that the metals are adsorbed on γ-FeOOH, and then subsequently incorporated to form the metal ion-bearing ferrites. The air oxidation of an $Fe(OH)_2$ suspension containing metal ions brings about the formation of the metal ion-bearing ferrites.[1-11] In previous reports,[12-15] we have suggested that the air-oxidation reaction involves a process in which the γ-FeOOH-layer is formed on the Fe_3O_4 by the oxidation of the adsorbed Fe(II) ion. The Fe_3O_4 particles will grow by the repetition of these processes during the air oxidation. When the other metal ion is present in the reaction suspension, the metal ion will be adsorbed along with the Fe(II) ion on the γ-FeOOH-layer, and the γ-FeOOH will be transformed into the metal

ion-bearing ferrites on the surface. For Cd(II), Mg(II), and Zn(II) ions, the pH dependence of their contents, as incorporated into the ferrites in the air-oxidation reaction[5-7], is very similar to the results in the present study (Fig. 4 and 5). These results suggest the validity of the above discussion.

References

1) T. Katsura, Y. Tamaura, and G. S. Chyo, *Bull. Chem. Soc. Jpn.*, **52**, 96 (1979).
2) Y. Tamaura and T. Katsura, *J. Chem. Soc., Dalton*, **1980**, 825.
3) Y. Tamaura, S. Mechaimonchit, and T. Katsura, *J. Inorg. Nucl. Chem.*, **43**, 671 (1981).
4) Y. Tamaura, U. Rasyid, and T. Katsura, *J. Chem. Soc., Dalton*, **1980**, 2125.
5) K. Kaneko and T. Katsura, *Bull. Chem. Soc. Jpn.*, **52**, 747 (1979).
6) K. Kaneko, T. Takei, Y. Tamaura, T. Kanzaki, and T. Katsura, *Bull. Chem. Soc. Jpn.*, **52**, 1080 (1979).
7) T. Kanzaki, J. Nakajima, Y. Tamaura, and T. Katsura, *Bull. Chem. Soc. Jpn.*, **54**, 135 (1981).
8) K. Ito, T. Kanzaki, Y. Tamaura, and T. Katsura, *J. Chem. Soc., Dalton*, **1981**, 2217.
9) T. Kanzaki, H. Furukawa, and T. Katsura, *J. Chem. Soc., Dalton*, **1983**, 1197.
10) Y. Tamaura, T. Kanzaki, and T. Katsura, Proc. Third Int. Conf. on Ferrites, Kyoto (1980), p. 15.
11) M. Kiyama, *Bull. Chem. Soc. Jpn.*, **51**, 134 (1978).
12) Y. Tamaura, P. V. Buduan, and T. Katsura, *J. Chem. Soc., Dalton*, **1981**, 1807.
13) Y. Tamaura, K. Ito, and T. Katsura, *J. Chem. Soc., Dalton*, **1983**, 189.
14) K. Ito, Y. Tamaura, and T. Katsura, *J. Chem. Soc., Dalton*, **1983**, 987.
15) Y. Tamaura, Y. Kobori, and T. Katsura, *Nippon Kagaku Kaishi*, **1983**, 1433.
16) I. Iwasaki, T. Katsura, T. Ozawa, M. Mashima, H. Haramura, and B. Iwasaki, *Bull. Volc. Soc. Jpn., Ser. II*, **5**, 75 (1960).
17) D. C. Dobson, J. W. Linnett, and M. M. Rahman, *J. Phys. Chem. Solids*, **31**, 2727 (1970).
18) X-ray Data Card, 19-629, Powder Diffraction File, Joint Committee on Powder Diffraction Standards (JCPDS).
19) P. P. Kirichok, L. G. Kustovskii, G. S. Podvalnykh, M. A. Shamanov, and V. P. Bibik, *Bull. Acad. Sci. USSR, Phys. Ser.*, **38**, 618 (1974).
20) R. Schrader and G. Büttner, *Z. Anorg. Allg. Chem.*, **320**, 205 (1963).
21) H. S. Roberts and H. E. Merwin, *Am. J. Sci.*, **21** 145 (1931).

Nitrogen-14 Magnetic Resonance Studies of the Exchange of Solvent Pyridine on Bis(β-diketonato)bis(pyridine)nickel(II) and -cobalt(II) Complexes

Seiko Ito[††] and Yoshiko Yano*,[†]

Institute of Chemistry, The University of Tsukuba, Sakuramura, Ibaraki 305

[†]*Laboratory of Chemistry, Wayo Women's University, Kohnodai Ichikawa, Chiba 272*

(Received December 26, 1983)

The analysis of linewidth and shift data of the nitrogen-14 magnetic resonance gave the following activation parameters for the exchange reaction of pyridine (py) on $CoA_2(py)_2$ (A=acac, tfa, and tta) and $Ni(acac)_2(py)_2$ with a pyridine molecule as bulk solvent: $\Delta H^{\neq}$=41.4, 51.1, 48.3, and 47.2 kJ mol^{-1}, $\Delta S^{\neq}$=18, 17, 3, and 10 JK^{-1} mol^{-1}, and k_1(298K)=2.9×10^6, 5.3×10^4, 2.9×10^4, and 1.3×10^5 s^{-1}. Here acac=acetylacetonate, tfa=trifluoroacetylacetonate and tta=thenoyltrifluoroacetonate. The electron-withdrawing power of substituent groups on the β-diketonate rings was correlated with more favorable activation of the exchange, that is, the stronger electron withdrawal causes less dissociative activation. This explains qualitatively even the negative $\Delta S^{\neq}$ values observed for similar pyridine exchange in the cases of $Co(hfa)_2(py)_2$ (hfa=hexafluoroacetylacetonate) and $Ni(tta)_2(py)_2$.

Exchange reactions of a coordinated solvent molecule (S) on bis(β-diketonato) complexes of Ni^{II} and Co^{II}(M), represented by Eq. 1, have been kinetically studied by several authors[1-7] using NMR techniques.

$$MA_2S_2 + S^* \longrightarrow MA_2SS^* + S. \quad (1)$$

In most of the cases, the exchange rates were discussed in terms of the nature of β-diketone rings; that is, electron-withdrawing substituents on the rings were shown to be a major factor retarding the exchange and the trend was described quantitatively by the Hammet equation. On the other hand, only a few attempts have been made[4-7] to clarify the reaction mechanism, mainly because observed activation parameters contained rather large uncertainties. The FT-NMR systems enables us to reduce the uncertainties originated from previous instrumental problems and ^{14}N NMR is more favorable; its advantage has already been pointed out.[8] In the present work, we first focus our attention on a series of bis(β-diketonato)cobalt(II) complexes in pyridine solvent, since ^{14}N NMR studies of an analogous series of Ni^{II} were already reported by Lincoln *et al.* using CW wideline spectrometer.[6] Nickel(II) complexes with acac and tta are also examined; the former is considered as a standard complex for comparison to other works. The tta complexes of both Co^{II} and Ni^{II} appear in similar solvent exchange studies.

Experimental

Materials. Anhydrous $M(acac)_2$ and $M(tta)_2$ were prepared by the method of Cotton *et al.*[9] or by a slightly modified version of it. $Co(tfa)_2(py)_2$ and $Co(hfa)_2(py)_2$ were obtained by repeated recrystalization of the corresponding diaqua complexes from pyridine solution. The values of chemical analysis of all products were in good agreement with the theoretical values. Pyridine used as a solvent was dried over pottasium hydroxide for several days and then doubly distilled in the presence of a small amount of suspended barium oxide. Deuterated pyridine was obtained in ampules from CEA France and an ampule was freshly opened just before each use,without any purification.

Solutions for NMR experiments were prepared under a nitrogen atmosphere by dissolution of complexes into pyridine which contained 13 v.% of pyridine-d_5. The concentration range of the paramagnetic ions was 0.01—0.15 mol dm^{-3}; this was quantitatively determined by EDTA titration. The water content of the solutions was found by the GC method[10] to be less than 2ppm, which means the content was negligible.

The electronic absorption spectra of the solution were recorded and the molecular weight measurements were carried out for the preliminary characterization of the solvated complexes in pyridine: a JASCO UVDEC-1 spectrometer and a Corona-117 apparatus for vapor pressure depression method were used.

NMR Measurements. A JEOL FX-90Q FT-NMR spectrometer operated at 6.42 MHz for ^{14}N was used in the ^{2}H lock mode. Typically,the free induction decay(FID) spectrum was accumulated over 1000 to 4000 pulses of 20 μs with a spectral width of 6 kHz. Since a WIND function was applied, linewidths of plotted spectra were necessarily corrected with subtraction by the corresponding broadening factors in Hz. The temperatures(−18—113 °C) were measured by using a copper-constantan thermocouple in a 10φ o.d. NMR tube with silicone oil before and after pulsing; while accumulation was being performed, temperature drift was monitored by a thermocouple installed inside JEOL temperature control unit; correspondence between temperature readings from two thermocouples had been investigated before accumulation. The accumulated FID's were used for data analysis only when the temperature deviation during the accumulations had been less than ±0.3 °C.

Results

Relaxation Data. The ^{14}N transverse relaxation time due to the interaction between pyridine solvent and a paramagnetic β-diketonato complex (T_{2p}) is defined as Eq. 2:

$$T_{2p} = (1/T_2 - 1/T_{2A})^{-1} P_m (1-P_m)^{-1}. \quad (2)$$

Here T_2 is the observed relaxation time of paramagnetic solution and T_{2A} is that of the pure solvent, both derived from the observed half-height widths in Hz, $W(=\pi^{-1}T_2^{-1})$ and $W_A(=\pi^{-1}T_{2A}^{-1})$. P_m is the mole fraction of the solvent in the first coordination sphere, assuming an additional coordination number of 2. The values of it were small enough in the present work to treat $(1-P_m)$ in Eq. 2 as 1. According to Swift and Connick,[11] T_{2p} can be represented in a reduced form as follows:

$$T_{2p}^{-1} = [\tau_m + \{\tau_m(\Delta\omega_m)^2\}^{-1}]^{-1} + (T_2^*)^{-1}. \quad (3)$$

[††]Present address: Seiko Nomura, Utsunomiya Kaisei Joshigakuin High-school, Utsunomiya, Tochigi 321-32

Here τ_m is the mean lifetime of coordinated pyridine and $\Delta\omega_m$ is the chemical shift in radian/s of ^{14}N of complexed solvent relative to free solvent.

$$\tau_m = h(k_B T)^{-1} \exp\{\Delta H^{\neq}(RT)^{-1} - \Delta S^{\neq} R^{-1}\} \quad (4)$$

$$\Delta\omega_m = (2\pi)^2 (A/h)\omega\mu_{eff}\mu_B\{S(S+1)\}^{1/2} T^{-1}(3k_B\gamma_N). \quad (5)$$

Here A/h is the scalar coupling constant, μ_{eff} the effective magnetic moment (3.13 and 4.82 BM for Ni and Co complexes), S the net electron spin of the paramagnetic ions, ω the radio frequency(Hz) of operation, k_B the Boltzman constant and γ_N the gyromagnetic ratio of ^{14}N; other symbols have their usual meanings. The first term of Eq. 3 is a reduced form of the full equation of Swift and Connick assuming that $\Delta\omega_m^2 \gg T_{2m}^{-2}$, τ_m^{-2}, in the relatively lower temperature range and that $\tau_m^{-2} \gg \Delta\omega_m^2 \gg (T_{2m}\tau_m)^{-1}$, in the higher temperature range, where T_{2m} is the relaxation time of ^{14}N in pyridine coordinated to M in the absence of chemical exchange. The former condition was experimentally confirmed by the constant chemical shift of the bulk pyridine peak. The latter was not sure since the pyridine peak was not recognized while coordinated to the paramagnetic ion, even at the lowest temperature, because of the small P_m and the broadening of the line. It seemed reasonable, however, that T_{2m} in pyridine case could be replaced by that in acetonitrile, which had been already found to meet the latter condition.[8] The T_2^* term of Eq. 3 is the additional contribution from the outer coordination sphere or the fast exchange region.

The circles in Figs. 1 to 6 are the observed T_{2p}'s and they are shown along with full lines of the computed best fits. The full lines in Figs. 2 and 3 were obtained by use of the SALS (Statistical Analysis with Least-Squares Fittings)[17] program applied to Eq. 3 in which $\Delta H^{\neq}$, $\Delta S^{\neq}$, and A/h were treated as parameters and the T_2^* term was ignored. In Figs. 1 and 5, SALS computation was first performed about the temperature range in which the T_2^* was negligible. The term was treated as an additional parameter which caused the deviation of the observed points; it affected the first term in brackets at the lowest temperature and/or $\tau_m(\Delta\omega_m)^2$ in the highest temperature range. In Figs. 4 and 6, only the τ_m term in brackets of Eq. 3 was used for the computation. The activation parameters and the A/h values obtained

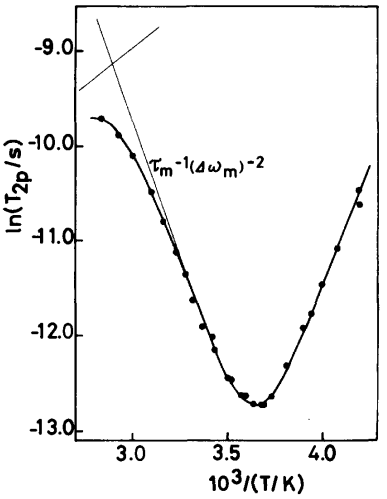

Fig. 1. Temperature dependence of the reduced ^{14}N NMR linewidth(T_{2p}) for the bulk-solvent pyridine resonance in the $Co(acac)_4(py)_2$ system.

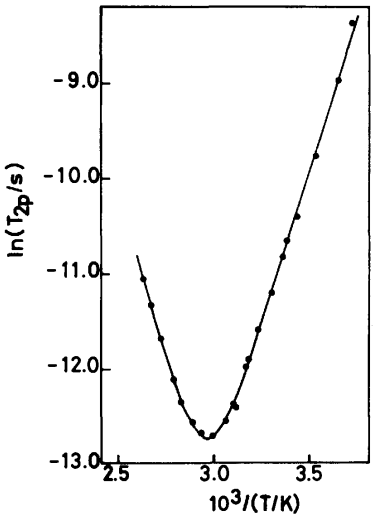

Fig. 2. Temperature dependence of T_{2p} in the $Co(tfa)_2(py)_2$ system.

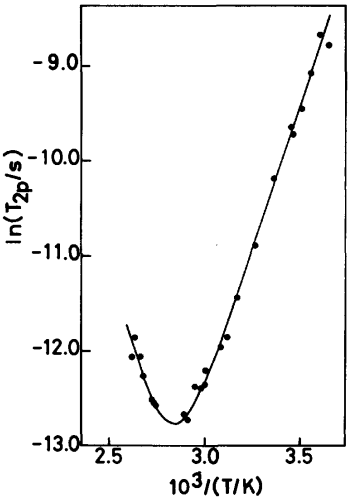

Fig. 3. Temperature dependence of T_{2p} in the $Co(tta)_2(py)_2$ system.

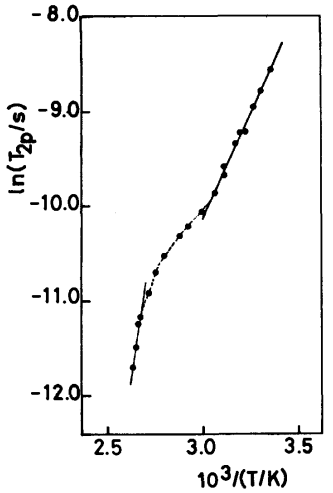

Fig. 4. Temperature dependence of T_{2p} in the $Co(hfa)_2(py)_2$ system.

from the computation are summarized in Table 1.

Shift Data. The chemical shift of the paramagnetic solutions is represented also in terms of τ_m, $\Delta\omega_m$, and T_{2m} by Swift and Connick.[11] Assuming the same two conditions as in the case of the T_{2p} data analysis, Eq. 6 can be derived:

$$S_p = (S-S_0)P_m^{-1} = -(\Delta\omega_m/2\pi)\{1+(\Delta\omega_m\tau_m)^2\}^{-1}. \quad (6)$$

Here S(in Hz) is the observed chemical shift of the paramagnetic solution and S_0(in Hz) is that of the pure solvent. The observed shift data of the present systems are illustrated in Figs. 7 and 8 along with the calculated one(full lines in the Figs.). The latter were obtained from Eq. 6 by using the results of the relaxation data analysis already mentioned. The agreement between them indicated the validity of the relaxation data analysis again. The dashed lines denote cases in which the prediction by Eq. 6 was impossible, since the relaxation data lacked any contribution from the $\tau_m(\Delta\omega_m)^2$ term. (See Figs. 4 and 6.)

It should be noted that A/h values could be also obtained, roughly but absolutely independently from the relaxation data, from the observed S_p values. In the Figs. 7 and 8, the values of S_pT on the ordinate become constant as the temperature approaches the highest values, except in Co(hfa)$_2$(py)$_2$ and Ni(tta)$_2$(py)$_2$ cases. The constant values must be $-\Delta\omega_m T/2\pi$. That is because the $(\Delta\omega_m\tau_m)^2$ term in the Eq. 6 was negligible at temperature high enough for τ_m to be very small. A/h values were, therfore, derived from Eq. 5; they are shown in parentheses in Table 1.

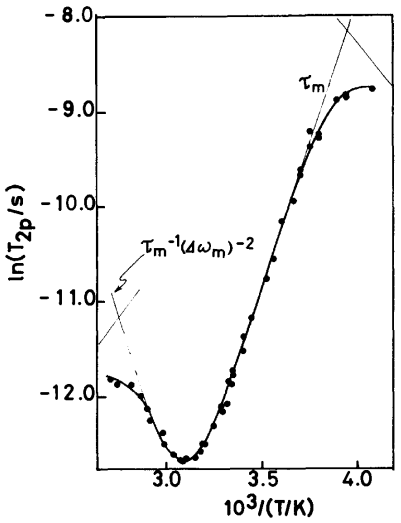

Fig. 5. Temperature dependence of T_{2p} in the Ni(acac)$_2$(py)$_2$ system.

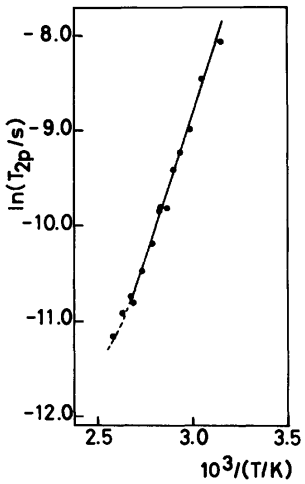

Fig. 6. Temperature dependence of T_{2p} in the Ni(tta)$_2$(py)$_2$ system.

Table 1. Kinetic parameters for pyridine exchange

	ΔH^*	ΔS^*	$k_{1,298}$*a	A/h
	kJ mol^{-1}	JK^{-1}mol^{-1}	s^{-1}($\sum\sigma^*$)*b	10^6Hz
Co(acac)$_2$(py)$_2$	41.4(0.5)*c	17.7(2.1)*c	2.9×10^6(0)	6.7(6.9)*d
Co(tfa)$_2$(py)$_2$	51.1(0.6)	16.9(1.9)	5.3×10^4(2.75)	8.2(7.9)
Co(tta)$_2$(py)$_2$	48.3(0.8)	2.6(2.7)	2.9×10^4(3.55)	9.0(9)
Co(hfa)$_2$(py)$_2$	33.8(3.0)	−60.1(9.7)	5.4×10^3(5.50)	[~7]*e
Ni(acac)$_2$(py)$_2$	47.2(0.8)	10.3(2.5)	1.3×10^5(0)	18(18)
Ni(tta)$_2$(py)$_2$	48.6(1.4)	−27.4(3.9)	7.1×10^2(3.55)	[~11]

*a: Defined as τ_m^{-1} at 298K and evaluated from ΔH^* and ΔS^* results. *b: Sum of Taft parameters. *c: Standard deviation. *d: Values in parenthses from shift data. *e: Values in brackets are estimated(see text).

Table 2. Absorption spectra of pyridine solution of complexes: λ_{max} in cm^{-1} with ε in mol^{-1}cm^{-1} in parentheses

	$^4T_{2g}\leftarrow{}^4T_{1g}$	$^4A_{2g}\leftarrow{}^4T_{1g}$	$^4T_{1g}(P)\leftarrow{}^4T_{1g}$
Co(acac)$_2$(py)$_2$*	9730(6.06)	18420(18.63)	19800(26.24) 20880(33.84)
Co(tfa)$_2$(py)$_2$	9600(5.48)	18520(23.51)	19760(36.87) 21370(43.84)
Co(tta)$_2$(py)$_2$	9600(10.54)	18400(70.66)	**
Co(hfa)$_2$(py)$_2$	9380(6.50)	**	**
	$^3T_{2g}\leftarrow{}^3A_{2g}$	$^1E_g\leftarrow{}^3A_{2g}$	$^3T_{1g}\leftarrow{}^3A_{2g}$
Ni(acac)$_2$(py)$_2$	10000(7.30)	12990(1.45)	16900(8.17)
	9750(6.8)	13100(v.w.)	16650(8.0)***
Ni(tta)$_2$(py)$_2$	10000(9.78)	12950(1.97)	16890(17.25)

* The crystal shows isomorphism with Ni(acac)$_2$(py)$_2$ (Ref. 12). ** Overlapped by intense UV absorption. *** Ref. 12.

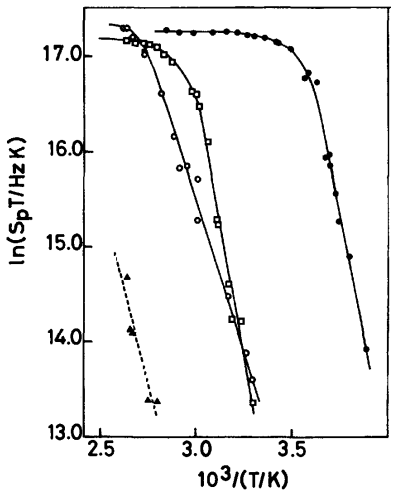

Fig. 7. Temperature dependence of the shift for the pyridine solutions containing Co(II) complexes.

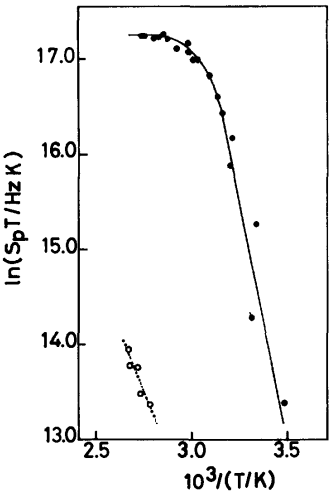

Fig. 8. Temperature dependence of the shift for the pyridine solutions of Ni(II) complexes.

In the case of either $Co(hfa)_2(py)_2$ or $Ni(tta)_2(py)_2$, A/h was only estimated from the observed S_p and the τ_m value derived from the relaxation data, by the use of Eq. 6. The results are shown in brackets in Table 1.

Discussion

Table 1 reveals that the pyridine exchange is retarded by electron-withdrawing substituents of chelate rings, which can be described by the Hammett equation:[1] $\log(k/k_0)=\rho\sigma$, where σ is the sum of the Taft σ^* parameters for the substituents of β-diketons. The trend is consistent with other authors' observations.[1,2,6] The σ^* values of tta was obtained by interpolation of the present observations, resulting in the value of 0.9 for σ^* of thienyl group. This seems quite suitable,in comparison with the value of 0.6 of the phenyl group.

The $\Delta S^{\neq}$ values listed in Table 1 suggest that, among a series of β-diketonato complexes of the metals, the electron-withdrawing power of the substituents have an effect also on the activation mechanism of the pyridine exchange. The stronger electron withdrawal causes the lower electron density within a chelate ring and the larger effective oxidation number of a central metal. It is reasonable in an activated state that the central metal with a larger effective oxidation number would interact with both leaving and entering pyridine molecules to form virtually two bonds. This case might be called an "associatively" activated mechanism. When the effective oxidation number is much smaller, the interaction between the central metal and any leaving or entering solvent is weak enough to lead all the present complexes, except $Co(hfa)_2(py)_2$ and $Ni(tta)_2(py)_2$, to dissociative activation. It should be noted here that actual activated states cannot be clearly visualized as either associative(ly) or dissociative. There might be possibilities of β-diketonates as unidentate ligands at an activated state and/or of a *trans-cis* equiliblium with their mutual conversion. A straight comparison, therefore, between the cases of simply solvated ions by six solvent molecules[13,14] and the present case is of little significance.

Taking into account the fact that the $\Delta H^{\neq}$ values reflect the crystal field theory activation energies (C.F.A.E),[15,16] the $\Delta H^{\neq}$ values in Table 1 support partly the trend of the activation mechanism already suggested by the $\Delta S^{\neq}$ values. The smaller effective oxidation number of a central ion causes the smaller C.F.A.E., assuming a dissociatively activated state. Assuming an associatively activated one, the circumstances are exactly the reverse. (The smaller C.F.A.E. must be the reflection of either the easier bond rupture or the more difficult bond formation.) In the actual series of Co complexes, the acac complex has a smaller $\Delta H^{\neq}$ compare to the tfa analogue, which has a larger effective oxidation number. This behavior is consistent with their dissociative activations predicted by $\Delta S^{\neq}$ values. That the $\Delta H^{\neq}$ value of the hfa analogue is smaller than the tta one can be explained as follows: The activation mechanism of the former complex is associative and that of the latter has a transient feature. They are consistent with what the $\Delta S^{\neq}$ values suggested. Furthermore, the differences in the $\Delta H^{\neq}$ values between $Co(acac)_2(py)_2$ and the Ni analogue and between $Co(tta)_2(py)_2$ and its Ni analogue are roughly parallel to C.F.A.E. calculated by Basolo and Pearson,[15] assuming a trigonal bipyramidal five coordinate and an octahedral wedge seven coordinate transition state.

Since it proved significant that solvent molecules interact with the effective charge of a central metal ion, not only the nature of the ligand but also the basicity of the solvents should be one of the alternate factors to predict the nature of activation. Trimethyl phosphate seems suitable as a solvent with small basicity and enough affinity to solvate to bis(β-diketonato) complexes in the present work. In any case, even a strong electron-withdrawing substituent induces an effective charge on a central ion which is not large enough to cause "associative" activation. A precise report will be submitted soon.

The authors wish to thank Prof. Kozo Nagashima of Institute of Chemistry, The University of Tsukuba, for his continuing support and encouragement during the course of this work. Thanks are also due to Mr. Hideto Suzuki and Dr. Shigeo Tanuma for their assist-

ance in instrumental problems and in computing.

References

1) R. W. Kluiber, R. Kukla, and W. D. Horrocks, Jr., *Inorg. Chem.*, **9**, 1319 (1970).
2) R. W. Kluiber, F. Thaller, R. W. Low, and W. D. Horrocks, Jr., *Inorg. Chem.*, **9**, 2592 (1970).
3) M. J. Petrin and W. L. Reynolds, *J. Inorg. Nucl. Chem.*, **33**, 3978 (1971).
4) R. W. Kluiber, R. Kukla, and F. Thaller, *J. Coord. Chem.*, **3**, 39 (1973).
5) S. F. Lincoln, *J. Chem. Soc., Dalton*, **1973**, 1896.
6) J. Crea and S. F. Lincoln, *Aust. J. Chem.*, **28**, 1523 (1975).
7) C. L. Watkins and M. E. Harris, *J. Inorg Nucl. Chem.*, **40**, 1769 (1978).
8) Y. Yano, M. T. Fairhurst, and T. W. Swaddle, *Inorg. Chem.*, **19**, 3269 (1978).
9) F. A. Cotton and R. H. Soderberg, *Inorg. Chem.*, **4**, 1145 (1965).
10) J. M. Hogen, R. A. Engel, and H. F. Stevenson, *Anal. Chem.*, **42**, 249 (1970).
11) T. J. Swift and R. E. Connick, *J. Chem. Phys.*, **37**, 307 (1962); erratum, **41**, 2553 (1964).
12) J. T. Hashgen and J. P. Fackler,Jr., *J. Am. Chem. Soc.*, **87**, 2821 (1965).
13) A. E. Merbach, *Pure Appl. Chem.*, **54**, 1479 (1983).
14) M. J. Sisley, Y. Yano, and T. W. Swaddle, *Inorg. Chem.* **21**, 1141 (1982).
15) F. Basolo and R. G. Pearson, "Mechanisms of Inorganic Reactions," tr. by H. Okuno *et al.*, Tokyo Kagaku Dozin, (1971), p. 155.
16) T. R. Stengel and C. H. Langford, *Coord. Chem. Rev.*, **2**, 363 (1967).
17) T. Nakagawa and Y. Oyanagi, "SALS," Tokyo Univ. Computer Centre (1979).

Thermal Square Planar-to-octahedral Transformation of Nickel(II) Complexes Containing 1,2-Diphenyl-1,2-ethanediamine in the Solid Phase

Yoshinori IHARA* and Ryokichi TSUCHIYA†

Laboratory of Chemistry, Faculty of Education, Kanazawa University, Kanazawa 920

†*Department of Chemistry, Faculty of Science, Kanazawa University, Kanazawa 920*

(Received January 5, 1984)

The following ten nickel(II) complexes with *meso*- or *dl*-1,2-diphenyl-1,2-ethanediamine (abbreviated as *meso*-stien and *dl*-stien, respectively) were prepared, and their thermal behavior was investigated in the solid phase: $[Ni(meso\text{-stien})_2]X_2$ (X=Cl, Br, I, NO_3, or ClO_4), $[Ni(dl\text{-stien})_2]X_2$ (X=I or ClO_4), and $[Ni(H_2O)_2(dl\text{-stien})_2]X_2$ (X=Cl, Br, or NO_3). The square planar bis(*dl*-stien) complex chloride, bromide, and nitrate obtained by thermal dehydration of their respective octahedral diaqua complexes were found by various techniques to be transformed, upon further heating, to the octahedral diacido bis(*dl*-stien) complexes. The complexes containing *dl*-stien have a stronger tendency to show such structural transformations than those containing *meso*-stien. The reason for this difference is discussed.

Nickel(II) ion forms complexes with various structures, *e.g.* octahedral, tetrahedral, and square planar, depending upon the nature of the ligands, and mutual transformation among these structures often occurs in solution.[1,2] Up to the present, however, a few studies[3-5] have dealt with the thermal reaction of octahedral diaqua complexes, $[Ni(H_2O)_2(diamine)_2]X_2$, in the solid phase. These complexes were found to lose $2H_2O$ upon heating to form either square planar bis-diamine complexes by mere deformation or octahedral diacido complexes by anation of counter ions.

An interesting example of thermal transformation from the square planar to the octahedral geometry was found in the anation of $[Ni(bimd)_4](NO_3)_2 \cdot 2.5C_2H_5OH$, where bimd denotes benzimidazole.[6] Similar transformations were also reported for the nickel(II) complexes with 2-aminobenzimidazole[7] and 2,3-butanediamines.[8] The purpose of the present study is to find whether or not the nickel(II) complexes with stien undergo the thermal square planar-to-octahedral transformation in the solid phase depending upon the structure of stiens and counter anions. Another purpose is to confirm the stronger tendency toward the transformation of the complexes with *dl*-stien than those with *meso*-stien, which was found for the complexes of *dl*- and *meso*-2,3-butanediamine.[8]

Experimental

Preparation. The ligands, *meso*-stien and *dl*-stien, were obtained by the methods described in the literature.[9,10] Aqueous solutions of nickel(II) chloride, bromide, iodide, nitrate, or perchlorate were added to ethanolic solutions of the ligands in the molar ratio of 1:2 to prepare the desired bis-type complexes. The resulting yellow or violet crystals were collected by filtration and washed with ethanol and diethyl ether. The formulas determined by elemental analyses and also by spectral and magnetic measurements (Table 1) are as follows: $[Ni(meso\text{-stien})_2]X_2$ (X=Cl, Br, I, NO_3, or ClO_4), $[Ni(dl\text{-stien})_2]X_2$ (X=I or ClO_4), and $[Ni(H_2O)_2(dl\text{-stien})_2]X_2$ (X=Cl, Br, or NO_3).

Measurements. Simultaneous TG and DSC measurements were carried out with a Rigaku Denki standard TG-DSC apparatus under a constant flow of nitrogen. The heating rates and amounts of samples used are given in Fig. 1. The complexes shown in Table 2 were obtained by isothermal heating at the temperatures corresponding to the respective DSC peaks.

The electronic spectra in the solid phase were measured by the diffuse reflectance method on a JASCO UNIDEC-410 spectrophotometer. The effective magnetic moments were evaluated from the susceptibilities measured by Gouy's method at room temperature.

Results and Discussion

Thermal Analyses. Of the ten complexes studied, all the yellow *meso*-stien complexes, and *dl*-stien iodide and perchlorate, did not show expected color changes. Heating of the remaining three diaqua complexes, however, led to an irreversible thermochromism consisting of two steps from violet to blue through yellow before decomposition.

The results of the simultaneous TG-DSC measure-

TABLE 1. DATA ON THE ELEMENTAL ANALYSES, ELECTRONIC SPECTRA AND MAGNETIC MOMENTS OF THE ORIGINAL COMPLEXES

Complexes	Color	Analytical data[a]			Absorption maxima	μ_{eff}
		H(%)	C(%)	N(%)	$\bar{\nu}/10^3\,cm^{-1}$	BM
$[Ni(meso\text{-stien})_2]Cl_2$	yellow	5.80(5.82)	60.45(60.68)	10.12(10.11)	22.5	diamag.
$[Ni(meso\text{-stien})_2]Br_2$	yellow	5.07(5.02)	52.33(52.30)	8.70(8.71)	22.3	diamag.
$[Ni(meso\text{-stien})_2]I_2$	yellow	4.36(4.38)	45.49(45.63)	7.67(7.60)	22.1 sh	diamag.
$[Ni(meso\text{-stien})_2](NO_3)_2$	yellow	5.31(5.31)	55.46(55.38)	13.63(13.84)	22.6	diamag.
$[Ni(meso\text{-stien})_2](ClO_4)_2$	yellow	4.70(4.73)	49.30(49.30)	8.04(8.21)	22.5	diamag.
$[Ni(H_2O)_2(dl\text{-stien})_2]Cl_2$	violet	5.96(6.15)	56.86(56.98)	9.42(9.49)	13.5 18.5 27.7 sh	3.30
$[Ni(H_2O)_2(dl\text{-stien})_2]Br_2$	violet	5.31(5.34)	49.25(49.52)	8.51(8.25)	13.7 18.3 27.8 sh	3.31
$[Ni(dl\text{-stien})_2]I_2$	yellow	4.17(4.38)	45.37(45.63)	7.58(7.60)	22.2	diamag.
$[Ni(H_2O)_2(dl\text{-stien})_2](NO_3)_2$	violet	5.35(5.64)	51.40(52.28)	12.98(13.06)	13.5 18.3 27.6 sh	3.33
$[Ni(dl\text{-stien})_2](ClO_4)_2$	yellow	4.96(4.73)	49.28(49.30)	8.28(8.21)	22.1	diamag.

a) Calculated values are in parentheses.

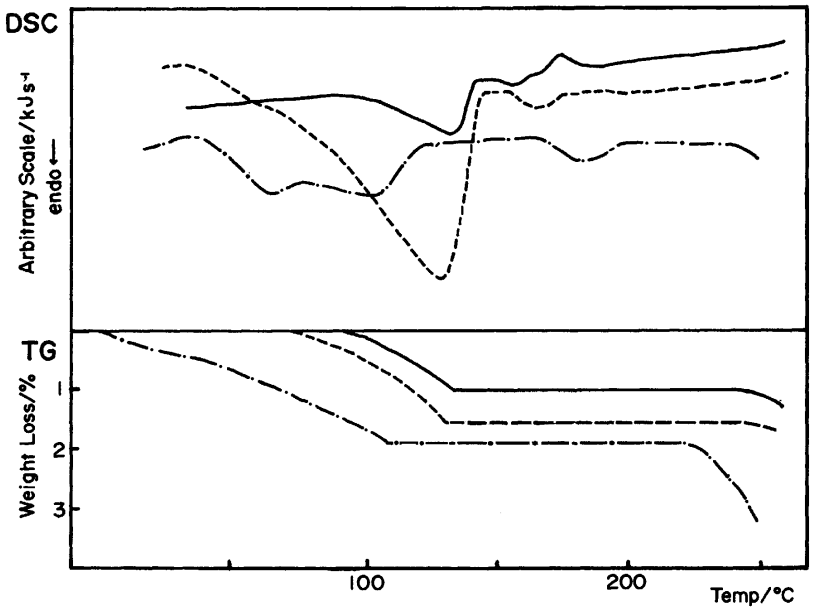

Fig. 1. TG-DSC patterns of $[Ni(H_2O)_2(dl\text{-stien})_2]Cl_2$ (——), $[Ni(H_2O)_2(dl\text{-stien})_2]Br_2$ (------), and $[Ni(H_2O)_2(dl\text{-stien})_2](NO_3)_2$ (—·—). The heating rate and amount of sample used were as follows: 1.25 °C min^{-1}, 17.5 mg for chloride, 2.5 °C min^{-1}, 40.4 mg for bromide, and 1.25 °C min^{-1}, 32.5 mg for nitrate, respectively.

TABLE 2. DATA ON THE ELEMENTAL ANALYSES, ELECTRONIC SPECTRA, AND MAGNETIC MOMENTS OF THE COMPLEXES OBTAINED BY HEATING

Complexes	Color	Analytical data[a)]			Absorption maxima	μ_{eff}
		H(%)	C(%)	N(%)	$\bar{\nu}/10^3\,cm^{-1}$	BM
$[Ni(dl\text{-stien})_2]Cl_2$	yellow				22.7	diamag.
$[NiCl_2(dl\text{-stien})_2]$	blue	5.57(5.82)	61.32(60.68)	10.16(10.11)	14.3 17.9 26.5 sh	3.28
$[Ni(dl\text{-stien})_2]Br_2$	yellow				22.5	diamag.
$[NiBr_2(dl\text{-stien})_2]$	blue	5.16(5.02)	52.16(52.30)	8.81(8.71)	13.9 18.1 26.1 sh	3.33
$[Ni(dl\text{-stien})_2](NO_3)_2$	yellow				22.9	diamag.
$[Ni(NO_3)_2(dl\text{-stien})_2]$	blue	5.43(5.31)	54.34(55.38)	13.55(13.84)	14.3 18.4 26.6 sh	3.22

a) Calculated values are in parentheses.

ments are shown in Fig. 1. The weight losses in TG curves correspond to two moles of coordinated water (obsd 6.06%, calcd 6.10% for chloride; 4.11%, 5.31% for bromide; and 5.85%, 5.60% for nitrate). The dehydration proceeds endothermically; thereafter, a small endothermic peak appears at 145 °C, 150 °C, and 170 °C for the chloride, bromide, and nitrate, respectively, without any change in TG curves. The yellow complexes obtained by the loss of the coordinated water were converted to blue after the second endothermic peaks, which indicated the thermochromism from violet to blue through yellow.

Cooling of the blue products did not cause the reverse color change. However, the yellow products absorbed water molecules relatively easily in the coordination sphere, and after cooling and standing in the air for several hours, they changed completely to the original octahedral complexes. This change was confirmed by the data of elemental analyses, electronic spectra, and magnetic moments.

The exothermic peak observed only for the chloride at 172 °C did not seem to correspond to a fundamental structural change, because the complex did scarcely show any color change, and the IR spectra measured at 165 °C and 180 °C, *i.e.* before and after the peak, were

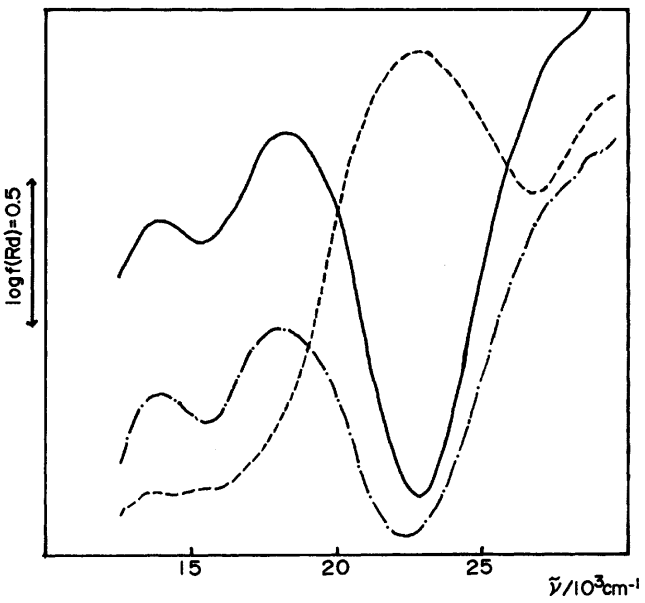

Fig. 2. Electronic spectra of $[Ni(H_2O)_2(dl\text{-stien})_2]Br_2$ before heating (——) and after heating at 120 °C (------) and at 170 °C (—·—).

TABLE 3. THE ENTHALPY CHANGES AND INITIATION TEMPERATURES OF THE SQUARE PLANAR-TO-OCTAHEDRAL TRANSFORMATION

X\NN	*dl*-stien	*meso*-bn[8]	*dl*-bn[8]
Cl	4.1 kJ/mol 145 °C		17.6 kJ/mol 159 °C
Br	2.4 kJ/mol 150 °C		16.0 kJ/mol 175 °C
NO_3	10.0 kJ/mol 170 °C	9.7 kJ/mol 188 °C	

nearly the same.

Electronic Spectra. The electronic spectra corresponding to the color change of the solid bromide upon heating are shown in Fig. 2. The spectral data are summarized in Table 2, together with the magnetic moments and analytical data.

The blue product has a spectral pattern identical with that of the original octahedral structure. On the other hand, the pattern of the yellow product, which is completely different from others, coincides with that of characteristic square planar nickel(II) complexes which have usually a broad and strong absorption band in the same frequency region. The chloride and nitrate show similar changes in the absorption spectra (Table 2).

Magnetic Moments. The yellow products are diamagnetic, whereas the blue products paramagnetic (3.22—3.33 BM). These facts, together with the above absorption spectral data, suggest that the yellow and blue products are the square planar and octahedral complexes, respectively. The stepwise thermochemical changes observed for the three diaqua *dl*-stien complexes are represented by the following scheme:

$$[Ni(H_2O)_2(dl\text{-stien})_2]X_2 \xrightarrow[\Delta]{-2H_2O} [Ni(dl\text{-stien})_2]X_2 \xrightarrow[\Delta]{}$$

$$[NiX_2(dl\text{-stien})_2] \quad (X=Cl, Br, \text{or } NO_3)$$

Comparison with the Butanediamine Complexes. In Table 3 the enthalpy changes and the initiation temperatures of the square planar-to-octahedral transformation estimated from the DSC peaks are compared with those of the corresponding 2,3-butanediamine (bn) complexes. The blank space in the Table means the absence of the transformation. The data show that the heat required to cause the transformation is smaller for the stien complexes than for the bn complexes.

In conclusion, the present study confirmed the stronger tendency of the complexes containing the *dl*-form toward the square planar-to-octahedral transformation than those of the *meso*-form. It was also found that the smaller anion is more advantageous for the configurational change, *i. e.* the order, $Cl^->Br^->I^-$ holds for the complex halides.

The nitrate complexes seem to have a somewhat higher inclination to cause the transformation irrespective of the ligand configuration (*meso*- or *dl*-), as was recognized for benzimidazole[6] and 2-aminobenzimidazole.[7] Additional stabilization due to the formation of hydrogen bonding between nitrate ion and diamines during the thermal structural change seems to be a plausible reason for the special property of the nitrate complex.

The discussion developed in the preceding paper[8] can be applied similarly to the difference in reactivity between the *meso*- and *dl*-stien complexes. In the *dl*-stien complexes containing two moles of stien with a square planar structure, four phenyl groups are able to occupy the equatorial positions, whereas for the *meso*-stien complexes at least two of four phenyl groups are forced to occupy the axial positions. The latter conformation will make the apical approach of the counter ion to the central metal ion difficult because of the steric hindrance.

References

1) R. H. Holm, *J. Am. Chem. Soc.*, **83**, 4683 (1961).
2) D. R. Eaton, W. D. Philips, and D. J. Caldwell, *J. Am. Chem. Soc.*, **85**, 397 (1963).
3) R. Tsuchiya, S. Joba, A. Uehara, and E. Kyuno, *Bull. Chem. Soc. Jpn.*, **46**, 1454 (1973).
4) H. Nishimoto, T. Yoshikuni, A. Uehara, E. Kyuno, and R. Tsuchiya, *Bull. Chem. Soc. Jpn.*, **51**, 1068 (1978).
5) Y. Ihara, E. Izumi, A. Uehara, R. Tsuchiya, S. Nakagawa, and E. Kyuno, *Bull. Chem. Soc. Jpn.*, **55**, 1028 (1982).
6) R. Tsuchiya, E. Kyuno, A. Uehara, S. Joba, and S. Ohba, *Chem. Lett.*, **1976**, 911.
7) Y. Ihara and R. Tsuchiya, *Bull. Chem. Soc. Jpn.*, **53**, 1614 (1980).
8) Y. Ihara, T. Kamishima, and R. Tsuchiya, *Thermochim. Acta*, **67**, 23 (1983).
9) S. Tripett, *J. Chem. Soc.*, **1957**, 4407.
10) O. F. Williams and J. C. Bailar, Jr., *J. Am. Chem. Soc.*, **81**, 4464 (1959).

 © 1984 The Chemical Society of Japan Bull. Chem. Soc. Jpn., 57, 2832—2834 (1984) [Vol. 57, No. 10

Recovery of Heavy Metals with Calcium Silicon Alloy. III. Stoichiometric Discussion on the Reduction of Copper(II) Ions

Shuzo TOKUNAGA
National Chemical Laboratory for Industry, Yatabe, Ibaraki 305
(Received February 10, 1984)

For the reduction of Cu^{2+} ions with Ca-Si alloy in aqueous solutions, the following elementary reactions were postulated:

$$Ca^0+Cu^{2+}=Ca^{2+}+Cu^0, \quad (1)$$
$$Ca^0+2H_2O=Ca^{2+}+H_2+2OH^-, \quad (2)$$
$$Si^0+2Cu^{2+}+3H_2O=H_2SiO_3+2Cu^0+4H^+, \quad (3)$$
$$Si^0+3H_2O=H_2SiO_3+2H_2. \quad (4)$$

From these reactions, amounts of Si^{IV} species were estimated by using those of H_2 and increments of H^+ ions. Total equivalents of the reduction products showed good agreement with those of the oxidation products, indicating the validity of the elementary reactions. The remained problems of the stoichiometric disagreement and the phenomenon of pH decrease indicated in Part II could be solved by using these elementary reactions. At the beginning of the reaction, a small amount of Cu^+ ions formed. Decomposition of water occurred subsequently to the Cu^{2+} reduction. A contribution of Si^0 to the reaction became greater than that of Ca^0 at higher Cu^{2+} concentrations than *ca.* 10 matom dm^{-3}. Thus, it proved that Si^0 in the alloy exhibits a great reducing effect.

Various metal ions having high standard electrode potentials are reduced effectively with Ca-Si alloy.[1-3] In Part II,[3] discussions were made on the reduction of Cu^{2+} ions about the reaction rate and the effects of acids, salts, and other metal ions. The following phenomena have remained uninterpreted. At lower Cu^{2+} concentrations than 5 matom dm^{-3}, equivalents of Cu^{2+} ions reduced well accounted for total equivalents of Ca^{II} and Si^{IV} species dissolved in the solution, and the pH tended to increase as the reaction proceeded. On the other hand, at higher Cu^{2+} concentrations, the equivalents of Cu^{2+} ions reduced became considerably greater than the total equivalents of Ca^{II} and Si^{IV} species dissolved in the solution, and the pH decreased from 4 to 2 or lower. The objectives of the present study are to solve these problems and, at the same time, to elucidate the mechanism of the whole reaction inclusive of decomposition of water as a side reaction. To this end, potential elementary reactions were postulated basing on the observed phenomena, and stoichiometric discussions were made on the reaction products.

Experimental

One dm^3 of *ca.* 2.5—40-matom dm^{-3} Cu^{2+} solutions was prepared and the pH was adjusted to 4.0 with HCl or NaOH. The sample solution was placed in a 25 °C thermostat. Prior to a run, nitrogen was bubbled thoroughly to purge dissolved oxygen. To the solution was added 3.0 g of Ca-Si alloy powder, and nitrogen bubbling and magnetic stirring were continued. An aliquot of the solution was taken at intervals and filtered quickly under reduced pressure through a membrane filter 0.30 μm in pore size. Then, analyses were made on the filtrate. The increment of H^+ or OH^- ions was determined by titration with either *ca.* 0.01-mol dm^{-3} standard NaOH or HCl solution, respectively. Cu^+ ions were determined by colorimetry with Bathocuproinesulfonate (disodium 2,9-dimethyl-4,7-diphenyl-1,10-phenanthroline-disulfonate).[4] Cu^{2+} and Ca^{2+} ions and dissolved silicate were determined in the same way as reported previously.[3] Separately, similar runs were made in a closed system to determine the volume of H_2 being collected in a graduated cylinder. The same materials were used as those in the previous report.

Results and Discussion

Postulation of Elementary Reactions. On adding Ca-Si alloy, Cu^{2+} ions are reduced effectively and recovered entirely from the solid phase as Cu^0. At the beginning of the reaction, a small amount of Cu^+ ions form. At the same time, decomposition of water occurs generating H_2. On the other hand, the alloy is oxidized to form Ca^{II}, Si^{IV} species, H^+, and OH^- ions in the solution.

It was indicated previously that, at high Cu^{2+} concentrations, equivalents of Cu^0 were greater than the total equivalents of Ca^{II} and Si^{IV} species dissolved in solution. The main causes of such disagreement are considered to be the neglect of effects of water decomposition and the possibility of existence of oxidation products (Ca^{II} and/or Si^{IV} species) also in the solid phase. For the former cause, H_2 and the increment of H^+ or OH^- ions were determined in the present study. As for the latter, their existence was not recognized in the X-ray diffraction pattern of the solid product. There is little possibility of formation of insoluble amorphous calcium silicate under the present experimental conditions of low pH (4—2 or lower). Consequently, Ca^{II} species exists entirely in the dissolved form, Ca^{2+} ions. The IR absorption spectrum of the solid products showed a broad and strong absorption band in the wave number range from *ca.* 900 to 1350 cm^{-1}. It is characteristic of amorphous silica, and was not found in the spectrum of the original alloy. It is, therefore, necessary to take into account the amount of silica present in the solid phase for the stoichiometric discussion. However, it was practically impossible to determine its amount at the time of interruption of the reaction by solid-liquid separation, since oxidation of unreacted alloy by water proceeded under the wet condition even after the separation.

Then potential elementary reactions were postulated on the basis of the observed phenomena, and are shown in Fig. 1. The elementary reactions are composed of reduction of Cu^{2+} ions and decomposition of water

$$Ca^0 + Cu^{2+} = Ca^{2+} + Cu^0 \quad (1)$$
$$a \qquad\qquad a \quad a$$
$$Ca^0 + 2H_2O = Ca^{2+} + H_2 + 2OH^- \quad (2)$$
$$b \qquad\qquad b \quad b \quad 2b$$
$$Si^0 + 2Cu^{2+} + 3H_2O = H_2SiO_3 + 2Cu^0 + 4H^+ \quad (3)$$
$$c \qquad\qquad\qquad\qquad c \quad 2c \quad 4c$$
$$Si^0 + 3H_2O = H_2SiO_3 + 2H_2 \quad (4)$$
$$d \qquad\qquad d \quad 2d$$

Fig. 1. Elementary reactions and stoichiometric relations for the reduction of Cu^{2+} ions with Ca-Si alloy in aqueous solution.

by Ca^0, reactions 1 and 2 respectively, and of Cu^{2+} reduction and water decomposition by Si^0, reactions 3 and 4 respectively. In reaction 3, Si^0 is oxidized to form silicic acid, when decomposition of water occurs inevitably to form H^+ ions. This can interpret the unsolved phenomenon of decrease in pH accompanying the reduction of Cu^{2+} ions. Silicic acid may exist in other forms, which can be ignored in the stoichiometric discussion. Reduction of one atom of Si^0 always results in formation of four H^+ ions. Part of silicic acid forming in reactions 3 and 4 exists in the form of amorphous silica in the solid phase. In addition, there exist consecutive reactions $Cu^{2+}+e=Cu^+$ and $Cu^++e=Cu^0$ in the initial stage of the reaction. For the sake of simplification, these elementary reactions were discussed stoichiometrically at the time when the reduction of Cu^{2+} ions to Cu^0 had been complete.

In these elementary reactions, Ca^{2+} and H_2 can be determined directly. The increment of either H^+ or OH^- ions can be determined by neutralization titration. The amount of Cu^0 can be estimated from residual Cu^{2+} concentration. Then the total amount of Si^{IV} species forming in both liquid and solid phases at the time of the interruption of the reaction was estimated by using amounts of other determinable components dissolved in the solution as follows: Let a and b be numbers of atoms of Ca^0 oxidized in reactions 1 and 2, respectively. And let c and d be those of Si^0 in reactions 3 and 4, respectively. Then, we get

$$a + b = Ca^{2+},$$
$$a + 2c = Cu^0,$$
$$b + 2d = H_2,$$
$$4c - 2b = \Delta H^+ \text{ (or } -\Delta OH^-).$$

Solving these equations for Si^{IV}, we get

$$Si^{IV} = c + d = 1/2H_2 + 1/4\Delta H^+ \text{ (or } -1/4\Delta OH^-).$$

Unfortunately, a, b, c, and d cannot be determined individually by this method. But it became possible to discuss the whole reaction only with the reaction products in the solution and H_2.

Stoichiometric Discussion. The validity of these deductions was examined by comparing the total equivalents of the reduction and oxidation products of *ca.* 2.5—40-matom dm^{-3} Cu^{2+} solutions. Values at the time when the Cu^{2+} reduction was almost complete (*ca.* 3—8 min after the alloy addition) were used in order to minimize the effects of water decomposition and to exclude those of Cu^+ formation. Equivalents of Ca^{2+} and Si^{IV} as the oxidation products and the total of both values are plotted against total equivalents of Cu^0 and H_2 as the reduction products in Fig. 2. In addition, equivalents of H_2 are plotted to show the degree of water decomposition. The results show that the total of the found Ca^{2+} and the calculated Si^{IV} values are approximately on a straight line with a slope of 1.0 passing the origin 0. This indicates the validity of postulated elementary reactions 1—4, and consequently that of estimation of the amount of Si^{IV}. Thus, the remained problems of stoichiometric disagreement and pH decrease phenomenon are solved. The stoichiometric agreement at low Cu^{2+} concentrations in the previous study may be due to entire dissolution of Si^{IV} species and little water decomposition. It has been considered that Cu^{2+} ions are reduced mainly by Ca^0. But, as a matter of fact, the contribution of Si^0 to the reduction was greater than that of Ca^0 at high Cu^{2+} concentrations. It was very small at 2.5 matom dm^{-3} but increased linearly with the amounts of reduction. On the other hand, the contribution of Ca^0 became small relatively at high reduction values, where Ca^0 in the alloy was mostly consumed. Thus, it proved that Si^0, practically an inactive element due to passivation by silica film on the surface, exhibits its original strong reducing power in Ca-Si alloy when the fresh surface appears after dissolution of Ca^0. Proportion of H_2 in the reduction values became smaller at higher values, indicating that the alloy was used more effectively for the reduction of Cu^{2+} ions.

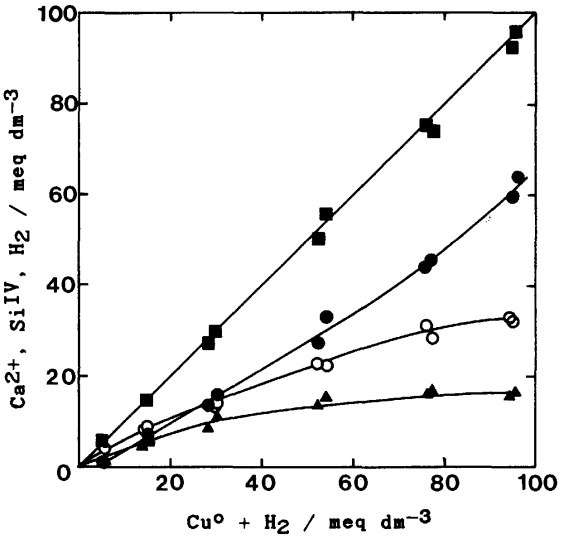

Fig. 2. Relation between equivalents of reduction products (Cu^0 and H_2) and oxidation products (Ca^{2+} and Si^{IV}).
O: Ca^{2+}, ●: Si^{IV}, ■: $Ca^{2+}+Si^{IV}$, ▲: H_2.

Behavior of Reaction Products. In order to know the whole aspect of the reaction, behavior of all the products was studied with the 10.0-matom dm^{-3} Cu^{2+} solution. Concentrations of the products in meq dm^{-3} are plotted in Fig. 3 against the time after addition of the alloy. At the beginning of the reaction (after *ca.* 1.5 min), pH decreased from 4.0 to 2.2 because of formation of H^+ ions in the reduction of Cu^{2+} ions

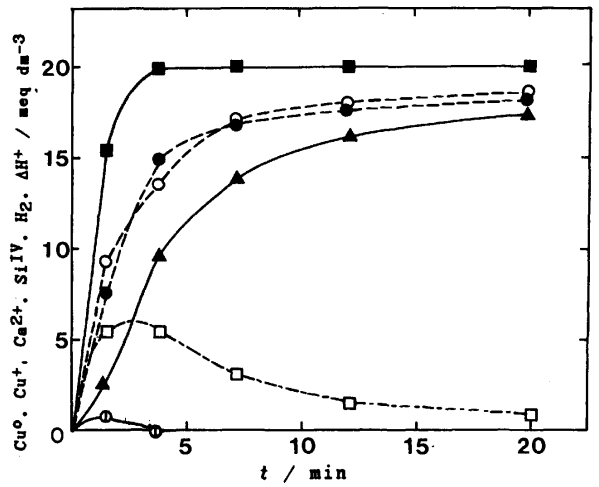

Fig. 3. Behavior of the reaction products in the reduction of 10.0-matom dm^{-3} Cu^{2+} solution.
■: Cu^0, Φ: Cu^+, ○: Ca^{2+}, ●: Si^{IV}, ▲: H_2, □: ΔH^+.

by Si^0. Then, *ca.* 0.8 and 2.3 matom dm^{-3} of Cu^+ and Cu^{2+} ions, respectively, were found in the solution. The remainder of copper species was recovered from the solid phase as Cu^0. According to Charlot,[5] the reduction process of Cu^{2+} to Cu^0, potentially including formation of Cu^+ species, is subject to pH value and the concentration of Cl^- ion. Therefore, the details of the reduction process of Cu^{2+} through Cu^+ are unknown with the present data. After *ca.* 4 min, the Cu^{2+} reduction was almost complete when Cu^+ and Cu^{2+} ions were undetectable in the solution. The reduced Cu^{2+} was entirely recovered from the solid phase.

Decomposition of water proceeded almost simultaneously with the Cu^{2+} reduction, and became slow in rate after completion of the Cu^{2+} reduction. A considerable amount of alloy was consumed in the decomposition of water. Calculated values of Si^{IV} species were much greater than those found in the solution. Ca^0 and Si^0 exhibited almost similar contribution to the entire reaction. After *ca.* 4 min, the increment of H^+ ions decreased because of completion of Cu^{2+} reduction by Si^0 and because of formation of OH^- ions in the decomposition of water by Ca^0.

References

1) S. Tokunaga and K. Uematsu, *Nippon Kagaku Kaishi*, **1978**, 619.
2) S. Tokunaga, K. Uematsu, and Y. Nagawa, *Bull. Chem. Soc. Jpn.*, **54**, 733 (1981).
3) S. Tokunaga, *Bull. Chem. Soc. Jpn.*, **55**, 95 (1982).
4) D. Blair and H. Diehl, *Talanta*, **7**, 163 (1961).
5) G. Charlot, "Teisei Bunseki Kagaku," Revised ed., Kyoritsu, Tokyo (1974), pp. 168—170 and pp. 379—380.

 © 1984 The Chemical Society of Japan Bull. Chem. Soc. Jpn., 57, 2835—2838 (1984)

Ylide-Metal Complexes. IX.[1] The Preparation and Properties of Metal (Be, Mg, Zn, Cd, Hg, Al, In, Sn, and Pb) Complexes with Methylenetriphenylarsorane

Yoshihisa YAMAMOTO

Faculty of Pharmaceutical Science, Higashi Nippon Gakuen University, Ishikari-Tobetsu, Hokkaido 061-02

(Received February 13, 1984)

The reactions of methylenetriphenylarsorane, $(C_6H_5)_3As{=}CH_2$ (**L**), with $ZnCl_2$ or $HgCl_2$ in the mole ratio 2:1 yield new monomeric compounds of bis(methylenetriphenylarsorane)metal dichloride, $[(C_6H_5)_3AsCH_2\text{-}M\text{-}CH_2As(C_6H_5)_3]Cl_2$. The reactions of **L** with $BeCl_2$ or $MgCl_2$ in the mole ratio 2:2 yield dimeric trigonal compounds of di-μ-chloro-bis[(methylenetriphenylarsorane)metal] dichloride, $[(C_6H_5)_3AsCH_2\text{-}M\langle^{Cl}_{Cl}\rangle M\text{-}CH_2As(C_6H_5)_3]Cl_2$. The reactions of **L** with $AlCl_3$ or $InCl_3$ in the mole ratio 4:2 yield dimeric tetrahedral compounds of di-μ-chloro-bis[bis(methylenetriphenylarsorane)metal] tetrachloride, $[\{(C_6H_5)_3AsCH_2\}_2\text{-}M\langle^{Cl}_{Cl}\rangle M\text{-}\{CH_2As(C_6H_5)_3\}_2]Cl_4$. The reactions of **L** with $(C_6H_5)_3MCl$ (M: Sn and Pb) in the mole ratio 1:1 yield new monomeric compounds of (methylenetriphenylarsorane)triphenyl-metal chloride, $[(C_6H_5)_3AsCH_2\text{-}M(C_6H_5)_3]Cl$. They are thermally stable complexes and their properties are compared with those of the methylenetriphenylphosphorane metal compounds.

A previous paper,[1] in this series, was concerned with the preparation and properties of Cu, Ag, Au, Zn, Cd, Hg, Ge, Sn, Pb, Pd, and Pt complexes with methylenetris(dimethylamino)phosphorane, $(Me_2N)_3P{=}CH_2$.

Many investigations of organometallic compounds between unstable phosphonium ylides and metals have been reported concerning their preparation, structure, general properties, stability and NMR spectra. The metal compounds with methylenetriphenylphosphorane, $(C_6H_5)_3P{=}CH_2$, have a linear structure,[2-7] *e.g.*,

$$[(C_6H_5)_3\overset{+}{P}CH_2\text{–}\overset{-}{M}\text{–}CH_2\overset{+}{P}(C_6H_5)_3]Cl^- \quad (M: Cu, Ag, Au).$$

On the other hand, the metal compounds with methylenetrimethylphosphorane, $(CH_3)_3P{=}CH_2$, and the related phosphoranes, $R_2(CH_3)P{=}CH_2$ (R: C_2H_5, C_6H_5), are cyclic[8-21] such as

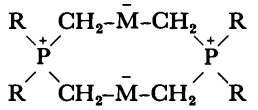

(M: Cu, Ag, Au).

The cyclic structure compound is formed by a rapid intermolecular proton exchange[22] of the phosphoranes.

In the arsenic ylide series, many researchers tried to isolate methylenetriphenylarsorane, $(C_6H_5)_3As{=}CH_2$.[22-25] However, it was not isolated until 1975,[26] because of its sensitivity to air, water, and temperature. Even now, the investigation of organometallic compounds with methylenetriphenyl(or trimethyl)arsorane is limited to the Cu, Ag, Au compounds.[3,28-30] Very little is known of the physical properties and general chemistry of the arsorane metal compounds, in contrast to the information on phosphorane metal compounds. The present paper deals with the preparation and properties of bis(methylenetriphenylarsorane)metal dichloride, $[(C_6H_5)_3AsCH_2\text{-}M\text{-}CH_2As(C_6H_5)_3]Cl_2$ (M: Zn, Cd, Hg), di-μ-chloro-bis[(methylenetriphenylarsorane)metal] dichloride, $[(C_6H_5)_3AsCH_2\text{-}M\langle^{Cl}_{Cl}\rangle M\text{-}CH_2As(C_6H_5)_3]Cl_2$ (M: Be, Mg), di-μ-chloro-bis[bis(methylenetriphenylarsorane)-metal] tetrachloride, $[\{(C_6H_5)_3AsCH_2\}_2\text{-}M\langle^{Cl}_{Cl}\rangle M\text{-}\{CH_2As(C_6H_5)_3\}_2]Cl_4$ (M: Al, In), and (methylenetriphenylarsorane)triphenylmetal chloride, $[(C_6H_5)_3AsCH_2M(C_6H_5)_3]Cl$ (M: Sn, Pb).

Results and Discussion

Zinc, Cadmium, and Mercury Complexes. Bis(methylenetriphenylarsorane)zinc dichloride (**1**) and the corresponding mercury(II) chloride (**3**) have been isolated from a reaction mixture of arsorane, $(C_6H_5)_3As{=}CH_2$ (**L**), and $ZnCl_2$ or $HgCl_2$ in the mole ratio of 2:1. The corresponding cadmium complex (**2**) was not isolated (*cf.* Experimental section). Complexes **1** and **3** are soluble in chloroform, dichloromethane, *N*,*N*-dimethylformamide (DMF), dimethyl sulfoxide(DMSO) and methanol but insoluble in acetone, ether, pentane, tetrahydrofuran (THF), ethyl acetate, acetic acid, hydrochloric acid and water.

$$2(C_6H_5)_3As{=}CH_2 + MCl_2 \longrightarrow [(C_6H_5)_3AsCH_2\text{-}M\text{-}CH_2As(C_6H_5)_3]Cl_2$$

1, 3

1: M=Zn, **3**: M=Hg

Complex **3** is unstable in dichloromethane at room temperature, but stable at −80 °C. On the other hand, complex **1** was slowly changed to methyltriphenylarsonium chloride $[(C_6H_5)_3AsCH_3]Cl$ (**4**) in dichloromethane at −80 °C. They are highly hygroscopic. The ^1H NMR spectrum of **3** showed a singlet signal for the CH_2As at δ 2.9 and the multiplet signal for the phenyl groups at δ 7.1—9.2 in a ratio of 2:15 in dichloromethane-d_2 at −80 °C as is shown in Table 1. The chemical shift of the methylene protons of **3** is at a lower field than that[26] (δ 0.93) of arsorane (**L**). This property is similar to those of bis(methylenetriphenylarsorane)gold(I) chloride[3] $[(C_6H_5)_3AsCH_2\text{-}Au\text{-}CH_2As(C_6H_5)_3]Cl$ (**5**) and bis(methylenetriphenylphosphorane)metal(II) dichloride,[4] $[(C_6H_5)_3PCH_2\text{-}M\text{-}CH_2P(C_6H_5)_3]Cl_2$ M: Zn, Cd,

Hg (**6**). The arsorane (**L**) is bonded to the metal atom through the carbanionic donor atom. Complexes **1** and **3** have free anion from the equivalent conductance, and the chloride is precipitated by silver nitrate in methanol–water solution. Thus, we suggest that the structures of **1** and **3** are linear similar to those of complexes **5** and **6**.

Beryllium and Magnesium Complexes. Di-μ-chloro-bis(methylenetriphenylarsorane)beryllium dichloride (**7**) and the corresponding magnesium dichloride (**8**) have been isolated from a reaction mixture of arsorane (**L**) with $BeCl_2$ or $MgCl_2$ in the mole ratio of 2:2. Complex **7** is somewhat soluble in nitric acid and hydrochloric acid, and very slightly soluble in chloroform and dichloromethane. Complex **8** is soluble in DMF, DMSO, methanol, and water, and very slightly soluble in chloroform and dichloromethane, though insoluble in acetic acid, benzene,

$$2(C_6H_5)_3As{=}CH_2 + 2MCl_2 \longrightarrow [(C_6H_5)_3AsCH_2\text{-}M(\mu\text{-}Cl)_2M\text{-}CH_2As(C_6H_5)_3]Cl_2$$

7, 8

7: M=Be, **8**: M=Mg

ether, ethyl acetate and THF. They are highly hygroscopic. Complexes **7** and **8** were slowly changed to the corresponding arsonium salt (**4**) in dichloromethane at −80°C, showing signals of both **4** and **7** or **8** in the NMR spectra. The NMR spectra of **7** and **8** showed a singlet signal for the CH_2As at δ 2.79 and 2.84, respectively and the multiplet signal for phenyl groups at δ 7.2—8.7 as is shown in Table 1. The chemical shifts of the methylene protons of **7** and **8** are at a lower field than that of **L**. The arsorane is bonded to the metal atom. Two structures for the beryllium compounds have been considered possible: either a tetrahedral (monomeric,[30] dimeric,[31] and polymeric[32,33]) or trigonal (monomeric,[34] dimeric,[35] and trimeric[36,37]) structure. Complexes **7** and **8** are not polymeric, because they are soluble in methanol. They have free anion from the equivalent conductance. Their solubility in chloroform and dichloromethane is different from that of **1**, **3**, **5**, and **6** (linear structure) and di-μ-chloro-bis[bis(methylenetriphenylphosphorane)-metal] tetrachloride,[7] $[\{(C_6H_5)_3PCH_2\}_2\text{-}M(\mu\text{-}Cl)_2M\text{-}\{CH_2P(C_6H_5)_3\}_2]Cl_4$ M:Al, Ga, In (**9**), and the corresponding arsorane complexes (**11**, **12**) (tetrahedral structure). Their elemental analyses agreed with that of $[LMCl_2]_2$. These properties resemble those of di-μ-chloro-bis(methylenetriphenylphosphorane)metal dichloride, $[(C_6H_5)_3PCH_2\text{-}M(\mu\text{-}Cl)_2M\text{-}CH_2P(C_6H_5)_3]Cl_2$ M:Be and Mg (**10**), of dimeric trigonal structure,[7] reported previously. Thus, we suggest that their structure can be neither linear nor tetrahedral but a dimeric trigonal structure bridged by chloride.

Aluminium and Indium Complexes. Di-μ-chloro-bis[bis(methylenetriphenylarsorane)aluminium] tetrachloride (**11**) and the corresponding indium tetrachloride (**12**) have been isolated from a reaction mixture of arsorane (**L**) and $AlCl_3$ or $InCl_3$ in the mole ratio of 4:2. Complexes **11** and **12** are soluble in chloroform, dichloromethane, DMF, DMSO, methanol and water, though insoluble in acetone, benzene, acetic acid, and THF. They are highly hygroscopic. The ^1H NMR

$$4(C_6H_5)_3As{=}CH_2 + 2MCl_3 \longrightarrow [(C_6H_5)_3AsCH_2(\mu\text{-}Cl)_2M(\mu\text{-}CH_2As(C_6H_5)_3)_2]Cl_4$$

11, 12

11: M=Al, **12**: M=In

spectra of complexes **11** and **12** showed a singlet signal for the CH_2As at about δ 2.9 and a multiplet signal for the phenyl groups at δ 7.3—8.3, though both complexes were slowly changed to salt **4** in dichloromethane at −80°C. Complexes **11** and **12** are not polymeric, because they are soluble in dichloromethane and methanol. The elemental analyses of **11** and **12** agreed with that of $[L_2MCl_3]_2$. Their colors are white. They have free anions from the equivalent conductance. Their properties resemble those of complex **9**.[7] The structure of $AlCl_3$, $InCl_3$ and related compounds are of a dimeric, tetrahedral structure bridged by chloride.[38–42] Then, we suggest that their structure is dimeric bridged by chloride and tetrahedral.

Tin and Lead Complexes. (Methylenetriphenylarsorane)triphenyltin chloride (**13**) and the corresponding lead chloride (**14**) have been isolated from a reaction mixture of the arsorane (**L**) and triphenyltin chloride or triphenyllead chloride in the mole ratio of 1:1. Complexes **13** and **14** are soluble in alcohols,

$$(C_6H_5)_3As{=}CH_2 + (C_6H_5)_3MCl \longrightarrow [(C_6H_5)_3AsCH_2\text{-}M(C_6H_5)_3]Cl$$

13, 14

13: M=Sn, **14**: M=Pb

chloroform, dichloromethane, DMF, DMSO, and THF, but insoluble in benzene, ether, and water. They are hygroscopic. Complex **14** is soluble in chloroform and dichloromethane, though complex **13** is slightly soluble in both solvents. The ^1H NMR spectra of **13** and **14** showed a singlet signal for the methylene group

TABLE 1. ^1H NMR DATA OF COMPLEXES

No	CH_2As δ	C_6H_5 δ	Temp °C	Solvent and Standard
1	2.88 s	7.1—8.7 m	−80	1)
3	2.90 s (4H)	7.1—9.2 m (30H)	−80	1)
7	2.79 s	7.3—8.1 m	−80	1)
8	2.84 s	7.2—8.7 m	−80	1)
11	2.90 s	7.3—8.3 m	−80	1)
12	2.88 s	7.3—8.3 m	−80	1)
13	2.32 s (2H)	6.9—8.0 m (30H)	r.t.	1)
14	2.45 s (2H)	6.8—8.0 m (30H)	r.t.	1)
L[a]	0.93 s (2H)	7.1—8.2 m (15H)	r.t.	2)
4	3.2 s (3H)	7.7 m (15H)	r.t.	1)

Solvents: 1) CD_2Cl_2, 2) $C_6D_5CD_3$. Standard: internal TMS (δ=0). a) Ref. 26.

(CH_2As) at δ 2.32 for **13** (δ 2.45 for **14**) and a multiplet signal for the phenyl group at δ 6.9—8.0 in a ratio of 2:30 in dichloromethane at room temperature as is shown in Table 1. The chemical shifts of their methylene protons are at a lower field than that of **L**. Complexes **13** and **14** have free anion from the equivalent conductance, and the chloride is precipitated by silver nitrate in ethanol–water solution. Thus, their structure is monomeric tetrahedral. The chemical shift of methylene protons of **14** is different from that (δ 2.68)[5] of the corresponding phosphorane lead complex, $[(C_6H_5)_3PCH_2Pb(C_6H_5)_3]Cl$ (**15**), and complex **13** is stable in dichloromethane at room temperature, though the corresponding phosphorane tin complex[5] (**16**) is unstable at −80°C. This can be ascribed to a property of the As or P in the complexes. The configuration (sp^3-sp^3) of the CH_2–M bonds of **13** and **14** is similar to those of **11** and **12** but complexes **11** and **12** are not so stable as complexes **13** and **14** in dichloromethane.

The monomeric complexes have a linear and tetrahedral structure. The structure of the dimeric complexes is trigonal and tetrahedral. All complexes are thermally stable. The Ag, Au, Hg, Sn, and Pb arsorane complexes are stable but the Cu, Be, Mg, Zn, Al, and In complexes are unstable. In the other hand, the Cu, Ag, Au, Mg, Zn, Cd, Al, Ga, In, and Pb phosphorane complexes are stable in dichloromethane, but the Be, Hg, and Sn complexes are not. The stable and unstable metal complexes with arsorane are the unstable and stable metal complexes of phosphorane, respectively, except for Ag, Au, Pb, and Be complexes. This difference is ascribed to both ylides, *i.e.*, the carbanionic carbon of the arsorane can be tetrahedral[26] and that of the phosphorane is trigonal.[43,44]

Experimental

Measurements. The NMR spectra were recorded with an R-40 spectrometer (Hitachi), Varian XL-200 spectrometer for ^1H NMR. The electric conductivities of solutions were determined by the use of a conductometric meter, CM-30 (Shimadzu) in dichloromethane at −80°C for **1**, **3**, **7**, **8**, **11**, **12** and room temperature for **13**, **14**.

Starting Materials. Methylenetriphenylarsorane (**L**) was prepared from a reaction mixture of methyltriphenylarsonium bromide[45] and sodium amide in dry THF by the method of the previous paper.[26,28]

Ylide-metal Complexes. Bis(methylenetriphenylarsorane)-zinc Dichloride (1): Zinc dichloride (0.15 g, 1.10 mmol) was added to a dry THF solution (15 cm^3) of arsorane (0.71 g, 2.22 mmol). The mixture was stirred for 1 d at room temperature. The color of the ylide changed to colorless from yellow. The white complex which formed was filtered, washed with pentane and dried. Yield: 0.54 g (62.3%). Found: C, 58.78; H, 4.50%. Calcd for $C_{38}H_{34}As_2ZnCl_2$ (MW 776.82) C, 58.76; H, 4.41%. Mp 117—120°C.

Bis(methylenetriphenylarsorane)cadmium Dichloride (2): Cadmium dichloride (0.22 g, 1.20 mmol) was added to a dry THF solution (10 cm^3) of arsorane (0.78 g, 2.44 mmol). The mixture was stirred for 1—24 h at room temperature. Complex **2** was not isolated from the reaction mixture, because the precipitate was a gum.

Bis(methylenetriphenylarsorane)mercury Dichloride (3): Mercury(II) chloride (0.33 g, 1.22 mmol) was added to a dry THF solution (11 cm^3) of arsorane (0.78 g, 2.44 mmol). The mixture was stirred for 12 h at room temperature. The color of the ylide changed to colorless from yellow. The white complex precipitate was filtered, washed with pentane and dried. Yield: 0.7 g (62.9%). Found: C, 49.81; H, 4.03%. Calcd for $C_{38}H_{34}As_2HgCl_2$ (MW 912.03) C, 50.04; H, 3.76%. Mp 196—198°C.

Di-μ-chloro-bis[(methylenetriphenylarsorane)beryllium] Dichloride (7): The arsorane **L** (0.44 g, 1.37 mmol) was added to dry THF (14 cm^3), and beryllium dichloride (0.11 g, 1.38 mmol) was added to the solution. The mixture was stirred for 20 h at room temperature, the white complex which precipitated was filtered, washed with pentane and dried. Yield: 0.28 g (51.1%). Found: C, 57.28; H, 4.62%. Calcd for $C_{38}H_{34}As_2Be_2Cl_4$ (MW 800.37) C, 57.03; H, 4.28%. Mp 133—135°C.

Di-μ-chloro-bis[(methylenetriphenylarsorane)magnesium] Dichloride (8): To a dry THF (10 cm^3) solution of arsorane (0.35 g, 1.09 mmol), magnesium dichloride (0.1 g, 1.05 mmol) was added and the mixture was stirred for 1 d at room temperature. The white complex which formed was filtered, washed with pentane and dried. Yield: 0.4 g (88.3%). Found: C, 54.85; H, 4.50; Cl, 16.14%. Calcd for $C_{38}H_{34}As_2Mg_2Cl_4$ (MW 830.96) C, 54.93; H, 4.12; Cl, 17.06%. Dp 190°C.

Di-μ-chloro-bis[bis(methylenetriphenylarsorane)aluminium] Tetrachloride (11): Aluminium trichloride (0.18 g, 1.35 mmol) was added to a dry THF (10 cm^3) solution of arsorane (0.87 g, 2.72 mmol) and the mixture stirred for 2 h at room temperature. The white complex precipitate was filtered and washed with pentane and dried. Yield: 0.56 g (53.2%). Found: C, 58.98; H, 4.40; Cl, 13.48%. Calcd for $C_{76}H_{68}As_4Al_2Cl_6$ (MW 1547.74) C, 58.98; H, 4.43; Cl, 13.74%. Mp 157—160°C.

Di-μ-chloro-bis[bis(methylenetriphenylarsorane)indium] Tetrachloride (12): Indium trichloride (0.20 g, 0.904 mmol) was added to a dry THF (10 cm^3) solution of arsorane (0.58 g, 1.81 mmol) and the mixture stirred for 3 h at room temperature. The white complex which formed was filtered, washed with pentane and dried. Yield: 0.55 g (70.5%). Found: C, 52.61; H, 4.11; Cl, 11.89%. Calcd for $C_{76}H_{68}As_4In_2Cl_6$ (MW 1723.42) C, 52.97; H, 3.98; Cl, 12.34%. Mp 122—125°C.

Methylenetriphenylarsorane(triphenyl)tin Chloride (13): The arsorane **L** (0.67 g, 2.09 mmol) was added to dry THF (12 cm^3) under nitrogen, and triphenyltin chloride (0.80 g, 2.08 mmol) was added to the solution. The mixture was stirred for 2 h at −40°C. The color of the ylide changed from yellow to colorless. Dry ether was then added to the solution at −40°C. The white complex precipitate was filtered at −40°C, washed with dry ether and dried under vacuum. Yield: 0.56 g (38.0%). Found: C, 62.80; H, 4.45%. Calcd for $C_{37}H_{32}AsSnCl$ (MW 705.73) C, 62.97; H, 4.57%. Dp 120°C.

Methylenetriphenylarsorane(triphenyl)lead Chloride (14): The arsorane **L** (0.74 g, 2.31 mmol) was added to dry THF (12 cm^3) under nitrogen, and triphenyllead chloride (1.1 g, 2.32 mmol) was added to the solution. The mixture was stirred 1 h at room temperature. The color of the ylide changed to colorless from yellow. Dry pentane was added to the solution, and the white complex precipitate was filtered, washed with pentane and dried under vacuum. Yield: 0.51 g (27.8%). Found: C, 55.69; H, 4.04%. Calcd for $C_{37}H_{32}AsPbCl$ (MW 794.16) C, 55.96; H, 4.06%. Mp 157°C.

References

1) Part VIII: Y. Yamamoto, *Bull. Chem. Soc. Jpn.*, **57**, 43 (1984).

2) Y. Yamamoto and H. Schmidbaur, *J. Organomet. Chem.*, **96**, 133 (1975).

3) Y. Yamamoto and Z. Kanda, *Bull. Chem. Soc. Jpn.*, **52**, 2560 (1979).

4) Y. Yamamoto and H. Sugimoto, *Bull. Chem. Soc. Jpn.*, **53**, 3176 (1980).

5) Y. Yamamoto, *Bull. Chem. Soc. Jpn.*, **55**, 3025 (1982).
6) D. Seyferth and S. O. Grim, *J. Am. Chem. Soc.*, **83**, 1610 (1961).
7) Y. Yamamoto, *Bull. Chem. Soc. Jpn.*, **56**, 1772 (1983).
8) H. Schmidbaur, J. Adlkofer, and M. Heimann, *Chem. Ber.*, **107**, 3697 (1974).
9) H. Schmidbaur, J. Adlkofer, and W. Buchner, *Angew. Chem. Int. Ed. Engl.*, **12**, 415 (1973).
10) H. Schmidbaur, J. Adlkofer, and W. Buchner, *Angew. Chem.*, **85**, 448 (1973).
11) H. Schmidbaur, J. R. Mandl, A. Frank, and G. Huttner, *Chem. Ber.*, **109**, 466 (1976).
12) H. Schmidbaur and R. Franke, *Inorg. Chim. Acta.*, **13**, 85 (1975).
13) H. Schmidbaur and R. Franke, *Angew. Chem.*, **85**, 449 (1973).
14) H. Schmidbaur and J. Eberlein, *Z. Anorg. Allg. Chem.*, **434**, 145 (1977).
15) H. Schmidbaur and H.-J. Füller, *Chem. Ber.*, **107**, 3674 (1974).
16) D. J. Brauer, C. Krüger, P. J. Roberts, and Y.-H. Tsay, *Chem. Ber.*, **107**, 3706 (1974).
17) H. H. Karsch and H. Schmidbaur, *Chem. Ber.*, **107**, 3684 (1974).
18) H. H. Karsch, H.-F. Klein, and H. Schmidbaur, *Chem. Ber.*, **107**, 93 (1974).
19) H. H. Karsch and H. Schmidbaur, *Angew. Chem.*, **85**, 910 (1973).
20) E. Karras, U. Rosenthal, H. Mennenga, and G. Oehme, *Angew. Chem.*, **85**, 913 (1973).
21) H. Schmidbaur and W. Wolfsberger, *Angew. Chem. Int. Ed. Engl.*, **6**, 448 (1967).
22) P. S. Kendurkar and R. S. Tewari, *J. Organomet. Chem.*, **102**, 141 (1975).
23) D. Seyferth and H. M. Cohen, *J. Inorg. Nucl. Chem.*, **20**, 73 (1961).
24) M. C. Henry and G. Wittig, *J. Am. Chem. Soc.*, **82**, 563 (1960).
25) S. O. Grim and D. Seyferth, *Chem. and Ind. Rev.*, 849 (1959).
26) Y. Yamamoto and H. Schmidbaur, *J. Chem. Soc., Chem. Commun.*, **1975**, 668.
27) S. Schmidbaur and W. Richter, *Chem. Ber.*, **108**, 2656 (1975).
28) W. Richter, Y. Yamamoto, and H. Schmidbaur, *Chem. Ber.*, **110**, 1312 (1977).
29) H. Schmidbaur, J. E. Mandl, W. Richter, V. Bejenke, A. Frank, and G. Huttner, *Chem. Ber.*, **110**, 2236 (1977).
30) V. Amirthalingham, V. M. Padmanabhan, and J. Shanker, *Acta Crystallogr., Sec. B*, **16**, 201 (1960).
31) O. Rahlfs and W. Fischer, *Z. Anorg. Chem.*, **211**, 349 (1933).
32) R. E. Rundle and P. H. Lewis, *J. Chem. Phys.*, **20**, 132 (1952).
33) H. Steinfink and G. D. Brunton, *Acta Crystallogr., Sec. B*, **24**, 807 (1968).
34) L. G. Brisseau, M. G. B. Drew, and J. E. Goulter, *J. Chem. Soc., Chem. Commun.*, **1972**, 916.
35) G. E. Coates and F. Glockling, *J. Chem. Soc.*, **1954**, 22.
36) J. L. Atwood and G. D. Stucky, *J. Am. Chem. Soc.*, **91**, 4426 (1969).
37) J. L. Atwood and G. D. Stucky, *J. Chem. Soc., Chem. Commun.*, **1967**, 1169.
38) H. Kato, K. Yamaguchi, and T. Yonezawa, *Bull. Chem. Soc. Jpn.*, **39**, 1377 (1966).
39) J. D. Forrester, A. Zalkin, and D. H. Templeton, *Inorg. Chem.*, **3**, 63 (1964).
40) M. P. Groenewege, J. Smidt, and H. De Vries, *J. Am. Chem. Soc.*, **82**, 4425 (1960).
41) L. O. Brockway and N. R. Davidson, *J. Am. Chem. Soc.*, **63**, 3287 (1941).
42) K. J. Palmer and N. Elliott, *J. Am. Chem. Soc.*, **60**, 1852 (1938).
43) J. C. J. Bart, *J. Chem. Soc. (B)*, **1969**, 350.
44) J. C. J. Bart, *Angew. Chem. Int. Ed. Engl.*, **7**, 730 (1968).
45) A. Michaelis, *Liebigs Ann. Chem.*, **321**, 141 (1902).

 © 1984 The Chemical Society of Japan Bull. Chem. Soc. Jpn., 57, 2839—2846 (1984)

Syntheses and Chelating Properties of Sulfonamidoquinolines

Hiroshi NAKAMURA, Tsukasa YOSHIDA, Masaaki TODOKO, Keihei UENO,† and Makoto TAKAGI*

Department of Organic Synthesis, Faculty of Engineering, Kyushu University, Fukuoka 812

†*Department of Industrial Chemistry, Kumamoto Institute of Technology, 4-22-1, Ikeda, Kumamoto 860*

(Received March 31, 1984)

Seven chelating agents were synthesized. The complexation properties of these reagents with divalent metals (Cu^{2+}, Co^{2+}, Ni^{2+}, Zn^{2+}) were investigated in dioxane-water (75% dioxane, 25% water), and the complex formation constants were compared with those of 8-quinolinol as a reference chelating agent. These sulfonamidoquinoline reagents formed ML and ML_2 type complexes, and the order of complex stabilities followed Irving-Williams' order except for 2-methyl substituted derivatives. With 2-methyl derivatives, Ni^{2+} complexes were less stable than Co^{2+} complexes. Structural characteristics of sulfonamides as chelating agent were discussed in detail.

We have synthesized a series of new sulfonamide reagents, and studied their properties as regards the complexation and the solvent extraction of metal ions.[1-4] The acidity of an amide proton of sulfonamide is comparable to that of phenol, and in this respect sulfonamide-type chelating agents are expected to show a similar complex-forming ability to ordinary phenol-based chelating agents. Experimental studies showed that this is in fact the case.[1-7]

8-Sulfonamidoquinoline derivatives extract transition metal ions as 8-quinolinol do, but they strongly prefer the extraction of copper(II) and do not extract iron(III).[1,3,8,9] To understand somewhat unusual metal extraction behavior of 8-sulfonamidoquinoline as compared with phenolic or β-diketone-type extractants, a measurement of complex formation constants of this series of chelating agents is highly desirable.

In this study, the complex formation constants with divalent metals of sulfonamidoquinolines, 8-(methanesulfonamido)quinoline (**MQ**), 8-(2,4,6-trimethylbenzenesulfonamido)quinoline (8-(mesitylenesulfonamido)quinoline; **MsQ**), 8-(trifluoromethanesulfonamido)-quinoline (**FQ**), 8-(*p*-toluenesulfonamido)quinoline (*p*-**TQ**), 2-methyl-8-(methanesulfonamido)quinoline (**MMQ**), 2-methyl-8-(mesitylenesulfonamido)quinoline (**MMsQ**), and 2-methyl-8-(trifluoromethanesulfonamido)-quinoline (**MFQ**), were investigated by potentiometric method.

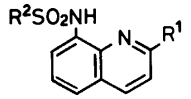

R^1	R^2	Abbrev.
H	CH_3	MQ
CH_3	CH_3	MMQ
H	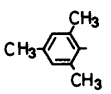	MsQ
CH_3	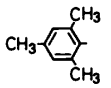	MMsQ
H	CF_3	FQ
CH_3	CF_3	MFQ
H	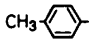	p-TQ

Experimental

*Syntheses of Sulfonamide Reagents. 2-Methyl-8-methanesulfonamidoquinoline (**MMQ**).* To a pyridine solution (15 ml) of 8-amino-2-methylquinoline (1.0 g, 6.32 mmol) was added dropwise a benzene solution of methanesulfonyl chloride (0.793 g, 6.92 mmol) in an ice bath during 1 h. The reaction mixture was gradually warmed to 60°C, and 1 ml of water was added. After stirring for 30 min, the reaction mixture was evaporated under reduced pressure. The residue was dissolved in chloroform, and was washed with diluted sulfuric acid, water, 5% sodium carbonate solution and water, successively. The chloroform solution was dried with sodium sulfate, concentrated, and was chromatographed on a silica-gel column (WAKOGEL C-200, 17×40 mm) with chloroform as an eluent. The main band was collected, and the product was recrystallized from methanol. Yield, 0.83 g (55%). Pale yellow needles. Mp 142.5—143.5°C. IR (KBr disk) 3300 (NH), 1328, 1147 cm^{-1} (SO_2). ^1H NMR (δ ppm from TMS; $CDCl_3$); δ=2.70 (3H, s, CH_3-2), 3.00 (3H, s, CH_3SO_2-), 7.35—8.12 (5H, m, Ar-H). Found: C, 55.90; H, 5.16; N, 11.77%. Calcd for $C_{11}H_{12}N_2O_2S$: C, 55.91; H, 5.12; N, 11.86%.

*8-(Trifluoromethanesulfonamido)quinoline (**FQ**).* To a dichloromethane solution (70 ml) of 8-aminoquinoline (7.2 g, 50 mmol) was slowly added a dichloromethane solution (10 ml) of freshly distilled trifluoromethanesulfonic anhydride (15.3 g, 54 mmol) in the period of 30 min. The mixture was stirred for 1.5 h in an ice bath, and then gradually warmed to 60°C (1h). After the removal of solvent under reduced pressure, the reaction mixture was dissolved in chloroform, and was washed with water. The chloroform solution was dried with sodium sulfate, concentrated, and was chromatographed on a silica-gel column (WAKOGEL C-200, 20×40 mm) with chloroform as an eluent. The main band was collected and the product was recrystallized from chloroform. Yield, 10.8 g (78%). Yellow prisms. Mp 146—147°C. IR (KBr disk) 3140 (NH), 1295, 1145 cm^{-1} (SO_2). ^1H NMR ($CDCl_3$); δ= 7.30—7.75 (3H, m, H-3, -5, and -6), 7.90 (1H, dd, H-7, J=2.6, 6.0 Hz), 8.23 (1H, dd, H-4, J=1.6, 7.8 Hz), 8.81 (1H, dd, H-2, J=4.1, 1.6 Hz). Found: C, 43.35; H, 2.60; N, 10.17%. Calcd for $C_{10}H_7F_3N_2O_2S$: C, 43.38; H, 2.55; N, 10.14%.

*2-Methyl-8-(trifluoromethanesulfonamido)quinoline (**MFQ**).* This compound was prepared in a similar manner to **FQ**. Recrystallized from methanol-chloroform. Yield, 80%. Yellow needles. Mp 137.0—137.5°C. IR (KBr disk) 3165 (NH), 1290, 1154 cm^{-1} (SO_2). ^1H NMR ($CDCl_3$); δ=2.75 (3H, s, CH_3-), 7.37 (1H, d, H-3, J=8.0 Hz), 7.40—7.70 (2H, m, H-5 and -6), 7.85 (1H, dd, H-7, J=6.5, 2.5 Hz), 8.10 (1H, d, H-4, J=8.0 Hz). Found: C, 45.54; H, 3.21; N, 9.65%. Calcd for $C_{11}H_9F_3N_2O_2S$: C, 45.52; H, 3.13; N, 9.65%.

*8-Mesitylenesulfonamidoquinoline (**MsQ**) and 2-Methyl-8-mesitylenesulfonamidoquinoline (**MMsQ**).* These compounds were prepared in a similar manner to **MMQ**. Recrystallized from methanol-chloroform.

MsQ: Yield, 90%. Colorless prisms. Mp 178—179°C. IR (KBr disk) 3305 (NH), 1359, 1150 cm^{-1} (SO_2). ^1H NMR ($CDCl_3$); δ=2.15 (3H, s, CH_3-4'), 2.74 (6H, s, CH_3-2' and -6'),

6.81 (2H, s, H-3′ and -5′), 7.25—7.70 (4H, m, H-3, -5, -6, and -7), 8.11 (1H, dd, H-4, J=2.0, 8.5 Hz), 8.80 (1H, dd, H-2, J=5.0, 2.0 Hz). Found: C, 65.67; H, 5.67; N, 8.48%. Calcd for $C_{12}H_{18}N_2O_2S$: C, 66.23; H, 5.56; N, 8.58%.

MMsQ: Yield 71%. Pale yellow needles. Mp 169—170.5 °C. IR (KBr disk) 3295 (NH), 1157 cm^{-1} (SO_2). ^1H NMR ($CDCl_3$); δ=2.16 (3H, s, CH_3-4′), 2.67 (6H, s, CH_3-2′ and -6′), 2.74 (3H, s, CH_3-2), 6.79 (2H, s, H-3′ and -5′), 7.17—7.68 (4H, m, H-3, -5, -6, and -7), 7.92 (1H, d, H-4, J=8.2 Hz). Found: C, 66.84; H, 6.03; N, 8.22%. Calcd for $C_{19}H_{20}N_2O_2S$: C, 67.03; H, 5.92; N, 8.23%.

*8-(Methanesulfonamido)quinoline (**MQ**) and 8-(p-Toluenesulfonamido)quinoline (p-**TQ**).* These compounds were prepared according to the reported procedure.[7]

Measurement of Acid Dissociation Constants and Complex Formation Constants. Reagent: Dioxane was used immediately after purification. Standard potassium hydroxide (0.1 M (1 M=1 mol dm^{-3})) solution was prepared by the Albert's method.[10] Metal nitrate solutions (0.01 M) were prepared by dissolving the metal nitrate (guaranteed reagents) in distilled water. The concentration was determined by chelatometric titration.[11] Other reagents were of guaranteed grade.

Measurement. Two milliliters of 0.01 M perchloric acid, 2 ml of 0.1 M potassium nitrate, 1 ml of 0.01 M metal nitrate aqueous solution, 2 ml of 0.01 M ligand solution in dioxane, and 13 ml of dioxane were taken in a titration vessel (75% dioxane solution). When acid dissociation constants were determined, 1 ml of water was taken instead of 1 ml of 0.01 M metal nitrate solution. The titration vessel was maintained at 30±0.1 °C. Nitrogen gas which was pre-passed through 75% dioxane-water was slowly passed over the solution throughout the titration. The standard potassium hydroxide solution was added to the stirred solution with small portions together with three times volume of pure dioxane in order to keep the solvent composition constant. All pH measurements were made with GC-195C combined pH electrode (TOA Elect. Ltd.) on HM-15A digital pH meter (TOA Elect. Ltd.).

Evaluation of Acid Dissociation Constants. Since the sulfonamide ligand has one dissociable amide proton and one quinolinic nitrogen, two proton dissociation constants are defined as in Eqs. 1 and 2. Ka_1 and Ka_2 correspond to the dissociation of quinolinium and amide protons, respectively.

$$H_2L^+ \rightleftarrows HL + H^+ : \quad Ka_1 = \frac{[HL][H^+]}{[H_2L^+]}, \tag{1}$$

$$HL \rightleftarrows L^- + H^+ : \quad Ka_2 = \frac{[L^-][H^+]}{[HL]}. \tag{2}$$

First, the pH meter was calibrated in a usual manner against phthalate and phosphate buffers. Then, a standard solution of perchloric acid in 75% dioxane was titrated by standard potassium hydroxide solution while keeping the composition of the solvent constant. A certain constant value (0.55) was found to be added in order to convert the measured (apparent) pH values to $-\log [H^+]$ values, *i.e.*,

$$-\log [H^+] = pH_{app} + 0.55. \tag{3}$$

A titration of standard perchloric acid solution beyond an equivalence point or of pure mixed solvent (with added potassium perchlorate) by standard potassium hydroxide gave an estimation of "conditional" ionic product Kw for the dissociation of water. Thus, for known concentrations of OH^- ion, $-\log [H^+]$ values were obtained according to Eq. 3 from the measured pH_{app} values for the solution. The relationship between $[OH^-]$ and $[H^+]$ was found to be

$$Kw = [H^+][OH^-] = 10^{-17.4}. \tag{4}$$

The conditional Kw value is close to the value of $10^{-17.70}$ reported for the similar solvent (30% water −70% dioxane (v/v)) without added salt.[12]

A conventional treatment of mass balance and equilibrium in solution leads to the following expressions (under conditions, $Ka_1 \gg Ka_2$) which relate proton dissociation constants to the experimentally observable variables. When $0<a<1$,

$$T_{OH} = \frac{-[H^+]^3 - Ka_1[H^+]^2 + (Kw + Ka_1 \cdot T_L)[H^+] + Ka_1 \cdot Kw}{[H^+](Ka_1 + [H^+])}, \tag{5}$$

and when $1<a<2$,

$$T_{OH} = \frac{-[H^+]^3 - Ka_2[H^+]^2 + (Kw + Ka_2 \cdot T_L)[H^+] + Ka_2 \cdot Kw}{[H^+](Ka_2 + [H^+])} + T_L, \tag{6}$$

where T_{OH} is a total concentration of added potassium hydroxide, T_L is a total concentration of ligand, and a is equal to T_{OH}/T_L.

Ka_1 and Ka_2 values were calculated from titration data of ligands in the absence of metal ions (Figs. 1a—1h) by using Marquardt nonlinear least squares method[14] according to Eqs. 5 and 6.

Evaluation of Complex Formation Constants. The complex formation equilibria of sulfonamide reagents in this study with divalent metal ion are generally formulated as follows:

$$M^{2+} + L^- \rightleftarrows ML^+ : \quad K_1 = \frac{[ML^+]}{[M^{2+}][L^-]}, \tag{7}$$

$$ML^+ + L^- \rightleftarrows ML_2 : \quad K_2 = \frac{[ML_2]}{[ML^+][L^-]}. \tag{8}$$

In this study, however, the second proton dissociation constant Ka_2 was sometimes too low to be measured accurately, and it is generally inconvenient to treat the complex formation in terms of the concentration of L^- species. Thus, the equilibria were described in a different way as follows:

$$M^{2+} + HL \rightleftarrows ML^+ + H^+ : \quad K_1' = \frac{[ML^+][H^+]}{[M^{2+}][HL]}, \tag{9}$$

$$ML^+ + HL \rightleftarrows ML_2 + H^+ : \quad K_2' = \frac{[ML_2][H^+]}{[ML^+][HL]}. \tag{10}$$

Then, K_1 and K_2 are related to K_1' and K_2', respectively, as follows:

$$K_1 = K_1'/Ka_2, \tag{11}$$

$$K_2 = K_2'/Ka_2. \tag{12}$$

A treatment of complex formation equilibria leads to Eq. 13, and K_1' and K_2' were calculated from the titration data by nonlinear least squares method in a usual manner.

$$T_{OH} = T_L - A - [H^+] + Kw/[H^+], \quad (13)$$

where,

$$A = \frac{-C+\sqrt{C^2-4BD}}{2B}, \quad (14)$$

$$B = K_1' \cdot K_2'(Kw - T_{OH}[H^+] - [H^+]^2 + 2T_M[H^+]), \quad (15)$$

$$C = K_1'[H^+](Kw - T_{OH}[H^+] - [H^+]^2 + T_M[H^+]), \quad (16)$$

$$D = [H^+]^2(Kw - T_{OH}[H^+] - [H^+]^2). \quad (17)$$

Results and Discussion

Acid Dissociation Constants. Titration curves of sulfonamide ligands in 75% dioxane–water are illustrated in Figs. 1a—1h including 8-quinolinol (**HQ**) as a reference ligand. The ligand concentration could not be increased over 10^{-3} M because of the solubility limitation of the ligand itself or metal complexes derived. At such relatively low concentrations, the proton dissociation constants (p*K*a) lower than 3 or higher than 14 can not be accurately determined by pH measurement; a computer simulation study indicated that pH measurement error of 0.02 pH unit can result in artificial proton dissociation constants of that order of acid strength. Thus, such low or high p*K*a values numerically obtained were not adopted as real constants.

Few equilibrium data have been reported on the complex formation in 75% dioxane–water medium. 8-Quinolinol (**HQ**) and 2-methyl-8-quinolinol (**MHQ**)

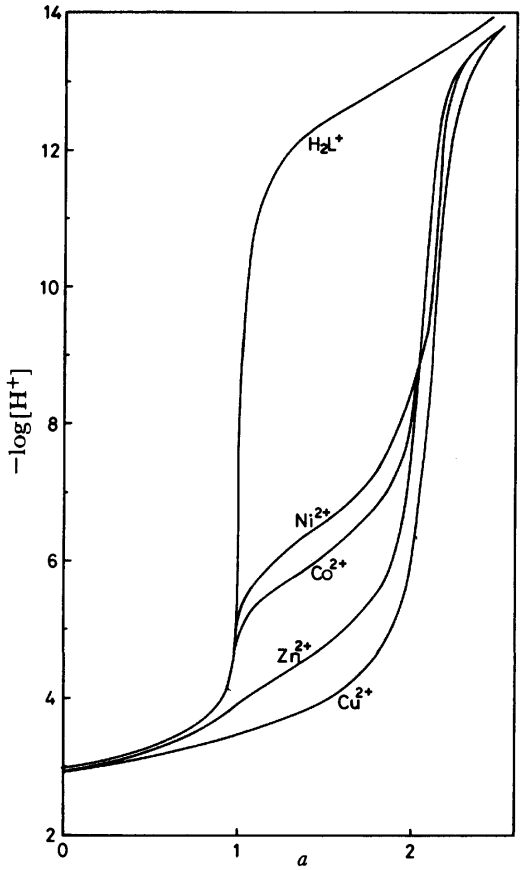

Fig. 1b.

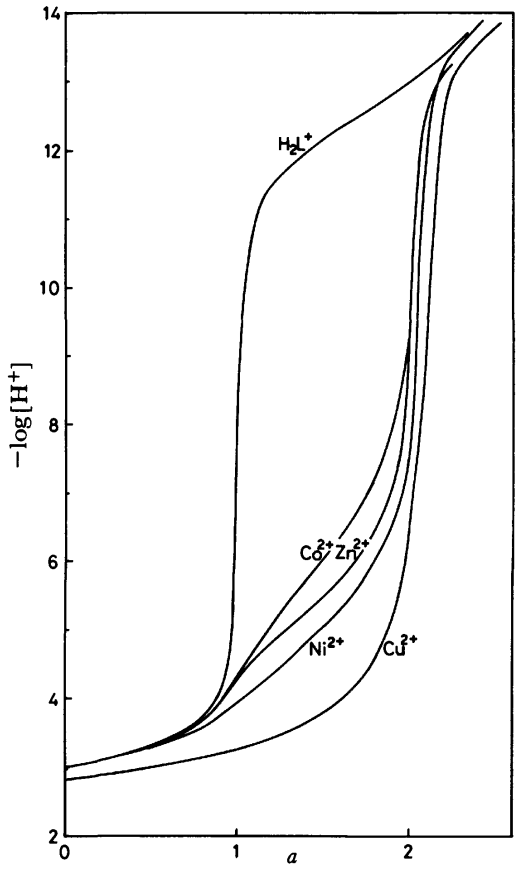

Fig. 1a.

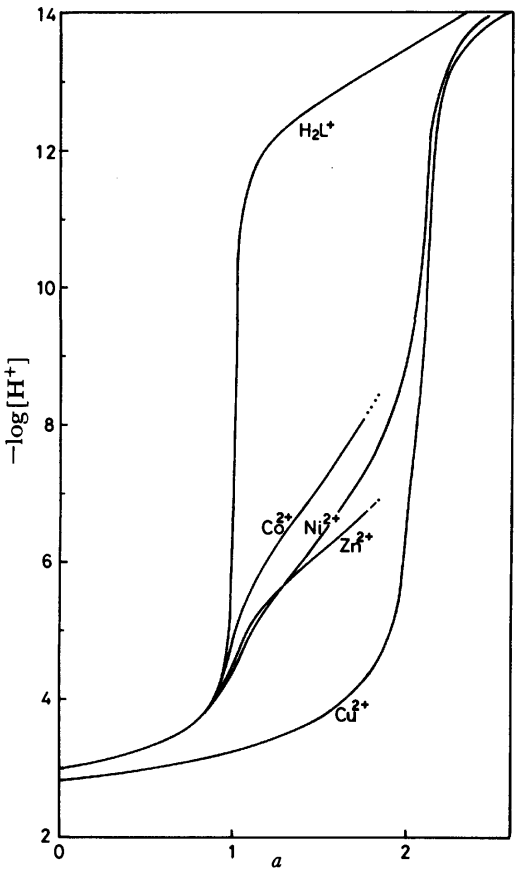

Fig. 1c.

Fig. 1. Titration curves for sulfonamidoquinolines in the absence and presence of metal ions in 75% dioxane–water (v/v) at 30°C: a) **MQ**; b) **MMQ**; c) **MsQ**; d) **MMsQ**; e) **FQ**; f) **MFQ**; g) *p*-**TQ**; h) **HQ**. $[M^{2+}]=[H_2L^+]=1\times10^{-3}$ M, μ=0.1 (KNO_3).

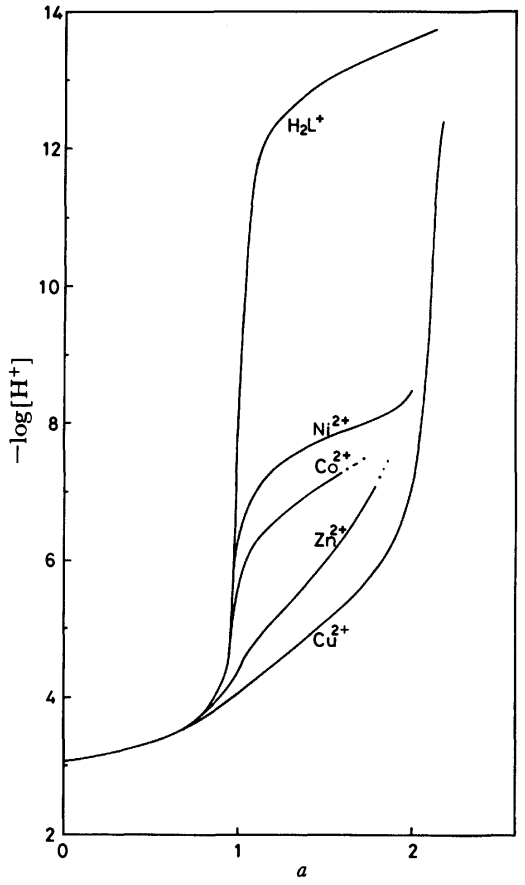

Fig. 1d.

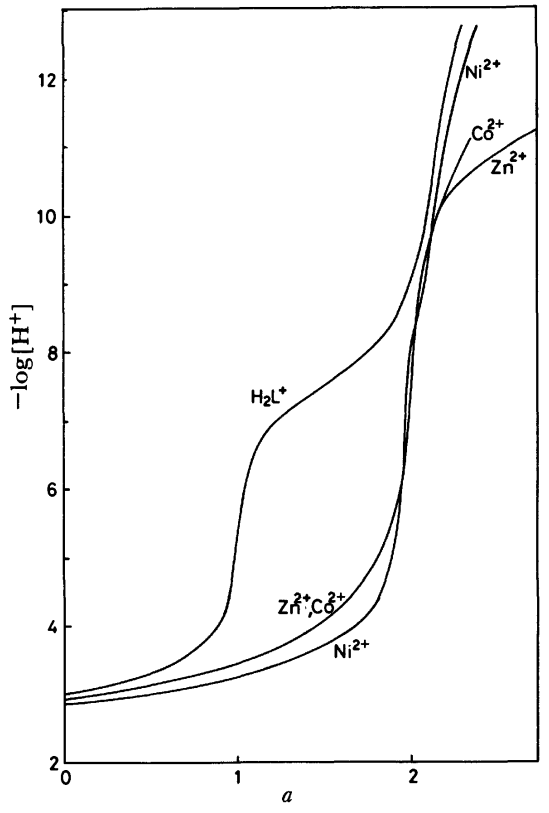

Fig. 1e.

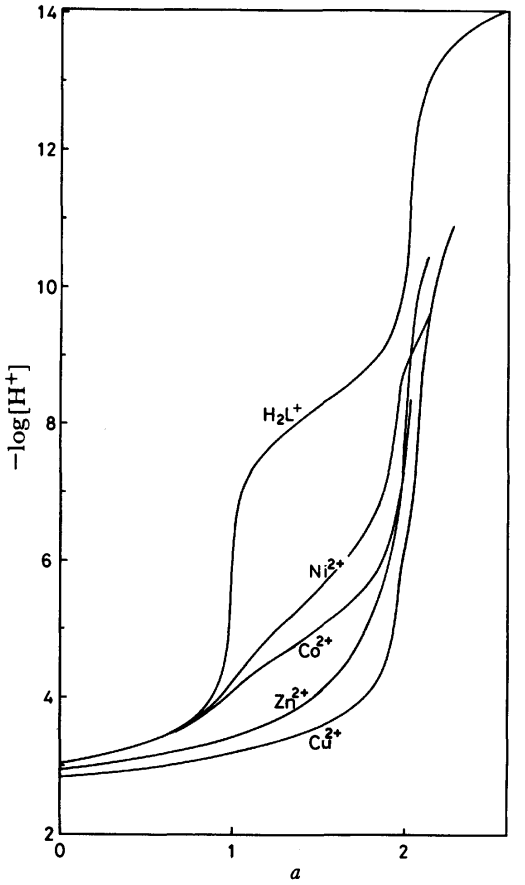

Fig. 1f.

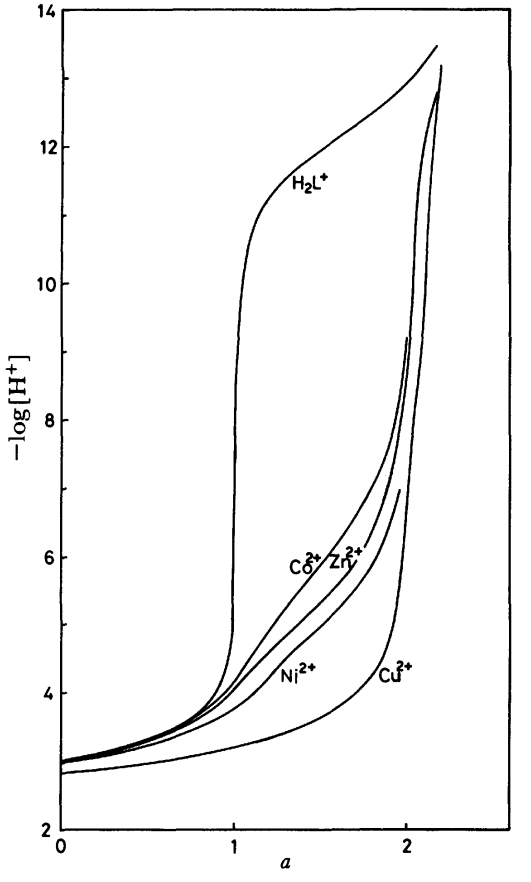

Fig. 1g.

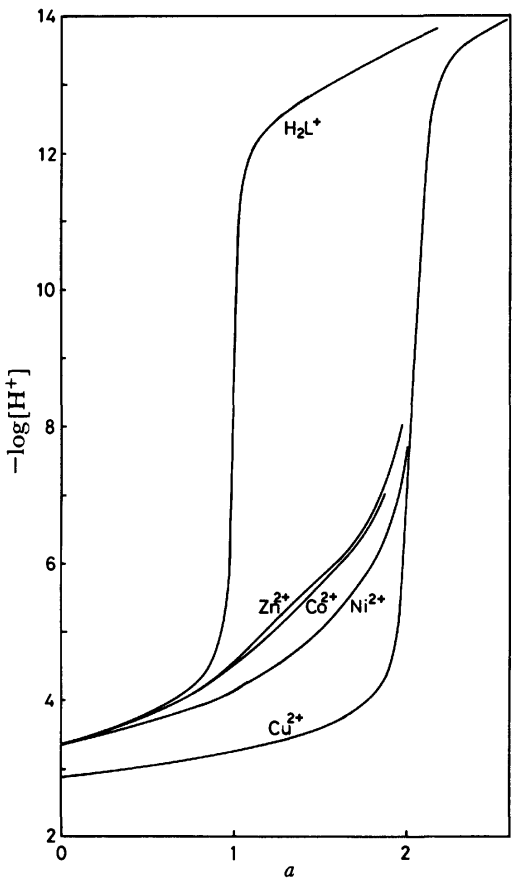

Fig. 1h.

were studied in 50% dioxane-water,[9] and the reported constants are listed in Table 1 for comparison. In the case of 8-quinolinol, the change of 50 to 75% for the volume fraction of dioxane in the medium caused a decrease of 0.56 in pKa_1 and an increase of 1.8 in pKa_2. This is explained that charged species, H_2L^+ and L^- are less stable in organic-rich medium than in water rich solvent.

Complex Formation Constants. Titration curves of the chelating agents in the presence of divalent metal ions are illustrated in Figs. 1a—1h. It is evident from these curves that most ligands including 8-quinolinol form ML and ML_2 type, stable complexes with divalent metal cations. The complex formation constants calculated from these data are summarized in Table 1, K_1 and K_2 values rather than K_1' and K_2' are shown. As mentioned before, the latter values are experimentally more reliable for ligands with high pKa_2 values (log K_2 values for proton association)(>13) since they are free from the ambiguity in the determination of Ka_2. K_1 and K_2 values are obtained by using Eqs. 11 and 12.

The formation constants suffer a considerable medium effect (composition of solvent). Thus, except for Cu^{2+} all of log K_1, log K_2, and log β value are greater in 75% dioxane-water than in 50% dioxane-water. This may be explained in a usual manner that the complex state M-L is more stable than the free metal cation plus L^- state which is more stabilized by hydration in water-rich medium. The increased stability of the complexes in 75% dioxane-water probably holds in sulfonamide ligands.

The orders of stabilities, log K_1, log K_2, log β of 8-sulfonamidoquinolines which do not carry 2-methyl group all follow Irving-Williams' order (*i.e.* $Cu^{2+}>Ni^{2+}>Co^{2+}$). Since **FQ** and Cu^{2+} formed a complex insoluble in 75% dioxane, the stability constants could not be obtained.

The order of metal complex stabilities of 2-methylquinoline derivatives (including 2-methy-8-quinolinol) are $Cu^{2+}>Co^{2+}>Ni^{2+}$, the order of Ni^{2+} and Co^{2+} being reversed from that of Irving-Williams. The difference of log K_1 between Ni^{2+} and Co^{2+} is smaller than that of log K_2. This may be considered that the ML_2 type Co^{2+} complex can assume either tetrahedral or octahedral configuration (chelating ligands of square planar configuration, with coordinated water molecules in axial position), while Ni^{2+} complex takes (distorted) octahedral configuration.[15]

If two 8-sulfonamidoquinoline chelating ligands take square planar configuration around a metal ion, a steric interaction between 2-methyl group of one ligand and 8-sulfonamide group of the other is expected from a molecular model consideration. 2-Methyl group may interact with a coordinated water in the same plane even when a single chelating ligand is bound to the metal. The complex formation constants (log β) for Cu^{2+} and Ni^{2+} are unanimously lowered on introduction of 2-methyl group in 8-sulfonamidoquinoline or 8-quinolinol, inspite of the increased basicity of L^- associated with the methyl substitution. For **MMsQ** where an extremely bulky mesitylenesulfonyl group comes close to the ligand on the opposite side of the plane, nickel complex is expected to become especially unstable. The titration curve (Fig. 1d), however, indicates a considerable pH depression at *a* value above 1. Around this pH region, however, proton dissociation from coodinated water is also expected to take place as a side reaction. In accordance with this, the titration data did not give well-defined K_1 and K_2 values.

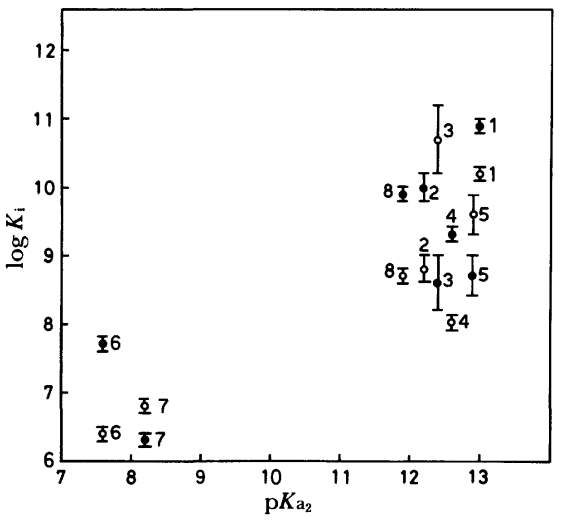

Fig. 2. The relation of log K_1 and log K_2 of Co^{2+} *vs.* pKa_2: ● K_1, ○ K_2; 1) **HQ**, 2) **MQ**; 3) **MMQ**; 4) **MsQ**; 5) **MMsQ**; 6) **FQ**; 7) **MFQ**; 8) *p*-**TQ**.

Table 1. Complex formation constants

Ligand		H^{+} [a]	Cu^{2+}	Zn^{2+}	Co^{2+}	Ni^{2+}
MQ	log K_1	<2	13.6±0.2	10.1±0.1	10.0±0.2	10.8±0.1
	log K_2	12.2±0.1	11.4±0.2	9.8±0.2	8.8±0.2	9.9±0.1
	log β		24.7±0.4	19.7±0.3	18.6±0.4	20.6±0.2
MMQ	log K_1	<2	11.7±0.1	10.9±0.1	8.6±0.4	8.8±0.1
	log K_2	12.4±0.1	12.0±0.2	11.0±0.3	10.7±0.5	9.4±0.1
	log β		23.9±0.3	22.0±0.4	19.3±0.9	18.3±0.2
MsQ	log K_1	<2	14.7±0.3	10.0±0.1	9.3±0.1	10.0±0.1
	log K_2	12.6±0.1	12.1±0.1	9.4±0.2	8.0±0.1	8.7±0.1
	log β		26.9±0.4	19.5±0.3	17.5±0.2	18.8±0.2
MMsQ	log K_1	<2	11.3±0.2	10.7±0.2	8.7±0.3	—[c]
	log K_2	12.9±0.2	11.0±0.2	9.8±0.2	9.6±0.3	—[c]
	log β		22.3±0.4	20.6±0.4	18.3±0.6	—[c]
FQ	log K_1	<2	—[d]	7.7±0.1	7.7±0.1	8.8±0.1
	log K_2	7.6±0.1	—[d]	6.4±0.1	6.4±0.1	7.2±0.1
	log β		—[d]	14.0±0.2	14.1±0.2	16.0±0.2
MFQ	log K_1	<2	9.3±0.2	8.5±0.3	6.3±0.1	6.3±0.1
	log K_2	8.2±0.1	8.4±0.1	7.2±0.2	6.8±0.1	5.5±0.1
	log β		17.7±0.3	15.7±0.4	13.1±0.2	11.8±0.2
***p*-TQ**	log K_1	<2	13.6±0.1	10.2±0.1	9.9±0.1	10.7±0.1
	log K_2	11.9±0.1	11.7±0.1	9.5±0.2	8.7±0.1	9.8±0.1
	log β		25.3±0.2	19.8±0.3	18.6±0.2	20.5±0.2
HQ	log K_1	3.6±0.1	13.0±0.6	10.8±0.1	10.9±0.1	11.6±0.1
	log K_2	13.0±0.1	13.7±0.2	10.2±0.2	10.2±0.1	10.7±0.2
	log β		27.0±0.8	21.0±0.3	21.2±0.2	22.3±0.3
HQ[b]	log K_1	4.16	13.29	9.45	9.65	10.50
	log K_2	11.2	12.61	8.70	8.40	9.77
	log β		25.90	18.15	18.05	20.27
MHQ[b]	log K_1	4.68	11.92	9.06	8.59	8.96
	log K_2	11.3	10.90	8.84	8.79	7.98
	log β		22.82	17.90	17.38	16.94

a) These values listed in the row of log K_1 and log K_2 are for pKa_1 and pKa_2, respectively. b) Data in 50% dioxane-water (v/v), μ=0.1 (Ref. 13). c) The value could not be calculated. d) Precipitated.

Table 2. Complex formation equilibrium constants according to equation 18—20

Ligand		Cu^{2+}	Zn^{2+}	Co^{2+}	Ni^{2+}
MQ	log K_1'	1.4±0.2	−2.1±0.1	−2.2±0.1	−1.4±0.1
	log K_2'	−0.8±0.2	−2.3±0.2	−3.4±0.1	−2.2±0.1
	log β'	0.6	−4.4	−5.6	−3.6
MMQ	log K_1'	−0.7±0.1	−1.5±0.1	−3.8±0.4	−3.6±0.1
	log K_2'	−0.4±0.2	−1.4±0.3	−1.7±0.5	−3.0±0.1
	log β'	−1.1	−2.9	−5.5	−6.6
MsQ	log K_1'	2.1±0.3	−2.6±0.1	−3.2±0.1	−2.5±0.1
	log K_2'	−0.5±0.1	−3.2±0.2	−4.5±0.1	−3.8±0.1
	log β'	1.6	−5.8	−7.7	−6.3
MMsQ	log K_1'	−1.6±0.1	−2.2±0.1	−4.3±0.3	—[a]
	log K_2'	−1.9±0.1	−3.1±0.1	−3.3±0.3	—[a]
	log β'	−3.5	−5.3	−7.6	
FQ	log K_1'	—[b]	0.1±0.1	0.1±0.1	1.2±0.1
	log K_2'	—[b]	−1.2±0.1	−1.2±0.1	−0.4±0.1
	log β'		−1.1	−1.1	0.8
MFQ	log K_1'	1.1±0.2	0.2±0.3	−1.9±0.1	−2.0±0.1
	log K_2'	0.1±0.1	−1.2±0.1	−1.5±0.1	−2.8±0.1
	log β'	1.2	−1.0	−3.4	−4.8
***p*-TQ**	log K_1'	1.7±0.1	−1.8±0.1	−2.1±0.1	−1.3±0.1
	log K_2'	−0.2±0.1	−2.4±0.2	−3.2±0.1	−2.1±0.1
	log β'	1.5	−4.2	−5.3	−3.4
HQ	log K_1'	0.1±0.5	−2.2±0.1	−2.1±0.1	−1.4±0.1
	log K_2'	0.7±0.2	−2.8±0.2	−2.7±0.1	−2.3±0.2
	log β'	0.8	−5.0	−4.8	−3.7
HQ[c]	log K_1'	2.1	−1.75	−1.55	−0.70
	log K_2'	1.4	−2.50	−2.80	−1.43
	log β'	3.5	−4.25	−4.35	−2.13
MHQ[c]	log K_1'	0.6	−2.24	−2.71	−2.34
	log K_2'	−0.4	−2.46	−2.51	−3.32
	log β'	0.2	−4.70	−5.22	−5.66

a) The value could not be calculated. b) Precipiated. c) Data in 50% dioxane-water (v/v), μ= 0.1 (Ref. 13).

The plots of log K_1 or log K_2 against pKa_2 are shown in Fig. 2. The points are classified in two groups, trifluoromethane-sulfonamides and the rest of the sulfonamides. Both log K_1 and log K_2 decrease as pKa_2 decreases when the two groups are compared, indicating that a large decrease in basicity of the ligand inevitably leads to a decrease in nucleophilicity toward metal cations. However, there is no obvious correlation between the complex formation constants and the second proton dissociation constants within the individual group. Similar trends were observed for other metal ions when log K_1 and log K_2 values were plotted against pKa_2.

It is more convenient to consider the structural factors of complex formation in terms of the ion exchange-type equilibria formulated in Eqs. 9 and 10, the equilibrium constants of which do not involve the contribution from the second proton dissociation constants, *i.e.*,

$$\log K_1' = \log K_1 - \mathrm{p}Ka_2, \quad (18)$$

$$\log K_2' = \log K_2 - \mathrm{p}Ka_2, \quad (19)$$

$$\log \beta' = \log K_1 + \log K_2 - 2\mathrm{p}Ka_2. \quad (20)$$

In other words, log K_1' (or log K_2') is expected to reflect the contribution of (i) nucleophilicity of quinoline nitrogen and (ii) steric factors to the free energy of 1:1 (or 1:2) complex formation. In addition, log K_1' and log K_2' can be an indirect measure of an ease of solvent extraction, since the reagents with higher K_1' and K_2' values can extract metal ions under lower pH conditions. Table 2 summarizes these constants.

One first can compare the simplest sulfonamide homologue **MQ** with **HQ**. For clarity, log K_1' and log K_2' values for **MQ** and **HQ** are shown in Fig. 3. The constants K_1' almost parallel in the two chelating agents (for the four metal ions studied). The magnitude of the constants are also quite close to each other. This suggests the chelating behavior of the agents **MQ** and **HQ** toward the four metal ions are similar in nature toward the four metal ions in spite of the difference in the coordinating atoms.

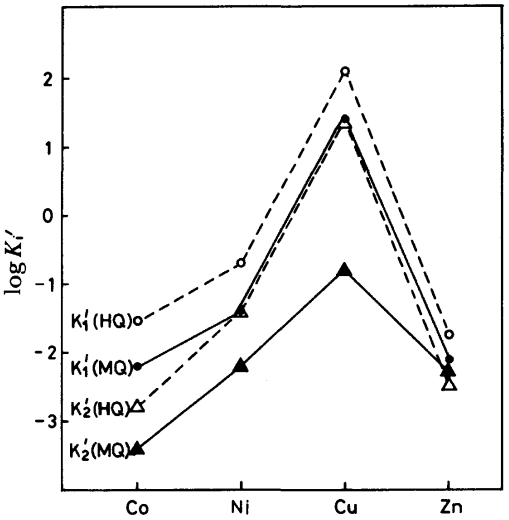

Fig. 3. Comparison of complex formation equilibrium constants K_i' between 8-(methanesulfonamido)quinoline (**MQ**) and 8-quinolinol (**HQ**).

One now looks in Fig. 3 at the log K_2' values of **HQ**, and finds that they almost parallel with the log K_1' values. On the other hand, however, there is no such parallelism in **MQ** metal chelates, *i.e.*, for Cu^{2+} the K_2' value is too low and for Zn^{2+} the value is too high. This suggests that there are some structural factors which lower the formation constant of 1:2 copper(II)-**MQ** chelate. Such structural factors are not easily foreseeable from the analogy between **MQ** and **HQ** mentioned just above. In the same notion, there seems to be some stabilizing factor for the 1:2 zinc(II)-**MQ** chelate as compared with the corresponding **HQ** chelate. A destabilizing effect in 1:2 copper(II) chelate has already been noticed for the sulfonamide chelating agents derived from 2-(aminomethyl)pyridine,[2] and a steric bulkiness of sulfonamido group may be the reason of the destabilization. As to the stabilizing effect in 1:2 zinc(II) chelate (as compared with the corre-

Table 3. Effect of substituents on the stability of metal complexes of 8-sulfonamidoquinolines and 8-Quinolinol[a]

Difference	Constant(K) concerned	Cu^{2+}	Zn^{2+}	Co^{2+}	Ni^{2+}
log K(**MQ**)-log K(**MMQ**)	K_1'	2.1	−0.6	1.6	2.2
	K_2'	−0.4	−0.9	−1.7	0.8
	β'	1.7	−1.5	−0.1	3.0
log K(**MsQ**)-log K(**MMsQ**)	K_1'	3.7	−0.4	1.1	—
	K_2'	1.4	−0.1	−1.2	—
	β'	5.1	−0.5	−0.1	—
log K(**FQ**)-log K(**MFQ**)	K_1'	—	−0.1	2.0	3.2
	K_2'	—	0.0	0.3	2.4
	β'	—	−0.1	2.3	5.6
log K(**p-TQ**)-log K(**MsQ**)	K_1'	−0.4	0.8	1.1	1.2
	K_2'	0.3	0.8	1.3	1.7
	β'	−0.1	1.6	2.4	2.9
log K(**HQ**)-log K(**MHQ**)[b]	K_1'	1.5	0.49	1.16	1.64
	K_2'	1.8	−0.04	−0.29	1.89
	β'	3.3	0.45	0.87	3.53

a) Calculated from the data in Table 2. b) Data in 50% dioxane-water.

sponding 8-quinolinol chelate), there is no reasonable explanation at present.

Table 3 summarizes the effect of substituent (mainly 2-methyl substitution on quinoline ring) on the stability of metal complexes. The positive values indicate destabilization of the complex on methyl-substitution, and the negative values, stabilization. The major effect of substitution shown in the table may be assumed to be those of steric interaction and not those of electronic effect, since, as discussed before, K' value does not include a contribution from the basicity of sulfonamide anion or the proton dissociation constant Ka_2. Electron-donating effect of methyl group which increases the basicity of quinoline nitrogen (see Table 1 for pKa_1 values of **HQ** and **MHQ**) should not be treated lightly, but the net effect of the increase in basicity is to increase the stability of the metal complex in rather a uniform manner irrespective of the nature of metal ion.

It is seen in Table 3 that 2-methyl group on quinoline ring causes a strong overall destabilizing effect (large positive value for β' row in Table 3) on copper(II) and nickel(II) chelates of both 8-sulfonamidoquinoline and 8-quinolinol. A moderate to none destabilizing effect is observed with cobalt(II) chelates, while a stabilizing effect is noticed for zinc(II) chelates of sulfonamides. The increase of stability in zinc(II) chelates of 2-methyl-substituted sulfonamide reagents is at least partially due to the increase in basicity (nucleophilicity) of quinoline nitrogen, since no steric constraints due to methyl substitution are expected in tetrahedral configuration of zinc(II) chelates. However, **HQ** and **MHQ** chelates in Table 3 indicate that the introduction of methyl group causes a decrease in stability even for zinc(II) chelate (though small as compared with copper(II) and nickel(II)). A stabilization of zinc(II) complex with 8-sulfonamide chelating agent as compared with 8-quinolinol has been pointed out earlier. It may deserve further study.

It is important to note that the destabilization by 2-methyl substitution is already pronounced at the formation of *1:1* complex for some metal-ligand combination (Cu-**MMsQ** and Ni-**MFQ** in Table 3). This means that the effect of methyl substitution —whether it can be purely steric or not— is operating not only between the coordinated chelating ligands but also between the chelating ligand and the water both coordinated on the metal.

A change from *p*-toluenesulfonyl to mesitylenesulfonyl group causes a moderate over-all destabilization of the complex except for copper(II) (see β' row in Table 3). In this case, a steric interaction between the chelating ligands seems to be an important factor, since contributions from K_2' term (the value of K_2' row, Table 3) are positive for all the metal ions.

In summary, it is concluded that (i) the coordination behavior toward Co^{2+}, Ni^{2+}, Cu^{2+}, and Zn^{2+} of 8-sulfonamidoquinoline chelating agents quite resemble 8-quinolinol, but (ii) a steric bulkiness of sulfonamido group exerts a destabilizing effect when the configuration of the complex is not tetrahedral. An introduction of methyl group on 2-position of quinoline ring further amplifies the latter effect through a chelating ligand-ligand interaction and through a chelating ligand-coordinated water interaction, leading to destabilization in zinc(II) chelates. The point (ii) above seems to be the most notable feature of sulfonamide reagents, but it is likely that the effect did not work in full for the metal ions herein studied. For metal cations of smaller ionic radius such as Fe^{3+}, a destabilizing effect is expected to be more pronounced. Unfortunately, rather unusual medium used in the present work (75% dioxane) hampered a detailed study on iron(III) chelates.

References

1) M. Takagi, T. Omori, S. Matsuo, S. Matsuno, K. Ueno, and S. Ide, *Chem. Lett.*, **1980**, 387.

2) Y. Moriguchi, T. Yoshimatsu, M. Takagi, and K. Ueno, *Bunseki Kagaku*, **31**, 318 (1982).

3) S. Ide, T. Yoshida, S. Matsuno, M. Takagi, and K. Ueno, *Anal. Chim. Acta*, **149**, 235 (1983).

4) Y. Moriguchi, T. Yoshida, and M. Takagi, *Bunseki Kagaku*, in press.

5) S. U. Kreingol'd, E. A. Bozhevol'nov, and G. V. Serebryakova, *Tr. Vses. Nauchno-Issled. Inst. Khim.* Reaktivov, **25**, 422 (1963); *Chem. Abstr.*, **61**, 82a (1964).

6) D. Betteridge and R. Rangaswamy, *Anal. Chim. Acta*, **42**, 293 (1968).

7) J. H. Billman, N. S. Janetos, and R. Chernin, *Anal. Chem.*, **32**, 1342 (1960); J. H. Billman and R. Chernin, *ibid.*, **34**, 409 (1962).

8) G. A. Kordosky, K. D. Mac Kay, and M. J. Virnig, *Trans. Soc. Min. Eng. AIME*, **262**, 36 (1977).

9) M. Matsumoto, K. Yoshizuka, K. Kondo, F. Nakashio, *J. Chem. Eng. Jpn.*, **17**, 89 (1984).

10) A. Albert and E. P. Serjeant; "Ionization Constants of Acids and Bases, a Laboratory Manual," Methuen & Co., Ltd. (1962).

11) K. Ueno, "Chelatometric Titration," 2nd ed., Nankodo, Tokyo, (1972).

12) H. S. Harned and B. B. Owen; "the Physical Chemistry of Electrolytic Solutions" 3rd ed., Reinhold Publ. Corp., N. Y. (1958) p. 756.

13) R. L. Stevenson and H. Freiser, *Anal. Chem.*, **39**, 1354 (1967).

14) D. W. Marquardt, *J. Soc. Indust. Appl. Math.*, **11**, 431 (1963).

15) The sulfonamide chelating agents formed only "green" complexes with Ni^{2+} in a medium containing water. When the isolated green complex was heated in an organic solvent such as acetone, the complex turned brown (square planar complex) which on addition of water reverted to green complex.

 © 1984 The Chemical Society of Japan Bull. Chem. Soc. Jpn., 57, 2847—2851 (1984)

Solvent Effects on Dimerization of Copper(II) Decanoate in Ketone Solvents

Hiromichi YAMADA,* Kaoru TAKAHASHI, Yukio FUJII, and Masateru MIZUTA
Faculty of Engineering, Gifu University, 1-1, Yanagido, Gifu 501-11
(Received April 9, 1984)

The extraction of copper(II) with decanoic acid in some ketone solvents was carried out at 25 °C and at 0.1 mol/dm^3 ($NaClO_4$) aqueous ionic strength. Organic solvents used are 2-pentanone, 3-pentanone, 2-hexanone, 4-methyl-2-pentanone, 5-methyl-2-hexanone, and 2-octanone. For all solvents, the extracted species are CuA_2, CuA_2HA, Cu_2A_4, and $Cu_2A_4(HA)_2$ (HA: decanoic acid). The dimerization and adduct formation of copper(II) decanoates in each organic phase can be formulated as:

$$CuA_2 + HA \overset{K_{ad,monomer}}{\rightleftharpoons} CuA_2HA,$$

$$Cu_2A_4 + 2HA \overset{\beta_{ad,dimer}}{\rightleftharpoons} Cu_2A_4(HA)_2,$$

$$2CuA_2 \overset{K_{dim-1}}{\rightleftharpoons} Cu_2A_4,$$

$$2CuA_2HA \overset{K_{dim-2}}{\rightleftharpoons} Cu_2A_4(HA)_2.$$

The solvent effects on the dimerization of copper(II) decanoate can be interpreted in terms of the regular solution theory. It was proved that the number of solvent molecules liberated in the formation of the dimeric copper(II) decanoate in ketones was less than that in alcohols.

In a series of investigations[1–7] on the extraction of copper(II) with aliphatic carboxylic acids in various inert solvents, the extracted species has been established to be the dimeric copper(II) carboxylates. On the other hand, by using 1-octanol as solvating solvent, the monomeric copper(II) decanoates were extracted together with the dimeric ones.[8] In the previous work,[9] it has been shown that the monomeric (CuA_2) and dimeric copper(II) decanoates (Cu_2A_4, and $Cu_2A_4(HA)_2$) are responsible for the extraction with decanoic acid in some alcohol solvents and the solvent effects on the dimerization of copper(II) decanoate in the alcohol phase can be interpreted by means of the regular solution theory.

The present paper describes the results of the extraction of copper(II) with decanoic acid in some ketone solvents. Through the comparison of the present results with those obtained for alcohol solvents, it was found that the dimerization constants of copper(II) decanoates in ketones was much larger than those in alcohols and the number of solvent molecules set free in the dimerization of copper(II) decanoate in ketones was less than that in alcohols.

Experimental

Reagents. *Solvents*: 2-Pentanone, 3-pentanone, 2-hexanone, 4-methyl-2-pentanone, 5-methyl-2-hexanone, and 2-octanone of reagent grade were purified by distillation and saturated with distilled water at 25 °C.

Reagent grade 8-quinolinol was used for the spectrophotometric determination of lower concentration of copper in the organic phase.

Copper(II) perchlorate was prepared in the same manner as presented previously.[8]

Sodium perchlorate and decanoic acid were purified by the method described previously.[8]

All other reagents were reagent grade and used without further purification.

Procedure. Experiments were carried out in the same manner as was stated in the previous work.[8]

Apparatus. For mechanical shaking in a thermostat, Taiyo Incubator M-100^N (Taiyokagaku-Kogyo Co., Tokyo) was used. A Orion Research Microprocessor Ionalyzer 901 (Orion Research Inc., USA) and Horiba pH Analyzer F-80 (Horiba Seisakusho Ltd., Kyoto) were used for the determination of hydrogen ion concentration in the aqueous phase. Spectrophotometric determination was carried out on a Shimadzu double-beam type UV-210A Spectrophotometer (Shimadzu Seisakusho Ltd., Kyoto).

Results and Discussion

Distribution of Decanoic Acid. Distribution ratio of decanoic acid between water and the organic solvent is written as follows:

$$D = \frac{C_{HA,o}}{C_{HA,w}} = \frac{K_{D,HA}(1+2K_{dim,HA}K_{D,HA}[HA])}{1+\frac{K_a}{[H^+]}}, \quad (1)$$

where K_a, $K_{dim,HA}$, and $K_{D,HA}$ denote the dissociation constant in the aqueous phase, the dimerization constant in the organic phase, and the partition constant of decanoic acid, respectively. At lower pH where the dissociation of decanoic acid in the aqueous phase is negligible, Eq. 1 is rewritten as:

$$\log D = \log K_{D,HA} + \log (1+2K_{dim,HA}K_{D,HA}[HA]). \quad (2)$$

Distribution ratio of decanoic acid between water and 4-methyl-2-pentanone was illustrated in Fig. 1 as a function of the concentration of decanoic acid in the aqueous phase. In Fig. 1, the concentration of hydrogen ion in the aqueous phase is 10^{-3} mol/dm^3 and the ionic strength in the aqueous phase is 0.1 mol/

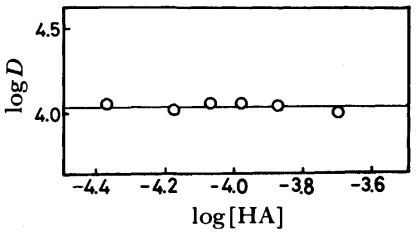

Fig. 1. Distribution of decanoic acid between water and 4-methyl-2-pentanone.
The ionic strength and $[H^+]$ in the aqueous phase are 0.1 mol/dm^3 and 10^{-3} mol/dm^3, respectively.

dm^3 ($NaClO_4$). Under the present experimental conditions the distribution ratio of decanoic acid can be approximated by Eq. 2. As demonstrated in Fig. 1, the distribution ratio of decanoic acid seems to be constant, independent of the concentration of decanoic acid in the aqueous phase. This suggests that the dimerization of decanoic acid in the organic phase (4-methyl-2-pentanone) does not occur to any appreciable extent. Then, the distribution ratio of decanoic acid is equal to the partition constant: $D=K_{D,HA}$. From Fig. 1, the value of log $K_{D,HA}$ obtained was to be 4.04. G. K. Schweitzer and D. K. Morris[10] have reported that the partition constant of octanoic acid between water and 4-methyl-2-pentanone is about 10^3. In addition, it is evident that the increment of the partition constant of carboxylic acid for each methylene group is nearly constant irrespective of solvent, that is, $\Delta\log K_{D,HA}/-CH_2-=0.56$—$0.60$.[11] Then, from these results, the partition constant of decanoic acid between water and 4-methyl-2-pentanone can be expected to be $10^{4.12-4.20}$. This is in fairly good agreement with the present value.

Consequently, under the present experimental conditions, the concentration of the monomeric decanoic acid in the 4-methyl-2-pentanone phase can be adequately approximated by the total concentration of decanoic acid: $[HA]_o=C_{HA}$. For the other ketones used the similar relations are expected to hold.

Distribution of Sodium Perchlorate. In the present work, the ionic strength in the aqueous phase was kept constant by sodium perchlorate. Then, the distribution ratio of sodium perchlorate between water and some ketones were determined under the following experimental conditions: $C_{NaClO_4}=0.1$ mol/dm^3 and $-\log[H^+]=3.5$. The results are summarized in Table 1. The distribution ratio of sodium perchlorate between water and 4-methyl-2-pentanone is reported[12] to be $10^{-2.60}$. The value for 4-methyl-2-pentanone in Table 1 is in fair agreement with this. As shown in Table 1, the distribution ratio of sodium perchlorate for any ketone is extremely small. Thus, the effect of perchlorate ion on the present extraction systems was proved to be negligible.

TABLE 1. DISTRIBUTION RATIO OF SODIUM PERCHLORATE BETWEEN WATER AND SOME KETONES

Solvent	log$D$[a)]
2-Pentanone	−2.24
3-Pentanone	−2.50
2-Hexanone	−2.70
4-Methyl-2-pentanone	−2.82
5-Methyl-2-hexanone	−3.06
2-Octanone	−3.27

a) $C_{NaClO_4}=0.1$ mol/dm^3 and $-\log[H^+]=3.5$.

Extraction of Copper(II) with Decanoic Acid. The extraction equilibrium in the present systems was elucidated according to the previously described manner.[9]

As previously reported, if a j-merized copper(II) decanoate, $Cu_jA_{2j}(HA)_a$ is responsible for the extraction, the extraction equilibrium can be expressed as follows:

$$jCu^{2+} + (2j+a)(HA)_o \rightleftharpoons (Cu_jA_{2j}(HA)_a)_o + 2jH^+,$$

with the extraction constant:

$$K_{ex(ja)} = \frac{[Cu_jA_{2j}(HA)_a]_o[H^+]^{2j}}{[Cu^{2+}]^j[HA]_o^{(2j+a)}}, \quad (3)$$

where the subscript o refers to the organic phase.

From the results obtained for alcohols,[9] it is expected that the monomeric and dimeric copper(II) decanoates are responsible for the extraction of copper(II) with decanoic acid in ketones. Then, the following equation can be expected to hold for the present extraction systems:

$$\log C_{Cu,o} - (\log C_{Cu,w} - 2\log[H^+]) = (2+a)\log[HA]_o + \log K_{ex(1a)} + \log\left(1+\frac{2K_{ex(2p)}}{K_{ex(1a)}}[HA]_o^{(2+p-a)} \cdot C_{Cu,w}[H^+]^{-2}\right), \quad (4)$$

where the subscript w refers to the aqueous phase, and $K_{ex(1a)}$ and $K_{ex(2p)}$ represent the extraction constants of the monomer $CuA_2(HA)_a$ and the dimer $Cu_2A_4(HA)_p$, respectively. By comparing the plot of the values of the left-hand side of Eq. 4 against $(\log C_{Cu,w}-2\log[H^+])$ at constant $[HA]_o$ with the normalized curve, $\log(1+X)$ *vs.* $\log X$, it is confirmed that the monomeric and dimeric copper(II) decanoates are responsible for the extraction. The results obtained for 2-hexanone are shown in Fig. 2. As expected, it was proved that the monomer $CuA_2(HA)_a$ and the dimer $Cu_2A_4(HA)_p$ were extracted into the 2-hexanone phase. The same results were obtained for the other ketones.

In the region where the monomer prevails, it was found by the same approach as in the previous work[9] that the two monomeric copper(II) decanoates were responsible for the extraction and they were CuA_2 and $CuA_2(HA)_a$ ($a \geqq 1$). Then, we have the following expression in the similar manner described in the previous report:[9]

$$\log C_{Cu,o} - (\log C_{Cu,w} - 2\log[H^+]) - 2\log[HA]_o = \log K_{ex(10)} + \log\left(1+\frac{K_{ex(1a)}}{K_{ex(10)}}[HA]_o^a\right), \quad (5)$$

where $K_{ex(10)}$ and $K_{ex(1a)}$ represent the extraction constants of the monomeric species, CuA_2 and $CuA_2(HA)_a$, respectively. By comparing the plot of the values of

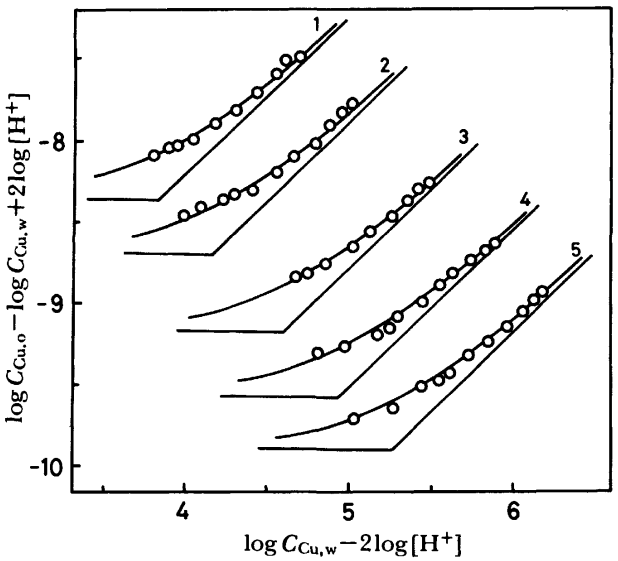

Fig. 2. The identification of the degree of polymerization of Cu(II) decanoates.
C_{HA}; No. 1: 2.0, No. 2: 1.5, No. 3: 1.0, No. 4: 0.7, No. 5: 0.5 mol/dm³. Solvent: 2-hexanone.
Solid curves are the normalized curves, log(1+X) *vs.* log$X$. Solid lines are the asymptotes of the normalized curves.

the left-hand side of Eq. 5 against log[HA]$_o$ with the following normslized curves: log(1+X^n) *vs.* log$X$, we can find the number of decanoic acid molecules involved in another monomeric copper(II) decanoate. The results are shown in Figs. 3a and 3b. As can be seen in Figs. 3a and 3b, for all the solvents the plots fit well the normalized curve with n=1, that is, a=n=1. Thus, CuA_2 and CuA_2HA are found to be responsible for the extraction. From Figs. 3a and 3b, we can also obtain the respective extraction constants $K_{ex(10)}$ and $K_{ex(11)}$ by fitting the normalized curve to the observed values. The results obtained for each solvent are listed in Table 2 together with the other constants.

Subsequently, the composition of the dimeric copper(II) decanoates was determined by the same manner as in the previous paper.[9] It was proved that the dimeric species in each ketone phase were Cu_2A_4 and $Cu_2A_4(HA)_p$($p \geqq 1$). Then, we can obtain the following expression:

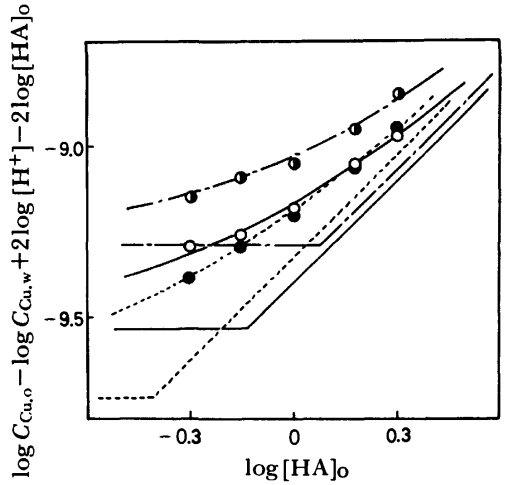

Fig. 3a. Determination of the number of decanoic acid molecules involved in the monomeric Cu(II) decanoates.
Curves are the normalized curves, log(1+X) *vs.* log$X$. Straight lines are the asymptotes of the normalized curves. Solvent; ◑: 3-pentanone, ○: 2-hexanone, ●: 2-octanone.

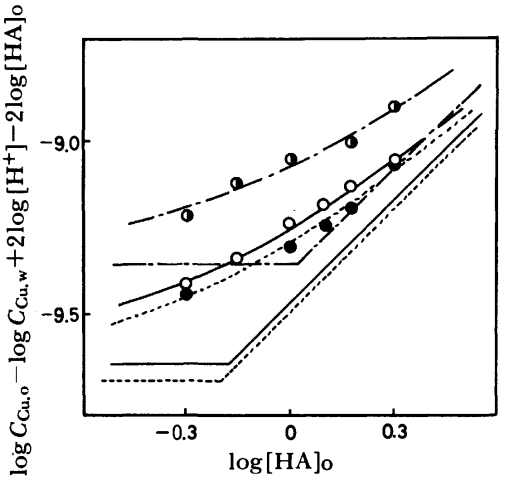

Fig. 3b. Determination of the number of decanoic molecules involved in the monomeric Cu(II) decanoates.
Curves and straight lines are the same as in Fig. 3a. Solvent; ◑: 2-pentanone, ○: 4-methyl-2-pentanone, ●: 5-methyl-2-hexanone.

Table 2. Extraction, dimerization, and adduct formation constants of copper(II) decanoates

	3-Pentanone	2-Pentanone	2-Hexanone	4-Methyl-2-pentanone	5-Methyl-2-hexanone	2-Octanone
$\delta^{a)}$/J$^{1/2}$cm$^{-3/2}$	18.5	18.4	17.7	17.6	17.7	17.8
$V^{b)}$/cm³	106	108	124	126	141	158
log $K_{ex(10)}$	−9.29	−9.36	−9.54	−9.65	−9.70	−9.74
log $K_{ex(11)}$	−9.37	−9.39	−9.40	−9.47	−9.50	−9.33
log $K_{ex(20)}$	−14.70	−14.74	−14.35	−14.34	−14.18	−13.88
log $K_{ex(22)}$	−14.50	−14.74	−14.43	−14.58	−14.44	−14.22
log K_{dim-1}	3.88	3.98	4.73	4.96	5.22	5.60
log K_{dim-2}	4.24	4.04	4.37	4.36	4.56	4.44
log $K_{ad,monomer}$	−0.08	−0.03	0.14	0.18	0.20	0.41
log $\beta_{ad,dimer}$	0.20	0.00	−0.08	−0.24	−0.26	−0.34

a) : Solubility parameter. b) : Molar volume.

$$\log C_{Cu,o} - 2(\log C_{Cu,w} - 2\log[H^+]) - 4\log[HA]_o = \log\left(1+\frac{K_{ex(2p)}}{K_{ex(20)}}[HA]_o^p\right) + \log K_{ex(20)} + \log 2, \quad (6)$$

where $K_{ex(20)}$ and $K_{ex(2p)}$ refer to the extraction constants of Cu_2A_4 and $Cu_2A_4(HA)_p$, respectively. The values of the left-hand side of Eq. 6 were plotted against $\log[HA]_o$. As shown in Figs. 4a and 4b, for all the solvents the plots fit well the normalized curve, $\log(1+X^2)$ *vs.* $\log X$, that is, $p=n=2$. As expected, the dimeric species were Cu_2A_4 and $Cu_2A_4(HA)_2$ irrespective of the solvent. From Figs. 4a and 4b we can also obtain the respective extraction constants, $K_{ex(20)}$ and $K_{ex(22)}$ by fitting the normalized curve to the observed values. The results are summarized in Table 2 together with the other constants.

Consequently, we conclude that the extraction equilibria for the present extraction systems are written as follows:

$$Cu^{2+} + 2(HA)_o \overset{K_{ex(10)}}{\rightleftharpoons} (CuA_2)_o + 2H^+,$$

$$Cu^{2+} + 3(HA)_o \overset{K_{ex(11)}}{\rightleftharpoons} (CuA_2HA)_o + 2H^+,$$

$$2Cu^{2+} + 4(HA)_o \overset{K_{ex(20)}}{\rightleftharpoons} (Cu_2A_4)_o + 4H^+,$$

$$2Cu^{2+} + 6(HA)_o \overset{K_{ex(22)}}{\rightleftharpoons} (Cu_2A_4(HA_2)_o) + 4H^+.$$

Then, the adduct formation and dimerization of copper(II) decanoates in the present ketone solutions can be formulated as:

$$CuA_2 + HA \overset{K_{ad,monomer}}{\rightleftharpoons} CuA_2HA,$$

$$Cu_2A_4 + 2HA \overset{\beta_{ad,dimer}}{\rightleftharpoons} Cu_2A_4(HA)_2,$$

$$2CuA_2 \overset{K_{dim-1}}{\rightleftharpoons} Cu_2A_4,$$

$$2CuA_2HA \overset{K_{dim-2}}{\rightleftharpoons} Cu_2A_4(HA)_2.$$

We can readily calculate the corresponding adduct formation and dimerization constants from the respective extraction constants for each solvent. The values obtained are listed in Table 2 together with the extraction constants. In addition, the dimerization constants of copper(II) decanoate in alcohols[9] are shown in Table 3 for comparison.

Solvent Effects on the Dimerization of Copper(II) Decanoate in the Ketone Solutions. According to the regular solution theory,[13,14] the dimerization constant of copper(II) decanoate, K_{dim-1} is given as follows by the same approach as in the previous work:[9]

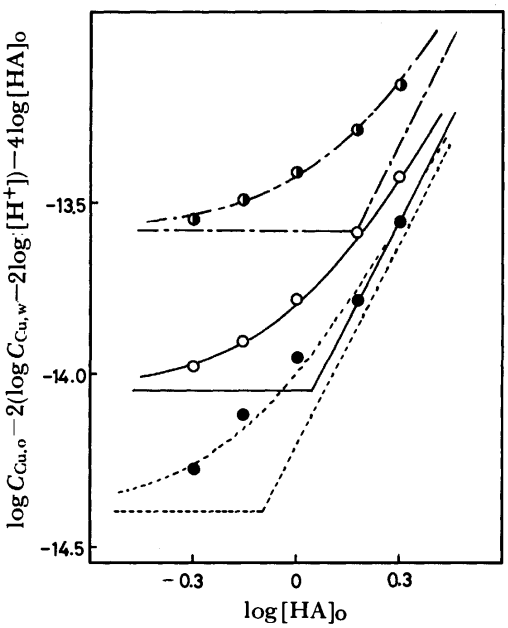

Fig. 4a. Determination of the number of decanoic acid molecules involved in the dimeric Cu(II) decanoates.
Curves and straight lines are the normalized curves, $\log(1+X^2)$ *vs.* $\log X$ and their asymptotes, respectively. Solvent; ◑: 2-octanone, ○: 2-hexanone, ●: 3-pentanone.

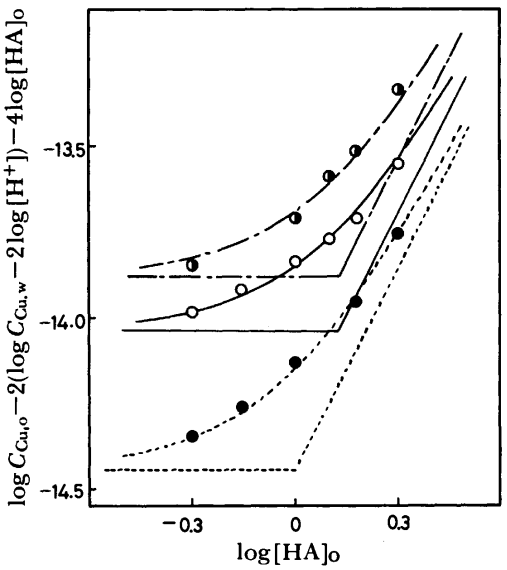

Fig. 4b. Determination of the number of decanoic acid molecules involved in the dimeric Cu(II) decanoates.
Curves and straight lines are the same as in Fig. 4a. Solvent; ◑: 5-methyl-2-hexanone, ○: 4-methyl-2-pentanone, ●: 2-pentanone.

TABLE 3. DIMERIZATION CONSTANTS OF COPPER(II) DECANOATE IN ALCOHOLS[9]

	Cyclohexanol	1-Pentanol	1-Hexanol	1-Heptanol	1-Octanol[8]
$\delta^{a)}/J^{1/2}cm^{-3/2}$	23.3	22.7	22.0	21.5	21.1
$V^{b)}/cm^3$	103	108	125	142	158
$\log K_{dim-1}$	2.23	2.26	2.77	3.04	3.46

a) : Solubility parameter. b) : Molar volume.

$$\log K_{\text{dim}-1} - \log V_s = 0.43nV_s(\delta_s-\delta')^2/RT + \log K_{\text{dim}-1}^\circ - 3, \quad (7)$$

where V_s and δ_s represent the molar volume and the solubility parameter of the solvent, δ' refers to the solubility parameter of copper(II) decanoate, $K_{\text{dim}-1}^\circ$ denotes the dimerization constant of copper(II) decanoate in an ideal solution, and n denotes the number of solvent molecules set free in the dimerization of copper(II) decanoate, that is, $nV_s=2V_{CuA_2}-V_{Cu_2A_4}$, where V_{CuA_2} and $V_{Cu_2A_4}$ represent the molar volume of the monomeric and dimeric copper(II) decanoates, respectively. The optimum δ' value based on the assumption, that the monomeric and dimeric copper(II) decanoates have the same solubility parameter, was found to be 24.1 ($J^{1/2}cm^{-3/2}$) from the previous work.[9] According to Eq. 7, the plot of ($\log K_{\text{dim}-1} - \log V_s$) against $0.43V_s(\delta_s-\delta')^2/RT$ should result in a straight line with a slope of n. The straight line shown in Fig. 5 leads to the validity of Eq. 7. The previous results for alcohol solvents are also implied in Fig. 5 for comparison. The values of n and $\log K_{\text{dim}-1}^\circ$ were calculated to be 2.8 and 3.19, respectively, by the least squares method. The value of n for alcohols was revealed to be 4.5 in the previous paper.[9] Thus, it was proved that the number of solvent molecules liberated in the formation of the dimeric copper(II) decanoate in ketones was less than that in alcohols. This suggests that the solvation of copper(II) decanoates in these two kinds of solvents differs from each other. Taking into account the hydrogen bonding abilities of the two types of solvents, it can be expected that in alcohols the copper(II) decanoates are much more solvated than in ketones. Further, judging from the difference in the n value between alcohols and ketones, the monomeric copper(II) species in alcohols seems to be more extensively solvated compared to the dimeric species. This is consistent with the view that the lower dimerization constant of copper(II) decanoate in alcohols is attributable to the more favorable solvation of the monomeric copper(II) decanoate by alcohol molecules.

On the other hand, as seen in Fig. 5, the intercept of the respective straight lines for alcohols and ketones agreed closely with one another. Then, the dimerization constant of copper(II) decanoate in an ideal solution, which was estimated by the extrapolation of the respective linear plots for alcohols and ketones, were found to be practically equal: $\log K_{\text{dim}-1}^\circ$=3.14 and 3.19, respectively.

Thus, the dimerization of copper(II) decanoate in the organic solvent seems to be strongly influenced by the solvation. The difference between the solvation of copper(II) decanoates in alcohols and ketones can be primarily attributable to the hydrogen bonding abilities of these two types of solvents.

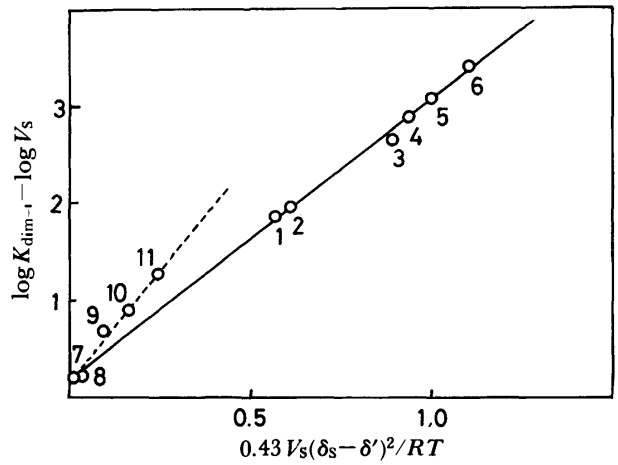

Fig. 5. Correlation of the dimerization constant of Cu(II) decanoate with the solubility parameter of solvents. Solid and dotted lines are the straight lines with a slope of 2.8 and 4.5, and with a intercept of 0.19 and 0.14, respectively. δ'=24.1 ($J^{1/2}cm^{-3/2}$). Ketones; No. 1: 3-pentanone, No. 2: 2-pentanone, No. 3: 2-hexanone, No. 4: 4-methyl-2-pentanone, No. 5: 5-methyl-2-hexanone, No. 6: 2-octanone, Alcohols; No. 7: cyclohexanol, No. 8: 1-pentanol, No. 9: 1-hexanol, No. 10: 1-heptanol, No. 11: 1-octanol.

The authors wish to thank Professor Motoharu Tanaka of Nagoya University for his valuable discussion.

References

1) D. P. Graddon, *Nature*, **186**, 715 (1960).
2) A. W. Fletcher and D. S. Flett, *J. Appl. Chem.*, **14**, 250 (1964).
3) M. Tanaka and T. Niinomi, *J. Inorg. Nucl. Chem.*, **27**, 431 (1965).
4) W. J. Haffenden and G. J. Lawson, *J. Inorg. Nucl. Chem.*, **29**, 1133 (1967).
5) I. Kojima, M. Uchida, and M. Tanaka, *J. Inorg. Nucl. Chem.*, **32**, 1333 (1970).
6) M. J. Jaycock, A. D. Jones, and C. Robinson, *J. Inorg. Nucl. Chem.*, **36**, 887 (1974).
7) H. Yamada and M. Tanaka, *J. Inorg. Nucl. Chem.*, **38**, 1501 (1976).
8) H. Yamada, S. Suzuki, and M. Tanaka, *J. Inorg. Nucl. Chem.*, **43**, 1873 (1981).
9) H. Yamada, R. Kitazaki, and I. Kakimi, *Bull. Chem. Soc. Jpn.*, **56**, 3302 (1983).
10) G. K. Schweitzer and D. K. Morris, *Anal. Chim. Acta*, **45**, 65 (1969).
11) I. Kojima, M. Yoshida, and M. Tanaka, *J. Inorg. Nucl. Chem.*, **32**, 987 (1970).
12) Y. Hasegawa, T. Ishii, and T. Sekine, *Bull. Chem. Soc. Jpn.*, **44**, 275 (1971).
13) J. H. Hildebrand, J. M. Prausnitz, and R. L. Scott, "Regular and Related Solutions," Van Nostrand Reinhold, New York (1970).
14) M. Tanaka, *Z. Phys. Chem.*, N. F., **96**, 239 (1975).

Synthesis and Stereochemistry of (Diamine)(2,9-dimethyl-4,7-diazadecane-2,9-dithiolato)cobalt(III) Complexes and Their Derivatives

Kazuaki YAMANARI,* Norimatsu TAKESHITA, and Yoichi SHIMURA
Department of Chemistry, Faculty of Science, Osaka University, Toyonaka, Osaka 560
(Received April 24, 1984)

Several (diamine)(2,9-dimethyl-4,7-diazadecane-2,9-dithiolato)cobalt(III) complexes, $[Co(SNNS)(diamine)]^+$ (diamine=1,2-ethanediamine and (*R,R*)-1,2-cyclohexanediamine), were prepared and characterized by the visible-UV absorption, circular dichroism(CD), and ^{13}C NMR spectra. The above SNNS quadridentate ligand gave only the *cis-β* geometrical isomer, which was chromatographically separated into two diastereomers owing to the configurations of chiral nitrogen atoms. All the thiolato and the corresponding sulfinato complexes exhibited two CD bands of opposite signs in the $Co(\sigma^*)\leftarrow S(\sigma)$ ligand-to-metal charge transfer band region. The sign pattern was found to be in connection with the absolute configurations of these complexes.

For the complex $[Co(SNNS)(diamine)]^+$ where SNNS denotes a quadridentate ligand having SNNS donor set, three geometrical isomers, *cis-α*-(R^NR^N/S^NS^N), *cis-β*-(R^NR^N/S^NS^N), and *cis-β*-(R^NS^N/S^NR^N), are possible as shown in Fig. 1. One of such quadridentate ligands 3,6-dimethyl-3,6-diazaoctane-1,8-dithiol (H_2endet) gave *cis-α* and *cis-β*-(R^NS^N/S^NR^N) isomers together and the other (*R*)-3,4,6-trimethyl-3,6-diazaoctane-1,8-dithiol(*R*-H_2pndet) gave *Δ-cis-α*-(R^NR^N) and *Δ-cis-β*-(S^NR^N) isomers only.[1] However, the complexes containing these ligands were generally prepared in low yield and unstable in aqueous solutions owing to the air-oxidation. This may be mainly due to the high reactivity of the thiolato group bonded to the primary carbon.

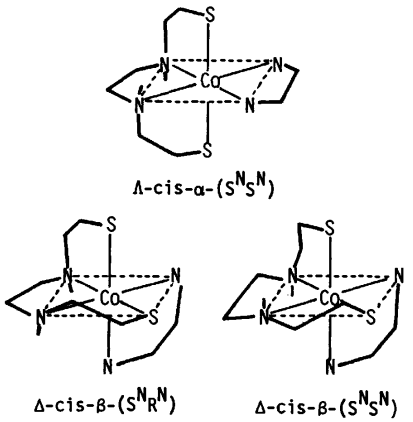

Fig. 1. Three geometrical isomers of [Co(SNNS)-(diamine)]$^+$.

In this paper, a new SNNS quadridentate ligand 2,9-dimethyl-4,7-diazadecane-2,9-dithiol (H_2dddt), where the thiols are attached to the tertiary carbon, was used to prepare several cobalt(III) complexes [Co(SNNS)-(diamine)]$^+$ (diamine=en, *R*-pn, *RR*-chxn, tn, *NN'*-Me_2en, meso-bn, and phen)[2] and their oxidation derivatives. The geometrical and optical isomers were chromatographically separated and characterized by the visible-UV absorption, circular dichroism(CD), and ^{13}C NMR spectra. In this system, only two kinds of *cis-β* isomers, *cis-β*-(R^NR^N/S^NS^N) and *cis-β*-(R^NS^N/S^NR^N), were found. The absolute configurations of the optical isomers were discussed in relation to the CD signs in the first d-d and the $Co(\sigma^*)\leftarrow S(\sigma)$ ligand-to-metal charge transfer (LMCT) band regions.

Experimental

Preparation of 2,9-Dimethyl-4,7-diazadecane-2,9-dithiol (H_2dddt), [$HSC(CH_3)_2CH_2NHCH_2-]_2$: This ligand was prepared according to the reference.[3] ^{13}C NMR (benzene): δ 31.03 (-C(CH_3)$_2$SH), 45.82 (-C(CH_3)$_2$SH), 50.04 (-NHCH_2C-(CH_3)$_2$SH), and 63.80 (-NHCH_2CH_2NH-). Found: C, 51.84; H, 10.21; N, 11.65%. Calcd for H_2dddt·0.07 C_6H_6=$C_{10.42}H_{24.42}N_2S_2$: C, 51.74; H, 10.08; N, 11.56%.

Preparation of cis-β-*[Co(dddt)(diamine)]ClO_4 (Diamine=en,* R-*pn,* RR-*chxn, tn,* NN'-*Me_2en, meso-bn, and phen)*: To a solution of 0.5 g of $[Co(NH_3)_6]Cl_3$ in 30 cm^3 of water was added a mixture of 0.46 g of H_2dddt and 0.24 g of en in 10 cm^3 of water and then a small amount of activated charcoal. The mixed solution was stirred at 70°C for 1 h. After removing the precipitate the filtrate was poured onto a column of SP-Sephadex C-25 (Na^+ form) and eluted with water and then 0.1 mol dm^{-3} $NaClO_4$ to give a dark violet band, which was assigned to *cis-β* isomer by the absorption spectrum. The eluate was concentrated on a rotary evaporator and cooled to give the perchlorate salt. The presence of *cis-α* isomer was undetectable in spite of the repeated experiments. Found for en complex: C, 32.09; H, 6.65; N, 12.30%. Calcd for *cis-β*-[Co(dddt)(en)]ClO_4=$C_{12}H_{30}N_4S_2O_4ClCo$: C, 31.82; H, 6.68; N, 12.37%.

The other complexes of *R*-pn, *RR*-chxn, tn, *NN'*-Me_2en, and meso-bn were prepared according to the same method as that of *cis-β*-[Co(dddt)(en)]ClO_4 except for the use of an appropriate diamine instead of en. Found for *R*-pn complex: C, 33.61; H, 6.91; N, 12.01%. Calcd for *cis-β*-[Co(dddt)(*R*-pn)]ClO_4=$C_{13}H_{32}N_4S_2O_4ClCo$: C, 33.44; H, 6.91: N, 12.00%. Found for *RR*-chxn complex: C, 38.01; H, 7.18; N, 11.03%. Calcd for *cis-β*-[Co(dddt)(*RR*-chxn)]ClO_4=$C_{16}H_{36}N_4S_2O_4$-ClCo: C, 37.91; H, 7.16; N, 11.05%. Found for tn complex: C, 33.65; H, 6.92; N, 12.06%. Calcd for *cis-β*-[Co(dddt)(tn)]ClO_4=$C_{13}H_{32}N_4S_2C_4ClCo$: C, 33.44; H, 6.91; N, 12.00%. Found for meso-bn complex: C, 35.04; H, 7.09; N, 11.68%. Calcd for *cis-β*-[Co(dddt)(meso-bn)]ClO_4=$C_{14}H_{34}N_4S_2O_4ClCo$: C, 34.96; H, 7.13; N, 11.65%. Found for *NN'*-Me_2en complex: C, 35.00; H, 7.16; N, 11.56%. Calcd for *cis-β*-[Co(dddt)(*NN'*-Me_2en)]ClO_4=$C_{14}H_{34}N_4S_2O_4ClCo$: C, 34.96; H, 7.13; N, 11.65%.

The complex *cis-β*-[Co(dddt)(phen)]ClO_4 was prepared as follows: to a solution of 0.5 g of $[Co(CO_3)(phen)_2]Cl$ in 15 cm^3 of water was added a mixture of 0.23 g of H_2dddt and 0.2 g of $(C_2H_5)_3N$ in 5 cm^3 of water. The mixed solution was stirred at 40°C for 1 h and filtered. The filtrate was poured onto a column of SP-Sephadex C-25(Na^+ form) and eluted with 0.1 mol dm^{-3} $NaClO_4$. The brown band was evaporated on a rotary evaporator and cooled to give the desired perchlorate. Found: C, 45.47; H, 5.25; N, 9.64%. Calcd for *cis-β*-[Co-(dddt)(phen)]ClO_4·0.5H_2O=$C_{22}H_{31}N_4S_2O_{4.5}ClCo$: C, 45.40; H, 5.37; N, 9.63%.

Diastereomer Separation of cis-β-*[Co(dddt)(diamine)]$^+$ (Diamine=en and* RR-*chxn)*: An aqueous solution of *cis*-β-[Co(dddt)(en)]ClO_4 was poured onto a column of Dowex 50W×2 (Na^+ from, φ4×5 cm) and eluted with 0.2 mol dm^{-3} Na_2SO_4. Two bands, dark violet (**A1**) and brown (**A2**), were eluted in this order. Each eluate was concentrated by a vacuum evaporator. After repeated removal of Na_2SO_4 deposited, a small amount of NaCl was added to the filtrate to yield the desired crystals. The formation ratio **A1**/**A2** was *ca.* 8, which was almost identical to that determined by the column chromatography of the reaction solution. Found for **A1** isomer: C, 36.74; H, 7.78; N, 14.13%. Calcd for *cis*-β-[Co(dddt)(en)]Cl: $0.25H_2O$=$C_{12}H_{30.5}N_4S_2O_{0.25}ClCo$: C, 36.64; H, 7.81; N, 14.24%. Found for **A2** isomer: C, 36.41; H, 7.70; N, 14.03%. Calcd for *cis*-β-[Co(dddt)(en)]Cl·$0.5H_2O$=$C_{12}H_{31}N_4S_2O_{0.5}ClCo$: C, 36.22; H, 7.85; N, 14.08%.

The column separation using SP-Sephadex C-25 (Na^+ form, φ4×60 cm) was ineffective. The use of $NaClO_4$ or NaCl as an eluent was troublesome because in the former case the desired perchlorate salt crystallized in the column and in the latter case evaporation of the eluate caused coprecipitation of the complex chloride and NaCl. Acidic eluent has been usually used to prevent the racemization *via* proton exchange at secondary nitrogen centers. However, it is well known that the thiolato cobalt(III) complexes give the protonated species in an acid media.[4] In this system, the protonated species caused the band broadening and the significant decrease of the elution rate. Therefore, the column chromatography was achieved under neutral conditions.

In *cis*-β-[Co(dddt)(*RR*-chxn)]$^+$, the Dowex chromatography of the reaction mixture gave two bands, dark violet (**B1**) and brown (**B2**), in this order. The absorption and CD spectral measurements confirmed that the former band contains two species (**B1-I** and **B1-II**) and the latter single one. No solid complex **B1-I** or **B1-II** was isolated because the less soluble pseudo racemate composed of **B1-I** and **B1-II** tended to deposit. The CD spectra of **B1-I** and **B1-II** were measured with the fractionated solutions, whose concentrations were calculated from the measured absorbance using the absorption coefficient of **B1** complex. The formation ratio **B1**/**B2** was 2.8. Found for **B1** complex: C, 37.84; H, 7.17; N, 11.06%. Found for **B2** complex: C, 37.86; H, 7.13; N, 10.97%. Calcd for *cis*-β-[Co(dddt)(*RR*-chxn)]ClO_4=$C_{16}H_{36}N_4S_2O_4ClCo$: C, 37.90; H, 7.16; N, 11.05%.

Preparation and Diastereomer Separation of cis-β-*[Co(dddsi)(diamine)]$^+$ (H_2dddsi=2,9-dimethyl-4,7-diazadecane-2,9-disulfinic Acid, $[HO_2SC(CH_3)_2CH_2NHCH_2-]_2$ and Diamine=en and* R,R-*chxn)*: In general, sulfinato complexes can be prepared *via* H_2O_2 oxidation of the corresponding thiolato complexes. To the reaction mixture of *cis*-β-[Co(dddt)(en)]$^+$ was added an excess H_2O_2 and the resulting solution was kept standing for 3 d. The resulting yellow solution was poured onto a column of SP-Sephadex C-25 (Na^+ form, φ4×60 cm) and eluted with 0.1 mol dm^{-3} Na_2SO_4 to give two yellow bands (**C1** and **C2** in this order). The formation ratio **C1**/**C2** was about 8. Both isomers showed twelve ^{13}C NMR signals and therefore have the *cis*-β geometry. The oxidation of the pure isomer **A1**-*cis*-β-[Co(dddt)(en)]$^+$ yielded only **C1** sulfinato complex. These facts indicate that no isomerization occurs during the oxidation reaction. The solid complexes were isolated by the same way as described above. Found for **C1** isomer: C, 27.04; H, 6.02; N, 10.57%. Found for **C2** isomer: C, 26.85; H, 6.03; N, 10.40%. Calcd for *cis*-β-[Co(dddsi)(en)]ClO_4·H_2O=$C_{12}H_{32}N_4S_2O_9ClCo$: C, 26.94; H, 6.03; N, 10.47%.

The oxidized solution of **B1**-*cis*-β-[Co(dddt)(*RR*-chxn)]$^+$ was separated by a column of Dowex 50W×2 (Na^+ form, φ4×8 cm; 0.15 mol dm^{-3} Na_2SO_4). The earlier eluted fractions (**D1-I**) showed a positive CD band in the spin-allowed first d-d absorption band region and the latter fractions (**D1-II**) a negative and a positive band from the lower energy in the same region. Found for **D1-I** isomer: C, 32.01; H, 6.59; N, 9.21%. Calcd for *cis*-β-[Co(dddsi)(*R*,*R*-chxn)]ClO_4·$1.5H_2O$=$C_{16}H_{39}N_4S_2O_{9.5}ClCo$: C, 32.14; H, 6.57; N, 9.37%. The concentration of **D1-II** was calculated from the measured absorbance by assuming that the absorption coefficient of **D1-II** is the same as that of **D1-I**. The complex **D2**-*cis*-β-[Co(dddsi)(*R*,*R*-chxn)]ClO_4 was obtained by the oxidation reaction of the corresponding **B2** complex. Found: C, 32.74; H, 6.24; N, 9.56%. Calcd for *cis*-β-[Co(dddsi)(*RR*-chxn)]ClO_4·H_2O=$C_{16}H_{38}N_4S_2O_9ClCo$: C, 32.63; H, 6.50; N, 9.51%.

Measurement. The visible and ultraviolet absorption spectra were measured on a Hitachi 330 spectrophotometer and CD spectra with a JASCO MOE-1 spectropolarimeter in

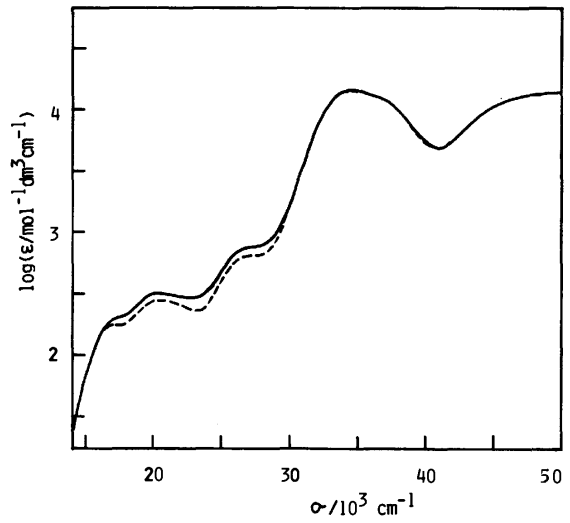

Fig. 2. Absorption spectra of *cis*-β-[Co(dddt)(en)]$^+$: **A1** isomer (——) and **A2** isomer (----).

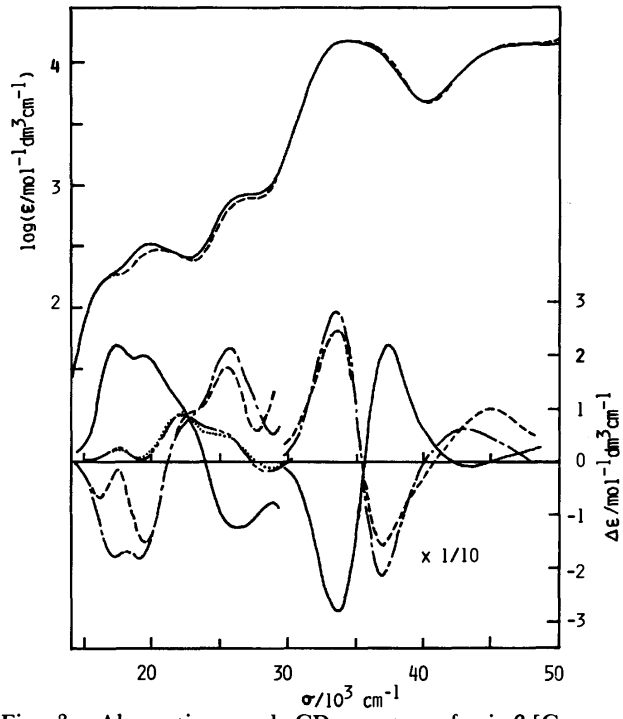

Fig. 3. Absorption and CD spectra of *cis*-β-[Co(dddt)(*RR*-chxn)]$^+$: **B1-I** isomer (——), **B1-II** isomer (———), **B1** isomer (———·———), the calculated curve by the equation $(\Delta\varepsilon_{B1\text{-}I}+\Delta\varepsilon_{B1\text{-}II})/2$ (·····), and **B2** isomer (----).

TABLE 1. ABSORPTION DATA OF *cis*-β-[Co(SNNS)(DIAMINE)]$^+$

SNNS	Diamine	Isomer	Assignment	σ_{max}(log ε)	
				d-d band[a]	CT band[a]
dddt	en	**A1**	(R^NR^N/S^NS^N)	17.2(2.30)[c]	34.42(4.198)
				20.35(2.525)	37.0(4.11)[c]
				27.0(2.90)[c]	47.0(4.15)[c]
		A2	(R^NS^N/S^NR^N)	17.2(2.27)[c]	34.36(4.184)
				20.51(2.470)	37.0(4.10)[c]
				27.0(2.83)[c]	47.0(4.15)[c]
	RR-chxn	**B1**	Λ-$(R^NR^N)(R^CR^C)$	17.2(2.26)[c]	34.42(4.184)
			Λ-$(S^NS^N)(R^CR^C)$	20.20(2.515)	37.0(4.06)[c]
				27.0(2.92)[c]	47.4(4.16)
		B2	Λ-$(S^NR^N)(R^CR^C)$	17.2(2.26)[c]	34.36(4.184)
				20.40(2.464)	37.0(4.09)[c]
				27.0(2.88)[c]	47.4(4.17)
	R-pn[b]			17.1(2.29)[c]	34.41(4.214)
				20.35(2.494)	36.9(4.12)[c]
				27.32(2.861)	47.0(4.16)[c]
	tn[b]			16.8(2.31)[c]	34.08(4.148)
				20.02(2.516)	37.0(4.05)[c]
				26.7(2.91)[c]	46.99(4.111)
	NN'-Me$_2$en[b]			16.26(2.24)[c]	33.66(4.158)
				20.02(2.517)	36.2(4.07)[c]
				26.0(2.87)[c]	45.37(4.115)
	phen[b]			16.61(2.195)	33.44(4.28)[c]
				20.7(2.71)[c]	36.79(4.525)
				27.7(3.50)[c]	39.5(4.28)[c]
					43.96(4.583)
dddsi	en	**C1**	(R^NR^N/S^NS^N)	22.91(2.765)	30.92(4.278)
					34.0(4.15)[c]
					44.94(4.031)
		C2	(R^NS^N/S^NR^N)	22.94(2.747)	30.96(4.260)
					34.0(4.13)[c]
					45.05(4.028)
	RR-chxn	**D1-I**	Λ-$(R^NR^N)(R^CR^C)$	22.73(2.795)	30.63(4.243)
					33.3(4.15)[c]
					44.15(4.028)
		D2	Λ-$(S^NR^N)(R^CR^C)$	22.30(2.770)	30.49(4.246)
					33.5(4.12)[c]
					43.86(4.043)

a) Wave numbers and ε values are given in 10^3 cm^{-1} and cm^{-1} mol^{-1} dm^3, respectively. b) No chromatographic separation for these complexes was attempted. c) Shoulder.

aqueous solutions. The ^{13}C NMR spectra were recorded with a JEOL FX-90Q NMR spectrometer.

Results and Discussion

Characterization of Geometrical Isomers. The absorption spectra and data of [Co(N)$_4$(thiolato)$_2$] type complexes are shown in Figs. 2 and 3 and Table 1. Both isomers **A1**- and **A2**-[Co(dddt)(en)]$^+$ showed very similar absorption spectra. The intense band in 30000—40000 cm^{-1} region, which is assigned to the Co(σ^*)←S(σ) LMCT transition,[5] is composed of two components at 34400 and *ca.* 37000 cm^{-1} for each isomer. Such a spectral pattern is characteristic of *cis(S)* geometry.[1] Therefore, both isomers can be assigned to the *cis*-β geometry. This assignment was confirmed by the ^{13}C NMR spectra (Table 2): each isomer showed twelve or eleven signals, which is consistent with the *cis*-β geometry of C_1 symmetry. The thiolato complexes containing the other diamines were also assigned to *cis*-β isomer on the basis of the absorption spectra.

The yield of the first eluted isomer is considerably higher than that of the second one in either *cis*-β-[Co(dddt)(en)]$^+$ or *cis*-β-[Co(dddt)(*RR*-chxn)]$^+$. For the complexes containing triethylenetetramine (trien) as a quadridentate ligand, the strain minimization cal-

TABLE 2. ^{13}C NMR DATA (ppm FROM Me$_4$Si)[a]

Complex	Chemical shift
A1-[Co(dddt)(en)]$^+$	31.35, 32.94, 36.41, 36.63, 43.29, 46.38, 48.06, 50.28, 52.66, 53.42, 66.69, 68.10
A2-[Co(dddt)(en)]$^+$	31.87, 33.36,[b] 37.20, 44.06, 46.44, 47.50, 49.45, 52.75, 56.08, 66.70, 70.33
C1-[Co(dddsi)(en)]$^+$	20.49, 22.33, 25.90, 26.39, 44.43, 44.81, 51.74, 52.99, 58.57, 60.03, 76.12, 78.94
C2-[Co(dddsi)(en)]$^+$	20.49, 22.33, 25.90, 26.39, 44.16, 44.59, 51.74, 53.04, 58.57, 60.03, 76.07, 78.94

a) All complexes were converted into the soluble sulfate salts for measurement. b) The intensity is *ca.* twice those of others.

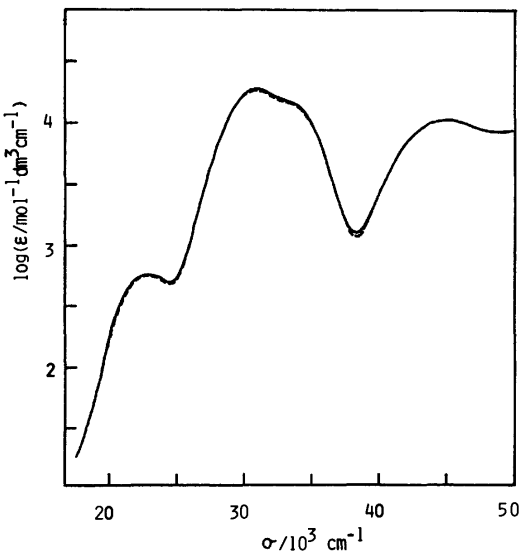

Fig. 4. Absorption spectra of *cis*-β-[Co(dddsi)(en)]$^+$: **C1** isomer (——) and **C2** isomer (----).

culations were carried out by several groups.[6] These calculations indicated that *cis*-β-(R^NR^N/S^NS^N) isomer is more stable than *cis*-β-(R^NS^N/S^NR^N) one. This was experimentally confirmed by the higher yield of *cis*-β-(R^NR^N/S^NS^N) isomer in $[CoX_2(trien)]^{n+}$ (X_2=$NH_2CH_2CO_2^-$,[6b] $2NH_3$,[6c] $2NCS^-$,[7] and $2CN^-$[8]). Therefore, it is reasonable to consider that **A1** isomer has the *cis*-β-(R^NR^N/S^NS^N) structure and **A2** isomer the *cis*-β-(R^NS^N/S^NR^N) one. Similarly **B1** isomer was assigned to a pair of the diastereomers of *Λ-cis*-β-(R^NR^N)(R^CR^C) and *Δ-cis*-β-(S^NS^N)(R^CR^C), but **B2** isomer was found to be stereoselectively composed of *Δ-cis*-β-(S^NR^N)(R^CR^C) as described later. Another empirical criterion of the geometry assignment may be derived from ^{13}C NMR spectra. The chemical shift of *cis*-β-(R^NR^N/S^NS^N) isomer always locates at the higher magnetic field than that of the corresponding *cis*-β-(R^NS^N/S^NR^N) one in all $[CoX_2(trien)]^{n+}$ complexes so far isolated (X_2=$2NH_3$,[6c] $2NCS^-$,[7] $2CN^-$,[8] and en[9]). In the present system, **A1** isomer exhibited the ^{13}C NMR resonances at somewhat higher magnetic field than **A2** one, which leads to the assignment that **A1** and **A2** isomers are *cis*-β-(R^NR^N/S^NS^N) and *cis*-β-(R^NS^N/S^NR^N), respectively. Thus, the same assignment was derived from the formation ratio and the relative position of ^{13}C NMR chemical shift.

The absorption spectra of sulfinato complexes are shown in Figs. 4 and 5 and Table 1. All sulfinato complexes showed the intense LMCT band of two components at 27000—37000 cm^{-1}, which is characteristic for the S-bonded sulfinato complex.[10] Both isomers **C1**- and **C2**-[Co(dddsi)(en)]$^+$ could be assigned to the *cis*-β geometry based on the ^{13}C NMR spectra (Table 2) and the absorption spectral resemblance to *cis*-β-[Co(endesi)(diamine)]$^+$.[1] The formation ratio **C1**/**C2** in the sulfinato complex was almost identical to the ratio **A1**/**A2** in the starting thiolato complex and the oxidation of *cis*-β-(R^NR^N/S^NS^N)-[Co(dddt)(en)]$^+$ (**A1** isomer) gave only **C1** isomer. Therefore, **C1** isomer is assignable to *cis*-β-(R^NR^N/S^NS^N) and **C2** one to *cis*-β-(R^NS^N/S^NR^N). From a similar argument, **D1** isomer was attributed to a pair of diastereomers of *Λ-cis*-β-

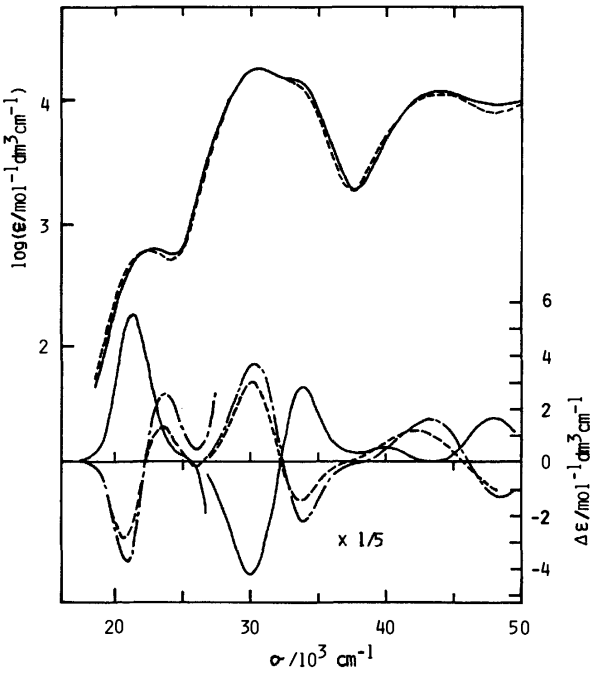

Fig. 5. Absorption and CD spectra of *cis*-β-[Co(dddsi)(*RR*-chxn)]$^+$: **D1-I** isomer (——), **D1-II** isomer (— — —), and **D2** isomer (----).

(S^NS^N)(R^CR^C) and *Λ-cis*-β-(R^NR^N)(R^CR^C), and **D2** isomer to *Λ-cis*-β-(S^NR^N)(R^CR^C).

Synthesis and Property of Cobalt(III) Complexes with SNNS Ligand. Several cobalt(III) complexes of [Co(SNNS)(diamine)]$^+$ type could be prepared using the dddt quadridentate ligand $^-SC(CH_3)_2CH_2NHCH_2CH_2NHCH_2C(CH_3)_2S^-$. This ligand did not react directly with the tris(diamine)cobalt(III) complexes such as $[Co(en)_3]^{3+}$ and $[Co(RR\text{-chxn})_3]^{3+}$, though the endet (R=H) and *R*-pndet ($R=CH_3$) ligands having general skeleton $^-SCH_2CH_2N(CH_3)CH_2CHRN(CH_3)CH_2CH_2S^-$ reacted immediately with these complexes.[1] In the latter ligands, it was found that the mononuclear complex formation is possible only when the remaining two coordination sites are occupied by such tightly bound ligands as diamine, $2CN^-$, and $NH_2CH_2CH_2S^-$. However, in the present dddt ligand, the formation of $[Co(dddt)ox]^-$ ($ox=^-O_2CCO_2^-$) was confirmed by the absorption spectrum. The thiolato complexes with endet or *R*-pndet were liable to oxidation by air in aqueous solutions but the dddt complexes were not. The complete oxidation of the thiolato complex to the sulfinato one with an excess of H_2O_2 necessitated *ca.* 3 d at room temperature in the dddt complex. Such long time was not needed for the endet complexes.[1] These facts indicate that the dddt ligand has not so higher reactivity as the endet or *R*-pndet. This is attributable to the structure of dddt where the thiolate are bonded to the tertiary carbon. A similar situation is encountered between cysteinate(cyst) $NH_2CH(CO_2^-)CH_2S^-$ and penicillaminate(pen) $NH_2CH(CO_2^-)C(CH_3)_2S^-$: The former ligand and its analog $NH_2CH_2CH_2S^-$, where the thiolate is bonded to the primary carbon, tend to form polymeric complexes with μ-thiolato structure because of residual reactivity after coordination.[11] Bis(terdentato)cobalt(III) complex has been

reported only for the penicillaminate.[12]

The endet and *R*-pndet ligands gave both *cis*-α and *cis*-β isomers[1] but the dddt only *cis*-β one. In general, cobalt(III) complexes containing two or three thiolato groups prefer the *cis(S)* geometry as found in *trans(N)*- and *trans(O)*-[Co(D-pen)$_2$]$^-$,[12b] *fac(S)*-[Co($NH_2CH_2CH_2S$)$_3$],[5] and *fac(S)*-[Co(L-cyst)$_3$]$^{3-}$,[5] because of the strong structural trans effect of the thiolato sulfur atom.[13] The fact that only *cis*-β isomers with the *cis(S)* geometry were found in the dddt ligand agrees well with the above general tendency of the thiolato complexes. The endet and *R*-pndet ligands have the methyl group on the nitrogen atoms. The steric repulsion between the two methyl groups may be weakened in the *cis*-α structure rather than in the *cis*-β one, which is responsible for the formation of *cis*-α isomer in the endet and *R*-pndet complexes. A similar substituent effect has been observed for the edda complexes [Co(edda)X_2]$^+$ (edda= ethylenediamine-*N*,*N*′-diacetate and X_2=en or $2NH_3$):[14] A trace of *cis*-β isomer was found for the edda complexes but no *cis*-β isomers for the *N*,*N*′-dimethyl- and *N*,*N*′-diethyl-edda complexes.

A linear flexible edda-type ONNO ligand apparently resembles the present SNNS ligand. In the edda complexes, *cis*-α isomer is dominantly formed[14] and the formation of *cis*-β isomer depends mainly on the properties of the bidentate ligands[15] and the reaction temperature.[16] No couple of *cis*-β isomers, *cis*-β-(R^NR^N/S^NS^N) and *cis*-β-(R^NS^N/S^NR^N), has been known so far,[17] though the possible existence of two *cis*-β isomers in [Co(edda)(H_2O)$_2$]$^+$ and [Co(edda)CO_3]$^-$ was suggested by a ^{1}H NMR study.[15c] The X-ray structural study showed that *cis*-β-[Co(edda)(H_2O)$_2$]ClO_4 is the racemate consisting of Λ-*cis*-β-(R^NS^N) and Δ-*cis*-β-(S^NR^N)[15c] and Δ-*cis*-β-[Co(edda)(*R*-pn)]Cl takes the (S^NR^N) configuration[18] in the crystalline state. Thus, it has been concluded that the (S^NR^N) configuration represents the thermodynamically stable isomer in solution as well as in the solid state.[18] Such conclusion is in good agreement with that for the endet and *R*-pndet complexes where *cis*-α and only *cis*-β-(R^NS^N/S^NR^N) isomers were found. However, two *cis*-β isomers have been found for the present dddt complexes, the *cis*-β-(R^NR^N/S^NS^N) configuration being predominant. The stereochemistry of the dddt complexes resembles that of the trien complexes rather than the edda complexes.

Absolute Configurations of Thiolato and Sulfinato Complexes. The CD spectra are shown in Figs. 3 and 5. **B1-I** isomer showed three positive CD components in the first d-d absorption band region and therefore is assigned to the Λ-*cis*-β-(R^NR^N)(R^CR^C) configuration.[1] Since **B1-II** isomer showed main two negative CD components in the same region, it can be assigned to the Δ-*cis*-β-(S^NS^N)(R^CR^C) configuration. The CD spectrum of less soluble **B1** isomer is the same as that calculated from equimolecular amount of **B1-I** and **B1-II**, which means that **B1** isomer is a pseudoracemate composed of **B1-I** and **B1-II**. Only one diastereomer **B2** was found for the later eluted band. On the basis of the two negative CD bands in the first d-d absorption band region, the Δ-*cis*-β-(S^NR^N)(R^CR^C) configuration is assigned to it. It is noteworthy that such complete stereoselectivity was found in other sys-

TABLE 3. CD DATA OF *cis*-β-[Co(SNNS)(*RR*-CHXN)]$^+$

SNNS	Isomer	Assignment	$\sigma_{ext}(\Delta\varepsilon)$[a]	
			d-d band region	CT region
dddt	**B1-I**	Λ-(R^NR^N)(R^CR^C)	17.39(+2.19)	33.67(−28.2)
			19.34(+1.99)	37.38(+22.0)
			22.4(+1.0)[b]	43.10(−1.03)
			26.25(−1.24)	
	B1-II	Δ-(S^NS^N)(R^CR^C)	17.24(−1.78)	33.56(+28.2)
			19.16(−1.82)	36.90(−21.4)
			22.4(+0.7)[b]	43.1(+6.15)
			25.64(+2.13)	
	B1(B1-I+B1-II)		17.39(+0.27)	
			22.35(+0.90)	
			25.0(+0.59)[b]	
			28.5(−0.18)	
	B2	Δ-(S^NR^N)(R^CR^C)	16.13(−0.67)	33.44(+24.8)
			19.49(−1.53)	36.92(−15.8)
			22.5(+0.88)[b]	45.2(+9.8)
			25.38(+1.78)	
dddsi	**D1-I**	Λ-(R^NR^N)(R^CR^C)	21.32(+5.61)	29.99(−22.1)
				33.84(+14.9)
				40.0(+2.89)
				48.0(+8.66)
	D1-II	Δ-(S^NS^N)(R^CR^C)	20.88(−3.95)	30.30(+19.4)
			23.61(+2.68)	33.96(−11.6)
				43.2(+8.46)
				48.5(+6.72)
	D2	Δ-(S^NR^N)(R^CR^C)	20.75(−2.90)	30.13(+15.1)
			23.53(+1.23)	33.67(−7.12)
			25.9(−0.18)	42.19(+5.97)

a) Wave numbers and $\Delta\varepsilon$ values are given in 10^3 cm^{-1} and cm^{-1}mol^{-1}dm^3, respectively. b) Shoulder.

TABLE 4. THE RELATIONSHIP BETWEEN CD SIGN PATTERNS AND ABSOLUTE CONFIGURATIONS IN THE THIOLATO AND SULFINATO COMPLEXES WITH TWO OR MORE SULFUR DONOR ATOMS

Complex[a]	Structure	$\sigma_{ext}(\Delta\varepsilon)$[b] First d-d band region[c]	$\sigma_{ext}(\Delta\varepsilon)$[b] LMCT region	Ref.
Thiolato complexes				
[Co(endet)(*R*-pn)]$^+$	Λ-*cis*-β-(S^NR^N)(R^C)	16.47(−1.50) 20.75(−1.65)	32.31(+28.2) 36.04(−33.3)	1)
[Co(endet)(*RR*-chxn)]$^+$	Λ-*cis*-β-(S^NR^N)(R^CR^C)	16.31(−1.64) 20.62(−1.85)	32.27(+29.3) 35.84(−31.8)	1)
[Co(*R*-pndet)(en)]$^+$	Λ-*cis*-β-($S^NR^CR^N$)	16.35(−1.32) 20.62(−1.87)	32.21(+26.6) 35.91(−34.0)	1)
[Co(*R*-pndet)(*RR*-chxn)]$^+$	Λ-*cis*-β-($S^NR^CR^N$)(R^CR^C)	16.31(−1.82) 20.64(−2.43)	32.27(+33.5) 35.91(−36.6)	1)
[Co(dddt)(*RR*-chxn)]$^+$	Λ-*cis*-β-(R^NR^N)(R^CR^C)	17.39(+2.19) 19.34(+1.99)	33.67(−28.2) 37.38(+22.0)	e)
	Δ-*cis*-β-(S^NS^N)(R^CR^C)	17.24(−1.78) 19.16(−1.82)	33.56(+28.2) 36.90(−21.4)	e)
	Δ-*cis*-β-(S^NR^N)(R^CR^C)	16.13(−0.67) 19.49(−1.53)	33.44(+24.8) 36.92(−15.8)	e)
[Co(D-pen)$_2$]$^-$	*trans*(*O*)[d]	17.03(+6.96)	34.13(−10.2) 38.03(+12.5)	12b)
	trans(*N*)[d]	19.73(−8.68)	33.73(+36.9) 37.93(−19.5)	12b)
[Co(dpt)$_2$]$^+$	*cis*(*S*)[d]	16.89(+0.79)	33.90(−5.98) 38.68(+10.9)	21)
Sulfinato complexes				
[Co(dddsi)(*RR*-chxn)]$^+$	Λ-*cis*-β-(R^NR^N)(R^CR^C)	21.32(+5.61)	29.99(−22.1) 33.84(+14.9)	e)
	Λ-*cis*-β-(S^NS^N)(R^CR^C)	20.88(−3.95)	30.30(+19.4) 33.96(−11.6)	e)
	Λ-*cis*-β-(S^NR^N)(R^CR^C)	20.75(−2.90)	30.13(+15.1) 33.67(−7.12)	e)
[Co(dti)$_3$]$^{3-}$	Λ	23.8(−3.92)	27.4(+11.2) 35.0(−5.99)	22)
[Co(aesi)$_3$]	Λ-*fac*(*S*)	22.7(+2.04)	31.7(−10.9) 36.4(+7.86)	5)
[Co(L-cysi)(aesi)$_2$]$^-$	Δ-*fac*(*S*)	22.7(−2.87)	31.7(+15.5) 35.7(−13.3)	5)
[Co(L-cysi)$_3$]$^{3-}$	Δ-*fac*(*S*)	22.7(−3.16)	31.8(+18.0) 35.7(−17.2)	5)
[Co(L-cymi)$_3$]	Δ-*fac*(*S*)	22.5(−2.91)	31.7(+15.1) 35.6(−14.8)	5)
[Co(SO$_3$)$_2$(en)$_2$]$^-$	Λ-*cis*(*S*)	21.05(−1.83)	34.25(+25.7) 38.02(−28.7)	19)

a) Ligand abbreviations: Hdpt=$NH_2CH_2CH(SH)CH_2NH_2$, H_2dti=$HO_2SCH_2CH_2SO_2H$, Haesi=$NH_2CH_2CH_2SO_2H$, L-H_2cysi=$NH_2CH(CO_2H)CH_2SO_2H$, and L-Hcymi=$NH_2CH(COOCH_3)CH_2SO_2H$. b) Wave numbers and $\Delta\varepsilon$ values are given in $10^3\,cm^{-1}$ and $cm^{-1}mol^{-1}dm^3$, respectively. c) Only dominant bands are shown. d) The definition of absolute configuration based on the skew pairs of chelate rings is ineffective for these complexes. e) This work.

tem of Λ-*cis*-β-(S^NR^N)-[Co(endet)(*R*-pn or *RR*-chxn)]$^+$ and Λ-*cis*-β-(S^NR^N)-[Co(*R*-pndet)(en or *RR*-chxn)]$^+$.[1] The corresponding Λ-*cis*-β-(R^NS^N) structure has been considered to be less stable in these complexes because of a steric repulsion between the two amine protons on bidentate diamine and the two methylene protons adjacent to the tertiary amine of the quadridentate. The same discussion is effective for the present complex *cis*-β-[Co(dddt)(*RR*-chxn)]$^+$. The configurations of the sulfinato complexes were determined by the CD sign in the first absorption band region, being in agreement with those based on the oxidation reaction of the corresponding thiolato complexes: **D1-I** and **D1-II** isomers are Λ-*cis*-β-(R^NR^N)(R^CR^C) and Δ-*cis*-β-(S^NS^N)-(R^CR^C), respectively, and **D2** isomer Δ-*cis*-β-(S^NR^N)-(R^CR^C).

A clear relationship between absolute configuration and CD sign could be found in the LMCT band region. All the present complexes showed two intense CD bands of opposite signs at 30000—40000 cm^{-1} for the thiolato complexes and at 27000—37000 cm^{-1} for the sulfinato complexes. The sign pattern in this region always relates to that in the first d-d band region, that is, (+)(−)CT from the lower energy corresponds to (−)d-d, and (−)(+)CT to (+)d-d. Therefore, the complexes with (+)(−) and (−)(+) patterns from the lower energy in the LMCT band region can be assigned to the Δ and Λ configurations, respectively.

Table 4 collects the thiolato and sulfinato complexes with two or more sulfur donor atoms. All complexes

have the *cis(S)* geometry and showed two intense CD bands of opposite signs as well as characteristic LMCT absorption band with two components. It is very interesting that the above empirical relationship about absolute configuration is applicable to all thiolato and sulfinato complexes with two or more sulfur donor atoms no matter what the ligands may be. This is exemplified in the system containing monodentate ligand $[Co(SO_3)_2(en)_2]^-$.[19] The thiolato and sulfinato complexes in Table 4 have only CD contribution owing to the skew pairs of chelate rings and their LMCT transitions overlap neither with two d-d transitions nor with the other LMCT transitions such as Co(σ^*)←N(σ), the situations being responsible for the above result. The empirical relationship does not hold for the *trans(S)* complexes such as *cis*-α-[Co(endet)(diamine)]$^+$,[20] *cis*-α-[Co(*R*-pndet)(diamine)]$^+$,[1] and *trans(S)*-$[Co(mp)_2(en)]^+$ (mp=2-pyridinethiolate), because they show the single LMCT band at relatively lower energy. In the complexes containing sulfenato and/or thioether groups, there is also no simple relationship because another CD contribution owing to the chiral sulfur donor atoms adds to that owing to the skew pairs of chelate rings.

References

1) K. Yamanari, N. Takeshita, and Y. Shimura, *Bull. Chem. Soc. Jpn.*, **57**, 1227 (1984).

2) Abbreviations used for ligands are as follows: en=1,2-ethanediamine, *R*-pn=(*R*)-1,2-propanediamine, *RR*-chxn=(*R*,*R*)-1,2-cyclohexanediamine, tn=1,3-propanediamine, *N*,*N*′-Me_2en=*N*,*N*′-dimethyl-1,2-ethanediamine, meso-bn=(2*R*, 3*S*)-2,3-butanediamine, and phen=1,10-phenanthroline.

3) J. Corbin and D. E. Worke, *J. Org. Chem.*, **41**, 489 (1976).

4) I. K. Adzamli, D. L. Nosco, and E. Deutsch, *J. Inorg. Nucl. Chem.*, **42**, 1364 (1980).

5) M. Kita, K. Yamanari, and Y. Shimura, *Bull. Chem. Soc. Jpn.*, **55**, 2873 (1982).

6) a) D. A. Buckingham, P. A. Marzilli, and A. M. Sargeson, *Inorg. Chem.*, **6**, 1032 (1967); b) D. A. Buckingham, M. Dwyer, G. J. Gainsford, V. Jansen, L. G. Marzilli, W. T. Robinson, A. M. Sargeson, and K. R. Turnbull, *ibid.*, **14**, 1739 (1975); c) S. Utsuno, Y. Sakai, Y. Yoshikawa, and H. Yamatera, presented at the 30th Symposium on the Coordination Chemistry of Japan, Tokyo, 1981, Abstract No. 1C18.

7) Y. Sakai, Y. Nokami, H. Kanno, and S. Utsuno, *Chem. Lett.*, **1981**, 371.

8) Y. Nokami, M. Irimichi, Y. Tahata, and S. Utsuno, presented at the 31st Symposium on the Coordination Chemistry of Japan, Sendai, 1981, Abstract No. 3B14.

9) N. Kato, Y. Yoshikawa, and H. Yamatera, presented at the Symposium on the Stereoselectivity and Optical Resolution in Metal Complexes, Nagoya, 1981, Abstract p. 57.

10) C. P. Sloan and J. H. Krueger, *Inorg. Chem.*, **14**, 1481 (1975); B. A. Lange, K. Libson, E. Deutsch, and R. C. Elder, *ibid.*, **15**, 2985 (1976).

11) B. J. McCormick and G. Gorin, *Inorg. Chem.*, **2**, 928 (1963); K. Hori, *Nippon Kagaku Zasshi*, **90**, 561 (1969).

12) a) H. M. Helis, P. de Meester, and D. J. Hodgson, *J. Am. Chem. Soc.*, **99**, 3309 (1977); b) K. Okamoto, K. Wakayama, H. Einaga, S. Yamada, and J. Hidaka, *Bull. Chem. Soc. Jpn.*, **56**, 165 (1983).

13) R. C. Elder, L. R. Florian, R. E. Lake, and A. M. Yacynych, *Inorg. Chem.*, **12**, 2690 (1973); M. Kita, K. Yamanari, K. Kishi, S. Ikeda, and Y. Shimura, *Chem. Lett.*, **1981**, 337.

14) J. I. Legg and D. W. Cooke, *Inorg. Chem.*, **4**, 1576 (1965).

15) a) P. J. Garnett, D. W. Watts, and J. I. Legg, *Inorg. Chem.*, **8**, 2534 (1969); b) P. F. Coleman, J. I. Legg, and J. Steele, *ibid.*, **9**, 937 (1970); c) P. J. Garnett and D. W. Watts, *Inorg. Chim. Acta*, **8**, 293 (1974).

16) K. Kuroda and K. Watanabe, *Bull. Chem. Soc. Jpn.*, **44**, 1034 (1971).

17) D. J. Radanović, *Coord. Chem. Rev.*, **54**, 159 (1984).

18) L. J. Halloran, R. E. Caputo, R. D. Willett, and J. I. Legg, *Inorg. Chem.*, **14**, 1762 (1975).

19) K. Akamatsu, J. Hidaka, and Y. Shimura, *Bull. Chem. Soc. Jpn.*, **50**, 533 (1977).

20) M. Kita, K. Yamanari, and Y. Shimura, *Chem. Lett.*, **1983**, 141.

21) K. Yamanari, N. Takeshita, T. Komorita, and Y. Shimura, *Chem. Lett.*, **1981**, 861.

22) M. Kita, K. Yamanari, and Y. Shimura, presented at the 31st Symposium on the Coordination Chemistry of Japan, Sendai, 1981, Abstract No. 3B15.

 © 1984 The Chemical Society of Japan Bull. Chem. Soc. Jpn., 57, 2859—2862 (1984)

Selective Adsorption of Molybdenum(VI) and/or Vanadium(V) Using Cross-linked Polystyrene Resins with Bis(2-hydroxyethyl)-amino, Bis(carboxymethyl)amino, and Bis-(phosphonomethyl)amino Groups

Masato NISHIZAWA,* Toshiro YOKOYAMA, Tetsuo KIMURA, and Toshishige M. SUZUKI*
Government Industrial Research Institute, Tohoku. 4-2-1, Nigatake, Sendai 983
(Received April 27, 1984)

Styrene–divinylbenzene copolymers containing $-N(CH_2CH_2OH)_2$, $-N(CH_2CO_2H)_2$, and $-N(CH_2PO(OH)_2)_2$ moieties have been synthesized and applied to the selective adsorption of molybdenum and/or vanadium from aqueous solution. The equilibrium adsorption capacity *vs.* pH correlation and exchange kinetics of the resins for Mo^{VI} and V^{V} have been studied. The resin containing bis(2-hydroxyethyl)amino group is particularly effective for the selective recovery of Mo^{VI} and/or V^{V} by column operation due to its high adsorption capacity and faster exchange rate, whereas other resins required much longer time to attain adsorption equilibrium. The bis(2-hydroxyethyl)amino resin was used for the selective recovery of molybdenum from an acid-leaching solution of waste desulfurization catalyst.

In all industrialized countries a significant proportion of the metals consumed by industry should be provided by recycling of used metals. Therefore it is important to achieve a process to recover metals from scrap and industrial wastes. Waste catalysts used in the desulfurization of petroleum contain appreciable amounts of molybdenum and vanadium.[1] We have been searching for highly selective chelating resins in order to recover these metals from acid-leaching solution. Multidentate ligands containing bis(carboxymethyl)amino group(s) are known to form stable complexes with oxomolybdenum(VI) and oxovanadium(V) ions.[2,3] The selective adsorption of these metal ions has been demonstrated by polymer-immobilized iminodiacetic acid[4,5] and *N*-[2-(2-pyridyl)ethyl]ethylenediamine-*N*,*N*′-diacetic acid.[5]

We have recently prepared cross-linked polystyrene resins containing a series of multidentate ligands as discrete units to attain a high adsorption capacity and selectivity.[6,7] In our preliminary work we found that those resins which contain bis(2-hydroxyethyl)amino and bis(phosphonomethyl)amino moieties have a potential utility for selective adsorption of oxometal ions.[8] In the present paper we deal with a detailed study on the adsorption of Mo^{VI} and/or V^{V} using chelating resins having bis(2-hydroxyethyl)amino (HEA), bis(carboxymethyl)amino (CMA), and bis(phosphonomethyl)amino (PMA) moieties as depicted in Fig. 1 to elucidate the correlation of the adsorption characteristics with the properties of the functional groups. The application of the resins for the selective recovery of molybdenum from the acid-leaching solution of waste catalyst has been studied.

Experimental

Materials. Reagent grade $Na_2MoO_4 \cdot 2H_2O$, $K_2MoO_4 \cdot 5H_2O$, NH_4VO_3, and ethylenediamine-*N*,*N*,*N*′,*N*′-tetraacetic acid (EDTA) were used without further purification. *N*,*N*,*N*′,*N*′-Tetrakis(2-hydroxyethyl)ethylenediammonium bis(perchlorate) (THEED·$2HClO_4$)[9] and *N*,*N*,*N*′,*N*′-tetrakis-(phosphonomethyl)ethylenediamine (EDTPO)[10] were prepared by the reported methods and identified by ^{1}H-NMR and ^{13}C-NMR spectroscopy. Gel-type of polystyrene-2%-divinylbenzene copolymer beads (200—400 mesh, Kanto Chemical Co.) were used as the polymer matrix of the chelating resins.

Leaching Solution of Desulfurization Catalyst. Metal ions were leached from waste desulfurization catalyst by treatment with 4 M HCl (1 M = 1 mol dm^{-3}) as described previously.[5] The main components in the leaching solution were molybdenum, vanadium, and aluminium, of which the latter two metals originated from crude oil and catalyst support (Al_2O_3), respectively.

Preparation of the Chelating Resins. Polystyrene beads were chloromethylated followed by functionalization with diethylenetriamine (*dien*) to give a *dien*-resin in which *dien* is linked to the polymer uniquely through the imino group.[6,7] The *dien*-resin was used as the starting material for the preparation of *N*-substituted derivatives.

HEA Resin: The *dien*-resin (11 g) was stirred with aqueous ethylene oxide (9.6 g in 100 cm^3) for 3 h under ice-cooling. After standing overnight at room temperature, the resin beads were filtered, washed throughly with water, ethanol, and diethyl ether, and then dried *in vacuo* at 50°C. Yield: 19.5 g. Nitrogen analysis: 7.3%.

CMA and PMA resins were prepared by carboxymethylation and phosphonomethylation of the *dien*-resin as described previously.[7] Nitrogen analyses of CMA and PMA resins were 7.7 and 6.5%, respectively.

Determination of Adsorption Capacity. A batchwise technique was used to determine the equilibrium adsorption capacity (amount of metal adsorbed on one gram of dry resin) with metal ion always being excess over the resin capacity.

Typically, 100 mg of dry resin was added to 100 cm^3 of metal

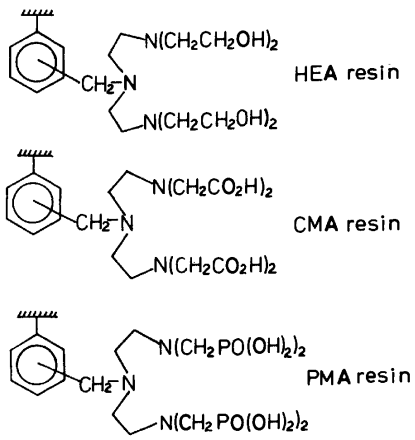

Fig. 1. Polymer-immobilized multidentate ligands.

ion solution of various pH and the mixture was shaken at room temperature. After equilibrium was attained, the concentration of the remaining metal ion in the supernatant was analyzed by atomic absorption spectrometry. The capacity of the resins was calculated by the change in the metal concentration observed.

Adsorption Rate. Time-course experiments for the adsorption of metal ion were carried out under a batchwise procedure: To a buffered metal solution (2—4 mM) was added 500 mg of resin which was swollen with water in advance. While stirring, small portions of the samples were withdrawn at appropriate intervals and analyzed as described above.

Kinetic Runs. Complex formation kinetics of THEED, EDTPO, and EDTA with Mo^{VI} was studied at 25 °C in the pH regions 3.9—5.6, 3.7—6.1, and 4.5—6.8, respectively. The reaction was followed spectrophotometrically at 270 nm by a stopped-flow technique. The kinetic runs were carried out under pseudo-first-order conditions, ligand concentration being in excess (3×10^{-3} M) over Mo^{VI} (1×10^{-4} M). The pH was adjusted with perchloric acid and sodium hydroxide solution at an ionic strength of 0.5 ($NaClO_4$). Plots of log $(A_\infty-A_t)$ against time gave straight lines until the reaction reached 85% completion.

Column-breakthrough Experiments. A 5 g sample of chelating resin was swollen with water and poured onto a glass column (ϕ 1.3 cm). The column was conditioned with dilute HCl (pH 1) in advance, then the metal ion solution was passed through the column continuously at a rate of 1.5 $cm^3\,min^{-1}$. The effluent was fractionated into 10 cm^3 portions and the amount of metal ion was determined. The adsorbed molybdenum and/or vanadium was liberated from the column by elution with 1 M sodium hydroxide solution. The resin was regenerated by this procedure and used in the successive operation.

A similar column operation was applied to the actual leaching solution of waste catalyst in which various foreign metal ions other than molybdenum and vanadium were also present. The concentration of the components in the feed solution were 360, 220, 53, 15, 4, and 3 ppm for Mo, V, Al, Co, Ni, and Fe, respectively.

Measurements. The ^1H-NMR and ^{13}C-NMR were obtained with a JEOL FX-100 spectrometer with sodium 3-(trimethylsilyl)-1-propanesulfonate as the internal standard. UV spectra were recorded with a Hitachi 100-60 spectrophotometer. The metal ion concentration was determined with a Shimadzu atomic absorption/flame photometer Model AA-610S. The complexation reaction was followed by a stopped-flow method using a Union Giken RA 601 with a data processor and an X-Y recorder.

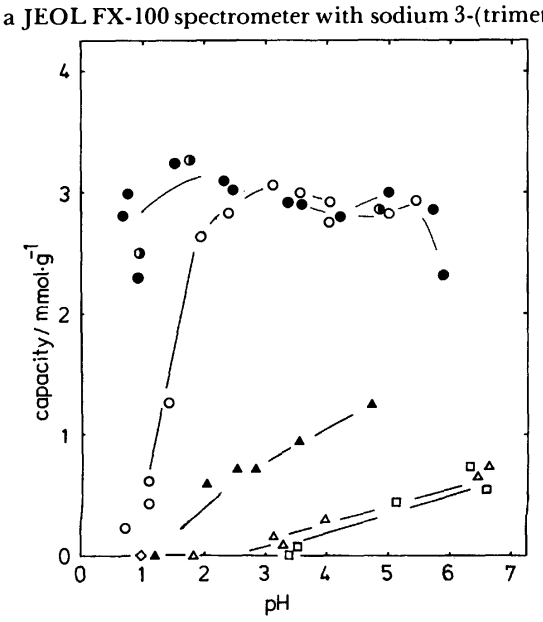

Fig. 2. Adsorption capacity of HEA resin as a function of pH.
-●-: Mo^{VI}, -○-: V^V, -▲-: Cu^{2+}, -△-: Ni^{2+}, -□-: Co^{2+}, -◇-: Al^{3+}, -◑-: Mo^{VI}, in the presence of 1500 ppm of SO_4^{2-}.

Results

Preparation of the Chelating Resins. The chelating resins used in the present study were derived from diethylenetriamine which was immobilized on polystyrene through the imino nitrogen.[6,7] The HEA resin was prepared by treatment of the *dien*-resin with aqueous ethylene oxide solution. *N*-Carboxymethylation and *N*-phosphonomethylation of the *dien*-resin yielded the CMA resin and PMA resin, respectively. Nitrogen analyses indicated that the HEA, CMA, and PMA resins formally contain 1.7, 1.8, and 1.6 mmol of the functional group per gram resin, respectively. All the resins have a satisfactory stability over a wide pH range.

Equilibrium Adsorption. The adsorption capacity *vs.* pH profiles of the resins are given in Figs. 2, 3. The amount of Mo^{VI} adsorbed on one gram of resin are approximately 3 mmol over pH 1—6 irrespective of the functional group. Thus, the ratios of Mo^{VI} capacity to the content of functional group are in the range 1.8—2.0. Previously we reported the capacity of the CMA resin for Mo^{VI} to be 1—1.5 mmol g^{-1} by allowing the resin for 3 h in a metal solution.[5] However a slower adsorption step took place subsequently and the equilibrium was attained after seven days. In any case, the capacities for Mo^{VI} and V^V are markedly decrease in alkaline solution (pH 10) in which pH region the functional groups coordinate to the metal species with difficulty.[11] Therefore adsorbed Mo^{VI} and V^V were readily liberated from the resin on treatment with dilute sodium hydroxide solution. The adsorption capacities

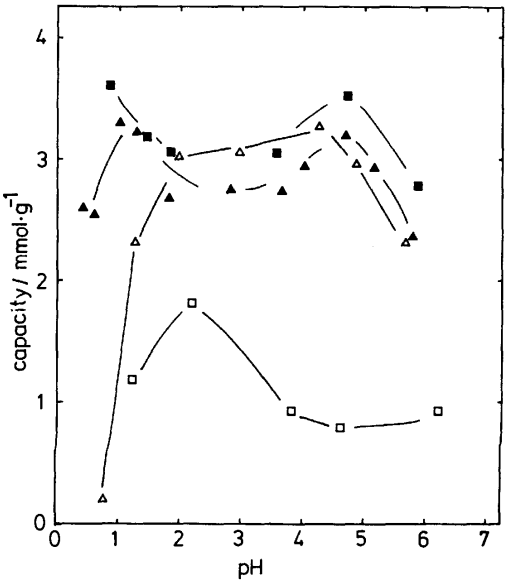

Fig. 3. Adsorption capacity of CMA and PMA resins for Mo^{VI} and V^V as a function of pH.
-■-: Mo^{VI}-CMA resin, -□-: V^V-CMA resin, -▲-: Mo^{VI}-PMA resin, -△-: V^V-PMA resin.

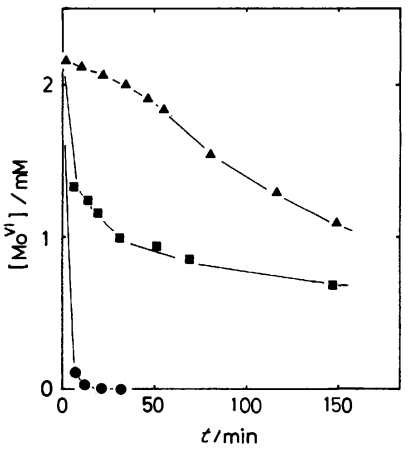

Fig. 4. Adsorption time-course of Mo^{VI} at pH 4.
-●-: HEA resin, -■-: CMA resin, -▲-: PMA resin.

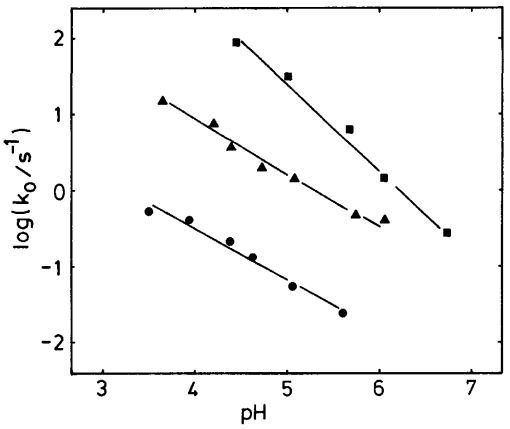

Fig. 5. Conditional first-order rate constant of Mo^{VI} complex formation as a function of pH.
-●-: THEED, -▲-: EDTPO, -■-: EDTA.

of the present resins were reproducible over several adsorption-regeneration cycles. Apparent selectivity was observed for all the resins, the capacities for vanadium at pH below 2.0 is remarkably lower than those for molybdenum. In addition, these resins revealed very little affinity for the common metal cations including Al^{3+}, Cu^{2+}, Co^{2+}, Ni^{2+}, Fe^{2+}, at pH lower than 3.0.

Complexation Kinetics. The time-course of Mo^{VI} adsorption on the present resins was followed by monitoring the concentration in the aqueous phase at pH 4 and the results are shown in Fig. 4. The HEA resin can adsorb the metal ion rapidly and equilibrium was attained within 3 min, while the CMA and PMA resins required much longer time for equilibration under identical conditions. A similar trend was observed at pH 1 for Mo^{VI} uptake and at pH 4 for V^{V}. As mentioned above, the adsorption of Mo^{VI} by CMA resin involves two steps, *i.e.*, rapid adsorption took place in the initial 1 or 2 h followed by a second slower step which required extremely long time for equilibration.

The rate of complexation between functional groups and Mo^{VI} was estimated by model reactions employing ethylenediamine derivatives, THEED, EDTA, and EDTPO. The absorption intensity of aqueous Mo^{VI} solution at 300—200 nm region increases on addition of the ligands and was monitored spectrophotometrically. Figure 5 shows the profile of the pseudo-first-order rate constants against pH. EDTA coordinates to Mo^{VI} in one order of magnitude faster than EDTPO and two orders of magnitude than THEED. In every case the rate was enhanced as the concentration of proton increased, however the spectral change became complicated at pH lower than 3.5 due to side reactions.

Column Breakthrough. In the batch experiments present resins showed an apparent selectivity toward Mo^{VI} at pH lower than 1.5 suggesting the possibility of selective recovery of the metal ion. When a model solution containing equimolar Mo^{VI} and V^{V} (4 mM each, pH 1.0) was passed continuously through the column of HEA resin, Mo^{VI} was quantitatively adsorbed on the resin while V^{V} was found in the eluate. The amount of Mo^{VI} adsorbed on one gram of the resin at breakthrough point (breakthrough capacity) is approximately 90% of the equilibrium capacity obtained by batch experiment. Vanadium was then quantitatively

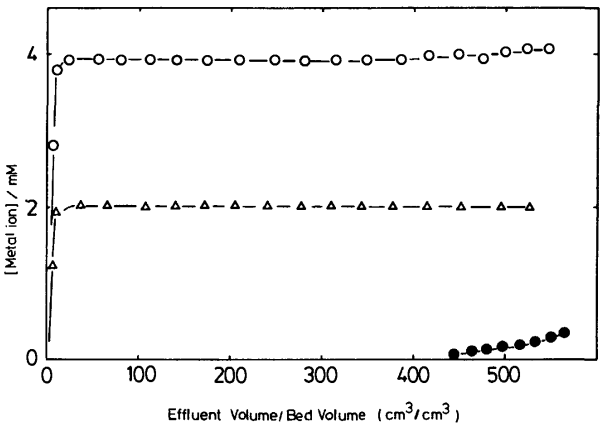

Fig. 6. Breakthrough profile of the acid-leaching solution of waste catalyst.
-●-: Mo, -Δ-: Al, -○-: V.
Bed resin: HEA resin, 5 g (wet volume 13 cm^3), pH of the feed: 1.0, Flow rate: 1.5 $cm^3\,min^{-1}$.

collected from the eluate upon subsequent column operation at pH 2—3. Using the column with CMA and PMA resins, on the other hand, both Mo^{VI} and V^{V} leaked through the column in the early stage regardless of the pH of the feed solution.

Based on the column experiments we chose HEA resin for selective recovery of molybdenum and/or vanadium from the acid-leaching solution of desulfurization catalyst. Using the column operation described above, molybdenum was quantitatively adsorbed on the resin, while other metals leaked through the column. The breakthrough curves are given in Fig. 6. Small amount of vanadium was cosorbed in a molar ratio Mo/V *ca.* 5/1. The adsorbed ion was liberated in concentrated form, 60-fold over the feed solution, on elution with 1 M sodium hydroxide. Repeated column operation for the eluate greatly improved the Mo/V ratio to be 50/1.

Discussion

EDTA is known to form 1:2 (ligand:metal) complex with oxomolybdenum(VI) ion in the presence of excess metal ion. The facial tridentate coordination of each iminodiacetate arm to the trioxomolybdenum-

(VI) was suggested by ^{1}H- and ^{13}C-NMR studies[12-14] and confirmed in the solid state for $Na_4(MoO_3)_2$-EDTA·$8H_2O$.[15] The HEA, CMA, and PMA resins formally contain two sets of tridentate ligand, bis(2-hydroxyethyl)amino, bis(carboxymethyl)amino, and bis(phosphonomethyl)amino moieties, respectively. It appears that each of the tridentate ligand units forms a 1:1 complex with Mo^{VI} in a similar fashion to that for the EDTA-Mo^{VI} complex since the metal capacity values in equilibrium are approximately twice the value of the ligand capacity.

The coordination of the hydroxyl arm onto the Mo^{VI} center has been demonstrated by Freeman *et al.*, using *N*-methyl-*N*-hydroxyglycine (MHEG) and *N*-(2-hydroxyethyl)ethylenediaminetriacetic acid (HEDTA).[14] They reported that ^{13}C peaks of 2-hydroxyethyl carbons shift *ca.* δ=13 (hydroxyl carbon) and δ=5 (carbon adjacent to N) down field upon coordination to Mo^{VI}. The ^{13}C-signals of THEED appear at δ 50.5, 57.9, and 58.4 in which the latter two peaks correspond to the 2-hydroxyethyl carbons. On addition of Mo^{VI} (Mo:L=2:1) at pH 5.0 seven peaks are observed in which two peaks at δ 63.0 and 73.9 can be assigned to the coordinated 2-hydroxyethyl carbons. Therefore Mo^{VI} seems to be retained on HEA resin *via* chelate formation with the bis(2-hydroxyethyl)amino moiety.

Although equilibrium capacity is of fundamental importance in characterizing the resin, the rate at which equilibrium is achieved is extremely important from a practical point of view. If the adsorption rate is not sufficiently rapid, the concentration of a metal on the resin is unlikely owing to the short contact time between the resin and the solution. In fact effective column separation of Mo^{VI}/V^{V} was realized only by use of the HEA resin which is superior to other resins with respect to the adsorption rate. On the other hand, CMA and PMA resins were not applicable for column separation due to their slow adsorption rates. In those cases, a batch extraction with a large excess of resin could be conducted over an extended period.

The metal adsorption process of a chelating resin may include the following steps, i) diffusion of the metal ion into the polymer matrix, ii) complex formation with the functional group. The rate for the latter step was estimated by measuring the conditional rate constant of Mo^{VI} complex formation using model ligands. The observed pH dependence of the rates could be accounted for by a mechanism involving protonation to the oxo groups in the activated complexes.[16] The complexation rates are, in any extent, appreciably rapid, especially in the low pH region. Moreover the order of the complexation rate in a homogeneous solution was not in accord with the order of the adsorption rate of the respective resins. Thus, this step is unlikely to play a rate-determining role in the adsorption process.

Since Mo^{VI} was adsorbed on an anion exchange resin at pH 1—2, Mo^{VI} must, principally, exist as anionic form(s) in this pH region. Under acidic conditions, HEA resin is expected to be positively charged due to protonation of the amine nitrogen. The local charge density must be highly concentrated inside the polymer beads where the functional groups are fixed closely, and hence the migration of oxoanion into polymer matrix may be facilitated. On the other hand, the functional group in the PMA resin holds a negative charge on the phosphonomethyl group.[17] Then, the migration of anionic species into the polymer would be retarded due to charge repulsion. Our view is consistent with the observation that PMA resin readily adsorb a wide range of metal cations.[7] Although bis(carboxymethyl)amino moiety itself has a strong affinity toward Mo^{VI},[18] an efficient adsorption of the ion was not achieved by CMA resin. Currently we have no clear explanation for the stepwise adsorption of Mo^{VI} by the CMA resin.

In addition to the high selectivity and rapid adsorption rate toward oxometal ions, HEA resin has little or no affinity for the common cations which are usually contained in the acid-leaching solution. Therefore HEA resin is the most promising agent for practical recovery of oxometal ions from industrial wastes.

The authors thank Professor K. Saito for his permission to use the stopped-flow apparatus at Tohoku University.

References

1) "Proceeding of the Climax Third International Conference on the Chemistry and Uses of Molybdenum," ed by H. F. Barry and P. C. H. Mitchell, Climax Molybdenum Company, Ann Arbor, Michigan, (1979), pp. 73—113.
2) E. I. Stiefel, *Prog. Inorg. Chem.*, **22**, 1 (1977).
3) K. Saito and Y. Sasaki, *Adv. Inorg. Bioinorg. Mechanisms*, **1**, 179 (1982).
4) N. Rokkawa, *Nippon Kagaku Kaishi*, **1981**, 1227.
5) T. Yokoyama, A. Kikuchi, T. Kimura, and T. M. Suzuki, *Nippon Kagaku Kaishi*, **1983**, 363.
6) T. M. Suzuki and T. Yokoyama, *Polyhedron*, **2**, 127 (1983).
7) T. M. Suzuki and T. Yokoyama, *Polyhedron*, in the press.
8) M. Nishizawa, T. Yokoyama, T. Kimura, and T. M. Suzuki, *Chem. Lett.*, **1983**, 1413.
9) L. Knorr and H. W. Brownsdon, *Chem. Ber.*, **35**, 4470 (1902); D. B. Rorabacher and D. B. Moss, *Inorg. Chem.*, **9**, 1314 (1970).
10) K. Moedritzer and R. R. Irani, *J. Org. Chem.*, **31**, 1603 (1966).
11) S. I. Chan, R. J. Kula, and D. T. Sawyer, *J. Am. Chem. Soc.*, **86**, 377 (1964).
12) R. J. Kula, *Anal. Chem.*, **39**, 1171 (1967).
13) R. J. Kula, *Anal. Chem.*, **38**, 1581 (1966).
14) M. A. Freeman, F. A. Schultz, and C. N. Reilley, *Inorg. Chem.*, **21**, 567 (1982).
15) J. J. Park, M. D. Glick, and J. L. Hoard, *J. Am. Chem. Soc.*, **91**, 301 (1969).
16) S. Funahashi, Y. Kato, M. Nakayama, and M. Tanaka, *Inorg. Chem.*, **20**, 1752 (1981).
17) R. J. Motekaitis, I. Murase, and A. E. Martell, *J. Inorg. Nucl. Chem.*, **33**, 3353 (1971).
18) R. J. Kula, *Anal. Chem.*, **38**, 1934 (1966).

Fragmentation of Human Erythrocyte Ghosts and Their Application as a Carrier of Heme Complex

Noriko SEKI, Hiroyuki OHNO, Eishun TSUCHIDA,* and Shigeru SASAKAWA†
Department of Polymer Chemistry, Waseda University, Tokyo 160
†*Department of Research, Central Blood Center, Japanese Red Cross, Tokyo 150*
(Received December 27, 1983)

Human erythrocyte ghosts were taken into fragments by sonication. The average radius of the fragmented ghosts gradually decreased with the sonication time. The fragmented ghosts were obtained as spheres and reached to about 0.1 μm. In spite of the change in radius, their membrane fluidity was the same as that of the unsonicated ghost membrane. The [*meso*-α,α,α,α-tetrakis(*o*-pivalamidophenyl)porphinato]iron(III)-*mono* (1-dodecyl-2-methylimidazole) complex was incorporated into the hydrophobic region of the fragmented ghost membrane. This hybrid showed a semistable oxygen adduct in pH 7.0 phosphate buffer solution.

Human erythrocyte ghost membranes have been widely used in many fields due to their interesting character and brief preparation method.[1] The purified ghosts could be obtained easily in large quantities by direct hemolysis. They have also been studied extensively as a typical model for cell membranes. Ghost membranes are turned into liposomes by treating them in hypotonic buffer solution. These liposomes become inside-out when they were prepared in hypotonic alkaline buffer solution, but right side out liposomes were generally obtained by treating them in hypotonic Tris buffer solution.[2,3]

It is known that bilayer membranes can be used as vehicles for biological-active materials. The authors succeeded in oxygen-binding by incorporating the [*meso*-α,α,α,α-tetrakis(*o*-pivalamidophenyl)porphinato]-iron(III)-*mono*(1-dodecyl-2-methylimidazole) complex (abbreviated as "heme") into phosphatidylcholine liposomes.[4] Human erythrocyte ghost membranes were expected to carry the heme complex instead of synthetic lipid liposomes, because the fluidity of ghost membranes was relatively low. This paper describes the fragmentation of human erythrocyte ghost and the oxygen-binding ability of the heme embedded in the fragmented ghost membrane.

Experimental

Preparation of Ghost Membranes. Human erythrocytes were isolated from whole blood of healthy donors. Erythrocytes were centrifuged (3000 min^{-1} for 5 min at 4 °C) three times with 10 volumes of 0.9% NaCl solution to remove buff coating. The erythrocytes were lysed with hypotonic Tris buffer solution (pH 7.4).[1] Erythrocyte white ghosts were collected by centrifugation (13000 min^{-1} for 20 min at 4 °C). Then this pellet was dispersed in isotonic Tris buffer solution and was incubated at 37 °C for 1 h before use.

Incorporation of Glycoprotein in Liposome. Bovine glycoprotein (fraction IV) and dimyristoyl phosphatidylcholine (DMPC) were purchased from Sigma. The phospholipid liposomes with glycoprotein incorporated could be prepared by the dialysis with cholic acid.[5] A suitable amount of purified glycoprotein was added to 50 mg DMPC in isotonic Tris buffer solution (pH 7.0). The detergent solution containing the glycoprotein and phospholipid was then extensively dialyzed against a Tris buffer solution at 37 °C for 48 h. The final concentration of DMPC was set to 0.1 wt% in the buffer solution. Glycoprotein was set to 1—25% (wt/wt DMPC).

Sonication. Fragmented white ghosts were prepared by sonication (Tomy Seiko Co., Ltd., UR-200P) with different sonication times from 0 to 30 min at 25 W in an ice bath.

Scanning Electron Microscopy. Fragmented ghosts were fixed with 1% glutaraldehyde. Radius of each of the fragmented ghosts was measured directly by Hitachi S-800 scanning electron microscope without spattering.

Fluorescence Depolarization Measurement. Fluorescence probes sodium 8-anilino-1-naphthalenesulfonate (ANS) and 1,6-diphenyl-1,3,5-hexatriene (DPH) were purchased from Tokyo Kasei Co., Ltd. Erythrocyte ghosts were labeled with ANS or DPH by incubation with gentle shaking at 37 °C for 12 h. The stained erythrocyte ghosts were washed once with isotonic Tris buffer solution. The ghosts were centrifuged at 10000 min^{-1} for 30 min at 4 °C, and then were resuspended in the same buffer. The labeled ghosts were sonicated for a suitable period of time and the molecular motion of component lipids were measured by means of fluorescence depolarization measurements (JASCO FP-550 fluorescence spectrophotometer). Lights with wavelengths of 375 nm and 366 nm were used for excitation of membrane-incorporated ANS and DPH respectively. The emission intensities from ANS and DPH were detected at 480 nm and 432 nm. The fluorescence polarization was evaluated from averaging the fluorescence intensities polarized parallel ($I_{\parallel}$) and perpendicular ($I_{\perp}$) to the direction of the polarized excitation beam. The degree of polarization (P) is defined in the following equation:

$$P = (I_{\parallel} - I_{\perp})/(I_{\parallel} + I_{\perp})$$

The $1/P$-value represents the membrane fluidity.

Incorporation of Heme. Dichloromethane solution of the iron(III) derivative of heme ([Fe]=0.05 mM (1 M=1 mol dm^{-3}), [1-dodecyl-2-methylimidazole]=2.25 mM) was evaporated to prepare a thin film on a glass flask under nitrogen gas flow. A phosphate buffer solution containing 10 vol% of the white ghost (pH 7.0) was mixed with the thin film, then it was sonicated for a suitable period of time under nitrogen atmosphere. In degassed solution, the incorporated iron(III) derivative of heme was reduced by L-ascorbic acid. The resulting solution was incubated at 37 °C for 1 h. Oxygen gas was bubbled through the solution for 15 s to induce the oxygen-binding of heme. The reduction and oxygen-binding were detected by visible absorption spectrometry (Hitachi-320 UV. *vis.* spectrophotometer).

Results and Discussion

Fragmentation of Human Erythrocyte Ghosts. Human erythrocyte ghosts turned into fragments by the sonication, and they formed smaller liposomes than the initial ghosts. The shape and radius of fragmented

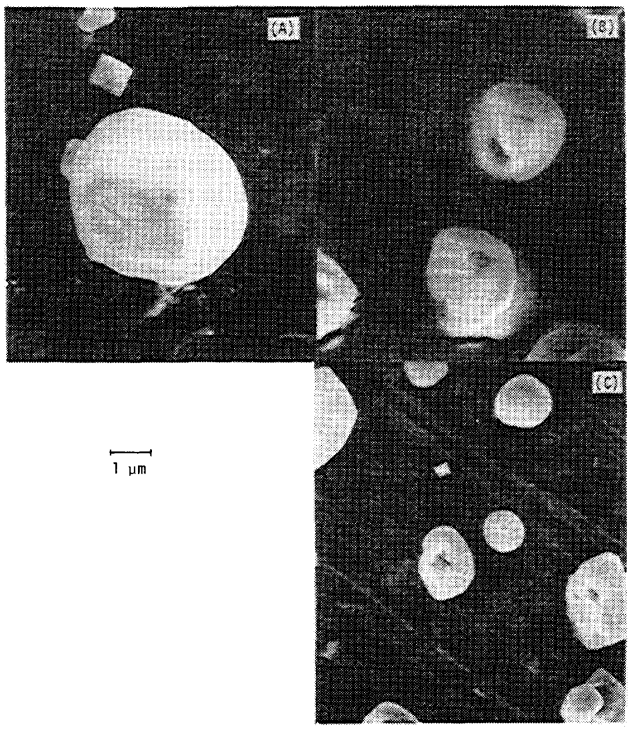

Fig. 1. Scanning electron micrographs of fragmented ghost.
Sonication time was 10 s (A), 60 s (B), 5 min (C) respectively.

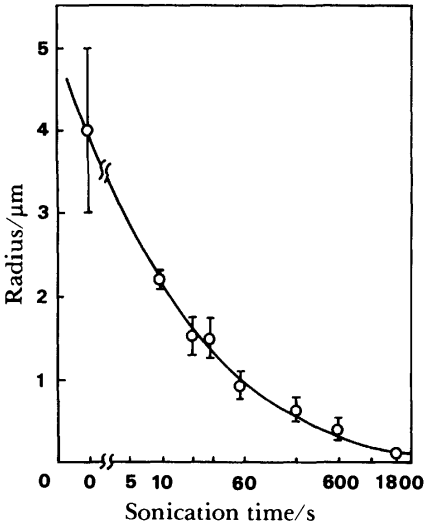

Fig. 2. Effect of sonication time on the average radius of fragmented ghost.
Average radius was directly measured by SEM. Sonication (25 W, in ice bath)

ghosts were detected directly by means of high resolution scanning electron microscopy. The fragmented ghost was generally observed as a sphere, as shown in Fig. 1. The average radius greatly depended on the sonication time. Figure 2 shows the effect of sonication time on the radius of the fragmented ghosts. The average radius of the intact white ghost was about 4 μm, which decreased with increasing sonication time and turned about 1 μm after 60 s sonication. Finally it reached to about 0.1 μm by 30 min sonication.

The motion of membrane-constituted molecules

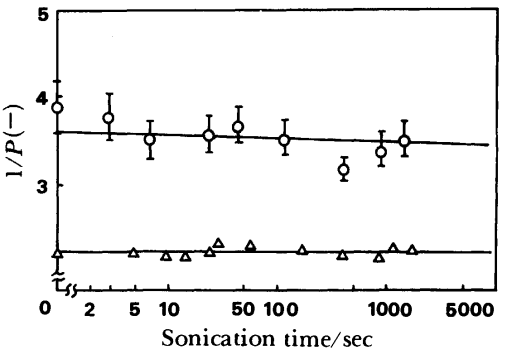

Fig. 3. Effect of sonication time on the membrane fluidity of fragmented ghosts.
Sonication (25 W, in ice bath), ○: ANS, △: DPH, [ANS]=[DPH]=10^{-6} M.

Table 1. Membrane fluidity of fragmented ghost and DMPC liposome with or without glycoprotein

Liposome	Membrane fluidity (1/P)	
	ANS	DPH
DMPC	8.24	3.75
Glycoprotein incorporated	2.85	2.11
Fragmented ghost	3.68	2.20

[DMPC]=0.1 wt%; [Glycoprotein]=10% (wt/wt DMPC); [ghost]=1 vol%; [DPH]=1.0×10^{-6} M; at 37°C

could be detected by the fluorescence depolarization measurements.[6,7] Fluorescence measurements with different types of probe molecules gave us important information for membrane fluidity at molecular level, because the location of the incorporated probe molecules depends on their molecular structure.[6] As an ANS molecule dissociates to give an anion, ANS can be incorporated into the hydrophobic region closest to the surface of the membrane.[8] On the other hand, as DPH is a conjugated aromatic hydrocarbon, it is located at the center of the hydrophobic hydrocarbon of cell membranes.[9] It was observed that the membrane fluidity of the fragmented ghosts was independent of their radius and was almost the same as that of unsonicated ghost membrane, as shown in Fig. 3. This shows that the network structure of the ghost membrane was taken off by sonication but the composition of membrane-constituted molecules was almost unchanged.

The membrane fluidity of the fragmented ghosts was compared with that of the DMPC liposome and DMPC liposome with glycoprotein incorporated. Results are summarized in Table 1. When the liposomes are labeled with ANS, the membrane fluidity of the fragmented ghost was higher than that of DMPC liposome with glycoprotein incorporated. But it was suppressed more strongly than that of DMPC liposome only. On the other hand, the membrane fluidity of fragmented ghost was almost the same as that of DMPC liposome with 10% (wt/wt DMPC) of glycoprotein when labeled by DPH. These results show that the effect of sonication in fragmented ghost membrane was more remarkable in the surface region than in the hydro-

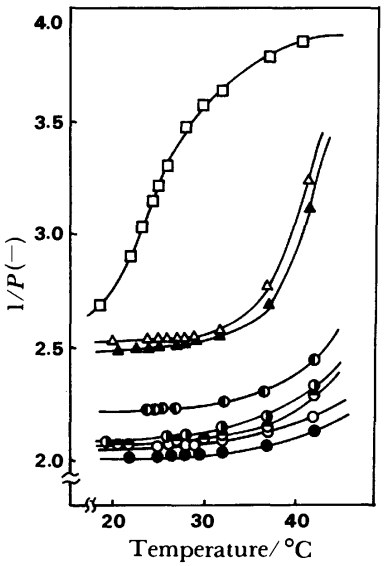

Fig. 4. Temperature dependence of the membrane fluidity of the DMPC liposome with the glycoprotein incorporated.
[DMPC]=0.1 wt%, [DPH]=10^{-6} M, Sonication (25 W, for 30 sec), [glycoprotein]=0.0 (□), 1.0 (△), 2.5 (▲), 5.0 (◐), 10 (◑), 15 (◓), 20 (○), 25 (●) % (wt/wt DMPC)

phobic region. The membrane fluidity of the initial ghost membranes was considered to be higher than that of human erythrocytes. The membrane fluidity of erythrocytes was reduced by the existence of the network structure. Though the network structure of spectrin in the fragmented ghost was destroyed by the sonication, the membrane fluidity in the hydrophobic region was kept lower because of the existence of the membrane proteins. Figure 4 shows the temperature dependence of the fluidity of the DMPC liposome with or without glycoprotein. The membrane fluidity of the DMPC liposome increased remarkably at 24°C. This temperature corresponded to the gel to liquid-crystalline phase transition temperature (T_c). On the other hand, the membrane fluidity of DMPC liposome with glycoprotein incorporated was gradually increased at temperature higher than T_c, and the transition point became unclear with increasing concentration of the incorporated glycoprotein, as shown in Fig. 4. So, it is clear that the membrane fluidity of DMPC liposome with glycoprotein incorporated remarkably depended on the concentration of the incorporated glycoprotein. The effect of the concentration was particularly, dramatic when the concentration of incorporated glycoprotein was less than 5.0% (wt/wt DMPC). The molecular motion of lipids was considered to be suppressed through the interaction with the incorporated glycoprotein. When 10% (wt/wt DMPC) of glycoprotein was incorporated to DMPC liposome, the membrane fluidity in the hydrophobic region was almost the same as that of fragmented ghost membrane, as shown in Table 1. It is expected that these fragmented ghosts could be applicable as a membrane model when synthetic pospholipid hybrid liposomes are prepared. This is because fragmented ghost liposomes could be prepared easily and their membrane fluidity was adequately suppressed, in almost the same

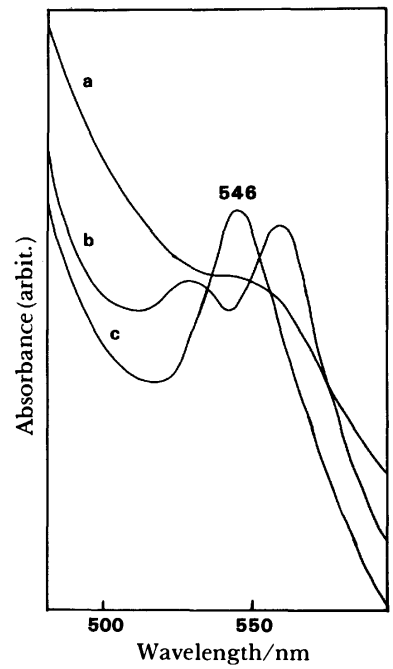

Fig. 5. Visible absorption spectra of ghost-embedded heme in fragmented ghost.
[Fe]=0.05 mM, [Ligand]/[Fe]=50, [ghost]=10 vol%.

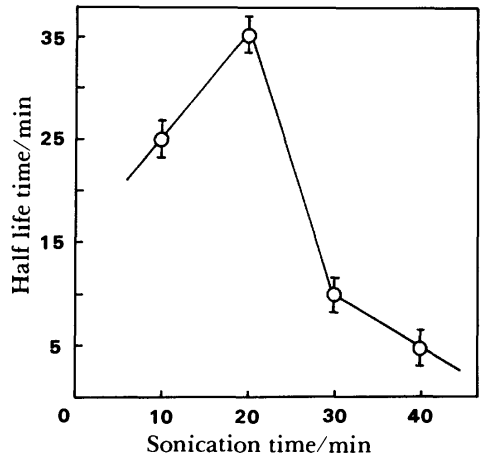

Fig. 6. Relation between the dispersion state and the life time of oxygen adduct on ghost-embedded heme. Sonication (25 W, in ice bath)

way as that of ghost membranes or phospholipid liposomes containing glycoprotein.

Application as a Carrier of Heme Complex. The fragmented ghost containing heme in the hydrophobic region (ghost-embedded heme) was prepared by a sonication method. The stability and oxygen-binding ability of the ghost-embedded heme suspension was measured by means of visible absorption spectrometry, as shown in Fig. 5. Fig. 5 (a) shows the visible spectra of the ghost-embedded heme before reduction. They were incubated at 37°C for 1 h after adding a reducing agent. The absorption bands of the ghost-embedded heme were observed at 535 nm and 555 nm, corresponding to the penta-coordinated heme, as shown in Fig. 5 (b). The oxygen adducts were obtained after bubbling oxygen gas for 15 sec through that solution. The formation of oxygen adducts was

detected by the appearance of a single peak at 546 nm, as shown in Fig. 5 (c). This peak coincided with that of semistable oxygen adducts of the liposome-embedded heme.[4] In this system, it is important to analyze the effect of sonication time of the dispersion state of ghost-embedded heme and of the life time of its oxygen adduct. These results are summarized in Fig. 6. It was found that ghost-embedded heme could be dispersed relatively homogeneously by a suitable period of sonication time. The life time of the semistable oxygen adducts turns longer (35 min) when they were sonicated for 20 min at 25 W. But most of ghost-embedded heme phase-separated (aggregated) when incubated overnight. Contrary to this, the life time of the semistable oxygen adducts was only for 20 min when ghosts were fragmented by 30 min sonication. But, they were quite stable and the dispersion state was maintained over several days. As the fluidity was completely independent of the sonication time, it was better for the vehicle size to be as small as possible. The reason of the effect of sonication time on the life time of oxygen adducts has not been clarified yet. It is expected that more stable oxygen adducts with longer life time should be obtained by the improvement of the composition of iron heme/complex/the membrane-constituted molecules as well as the physicochemical conditions.

This work was partially supported by the Grant-in-Aid for Special Project Reserch (No. 58211018) from the Ministry of Education, Science and Culture, Japan. Grateful acknowledgement is also made to Dr. H. Shii and Dr. H. Koyama, Central Research Laboratory, Furukawa Electric Co., for taking the electron micrographs.

References

1) J. T. Dodge, C. Mitchell, and D. J. Hanahan, *Arch. Biochem. Biophys.*, **100**, 119 (1963).
2) K. Honda, Y. Maeda, S. Sasakawa, H. Ohno, and E. Tsuchida, *Biochem. Biophys. Res. Commun.*, **101**, 165 (1981).
3) T. L. Steck, R. S. Weinstein, J. H. Straus, and D. F. H. Wallach, *Science*, **10**, 255 (1970).
4) E. Hasegawa, Y. Matsushita, M. Kaneda, K. Ejima, and E. Tsuchida, *Biochem. Biophys. Res. Commun.*, **105**, 1416 (1982).
5) W. A. Petri, T. N. Estep, R. Pal, T. E. Thompson, L. R. Biltion, and R. R. Wagner, *Biochemistry*, **19**, 3088 (1980).
6) H. Ohno, T. Sakai, E. Tsuchida, K. Honda, and S. Sasakawa, *Biochem. Biophys. Res. Commun.*, **102**, 426 (1981).
7) H. Ohno, N. Shimidzu, E. Tsuchida, S. Sasakawa, and K. Honda, *Biochem. Biophys. Acta*, **649**, 221 (1981).
8) D. H. Haynes and H. Staerk, *J. Membrane Biol.*, **17**, 313 (1974).
9) M. Shinitzky and M. Inbar, *J. Mol. Biol.*, **85**, 603 (1974).

The Platinum Catalyzed Reduction of Nitroarenes to Aminoarenes with Carbon Monoxide and Water

Yoshihisa WATANABE,* Yasushi TSUJI, Tatsuya OHSUMI, and Ryo TAKEUCHI
Department of Hydrocarbon Chemistry, Faculty of Engineering, Kyoto University, Sakyo-ku, Kyoto 606
(Received January 27, 1984)

Nitroarenes were transformed into the corresponding aminoarenes in high yields at 80 °C with carbon monoxide (an initial pressure 30—60 kg cm^{-2}) and water in the presence of a catalytic amount of a platinum catalyst. The platinum catalyst was combined with tin(IV) chloride, triphenylphosphine and triethylamine. This combination was essential for the high catalytic activity.

The homogeneous water gas shift reaction (WGSR) with transition metal catalysts is of current interest[1] (Eq.1).

$$CO + H_2O \xrightarrow{[cat]} H_2 + CO_2 \quad (1)$$

The application of WGSR to the reduction of organic compounds such as nitroarenes,[2-7] aldehydes[8,9] and olefins[10] has been widely attempted. In these reductions, iron,[2,8] rhodium[2-5,8,9] and ruthenium[2,6-8] clusters have been mostly employed as effective catalysts. With these catalyst systems, however, reaction temperatures are rather high[2,4,8] or a large amount of the catalyst is required under the mild conditions.[4-6]

Concerning the related platinum-catalyzed reaction, Yoshida *et al.* have reported that WGSR can be catalyzed by platinum(0) phosphine complexes.[11] Eisenberg and co-workers described the reduction of olefins with carbon monoxide and HCl aq in the presence of a platinum complex.[10] They also have reported the platinum-catalyzed WGSR and discussed the mechanism of hydrogen and carbon monoxide evolution.[12] The activities of these platinum catalysts, however, were rather low.

In this paper, we describe the platinum-catalyzed reduction of nitroarenes with carbon monoxide and water.[13] The nitroarenes were converted into the corresponding aminoarenes under mild reaction conditions (Eq. 2).

$$Ar\text{-}NO_2 + 3CO + H_2O \longrightarrow Ar\text{-}NH_2 + 3CO_2 \quad (2)$$

Results and Discussion

The results of nitrobenzene are listed in Table 1. Nitrobenzene was converted into aniline almost quantitatively with dichlorobis(triphenylphosphine)-platinum(II) combined with triethylamine and tin(IV) chloride (Runs 1, 2).

When triethylamine was removed from the catalyst system, the reduction did not take place at all (Run 3). The conversion of nitrobenzene was considerably decreased without tin(IV) chloride or triphenylphosphine (Runs 5, 6). In the absence of water or platinum complex, reduction did not proceed (Runs 7, 8). Thus, for the high activity by the present catalyst system, the presence of triethylamine, tin(IV) chloride, and triphenylphosphine is essential.

The effect of the reaction temperature and the initial carbon monoxide pressure are summarized in Table 2. Nitrobenzene was reduced to aniline almost

TABLE 1. THE PLATINUM-CATALYZED REDUCTION OF NITROBENZENE BY USE OF CARBON MONOXIDE WATER.[a] EFFECTS OF COMPONENTS IN THE CATALYST SYSTEM

Run	$SnCl_4$ /mmol	Et_3N /mmol	Conv.[b] /%	Selectivity to[b] aniline/%
1	2.0	2.0	100	98
2	2.0	1.0	100	97
3	2.0	—	9	0
4	1.0	1.0	88	64
5	—	1.0	53	98
6[c]	2.0	1.0	75	99
7[d]	2.0	1.0	3	0
8[e]	2.0	—	4	0

a) A mixture of nitrobenzene (20 mmol), [$PtCl_2(PPh_3)_2$] (0.10 mmol; 0.5 mol% based on nitrobenzene used.), $SnCl_4$, Et_3N, H_2O (1 ml), and dioxane (10 ml) was stirred under carbon monoxide (initial pressure of 60 kg cm^{-2}) for 4 h. b) Based on the amount of charged nitrobenzene by GLC. c) [$PtCl_2(PhCN)_2$] (0.10 mmol) as a platinum complex. d) Without water. e) Without platinum catalyst.

TABLE 2. THE PLATINUM-CATALYZED REDUCTION OF NITROBENZENE WITH CARBON MONOXIDE AND WATER UNDER VARIOUS REACTION CONDITIONS[a]

Run	Reaction Temp/°C	CO Pres. /kg cm^{-2}	Reaction Time/h	Nitrobenzene /mmol	Conv.[b] /%	Selectivity[b] to Aniline/%
2	80	60	4	20	100	97
9	50	60	7	20	83	88
10	20	60	22	20	31	71
11	80	30	4	20	100	91
12	80	15	4	10	58	93
13	80	15	20	10	63	86
14	80	bubbling	14	20	32	41

a) Nitrobenzene: [$PtCl_2(PPh_3)_2$]: $SnCl_4$: Et_3N: H_2O: Dioxane=20:0.10:2.0:1.0:56:118 (molar ratio). b) Determined by GLC.

TABLE 3. EFFECT OF SEVERAL LEWIS ACIDS ON THE REACTION[a]

Run	Et_3N	Lewis acid	Conv./%	Selectivity/%
2	+	$SnCl_4$	100	97
15	+	$SnCl_2 \cdot 2H_2O$	78	87
16	+	$FeCl_3$	40	78
3	−[b]	$SnCl_4$	9	0
17	−	$SnCl_2 \cdot 2H_2O$	78	100
18[c]	−	$SnCl_2 \cdot 2H_2O$	79	95
19	−	$FeCl_3$	15	93
20	−	$AlCl_3$	15	0
21	−	$ZnCl_2$	37	84

a) Nitrobenzene 20 mmol, $[PtCl_2(PPh_3)_2]$ 0.10 mmol, Lewis acid 2.0 mmol, Et_3N 1.0 mmol, dioxane 10 ml, carbon monoxide 60 kg cm^{-2} at 80 °C for 4h. b) Without Et_3N. c) Reaction time 8h.

quantitatively at 80 °C (Run 2). Lower temperatures, 50 °C and 20 °C, gave only low conversions of nitrobenzene and low selectivities to aniline (Runs 9, 10). The reaction temperature over 80 °C is desired for the high conversion and the high selectivity. The activity of the catalyst system was also affected by the initial carbon monoxide pressure. A higher pressure (60 kg cm^{-2}) of the initial carbon monoxide was more favorable for the reaction (Run 2). The selectivity to aniline slightly reduced to 91% under 30 kg cm^{-2} of the initial carbon monoxide pressure (Run 11). Under 15 kg cm^{-2} of the initial pressure, the conversion of nitrobenzene was not improved even by prolonging the reaction time to 20 h (Runs 12,13). The reduction was also sluggish with bubbling carbon monoxide and expelling the resultant carbon dioxide from the reaction system (Run 14).

Tin(IV) chloride played an important role in the present catalyst system. Effects of the presence of Lewis acids as co-catalysts with or without triethylamine are summarized in Table. 3. In the presence of triethylamine, tin(IV) chloride was the most favorable. Tin(II) chloride and iron(III) chloride were less effective (Runs 15,16). On the other hand, the reaction without triethylamine showed an interesting contrast. Employing tin(IV) chloride, aniline was not obtained at all, as mentioned above. However, employing tin(II) chloride, aniline was produced with 100% selectivity and 78% conversion even without the amine (Run 17), although the conversion was not improved by prolonging the reaction time (Run 18). Other Lewis acids, such as iron(III) chloride, aluminum chloride, and zinc chloride were less effective and the conversion was decreased considerably (Runs 19—21).

Various nitroarenes could be converted to the corresponding aminoarenes by this procedure (Table 4). 4-Methylaniline was obtained from 1-methyl-4-nitrobenzene in 71% yield (80% selectivity and 89% conversion) (Run 22). The yield of the product was improved to 100% in the presence of less water (Run 23). 1-Chloro-4-nitrobenzene was converted to 4-chloroaniline in 89% yield (94% selectivity and 95% conversion) at 80 °C (Run 24). The yield increased to 95% (99% selectivity and 96% conversion) by elevating the reaction temperature to 100 °C (Run 25). 3-Methoxyaniline was reduced to 3-methoxyaniline in high yield (Run 26). However, for ortho-substituted nitroarenes, the

TABLE 4. REDUCTION OF VARIOUS NITROARENES WITH CARBON MONOXIDE AND WATER[a]

Run	Nitroarene	Conv./%[b]	Selectivity to[b] aminoarene
22	4-Methylnitrobenzene	89	80(79)
23[c]	4-Methylnitrobenzene	100	100
24	4-Chloronitrobenzene	95	94
25[d]	4-Chloronitrobenzene	96	99(98)
26	3-Methoxynitrobenzene	100	96(95)
27	2-Methylnitrobenzene	87	64
28	2-Methoxynitrobenzene	100	32

a) Nitroarene (20 mmol), $[PtCl_2(PPh_3)_2]$ (0.10 mmol), $SnCl_4$ (2.0 mmol), Et_3N (1.0 mmol), H_2O (1.0 ml), Dioxane (10 mmol), CO(initial 60 kg cm^{-2} at r.t.)for 4h. b) By GLC, figures in parentheses were determined based on the isolated products. c) H_2O (0.5 ml). d) at 100 °C.

selectivities to the corresponding aminoarenes were low (Runs 27, 28). The steric effect of the ortho-substituents would cause these low selectivities.

After the reaction, analysis of the gas phase by gas chromatography revealed that only carbon dioxide was produced. Furthermore, a control experiment showed that the present catalyst system could not catalyze the WGSR.[14] These observations clearly indicated that the nitroarenes were not reduced to aminoarenes by the hydrogen produced by the WGSR (Eq. 1). In fact, aniline was obtained from nitrobenzene only in 34% yield with the same catalyst system under 60 kg cm^{-2} of hydrogen pressure in place of carbon monoxide and water. This result indicates that carbon monoxide and water is a more effective reductant than hydrogen with the present catalyst system.

Other substrates such as 1-nitropropane, 2-ethyl-2-hexenal, phenylacetylene and diphenylacetylene were not reduced by this procedure. The competitive reduction of nitrobenzene and diphenylacetylene by this procedure[15] gave only aniline as the reaction product in 88% selectivity and 80% conversion, while diphenylacetylene was recovered quantitatively. Thus, by the present reaction, the nitroarenes appeared to be reduced chemoselectively. This chemoselectivity is an outstanding feature which was not seen in the previous studies.[2-9]

A possible route for the present reaction is as follows. The nitroarenes is deoxygenated with carbon monoxide to an arylnitrene intermediate (Eq. 3). The carbonylation of the nitrene intermediate successively occurs and generates the phenyl isocyanate intermediate (Eq. 4). Iqbal[16] has reported the transition metal catalyzed deoxygenation of nitroarenes with carbon monoxide and proposed the nitrene intermediate for the reaction. Bennett *et al.*[17] and Collman *et al.*[18] have reported the formation of phenyl isocyanate from phenyl azide under carbon monoxide pressure and Bennett *et al.* have suggested that arylnitrene was the reaction intermediate. Furthermore, we have recently reported that the present platinum catalyst system catalyzed the reductive carbonylation of nitroarenes in ethanol and the corresponding ethyl phenylcarbamates were obtained in high yield[19] (Eq. 6). We have proposed the arylnitrene and phenyl

isocyanate as key intermediates in that reaction. Although that reaction required the elevated reaction temperature (at 180°C), we recently found that the reaction temperature can be lowered to 150°C by employing 1 equiv ethanol in benzene.[20] In the

$$Ar\text{-}NO_2 + 2CO \longrightarrow Ar\text{-}N: + 2CO_2 \quad (3)$$

$$Ar\text{-}N: + CO \longrightarrow Ar\text{-}NCO \quad (4)$$

$$Ar\text{-}NCO + H_2O \longrightarrow [Ar\text{-}NHCOOH] \xrightarrow{-CO_2} Ar\text{-}NH_2 \quad (5)$$

$$Ar\text{-}NO_2 \xrightarrow{[Pt]} [Ar\text{-}NCO] \xrightarrow{ROH} Ar\text{-}NHCOOR \quad (6)$$

present reduction of nitroarenes, we propose the phenyl isocyanate as a key intermediate as mentioned above (Eq. 4). The phenyl isocyanate can react with water to give phenylcarbamic acid which easily decarboxylates to aminoarene (Eq. 5). Tarakanov *et al.* have reported a phenylcarbamic acid intermediate in the reaction of phenyl isocyanate and water.[21] In this reaction, nitroarenes were chemoselectively reduced to aminoarene. This chemoselectivity must be originated in the reaction pathway including the phenylcarbamic acid intermediate.

There is another possible route, in which the nitrene intermediate abstracts hydrogen from the solvent or other hydrogen source.[22] As indicated by Run 7 (Table 1), the aminoarene was not obtained at all in the absence of water. This result clearly shows that water is the only possible hydrogen source. However, there is no example that nitrene intermediate abstract hydrogen from water, although it is well known that hydrocarbon solvents are good hydrogen donors.[22] Therefore, it is rather hard to accept that the aminoarenes were generated *via* the nitrene intermediate by hydrogen abstraction from water.

In this reaction, characterization of the active catalyst species was not done. Several studies have indicated that Lewis acid promotes migratory insertion of coordinated carbon monoxide to a carbon-metal bond.[23] In the present reaction, tin(IV) chloride may be operative in promoting the insertion of carbon monoxide into a nitrogen-metal bond to generate the phenyl isocyanate intermediate (Eq. 4).

Experimental

Materials. The reagents employed in this study were purified by distillation or recrystallization before use. Carbon monoxide (>99.9%) was used without further purification. Platinum complexes were prepared by the methods in the literature.[24,25]

General Procedure. A 100 ml stainless steel autoclave (Nitto Koatsu SUS 316) equipped with a magnetically driven stirrer was used. A glass liner was set in the autoclave. The reagents were charged in the glass liner in the following order: dioxane (10 ml), water (1 ml), nitroarene (20 mmol), triethylamine (0.14 ml, 1.0 mmol), $PtCl_2(PPh_3)_2$ (79 mg, 0.10 mmol) and $SnCl_4$ (0.24 ml, 2.0 mmol). After sealing and flushing with carbon monoxide, the reactor was pressurized with carbon monoxide to 60 kg cm^{-2} at r.t. The autoclave was heated to 80°C in 10 min and then held at this temperature for 4 h. The reaction was terminated by rapid cooling and the autoclave was discharged. The resultant clear brown solution was analyzed with GLC.

Product Isolation. The solvent, dioxane, was evaporated off from the reaction mixture and benzene (20 ml) was added. The benzene solution was shaken with 10% HCl aq and the benzene layer was discarded. Then the aqueous layer was neutralized with 20% NaOH aq and extracted with benzene (20 ml). After filtering the whole mixture, the oil layer was separated and dried. Evaporation of benzene from the solution give a pure aminoarene.

Analytical Procedure. The GLC analyses were performed on Shimadzu GC-3BT (with thermal conductivity detector) or GC-4CM (with flame ionization detector) with columns (3 mmϕ×3 m) packed with Versamide 900 (10% on Neopak 1A 60—80 mesh), PEG 20 M TPA (10% on Chromosorb W AW 60—80 mesh) or Apieson Grease L (5% on Neopak 1A). The conversion of the substrate and the selectivity to the product were determined by the internal standard method with naphthalene according to the calibration curve obtained for each sample. The analysis of gas phase was performed on Shimadzu GC-3BT with a column (3 mm ϕ×3 m) packed with Active Carbon 60—80 mesh.

The identification of the products was confirmed by comparing the spectral data (^{13}C-, ^{1}H-NMR and IR spectra) with those of the authentic samples.

The ^{13}C- and ^{1}H-NMR spectra were recorded 25.05 MHz and 100 MHz with a JEOL JNM FX 100 spectrometer. The IR spectra were measured on a Hitachi model 215 grating spectrometer.

Reduction under Hydrogen Pressure. Nitrobenzene (20 mmol) was reduced in the presence of the platinum catalyst system ($PtCl_2(PPh_3)_2$ 0.10 mmol; Et_3N 1.0 mmol; $SnCl_4$ 2.0 mmol) in dioxane (10 ml) under hydrogen pressure (initial pressure 60 kg cm^{-2} at r.t.) at 80°C for 4 h. After the reaction, GLC analysis indicated that the conversion of nitrobenzene was 39% and the selectivity to aniline was 87% (yield 34%).

Synthesis of Ethyl Phenylcarbamate. A mixture of nitrobenzene (20 mmol), ethanol (20 mmol), $PtCl_2(PPh_3)_2$ (0.20 mmol), $SnCl_4$ (2.0 mmol), Et_3N (3.6 mmol) and benzene (18.5 ml) was stirred under carbon monoxide pressure (initial 60 kg cm^{-2}) at 150°C for 4 h. The GLC analysis of the reaction mixture showed that ethyl phenylcarbamate was obtained in 70% yield (100% conversion).

References

1) P. C. Ford ed. "Catalytic Activation of Carbon Monoxide," ch. 5, 6, 7, 8, and 21, ACS symposium series 152, American Chemical Society (1981), and references cited therein.

2) K. Cann, T. Cole, W. Selegeir, and R. Pettit, *J. Am. Chem. Soc.*, **100**, 3969 (1978).

3) A. F. M. Iqbal, *Tetrahedron Lett.*, **1971**, 3385.

4) R. C. Ryan, G. M. Wilemon, M. P. Dalsanto, and C. V. Pittman, Jr., *J. Mol. Catal.*, **5**, 319 (1979).

5) K. Kaneda, M. Hiraki, T. Imanaka, and S. Teranishi, *J. Mol. Catal*, **12**, 385 (1981).

6) T. Okano, K. Fujiwara, H. Konishi, and J. Kiji, *Chem. Lett.*, **1981**, 1083.

7) H. Alper and S. Amaratunga, *Tetrahedron Lett.*, **21**, 2603 (1980).

8) W. J. Thomson and R. M. Lain, ch. 9 in Ref. 1.

9) K. Kaneda, M. Yasumura, T. Imanaka, and S. Teranishi, *J Chem. Soc., Chem. Commun.*, **1982**, 935.

10) C.-H. Cheng, L. Kuritzekes, and R. Eisenberg, *J. Organomet. Chem.*, **190**, C21 (1980).

11) T. Yoshida, Y. Ueda, and S. Otsuka, *J. Am. Chem. Soc.*, **100**, 3941 (1978).

12) C.-H. Cheng and R. Eisenberg, *J. Am. Chem. Soc.*,

100,5968 (1978).
13) Y. Watanabe, Y. Tsuji, T. Ohsumi, and R. Takeuchi, *Tetrahedron Lett.*, **24**, 4121 (1983).
14) A mixture of $[PtCl_2(PPh_3)_2]$ (0.10 mmol), $SnCl_4$ (2.0 mmol), triethylamine (1.0 mmol) and water (1.0 ml) was stirred in dioxane (10 ml) under carbon monoxide pressure (initial 60 kg cm^{-2} at r.t.) at 80 °C for 4 h. After the reaction, GC analysis of gas phase showed that no hydrogen and no carbon dioxide were produced.
15) A mixture of nitrobenzene (20 mmol), diphenylacetylene (10 mmol), $[PtCl_2(Ph_3)_2]$ (0.10 mmol), $SnCl_4$ (2.0 mmol), triethylamine (1.0 mmol) and water (1.0 ml) was stirred in dioxane (10 ml) under carbon monoxide pressure (initial 60 k cm^{-2} at r.t.) at 80 °C for 4 h.
16) A. F. M. Iqbal, *J. Org. Chem.*, **37**, 2791 (1972) ; *Helv. Chim. Acta.*, **55**, 2637 (1972).
17) R. B. Bennett and W. B. Hardy, *J. Am. Chem. Soc.*, **90**, 3295 (1968).
18) J. P. Collman, M. Kubota, D. F. Vastine, T. Y. Sun, and W. J. Kong, *J. Am. Chem. Soc.*, **90**, 5430 (1968).
19) Y. Watanabe, Y. Tsuji, and N. Suzuki, *Chem. Lett.*, **1982**, 105; Y. Watanabe, Y. Tsuji, R. Takeuchi, and N. Suzuki, *Bull. Chem. Soc. Jpn.*, **56**, 3343 (1983).
20) When ethanol was employed in larger molar excess and the reaction was carried out at 160 °C, the yield of ethyl phenylcarbamate was 30%. However, with 1 equiv ethanol, the product was obtained in 70% yield even by the reaction at 150 °C (see Experimental Section).
21) O. G. Tarakanov, Yu. V. Aleksandrova, and F. A. Kryuchkov, *Khim. Tekhnol. Vespenen. Plastmass*, **1970**, 14.
22) E. F. V. Scriven, "Reaction Intermediate" Vol. 2, p. 18, ed by R. A. Abramovitch, Plenum Press, New York (1982).
23) S. B. Butts, S. H. Straus, E. M. Holt, R. E. Stimson, N. W. Alcock, and D. F. Shriver, *J. Am. Chem. Soc.*, **102**, 5093 (1980); F. Correa, R. Nakamura, R. E. Stimson, R. L. Burwell, Jr., and D. F. Shriver, *ibid.*, **102**, 5114 (1980); S. B. Butts, T. G. Richmond, and D. F. Shriver, *Inorg. Chem.*, **20**, 278 (1981); S. J. La Croce and A. R. Culter, *J. Am. Chem. Soc.*, **104**, 2312 (1982).
24) J. C. Bailar and H. Itatani, *Inorg. Chem.*, **4**, 1618(1965).
25) F. R. Hartley," The Chemistry of Platinum and Palladium." Applied Science, London, 1973, p. 462.

 © 1984 The Chemical Society of Japan Bull. Chem. Soc. Jpn., 57, 2871—2878 (1984)

Gas Chromatography-Mass Spectrometry of Trimethylsilyl Derivatives of Some Iminodicarboxylic Acids

Katsuhiro KAWASHIRO,* Shiro MORIMOTO, and Hideyuki YOSHIDA

Department of Chemical Engineering, Faculty of Engineering, Tokushima University, Minamijosanjima, Tokushima 770

(Received February 20, 1984)

Trimethylsilylation of eight iminodicarboxylic acids (IDCAs) with *N,O*-bis(trimethylsilyl)trifluoroacetamide (BSTFA) or *N,O*-bis(trimethylsilyl)acetamide was studied under various reaction conditions. The IDCAs include iminodiacetic acid (**1**), 2- and 3-(carboxymethylamino)propionic acids (**2** and **3**), 2,2′-, 2,3′-, and 3,3′-iminodipropionic acids (**4—6**), *N*-methyliminodiacetic acid (**7**), and nitrilotriacetic acid (**8**). For **1—6**, both bis- and tris(trimethylsilyl) (TMS) derivatives were formed under usual silylating conditions, although the proportion of amounts of the two derivatives varied depending on reaction conditions. This double derivatization was due to the steric hindrance of *N*-substituent group. However, under mild silylating conditions (BSTFA alone, 120 °C, 30 min), **1—6** yielded only the di-TMS derivatives. Upon electron impact at 20 eV, both the di- and tri-TMS derivatives showed simple spectra with a molecular (M^+) ion and M −15 (loss of CH_3). The α,α'-IDCAs (**1**, **2**, **4**, **7**, and **8**) are characterized by fragments M −43 (loss of CH_3 and CO) and M −117 (loss of COOTMS) (base peak). On the other hand, the β,β'-IDCA (**6**) is characterized by fragments M −57 (loss of CH_3, CH_2, and CO) and prominent M −131 (loss of $CH_2COOTMS$). The α,β'-IDCAs (**3** and **5**) exhibit both the fragments characteristic of α,α'- and β,β'-IDCAs, M −43, M −57, M −117, and M −131. However, base beaks are usually the fragment M −117 and not M −131.

In recent years, gas chromatography-mass spectrometry (GC-MS) has become an important method for unequivocal identification of amino acids and related compounds. Amino acids themselves are nonvolatile and cannot be analyzed by GC without their prior conversion into suitable volatile derivatives. Preparations of a number of such volatile derivatives have been reported by many investigators, which have been reviewed by Hušek and Macek.[1] Of these volatile derivatives for GC, *N*-trifluoroacetyl (TFA) alkyl ester and trimethylsilyl (TMS) derivatives are used most widely at present.

In our previous paper,[2] we reported on mass spectra (electron impact at 20 eV) of both butyl and *N*-TFA butyl esters of some iminodicarboxylic acids (IDCAs) as shown in Fig. 1. The mass spectra of the butyl ester derivatives are rather simple, but those of the *N*-TFA butyl ester derivatives are very complicated due to the presence of rearrangement peaks. For this reason, we undertook a GC-MS study of TMS derivatives of IDCAs, which are expected to give much simpler spectra than the *N*-TFA butyl ester derivatives.

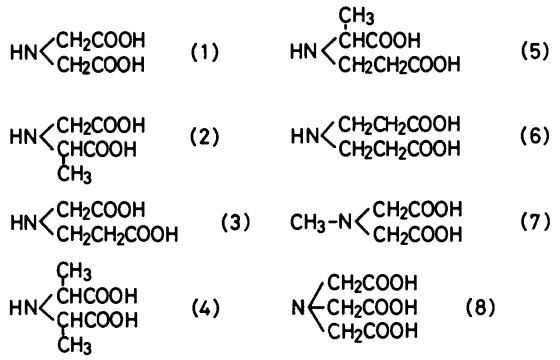

Fig. 1. Iminodicarboxylic acids.

TMS derivatives of amino acids have received great interest since Rühlmann and Giesecke[3] first reported on the preparation of some of them and their resolution by GC in 1961, because of the thermal stability and simplicity of preparation. In general, the TMS derivative can be prepared by use of a silylating reagent with heating (one-step derivatization), whereas multiple procedures are necessary for many other volatile derivatives such as the *N*-TFA butyl ester derivative. At present, many silylating reagents are easily available. Of these reagents, *N,O*-bis(trimethylsilyl)acetamide (BSA)[4] and *N,O*-bis(trimethylsilyl)trifluoroacetamide (BSTFA)[5] are known to be strong TMS donors and have been used most frequently by many investigators. Gehrke *et al.*[6,7] reported on derivatization conditions using BSTFA and single-column resolution of protein amino acids for rapid and quantitative analysis of protein hydrolyzates.

The GC-MS of TMS derivatives of protein amino acids has been studied by several investigators[8–13] for unequivocal identification of amino acids present in biological samples. In most instances, mass spectra exhibited easily recognizable molecular (M^+) and M−15 ions, which are useful for molecular weight determination. However, double derivatization[8,12,13] due to steric hindrance has been found to take place for certain amino acids such as glycine and lysine.

The GC-MS of TMS derivatives of nonprotein amino acids[14–17] has far less been studied. Mařik *et al.*[16] studied silylation of some ω-amino acids with BSA in the presence of catalyst such as HCl. In most instances, both di- and tri-TMS derivatives were formed. However, they established the derivatization conditions under which only the tri-TMS derivative can be prepared.

This investigation reports on silylation of some IDCAs as shown in Fig. 1, with BSA or BSTFA under various conditions, and on mass spectra of the TMS derivatives obtained upon electron impact at 20 eV. The IDCAs include iminodiacetic acid (**1**), 2- and 3-(carboxymethylamino)propionic acids (**2** and **3**), 2,2′-2,3′-, and 3,3′-iminodipropionic acids (**4—6**), *N*-methyliminodiacetic acid (**7**), and nitrilotriacetic acid (**8**).

Results and Discussion

Trimethylsilylation. The silylation of the IDCAs was carried out under various conditions with or without solvent. In general, hydrogen atoms attached to heteroatoms (active hydrogens) can be replaced by TMS groups. In most instances, a suspended IDCA was dissolved into a reagent solution completely during silylation. This fact suggests that free IDCA remaining in the reaction mixture was of a negligible amount. For **1—6**, both di- and tri-TMS derivatives were found to be present by means of GC–MS, although the proportion of their amounts varied depending on silylating conditions. However, any GC peaks corresponding to a mono-TMS derivative could not be detected. These findings indicate that the silylation takes place in two steps, the first formation of di-TMS derivative and its successive conversion into tri-TMS derivative (*N*-TMS di-TMS ester). In the di-TMS derivative, the two TMS groups are considered to be present as silyl esters (di-TMS ester), because it is known that silylation of amines is more difficult than carboxyl groups.

Table 1 gives retention times of the two derivatives of the IDCAs on GC. As expected, the di-TMS derivative has a consistently shorter retention time than the corresponding tri-TMS derivative. Both the two derivatives gave sharp and symmetrical GC peaks on a glass column (1 m) packed with 1.5% OV-101 on Chromosorb G HP. Of these TMS derivatives, the tri-TMS derivative of **4** was found to give two GC peaks, which were evidenced on the basis of mass spectral data. This is ascribable to the separation between diastereomers, as **4** has two asymmetric carbons. However, such separation was not observed for the di-TMS derivative of **4**.

Table 1. Retention times of the TMS derivatives of **1—8** on GC[a]

Parent IDCA	Retention time/min	
	Di-TMS	Tri-TMS
1	10.2	12.5
2	10.0	13.3
3	12.1	15.2
4	9.6	14.2, 15.1
5	11.8	16.1
6	14.2	17.9
7	10.2	—
8	20.0[b]	—

a) Initial temp: 100°C. Initial hold: 5 min. Program rate: 5°C/min. Final temp: 230°C. Injector: 230°C. Column: 3 mmϕ×1 m(glass). Packing: OV-101 1.5% on Chromosorb G HP (100/120 mesh). Retention time of phenanthrene: 17.0 min. b) A tri-TMS ester.

Table 2. Silylation of **1—6** in BSTFA-CH_3CN[a,b]

Parent IDCA	Immediately after silylation		After 1 d	
	Di-TMS/%	Tri-TMS/%	Di-TMS/%	Tri-TMS/%
1	2	98	2	98
2	10	90	7	93
3	11	89	10	90
4	79	21	78	22
5	82	18	56	44
6	12	88	8	92

a) Silylation was carried out at 140°C for 30 min (IDCA, 50 μmol; BSTFA, 0.25 ml; CH_3CN, 0.25 ml) and then the reaction mixture was allowed to stand at room temperature. b) Values indicate peak area ratios.

Table 2 gives the results of silylation of **1—6** in BSTFA-acetonitrile (1:1, v/v), which has been recommended by Gehrke *et al.*[5-7] for silylation of amino acids. Although the reaction conditions (140°C, 30 min) are rather severe, both the di- and tri-TMS derivatives were formed for **1—6**. It is well known that the proportion of the amounts of TMS derivatives varies with the standing time after silylation[8,16] when double derivatization occurs. Therefore, aliquots of the reaction mixture were analyzed by GC immediately after silylation and subsequently after standing for about 1 d at room temperature. A small amount of the di-TMS derivative (2%) still remains even for **1**, the imino group of which is least hindered of the IDCAs. The amounts of the tri-TMS derivatives are much smaller than those of the corresponding di-TMS derivatives for **4** and **5**, the imino groups of which are much more hindered than **1**. Under mild conditions (120°C, 30 min), **4** and **5** gave only the di-TMS derivatives immediately after silylation. These findings indicate that the conversion of the di-TMS derivatives into the corresponding tri-TMS derivatives is governed by the steric hindrance of *N*-substituted groups.

Gehrke and Leimer[18] studied the effect of different solvents on silylation of glycine with BSTFA. They found that polar solvents such as acetonitrile, *N,N*-dimethylformamide (DMF), and pyridine, gave both *N,O*-di-TMS and *N,N,O*-tri-TMS derivatives, whereas nonpolar solvents (dichloromethane, 1,2-dichloroethane, hexane, *etc.*) gave consistently only the di-TMS derivative, under the conditions studied. Table 3 presents the solvents used and their effects on silylation of **1** with BSA. Of these solvents, pyridine gives the highest yield of tri-TMS derivative. The amount of the derivative is 97% immediately after silylation and increases up to 98% after subsequent standing at room temperature for 1 d. It is interesting to note that tetrahydrofuran (THF) gives an extraordinarily high yield of tri-TMS derivative (93%) immediately after silylation, of the nonpolar solvents. In instances of nonpolar solvents such as 1,2-dichloroethane and hexane, as expected, the amount of tri-TMS derivative formed is rather small immediately after silylation, but it increases up to 95—97% on standing at room temperature for 1 d. The amount of tri-TMS derivative after 1 d is somewhat larger than that formed under comparable conditions in polar solvents such as acetonitrile and DMF, which have been used as preferable solvents most frequently. This complicated solvent effect cannot be explained in terms of the polarity of a solvent used, and other factors controlling silylation must be considered.

Figure 2 shows the catalytic effect of HCl on silylation of **1** using BSA or BSTFA in the absence of solvent. It is evident that the silylation is greatly enhanced by the presence of HCl as demonstrated by

Mařik *et al.*[16] for ω-amino acids. In the instance of the HCl salt of **1** and BSA (A), the amount of tri-TMS derivative is 96% immediately after silylation and then gradually increases up to 98% on standing for 3 d at room temperature. Further changes in composition were not observed over the next 4 d at room temperature. This finding indicates that the silylation reaches an equilibrium. As shown in Fig. 2, silylation in other three instances (B, C, and D) also has a tendency to proceed to an equilibrium slowly. These facts are consistent with results obtained by Bergström *et al.*,[8] that silylation of certain amino acids (glycine and lysine) proceeds to an equilibrium in which a few percent of a less silylated derivative still remains. Although Mařik *et al.*[16] have reported that only a tri-TMS derivative was obtained reproducibly in silylation of certain ω-amino acids under comparable conditions (*i.e.*, in silylation by BSA alone in the presence of HCl at 90 °C for 0.5—1 h followed by standing for 1 d at room temperature), we failed to find such conditions under which only the tri-TMS derivative can be formed for **1—6**. A comparison of A with C and of B with D in Fig. 2, indicates obviously that BSA is a stronger TMS donor than BSTFA.

The solvent effect on the silylation of **1**·HCl with BSA was also studied. The addition of pyridine accelerated the silylation to a slight extent. On the other hand, the addition of acetonitrile resulted in a decrease in the amount of the tri-TMS derivative ; this is consistent with results obtained by Mařik *et al.*[16] for the silylation of ω-amino acids. These findings suggest that pyridine is an effective solvent for silylation of hydrochlorides of IDCAs with BSA.

As described above, it seemed impossible to prepare only the tri-TMS derivative for **1—6** under the present conditions. Therefore, silylating conditions under which only the di-TMS derivative can be prepared selectively, were studied. When silylation was carried out with BSTFA alone at 120 °C for 30 min, only the di-TMS derivative was detected for **1—6** immediately after silylation. For **4—6**, the conversion into the tri-TMS derivative did not take place during subsequent standing at room temperature for several days. On the other hand, for **1—3** which have less bulky *N*-substituted groups, the formation of the tri-TMS derivative was observed as shown in Table 4. Therefore, when these IDCAs are analyzed as their di-TMS derivatives, the derivatized solution should be injected into a GC column as soon as possible after silylation. Under the same conditions, BSA was found to give both the

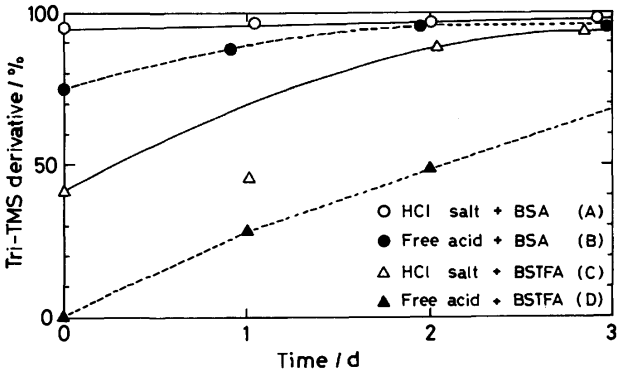

Fig. 2. Catalytic effect of HCl on silylation of **1**. Silylation was carried out at 120 °C for 30 min (**1** or **1**·HCl, 25 μmol; BSA or BSTFA, 0.25 ml) and then the reaction mixture was allowed to stand at room temperature.

Table 3. Solvent effect on silylation of **1** with BSA[a]

Solvent	Dielectric constant (20 °C)[b]	Immediately after silylation		After 1 d	
		Di-TMS/%	Tri-TMS/%	Di-TMS/%	Tri-TMS/%
CH_3CN	37.5	20	80	8	92
DMF	36.7[c]	9	91	10	90
Pyridine	12.3[c]	3	97	2	98
CH_2Cl-CH_2Cl	10.5	39	61	5	95
CH_2Cl_2	9.1	11	89	5	95
THF	7.6[c]	7	93	4	96
Hexane	1.9	28	72	3	97
None	—	25	75	12	88

a) Silylation was carried out at 120 °C for 30 min (**1**, 50 μmol; solvent, 0.25 ml; BSA, 0.25 ml) and then the reaction mixture was allowed to stand at room temperature. b) Cited from Ref. 19. c) At 25 °C.

Table 4. Silylation of **1—6** with BSTFA alone[a]

Parent IDCA	Immediately after silylation		After 1 d		After 2 d	
	Di-TMS/%	Tri-TMS/%	Di-TMS/%	Tri-TMS/%	Di-TMS/%	Tri-TMS/%
1	100	—	72	28	52	48
2	100	—	99	1	96	4
3	100	—	91	9	72	28
4	100	—	100	—	100	—
5	100	—	100	—	100	—
6	100	—	100	—	100	—

a) Silylation was carried out at 120 °C for 30 min (IDCA, 25 μmol; BSTFA, 0.25 ml) and then the reaction mixture was allowed to stand at room temperature. In the instances of **4** and **5**, 0.5 ml of BSTFA was used.

di- and tri-TMS derivatives for **1**—**3**, even immediately after silylation. This fact also indicates that BSA is a stronger silylating reagent than BSTFA.

Figure 3 shows the time course of the silylation of **2** with BSTFA alone at 120 °C, as a typical example. The peak area ratio of the di-TMS derivative to an internal standard (phenanthrene) becomes almost constant after reaction time of 20 min, and its conversion into the tri-TMS derivative was not observed. This fact indicates that **2** can be converted quantitatively into the di-TMS derivative under the silylating conditions (BSTFA alone, 120 °C, and 30 min) described above, and also that the amounts of free **2** and the mono-TMS derivative remaining in the reaction mixture are negligible.

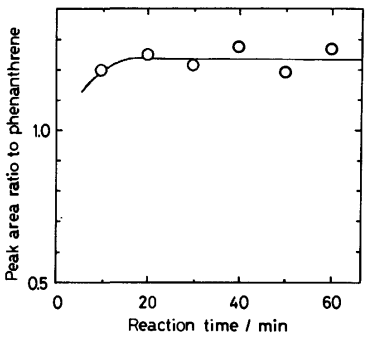

Fig. 3. Time course of the silylation of **2** with BSTFA alone at 120 °C (**2**, 25 mmol; BSTFA, 0.5 ml; phenanthrene, 1.8 mg).

As shown in Table 1, the GC separation of the di-TMS derivatives of the IDCAs is rather poor on the 1 m column. A longer column (2 m), however, showed an indication of partial decomposition of the TMS derivatives of **6** and **8** having longer retention times.

Mass Spectra. Since the IDCAs (**1**—**8**) are regarded as α- or β-amino acids, their TMS derivatives are expected to behave in the same manner as those of α- or β-amino acids upon electron impact. Compounds **7** and **8** are *N*-substituted IDCAs, so that only one derivative, a silyl ester, was formed for each compound.

A) Tri-TMS Derivatives (N-TMS TMS Esters): Figures 4a—f show the mass spectra of the tri-TMS deriv-

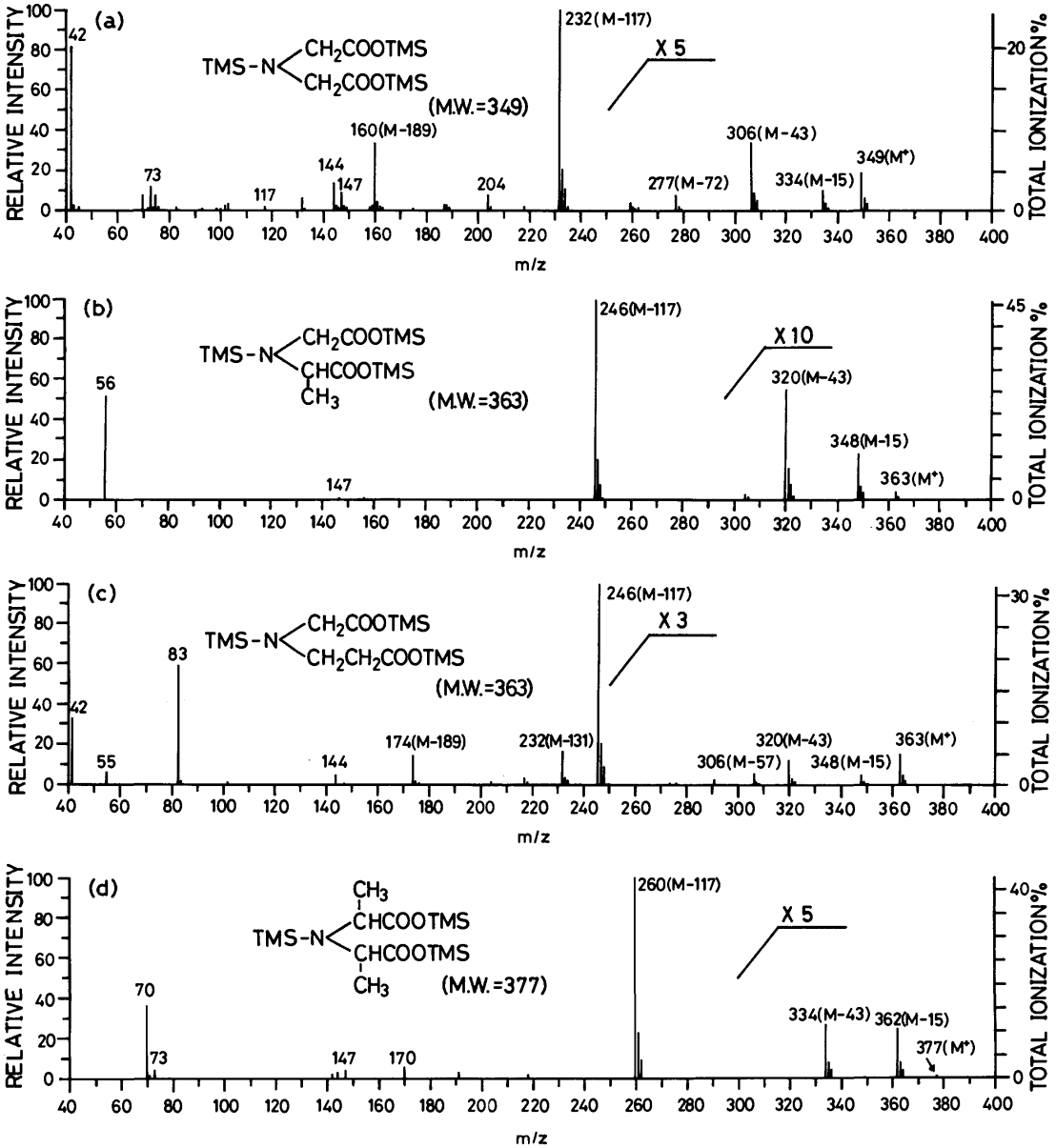

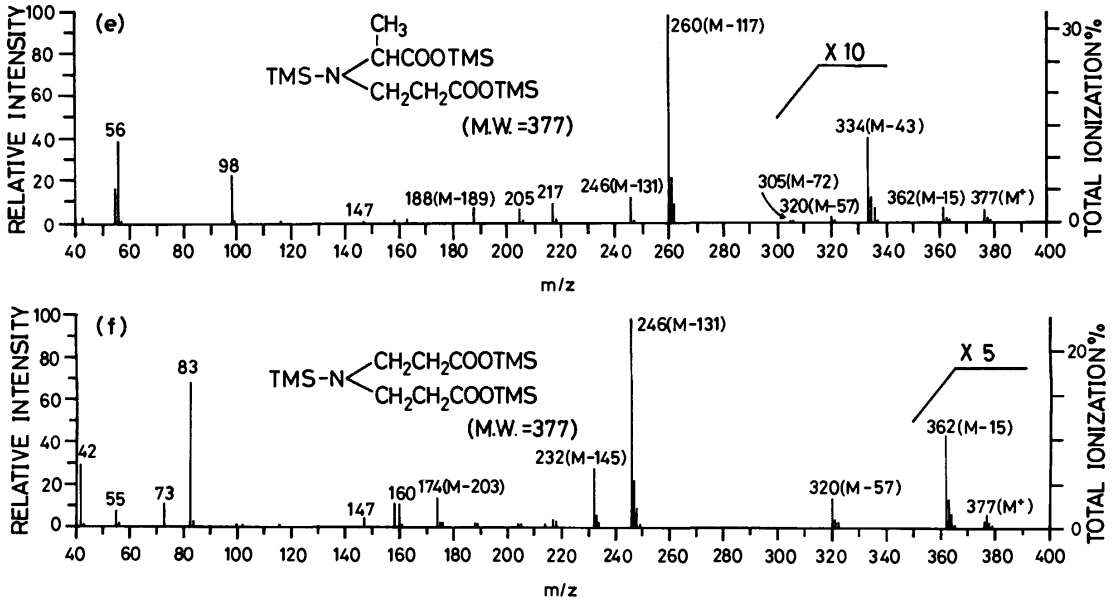

Fig. 4. Mass spectra of the tri-TMS derivatives of IDCAs.
a: **1**, b: **2**, c: **3**, d: **4**, e: **5**, and f: **6**.

atives of **1**—**6**. Both the M^+ and M−15 (CH_3) ions characteristic of TMS derivatives are present in all the spectra. These spectra are much simpler than those of the corresponding *N*-TFA butyl ester derivatives previously reported.[2]

The α,α'-IDCAs (**1**, **2**, and **4**) exhibit characteristic ions such as M^+, M−15, M−43 (CH_3+CO), and M−117 (COOTMS). The M−117 ion constitutes a base peak, which results from the M^+ ion by the loss of a COOTMS group with charge retention on the imino nitrogen as follows:

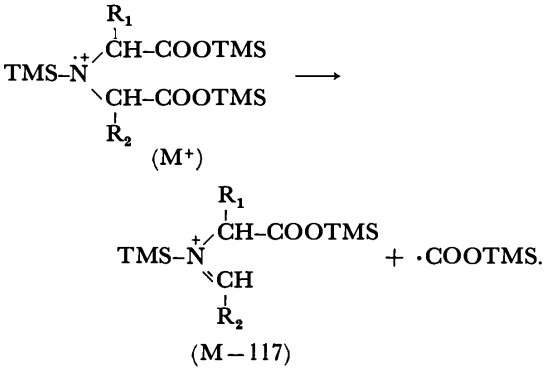

This fragment is very prominent due to the resonance stabilization of the resultant ion. An analogous fragmentation has been described for α-amino acids.[8,13,14] The M−43 ion is difficult to be explained in terms of simple cleavage of the M^+ ion and may be a result of a certain rearrangement process.[14,17] This ion appears for the α,α'- and α,β'-IDCAs but not for the β,β'-IDCA (**6**), indicating the presence of an $\geq NCH_2COOTMS$ group in the molecule. Additional characteristic ions are observed at *m/z* 277 (M−72) and 160 (M−189) for **1**. The M−72 and M−189 ions may result from the M^+ and M−117 ions, respectively, by the loss of a neutral molecule, $CH_2{=}Si(CH_3)_2$, from the ester portion.[14]

On the other hand, the β,β'-IDCA is characterized by the M^+, M−15, M−57 (CH_3+CH_2+CO), and M−131 ($CH_2COOTMS$) ions. The M−131 fragment at *m/z* 246 constitutes a base peak, which arises from the M^+ ion by the loss of a $CH_2COOTMS$ group due to the alpha-beta bond cleavage (α-cleavage) to the imino nitrogen. Because of the stability of this ion due to resonance, the fragmentation losing a COOTMS group which is typical of α,α'-IDCAs does not take place to any appreciable extent. This fragment then gives an M−203 ion at *m/z* 174 by loss of a neutral molecule, $CH_2{=}Si(CH_3)_2$, from the residual ester portion. The elementary composition of the M−57 ion was confirmed by a high-resolution mass measurement. This ion is observed for β,β'- and α,β'-IDCAs, but not for α,α'-IDCAs, indicating the presence of an $\geq NCH_2$-$CH_2COOTMS$ group in the molecule. The M−57 ion also is difficult to be explained in terms of simple cleavage of the M^+ ion as with the M−43 ion described for α,α'-IDCAs. It can therefore be presumed that a rearranged M−15 ion may break down to this ion by the loss of CH_2 and CO.

It is interesting to note that α,β'-IDCAs (**3** and **5**) are characterized by both the ions typical of α,α'- and β,β'-IDCAs. However, the M−117 ion constitutes a base peak as with α,α'-IDCAs. The M−131 ion which is a base peak for **6**, is much less intense than the M−117 ion. This fact indicates that a silylated carboxyl group (a), defined below, is more preferentially split off than

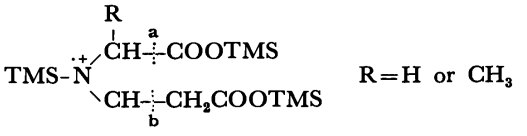

an *O*-silylated methylcarboxyl one (b), also defined above, due to α-cleavage to the imino nitrogen. Additional characteristic ions, the M−72 ($CH_2{=}Si(CH_3)_2$) and M−189 (COOTMS+$CH_2{=}Si(CH_3)_2$), appear for both **3** and **5**. The M−203 ($CH_2COOTMS$+$CH_2{=}Si(CH_3)_2$) ion

typical of **6**, however, is not observed in these instances. Scheme 1 presents the fragmentation pathways for α,β'-IDCAs as an illustrative example, which also involves the characteristics of both α,α'- and β,β'-IDCAs.

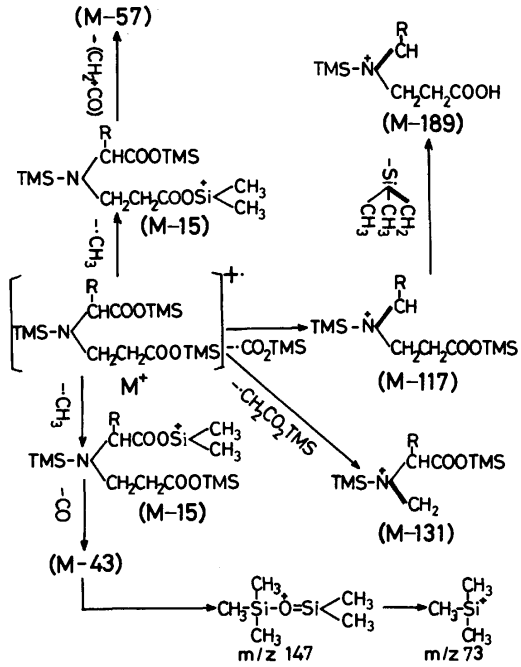

Scheme 1. Fragmentation pathways for the tri-TMS derivatives of α,β'-IDCAs.

B) Di-TMS Derivatives (TMS Esters): Figures 5a—c show the mass spectra of the di-TMS derivatives of 2,2′-, 2,3′-, and 3,3′-iminodipropionic acids (**4**—**6**). In general, the mass spectra of the di-TMS derivatives of **1**—**6** are more complex than those of the corresponding tri-TMS derivatives. For **1**—**6**, the absence of M−45 (COOH) ion indicates that the two TMS groups exist as silyl esters in the molecule, and therefore that the imino nitrogen is not silylated. Characteristic ions for **1**—**8** are listed in Table 5.

α,α'-IDCAs (**1**, **2**, **4**, **7**, and **8**) are characterized by the M^+, M−15, M−43, and M−117 (base peak) ions. On the other hand, β,β'-IDCA (**6**) exhibits a more complex spectrum with characteristic ions such as M^+, M−15, M−57, and M−131. The M−131 ion is very prominent but not a base peak. $\alpha;\beta'$-IDCAs (**3** and **5**) exhibit both the ions characteristic of α,α'- and β,β'-IDCAs. The M−117 ion constitutes a base peak in these instances. These facts indicate that the fragmentation pathways for the di-TMS derivatives are similar to those for the corresponding tri-TMS derivatives.

However, some differences are noted between these two TMS derivatives. The M+1 ion appears only for the di-TMS derivatives, the intensity of which is higher than the corresponding M^+ ion in certain instances (**4** and **5**). An ion *m/z* 172 observed for **4** (Fig. 5a), was confirmed to be M−133 (CH_3+CO+$(CH_3)_3SiOH$) by a high-resolution mass measurement. This fact suggests that this ion results from the M−43 ion by the loss of a $(CH_3)_3SiOH$ group. The M−133 ion is characteristic of α,α'-IDCAs, indicating the presence of an

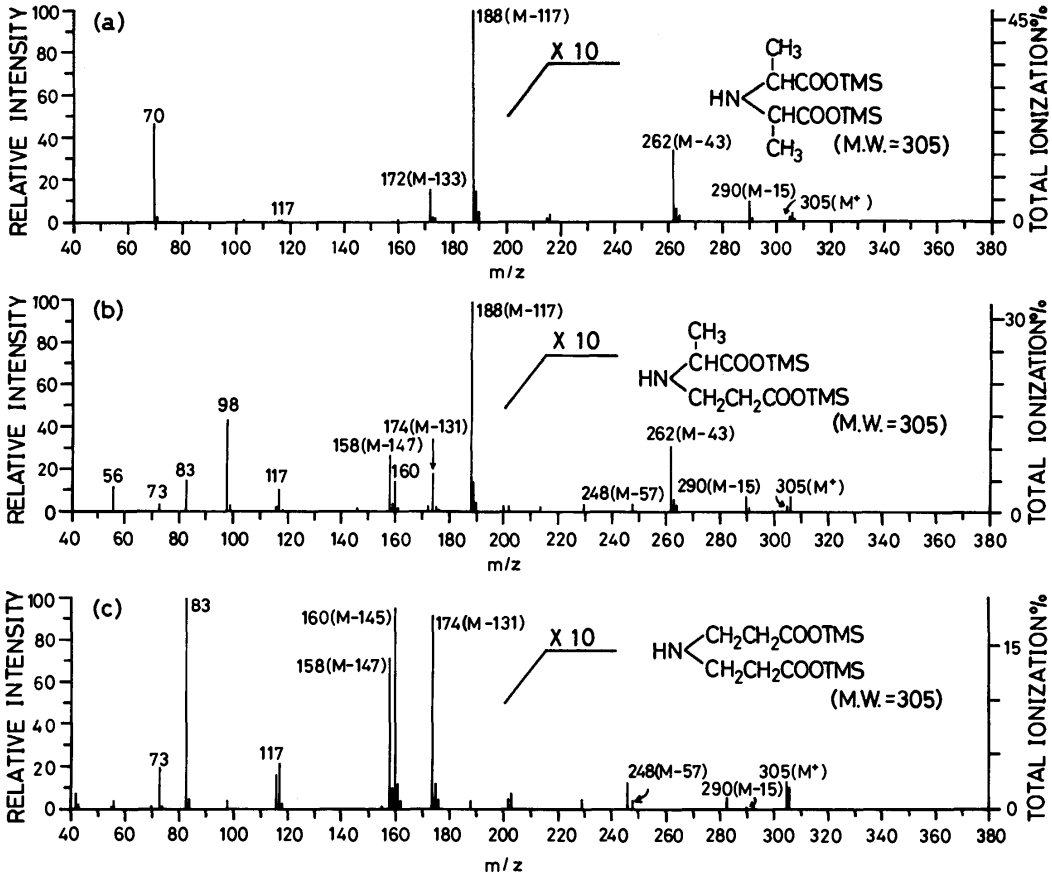

Fig. 5. Mass spectra of the di-TMS derivatives of IDCAs.
a: **4**, b: **5**, and c: **6**.

$\geq NCH_2COOTMS$ group in the molecule. This fragmentation has been described for TMS derivatives of amino acids and peptides.[13,20] On the other hand, two prominent unusual ions are observed at *m/z* 160 and 158 for **6** (Fig. 5c). The elementary composition of the latter ion was determined as $C_6H_{12}NO_2Si$ by a high-resolution mass measurement, which corresponds to M−147 (CH_3+CH_2+CO+$(CH_3)_3SiOH$). This fact suggests that the M−147 ion results from the M−57 ion by the loss of a $(CH_3)_3SiOH$ group as with the M−133 ion described for α,α'-IDCAs. The M−147 ion characteristic of β,β'-IDCA indicates the presence of an $\geq NCH_2CH_2COOTMS$ group in the molecule. Another prominent ion at *m/z* 160 was determined as $C_6H_{14}NO_2Si$ also by a high-resolution mass measurement, which corresponds to M−145 ($2CH_2$+COOTMS). This observation suggests that the M−145 ion results from the M^+ ion by the loss of a $CH_2CH_2COOTMS$ group *via* the N-C bond cleavage. The M−145 ion is characteristic of β,β'-IDCA and also observed at *m/z* 232 with a relative intensity of 29% for the tri-TMS derivative of **6** (Fig. 4f). As expected, α,β'-IDCAs (**3** and **5**) are characterized by the M−133, M−145, and M−147 ions.

Other characteristic ions such as M−89, M−90, M−102, M−103, M−104, and M−105 appear with a low intensity for the di-TMS derivatives. In the instance of **1**, however, the M−89 ion at *m/z* 188 is very prominent (Table 5). Of them, the M−89 and M−90 ions were determined to correspond to fragments M−$(CH_3)_3SiO$ and M−$(CH_3)_3SiOH$, respectively, by a high-resolution mass measurement. The characteristic ions described above have been observed for TMS derivatives of amino acids and peptides[13,20] except the M−103 ion. The disiloxynium ion ($(CH_3)_2Si{=}\dot{O}{-}Si(CH_3)_3$)[8,14,16] at *m/z* 147 indicating the presence of an -OTMS group, appears for all the tri-TMS derivatives, though as a minor peak. This ion is not observed for all the di-TMS derivatives. On the other hand, the ion *m/z* 117 with the structure $\dot{O}{\equiv}CO$-TMS[8,16] is observed for all the di-TMS derivatives but not for the tri-TMS derivatives except **1**. The ion at *m/z* 83 appears for most of the di-TMS derivatives with different intensities, which is a base peak for **6**. This ion is observed also for certain tri-TMS derivatives (**1**, **3**, and **6**).

As shown in Table 6, the total ionization of the base peak (M−117) for α,α'- and α,β'-IDCAs, generally depends on the structure of IDCA. The IDCAs with a methyl group on an α-carbon or an imino nitrogen atom have larger total ionization. Since **7** is an isomer of **2**, the mass spectra of their di-TMS derivatives resemble each other. However, **7** carrying a methyl group on its imino nitrogen is characterized not only by a more intense M^+ ion but also by a larger total ionization of the base peak (M−117) (Tables 5 and 6).

Previous investigators[13,16] have found that, for amino acids which do form double derivatives, the relative intensity of the M^+ ion was higher than that of more highly silylated derivatives, but this is not true for the TMS derivatives of **1**—**6**.

In the present study, the TMS derivatives of the IDCAs are shown to have advantages over the *N*-TFA butyl ester derivatives[2] in both the simplicity of preparation and the simple mass spectra containing the M^+, M−15, and additional characteristic ions. However, double derivatization was found to occur for **1**—**6**, which is often observed for TMS derivatives. This is possibly because of the bulkiness of TMS group. This double derivatization may be overcome by introducing TFA to the imino nitrogen instead of TMS group, which is less bulky and also known to be a good *N*-masking group for amino acids for GC

Table 6. Total ionization of base peaks of the di-TMS derivatives of **1**—**8**

Parent IDCA	Base peak/*m/z*	Origin	Total ionization/%
1	160	M−117	19
2	174	M−117	41
3	174	M−117	22
4	188	M−117	47
5	188	M−117	32
6	83		20
7	174	M−117	49
8[a]	290	M−117	22

a) A tri-TMS ester.

Table 5. Characteristic ions of the di-TMS derivatives of **1**—**8**[a]

Parent IDCA	M^+	M−15	M−43	M−57	M−117	M−131	M−133	M−147	Others
1	277	262	234	—	160	146	144	130	188[M−89], 98
	(4.0)	(2.9)	(4.8)		(100)	(3.9)	(29.1)	(1.0)	(84.9) (48.1)
2	291	276	248	—	174	160	158	144	83
	(0.5)	(0.5)	(3.4)		(100)	(7.4)	(20.6)	(3.7)	(14.4)
3	291	276	248	234	174	160	158	144	188[M−103], 83
	(2.9)	(0.9)	(3.2)	(2.7)	(100)	(38.3)	(13.4)	(34.5)	(19.8) (93.1)
4	305	290	262	—	188	—	172	—	70
	(0.2)	(1.0)	(3.4)		(100)		(15.2)		(46.5)
5	305	290	262	248	188	174	172	158	160[M−145], 98
	(0.2)	(0.7)	(3.1)	(0.3)	(100)	(18.7)	(2.0)	(27.4)	(14.8) (44.0)
6	305	290[b]	—	248	—	174	—	158	160[M−145], 83
	(1.2)			(0.4)		(92.0)		(71.4)	(95.4) (100)
7	291	276	248	—	174	160[b]	158[b]	—	103
	(4.2)	(1.5)	(5.5)		(100)				(11.6)
8[c]	407	392	364	—	290	276	274	—	232, 174, 103
	(7.8)	(14.6)	(8.5)		(100)	(2.9)	(1.4)		(25.9)(20.6)(26.2)

a) Values in parentheses indicate relative intensity. b) Relative intensity of this ion is less than 0.1%. c) A tri-TMS ester.

analysis. However, one-step derivatization of such *N*-TFA TMS esters of amino acids[21] is not established at present. Further study must be undertaken along this line.

Experimental

Materials. BSA and BSTFA were obtained from Wako Pure Chemical Industries, Ltd. and Nakarai Chemicals, Ltd., respectively. Acetonitrile, DMF, pyridine, dichloromethane, 1,2-dichloroethane, and hexane were obtained from Wako Pure Chemical Industries, Ltd. as S grade reagents and used as silylation solvents without further purification. Compounds **1**—**8** were the same as previously reported.[2]

Silylation. About 50 μmol of each IDCA was weighed into a 1 ml screw vial. Then, 0.25 ml of a silylating reagent and 0.25 ml of a solvent were added to the vial. It was closed tight with a silicone cap and then heated at different temperatures for different durations in a constant-temperature air bath (Yamato Drying-Oven, DX-58). When silylation was performed with a silylating reagent alone in the absence of solvent, about 25 μmol of each IDCA was heated with 0.25 or 0.50 ml of a silylating reagent. The hydrochloride of **1** was prepared by treating **1** with distilled 6 M HCl (1 M=1 mol dm^{-3}). After reaction, the solution was evaporated completely to dryness under reduced pressure. The hydrochloride obtained was purified by recrystallization. Usually, 1 μl portions of silylated solutions were injected into a GC column.

GC. GC was carried out with a Hitachi gas chromatograph 163 equipped with a flame ionization detector. The conditions were the same as previously reported.[2]

GC-MS. GC-MS was carried out with a JEOL JMS-D 300 mass spectrometer connected with a JGC-20 KP gas chromatograph and mass spectra upon electron impact at 20 eV were obtained. The GC-MS conditions were the same as previously reported.[2]

Note added in proof

Better GC separation of the di-TMS derivatives of the IDCAs was obtained when a fused silica capillary column (OV-101 FS-WCOT, 0.35 mmϕ×25 m, Gasukuro Kogyo Co., Ltd.) was used instead of the packed column. In this instance, the separation between diastereomers was observed for **4**. Decomposition of the di-TMS derivatives did not take place on the capillary column because of the absence of solid support.

References

1) P. Hušek and K. Macek, *J. Chromatogr.*, **113**, 139 (1975).
2) K. Kawashiro, S. Morimoto, and H. Yoshida, *Bull. Chem. Soc. Jpn.*, **57**, 1097 (1984).
3) K. Rühlmann and W. Giesecke, *Angew. Chem.*, **73**, 113 (1961).
4) J. F. Klebe, H. Finkbeiner, and D. M. White, *J. Am. Chem. Soc.*, **88**, 3390 (1966).
5) D. L. Stalling, C. W. Gehrke, and R. W. Zumwalt, *Biochem. Biophys. Res. Commun.*, **31**, 616 (1968).
6) C. W. Gehrke, H. Nakamoto, and R. W. Zumwalt, *J. Chromatogr.*, **45**, 24 (1969).
7) C. W. Gehrke and K. R. Leimer, *J. Chromatogr.*, **57**, 219 (1971).
8) K. Bergström, J. Gürtler, and R. Blomstrand, *Anal. Biochem.*, **34**, 74 (1970).
9) J. L. Laseter, J. D. Weete, A. Albert, and C. H. Walkinshaw, *Anal. Lett.*, **4**, 671 (1971).
10) R. Mitra, J. Burton, and J. E. Varner, *Anal. Biochem.*, **70**, 1 (1976).
11) F. P. Abramson, M. W. McCaman, and R. E. McCaman, *Anal. Biochem.*, **57**, 482 (1974).
12) H. Iwase, Y. Takeuchi, and A. Murai, *Chem. Pharm. Bull.*, **27**, 1307 (1979).
13) K. R. Leimer, R. H. Rice, and C. W. Gehrke, *J. Chromatogr.*, **141**, 355 (1977).
14) K. Bergström and J. Gürtler, *Acta. Chem. Scand.*, **25**, 175 (1971).
15) O. Vitzthum and P. Werkhoff, *J. Chromatogr.*, **95**, 39 (1974).
16) J. Mařik, A. Čapek, and J. Králičcek, *J. Chromatogr.*, **128**, 1 (1976).
17) P. V. Fennessey and S. S. Tjoa, *Org. Mass Spectrom.*, **15**, 202 (1980).
18) C. W. Gehrke and K. Leimer, *J. Chromatogr.*, **53**, 201 (1970).
19) "Yôzai Handbook," ed by T. Asahara *et al.*, Kodansha, Tokyo (1976).
20) K. M. Baker, M. A. Shaw, and D. H. Williams, *J. Chem. Soc., Chem. Commun.*, **1969**, 1108.
21) G. Michael, *J. Chromatogr.*, **196**, 160 (1980).

 © 1984 The Chemical Society of Japan Bull. Chem. Soc. Jpn., 57, 2879—2884 (1984)

Photoresponsive Crown Ethers. 13. Synthesis of Photoresponsive NS_2O Crown Ethers and Application of the Cu(I) Complexes to O_2-Binding

Seiji SHINKAI,* Kazuyoshi SHIGEMATSU, Yoshihiro HONDA, and Osamu MANABE*
Department of Industrial Chemistry, Faculty of Engineering, Nagasaki University, Nagasaki 852
(Received March 10, 1984)

Photoresponsive crown ethers with heavy metal affinity were synthesized: They are the NS_2O crowns bound to photofunctional azobenzene at 4,4′-positions *via* X(CH_2 or CO) (**1**(X=CH_2) and **1**(X CO), respectively). They efficiently extracted heavy metal ions from aqueous phase to organic(dichloromethane) phase. The continuous variation method established that both *trans*-**1** and photoisomerized *cis*-**1** bind two Cu(II) ions forming 1:1 metal/NS_2O crown complexes. The *trans*-**1**(X=CH_2)·$Cu(I)_2$ complex was irreversibly oxidized by O_2 to the $Cu(II)_2$ complex, whereas the *cis*-**1**(X=CH_2)·$Cu(I)_2$ complex bound O_2 in a partly reversible manner like Osborn's complex. Thus, a photoinduced change in the Cu(I)·····Cu(I) interatomic distance is responsible for the stability of the O_2 complex. These results show that the extraction of heavy metal ions and the O_2-complexation can be controlled by light with the mediation of photoresponsive NS_2O crown ethers.

Chemical substances which exhibit photoinduced structural changes are potential candidates not only for the storage of light energy but also as mediators for the conversion of light into other forms of energy. Further, if the structural changes occurring in the photoresponsive chromophores can be transmitted to functional molecules, the fundamental functions of photoresponsive systems in nature may be mimicked in artificial systems. Azobenzene derivatives which exhibit photoinduced reversible cis-trans isomerism have frequently been employed as photoantennae which trigger subsequent events of a number of functional molecules.[1-6]

The purpose of our investigation has been to control the functions of a crown ether family by an on-off light switch, which would lead to photoregulated ion-extraction and membrane transport.[7-12] It was shown that in these photoresponsive crown ethers, not only the binding ability but also the ion selectivity was markedly changed by photoirradiation.[7-16] Two different techniques have been developed to change the binding ability of crown ethers by light. One method is to induce a conformational change in the crown ether moiety in conjugation with a photoinduced configurational change in the azobenzene moiety. The other method is associated with a change in the spatial position between two crown rings which leads to interconversion between 1:1 and 2:1 crown/cation complexes. It is known that a thiacrown family exhibits a significant affinity toward heavy metal cations.[17,18] Thus, if one can extend the above concept to the thiacrown family, it would lead to photocontrol of the ion-binding ability toward heavy metal cations. As a related system, Blank *et al.*[19] recently reported the photoresponsive binding of Zn(II) to 4,4′-bis(α-iminodiacetic acid) azotoluene. We considered that in photoresponsive thiacrown ethers, the heavy metal complexes would have affinity toward small molecules such as O_2 and CO, and thus the affinity might be also photocontrolled. With these objects in view, we synthesized **1**—**3** and evaluated the reversible O_2 binding to the Cu(I) complexes.

Experimental

Materials. 1-Oxa-4,10-dithia-7-azacyclododecane (NS_2O crown) was prepared from equimolar amounts of 3-oxapentane-1,5-dithiol and 1,5-dibromo-3-azapentane hydrobromide in absolute ethanol in the presence of sodium ethoxide: Mp 64—67 °C (lit,[20] 64 °C), yield 31.5%. $M^+(m/z)$: 207. IR (Nujol): ν_{NH} 3255, 3230 cm^{-1}, ν_{C-O-C} 1280, 1115 cm^{-1}. Found: C, 46.05; H, 8.36; N, 6.67; S, 30.70%. Calcd for $C_8H_{17}NOS_2$: C, 46.33; H, 8.26; N, 6.75; S, 30.92%.

4,4′-Bis(1-oxa-4,10-dithia-7-azacyclododec-7-ylmethyl)azobenzene **1**(X=CH_2)) was synthesized from the NS_2O crown and 4,4′-bis(chloromethyl) azobenzene in acetonitrile in the presence of excess powdered K_2CO_3. The detailed procedure is essentially similar to that described for the synthesis of the crown ether analogue.[9] The product was isolated by a TLC method (silica gel and chloroform-ethanol (10:1 by volume)) and finally recrystallized from benzen-ligroin: Mp 117—118 °C, yield 43%. $M^+(m/z)$: 620. ^{1}H-NMR ($CDCl_3$, δ): SCH_2 and NCH_2 in the rings, 2.63—3.10, 24H; OCH_2 and $ArCH_2N$, 3.70—3.90, 12H; 3,3′-ArH, 7.44, 4H; 2,2′-ArH, 7.82, 4H.

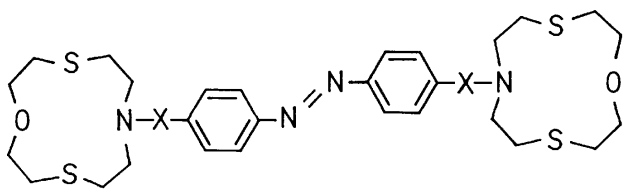

trans-1(X=CH_2 or CO)

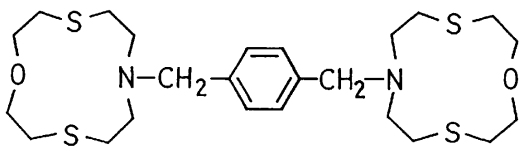

2

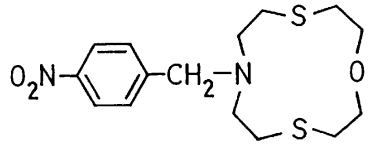

3

Found: C, 57.83; H, 7.12; N, 8.87; S, 20.50%. Calcd for $C_{30}H_{44}N_4O_2S_4$: C, 58.03; H, 7.14; N, 9.02; S, 20.65%.

4,4'-Bis(1-oxa-4,10-dithia-7-azacyclododec-7-ylcarbonyl)azobenzene (**1**(X=CO)) was synthesiszed from the NS_2O crown and 4,4'-*bis*(*chloroformyl*)*azobenzene* in benzene in the presence of excess triethylamine. A similar procedure was described previously for the synthesis of the crown ether analogue.[9] The product was isolated by a TLC method(silica gel and chloroform–ethanol (10:1 by volume)) and recrystallized from benzene–ether: Mp 246—247 °C, yield 54%. $M^+(m/z)$: 648. ^{1}H-NMR($CDCl_3$, δ): SCH_2, 2.5—3.2, 16H; OCH_2 and NCH_2 in the rings, 3.5—4.2, 16H; 3,3'-ArH, 7.52, 4H; 2,2'-ArH, 7.97, 4H. Found: C, 55.12; H, 6.21; N, 8.66; S, 19.56%. Calcd for $C_{30}H_{40}N_4O_4S_4 \cdot 0.25\ H_2O$: C, 55.15; H, 6.25; N, 8.57; S, 19.63%.

1,4-Bis(1-oxa-4,10-dithia-7-azacyclododec-7-ylmethyl)benzene (**2**)was prepared from the NS_2O crown and α,α'-dibromo-*p*-xylene in acetonitrile in the presence of excess powdered K_2CO_3. The method is analogous to that employed for the synthesis of **1**(X=CH_2). The product was isolated by a TLC method (silica gel and chloroform–ethanol (10:1 by volume)) and recrystallized from benzene–petroleum ether: Mp 109—110 °C, yield 34%. $M^+(m/z)$: 516. ^{1}H-NMR($CDCl_3$, δ): SCH_2 and NCH_2 in the rings, 2.65—3.05, 24H; $ArCH_2N$, 3.64, 4H; OCH_2, 3.78, 8H; ArH, 7.26, 4H. Found: C, 55.84; H, 7.92; N, 5.35; S, 24.65%. Calcd for $C_{24}H_{40}N_2O_2S_4$: C, 55.78; H, 7.80; N, 5.42; S, 24.81%.

N-(*p*-Nitrobenzyl)-1-oxa-4,10-dithia-7-azacyclododecane (**3**-(X=NO_2)) was synthesized from the NS_2O crown and *p*-nitrobenzyl chloride in acetonitrile in the presence of excess powdered K_2CO_3 in a manner similar to that described previously.[9] After TLC separation (silica gel and chloroform–ethanol (10:1 by volume)), the product was recrystallized from benzen–ligroin: Mp 133—134 °C, yield 60%. $M^+(m/z)$: 342. ^{1}H-NMR($CDCl_3$, δ): SCH_2 and NCH_2 in the ring, 2.61—3.00, 12H; OCH_2 and $ArCH_2N$, 3.72, 6H; *o*-ArH, 7.44, 2H; *m*-ArH, 8.08, 2H. Found: C, 52.51; H, 6.54; N, 8.19; S, 18.84%. Calcd for $C_{15}H_{22}N_2O_3S_2$: C, 52.61; H, 6.47; N, 8.18; S, 18.72%.

N-Benzyl-1-oxa-4,10-dithia-7-azacyclodedecane (**3**(X=H)) was similarly synthesized from the NS_2O crown and benzyl chloride: Mp 108—110 °C, yield 65%. Found: C, 60.66; H, 7.80; N, 4.77%. Calcd for $C_{15}H_{23}NOS_2$: C, 60.56; H, 7.79; N, 4.71%.

Miscellaneous. The methods of solvent extraction and the rate determination of thermal cis-to-trans isomerization were described previously.[7-12] As a UV-light source for the trans-to-cis isomerization, a 500 W high-pressure Hg-lamp with a colour glass filter (330 nm<λ<380 nm) was used. In the solvent extraction of Cu(II) with **1**(X=CH_2), we measured the concentrations of picrate ion (by absorption spectroscopy) as well as Cu(II) (by atomic absorption spectroscopy) extracted into the dichloromethane phase. It was found that the concentration of Cu(II) is very close to that of picrate ion, indicationg that Cu(II) is extracted as Cu·picrate·Cl.

The O_2-absorption experiments of **1**—**3** were carried out by using a Thunberg cuvette. The thiacrown ether dissolved in propylene carbonate (PC) was placed in the bottom cell of the Thunberg cuvette and $[Cu(CH_3CN)_4]BF_4$ in PC was deposited in the side arm. After N_2-substitution by repeating a freezing-and-thawing, two solutions were mixed and subjected to spectral measurement at 30 °C. At this time, there was no absorption maximum at around 700 nm. An O_2 stream was introduced into the cell for 5 min at 40—50 °C, and the spectrum was recorded at 30 °C. Then, the mixture was evacuated at 1.0 mmHg for 1h at 70 °C (for *cis*-**1**, for 20 min at 40 °C in order to suppress the cis-to-trans thermal isomerization). The fraction of the oxygenation product was estimated from the decrease in the absorption band at around 700 nm.

Results and Discussion

Spectral Examination of Metal-crown Interactions. The spectroscopic properties of *trans*-**1** are summarized in Table 1. Since the π-π^* band of *trans*-**1** and the n-π^* band of *cis*-**1** are clearly separated, one may expect that trans-to-cis and cis-to-trans isomerizations are controlled by irradiation of UV and visible light, respectively. Under UV-light irradiation, the absorbance of the π-π^* band decreased and that of the n-π^* band increased gradually with tight isosbestic points and finally reached a photostationary state. The cis concentration at the photostationary state was estimated (Table 1) by the decrease in the OD of the absorption maxima, assuming that the OD of *cis*-**1** at these wavelengths is negligible in comparison with that of *trans*-**1**. The cis-forms of **1**(X=CH_2) and **1**(X=CO) isomerized thermally to the trans-forms with k(first-order rate constant)=0.0347 and 0.0958 h^{-1}, respectivery, at 30 °C in dichloromethane. Under visible light irradiation (200 W tungsten-lamp, 15 s at intervals of 10 min), the isomerization reaction was speeded up to 1.24 and 4.90 h^{-1}, respectively.

The addition of $CuCl_2$ to a dichloromethane solution of **1**(X=CH_2) gave rise to a new shoulder at 390—420 nm region as well as to an absorption maximum at around 700 nm. Since a similar spectral change was observed for **2**[18] and **3**, these absorption bands are attributed to the $CuCl_2$–NS_2O crown interaction. On the other hand, the spectral change of **1**(X=CO) occurred to a relatively smaller extent. We chose 390 nm to conduct the continuous variation method of *trans*- and *cis*-**1**(X=CH_2), because this band is relatively stronger than the 700 nm band and corresponds to an isosbestic point of the cis-trans isomerism. Thus, one may estimate the extent of the Cu(II)-crown association directly from the observed OD without regard to the cis percentage. Figure 1 shows that the maxima appear at $[CuCl_2]/[\mathbf{1}(X=CH_2)]=2$, indicating that both *trans*- and *cis*-**1**(X=CH_2) form the 2:1 copper/**1** complexes. This means that each NS_2O crown binds one Cu(II) and the composition is not changed by the photoisomerization.

Metal Ion Catalyses in the Thermal Cis-to-Trans Isomerization. We have described that the photoinduced cis-trans interconversion of **1** occurs reversibly. It is known that some heavy metal ions can catalyze the thermal isomerization of azo-linkages[12,21,22] probably because of the stabilization of the transition state through metal ion coordination to the azo linkages. In Table 2, typical first-order rate constants in the presence of metal ions are summarized. From Table 2, most of the heavy metal ions used are capable of catalyzing the thermal isomerization and, in particular, Cu(II) provides the greatest catalytic effect. We thus carried out further detailed investigation on the Cu(II) catalysis. In Fig. 2, the first-order rate constants for **1** are plotted against the Cu(II) concentration. The plots for **1** give a biphasic dependence which consists of no rate increase at $[CuCl_2]/[\mathbf{1}]<2$ and marked rate increase at $[CuCl_2]/[\mathbf{1}]>2$. The result suggests that Cu(II) is selectively bound to the two NS_2O crown ethers in the first phase and the interaction with the azo

Table 1. λ_{max} and ε_{max} of *trans*-**1**, cis/trans ratio at the photostationary state, and first-order rate constants(k) for theramal isomerization[a]

Crown	Solvent	$\lambda_{max}(\varepsilon_{max})$	cis/trans[b]	k[c]/h^{-1}
1(X=CH_2)	CH_2Cl_2	325(20000) 436(520)	68/32	0.0347
1(X=CH_2)	PC[d]	330(22900) 440(770)	72/28	
1(X=CO)	CH_2Cl_2	330(28600) 445(780)	49/51	0.0958
1(X=CO)	PC[d]	330(29000) 435(870)	63/37	

a) 30°C. b) It takes about 10 min for 2.50×10^{-5} M(1M=1 mol dm^{-3}) of the crown solutions to reach the photostationary state by light from a 500 W high-pressure Hg-lamp through a glass filter (330 nm<λ<380 nm). c) CH_2Cl_2 containing 3.1 vol% of ethanol. d) Propylene carbonate.

Table 2. Influence of heavy metal ions on the first-order rate constants(k, h^{-1}) for the thermal cis-to-trans isomerization(30°C)[a]

Metal salt	**1**(X=CH_2)	**1**(X=CO)
None	0.0347	0.0958
$CuCl_2$	1.15	0.594
$HgCl_2$	0.067	0.126
$CoCl_2$	0.033	0.358
$Ni(OCOCH_3)_2$	0.033	0.094

a) Solvent: dichloromethane: ethanol=96.9: 3.1 by volume, [metal salt]=1.00×10^{-4} M. [**1**]=2.50×10^{-5} M.

linkage which is associated with the rate enhancement begins at $[CuCl_2]/[1]>2$. This is second evidence that each NS_2O crown binds one Cu(II).

Solvent Extraction of Heavy Metal Ions. In Table 3, the influence of photoirradiation on the extractability of **1** and related compounds **2** and **3**(X=NO_2) is summarized. **3**(X=NO_2) was mainly used because of the analogy between NO_2 and azobenzene as electron-withdrawing substituents. It is seen from extractabilities (Ex%) of **2** and **3**(X=NO_2) that Hg(II) has a contrasting characteristic to other metal ions: Cu(II), Co(II), Ni(II), and Pb(II) give the smaller Ex% in **3**(X=NO_2) than in **2**, while the Ex% for Hg(II) is slightly enhanced in **3**(X=NO_2). The result means that the basicity of the nitrogen in the NS_2O crown ring plays a decisive role in the complexation with the four metal ions, while the affinity with the sulfur atoms is

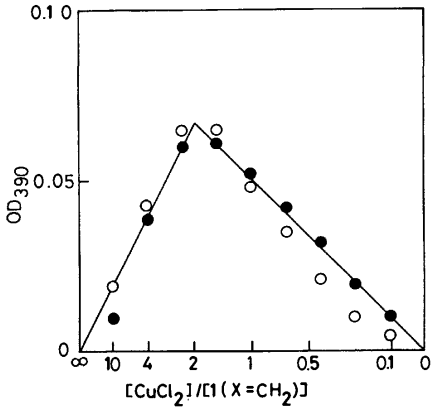

Fig. 1. Continuous variation plots of OD_{390}. 30°C, CH_2Cl_2 (containing 3.1 vol% ethanol), [**1**(X=CH_2)]+[$CuCl_2$]=2.50×10^{-5} M.
● *trans*-**1**(X=CH_2); ○ Photoirradiated **1**(X=CH_2) where cis/trans=68/32.

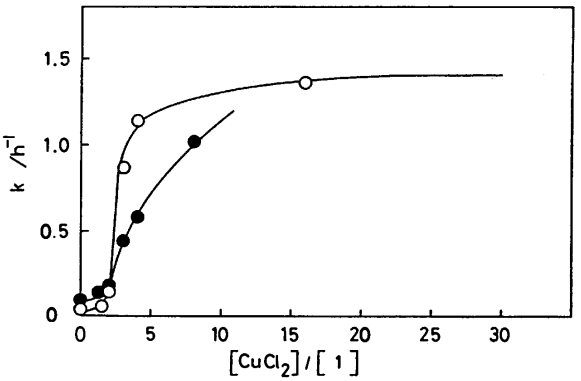

Fig. 2. Influence of added $CuCl_2$ on the thermal cis-to-trans isomerization (30°C). ○ and● [**1**(X=CH_2)]=[**1**(X=CO)]=2.50×10^{-5} M, (respectively) in CH_2Cl_2 containing 3.1 vol% ethanol.

most important in the Hg(II)-binding. Most important in Table 3 is the fact that the Ex% for **1** is scarcely affected by photoirradiation. This means that two NS_2O crown rings act rather independently. We previously examined the photoresponsive behaviors of 4,4′-bis(1,4,7,10-tetraoxa-13-azacyclopentadec-13-ylmethyl)-azobenzene and 4,4′-bis(1,4,7,10-tetraoxa-13-azacyclopentadec-13-ylmethyl)azobenzene and 4,4′-bis(1,4,7,10-tetraoxa-13-azacyclopentadec-13-ylcarbonyl)azobenzene (monoaza-15-crown-5 analogues of **1**(X=CH_2) and **1**(X=CO)).[9] The photoisomerized cis-forms of these

Table 3. Influence of photoirradiation on the extraction of heavy metal ions to the organic phase (dichloromethane) with **1**, **2**, and **3**(X=NO_2) at 30°C[a]

Crown	Extracted picrate/%				
	Cu^{2+}	Hg^{2+}	Co^{2+}	Ni^{2+}	Pb^{2+}
trans-**1**(X=CH_2)	77.6	78.2	17.9	20.3	38.5
Photoirradiated **1**(X=CH_2)[b]	86.4	84.4	20.4	28.0	35.1
trans-**1**(X=CO)	14.2	18.6	13.7	12.7	
Photoirradiated **1**(X=CO)[c]	15.0	19.6	14.7	13.1	
2	100	74.0	22.8	25.6	73.9
3(X=NO_2)	10.2	91.4	14.2	14.9	17.5

a) Extraction conditions: aqueous phase, [metal salt]=0.010 M, [picric acid]=1.00×10^{-4} M, pH4.0—4.1 with Et_4NOH(*ca.* 10^{-4} M); organic phase, [**1** or **2**]=6.06×10^{-4} M or [**3**(X=NO_2)]=1.21×10^{-3} M. Chloride salts are used except Pb^{2+}(acetate salt). b) cis-Form 76%. c) cis-Form 49%.

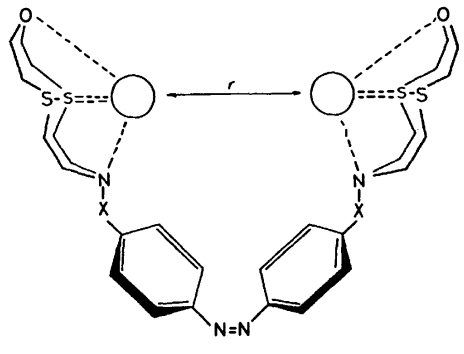

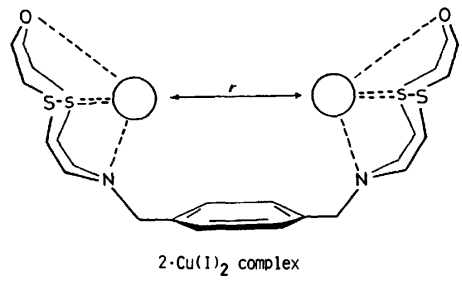

Fig. 3. Ear-muff conformation of the Cu(I) complexes of **2** and *cis*-**1**(X=CH_2).

crown ethers bound Rb^+ and Cs^+ with relatively large ion radii more efficiently than the trans-forms, but no significant difference could be seen for Na^+. One may presume, therefore, that the caity constructed by two intramolecular crown rings is pretty large. The ion radius of Cu(II) (0.76—0.87 Å) is much smaller than that of Na^+ (1.13—1.16 Å). Provided that the cis-forms of **1**(X=CH_2) and **1**(X=CO) construct the cavity similar to these crown ethers, it is very likely that two NS_2O crown rings in *cis*-**1** cannot coordinate to one Cu(II) ion cooperatively.

The results indicate, together with the result of the continuous variation experiment (Fig. 1), that both *trans*- and *cis*-**1** form the 2:1 (*i.e.*, 1:1 metal/crown) complexes with metal ions. Based on the foregoing informations, we conducted photocontrol studies of reversible O_2 adsorption to the **1**(X=CH_2)·$Cu(I)_2$ complex.

Oxygen Adsorption to the Cu(I)-complexes of 1, 2, and 3. The preparation of complexes which contain two transition metal ions separated by distances of 3.5—6 Å has been of much concern in recent years. Interest in such complexes stems from their potential for the functionality to flank small molecules in a sandwich manner as a so-called cascade complex.[23] In particular, the systems which are capable of binding O_2 or N_2 are of special interest because of their relevance to biological systems, such as haemocyanin, hemerythrin, and perhaps nitrogenase. There are several precedents for bi-metallic copper complexes which bind O_2 or CO, although the revesibility is not satisfactory yet.[18,24-26] Osborn *et al.*[18] reported **2**·$Cu(I)_2$ complex, in which the oxygenation-deoxygenation sequence in the solid state can be repeated several times although the reversibility in solution is not as complete as in the solid state.

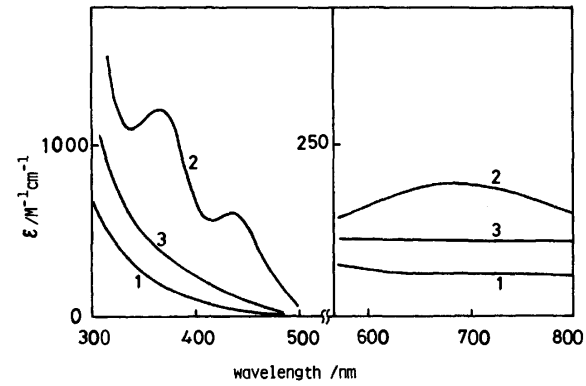

Fig. 4. Spectral change for the reaction of **2**·$Cu(I)_2$ (1.00×10^{-3} M) and O_2 in propylene carbonate. **2**·$Cu(I)_2$; was prepared from 1.00 mM of **2** and 4.00 mM of $[Cu(CH_3CN)_4]BF_4$. 1, **2**·$Cu(I)_2$; 2, after introduction of O_2; 3, after evacuation.

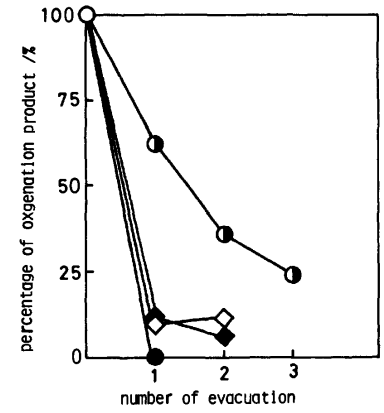

Fig. 5. Reversibility in O_2-binding in propylene carbonate.
◑ [**2**]=1.00×10^{-3} M, [$Cu(CH_3CN)_4\cdot BF_4$]=4.00×10^{-3} M; ◇ [**3**(X=NO_2)] and ◆ [**3**(X=H)]=1.00×10^{-3} M, [$Cu(CH_3CN)_4\cdot BF_4$]=3.83×10^{-3} M; ● [*trans*-**1**(X=CH_2)]=2.50×10^{-4} M, [$Cu(CH_3CN)_4\cdot BF_4$]=2.66×10^{-3} M.

It occurred to us that as the ability of the bi-metallic complexes to bind O_2 is largely governed by the distance between two metal ions, a change in this would directly induce a change in the stability of the O_2-complex. Molecular models show that for preferred ear-muff conformation of **2** (Fig. 3) the two Cu(I) ions are separated by 3.5—5 Å: the later X-ray study of the **2**·$Cu(I)_2$·OH complex gave a distance of 3.384 Å.[27] We estimated on the basis of the CPK model building that the Cu(I)···Cu(I) interatomic distance in the *cis*-**1**(X=CH_2)·$Cu(I)_2$ complex is in the range 3.0—9.0 Å. The wide distance range is due to the conformational freedom of the thiacrowns. The ear-muff conformation of **1**(X=CH_2) and **2** may not be the stable one, but one may expect for the O_2-complexes the "lock-in" effect[8,16] of O_2 that enforces the ear-muff conformation. Therefore, the Cu(I) complex of **1**(X=CH_2) and **2** may allow the reversible binding of O_2 only when it is photoisomerized to cis and adopts the preferred ear-muff conformation (Fig. 3). On the other hand, such favorable distance between the two intramolecular Cu(I) ions is not expected for the complex with *trans*-**1**(X=CH_2).

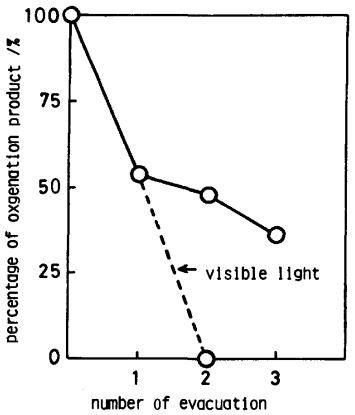

Fig. 6. Reversibility in O_2-binding to *cis*-**1**(X=CH_2) in propylene carbonate. [photoirradiated **1**(X=CH_2) (*cis* 72%)]=2.50×10^{-4} M, [$Cu(CH_3CN)_4\cdot BF_4$]=2.66×10^{-3} M. Photoirradiation was carried out before mixing with the Cu(I) solution.

In an optical cell, the appropriate amount of thiacrown ethers (*trans*-**1**, **2**, and **3**) was mixed with $[Cu(CH_3CN)_4]BF_4$ in propylene carbonate (PC) under anaerobic conditions. An oxygen stream was introduced into the optical cell at 40—50°C for 5 min and the mixture was subjected to spectral measurement at 30°C. A new broad absorption maximum appeared at around 700 nm (Fig. 4), which was scarcely affected by further introduction of oxygen. This band is attributable either to a reversible oxygenation product (Cu(I)·····O_2·····Cu(I)) or to an irreversible oxidation product (Cu(II)).[18,24-26] The fraction of the reversible oxygenation product was evaluated from the disappearance of the absorption maximum on evacuation[18] (1.0 mmHg, 70°C, 1 h). The results are illustrated in Fig. 5. When the treatment was repeated several times, oxygen was newly introduced after evacuation. It is seen from Fig. 5 that the Osborn's complex **2**·$Cu(I)_2$(λ_{max} of the O_2-complex 686 nm) is capable of binding O_2 in a reversible manner for several times: the fractions of the oxygenated product are 62 (1st evacuation), 36 (2nd evacuation), and 23% (3rd evacuation). Thus, the reversibility becomes inferior as the repeated number of evacuation and the irreversible oxidation product is accumulated. The reversibility of the mononuclear complexes **3**·Cu(I) (λ_{max} of the O_2-complex 694 nm for **3**(X=NO_2) and 684 nm for **3**(X=H)) was found to be much inferior: 9 (1st evacuation) and 11% (2nd evacuation) for **3**(X=NO_2) and 12 (1st evacuation) and 6% (2nd evacuation) for **3**(X=H). As expected, no decrease in the absorbance was observed for the *trans*-**1**(X=CH_2)·$Cu(I)_2$ complex ((λ_{max} 710 nm), indicating that the irreversible oxidation to Cu(II) is the sole reaction path.

In contrast, we found that *cis*-**1**·$Cu(I)_2$ complex ((λ_{max} 708 nm) is capable of forming the significant fraction of the reversible oxygenation product. The evacuation was carricd out under milder conditions (1.0 mmHg, 40°C, 20 min) where the progress of the thermal cis-to-trans isomerization is almost negligible (k=0.12 h^{-1} at 40°C: for the conditions see the figure caption to Fig. 5). We used photoisomerized **1**(X=CH_2) containing 72% of *cis*-**1**(X=CH_2) at the beginning. We observed 54% decrease in the absorbance after first evacuation. This value indicates that 75% of *cis*-**1**(X=CH_2) form the oxygenation product (Fig. 6). Second and third evacuations gave 48 and 36% decrease, respectively. In a separate study, we irradiated the sample by visible light for 5 min after first evacuation. The spectral measurement showed that by this treatment the remaining cis-form has been isomerized to the trans-form. Then, O_2 was introduced. As shown in Fig. 6, no oxygenated product was detected on second evacuation. The marked difference in the reversibility between the the *trans*- and *cis*-**1**(X=CH_2)·$Cu(I)_2$ complexes suggests that this process may be controlled by a light switch through the photoinduced cis-trans interconversion of **1**(X=CH_2).

Conclusions. In this article we have indicated that the concept to photocontrol the chemical and physical functions of a crown ether family can be extended to a thiacrown ether family which acts as receptors for heavy metal ions. Being different from "inactive" alkali metal ions, some kinds of heavy metal ions are "active" for small molecules and others as seen in metalloproteins. We thus consider that the activities of heavy metal ions could be photocontrolled by use of thiacrown ethers or azacrown ethers linked to photofunctional groups. One example is the reversible O_2-binding reported here. Although the frameworks of the photoresponsive thiacrown ethers are still to be improved, the results indicate that the affinity of heavy metal ions with O_2 can be controlled, in principle, by switching the light source on and off. Further investigation is currently in progress in this laboratory.

This research was supported by a grant from the Ministry of Education of Japan. We thank Professor H. L. Ammon and Professor K. T. Douglas for helpful discussions. Appreciation is also expressed to Professor J. A. Osborn for teaching the experimental conditions.

References

1) D. Balasubramanian, S. Subramani, and S. Kumar, *Nature (London)*, **254**, 252 (1975).
2) K. Kano, Y. Tanaka, T. Ogawa, M. Shimomura, Y. Okahata, and T. Kunitake, *Chem. Lett.*, **1980**, 421.
3) A. Ueno, J. Anzai, T. Osa, and Y. Kodama, *Bull. Chem. Soc. Jpn.*, **50**, 2995 (1977).
4) A. Ueno, H. Yoshimura, R. Saka, and T. Osa, *J. Am. Chem. Soc.*, **101**, 2779 (1979).
5) M. Irie and K. Hayashi, *J. Macromol. Sci., Chem.*, **A13**, 511 (1979).
6) C. D. Eisenbach, *Makromol. Chem.*, **179**, 2489 (1978).
7) S. Shinkai, T. Ogawa, T. Nakaji, Y. Kusano, and O. Manabe, *Tetrahedron Lett.*, **1979**, 4569; S. Shinkai, T. Nakaji, Y. Nishida, T. Ogawa, and O. Manabe, *J. Am. Chem. Soc.*, **102**, 5860 (1980).
8) S. Shinkai, T. Nakaji, T. Ogawa, K. Shigematsu, and O. Manabe, *J. Am. Chem. Soc.*, **103**, 111 (1981).
9) S. Shinkai, T. Nakaji, T. Ogawa, K. Shigematsu, and O. Manabe, *J. Chem. Soc., Perkin Trans. 1*, **1981**, 3279.
10) S. Shinkai, T. Minami, Y. Kusano, and O. Manabe, *J. Am. Chem. Soc.*, **104**, 1967 (1982).
11) S. Shinkai, K. Shigematsu, M. Sato, and O. Manabe, *J. Chem. Soc., Perkin Trans. 1*, **1982**, 2735.
12) S. Shinkai, T. Kouno, Y. Kusano, and O. Manabe, *J. Chem. Soc., Perkin Trans. 1*, **1982**, 2741.

13) I. Yamashita, M. Fujii, T. Kaneda, S. Misumi, and T. Otsubo, *Tetrahedron Lett.*, **1980**, 541.
14) M. Shiga, M. Takagi, and K. Ueno, *Chem. Lett.*, **1980**, 1021.
15) S. Shinkai, T. Minami, Y. Kusano, and O. Manabe, *Tetrahedron Lett.*, **23**, 2581 (1982); Idem, *J. Am. Chem. Soc.* **105**, 1851(1983).
16) J.-P. Desvergne and H. Bouas-Laurent, *J. Chem. Soc., Chem. Commun.*, **1978**, 403.
17) J. J. Christensen, D. J. Eatough, and R. M. Izatt, *Chem. Rev.*, **74**, 351 (1974).
18) J. E. Bulkowski, P. L. Burk, M.-R. Ludmann, and J. A. Osborn, *J. Chem. Soc., Chem. Commun.*, **1977**, 498.
19) M. Blank, L. M. Soo, N. H. Wasserman, and B. F. Erlanger, *Science*, **214**, 70 (1981).
20) D. S. C. Black and I. A. McLean, *Aust, J. Chem.*, **24**, 1401 (1971).
21) D. P. Fisher, V. Piermattie, and J. C. Dabrowiak, *J. Am. Chem. Soc.*, **99**, 2811 (1977).
22) A. Nakamura, M. Aotake, and S. Otsuka, *J. Am. Chem. Soc.*, **96**, 3456 (1974).
23) J.-M. Lehn, *Acc. Chem. Res.*, **11**, 49 (1978) and references cited therein.
24) J. Powell and C. J. May, *J. Am. Chem. Soc.*, **104**, 2636 (1982).
25) H. M. J. Hendricks, J. J. M. W. Birker, J. van Rijn, G. G. Vershoor, and J. Reedijk, *J. Am. Chem. Soc.*, **104**, 3607 (1982).
26) M. S. Haddad, S. R. Wilson, D. J. Hodgson, and D. N. Hendrickson, *J. Am. Chem. Soc.*, **103**, 384 (1981).
27) P. L. Burk, J. A. Osborn, M.-T. Youinou, Y. Agnus, R. Louis, and R. Weiss, *J. Am. Chem. Soc.*, **103**, 1273 (1981).

Structure Determination of Bitter Principles of *Ailanthus altissima*. Structures of Shinjulactones F, I, J, and K[1)]

Masami Ishibashi, Shin Yoshimura, Takahiko Tsuyuki, Takeyoshi Takahashi,*
Akiko Itai†, and Yoichi Iitaka†
Department of Chemistry, Faculty of Science, The University of Tokyo, Hongo, Bunkyo-ku, Tokyo 113
†*Faculty of Pharmaceutical Sciences, The University of Tokyo, Hongo, Bunkyo-ku, Tokyo 113*
(Received May 25, 1984)

Four new quassinoids, shinjulactones F, I, J, and K were isolated from *Ailanthus altissima* Swingle. The structure of shinjulactone F was established to be 1α,11-epoxy-1β,20-dihydroxy-5β*H*-picrasa-3,9(11)-diene-2,12,16-trione by X-ray diffraction analysis. The structures of shinjulactones I, J, and K were determined to be 11α-acetoxy-2α,12α-dihydroxypicrasane-1,16-dione, 1β,12β-dihydroxypicrasane-2,11,16-trione, and 12α-acetoxy-2α,11α-dihydroxypicrasane-1,16-dione, respectively, by spectral and chemical means.

Bitter principles of Simaroubaceous plants have been extensively investigated from the interest in structure determination and their useful biological activities. In previous papers we have reported the isolation and structure elucidation of several quassinoids from *Ailanthus altissima* Swingle (Japanese name: Shinju or Niwaurushi).[2-5)] Recently quassinoid glycosides have been isolated from seeds of this plant.[6)] This paper describes structure determination of four new bitter principles, shinjulactones F, I, J, and K (**1**, **2**, **3**, and **4**), isolated from the same plant.

Aqueous extract of the root bark of *A. altissima* was continuously extracted with dichloromethane. The organic layer was subjected to separation by a silica-gel column chromatography and then further purified by a partition column chromatography on silicic acid to afford four minor bitter quassinoids, shinjulactones F (**1**, *ca.* 0.003% yield), I (**2**, *ca.* 0.0002% yield), J (**3**, *ca.* 0.0001% yield), and K (**4**, *ca.* 0.0005% yield) together with other known quassinoids.[2-5)]

Shinjulactone F (**1**), mp 201—203 °C, was shown to have a molecular formula, $C_{20}H_{22}O_7$, by elemental analysis and high-resolution mass spectrum. IR and UV spectra indicated the presence of hydroxyl(s) (ν_{max} 3450 cm^{-1}), δ-lactone (ν_{max} 1735 cm^{-1}), and two α,β-unsaturated carbonyls (ν_{max} 1685 cm^{-1}; λ_{max} 244 nm and 291 nm). Investigation on ^1H and ^{13}C NMR spectra of **1** revealed that shinjulactone F (**1**) possesses a vinyl methyl, a tertiary methyl, a secondary methyl, and a hydroxymethyl group.

Spectral comparison with known quassinoids such as ailanthone (**5**)[3)] and shinjulactone B (**6**)[5)] suggested the presence of partial structures **A** and **B** for shinjulactone F (**1**). The A ring of shinjulactone F (**1**) was shown to resemble that of ailanthone (**5**) except for the facts described below. ^{13}C NMR of **1** showed a signal assignable to a hemiacetal carbon (δ 120.6 s) instead of a signal (δ 84.4 d) due to C-1 for **5**. In ^1H NMR spectrum of **1** a signal due to a proton attached to C-1 was not observed. Thus the partial structure **A** was proposed for the A ring of shinjulactone F (**1**). In the part of the C ring the presence of the partial structure **B** was inferred from the following evidence. In ^{13}C NMR spectrum of **1** signals ascribable to the partial structure **B** were observed at δ 135.9 s, 149.9 s, and 194.3 s. These signals are similar to those assignable to a diosphenol part (δ 138.5 s; C-9, δ 145.1 s; C-11, and δ 195.9 s; C-12) of shinjulactone B (**6**) in its

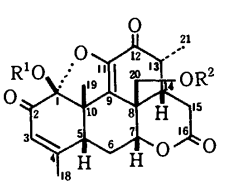

1 R^1-R^2-H
7 R^1-R^2-Ac
12 R^1-CH_3, R^2-H
14 R^1-CH_3, R^2-Ac

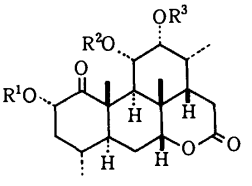

2 R^1-R^3-H, R^2-Ac
4 R^1-R^2-H, R^3-Ac
18 R^1-R^2-Ac, R^3-H
26 R^1-R^2-R^3-Ac

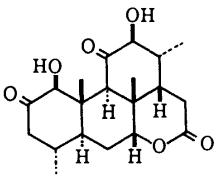

3

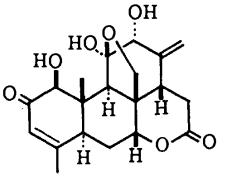

5

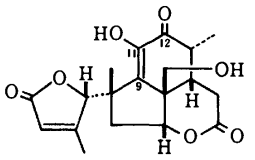

6

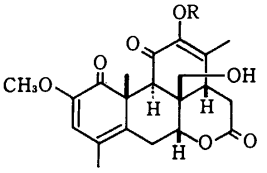

8 R=CH_3
9 R=H

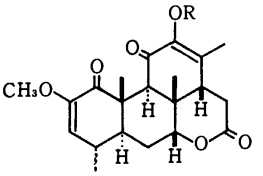

10 R=CH_3
11 R=H

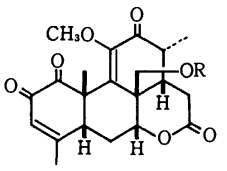

13 R=H
15 R=Ac

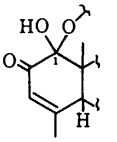

A

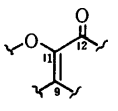

B

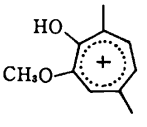

C

^{13}C NMR spectrum.

Acetylation of **1** gave a diacetate (**7**), which did not show the IR absorption band due to hydroxyl groups, indicating the presence of two hydroxyl groups for **1**. Assuming the picrasane skeleton, the presence of a 1,11-epoxide structure would be proposed for **1**, because the nature of all the seven oxygen atoms including the hemiacetal one at C-1 and nine of the ten unsaturation degrees have been clarified. Polonsky *et al.*[7] isolated karinolide from *Simaba multiflora*, for which 1α,11α-epoxypicrasane structure has been proposed. Treatment of **1** with hydrogen chloride in methanol afforded a reaction mixture, from which a dimethoxy derivative (**8**) and a monomethoxy derivative (**9**) were obtained by preparative TLC separation. The presence of a dienone moiety in the A ring of both **8** and **9** was indicated by UV (λ_{max} 325 nm) and MS (*m/z* 165; fragment ion **C**) spectra. In the UV spectra **8** exhibited an absorption maximum at 252 nm, while **9** showed it at 276 nm. These absorption maxima were reminiscent of quassin (**10**; 255 nm) and the diosphenol (**11**; 270 nm), respectively.[8] These observations indicated the presence of an enone moiety in the C ring for **8** and **9**. On methylation with diazomethane shinjulactone F (**1**) afforded 1-*O*-methyl derivative (**12**) and 11-*O*-methyl derivative (**13**), which were acetylated to give the corresponding acetates, **14** and **15**, respectively. Formation of these compounds adequately demonstrates the presence of the hemiacetal functionality at C-1 position for shinjulactone F (**1**).

The ^1H NMR spectrum of shinjulactone F (**1**) showed a multiplet signal at δ 2.71 due to a methine proton

Table 1. ^1H NMR Spectra of Shinjulactones F, I, J, and K (**1**, **2**, **3**, and **4**)

	δ (*J*/Hz)			
	1[a]	**2**[b]	**3**[b]	**4**[b]
1-H			3.82 br s	
2-H		4.72 ddd (10.5, 7.6, 7)		4.75 ddd (11.6, 7.6, 5.5)
3α-H	6.26 br s	*	*	*
3β-H		2.50 ddd (12.8, 7.6, 4.3)	2.58 dd (14.6, 4.8)	2.50 ddd (12.8, 7.6, 3.9)
5-H	2.71 m	1.53 ddd (13, 12.8, 3.6)	*	1.54 ddd (12.8, 12, 3.4)
6α-H	2.65 ddd (16, 3, 2.9)	1.97 ddd (14.5, 3.6, 3.3)	*	2.01 dt (14.6, 3.4)
6β-H	2.52 ddd (16, 5.5, 2.1)	1.79 ddd (14.5, 12.8, 2.1)	*	1.85 ddd (14.6, 12, 2.1)
7-H	5.20 dd (2.9, 2.1)	4.15 dd (3.3, 2.1)	4.39 dd (4.0, 1.8)	4.15 dd (3.4, 2.1)
9-H		3.35 d (11.9)	2.80 s	2.83 d (11.3)
11-H		5.15 dd (11.9, 2.7)		3.88 dd (11.3, 3.1)
12-H		3.97 t (2.7)	3.95 br d (11.0)	5.37 t (3.1)
13-H	3.34 dq (3.7, 7)	2.15 m	*	2.27 m
14-H	3.18 ddd (12.5, 6.4, 3.7)	*	*	1.67 ddd (12.8, 7.0, 5.2)
15α-H	2.10 dd (18, 12.5)	3.55 dd (19.2, 12.2)	2.69 dd (19.2, 12.8)	3.06 dd (19.2, 12.8)
15β-H	2.60 dd (18, 6.4)	2.59 dd (19.2, 6.7)	2.86 dd (19.2, 7.0)	2.56 dd (19.2, 7.0)
20-H	4.22 d (11.9)			
20-H′	4.16 d (11.9)			
4-CH_3	2.08 br s	0.90 d (6.4)	1.05 d (6.4)	0.94 d (6.7)
8-CH_3		1.25 s[c]	1.24 s[c]	1.42 s[c]
10-CH_3	1.69 s	1.21 s[c]	1.10 s[c]	1.22 s[c]
13-CH_3	0.98 d (7)	1.10 d (7.0)	1.17 d (6.7)	0.95 d (7.3)
CH_3CO-		1.93 s		2.24 s
1-OH	*		3.49 br s	
2-OH		3.60 d (7)		3.41 d (5.5)
12-OH		*	3.53 br s	*

a) 400 MHz in C_5D_5N. b) 400 MHz in $CDCl_3$. c) Signals may be reversed.
* not assigned

at C-5, which is coupled with methylene protons at C-6 with coupling constants, $J_{5,6\alpha}$=3 Hz and $J_{5,6\beta}$=5.5 Hz (see Table 1). These coupling patterns have never been observed in ^{1}H NMR of any known quassinoids. However this observation could be reasonably explained if an inversion of a chiral center at C-5 occurs so as to form the 1,11-epoxide ring with a less strain. Configurations of the hydroxyl group at C-1 and the hydrogen at C-5 could be determined by NOE measurement of 1-*O*-methyl monoacetate (**14**). On saturation of the signal due to $C_{(10)}$-CH_3, the signals due to $C_{(1)}$-OCH_3 and $C_{(5)}$-H showed increase in area by 3 and 9%, respectively. This observation implies the $C_{(1\beta)}$-OCH_3 and $C_{(5\beta)}$-H orientations.

Unambiguous proof for the structure of shinjulactone F (**1**) was provided by X-ray diffraction analysis. The crystal of **1** obtained from benzene–acetone solution belongs to a monoclinic space group $P2_1$ with the cell parameters of a=8.392(2), b=14.920(4), c=7.581(2) Å, and β=105.3(2)°. Two molecules of **1** and two water molecules are contained in the unit cell to give D_c=1.42 g·cm^{-3}. Intensity data were measured on a Philips PW1100 automatic four-circle diffractometer using monochromated Cu $K\alpha$ radiation. A total of 1883 independent structure factors with $F_o \geq 2.5\sigma(F_o)$ within 2θ=156° were obtained by the 2θ–θ scanning mode. The structure was solved by the direct method using MULTAN 80 program. An E-map revealed the positions of all the non-hydrogen atoms, and the hydrogen atoms except those of water molecule were located in a difference electron density map. The structure was refined by the block-diagonal least-squares calculations assuming anisotropic thermal motions for non-hydrogen atoms and isotropic ones for hydrogen atoms. The final R-factor was 0.036. The final atomic coordinates are listed in Table 2 and bond lengths and bond angles are listed in Tables 3 and 4[9]. The hemiacetal structure and the $C_{(5\beta)}$-H configuration were clearly established as shown in Fig. 1. Thus the structure of shinjulactone F (**1**) was established to be 1α,11-epoxy-1β,20-dihydroxy-5βH-picrasa-3,9(11)-diene-2,12,16-trione.

Table 2. Atomic positonal parameters (×10^4) and isotropic temperature factors (×10^2) for non-hydrogen atoms of shinjulactone F (**1**) with estimated standard deviations in parentheses

Atom	x	y	z	B_{eq}[a]
C(1)	3603(3)	2317(0)	7089(3)	208(3)
C(2)	4687(3)	2338(2)	5734(3)	242(3)
C(3)	6335(3)	2700(2)	6342(4)	284(4)
C(4)	6947(3)	3095(2)	7954(3)	263(3)
C(5)	5941(3)	3258(2)	9309(3)	231(3)
C(6)	6137(3)	4222(2)	10102(3)	271(4)
C(7)	5358(3)	4960(2)	8752(3)	254(3)
C(8)	3516(3)	4806(2)	7824(3)	208(3)
C(9)	3170(3)	3829(2)	7489(3)	184(3)
C(10)	4078(3)	3052(2)	8594(3)	196(3)
C(11)	1982(3)	3508(2)	6088(3)	212(3)
C(12)	907(3)	4054(2)	4667(3)	249(3)
C(13)	1131(3)	5061(2)	4957(3)	232(3)
C(14)	2935(3)	5298(2)	5974(3)	220(3)
C(15)	4095(3)	5083(2)	4762(4)	269(4)
C(16)	5903(3)	5097(2)	5698(4)	287(4)
C(18)	8753(3)	3343(3)	8545(5)	428(5)
C(19)	3350(3)	2804(2)	10190(3)	302(4)
C(20)	2545(3)	5150(2)	9190(3)	281(4)
C(21)	484(3)	5582(2)	3182(4)	331(4)
O(1)	3552(2)	1471(1)	7775(2)	272(3)
O(2)	4154(3)	1984(2)	4226(3)	374(3)
O(3)	1937(2)	2584(1)	6009(2)	251(2)
O(4)	−73(3)	3712(2)	3348(3)	445(4)
O(5)	6955(3)	5154(2)	4855(3)	419(4)
O(6)	6427(2)	5022(1)	7497(3)	317(3)
O(7)	2671(3)	6080(2)	9461(3)	394(3)

a) $B_{eq}=8\pi^2(u_1^2+u_2^2+u_3^2)/3$

Table 3. Bond lengths of shinjulactone F (**1**) with estimated standard deviations in parentheses

Bond length		l/Å
Atom 1	Atom 2	
C(1)	−C(2)	1.542 (4)
C(1)	−C(10)	1.556(3)
C(1)	−O(1)	1.370(2)
C(1)	−O(3)	1.475(3)
C(2)	−C(3)	1.442(4)
C(2)	−O(2)	1.231(3)
C(3)	−C(4)	1.332(4)
C(4)	−C(5)	1.511(4)
C(4)	−C(18)	1.509(4)
C(5)	−C(6)	1.551(4)
C(5)	−C(10)	1.544(3)
C(6)	−C(7)	1.528(4)
C(7)	−C(8)	1.538(3)
C(7)	−O(6)	1.473(4)
C(8)	−C(9)	1.494(3)
C(8)	−C(14)	1.543(3)
C(8)	−C(20)	1.564(4)
C(9)	−C(10)	1.514(3)
C(9)	−C(11)	1.338(3)
C(10)	−C(19)	1.538(4)
C(11)	−C(12)	1.458(3)
C(11)	−O(3)	1.381(3)
C(12)	−C(13)	1.523(4)
C(12)	−O(4)	1.226(3)
C(13)	−C(14)	1.548(3)
C(13)	−C(21)	1.523(4)
C(14)	−C(15)	1.538(4)
C(15)	−C(16)	1.496(3)
C(16)	−O(5)	1.222(4)
C(16)	−O(6)	1.322(3)
C(20)	−O(7)	1.403(4)

Shinjulactone F (**1**) contains several interesting structural features. 1,11-Epoxypicrasanes are rarely found and only two types have been reported; artificial bisnorquassin and its derivatives[10] and karinolide.[7] It is noteworthy that shinjulactone F (**1**) is the first example of 5β-H picrasane skeleton with all-*cis* configurations at A/B, B/D, and C/D ring junctures to form a unique folded-shape molecule.

Shinjulactone I (**2**) crystallized from acetone as colorless prisms, mp 220—223 °C. High-resolution mass spectrum indicated the molecular formula $C_{22}H_{32}O_7$. IR spectrum showed the presence of hydroxyl(s) (3430 cm^{-1}), a δ-lactone (1725 cm^{-1}), and an isolated carbonyl group (1705 cm^{-1}). ^{1}H (Table 1) and ^{13}C NMR spectra revealed that shinjulactone I (**2**) possesses two

Table 4. Bond angles of shinjulactone F (**1**) with estimated standard deviations in parentheses

Bond angle			ϕ/°
Atom 1	Atom 2	Atom 3	
C(2)	−C(1)	−C(10)	113.1(2)
C(2)	−C(1)	−O(1)	110.7(2)
C(2)	−C(1)	−O(3)	105.3(2)
C(10)	−C(1)	−O(1)	113.5(2)
C(10)	−C(1)	−O(3)	103.8(2)
O(1)	−C(1)	−O(3)	109.8(2)
C(3)	−C(2)	−C(1)	118.7(2)
C(3)	−C(2)	−O(2)	122.7(2)
C(1)	−C(2)	−O(2)	118.5(2)
C(4)	−C(3)	−C(2)	124.3(3)
C(5)	−C(4)	−C(3)	123.1(2)
C(5)	−C(4)	−C(18)	117.1(2)
C(3)	−C(4)	−C(18)	119.7(3)
C(6)	−C(5)	−C(4)	113.1(2)
C(6)	−C(5)	−C(10)	108.4(2)
C(4)	−C(5)	−C(10)	115.1(2)
C(7)	−C(6)	−C(5)	115.2(2)
C(8)	−C(7)	−C(6)	113.5(2)
C(8)	−C(7)	−O(6)	115.1(2)
C(6)	−C(7)	−O(6)	104.6(2)
C(9)	−C(8)	−C(7)	110.5(2)
C(9)	−C(8)	−C(14)	108.0(2)
C(9)	−C(8)	−C(20)	108.7(2)
C(7)	−C(8)	−C(14)	112.4(2)
C(7)	−C(8)	−C(20)	106.5(2)
C(14)	−C(8)	−C(20)	110.5(2)
C(10)	−C(9)	−C(8)	127.3(2)
C(10)	−C(9)	−C(11)	109.0(2)
C(8)	−C(9)	−C(11)	123.7(2)
C(19)	−C(10)	−C(1)	109.2(2)
C(19)	−C(10)	−C(5)	110.4(2)
C(19)	−C(10)	−C(9)	111.9(2)
C(1)	−C(10)	−C(5)	115.9(2)
C(1)	−C(10)	−C(9)	98.0(2)
C(5)	−C(10)	−C(9)	110.9(2)
C(12)	−C(11)	−C(9)	124.9(2)
C(12)	−C(11)	−O(3)	121.5(2)
C(9)	−C(11)	−O(3)	113.4(2)
C(13)	−C(12)	−C(11)	114.6(2)
C(13)	−C(12)	−O(4)	124.0(2)
C(11)	−C(12)	−O(4)	121.4(2)
C(14)	−C(13)	−C(12)	111.3(2)
C(14)	−C(13)	−C(21)	113.4(2)
C(12)	−C(13)	−C(21)	112.0(2)
C(15)	−C(14)	−C(8)	110.2(2)
C(15)	−C(14)	−C(13)	110.2(2)
C(8)	−C(14)	−C(13)	112.1(2)
C(16)	−C(15)	−C(14)	115.9(2)
O(6)	−C(16)	−C(15)	120.5(2)
O(6)	−C(16)	−O(5)	117.1(3)
C(15)	−C(16)	−O(5)	122.4(3)
O(7)	−C(20)	−C(8)	112.9(2)
C(1)	−O(3)	−C(11)	103.6(2)
C(7)	−O(6)	−C(16)	125.3(2)

tertiary methyls, two secondary methyls, and an acetoxyl group. Since five oxygen atoms were characterized by a lactone, an isolated carbonyl, and an acetoxyl group, the remaining two oxygen atoms were shown to be those of hydroxyl groups. Spectral comparison with amarolide (**16**)[11] suggests that

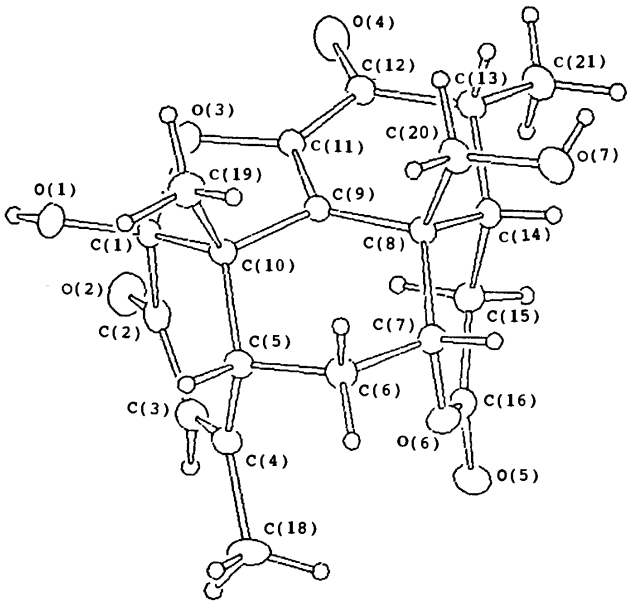

Fig. 1. Perspective view of shinjulactone F (**1**).[a]
a) For clarity hydrogen atoms are represented by spheres of arbitrary radius.

shinjulactone I (**2**) possesses the same structure as **16** in respect of A ring. In the part of C ring the presence of a partial structure **D** was proposed by ^{1}H NMR double resonance experiment for **2** at 90 MHz. Irradiation on a double doublet signal at δ 5.15 (11-H) caused a collapse of a triplet at δ 3.97 (12-H) into a doublet and changed a doublet at δ 3.35 (9-H) into a singlet. Irradiation on a multiplet at δ 2.15 (13-H) changed a doublet methyl-signal at δ 1.10 (13-CH_3) into a singlet and the triplet at δ 3.97 (12-H) into a doublet. The configurations of the four adjacent protons were, therefore, deduced to be 9α-axial, 11β-axial, 12β-equatorial, and 13β-axial orientations from the coupling constants, $J_{9,11}$=11.9, $J_{11,12}$=2.7, and $J_{12,13}$=2.7 Hz, respectively. A low magnetic field resonance due to $C_{(11)}$-H implies that the acetoxyl group is attached to C-11 position. From these observations the structure **2** might be formulated for shinjulactone I. The structure of shinjulactone I (**2**) was firmly established by a conversion into known amarolide diacetate (**17**).[11] Acetylation of shinjulactone I (**2**) at 0°C for 6h afforded its monoacetate (**18**). A signal at δ 4.72 due to $C_{(2)}$-H in ^{1}H NMR spectrum of **2** was shifted to a lower magnetic field at δ 5.56 in that of **18**. Protons at C-12 of **2** and **18** resonated at nearly the same magnetic fields (δ 3.97 and δ 3.90, respectively). This fact shows that the hydroxyl group at C-12 position remained intact. Jones oxidation of the monoacetylated derivative (**18**) afforded amarolide diacetate (**17**), which was completely identical with an authentic sample. Thus the structure of shinjulactone I (**2**) was determined to be 11α-acetoxy-2α,12α-dihydroxypicrasane-1,16-dione.

The molecular formula, $C_{20}H_{28}O_6$, of shinjulactone J (**3**), mp 127—130°C, was determined by high-resolution mass spectrum. IR spectrum revealed characteristic absorptions for hydroxyl(s) (3510 cm^{-1}),

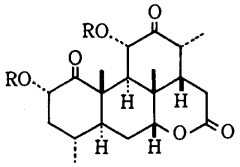

16 R=H
17 R=Ac

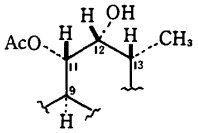

D

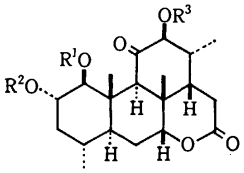

19 R^1=R^2=R^3=H
20 R^1=R^3=H, R^2=$SiMe_2{}^tBu$
21 R^1=H, R^2=R^3=$SiMe_2{}^tBu$
22 R^1=H, R^2=$SiMe_2{}^tBu$, R^3=Ac

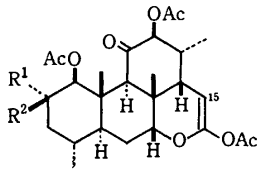

23 R^1=$OSiMe_2{}^tBu$, R^2=H
24 R^1=OH, R^2=H
25 R^1,R^2=O

isolated carbonyl(s) (1715 cm^{-1}), and a δ-lactone (1725 cm^{-1}). ^1H (Table 1) and ^{13}C NMR spectra showed the presence of two secondary methyls, two tertiary methyls, two isolated carbonyls, and a lactone grouping. Four of six oxygen atoms were thus explained and the presence of two hydroxyl groups was indicated by two broad singlet signals at δ 3.49 and δ 3.53 due to hydroxyl protons, which disappeared on addition of D_2O. Signals due to protons attached to carbons with hydroxyl groups were observed as a singlet at δ 3.82 and a doublet at δ 3.95, respectively, the both signals being coupled with hydroxyl protons with small coupling constants. A signal assignable to $C_{(9)}$-H was observed at δ 2.80 as a singlet. These findings suggest that hydroxyl groups exist at C-1 and C-12 positions and isolated carbonyl groups are located at C-2 and C-11 positons. This is also supported by comparison with other quassinoids. Most of quassinoids with six oxygen atoms possess oxygenated functionalities at C-1, C-2, C-11, and C-12 positions other than a δ-lactone moiety. Configurations of hydroxyl groups of shinjulactone J (**3**) was determined by NOE experiment at 400 MHz. On saturation of the proton singlet due to $C_{(9)}$-H, the signals due to $C_{(1)}$-H and $C_{(12)}$-H showed increase in area by 14 and 7%, respectively. This observation indicates the $C_{(1\beta)}$-OH and $C_{(12\beta)}$-OH orientations. From these results the structure **3** was proposed for shinjulactone J.

In order to confirm the proposed structure **3**, a preparation of shinjulactone J (**3**) from known chaparrolide (**19**)[12] was carried out as follows. Treatment of chaparrolide (**19**) with *t*-butyldimethylsilyl chloride in the presence of imidazole in *N*,*N*-dimethylformamide afforded a monosilyl derivative (**20**; yield 40%) and a disilyl derivative (**21**; yield 17%). The monosilyl derivative (**20**) was acetylated at room temperature for 4 d to give 2-siloxy monoacetate (**22**; yield 96%), which was further acetylated at 110 °C for 40 h to afford 2-siloxy triacetate (**23**; yield 51%). The ^1H NMR spectrum of **23** showed a signal due to an olefinic proton (δ 5.51 br s; 15-H) and three singlet methyl-signals due to acetyl groups (δ 2.14, 2.16, and 2.30). The ^{13}C NMR of **23** showed a signal at δ 202.9 assignable to a carbonyl carbon atom at C-11 position and a signal at δ 110.6 due to sp^2 carbon atom at C-15. The IR spectrum of **23** revealed no absorption band due to hydroxyl groups, while an absorption at 1670 cm^{-1} with a middle intensity ascribable to $\Delta^{15(16)}$-double bond with two oxygen functions was observed. Since the dihedral angle between $C_{(14)}$-H and $C_{(15)}$-H was estimated to be *ca.* 90° from the Drieding model, the fact that the olefinic proton at C-15 appeared as a singlet signal was well explained. From these observations the structure of 2-siloxy triacetate (**23**) was firmly established. Treatment of **23** with AcOH–H_2O–THF afforded 2-hydroxy triacetate (**24**; yield 64% based on consumed **23**), which was subjected to Jones oxidation to give 2-keto triacetate (**25**; yield *ca.* 80%). Finally this compound (**25**) was hydrolyzed under acidic conditions to afford shinjulactone J (**3**; yield *ca.* 50%), whose spectral data showed good agreements with those of a natural specimen. The structure of shinjulactone J (**3**) was, therefore, concluded to be 1β,12β-dihydoxypicrasane-2,11,16-trione.

Shinjulactone K (**4**), mp 135—139 °C, crystallized from chloroform–hexane as colorless prisms. The molecular formula, $C_{22}H_{32}O_7$, was determined by high-resolution mass spectrum. ^1H (Table 1) and ^{13}C NMR spectra showed that shinjulactone K (**4**) possesses two secondary methyls, two tertiary methyls, an isolated carbonyl, a lactone, and an acetoxyl group. The IR absorption band at 3430 cm^{-1} suggested that the remaining two oxygen atoms are ascribed to hydroxyl groups. These spectral features were very similar to those of shinjulactone I (**2**). The ^1H NMR spectral comparison between shinjulactones I (**2**) and K (**4**) is indicative of a difference in the relative position of hydroxyl and acetoxyl groups in C ring. Shinjulactone K (**4**) showed a double doublet at δ 3.88 and a triplet at δ 5.37, which were assignable to protons attached to carbons with hydroxyl and acetoxyl groups, respectively. The shapes of these signals were quite parallel to those of the signals due to $C_{(11)}$-H and $C_{(12)}$-H of shinjulactone I (**2**), respectively, and their chemical shifts seemed to be just reversed. Double resonance experiment on shinjulactone K (**4**) was carried out in the same way as developed in the case of shinjulactone I (**2**). Irradiation on the double doublet at δ 3.88 (11-H) changed the triplet at δ 5.37 (12-H) into a doublet and a doublet at δ 2.83 (9-H) into a singlet. Irradiation on a multiplet at δ 2.27 (13-H) changed a doublet methyl-signal at δ 0.95 (13-CH_3) into a singlet and the triplet at δ 5.37 (12-H) into a doublet. These observations could propose the structure **4** for shinjulactone K.

Finally shinjulactones I (**2**) and K (**4**) were chemically correlated to each other. Acetylation of shinjulactone I (**2**) with acetic anhydride in pyridine in the presence of 4-dimethylaminopyridine at room temperature for 6 d gave its diacetate (**26**) together with the monoacetylated product (**18**). Shinjulactone K (**4**) was also acetylated under similar conditions to afford a diacetyl derivative

(**26**), which was completely identical with the diacetyl derivative (**26**) derived from shinjulactone I (**2**). Thus the structure of shinjulactone K (**4**) was established to be 12α-acetoxy-2α,11α-dihydroxypicrasane-1,16-dione.

Experimental

General Procedure. All melting points were measured on a Mel-temp capillary melting apparatus (Laboratory devices) and uncorrected. Optical rotations were determined on a JASCO polarimeter DIP-181. Ultraviolet absorption (UV) spectra and infrared (IR) spectra were measured on a Hitachi 340 and a Hitachi 260-30 spectrometer, respectively. Mass (MS) spectra were run on a JEOL JMS D-300 mass spectrometer operating at 70 eV. Proton nuclear magnetic resonance (^{1}H NMR) spectra (90 MHz) were taken using a Varian EM 390 or a JEOL FX 90Q and carbon-13 nuclear magnetic resonance (^{13}C NMR) spectra (22.5 MHz) were measured on a JEOL FX 90Q unless otherwise stated. Measurement of ^{1}H NMR spectra at 400 MHz and ^{13}C NMR at 100 MHz was carried out on a JEOL JMN GX 400 spectrometer. Chemical shifts were expressed in ppm downfield from tetramethylsilane as an internal standard (δ value) and coupling constants in Hz. Thin-layer chromatography (TLC) was carried out on Kieselgel 60 GF_{254} coated in 0.25 mm- or 0.5 mm-thickness. Wakogel C-200 (Wako) or Silicic acid AR (Mallinckrodt) was used for column chromatography.

Plant Material. Roots of *Ailanthus altissima* Swingle were collected at the Botanical Gardens, Faculty of Science, the University of Tokyo in August 1982. Bark was stripped off from the root, air-dried, and chipped to afford 6.2 kg of materials.

Extraction and Separation. The root bark (6.2 kg) was extracted with hot water overnight. The aqueous layer was concentrated and continuously extracted with dichloromethane. The organic layer was evaporated to give a residue (40 g), which was separated by a silica-gel column chromatography. Gradient elution with 7 and 13% methanol-chloroform gave fractions A and B, respectively.

Fraction A was subjected to a partition column chromatography of silicic acid (250 g) on which water (150 ml) was adsorbed. Gradient elution with 1—2 and 4—8% 1-butanol-benzene afforded fractions C and D, respectively. Fraction C was further purified by a silica-gel column chromatography eluted with benzene-acetone (3:1) to afford shinjulactone K (**4**; *ca.* 20 mg). Fraction D was also purified by a silica-gel column chromatography eluted with benzene-acetone (3:1) to give shinjulactone I (**2**; *ca.* 10 mg) and shinjulactone J (**3**; *ca.* 6 mg) together with shinjulactone H.[4]

Fraction B was separated by a partition column chromatography eluted with 0—16% ethanol-chloroform. The fraction eluted with 8% ethanol-chloroform was further purified by a silica-gel column chromatography eluted with 3% methanol-ethyl acetate to give shinjulactone F (**1**; *ca.* 170 mg) together with shinjulactone G.[4]

Shinjulactone F (1). Colorless prisms cryltallized from ethanol-chloroform or benzene-acetone, mp 201—203 °C, $[\alpha]_D^{20}$ −148° (*c* 2.1, pyridine); IR (KBr) 3450, 1735, 1685, 1220, and 1040 cm^{-1}; UV(ethanol) 244 nm (ε 7400) and 291 nm (ε 3400); ^{1}H NMR (Table 1); ^{13}C NMR (C_5D_5N) δ=11.4q, 20.3q, 23.2q, 27.2t, 27.6t, 30.1d, 38.8d, 40.8s, 41.9d, 47.8s, 63.0t, 78.1d, 120.6s, 126.8d, 135.9s, 149.9s, 164.3s, 168.0s, 190.4s, and 194.3s; MS *m/z* (%) 374 (M^+; 1.5), 356 (7), 340 (5), 282 (100), 266 (25), 253 (35), 236 (50), 189 (50), and 177 (45); Found: *m/z* 374.1364. Calcd for $C_{20}H_{22}O_7$: M 374.1366. Found: C, 62.03; H, 5.93%. Calcd for $C_{20}H_{22}O_7 \cdot 2/3H_2O$: C, 62.17; H, 6.09%.

1,20-Di-O-acetylshinjulactone F (7). Shnjulactone F (**1**; 12 mg) was acetylated with acetic anhydride (0.5 ml) in pyridine (2 ml) at room temperature for 40 h. Addition of methanol and the usual work-up afforded a reaction mixture, which was purified by preparative TLC developed with *ca.* 2% methanol-ethyl acetate to give 1,20-di-*O*-acetylshinjulactone F (**7**; 4 mg), mp 128—132 °C (acetone); IR (Nujol) 1740, 1685, 1675, and 1220 cm^{-1}; UV (ethanol) 245 nm (ε 8000) and 285 nm (ε 2900); ^{1}H NMR ($CDCl_3$) δ=1.11 (3H, d, *J*= 7 Hz), 1.40 (3H, s), 2.19 (9H, br s), 4.36 (2H, s), 4.63 (1H, t, *J*= 2.5 Hz), and 6.21 (1H, br s); MS *m/z* (%) 458 (M^+; 30), 416 (100), 398 (45), 356 (50), 193 (55), and 151 (75); Found *m/z* 458.1554. Calcd for $C_{24}H_{26}O_9$: M 458.1576.

Reaction of 1 with Hydrogen Chloride. To a solution of shinjulactone F (**1**; 31 mg) in dry methanol (6 ml), acetyl chloride (0.3 ml) was added and the mixture was stirred at room temperature for 3 h to give a complex mixture, from which a dimethoxy derivative (**8**; *ca.* 1.5 mg) and a monomethoxy derivative (**9**; *ca.* 1.5 mg) were obtained by preparative TLC developed with 2% methanol-ethyl acetate. **8**: Mp 166—169 °C (acetone); UV(ethanol) 252 nm and 325 nm; ^{1}H NMR ($CDCl_3$) δ=1.45 (3H, s), 1.81 (3H, s), 1.93 (3H, br s), 3.64 (3H, s), 3.75 (3H, s), 4.63 (1H, m), and 5.96 (1H, br s); MS *m/z* (%) 402 (M^+; 75), 388 (20), 370 (18), and 165 (100); Found: *m/z* 402.1682. Calcd for $C_{22}H_{26}O_7$: M 402.1677. **9**: Mp 157—160 °C (acetone); UV(ethanol) 276 nm and 325 m; ^{1}H NMR ($CDCl_3$) δ=1.45 (3H, s), 1.80 (3H, s), 1.93 (3H, br s), 3.34 (1H, s), 3.73 (3H, s), 3.78 (2H, br s), 4.81 (1H, m), and 5.94 (2H, br s); MS *m/z* (%) 388 (M^+; 100), 370 (10), 356 (18), 280 (45), and 165 (80); Found: *m/z* 388.1515. Calcd for $C_{21}H_{24}O_7$: M 388.1520.

Methylation of 1 with Diazomethane. Shinjulactone F (**1**; 38 mg) in THF (10 ml) was treated with diazomethane in ether and the reaction mixture was allowed to stand at room temperature for 12 h. Usual work-up and separation by preparative TLC (7% methanol-chloroform) afforded 1-*O*-methyl derivative (**12**; 9.5 mg) and 11-*O*-methyl derivative (**13**; 11 mg). **12**: Mp 200—201 °C (chloroform); IR(KBr) 3450, 1720, 1710, 1680, and 1225 cm^{-1}; UV(ethanol) 245 nm (ε 8200) and 295 nm (ε 3000); ^{1}H NMR ($CDCl_3$) δ=1.09 (3H, d, *J*=7 Hz), 1.40 (3H, s), 2.10 (3H, br s), 3.53 (3H, s), 3.90 (2H, br s), 4.84 (1H, m), and 6.02 (1H, br s); MS *m/z* (%) 388 (M^+; 20), 358 (100), 343 (15), 329 (20), and 314 (45); Found: *m/z* 388.1472. Calcd for $C_{21}H_{24}O_7$: M 388.1520. **13**: Mp 118—122 °C (ethanol-ethyl acetate); IR (KBr) 3450, 1720, 1680, 1275, and 1040 cm^{-1}; UV (ethanol) 256 nm (ε 7200); ^{1}H NMR ($CDCl_3$) δ=1.11 (3H, d, *J*=7 Hz), 1.55 (3H, s), 2.19 (3H, br s), 3.65 (3H, s), 3.77 and 3.98 (each 1H, d, *J*=10 Hz), 4.85 (1H, m), and 6.08 (1H, br s); ^{13}C NMR ($CDCl_3$) δ=12.2, 21.2, 23.6, 27.6, 29.3, 36.9, 40.5, 42.1, 48.3, 51.8, 60.1, 66.3, 77.5, 128.9, 135.8, 151.4, 166.7, 167.9, 188.9, 193.9, and 198.8; MS *m/z* (%) 388 (M^+; 70), 358 (100), 329 (75), and 283 (50); Found: *m/z* 388.1540. Calcd for $C_{21}H_{24}O_7$: M 388.1520.

Acetylation of 12 and 13. A crude mixture (*ca.* 60 mg) of 1-*O*-methyl derivative (**12**) and 11-*O*-methyl derivative (**13**) was acetylated with acetic anhydride (2 ml) in pyridine (5 ml) at room temperature for 16 h. Addition of methanol and the usual work-up afforded a reaction mixture, which was separated by preparative TLC developed with chloroform-ethyl acetate (9:1) to afford 1-*O*-methyl monoacetate (**14**; 15 mg) and 11-*O*-methyl monoacetate (**15**; *ca.* 6 mg). **14**: Mp 193—195 °C (acetone-ether); IR(KBr) 1740, 1685, 1380, and 1220 cm^{-1}; UV(ethanol) 243 nm (ε 12000) and 291 nm (ε 4500); ^{1}H NMR ($CDCl_3$, 400 MHz) δ=1.12 (3H, d, *J*= 7 Hz; 13-CH_3), 1.42 (3H, s; 10-CH_3), 1.85 (1H, dd, *J*=18, 12.5 Hz; 15α-H), 2.09 (3H, br s; 4-CH_3), 2.15 (3H, s; CH_3CO-), 2.34 (1H, ddd, *J*=16, 6, 2.5 Hz; 6β-H), 2.52 (1H, dd, *J*=18, 6 Hz; 15β-H), 2.59 (1H, m; 5-H), 2.66 (1H, ddd, *J*=16, 3.5, 2.5 Hz; 6α-H), 2.69 (1H, ddd, *J*=12.5, 6, 3.5 Hz; 14-H), 3.06 (1H, dq, *J*=3.5, 7 Hz; 13-H), 3.53 (3H, s; CH_3O-), 4.32 and 4.36 (each 1H, d, *J*=12 Hz; 20-H), 4.62 (1H, t, *J*=2.5 Hz; 7-H), and 6.05 (1H, br s; 3-H); ^{13}C NMR ($CDCl_3$) δ=11.3q, 20.1q,

20.7q, 22.9q, 26.7t, 26.9t, 38.4s, 39.2d, 41.0d, 41.8d, 47.5s, 54.7q, 62.7t, 76.6d, 108.2s, 126.6d, 133.1s, 148.5s, 162.4s, 167.0s, 170.1s, 188.5s, and 191.0s; MS *m/z* (%) 430 (M^+; 72), 402 (75), 361 (70), 329 (100), and 301 (80); Found: *m/z* 430.1622. Calcd for $C_{23}H_{26}O_8$: M 430.1627. **15**: amorphous solid from ether, mp *ca.* 80—85 °C; IR(film) 1740, 1680, and 1220 cm^{-1}; UV (ethanol) 258 nm (ε 9200); ^1H NMR ($CDCl_3$) δ=1.16 (3H, d, *J*=7 Hz), 1.58 (3H, s), 2.13 (6H, s), 3.70 (3H, s), 4.13 and 4.51 (each 1H, d, *J*=12 Hz), 4.63 (1H, m), and 6.13 (1H, br s); MS *m/z* (%) 430 (M^+; 60), 402 (100), 387 (45), 371 (40), and 329 (93); Found: *m/z* 430.1611. Calcd for $C_{23}H_{26}O_8$: M 430.1627.

Shinjulactone I (2). Colorless prisms crystallized from acetone, mp 220—223 °C; $[\alpha]_D^{16}$+33° (*c* 0.67, $CHCl_3$); IR(KBr) 3430, 1725, 1705, and 1245 cm^{-1}; ^1H NMR (Table 1); ^{13}C NMR ($CDCl_3$) δ=13.4q, 13.9q, 18.3q, 21.1q, 21.7q, 26.4t, 28.8d, 29.4t, 30.5d, 32.1d, 35.9s, 44.8d, 48.0d, 48.6s, 49.0t, 70.1d, 72.8d, 73.4d, 82.3d, 170.0s, 171.1s, and 214.3s; MS *m/z* (%) 408 (M^+; 1.3), 390 (4.5), 380 (7), 352 (8), 348 (12), 330 (10), 320 (15), 302 (29), 258 (76), 242 (62), and 171(100); Found: *m/z* 408.2162. Calcd for $C_{22}H_{32}O_7$: M 408.2146.

2-O-Acetylshinjulactone I (18). Shinjulactone I (**2**; 6 mg) was treated with acetic anhydride (1 ml) in pyridine (2 ml) at 0 °C for 6 h. After addition of methanol and the usual work-up, the reaction mixture was separated by silica-gel column chromatography eluted with benzene–acetone (9:1) to afford the starting shinjulactone I (**2**; 1 mg) and 2-*O*-acetylshinjulactone I (**18**; 4.5 mg), mp 285—288 °C (benzene–acetone); IR (film) 3480, 1720, and 1250 cm^{-1}; ^1H NMR ($CDCl_3$) δ=0.95 (3H, d, *J*=5.5 Hz), 1.07 (3H, d, *J*=7 Hz), 1.24 (3H, s), 1.28 (3H, s), 2.04 (3H, s), 2.14 (3H, s), 3.26 (1H, d, *J*=12 Hz), 3.90 (1H, m), 4.10 (1H, t, *J*=2.5 Hz), 5.14 (1H, dd, *J*=12, 3 Hz), and 5.56 (1H, dd, *J*=12, 7 Hz); MS *m/z* (%) 450 (M^+; 11), 406 (10), 390 (65), 330 (100), and 274 (54); Found: *m/z* 450.2228. Calcd for $C_{24}H_{34}O_8$: M 450.2253.

Oxidation of 18 with Jones Reagent. 2-*O*-Acetylshinjulactone I (**18**; 3 mg) was treated with Jones reagent (in excess) in acetone (5 ml) at 0 °C for 1 h. After addition of 2-propanol (*ca.* 3 ml) and sodium hydrogencarbonate (*ca.* 1 g), the reaction mixture was filtered through Florisil (Wako, 100—200 mesh; *ca.* 5 g). After evaporation, brine and dichloromethane were added. Extraction with dichloromethane, evaporation, and purification by silica-gel column chromatography eluted with benzene–acetone (4:1) afforded amarolide diacetate (**17**), which was identified with an authentic sample by TLC, ^1H NMR, IR and mass spectra.

Shinjulactone J (3). White powder from benzene, mp 127—130 °C; $[\alpha]_D^{13}$−41° (*c* 0.4, $CHCl_3$); IR (film) 3510, 1725 (shoulder), 1715, and 1120 cm^{-1}; ^1H NMR (Table 1); ^{13}C NMR ($CDCl_3$, 100 MHz) δ=11.0q, 15.0q, 19.7q, 22.2q, 25.9t, 27.8t, 31.4d, 40.7s, 41.5d, 42.1d, 44.5d, 45.0s, 46.9t, 51.3d, 77.0d, 82.3d, 85.5d, 169.6s, 208.2s, and 208.7s; MS *m/z* (%) 364 (M^+; 23), 346 (19), 320 (66), 292 (17), and 206 (100); Found: *m/z* 364.1859. Calcd for $C_{20}H_{28}O_6$: M 364.1884.

t-Butyldimethylsilylation of Chaparrolide (19). Chaparrolide (**19**; 71 mg) was treated with *t*-butyldimethylsilyl chloride (53 mg; 1.8 equiv) in the presence of imidazole (63 mg; 4.7 equiv) in DMF (3 ml) at room temperature for 17 h. After addition of water (2 ml), evaporation under reduced pressure, dichloromethane and 2 M (1 M=1 mol dm^{-3}) hydrochloric acid were added. After extraction with dichloromethane, the organic layer was washed with a saturated solution of sodium hydrogencarbonate, dried over magnesium sulfate, and subjected to separation by a silica-gel column chromatography eluted with benzene–acetone (3:1) to give a monosilyl derivative (**20**; 37 mg) and a disilyl derivative (**21**; 20 mg). 2-*O*-(*t*-Butyldimethylsilyl)chaparrolide (**20**): Mp 178—179 °C (acetone–hexane); IR(KBr) 3460, 1720, 1250, and 1065 cm^{-1}; ^1H NMR ($CDCl_3$) δ=0.06 (6H, s), 0.87 (9H, s), 0.90 (3H, d, *J*=*ca.* 6 Hz), 1.09 (3H, s), 1.14 (3H, d, *J*=6 Hz), 1.34 (3H, s), 2.46 (1H, br s), 2.53 (1H, s), 2.92 (1H, br d, *J*=9 Hz), 3.52 (1H, d, *J*=5 Hz), 3.65 (1H, m), 3.88 (1H, dd, *J*=10.5, 5 Hz), and 4.31 (1H, t, *J*=3 Hz); MS *m/z* (%) 465 (M^+-CH_3; 0.8), 423 (63), 331 (100), 313 (70), and 75 (66); Found: *m/z* 465.2695. Calcd for $C_{25}H_{41}O_6Si$ ($M-CH_3$): 465.2672. 2,12-Bis(*O-t*-butyldimethylsilyl)chaparrolide (**21**): Mp 247 °C (chloroform–hexane); IR(film) 3550, 1730, and 1255 cm^{-1}; ^1H NMR ($CDCl_3$) δ=0.01 (3H, s), 0.05 (6H, s), 0.12 (3H, s), 0.86 (9H, s), 0.90 (9H, s), 1.05 (3H, d, *J*=7 Hz), 1.10 (3H, s), 1.33 (3H, s), 2.35 (1H, d, *J*=2.5 Hz), 2.38 (1H, s), 2.89 (1H, dd, *J*=9, 2.5 Hz), 3.65 (1H, m). 3.91 (1H, d, *J*=11 Hz), and 4.26 (1H, t, *J*=2.5 Hz); MS *m/z* (%) 579 (M^+-CH_3; 2), 561 (1) 537 (90), 519 (30), and 75 (100); Found: *m/z* 579.3548. Calcd for $C_{31}H_{55}O_6Si_2$ ($M-CH_3$): 579.3537.

Acetylation of 2-O-(t-Butyldimethylsilyl)chaparrolide (20). 2-*O*-(*t*-Butyldimethylsilyl)chaparrolide (**20**; 49 mg) was acetylated with acetic anhydride (1 ml) in pyridine (2 ml) in the presence of a catalytic amount of 4-dimethylaminopyridine at room temperature for 4 d. After the usual work-up, purification by a silica-gel column chromatography eluted with benzene–acetone (9:1) afforded 2-*O*-(*t*-butyldimethylsilyl)-12-*O*-acetylchaparrolide (**22**; 51 mg) as an amorphous solid, IR (film) 3580, 1730, and 1235 cm^{-1}, ^1H NMR ($CDCl_3$) δ=0.05 (6H, s), 0.87 (9H, s), 0.87 (3H, d, *J*=*ca.* 7 Hz), 1.02 (3H, d, *J*=7 Hz), 1.13 (3H, s), 1.31 (3H, s), 2.15 (3H, s), 2.96 (1H, d, *J*=9 Hz), 3.63 (1H, m), 4.30 (1H, t, *J*=3 Hz), and 4.90 (1H, d, *J*=12 Hz); MS *m/z* (%) 507 (M^+-CH_3; 1.2), 465 (32), 373 (42), 331 (13), 313 (66), and 75 (100); Found: *m/z* 507.2742. Calcd for $C_{27}H_{43}O_7Si$ ($M-CH_3$): 507.2777. 2-*O*-(*t*-Butyldimethylsilyl)-12-*O*-acetylchaparrolide (**22**; 51 mg) was further acetylated with acetic anhydride (2 ml) in pyridine (2 ml) in the presence of a catalytic amount of 4-dimethylaminopyridine at 110 °C for 40 h. After the same work-up as above, the reaction mixture was purified by a silica-gel column chromatography eluted with chloroform–ethyl acetate (4:1) to give 2-siloxy triacetate (**23**; 30 mg) as an amorphous solid, IR (film) 1735, 1670, and 1230 cm^{-1}; ^1H NMR ($CDCl_3$) δ=0.04 (6H, s), 0.84 (9H, s), 0.93 (3H, d, *J*=6 Hz), 0.98 (3H, d, *J*=6 Hz), 1.14 (3H, s), 1.42 (3H, s), 2.14 (3H, s), 2.16 (3H, s), 2.30 (3H, s), 3.75 (1H, m), 4.30 (1H, t, *J*=3 Hz), 4.60 (1H, d, *J*=9 Hz), 5.11 (1H, d, *J*=12 Hz), and 5.51 (1H, br s); ^{13}C NMR ($CDCl_3$) δ=−4.8, −4.3, 12.0, 14.7, 17.8, 18.1, 19.5, 20.3, 21.0, 23.2, 25.6, 25.6, 25.6, 27.6, 27.7, 37.1, 39.9, 41.8, 43.0, 43.5, 45.1, 52.9, 68.9, *ca.* 77.0(overlapped with the signal of $CDCl_3$), 82.6, 84.2, 110.6, 164.1, 166.0, 167.6, 169.1, and 202.9; MS *m/z* (%) 591 (M^+-CH_3; 12), 549 (3), 507 (10), 465 (17), 447 (14), 405 (6), 387 (21), 373 (30), 313 (50), 159 (100), and 75 (44); Found: *m/z* 591.3031. Calcd for $C_{31}H_{47}O_9Si$ ($M-CH_3$): 591.2989.

Desilylation of 2-Siloxy Triacetate (23). 2-Siloxy triacetate (**23**; 17 mg) was treated with AcOH (4 ml), H_2O (2 ml), and THF (2 ml) at room temperature for 6 d. The reaction mixture was evaporated and separated by a silica-gel column chromatography to afford the starting 2-siloxy triacetate (**23**; 4.5 mg) and 2-hydroxy triacetate (**24**; 6.5 mg), mp 94—98 °C (chloroform–hexane); IR(film) 3460, 1750, 1735, 1670, and 1235 cm^{-1}; ^1H NMR ($CDCl_3$) δ=0.92 (3H, d, *J*=7 Hz), 0.96 (3H, d, *J*=6.5 Hz), 1.12 (3H, s), 1.39 (3H, s), 2.13 (3H, s), 2.15 (3H, s), 2.33 (3H, s), 3.80 (1H, m), 4.26 (1H, br s), 4.50 (1H, d, *J*=10 Hz), 5.01 (1H, d, *J*=12 Hz), and 5.54 (1H, s); MS *m/z* (%) 492 (M^+; 1.1), 451 (1.7), 433 (4), 390 (32), 373 (46), 330 (74), 313 (78), and 55 (100); Found: *m/z* 492.2353. Calcd for $C_{26}H_{36}O_9$: M 492.2358.

Oxidation of 24 with Jones Reagent. 2-Hydroxy triacetate (**24**; 6 mg) was treated with Jones reagent (in excess) in acetone (3 ml) at 0 °C for 30 min. The usual work-up afforded 2-keto triacetate (**25**; 5 mg), mp 131—135 °C, IR (film) 1730, 1670, and 1225 cm^{-1}; ^1H NMR ($CDCl_3$) δ=1.00 (3H, d, *J*=7 Hz), 1.03 (3H, d, *J*=5.5 Hz), 1.13 (3H, s), 1.34 (3H, s), 2.13 (3H, s), 2.15 (3H, s), 2.33 (3H, s), 4.35 (1H, br s), 4.80

(1H, d, J=12.5 Hz), 4.95 (1H, s), and 5.60 (1H, s); MS m/z (%) 490 (M^+; 72), 406 (82), 362 (74), 206 (64), and 85 (100); Found: m/z 490.2214. Calcd for $C_{26}H_{34}O_9$: M 490.2203.

Acidic Hydrolysis of ***25***. A solution of 2-keto triacetate (**25**; 2 mg) in 1.5 M sulfuric acid–THF (each 1.5 ml) was refluxed for 5.5 h. After evaporation and addition of dichloromethane and brine, the mixture was extracted with dichloromethane. The organic layer was dried over magnesium sulfate, and evaporated to give a residue. Purification by silica-gel column chromatography eluted with benzene–acetone (7:3) afforded shinjulactone J (**3**; *ca.* 1 mg), which was identified with a natural specimen by TLC, ^{1}H NMR, IR, and mass spectra.

*Shinjulactone K (****4****).* Colorless prisms from chloroform-hexane, mp 135—139°C, $[\alpha]_D^{24}$+33° (c 1.0, $CHCl_3$); IR (KBr) 3430, 1730, and 1230 cm^{-1}; ^{1}H NMR (Table 1); ^{13}C NMR ($CDCl_3$) δ=13.4q, 13.9q, 18.5q, 21.0q, 21.8q, 26.4t, 28.7d, 28.9t, 31.9d, 33.8d, 35.9s, 44.9d, 47.2d, 47.9t, 49.7s, 69.1d, 70.6d, 77.1d, 82.5d, 170.3s, 170.7s, and 221.9s; MS m/z (%) 408 (M^+; 1.1), 390 (12), 380 (8), 362 (7), 348 (20), 302 (15), 258 (32), 222 (58), and 198 (100); Found: m/z 408.2139. Calcd for $C_{22}H_{32}O_7$: M 408.2146.

*2,12-Di-O-acetylshinjulactone I (****26****).* Shinjulactone I (**2**; 2 mg) was treated with acetic anhydride (1 ml) in pyridine (2 ml) in the presence of a catalytic amount of 4-dimethylaminopyridine at room temperature for 6 d. After addition of methanol and evaporation under a reduced pressure, the reaction mixture was separated by a silica-gel column chromatography to give 2-*O*-acetylshinjulactone I (**18**; *ca.* 1 mg) and 2,12-di-*O*-acetylshinjulactone I (**26**; *ca.* 1 mg), mp 258—260°C (chloroform–hexane); IR (film) 1735 and 1250 cm^{-1}; ^{1}H NMR ($CDCl_3$) δ=0.97 (6H, d, J=7 Hz), 1.30 (6H, s), 1.90 (3H, s), 2.15 (3H, s), 2.24 (3H, s), 3.18 (1H, d, J=12 Hz), 4.14 (1H, t, J=3 Hz), 5.18 (1H, dd, J=12, 3 Hz), 5.29 (1H, t, J=3 Hz), and 5.57 (1H, dd, J=12, 7 Hz); MS m/z (%) 492 (M^+; 18), 450 (5), 432 (29), 407 (32), 390 (100), 330 (68), and 258 (69); Found: m/z 492.2378. Calcd for $C_{26}H_{36}O_9$: M 492.2358.

*2,11-Di-O-acetylshinjulactone K (****26****).* Shinjulactone K (**4**; 10 mg) was acetylated with acetic anhydride (1 ml) in pyridine (2 ml) in the presence of a catalytic amount of 4-dimethylaminopyridine at room temperature for a week. The usual work-up and purification by a silica-gel column chromatography eluted with 0—10% acetone–benzene afforded 2,11-di-*O*-acetylshinjulactone K (**26**; 7 mg), which was identified with 2,12-di-*O*-acetylshinjulactone I (**26**) by TLC, ^{1}H NMR, IR, and mass spectra.

The authors wish to thank Mr. Kazuhiro Matsushita of JEOL Co. Ltd. for measurement of NMR spectra and Mr. Eiichi Ishii of the Botanical Gardens, Faculty of Science, the University of Tokyo, for collecting *Ailanthus altissima* Swingle.

References

1) A part of this work was reported in a preliminary form: M. Ishibashi, S. Yoshimura, T. Tsuyuki, T. Takahashi, A. Itai, Y. Iitaka, and K. Matsushita, *Chem. Lett.*, **1984**, 555.

2) M. Ishibashi, T. Tsuyuki, T. Murae, H. Hirota, T. Takahashi, A. Itai, and Y. Iitaka, *Bull. Chem. Soc. Jpn.*, **56**, 3683 (1983).

3) H. Naora, M. Ishibashi, T. Furuno, T. Tsuyuki, T. Murae, H. Hirota, T. Takahashi, A. Itai, and Y. Iitaka, *Bull. Chem. Soc. Jpn.*, **56**, 3694 (1983).

4) M. Ishibashi, S. Yoshimura, T. Tsuyuki, T. Takahashi, and K. Matsushita, *Bull. Chem. Soc. Jpn.*, **57**, 2013 (1984).

5) T. Furuno, M. Ishibashi, H. Naora, T. Murae, H. Hirota, T. Tsuyuki, T. Takahashi, A. Itai, and Y. Iitaka, *Bull. Chem. Soc. Jpn.*, **57**, 2484 (1984).

6) S. Yoshimura, M. Ishibashi, T. Tsuyuki, T. Takahashi, and K. Matsushita, *Bull. Chem. Soc. Jpn.*, **57**, 2496, (1984).

7) J. Polonsky, J. Gallas, J. Varenne, T. Prangé, C. Pascard, H. Jacquemin, and C. Moretti, *Tetrahedron Lett.*, **23**, 869 (1982).

8) T. Murae, T. Tsuyuki, T. Ikeda, T. Nishihama, S. Masuda, and T. Takahashi, *Tetrahedron*, **27**, 1545 (1971).

9) The complete F_o–F_c data, anisotropic thermal parameters for non-hydrogen atoms, atomic positional parameters and isotropic thermal parameters for hydrogen atoms, and bond lengths and bond angles containing hydrogen atoms are deposited as Document No. 8448 at the Office of the Editor of *Bull. Chem. Soc. Jpn.*

10) J. A. Findlay, R. F. Langler, and J. S. Tandon, *Can. J. Chem.*, **48**, 313 (1970).

11) W. Stöcklin M. Stefanović, T. A. Geissman, and C. G. Casinovi, *Tetrahedron Lett.*, **1970**, 2399.

12) R. E. Mitchell, W. Stöcklin, M. Stefanović, and T. A. Geissman, *Phytochemistry*, **10**, 411 (1971).

 © 1984 The Chemical Society of Japan Bull. Chem. Soc. Jpn., 57, 2893—2896 (1984)

Structure and Synthesis of Miyaginin, a *p*-Allylphenyl Glycoside from *Lespedeza thunbergii* forma *macrantha*

Makoto OJIKA, Hiroki KUYAMA, Haruki NIWA, and Kiyoyuki YAMADA*
Department of Chemistry, Faculty of Science, Nagoya University, Chikusa-ku, Nagoya 464
(Received May 14, 1984)

The structure of miyaginin previously reported as *p*-vinylphenyl *O*-D-xylosyl-(1→6)-D-glucoside without stereochemical assignment of two glycosidic linkages was reinvestigated by spectral and chemical means and shown to be revised as *p*-allylphenyl *O*-β-D-xylopyranosyl-(1→6)-β-D-glucopyranoside (*p*-allylphenyl β-primeveroside). In order to confirm the revised structure, an unambiguous synthesis of miyaginin was performed.

Miyaginin was first isolated from *Lespedeza thunbergii* (Miyaginohagi in Japanese) and its structure was reported to be *p*-vinylphenyl *O*-D-xylosyl-(1→6)-D-glucoside (**1**) without configurational assignment of two glycosidic linkages.[1] In connection with the carcinogenicity of bracken, *Pteridium aquilinum* var. *latiusculum*, we have examined the constituents of a carcinogenic fraction obtained from the aqueous extract of bracken and isolated a new *p*-hydroxystyrene glycoside, ptelatoside-A (**4**).[2] While the planar structure of ptelatoside-A (**4**) was the same as the previously assigned structure[1] of miyaginin (structure **1**), both compounds were found to be different by comparison of the spectral and physical properties.

In order to establish the complete structure of miyaginin we have isolated miyaginin from *Lespedeza thunbergii* forma *macrantha* [Kehagi in Japanese, a wild type of Miyaginohagi (*L. thunbergii*)] and reinvestigated the structure by chemical and spectral means. As the result the structure of miyaginin previously reported as **1** was shown to be revised to *p*-allylphenyl *O*-β-D-xylopyranosyl-(1→6)-β-D-glucopyranoside (*p*-allylphenyl β-primeveroside) (**2**). We describe the details of structural determination of miyaginin (**2**) and its unambiguous synthesis.

Results and Discussion

Isolation of Miyaginin (2). The ethanolic extract of *L. thunbergii* forma *macrantha* dissolved in water was washed successively with hexane, ether, and ethyl acetate. The aqueous layer was then extracted repeatedly with 1-butanol. The 1-butanol extract was chromatographed on silica gel and then alumina to give crude miyaginin (**2**). Further purification with preparative HPLC afforded pure miyaginin (**2**) (0.07% yield based on dried plant material), mp 215—216°C, $[\alpha]_D^{21}$ −81.0°. Spectral (UV, IR, and ^{1}H NMR) and physical (mp and $[\alpha]_D$) properties of miyaginin (**2**) were identical with those of the authentic sample[1] isolated previously from *L. thunbergii*. Although, in search for miyaginin (**2**), we have examined the constituents of the ethanolic extract of *L. thunbergii* collected in the botanical garden of Tohoku University, **2** was not detected.

Structure of Miyaginin (2). The molecular formula of miyaginin (**2**) was determined to be $C_{20}H_{28}O_{10}$ based on the elemental analysis of **2** and the hexaacetate **3** coupled with FAB-MS of **2**. The spectral data of miyaginin (**2**) suggested the presence of a *p*-(substituted oxy)allylbenzene moiety in **2**: ^{1}H NMR δ=5.00 (2H, m, H-9), 5.96 (1H, ddt, *J*=17.6, 9.5, and 6.4 Hz, H-8), and 7.07 (4H, m, aromatic protons); ^{13}C NMR δ=156.0 (s, C-1), 117.9 (d, C-2 and 6), 130.6 (d, C-3 and 5), 135.7 (s, C-4), 39.6 (t, C-7), 138.8 (d, C-8), and 116.4 (t, C-9); UV 221 (ε 9900), 272 (1200), and 279 nm (1000).

On acidic methanolysis miyaginin (**2**) afforded an aglycone, *p*-allylphenol (chavicol)(**5**)[3,13] and a mixture of methyl glycosides of D-xylose and D-glucose. After acetylation followed by chromatographic separation the methyl glycosides were identified as methyl 2,3,4-tri-*O*-acetyl-α-D-xylopyranoside and methyl 2,3,4,6-tetra-*O*-acetyl-α-D-glucopyranoside, respectively by comparison with authentic specimens. The aglycone, *p*-allylphenol (**5**) was identified by comparison of the spectral data with those of the authentic sample, the synthesis of which is described later and also by conversion into the known 3,5-dinitrobenzoate **6**.[4] Acetylation of miyaginin (**2**) gave the corresponding hexaacetate **3** as colorless needles, mp 163—164°C, spectral and physical properties of which were identical with those of the authentic sample.[1] The signals at δ=68.9 (t, C-6′), 101.6 (d, $^1J_{CH}$=164 Hz, C-1′), and 104.2 (d, $^1J_{CH}$=163 Hz, C-1″) in the ^{13}C NMR spectrum of miyaginin (**2**) and the signals at δ=4.89 (1H, d, *J*=7.9 Hz, H-1′), 4.38 (1H, d, *J*=6.8 Hz, H-1″), and 3.50—3.80 (2H, m, H-6′) in the ^{1}H NMR spectrum of the hexaacetate **3** suggested the sugar moiety of miyaginin to be represented as β-D-xylopyranosyl-(1→6)-β-D-glucopyranosyl (β-primeverosyl). The structure of miyaginin was therefore determined to be *p*-allylphenyl β-primeveroside (**2**). In order to confirm the structure of miyaginin, the unambiguous synthesis of **2** was performed as described below.

Synthesis of Miyaginin (2). *p*-Allylphenol (**5**) was previously reported to be synthesized from allylbenzene in very low yield.[13] In the present study we have executed a new synthesis of **5** in 80% overall yield starting from commercially available 3-(4-hydroxyphenyl)-1-propanol (**7**). The alcohol **7** was converted by the procedure developed by Sharpless[5] into the selenide **8** in quantitative yield. Oxidation of **8** with hydrogen peroxide and subsequent elimination of *o*-nitrobenzeneselenenic acid from the resulting selenoxide gave *p*-allylphenol (**5**) in 80% yield. Glycosylation of **5** with penta-*O*-acetyl-β-D-glucopyranose under the Helferich's conditions[6] gave *p*-allylphenyl 2,3,4,6-tetra-*O*-acetyl-β-D-glucopyranoside-(**9**)[7] in 56% yield. Methanolysis of **9** with sodium methoxide in

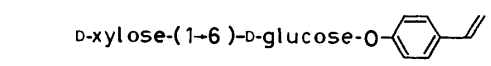

1

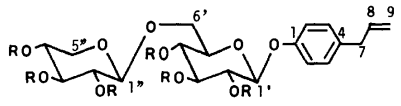

2 : R=H

3 : R=Ac

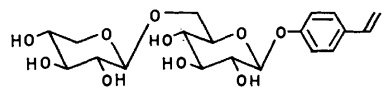

4

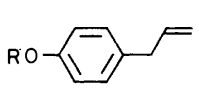

5 : R = H

6 : R = CO-

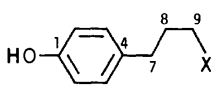

7 : X = OH

8 : X = Se- 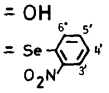

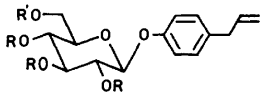

9 : R=R'=Ac

10 : R=R'=H

11 : R=Ac, R'=H

methanol afforded *p*-allylphenyl β-D-glucopyranoside (**10**), a natural glucoside previously isolated from *Pinus contorta*,[7] in 84% yield. The glucoside **10** was then converted to *p*-allylphenyl 2,3,4-tri-*O*-acetyl-β-D-glucopyranoside (**11**) in 40% overall yield by the following three-step sequence;[8] (i) tritylation with trityl chloride–pyridine, (ii) acetylation with acetic anhydride–pyridine, (iii) detritylation with aqueous acetic acid. Glycosylation of **11** with 2,3,4-tri-*O*-acetyl-α-D-xylopyranosyl bromide under the Helferich's conditions[9] gave miyaginin hexaacetate (**3**) in 88% yield. The physical and spectral properties of synthetic **3** were identical with those of the authentic sample derived from natural miyaginin (**2**) in all respects. Finally, methanolysis of **3** with sodium methoxide in methanol afforded *p*-allylphenyl β-primeveroside (**2**), colorless needles, mp 211.5—213 °C, $[\alpha]_D^{14}$ −81.6° in 89% yield. The physical and spectral properties as well as chromatographic mobilities of synthetic **2** were completely identical with those of natural miyaginin in all respects. Thus, the structure of miyaginin was unambiguously established to be *p*-allylphenyl *O*-β-D-xylopyranosyl-(1→6)-β-D-glucopyranoside (*p*-allylphenyl β-primeveroside) (**2**).

So far, there have been known a few *p*-allylphenyl glycosides in nature: *p*-allylphenyl rutinoside,[10] *p*-allylphenyl *O*-α-L-arabinofuranosyl-(1→6)-β-D-glucopyranoside,[11] *p*-allylphenyl *O*-[3-*C*-(hydroxymethyl)-β-D-erythrofuranosyl]-(1→6)-β-D-glucopyranoside (furcatin),[12] and *p*-allylphenyl β-D-glucopyranoside (**10**).[7] *p*-Allylphenol (**5**) itself was also isolated from the plant, *Viburnum japonicum*.[3]

Experimental

Boiling point and melting points were uncorrected. Optical rotations were measured with a JASCO DIP-4 or a JASCO DIP-181 digital polarimeter. IR and UV spectra were recorded on a JASCO model IR-S spectrophotometer and a JASCO UVIDEC-510 spectrophotometer, respectively. ^1H and ^{13}C NMR spectra were measured at 90 MHz and 22.5 MHz, respectively with a JEOL FX-90QE spectrometer: the chemical shifts are given in δ using Me_4Si as internal standard except for the ^{13}C-chemical shifts measured in D_2O, which are reported in ppm downfield from Me_4Si by assigning the resonance from internal dioxane to 67.4 ppm. Mass spectra and the fast atom bombardment mass spectrum (FAB-MS) were taken on a Hitachi RMU-6C mass spectrometer and a JEOL JMS-DX300 mass spectrometer, respectively. For column chromatography Fuji-Davison silica gel (BW-820 MH) and Merck neutral alumina (Aluminiumoxid 90, activity II-III) were used. Preparative thin layer chromatography (TLC) was carried out using Merck silica gel PF_{254}. A high performance liquid chromatography (HPLC) was performed with a JASCO TRI ROTAR-II apparatus equipped with a UV detector (JASCO UVIDEC-100-II) set at 221 nm.

Isolation of Miyaginin (2). The air-dried and chopped leaves and stems (278 g) of *L. thunbergii* forma *macrantha* collected in the Higashiyama botanical garden (Nagoya city) in June, 1983, were immersed in ethanol (2.4 L) at room temperature for 10 d. The ethanol extract was concentrated to dryness under reduced pressure. The residue (20 g) was diluted with water (200 mL) and the mixture was washed successively with hexane (10×200 mL), ether (7×200 mL), and ethyl acetate saturated with water (19×100 mL). The aqueous layer was then extracted with 1-butanol saturated with water (5×100 mL). The 1-butanol layer was concentrated to dryness under reduced pressure. The residue (2.6 g) was chromatographed on silica gel (55 g). Elution with chloroform–methanol (4:1) gave a fraction (0.5 g) containing **2**, which was subsequently chromatographed on alumina (20 g) with methanol–water (9:1) to afford crude **2** (320 mg). Further purification by preparative HPLC on Develosil ODS-5 (250×10 mm I.D.) using ethanol–water (30:70) (flow rate, 3 mL/min) afforded **2** (retention time, 12.4 min) as an amorphous powder (208 mg, 0.07% based on dried plant material). Recrystallization from aqueous acetone gave **2** as colorless needles, mp 215—216 °C (lit,[1] mp 212—214 °C); $[\alpha]_D^{21}$ −81.0° (*c* 1.0, H_2O) [lit,[1] $[\alpha]_D^{20}$ −86.25° (*c* 2.0, H_2O)]; UV (MeOH) 221 (ε 9900), 272 (1200), and 279 nm (1000); IR (KBr) 3440, 1636, 1610, 1511, 1231, 1100, 1075, 1038, and 908 cm^{-1}; ^1H NMR (CD_3OD) δ=4.32 (1H, d, *J*=7.3 Hz, H-1″), 5.00 (2H, m, H-9), 5.96 (1H, ddt, *J*=17.6, 9.5, and 6.4 Hz, H-8), and 7.07 (4H, m, aromatic protons); ^{13}C NMR (D_2O) δ=39.6 (t, C-7), 65.9 (t, C-5″), 68.9 (t, C-6′), 69.9 (d), 70.1 (d), 73.8 (d), 75.8 (d), 76.5 (d), 101.6 (d, $^1J_{CH}$=164 Hz, C-1′), 104.2 (d, $^1J_{CH}$=163 Hz, C-1″), 116.4 (t, C-9), 117.9 (d, C-2 and 6), 130.6 (d, C-3 and 5), 135.7 (s, C-4), 138.8 (d, C-8), and 156.0 (s, C-1); FAB-MS *m/z* 451 (M^++Na), 429 (M^++1), 427 (M^+−1). Found: C, 55.18; H, 6.74%. Calcd for $C_{20}H_{28}O_{10}\cdot 1/2H_2O$: C, 54.91; H, 6.68%.

Acetylation of 2. A solution of **2** (40 mg) in acetic anhydride (2 mL) and pyridine (2 mL) was stirred at room temperature for 2 h. The mixture was evaporated under reduced pressure and the residue was purified by column chromatography on silica gel (30 g) with benzene–ether (3:1)

to give miyaginin hexaacetate (**3**). Recrystallization from methanol gave pure **3** (30 mg) as colorless needles, mp 163—164 °C (lit,[1] mp 164—165 °C); $[\alpha]_D^{21}$ −46.4° (*c* 0.41, $CHCl_3$); UV (MeOH) 220 (ε 10800), 272 (1000), and 278 nm (800); IR ($CHCl_3$) 3050, 1760, 1635, 1604, 1508, 1220, 1052, 986, and 907 cm^{-1}; ^1H NMR (C_6D_6) δ=1.58 (3H, s, $COCH_3$), 1.65 (3H, s, $COCH_3$), 1.72 (6H, s, 2×$COCH_3$), 1.74 (6H, s, 2×$COCH_3$), 2.89 (1H, dd, *J*=11.7 and 8.8 Hz, H-5″), 3.26 (2H, d, *J*=6.6 Hz, H-7), 3.50 (2H, m, H-5′ and 6′), 3.80 (1H, m, H-6′), 3.87 (1H, dd, *J*=11.7 and 5.1 Hz, H-5″), 4.38 (1H, d, *J*=6.8 Hz, H-1″), 4.89 (1H, d, *J*=7.9 Hz, H-1′), 5.00—5.60 (complex pattern), 5.94 (1H, ddt, *J*=17.2, 9.3, and 6.6 Hz, H-8), 7.00 and 7.17 (2H each, AA′BB′ system, aromatic protons); ^{13}C NMR ($CDCl_3$) δ=20.5 (q, 6×$CO\underline{C}H_3$), 39.3 (t, C-7), 62.0 (t, C-5″), 67.5 (t, C-6′), 68.9 (d, 2C), 70.7 (d), 71.3 (d), 71.5 (d), 72.8 (d), 73.8 (d), 99.3 (d, $^1J_{CH}$=163 Hz, C-1′), 100.4 (d, $^1J_{CH}$=161 Hz, C-1″), 115.6 (t, C-9), 116.8 (d, C-2 and 6), 129.8 (d, C-3 and 5), 135.0 (s, C-4), 137.5 (d, C-8), 155.4 (s, C-1), 169.2, 169.3, 169.4, 169.7, 169.8, and 170.0 (s each, 6×$COCH_3$). Found: C, 56.35; H, 6.05%. Calcd for $C_{32}H_{40}O_{16}$: C, 56.46; H, 5.92%.

Methanolysis of Miyaginin (2). To a solution of **2** (41 mg) in methanol (3 mL) was added concd H_2SO_4 (0.09 mL) and the mixture was refluxed for 14 h. After cooling, the mixture was neutralized with a saturated aqueous $NaHCO_3$ solution and concentrated. The residue was diluted with water (2 mL) and the mixture was extracted with chloroform (3×20 mL); the aqueous layer was saved for further experiment. The chloroform layer was dried (Na_2SO_4) and concentrated under reduced pressure to give an oily residue, which was purified by preparative TLC ($CHCl_3$–MeOH, 4:1), affording *p*-allylphenol (**5**) as colorless oil (9 mg). The ^1H NMR spectrum of **5** (see the experimental section of synthesis of **5**) was identical with that of the authentic sample. For identification **5** was converted with 3,5-dinitrobenzoyl chloride in pyridine to the corresponding *p*-allylphenyl 3,5-dinitrobenzoate **6**, mp 102.5—103 °C (benzene–hexane) (lit,[4] mp 103.5—104.5 °C). The aqueous layer obtained after extraction of the aglycone **5** described above was concentrated under reduced pressure and the residue (*ca.* 200 mg) was treated with acetic anhydride (2 mL) and pyridine (2 mL) at room temperature for 14 h. The mixture was concentrated under reduced pressure to dryness. The residue was diluted with chloroform and the insoluble materials were removed by filtration and washed with chloroform. The filtrate and washings were combined and concentrated under reduced pressure to afford a syrup, which was purified by preparative TLC (hexane–EtOAc, 1:1) to give methyl 2,3,4-tri-*O*-acetyl-α-D-xylopyranoside (9.3 mg) and methyl 2,3,4,6-tetra-*O*-acetyl-α-D-glucopyranoside (13 mg). Methyl 2,3,4-tri-*O*-acetyl-α-D-xylopyranoside (ether–hexane): mp 82—83 °C; $[\alpha]_D^{24}$ +122° (*c* 0.26, $CHCl_3$); ^1H NMR (C_6D_6) δ=1.70, 1.74, 1.78, and 3.06 (3H each, s), 3.41 (1H, dd, *J*=10.9 and 10.8 Hz), 3.66 (1H, dd, *J*=10.9 and 6.5 Hz), 4.79 (1H, d, *J*=3.6 Hz), 4.89 (1H, dd, *J*=10.2 and 3.6 Hz), 5.00 (1H, ddd, *J*=10.8, 10.1, and 6.5 Hz), and 5.65 (1H, dd, *J*=10.2 and 10.1 Hz). Methyl 2,3,4,6-tetra-*O*-acetyl-α-D-glucopyranoside (ether–hexane): mp 63.5—64.5 °C; $[\alpha]_D^{24}$ +129° (*c* 0.24, $CHCl_3$); ^1H NMR (C_6D_6) δ= 1.70, 1.75, 1.76, 1.79, and 3.04 (3H each, s), 3.80 (1H, ddd, *J*=9.9, 4.3, and 2.7 Hz), 4.00 (1H, dd, *J*=11.9 and 2.7 Hz), 4.24 (1H, dd, *J*=11.9 and 4.3 Hz), 4.86 (1H, d, *J*=3.7 Hz), 4.96 (1H, dd, *J*=9.9 and 3.7 Hz), 5.18 (1H, dd, *J*=9.9 and 9.0 Hz), and 5.70 (1H, dd, *J*=9.9 and 9.0 Hz); these data were identical with those of the authentic samples derived from D-xylose and D-glucose, respectively.

Preparation of p-*Allylphenol (5).* To a stirred solution of 3-(4-hydroxyphenyl)-1-propanol (**7**) (1.0 g, 6.6 mmol) and *o*-nitrophenyl selenocyanate (1.93 g, 8.46 mmol) in anhydrous tetrahydrofuran (50 mL) was added tributylphosphine (3.2 mL, 12.8 mmol) at room temperature under nitrogen. After stirring for 5 h, the mixture was diluted with ether and the insoluble materials were removed by filtration and washed with ether. The filtrate and washings were combined and concentrated under reduced pressure to afford a brown syrup, which was purified by column chromatography on silica gel (150 g) using cyclohexane–ether (2:1) to give a crystalline selenide **8** (2.4 g, quantitative yield), mp 45—47 °C (without recrystallization); UV (MeOH) 226 (ε 13900), 255 (13600), 275 (sh, 7600), and 389 nm (3600); IR ($CHCl_3$) 3630, 3380, 1613, 1594, 1570, 1514, and 1334 cm^{-1}; ^1H NMR ($CDCl_3$) δ=2.08 (2H, quintet, *J*=7.2 Hz, H-8), 2.72 and 2.88 (2H each, t, *J*=7.2 Hz, H-7 and 9), 6.74 and 7.04 (2H each, AA′BB′ system, H-2, 3, 5, and 6), 7.36 (3H, m, H-4′, 5′, and 6′), and 8.24 (1H, br d, *J*=7.2 Hz, H-3′); MS (70 eV) *m/z* (rel intensity) 337 (M^+, $C_{15}H_{15}NO_3{}^{80}Se$; 26), 202 (13), 186 (18), 133 (97), and 107 (100). Found: *m/z* 337.0195. Calcd for $C_{15}H_{15}NO_3{}^{80}Se$: M, 337.0217.

To a stirred solution of **8** (2.2 g, 6.5 mmol) in tetrahydrofuran (50 mL) was added dropwise a 30% hydrogen peroxide solution (6.8 mL, 65 mmol) at room temperature. After stirring at 40 °C for 3.5 h, the mixture was extracted with ether (4×30 mL). The ethereal extracts were washed with 1 M (1 M=1 mol dm^{-3}) $Na_2S_2O_3$ (5×15 mL) and a saturated NaCl solution, dried (Na_2SO_4), and evaporated. The residue was purified by column chromatography on silica gel (40 g) with ether–hexane (1:3) to give a crude oil (863 mg) of **5**. By the same procedure described above 937 mg of oily **5** was obtained from 2.20 g of the selenide **8**. The combined crude oil (1800 mg) was distilled to afford pure **5** (1.40 g, 80%) as a colorless liquid, bp 100.5—101.5 °C/7.5 mmHg (1 mmHg≈ 133.322 Pa) (lit,[13] bp 105—110 °C/11 mmHg); ^1H NMR ($CDCl_3$) δ=3.31 (2H, br d, *J*=6.8 Hz, H-7), 4.84 (1H, br s, OH), 5.02 (2H, m, H-9), 5.95 (1H, ddt, *J*=17.3, 9.4, and 6.8 Hz, H-8), 6.75 and 7.05 (2H each, AA′BB′ system, aromatic protons).

p-*Allylphenyl 2,3,4,6-Tetra-O-acetyl-β-D-glucopyranoside (9).* A mixture of penta-*O*-acetyl-β-D-glucopyranose (512 mg, 1.31 mmol), *p*-allylphenol (**5**) (370 mg, 2.76 mmol), acetic anhydride (0.12 mL, 1.3 mmol), and anhydrous *p*-toluenesulfonic acid (12 mg, 0.07 mmol) was stirred at 100—110 °C for 50 min under reduced pressure (20 mmHg). After cooling, the mixture was diluted with benzene (20 mL) and washed successively with water (3 mL), 0.25 M NaOH (15 mL), and water (10 mL). The benzene layer was dried (Na_2SO_4) and evaporated under reduced pressure to give a residue, which was chromatographed on silica gel (20 g) with benzene–ether (5:1), affording crude crystals of **9**. Recrystallization from methanol afforded **9** (337 mg, 56%) as colorless needles, mp 141—142 °C (lit,[7] mp 136—138 °C); $[\alpha]_D^{16}$ −21.1° (*c* 0.78, $CHCl_3$); IR (Nujol) 1756, 1640, 1610, 1590, 1514, 1230, 1043, 990, and 910 cm^{-1}; ^1H NMR (C_6D_6) δ=1.68, 1.69, 1.72, and 1.73 (3H each, s, 4×$COCH_3$), 3.15 (2H, d, *J*=6.5 Hz, H-7), 3.20 (1H, m, H-5′), 3.94 (1H, dd, *J*=12.3 and 2.6 Hz, H-6′), 4.18 (1H, dd, *J*=12.3 and 4.8 Hz, H-6′), 4.82 (1H, d, *J*=7.7 Hz, H-1′), 4.97 (2H, m, H-9), 5.00—5.60 (3H, complex pattern), 5.82 (1H, ddt, *J*=17.6, 9.0, and 6.5 Hz, H-8), and 6.95 (4H, s, aromatic protons).

p-*Allylphenyl β-D-Glucopyranoside (10).* To a stirred solution of **9** (100 mg, 0.22 mmol) in anhydrous methanol (2 mL) was added a solution of 1 M sodium methoxide in methanol (0.04 mL) at room temperature under nitrogen. After stirring for 2 h, the mixture was neutralized by adding ion-exchange resin, Amberlite IRC-50 (260 mg). The resin was removed by filtration and washed with methanol. The filtrate and washings were combined and concentrated to afford an amorphous powder. Purification by column chromatography on silica gel (20 g) with chloroform–methanol (6:1) gave **10** (54 mg, 84%) as a colorless solid, which was recrystallized from water to give crystalline **10**, mp 149—150 °C (lit,[12] mp 148—149 °C); $[\alpha]_D^{15}$ −56.3° (*c* 0.39, MeOH)

[lit,[12] $[\alpha]_D^{20}$ −61.8° (*c* 0.275, MeOH)]; UV (MeOH) 222 (ε 6800), 273 (900), and 279 nm (700); IR (KBr) 3350, 1633, 1610, 1590, 1507, 1230, and 910 cm^{-1}; ^1H NMR (CD_3COCD_3) δ=3.32 (2H, d, *J*=6.6 Hz, H-7), 4.91 (1H, d, *J*=7.0 Hz, H-1′), 5.00 (2H, m, H-9), 5.96 (1H, ddt, *J*=16.9, 10.1, and 6.6 Hz, H-8), 6.97 and 7.12 (2H each, AA′BB′ system, aromatic protons).

p-Allylphenyl 2,3,4-Tri-O-acetyl-β-D-glucopyranoside (11). A solution of **10** (51 mg, 0.17 mmol) and trityl chloride (147 mg, 0.527 mmol) in anhydrous pyridine (1 mL) was stirred at 100°C for 7 h. After cooling, acetic anhydride (0.5 mL) was added to the mixture. The mixture was stirred for additional 4.5 h at room temperature and concentrated under reduced pressure. The residue was diluted with 80% acetic acid (3 mL) and the mixture was stirred at 100°C for 30 min and then at room temperature for several hours. The crystalline precipitates in the mixture were removed by filtration and washed with 75% methanol (20 mL). The combined filtrate and washings were concentrated under reduced pressure to leave a solid, which was purified by column chromatography on silica gel (20 g) with benzene–ether (2:1) to give crude **11**. Recrystallization from ether–hexane afforded **11** (29 mg, 40% overall yield) as colorless needles, mp 79—80°C; $[\alpha]_D^{12}$ −9.40° (*c* 0.24, $CHCl_3$); UV (MeOH) 221 (ε 10400), 272 (1300), and 278 nm (1000); IR ($CHCl_3$) 3400, 3040, 1760, 1638, 1607, 1510, 1220, 993, and 910 cm^{-1}; ^1H NMR (C_6D_6) δ=1.57, 1.61, and 1.73 (3H each, s, 3×$COCH_3$), 3.15 (2H, br d, *J*=6.4 Hz, H-7), 3.15 (1H, m, H-5′), 3.40 (2H, m, H-6′), 4.80—5.60 (6H, complex pattern), 5.86 (1H, ddt, *J*=17.8, 9.2, and 6.4 Hz, H-8), 6.94 (4H, s, aromatic protons); ^{13}C NMR ($CDCl_3$) δ=20.5 (q, 3×$CO\underline{C}H_3$), 39.3 (t, C-7), 61.3 (t, C-6′), 68.7 (d), 71.4 (d), 72.8 (d), 74.4 (d), 99.2 (d, $^1J_{CH}$=162 Hz, C-1′), 115.7 (t, C-9), 116.8 (d, C-2 and 6), 129.7 (d, C-3 and 5), 135.0 (s, C-4), 137.3 (d, C-8), 155.2 (s, C-1), 169.2, 169.8, and 170.2 (s each, 3×$\underline{C}OCH_3$); MS (70 eV) *m/z* (rel intensity) 422 (M^+, 1), 331 (14), 289 (91), 229 (100), 187 (35), 169 (72), 134 (84), 127 (98), and 109 (71). Found: C, 59.12; H, 6.29%. Calcd for $C_{21}H_{26}O_9$: C, 59.71; H, 6.20%.

Miyaginin Hexaacetate (3). A solution of **11** (43 mg, 0.10 mmol), 2,3,4-tri-*O*-acetyl-α-D-xylopyranosyl bromide (100 mg, 0.29 mmol), mercury(II) bromide (91 mg, 0.25 mmol), and mercury(II) cyanide (64 mg, 0.25 mmol) in dry acetonitrile (3 mL) was stirred at room temperature under nitrogen in the dark. After stirring for 5 h, the mixture was concentrated under reduced pressure. The residue was dissolved in chloroform (20 mL) and the insoluble materials were removed by filtration and washed with chloroform. The filtrate and washings were combined and washed with a saturated KBr solution, until washings showed no coloration with an aqueous ammonium sulfide solution. The chloroform layer was dried (Na_2SO_4) and concentrated under reduced pressure to leave a syrup. Purification by column chromatography on silica gel (25 g) with benzene–ether (3:1) gave **3** (60 mg, 88%) as a colorless solid. Recrystallization from methanol gave **3** as colorless needles, mp 163—164°C; $[\alpha]_D^{21}$ −44.9° (*c* 0.55, $CHCl_3$). The physical (mp and $[\alpha]_D$) and spectral (IR, UV, ^1H NMR, and ^{13}C NMR) properties of synthetic **3** were identical with those of **3** derived from natural miyaginin (**2**).

Miyaginin (2). Methanolysis of **3** (23 mg, 0.034 mmol) was performed by essentially the same procedure as described in the preparation of **10**. The crude product was purified by column chromatography on silica gel (20 g) with chloroform–methanol (4:1) to give **2** (13 mg, 89%) as an amorphous solid. Recrystallization from aqueous acetone afforded crystalline **1** as colorless needles, mp 211.5—213°C; $[\alpha]_D^{14}$ −81.6° (*c* 0.36, H_2O). The physical (mp and $[\alpha]_D$) and spectral (UV, IR, ^1H NMR, and ^{13}C NMR) properties and chromatographic mobilities of synthetic **2** were completely identical with those of natural **2** in all respects.

We are grateful to Dr. Hiroaki Matsuda, the University of Tokyo for providing us with authentic samples of miyaginin and the hexaacetate, and to Emeritus Prof. Arika Kimura, Tohoku University and Prof. Hiroyoshi Ohashi, Tohoku University for their kind assistance in the collection and the identification of the plant materials.

References

1) M. Kanao and H. Matsuda, *Yakugaku Zasshi*, **98**, 366 (1978).
2) M. Ojika, K. Wakamatsu, H. Niwa, K. Yamada, and I. Hirono, *Chem. Lett.*, **1984**, 397.
3) H. Ohigashi and K. Koshimizu, *Agr. Biol. Chem.*, **40**, 2283 (1976).
4) S. Palkin and P. A. Wells, *J. Am. Chem. Soc.*, **55**, 1556 (1933).
5) K. B. Sharpless and M. W. Young, *J. Org. Chem.*, **40**, 947 (1975).
6) B. Helferich and E. Schmitz-Hillebrecht, *Chem. Ber.*, **66**, 378 (1933); A. L. Clingman, *J. Med. Chem.*, **7**, 242 (1964).
7) R. Higuchi and D. M. X. Donnelly, *Phytochemistry*, **16**, 1587 (1977).
8) This three-step sequence was originally employed for the preparation of 1,2,3,4-tetra-*O*-acetyl-β-D-glucopyranose from D-glucose: B. Helferich and W. Klein, *Justus Liebigs Ann. Chem.*, **450**, 219 (1926).
9) B. Helferich and W. Ost, *Chem. Ber.*, **95**, 2612 (1962).
10) H. Herissey, *C. R. Acad. Sci.*, **198**, 265 (1934).
11) R. Higuchi, M. Aritomi, and D. M. X. Donnelly, *Phytochemistry*, **16**, 1007 (1977).
12) T. Hase and T. Iwagawa, *Bull. Chem. Soc. Jpn.*, **55**, 3663 (1982).
13) C. D. Hurd and W. W. Jenkins, *J. Org. Chem.*, **22**, 1418 (1957).

 © 1984 The Chemical Society of Japan Bull. Chem. Soc. Jpn., 57, 2897—2904 (1984)

Reactions of Enolates with Vinyl Selenoxides and Vinyl Selenones. One-step Synthesis of Cyclopropylcarbonyl Compounds

Ryoichi ANDO, Tomoo SUGAWARA, Makoto SHIMIZU,† and Isao KUWAJIMA*
Department of Chemistry, Tokyo Institute of Technology, Meguro, Tokyo 152
(Received May 22, 1984)

In the reactions with enolate anions, organoselenium moieties of aryl vinyl selenoxides and selenones have exhibited two important roles, *e.g.*, activation of C=C bonds for conjugate addition reaction and behaviors as excellent leaving groups. Owing to such characteristic features, ketone enolates react with *p*-chlorophenyl vinyl selenoxide to afford the corresponding cyclopropyl ketones through an initial conjugate addition followed by substitution processes. On the other hand, use of vinyl selenones usually gives much better results with anionic species of active methylene compounds. Vinyl selenones bearing hydroxyl, ketone, and ester groups can also be employed equally well for this type of transformation.

Cyclopropylcarbonyl compounds have recently received much attention because of their versatility in synthetic organic reactions.[1,2] Reactive conjugate receptors in which electron-withdrawing activator **X** also acts as a good leaving group may be used as versatile ethylene transfer reagents for enolates (dibasic nucleophiles) to yield the corresponding cyclopropyl ketones as shown in Scheme 1. Relatively few examples of reactions of this type are known. Gosselck and his collaborators reported the formation of cyclopropanes in the reaction of active methylene compounds with substituted dimethylvinylsulfonium salts.[3] Johnson and Lockard observed the cyclopropane ring formation in the reaction between [(dimethylamino)phenyl](2-phenylvinyl)oxosulfonium tetrafluoroborate and active methylene compounds.[4] More recently it was reported that the reaction of lithium enolate of acetophenone with dimethylvinylsulfonium perchlorate gave the corresponding cyclopropyl ketones.[5]

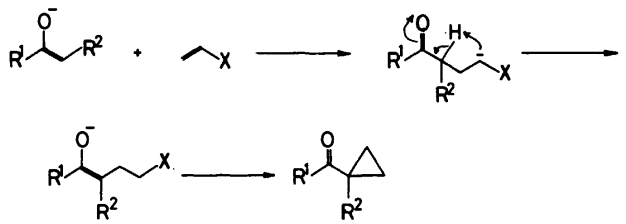

Scheme 1.

However, these procedures have only limited applicability due to the difficulty encountered for the preparation of vinylsulfonium salts and to the fact that only active methylene compounds are employable for the former two examples. In the latter case only acetophenone meets with success. It is, therefore, desirable to develop an easy and reliable ethylene transfer methodology to a variety of carbonyl compounds.

A few years ago, we began to study on use of vinyl selenoxide or vinyl selenones for such kind of organic transformations. In contrast to studies on the reactivities of vinyl sulfoxides,[6] those on vinyl selenoxides have limited numbers of investigation,[7] because alkyl aryl selenoxides are in usual quite unstable if they bear β-hydrogens. A well-documented *syn*-elimination of selenoxides always takes place at low temperature in such case, leading to the formation of olefins.[8,9] Selenoxides become relatively stable when there is no β-hydrogen available or areneseleninyl groups are attached to sp^2 or sp hybridized carbons.[7a,10] Further it has been reported that selenoxides are more polar and more basic than sulfoxides are.[11] In this regard, vinyl selenoxides appear to be more reactive than vinyl sulfoxides toward nucleophiles.

In this paper, we describe our results for the preparation of cyclopropylcarbonyl compound in full details by using organoselenium compounds.[12,13]

Results and Discussion

Although to date no reports deal with S_N2 type substitution of areneseleninyl groups, the weak C–Se bonds appear to make this type transformation feasible, which will lead to an introduction of a new functional group to the carbon bearing areneseleninyl group. In light of polar character of selenoxides[11] coupled with weak C–Se bonds, it is then expected that when **X** in Scheme 1 is displaced with areneseleninyl group, a cyclopropane ring may be formed through conjugate addition followed by substitution in the reaction between ketone enolates and aryl vinyl selenoxides.

Aryl vinyl selenoxides are readily prepared by oxidation of the corresponding aryl vinyl selenides with either 1 equiv of *m*-CPBA or sodium periodate.[7a] For the preparation of the starting materials, aryl vinyl selenides, two methods are now available[7a,14,15]: One involves an addition of an areneselenenyl halide to olefins followed by elimination of hydrogen halide with an appropriate base, and the other is the transformation from selenoacetals obtained from aldehydes and areneselenol.

Treatment of 1-dodecenyl phenyl selenoxide thus obtained with sodium diethyl malonate indeed gave rise to the 1,1-cyclopropanedicarboxylic ester in 47% yield.

It has been reported that the reaction of sodium diethyl malonate to tolyl vinyl sulfoxide proceeds in refluxing tetrahydrofuran (THF) to afford the addition product (not the cyclopropane derivative).[6] In strong contrast to the sulfoxide, vinyl selenoxides seem to be much more reactive toward this nucleophile, and the reaction proceeds at as low as −20°C.

†Present address: The Institute of Physical and Chemical Research, Wako, Saitama 351-01.

The reaction of the selenoxide with lithium enolate of acetophenone gave the cyclopropyl ketone **1** in much higher yield than the case with diethyl malonate. This conversion, however, is not free from side-reactions: Major by-product formed during the reaction is α-

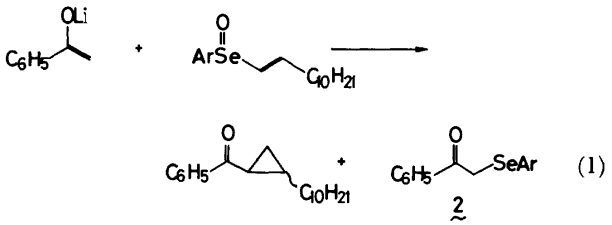

(1)

phenylselenoacetophenone **2** arising from selenenylation of the enolate. To improve the procedure more precisely, effects of substituents on the benzene ring of areneseleninyl group as well as the reaction solvent were examined on the reaction of aryl 1-dodecenyl selenoxide with lithium enolate of acetophenone. Results are shown in Table 1.

As shown in the Table 1, significant effects of substituents on aryl selenoxides together with those of solvents were observed. An electron-withdrawing substituent such as *m*-trifluoromethyl or *p*-chloro group facilitates the reaction remarkably (runs 6 and 9), whereas electron-donating *o*-methyl group decreased the product yield (run 5). In the *syn*-elimination reaction of selenoxides, *o*-nitro group has been known to facilitate the reaction.[16] In the present case, however, no detectable amount of the desired product was obtained (run 7). The use of ether as solvent proved to be most suitable because the undesired selenenylation of the enolate could be practically excluded. When THF is employed as the solvent, areneselenenylation of acetophenone usually accompanies up to 15% yield. It is likely that in ether the eliminated selenium species has poor solubility, which seems to make this species incapable of selenenylation.

A variety of lithium enolates were subjected to the reaction with three types of *p*-chlorophenyl vinyl selenoxides **3a**, **3b**, and **3c**. Table 2 lists the results.

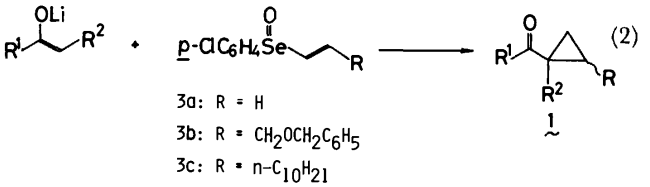

(2)

Relatively hard nucleophiles such as ketone or α-phenylthio ester enolates gave better results, whereas the yields of cyclopropylcarbonyl compounds were decreased with soft nucleophiles such as α-phenylsulfinyl or α-phenylsulfonyl ester enolates and lithium diethyl malonate (runs 25, 26, 27, and 28).

The present reaction proceeds most probably *via* conjugate addition of enolates to vinyl selenoxides followed by proton transfer from **4** to **5** and displacement of areneseleninyl group as outlined in Scheme 2.

The first conjugate addition step appears to be favored with relatively hard nucleophiles. With soft

Table 1. Effects of aryl substituents for cyclopropanation[a]

Run	Ar	Solvent	Yield/% of **1**
1	C_6H_5[b]	THF	65
2	C_6H_5[c]	THF	20
3	C_6H_5[d]	THF-HMPA	51
4	C_6H_5	Ether	63
5	*o*-$CH_3C_6H_4$	THF	17
6	*m*-$CF_3C_6H_4$	Ether	73
7	*o*-$NO_2C_6H_4$	Ether	Trace
8	*p*-ClC_6H_4	THF	69
9	*p*-ClC_6H_4	Ether	81
10	*p*-ClC_6H_4[e]	THF	91

a) A reactant ratio, ketone: selenoxide: LDA=1.2—1.25:1.0:1.5. b) Ketone: selenoxide: LDA=1.1:1.0:2.2. c) Sodium hexamethyldisilazide (1.4 equiv) was used. d) Ketone: selenoxide: LDA=1.1:1.0:1.4. e) An excess amount of enolate (1.7 equiv) was used.

Table 2. Reactions of vinyl selenoxides with ketone enolates[a]

Run	Ketone	Selenoxide	Yield/% of **1**	
11	Acetophenone	**3a**	**1a**	72[b]
12	Acetophenone	**3b**	**1b**	70
13	Acetophenone	**3c**	**1c**	81
14	Propiophenone	**3a**	**1d**	59[b]
15	Propiophenone	**3b**	**1e**	84[b]
16	Propiophenone	**3c**	**1f**	62[b]
17	Ethyl (phenylthio)acetate	**3a**	**1g**	65[b]
18	Ethyl (phenylthio)acetate	**3b**	**1h**	72
19	Ethyl (phenylthio)acetate	**3c**	**1i**	71
20	Cyclododecanone	**3b**	**1j**	55
21	Cyclohexanone	**3c**	**1k**	51[b]
22	*t*-Buty methyl ketone	**3c**	**1l**	72
23	*t*-Butyl acetate	**3c**	**1m**	52
24	Isopropyl methyl ketone	**3c**	**1n**	56
25	1-Phenylthio-2-heptanone	**3c**	**1o**	47
26	Ethyl phenylsulfinylacetate	**3c**	**1p**	35
27	Ethyl phenylsulfonylacetate	**3c**	**1q**	13
28	Diethyl malonate	**3c**	**1r**	23

a) A reactant ratio, ketone: selenoxide: LDA=1.20—1.25:1.0:1.5. b) Ketone: selenoxide: LDA=1.0: 1.2:1.5.

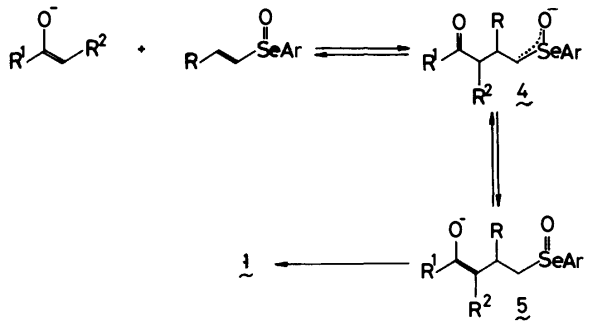

Scheme 2.

nucleophiles, the conjugate addition seems to proceed under equilibrium conditions. The equilibrium is usually favored on the left side (Scheme 2) and the other side reactions, *e.g.*, attack of enolates to areneseleninyl moiety or proton abstraction from vinyl selenoxide, may cause the low yield of the desired product.

As the third step, the displacement of areneseleninyl group, this type of intramolecular substitution has closely related precedents in sulfone chemistry, where an approach to chrysanthemic acid represents an outstanding example.[17]

Although the formation of a cyclopentanone derivative might also be conceivable when the parent ketone is enolizable on both sides, such products were not obtained in any cases.

Further application to cyclohexenone, β-ionone, and camphor shows the utility of the present method.

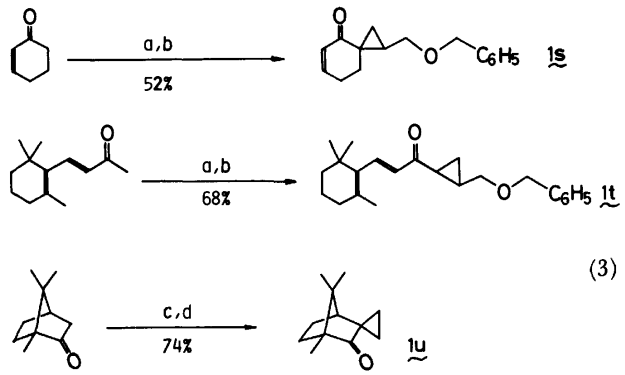

(3)

a) LDA (1.5 eq), ether. b) 3b (1.2 eq)
c) LDA (1.5 eq), DME. d) 3a (1.2 eq)

Cyclopropanation of camphor in THF gave rise to the desired ketone in only 38% yield along with concomitant formation of α-selenenylated ketone (18%). 1,2-Dimethoxyethane (DME) was proved to be a solvent of choice in that case.

Cory and his collaborators have reported the reaction of bicycloannulation of cyclohexenone derivatives with vinyltriphenylphosphonium salts[18] or vinyl sulfones.[19] In the present system, enolates of α,β-unsaturated ketones underwent cyclopropanation solely as indicated in the case with cyclohexenone. Relatively low efficacy of active methylene compounds as dibasic nucleophiles for this type of transformation may be attributable to insufficient activation of the neighboring C=C bonds with areneseleninyl group as well as its less efficient character as the leaving group.

Recently, we described preparation of vinyl selenones **6**: They can be easily prepared by oxidation of the corresponding vinyl selenides with 2—2.2 equiv of *m*-CPBA in an alcoholic media.[20] Further, in their reactions with alkoxides, *e.g.*, oxetane formation[20a] and fragmentation reactions,[20b] the selenonyl group has exhibited such similar characters as the seleninyl group described above, *e.g.*, activation of C=C bonds and as excellent leaving groups. By using such features of vinyl selenones, we have also examined the cyclopropanation reaction of enolate anions. Various examinations revealed that reactivity of a C=C bond to active methylene compounds has been greatly improved to form a cyclopropane ring on that linkage efficiently. For example, 1-hexenyl phenyl selenone was treated with an equimolar amount of sodium dimethyl malonate in THF at room temperature for 4 h, which gave the corresponding cyclopropanedicarboxylic ester in 92% yield. Various kinds of active methylene compounds can also be used equally well to give the corresponding cyclopropane **7** in good yields (see Table 3).

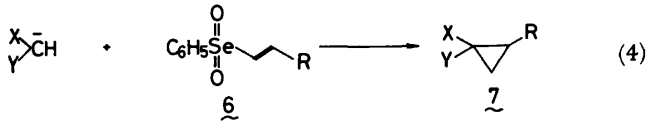

(4)

A transition metal-catalyzed reaction of olefins with diazo compounds has also been widely employed for

Table 3. Reactions of active methylene compounds with phenyl vinyl selenones **6**[a]

X	Y	R	Conditions	Yield/% of 7	
CO_2CH_3	CO_2CH_3	C_4H_9	r.t., 4 h	**7a**	92(87[b])
$COCH_3$	CO_2CH_3	C_4H_9	r.t., 1.5 h	**7b**	77
$COCH_3$	CONH-*t*-Bu	C_4H_9	r.t., 1.5 h	**7c**	98
CO_2CH_3	CN	C_4H_9	r.t., 1 h	**7d**	91
NO_2	H	C_4H_9	65 °C, 1 h	**7e**	75
$COCH_3$	C_6H_5S	C_4H_9	r.t., 1 h	**7f**	83
$CO_2C_2H_5$	C_6H_5S	C_4H_9	r.t., 2.5 h	**7g**	56
$CO_2C_2H_5$	$CO_2C_2H_5$	$(CH_2)_5C(OH)CH_2$	r.t., 4 h,	**7h**	72[b]
CO_2CH_3	CO_2CH_3	$C_5H_{11}CH(OH)$-$(CH_2)_3$-	r.t., 4 h	**7i**	80
CO_2CH_3	CO_2CH_3	$C_5H_{11}CO$-$(CH_2)_3$-	r.t., 2 h	**7j**	86
CO_2CH_3	CO_2CH_3	C_4H_9CO-$(CH_2)_8$-	r.t., 1.2 h	**7k**	91
CO_2CH_3	CO_2CH_3	CH_3O_2C-$(CH_2)_8$-	r.t., 2 h	**7l**	86
CO_2CH_3	CO_2CH_3	$CH_3O_2CCH(C_4H_9)$-$(CH_2)_3$-	r.t., 2 h,	**7m**	87

a) A reactant ratio, ketone:selenone=1.2:1.0. b) Lithium enolate was used.

this type of transformation,[20] but there exist serious drawbacks on the following two points; (i) use of an excess amount of olefin is usually required for moderate success, and (ii) a range of its application suffers from severe limitation because oxygen-containing functional groups prevent the cyclopropanation reaction.[21a]

Both of them have been overcome efficiently by the present method using vinyl selenones. First, olefins can be converted to the corresponding vinyl selenones effectively *via* vinyl selenides, and active methylene compounds undergo cyclopropanation with a stoichiometric amount of the vinyl selenones. In the second, various oxygen-containing functionalities do not disturb this olefin unit transfer to active methylene sites to give the corresponding cyclopropane in excellent yields as exemplified in formation of **7h—m**.

Further, the following example has demonstrated site-selective activation of terminal olefins. When started from a diene, selenenylation takes place selectively on the terminal C=C bond.[14,22] Although an internal one also undergoes oxidation to the oxirane during conversion of a selenide to the selenone, selective formation of cyclopropane ring has been executed on the parent terminal C=C bond under the reaction conditions where the oxirane survives as shown in Eq. 5.

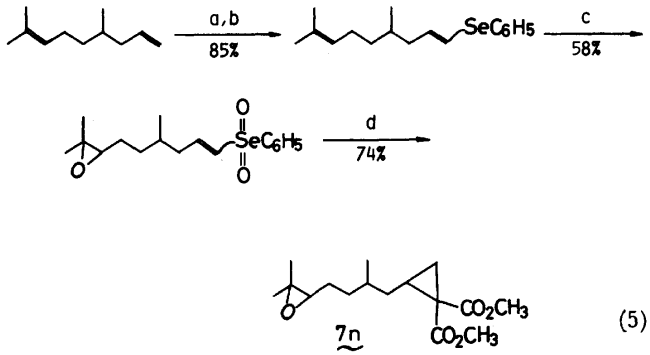

(5)

a) C_6H_5SeBr. b) t-BuOK. c) m-CPBA (2.2 eq). d) $NaCH(CO_2CH_3)_2$

Conclusion

As shown above, various kinds of enolate anions behave as dibasic nucleophiles toward vinyl selenoxides and vinyl selenones due to characteristic features of seleninyl and selenonyl groups. Difference between vinyl selenoxides and vinyl selenones should be noted here. As described earlier, the formers in general give much better results with usual enolates than with anionic species of active methylene compounds. On the contrary, vinyl selenones has exhibited slight different behavior toward enolate nucleophiles. Thus, in addition to activation of a neighboring C=C bond to nucleophiles, a selenonyl group appears to enhance the acidity of vinyl proton, which sometimes results in undesired side-reactions such as decomposition to the corresponding acetylene[23] when anionic species of less acidic substrates are used as nucleophiles. For example, treatment of 1-dodecenyl phenyl selenone with lithium enolate of acetophenone led to the formation of the cyclopropane in 41% yield together with 1-dodecyne (19%). Such a feature clearly disfavors use of vinyl selenones for the preparation of cyclopropyl ketones, and use of vinyl selenoxides should be recommended.

There have been developed several types of procedures for cyclopropanation of olefins, *e.g.*, use of oxosulfonium,[24] phosphonium[25] selenium ylides,[26] or Simmons-Smith reagent.[27] In regard to the accessibility of the starting material, the present procedure, complementary to these methods, offers a simple and useful approach to cyclopropylcarbonyl compounds.

Experimental

General Methods. Boiling points and melting points are uncorrected. Infrared (IR) spectra were recorded on a Hitachi EPI-G3 spectrometer; absorptions are given in reciprocal centimeters. Proton nuclear magnetic resonance spectra (^1H NMR) were obtained on a Hitachi R-24B spectrometer; chemical shifts (δ) are expressed in parts per million downfield from internal tetramethylsilane. Mass spectra (70 eV) were determined on a Hitachi RMU-6C or RMU-7M spectrometer. Microanalysis were performed with a Perkin Elmer 240 at the Microanalysis Laboratory, Tokyo Institute of Technology.

Reactions involving air- or moisture-sensitive compounds were carried out in appropriate round-bottomed flasks with magnetic stirring bars under nitrogen or argon. Bulb-to-bulb distillation was performed with a Büchi Kügelrohr apparatus.

Preparative thin-layer chromatography (TLC) was carried out on glass plates (20×20 cm) coated with Merck silica gel PF 254 (1 mm thick). Column chromatography was performed on Merck Kieselgel or Wakogel C-200.

Ether, tetrahydrofuran (THF), and 1,2-dimethoxyethane were distilled from sodium-benzophenone ketyl in a recycling still immediately before use. *m*-Chloroperbenzoic acid (*m*-CPBA, 85% pure), purchased from Aldrich Chemical Co., was used directly without purification.

Preparation of Aryl Vinyl Selenides. The preparation

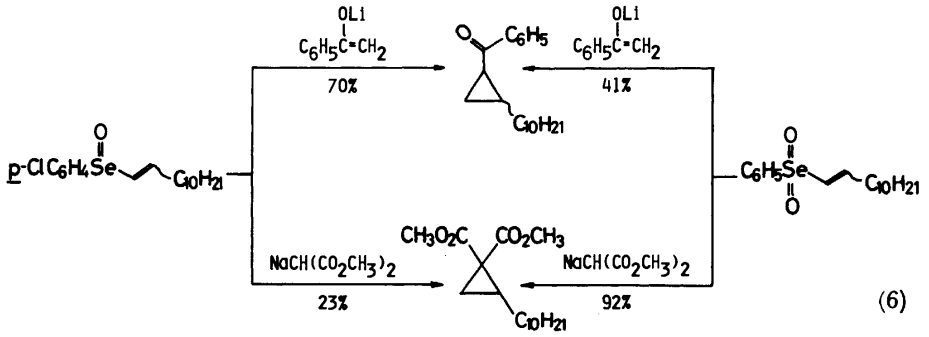

(6)

of 1-dodecenyl *p*-chlorophenyl selenide, which was prepared by a similar method developed by Raucher *et al*,[14a] represents a typical procedure. To a solution of *p*-chlorobenzeneselenenyl bromide prepared from bis(*p*-chlorophenyl) diselenide (2.29 g, 6.0 mmol) and bromine (6 mL of 1 M (1 M=1 mol dm^{-3}) carbon tetrachloride solution, 6.0 mmol) in 5 mL of acetonitrile was added a solution of 1-dodecene (2.02 g, 12 mmol) in 35 mL of acetonitrile, and the reaction mixture was stirred for 2.5 h at room temperature. After all the solvent was removed, potassium *t*-butoxide (2.7 g, 24 mmol) and THF (50 mL) were added to the crude mixture, and the resulting brown-colored mixture was stirred for 1 h at room temperature. Then, it was washed with satd aq NaCl, and the aqueous layer was extracted with ethyl acetate. The combined extracts were dried and concentrated to give an oil, which was distilled to afford a mixture of (*E*)- and (*Z*)-1-dodecenyl *p*-chlorophenyl selenide (2.98 g, 69%); bp 105 °C/0.08 mmHg**; IR (neat) 2900, 1600, 1470, 1380, 1090, 1010, 950, 810, 725; NMR (CCl_4) 0.80—1.70 (m, 19H), 1.90—2.33 (m, 2H), 5.73—6.50 (m, 2H), 7.03—7.60 (m, 4H). Calcd for $C_{18}H_{27}SeCl$: C, 64.42; H, 7.61%. Found: C, 64.72; H, 7.79%.

1-Dodecenyl Phenyl Selenide. IR (neat) 2919, 1580, 1480, 1440, 1075, 1025, 1000, 955, 740, 690; NMR (CCl_4) 0.70—1.60 (m, 19H), 1.90—2.63 (m, 2H), 5.70—6.50 (m, 2H), 7.00—7.50 (m, 5H). Calcd for $C_{18}H_{28}Se$: C, 66.86; H, 8.73%. Found: C, 66.82; H, 8.67%.

1-Dodecenyl o-Tolyl Selenide. IR (neat) 2900, 1605, 1585, 1565, 1460, 1375, 1050, 1035, 950, 740; NMR (CCl_4) 0.70—1.70 (m, 19H), 1.57—2.50 (m, 2H), 2.37 (s, 3H), 5.73—6.50 (m, 2H), 6.83—7.50 (m, 4H). Calcd for $C_{19}H_{30}Se$: C, 67.63; H, 8.96%. Found: C, 67.72; H, 9.04%.

1-Dodecenyl o-Nitrophenyl Selenide. IR (neat) 2890, 1580, 1465, 1445, 1330, 1300, 1100, 1040, 970, 860, 790, 735; NMR (CCl_4) 0.70—1.70 (m, 19H), 2.00—2.50 (m, 2H), 6.20—6.50 (m, 2H), 7.00—7.57 (m, 3H), 8.03—8.90 (m, 1H). Calcd for $C_{18}H_{27}NO_2Se$: C, 58.69; H, 7.39; N, 3.80%. Found: C, 58.99; H, 7.55; N, 3.95%.

1-Decenyl m-Trifluoromethylphenyl Selenide. IR (neat) 2905, 1575, 1465, 1420, 1315, 1270, 1160, 1125, 1095, 1080, 1065, 995, 960, 890, 790, 690; NMR (CCl_4) 0.50—1.70 (19H), 2.00—2.67 (m, 2H), 6.13—6.23 (m, 1H), 6.50—6.70 (m, 1H), 7.50—8.10 (m, 4H). Calcd for $C_{19}H_{27}F_3Se$: C, 58.31; H, 6.95%. Found: C, 58.59; H, 7.29%.

3-Benzyloxy-1-propenyl p-Chlorophenyl Selenide. To a solution of sodium *p*-chlorobenzeneselenolate prepared by reduction of bis(*p*-chlorophenyl) diselenide (7.6 g, 20 mmol) with sodium borohydride (1.5 g, 40 mmol) in ethanol (100 mL) was added a solution of epichlorohydrin (11.1 g, 120 mmol) in ethanol (20 mL) at −78 °C and the reaction mixture was allowed to stand at room temperature for 20 h. Then all the solvent was removed *in vacuo*. The resulting residue was washed with satd aq NaCl, and the aqueous layer was extracted with ethyl acetate. The combined extracts were dried and concentrated to give an oil. To a suspension of sodium hydride (45 mmol) in THF (10 mL) was added a solution of the crude oil obtained above in 40 mL of THF, and the mixture was stirred under refluxing for 1.5 h. Then a solution of benzyl bromide (6.7 g, 39.2 mmol) in THF (20 mL) was added to the ice-cooled mixture. After allowed to stand for 16 h at room temperature, the reaction mixture was washed with satd aq NaCl and dried. Removal of the solvent gave an oil, which was distilled to yield the title compound (8.8 g, 67%) as a mixture of (*E*)- and (*Z*)-isomers: bp 122 °C (bath temp)/0.08 mmHg; IR (neat) 3000, 2900, 2830, 1605, 1475, 1450, 1390, 1360, 1305, 1210, 1095, 1015, 950, 820, 740, 700; NMR (CCl_4) 3.93, 3.96 (unresolved dd, *J*=5 and 6 Hz, 2H), 4.47 (unresolved, s, 2H), 5.70—6.80 (m, 2H), 7.00—7.60 (m, 4H). Calcd for $C_{16}H_{15}OSeCl$: C, 56.91; H, 4.48%. Found: C, 56.67; H, 4.32%.

p-Chlorophenyl Vinyl Selenide. To a solution of sodium *p*-chlorobenzeneselenolate prepared from bis(*p*-chlorophenyl) diselenide (3.81 g, 10 mmol) and sodium borohydride (758 mg, 20 mmol) in ethanol (29 mL) was added 1,2-dichloroethane (78 mL) at room temperature, and the mixture was allowed to stand for 24 h at that temperature. After usual work-up, potassium *t*-butoxide (3.36 g, 30 mmol) was added to a THF (50 mL) solution of the crude oil obtained above, and it was stirred for 1 h at room temperature. Usual work-up of the reaction mixture followed by distillation gave the title compound (2.6 g, 60%) as a colorless oil: bp 115 °C (bath temp)/0.2 mmHg; IR(neat) 2910, 1585, 1475, 1390, 1250, 1100, 1020, 965, 895, 870, 820, 795, 770; NMR (CCl_4) 5.12 (dd, *J*=16 and 2Hz, 1H), 5.40 (dd, *J*=10 and 2 Hz, 1H), 6.30 (dd, *J*=16 and 10 Hz, 1H), 6.87—7.10 (m, 4H). Calcd for C_8H_7SeCl; C, 44.17; H, 3.24%. Found: C, 43.95; H, 3.18%.

Preparation of 1-Dodecenyl p-Chlorophenyl Selenoxide 3c. General Procedure for the Preparation of Vinyl Selenoxide. A solution of 1-dodecenyl *p*-chlorophenyl selenide (179 mg, 0.5 mmol) in dichloromethane (4 mL) was added to a solution of *m*-CPBA (152 mg of 85% pure material, 0.75 mmol) in 1 mL of dichloromethane. After allowed to stand for 30 min at room temperature, the reaction mixture was washed with satd aq $NaHCO_3$ and dried. Removal of the solvent from organic layer gave the title compound as a colorless oil (176 mg, 94%) which was homogeneous in tlc; IR (neat) 2905, 1980, 1470, 1090, 1015, 820, 730; NMR (CCl_4) 0.70—1.70 (m, 19H), 2.23—2.56 (m, 2H), 6.17—6.30 (m, 1H), 6.33—6.80 (m, 1H), 7.10—7.70 (m, 4H).

p-Chlorophenyl Vinyl Selenoxide 3a. IR (neat) 2890, 2830, 1590, 1570, 1470, 1390, 1360, 1175, 1090, 1020, 970, 940, 890, 830, 735; NMR(CCl_4) 6.03 (dd, *J*=9 and 1 Hz, 1H), 6.27 (dd, *J*=17 and 1 Hz, 1H), 6.93 (dd, *J*=17 and 9 Hz, 1H), 7.30—7.67 (m, 4H).

3-Benzyloxy-1-propenyl p-Chlorophenyl Selenoxide 3b. IR (neat) 2880, 1465, 1380, 1085, 1010, 820, 730, 695; NMR (CCl_4) 4.00 (unresolved s, $CH_2C_6H_5$), 4.13 (unresolved s, $CH_2C_6H_5$), 4.36—4.57 (m, 2H), 6.20 (unresolved s, 1H), 6.70 (unresolved s, 1H), 6.80—7.70 (m, 4H).

2-Decylcyclopropyl Phenyl Ketone 1c. General Procedure for the Reactions in Tables 1 and 2. A solution of acetophenone (66 mg, 0.55 mmol) in ether (3 mL) was added to a solution of lithium diisopropylamide (LDA) (0.75 mmol) in ether (2 mL) at −30 °C, and the mixture was stirred for 30 min at that temperature. An ethereal solution (5 mL) of 1-dodecenyl *p*-chlorophenyl selenoxide (164 mg, 0.44 mmol) was added to the solution of enolate, and it was stirred for 1 h at the same temperature. Then, after allowed to stand at room temperature for 5 h, the reaction mixture was washed with satd aq NaCl and dried. Removal of the solvent from organic layer followed by purification by preparative tlc gave the title compound (102 mg, 81%) as a colorless oil; bp 114 °C (bath temp)/0.04 mmHg; IR (neat) 1655; NMR (CCl_4) 0.60—1.80 (m, 24H), 2.10—2.50 (m, 1H), 7.25—7.50 (m, 3H), 7.65—8.00 (m, 2H). Calcd for $C_{20}H_{30}O$: C, 83.86; H, 10.56%. Found: C, 83.57; H, 10.47%.

Cyclopropyl Phenyl Ketone 1a. IR (neat) 1660; NMR (CCl_4) 0.50—1.70 (m, 4H), 2.35—2.85 (m, 1H), 7.00—7.60 (m, 5H). These spectroscopic properties were identical with those of the commercially available sample from Aldrich Chemical Co.

2-Benzyloxymethylcyclopropyl Phenyl Ketone 1b. IR (neat) 1660; NMR (CCl_4) 0.70—2.00 (m, 3H), 2.35—2.70 (m, 1H), 3.20—3.50 (m, 2H), 4.43 (s, 2H), 6.90—7.60 (m, 8H), 7.60—8.10 (m, 2H); mass spectrum *m/z* (relative %) 266 (M^+, 1), 234 (1), 160 (10), 145 (9), 115 (5), 105 (100), 91 (93), 77 (64), 65 (29), 51 (36).

** 1 mmHg=133.322 Pa

1-Methylcyclopropyl Phenyl Ketone **1d.** Bp 55 °C (bath temp)/0.2 mmHg; IR (neat) 1670; NMR (CCl_4) 0.50—1.70 (m, 7H including a singlet (3H) at 1.40), 7.10—7.55 (m, 3H), 7.55—7.90 (m, 2H). Calcd for $C_{11}H_{12}O$: C, 82.46; H, 7.54%. Found: C, 82.84; H, 7.55%.

2-Benzyloxymethyl-1-methylcyclopropyl Phenyl Ketone **1e.** IR (neat) 1670; NMR (CCl_4) 0.70—2.00 (m, 6H including a singlet (3H) at 1.40), 3.10—3.55 (m, 1H), 3.70—4.00 (m, 1H), 4.50 (s, 2H), 7.00—7.50 (m, 8H), 7.70—8.50 (m, 2H).

2-Decyl-1-methylcyclopropyl Phenyl Ketone **1f.** IR (neat) 1670; NMR (CCl_4) 0.70—1.80 (m, 27H), 7.20—7.50 (m, 3H), 7.50—7.80 (m, 2H); mass spectrum *m/z* (relative %) 300 (M^+, 12), 285 (2), 215 (2), 201 (9), 173 (14), 145 (4), 134 (12), 105 (100), 91 (9), 77 (27).

Ethyl 1-(Phenylthio)cyclopropanecarboxylate **1g.** Bp 85 °C (bath temp)/0.1 mmHg; IR (neat) 1705; NMR (CCl_4) 0.70—2.00 (m, 7H), 4.03 (q, J=9 Hz, 2H), 6.85—7.50 (m, 5H); Anal. Calcd for $C_{12}H_{14}O_2S$: C, 64.85; H, 6.35; S, 14.43%. Found: C, 65.18; H, 6.21; S, 14.43%.

Ethyl 2-Benzyloxymethyl-1-(phenylthio)cyclopropanecarboxylate. **1h.** Bp 135 °C (bath temp)/0.04 mmHg; IR (neat) 1705; NMR (CCl_4) 0.75—1.30 (m, 4H including a triplet (J=7 Hz, 3H) at 1.33), 1.55—2.50 (m, 2H), 3.40—3.80 (m, 2H), 4.00 (q, J=7 Hz, 2H), 4.30 (s, 2H), 6.70—7.40 (m, 10H). Calcd for $C_{20}H_{22}O_3S$: C, 70.16; H, 6.48; S, 9.37%. Found: C, 70.20; H, 6.43; S, 9.39%.

Ethyl 2-Decyl-1-(phenylthio)cyclopropanecarboxylate **1i.** IR (neat) 1705; NMR (CCl_4) 0.70—2.00 (m, 27H), 4.05 (q, J= 7 Hz, 2H), 7.13 (s, 5H).

1-(Benzyloxymethyl)spiro[2.11]pentadecan-4-one **1j.** IR (neat) 1670; NMR (CCl_4) 0.70—2.70 (m, 13H), 3.15—3.75 (m, 2H), 4.43 (unresolved s, 2H), 7.23 (unresolved s, 5H).

1-Decylspiro[2.4]octan-4-one **1k.** IR (neat) 1675; NMR (CCl_4) 0.70—2.10 (m, 32H).

t-*Butyl 2-Decylcyclopropyl Ketone* **1l.** Bp 87 °C (bath temp)/0.08 mmHg; IR (neat) 1680; NMR (CCl_4) 0.70—2.00 (m, 34H including a singlet (9H) at 1.10). Calcd for $C_{18}H_{34}O$: C, 81.13; H, 12.86%. Found: C, 81.10; H, 12.72%.

t-*Butyl 2-Decylcyclopropanecarboxylate* **1m.** Bp 86 °C (bath temp)/0.01 mmHg; IR (neat) 1715; NMR (CCl_4) 0.50—1.90 (m, 34H including a singlet (9H) at 1.30). Calcd for $C_{18}H_{34}O_2$: C, 76.54; H, 12.13%. Found: C, 76.29; H, 12.09%.

2-Decylcyclopropyl Isopropyl Ketone **1n.** IR (neat) 1680; NMR (CCl_4) 0.50—1.85 (m, 30H), 1.85—2.30 (m, 1H), 2.30—3.00 (m, 1H).

2-Decyl-1-(phenylthio)cyclopropyl Hexyl Ketone **1o.** IR (neat) 1680; NMR (CCl_4) 0.50—2.10 (m, 33H), 2.80 (t, J= 6 Hz, 2H), 7.10 (s, 5H); mass spectrum *m/z* (relative %) 388 (M^+, 15), 217 (12), 208 (6), 154 (18), 148 (12), 110 (65), 109 (41), 105 (29), 91 (59), 85 (32), 77 (35), 71 (53), 69 (53), 57 (100), 55 (82).

Ethyl 2-Decyl-1-(phenylsulfinyl)cyclopropanecarboxylate **1p.** IR (neat) 1725, 1710; NMR (CCl_4) 0.50—2.00 (m, 27H), 4.03 (q, J=6 Hz, 2H), 7.00—7.83 (m, 5H).

Ethyl 2-Decyl-1-(phenylsulfonyl)cyclopropanecarboxylate **1q.** IR (neat) 1720; NMR (CCl_4) 0.50—2.20 (m, 27H), 4.07 (q, J= 6 Hz, 2H), 7.17—8.00 (m, 5H).

Diethyl 2-Decyl-1,1-cyclopropanedicarboxylate **1r.** Bp 110 ° C (bath temp)/0.03 mmHg; IR (neat) 1720; NMR (CCl_4) 0.67—1.83 (m, 30H), 4.13 (q, J=6 Hz, 4H); mass spectrum *m/z* (relative %) 281 (M^+−45, 13), 253 (17), 235 (7), 173 (73), 160 (100), 127 (93), 108 (27), 99 (33), 95 (27), 81 (23), 74 (40), 59 (73), 55 (53). Calcd for $C_{19}H_{34}O_4$: C, 69.90; H, 10.50%. Found: C, 69.67; H, 10.41%.

1-(Benzyloxymethyl)spiro[2.5]oct-5-en-4-one **1s.** IR (neat) 1665; NMR (CCl_4) 0.70—2.70 (m, 7H), 3.15—3.80 (m, 2H), 4.35—4.70 (m, 2H), 5.80—6.25 (m, 1H), 6.70—7.60 (m, 6H).

1-(2-Benzyloxymethylcyclopropyl)-3-(2,6,6-trimethyl-1-cyclohexenyl)-2-propen-1-one **1t.** IR (neat) 1670; NMR (CCl_4) 0.70—2.25 (m, 19H including singlets at 1.03 and 1.76), 3.35 (m, 2H), 4.17 (s, 2H), 4.13 (d, J=16 Hz, 1H), 7.17 (s, 5H), 7.23 (d, J=16 Hz, 1H).

4,7,7-Trimethylspiro[bicyclo[2.2.1]heptan-2,1'-cyclopropan]-3-one **1u.** IR (neat) 1720; NMR (CCl_4) 0.50—2.33 (m, 18H including three methyl singlets at 0.83, 0.87, and 0.97); mass spectrum *m/z* (relative %) 178 (M^+, 13), 162 (17), 135 (25), 109 (29), 95 (100), 83 (33), 74 (33), 69 (42), 59 (54), 55 (42).

1-Hexenyl Phenyl Selenone. General Procedure for the Preparation of Vinyl Selenones **6.** To a solution of 1-phenylseleno-1-hexene (1.50 g, 6.3 mmol) in methanol (20 mL) was added *m*-CPBA (2.8 g, 14 mmol) at 0 °C, and it was stirred overnight at room temperature. After the solvent was removed *in vacuo*, satd aq $NaHCO_3$ was added and it was extracted with chloroform. The combined extracts were dried and concentrated to give an oil, which was purified by column chromatography (hexane:ethyl acetate=1:1) to afford the title compound (1.30 g, 76%); IR (neat) 935, 885; NMR (CCl_4) 0.60—1.85 (m, 7H), 2.05—3.00 (m, 2H), 6.30—7.30 (m, 2H), 7.35—8.15 (m, 5H).

Dimethyl 2-Butyl-1,1-cyclopropanedicarboxylate **7a.** *General Procedure for an Olefin Unit Transfer to Active Methylene Compounds in Table 3.* To a suspension of NaH (0.33 mmol) in THF (0.5 mL) was added dimethyl malonate (48 mg, 0.37 mmol) at 0 °C and it was stirred for 10 min at that temperature. Then, a THF (1.0 mL) solution of 1-hexenyl phenyl selenone (83 mg, 0.30 mmol) was added to the resulting mixture, and it kept stirring 4 h at room temperature. The reaction mixture was quenched with water and the aqueous layer was extracted with ether. The combined extracts were washed with satd aq NaCl, dried over anhyd $MgSO_4$, and then concentrated to give an oil, which was purified by column chromatography to afford the title compound (60.0 mg, 92%); bp 62—64 °C (bath temp)/0.012 mmHg; IR (neat) 1710; NMR (CCl_4) 0.65—2.10 (m, 12H), 3.62 (s, 6H). Calcd for $C_{11}H_{18}O_4$: C, 61.66; H, 8.47%. Found: C, 61.40; H, 8.54%.

Methyl 1-Acetyl-2-butylcyclopropanecarboxylate **7b.** Bp 85 °C (bath temp)/9 mmHg; IR (neat) 1710; NMR (CCl_4) 0.60—2.15 (m, 12H), 2.26 (s, 3H), 3.69 (s, 3H). Calcd for $C_{11}H_{18}O_3$: C, 66.64; H, 9.15%. Found: C, 66.57; H, 9.11%.

N-t-*Butyl-1-acetyl-2-butyl-1-cyclopropanecarboxamide* **7c.** Two stereoisomers (**A** and **B**) were isolated. **A**; IR (neat) 3280, 1650; NMR (CCl_4) 0.65—1.65 (m, 12H), 1.30 (s, 9H), 2.14 (s, 3H), 6.70 (br s, 1H); Anal. Calcd for $C_{14}H_{25}NO_2$: C, 70.25; H, 10.53; N, 5.85. Found: C, 70.17; H, 10.43; N, 6.03. **B**; IR (neat) 3280, 1650; NMR (CCl_4) 0.60—1.70 (m, 12H), 1.33 (s, 9H), 2.01 (s, 3H), 7.38 (br s, 1H).

Methyl 2-Butyl-1-cyanocyclopropanecarboxylate **7d.** Bp 53—57 °C (bath temp)/0.012 mmHg; IR (neat) 2230, 1730; NMR (CCl_4) 0.70—2.10 (m, 12H), 3.74 (s, 3H). Calcd for $C_{10}H_{15}NO_2$: C, 66.27; H, 8.34; N, 7.73%. Found: C, 65.94; H, 8.31; N, 7.52%.

1-Butyl-2-nitrocyclopropane **7e.** Bp 80 °C (bath temp)/9 mmHg; IR (neat) 1530; NMR (CCl_4) 0.60—2.05 (m, 12H), 3.87 (m, 1H). Calcd for $C_7H_{13}O_2N$: C, 58.72; H, 9.15; N, 9.78%. Found: C, 58.94; H, 9.34; N, 9.72%.

2-Butyl-1-(phenylthio)cyclopropyl Methyl Ketone **7f.** Bp 110 °C (bath temp)/3 mmHg; IR (neat) 1685; NMR (CCl_4) 0.65—2.15 (m, 12H), 2.31 (s, 3H), 6.85—7.20 (m, 5H). Calcd for $C_{15}H_{20}OS$: C, 72.54; H, 8.12; S, 12.91%. Found: C, 72.45; H, 7.88; S, 12.96%.

Ethyl 2-Butyl-1-(phenylthio)cyclopropanecarboxylate **7g.** Bp 140 °C (bath temp)/3 mmHg; IR (neat) 1708; NMR (CCl_4) 0.68—2.10 (m, 15H), 4.06 (q, J=7 Hz, 2H), 6.87—7.50 (m, 5H). Calcd for $C_{16}H_{22}O_2S$: C, 69.03; H, 7.96; S, 11.52%. Found: C, 68.80; H, 7.92; S, 11.07%.

Diethyl 2-[(1-Hydroxycyclohexyl)methyl]-1,1-cyclopropanedicarboxylate **7h.** To a THF (0.3 mL) solution of lithio

diethyl malonate prepared from diethyl malonate (26.4 mg, 0.17 mmol) and butyllithium (0.11 mL of 1.57 M hexane solution, 0.17 mmol) was added a THF (0.3 mL) solution of 1-(3-phenylselenonyl-1-propenyl)-1-cyclohexanol (45.1 mg, 0.14 mmol), and it was stirred for 4 h at room temperature. Then, the reaction mixture was quenched with water, and the aqueous layer was extracted with ethyl acetate. The combined extracts were washed with satd aq NaCl and were dried over anhyd $MgSO_4$. Removal of the solvent followed by purification with column chromatography afforded the title compound (29.6 mg, 72%); bp 114 °C (bath temp)/0.08 mmHg; IR (neat) 3475, 1724; NMR (CCl_4) 1.0—2.2 (m, 22H), 4.07 (q, J=7.0 Hz, 4H). Calcd for $C_{16}H_{26}O_5$: C, 64.40; H, 8.76%. Found: C, 64.23; H, 8.81%.

Dimethyl 2-(4-Hydroxynonyl)-1,1-cyclopropanedicarboxylate **7i**. Bp 120 °C (bath temp)/0.019 mmHg; IR (neat) 3350, 1710; NMR (CCl_4) 0.65—1.95 (m, 21H), 3.20—3.55 (br s, 1H), 3.59 (s, 6H). Calcd for $C_{16}H_{28}O_5$: C, 63.97; H, 9.39%. Found: C, 63.90; H, 9.47%.

Dimethyl 2-(4-Oxononyl)-1,1-cyclopropanedicarboxylate **7j**. Bp 114 °C (bath temp)/0.013 mmHg; IR (neat) 1705; NMR (CCl_4) 0.65—1.90 (m, 16H), 2.10—2.50 (m, 4H), 3.58 (s, 3H), 3.61 (s, 3H). Calcd for $C_{16}H_{26}O_5$: C, 64.41; H, 8.78%. Found: C, 64.28; H, 8.75%.

Dimethyl 2-(9-Oxotridecyl)-1,1-cyclopropanedicarboxylate **7k**. Bp 134 °C (bath temp)/0.024 mmHg; IR (neat) 1720, 1705; NMR (CCl_4) 0.70—1.85 (m, 24H), 2.10—2.45 (m, 4H), 3.60 (s, 6H). Calcd for $C_{20}H_{34}O_5$: C, 67.77; H, 9.67%. Found: C, 67.83; H, 9.96%.

Dimethyl 2-(8-Methoxycarbonyloctyl)-1,1-cyclopropanedicarboxylate **7l**. Bp 116 °C/0.015 mmHg; IR (neat) 1725; NMR (CCl_4) 1.05—2.35 (18H), 2.83 (s, 3H), 2.93 (s, 6H). Calcd for $C_{17}H_{28}O_6$: C, 62.18; H, 8.59%. Found: C, 62.36; H, 8.45%.

Dimethyl 2-(4-Methoxycarbonyloctyl)-1,1-cyclopropanedicarboxylate **7m**. Bp 138 °C/0.14 mmHg; IR (neat) 1725; NMR (CCl_4) 0.70—2.30 (m, 22H), 3.62 (s, 6H), 3.98 (q, J=7.0 Hz, 2H). Calcd for $C_{18}H_{30}O_6$: C, 63.14; H, 8.83%. Found: C, 63.00; H, 8.75%.

Dimethyl 2-(5,6-Epoxy-2,6-dimethylheptyl)-1,1-cyclopropanedicarboxylate **7n**. Bp 96 °C (bath temp)/0.02 mmHg; IR (neat) 1735; NMR (CCl_4) 0.75—1.95 (m, 18H), 2.30—2.50 (m, 1H), 3.58 (s, 6H). Calcd for $C_{16}H_{26}O_5$: C, 64.41; H, 8.78%. Found: C, 64.63; H, 8.84%.

This work is supported by a Grant-in-Aid from the Ministry of Education, Science, and Culture of Japanese Government.

References

1) G. Stork and M. Marx, *J. Am. Chem. Soc.*, **91**, 2371 (1969); G. Stork and M. Gregson, *ibid.*, **91**, 2373 (1969); G. Stork and P. A. Grieco, *ibid.*, **91**, 2407 (1969); E. J. Corey and R. D. Balanson, *Tetrahedron Lett.*, **1973**, 3153.

2) S. Danishefsky, *Acc. Chem. Res.*, **12**, 66 (1979); R. V. Stevens, *Pure Appl. Chem.*, **51**, 1317 (1979).

3) J. Gosselck, L. Beress, and H. Schenk, *Angew. Chem.*, **78**, 606 (1966); J. Gosselck, H. Ahlbrecht, F. Dost, H. Schenk, and G. Schmidt, *Tetrahedron Lett.*, **1968**, 995; G. Schmidt and J. Gosselck, *ibid.*, **1969**, 3445.

4) C. R. Johnson and P. J. Lockard, *Tetrahedron Lett.*, **1971**, 4589.

5) K. Takaki and T. Agawa, *J. Org. Chem.*, **42**, 3303 (1977); K. Takaki, K. Negoro, and T. Agawa, *J. Chem. Soc., Perkin Trans I*, **1979**, 1490.

6) G. A. Russel and H.-D. Becker, *J. Am. Chem. Soc.*, **85**, 3406 (1963); G. Tsuchihashi, S. Mitamura, S. Inoue, and K. Ogura, *Tetrahedron Lett.*, **1973**, 323; G. A. Koppel and M. D. Kinnick, *J. Chem. Soc., Chem. Commun.*, **1975**, 473; G. Tsuchihashi, S. Mitamura, and K. Ogura, *Tetrahedron Lett.*, **1976**, 855.

7) a) M. Sevrin, W. Dumont, and A. Krief, *Tetrahedron Lett.*, **1977**, 3835. Benzeneseleninyl group stabilized carbanions undergo several versatile reactions: b) H. J. Reich and S. K. Shah, *J. Am. Chem. Soc.*, **97**, 3250 (1975); c) H. J. Reich and F. Chow, *J. Chem. Soc., Chem. Commun.*, **1975**, 790; d) H. J. Reich, S. K. Shah, and F. Chow, *J. Am. Chem. Soc.*, **101**, 6648 (1979).

8) D. N. Jones, D. Mundy, and R. D. Whitehouse, *J. Chem. Soc., Chem. Commun.*, **1970**, 86; R. Walter and J. Roy, *J. Org. Chem.*, **36**, 2561 (1971); D. L. J. Clive, *J. Chem. Soc., Chem. Commun.*, **1973**, 695; K. B. Sharpless, M. W. Young, and R. F. Lauer, *Tetrahedron Lett.*, **1973**, 1979; H. J. Reich, I. L. Reich, and J. M. Renga, *J. Am. Chem. Soc.*, **95**, 5813 (1973).

9) For recent reviews: D. L. J. Clive, *Tetrahedron*, **34**, 1049 (1978); H. J. Reich, *Acc. Chem. Res.*, **12**, 22 (1979).

10) H. J. Reich and W. W. Willis, Jr., *J. Am. Chem. Soc.*, **102**, 5967 (1980).

11) P. Nylen, *Z. Anorg. Allg. Chem.*, **246**, 227 (1941).

12) M. Shimizu and I. Kuwajima, *J. Org. Chem.*, **45**, 2921 (1980).

13) I. Kuwajima, R. Ando, and T. Sugawara, *Tetrahedron Lett.*, **24**, 4429 (1983).

14) a) S. Raucher, *J. Org. Chem.*, **42**, 2950 (1977); b) S. Raucher and G. A. Koolpe, *ibid.*, **43**, 3794, 4252 (1978); c) S. Raucher, M. R. Hansen, and M. A. Colter, *ibid.*, **43**, 4885 (1978).

15) For other preparation see: H. J. Reich and F. Chow, *J. Chem. Soc., Chem. Commun.*, **1975**, 790; J. Hooz and R. Rodrigues, *Tetrahedron Lett.*, **1976**, 805; N. Petragnani, R. Rodrigues, and J. V. Comassetto, *J. Organomet. Chem.*, **114**, 281 (1976); B.-T. Grobel and D. Seebach, *Chem. Ber.*, **110**, 852 (1977); B. Harirchian and P. Magnus, *J. Chem. Soc., Chem. Commun.*, **1977**, 522, and Ref. 7c.

16) K. B. Sharpless and M. W. Young, *J. Org. Chem.*, **40**, 47 (1975); P. A. Grieco, Y. Masaki, and D. Boxler, *J. Am. Chem. Soc.*, **95**, 1579 (1975); P. A. Grieco, J. A. Noguez, and Y. Masaki, *Tetrahedron Lett.*, **1975**, 4213; H. J. Reich, J. M. Renga, and I. L. Reich, *J. Am. Chem. Soc.*, **97**, 5434 (1975).

17) L. Velluz, J. Martel, and G. Namine, *C. R. Acad. Sci. Ser. C*, **268**, 2199 (1965); J. Martel and C. Huynh, *Bull. Soc. Chim. Fr.*, **1967**, 985; M. Julia and A. Guy-Rouault, *ibid.*, **1967**, 1411; R. V. M. Campbell, L. Crombie, and G. Pattenden, *J. Chem. Soc., Chem. Commun.*, **1971**, 218; L. Crombie, D. A. R. Findley, and D. A. Whiting, *ibid.*, **1972**, 1045.

18) R. M. Cory, D. M. T. Chan, Y. M. A. Naguib, M. H. Rastall, and R. M. Renneboog, *J. Org. Chem.*, **45**, 1852 (1980).

19) R. M. Cory and R. M. Renneboog, *J. Chem. Soc., Chem. Commun.*, **1980**, 1081.

20) a) M. Shimizu and I. Kuwajima, *J. Org. Chem.*, **45**, 4063 (1980); b) M. Shimizu, R. Ando, and I. Kuwajima, *ibid.*, **46**, 5246 (1981); c) M. Shimizu, R. Ando, and I. Kuwajima, *ibid.*, **49**, 1230 (1984).

21) a) B. W. Peace and D. S. Wulfman, *Synthesis*, **1973**, 137; b) T. Livinghouse and R. V. Stevens, *J. Am. Chem. Soc.*, **100**, 6479 (1978); c) J. Cuffe, R. J. Gillwspie, and E. A. Porter, *J. Chem. Soc., Chem. Commun.*, **1978**, 641; d) N. Kawabata and M. Tanimoto, *Tetrahedron*, **36**, 3517 (1980); e) J. Ohishi, *Synthesis*, **1980**, 690; f) A. Nakamura, A. Konishi, Y. Tatsuno, and S. Otsuka, *J. Am. Chem. Soc.*, **100**, 3443, 3449 (1978).

22) J. N. Denis, J. Vincens, and A. Krief, *Tetrahedron Lett.*, **1979**, 2697.

23) On α-deprotonation of vinyl selenides see: H. J. Reich, W. W. Willis, Jr., and P. D. Clark, *J. Org. Chem.*, **46**, 2775 (1981), and Ref 14b.

24) E. J. Corey and M. Chaykovsky, *J. Am. Chem. Soc.*, **87**, 1353 (1965).

25) J. P. Freeman, *J. Org. Chem.*, **31**, 538 (1966); P. A. Grieco and R. S. Finkelhor, *Tetrahedron Lett.*, **1972**, 3781; W. G. Dauben, D. J. Hart, J. Ipaktschi, and A. P. Kosikowski, *ibid.*, **1973**, 4425; R. F. Heldeweg, H. Hogeveen, and E. P. Schudde, *J. Org. Chem.*, **43**, 1912 (1978); M. J. Devos, J. N. Denis, and A. Krief, *Tetrahedron Lett.*, **1978**, 1847; **1979**, 1511, 1515.

26) W. W. Lotz and J. Gosselck, *Tetrahedron Lett.*, **1973**, 29, 917.

27) H. E. Simmons, T. L. Cairns, S. A. Vladuchick, and C. M. Hoiness, *Org. Reactions*, **20**, 1 (1973).

 © 1984 The Chemical Society of Japan Bull. Chem. Soc. Jpn., 57, 2905—2909 (1984)

The Electronic Spectrum of Diphenylhexatriyne. The Interaction of Mutually Perpendicular π and π′ Systems

Michio KOBAYASHI,* Toshihiko HOSHI,† Jun OKUBO,† Hiroshi HIRATSUKA,†† Toshie HARAZONO,††
Masazumi NAKAGAWA,††† and Yoshie TANIZAKI

Department of Materials Science and Technology, Technological University of Nagaoka, Nagaoka-shi 949-54
†*Department of Chemistry, College of Science and Engineering, Aoyama Gakuin University, Chitosedai, Setagaya-ku, Tokyo 157*
††*Department of Chemistry, Tokyo Institute of Technology, Meguro-ku, Tokyo 152*
†††*Department of Chemistry, Faculty of Science, Osaka University, Toyonaka-shi, Osaka 560*
(Received January 30, 1984)

The electronic absorption spectrum of diphenylhexatriyne has been divided into two components polarized along the long and the short molecular axes by means of dichroism analysis using the stretched-polymer-film technique; *i.e.*, a reduced polarization spectrum has been obtained. This reduced polarization spectrum can be explained by a modified PPP calculation including the interaction between mutually perpendicular π and π′ systems in the conjugated system. It has been clarified that the relative intensities of the first and second bands of diphenylhexatriyne reflect the magnitude of interaction between mutually perpendicular π and π′ systems, which is quite great. The magnitude of the electron-repulsion integral between π and π′ electrons is estimated to be about 20—30 per cent of that between ordinary π (or π′) electrons.

Armitage *et al.* synthesized a series of diphenylpolyynes (Ph-(C≡C)$_n$-Ph) and determined the electronic and vibrational absorption spectra.[1] They have shown that the Lewis-Calvin equation,[2] $\lambda^2=kn$, should be kept for the wavelength (λ) of the first band and the number (n) of polyynes, as in the case of polyenes, and, moreover, that the second bands increase in intensity as n increases, while the first bands become less intense. On the other hand, for the case of polyynes with terminal groups other than phenyl, Akiyama *et al.* found relationships different from the above equation between λ and n, depending on the kinds of terminal groups.[3] As has been mentioned above, studies of the electronic spectra of the polyynes have been concerned merely with phenomenological interpretations. In order to obtain more detailed information on the electronic structures and spectra of the conjugated polyynes, we measured a polarized absorption spectrum of diphenylhexatriyne using the stretched-polymer-film technique[4,5] and performed a modified PPP calculation which includes the interaction between mutually perpendicular π and π′ systems in the conjugated system including conjugated triple bonds.

Experimental

Diphenylhexatriyne was synthesized by the method described previously.[3] The polarized absorption spectrum in a stretched poly(vinyl alcohol)(PVA) film was measured in a way described elsewhere.[6] In the figure of the polarized absorption spectrum, $D_{\parallel}$ and $D_{\perp}$ denote the optical densities for the polarized-light beams, whose electric vectors are parallel to and perpendicular to the stretched direction of the PVA film respectively. The dichroic ratio (R_d) is defined as $R_d=D_{\parallel}/D_{\perp}$. R_s is the stretching ratio of the film.

Theoretical

In a PPP approximation,[7,8] each atom is considered to offer only one atomic p orbital for conjugation. It is, therefore, impossible to treat simultaneously the $\pi(2p_x)$ and $\pi'(2p_y)$ conjugated systems, which are contained, for example, in diphenylhexatriyne, by the conventional PPP method. This is because the π and π′ systems are mutually perpendicular, as is shown below, where both terminal phenyl rings are on the same plane. π means an ordinary conjugated system delocalized over the whole molecule, and π′, another conjugated system localized on the conjugated triple bonds of the hexatriyne moiety.

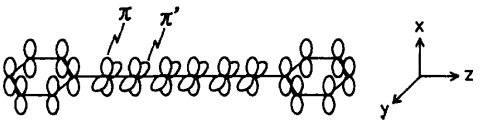

Thus, a modified PPP calculation which includes both π and π′ systems should be performed.[9] In this calculation, the interaction of π and π′ systems is taken into account in terms of the electron-repulsion integrals $(\pi_{2p}(r)\pi_{2p}(r)|\pi'_{2p}(s)\pi'_{2p}(s))$ between π and π′ electrons, the magnitudes of which are estimated by means of this equation;

$$(\pi_{2p}(r)\pi_{2p}(r)\,|\,\pi'_{2p}(s)\pi'_{2p}(s))=(\pi_{2p}(r)\pi_{2p}(r)\,|\,\pi'_{2p}(s)\pi'_{2p}(s))_0\times F.$$

Here, F is a parameter to be evaluated semiempirically, and $\pi_{2p}(r)$ and $\pi'_{2p}(s)$ stand for 2p atomic orbitals on the r and s atoms respectively. The values of the atomic integrals $(\pi_{2p}(r)\pi_{2p}(r)\,|\,\pi'_{2p}(s)\pi'_{2p}(s))_0$ are evaluated by assuming, after the manner of the CNDO/2 method,[15] that $(\pi_{2p}(r)\pi_{2p}(r)\,|\,\pi'_{2p}(s)\pi'_{2p}(s))_0=(\pi_{2p}(r)\pi_{2p}(r)\,|\,\pi_{2p}(s)\pi_{2p}(s))_0$. Here, the values of the atomic integrals $(\pi_{2p}(r)\pi_{2p}(r)\,|\,\pi_{2p}(s)\pi_{2p}(s))_0$ are obtained by the semiempirical method ordinarily used.[8,10] The resonance integrals between π_{2p} and π'_{2p} are all neglected, while those between 2p atomic orbitals within the π or π′ system are estimated using the variable β method.[11]

Results and Discussion

Figures 1 and 2 show the absorption spectra of diphe-

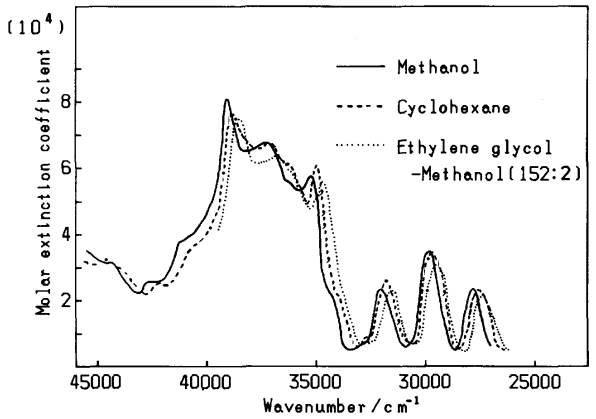

Fig. 1. Absorption spectra of diphenylhexatriyne in various solvents.

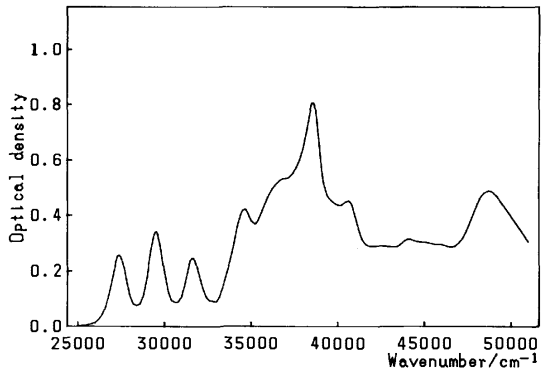

Fig. 2. Absorption spectrum of diphenylhexatriyne in the unstretched PVA film.

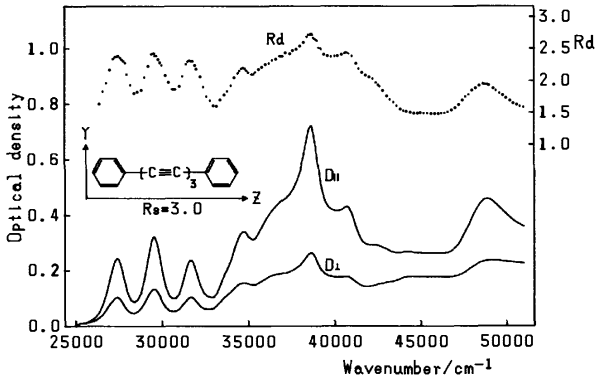

Fig. 3. The polarized absorption spectrum of diphenylhexatriyne in the stretched PVA film at room temperature.

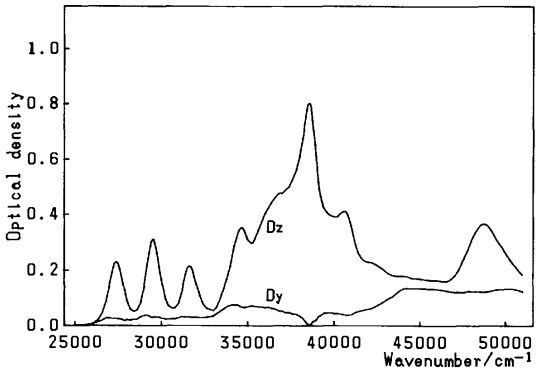

Fig. 4. The reduced polarization spectrum of diphenylhexatriyne.

nylhexatriyne in various solvents and in the unstretched PVA film respectively. The comparison of these two figures reveals that the peculiar band contour of the intense peaks in the range of 34000—41000 cm^{-1} in the PVA film is significantly different from that of the corresponding band peaks in the other solvents. This may be due to something like the Shpol'skii effect,[12,13] which is usually observed in *n*-paraffine matrices and which gives rise to very fine vibrational structures. The band peaks concerned are, therefore, considered to be members of a vibrational progression of the purely single electronic absorption band, whose 0-0 transition is at 34600 cm^{-1}. The first three peaks in the range of 27000—33000 cm^{-1} are, judging from the regularities in their shapes and positions, also considered to be members of a vibrational progression of the 27400-cm^{-1} electronic transition. These considerations are supported by the results of the modified PPP calculation discussed below; *i.e.*, there are only two allowed electronic transitions that can be assigned to the band peaks in the range of 27000—41000 cm^{-1}.

Figure 3 shows the polarized $S_n \leftarrow S_0$ absorption spectrum of diphenylhexatriyne in the stretched PVA film. In the spectrum of this compound, as has been discussed above, there are two electronic band systems whose 0-0 transitions are at 27400 and 34600 cm^{-1}. In Fig. 3, an additional electronic band is obvious at 48800 cm^{-1}. It is known that molecules adsorbed in the PVA film have a tendency that the molecular long axis inclines, on uniaxial stretching of the film, preferentially to the stretching direction of the film. Thereby, R_d values for a long-axis-polarized band are high, while those for a short-axis-polarized one are low. The R_d curve is high and takes a peak at the position of each 0-0 transition, indicating that the transitions at 27400, 34600, and 48800 cm^{-1} are polarized along the long axis (Z) of the molecule. The R_d value is highest for the most intense peak at 38600 cm^{-1}, which indicates that the intense peak at 38600 cm^{-1} may be regarded as being due purely to a longer-molecular-axis-polarized transition. Thus, taking this R_d value as a standard, the absorption spectrum of diphenylhexatriyne measured in the unstretched PVA film (Fig. 2) has been divided into two components polarized along the long (Z) and short (Y) axes by means of dichroism analysis.[4] That is, a reduced polarization spectrum has been obtained (Fig. 4). It is evident from this figure that the vibrational progressions of the two band systems, the one in the range of 27000—33000 cm^{-1}, and the other, in that of 34000—41000 cm^{-1}, and the band at 48800 cm^{-1} are all indeed polarized along the long axis of the molecule. This figure also shows that the short-axis-polarized bands are at 44000 cm^{-1} and at around 50000 cm^{-1}. Besides, a long-axis-polarized band might exist around 45000 cm^{-1}. These observations are summarized in the right column of Table 1.

In order to explain the above experimental results,

TABLE 1. COMPARISON OF THE CALCULATED AND OBSERVED RESULTS

Calc. 1				Calc. 2 F=0.0				Calc. 3 F=1.0				Calc. 4 F=0.2				Obs.			
	T.E. (cm^{-1})	f	Po.		T.E. (cm^{-1})	f	Po.		T.E. (cm^{-1})	f	Po.		T.E. (cm^{-1})	f	Po.	T.E. (cm^{-1})	f	Po.
S_1, $^1B_{1u}$	26100	2.237	Z	S_1, $^1B_{1u}$	26200	2.248	Z	S_1, $^1B_{1u}$	12300	0.057	Z	S_1, $^1B_{1u}$	25300	1.250	Z	27400	0.478	Z
⋮				⋮				⋮				⋮						
				S_4, $^1B_{1u}$	35000	1.366	Z	S_9, $^1B_{1u}$	35100	2.964	Z	S_4, $^1B_{1u}$	35100	2.589	Z	34600	1.980	Z
⋮				⋮				⋮				⋮						
S_8, $^1B_{2u}$	43000	0.475	Y	S_8, $^1B_{2u}$	43100	0.495	Y	S_{15}, $^1B_{2u}$	43100	0.495	Y	S_8, $^1B_{2u}$	43100	0.495	Y	44000		Y
S_9, $^1B_{1u}$	43500	0.008	Z	S_9, $^1B_{1u}$	43500	0.009	Z	⋮				⋮						
⋮				⋮				S_{19}, $^1B_{1u}$	45600	0.578	Z	S_{10}, $^1B_{1u}$	43900	0.182	Z	45000		Z
S_{14}, $^1B_{1u}$	49600	0.147	Z	S_{16}, $^1B_{1u}$	49800	0.154	Z	⋮				⋮						
S_{15}, $^1B_{1u}$	50100	0.750	Z	S_{17}, $^1B_{1u}$	50400	0.840	Z	S_{27}, $^1B_{1u}$	47800	0.719	Z	S_{18}, $^1B_{1u}$	49700	0.374	Z	48800		Z
⋮				⋮				⋮				⋮						
S_{18}, $^1B_{2u}$	53200	1.262	Y	S_{22}, $^1B_{2u}$	53300	1.239	Y	S_{35}, $^1B_{2u}$	53300	1.239	Y	S_{20}, $^1B_{1u}$	50700	0.406	Z			
⋮				⋮				⋮				⋮						
												S_{22}, $^1B_{2u}$	53300	1.239	Y	50000		Y

T.E.: Transition energy. f: Oscillator strength. Po: Polarization. Y: The short axis in the molecular plane. Z: The long axis in the molecular plane.

a standard PPP calculation, in which only the π system is included, has been carried out. The calculated results can not, however, explain the above experimental results; *i.e.*, the observed 34600 cm^{-1} band can not be reproduced by this calculation (Table 1, Calc. 1). Thus, we performed a modified PPP calculation, including both π and π′ systems. The calculated results are shown in Table 1 (Calc. 2—4). The calculated transition energies and polarizations of Calc. 2, in which 0.0 is used for the value of the parameter F, well explain the observed results. However, the calculated intensity of the first-band transition is too large compared to the observation. As a result, the relative intensity of the second-band transition with respect to that of the first one can not be explained by this calculation; *i.e.*, the calculated intensity for the second transition is smaller than that for the first one, while the observed intensity for the second band is three or four times greater than that for the first one. This may be due to the fact that the interaction between π and π′ systems is neglected in Calc. 2. That is, if there is no interaction between the π system (diphenylhexatriene) and the π′ system (hexatriene), their first transitions should remain unchanged to give the first and second transitions of the united (π+π′) system (diphenylhexatriyne). If this is the case, since the conjugation of the π system is longer than that of the π′ system, and since the first transitions of both systems are polarized along the long axis, the transition energy and the transition moment for the first transition of the π system are, respectively, smaller and larger than those of the π′ system. These values are represented diagrammatically in Fig. 5 as the positions and magnitudes of the transition moment. It is, therefore, a natural result in the case of Calc. 2 that the calculated intensity for the second band of the (π+π′) system, which stems from the π′ system, is smaller than that for the first band of the (π+π′), from the π system.

However, the interaction of π and π′ systems changes the intensities (transition moments) of the first and second transitions of the (π+π′) system, as is shown in Fig. 5. In this figure, the first transition moment of the π system (diphenylhexatriene) has been made to interact with that of π′ (hexatriene) to give the combined first and second transition moments of the (π+π′) system (diphenylhexatriyne). This type of interaction between the transition moments affects only the energy levels of the excited states; the result is that the lower lying $\psi_1^0(\pi\pi^*)$ energy level is stabilized, while the upper lying $\psi_1^0(\pi'\pi'^*)$ one is destabilized. In other words, in the transition-energy scale in Fig. 5, the location of the large transition-moment vector of the π system is lowered *via* the interaction with the upper-lying, moderately large transition-moment vector of the π′ system, with their vectors being opposite in direction. As a result, the two vectors are cancelled in part, resulting in a small transition moment, *i.e.*, a weak electronic transition for the first transition of the (π+π′) system. On the other hand, the moderately large transition-moment vector of the π′ system is heightened *via* the interaction with the lower-lying large transition-moment vector of the π system, with the two vectors being the same in direction. This destabilization is small, since the transition moment concerned is also interacting with the upper-lying transition moment of π. The sum of the two vectors results, therefore, in a very large transition moment, *i.e.*, a very strong electronic transition for the second transition of the (π+π′) system.

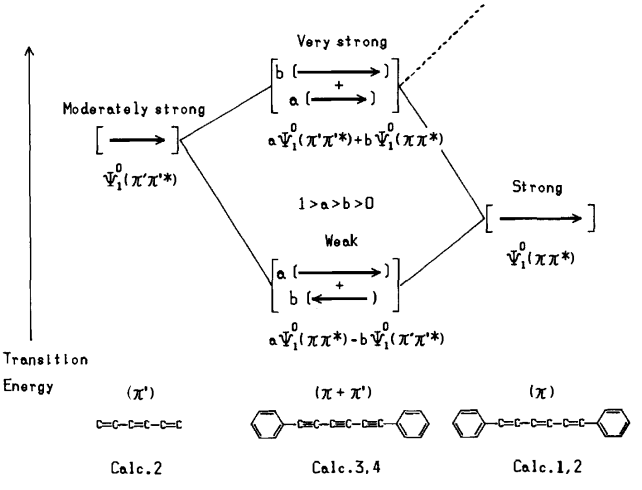

Fig. 5. The interaction of the first transition-moment vectors of the π and π′ systems, which gives the first and second transition-moment vectors of the united (π+π′) system.

TABLE 2. RESULTS OF THE CONFIGURATION ANALYSIS IN WEIGHT PER CENT

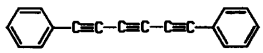

		ψ_G A_g	ψ_1 B_{1u} 27400*	ψ_2 B_{2u}	ψ_3 B_{3g}	ψ_4 B_{1u} 34600*	ψ_5 A_g	...	ψ_8 B_{2u} 44000*	ψ_9 B_{1u}	ψ_{10} B_{1u} 45000*	ψ_{11} A_u	...	ψ_{18} B_{1u} 48800*	ψ_{19} A_g	...	ψ_{22} B_{2u} 50000*
	ψ_G^0 A_g	100															
	ψ_1^0 B_{1u}		91.7			8.0											
	ψ_2^0 B_{2u}			100													
	ψ_3^0 B_{3g}				100												
	ψ_7^0 B_{2u}								100								
	ψ_8^0 B_{1u}					4.0					95.8						
	ψ_9^0 B_{1u}									100							
	ψ_{13}^0 A_g																
	ψ_{14}^0 B_{1u}												95.9				
	ψ_{15}^0 B_{1u}					1.1							2.8				
	ψ_{16}^0 B_{3g}																
	ψ_{17}^0 B_{2u}																100
	ψ_{18}^0 A_g													30.4			
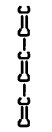	ψ_1^0 B_{1u}		7.9			86.1					3.7						
	ψ_2^0 A_g																
	ψ_3^0 A_g						3.2							42.9			

ψ_i: The total wavefunction of diphenylhexatriyne. ψ_i^0: The total wavefunction of the reference molecule.
*: The observed transition energy in wave number.

Thus, the relative intensities of the first and second bands of diphenylhexatriyne reflect the magnitude of the interaction between the π and π' systems. That is, the fact that the intensity of the second-band system is larger than that of the first-band system implies that there is a considerable interaction between the π and π' systems. The magnitude of the interaction between the two π systems is controlled by the magnitude of the parameter F used in the equation to obtain the electron-repulsion integral between π and π' electrons, and it is manifested by the mixing coefficients a and b given in Fig. 5. For zero interaction (F=0.0), a=1 and b=0. For non-zero interaction (F>0.0), the relation $1>a>b>0$ holds ($a^2+b^2=1$).

The calculated results for a large interaction (Calc. 3, F=1.0) deviate greatly from the observed results as to the location and intensity of the first transition. That is, the first transition moment of diphenylhexatriyne is stabilized too much and cancelled to an excessive degree. The appropriate value of the parameter F is 0.2—0.3 (Calc. 4), which yields reasonable intensities for the first and second transitions. The evaluation of the parameter F has already been discussed elsewhere.[9] In the CNDO/2 method, F is regarded as 1.0.[15] The results of Calc. 4 reproduce the observed spectrum fairly well. That is, the long-axis (Z) polarized bands observed at 27400, 34600, 45000, and 48800 cm^{-1} correspond to the calculated transitions ($^1B_{1u} \leftarrow {}^1A_g$, D_{2h}) from S_0 to S_1, S_4, S_{10}, and S_{18} respectively, while the short-axis (Y) polarized bands at 44000 and 50000 cm^{-1} correspond to the transitions ($^1B_{2u} \leftarrow {}^1A_g$) to S_8 and S_{22} respectively.

Incidentally, the interaction scheme given in Fig. 5 also gives an explanation of the finding made by Armitage *et al.* that, in a series of diphenylpolyynes (Ph-(C≡C)$_n$-Ph), the second bands increase in intensity as n increases, while the first bands become less intense. As n increases, the magnitudes of the transition moments of both the π and π' systems become larger, which results in a larger value (an increase in intensity) for the plus combination (the second bands) of the two vectors, but their difference may, though not easy to predict *a priori*, become smaller, which results in a smaller value (a decrease in intensity) for the minus combination (the first bands). F and the mixing coefficients (a and b) are now assumed to be constant, irrespective of n.

In order to ascertain the nature of each electronic transition of diphenylhexatriyne, configuration analysis[14] has been performed for the wavefunctions of Calc. 4 whose results are in good agreement with the observations as has been discussed above; some interesting results have thus been obtained (see Table 2). The main contributors to the S_1 and S_4 states are, respectively, the π-π^* and π'-π'^* configurations; *i.e.*, the $S_1 \leftarrow S_0$ observed at 27400 cm^{-1} is regarded as a typical π-π^* transition, and the $S_4 \leftarrow S_0$ at 34600 cm^{-1}, as a π'-π'^* within the π' framework perpendicular to the π system. The eighth excited state (S_8) corresponding to the short-axis polarized 44000 cm^{-1} band consists of the π-π^* configuration ($\psi_{7th}^0(\pi\pi^*)$=100%), in which the electronic transition occurs from the MO delocalized over the π system to the MO localized on the two phenyl rings, or *vice versa*.

It should, moreover, be noted that a mixing between mutually perpendicular π and π' electron systems results from a considerable degree of configuration interaction. That is, the S_1 ($\psi_{1st}^0(\pi\pi^*) \simeq 92\%$) state con-

tains about 8% of the π'–π'^* character ($\psi^0_{1st}(\pi'\pi'^*) \simeq 8\%$), and the S_4 ($\psi^0_{1st}(\pi'\pi'^*) \simeq 86\%$) state, about 12% of the π–π^* character ($\psi^0_{1st}(\pi\pi^*) \simeq 8\%$, $\psi^0_{5th}(\pi\pi^*) \simeq 4\%$).

References

1) J. B. Armitage, N. Entwistle, E. R. H. Jones, and M. C. Whiting, *J. Chem. Soc.*, **1954**, 147.

2) G. N. Lewis and M. Calvin, *Chem. Rev.*, **25**, 237 (1937).

3) S. Akiyama, K. Nakasuji, K. Akashi, and M. Nakagawa, *Tetrahedron Lett.*, **1968**, 1121.

4) Y. Tanizaki and S. Kubodera, *J. Mol. Spectrosc.*, **24**, 1 (1967).

5) T. Hoshi and Y. Tanizaki, *Z. Phys. Chem. N. F.*, **71**, 230 (1970).

6) M. Kobayashi, Y. Tanizaki, and T. Hoshi, *Can. J. Spectrosc.*, **6**, 165 (1974).

7) J. A. Pople, *Trans. Faraday Soc.*, **49**, 1375 (1953); *Proc. Phys. Soc. (London)*, **A68**, 81 (1955).

8) R. Pariser and R. G. Parr, *J. Chem. Phys.*, **21**, 466, 767 (1953).

9) T. Hoshi, H. Ito, J. Okubo, and S. Mori, *Nippon Kagaku Kaishi*, **1983**, 671.

10) M. Mataga and K. Nishimoto, *Z. Phys. Chem. N. F.*, **13**, 140 (1957).

11) K. Nishimoto and L. S. Forster, *Theoret. Chim. Acta (Berl.)*, **3**, 407 (1965); **4**, 155 (1966).

12) E. V. Shpol'skii, A. A. Wina, and L. A. Klimova, *Dokl. Akad. Nauk SSSR.*, **87**, 935 (1952).

13) E. V. Shpol'skii, *Soviet Phys. Usp.*, **3**, 372 (1960); **5**, 522 (1962); **6**, 411 (1963).

14) H. Baba, S. Suzuki, and T. Takemura, *J. Chem. Phys.*, **50**, 2078 (1969).

15) a) J. A. Pople, D. P. Santry, and G. A. Segal, *J. Chem. Phys.*, **43**, S129 (1965); b) J. A. Pople and G. A. Segal, *ibid.*, **43**, S136 (1965); c) J. A. Pople, *ibid.*, **44**, 3289 (1965).

The Radiopolarography of Gadolinium, Ytterbium, and Californium

Yoshinobu SHIOKAWA* and Shin SUZUKI
The Research Institute for Iron, Steel, and Other Metals, Tohoku University, Katahira, Sendai 980
(Received February 29, 1984)

The polarographic reduction of Gd, Yb, and Cf was investigated. It was found that the M(III)→Hg(M) reduction process in an aqueous solution, that cannot be detected by dc polarography, can be detected by radiopolarography. The polarographic behavior of Gd, Eu, Yb, and Cf in the presence of 1,4,7,10,13,16-hexaoxacyclooctadecane(18-crown-6) suggests that Cf(III) is reduced in two steps to Hg(Cf) in an aqueous solution.

The existence of divalent californium has been confirmed by the hydrogen reduction of CfI_3,[1] the polarographic reduction in an acetonitrile,[2] and the distribution between molten salts and liquid Bi.[3] However, concerning its existence in an aqueous solution there are conflicting observations. Musikas *et al.* observed through dc polarography and cyclic voltammetry that Cf(III) in 0.1 M $(CH_3)_4NI$ (1 M=1 mol dm^{-3}) was reduced in two steps.[4] On the other hand, David and Samhoun observed through radiopolarography Cf(III) in 0.1 M LiCl or 0.1 M $(CH_3)_4NClO_4$ was reduced in a single step.[5,6]

In the present work we wish to clarify the reduction process of Cf(III) in an aqueous solution. First, we performed the polarographic reduction of Gd(III) and Yb(III) in order to examine how the M(III)→Hg(M) process was observed by means of radiopolarography. Next, the reduction behavior of Gd, Eu, Yb, and Cf in the presence of 18-crown-6 was investigated.

Experimental

The ^{153}Gd, ^{169}Yd, and $^{250,252}Cf$ were purified by the standard ion exchange technique.[7,8] The tetramethylammonium iodide was used as a supporting electrolyte; in it Musikas *et al.* had observed the existence of Cf(II).[4] Aliquots of the gadolinium, ytterbium, or californium solution were evaporated to dryness and the residue was dissolved in 1 ml of 0.01 M H_2SO_4 and 5 ml of 0.2 M $(CH_3)_4NI$, and then the mixture was diluted to 10 ml. The pH value of the solution was adjusted by the use of 0.1 M H_2SO_4 or 0.1 M $(CH_3)_4NOH$.

In a conventional radiopolarographic cell, the aqueous solution examined is directly in contact with the insulating phase(CCl_4), in which the radioactive amalgam is accumulated. In such a cell, because of the direct contact with the organic solvent, the radiopolarographic reduction in an organic solvent or an aqueous solution which contains some soluble substance such as 18-crown-6 in the CCl_4, is difficult. In this experiment, however, we used a new radiopolarographic cell, shown in Fig. 1, in which the solution examined was not directly in contact with the CCl_4 phase. In this cell, the inner surface of the part of capillary E(inner diameter, 3 mm) below the stopcock F was treated with the vapor of dimethyldichlorosilane. The increased surface tension between the solution and the glass makes the solution hold above the argon phase.

The deoxidized CCl_4 and then the solution examined were introduced into the cell, and the tube connected to the needle valve I was filled with argon. A constant potential was imposed at the DME during 10 min, while the mercury drops were passed through the capillary E and the argon phase and then accumulated in the compartment on the stopcock G. Then, the stopcock F was closed and the needle valves I and J, and the stopcock G were opened. By the flow of CCl_4(J→G→I), the amalgam was rinsed in order to remove the radioactive solution adhered to it and falled into the compartment on the stopcock H. After the stopcock G was closed, the amalgam was taken out from cell with a small quantity of CCl_4. The dried amalgam was weighed, and then the amalgamated metal was extracted by shaking it with 1 ml of 0.5 M HCl or 0.5 M HNO_3 for 10 min. For the Gd and Yb runs, an aliquot of the extraction solution was determined by means of γ-ray spectrometry. For Cf, the sample, prepared by evaporating an aliquot of the solution on a dish of stainless steel, was determined by means of α-ray spectrometry.

There was no difference of more than 0.1 of the pH value between before and after experiments. The radiopolarographic cell was placed in a constant-temperature box with 25±1 °C. The polarograph and the DME knocker for obtaining a constant lifetime of a mercury drop were manufactured by ourselves. The DME knocker was used only in the dc polarography. The 18-crown-6 was a product of the Nippon Soda Co.,Ltd., and was dried by use of P_2O_5 in a vacuum desiccator with a liquid-nitrogen trap.

Results and Discussion

The dc polarogram of lanthanoid(III), except for

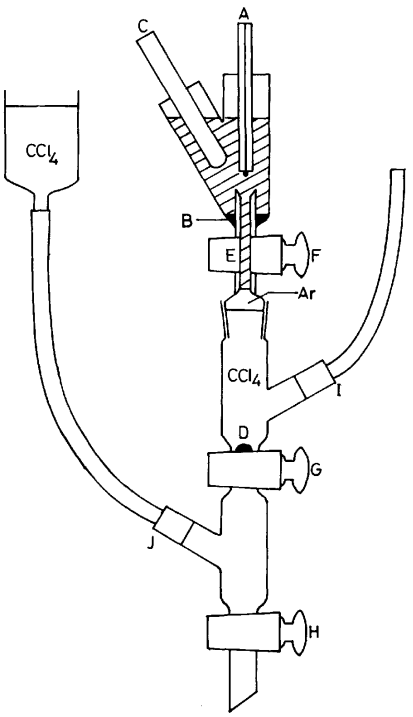

Fig. 1. Radiopolarographic cell.
A: dropping mercury electrode, B: mercury anode, C: reference electrode, D: amalgam, E: capillary, F, G and H: stopcocks, I and J: needle valves.

Eu(III) and Yb(III) in an aqueous solution, exhibits two waves, whose processes are not limited by the rate of diffusion, beyond the hydrogen discharge. According to Large and Timnick,[9] the first wave is attributed to the reduction of the hydrogen ions produced by the protolytic dissociation of the hydrated lanthanoid(III) at the electrode surface, while the second is due to the adsorption of the hydrolytic species of lanthanoid(III). Therefore, the reduction process of lanthanoid(III) cannot be detected by dc polarography.

In radiopolarography, the measured quantity is not the flux of electrons(current), but the amount of the amalgamated radioactive nuclide. That is, this quantity corresponds to the mass transfer associated by the electrode reaction and not to the electron transfer. Also, the concentration of the metal ions is much lower than that used in the dc polarography. It can, therefore, be expected that the reduction process of lanthanoid(III) in an aqueous solution can be detected by means of the radiopolarography.

Figure 2 shows the radio and dc polarograms of Yb(III). In the dc radiopolarogram, two waves due to the hydrogen discharge and reduction of Yb(III) to Yb(II) at about −1.5 V,[10] which, naturally, cannot be detected by the radiopolarography, are overlapped, while the wave at about −2.0 V is attributed to the reduction of Yb(II) to Hg(Yb). Its reciprocal of the slope of logarithmic analysis for the wave is 29—34 mV. On the other hand, the radiopolarographic wave is detected at about −2.0 V, and its reciprocal of the slope is 27—31 mv. Moreover, as is shown in Fig. 3, the limiting activity A_d, one at the plateaus of the radiopolarogram, is controlled by the rate of diffusion. Therefore, the radiopolarographic results are almost the same as the dc polarographic ones; nevertheless, the concentration of ytterbium on each solution examined differs by an order of four. The diffusion coefficient calculated from the limiting activity is 3—4×10^{-6} cm^2s^{-1}, which is lower than that calculated from the limiting current. This may be attributed to desamalgamation in CCl_4.[5]

However, there is a little difference in the half-wave potentials, $E_{1/2}$, obtained by the two methods. The potentials obtained by the dc polarography are more negative and dependent on the pH values; $E_{1/2}$=−2.033 V at pH=2.9, $E_{1/2}$=−2.059 V at pH=3.5. A similar dependence is observed by the dc polarographic reduction of Eu(II) to Hg(Eu).[11] On the other hand, the half-wave potentials obtained by the radiopolarography are independent of the pH values; $E_{1/2}$=−2.016 V at pH=2.8, $E_{1/2}$=−2.015 V at pH=3.5. The dependency of the potentials on the pH observed by the dc polarography have been explained by the formation of hydroxo complexes.[11] This explanation is not correctly but we ourselves cannot at present explain these differences in pH dependency.

Figure 4 shows the radio and dc polarograms of Gd(III). In the dc polarogram, except for the hydrogen discharge at about −1.5 V, two waves are observed, as has been mentioned above: One at about −1.80 V and another at about −2.07 V. In the radiopolarogram, the wave is found at about −2.15 V, and the half-wave potentials are independent of the pH; $E_{1/2}$=−2.154 V at pH=2.8, $E_{1/2}$=−2.149 V at pH=3.5. As is shown in Fig. 3, this process is limited by the rate of diffusion, while the reciprocal of the slope of logarithmic analysis for the wave is about 35 mV. Therefore, the radiopolarographic wave must be due to the reduction of Gd(III) to Hg(Gd) being irreversible.

By means of radiopolarography, in an aqueous

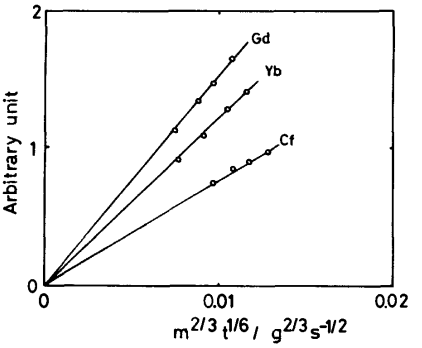

Fig. 3. Dependence of the limiting activity on the mercury column height.
Gd: at −2.202 V in 0.1 M $(CH_3)_4NI$, pH=3.0.
Yb: at −2.082 V in 0.1 M $(CH_3)_4NI$, pH=3.0.
Cf : at −1.845 V in 0.1 M LiCl, pH=2.9.

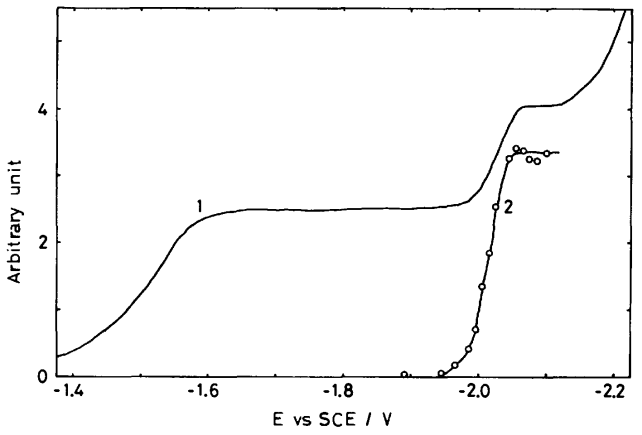

Fig. 2. Polarograms of Yb in 0.1 M $(CH_3)_4NI$, pH=3.0.
1: dc polarogram, [Yb]=1.46×10^{-3} M, 0.02% gelatin.
2: radiopolarogram, [Yb]=6×10^{-7} M.

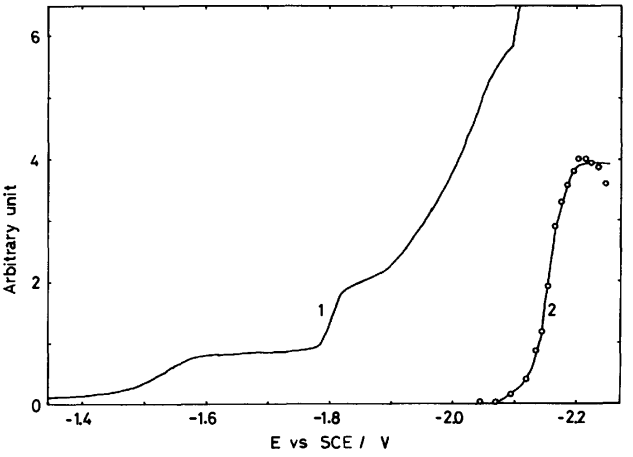

Fig. 4. Polarograms of Gd in 0.1 M $(CH_3)_4NI$, pH=3.0.
1: dc polarogram, [Gd]=1.30×10^{-3} M, 0.01% gelatin.
2: radiopolarogram, [Gd]=5×10^{-7} M.

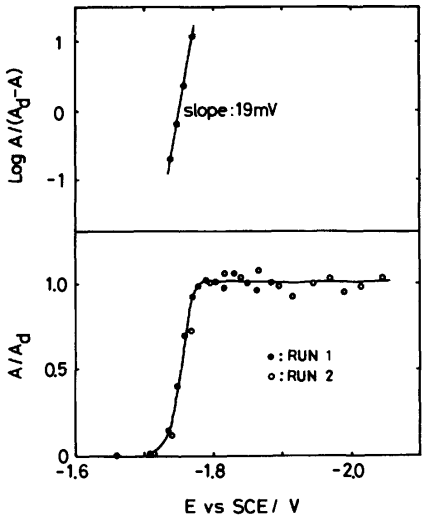

Fig. 5. Radiopolarogram and logarithmic analysis of Cf in 0.1 M $(CH_3)_4NI$, pH=3.0.
A: radioactivity in mercury drops. A_d: limiting activity.

solution the reduction wave of not only lanthanoid(II) but also lanthanoid(III) can be detected, as has been mentioned above. Thus radiopolarography can be expected to elucidate the reduction process of Cf(III) in an aqueous solution.

Figure 5 shows the radiopolarogram and logarithmic analysis of Cf(III). The half-wave potential and the reciprocal of the slope are −1.750 V and 19 mv respectively, and this process is limited by the rate of diffusion, as is shown in Fig. 3. The half-wave potential obtained is almost in agreement with that obtained by David and Shahoun through radiopolarography,[5,6] but not with that obtained by Musikas *et al.* through dc polarography.[4] According to Musikas *et al.*, the half-wave potential is −1.71 V for Cf(III)/Cf(II) and −1.93 V for Cf(II)/Hg(Cf). At this amalgamated potential, as is shown in Run 2 of Fig. 5, no appreciable change in the radiopolarogram is observed. The disagreement is not due to the difference in the concentration of Cf(III), because, as is shown in Fig. 2, the potentials obtained by radio and dc polarography are almost in agreement. The disagreement may be attributed to the difference in the specfic activity of a solution. In this work, the specific activity of $^{250,252}Cf$ was about 0.3 μCi/ml (the concentration of Cf: 4×10^{-9} M), while Musikas *et al.* carried out at about 0.5 mCi/ml (10^{-4}—10^{-3} M). The difference in the potentials, $E_{1/2}$, may be attributed to the influence of the α activity in the electrical double layer at the electrode.

From the logarithmic analysis of the radiopolarographic wave, David and Samhoun have drawn the conclusion that Cf(III) is reduced by a single step to Hg(Cf). Our reciprocal of the slope, as is shown in Fig. 5, supports their conclusion. However, as the reduction wave of Cf(III) to Cf(II), even if the reduction can occur, cannot be detected by radiopolarography, it is desirable to investigate the electrode reaction from a different viewpoint. In the present work, therefore, the shift of half-wave potentials in the presence of

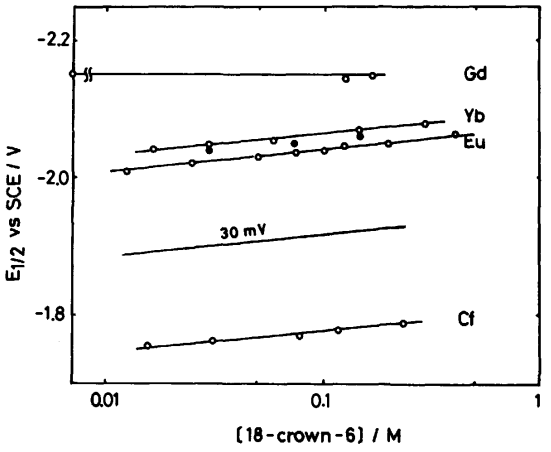

Fig. 6. $E_{1/2}$ of Eu, Gd, Yb, and Cf as a function of 18-crown-6 concentration.

18-crown-6 was investigated.

It is well known that 18-crown-6 forms stable complexes with cations whose ionic diameters are very close to the cavity diameter of 18-crown-6. Izatt *et al.* showed that, in an aqueous solution, 18-crown-6 with a cavity diameter of 280 pm[12] does not form complexes with La(III) with an ionic radius $r_{La^{3+}}$=103 pm[13] upon the calorimetry.[14] Therefore, it cannot form complexes with Cf(III) with a smaller radius $r_{Cf^{3+}}$=95 pm[13] than La(III). On the other hand, 18-crown-6 is expected to form complexes with Cf(II) because of two adavantages, its radius, $r_{Cf^{2+}}$=107 pm[13], is larger than that of Cf(III), and its hydration energy is lower than that of La(III).

Figure 6 shows the dependence of the half-wave potentials of the reduction to the amalgam on the concentration of 18-crown-6. The potentials $E_{1/2}$ of Gd, Cf, and a part of Yb (blackened circles in Fig. 6) were obtained by radiopolarography, and the others, by dc polarography.

For the case of Gd, the potentials $E_{1/2}$ shown in Fig. 6 are due to the reduction of Gd(III) to Hg(Gd); the potential $E_{1/2}$ in the absence of 18-crown-6 is also shown in this figure. No shift of potentials $E_{1/2}$ and no appreciable change in the irreversibility are observed, even in the presence of 18-crown-6.

For Eu and Yb, the potentials $E_{1/2}$ shown are due to the reversible reduction of M(II) to Hg(M). The observed slope of the half-wave potentials *vs.* the logarithmic concentration of 18-crown-6 is 30 mV, as is shown in Fig. 6. As is well known, if the reduction is reversible, such a plot has a slope of $P(RT/nF)$, where P is the coordination number of 18-crown-6. Figure 6 suggests that 18-crown-6 forms 1:1 complexes with Eu(II) and Yb(II). Their stability constants are estimated to be $\log K_{Eu^{2+}}$=2.7 and $\log K_{Yb^{2+}}$=2.4.

The observed shift of the half-wave potentials of Cf indicates that 18-crown-6 forms complexes with Cf(II), as has been mentioned above, and that Cf(II) reduces to Hg(Cf). However, the mean reciprocal of the slope of logarithmic analysis in the presence of 18-crown-6 is 23 mV, which is nealy equal to that in the absence of 18-crown-6, as is shown in Fig. 5, and corresponds to a Cf(III)→Hg(Cf) process, not a Cf(II)→Hg(Cf) process. We cannot interpret these conflicting results. Miranda *et al.* have pointed out, in their critical survey of radio-

polarography, that the logarithmic analysis of the radiopolarogram cannot always be taken at its face value.[15] Therefore, at the present time the results of the logarithmic analysis of Cf remain as the question to be solved later.

It is of interest that the observed dependence of the half-wave potentials of Cf on the concentration of 18-crown-6 has the same slope as that of Eu(II) to Hg(Eu) and that of Yb(II) to Hg(Yb). Therefore, we may suppose that the reduction of Cf is reversible. Figure 6 shows that 18-crown-6 forms 1:1 complexes with Cf-(II) and its stability constant is estimated to be log $K_{Cf^{2+}}$=2.0. The estimated stability constants of 18-crown-6 with Eu(II), Yb(II), and Cf(II) satisfy the relationship between the stability constants of alkaline-earth elements and their ionic radii.[12]

References

1) J. F. Wild, E. K. Hulet, R. W. Lougheed, W. N. Hayes, J. R. Peterson, R. L. Fellows, and J. P. Young, *J. Inorg. Nucl. Chem.*, **40**, 811 (1978).

2) H. A. Friedman, J. R. Stokeley, and R. D. Baybarz, *Inorg. Nucl. Chem. Lett.*, **8**, 433 (1972).

3) J. C. Mailen and L. M. Ferris, *Inorg. Nucl. Chem. Lett.*, **7**, 431 (1971).

4) C. Musikas, R. G. Haire, and J. R. Peterson, *J. Inorg. Nucl. Chem.*, **43**, 2935 (1981).

5) K. Samhoun and F. David, *J. Inorg. Nucl. Chem.*, **41**, 357 (1979).

6) F. David, K. Samhoun, and G. D. O'Kelley, *J. Inorg. Nucl. Chem.*, **43**, 2941 (1981).

7) E. K. Hulet, R. G. Gutmacher, and M. S. Coops, *J. Inorg. Nucl. Chem.*, **17**, 350 (1961).

8) G. R. Choppin, B. G. Harvey, and S. G. Thompson, *J. Inorg. Nucl. Chem.*, **2**, 66 (1956).

9) R. F. Large and A. Timnick, *Anal. Chem.*, **36**, 1258 (1964).

10) All electrode potentials in this paper are with respect to the saturated calomel electrode(SCE).

11) S. Misumi and Y. Ide, *Bull. Chem. Soc. Jpn.*, **32**, 1159 (1959).

12) J. D. Lamb, R. M. Izatt, J. J. Christensen, and D. J. Eatough, "Coordination Chemistry of Macrocyclic Compounds," ed by G. A. Melson, Plenum Press, New York (1979), Chapter 3.

13) R. D. Shannon, *Acta Cryst., Sect. A*, **32**, 751 (1976); N. B. Mikheev, *Radiochimica Acta.*, **32**, 69 (1983).

14) R. M. Izatt, R. E. Terry, B. L. Haymore, L. D. Hansen, N. K. Dalley, A. G. Avondet, and J. J. Christensen, *J. Amer. Chem. Soc.*, **98**, 7620 (1976).

15) C. F. Miranda, R. Muxart, J. Vernois, and G. Zuppiroli, *Radiochimica. Acta*, **19**, 153 (1973); **20**, 11 (1973).

The Synthesis and Thermal Decomposition of Calcium Phosphoramidate

Makoto WATANABE,* Yoshio MORII, and Shoji SATO
Department of Industrial Chemistry, Chubu University, Matsumoto-cho, Kasugai, Aichi 487
(Received March 5, 1984)

Calcium phosphoramidate monohydrate was made by adding an aqueous calcium chloride solution to an aqueous potassium hydrogenphosphoramidate solution at pH 9.0—9.5 below 5 °C. The product was stable at room temperature, but it was decomposed by heating. When the product was heated at 150 °C in air, the phosphoramidate decomposed to produce anhydrous calcium phosphoramide and also ortho- and diphosphates. The elimination of ammonia from amino groups to form a P-N(H)-P linkage was not observed at this temperature. The phosphoramidate decomposed in air to form ortho-, imidodi-, di-, and a small amount of higher polyphosphates at a temperature higher than 150 °C. Imidodiphosphate was decomposed to diphosphate by moisture in air. β-Calcium diphosphate was formed by heating the phosphoramidate at a temperature higher than 750 °C in air. When the phosphoramidate was heated in dried N_2, it showed the same thermal reaction as that in air below 250 °C, while the amount of imidodiphosphate in the thermal product was larger than that in air at a temperature higher than 400 °C

There are so many phosphorus-nitrogen compounds which have a P-N covalent bond. In the compounds, the phosphazens are maybe the best known and most intensively investigated compounds. There are a series of phosphorus-nitrogen compounds which have amino groups on a P atom. These compounds have potential for use as a new type of chemical fertilizer with a P-N covalent bond and as flameproof materials because they produce polyphosphates containing imino and amino groups when they are heated. They can also be used as starting materials for the preparation of many organic and inorganic phosphorus compounds.[1] In our previous paper,[2,3] the thermal decomposition of calcium or magnesium bis(hydrogenphosphoramidate) was studied. The two hydrogenphosphoramidates were unstable even at room temperature and were decomposed to polyphosphates at that temperature or at higher temperatures. This unstability was concluded to be due to the presence of an OH group in the phosphoramidates. This paper will describe the synthesis and the thermal decomposition of calcium phosphoramidate in order to ascertain the difference in thermal properties between the phosphoramidate and the hydrogenphosphoramidates.

Experimental

Preparation. The potassium hydrogenphosphoramidate was made by the method described in a previous paper;[4] 0.12 mol of the phosphoramidate was dissolved in 1.2 dm^3 of water. The aqueous solution of calcium chloride, which was made by dissolving 0.12 mol of calcium chloride dihydrate in 360 cm^3 of water, was added to the phosphoramidate solution below 5 °C to prevent the hydrolysis of the phosphoramidate. The resulting solution was stirred for 15 min. During the treatment, the pH of the solution was kept at 9.0—9.5 with 2.7% aqueous ammonia. The white precipitate thus produced was filtered off and washed with 50-V% aqueous ethanol, ethanol, and then acetone. The product was dried under 5330 Pa at 25 °C for 2 d.

Chemical Analysis. About 0.2 g of the product was dissolved in 20 cm^3 of 6-mol nitric acid, and the solution was heated on a water bath for 1 h. The orthophosphate in the solution was determined by the gravimetric method.[5] The nitrogen and calcium were estimated by, respectively, the Kjeldahl method and the EDTA (disodium dihydrogen ethylenediaminetetraacetate dihydrate) substitution-titration method with a BT indicator.

Paper Chromatography and Colorimetry of Phosphates. The paper-chromatographic separation of phosphate species in a sample and the determination of the phosphates on the chromatogram were run by the method described in our previous paper.[2]

X-Ray Diffractometry. An X-ray diffraction diagram of a powder sample was taken with nickel-filtered Cu $K\alpha$ radiation by using a Toshiba X-ray diffractometer, ADG-102.

IR Spectrophotometry. An IR spectrum of a sample was recorded on a JASCO IR spectrophotometer, A-3, by means of the KBr disc method.

DTA and TG. A sample was heated at a rate of 5 °C min^{-1} in air and dried N_2 by means of a Cho Balance TRDA$_1$-H apparatus.

^{31}P NMR Measurement. About 50 mg of a powder sample was put in 1.2 cm^3 of a 6% EDTA deuterated-water solution and stirred for 1—20 min, depending on the solubility of the sample, below 5 °C. The ^{31}P NMR spectrum of the solution was then measured by means of a JEOL JNM-FX-60-FT-NMR instrument.

Determination of Bound Water. The bound water in a sample was estimated by means of the Karl Fisher method with an MK-AII apparatus made by Kyoto Denshi.

Results and Discussion

Composition of the Product. The yield of the product was about 15 g. The ^{31}P NMR spectrum of the product gave only one peak of phosphoramidate at 3.4 ppm. (To get a single peak, the measuring time had to be as short as possible because the phosphoramidate was easily hydrolyzed to orthophosphate and the spectrum of the phosphoramidate solution also showed a peak of orthophosphate, depending on the experimental conditions.) Found: P, 19.9; N, 8.9; Ca, 27.1; H_2O, 12.1%. Calcd for $CaPO_3NH_2 \cdot H_2O$: P, 20.2; N, 9.2; Ca, 26.2; H_2O, 11.8%. Accordingly, it was found that the product was calcium phosphoramidate monohydrate, $CaPO_3NH_2 \cdot H_2O$. The product was stable at room temperature.

Thermal Reaction in Air. *(1) DTA and TG*: The DTA and TG curves of the product in air are presented in Fig. 1. The samples, numbered as in Fig. 1, were removed from the furnace, cooled in a silica-gel desiccator, and subjected to further analysis. The results are shown in Table 1 and Fig. 2. According to Table 1, the first large endothermic peak accompanying a rapid weight loss seemed to be mainly

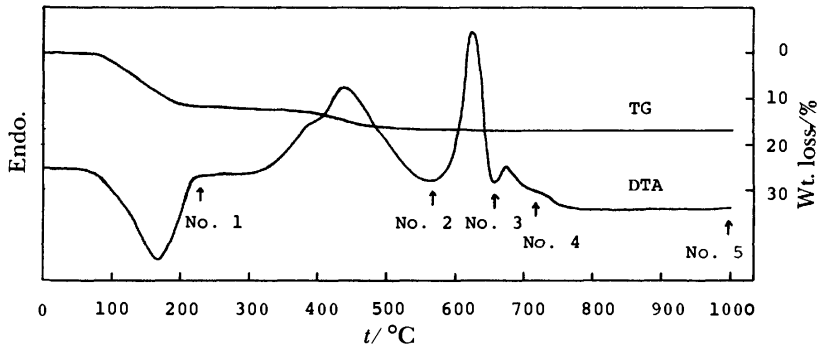

Fig. 1. DTA and TG curves of $CaPO_3NH_2 \cdot H_2O$ in air.

TABLE 1. WEIGHT LOSS OF THE PRODUCT, AND NITROGEN AND WATER CONTENT OF THE THERMAL DECOMPOSITION PRODUCTS IN AIR

Sample	Total N/%	Water/%	Wt. loss/%
Product	8.9	12.1	—
No. 1	9.1	1.4	11.3
No. 2	4.0	0	16.9
No. 3	1.6	0	17.1
No. 4	1.2	0	17.2
No. 5	0	0	17.2

caused by the elimination of bound water. The weight loss of the product at this stage was very close to the one calculated according to the following reaction:

$$CaPO_3NH_2 \cdot H_2O \longrightarrow CaPO_3NH_2 + H_2O, \quad (1)$$

but the thermal product, No. 1, still had 1.4% of water and its nitrogen content was a little less than that of $CaPO_3NH_2$. The IR spectrum of No. 1 showed a peak at 930 cm^{-1} which is considered to be due to a P-N(H)-P or a P-O-P linkage, and it was found that the endothermic reaction included condensation. The following condensation reaction is acceptable for the formation of a P-N(H)-P linkage:

$$2CaO_3P\text{-}NH_2 \longrightarrow CaO_3P\text{-}N(H)\text{-}PO_3Ca + NH_3. \quad (2)$$

There are two ways for the formation of a P-O-P linkage. One is:

$$2CaO_3P\text{-}NH_2 + 2H_2O \longrightarrow 2CaO_3P\text{-}ONH_4 \longrightarrow CaO_3P\text{-}O\text{-}PO_3Ca + 2NH_3 + H_2O; \quad (3)$$

the other is:

$$\left.\begin{aligned} &CaO_3P\text{-}N(H)\text{-}PO_3Ca + 2H_2O \longrightarrow 2CaO_3P\text{-}OH + NH_3 \\ &2CaO_3P\text{-}OH \longrightarrow CaO_3P\text{-}O\text{-}PO_3Ca + H_2O. \end{aligned}\right\} \quad (4)$$

It was, however, impossible to distinguish between the P-N(H)-P and the the P-O-P linkages according to the IR spectrum. There appeared a broad exothermic peak accompanying weight loss at 320—560 °C. After the reaction, the nitrogen content in the product decreased from 9.1 to 4.0, so the reaction includes the elimination of ammonia. As has been mentioned above, Reactions 2, 3, and 4 can be presented for the elimination of ammonia. As Fig. 2 shows, the No. 1 thermal product has a very weak peak of NH_4^+ at 1400 cm^{-1}. It is still

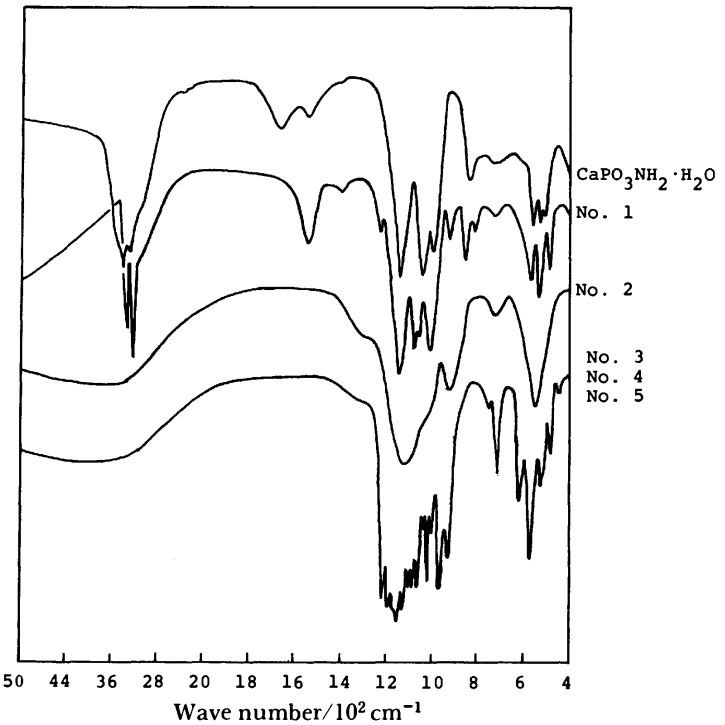

Fig. 2. IR spectra of the thermal decomposition products of $CaPO_3NH_2 \cdot H_2O$ in air.

difficult to say that Reaction 3 does not take place much, because the overall-reaction rate of Reaction 3 in that temperature range is obscure in these data. No detailed information about Reaction 4 could be obtained by the above data, either. The exothermic reaction may, however, be thought to include all these reactions at this stage. The formation of an ammonium ion in the thermal product will be discussed in the next section. The No. 1 sample showed an unkown X-ray diffraction pattern, while No. 2 was X-ray diffractometrically amorphous. The unknown pattern may be thought to be due to $CaPO_3NH_2$, because Reaction 1 may be predominant at this step. The IR spectrum of No. 2 showed a weak absorption of a $(PO_2)^-$ group at 1300 cm^{-1}, a strong absorption of a $(PO_3)^{2-}$ group at 1150 cm^{-1}, and absorptions of a P-N(H)-P or a P-O-P linkage at 930 and 730 cm^{-1}. The sample did not show any absorptions of an amino group in its spectrum. Accordingly, the main thermal product involved in No. 2 may be calcium diphosphate, $CaO_3P\text{-}O\text{-}PO_3Ca$, or calcium imidodi-

phosphate, $CaO_3P-N(H)-PO_3Ca$. If the sample is the imidodiphosphate, its nitrogen content should be 5.5%. Therefore, the sample No. 2 may be a mixture of the two diphosphates. To obtain proof of this, the ^{31}P NMR spectrum of No. 2 was taken; it is shown in Fig. 3. The peaks at about 0.9 and 10—11 ppm may be due to imidodiphosphate and diphosphate respectively. As has been described above, the sample No. 2 showed a weak IR absorption of a $(PO_2)^-$ group at 1300 cm^{-1}. This means that the thermal product contains polyphosphates or imidopolyphosphates with chain lengths longer than that of the dimer (diphosphate and imidodiphosphate). According to Reactions 2—4, the formation of such polyphosphates with a $(PO_2)^-$ group seems to be impossible at a relatively low-temperature range. The problem can be solved by assuming that the following disproportionation is taking place in the amorphous thermal decomposition products:

$$2\,Ca\text{-}O\text{-}P(=O)(O)\text{-}ONH_4 \longrightarrow Ca_{1/2}O\text{-}P(=O)(O)\text{-}ONH_4 + O\text{-}P(=O)(Ca\text{-}O)\text{-}OCa_{1/2}. \quad (5)$$

The $Ca_{1/2}(NH_4)_2PO_4$ species is bifunctional for thermal condensation in this temperature range and can produce tri- and higher polyphosphates. The sample No. 2 did not show any ^{31}P NMR peak of a $(PO_2)^-$ group. The sample contained an insoluble part, and so it could be concluded that the polyphosphates with a $(PO_2)^-$ group has a very low solubility. The NMR spectrum of No. 2 also exhibited a peak of phosphoramidate. It is found that the thermal product No. 2 is composed of these compounds. After the sharp large exothermic peak at around 630 °C, the sample showed an X-ray diffraction diagram of β-$Ca_2P_2O_7$ (ASTM cards, Nos. 9—346 and 20—24). It is clear that the thermal reaction is caused by the crystallization of amorphous calcium diphosphate to the β-form. It was difficult to understand the next small exothermic peak at about 670 °C because no definitive change in the IR spectrum or in the X-ray diffraction diagram of the sample after the exothermic peak was observed. As Table 1 shows, however, nitrogen was released from the sample during the crystallization, so it might be said that the amorphous calcium diphosphate produced according to Reactions 3 and/or 4 in this temperature range crystallizes at around 670 °C. The weight loss of the product was observed until about 620 °C; this seems to support the above discussion. The samples Nos. 3—5 did not indicate any IR absorption of a $(PO_2)^-$ group. The disappearance of the absorption may be explained by the following reorganization or degradation of amorphous phosphates to β-$Ca_2P_2O_7$;

$$Ca\text{-}O\text{-}P(=O)(O)\text{-}O\text{-}(P(=O)(O)\text{-}O)_n\text{-}P(=O)(O\text{-}Ca)\text{-}O\text{-}P(=O)(Ca\text{-}O)\text{-}O\text{-}Ca + n\,O\text{-}P(=O)(Ca\text{-}O)\text{-}OCa_{1/2}$$

$$\longrightarrow (n+1)\,O\text{-}P(=O)(Ca\text{-}O)\text{-}O\text{-}P(=O)(O\text{-}Ca)\text{-}O. \quad (6)$$

$(n \geqq 1)$

The sample No. 5 did not contain nitrogen. The nitrogen as an imino group in the thermal product may be converted to oxygen according to Reaction 4. Since the weight change associated with the reaction is very small, no increase in the weigh of the thermal product could be observed by the TG.

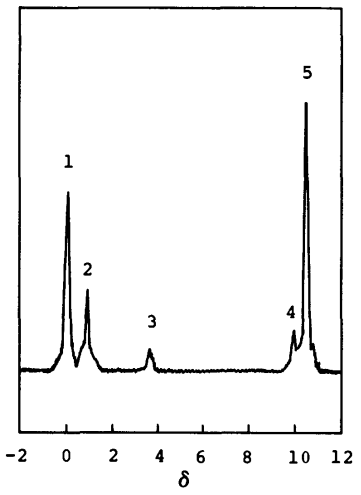

Fig. 3. ^{31}P NMR spectrum of the thermal product, No. 2.
1: Orthophosphate, 2: imidodiphosphate, 3: phosphoramidate, 4: and 5: diphosphate.[6]

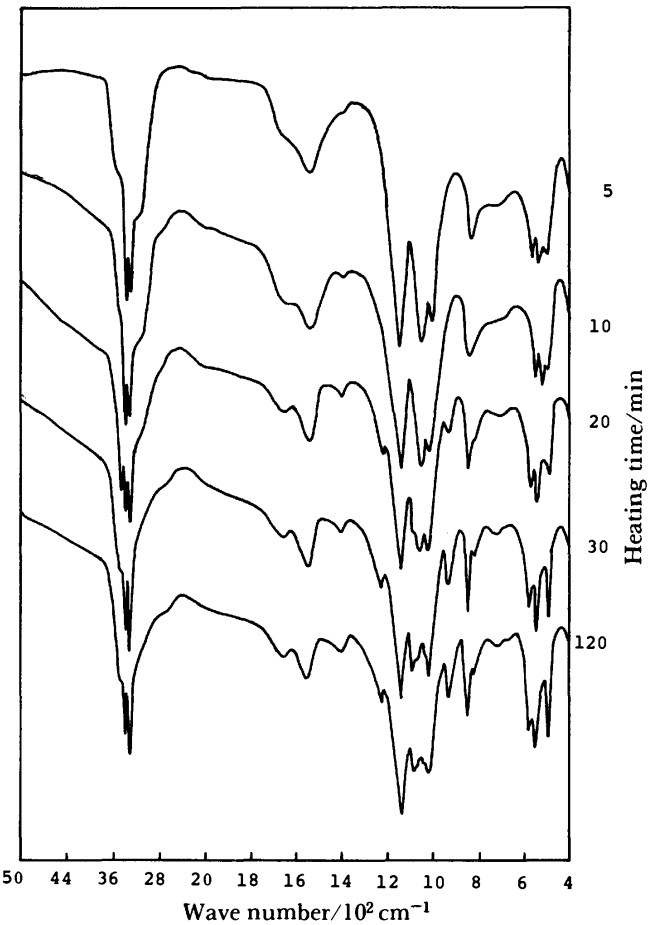

Fig. 4. IR spectra of the isothermal decomposition products in air at 150 °C.

(2) Isothermal Reaction at 150°C: As has been mentioned above, it was difficult to get clear information about the formation of an ammonium ion according to Reaction 3 by means of the DTA-TG instrument. Therefore, $CaPO_3NH_2 \cdot H_2O$ was isothermally heated at 150°C. This temperature seemed to be suitable for the analysis, because the thermal reaction was active and the elimination of ammonia from the product was very slow at this temperature. The IR spectra of the isothermal decomposition products in Fig. 4 indicate a very small peak due to NH_4^+ at 1400 cm^{-1}. This means that the amount of nitrogen present as NH_4^+ is very small. If only the dehydration of bound water from the product is taking place at this temperature according to Reaction 1, the nitrogen content in the thermal product should be 10.4%. As Table 2 shows, however, the nitrogen content was less than 10.4%. Therefore, ammonia must be released from the product. The ^{31}P NMR spectrum shows that the thermal product is composed of orthophosphate, phosphoramidate, and diphosphate. Reactions 2—4 can be responsible for the reaction. Imidophosphates were not made at all at this temperature. Therefore, Reactions 1 and 3 occur at 150°C. By the way, the thermal product heated at 150°C showed very small IR absorption of NH_4^+, while it had a large ^{31}P NMR peak of orthophosphate. The orthophosphate without NH_4^+ can be made by the elimination of ammonia as follows:

$$CaO_3PONH_4 \longrightarrow CaO_3POH + NH_3. \quad (7)$$

As has been mentioned above, phosphoramidate is hydrolyzed easily to orthophosphate in water. It is difficult to ascertain which reaction is responsible for the appearance of the large NMR peak of orthophosphate, but it seems reasonable that both reactions contribute to it. The other reactions do not occur at this temperature; they may take place at a temperature higher than 150°C.

Thermal Reaction in Dried N_2. According to Reactions 3 and 4, the presence of water causes the decomposition of the $P-NH_2$ and P-N(H)-P linkages. The water which brings about the decomposition comes from bound water and from moisture in the air. After the release of the bound water, the moisture in the air may give an important effect on the decomposition. To avoid its influence, the DTA and TG measurements of $CaPO_3NH_2 \cdot H_2O$ were made in dried N_2; the results are shown in Fig. 5. According to the results shown in Table 3, the first endothermic reaction, accompanied by a rapid weight loss, seemed to be mainly caused by the release of bound water. The weight loss of the product exhibited a value very close to the one calculated with Reaction 1, but the sample No. 6 still contained 1.5% of water and its nitrogen content was less than that of $CaPO_3NH_2$. Therefore, the elimination of ammonia seemed to take place at the same time. The IR spectrum of No. 6 had absorptions at 930 and 720 cm^{-1}. These absorptions were considered to be due to a P-N(H)-P or a P-O-P linkage. The ^{31}P NMR spectrum of No. 6 in Fig. 6 shows that the thermal product contains ortho- and diphosphates other than phosphoramidate. The sample also indicated a small IR peak of NH_4^+ at 1400 cm^{-1}. Accordingly, the thermal reactions taking place here are Reactions 1, 3, and 7. The other reactions may not occur at this stage. The X-ray diffraction pattern of No. 6 was the same as that of No. 1 and is concluded to be the pattern of $CaPO_3NH_2$. The sample No. 7 had the same X-ray diffraction diagram and IR spectrum as those of No. 6, while No. 7 indicated the loss of nitrogen and a ^{31}P NMR peak at 0.9 ppm which seemed to be due to imidodiphosphate. Therefore, reaction 2 may be taking place at this stage. The sample showed a small endothermic peak, accompanied by a fast weight loss, at around 450°C. The sample No. 8 was X-ray diffractometrically amorphous and had a small NMR peak of phosphoramidate and a large

Table 2. Weight loss of the product, and nitrogen and water content of the isothermal decomposition products at 150°C in air

Reaction time/min	Total N/%	Water/%	Wt. loss/%
5	8.9	11.4	0.6
10	8.8	10.1	2.2
20	8.8	4.5	7.9
30	8.7	1.3	11.0
60	8.7	1.2	11.4
120	8.5	1.1	11.6

Table 3. Weight loss of the product, and nitrogen and water content of the thermal decomposition products in dried N_2

Sample	Total N/%	Water/%	Wt. loss/%
No. 6	9.4	1.5	11.8
No. 7	8.3	0	13.2
No. 8	6.1	0	16.2
No. 9	4.0	0	17.1
No. 10	3.6	0	17.2

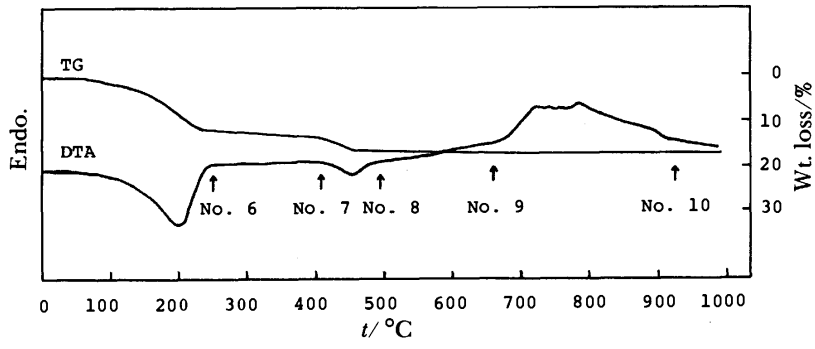

Fig. 5. DTA and TG curves of $CaPO_3NH_2 \cdot H_2O$ in dried N_2.

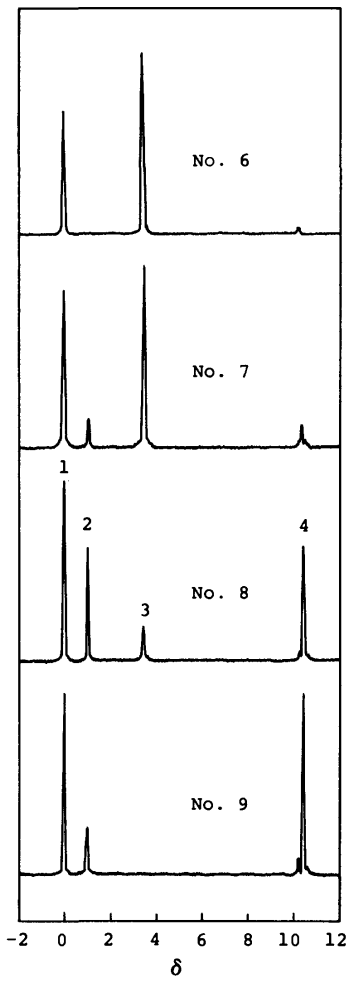

Fig. 6. ^{31}P NMR spectra of the thermal decomposition products in dried N_2.
1: Orthophosphate, 2: imidodiphosphate, 3: phosphoramidate, 4: diphosphate.

NMR peak of imidodiphosphate. The sample No.7 had a very small peak of NH_4^+. Therefore, reaction 2 may be taking place rapidly at this stage. According to the above discussion and the result that the DTA curve did not show any exothermic peak of the crystallization of calcium diphosphate at around 630°C, the main thermal decomposition product in No. 8 is concluded to be calcium imidodiphosphate, but the sample also indicated large NMR peaks of ortho- and diphosphates. The appearance of the two large ^{31}P NMR peaks can be explained by the hydrolysis of imidodiphosphate to ortho- and diphosphates as follows:

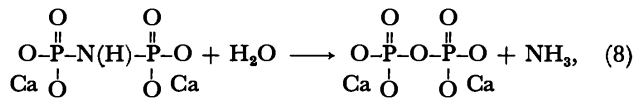

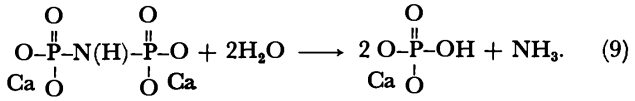

The samples Nos. 7 and 8 also had a weak IR absorption at 1300 cm^{-1} which seemed to be the absorption of a $(PO_2)^-$ group. The small amount of ammonium calcium orthophosphate which was produced by Reaction 3 may disproportionate according to Reaction 5 and then produce polyphosphates with chain lengths longer than that of diphosphate in this temperature range. As has been discussed above, the calcium polyphosphates seemed to have a very low solubility, for samples Nos. 7 and 8 did not exhibit any NMR peak of a $(PO_2)^-$ group. After the small endothermic peak at about 450°C, the weight loss of the product lasted until about 650°C. During the reaction, the nitrogen content of the thermal product decreased from 6.1 to 4.0. The sample No. 9 did not have any ^{31}P NMR peak of phosphoramidate at all. Therefore, the loss of nitrogen content at this stage may be mainly caused by Reaction 2. The sample No. 9 did not show any IR absorption of a $(PO_2)^-$ group. The reorganization of Reaction 6 may also be taking place at this stage. The sample No. 9 showed several complex exothermic reactions in the temperature range of 700—1000°C. The sample No. 9 was X-ray diffractometrically amorphous, while No. 10 showed an X-ray diffraction diagram of β-$Ca_2P_2O_7$ and the nitrogen content decreased a little after the exothermic reaction. It could be concluded, from the presence of slight amounts of water in the DTA-TG instrument, that the conversion of an imino group to oxygen seems to occur according to Reaction 4 at this stage. It was difficult to prevent such decomposition in the instrument used here.

Difference of Thermal Reaction Between Phosphoramidate and Hydrogenphosphoramidate. The calcium and magnesium bis (hydrogenphosphoramidate)[2,3] were unstable and decomposed to polyphosphates at room temperature. They also decomposed to polyphosphates and did not form a P-N(H)-P linkage at all upon the elimination of ammonia at a temperature higher than room temperature. On the other hand, the calcium phosphoramidate made in this study was stable at room temperature, and quite a bit of the phosphoramidate, especially in dried N_2, produced a P-N(H)-P linkage upon thermal condensation at a temperature higher than 150°C.

References

1) For example, D. E. C. Corbridge, "Phosphorus," Elsevier, Amsterdam (1980), p. 219.
2) M. Watanabe, T. Inagaki, and S. Sato, *Bull. Chem. Soc. Jpn.*, **56**, 458 (1983).
3) M. Watanabe, T. Inagaki, Y. Morii, and T. Yamada, *Setsuko To Setsukai*, No. 184, 111 (1983).
4) "Shin Zitsuken Kagaku Koza," ed by the Chemical Society of Japan, Maruzen, Tokyo (1976), Vol. 8-[I], p. 354.
5) "Bunseki Kagaku Binran," ed by the Chemical Society of Japan, Maruzen, Tokyo (1971), pp. 204 and 1492.
6) M. M. Crutchfield, C. H. Dungan, J. H. Letcher, V. Mark, and J. R. Van Wazer, "Topics in Phosphorus Chemistry," Interscience Publishers, New York (1967), Vol. 5, p. 227, and the references cited there in.

 © 1984 The Chemical Society of Japan Bull. Chem. Soc. Jpn., 57, 2919—2924 (1984)

The Syntheses, Properties, and Crystal and Molecular Structures of Bis(benzamide)tris(*O,O'*-diisopropyl dithiophosphato)neodymium(III), $[Nd\{(C_3H_7O)_2PS_2\}_3(C_6H_5CONH_2)_2]$, and Its Isomorphous Complexes of La, Ce, Pr, Sm, Eu, and Gd

Reiko NAKAMURA, Kiyofumi NAGAI,* Mamoru SHIMOI, and Akira OUCHI

Department of Chemistry, College of Arts and Sciences, The University of Tokyo, Komaba 3-8-1, Meguro-ku, Tokyo 153

(Received March 15, 1984)

The new complexes indicated in the title have been synthesized, and the crystal and molecular structure of the neodymium(III) complex has been determined by the X-ray diffraction method. The crystal is monoclinic, with the space group C2/c, $Z=16$, $a=28.887(4)$, $b=28.913(5)$, $c=24.814(5)$ Å, $\beta=106.72(1)°$. The final R value for 7761 reflections is 0.066. The central neodymium(III) atom of the complex is octa-coordinated and is in a dodecahedron geometry; three *O,O'*-diisopropyl dithiophosphato ligands, chelating by both of the sulfur atoms, span the two *m* edges of a trapezium as well as one *a* edge of the other trapezium, and two oxygen atoms of both the benzamide ligate at both tips of the base edge of the latter trapezium. The solid and the acetonitrile solution of the europium(III) complex are orange in color, and they show a charge-transfer band in their near-ultraviolet absorption spectra.

The lanthanoid metal complexes of sulfur-ligating ligands, such as *O,O'*-dialkyl dithiophosphate,[1-3] dialkyl dithiophosphinates,[4] and dialkyldithiocarbamates,[5] are very interesting compounds, because they are stable enough in spite of the fact that lanthanoid elements are known as "hard acids" according to the HSAB theory.[6] The structure of some complexes of the type have already been determined by means of X-ray analysis.[1,2,4,5,7]

Our group has already reported about the mixed complexes of lanthanoid(III) containing the *O,O'*-diisopropyl dithiophosphato (iPr_2dtp) ligand, as well as *N,N*-dimethylacetamide (dma).[1] Although we could obtain La, Ce, and Nd complexes of the type, all of which are isomorphous with each other, those of Sm and of the heavier members of lanthanoid were not synthesized in a stable crystalline state. Therefore, we tried to find more stable mixed complexes of the type. The adducts obtained this time, which are isomorphous with each other, were those of all members from La to Gd, except for Pm. All of them are stable, and all can be kept in air for several months at room temperature without decomposition.

Another interesting problem about the type of complexes is the coordination position of the oxygen atoms. As has been shown in the previous paper,[1] the two oxygen atoms take side-by-side positions in $[La(iPr_2dtp)_3(dma)_2]$, while in the case of $[La(Et_2dtp)_3\{(C_6H_5)_3PO\}_2]$ the two oxygen atoms are apart.[2c] We assumed that the difference is due mainly to the size of the ligand molecule;[1] consequently, the titled complexes, where the benzamide (bza) ligand is larger than dma, are expected to have different oxygen-atom positions around the central metal atom.

Among the series of titled complexes, the best crystals were obtained for Nd(III) complex. Therefore, its structure was determined by the single-crystal X-ray diffraction method.

Attempts to obtain similar complexes of lanthanoid heavier than gadolinium has not been successful until now; in these cases, other isomorphous complexes with the formula of $[M(iPr_2dtp)_2(bza)_3]^+(iPr_2dtp)^-$ (where M=Gd, Tb, Dy, Er, and Yb) were obtained. The details about them will be shown in a separate paper.[8]

Experimental

Synthesis of Bis(benzamide)tris(O,O'-diisopropyl dithiophosphato)neodymium(III). Neodymium(III) chloride hexahydrate (0.5 g, 1.4 mmol) and sodium *O,O'*-diisopropyl dithiophosphate (1.5 g, 6.3 mmol)[1] were dissolved in 25 cm^3 of 2-propanol, and the mixture was refluxed for about 20 min at 80 °C to complete the reaction. The solution was then filtered off, and about 0.5 g (4.1 mmol) of benzamide was added to the filtrate. It was warmed and kept at about 65 °C for 5 min to terminate the reaction. The solution was then evaporated almost to dryness by the use of a rotary vacuum evaporator at 65 °C. The residue was dissolved in 5 cm^3 of 2-propanol, the turbid materials were filtered off, and the clear filtrate was kept in a silica-gel desiccator for several days. The deposited crystals were filtered off, washed with small portions of 2-propanol and diisopropyl ether, in that order, and dried in a vacuum desiccator. The yield was about 0.7 g (0.7 mmol, 49%).

The isomorphous complexes of La, Ce, and Pr(III) were obtained in almost the same way. In the cases of the Sm and Eu(III) complexes, the crude product was obtained by adding 10 cm^3 of diisopropyl ether to the evaporating residue. Their crystals were obtained when they were dissolved in 5 cm^3 of 2-propanol; then were subsequently kept in the diisopropyl ether-vapor moiety. In all cases, the yield was about 50% calculated from the starting metal salt.

In the case of the Gd(III) complex, 0.49 g (1.3 mmol) of gadolinium chloride hexahydrate and 1.29 g (5.5 mmol) of sodium *O,O'*-diisopropyl dithiophosphate were used as the starting materials. The added benzamide should be less than 0.33 g (2.7 mmol). About 10 cm^3 of diisopropyl ether was added to the solution before it was placed in a desiccator to obtain the crystals. The yield was 0.63 g (0.6 mmol, 47%). (If the mol ratio of benzamide to the metal salt was higher, the $[Gd(iPr_2dtp)_2(bza)_3]^+(iPr_2dtp)^-$-type complex was mainly deposited).

The results of the elemental analyses, their average yields, and their magnetic moments as measured by a Gouy balance at the ambient temperature are shown in Table 1.

Intensity-data Collection. A crystal with dimensions of 0.4×0.4×0.25 mm^3 was used for the measurement without shaping. The crystallographic data are $NdC_{32}H_{56}N_2O_8P_3S_6$, $F.W.=1026.36$, monoclinic, space group C2/c, $Z=16$, $a=28.887(4)$, $b=28.913(5)$, $c=24.814(5)$ Å $\beta=106.72(1)°$, $U=$

TABLE 1. ANALYSES, YIELDS OF THE SYNTHESES, AND MAGNETIC MOMENTS OF THE $[M\{((CH_3)_2CHO)_2PS_2\}_3(H_2NCOC_6H_5)_2]$ COMPLEXES

M		M(%)	C(%)	H(%)	N(%)	Yield/%	μ_{eff}/BM[a)]
La	Found	13.60	37.54	5.49	2.69	62.0	(diamag.)
	Calcd	13.61	37.65	5.53	2.74		
Ce	Found	13.72	37.63	5.52	2.83	54.0	2.4_7
	Calcd	13.71	37.60	5.49	2.73		
Pr	Found	13.74	37.69	5.50	2.86	56.0	3.5_3
	Calcd	13.77	37.55	5.51	2.74		
Nd	Found	14.22	37.15	5.49	2.64	55.7	3.5_6
	Calcd	14.05	37.45	5.50	2.73		
Sm	Found	14.68	37.12	5.46	2.72	41.3	1.5_6
	Calcd	14.56	37.23	5.47	2.71		
Eu	Found	14.81	37.20	5.44	2.72	55.5	3.3_2
	Calcd	14.70	37.17	5.46	2.71		
Gd	Found	15.01	37.00	5.41	2.74	46.6	7.4_3
	Calcd	15.13	36.98	5.43	2.70		

a) 1 BM=$9.274078(36)\times10^{-24}$ J T^{-1}

19, 848(6) Å^3, D_x=1.37, D_m=1.36(3) Mg m^{-3}, μ(Mo $K\alpha$)=1.47 mm^{-1}. The reflections whithin the range of $3°<2\theta<48°$ were collected on a Rigaku AFC-6A automated four-circle diffractometer with graphite monochromated Mo $K\alpha$ radiation, the ω-scan technique being employed (scan speed: 4° min^{-1}; scan width: $1.40+0.5\tan\theta°$). The crystal was stable during the exposure to X-rays. From the 10017 independent reflections thus measured, 7761 with $|F_o|>3\sigma(|F_o|)$ were selected and used for the structure determination. The intensities were corrected for the Lorentz and polarization factors, but no correction was made for absorption and extinction.

Structure Determination. The structure was solved by the heavy-atom method. The positions of the Nd, P, and S atoms were deduced from a three-dimensional Patterson map; the other non-hydrogen atoms were located by means of successive Fourier syntheses. Their positional, isotropic, and then anisotropic thermal parameters were refined by the block-diagonal least-squares method. All the calculations were carried out on a HITAC M-200H computer at the Computer Center of the University of Tokyo, using the local version of the UNICS program system.[9] The atomic-scattering factors were taken from the tables.[10]

Although the positional and thermal parameters of the central Nd(III) atoms, as well as those of the other atoms near them, were exactly determined, those of some isopropyl groups and of some phenyl rings were found to have relatively large standard deviations; this may be due to the fact that they are not fixed tightly in the crystal. As is shown in Table 2, the thermal parameters of some isopropyl carbon atoms are very large; therefore, we can know only the probable domains, not the exact positions, of some atoms, even after the repeated-refinement process, although they converged to the respective values. The position of C(226) was not decided. The seven carbon atoms of the phenyl groups, C(11C), C(11D), C(11E), C(11F), C(31D), C(31E), and C(31F), were fixed at the positions calculated from those of the vicinal atoms; their isotropic temperature factors were assumed to be 16.0 Å^2. In the final cycle of the refinement, the parameter shifts of the atoms were less than one-third of the corresponding standard deviations.

The final R value was 0.066.[11]

Other Measurements. The X-ray powder patterns of these complexes were obtained by the use of a diffractometer, Model DX-GO-F JEOL, using Cu Kα radiation, in the range from 6° to 40° in 2θ. The infrared spectra of the samples were obtained by means of a JASCO A202 grating infrared spectrophotometer, using Nujol and hexachloro-1,3-butadiene mull. The near-ultraviolet absorption spectra of the complexes were measured with a Hitachi 124 spectrophotometer.

Results and Discussion

The final atomic parameters of the title complex are listed in Table 2.[12] The sixteen neodymium(III) atoms in one unit cell are divided into three groups. The Nd(1) atom is at a general equivalent position, while the Nd(2) as well as Nd(3) atoms and P(21) as well as P(31) atoms take special equivalent positions on the two-fold axes (Wyckoff notation: e). Some bond lengths and bond angles of the complex are shown in Table 3.[13] The general features of the three types of complex molecules are almost the same; their corresponding bond lengths and bond angles are compared in the table.

A perspective drawing of the complex around the central metal Nd(1) atom is shown in Fig. 1. The numbering scheme of the ligand atoms is shown in Fig. 2, and the configuration of the ligating atoms around the Nd(1) atom, in Fig. 3.

Each complex molecule is isolated, and no bridgings are found between them. However, as is shown in Table 2, some interatomic distances between S and N atoms are shorter than 3.5 Å; these may be the hydrogen bonds, since the S···H–N hydrogen bond length has been reported to be about 3.42 Å between S and N atoms.[14] As is shown in Fig. 3, the central Nd(III) atom is octa-coordinated and is in a distorted dodecahedron geometry, where three iPr_2dtp ligands span at two m edges of a trapezium and one a edge of the other trapezium, chelating by both of the sulfur atoms. Two oxygen atoms of bza ligands take the two tip positions of the base edge of the latter trapezium. Five atoms, including the central metal atom, of each trapezium of each complex are almost on one plane (the deviation of each atom's position from the plane was 0.267 Å in the maximum and 0.12 Å on the average), and the dihedral angle between the two planes of each complex is almost right-angled (88.7—90.2°).[13]

TABLE 2. FINAL ATOMIC COORDINATES ($\times 10^4$) AND EQUIVALENT ISOTROPIC TEMPERATURE FACTORS (B/Å^2) OF NON-HYDROGEN ATOMS WITH ESTIMATED STANDARD DEVIATIONS IN PARENTHESES

Atom	x	y	z	B_{eq}/Å$^{2a)}$	Atom	x	y	z	B_{eq}/Å$^{2a)}$
Nd(1)	2921.0(2)	4377.2(2)	2571.2(2)	4.9	P(22)	672(2)	2739(2)	3807(2)	8.8
S(111)	2137(1)	3842(1)	2853(2)	6.4	O(211)	327(4)	731(4)	2950(5)	8.9
S(112)	1979(1)	4880(1)	2273(2)	6.9	C(211)	168(8)	477(7)	3361(10)	12
P(11)	1693(1)	4360(1)	2580(2)	6.2	C(212)	274(11)	−24(7)	3310(12)	16
S(121)	2959(2)	4754(2)	3666(2)	9.1	C(213)	468(12)	701(11)	3924(12)	17
S(122)	3928(2)	4530(2)	3286(2)	9.0	O(221)	550(5)	2827(5)	4378(5)	12
P(12)	3661(2)	4712(2)	3910(2)	9.0	O(222)	1233(7)	2964(7)	3954(8)	17
S(131)	2459(2)	4006(2)	1463(2)	9.7	C(221)	50(9)	2738(9)	4398(9)	13
S(132)	3600(2)	4276(2)	1883(2)	9.1	C(222)	66(16)	2345(15)	4845(14)	26
P(13)	3070(2)	4039(2)	1275(3)	10	C(223)	−119(15)	3169(12)	4613(13)	24
O(111)	1482(4)	4572(4)	3029(6)	9.9	C(224)	1706(13)	2757(10)	4185(15)	21
O(112)	1242(3)	4147(4)	2135(5)	8.0	C(225)	1976(13)	3086(16)	4283(17)	25
C(111)	1391(8)	4292(7)	3518(10)	12	O(21)	693(3)	2469(3)	2204(4)	6.2
C(112)	842(9)	4392(9)	3466(12)	15	N(21)	1118(6)	3098(5)	2441(7)	11
C(113)	1731(11)	4425(14)	4045(9)	20	C(21A)	1006(5)	2739(5)	2155(7)	6.7
C(114)	892(7)	4413(7)	1743(8)	9.9	C(21B)	1246(5)	2660(5)	1724(7)	7.7
C(115)	395(7)	4313(9)	1742(14)	16	C(21C)	1118(8)	2280(7)	1388(10)	12
C(116)	975(11)	4304(12)	1199(13)	18	C(21D)	1323(13)	2200(9)	953(15)	22
O(121)	3876(8)	5204(6)	4179(9)	19	C(21E)	1615(10)	2532(8)	815(14)	18
O(122)	3851(5)	4393(5)	4432(5)	11	C(21F)	1735(9)	2907(7)	1200(11)	14
C(121)	4083(14)	5462(11)	4356(13)	19	C(21G)	1535(7)	3000(7)	1591(8)	10
C(122)	3983(15)	5927(9)	4115(15)	22	Nd(3)	5000	1477.0(3)	2500	5.4
C(123)	4431(17)	5347(14)	4948(13)	24	S(311)	4407(1)	2340(1)	2222(2)	7.4
C(124)	3703(9)	3892(7)	4360(8)	11	P(31)	5000	2709(2)	2500	6.9
C(125)	3392(12)	3783(10)	4717(12)	17	S(321)	5094(2)	1694(2)	1396(3)	11
C(126)	4222(14)	3669(11)	4533(12)	20	S(322)	4963(2)	647(2)	1793(3)	10
O(131)	3276(7)	3541(7)	1088(10)	20	P(32)	4994(2)	1055(2)	1169(3)	10
O(132)	2996(6)	4308(6)	699(5)	13	O(311)	5084(4)	3035(4)	2027(5)	9.7
C(131)	2931(13)	3286(18)	737(18)	25	C(311)	4704(7)	3268(6)	1582(8)	9.6
C(132)	3221(18)	2811(16)	949(21)	30	C(312)	4693(13)	3099(11)	1041(11)	18
C(133)	3096(28)	3237(20)	292(25)	40	C(313)	4812(9)	3776(7)	1572(12)	15
C(134)	2853(9)	4792(9)	679(10)	14	O(321)	4544(5)	995(5)	644(5)	11
C(135)	2442(15)	4843(15)	233(16)	24	O(322)	5426(6)	920(9)	888(8)	20
C(136)	3218(13)	5027(13)	497(14)	22	C(321)	4075(7)	1098(9)	660(9)	13
O(11)	3188(3)	3619(3)	2861(4)	7.1	C(322)	3799(12)	652(14)	441(16)	23
N(11)	3810(6)	3282(6)	2656(9)	15	C(323)	3877(11)	1521(12)	305(15)	20
C(11A)	3458(6)	3284(5)	2885(7)	7.3	C(324)	5650(11)	718(14)	698(14)	20
C(11B)	3414(8)	2880(7)	3215(15)	19	C(325)	5424(14)	630(15)	56(16)	23
C(11G)	3770(11)	2515(7)	3357(14)	19	C(326)	6159(10)	702(15)	962(16)	22
O(12)	3010(3)	5143(3)	2281(4)	6.5	O(31)	4161(3)	1291(3)	2209(5)	7.4
N(12)	3722(4)	5528(5)	2563(6)	8.8	N(31)	3863(6)	631(5)	2396(10)	14
C(12A)	3274(6)	5464(5)	2225(7)	6.9	C(31A)	3814(5)	1029(5)	2170(7)	7.4
C(12B)	3079(6)	5812(7)	1764(9)	9.7	C(31B)	3329(7)	1148(7)	1883(12)	15
C(12C)	3377(7)	6132(7)	1625(8)	10	C(31C)	2958(6)	847(8)	1749(10)	13
C(12D)	3197(8)	6432(9)	1183(11)	14	C(31G)	3291(10)	1553(12)	1741(27)	36
C(12E)	2702(9)	6370(11)	817(15)	20	C(11C)	2860	2676	2939	16
C(12F)	2419(9)	6028(11)	1007(14)	18	C(11D)	2750	2233	3102	16
C(12G)	2606(7)	5731(8)	1431(10)	13	C(11E)	3121	1931	3376	16
Nd(2)	0	2286.3(3)	2500	4.7	C(11F)	3603	2071	3488	16
S(211)	442(1)	1428(1)	2198(2)	6.2	C(31D)	2517	929	1413	16
P(21)	0	1059(2)	2500	5.5	C(31E)	2403	1403	1290	16
S(221)	643(2)	2083(2)	3605(2)	8.4	C(31F)	2770	1742	1421	16
S(222)	295(2)	3130(1)	3198(2)	8.3					

a) The equivalent isotropic temperature factors were computed using the following expression; $B_{eq}=4/3(B_{11}a^2+B_{22}b^2+B_{33}c^2+B_{13}ac\cos\beta)$. The B_{ij}'s are defined by; $\exp[-(h^2B_{11}+k^2B_{22}+l^2B_{33}+2klB_{23}+2hlB_{13}+2hkB_{12})]$.

As is shown in Table 3, all the Nd-S bond lengths are in the range from 2.888(6) to 2.988(5) Å; they are almost equal. Taking the difference in the ionic radii of La^{III} and Nd^{III} (1.160 and 1.109 Å respectively)[15] into consideration, they are comparable with the La-S bond lengths of $La(iPr_2dtp)_3(bza)_2$, which range from 2.998(3) to 3.046(7) Å.[1] All the P-S bond lengths are not very different, either; they are in the range of 1.943(8)—1.961(7) Å, except for S(122)-P(12) (1.982(8) Å); it is likely that the P=S double bond of the ligand is almost completely delocalized. Although in some cases the respective lengths of the pair of Nd-S and of P-S of each ligand are different from each other, there is probably no general rule such as that the sulfur

TABLE 3. SELECTED BOND LENGTHS AND BOND ANGLES OF THE COMPLEX, WITH ESTIMATED STANDARD DEVIATIONS IN PARENTHESES

Bond length	l/Å $n=1$[a]	Bond length	l/Å $n=2$[a]	$n=3$[a]
Nd(1)-S(111)	2.898(4)	Nd(n)-S(n11)	2.984(4)	2.933(4)
Nd(1)-S(112)	2.985(4)			
Nd(1)-S(121)	2.900(7)	Nd(n)-S(n21)	2.895(5)	2.898(8)
Nd(1)-S(131)	2.896(6)			
Nd(1)-S(122)	2.972(4)	Nd(n)-S(n22)	2.971(5)	2.956(6)
Nd(1)-S(132)	2.962(7)			
Nd(1)-O(11)	2.366(9)	Nd(n)-O(n1)	2.380(11)	2.381(9)
Nd(1)-O(12)	2.364(9)			
S(111)-P(11)	1.963(5)	S(n11)-P(n1)	1.970(6)	1.967(5)
S(112)-P(11)	1.970(6)			
S(121)-P(12)	1.945(7)	S(n21)-P(n2)	1.960(7)	1.929(9)
S(131)-P(13)	1.953(10)			
S(122)-P(12)	1.988(10)	S(n22)-P(n2)	1.950(8)	1.966(11)
S(132)-P(13)	1.940(8)			
P(11)-O(111)	1.542(17)	P(n1)-O(n11)	1.559(12)	1.579(16)
P(11)-O(112)	1.572(11)			
P(12)-O(121)	1.617(20)	P(n2)-O(n21)	1.576(21)	1.564(15)
P(13)-O(131)	1.671(23)			
P(12)-O(122)	1.556(16)	P(n2)-O(n22)	1.687(19)	1.641(27)
P(13)-O(132)	1.588(20)			
O(11)-C(11A)	1.233(18)	O(n1)-C(n1A)	1.228(18)	1.238(17)
O(12)-C(12A)	1.234(18)			
S(122)···N(12)	3.362(17)	S(n22)···N(n1)	3.428(22)	
S(132)···N(11)	3.412(21)			
S(322)···N(31^{ii})	3.409(18)	N(31)···S(112^{iii})	3.529(21)	
S(211)···N(12^{iii})	3.482(14)			

Bond angle	ϕ/° $n=1$[a]	Bond angle	ϕ/° $n=2$[a]	$n=3$[a]
S(111)-Nd(1)-S(112)	67.15(11)	S(n11)-Nd-S(n12)	67.41(11)	67.01(10)
S(111)-Nd(1)-S(121)	78.61(16)	S(n11)-Nd(n)-S(n21[b])	78.32(13)	78.72(18)
S(111)-Nd(1)-S(131)	81.75(15)	S(n11)-Nd(n)-S(n21[c])	82.18(13)	80.48(18)
S(121)-Nd(1)-S(122)	67.54(16)	S(n21)-Nd(n)-S(n22)	67.49(14)	67.13(20)
S(131)-Nd(1)-S(132)	67.46(18)			
S(111)-Nd(1)-O(11)	69.64(23)	S(n11)-Nd(n)-O(n1)	69.41(27)	69.73(22)
S(111)-Nd(1)-O(12)	135.46(24)	S(n11)-Nd(n)-O(n1[d])	136.05(27)	136.28(23)
Nd(1)-S(111)-P(11)	89.26(18)	Nd(n)-S(n11)-P(n1)	89.09(19)	89.34(15)
Nd(1)-S(112)-P(11)	89.22(19)			
S(111)-P(11)-S(112)	114.3(2)	S(n11)-Nd(n)-S(n12)	114.4(2)	114.3(2)
S(111)-P(11)-O(111)	114.0(6)	S(n11)-P(n1)-O(n11)	106.0(4)	111.6(5)
S(112)-P(11)-O(112)	112.5(4)			
Nd(1)-S(121)-P(12)	91.3(3)	Nd(n)-S(n21)-P(n2)	90.8(2)	91.2(3)
Nd(1)-S(131)-P(13)	90.4(2)			
Nd(1)-S(122)-P(12)	88.4(2)	Nd(n)-S(n22)-P(n2)	88.7(2)	88.8(2)
Nd(1)-S(132)-P(13)	88.8(2)			
S(121)-P(12)-S(122)	112.2(3)	S(n21)-P(n2)-S(n22)	113.0(3)	112.4(4)
S(131)-P(13)-O(131)	104.9(8)			
S(122)-P(12)-O(122)	111.6(6)	S(n22)-P(n2)-O(n22)	103.4(7)	113.9(9)
S(132)-P(13)-O(132)	113.5(7)			
Nd(1)-O(11)-C(11A)	152.7(9)	Nd(n)-O(21)-C(n1A)	151.6(10)	153.2(9)
Nd(1)-O(12)-C(12A)	149.7(9)			

a) $n=1$, 2 or 3 means the numbering of the central metal atom. Keys to the symmetry operations: i $-x$, y, $0.5-z$; ii $1.0-x$, y, $0.5-z$; iii $0.5-x$, $-0.5+y$, $0.5-z$. The symmetry operations for the atoms around Nd(n) ($n=2$ or 3) in the bond-angle columns are: b) i for $n=2$, and original for $n=3$; c) original for $n=2$, and ii for $n=3$; d) i for $n=2$, and ii for $n=3$.

atom of a longer P-S has the shorter Nd-S bond. The nitrogen atoms of bza ligands are not ligated to the central metal atom; the average Nd···N distance is 4.040 Å. The Nd-O bond lengths of this complex are about 0.047 Å shorter than those of the La(iPr$_2$dtp)$_3$-(dma)$_2$; this difference is also comparable to the difference in the ionic radii of Nd^{III} and La^{III}.[15] Therefore, the Nd-O bond lengths are shorter than those of the common oxygen-atom-ligating lanthanoid complexes (2.5 Å),[16,17,18] as in the case of the dma adduct of lanthanum.[1]

The positions of the coordinating oxygen atoms

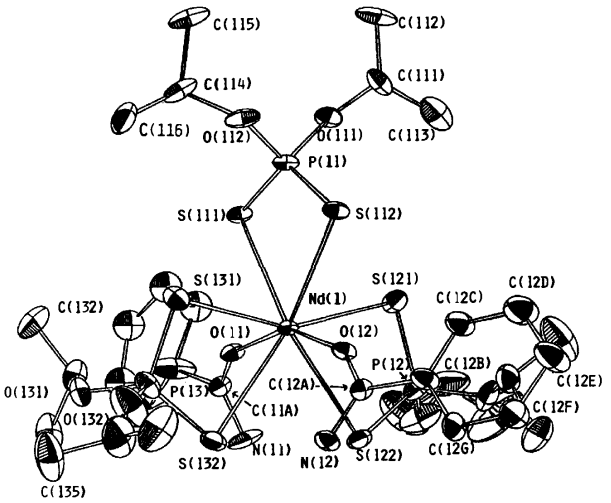

Fig. 1. A perspective drawing of the neodymium-(III) complex around Nd(1) atom with numbering scheme.

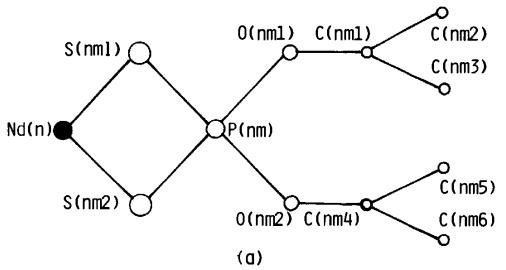

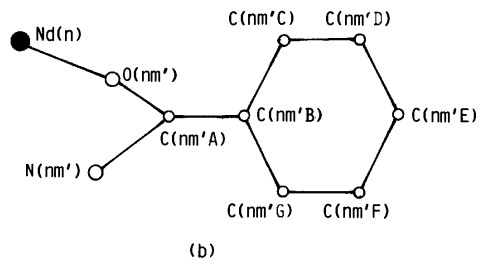

Fig. 2. Numbering scheme of the ligand atoms. a) iPr2dtp (where *n*: numbering of the central Nd(III) atom, 1—3; *m*: numbering of each iPr2dtp ligand, 1—3). b) bza (where *n*: numbering of the central Nd(III) atom, 1—3; *m'*: numbering of each bza ligand, 1—2).

of the title complex are different from those of the La(iPr2dtp)3(dma)2. This discrepancy is probably due to the bulkiness of the bza molecule. Although Pinkerton wrote that La(Et2dtp)3{(C6H5)3PO}2 is in a deformed square-antiprism geometry,[2c] it can also be regarded as in the deformed dodecahedron geometry. According to the latter aspect, two coordinating oxygen atoms of the complex take positions of the two tips of the base edge of a trapezium, like the titled complex.

The powder X-ray diffraction patterns of the M-(iPr2dtp)3(bza)2 (where M=La, Ce, Pr, Nd, Sm, Eu, and Gd) complexes show that they are all isomorphous.

The infrared-absorption spectral pattern of the title complex, benzamide, Na[Nd(iPr2dtp)4], and Na-

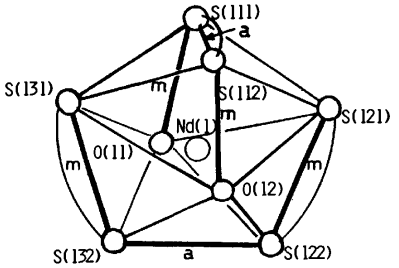

Fig. 3. Dodecahedron geometry around Nd(1) atom of the complex.

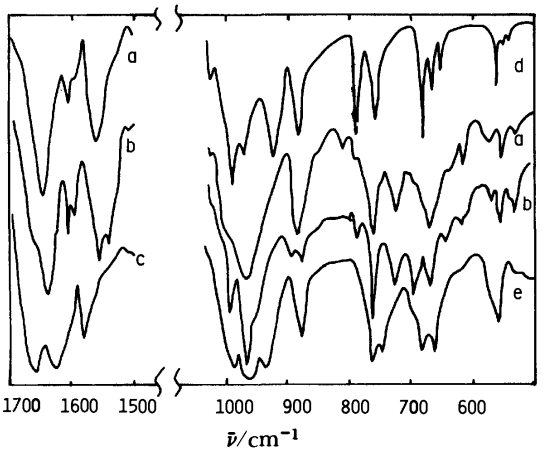

Fig. 4. Infrared spectra of the complex and some related compounds. a: [Nd(iPr2dtp)3(bza)2], b: [Er-(iPr2dtp)2(bza)3](iPr2dtp), c: bza, d: Na[Nd(iPr2dtp)4], e: Na(iPr2dtp).

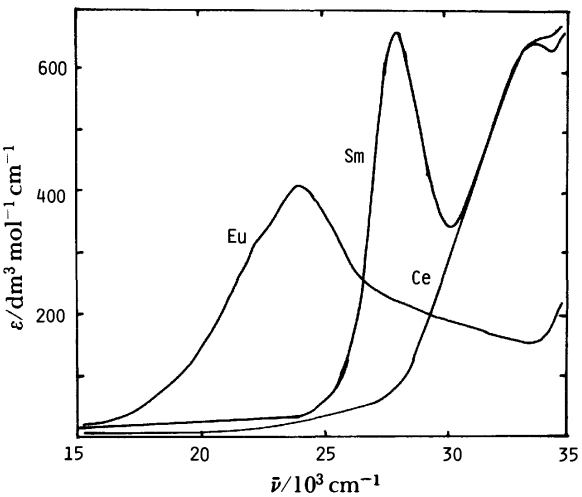

Fig. 5. Electronic spectra of [M(iPr2dtp)3(bza)2] type complexes (M=Ce, Sm, and Eu).

(iPr2dtp) are shown in Fig. 4. As all of the isomorphous complexes show almost the same spectral pattern, only the spectra of the neodymium(III) complex are shown. The amide I and II bands of bza appear at about 1660, 1623, and 1578 cm^{-1}, the former one seeming to split into two peaks. In the spectra of the neodymium complex, the corresponding peaks appear in a wave-number region about 20 cm^{-1} lower. The bands characteristic of the iPr2dtp ligand, ν_s(P–S)+ν_s(P–O), ν_{as}(P–O), and ν_{as}(P–S), which were expected to be found near the

700-cm^{-1} region, appeared at 783, 748, and 676 cm^{-1} in the spectra of the title complex. Their wave numbers are a little lower than those of the corresponding peaks of $Na[Nd(iPr_2dtp)_4]$.

The ultraviolet absorption spectra of the type of the cerium, samarium, and europium complexes in acetonitrile solutions (about 0.4—1.0×10^{-2} mol dm^{-3} in concentration) are shown in Fig. 5. The samarium and europium complexes show a very strong absorption in this region (Sm complex: ν_{max}=3.39×10^4 cm^{-1}, ε_{max}=6.4×10^2 dm^3 mol^{-1} cm^{-1}; Eu complex: ν_{max}= 4.27×10^4 cm^{-1}, ε_{max}=4.2×10^2 dm^3 mol^{-1} cm^{-1}). This kind of band has already been found in the spectra of the lanthanoid complexes where sulfur atoms ligate the central metal atom, and it has been assigned as a charge-transfer band.[3,5,19] However, these iPr_2dtp–bza mixed complexes are found to be more stable than any other compounds ever reported which show the absorption band.

The authors are greatly obliged to the Shin-Etsu Chemical Co., Ltd., for aiding this study by presenting the highly pure lanthanoid oxides. They also wish to thank Professor Yoichi Iitaka, The Faculty of Pharmaceutical Sciences, The University of Tokyo, for aiding in the calculations of this study. The present work was partially supported by a Grant-in-Aid for Scientific Research (No. 57430011) from the Ministry of Education, Science, and Culture.

References

1) K. Nagai, Y. Sato, S. Kondo, and A. Ouchi, *Bull. Chem. Soc. Jpn.*, **56**, 2605 (1983).
2) A. A. Pinkerton and D. Schwarzenbach, *J. Chem. Soc. Dalton Trans.*, a) **1981**, 1470; b) **1978**, 267; c) **1976**, 2466.
3) A. A. Pinkerton, Y. Meseri, and C. Rieder, *J. Chem. Soc., Dalton Trans.*, **1978**, 85.
4) A. A. Pinkerton and D. Schwarzenbach, *J. Chem. Soc. Dalton Trans.*, a) **1980**, 1300; b) **1976**, 2464.
5) M. Cianpolini, N. Nardi, P. Colamario, and P. Orioli, *J. Chem. Soc., Dalton Trans.*, **1977**, 379.
6) R. G. Pearson, *J. Chem. Educ.*, **45**, 581, 643 (1968).
7) Y. Meseri, A. A. Pinkerton, and G. Chapius, *J. Chem. Soc., Dalton Trans.*, **1977**, 725.
8) K. Nagai, R. Nakamura, M. Shimoi, and A. Ouchi, *Bull. Chem. Soc. Jpn.*, **57**, 2725 (1984).
9) "Universal Crystallographic Computation Program System (UNICS)," ed by T. Sakurai, Crystallographic Society of Japan, Tokyo (1967).
10) "International Tables for X-Ray Crystallography," Kynoch Press, Birmingham (1974), Vols III and IV.
11) $R=\sum||F_o|-|F_c||/\sum|F_o|$
12) The final thermal parameters and the final F_o–F_c table are deposited as Document No. 8438 at the Office of the Editor of Bull. Chem. Soc. Jpn.
13) Some additional data about bond lengths and bond angles, as well as the plane equations, the deviations of the atomic positions from the plane, and the dihedral angles between them of the trapezia of dodecahedrons, are also deposited as Document No. 8438 at the Office of the Editor of Bull. Chem. Soc. Jpn.
14) L. N. Kuleshova and P. M. Zorkii, *Acta Crystallogr., Sect B*, **37**, 1368 (1981).
15) R. D. Shannon, *Acta Crystallogr., Sect A*, **32**, 751 (1976).
16) L. A. Aslanov, M. A. Porai-Koshits, and M. O. Dekaprilevich, *Zh. Strukt. Khim.*, **12**, 470 (1971).
17) S. Kondo, M. Shimoi, A. Ouchi, and T. Takeuchi, *Bull. Chem. Soc. Jpn.*, **55**, 2840 (1982).
18) Y. Koizumi, H. Sawase, Y. Suzuki, M. Shimoi, and A. Ouchi, *Bull. Chem. Soc. Jpn.*, **57**, 1677 (1984).
19) L. J. Nugent, R. D. Baybarz, J. L. Brnett, and R. L. Ryan, *J. Phys. Chem.*, **77**, 1528 (1973).

A Nuclear Magnetic Resonance Study of the Kinetics of Ligand Exchange Reactions in Uranyl Complexes. VI. *N,N*-Dimethylformamide Exchange in Bis(acetylacetonato) (*N,N*-dimethylformamide)dioxouranium(VI)

Yasuhisa IKEDA, Hiroshi TOMIYASU, and Hiroshi FUKUTOMI*

Research Laboratory for Nuclear Reactors, Tokyo Institute of Technology, Ookayama, Meguro-ku, Tokyo 152

(Received May 4, 1984)

The exchange reaction of *N,N*-dimethylformamide(dmf) in $[UO_2(acac)_2dmf]$(acac=acetylacetonato) has been studied by the NMR line-broadening method in CD_3COCD_3 and CD_2Cl_2. In CD_3COCD_3, the rate of dmf exchange is independent of the free DMF concentration. The rate constant(s^{-1}) at 25 °C and activation parameters $\Delta H^{\ddagger}$(kJ mol^{-1}) and $\Delta S^{\ddagger}$(JK^{-1} mol^{-1}) are 1.19×10^3, 42.0±1.3, and −45.8±5.5, respectively. In CD_2Cl_2, the exchange rate depends on the free DMF concentration. The exchange rate constant (k_{ex}) is expressed by $k_{ex}=k_1+k_2$[DMF], where k_1(25 °C)$=1.90\times10^2$ s^{-1}, $\Delta H^{\ddagger}=32.8\pm1.7$ kJ mol^{-1}, and $\Delta S^{\ddagger}=-92.0\pm5.9$ JK^{-1} mol^{-1}, and k_2 (25 °C)$=5.66\times10^3$ M^{-1} s^{-1}(1M=1 mol dm^{-3}), $\Delta H^{\ddagger}=37.0\pm2.1$ kJ mol^{-1}, and $\Delta S^{\ddagger}=-49.6\pm8.8$ JK^{-1} mol^{-1}. The D and I mechanisms are proposed for the dmf exchange in $[UO_2(acac)_2$ dmf].

The uranyl β-diketonato complexes, $[UO_2(\beta$-diketonato$)_2L]$ (L=adduct ligand) have been studied extensively in view of the extraction of uranyl ions[1] and the IR laser separation of uranium isotopes.[2] In particular, the synergistic effect on the extraction[1] and the relationship between the bond-strength and basicity[3] have been studied for the adduct ligands. However, only limited kinetic data are available with respect to the reactivity of adduct ligands.[4,5]

Recently, we studied exchange reactions of dimethyl sulfoxide(dmso) in $[UO_2(acac)_2$dmso] and $[UO_2(dbm)_2$ dmso] (dbm=dibenzoylmethanate) by using NMR[6] and proposed the exchange mechanism to be either D or I.[7] The dmso exchange rates in these complexes are much slower than that in $[UO_2(dmso)_5]^{2+}$.[8] This result suggests that the steric hindrance is regarded as significant for the ligand exchange reactions in uranyl complexes. In order to examine the steric effect on the ligand exchange reaction in uranyl complexes and the relationship between the reactivity and basicity of adduct ligands, the exchange reaction of dmf in $[UO_2(acac)_2\cdot$dmf] was studied and compared with the dmso exchange in $[UO_2(acac)_2$dmso] and the dmf exchange in $[UO_2(dmf)_5]^{2+}$.[9]

Experimental

The $[UO_2(acac)_2$dmf] complex was prepared by the same method as described in a previous paper.[5] Calcd for $[UO_2(acac)_2$dmf]: C, 28.84; H, 4.28; N, 2.59. Found: C, 28.79; H, 3.89; N, 2.55. Acetone-d_6 (CD_3COCD_3, Merck 99.8%) and dichloromethane-d_2 (CD_2Cl_2, Merck 99%), which were used as solvents, were dried over 3A and 4A molecular sieves (Wako Pure Chemical Ind. Ltd.), respectively. *N,N*-Dimethylformamide (Wako) was distilled over barium oxide *in vacuo*, followed by distillation with molecular sieves, and stored over 3A molecular sieves. Sample solutions for NMR measurements were prepared by weighing the complex, DMF and solvents in a 1 cm^3 volumetric flask and some of each solution was placed in an NMR sample tube and sealed. All samples were prepared in a glove box filled with dried nitrogen. The measurement of the ^1H NMR spectra was carried out at 100 MHz on a JEOL JNM FX-100 FT-NMR spectrometer equipped with a JNM-VT-3B temperature controller. The infrared spectra of $[UO_2(acac)_2\cdot$dmf] in CD_2Cl_2 were recorded in the 200—4000 cm^{-1} range by using a JASCO DS-701G IR spectrophotometer. The dmf exchange reaction in $[UO_2(acac)_2$dmf] was measured by the NMR linebroadening method. The kinetic parameters were calculated by using a computer program on the assumption of a two-site exchange process as described in the previous paper.[5]

Results and Discussion

The Structure of $[UO_2(acac)_2dmf]$ in Solutions. Figure 1 shows the ^1H NMR spectrum of a solution containing $[UO_2(acac)_2\cdot$dmf], DMF, and CD_3COCD_3 at −75 °C. In the spectrum, signals (a) and (d) are assigned to the methyl protons and the 3-H protons of coordinated acac, respectively, and signals (b) and (c), and signals (e) and (f) are the methyl protons, and the formyl protons of free and coordinated DMF, respectively. The area ratio of (f) to (d) to (c) to (a) was 1:2:6:12, and this ratio remained constant in solutions i, ii, and iii listed in Table 1. This fact indicates

TABLE 1. SOLUTION COMPOSITION AND KINETIC PARAMETERS FOR THE EXCHANGE OF dmf IN $[UO_2(acac)_2$dmf]

Solution	$[UO_2(acac)_2dmf]$	[DMF][a]	$[CD_3COCD_3]$	$[CD_2Cl_2]$	$\Delta H^{\ddagger}$	$\Delta S^{\ddagger}$	k_{ex}(25 °C)[b]
	10^{-2} M	10^{-2} M	M	M	kJ mol^{-1}	J mol^{-1} K^{-1}	10^3 s^{-1}
i	3.25	3.83	13.6		42.0±1.3	−45.8±5.5	1.19
ii	6.45	6.57	13.4		42.0±1.3	−46.2±5.5	1.14
iii	6.61	11.2	13.3		43.7±1.1	−38.6±5.0	1.44
iv	2.73	2.87		15.2	k_1 pathway		
v	11.0	12.0		14.8	32.8±1.7	−92.0±5.9	0.190
vi	11.6	21.5		14.7	k_2 pathway		
vii	14.6	35.7		14.6	37.0±2.1	−49.6±8.8	5.66

a) Added as DMF. b) Calculated values from $\Delta H^{\ddagger}$ and $\Delta S^{\ddagger}$ at 25 °C.

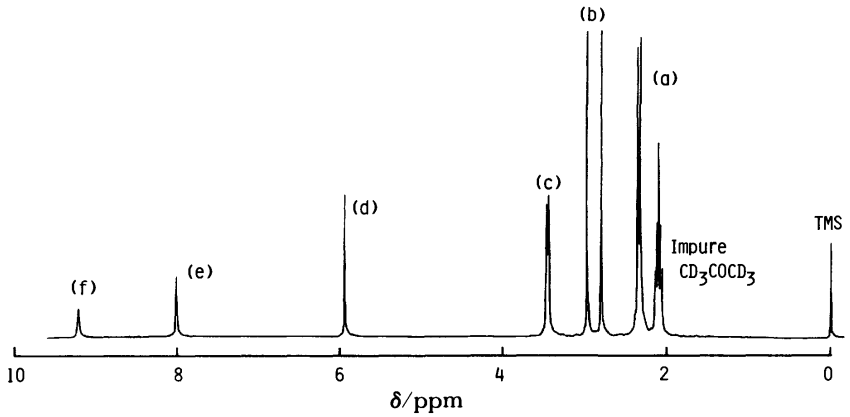

Fig. 1. The ^1H NMR spectrum of a solution containing of $[UO_2(acac)_2dmf]$ (0.0661 M), DMF (0.112 M), and CD_3COCD_3 (13.3 M) at −75°C.

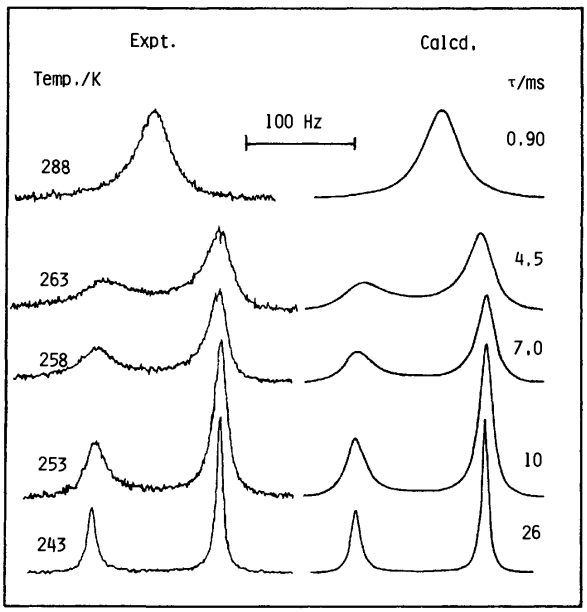

Fig. 2. Experimental (left side) and best-fit calculated lineshapes of a solution containing $[UO_2(acac)_2dmf]$ (0.0661 M), DMF (0.112 M), and CD_3COCD_3 (13.3 M). Temperatures and best-fit t values are shown at left and right sides of the figure, respectively.

that two acac ions and one DMF molecule coordinate to a uranyl ion. The singlet signal of the 3-H protons means that two coordinated acac ions are bidentate ligands. Therefore, the structure of $[UO_2(acac)_2dmf]$ is presumed to be pentagonal bipyramidal, which is the same as those of $[UO_2(acac)_2dmso]$ and $[UO_2(acac)_2\cdot H_2O]$.[6,10] This structure is supported by the separation of the methyl protons of the coordinated acac, because in such a structure the two methyl groups of the coordinated acac are in different magnetic environments, *i.e.* the nearest group to and the farthest group from the coordinated dmf.

In CD_2Cl_2, similar phenomena were also observed in the ^1H NMR spectra. The IR spectra of $[UO_2(acac)_2dmf]$ measured in CD_2Cl_2 showed that the C–O stretching for the coordinated dmf was observed at 1652 cm^{-1}, which was 27 cm^{-1} lower than that observed in pure DMF (1675 cm^{-1}). It has been known that the C–O stretching, so-called Amide I, will shift to a lower side when DMF coordinated through oxygen.[11,12] Hence, the observed band of C–O stretching indicates that dmf in $[UO_2(acac)_2dmf]$ is coordinated through oxygen. In addition, only one band corresponding to the carbonyl vibration of coordinated acac was observed at 1574 cm^{-1}. This result indicates that acac ions in $[UO_2(acac)_2dmf]$ are coordinated as the bidentate, since the frequency less than 1600 cm^{-1} is characteristic of the carbonyl vibration of chelated metal β-diketonato complexes.[13] On the basis of these results, it is concluded that $[UO_2(acac)_2dmf]$ has a pentagonal bipyramidal structure in CD_3COCD_3 and CD_2Cl_2.

dmf Exchange in $[UO_2(acac)_2dmf]$. The formyl proton signals of the coordinated and free DMF were measured at various temperatures. Results are shown in Fig. 2. This figure shows that DMF molecule exchanges between the coordinated and free sites. The best-fit life times (τ values) were determined by using a computer program for the two-site exchange[14] and are shown at the right side in Fig. 2 together with the corresponding line shapes. From these τ values, the first-order rate constants, k_{ex}, were calculated by the following equations, where τ and P with the subscripts f and c are the life times and mole fractions of the free and coordinated sites, respectively.

$$\tau = P_f\tau_c = P_c\tau_f \quad (1)$$

$$k_{ex} = 1/\tau_c = \text{rate}/[UO_2(acac)_2dmf] = (kT/h)\exp(-\Delta H^*/RT)\exp(\Delta S^*/R), \quad (2)$$

The same measurements were carried out for the solutions with different compositions listed in Table 1. In Fig. 3, the values of k_{ex} are plotted semi-logarithmically against the reciprocal temperature. The activation parameters obtained from Fig. 3 are listed in Table 1. As can be seen in Fig. 3 and Table 1, the exchange rate of dmf in CD_3COCD_3 is independent of [DMF], while that in CD_2Cl_2 is dependent on [DMF]. Plots of k_{ex} values against [DMF] are linear in CD_2Cl_2(Fig. 4) and result in the following equation.

$$k_{ex} = k_1 + k_2[DMF] \quad (3)$$

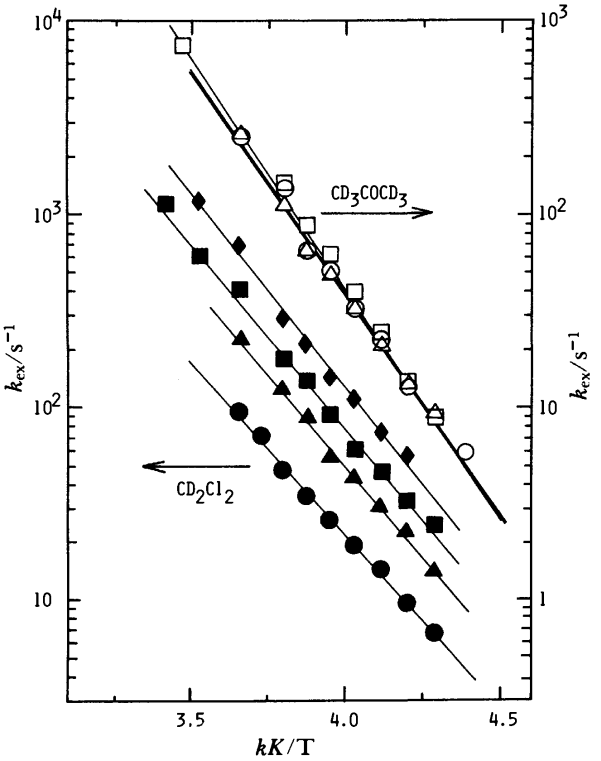

Fig. 3. Semilogarithmic plots of k_{ex} against the reciprocal temperature for the exchange of dmf in $[UO_2(acac)_2dmf]$ in CD_3COCD_3 and CD_2Cl_2. The symbols of ○, △, □, ●, ▲, ■, and ◆, correspond to i, ii, iii, iv, v, vi, and vii solutions in Table 1.

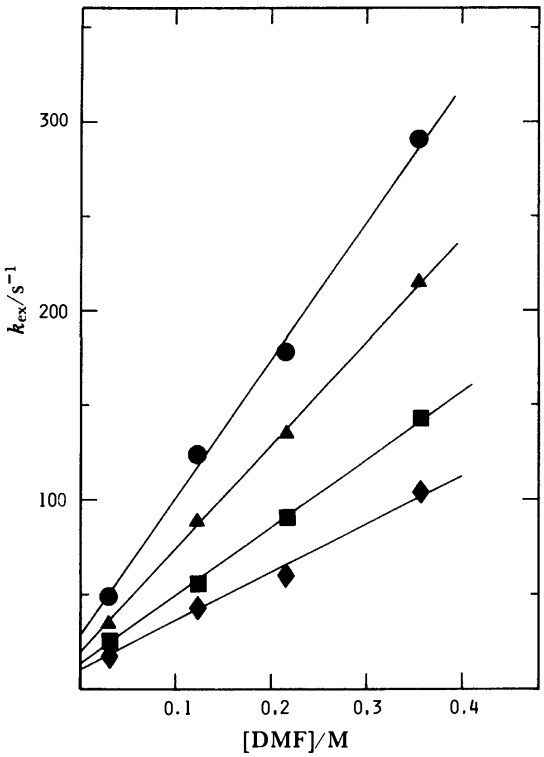

Fig. 4. plots of k_{ex} *vs.* [DMF] for the exchange of dmf in $[UO_2(acac)_2dmf]$ in CD_2Cl_2. ●: −10°C; ▲: −15°C; ■: −20°C; ◆: −25°C.

The values of k_1 and k_2 were obtained from the intercepts and the slopes of the plots in Fig. 4 by means of the least-squares method, and are listed in Table 2. The activation parameters for these pathways are given in Table 1.

Exchange Mechanism. The exchange rate of dmf in $[UO_2(acac)_2\cdot dmf]$ in CD_3COCD_3 is independent of the free DMF concentration. This result suggests that the dmf exchange in CD_3COCD_3 proceeds through either the D or I mechanism.[7] In the D mechanism, the exchange processes are expressed as

$$UO_2(acac)_2dmf + DMF^* \xrightarrow[\text{slow}]{k_d} UO_2(acac)_2 + DMF + DMF^* \xrightarrow[\text{fast}]{} UO_2(acac)_2dmf^* + DMF, \quad (4)$$

where an asterisk is used to denote the exchanging species. In this mechanism, the rate-determining step is the dissociation of the coordinated dmf from $[UO_2(acac)_2dmf]$. Thus, k_{ex} is given by

$$k_{ex} = k_d \quad (5)$$

In the I mechanism, the exchange processes are represented as follows.

$$UO_2(acac)_2dmf + DMF^* \underset{\text{fast}}{\overset{K_{os}}{\rightleftharpoons}} UO_2(acac)_2dmf\cdots DMF^* \xrightarrow[\text{slow}]{k_I} UO_2(acac)_2dmf^*\cdots DMF \longrightarrow UO_2(acac)_2dmf^* + DMF, \quad (6)$$

where K_{os} is the formation constant of the outer-sphere complex, $UO_2(acac)_2dmf\cdots DMF^*$, and k_I is the rate constant for the interchange of dmf molecule between the first and second coordination spheres. In this mechanism, k_{ex} is given by Eq. (7).

$$k_{ex} = k_I K_{os}[DMF]/(1+K_{os}[DMF]) \quad (7)$$

If $K_{os}[DMF] \gg 1$, Eq. (7) can be simplified as

$$k_{ex} = k_I. \quad (8)$$

Equations (5) and (8) are compatible with the experimental results. However, the I mechanism seems to be unlikely for the following reasons. In the I mechanism, the condition of $K_{os}[DMF] \gg 1$ must be satisfied over the DMF concentration range (0.0383—

Table 2. The values of k_1 and k_2 at various temperatures for the exchange of dmf in $[UO_2(acac)_2dmf]$ in CD_2Cl_2

Temp	k_1	k_2
°C	$10\,s^{-1}$	$10^2\,M^{-1}\,s^{-1}$
−10	2.82±0.72	7.26±0.33
−15	2.01±0.24	5.45±0.11
−20	1.44±0.13	3.56±0.58
−25	1.08±0.38	2.54±0.18

0.112 M) employed in this study. This indicates that K_{os} should be at least larger than 50 M^{-1}. However, such a value of K_{os} is too large considering that the reactants $[UO_2(acac)_2dmf]$ and DMF are both uncharged. On the other hand, the four-coordinated intermediate in the equatorial plane should be formed in the D mechanism. This is supported by the fact that some uranyl complexes, *e.g.* $[UO_2(H_2O)_4]^{2+}$,[15,16] $[UO_2(hmpa)_4]^{2+}$[17] (hmpa=hexamethylphosphoric triamide), exist in solution as a tetragonal bipyramidal structure.

In CD_2Cl_2, the dmf exchange occurs through two pathways as seen in Fig. 4. The k_1 pathway, where the exchange rate is independent of the free DMF concentration, is considered to be the same D mechanism as the dmf exchange in CD_3COCD_3. The k_2 pathway exhibits a first-order dependence with respect to the free DMF concentration and seems to proceed through either the I or A mechanism.[7] In the A mechanism, the dmf exchange processes are expressed as

$$UO_2(acac)_2dmf + DMF^* \xrightarrow[slow]{k_a} UO_2(acac)_2dmf\cdot dmf^* \xrightarrow[fast]{} UO_2(acac)_2dmf^* + DMF, \quad (9)$$

where the rate-determining step is the coordination of DMF to $[UO_2(acac)_2dmf]$, followed by the formation of six-coordinated intermediate in the equatorial plane. Hence, if the dmf exchange in CD_2Cl_2 proceeds through the D and A mechanisms, k_{ex} is given by Eq. (10).

$$k_{ex} = k_d + k_a[DMF] \quad (10)$$

On the other hand, if the dmf exchange proceeds through the D and I mechanisms, k_{ex} is given by Eq. (11).

$$k_{ex} = \frac{k_d + k_I K_{os}[DMF]}{1 + K_{os}[DMF]} \quad (11)$$

When $K_{os}[DMF] \ll 1$, Eq. (11) becomes Eq. (12).

$$k_{ex} = k_d + k_I K_{os}[DMF] \quad (12)$$

Both of Eqs. (10) and (12) are compatible with Eq. (3). Although it has been known that the uranyl ion forms six-coordinated complexes in the equatorial plane with small ligands,[18] the A mechanism for the k_2 pathway seems to be unlikely, because the coordinated acac is a bulky chelating ligand and may make it difficult to form a six-coordinated intermediate in the equatorial plane of $[UO_2(acac)_2dmf]$. On the other hand, if the k_2 pathway proceeds through the I mechanism, the condition of $K_{os}[DMF] \ll 1$ has to be satisfied. This condition seems to be fulfilled in the present exchange reaction, since both of $[UO_2(acac)_2dmf]$ and DMF are uncharged and hence the K_{os} vlaue is expected to be relatively small. In fact, the corresponding K_{os} value to the dmso exchange in$[UO_2(acac)_2dmso]$ in CD_2Cl_2 is *ca.* 5 M^{-1}.[6] Taking into account Gutmann's donor number[19] that the basicity of DMF is smaller than that of DMSO, the K_{os} value for tbe present exchange reaction is supposed to be smaller than 5 M^{-1} and satisfies the condition mentioned above in the DMF concentration range 0.0287 to 0.357 M (Table 1). Therefore, it is suggested that the dmf exchange in $[UO_2(acac)_2dmf]$ in CD_2Cl_2 proceeds through both the D and I mechanisms.

The difference in mechanisms observed in two solvents CD_3COCD_3 and CD_2Cl_2, which was also observed in the dmso exchange in $[UO_2(acac)_2dmso]$ and $[UO_2(dbm)_2dmso]$ in the same two solvents,[6] may primarily be due to the difference in basicity and dielectric constant of these solvents. Acetone has a relatively large basicity compared with dichloromethane and tends to preferentially solvate to the second coordination sphere of $[UO_2(acac)_2dmf]$ under the present experimental conditions. This preferential solvation may block the access of DMF molecule to the outer-sphere of $[UO_2(acac)_2dmf]$. Moreover, the dielectric constant of acetone (20.7) is fairly larger than that of dichloromethane(8.93). These factors may lead to the smaller K_{os} value in CD_3COCD_3 than that in CD_2Cl_2. This is consistent with the results that the dmf exchange in CD_3COCD_3 proceeds through only the D mechanism, while that in CD_2Cl_2 proceeds through both the D and I mechanisms. In spite of the result that the dmf exchange in $[UO_2(acac)_2dmf]$ proceeds through the D and I mechanisms, activation entropies have large negative values. This may be attributed to the contribution of solvent rearrangement around the complex as proposed by Benneto and Caldin.[20]

It is of interest to compare the dmf exchange in $[UO_2(acac)_2dmf]$ with that in $[UO_2(dmf)_5]^{2+}$ and the dmso exchange in $[UO_2(acac)_2dmso]$, whose kinetic parameters are summarized in Table 3. It was not clear which mechanism (I_d or I_a) is reasonable for the dmf exchange in $[UO_2(dmf)_5]^{2+}$. The fact that the dmf ex-

TABLE 3. KINETIC PARAMETERS FOR THIS WORK AND RELATED REACTIONS[a]

Reaction	Mechanism	ΔH^*	ΔS^*	Rate constant(25 °C)[b]	Ref.
		kJ mol^{-1}	JK^{-1} mol^{-1}	s^{-1}	
$[UO_2(dmf)_5]^{2+}$+DMF	D	42.0±2.1	−15.1±3.3	4.70×10^4	9
	I	48.3±0.9	38.6±2.6	2.34×10^6	9
$[UO_2(acac)_2dmf]$+DMF	D	32.8±1.7	−92.0±5.9	1.90×10^2	This work
	I	37.0±2.1[c]	−49.6±8.8[c]	$5.66\times10^3/M^{-1}$ [c]	This work
$[UO_2(acac)_2dmso]$+DMSO	D	47.9±5.2	−46.6±11.2	1.02×10^2	6
	I	35.4±12.4	−69.7±20.5	1.01×10^3	6

a) In CD_2Cl_2 solvent. b) Calculated values from ΔH^* and ΔS^* at 25 °C. c) The values of kinetic parameters for $k_I K_{os}$.

change rate in $[UO_2(acac)_2dmf]$ becomes slower than that in $[UO_2(dmf)_5]^{2+}$ suggests that the dmf exchange in $[UO_2(dmf)_5]^{2+}$ proceeds through the I_a mechanism, since if the exchange occurs associatively, the exchange rate is expected to be reduced with crowding at the reaction site. In the ligand(L) exchange in $[UO_2(acac)_2L]$ (L=dmso or dmf) proceeding through the D mechanism, the rate constant for the dmf exchange is larger than that for the dmso exchange. This may be due to the fact that the basicity of DMF is smaller than that of DMSO, and hence the bond-strength between UO_2^{2+} and dmf in $[UO_2(acac)_2dmf]$ is expected to be weaker than that between UO_2^{2+} and dmso in $[UO_2(acac)_2dmso]$, because the rate-determining step is the dissociation of dmf or dmso in the D mechanism. This is supported by the result that the ΔH^* value for the dmf exchange is smaller than that for the dmso exchange. Since the kinetic parameters in the I mechanism for the dmf exchange in $[UO_2(acac)_2dmf]$ are obtained for k_1K_{os}, it is difficult to compare directly with the kinetic parameters for the dmso exchange in $[UO_2(acac)_2dmso]$. The K_{os} value is considered to be smaller than that for the dmso exchange in $[UO_2(acac)_2dmso]$ (*ca.* $5\,M^{-1}$). Therefore,the k_1 value for the dmf exchange in $[UO_2(acac)_2dmf]$ should be larger than $1.01\times10^3\,s^{-1}$ (Table 3) for the dmso exchange in $[UO_2(acac)_2\cdot dmso]$. This suggests that the I mechanism for the exchange of L in $[UO_2(acac)_2L]$ (L=dmso or dmf) is not I_a but I_d on the basis of the same reasons as described above. It might be concluded that the D mechanism is the major process for the exchange of L in $[UO_2(\beta\text{-diketonato})_2L]$ complexes because of the steric hindrance.

The present work was partially supported by a Grant-in-Aid for Scientific Research No. 57470035 from the Ministry of Education, Science and Culture, and by the International Joint Research Program sponsored by the Japan Society for the Promotion of Science.

References

1) T. V. Healy, D. F. Peppard, and G. W. Mason, *J. Inorg. Nucl. Chem.*, **24**, 1429 (1962); M. S. Subramanian and A. Viswanatha, *ibid.*, **31**, 2575 (1969); J. M. Haigh and D. A. Thoronton, *ibid.*, **33**, 3001 (1971).

2) A. Kaldor, R. B. Hall, D. M. Cox, J. A. Horsley, P. Rabinowitz, and G. M. Kramer, *J. Am. Chem. Soc.*, **101**, 4465 (1979); D. M. Cox, R. B. Hall, J. A. Horsley, G. M. Kramer, P. Rabinowitz, and A. Kaldor, *Science*, **205**, 390 (1979); A. Ekstrom, H. J. Hurst, C. H. Randall, and H. Loeh, *J. Phys. Chem.*, **84**, 2626 (1980); R. G. Bray, D. M. Cox, R. B. Hall, J. A. Horsley, A. Kaldor, G. M. Kramer, M. R. Levy, and E. B. Priestley, *ibid.*, **87**, 429 (1983).

3) G. M. Kramer, E. T. Maas, Jr., and M. B. Dines, *Inorg. Chem.*, **20**, 1415, 1418 (1981); R. B. Bray and G. M. Kramer, *ibid.*, **22**, 1843 (1983).

4) G. M. Kramer, M. B. Dines, R. Kastrup, M. T. Melchior, and E. T. Maas, Jr., *Inorg. Chem.*, **20**, 3 (1981).

5) Y. Ikeda, H. Tomiyasu, and H. Fukutomi, *Inorg. Chem.*, **23**, 1356 (1984).

6) Y. Ikeda, H. Tomiyasu, and H. Fukutomi, *Bull. Chem. Soc. Jpn.*, **56**, 1060 (1983).

7) C. H. Langford and H. B. Gray, "Ligand Substitution Processes," Benjamin, London (1974).

8) Y. Ikeda, H. Tomiyasu, and H. Fukutomi, *Bull. Res. Lab. Nuclear Reactor (Tokyo Inst. Tech.)*, **4**, 47 (1979).

9) H. Doine, Y. Ikeda, H. Tomiyasu, and H. Fukutomi, *Bull. Chem. Soc. Jpn.*, **56**, 1989 (1983).

10) E. Frasson, G. Bombieri, and C. Panattoni, *Coord. Chem. Rev.*, **1**, 145 (1966).

11) C. D. Schmulbach and R. S. Drago, *J. Am. Chem. Soc.*, **82**, 4484 (1960).

12) S. T. Kuhn and J. S. McIntyre, *Can. J. Chem.*, **43**, 375 (1965).

13) K. Nakamoto, "Infrared and Raman Spectra of Inorganic and Coordination Compounds," John Wiley & Sons, New York (1978).

14) G. Binsch, *Top. Stereochem.*, **3**, 97 (1968).

15) Y. Ikeda, S. Soya, H. Tomiyasu, and H. Fukutomi, *J. Inorg. Nucl. Chem.*, **41**, 1333 (1979).

16) A. Fratiello, V. Kubo, and R. E. Schuster, *Inorg. Chem.*, **10**, 744 (1971).

17) A. Fratiello, G. A. Vidlich, C. Cheng, and V. Kubo, *J. Solution Chem.*, **1**, 433 (1972).

18) I. I. Chernyaev, "Complex Compounds of Uranium," (Translated from Russian), Israel Program for Scientific Translations, Jerusalem (1966).

19) V. Gutmann and R. Schmid, *Coord. Chem. Rev.*, **12**, 263 (1974).

20) H. P. Benneto and E. F. Caldin, *J. Chem. Soc., A*, **1971**, 2198.

Magnetic Circular Dichroism and Electronic Absorption Spectra of Mixed (Amine)(carboxylato) Complexes with the $[Pd(N)_n(O)_{4-n}]$-type (n=0—4)

Kazuhiko NAKAYAMA,* Takashi KOMORITA, and Yoichi SHIMURA
Department of Chemistry, Faculty of Science, Osaka University, Toyonaka, Osaka 560
(Received March 29, 1984)

Mixed-ligand $[Pd(N)_n(O)_{4-n}]$-type complexes constituting a long systematic series (n=0—4) were synthesized. Ammonia, ethylenediamine, *rac*-propylenediamine, trimethylenediamine, glycinate, β-alaninate, acetate, oxalate, and malonate were employed as ligands. Their magnetic circular dichroism (MCD) and electronic absorption spectra were discussed together with the CD spectra of the corresponding optically active complexes. The results strongly suggest that the dispersion of MCD observed in the spin-allowed d-d region is primarily a composite of B terms. Moreover, the MCD in the charge transfer region was found to be qualitatively additive with respect to contributions by the constituent ligands. From a detailed examination of the spin-allowed d-d absorption bands, it is noted that the substitution of an *N,O*-ligand for an *N,N*-ligand largely affects neither the band area nor band width whereas that of an *O,O*-ligand for an *N,O*-ligand does.

The concurrent examination of absorption, magnetic circular dichroism(MCD), and CD spectra furnished useful information on the electronic structures of *cis*- and *trans*- $[Pd(Cl)_2(N)_2]$-type complexes.[1] In the preceding paper,[2] we reported the synthesis of a large number of mixed-ligand $[Pd(N)_n(O)_{4-n}]$-type complexes with at least one optically active ligand and the detailed investigation of the CD spectra.

In the present work, optically inactive $[Pd(N)_n(O)_{4-n}]$-type complexes were synthesized corresponding to the previous optically active comlexes,[2] and their MCD spectra were examined. Although most of the former complexes were found to be more labile than the latter, the systematized synthetic methods developed previously[2] were effective. Ammonia, ethylenediamine(en), *rac*-propylenediamine(*rac*-pn), and trimethylenediamine(tn) were employed as *N*- or *N,N*-ligands; glycinate(gly) and β-alaninate(β-ala) were as *N,O*-ligands; and acetate, oxalate(ox), and malonate(mal) were as *O*- or *O,O*-ligands. Di-μ-hydroxodipalladium complexes were also obtained. Although these complexes, if approximated by a D_{4h} symmetry, are expected to exhibit A-term MCD based on $^1E_g \leftarrow {}^1A_{1g}$ in the d-d transition region, our spectral examination indicates that the contribution of the A term is minor and that inherent B terms generally predominate irrespective of the symmetries of the complexes, unlike in the case of $[MCl_4]^{2-}$ (M=Pt and Pd)[3] and *cis*-$[Pd(Cl)_2(N)_2]$-type complexes.[1] Although three or four spin-allowed d-d transitions should occur in a D_{4h} or lower symmetries, the spin-allowed d-d absorption bands of the series of complexes appear only as a single broad unsymmetrical band. These bands are analyzed in terms of band area and the band shape parameters,[1] and the influence of ligands on the band shape and band area is discussed.

Experimental

$[Pd(N)_4]$-type Complexes. *1) $[Pd(NH_3)_4](ClO_4)_2$*: This complex was obtained by metathesis of the corresponding chloride with the calculated amount of silver perchlorate. Found: H, 3.33; N, 14.97%. Calcd for $H_{12}N_4Cl_2O_8Pd$: H, 3.24; N, 15.00%.

2) $[Pd(en)(NH_3)_2]Cl_2$: This complex was prepared in the same manner as for $[Pd(S\text{-pn})(NH_3)_2]Cl_2$,[2] but ethanol was used for crystallization in place of ether. Yield: 70%. Found: C, 8.99; H, 5.20; N, 20.52%. Calcd for $C_2H_{14}N_4Cl_2Pd$: C, 8.85; H, 5.20; N, 20.64%.

3) $[Pd(en)(tn)]Cl_2$: This was prepared from $[PdCl_2(en)]$ in the same way as for $[Pd(S\text{-pn})(tn)]Cl_2$[2] but crystallized from a methanol–ethanol medium instead of an ethanol–ether one. Yield: 80%. Found: C, 19.23; H, 5.79; N, 17.94%. Calcd for $C_5H_{18}N_4Cl_2Pd$: C, 19.28; H, 5.82; N, 17.98%.

4) $[PdL(N,N\text{-}Et_2en)]Cl_2$ (L=en and tn): These complexes were prepared by methods similar to those for the corresponding (2*S*)-N^1,N^1-diethyl-1,2-propanediamine(N^1,N^1-Et_2-(*S*)-pn) complexes.[2] Yield: 75—85%. Found: C, 24.79; H, 7.20; N, 14.32%. Calcd for $[Pd(en)(N,N\text{-}Et_2en)]Cl_2\cdot 2H_2O$=$C_8H_{28}N_4Cl_2O_2Pd$: C, 24.66; H, 7.24; N, 14.38%. Found: C, 28.20; H, 7.31; N, 14.55%. Calcd for $[Pd(tn)(N,N\text{-}Et_2en)]Cl_2\cdot H_2O$=$C_9H_{28}N_4Cl_2OPd$: C, 28.03; H, 7.32; N, 14.53%.

5) $[PdL_2]Cl_2$ (L=N,N-Et₂en and N,N,C,C-Me₄en):[4] These were obtained in a way similar to that for $[Pd(N^1,N^1\text{-}Et_2\text{-}(S)\text{-pn})_2]Cl_2$.[5] Found: C, 35.15; H, 7.92; N, 13.63%. Calcd for $[Pd(N,N\text{-}Et_2en)_2]Cl_2$=$C_{12}H_{32}N_4Cl_2Pd$: C, 35.18; H, 7.87; N, 13.67%. Found: C, 32.40; H, 8.14; N, 12.61%. Calcd for $[Pd(N,N,C,C\text{-}Me_4en)_2]Cl_2\cdot 2H_2O$=$C_{12}H_{36}N_4Cl_2O_2Pd$: C, 32.33; H, 8.14; N, 12.57%.

6) Other Complexes: The complexes $[Pd(en)_2]Cl_2$ and $[Pd(tn)_2]Cl_2$ were obtained according to the method described in the literature[6] or the one similar to it. Found: C, 16.18; H, 5.43; N, 18.83%. Calcd for $[Pd(en)_2]Cl_2$=$C_4H_{16}N_4Cl_2Pd$: C, 16.15; H, 5.42; N, 18.83%. Found: C, 22.20; H, 6.24; N, 17.14%. Calcd for $[Pd(tn)_2]Cl_2$=$C_6H_{20}N_4Cl_2Pd$: C, 22.13; H, 6.19; N, 17.21%.

$[Pd(N)_3(O)]$-type Complexes. *1) $[Pd(gly)(NH_3)_2]ClO_4$*: Silver perchlorate (246 mg) and freshly prepared silver oxide (140 mg) were successively added to a suspension of 250 mg of *cis*-$[PdCl_2(NH_3)_2]$[7] in 10 cm^3 of water and the mixture was stirred at room temperature for 10 min in the dark. Immediately after removal of the silver chloride the filtrate was mixed with an aqueous solution (1 cm^3) of 89 mg of glycine, evaporated to *ca.* 4 cm^3 under reduced pressure, and chilled in an ice-bath. After 2 h lemon yellow crystals were collected, washed with cold water, and dried in air. Yield: 200 mg. Found: C, 7.73; H, 3.27; N, 13.34%. Calcd for $C_2H_{10}N_3ClO_6Pd$: C, 7.65; H, 3.21; N, 13.38%.

2) $[Pd(gly)L]ClO_4$ (L=en and tn): Each of these complexes was prepared by the method adopted for $[Pd(S\text{-ala})(S\text{-pn})]ClO_4$[2] but crystallized from a water–methanol medium. The crude product was recrystallized from warm water (*ca.* 60 °C). Yield: 55 (en) and 75% (tn complex). Found: C, 14.31; H, 3.60; N, 12.36%. Calcd for $[Pd(gly)(en)]ClO_4$=$C_4H_{12}N_3ClO_6Pd$: C, 14.13; H, 3.56; N, 12.36%. Found: C, 17.09; H, 4.03; N, 11.92%. Calcd for $[Pd(gly)(tn)]ClO_4$=$C_5H_{14}N_3ClO_6Pd$: C, 16.96; H, 3.99; N, 11.87%.

3) $[Pd(\beta\text{-ala})L]ClO_4$ (L=en and tn) and [Pd(N-Megly)(en)]-

ClO$_4$: These complexes were prepared and crystallized in the same way as for [Pd(*S*-ala)(*S*-pn)]ClO$_4$.[2] The β-ala complexes were recrystallized from warm water, by adding acetone if necessary. Yield: 50 (en) and 70% (tn) for the β-ala complexes; and 90% for the *N*-Megly (=sarcosinato) complex. Found: C, 17.15; H, 4.06; N, 11.76%. Calcd for [Pd(β-ala)(en)]ClO$_4$=$C_5H_{14}N_3ClO_6Pd$: C, 16.96; H, 3.99; N, 11.87%. Found: C, 19.68; H, 4.40; N, 11.37%. Calcd for [Pd(β-ala)(tn)]ClO$_4$=$C_6H_{16}N_3ClO_6Pd$: C, 19.58; H, 4.38; N, 11.42%. Found: C, 17.09; H, 4.05; N, 11.85%. Calcd for [Pd(*N*-Megly)(en)]ClO$_4$=$C_5H_{14}N_3ClO_6Pd$: C, 16.96; H, 3.99; N, 11.87%.

cis-[Pd(N)$_2$(O)$_2$]-type Complexes. *1) [Pd(CH$_3$CO$_2$)$_2$L] (L= en and tn)*: Each of these complexes was prepared by the same method as for [Pd(CH$_3$CO$_2$)$_2$(*S*-pn)][2] but crystallized from a water-acetone medium. Yield: 75—80%. Found: C, 24.19; H, 5.21; N, 9.37%. Calcd for [Pd(CH$_3$CO$_2$)$_2$(en)]·0.75H$_2$O= $C_6H_{15.5}N_2O_{4.75}Pd$: C, 24.17; H, 5.24; N, 9.40%. Found: C, 26.57; H, 5.74; N, 8.55%. Calcd for [Pd(CH$_3$CO$_2$)$_2$(tn)]·H$_2$O=$C_7H_{18}N_2O_5Pd$: C, 26.55; H, 5.73; N, 8.85%.

*2) [Pd(ox)L] (L=*rac-*pn and tn)*: These complexes were obtained by the reaction of [PdCl$_2$L] with silver oxalate,[2] in an 85—90% yield. Found: C, 22.36; H, 3.75; N, 10.44%. Calcd for [Pd(ox)(*rac*-pn)]=$C_5H_{10}N_2O_4Pd$: C, 22.36; H, 3.75; N, 10.43%. Found: C, 22.37; H, 3.76; N, 10.46%. Calcd for [Pd(ox)(tn)]=$C_5H_{10}N_2O_4Pd$: C, 22.36; H, 3.75; N, 10.43%.

3) [Pd(ox)(en)] and [Pd(mal)L] (L=cn, rac-*pn, and tn)*: These complexes were prepared by the method adopted for [Pd(mal)(*S*-pn)][2]. Yield: 70—85%. Found: C, 18.84; H, 3.21; N, 10.97%. Calcd for [Pd(ox)(en)]=$C_4H_8N_2O_4Pd$: C, 18.87; H, 3.17; N, 11.01%. Found: C, 22.29; H, 3.78; N, 10.31%. Calcd for [Pd(mal)(en)]=$C_5H_{10}N_2O_4Pd$: C, 22.36% H, 3.75; N, 10.43%. Found: C, 25.56; H, 4.28; N, 9.90%. Calcd for [Pd(mal)(*rac*-pn)]=$C_6H_{12}N_2O_4Pd$: C, 25.50; H, 4.28; N, 9.91%. Found: C, 24.96; H, 4.44; N, 9.72%. Calcd for [Pd(mal)(tn)]·0.33H$_2$O=$C_6H_{12.66}N_2O_{4.33}Pd$: C, 24.98; H, 4.42; N, 9.71%. The complexes [Pd(ox)(en)] and [Pd(mal)(en)] are almost insoluble in water.

4) [Pd(mal)(NH$_3$)$_2$]: A suspension of 200 mg of *cis*-[PdCl$_2$(NH$_3$)$_2$] in 6 cm^3 of water was stirred with 225 mg of freshly prepared silver oxide for 10 min at room temperature. After removal of the silver chloride the filtrate was evaporated to *ca.* 4 cm^3 under reduced pressure and mixed with an aqueous solution (1.5 cm^3) of 98 mg of malonic acid. The reaction mixture was allowed to stand at room temperature to give light orange crystals, which were washed with cold water and methanol and dried *in vacuo*. Yield: 180 mg. Found: C, 14.56; H, 3.47; N, 11.02%. Calcd for [Pd(mal)(NH$_3$)$_2$]·0.5H$_2$O= $C_3H_9N_2O_{4.5}Pd$: C, 14.33; H, 3.61; N, 11.14%. This complex is insoluble in water without decomposition.

5) [Pd(ox)L$_2$] (L=NH$_3$, CH$_3$NH$_2$, and (CH$_3$)$_2$NH): These complexes were prepared from *cis*- or *trans*-[PdCl$_2$L$_2$][1] in the same manner as in 4). Yield: 75—85%. Found: C, 10.20; H, 2.82; N, 11.64%. Calcd for [Pd(ox)(NH$_3$)$_2$]·0.5H$_2$O=$C_2H_7N_2O_{4.5}Pd$: C, 10.11; H, 2.97; N, 11.79%. Found: C, 17.44; H, 4.25; N, 9.95%. Calcd for [Pd(ox)(CH$_3$NH$_2$)$_2$]·H$_2$O= $C_4H_{12}N_2O_5Pd$: C, 17.50; H, 4.41; N, 10.20%. Found: C, 22.22; H, 5.57; N, 8.59%. Calcd for [Pd(ox){(CH$_3$)$_2$NH}$_2$]·2H$_2$O= $C_6H_{18}N_2O_6Pd$: C, 22.48; H, 5.66; N, 8.74%. Every complex is insoluble in water.

6) [Pd$_2$(μ-OH)$_2$L$_2$](ClO$_4$)$_2$ (L=en and tn): An aqueous solution containing each of these complexes was prepared in the same way as for [Pd$_2$(μ-OH)$_2$(*S*-pn)$_2$](ClO$_4$)$_2$.[2] The en complex was crystallized by mixing the concentrated solution with methanol-free acetone (because alcohols reduce the complex to deposit palladium metal), and the tn complex by evaporating and cooling the solution. Yield: 65% for both complexes. Found: C, 8.73; H, 3.29; N, 9.52%. Calcd for [Pd$_2$(μ-OH)$_2$(en)$_2$](ClO$_4$)$_2$=$C_4H_{18}N_4Cl_2O_{10}Pd_2$: C, 8.49; H, 3.21; N, 9.90%. Found: C, 12.28; H, 3.75; N, 9.38%. Calcd for [Pd$_2$(μ-OH)$_2$(tn)$_2$](ClO$_4$)$_2$=$C_6H_{22}N_4Cl_2O_{10}Pd_2$: C, 12.13; H, 3.73; N, 9.43%. The en complex is less stable than the corresponding *S*-pn one and decomposes in a basic aqueous solution, whereas the tn complex is more stable than the latter.

[Pd(N)(O)$_3$]-type Complexes. *1) K[Pd(CH$_3$CO$_2$)$_2$(gly)]*: The starting material K[PdCl$_2$(gly)] was prepared in the same way as for the corresponding *S*-ala complex.[8] Found: C, 7.88; H, 1.95; N, 4.58%. Calcd for K[PdCl$_2$(gly)]·H$_2$O=$C_2H_6NCl_2O_3KPd$: C, 7.79; H, 1.96; N, 4.54%. The electronic absorption (AB) and MCD data in a 0.20 M KCl aqueous solution (1 M=1 mol dm^{-3}) are as follows in $\sigma_{max}/10^3$ cm^{-1}(ε/mol^{-1} dm^3 cm^{-1}) and $\sigma_{ext}/10^3$ cm^{-1} ($\Delta\varepsilon_M$/mol^{-1} dm^3 cm^{-1} T^{-1}), respectively; AB: 19.6sh (13), 25.28 (312) [$\Delta\sigma^-$=2.56 and $\Delta\sigma^+$=2.63],[9] 37.8sh (1900), and 46.23 (19900) and MCD: 23.6 (+0.023), 26.8 (−0.027), 37.1 (+0.23), and 44.0 (−0.6).

The crude product which was obtained by the same method as for K[Pd(CH$_3$CO$_2$)$_2$(*S*-ala)][2] was considerably contaminated with bis(glycinato)palladium(II), and could not be purified by repeated recrystallizations from water-acetone. Orange-brown crystals deposited in the second recrystallization were mechanically separated from faint yellow needles [Pd(gly)$_2$]. Yield: 15%. Found: C, 21.45; H, 3.00; N, 4.17%. Calcd for $C_6H_{10}NO_6KPd$: C, 21.34; H, 2.98; N, 4.15%.

2) K[Pd(mal)(gly)]: This complex was prepared and separated in a manner similar to that in 1). Yield: 30%. Found: C, 18.52; H, 1.94; N, 4.32%. Calcd for $C_5H_6NO_6KPd$: C, 18.67; H, 1.88; N, 4.35%.

3) K[Pd(ox)(β-ala)]: The calculated quantity of a 1 M KOH aqueous solution was added drop by drop to an aqueous suspension containing equimolar amounts of palladium chloride and β-alanine, with stirring at *ca.* 45 °C. After continuous stirring a small amount of undissolved material was filtered off, and the filtrate was concentrated and mixed with acetone. The crude product K[PdCl$_2$(β-ala)] was recrystallized from water-acetone below 50 °C.[10] Found: C, 12.02; H, 2.04; N, 4.66%. Calcd for K[PdCl$_2$(β-ala)]= $C_3H_6NCl_2O_2KPd$: C, 11.83; H, 1.99; N, 4.60%. The AB and MCD data in 0.20 M KCl are as follows in the same format as in 1); AB: 20.0sh (12), 25.66 (360) [$\Delta\sigma^-$=2.23 and $\Delta\sigma^+$= 2.50], 38.4sh (2800), and 46.60 (17300) and MCD: 20 (+0.0008), 24.1 (+0.015), 27.3 (−0.027), 38.3 (+0.26), and 45.8 (−0.41).

An aqueous solution (20 cm^3) containing K[PdCl$_2$(β-ala)] (600 mg) and oxalic acid dihydrate (250 mg) was stirred with freshly prepared silver oxide (460 mg) for 10 min at room temperature. After removal of the silver chloride the filtrate was evaporated to *ca.* 4 cm^3. The product separated was dissolved again in the mother liquor at 50 °C and the resulting solution was allowed to stand at room temperature. Orange crystals were collected after 4 h, washed with a cold mixture of water-acetone, and dried *in vacuo*. Yield: 120 mg. Found: C, 18.59; H, 1.91; N, 4.27%. Calcd for $C_5H_6NO_6KPd$: C, 18.67; H, 1.88; N, 4.35%. Further crops obtained from the mother liquor were contaminated with bis(oxalato)palladium(II) and could not be purified perfectly by recrystallization.

4) K[Pd(mal)(β-ala)]: This complex was prepared in the same manner as in 3), but crystallized from a more concentrated solution. Although the crude product was contaminated with a small amount of [Pd(β-ala)$_2$], it was purified twice by recrystallization from warm water-acetone. Yield: 40%. Found: C, 20.23; H, 2.94; N, 3.94%. Calcd for K[Pd(mal)(β-ala)]·H$_2$O=$C_6H_{10}NO_7KPd$: C, 20.38; H, 2.85; N, 3.96%.

[Pd(O)$_4$]-type Complexes. The complexes K$_2$[Pd(ox)$_2$] and K$_2$[Pd(mal)$_2$] were prepared by a method similar to that reported for K$_2$[Pd(ox)$_2$],[11] but the number of water of crystallization was different from the literature values.[11-13]

Found: C, 12.09; H, 1.00%. Calcd for $K_2[Pd(ox)_2]\cdot 2H_2O$= $C_4H_4O_{10}K_2Pd$: C, 12.11; H, 1.02%. Found: C, 16.20; H, 2.29%. Calcd for $K_2[Pd(mal)_2]\cdot 3H_2O$=$C_6H_{10}O_{11}K_2Pd$: C, 16.28; H, 2.28%. The corresponding platinum(II) complexes, which were prepared for the purpose of comparison, turned out to have analogous compositions (Found: C, 9.99; H, 0.85%. Calcd for $K_2[Pt(ox)_2]\cdot 2H_2O$=$C_4H_4O_{10}K_2Pt$: C, 9.90; H, 0.83%. Found: C, 13.63; H, 1.95%. Calcd for $K_2[Pt(mal)_2]\cdot 3H_2O$= $C_6H_{10}O_{11}K_2Pt$: C, 13.56; H, 1.90%).

Measurements. Electronic absorption and MCD spectra were recorded with the same apparatus and in the same manner as described elsewhere.[3] Unless otherwise noted, all the measurements were made in aqueous solutions at room temperature. CD spectra were measured in our previous work.[2]

Results and Discussion

Synthesis. All the mixed-ligand palladium(II) complexes isolated in the present work were synthesized on the basis of the principle that a ligand with higher affinity for palladium(II) ion is made to coordinate in preference to a ligand with lower affinity.[2] However, disproportionation reactions were observed in the course of the synthesis of $[Pd(N)_3(O)]$- and $[Pd(N)(O)_3]$-type complexes, particularly in the latter. These complexes were usually contaminated with the corresponding bis(amino carboxylato) complexes, but $K[Pd(ox)(\beta\text{-ala})]$ was with the bis(oxalato) complex. The $[Pd(N)_3(O)]$-type complexes can be purified by recrystallization, whereas the $[Pd(N)(O)_3]$-type ones generally can not because a disproportionation reaction further proceeds during the course of recrystallization. The pure products of the latter type could be obtained only by careful crystallization under a mild condition followed by a mechanical separation. Although most of the complexes with every combination of the ligands were successfully isolated, the complexes $[Pd(tn)(NH_3)_2]Cl_2$, $[Pd(\beta\text{-ala})(NH_3)_2]ClO_4$, $K[Pd(ox)(gly)]$, and $K[Pd(CH_3CO_2)_2(\beta\text{-ala})]$ as well as mixed-ligand $[Pd(O)_4]$-type complexes could not be obtained.[14] As noticed easily, three of these complexes contain one six-membered chelate ring and two unidentate ligands. On the contrary, similar but neutral complexes, $[Pd(mal)(NH_3)_2]$ and $[Pd(CH_3CO_2)_2(tn)]$, could be isolated. This seems to be ascribed to the low solubilities of the mixed-ligand complexes relative to those of the disproportionation products.

The mixed-ligand complexes with en or gly are more labile than the corresponding complexes with *S*-pn or *S*-ala, judging from the degree of the disproportionation observed in the synthesis or recrystallization. This may be attributable to high flexibility of an en or gly chelate ring over an *S*-pn or *S*-ala one, but the following observations can not be explained so easily. The mixed-ligand complexes with tn or β-ala are also more labile than those with *S*-pn or *S*-ala when the remaining coordination sites are occupied by an *N,N*- or *N,O*-ligand, whereas they are comparable or more stable when the sites are occupied by an *O,O*- or two *O*-ligands.

MCD Spectra. *1) [Pd(N)$_4$]-type Complexes*: Figure 1 shows the absorption and MCD spectra of typical $[Pd(N)_4]$-type complexes together with the CD spectra of the corresponding optically active complexes. For convenience these spectra are divided into three regions: spin-forbidden d-d, spin-allowed d-d, and charge transfer (CT) regions (Tables 1 and 2). Each of the MCD spectra shows a positive band and a dispersion comprising a positive and a negative lobe in the spin-forbidden and -allowed d-d regions, respectively. The dispersion changes sign at $2\text{—}3\times10^3\,cm^{-1}$ lower energy than the peak position of the main negative CD band (*ca.* $35\times10^3\,cm^{-1}$), originating primarily from the $^1E_g\leftarrow{}^1A_{1g}$ transition (D_{4h}),[2] of the corresponding optically active complexes. The negative lobe lies at energies only by $0.2\text{—}0.5\times10^3\,cm^{-1}$ higher than the main CD band; and the positive lobe occurs at almost the same energy as the positive CD maximum of $[Pd(S\text{-pn})(tn)]^{2+}$ ($31.4\times10^3\,cm^{-1}$), which has been assigned to the $^1A_{2g}\leftarrow{}^1A_{1g}$ transition (D_{4h}).[2] These facts suggest that the possible A term based on the $^1E_g\leftarrow{}^1A_{1g}$ transition does not contribute so significantly to the dispersion. Therefore, it is reasonable to consider, in combination with the information from the CD spectra,[2] that the positive lobe of the dispersion is mainly composed of a negative B term assigned to the $^1A_{2g}\leftarrow{}^1A_{1g}$ transition and that the large negative lobe is a composite of two positive B terms ascribed to the ^1E_g and $^1B_{1g}\leftarrow{}^1A_{1g}$ transitions (D_{4h}). The same assignment is appropriate for the *N,N*-Et$_2$en complexes (Fig. 2).

The MCD spectra have various features in the CT region, depending on the kind of the ligands. Namely, the complexes $[Pd(NH_3)_4]^{2+}$, $[Pd(tn)_2]^{2+}$, and $[Pd(en)_2]^{2+}$ exhibit a weak positive, an intense positive, and a medium negative band, respectively; however, an additivity holds qualitatively for the MCD spectra of

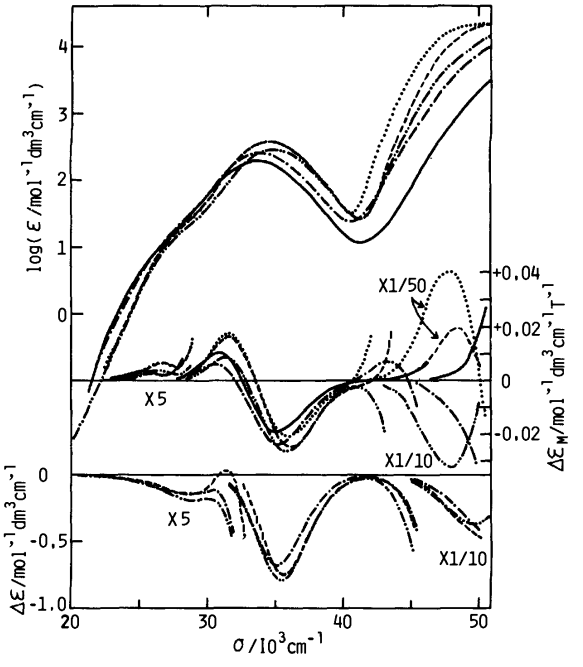

Fig. 1. Absorption and MCD spectra of $[Pd(NH_3)_4](ClO_4)_2$ (——), $[Pd(en)(NH_3)_2]Cl_2$ (—·—), $[Pd(en)_2]Cl_2$ (—· ·—), $[Pd(en)(tn)]Cl_2$ (------), and $[Pd(tn)_2]Cl_2$ (·····); and CD spectra of $[Pd(S\text{-pn})(NH_3)_2]Cl_2$ (—·—), $[Pd(S\text{-pn})(en)]Cl_2$ (—· ·—), and $[Pd(S\text{-pn})(tn)]Cl_2$ (------).

TABLE 1. ABSORPTION DATA[a] OF $[Pd(N)_4]$-TYPE COMPLEXES $[Pd(L_1)(L_2)]Cl_2 \cdot nH_2O$

$(L_1)(L_2)$	n	$\sigma_{max}/10^3\,cm^{-1}(\varepsilon/mol^{-1}\,dm^3\,cm^{-1})$			
		Spin-forbidden d-d	Spin-allowed d-d	Charge transfer	
$(NH_3)_4$[b]	0	27.8 sh(19)	33.68(193)		
$(NH_3)_4$[b,c]	0	27.6 sh(15)	33.67(211)		
$(en)(NH_3)_2$	0	28.4 sh(26)	34.03(253)		
$(en)_2$	0	28.8 sh(22)	34.83(286)		
(en)(tn)	0	28.6 sh(24)	34.60(374)		
$(tn)_2$	0	28.6 sh(23)	34.60(378)	50.76(20900)	
(*N*,*N*-Et_2en)(en)	2	28.2 sh(53)	34.13(395)	49.88(16000)	
(*N*,*N*-Et_2en)(tn)	1	28.0 sh(41)	33.90(477)	48.29(18800)	
$(N,N\text{-Et}_2en)_2$[d]	0	27.4 sh(42)	33.61(572)	44.25(14400)	48.2 sh(11600)
$(N,N,C,C\text{-Me}_4en)_2$[d]	2	27.6 sh(41)	33.68(596)	44.44(15300)	48.2 sh(12400)

a) sh: shoulder (ε is for the value σ given). b) Perchlorate. c) In acetonitrile. d) Another band was observed at *ca.* $22\times10^3\,cm^{-1}$ as a shoulder.

TABLE 2. MCD DATA[a] OF $[Pd(N)_4]$-TYPE COMPLEXES $[Pd(L_1)(L_2)]Cl_2$[b]

$(L_1)(L_2)$	$\sigma_{ext}/10^3\,cm^{-1}(\Delta\varepsilon_M/mol^{-1}\,dm^3\,cm^{-1}\,T^{-1})$		
	Spin-forbidden d-d	Spin-allowed d-d	Charge transfer
$(NH_3)_4$[c]	25.3(+0.0008)	30.8(+0.011)	
	26.8 m	35.0(−0.019)	
$(NH_3)_4$[c, d]	25.3(+0.0007)	30.6(+0.012)	46.5(−0.002)
	26.8 m	34.9(−0.021)	
$(en)(NH_3)_2$	26.0(+0.0006)	30.5(+0.006)	43.3(+0.008)
	26.9 m	35.2(−0.024)	
$(en)_2$	26.3(+0.0008)	31.3(+0.009)	48.0(−0.32)
	27.7 m	35.8(−0.026)	
(en)(tn)	26.8(+0.0014)	31.6(+0.016)	48.4(+0.93)
	27.8 m	36.1(−0.024)	
$(tn)_2$	26.6(+0.0014)	31.6(+0.018)	47.8(+2.0)
	27.7 m	36.0(−0.020)	
(*N*,*N*-Et_2en)(en)	26.2(+0.0013)	30.6(+0.011)	45.7(−0.28)
	27.5 m	35.2(−0.033)	
(*N*,*N*-Et_2en)(tn)	25.9(+0.0011)	30.8(+0.012)	46.4(+0.56)
	27.4 m	35.4(−0.026)	
$(N,N\text{-Et}_2en)_2$	25.5(+0.0019)	29.7(+0.011)	43.2(−0.26)
	26.5 m	34.4(−0.038)	48.9(+0.22)
$(N,N,C,C\text{-Me}_4en)_2$	25.6(+0.0017)	29.9(+0.011)	43.1(−0.38)
	26.6 m	34.5(−0.039)	48.6(+0.35)

a) m; minimum of $|\Delta\varepsilon_M|$. b) Water of crystallization is omitted (See Table 1). c) Perchlorate. d) In acetonitrile.

the mixed-ligand complexes (Fig. 1). An analogous situation is also observed for the mixed-ligand *N*,*N*-Et_2en complexes. A positive and a negative A term are correlated with the CT absorption bands around $50\times10^3\,cm^{-1}$ in the complexes of en and tn, respectively (Fig. 2). We previously found that the complexes having two *N*,*N*-dialkylamino groups in positions trans to each other exhibited a splitting both in the absorption and CD bands which were assigned to $Pd\leftarrow N(\sigma)$ transitions.[2] The spectra of such complexes show a negative and a positive band corresponding to the two split components (Fig. 2). These two B terms may be considered as a pseudo A term.[15] The MCD spectrum of $[Pd(en)(NH_3)_2]^{2+}$ shows a weak positive band on the lower edge of the CT absorption band, and it is presumably attributed to an orbitally-forbidden CT transition.

2) [Pd(N)$_3$(O)]-type Complexes: The spectra of the complexes containing gly or β-ala are shown in Fig. 3 or 4, respectively, and the numerical data in Tables 3 and 4. The MCD spectra showed a single positive or a couple of + and − bands in the spin-forbidden d-d region. Taking into account the overlapping of the neighboring intense positive band, all the complexes are expected to have the two (+ and −) bands in the region. The minimum around $26\times10^3\,cm^{-1}$ is considered to be formed by such an undetectable negative band, and included in Table 4; the main CD band of spin-forbidden nature occurs at almost the same energy as the minimum (Figs. 3 and 4). Such a correspondance is also found in the $[Pd(N)_4]$-type complexes (Figs. 1 and 2; Table 2).

The MCD spectra in the spin-allowed d-d region of the $[Pd(gly)(N)_2]$-type complexes are very similar to those of the corresponding $[Pd(en)(N)_2]$-type complexes (Figs. 3 and 1). The MCD spectra of the

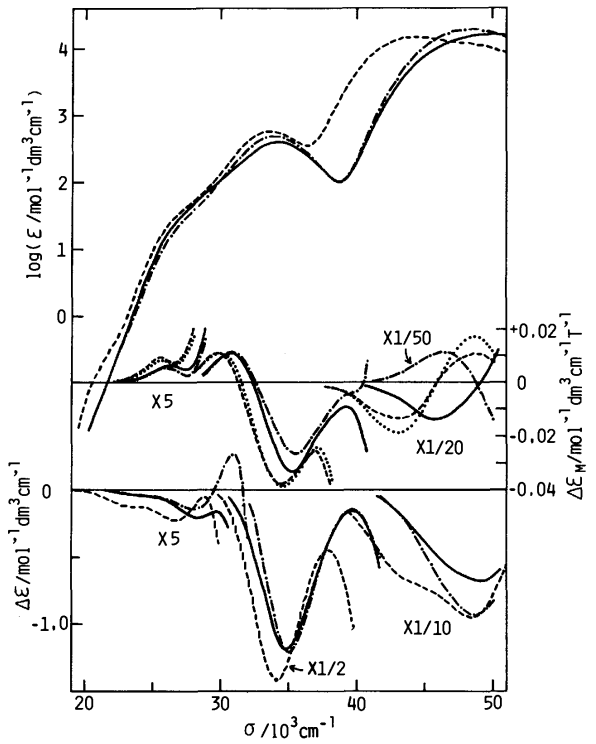

Fig. 2. Absorption and MCD spectra of [Pd(*N*,*N*-Et$_2$en)(en)]Cl$_2$ (——), [Pd(*N*,*N*-Et$_2$en)(tn)]Cl$_2$ (—·—), and [Pd(*N*,*N*-Et$_2$en)$_2$]Cl$_2$ (------); MCD spectrum of [Pd(*N*,*N*,*C*,*C*-Me$_4$en)$_2$]Cl$_2$ (·····) (the absorption spectrum is almost identical with that of [Pd(*N*,*N*-Et$_2$en)$_2$]Cl$_2$); and CD spectra of [Pd(*N*^{1},*N*^{1}-Et$_2$-(*S*)-pn)(en)]Cl$_2$ (——), [Pd(*N*^{1},*N*^{1}-Et$_2$-(*S*)-pn)(tn)]Cl$_2$ (—·—), and [Pd(*N*^{1},*N*^{1}-Et$_2$-(*S*)-pn)$_2$]Cl$_2$ (------).

[Pd(β-ala)(N)$_2$]-type complexes in the same region do not largely differ from those of the corresponding gly complexes (Figs. 4 and 3). Thus, these MCD spectra can be interpreted in analogy with those of the [Pd(N)$_4$]-type complexes. The complexes containing tn exhibit larger intensity ratios of the positive to the negative lobe of the dispersion, $|\Delta\varepsilon_M(+)/\Delta\varepsilon_M(-)|$, than the corresponding en complexes. Moreover it is noteworthy that the ratio is closely related to the sign and intensity of the MCD band in $45—50\times10^3$ cm^{-1}: the complexes which exhibit an intense positive MCD in the CT region do also an intense positive MCD band in the spin-allowed d-d region, and the complexes with a negative band in the former region exhibit a weak positive band in the latter region (Figs. 2 and 3). This fact is proved to hold likewise for the complexes of the other types, implying the mixing of a CT excited state with a d-d vibronic excited state.

Again in the CT region, the [Pd(gly)(N)$_2$]-type complexes generally exhibit MCD features similar to those of the corresponding en complexes, except for the positive band at 43.3×10^3 cm^{-1} in [Pd(en)(NH$_3$)$_2$]$^{2+}$. On the other hand, [Pd(β-ala)(en)]$^+$ exhibits a unique pattern of −, +, and −, and [Pd(β-ala)(tn)]$^+$ a pattern characteristic of the complexes containing tn. These observations indicate that gly and en ligands make an almost equivalent contribution to the MCD in the region but that a β-ala has a greater influence on the MCD than an en but smaller than a tn.

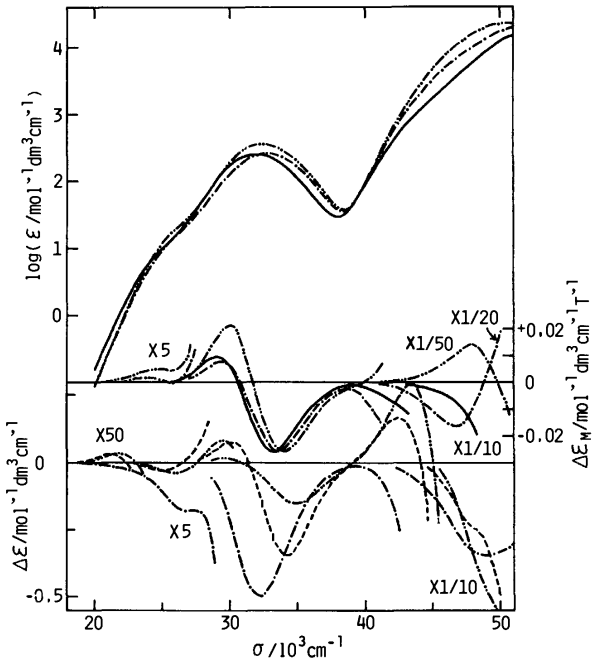

Fig. 3. Absorption and MCD spectra of [Pd(gly)L]ClO$_4$: L=(NH$_3$)$_2$ (——), L=en (—·—), and L=tn (—· ·—); and CD spectra of [Pd(gly)(*S*-pn)]ClO$_4$ (—·—), [Pd-(*S*-ala)(en)]ClO$_4$ (------), and [Pd(*S*-ala)(tn)]ClO$_4$ (—· ·—).

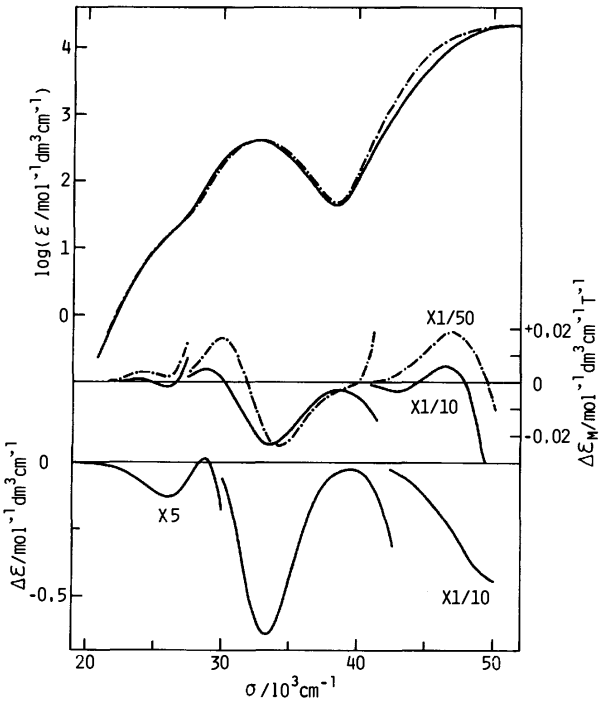

Fig. 4. Absorption and MCD spectra of [Pd(β-ala)L]ClO$_4$: L=en (——) and L=tn (—·—), and CD spectrum of [Pd(β-ala)(*S*-pn)]ClO$_4$ (——).

3) cis-[Pd(N)$_2$(O)$_2$]-type Complexes: The spectra of the complexes with this type are shown in Figs. 5—7, and the numerical data in Tables 5 and 6. The situation in the spin-forbidden d-d region is substantially the same as for the [Pd(N)$_3$(O)]- and [Pd(N)$_4$]-type complexes, but the negative MCD band in the higher energy side appears more explicitly. A comparison of the MCD spectrum of [Pd(ox)(*rac*-pn)] with the CD

TABLE 3. ABSORPTION DATA[a] OF $[Pd(N)_3(O)]$-TYPE COMPLEXES $[Pd(L_1)(L_2)]ClO_4$

$(L_1)(L_2)$	$\sigma_{max}/10^3\,cm^{-1}(\varepsilon/mol^{-1}\,dm^3\,cm^{-1})$		
	Spin-forbidden d-d	Spin-allowed d-d	Charge transfer
(gly)$(NH_3)_2$	25.4 sh(12)	31.81(254)	44.5 sh
(gly)(en)	26.4 sh(19)	32.70(259)	
(gly)(tn)	26.4 sh(23)	32.35(360)	50.61(22700)
(β-ala)(en)	26.2 sh(17)	32.46(406)	51.28(20600)
(β-ala)(tn)	26.6 sh(21)	32.68(410)	51.63(21600)
(*N*-Megly)(en)	26.4 sh(22)	32.83(284)	51.41(22500)

a) sh: shoulder (ε is for the value σ given).

TABLE 4. MCD DATA[a] OF $[Pd(N)_3(O)]$-TYPE COMPLEXES $[Pd(L_1)(L_2)]ClO_4$

$(L_1)(L_2)$	$\sigma_{ext}/10^3\,cm^{-1}(\Delta\varepsilon_M/mol^{-1}\,dm^3\,cm^{-1}\,T^{-1})$		
	Spin-forbidden d-d	Spin-allowed d-d	Charge transfer
(gly)$(NH_3)_2$	24 sh(+0.0003)	28.9(+0.010) 33.2(−0.026)	
(gly)(en)	23.8(+0.0004) 25.8(−0.00004)	29.3(+0.008) 33.5(−0.026)	46.7(−0.33)
(gly)(tn)	24.7(+0.0010) 25.8 m	30.0(+0.021) 34.0(−0.026)	47.8(+0.70)
(β-ala)(en)	24 sh(+0.0002) 25.9(−0.0004)	28.8(+0.005) 33.5(−0.023)	42.8(−0.03) 46.6(+0.06)
(β-ala)(tn)	24.1(+0.0008) 26.0 m	29.9(+0.017) 34.1(−0.024)	46.9(+0.94)
(*N*-Megly)(en)	24.5(+0.0008) 25.9 m	29.3(+0.010) 33.5(−0.028)	46.2(−0.30)

a) sh: shoulder ($\Delta\varepsilon_M$ is for the value σ given); m: minimum of $|\Delta\varepsilon_M|$.

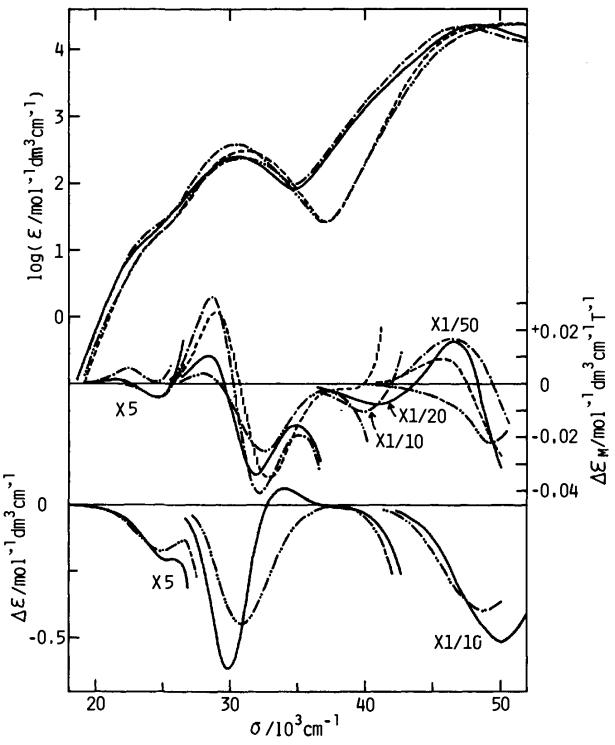

Fig. 5. Absorption and MCD spectra of [Pd(ox)(*rac*-pn)] (——), [Pd(ox)(tn)] (—·—), [Pd(mal)(*rac*-pn)] (—· ·—), and [Pd(mal)(tn)] (------); and CD spectra of [Pd(ox)(*S*-pn)] (——) and [Pd(mal)(*S*-pn)] (—· ·—).

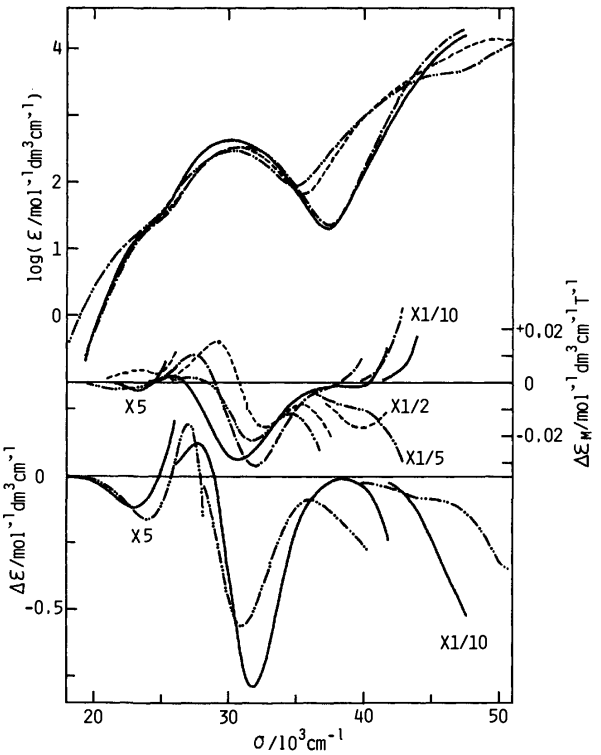

Fig. 6. Absorption and MCD spectra of $[Pd(CH_3CO_2)_2L]$ in 0.50 M CH_3CO_2Na: L=en (——) and L=tn (—·—), and $[Pd_2(\mu\text{-}OH)_2L_2](ClO_4)_2$ in H_2O: L=en (—· ·—) and L=tn (------); and CD spectra of $[Pd(CH_3CO_2)_2(S\text{-pn})]$ in 0.50 M CH_3CO_2Na (——) and $[Pd_2(\mu\text{-}OH)_2(S\text{-pn})_2](ClO_4)_2$ in H_2O (—· ·—).

one of [Pd(ox)(*S*-pn)] in the spin-allowed d-d region leads to the expectation that the A term based on the $^1E_g \leftarrow {}^1A_{1g}$ transition (D_{4h}) contributes to the dispersion of MCD more substantially than in the case of the $[Pd(N)_4]$- and $[Pd(N)_3(O)]$-type complexes (Fig. 5). The CD band at *ca.* $34\times10^3\,cm^{-1}$, which was assigned to the $^1B_{1g} \leftarrow {}^1A_{1g}$ transition (D_{4h}),[2] is correlated to a positive B term included in the negative lobe of the dispersion. The intensity ratio, $|\Delta\varepsilon_M(+)/\Delta\varepsilon_M(-)|$, is determined primarily by the kind of the *N*-ligand as seen in the previous section and secondarily by that of the *O*-ligand: it decreases in the order of the ox, mal, and CH_3CO_2 complexes when compared within the complexes with the same *N*-ligand. No such regularity is found for the complexes with μ-hydroxo or aqua ligands. The complex $[Pd(OH_2)_2(en)]^{2+}$ is so unique among the series of the complexes studied here as to exhibit only a negative band in the MCD of the spin-allowed d-d region (Fig. 7). The MCD band lies at the lower energy side of the main CD band of $[Pd(OH_2)_2(S\text{-pn})]^{2+}$; accordingly, a positive B term is expected for the $^1A_{2g} \leftarrow {}^1A_{1g}$ transition (D_{4h}) in this complex. The diacetato complex $[Pd(CH_3CO_2)_2(en)]$ is similarly situated, although it exhibits a weak positive MCD band. The weak band is considered to be the remainder of the positive lobe of the minor negative A term based on the $^1E_g \leftarrow {}^1A_{1g}$ transition canceled by the positive B term on the $^1A_{2g} \leftarrow {}^1A_{1g}$ one.

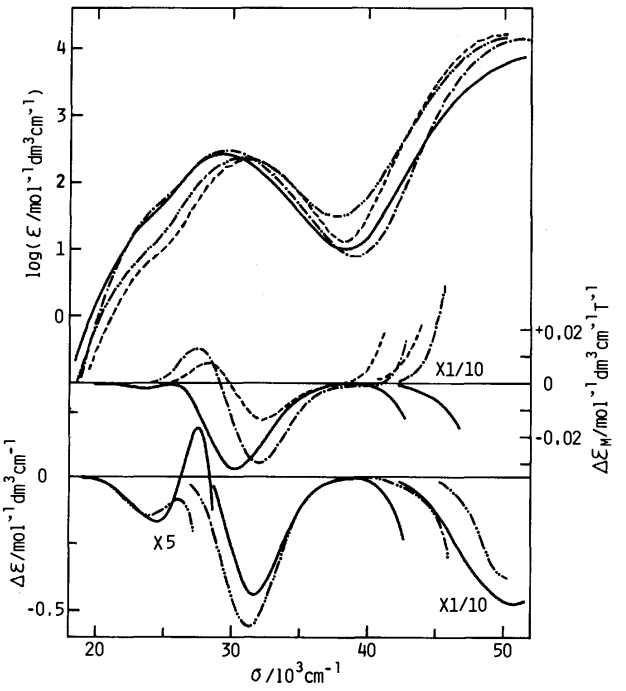

Fig. 7. Absorption and MCD spectra of $[Pd_2(\mu\text{-}OH)_2L_2](ClO_4)_2$ in 0.01 M $HClO_4$ (=2[$Pd(OH_2)_2L$]$(ClO_4)_2$): L=en (——) and L=tn (— · —), and in 0.01 M NaOH (=2[$Pd(OH)_2L$]): L=tn (------); absorption and CD spectra (— · · —) of $[Pd_2(\mu\text{-}OH)_2(S\text{-pn})_2](ClO_4)_2$ in 0.01 M NaOH (=2[$Pd(OH)_2(S\text{-pn})$]); and CD spectrum (——) of $[Pd_2(\mu\text{-}OH)_2(S\text{-pn})_2](ClO_4)_2$ in 0.01 M $HClO_4$ (=2[$Pd(OH_2)_2(S\text{-pn})$]$(ClO_4)_2$).

The MCD spectra in the CT region of the complexes with ox or mal are qualitatively additive with respect to the constituent ligands as noted in the $[Pd(N)_4]$-type complexes (Figs. 5, 1, and 9). This fact agrees with the expectation that two kinds of CT transitions, namely Pd←N(σ) and O(n, π, and/or σ), are present with small energy gaps. The absorption band which was observed as a shoulder around 42×10^3 cm^{-1} in the complexes with ox is readily assigned to the latter CT transitions, to which a positive B term corresponds. On the other hand, the CD spectra show no remarkable band in $35\text{—}45\times10^3\,cm^{-1}$; this can be explained by the fact that an asymmetric center is present only in the *N*-ligand, if such a chirality is more effective in Pd←N than in Pd←O CT transitions. A similar spectral behavior has been observed also for $[Pd(Cl)_2(N)_2]$-type complexes.[1] Therefore, the CD bands at *ca.* $50\times10^3\,cm^{-1}$ are attributable primarily to Pd←N(σ) transitions (Fig. 5).

4) [Pd(N)(O)$_3$]-type Complexes: The absorption and MCD spectra of the complexes of this type are shown in Fig. 8 together with the CD spectra of the relating complexes with *S*-ala, and the numerical data in Tables 7 and 8. The MCD spectra of the complexes with gly are very similar to those of the corresponding en (or *rac*-pn) complexes of *cis*-$[Pd(N)_2(O)_2]$-type over the range $20\text{—}50\times10^3\,cm^{-1}$ (Figs. 8, 5, and 6). Thus, the MCD spectra of the former complexes can be interpreted in analogy with those of the latter. The MCD spectrum of $[Pd(CH_3CO_2)_2(gly)]^-$ supports the idea proposed be-

TABLE 5. ABSORPTION DATA[a] OF *cis*-$[Pd(N)_2(O)_2]$-TYPE COMPLEXES

Complex	$\sigma_{max}/10^3\,cm^{-1}(\varepsilon/mol^{-1}\,dm^3\,cm^{-1})$			
	Solvent	Spin-forbidden d-d	Spin-allowed d-d	Charge transfer
$[Pd(CH_3CO_2)_2(en)]\cdot0.75H_2O$	0.50 M CH_3CO_2Na	24.2 sh(23)	30.11(430)	
$[Pd(CH_3CO_2)_2(tn)]\cdot H_2O$	0.50 M CH_3CO_2Na	24.6 sh(24)	31.00(340)	
[Pd(ox)(*rac*-pn)]	H_2O	24.4 sh(19)	30.53(253)	48.08(23100)
[Pd(ox)(tn)]	H_2O	24.8 sh(25)	30.40(384)	47.17(21800)
[Pd(mal)(*rac*-pn)]	H_2O	24.8 sh(18)	31.00(240)	51.36(23700)
$[Pd(mal)(tn)]\cdot0.33H_2O$	H_2O	25.2 sh(21)	31.14(311)	50.63(24400)
$[Pd_2(\mu\text{-}OH)_2(en)_2](ClO_4)_2$[b]	H_2O	23.8 sh(21)	30.44(291)	45.5 sh(4100)
	0.01 M $HClO_4$	24.4 sh(37)	29.21(270)	
$[Pd_2(\mu\text{-}OH)_2(tn)_2](ClO_4)_2$[b]	H_2O	24.4 sh(22)	30.71(332)	44 sh
				50.10(13700)
	0.01 M $HClO_4$	24.8 sh (53)	29.50(300)	51.49(13600)
	0.01 M NaOH	24.6 sh(9)	31.23(219)	

a) sh: shoulder (ε is for the value σ given). b) Molar absorption coefficient is based on palladium; another band was observed at *ca.* $39.5\times10^3\,cm^{-1}$ as a shoulder.

TABLE 6. MCD DATA[a] OF *cis*-[Pd(N)$_2$(O)$_2$]-TYPE COMPLEXES

Complex	Solvent	$\sigma_{ext}/10^3$ cm^{-1}($\Delta\varepsilon_M$/mol^{-1} dm^3 cm^{-1} T^{-1}) Spin-forbidden d-d	Spin-allowed d-d	Charge transfer
[Pd(CH$_3$CO$_2$)$_2$(en)]·0.75H$_2$O	0.50 M CH$_3$CO$_2$Na		25.9(+0.002)	
		23.2(−0.0006)	30.7(−0.029)	
[Pd(CH$_3$CO$_2$)$_2$(tn)]·H$_2$O	0.50 M CH$_3$CO$_2$Na		27.4(+0.010)	
			31.9(−0.031)	
[Pd(ox)(*rac*-pn)]	H$_2$O	21.7 sh(+0.0003)	28.4(+0.011)	40.8(−0.15)
		24.6(−0.001)	31.9(−0.034)	46.5(+0.32)
[Pd(ox)(tn)]	H$_2$O	22.4(+0.0011)	28.6(+0.032)	39.9(−0.10)
		24.5 m	32.1(−0.041)	46.4(+0.83)
[Pd(mal)(*rac*-pn)]	H$_2$O		28.0(+0.004)	49.3(−1.1)
		24.7(−0.001)	32.5(−0.025)	
[Pd(mal)(tn)]·0.33H$_2$O	H$_2$O		29.0(+0.027)	45.7(+0.45)
			32.9(−0.035)	
[Pd$_2$(μ-OH)$_2$(en)$_2$](ClO$_4$)$_2$[b]	H$_2$O	21.7(−0.0005)	27.2(+0.002)	39.5 sh(−0.05)
			31.6(−0.022)	
	0.01 M HClO$_4$		25.6 m	
		23.6(−0.002)	30.2(−0.032)	
[Pd$_2$(μ-OH)$_2$(tn)$_2$](ClO$_4$)$_2$[b]	H$_2$O		29.0(+0.015)	39.7(−0.034)
		23.5(+0.0009)	32.6(−0.017)	
	0.01 M HClO$_4$		27.4(+0.013)	
			32.0(−0.030)	
	0.01 M NaOH		28.2(+0.007)	
			32.2(−0.014)	

a) sh: shoulder ($\Delta\varepsilon_M$ is for the value σ given); m: minimum of $|\Delta\varepsilon_M|$. b) $\Delta\varepsilon_M$ is based on palladium.

fore that the vicinal CD contribution by *S*-ala exhibits a dispersion pattern of + and − for the $^1E_g \leftarrow {}^1A_{1g}$ transition (D_{4h}).[2] The MCD spectra of the two complexes with β-ala are similar to that of [Pd(β-ala)(en)]$^+$ in the d-d region, particularly in the intensity ratio $|\Delta\varepsilon_M(+)/\Delta\varepsilon_M(-)|$, and showed a composite of the patterns characteristic of the constituent ligands in the CT region (Figs. 8 and 4).

5) [Pd(O)$_4$]-type Complexes: The absorption and MCD spectra are shown in Fig. 9 and the numerical data in Tables 7 and 8. The MCD curves in the d-d region of [Pd(ox)$_2$]$^{2-}$ and [Pd(mal)$_2$]$^{2-}$ are very similar to each other, although the intensity for the former complex is about a half of that for the latter. Considering only coordinating atoms, the complexes of this type can be approximated by a D_{4h} symmetry; nevertheless the contribution of the A term based on the $^1E_g \leftarrow {}^1A_{1g}$ transition is considered to be small from the MCD features. This situation is similar to that in the [Pd(N)$_4$]-type complexes.

The MCD spectrum of [Pd(ox)$_2$]$^{2-}$ showed four bands in the CT region. The lowest-energy band, which was observed only as a shoulder, corresponds to the absorption band (shoulder) at 32.8×10^3 cm^{-1}. Neither the MCD nor the absorption band corresponding to the above respective band was observable in the complexes containing only one ox ligand because of the relatively high intensities of the neighboring bands. The three higher-energy bands are familiar in the complexes with ox (See also Figs. 5 and 8). The MCD spectrum of [Pd(mal)$_2$]$^{2-}$ showed two bands in the CT region; a positive B term and a positive A term correspond to

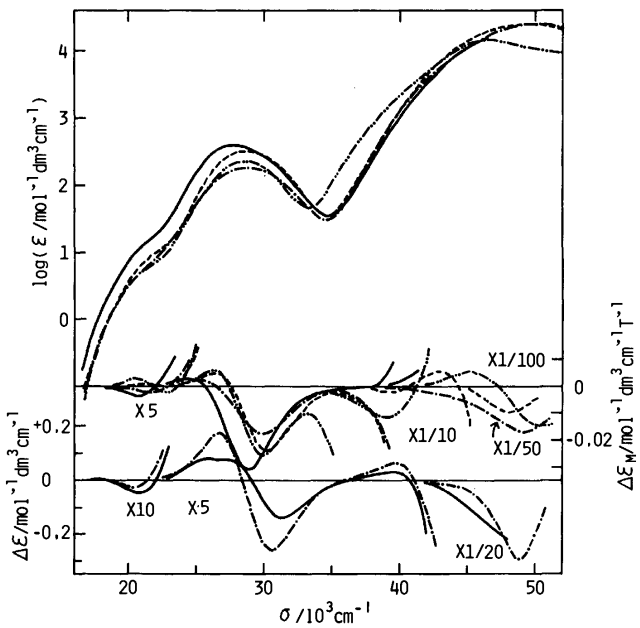

Fig. 8. Absorption and MCD spectra of K[Pd(CH$_3$CO$_2$)$_2$(gly)] in 0.50 M CH$_3$CO$_2$Na (——), K[Pd(mal)(gly)] in H$_2$O (—·—), K[Pd(ox)(β-ala)] in H$_2$O (—· ·—), and K[Pd(mal)(β-ala)] in H$_2$O (------); and CD spectra of K[Pd(CH$_3$CO$_2$)$_2$(*S*-ala)] in 0.50 M CH$_3$CO$_2$Na (——) and K[Pd(mal)(*S*-ala)] in H$_2$O (—·—).

the absorption bands at 44.5 and 48.5×10^3 cm^{-1}, respectively.

Ligand-field Absorption Spectra. Each absorption spectrum of the [Pd(N)$_n$(O)$_{4-n}$]-type complexes is

TABLE 7. ABSORPTION DATA[a] OF [Pd(N)(O)$_3$]- AND [Pd(O)$_4$]-TYPE COMPLEXES

Complex	$\sigma_{max}/10^3\,cm^{-1}(\varepsilon/mol^{-1}\,dm^3\,cm^{-1})$			
	Spin-forbidden d-d	Spin-allowed d-d	Charge transfer	
K[Pd(CH_3CO_2)$_2$(gly)][b]	21.6 sh(16)	27.77(402)		
K[Pd(mal)(gly)]	22.0 sh(9)	28.79(184)	44 sh	50.06(25200)
K[Pd(ox)(β-ala)]	21.8 sh(11)	28.58(372)	39.5 sh	46.45(22200)
K[Pd(mal)(β-ala)]·H_2O	22.4 sh(11)	28.69(326)		49.44(24900)
K_2[Pd(ox)$_2$]·$2H_2O$[c]	19.2 sh(4)	26.31(106)	37.5 sh(3400)	44.39(24100)
K_2[Pd(mal)$_2$]·$3H_2O$	20.4 sh(7)	26.99(164)	44.5 sh	48.53(27800)

a) sh: shoulder (ε is for the value σ given). b) In 0.50 M CH_3CO_2Na. c) Another band was observed at *ca.* 32.8×$10^3\,cm^{-1}$ (ε=150) as a shoulder.

TABLE 8. MCD DATA OF [Pd(N)(O)$_3$]- AND [Pd(O)$_4$]-TYPE COMPLEXES

Complex	$\sigma_{ext}/10^3\,cm^{-1}(\Delta\varepsilon_M/mol^{-1}\,dm^3\,cm^{-1}\,T^{-1})$		
	Spin-forbidden d-d	Spin-allowed d-d	Charge transfer
K[Pd(CH_3CO_2)$_2$(gly)][a]		24.4(+0.003)	
	20.7(−0.0007)	28.8(−0.031)	
K[Pd(mal)(gly)]		25.2(+0.0025)	49.2(−0.85)
	21.6(−0.0004)	30.0(−0.018)	
K[Pd(ox)(β-ala)]	20.4(+0.0006)	26.2(+0.0061)	39.0(−0.12)
	22.8(−0.0004)	29.9(−0.026)	45.1(+0.55)
			50.6(−1.5)
K[Pd(mal)(β-ala)]·H_2O	21.3(+0.0002)	26.4(+0.0050)	39.3(−0.02)
		30.2(−0.024)	42.9(+0.06)
			48.1(−1.0)
K_2[Pd(ox)$_2$]·$2H_2O$[b]		23.3(+0.0029)	36.9(−0.19)
	18.7(−0.0002)	27.1(−0.011)	43.8(+0.54)
			49.3(−0.90)
K_2[Pd(mal)$_2$]·$3H_2O$		24.7(+0.0067)	46.7(−1.1)
	20.2(−0.0003)	28.5(−0.020)	

a) In 0.50 M CH_3CO_2Na. b) Another band was observed at *ca.* 32.5×$10^3\,cm^{-1}$ ($\Delta\varepsilon_M$=−0.02) as a shoulder.

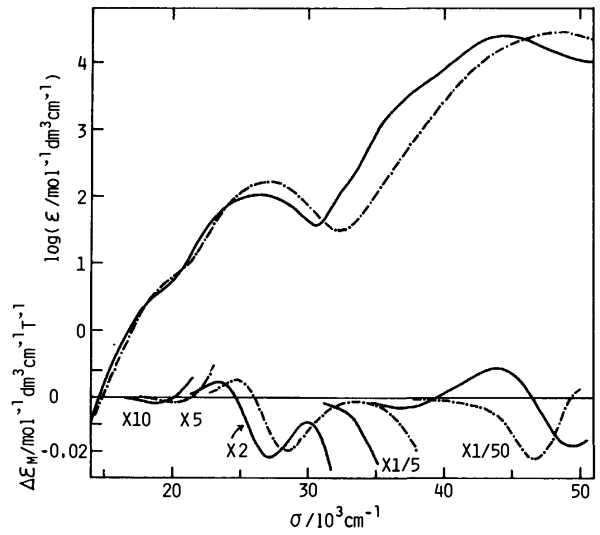

Fig. 9. Absorption and MCD spectra of K_2[Pd(ox)$_2$] (——) and K_2[Pd(mal)$_2$] (—·—).

composed of an unsymmetrical broad band and a lower-lying shoulder in the d-d transition region, and these bands are roughly assigned to a spin-allowed and a spin-forbidden band, respectively. The former band will be described in detail and discussed briefly hereafter. We previously demonstrated that such an unsymmetrical band could be characterized by the half-value-width parameters and the unsymmetry parameter.[1] The parameters are listed in Table 9 for the complexes studied here.

Figure 10 represents the complexes together with the relating optically active complexes[2] as a function of the molar absorption coefficient of the absorption peak and the half-value width $\Delta\sigma_{1/2}$; moreover it shows the approximate band area, which is proportional to the oscillator strength. The [Pd(N)$_4$]-type complexes composed of ammine, en (or *S*-pn) and/or tn are classified into four groups, *i.e.*, a tetraammine complex, diammine(five-membered chelate) complexes, bis(five-membered chelate) complexes, and tn-containing complexes; the half-value width decreases and the band area increases in this order. A similar behavior is also found among the [Pd(N)$_4$]-type complexes containing *N*,*N*-diethylethylene(or propylene)diamine. The [Pd(N)$_3$(O)]-type complexes can be classified into three groups: complexes containing no six-membered chelates, complexes composed of a five-membered N–O and a six-membered N–N chelate, and complexes containing a six-membered N–O chelate. Thus the complexes with β-ala form a single group in Fig. 10 irrespective of the sizes of the accompanying diamines, and this situation is very similar to that found for the [Pd(N)$_4$]-type complexes with tn.

TABLE 9. BAND SHAPE PARAMETERS FOR THE SPIN-ALLOWED d-d BAND OF $[Pd(N)_n(O)_{4-n}]$-TYPE COMPLEXES (n=0—4)

Complex	$\Delta\sigma^{-}$ [a]	$\Delta\sigma^{+}$ [a]	$\Delta\sigma_{1/2}$ [a]	Unsymmetry parameter [b]
	$10^3\,cm^{-1}$	$10^3\,cm^{-1}$	$10^3\,cm^{-1}$	
$[Pd(NH_3)_4]^{2+}$	2.73	2.88	5.61	2.7
$[Pd(NH_3)_4]^{2+}$ [c]	2.50	2.71	5.22	4.0
$[Pd(en)(NH_3)_2]^{2+}$	2.73	2.79	5.52	1.1
$[Pd(en)_2]^{2+}$	2.53	2.77	5.30	4.5
$[Pd(en)(tn)]^{2+}$	2.51	2.72	5.23	4.0
$[Pd(tn)_2]^{2+}$	2.48	2.68	5.16	3.9
$[Pd(N,N\text{-}Et_2en)(en)]^{2+}$	2.75	2.75	5.50	0.0
$[Pd(N,N\text{-}Et_2en)(tn)]^{2+}$	2.57	2.69	5.26	2.3
$[Pd(gly)(NH_3)_2]^{+}$	2.53	2.84	5.38	5.8
$[Pd(gly)(en)]^{+}$	2.70	2.77	5.47	1.3
$[Pd(gly)(tn)]^{+}$	2.48	2.81	5.29	6.2
$[Pd(\beta\text{-ala})(en)]^{+}$	2.42	2.66	5.08	4.7
$[Pd(\beta\text{-ala})(tn)]^{+}$	2.48	2.68	5.16	3.9
$[Pd(N\text{-Megly})(en)]^{+}$	2.78	2.73	5.51	−0.9
$[Pd(CH_3CO_2)_2(en)]$ [d]	2.63	3.01	5.65	6.7
$[Pd(CH_3CO_2)_2(tn)]$ [d]	3.05	2.80	5.85	−4.3
[Pd(ox)(*rac*-pn)]	2.58	2.74	5.32	3.0
[Pd(ox)(tn)]	2.31	2.54	4.85	4.7
[Pd(mal)(*rac*-pn)]	2.86	2.82	5.68	−0.7
[Pd(mal)(tn)]	2.64	2.70	5.35	1.1
$[Pd_2(\mu\text{-}OH)_2(en)_2]^{2+}$	3.06	2.73	5.79	−5.7
$[Pd_2(\mu\text{-}OH)_2(tn)_2]^{2+}$	2.70	2.67	5.37	−0.6
$[Pd(OH_2)_2(en)]^{2+}$ [e]	2.51	3.05	5.56	9.7
$[Pd(OH_2)_2(tn)]^{2+}$ [e]	2.61	3.07	5.68	8.1
$[Pd(OH)_2(tn)]^{0}$	2.68	2.78	5.47	1.8
$[Pd(CH_3CO_2)_2(gly)]^{-}$ [d]	2.41	2.99	5.40	10.7
[Pd(mal)(gly)]$^{-}$	2.95	3.05	6.00	1.7
[Pd(ox)(β-ala)]$^{-}$	2.38	2.40	4.79	0.4
[Pd(mal)(β-ala)]$^{-}$	2.53	2.78	5.32	4.7
$[Pd(ox)_2]^{2-}$	3.09	3.12	6.21	0.5
$[Pd(mal)_2]^{2-}$	2.75	2.76	5.52	0.2

a) $\varepsilon=\varepsilon_{max}/2$ at $\sigma=\sigma_{max}-\Delta\sigma^{-}$ and $\sigma_{max}+\Delta\sigma^{+}$; $\Delta\sigma_{1/2}=\Delta\sigma^{-}+\Delta\sigma^{+}$. b) unsymmetry parameter= $\{(\Delta\sigma^{+}-\Delta\sigma^{-})/\Delta\sigma_{1/2}\}\times100$. c) In acetonitrile. d) In 0.50 M CH_3CO_2Na. e) $[Pd_2(\mu\text{-}OH)_2(en\text{ or }tn)_2](ClO_4)_2$ in 0.01 M $HClO_4$. f) $[Pd_2(\mu\text{-}OH)_2(tn)_2](ClO_4)_2$ in 0.01 M NaOH.

The substitution of β-ala for tn largely affect neither the band area nor the band width, but that of mal for β-ala does. An analogous behavior is also found in the series of en(or pn)–gly(or *S*-ala)–ox complexes except a pair of [Pd(ox)(pn)] and [Pd(gly)(en)] (Fig. 10).

The complexes containing tn, β-ala, or CH_3CO_2 generally possess oscillator strengths higher than the corresponding en(or pn), gly, or mal(or ox) complexes, respectively (Fig. 10). The exceptions are limited to the complexes with one tn and two unidentate ligands: $[Pd(CH_3CO_2)_2(tn)]$, $[Pd(OH)_2(tn)]$, and $[PdCl_2(tn)]$.[16] These complexes are expected to be less distorted than the corresponding en or *S*-pn complexes mainly in terms of bond angle. In other complexes, ligand-ligand interactions are presumed to be predominant. The complex $K_2[Pd(ox)_2]$ has the lowest oscillator strength among the palladium(II) complexes which we have so far investigated $[(\Delta\sigma_{1/2}\times\varepsilon)/10^5\ mol^{-1}\ dm^3\ cm^{-2}=6.57$; *cf.* $K_2[PdCl_4]$ (6.66)]. This may be attributable to the high planarity of the complex ion.

Figure 11 displays the unsymmetrical shape of the spin-allowed d-d absorption band. The complexes which exhibit an absorption band with a swelling in the higher or lower energy side are located on the lower right or upper left of the line $\Delta\sigma^{+}=\Delta\sigma^{-}$ (See the footnote of Table 9), respectively; the farther the complexes are located away from the line, the more unsymmetrical their band shapes are. The introduction of *N*,*N*-Et_2en(or N^1,N^1-Et_2-(*S*)-pn) in place of en(or *S*-pn) increases the band width mainly through the increase in $\Delta\sigma^{-}$. This behavior can be explained by supposing an increased transition energy difference between $^1A_{2g}$ and $^1E_g\leftarrow{}^1A_{1g}$ and/or the enhanced oscillator strength of $^1A_{2g}\leftarrow{}^1A_{1g}$. The location of the di-μ-hydroxo complex of en or S-pn in Fig. 11 may be also attributable to the relative lowering of the transition energy of $^1A_{2g}\leftarrow{}^1A_{1g}$.

The en or pn complexes of μ-OH, OH, mal, and ox are correlated with the corresponding tn complexes in a similar fashion (Fig. 11): the substitution of tn for en or pn decreases the band width with the decrease of $\Delta\sigma^{-}$ which is more substantial than that of $\Delta\sigma^{+}$.

The band shapes of the diaqua complexes are similar to each other irrespective of the kind of diamine ligands, whereas the diacetato complex with tn exhibits a band shape largely different from that of the corresponding complex with en or pn; thus, aqua and the diamine ligands have a predominant influence on the band shape in the former and the latter case, respectively. Similarly, tn and β-ala ligands seem to have a overwhelming influence on the band shape

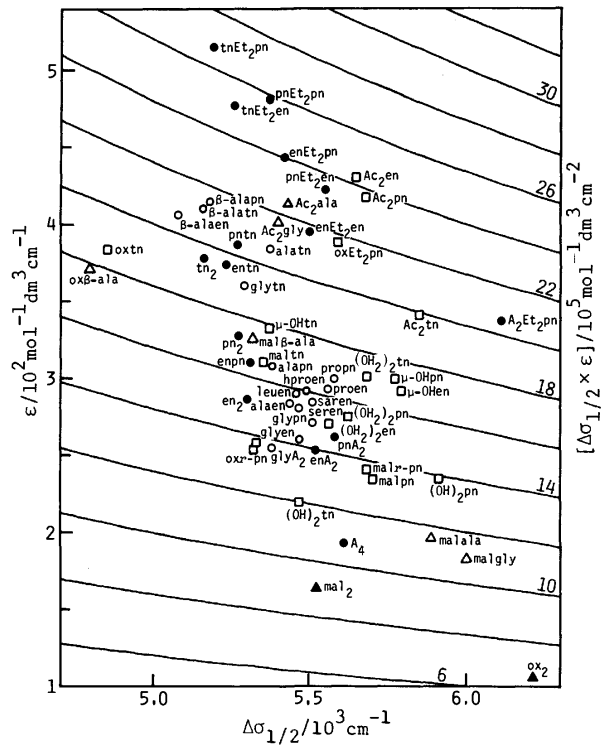

Fig. 10. Area intensity of the spin-allowed d-d absorption band represented as a function of the molar absorption coefficient of the absorption peak and the half-value width $\Delta\sigma_{1/2}$; ●: $[Pd(N)_4]$-, ○: $[Pd(N)_3(O)]$-, □: *cis*-$[Pd(N)_2(O)_2]$-, △: $[Pd(N)(O)_3]$-, and ▲: $[Pd(O)_4]$-type complexes; A=NH_3, pn=S-pn, *r*-pn=*rac*-pn, Et_2en=*N*,*N*-Et_2en, Et_2pn=N^1,N^1-Et_2-(*S*)-pn, ala=(*S*)-alaninato, ser=(*S*)-serinato, leu=(*S*)-leucinato, pro=(*S*)-prolinato, hpro=(*S*)-hydroxyprolinato, sar=sarcosinato, and Ac=acetato.

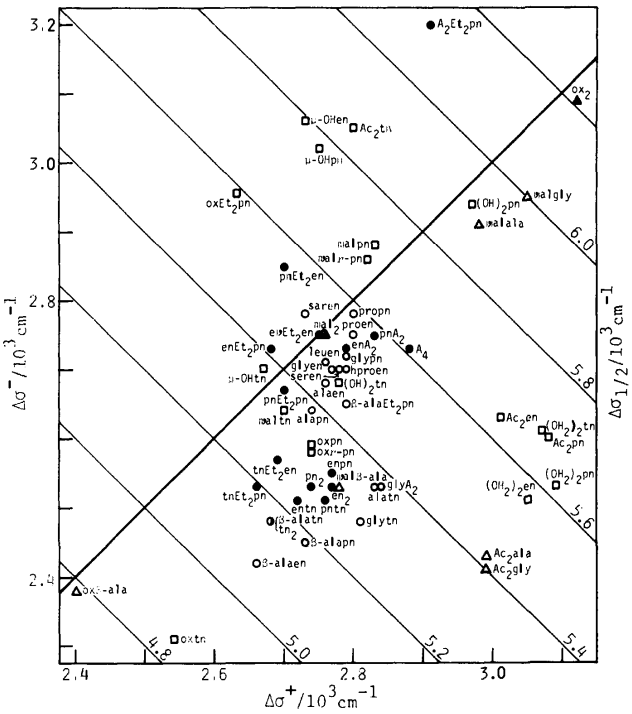

Fig. 11. Half-value width $\Delta\sigma_{1/2}$ (thin lines) represented as a function of $\Delta\sigma^+$ and $\Delta\sigma^-$; the thick line denotes $\Delta\sigma^+=\Delta\sigma^-$. See the footnote of Table 9 and the figure caption of Fig. 10 as to the marks and abbreviations.

in the $[Pd(N)_4]$- and $[Pd(N)_3(O)]$-type complexes, respectively.

The complexes containing tn, β-ala, or ox possess a band width narrower than the corresponding en(or pn), gly, or mal complexes, respectively, except $[Pd(OH_2)_2(tn)]^{2+}$, $[Pd(CH_3CO_2)_2(tn)]$, $[Pd(\beta\text{-ala})(tn)]^+$, and $[Pd(ox)_2]^{2-}$.

The relationship between the absorption band width $\Delta\sigma_{1/2}$ and the MCD intensity ratio $|\Delta\varepsilon_M(+)/\Delta\varepsilon_M(-)|$ is visualized in Fig. 12; which includes the data for $[Pd(Cl)_n(N)_{4-n}]$(n=1,2, and 4) and *cis*-$[Pd(Cl)_2(N)(O)]$-type complexes in addition to those for the $[Pd(N)_n(O)_{4-n}]$-type ones and reveals two facts. Firstly, the complexes with tn have a larger value of $|\Delta\varepsilon_M(+)/\Delta\varepsilon_M(-)|$ than the corresponding en or pn complexes without exception. Secondly, the complexes which possess a smaller $\Delta\sigma_{1/2}$ value exhibit a larger $|\Delta\varepsilon_M(+)/\Delta\varepsilon_M(-)|$ value and *vice versa*. This relationship implies a possibility of the mixing between d-d vibronic excited states by applied magnetic field; and such a mixing is presumed to give a negative B term for the $^1A_{2g}\leftarrow{}^1A_{1g}$ transition depending upon the magnitude of the mixing, which should be inversely proportional to the energy gap involved.[17] Thus, the MCD features predominated by B terms can be qualitatively explained by the mixing of this kind and by the mixing between a d-d vibronic excited state and a CT excited state as proposed in the previous section.

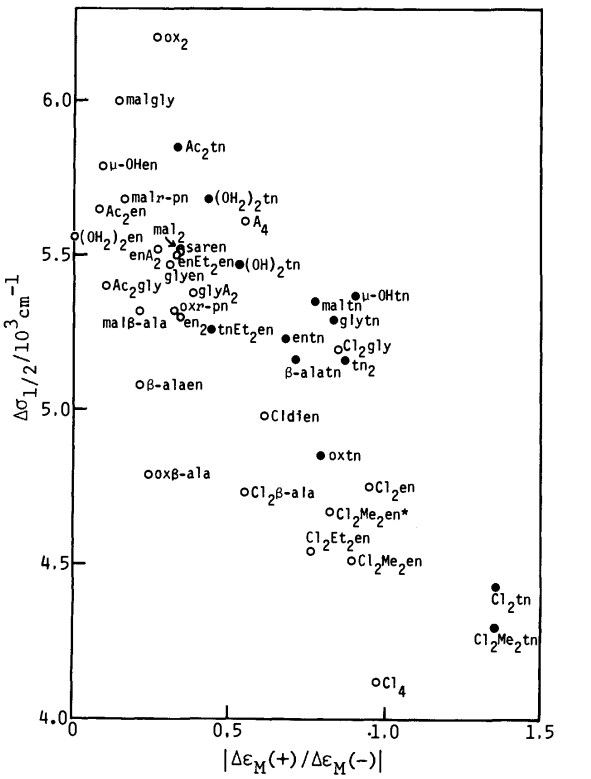

Fig. 12. Relationship between the half-value width $\Delta\sigma_{1/2}$ and the intensity ratio $|\Delta\varepsilon_M(+)/\Delta\varepsilon_M(-)|$; ●: complexes containing tn and ○: complexes not containing tn; Me_2en=*N*,*N*-Me_2en, Me_2en*=*N*,*N*'-Me_2en, Me_2tn=*N*,*N*-Me_2tn, and dien=diethylenetriamine, and see the figure caption of Fig. 10 as to the other abbreviations.

References

1) K. Nakayama, T. Komorita, and Y. Shimura, *Bull. Chem. Soc. Jpn.*, **57**, 1336 (1984).

2) K. Nakayama, T. Komorita, and Y. Shimura, *Bull. Chem. Soc. Jpn.*, **57**, 1240 (1984).

3) K. Nakayama, T. Komorita, and Y. Shimura, *Bull. Chem. Soc. Jpn.*, **57**, 972 (1984).

4) K. Nakayama, T. Komorita, and Y. Shimura, *Bull. Chem. Soc Jpn.*, **54**, 1056 (1981). *N,N,C,C*-Me$_4$en=N^2,N^2-dimethyl-2-methyl-1,2-propanediamine: $NH_2CH_2C(CH_3)_2N(CH_3)_2$; the abbreviation is based on the name for a substituted ethylenediamine.

5) M. Suzuki and Y. Nishida, *Inorg. Chim. Acta*, **34**, 61 (1979).

6) H. D. K. Drew, F. W. Pinkard, G. H. Preston, and W. Wardlaw, *J. Chem. Soc.*, **1932**, 1895.

7) J. S. Coe and J. R. Lyons, *Inorg. Chem.*, **9**, 1775 (1970).

8) E. A. Sullivan, *Can. J. Chem.*, **57**, 62 (1979).

9) The half-value-width parameters given in $10^3 cm^{-1}$: See the footnote of Table 9.

10) Prolonged heating gave the dimer complex [(β-ala)Pd(μ-Cl)$_2$Pd(β-ala)]. Found: C, 15.72; H, 2.74; N, 5.96%. Calcd for $C_6H_{12}N_2O_4Cl_2Pd_2$: C, 15.67; H, 2.63; N, 6.09%. This complex is sparingly soluble in water.

11) M. Vèzes, *Bull. Soc. Chim. Fr.*, **21**, 172 (1899).

12) G. Landesen, *Z. Anorg. Chem.*, **154**, 432 (1926).

13) M. J. Schmelz, I. Nakagawa, S. Mizushima, and J. V. Quagliano, *J. Am. Chem. Soc.*, **81**, 287 (1959).

14) The complex $[Pd(CH_3CO_2)_2(NH_3)_2]$ was excluded owing to its lability for isomerization.

15) S. B. Piepho, P. N. Schatz, and A. J. McCaffery, *J. Am. Chem. Soc.*, **91**, 5994 (1969).

16) $(\Delta\sigma_{1/2}\times\varepsilon)/10^5$ mol^{-1} $dm^3 cm^{-2}$=13.3, 17.2, and 17.5 for [$PdCl_2$(tn)], [$PdCl_2$(en)], and [$PdCl_2$(*S*-pn)], respectively.

17) P. N. Schatz and A. J. McCaffery, *Quart. Rev.*, **23**, 552 (1969).

Photoelectrochemical Behavior of the $Fe(CN)_5^{2-}$ Complexes Coordinated to the Poly(4-vinylpyridine) Film on Graphite Surfaces

Noboru OYAMA,* Hisao YAMAMOTO, Takeo OHSAKA, and Masao KANEKO†

Department of Applied Chemistry for Resources, Tokyo University of Agriculture and Technology, Koganei, Tokyo 184

†*The Institute of Physical and Chemical Research, Wako-shi, Saitama 351*

(Received April 19, 1984)

Photoelectrochemical reaction of the $Fe(CN)_5^{2-}$ complex ($PVP[Fe(CN)_5^{2-}]_n$) coordinated to the unprotonated poly(4-vinylpyridine) (PVP) film on a graphite electrode was examined in an aqueous solution. It was found that the carbon electrode coated with the $PVP[Fe(CN)_5^{2-}]_n$ generates the long-time responses of the photocurrents under irradiation of visible light and that the mechanism of its photochemical reaction is different from that for the photochemical reaction of $[Fe(CN)_6]^{3-}$ in a bulk solution, where the dissociation reaction of $[Fe(CN)_6]^{3-}$ to its aqua ion occurs.

Recently, the present authors have reported that the carbon surfaces coated with a couple of tris (2,2′-bipyridine)ruthenium(II) and methylviologen can generate the photocurrent.[1-3] As a series of papers regarding photoresponsive electrode prepared by coating of the photochemically active polymer, the present paper reports the photoelectrochemical investigation of the $Fe(CN)_5^{2-}$ complex (abbreviated as $PVP[Fe(CN)_5^{2-}]_n$) which is coordinated to the unprotonated poly(4-vinylpyridine) film coated on a basal plane pyrolytic graphite electrode in an aqueous solution. The photosensitivity of $[Fe(CN)_6]^{3-}$ and $[Fe(CN)_6]^{4-}$ was already known in 19th century and since then, a number of reports dealing with the photochemistry of $[Fe(CN)_6]^{3-}$ and $[Fe(CN)_6]^{4-}$ in aqueous solutions have appeared.[4] Moggi *et al.*[5] have studied the photochemical behavior of some cyanide complexes at various wavelengths in the ligand field spectral region and proposed a reaction mechanism involving a primary photoaquation reaction for the photolysis of the $[Fe(CN)_6]^{3-}$ ion both in neutral and in acidic solutions (see Scheme 1). Recently, Bowen and Hurlen[6] have studied the effect of irradiation on the electrode reactions of the $[Fe(CN)_6]^{4-}/[Fe(CN)_6]^{3-}$ couple at passive iron electrodes in borate solution and suggested that the rate of oxidation of $[FeCN)_6]^{4-}$ is markedly increased on irradiation, whereas the reduction of $[Fe(CN)_6]^{3-}$ is not affected. The overall photochemical reactions of $[Fe(CN)_6]^{3-}$ and $[Fe(CN)_6]^{4-}$ in aqueous solutions are composed of photoaquation, photooxidation-reduction and photosubstitution processes which sometimes occur simultaneously or successively. The photochemical reactions of these complexes are thus complicated, so that their photolysis has not been completely understood yet.

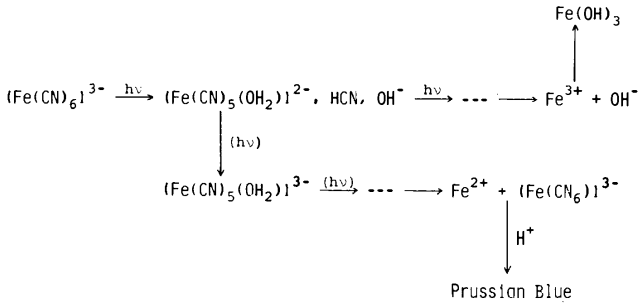

Scheme 1. $[Fe(CN)_6]^{3-}$ photolysis schematized by Ref. 5

The electrode reaction of $Fe(CN)_5^{2-/3-}$ redox couple, which is coordinated to the unprotonated PVP film coated on a graphite electrode, at the electrode/PVP film interfaces and the electron transfer reaction within the PVP film have been examined in previous papers,[7,8] where the special effect of the domain of the polymer film upon the electron transfer reactions has been demonstrated. Therefore, it is of interest to examine whether the polymeric domains influence upon the photochemical reaction of the $Fe(CN)_5^{2-/3-}$ complexes which are coordinated to the unprotonated PVP film or not.

Experimental

Electrochemical measurements were performed with a voltammetric analyzer (Model P-1000, Yanaco Co.). A 500 W Xenon lamp power supply (Model UI-501C, Ushio Electric Co.) was used as an irradiation source. The irradiation on the graphite electrode was performed with visible light (400—800 nm) through UV (Toshiba VY-42) and IR (Toshiba IRQ-80) cut-off filters. The intensity of the light could be varied by means of neutral density filters, and the wavelength could be varied using interference filters of bandpass 10 nm. IR spectra of $PVP[Fe(CN)_5^{2-}]_n$ film coated on electrode surface was measured by infrared spectrophotometer (A-302, Japan Spectroscopic Co., LTD.).

Poly(4-vinylpyridine) (PVP) (Bordon Inc., Philadelphia, PA) which was used in the present experiment unless otherwise described was reprecipitated twice from methanol-diethyl ether and its average molecular weight was 7.4×10^5.[9] Solutions containing PVP to which various quantities of $Fe(CN)_5^{3-}$ groups were coordinated were prepared, as described previously,[7] by mixing methanolic solutions of PVP having appropriate concentrations and aqueous solutions of $[Fe(CN)_5(OH_2)]^{3-}$ which were prepared by dissolving $Na_3[Fe(CN)_5(NH_3)]\cdot3H_2O$ (Tokyo Kasei Kogyo Co., Ltd.) in aqueous solutions under conditions where substitution of the NH_3 ligand by H_2O proceeds rapidly. Aliquots of the resulting solution of the polymer were transferred to the surface of a freshly cleaved basal plane graphite electrode (BPG, Union Carbide Corp.) and then the evaporation of the solvent was carried out at room temperature. The resulting coatings were swelled in an aqueous solution but remained insoluble. The thickness of the coating was calculated from the polymer densities (0.65 g cm^{-3}) estimated from the solvent-swelling measurements. The quantities of $Fe(CN)_5^{3-}$ moiety present in the coatings were measured by integrating the current from cyclic voltammograms which were observed at a low scan rate of 1—4 mV s^{-1}.[10] The exposed area of each electrode was 0.17 cm^2.

The test solution was made of a distilled water and a supporting electrolyte (0.2 M (1 M=1 mol dm^{-3}) CF_3COONa) and its pH was adjusted to desired pH value with NaOH and CF_3COOH solutions. Solutions were deaerated with prepurified argon and experiments were conducted at 25 °C under an atmosphere of argon. All potentials are reported with respect to a sodium chloride saturated calomel electrode (SSCE).

Results and Discussion

In previous papers,[7,8] we have succeeded in evaluation of the kinetic parameters of the electron-transfer reactions within the $PVP[Fe(CN)_5^{3-/2-}]_n$ film coated on a BPG and at the BPG/film interface in a solution containing only supporting electrolyte. Such a success depended upon the insolubility of the $PVP[Fe(CN)_5^{3-/2-}]_n$ film coated on electrodes in an aqueous solution. Figure 1 shows typical voltammetric response which is obtained with a pyrolytic graphite electrode coated with $PVP[Fe(CN)_5^{3-/2-}]_n$ film in a 0.2 M

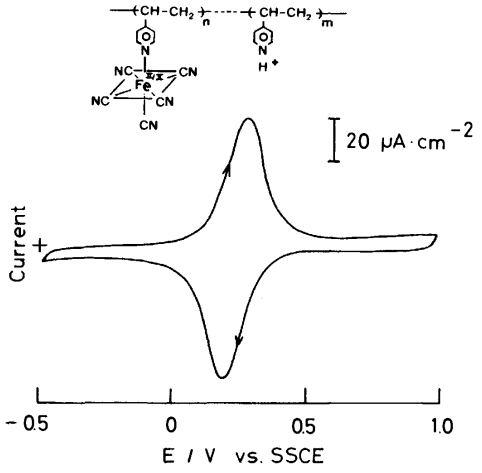

Fig. 1. Cyclic voltammogram for the $PVP[Fe(CN)_5^{2-}]_n$-coated BPG electrode in 0.2 M CF_3COONa aqueous solution adjusted to pH 3.0 at scan rate of 100 mV s^{-1}. $\Gamma_{PVP}=5.6\times10^{-7}$ mol cm^{-2} of pyridine units as PVP and $\Gamma_{Fe(CN)_5}=1.4\times10^{-9}$ mol cm^{-2} of electroactive $[Fe(CN)_5(pyridine)]$ moieties.

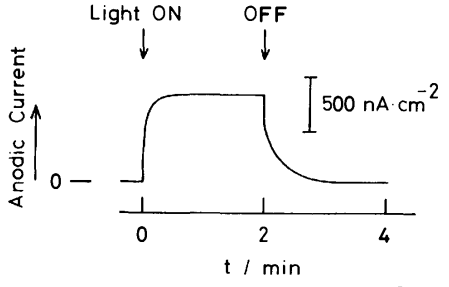

Fig. 2. Photocurrent responses to ON and OFF of irradiation on the $PVP[Fe(CN)_5^{2-}]_n$-coated BPG electrode in 0.2 M CF_3COONa solution adjusted to pH 3.0 at the electrode potential of +0.80 V *vs.* SSCE. $\Gamma_{PVP}=5.6\times10^{-7}$ mol cm^{-2} and $\Gamma_{Fe(CN)_5}=6.8\times10^{-9}$ mol cm^{-2}. Photocurrents were measured as the difference between the total current and its residual current measured with an uncoated BPG electrode at the same potential. Intensity of the visible light (400—800 nm) through UV and IR cut-off filters is 140 mW cm^{-2}.

CF_3COONa solution adjusted to pH 3.0 in dark or under irradiation. The anodic and cathodic peak potentials under irradiation were the same as those in dark. The voltammograms remained unchanged for several hours of continued cycling of the electrode potential in an acidic solution (pH 3.0) under the usual diffuse light, although the peak currents decreased gradually with increasing the irradiation time of visible light as mentioned below.

Figure 2 demonstrates the photoresponses induced by ON and OFF of the irradiation of visible light (400—800 nm) on the $PVP[Fe(CN)_5]_n$ coated BPG electrode in a 0.2 M CF_3COONa solution (pH 3.0) at +0.80 V *vs.* SSCE. The same photocurrent response to ON and OFF of irradiation was obtained repeatedly. The anodic photocurrent responses were observed at the positive-side potential more than *ca.* 0.3 V and the values increased as the applied potential shifts to the positive side. The photocurrent was also influenced by pH of the solution in which the electrode is soaked, and its maximum was observed in the solution of pH 3.0. In the case of the electrode coated with PVP film ($\Gamma_{PVP}=5.6\times10^{-7}$ mol cm^{-2}) to which the $Fe(CN)_5^{3-}$ moieties of $\Gamma_{Fe(CN)_5}=6.8\times10^{-9}$ mol cm^{-2} were coordinated, the anodic photocurrent of 0.9 μA cm^{-2} was obtained at the potential of 0.80 V under the irradiation with the intensity of 140 mW cm^{-2} in a 0.2 M CF_3COONa solution (pH=3.0). No photocurrent response under irradiation were observed with a bare BPG electrode and the BPG electrode coated with PVP coordinating no $Fe(CN)_5^{2-}$ complexes. The cathodic photocurrents were also observed at the negative-side potential more than about 0.2 V, although their values were smaller than the values of the anodic ones.

Figure 3 shows the action spectrum of the anodic photocurrent obtained with the coated electrode, coverages of which are $\Gamma_{PVP}=1.1\times10^{-6}$ mol cm^{-2} and $\Gamma_{Fe(CN)_5}=3.6\times10^{-8}$ mol cm^{-2}, at the electrode potential of 0.80 V under irradiation of monochromatic light. The shift (about 20 nm) of the action spectrum to longer wavelengths than the absorption spectrum in water

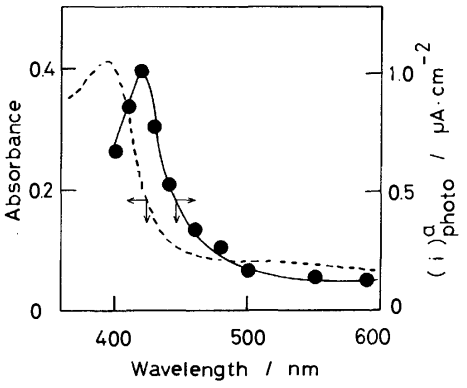

Fig. 3. Action spectrum for the anodic photocurrent observed with the $PVP[Fe(CN)_5^{2-}]_n$-coated electrode, coverages of which are $\Gamma_{PVP}=1.1\times10^{-6}$ mol cm^{-2} and $\Gamma_{Fe(CN)_5}=3.6\times10^{-8}$ mol cm^{-2}. (●) experimental; (----) absorption spectrum of 0.46 mM $[Fe(CN)_5^{2-}]_n$ coordinated to PVP of the average molecular weight 1980 in 0.2 M CF_3COONa aqueous solution adjusted to pH 3.0.

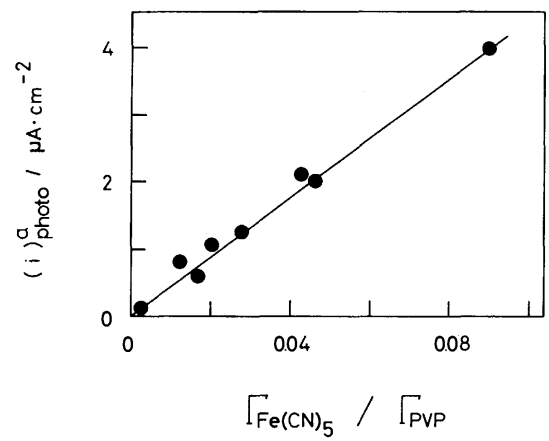

Fig. 4. Anodic photocurrent *vs.* $\Gamma_{Fe(CN)_5}/\Gamma_{PVP}$. Γ_{PVP} is constant (5.6×10^{-7} mol cm^{-2}). Other experimental conditions are the same as in Fig. 2.

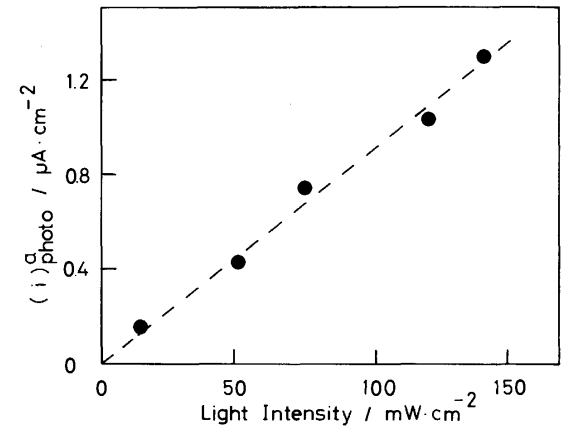

Fig. 5. Anodic photocurrent *vs.* light intensity. $\Gamma_{PVP}=5.6\times10^{-7}$ mol cm^{-2} and $\Gamma_{Fe(CN)_5}=1.6\times10^{-8}$ mol cm^{-2} at electrode potential +0.80 V *vs.* SSCE. Other experimental conditions are the same as in Fig. 2.

suggests some strong interaction[11] between the metal complex and PVP. Its shape almost agrees with that of the spectrum of the $PVP[Fe(CN)_5^{2-}]_n$ complexes formed with PVP of the average molecular weight 1980 in aqueous solutions, indicating that the excitation of the $Fe(CN)_5^{2-}$ complexes coordinated to the unprotonated PVP film is responsible for their photoelectrochemical behaviors.

Figure 4 shows the dependence of the anodic photocurrent, $(i)^a_{photo}$, upon the ratio $\Gamma_{Fe(CN)_5}/\Gamma_{PVP}$ at the constant concentration of pyridine ligand as PVP ($\Gamma_{PVP}=5.6\times10^{-7}$ mol cm^{-2}). The measurements were made in a 0.2 M CF_3COONa (pH 3.0) at the electrode potential of 0.80 V *vs.* SSCE under the irradiation of visible light with the intensity of 140 mW cm^{-2}. $(i)^a_{photo}$ was proportional to $\Gamma_{Fe(CN)_5}/\Gamma_{PVP}$. The dependence of the anodic photocurrent on the light intensity at the electrode potential of 0.80 V *vs.* SSCE was also measured and is shown in Fig. 5. $(i)^a_{photo}$ exhibits essentially linear dependence on the light intensity. The similar dependence of photocurrent on the light intensity has been reported in the photochemistry of an aqueous solution of $[Fe(CN)_6]^{4-}$.[6] At constant values of $\Gamma_{Fe(CN)_5}/\Gamma_{PVP}$, $(i)^a_{photo}$ increased with an increase in Γ_{PVP}.

Moggi *et al.*[5] have suggested that $[Fe(CN)_5(OH_2)]^{2-}$ is the main primary product of the photoreaction of $[Fe(CN)_6]^{3-}$ and the photochemical aquosubstitution reaction of $[Fe(CN)_5(OH_2)]^{2-}$ occurs simultaneously with the oxidation-reduction reaction which yields $[Fe(CN)_5(OH_2)]^{3-}$. They have confirmed that the products formed by a series of these reactions under long irradiation periods are $Fe(OH)_3$ (in neutral solution), prussian blue (in acidic solution), $[Fe(CN)_5(OH_2)]^{3-}$, Fe^{2+} and Fe^{3+}, and further that the pH of aqueous solutions slowly increases during irradiation in neutral solution and after some time tends to reach a constant value. On the basis of the mechanism (Scheme 1) proposed previously for photochemical reaction of the aqueous solution of $[Fe(CN)_6]^{3-}$, the mechanism of the photoelectrochemical reaction of $PVP[Fe(CN)_5]_n$ coated on the BPG can be expressed as follows:

$$PVP[Fe(CN)_5^{3-}]_n - e \rightleftharpoons PVP[Fe(CN)_5^{2-}]_n, \quad (1)$$

$$PVP[Fe(CN)_5^{2-}]_n \xrightarrow{h\nu} PVP[Fe(CN)_5^{2-}]^*_n, \quad (2)$$

$$PVP[Fe(CN)_5^{2-}]^*_n \longrightarrow PVP[Fe(CN)_{5-x}(OH_2)_x^{(2-x)-}]_n, \quad (3)$$

$$PVP[Fe(CN)_{5-x}(OH_2)_x^{(2-x)-}]_n \xrightarrow{OH^-} PVP, Fe(OH)_3, CN^-, \quad (4)$$

$$PVP[Fe(CN)_{5-x}(OH_2)_x^{(2-x)-}]_n \xrightarrow{H^+} PVPH^+, Fe^{2+}, HCN, \quad (5)$$

$$PVP[Fe(CN)_{5-x}(OH_2)_x^{(2-x)-}]_n \longrightarrow PVP[Fe(CN)_{5-x}(OH_2)_x^{(3-x)-}]_n, \quad (6)$$

where, Eq. 1 shows the electrode reaction of $PVP[Fe(CN)_5^{3-/2-}]_n$ couple, $PVP[Fe(CN)_5^{2-}]^*_n$ is the excited species formed from $PVP[Fe(CN)_5^{2-}]_n$ by the irradiation of visible light, $PVPH^+$ is the protonated PVP, Eqs. 3 and 6 denote aqua-substitution and thermal reduction reactions, respectively, and Eqs. 4 and 5 show the decomposition reactions in neutral and acidic solutions, respectively. If this series of the reaction mechanism is applicable to the present system, anodic photocurrent could not be observed for the longer irradiation time than that which is enough for the reaction expressed by Eq. 2 to be terminated. However, when the $PVP[Fe(CN)_5^{2-}]_n$ coated on electrode, the coverages of which were $\Gamma_{PVP}=2.8\times10^{-7}$ mol cm^{-2} and $\Gamma_{Fe(CN)_5}=1.9\times10^{-9}$ mol cm^{-2}, was irradiated with visible light for 30 h in a 0.2 M CF_3COONa solution (pH 3.0) at the electrode potential of 0.80 V *vs.* SSCE, total amount of electricity, Q_p, that flowed during irradiation was estimated to be 1.8×10^{-3} coulomb cm^{-2}, which corresponds to 1.9×10^{-8} mol cm^{-2}. After 30 h, $PVP[Fe(CN)_5^{2-}]_n$ of $\Gamma_{Fe(CN)_5}=2.0\times10^{-10}$ mol cm^{-2} remained still confined in the PVP film on electrode surface. The concentration of $Fe(CN)_5^{2-}$ moiety decreased to about 10% of its initial value, nevertheless the value of Q_p corresponded to about ten times the initial concentration of $Fe(CN)_5^{2-}$ moiety. The anodic photocurrent after 30 h was also about 10% of its initial value, although about 80% of its initial value was lost

within 1 h of irradiation. The decays in the current and in the concentration of the $Fe(CN)_5$ complex are rapid and almost exponential. Judging from the fact that the redox potentials of $[Fe(CN)_6]^{4-/3-}$ and $[Fe(CN)_5(py)]^{3-/2-}$ (where py=pyridine) couples were 0.20 V *vs.* SSCE and that of $[Fe(CN)_5(OH_2)]^{3-/2-}$ was 0.09 V *vs.* SSCE at a bare BPG in aqueous solutions, if the aquoated complex, *i.e.*, $[Fe(CN)_{5-x}(OH_2)_x]^{(2-x)-}$ formed during the photochemical reaction of $Fe(CN)_5^{2-}$ remains in the PVP film without any dissociation, the peak potentials of voltammograms would be different from those for $Fe(CN)_5^{3-/2-}$ couple coordinated to the unprotonated PVP film. However, the redox potential estimated from cyclic voltammogram obtained with the $PVP[Fe(CN)_5]_n$-coated electrode which was irradiated with visible light for 30 h was the same as that (0.2 V *vs.* SSCE) obtained with the same electrode before irradiation (see Fig. 1). Further, Fe^{2+} aqua ion as Prussian blue was undetected.

From these results, it seems unlikely that the similar mechanism (Eqs. 1—6) to the photochemical reaction of $[Fe(CN)_6]^{3-}$ in aqueous solution is applicable to the photoelectrochemical reaction of $PVP[Fe(CN)_5]_n$ coated on the BPG. In the place of reactions expressed by Eqs. 3—6, we can consider the following reaction mechanisms for the photochemical reaction under consideration:

$$PVP[Fe(CN)_5^{2-}]_n^* + H_2O \longrightarrow PVP[Fe(CN)_5^{3-}]_n + 1/2O_2 + 2H^+, \quad (7)$$

$$PVP[Fe(CN)_5^{2-}]_n^* \longrightarrow PVP^+[Fe(CN)_5^{3-}]_n, \quad (8)$$

$$PVP[Fe(CN)_5^{2-}]_n^* + (BPG) \longrightarrow PVP[Fe(CN)_5^{3-}]_n + (BPG)^+, \quad (9)$$

where, $PVP^+[Fe(CN)_5^{3-}]_n$ denotes the species resulting from oxidation of pyridine ring and/or vinyl group of PVP, $(BPG)^+$ denotes the product obtained from oxidation of the BPG material itself by the $PVP[Fe(CN)_5^{2-}]_n^*$. IR absorption spectra of the $PVP[Fe(CN)_5]_n$ coated on the BPG after long-time irradiation (30 h) demonstrated the new absorption peak which seems to be characteristic of carbonyl group at 1670 cm^{-1}. This suggests the formation of carbonyl group which is caused by Eq. 8 during the irradiation of visible light, although the details of this reaction mechanism are not clear. From the reaction expressed by Eq. 7, the evolution of oxygen is expected under long-time irradiation but has not been detected by gas chromatography. Figure 6 demonstrates the decay in the anodic photocurrent under the irradiation. As seen from this figure, the electricity, Q_p, that flows as a photocurrent during 35 h irradiation is estimated to be 9.4×10^{-3} coulomb cm^{-2}, which corresponds to 9.7×10^{-8} mol cm^{-2}. This value of Q_p corresponded to fifty times the initial concentration of the $Fe(CN)_5^{2-}$ complexes and about five times the initial concentration of pyridine ligand as PVP. Therefore, the process expressed by Eq. 9 (*i.e.*, the oxidation of the BPG electrode used as an anode) seems to be mainly responsible for the photochemical responses, since vinylpyridine moiety of PVP, not oxidized, is still on the BPG surfaces.

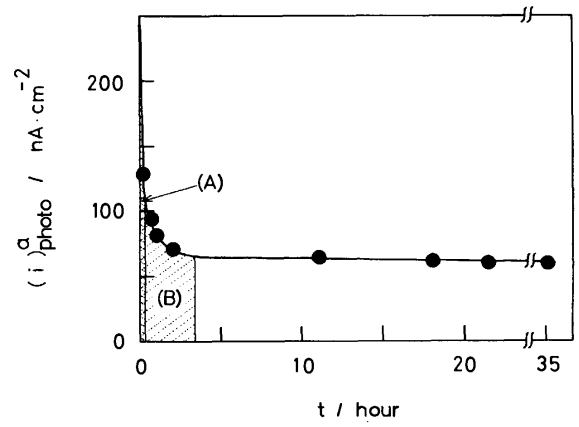

Fig. 6. Anodic photocurrent *vs.* irradiation time. Initial value of $\Gamma_{PVP}=1.8\times10^{-8}$ mol cm^{-2} and initial value of $\Gamma_{Fe(CN)_5}=1.9\times10^{-9}$ mol cm^{-2}. Other experimental conditions are the same as in Fig. 2. Area (A) corresponds to the initial value of $\Gamma_{Fe(CN)_5}$; area (B) corresponds to the initial value of Γ_{PVP}.

The present results conclude that the mechanism of the photochemical reaction following the oxidation of $PVP[Fe(CN)_5^{3-}]_n$ coated on the BPG surfaces is different from that of an aqueous solution of $[Fe(CN)_6]^{3-}$ [5] and photochemical processes are oxidation-reduction reactions expressed by Eqs. 8 and 9. Further, it became to be clear that the photoaquation and the subsequent dissociation reactions, which are very familiar in the photochemistry of aqueous solutions of $[Fe(CN)_6]^{3-}$ and $[Fe(CN)_6]^{4-}$, [4,5] seem to be suppressed in the polymer domains. However, some unsolved problems still remain: (1) A rapid, almost exponential decay in the anodic photocurrent occurred during the short-time (less than 1 h) irradiation. We have no idea to explain such a behavior at present. (2) Anodic photocurrents were influenced by pH of the solution in which the $PVP[Fe(CN)_5^{2-}]_n$-coated electrode was soaked, and their maxima were observed for the solution of pH 3.0. It seems to be considered that the change of morphology of the $Fe(CN)_5^{2-}$ complex polymer with pH results in the pH-dependence of the photocurrent. (3) The cathodic photocurrents were also observed at the negative-side potential more than about 0.20 V and their values were smaller than the anodic ones at the same coating electrode. The reduction of the BPG electrode by the $PVP[Fe(CN)_5^{3-}]_n^*$ may result in the cathodic photocurrents but we have no direct evidence to support this interpretation.

In conclusion, we emphasize that modification of the carbon electrode by coating the photosensitive species on it can generate the photocurrent.

The present work was partially supported by the Grant of the Nissan Science Foundation.

References

1) N. Oyama, S. Yamaguchi, M. Kaneko, and A. Yamada, *J. Electroanal. Chem.*, **139**, 215 (1982).

2) M. Kaneko, A. Yamada, N. Oyama, and S. Yamaguchi, *Makromol. Chem., Rapid Commun.*, **3**, 769 (1982).

3) M. Kaneko, S. Moriya, A. Yamada, H. Yamamoto, and N. Oyama, *Electrochim. Acta*, **29**, 115 (1984).
4) V. Balzani and V. Carassiti, "Photochemistry of Coordination Compounds," Academic Press, London and New York, (1967), Chapter 10.
5) L. Moggi, F. Bolletta, V. Balzani, and F. Scandola, *J. Inorg. Nucl. Chem.*, **28**, 2589 (1966).
6) W. R. Bowen and T. Hurlen, *Acta Chem. Scand., Ser. A* **35**, 359 (1981).
7) K. Shigehara, N. Oyama, and F. C. Anson, *J. Am. Chem. Soc.*, **103**, 2552 (1981).
8) N. Oyama, T. Ohsaka, M. Kaneko, K. Sato, and H. Matsuda, *J. Am. Chem. Soc.*, **105**, 6003 (1983).
9) N. Oyama and F. C. Anson, *J. Am. Chem. Soc.*, **101**, 739, 3450 (1979).
10) N. Oyama and F. C. Anson, *J. Electrochem. Soc.*, **127**, 640 (1980).
11) M. Kaneko, J. Motoyoshi, and A. Yamada, *Nature*, **289**, 468 (1980).

 © 1984 The Chemical Society of Japan Bull. Chem. Soc. Jpn., 57, 2947—2953 (1984)

Theory of Time-resolved Photon Absorption by Molecules after Radiationless Transition. Application to Benzene after $S_2 \rightsquigarrow S_0$.

Yuichi FUJIMURA,* Minoru ARAI, Nobuaki NAKASHIMA,† and Keitaro YOSHIHARA†
Department of Chemistry, Faculty of Science, Tohoku University, Sendai 980
†*Institute for Molecular Science, Myodaiji, Okazaki 444*
(Received May 18, 1984)

Expressions for the intensity of the time-resolved absorption (TRA) by molecules after radiationless transition have been derived. It is assumed that a non-equilibrium vibronic distribution is realized after the radiationless transition and relaxes to the equilibrium one. Two types of non-equilibrium distributions, Poisson distribution and canonical distribution with temperature higher than that of the heat bath are taken into account. The theory developed is applied to the TRA spectra ($S_3 \leftarrow S_0$) of benzene after the internal conversion $S_2 \rightsquigarrow S_0$ (N. Nakashima and K. Yoshihara, *J. Chem. Phys.* **79**, 2727, (1983)). It is shown that the expression for the intensity in the Sulzer-Wieland model is involved in the expression derived using the canonical distribution.

Recently Nakashima and Yoshihara[1] have observed the time-resolved absorption (TRA) spectra of gaseous benzenes after excitation to the $S_2(^1B_{1u})$ state. It has been shown that the transient spectra consist of the $S_3(^1E_{1u}) \leftarrow S_0(^1A_{1g})$ transition at high temperatures. The spectra reflect the vibronic energy distribution after the internal conversion from the S_2 state to the ground state. The spectral changes with time are mainly brought about by collisional deactivation processes of the hot benzene by inert gas and unexcited benzene. The transient spectrum at $t=0$ was explained by using the Sulzer-Wieland model[2] originally applied to absorption spectra of diatomic molecules with a large potential displacement at high temperatures. This model has been applied to analysis of the high temperature ultraviolet absorption spectra of polyatomic molecules in shock waves by Astholz *et al.*[3] and by Hippler *et al.*[4] as well. To our knowledge, however, there exists no any sufficient theoretical explanation for the applicability of the Sulzer-Wieland model to the polyatomic molecules in the highly excited vibronic states. The purpose of this paper is to develop a theory of the time-resolved absorption spectra of hot molecules produced by radiationless transition, and to apply the theory to the time-resolved absorption spectra of benzene observed previously.[1]

The TRA spectra of molecules strongly depend on the initial non-equilibrium vibronic energy distribution which is realized in a time scale of observation. The following scheme can account for the observed TRA spectra.

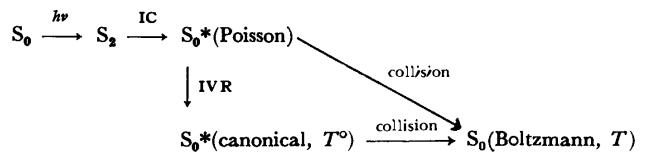

Two types of the vibronic energy distributions different from the thermal equilibrium distribution can be expected after radiationless transitions. One is a Poisson (intramolecular) vibronic energy distribution,[5,6] and the other is a canonical distribution characterized by a higher temperature $T°$ than that of the heat bath T. The former distribution is formed just after internal conversion (IC) following laser excitation. One of the evidences for the intramolecular vibronic energy distribution is seen in the TRA spectra ($^3B_{1g} \leftarrow {}^3B_{2u}$) after excitation to the S_1 state of naphthalene in vapor.[7] A vibronic structure associated with the triplet-triplet absorption appears in the TRA spectra just after the intersystem crossing takes place. A canonical vibronic energy distribution with $T°>T$, on the other hand, is expected to be realized when an intramolecular vibrational redistribution takes place following the radiationless transition. Taking into account the two types of the initial distributions we derive expressions for the absorption intensity of the TRA spectra of polyatomic molecules. In deriving the expressions for the intensity, it is assumed that the initial distributions relax to the Boltzmann distribution due to collisional deactivations and that the collision rates vary linearly with respect to the vibrational quantum number.[8] It is shown that the expression for the time-resolved absorption intensity of the molecular system with a canonical distribution as the initial distribution involves the expression derived by Sulzer and Wieland as a special case. A model calculation of the TRA spectra using the derived expressions supports the conclusion given in the previous paper:[1] the initial vibronic distribution is of the canonical one with a high temperature.

Theory

Let us consider a time-resolved absorption process from the vibrationally hot ground electronic state a to an electronically excited state b. The initial, vibrational state in the non-equilibrium condition is produced by internal conversion $S_2 \rightsquigarrow S_0^*$. The intensity per unit length, $D_{ab}(\omega_R, t)$, as a function of time, t, and the laser frequency, ω_R is expressed in the form,[5]

$$D_{ab}(\omega_R, t) = \sum_{\{v\}} k_{a\{v\}}(\omega_R)\chi_{\{v\}}(t), \qquad (1)$$

where $k_{a\{v\}}(\omega_R)$ represents the absorption coefficient from a single vibronic level $\{v\}$ in the ground state a, and $\chi_{\{v\}}(t)=\prod_j^N \chi_{vj}(t)$ in which $\chi_{vj}(t)$ denotes the vibronic energy distribution of the optical vibrational mode j

per unit volume at time t, and N is the number of the optical modes whose potential forms between a and b states are different. The distribution $\chi_{\{v\}}(t)$ depends on the dynamical behavior and the initial distribution. In this paper we consider Poisson and canonical distributions. First we treat the time-evolution of molecules characterized by a Poisson distribution which relaxes to the equilibrium distribution with T. In a previous paper,[6] a theoretical treatment of the TRA spectroscopy was presented in the case of the relaxation of the Poisson distribution to the lowest vibronic state in the low temperature limit.

Poisson Vibronic Energy Distribution. We assume that at $t=0$ a non-equilibrium state originating from an intramolecular radiationless transition has been prepared. It has been shown that the distribution of the vibrational mode j with frequency ω_j after the radiationless transition from the lowest vibronic level is expressed as[5,6]

$$\chi_{v_j}(0) = S_{0_j'v_j} \exp\left[-v_j\bar{\beta}\hbar\omega_j + \frac{\bar{\Delta}_j^2}{2}\{1-\exp(-\bar{\beta}\hbar\omega_j)\}\right], \quad (2)$$

where the displaced harmonic oscillator model has been used. $S_{0_j'v_j}$ is the optical Franck-Condon factor between $0_j'$ and v_j states, and given by $S_{0_j'v_j}=(\bar{\Delta}_j/\sqrt{2})^{2v_j}$ $\exp(-\bar{\Delta}_j^2/2)/v_j!$. $\bar{\Delta}_j$ is the displacement of the mode j in the equilibrium points between the relevant two electronic states. $\bar{\beta}$ in Eq. (2) is a parameter which is determined from the condition of the energy conservation for the radiationless transition. Equation (2) satisfies $\sum_{v_j}\chi_{v_j}(0)=1$. Equation (2) can be rewritten in the form of a Poisson distribution,

$$\chi_{v_j}(0) = \frac{\alpha_j^{v_j}}{v_j!}\exp(-\alpha_j), \quad (3)$$

with the average vibrational quantum number[5] given by

$$\alpha_j = \frac{\bar{\Delta}_j^2}{2}\exp(-\bar{\beta}_j\hbar\omega_j). \quad (4)$$

In the case of the radiationless transition from v_j' level, the expression for the distribution can approximately be represented by Eq. (2) in which $S_{0_jv_j}$ is replaced by $S_{v_j'v_j}$.

If we assume that the molecular system undergoes only a collisional vibrational energy exchange between the system and the heat bath, and interactions between the vibrational modes of the system are neglected, *i.e.* each vibrational mode relaxes to its equilibrium distribution, then the time-dependent distribution χ_{v_j} satisfies the master equation,[8]

$$\begin{aligned}\frac{d\chi_{v_j}(t)}{dt} = {} & \kappa_j\{1-\exp(-\theta_j)\}^{-1}[v_j\exp(-\theta_j)\chi_{v_j-1}(t) \\ & - \{v_j+(v_j+1)\exp(-\theta_j)\}\chi_{v_j}(t) \\ & + (v_j+1)\chi_{v_j+1}(t)], \end{aligned} \quad (5)$$

where κ_j is the transition probability per unit time between levels $v_j=1$ and 0 of mode j, and $\theta_j=\hbar\omega_j/kT$. T denotes temperature of the heat bath consisting of unexcited benzenes. The master equation with the initial condition as given by Eq. (3) is solved as[8]

$$\begin{aligned}\chi_{v_j}(\tau_j) = {} & \left\{\frac{1-\exp(\theta_j)}{\exp(-\tau_j)-\exp(\theta_j)}\right\} \\ & \times \exp\left[\frac{\alpha_j\exp(-\tau_j)\{\exp(\theta_j)-1\}}{\exp(-\tau_j)-\exp(\theta_j)}\right] \\ & \times \left\{\frac{1-\exp(-\tau_j)}{\exp(\theta_j)-\exp(-\tau_j)}\right\}^{v_j} L_{v_j}(y_j), \end{aligned} \quad (6)$$

in which $L_{v_j}(y_j)$ is the Laguerre polynomials,

$$y_j = \frac{\alpha_j\exp(-\tau_j)\{\exp(\theta_j)-1\}^2}{\{1-\exp(-\tau_j)\}\{\exp(-\tau_j)-\exp(\theta_j)\}}, \quad (7)$$

and

$$\tau_j = \kappa_j t\{1-\exp(-\theta_j)\}. \quad (8)$$

In the case in which the vibronic band is characterized by a Lorentzian envelope, the absorption coefficient $k_{a\{v\}}$ in Eq. (1) is given by

$$k_{a\{v\}}(\omega_R) = \frac{4\pi\omega_R}{3\hbar c}\mathrm{Re}\sum_{\{v''\}}\frac{|R_{bv'',av}|^2}{i(\omega_{bv'',av}-\omega_R)+\Gamma_{ba}}, \quad (9)$$

where $\omega_{bv'',av}$ is the frequency difference between two vibronic levels, bv'' and av, $R_{bv'',av}$, the matrix element of the electric transition dipole moment, and Γ_{ba}, the damping constant associated with the interactions between the optical and other vibrational modes. We invoke the adiabatic and Condon approximations since we are interested in the allowed electronic transition $S_3(E_{1u})\leftarrow S_0(A_{1g})$ of benzene. In these approximations, Eq. (9) can be expressed as

$$k_{a\{v\}}(\omega_R) = C\sum_{\{v''\}}\frac{\Gamma_{ba}|\langle\eta_{bv''}|\eta_{av}\rangle|^2}{(\omega_{bv'',av}-\omega_R)^2+\Gamma_{ba}^2}, \quad (10)$$

where $C=4\pi\omega_R|R_{ab}^0|^2/(3\hbar c)$, and η denote the vibrational wavefunctions. We adopt a displaced harmonic oscillator model for the optical modes.

Carrying out the summation over the vibronic states in Eq. (1), we express the absorption coefficient, Eq. (10), as:

$$\begin{aligned}k_{a\{v\}}(\omega_R) = {} & \frac{C}{2}\exp(-S)\int_{-\infty}^{\infty}d\xi\exp[i\xi(\omega_{ba}-\omega_R)-\Gamma_{ba}|\xi| \\ & + \sum_{j=1}^{N}\frac{\Delta_j^2}{2}\exp(i\omega_j\xi)]\sum_{n_1=0}^{v_1}\cdots\sum_{n_j=0}^{v_j}\cdots\sum_{n_N=0}^{v_N}\prod_j \\ & \times\frac{v_j!\Delta_j^{2n_j}}{(v_j-n_j)!(n_j!)^2}(\cos\omega_j\xi-1)^{n_j}, \end{aligned} \quad (11)$$

where S $(=\sum_{j=1}^{N}\bar{\Delta}_j^2/2)$ is the coupling strength in the low temperature limit. Substituting Eqs. (6) and (11) into Eq. (1), we can derive an analytical expression for the time-dependent intensity:

$$\begin{aligned}D_{ab}(\omega_R,\tau) = {} & C\exp[-S-\sum_{j=1}^{N}a(\tau_j)]\sum_{n_1=0}^{\infty}\cdots\sum_{n_j=0}^{\infty}\cdots\sum_{n_N=0}^{\infty} \\ & \times\sum_{l_1=0}^{\infty}\cdots\sum_{l_j=0}^{\infty}\cdots\sum_{l_N=0}^{\infty}\sum_{m_1=0}^{l_1}\cdots\sum_{m_j=0}^{l_j}\cdots\sum_{m_N=0}^{l_N}\sum_{k_1=0}^{l_1-m_1}\cdots\sum_{k_j=0}^{l_j-m_j}\cdots\sum_{k_N=0}^{l_N-m_N}\end{aligned}$$

$$\times \sum_{p_1=0}^{2(m_1+k_1)} \cdots \sum_{p_j=0}^{2(m_j+k_j)} \cdots \sum_{p_N=0}^{2(m_N+k_N)} \left[\prod_{j=1}^{N} \binom{l_j}{m_j} \binom{l_j-m_j}{k_j} \binom{2m_j+2k_j}{p_j} \right.$$
$$\times \frac{(-1)^{p_j}}{n_j!\,(m_j+k_j)!\,(l_j-m_j)!} \left(\frac{\Delta_j^2}{2}\right)^{n_j+m_j+k_j}$$
$$\left. \times a(\tau_j)^{l_j-m_j} \left\{ \frac{1-\exp(-\tau_j)}{\exp(\theta_j)-1} \right\}^{m_j} \right]$$
$$\times \frac{\Gamma_{ba}}{\{\omega_{ba}+\sum_{j=1}^{N} \omega_j(n_j+k_j+m_j-p_j)-\omega_R\}^2+\Gamma_{ba}^2}, \quad (12)$$

where $\tau \equiv \{\tau_j\}$, $j=1, 2, \cdots, N$, and

$$a(\tau_j) = \frac{\alpha_j \exp(-\tau_j)\{\exp(\theta_j)-1\}}{\exp(\theta_j)-\exp(-\tau_j)}. \quad (13)$$

A detailed derivation of Eq. (12) is presented in Appendix A.

In the case in which $a(\tau_j)>1$ is satisfied, it is appropriate to use the following approximate expression for the intensity:

$$D_{ab}(\omega_R, \tau) = C \exp[-S] \sum_{n_1=0}^{\infty} \cdots \sum_{n_j=0}^{\infty} \cdots \sum_{n_N=0}^{\infty} \sum_{l_1=0}^{\infty} \cdots \sum_{l_j=0}^{\infty} \cdots \sum_{l_N=0}^{\infty}$$
$$\times \sum_{m_1=0}^{l_1} \cdots \sum_{m_j=0}^{l_j} \cdots \sum_{m_N=0}^{l_N} \sum_{k_1=0}^{l_1-m_1} \cdots \sum_{k_j=0}^{l_j-m_j} \cdots \sum_{k_N=0}^{l_N-m_N} \sum_{p_1=0}^{m_1+k_1} \cdots \sum_{p_j=0}^{m_j+k_j} \cdots \sum_{p_N=0}^{m_N+k_N}$$
$$\times \sum_{q_1=0}^{p_1} \cdots \sum_{q_j=0}^{p_j} \cdots \sum_{q_N=0}^{p_N} \sum_{r_1=0}^{m_1+k_1-p_1} \cdots \sum_{r_j=0}^{m_j+k_j-p_j} \cdots \sum_{r_N=0}^{m_N+k_N-p_N}$$
$$\times \left\{ \prod_{j=1}^{N} \frac{(-1)^{p_j-q_j+r_j}}{n_j!\,(m_j+k_j)!} \left(\frac{\Delta_j^2}{2}\right)^{n_j+m_j+k_j} \right.$$
$$\times \binom{l_j}{m_j} \binom{l_j-m_j}{k_j} \binom{m_j+k_j}{p_j} \binom{p_j}{q_j} \binom{m_j+k_j-p_j}{r_j}$$
$$\times \left[\frac{1-\exp(-\tau_j)}{\exp(\tau_j)-1} \right]^{m_j} \exp\left[-\frac{\{l_j-m_j-a(\tau_j)\}^2}{2a(\tau_j)} \right] \Bigg\}$$
$$\times \frac{\Gamma_{ba}}{\{\omega_{ba}+\sum_{j=1}^{N} \omega_j(n_j+k_j+m_j-p_j)-\omega_R\}^2+\Gamma_{ba}^2}. \quad (14)$$

Canonical Vibronic Energy Distribution. It is assumed that at $t=0$, a local equilibrium characterized by a canonical distribution with T° ($>T$) has been prepared. The solution of the master equation Eq. (5) in this case is given[8] by

$$\chi_{v_j}(\tau_j) = \{1-\exp[-u(\tau_j)]\} \exp[-v_j u(\tau_j)], \quad (15)$$

with

$$u(\tau_j) = \log\left[\frac{\exp(-\tau_j)\{1-\exp(\theta_j-\theta_j^0)\}-\exp(\theta_j)\{1-\exp(-\theta_j^0)\}}{\exp(-\tau_j)\{1-\exp(\theta_j-\theta_j^0)\}-\{1-\exp(-\theta_j^0)\}} \right]. \quad (16)$$

The expression for the intensity of the TRA spectra can be written as

$$D_{ab}(\omega_R, \tau) = \frac{C}{2} \exp[-S(\tau)] \int_{-\infty}^{\infty} d\xi \exp[i\xi(\omega_{ba}-\omega_R)-\Gamma_{ba}|\xi|$$
$$+ \sum_{j=1}^{N} \frac{\Delta_j^2\{n(\tau_j)+1\}}{2} \exp(i\omega_j\xi)$$
$$+ \sum_{j=1}^{N} \frac{\Delta_j^2 n(\tau_j)}{2} \exp(-i\omega_j\xi)], \quad (17)$$

where $S(\tau)$, time dependent coupling strength, is defined as

$$S(\tau) = \sum_{j=1}^{N} \{2n(\tau_j)+1\} \frac{\Delta_j^2}{2}. \quad (18)$$

Equation (17) has the same structure as that of the absorption band shape in the equilibrium condition. In Eq. (17), $n(\tau_j)$, the time-dependent occupation number of the optical mode j, is given as

$$n(\tau_j) = [\exp\{u(\tau_j)\}-1]^{-1}. \quad (19)$$

From Eqs. (16) and (19), we obtain $n(0)=[\exp(\theta^0)-1]^{-1}$ and $n(\infty)=[\exp(\theta)-1]^{-1}$ which are the occupation numbers at the initial time and in the equilibrium state, respectively.

Applying the Tayler expansions to Eq. (17), and carrying out the integration of the resulting expression over ξ, we can derive an analytical expression for the intensity as

$$D_{ab}(\omega_R, \tau) = C \exp[-S(\tau)] \sum_{k_1=0}^{\infty} \cdots \sum_{k_j=0}^{\infty} \cdots \sum_{k_N=0}^{\infty} \sum_{l_1=0}^{\infty} \cdots \sum_{l_j=0}^{\infty} \cdots \sum_{l_N=0}^{\infty}$$
$$\times \left[\prod_{j=1}^{N} \frac{\left[\{n(\tau_j)+1\}\frac{\Delta_j^2}{2}\right]^{k_j} \left\{n(\tau_j)\frac{\Delta_j^2}{2}\right\}^{l_j}}{k_j!\,l_j!} \right]$$
$$\times \frac{\Gamma_{ba}}{\{\omega_{ba}+\sum_{j=1}^{N} \omega_j(k_j-l_j)-\omega_R\}^2+\Gamma_{ba}^2}. \quad (20)$$

Equation (20) can be applied to both weak and strong coupling cases in principle. A fast convergence for the summations over k_j and l_j in Eq. (20) can be expected for the weak coupling case in which $S(\tau)\leq 1$. In the strong coupling case in which $S(\tau)>1$, on the other hand, we cannot expect the fast convergence. The classification for these coupling cases depend on time, as well as temperature, the frequency of the mode and the potential displacement. In the time domain in which the strong coupling case is satisfied and further $\Gamma_{ba}^2 < \sum_j \omega_j^2 \Delta_j^2 \{2n(\tau_j)+1\}$, it is better to use an approximate expression for the absorbance rather than Eq. (20). Neglecting Γ_{ba}, expanding $\exp(\pm i\omega_j\xi)$ to the second order of ξ in Eq. (17), and carrying out the integration of the equation over ξ we obtain

$$D_{ab}(\omega_R, \tau) = \frac{\sqrt{2\pi}C}{\sigma(\tau)} \exp\left[-\frac{\left(\omega_{ba}+\sum_{j=1}^{N} \frac{\omega_j\Delta_j^2}{2}-\omega_R\right)^2}{2\sigma^2(\tau)} \right], \quad (21)$$

where $\sigma(\tau)$, the time-dependent half-width of the TRA spectrum, is given as

$$\sigma(\tau) = \left[\sum_{j=1}^{N} \frac{\omega_j^2\Delta_j^2}{2} \{2n(\tau_j)+1\} \right]^{1/2}, \quad (22)$$

or

$$\sigma(\tau) = \left[\sum_{j=1}^{N} \frac{\omega_j^2\Delta_j^2}{2} \coth\frac{u(\tau_j)}{2} \right]^{1/2}. \quad (23)$$

It should be noted that the expression for the intensity in the Sulzer-Wieland model is involved in Eq. (21), that is, by setting $\tau=0$ in Eq. (21) we can obtain the expression given by Sulzer and Wieland[2] for one vibrational mode case:

$$D_{ab}(\omega_R, 0) \propto \left\{\tanh\frac{\hbar\omega}{2kT}\right\}^{1/2} \times \exp\left[-\tanh\frac{\hbar\omega}{2kT}\left\{\frac{\omega_{ba}+\omega\Delta^2/2-\omega_R}{\omega\Delta}\right\}^2\right]. \quad (24)$$

For the multimode case we can obtain the intensity expression simillar to that given by Asholz *et al.*[3]

Discussion

In order to clarify the initial vibronic distribution reflected in the TRA spectra we apply the derived expressions for the absorbance to benzene S_0* produced by internal conversion after the $S_2 \leftarrow S_0$ excitation.[1] We shall first calculate the TRA spectra assuming that Poisson distribution is realized and relaxes to the equilibrium one. It is necessary to estimate the parameter set for constructing vibronic distribution given by Eq. (3) after the internal conversion ($^1B_{1u} \rightsquigarrow {}^1A_{1g}$). Though it is recognized that benzene in the $^1B_{1u}$ state is subjected to the pseudo Jahn-Teller effect and the geometry of the $^1B_{1u}$ state may belong to D_{2h} symmetry, we neglect the geometry reduction. We simply adopt a model in which there are two displaced optical modes, one is a carbon-carbon stretching mode with frequency $\omega_{C\text{-}C}=1000\,cm^{-1}$, and the other is a carbon-hydrogen stretching mode with $\omega_{C\text{-}H}=3000\,cm^{-1}$. It was tentatively assumed that $\Delta_{C\text{-}C}=1.5$ and $\Delta_{C\text{-}H}=0.3$ for the dimensionless displacements.[9,10] Using these parameters we obtained $\alpha_{C\text{-}C}=6.8$ and $\alpha_{C\text{-}H}=12.5$ in Eq. (3) from the constraint of the energy conservation of the internal conversion with the electronic energy gap of 6.43 eV. Figure 1 shows the TRA spectra ($S_3 \leftarrow S_0$) calculated by using Eq. (12). Here the same molecular parameters of the S_3 state as those of the S_2 state were assumed.[11] The TRA spectra for the case of $\tau=0$, 0.5 (which corresponds to $t\simeq 0.5\times10^{-6}$ s) and 1 are indicated by solid, broken and dotted-broken lines, respectively. The remaining parameters have been assumed as follows: $\kappa_{C\text{-}C}=10^6\,s^{-1}$, $\kappa_{C\text{-}H}=2\times10^4\,s^{-1}$, $\Gamma_{ba}=500\,cm^{-1}$, and $T=300$ K. In Fig. 1 we can see the vibronic structure originating from the C-C stretching mode in the wavelength region of 180~200 nm even at early times. The carbon-hydrogen mode is, on the other hand, almost inactive in the TRA spectra because of its small magnitude of the displacement though this mode acts as the effective accepting mode for the internal conversion.[12] The TRA spectrum calculated at $\tau=0$ is different from the structureless spectrum which has been observed by Nakashima and Yoshihara.[1]

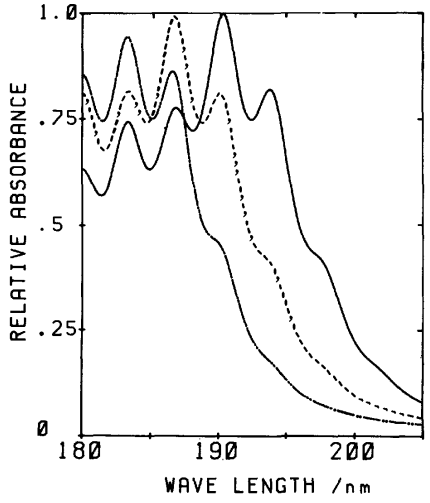

Fig. 1. The calculated TRA spectra ($S_3 \leftarrow S_0$) of benzene. Poisson distribution is adopted as the initial vibronic distribution. The calculation has been carried out by using Eq. (12). The solid, broken and dotted-broken lines denote TRA spectra at $\tau=0$, 0.5 and 1, respectively. See text for the parameter set.

Assuming that the canonical distribution with temperature higher than that of the heat bath is produced and relaxes to the equilibrium one, we now calculate the TRA spectra of benzene by using Eq. (21). Figure 2 shows the calculated spectra. The solid, broken and dotted-broken lines denote the TRA spectra at $\tau=0$, 0.5 ($t\simeq 0.14\times10^{-6}$ s) and 1, respectively. Here we, for simplicity, adopt an approximate expression for the half-width given by Eq. (23): $\sigma(0)\approx\overline{(\omega\Delta)^2}kT^\circ/\hbar\bar{\omega}$ at $\tau=0$, where the bars indicate magnitudes of the quantities averaged over the vibrational modes: we use $\overline{\omega\Delta}=2600\,cm^{-1}$, $\bar{\omega}=200\,cm^{-1}$, $T^\circ=3400$ K and $T=300$ K which were estimated in a previous paper.[1] The collisional vibrational transition probability κ is taken as $6\times10^6\,s^{-1}$. The closed circles in Fig. 2 denote experimental values for 2 Torr benzene at $\tau=0$.[1] In order to compare the experimental values with the calculated ones at $\tau=0$ the calculated molar extinction coefficient at 230 nm was taken to be equal to the experimental one. From Fig. 2 we can see that the initial vibronic distribution is of the canonical one rather than the Poisson one. In other words, lifetime of the vibronic states just after the internal conversion

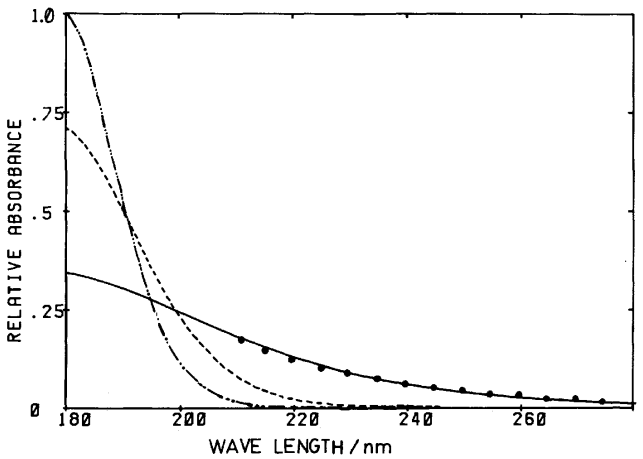

Fig. 2. The calculated TRA spectra of benzene when a canonical distribution is adopted as the initial distribution. The calculation has been carried out by using Eq. (21). The solid, broken and dotted-broken lines denote TRA spectra at $\tau=0$, 0.5, and 1, respectively. The closed circles represent experimental values for 2 Torr benzene at $\tau=0$.

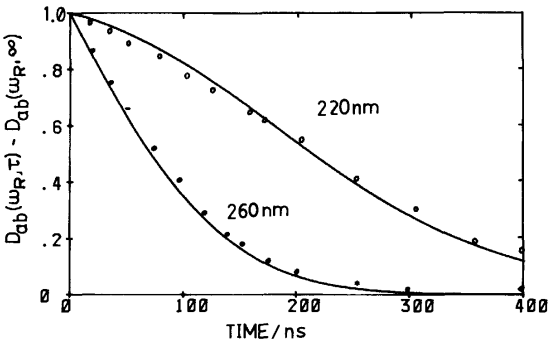

Fig. 3. The calculated decay curves, $D_{ab}(\omega_R, \tau)-D_{ab}(\omega_R, \infty)$ at 220 and 260 nm. The measured values of the absorbances of the 2 Torr (1 Torr≈133.322 Pa) benzene and 10 Torr propane are denoted at 220 nm (○) and 260 nm (●). See text for detail.

$S_2 \rightsquigarrow S_0$ is too short to observe the Poisson distribution because of a fast vibrational redistribution in the high vibronic state of S_0. The vibrational redistribution is caused by intramolecular couplings such as the ones caused by anharmonicities and mode mixings. This explains why the low vibrational frequency and the large potential displacement within the harmonic approximation has to be included in simulating the TRA spectra of benzene with the canonical distribution.

In Fig. 3 are shown decay curves, $D_{ab}(\omega_R,\tau)-D_{ab}(\omega_R,\infty)$ at 220 and 260 nm calculated by using Eq. (21). The same parameters as those in Fig. 2 are adopted except for $\kappa=9\times10^6\,s^{-1}$. The measured absorbances of the 2 Torr benzene and 10 Torr propane are plotted at 220 nm (○) and 260 nm (●).[13] The calculated decay curves are in fairly good agreement with the observed values. This suggests the validity of the linear collisional deactivation mechanism for the vibrationally hot benzene. In the previous paper, an energy-dependent energy transfer model has been adopted in order to explain the decay curves.

In summary we have developed a theory of the TRA spectra of molecules after radiationless transition. Two types of the initial vibronic distribution, Poisson and canonical ones are taken into account. The theory developed has been applied to the TRA spectra ($S_3 \leftarrow S_0$) of benzene produced by the internal conversion $S_2 \rightsquigarrow S_0$. It has been shown that the canonical distribution can explain the transient behavior of benzene after the internal conversion. Finally it should be noted that we can semi-quantitatively explain both time-resolved spectra and decay curves of benzenes in a foreign gas by using the derived expressions for the time-dependent absorption intensity. These expressions can be applied to the investigation of the relaxation processes in hot molecules, such as hexafluorobenzene[14] and other polyatomic molecules as well.

Appendix

A. Time-resolved absorption intensity for a Poisson distribution.

In this appendix, analytical expressions for the intensity $D_{ab}(\omega_R,\tau)$ are derived for the molecular system characterized by a Poisson distribution. Two cases depending on the magnitudes of the coupling strength $\sum_j \Delta_j^2/2 \gtrless 1$ will be considered.

Substituting Eqs. (6) and (11) into Eq. (1) yields

$$D_{ab}(\omega_R, \tau) = \frac{C}{2}\sum_{v_1=0}^{\infty}\cdots\sum_{v_j=0}^{\infty}\cdots\sum_{v_N=0}^{\infty} \times \exp(-S)\int_{-\infty}^{\infty} d\xi \exp[i\xi(\omega_{ba}-\omega_R)-\Gamma_{ba}|\xi| + \sum_{j=1}^{N}\frac{\Delta_j^2}{2}\exp(i\omega_j\xi)]\Big[\prod_{j=1}^{N} L_{v_j}\{\Delta_j^2(1-\cos\omega_j\xi)\} \times \frac{1-\exp(\theta_j)}{\exp(-\tau_j)-\exp(\theta_j)}\exp\left[-\frac{\alpha_j\exp(-\tau_j)\{\exp(\theta_j)-1\}}{\exp(\theta_j)-\exp(-\tau_j)}\right] \times \left\{\frac{1-\exp(-\tau_j)}{\exp(\theta_j)-\exp(-\tau_j)}\right\}^{v_j} L_{v_j}(y_j)\Big], \quad (A.1)$$

or

$$D_{ab}(\omega_R, \tau) = \frac{C}{2}\exp(-S) \times \left\{\prod_{j=1}^{N}\exp\left[-\frac{\alpha_j\exp(-\tau_j)\{\exp(\theta_j)-1\}}{\exp(\theta_j)-\exp(-\tau_j)}\right]\right\} \times \int_{-\infty}^{\infty} d\xi \exp[i\xi(\omega_{ba}-\omega_R)-\Gamma_{ba}|\xi| + \prod_{j=1}^{N}\frac{\Delta_j^2}{2}\exp(i\omega_j\xi)] \times \prod_{j=1}^{N}\frac{1-\exp(\theta_j)}{\exp(-\tau_j)-\exp(\theta_j)}\sum_{v_j=0}^{\infty}\sum_{n_j=0}^{v_j}\frac{v_j!\,x_j^{n_j}(\xi)}{(v_j-n_j)!\,(n_j!)^2} \times \sum_{m_j=0}^{v_j}\frac{v_j!\,(-y_j)^{m_j}}{(v_j-m_j)!\,(m_j!)^2}\left\{\frac{1-\exp(-\tau_j)}{\exp(\theta_j)-\exp(-\tau_j)}\right\}^{v_j}, \quad (A.2)$$

where $x_j(\xi)=\Delta_j^2(\cos\omega_j\xi-1)$, $y_j=\alpha_j\exp(-\tau_j)\{\exp(\theta_j)-1\}^2/[\{1-\exp(-\tau_j)\}\{\exp(-\tau_j)-\exp(\theta_j)\}]$, and the following expression for the Laguerre polynomials has been used,

$$L_v(y) = \sum_{m=0}^{v}\frac{v!\,(-y)^m}{(v-m)!\,(m!)^2}. \quad (A.3)$$

Applying the identity

$$\frac{1}{n!} = \frac{1}{2\pi i}\oint\frac{\exp(z)}{\cdot\, z^{n+1}}dz \quad (A.4)$$

to Eq. (A. 2) and after taking summations over m_j and n_j, one obtains

$$D_{ab}(\omega_R, \tau) = \frac{C}{2}\exp(-S) \times \left\{\prod_{j=1}^{N}\exp\left[-\frac{\alpha_j\exp(-\tau_j)\{\exp(\theta_j)-1\}}{\exp(\theta_j)-\exp(-\tau_j)}\right]\right\} \times \int_{-\infty}^{\infty} d\xi \exp[it(\omega_{ba}-\omega_R)-\Gamma_{ba}|\xi| + \prod_{j=1}^{N}\frac{\Delta_j^2}{2}\exp(i\omega_j\xi)] \times \prod_{j=1}^{N}\frac{1-\exp(\theta_j)}{\exp(-\tau_j)-\exp(\theta_j)}\Lambda_j(\xi), \quad (A.5)$$

where

$$\Lambda_j(\xi) = \left(\frac{1}{2\pi i}\right)^2\oint dz_1\oint dz_2\frac{\exp(z_1+z_2)}{z_1z_2}\sum_{v_j=0}^{\infty}\left\{1+\frac{x_j(\xi)}{z_1}\right\}^{v_j} \times \left(1-\frac{y_j}{z_2}\right)^{v_j}\left\{\frac{1-\exp(-\tau_j)}{\exp(\theta_j)-\exp(-\tau_j)}\right\}^{v_j}. \quad (A.6)$$

Assuming convergence of the summation over v_j in Eq. (A. 6), one can express Eq. (A. 6) as

$$\Lambda_j(\xi) = \left(\frac{1}{2\pi i}\right)^2 \oint dz_1 \oint dz_2 \frac{\exp(z_1+z_2)}{z_1 z_2 (1-A_j)} \times \left\{1 - \frac{A_j x_j(\xi)}{(1-A_j)z_1} + \frac{A_j y_j}{(1-A_j)z_2} + \frac{A_j x_j(\xi) y_j}{(1-A_j)z_1 z_2}\right\}^{-1}, \quad (A.7)$$

where

$$A_j = \{1-\exp(-\tau_j)\}/\{\exp(\theta_j)-\exp(-\tau_j)\}. \quad (A.8)$$

Equation (A. 7) can be expanded as

$$\Lambda_j(\xi) = \left(\frac{1}{2\pi i}\right)^2 \oint dz_1 \oint dz_2 \frac{\exp(z_1+z_2)}{z_1 z_2 (1-A_j)} \times \sum_{l_j=0}^{\infty} \left\{\frac{A_j x_j(\xi)}{(1-A_j)z_1} - \frac{A_j y_j}{(1-A_j)z_2} - \frac{A_j x_j(\xi) y_j}{(1-A_j)z_1 z_2}\right\}^{l_j}. \quad (A.9)$$

In order to obtain the correct values of the intensity for the limiting cases, $\tau \to 0$ and $\tau \to \infty$, it is necessary to define

$$B_j = -A_j y_j = \frac{\alpha_j \exp(-\tau_j)\{\exp(\theta_j)-1\}^2}{\{\exp(\theta_j)-\exp(-\tau_j)\}^2}. \quad (A.10)$$

Utilizing the binomial expansion and Eq. (A. 4) one can rewrite Eq. (A. 9) as

$$\Lambda_j(\xi) = \frac{\exp(-\tau_j)-\exp(\theta_j)}{1-\exp(\theta_j)} \sum_{l_j=0}^{\infty} \sum_{m_j=0}^{l_j} \sum_{k_j=0}^{l_j-m_j} \binom{l_j}{m_j} \binom{l_j-m_j}{k_j} \times \left(\frac{A_j}{1-A_j}\right)^{m_j} \left(\frac{B_j}{1-A_j}\right)^{l_j-m_j} \frac{\{x_j(\xi)\}^{m_j+k_j}}{(m_j+k_j)!\,(l_j-m_j)!}. \quad (A.11)$$

Here it should be noted that one has $m_j=0$ for $\tau_j \to 0$ that is, $A_j=0$, and $k_j=0$ and $l_j=m_j$ for $\tau_j \to \infty$, that is, $B_j=0$.

One uses the following expansions,

$$\{x_j(\xi)\}^{m_j+k_j} = \left(\frac{\Delta_j^2}{2}\right)^{m_j+k_j} \sum_{p_j=0}^{m_j+k_j} \sum_{q_j=0}^{p_j} \sum_{r_j=0}^{m_j+k_j-p_j} \binom{m_j+k_j}{p_j} \binom{p_j}{q_j} \times \binom{m_j+k_j-p_j}{r_j} (-1)^{m_j+k_j-q_j-r_j} \exp[i\omega_j(q_j-r_j)\xi], \quad (A.12a)$$

or

$$\{x_j(\xi)\}^{m_j+k_j} = \left(\frac{\Delta_j^2}{2}\right)^{m_j+k_j} \sum_{p_j=0}^{2(m_j+k_j)} (-1)^{p_j} \binom{2(m_j+k_j)}{p_j} \times \exp\{i\omega_j(k_j+m_j-p_j)\xi\}, \quad (A.12b)$$

Substituting Eq. (A. 11) with Eq. (A. 12b) into Eq. (A. 5) yields

$$D_{ab}(\omega_R, \tau) = \frac{C}{2} \exp\left[-S - \sum_{j=1}^{N} \frac{\alpha_j \exp(-\tau_j)\{\exp(\theta_j)-1\}}{\exp(\theta_j)-\exp(-\tau_j)}\right] \times \sum_{l_1=0}^{\infty} \cdots \sum_{l_j=0}^{\infty} \cdots \sum_{l_N=0}^{\infty} \sum_{m_1=0}^{l_1} \cdots \sum_{m_j=0}^{l_j} \cdots \sum_{m_N=0}^{l_N} \sum_{k_1=0}^{l_1-m_1} \cdots \sum_{k_j=0}^{l_j-m_j} \cdots \sum_{k_N=0}^{l_N-m_N} \times \sum_{p_1=0}^{2(m_1+k_1)} \cdots \sum_{p_j=0}^{2(m_j+k_j)} \cdots \sum_{p_N=0}^{2(m_N+k_N)} \left[\prod_{j=1}^{N} \left(\frac{\Delta_j^2}{2}\right)^{m_j+k_j} \binom{l_j}{m_j} \binom{l_j-m_j}{k_j} \times \left\{\frac{1-\exp(-\tau_j)}{\exp(\theta_j)-1}\right\}^{m_j} \left\{\frac{\alpha_j \exp(-\tau_j)[\exp(\theta_j)-1]}{\exp(\theta_j)-\exp(-\tau_j)}\right\}^{l_j-m_j} \times \frac{(-1)^{p_j}\binom{2m_j+2k_j}{p_j}}{(m_j+k_j)!\,(l_j-m_j)!}\right] \int_{-\infty}^{\infty} d\xi \exp\left[i\xi\{\omega_{ba} + \sum_{j=1}^{N} \omega_j(k_j+m_j-p_j) - \omega_R\} + \sum_{j=1}^{N} \frac{\Delta_j^2}{2} \exp(i\omega_j\xi) - \Gamma_{ba}|\xi|\right]. \quad (A.13)$$

Integration over ξ in Eq. (A. 13) will be carried out in the weak coupling case, $S \leq 1$ and the strong coupling case, $S > 1$, separately.

i. Weak Coupling Case. In this case, utilizing the Tayler expansion and integrating the expression over ξ, one can obtain the analytical expression for the absorption intensity,

$$D_{ab}(\omega_R, \tau) = C \exp\left[-S - \sum_{j=1}^{N} \frac{\alpha_j \exp(-\tau_j)\{\exp(\theta_j)-1\}}{\exp(\theta_j)-\exp(-\tau_j)}\right] \times \sum_{n_1=0}^{\infty} \cdots \sum_{n_j=0}^{\infty} \cdots \sum_{n_N=0}^{\infty} \sum_{l_1=0}^{\infty} \cdots \sum_{l_j=0}^{\infty} \cdots \sum_{l_N=0}^{\infty} \sum_{m_1=0}^{l_1} \cdots \sum_{m_j=0}^{l_j} \cdots \sum_{m_N=0}^{l_N} \times \sum_{k_1=0}^{l_1-m_1} \cdots \sum_{k_j=0}^{l_j-m_j} \cdots \sum_{k_N=0}^{l_N-m_N} \sum_{p_1=0}^{2(m_1+k_1)} \cdots \sum_{p_j=0}^{2(m_j+k_j)} \cdots \sum_{p_N=0}^{2(m_N+k_N)} \times \left[\prod_{j=1}^{N} \left(\frac{\Delta_j^2}{2}\right)^{n_j+m_j+k_j} \binom{l_j}{m_j} \binom{l_j-m_j}{k_j} \frac{(-1)^{p_j}\binom{2m_j+2k_j}{p_j}}{n_j!\,(m_j+k_j)!\,(l_j-m_j)!} \times \left\{\frac{\alpha_j \exp(-\tau_j)[\exp(\theta_j)-1]}{\exp(\theta_j)-\exp(-\tau_j)}\right\}^{l_j-m_j} \left\{\frac{1-\exp(-\tau_j)}{\exp(\theta_j)-1}\right\}^{m_j}\right] \times \frac{\Gamma_{ba}}{\{\omega_{ba} + \sum_{j=1}^{N} \omega_j(n_j+k_j+m_j-p_j) - \omega_R\}^2 + \Gamma_{ba}^2}. \quad (A.14)$$

ii. Strong Coupling Case. In this case, one can use the expansion of $\exp(i\omega_j\xi)$ to the second order,

$$\exp(i\omega_j\xi) \fallingdotseq 1 + i\omega_j\xi - \frac{\omega_j^2\xi^2}{2}. \quad (A.15)$$

In the strong coupling case the following relation is satisfied for the optical transition between two electronic states of molecules,

$$\sum_{j=1}^{N} \frac{\omega_j^2 \Delta_j^2}{4} > \Gamma_{ba}^2, \quad (A.16)$$

that is, effect of the damping on the spectrum can be neglected.

Substituting Eq. (A. 15) into Eq. (A. 13) and integrating the expression over ξ yield

$$D_{ab}(\omega_R, \tau) = D_{ab}(\omega_{max}, \infty)_{T=0} \times \exp\left[-\sum_{j=1}^{N} \frac{\alpha_j \exp(-\tau_j)\{\exp(\theta_j)-1\}}{\exp(\theta_j)-\exp(-\tau_j)}\right] \sum_{l_1=0}^{\infty} \cdots \sum_{l_j=0}^{\infty} \cdots \sum_{l_N=0}^{\infty} \times \sum_{m_1=0}^{l_1} \cdots \sum_{m_j=0}^{l_j} \cdots \sum_{m_N=0}^{l_N} \sum_{k_1=0}^{l_1-m_1} \cdots \sum_{k_j=0}^{l_j-m_j} \cdots \sum_{k_N=0}^{l_N-m_N} \sum_{p_1=0}^{2(m_1+k_1)} \cdots \sum_{p_j=0}^{2(m_j+k_j)} \cdots \sum_{p_N=0}^{2(m_N+k_N)} \times \left[\prod_{j=1}^{N} \left(\frac{\Delta_j^2}{2}\right)^{m_j+k_j} \binom{l_j}{m_j} \binom{l_j-m_j}{k_j} \frac{(-1)^{p_j}\binom{2m_j+2k_j}{p_j}}{(m_j+k_j)!\,(l_j-m_j)!} \times \left\{\frac{\alpha_j \exp(-\tau_j)[\exp(\theta_j)-1]}{\exp(\theta_j)-\exp(-\tau_j)}\right\}^{l_j-m_j} \left\{\frac{1-\exp(-\tau_j)}{\exp(\theta_j)-1}\right\}^{m_j}\right] \times \exp\left[-\frac{\left\{\omega_{ba} + \sum_{j=1}^{N} \omega_j\left(\frac{\Delta_j^2}{2}+k_j+m_j-p_j\right) - \omega_R\right\}^2}{2\sum_{j=1}^{N} \frac{\omega_j^2\Delta_j^2}{2}}\right] \quad (A.17)$$

where $D_{ab}(\omega_{max}, \infty)_{T=0} = \sqrt{2\pi}C/\{\sum_{j=1}^{N} \omega_j^2\Delta_j^2/2\}^{1/2}$ is the maximum absorption intensity at 0 K in the equilibrium state.

References

1) N. Nakashima and K. Yoshihara, *J. Chem. Phys.*, **79**,

2727 (1983).
2) P. Sulzer and K. Wieland, *Helv. Phys. Acta*, **25**, 653 (1952).
3) D. C. Astholz, L. Brouwer and J. Troe, *Ber. Bunsenges. Phys. Chem.*, **85**, 559 (1981).
4) H. Hippler, J. Troe, and H. J. Wendelken, *J. Chem. Phys.*, **78**, 5351 (1983).
5) Y. Fujimura, S. H. Lin, H. Schröder, H. J. Neusser, and E. W. Schlag, *Chem. Phys.*, **43**, 205 (1979).
6) Y. Fujimura, T. Nakajima, S. H. Lin, and E. W. Schlag, *Chem. Phys. Lett.*, **67**, 299 (1979).
7) H. Schröder, H. J. Neusser, and E. W. Schlag, *Chem. Phys. Lett.*, **48**, 12 (1977); **54**, 4 (1978).
8) E. W. Montroll and K. E. Shuler, *J. Chem. Phys.*, **26**, 454 (1957).
9) S. Fischer, *Chem. Phys. Lett.*, **11**, 577 (1971).
10) Y. Fujimura and T. Nakajima, *Chem. Phys. Lett.*, **14**, 108 (1972).
11) Y. Fujimura, H. Yamaguchi, and T. Nakajima, *Bull. Chem. Soc. Jpn.*, **45**, 384 (1972).
12) E. W. Schlag, S. Schneider, and S. F. Fischer, *Ann. Rev. Phys. Chem.*, **22**, 465 (1971).
13) The vibrational energy of the hot benzene in the presence of foreign molecules can be exchanged with the translational degree of freedom of the foreign molecule. In this case within the linear interaction model the collision-induced vibrational relaxation can be explained by using the master equation given by Eq. (5) in which $\kappa_j(1-e^{-\theta})^{-1}$ is replaced by $\kappa_j(1-e^{-\theta})^{-1}+\kappa_j'$ where κ_j' is the transition probability between levels $v_j=1$ and $v_j=0$ of mode j of the hot benzene for the vibration-translation energy exchange.[8)]
14) T. Ichimura, Y. Mori, N. Nakashima, and K. Yoshihara, *Chem. Phys. Lett.*, **104**, 533 (1984).

Synthesis of Pharmaceutically Important Heteroaromatics from Methyl Phenyl Sulfone

Masataka YOKOYAMA,* Kouichi TSUJI, and Tsuneo IMAMOTO
Department of Chemistry, Faculty of Science, Chiba University, Yayoi-cho, Chiba 260
(Received April 26, 1984)

Some 5-substituted pyrazoles and pyrimethamine were prepared from 3-methylthio-1-phenyl-4-phenylsulfonyl-2-buten-1-one (**5a**) or (*E*)-1-*p*-chlorophenyl-1-cyano-2-methylthio-3-phenylsulfonylpropene (**6b**) which could be easily synthesized from methyl phenyl sulfone.

Pyrazole derivatives are found in several febrifuges, weed killers, and insecticides. And pyrimethamine is a useful antimalarial agent, which is about 1000 times as active as quinine.[1] Thus, improvement of the synthetic method for these compounds is important. We found that 1,1-bis(methylthio)-2-phenylsulfonylethene (**1**), derived easily from methyl phenyl sulfone, was a useful starting material for the synthesis of these pharmaceutical heteroaromatics. In this paper we describe an efficient method for the synthesis of 5-[(*Z*)-1,3-butadienyl]-3-phenylpyrazole (**2**), 5-methyl-3-phenylpyrazole (**3**), and pyrimethamine (**4**) from methyl phenyl sulfone.

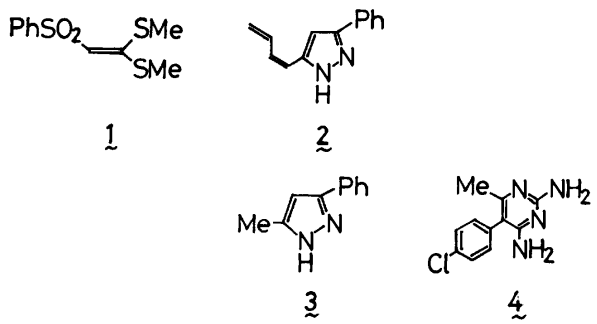

Fig. 1.

Results and Discussion

Reaction of (1) with α-Metalated Ketones or Nitriles. Compound (**1**) was prepared by means of the condensation between methyl phenyl sulfone and methyl trithiocarbonate, followed by methylation in 50% yield. Although Vialle *et al.* have already prepared this compound,[2] our method has a better yield.

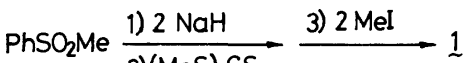

Fig. 2.

When treated with α-metalated ketones[3] or nitriles, **1** was converted to 3-(methylthio)vinyl ketones (**5**) or nitriles (**6**) in moderate yields. The results are summarized in Table 1.

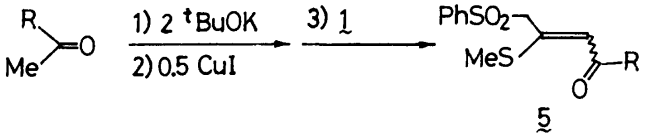

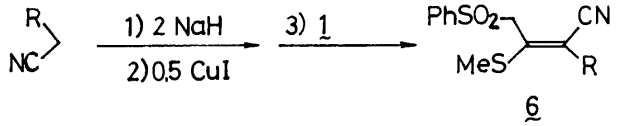

Fig. 3.

TABLE 1. PREPARATION OF **5** AND **6**

Product	R	Yield/%
5a	Phenyl	72
5b	2-Thienyl	64
5c	2-Pyridyl	38
5d	2-Naphthyl	78
5e	Methyl	57
6a	Phenyl	61
6b	*p*-Chlorophenyl	71

In this reaction, copper(I) iodide acted as an inhibitor of the formation of 1,1,2-tris(methylthio)ethene[4] which was generated in the side reaction.[5] But in the case of the reaction with methyl 2-pyridyl ketone, product **5c** could not be obtained in the presence of copper(I) iodide, probably due to the reduced reactivity of the carbanion by chelation of the pyridine nitrogen toward the copper. Compounds (**5**) were obtained as *E,Z* mixtures, while compounds (**6**) were given almost stereoselectively owing to the steric hindrance.

Preparation of Pyrazole Derivatives. Compound (**5a**) reacted with hydrazine hydrate in ethanol at refluxing temperature in the presence of a catalytic amount of sulfuric acid to give 3-phenyl-5-(phenylsulfonylmethyl)-pyrazole (**7**)[6] in 98% yield. When **7** was treated with 2 equivalents of *n*-BuLi, followed by addition of allyl bromide, **8** was obtained in 81% yield. Then **8** could easily be converted to 5-[(*Z*)-1,3-butadienyl]-3-phenylpyrazole (**2**) in 89% yield by treatment with 2 equivalents of *t*-BuOK. By the reaction of dianion of **7** with *p*-chlorobenzaldehyde, 5-[2-(*p*-chlorophenyl)-2-hydroxy-1-(phenylsulfonyl)ethyl]-3-phenylpyrazole (**9**) was afforded in 71% yield. Furthermore **7** could also give 5-methyl-3-phenylpyrazole (**3**) in 78% yield on treatment with 5% sodium-amalgam (Na/Hg).[7] In this way, **7** could be converted into various pyrazoles which have an alkadienyl, alkyl, or other functional group at 5-position. This is the principal advantage of the present method over known preparative methods for pyrazoles.[8]

Preparation of Pyrimethamine. When **6b** was treated with 2 equivalents of guanidine, 5-(*p*-chlorophenyl)-2,4-diamino-6-(phenylsulfonylmethyl)pyrimidine (**10**) was obtained in 92% yield. And **10** could be converted to pyrimethamine (**4**) on treatment with

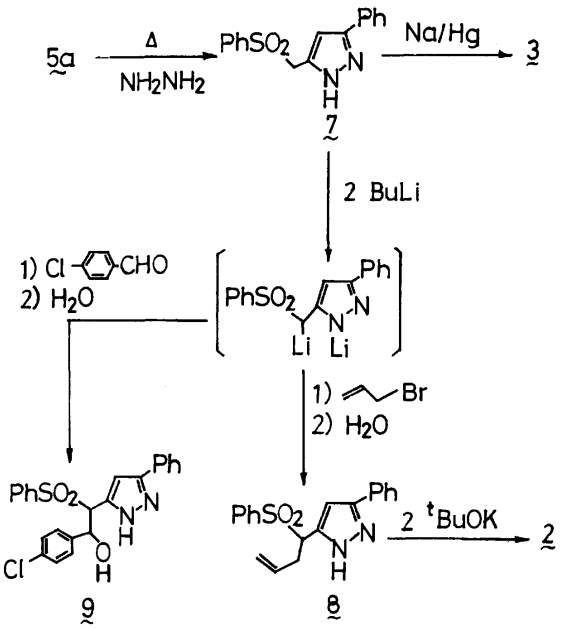

Fig. 4.

Na/Hg quantitatively. The attempts to introduce electrophiles into 6-position failed, owing to low reactivity of the corresponding carbanaion and the presence of free amino groups. However our preparative method for **4** can compete in terms of simple preparation and yield with hitherto known ones.[1]

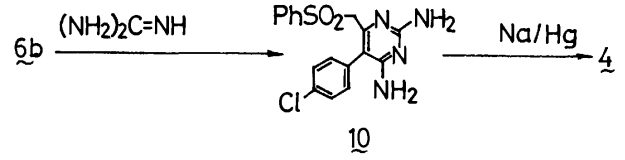

Fig. 5.

Experimental

Microanalyses were performed with Perkin-Elmer 240 elemental analyser at the Chemical Analysis Center of Chiba University. IR, UV, Mass, and ^{1}H-NMR spectra were measured with Japan Spectroscopic Co. DS 403G, Hitachi EPS-3T, RMU 6MC instruments, and Japan Electron Optics Lab. Co. C-60HL instruments, respectively. The silica gel used for TLC was Wakogel B-5F.

Preparation of 1,1-Bis(methylthio)-2-phenylsulfonylethene (1). A solution of methyl phenyl sulfone (9.4 g, 0.06 mol) in 60 ml of THF was added to 60% NaH (5.3 g, 0.13 mol) under nitrogen. After reflux for 1 h and then cooling to 0 °C, methyl trithiocarbonate (8.3 g, 0.06 mol) in 20 ml of THF was added to the mixture. It was stirred for 30 min at 0 °C and at room temperature for an additional 12 h. After addition of methyl iodide (0.12 mol), the resulting mixture was stirred for 3 h, quenched with water, and extracted with chloroform. The chloroform extract was dried over sodium sulfate and evaporated. The yellow powder was obtained and recrystallized from ethanol to give 7.8 g (50% yield) of **1** as white needles, mp 122—123 °C (lit,[2] 119 °C).

Reaction of 1 with α-Metalated Ketones. To a suspension of ketone (1.0 mmol), *t*-BuOK (274 mg, 2.2 mmol), and copper (I) iodide (100 mg, 0.5 mmol) in 5 ml of THF was added a solution of **1** (260 mg, 1.0 mmol) in 5 ml of THF. After stirring for 15 h, water and chloroform were added to the mixture, and acidified with 2M HCl(1 M=1 mol dm^{-3}). The resulting mixture was filtered through Celite, and the organic layer was dried over sodium sulfate and rotary-evaporated. The resulting brown oil was purified by TLC on silica gel using AcOEt–hexane (2:3) as a developing solvent to afford **5**. In the case of methyl 2-pyridyl ketone, copper (I) iodide was not used in the reaction.

3-Methylthio-1-phenyl-4-phenylsulfonyl-2-buten-1-one (5a): Yellow needles (from EtOH); 239 mg (72%); a 1:4 mixture of two stereoisomers; IR (KBr): 3050 (arom CH), 2960, 2900 (CH), 1640 (C=O), 1320 and 1150 cm^{-1} (SO_2); NMR ($CDCl_3$): δ=7.85 (2H, m, $PhSO_2$), 7.63 (2H, m, Ph), 7.40 (6H, m, 2Ph), 6.70, 6.58 (1H, s, CH), 5.00, 4.30 (2H, s, CH_2), 2.43, 2.38 (3H, s, CH_3); MS: *m/z* 332 (M^+). Found: C, 61.39; H, 4.86%. Calcd for $C_{17}H_{16}O_3S_2$: C, 61.42; H, 4.85%.

3-Methylthio-4-phenylsulfonyl-1-(2-thienyl)-2-buten-1-one (5b): White prisms (from $CHCl_3$); 217 mg (64%); a 1:4 mixture of two stereoisomers; IR (KBr): 3080 (arom CH), 2950, 2900 (CH), 1620 (C=O), 1320 and 1140 cm^{-1}(SO_2); NMR ($CDCl_3$): δ=7.88 (2H, m, C_6H_5), 7.48 (5H, m, C_6H_5, C_4H_3S), 7.02 (1H, m, C_4H_3S), 6.45 (1H, s, CH), 5.01, 4.25 (2H, s, CH_2), 2.48, 2.38 (3H, s, CH_3); MS: *m/z* 338 (M^+). Found: C, 53.02; H, 4.15%. Calcd for $C_{15}H_{14}O_3S_3$: C, 53.23; H, 4.17%.

3-Methylthio-4-phenylsulfonyl-1-(2-pyridyl)-2-buten-1-one (5c): Greenish brown needles (from acetone); 127 mg (38%); a 1:5 mixture of two stereoisomers; IR (KBr): 3050 (arom CH), 2970, 2890 (CH), 1650 (C=O), 1310 and 1140 cm^{-1}(SO_2); NMR ($CDCl_3$): δ=8.63 (1H, m, C_5H_4N), 7.93 (4H, m, C_6H_5, C_5H_5N), 7.63 (1H, s, CH), 7.47 (4H, m, C_6H_5, C_5H_4N), 5.08, 4.38 (2H, s, CH_2), 2.52, 2.48 (3H, s, CH_3); MS: *m/z* 286 ($M-47$)$^+$. Found: C, 57.61; H, 4.51; N, 4.13%. Calcd for $C_{16}H_{15}NO_3S_2$: C, 57.64; H, 4.53; N, 4.20%.

3-Methylthio-1-(2-naphtyl)-4-phenylsulfonyl-2-buten-1-one (5d): Yellow needles (from EtOH); 298 mg (78%); a 2:5 mixture of two stereoisomers; IR (KBr): 3050 (arom CH), 2990, 2900 (CH), 1640 (C=O), 1310 and 1150 cm^{-1}(SO_2); NMR ($CDCl_3$): δ=8.30—7.20 (12H, m, C_6H_5, $C_{10}H_7$), 6.78, 6.72 (1H, s, CH), 5.05, 4.33 (2H, s, CH_2), 2.45, 2.38 (3H, s, CH_3); MS: *m/z* 382 (M^+). Found: C, 65.90; H, 4.82%. Calcd for $C_{21}H_{18}O_3S_2$: C, 65.94; H, 4.74%.

4-Methylthio-5-phenylsulfonyl-3-penten-2-one (5e): White plates (from EtOH); 154 mg (57%); a 3:5 mixture of two stereoisomers; IR (KBr): 3050 (arom CH), 2970, 2900 (CH), 1660 (C=O), 1300 and 1150 cm^{-1} (SO_2); NMR ($CDCl_3$): δ=7.88 (2H, m, Ph), 7.23 (3H, m, Ph), 5.93 (1H, s, CH), 4.85, 4.18 (2H, s, CH_2), 2.35 (3H, s, SCH_3), 2.00 (3H, s, CH_3); MS: *m/z* 270 (M^+). Found: C, 53.35; H, 5.18%. Calcd for $C_{12}H_{14}O_3S_2$: C, 53.31; H, 5.22%.

Reaction of 1 with α-Metalated Nitriles. To a solution of nitrile (1.0 mmol) and **1** (260 mg, 1.0 mmol) in 10 ml of THF was added 60% NaH (88 mg, 2.2 mmol) and copper (I) iodide (100 mg, 0.5 mmol). The treatment described above gave **6**.

(E)-3-Methylthio-2-phenyl-4-phenylsulfonyl-2-butenenitrile (6a): Colorless plates; mp 116—118 °C (from EtOH); IR (KBr): 3050 (arom CH), 2900 (CH), 2200 (CN) 1330 and 1160 cm^{-1} (SO_2); NMR ($CDCl_3$): δ=8.03 (2H, m, $PhSO_2$), 7.57 (3H, m, $PhSO_2$), 7.33 (5H, s, Ph), 4.61 (2H, s, CH_2), 2.48 (3H, s, CH_3); MS: *m/z* 329 (M^+). Found: C, 61.94; H, 4.62; N, 4.22%. Calcd for $C_{17}H_{15}NO_2S_2$: C, 61.98; H, 4.59; N, 4.25%.

(E)-2-(p-Chlorophenyl)-3-methylthio-4-phenylsulfonyl-2-butenenitrile (6b): White plates; mp 131—132 °C (from $CHCl_3$); IR (KBr): 3040 (arom CH), 2900 (CH), 2200 (CN), 1330 and 1160 cm^{-1} (SO_2); NMR ($CDCl_3$): δ=8.03 (2H, m, Ph), 7.60 (3H, m, Ph), 7.30 (4H, s, *p*-ClC_6H_4), 4.58 (2H, s, CH_2), 2.50 (3H, s, CH_3); MS: *m/z* 363 (M^+). Found: C, 55.84; H, 3.87; N, 3.79%. Calcd for $C_{17}H_{14}ClNO_2S_2$: C, 56.11; H, 3.88; N, 3.85%.

Preparation of 3-Phenyl-5-(phenylsulfonylmethyl)pyrazole (7). To a solution of **5a** (500 mg, 1.5 mmol) in 40 ml of EtOH was added hydrazine hydrate (150 mg, 3.0 mmol) in 10 ml of

EtOH and a few drops of 5% sulfuric acid. When stirred at refluxing temperature for about 2 h, the yellow solution turned colorless. After being quenched with water, the mixture was extracted with chloroform. The chloroform extract was dried over sodium sulfate and evaporated. A white powder was obtained (439 mg, 98%) and recrystallized from chloroform to give **7** as white plates, mp 170—171 °C (lit, [6] 173 °C).

Preparation of 3-Phenyl-5-(1'-phenylsulfonyl-3'-butenyl)-pyrazole (8). To a solution of **7** (388 mg, 1.3 mmol) in 10 ml of THF was added 1.4 M solution of *n*-BuLi in hexane (2.0 ml, 2.86 mmol) at −70 °C under nitrogen. After stirring for 30 min, allyl bromide (0.12 ml, 1.43 mmol) was added to the mixture and it was stirred for 10 min at −70 °C, and then for 1 h at room temperature. After being quenched with saturated solution of ammonium chloride, the mixture was extracted with ethyl acetate. The ethyl acetate extract was dried over sodium sulfate and rotary-evaporated. The resulting colorless oil was purified by TLC on silica gel using AcOEt–hexane (1:1) as a developing solvent to give 356 mg (81%) of **8** as a colorless oil; bp 130 °C/13.3 Pa; IR (KBr): 3300 (NH), 1300 and 1150 cm^{-1} (SO_2); NMR ($CDCl_3$): δ= 11.68 (1H, br, NH), 7.55 (10H, m, 2Ph), 6.60 (1H, s, CH), 6.20—5.37 (1H, m, CH_2=C<u>H</u>CH_2), 5.10 (1H, dd, J_{trans}=18 Hz, J_{gem}=1 Hz, C<u>H</u>$_2$=CH), 5.02 (1H, dd, J_{cis}=10 Hz, J_{gem}=1 Hz, C<u>H</u>$_2$=CH), 4.59 (1H, t, J=8 Hz, $PhSO_2CH$), 3.07 (2H, m, CH_2=CH-C<u>H</u>$_2$); MS: *m/z* 338 (M^+).

Preparation of 5-[(Z)-1,3-Butadienyl]-3-phenylpyrazole (2). To a solution of **8** (203 mg, 0.6 mmol) in 5 ml of THF was added *t*-BuOK (165 mg, 1.32 mmol), the mixture was stirred for 3 h. The treatment described above gave white powder. It was purified by TLC on silica gel using AcOEt–hexane (2:3) as a developing solvent to give 105 mg (89%) of **2** as white needles; mp 50 °C (decomp.); IR (KBr): 3200 cm^{-1} (NH); NMR ($CDCl_3$): δ=12.15 (1H, br, NH), 7.61 (2H, m, Ph), 7.26 (3H, m, Ph), 6.57 (1H, s, CH), 6.55 (1H, m, CH_2=C<u>H</u>), 6.54 (1H, d, J_{cis}=8 Hz, CH_2=CHC<u>H</u>=CH), 6.20 (1H, dd, J_{cis}=8 Hz, J=10 Hz, CH_2=CHC<u>H</u>=CH), 5.29 (1H, dd, J_{cis}=10 Hz, J_{gem}= 1 Hz, C<u>H</u>$_2$=CH), 5.20 (1H, dd, J_{trans}=17 Hz, J_{gem}=1 Hz, C<u>H</u>$_2$=CH); MS: *m/z* 196 (M^+). Found: C, 79.35; H, 6.21; N, 14.20%. Calcd for $C_{13}H_{12}N_2$: C, 79.56; H, 6.16; N, 14.27%.

Preparation of 5-[2-(p-Chlorophenyl)-2-hydroxy-1-(phenylsulfonyl)ethyl]-3-phenylpyrazole (9). The compound was prepared from **7** (149 mg, 0.5 mmol) in 2 ml of THF by the same method as described in the preparation of **8**; white prisms; mp 164—165 °C (from acetone); IR (KBr): 3650—3010 (NH, OH), 1310 and 1130 cm^{-1}(SO_2); NMR (CD_3CO-CD_3): δ=8.00—6.88 (15H, m, $2C_6H_5$, *p*-ClC_6H_4, NH), 6.72 (1H, s, CH), 6.01 (1H, d, J=2 Hz, C<u>H</u>(OH)), 5.45 (1H, br, OH), 4.78 (1H, d, J=2 Hz, $PhSO_2CH$); MS: *m/z* 421 $(M-17)^+$. Found: C, 62.97; H, 4.39; N, 6.44%. Calcd for $C_{23}H_{19}$-ClN_2O_3S: C, 62.94; H, 4.36; N, 6.38%.

Preparation of 5-Methyl-3-phenylpyrazole (3). To a solution of **7** (89.1 mg, 0.3 mmol) and anhydrous disodium hydrogenphosphate (170 mg, 1.2 mmol) in 10 ml of dry MeOH was added 5% sodium amalgam (1 g). After stirring for 2 h, water and ether were added to the reaction mixture. The resulting mixture was filtered through Celite, and the organic layer was dried over sodium sulfate and rotary-evaporated. The resulting white powder was purified by TLC on silica gel using AcOEt–hexane (1:1) as a developing solvent to afford 37 mg (78%) of **3** as white crystals, mp 123—124 °C (lit,[9] 127 °C).

Preparation of 5-(p-Chlorophenyl)-2,4-diamino-6-(phenylsulfonylmethyl)pyrimidine (10). NaOEt (74.9 mg, 1.1 mmol) was added to the solution of **6b** (182 mg, 0.5 mmol) and guanidine hydrochloride (105 mg, 1.1 mmol) in 10 ml of absolute EtOH. The resulting mixture was refluxed for 24 h. The reaction was quenched with 10% sodium hydroxide solution. An organic substance was extracted with chloroform, and the extract was dried over sodium sulfate. After removal of the solvent under reduced pressure, the red powder was purified by TLC on silica gel using AcOEt–MeOH (9:1) as a developing solvent to afford 172 mg (92%) of **10** as white needles; mp 206—207 °C (from $CHCl_3$); IR (KBr): 3340, 3150 (NH), 1300 and 1160 cm^{-1}(SO_2); NMR ($CDCl_3$): δ=7.70 (5H, m, Ph), 7.48 (2H, B part of AB quartet, J=8 Hz), 7.12 (2H, A part of AB quartet, J=8 Hz), 5.75, 5.38 (4H, br, $2NH_2$), 4.17 (2H, s, CH_2); MS: *m/z* 374 (M^+). Found: C, 54.40; H, 4.06; N, 15.14%. Calcd for $C_{17}H_{15}ClN_4O_2S$: C, 54.47; H, 4.03; N, 14.95%.

Preparation of 5-(p-Chlorophenyl)-2,4-diamino-6-methylpyrimidine (4). 5% Sodium amalgam (3g) was added to the solution of **10** (150 mg, 0.4 mmol) and anhydrous disodium hydrogenphosphate (227 mg, 1.6 mmol) in 10 ml of dry MeOH. After stirring for 2 h, the reaction was quenched with water and filtered through Celite. The resulting mixture was acidified with 2 M HCl, and washed with ether three times. After neutralization, the solvent was evaporated, and the residue was washed with hot MeOH three times. Removal of MeOH from the washings gave 93.9 mg (100%) of **4** as white needles, mp 269—271 °C (from MeOH) (lit,[1] 264—265 °C).

References

1) P. B. Russell and G. H. Hitchings, *J. Am. Chem. Soc.*, **73**, 3763 (1951).

2) D. Laduree, P. Rioult, and J. Vialle, *Bull. Soc. Chim. Fr.*, **1973**, 637.

3) K. T. Potts, M. J. Cipullo, P. Ralli, and G. Theodoridis, *J. Am. Chem. Soc.*, **103**, 3584 (1981).

4) K. Hartke and J. Quante, *Arch. Parm.*, **313**, 1029 (1980).

5) Phenylsulfonyl group was displaced by methylthio anion which was generated by the nucleophilic substitution as shown bellow.

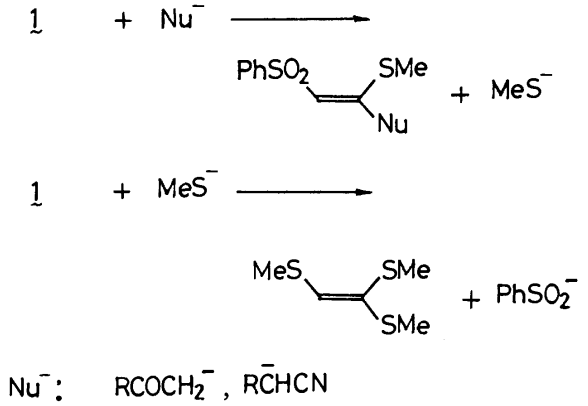

Fig. 6.

6) W. I. O'Sullivan, D. F. Tavares, and C. R. Hauser, *J. Am. Chem. Soc.*, **83**, 3453 (1961).

7) B. M. Trost, H. C. Arndte, P. E. Strege, and T. R. Verhoeven, *Tetrahedron Lett.*, **1976**, 3477.

8) A. R. Katritzky ed, "Advances in Heterocyclic Chemistry," Academic Press, New York (1966), Vol. 6, p. 347.

9) K. V. Auwers and H. Stuhlmann, *Ber.* **59B**, 1043 (1926).

 © 1984 The Chemical Society of Japan Bull. Chem. Soc. Jpn., 57, 2957—2961 (1984)

Synthesis of Fluorescent Peptides and Their Phosphorylation by the Catalytic Subunit of cyclicAMP-dependent Protein Kinase†

Hiroki KONDO,* Katsunori TAKAKI, Ryoichi KUROKI, Akihiro TADA, Kunihiro FUKUMOTO, and Junzo SUNAMOTO

Department of Industrial Chemistry, Faculty of Engineering, Nagasaki University, Nagasaki 852

(Received May 1, 1984)

The following two fluorescent peptides were prepared as substrates of the cyclicAMP-dependent protein kinase reaction: Leu-Arg-Arg-Ala-Ser-Leu-X; **1** (X= 2-(dansylamino)ethylamino or DAE) and **2** (X=4-methyl-2-oxo-7-chromenylamino or MCA). Both peptides were phosphorylated by ATP and the catalytic subunit of cyclicAMP-dependent protein kinase from bovine heart in a stoichiometric manner. Phosphorylation of peptide **1** is accompanied by a 10% increase in the fluorescence intensity at 550 nm. This enables one to assay peptide phosphorylation by fluorescence spectroscopy. The kinetic parameters obtained by this and the conventional phosphocellulose paper method for this phosphorylation were the following: K_m 7.8 μM and V_{max} 35 μmol·min^{-1}·mg^{-1} for **1**, and K_m 7.4 μM and V_{max} 16 μmol·min^{-1}·mg^{-1} for **2**.

Phosphorylation and dephosphorylation of proteins are one of the major mechanisms by which functions of proteins are regulated in biological systems.[1,2] A number of protein kinases, which mediate protein phosphorylation by ATP, are now known, but despite their importance in cellular regulation the detailed mechanism of enzymatic phosphoryl transfer reactions remains largely obscure. cAMP-dependent protein kinase is one of the most ubiquitous protein kinases[3] and is the only protein kinase whose primary structure has been reported.[4-6] This enzyme recognizes the two successive basic amino acid residues placed N-terminal to the phosphorylatable Ser or Thr of a protein.[7-9] Model peptides such as **3** that bears this feature of the amino acid sequence serve as good a substrate as do the natural protein substrates.[8] This fact as well as

Leu-Arg-Arg-Ala-Ser-Leu-Gly

3

the known primary sequence of the protein makes this enzyme system suitable for mechanistic studies. We have undertaken a study of enzyme-substrate interaction by use of fluorescent peptides and fluorescence spectroscopy. Besides mechanistic studies, such peptides are useful for assaying peptide phosphorylation spectroscopically and continuously. To date a few peptides bearing a fluorophore or chromophore at the N-terminus or in the middle of the sequence of **3** have been reported.[10-12] Unfortunately, however, a large spectral change was not observed before and after phosphorylation of the peptide and in the presence or absence of enzyme. In this aritcle we have attempted a C-terminal modification of peptide **3** with a fluorophore to examine if the resulting peptide is a sensitive probe of phosphorylation and/or the polarity of the enzyme active site.

† Abbreviations: cAMP, adenosine 3′,5′-cyclic monophosphate; DCC, dicyclohexylcarbodiimide; HOBt, 1-hydroxybenzotriazole; EEDQ, *N*-ethoxycarbonyl-2-ethoxy-1,2-dihydroquinoline; TFA, trifluoroacetic acid; Boc, *t*-butoxycarbonyl; Bzl, benzyl (ester); DCUrea, dicyclohexylurea; NEM, *N*-ethylmorpholine; Mops, 4-morpholinepropanesulfonic acid; EGTA, ethyene glycol bis (β-aminoethyl ether)-*N,N,N′,N′*,-tetraacetic acid; BSA, bovine serum albumin; SDS-PAGE, sodium dodecyl sulfate-polyacrylamide gel electrophoresis. The abbreviations used for amino acids follow the nomenclature recommended by the IUPAC-IUB Joint Commission on Biochemical Nomenclature (*Eur. J. Biochem.*, **138**, 9 (1984)).

Results and Discussion

Synthesis. The synthesis of peptides **1** and **2** has been accomplished by the route illustrated in Fig. 1. The peptides were bisected between Ala and Ser. The resulting two fragments were prepared separately and then combined at the late stage of the synthesis. The C-terminal fragment which contains the fluorophore was assembled by a stepwise elongation of the sequence from the C terminus. The N-terminal fragment was further divided into two dipeptides mainly for synthetic reasons. It was first attempted to synthesize the tetrapeptide also by the stepwise elongation method, but a difficulty was encountered at the synthesis of tripeptide Boc-Arg(NO_2)-Arg(NO_2)-Ala-OMe(**4**). A coupling of Boc-Arg(NO_2)-OH with H-Arg(NO_2)-Ala-OMe by the DCC method or the mixed anhydride method with ethyl chloroformate gave impure **4** in a low yield (<30%, depending on the coupling method). The poor solubility of **4** in most common solvents except MeOH hampered purification by recrystallization or chromatograpy. In one case, tetrapeptide

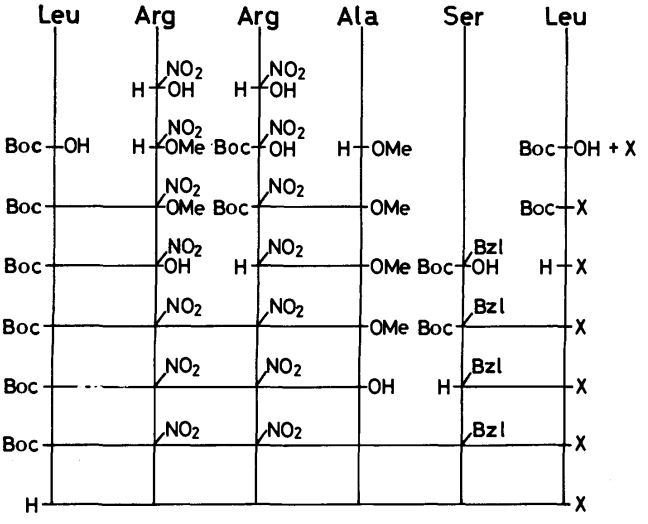

Fig. 1. Synthetic route to peptides **1** and **2** (X=DAE or MCA).

TABLE 1. ANALYTICAL DATA FOR PEPTIDES 1 AND 2

Peptide	TLC R_f		Paper electrophoresis[b]
	Solvent[a] A	B	F(pH 3.6)
1	0.49	0.23	0.85
2	0.47	0.40	0.88

a) For solvents see text. b) Mobility relative to Arg.

Boc-Leu-Arg(NO_2)-Arg(NO_2)-Ala-OMe was prepared by coupling of Boc-Leu-OH with H-Arg(NO_2)-Arg-(NO_2)-Ala-OMe, derived from partially purified **4**, by the DCC-HOBt method. The product purified by recrystallization from CH_3CN-ether was analytically pure and identical within experimental error in optical rotations with the peptide obtained by the fragment condensation of Boc-Leu-Arg(NO_2)-OH and H-Arg-(NO_2)-Ala-OMe; the former product, $[\alpha]_D^{26}$ −26.8° (*c* 1.0, MeOH); the latter peptide, $[\alpha]_D^{27}$ −27.7° (*c* 1.0, MeOH). This suggests that racemization of Arg has been suppressed in the DCC fragment condensation of dipeptides in the presence of HOBt.

A final condensation of the N-terminal tetrapeptide with the C-terminal fragment by either EEDQ or DCC-HOBt method afforded fully protected hexapeptides with the fluorophore at their C-termini in moderate yields (50—70%). The peptides were subjected to HF cleavage followed by chromatography on Sephadex G-10 and CM-cellulose. The purified peptides were characterized by various analytical techniques such as TLC and ^1H NMR. The data obtained were consistent with the proposed structure for the peptides (Table 1). Peptides **1** and **2** exhibit absorption maxima at 333 and 327 nm, respectively, and when excited at their respective absorption maximum wavelength, they emit strong fluorescence with maxima at 550 and 393 nm. This observation and the ready phosphorylation by the enzyme provide final proof of the identity of both peptides.

Fluorescence Assay of Phosphorylation. Both peptides **1** and **2** are phosphorylated by ATP and the catalytic subunit of cAMP-dependent protein kinase from bovine heart. Phosphorylation of peptide **1** gives rise to a slight blue shift (4 nm) of the emission maximum and a 10% increase in the fluorescence intensity (Fig. 2), while no discernible change was observed in the fluorescence spectrum of **2** before and after phosphorylation (data not shown). The magnitude of intensity change in **1** is half of that observed for the peptide bearing a Trp residue just N-terminal to the phosphorylatable Ser.[12] Peptide phosphorylation can be assayed by taking advantage of the spectral change in **1** as well as by the conventional phosphocellulose paper method.[13] As the time course experiment given in Fig. 3 demonstrates, phosphorylation of **1** in the presence of a saturating concentration of ATP, *i.e.*, about fifty times the $K_{m,ATP}$,[14] is rapid and stoichiometric; 0.96±0.03 mol of phosphate is incorporated to **1** and **2** in ≈10 min. For identification of the phosphorylated peptides, the reaction mixture was subjected to high voltage paper electrophoresis at pH 3.6. As the reaction progresses, a spot migrating toward the cathode more slowly than

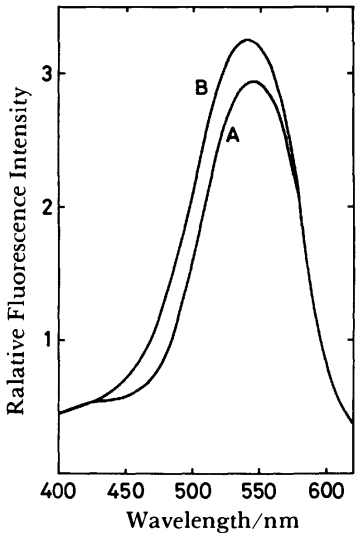

Fig. 2. Fluorescence spectra of peptide **1** in 50 mM Mops, pH 7.0, before (A) and after phosphorylation (B).

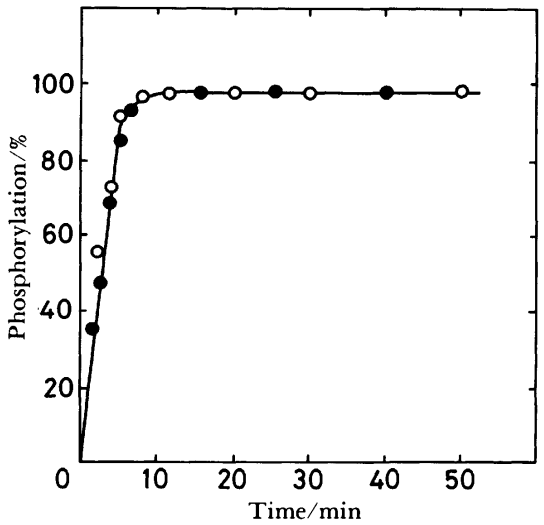

Fig. 3. Time course of peptide **1** phosphorylation at 30°C.
The extent of reaction was determined by the fluorescence (○) or phosphocellulose paper method (●). The assay mixture consisted of 250 μM [γ-^{32}P]ATP, 12.5 mM magnesium acetate, 0.25 mM EGTA, 140 μM **1**, 0.1 mg/ml BSA, and 1.8 μg/ml enzyme in 50 mM Mops, pH 7.0.

the unphosphorylated peptide becomes visible (data not shown). This is as expected, since phosphorylation introduces 1—2 negative charges into substrate.

Initial rate data of peptide phosphorylation at a low enzyme concentration were analyzed in terms of Henri-Michaelis-Menten formulation.[15] The results are summarized in Table 2. The kinetic parameters for **1** obtained by the fluorescence assay are identical within experimental error with those determined by the phosphocellulose paper method; *e.g.*, K_m was 7.5 μM for the former and 7.8 μM for the latter. The K_m values for **1** and **2** are smaller than that of peptide **3**. This result is consistent with the previous observation that a hydrophobic substituent placed C-terminal to the

Table 2. Kinetic parameters for phosphorylation of peptides **1** and **2** by ATP and the catalytic subunit of cAMP-dependent protein kinase at pH 7.0 and 30 °C

Peptide	K_m/μM	V_{max}/μmol·min^{-1}·mg^{-1}	Reference
1	7.8	35	This work
2	7.4	16	This work
3	16	20	8

phosphorylatable Ser increases the binding ability of peptide substrate to the enzyme.[16] In addition to K_m, the catalytic rates (V_{max}) are high and comparable with those of peptide **3** and protein substrates. This excellent substrate activity of peptides **1** and **2** makes them useful in mechanistic studies of enzyme-substrate interaction by, for example, fluorescence spectroscopy.

Experimental

Materials. L-Amino acids were obtained from Protein Research Foundation or Wako Pure Chemical Ind. Co., both Osaka. DCC, HOBt, and EEDQ were purchased from the former source, while TFA and dansyl chloride were from the latter. Sephadex G-10 and CM-cellulose were obtained from Pharmacia and Brown, respectively. Carrier-free [^{32}P] inorganic phosphate was the product of Japan Atomic Energy Research Institute. Scintillation reagents 2,5-diphenyloxazole (PPO) and 2,2′-(*p*-phenylene)bis[5-phenyloxazole] (POPOP) were obtained from Nakarai Chemical Ltd., Kyoto. 4-Methyl-7-aminocoumarin was prepared according to the literature,[17] whereas 2-(dansylamino)ethylamine was synthesized by the route illustrated in the Scheme. [γ-^{32}P]ATP of specific radioactivity 20—200 cpm/pmol was prepared by the method of Glynn and Chappell.[18]

Apparatus. Electronic absorption and fluorescence spectra were taken on a Shimadzu UV-150 and Hitachi 650-10S spectrophotometer, respectively. ^{1}H NMR spectra were recorded on a Jeol JNM-MH-100 spectrometer. Optical rotations were read on a Jasco DIP-4. Paper electrophoresis was run with a Toyo HPE-406 apparatus. Radioactivity was determined on an Aloka liquid scintillation counter LSC-703.

Miscellaneous. TLC was run on a silica-gel plate in the following solvent systems: (A) AcOH: Pyridine: *n*-BuOH: H_2O=1:1:4:2 (B) AcOH:*n*-BuOH:H_2O=4:2:1 (C) MeOH (D) $CHCl_3$:MeOH=5:1 (E) $CHCl_3$:MeOH:benzene=5:1:1. Paper chromatography was carried out on a Toyo Roshi filter paper No.51 in one of the solvents described above. High-voltage paper electrophoresis was run on the same filter paper in AcOH:Pyridine:H_2O=10:1:99 (solvent F) at pH 3.6 and 2,500 V for ≈2 h. Peptide concentrations were determined spectroscopically by using ε_{329} 4780 of *N*-ethyl-5-dimethylamino-1-naphthalenesulfonamide[19] for **1** and ε_{324} 26800 of Leu-MCA·HCl[20] for **2**.

Enzyme Preparation and Assay. The catalytic subunit of bovine heart cAMP-dependent protein kinase was prepared by the method of Demaille *et al.*[16] The preparation gave a single band on SDS-PAGE that corresponds to a molecular weight of ≈41000.[4] The enzyme concentration was determined on the basis of $A_{280}^{1\%}$14.9.[16] The enzyme activity was assayed by the phosphocellulose paper method of Witt and Roskoski[13] with a slight modification.[21,22] The components of an assay solution and the assay conditions are given in the caption of Fig. 3. The radioactivity associated with the peptide was counted with 5 ml of a toluene solution of 4 g/l PPO and 0.1 g/l POPOP.

Boc-Arg(NO$_2$)-Ala-OMe (5). A mixture of Boc-Arg(NO$_2$)-OH (9.6 g, 30 mmol), HOBt (4.1 g, 30 mmol), and DCC (6.2 g, 30 mmol) in CH_3CN (50 ml)-DMF (20 ml) was stirred at −5 °C for 20 min. A pre-cooled solution of H-Ala-OMe·HCl (4.2 g, 30 mmol) and NEM (3.8 ml, 30 mmol) in CH_2Cl_2 (50 ml) was added and the whole mixture was stirred at −5 °C for 1 h and then at room temperature overnight. The precipitate formed (DCUrea) was removed by filtration. The filtrate was kept in a refrigerator for 4 h and DCUrea was filtered off again. Evaporation of the solvent *in vacuo* gave a semi-solid. It was taken up in AcOEt (300 ml) and the insoluble material was removed by filtration. The filtrate was washed with 70 ml each of the following ice-cold solutions three times; 4% $NaHCO_3$, aq saturated NaCl, 10% citric acid, aq saturated NaCl. After drying over Na_2SO_4, the solvent was evaporated *in vacuo* to yield a solid. It was recrystallized from CH_3CN-Et_2O (7.0 g, 58%), mp. 149.5—151 °C. Found: C, 44.66; H, 7.11; N, 20.63%. Calcd for $C_{15}H_{28}N_6O_7$: C, 44.55; H, 6.98; N, 20.78%. Use of 1.5-equiv DCC and HOBt increased the yield to 62%.

Boc-Leu-Arg (NO$_2$)-OMe (6). To a stirred solution of Boc-Leu-OH·H_2O (7.5 g, 30 mmol) and NEM (3.8 ml, 30 mmol) in THF (40 ml) chilled at −15 °C was added isobutyl chloroformate (4.0 ml, 30 mmol). Ten min later, a pre-cooled solution of H-Arg(NO$_2$)-OMe·HCl (8.1 g, 30 mmol) and NEM (3.8 ml, 30 mmol) in CH_2Cl_2 (40 ml)-DMF (50 ml) was added. The mixture was stirred at −15 °C for 2 h and then at room temperature overnight. The precipitate formed was filtered off and washed with CH_2Cl_2. The solvents were evaporated *in vacuo*. The resulting syrup was taken up in 500 ml of AcOEt. The solution was washed and worked up essentially as described above. The crude product was recrystallized from aqueous ethanol (12.1 g, 90%), mp 146—148 °C. Found: C, 48.36; H, 7.82; N, 18.95%. Calcd for $C_{18}H_{34}N_6O_7$: C, 48.42; H, 7.67; N, 18.82%.

Boc-Leu-Arg(NO$_2$)-Arg(NO$_2$)-Ala-OMe(7). A sample of **6** (4.2 g, 10 mmol) was treated with 20 g of TFA (175 mmol) in 35 ml of CH_2Cl_2 at room temperature for 40 min. The solvent and excess TFA were evaporated *in vacuo*. The residual syrup was taken up in CH_2Cl_2 and the solvent was

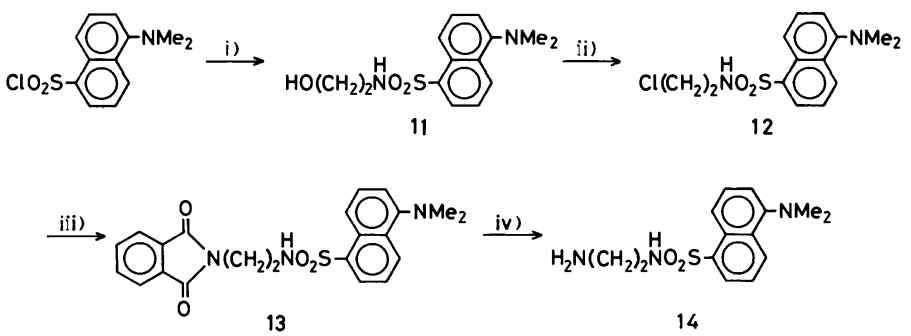

Scheme. Reagents: i, $HO(CH_2)_2NH_2$; ii, $SOCl_2$; iii, potassium phthalimide; iv, H_2NNH_2.

evaporated *in vacuo*. This procedure was repeated until constant weight was reached for H-Arg(NO_2)-Ala-OMe (**8**)·2TFA. Boc-Leu-Arg(NO_2)-OH (**9**) was preapred by saponification of **6** in the way identical with that described for **10** below. A mixture of **8**·2TFA (1.5 g, 2.8 mmol), **9** (1.2 g, 2.8 mmol), NEM (0.65 g, 5.6 mmol), HOBt (0.38 g, 2.8 mmol), and DCC (0.58 g, 2.8 mmol) in 30 ml of THF was allowed to react at 0°C for 2 h and then at room temperature overnight. The precipitate formed was filtered off. The filtrate was concentrated to dryness. The residue was taken up as much as possible in 1 l each of AcOEt. The insoluble material was extracted three more times with 1 l each of AcOEt. The extract was washed and worked up as described above for **5**. The product was recrystallized from CH_3CN-Et_2O (1.9 g, 93%), mp 140—142°C. TLC R_f 0.69 (C).

Boc-Leu-Arg(NO_2)-Arg(NO_2)-Ala-OH (10). A sample of **7** (0.72 g, 1.0 mmol) in 20 ml of MeOH was allowed to react with 1.7 ml of 1 M NaOH at room temperature for 7 h. The solution was diluted with 20 ml of water and MeOH was evaporated *in vacuo*. After washing with Et_2O, the aqueous solution was chilled in ice and the pH was brought to 3—4 with ice-cold 10% citric acid. The precipitate formed was collected by filtration and recrystallized from MeOH-Et_2O (0.69 g, 98%), mp 205—208°C. TLC R_f 0.53 (C). Found: C, 43.31; H, 6.90; N, 23.01%. Calcd for $C_{26}H_{48}N_{21}O_{11}\cdot H_2O$: C, 43.21; H, 6.97; N, 23.26%.

2-(5-Dimethylamino-1-naphthalenesulfonamido)ethanol (11) Dansyl chloride (2.0 g, 7.4 mmol) was added dropwise to a 33% aqueous 2-aminoethanol solution (2 ml). The mixture was heated at 80°C until the dansyl chloride disappeared as inspected by TLC. The solution was made weakly acidic (pH 3—4) and the product was extracted with AcOEt. The extract was dried over Na_2SO_4 and then concentrated to dryness. The crude product obtained was recrystallized from ether-petroleum ether (2.10 g, 96%), mp 102.5—104°C. TLC R_f 0.71 (D), 0.55 (E). Found: C, 56.66; H, 6.21; N, 9.23%. Calcd for $C_{14}H_{18}N_2O_3S$: C, 57.12; H, 6.16; N, 9.52%.

1-Chloro-2-(5-dimethylamino-1-naphthalenesulfonamido)ethane (12). To a solution of **11** (0.42 g, 1.4 mmol) in chloroform (30 ml) was added dropwise 1.7 g (14 mmol) of thionyl chloride in chloroform (25 ml). The mixture was refluxed for 4 h. The excess reagent and solvent were evaporated *in vacuo* to leave a solid, which was taken up in water. The solution was made weakly alkaline and the precipitate formed was extracted with AcOEt and treated as above for **11** (yield 95%), mp 87—90°C. TLC R_f 0.75 (E).

N-[(5-Dimethylamino-1-naphthalenesulfonamido)ethyl]phthalimide (13). A mixture of **12** (0.42 g, 1.3 mmol) and potassium phthalimide (0.29 g, 1.5 mmol) in 30 ml of DMF was stirred at 100°C for 3 h. The solution was mixed with 200 ml of 0.1 M NaOH (1 M=1 mol dm^{-3}) and extracted with 50 ml each of chloroform four times. The extract was washed with 0.2 M NaOH and water, and dried over Na_2SO_4. The following work-up procedures were the same as that for **11**. The product was obtained in 76% yield, mp 160—165°C. TLC R_f 0.81 (D).

2-(5-Dimethylamino-1-naphthalenesulfonamido)ethylamine (14). A methanolic solution (25 ml) of **13** (0.43 g, 1.0 mmol) and hydrazine hydrate (0.10 g, 2.0 mmol) was refluxed for 2 h. The mixture was diluted with water (25 ml) and methanol was removed *in vacuo*. The turbid solution left was heated with conc. HCl for 2 h. The solution was made alkaline and the precipitate formed was extracted with AcOEt. The product was obtained in 72% yield by the usual work-up described above, mp 155—157°C. TLC R_f 0.10 (E). Found: C, 57.24; H, 6.53; N, 13.71%. Calcd for $C_{14}H_{19}N_3O_2S$: C, 57.32; H, 6.53; N, 14.32%.

Boc-Leu-DAE (15). A mixture of **14** (0.58 g, 2.0 mmol), Boc-Leu-OH·H_2O (0.55 g, 2.2 mmol), HOBt (0.30 g, 2.2 mmol), NEM (2.2 mmol), and DCC (0.45 g, 2.2 mmol) in 25 ml of CH_2Cl_2 was stirred at 0°C for 2 h and then at room temperature overnight. The precipitated DCUrea was filtered off. The filtrate was concentrated, diluted with 200 ml of AcOEt and washed as described earlier for **5**. After drying over Na_2SO_4, the solution was concentrated to dryness, 0.94 g (94%), mp 63—64.5°C. TLC R_f 0.53 (E). Found: C, 59.11; H, 7.63; N, 10.47%. Calcd for $C_{25}H_{38}N_4O_5S$: C, 59.26; H, 7.56; N, 11.06%.

Boc-Ser(Bzl)-Leu-DAE (17). H-Leu-DAE (**16**)·3TFA was prepared from **15** as described for **8**. The reaction of **16**·3TFA (1.25 g, 1.7 mmol) with Boc-Ser(Bzl)-OH (0.54 g, 1.8 mmol) in the presence of NEM (0.58 g, 5.0 mmol), HOBt (0.25 g, 1.8 mmol), and DCC (0.38 g, 1.8 mmol) in CH_2Cl_2 (5 ml) and AcOEt (25 ml) and the usual work-up of the reaction mixture gave 1.1 g (94%) of **17** (AcOEt-petroleum ether), mp 68—70°C. TLC R_f 0.63 (E). Found: C, 60.94; H, 7.25; N, 10.22%. Calcd for $C_{35}H_{49}N_5O_7S$: C, 61.47; H, 7.22; N, 10.24%.

Boc-Leu-Arg(NO_2)-Arg(NO_2)-Ala-Ser(Bzl)-Leu-DAE (19). H-Ser(Bzl)-Leu-DAE (**18**)·3TFA was prepared from **17** as described for **8**. A mixture of **18**·3TFA (1.3 g, 1.4 mmol), **10** (1.1 g, 1.5 mmol), NEM (0.49 g, 4.2 mmol), DCC (0.31 g, 1.5 mmol), and HOBt (0.21 g, 1.5 mmol) was allowed to react at 2°C for 2 h and then at room temperature overnight. The precipitate formed was filtered off. The filtrate was kept in a refrigerator for 4 h to ensure precipitation of DCUrea, which was again removed by filtration. The filtrate was concentrated to a small volume and the product was precipitated with 100 ml of AcOEt in 52% yield (0.93 g), mp 211—212°C. TLC R_f 0.31 (E).

Boc-Ser(Bzl)-Leu-MCA (21). H-Leu-MCA (**20**) was prepared by the deprotection of Boc-Leu-MCA[20] with TFA in CH_2Cl_2. A mixture of **20**·TFA (1.37 g, 3.4 mmol), Boc-Ser(Bzl)-OH (1.0 g, 3.4 mmol), NEM (0.43 ml, 3.4 mmol), and EEDQ (0.84 g, 3.4 mmol) in DMF (5.5 ml) was stirred at room temperature for 12 h. Following evaporation of the solvent, the residue was taken up in AcOEt and washed with acid and alkaline solutions as above to give 1.5 g of the product in 78% yield. Recrystallized from MeOH-ether, mp 152—154°C. Found: C, 65.25; H, 7.25; N, 7.30%. Calcd for $C_{31}H_{39}N_3O_7\cdot 0.5\ H_2O$: C, 64.79; H, 7.02; N, 7.31%.

Boc-Leu-Arg(NO_2)-Arg(NO_2)-Ala-Ser(Bzl)-Leu-MCA (23). H-Ser(Bzl)-Leu-MCA (**22**)·TFA was prepared from **21** as above. An equimolar mixture (1.9 mmol) of **10**, **22**·TFA, and NEM was allowed to react with EEDQ in DMF at room temperature for 12 h. The solvent was evaporated *in vacuo* and the product was precipitated with EtOAc in 70% yield. Recrystallized from MeOH-ether, mp 176—178°C. TLC R_f 0.36 (E).

Peptide 2. A sample of **23** (550 mg) was treated with 20 ml of HF and 8 ml of anisole at 0°C for 50 min. The HF was removed *in vacuo* and the residue was taken up in 10% AcOH. Anisole was removed by extraction with 10 ml each of AcOEt three times. The aqueous phase was concentrated to *ca.* 5 ml and then applied to a column of Sephadex G-10 (3.2×56 cm). The column was eluted with 1% AcOH and the peak fractions were pooled and lyophilized. The peptide was further purified by chromatography on a column of CM-cellulose (1.8×24 cm) with a linear gradient elution with 25 mM ammonium acetate, pH 5.0, and 700 mM ammonium acetate, pH 6.0. The desired fractions were combined, concentrated to *ca.* 10 ml, and then applied to the same Sephadex G-10 column. The column was first washed with water for desalting and the peptide was eluted with 1% AcOH.

Peptide **1** was obtained also by an analogous treatment of **19**.

The authors are grateful to Professor E. T. Kaiser

for helpful advice in initiating this project. They are also indebted to Mr. H. Maruta for expert technical assistance. They also thank Professors M. Sugii and M. Koida, Nagasaki University, for making them accessible to a scintillation counter. This work was supported by the Naito Foundation Subsidy for Inter-Institute Researches and in part by the Eighteenth Bank Fund for Community Development and Promotion.

References

1) E. G. Krebs and J. A. Beavo, *Annu. Rev. Biochem.*, **48**, 923 (1979).
2) P. Cohen, *Nature*, **296**, 613 (1982).
3) D. A. Walsh, J. P. Perkins, and E. G. Krebs, *J. Biol. Chem.*, **243**, 3763 (1968).
4) S. Shoji, D. C. Parmelee, R. D. Wade, S. Kumar, L. H. Ericsson, K. A. Walsh, H. Neurath, G. L. Long, J. G. Demaille, E. H. Fischer, and K. Titani, *Proc. Natl. Acad. Sci. U.S.A.*, **78**, 848 (1981).
5) K. Takio, S. B. Smith, E. G. Krebs, K. A. Walsh, and K. Titani, *Proc. Natl. Acad. Sci. U.S.A.*, **79**, 2544 (1982).
6) S. A. Carr, K. Biemann, S. Shoji, D. C. Parmelee, and K. Titani, *Proc. Natl. Acad. Sci. U.S.A.*, **79**, 6128 (1982).
7) Ö. Zetterqvist, U. Ragnarsson, E. Humble, L. Berglund, and L. Engström, *Biochem. Biophys. Res. Commun.*, **70**, 696 (1976).
8) B. E. Kemp, D. J. Graves, E. Benjamini, and E. G. Krebs, *J. Biol. Chem.*, **252**, 4888 (1977).
9) A. H. Pomerantz, V. G. Allfrey, R. B. Merrifield, and E. M. Johnson, *Proc. Natl. Acad. Sci. U.S.A.*, **74**, 4261 (1977).
10) B. E. Kemp, *J. Biol. Chem.*, **255**, 2914 (1980).
11) H. N. Bramson, N. Thomas, W. F. DeGrado, and E. T. Kaiser, *J. Am. Chem. Soc.*, **102**, 7156 (1980).
12) D. E. Wright, E. S. Noiman, P. B. Chock, and V. Chau, *Proc. Natl. Acad. Sci. U.S.A.*, **78**, 6048 (1981).
13) J. J. Witt and R. Roskoski, Jr., *Biochemistry*, **14**, 4503 (1975).
14) R. N. Armstrong, H. Kondo, and E. T. Kaiser, *Proc. Natl. Acad. Sci. U.S.A.*, **76**, 722 (1979).
15) I. H. Segel, "Enzyme Kinetics," Chap. 6, Wiley, New York, (1975).
16) J. G. Demaille, K. A. Peters, and E. H. Fischer, *Biochemistry*, **16**, 3080 (1977).
17) M. Zimmerman, E. Yurewicz, and G. Patel, *Anal. Biochem.*, **70**, 258 (1976).
18) I. M. Glynn and J. B. Chappell, *Biochem. J.*, **90**, 147 (1964).
19) B. S. Hartley, *Biochem. J.*, **119**, 805 (1970).
20) Y. Kanaoka, T. Takahashi, and H. Nakayama, *Chem. Pharm. Bull.*, **25**, 362 (1977).
21) D. B. Glass, R. A. Masaracchia, J. R. Feramisco, and B. E. Kemp, *Anal. Biochem.*, **87**, 566 (1978).
22) R. N. Armstrong, H. Kondo, J. Granot, E. T. Kaiser, and A. S. Mildvan, *Biochemistry*, **18**, 1230 (1979).

Reaction of Trifluoronitrosomethane with Arenesulfonohydrazides. Synthesis of *N*-Trifluoromethyl-*N*-hydroxyarenesulfonamides

Akira SEKIYA and Teruo UMEMOTO*

Sagami Chemical Research Center, Nishi-Ohnuma 4-4-1, Sagamihara, Kanagawa 229

(Received May 10, 1984)

The reaction of trifluoronitrosomethane **1** with arenesulfonohydrazides resulted in the formation of *N*-trifluoromethyl-*N*-hydroxyarenesulfonamides **3** which were characterized by spectral and elemental analyses. It showed a sharp contrast to the reaction of **1** with acyl- or carbamoylhydrazines, which afforded the corresponding trifluoromethylazo compounds. As an alternative route, **3** could be synthesized by the reaction of **1** with arenesulfinic acids or their salts. The sulfonamides **3** were converted to the corresponding methyl ethers or tosylates.

Trifluoronitrosomethane[1] **1** is an interesting blue gas, which is expected to have high reactivity because of a combination of a reactive nitroso group and a highly electronegative trifluoromethyl group. It has been known that **1** condensed with amino compounds such as aromatic amines,[2] alkylamines,[3] amino acids,[4] and other amines[5] to give the corresponding trifluoromethylazo compounds. Recently, we reported that electron-deficient amino compounds, arenesulfonamides, condensed with **1** only in the presence of a base to give trifluoromethylazosulfonylarenes in high yields.[6] This paper described that the reaction of arenesulfonohydrazides **2** with **1** led to unexpected compounds, *N*-trifluoromethyl-*N*-hydroxyarenesulfonamides **3.**

Results and Discussion

Benzenesulfonohydrazide **2a** in *N*,*N*-dimethylformamide (DMF) reacted with two molar equivalent amount of **1** at room temperature. After the solvent was removed under vacuum, the residue was column-chromatographed on silica gel using ether as an eluent to give a stable colorless compound. The ^{19}F NMR spectrum showed a singlet at 65.00 ppm which could be assigned to trifluoromethyl group bonding to a nitrogen atom. The ^{1}H NMR showed a AB_2X_2 pattern in the region of aromatic protons, characteristic of benzenesulfonyl group, and a broad peak at 7.88 ppm which was assigned to a hydroxyl group by deuterium oxide exchange experiment. The infrared spectrum showed strong absorption bands at 3410 and 1370 cm^{-1} due to OH and SO_2 stretching vibration, respectively. It was found that the compound contains a nitrogen atom in the molecule from the elemental analysis. From the above results, the structure of the product was assigned to be entirely unexpected *N*-trifluoromethyl-*N*-hydroxybenzenesulfonamide **3a**.

$$2\,CF_3NO + ArSO_2NHNH_2 \longrightarrow CF_3\text{-}\overset{OH}{\overset{|}{N}}\text{-}SO_2Ar$$

1 **2a—f** **3a—f**

The reaction proceeded smoothly in several kinds of solvents (Table 1). As a result, methanol was the best solvent because of its low boiling point and shorter reaction time. Several *N*-trifluoromethyl-*N*-hydroxyarenesulfonamides **3a—f** were synthesized under the conditions in high yields (Table 1).

p-Toluenesulfonohydrazide **2b** was allowed to react with **1** in DMF, and the same post-treatment gave 61% yield of **3b** and 28% yield of a 2:1 complex of **3b** with DMF. The complex was characterized by IR, NMR, and elemental analyses.

From the fact that two molar equivalent amount of **1**

TABLE 1. SYNTHESIS OF **3a—f** FROM **1** AND **2a—f**

Run	Ar		Solv.	Time / min	Yield of **3a—f**[a]/%
1	Ph-	**3a**	DMF	50	96
2	Ph-	**3a**	CH_3CN	540	92
3	Ph-	**3a**	THF	90	99
4	Ph-	**3a**	CH_3COOH	90	94
5	Ph-	**3a**	CH_3OH	15	96
6	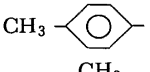	**3b**	CH_3OH	40	97
7	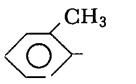	**3c**	CH_3OH	35	88
8	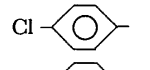	**3d**	CH_3OH	35	87
9	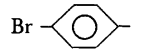	**3e**	CH_3OH	35	74
10	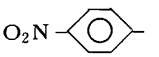	**3f**	CH_3OH	35	91

a) Based on the amount of **2a—f**.

to **2** was consumed in the reaction, it is clear that the reaction consists of at least two steps. In order to isolate the intermediate, the reaction of **1** with an equimolar amount of **2** was carried out. The reaction solution contained no intermediate but a 1:1 mixture of **3** and **2**, which indicated that the second reaction with **1** should be faster than the first one.

Interestingly, these results showed a sharp contrast to the reaction of **1** with acyl- or carbamoylhydrazines.

$$\underset{\mathbf{4}}{PhCONHNH_2} \xrightarrow{1} \underset{\mathbf{5}}{CF_3N{=}NNHCOPh} \quad 97\%$$

$$\underset{\mathbf{6}}{CH_3CONHNH_2} \xrightarrow{1} \underset{\mathbf{7}}{CF_3N{=}NNHCOCH_3}^{5a)} \quad 50\%$$

$$\underset{\mathbf{8}}{PhNHCONHNH_2} \xrightarrow{1} \underset{\mathbf{9}}{CF_3N{=}NNHCONHPh} \quad 98\%$$

Hydrazines **4**, **6**, and **8** were treated with two molar equivalent of **1** in methanol at room temperature for 3 d to produce normal condensation products **5**, **7**, and **9** with recovery of one molar equivalent of **1**.

From a different point of view, **3** can be regarded as the combination of **1** and arenesulfinic acid. As an alternative route, we tried the reaction of **1** with arenesulfinic acid. Benzene- and toluenesulfinic acids

$$\mathbf{1} + ArSO_2H \longrightarrow \underset{\mathbf{3a}\ (95\%)\\ \mathbf{3b}\ (91\%)}{CF_3\text{-}\overset{OH}{\overset{|}{N}}\text{-}SO_2Ar}$$

absorbed smoothly an equivalent amount of **1** at room temperature to produce **3a** and **3b** in high yields. This experimental result afforded another proof of the structural assignment of **3** and suggested the following reaction mechanism for the formation of **3** in the reaction of **1** with hydrazides **2**. Probably, the intermediate resulting from the first step decomposes so as to produce arenesulfinic acid, which reacts with **1** to afford **3**. Unfortunately, an attempt to isolate the other part of decomposition products from the intermediate was failed. This result demonstrates the quite difference in the reactions between **2** and other hydrazines **4**, **6**, and **8**. This may be because acyl or carbamoyl groups cannot act as leaving groups, while arenesulfonyl groups are relatively strong leaving groups.[7]

On the other hand, sodium benzenesulfinate gave **3a** in a low yield in its reaction with **1** in methanol. The salt absorbed **1** very smoothly, but several undetermined by-products were produced in addition to **3a**. It indicates that high nucleophilicity of the salt compared to the sulfinic acid causes side reactions.

$$\mathbf{1} + PhSO_2Na \longrightarrow \mathbf{3a} \quad 40\%$$

Since **3** have free hydroxyl groups, it is possible to derive some ethers or esters as follows. Treatment of **3** with methyl iodide afforded the methyl ethers **10a—c** in 33—85% yields. Tosyl chloride gave the esters **11a** and **11b** in 20 and 55% yields, respectively.

$$\mathbf{3} \xrightarrow{CH_3I} \underset{33\text{—}85\%}{CF_3\text{-}\overset{OCH_3}{\overset{|}{N}}\text{-}SO_2Ar} \quad \begin{matrix}\mathbf{10a}\ (Ar{=}Ph)\\ \mathbf{10b}\ (Ar{=}p\text{-Tolyl})\\ \mathbf{10c}\ (Ar{=}o\text{-Tolyl})\end{matrix}$$

$$\mathbf{3} \xrightarrow{TsCl} \underset{20\text{—}55\%}{CF_3\text{-}\overset{OTs}{\overset{|}{N}}\text{-}SO_2Ar} \quad \begin{matrix}\mathbf{11a}\ (Ar{=}Ph)\\ \mathbf{11b}\ (Ar{=}p\text{-Tolyl})\end{matrix}$$

Experimental

General. Melting and boiling points were uncorrected. ^1H NMR spectra were determined with a Varian HA-100 NMR spectrometer or a Varian EM 390 NMR spectrometer. ^{19}F NMR spectra were determined with a Varian XL-100A NMR spectrometer or a Hitachi R-20B NMR spectrometer. ^{19}F chemical shifts are given in ppm upfield from trichlorofluoromethane as an internal standard. IR spectra were measured on a Jasco A-202 diffraction grating infrared spectrophotometer.

Materials. Trifluoronitrosomethane **1** was prepared as previously.[8] Arenesulfonohydrazides, *p*-toluenesulfinic acid, and sodium benzenesulfinate used were commercial products and used without further purification.

N-Trifluoromethyl-N-hydroxyarenesulfonamides 3a—f. The reactions were carried out in 200 ml glass vessels fitted with valves. Arenesulfonohydrazide **2** (5.5 mmol) was dissolved in a solvent (10 ml) in the reactor and the vessel was cooled to −196 °C and then evacuated. The amount of **1** (11.1 mmol) was determined by PVT measurements assuming ideal gas behavior and it was condensed into the reactor. The vessel was warmed to room temperature with a water bath and the solution was stirred by magnetic stirrer. After the blue color of **1** disappeared, the solvent was removed under vacuum. The residue was column-chromatographed on silica gel eluted with ether to give **3**. The results are summarized in Table 1.

3a: Bp 146—148 °C/800 Pa, mp 42—43 °C; IR (KBr, cm^{-1}) 3410 (OH), 1370 (SO_2); ^{19}F NMR ($CDCl_3$) 65.00 (s); ^1H NMR ($CDCl_2$); δ=7.4—7.8 (3H, m, ArH), 7.88 (1H, bs, OH), 7.98 (2H, m, ArH). Found: C, 34.78; H, 2.46; N, 5.83%. Calcd for $C_7H_6F_3NO_3S$: C, 34.86; H, 2.51; N, 5.81%.

3b: Mp 65—71 °C; IR (KBr, cm^{-1}) 3370 (OH), 1370 (SO_2); ^{19}F NMR ($CDCl_3$) 65.74 (s); ^1H NMR ($CDCl_3$); δ=2.44 (3H, s, CH_3), 7.35 (2H, d, J=8.0 Hz, ArH), 7.68 (1H, bs, OH), 7.86 (2H, d, J=8.0 Hz, ArH). Found: C, 37.71; H, 3.18; N, 5.48%. Calcd for $C_8H_8F_3NO_3S$: C, 37.65; H, 3.17; N, 5.49%.

3c: Mp 79.5—80 °C; IR (KBr, cm^{-1}) 3320 (OH), 1355 (SO_2); ^{19}F NMR (CD_3CN) 63.25 (s); ^1H NMR (CD_3CN); δ=2.70 (3H, s, CH_3), 7.2—8.1 (4H, m, ArH), 8.56 (1H, s, OH). Found: C, 37.48; H, 3.21; N, 5.46%. Calcd for $C_8H_8F_3NO_3S$: C, 37.65; H, 3.16; N, 5.49%.

3d: Mp 114—114.5 °C; IR (KBr, cm^{-1}) 3320 (OH), 1375 (SO_2); ^{19}F NMR (CD_3CN) 64.33 (s); ^1H NMR (CD_3CN); δ=7.68 (2H, d, J=9.0 Hz, ArH), 7.95 (2H, d, J=9.0 Hz, ArH), 9.27 (1H, bs, OH). Found: C, 30.56; H, 1.95; N, 5.11%. Calcd for $C_7H_5ClF_3NO_3S$: C, 30.50; H, 1.83; N, 5.08%.

3e: Mp 134—134.5 °C; IR (KBr, cm^{-1}) 3360 (OH), 1370 (SO_2); ^{19}F NMR (CD_3CN) 64.15 (s); ^1H NMR (CD_3CN); δ=7.85 (4H, s, ArH), 9.26 (1H, bs, OH). Found: C, 26.40; H, 1.69; N, 4.34%. Calcd for $C_7H_5BrF_3NO_3S$: C, 26.27; H, 1.57; N, 4.38%.

3f: Mp 116—116.5 °C; IR (KBr, cm^{-1}) 3370 (OH), 1530 (NO_2), 1385 (SO_2), 1345 (NO_2); ^{19}F NMR (CD_3CN) 66.33 (s); ^1H NMR (CD_3CN); δ=8.38 (4H, m, ArH), 9.48 (1H, bs, OH). Found: C, 29.45; H, 1.81; N, 9.50%. Calcd for $C_7H_5F_3N_2O_5S$: C, 29.38; H, 1.76; N, 9.79%.

DMF Complex of 3b. *p*-Toluenesulfonohydrazide **2b**

in DMF was treated with **1** in a similar manner as described above. After removing the solvent under vacuum, the residue was washed with water, extracted with benzene, and the benzene solution was dried with magnesium sulfate. The compound **3b** and the complex **3b**·1/2DMF were isolated by column chromatography on silica gel eluted with benzene in 61 and 28% yields, respectively. **3b**·1/2DMF: Mp 55—56 °C (hexane); IR (KBr, cm^{-1}) 3390 (OH, sh), 3160 (OH), 2890 (CH), 1645 (C=O), 1380 (SO_2); ^{19}F NMR ($CDCl_3$) 64.75 (s); ^1H NMR ($CDCl_3$); δ=2.45 (3H, s, CH_3), 2.90 (1.5H, s, 1/2CH_3), 3.00 (1.5H, s, 1/2CH_3), 7.35 (2H, d, J=9.0 Hz, ArH), 7.85 (2H, d, J=9.0 Hz, ArH), 8.02 (0.5H, s, 1/2CHO), 9.65 (1H, bs, OH). Found: C, 39.01; H, 3.87; N, 7.23%. Calcd for $C_{9.5}H_{11.5}F_3N_{1.5}O_{3.5}S$: C, 39.11; H, 3.97; N, 7.20%.

Trifluoromethylazo Compounds **5**, **7**, *and* **9**. The reaction between 5.5 mmol of hydrazides **4**, **6**, or **8** and 11.1 mmol of **1** in 11 ml of methanol was carried out in a similar way as described above. The blue color of **1** didn't disappear even after stirring for 3 days at room temperature and 4 mmol of **1** was recovered by trap to trap separation. After removing methanol under vacuum, the residue was column-chromatographed on silica gel eluted with ether to give the normal condensation products **5**, **7**, and **9** in the yields of 97, 50, and 98%, respectively.

5: Mp 110—111 °C; IR (KBr cm^{-1}) 3150 (NH), 1680 (C=O); ^{19}F NMR (CCl_4) 67.5 (s); ^1H NMR (CCl_4); δ=7.4—8.1 (5H, m, ArH), 11.1 (1H, bs, NH). Found: C, 44.18; H, 2.83; N, 19.60%. Calcd for $C_8H_6F_3N_3O$: C, 44.25; H, 2.79; N, 19.35%

7: Mp 42—43 °C (lit,[5a] 51 °C); IR (KBr, cm^{-1}) 3110 (NH), 1715 (C=O); ^{19}F NMR (CCl_4) 67.5 (s); ^1H NMR (CCl_4) δ=2.40 (3H, s, CH_3), 11.30 (1H, bs, NH). Found: C, 23.48; H, 2.73; N, 26.80%. Calcd for $C_3H_4F_3N_3O$: C, 23.24; H, 2.60; N, 27.10%.

9: Mp 136—136.5 °C; IR (KBr, cm^{-1}) 3310 (NH), 3165 (NH), 1680 (C=O); ^{19}F NMR (CCl_4) 67.5 (s); ^1H NMR (CCl_4) δ=7.1—7.6 (5H, m, ArH), 7.8 (1H, bs, NH), 11.5 (1H, bs, NH). Found: C, 41.68; H, 3.13; N, 24.43%. Calcd for $C_8H_7F_3N_4O$: C, 41.39; H, 3.04; N, 24.13%.

The Reaction of **1** *with* p-*Toluenesulfinic Acid*. Into a flask containing a solution of 0.50 g (3.2 mmol) of *p*-toluenesulfinic acid in 6 ml of methanol, **1** was gradually introduced at room temperature till the absorption of **1** stopped. The methane **1** (0.3 g, 3 mmol) was absorbed and 20 min was needed as the reaction time. After evaporation of the solvent, the residue was column-chromatographed on silica gel using a mixture of ethyl acetate and pentane (15:85) as an eluent, giving 0.74 g (91%) of **3b**.

The Reaction of **1** *with Benzenesulfinic Acid*. Benzenesulfinic acid derived from sodium benzenesulfinate (2 hydrates) by treatment with hydrochloric acid was treated with **1** in a similar manner as described above, except that THF was used as a solvent instead of methanol. The yield of **3a** was 95%.

The Reaction of **1** *with Sodium Benzenesulfinate*. Sodium benzenesulfinate (2 hydrates) (11.1 mmol) in 10 ml of methanol was treated with **1** (11.1 mmol) in a similar manner as the case of the reaction of **1** with arenesulfonohydrazides **2**. After 3 min at room temperature, the absorption of **1** was completed. The solvent was then evaporated under vacuum. The residue was extracted with ether, washed with water, and dried with magnesium sulfate. Evaporation of ether gave an oily product, of which TLC analysis indicated that it contained at least six components. Distillation gave 1.07 g (40%) of pure **3a**. Bp 141—142 °C/1600 Pa.

N-*Trifluoromethyl*-N-*methoxyarenesulfonamides* ***10a—c***. Into a solution of **3** (4 mmol) in methyl iodide (1 ml) and DMF (7 ml), sodium carbonate (10 mmol) was added, and the mixture was stirred for 5 days at room temperature. The reaction mixture was poured into water and extracted with ether. The ether layer was dried over magnesium sulfate. Methyl ethers **10** were obtained by column chromatography on silica gel eluted with benzene. **10a**: Ar=phenyl 52%; **10c**: Ar=*o*-tolyl 33%; **10b**: Ar=*p*-tolyl 85% yield (in this case, 4.5 mmol of calcium oxide was employed instead of sodium carbonate).

10a: Liquid; IR (neat, cm^{-1}) 1392 (SO_2); ^{19}F NMR (CCl_4) 65.00 (s); ^1H NMR (CCl_4); δ=3.98 (3H, s, CH_3), 7.60 (3H, m, ArH), 7.93 (2H, d, J=8.0 Hz, ArH). Found: C, 37.62; H, 3.04; N, 5.41%. Calcd for $C_8H_8F_3NO_3S$: C, 37.65; H, 3.16; N, 5.49%.

10b: Mp 30—30.5 °C; IR (KBr, cm^{-1}) 1392 (SO_2); ^{19}F NMR (CCl_4) 65.25 (s); ^1H NMR (CCl_4); δ=2.45 (3H, s, CH_3), 3.98 (3H, s, OCH_3), 7.27 (2H, d, J=9.0 Hz, ArH), 7.75 (2H, d, J=9.0 Hz, ArH). Found: C, 39.90; H, 3.62; N, 5.12%. Calcd for $C_9H_{10}F_3NO_3S$: C, 40.15; H, 3.74; N, 5.20%.

10c: Liquid; IR (neat, cm^{-1}) 1380 (SO_2); ^{19}F NMR (CCl_4) 64.88 (s); ^1H NMR (CCl_4); δ=2.69 (3H, s, CH_3), 3.87 (3H, s, OCH_3), 7.2—7.65 (3H, m, ArH), 8.0 (1H, m, ArH). Found: C, 40.00; H, 3.61; N, 5.01%. Calcd for $C_9H_{10}F_3NO_3S$: C, 40.15; H, 3.74; N, 5.20%.

N-*Trifluoromethyl*-N-*(p-tolylsulfonyloxy)arenesulfonamides* ***11a—b***. The reaction of **3** (5 mmol) with *p*-toluenesulfonyl chloride (5 mmol) in pyridine (15 ml) were carried out for 23 h at 5 °C. The reaction mixture was treated in a similar manner as described in the preparation of **10**. Tosylates **11a** and **11b** were obtained from **3a** and **3b** in 20 and 55% yields, respectively.

11a: Mp 60—62 °C; IR (KBr, cm^{-1}) 1400 (SO_2); ^{19}F NMR ($CDCl_3$) 62.63 (s); ^1H NMR ($CDCl_3$); δ=2.47 (3H, s, CH_3), 7.3—8.0 (9H, m, ArH). Found: C, 42.14; H, 3.06; N, 3.41%. Calcd for $C_{14}H_{12}F_3NO_5S_2$: C, 42.53; H, 3.06; N, 3.54%.

11b: Mp 110—111 °C; IR (KBr, cm^{-1}) 1400 (SO_2); ^{19}F NMR ($CDCl_3$) 62.50 (s); ^1H NMR ($CDCl_3$); δ=2.45 (6H, s, 2×CH_3), 7.2—8.0 (8H, m, ArH). Found: C, 44.16; H, 3.54, N, 3.42%. Calcd for $C_{15}H_{14}F_3NO_5S_2$: C, 44.01; H, 3.45; N, 3.42%.

References

1) a) R. N. Haszeldine, *J. Chem. Soc.*, **1953**, 2075; b) J. Jander and R. N. Haszeldine, *J. Chem. Soc.*, **1954**, 912.

2) S. P. Makarov, A. S. Filatov, and A. Ya. Yakubovich, *Zh. Obsh. Khim.*, **37**, 158 (1967).

3) a) A. H. Dinwoodie and R. N. Haszeldine, *J. Chem. Soc.*, **1965**, 2266; b) A. S. Filatov, S. P. Makarov, and A. Ya. Yakubovich, *Zh. Obsh. Khim.*, **37**, 837 (1967); c) P. Gölitz and A. de Meijere, *Angew. Chem. Int. Ed. Engl.*, **16**, 854 (1977).

4) V. A. Ginsburg and M. N. Vasil'eva, *Zh. Org. Khim.*, **9**, 2028 (1973).

5) a) S. P. Makarov, A. Ya. Yakubovich, V. A. Ginsburg, A. S. Filatov, M. A. Englin, N. F. Privezentseva, and T. Ya. Nikiforova, *Dokl. Akad. Nauk SSSR* **141**, 357 (1961); C. A. 11425g (1962); b) S. P. Makarov, A. Ya. Yakubovich, A. S. Filatov, M. A. Englin, and T. Ya. Nikiforova, *Zh. Obsh. Khim.*, **38**, 709 (1968); c) T. Umemoto and O. Miyano, *J. Fluorine Chem.*, **22**, 91 (1983); d) T. Umemoto and O. Miyano, *Tetrahedron Lett.*, **23**, 3929 (1982); e) U. Hartkopf and A. de Meijere, *Angew. Chem. Int. Ed. Engl.*, **21**, 443 (1982).

6) A. Sekiya and T. Umemoto, *Chem. Lett.*, **1982**, 1519.

7) a) L. F. Fieser and M. Fieser, "Reagents for Organic Synthesis," John Wiley and Sons, Inc., New York (1967), Vol. 1, pp. 1185—1186; b) A. M. Van Leusen, B. E. Hoogenboom, and H. Siderius, *Tetrahedron Lett.*, **1972**, 2369.

8) T. Umemoto and H. Tsutsumi, *Bull. Chem. Soc. Jpn.*, **56**, 631 (1983).

Mechanism of Dipeptidyl Carboxypeptidase Activity of Thermolysin

Mitsuhiro FUKUDA* and Shigeru KUNUGI†
Department of Polymer Chemistry, Kyoto University, Sakyo-ku, Kyoto 606
†*Department of Applied Chemistry, Fukui University, Bunkyo, Fukui 910*
(Received May 18, 1984)

Steady state and presteady state kinetic analyses were performed for thermolysin-catalyzed hydrolysis of chromophoric tripeptide substrates with free carboxyl terminal. The pH dependence of k_{cat} showed fairly higher pK_a (≃7) than that of the second-order rate parameter(k_{cat}/K_m)(≃5) and the pH-dependence of K_m resembled that of K_i for *N*-blocked dipeptidyl inhibitor observed before (S. Kunugi *et al.*, *Eur. J. Biochem.* **124**, 157 (1982)). These findings indicated that the reaction with this type of substrate involves a nonproductive binding mode. In a presteady state kinetic study by stopped-flow method, a burst process of 10—20 ms order was observed before the linear steady state at a relatively low pH and temperature. This process showed moderate pH dependence. Considering these experimental results coupled with those accumulated so far on this enzyme, a unified mechanism including a nonproductive binding and an isomerization process in prior to the cleavage of the peptide bond was proposed for the dipeptidyl carboxypeptidase activity of this enzyme.

Thermolysin is a microbial thermostable zinc-containing protease.[1] This enzyme shows no exo-activity. Dipeptides or *N*-blocked amino acids act as inhibitors.[2] It shows, however, dipeptidyl carboxypeptidase activity towards certain *N*-blocked peptides with free carboxyl terminal, such as *N*-(benzyloxycarbonyl)glycyl-L-leucyl-L-leucine (ZGlyLeuLeu), *N*-benzyloxycarbonyl-L-phenylalanylglycyl-L-leucyl-L-alanine (ZPheGlyLeuAla)[3] and 3-(2-furyl)acrylolglycyl-L-leucyl-L-alanine (FuaGlyLeuAla).[4] The K_m values of thermolysin against several synthetic peptides are relatively high: that for 3-(2-furyl)acryloylglycyl-L-leucinamide (FuaGlyLeuNH_2) or 3-(2-furyl)acryloylglycyl-L-phenylalaninamide (FuaGlyPheNH_2), widely used for the assay of the activity of this enzyme, is around 0.5 mM (1M=1 mol dm^{-3}) at acidic pH and 5 mM at neutral pH.[5] These low affinities limited detailed kinetic analysis of the catalytic reactions. Analysis of the presteady state in this enzyme reaction was performed only for special tripeptide or pentapeptide substrates having fluorescent acyl group[6,7] and thorough discussions of the reaction processes have not been given as yet.

In the research on the interaction of various substrate analogues with several zinc-containing proteases[5,8,9] we noticed that the C-free amino acid or dipeptide inhibited these enzymes very strongly at acidic pH and showed very steep pH dependences. An X-ray crystallographic study by Kester *et al.*[10] showed that an anionic inhibitors of this type binds on the active site of thermolysin in an inversed manner with the carboxylate directly coordinating on the active site zinc, which is to have strong relation with the peculiar pH dependence of the inhibition. Such a binding mode could be common in the case of the substrates having free carboxyl end, such as *N*-acylated tripeptides. Thus we report here results of detailed steady-state kinetic analysis of the hydrolysis of 3-(2-furyl)acryloyl tripeptide substrates catalyzed by thermolysin, as well as the observation of the presteady state process of the reaction and discuss the mechanisms of the dipeptidyl carboxypeptidase activity of this enzyme.

Experimental

Materials. Thermolysin was obtained from Daiwa Kasei (Osaka), (lot. T8CA81), and its active concentration was determined as described previously.[5] Four chromophoric substrates, 3-(2-furyl)acryloylglycyl-L-phenylalanyl-L-alanine (FuaGlyPheAla), FuaGlyLeuAla, FuaGlyPheNH_2 and FuaGlyLeuNH_2 were the same samples as used in the previous studies.[5,9] Good's buffers (Mes and Hepes) were purchased from Dojindo Laboratories (Kumamoto). Other chemicals were of reagent grade and used without further purifications. Deionized and distilled water was used in the present work.

Methods. The steady-state kinetics were followed by an ultraviolet/visible spectrophotometer (Union SM401, Union Giken, Hirakata). The difference spectrum between the chromophoric substrate(FuaGlyPheAla) and the products (FuaGly and PheAla) was referred to in the previous paper.[9]

The second-order rate constant (k_{cat}/K_m) was obtained from the initial velocity of the pseudo-first order rate at a low substrate concentration. The k_{cat} and K_m values were evaluated from Eadie-type plot of the velocities at various substrate concentrations. At lower pH the K_m for FuaGlyPheAla was so low that its concentration could not be reduced enough to evaluate K_m and k_{cat}/K_m. In such a case, the velocity devided by initial enzyme concentration at saturated substrate condition ([S]>0.3 mM) was considered as the k_{cat} (for details see result). The reactions were studied in 0.1 M buffer solution containing 0.01 M $CaCl_2$ unless otherwise mentioned.

The presteady state of the reaction was measured on a stopped-flow spectrophotometer (Union RA1100, Union Giken, Hirakata). The dead-time of this apparatus attached with a 10 mm cell has been determined as 3.0 ms.[11] The strong back ground absorbance of the substrate at high concentration limited observation at wavelengths higher than 330 nm. The temperature of the solution was controlled by circulating thermostated water (Neslab RTE-8) through the cell compartments of the spectrophotometers and occasionally checked with a thermister(±0.1 °C).

Results and Discussion

Steady State Kinetics. In Fig. 1, the pH dependences of k_{cat}/K_m, k_{cat}, and K_m[12] for FuaGlyPheAla are shown. At pH lower than 6, where the K_m becomes very low, we show only the apparent second-order rate constant at $[S]_0$=10 μM (which is the lowest concentration to get a reliable rate) in Fig. 1-a, the rate constant at $[S]_0$>0.3 mM in Fig. 1-b and the ratio of the above two quantities in Fig. 1-c. In Fig. 1-a the left half of

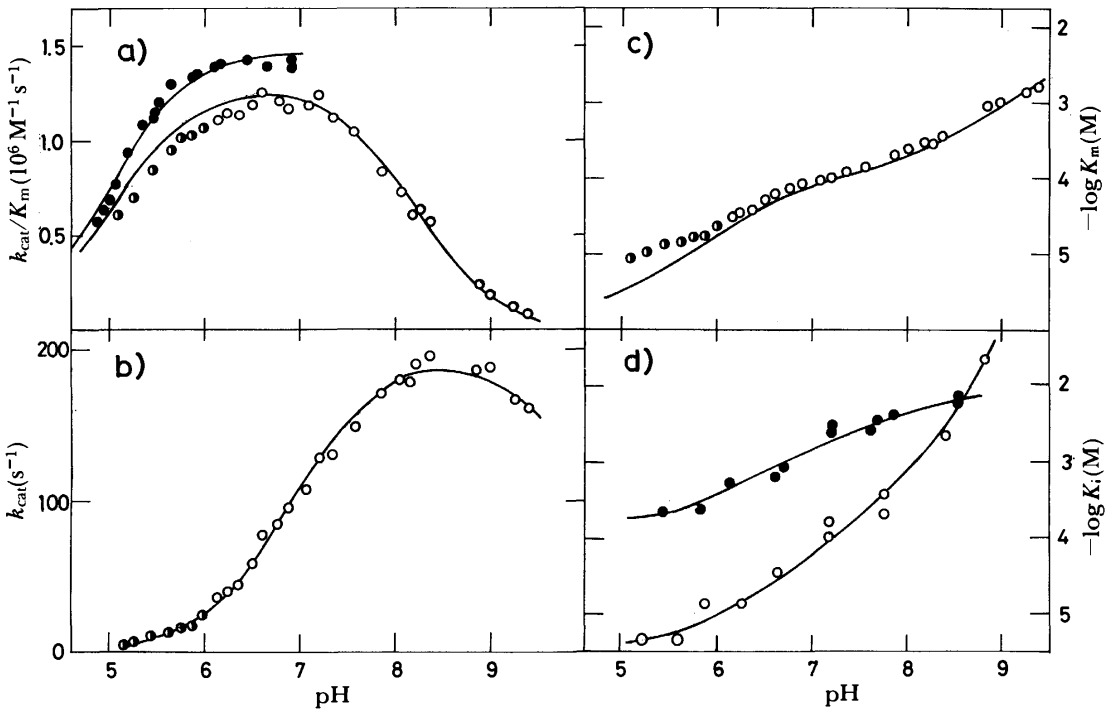

Fig. 1. pH-dependence of k_{cat}/K_m, k_{cat}, and K_m for FuaGlyPheAla and FuaGlyLeuAla at 25°C.
a) k_{cat}/K_m (○, ◑) FuaGlyPheAla; (●) FuaGlyLeuAla. ○, obtained from Eadie plot; ◑, ● rate at [substrate]=10 μM. b) k_{cat} for FuaGlyPheAla. (○) obtained from Eadie-plot with [substrate]=20 μM–2 mM; (◑) velocity at [substrate]>0.3 mM. c) K_m for FuaGlyPheAla. (○) from Eadie-plot; (◑) ratio of velocity at [substrate]=10 μM to that at [substrate]>0.3 mM. Due to the insufficiently low concentration of the substrate for the determination of k_{cat}/K_m, K_m data deviated downward from the curve calculated on the pK_1 obtained from FuaGlyLeuAla especially at low pH. d) pH dependence of two inhibitors for comparison. (○) ZPhe; (●) ZLeuGly. Both are taken from Ref. 5.

the pH profile of the second-order rate for FuaGly-LeuAla at $[S]_0=10\,\mu M$, which satisfies the condition of $[S] \ll K_m$ for this substrate, was also given. The pH dependence is apparently explained by assuming two pK_a's (pK_{a1} for the lower side and pK_{a2} for the higher side) and one limiting rate constant. The pK_{a1} was evaluated from the data of FuaGlyLeuAla to be 5.00 ± 0.03 and pK_{a2} was from those of FuaGlyPheAla as 8.18 ± 0.02, both of which are consistent to the values obtained for the neutral dipeptide substrates, FuaGly-PheNH$_2$ and FuaGlyLeuNH$_2$.[5] Compared with this pK_{a1}, the pH profile of k_{cat} value gave a high apparent pK_a. Accordingly K_m showed a very characteristic pH dependence, the value being approximately proportional to the 1/2 power of $[H^+]$. This resembles the pH dependence of the K_i of dipeptide substrate analogue[5] (Fig. 1-d, ●).

In the study of the pH dependence of K_i of *C-free N-benzyloxycarbonyl amino acids*, such as ZPhe and ZLeu,[5] it was made clear that these inhibitors are bound only to the enzyme form which is protonated at catalytic site with the carboxylato group coordinating on the active site zinc and they show a very strong pH dependence of K_i as an example given in Fig. 1-d, (○ for ZPhe). This result was formally represented by Scheme 1, where the cationic form of the enzyme is written as EH_2. K_n's and K_I^* denote the proton dissociation constants and the dissociation constant for the inhibitor(I)-enzyme complex, respectively. The pH profile for *dipeptide inhibitor* (● for ZLeuGly) is, as well, explained by Scheme 2, where two binding modes are assumed. A K_I/K_I^* ratio of 22 gave a satisfactory curve as fitted to the data in Fig. 1-d.

Based on these schemes, the presently observed pH dependence of K_m of the *tripeptide substrates* can be explained by Scheme 3, where S written in the left-hand side of E (SEH_2) indicates that the substrate is bound on the active site in a different manner. That is, this type of substrate can be bound on the enzyme

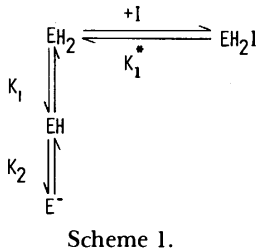

Scheme 1.

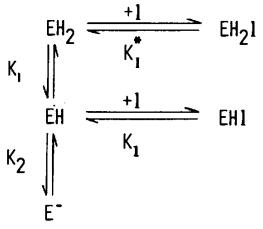

Scheme 2.

active site in two different manners. The one is a normal (productive) mode (K_s) in which the carbonyl carbon of the scissile bond is located on the zinc and the amino acid side residues are located in their respective subsites.[10] The other (K_S^*) is considered similar to that seen in C-free *N*-blocked amino acids and the terminal carboxylate is coordinating on the zinc. In the kinetic formula, however, this scheme is identical with the one given for Scheme 4, where $1/K_3^* = 1/K_3 + K_S/K_S^*/K_1$. A nonlinear regression of the data in Fig. 1 gave the parameters for Scheme 4 as: $pK_1 = 5.3 \pm 0.1$, $pK_2 = 8.2 \pm 0.02$, $pK_3^* = 6.9 \pm 0.05$, $pK_4 = 10.0 \pm 0.1$. Insufficiently low concentration of FuaGlyPheAla gave slightly higher pK_1 for this substrate than the intrinsic value(5.0).[5] The solid curves in Fig. 1 are reconstituted on these parameters. When we *a priori* assume that the pK_a for the protonation of the productive enzyme-susbtrate complex is not so much different from that of the free enzyme, then we get the K_S/K_S^* ratio around $10-10^2$, which is not inconsistent to the value evaluated in Fig. 1-d.

Presteady State Kinetics. Mixing FuaGlyPheAla with the enzyme in a stopped-flow apparatus, we observed the reaction traces as shown in Fig. 2. A presteady state relaxation process was observed before the steady state linear decrease in absorbance. To get clearer traces the temperature was lowered. The relevant parameters under some experimental conditions are summarized in Table 1. The inverse of the observed relaxation time of the presteady part is k_{burst} and the difference in the optical density during this burst process, which is obtained by an extrapolation of the steady state linear portion to time zero with consideration of the dead time of the apparatus, is the burst amplitude (ΔOD_{burst}). The steady state parameters obtained under this stopped-flow conditions ($v_{steady}/[E]_0$) were consistent with those measured by the conventional method. The strong background absorbance due to the substrate of higher concentrations, the small absorbance change accompanied by the large change of the steady state, and the rapidness of the process, all of these unfortunately limited the conditions and the accuracy of the observation of the presteady state process, but we can point the following features for the process detected here.

1) The apparent rate slowly increased with an increase in the substrate concentration,

2) it increased only 2.5 times by an increase in the pH from 5.3 to 6.75, and,

3) the burst amplitude did not strongly depend on the substrate concentration or pH of the solution, at least within the range studied here.

By this observation of the presteady process we must modify the reaction Scheme of 4 or 3 into what allows the existence of a certain burst process. Morgan and Frouton observed a presteady process in thermolysin catalysis of the hydrolyis of fluorescent tripeptide or pentapeptide substrate[6] and explained the process as the binding of the substrate, having k_{bind} of 3×10^6 $M^{-1}s^{-1}$ and $k_{dissociate}$ of $55\,s^{-1}$ at 25 °C and pH 8.5. Lobb

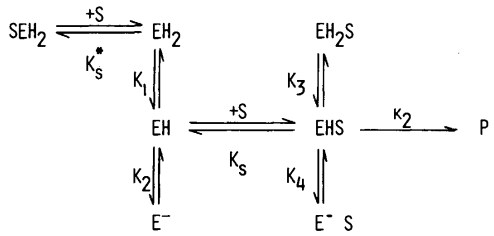

Scheme 3.

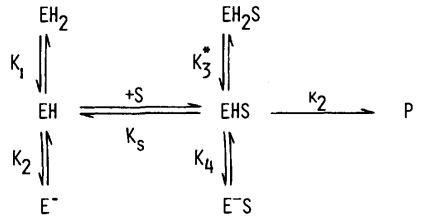

Scheme 4.

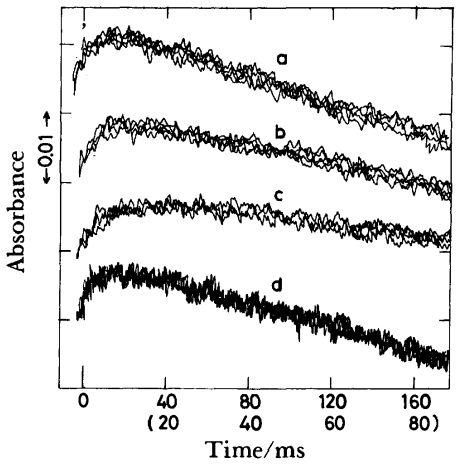

Fig. 2. Stopped-flow traces of the burst process observed in the hydrolysis of FuaGlyPheAla. Ordinate scale is 0.01 OD/scale.

	Temp. (°C)	pH	[S]o mM	[E]o μM	abscissa scale(ms)
a)	25.0	5.35	0.1	10.1	40
b)	15.5	5.35	0.1	10.1	40
c)	7.5	5.35	0.1	10.1	40
d)	7.7	6.75	0.09	10.7	20

Table 1. Parameters of the burst process of thermolysin catalysed hydrolysis of FuaGlyPheAla

pH	Temp °C	[S]o mM	[E]o μM	ΔOD_{burst} $10^{-3}\,cm^{-1}$	k_{burst} s^{-1}	$v_{steady}/[E]_0$ s^{-1}
5.35	25.0	0.1	10.1	7	100	6.3
5.35	15.5	0.1	10.1	8	100	4.2
5.35	7.5	0.1	10.1	6	50	3.6
5.35	7.5	0.05	10.1	7	38	3.1
5.35	7.5	0.2	10.1	6	65	4.1
6.75	7.7	0.09	10.7	10	180	11.5

and Auld also observed a similar presteady state process for a *N*-dansylated tripeptide and an apparent rate constant was $50\,s^{-1}$ at 15 °C, pH 6.0 and [substrate] $=0.045\,mM$.[7] If the presently observed burst process was the binding of the substrate, then k_{bind} would be calculated as around $2\times10^5\,M^{-1}s^{-1}$ and $k_{dissociate}$ around $30\,s^{-1}$. The former one is considerably small for a molecular complex formation process, even at a reduced temperature.[14] Furthermore in the case of chromophoric substrate such as the present one, binding on the enzyme active site generally results in a far smaller difference spectrum than the fluorescent one, as was exemplified for the Fua-substituted amino acid ester bound on α-chymotrypsin, where the difference extinction coefficient was less than a few hundreds.[14] The positive concentration dependence of the inverse of the relaxation time will discourage the possibility that the observed process is the conformational change of the enzyme protein prior to the binding of the substrate on it. Therefore we would like to conclude that the presently observed burst process is an isomerisation subsequent to the substrate binding. Since the observed process is clearly an upward change in the absorbance, it is neither due to a mere time lag of the final product appearance (see Appendix).

Possible Reaction Mechanism. The first possible and simplest mechanism we can postulate is such as Scheme 5. This scheme qualitatively explains the pH independence of the burst amplitude, by assuming that both EHS′ and EH_2S' have (positive) difference extinction coefficients against free substrate, and also the pH dependences of steady state parameters. It cannot, however, explain the moderate pH dependence of the burst rate in the measured pH range. There could be, of course, a number of possible reaction schemes, which explain all of these quantities, when several reaction processes and kinetic parameters are assumed. The simplest and most reasonable one which is consistent to the present data is that given in Scheme 6, containing the second pathway from EH_2S to EH_2S'.

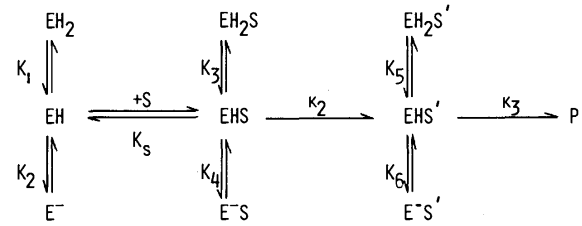

Scheme 5.

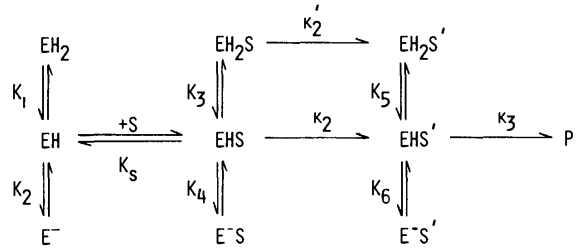

Scheme 6.

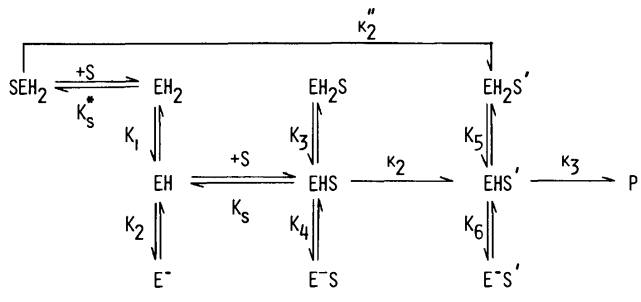

Scheme 7.

In contrast to the precise data regression for the steady state result in the former section, the limited number and rather high deviations of the presteady state data provided us only a semi-quantitative parametrization of the Scheme, and the calculated pH dependences of the several quantities from Scheme 6 are given in Fig. 3 for a plausible set of the parameters. In analogy to the relation of Scheme 3 and 4, Scheme 6 is formally equivalent to the reaction mechanism of Scheme 7, where the nonproductively bound substrate, as postulated in the steady state analysis, has a route to be converted to the productive mode and the actual reaction is likely to occur by such a mechanism. At relatively low pH the second route becomes important.

Then the problem is the molecular description of the EHS′ intermediate. Regarding several discussions so far given on the mechanism of zinc-containing proteases, at least three possibilities are to be considered;

1) conversion of the noncovalently bound substrate-enzyme complex to an intermediate covalently attached to the enzyme (such as acid anhydride acylenzyme),[15-17] 2) formation of the tetrahedral intermediate on the carbonyl carbon of the scissile bond, and 3) a conformational transition of the enzyme

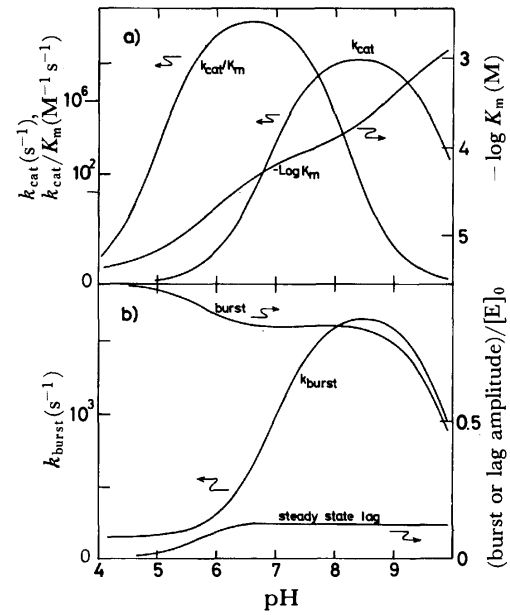

Fig. 3. Simulation of the pH dependences of several quantities at saturated substrate level calculated on the basis of the reaction Scheme 6 with following parameters, which are considered most plausible for the hydrolysis of FuaGlyPheAla at 25 °C.
$pK_1=5$, $pK_2=8.2$, $pK_3=7$, $pK_4=10$, $pK_5=6.8$, $pK_6=10$, $K_s=0.001$ M, $k_2=1500\,s^{-1}$, $k_{2'}=150\,s^{-1}$, $k_3=250\,s^{-1}$. (a) k_{cat}/K_m, k_{cat}, and K_m (b) k_{burst}, burst and the steady state lag.
Burst amplitude and lag are normalized to $[E]_0$ value.

protein or 3') that of the substrate.

The positive absorbance change due to the burst process will discourage reduction of the process to a purely conformational change of the protein. A change in the absorbance of the Fua-modified substrate due to the formation of an acyl intermediate have been observed in the case of serine proteases such as α-chymotrypsin[18] and trypsin[19] and have provided fruitful analyses of the presteady state kinetics for these enzymes. In those instances the difference extinction coefficients($\Delta\varepsilon$) of the acyl intermediate against the free substrate were around 3000—3500($M^{-1}cm^{-1}$) at 330nm and ≈3000 ($M^{-1}cm^{-1}$) at 335nm.[14] When we apply the reaction scheme 6 or 7 to the presently observed burst amplitude, the expected $\Delta\varepsilon_{335}$ values is calculated as only around 1000 ($M^{-1}cm^{-1}$) at saturated substrate concentration (see Appendix). Furthermore the k_{burst} expected at very large substrate concentration would be around $200\,s^{-1}$ at pH 6.75 and 7.5 °C and $>100\,s^{-1}$ at pH 5.15 and 25 °C. That at optimum conditions would be near $1000\,s^{-1}$, which is considerably large for an acyl transfer step from a peptide substrate. Even the rate constant for the acyl transfer from the ester to Glu270 of carboxypeptidase A under similar conditions[16] was estimated in the order of $10^1\,s^{-1}$ and the highest $k_{acylation}$ value observed for the acylation of Ser-195 of α-chymotrypsin[13] by normal alkyl ester of amino acid was no more than $10^3\,s^{-1}$.

On the basis of the temperature dependence of the pK_a values controlling the second-order rate constant of thermolysin catalysis and several experimental data given by other investigators,[10,20] we proposed the general-base mechanism including the zinc-coordinated water molecule for this enzyme. Recent X-ray studies on inhibitor or interaction with thermolysin also ruled out the anhydride mechanism.[21] Considering all these, the observed burst process is to be related to the possibility 2) or 3'). As for the hydrolysis of Fua-TrpNH$_2$ by α-chymotrypsin, Hess's group observed some presteady state process by using a temperature jump and stopped flow apparatus.[22] The k_{burst} was $31\,s^{-1}$ at pH 6.7 and 15 °C and the authors speculated that the observed intermediate is the tetrahedral intermdiate accumulated during the acylation reaction, since the acylation step is the rate limiting in the overall hydrolytic reaction of amide substrate catalyzed by this enzyme. Also in the cases of thermolysin and carboxypeptidase A, the general-base reaction can proceed *via* such an intermediate and for the specific substrates the accumulated amount of the intermediate could be significant.

On the other hand, Lipscomb[23] and Clealand[13] have postulated that in the carboxypeptidase A catalyzed hydrolysis of peptide the entry of the C-terminal residue into its subsite which places the carboxylato group on Arg145 and causes a strain in the peptide bond of the substrate, is rate-limiting. Though there is no evidently working electrostatic interaction in the case of thermolysin and the substrate binding force is mainly hydrophobic, the reactivity of the enzyme-bound substrate may also be raised by forcing the peptide bond to have a strained structure and to increase proton-acceptability of the imino group;[24] geometric destabilization, just we have seen in the α-chymotrypsin-catalyzed hydrolysis of activated peptide-model compounds.[25] In the case of thermolysin the destablization process might not be so slow to limit the overall reaction but it might limit the presteady process. The absorbance of the bound substrate could be altered with breakage of the resonance structure along the peptide bond to provide an observable burst process.

Though we cannot conclusively discriminate the two possibilities[26] given above, an isomerization process of the enzyme-bound substrate was observed as a presteady state process in the hydrolysis of tripeptide substrate and especially at lower pH, the conversion from the nonproductively (inversely) bound substrate to a productive one might be significant to this burst process.

Appendix

When we assume the reaction mechanism of Scheme 6, the time dependences of EHS'+EH$_2$S' and P are given as follows;

$$[EHS'+EH_2S'] = (C_1/C_2)(1-\exp(-C_2t))(1+[H^+]/K_6), \quad (1)$$

$$[P] = k_3(C_1/C_2)t + k_3(C_1/C_2^2)(\exp(-C_2t)-1), \quad (2)$$

where

$$C_1 = (k_2+k_2'[H^+]/K_4)[E]_o/(A(1+[H^+]/K_6))$$

$$C_2 = (k_2+k_2'[H^+]/K_4)(1+[H^+]/K_6+K_5/[H^+])/(A(1+[H^+]/K_6))+k_3/(1+[H^+]/K_6)$$

$$A = 1+[H^+]/K_4+K_3/[H^+]+(1+[H^+]/K_2+K_1/[H^+])K_5/[S]_o.$$

The first term of Eq. 2 corresponds to the steady state change and the second term is the burst process. Assuming that the amount of ES is very small and stationary, the observed change in optical density is written

$$\Delta OD(t) = \Delta\varepsilon_{EHS'}[EHS'] + \Delta\varepsilon_{EH_2S}[EH_2S'] + \Delta\varepsilon_P[P]. \quad (3)$$

If the extinction coefficients of EHS' and EH$_2$S' can be considered equal($\Delta\varepsilon_x$), then Eq. 3 is reduced to

$$\Delta OD(t) = \Delta\varepsilon_x[EHS'](1+[H^+]/K_6) + \Delta\varepsilon_P[P]. \quad (4)$$

The change in the optical density as given in Fig. 2 means $\Delta\varepsilon_x>0$ and $\Delta\varepsilon_P<0$. $\Delta\varepsilon_P$ at 335 nm was evaluated as −1540 at 25 °C pH 5.35. The burst amplitude(ΔOD_{burst}), which is obtained experimentally by an extrapolation of the steady-state part to time zero, is derived from Eqs. 1, 2, and 4 as

$$\Delta OD_{burst} = \Delta\varepsilon_x(1+[H^+]/K_6)C_1/C_2 - \Delta\varepsilon_P k_3 C_1/C_2^2, \quad (5)$$

where the first term is from the formation of the intermediate(s) and the second term is due to the lag period of the product formation. According to Scheme 6, the amount of the intermediates formed at saturated substrate concentration becomes 90% of the total enzyme at acidic to neutral pH (Fig. 3) and therefore the fact that the burst amplitude(in O.D.) observed at saturated substrate concentration was the order of 0.01 at the present enzyme concentration means that the difference extinction coefficient of the intermediate is around 1000($M^{-1}cm^{-1}$).

We gratefully acknowledge Professor Norio Ise, Kyoto University, for his advice and encouragement throughout the work.

References

1) S. Endo, *J. Ferment. Technol.* **40**, 346 (1961).
2) J. Feder, L. R. Brougham, and B. S. Wildi, *Biochemistry*, **13**, 1186 (1974).
3) K. Morihara and H. Tsuzuki, *Eur. J. Biochem.*, **15**, 374 (1970).
4) S. Blumberg and B. L. Vallee, *Biochemistry*, **14**, 2410 (1975).
5) S. Kunugi, H. Hirohara, and N. Ise, *Eur. J. Biochem.*, **124**, 157 (1982).
6) G. Morgan and J. S. Frouton, *Biochemistry*, **17**, 3562 (1978).
7) R. R. Lobb and D. S. Auld, *Proc. Natl. Acad. Sci. U.S.A*, **76**, 2684 (1979).
8) M. Fukuda, S. Kunugi, and N. Ise, *Bull. Chem. Soc. Jpn.*, **56**, 3308 (1983).
9) M. Fukuda and S. Kunugi, *Eur. J. Biochem.*, **142**, 565 (1984).
10) W. R. Kester and B. W. Matthews, *Biochemistry*, **16**, 2506 (1977).
11) S. Kunugi, Ph. D Thesis for Kyoto University (1978).
12) Among the three parameters of k_{cat}/K_m, k_{cat}, and K_m, K_m, was claimed to be nothing more than a ratio of the former two and has no significant meaning.[13] However to be compared with the parameters such as K_i, which is a useful measure of the affinity of the substrate analogues toward the enzyme, K_m is still an important parameter.
13) W. W. Cleland, *Adv. Enzymol.* **45**, 273 (1977).
14) S. Kunugi, H. Hirohara, and N. Ise, *J. Amer. Chem. Soc.*,**101**, 3640 (1979).
15) B. Holmquist and B. L. Vallee, *Biochemistry*, **15**, 101 (1976).
16) M. W. Makinen, L. C. Kuo, J. J. Dymowski, and S. Jaffers, *J. Biol. Chem.*, **254**, 350 (1979).
17) L. C. Kuo and M. W. Makinen, *J. Biol. Chem.*, **257**, 24 (1982).
18) C. G. Miller and M. L. Bender, *J. Amer. Chem. Soc.*, **90**, 6850 (1968).
19) S. A. Bernhard, "The structure and function of Enzymes", W. A. Benjamin Inc., New York, N. Y. (1968) Chap. 8.
20) R. Breslow and D. L. Wernick, *J. Amer. Chem. Soc.*, **98**, 259 (1976); R. Breslow and D. L. Wernick, *Proc. Natl. Acad. Sci. U.S.A*, **74**, 1303 (1977).
21) M. A. Holmes and B. W. Matthews, *Biochemistry*, **20**, 6912 (1981); M. A. Holmes, D. E. Tronrad and B. W. Matthews, *Biochemistry*, **22**, 236 (1983).
22) G. P. Hess, J. McConn, E. Ku, and G. McConkey, *Phil. Trans. Roy. Soc. London*, **B257**, 89 (1970); G. P. Hess, "The Enzymes, vol. 3," 3rd. ed, ed by P. D. Boyer., Academic Press, New York, N.Y. (1971) Chap. 7.
23) W. N. Lipscomb, *Proc. Natl. Acad. Sci., U.S.A*, **77**, 3875 (1980); D. G. Rees and W. N. Lipscomb, *ibid.*, **78**, 5455 (1981).
24) W. P. Jencks, *Adv. Enzymol.*, **43**, 219 (1975).
25) K. Ikeda and S. Kunugi, *J. Biochem.*, **88**, 977 (1980).
26) In either case of tetrahedral intermediate or strained peptide bond, an apparent difficulty of the mechanism of Scheme 6 or scheme 7 is in the observed similarity in the pH dependence and the magnitude of K_i of the several inhibitors with those of K_m of the substrate. However, in many substrate-analogues, inhibition of the hydrolysis of the chromophoric substrate is as the result of the very slow reaction of the nonchromophoric substrate (considered as inhibitor) and therefore the evaluation of the K_i values always include the contribution from the (small fraction of) further reacting intermediate such as EHS'. Furthermore the significant contribution of inversely bound substrate is limited at lower pH. Therefore the discussion on the binding step of this enzyme in the previous paper[9] based on the pressure dependence of K_m is not influenced by the present finding of the presteady state process.

 © 1984 The Chemical Society of Japan Bull. Chem. Soc. Jpn., 57, 2971—2975 (1984)

400 MHz Proton Nuclear Magnetic Resonance Study of Magydardienediol, a Diterpene from *Magydaris panacifolia*

Hajime NAGANO,* Motoo TORI,† Michio SHIOTA, and Joaquín DE PASCUAL TERESA††
Department of Chemistry, Faculty of Science, Ochanomizu University, Otsuka, Bunkyo-ku, Tokyo 112
†*Faculty of Pharmaceutical Sciences, Tokushima Bunri University, Yamashiro-cho, Tokushima 770*
††*Departamento de Química Orgánica, Facultad de Química, Universidad de Salamanca, Spain*
(Received May 18, 1984)

A detailed analysis of the 400 MHz ^{1}H-NMR spectrum of magydardienediol (**1**), a diterpene isolated from *Magydaris panacifolia* (Vahl) Lange, has been performed by use of a combination of proton homonuclear spin decoupling, COSY, NOE difference, and NOESY techniques. This ^{1}H-NMR spectral analysis, in conjunction with the mass spectral analysis of some derivatives of **1**, revealed that the structure of **1** should be revised to *t*-6-hydroxymethyl-1,*t*-3-dimethyl-*t*-2-(3-methyl-2-butenyl)-3-(4-methyl-3-pentenyl)-*r*-1-cyclohexanol.

Magydardienediol, magydartrienol, and magydartrienyl acetate[1] are diterpenes isolated from *Magydaris panacifolia* (Vahl) Lange (Umbelliferae) and have been formulated as **2**, **3**, and **4**, respectively.[2] Recently, it was found that the ^{1}H-NMR spectral data of the diastereomers with structure **3** prepared from α-santonin were different from those reported for magydartrienol.[3] This finding prompted us to reinvestigate the structures of these natural diterpenes.[4]

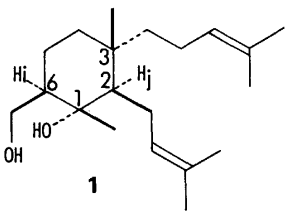

1

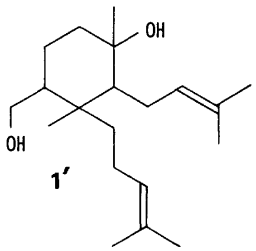

1′

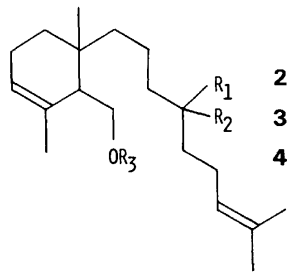

2 $R_1 = CH_3$ $R_2 = OH$ $R_3 = H$
3 $R_1, R_2 = CH_2$ $R_3 = H$
4 $R_1, R_2 = CH_2$ $R_3 = COCH_3$

We now wish to present a detailed analysis of the 400 MHz ^{1}H-NMR spectrum of magydardienediol (**1**) (Fig. 1) by use of a combination of ^{1}H-NMR spectroscopic techniques, *i.e.* proton homonuclear spin decoupling, two-dimensional proton-proton correlation (COSY)[5] (Fig. 3), NOE difference (Figs. 5 and 6), and two-dimensional NOE (NOESY)[6] (Fig. 7) spectroscopies, together with the mass spectral fragmentations of some derivatives of **1**. This spectral analysis showed unequivocally that the structure of magydardienediol should be revised to *t*-6-hydroxymethyl-1,*t*-3-dimethyl-*t*-2-(3-methyl-2-butenyl)-3-(4-methyl-3-pentenyl)-*r*-1-cyclohexanol (**1**),[7] and corroborated the structural revision of this diterpene preliminarily reported very recently by one of us and his associates.[8]

Magydardienediol (**1**), mp 55—56 °C (from hexane); $[\alpha]_D^{24}$ +24.0° (*c* 1.2, $CHCl_3$); EI-MS (*m/z* 308.2705. Calcd for $C_{20}H_{36}O_2$: M^+, *m/z* 308.2714); ^{13}C-NMR (see Experimental), is a monocyclic diterpene posessing two trisubstituted double bonds and two hydroxyl groups (one primary and one tertiary).[2] Its ^{1}H-NMR spectrum at 400 MHz (Fig. 1) showed distinctly four olefinic methyl peaks at δ 1.71, 1.70, 1.68, and 1.60; this indicated that the structure of **1** was quite different from that reported previously.[2]

It was found firstly that **1** had partial structures **A**, **B**, and **C**, along with two tertiary methyls (partial structures **D** and **E**), by the proton homonuclear spin decoupling experiments in conjunction with the COSY analysis (Fig. 2).

Partial structure **A**. The resonances at δ 2.30 (H_e) and δ 2.05 (H_f) were assigned to the two nonequivalent allylic methylene protons spin-coupled to the olefinic proton observed at δ 5.30 (H_a). Although the methine proton H_j signal at δ 1.59 (dd, J=8.5 and 3 Hz) was partially (one of the four-lines) overlapped by the olefinic methyl peak (δ 1.60), the cross peaks, H_e—H_j, in the COSY spectrum (Fig. 3) indicated unambiguously the vicinal spin couplings between these protons. The methine group (CH_j) had two quaternary carbon neighbors, because the irradiation at δ 1.59 (H_j) changed only the signals at δ 2.30 (H_e) and 2.05 (H_f).[9] Long-range spin couplings were observed between H_a and the olefinic methyls (δ 1.71 and 1.70) in both the decoupling and the COSY experiments. The broader peak at δ 1.70 was assigned to the olefinic methyl *cis* to H_a by analogy with the preceding examples[10] and also by the NOESY spectrum.

Partial structure **B**. Another spin system $(CH_3)_2C=CH_bCH_gH_h$ was identified by spin decoupling. The methylene protons (H_n and H_o) hidden among other multiplets were revealed by irradiation of the equivalent allylic methylene protons (H_g and H_h, δ 1.91) and analysis of the COSY spectrum (Fig. 3). The multiplicities of H_n (δ 1.32, d, J=15 Hz) and H_o (δ 1.21, d,J=15 Hz) in the spin decoupled spectrum showed that the methylene group (CH_nH_o) was connected to a quaternary carbon atom.

Partial structure **C**. The starting point in the analysis of this spin system was the two nonequivalent methylene protons, (H_c, δ 3.78) and (H_d (δ 3.50), of the hydroxymethyl group. For this analysis the COSY spectrum (Fig. 3) was very efficient and the spin network $HOCH_2CHCH_2CH_2$ was deduced as the sole spin system consistent with the observation of the cross peaks, H_c-H_d, H_c-H_i, H_d-H_i, H_i-H_p, H_p-H_k, H_p-H_m, H_p-H_l, H_k-H_l, and H_k-H_m, Extensive decoupling

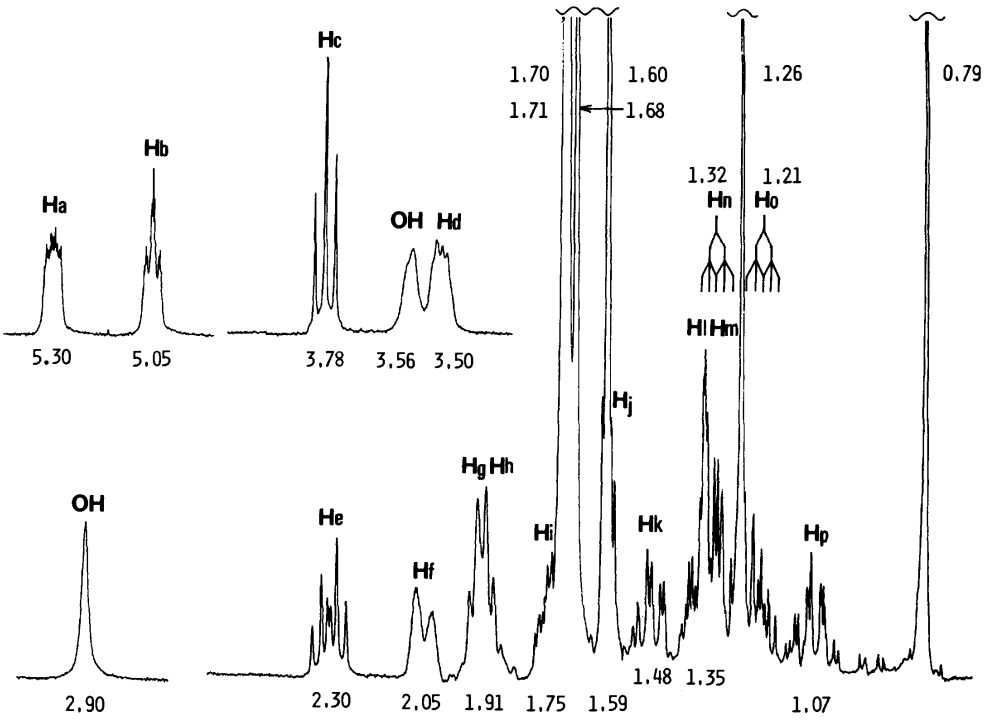

Fig. 1. 400 MHz ^{1}H-NMR Spectrum of magydardienediol (**1**) in $CDCl_3$.

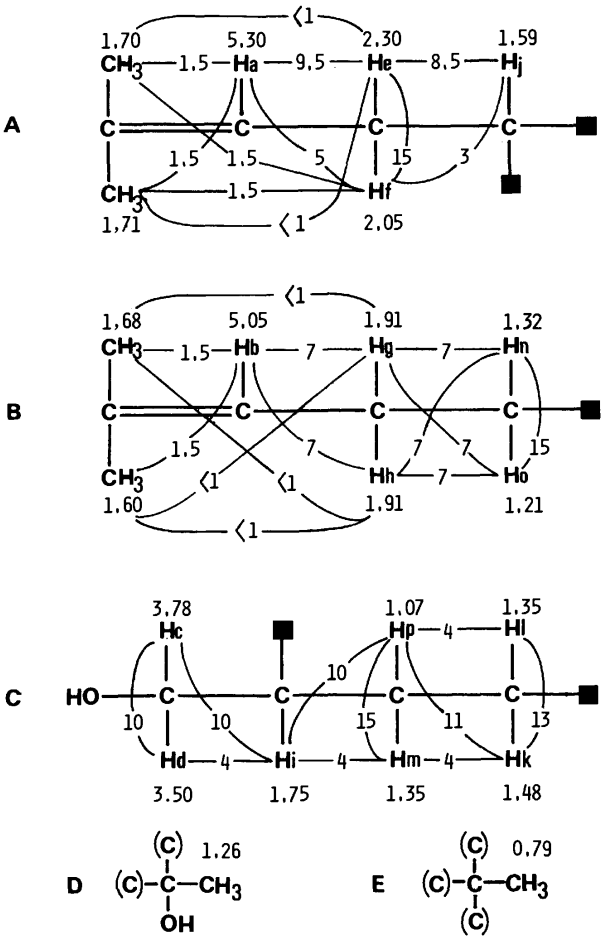

Fig. 2. Partial structures **A**—**E** and ^{1}H-NMR spectral data (chemical shifts (δ) and coupling constants (in Hz)).

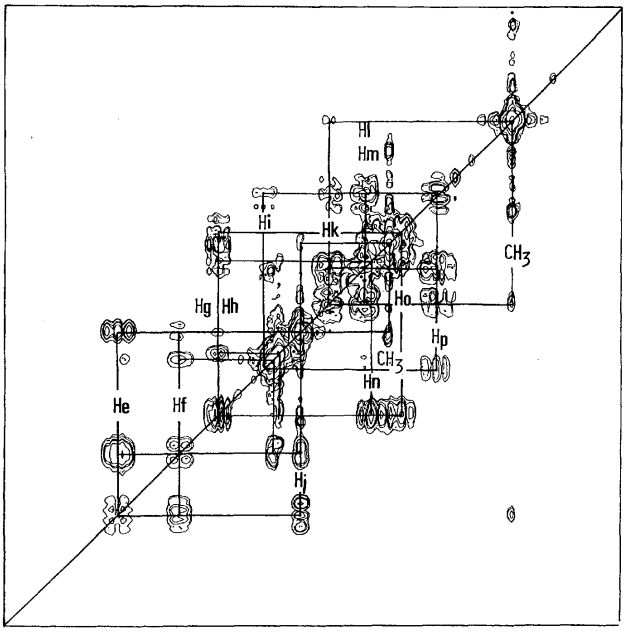

Fig. 3. Contour plot (high-field region) of the two-dimensional proton-proton correlation spectrum (COSY) of magydardienediol (**1**). The spectral width (total region) was 2000 Hz (1024×512 data points). Pulse delay time was 0.8 s and 16 times accumulation was used.

experiments revealed the multiplicities and the coupling constants of these protons. In particular, irradiation of H_l, (δ 1.35) and H_m (δ 1.35) observed in a highly congested region changed the signal patterns of H_p, (δ 1.07, dddd, J=15, 11, 10, and 4 Hz), H_k (δ 1.48, ddd, J=13, 11, and 4 Hz),[9] and H_i (δ 1.75, tt, J=10 and 4 Hz) into a double doublet (J=11 and 10 Hz), a doublet (J=11), and a triple doublet (J=10 and 4 Hz; two

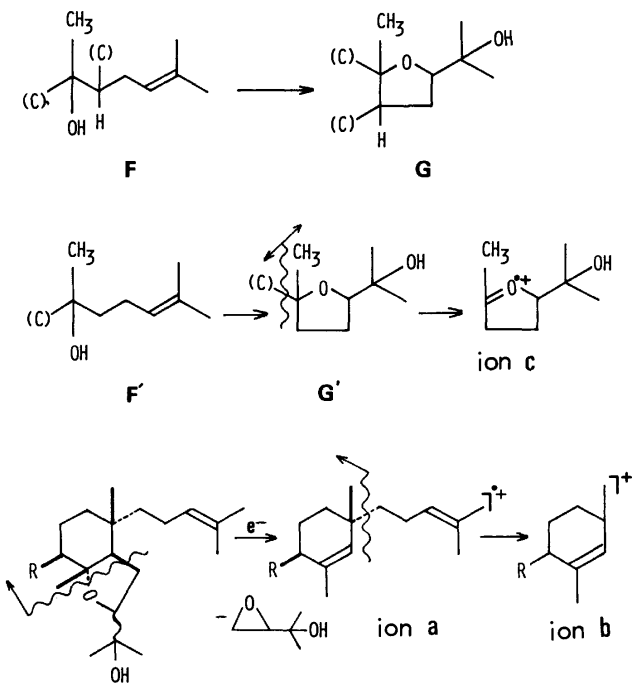

5a 5b R = CO_2CH_3

6a 6b R = CH_2OH

Fig. 4. Mass spectral fragmentations of **5a**, **5b**, **6a**, and **6b**.

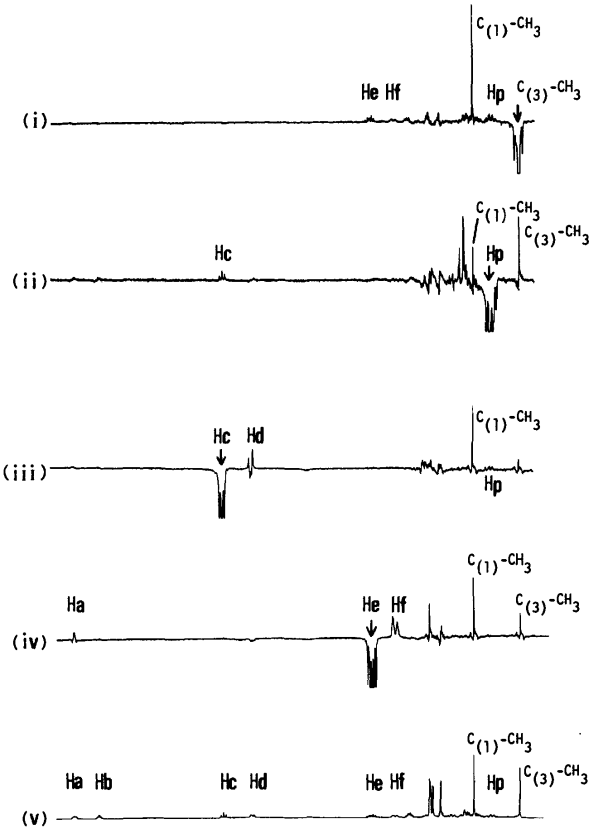

Fig. 5. Normal spectrum (v) and NOE difference spectra (i)—(iv) of magydardienediol (**1**). Irradiation protons are indicated by an arrow. The sum of the spectra obtained by irradiation of the downfield and the upfield components of H_e is shown in (iv).[17]

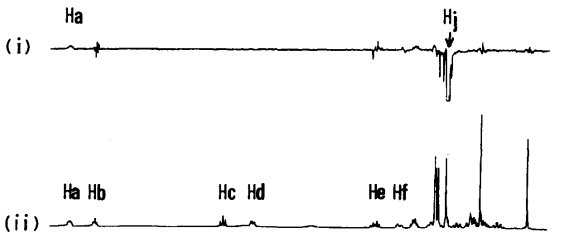

Fig. 6. Normal spectrum (ii) and NOE difference spectrum (i) of magydardienediol (**1**). Irradiation proton is indicated by an arrow.

of the six-lines in higher field part were hidden among the olefinic methyls), respectively. The values of the geminal and vicinal coupling constants indicated that this grouping could be part of a five or six-membered ring system. The multiplicities of H_i and H_k suggested that both the methine (CH_i) and the methylene (CH_kH_l) groups had a quaternary carbon neighbor.

The following mass spectral analysis (Fig. 4) was very indicative of the connections among the spin systems (partial structures **A**—**E**) separated by the quaternary carbon atoms. Oxidation of magydardienediol (**1**) with Jones reagent, followed by methylation with diazomethane, gave a diastereomeric mixture (*ca.* 1 : 1) of tetrahydrofuran derivatives, **5a** and **5b**. The tetrahydrofuran ring moiety can be derived from either partial structure **F** (**A**+**D**) or **F'** (**B**+**D**).[2,11] Both the mass spectra of **5a** and **5b** exhibited two characteristic intense peaks at *m/z* 250 (ion **a** (R=CO_2CH_3)) and *m/z* 167 (ion **b** (R=CO_2CH_3)). The complete lack of the peaks at *m/z* 143 (ion **c**) and 209 ([M−143]$^+$) expected for partial structure **G'** disproved the presence of partial structure **F'** in **1**.[12] Ion **b** may be formed by cleavage of the tetrahydrofuran ring moiety followed by loss of the 4-methyl-3-pentenyl side chain.[13,14] Thus, it was shown that partial structures **F** and **B** were present in the diterpene (**1**).

From the foregoing evidence either **1** or **1'** could be deduced as the gross structure of magydardienediol. The diol (**1**) exhibited an IR absorption at 3520 cm^{-1} (5×10^{-3} mol dm^{-3} in CCl_4) due to an intramolecular hydrogen bond.[15] As the hydroxymethyl group has already been shown to be equatorial (*i.e.* axial H_i), only **1** can take up a conformation in which the hydroxyl groups are sufficiently close in space for intramolecular hydrogen bonding. In further support of the structure, the proximity of the hydroxymethyl group to $C_{(1)}$-CH_3 was ascertained by the NOE experiments (Figs. 5(iii) and 7) and the long-range spin couplings between H_k and $C_{(3)}$-CH_3 and between H_j and $C_{(1)}$-CH_3 were shown in the COSY (Fig.3) and the proton-proton long-range COSY[16] spectra.

The stereochemistry of magydardienediol (**1**) was established as that shown in Fig. 8 based on the NOE difference spectra and the NOESY spectral analysis (Fig. 7). When $C_{(3)}$-CH_3 was irradiated the $C_{(1)}$-CH_3 and the H_p signals were enhanced (Fig. 5(i)) and furthermore when H_p was irradiated both the peaks of the tertiary methyls were enhanced (Fig. 5(ii)); this indicated that the tertiary methyls and H_p were 1,3-diaxially oriented on a chair cyclohexane ring. The

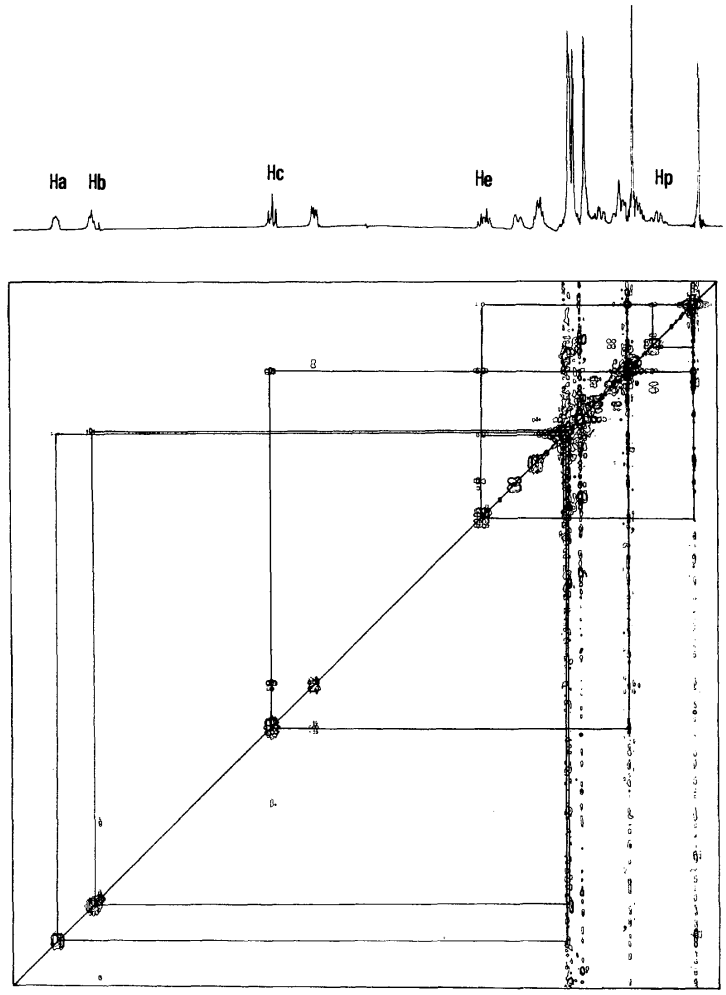

Fig. 7. Contour plot of the two-dimensional NOE spectrum (NOESY) of magydardienediol (**1**). The spectral width was 2000 Hz (1024×512 data points). Pulse delay and mixing times were 5 s and 1000 ms, respectively.

W-rule long-range spin coupling between $C_{(3)}$-CH_3 and the axial proton H_k (Fig. 3) gave additional evidence of the axial nature of the tertiary methyl.

As for the torsional isomerism about the single bond between the equatorial hydroxymethyl group and $C_{(6)}$, the intramolecular hydrogen bonding favored the conformation in which H_c and H_i were in antiperiplanar relation. This conformation was defined by the value of the vicinal coupling constant (J=10 Hz) observed between H_c and H_i and was well consistent with the NOE connectivities of H_c to $C_{(1)}$-CH_3 and H_p (Fig. 5(ii)(iii)).[15]

Finally, the *cis* relation of the 3-methyl-2-butenyl side chain to the tertiary methyls was revealed by the NOE experiments (Fig. 5(i) (iv)) which showed the proximity of H_e to the tertiary methyls. The axial nature of H_j was further shown by the W-rule long-range spin coupling between the axial $C_{(1)}$-CH_3 and H_j. The preferred conformation of the 3-methyl-2-butenyl side chain and the assignment of H_e and H_f were deduced as shown in Fig. 8 based on the NOE difference and NOESY experiments (Figs. 5(i) (iv), 6, and 7). The lower shift of the olefinic methyl resonance (δ 1.71) may be due to an anisotropy of the tertiary hydroxyl group in close proximity.[10]

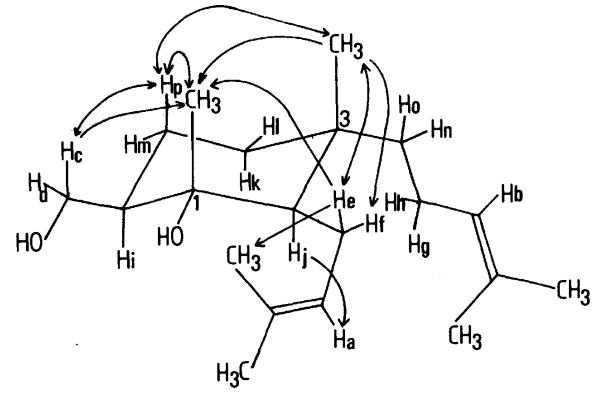

Fig. 8. Conformation and NOE connectivities of magydardienediol (**1**) (arrow heads show enhanced signals in the NOE difference spectra). The NOESY spectrum showed cross peaks corresponding almost to the above connectivities.

The structure of magydardienediol (**1**), a diterpene with a novel carbon skeleton, was thus established as *t*-6-hydroxymethyl-1,*t*-3-dimethyl-*t*-2-(3-methyl-2-butenyl)-3-(4-methyl-3-pentenyl)-*r*-1-cyclohexanol.

Experimental

Both ^{1}H-NMR and ^{13}C-NMR spectra were recorded on a JEOL GX-400 spectrometer with tetramethylsilane as internal standard. Mass and IR spectra were obtained using JEOL DX-300 and JASCO A-3 spectrometers, respectively.

^{13}C-NMR Spectral Data of Magydardienediol (1) Derived from the Complete Decoupling and INEPT Spectroscopies (100 MHz, $CDCl_3$). δ 132.10 (C=), 131.30 (C=), 126.42 (CH=), 124.79 (CH=), 78.87 ($C_{(1)}$), 65.73 (CH_2OH), 54.81 (CH), 49.90 (CH), 43.81 (CH_2), 37.20 ($C_{(3)}$), 36.96 (CH_2), 25.91 (CH_3), 25.74 (CH_3), 23.92 (CH_2), 22.65 (CH_2), 22.00 (CH_2), 20.47 (CH_3), 19.11 (CH_3), 18.04 (CH_3), and 17.65 (CH_3).

Preparation of 5a and 5b. Magydardienediol (**1**) (15 mg) was treated with an excess of Jones reagent and the resulting carboxylic acids were methylated with diazomethane in ether. The crude product was chromatographed on silica gel (1 g) using hexane–ethyl acetate (3:1) as eluent to give a mixture of **5a** and **5b** (3 mg); one spot on TLC; IR spectrum of the mixture (neat): 3460 and 1730 cm^{-1}; GLC: retention times, 14.8 (**5a**) and 18.8 (**5b**) min (Carbowax 20M (20%, 2 m), 200 °C); GC–MS (Carbowax 20M (1.2 m), 70 eV) *m/z* (rel intensity) 352 (M^+; 0.7 (**5a**) and nil (**5b**)), 337 ($[M-CH_3]^+$; 1 (**5a**) and 1 (**5b**)), 334 ($[M-H_2O]^+$; 3.6 (**5a**) and 0.4 (**5b**)), 321 ($[M-OCH_3]^+$; 3 (**5a**) and 3 (**5b**)), 294 (12 (**5a**) and 15 (**5b**)), 250 (27 (**5a**) and 24 (**5b**)), 167 (41 (**5a**) and 30 (**5b**)), and 69 (100 (**5a**) and 100 (**5b**)); High-resolution mass spectrum of the mixture *m/z* 337.2369 (Calcd for $C_{20}H_{33}O_4$: *m/z* 337.2378), 250.1906 (Calcd for $C_{16}H_{26}O_2$: 250.1932), and 167.1069 (Calcd for $C_{10}H_{15}O_2$: 167.1071).

References

1) In the previous papers (Refs. 2 and 3) "magydar-2,13-diene-10,17-diol" and "magydar-2,10(20),13-trien-17-ol" were used for the names of magydardienediol and magydartrienol, respectively.

2) J. de Pascual Teresa, C. Grande, and M. Grande, *Tetrahedron Lett.*, **1978**, 4563.

3) H. Nagano, Y. Ishikawa, Y. Matsuo, and M. Shiota, *Chem. Lett.*, **1982**, 1947.

4) Our hope to establish the structures of these diterpenes by X-ray crystallography was frustrated by our inability to prepare suitable crystals of **1** or its *p*-bromobenzoate derivative (mp 69—71 °C, fine needles).

5) a) J. Jeener, *Ampère International Summer School*, Basko, Polje, Yugoslavia (1971); b) W. P. Aue, E. Bartholdi, R. R. Ernst, *J. Chem. Phys.*, **64**, 2229 (1976); c) A. Bax and R. Freeman, *J. Magn. Reson.*, **44**, 542 (1981).

6) S. Macura and R. R. Ernst, *Mol. Phys.*, **41**, 95 (1980).

7) Numbering of the cyclohexane ring reported in the previous paper (Ref. 8) was revised according to the IUPAC rules.

8) J. de Pascual Teresa, C. Grande, J. R. Moran, and M. Grande, *Chem. Lett.*, **1984**, 247.

9) Although the COSY (Fig. 3) and the proton–proton long-range COSY spectra showed furthermore the presence of long-range spin couplings between $C_{(1)}$–CH_3 and H_j and between $C_{(3)}$–CH_3 and H_k, their accurate coupling constants (<0.5 Hz) were not obtained.

10) R. B. Bates, R. H. Carnighan, R. O. Rakutis, and J. H. Schauble, *Chem. Ind. (London)*, **1962**, 1020; R. B. Bates and D. M. Gale, *J. Am. Chem. Soc.*, **82**, 5749 (1960).

11) E. W. Warnhoff and C. M. M. Halls, *Can. J. Chem.*, **43**, 3311 (1965).

12) C. R. Enzell, R. A. Appleton, and I. Wahlberg, "Biochemical Applications of Mass Spectrometry," ed by G. R. Waller, John Wiley, Chap. 13, p. 372.

13) Reduction of the mixture of **5a** and **5b** with lithium aluminium hydride gave a mixture of **6a** and **6b**, whose mass spectrum also exhibited intense peaks at *m/z* 222.1966 (52%, ion **a** (R=CH_2OH). Calcd for $C_{15}H_{26}O$: *m/z* 222.1983) and 139.1123 (40%, ion **b** (R=CH_2OH). Calcd for $C_9H_{15}O$: 139.1123). Catalytic hydrogenation (10% Pd-C, ethanol) of the mixture of **5a** and **5b** gave a mixture of dihydro derivatives and both the products exhibited a peak at *m/z* 167 (ion **b** (R=CO_2CH_3): 100%) in GC–MS analysis.

14) Catalytic hydrogenation (10% Pd-C, ethanol) of **1** gave a tetrahydro derivative, IR (neat) 3350 cm^{-1}; MS *m/z* 312.2929 (21%. Calcd for $C_{20}H_{40}O_2$: M^+, *m/z* 312.3027. Its mass spectrum (base peak, *m/z* 57) showed an intense peak (78%) at *m/z* 209.1859 (Calcd for $C_{14}H_{25}O$: *m/z* 209.1909) which must arise by dehydration of the molecular ion followed by loss of the 4-methylpentyl side chain.

15) A. Balsamo, P. Crotti, and F. Macchia, *J. Chem. Soc., Perkin Trans., 1*, **1982**, 3065.

16) Delay time (300 ms) was introduced at the beginning of the evolution and detection periods. Delay time between each pulse sequence was 0.8 s. (See Ref. 5c).

17) D. Neuhause, R. N. Sheppard, and I. R. C. Bick, *J. Am. Chem. Soc.*, **105**, 5996 (1983).

Phenanthraquinone Monothiosemicarbazone as Sensitive Reagent for the Spectrophotometric Determination of Zinc(II)

Prem Prakash SINHA, Sharwan Kumar SINDHWANI,* and Rajendra Pal SINGH
Department of Chemistry, University of Delhi, Delhi-7, India
(Received April 23, 1983)

Phenanthraquinone monothiosemicarbazone has been found to be a sensitive and selective reagent for the spectrophotometric determination of zinc(II) in the pH range 7.0—8.6. The red complex formed shows maximal absorbance at 510 nm. Beer's law is obeyed up to 1.96 ppm and optimum range of concentration being 0.22—1.70 ppm. The sandell sensitivity is 0.0018 μg Zn^{II} cm^{-2}, with molar extinction coefficient being 3.52×10^4 mol^{-1} cm^{-1}. The method has been applied to the determination of zinc in 6% Zn–Al alloy.

Several organic reagents[1] have been used for the determination of micro amounts of zinc. Recently introduced reagents are 5,10,15,20-tetrakis(1-methylpridinium-4-yl)porphine,[2] 2-(3-sulfobenzoyl)pyridine thiosemicarbazone,[3] and 2-(5-nitro-2-pyridylazo)-1-naphthol.[4] But most of them suffer from various disadvantages.

Preliminary investigations have shown that phenanthraquinone monothiosemicarbazone (PTS) forms coloured complexes with several metal ions such as iron (II and III) (λ_{max}=510 nm), cobalt(II) (λ_{max}=500 nm), nickel (II) (λ_{max}=520 nm), copper (I and II) (λ_{max}=530 nm), cadmium(II) (λ_{max}=500 nm), ruthenium(III) (λ_{max}=660 nm), rhodium(III) (λ_{max}=510 nm), palladium(II) (λ_{max}=590 nm, when the final concentration of hydrochloric acid is in the range 0.28—1.14 M+ and λ_{max}=540 nm at pH 8.0—9.5), osmium(VIII) (λ_{max}=530 nm), iridium(III) (λ_{max}=520 nm) and platinum(IV) (λ_{max}=510 nm). The present study deals with spectrophotometric determination of zinc with PTS. Zinc(II) reacts with PTS and forms red complex which is soluble in methanol and shows maximum absorbance at 510 nm.

Experimental

Apparatus. A Unichem SP 600 spectrophotometer with matched glass cells of 10 mm light path was used for absorbance measurements. An ECIL (PH 821 A) expanded scale pH-meter was used for pH measurements.

Reagents. *Synthesis of PTS*: Phenanthraquinone monothiosemicarbazone (PTS) was prepared by refluxing equimolar amounts of phenanthraquinone and thiosemicarbazide in methanol for 3 h on a boiling water bath. The hot solution was filtered under suction and cooled in refrigerator. Red crystals of PTS obtained, were recrystallized from methanol (yield, 80%). The purity was checked by thin-layer chromatography and elemental analysis. A 2.5×10^{-3} M PTS solution was prepared in *N*,*N*-dimethylformamide (DMF). Though the solution is stable for at least two days, a fresh solution was prepared each day to avoid possible decomposition.

Zinc(II) Solution. 0.1 M zinc (II) solution was prepared by dissolving zinc sulfate heptahydrate (AnalR BDH) in double distilled water, containing 0.5 ml of sulfuric acid in one liter of the solution. The solution was standardized volumetrically.

Sodium Tetraborate Solution. 0.01 M in double distilled water. All other solutions of cations and anions were prepared from A.R. grade chemicals in double distilled water.

Separation of Zinc. The separation of zinc from other cations by diethyldithiocarbamate has been suggested.[5] Zinc (II) solution was buffered with ammonium citrate and ammonium hydroxide at pH 8.5; the final solution containing approximately 1% citrate. The solution was then extracted with 5.0 ml portions of diethyldithiocarbamate in chloroform until the chloroform no longer changes colour. Zinc was again re-extracted from the combined chloroform extact with aqueous 0.16 M hydrochloric acid and determined spectrophotometrically with PTS.

Recommended Procedure for the Determination of Zinc. To an aliquot containing 2.24 to 17.0 μg of zinc(II), add 1 ml of 2.5×10^{-3} M PTS solution in DMF. Adjust the pH between 7.0—8.6 with 0.01 M sodium tetraborate. Add 5 ml of methanol and dilute the solution to 10 ml with distilled water. Measure absorbance at 510 nm against corresponding reagent blank prepared under identical conditions. Calculate the amount of zinc from the calibration curve.

Determination of Zinc in 6% Zn–Al Alloy (BCS No. 300). Dissolve 0.1 g alloy in about 5 ml of aqua regia and evaporate to almost dryness. Dissolve the residue in about 2 ml of hydrochloric acid and dilute to 100 ml . Take suitable aliquot and determine the amount of zinc following the recommended procedure after masking iron with fluoride.

The results obtained for three determinations are shown in Table 1.

TABLE 1. DETERMINATION OF ZINC IN 6% Zn–Al ALLOY

Composition of 6% Zn–Al alloy (%)	Zinc found (ppm)	Zinc calculated (ppm)	Error (%)
C=1.28, Mn=0.41	0.594	0.598	−0.67
Si=0.16, Mg=2.76 Fe=0.30, Ti=0.15	0.890	0.897	−0.78
Zn=5.98, Cr=0.15 Pb=0.003 and Sn=0.006	1.122	1.196	−0.53

Results

Absorbance Spectra and Stability of the Complex. A study of the effect of pH on the complexation of zinc(II) with PTS showed that the red complex gives maximum absorbance at 510 nm (Fig. 1) which is constant in the pH range 7.0—8.6 (Fig. 2). Subsequent studies were carried out at pH 7.5±0.1. The complex is stable for 2 h.

* 1M=mol dm^{-3}.

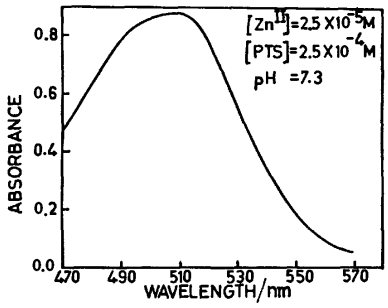

Fig. 1. Absorption spectra of Zn^{II}–PTS complex.

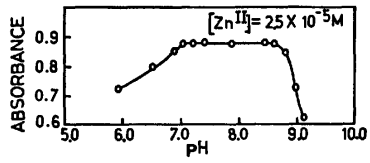

Fig. 2. Effect of pH on Zn^{II}–PTS compex.

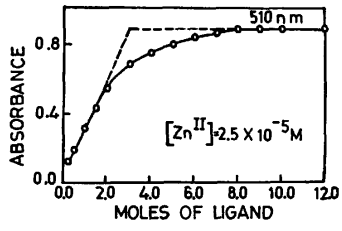

Fig. 3. Composition of Zn^{II}–PTS complex by mole ratio method.

Effect of Reagent Concentration. The ratio of reagent to metal ion necessary for maximum colour formation was ascertained. It was found that eight fold excess of reagent is required for the complete complexation (Fig. 3) but however 10 times PTS was used during all studies. Since the absorbance of the ligand at 510 nm is very small therefore the excess of the reagent is not critical.

Physical Constants of the Complex. Under the optimal conditions describred above, Beer's law obeyes up to 1.96 ppm of zinc(II). The potimum range of concentration of zinc(II) for accurate determination, as deduced from Ringbom plot[6] (Fig. 4) is 0.22—1.70 ppm. The molar absorptivity is 35200 l mol^{-1} cm^{-1} at 510 nm with Sandell's sensitivity of 0.0018 μg Zn cm^{-2} for log I_0/I=0.001.

Precision of the Method. Measured under optimum conditions, eight samples containing 1.63 ppm of zinc, the average relative deviation was found to be 0.26% with maximum relative deviation of 0.41% and mean absorbance of 0.880. The standard deviation is 5.4×10^{-3}.

Stoichiometry of the Complex. The stoichiometry of the complex was determined by Job's method of continuous variations[7] (Fig. 5) and mole ratio method[8] (Fig. 3). Both showed the formation of 1:3 complex (metal:ligand).

Effect of Diverse Ions. Synthetic solutions containing 1.63 ppm of zinc(II) and different amounts of diverse ions were prepared and analyzed by the

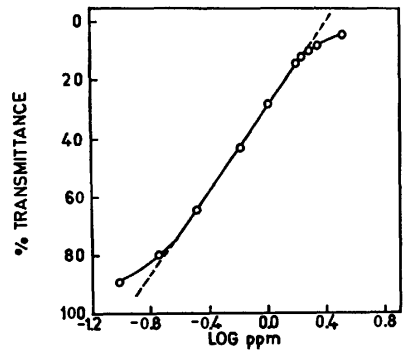

Fig. 4. Ringbom plot for Zn^{II}–PTS complex.

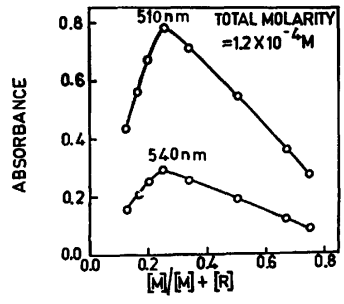

Fig. 5. Composition of Zn^{II}–PTS complex by Job's method.

recommended procedure. An error of ±2% absorbance reading was neglected. The amounts (in ppm) of ions tolerated with masking ion if any, are given in parentheses:

Chloride, bromide, and nitrate (1000 each); fluoride and thiourea (700 each); nitrite (350); thiocyanate (250); tartrate (100): iodide (100); thiosulfate (300); oxalate (30); sulfite (500); magnesium(II), calcium (II), barium(II), and strontium(II) (150 each); aluminium(III) (75); uranyl(VI) (100); molybdenum (VI) and tungsten(VI) (50 each); manganese(II) (F^-, 15); vanadium(V) (F^-, 20); thorium(IV) and titanium(IV) (50 each); silver(I) (Cl^-, 10); rhodium (III) (thiourea, 5); iridium(III) (SCN^-, 1); osmium (VIII) (SCN^-, 5); platinum(IV) (I^-, 5); nickel(II) (SCN^-, 10); lead(II) (15); tin(II) (10); copper(II) (thiourea, 2); iron(II) (F^-, 5); mercury(II) (I^-, 10); cadmium(II) ($C_2O_4^{2-}$, 5) and chromium(III) (5).

EDTA, phosphate, citrate, and cyanide interfere seriously.

Discussion

Among various reagents reported for the determination of zinc, dithizone[9-11] is notable. The reagent is highly sensitive but excess of dithizone has to be removed by shaking with very dilute ammonia solution which can often contain traces of zinc. It is important in the determination of traces of zinc and the procedure is tedious. Zincon[12,13] is another important reagent but the sensitivity is low, and a large number of metals interfere, making it necessary to separate the zinc first. PAN[14,15] and Chrome Azurol S[16] are sensitive reagents but highly unselective. The disadvantage of 5, 10, 15, 20-tetrakis-(1-methyl-

TABLE 2. SENSITIVITIES OF REAGENTS FOR THE SPECTROPHOTOMETRIC DETERMINATION OF ZINC(II)

Reagent	Sensitivity (μg Zn cm^{-2})
Dithizone	0.0007/538 nm
Zincon	0.0032/625 nm
1-(2-Pyridylazo)-2-naphthol	0.0012/550 nm
Chrome Azurol S	0.0015/510 nm
Methylthymol Blue	0.0047/584 nm
2-(2-Pyridylazo)-*p*-cresol	0.0022/580 nm
Arsenazo III	0.0023/570 nm
Thiodibenzoylmethane	0.0019/410 nm
Biacetyl bis[4-phenyl-(thiosemicarbazone)]	0.003/440 nm
2-(3-Sulfobenzoyl)pyridine thiosemicarbazone	0.0022/390 nm
5,10,15,20-tetrakis-(1-methyl-pyridinium-4-yl)porphine	0.0028/437 nm
Phenanthraquinone monothiosemicarbazone (PTS)	0.0018/510 nm

pyridinium-4-yl) porphine[2] is that free reagent which absorbs at 423 nm has to be removed by forming the lead complex (λ_{max}=476 nm) before measuring the absorbance of the zinc complex. Among thiosemicarbazones, 2-(3-sulfobenzoyl) pyridine thiosemicarbazone[3] is fairly sensitive but effect of diverse of ions, in the determination of zinc, has not been investigated.

In the present investigation, PTS compares favourably with other well-known reagents. The procedure is simple and large amounts of ligand do not interfere, which is an advantage over dithizone. The reagent is more selective than PAN and Chrome Azurol S. There is no extraction *etc.* which is an advantage over other methods. Although small amounts of the metals such as copper, iron, nickel *etc.* can be masked, they should be separated if present in large amounts before the determination of zinc. The sensitivity of the different methods for the determination of zinc are compared in Table 2.

One of the authors (PPS) is thankful to University Grants Commission, New Delhi, India for the award of a teacher fellowship to him.

References

1) Z. Marczenko, "Spectrophotometric Determination of Elements," John Willey & Sons, New York (1976), p. 601.
2) S. Igarashi, J. Kobayshi, T. Yotsuyanagi, and K. Aomura, *Nippon Kagaku Kaishi*, **1979**, 602.
3) J. M. Bautista and J. M. Cano Pavon. *Talanta*, **27**, 923 (1980).
4) Y. Sokai and M. Daigaku, *Shizen Kagaku*, **45**, 11 (1979).
5) J. A. Stewart and J. C. Bartlet, *Anal. Chem.*, **30**, 404 (1958).
6) A. Z. Ringbom, *Anal. Chem.*, **115**, 332 (1939).
7) P. Job, *Annls. Chim.*, **9**, 113 (1928).
8) J. A. Yoe and A. L. Jones, *Ind. Eng. Chem., Anal Ed.*, **16**, 111 (1944).
9) G. K. Schweitzer and C. B. Honaker, *Anal. Chim.* Acta, **19**, 224 (1958).
10) J. Stary and L. Ružička, *Talanta*, **8**, 296 (1961).
11) P. R. Subbaraman, S. M. Cordes, and H. Freiser, *Anal. Chem.*, **41**, 1878 (1969).
12) J. H. Yoe, and R. M. Rush, *Anal. Chim. Acta*, **6**, 526 (1952).
13) R. M. Rush and J. H. Yoe, *Anal. Chem.*, **26**, 1349 (1954).
14) H. Flaschka and R. Weiss, *Microchem. J.*, **14**, 318 (1969).
15) T. T. Bykhortsova, *Zavod. Lab.*, **40**, 512 (1974).
16) Y. Horiuchi and H. Nishida, *Bunseki Kagaku*, **16**, 756 (1967).

 © 1984 The Chemical Society of Japan Bull. Chem. Soc. Jpn., 57, 2979—2983 (1984)

A Rapid Pulse Nebulization Technique for Flame Atomic Fluorescence Spectrometry

Edet Joseph EKANEM
School of Basic Studies, Ahmadu Bello University, Zaria, Nigeria
(Received July 21, 1983)

A simple and rapid pulse nebulization technique in which 200 μl sample volume is injected and aspirated into a flame-nebulizer is described for the determination of cadmium by line source atomic fluorescence spectrometry (AFS) and for magnesium and other elements by continuum source AFS. The volume of blood and serum samples required for replicate analysis is reduced below 1 ml; nebulizer clogging by heavy sample matrices is reduced; small volumes of rare samples can be analysed in the same batch as bulky samples using this technique. The technique is also applicable to flame AES which can also be performed with the instrumentation used in this work.

In the flame atomic fluorescence spectrometric determination of cadmium, the high sample uptake rate of about 9 ml min^{-1} requires large sample volumes for replicate analysis. In the nitric acid deproteinisation procedure already reported for the determination of low cadmium levels in blood,[1] a 2 ml minimum blood volume was required for replicate analysis by continuously aspirating the analytical sample into the nitrogen-separated air-acetylene flame. This demand on sample is unsatisfactory for rare samples especially in cases like cadmium determination where sample dilution must be minimised to improve analytical sensitivity. The possibility of using a pulse nebulization technique with small sample volumes has, therefore, been explored in the line source AFS determination of cadmium and the continuum source AFS determination of other elements as exemplified by magnesium in clinical samples.

The application of pulse nebulization to flame spectrometry has been reported by various workers[2–11] and reviewed by Berndt *et al.*[11] This includes microsampling techniques employing small Teflon funnels[9] and a Teflon sampling manifold for use with small sample injections.[10] Applications specific to flame AFS have also been reported.[2,8]

Experimental

Chemicals and Samples. The procedure reported was applied to whole blood, serum, and urine samples after appropriate pretreatment, Whole blood and serum samples were deproteinised by shaking the sample and 2 M† nitric acid in equal volumes and centrifuging. The supernatant was analyzed for cadmium by line source AFS without further dilution; it was, however, further diluted 100 times with deionised water before determining magnesium by continuum source AFS. Urine samples were only acidified to 0.04 M with hydrochloric acid for cadmium determination, while they were diluted 200 times with deionised water and similarly acidified for magnesium analysis. It has previously been shown that hydrochloric acid enhances the measurement sensitivity for both cadmium[12] and magnesium.[1]

Instrumentation. The spectrometer used for these studies was the laboratory-constructed one already described.[1,12] It consisted of a SPEX double monochromator with a photomultiplier detector and a Brookdeal 5C14 photon counter for signal processing. A nitrogen-separated air-acetylene flame was used as atom cell. A thermostated electrodeless discharge lamp excited by microwave in a 3/4 wave Broida cavity was used as a line source. The continuum source was a 300 W Xenon arc lamp. For line source AFS, a mechanical chopper was applied for background correction by intensity modulation while, for continuum source AFS, the rotating circular quartz plate with different quadrant thicknesses[13] was used for background correction by wavelength modulation. Though the continuum source was used as a primary source in continuum source work, it was also employed as a secondary source for effecting scatter correction in line source AFS work, operating at low power. The layout of the spectrometer for line source and continuum source AFS is presented in Figs. 1 and 2 respectively.

To modify the spectrometer for pulse nebulization, a polypropylene micro-pipette tip was attached to the nebulizer capillary tubing as shown in Fig. 3 to serve as a sample pulse reservoir, taking care to obtain a leakproof connection. It was ensured that the end of the capillary tubing did not project into the pipette tip so that each sample pulse injected into it was completely uptaken into the nebulizer without any dead volume. Micro-pipettes of various volumes were employed to deliver sample pulses into the reservoir. Figure 3 is not drawn to scale but typical dimensions for the device are indicated.

Procedure. The instrument was aligned and optimised for line source AFS, continuum source AFS, or flame AES as required. The measurement cycle time, usually 1 s, for collecting the signals was selected on the photon counter as explained later and the optimum uptake rate was measured. An aliquot of the sample to be measured was injected rapidly into the sample reservoir from a micropipette so that it was aspirated into the nebulizer in a single unbroken stream. The highest signal displayed soon after the injection was recorded. This was repeated for 3 or 4 aliquots of each sample and the mean signal for the sample was obtained as the average of the 3 or 4 replicate results. Between injections, deionised water or an appropriate blank solution was continuously aspirated to prevent inter-sample memory effects. A sample blank was also analyzed by the same procedure and its signal was subtracted from all sample results.

Alternatively the signal from each aliquot was traced on a chart recorder. It was then necessary to determine the appropriate measurement cycle time to obtain a representative signal trace.

Optimization of Measurement System. The optimum measurement cycle time constant was selected from a range of options provided on the photon counter. The optimum time constant, however, depended on other system para-

† 1 M = 1 mol dm^{-3}.

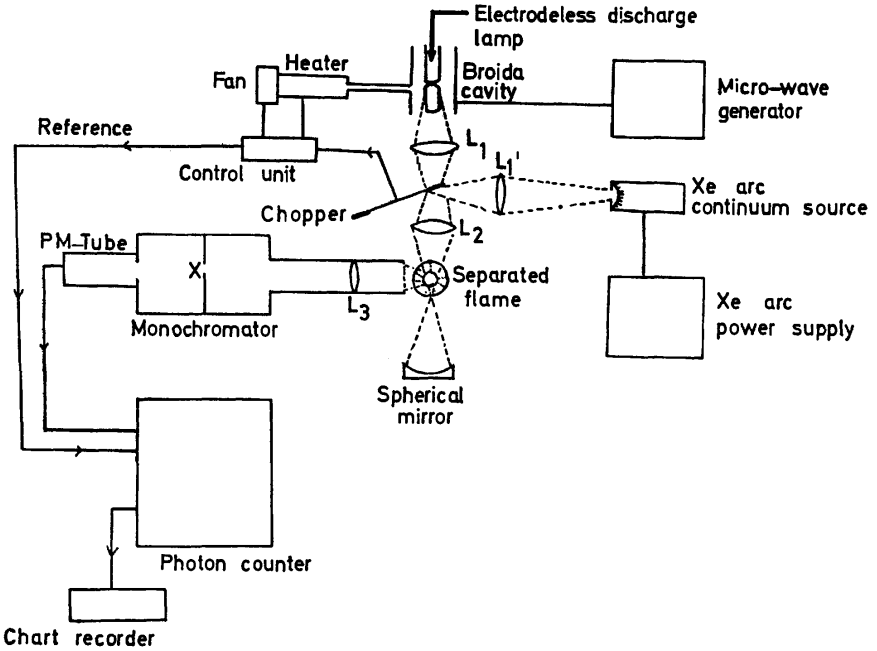

Fig. 1. The AFS instrumentation. (X)=Rotating quartz chopper. L=Lenses.

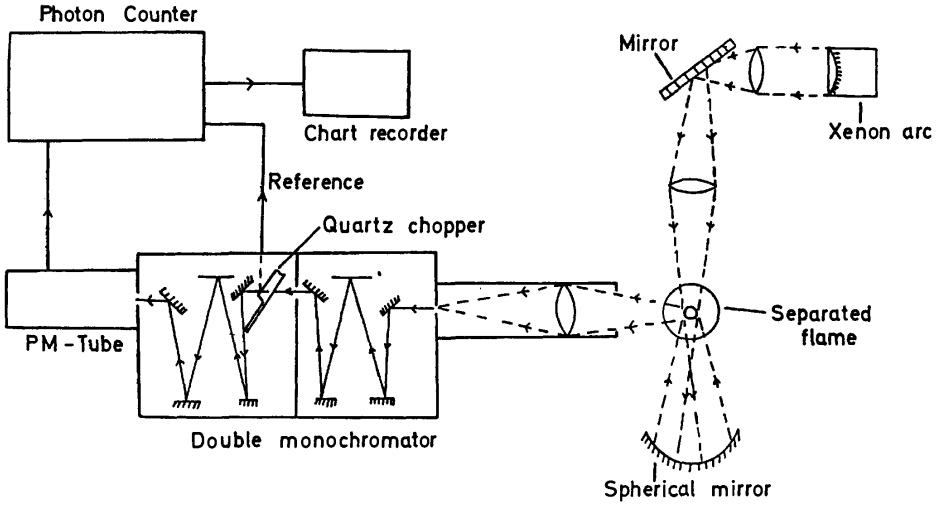

Fig. 2. The modified instrumentation for continuum source AFS.

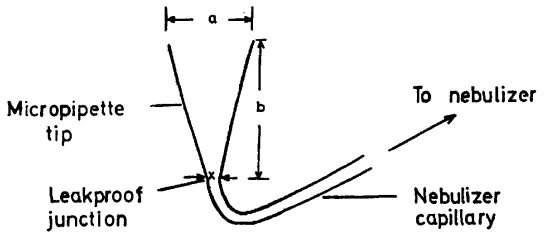

Fig. 3. Reservoir for sample injection. (a)=0.6 cm (b)=5 cm x=0.5 mm

meters defined below for purposes of this pulse nebulization technique.

Uptake Rate (R_u): The optimum uptake rate was similar to that obtained for continuous sample aspiration. It was measured at the nebulizer screw setting that gave the highest signal for pulses of a suitable standard solution.

Sampling Time (t_s): This was the time required for a sample pulse to be completely sucked up from the reservoir. It was measured approximately with a stopwatch and averaged for a large number of equal pulses; it was directly related to the sample uptake rate and pulse volume as

$$t_s = \frac{V_p}{R_u}, \tag{1}$$

where V_p is the pulse volume; and R_u is the uptake rate.

Peak Time (t_p): This was the total time required to attain a peak analyte concentration in the measurement zone of the flame, after sample injection into the reservoir. Usually this time was slightly longer than t_s as in the expression

$$t_p = t_s + x.$$

where x is the time between the complete uptake of the pulse and the attainment of a stable peak signal level in the flame.

Readout Time (t_r): This was the period between sample injection and the digital display of the relevant signal. The value of t_r depended on the measurement cycle time constant selected on the photon counter.

For a given sample pulse volume and uptake rate, some measurement cycle time constants were more suitable than others. The option selected for a given application was determined by the way in which the signal was obtainable from pulse operation.

From a measurement of the uptake rate (R_u), Eq. 1 could be used to derive t_s for any pulse volume used. t_r could be measured directly for a given uptake rate and pulse volume. Usually t_r exceeded t_s by a fraction that could be estimated, the excess depending solely on the measurement cycle time selected.

At the measurement zone, the atoms from a pulse just injected arrived according to the profile illustrated in Fig. 4 and a peak signal was observed for a pulse only if t_r bracketted t_p.

In selecting the measurement cycle time (t_{mc}), three possibilities could be applied as follows:

I. $t_{mc} \ll t_p$: During the period t_p, when the pulse is passing through the measurement zone, a counting cycle is executed and repeated many times with progressively increasing total counts as t_p is approached and progressively decreasing totals as t_p is exceeded. These signals which are digitally displayed in sequence can be plotted to obtain a peak profile as shown in Fig. 4. Alternatively the signals accumulated during t_p may activate a chart recorder to plot a peak as in the profile. For a pulse volume of 200 μl and the 9 ml min^{-1} uptake rate routinely employed in these measurements, the 0.1 s measurement cycle typified this condition.

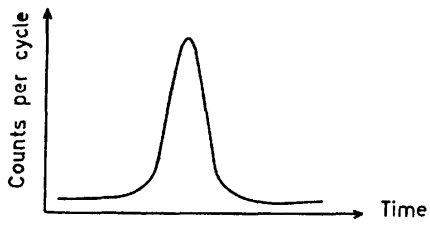

Fig. 4. The Peak Profile when $t_{mc} \ll t_p$.

II. $t_{mc} \gg t_p$: In this case the sample passes through the flame rather quickly while the counting continues for much longer. The signal collected during a short period is ascribed to a much longer period during most of which sample is not passing through the measurement zone. Sensitivity is poorer and higher chances exist of noise signals being counted. The 10 s measurement cycle typified this condition.

III. $t_{mc} \approx t_p$: In this option, sample presentation may get so locked to the measurement cycle that signal collection takes place only at the time when sample is passing the measurement zone. The signal is registered as one total at the end of the measurement cycle and offers increased sensitivity. The 1 s count time was typical.

It is to be noted that in case I where a definite peak can be traced as the measurement is repeated many times while sample is passing through the flame, the peak value does not follow the sample presentation immediately. There are a number of lower signals before the peak value. Therefore the peak signal needs to be selected from others that arise from the same sample pulse. Alternatively the signal is traced on a chart recorder and the peak height measured from the trace. In the other cases, the signal displayed immediately following the injection of the sample pulse is the peak signal. Only one measurement cycle is executed while sample is passing through the measurement zone and only one signal is output at the end of the cycle. This signal, however, is much higher than even the peak value in case I.

In this instrumentation, all three options are possible but only option III provides good sensitivity and precision. Option I suffers from reduction in sensitivity because of a reduced counting time, while option II suggests lower precision.

Results and Discussion

Line Source AFS. The experimental conditions of the flame are shown in Table 1. The sample uptake rate and other parameters for signal retrieval were measured with a stopwatch for a measurement cycle time of 1 s. Pulses of a 10 μg l^{-1} Cd standard solution were injected while adjusting the uptake rate until a maximum signal was obtained. The uptake rate was then measured by continuous nebulization. The sampling time, t_s, was measured by noting the time between the sample delivery into the reservoir and sample disappearance from the reservoir into the nebulizer capillary tubing. The calculated values also shown in Table 2 were based on the measured uptake rate of 9.2 ml min^{-1}. The readout time, t_r, was measured by noting the time between the delivery of the pulse into the reservoir and the display of the relevant signal on the photon counter readout. The mean values of these parameters were based on 15 measurements of each and are reported in Table 2.

The Optimum Pulse Volume and Measurement Cycle. Measurements were repeated for various pulse volumes of an aqueous 4 μg l^{-1} cadmium standard solution and the results shown in Table 3 were obtained for measurement times of 1 s and 0.1 s. The trends were similar for both measurement cycle times and also for a 10 μg l^{-1} cadmium standard solution.

In the 20—200 μl range of pulse volumes, the 200 μl pulse produced the highest sensitivity. As indicated in Table 3, it also yielded a more satisfactory detection limit than smaller sample volumes investigated. So

Table 1. Optimised flame conditions

Factor	Optimum values
Flame type	Nitrogen-separated air-acetylene flame
Flame composition	Stoichiometric-fuel rich
Nitrogen pressure	1 psi
Acetylene back pressure	12 psi
Acetylene feed pressure	8 psi
Air feed pressure	40—45 psi
Flame height	28 mm

Table 2. Parameters for signal retrieval

Parameter	Pulse volume/μl	Measured	Calculated
t_s	200	1.31 s	1.30 s
t_s	50	—[a)]	0.33 s
t_r	200	1.58 s	
R_u		9.2 ml min^{-1}	

a) t_s was too short to measure accurately for 50 μl pulses.

TABLE 3. VARIATION OF Cd FLUORESCENCE SENSITIVITY WITH PULSE VOLUME AND COUNTING TIME CONSTANTS

Pulse volume	Signal (counts/cycle)		Detection limit/μg l^{-1}	
μl	1 s cycle	0.1 s cycle	1 s cycle	0.1 s cycle
200	226	42	0.76	1.36
100	65	35	2.66	1.63
50	54	21	3.21	2.72
20	51	8	3.41	7.14

the 200 μl pulse volume was selected for routine analysis. For similar reasons, a measurement time of 1 s was preferred to 0.1 s. In this case, the measurement time was similar in magnitude to t_s and t_p. That t_s, t_p, and t_r exceeded the measurement cycle time, t_{mc}, of 1 s offered optimum sensitivity as it ensured that sample was present in the measurement zone throughout the counting cycle. Otherwise there would be no sample in the flame for some part of the counting cycle and reduced sensitivity would result.

Measurements With a Chart Recorder. The smallest pulse volume that gave a trace with well defined peaks was the 200 μl pulse volume. Only the 0.1 s time constant yielded peak traces. The precision and the linearity of calibration curves were satisfactory but the detection limit was three times worse than that obtained when the signal was obtained directly from the photon counter display using a 1 s measurement time constant. The value increased from 0.7 μg l^{-1} to 2.0 μg l^{-1} for cadmium. Samples could still be compared by this procedure if they contained more than the 2 μg l^{-1} level.

Comparison of Procedures. Pulse nebulization was compared with continuous nebulization by applying each sampling technique to exactly the same solutions, instrumental settings and analysis conditions. A measurement time of 1 s and 200 μl sample were employed for all pulse nebulization measurements. Parameters considered for comparison included overall sensitivity, precision, accuracy, detection limit, and linear range of calibration curve.

To compare overall sensitivity, a number of samples were measured using both techniques and the signal levels were compared. The detection limits calculated for each sample introduction technique were also compared.

Pulse nebulization generally provided 40—52% less sensitivity than continuous nebulization when 200 μl sample pulses were applied. As shown in Table 4, detection limits were twice worse for pulse nebulization than for continuous nebulization.

Precisions calculated as relative standard deviations for 15 replicate measurements were compared for pulse and continuous nebulizations. Very similar results were obtained for the two techniques.

The calibration curve obtained for pulse operation was linear up to 8 ppm, while the linear range for continuous nebulization was only up to 2 ppm.

Larger Pulse Volumes. The disparity indicated between pulse and continuous nebulization was further investigated by observing pulse volumes above 200 μl.

TABLE 4. COMPARISON OF DETECTION LIMIT FOR CADMIUM

Sample	Detection limit/ppb	
	Pulse nebulization	Continuous nebulization
Aqueous	0.11	0.05
Water diluted blood	0.48	0.24
Blood Deproteinate	0.22	0.11
Urine	0.16	0.08

TABLE 5. DEPENDENCE OF ANALYTICAL FIGURES OF MERIT ON PULSE VOLUMES

Pulse volume	Signal	Detection limit	Precision
μl	(counts/s^{-1})	μg l^{-1}	%
100	80	0.39	4.9
200	223	0.11	3.6
400	285	0.08	3.1
600	401	0.05	2.9
700	398	0.05	3.1
800	396	0.05	3.1
1000	409	0.05	2.4
1200	420	0.05	2.9
1500	406	0.05	3.2

The respective signals for an aqueous 4 μg l^{-1} cadmium standaed solution and the corresponding detection limits are shown in Table 5; the measurement precision provided by each pulse volume is also indicated. A 1 s measurement cycle was employed in all cases.

As can be seen from Table 5, the sensitivity was improved with the increase of pulse volume and became constant over about 600 μl. There was a progressive improvement in both measurement precision and detection limit until 600 μl. Thereafter these parameters attained identical values to those obtained by continuous nebulization. Then, the nebulization ceased to be strictly pulse but semicontinuous, as the sample volume was enough to maintain a steady signal level over several counting cycles. Instead of achieving reasonable sensitivity and precision using a microvolume of rare samples, 600 μl of sample, when continuously aspirated, became insufficient for three replicate measurements as achieved by the pulse technique.

Comparison of Accuracy. The same whole blood samples were analyzed for cadmium by flame AFS employing pulse and continuous nebulization in turn and the results are campared in Table 6. A comparison of other results for cadmium in whole blood obtained by this pulse AFS technique with those obtained independently in a different laboratory by carbon furnance AAS showed satisfactory agreement. Whole blood samples which had been analyzed for cadmium by many laboratories were also analyzed by this pulse AFS technique and the results were in good agreement with the laboratory means.

Continuum Source AFS. The application of pulse nebulization to the continuum source AFS technique was also investigated in detail for the determination of magnesium. Various pulse volumes of a 400 μg l^{-1} Mg aqueous standard were measured by the con-

Table 6. Determination of cadmium in whole blood by pulse and continuous nebulization

Sample No.	Concentration/μg l^{-1}	
	Pulse nebulization	Continuous nebulization
1	15.4	21.4
2	10.8	8.0
3	10.0	8.8
4	14.8	14.8
5	27.0	29.2

Table 7. Comparison of analytical results for magnesium by pulse continuous nebulization

Sample	Mg results/μg ml^{-1}	
	Pulse nebulization (y)	Continuous nebulization (x)
Blood 1	40.5	40.5
Blood 2	40.7	40.8
Blood 3	47.5	47.3
Blood 4	44.6	44.5
Urine 5	99.8	99.5
Urine 6	97.9	98.6
Urine 7	114.0	113.4
Urine 8	111.2	110.9
Urine 9	108.9	109.6
Serum 10	20.5	20.2
Serum 11	17.3	17.6
Serum 12	18.5	18.7
Serum 13	24.1	23.9

Regression line: $y=x+0.01$; $r=0.9999$.

tinuum source AFS procedure using the measurement cycles of 0.1 and 1 s. From the results, the 1 s counting time provided higher sensitivity than the 0.1 s counting time. The 200 μl pulse volume was also superior to smaller pulse volumes in sensitivity and precision. As in the determination of cadmium by pulse nebulization, the detection limit, overall sensitivity, and precision for magnesium were improved with increasing pulse volume and were similar to values obtained by continuous nebulization for pulse volumes larger than 600 μl.

Using 200 μl pulses and a measurement cycle of 1 s, the pulse technique was employed to determine magnesium in various samples which were also measured by continuous nebulization. A comparison of the results is presented in Table 7. The blood, serum, and urine samples were appropriately diluted and acidified with hydrochloric acid as already described. The calibrations were achieved for all samples using aqueous magnesium standards acidified to 0.04 M with hydrochloric acid. The linear range extended from 4 μg l^{-1} to 10 μg ml^{-1} for pulse nebulization while it was in the range of 2 μg l^{-1}—2 μg ml^{-1} for continuous nebulization.

Other Applications. A broader scope for pulse nebulization in AFS and other techniques developed with the present instrumentation was demonstrated in other application as summarized in Table 8. A pulse size of 200 μl was employed in all cases. The technique was suitable for the determination of both major and minor elements in clinical samples.

Table 8. Other applications of pulse nebulization

Element	Technique	Detection limit μg l^{-1}	% Precision at (aqueous level)
Mg	CSAFS	4	2.5 (400 μg l^{-1})
Zn	CSAFS	80	2.3 (500 μg l^{-1})
Fe (248.3 nm)	CSAFS	10	2.6 (500 μg l^{-1})
Na (589 nm)	FAES	3	1.8 (10 μg ml^{-1})
P (246.4 nm)	FMFS	21000	2.3 (200 μg ml^{-1})

(FMFS) = Flame molecular fluorescence spectrometry.

Conclusion

The pulse nebulization device was very simple and easily attached to the pneumatic nebulizer, yielding zero dead volume during operation. The sensitivity and analytical precision were comparable to those attainable with large sample volumes aspirated continuously. The procedure was rapid and the volume of sample required for replicate analysis was effectively reduced. Employing the deproteinisation procedure for blood sample pretreatment, this sample introduction technique reduced system clogging with heavy sample matrices, compared to the normal continuous nebulization since less total amount of matrix per sample was introduced into the system. Accuracy was not impaired by the pulse technique.

References

1) E. J. Ekanem, "The Development of Atomic Fluorescence Spectrometric Methods for Clinical Analysis," Ph. D. Thesis, Strathclyde University, (1981)
2) J. R. Sarbeck, St. P. A. John, and J. D. Winefordner, Mikrochim. Acta, **1972**, 55.
3) E. Sebastiani, K. Ohls, and G. Riemer, Fresenius *Z. Anal. Chem.*, **264**, 105 (1973)
4) N. E. Korte, J. L. Moyers, and M. B. Denton, *Anal. Chem.*, **45**, 530 (1973)
5) D. C. Manning, *At. Absorpt. Newsl.*, **14**, 169, (1975)
6) H. Berndt and E. Jackwerth, *Spectrochim. Acta*, **30B**, 169 (1975).
7) K. C. Thompson and R. G. Godden, *Analyst*, **101**, 96 (1976)
8) K. C. Thompson and R. G. Godden, *Analyst*, **101**, 174 (1976)
9) R. C. Fry, S. J. Northway, and M. B. Denton, *Anal. Chem.*, **50**, 1719 (1978)
10) A. Eaton and E. Schiemer, *At. Absorpt. Newsl.*, **17**, 113 (1978)
11) H. Berndt and W. Slavin, *At. Absorpt. Newsl.*, **17**, 109, (1978)
12) R. G. Michel, M. L. Hall, S. A. K. Rowland, J. Sneddon. J. M. Ottaway, and G. S. Fell, *Analyst*, **104**, 505 (1979)
13) R. G. Michel, J. Sneddon, J. K. Hunter, J. M. Ottaway, and G. S. Fell, *Analyst*, **106**, 288 (1981).

A New Synthesis of Pyrazolo[3,4-*b*]quinoline Derivatives†

D. C. Holla and S. Seshadri*

Dyes Research Laboratory, University Department of Chemical Technology, Matunga, Bombay 400019, India

(Received August 29, 1983)

A new synthesis of pyrazolo[3,4-b]quinoline-4-carboxylic acid derivatives is described. This involves the Pfitzinger reaction of pyrazolone derivatives with isatic acid under controlled conditions. The pyrazoloquinolinecarboxylic acids were converted to their corresponding amides and nitriles, and their absorption and emission characteristics are recorded.

The use of pyrazolo[3,4-*b*]quinoline derivatives as fluorescent brighteners is well known.[1] The major synthetic approach has been the cyclization of appropriately substituted *N*-(1-alkyl-5-pyrazolyl)anthranilic acids by phosphoryl chloride. 5-Chloro-4-formylpyrazoles and substituted aromatic amines on heating form respective 1-phenylpyrazolo[3,4-*b*]-quinoline derivatives which are reported[2,3] to be optical brightening agents.

An obvious alternate synthetic route would be the reaction of pyrazolone derivatives with isatin under the Pfitzinger conditions which would yield the pyrazolo [3,4-*b*]quinoline-4-carboxylic acid. Rather surprisingly, this simple synthetic scheme has not been previously described in the literature. This synthetic scheme has the advantage that different pyrazolones can be employed and further the resultant carboxylic acid could also be further converted to different derivatives such as amide or nitrile.

The Pfitzinger reaction on 3-methyl-1-phenyl-5-pyrazolone (**IIb**) was carried out under normal conditions, employing isatin (**I**) in 40% sodium hydroxide solution. Under these conditions the reaction did not occur even when the reaction mixture was heated for several hours. It was thought that the failure of the reaction might be due to the existence of the pyrazolone in the enolic form in the alkaline conditions, tending to make the pyrazolone inactive for the reaction with isatic acid (2-aminophenylglyoxylic acid). We, therefore carried out the reaction at a certain level of basicity (pH 10—11) so that the enolization would not be complete and the active methylene group would be able to react with isatic acid. Indeed, under these conditions the reaction did take place and on work-up by acidification a yellow product was obtained which was characterized as the expected 3-methyl-1-phenyl-pyrazolo[3,4-*b*]quinoline-4-carboxylic acid (**IIIb**). The structure of this product was established by its acidic character, infrared spectrum (carboxylic acid at 1695 cm^{-1}) and elemental analysis and also by conversion into its derivatives like amide (**IVb**) and nitrile (**Vb**).

Rather surprisingly, the fluorescence of this acid was weak and we therefore wished to study the fluorescence of the derivatives of this acid. Thus the amide (**IVb**) was prepared by the usual method and the amide (**IVb**) was converted to nitrile (**Vb**). The nitrile (**Vb**) was expected to show enhanced fluorescence compared to the carboxylic acid (**IIIb**) but we found that there was no improvement in the fluorescence intensity.

We then proceeded to synthesise other pyrazolo [3,4-*b*]quinoline derivatives by this route. Thus, 3-methyl-5-pyrazolone (**IIa**) was reacted with isatin and 1-unsubstituted pyrazoloquinolinecarboxylic acid (**IIIa**) was obtained. This was further alkylated by dimethyl sulfate to yield the *N*-methyl derivative (**VIa**) and by acrylonitrile to yield *N*-(2-cyanoethyl) derivative (**VIb**). The alkylation products have been given the structures as indicated since there was only a slight bathochromic shift on alkylation. Alkylation on the 2-nitrogen atom would have yielded a quinonoid structure, which would have given a larger bathochromic shift. Thus the compounds (**IIIa, VIa, VIb, IIIb**) showed absorption maxima 382, 386, 392, and 386 nm respectively whereas 2-phenyl derivative (**X**) prepared by us earlier[4] had maximum at 420 nm (Chart 2).

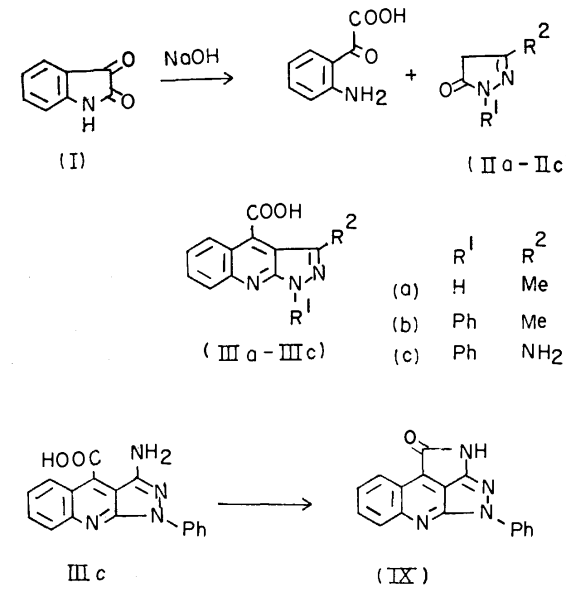

Chart 1.

We found to our satisfaction that the *N*-alkyl derivatives showed much stronger fluorescence and even the *N*-unsubstituted derivative (**IIIa**) showed stronger fluorescence than the *N*-phenyl derivative (**IIIb**). The N-unsubstituted pyrazoloquinolinecarboxylic acid and the two *N*-alkyl derivatives were also converted into the corresponding amides (**VIIa** and **VIIb**) and nitriles (**VIIIa** and **VIIIb**). The absorption and fluorescence efficiencies of these compounds were also studied (Table 1)

From our studies, it can be seen that the *N*-alkylpyrazolo[3,4-*b*]quinoline derivatives are strong

† Abstracted in part from the Ph. D. thesis of D. C. Holla, University of Bombay, 1976.

TABLE 1. PHYSICAL DATA OF VARIOUS PYRAXAZOLO[3,4-*b*]QUINOLINE-4-CARBOXYLIC ACIDS AND DERIVATIVES

Compound	Yield %	Mp θ_m/°C	Recrystallization solvent	λ_{max} absorption/nm	log *E*	λ_{max} emission/nm
Carboxylic acid						
IIIa	65	>300	EtOH	382	3.74	425
IIIb	62	188—190	EtOH	386	3.81	480
IIIc	58	214—215	EtOH			
Amides						
IVa	78	276—280	EtOH	388	3.74	434
IVb	80	>300	EtOH	394	3.54	494
VIIa (*N*-CH_3)	80	226—228	EtOH	394	3.93	456
VIIb (*N*-CH_2CH_2CN)	82	246—248	EtOH	392	3.86	434
Nitriles						
Va	86	180—182	C_6H_6	418	3.69	470
Vb	84	>300	EtOH	428	3.36	494
VIIIa (*N*-CH_3)	79	260—262	EtOH	396	3.59	490
VIIIb (*N*-CH_2CH_2CN)	83	166—168	EtOH	400	3.50	472

fluorophores but comparison with a commercial fluorescent brightener (7-diethylamino-4-methylcoumarin) showed them to be very much inferior. These compounds were also evaluated by application to polyester fibre but they did not produce significant brightening.

We also carried out the Pfitzinger reaction on 3-amino-1-phenyl-5-pyrazolone (**IIc**) and the product obtained was the expected 3-aminopyrazolo[3,4-*b*]-quinoline-4-carboxylic acid (**IIIc**) as shown by its amphoteric properties, infrared spectrum (doublet for the amino group at 3200 and 3100 cm^{-1} and carboxyl carbonyl at 1650 cm^{-1}) and elemental analysis. This compound could be converted to the lactam (**IX**) by treatment with conc. hydrochloric acid. The structure of the lactam (**IX**) was established by elemental analysis and infrared spectrum (lactam carbonyl at 1720 cm^{-1}). The amino acid (**IIIc**) and the lactam (**IX**) were strongly colored and did not show any fluorescence (Chart 1).

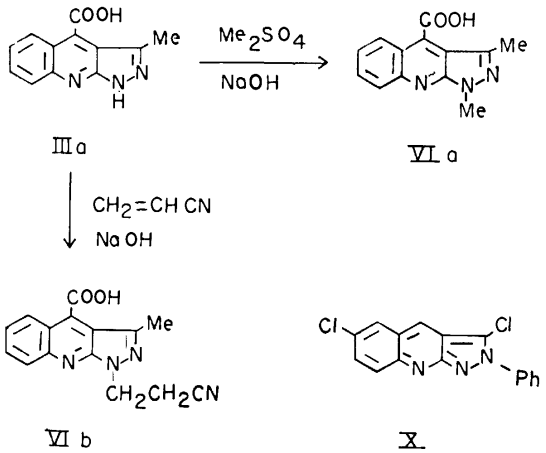

Chart 2.

Experimental

All melting points are uncorrected. The IR spectra were recorded on different spectrophotometers as Nujol mull and the UV spectra were recorded on Pye-Unicam SP8000.

General Procedure for the Synthesis of Pyrazolo[3,4-b]quinoline Derivatives. To a clear solution of isatin (6.8 mmol) in NaOH (10 ml, 10%) pyrazolone derivative (**IIa—IIc**) (7 mmol) was added and stirred till a homogeneous solution was obtained. The pH of the solution was adjusted between 10 and 11 by adding a few drops of HOAc. The solution was refluxed for 5 to 6 h and cooled . On acidification (with HCl 1:1 in the case of 3-Methyl-1-phenyl-5-pyrazolone and 3-methyl-5-pyrazolone and with HOAc to pH 6 in the case of 3-amino-1-phenyl-5-pyrazolone). The products separated were isolated. The yield, mp, recrystallization solvent and molecular formula are given in the Table.

*1,3-Dimethylpyrazolo[3,4-b]quinoline-4-carboxylic Acid (**VIa**).* To the solution of **IIIa** (4.4 mmol) in NaOH (20 ml, 5%) dimethyl sulfate (5.3 mmol) was added and the reaction mixture was heated in a water bath at 60—70 °C for 2 h. The resulting yellow solution was cooled and acidified with dil. HCl (2M). A yellow precipitate of **VIa** was obtained in 86% yield and was recrystallized from ethanol as yellow crystals mp >300° (Found: C, 65.1; H, 4.9; N, 17.1%, Calcd for $C_{13}H_{11}N_3O_2$: C, 65.0, H, 4.6, N, 17.5%).

*1-(2-Cyanoethyl)-3-methylpyrazolo[3,4-b]quinoline-4-carboxylic Acid (**VIb**).* To the solution of **IIIa** (4.4 mmol) in NaOH (20 ml, 5%) containing 0.1 g of Triton B as the catalyst acrylonitrile (5.3 mmol) was added and the reaction mixture was stirred at room temperature for 3 h. The sodium salt that separated was acidified with dil. HCl (2M (1M=1 mol dm^{-3})) and the product **VIb** was obtained in 89% yield. This was recrystallized from ethanol mp >236—237 °C (Found: N, 19.7%, Calcd for $C_{15}H_{12}N_4O_2$: N, 20.0%).

*Synthesis of the Lactam (**IX**).* The acid **IIIc** (3.2 mmol) was taken in concd HCl (10 ml) and kept at room temperature for 3 to 4 h. It was diluted with water, when a brown-colored solid **IX** was obtained in 74% and was recrystallized from EtOAc mp >300 °C (Found: N. 19.1%, Calcd for $C_{17}H_{10}N_4O$: N, 19.6%).

General Procedure for the Synthesis of Pyrazolo[3,4-b]quinoline-4-carboxamides. A mixture of the acid (1 g), dry benzene (5 ml), and freshly-distilled thionyl chloride (10 ml) was refluxed for 2 to 3 h. The acid chloride, obtained after removing excess thionyl chloride and benzene, was

treated with liquid ammonia and kept overnight at room temperature. The amide obtained was filtered. The yield, mp, recrystallization solvent, molecular formula of the various amides prepared are given in the Table.

General Procedure for the Synthesis of Pyrazolo[3,4-b]quinoline-4-carbonitriles. These were prepared by refluxing the amide (1 g) with $POCl_3$ (6 ml) in an oil bath at 110—115 °C for 2 h. After the usual work-up, the product separated was isolated. The yield, mp, recrystallization solvent, molecular formula of the various nitriles prepared are given in the Table.

We are thankful to Prof. M.R. Padhye for recording the IR and UV spectra and to the Microanalytical section of our department for the analyses. One of us (D.C.H.) is thankful to C.S.I.R., New Delhi for the award of a junior research fellowship.

References

1) H, Gold, "The Chemistry of Synthetic Dyes", ed by K. Venkatraman, Academic Press, New York and London 1971, Vol. V, Page 659.

2) A. Brack (Farben fabriken Bayer A. G.) Belg. Pat. 617180, *Chem. Abstr.* **59**, 636 (1963).

3) A. Brack (Farben fabriken Bayer, Laver Kusa Ger) *Ann. Chem.*, **681**, 105—110 (1965) *Chem. Abstr.*, **62**, 11799 (1965).

4) V. Purnaprajna and S, Seshadri, *Ind. J. Chem. Sect. B*, **14B**, 971—2 (1976).

The Self-condensation of Methyl Iodide. The Intermediacy of Methylium Ions in C-C Bond Formation

Yoshio ONO* and Masahiko KOGAI

Department of Chemical Engineering, Tokyo Institute of Technology, Ookayama, Meguro-ku, Tokyo 152

(Received November 22, 1983)

Synopsis. Hydrocarbons are formed by the reaction of methyl iodide vapor with solid-silver dodecatungstophosphate. The self-condensation is plausibly initiated by the attack of the methylium ion on the C-H bond of methyl iodide. It is suggested that the methylium ion is a key intermediate also in the conversion of methanol into hydrocarbons.

Since the conversion of methanol into hydrocarbons over ZSM-5 zeolites was discovered, many discussions have been reported on the mechanism of the reaction, especially with regard to the first C-C bond formation.[1] As for the first C-C bond formation, three major intermediates proposed are carbenoid species,[2] the trimethyloxonium ion,[3] and the methylium ion.[4]

Ono and Mori[4] proposed the intermediacy of the methylium ion, which attacks the C-H bond of methanol or dimethyl ether by forming a three center-two electron bond. The methylium ion would be generated by the reaction of the acidic sites and methanol (or dimethyl ether).

$$H^+ + CH_3OH \longrightarrow CH_3^+ + H_2O$$

$$CH_3^+ + CH_3OR \longrightarrow \left[\begin{array}{l} H \\ CH_3 \end{array}\!\!>\!\!\!-\!\!-CH_2OR\right]^+$$

$$\longrightarrow CH_3CH_2OR + H^+$$

The carbon-carbon bond formation *via* the direct attack of the methylium ion on a C-H bond has been established in superacid chemistry, as examplified by the polymerization of methane.[5] According to the above shceme, the C-C bond formation should occur even without acid centers if the methylium ion is provided in some another way. We have attempted such experiments.

As the source of methylium ions, the reaction of methyl iodide and silver cation was selected, since combinations of methyl iodide and a metal cation are known to be good methylating reagents.

$$CH_3I + Ag^+ \longrightarrow CH_3^+ + AgI \qquad (1)$$

As a silver salt, silver dodecatungstophosphate ($Ag_3PW_{12}O_{40}$, AgTP) was selected. The ease of the reaction between methyl iodide and AgTP is evidently shown by the fact that the immediate precipitation of silver iodide is observed when methyl iodide is added to a methanol solution of AgTP at room temperature.

If methylium ions are generated by Reaction (1), they would attack C-H bonds of methyliodide molecules to form C-C bonds.

We wish to report here the formation of hydrocarbons by the reaction of methyl iodide vapor with solid AgTP.

The reaction was carried out as follows: The powder of AgTP (1 g=8.3×10^{-4} mol of Ag^+) was placed in a reactor which was a part of a closed-recirculation system (dead volume, 234 ml), heated under a vacuum at 573 K, and then kept at the reaction temperature. Methyl iodide vapor (17.7×10^{-4} mol) was then admitted to the system, and the change in the gas phase composition was monitored with the time by withdrawing small portions of the gas at appropriate intervals.

In Fig. 1, the amount of methyl iodide which disappeared from the gas phase and the amount of hydrocarbons which appeared in the gas phase at 373 K are plotted as functions of the reaction time. The distribution of hydrocarbons produced is also shown. Both the yield and the distribution of hydrocarbons are expressed on a carbon-number basis. The amount of methyl iodide consumed and that of hydrocarbons produced increased gradually with the time, until the reaction almost ceased after 5 h, when hydrocarbons amounting to 6.6×10^{-4} mol of carbon atoms appeared in the gas phase. This amount corresponds to about 80% of that Ag^+ ions in the salt, indicating that the reaction is a stoichiometric one.

The amount of methyl iodide disappearing from the gas phase was more than the amount of hydro carbons and even more than the amount of Ag^+ in the salt. The difference may be due to the sorption of unreacted methyl iodide in the bulk of the solid and/or the accumulation of part of the hydrocarbon prod-

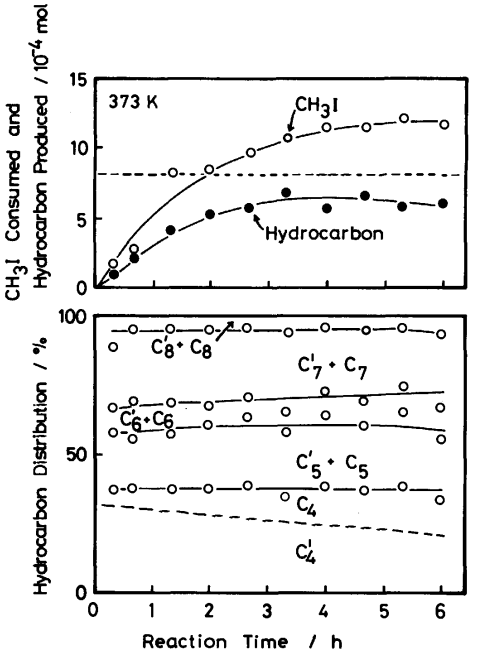

Fig. 1. Change in the amount of CH_3I consumed and hydrocarbons produced with time in the reaction of CH_3I and $Ag_3PW_{12}O_{40}$ at 373 K.

ucts in the solid. The main hydrocarbon products at this temperature are aliphatic hydrocarbons with carbon atoms of 4—7.

At 423 K, the reaction procceded faster. The methyl iodide disappearing from the gas phase amounted to 10.6×10^{-4} mol after 1.5 h. The amount of hydrocarbon produced was 8.3×10^{-4} mol after a reaction of 15 min.

At 573 K, the stoichiometric amount of methyl iodide was consumed within 5 min, as is shown in Fig. 2. The further consumption of methyl iodide continued for another 30 min, even though the amount of hydrocarbons in the gas phase did not increase any longer. At this temperature, the main hydrocarbon products were propane and isobutane. Propylene and butenes found at the early stage disappeared after 1 h, probably because of their further reactions with methyl iodide. This may be account for the consumption of methyl iodide beyond the stoichiometry based on the silver cation.

The fact that hydrocarbons are formed from methyl iodide in the presence of AgTP strongly indicates the importance of the methylium ion in forming C–C bonds from one-carbon molecules. The reaction is essentially a stoichiometric one. The reaction mechanism may be expressed as follows:

$$CH_3I + Ag^+ \longrightarrow CH_3^+ + AgI$$

$$CH_3^+ + CH_3I \longrightarrow \left[\begin{array}{l} H \\ CH_3 \end{array}\!\!>\!\!\cdots CH_2I\right]^+ \longrightarrow CH_3CH_2I + H^+$$

$$CH_3CH_2I + Ag^+ \longrightarrow CH_2{=}CH_2 + AgI + H^+$$

$$CH_2{=}CH_2 + CH_3I \longrightarrow CH_3CH_2CH_2I$$

$$n CH_3I + n Ag^+ \longrightarrow (CH_2)_n + n AgI \text{ (overall)}$$

Besides the reactions described above, various reactions involving carbenium-ion intermediates, like H-transfer, alkylation, and dimerization, may well occur, resulting in the formation of paraffins. It should be noted that a similar mechanism for the C–C bond formation has been proposed for the self-condensation of methyl fluoride in neat antimony fluoride.[9,10]

AgTP is an effective catalyst for converting methanol into hydrocarbons.[11–13] It has been eatablished that the active centers in this system are Brönsted-acid sites, which are produced by the reduction of silver cations by hydrogen molecules (or atoms) provided by the partial decomposiiton of methanol under the present reaction conditions.[12–14]

The distribution of hydrocarbons in the catalytic conversion of methanol over AgTP at 573 K is very similar to that in the stoichiometric reaction of methyl iodide and AgTP at the same temperature, indicating that the mechanism of the propagation of the C–C chain is the same in the two systems. This again argues favorably for the intermediacy of

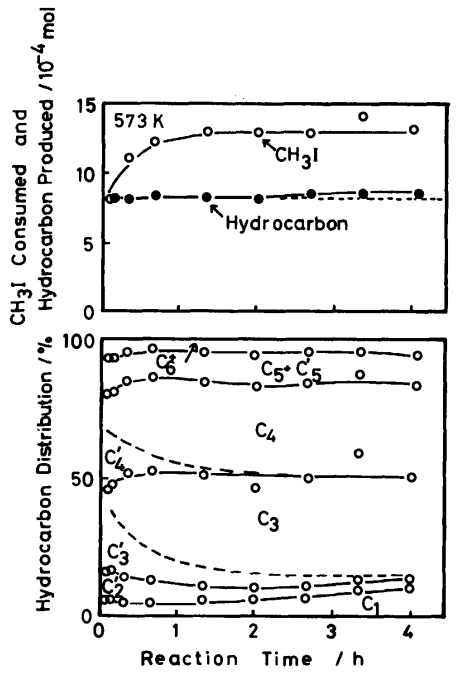

Fig. 2. Change in the amount of CH_3I consumed and hydrocarbons produced with time in the reaction of CH_3I and $Ag_3PW_{12}O_{40}$ at 573 K.

methylium ions in the conversion of methanol into hydrocarbons over acidic catalysts.

It is important to note that hydrocarbons are formed from methyl iodide at temperature at which the hydrocarbon formation from methanol over zeolites or heteropolyacids is practically unobservable. The easier formation of the C–C bonds in the methyl iodide-Ag^+ system may be attributed to the facile generation of incipient methylium ions.

References

1) For a recent review, see C. D. Chang, *Catal. Rev.*, **25**, 1 (1983).

2) C. D. Chang and A. J. Silvestri, *J. Catal.*, **47**, 249 (1977).

3) J. P. van den Berg, J. P. Wilthuizen, and J. H. C. van Hooff, in L. V. Rees (ed.), Proc. 5th Int. Conf. Zeolites (1980), p. 649.

4) Y. Ono and T. Mori, *J. Chem. Soc., Faraday Trans. 1*, **77**, 2209 (1981).

5) G. A. Olah, G. Klopman, and R. H. Schlosberg, *J. Am. Chem. Soc.*, **91**, 3261 (1977).

6) G. A. Olah, J. R. DeMember, and R. H. Schlosberg, *J. Am. Chem. Soc.*, **91**, 2112 (1969).

7) G. A. Olah, J. R. DeMember, R. H. Schlosberg, and Y. Halpern, *J. Am. Chem. Soc.*, **94**, 156 (1972).

8) Y. Ono, T. Baba, J. Sakai, and T. Keii, *J. Chem. Soc., Chem. Comm.*, **1981**, 400.

9) T. Baba, J. Sakai, and Y. Ono, *Bull. Chem. Soc. Jpn.*, **55**, 2633 (1982).

10) Y. Ono, M. Kogai, and T. Baba, in Proc. Pan-Pacific Synfuel Conf. Vol. 1, Japan Petroleum Institute (1982), Tokyo, p. 115.

11) T. Baba and Y. Ono, *J. Phys. Chem.*, **87**, 2406 (1983).

Formation of Aluminosilicate by Adsorption of Silicic Acid on Aluminium Hydroxide

Takushi YOKOYAMA,* Osamu NAKAMURA,† and Toshikazu TARUTANI
Department of Chemistry, Faculty of Science, Kyushu University 33, Hakozaki, Higashiku, Fukuoka 812
(Received February 15, 1984)

Synopsis. When monosilicic acid was adsorbed on aluminium hydroxide, allophane-like compound rapidly formed and the monosilicic acid adsorbed was consumed by the formation of the allophane-like compound until the Si/Al mole ratio of the sample reached 0.33—0.39. Above these ratio, the formation of polysilicic acid occured.

Some reports have been published on the formation of surface products by adsorption of silicic acid on solids. Huang[1] suggested the formation of phyllite sheets on γ-alumina from a kinetic study. Muraishi and Kitahara[2] confirmed the formation of magnesium silicate on the surface of magnesium hydroxide by differential thermal analysis (DTA) and infrared absorption.

In a previous paper,[3] the authors reported that aluminium hydroxide, which had adsorbed monosilicic acid, showed an endothermic peak between 100 and 300 °C and an exothermic peak at around 1000 °C on the DTA curve. The DTA curve is similar to the thermal curve of allophane, indicating amorphous aluminosilicate.[4]

In this paper, the formation of an allophane-like compound by the adsorption of monosilicic acid on aluminium hydroxide and the effect of the composition of the samples on the exothermic peak intensity are discussed.

Experimental

All the reagents used were of analytical reagent grade. Monosilicic acid solution and aluminium hydroxide were prepared as described previously.[3,5]

Adsorption experiments were carried out using a batch method[3] and a continuous flow method.[5] In the batch method, a known amount of aluminium hydroxide was introduced into a monosilicic acid solution (500 cm^3) of pH 5. In the continuous flow method, aluminium hydroxide was introduced into a flask and then 150 ppm (SiO_2) monosilicic acid solution of pH 5 was continuously flowed through the flask with a flow rate of 2 dm^3/d. Adsorption experiments were carried out at 25 °C. In both methods, after 5 h or at appropriate intervals, an aliquot of aluminium hydroxide, which had adsorbed silicic acid, was pipetted and filtered, and the composition of the sample was determined. The sample dried at 25 °C for 10 d was used for differential thermal analysis. Si(M)/Al(A) and Si(T)/Al(A) ratios are the mole ratios of monosilicic acid and total silicic acid to aluminium in the sample, respectively. The difference between the two ratios indicates the formation of polysilicic acid on the aluminium hydroxide. Si/Al(MR) ratio is the mole ratio of monosilicic acid to aluminium hydroxide in the initial solution in the batch method.

Differential thermal analysis was performed using a Rigaku Denki Thermoflex 8002 H/D thermoanalyzer. The sample (13.5 mg) in a shallow platinum crucible was heated in air at a heating rate of 10 °C/min. The water content was almost the same in all samples (*ca.* 40%). The reference material was γ-alumina.

Results and Discussion

In a preliminary experiment, it was found that the exothermic peak height decreased steeply with increasing pH of the mother solutions over the pH range 5—10. Therefore, the adsorption experiments were carried out at pH 5. A DTA curve of the sample prepared at pH 5 is shown in Fig. 1. In this study the exothermic peak similar to that of allophane was observed for all samples.

The adsorption experiment (batch method) was carried out under the condition of a 2.1 Si/Al(MR) ratio. The results of the differential thermal analysis of the samples are shown in Fig. 2. The exothermic peak height increased with adsorption time and attained a constant value after 2 h. This indicates that the allophane-like compound rapidly formed by the reaction of the adsorbed monosilicic acid and aluminium hydroxide.

In order to examine the effect of the Si(T)/Al(A) ratio of a sample on the exothermic peak height, adsorption experiments (batch method) were carried out by changing the Si/Al(MR) ratio in 100 and 300 ppm (SiO_2) monosilicic acid solutions. Figure 3 shows the variation of the exothermic peak height with the Si(T)/Al(A) ratio. The maximum peak height occurred at a 0.33 Si(T)/Al(A) ratio. The sample (Si(T)/Al(A)=0.36, Si(M)/Al(A)=Si(T)/Al(A))

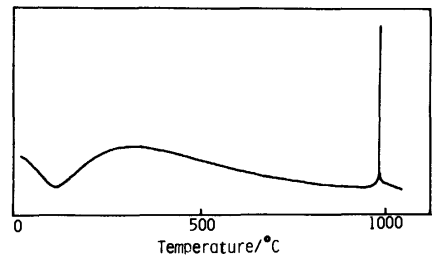

Fig. 1. DTA curve of the sample prepared at pH 5.

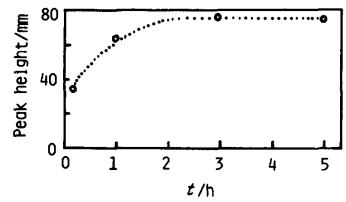

Fig. 2. Variation with adsorption time of exothermic peak height. Initial monosilicic acid concentration: 300 ppm (SiO_2). Si/Al(MR): 2.1. pH: 5.

† Present address: Department of Commerce and Industry, Fukuoka Prefectual Government, Hakataku, Fukuoka 812.

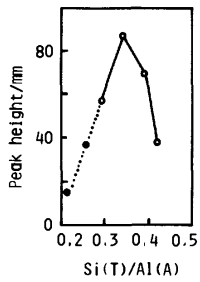

Fig. 3. Variation of exothermic peak height with Si(T)/Al(A) ratio. Initial monosilicic acid concentration: ···●··· 100 ppm, —○— 300 ppm. Reaction time: 5 h. pH: 5.

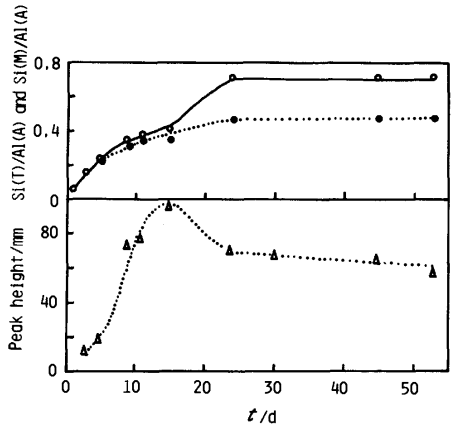

Fig. 4. Variations with time of Si(M)/Al(A) and Si(T)/Al(A) ratios and exothermic peak height. Flowing solution: 150 ppm monosilicic acid solution of pH 5. ···●···: Si(M)/Al(A), —○—: Si(T)/Al(A), ···△···: Exothermic peak height.

was heated at 1000°C for 5 h and the heated sample was analyzed by powder X-ray diffraction. The diffractogram showed the formation of mullite ($3Al_2O_3 \cdot 2SiO_2$). This result also suggests that the sample is an allophane-like compound.[4]

The results obtained by the continuous flow method are shown in Fig. 4. The exothermic peak height increased steeply until the Si(T)/Al(A) ratio reached 0.39 and then declined with further increase in the Si(T)/Al(A) ratio. At an early stage of adsorption the Si(T)/Al(A) and Si(M)/Al(A) ratios increased with time, and the Si(T)/Al(A) ratio was nearly equal to the Si(M)/Al(A) ratio below 15 d. Subsequently the Si(T)/Al(A) ratio became larger than the Si(M)/Al(A) ratio with time, indicating that a part of the silicic acid adsorbed on the aluminium hydroxide polymerized.

As shown in Figs. 3 and 4, the exothermic peak height was strongly influenced by the Si(T)/Al(A) ratio of the sample and the maximum peak height occurred at Si(T)/Al(A) ratios of 0.33 and 0.39. These values are similar to that of mullite. In the sample having the 0.33 Si(T)/Al(A) ratio, the largest amount of the allophane-like compound may exist.

The behavior of monosilicic acid adsorbed on aluminium hydroxide can be explained as follows. When monosilicic acid is adsorbed on aluminium hydroxide, the allophane-like compound rapidly forms and the adsorbed monosilicic acid is consumed by the formation of an allophane-like compound until the Si(T)/Al(A) ratio reaches 0.33. Most of the aluminium hydroxide transforms to the allophane-like compound after a short time. Monosilicic acid is still adsorbed on the allophane-like compound formed, and the adsorbed monosilicic acid polymerizes with time above a Si(T)/Al(A) ratio of *ca.* 0.4.

References

1) C. P. Huang, *Earth Planet. Sci. Lett.*, **27**, 265 (1975).
2) H. Muraishi and S. Kitahara, *Nippon Kagaku Kaishi*, **1978**, 1457.
3) T. Yokoyama and T. Tarutani, *Bull. Chem. Soc. Jpn.*, **55**, 975 (1982).
4) K. Wada, "Clays and Clay minerals of Japan," ed by T. Sudo and S. Shimoda, Kodansha, Tokyo (1978). Chap. 4, p. 160.
5) T. Yokoyama and T. Tarutani, *Mem. Fac. Sci., Kyushu Univ., Ser. C*, **13**, 23 (1981).

Solvent Effects on the $n\rightarrow\pi^*$ Absorption Intensities of Acetone and Cyclopentanone

Tai-ichi SHIBUYA

Department of Chemistry, Faculty of Textile Science and Technology, Shinshu University, Ueda, Nagano 386

(Received April 13, 1984)

Synopsis. The recently proposed theory [*J. Chem. Phys.* **78**, 5175 (1983)] for the solvent effect on the absorption intensity has been successfully applied to the $n\rightarrow\pi^*$ bands of acetone and cyclopentanone in various organic solvents observed by Nakashima, *et al.* [*Bull. Chem. Soc. Jpn.* **55**, 415 (1982)].

Nakashima *et al.*, in their recent paper,[1] correlated the intensities of the $n\rightarrow\pi^*$ absorption bands of acetone and cyclopentanone in various organic solvents to $(\bar{\alpha}/\bar{r}^6)^2$ of the solvents, $\bar{\alpha}$ being the mean molecular polarizability of the solvent and $\bar{r}$ the mean distance between the solute and solvent molecules.[2] The $n\rightarrow\pi^*$ absorption of ketones is usually observed as very weak bands. It is electric-dipole forbidden, but is vibrationally induced.[3,4]

Recently we[5] have shown that the energy density of light acting on the solute molecule is different from that outside of the solution and that the ratio of the observed oscillator strength (f'') to the *true* oscillator strength (f) of the solute molecule is given by

$$f''/f = [s(n^2-1)+1]^2/n. \quad (1)$$

In this expression, n is the refractive index of the medium, and s is a shape parameter between zero and unity depending upon the shape of the cavity in which the solute molecule is supposed to lie and upon the relative direction of the transition moment in the cavity. Eq. (1) may also be written as

$$\sqrt{nf''} = \sqrt{f}s(n^2-1) + \sqrt{f}, \quad (2)$$

which expresses a linear relationship between $\sqrt{nf''}$ and (n^2-1).

Nakashima *et al.*, measured absorption spectra at room temperature. The observed oscillator strengths (f'') of acetone and cyclopentanone in various solvents were estimated from Figs. 6 and 7 in their paper.[1] These values are listed in Table 1. Also listed are the refractive indices (n_{20}^{D}) of these solvents measured[6] at 20°C with the Na-D line. Using these values for n in Eq. (2), we plotted $\sqrt{nf''}$ *vs.* n^2-1 in Figs. 1 and 2. The least-squares fittings give s=0.88 and $f=1.80\times10^{-4}$ for acetone and $s=0.71_5$ and $f=2.27\times10^{-4}$ for cyclopentanone.

These values of s are reasonable since the transition moments of the vibrationally induced $n\rightarrow\pi^*$ transitions of these molecules are supposed to be perpendicular to the plane of the sp^2-hybrid planar structure in the carbonyl group. Note that $s=1$ if the flat molecule is very large compared with the size of the solvent molecules and that $s=1/3$ when the cavity is spherical.[5]

The relation Eq. (1) or (2) was derived in Ref. 5 on the assumptions (i) that both solute and solvent are nonpolar and mutually innert and (ii) that the absorption band is strong enough so that the imaginary part of the polarizability in the frequency region of the absorption is well approximated by this absorption band alone. These conditions are not strictly satisfied here, but the reasonable results obtained here imply that these conditions are fairly well satisfied. It may be interesting to compare the values of f with the gas-phase oscillator strengths ($f°$). Values of $f°$ are, however, not known for the $n\rightarrow\pi^*$ transitions of these molecules.

Solvent effects on the absorption intensity are of two-fold:[5] (a) The effective density of radiation energy "seen" by the solute molecule is different from the energy density when the dielectric medium is eliminated, and (b) the transition moment and the absorption frequency of the solute molecule are different from one solution to another and also different from those of the isolated molecule because of the solute-solvent interaction in the solution systems. In the present paper, only the solvent effect of type (a) was considered. On the other hand, the effect considered

TABLE 1. OBSERVED OSCILLATOR STRENGTHS[a] (f'') AND THE QUANTITIES $\sqrt{nf''}$ OF THE $n\rightarrow\pi^*$ TRANSITIONS OF ACETONE AND CYCLOPENTANONE IN VARIOUS SOLVENTS

Solvent[b]	n[c]	n^2-1	Acetone		Cyclopentanone	
			$f''/10^{-4}$	$\sqrt{nf''}/10^{-2}$	$f''/10^{-4}$	$\sqrt{nf''}/10^{-2}$
(1) C_6F_{14}	1.2514	0.5660	3.33_5	2.04_3	3.56_7	2.11_3
(7) CH_3CN	1.344_{1_1}	0.806_6	4.03_9	2.33_0	4.34_3	2.41_6
(2) C_6H_{14}	1.3748_6	0.890_2	4.15_7	2.39_1	4.15_0	2.38_9
(6) CH_2Cl_2	1.4246	1.029_5	4.43_3	2.51_3	4.87_4	2.63_5
(3) C_6H_{12}	1.4262_3	1.034_1	4.18_9	2.44_4	4.47_2	2.52_5
(5) $CHCl_3$	1.4485_8	1.098_4	4.73_2	2.61_8	5.29_5	2.77_0
(4) CCl_4	1.4603_0	1.132_5	5.26_8	2.77_4	5.55_1	2.84_7
(9) $C_6H_5CH_3$	1.4969_3	1.240_8			5.13_8	2.77_3
(8) C_6H_6	1.5011_2	1.253_4	5.55_1	2.88_7	5.37_4	2.84_0
(10) C_6H_5CN	1.5282	1.335_4			5.64_6	2.93_7

a) Estimated from Figs. 6 and 7 in Ref. 1. b) The numbering of solvents coincides with that of Ref. 1. Here, solvents are in the order of increasing n. c) Refractive indices of solvents, n_{20}^{D} taken from Ref. 6.

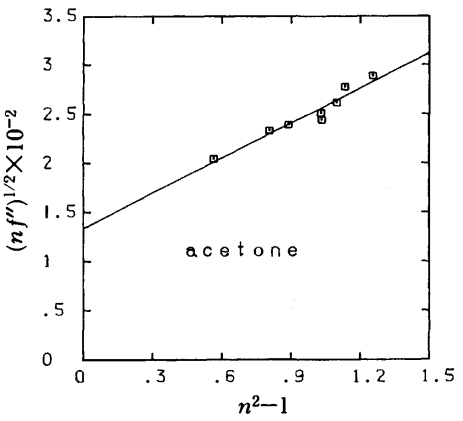

Fig. 1. Plot of $\sqrt{nf''}$ *vs.* n^2-1 for the $n\rightarrow\pi^*$ transition of acetone in various organic solvents. The solid line indicates the least-squares fitted Eq.(2) with $s=0.884$ and $f=1.80_1\times10^{-4}$.

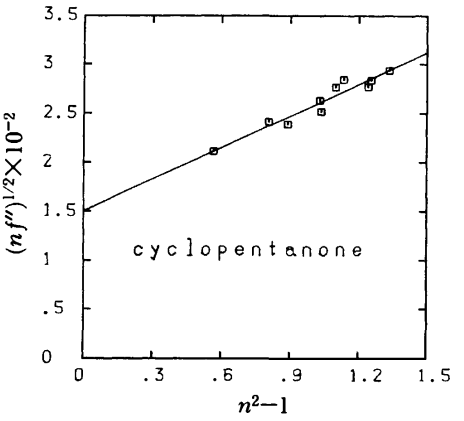

Fig. 2. Plot of $\sqrt{nf''}$ *vs.* n^2-1 for the $n\rightarrow\pi^*$ transition of cyclopentanone in various organic solvents. The solid line indicates the least-squares fitted Eq. (2) with $s=0.715$ and $f=2.27_0\times10^{-4}$.

by Nakashima *et al.*[1] is of type (b). The fact that the linearity of Eq. (2) has been observed fairly well as shown in Figs. 1 and 2 indicates that the effect of type (a) is significant in the solution systems studied here. This, however, does not exclude the possibility that f may be significantly different from f° as the result of the solvent effect of type (b). It is therefore desirable to have experimental values of f° for the $n\rightarrow\pi^*$ transitions of acetone and cyclopentanone.

References

1) K. Nakashima, K. Uchida-Kai, M. Koyanagi, and Y. Kanda, *Bull. Chem. Soc. Jpn.*, **55**, 415 (1982).
2) M. Koyanagi, *J. Mol. Spectrosc.*, **25**, 273 (1968).
3) J. W. Sidman, *Chem. Rev.*, **58**, 686 (1958); J. H. Callomon and K. K. Innes, *J. Mol. Spectrosc.*, **10**, 166 (1963); W. D. Chandler and L. Goodman, *ibid.*, **36**, 141 (1970) and **37**, 33 (1971).
4) J. D. Swalen and C. C. Costain, *J. Chem. Phys.*, **31**, 1562 (1959); M. Koyanagi and L. Goodman, *Chem. Phys.*, **5**, 107 (1974).
5) T. Shibuya, *J. Chem. Phys.*, **78**, 5175 (1983).
6) "Handbook of Chemistry and Physics," 56th ed.. edited by R. C. Weast (CRC Press, Cleveland, 1975—1976).

A Molecular Orbital Study of the 1,2-Migration Reaction of Substituted Cyclohexadienyl Radicals

Osamu KIKUCHI* and Satoshi SHIMOMURA
Department of Chemistry, The University of Tsukuba, Sakura, Ibaraki 305
(Received April 20, 1984)

Synopsis. The 1,2-migration reaction of cyclohexadienyl radicals was examined on the basis of an open-shell restricted self-consistent field (SCF) MINDO/3 calculation. For the NO_2- and OH-substituted cyclohexadienyl radicals, the 6-substituted isomers (**1**; X=H, Y=NO_2 or OH) were calculated to be the least stable and apt to undergo a 1,2-hydrogen shift. The electron-withdrawing groups were predicted to have high migratory aptitude.

The cyclohexadienyl radical, **1**, is considered to be an intermediate in the radical aromatic substitution reaction.[1] The isomer distribution of the reaction products in the radical substitution reaction of substituted benzenes is affected by the stabilities of isomeric cyclohexadienyl radicals.[2]

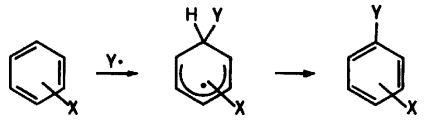

1

Another factor which affects the product distribution is the 1,2-migration reaction of the intermediate radical to give another cyclohexadienyl radical. *p*-Bromonitrobenzene reacts with the Cl radical to give 2-bromo-1-chloro-4-nitrobenzene.[3]

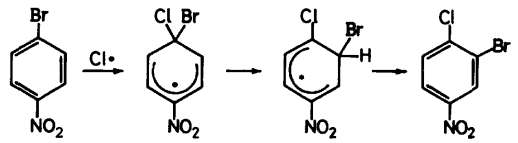

2 **3**

This suggests that the intermediate ipso radical, **2**, rearranges to **3** by the bromo 1,2-shift. The reaction of the adamantyl radical with **4** to give **5** also suggests the 1,2-shift of the CHO group in the intermediate ipso radical.[4]

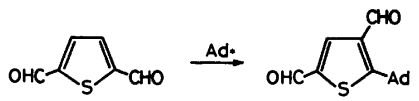

4 **5**

In this note the 1,2-migration reaction of cyclohexadienyl radicals is examined theoretically. The open-shell restricted SCF method[5] with MINDO/3 approximation[6] was applied to substituted cyclohexadienyl radicals, **1**, and to the bridged radicals, **6**, which are the transition states of the 1,2-migration reaction.

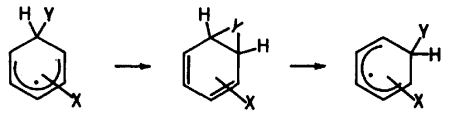

1 **6**

Results and Discussion

1,2-Shift of Cyclohexadienyl Radical. The structures of unsubstituted cyclohexadienyl radical, **1** (X=Y=H), and the transition state bridged radical, **6** (X=Y=H), were optimized by assuming a planar carbon skeleton,[7] C_{2v} symmetry for **1** and C_s symmetry for **6**. The structures obtained are shown in Fig. 1. Structure **II** is that of the transition state, since a small deviation of the migrating H atom out of the C_s symmetry plane results in energy lowering. The schematic representation of the singly-occupied molecular orbitals (SOMO) of **I** and **II** are shown in Fig. 2. The energy difference between **I** and **II**, 156 kJ/mol, is the activation energy of the 1,2-hydrogen shift of **I**.

Substituent Effect. The substituent effect on the 1,2-hydrogen shift was examined by using the NO_2 and OH groups as the substituent. The **I** and **II** structures were employed and partial optimization was performed for the substituent structure. The calculated heats of formation are listed in Table 1. The activation energies are shown in Fig. 3. For the NO_2- and OH-substituted cyclohexadienyl radicals, the 3-substituted isomer was predicted to be the most stable, while the 6-substituted isomer was the least stable. The stability of the 3-substituted isomer may be understood from the interaction between the SOMO of **I** (Fig. 2-a) and the substituent. The energy differences among the transition states are small in comparison with those among the reactant isomers, suggesting that the liability of the 1,2-shift is determined by the instability of the reactant radical.

Migratory Aptitude. The migratory ability of migration groups was estimated from the energy differences between **1** (X=H) and **6** (X=H) for Y=CH_3, H, NO_2, and CHO. The structure of **6** was optimized for each migration group. The calculated activation energies are listed in Table 2. The activation energies for the 1,2-shift of electron-withdrawing groups (NO_2 and CHO) are smaller than those for the H and CH_3 groups. This trend is well explained by the stability of the SOMO at the transition state. In the H shift, the unpaired electron localizes on the six-membered carbon ring (Fig. 2-b). On the other hand, in the case of the CHO shift, the unpaired electron delocalizes into the antibonding π-orbital of the carbonyl group (Fig. 4); this delocalization lowers the SOMO energy. The easy transformation of the electron-withdrawing

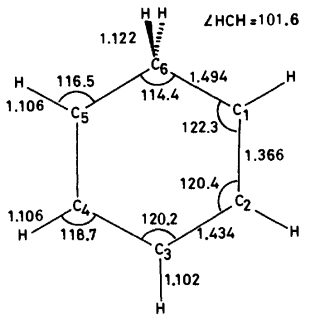

I

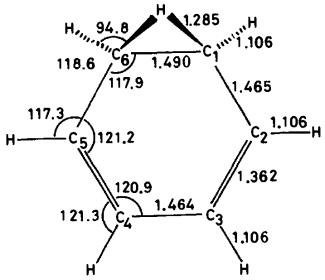

II

Fig. 1. The optimized structures of cyclohexadienyl radical, I, and the transition state of the 1,2-hydrogen shift, II. Bond lengths are in A and bond angles in degrees.

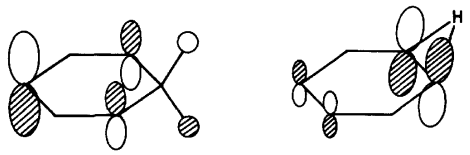

a b

Fig. 2. Schematic representations of (a) SOMO of I and (b) SOMO of II.

group, as is observed in the **4**→**5** reaction, is caused by the stabilization of the transition state due to the delocalization of the unpaired electron into the migrating group.

References

1) M. J. Perkins, "*Aromatic Substitution*" in "*Free Radicals II*," ed by J. K. Kochi, John Wiley & Sons, New York (1973), p. 231.

2) The recent theoretical works calculated relative stabilities of substituted cyclohexadienyl radicals: A. J. Birch, A. L. Hinde, and L. Radom, *J. Am. Chem. Soc.*, **102**, 4074 (1980); R. G. Gandour, *Tetrahedron*, **36**, 1001 (1980).

3) C. R. Everly and J. G. Traynham, *J. Am. Chem. Soc.*, **100**, 4316 (1978).

4) M. Tiecco, *Acc. Chem. Res.*, **13**, 51 (1980).

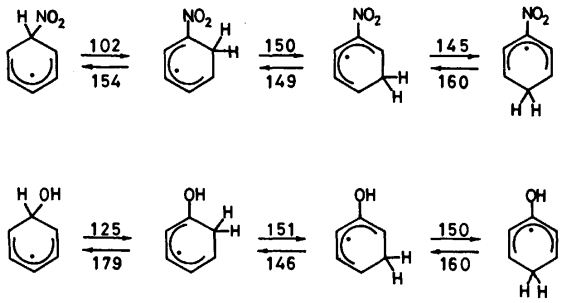

Fig. 3. Activation energies for the 1,2-hydrogen migration reactions of the NO_2 or OH substituted cyclohexadienyl radicals. Values are in kJ/mol.

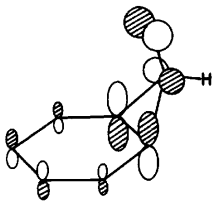

Fig. 4. Schematic representation of SOMO of the transition state of the 1,2-CHO shift.

TABLE 1. CALCULATED HEATS OF FORMATION (KJ/mol) OF NO_2 AND OH SUBSTITUTED CYCLOHEXADIENYL RADICALS AND OF THE TRANSITION STATE FOR THE 1, 2-HYDROGEN SHIFT

Cyclohexadienyl[a]			
1-NO_2	124	1-OH	−59
2-NO_2	125	2-OH	−54
3-NO_2	110	3-OH	−64
6-NO_2	176	6-OH	−5
Transition state[b]			
1-NO_2	278	1-OH	120
2-NO_2	274	2-OH	92
3-NO_2	270	3-OH	96

a) Numbering is shown in I of Fig. 1. b) Numbering is shown in II of Fig. 1.

TABLE 2. CALCULATED ACTIVATION ENERGIES(KJ/mol) FOR THE 1,2-SHIFT

Migration group	Activation energy
CH_3	181
H	156
NO_2	96
CHO	66

5) K. Hirao and H. Nakatsuji, *J. Chem. Phys.*, **59**, 1457 (1973).

6) R. C. Bingham, M. J. S. Dewar, and D. H. Lo, *J. Am. Chem. Soc.*, **97**, 1285 (1975).

7) CNDO/2 calculation of a 6-substituted cyclohexadienyl radical showed a small out-of-plane distortion of the CHY group (4° for Y=$SiMe_3$): M. Kira and H. Sakurai, *J. Am. Chem. Soc.*, **99**, 3892 (1977).

The Cooperative Binding Isotherms of Sodium Alkanesulfonates to Poly(1-methyl-4-vinylpyridinium chloride)

Iwao SATAKE,* Katumitu HAYAKAWA, Mayumi KOMAKI, and Tamaki MAEDA
Department of Chemistry, Faculty of Science, Kagoshima University, Korimoto, Kagoshima 890
(Received May 1, 1984)

Synopsis. Binding isotherms of nonane-, decane-, and undecane- sulfonate ions to poly (1-methyl-4-vinylpyridinium chloride) were determined by using nitrobenzene-membrane electrode. It was shown that an increase in alkyl chain length is accompanied not only by a rapid increase in the cooperativity parameter but by a regular decrease in an equilibrium surfactant concentration at half binding.

Recently, much attention has been paid to the potentiometric determination of the cooperative binding isotherms of the surfactant ion to polyions such as ionic polypeptide,[1,2] synthetic polyelectrolyte,[3-7] polysaccharide,[5-8] and DNA.[9] In all cases, the binding isotherm has been found to rise steeply in quite narrow range of the equilibrium surfactant concentration. It is now well recognized that the hydrophobic interaction among the bound surfactant molecules plays an important role in determining the nature of the cooperative binding isotherm. In order to make this point clear, we studied in this communication the effect of the surfactant chain length on the cooperative binding isotherm of sodium alkanesulfonate to poly (1-methyl-4-vinylpyridinium chloride) (PVMP) in the presence of added salt.

Experimental

Sodium alkanesulfonates (SAS) with carbon atoms (n) of 9, 10, and 11 were synthesized from the alkyl bromides purified by vacuum distillation.[10] The products were purified by the recrystallization from water, then from methanol and finally by extraction with petroleum ether for 20 h. PVMP was prepared by quaternization of poly (4-vinylpyridine) with methyl bromide.[11] The product was then converted to the chloride through dialysis against NaCl solution. An infrared spectrum showed that virtually all of the pyridine moiety was quaternized. The concentration (C_p) of PVMP in molarity of ionic groups was determined by titrating the corresponding polybase with HCl.

The binding isotherm of SAS to PVMP was determined potentiometrically at 25 °C by using the following cell. Reference electrode (Ag-AgCl)| NH_4NO_3 agar bridge| Reference solution (SAS, C_r)| Nitrobenzene (DTAAS, 1×10^{-4} mol dm^{-3})| Sample solution (PVMP, C_p; SAS, C; NaCl, C_s)| NH_4NO_3 agar bridge| Reference electrode (Ag-AgCl) where DTAAS denotes an ion exchanger, dodecyltrimethylammonium alkanesulfonate, and C_r and C the concentrations of SAS in reference and sample solutions, respectively. The concentrations of PVMP and NaCl were kept constant throughout whole experiments. The electromotive force (E) of the cell was measured with an Orion digital pH meter model 701 A with an accuracy of ±0.1 mV.

Results and Discussion

Prior to the measurements on PVMP solutions, the membrane electrode was calibrated with solutions of SAS. In the absence of PVMP, a plot of E *vs.* log C gave a straight line with a slope of 58.6 mV for n=9, 58.8 mV for n=10, and 59.7 mV for n=11, respectively. The linear relation was found to hold in the concentration range above 2×10^{-5} mol dm^{-3} for n=11 and 10, and 2×10^{-4} mol dm^{-3} for n=9. These calibration curves permit the determination of an equilibrium surfactant concentration (C_f) in solution of SAS with PVMP. The degree of binding of the surfactant ion by PVMP (β) can then be given by $\beta=(C-C_f)/C_p$.

The binding isotherms of SAS to PVMP thus determined are shown in Fig. 1. In conformity with the results obtained for a variety of surfactant ion-polyion systems,[1-9] the binding isotherm rises steeply in narrow range of C_f, reflecting the highly cooperative nature of the binding process of alkanesulfonate ion to PVMP. An important feature of Fig. 1 is the striking effect of the surfactant chain length on the critical range of C_f where the steep rise in binding isotherm occurs. Indeed, the successive decrease in n causes approximately four-fold increase of the value of C_f at β=0.5. Moreover, the steepness of the binding isotherm tends to decrease regularly with decreasing alkyl chain length. According to the theoretical treatment of the surfactant ion-polyion interactions, the surfactant ion is considered to cluster side by side onto the ionic groups of the polyion.[1] Hence, the regular dependence of the cooperativity on alkyl chain length may reasonably be ascribed to a change in hydrophobic interaction among the bound surfactant ions.

The cooperative binding isotherm in excess salt solution can well be described by the following expressions.[1]

$$2\beta - 1 = (y-1)/[(1-y)^2+4y/u]^{1/2} \quad (1)$$

$$KuC_f(\beta=0.5) = 1 \quad (2)$$

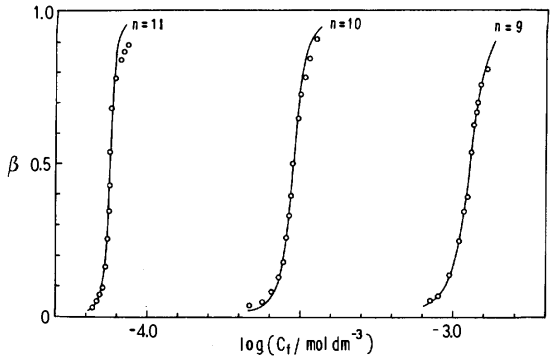

Fig. 1. The binding isotherms of alkanesulfonate ions to PVMP at 25 °C. $C_p=2.55\times10^{-4}$ mol dm^{-3}, $C_s=2.12\times10^{-2}$ mol dm^{-3}. O, observed; solid line, calculated isotherm from Eq. 1 with u=220 for n=9, 480 for n=10, and 2000 for n=11, respectively.

Here, y refers to $C_f/[C_f(\beta=0.5)]$, K is the apparent binding constant of the surfactant ion to a site which has two unoccupied neighbors, and Ku is that to a site which has one or more occupied neighboring sites, respectively. Equation 1 can easily be rearranged to

$$2\beta - 1 = u^{1/2}(y-1)[\beta(1-\beta)/y]^{1/2}. \quad (3)$$

This equation implies that the plot of β *vs.* $(y-1)[\beta(1-\beta)/y]^{1/2}$ gives a straight line with a slope of, $u^{1/2}/2$. As is shown in Fig. 2, such a plot gives in fact a straight line over a wide range of β. A least squares treatment leads to the most reliable value of the cooperativity parameter, u, of 220 for n=9, 480 for n=10, and 2000 for n=11, respectively. The calculated binding isotherms from Eq. 1 with the values of u so determined are shown in Fig. 1. In all cases, the agreement is satisfactory up to about β=0.8. As may be expected, the value of u increases rapidly with increasing alkyl chain length. This, in turn, suggests that the hydrophobic interaction among the bound surfactant ions is of primary importance in determining the cooperativity of the binding process of a homologous series of surfactant ions to a given polyion. An interesting comparison may be made here among the values of u for surfactant ions with the same alkyl chain length. For example with sodium decyl sulfate, the value of u was found to be 77 for helical poly(L-ornithine),[1] 161 for poly (D,L-ornithine),[1] and 26 for a copolymer of diallyldimethylammonium chloride and sulfur dioxide.[3] In the case of cationic surfactants, the value of u was estimated to be 40 for decylammonium chloride in a helical poly (L-glutamic acid) solution[2] and 200 for 1-decylpyridinium bromide in a sodium poly (vinyl sulfate) solution.[4] These observations indicate that the cooperativity parameter depends also on the polyion conformation as well as the hydrophobic character of the polyion residue.

According to Eq. 2, the logarithm of C_f (β=0.5) is anticipated to depend linearly on n, since an increment in $-RT$ ln Ku per CH_2 group represents the free energy of transfer, w, of a methylene group from aqueous medium to the surfactant ion cluster on the polyion. Indeed, the plot of ln $[C_f(\beta=0.5)/\text{mol dm}^{-3}]$ *vs.* n gives a straight line with a slope of -1.36 which corresponds to w of -3370 J mol^{-1} at 25 °C. The fact that the estimated value of w is comparable to that of -3700 J mol^{-1} from aqueous medium to liquid hydrocarbons[12] reflects well the hydrophobic character of the bound surfactant ion cluster on the polyion chain. In their study

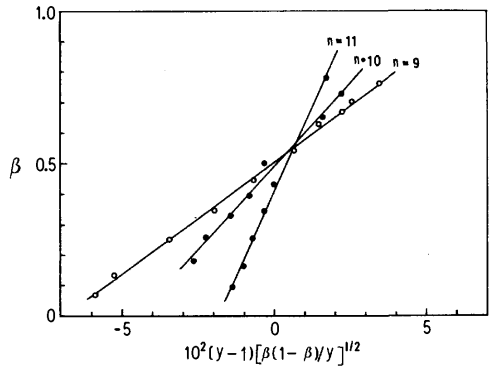

Fig. 2. Plots of β *vs.* $(y-1)[\beta(1-\beta)/y]^{1/2}$.

of the cooperative binding isotherms of dodecyl- and tetradecyltrimethylammonium ions to alginate, pectate, and carboxymethylcellulose, Hayakawa *et al.*[7] obtained the values of w of $-$(3150—3330) J mol^{-1} at 30 °C. Thus, the local environment around the alkanesulfonate ions bound to PVMP is supposed to be similar in its hydrophobicity to those around the alkyltrimethylammonium ions bound to the ionic polysaccharides.

References

1) I. Satake and J. T. Yang, *Biopolymers*, **15**, 2263 (1976).
2) I. Satake, T. Gondo, and H. Kimizuka, *Bull. Chem. Soc. Jpn.*, **52**, 361 (1979).
3) K. Shirahama, H. Yuasa, and S. Sugimoto, *Bull. Chem. Soc. Jpn.*, **54**, 375 (1981).
4) K. Shirahama and M. Tashiro, *Bull. Chem. Soc. Jpn.*, **57**, 377 (1984).
5) K. Hayakawa and J. C. T. Kwak, *J. Phys. Chem.*, **86**, 3866 (1982).
6) K. Hayakawa and J. C. T. Kwak, *J. Phys. Chem.*, **87**, 506 (1983).
7) K. Hayakawa, J. P. Santerre, and J. C. T. Kwak, *Macromolecules*, **16**, 1642 (1983).
8) K. Hayakawa, A. Latiff Ayub, and J. C. T. Kwak, *Colloids and Surfaces*, **4**, 389 (1982).
9) K. Hayakawa, J. P. Santerre, and J. C. T. Kwak, *Biophys. Chem.*, **17**, 175 (1983).
10) S. Zuffanti, *J. Am. Chem. Soc.*, **62**, 1044 (1940).
11) Yu. E. Kirsh, V. Ya. Kovner, A. I. Kokorin, K. I. Zamaraev, V. Ya. Chernyak, and V. A. Kabanov, *Eur. Polym. J.*, **10**, 671 (1974).
12) C. Tanford "The Hydrophobic Effect: Formation of Micelles and Biological Membranes," John Wiley & Sons, New York (1973), Chap. 2.

Fermi Resonance Effects on the ν_1 Raman Bands of Liquid CH_2Br_2 and CH_3Br

Kazuyoshi FUJITA, Takuya FUKUDA, Kohji FUKUSHI, and Masao KIMURA*
Department of Chemistry, Faculty of Science, Hokkaido University, Sapporo 060
(Received May 16, 1984)

Synopsis. Applying Fermi-resonance-band-shape functions to the isotropic Raman band profiles of liquid CH_2Br_2 and CH_3Br in the ν_1 region, the peak frequencies, band-widths, and coupling constants of the ν_1 and combination vibrations have been determined.

In a previous paper on the Raman spectra of halogenated methanes in the liquid state,[1] Fukushi and Kimura have proposed the interpretation that the band around 2990 cm^{-1} of CH_2Br_2 is caused by Fermi resonance (FR) between the fundamental ν_1 and combination $2\nu_3+\nu_8+\nu_9$ vibrations. This interpretation was made on the basis of the fact that the band was observed in both the liquid[1] and solid[2] states as a doublet comprized of two components with comparable intensities. The band around 2960 cm^{-1} of liquid CH_3Br has an unsymmetric profile with a satellite on the high-frequency side.[1] The band was also considered to be a FR band between the ν_1 and $\nu_3+\nu_5+\nu_6$ vibrations, because its profile did not vary much with the temperature.[3] The decomposition of these bands into two components with the Voigt profile yielded the half-widths at half-height (hwhh) of 4.2 and 2.4 cm^{-1} for CH_2Br_2 and CH_3Br respectively.[4] These values are quite different from each other even though the bands belong to the same vibrational species. However, the Fermi-resonance band must be described by a linear combination of two Lorentzians and an unsymmetric function,[5] and the hwhh and peak frequency of each Lorentzian component are not equivalent to those of either the active or the passive band. Therefore, the hwhh values previously reported, especially for CH_2Br_2, may not be true, but only apparent. Thus, these bands have been reanalyzed using functions for the Fermi-resonance band shape (FRBS) proposed previously.[5]

Experimental and the Results of Band Analysis

The details of the experimental unit and technique have been published elsewhere.[1,3] The true power spectra were determined from the observed spectra by deconvoluting a slit function.

TABLE 1. RESULTS OF ANALYSIS FOR THE ν_1 ISOTROPIC RAMAN BANDS OF CH_2Br_2 AND CH_3Br(in cm^{-1} units)

	CH_2Br_2[a]		CH_3Br[a]	
	F[b]	L[c]	F[b]	L[c]
Ω^A	2988.0	2987.9	2956.1	2956.0
Ω^P	2989.3	2989.0	2963.5	2959.5
Γ^A	2.3	3.9	2.3	2.3
Γ^P	6.6	—	8.9	—
$\lvert\omega_\lambda\rvert$	6.2	4.6	4.1	2.1

a) Apparent peak frequencies: CH_2Br_2, 2983 and 2993 cm^{-1}; CH_3Br, 2955 cm^{-1}. b) Fermi-resonance-band shape (Figs. 1a and 2a). c) Two Lorentzians (Figs. 1b and 2b).

The band parameters of the two Lorentzian components; the hwhh, Γ_+ and Γ_-, the peak frequencies, Ω_+ and Ω_-, and the integrated intensities S_+ and S_-, are related to those for active (A) and passive (P) bands in the uncoupled state by these equations:[5]

$$\Gamma_\pm = \bar{\Gamma}_+/2 \pm (1/\sqrt{2})[(u^2+v^2)^{1/2}-v]^{1/2},$$

$$\Omega_\pm = \bar{\Omega}_+/2 \pm (1/\sqrt{2})[(u^2+v^2)^{1/2}+v]^{1/2},$$

$$S_\pm = (1/2) \pm [\bar{\Omega}_- u/2+\bar{\Gamma}_- v/2][u^2+v^2]^{-3/4},$$

where $\bar{\Gamma}_\pm=\Gamma^A\pm\Gamma^P$, $\bar{\Omega}_\pm=\Omega^A\pm\Omega^P$, $u=[\bar{\Omega}_-/2]^2-\bar{\Gamma}_-^2+|\omega_\lambda|^2$, and $v=2\bar{\Omega}_-\bar{\Gamma}_-$, and where ω_λ is the coupling constant. The unsymmetric part is also expressed in terms of these parameters.[5] The parameter values were determined by the least-squares method applied to the band profiles. The true peak frequencies and band-widths for the active and passive modes and the coupling constants were calculated from the $\Gamma_\pm$, $\Omega_\pm$, and $S_\pm$ values thus obtained; they are listed in Table 1, Column F. Table 1, Column L, lists peak frequencies and band-widths obtained by analyzing the bands with two Lorentzians and the coupling constants estimated using equation usually quoted.[6] Figures 1 and 2 show the results of simulation for the ν_1 bands of CH_2Br_2 and CH_3Br at 290 K respectively, while (a) and (b) compare the results from the FRBS and Lorentz functions.

Discussion

As may be seen in Fig. 1, it is clear that the ν_1 band of CH_2Br_2 cannot be described as a superposition of two independent Lorentzians. The unsymmetric component of the FRBS makes a fairly large contribution to the whole band shape. The apparent band-widths, Ω_+ and Ω_- and the relative intensity of the two symmetric components, S_+ and S_-, shown in Figs. 1 (a) and (b) are not very different from each other, but the resulting band-widths, Γ^A, and coupling constants, $|\omega_\lambda|$, are quite different, as Table 1 shows.

For the ν_1 band of CH_3Br, both theoretical curves seem to reproduce the experiment, as is shown in Figs. 2 (a) and (b). On close examination, however, a difference between the two sets of results appears in the high-frequency region. In the results of analysis with the FRBS function, the unsymmetric component contributes significantly to the band profile and, as a result, the peak frequency of the satellite band, Ω^P, is high and the coupling constant, $|\omega_\lambda|$, is large compared with the results based on the two Lorentzians. The unperturbed frequency of the passive mode obtained by the FRBS analysis, 2963.5 cm^{-1}, is very close to the frequency of the combination band, $\nu_3+\nu_5+\nu_6$, calculated from the fundamental frequencies, 2965 cm^{-1}. As far as the Ω^A and Γ^A values are concerned, both analyses yielded the same results. The present results for CH_3Br are also coincident with the results obtained in the previous study,[3] where the band was

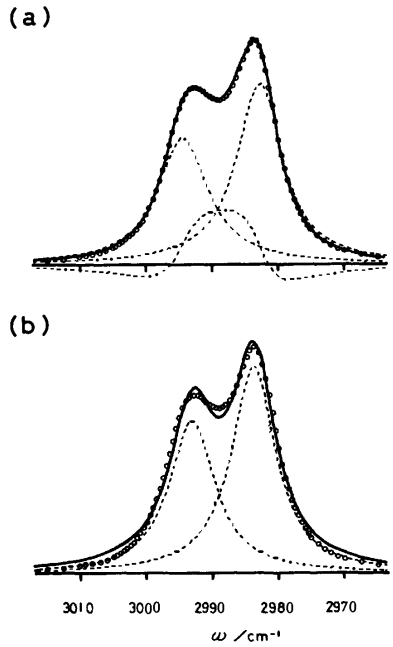

Fig. 1. Band simulation for the ν_1 isotropic Raman band of CH_2Br_2 with (a) Fermi resonance band shape function and (b) two Lorentzians; o observed, —— simulated curves, and ---- components.

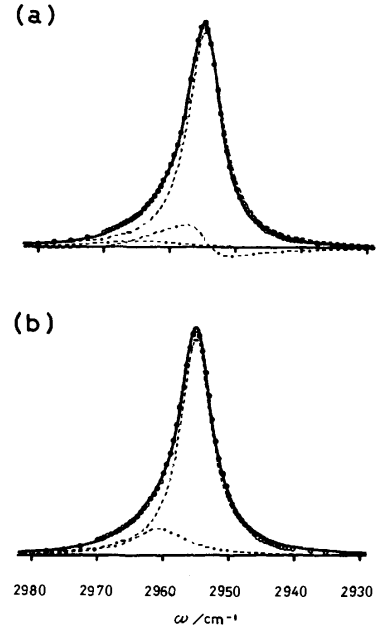

Fig. 2. Band simulation for the ν_1 isotropic Raman band of CH_3Br with (a) Fermi resonance band shape function and (b) two Lorentzians; o observed, —— simulated curves, and ---- components.

not deconvoluted and was analyzed with two Voigt functions. This indicates that the Fermi resonance effect on the band shape is insignificant for two bands with such a large separation and a weak coupling. The hwhh values of the ν_1 bands obtained for CH_2Br_2 and CH_3Br agree perfectly with each other. This suggests that the vibrational relaxation mechanisms of the ν_1 modes are similar to each other.

References

1) K. Fukushi and M. Kimura, *J. Raman Spectrosc.*, **8**, 125 (1979).
2) M. Ito, *J. Chem. Phys.*, **42**, 391 (1965).
3) T. Fukuda, K. Fukushi, and M. Kimura, the 42nd Annual Meeting of the Chemical Society of Japan, Sendai, Oct.,1980.
4) K. Fukushi and M. Kimura, *J. Raman Spectrosc.*, **13**, 9 (1982).
5) K. Fujita and M. Kimura, *Mol. Phys.*, **41**, 1203 (1980).
6) Peak frequencies; $\omega=\bar{\Omega}_+\pm(\bar{\Omega}_-^2+|\omega_\lambda|^2)^{1/2}$ and $S_+/S_-=[(\bar{\Omega}_-^2+|\omega_\lambda|^2)^{1/2}+\bar{\Omega}_-]/[(\bar{\Omega}_-^2+|\omega_\lambda|^2)^{1/2}-\bar{\Omega}_-]$; G. Herzberg, "Molecular Spectra and Molecular Structure," Vol. II, Infrared and Raman Spectra of Polyatomic Molecules, D. Van Nostrand Co., New York (1945), p. 215.

A Modification of the Method of Spectrophotometric Determination of Iron with Ethylenediamine-*N,N'*-bis(2-hydroxyphenylacetic acid)

Tetsuo KATSUYAMA* and Kyoko WATANABE
Department of Basic Technology, Faculty of Engineering, Yamagata University, Yonezawa, Yamagata 992
(Received January 9, 1984)

Synopsis. Etylenediamine-*N,N'*-bis(2-hydroxyphenylacetic acid) (H_4eddha) reacts with iron to form a 1:1 complex having an absorption maximum at 480 nm. The method of the spectrophotometric determination of iron with eddha was modified by heating the colored solution in a boiling water bath for a few minutes. The molar absorption coefficient of the Fe^{III}-eddha complex formed was 4.72×10^3 l mol^{-1} cm^{-1} and the relative standard deviation for determination of 5.90×10^{-5} mol dm^{-3} (3.29 μg cm^{-3}) of iron was 0.21%. The effect of 45 diverse ions was examined; only a few metal ions interfered. Aluminium alloys were analyzed for iron by the present method.

Ethylenediamine-*N,N'*-bis(2-hydroxyphenylacetic acid) (H_4eddha) has been used for the spectrophotometric determination of iron.[1-4] This reagent reacts with either iron(III) or iron(II) in the molar ratio 1:1 to form a red iron (III) complex.[5] The stability constant of the Fe^{III}-eddha complex is particularly large among metal-eddha complexes,[6] and the iron(III) complex is so stable that the color development is maximal over a wide pH range and a large excess of the reagent is not necessary for the determination.

This reagent has desirable properties for the spectrophotometric determination of iron. However it is not widely used for this purpose in spite of it being available for analytical use at a reasonable cost. This can be attributed to the following facts. (1) The color reaction of eddha with iron is slow; (2) the effect of diverse ions has not previously been examined sufficiently.

Gordon V. Johnson *et al.* reported that when the resultant colored solution was allowed to stand 18 h before absorbance was measured, the adverse effect of foreign metals on the accuracy of the analysis could be minimized.[4] However, their method is not convenient for usual spectrophotometric analysis since the color-developing period is long. Recently we have found that when the resultant colored solution not showing maximum color intensity was heated in a boiling water bath for a few minutes, the maximum color development was obtained and the color, once developed, was stable. Further, when the heating treatment was used, the existence of moderately large amounts of diverse ions was permited and accurate results were obtained. The present method can be also applied to the determination of iron in aluminium alloys.

Experimental

Reagents. A 1×10^{-2} M (1 M=1 mol dm^{-3}) iron(III) solution was prepared by dissolving guranteed reagent grade iron(III) nitrate in 0.02 M nitric acid. The concentration of the iron(III) ion was determined titrimetrically with edta. This solution was diluted with 0.02 M nitric acid as required.

A 1×10^{-3} M eddha solution was prepared by dissolving the known amount of the reagent obtained from Dojindo Laboratories in dilute sodium hydroxide solution; the molar ratio of eddha to sodium hydroxide was one to two. The reagent solution is colorless. However it changes to light yellow on standing for about 15 d. Thus it is recommended that fresh reagent solution be prepared every two weeks.

Apparatus. Absorbance and absorption spectra were measured with a Hitachi Perkin Elmer 139 spectrophotometer using 10 mm quartz cells. The pH values were measured with a Toa Electronics Model HM-15A digital pH-meter.

Standard Procedure. A sample solution containing less than about 8 μmol (450 μg) of iron was taken into a 50 cm^3 Erlenmeyer flask. Then, 12 cm^3 of 1×10^{-3} M eddha, 2 cm^3 of 1 M acetic acid, and 5 cm^3 of 1 M sodium acetate were added to the solution. After the Erlenmeyer flask was kept for three minutes in a boiling water bath, the solution was cooled with running water. The cooled solution was then transfered to a 50 cm^3 volumetric flask and diluted to the mark with water; final pH was 5.1. The absorbance of the solution was measured at 480 nm against water.

Results and Discussion

The solutions for absorbance measurements were prepared by the heating method unless otherwise stated.

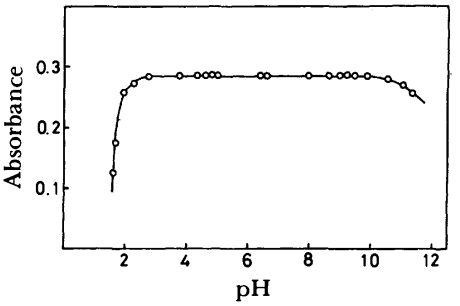

Fig. 1. Effect of pH on formation of the Fe^{III}-eddha complex.
Fe^{III}: 6.04×10^{-5} M (3.37 μg cm^{-3}), eddha: 2.40×10^{-4} M, wavelength: 480 nm, reference: water.

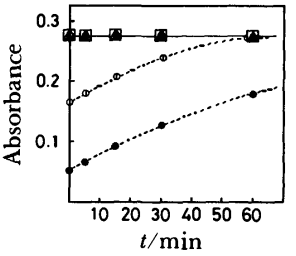

Fig. 2. The changes in absorbance of iron(III) eddha solution with time.
Fe^{III}: 5.83×10^{-5} M eddha: 2.40×10^{-4} M, Ni^{II}: 1.70×10^{-2} M pH: 5.0, room temperature (20 °C), wavelength: 480 nm, reference: water.
Heating time: ---●---, 0 min; ---Ⓘ---, 1 min; —▲—, 2 min; —○—, 3 min; —△—, 5 min; —□—, 8 min.
The quantity of the solution heated was 25 cm^3.

Absorption Spectra and Effect of pH. The solution of Fe^{III}-eddha had an absorption maximum at 480 nm. The absorbance of the solution at 480 nm remained constant over a wide pH range 2.5—10.0 (Fig. 1).

Color Development. Without the heat treatment, the time to obtain the maximum color development was varied by changing the conditions.[7] However, when the solution not showing maximum color intensity was kept for a few minutes in a boiling water bath the color reaction was completed. Examples are shown in Fig. 2, in which it is seen that the maximum color development is obtained by the heat treatment of two minutes and above. As a rule, a heat treatment of three minutes was adequate for full color development if the quantity of the solution for the color reaction was less than 40 cm^3. The color, once developed, was stable; the absorbance remained constant over a period of 5 h. The absorbance was independent of the temperature of measurement (10—35 °C).

Composition of the Complex and Effect of eddha Concentration. The composition of the complex was determined by a molar ratio study: The absorbance was plotted as ordinate against the [eddha]/[Fe^{III}] ratio (iron concentration constant; ratio, 0.3—6.0). The absorbance increased linearly with the ratio but became constant above a ratio of unity. This suggests that iron(III) forms a 1:1 complex with eddha and a large excess of reagent is not needed for full color development.

Effects of Amount of Buffer Solution and Ionic Strength. A buffer solution was prepared by mixing 1 M acetic acid solution with 1 M sodium acetate solution in 1:2.5 ratio. The color intensity of the iron(III) complex was not affected by the addition of from 2 to 20 cm^3 of the buffer solution (for 2.95 μmol of iron(III) in 50 cm^3 solution). The color intensity of the iron(III) complex was also not affected by an ionic strength change of from 0.1 to 1.4 M.

Calibration Curve. The calibration curve under the conditions described in the standard procedure was linear in the concentration range 1×10^{-5}—1.6×10^{-4} M (0.6—9 μg cm^{-3}) of iron(III). The molar absorption coefficient of the Fe^{III}-eddha complex was 4.72×10^3 l mol^{-1} cm^{-1} (at 480 nm). These values are somewhat smaller than those reported in the literature,[1] in which it is stated that the linear concentration range and the molar absorption coefficient of the Fe^{III} -eddha complex are 0—2.5×10^{-4} M and about 5.6×10^{-3} l mol^{-1} cm^{-1} (at 470) respectively. The relative standard deviation of the absorbance was 0.21% for 5.90×10^{-5} M (3.29 μg cm^{-3}) of iron(III) (12 determinations). This value is smaller than that of the method of A. L. Underwood (0.5%).[1]

Effect of Diverse Ions. The effect of 45 diverse ions was examined by the standard procedure stated. The ion in question was introduced into the iron sample solution before addition of other reagents. The results are shown in Table 1.

A. L. Underwood tested several metal ions for interference in the measurement of 5.4 μmol (in 50 ml) of iron(III);[1] it was shown that the presence of the metal ions in the following amounts did not interfere with the determination of the iron(III). Ca^{2+}, 5000 μmol; Cu^{2+}, 32 μmol; Hg^{2+}, 100 μmol; Mg^{2+}, 8200 μmol; Mn^{2+}, 3600 μmol; Ni^{2+}, 34 μmol; Pb^{2+}, 97 μmol; UO_2^{2+}, 8 μmol; Zn^{2+}, 31 μmol; Al^{3+}, 7400 μmol; Th^{4+}, 9 μmol in 50 ml. Comparing Table 1 with the results tested by A. L. Underwood, it seems that in many cases the interferences in the present method are smaller than those in A. L. Underwood's results. Thus, it may be said that the tolerance limit of diverse ions increases by use of heat treatment.

TABLE 1. EFFECT OF DIVERSE IONS ON THE DETERMINATION OF IRON(III)[a]

Ions added	Tolerance amount added to 50 cm^3 / μmol
K^+, Li^+, Na^+, NH_4^+, Rb^+, Tl^+, Ba^{2+}, Be^{2+}, Ca^{2+}, Cd^{2+}, Mg^{2+}, Pb^{2+}, Sr^{2+}, Zn^{2+}, Ce^{3+}, La^{3+}	6000[b]
Al^{3+}	5400
Mn^{2+}	3000
Th^{4+}	1800
Ni^{2+}	1200
Hg^{2+}	900
Ag^+	450
UO_2^{2+}, Cu^{2+}	80
Co^{2+}, Cr^{3+}	3
Br^-, Cl^-, ClO_3^-, ClO_4^-, HCO_3^-, CH_3COO^- I^-, NO_3^-, $H_2PO_4^-$, SCN^-, SO_4^{2-}, thiourea	6000[b]
F^-	3000
tartrate	1500
citric acid, $P_2O_7^{4-}$	300
NO_2^-, oxalate	90
CN^-	60

a) Iron(III) taken in 50 cm^3 was 2.95 μmol (165 μg). The tolerance limit was taken as the value in which an error is not more than 1%. Foreign ions were added as nitrates and sodium salts except following: K^+, KCl; NH_4^+, NH_4Cl; Hg^{2+}, $HgCl_2$; Al^{3+}, $K_2Al_2(SO_4)_4$; SCN^-, NH_4SCN; CN^-, KCN; tartrate, sodium potassium tartrate. b) Maximum tested.

Determination of Iron in an Aluminium Alloy. Aluminium alloys furnished by the National Bureau of Standards were analyzed for iron. The sample solution was prepared by dissolving the aluminium alloy (NBS 85: 1.2 g, NBS 87a: 0.5 g) in perchloric acid using the method described previously.[8] The results of the three repeated determinations of iron (starting from the weighing of the alloy) were as follows. NBS 85 (certified, 0.24%): 0.24, 0.23, and 0.24%. NBS 87a (certified, 0.61%): 0.61, 0.61, and 0.61%. Satisfactory results were obtained.

References

1) A. L. Underwood, *Anal. Chem.*, **30**, 44 (1958).

2) A. L. Underwood, *Anal. Chim. Acta*, **20**, 228 (1959).

3) R. Kono and T. Maikawa, *Kei Kinzoku*, **51**, 35 (1962).

4) G. V. Johnson and R. A. Young, *Anal. Chem.*, **40**, 354 (1968).

5) Fe^{II}-eddha complex formed is oxidixed instantly to Fe^{III}-eddha complex even without addition of any oxidizing agent.

6) $\log K_{Fe^{III}\text{-eddha}}=33.9$,[a] $\log K_{Mg^{II}\text{-eddha}}=8.0$,[b] $\log K_{Ca^{II}\text{-eddha}}=7.2$,[b] $\log K_{Ni^{II}\text{-eddha}}=19.7$,[b] $\log K_{Cu^{II}\text{-eddha}}=23.9$,[b] $\log K_{Zn^{II}\text{-eddha}}=16.8$,[b] $\log K_{Cd^{II}\text{-eddha}}=13.1$[b]: a) G. Anderegg and F. L'Eplattenier, *Helv. Chim. Acta*, **47**, 1067 (1964); b) A. E. Frost, H. H. Freedman, S. J. Westerback, and A. E. Martell, *J. Am. Chem. Soc.*, **80**, 530 (1958).

7) When a buffer was added to an iron solution before the reagent was added, or the pH was raised to about 5 in the absence of reagent, and/or an excess of foreign species was present, long color-developing periods were necessary in order to attain maximal color intensity.

8) T. Katsuyama and T. Kumai, *Bull. Chem. Soc. Jpn.*, **54**, 1544 (1981).

On the Crystal-Structure Change of Manganese Dioxide (CMD) during the Acid Digestion in $MnSO_4$-H_2SO_4 System

Tsutomu OHZUKU* and Taketsugu HIRAI†

Department of Synthetic Chemistry, Faculty of Engineering, Okayama University, Tsushima, Okayama 700
†*Department of Applied Chemistry, Faculty of Engineering, Osaka City University, Sumiyoshi, Osaka 558*

(Received February 23, 1984)

Synopsis. The wet method to convert chemically prepared manganese dioxides (MnO_2s) into β-MnO_2 was reported. Chemically prepared MnO_2s, such as I. C. Sample Nos. 5, 8, 11, and 12, were converted into β-MnO_2 by using a proton-assisted rearrangement reaction in a boiling dil. H_2SO_4 solution containing Mn^{2+} ion at 100±10 °C.

In a previous paper,[1] the wet method to change crystal structures from several MnO_2s, such as δ-MnO_2, α-MnO_2, electrolytic MnO_2s (EMDs) and heat-treated EMDs to β-MnO_2 was reported and a complex situation in classifying artificial MnO_2s, especially prepared by wet methods, was discussed. In recent years, so-called chemically prepared MnO_2s (CMDs) in addition to EMDs became available for experimental use in batteries. In this paper, we report an extension of the method to some CMDs.

Experimental

CMDs, I. C. Sample Nos. 5, 8, 11, and 12, obtained from the International MnO_2 Sample Office (c/o Union Carbide Corp., Parma Technical Center, P. O. Box 6116, Cleveland, Ohio 44101, USA) were used as received. A reaction vessel was consisted of a 500 ml round-bottom flask joined to a condenser with the standard taper joint and a heating mantle at the bottom. A 250 ml of 0.5 mol dm^{-3} H_2SO_4 with 10 g of $MnSO_4$ (4—5)H_2O in a round-bottom flask was heated at 100±10 °C and then 10 g of MnO_2 sample was added into the flask. After the reaction period of a week, a reaction product was filtered and well-washed with cool distilled water. The washed reaction product was dried at about 60 °C in the air.

X-Ray data on starting materials and reaction products were obtained by using a Shimadzu XD-3A X-ray diffractometer with iron $K\alpha$ radiation (30 kV, 10 mA) filtered with manganese.

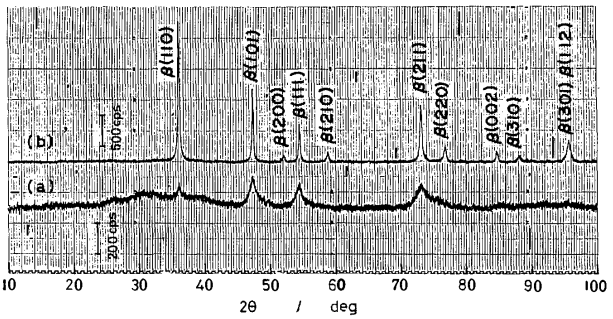

Fig. 1. X-Ray diffractional patterns of I.C. Sample No. 5 (a) and a reaction product (b) after the acid digestion of I.C. Sample No. 5 in 0.5 M H_2SO_4 (1 M= 1 mol dm^{-3}) with $MnSO_4$ at 100±10 °C for a week.

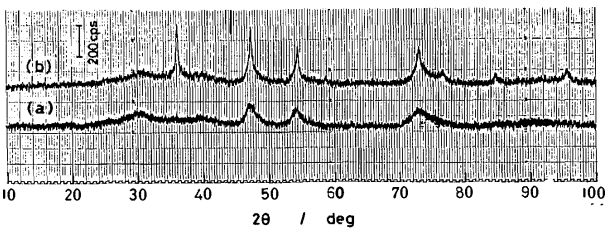

Fig. 2. X-Ray diffractional patterns of I.C. Sample No. 8 (a) and a reaction product (b) after the acid digestion of I.C. Sample No. 8 in 0.5 M H_2SO_4 with $MnSO_4$ at 100±10 °C for a week.

Since the location of line in terms of diffraction angle (2θ) and the shape of line were important in identifying the crystal structure of MnO_2, observed XRD patterns are shown in Figs. 1—4. The reaction product was identified as β-MnO_2 (pyrolusite) from both 2θ value (tetragonal system, a=4.39 Å and c=2.87 Å) and the intensities of lines ($P4_2/mnm$-D_{4h}^{14} with the positional parameter of anion u=0.31), and the indices (h, k, l) are given in figures.

CMDs, such as I. C. Sample Nos. 5, 8, and 12, have almost the same XRD patterns, which may be

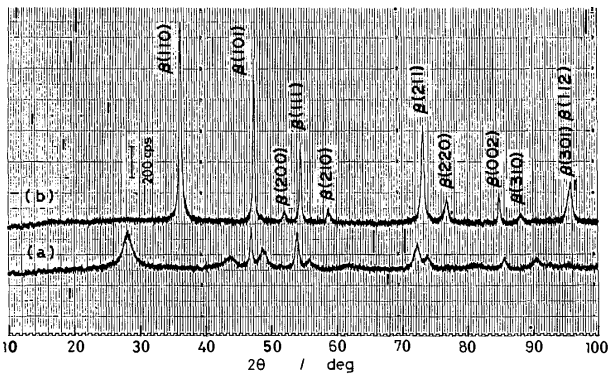

Fig. 3. X-Ray diffractional patterns of I.C. Sample No. 11 (a) and a reaction product (b) after the acid digestion of I.C. Sample No. 11 in 0.5 M H_2SO_4 with $MnSO_4$ at 100±10 °C for a week.

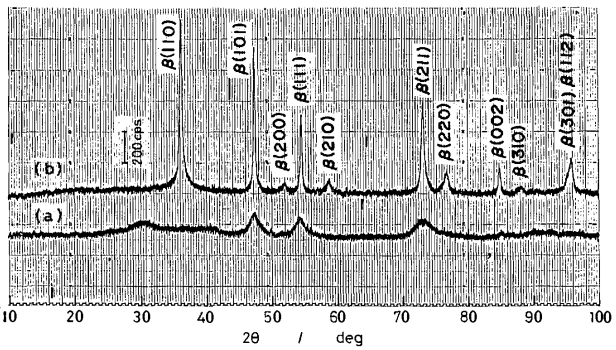

Fig. 4. X-Ray diffractional patterns of I.C. Sample No. 12 (a) and a reaction product (b) after the acid digestion of I.C. Sample No. 12 in 0.5 M H_2SO_4 with $MnSO_4$ at 100±10 °C for a week.

characterized by diffused lines at *ca.* 30 and 40° as shown in Figs. 1, 2, and 4. According to Gattow and Glemser,[2] they may be classified as γ-MnO_2.

The XRD pattern of I. C. Sample No. 11 has almost the identical 2θ values with those of ramsdellite[3] but the intensities are quite different, suggesting that the crystal structure is very close to ramsdellite but not exactly the same, which is probably due to the intergrowth of pyrolusite and ramsdellite domains[4] like nsutite.[5]

As can be seen in Figs. 1, 3, and 4, both types of CMDs, *i.e.*, I. C. Sample Nos. 5, 11, and 12, were converted into β-MnO_2. Although the XRD pattern of β-MnO_2 uncontaminated by the lines of starting material has not been obtained yet for some reasons, I. C. Sample No. 8 seems to be converted into β-MnO_2 after the acid digestion as is shown in Fig. 2. Without addition of $MnSO_4$ in a reaction mixture, none of the changes in XRD patterns was observed after the acid digestion.

Then, we conclude that CMDs available in the I. C. Sample Office can be converted into β-MnO_2 by using the proton-assisted rearrangement reaction in a boiling dil. H_2SO_4 solution containing Mn^{2+} ion at 100 ± 10°C. The mechanism of the proton-assisted rearrangement reaction with Mn^{2+} ion is still under investigation by using spectro-electrochemical techniques combined with conventional analytical techniques.

The authors wish to thank Mr. I. Matsuhisa and Mr. K. Ogino for their assistance in sample preparation. This work was partially supported by a grant in aid for Scientific Research from the Ministry of Education, Science and Culture.

References

1) T. Ohzuku, H. Higashimura and T. Hirai, *Electrochim. Acta*, **29**, 779 (1984).
2) G. Gattow and O. Glemser, *Z. Anorg. Allg. Chem.*, **309**, 20 (1961).
3) A. M. Byström, *Acta Chem. Scand.*, **3**, 163 (1949).
4) P. M. de Wolff, *Acta Cryst.*, **12**, 341 (1959).
5) W. K. Zwicker, W. O. J. Meijer and H. W. Jasse, *Amer. Min.*, **47**, 246 (1962).

A Study of Inorganic Ion Exchangers. IX.[1] The Synthesis of $Al_xZrH_{2-3x}(PO_4)_2 \cdot yH_2O$ and Its Characteristics

Etsuro KOBAYASHI

National Chemical Laboratory for Industry, Yatabemachi, Tsukuba-gun, Ibaraki 305

(Received April 9, 1984)

Synopsis. To make a material with specific functions such as those of a catalyst, a layer-structure compound with the formula of $Al_xZrH_{2-3x}(PO_4)_2 \cdot yH_2O$ ($x \leqq 2/3$) was synthesized by a hydrothermal reaction between $ZrOCl_2 \cdot 8H_2O$ and $Al(H_2PO_4)_3$ at 200—270 °C. The product had a layer spacing of 7.75 Å, slightly longer than α-$Zr(HPO_4)_2 \cdot H_2O$ (7.62 Å), and fairly good thermal stability at 250—500 °C. However, the above objective was not attained by ion-exchange between various zirconium phosphates and an aqueous solution of aluminium chloride.

Inorganic layer-structure compounds with thermal stability have specific functions of ion-exchangers or catalysts. In this study, crystalline alminium zirconium phosphate, $Al_xZrH_{2-3x}(PO_4)_2 (x \leqq 2/3)$, was synthesized by the hydrothermal reaction of zirconium(IV) chloride oxide with tris(dihydrogenphosphate) aluminium, and the properties of the product were examined. An attempt was also made to obtain such a material by means of ion exchange between various zirconium phosphates and aluminium chloride.

Experimental

The reaction product, $Al_xZrH_{2-3x}(PO_4)_2 \cdot yH_2O$, was synthesized by means of a hydrothermal reaction between $ZrOCl_2 \cdot 8H_2O$ and an $Al(H_2PO_4)_3$ aqueous solution (P_2O_5, 34.8%; Al_2O_3, 8.6%; specific gravity, 1.499; Nippon Chemical Co.) in an autoclave, according to the previously reported method.[1]

The formation of $Al_xZrH_{2-3x}(PO_4)_2$ was also examined by means of ion exchange between one gram of α-$Zr(HPO_4)_2 \cdot H_2O$. γ-$Zr(HPO_4)_2 \cdot 2H_2O$, or $Zr[(C_4H_9)_3NH]_xH_{2-3x}(PO_4)_2$[1] and 100 cm^3 of M/10 (1 M=1 mol dm^{-3}) $AlCl_3$. In this process, the pH change of the mother liquor was measured for 18 h at 20 °C, and the Al^{3+} ions adsorbed onto the zirconium phosphate were determined. The analysis of the above products was carried out as follows. The H_2O was estimated from the weight loss of the sample heated at 800 °C. After the heated product had been dissolved by alkali fusion, the ZrO_2, Al_2O_3, and P_2O_5 components were separated from each other and determined by means of gravimetric analysis. The reaction products were characterized by means of X-ray diffraction and thermal analysis (DTA, TG).

Results and Discussion

The conditions for the hydrothermal reaction of $ZrOCl_2$ with $Al(H_2PO_4)_3$ and the analytical data of the products are shown in Table 1.

The influence of the reaction temperatures was examined in Nos. 1—4 of Table 1. An amorphous product was formed in the mother liquor at temperatures lower than 150 °C. The crystallinity was augmented, and a crystalline product was obtained at 200 °C or higher.

The influence of the Al $(H_2PO_4)_3/ZrOCl_2$ (Al/Zr) mole ratios on the hydrothermal reaction was examined in Nos. 2, 5—7; the X-ray diffraction patterns of the reaction products are shown in Fig. 1.

At an Al/Zr mole ratio of 3 (No. 5), an amorphous product was formed, though the crystalline product was obtained with an increase in the mole ratio. However, the diffraction peaks (2θ; 20.6°, 26.3°) attributed to $Al_2(HPO_4)_3$ appeared in the X-ray diffraction pattern of the product at an Al/Zr mole ratio of 12 (No. 7). Thus, the reaction product is apparently intermingled with $Al_2(HPO_4)_3$. This is also evident from the increase in the Al_2O_3 content of the reaction product. Under suitable conditions (200—250 °C, Al/Zr=8) for the synthesis, the $ZrO_2 : P_2O_5$ mole ratio of the reaction product was 1:1, and then the Al^{3+}-ion content was about 5%. The product composition can be written as $Al_{0.2-0.3}ZrH_{2-3(0.2-0.3)}(PO_4)_2 \cdot 0.7-1.4H_2O$.

The X-ray diffraction pattern of this product was quite similar to that of α-$Zr(HPO_4)_2 \cdot H_2O$, but the layer

TABLE 1. SYNTHESIS AND ANALYSIS OF $Al_xZrH_{2-3x}(PO_4)_2$

No.	Reaction conditions: $ZrOCl_2 \cdot 8H_2O$ (g)	$Al(H_2PO_4)_3$ (ml)	H_2O a) (ml)	Al:Zr:P Atomic ratio	Temp °C	Time h	Mother riquor (pH)	Reaction products: ZrO_2 (%)	P_2O_5 (%)	Al_2O_3 (%)	H_2O (%)	$ZrO_2 : P_2O_5 : Al_2O_3 : H_2O$ (mole ratio)
1	1.61	5.3	4.7	8:1:24	150	96	1.55	38.2	34.8	11.3	15.7	1.0:0.8:0.4:2.8
2	1.61	5.3	4.7	8:1:24	200	96	1.69	38.7	42.6	7.7	11.0	1.0:1.0:0.3:2.0
3	1.61	5.3	5.0	8:1:24	250	96	1.70	40.7	44.5	6.7	8.07	1.0:1.0:0.2:1.4
4	16.1	53	0.0	8:1:24	270	96	2.01	40.0	46.4	5.8	7.84	1.0:1.0:0.2:1.9
5	1.61	2.0	8.0	3:1:9	200	96	1.76	35.7	41.4	3.5	19.4	1.0:1.0:0.1:3.7
6	1.61	3.3	7.7	5:1:15	200	96	1.74	36.6	42.6	8.0	12.8	1.0:1.0:0.3:2.4
7	1.61	8.0	3.0	12:1:36	200	96	1.57	32.1	39.7	19.4	8.84	1.0:1.1:0.7:1.9
8	16.1	53	0.0	8:1:24	200	130	1.83	38.5	40.8	8.8	11.9	1.0:0.9:0.3:2.1
9	16.1	53	50	10.7:1:24 +10.4(g)$Al(OH)_3$	200	66	2.41	22.0	35.8	30.8	11.4	1.0:1.4:1.7:3.5
10	1.61	0.53	2.5	8:1:24 +3.71(g)n-$(C_4H_9)_3N$	160	115	2.27	23.0	38.3	23.5	11.1	1.0:1.4:1.2:3.3 :0.02:$(C_4H_9)_3N$ (4.1)

a) Aqueous solution of $Al(H_2PO_4)_3$ containing 34.8% of P_2O_5 and 8.6% of Al_2O_3.

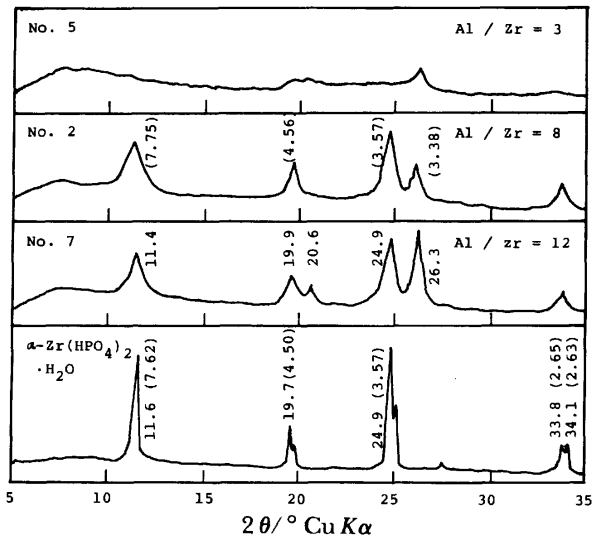

Fig. 1. X-Ray diffraction patterns of $Al_xZrH_{2-3x}(PO_4 \cdot yH_2O$ and α-$Zr(HPO_4)_2 \cdot H_2O$. Effect of $Al(H_2PO_4)_2$ mole/$ZrOCl_2$ mole (Al/Zr) on the synthesis Numerals on peaks indicate 2θ/degrees and lattice distances Cl/Å).

spacing of 7.75 Å, determined from the first d value (002) of the reaction product, was slightly longer than that of 7.62 Å for α-$Zr(HPO_4)_2 \cdot H_2O$.

The results of adding $Al(OH)_3$ (No. 9), or $(C_4H_9)_3N$ (No. 10) to this reaction system were investigated. The pH of the reaction mixture containing $Al(OH)_3$ was slightly higher than that to which no addition was made, but the reaction product was possibly contaminated by metal ions dissolved by the corrosion of the autoclave. The X-ray diffraction patterns of the reaction products of Nos. 9 and 10 were shown to be intermingled with $Al_2(HPO_4)_3$ as a by-product. In Experiment No. 10, the crystalline zirconium phosphate connected to $(C_4H_9)_3N$ could not be obtained as a result of the formation of an oily tertiary amine phosphate.

The DTA and TG curves of $Al_xZrH_{2-3x}(PO_4)_2 \cdot H_2O$ and α-$Zr(HPO_4)_2 \cdot H_2O$ are shown in Fig. 2.

The thermal decomposition in the reaction product showed a behavior similar to that of α-$Zr(HPO_4)_2 \cdot H_2O$. A broad endothermic peak attributed to the dehydration of the water of layer spacing appeared at 130—150 °C. The change in the weight of the heating

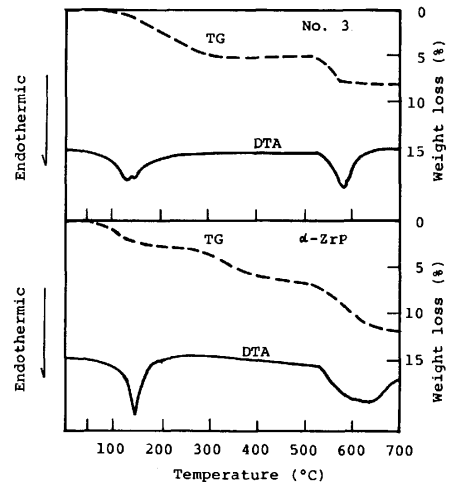

Fig. 2. DTA and TG curves of $Al_xZrH_{2-3x}(PO_4 \cdot yH_2O$ and α-$Zr(HPO_4)_2 \cdot H_2O$.

product could not be detected on the TG curve at 250—500 °C. In this temperature range, the condensation was obstructed by aluminium ions present in the layer-spacing of the phosphate. The thermal stability of $Al_xZrH_{2-3x}(PO_4)_2 \cdot yH_2O$ at 250—500 °C could also be observed from the X-ray diffraction pattern of the heated product.

When a reaction between zirconium phosphate and aluminium ions occurs easily, the method of synthesizing $Al_xZrH_{2-3x}(PO_4)_2 \cdot yH_2O$ directly becomes less necessary. Accordingly, the reactions of zirconium phosphates (α-$Zr(HPO_4)_2 \cdot H_2O$, γ-$Zr(HPO_4)_2 \cdot 2H_2O$ or $Zr[(C_4H_9)_3NH]_xH_{2-x}(PO_4)_2 \cdot yH_2O$) with an aqueous solution of $AlCl_3$ were examined. The pH values were found to decrease from about 4.5 to 2.5, followed by the adsorption of Al^{3+} ions onto the solid phase by 1.66% in the case of the butyl amine salt (17.0 Å), 0.81% for γ-$Zr(HPO_4)_2 \cdot 2H_2O$ (12.3 Å), and 0.24% for α-$Zr(HPO_4)_2 \cdot H_2O$ (7.6 Å). The adsorbed Al^{3+} ions slightly increased in proportion to the layer-spacing of the phosphates. Thus, the direct synthesis is significant for the indicated purpose.

References

1) a) Presented at the 49th National Meeting of the Chemical Society of Japan, Tokyo, April, 1984; b) Part VIII of this series: E. Kobayashi and S. Shin, *Bull. Chem. Soc. Jpn.*, **57**, 465 (1983).

Thermal Decomposition of Cobalt(II) Halide Complexes of Tetramethylurea and Related Cyclic Ureas

Kozo SONE,* Masae KIKUCHI,† Kaede OGASAWARA, Miuaco Kawashita KUYA,†† and Anamaria Dias PEREIRA††

Department of Chemistry, Faculty of Science, Ochanomizu University, Otsuka 2-1-1, Bunkyo-ku, Tokyo 112

†*Institute for Iron, Steel and Other Metals, Tohoku University, Katahira-cho, Sendai 980*

††*Instituto de Química, Universidade de São Paulo, Cidade Universitária, C.P.20.780, São Paulo, Brazil*

(Received May 1, 1984)

Synopsis. TG-DTA studies revealed that the complexes CoX_2L_2 (L=tmu, dmeu or dmpu (see text); X=Cl, Br or I) decompose into CoX_2 and 2L by slight heating. The ease of this decomposition decreases in the orders of tmu>dmeu>dmpu and Cl>Br>I, corresponding to the orders of coordination abilities of these ligands.

In connection with the recent studies of Kuya *et al.* on the cobalt (II) halide complexes of dimethyl ethyleneurea (dmeu) and dimethyl trimethyleneurea (dmpu),[1,**] we carried out a comparative study on the thermal behaviors of these complexes and also those of the corresponding complexes of tetramethylurea (tmu), reported formerly by King.[2] All these complexes are of the general formula CoX_2L_2 (L= tmu, dmeu or dmpu; X=Cl, Br or I), and their spectral, magnetic and conductometric studies indicated that they are composed of tetrahedral, high-spin and uncharged species, *i.e.*, $[CoX_2L_2]$, in which the L molecules are coordinated to Co (II) at their C=O groups.[1,2]

Experimental

Preparation of the Complexes. The complexes of dmpu, and the Cl- and Br-complexes of dmeu, were prepared as reported elsewhere.[1] The remaining complexes were prepared by stirring anhydrous CoX_2 with 1,2-dichloroethane, in which it is nearly insoluble, and dropping L into the mixture, until complete dissolution of CoX_2 took place. The blue or bluish green solution formed was then evaporated under vacuum, until large crystals of the same color separated out. The purity of the crystals was confirmed by elementary analysis, and also by the TG data (especially Δw in vacuum; *cf.* Table 1).

TG-DTA Measurements. The thermogravimetric (TG) and differential thermal analysis (DTA) measurements were carried out with a Sinku-Riko TGD-3000 Differential Thermobalance, in static air, in flowing N_2 (flow rate: 50 $cm^3 min^{-1}$) and in vacuum (3 Torr; 1 Torr=133 $N m^{-2}$). 15—20 mg of the sample was taken for each run, and heated at a rate of 4 °C min^{-1}.

Results and Discussion

Figure 1 shows the TG curves of the dmpu complexes, and the DTA curve of $[CoBr_2(dmpu)_2]$, both measured in flowing N_2. The TG and DTA curves of the remaining complexes are essentially similar to these. All the TG curves show a wide decomposition step, and the weight loss for it agrees, in each case, reasonably well with the stoichiometry of the following decomposition (1):

$$[CoX_2L_2] \longrightarrow CoX_2 + 2L, \quad (1)$$

in which all the organic ligands are driven off in the gas phase, leaving cobalt halides behind. On the other hand, the DTA curves are composed of a sharp endothermic peak appearing at 90—150 °C, and another endothermic peak near the end of the decomposition step on the TG curve. Visual observation confirmed that the former corresponds to the melting point; the fact that it is so low indicates that these complexes are essentially molecular crystals, supporting their formulation.[1,2] The latter corresponds apparently to the absorption of heat of the decomposition, together with the heat of vaporization of evolved L. In certain cases, another very weakly endothermic peak appears before melting (mostly at 70—80 °C), which may be due to some phase transition in the solid.

Comparing all these data, which are also summarized in Table 1, we can readily recognize that the ease of the reaction (1) in N_2 decreases in the following orders of L and X:

L: tmu>dmeu>dmpu

X: Cl>Br>I

The meaning of these orders can be explained as follows. In the course of the decomposition (1), the ligands L are driven out of the coordination sphere, but the driving force for it must be the attack by the anions X^- belonging to the surrounding complexes, which tend to form Co-X-Co bridges leading, eventually, to the formation of the layer lattice structure of CoX_2. In other words, we can say that the ligands L are squeezed out of the coordination sphere by the anions X^-. The ease of the decomposition will then increase with the

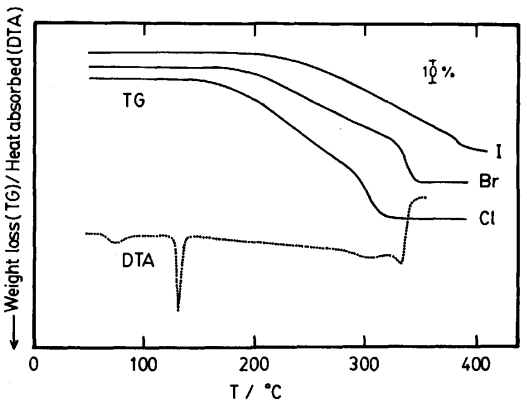

Fig. 1. TG curves of the dmpu complexes, and DTA curve of $[CoBr_2(dmpu)_2]$, in flowing N_2.

**) According to the IUPAC nomenclature, dmeu and dmpu are 1,3-dimethyl-2-imidazolidinone and 1,3-dimethylhexahydro-2-pyrimidinone, respectively.

TABLE 1. TG-DTA DATA OF THE COMPLEXES: TEMPERATURE RANGES AND WEIGHT LOSSES(Δw) FOR THE DECOMPOSITION STEP, AND DTA PEAK POSITIONS

Complex	In N_2			In vacuum		Δw/% (Calcd)[b]
	Temp range/°C	Δw/%	DTA peaks[a]/°C	Temp range/°C	Δw/%	
$[CoCl_2(tmu)_2]$	80—260	61.4	*91*, 239	50—205	64.7	64.1
$[CoBr_2(tmu)_2]$	100—300	48.5	*97*, 289	65—180	49.2	51.5
$[CoI_2(tmu)_2]$	120—380	46.6	*131*, —[c]	85—245	41.3	42.6
$[CoCl_2(dmeu)_2]$	125—350	60.0	(76), *127*, 252	70—220	62.0	63.7
$[CoBr_2(dmeu)_2]$	125—310	49.4	(72), *138*, 290	85—255	48.9	51.1
$[CoI_2(dmeu)_2]$	110[d]—430	43.0	*134*, —[c]	70—245	41.4	42.2
$[CoCl_2(dmpu)_2]$	120—340	64.9	(101), *127*, 313	85—220	65.2	66.4
$[CoBr_2(dmpu)_2]$	150—365	52.8	(70), *130*, 344	100—260	53.0	54.0
$[CoI_2(dmpu)_2]$	170—410	45.2	*146*, 384	115—250	43.6	45.0

a) The peaks for melting points are italicized, and those for solid phase transitions are in parentheses. b) Calculated according to the eq.(1). c) Scarcely perceptible. d) Sizable decomposition begins at *ca.*160°C.

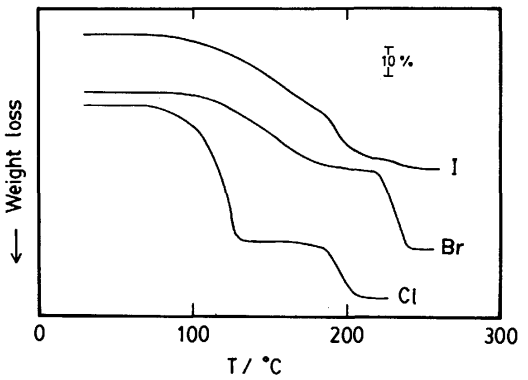

Fig. 2. TG curves of the dmeu complexes in vacuum.

increase of the coordination ability of X^-, *i.e.*, in the direction of $I^- \rightarrow Br^- \rightarrow Cl^-$, and also with the decrease of the coordination ability of L. As one can easily see from their dipole moments (tmu: 3.49D, dmeu: 4.09D, dmpu: 4.23D; solvent: dioxane, 1 D=3.33×10^{-30} Cm), the latter ability will be the lowest with tmu, and will increase through dmeu to dmpu.[3,4]

Similar measurements were also made in static air and in vacuum. The data in air was found to be essentially similar to those in N_2, but those in vacuum were notably different. As can be seen from Table 1, the temperature range for the decomposition is notably lowered by evacuation, and, although the general appearance of the TG curves indicate that the two orders of L and X still approximately hold, small shoulders indicating stepwise release of L are observed on most of them. The most significant ones are those of $[CoX_2(dmeu)_2]$ shown in Fig. 2, which reveal that Cl- and Br-complexes of definite intermediate compositions, *i.e.*,$CoCl_2(dmeu)_{2/3}$ and $CoBr_2(dmeu)$, are formed in the course of the decomposition (1). Intermediate complexes of similar stoichiometries, with probably polymeric structures, have been observed in the thermal decompositions of other CoX_2L_2-type complexes.[5,6] The DTA curves in vacuum are rather complicated, with several endothermic peaks corresponding to the successive steps.

We can thus conclude that this decomposition can be understood as the competition of the coordination tendencies of the leaving and entering groups, as is commonly encountered among the ligand exchange reactions.[7,8]

References

1) M. K. Kuya, A. D. Pereira, E. Giesbrecht, and K. Sone, *Anais Acad. Brasil. Ciênc.*, **56**, 147 (1984).
2) T. M. King, Ph. D. Thesis, Univ. of Tennessee (1966).
3) A. L. McClellan, "Tables of Experimental Dipole Moments," Freeman, San Francisco (1963), p. 153.
4) E. J. Lien and W. D. Kumler, *J. Med. Chem.*, **11**, 214 (1968).
5) J. R. Allan, D. H. Brown, R. H. Nuttall, and D. W. A. Sharp, *J. Inorg. Nucl. Chem.*, **26**, 1895 (1964).
6) D. H. Brown, R. H. Nuttall, and D. W. A. Sharp, *ibid.*, **26**, 1151 (1964).
7) As to a related TG-DTA study on the tmu complexes of lanthanoids, *cf.* K. Sone, K. Nagase, M. K. Kuya, and E. Giesbrecht, *Bull. Chem. Soc. Jpn.*, **55**,449 (1982).
8) It may be added that the fully alkylated ureas studied here are all liquids which boil near or above 200°C, and are thermally very stable. Further decomposition of the released ligand will thus be quite unlikely, at least for the most part of the decomposition step.

A Solubility Phase Diagram Study on Optical Resolution of Bis(ethylenediamine)oxalatocobalt(III) (1+) by L-α-Amino Dicarboxylate(1−)

Kazuaki YAMANARI,* Michihito IGAKI,† and Yoichi SHIMURA
Department of Chemistry, Faculty of Science, Osaka University, Toyonaka, Osaka 560
(Received May 1, 1984)

Synopsis. The binary and ternary solubility phase diagrams for the system of Δ- and Λ-[Co(ox)(en)$_2$]X (X=L-glutamate (L-Hglu$^-$) and L-aspartate (L-Hasp$^-$)) were determined in water. It was found that the former anion L-Hglu$^-$ behaves as an excellent resolving agent for [Co(ox)(en)$_2$]$^+$ but the latter anion L-Hasp$^-$ forms a pseudoracemate *rac*-[Co(ox)(en)$_2$](L-Hasp).

An application of L-amino acid cation as a resolving agent for metal complexes has been reported.[1] In this note, L-α-amino acid anion, L-glutamate (L-Hglu$^-$) and L-aspartate (L-Hasp$^-$), are examined as a resolving agent for the resolution of [Co(ox)(en)$_2$]$^+$, the former anion leading to the successful optical resolution. The binary and ternary solubility phase diagrams of these systems are presented here.

Experimental

Δ- and Λ-[Co(ox)(en)$_2$](L-Hglu)·5.5H$_2$O: To a solution of *rac*-[Co(ox)(en)$_2$]CH$_3$CO$_2$[2] (100 g, 0.307 mol) dissolved in 300 cm^3 of water was added a solution of Na(L-Hglu)·H$_2$O (57.4 g, 0.307 mol) in 200 cm^3 of water. The mixed solution was evaporated to *ca.* 450 cm^3 and cooled in an ice bath. The less soluble Λ-diastereomer deposited was filtered, washed with methanol and acetone and then air-dried at room temperature. Further concentration of the filtrate gave the second crop (the final filtrate was reserved for Δ-diastereomer). The total yield was 72 g. The diastereomer was recrystallized from hot water. Found: C, 25.97; H, 6.78; N, 13.64%. Calcd for Λ-[Co(ox)(en)$_2$](L-Hglu)·5.5H$_2$O=C$_{11}$H$_{35}$N$_5$O$_{13.5}$Co: C, 25.79; H, 6.89; N, 13.67%. $\Delta\varepsilon_{523}$=+2.88 and ε_{497}=119.6 mol^{-1} dm^3 cm^{-1}.

An excess of conc. HCl was added to the above filtrate to give Δ-[Co(ox)(en)$_2$]Cl·3H$_2$O. The chloride salt was converted into the L-Hglu salt using a column of QAE-Sephadex A-25 (L-Hglu$^-$ form). Found: C, 25.94; H, 6.73; N, 13.63%. Calcd for Δ-[Co(ox)(en)$_2$](L-Hglu)·5.5H$_2$O=C$_{11}$H$_{35}$N$_5$O$_{13.5}$Co: C, 25.79; H, 6.89; N, 13.67%. $\Delta\varepsilon_{523}$=−2.91 and ε_{497}=120.3 mol^{-1} dm^3 cm^{-1}.

rac-, Δ-, *and Λ-[Co(ox)(en)$_2$](L-Hasp)·nH$_2$O*: The same process as described above except for the use of Na(L-Hasp)·H$_2$O instead of Na(L-Hglu)·H$_2$O gave the pseudoracemate *rac*-[Co(ox)(en)$_2$](L-Hasp). Found: C, 29.96; H, 5.57; N, 17.52%. Calcd for *rac*-[Co(ox)(en)$_2$](L-Hasp)=C$_{10}$H$_{22}$N$_5$O$_8$Co: C, 30.08; H, 5.55; N, 17.54%. ε_{497}=119.4 mol^{-1} dm^3 cm^{-1}.

The active diastereomers Δ-and Λ-[Co(ox)(en)$_2$](L-Hasp) were prepared from the corresponding active complexes Δ-[Co(ox)(en)$_2$]Cl·3H$_2$O and Λ-[Co(ox)(en)$_2$](L-Hglu)·5.5H$_2$O, respectively, using a column of QAE-Sephadex A-25 (L-Hasp$^-$ form). Found for Δ-diastereomer: C, 26.66; H, 6.22; N, 15.56%. Found for Λ-diastereomer: C, 26.69; H, 6.20; N, 15.55%. Calcd for [Co(ox)(en)$_2$](L-Hasp)·3H$_2$O=C$_{10}$H$_{28}$N$_5$O$_{11}$Co: C, 26.50; H, 6.23; N, 15.45%. $\Delta\varepsilon_{523}$=−2.86 and ε_{497}=119.3 mol^{-1} dm^3 cm^{-1} for Δ-diastereomer, and $\Delta\varepsilon_{523}$=+2.85 and ε_{497}=118.7 mol^{-1} dm^3 cm^{-1} for Λ- one.

Measurement. Solubility in water was determined according to the previously reported method.[3] The solid phases were identified by elemental analysis, absorption,

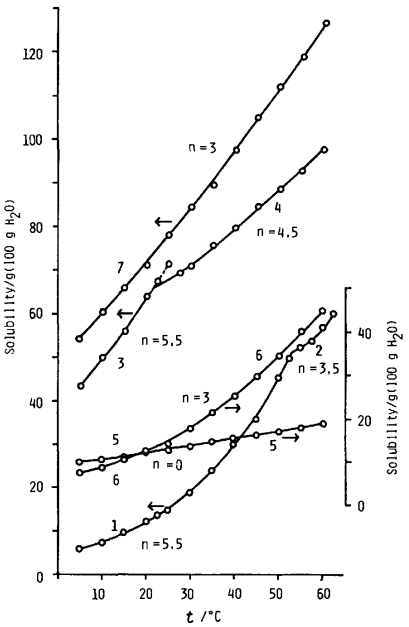

Fig. 1. Binary solubility curves of [Co(ox)(en)$_2$]X·nH$_2$O; X=L-Hglu: Λ form (**1**, **2**) and Δ form (**3**, **4**), and X=L-Hasp: racemic form (**5**), Λ form (**6**), and Δ form (**7**).

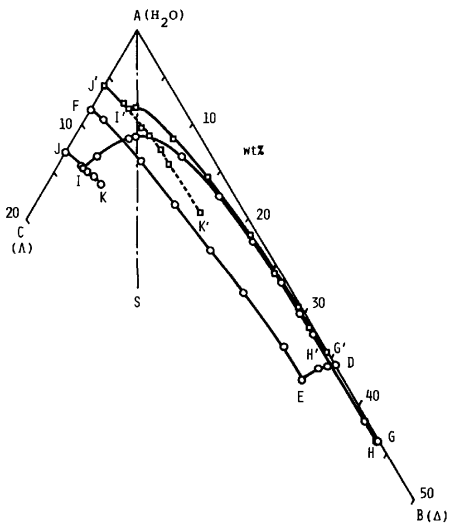

Fig. 2. Solubility isotherm of the ternary system, (A) H$_2$O—(B) Δ-[Co(ox)(en)$_2$]X—(C) Λ-[Co(ox)(en)$_2$]X; DEF: X=L-Hglu at 15 °C (○), GHIJ: X=L-Hasp at 25 °C (○), and G'H'I'J': X=L-Hasp at 2 °C (□). See Table 2 for the solid phase compositions.

† Present address: Department of Chemistry, Faculty of Science, Kobe University, Nada-ku, Kobe 657.

Table 1. Solubility of the complex salts (grams of anhydrous salt in 100 g of water)

t/°C	No. of complex salt[a]						
	1	2	3	4	5	6	7
5	5.90		43.3		9.87	7.26	54.5
10	7.40		49.9		10.2	8.47	60.6
15	9.49		56.0		10.9	10.4	66.0
20	12.1		63.8		11.9	12.4	71.0
22.5	13.5		67.5				
25	14.9		71.3		12.5	14.9	78.2
27.5				69.4			
30	18.9			71.0	13.5	17.6	84.6
35	24.1			75.6	14.6	21.4	89.7
40	30.0			79.6	15.4	25.2	97.9
45	36.0			84.7	16.1	29.5	105
50	45.5			88.7	17.0	34.4	112
52.5	50.0						
55		52.6		93.0	18.0	40.0	119
57.5		54.0					
60		57.1		97.8	18.8	44.8	127
62.5		60.4					

a) **1**: *Λ*-[Co(ox)(en)$_2$](L-Hglu)·5.5H$_2$O, **2**: *Λ*-[Co(ox)(en)$_2$](L-Hglu)·3.5H$_2$O, **3**: *Δ*-[Co(ox)(en)$_2$](L-Hglu)·5.5H$_2$O, **4**: *Δ*-[Co(ox)(en)$_2$](L-Hglu)·4.5H$_2$O, **5**: *rac*-[Co(ox)(en)$_2$](L-Hasp), **6**: *Λ*-[Co(ox)(en)$_2$](L-Hasp)·3H$_2$O, and **7**: *Δ*-[Co(ox)(en)$_2$](L-Hasp)·3H$_2$O.

and circular dichroism (CD) spectra. Optical densities were measured with a Hitachi 330 spectrophotometer and CD with a JASCO MOE-1 spectropolarimeter.

Results and Discussion

The solubility data for the binary and ternary systems are given in Tables 1 and 2, respectively.

System containing L-*Hglu*$^-$. The binary solubility curves are shown in Fig. 1. The solubility of *Δ*-diastereomer is very higher than that of *Λ*-one at 5—60 °C. The *Δ*-diastereomer showed an inflection at *ca.* 21.5 °C, where solid phase changes from 5.5-hydrate to 4.5-hydrate. A similar inflection appeared at *ca.* 53.5 °C for *Λ*-diastereomer, corresponding to the transition from 5.5-hydrate to 3.5-hydrate. The ternary isotherm at 15 °C showed one invariant point E near the *Δ*-diastereomer side (Fig. 2). Therefore, when an aqueous solution of pseudoracemic mixture is concentrated at 15 °C, the less soluble *Λ*-diastereomer will be obtained as solid deposit. The maximum yield of optical resolution calculated from the liquid phase composition at point E is 89%,[4] which ranks with those of the most excellent resolving agents such as *Δ*(or *Λ*)-[Co(edta)]$^-$(93%) and hydrogen tartrate (*R,R*)-C$_4$H$_5$O$_6^-$ (79%).[3]

System containing L-*Hasp*$^-$. The binary solubility curves are shown in Fig. 1. The solubility of *Δ*-diastereomer is the highest among three complexes. The curve of pseudoracemate intersects that of *Λ*-diastereomer at *ca.* 19 °C, the solubility of the latter being less than that of the former below this temperature. The ternary isotherm at 25 °C (Fig. 2) showed two invariant points H and I in agreement with the preparative formation of pseudoracemate *Δ*-[Co(ox)(en)$_2$]· *Λ*-[Co(ox)(en)$_2$](L-Hasp)$_2$=*rac*-[Co(ox)(en)$_2$](L-Hasp). The fundamental feature of the ternary isotherm was unaltered at 2 °C in equilibrium conditions. However, certain metastable states, which were at least maintained for several hours, were observed at this temperature. Especially, it is noteworthy that the curve I'K' intersects the racemic line AS, which means that the pseudoracemic mixture is optically resolvable in metastable state at 2 °C.

Table 2. Solubility in the ternary systems (H_2O—*Δ*-[Co(ox)(en)$_2$]X—*Λ*-[Co(ox)(en)$_2$]X)

X	a)	Liquid phase composition (wt%) *Δ*-salt	*Λ*-salt	Solid phase[b]	X	a)	Liquid phase composition (wt%) *Δ*-salt	*Λ*-salt	Solid phase[b]
L-Hglu	D	35.5	0	**3**	L-Hasp		3.05	12.0	**6**
15 °C		34.9	0.73	**3**	25 °C[c]		3.93	11.6	**6**
		34.2	1.58	**3**		K	4.93	11.4	**6**
	E	33.5	3.71	**1+3**					
		29.9	3.76	**1**	L-Hasp	G'	34.2	0	**7**
		23.4	4.54	**1**	2 °C	H'	34.4	0.08	**5+7**
		18.3	5.10	**1**			31.2	0.31	**7**
		12.7	5.85	**1**			29.2	0.20	**7**
		7.27	6.73	**1**			25.3	0.55	**7**
		1.64	7.94	**1**			21.1	0.72	**7**
	F	0	8.55	**1**			14.2	1.39	**7**
							8.97	2.64	**7**
L-Hasp	G	43.6	0	**7**			3.93	4.27	**7**
25 °C	H	43.5	0.22	**5+7**			3.28	4.91	**7**
		41.2	0.19	**5**		I'	3.31	5.03	**5+6**
		32.0	0.31	**5**			2.61	5.16	**6**
		29.6	0.47	**5**		J'	0	5.88	**6**
		26.3	0.43	**5**					
		21.6	0.77	**5**	L-Hasp		33.6	1.34	**7**
		16.2	1.28	**5**	2 °C[c]		5.48	4.86	**6**
		10.7	2.70	**5**			6.71	4.56	**6**
		5.37	5.78	**5**			8.39	4.34	**6**
		4.97	6.54	**5**			9.98	4.27	**6**
		3.03	10.4	**5**		K'	15.4	3.96	**6**
	I	2.42	12.2	**5+6**					
		2.10	12.2	**6**					
	J	0	12.9	**6**					

a) The capital letters D, E, ···K, K' are identical to those in Fig. 2. b) Nos. of solid phase denote the complex salts in Table 1. c) Metastable phase.

References

1) R. D. Gillard, P. R. Mitchell, and C. F. Weick, *J. Chem. Soc., Dalton Trans.*, **1974**, 1635.

2) This complex was prepared by N. Koine (private communication): the reaction solution of *rac*-[Co(ox)(en)$_2$]-CH$_3$CO$_2$ prepared by the procedure of Dwyer *et al.* (*J. Am. Chem. Soc.*, **83**, 1285 (1961)) was concentrated without any addition of H$_2$SO$_4$ and HCl to give the crystals of the desired salt.

3) Y. Shimura and K. Tsutsui, *Bull. Chem. Soc. Jpn.*, **50**, 145 (1977).

4) The general equation of resolution yield in ternary system has been given by A. Fuyuhiro (D. Thesis, Univ. of Osaka (1982), p. 95). If the angle between AE and AS in Fig. 2 is θ, the resolution yield is represented as follows: yield(%)=$\{\sin\theta/(\cos\theta/2\sqrt{3}+\sin\theta/2)\}\times 100$.

Immunoassay Using a Metal-complex Compound as a Chemiluminescent Catalyst. IV. The Investigation of a Metal Porphine Complex as a Labeling Reagent

Tadashi HARA,* Motohiro TORIYAMA, Hisayo MIYOSHI, and Shinji SYOGASE
Department of Chemical Engineering, Faculty of Engineering, Doshisha University, Karasuma Imadegawa, Kamigyo-ku, Kyoto 602
(Received May 7, 1984)

Synopsis. Among the metal porphine and phthalocyanine complexes synthesized by the present authors, a iron(III) complex of 5,10,15,20-tetrakis(4-carboxyphenyl)-porphine was found to be most sensitive for the chemiluminescence reaction of luminol-H_2O_2; it was successfully used in the determination of albumin as a protein model, with a detection limit of about 130 pg.

A chemiluminescence complex catalyst immunoassay (CLCCIA), in which a synthesized iron(III) phthalocyanine complex compound, acting as a catalyst in the chemiluminescence(CL) reaction of 5-amino-2,3-dihydro-1,4-phthalazinedione(luminol) hydrogen peroxide(H_2O_2), was used as a labeling reagent, was previously described for practical use by the present authors.[1-3] This method has the advantages of being sensitive and of enabling one to select the desired chemical structure of the labeling reagent[2] since it is based on the use of the catalytic reaction of a synthesized metal-complex compound. In order to make this method very useful as an immunoassay, the preparation of a more sensitive complex compound than a iron(III) phthalocyanine complex compound as a labeling reagent is necessary.

It is well known that the natural substances having a porphine skeleton in their active centers, that is, peroxidase, microperoxidase, hemin, and hematin, act as sensitive catalysts for the CL reaction of luminol-H_2O_2. Several metal porphine complexes with a skeleton similar to those of the above natural substances were, therefore, synthesized by the present authors, and their catalytic activities were compared with each other; our studies included hematin, which had been previously reported[4] to show the highest catalytic activity among the above natural substances. Here, the catalytic activity was compared for a liberated catalyst and a catalyst-albumin conjugate obtained by the carbodiimide method.

Experimental

A metal 5,10,15,20-tetrakis(4-carboxyphenyl)porphine (TCPP) complex was prepared by synthesizing TCPP by Adler's procedure[5] and by reacting it with the desired metal salt under refluxing in an acetic-acid medium.[6] The labeling of human serum albumin(HSA) as a protein model with a metal-complex compound except for iron(III) 1,8,15,22-tetracarboxyphthalocyanine (TCP-Fe(III)) was carried out by the carbodiimide method used by Karube *et al.*[7] Here, 1-ethyl-3-(3-dimethylaminopropyl)carbodiimide hydrochloride (EDC) or *N*-cyclohexyl-*N'*-(2-morpholinoethyl)carbodiimide-methyl *p*-toluenesulfonate(CMC) as a water-soluble carbodiimide was used and the column charged with TOYOPEARL HW-50 was used for the gel filtration. The labeling of TCP-Fe(III) was carried out as follows: A 5-cm³ phosphate buffer solution(pH 7.2) containing 25 mg of HSA was added to the solution immediately after 5 mg of iron(III) 1,8,15,22-tetrakis (chlorocarbonyl)phthalocyanine had been dissolved in 1 cm³ of dimethyl sulfoxide. The contents were made to react at room temperature for 1 h and then at 4 °C for 18 h. Thereafter, the contents were treated much as in the method used by Karube *et al.*

The catalytic activity was measured by diluting a sample solution with a borate buffer solution(pH 10.2) and by subjecting the diluted solution to the flow-injection analysis apparatus shown in Fig. 1. By the use of the peristaltic pumps (d) in Fig. 1, a 1.0×10^{-3} mol/dm³ luminol solution (pH 10.2) (a), a 7.5×10^{-3} mol/dm³ H_2O_2 solution(b), and a borate buffer solution (pH 10.2) (c) were delivered at the rate of 2.5 cm³/min. A definite volume of the sample solution was taken by means of the sampling loop (200 mm³) (f) and injected into the flow line by operating a six-way cock (e). Then the CL emitted was measured with a photon counter (Hamamatsu TV, C-1230, R-464) (i).

Results and Discussion

It has been established that the salts of Fe^{III}, Co^{II}, and Os^{VIII}, belonging to the eighth-group of the periodic table, and natural substances with a iron porphine skeleton, such as peroxidase, microperoxidase, hemoglobin, hematin, and hemin, show high catalytic activities for the CL reaction of luminol-H_2O_2. Several water-soluble porphine complexes of the eighth-group elements were synthesized, and their catalytic activities were examined. A useful labeling reagent for CLCCIA was required to satisfy the following conditions: 1) the labeling reagent should be soluble in an alkaline solution when the CL of luminol-H_2O_2 gave a high quantum yield, and 2) the labeling reagent should contain a functional group by which the labeling reagent could be covalently bonded to the desired constituent, such as protein, under mild conditions. From these points of view, the TCPP complex was selected as the labeling reagent in the pres-

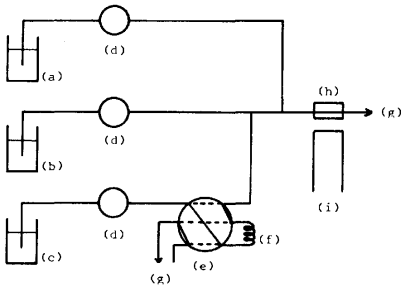

Fig. 1. A flow diagram of the flow-injection system for the measurement of catalytic activity.
a: Luminol, b: H_2O_2, c: buffer solution, d: pump, e: six-way cock, f: sampling loop, g: waste, h: flow-cell, and i: photon counter.

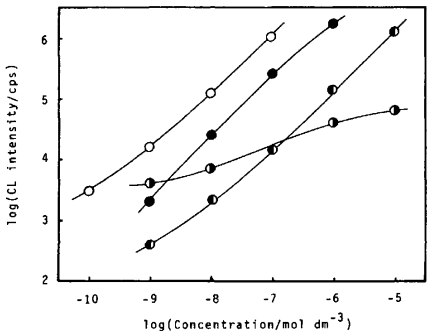

Fig. 2. The relationship between catalyst concentration and CL intensity.
O: TCPP-Fe(III), ◑: TCPP-Pd(II), ◐: TCPP-Pt(II), and ●: TCP-Fe(II).

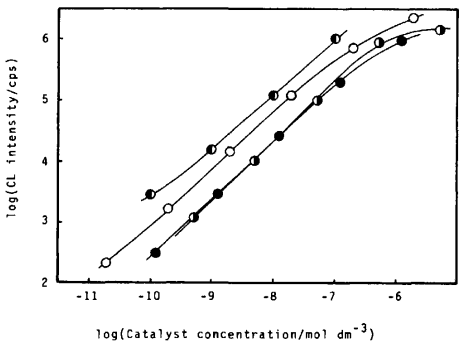

Fig. 3. The catalytic activities of labeled HSA on the basis of catalyst concentration.
Liberated TCPP-Fe(III) (◐), and HSA labeled with TCPP-Fe(III) (O), TCP-Fe(III) (●), and hematin (◑), respectively, by the use of CMC as a carbodiimide.

ent study. Though Co^{II} belonged to the eighth-group, its complexes[1] did not show very high catalytic activity. The catalytic activities of the TCPP complexes of Fe^{III}, Pt^{II}, and Pd^{II}, all belonging to the eighth-group, were examined (Fig. 2). The TCPP-Fe(III) was found to be most sensitive among them; its catalytic activity was higher than that of TCP-Fe(III),[1] which had been previously reported to be most sensitive, and that of hematin,[4] which had been reported to be the most sensitive among the natural-substance catalysts. The TCPP complexes of Mn^{III} and Sn^{IV} other than the eighth-group elements were also synthesized in order to examine their catalytic activities. The catalytic activity of TCPP-Mn(III) was about one-three hundredth that of TCPP-Fe(III), and TCPP-Sn(IV) showed a slight catalytic activity.

HSA as a model protein, was labeled with TCPP-Fe(III), TCP-Fe(III), and hematin, and the catalytic activities of the labeled HSA were examined. Each concentration of the HSA and the catalyst in the labeled HSA was determined by the use of the calibration curves of TCPP-Fe(III) at 414 nm and 280 nm, of TCP-Fe(III) at 637 nm and 280 nm, of hematin at 384 nm and 280 nm, and of HSA at 280 nm, on the assumption that the absorption of each constituent remained unchanged before and after the labeling. The catalytic activities of the labeled HSA are shown in relation to

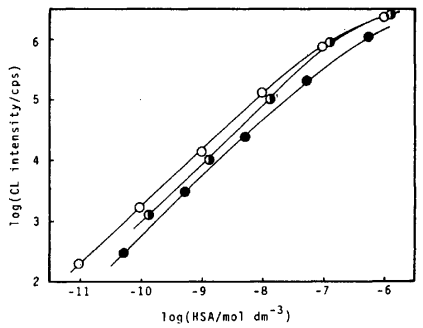

Fig. 4. The catalytic activities of labeled HSA.
HSA labeled with TCPP-Fe(III) (O), TCP-Fe(III) (●), and hematin (◑), respectively, by the use of CMC as a carbodiimide.

the catalyst concentration in Fig. 3. It was concluded from the absorbance measurement that the mole ratio of HSA to TCPP-Fe(III) was 1:3 or 1:2 for the HSA labeled with TCPP-Fe(III) by the use of EDC or CMC as a carbodiimide. The HSA labeled with TCPP-Fe(III) was not so sensitive as the value to be expected from the above mole ratio. As can be seen from Fig. 3, the catalytic activities of a liberated TCPP-Fe(III) and the TCPP-Fe(III) labeled onto HSA were not as similar as TCP-Fe(III) and hematin.

The catalytic activities of TCPP-Fe(III), TCP-Fe(III), and hematin, based on the HSA concentration, were also compared with each other (Fig. 4). The detection limit of the HSA labeled with TCPP-Fe(III) gave the lowest value among them, and a linear calibration curve was obtained at the concentration range of 9.4×10^{-12}—9.4×10^{-8} mol/dm^3-labeled HSA, with a detection limit of about 130 pg HSA. The HSA labeled with TCPP-Fe(III) was about 5.6 times as sensitive as the HSA labeled with TCP-Fe(III), since the detection limit of the latter was about 730 pg; it was also about twice as sensitive as the HSA labeled with hemin reported by Ikariyama *et al.*[8]

It was concluded from the above results that TCPP-Fe(III) was a more sensitive and more excellent labeling reagent for the determination of protein than those reported so far, though the catalytic activity of TCPP-Fe(III) was lowered by the labeling, unlike the case of the other chemiluminescence complex catalysts.

References

1) T. Hara, M. Toriyama, and K. Tsukagoshi, *Bull. Chem. Soc. Jpn.*, **56**, 2267 (1983).
2) T. Hara, M. Toriyama, and K. Tsukagoshi, *Bull. Chem. Soc. Jpn.*, **56**, 2965 (1983).
3) T. Hara, M. Toriyama, and K. Tsukagoshi, *Bull. Chem. Soc. Jpn.*, **57**, 587 (1984).
4) H. A. Neufeld, C. J. Conklin, and R. D. Towner, *Anal. Biochem.*, **12**, 303 (1965).
5) A. D. Adler, *J. Org. Chem.*, **32**, 476 (1967).
6) T. Osa, "Porphyrin no Kagaku," Kyoritsu Shuppan, Tokyo (1982), pp. 57—58.
7) I. Karube, T. Matsunaga, T. Satoh, and S. Suzuki, *Anal. Chim. Acta*, **156**, 283 (1984).
8) Y. Ikariyama, S. Suzuki, and M. Aizawa, *Anal. Chim. Acta*, **156**, 245 (1984).

The Platinum Complex-catalyzed Reductive *N*-Carbonylation of Dinitroarenes to the Biscarbamates

Yoshihisa WATANABE,* Yasushi TSUJI, and Ryo TAKEUCHI
Department of Hydrocarbon Chemistry, Faculty of Engineering, Kyoto University, Sakyo-ku, Kyoto 606
(Received December 21, 1984)

Synopsis. Dichlorobis(triphenylphosphine) platinum(II) shows good catalytic activity for the reductive *N*-carbonylation of dinitroarenes in ethanol in the presence of a Lewis acid and triethylamine. From 2,4-dinitrotoluene, diethyl 4-methyl-1,3-phenylenebiscarbamate is obtained in 50% yield at 190 °C under carbon monoxide pressure of 60 kg cm^{-2}.

Much attention has been paid to the reductive *N*-carbonylation of dinitroarenes and intensive effort is focused on finding an effective catalyst system.[1] We have recently demonstrated that a homogeneous platinum catalyst system including tertiary amine and a Lewis acid has high catalytic activity for the reductive *N*-carbonylation of mononitroarenes,[2] where ethyl phenylcarbamate derivatives are obtained in high yields in ethanol medium. In the present paper, dinitroarenes such as 2,4-dinitrotoluene, 2,6-dinitrotoluene, and *m*-dinitrobenzene are employed as a substrate (Eq. 1).

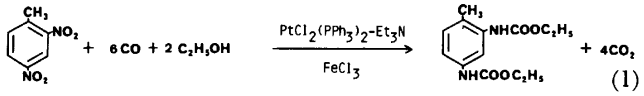

(1)

Results and Discussion

Dichlorobis (triphenylphosphine) platinum(II) is effective for the catalytic transformation of 2,4-dinitrotoluene into diethyl 4-methyl-1,3-phenylenebiscarbamate in the presence of tertiary amine and a Lewis acid. The combination of the platinum complex with a Lewis acid, tertiary amine, and triphenylphosphine is essential for the high catalytic activity , as in the previous paper.[2] The effectiveness of the catalyst system is highly affected by the nature of and the ratio between those components.

The most dominant factor is the nature of a Lewis acid (Table 1). Without a Lewis acid, the platinum catalyst system does not show any catalytic activity and dinitroarenes are recovered unchanged. Iron(III) chloride is the most favorable for giving the biscarbamate, diethyl 4-methyl-1,3-phenylenebiscarbamate, in a good yield (Run 1). Different from the previous paper,[2] tin(IV) chloride and aluminum chloride are less effective. The additions of vanadium(V) trichloride oxide or titanium(IV) chloride were also less effective. With iron(II) chloride trihydrate or pentacarbonyliron(0) or molybdenum(V) chloride, the biscarbamate is not obtained.

The catalytic activity is strongly influenced by the amount of the Lewis acid in the catalytic system (Table 2). The yield of the biscarbamate was nearly zero and only 8% with a small amount of iron(III) chloride. In order to maintain the high catalytic activity, more than tenfold excess of the Lewis acid to the platinum complex is required.

The molar ratio of triethylamine to iron(III) chloride is also a major factor determining the catalytic activity (Fig. 1). The yield of the biscarbamate showed a maximum at the molar ratio of 1.8. The biscarbamate was not obtained at all at the molar ratio over 3. Excess triethylamine would coordinate the platinum complex and saturate the active catalyst sites.

The reaction proceeded with reasonable conversion at 180 °C and 190 °C. At lower temperatures, the yield of the biscarbamate is low and cannot be improved by prolonging the reaction time. The reaction completed at 190 °C for 4 h. Elevating the reaction temperature to 200 °C decreased the yield of biscarbamate to 37%. The optimum initial carbon monoxide pressure is 60 kg cm^{-2}. Under both lower and higher pressures the yield of biscarbamate decreased (yield 29% both under 85 and 45 kg cm^{-2}). The reaction was performed with other dinitroarenes. *m*-Dinitrobenzene and 2,6-dinitrotoluene were converted to the corresponding biscarbamate, although the yields were rather low (diethyl 1,3-phenylenebiscarbamate 28%, diethyl 2-methyl-1,3-phenylenebiscarbamate 30%).

TABLE 1. THE PLATINUM- COMPLEX- CATALYZED REDUCTIVE *N*-CARBONYLATION OF 2, 4- DINITROTOLUENE[a]. THE EFFECT OF VARIOUS LEWIS ACIDS

Run	Lewis acid	Temp	Time	Yield[b]
		°C	h	%
1[c]	$FeCl_3$	190	4	50
2[c]	$FeCl_3$	190	8	40
3	$FeCl_3$	180	4	44
4	$SnCl_4$	180	4	27
5	$AlCl_3$	180	4	6
6	$TiCl_4$	180	4	13

a) A mixture of 2, 4-dinitrotoluene(10 mmol), [$PtCl_2(PPh_3)_2$](0.1 mmol; 1 mol% based on 2, 4-dinitrotoluene used), Lewis acid(2.0 mmol), triethylamine(3.6 mmol) and ethanol(20 ml) was stirred under 60 kg cm^{-2} carbon monoxide. b) Product: Diethyl 4-methyl-1, 3-phenylenebiscarbamate. Determined by HPLC based on the amount of 2, 4-dinitrotoluene charged. c) Iron(III) chloride(1.0 mmol), triethylamine(1.8 mmol).

Table 2. The effect of molar ratio of iron(III) chloride to platinum complex[a]

Run	Molar ratio of $[PtCl_2(PPh_3)_2]$ to Iron(III) Chloride	Yield[b]/%
7	1: 2	0
8	1: 5	8
9	1:10	44
3	1:20	44
10	1:40	40

a) 2, 4-Dinitrotoluene(10 mmol), $[PtCl_2(PPh_3)_2]$(0.1 mmol), iron(III) chloride(0.2-4 mmol), triethylamine(0.36-7.2 mmol; fixing $FeCl_3/Et_3N=1/1.8$), EtOH(20 ml) at 180 °C for 4 h under 60 Kg cm^{-2}. b) Product: Diethyl 4-methyl-1, 3-phenylenebiscarbamate. Determined by HPLC based on the amount of 2, 4-dinitrotoluene charged.

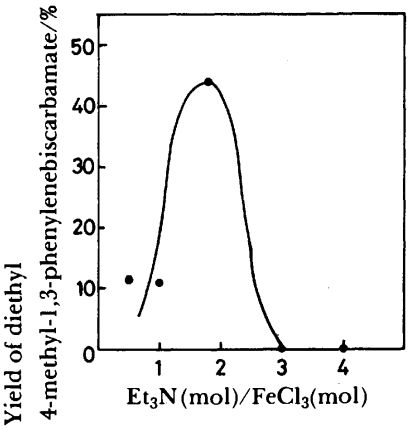

Fig 1. The *N*-Carbonylation of 2,4-Dinitrotoluene. The Effect of the Molar Ratio, $Et_3N/FeCl_3$. 2,4-Dinitrotoluene (10 mmol), $PtCl_2(PPh_3)_2$ (0.1 mmol), $FeCl_3$ (1.0 mmol), triethylamine (0.5—4.0 mmol), EtOH (20 ml) at 180 °C for 4 h under the initial pressure of 60 kg cm^{-2} carbon monoxide. Yields are determined by HPLC based on the amount of 2,4-dinitrotoluene charged.

In the present *N*-carbonylation, the nitrene intermediate would be generated by the deoxygenation of dinitroarene with carbon monoxide, and the carbonylation of the nitrene intermediate will follow (Eq. 2).[2]

$$ArNO_2 \xrightarrow[-CO_2]{+CO} (ArN)(Pt) \xrightarrow{+CO} (ArNCO)(Pt) \xrightarrow{+EtOH} ArNHCOOEt + (Pt) \quad (2)$$

Experimental

General Procedure. A glass liner was set in a 100 ml stainless steel autoclave. The reagents were charged in the following order: Dinitroarene (10 mmol), ethanol (20 ml), triethylamine (0.25 ml, 1.8 mmol), $[PtCl_2(PPh_3)_2]$ (79 mg, 0.1 mmol), and $FeCl_3$ (162 mg, 1.0 mmol). After being sealed and flushed with carbon monoxide, the reactor was pressurized with carbon monoxide to 60 kg cm^{-2}. The autoclave was heated to 190 °C in 20 min and then held at this temperature for 4 h.

Product Isolation. Ethanol was removed from the reaction mixture *in vacuo* at 50 °C. Then, benzene was added to the residue. Aminoarenes were extracted by 60 ml of 10% HClaq three times and the aqueous layer was discharged. Evaporation of benzene afforded the biscarbamate.

Analytical Procedure. The melting points were uncorrected. The HPLC analysis was performed on a Shimadzu LC-5A equipped with a column (μ-Bondapak C_{18}) and $MeOH/H_2O=6/4$ as an eluent. Naphthalene was employed as an internal standard and the yield of the product was determined according to the calibration curve obtained for each sample. The IR spectra were measured on a Hitachi model 215 grating spectrophotometer. The ^{13}C and ^1H-NMR spectra were recorded at 25.05 MHz and 100 MHz respectively with a JEOL JNM FX- 100 spectrometer. Elemental analyses were performed at the Microanalytical Center of Kyoto University. The mass spectra were recorded on a JMS OISG mass spectrometer.

The analytical data of the products are described below. The phenyl carbon resonances in the ^{13}C-NMR spectra were tentatively assigned by calculating their chemical shifts with additive parameters.[4]

Diethyl 4-Methyl-1,3-phenylenebiscarbamate. White crystals, mp 136—138 °C. (lit,[4] mp 137 °C) ^1H-NMR (100 MHz) ($CDCl_3$): 1.29 (t, 3H, $-OCH_2CH_3$), 1.30 (t, 3H, $-OCH_2CH_3$), 2.18 (s, 3H, $-CH_3$), 4.20 (q, 2H, $-OCH_2CH_3$), 4.21 (q, 2H, $-OCH_2CH_3$), 4.74 (br, 1H, -NH), 6.42 (br, 1H, -NH), 7.14 (d, 1H, phenyl), 7.30 (d, 1H, phenyl), 7.76 (d, 1H, penyl). ^{13}C-NMR (25.05 MHz) ($CDCl_3$): 14.6 (q, $-OCH_2CH_3$), 16.7 (q, $-CH_3$), 61.1 (t, $-OCH_2CH_3$), 61.4 (t, $-OCH_2CH_3$), 111.3 (d, phenyl 2), 114.3 (d, phenyl 6), 121.9 (s, phenyl 4), 130.7 (d, phenyl 5), 136.3 (s, phenyl 1), 136.7 (s, phenyl 3), 153.6 (s, C=O). IR (KBr): 3330 cm^{-1} (ν_{N-H}), 3280 cm^{-1} (ν_{N-H}), 1690 cm^{-1} ($\nu_{C=O}$), 1680 cm^{-1} ($\nu_{C=O}$). MS (*m/z*): 266 (M^+). Calcd for $C_{13}H_{18}N_2O_4$: C, 58.64; H, 6.81; N, 10.52%. Found: C, 58.50, H, 6.81, N, 10.05%.

Diethyl 2-Methyl-1,3-phenylenebiscarbamate. White crystals, mp 168—169 °C. ^1H-NMR (100 MHz) ($CDCl_3$): 1.30 (t, 6H, $-OCH_2CH_3$), 2.10 (s, 3H, $-CH_3$), 4.20 (q, 4H, $-OCH_2CH_3$), 6.39 (br, 2H, -NH), 7.09—7.49 (m, 3H, phenyl). ^{13}C-NMR (25.05 MHz) ($CDCl_3$): 12.0 (q, $-CH_3$), 14.5 (q, $-OCH_2CH_3$), 61.3 (t, $-OCH_2CH_3$), 119.5 (d, phenyl 4,6), 126.3 (d, phenyl 5), 135.9 (s, phenyl 1, 2, 3), 153.9 (s, C=O). IR (KBr): 3270 cm^{-1} (ν_{N-H}), 1685 cm^{-1} ($\nu_{C=O}$). MS (*m/z*): 266 (M^+). Calcd for $C_{13}H_{18}N_2O_4$: C, 58.64; H, 6.81; N; 10.52%. Found: C, 58.89; H, 6.69; N, 10.00%.

Diethyl 1,3-Phenylenebiscarbamate. White crystals, mp 142—145 °C. (lit,[5] mp 143—145 °C) ^1H-NMR (100 MHz) ($CDCl_3$): 0.95 (t, 6H, $-OCH_2CH_3$), 4.00 (q, 4H, $-OCH_2CH_3$), 7.04—7.16 (m, 4H, phenyl), 7.82 (br, 2H, -NH). ^{13}C-NMR (25.05 MHz) ($CDCl_3$): 14.6 (q, $-OCH_2CH_3$), 61.4 (t, $-OCH_2CH_3$), 109.1 (d, phenyl 2), 113.5 (d, phenyl 4,6), 129.5 (d, phenyl 5), 139.5 (s, phenyl 1,3), 153.4 (s, C=O). IR (KBr): 3270 cm^{-1} (ν_{N-H}), 1700 cm^{-1} ($\nu_{C=O}$), 1680 cm^{-1} ($\nu_{C=O}$). MS (*m/z*): 252 (M^+). Calcd for $C_{12}H_{16}N_2O_4$: C, 57.13; H, 6.39; N, 11.1%. Found: C,57.39; H, 6.37; N, 10.97%.

References

1) a) V. I. M. Yuvenskii and B. K. Nefedov, *Russ. Chem. Rev.*, **50**, 470, (1980); b) K. Miyata, *Shokubai*, **23**, 29, (1980).

2) Y. Watanabe, Y. Tsuji, R. Takeuchi, and N. Suzuki, *Bull. Chem. Soc. Jpn.*, **56**, 3343 (1983).

3) J. B. Stothers, "Carbon-13 NMR Spectroscopy," Academic Press, New York (1972). p. 197.

4) Beilsteins Handbuch der Organischen Chemie, **13**, 137 (1930).

5) M. Michman, S. Patai, and Y. Wiesel, *J. Chem. Soc. Perkin I*, **1977**, 1705.

A Convenient Method for the Preparation of Conjugated Olefins from Allylic Acetates and Aldehydes. Synthesis of Pellitorine

Yuhko TSUKAHARA, Hideki KINOSHITA,* Katsuhiko INOMATA, and Hiroshi KOTAKE
Department of Chemistry, Faculty of Science, Kanazawa University, Kanazawa 920
(Received March 28, 1984)

Synopsis. A variety of allylic acetates were treated with sodium bromide and triphenylphosphine in the presence of 5 mol% of [Pd(PPh$_3$)$_4$] to give the phosphonium salts, which were converted to the ylids *in situ* and allowed to react with various aldehydes to afford the corresponding conjugated olefins in good yields. Furthermore, this procedure was applied to the synthesis of an insecticidal substance, Pellitorine.

In the previous paper,[1] it was reported that the reaction of allylic acetates with sodium *p*-toluenesulfinate in THF–MeOH catalyzed by [Pd(PPh$_3$)$_4$] gave regiocontrolled allylic sulfones in good yields. On the basis of this finding, we thought that the reaction of allylic acetates with alkali halides such as NaBr and LiI instead of sodium *p*-toluenesulfinate would give the corresponding allylic halides under the same reaction conditions. When geranyl acetate was treated with NaBr in the presence of a catalytic amount of [Pd(PPh$_3$)$_4$] and one equiv of triphenylphosphine, the corresponding phosphonium salt (**1**) was actually isolated.[2]

In this paper, we wish to report an efficient procedure for the preparation of conjugated olefins in one-pot from allylic acetates *via* the formation of the triphenylphosphonium salts (**1**). Thus, to a solution of one equiv of PPh$_3$ and 5 mol% of [Pd(PPh$_3$)$_4$] in dry THF were added a solution of one equiv of cinnamyl acetate in dry THF and a solution of two equiv of NaBr in dry MeOH under N_2. After the reaction mixture was stirred for 1.5 h at room temperature, it was successively treated with 1.2 equiv of BuLi and 1.1 equiv of benzaldehyde at −17 °C and stirred for 4 h at room temperature. The usual work-up gave the desired 1,4-diphenyl-1,3-butadiene (**2a**) in 83% yield.

In a similar manner, various conjugated olefins (**2b—g**) were prepared in good yields as shown in Table.

Next, the present method was applied to the synthesis of Pellitorine (**5**),[3] a crystalline insecticidal substance isolated from *Anacyclus pyrethrum DC.* roots, from the allylic acetate(**4**) prepared by oxidation of (*E*)-*N*-isobutyl-2-butenamide (**3**) and hexanal according to the following scheme. Pellitorine (**5**, 2*E*, 4*E*-) and its 2*E*,4*Z*-isomer were obtained in 31% and 24% yields, respectively. The latter isomer could be converted into Pellitorine (**5**) in a quantitative yield by treatment with a catalytic amount of I_2.

As mentioned above, the present method proved to be a very useful procedure for the preparation of conjugated olefins[4] from easily available acetates.

Experimental

HPLC analyses were performed with a Waters M6000 A instrument using a 30 cm×3.9 mm column (μ-Polasil, particle size-10 μm, detection 254 nm). Thin-layer chromatography (TLC) was performed on Merck's silica gel 60 PF_{254}

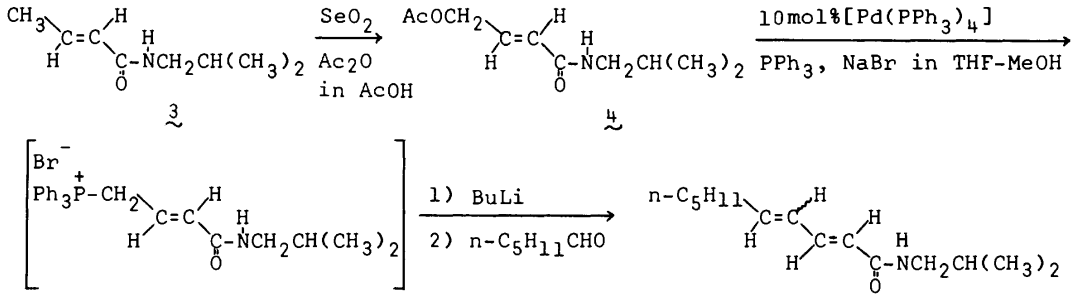

Scheme 1. Synthesis of Pellitorine

TABLE 1. CONVERSION OF ALLYLIC ACETATES TO CONJUGATED OLEFINS

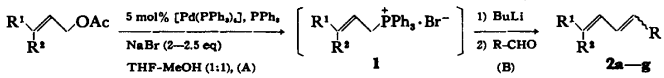

Allylic acetate	R-CHO	Reaction conditions (A)	Reaction conditions (B)	Yield of 2/%	Stereochemistry
Ph/\/OAc	Ph-CHO	r.t., 1.5 h	−17°—r.t., then r.t., 4 h	83 (2a)	1*E*, 3*Z*: 1*E*, 3*E* (79:21)
Ph/\/OAc	O_2N-C$_6$H$_4$-CHO	r.t., 1.5 h	−17°—r.t., then r.t., 3 h	84 (2b)	1*E*, 3*E* only
Ph/\/OAc	Ph/\/CHO	r.t., 1.5 h	−17°—r.t., then r.t., 3 h	82 (2c)	1*E*, 3*Z*, 5*E*: 1*E*, 3*E*, 5*E* (77:23)
Ph/\/OAc	CH_3CH_2CHO	r.t., 1.5 h	−17°—r.t., then r.t., 4 h	81 (2d)	1*E*, 3*Z*: 1*E*, 3*E* (47:53)
/\/\/OAc	Ph-CHO	reflux, 2 h	−17°—r.t., then r.t., overnight	85 (2e)	1*Z*, 3*E*: 1*E*, 3*E* (70:30)
/\/\/OAc	/\/\/CHO	reflux, 2 h	−17°—r.t., then r.t., overnight	76 (2f)	6*E*, 8*Z*, 10*E*: 6*E*, 8*E*, 10*E* (50:50)
/\/OAc	Ph-CHO	reflux, 2 h	−17°—r.t., then r.t., overnight	73 (2g)	1*Z*: 1*E* (45:55)

(Art. 7749).

Preparation of Conjugated Olefins (2a—g). **2a**: To a solution of PPh_3 (131 mg, 0.5 mmol) and $[Pd(PPh_3)_4]$ (29 mg, 0.025 mmol) in dry THF (1.5 ml) were added a solution of cinnamyl acetate (88 mg, 0.5 mmol) in dry THF (0.5 ml) and a solution of NaBr (103 mg, 1 mmol) in dry MeOH (2 ml) under N_2. After stirring for 1.5 h at room temperature, the reaction mixture was cooled to −17 °C and a hexane solution (*ca.* 15%) of 1.2 equiv of BuLi was added at the temperature. The mixture was stirred for 30 min at room temperature and cooled to −17 °C again. Then, a solution of benzaldehyde (59 mg, 0.55 mmol) in dry THF (0.5 ml) was added. The reaction mixture was gradually warmed and kept at room temperature for 4 h. After quenching the reaction with aq KCN (7 mg, 0.1 mmol), the product was extracted with AcOEt and subjected to preparative TLC (solvent; hexane) to give **2a** consisting of two isomers in 83% yield (86 mg). They were separable with a pre-coated TLC plate (Merck's silica gel $60F_{254}$, Art.5715, solvent; hexane) and their stereochemistry was assigned by comparison of UV spectra and melting point with those reported in literatures. Ratio of the isomers was determined by HPLC analysis of the crude product (solvent; hexane, flow rate 1 ml/min). 1*E*,3*E*-isomer: Mp 144—149 °C (lit, 147—149 °C).[5] UV (hexane) 329 nm (lit, 328 nm).[6] 1*E*,3*Z*-isomer: An oil; IR (neat) 980, 745, 720, 692, and 680 cm^{-1}. The 1*E*,3*Z*-isomer was readily converted to the 1*E*,3*E*-isomer with the aid of a catalytic amount of I_2 in benzene-ether.

2b: Mp 177.0—178.5 °C (lit, 172 °C).[7]

2c: Ratio of the isomers was determined by HPLC analysis using "iso-octane" as eluent. The stereochemistry of the isomers was assigned by UV spectra comparing with the reported ones.[8]

2d: An oil. The stereochemistry and ratio of the isomers were determined by 100 MHz ^{1}H-NMR spectrum. 1*E*,3*E*-isomer: NMR ($CDCl_3$) δ=1.05 (t, *J*=7.4 Hz, 3H), 2.17 (m, 2H), 5.85 (dt, *J*=6.3, 14.8 Hz, 1H), 6.18 (dd, *J*=9.4, 14.8 Hz, 1H), 6.42 (d, *J*=15.4 Hz, 1H), 6.76 (dd, *J*=9.4, 15.4 Hz, 1H), and 7.10—7.45 (m, 5H). 1*E*,3*Z*-isomer: NMR ($CDCl_3$) δ=1.05 (t, *J*=7.4 Hz, 3H), 2.17 (m, 2H), 5.54 (dt, *J*=7.4, 10.5 Hz, 1H), 5.98—6.25 (m, 1H), 6.42 (d, *J*=15.4 Hz, 1H), 6.76 (dd, *J*=9.4, 15.4 Hz, 1H), and 7.10—7.45 (m, 5H). MS (of the mixture) *m/z* 158 (M^+) and 129 ($M^+-C_2H_5$). IR (of the mixture, neat) 980 736, and 680 cm^{-1}.

2e: An oil. Ratio of the isomers was determined by HPLC analysis (solvent; "iso-octane." flow rate 0.5 ml/min). 1*E*,3*E*-isomer: IR (neat) 951, 740, and 680 cm^{-1}.[2] 1*Z*,3*E*-isomer: IR (neat) 790 and 690 cm^{-1}; NMR ($CDCl_3$) δ=1.60 (s, 3H), 1.68 (s, 3H), 1.81 (s, 3H), 2.00—2.30 (m, 4H), 5.04 (br, 1H), and 5.83—7.57 (m, 8H). MS (of the mixture) *m/z* 226 (M^+) and 157 ($M^+-CH_2CH{=}C(CH_3)_2$).

2f: An oil. Ratio of the isomers was determined by GLC analysis (Shimazu GC 6A, 10% Silicone SE-30 on 60-80 mesh Shimalite W, 210 °C). The mixture was separated by preparative TLC (30% silver nitrate-impregnated silica gel). 6*E*,8*E*,10*E*-isomer: IR (neat) 986 and 951 cm^{-1}.[2] 6*E*,8*Z*,10*E*-isomer: IR (neat) 760 cm^{-1}. NMR (of the mixture, $CDCl_3$) δ=1.58 (s, 6H), 1.65 (s, 6H), 1.73 (s, 6H), 1.93—2.30 (m, 8H), 5.05 (br, 2H), and 5.07—6.50 (m, 4H).

2g: An oil. Determination of the stereochemistry and ratio of the isomers were performed as described for **2e**. 1*E*-isomer: IR (neat) 980 and 950 cm^{-1}.[3] 1*Z*-isomer: IR (neat) 783, 740, and 686 cm^{-1}. MS (of the mixture) *m/z* 158 (M^+) and 143 (M^+-CH_3). NMR (of the mixture, $CDCl_3$) δ=1.80 (s, 6H), and 5.72—7.63 (m, 8H).

(E)-N-Isobutyl-2-butenamide (3). To a solution of triethylamine (1.518 g, 15 mmol) and isobutylamine (1.646 g, 22.5 mmol) in dry CH_2Cl_2 (20 ml) was added dropwise a solution of crotonoyl chloride (1.568 g, 15 mmol) in dry CH_2Cl_2 (10 ml) at 0 °C under N_2. Usual work-up gave the desired product which was recrystallized from hexane. Yield, 2.063 g (97%). Mp 70.5—72.0 °C. IR (KBr) 3240, 2960, 1660, 1615, 1550, 1230, and 978 cm^{-1}. NMR ($CDCl_3$) δ=0.92 (d, *J*=6.5 Hz, 6H), 1.47—2.26 (m, 1H), 1.83 (dd, *J*=2.0, 7.0 Hz, 3H), 3.13 (dd, *J*=6.0, 6.0 Hz, 2H), 5.87 (dd, *J*=2.0, 15.0 Hz, 1H), 6.14 (br, 1H), and 6.81 (dq, *J*=7.0, 15.0 Hz, 1H). Found: C, 67.78; H, 10.89; N, 9.74%. Calcd for $C_8H_{15}NO$: C, 68.04; H, 10.71; N, 9.92%.

(E)-Isobutyl-4-acetoxy-2-butenamide (4). A mixture of **3** (565 mg, 4 mmol), acetic anhydride (449 mg, 4.4 mmol), water (73 mg, 4 mmol), and acetic acid (5 g, 83 mmol) was refluxed for 75 min under N_2. Selenium(IV) oxide (533 mg, 4.8 mmol) was added to it by portions. The mixture was refluxed for about 10 h and worked up in the usual way. The product was isolated by preparative TLC (solvent; hexane:AcOEt= 1:1 v/v). Yield, 120 mg (15%). IR (neat) 3293, 2960, 1740, 1670, 1630, 1550, 1270, 1235, and 980 cm^{-1}; NMR ($CDCl_3$) δ=0.92 (d, *J*=6.5 Hz, 6H), 1.47—2.14 (m, 1H), 2.07 (s, 3H), 3.11 (dd, *J*=6.0, 6.0 Hz, 2H), 4.65 (dd, *J*=1.5, 5.0 Hz, 2H), 6.06 (dd, *J*=2.0, 15.4 Hz, 1H), 6.12 (br, 1H), and 6.73 (dt, *J*=5.0, 15.4 Hz, 1H); CI-MS *m/z* 200 (M^++1).

Preparation of Pellitorine (5). To a solution of PPh_3 (110 mg, 0.42 mmol) and $[Pd(PPh_3)_4]$ (42 mg, 0.036 mmol) in dry THF (1.5 ml) were added a solution of **4** (71 mg, 0.36 mmol) in dry MeOH (3 ml) and a solution of NaBr (86 mg, 0.84 mmol) in dry MeOH (1.5 ml) under N_2. The mixture was refluxed for 4 h and cooled to −17 °C. Then, a hexane solution of BuLi (0.396 mmol) was added with vigorous stirring followed by the addition of a solution of hexanal (40 mg, 0.396 mmol) in dry THF (1 ml). The reaction mixture was gradually warmed up to room temperature and worked up in the usual way. Two fractions were obtained by preparative TLC (Merck's Aluminum oxide 60 PF_{254}, Type E, solvent; benzene:AcOEt=8:1 v/v). From the first fraction of lower R_f value, Pellitorine (**5**) was obtained in 31% yield (25 mg). Its Mp, IR, and NMR data were identical with those of the reported ones.[9] Mp 89—90 °C (lit, 89—90 °C). 4*Z*-isomer was obtained from the second fraction of higher R_f value as an oil. It could be converted to Pellitorine in a quantitative yield by treatment with a catalytic amount of I_2 in benzene for 1 h at room temperature. Yield, 19 mg (24%, an oil); IR (neat) 3250, 1635, 1598, 1528, 1262, 982, and 858 cm^{-1}; NMR ($CDCl_3$) δ=0.66—1.10 (t, 3H), 0.92 (d, *J*=6.0 Hz, 6H), 1.10—2.53 (m, 9H), 3.12 (dd, *J*=6.0, 6.0 Hz, 2H), 5.37—6.27 (m, 4H), and 7.27—7.70 (m, 1H); MS *m/z* 223 (M^+).

References

1) K. Inomata, T. Yamamoto, and H. Kotake, *Chem. Lett.*, **1981**, 1357.

2) L. Barlow and G. Pattenden, *J. Chem. Soc., Perkin Trans.* I, **1976**, 1021.

3) L. Crombie, *J. Chem. Soc.*, **1955**, 999.

4) M. Moreno-Manâs and A. Trius, *Bull. Chem. Soc. Jpn.*, **56**, 2154 (1983).

5) C. Piechuki, *Synthesis*, **1976**, 187.

6) J. H. Pinkard, B. Wille, and L. Zeichmeister, *J. Am. Chem. Soc.*, **70**, 1938 (1948).

7) F. Bergmann amd Z. Weinberg, *J. Org. Chem.*, **6**, 134 (1941).

8) K. Lunde and L. Zeichmeister, *J. Am. Chem. Soc.*, **76**, 2308 (1954).

9) T. Sasaki, K. Seko, A. Tsuji, M. Utaka, and A. Takeda, *J. Org. Chem.*, **47**, 1101 (1982).

Studies on Pyrazines. 11.[1] A Novel Formation of 2-Aminopyrazine from the Reaction of Pyrazine 1-Oxide with Phosphoryl Chloride

Nobuhiro SATO* and Michio KOBAYASHI†

Department of Chemistry, Yokohama City University, Seto, Kanazawa-ku, Yokohama 236

†*Department of Chemistry, Tokyo Metropolitan University, Fukasawa, Setagaya-ku, Tokyo 158*

(Received March 29, 1984)

Synopsis. The reaction of pyrazine 1-oxide with phosphoryl chloride gave a 49% yield of 2-chloropyrazine and a small amount of 2-aminopyrazine. The precursor of aminopyrazine was elucidated to be a 1-(2-pyrazinyl)-pyrazinium salt. The orientation of substitution in the formation of the salt was determined by reaction of deuterium labelled pyrazine *N*-oxides with phosphoryl chloride.

As part of our continuing program directed toward the reaction of pyrazine *N*-oxides,[1] we now report a novel formation of 2-aminopyrazine (**3**) from the reaction of pyrazine 1-oxide (**1**) with phosphoryl chloride.

It has been known that treatment of pyrazine 1-oxide **1** with two equivalents of phosphoryl chloride at 55 °C followed by brief reflux gives a 25% yield of 2-chloropyrazine (**2**).[2] The yield of **2**, however, was increased to 49% when **1** was treated in a large excess of the reagent at 70 °C for 2 h. Surprisingly, a small amount of 2-aminopyrazine (**3**) was isolated on hydrolytic workup of the reaction mixture. The precursor of **3** was elucidated to be a 1-(2-pyrazinyl) pyrazinium salt (**4**) from the ^{1}H NMR spectrum of the reaction mixture prior to hydrolysis (see Fig.). The doublet of doublets having the coupling constants of 4.5 and 1.5 Hz at δ 9.47 and 8.76, which correspond to C-2,6 and C-3,5 protons of the pyrazinium moeity of **4**, respectively, are characteristic for those of pyrazine 1-oxide **1** or 1-methylpyrazinium iodide.[3] Presumably the counter ion of **4** is the chloride ion but it was not established because of difficult separation of **4** from the reaction mixture. Thus, **3** was formed by decomposition of the pyrazinium group of the salt **4** under hydrolytic conditions. In addition, the NMR spectrum of the reaction mixture indicated that **2** and **4** were formed in 50% yields each. These results are illustrated in Scheme 1.

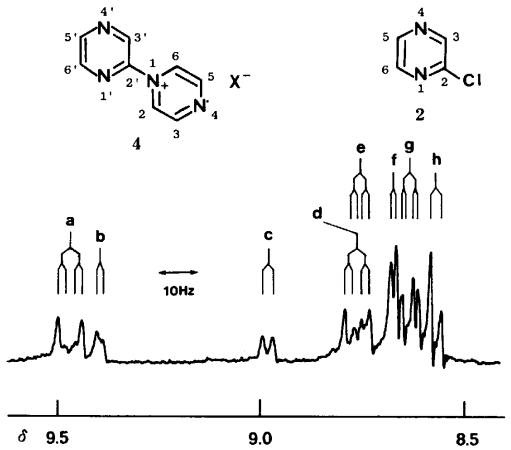

Fig. 1. The ^{1}H NMR spectrum (100 MHz) of reaction mixture formed by treatment of **1** with phosphoryl chloride at 70 °C for 2 h. Assignment of signals: a, δ 9.47, H-3,5 of **4**; b, 9.40, H-3′ of **4**; c, 8.98, H-5′ of **4**; d, 8.76, H-2,6 of **4**; e, 8.75, H-6′ of **4**; f, 8.68, H-3 of **2**; g, 8.63, H-6 of **2**; h, 8.57, H-5 of **2**. The counter ion of **4**, X^-, is chloride ion or an unidentified ion.

The pyrazinium salt **4** having the counter ion of $P_2O_3Cl_2^-$, which would seem to consist of several complex hydrolysates of phosphoryl chloride,[4] was isolated from the reaction mixture of **1** with phosphoryl chloride at room tempeature for 30 min. The isolated salt **4** gave satisfactory analysis for C, H, and N, and ^{1}H and ^{13}C NMR spectra. The other products of the reaction at room temperature were a 13% yield of **2**, and an approximate 30% yield of the hydrochloride of **1**.

The direction of substitution in formation of the salt **4** was significantly demonstrated by reactions of deuterium labelled *N*-oxides, pyrazine-2,6-d_2 and -3,5-d_2 1-oxides, which were obtained by treatment of the corresponding dichloropyrazine 1-oxides with deuterium. The NMR spectra of those reaction mixtures showed that the substitution reaction took place at carbons both α and β to the *N*-oxide function, and the pyrazinium nitrogen atom was derived from the nitrogen atom originally oxidized in another molecule of **1**. For example, pyrazine-2,6-d_2 1-oxide gave a pair of isomers (*ca.* 1:1) of the salts as shown in Scheme 2.

1-(2-Pyridyl)pyridinium salts have been prepared by treatment of pyridine 1-oxide with tosyl chloride in pyridine, and the hydrolysis of these salts gives aminopyridines.[5] The formation of the salt is believed to involve the nucleophilic attack of pyridine on (1-pyridinio) tosylate. The regiospecificity of the pyrazinium nitrogen of **4**, however, rules out the mechanism in which pyrazine is formed by deoxygena-

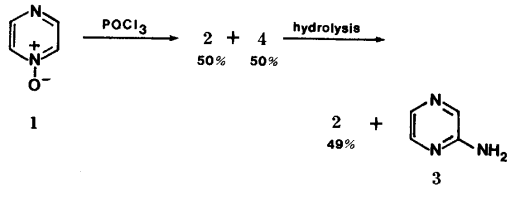

Scheme 1.

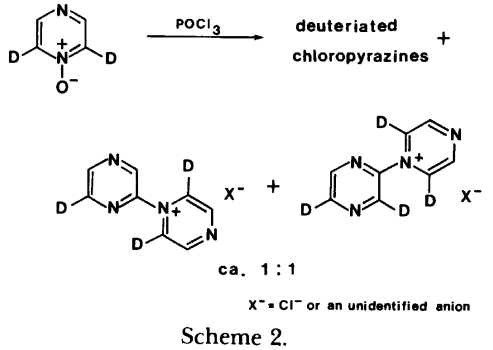

Scheme 2.

tion of the *N*-oxide **1** with phosphoryl chloride. In addition, the basicity (pK_a 0.65)[6] of the nitrogen in pyrazine is not enough to bring about the nucleophilic attack of the nitrogen atom on pyrazine *N*-phosphorodichloridate which initially formed, or chloropyrazine **2**. Actually, no incorporation of unlabelled pyrazine was observed when the reaction of deuteriopyrazine *N*-oxide was conducted in the presence of unlabelled pyrazine. We have not yet determined the mechanism which accounts for the observed regiochemistry but now the work is in progress.

Experimental

Materials. Phosphoryl chloride was used after being distilled twice at 106—107°C. Pyrazine 1-oxide (**1**) was prepared according to the procedure of Koelsch and Gumprecht.[7] The crude product was extracted with hot benzene, and the solution was passed through a column of 100/200 Florisil eluted with chloroform to remove a small amount of pyrazine 1,4-dioxide. Further purifications were carried out by sublimation at *ca.* 100°C/1 Pa and recrystallization from benzene to give **1** of mp 113—114°C (lit, 113—114°C;[7] ^{1}H NMR ($CDCl_3$): δ=8.50 (2H, dd, J=3.4 and 1.6 Hz), 8.17 (2H, dd). Deuterium labelled pyrazine 1-oxides were prepared by replacement of the corresponding dichloropyrazine *N*-oxides[8,9] (0.01 mol) in acetonitrile (50 ml) with deuterium (99.5 atom% D, 1.1 equivalents) in the presence of 5% palladium on carbon (0.1 g/1.0 g) and triethylamine (1.05 equivalents) under atmospheric pressure at 20°C. The mixture was filtered and evaporated to dryness *in vacuo*. The residue was worked up by our earlier procedure[10] to give 60—70% of the labelled *N*-oxide, which was purified by sublimation at *ca.* 100°C/1 Pa. Isotopic purity was determined by ^{1}H NMR spectrum to be 80%d_2 and 95%d_2 for pyrazine-2,6-d_2 and -3,5-d_2 1-oxides, respectively. The starting material for pyrazine-3,5-d_2 1-oxide, 3,5-dichloropyrazine 1-oxide, was prepared by N-oxidation of 2,6-dichloropyrazine with peracetic acid in acetic acid but the yield was very low (1.2—4%).[8,9] We found that the *N*-oxide was obtained in 64% yield by treatment of the dichloropyrazine with *m*-chloroperbenzoic acid (1.2 equivalents) in chloroform (reflux, 24 h).

Reaction of 1 with Phosphoryl Chloride. At 70°C for 2 h: A mixture of **1** (0.480 g, 5.0 mmol) in 9.0 ml of phosphoryl chloride was stirred and heated at 70°C for 2 h. After cooling to room temperature, the solution was poured into ice-water and basified at pH 9 with 30% aqueous sodium hydroxide. The solution was extracted with four 10-ml portions of chloroform, and the extracts were washed with two 20-ml portions of water and dried over magnesium sulfate. The yield of **2** was determined by GLC analysis of the chloroform extract.[11] The aqueous layer and washings were further basified at pH 10 with sodium carbonate and evaporated to dryness *in vacuo*. The residue was sublimed at 100°C/1 Pa to give 0.026 g (11%) of **3**, mp 114—116°C. This compound was identified by comparison with the IR and NMR spectra of the authentic sample, mp 119—120°C, purchased from Aldrich Chem. Co.

At Room Temperature: A mixture of **1** (0.480 g, 5.0 mmol) in 9.0 ml of phosphoryl chloride was stirred at room temperature for 30 min, and then 20 ml of dry chloroform was added to the mixture. Insoluble material was collected by filtration and the filtrate was worked up as described. The insoluble material was dried at room temperature *in vacuo* and triturated in dry nitromethane. Insoluble material (hydrochloride of **1**, 0.2 g, 30%; Found: C, 35.73; H, 3.67; N, 21.13; Cl, 26.97%. Calcd for $C_4H_5N_2OCl$: C, 36.24; H, 3.80; N, 21.14; Cl,26.75%) was collected by filtration, and dry carbon tetrachloride was added to the filtrate to give 0.44 g of **4**. Several purifications in the predescribed fashion gave an unstable solid of **4**, mp 126—128°C (decomp); IR (KBr): 1606 cm^{-1} (P=O); ^{1}H NMR (nitromethane-d_3): δ=9.51 (2H, dd, J=4.5 and 1.5 Hz), 9.41 (1H, d, J=1.5 Hz), 9.02 (1H, d, J=2.6 Hz), 8.84 (2H, dd, J=4.5 and 1.5 Hz), 8.80 (1H, dd, J=2.6 and 1.5 Hz); ^{13}C NMR (nitromethane-d_3): 149.5, 145.2, 141.4 (C-3′, 4′, 5′), 147.3 (C-2′), 139.0, 138.7 (C-2,6 and C-3,5); Found: C, 28.30; H, 2.38; N, 16.69; Cl, 19.46%. Calcd for $C_8H_7N_4P_2O_3Cl_2$: C, 28.26; H, 2.08; N, 16.48; Cl, 20.85%.

References

1) Part 10: N. Sato, *J. Chem. Research*, in press.
2) B. Klein, N. E. Hetman, and M. E. O'Donnell, *J. Org. Chem.*, **28**, 1682 (1963).
3) T. Goto, M. Isobe M. Ohtsuka, and K. Tori, *Tetrahedron Lett.*, **1968**, 1511.
4) H. Roux and A. Couzinie, *Experientia*, **10**, 168 (1954).
5) E. Ochiai, "Aromatic Amine Oxides," Elsevier, Amsterdam (1967), pp. 285—286.
6) G. W. H. Cheeseman and E. S. G. Werstiuk, *Adv. Heterocycl. Chem.*, **14**, 99 (1972).
7) C. F. Koelsch and W. H. Gumprecht, *J. Org. Chem.*, **23**, 1603 (1958).
8) G. Palamidessi, L. Bernardi, and A. Leone, *Farmaco, Ed Sci.*, **21**, 805 (1966); *Chem. Abstr.*, **66**, 37885 (1967).
9) C. E. Mixan and R. G. Pew, *J. Org. Chem.*, **42**, 1869 (1977).
10) N. Sato, *J. Org. Chem.*, **43**, 3367 (1978).
11) A. Marchese, L. Cere, and P. F. Rose, *Rass. Chim.*, **27**, 70 (1975); *Chem. Abstr.*, **84**, 12123 (1967).

Synthesis and Reactions of 1-(Trimethylsilyl)allyl Chloride[1]

Nobujiro SHIMIZU,* Fumihiro SHIBATA, and Yuho TSUNO
Department of Chemistry, Faculty of Science, Kyushu University 33, Hakozaki, Higashi-ku, Fukuoka 812
(Received April 13, 1984)

Synopsis. 1-(Trimethylsilyl)allyl chloride prepared conveniently from 1,3-dichloropropene reacted smoothly with organocopper compounds yielding terminal alkenylsilanes, while its Grignard reactions with carbonyl compounds gave the corresponding alcohols with the regioselection depending sensitively on substrates.

Silylated allyl halides are useful synthetic intermediates.[2] 3-Silylallyl halides are obtainable from allylsilanes or 3-silylallyl alcohols[3,4] but no practical method is so far available for 1-silylallyl halides, although 3-chloro-3-(trimethylsilyl)allyltriphenyllead was reported to yield 1-(trimethylsilyl)allyl chloride (**1**) as a minor product on treating with butyllithium followed by hydrolysis.[5,6] We here describe a convenient route to **1** and several reactions of this material.

1,3-Dichloropropene reacted with chlorotrimethylsilane on mixing in the presence of magnesium at room temperature in a THF/ether (1:1) solution to give **1** in 40% yield.[7] The product contained a small amount of 1-chloro-3-trimethylsilylpropene as an impurity which was difficult to be removed.[8]

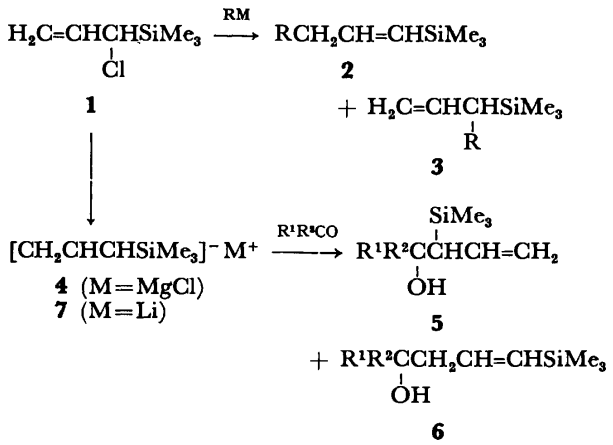

Treatment of **1** with organocopper compounds led to the regioselective γ-alkylation affording terminal alkenylsilanes **2** (**2**/**3**>97/3 in most cases) in good yields. The results are given in Table 1. Stereochemistry of the product **2** was dependent on the organometallic species involved. For example, lithium dibutylcuprate(I) reacted with **1** to give *trans*-1-trimethylsilylheptene predominantly, whereas butylcopper yielded the *cis*-isomer as the major product. In the alkylation with Grignard reagents (RMgX) in the presence of a catalytic amount of copper(I) iodide, *cis*-products significantly increased when RMgX was slowly added to a mixture of **1** and CuI instead of the addition of **1** to an admixture of RMgX and CuI. Probably, RCu is involved as a reactive species under the former conditions; a cuprate(I) may be operative under the latter conditions.

A Grignard reagent **4** prepared from **1** added regioselectively to aldehydes to give the corresponding α-alcohols **5** together with a small amount of regioisomeric γ-alcohols **6**. Low reaction temperature favored the formation of **5** and so did THF as compared to ether as solvent. In contrast, the reagent **4** reacted with ketones yielding **6** exclusively irrespective of the reaction conditions, as shown in Table 2. The silylated carbon terminus of the species **4** is probably more electronegative than is the unsubstituted CH_2-terminus; so electronically a carbonyl group would preferentially attack the former site, as is indeed observed for aldehydes. A marked change in the regioselectivity for ketones presumably arises from the steric hindrance around a carbonyl group. The regioselection also depends on a counter cation of the allyl anion. Thus, the present results contrast with the fact that a related species **7** reacts with both aldehydes and ketones to give **6** as the sole product.[9] This is probably associated with the difference in the ionic character of a carbon-metal bond.

TABLE 1. REACTIONS OF **1** WITH ORGANOMETALLIC REAGENTS[a]

Reagent	Yield/% of **4**[f]	Isomer ratio (*Z*)/(*E*)
n-BuMgBr/CuI (10 mol%)	83	0.72[i], 0.43[j]
PhMgBr/CuI (10 mol%)	84[g]	1.4[i], 0.67[j]
c-C_6H_{11}MgBr/CuI (10 mol%)	69	0.79[i], 0.32[j]
t-BuMgCl/CuI (10 mol%)	84	0.63[i]
n-BuMgBr[b]	36[h]	0.49
n-Bu_2CuLi[c]	68	0.67
n-BuCu[c]	97	2.1
$NCCH_2Cu$[d]	72	0.79
$PhCOCH_2CH_2CH_3$/NaH[e]	21	k)

a) Reactions were carried out in THF at 0 °C for 30 min under nitrogen unless otherwise noted. b) At room temperature for 3 h. c) At −50 °C. d) At −25 °C. e) In 1, 2-dimethoxyethane under reflux. f) GLC yield. g) **2**/**3**=92/8. h) **2**/**3**=70/30. i) RMgX was added to a mixtue of **1** and CuI. j) **1** was added to a mixture of RMgX and CuI. k) Not determined.

Table 2. Reactions of **4** with carbonyl compounds

Substrate	Conditions	Product ratio **5**:**6**	Yield/%[a]
i-PrCHO	ether, 0 °C	76:24	76
	THF, 0 °C	84:16	67
	THF, −75 °C	94:6	b)
PhCHO	ether, 0 °C	66:34	81
	THF, 0 °C	79:21	73
	THF, −75 °C	82:18	b)
cyclohexanone	ether, 0 °C	~0:100	83
	THF, 0 °C	~0:100	88
	THF, −75 °C	~0:100	b)
$PhCOCH_3$	ether, 0 °C	~0:100	79

a) GLC yield. b) Not determined.

Experimental

NMR spectra were determined in carbon tetrachloride solutions with a Hitachi R-600 spectrometer and IR spectra were recorded on a Hitachi 260-10 spectrophotometer.

1-(Trimethylsilyl)allyl Chloride (1). A mixture of 1,3-dichloropropene (Tokyo Chemical Industry, 43 g, 0.39 mol), chlorotrimethylsilane (42 g, 0.39 mol), and 1,2-dibromoethane (0.1 cm^3) was added to a stirred mixture of magnesium (13 g) and chlorotrimethylsilane (20 g) in THF/ether (1:1) (400 cm^3) over a period of 4 h at room temperature. The mixture was stirred for further 4h at room temperature and quenched with a sodium hydrogencarbonate solution. Usual workup gave a colorless oil (23 g), bp 73—76 °C (100 Torr: 1 Torr=133.3 Pa), which was a mixture of **1** and 1-chloro-3-trimethylsilylpropene in the ratio 93:7. The spectral data for these two compounds were superimposable with those reported.[5,10]

Reactions of 1 with Organometallic Reagents. The following example is representative.

Butylmagnesium bromide (16 mmol) in THF (20 cm^3) was added to a mixture of **1** (0.79 g, 5.3 mmol), copper(I) iodide (0.3 g, 1.5 mmol), and ethylbenzene (50 mg, as an internal standard) in THF (5 cm^3) over a period of 15 min at 0 °C. Aqueous workup of the mixture gave 1.01 g of 1-trimethylsilylheptene (*E*/*Z*=1.08) (37%; 84% based on GLC), bp 90—97 °C (47 Torr) (Found: C, 70.50; H, 13.06%). An analytical sample of each isomer was obtained by GLC. (*E*): IR 1620 (C=C) cm^{-1}; NMR δ=0.03 (9H, s), 0.7—1.6 (9H, m), 1.8—2.3 (2H, m), 5.48 (1H, d, *J*=17 Hz), 5.7—6.2 (1H, m). (*Z*): IR 1610 cm^{-1}; NMR δ=0.09 (9H, s), 0.7—1.6 (9H, m), 1.75—2.35 (2H, m), 5.35 (1H, d, *J*=13 Hz), 6.25 (1H, d of t, *J*=13 and 6 Hz).

Similarly, the following alkenylsilanes (RCH_2CH=$CHSiMe_3$) were prepared and characterized. R=*t*-Bu (*E*/*Z*=1.6), bp 100—107 °C (135 Torr) (Found: C, 70.84; H, 13.02%): NMR (Signals for the (*Z*)-isomer were shown in italics.) δ= 0.03 and *0.10* ($SiMe_3$), *5.46* (d, *J*=14 Hz) and 5.55 (d, *J*=18 Hz) (=$CHSiMe_3$). R=*c*-C_6H_{11} (*E*/*Z*=1.3), bp 102—107 °C (11 Torr): NMR δ=0.03 and *0.08* ($SiMe_3$), *5.37* (d, *J*=13 Hz) and 5.46 (d, *J*=18 Hz) (=$CHSiMe_3$). R=CH_2CN (*E*/*Z*=1.3), bp 134—136 °C (82 Torr) (Found: C, 62.50; H, 9.85; N, 9.01%): NMR δ=0.08 and *0.15* ($SiMe_3$), *5.66* (d, *J*=14 Hz) and 5.4—6.1 (complicated due to coalescence of the two olefinic protons) (=$CHSiMe_3$). R=Ph (*E*/*Z*=0.7), bp 95—99 °C (25 Torr): NMR δ=0.05 and *0.17* ($SiMe_3$), *5.55* (d, *J*=13 Hz) and 5.60 (d, *J*= 16 Hz) (=$CHSiMe_3$). These alkenylsilanes showed an IR band (C=C) near 1605 (for *Z*-isomer) or near 1620 cm^{-1} (for *E*-isomer). R=PhCOCHEt: IR 1680 and 1620 cm^{-1}; NMR δ=−0.04 (9H, s), 0.87 (3H, t), 1.7 (2H, m), 2.4 (2H, m), 3.37 (1H, m), 5.4—6.1 (2H, m), 7.3—8.0 (5H, m)

Reactions of 1-(Trimethylsilyl)allylmagnesium Chloride (4) with Carbonyl Compounds. The Grignard reagent **4** prepared from **1** (0.4 g, 2.7 mmol) in ether (20 cm^3) was added to a solution of isobutyraldehyde (240 mg) and decane (54 mg, internal standard) in ether (10 cm^3) at 0 °C. Usual workup gave 127 mg of two isomeric alcohols **5** and **6** (R^1=*i*-Pr, R^2=H) (76:24), bp 95—96 °C (41 Torr). Each alcohol was isolated by GLC. **5**: IR 3500, 1635 cm^{-1}; NMR δ=0.02 (9H, s), 0.7—1.0 (6H, m), 3.1—3.5 (1H, m), 4.6—5.1 (2H, m), 5.5—6.2 (1H, m) (Found: C, 64.04; H, 11.87%). **6**: IR 3410, 1625 cm^{-1}; NMR δ=0.05 (9H, s), 0.88 (6H, d, *J*=6 Hz), 2.20 (2H, m), 3.30 (1H, m), 5.64 (1H, d, *J*=18 Hz), 5.6—6.4 (1H, m).

The following alcohols were also characterized. **5** (R^1=Ph, R^2=H): IR 3400, 1620 cm^{-1}; NMR δ=−0.02 (9H, s), 1.7 (1H, broad s), 1.88 (1H, d of d, *J*=9 and 6 Hz), 4.2—6.2 (3H, m), 7.2 (5H, s). **6** (R^1=Ph, R^2=Me): IR 3450, 1620 cm^{-1}; NMR δ=0.09 (9H, s), 1.7 (1H, s), 2.55 (2H, m), 5.6—5.9 (2H, m), 7.1—7.5 (5H, m) (Found: C, 71.49; H, 9.47%).

References

1) F. Shibata, N. Shimizu, and Y. Tsuno, presented at the Kyushu Chugoku-Shikoku Regional Meeting of the Chemical Society of Japan, Kitakyushu, October 1983, Abstr. No. 2A09.

2) W. P. Weber, "Silicon Reagents for Organic Synthesis," Springer-Verlag, Berlin Heidelberg (1983).

3) R. J. P. Corriu, J. Masse, and D. Samate, *J. Organomet. Chem.*, **93**, 71 (1975).

4) G. Stork, M. E. Jung, E. Colvin, and Y. Noel, *J. Am. Chem. Soc.*, **96**, 3684 (1974).

5) D. Seyferth and R. E. Mammarella, *J. Organomet. Chem.*, **156**, 279 (1978).

6) Another route to 1-silylallyl halides has been reported recently: M. Ando, A. Hosomi, and H. Sakurai, 49th National Meeting of the Chemical Society of Japan, Tokyo, March 1984, Abstr. No. 1229.

7) The coupling reaction in THF in place of THF/ether gave 1,3-bis(trimethylsilyl)propene as the major product.

8) The impurity was inert to organometallic reagents as well as metallic magnesium.

9) D. A-Chass, E. Ehlinger, and P. Magnus, *J. Chem. Soc., Chem. Commun.*, **1977**, 772; P. W. K. Lau and T. H. Chan, *Tetrahedron Lett.*, **1978**, 2383.

10) M. Ochiai and E. Fujita, *J. Chem. Soc., Chem. Commun.*, **1980**, 1118.

Electronic Spectra of Cyclotrisilane (Si_3) and Disilene (Si=Si) Frameworks

Hamao WATANABE,* Yuichi KOUGO, Motohiko KATO, Haruyoshi KUWABARA, Tadashi OKAWA, and Yoichiro NAGAI*

Department of Chemistry, Faculty of Engineering, Gunma University, Kiryu, Gunma 376

(Received May 16, 1984)

Synopsis. Photolyses of a series of octaalkylcyclotetrasilanes (**1**) in a hydrocarbon solvent successively afforded hexaalkylcyclotrisilanes (**2**) and tetraalkyldisilenes (**3**). Compounds **2** and **3** were found to exhibit their absorption bands corresponding to the lowest energy transitions at λ_{max} 300—330 and 390—440 nm, respectively.

Recently we succeeded to isolate the first peralkylcyclotrisilane, hexaneopentylcyclotrisilane $[(Bu^tCH_2)_2Si]_3$ which gave on photolysis the first peralkyldisilene, tetraneopentyldisilene $(Bu^tCH_2)_2Si{=}Si(CH_2Bu^t)_2$.[1,2] It was found that the both Si_3 and Si=Si frameworks behave as chromophores *per se*, showing their longest-wavelength absorption maxima at λ_{max} 310 and 400 nm, respectively. Further, it was also demonstrated in our subsequent work that irradiation of octaisopropylcyclotetrasilane $[Pr^i_2Si]_4$ successively yielded hexaisopropylcyclotrisilane $[Pr^i_2Si]_3$ (λ_{max} 300—330 and tetraisopropyldisilene $(Pr^i_2Si{=}SiPr^i_2)$ (λ_{max} 400 nm).[3] Shortly after our publication,[1] Masamune and coworkers reported that photolysis of 5,6-benzo-2,2,3,3-tetra-*t*-butyl-2,3-disilabicyclo[2.2.2]octa-5,7-diene leads to the formation of tetra-*t*-butyl-disilene $(Bu^t_2Si{=}SiBu^t_2)$ (λ_{max} 433 nm),[4] and also that hexakis(1-ethylpropyl)cyclotrisilane $[(Et_2CH)_2Si]_3$ (λ_{max} 328 nm) undergoes photolysis to furnish the corresponding peralkyldisilene (λ_{max} 390 nm).[5] This note describes a photochemical reaction of peralkylcyclotetrasilanes $[R^1R^2Si]_4$ having various alkyl groups other than isopropyl group in order to observe spectrophotometric properties of cyclotrisilane (Si_3) and disilene (Si=Si) frameworks.

Photolyses of peralkylcyclotetrasilanes (**1a—1e**) were carried out by using a cyclohexane solution in an evacuated UV cell, as shown previously.[3] In general, upon irradiation (254 nm) at room temperature, the longest-wavelength absorption band (290—310 nm) of a starting cyclotetrasilane diminished rapidly and a new intense band appeared at λ 300—330 nm. The intensity of the band increased and attained the highest value. This band began to diminish and instead a new weak band at λ 390—400 nm appeared. The colorless solution turned to yellow and the new band became more intense. On further irradiation, the both bands completely dissipated and the solution became colorless again, showing an absorption band in a shorter wavelength region (<275 nm). This spectral change during the irradiation was similar to that of octaisopropylcyclotetrasilane.[3] Thus, it is clearly demonstrated that the two absorption maxima at λ 300—330 nm and 390—400 nm regions in the present cases are also due to peralkylcyclotrisilanes $[R^1R^2Si]_3$ (**2a—2e**) and peralkyldisilenes $[R^1R^2Si{=}SiR^1R^2]$ (**3a—3e**), respectively. The absorption bands observed for these cyclotrisilanes and disilenes, together with the data reported by Masamune and coworkers,[4,5] are summarized in Table 1.

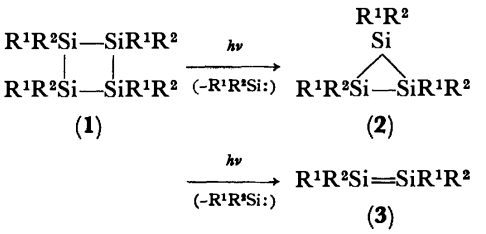

a: $R^1{=}Bu^t$, $R^2{=}Me$ **b**: $R^1{=}Bu^t$, $R^2{=}Pr^n$
c: $R^1{=}R^2{=}Bu^s$ **d**: $R^1{=}R^2{=}Bu^t$
e: $R^1{=}R^2{=}Me_3SiCH_2$

The absorption wavelength for tetra-*t*-butyldisilene[4] in Table 1 is longer than those for the other disilenes and comparable with those for peraryldisilenes (420—440 nm).[6] Masamune *et al.* interpreted this red shift in terms of the molecular geometry for the former disilene and also suggested that the four quaternary carbon atoms of the bulky substituents may not attain coplanality due to steric repulsion.[4]

Our previous observation that peralkylcyclotetrasilanes undergo photolysis to yield successively cyclotrisilanes and disilenes with extrusion of dialkylsilanediyls (eqn) was further confirmed in the present study.

TABLE 1. SPECTRAL BEHAVIORS OF CYCLOTRISILANES AND DISILENES (ABSORPTION BANDS CORRESPONDING TO LOWEST ENERGY TRANSITIONS)

No.	Substituents		Absorption maximum (nm)		
	R^1	R^2		Si=Si	Ref.
1	Bu^tCH_2	Bu^tCH_2	310(sh)	400	1)
2	Pr^i	Pr^i	320	400	3)
3	Bu^t	Me	328(sh)	390—400	This work
4	Bu^t	Pr^n	302	390—400	This work
5	Bu^s	Bu^s	323	400	This work
6	Bu^i	Bu^i	303	390—400	This work
7	Bu^t	Bu^t	..	433	4)
8	Me_3SiCH_2	Me_3SiCH_2	316	400	This work
9	Et_2CH	Et_2CH	328	390	5)

Experimental

Melting points are uncorrected. UV spectra were obtained by using a Hitachi 200-100 spectrometer. IR spectra were recorded on a JASCO A-102 spectrometer. NMR spectra were recorded in $CDCl_3$ at 400 MHz for ^1H NMR and 22.6 MHz for ^{13}C NMR by using a JEOL JNM FX-400FT and a Hitachi R-90H FT spectrometer, respectively. MS spectral analyses were conducted by using a JEOL JMS-07 spectrometer.

Materials. Octaalkylcyclotetrasilanes $[R^1R^2Si]_4$ ($R^1=R^2=Pr^i$;[7] $R^1=R^2=Bu^i$;[7] $R^1=R^2=Bu^s$; $R^1={}^t$Bu, $R^2=$Me;[7,8] $R^1=Bu^t$, $R^2=Pr^n$[7]) were prepared by the method described in the literatures.

$[(Me_3SiCH_2)_2Si]_4$: Bis(trimethylsilylmethyl)dichlorosilane $[(Me_3SiCH_2)_2SiCl_2]$ (bp 110—130 °C/55 Torr(1 Torr≈133.322 Pa)) (2.74 g, 10 mmol) and lithium (0.16 g, 23 mg-atom) in THF (20 ml; anhydrous and oxygen-free) was allowed, under Ar, to react with magnetic stirring at room temperature for 3 h, during which time the mixture was dark-brown in color and at the end of this time, the starting chlorosilane was consumed completely (by GLC analyses). After addition of cyclohexane (10 ml), the resulting light-yellow mixture gave on standing a yellow viscous liquid containing crystalline solid. Upon trituration with a small amount of hot ethanol, the crystalline solid was obtained, which was recrystallized from ethanol to give colorless fine needles of octakis(trimethylsilylmethyl)cyclotetrasilane $[(Me_3SiCH_2)_2Si]_4$; 0.25 g (12%), mp 290—301 °C (sealded capillary); UV (cyclohexane), λ_{max} 308 (ε 260), 263 sh (1800), and 223 nm (31000); ^1H NMR ($CDCl_3$) δ=0.106 (s, 16H, CH_2) and 0.094 (s, 72H, CH_3); ^{13}C NMR ($CDCl_3$) δ=2.47 ($\underline{C}H_3$, q) and 1.25 ($\underline{C}H_2$ t); IR (KBr pellet) 2960 s, 2900 m, 1440 m, 1400 w, 1350 w, 1242 vs (SiMe), 1043 sh, 1038 s, 990 w, 845 s, 770 s, 746 s, and 683 m cm^{-1}; MS (23 eV) *m/z* 810 M^+ (21), 289 (5), 217 (21), 201 $[(Me_3SiCH_2)_2\text{-}1]^+$ (100), 145 (19), and 73 $[Me_3Si]^+$ (14). Found; C, 47.87; H, 11.41%. Calcd for $C_{32}H_{88}Si_{12}$: C, 47.45; H, 10.95%.

$[Bu^tPr^nSi]_4$: UV (cyclohexane) λ_{max} 294 (ε 370), 257 sh (2600), and 217 nm (16900).

Photolyses of $[R^1R^2Si]_4$ giving $[R^1R^2Si]_3$ and $R^1R^2Si{=}SiR^1R^2$. All the photolyses of peralkylcyclotetrasilanes were performed by a similar manner to that for octaisopropylcyclotetrasilane $[Pr^i_2Si]_4$.[3]

We are grateful to Mr. M. Yanagisawa and Ms. K. Hiraizumi of the National Chemical Laboratory for Industry for the measurements of the high-resolution ^1H NMR spectra.

References

1) H. Watanabe, T. Okawa, M. Kato, and Y. Nagai, *J. Chem. Soc., Chem. Commun.*, **1983**, 781.

2) H. Watanabe, M. Kato, T. Okawa, Y. Nagai, and M. Goto, *J. Organomet. Chem.*, **271**, 225 (1984).

3) H. Watanabe, Y. Kougo, and Y. Nagai, *J. Chem. Soc., Chem. Commun.*, **1984**, 66.

4) S. Masamune, S. Murakami, and H. Tobita, *Organometal.*, **2**, 1464 (1983).

5) S. Masamune, H. Tobita, and S. Murakami, *J. Am. Chem. Soc.*, **105**, 6524 (1983).

6) R. West, M. J. Fink, and J. Michl, *Science*, **214**, 1343 (1981); S. Masamune, Y. Hanzawa, S. Murakami, T. Bally, and J. F. Blount, *J. Am. Chem. Soc.*, **104**, 1150 (1982); P. Boudjouk, B. -H. Han, and K. R. Anderson, *J. Am. Chem. Soc.*, **104**, 4992 (1982).

7) H. Watanabe, T. Muraoka, M. Kageyama, K. Yoshizumi, and Y. Nagai, *Organometal.*, **3**, 141 (1984); H. Watanabe, T. Muraoka, Y. Kohara, and Y. Nagai, *Chem. Lett.*, **1980**, 735.

8) M. Biernbaum and R. West, *J. Organomet. Chem.*, **131**, 179 (1977); B. J. Helmer and R. West, *Organometal.*, **1**, 1458 (1982).

N-Allylation of Imides Catalyzed by Palladium(0)

Yoshio INOUE,* Masaaki TAGUCHI, Masanori TOYOFUKU, and Harukichi HASHIMOTO
Department of Applied Chemistry, Faculty of Engineering, Tohoku University, Aoba, Aramaki, Sendai 980
(Received May 18, 1984)

Synopsis. Palladium(0)-triphenylphosphine complexes catalyzed the allylic exchange reaction of allylic esters, phenyl ethers, and isoureas with imides such as phthalimide to give *N*-allylic products. Among them, *O*-allylic isoureas were most effective in exchanging the allylic group of more complex structure. *N*-Allylic derivatives were also obtained by the telomerization of butadiene or allene with phthalimide catalyzed by a palladium(0) species.

Palladium-catalyzed allylic exchange reaction of esters and ethers with various nucleophiles occurs smoothly usually in the presence of bases. Alcohols, amines, active methylene compounds, and carboxylic acids are typical nucleophiles.[1] However there are no reports so far on the use of imides as the nucleophile. If it could be achieved, the product would be *N*-allylic imide. The removal of the dioyl group affords the primary allylic amine. The overall procedure is a modification of the Gabriel synthesis to obtain a primary amine. Primary allylic amine function exists in many natural products and is considerably of preparative importance.[2]

On the other hand, the dimerization of 1,3-butadiene or allene by palladium catalysts occurs with incorporation of various nucleophiles to produce functionalyzed allylic derivatives.[1] The similar nucleophiles to those employed in the allylic exchange reaction can be used. In this paper we describe the *N*-allylation of imides through allylic exchange reaction or through telomerization of dienes with imides catalyzed by a palladium(0) species.

Results and Discussion

Allylic Exchange Reaction. Allylic esters and phenyl ethers underwent allylic exchange reaction with imides such as phthalimide and succinimide to yield the *N*-allylic imides in the presence of palladium(0)-triphenylphosphine species. Although *N*-allylation of saccharin was achieved by this catalyst system, amides such as benzamide and acetanilide did not participate in the reaction. Results are shown in Table 1. The feature of this reaction is that this proceeds even in the absence of bases. The employment of phthalimide potassium salt affords the product in an increased yield. Allylic acetate needed slightly severe conditions to carry out the reaction compared to allyl phenyl ether.

2-Cyclohexenyl, geranyl, and linaryl acetate did not give the products. The lack of regio- and stereoselectivity shown in the case of crotyl acetate and the dull reactivity mentioned above indicated that the reaction using allylic acetate had limited value.

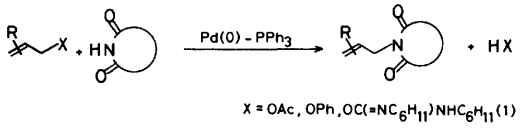

X = OAc, OPh, OC(=NC6H11)NHC6H11 (1)

To overcome these defects, *O*-allylic isourea **1** was employed as the allylating reagent, which was formed[3] by treating the allylic alcohol with dicyclo-

TABLE 1. *N*-ALLYLATION OF IMIDES

Imide	Allylic compound	Reaction temp/°C	Product[a]	Yield %
Phthalimide	CH_2=CHCH_2OAc	100	CH_2=CHCH_2NPth	76[b]
		100		82[c]
	CH_2=CHCH_2OPh	100		84
		60		81
		r.t.		27
	O-Allylisourea	r.t.		74
	(*E*)-CH_3CH=CHCH_2OAc	120	CH_2=CHCH(CH_3)NPth[d]	52
	(*E*)-PhCH=CHCH_2OAc	120	(*E*)-PhCH=CHCH_2NPth	79
	Octadienyl propionate[e]	100	OctadienylNPth[f]	63
	O-Geranylisourea	60	GeranylNPth	65
	O-Nerylisourea	60	NerylNPth	71
Succinimide	CH_2=CHCH_2OAc	100	CH_2=CHCH_2NSuc	60
	CH_2=CHCH_2OPh	60		72
	(*E*)-PhCH=CHCH_2OAc	100	(*E*)-PhCH=CHCH_2NSuc	50
Saccharin	CH_2=CHCH_2OAc	100	*N*-Allylsaccharin	51

Imide (10 or 5 mmol), allylic compound (1 equiv), $Pd(PPh_3)_3$ (2 mol%), DMF (20 or 10 cm^3); 5 h: a) Pth=phthaloyl, Suc=succinyl; all gave satisfactory elemental and spectral data. b) $Pd(dba)_2$ (2 mol%)(dba=dibenzylideneacetone) and PPh_3 (4 mol%) were used; 10 h. c) Phthalimide potassium salt (5 mmol) was used in place of phthalimide. d) In addition, (*E*)-and (*Z*)-2-butenyl isomers were formed in 6 and 4% yield, respectively. e) A mixture of (*E*)-2,7-octadienyl propionate (69%) and 1-vinyl-5-hexenyl propionate (30%). f) **2**:**3**=61:39.

hexylcarbodiimide. The reaction of geranyl and neryl derivatives of **1** with phthalimide proceeded smoothly at 60 °C regio- and stereo-selectively with the deposition of *N,N'*-dicyclohexylurea.

This reaction presumably proceeds by oxidative addition to the allylic substrate to palladium(0) to generate a π-allylpalladium species followed by nucleophilic attack of the imide to give the product.[1] Phthalimide and succinimide are quite acidic and cannot be nucleophiles. So the actual attacking species is the imide anion arised intermediately from the abstraction of the imide hydrogen by the allylic leaving group. The more basic the anion X^- is, the more facile the generation of the imide anion is. The increased reactivity of **1** is ascribed to the high basicity of the dicyclohexylurea anion[4] generated intermediately.

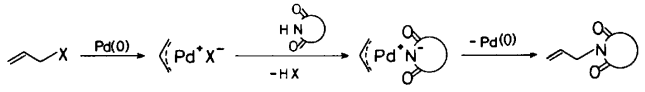

Telomerization of Dienes with Phthalimide. The reaction of 1,3-butadiene with phthalimide took place in the presence of $Pd(PPh_3)_3$ yielding *N*-(2,7-octadienyl)phthalimide (**2**) and *N*-(1-vinyl-5-hexenyl)-phthalimide (**3**). The reaction was rather sluggish at 100 °C. Employment of a slightly higher temperature (120 °C) and addition of 10 mol% of phthalimide potassium salt gave reasonable yields of the telomers, **2** and **3**. Longer reaction time (20 h) caused the degradation of the products.[5] Telomerization of isoprene with phthalimide did not occur even under forced conditions. Allene also reacted with phthalimide at 100 °C to give *N*-(3-methy-2-methylene-3-butenyl)phthalimide (**4**) by $Pd(PPh_3)_3$ catalyst in a moderate yield.

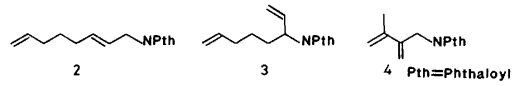

TABLE 2. TELOMERIZATION OF BUTADIENE WITH PHTHALIMIDE

Reaction temp/°C	Reaction time/h	Total yield/%[a]	Composition **2**:**3**
100	5	24	58:42
100	5	39[b]	58:42
120	5	74[b]	44:56
100	20	7	78:22

Butadiene (14—22 mmol), phthalimide (5 mmol), $Pd(PPh_3)_3$ (0.1 mmol), DMF (10 cm^3): a) Based on phthalimide. b) Phthalimide potassium salt (0.5 mmol) was added.

Experimental

General Procedure for the Allylic Exchange Reaction of Allylic Ester, Phenyl Ether, and Isourea with Imide. Imides and allylic compounds were reacted in DMF under nitrogen atmosphere in the presence of Pd(0)-PPh_3 catalyst. After the reaction, the DMF was evaporated under reduced pressure. The residue was taken up in benzene (*ca.* 10 cm^3) and the mixture was filtered to eliminate the unreacted imide. The pure products were obtained by column chromatography on silica gel.

N-Geranylphthalimide. Mp: 58.5—59.2 °C (60—61.5 °C).[6] Anal. ($C_{18}H_{21}NO_2$) C, H, N. IR (KBr) 1760 and 1700 cm^{-1}. ^1H NMR ($CDCl_3$) δ=1.52 (3H, s), 1.58 (3H, s), 1.79 (3H, s), 2.02 (4H, m), 4.02 (2H, d, J=7.2 Hz), 4.92—5.42 (2H, m), and 7.68 (4H, m). ^{13}C NMR ($CDCl_3$) δ=167.68, 140.29, 133.52, 132.35, 131.38, 123.72, 118.07, 39.42, 35.72, 26.31, 25.49, and 17.54.

N-Nerylphthalimide. Mp: 57.3—58.1 °C (59—60.5 °C).[6] Anal. ($C_{18}H_{21}NO_2$) C, H, N. IR (KBr) 1765 and 1700 cm^{-1}. ^1H NMR ($CDCl_3$) δ=1.65 (3H, s), 1.68 (3H, s), 1.70 (3H, s), 2.24 (4H, m), 4.27 (2H, d, J=7.2 Hz), 4.97—5.50 (2H, m), and 7.72 (4H, m). ^{13}C NMR ($CDCl_3$) δ=166.09, 140.48, 133.66, 131.91, 131.31, 123.87, 123.04, 118.90, 35.67, 32.06, 26.61, 25.68, 23.29, and 17.69.

Reaction of Butadiene with Phthalimide. The reaction was carried out in DMF in the presence of $Pd(PPh_3)_3$ in an autoclave. The products were purified by column chromatography on silica gel (benzene).

N-[(E)-2,7-Octadienyl]phthalimide (2). Liquid. Anal. ($C_{16}H_{17}NO_2$) C, H, N. IR (neat) 1770, 1700, 1640, 1470, 1420, 990, 960, and 910 cm^{-1}. ^1H NMR ($CDCl_3$) δ=1.2—1.6 (2H, m), 1.7—2.2 (4H, m), 4.1 (2H, d), 4.6—5.05 (2H, m), 5.1—6.0 (3H, m), and 7.65 (4H, m).

N-(1-Vinyl-5-hexenyl)phthalimide (3). Liquid. Anal. ($C_{16}H_{17}NO_2$) C, H, N. IR (neat) 1770, 1700, 1640, 1470, 990, and 910 cm^{-1}. ^1H NMR ($CDCl_3$) δ=1.1—1.7 (2H, m), 1.7—2.3 (4H, m), 4.6 (1H, m), 4.85 (1H, d), 4.86 (1H, d), 5.05 (1H, d), 5.15 (1H, d), 5.7 (1H, m), 6.15 (1H, m), and 7.65 (4H, m).

Reaction of Allene with Phthalimide. Phthalimide (5.0 mmol), $Pd(PPh_3)_3$ (0.1 mmol), and allene (10.0 mmol) were reacted in DMF (10 cm^3) at 100 °C for 5 h in an autoclave. Isolation by column chromatography on silica gel (hexane: ethyl acetate=10:1) gave the product, *N*-(3-methyl-2-methylene-3-butenyl)phthalimide (**4**); yield 0.56 g (49 %). Mp: 108.0—109.0 °C. Anal. ($C_{14}H_{13}NO_2$) C, H, N. IR (KBr) 1770, 1700, 1430, and 880 cm^{-1}. ^1H NMR ($CDCl_3$) δ=1.9 (3H, s), 4.5 (2H, s), 4.95 (2H, m), 5.25 (2H, m),and 7.8 (4H, m).

References

1) For reviews, see: J. Tsuji, "Organic Synthesis with Palladium Compounds," Springer-Verlag, Berlin Heidelberg New York, 1980; B. M. Trost, *Pure Appl. Chem.*, **53**, 2357 (1981).

2) N. J. Malek and A. E. Moormann, *J. Org. Chem.*, **47**, 5395 (1982); R. B. Cheikh, R. Chaabouni, A. Laurent, P. Mison, and A. Nafti, *Synthesis*, **1983**, 685.

3) E. Vowinkel and I. Büthe, *Chem. Ber.*, **107**, 1353 (1974).

4) A. F. Hegarty, "Comprehensive Organic Chemistry," ed by I. O. Sutherland, Pergamon Press, Oxford, New York, Toronto, Sydney, Paris, Frankfurt (1979), Vol. 2, Part 9. 10.

5) The degradation of allylic compounds, for example: E. J. Smutny, *J. Am. Chem. Soc.*, **89**, 6793 (1967).

6) D. L. Hachey and J.-P. Leresche, *J. Org. Chem.*, **37**, 4036 (1972).

Second-order Rate Constants for the Decomposition of Methyl Iodide in Different Rare Gases

Ko SAITO,* Hiroyuki TAHARA, and Ichiro MURAKAMI
Department of Chemistry, Faculty of Science, Hiroshima University, Higashisenda-machi, Naka-ku, Hiroshima 730
(Received February 24, 1984)

Synopsis. The thermal gas-phase decompostion of methyl iodide was studied in He and Kr over the temperature range of 1025—1520 K and the total-density range of (0.96—2.3)×10^{-5} mol cm^{-3}. The results showed that, at high temperatures, these inert gases act as "weak colliders." From the low-pressure limit rate constants, the relative values of the collision efficiency, β_c(M), were evaluted as;

$$\beta_c(\mathrm{He}):\beta_c(\mathrm{Ar}):\beta_c(\mathrm{Kr})=1.7:1.0:0.46$$

by connecting them with the previously reported data for an Ar mixture.

Studies of thermal decomposition in the low-pressure region provide important information of collisional intermolecular energy transfers. Although, at low temperatures, inert gas effects have been reported in many thermal systems,[1] at high temperatures (above 1000 K), only a few data are available from shock-tube studies, mostly in rare gases.[2]

In our previous study,[3] the thermal decomposition of methyl iodide in Ar was found to be controlled by the collisional activation step at temperatures above 1000K and at around atmospheric pressure. On the basis of the kinetic data, weak collision parameters were evaluated, and the energy-transfer behavior in collisions was discussed. In the present work, further investigations are made with regard to the thermal decomposition of CH_3I in Kr and Kr–He systems.

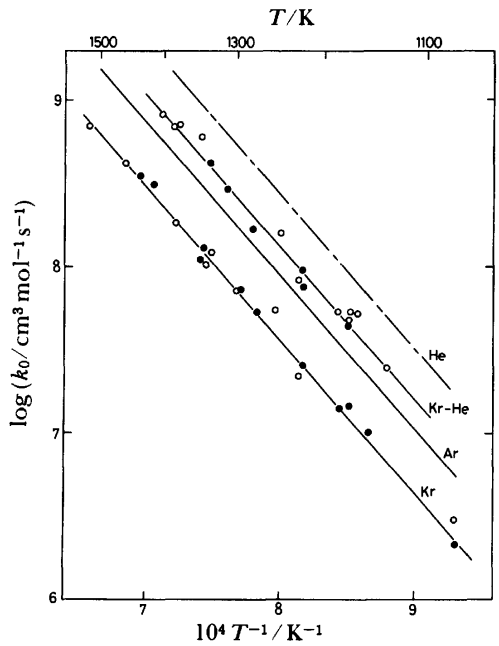

Fig. 1. Arrhenius plots of k_0 for different heat bath gases. Total density; ●: (1.0±0.1)×10^{-5} mol cm^{-3}, ○: (2.2± 0.1)×10^{-5} mol cm^{-3}. k_0(Ar) was cited from Ref. 3.

Experimental

The experiments were performed in a shock tube 9.4 cm in inner diameter. A detailed explanation of the equipment and the procedures has been given in the previous paper.[3] The decomposition rate of CH_3I was measured by monitoring the time dependent UV absorption at 275 nm.

Purified methyl iodide was diluted by the use of Kr (>99.95%) and He (>99.995%). As it was difficult to generate adequate shock conditions in He, a mixture of 50%Kr—50%He was used as the diluent to obtain the rate data in He. The temperature range behind the shock waves was from 1025 to 1520K, while the total density range was 9.6×10^{-6}—2.3×10^{-5} mol cm^{-3}.

Results and Discussion

The absorption profiles of methyl iodide behind the shock waves in Kr and Kr–He were essentially the same as those of the experiment in Ar.[3] In the present experiment, Lambert-Beer's law was also ascertained to hold in the present concentration range. In Fig. 1, Arrhenius plots of the second-order rate constants, $k_0=k/[\mathrm{M}]$, are shown for the different systems, where $k=\ln([CH_3I]_0/[CH_3I]_t)/t$ and where [M] denotes the concentration of the diluent gas M. The data for the Ar mixture, which were measured in the previous work, are also included in Fig. 1. From the facts that, in the Ar system, the decomposition occurred in the low-pressure region and that the k_0 values in Kr and Kr–He are of the same order as those of the Ar system, the decomposition in the present systems may be regarded as being in the low-pressure region. In fact, the estimated high-pressure rate constant was higher than the k_0 value by more than two orders of magnitude.

In the Kr and Kr–He systems, the reaction scheme for the overall decomposition is considered to be the same as in the Ar system, for there is no reason to consider that some of the secondary reactions are greatly enhanced by the change in the diluent gas from Ar to Kr or He. Thus, we obtain the low-pressure rate constants for the initiation reaction in Kr and He in the same manner as in the Ar system. The decomposition rate at the early stage of the reaction is written for the Kr system as;

$$-\mathrm{d}[CH_3I]/\mathrm{d}t = k_0(\mathrm{Kr})[CH_3I][\mathrm{Kr}],$$

where

$$k_0(\mathrm{Kr}) = 10^{15.0}\exp(-178\ \mathrm{kJ\ mol^{-1}}/RT)\ \mathrm{cm^3\ mol^{-1}\ s^{-1}}.$$

On the other hand, for the Kr–He system the decomposition rate is expressed as;

$$-d[CH_3I]/dt = k_0(Kr)[CH_3I][Kr] + k_0(He)[CH_3I][He],$$

provided that there are no additional interactions due to the mixing of the rare gases. Thus, the value of k_0(He) was evaluated from k_0(Kr) and k_0(Kr–He) as;

$$k_0(He) = 10^{15.88} \exp(-178\,kJ\,mol^{-1}/RT)\ cm^3\ mol^{-1}\ s^{-1}.$$

These rate constants have error limits of 20% in the temperature range of 1100—1500 K. In Fig. 1, the k_0(He) value is shown by a dashed line.

The collision efficiency, β_c, and the average energy, $<\Delta E>$, transferred per activating and deactivating collision were evaluated by the procedure described in the previous paper.[3,4] In Table 1, the evaluated values for these parameters are listed at four temperatures; the data for the Ar system are included. From Table 1, the importance of the weak collision effects is clearly demonstrated in these systems by the fact that $\beta_c \ll 1$. The temperature dependence of β_c for these weak colliders is expressed as $\beta_c \propto T^{-2}$, as in the previous papers.[3,5] This temperature dependence is larger than the theoretical prediction ($\beta_c \propto T^{-1}$).[6] Accordingly, we have found the temperature dependence of $<\Delta E>$ to be proportional to T^{-1} for the present systems. Large temperature dependences of $<\Delta E>$ are not unusual in the case of low collision effciencies at high temperatures.[7]

In general, the relative ordering of the energy-transfer efficiency in different bath gases depends on several limitations on the effective collisions, such as the relative masses, the relative translational energy of the colliding molecules, and the direction of the colliding molecules or the local position to be attacked. In the present systems, the ordering is β_c(He)$>\beta_c$(Ar)$>\beta_c$(Kr); this is the same as for the $-<\Delta E>$ values. That is, the average energy transferred per collision is larger for a lighter collision partner in the decomposition of CH_3I. This means that a fast collision is more effective in the enrgy transfer between translation and vibration modes. In this respect, it is of interest to compare the present results with such similar molecule-Ar systems as CH_3Cl–Ar[5] and CF_3I–Ar.[8] In the CH_3Cl–Ar system, $-<\Delta E>$ is as twice as large as that in the CH_3I–Ar system.[9] On the other hand, in the CF_3I–Ar system, $<\Delta E>$ is nearly the same as that in the CH_3I–Ar system. These facts also establish the effectiveness of fast collisions in T–V energy transfers at high temperatures in these systems. For different types of reactions, however, fast collisions are not necessarily dominant. For example, in the data for the decomposition of triatomic molecules, such as N_2O, NO_2, NOCl, and O_3, in different heat baths, Ar is less effective than Kr (except for N_2O).[2] This seems to suggest that some other factors are more important in these systems.

Table 1. Weak collision parameters

T/K	β_c			$-\langle\Delta E\rangle$/J mol^{-1}		
	He	Ar	Kr	He	Ar	Kr
1100	0.049	0.028	0.014	730	400	180
1200	0.037	0.022	0.010	600	330	150
1300	0.030	0.018	0.009	540	300	140
1400	0.027	0.016	0.008	510	290	130

References

1) For example, D. C. Tardy and B. S. Rabinovitch, *Chem. Rev.*, **77**, 369 (1977).

2) H. Endo, K. Glänzer, and J. Troe, *J. Phys. Chem.*, **83**, 2083 (1979).

3) K. Saito, H. Tahara, O. Kondo, T. Yokubo, T. Higashihara, and I. Murakami, *Bull. Chem. Soc. Jpn.*, **53**, 1335 (1980).

4) Input data for the calculations of the strong collision-rate constants: threshold energy, E_0=234 kJ mol^{-1}; Lennard-Jones collision parameters, $\sigma(CH_3I)$=4.23Å, σ(He)=2.551Å, σ(Ar)=3.542Å, σ(Kr)=3.665Å, $\varepsilon(CH_3I)/k$=519K, ε(He)/k=10.22K, ε(Ar)/k=93.3K, ε(Kr)/k=178.9K; vibrational frequencies of CH_3I=2969.8, 3060.1(2), 1251.5, 1435.5(2), 532.8, 882.4(2) cm^{-1}.

5) O. Kondo, K. Saito, and I. Murakami, *Bull. Chem. Soc. Jpn.*, **53**, 2133 (1980).

6) J. Troe, *J. Chem. Phys.*, **66**, 4745, 4758 (1977).

7) G. Kohlmaier and B. S. Rabinovitch, *J. Chem. Phys.*, **38**, 1962 (1963); D. W. Setser, B. S. Rabinovitch, and J. W. Simons, *J. Chem. Phys.*, **40**, 1751 (1964); J. A. Barnard and T. K. Parrott, *Int. J. Chem. Kinet.*, **9**, 387 (1977).

8) K. Saito, Y. Yoneda, H. Tahara, S. Kidoguchi, and I. Murakami, *Bull. Chem. Soc. Jpn.*, **57**, 2661 (1984).

9) The $<\Delta E>$ value for the CH_3Cl–Ar system at 1100K was estimated roughly by extrapolation using the relation $\beta_c \propto T^{-2}$, which was determined experimentally in the range of 1800—2100K.[5]

Dynamic NMR as a Nondestructive Method for the Determination of Rates of Dissociation. VIII. Proton Affinities of Anions Derived from Strong Acids in Chloroform[1)]

Michinori Ōki* and Manabu Ohira
Department of Chemistry, Faculty of Science, The University of Tokyo, Bunkyo-ku, Tokyo 113
(Received April 11, 1984)

Synopsis. Dynamic NMR study of topomerization by dissociation of *N,N*-dibenzylanilinium salt was applied to the determination of proton affinities of anions derived from strong acids in chloroform-*d*. The total line shape analysis of the benzylic proton signals gave the following order of proton affinity:

$$Cl^- > p\text{-}CH_3C_6H_4SO_3^- > CH_3SO_3^- > Br^-.$$

In a previous paper, we reported that the rates of proton exchange between *p*-substituted *N,N*-dibenzylanilinium and chloride ions could be determined by the dynamic NMR technique.[2)] That paper was concerned about the proton affinity of amines affected by substituents. However, it is expected that we can determine the proton affinity of anions, if we fix the *N,N*-dibenzylanilinium ion and vary the anion which forms an ion pair with the former, because the anion in the ion pair is the proton acceptor in the exchange reaction. In turn, the proton affinity of anions affords information about the acidity of the conjugate acids. Although it is possible to titrate acids in nonaqueous solutions against indicators, the knowledge of "intrinsic acidity", that means the acidity without foreign materials, will be of value, especially because acids very often act as catalysts in organic reactions. To contribute to this area, we have compared proton affinity of chloride, bromide, methanesulfonate, and *p*-toluenesulfonate anions. This paper is to report the results.

The kinetic parameters for the proton exchange between *N,N*-dibenzylanilinium ion and some anions are summarized in Table 1. Although iodide salt was also prepared, it discolored easily. The data are not included in Table 1 because of the low reliability, but broadening of lines was observed at temperatures close to the boiling point of chloroform. The coalescence temperature was estimated to be 70—80 °C.

The results indicated that the bromide ion has less proton affinity than the chloride anion and probably the iodide ion has the least proton affinity among the anions examined. This result is in conformity with the acidity data in water.[3)]

Comparison of the proton affinity of sulfonate anions and halide anions in water has some difficulty. Although Bessière calculated pK_a's of various inorganic acids and sulfonic acids from the data in trifluoroacetic acid,[4)] the p*Ka*'s are not in conformity with other standard values. One point which is certain from the report by Bessière is that methanesulfonic acid and *p*-toluenesulfonic acid have comparable acidity. Our data confirm this point and establish that the acidity of the sulfonic acids can be placed between hydrochloric acid and hydrobromic acid in chloroform. The order of acidity, $HBr > CH_3SO_3H > HCl$, obtained by titration in chloroform,[5)] agrees with the present results as well.

The interesting point in the kinetic data is that, whereas the anilinium halides give large positive entropy of activation, the sulfonates give small negative entropy of activation. We have shown that an ammonium perchlorate gives negative entropy of activation on dissociation of the C–N bond in it and have developed a hypothesis that the origin of the negative entropy of activation is the loss of freedom of motion of the perchlorate ion in the transition state.[1)] The data shown in Table 1 suggest that the negative entropy of activation is common when the anion carries more than two negatively charged, equivalent oxygens. The reason for this must be, as suggested in the previous paper, the loss of freedom of motion of the anion in the transition state by forming a partial O–H bond, whereas the anion is rotating in the ground state due to the presence of three or four negatively charged oxygen atoms. We may now conclude that the entropy of activation for the dissociation of the N–H or N–C bond in ammonium salts is large positive when the anion is halide, while it is small negaitve if the anion is sulfonate or perchlorate.

So far, we have discussed the proton exchange of *N,N*-dibenzylanilinium ions and anions. The data are confined to strong acids. This has a special meaning because it is difficult to obtain exact p*Ka* values of strong acids in water. A book which compiles acidities of organic substances cites the p*Ka* of methanesulfonic acid (−1∼−2) as uncertain.[6)] This technique is expected to provide a method of approach to acidities of very strong acids.

Table 1. Kinetic parameters and related data for the proton exchange between *N,N*-dibenzylanilinium ion and anions derived from strong acids in chloroform-*d*

Anions	Cl^-[b)]	Br^-	$CH_3SO_3^-$	$p\text{-}CH_3C_6H_4SO_3^-$
T_c/°C	−0.7	47.8	12.3	10.6
Correlatior Coeff.	0.999	0.998	0.999	0.999
ΔH^*/kcal mol^{-1}[a)]	18.5±0.7	21.1±1.1	14.1±0.3	11.6±0.5
ΔS^*/e.u.	18.0±2.6	15.5±3.3	−0.2±1.2	−8.9±1.7
ΔG^*_{273}/kcal mol^{-1}	13.6	16.9	14.2	14.0

a) 1 cal=4.184 J. b) The data were obtained in the previous paper.[2)]

However, this technique should not be limited to the anilinium salt. If a more basic amine, which fulfil the following conditions, is used, the proton affinity of anions, of which conjugate acid is less acidic than those described here, should be obtained. The necessary conditions are, 1) possession of diastereotopic nuclei which are NMR-active, and 2) exchange of their sites by dissociation followed by inversion. Thus this technique is potentially useful for determining acidity of various acids in aprotic solvents.

Experimental

N,N-Dibenzylaniline was commercially available from Tokyo Kasei Co. and was used as received. Preparation and acquisition of kinetic data of hydrochloride were described in the previous paper.[2]

Hydrobromide was prepared by mixing 1 g of *N,N*-dibenzylaniline in 50 mL of carbon tetrachloride with 2 mL of 47% hydrobromic acid followed by recrystallization of the precipitate from tetrahydrofurane–hexane, colorless crystals. ^{1}H NMR ($CDCl_3$, δ): 4.72 and 5.03 (4H, m), 7.1—7.7 (15H, m).

Hydriodide was prepared similarly from 57% hydriodic acid. It discolored easily under normal protections against oxygen and light. Removal of the brown color was difficult, brown crystals. ^{1}H NMR ($CDCl_3$, δ): 4.79—5.11 (4H, m), 7.0—7.8 (15H, m).

p-Toluenesulfonate was prepared by mixing an ethanolic solution of *N,N*-dibenzylaniline with *p*-toluenesulfonic acid in ethanol. The salt was recrystallized from chloroform–hexane, colorless crystals which discolor easily. ^{1}H NMR ($CDCl_3$, δ): 2.36 (3H, s), 4.88 (4H, br s), 7.0—8.0 (19H, m).

Methanesulfonate was prepared similarly, colorless oil. ^{1}H NMR ($CDCl_3$, δ): 2.97 (3H, s), 4.83 (4H, br s), 7.0—7.4 (15H, m).

Dynamic NMR measurement was performed as reported previously with chloroform-*d* solutions.[2] The following chemical shift differences ($\Delta\nu_{AB}$) and coupling constants (J_{AB}) were used throughout the total line shape analyses because they did not change at several temperatures where the exchange of protons was negligibly slow. J_{AX} and J_{BX} of which low temperature values are shown below, were treated as reciprocally variable with temperature.

HBr salt: $\Delta\nu_{AB}$ 25.9 Hz, J_{AB} −12.7 Hz, J_{AX} 3.2 Hz, J_{BX} 7.0 Hz.

CH_3SO_3H salt: $\Delta\nu_{AB}$ 34.0 Hz, J_{AB} −12.5 Hz, J_{AX} 2.4 Hz, J_{BX} 7.3 Hz.

p-$CH_3C_6H_4SO_3H$ salt: $\Delta\nu_{AB}$ 33.0 Hz, J_{AB} -12.5 Hz, J_{AX} 2.4 Hz, J_{BX} 7.3 Hz.

The following rate constants (s^{-1}) were obtained (temperature in °C in parentheses).

HBr salt: 28.0 (40.5), 39.0 (42.9), 49.0 (45.5), 63.0 (47.8), 81.0 (50.2), 107.0 (52.7)

CH_3SO_3H salt: 24.0 (-0.7), 37.0 (3.6), 40.0 (4.5), 49.0 (6.7), 57.0 (8.4), 72.0 (11.0), 82.0 (12.3), 103.0 (14.5)

p-$CH_3C_6H_4SO_3H$ salt: 30.0 (-2.4), 40.0 (1.0), 54.0 (4.9), 65.0 (6.7), 77.0 (9.7), 85.0 (10.6), 106.0 (13.6)

The kinetic parameters were obtained by the usual manner with the use of these rate constants and temperatures.

This work was supported by a Grant in Aid from Ministry of Education, Science and Culture.

References

1) Part VII: M. Ōki and T. Morita, *Chem. Lett.*, **1984**, 989.
2) M. Ōki, M. Ohira, Y. Yoshioka, T. Morita, H. Kihara, and N. Nakamura, *Bull. Chem. Soc. Jpn.*, **57**, 2224 (1984).
3) D. D. Perrin, "Ionisation Constants of Inorganic Acids and Bases in Aquecus Solution," 2nd ed, IUPAC Chemical Data Series, No. 29, Pergamon Press, Oxford (1982).
4) J. Bessière, *Anal. Chim. Acta*, **52**, 55 (1970).
5) M. Rumeau, *Ann. Chim (Paris)*, **8**, 131 (1973): *CA*, **79**, 70739c (1973).
6) E. P. Serjeant and B. Dempsey, "Ionisation Constants of Organic Acids in Aqueous Solution," IUPAC Chemical Data Series, No. 23, Pergamon Press, Oxford (1979).

 © 1984 The Chemical Society of Japan Bull. Chem. Soc. Jpn., 57, 3027—3031 (1984)

Effect of Hydrogenation on Solubility of Carbonized Pitch

Yoshio YAMADA,* Minoru SHIRAISHI, Takeshi FURUTA,
Toshio YAMAKAWA, and Yuzo SANADA†
National Research Institute for Pollution and Resources, Yatabe, Ibaraki 305
(Received December 12, 1983)

The effect of hydrogenation of carbonized pitch on its solubility in quinoline was investigated in connection with structural changes of the pitch during carbonization. Naphtha-tar pitch (NTP) and acenaphthylene were carbonized at 673 and 703 K, respectively, for various periods of time. The pitches thus heat-treated were hydrogenated by BenKeser reaction and the amount of quinoline insolubles (QI) in the hydrogenated pitch was determined. An acenaphthylene pitch (ACP) heat-treated for 24 h was rendered completely soluble into quinoline by the hydrogenation, whereas a considerable amount of insolubles was left in the case of NTP treated for longer residence times than 8 h. This can be explained in terms of the difference in interaction among aromatic molecules constituting the QI components derived from NTP and ACP. ACPs doped with elemental sulfur left a significant quantity of QI after the hydrogenation. The addition of sulfur is considered to form crosslinking bonds between aromatic molecules through hydrogen abstraction by the sulfur. When QI separated from carbonized NTP was hydrogenated, the degree of conversion into quinoline solubles (QS) was low as compared with that for the whole sample of the same NTP. The presence of QS in the pitch plays a very important role for the hydrogenation.

Since mesophase transformation occurring in the early stage of carbonization of pitch is a key step to determine physical and chemical properties of resultant coke and carbon products, much attention has so far been focused on the carbonization behavior of various pitches and related materials. The texture of optically anisotropic mesophase formed during the carbonization process is influenced by various factors, *e.g.*, molecular structures, their distribution in starting materials, and the fluidity of the system.[1] One of procedures controlling mesophase textures is modification by means of hydrogenation of pitch.[2,3] The effect of the hydrogenation is considered as increasing the fluidity of the system in the temperature range where mesophase is formed and thereby developing optical textures.

Hydrogenation under severe conditions such as high temperature and high pressure of hydrogen induces cracking and consequently, gives products different from original constituents. On the other hand, a mild reaction using lithium in ethylenediamine, *i.e.*, the BenKeser reduction, is suitable for modification of pitch[4] because aromatic rings in molecules are converted mainly to hydroaromatics in which hydrogens attached to naphthenic rings are transferrable during the carbonization. Such a hydrogenation of heat-treated pitch which contains partly anisotropic textures in an isotropic matrix, is also effective for controlling the development of mesophase by converting all anisotropic textures into isotropic ones.[5]

In this study, in order to obtain structural information on mesophase, pitches have been subjected to heat-treatment to different degrees prior to hydrogenation and then hydrogenated by the BenKeser reaction. The solubility of pitches thus obtained was determined for quinoline. In addition, influences on the hydrogenation have been investigated of sulfur doped in acenaphthylene pitch and of quinoline-soluble components in naphtha-tar pitch.

Experimental

Carbonization. Naphtha-tar pitch (NTP) obtained by thermal cracking of naphtha was supplied from Kureha Chemical Industry. Acenaphthylene of reagent grade was commercially available from Tokyo Kasei Kogyo Co., Ltd. and used without further purification. NTP and acenaphthylene were carbonized at 673 and 703 K, respectively, at a heating rate of 3 K min^{-1} and maintained at each temperature for 1—24 h in a nitrogen stream. Sumatora Light (Minas) vacuum residue (SL) treated at 703 K for 1—24 h[6] was used for comparison.

Doping of sulfur into acenaphthylene pitch (ACP) was carried out in the following way: Elemental sulfur was added to acenaphthylene with a ratio of 1 : 5 by weight and the mixture was heat-treated at 623 K for 3 h in a nitrogen atmosphere in an autoclave with a magnetic stirrer. After the treatment unreacted sulfur was removed by washing with ethanol. The pitch obtained was carbonized in a similar procedure as described above.

Hydrogenation. These pitches carbonized as above were hydrogenated by a method reported by Brooks and Silberman:[7] Lithium was added in small portions to a stirred suspension of a finely ground sample in anhydrous ethylenediamine in a nitrogen atmosphere. The weight of lithium was equal to that of the pitch. After 3 h reaction, the mixture was cooled and hydrolyzed with ice and water. The reaction product was recovered by centrifugation and washed repeatedly with water until lithium ion was removed. The product was dried below 383 K for 24 h in an oven.

Determination of Quinoline Insolubles (QI) and Elemental Analysis. The amount of QI was determined according to the filtration method of JIS-K2425. Analysis of carbon, hydrogen, and nitrogen was carried out with a Yanaco MT-3 CHN Corder and sulfur content was measured by using a LECO Corporation IR-33.

X-Ray Diffraction. The average size of molecules for carbonized pitches was calculated from the (11) band of X-ray diffraction profile according to Diamond's method.[8]

Results

Structural Change with Carbonization. Amounts

† Present address: Hokkaido University, Faculty of Engineering, Sapporo 060.

of quinoline insolubles in NTP and ACP carbonized at 673 and 703 K, respectively, are plotted against carbonization time in Fig. 1, together with those for hydrogenated pitches described in the next section. NTP forms easily QI at a higher rate than ACP does in spite of its lower carbonization temperature. Both pitches consist of almost all QI components at longer residence times. In order to obtain structural information on heat-treated pitches, the average size of molecules, *La*, was calculated from the (11) band of X-ray diffraction pattern (Table 1). It seems that the molecular size increases with residence time although the values listed in Table 1 somewhat scatter. An obvious difference between NTP and ACP is that NTP before carbonization is composed of larger molecules (10.2 Å). This is because the original pitch was subjected to thermal treatment at a higher temperature.[9] The number of stacking units as obtained from the (002) band of X-ray profile for the carbonized pitches of NTP ranges from 2.4 to 2.8 under these experimental conditions.*1)

Hydrogenation of Carbonized Pitch, QI of NTP, and ACP Containing Sulfur. Hydrogen to carbon atomic ratios for pitches carbonized and hydrogenated

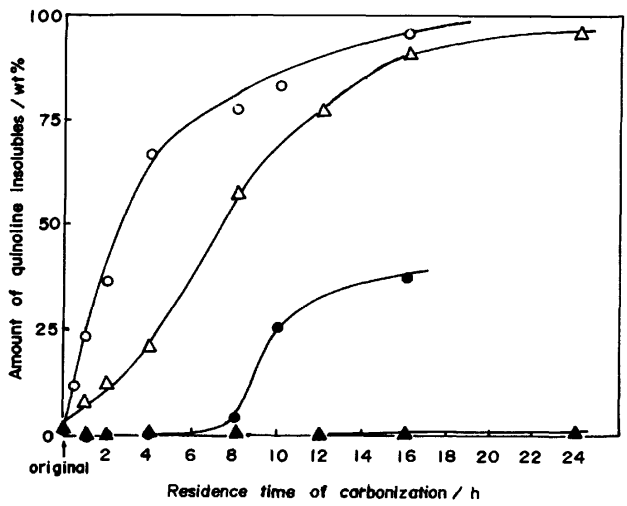

Fig. 1. Changes of the amount of QI for pitches carbonized and hydrogenated against carbonization time.
○: NTP carbonized at 673 K, ●: NTP hydrogenated after the carbonization, △: ACP carbonized at 703 K, ▲: ACP hydrogenated after the carbonization

Table 1. Average sizes (*La*) of molecules for NTP and ACP carbonized at 673 and 703 K, respectively, for various hours

Residence time	*La*/Å	
h	NTP	ACP
original	10.2	—
0.5	10.6	—
1	10.3	9.6
2	11.7	9.8
4	11.1	9.8
6	—	9.8
8	11.4	10.8
10	11.2	—
12	—	10.4
16	11.1	—
24	—	11.4

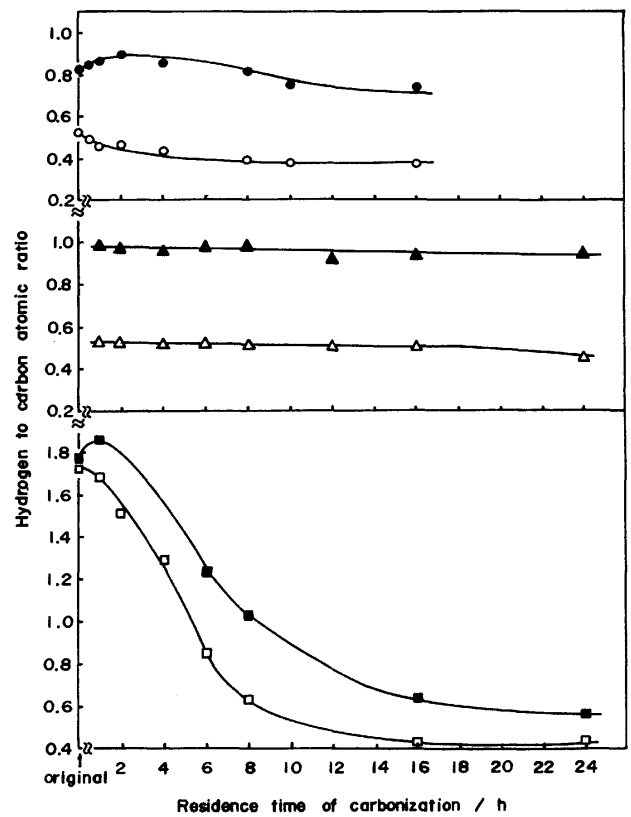

Fig. 2. Changes of hydrogen to carbon atomic ratio against carbonization time.
○: NTP carbonized at 673 K, △: ACP carbonized at 703 K, □: SL carbonized at 703 K, ●: Hydrogenated product of NTP carbonized at 673 K for various periods, ▲: Hydrogenated product of ACP carbonized at 703 K for various periods, ■: Hydrogenated product of SL carbonized at 703 K for various periods.

Table 2. Amounts of QI for NTP and hydrogenated NTP (NTP-BK)

Carbonization time at 673 K before hydrogenation	QI/wt%	
h	NTP	NTP-BK
4	66.9	0.4(25.7)a)
8	76.3	3.9(44.1)a)
10	83.3	26.6(28.1)a)
16	95.7	38.7(37.5)a)

a) Values were obtained when QI isolated from NTP was hydrogenated.

*1) Reliable values could not be obtained in the case of an ACP due to the presence of an additional band at a lower diffraction angle.

Table 3. Changes in H/C atomic ratio and sulfur content for ACP containing sulfur (ACP-S) and hydrogenated ACP-S (ACP-S-BK)

Sample	Treatment	Residence time at 703 K/h	H/C atomic ratio	Sulfur content wt%
ACP-S	Carbonization	4	0.501	1.00
		8	0.487	1.55
		12	0.484	1.72
ACP-S-BK	Carbonization/ Hydrogenation	4	0.816	0.39
		8	0.761	0.47
		12	0.740	0.49

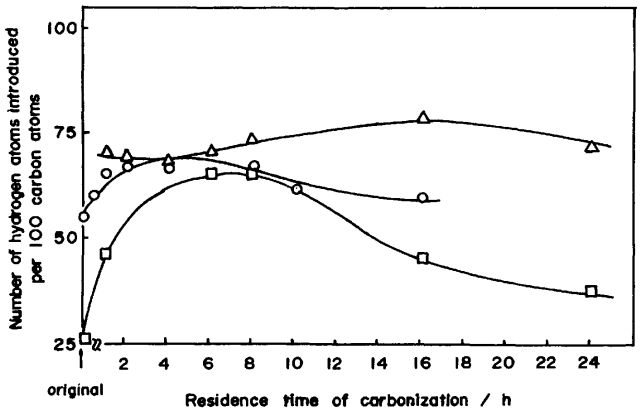

Fig. 3. Changes of hydrogen addition for carbonized pitches of NTP, ACP, and SL with carbonization time.
○: NTP carbonized at 673 K, △: ACP carbonized at 703 K, □: SL carbonized at 703 K.

Table 4. Amounts of QI for ACP containing sulfur (ACP-S) and hydrogenated ACP-S (ACP-S-BK)

Carbonization time at 703 K before hydrogenation h	QI/wt% ACP-S	ACP-S-BK
4	51.4	8.0
8	67.7	21.7
12	78.9	32.7

samples are plotted against residence time in Fig. 2. Values for SL pitch obtained in the same procedure are added there for comparison. When carbonized pitches of NTP and ACP were hydrogenated, the H/C ratio increased from 0.5 to 0.8—1.0. The number of hydrogen atoms introduced per 100 carbon atoms can be calculated from the difference between measurements of elemental analysis. The data are shown in Fig. 3. ACP maintains almost a constant value over the ranges of residence time adopted. On the other hand, the hydrogenation susceptivity of NTP is different from that of ACP; a remarkable hydrogen addition for NTP was recognized with its pitches produced in the early stage of carbonization. After a maximum was reached near 4 h carbonization, the number of hydrogens introduced was caused to decrease with residence time. SL exhibits a similar curve with a steeper slope than NTP.

When a series of ACPs heat-treated for various periods of time was hydrogenated, all carbonization products were completely converted to QS even in the case of the ACP carbonized at 703 K for 24 h, which consisted entirely of quinoline-insoluble fractions (Fig. 1). On the other hand, the whole components of the NTP samples carbonized at shorter residence times than 4 h were made soluble in quinoline by the hydrogenation, but further heat-treatment left a considerable amount of QI in the hydrogenated pitches, as can be seen in Fig. 1 and Table 2. The values designated in parentheses in Table 2 represent the amounts of QI when the insolubles isolated from NTP pitches were hydrogenated. When the whole NTP pitch treated for 10 or 16 h and the QI separated from the corresponding sample were hydrogenated, there was no significant difference between them. In the case of NTP carbonized for 4 or 8 h, however, a considerable difference is recognized between them (Table 2).

The ACP containing sulfur was prepared in order to investigate the effect of sulfur doping on carbonization. The amount of residual sulfur in the pitch is given in the last column of Table 3. The amount of the sulfur remaining increased with residence time, but after the hydrogenation the sulfur content in the pitch decreased because part of the sulfur had reacted with hydrogen to produce hydrogen sulfide. Values of QI for these pitches are given in Table 4. In contrast to the data of ACPs without sulfur (Fig. 1), ACPs containing sulfur left a large amount of QI after the hydrogenation.

Discussion

The structure and reactivity of insolubles present in original pitches have been investigated in detail by Mochida *et al.*[10,11] They found that the QI fraction with optical isotropy is different in chemical structure from the other fractions and can be modified by means of reductive alkylation and hydrogenation. Since the QI matters generated in the carbonization process of pitch are anisotropic in optical texture, they are fundamentally different from QIs involved in pitches without

heat-treatment. Therefore, it is interesting to consider structural changes associated with the increase in QI on the basis of the extent of hydrogenation of NTP and ACP carbonized to different degrees.

According to the pyrolysis scheme of acenaphthylene reported by Singer and Lewis[12] and others,[13,14] acenaphthylene polymerizes when subjected to heat-treatment at lower temperatures than 503 K, and then decomposes to produce fluorocyclene, decacyclene, *etc.* when heated over a temperature range of 600 to 650 K. As the temperature is raised further, zethrene which has a unit structure favorable for formation of higher aromatic sheet molecules, appears from 703 to 723 K. It was found from the X-ray result (Table 1) that a series of ACPs carbonized at 703 K for various periods of time has average sizes of 9.6—11.4 Å, which are roughly comparable to the size of zethrene-like molecules (≈10.6 Å). The hydrogen to carbon atomic ratios are kept at almost the same values (Fig. 2), whereas the QI content steadily increases with residence time (Fig. 1). These results suggest that the treatment for a prolonged period at this temperature does not bring about any drastic structural change in the constituent molecules of QI.[15] When the carbonized pitches of ACP were hydrogenated, the number of hydrogens introduced into aromatic molecules was almost constant over the carbonization-time range of 1—24 h and the whole samples were completely rendered soluble in quinoline. The above evidence suggests that the arrangement of aromatic molecules would be destroyed by the hydrogenation due to a reduction in the interaction among the molecules. Thus, it seems that the QI matters of ACP consist of components with such smaller molecular weights as to get dissolved into quinoline by the BenKeser reaction.

In contrast, hydrogenated NTP and SL behave in a manner different from that of ACP described above. Since both samples originate from petroleum oil, they contain alkyl chains attached to hydroaromatic rings before the carbonization. The less degree of hydrogenation on the pitches without heat-treatment might result from the presence of the alkyl groups inhibiting the effective hydrogenation of aromatic ring molecules.[7] When they are heat-treated, elimination and/or cyclization of the alkyl groups occur and at the same time the resultant molecules become more aromatic.

It is well known that the BenKeser reaction mainly converts aromatic hydrocarbons into partially hydrogenated ones without cleavage of rings.[4,7] However, the stronger the interaction between aromatic layers becomes, the lower the degree of hydrogenation is rendered because of the decrease in the dispersibility of molecules in solvent. Therefore, the considerable decrease in the ratio H/C of NTP and SL for longer residence times (Fig. 2) may suggest the presence of such a strong intermolecular force among aromatic layers in QI. In fact, the aromaticity of NTP carbonized at 673 K for 16 h was estimated to be roughly unity from data of H/C and helium density.[16] This value is higher than that obtained for ACP treated at 703 K for 24 h (0.95). Therefore, as the residence time becomes longer, NTP is considered to produce matters with high contents of QI, in which the interaction among stacked molecules is strong enough to prevent the solvent penetration. In other words, the degree of solubility in quinoline after the hydrogenation may reflect the quality of QI in pitch before the hydrogenation.

The influence of the sulfur present in the original NTP was taken into account as another factor in order to understand the difference in hydrogenation behavior between NTP and ACP. As already described, the result in Table 4 reveals that the sulfur addition to ACP produces residues which leave some amounts of QI after the hydrogenation. It may be associated with formation of crosslinkages during carbonization.[17]

Marsh and Crawford[18] reported that mesophase spherules formed in the early stage of carbonization include small soluble molecules between lamellae. When the carbonized pitch is treated with quinoline, the small molecules incorporated between mesophase layers are considered to get dissolved into quinoline. Consequently, it is expected that the interaction between the layers becomes stronger and that the solvent such as ethylenediamine cannot penetrate into these layers on the hydrogenation. Hydrogenation of only the QI fraction from NTP carbonized for 4 or 8 h left a considerable amount of insolubles (Table 2). Thus, the result supports the above assumption and furthermore, suggests that the soluble components in the present system contribute to the solubility of QI after the hydrogenation, as pointed out by Mochida *et al.*[11]

References

1) H. Marsh and P. L. Walker, Jr., "Chemistry and Physics of Carbon," ed by P. L. Walker, Jr., Marcel Dekker, Inc., New York (1979), Vol. 15, p. 230.
2) I. Mochida and H. Marsh, *Fuel*, **58**, 790 (1979).
3) T. Obara, T. Yokono, K. Miyazawa, and Y. Sanada, *Carbon*, **19**, 263 (1981).
4) I. Mochida, H. Matsuoka, H. Fujitsu, Y. Korai, and K. Takeshita, *Carbon*, **19**, 213 (1981); I. Mochida, K. Tamaru, Y. Korai, H. Fujitsu, and K. Takeshita, *ibid.*, **20**, 231 (1982).
5) Y. Yamada, M. Shiraishi, T. Furuta, Y. Yamashita, and T. Yamakawa, Symposium on Carbon, Toyohashi, November 1982, Extended Abstr., p. 135.
6) Y. Yamada and Y. Sanada, *Sekiyu Gakkai Shi*, **22**, 350 (1979).
7) J. Brooks and H. Silberman, *Fuel*, **41**, 67 (1962).
8) M. Shiraishi and K. Kobayashi, *Nippon Kagaku Kaishi*, **1972**, 1135.
9) S. Gomi, *Sekiyu Gakkai Shi*, **8**, 24 (1965).
10) I. Mochida, K. Kudo, K. Takeshita, R. Takahashi, Y. Suetsugu, and J. Furumi, *Fuel*, **53**, 253 (1974); I. Mochida, Y. Tomari, Y. Iwanaga, K. Maeda, and K. Takeshita, *Nenryo Kyokai Shi*, **54**, 994 (1975); I. Mochida, K. Maeda, and K. Takeshita, *Fuel*, **55**, 70 (1976); I. Mochida, K. Maeda, and K. Takeshita, *Sekiyu Gakkai Shi*, **21**, 52 (1978).
11) I. Mochida, Y. Tomari, K. Maeda, and K. Takeshita, *Fuel*, **54**, 265 (1975).
12) L. S. Singer and I. C. Lewis, *Carbon*, **2**, 115 (1964).
13) Y. Yamada and S. Toyoda, *Bull. Chem. Soc. Jpn.*, **46**, 3571 (1973).
14) E. Fitzer, K. Mueller, and W. Schaefer, "Chemistry and Physics of Carbon," ed by P. L. Walker, Jr., Marcel Dekker Inc., New York (1971), Vol. 7, p. 298.
15) I. Mochida, K. Maeda, and K. Takashita, *Carbon*, **16**, 459 (1978).

16) D. W. van Krevelen and H. A. G. Chermin, *Fuel*, **33**, 79 (1954).
17) H. Akamatu and H. Inokuchi, *Carbon*, **21**, 337 (1983).
18) H. Marsh and D. Crawford, Carbon'76, Deutscke Keremische Gesellschaft, 1976, p. 231.

Decomposition of Blue Orthorhombic Hydrogen Molybdenum Bronze, $H_{0.30}MoO_3$, by Heating *in vacuo* and in Helium Gas

Noriyuki SOTANI,* Noritetsu YOSHIDA,† Yoji KAWAMOTO,† Shozo KISHIMOTO,† and Masatomo HASEGAWA
College of Liberal Arts, Kobe University, Tsurukabuto, Nada, Kobe 657
†*Department of Chemistry, Faculty of Science, Kobe University, Rokkodai, Nada, Kobe 657*
(Received December 28, 1983)

The decomposition process of orthorhombic hydrogen molybdenum bronze, $H_{0.30}MoO_3$, was studied by the temperature programmed decomposition (TPD) technique *in vacuo* and in helium gas. The only gas liberated during the decomposition was H_2O and no other gas was detected. The TPD spectrum above 150 °C was composed of three bands (PII, PIII, and PIV). The PII band corresponded to the process from $H_{0.30}MoO_3$ to $H_{0.21}MoO_{2.95}$ without any structural change. The PIII band corresponded to the process from $H_{0.21}MoO_{2.95}$ to $H_{0.06}MoO_{2.88}$ with the structural change and the PIV band, to the process from $H_{0.06}MoO_{2.88}$ to $MoO_{2.85}$.

It is well known that hydrogen molybdenum bronzes are formed by reduction of MoO_3 in an aqueous medium[1] or by atomic hydrogen.[2] There are many phases which may be formulated as $H_xMoO_3(0<x\leqq2.0)$. The existence of four phases has been confirmed by Birtill and Dickens.[3] According to them, the ranges of homogeneity of these phases with the approximate limits are as follows; (i) blue orthorhombic ($0.23<x<0.40$), (ii) blue monoclinic ($0.85<x<1.04$), (iii) red monoclinic ($1.55<x<1.72$), and (iv) green monoclinic ($x=2.0$). In the hydrogen molybdenum bronze, hydrogen is inserted into the MoO_3 layers as atoms[4-6] and occupies available sites near the zigzag oxygen atoms of the intralayers.[6]

The authors have studied the structural and compositional changes of the blue orthorhombic bronze heated *in vacuo* and found that the bronze is decomposed to a nonstoichiometric compound with a rhombic MoO_3 structure with the evolution of H_2O.[7]

Sermon *et al.*[8] and Marcq *et al.*[9] studied the catalytic hydrogenation reaction for 1-pentene and ethylene on the red monoclinic bronze, $H_{1.6}MoO_3$, obtained from Pt-supported MoO_3 by hydrogen spillover. They concluded that atomic hydrogen plays an important role in the catalytic hydrogenation. The hydrogen in the blue orthorhombic bronze is also effective for 1-butene isomerization.[10]

It is important in studying the catalytic reaction to reveal the decomposition process of the bronze and the behavior of hydrogen in the bronze on heating. The authors have reported[11] the kinetics of isothermal decomposition of the blue orthorhombic bronze. In the present work, the decomposition was studied by the temperature programmed decomposition (TPD) technique *in vacuo* and in helium gas.

Experimental

The sample was prepared by the Glemser's method.[1] Its structure was confirmed by X-ray diffraction analysis to be identical with the blue orthorhombic phase reported by Birtill and Dickens.[3] The composition was determined to be $H_{0.30}MoO_3$ by chemical analysis[12] and by thermogravimetry.

A conventional high vacuum system equipped with a Cahn microbalance, a Pirani gauge, and a quadrupole gas analyzer was used for the measurements of the changes in weight and pressure. The rate of heating, β, was controlled by a temperature programmed controller.

The decomposition of the blue orthorhombic bronze on heating in helium gas was also studied by a gas chromatograph.

A differential scanning calolimeter (DSC) was used for measuring the heat of decomposition in helium gas.

Results

Temperature Programmed Decomposition in vacuo (TPD(v)). The bronze, $H_{0.30}MoO_3$, was degassed at room temperature under a vacuum of 10^{-4} Torr for 2 h and then heated at various heating rates (β=3.5—13.7 °C min^{-1}). The change in pressure was recorded with a Pirani gauge. The TPD(v) spectra at the various heating rates are shown in Fig. 1. A small band appeared below 150 °C. The TPD (v) spectrum above 150 °C showed clearly three peaks as the rate of heating was slow. Indeed, the spectrum obtained at a heating rate of 3.5 °C min^{-1} showed three distinct peaks, suggesting that the spectrum may be composed of three bands and the line shapes of each band may

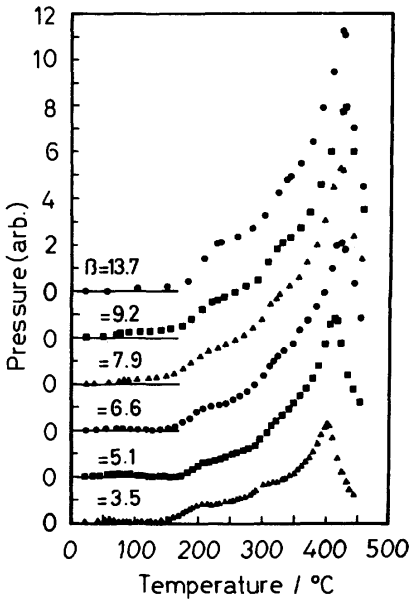

Fig. 1. TPD(v) spectra of the blue orthorhombic bronze, $H_{0.30}MoO_3$.

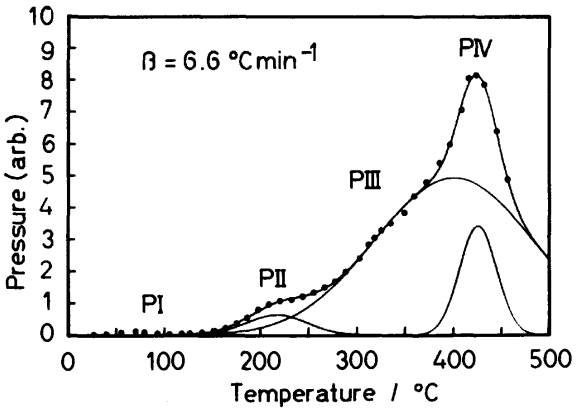

Fig. 2. Analysis of TPD(v) spectrum of the blue orthorhombic bronze, $H_{0.30}MoO_3$.

be symmetrical. Therefore, the spectra above 150 °C could be analyzed by a curve resolver. One of the results is shown in Fig. 2. This shows that the spectrum above 150 °C consists of three bands (PII, PIII, and PIV). All the spectra in Fig. 1 were analyzed by the same technique. The shifts of each peak temperature (Tm) to higher temperatures were observed when the heating rates were increased. The peak temperatures, Tm(II) of the PII band appeared over a temperature range of 185—238 °C. Tm(III) of the PIII band and Tm(IV) of the PIV band appeared at 356—408 and 392—429 °C, respectively.

The gas liberated in these experiments was H_2O and no other gas was detected by the quadrupole gas analyzer. The above results suggest that hydrogen in the bronze reacted with the lattice oxygen to produce H_2O in three steps.

Activation energies of 18.4(PII), 28.4(PIII), and 39.6(PIV) kcal mol^{-1} were estimated from the shifts of the peak temperatures (Tm(II), Tm(III), and Tm (IV)).[13]

Thermogravimetry. The weight-loss of the blue orthorhombic bronze was measured by a Cahn microbalance at various heating rates (β=3.5—13.7 °C min^{-1}) *in vacuo*. The X-ray and thermogravimetric results showed that on the vacuum heating the bronze transformed to $MoO_{2.85}$, a nonstoichiometric compound with rhombic MoO_3 structure, through a mixture of the orthorhombic and rhombic structures[7] as follows;

$$\text{(I)}\quad H_{0.30}MoO_3\cdot nH_2O \xrightarrow{\text{below 150 °C}} H_{0.30}MoO_3$$

$$\text{(II)}\quad \xrightarrow{\approx 286\ ^\circ C} H_{0.21}MoO_{2.95}^{**}$$

$$\text{(III)}\quad \xrightarrow{\approx 390\ ^\circ C} H_{0.06}MoO_{2.88}^{***}$$

$$\text{(IV)}\quad \xrightarrow{\approx 446\ ^\circ C} MoO_{2.85}\ .$$

**: Orthorhombic bronze with the lowest hydrogen content.

***: Isomorphous with rhombic MoO_3.

The rising temperature technique has been widely used in kinetic investigation of thermal decomposition and other reactions of solid.[13-16] By this technique, Ozawa[16] formulated a simple and useful method to analyze the thermogravimetric data and determined the activation energies of the decomposition of calcium oxalate and the degradation of Nylon 6. According to his method, activation energies are easily determined as follows; initially the fraction reacted, α, is plotted against the reciprocal absolute temperature ($1/T$), and the value of $1/T$ corresponding to $1-\alpha$ of each heating rate curve can be estimated. Secondly, the activation energies can be determined from the plots of the logarithms of the heating rate, $\log \beta$, *vs.* $1/T$ obtained from the above plots.

Figure 3 shows the typical thermogravimetric curves of the bronze plotted against $1/T$. If the decomposition proceeds in one step, activation energies estimated from the plots of $\log \beta$ *vs.* $1/T$ should be equal at every α. However, the results suggest that the activation energies for different α differ from one another. The value of $1-\alpha$ at the peak temperatures (Tm(II), Tm(III), and Tm(IV)) of each band of the TPD(v) spectra were 0.86±0.05(PII), 0.31±0.08(PIII), and 0.12±0.03(PIV), respectively. Figure 4 shows the plots of $\log \beta$ *vs.* $1/T$ which gives the same value of $1-\alpha$, corresponding to Tm(II), Tm(III), and Tm(IV). From these

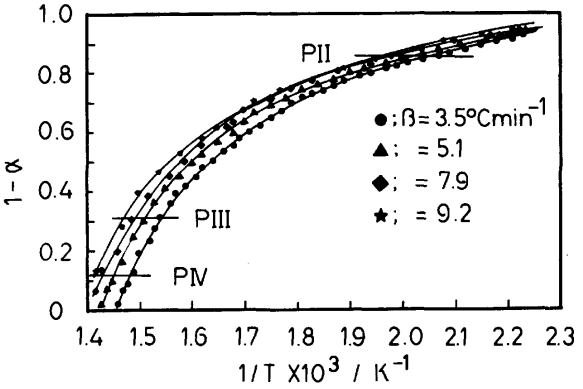

Fig. 3. The thermogravimetric curves of $H_{0.30}MoO_3$ plotted against the reciprocal absolute temperatures.

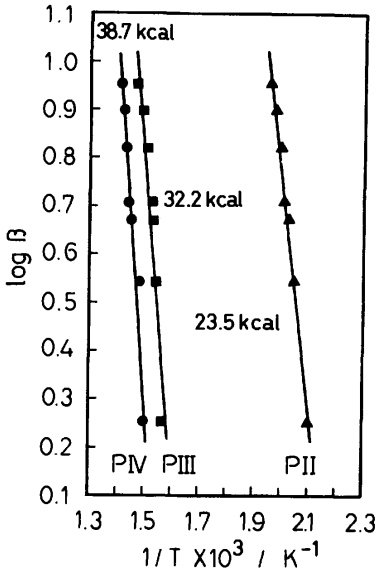

Fig. 4. The plots of logarithms of heating rates against the reciprocal absolute temperatures.

plots, the activation energies were determined to be 23.5(PII), 32.2(PIII), and 38.7(PIV) kcal mol^{-1}, respectively. These values are in good agreement with those determined from the TPD(v) spectra.

Temperature Programmed Decomposition in Helium Gas (TPD(h)). The bronze was also heated in helium gas with the flow rate of 90 ml min^{-1} and was studied by means of the gas chromatograph. The heating rates employed were 3, 7.5, and 10 °C min^{-1}. No peak appeared below 200 °C. Above this temperature, however, three peaks appeared as in the case of vacuum heating. The range of Tm(II) was 259—283 °C, which was higher compared with that obtained by TPD(v) spectra. Those of Tm(III) and Tm(IV) were 296—315 and 352—380 °C. These were lower than those obtained by TPD(v) spectra. These differences in Tm may be attributed to the difference in the experimental methods.

The activation energies were also estimated from the shifts of Tm and the heating rates and were determined to be 27.5(PII), 32.2(PIII), and 38.0(PIV) kcal mol^{-1}, respectively. The activation energy of PII is a little higher than those determined by TPD(v) spectra and by thermogravimetry, but those of PIII and PIV are in good agreement.

DSC Measurement. The heat of decomposition of the bronze was measured by DSC with the heating rates of 5, 7, and 10 °C min^{-1}, which were treated in helium gas with the flow rate of 90 ml min^{-1}. Three endothermal peaks appeared at 240—250, 310—321, and 353—364 °C, and were in good agreement with those of the Tm(II), Tm(III), and Tm(IV) of TPD(h) spectra obtained by heating in helium gas. The total endothermal heat was determined by the peak area to be 5.82±0.13 cal g^{-1}. If this value were proportioned to each band area of PII, PIII, and PIV, the alloted values would be 0.81±0.02(PII), 1.98±0.04(PIII), and 3.03±0.07(PIV) cal g^{-1}, respectively. These energies produce many effects; heat of reaction between hydrogens and lattice oxygens, heat of desorption of H_2O, *etc.* Therefore, it is difficult to conclude that the endothermal heats are directly related to the binding energies of hydrogen in the bronze.

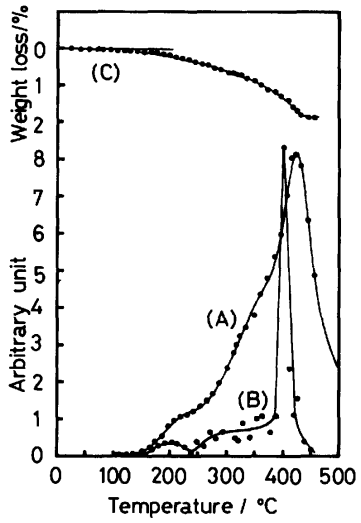

Fig. 5. Comparison between the TPD(v) spectrum and the differential curve obtained from the change in weight. (A); TPD(v) spectrum, (B); differential curve, and (C); change in weight.

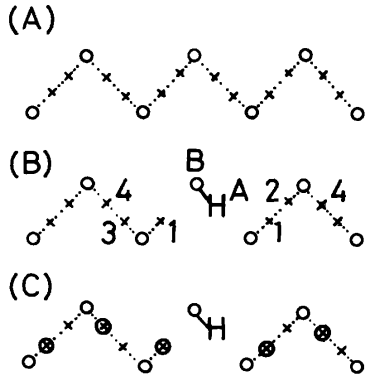

○: Oxygen atom, ×: available hydrogen site, ⊗: most available hydrogen site.

Fig. 6. Model of the available hydrogen atom sites in the blue orthorhombic bronze. (A); The average structure, (B); four kinds of available hydrogen atom sites apart from the A site occupied by a hydrogen atom near the oxygen(B), and (C); most available hydrogen atom sites.

Discussion

Figure 5(A) shows the typical TPD(v) spectrum obtained by the Pirani gauge, while Fig. 5(B) is the differential curve calculated from the weight change (Fig. 5(C)) of the bronze on vacuum heating. As shown in Fig. 5(B), the fluctuation is recognized above 250 °C and it is difficult to obtain a smooth curve. On the other hand, the TPD(v) spectrum is very smooth. However, the Tm's are somewhat higher than those obtained from the differentiation of the weight changes. The pirani gauge method to detect pressure change is somewhat different from the microbalance for measuring weight changes and, therefore, there might be a temperature lag between the both measurements. However, the Tm's obtained from both measurements might occur with a similar temperature lag in all the steps. The TPD method gives the smooth spectrum, and is the simplest and most useful method for studying the decomposition of the bronze.

According to the proton NMR result,[11] there is no difference in the behavior of the protons in the original bronze and in the bronze treated at 350 °C under a vacuum of 10^{-4} Torr (1 Torr=133.322 Pa). This suggests that the environment surrounding the protons does not change during heating at 350 °C. The hydrogen atom sites in the bronze are surrounded by oxygen atoms making zigzag chains in the MoO_3 layers, as is illustrated in Fig. 6(A). Two hydrogen atom sites on a given O···O line are too close for two hydrogen atoms to occupy them simultaneously and inelastic neutron scattering has confirmed that there is no OH_2 groups in this phase.[17] If one hydrogen atom occupied the A site near oxygen (B) as shown in Fig. 6(B), there would be four available sites for the hydroxyl hydrogen.[6] Most of the hydrogen atom must have a neighbouring site 1 in

pairs.[6] Therefore, the most available site must be the site 1 or 4 as shown in Fig. 6(C).

The PI band which appears below 150 °C in the TPD(v) spectra may result from the desorption of a small amount of adsorbed water. This corresponds exactly to the I process.

The orthorhombic bronze retains its original crystal structure up to about 287 °C although the hydrogen content (x) changes from 0.30 to 0.21. This suggests that the reaction occurs sporadically and the nearest two hydrogen atoms in the sites 1 and 4 react with the nearest lattice oxygens to produce H_2O. This temperature range falls in that of the PII band in the TPD spectra and, therefore, the PII band corresponds to the PII process.

The weight-loss in the temperature range of about 287 and 390 °C was about a half of the total weight-loss, and the product was confirmed to be the mixture of the orthorhombic and rhombic MoO_3 structures. It might be considered that the dehydration of the PII process involves nucleation and the nuclei produced might accelerate the dehydration successively. On the other hand, the PIII band is broad and the integrated area is much larger than those of the PII and PIV. Considering the above results, it is concluded that the PIII band corresponds to the PIII process.

$H_{0.06}MoO_{2.88}$ was isomorphous with the rhombic MoO_3 and the hydrogen atoms were considered to be sparsely distributed. Therefore, even though $H_{0.06}MoO_{2.88}$ was decomposed completely to $MoO_{2.85}$ at about 446 °C with the evolution of H_2O, no structural change was observed. The decrease in weight was small and the PIV band was narrow and small. It is reasonable to conclude that the PIV band corresponds to the IV process.

The authors thank to Professor Makoto Kaburagi of Kobe University for writing the program to analyze TPD spectra.

References

1) O. Glemser and G. Lutz, *Z. Anorg. Allg. Chem.*, **264**, 17 (1951); **285**, 173 (1956).
2) O. Glemser and G. Lutz, *Z. Anorg. Allg. Chem.*, **269**, 93 (1952).
3) J. J. Birtill and P. G. Dickens, *Mater. Res. Bull.*, **13**, 311 (1978).
4) K. A. Wilhelm, *Acta Chem. Scand.*, **23**, 419 (1969).
5) F. A. Schroeder and H. Weitzel, *Z. Anorg. Allg. Chem.*, **435**, 247 (1977).
6) R. C. Slade, T. K. Halstead, and P. G. Dickens, *J. Solid State Chem.*, **34**, 183 (1980).
7) N. Sotani, Y. Kawamoto, and M. Inui, *Mater. Res. Bull.*, **18**, 797 (1983).
8) P. A. Sermon and G. C. Bond, *J. Chem. Soc., Faraday Trans. 1*, **72**, 730 (1976).
9) J. P. Marcq, X. Wispenninckx, G. Poncelet, D. Keravis, and J. J. Fripiat, *J. Catal.*, **73**, 309 (1982).
10) N. Sotani *et al.*, unpublished data.
11) N. Sotani, M. Kunitomo, and M. Hasegawa, *Chem. Lett.*, **1983**, 647.
12) C. Choain and F. Marion, *Bull. Soc. Chim. Fr.*, **1963**, 212.
13) "Comprehensive Chemical Kinetics," ed by C. H. Banford and C. F. H. Tippen, Vol. 22, Elsevier Scientific Publishing Co., Amsterdam (1980).
14) C. D. Doyle, *J. Appl. Polym. Sci.*, **5**, 285 (1961); **6**, 639 (1962).
15) A. W. Coats and J. P. Redfern, *Nature (London)*, **201**, 68 (1964).
16) T. Ozawa, *Bull. Chem. Soc. Jpn.*, **38**, 1881 (1965).
17) P. G. Dickens, J. J. Birtill, and C. J. Wright, *J. Solid State Chem.*, **28**, 185 (1979).

Fluorescence of Europium Tris(bromate) Enneahydrate with Ar^+ Laser Excitation

Masahiko HASUNUMA, Keiko OKADA,* and (the late) Yoshifumi KATO
Department of Chemistry, Faculty of Science, Kobe University, Nada-ku, Kobe 657
(Received January 9, 1984)

The (f,f^*) transitions of europium tris(bromate) enneahydrate crystal between 12000 and 20000 cm^{-1} were measured at 95 K by laser-excited fluorescence spectroscopy. The crystal field components of the ground ($^7F_{0,1\cdots6}$) and the excited states ($^5D_{0,1}$) participating in the transitions were analyzed in terms of the tensor-operator method. Besides electric-dipole transitions, a number of magnetic-dipole transitions were detected in compliance with the selection rule. The theory could reproduce the observed wavenumbers and intensities both for the σ- and π-transitions. The population ratio of the $^5D_0$ to the $^5D_1$ was estimated to be 14.1 from the intensity calculations and the observed results. The result suggests that mixing of g-orbitals is significant for the forced electric-dipole transitions.

The trivalent europium ion of $4f^6$ electronic configuration has a ground ^7F multiplet with a width of about 5000 cm^{-1} and the next low energy levels of ^5D multiplet about 17000—24000 cm^{-1} above. The Eu^{3+} ion in crystals displays characteristic emission in the visible region which arises from the (f,f^*) transitions between these states. In the last decade, a considerable number of studies have been made on the fluorescence of Eu^{3+} doped in a variety of host lattices. So far, however, no work has been reported on the electronic structure of europium tris(bromate) enneahydrate crystals of $Eu(BrO_3)_3\cdot9H_2O$, which has a typical coordination structure of $[Eu(OH_2)_9]^{3+}$. In a previous work,[1] the fluorescence spectrum excited by an Ar^+ laser on the europium tris(ethyl sulfate) enneahydrate crystal (Eu(ES)) was studied. In this structure the Eu^{3+} ion is in the C_{3h} crystal field of $[Eu(OH_2)_9]^{3+}$. Besides the confirmation of the crystal field splittings of the ground ^7F multiplet and the excited $^5D_0$ and $^5D_1$ states, a successful interpretation of the spectral intensities was made by applying the Judd-Ofelt theory.[2,3]

The present study is concerned with the electronic structure of $Eu(BrO_3)_3\cdot9H_2O$ obtained by analysing the laser-excited fluorescence spectra. In this host, the Eu^{3+} ion is in the D_{3h} crystal field of $[Eu(OH_2)_9]^{3+}$ according to X-ray crystallography.[4,5] The transition probabilities for both the electric-dipole (ED) and magnetic-dipole (MD) transitions were also calculated by using the tensor-operator method. Some discussions are given of the calculated and observed relative intensities.

Experimental

Single crystals of $La(BrO_3)_3\cdot9H_2O$ and $Eu(BrO_3)_3\cdot9H_2O$ were prepared by the method described in a previous paper.[6] The fluorescence spectra of the crystals were measured through an analyser to obtain polarization of the emitted radiations whose polarizing planes are perpendicular (σ-) and parallel (π-spectrum) to the principal axis of the crystal. The experimental procedure was the same as in our previous report.[1]

Results and Discussion

Selection Rules. In view of the X-ray crystallographic studies,[4,5] it may appear adequate to assume the D_{3h} crystal field of $[Eu(OH_2)_9]^{3+}$. However, D_3 symmetry was adopted for the theoretical calculations, since it is convenient for the spectral assignments. The crystal field mixes the states which differ in J and J_z, whereupon J and J_z cease to be good quantum numbers. Then the crystal quantum number μ is used to classify the crystal field energy levels. The classification of the crystal quantum number for different

Table 1. Basis functions for the irreducible representations of D_3 symmetry

J	Crystal quantum number μ		
	0^+ (A_1)	0^- (A_2)	±1 (E)
0	$\|0,0\rangle$		
1		$\|1,0\rangle$	$\|1,\pm1\rangle$
2	$\|2,0\rangle$		$\|2,\pm1\rangle$ $\|2,\mp2\rangle$
3	$\frac{1}{\sqrt{2}}(\|3,3\rangle-\|3,-3\rangle)$	$\|3,0\rangle$ $\frac{1}{\sqrt{2}}(\|3,3\rangle+\|3,-3\rangle)$	$\|3,\pm1\rangle$ $\|3,\mp2\rangle$
4	$\|4,0\rangle$ $\frac{1}{\sqrt{2}}(\|4,3\rangle+\|4,-3\rangle)$	$\frac{1}{\sqrt{2}}(\|4,3\rangle-\|4,-3\rangle)$	$\|4,\pm1\rangle$ $\|4,\mp2\rangle$ $\|4,\pm4\rangle$
5	$\frac{1}{\sqrt{2}}(\|5,3\rangle-\|5,-3\rangle)$	$\|5,0\rangle$ $\frac{1}{\sqrt{2}}(\|5,3\rangle+\|5,-3\rangle)$	$\|5,\pm1\rangle$ $\|5,\mp2\rangle$ $\|5,\pm4\rangle$ $\|5,\mp5\rangle$
6	$\|6,0\rangle$ $\frac{1}{\sqrt{2}}(\|6,3\rangle+\|6,-3\rangle)$ $\frac{1}{\sqrt{2}}(\|6,6\rangle+\|6,-6\rangle)$	$\frac{1}{\sqrt{2}}(\|6,3\rangle-\|6,-3\rangle)$ $\frac{1}{\sqrt{2}}(\|6,6\rangle-\|6,-6\rangle)$	$\|6,\pm1\rangle$ $\|6,\mp2\rangle$ $\|6,\pm4\rangle$ $\|6,\mp5\rangle$

Table 2. Selection rules for D_3 symmetry in the case of an even number of electrons

(ED transition)				(MD transition)			
	μ				μ		
μ	0^+	0^-	±1	μ	0^+	0^-	±1
0^+	—	π	σ	0^+	—	σ	π
0^-	π	—	σ	0^-	σ	—	π
±1	σ	σ	σ,π	±1	π	π	σ,π

$|J,J_z>$ states are given for D_3 symmetry in Table 1.[7] The selection rules in terms of the crystal quantum number μ for ED and MD transitions are shown in Table 2.[8]

Spectra. The fluorescence spectra of $Eu(BrO_3)_3 \cdot 9H_2O$ at 95 K excited by a 457.9 nm line of an Ar^+ laser are shown in Figs. 1 and 2. The Raman lines of the vibrational modes were distinguished from the fluorescence lines by reference to the spectrum of $La(BrO_3)_3 \cdot 9H_2O$, which is isomorphous with $Eu(BrO_3)_3 \cdot 9H_2O$ and gives no (f,f^*) transitions, since it has no f-electron in the ground configuration. The σ- and π-polarized spectra exhibit fluorescence lines at the same wavenumbers but with different relative intensities. The intensities were measured by the areas under the curves of the spectra. The lines were assigned to ED and MD transitions between "crystal field levels" on the basis of the selection rules and the calculated transition energies and intensities. The observed wavenumbers and relative intensities of the fluorescence lines of $Eu(BrO_3)_3 \cdot 9H_2O$ are listed in Table 3. Eight strong MD transitions are allowed according to the selection rules for the "ion levels" (*i.e.* $|\Delta J| \leqq 1$) and 12 weak MD transitions are forbidden transitions with $|\Delta J|>1$. While the former strong transitions were already reported by Hellwege,[9] Axe,[10] and Sayre and Freed[11] for Eu(ES), the latter weak transitions were first observed in our previous research applying the laser as a light source.[1] The forbidden transitions occur when there exists a considerable interaction of the free ion with the crystal field, that is, when the influence of J-mixing is appreciable. Table 4 summarizes the crystal field levels of $Eu(BrO_3)_3 \cdot 9H_2O$ determined by the present analysis.

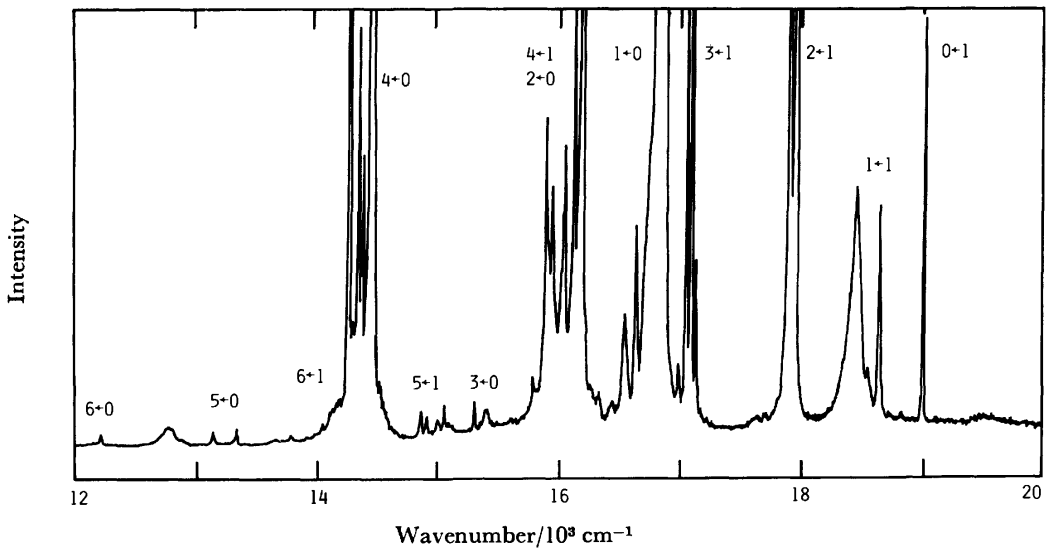

Fig. 1. σ-polarized fluorescence spectra of $Eu(BrO_3)_3 \cdot 9H_2O$ at 95 K excited by the 457.9 nm line of Ar^+ laser. Fluorescence lines assigned to the transitions between the ground ($^7F_{J'}$) and excited substates (^5D_J) are shown as ($J' \leftarrow J$).

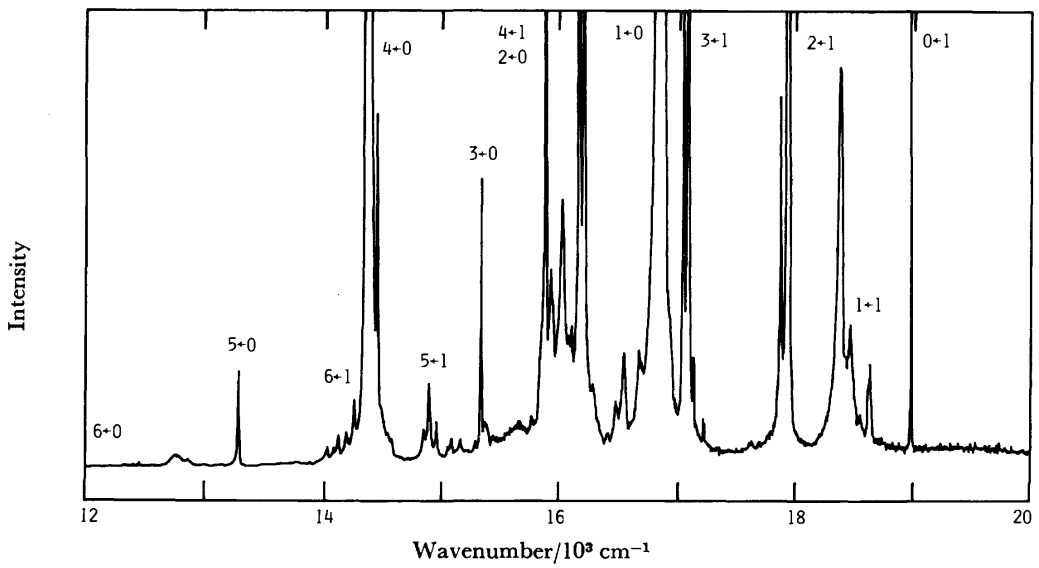

Fig. 2. π-polarized fluorescence spectra of $Eu(BrO_3)_3 \cdot 9H_2O$. Notations are the same as in Fig. 1.

Table 3. Assignments of the fluorescence spectra of $Eu(BrO_3)_3 \cdot 9H_2O$

	$5D_0(0^+)$			$5D_1(\pm1)$			$^5D_1(0^-)$			Averaged energy /cm^{-1}
	σ[b]/cm^{-1}	I_r[c]	Energy[d] /cm^{-1}	σ/cm^{-1}	I_r	Energy /cm^{-1}	σ/cm^{-1}	I_r	Energy /cm^{-1}	
$^7F_0(0^+)$				*19012.2π	1.00	0.0	*19019.7σ	0.81	0.0	0.0±0.2
$^7F_1(\pm1)$	*16900.6π	25.1	352.2	18658.9σ	0.24	352.3	*18666.0π	0.02	353.8	352.7±1.1
(0^-)	*16846.6σ	17.5	404.8							404.8
$^7F_2(\pm2)$	16229.4σ	4.51	1023.4	17986.2π	3.20	1024.8	17995.2σ	0.15	1024.3	1024.2±0.6
(±1)	*16215.0π	1.52	1038.0	17974.0σ	3.41	1037.0	*17982.5π	3.60	1037.1	1037.5±0.5
(0^+)				*17928.0π	0.52	1083.0	*17934.8σ	2.12	1084.0	1083.5±0.5
$^7F_3(3^+)$	15410.7π	2.85	1842.1	17168.1σ	0.95	1842.7				1842.4±0.4
(0^-)				*17128.4π	0.01	1882.4				1882.4
(±2)	15363.0σ	0.08	1889.7	17120.5π	7.81	1890.2	17128.4σ	3.10	1891.0	1890.4±0.7
(±1)	*15335.0π	0.13	1917.7	17092.8σ	2·09	1918.0	*17101.5π	0.12	1918.0	1917.9±0.2
(3^-)				17077.3σ	0.60	1933.8	17085.4π	1.51	1933.9	1933.8±0.1
$^7F_4(\pm2)$	14504.0σ	70.5	2748.5	16260.8π	4.93	2749.8				2749.2±0.7
(3^+)	14440.1π	103.	2812.5	16198.2σ	2.91	2812.3				2812.4±0.1
(±1)	*14407.0π	0.24	2845.5	16163.8σ	3.12	2846.5	*16172.6π	0.04	2845.9	2845.9±0.5
(0^+)				*16103.3π	0.51	2911.2				2911.2
(±2)	14324.4σ	22.5	2928.1	16083.4π	3.22	2927.1	16089.6σ	1.83	2929.5	2928.2±1.3
(3^-)				15936.5σ	1.21	3074.1	15944.2π	3.92	3074.9	3074.5±0.4
$^7F_5(\pm2)$	13408.7σ	0.61	3843.5	15165.8π	0.12	3844.2	15174.4σ	0.11	3843.8	3843.8±0.4
(0^-)	*13402.0σ	0.05	3850.2							3850.2
(±1)				15150.1σ	0.04	3860.1	15158.3π	0.04	3859.9	3860.1±0.1
(3^+)	13371.9π	1.51	3880.3	15128.7σ	0.36	3881.4				3880.8±0.6
(±1)	*13273.6π	0.10	3978.7	15031.3σ	0.01	3978.9				3978.8±0.1
(±2)	13215.0σ	1.21	4037.1	14972.4π	0.97	4037.7	14979.3σ	0.27	4039.4	4037.6±1.8
(3^-)				14932.0σ	0.52	4078.1	14939.6π	0.28	4079.1	4078.6±0.5
$^7F_6(3^+)$	12324.4π	1.80	4927.5	14082.0σ	0.15	4927.9				4927.9±0.5
(±2)	12308.5σ	4.05	4943.4	14067.0π	0.01	4943.0				4943.2±0.2
(±1)				14030.5σ	0.25	4979.4				4979.4
(0^+)				*14027.0π	0.01	4983.7				4983.7
(3^-)				14018.5σ	0.05	4991.4	14028.9π	0.05	4989.7	4990.5±0.9
(±2)	12248.9σ	1.01	5002.9							5002.9
(±1)				13959.5σ	0.05	5050.3				5050.3
(0^+)				*13900.2π	0.02	5109.6				5109.6
(0^-)	*12140.0σ	0.28	5111.8							5111.8

a) The lines with asterisk are due to MD transitions. b) Transition energies in air. c) Relative intensity in case of the intensity of the $^7F_0(0) \leftarrow {}^5D_1(0)$ transition being taken as 1.00. d) Energies of levels in vacuum.

Energy Levels. The procedure for calculating the energies of the 4*f*-orbitals in $[Eu(OH_2)_9]^{3+}$ will be briefly described here. In the case of strong spin-orbit interactions, the wavefunctions for the electrons of the free ion can be written as

$$|\phi) = \sum_n C_n |f^N : qSLJ), \quad (1)$$

where q is an additional quantum number specifying the state. In the presence of the crystal field, the wavefunctions should be rewritten as

$$|\psi_a) = \sum_i a_i |f^N : qSLJM). \quad (2)$$

In taking the summation, a basis set was restricted to the 64 states strongly interacting with ^5D_J and ^7F_J, that is, ^7F_J, $3(^5D_J)$, $2(^5F_J)$, $3(^5G_J)$, ^5H_J, $6(^3P_J)$, ^3D_J, ^3F_J, and ^3H_J states, where the numbers in front of the parentheses are the numbers of states with different q in Eqs. 1 and 2.[12]

The total Hamiltonian of a rare earth ion placed in a crystal field may be written as

$$H = H_{ion} + H_{cry}, \quad (3)$$

where H_{ion} is the Hamiltonian of the free ion and H_{cry} is the potential term provided by the crystal environment around the ions of interest. H_{ion} can be split into

$$H_{ion} = H_0 + H_{es} + H_{so}, \quad (4)$$

where H_0 is the sum of the kinetic energy and the potential energy due to the field of all the inner shell electrons and the nucleus, H_{es} is the electrostatic repulsive potential due to the coulomb and exchange interactions between pairs of the outer shell electrons, and H_{so} is the spin-orbit interaction. H_0 contributes only to a common energy shift for all the levels of a given configuration. Hence the energy levels of the $4f^6$ configuration can be evaluated by diagonalizing the interaction matrix elements of $H_{es}+H_{so}+H_{cry}$. The electrostatic interaction and the spin-orbit interaction can be expressed by a linear combination of the terms of the

Slater radial integrals F_n (n=2, 4, 6) and the spin-orbit coupling constant ζ_{4f}, respectively. The scalar two-body electrostatic interactions arising from the second-order perturbation energies were next considered. They give an additional term to H_{ion} with three configuration interaction (CI) parameters α, β, and γ.[8] The crystal field potential for D_3 symmetry may be expanded in terms of the tensor operator $C_n^{(k)}$ to give in which B_n^k is a

$$H_{cry} = B_0^2C_0^2 + B_0^4C_0^4 + B_3^4(C_3^4+C_{-3}^4) + B_0^6C_0^6 + B_3^6(C_3^6+C_{-3}^6) + B_6^6(C_6^6+C_{-6}^6), \quad (5)$$

crystal field parameter to be determined. First, the matrix concerned with the free ion part was diagonalized by fitting the calculated ion levels to the experimental centers of gravity of the J-manifolds. Next, the crystal field parameters were determined to reproduce the observed crystal field levels for each ion level. Finally, the matrix as a whole was diagonalized by readjusting all the parameters. Table 5 lists the optimum parameters thus obtained. The calculated eigenvalues are in close agreement with the observed ones within root mean square (rms) deviations of 24.0 cm^{-1} and 5.6 cm^{-1} for ion levels and crystal field levels, respectively.

The wavefunctions thus obtained were used to calculate the transition probabilities between crystal field levels.

Intensities. The intensity of radiation for the $\psi_b \leftarrow \psi_a$ transition is given by

$$I(\psi_a:\psi_b) \propto \sigma^4 g(\psi_a)N(\psi_a)[|(\psi_a|\boldsymbol{D}_e|\psi_b)|^2 + |(\psi_a|\boldsymbol{D}_m|\psi_b)|^2]/(2J+1), \quad (6)$$

where σ is the transition energy in wavenumber, $g(\psi_a)$ and $N(\psi_a)$ are the degeneracy and the population of the initial state ψ_a, and $\boldsymbol{D}_e$ and $\boldsymbol{D}_m$ are the ED and MD operators, respectively. The ED operator is written as

Table 4. Observed crystal field levels in $Eu(BrO_3)_3 \cdot 9H_2O$

Level		μ	Energy/cm^{-1}
$^7F_0$	0+	(A_1)	0.0±0.2
$^7F_1$	±1	(E)	352.7±1.1
	0−	(A_2)	404.8
$^7F_2$	±2	(E)	1024.2±0.6
	±1	(E)	1037.5±0.5
	0+	(A_1)	1083.5±0.5
$^7F_3$	3+	(A_2)	1842.4±0.4
	0−	(A_2)	1882.4
	±2	(E)	1890.4±0.7
	±1	(E)	1917.9±0.2
	3−	(A_1)	1933.8±0.1
$^7F_4$	±2	(E)	2749.2±0.7
	3+	(A_2)	2812.4±0.1
	±1	(E)	2845.9±0.5
	0+	(A_1)	2911.2
	±2	(E)	2928.2±1.3
	3−	(A_1)	3074.5±0.4
$^7F_5$	±2	(E)	3843.8±0.4
	0−	(A_2)	3850.3
	±1	(E)	3860.1
	3+	(A_2)	3880.8±0.6
	±1	(E)	3978.8±0.1
	±2	(E)	4037.6±1.8
	3−	(A_1)	4078.6±0.5
$^7F_6$	3+	(A_2)	4927.9±0.5
	±2	(E)	4943.2±0.2
	±1	(E)	4979.4
	0+	(A_1)	4983.7
	3−	(A_1)	4990.5±0.9
	±2	(E)	5002.9
	±1	(E)	5050.3
	0+	(A_1)	5109.6
	0−	(A_2)	5111.8
$^5D_0$	0+	(A_1)	17248.3
$^5D_1$	±1	(E)	19005.8
	0−	(A_2)	19014.4

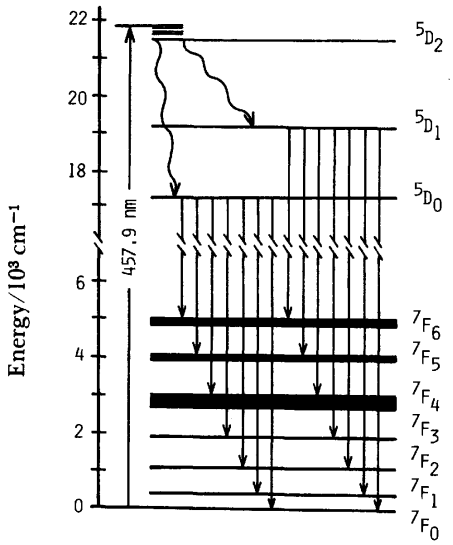

Fig. 3. The energy level diagram of $Eu(BrO_3)_3 \cdot 9H_2O$. Straight and waved arrows indicate the radiative and nonradiative transitions, respectively.

Table 5. Parameter values used in the calculation of energy levels

Parameter/cm^{-1}	
$F2$	179.
$F4$	55.05
$F6$	4.79
ζ_{4f}	1317.
α	49.5
β	998.
γ	995.
$B(2,0)$	202.
$B(4,0)$	−282.
$B(4,3)$	−3.00
$B(6,0)$	−522.
$B(6,3)$	77.
$B(6,6)$	859.
r.m.s. deviation/cm^{-1}	
"ion level"	24.5
"crystal field level"	5.6

$$\boldsymbol{D}_e = -e\sum_i \boldsymbol{r}_i(\mathbf{C}_\rho^{(1)})_i, \tag{7}$$

where $\mathbf{C}_\rho^{(1)}$ is an irreducible tensor of rank 1. The z-component of the ED moment corresponding to the π-polarized emission is obtained with $\rho=0$, and the $(x\pm iy)$-components corresponding to the σ-polarized emission are obtained with $\rho=\pm1$. The ED mechanism of the (f,f^*) transitions has been considered to be of a forced electric dipole origin by Judd[2] and Ofelt.[3] They occur due to the mixing of $nl^{N-1}n'l'$ configurations of opposite parity through the odd terms of the crystal field potential V_{odd}. Then the perturbed state $|\psi_a'\rangle$ is expressed as

$$|\psi_a'\rangle = |\psi_a\rangle - \sum_\eta \left[\frac{(nl^{N-1}n'l':\eta|V_{odd}|\psi_a)}{\Delta E(\eta)}\right]|nl^{N-1}n'l':\eta), \tag{8a}$$

$$\Delta E(\eta) = E(nl^{N-1}n'l':\eta) - E(\psi_a) \simeq \Delta E(n'l'), \tag{8b}$$

where the perturbing potential V_{odd} is defined by

$$V_{odd} = \sum_i \sum_{t,p} A_{tp}\boldsymbol{r}_i^t(\mathbf{C}_p^{(t)})_i. \tag{9}$$

For D_3 symmetry the odd potential has the form

$$V_{odd}(D_3) = \sum_i \sum_t A_{t3}\boldsymbol{r}_i^t(\mathbf{C}_3^{(t)} - \mathbf{C}_{-3}^{(t)})_i. \tag{10}$$

The matrix elements of $\boldsymbol{D}_e$ may be expanded in terms of LS multiplets by the application of the tensor-operator technique to yield

$$\begin{aligned}(\psi_a'|\boldsymbol{D}_e|\psi_b') = {} & \sum_{i,j}\sum_\lambda\sum_{t,p} a_i^* b_j (-1)^{2J+S+L'+\lambda-M+p+\rho}\delta(S,S') \\ & \times (2\lambda+1)[(2J+1)(2J'+1)]^{1/2} \\ & \begin{bmatrix}1 & \lambda & t\\ \rho & -p-\rho & p\end{bmatrix}\begin{bmatrix}J & \lambda & J'\\ -M & P+\rho & M'\end{bmatrix} \\ & \times \begin{Bmatrix}J & J' & \lambda\\ L' & L & S\end{Bmatrix} T_c(t,\lambda)(qSL||\boldsymbol{U}^{(\lambda)}||q'SL'),\end{aligned} \tag{11a}$$

$$\begin{aligned}T_c(t,\lambda) = {} & A_{tp_{l'}}\sum(-1)^{l+l'}2(2l+1)(2l'+1)\begin{bmatrix}l & l & l'\\ 0 & 0 & 0\end{bmatrix}\begin{bmatrix}l & t & l'\\ 0 & 0 & 0\end{bmatrix} \\ & \times \begin{Bmatrix}1 & \lambda & t\\ l & l' & l\end{Bmatrix}(R_{nl}|r|R_{n'l'})(R_{n'l'}|r^t|R_{nl})/\Delta E(\eta),\end{aligned} \tag{11b}$$

where A_{tp} is a perturbing crystal field parameter. From the triangular condition for n-j symbols with $l=3$, Eq. 11 has nonzero matrix elements only if

$$\lambda = 2,\ 4,\ 6,\quad t = \lambda\pm1,\quad l' = 2,\ 4. \tag{12}$$

Therefore, the five parameters $T_c(3,2)$, $T_c(3,4)$, $T_c(5,4)$, $T_c(5,6)$, and $T_c(7,6)$ are required. The $T_c(t,\lambda)$ contains theoretically undeterminable factors by the present method, namely, the crystal field parameter A_{tp}, the radial wavefunction and the energy of the $n'l'$ orbital. Hence, an alternative parametrization proposed by Axe[10] was adopted; this is appropriate to describe the relative intensities of transitions between the crystal field levels by taking the $T_c(t,\lambda)$ as adjustable parameters. A line strength[13] for transitions between ion levels was defined by Judd-Axe[2,10] as

$$S(\phi_nJ:\phi_mJ') = \sum_t\sum_\lambda (2\lambda+1)T_i(t,\lambda)^2|(\phi_nJ|\boldsymbol{U}^{(\lambda)}|\phi_mJ')|^2/(2t+1). \tag{13}$$

The $T_i(t,\lambda)$ is a parameter concerned with the transition between ion levels and should be distinguished from $T_c(t,\lambda)$ for the crystal field levels. The matrix elements of the unit tensor of rank λ can be calculated using the eigenvectors in Eq. 1:

$$\begin{aligned}(\phi_nJ|\boldsymbol{U}^{(\lambda)}|\phi_mJ') = {} & \sum_{n,m} c_n^* c_m \delta(S,S')(-1)^{S+L'+J-\lambda} \\ & \times [(2J+1)(2J'+1)]^{1/2} \\ & \times \begin{Bmatrix}J & J' & \lambda\\ L' & L & S\end{Bmatrix}(f^N:qSL||\boldsymbol{U}^{(\lambda)}||f^N:q'SL').\end{aligned} \tag{14}$$

Consequentry, the parameters $T_i(t,\lambda)$ may be estimated from the observed line strengths using Eq. 13:

$$\begin{aligned}&T_i(3,2) = \pm0.58,\quad T_i(3,4) = \pm0.20,\quad T_i(5,4) = \pm2.39,\\ &T_i(5,6) = \pm0.05,\quad T_i(7,6) = \pm1.46.\end{aligned} \tag{15}$$

An MD transition within the $4f^N$ configuration is allowed since an MD operator $\boldsymbol{D}_m$ is of even parity having the form

$$\begin{aligned}\boldsymbol{D}_m &= -\beta(2S+L),\\ \beta &= -e\hbar/(4\pi mc).\end{aligned} \tag{16}$$

The matrix element of $\boldsymbol{D}_m$ reduces to

$$\begin{aligned}(\psi_a|(\boldsymbol{D}_m)_\rho|\psi_b) = {} & \sum_{i,j} a_i^* b_j (-1)^{J-M}\begin{bmatrix}J & 1 & J'\\ -M & \rho & M'\end{bmatrix} \\ & \times (f^N:qSLJ||\boldsymbol{D}_m||f^N:q'S'L'J'),\end{aligned} \tag{17}$$

where $\rho=0$ and ±1 correspond to σ- and π-polarized radiations, respectively, contrary to ED transitions. According to Condon and Shortley,[13] the matrix elements are nonzero only when they are diagonal in the quantum numbers q, S, and L, and furthermore J satisfies the following three cases ($\Delta J=0,\ \pm1$):

1) $J'=J$,

$$(qSLJ||\boldsymbol{D}_m||qSLJ') = g[J(J+1)(2J+1)]^{1/2}, \tag{18}$$

where

$$q = 1 + [J(J+1) + S(S+1) - L(L-1)]/[2J+1].$$

2) $J' = J-1$,

$$(qSLJ||\boldsymbol{D}_m||qSLJ') = \left[\frac{(S+L+J+1)(S+L+1-J)(J+S-L)(J+L-S)}{4J}\right]^{1/2}. \tag{19}$$

3) $J' = J+1$,

$$(qSLJ||\boldsymbol{D}_m||qSLJ') = \left[\frac{(S+L+J+2)(S+J+1-L)(L+J+1-S)(S+L-J)}{4(J+1)}\right]^{1/2}. \tag{20}$$

Thus, the MD transition probability can be evaluated straightforwardly by using Eqs. 1 and 2 for ion levels and crystal field levels, respectively.

The calculated values of the relative line strengths are contrasted with the observed ones in Table 6. The comparison enables us to estimate the population of the initial levels by Eq. 6. The two components of the $^5D_1$ state, $^5D_1(0)$ and $^5D_1(\pm1)$, were assumed to be equal in population since they are separated by only 8.6 cm^{-1}. On the other hand, the $^5D_0(0)$ state lies about 1750 cm^{-1}

Table 6. Comparison of the calculated and observed line strength of $^7F_{J'} \leftarrow {}^5D_J$ transitions in $Eu(BrO_3)_3 \cdot 9H_2O$

Upper state	S_{obsd}		S_{theo}	
Lower state	$^5D_0$	$^5D_1$	$^5D_0$	$^5D_1$
$^7F_0$				
$^7F_1$		0.62		$1.86T_1(3,2)^2$
$^7F_2$	14.0		$3.01T_1(3,2)^2$	$0.56T_1(3,2)^2$
$^7F_3$	3.15	19.6		$4.68T_1(3,2)^2+7.88T_1(3,4)^2+5.02T_1(5,4)^2$
$^7F_4$	260.0	21.4	$9.84T_1(3,4)^2+6.26T_1(5,4)^2$	$12.3T_1(3,4)^2+7.84T_1(5,4)^2$
$^7F_5$	4.63	4.18		$4.32T_1(3,4)^2+2.75T_1(5,4)^2+0.15T_1(5,6)^2+0.11T_1(7,6)^2$
$^7F_6$	11.7	1.07	$0.60T_1(5,6)^2+0.45T_1(7,6)^2$	$0.69T_1(5,6)^2+0.50T_1(7,6)^2$

Table 7. Comparison of the theoretical and observed transition intensities of the fluorescence spectra of $Eu(BrO_3)_3 \cdot 9H_2O$

Upper state	$^5D_0(0^+)$			$^5D_1(\pm1)$			$^5D_1(0^-)$		
Lower state	theo. ED	theo. MD	obsd	theo. ED	theo. MD	obsd	theo. ED	theo. MD	obsd
$^7F_0(0^+)$					1.59	1.00		1.28	0.81
$^7F_1(\pm1)$		1.21	1.78	0.38		0.24		0.02	0.02
(0^-)		0.78	1.24						
$^7F_2(\pm2)$	0.24		0.32	0.07	3.19	3.20	0.15		0.15
(±1)		0.11	0.11	0.02	3.35	3.40		3.62	3.60
(0^+)					0.51	0.51		2.40	2.12
$^7F_3(3^+)$	~0		0.20	0.89		0.95			
(0^-)		~0			~0	0.005			
(±2)	~0			7.85	0.02	7.81	4.71		3.10
(±1)		0.08	0.01	1.21	0.02	2.09		0.34	0.12
(3^-)				0.90		0.60	0.54		1.51
$^7F_4(\pm2)$	4.75		5.00	4.54	0.01	4.93	~0		
(3^+)	6.15		7.30	2.28		2.91			
(±1)		0.02	0.02	4.53	~0	3.12		0.03	0.04
(0^+)					~0	0.51		~0	
(±2)	1.65		1.57	5.71	~0	3.22	2.16		1.83
(3^-)				2.27		1.21	2.90		3.92
$^7F_5(\pm2)$	0.02		0.04	0.17	~0	0.12	0.25		0.11
(0^-)		0.006	0.004		~0				
(±1)		~0		0.65	~0	0.10	0.02	~0	0.04
(3^+)	0.05		0.11	0.55		0.36			
(±1)		0.03	0.007	0.20	~0	0.01		~0	
(±2)	0.01		0.08	0.37	~0	0.97	1.02		0.52
(3^-)				0.92		0.52	0.66		0.81
$^7F_6(3^+)$	0.01		0.13	0.03		0.15			
(±2)	0.02		0.28	0.06		0.01	~0		
(±1)		~0		0.26	~0	0.25		~0	
(0^+)					0.01	0.01		~0	
(3^-)				0.06		0.05	0.03		0.05
(±2)	0.04		0.07	~0	~0		~0		
(±1)		~0		0.02	~0	0.05		~0	
(0^+)				~0	0.02	0.02		~0	
(0^-)		0.02	0.02		~0				

below the $^5D_1$ state. The ratio of the population of $^5D_0$ to that of $^5D_1$ is given by

$$\frac{N(^5D_0)}{N(^5D_1)} = \frac{S_{obsd}(^5D_0:{}^7F_J)/S_{calcd}(^5D_0:{}^7F_J)}{S_{obsd}(^5D_1:{}^7F_{J'})/S_{calcd}(^5D_1:{}^7F_{J'})} = R(^5D_0 \rightarrow {}^7F_J:{}^5D_1 \rightarrow {}^7F_{J'}), \quad (21)$$

where $N(^5D_J)$ stands for the sum of populations overall the components of the J-manifold. Since the fluorescence intensity is proportional to the population difference between the initial and the final states, the population ratio can be estimated from the intensities of two transitions involving the same final state. Thus, the population ratio was calculated from the line strengths in Table 6 to be

$$R(^5D_0 \rightarrow {}^7F_2:{}^5D_1 \rightarrow {}^7F_2) = 14.1, \quad (22a)$$

$$R(^5D_0 \rightarrow {}^7F_4:{}^5D_1 \rightarrow {}^7F_4) = 15.5, \quad (22b)$$

$$R(^5D_0 \rightarrow {}^7F_6:{}^5D_1 \rightarrow {}^7F_6) = 12.6. \quad (22c)$$

The average of these values gives 14.1 as the population ratio $^5D_0$ to $^5D_1$. The result differs from the Boltzmann distribution at 77k.

The values of $T_i(t,\lambda)$ of Eq. 15 for free ion levels were revalued for crystal field levels by a least-squares method.

$$T_c(3,2) = 0.25,\quad T_c(3,4) = -0.10,\quad T_c(5,4) = -2.71,$$
$$T_c(5,6) = -0.02,\quad T_c(7,6) = -0.10. \quad (23)$$

The calculated relative intensities are compared with the observed ones in Table 7, where the intensity of the line $^7F_0(0^+) \leftarrow {}^5D_1(\pm 1)$ is taken to be unity. The observation is well reproduced by the calculation.

Since $T_c(t,\lambda)$ is related to the radial wavefunction $R_{n'l'}$, the contribution of the admixing orbital $n'l'$ can be estimated. Then a parameter

$$\Gamma = \sum_{n'} \Omega(n'g)/[\sum_{n'} \Omega(n'g) + \sum_{n'} \Omega(n'd)], \quad (24)$$

proposed by Axe[10] may be introduced, where

$$\Omega(n'l') = (R_{4f}|r|R_{n'l'})(R_{n'l'}|r^t|R_{4f})/\Delta E(n'l'). \quad (25)$$

The parameter Γ may be considered as a kind of measure of the contribution of the admixing orbital $n'l'$, *i.e.*, if only d-orbitals contribute, Γ=0, and if only g-orbitals contribute, Γ=1. Approximate ratios between $T_c(t,\lambda)$ values given by Eq. 11b are shown as function of Γ as

$$\frac{T_c(3,4)}{T_c(3,2)} = \frac{1.95-1.42\Gamma}{1.0+1.44\Gamma}, \quad (26a)$$

$$\frac{T_c(5,6)}{T_c(5,4)} = \frac{6.08-6.19\Gamma}{1.0+5.00\Gamma}. \quad (26b)$$

From the $T_c(t,\lambda)$ values in Eq. 23 the value of Γ was calculated to be 0.968 and 0.987 for the t=3 (Eq. 26a) and t=5 (Eq. 26b), respectively. Consequently, it is concluded that the $n'g$-orbital plays a dominant role in configuration mixing for ED transitions.

This work was partially supported by a Grant-in-Aid for Scientific Research to Y. K. from the Ministry of Education, Science and Culture (No. 58350049).

References

1) T. Ohoka and Y. Kato, *Bull. Chem. Soc. Jpn.*, **56**, 1289 (1983).
2) B. R. Judd, *Phys. Rev.*, **127**, 750 (1962).
3) G. S. Ofelt, *J. Chem. Phys.*, **37**, 511 (1962).
4) L. Helmholz, *J. Am. Chem. Soc.*, **61**, 1544 (1939).
5) S. K. Sikka, *Acta Crystallogr., Sect. A*, **25**, 621 (1969).
6) Y. Kato, K. Okada, H. Fukuzaki, and T. Takenaka, *J. Mol. Struct.*, **49**, 57 (1978).
7) G. H. Dieke, "Spectra and Energy Levels of Rare Earth Ions in Crystals," Interscience Publ., New York (1968).
8) B. G. Wybourne, "Spectroscopic Properties of Rare Earths," Interscience Publ., New York (1965).
9) K. H. Hellwege, U. Johnsen, H. G. Kahle, and G. Schaack, *Z. Phys.*, **148**, 112 (1957).
10) J. D. Axe, Jr., *J. Chem. Phys.*, **39**, 1154 (1963).
11) E. V. Sayre and S. Freed, *J. Chem. Phys.*, **24**, 1213 (1956).
12) C. W. Nielson and G. F. Koster, "Spectroscopic Coefficients for the p^n, d^n, and f^n configurations," M. I. T. Press, Cambridge, Mass. (1964).
13) E. U. Condon and G. H. Shortley, "The Theory of Atomic Spectra," Cambridge Univ. Press, Cambridge, England (1964).

Reflection and Photoconduction Spectra of the Single Crystals of Perylene-TCNQ 1:1 and 3:1 Molecular Complexes

Kikujiro Ishii,* Kyuya Yakushi,† Haruo Kuroda,† and Hiroo Inokuchi††
Department of Chemistry, Faculty of Science, Gakushuin University, Mejiro, Toshima-ku, Tokyo 171
†*Department of Chemistry, Faculty of Science, The University of Tokyo, Hongo, Bunkyo-ku, Tokyo 113*
††*Institute for Molecular Science, Myodaiji-cho, Okazaki 444*
(Received January 27, 1984)

Crystal absorption spectra of the two modifications of the perylene-TCNQ (7,7,8,8-tetracyanoquinodimethan) complex were derived from reflection spectra by the Kramers-Kronig transformation and are discussed in relation to the differences in the crystal structures. The spectral response of photoconduction does not show any efficient photocarrier generation in the lowest charge-transfer band region in either modification. However, the rise of the photocurrent of both modifications was found to obey an empirical equation, $Y \propto (E-E_{th})^{2.5}$, where Y is the quantum yield of the photocarrier generation, E is the photon energy, and E_{th} is the threshold energy. E_{th} of the two modifications is almost the same and falls in the energy region a little above the lowest charge-transfer band. Efficiencies of the carrier generation, on the other hand, are quite different for the two modifications. These photoelectrical characters are discussed in connection with the optical spectra and also with the data of photoelectron emission.

Photoconduction in the charge-transfer (CT) complex has been studied for a number of complexes since Akamatu and Kuroda reported the photoconduction in the complexes of pyrene with some electron acceptors.[1-17] As for the mobility of the charge carriers, some features arising from the one-dimensionality of the crystal structure have been observed for some complexes.[15-17] However much less has been known about the mechanism of the carrier generation.[14] Photoelectric responses have been observed for some complexes in the region of the lowest CT-band, while some other complexes show photoelectric response only in the higher-energy regions. It has been inferred that the higher CT-states, in which the charge transfer occurs to acceptor molecules farther than the nearest neighbor of a donor, play an important role in the carrier generation.[10] However, no clear evidence has been obtained for such an inference.

Perylene and TCNQ have been found to form a 3:1 complex[18] as well as the well known 1:1 modification.[7,19] The crystal structure of the former (Fig. 1b)[20] has two characteristics as compared with the usual CT-complexes. First, the stacks of perylene-the donor(D)- and TCNQ-the acceptor(A)- are composed of DAD units. The CT-interaction between the donor and acceptor molecules seems to be confined within a DAD unit. Secondly, there are additional arrays of perylene molecules between the stacks of perylene and TCNQ, the orientation of those perylene molecules being almost perpendicular to the molecules forming the stacks. Consequently, the interaction between the stacks is blocked by those additional perylene molecules, which are hereafter called *interstitial* perylene molecules.

In this paper, we report the reflection and photoconduction spectra of the single crystals of the two modifi-

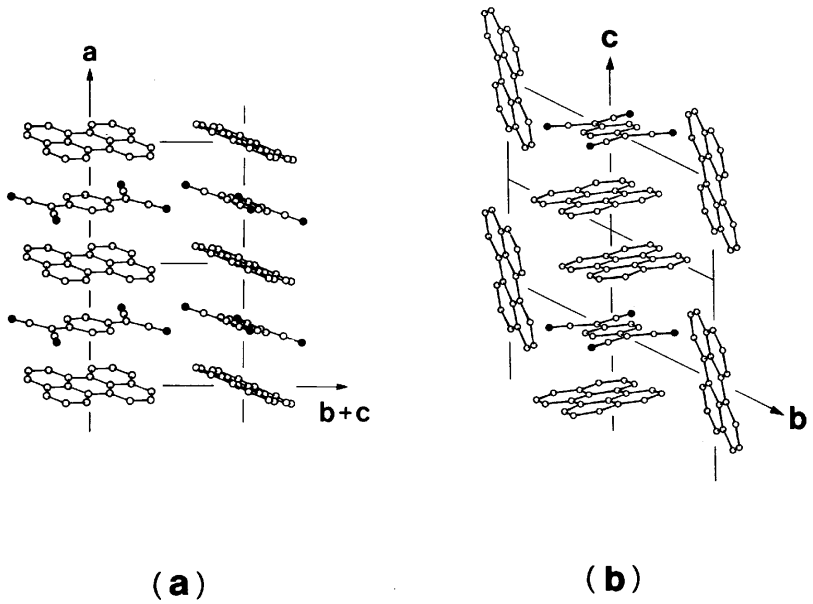

Fig. 1. Crystal structures of the two modifications of the perylene-TCNQ complex, (a) 1 : 1, (b) 3 : 1.

cations of the perylene-TCNQ complex, and discuss the threshold energies of the photocarrier generation in these crystals. The nature of the higher CT-states and the process of the carrier generation through those states are also discussed in connection with the crystal structures.

Experimental

Perylene was purified from Aldrich gold-label reagent by column chromatography on active alumina using xylene as the eluent, and then by the sublimation in the vacuum. TCNQ obtained from Tokyo Kasei was purified successively by the recrystallization from acetonitrile and by the repeated sublimation in the vacuum.

Crystals of the 1:1 modification were obtained by the recrystallization from an equimolar solution in tetrahydrofuran or by the sublimation in the vacuum. Crystals of the 3:1 modification were obtained by the diffusion method in benzene or by the recrystallization in the same solvent. In the diffusion method, perylene and TCNQ were separately charged in two branches of a sealed U-shaped tube filled with benzene, and then it was maintained at about 30 °C for several weeks. The 3:1 modification was also obtained by slowly evaporating the benzene solution containing an excess amount of perylene.

Both the 1:1 and 3:1 crystals were dark-blue crystals with metallic lusters, but their crystal-formation habits were totally different. The 1:1 modification usually crystallizes as needle-like crystals elongated along the c-axis, whereas the 3:1 modification crystallizes as small blocks. The above-mentioned two kinds of crystals were confirmed by X-ray diffraction to be identical with the known 1:1 and 3:1 modifications.[19,20]

Polarized reflection spectra of single crystals of the two modifications were measured at room temperature with a microspectrophotometer, details of which have been previously reported.[21] Single crystals of silicon were used as the standard of the reflectivity.[22]

The photocurrent of the single crystals was measured at room temperature with a Keithley 602 electrometer or a Cary 401 vibrating-reed electrometer by a two-probe method with an arrangement of the so-called surface type. Electrical contacts onto the crystals were made with colloidal silver. Typical conditions of the electric field and the cross section of the crystal were 100 V across an electrode gap of 1 mm and 0.2 mm^2. Measurements were carried out in a nitrogen atmosphere. Spectral response of the photocurrent was measured with a monochromatized light source equipped with a 150 W tungsten-iodine lamp and a neutral filter with a variable density. It gave a constant flux of photons at any wavelength in the visible and near-infrared regions. The spectral width of the monochromator was about 6 nm (240 cm^{-1}) at 500 nm.

Results and Discussion

Reflection Spectra. Figures 2 and 3 show the reflection spectra of the (01$\bar{1}$) face of the 1:1 modification and of the (100) face of the 3:1 modification, respectively. Each figure shows the spectra measured respectively for the light polarizations parallel and perpendicular to the stacking axis (a-axis of the 1:1 modification and c-axis of the 3:1 modification). Recently, Bandrauk and his coworkers[23] reported the reflection spectra of the two modifications of the perylene-TCNQ complex. Their results are different in some respects from ours. In their c-polarized spectrum of the bc-plane of the 3:1 modification, the peak reflectances of the

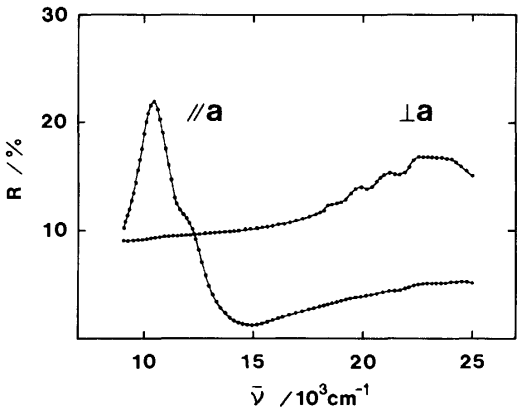

Fig. 2. Reflection spectra of the (01$\bar{1}$) face of the 1 : 1 modification with the polarizations along and perpendicular to the stacking axis (a-axis).

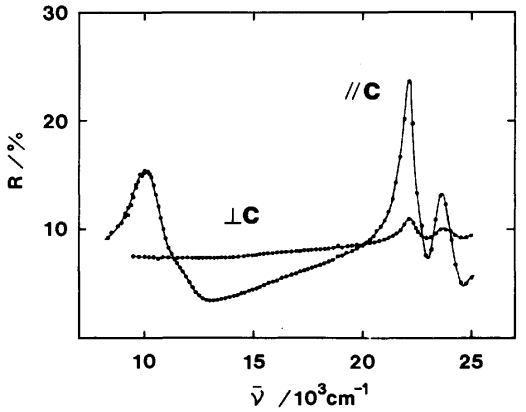

Fig. 3. Reflection spectra of the (100) face of the 3 : 1 modification with the polarizations along and perpendicular to the stacking axis (c-axis).

CT-band as well as those of the local-excitation bands are much smaller than our results. In addition, there appears a small dispersion around 500 nm in their spectrum obtained for another light polarization on the same crystal plane. We could not observe such a dispersion for any light polarization on the (100) face (bc-plane) of the 3:1 modification, but observed a similar dispersion in the spectra taken on another crystal face which is considered to be the (00$\bar{1}$) face (ab-plane).

From the observed reflectivity data, we calculated the optical constants by the Kramers-Kronig transformation, assuming simple dispersions of the optical constants outside of the energy region where the measurement was carried out.[21] Optical constants near the upper limit of the experiment (25×10^3 cm^{-1}), therefore, naturally contain some ambiguity on account of this assumption. Absorption spectra thus calculated of the (01$\bar{1}$) face of the 1:1 modification are shown in Fig. 4. The lowest-energy band is almost completely polarized along the stacking axis (a-axis). It has the peak at 10.6×10^3 cm^{-1} and a shoulder around 12×10^3 cm^{-1}. The peak molar extinction coefficient is 2.4×10^4 dm^3 mol^{-1} cm^{-1}. According to the polarization, this band must arise from the CT-transition between the perylene and TCNQ stacking in a column.

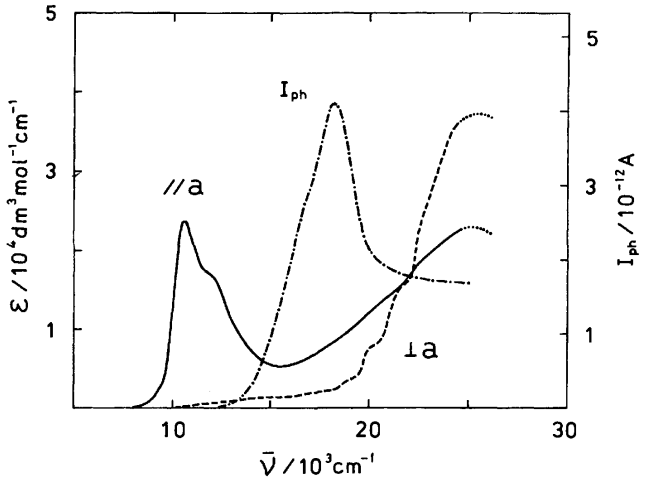

Fig. 4. Absorption spectra on the (01$\bar{1}$) face of the 1 : 1 modification with the polarization along (——) and perpendicular (----) to the stacking axis (a-axis), and photoelectric response (—·—) of the same modification.

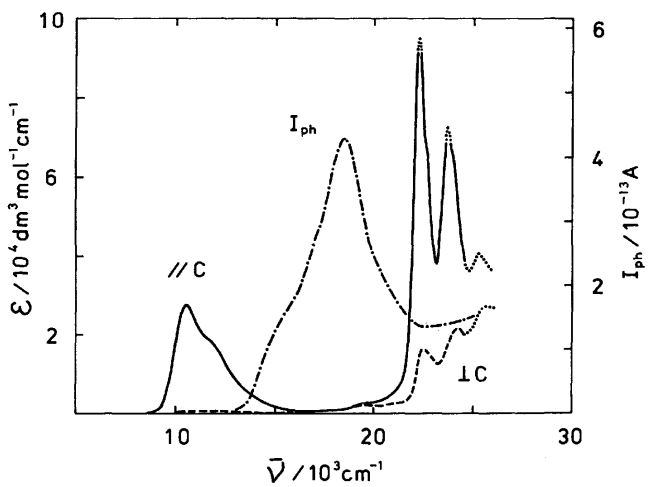

Fig. 5. Absorption spectra on the (100) face of the 3 : 1 modification with the polarizations along (——) and perpendicular (----) to the stacking axis (c-axis), and photoelectric response (—·—) of the same modification.

The energy difference between the peak and the shoulder suggests that this shoulder may be a vibrational structure, but there remains a possibility that it is related to a higher CT-state. The nature of this shoulder will be discussed later in connection with the spectrum of the 3:1 modification. As is seen in the ⊥a spectrum, local-excitation transitions of the perylene and TCNQ arise above 19×10^3 cm^{-1}. Note that the absorption at the higher-energy side of the CT-band in the //a spectrum does not completely decay but is followed by an absorption which gradually increases its intensity until the local-excitation region above 19×10^3 cm^{-1}. This implies that, in the above-mentioned region, there are some more electronic transitions polarized along the stacking axis. They may be mixed states between higher CT-states and the local-excitation states.

Absorption spectra on the (100) face of the 3:1 modification were similarly calculated from the reflection spectra (Fig. 5). The lowest-energy band of this modification, polarized along the c-axis, has a strong resemblance to the corresponding band of the 1:1 modification, and can be assigned to the CT-transition between perylene and TCNQ stacking in a column. It has the peak at 10.5×10^3 cm^{-1} and a shoulder around 12×10^3 cm^{-1}. The peak molar extinction coefficient is 2.8×10^4 dm^3 mol^{-1} cm^{-1}. The higher-energy side of the above shoulder decays clearly, and does not show any absorption which continues to the local-excitation region.

The similarity and the differences between the CT-bands of these two modifications may be understood by comparing their crystal structures[19,20] which have already been described. Electronic overlaps between the donor and acceptor of the nearest neighbor are similar in the two modifications. However, the interactions with the molecules in the second nearest unit and the farther units are by no means the same. It is therefore inferred that the lowest CT-states in the two modifications are similar, but that some differences may be seen for the higher CT-states. These are the features seen in the observed spectra if we consider that the shoulders around 12×10^3 cm^{-1} are the vibrational structures of the lowest CT-bands and that the absorption in the region of 15×10^3—20×10^3 cm^{-1} in the //a spectrum of the 1:1 modification is associated with the higher CT-states. Very weak absorption in the same region in the spectra of the 3:1 modification suggests the small transition probabilities to the higher CT-states in this modification.

Pronounced peaks are seen in the local-excitation region in the //c spectrum of the 3:1 modification. The peak wave numbers, 22.2 and 23.7×10^3 cm^{-1}, fall between the corresponding wave numbers[24] of the absorption peaks of perylene in the solution and the α-perylene crystal which is composed of perylene molecules with a dimer-type conformation. Taking account of the polarization of the above peaks and the crystal structure, those peaks are assigned to the transitions in the interstitial perylenes. Molar extinction coefficients at the peaks of these bands could not be estimated accurately because the interval of the experimental points of the reflection spectrum was not small enough compared with the band width. However, they seem to be almost three times as large as the extinction coefficients of the corresponding peaks in the solution spectrum,[24] which is in harmony with a simple expectation based on the oriented-gas model. These observations indicate the weakness of the interaction of the interstitial perylenes with other molecules in the stacks.

Photoconduction of the 1:1 Modification. The spectral response of the photocurrent of the 1:1 modification obtained by the recrystallization from tetrahydrofuran is shown in Fig. 4. A crystal obtained by the sublimation method gave an almost similar result. These spectral-response curves qualitatively agree with those of needle crystals reported by Vincent and Wright.[7,25] The curve shows a peak around 18×10^3

cm^{-1} with a long tail in the small wave-number side. Note that excitation in the lowest CT-band region seemingly does not give rise to a photocurrent efficiently. The photocurrent, I_{ph}, changed nonlinearly against the intensity of the excitation light, L, as follows:

$$I_{ph} = aL^n, \tag{1}$$

where a is a constant and n was 0.4—0.6 depending on the crystal. This result indicates that the steady-state photocurrent in our crystals was affected by the presence of charge-carrier traps.[26] However the dominant mechanism of the carrier generation may not be the detrapping of the carriers by the excitons, because no large photoelectric response was observed around the lowest CT-band region.

Energy for the charge-carrier generation in molecular crystals has been estimated by Lyons' scheme.[27,28] This scheme also seems applicable to weak molecular complexes.[29,30] Figure 6 illustrates this idea for the perylene-TCNQ complexes, where I_c=5.7 eV[31] is the adiabatic photoelectron-emission threshold and E_A=2.8 eV[32] is the electron affinity of TCNQ. Since the direct measurement of P^-, the polarization energy of the TCNQ anion in the complex, is practically difficult,[30] we roughly estimated it by assuming that P^- is the same as P^+, the polarization energy of the perylene cation in the complex. The latter was estimated to be 1.2 eV from the difference between I_c and the ionization potential of perylene molecule.[33-35] Thus the energy for generating a pair of thermally relaxed charge carriers, $I_c - E_A - P^-$, is estimated to be 1.7 eV (14×10^3 cm^{-1}). The photocurrent in Fig. 4 does not show efficient response at this energy. One must, however, examine the threshold region of the spectral response more precisely.

It has been empirically found[27] that the quantum yield, Y, of the photocarrier generation in some molecular crystals around the threshold is given by

$$Y = b(E - E_{th})^{2.5}, \tag{2}$$

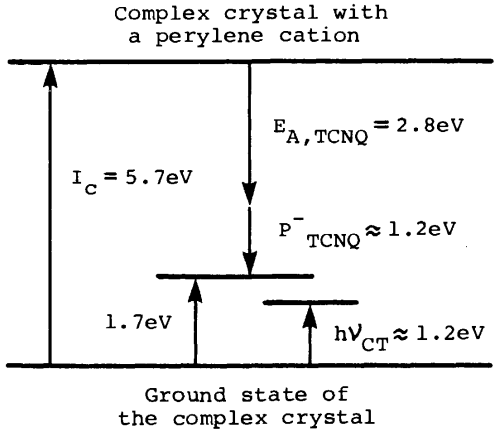

Fig. 6. Energy diagram for estimating the threshold energy of the carrier generation in the 1 : 1 modification, where I_c is the ionization potential of the 1 : 1 complex, $E_{A,TCNQ}$ is the electron affinity of TCNQ, and P^-_{TCNQ} is the assumed polarization energy for $TCNQ^-$ in the complex crystal (see the text). Threshold energy is estimated to be 1.7 eV. $h\nu_{CT}$ shows the approximate level of the lowest CT-state.

where E is the photon energy, E_{th} is the threshold energy of the carrier generation, and b is a constant. In our experiment, we utilized a light source by which a constant photon flux, L_0, was obtained at each wavelength studied. The photocurrent spectrum reflects, then, the quantum yield of the carrier generation, as follows:

$$I_{ph}(E) = c\{L_0 Y(E)\}^n, \tag{3}$$

where n is the number appeared in Eq. (1), and c is a constant. We therefore plotted $I_{ph}^{1/2.5n}$ against the photon energy. Curve A in Fig. 7 shows the result thus plotted in the threshold region for the 1 : 1 modification. A straight line can been seen in the region above 14×10^3 cm^{-1}. Extrapolation of this line gives the value of E_{th} to be 13.8×10^3 cm^{-1} (1.71 eV). Deviation from the line in the smaller-energy region may arise from some extrinsic carrier generations which involve the carrier traps at the impurity sites. The E_{th} value obtained above agrees well with the energy for the carrier generation estimated from the photoemission data and is a little larger than the peak energy of the lowest CT-band.

CT-Excitons have the character of a Wannier exciton. If one took a one-electron scheme,[27] the threshold of the carrier generation might be found at an energy where the series of the higher CT-states (larger Wannier excitons) converges. A simple consideration indicates that the lowest CT-state is more stable by approximately $e^2/2\varepsilon R$ than this energy, where R is the distance between the nearest donor-acceptor couple and ε is the dielectric constant of the crystal along the stacking axis. This difference may be as large as 1 eV. The threshold of the photoconduction, then, would be expected at an energy much higher than the lowest CT-band. This does not agree with the experimental observation. This discrepancy may be understood if one thinks about the relaxation from higher CT-states to the pair of the thermally relaxed charge carriers. In CT-complexes, CT-excitations contribute an non-negligible amount to the total polarizability of the crystal.[21] The polarization energy gained by localizing a unit charge in a molecular crystal is as large as 1 eV.[34]

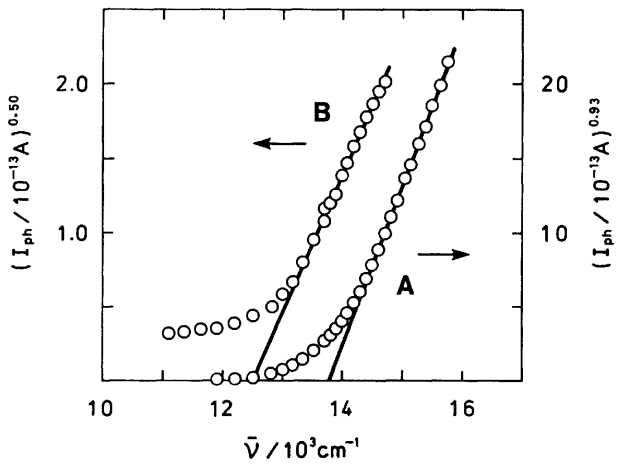

Fig. 7. (A) Plot of $I_{ph}^{1/2.5n}$ for the 1 : 1 modification. The number n (see the text) was 0.43 for this crystal. (B) $I_{ph}^{1/2.5n}$ for the 3 : 1 modification. n was 0.80 for this crystal.

Then the energy gain by relaxing the higher CT-states to a pair of charge carriers may be as large as several tenths of 1 eV. This energy may compensate a considerable part of the energy difference between the higher CT-states and the lowest CT-state. This may be the reason why we observed the threshold of the photocarrier generation only a little above the lowest CT-band.

Photoconduction of the 3:1 Modification. The spectral response of the photoconduction of the 3:1 modification is shown in Fig. 5. Although this spectrum is similar to that of the 1:1 modification, the photocurrent is smaller by one or two orders of magnitude, though the experimental conditions were similar. $I_{ph}^{1/2.5n}$ plotted for the threshold region is shown in Fig. 7 (curve B). There seems a threshold of the carrier generation at 12.5×10^3 cm^{-1} (1.55 eV). Small shoulders of photocurrent are seen around 15 and 17×10^3 cm^{-1} in Fig. 5. They suggest that some density of states related to the initial step of carrier generation are located around those energies. These may be mixed states of the higher CT-states and the local-excitation states. The threshold energy is smaller than that of the 1:1 modification, but the difference is not large. This is reasonable because the stabilization of the valence electrons in the crystal and also the polarization energies of the charge carriers are inferred to be almost the same in the two modifications.

The spectral response shows that the efficiency of the photocarrier generation is small around the threshold region and larger in the region of the higher CT-states. This may be easily understood if one considers a competition between the carrier generation through the CT-states and the deactivation of these states. The molar extinction coefficient of the lowest CT-band is very large although it is an intermolecular transition. Then, the radiative deactivation may be fast and the probability of the carrier generation from this state may be small, even if the thermal energy required to activate the carrier generation from this state were very small. For the higher CT-states, the transition dipoles to the ground state are small, and the thermal relaxation easily causes the localization of the electron and generates the charge carriers.

The small photoelectric response of the 3:1 modification compared with the 1:1 modification may be explained in terms both of the carrier generation and of the mobility. The weak absorption in the intermediate region between the lowest CT-band and the local excitation region in the absorption spectra of the 3:1 modification (Fig. 5) seems to indicate the small transition probabilities to the higher CT-states and then the smaller probability of the photocarrier generation. The crystal structure of the 3:1 modification obviously does not favor the carrier transport either.

References

1) H. Akamatu and H. Kuroda, *J. Chem. Phys.*, **39**, 3364 (1963).
2) See Ref. 7 for other references in the earlier period.
3) J. H. Sharp, *J. Phys. Chem.*, **71**, 2587 (1967).
4) T. K. Mukherjee, *J. Phys. Chem.*, **74**, 3006 (1970).
5) O. V. Kolninov, V. M. Vozzhennikov, Z. V. Zvonkova, L. F. Rybakova, R. S. Sorokina, E. M. Panov, and K. A. Kocheshkov, *Dokl. Akad. Nauk SSSR*, **202**, 844 (1972).
6) O. V. Kolninov, Y. P. Popov, V. M. Vozzhennikov, A. V. Dzyabchenko, and Z. V. Zvonkova, *Dokl. Akad. Nauk SSSR*, **205**, 110 (1972).
7) V. M. Vincent and J. D. Wright, *J. Chem. Soc., Faraday Trans. 1*, **70**, 58 (1974).
8) N. Karl and J. Ziegler, *Chem. Phys. Lett.*, **32**, 438 (1975).
9) H. Kaino, *J. Phys. Soc. Jpn.*, **41**, 570 (1976).
10) E. L. Frankevich, M. M. Tribel, I. A. Sokolik, and B. V. Kotov, *Phys. Status Solidi A*, **40**, 655 (1977).
11) J. B. Webb, N. S. Dalal, and D. F. Williams, *Mol. Cryst. Liq. Cryst.*, **41 Lett.**, 203 (1978).
12) J. Zieglar and N. Karl, *Chem. Phys.*, **40**, 207 (1979).
13) R. Anthoj, N. Karl, R. F. Robertson, and J. J. Stezowski, *J. Chem. Phys.*, **72**, 1244 (1980).
14) M. Samoc and D. F. Williams, *J. Chem. Phys.*, **78**, 1924 (1983).
15) H. Mohwald, D. Haarer, and G. Castro, *Chem. Phys. Lett.*, **32**, 433 (1975).
16) D. Haarer and H. Mohwald, *Phys. Rev. Lett.*, **34**, 1447 (1975).
17) Z. Zboinski, *Phys. Status Solidi B*, **74**, 561 (1976).
18) K. D. Truong and A. D. Bandrauk, *Chem. Phys. Lett.*, **44**, 232 (1976).
19) I. J. Tickle and C. K. Prout, *J. Chem. Soc., Perkin Trans. 2*, **1973**, 720.
20) A. W. Hanson, *Acta Crystallogr., Sect. B*, **34**, 2339 (1978).
21) K. Yakushi, M. Iguchi, and H. Kuroda, *Bull. Chem. Soc. Jpn.*, **52**, 3180 (1979).
22) H. W. Verleur, *J. Opt. Soc. Am.*, **58**, 1356 (1968).
23) A. D. Bandrauk, K. D. Truong, and C. Carlone, *Can. J. Chem.*, **60**, 558 (1982).
24) K. Fuke, K. Kaya, T. Kajiwara, and S. Nagakura, *J. Mol. Spectrosc.*, **63**, 98 (1976).
25) Unlike the authors in Ref. 7, we did not obtain plate crystals which show a large shoulder of photocurrent around 15×10^3 cm^{-1}.
26) R. H. Bube, "Photoconductivity of Solids," R. E. Krieger Pub. Co., New York (1978).
27) E. A. Silinsh, "Organic Molecular Crystals," Springer-Verlag, Berlin (1980).
28) L. E. Lyons, *J. Chem Soc.*, **1957**, 5001.
29) K. Ishii, K. Sakamoto, K. Seki, N. Sato, and H. Inokuchi, *Chem. Phys. Lett.*, **41**, 154 (1976).
30) N. Karl, N. Sato, K. Seki, and H. Inokuchi, *J. Chem. Phys.*, **77**, 4870 (1982).
31) K. Ishii, N. Sato, K. Seki, and H. Inokuchi, unpublished data.
32) R. N. Compton and C. D. Cooper, *J. Chem. Phys*, **66**, 4325 (1977).
33) R. Boschi, J. N. Murrell, and W. Schmidt, *Faraday Discuss. Chem. Soc.*, **54**, 116 (1972).
34) N. Sato, K. Seki, and H. Inokuchi, *J. Chem. Soc., Faraday Trans. 2*, **77**, 1621 (1981).
35) Valence electrons in the highest occupied molecular orbital of the donor are considered to be stabilized by the CT-interaction with the acceptor and are by no means the same as in the free donor molecule. This stabilization seems small in the weak CT-complexes studied before (Refs. 28, 29), but it is uncertain in the complexes studied here. However, we have tried to estimate the threshold energy of the photocarrier generation very roughly in this paper.

The Crystal Structure of 13*H*-Dibenz[*a*,*de*]anthracen-13-one

Isao OONISHI,* Shoji FUJISAWA, Junji AOKI, Yuji OHASHI,† and Yoshio SASADA†

Department of Chemistry, Faculty of Science, Toho University, Funabashi, Chiba 274

†*Laboratory of Chemistry for Natural Products, Tokyo Institute of Technology, Nagatsuta, Midori-ku, Yokohama 227*

(Received February 27, 1984)

Crystals of the title compound, $C_{21}H_{12}O$, are orthorhombic, belong to the space group $Pn2_1a$, have lattice constants of a=14.227(3), b=15.551(4), c=12.436(3) Å, and also have Z=8. The structure was determined using the direct method and was refined by using a full-matrix least-squares method to an R value of 0.106 on the basis of 1964 reflections with $|F_o|>3\sigma(|F_o|)$. The molecules is slightly distorted from the planar conformation owing to a steric repulsion between the O and H atoms. The molecules are stacked in pairs and two pairs with different overlapping modes are randomly arranged with different populations. It has been qualitatively explained that the populations of disordered molecules reflect the difference in their lattice energies.

It has been assumed that the glycerol condensation of benz[*a*]anthracene-9,10-dione results in the formation of two isomeric products: 7*H*-benzo[*h*,*i*]chrysen-7-one (8,9-BzBT)†† and 13*H*-dibenz[*a*,*de*]anthracen-13-one (5,6-BzBT)††. The crystal and molecular structure of 8,9-BzBT has been determined using the X-ray diffraction method.[1] The molecule is distorted from the planar conformation owing to a steric repulsion between the O* and H* atoms. Around an inversion center, the molecules are stacked in pairs. Two pairs with different overlapping mode are randomly arranged with different populations. The present work was undertaken to confirm the structure of another isomer, 5,6-BzBT, and to compare its crystal and molecular structure with that of 8,9-BzBT.

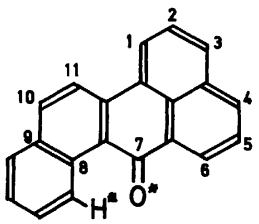

7*H*-benzo[*h*,*i*]chrysen-7-one (8,9-BzBT)††

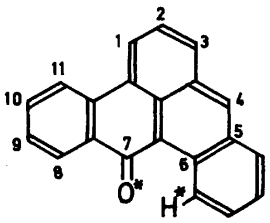

13*H*-dibenz[*a*,*de*]anthracen-13-one (5,6-BzBT)††

Scheme

†† The names in common use.

Experimental

The title compound was prepared by a method which has been reported previously.[1] The crystals used for X-ray work were grown by slow sublimation in a sealed glass tube with a nitrogen atmosphere (100 Pa). Crystal data are as follows: $C_{21}H_{12}O$; M.W. 280.1; orthorhombic; a=14.227(3), b=15.551(4), c=12.436(3) Å, and U=2751.4(9) Å^3; D_x=1.352 g cm^{-3}; Z=8; space group $Pn2_1a$; μ(Cu $K\alpha$)=42.6 cm^{-1}. The intensity data were collected on a Rigaku automated four-circle diffractometer using the $\omega/2\theta$ scan technique with a scanning rate of 4°(2θ) min^{-1}. The dimensions of the crystal used for data collection were 0.4×0.35×0.3 mm. A total of 2569 independent reflections were measured (up to 2θ=125.0°) using graphite monochromated Cu $K\alpha$ radiation, of which 1694 reflections with $|F_o|>3\sigma(|F_o|)$ were used for the analysis. Corrections were made for Lorentz and polarization factors, but not for absorption.

Structure Determination

Systematic absences of $0kl$, $k+l=2n+1$ and $hk0$, $h=2n+1$ indicated the space group to be Pnma or $Pn2_1a$. The packing consideration suggested a non-centrosymmetric arrangement and the structure was successfully refined on the basis of the space group $Pn2_1a$. There are two crystallographically independent molecules in an asymmetric unit, which are denoted as A and B. The structure was determined using the direct method, with the MULTAN 78 program.[2] This structure was refined using the block-diagonal least-squares method with isotropic thermal parameters. After 6 cycles of refinement (R=0.20), 20 small peaks due to the disordered B molecule were found on the difference map*. This molecule is denoted as C. Further refinement was performed using the full-matrix least-squares method with the SHELX 76 program.[3] The anisotropic thermal parameters were used for the non-hydrogen atoms of the A and B molecules and the isotropic thermal parameters were used for the atoms of the C molecules and H atoms. The C molecule was constrained to have the same structure as that of A. The final R became 0.106. The population factors of the B and C molecules were refined to be 0.80(1) and 0.20(2), respectively. No peaks higher than 0.3 eÅ^{-3} were found on the final difference map. The atomic scattering factors were taken from Ref. 4. The final atomic parameters with their standard deviations are listed in Table 1.**

Results and Discussion

Figure 1 illustrates the crystal structure of 5,6-BzBT viewed along the b axis. One of the two crystallographically independent molecules takes a disordered structure, B and C, which are situated on nearly the same plane and have different orientations. The two

* No diffuse scattering was observed on the Weissenberg photographs.

** Lists of the observed and calculated structure factors, anisotropic thermal parameters for non-H atoms and positional parameters for H atoms are deposited as Document No. 8444 at the office of the Chemical Society of Japan.

TABLE 1. FINAL ATOMIC COORDINATES WITH THEIR ESTIMATED STANDARD DEVIATIONS IN PARENTHESES, MULTIPLIED BY 10^4 FOR ATOMS OF MOLECULE A AND B, AND 10^3 FOR ATOMS OF MOLECULE C

Atom	x	y	z	B or B_{eq}/Å	Atom	x	y	z	B or B_{eq}/Å
C(1A)	3431(8)	3260(8)	7395(10)	6.4	C(12B)	8978(8)	−145(9)	4617(10)	4.8
C(2A)	3822(9)	2421(6)	7311(8)	5.3	C(13B)	8530(9)	−982(9)	4659(10)	4.9
C(3A)	4626(9)	2267(7)	6787(10)	6.1	C(14B)	7653(8)	−1157(7)	5260(8)	3.2
C(4A)	5911(8)	2885(7)	5754(8)	5.2	C(15B)	7282(10)	−1999(9)	5303(10)	5.1
C(5A)	6388(9)	3555(8)	5236(8)	5.7	C(16B)	7222(8)	−452(7)	5838(10)	3.7
C(6A)	5989(7)	4422(6)	5203(8)	4.4	C(17B)	8460(8)	497(8)	5148(9)	3.9
C(7A)	4721(8)	5427(6)	5925(9)	5.6	C(18B)	5218(10)	−1737(10)	7013(11)	6.0
C(8A)	3426(7)	6324(6)	6630(8)	4.4	C(19B)	4717(10)	−1095(10)	7594(10)	6.1
C(9A)	2606(8)	6465(6)	7200(8)	5.1	C(20B)	5105(9)	−286(11)	7587(11)	5.9
C(10A)	2201(7)	5775(8)	7652(9)	6.1	C(21B)	5839(10)	−22(10)	7056(10)	5.4
C(11A)	2549(9)	4949(7)	7580(9)	5.9	O(B)	7205(6)	1026(6)	6175(7)	5.8
C(12A)	3389(7)	4819(6)	7007(7)	4.1	C(1C)	711(3)	−251(3)	535(3)	2.7(8)
C(13A)	3823(7)	3927(7)	6936(8)	4.8	C(2C)	791(5)	−286(5)	469(5)	7.4(17)
C(14A)	4682(7)	3851(7)	6359(8)	4.6	C(3C)	858(4)	−229(4)	436(5)	5.9(14)
C(15A)	5088(8)	3022(7)	6300(8)	4.9	C(4C)	922(3)	−90(3)	424(4)	3.6(9)
C(16A)	5118(7)	4579(7)	5827(8)	5.1	C(5C)	929(4)	−1(4)	451(5)	5.4(12)
C(17A)	3815(6)	5524(7)	6540(7)	4.0	C(6C)	857(4)	41(4)	509(5)	5.6(12)
C(18A)	7247(9)	3422(9)	4706(10)	7.1	C(7C)	706(3)	17(3)	627(4)	3.8(9)
C(19A)	7662(8)	4078(12)	4139(12)	9.0	C(8C)	564(4)	−9(3)	737(4)	5.1(11)
C(20A)	7231(11)	4834(8)	4068(10)	7.5	C(9C)	493(3)	−69(3)	779(4)	3.4(9)
C(21A)	6468(7)	5031(7)	4596(9)	4.8	C(10C)	501(3)	−147(3)	743(3)	3.1(8)
O(A)	5113(6)	6046(5)	5559(7)	6.8	C(11C)	566(3)	−187(3)	674(4)	4.0(10)
C(1B)	8892(11)	−1666(9)	4121(11)	5.8	C(12C)	632(3)	−125(3)	638(4)	4.3(10)
C(2B)	8497(9)	−2528(9)	4139(12)	5.6	C(13C)	709(3)	−167(3)	560(4)	3.9(10)
C(3B)	7702(10)	−2710(9)	4708(12)	5.8	C(14C)	781(3)	−104(3)	530(4)	3.6(9)
C(4B)	6511(10)	−2171(9)	5847(10)	4.9	C(15C)	847(3)	−146(2)	465(3)	2.3(7)
C(5B)	6075(7)	−1495(8)	6398(9)	3.8	C(16C)	781(3)	−15(3)	547(4)	3.5(9)
C(6B)	6354(9)	−634(9)	6427(10)	4.5	C(17C)	637(3)	−39(3)	668(3)	2.9(8)
C(7B)	7615(8)	408(9)	5764(9)	4.2	C(18C)	1009(4)	50(4)	407(4)	4.9(11)
C(8B)	8840(10)	1335(10)	5073(10)	5.4	C(19C)	1004(3)	139(3)	431(3)	3.4(9)
C(9B)	9596(10)	1519(10)	4571(12)	6.3	C(20C)	918(4)	178(4)	485(5)	5.3(12)
C(10B)	10118(10)	928(11)	4134(11)	6.6	C(21C)	854(4)	123(4)	525(5)	5.9(13)
C(11B)	9821(11)	70(10)	4133(11)	5.9	O(C)	709(2)	88(2)	667(3)	4.8(8)

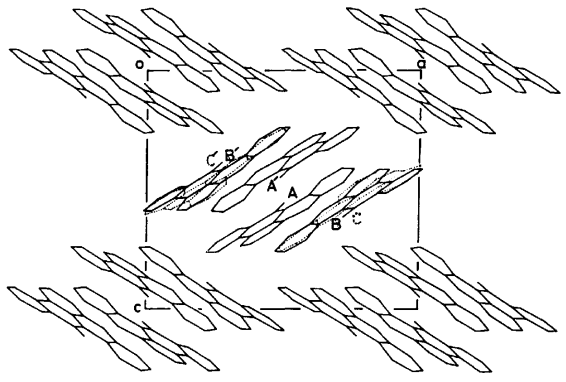

Fig. 1. Projection of the crystal structure along the b axis.
A and B′, and A and C′ form dimer pairs; A and A′ *etc.* are related to each other by the symmetry 2_1.

crystallographically independent molecules are stacked on each other as shown in Fig. 2. The mean interplanar distances between A and B′, and A and C′, are 3.47(2) and 3.58(2) Å, respectively, which are similar to 3.47(1) and 3.52(3) Å observed in the 8,9-BzBT crystal.[1] There is no unusually short contacts between the molecules.

The deviations of the atoms from the mean molecular plane are shown in Fig. 3. The bond distances and angles are listed in Tables 2 and 3, respectively. The molecules are significantly distorted from a planar conformation owing to the overcrowding around the O atom, which is also found in the 8,9-BzBT crystal. The steric repulsion between O and C(21)–H(21) is released mainly by the enlargement of the O–C(7)–C(16) angle and the twisting of the C(7)–O and C(6)–C(21) bonds. The angle of O–C(7)–C(16) and the twisting angle of O–C(7)···C(6)–C(21) are 126° and 8.2° in A, and 125° and 6.3° in B, respectively. They are comparable to 123° and 6° in 8,9-BzBT.

The interplanar distances between A and B′ or A and C′ seems to indicate that the interaction between the two molecules should be weak. This suggests that the difference in populations of the disordered molecules, B and C, is brought about by the crystalline field. A similar disordering is also found in the 8,9-BzBT

crystal. In order to clarify the effect of the crystalline field, the lattice energies were calculated for the two ordered structures using the program PCK5;[5] one is composed of A and B, and the other of A and C. Only the nonbonded interatomic repulsive force was taken into account. The orientation and translation of the molecules were refined to obtain the minimum lattice energy, the molecular geometry being fixed. Several starting structures were constructed by rotating and translating the molecules to a small extent from the position determined by X-ray analysis. Figure 4 shows the structures with the minimum lattice energies and the structure studied by X-ray analysis. The structure

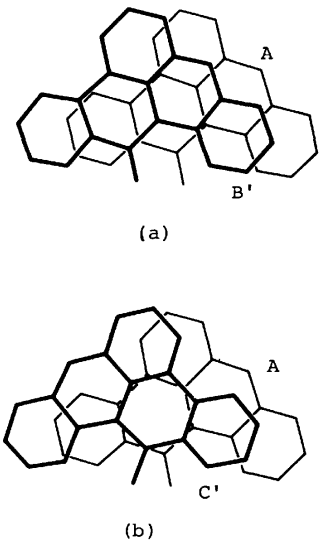

Fig. 2. Overlapping modes.
(a) Dimer pair of A and B'.
(b) Dimer pair of A and C'.

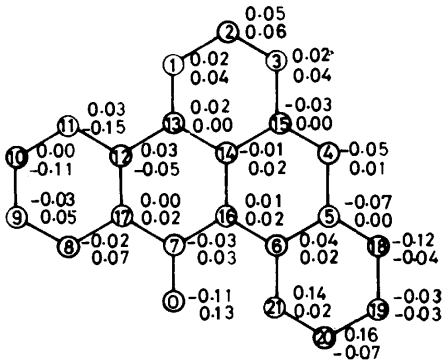

Fig. 3. Numbering scheme and atomic shifts (l/Å) from the mean planes of molecules ; the upper and lower values refer to the A and B molecules, respectively.

Table 2. Bond lengths (l/Å)

	A	B		A	B
C (1) - C (2)	1.42	1.45	C (8) - C (9)	1.38	1.28
C (1) - C (13)	1.31	1.36	C (8) - C (17)	1.37	1.41
C (2) - C (3)	1.34	1.36	C (9) - C (10)	1.34	1.30
C (3) - C (15)	1.48	1.46	C (10) - C (11)	1.38	1.40
C (4) - C (5)	1.40	1.40	C (11) - C (12)	1.41	1.38
C (4) - C (15)	1.37	1.32	C (12) - C (13)	1.52	1.45
C (5) - C (6)	1.46	1.40	C (12) - C (17)	1.38	1.41
C (5) - C (18)	1.40	1.49	C (13) - C (14)	1.42	1.48
C (6) - C (16)	1.48	1.46	C (14) - C (15)	1.42	1.41
C (6) - C (21)	1.39	1.43	C (14) - C (16)	1.45	1.45
C (7) - C (16)	1.44	1.45	C (18) - C (19)	1.37	1.42
C (7) - C (17)	1.51	1.43	C (19) - C (20)	1.33	1.37
C (7) - O	1.20	1.24	C (20) - C (21)	1.30	1.30

The values of e.s.d.'s are 0.01—0.02 in A and 0.02—0.03 in B.

Table 3. Bond angles (ϕ/°)

	A	B		A	B
C (2) - C (1) - C (13)	122	125	C (1) - C (13) - C (12)	122	121
C (1) - C (2) - C (3)	122	121	C (1) - C (13) - C (14)	121	115
C (2) - C (3) - C (15)	116	117	C (12) - C (13) - C (14)	117	124
C (5) - C (4) - C (15)	122	118	C (13) - C (14) - C (15)	117	120
C (4) - C (5) - C (6)	121	127	C (13) - C (14) - C (16)	122	118
C (4) - C (5) - C (18)	122	115	C (15) - C (14) - C (16)	121	122
C (6) - C (5) - C (18)	117	118	C (3) - C (15) - C (4)	117	117
C (5) - C (6) - C (16)	118	114	C (3) - C (15) - C (14)	121	122
C (5) - C (6) - C (21)	117	120	C (4) - C (15) - C (14)	121	121
C (16) - C (6) - C (21)	126	125	C (6) - C (16) - C (7)	122	122
C (16) - C (7) - O	122	121	C (6) - C (16) - C (14)	118	117
C (17) - C (7) - O	121	123	C (7) - C (16) - C (14)	121	120
C (16) - C (7) - C (17)	118	117	C (7) - C (17) - C (18)	119	117
C (9) - C (8) - C (17)	122	124	C (7) - C (17) - C (12)	121	128
C (8) - C (9) - C (10)	117	122	C (8) - C (17) - C (12)	121	115
C (9) - C (10) - C (11)	124	120	C (5) - C (18) - C (19)	120	120
C (10) - C (11) - C (12)	118	119	C (18) - C (19) - C (20)	120	116
C (11) - C (12) - C (13)	120	128	C (19) - C (20) - C (21)	124	128
C (11) - C (12) - C (17)	118	119	C (6) - C (21) - C (20)	121	119
C (13) - C (12) - C (17)	121	113			

The values of e.s.d.'s are 1°.

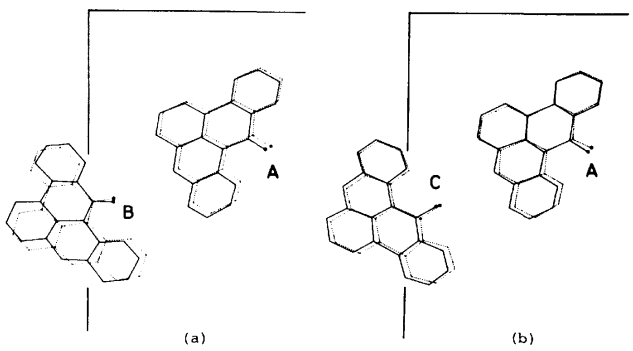

Fig. 4. Results of the packing analysis for 5,6-BzBT. The structures with minimum energies and the ones obtained by the X-ray analysis are dotted and solid lines, respectively.

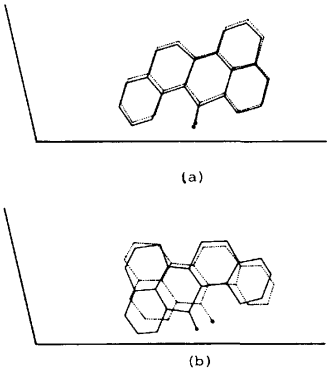

Fig. 5. Results of the packing analysis for 8,9-BzBT. (a) and (b) correspond to the molecules (I) and (II),[1] respectively.
The stuctures with minimum energies and the ones obtained by the X-ray analysis are dotted and solid lines, respectively.

calculated for B is considerably different from the X-ray structure. The lattice energies calculated are 25.1 and 31.8 KJ mol^{-1} for (a) and (b), respectively. This result qualitatively explains the smaller population of the C molecule.

Similar calculations were also performed for the disordered structure of 8,9-BzBT. In this case, the asymmetric unit of the space group $P2_1/c$ contains one molecule, which is disordered with a ratio of about 4:1. Figure 5(a) shows the structure obtained by X-ray analysis and by the minimum-energy calculation for the molecule with the greater population, whereas Fig. 5(b) is the corresponding one for the molecule with the smaller population. The minimum lattice energies are 13.8 and 31.0 KJ mol^{-1} for (a) and (b), respectively. These results suggest that several packing modes have energies similar to each other in the crystals of such condensed polycyclic aromatic compounds and the populations of the disordered molecules reflects the difference in their lattice energies.

References

1) S. Fujisawa, S. Sato, and Y. Saito, *Acta Crystallogr., Sect. B*, **37**, 2194 (1981).
2) P. Main, L. Lessinger, M. M. Woolfson, G. Germain, and J. P. Declercq (1978). MULTAN 78. A System of Computer Programs for the Automatic Solution of Crystal Structure from X-ray Diffraction Data. Univ. of York, England, and Lauvain, Belgium.
3) G. M. Scheldrick, SHELX. A program for crystal structure determination. Univ. of Cambridge, England (1976).
4) "International Tables for X-ray Crystallography," Vol. **IV**, Birmingham, Kynoch Press (1974).
5) D. E. Williams, *Acta Crystallogr., Sect. A.* **25**, 464 (1969).

Temperature Effect on Decay of Ions and Radicals in Supercooled Liquids as Studied by Pulse Radiolysis and γ-Radiolysis: 1-Propanol and Ethanol

Noriyuki KATO,* Tetsuo MIYAZAKI, Yukihiro KAWAI, and Kenji FUEKI
Department of Synthetic Chemistry, Faculty of Engineering, Nagoya University, Chikusa-ku, Nagoya 464
(Received March 9, 1984)

The decay-rate constants, k, of dipentyl disulfide anions or benzyl radicals in 1-propanol and ethanol were measured over a temperature range of 107—230 K by pulse- and γ-radiolysis method. The decay-rate constants were found to range over nine orders of magnitude. The decay kinetics is a composite first-order reaction. Since the decay rates of reaction intermediates observed are diffusion-controlled, the decay-rate constants represent directly the rates of molecular transport in the supercooled liquids. It was found that the temperature dependence of the decay-rate constants could be expressed by the following equation.

$$\log\frac{k}{T} = -\frac{A}{T-T_g} + B,$$

where T is the absolute temperature, A and B are constants. T_g is the glass transition temperature. The molecular diffusion of the ions or radicals in the supercooled liquids was completely suppressed at the glass transition temperature. The temperature dependence of the decay-rate constant was compared with that of the viscosity of the matrix. It was found that the temperature, at which the molecular diffusion is completely suppressed is much higher than the temperature at which the viscosity is infinite.

1-Propanol and ethanol form supercooled liquids at low temperature. Reaction intermediates, such as ions and free radicals, are produced in these alcohols by exposure to γ-rays or high-energy electrons. When the ions or radicals do not react with the solvent, they diffuse in the solvent to recombine with other reactive species. The diffusion of the reaction intermediates in the supercooled liquids is an important process in condensed-phase radiation chemistry.

The temperature dependence of the rate constants of reaction intermediates in condensed media has been studied by several workers: Leone and Hamill,[1] Fuller *et al.*,[2] Gilles and Boyd,[3] and Čerček[4] reported that the rate constants for reactions of ionic species produced by pulse radiolysis were correlated with the viscosity of the solvents. The decay of free radicals produced by γ-radiolysis of organic solutions has been investigated at low temperatures by Dainton *et al.*[5] and Willard *et al.*[6] Since the previous studies on the decay of reaction intermediates were undertaken only by the use of either pulsed-electron beams or γ-rays, the decay-rate constants were obtained over at most three orders of magnitude.

Recently we have reported the decay-rate constants of solute ions produced by both the pulse- and γ-radiolysis of 2-methyltetrahydrofuran(MTHF) and of a methylcyclohexane(MCH)-2-methylbutane(2MB) mixture over wide temperature (88—230 K) and viscosity ranges.[7] By use of both pulse- and γ-radiolysis the decay-rate constants of the reaction intermediates were obtained over the range of nine orders of magnitude, and then it was found that the temperature dependence of the decay-rate constants is closely related to the glass transition temperature, T_g, of the solvents. However, the relation between the decay-rate constants and the viscosity could not be discussed in the previous paper,[7] since the viscosity of MTHF or a MCH–2MB mixture was not known over a wide temperature range.

The viscosity of 1-propanol or ethanol was measured over a wide temperature range.[8,15] In order to compare the decay-rate constants of reaction intermediates with the viscosity, we have now studied the decay of ions and radicals produced in the temperature range 107—230 K. The decay-rate constants were also obtained over nine orders of magnitude. The decay-rate constant of reaction intermediates represents directly a microscopic molecular transport property, while the viscosity reflects a macroscopic transport phenomenon. Thus, it was found that the diffusible behavior obtained by the measurement of such rate constants provides us with direct information on microscopic molecular transport in the supercooled liquid, in contrast to the viscosity behavior as a macroscopic transport phenomenon in the supercooled liquid.

Experimental

Spectrograde ethanol, supplied by Nakarai Kagaku Co., and standard pure 1-propanol, supplied by Hayashi Junyaku Co., were used as received. Standard pure dipentyl disulfide (DPDS) was used after the distillation *in vacuo* and standard pure benzyl chloride was used without further purification. The sample was degassed on a vacuum line and sealed off.

Pulsed-electron beams were generated with a Febetron 707 accelerator operated at an electron energy of 2 MeV, and the duration time of a pulse was 20 ns. The radiation dose of one pulse is about 6×10^4 rad. The dose was controlled by inserting a brass mesh between the sample and the electron beam exit. The sample, sealed into a quartz cell, is fixed in a sample holder of a metal Dewar which was described in a previous paper.[9] The temperature of the sample can be controlled within an error limit of ±0.1 K. The temperature rise of the sample was less than 0.5 K immediately after the pulse irradiation. An apparatus for optical absorption measurements consists of a Xenon lamp, a monochromator, a photomultiplier, an oscilloscope, and a polaroid camera.[10] The signals obtained from pulse radiolysis were analyzed by use of a UP10E personal computer (Nippon Univac Co., Ltd.).

γ-Irradiation was made with ^{60}Co γ-rays at a dose rate of 5×10^5 rad/h. The dose given to the n-C_3H_7OH–DPDS system

was 3.5×10^5 rad, while that of the n-C_3H_7OH-$C_6H_5CH_2Cl$ and the C_2H_5OH-$C_6H_5CH_2Cl$ system was 1.0×10^5 rad.

After γ-irradiation in liquid nitrogen at 77 K, the sample was stored in liquid methane (100—111 K) or a liquid isopentane-methane mixture (112—120 K). The temperature of the liquid methane or liquid isopentane-methane mixture was controlled by addition of liquid nitrogen. The temperature of the sample can be fixed within an error limit of ±0.5 K. All optical absorption measurements on γ-irradiated samples were carried out at 77 K.

Results

Figure 1 shows optical absorption spectra of the irradiated n-C_3H_7OH containing 1 mol% DPDS (Fig. 1-a) and 3 mol% $C_6H_5CH_2Cl$ (Fig. 1-b). The absorption observed in the γ-radiolysis, shown by a solid line, was obtained at 77 K. Absorption bands around 420 nm (Fig 1-a) and 318 nm (Fig. 1-b) are attributed to DPDS anions[11] and benzyl radicals,[12] respectively. The absorption observed in the pulse radiolysis at 140 K, denoted by circles, indicates clearly the formation of DPDS anions (Fig. 1-a) and benzyl radicals (Fig. 1-b). When the C_2H_5OH-$C_6H_5CH_2Cl$ (3 mol%) system was irradiated by γ-rays at 77 K or pulsed-electron beams in the temperature ranges of 125—200 K, the optical absorption spectrum of benzyl radicals was also observed.

The decay of DPDS anions or benzyl radicals in the present systems, represented by the optical density of their absorption maxima, were similar to those of pyrene anions observed in the MCH-2MB(3:1 in volume)-pyrene and the MTHF-pyrene systems.[7]

Discussion

Decay Kinetics of Dipentyl Disulfide Anions and Benzyl Radicals. When DPDS anions and benzyl radicals decay by a first-order reaction or a second-order reaction, the decay should be described by Eq. 1 for the first-order reaction or Eq. 2 for the second-order reaction.

$$\log (OD/OD_o) \propto -kt, \quad (1)$$

$$(1/OD) - (1/OD_o) \propto kt, \quad (2)$$

where OD_o is the initial optical density of the absorption of the anions or radicals, and OD is the optical density at a time, t, after irradiation. Figure 2 shows $[(1/OD)-(1/OD_o)]$ of DPDS anions against time in the radiolysis of n-C_3H_7OH-DPDS(1 mol%) at 140 K. The slope at a dose of 1.7×10^4 rad does not coincide with that at 6×10^4 rad, indicating that the slope depends upon the initial concentration of DPDS anions. Thus, the second-order reaction plays a minor role in the decay of DPDS anions. Figure 3 shows $\log (OD/OD_o)$ of DPDS anions against time in the radiolysis of n-C_3H_7OH-DPDS(1 mol%) at 140 K. The decay curves at different initial anion concentrations (resulting from different doses) roughly superimposed on each other, but show a curvature convex to the origin, rather than the straight line for a "pure" first-order decay. Thus, the DPDS anions in n-C_3H_7OH decay by a composite first-order kinetics which was proposed previously by Willard *et al.* for the decay of alkyl radicals in γ-irradiated alkyl iodides.[13] The decay of benzyl radicals in the radiolysis of n-C_3H_7OH-$C_6H_5CH_2Cl$(3 mol%) and C_2H_5OH-$C_6H_5CH_2Cl$(3 mol%) was also expressed by a composite first-order kinetics. As was reported in our previous paper,[7] the pyrene anions in MTHF and in a MCH-2MB mixture decay by a composite first-order kinetics. Thus, it can be said that the anions and radicals in the supercooled liquids, such as 1-propanol, ethanol, MTHF, and a MCH-2MB mixture, do not decay by a simple first-order process but a composite first-order process.

Since the shape of the composite first-order decay curve probably arises from various distances of intraspur diffusion before reactions, the observed decay curve consists of a differential decay rate. For analytical convenience the apparent decay-rate constants, k_{75}, k_{50}, and k_{35} are defined here to be $(-\ln 0.75)/t_{75}$, $(-\ln 0.5)/t_{50}$, and $(-\ln 0.35)/t_{35}$, where t_m is the time required for the decay to m% of the initial amount of ions or radicals.

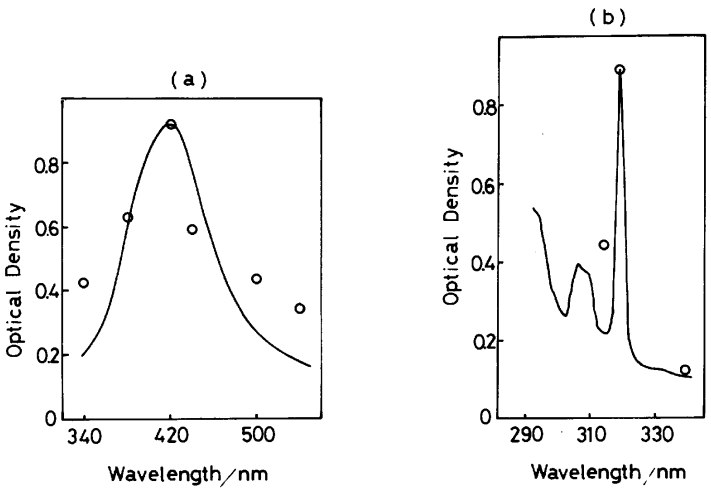

Fig. 1. a. Optical absorption spectrum of the 1-propanol-dipentyl disulfide (1 mol%) system. ——: After γ-irradiation at 77 K; ○: After pulse irradiation at 140 K. b. Optical absorption spectrum of the 1-propanol-benzyl chloride (3 mol%) system. ——: After γ-irradiation at 77 K; ○: After pulse irradiation at 140 K.

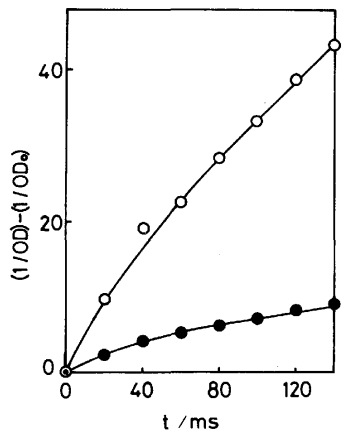

Fig. 2. The second-order kinetic plots of the decay of dipentyl disulfide anions in the pulse radiolysis of 1-propanol-dipentyl disulfide (1 mol%) at 140 K. ●: Irradiation dose; 6×10^4 rad, ○: Irradiation dose; 1.7×10^4 rad. OD and OD_0 are the optical density at time t and the initial optical density, respectively.

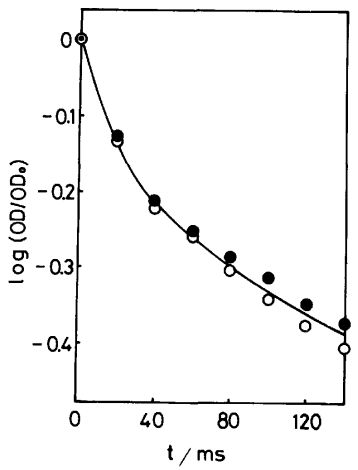

Fig. 3. The first-order kinetics plots of the decay of dipentyl disulfide anions in the pulse radiolysis of 1-propanol-dipentyl disulfide (1 mol%) at 140 K. ●: Irradiation dose; 6×10^4 rad, ○: Irradiation dose; 3.1×10^4 rad. OD and OD_0 are the optical density at time t and the initial optical density, respectively.

Since the temperature dependences of k_{75} and k_{35} coincide with that of t_{50}, the discussion on the decay-rate constant is limited here to k_{50}.

Decay of Dipentyl Disulfide Anions in Irradiated 1-Propanol. The formation of DPDS anions in the radiolysis of n-C_3H_7OH–DPDS(1 mol%) are described by the following reactions:

$$n\text{-}C_3H_7OH \rightsquigarrow n\text{-}C_3H_7OH^+ + e^-, \quad (3)$$

$$e^- + DPDS \longrightarrow DPDS^-. \quad (4)$$

They decay by the following neutralization reaction.

$$DPDS^- + M^+ \longrightarrow P, \quad (5)$$

where M^+ means the n-C_3H_7OH cation or DPDS cation formed by hole capture, and P denotes some products. Since the DPDS anions decay by a composite first-order reaction, they decay by recombination with cationic species in a spur. That is, most of DPDS anions decay by recombination with M^+ in close proximity.

An apparent activation energy, E, for the decay of DPDS anions is evaluated by $E=R\times d(\ln k)/d(1/T)$, where R is the gas constant. k is the apparent decay-rate constant for DPDS anions, defined by $(\ln 2)/t_{1/2}$ (*cf.* previous section). Then E=17, 29, and 71 kJ mol^{-1} are obtained for the temperature ranges of 170—155 K, 155—135 K, and 125—111 K, respectively. This implies that the Arrhenius-type activation energy is inappropriate to be defined under our experimental conditions. Since recombination of the anions in reaction (5) needs no activation energy, the apparent activation energy for the decay of DPDS anions arises from the diffusion controlled processes before recombination. The apparent activation energy (71 kJ mol^{-1}) for the decay of DPDS anions at 125—111 K may correspond to the barrier height for the molecular diffusion of DPDS anions at low temperature rather than for the tunneling neutralization. The tunneling neutralization may play a minor role in the decay of DPDS anions.

The temperature effect on the decay of reaction intermediates in the radiolysis will be discussed in terms of the relation between the decay-rate constant and the viscosity. When the rate constant for a bimolecular diffusion-controlled process expressed by Eq. 6 is connected with the diffusion coefficient expressed by the Stokes-Einstein relation (Eq. 7), Eq. 8 can be obtained.

$$k = 4\pi r_{ab} D_{ab}, \quad (6)$$

$$D = k_B T/6\pi r\eta, \quad (7)$$

$$k/T \propto \eta^{-1}, \quad (8)$$

where r_{ab} is the separation distance between two molecular species in collision, and $D_{ab}=D_a+D_b$ is the relative diffusion coefficient of the two species (a, b), and k_B is the Boltzmann's constant, r is the radius of a molecular species as a moving sphere, and η is the viscosity of solvent. The viscosity is related to the solvent-solvent molecular interaction, whereas the diffusion processes of reaction intermediates are related to the solute-solvent interaction. Equation 9 applies to the latter case.

$$k/T \propto \eta^{-n}, \quad (9)$$

where n is equal to or less than unity.[2]

Since the decay of pyrene anions in the irradiated MTHF or a MCH–2MB mixture can be expressed by the Doolittle-type equation[7,14] which has often been used for relaxation phenomena in supercooled liquids, we will examine whether the temperature effect on the decay-rate constant for DPDS anions can also be expressed by this type of equation (Eq. 10).

$$\log\frac{k}{T} = -\frac{A}{T-T_d^\circ} + B, \quad (10)$$

where A and B are constants. T_d° is the temperature at which the molecular transport of reaction intermediates is completely suppressed. T_d°, A, and B were

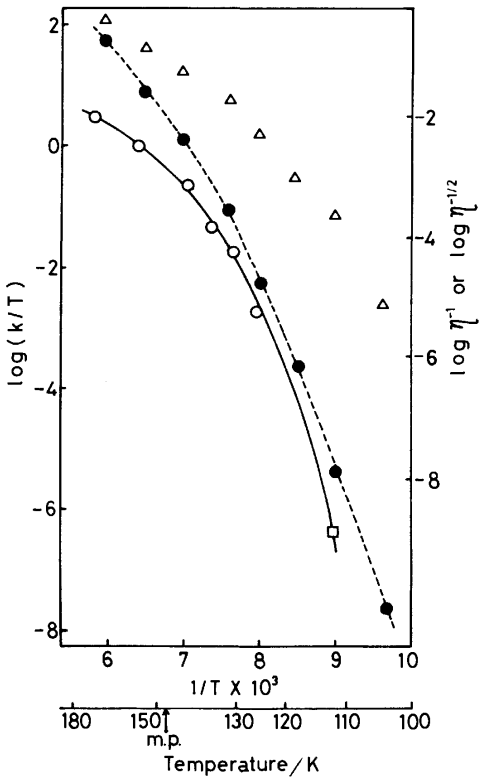

Fig. 4. Temperature dependence of the decay-rate constant of dipentyl disulfide anions in the irradiated 1-propanol-dipentyl disulfide (1 mol%). ○: Pulse radiolysis, □: γ-radiolysis, ——: Eq. 11 in text, ●: $\log \eta^{-1}$, ----: Eq. 12 in text, △: $\log \eta^{-1/2}$. The viscosity, η (in poise), of 1-propanol was quoted from Ref. 8.

determined so that they could best reproduce the experimental decay-rate constants.

Equation 11 is obtained for the decay of DPDS anions in n-C_3H_7OH which is illustrated by a solid line in Fig. 4.

$$\log \frac{k}{T} = -\frac{157.6}{T-94} + 2.577, \qquad (11)$$

where k is in units of s^{-1}. The error limit of T_g is ±2 K. The curve drawn by using Eq. 11 fits well the experimental (k/T) (*cf.* Fig. 4). The reported viscosity[8] of n-C_3H_7OH is also shown in the figure. It is well-known that the viscosity can be expressed by the Doolittle-type equation,[14] in which T_g in Eq. 10 is replaced by T_v°, a characteristic temperature in viscosity. The reported viscosity,[8] η (in poise), of n-C_3H_7OH can be expressed by the following equation as a function of temperature.

$$\log \eta^{-1} = -\frac{409.3}{T-75} + 3.501 \qquad (12)$$

Figure 4 shows that the temperature dependence of $\log (k/T)$ is different from those of $\log \eta^{-1/2}$ and $\log \eta^{-1}$.

Decay of Benzyl Radicals in Irradiated 1-Propanol and Ethanol. When n-C_3H_7OH containing 3 mol% $C_6H_5CH_2Cl$ or C_2H_5OH containing 3 mol% $C_6H_5CH_2Cl$ is irradiated by pulsed-electron beams or γ-rays, benzyl

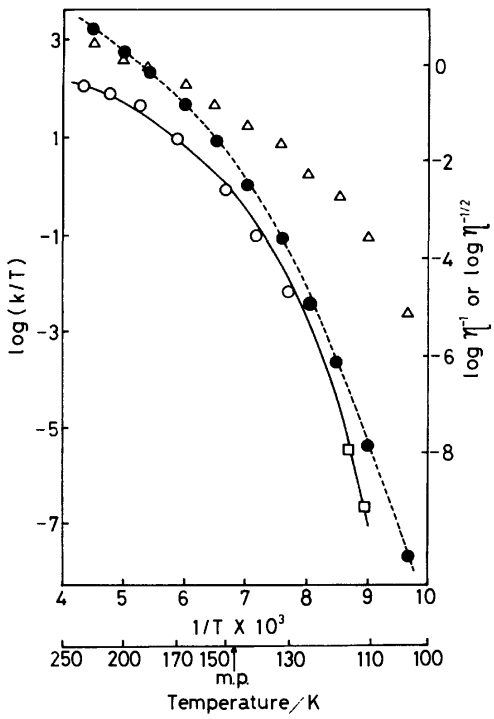

Fig. 5. Temperature dependence of the decay-rate constant of benzyl radicals in the irradiated 1-propanol-benzyl chloride (3 mol%). ○: Pulse radiolysis, □: γ-radiolysis, ——: Eq. 14 in text, ●: $\log \eta^{-1}$, ----: Eq.12 in text, △: $\log \eta^{-1/2}$. The viscosity, η (in poise), of 1-propanol was quoted from Ref. 8.

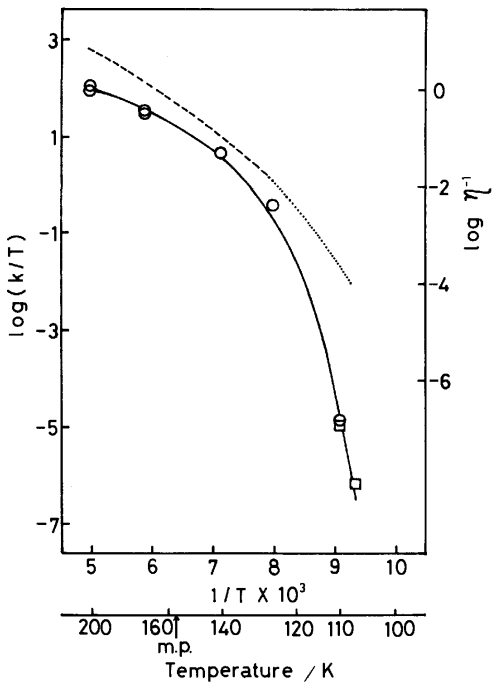

Fig. 6. Temperature dependence of the decay-rate constant of benzyl radicals in the irradiated ethanol-benzyl chloride (3 mol%). ○: Pulse radiolysis, □: γ-radiolysis, ——: Eq.15 in text, ----: $\log \eta^{-1}$, ·····: $\log \eta^{-1}$ extrapolated by Eq. 16, see text. The viscosity, η (in poise), of ethanol was quoted from Ref. 15.

radicals are produced by the dissociative electron attachment.

Since the benzyl radicals decay by a composite first-order reaction, they may decay by the following geminate recombination with the Cl^- ion rather than random recombination with other radicals.

$$C_6H_5CH_2 + Cl^- \longrightarrow C_6H_5CH_2Cl^- \quad (13)$$

Willard *et al.* reported previously that the C_2H_5 radicals produced from dissociative electron capture by ethyl iodide at 77 K decay by geminate recombination of the $(C_2H_5+I^-)$ pair.[13] $C_6H_5CH_2Cl^-$ produced by reaction (13) decays by the recombination with n-$C_3H_7OH^+$ or $C_2H_5OH^+$. Another possibility that the benzyl radicals react with a small amount of impurities, such as oxygen, in the alcohol cannot be ruled out in this system. Since the reaction of a benzyl radical with 1-propanol or ethanol is endothermic, the benzyl radical cannot react with the solvent at such low temperatures as those in the present experiments.

Though ethanol is liquid at 170 K, the viscosity (0.62 poise) at this temperature is much higher than that (0.01 poise) at room temperature.[15] Thus, the random diffusion of benzyl radicals may be suppressed at 170 K, resulting in geminate recombination.

Figure 5 shows the apparent decay-rate constants ($\log(k/T)$) for benzyl radicals in the n-C_3H_7OH-$C_6H_5CH_2Cl$ (3 mol%) system. The experimental (k/T) can be well expressed by the following equation, as shown by a solid line.

$$\log\frac{k}{T} = -\frac{202.6}{T-92} + 3.500, \quad (14)$$

where k is in units of s^{-1}. It is noted that the value of T_d° (92 K) in Eq. 14 is approximately the same as that in Eq. 11 (T_d°=94 K) within an error limit.

Figure 6 shows the apparent decay-rate constants of benzyl radicals in the C_2H_5OH-$C_6H_5CH_2Cl$ (3 mol%) system. It is noted that the decay-rate constant at 110 K obtained by pulse radiolysis almost agrees with that by the γ-radiolysis. Equation 15 is obtained for the decay of benzyl radicals in the C_2H_5OH-$C_6H_5CH_2Cl$ system

$$\log\frac{k}{T} = -\frac{115.9}{T-95} + 3.144, \quad (15)$$

where k is expressed in units of s^{-1}. It was reported that the viscosity, η (in poise), of C_2H_5OH at the temperature T K can be expressed by Eq. 16 in the temperature range of 124—273 K.[15]

$$\log\eta^{-1} = -\frac{343.8}{T-59.7} + 3.325 \quad (16)$$

The temperature dependence of the viscosity is shown by a dashed line in Fig. 6. The viscosity values extrapolated below 124 K by using Eq. 16 are also shown by a dotted line. The temperature dependence of $\log(k/T)$ for the decay of benzyl radicals is different from that of $\log\eta^{-1}$ for C_2H_5OH.

Molecular Transport of Reaction Intermediates and Viscosity in Supercooled Liquids. The decay of reaction intermediates represents directly their molecular transport properties. It should be emphasized that the decay-rate constants in the supercooled liquids can be expressed by Eq. 10 over the wide temperature range in which the decay-rate constants change by nine orders of magnitude. Table 1 shows T_d° obtained from Eq. 10 together with the reported glass transition temperatures, T_g, of the supercooled liquids. It is interesting to note that T_d° corresponds well to T_g, though the reported values of T_g slightly differ to each other due to the different methods of measurement. Thus, Eq. 10 can be rewritten as follows:

TABLE 1. CHARACTERISTIC TEMPERATURE, T_d°, T_g, AND T_v° IN SUPERCOOLED LIQUIDS

Solvent	Diffusible intermediate	T_d°/K[a]	T_g/K	T_v°/K[b]
n-C_3H_7OH	Dipentyl	94	86—100[c], 93—100[d]	75
	Disulfide anion		94[e], 98[f]	
	Benzyl radical	92		
C_2H_5OH	Benzyl radical	95	90—96[c], 92—96[g]	60
			93—97[h], 93[e], 95[i], 96[f]	
MCH-2MB	Pyrene anion	80[j]	81[k]	63
MTHF	Pyrene anion	88[j]	88[l]	—

a) T_d° is the temperature at which the molecular diffusion of reaction intermediates is completely suppressed (*cf.* Eq. 10 in text). The error limit of T_d° is ± 2 K. b) The viscosity can generally be expressed by the Doolittle-type equation of $\log\eta^{-1}=C/(T-T_v^\circ)+D$ where C and D are constants. T_v° is the temperature at which the viscosity is infinite. c) W. Kauzmann, *Chem. Rev.*, **43**, 219 (1948). d) The value was obtained from specific heat measurements (G. S. Parks and H. M. Huffmann, *J. Phys. Chem.*, **31**, 1842 (1927)). e) The value was taken as the temperature at which the viscosity is $\approx 10^{13}$ poise, based on data in Ref. 9. f) The value quoted from Ref. 17. g) The value was obtained from specific heat measurements (G. S. Parks, *J. Am. Chem. Soc.*, **47**, 338 (1925)). h) The value was obtained from specific heat measurements (K. K. Kelley, *J. Am. Chem. Soc.*, **51**, 779 (1929)). i) The value was determined from the differential thermal analysis method (O. Haida, H. Suga, and S. Seki, *Proc. Japan Acad.*, **48**, 683 (1972)). j) The value was obtained from Ref. 7. k) The glass transition temperature of the mixture was estimated by interpolation from the T_g values of neat MCH and 2MB (*cf.* C. A. Angell, J. M. Sare, and E. J. Sara, *J. Phys. Chem.*, **82**, 2622 (1978)). l) The value was taken as the temperature at which the viscosity is $\approx 10^{13}$ poise, based on data from A. C. Ling and J. E. Willard (*J. Phys. Chem.*, **72**, 3349 (1968)).

$$\log\frac{k}{T} = -\frac{A}{T-T_g} + B. \quad (17)$$

Therefore, it is concluded that the decay-rate constant for reaction intermediates in the supercooled liquids can be expressed by Eq. 17 and that the molecular diffusion is completely suppressed at the glass transition temperature.

The viscosity can be expressed by the Doolittle-type equation, and the temperature, T_v^0, at which the viscosity is infinite, is also shown in Table 1. It is interesting to note that T_g^0 (or T_g) does not agree with T_v^0. It should be pointed out that the viscosity represents a macroscopic transport property of the solvent, while the decay rate of reaction intermediates represents the microscopic molecular transport of solutes in the solvent.

This work was supported in part by a Grant-in-Aid for Scientific Research from the Ministry of Education, Science and Culture.

References

1) J. A. Leone and W. H. Hamill, *J. Chem. Phys.*, **49**, 5294 (1968).
2) J. Fuller, N. Poteleski, D. Ruppel, and M. Tomlinson, *J. Phys. Chem.*, **74**, 3066 (1970).
3) L. Gilles and A. W. Boyd, *Can. J. Chem.*, **54**, 531 (1976).
4) Čerček, *Int. J. Radiat. Phys. Chem.*, **7**, 223 (1975).
5) a) F. R. S. Dainton and G. A. Salmon, *Proc. R. Soc. London, Ser. A*, **285**, 319 (1965); b) F. R. S. Dainton, G. A. Salmon, and V. F. Zucker, *Proc. R. Soc. London, Ser. A*, **325**, 23 (1971).
6) a) J. E. Willard, *Science*, **180**, 553 (1973); b) D. D. Wilkey, H. W. Fenrick, and J. E. Willard, *J. Phys. Chem.*, **81**, 220 (1977).
7) N. Kato, T. Miyazaki, K. Fueki, S. Miyata, and Y. Kawai, *J. Phys. Chem.*, **88**, 1445 (1984).
8) A. C. Ling and J. E. Willard, *J. Phys. Chem.*, **72**, 1918 (1968).
9) T. Miyazaki, N. Kato, and K. Fueki, *Radiat. Phys. Chem.*, **21**, 489 (1983).
10) T. Miyazaki, Y. Fujitani, and Z. Kuri, *Bull. Chem. Soc. Jpn.*, **47**, 1070 (1974).
11) T. Shida, *J. Phys. Chem.*, **74**, 3055 (1970).
12) a) G. Porter and E. Strachan, *Trans. Faraday Soc.*, **54**, 1595 (1958); b) W. H. Hamill, "Radical Ions," ed by E. T. Kaiser, and L. Kevan, John Willey and Sons, New York (1968), 321.
13) H. W. Fenrick, N. B. Nazhat, P. J. Ogren, and J. E. Willard, *J. Phys. Chem.*, **75**, 472 (1971).
14) A. K. Doolittle, *J. Appl. Phys.*, **22**, 1471 (1951).
15) M. R. Carpenter, D. B. Davies, and A. J. Matheson, *J. Chem. Phys.*, **46**, 2451 (1967).

Thermochemical Studies on 3- and 4-Nitroanilines and Their *N,N*-Dimethyl Derivatives†

Junichi FURUKAWA, Shigeo MURATA, Minoru SAKIYAMA,* and Syûzô SEKI**
Chemical Thermodynamics Laboratory and Department of Chemistry, Faculty of Science, Osaka University, Toyonaka 560
(Received April 2, 1984)

Standard enthalpies of combustion and of sublimation at 298.15 K were determined and standard enthalpies of formation in crystalline and gaseous states were derived for *N,N*-dimethyl-3- and *N,N*-dimethyl-4-nitroanilines by calorimetric measurements. Stabilization energies due to the intramolecular interaction between substituents were evaluated and discussed for these compounds and 3- and 4-nitroanilines.

For most of disubstituted benzenes, dipole moment in benzene solution may be approximated by the vector sum of the dipole moments of the appropriate monosubstituted benzenes.[1] However, there are a group of exceptional compounds, 2- and 4-nitroanilines and *N,N*-dimethyl derivative of the latter being examples of such compounds. Observed dipole moments in benzene solution are by 16 and 20 per cent higher than the calculated values for 2- and 4-nitroanilines, respectively, whereas that of 3-nitroaniline is only 3 per cent higher than the calculated value.[1] The corresponding deviations are 23 and 4 per cent for *N,N*-dimethyl-4- and *N,N*-dimethyl-3-nitroanilines, respectively.[1]

The unusual dipole moments were attributed to the enhanced contribution of the following polar ortho- and para-quinonoid resonance structures to the ground state configurations of these molecules:[2]

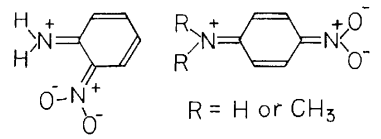

These resonance structures are characterized by the intramolecular charge transfer interaction between (dimethyl) amino and nitro substituents through the benzene ring. In this sense, the resonance has been called "interaction resonance" or "through resonance" between "push" (electron-donating) and "pull" (electron-accepting) substituents. For 3-nitroaniline and its *N,N*-dimethyl derivative, meta-quinonoid structures are available, but their contributions to the ground state configurations were considered to be small owing to the presence of a transannular bond. The normal dipole moments of 3-nitroaniline and its *N,N*-dimethyl derivative were explained along this line.

In a previous paper,[3] standard enthalpies of formation at 298.15 K were reported for 3- and 4-nitroanilines (**1** and **2**, respectively) in gaseous state by the present authors. In this paper, standard enthalpies of combustion and sublimation are reported and standard enthalpies of formation in crystalline and gaseous states are derived for *N,N*-dimethyl-3- and *N,N*-dimethyl-4-nitroanilines (**3** and **4**, respectively). Stabilization energies have been evaluated and discussed for these molecules.

Experimental

Materials. Commercial **3** (Tokyo Kasei, G.R.) was purified by recrystallization from ethanol solution, preliminary sublimation *in vacuo*, zone melting, and fractional sublimation *in vacuo*. Commercial **4** (Tokyo Kasei, G.R.) was purified by recrystallization from ethanol, ethyl acetate, and benzene solutions, and fractional sublimation *in vacuo*. The purified sample of **4** is highly pure as revealed by the results of CO_2 determination to be shown later. That of **3** is slightly less pure as compared with the former, judging from DSC curves in the melting region.

Combustion Calorimetry. A constant temperature jacket type rotating bomb calorimeter with a platinum-lined bomb, described elsewhere,[4] was used without rotating the bomb. The calorimeter was calibrated by burning thermochemical standard benzoic acid (N. B. S. SRM 39i) under certificate conditions. Mean and standard deviation of mean of observed energy equivalents for the empty calorimeter were (15161.76±0.90) J K^{-1} (8 experiments) and (15162.9±1.3) J K^{-1}(4 experiments) for 3 and 4, respectively. In contrast to **1** and **2**,[3] **3**, and **4** in pellet form could be burnt completely without using a promoter, in most cases, in an ordinary open crucible at 3 MPa of oxygen pressure. Carbon monoxide was barely detected for **3** and **4**. Nitric acid was determined by titration with aqueous sodium hydroxide. For **4**, carbon dioxide recovery was determined by the method described elsewhere.[4b]

Sublimation Calorimetry. A sublimation calorimetric system incorporating a Calvet microcalorimeter, described elsewhere,[5] was employed. Apparatus Mark II with sample containers Mark B and apparatus Mark I with sample containers Mark A were used for **3** and **4**, respectively.

Auxiliary Quantities. Relative atomic masses were taken from the recommendation of IUPAC Commission on Atomic Weights (1977). Densities, specific heat capacities,

TABLE 1. AUXILIARY DATA FOR THE CALCULATION OF STANDARD ENERGIES OF COMBUSTION

Material	Formula	ρ / g cm^{-3}	c_p[a] / J K^{-1} g^{-1}	$(\partial U/\partial p)_T$[a] / J g^{-1} MPa^{-1}
3	$C_8H_{10}O_2N_2$	1.313	(1.21)	(−0.0524)
4	$C_8H_{10}O_2N_2$	1.35	(1.21)	(−0.0519)
Cotton fuse	$CH_{1.86}O_{0.93}$	1.5	1.70	−0.0290

a) Parenthesized values are estimated ones.

** Present address: School of Science, Kwansei Gakuin University, Nishinomiya 662.

† Contribution No. 64 from Chemical Thermodynamics Laboratory, Faculty of Science, Osaka University.

and $(\partial U/\partial P)_T$ values, which were used to reduce weights to masses in vacuum and to deduce standard energies of combustion from calorimetric data, are presented in Table 1. Other auxiliary quantities are as follows: T_h=298.15 K, V(bomb)=0.3469 dm^3, and $\Delta U_c^\circ/M$(fuse)=−16507 J g^{-1}.

Results

Standard Energies of Combustion. Molar standard energies and enthalpies of combustion, given in this paper, refer to the following idealized combustion reactions at 298.15 K:

$$C_8H_{10}O_2N_2(c) + (19/2)O_2(g) = 8CO_2(g) + 5H_2O(l) + N_2(g).$$

Details of the combustion calorimetric results are presented in Table 2 and 3 for **3** and **4**, respectively. Most of the symbols in these tables are similar to those used by Hubbard *et al.*[6] Mean and standard deviation of the mean for the observed standard energies of combustion, ΔU_c°(c), were −(4555.91±0.66) and −(4540.63±0.22) kJ mol^{-1}, for **3** and **4**, respectively. Relative total carbon dioxide recovery, [m(CO_2, obsd)/m(CO_2, calcd)], where m(CO_2, obsd) and m(CO_2, calcd) are the observed and calculated total masses of recovered carbon dioxide, respectively, was (1.0000±0.0002) for **4**, where uncertainty is the standard deviation of the mean.

Standard Enthalpies of Sublimation. Details of the sublimation calorimetric results are presented in Table 4 for both compounds. Observed enthalpies of sublimation for each substance were subjected to a regression analysis for linear relations between two variables.[7] Derived expressions are as follows:

Table 2. Summary of combustion calorimetric results on *N,N*-dimethyl-3-nitroaniline

Experiment	1	2	3	4	5
m'(compd)/g	1.01048	1.01128	1.01032	1.00732	1.00960
m'''(fuse)/g	0.00217	0.00227	0.00223	0.00226	0.00226
m^i(H_2O)/g	2.98	2.99	2.99	2.99	3.03
p^i(gas)/MPa	3.039	3.040	3.043	3.044	3.046
(T_i/K) − 273.15	23.12877	23.12670	23.12545	23.12295	23.12771
(T_f/K) − 273.15	24.98213	24.98114	24.97820	24.97007	24.98006
ΔT_{corr}/K	0.02157	0.02139	0.02157	0.02149	0.02181
n^f(HNO_3)/mmol	1.014	0.982	0.975	0.999	0.997
ΔU_{ign}/J	7.5	4.0	7.8	4.7	7.4
ΔU_Σ/J	17.9	17.9	17.9	17.8	18.0
ΔU_d(HNO_3)/J	59.7	57.8	57.4	58.7	58.7
ε^i(cont)/J K^{-1}	25.4	25.5	25.5	25.5	25.7
ε^f(cont)/J K^{-1}	26.8	26.8	26.9	26.8	27.0
$-\Delta U_{IBP}$/J	27812.2	27835.1	27825.5	27721.6	27793.7
$-\{\Delta U_c^\circ/M$(compd)$\}$/kJ g^{-1}	27.4115	27.4127	27.4303	27.4071	27.4116
$-\Delta U_c^\circ$(compd)/kJ mol^{-1}	4555.22	4555.41	4558.35	4554.49	4556.06

Table 3. Summary of combustion calorimetric experiments on *N,N*-dimethyl-4-nitroaniline

Experiment	1	2	3	4	5	6	7
m'(compd)/g	0.97711	0.99630	1.00090	1.00228	1.00831	1.00644	1.00778
m'''(fuse)/g	0.00227	0.00218	0.00224	0.00216	0.00226	0.00227	0.00221
m^i(H_2O)/g	3.37	2.89	2.99	3.01	2.96	2.96	3.01
p^i(gas)/MPa	3.041	3.040	3.045	3.040	3.043	3.040	3.048
(T_i/K) − 273.15	23.12454	23.12655	23.12796	23.12511	23.12655	23.12440	23.12761
(T_f/K) − 273.15	24.91463	24.94944	24.95898	24.95885	24.97036	24.96512	24.97065
ΔT_{corr}/K	0.02444	0.02248	0.02249	0.02273	0.02192	0.02190	0.02172
n^f(HNO_3)/mmol	1.014	1.020	1.067	1.039	1.079	1.043	1.063
ΔU_{ign}/J	7.2	2.7	3.3	7.4	7.6	7.6	7.5
ΔU_Σ/J	17.8	17.5	17.7	17.7	17.8	17.7	17.9
ΔU_d(HNO_3)/J	59.7	60.1	62.8	61.2	63.5	61.4	62.6
ε^i(cont)/J K^{-1}	27.0	25.1	25.5	25.5	25.4	25.4	25.6
ε^f(cont)/J K^{-1}	28.3	26.4	26.8	26.9	26.7	26.7	26.9
$-\Delta U_{IBP}$/J	26812.7	27341.9	27465.2	27499.0	27663.6	27617.0	27655.4
$-\{\Delta U_c^\circ$/M(compd)$\}$/kJ g^{-1}	27.3231	27.3295	27.3231	27.3221	27.3180	27.3244	27.3259
$-\Delta U_c^\circ$(compd)/kJ mol^{-1}	4540.53	4541.58	4540.52	4540.36	4539.67	4540.74	4540.99
$\left\{\frac{m(CO_2, \text{obs})}{m(CO_2, \text{calc})}\right\}$	0.9997	0.9996	1.0003	—	0.9998	1.0009	0.9998

$$\Delta H^{\circ}_{sub}(T)/\text{kJ mol}^{-1} = -(0.046\pm0.010)(T/\text{K}) + (106.4\pm3.1), \quad (1)$$

and

$$\Delta H^{\circ}_{sub}(T)/\text{kJ mol}^{-1} = -(0.031\pm0.012)(T/\text{K}) + (111.9\pm4.5), \quad (2)$$

for **3** and **4**, respectively, where associated uncertainties are those at the 95 per cent confidence level. Estimated standard deviation from the fit, s_f, was 0.04 kJ mol^{-1} and 0.22 kJ mol^{-1}, for **3** and **4**, respectively. ΔH°_{sub} (298.15 K) values, obtained by extrapolation of the fits given above to 298.15 K, were (92.72±0.27) kJ mol^{-1} and (102.7±1.0) kJ mol^{-1} for **3** and **4**, respectively.[8]

Standard Thermodynamic Quantities. Derived thermodynamic quantities are presented in Table 5. Uncertainties for ΔU°_{c}(c) and ΔH°_{c}(c) are the uncertainty intervals, defined by Rossini.[9] CODATA key values for thermodynamics[10] were used to calculate ΔH°_{f}(c). Uncertainties for ΔH°_{f}(c) and ΔH°_{f}(g) were calculated by using the equation of error propagation.

Table 4. Summary of sublimation calorimetric results on *N,N*-dimethyl-3-nitroaniline (**3**) and *N,N*-dimethyl-4-nitroaniline (**4**)

T/K	t/ks	m/mg	E_{calib}/J	S_T/S_B	$\Delta H^{\circ}_{sub}(T)$/kJ mol^{-1}
			(**3**)[a]		
320.9	79.00	87.86	3.6478	13.283	91.64
320.9	89.80	100.44	6.9432	7.9823	91.70
325.5	42.20	79.87	3.9675	11.220	91.46
325.8	31.00	61.93	16.436	2.0745	91.50
325.8	50.90	100.28	6.4565	8.5465	91.44
330.7	32.40	109.97	8.8955	6.7825	91.17
330.7	69.60	239.22	10.576	12.423	91.28
330.7	15.20	53.08	5.2880	5.5097	91.21
			(**4**)[b]		
350.3	39.60	39.04	2.406	9.791	101.10
350.4	50.40	48.88	1.946	15.439	101.12
372.7	19.44	65.47	6.954	5.683	100.30
372.7	22.32	77.48	10.393	4.509	100.51
402.6	29.76	87.49	11.255	4.641	99.22
402.0	29.52	86.81	8.340	6.252	99.82

a) Both the diameter and the depth of the orifice were 1.0 mm. b) The diameter and the depth of the orifice were 2.0 and 0.1 mm, respectively, for experiments at 350 and 373 K, and 2.0 and 0.1 mm, respectively, for experiments at 402 K.

Table 5. Derived standard thermodynamic quantities at 298.15 K of *N,N*-dimethyl-3-nitroaniline (**3**) and *N,N*-dimethyl-4-nitroaniline (**4**)

	3	**4**
$-\Delta U^{\circ}_{c}$(c)/kJ mol^{-1}	4555.9±1.5	4540.63±0.94
$-\Delta H^{\circ}_{c}$(c)/kJ mol^{-1}	4557.2±1.5	4541.87±0.94
$-\Delta H^{\circ}_{f}$(c)/kJ mol^{-1}	20.1±1.8	35.4±1.4
ΔH°_{sub}/kJ mol^{-1}	92.72±0.27	102.7±1.0
ΔH°_{f}(g)/kJ mol^{-1}	72.6±1.8	67.3±1.7

Discussion

For **3** and **4**, neither ΔH°_{f}(c) nor ΔH°_{f}(g) has been reported. ΔH°_{f}(g) values reported in the previous paper[3] are (62.5±1.8) kJ mol^{-1} and (55.2±1.8) kJ mol^{-1} for **1** and **2**, respectively.

The difference in ΔH°_{f} (g) between **1** and **2** and between **3** and **4** are (7.3±2.5) kJ mol^{-1} and (4.7±2.5) kJ mol^{-1}, respectively. This shows that **2** and **4** are significantly more stable than **1** and **3**, respectively, in accordance with the resonance picture in terms of the quinonoid structures.

In this paper, stabilization energies E_{stb} of the disubstituted benzenes due to the intramolecular interaction between the substituents are defined as ΔH° (=ΔU°) at 298.15 K of the following type of hypothetical gas-phase redistribution reaction:

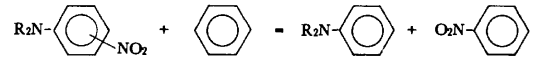

where R is H or CH_3. This type of reactions involves the fission and formation of a C_{ar}–NO_2 (or C_{ar}–NR_2) bond and a C_{ar}–H bond ,where C_{ar} denotes the aromatic ring carbon atom. The kind and number of the cleaved bonds are identical with those of the formed ones; the only change being the one from di- and un-substituted benzenes on the left-hand side to two mono-substituted benzenes on the right-hand side. In this sense, ΔH° of this type of reaction may be considered to be a reasonable measure of the degree of intramolecular interaction between the substituents through a benzene ring leading to the stabilization of the disubstituted benzene molecule with reference to benzene, aniline (or *N,N*-dimethylaniline), and nitrobenzene molecules.

Derived (E_{stb}/kJ mol^{-1}) values are (9.3±2.2), (16.6±2.2), (12.6±3.0), and (17.9±3.5) for **1**, **2**, **3**, and **4**, respectively. The following [ΔH°_{f}(g)/kJ mol^{-1}] values were employed in this calculation: (67.6±1.0),[11] (87.8±0.8),[11] (100.5±2.9),[12] and (82.9±0.3)[11] for nitrobenzene, aniline, *N,N*-dimethylaniline, and benzene, respectively.

Parr and Wasylishen briefly reported the result of MINDO/3 calculation on **2**.[13] The reported value of ΔH°_{f}(g) was 26.51 kJ mol^{-1}, which is by 29 kJ mol^{-1} less positive than the value reported by the present authors.[3] Hehre *et al.*[14] calculated the interaction energy of **2**, which may be identified with ΔH° (=ΔU°) at 0 K of the redistribution reaction described above, from calculated atomization energies of the relevant species based on *ab initio* MO theory, employing the STO-3G minimal set. They reported 9.2 and 12.6 kJ mol^{-1} for pyramidal and planar forms of the amino group, respectively. These values are comparable with the present result.

Comparison of E_{stb} between **1** and **3** and between **2** and **4** shows that the effect of *N,N*-dimethyl substitution on E_{stb} is not significant. It is to be noted that **1** and **3** as well as **2** and **4** have been shown to have positive stabilization energies by the present analysis. From the viewpoint of the resonance theory, the 1,3-isomers are expected to be barely stabilized with respect

to benzene, aniline (or its *N,N*-dimethyl derivative), and nitrobenzene, since the contribution from the meta-quinonoid resonance structure would be small. The present result is not in accord with this expectation.

References

1) C. P. Smyth, "Dielectric Behavior and Structure," McGraw-Hill, New York (1955), Chap. 10.

2) L. N. Ferguson, "The Modern Structure Theory of Organic Chemistry," Prentice-Hall, Engelwood Cliffs (1963), Chap. 4.

3) K. Nishiyama, M. Sakiyama, and S. Seki, *Bull. Chem. Soc. Jpn.*, **56**, 3171 (1983).

4) a) M. Sakiyama, T. Nakano, and S. Seki, *Bull. Chem. Soc. Jpn.*, **48**, 705 (1975); b) K. Nishiyama, M. Sakiyama, S. Seki, H. Horita, T. Otsubo, and S. Misumi, *Bull. Chem. Soc. Jpn.*, **53**, 869 (1980).

5) S. Murata, M. Sakiyama, and S. Seki, *J. Chem. Thermodyn.*, **14**, 707 (1982).

6) W. N. Hubbard, D. W. Scott, G. Waddington, "Experimental Thermochemistry," Vol. 1, ed by F. D. Rossini, Interscience, New York (1956), Chap. 5.

7) O. L. Davies and P. L. Goldsmith (eds.), "Statistical Method in Research and Production with Special Reference to Chemical Industry," 4-th ed., Longman, London (1977).

8) Temperature dependence of vapor pressure has also been determined for **4** by using a DuPont Thermal Evolution Analyzer.[4b] Derived standard enthalpy of sublimation was 101.2 kJ mol^{-1} at the mid-range temperature of 376.1 K. The value calculated from equation (2) is (101.3±0.3) kJ mol^{-1}, with which the former value agrees well.

9) F. D. Rossini, "Experimental Thermochemistry," ed by F. D. Rossini, Interscience, New York (1956), Chap. 12.

10) CODATA Task Group on Key values for Thermodynamics, 1977, *CODATA Bull.*, **1978**, 28; *J. Chem. Thermodyn.*, **10**, 903 (1978).

11) J. B. Pedley and J. Rylance, "Sussex-N.P.L. Computer Analysed Thermochemical Data; Organic and Organometallic Compounds," Univ. of Sussex, Brighton (1977).

12) J. Furukawa, M. Sakiyama, S. Seki, Y. Saito, and K. Kusano, *Bull. Chem. Soc. Jpn.*, **55**, 3329 (1982).

13) W. J. E. Parr and R. E. Wasylishen, *J. Mol. Struct.*, **38**, 272 (1977).

14) W. J. Hehre, L. Radom, and J. A. Pople, *J. Chem. Soc., Chem. Commun.*, **1972**, 669.

Kinetic Study of Excited Diatomic Molecules of Krypton and Xenon

Yoshiro Ito and Shigeyoshi Arai*
The Institute of Physical and Chemical Research, Wako-shi, Saitama 351-01
(Received April 17, 1984)

Excited diatomic molecules of krypton and xenon in $1^3\Sigma_u^+$ states, Kr_2^* and Xe_2^*, were produced by irradiating krypton and xenon in the presence of an excess of argon with short electron-beam pulses. The kinetic behaviors of Kr_2^* and Xe_2^* (monitored by near-IR absorption spectrophotometry) are explained quantitatively in terms of mechanisms involving three-body association and radiative decay. The rate constants were found to be $(6.5\pm0.8)\times10^{-33}$ cm^6 s^{-1} for $Kr^*+Kr+Ar\rightarrow Kr_2^*+Ar$ and $(1.6\pm0.3)\times10^{-32}$ cm^6 s^{-1} for $Xe^*+Xe+Ar\rightarrow Xe_2^*+Ar$. The rate constants for the quenching reactions of Kr_2^* were determined for Xe, H_2, O_2, N_2, CO, and NO.

The irradiation of rare gases with ionizing radiations results in the formation of excited atoms *via* direct excitation or ionization followed by charge neutralization. When pressures of rare gases are sufficiently high (10^2 Torr or higher), excited atoms are rapidly converted into excited diatomic molecules in a three-body association reaction involving one excited and two ground-state atoms.[1-3] Excited diatomic molecules of rare gases have broad and continuous vacuum UV emissions, which are attributed to the optical transitions between the bound excited and repulsive ground states.[4,5] Arai, Firestone, and their co-workers have demonstrated that rare gases irradiated with electron pulses exhibit two types of intense transient absorptions due to excited diatomic molecules in the near-IR region.[6-9] A comparison of the observed optical data with theoretical values leads to an assignment of the first absorption (at shorter wavelengths) and the second absorption (at longer wavelengths) to the transition $1^3\Sigma_u^+$ to $2^3\Pi_g$ and $1^3\Sigma_g^+$, respectively (potentical curves of diatomic molecules).[10] The two near-IR absorptions and the principal vacuum UV emission originate from a molecule in the same electronic state, *i.e.*, the lowest triplet state $1^3\Sigma_u^+$.

By observing the time dependence of the first absorption, several kinetic parameters have been determined for the excited diatomic molecules of rare gases in the $1^3\Sigma_u^+$ state.[7,9,11,12] The parameters are the rate constants of the formation and decay processes, together with quenching processes by many simple molecules. The absorption spectrophotometric method has also been applied to the kinetic study of helium molecules in the $1^3\Sigma_u^+$ state.[13]

The present paper reports on the kinetic parameters of the excited diatomic molecules of krypton and xenon. These parameters were determined by time-dependent observations of their first absorptions under various experimental conditions. The chemical reactions of excited atoms or excited diatomic molecules of rare gases should be studied more extensively, since information from such studies is important for constructing or testing theoretical models used in chemical kinetics.

Experimental

The experimental apparatus and procedures are essentially the same as those described in previous studies.[8,9,11-13] Therefore, only a few fundamental points will be briefly described.

All the samples were irradiated with 600-keV electron pulses generated from a Febetron 706. The profile had a pulse width of about 5 ns. The absorptions due to excited diatomic molecules of rare gases were measured spectrophotometrically as a function of time under various experimental conditions. The photomultiplier used was a Hamamatsu TV R316. The total rise time of the detection system was about 20 ns. Molecular absorptions were measured at a slit width of 0.30 mm, *i.e.*, a wavelength resolution of about 0.9 nm using a Narumi R23 monochromator. The widths of the 983-nm band due to an excited krypton molecule and the 1032-nm band due to an excited xenon molecule are much larger than the wavelength resolution.

Krypton and xenon purchased from Teikoku Sanso Co. and Takachiho Shoji Co., respectively, were of the highest grade and were used without further purification. The krypton used in the previous study contained xenon as an impurity. For the krypton used here, however, we could not detect any absorption due to an excited xenon atom, when 800 Torr (1 Torr=133.322 Pa) of krypton was irradiated with electron pulses. Since the energy transfer from excited krypton to xenon occurs very efficiently, the absence of excited xenon guarantees the high purity of krypton. Argon purchased from Nihon Sanso Co. did not show any sign of an impurity throughout all the observations. The other gases were obtained from Takachiho Shoji Co. and were used without further purification.

Results and Discussion

In this paper, the excited rare-gas atoms with an electronic configuration of $np^5(n+1)s^1$ are denoted by $X^*(^1P_1)$, $X^*(^3P_0)$, $X^*(^3P_1)$, and $X^*(^3P_2)$ in the L-S coupling notation, where X is a rare-gas atom and n is the principal quantum number of the outer shell of the ground state atom X. The excited diatomic molecules in the $1^3\Sigma_u^+$ state are denoted by X_2^*.

Formation of Excited Diatomic Molecules in Mixtures. The formation processes of Kr_2^* and Xe_2^* in the presence of excess argon were studied by measuring their near-IR absorptions as a function of time. Kr_2^* has its first absorption bands at 965.5, 974.3, 983.3, and 988.6 nm, and Xe_2^* has corresponding bands in the region of 1000—1120 nm.[6-9] The time dependencies of the absorptions were monitored at 983.3 nm for Kr_2^* and at 1032.0 nm for Xe_2^*. No change in shape was observed for the first absorption bands of Kr_2^* and Xe_2^* through their formation and decay processes in previous studies.[8,9]

Although the ionizing radiation interacts mainly

with the excess argon at an initial stage, excitation energies are expected to be transferred rapidly to krypton and xenon in the mixtures examined here. For example, the energy-transfer rates from $Ar^*(^3P_0)$ and $Ar^*(^3P_2)$ to $Kr(^1S_0)$ are estimated to be 1.5×10^6 and 3.7×10^6 s^{-1}, respectively, in a mixture of 930-Torr argon and 20-Torr krypton.[14] Our time-dependent absorption measurements for $Ar^*(3p^54s^1)$ indicated a rapid disappearance (within 1 μs or so) after a pulse in the same mixture. Chang and Setser have measured two-body deactivation rate constants for $Ar^*(3p^54p^1)$, which were produced by the laser-pulse excitation of $Ar^*(3p^54s^1)$.[15] The constants range from 1×10^{-10} to 2×10^{-11} cm^3 s^{-1}. Therefore, the lifetimes of $Ar^*(3p^54p^1)$ are estimated to be less than about 2 ns in 760-Torr argon at room temperature. We observed several visible and near-IR emission lines originating from $Ar^*(3p^54p^1)$ and $Kr^*(4p^55p^1)$ in irradiated argon-krypton mixtures. In all the mixtures examined, emissions terminated immediately after irradiation ceased. The excited argon and krypton atoms in higher states are, if produced, degraded almost instantaneously into those in the four lower states *via* radiative or collision processes. Although there are many visible and near-IR emission lines caused by excited rare-gas atoms at various high levels, such lines have not been observed in electron-irradiated rare gases at about 760 Torr except for those by $X^*(np^5(n+1)p^1)$.[6] The energy-transfer rate from Ar_2^* to $Kr(^1S_0)$ is 6.4×10^7 s^{-1} in a mixture of 930-Torr argon and 20-Torr krypton.[11]

Charged species disappear very rapidly after irradiation ceases. Ion recombination coefficients for X_2^+ and e^- have been summerized in the review by Bardsley and Biondi.[16] The coefficients are 7.5×10^{-7} cm^3 s^{-1} for Ar_2^+, 12×10^{-7} cm^3 s^{-1} for Kr_2^+, and 14×10^{-7} cm^3 s^{-1} fox Xe_2^+. Assuming that the electron pulse has an accelerating energy of 600 keV, a total output of 10 J, and a beam cross section of 2 cm^2, one can roughly estimate the initial ion concentration (n_0) from the energy loss of the incident electrons in 950-Torr argon.[17] The calculated initial lifetimes of X_2^+, *i.e.*, (recombination coefficient$\times n_0)^{-1}$ are less than 0.22 ns, indicating a rapid disappearance of charged species.

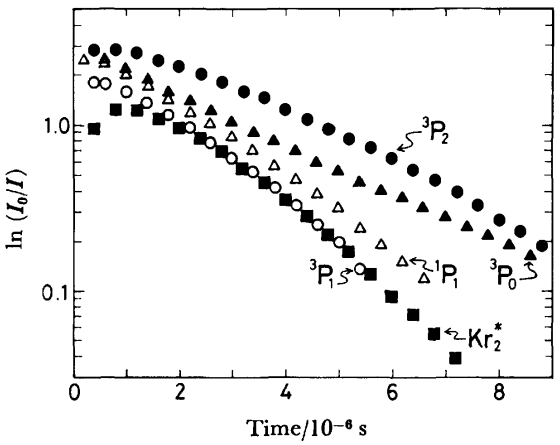

Fig. 1. Logarithmic plots of optical densities against time for Kr_2^* and $Kr^*(^1P_1, ^3P_0, ^3P_1,$ and $^3P_2)$ in the mixture of 60 Torr Kr and 890 Torr Ar. I_0, intensity of analyzing light transmitted in the absence of absorbing species; I, that in the presence of absorbing species. Absorption measurements, see text.

Figure 1 shows logarithmic plots of optical densities *vs.* time for Kr_2^*, $Kr^*(^1P_1)$, $Kr^*(^3P_0)$, $Kr^*(^3P_1)$, and $Kr^*(^3P_2)$ in the mixture of 890-Torr argon and 60-Torr krypton. $Kr^*(^1P_1)$, $Kr^*(^3P_0)$, $Kr^*(^3P_1)$, and $Kr^*(^3P_2)$ were monitored by observing absorption lines at 828.1, 785.4, 819.0, 892.9 nm, respectively (Fig. 1). The apparent lifetimes of these excited species range from 1.5 to 3 μs in the mixture. However, the Lambert-Beer law does not hold between optical density and concentration, because the bandpass of analyzing light used here (*i.e.*, about 0.35 nm) is larger than the widths of the atomic absorption lines. The net lifetimes should be shorter than the apparent ones by a factor between 1 and 2.[18]

The time dependence of the concentration of an excited diatomic molecule in a mixture can be explained by the following mechanism:

$$\text{X in excess argon} \rightsquigarrow X^* \tag{1}$$

$$X^* \longrightarrow X, \tag{1}$$

$$X^* + X + M \longrightarrow X_2^* + M, \tag{2}$$

$$X_2^* \longrightarrow 2X + h\nu, \tag{3}$$

where M is a third body. The mechanism leads to the equation:

$$[X_2^*] = \frac{k_2[X][M][X^*]_0}{k_1+k_2[X][M]-k_3}\{\exp[-k_3t] - \exp[-(k_1+k_2[X][M])t]\}, \tag{4}$$

where k_n is the rate constant of the corresponding reaction and $[X^*]_0$ is an initial concentration of X^*. The absorption intensity *vs.* time curves observed for Kr_2^* and Xe_2^* exhibit an early growth and a subsequent slow decay after passing a maximum. The apparent decay and growth should correspond to the first and second exponential terms of Eq. 4, respectively, in the high-pressure region where $\{k_1+k_2[X][M]\}$ is larger than k_3. On the other hand, the relation is reversed in the low-pressure region where $\{k_1+k_2[X][M]\}$ is smaller than k_3, since the sign of Eq. 4 changes. As the result, the apparent first-order decay rate is equal to $\{k_1+k_2[X][M]\}$.

On the basis of Eq. 4, we have analyzed a series of absorption-intensity *vs.* time curves obtained with Kr_2^* and Xe_2^* in mixtures, where the total pressures were kept nearly constant and the partial pressures of krypton and xenon were varied over a wide range. In fact, the observed curves were found to approximately fit the difference of the two exponential terms, as shown in Fig. 2. Since the partial pressures of krypton and xenon are relatively low, the apparent first-order decay rates obtained here are expected to correspond to $\{k_1+k_2[X][M]\}$ in the second term. We determined the first-order decay rates from late portions of absorption-intensity *vs.* time curves, *i.e.*, portions later than 2 μs after pulses. Figures 3 and 4 present plots of $\{k_1+k_2[X][M]\}$ against [X] for krypton and xenon, respectively, where good linear relations are seen for both gases. The radiative decay rates, *i.e.*, k_3's of Kr_2^*

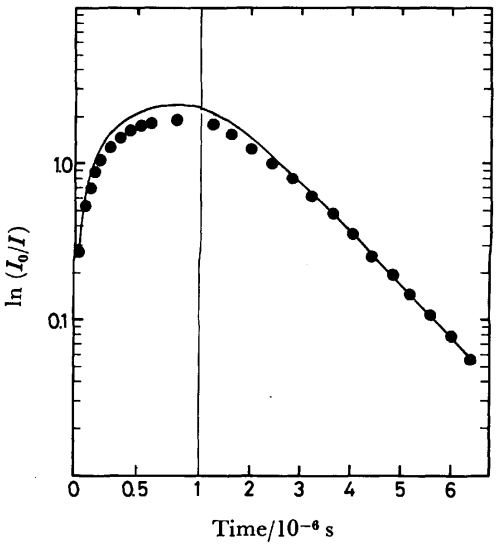

Fig. 2. Logarithmic plots of optical density at 983.3 nm against time for Kr_2^* in the mixture of 76 Torr Kr and 874 Torr Ar. Time scales are different between the regions before and after 1 μs. Solid curve was calculated from Eq. 4, where $k_3=1.8\times10^6$ s^{-1} and $k_1+k_2[M][Kr]=7.7\times10^5$ s^{-1}.

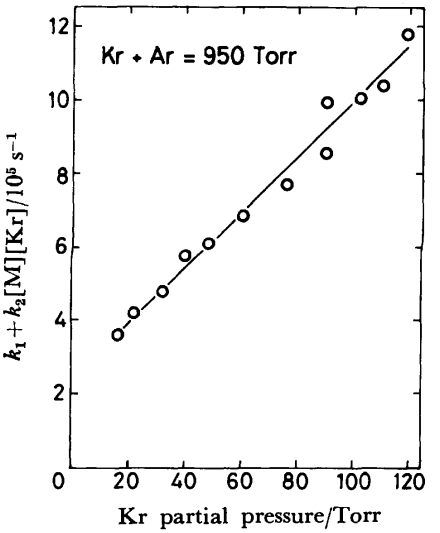

Fig. 3. Plot of $k_1+k_2[M][Kr]$ against partial pressure of Kr.

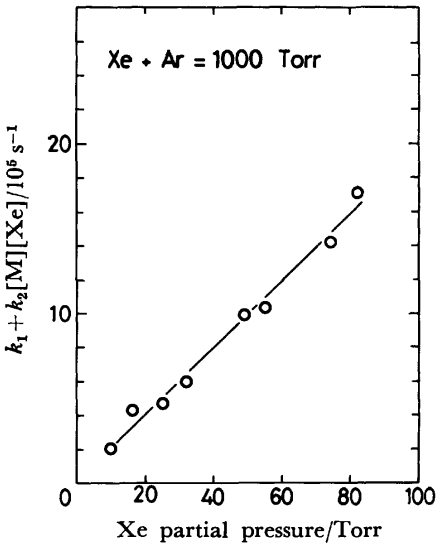

Fig. 4. Plot of $k_1+k_2[M][Xe]$ against partial pressure of Xe.

and Xe_2^* have been reported to be 2.83×10^6 s^{-1} and 1.0×10^7 s^{-1}, respectively.[7,19] The decay rates are much larger than the apparent first-order decay rates shown in Figs. 3 and 4. The rate constants for the formation of Kr_2^* and Xe_2^* are tabulated in Table 1, together with those reported previously.[3,20,21] The rate constant determined here for Xe_2^* is a little smaller than that reported in the vacuum UV-emission study by Rice and Johnson.[20] However, it agrees with more recent determination by Gleason *et al.* within the error limits.[21]

It is generally accepted that the precursor responsible for the formation of X_2^* in the $1^3\Sigma_u^+$ state is one or more of the excited atoms $X^*(^1P_1)$, $X^*(^3P_0)$, $X^*(^3P_1)$, and $X^*(^3P_2)$. The observed results presented in Figs. 3 and 4 indicate that X_2^* is produced in a three-body reaction involving X, X*, and M, where the rate constant is given by the slope in each figure. If two or more precursors are involved in the formation of X_2^*, the corresponding three-body reactions should have almost the same rate constant among different precursors. There might be a possibility that some collisional processes induce the degradation of higher excited atoms, *i.e.*, $X^*(^1P_1)$, $X^*(^3P_0)$, and $X^*(^3P_1)$ into $X^*(^3P_2)$, and the resulting excited atom $X^*(^3P_2)$ acts as a precursor in the formation of X_2^*. However, it seems difficult to reconcile such a complicated mechanism with the simple relations presented in Figs. 3 and 4, except for the extreme case that collisional processes proceed much more rapidly than the three-body formation process of X_2^*. The results (Fig. 1) are inconsistent with the extreme case. The excited diatomic molecule in the $1^3\Sigma_u^+$ state is correlated to $X^*(^3P_2)$ and $X(^1S_0)$ at an infinite nuclear distance in theoretical studies.[10,22-27] The molecule in the $1^1\Sigma_u^+$ state is correlated to $X^*(^3P_1)$ and $X(^1S_0)$. Further, the combination of $X^*(^1P_1)$ and $X(^1S_0)$ leads to molecules in other states and that of $X^*(^3P_0)$ and $X(^1S_0)$ leads to repulsive potentials. These studies suggest that the most probable precursor is $X^*(^3P_2)$. The other excited atoms do not contribute appreciably to the formation of $X_2^*(1^3\Sigma_u^+)$, although they might produce $X_2^*(1^1\Sigma_u^+)$ in a similar three-body reaction.

Table 1. Rate constants of three-body association reactions

Reaction	Rate constant/cm^6 s^{-1}	
$Kr^*+Kr+Ar\rightarrow Kr_2^*+Ar$	$(6.5\pm0.8)\times10^{-33}$	This work
$Xe^*+Xe+Ar\rightarrow Xe_2^*+Ar$	$(1.6\pm0.3)\times10^{-32}$	This work
	$(2.15\pm0.25)\times10^{-32}$	Ref. 21
	$(2.35\pm0.02)\times10^{-32}$	Ref. 20

Quenching Reactions of Excited Krypton Molecule. Excited diatomic molecules of rare gases are very reac-

tive with other molecules since they have large internal excitation energies. The energies are estimated to be 16.1 eV for Ne_2^*, 10.8 eV for Ar_2^*, 9.2 eV for Kr_2^*, and 7.7 eV for Xe_2^*. These values can be derived from the well depths of excited molecules in the $1^3\Sigma_u^+$ state and energy levels of excited atoms in $^3P_2$ states.[10,25,27,28] Rate constants of quenching reactions of He_2^*, Ne_2^*, and Ar_2^* by a number of simple gases were already determined using an absorption spectrophotometric technique.[11-13] However, those of Kr_2^* have been scarcely known in both absorption and emission studies.

The decay rate of Kr_2^* in pure krypton increases with increasing pressure of krypton (at low pressures). The apparent decay reflects the three-body association (similarly for the mixtures of argon and krypton). However, the decay becomes constant at pressures above 600 Torr. The radiative process now corresponds to the observed decay in the pressure region. This result is consistent with the previous one.[7] The rate was found to be 2.9×10^6 s^{-1}. In 800-Torr krypton, Kr_2^* is produced much more rapidly as compared with the radiative decay process. The addition of a small amount of quenchers into 800-Torr krypton enhanced the decay rate of Kr_2^*. Plots of decay rates against partial pressures of quenchers gave straight lines for the quenchers examined here. Table 2 tabulates the rate constants and cross-sections obtained with Xe, H_2, O_2, N_2, CO, and NO. The reactivities of Kr_2^* toward these gases are more or less similar to those of Ar_2^*; the rate constants are relatively small for H_2 and N_2 in both Kr_2^* and Ar_2^*.[11]

Table 2. Rate constants and cross sections of quenching reactions of $Kr_2^*(1^3\Sigma_u^+)$

Quencher	Rate constant 10^{-11} cm^3 s^{-1}	Cross section 10^{-2} nm^2
Xe	14±3	40±8
H_2	4.0±0.8	2.2±0.4
N_2	0.62±0.12	1.1±0.2
O_2	37±7	70±14
CO	12±2	21±4
NO	35±7	65±13

References

1) G. S. Hust and C. E. Klots, "Advances in Radiation Chemistry," ed by M. Burton and J. L. Magee, Wiley, New York (1976), Vol. 5, p. 1.
2) M. F. Golde, *Gas Kinet. Energy Transfer*, **2**, 123 (1977).
3) M. Krauss and F. H. Mies, "Excimer Lasers," ed by Ch. K. Rhodes, Springer-Verlag, New York (1979), p. 5; M. V. McCusker, *ibid.*, p. 47; Ch. A. Brau, *ibid.*, p. 87.
4) R. E. Huffman, Y. Tanaka, and J. C. Larrabee, *Appl. Opt.*, **2**, 617 (1963).
5) R. E. Huffman, J. C. Larrabee, and Y. Tanaka, *Appl. Opt.*, **4**, 1581 (1965).
6) S. Arai and R. F. Firestone, *J. Chem. Phys.*, **50**, 4575 (1969).
7) T. Oka, K. V. S. R. Rao, J. L. Redpath, and R. F. Firestone, *J. Chem. Phys.*, **61**, 4740 (1974).
8) S. Arai, T. Oka, M. Kogoma, and M. Imamura, *J. Chem. Phys.*, **68**, 4595 (1978).
9) K. Kasama, T. Oka, S. Arai, H. Kurusu, and Y. Hama, *J. Phys. Chem.*, **86**, 2035 (1982).
10) S. Iwata, *Chem. Phys.*, **37**, 251 (1979).
11) T. Oka, M. Kogoma, M. Imamura, S. Arai, and T. Watanabe, *J. Chem. Phys.*, **70**, 3384 (1979).
12) T. Doba and S. Arai, *J. Chem. Phys.*, **75**, 488 (1981).
13) S. Takao, M. Kogoma, T. Oka, M. Imamura, and S. Arai, *J. Chem. Phys.*, **73**, 148 (1980).
14) J. E. Velazco, J. H. Kolts, and D. W. Setser, *J. Chem. Phys.*, **69**, 4357 (1978).
15) R. S. F. Chang and D. W. Setser, *J. Chem. Phys.*, **69**, 3885 (1978).
16) J. N. Bardsley and M. A. Biondi, *Adv. At. Mol. Phys.*, **6**, 2 (1970).
17) L. Pages, E. Bertel, H. Joffre, and L. Sklavenitis, *Atomic Data*, **4**, 1 (1972).
18) T. Oka, *Res. Rep. Nagaoka Tech. Coll.*, **13**, 207 (1977).
19) J. W. Keto, R. E. Gleason, Jr., and G. K. Walters, *Phys. Rev. Lett.*, **33**, 1365 (1974).
20) J. K. Rice and A. W. Johnson, *J. Chem. Phys.*, **63**, 5235 (1975).
21) R. E. Gleason, T. D. Bonifield, J. W. Keto, and G. K. Walters, *J. Chem. Phys.*, **66**, 1589 (1977).
22) R. S. Mulliken, *J. Chem. Phys.*, **52**, 5170 (1970).
23) J. S. Cohen and B. Schneider, *J. Chem. Phys.*, **61**, 3230 (1974).
24) R. P. Saxon and B. Liu, *J. Chem. Phys.*, **64**, 3291 (1976).
25) F. Spiegelman and J. P. Malrieu, *Chem. Phys. Lett.*, **57**, 214 (1978).
26) W. C. Ermler, Y. S. Lee, K. S. Pitzer, and N. W. Winter, *J. Chem. Phys.*, **69**, 976 (1978).
27) O. Vallee, N. Tran Minh, and J. Chapelle, *J. Chem. Phys.*, **73**, 2784 (1980).
28) C. E. Moore, Selected Tables of Atomic Spectra; *Natl. Stand. Ref. Data Ser. Natl. Bur. Stand.*, **3**, Sec. 7 (1976).

 © 1984 The Chemical Society of Japan Bull. Chem. Soc. Jpn., 57, 3066—3069 (1984) [Vol. 57, No. 11

Photocatalytic Reactions of Azide Ions on Platinized Titanium Dioxide Powders in Solutions

Yoshio NOSAKA,* Yutaka ISHIZUKA, Kohji NORIMATSU, and Hajime MIYAMA
Department of Chemistry, The Technological University of Nagaoka, Kamitomioka, Nagaoka 949-54
(Received April 28, 1984)

Ammonia was formed photocatalytically from an aqueous solution of azide ion by using illuminated Pt/TiO_2 semiconductor powder. The reaction products, NH_3, N_2, and small amounts of N_2O and NO_3^-, were detected. Hydrogen, O_2 and N_2H_4 were not formed in the primary reaction products. From these results, together with photoelectrochemical measurements, a mechanism of the ammonia formation from azide ion and water is presented.

From the viewpoint of the chemical conversion of solar energy, much attention has been paid to the synthesis of ammonia from molecular nitrogen and water with the aid of light energy. Photocatalytic synthesis of ammonia from N_2 on illuminated semiconductors has been reported by several researchers.[1-5] Schrauzer and Guth[1] first reported the ammonia synthesis on moist iron doped TiO_2 powders. Miyama *et al.*[2] described the synthesis of ammonia from N_2 saturated water by using various kinds of semiconductors as photocatalysts. Recently, $SrTiO_3$ doped with RuO_2 and NiO has been used by Tamaru and coworkers.[5] Yoneyama *et al.*[6] described the formation of a considerable amount of ammonia from nitrogen monoxide instead of N_2. Nitrogenase, which is a well known catalyst for ammonia synthesis, catalyzes the ammonia production from N_3^- and other nitrogen compounds as well as from N_2.[7] Since N_3^-, which is a halogen-like ion, has an oxidized state between N_2 and NH_3, it may be expected to have some connection with intermediate spieces of the NH_3 synthesis from N_2. However, there has been no report for the photocatalytic reaction of aqueous azide ions. Therefore, we studied the photocatalytic ammonia synthesis from N_3^- aqueous solution and examined the reaction mechanism.

Experimental

The platinized TiO_2 used in the present study was prepared by the following procedure. Titanium dioxide powder (anatase, 99.95%, Kojundo Kagaku Co., Ltd.) was mixed with a platinum tetrachloride aqueous solution, dried and fired at 600 °C in flowing argon. Then, the powder was reduced in flowing hydrogen at 600 °C for 4 h. The catalysts were washed thoroughly with pure water. The 5%-platinized TiO_2 was used, unless otherwise stated. In a typical experiment, 0.2 g of catalyst and 10 cm^3 of 0.1 mol/dm^3 sodium azide solution was placed in a Pyrex vessel of 30 mm diameter, and the mixture was vigorously stirred throughout the reaction. Irradiation was performed with a 500 W high pressure mercury lamp focused through two water-filled round flasks. The temperature of the reaction mixture was about 43 °C. The catalyst in the reaction tube was removed with a centrifuge before the quantitative analysis of the products in the solution. The amount of ammonia was determined by measuring the absorbance at 640 nm after the reaction with Indophenol Blue. Hydrazine and NO_3^- were analysed from the absorbance at 458 nm and 410 nm with *p*-dimethylaminobenzaldehyde and brucine, respectively. The amount of unreacted N_3^- was determined as FeN_3^{2+} with 460-nm absorbance, which was formed by passing N_3H gas evolved by heating the acidified sample solution through a $Fe(NO_3)_3$ solution. Gaseous products were analyzed by gas chromatography with a thermal conductivity detector. A molecular sieve 5A column was used for the analysis of H_2, O_2, and N_2. For N_2O an active carbon column was used. The carrier gases were argon and helium for the analysis of H_2 and the other gases, respectively. Ammonia could not be detected by the columns used in the present study.

The TiO_2 film electrodes used for electrochemical measurements were prepared by painting $TiCl_4$ solution on polished titanium plate and firing at 500 °C. The platinization on the electrode was performed by a similar method described above for TiO_2 powder. The method of the electrochemical measurements is the same as described previously.[8]

Results

Table 1 summarizes a part of experimental results. Platinization of TiO_2 caused marked ammonia formation from N_3^-. The effect of platinization could be observed for the catalyst made by mixing in an agate mortar. The activity of the catalysts prepared by the impregnation method was comparable to those by the photodeposition method.[9] Accordingly, the impregnation method was used in further experiments because of the simplicity of the preparation. The reproducibil-

TABLE 1. RATE OF AMMONIA FORMATION[a]

Pt content wt%	Atmosphere	$NH_3/(\mu mol/h)$ light	$NH_3/(\mu mol/h)$ dark	Remarks
0	air	<0.01	<0.01	
1.0[b]	air	0.76	—	
3.0[b]	air	5.5	—	
5.0[b]	air	11.7	0.10	
5.0	air	0.17	—	Pt mixed
5.0	air	10.5	<0.01	Pt photodeposited
3.6	He	15.5	—	
5.0	He	31.0	—	
5.0	air	0.61	—	N_3^-: 100 μmol
5.0	air	<0.01		N_3^-: 10 μmol

a) Unless otherwise remarked, platinization of TiO_2 powder was done by the impregnation method, and 1 mmol N_3^-, 10 cm^3 water, and 0.2 g of catalysts were used. b) These catalysts were prepared in the same process.

ity in the activity measurements was within ±5% for the same catalysts. However, the activity of catalysts was different from preparation to preparation up to about 3 times. The maximum quantum yield obtained for the ammonia production was estimated to be about 0.5%. The effect of different compounded metals on the catalytic activity has been described already.[10] The activity of 1.0% platinized TiO_2 is much smaller than that of 3.0% or 5.0% platinized TiO_2. Sakata *et al.*[11] reported the effect of the platinum content on the photocatalytic activity for hydrogen evolution from alcohol and water. They have shown that the activity increases rapidly with the amount of platinum up to 0.05%, and the increase becomes gradual above this content. The difference in the dependence of the platinum content on the catalytic activity may be attributed to the difference in platinization method. The dependence on the platinum content is similar to that of the photoconductivity of Pt/TiO_2 powders prepared by the impregnation method.[12] One of the factors controlling the photoconductivity is the rate of recombination of photoinduced electron-hole pairs. Therefore, the present result suggests that the rate of the decomposition of N_3^- is determined by the separation of the photoinduced electron-hole pairs, as has been proposed in the previous paper.[10]

When the reaction mixture had been deaerated, the rate of ammonia formation increased to three times that for the aerated conditions. This indicates that reduction of N_3^- competes with that of O_2 in the air. In order to clarify this observation, photocatalytic reaction was performed in various atmospheres with the same Pt/TiO_2 catalyst. The product yields are shown in Table 2 and the growth features of gaseous products are shown in Fig. 1. In the He atmosphere, N_2O was formed gradually with irradiation time. When the reactant mixture was bubbled with O_2 gas thoroughly, the amount of ammonia formed was very low. In this case, a large amount of N_2O was formed. In a N_2O atmosphere, the N_2 yield did not increase, although the ammonia yield was greater than that in the O_2 atmosphere, indicating that N_2O formed in the reaction with O_2 was not responsible for the decrease in the ammonia yield. Under any reaction conditions, O_2 and H_2 were not detected as a primary product. After the mitigation of the evolution of N_2, molecular hydrogen was observed in the He atmosphere. Since aqueous ammonia is known to be decomposed into N_2 and H_2 with photocatalysts,[5] the delayed formation of H_2 is attributed to the decomposition of the ammonia produced. The amount of remaining N_3^- was measured at the end of the growth of N_2 in the reaction under He atmosphere. The amount of N_3^- was 100 μmol when 1240 μmol of N_2 and 180 μmol of ammonia had been

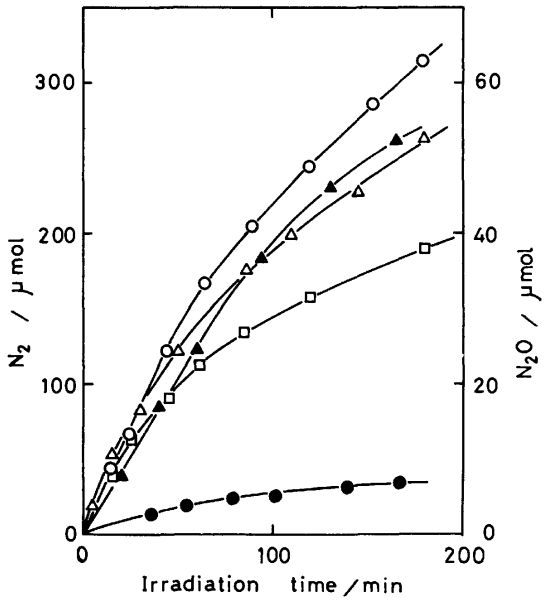

Fig. 1. The formation of N_2 (○, △, and □) and N_2O (● and ▲) as a function of the irradiation time in various atmospheric conditions; He (○ and ●), O_2 (△ and ▲), and N_2O (□).

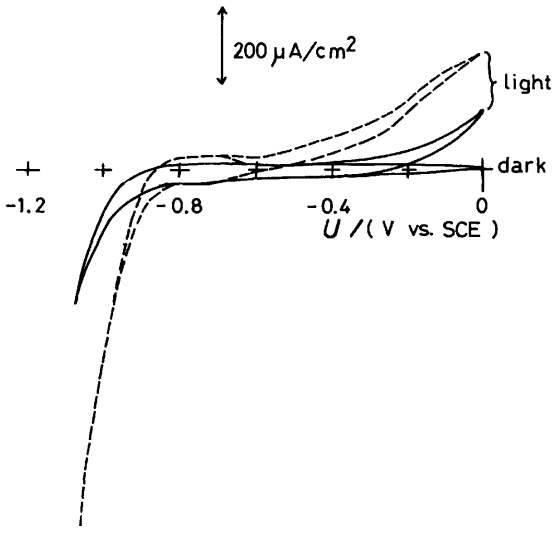

Fig. 2. Current-potential curves obtained for a Pt/TiO_2 polycrystalline electrode with and without illumination. Electrolyte; ----: 0.1 mol/dm³ NaN_3, ——: 0.05 mol/dm³ Na_2SO_4+KOH (pH 8.4).

Table 2. Yield of products for the reactions in various atmospheres[a)]

Atmosphere[b)]	NH_3/μmol	N_2/μmol	N_2O/μmol	O_2/μmol	H_2/μmol
He	80	324	6.7	0.0	0.0
O_2	2.0	278	53	—	0.0
N_2O	12	190	—	0.0	0.0

a) Solutions containing 1 mmol of N_3^- and 0.2 g of 5%-platinized TiO_2 powder in 10 cm³ of water were irradiated for 3 h. b) Thoroughly bubbled and saturated with these gases.

produced. Since the initial amount of N_3^- has been 1 mmol, this result suggests that all of the consumed N_3^- turned into ammonia or N_2. For confirmation, the by-products possibly formed in the solutions were analyzed. Hydrazine was not detected to a sensitivity of about 0.01 μmol, and the amount of NO_3^- was less than 0.5 μmol. Under the aerated conditions, these nitrogen compounds were not increased.

In order to clarify the mechanism of the photocatalytic reaction, electrode reactions were measured with a platinized TiO_2 polycrystalline film electrode. For aqueous solutions of 0.1 mol/dm^3 NaN_3 and 0.05 mol/dm^3 Na_2SO_4, current-potential curves were measured and some of them are shown in Fig. 2. The pH value of sulfate solution had been adjusted to that of azide solution (pH 8.4) by the addition of a small amount of KOH. A reduction current accompanied by the evolution of a gas was observed at less cathodic potential in the presence of N_3^-. After the reduction with the Pt/TiO_2 electrode, ammonia was detected in the solution. The gas evolved was determined to be nitrogen by a separate experiment using a platinum electrode. By the irradiation on the Pt/TiO_2 electrode, the feature of the reduction current was almost unchanged. On the other hand, at anodic potentials photoinduced oxidation currents were observed for both of the solutions. In the presence of N_3^-, the photocurrent appeared at less anodic potential, indicating that N_3^- is more easily oxidized than OH^- at TiO_2 surface. This experimental result is consistent with the report for the oxidation of N_3^- on platinum electrodes.[13]

Discussion

Bard has pointed out that an illuminated platinized TiO_2 powder works as a microelectrode.[14] Consequently, the surface reactions on the photocatalyst are predicted by those of cathodic and anodic processes observed in the photoelectrochemical measurements. In the present study, the current-potential curves in Fig. 2 show that N_3^- is oxidized before the oxidation of OH^-. The oxidation potential of N_3^- on a platinum electrode is 0.78 V (*vs.* SCE).[13] The azide radical, $N_3\cdot$, formed by the oxidation of N_3^- becomes, instantly, the dimer, $(N_3)_2$, followed by the evolution of N_2.[13] Therefore, at the oxidation site on the photocatalysts the following reaction is expected to occur.

$$2N_3^- \longrightarrow 3N_2 + 2e^- \quad (1)$$

On the other hand, the reduction of N_3^- aqueous solution on solid electrodes has not been reported. However, Fig. 2 shows that N_3^- is reduced before the formation of H_2. Since the formation of adsorbed hydrogen atoms precedes the evolution of H_2, the hydrogen atoms seem to react with N_3^-. The reductive decomposition may occur in succession as indicated by the current-potential curve having no shoulder. As mentioned above, the evolution of N_2 gas was observed during the electrode reduction, then the reduction of N_3^- accompanied by the reaction with water may be expressed by Eq. 2;

$$N_3^- + 3H_2O + 2e^- \rightarrow NH_3 + N_2 + 3OH^-. \quad (2)$$

The standard potential for the electrode reduction of N_3H was reported to be 1.82 V (*vs.* NHE) in acidic solution,[15] so that of Eq. 2 can be estimated as 0.97 V at pH 8.4. At this pH, the standard potential for the reduction of water is −0.50 V. Therefore, from a thermodynamical view point, Eq. 2 is more likely to occur than the reduction of water.

The total stoichiometric equation for the photocatalytic reaction of N_3^- and water should be expressed by the combination of Eqs. 1 and 2; *viz.*,

$$3N_3^- + 3H_2O \longrightarrow NH_3 + 4N_2 + 3OH^-. \quad (3)$$

This equation is consistent with the present experimental results that the formation of ammonia involves N_2 gas evolution and that N_2 has not been detected for the undoped TiO_2 photocatlyst which did not yield ammonia. This stoichiometric equation implies that the ratio of the products $N_2 : NH_3$ is to be 4:1. The experimental result in Table 2 shows that the amount of ammonia formed was really about a quarter of that of N_2 in the early stage of the reaction. However, in the later stage, the amount of ammonia was smaller than that of stoichiometry. This may be attributed to the decomposition of produced ammonia into N_2 and H_2, as mentioned above.

In the helium atmosphere, N_2O was the major by-product. The formation of N_2O from N_3^- aqueous solution was studied by the method of radiolysis.[16] As a reaction intermediate, the presence of HNO, which gives $H_2N_2O_2$ followed by the formation of N_2O, has been assumed. When this assumption is adopted in the present system, the intermediate HNO may arise from N_3OH^- which is formed from $N_3\cdot$ and OH^-. The formation of N_3OH^- is probable,[17] because N_3^- is known to behave in chemical properties like halogen ions.[15] Since the yield of N_2O was very low, it is also probable that the oxygen of N_2O may originate from the possible absorbed oxygen on the catalysts.

In the oxygen atmopsphere, the NH_3 yield was very low while N_2O was formed largely. This indicates that at the reduction site the reactions of Eqs. 4 and 5 may happen instead of Eq. 2.

$$O_2 + H^+ + e^- \longrightarrow HO_2\cdot \quad (4)$$

$$2HO_2\cdot \longrightarrow H_2O_2 + O_2 \quad (5)$$

The hydrogen peroxide may produce N_2O by the following exothermic reactions[16];

$$H_2O_2 + N_3^- \longrightarrow HNO + N_2 + OH^- \quad (6)$$

$$2HNO \longrightarrow N_2O + H_2O. \quad (7)$$

Since N_2O is considered to be formed through some intermediates, there must be a delay for the formation of N_2O. Fig. 1 shows that the formation of N_2O delays from that of N_2. This reaction mechanism for N_2O formation predicts that the product ratio of $N_2 : N_2O$ is 8:1. The observed ratio was, however, nearly equal to 5:1. Then, another process such as the reaction of $N_3\cdot$ radical with O_2 at the oxidation site may be taken into account.

Since the standard free energy change for Eq. 3 is negative, the photocatalytic ammonia production *via*

azide ion is not suitable for storage of solar energy. Further investigation concerning the mechanism of the formation of ammonia may provide a clue to improving the yield of ammonia synthesis from N_2 and water.

This work was supported in partly as Grants-in-Aid for Scientific Research (No. 57045043 and 58045056) from the Ministry of Education, Science and Culture.

References

1) G. N. Schrauzer and T. D. Guth, *J. Am. Chem. Soc.*, **99**, 7189 (1977).
2) H. Miyama, N. Fujii, and Y. Nagae, *Chem. Phys. Lett*, **74**, 523 (1980).
3) F. Khan, P. L. Yue, L. Rizzuti, V. Augugliaro, and M. Schiavello, *J. Chem. Soc., Chem. Commun.*, **1981**, 1049.
4) P. P. Radford and C. G. Francis, *J. Chem. Soc., Chem. Commun.*, **1983**, 1520.
5) Q. Li, K. Domen, S. Naito, T. Onishi, and K. Tamaru, *Chem. Lett.*, **1983**, 321.
6) M. Yoneyama, H. Shiota, and H. Tamura, *Bull. Chem. Soc. Jpn.*, **54**, 1308 (1981).
7) R. W. F. Hardy, R. C. Burns, and G. W. Parshall, *Adv. Chem. Ser.*, **100**, 219 (1971).
8) Y. Nosaka, H. Sasaki, K. Norimatsu, and H. Miyama, *Chem. Phys. Lett.*, **105**, 456 (1984).
9) B. Kreutler and A. J. Bard, *J. Am. Chem. Soc.*, **100**, 4317 (1978).
10) Y. Nosaka, K. Norimatsu, and H. Miyama, *Chem. Phys. Lett.*, **106**, 128 (1984).
11) T. Sakata, T. Kawai, and K. Hashimoto, *Chem. Phys. Lett.*, **88**, 50 (1982).
12) J. Disdier, J. M. Hermann, P. Pichat, *J. Chem. Soc., Faraday Trans. 1*, **79**, 651 (1983).
13) V. Plzak and H. Wendt, *Ber. Bunsenges. Phys. Chem.*, **83**, 481 (1979).
14) A. J. Bard, *J. Photochem.*, **10**, 59 (1979).
15) K. Jones, "Comprehensive Inorganic Chemistry," ed by J. C. Bailar Jr., H. J. Emeleus, R. Nyholm, and A. F. Trotman-Dickenson, Pergamon, Oxford (1973), Vol. 2.
16) P. Kelly and M. Smith, *J. Chem. Soc.*, **1961**, 1479.
17) A. Singh, G. W. Koroll, and R. B. Cundall, *Radiat. Phys. Chem.*, **19**, 137 (1982).
18) G. Munuera, A. R. Gonzalez-Elipe, J. Soria, and J. Sanz, *J. Chem. Soc., Faraday Trans. 1*, **76**, 1535 (1980).

The Crystal Structure of 3-(Adenin-9-yl)-*N*-(2-succinimidyl)-propionamide and Hydrogen Bonding Scheme of Anticonvulsant Drugs with Adenine

Midori TAKIMOTO, Akio TAKENAKA, and Yoshio SASADA*
Laboratory of Chemistry for Natural Products, Tokyo Institute of Technology, Nagatsuta, Midori-ku, Yokohama 227
(Received May 28, 1984)

3-(Adenin-9-yl)-*N*-(2-succinimidyl)propionamide† has been synthesized as a model for studying the interaction between cyclic ureide and adenine, and its crystal structure examined. The crystals are monoclinic, the space group $P2_1/c$, with unit-cell dimensions of a=10.861(1), b=12.766(1), c=9.753(1) Å, β=91.10(1)°, and Z=4. The ureide moiety is hydrogen bonded to adenine with NH···N(1) (2.903(3) Å) and O···HN(6) (2.955(3) Å). A comparison of the hydrogen bonding patterns of the related compounds with adenine suggests that cyclic ureide anticonvulsant drugs possess the capability of interacting with N(1) and N(6) sites of adenine.

Many compounds containing cyclic ureide skeleton, such as barbiturate, hydantoin and succinimide derivatives, have been used extensively as anticonvulsant and antiepileptic drugs.[1] It is known that barbiturate/hydantoin derivatives form stronger hydrogen bonds with adenine than the other nucleic acid bases.[2] This is an interesting observation because it is suspected that some adenine-related complexes play a role in nerve transmission.[3]

To understand the structural aspects of their interaction, we have synthesized 3-(adenin-9-yl)-*N*-(2-succinimidyl)propionamide as a model and determined its crystal structure.

Experimental and Structure Determination

3-(Adenin-9-yl)propionic acid (**1**) was prepared by the method reported by Kondo, Miyata, and Takemoto[4] and DL-asparagine methyl ester hydrochloride (**2**) was derived from DL-asparagine. The condensation of **1** and **2** by dicyclohexylcarbodiimide method gave *N*-[3-(adenin-9-yl)propionyl]-DL-asparagine methyl ester, and the product was spontaneously converted into 3-(adenin-9-yl)-*N*-(2-succinimidyl)propionamide in a methanol solution saturated with ammonia.

Colourless plate crystals were obtained from an aqueous solution. Density was measured by flotation in a mixture of cyclohexane and carbon tetrachloride. A crystal, 0.35×0.35×0.1 mm³ in size, was mounted on a Rigaku automated four-circle diffractometer. Nickel-filtered Cu $K\alpha$ radiation (λ=1.54184 Å) was used. The accurate unit-cell dimensions were derived from the 2θ values of 34 high-angle reflexions. Crystallographic data are summarized in Table 1. Intensities were measured on the diffractometer by means of ω scanning ($2°<2\theta<125°$), the scan speed being 4°/min and scan width 1.2° plus α_1–α_2 divergence. Five reference reflexions monitored periodically showed no significant intensity deterioration. Corrections were made for Lorentz and polarization factors, but not for absorption effects. A total of 2153 independent reflexions were obtained, 378 of which had no net intensities; the observational threshold value, F_{lim}, was 1.96. The standard deviations were estimated by the equations $\sigma^2(F_o)=\sigma_P^2(F_o)+qF_o^2$, where $\sigma_P(F_o)$ was evaluated by counting statistics and q(1.22×10^{-5}) was derived from the variations of the monitored reflexions.

TABLE 1. CRYSTAL DATA FOR 3-(ADENIN-9-YL)-*N*-(2-SUCCINIMIDYL)PROPIONAMIDE

Chemical formula: $C_{12}H_{13}N_7O_3$	
Space group: $P2_1/c$	
a/Å=10.861(1)	V/Å³=1683.5(1)
b/Å=12.766(1)	Z=4
c/Å=9.753(1)	D_m/g cm^{-3}=1.49
β/°=91.10(1)	D_x/g cm^{-3}=1.490

† 2-Succinimidyl=2,5-dioxo-3-pyrrolidinyl

The structure was solved by the direct method using MULTAN 78 programme[5] and the atomic parameters were refined by the full-matrix least-squares method. The quantity minimized was $\sum\omega(|F_o|-|F_c|)^2$, where $\omega=1/\sigma^2(F_o)$. In the refinement, the zero-reflexions with $|F_c|>F_{lim}$ were included by assuming $F_o=F_{lim}$ and $\omega=\omega(F_{lim})$. All the hydrogen atoms were found on a difference map and included in the refinement.

The final R value was 0.059 for 1875 reflexions with $|F_o|>3\sigma(F_o)$; the maximum shift of parameters in the last cycle was 0.1σ for C, N, O, and 0.3σ for H. Atomic scattering factors were taken from Ref. 6. The atomic parameters of the non-hydrogen atoms are listed in Table 2.[7]

Results and Discussion

Molecular Structure. Figure 1 shows a stereoscopic view of 3-(adenin-9-yl)-*N*-(2-succinimidyl)propionamide molecule. Bond lengths and angles are shown in Fig. 2.

The dimensions of the adenine moiety are in good agreement with those found in 9-methyladenine,[8] 3-(adenine-9-yl)propionamide[9] and 3-(adenin-9-yl)propionic acid.[10] The adenine moiety is planar with maximum displacement of 0.016 Å for N(9) from the least-squares plane. The bond lengths and angles of the succinimide moiety are similar to those found in 2-(3-bromo-4-ethoxyphenyl)succinimide.[11] The succinimide moiety has a half-chair form; the value of P defined by Pitzer and Dorath[12] is −13.3°, which is between those of E_2 and ${}_1T_2$. The deviations of C(15) and C(16) from the plane [C(17), N(18), C(19)] are 0.150 Å and −0.083 Å, respectively. This conformation is different from the envelope form of 2-(3-bromo-4-ethoxyphenyl)succinimide. The dihedral angle between two amide planes [C(19), O(19), N(18)] and [C(17), O(17), N(18)] is 5.7°.

As shown in Fig. 1, the molecule is extended; torsion

angles, N(9)-C(11)-C(12)-C(13) and C(11)-C(12)-C(13)-N(13) are 69.5° and −149.5°, respectively. The conformation is similar to that found in the complex 3-(adenin-9-yl)propionamide : 1-methylthymine dihydrate[13] and 3-(adenin-7-yl)propionamide monohydrate.[14] The dihedral angle between the adenine and the mean plane of succinimide moiety (C(15), C(16), C(17), O(17), N(18), C(19), O(19)) is 6.2(1)°.

TABLE 2. FRACTIONAL COORDINATES AND EQUIVALENT ISOTROPIC TEMPERATURE FACTORS OF THE NON-HYDROGEN ATOMS IN 3-(ADENIN-9-YL)-*N*-(2-SUCCINIMIDYL)PROPIONAMIDE

Atom	*x*	*y*	*z*	*B*/Å²
N (1)	0.8782 (2)	0.3078 (2)	0.3446 (3)	2.9⟨10⟩
C (2)	0.9222 (3)	0.3974 (2)	0.2916 (4)	3.4⟨13⟩
N (3)	1.0051 (2)	0.4102 (2)	0.1940 (3)	3.2⟨12⟩
C (4)	1.0454 (3)	0.3171 (2)	0.1478 (3)	2.6⟨5⟩
C (5)	1.0107 (3)	0.2194 (2)	0.1935 (3)	2.5⟨4⟩
C (6)	0.9226 (3)	0.2160 (2)	0.2955 (3)	2.6⟨8⟩
N (6)	0.8799 (3)	0.1266 (2)	0.3494 (3)	3.2⟨15⟩
N (7)	1.0728 (2)	0.1418 (2)	0.1249 (3)	3.2⟨9⟩
C (8)	1.1426 (3)	0.1926 (2)	0.0392 (3)	3.2⟨8⟩
N (9)	1.1295 (2)	0.3005 (2)	0.0480 (2)	2.7⟨7⟩
C (11)	1.2000 (3)	0.3806 (2)	−0.0248 (3)	3.0⟨7⟩
C (12)	1.3096 (3)	0.4157 (2)	0.0628 (4)	3.0⟨8⟩
C (13)	1.4045 (3)	0.3295 (2)	0.0753 (3)	2.9⟨6⟩
O (13)	1.4321 (2)	0.2750 (2)	−0.0233 (2)	3.5⟨9⟩
N (14)	1.4604 (2)	0.3174 (2)	0.1977 (3)	3.1⟨8⟩
C (15)	1.5612 (3)	0.2446 (3)	0.2131 (3)	3.2⟨7⟩
C (16)	1.5306 (3)	0.1267 (3)	0.1994 (4)	3.7⟨15⟩
C (17)	1.6315 (3)	0.0833 (3)	0.1116 (3)	3.7⟨5⟩
O (17)	1.6519 (2)	−0.0086 (2)	0.0884 (2)	4.9⟨19⟩
N (18)	1.6973 (2)	0.1665 (2)	0.0572 (3)	3.2⟨8⟩
C (19)	1.6574 (3)	0.2628 (3)	0.1038 (3)	3.1⟨6⟩
O (19)	1.6951 (2)	0.3466 (2)	0.0651 (2)	3.9⟨13⟩

The equivalent isotropic temperature factors are calculated from anisotropic thermal parameters using the equation $B=8\pi^2(U_1+U_2+U_3)/3$, where U_1, U_2, and U_3 are principal components of the mean square displacement matrix U. Values in ⟨ ⟩ are anisotropicity defined by $(\Sigma(B-8\pi^2U_i)/3)^{1/2}$ and those in ( ) are e.s.d.'s; they refer to the last decimal places.

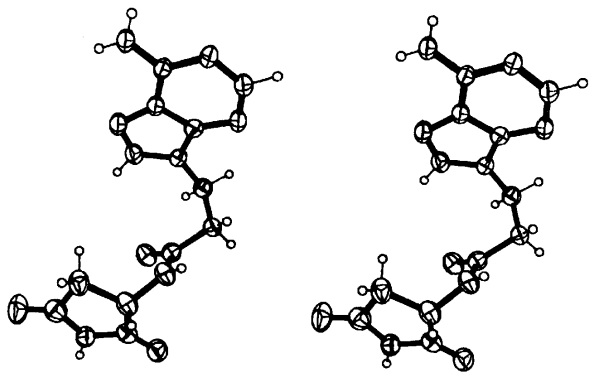

Fig. 1. Stereoscopic view of 3-(adenin-9-yl)-*N*-(2-succinimidyl)propionamide with 50% probability ellipsoids.

Crystal Structure. The crystal structure viewed along the b axis is shown in Fig. 3. The geometries of hydrogen bonds are given in Table 3. The succinimide moiety is linked to the adenine moiety at (1+*x*, 1/2−*y*, 1/2+*z*) by the hydrogen bonds, N(18)H···N(1) and O(19)···HN(6). The dihedral angle between the least-squares planes of these two moieties is 5.2(1)°. These and the N(6)H···N(3) hydrogen bonds between the molecules related by the two-fold screw make sheets parallel to (101) as shown in Fig. 4.

Another hydrogen bond N(14)H···O(13) between peptide groups links the sheets together. This N(14)H seems to make a bifurcated hydrogen bond, though the N(14)H···O(17) distance is rather long (3.297(4) Å).

The adenine moieties related by the c glide are stacked on each other at the distance of 3.558(5) Å for C(2)···C(8) and 3.412(4) Å for N(1)···C(8). Another closest contact is 3.456(4) Å between C(6) at (*x*, *y*, *z*) and C(8) at (−1+*x*, *y*, *z*).

Interaction between Cyclic Ureide and Adenine. Figure 5 shows the hydrogen bonding patterns found

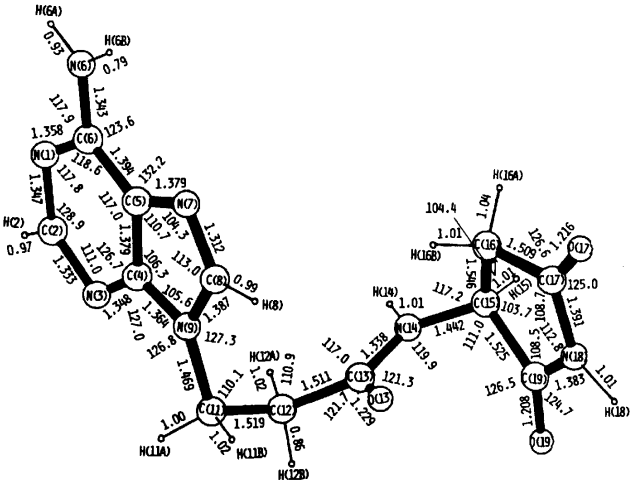

Fig. 2. Atomic numbering and bond lengths (*l*/Å) and angles (*φ*/°) in 3-(adenin-9-yl)-*N*-(2-succinimidyl)-propionamide. E.s.d.'s for bond lengths and angles are 0.004–0.005 Å and 0.3°, respectively.

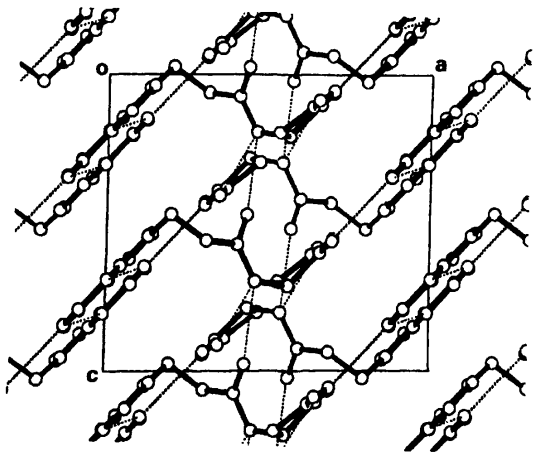

Fig. 3. Crystal structure of 3-(adenin-9-yl)-*N*-(2-succinimidyl)propionamide projected along the b axis.

in the adenine complexes with several cyclic ureide derivatives. Barbiturates interact with adenine through the two kinds of double hydrogen bonds; type 1 is a combination of NH···N(1) and O···HN(6) and type 2 is NH···N(7) and O···HN(6).[15,16] The present crystal exhibits the hydrogen bonds of type 1, while the scheme in parabanic acid with a similar cyclic ureide skeleton is type 2.[17] Recently it has been reported that 2-thiohydantoin interacts with adenine at the N(3) or N(7) site.[18]

In order to examine the preferential hydrogen bonding sites of adenine, the formation energies of possible complexes were calculated by CNDO/2 approximation[19] (Table 4). The formation energies with barbi-

Table 3. Hydrogen bonds in 3-(adenine-9-yl)-*N*-(2-succinimidyl)propionamide

E.s.d.'s are given in parentheses referring to the last decimal places.

X-H···Y	X···Y(*l*/Å)	XHY(*φ*/°)
N(6)-H(6A)···O(19)[i]	2.955(3)	172(2)
N(6)-H(6B)···N(3)[ii]	3.064(4)	170(3)
N(14)-H(14)···O(13)[iii]	2.986(3)	114(2)
N(14)-H(14)···O(17)[iv]	3.297(4)	156(3)
N(18)-H(18)···N(1)[v]	2.903(3)	165(3)

Symmetry codes:

i) $-1+x, \frac{1}{2}-y, \frac{1}{2}+z$ iv) $3-x, \frac{1}{2}+y, \frac{1}{2}-z$

ii) $2-x, -\frac{1}{2}+y, \frac{1}{2}-z$ v) $1+x, \frac{1}{2}-y, \frac{1}{2}+z$

iii) $x, \frac{1}{2}-y, \frac{1}{2}+z$

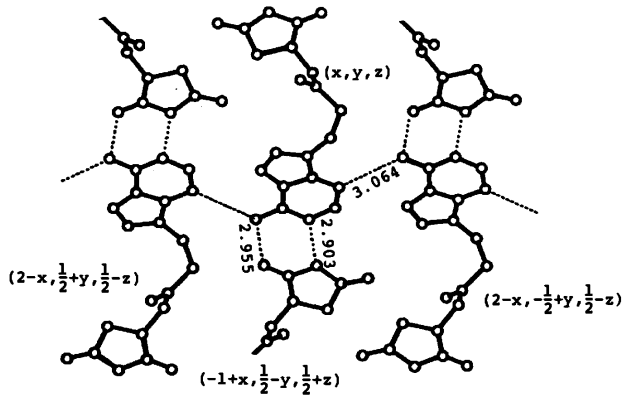

Fig. 4. Hydrogen bonds in the molecular sheet of 3-(adenin-9-yl)-*N*-(2-succinimidyl)propionamide.

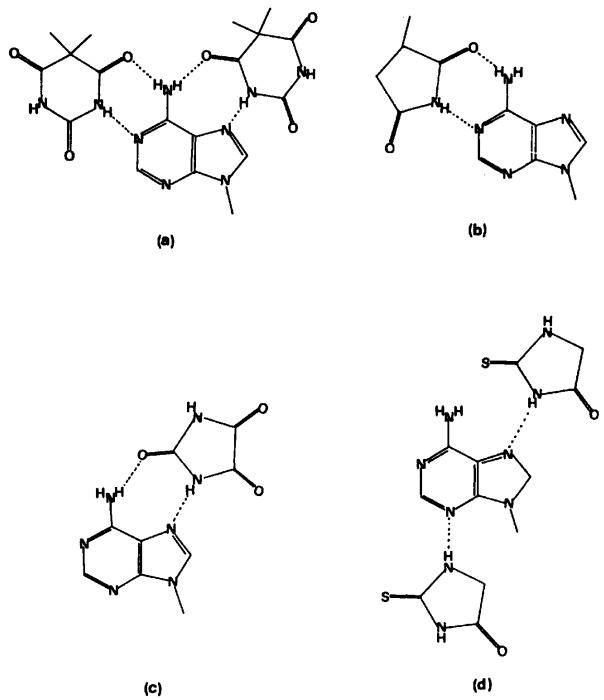

Fig. 5. The hydrogen bonding patterns of (a) adenine-barbiturate[15,16] (b) adenine-succinimide (the present study), (c) adenine-parabanic acid[17] and (d) adenine-2-thiohydantion[18].

Table 4. The difference in formation energy (ΔE/kcal mol^{-1}) between type 1 and type 2 of some cyclic ureides and 9-methyladenine by CNDO/2 calculation

Type 1 is a combination of NH···N(1) and O···NH(6) and type 2 is NH···N(7) and O···NH(6). 1 cal=4.186 J.

	Barbiturate	Parabanic acid	2-Methylsuccinimide
E(Type 2)-*E*(Type 1)	+0.2	−1.6(I) −2.0(I')	−0.4

In the calculation, hydrogen bond geometries are taken from Ref. 15, Ref. 17, and the present study. Type 1 of parabanic acid (two modes, I and I') and type 2 of 2-methylsuccinimide are hypothetical structures.

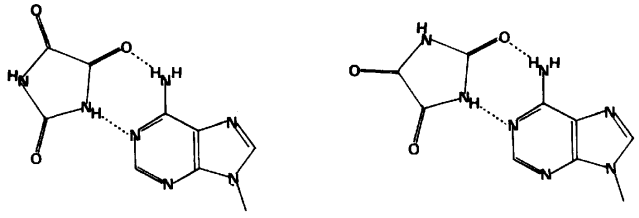

(I) (I')

turate are almost the same for the two types of hydrogen bonding. In the case of the parabanic acid, however, the type 1 is distinctly less stable than the type 2. These results are consistent with the hydrogen bonding patterns found in the respective crystals, suggesting that the hydrogen bonding scheme in model crystals comes from the inherent nature of the components. In the present combination of adenine and succinimide, there is no significant difference in formation energy so that the other type (type 2) would be found if the crystallizing condition is adjusted suitably.

While barbiturate and succinimide derivatives have anti-convulsant effect, parabanic acid and 2-thiohydantoin containing similar molecular skeleton do not exhibit such effect.[1] Activity and inactivity seem to be associated with the different hydrogen bonding patterns; that is cyclic ureide anticonvulsant drugs possess the capability of interacting with N(1) and N(6) sites of adenine.

Recently, it has been reported that diphenyl hydantoin and pentobarbital inhibit the protein synthesis in rat brain.[20-22] This side effect can be explained by the argument that they might interact with adenine at N(1) and N(6), which are the sites forming the Watson-Crick base pair.

The present work was partially supported by a Grant-in-Aid for Fundamental Scientific Research from the Japan Society for the Promotion of Science (M. T).

References

1) J. A. Vida and E. H. Gerry, "Medical Chemistry," ed by J. A. Vida, Academic Press, New York (1977), Vol. 15, p. 151.
2) Y. Kyogoku, R. C. Lord, and A. Rich, *Nature (London)*, **218**, 69 (1968).
3) a) A. Sattin and J. W. Rall, *Mol. Pharmacol.*, **6**, 13 (1970); b) G. Burnstock, "Physiological and regulatory function of adenosine and adenine nucleotide," ed by H. P. Baer and G. I. Drummond, Raven Press, New York (1979), p. 3.
4) K. Kondo, M. Miyata, and K. Takemoto, *Bull. Chem. Soc. Jpn.*, **44**, 2554 (1971).
5) P. Main, S. E. Hull, L. Lessinger, G. Germain, J-P. P. Declercq, and M. M. Woolfson, "MULTAN 78. A System of Computer Programs for the Automatic Solution of Crystal Structure from X-Ray Diffraction Data." Univ. of York, England, and Louvain, Bergium (1978).
6) "International Tables for X-ray Crystallography," Kynoch Press, Birmingham, Vol. 4, p. 71 (1974).
7) Lists of structure factors, anisotropic thermal parameters of C, N, and O atoms, atomic parameters of H atom, bond lengths and angles including H atoms and the least-squares planes for the adenine, succinimide and peptide moieties have been deposited as Document No. 8449 at the office of Chemical Society of Japan.
8) J. J. Kistenmacher and M. Ross, *Acta Crystallogr., Sect. B*, **33**, 253 (1977).
9) M. Takimoto, A. Takenaka, and Y. Sasada, *Bull. Chem. Soc. Jpn.*, **54**, 1635 (1981).
10) A. Takenaka and Y. Sasada, 38th Meeting of the Chemical Society of Japan, Abst. p. 1006 (1978).
11) A. A. Karapetyan, V. G. Andrianov, and Y. T. Struchkov, *Cryst. Struct. Commun.*, **9**, 417 (1980).
12) K. S. Pitzer and W. E. Donath, *J. Am. Chem. Soc.*, **81**, 3213 (1959).
13) M. Takimoto, A. Tekenaka, and Y. Sasada, *Bull. Chem. Soc. Jpn.*, **55**, 2734 (1982).
14) M. Takimoto, A. Tekenaka, and Y. Sasada, *Acta Crystallogr., Sect. C*, **39**, 73 (1983).
15) D. Voet, *J. Am. Chem. Soc.*, **94**., 8213 (1972).
16) D. Voet and A. Rich, *J. Am. Chem. Soc.*, **94**, 5888 (1972).
17) H-S. Shieh and D. Voet. *Acta Crystallogr., Sect. B*, **32**, 2361 (1976).
18) R. E. Cassady and S. W. Hawkianson, *Acta Crystallogr., Sect. B*, **38**, 2206 (1982).
19) J. A. Pople and G. A. Segal, *J. Chem. Phys.*, **44**, 3289 (1966).
20) J. Fontenot, *Subst. Alcohol Actions*, **2**, 249 (1981).
21) J. Fontenot, *Diss. Abstr. Int.*, **42**, 3648-B (1982).
22) T. Yanagihara and A. Henberger, *Exp. Neurol.*, **31**, 87 (1971).

 © 1984 The Chemical Society of Japan Bull. Chem. Soc. Jpn., 57, 3074—3076 (1984) [Vol. 57, No. 11

Acid Dissociation Constants of Alkyl Xanthic Acids and Formation Constants of Cadmium(II) and Zinc(II) Xanthato Complexes in 1:1 v/v H_2O-DMF Medium

Kenjiro HAYASHI,* Yoshiaki SASAKI, Shigehiro INOMATA, and Takagimi YANAGIDANI
Department of Chemistry, Faculty of Science, Yamaguchi University, Yoshida, Yamaguchi-shi 753
(Received December 27, 1983)

The overall formation constants, β_3, of cadmium(II) and zinc(II) complexes with alkyl xanthates (*O*-alkyl dithiocarbonates) were determined by polarography in the 1:1 v/v water-*N*,*N*-dimethylformamide mixture. The values of these constants increase in the order, methyl<ethyl<propyl<butyl<2-methylpropyl<1-methylethyl xanthate. This order agrees entirely with the order of the basicity of alkyl xanthates determined by using the kinetic parameter of the acid decomposition of xanthates.

Alkyl xanthates (*O*-alkyl dithiocarbonates, $ROC(S)S^-$, abbreviated as X^-) have been used as chelating reagents for the solvent extraction of metal ion.[1] However, the thermodynamical property of the metal xanthato complexes has not yet become clear sufficiently.

The present authors have studied the solvent extraction of several metal xanthato complexes, and reported the compositions and the formation constants of the extracted complexes.[2-5] Furthermore, the water-soluble complexes having a formula MX_3^- or MX_4^{2-} ($M=Cd^{2+}$, Zn^{2+}) were found to be formed only with methyl and ethyl xanthates in the presence of a large excess of xanthate[6,10].

All the cadmium(II) and zinc(II) xanthato complexes formed in the water-*N*,*N*-dimethylformamide(DMF) mixture were soluble in this mixture. Therefore, the compositions and the stability constants of these soluble complexes were determined by polarography. The apparent acid dissociation constants of alkyl xanthic acids (*O*-alkyl dithiocarbonic acids, HX) in the same medium were also determined, and the effect of the basicity of the ligand on the stability of the complex was studied.

Experimental

Reagents. Potassium salts of alkyl xanthates were synthesized from corresponding alkanols, carbon disulfide, and potassium hydroxide as described previously.[6] The solutions of xanthates were prepared immediately before use.

The stock solutions (0.02 mol dm^{-3}) of cadmium(II) and zinc(II) were prepared by dissolving each nitrate salt in 0.1 mol dm^{-3} nitric acid. These solutions were standardized volumetrically with EDTA.

Apparatus and Procedures. (1) The decomposition rate of xanthate in the 1:1 v/v water-DMF medium was measured spectrophotometrically at 305 nm which is an absorption maximum wavelength of xanthate on a Hitachi Model 139 spectrophotometer (for moderate decomposition) and a Union Giken Model RA-401 stopped-flow spectrophotometer (for fast decomposition). Each cell chamber was thermostated at 25 °C with a water jacket. The ionic strength of test solutions was kept at 0.4 mol dm^{-3} with potassium chloride (the use of nitrate salt was unfavorable because of the absorption of light in ultraviolet region and the oxidation of the xanthates in an acid solution). The pH of the solutions was controlled by using the potassium acetate-hydrochloric acid buffer solution.

(2) Direct current polarographic waves were recorded with a Yanaco Model P8 polarograph using a three-electrodes format with mercury as an auxiliary electrode and saturated calomel electrode as a reference electrode. The dropping mercury electrode used had an m value of 1.18 mg s^{-1} and a drop time of 5.67 s at open circuit at a height of mercury reservoir of 69.0 cm. All polarographic measurements were made in the 1:1 v/v water-DMF medium containing 5×10^{-4} mol dm^{-3} metal ion, proper amount of xanthate, and 0.002% Triton X-100 as a maximum suppressor at 25.0±0.2 °C under the air-free condition. The ionic strength of the test solutions was made 0.4 mol dm^{-3} by the addition of potassium nitrate, and pH was adjusted with nitric acid or potassium hydroxide solution.

Results and Discussion

(1) Acid Dissociation Constant of Xanthic Acid. Alkyl xanthates are quite unstable in an acid solution and decompose. The dissociation constant of xanthic acid in the water-DMF mixture system was determined according to the method of Iwasaki and Cooke,[7] who determined the constant in an aqueous medium.

The decomposition rate equation introduced by them is as follows:

$$-\frac{d\ln([X^-]+[HX])}{dt}=\frac{k_3}{1+K_a[H^+]^{-1}}\equiv\kappa \quad (1)$$

or

$$\log\frac{(\text{Absorbance})_1}{(\text{Absorbance})_2}=\frac{\kappa}{2.303}(t_2-t_1), \quad (2)$$

where k_3 and K_a are the decomposition rate and dissociation constants of xanthic acid, and $(\text{Absorbance})_1$ and $(\text{Absorbance})_2$ denote the absorbances at time t_1 and t_2, respectively.

A linear relationship of Eq. (2) held between the time elapsed after the preparation of xanthate solution and the absorbance at 305 nm. It is satisfactory to consider that Eq. (2) is valid not only in an aqueous medium but also in the 1:1 v/v water-DMF mixture.

The log-values of κ were calculated on the basis of the slopes of plots according to Eq. (2) and are given in Table 1. The acid dissociation and decomposition rate constants of xanthic acids were obtained by the analysis of $\log\kappa$ as a function of pH according to Eq. (1). Results are given in Table 2.

TABLE 1. LOG-VALUE OF κ/min^{-1} AS A FUNCTION OF pH

Methyl xanthate		Ethyl xanthate		Propyl xanthate		1-Methylethyl xanthate		Butyl xanthate		2-Methylpropyl xanthate	
pH	log κ	pH	log κ	pH	log κ	pH	log κ	pH	log κ	pH	log κ
1.23	1.47	1.23	1.39	1.23	1.40	1.20	1.35	1.17	1.40	1.20	1.17
1.57	1.39	1.57	1.33	1.57	1.34	1.73	1.31	1.70	1.33	1.70	1.12
1.76	1.32	1.76	1.29	1.76	1.31	2.00	1.26	2.40	1.05	1.95	1.10
1.99	1.21	1.99	1.20	1.99	1.23	2.20	1.14	2.70	0.83	2.23	0.98
2.52	0.84	2.52	0.90	2.52	0.97	2.65	0.87	3.25	0.39	2.70	0.72
2.75	0.63	2.75	0.68	2.75	0.79	2.94	0.68	3.45	0.16	2.95	0.53
2.93	0.57	2.93	0.63	2.93	0.65	3.06	0.56	4.07	−0.40	3.15	0.38
4.45	−0.89	4.47	−0.83	4.50	−0.89	4.47	−0.81	4.50	−0.82	4.50	−0.92
5.08	−1.49	5.11	−1.50	5.19	−1.50	5.08	−1.45	5.28	−1.62	5.08	−1.44
5.80	−2.24	5.82	−2.21	5.84	−2.19	5.80	−2.17	5.82	−2.18	5.84	−2.20

(2) Formation Constant of Metal Xanthato Complex. The polarographic determination of the compositions and the formation constants of the cadmium and zinc xanthato complexes was carried out by using Lingane's equation:[8]

$$(E_{1/2})_s - (E_{1/2})_c = \frac{2.303RT}{nF}\log\beta_j + j\frac{2.303RT}{nF}\log[X^-], \quad (3)$$

assuming the activity and diffusion coefficients of the simple and complexed metal ions to be equal to each other; where n is the number of moles of electrons involved in the electrode reaction, F the faraday, R the gas constant, T the absolute temperature, j the number of ligands coordinated to metal ion, and β_j the overall formation constant of MX_j. $(E_{1/2})_s$ and $(E_{1/2})_c$ denote the half-wave potentials of the simple and complexed metal ions, respectively.

The effect of pH on the diffusion current and the half-wave potential of simple metal ions was preliminarily studied. The half-wave potential was not affected by pH but the diffusion current decreased in a higher pH region than 8.2 for cadmium ion and 7.5 for zinc ion. Polarography for the metal xanthato complexes was therefore carried out in the pH ranging from 7.0 to 8.0 for the cadmium(II) system and from 7.0 to 7.3 for the zinc(II) system. The reversible half-wave potential was obtained graphically by the method of Matsuda and Ayabe.[9]

As shown in Figs. 1 and 2, there was a linear relationship between the half-wave potential and the logarithm of the free xanthate ion concentration which was estimated by subtracting three times of metal concentration from the total concentration of xanthate. The values of the slope of these plots obtained for the cadmium(II) system were 90, 88, 91, 89, 88, and 89 mV for methyl, ethyl, propyl, 1-methylethyl, butyl, and 2-methylpropyl xanthates, respectively. And the values for the zinc(II) system were 85, 93, 96, 95, 94, and 91 mV, respectively. These values of the slope were in agreement with those expected from Eq. (3) in which j was 3. The overall formation constants, β_3, calculated from Eq. (3) are given in Table 2.

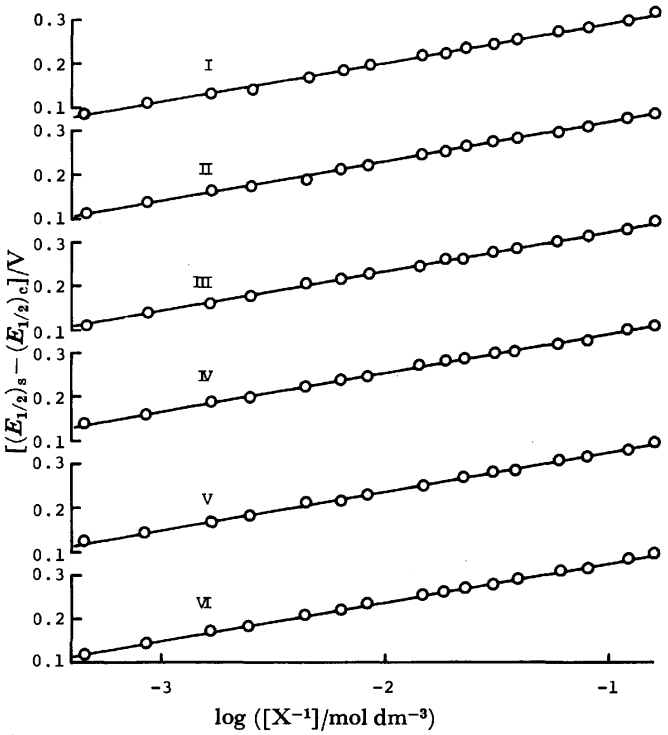

Fig. 1. Shift in the half-wave potential of cadmium(II) ion by the presence of alkyl xanthates in the 1 : 1 v/v water–DMF mixture.
I: methyl xanthate, II: ethyl xanthate, III: propyl xanthate, IV: 1-methylethyl xanthate, V: butyl xanthate, VI: 2-methylpropyl xanthate.

One of the authors (K. H.) has already studied the formation of ethyl xanthato complexes of cadmium and zinc in the 1 : 1 v/v water–DMF medium.[10] According to him, the β_3 values for cadmium and zinc complexes were $10^{14.40}$ and $10^{4.63}$, respectively. The β_3 value for cadmium in Table 2 was in fair agreement with the above value, but the β_3 value for zinc complex obtained in this work was significantly larger than that reported previously. In the previous paper, lithium perchlorate (0.5 mol dm^{-3})–potassium nitrate (1.0—1.5 mol dm^{-3}) was used as the supporting electrolyte for the cadmium system, while potassium chloride (0.5—1.0 mol dm^{-3})

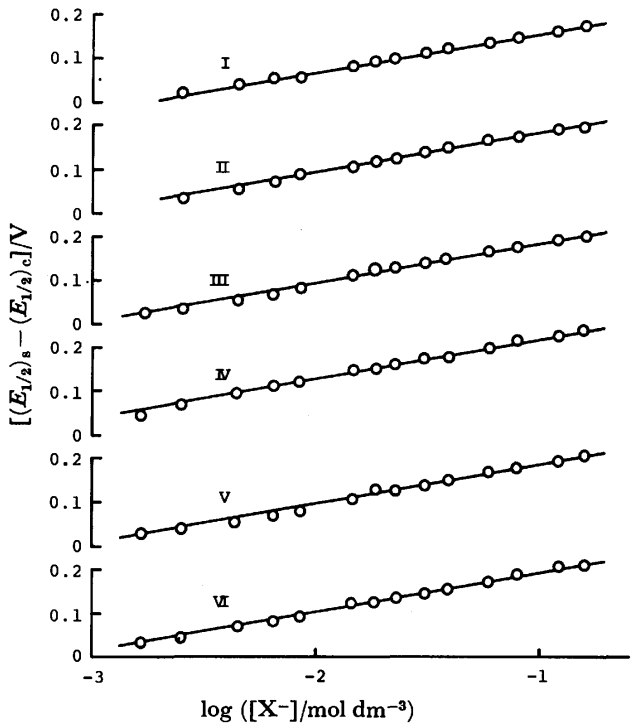

Fig. 2. Shift in the half-wave potential of zinc (II) ion by the presence of alkyl xanthates in the 1 : 1 v/v water-DMF mixture.
I: methyl xanthate, II: ethyl xanthate, III: propyl xanthate, IV: 1-methylethyl xanthate, V: butyl xanthate, VI: 2-methylpropyl xanthate.

was employed for the zinc system. Therefore, the apparent inconsistency seems to be caused by the formation of a zinc–chloro complex which was not considered in the previous paper.

As shown in Table 2, the basicity of xanthates increased in the order, methyl<ethyl<propyl<butyl<2-methylpropyl<1-methylethyl. This order is in agreement with the order reported in the aqueous medium[11] except for 2-methylpropyl and 1-methylethyl derivatives. The stability of complexes increased in the same order of the basicity of the ligands (Table 2), and this result is quite reasonable because a metal ion should form a more stable complex with a more basic ligand.

Table 2. Acid dissociation constant(K_a) and decomposition rate constant(k_3) of alkyl xanthic acid, and formation constant(β_3) of cadmium and zinc xanthato complexes

Xanthate	pK_a	k_3 / min^{-1}	log β_3 (for Cd)	log β_3 (for Zn)
Methyl	2.07	32.4	12.86	8.05
Ethyl	2.20	26.3	13.87	8.93
Propyl	2.22	27.5	13.94	9.00
1-Methylethyl	2.44	14.8	14.55	10.15
Butyl	2.23	27.5	14.04	9.04
2-Methylpropyl	2.25	26.9	14.04	9.20

The decomposition rate constant of methyl xanthate was the maximum and that of 1-methylethyl derivative was the minimum, and it can be said roughly that more basic xanthate is more stable in an acid solution.

The complexes of cadmium are always more stable than the corresponding zinc complexes. The difference in log β_3 was about 4.8. As cadmium(II) ion is more "soft" as Lewis acid than zinc(II) ion, the former should give a more stable complex with xanthate which coordinates through two sulfur atoms.

References

1) E. M. Donaldson, *Talanta*, **23**, 417 (1976).
2) K. Hayashi, Y. Sasaki, S. Tagashira, and E. Yamate, *Bunseki Kagaku*, **27**, 712 (1978).
3) K. Hayashi, Y. Sasaki, S. Tagashira, T. Tanaka, and K. Imada, *Bunseki Kagaku*, **28**, 106 (1979).
4) K. Hayashi, Y. Sasaki, S. Tagashira, K. Morishita, M. Ito, and Y. Soma, *Bunseki Kagaku*, **30**, 56 (1981).
5) Y. Sasaki, *Bunseki Kagaku*, **31**, E107 (1982).
6) Y. Sasaki, *Bunseki Kagaku*, **32**, E17 (1983).
7) I. Iwasaki and S. R. B. Cooke, *J. Am. Chem. Soc.*, **80**, 285 (1958).
8) J. J. Lingane, *Chem. Rev.*, **29**, 1 (1941).
9) H. Matsuda and Y. Ayabe, *Z. Elektrochem.*, **63**, 1164 (1959).
10) H. Kodama and K. Hayashi, *J. Electroanal. Chem.*, **14**, 209 (1967).
11) H. Majima, *Sci. Rep. Res. Inst. Tohoku Univ., Ser. A*, **13**, 183 (1961).

 © 1984 The Chemical Society of Japan Bull. Chem. Soc. Jpn., 57, 3077—3082 (1984)

Structural Characterization of Several Metal(II) 2-Methyl-8-quinolinolato Complexes in Several Organic Solvents

Hiroyuki NARIAI,* Yoshitaka MASUDA,† and Eiichi SEKIDO†
Department of Chemistry, College of General Education, Kobe University, Tsurukabuto, Nada-ku, Kobe 657
†*Department of Chemistry, Faculty of Science, Kobe University, Rokkodai-cho, Nada-ku, Kobe 657*
(Received February 3, 1984)

Bivalent metal complexes of cobalt(II), nickel(II), copper(II), and zinc(II) with 2-methyl-8-quinolinol (2MeHql) were prepared. Their properties, such as those shown by thermogravimetry (TG) and differential thermal analysis (DTA), X-ray diffraction, magnetic susceptibility, and the optical spectra, were measured and compared with those of 8-quinolinolato complexes. All the metal complexes prepared here are monohydrates, whereas their 8-quinolinolato complexes are dihydrates. The methyl group at the 2-position of the quinoline ring caused a shift of about 40—80 °C in the dehydration temperature, and, as a result of the dehydration, a dimer anhydrate was produced. The dimer-formation conditions were established in chloroform and dioxane solutions. However, the addition of such basic solvents as pyridine, water, and methanol cleaved the bridge linkages in complexes and produced a distorted octahedral configuration by solvent-binding in the axial position. The existence of a copper complex with a dimer structure such as has been shown in other metal complexes was not verified in any of the solvents used here.

8-Quinolinol (Hql) has been widely used as a useful analytical reagent to evoke insoluble stoichiometric precipitation with many bivalent metals.[1-5] Many studies have been done on the absorption spectra and the infrared (IR) analysis of their metal complexes.[6-10] However, from the standpoint of explaining the reaction mechanism involved in solvent extraction, the investigation of the solution state of their metal complexes in organic solvents has come to be especially important. However, there have been few reports on them.[11-13] In this work, 2-methyl-8-quinolinolato complexes of bivalent metals (Co, Ni, Cu, and Zn) have been prepared and studied in relation to their physical and chemical properties, their characterization in several organic solvents, and the mechanism of adduct formation. Furthermore, they have been compared with the metal 8-quinolinolato complexes.

Experimental

Reagents. The organic solvents, *e.g.*, chloroform, dioxane, and methanol, were of a reagent grade and were used after further purification, according to the handling methods of Sekido and Kunikida[13] or of Fieser.[14] The other reagents were of an analytical grade.

Preparation of Complexes. Preparation of several metal 2-methyl-8-quinolinolates: $M(2Meql)_2 \cdot H_2O$ (M=Co, Ni, Cu, and Zn). A definite quantity of each metal salt was placed in an acetic acid-acetate buffer solution at pH 5.0 (cobalt(II) and nickel(II)) or 6.2 (copper(II) and zinc(II)), and then the solution was added to an ethanolic 2-methyl-8-quinolinol solution to cause stoichiometric precipitation; the precipitate was filtered, washed several times with hot water to remove the excess 2-methyl-8-quinolinol, and dried in air. Their metal-complex anhydrates were prepared after heating their hydrates at a constant temperature (cobalt(II): 250 °C, nickel(II): 300 °C, copper(II): 150 °C, and zinc(II): 200 °C) for 3 h.

Apparatus and Procedures. A Rigaku Denki Differential Thermobalance TG-DSC was used for the measurement of the TG and DTA. A portion of about ten grams of each complex was heated in a small platinum dish in air and at the heating rate at 10 °C min^{-1}.

X-Ray analysis was carried out with a Rigaku Denki Geigerflex D-1 X-ray Diffractometer, using nickel-filtered Cu $K\alpha$ radiation, except for the cobalt(II) complexes, for which iron-filtered Co $K\alpha$ radiation was used.

The magnetic susceptibilities were measured by means of the Gouy method at room temperature.

The visible and ultraviolet spectra were measured with a Hitachi-124 Spectrophotometer, using the pure solvent as a blank, for cell path-lengths of 1, 10, 50, and 100-mm. A definite amount of a metal-complex anhydrate was dissolved in the appropriate solvent to give the desired concentration. The visible and ultraviolet spectra of the solution were measured within three hours after it had been prepared with the above method. Measurements with other solvents, *e.g.*, dioxane, pyridine, methanol, and their mixed solvents, were carried out with the same procedure.

Results and Discussion

Physical Properties of Several Metal 2-Methyl-8-quinolinolato Complexes. TG and DTA: Typical representative TG and DTA curves of the prepared complexes ($Co(2Meql)_2 \cdot H_2O$ and $Ni(2Meql)_2 \cdot H_2O$) are shown in Fig. 1. It can be seen that one molecule of hydration water is lost in the first step in the range of 170—210 °C for the cobalt(II) complex and in that of

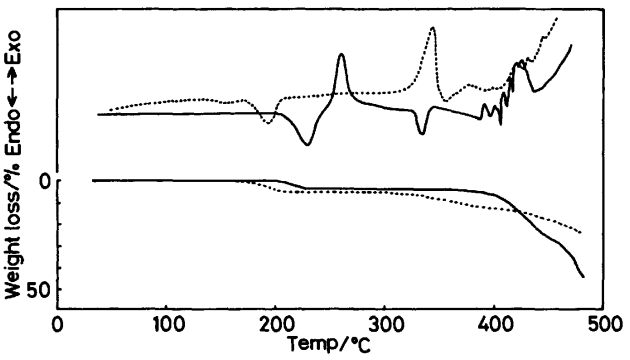

Fig. 1. TG and DTA curves of $Ni(2Meql)_2 \cdot H_2O$(——) and $Co(2Meql)_2 \cdot H_2O$(----) in air.

200—230 °C for the nickel(II) complex. The same patterns were also obtained for other metal (copper(II) and zink(II)) complexes. The composition and range of the dehydration temperatures of the hydrated complexes are shown in Table 1. As a reference, those of 8-quinolinolate hydrates are shown, too. From a comparison with hydrated 8-quinolinolato complexes, it can be seen, first, that hydrated 2-methyl-8-quinolinolato complexes have one molecule of hydration water and that the dehydration temperatures were 40—80 °C higher than those of the 8-quinolinolato complex dihydrates. This shows that the steric hindrance of the 2-methyl group prevents the complex formation;[15] consequently, the bond strength and length of M-N and M-O are rather weakened and lengthened in comparison with those of the 8-quinolinolato complex dihydrates, resulting in an increase in the bond strength from the axial directions; in other words, coordination becomes easier. The above discoveries enhanced the possibility of the formation of dimerization or polymer complexes and an adduct with a basic substance.

Second, the complexes which have one hydrated water molecule, $M(2Meql)_2 \cdot H_2O$, probably prefer a dimer geometry coordinated with two molecules of hydrated water above and below the two molecules of metal as is shown in Scheme 1, to a five-coordinated geometry (square pyramidal). However, since the dehydration temperature was much higher (about 200—230 °C) than those of other metal complexes, since the exothermic peak appeared upon dehydration, and since no loss in gravimetric quantity involving the exothermic reaction was observed, the geometry of the nickel(II) complex may be different from the structure described above (Scheme 1). The X-ray diffraction pattern of the amorphous sample and exchange by means of dehydration with heating, were not observed; still, it seems that dimer anhydrates were formed as a result of the dehydration of water coordinated above and below the metals.

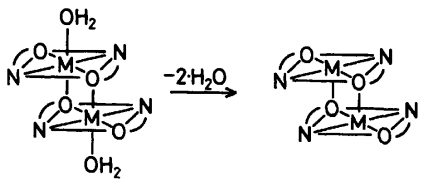

Scheme 1.

Table 1. Thermal analytical data

Molecular formula	Range of dehydration (°C)
$Cu(2Meql)_2 \cdot H_2O$	100—120
$Zn(2Meql)_2 \cdot H_2O$	130—160
$Co(2Meql)_2 \cdot H_2O$	170—210
$Ni(2Meql)_2 \cdot H_2O$	200—230
$Cuql_2 \cdot 2H_2O$	50— 80
$Znql_2 \cdot 2H_2O$	80—120
$Coql_2 \cdot 2H_2O$	110—145
$Niql_2 \cdot 2H_2O$	110—145

Susceptibility of Complexes: Table 2 shows the results of elemental analysis, the magnetic moments of metal 2Meql complex monohydrates, and their anhydrates compared with those of the 8-quinolinolato complexes. All the metal complexes have a high-spin magnetic moment;[16] these results suggest the possibility of dimer geometry.

X-Ray-diffraction-pattern Analysis: Figures 2 and 3 shows the X-ray diffraction patterns of metal 2Meql complex monohydrates and anhydrates. All the patterns of the cobalt(II), copper(II), and zinc(II) complex monohydrates, except for the nickel(II) complex, are similar, with some peaks of the same diffraction angles; the nickel(II) complex displayed different, rather complicated patterns. Metal-complex anhydrates of cobalt(II), copper(II), and zinc(II), except for nickel(II), also show very similar patterns; three peaks appeared at about $2\theta=10°$, and three or five peaks, at about $2\theta=30—40°$.

The Characterization of Several Metal 2Meql Complexes in Aqueous and Organic Solvents. Optical Spectra of 2MeHql in Aqueous Solutions: Figure 4 shows the optical spectra of 2MeHql in aqueous solutions. From the increase in the basicity of the oxygen and nitrogen atoms upon the substitution of the 2-position with the methyl group, the peaks showed a blue shift.[17] The substitution of the methyl group for hydrogen at the 2-position brought about an increase in the basicity of oxygen and nitrogen, resulting in a blue shift.

Table 2. Analytical data and magnetic susceptibilities of several metal 2-methyl-8-quinolinolato complexes

Compound	Found (%)			Calcd (%)			μ_{eff} (BM)		Compound	μ_{eff} (BM)
	C	H	N	C	H	N	Found	Calcd		Found
$Co(2Meql)_2 \cdot H_2O$	60.12	4.96	7.05	61.08	4.61	7.12	4.06	3.87	$Coql_2 \cdot 2H_2O$	4.88
$Co(2Meql)_2$	63.20	4.59	7.39	64.01	4.30	7.46	4.72	3.87	$Coql_2$	4.64
$Ni(2Meql)_2 \cdot H_2O$	60.61	4.85	7.35	61.12	4.62	7.13	3.19	2.83	$Niql_2 \cdot 2H_2O$	3.18
$Ni(2Meql)_2$	62.84	4.69	7.56	64.05	4.30	7.47	3.19	2.83	$Niql_2$	3.25
$Cu(2Meql)_2 \cdot H_2O$	60.78	5.25	7.00	60.37	4.56	7.04	2.00	1.73	$Cuql_2 \cdot 2H_2O$	1.93
$Cu(2Meql)_2$	62.67	4.34	7.60	63.23	4.25	7.37	1.74	1.73	$Cuql_2$	1.84
$Zn(2Meql)_2 \cdot H_2O$	60.00	4.93	6.99	60.10	4.54	7.01			$Znql_2 \cdot 2H_2O$	
$Zn(2Meql)_2$	62.50	4.44	7.39	62.93	4.23	7.34			$Znql_2$	

μ: Bohr magneton at room temperature.

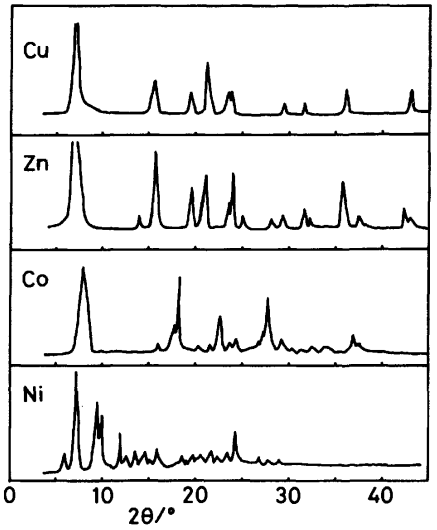

Fig. 2. X-Ray diffraction patterns of $M(2Meql)_2 \cdot H_2O$.

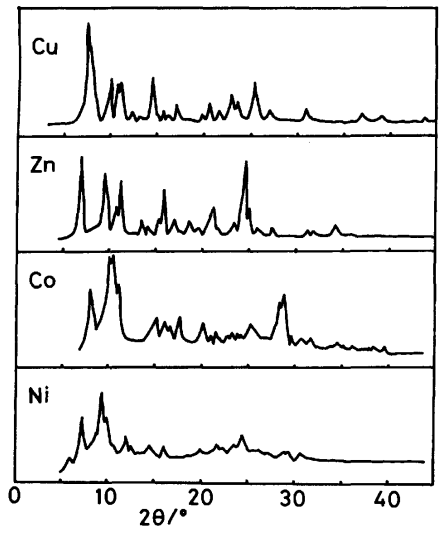

Fig. 3. X-Ray diffraction patterns of $M(2Mqel)_2$.

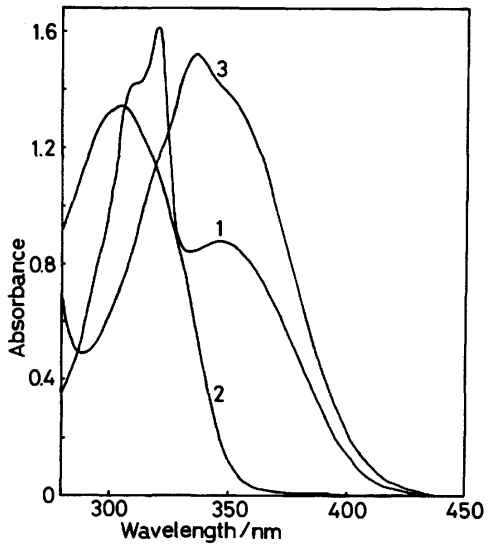

Fig. 4. Optical spectra of 2-methyl-8-quinolinol (2MeHql). 1: in 1M-HCl, 2: in CH_3OH, 3: in 1M-NaOH. $[2MeHql]=5.0\times10^{-4}$M.

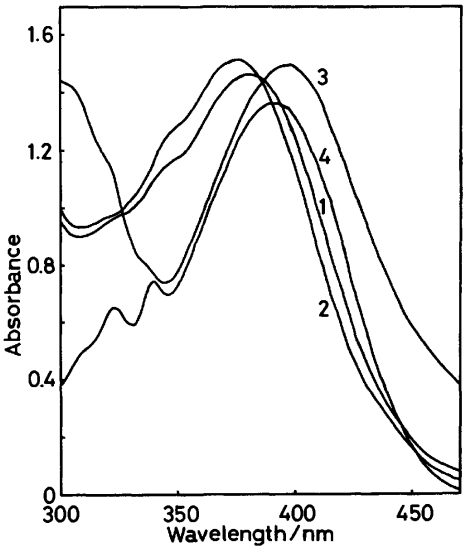

Fig. 5. Optical spectra of some metal(II) 2-methyl-8-quinolinolato complexes in chloroform. 1: Co(2.66×10^{-4} M), 2: Ni(3.04×10^{-4} M), 3: Cu(3.00×10^{-4} M), 4: Zn(3.04×10^{-4} M).

Optical Spectra of the Complexes in a Pure Organic-solvent Medium: It is important, from the standpoint of explaining the reaction mechanism involved in solvent extraction, to know whether or not the dimeric geometry of the cobalt(II), nickel(II), copper(II), and zinc(II) 2Meql complexes in organic solvents is kept. Figure 5 shows the optical spectra of the complexes in chloroform. In a previous paper,[13] Sekido and Kunikida have reported that a trace amount of water affects the optical spectra of nickel 8-quinolinolate anhydrate. We have been measured the optical spectra of metal complexes in chloroform treated with various desiccants; we have found that the red shifts of the optical maximum increase in this order: Ni(376 nm)<Co(381 nm)<Zn(391 nm)<Cu(397 nm), and that a variety of desiccants does not affect the optical spectra; that is, the dimer geometry of an anhydrate is maintained in a chloroform solution. Further, the behavior of the optical spectra in a dioxane solution is the same as in chloroform.

Optical Spectra of the Complexes in Mixed Solvents: From the viewpoint of adduct formation and configuration variation, the optical spectra of mixed solvents-in dioxane-pyridine, dioxane-methanol, and dioxane-water systems, were examined using the same preparing procedure in a chloroform solvent.[18] For example, the optical spectra of copper complexes are shown in Figs. 6, 7, and 8. In Fig. 6, with an increase in the amount of pyridine, the optical maximum at about 400 nm shifted toward 385 nm, involving only one isosbestic point at 394 nm. In Fig. 7, with an increase in the amount of methanol, the absorption maximum at about 400 nm shifted toward 385 nm, while the optical density decreased, and then the optical maximum at 339 nm turned into a shoulder. Isosbestic points were observed at 386 and 330 nm, so at least two species of metal complexes were present. In Fig. 8, a similar behavior of the optical spectra was

observed in dioxane-water; however, the optical maximum at 339 nm completely disappeared. In this system, the precipitation of hydrate was observed at a water concentration of about 33.3 M (1M=1 mol dm^{-3}). From the results of the optical spectra of other mixed-solvent systems, it seems that the optical spectra of complex anhydrates depend upon their nature, the molar ratio, the concentration of the solvents, and the analytical concentration of the complexes. The results of the optical spectra of complex anhydrates in various organic solvents are shown in Table 3. The optical spectra in the dioxane solution of copper-

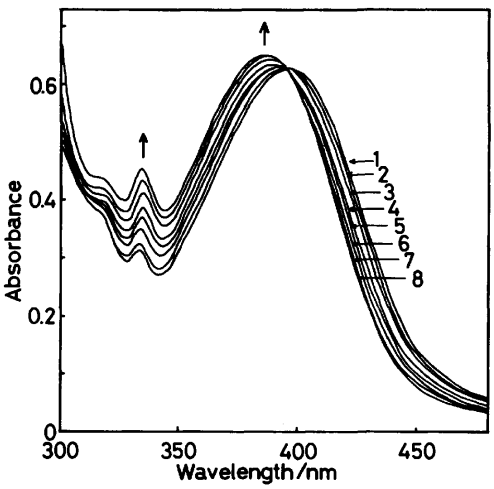

Fig. 6. Optical spectra of $Cu(2Meql)_2$ in dioxane containing various amounts of pyridine. 1: [py]= 0 M, 2: 6.19×10^{-2} M, 3: 1.86×10^{-1} M, 4: 3.72×10^{-1} M, 5: 6.19×10^{-1} M, 6: 1.24 M, 7: 2.48 M, 8: 4.96 M. $[Cu(2Meql)_2]=1.15\times10^{-4}$ M. Trends of spectral change with increase in base concentration are shown by arrows.

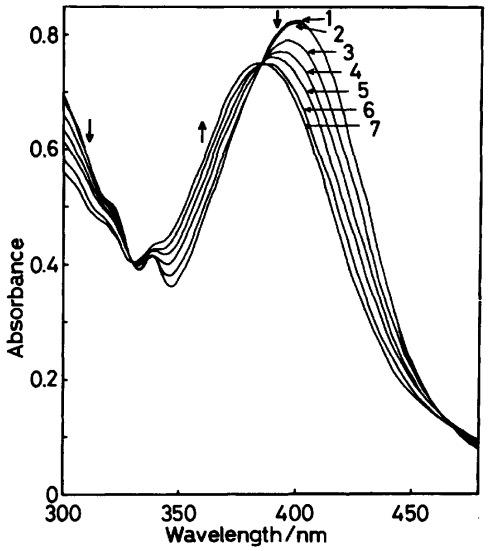

Fig. 7. Optical spectra of $Cu(2Meql)_2$ in dioxane containing various amounts of methanol. 1: [MeOH]= 0M, 2: 0.49M, 3: 2.47M, 4: 4.94M, 5: 7.41M, 6: 9.88M, 7: 12.35 M. $[Cu(2Meql)_2]=1.47\times10^{-4}$ M. Trends of spectral change with increase in base concentration are shown by arrows.

Table 3. Optical spectra data for several metal 2-methyl-8-quinolinolato complexes in various organic solvents

Solvent	Added reagent and its concn range (M)	λ at Absorption maxima (nm)			
		No reagent (Added reagent)		[Isosbestic points]	
		$Co(2Meql)_2$	$Ni(2Meql)_2$	$Cu(2Meql)_2$	$Zn(2Meql)_2$
Dioxane		392	388	400	388
		342	343	339	340
	Pyridine	387 (389)	390 (399)	396 (385)	385 (381)
	(0—7.4 M)	336 (338)	343 (345)	334	334 (336)
		[366, 423]	[387, 425]	[394]	[412]
	Methanol	389 (400)	390 (380)	400 (385)	390 (387)
	(0—12.4 M)	0—0.7 M			0—1.2 M
		400 (380)			387 (372)
		0.7—12.4 M			1.2—12.4 M
		342 (sh)	343 (341)	339 (sh)	
		[403, 348]	[394, 373, 339, 333, 320]	[386, 330]	[384, 330]
	Water	390 (405)	392 (384)	400 (378)	390 (381)
	(0—27.8 M)	0—0.5 M			0—4.7 M
		405 (391)			381 (370)
		0.5—2.5 M			4.7—16.7 M
		342	344 (341)	338 (sh)	339 (sh)
					324 (sh)
			[386, 353]	[328]	

(sh: shoulder).

(II) complex anhydrates were changed upon the addition of basic solvents, which resulted in a shifting of the isosbestic point. In other words, the configuration of the complex anhydrates in a dioxane solution turned into something else. However, in the case of other metal-complex anhydrates, upon the addition of basic solvents a new isosbestic point appears, so two equilibrium states at least are present. Depending on the amount of basic solvents added, the configuration of the complex anhydrate [1] in a dioxane solvent turns into a different structure [3a, 3b, or 3c] through a middle species [2a, 2b, or 2c] as is shown in Fig. 9. The amount of Lewis base added depended upon the strength of the basicity; it was preferred to the order of pyridine<water<methanol. For example, in nickel-complex anhydrate, the amounts of the basic solvents needed to change from one configuration to another were 2.5×10^{-3} M for pyridine, 1.1 M for water, and 4.9 M for methanol.

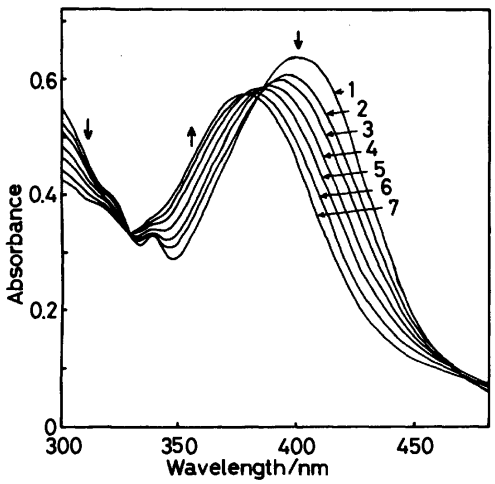

Fig. 8. Optical spectra of $Cu(2Meql)_2$ in dioxane containing various amounts of water. 1: $[H_2O]=0$ M, 2: 2.78 M, 3: 5.56 M, 4: 11.11 M, 5: 16.67 M, 6: 22.22M, 7: 27.78 M. $[Cu(2Meql)_2]=1.13\times10^{-4}$ M. Trends of spectral change with increase in base concentration are shown by arrows.

Effect of the Concentration of a Complex on Its Optical Spectra: The optical spectra of the nickel(II) 8-quinolinolato complex at various concentrations in dried chloroform were examined in a previous paper.[13] The monomer complex exists below 1×10^{-5} M, but the binuclear or trinuclear complex exists at concentrations above 1×10^{-5} M, and for the binuclear complex, the formation constant was calculated at $K=2000$:

$$2\cdot Niql_2 \overset{K}{\rightleftharpoons} (Niql_2)_2.$$

In the case of the metal 2Meql complexes, not enough change in the optical spectra upon the addition of basic solvents was obtained, so the equilibrium constant could not be calculated accurately. However, the dimeric complex of cobalt(II), nickel(II), or zinc(II) probably exists at concentrations above 2×10^{-5} M. The solvents added at lower concentrations coordinated at the axial positions of the dimer complex, and at higher concentrations the bridge linkages by 2Meql were broken by added solvents (refer to Fig. 9) and the axial positions were coordinated, resulting in a distorted octahedral geometry, as is shown in Fig. 9. The stability of dimer geometry increased in the order of: cobalt(II)≃nickel(II)>zinc(II); the dimer⇄monomer order

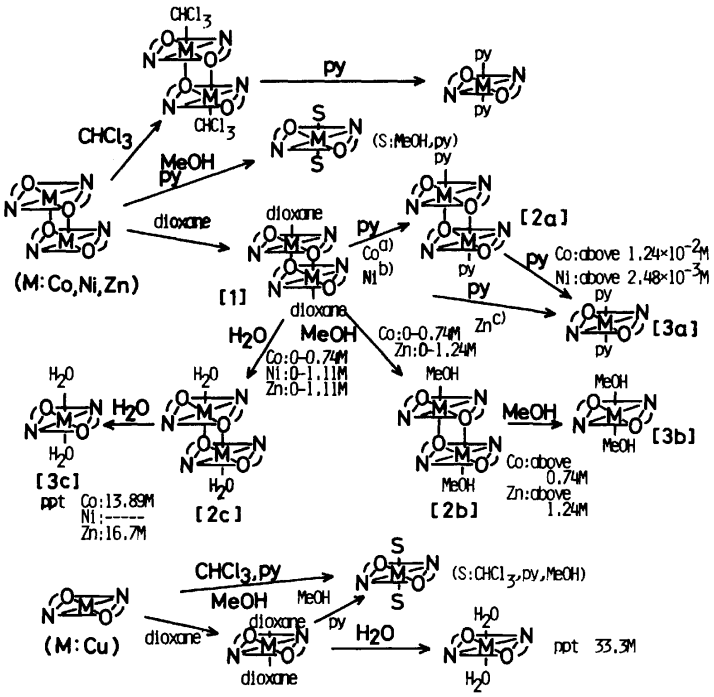

Fig. 9. Proposed structures of several metal(II) 2-methyl-8-quinolinolato complexes in various organic solvents. a) Co: 0—1.24×10^{-2} M, b) Ni: 0—2.48×10^{-3} M, c) Zn: above 0.743×10^{-3} M.

was affected by the nature of the basicity, and the dimer formed rapidly at low concentrations when a strong base such as in the pyridine solvent, was added. On the other hand, in the case of the copper(II) complex, from the optical spectra of all the organic solvents used here and the variation in the concentration of the copper(II) complex, it seems that the dimer structure did not exist; that is, an adduct complex with a planar geometry has formed.

This work was presented in part at the 37th Annual Meeting of the Chemical Society of Japan, Yokohama, April, 1978, Abstr. No. 2I29.

References

1) H. Hashitani, H. Yoshida, and K. Motojima, *Bunseki Kagaku*, **18**, 136 (1969).
2) T. Honjo, H. Imura, S. Shima, and T. Kiba, *Anal. Chem.*, **50**, 1545 (1978).
3) H. Hellwege and G. K. Schweitzer, *Anal. Chim. Acta*, **28**, 236 (1963).
4) K. Takiyama, *Bunseki Kagaku*, **22**, 291 (1973).
5) S. Oki and I. Terada, *Anal. Chim. Acta*, **66**, 201 (1973).
6) E. Sekido, *Nippon Kagaku Zasshi*, **80**, 375 (1959).
7) E. Sekido, *Nippon Kagaku Zasshi*, **80**, 379 (1959).
8) E. Sekido, *Nippon Kagaku Zasshi*, **80**, 383 (1959).
9) N. Ohkaku and K. Nakamoto, *Inorg. Chem.*, **10**, 798 (1971).
10) B. C. Baker and D. T. Sawyer, *Anal. Chem.*, **40**, 1945 (1968).
11) E. Sekido and Y. Yoshimura, *J. Inorg. Nucl. Chem.*, **38**, 1187 (1976).
12) E. Sekido and K. Fujita, *Bull. Chem. Soc. Jpn.*, **49**, 3073 (1976).
13) E. Sekido and K. Kunikida, *Anal. Chim. Acta*, **92**, 183 (1977).
14) L. F. Fieser, "Experiments in Organic Chemistry," trans. by K. Nakanishi and Y. Hirata, Maruzen, Tokyo (1971), Chap. 48, pp. 266—276.
15) L. G. Sillen and A. E. Martell, "Stability Constants of Metal-Ion Complexes," The Chemical Society, London (1964), pp. 719, 817.
16) F. P. Dwyer and D. P. Mellor, "Chelating Agents and Metal Chelates," Academic Press, New York (1964), p. 23.
17) H. Nakamura, Y. Shimura, and R. Tsuchida, *Bull. Chem. Soc. Jpn.*, **34**, 1143 (1961).
18) K. Sone, *J. Am. Chem. Soc.*, **75**, 5207 (1953).

Kinetics of Ligand Exchange of Tris(β-diketonato)iron(III) with Acetylacetone, Trifluoroacetylacetone, and 2-Thenoyltrifluoroacetone in Carbon Tetrachloride

Tatsuya SEKINE* and Kazuho INABA
Department of Chemistry, Science University of Tokyo, Kagurazaka, Shinjuku-ku, Tokyo 162
(Received February 17, 1984)

The ligand of tris(β-diketonato)iron(III) with acetylacetone (Hacac), trifluoroacetylacetone (Htfa), or 2-thenoyltrifluoroacetone (Htta) in carbon tetrachloride was exchanged with another ligand among these. The rate was measured in order to learn about the reaction mechanism in this medium; one in which no intermediates with the solvent molecules were expected. From the dependence of the rate on the particular leaving and entering ligand and from the values of ΔH^* and ΔS^*, it was concluded that in an exchange involving [Fe(acac)$_3$] there is always a proceeding dissociative mechanism and for [Fe(tta)$_3$] and [Fe(tfa)$_3$] with Hacac there is an interchange mechanism. Exchanges with a fluorinated β-diketone is thought to have a character intermediate to these two mechanisms.

Kinetic studies on the ligand exchange of metal complexes have been, in most cases, carried out in aqueous solutions and several explanations for models in which the solvent molecules also react as ligands to form intermediate species have been proposed from the experimental results. When nonpolar- and non-solvating-type solvents are employed instead of water, however, it is expected that more direct information about the effects of the chemical properties of the leaving and entering ligand on the reaction mechanism can be obtained.[1,2] For this reason, the rates of nonisotopic ligand exchanges for three tris(β-diketonato)iron(III) complexes in carbon tetrachloride were determined in the present study. Considerations are made on the reaction mechanism for situations where the effect of the solvent molecules is considered slight.

Experimental

Materials. All reagents were reagent grade. The β-diketones, 2,4-pentanedione (acetylacetone; Hacac), 1,1,1-trifluoro-2,4-pentanedione (trifluoroacetylacetone; Htfa), and 1-(2-thienyl)-4,4,4-trifluoro-1,3-butanedione (2-thenoyltrifluoroacetone; Htta) were supplied by Dojindo Co., Kumamoto. The Htta was recrystallized from benzene–petroleum ether before use. Iron(III) complexes of these β-diketones were synthesized by the conventional method[3] and recrystallized from benzene–petroleum ether. The purity was checked by an elementary analysis as: [Fe(acac)$_3$] (Found: C 51.25, H 6.02%, Calcd: C 51.01, H 5.99%), [Fe(tfa)$_3$] (Found: C 34.95, H 2.34, F 33.10%, Calcd: C 34.98, H 2.35, F 33.20%), and [Fe(tta)$_3$] (Found: C 40.11, H 1.71, S 13.25, F 23.62%, Calcd: C 40.07, H 1.68, S 13.37, F 23.77%). The carbon tetrachloride was washed three times with water, treated with a dehydrating resin, (SK1B, Mitsubishi Kasei Co., Tokyo) and distilled.

Procedures. The experiments were carried out in a thermostated bath (±0.3 K) located in a thermostated room (±0.6 K). A carbon tetrachloride solution containing 1×10^{-5} to 4×10^{-4} mol dm^{-3} of one of the iron(III) complexes (FeA$_3$) and an excess amount of the ligand (HA) was mixed with a solution containing 1×10^{-4} to 1 mol dm^{-3} of another entering ligand (HB). In order to study ligand exchange equilibrium, the mixed solution was left standing and its optical absorption was measured at 375 nm (exchange of [Fe(acac)$_3$] with Htfa), or 550 nm (for all of the other reactions) after it had become a certain constant value. This was repeated for several molar ratios of the two ligands, HA and HB. While the rate of ligand exchange was being studied, the optical absorption of the solution was measured several times.

Data Treatment. The exchange equilibrium of the iron(III) complex with the entering ligand in the solution may be expressed as;

$$FeA_3 + nHB \rightleftharpoons FeA_{3-n}B_n + nHA$$
$$K_n = [FeA_{3-n}B_n][HA]^n[FeA_3]^{-1}[HB]^{-n}. \quad (1)$$

The optical absorption of the solution at equilibrium is given by;

$$E = [Fe(III)](\varepsilon_0+\varepsilon_1K_1R+\varepsilon_2K_2R^2+\varepsilon_3K_3R^3) \times (1+K_1R+K_2R^2+K_3R^3)^{-1}, \quad (2)$$

where ε_n is the molar extinction coefficient of the $FeA_{3-n}B_n$ complex and R is the concentration ratio (R=[HB][HA]$^{-1}$). The values of K_n and ε_n were obtained by analyzing the data using a successive-approximation program.[4]

The kinetic data on ligand exchange can be treated as follows. When the whole exchange reaction is controlled by the exchange of the first ligand of FeA$_3$, the successively formed three species, FeA$_2$B, FeAB$_2$, and FeB$_3$, should be in equilibrium with each other. Under such conditions, the following conditional over-all extinction coefficient can be defined if R is kept constant, since the molar ratios of the three successive complexes should always be constant;[5]

$$\varepsilon_T = (\varepsilon_1K_1R+\varepsilon_2K_2R^2+\varepsilon_3K_3R^3)(K_1R+K_2R^2+K_3R^3)^{-1}. \quad (3)$$

This conditional constant can be calculated on the basis of Eqs. 1 and 2 and, at the same time, can be determined from the absorption at equilibrium if the starting complex, FeA$_3$, is nearly completely changed into the ligand exchanged species. Thus, from information on absorption and the total concentration of iron(III) in the solution, the concentration of the FeA$_3$ species after a certain time interval can be written as;

$$[FeA_3] = (E-\varepsilon_T\times[Fe(III)])(\varepsilon_0-\varepsilon_T)^{-1}. \quad (4)$$

From the decrease in the FeA$_3$ concentration, the rate of ligand exchange can be expressed as;

$$V = -d[FeA_3]/dt = k_{obsd}[FeA_3], \quad (5)$$

where k_{obsd} is the observed rate constant of the exchange reaction.

Results

Ligand Exchange Equilibria. From the absorption data of the equilibrated solutions, the values of K_n and ε_n were obtained as listed in Table 1.

Rate of Ligand Exchange of [Fe(acac)$_3$]. The rate of ligand exchange of [Fe(acac)$_3$] with Htfa or Htta was found to be first order with respect to [Fe(acac)$_3$] and independent of the leaving ligand. Figure 1 gives the results as a function of the concentration of the entering ligand at 298 K. When the entering ligand was Htta, the value of k_{obsd} was independent of its concentration in the range of 10^{-3} to 10^{-2} mol dm^{-3}, though a first-order dependence appeared below and above this range. When the entering ligand was Htfa, on the other hand, no region was apparently found where the rate was independent of its concentration. However, both data could be explained well by assuming the same type of reaction if the effect of the entering ligand as an acid catalyzer, as will be described later, is corrected.

Rate of Ligand Exchange of [Fe(tfa)$_3$]. In the course of the study of the ligand exchange of [Fe(tfa)$_3$] with Hacac, it was found that absorption at 375 nm rapidly increased just after the addition of a Hacac solution to the [Fe(tfa)$_3$] solution. This enhancement in the absorption was concluded to be due to an association of [Fe(tfa)$_3$] and Hacac which proceeded much more rapidly than the ligand exchange. Spectrometric data were analyzed after a correction for this intermediate was made. Figure 2 gives the results at 298 K as a function of the entering ligand. In the higher ligand concentration range, the value of the observed rate constant is independent of the entering ligand, but in the lower region it is proportional to its concentration.

Rate of Ligand Exchange of [Fe(tta)$_3$]. A similar type of increased absorption at 550 nm was also found upon the addition of Hacac to the [Fe(tta)$_3$] solution. The rate of ligand exchange of [Fe(tta)$_3$] with Hacac or Htfa was found to be first order with respect to the iron(III) complex and independent of the leaving ligand. The dependence on each entering ligand was first order when the concentration was lower than 0.2 mol dm^{-3} and independent above this value. Figure 3 gives the results.

The results in Figs. 1 to 3 can be represented by the following general equation;

$$k_{obsd} = \frac{k_A(1+k_C[HB])[HB]}{k_B+[HB]}. \quad (6)$$

TABLE 1. SUMMARY OF EQUILIBRIUM CONSTANTS

	[Fe(acac)$_3$] +Htfa (375 nm)	[Fe(acac)$_3$] +Htta (550 nm)	[Fe(tfa)$_3$] +Htta (550 nm)
log K_1	1.83	2.31	0.90
log K_2	2.73	3.45	1.35
log K_3	2.73	3.59	1.17
ε_0/mol^{-1} dm^3 cm^{-1}	2020	160	270
ε_1/mol^{-1} dm^3 cm^{-1}	2600	460	720
ε_2/mol^{-1} dm^3 cm^{-1}	3100	1010	1240
ε_3/mol^{-1} dm^3 cm^{-1}	3530	2150	2150

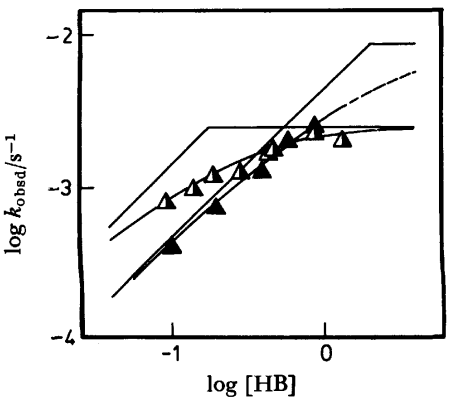

Fig. 2. Rate of [Fe(tfa)$_3$] reaction with Hacac (▲) and Htta (▲) as a function of the entering ligand concentration at 298 K. The curves are calculated by introducing the constants in Table 2 into Eq. 6. The straight lines are the asymptotes for the curves.

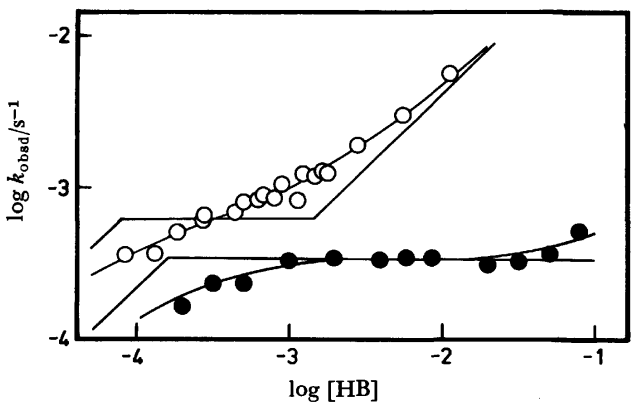

Fig. 1. Rate of [Fe(acac)$_3$] reaction with Htfa (○) and Htta (●) as a function of the entering ligand concentration at 298 K. The curves are caluclated by introducing the constants in Table 2 into Eq. 6. The straight lines are the asymptotes for the curves.

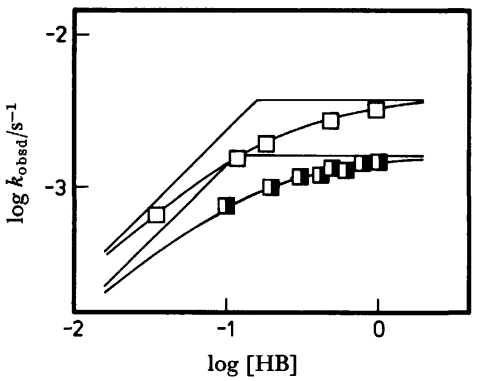

Fig. 3. Rate of [Fe(tta)$_3$] reaction with Hacac (■) and Htfa (□) as a function of the entering ligand concentration at 298 K. The curves are calculated by introducing the constants in Table 2 into Eq. 6. The straight lines are the asymptotes for the curves.

TABLE 2. SUMMARY OF CONSTANTS AND ACTIVATION PARAMETERS

	$[Fe(acac)_3]$		$[Fe(tfa)_3]$		$[Fe(tta)_3]$	
	+Htfa	+Htta	+Hacac	+Htta	+Hacac	+Htfa
$\log (k_A/s^{-1})$	−3.2	−3.5	−2.6	−2.1	−2.8	−2.4
$\log (k_B/\text{mol dm}^{-3})$	*ca.* −4	*ca.* −4	−0.8	0.3	−0.9	−0.8
$\log (k_C/\text{mol}^{-1}\text{ dm}^3\text{ s}^{-1})$	2.8	0.7	—	—	—	—
$\Delta H^*/\text{kJ mol}^{-1}$ †	83	82	56	63	62	68
$\Delta S^*/\text{J K}^{-1}\text{ mol}^{-1}$ †	−27	−38	−106	−74	−89	−64

† The estimated errors of ΔH^* and ΔS^* for the reactions of $[Fe(tfa)_3]$ and $[Fe(tta)_3]$ are around ±1 and ±5 while that for the reactions of $[Fe(acac)_3]$ are ±5 to 10 and ±20 to 30, respectively.

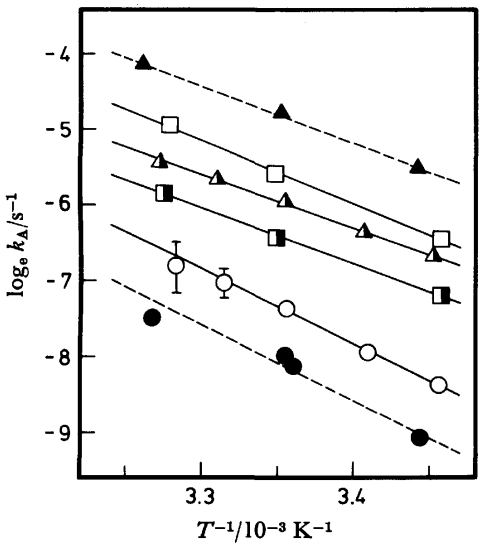

Fig. 4. Arrhenius plot of the rate constant k_A of the reaction of $[Fe(acac)_3]$ with Htfa (○) and Htta (●), $[Fe(tfa)_3]$ with Hacac (△) and Htta (▲), and $[Fe(tta)_3]$ with Hacac (◨) and Htfa (□).

From the information in Fig. 1, the value of the constant k_C was obtained. From the results expressed in Figs. 2 and 3, this term was concluded to be negligible. The values of the constants obtained are listed in Table 2.

Activation Parameters of Ligand Exchange Reactions. The rate of ligand exchange was also measured at 288 and 306 K (and 293 and 302 K for $[Fe(acac)_3]$ and Htfa or $[Fe(tfa)_3]$ and Hacac reaction). Figure 4 gives the $\log_e k_A$ *vs.* $1/T$ plot. The results regarding the reaction of $[Fe(acac)_3]$ with Htfa and Htta were found to be somewhat more erroneous than those of other reactions, especially at higher temperatures. The activation parameters, ΔH^* and ΔS^*, obtained from these data are listed in Table 2.

Effect of Trichloroacetic Acid. In a previous study, it was found that the rate of ligand exchange of $[Fe(acac)_3]$ with Htta in carbon tetrachloride was accelerated by the presence of several acids.[2] In the present study, the effect of trichloroacetic acid was measured. The reactions of $[Fe(acac)_3]$ with both Htta and Htfa were accelerated by trichloroacetic acid already at a concentration of 10^{-5} mol dm^{-3} and that of $[Fe(tta)_3]$ with Htfa was also accelerated by a presence of 10^{-3} mol dm^{-3}. The rates of other reactions were not affected by trichloroacetic acid in a concentration range of 10^{-5} to 10^{-3} mol dm^{-3}.

Discussion

It was concluded from the absorption data of the mixed sample solutions at equilibrium that more than 99% of the starting complex, FeA_3, had been changed to the ligand exchanged species under the conditions of the R employed for the kinetic experiments. Thus from the total concentration of iron(III) and the absorption at equilibrium, the value of ε_T in Eq. 3 should be obtained. This was confirmed since the values calculated by introducing the constants in Table 1 into Eq. 3 agreed well with this observed value. From this, the analysis of the kinetic data in the present study by using Eq. 4 and the values of ε_T should be reasonable.

Some experiments were made under conditions of R where the chemical species formed from FeA_3 were only of the FeA_2B type complex and $FeAB_2$ and FeB_3 were negligible. The rate was always similar to that obtained at values of R where exchange was complete. Thus, the rates of ligand exchange of the FeA_2B and of $FeAB_2$ species were much higher than that of the FeA_3 species. This should support the assumption already made that the rate was, in all the cases, not affected by the concentration of the leaving ligand and, consequently, the controlling step was the exchange of the first ligand of FeA_3. Thus, the discussion below is made on the basis of this assumption.

In the present study, it is assumed that (i) the solvation with carbon tetrachloride should be very weak and, thus, any intermediate species containing the solvent molecules is negligible, and (ii) the presence of any charged species is negligible in the solution. The results in Figs. 1 to 3 are generally represented by Eq. 6, but since the term k_C represents a catalytic effect with the entering ligand itself, as will be seen later, the results should be given by the following equation if this effect is statistically substracted;

$$k_{obsd} = \frac{k_A[HB]}{k_B + [HB]}. \quad (7)$$

This equation suggests that the reaction may possibly proceed by two types of ligand-exchange mechanisms. One is the dissociative mechanism which is represented by;

$$MA_3 \underset{k_{-1}}{\overset{k_1}{\rightleftharpoons}} MA_3^* \xrightarrow[+HB]{k_2} MA_2B + HA,$$

where the superscript "*" denotes a complex one of whose chelate ring is open. When the rate constant for the ring opening is given by k_1, that for its backward reaction by k_{-1} and that for the entering of HB by k_2, the following equation is obtained;

$$V = \frac{k_1[\mathrm{HB}][\mathrm{FeA_3}]}{(k_{-1}/k_2)+[\mathrm{HB}]}. \quad (8)$$

The other is the interchange mechanism which is represented by;

$$\mathrm{MA_3} + \mathrm{HB} \overset{K}{\rightleftharpoons} \mathrm{MA_3{*}HB} \overset{k}{\longrightarrow} \mathrm{MA_2B} + \mathrm{HA},$$

$$V = \frac{k[\mathrm{HB}][\mathrm{FeA_3}]}{K^{-1}+[\mathrm{HB}]}. \quad (9)$$

Here, MA_3 is in equilibrium with its associate with HB and the reaction is controlled by the formation of the first chelate ring with the anion of the entering ligand B^- involving a proton-transfer from the entering HB to the leaving A^-.

It is known that if a reaction proceeds by a dissociative mechanism, the value of ΔH^* is large and ΔS^* is positive or nearly zero while if it proceeds by an interchange mechanism, the ΔH^* is smaller than that by a dissociative mechanism and the ΔS^* is negative. After observing this general tendency and the values in Table 2, it may be concluded that the ligand exchange of the [Fe(acac)$_3$] complex proceeds by a dissociative mechanism while that of [Fe(tfa)$_3$] and [Fe(tta)$_3$] proceeds by an interchange mechanism, although the ligand exchange of [Fe(tta)$_3$] with Htfa may have an intermediate character of these two becasue of the intermediate magnitude of the values of ΔH^* and ΔS^*. Although the reactions of [Fe(acac)$_3$] with Htta and Htfa are assumed to proceed by a dissociative mechanism, the values of k_1 are not similar. One explanation for this may be that the amount and/or the effect on the rate of the minor contents in the systems such as water, impurities in the reagents *etc.*, are not identical. However, further experiments seem to be necessary in order to solve this problem.

It seems to be reasonable that a catalytic effect of the acids, including that with the entering β-diketone to the complex which is also a weak acid, appears only in the exchange reaction of [Fe(acac)$_3$] with the fluorinated β-diketones and not in the exchange of [Fe(tta)$_3$] or [Fe(tfa)$_3$] with acetylacetone or with the other fluorinated β-diketone if the former reaction proceeds by a dissociative mechanism and the latter by an interchange mechanism. When the reaction proceeds by a dissociative mechanism, the leaving ligand, $acac^-$, easily accepts a proton from a stronger acid. This should help in the dissociation of the ligand from the complex, but acetylacetone in an acid form, Hacac, may not give up a proton so easily to the leaving ligand. On the other hand, when the reaction proceeds by an interchange mechanism and when the dissociation of the proton from the entering ligand which is accompanied by the closure of the chelate ring controls the whole reaction, another acid whether it is stronger or weaker can not assist the leaving of the proton and, thus, can not catalyze the reaction.

The enhancement of the absorption properties of a solution of [Fe(tfa)$_3$] or [Fe(tta)$_3$] just after the addition of acetylacetone has been explained by a mechanism involving the interaction of the complex with the β-diketone from the statistical treatment of optical data. This may support the conclusion that the ligand exchange in these cases proceeds by an interchange mechanism, although such a change was not clearly observed with the addition of Htfa to the [Fe(tta)$_3$] solution or with the addition of Htta to the [Fe(tfa)$_3$] solution. A similar change in the absorption, but probably due to a somewhat different cause, was also found in the "inert" solvent, benzene, in the previous paper.[6]

Adduct formation of uncharged chelate complexes in nonpolar solvents with an uncharged ligand has been studied from the stand point of the "synergistic effect" of solvent extraction.[7] The tendency of metal chelates with acetylacetone to accept a neutral ligand is generally smaller than of those with fluorinated β-diketones. It is also known that the neucleophilic tendency of ligands to form such adducts is greater with those ligands to form more stable complexes and, thus, Hacac should be more neucleophilic than the other two. From these, the interactions of the complex and the entering ligand should be stronger with the chelates with the fluorinated β-diketones and, thus, it seems to be reasonable that they tend to exchange by an interchange mechanism while that with acetylacetone exchanges by a dissociative mechanism. The values k_B for the reaction of [Fe(tfa)$_3$] and [Fe(tta)$_3$] in Table 2 correspond to the inverse of the formation constant of the interacted species. The value is smaller for reactions with [Fe(tfa)$_3$] with Hacac than with Htta (the former forms a larger amount of interacted species), and is nearly the same in the reactions of [Fe(tfa)$_3$] and [Fe(tta)$_3$] with Hacac and, thus, the adducts are similarly stable.

In the previous work,[2] a set of values of ΔH^* and ΔS^* for the ligand exchange of [Fe(acac)$_3$] with Htta in carbon tetrachloride was reported. However, from recalculations made using data obtained in both the previous and present work, it was concluded that the values in Table 2 should be employed. In the present study, the results of experiments with Htta were found to be less reproducible than those with other β-diketones.

In aqueous solutions, the water molecules might also act as an entering ligand whose concentration is constant and much higher than any other entering ligands present. Thus, formation of intermediates with water molecules is expected prior to the entrance of the ligand to be studied. Since no such intermediates with solvent molecules could be formed in carbon tetrachloride, the effect of the chemical properties of the ligands on the reaction mechanism could be recognized more clearly than in aqueous solutions. The use of benzene in the kinetic study of the ligand exchange of iron(III) complexes was reported[6] but since the ligands are different, no direct comparison of this previous study with the present one seems to be possible.

Isotopic ligand exchange of tris(acetylacetonato)-iron(III) in an acetylacetone medium was studied and the reaction mechanism was reported to be associative.[3] However, since the nature of the solvent and the enter-

ing ligand is different, the present results may not be compared directly with the previous study.

In a previous kinetic study of the isotopic ligand exchange of aluminium(III), indium(III), gallium(III), and beryllium(II) complexes where the ligand was 2,4-pentanedione, 1-phenyl-1,3-butanedione, or 1,3-diphenyl-1,3-propanedione in tetrahydrofuran, the rate was always lower when the acidity of the ligand was weaker (pK_a is greater).[8]

There have been other reports on the isotopic and non-isotopic ligand exchange of complexes of other metal ions in organic solvents (for example Refs. 9—14). However, direct comparison of the present data with these previous results does not seem to be possible because of the difference of the medium.

We are grateful to Dr. Shigeru Suzuki of the Tokyo College of Pharmacy, for the elementary analysis of the complexes.

References

1) T. Sekine and K. Inaba, *Chem. Lett.*, **1983**, 1669.
2) T. Sekine, H. Honda, M. Kokiso, and T. Tosaka, *Bull. Chem. Soc. Jpn.*, **52**, 1046 (1979).
3) H. Kido and K. Saito, *Bull. Chem. Soc. Jpn.*, **53**, 424 (1980).
4) T. Sekine and K. Inaba, *Bunseki Kagaku*, **31**, E291 (1982).
5) T. Sekine and K. Inaba, *Bull. Chem. Soc. Jpn.*, **55**, 3773 (1982).
6) G. Carta, F. Cristiani, P. Deplano, A. Diaz, and E. F. Trogu, *Inorg. Chim. Acta*, **59**, 101 (1982).
7) T. Sekine and Y. Hasegawa, "Solvent Extraction Chemistry," Marcel Dekker, New York (1977).
8) C. Chatterjee, K. Matsuzawa, H. Kido, and K. Saito, *Bull. Chem. Soc. Jpn.*, **47**, 2809 (1974).
9) D. L. Pisaniello, L. Helm, P. Meier, A. E. Merbach, *J. Am. Chem. Soc.*, **105**, 4528 (1983).
10) S. F. Lincoln, J. H. Coates, B. G. Doddridge, A. M. Hounslow, and D. L. Pisaniello, *Inorg. Chem.*, **22**, 2869 (1983).
11) Y. Ikeda, S. Soya, H. Fukutomi, and H. Tomiyasu, *J. Inorg. Nucl. Chem.*, **41**, 1333 (1979).
12) Y. Ikeda, H. Tomiyasu, and H. Fukutomi, *Bull. Chem. Soc. Jpn.*, **56**, 1061 (1983).
13) H. Doine, Y. Ikeda, H. Tomiyasu, and H. Fukutomi, *Bull. Chem. Soc. Jpn.*, **56**, 1989 (1983).
14) K. Ishihara, S. Funahashi, and M. Tanaka, *Inorg. Chem.*, **22**, 3589 (1983).

 © 1984 The Chemical Society of Japan Bull. Chem. Soc. Jpn., 57, 3088—3093 (1984) [Vol. 57, No. 11

Preparation of {*N*-(2-Aminoethyl)-1,3-propanediamine}(diethylenetriamine)-cobalt(III) Complex, and Separation and Optical Resolution of the Isomers

Minoru Ishii

Department of Chemistry, College of Science, Rikkyo (St. Paul's) University, Nishi-ikebukuro, Toshima-ku, Tokyo 171

(Received February 24, 1984)

The mixed ligand complex {*N*-(2-aminoethyl)-1,3-propanediamine}(diethylenetriamine)cobalt(III) was prepared. Of the five possible geometrical isomers, two were isolated by column chromatography; their formation ratio was *ca.* 6:4. Both isomers were completely resolved by chromatography. Their configurations were assigned to the meridional type on the basis of electronic, infrared, and circular dichroism spectroscopy, and the X-ray analysis data.

The linear triamine, *N*-(2-aminoethyl)-1,3-propanediamine ($NH_2CH_2CH_2CH_2NHCH_2CH_2NH_2$; abbreviated as aepn), can act as a terdentate ligand. It coordinates to the central metal ion in two topological ways. The mixed complex, $[Co(aepn)(dien)]^{3+}$ (dien; diethylenetriamine), exists in five geometrical isomers: Three *facial* (*fac*) isomers and two *meridional* (*mer*) isomers (Fig. 1). The difference between the two *mer*-geometries arises from the orientation of the N (secondary)–H bond in the dien ligand. Further, there are the optically active antipodes arising from an alternative configuration (*R*/*S*) of the secondary nitrogen atom in the aepn (Fig. 2). Thus, this isomerism can be expected to hold for the *mer*-isomers, and it should be recognized as a new type.

As a few examples of complexes which can be expected to show similar stereochemistry and isomerism, $[Co(dien)_2]^{3+}$,[1] $[Co(dema)(dien)]^{3+}$, $[Co(dema)_2]^{3+}$ (dema; *N*-methylbis(2-aminoethyl)amine),[2] and $[Co(dpt)_2]^{3+}$ (dpt; bis(3-aminopropyl)amine)[3] have been prepared and their spectroscopic data reported. Among these complexes, all three of the possible isomers of $[Co(dien)_2]^{3+}$ were isolated,[1] and the molecular structures were determined by the X-ray analysis of the *sym-fac*-$[Co(dien)_2]Br_3$,[4] $(-)_{589}$ *unsym-fac*-$[Co(dien)_2][Co(CN)_6]\cdot 2H_2O$[5] and $(+)_{589}$ *mer*-$[Co(dien)_2]Br_3\cdot 1.6H_2O$[6] crystals.

Various types of optically active complexes also have been reported recently and studied for their stereochemical geometries. With respect to the polyamine cobalt(III) complexes, a considerable number of determinations of absolute configurations were accomplished by an X-ray analysis technique. On the basis of these results, attempts to relate the spectroscopic data with the geometrical structures were carried out. Hence, it has become feasible to discuss quantitative details, such as the relationship between the absolute configuration and the circular dichroism (CD) spectrum, and the estimation of the contributions in the CD spectrum. This discussion is, however, limited to special types. Most of the empirical and quasi-empirical rules are useful for the complexes containing a five-membered chelate or planar six-membered chelate rings, but no

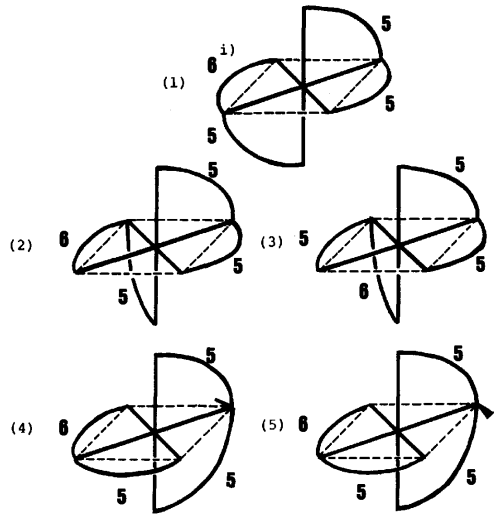

Fig. 1. Geometrical isomers of $[Co(aepn)(dien)]^{3+}$. (1): *sym-fac* type, (2),(3): *unsym-fac* type, (4),(5): *mer* type.
i) The numbers 5, 6 mean the number of chelate ring members.

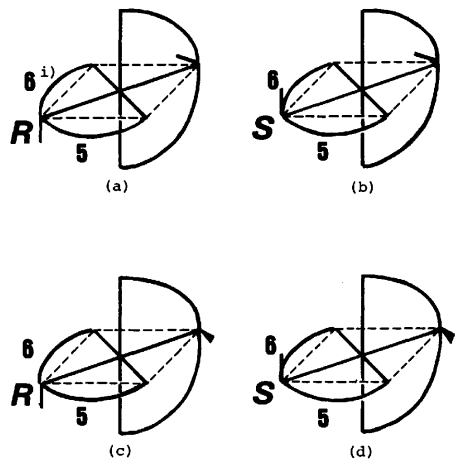

Fig. 2. Two types of *mer*-$[Co(aepn)(dien)]^{3+}$ and their antipodes.
mer-I type: (a) *trans*-δ-NH(*R*),[11] (b) *trans*-λ-NH (*S*), *mer*-II type : (c) *trans*-λ-NH(*R*), (d) *trans*-δ-NH(*S*).
i) The numbers 5, 6 mean the number of chelate ring members.
ii) See Appendix of Ref. 12.

rule is useful for the nonplanar six-membered chelate and larger chelate ring systems. In the [Co(aepn)(dien)]$^{3+}$ complex, three five-membered chelate rings and a six-membered one may coexist and be fused. From this viewpoint, it seemed that it would be interesting to investigate this complex. Moreover, the very fact that this is a new type of isomerism for the *mer*-isomers is worth noting.

In this paper, the preparation of [Co(aepn)(dien)]$^{3+}$, and its d-d absorption, CD and infrared spectra will be presented.

Experimental

Ligands and Reagents. The aepn and dien ligands were obtained from the Aldrich Chemical Co., Inc., and the Tokyo Kasei Co., Inc., respectively, and were used without further purification. The *mer*-[$CoCl_3$(dien)] complex was prepared according to the method described in the literature.[7] An ion-exchange resin (SP-Sephadex C-25) was obtained from Pharmacia Fine Chemicals Co., Inc. All the other reagents were obtained commercially.

Measurements. The elution curves were recorded with a Hitachi Perkin Elmer 139 spectrophotometer. The visible and near-ultraviolet absorption spectra were measured with a Hitachi EPS 3T spectrophotometer using 10-mm quartz cells. The CD spectra were obtained on a JASCO J-500 automatic spectropolarimeter using attached 10-mm quartz cells. The infrared spectra were measured with a JASCO A 202 infrared spectrophotometer by using Nujol mulls. All the spectral measurements were carried out at room temperature.

Analytical. The content of cobalt was colorimetrically determined by the nitroso-R method, while the contents of the other elements, C, H, N, and Cl, were measured at the Organic Analysis Center of the Institute of Physical and Chemical Research.

Preparation of the Complex, and Separation and Resolution of the Isomer. To 2.7 g of finely ground *mer*-[$CoCl_3$(dien)][7] suspended in 5 cm^3 of dimethyl sulfoxide (DMSO), 1.5 g of aepn was added in small portions, after which the mixture was stirred for 3 h at room temperature. The resulting orange solution was diluted with a small amount of water, and then the unreacted material was filtered off rapidly. The filtrate was poured into a SP-Sephadex C-25 column (H^+ form, ϕ 4 cm×*ca.* 30 cm) in several portions. After washing with 1.0 dm^3 of water and 1.0 dm^3 of 0.01 mol dm^{-3} hydrochloric acid, the elution was carried out with 0.10 mol dm^{-3} hydrochloric acid. The eluate was collected and evaporated to dryness with an evaporator (35 °C) to remove the hydrochloric acid. The residue was dissolved in a small amount of water. Upon the addition of $NaClO_4$, the resulting solution gave 3.7 g of the desired product in a 64% yield for perchlorate. This product was then dissolved in a small amount of water, and the solution was poured into a column containing the SP-Sephadex C-25 resin (H^+ form, ϕ 2.0 cm×*ca.* 100 cm) and washed with a large amount of water. When the elution was carried out with an acidic solution (pH≈2, 0.20 mol dm^{-3} Na_2SO_4+H_2SO_4), two orange-colored bands descended (the elution order: I, II).[8] The two eluates of these bands were independently collected and once more charged on a column of SP-Sephadex C-25 resin (H^+ form, ϕ 2.0 cm×*ca.* 100 cm). By elution with a 0.20 mol dm^{-3} sodium bis[(+)$_{589}$tartrato]diantimonate(III) solution, the two orange bands were separated. The four layers thus obtained (I-(1), I-(2), II-(1), and II-(2)) were optically active. The four eluents corresponding to these layers were independently collected and poured into a column of SP-Sephadex C-25 resin (H^+ form, ϕ 4.0 cm×*ca.* 30 cm). After having been washed with 2.0 dm^3 of water and 1.0 dm^3 of 0.01 mol dm^{-3} hydrochloric acid, elution with 0.10 mol dm^{-3} hydrochloric acid was carried out. The eluted solutions were evaporated to dryness at a low temperature (35 °C) and *in vacuo*. After the removal of the hydrochloric acid by evaporation, the residue was dissolved in a small amount of water. To this orange solution, $NaClO_4$ was added, after which the mixture was kept in a refrigerator. The orange precipitate was recrystallized from warm water. The analytical data of the four isomers thus obtained (I-(1), I-(2), II-(1), and II-(2)) are listed in Table 1.

Results and Discussion

The elution curves obtained at each step are shown in Fig. 3. Only two single bands are found in the first elution as shown in Fig. 3 (a) (the area ratio I:II is *ca.* 6:4); no indication of further separation can be recognized. On the preparation of complexes containing diverse ligands, it is generally known that a series of complexes which differ in the composition of the ligands is obtained as by-products. However, in the present reaction, there is little expectation that any [Co(dien)$_2$]$^{3+}$[9] and [Co(aepn)$_2$]$^{3+}$[10] can be obtained. In order to examine the behavior of these impurities in SP-Sephadex chromatography, these complexes were added beforehand to [Co(aepn)(dien)]$^{3+}$, and then the mixed samples (Fig. 4 (a), (b)) and a sample containing [Co(dien)$_2$]$^{3+}$ (Fig. 4 (c)) were eluted independently in a manner similar to the above. It was found that the behavior of *mer*-[Co(dien)$_2$]$^{3+}$ and the mixture of

Table 1. Elemental analysis of isomers

Isomer	Formula	Found (Calcd) (%)				
		Co	C	H	N	Cl
I-(1)	$CoC_9H_{28}N_6Cl_3O_4 \cdot H_2O$	12.78	23.48	6.30	17.73	22.30
		(12.60)	(23.11)	(6.47)	(17.97)	(22.74)
I-(2)	$CoC_9H_{28}N_6Cl_3O_4 \cdot H_2O$	12.35	22.39	5.97	17.34	22.55
		(12.60)	(23.11)	(6.47)	(17.97)	(22.74)
II-(1)	$CoC_9H_{28}N_6Cl_3O_{12} \cdot 1/2H_2O$	9.77	18.53	4.87	14.42	18.27
		(10.04)	(18.43)	(4.98)	(14.33)	(18.12)
II-(2)	$CoC_9H_{28}N_6Cl_3O_8 \cdot 1/2H_2O$	11.69	21.01	5.49	15.77	19.58
		(11.28)	(20.68)	(5.59)	(16.08)	(20.35)

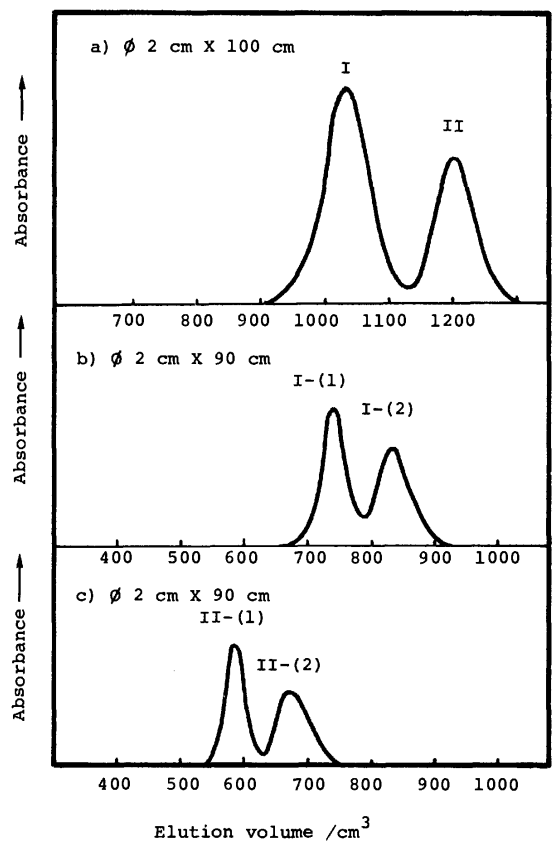

Fig. 3. Elution curves of the isomers of [Co(aepn)-(dien)]$^{3+}$ at 475 nm.
Eluents are as follows :
a) 0.20 mol dm^{-3} $Na_2SO_4+H_2SO_4$ acidic solution (pH≈2). b),c) 0.20 mol dm^{-3} sodium bis[(+)$_{589}$-tartrato]diantimonate(III) solution.

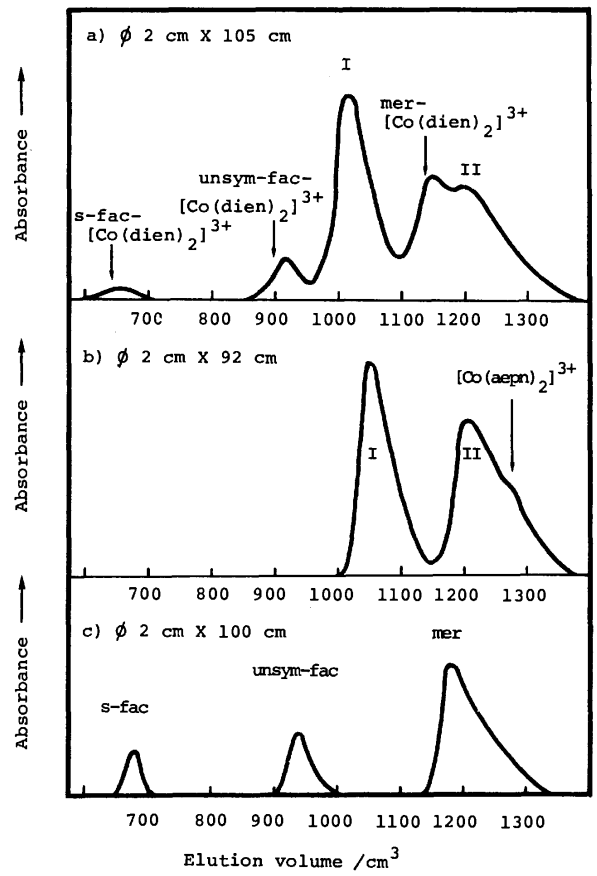

Fig. 4. Behavior of relevant complexes in column chromatography.
a): [Co(aepn)(dien)]$^{3+}$+[Co(dien)$_2$]$^{3+}$, b): [Co(apen)-(dien)]$^{3+}$+[Co(aepn)$_2$]$^{3+}$, c): [Co(dien)$_2$]$^{3+}$.
The eluent is 0.20 mol dm^{-3} $Na_2SO_4+H_2SO_4$ acidic solution (pH≈2).

isomers of [Co(aepn)$_2$]$^{3+}$ was somewhat analogous to that of the I and II isomers in chromatogram. However, careful and repeated elution of the I and II isomers of [Co(aepn)(dien)]$^{3+}$ did not provide any evidence indicating any further separation of other species. In the following elution, two bands with the area ratio of *ca.* 1:1 descended (Fig. 3 (b), (c)). From these facts, it was concluded that little or no [Co-(dien)$_2$]$^{3+}$ and [Co(aepn)$_2$]$^{3+}$ were obtained by this synthetic process; hence, the process was effective for the preparation of [Co(aepn)(dien)]$^{3+}$.

The absorption and CD spectra of the isolated isomers in the visible and near-ultraviolet region (18000—46000 cm^{-1}) are shown in Figs. 5 and 6 respectively, while their spectroscopic data are listed in Table 2. Among the absorption spectra, the positions and intensities of all the bands were approximately the same. In the three isomers (*mer-*, *unsym-fac-*, and *sym-fac-*) of [Co(dien)$_2$]$^{3+}$,[1] differences in the maxima of the absorption bands were observed. These facts indicate that the four isomers (I-(1), I-(2), II-(1), and II-(2)) of [Co(aepn)-(dien)]$^{3+}$ have a structural resemblance. Compared with the known complexes of the [Co(triamine)$_2$]$^{3+}$ type, the maximum of the first absorption band is at a lower energy side than those of the three isomers of [Co(dien)$_2$]$^{3+}$[1] and at a higher energy side than those of

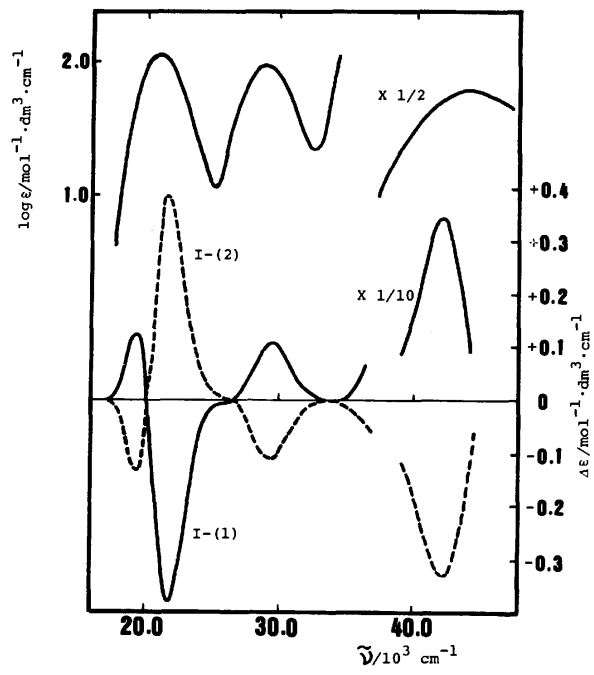

Fig. 5. Absorption and CD spectra of isomer I of [Co(aepn)(dien)]$^{3+}$.

$[Co(aepn)_2]^{3+}$ [10] and *mer*-$[Co(dpt)_2]^{3+}$.[3] These differences in absorption bands were concluded to be due to aepn which was located at a lower position than dien and at a higher position than dpt in the spectrochemical series. In a series of complexes of the $[Co(en)_x(tn)_y(tmd)_z]^{3+}$ type (x=0—3, y=0—3, z=0—3, $x+y+z$=3: tn=1,3-propanediamine, tmd=1,4-butanediamine), it was observed by Kojima *et al.*[11] that the maximum of the absorption bands shifted to the lower energy side as the number of ring members increased. A similar shift is observed for the complexes of the $[Co(triamine)_2]^{3+}$ type as the number of ring members increases from 5 to 6.

In the CD spectra as well as in the absorption spectra, a similarity in the band positions is also found for the four isomers. The pattern and magnitude of two pairs of the spectra, (I-(1) and I-(2), and II-(1) and II-(2)), are mirror images of each other. These findings indicate that they are two pairs of enantiomers with a structural resemblance; this fact agrees with the results obtained from chromatography.

The present author and his associates have already determined the molecular and absolute structures of the I-(1) isomer to be *mer-trans*-δ-NH(R) (corresponding to the *mer*-I type in Fig. 2 (a)) by the X-ray crystal analysis of the iodide monohydrate crystal.[12] Therefore, the structure of the antipode I-(2) can naturally be assigned to *mer-trans*-λ-NH(S) and, further, that of other pair (II-(1) and II-(2)), to the *mer*-II type isomers (Fig. 2 (c), (d)). The magnitudes of the CD spectra are rather weaker than those of the tris(chelate)cobalt(III) complexes in the d-d transition region. The values of $\Delta\varepsilon$ are of the same order of magnitude as those of the optically active forms of *mer*-$[Co(dien)_2]^{3+}$,[1] *mer*-[Co(dema)(dien)]$^{3+}$,[2] and *mer*-$[Co(dpt)_2]^{3+}$,[3] except that the major peak in the first absorption band region is somewhat intense. This finding is consistent with the assignment of the configuration presented above.

The infrared spectra of the I and II isomers are shown in Fig. 7. The similarity of these spectra also indicates that the structures of the two isomers

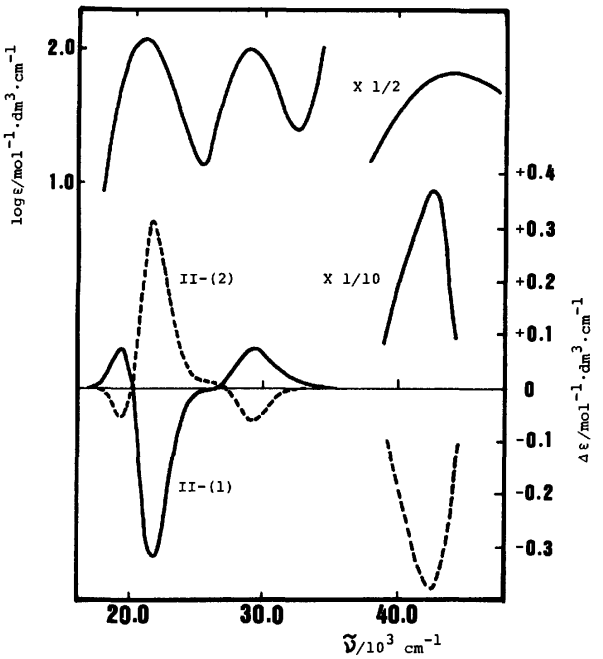

Fig. 6. Absorption and CD spectra of isomer II of [Co(aepn)(dien)]$^{3+}$.

Table 2. Absorption and CD spectra

Isomer	Absorption spectra		CD spectra	
	$\tilde{\nu}_{max}$ / cm^{-1}	log ε / mol^{-1} dm^3 cm^{-1}	$\tilde{\nu}_{max}$ / cm^{-1}	$\Delta\varepsilon$ / mol^{-1} dm^3 cm^{-1}
I-(1)	21150	2.05	19450	+0.128
			21700	−0.384
	29100	1.99	29500	+0.107
	44200	4.30	42400	+3.42
I-(2)	21150	2.05	19450	−0.140
			21700	+0.386
	29100	1.99	29500	−0.110
	44200	4.30	42200	−3.30
II-(1)	21160	2.06	19450	+0.078
			21750	−0.322
	28950	2.00	29100	+0.074
	44200	4.30	42400	+3.76
II-(2)	21160	2.06	19450	−0.056
			21750	+0.310
	28950	2.00	29100	−0.060
	44200	4.30	42400	−3.76

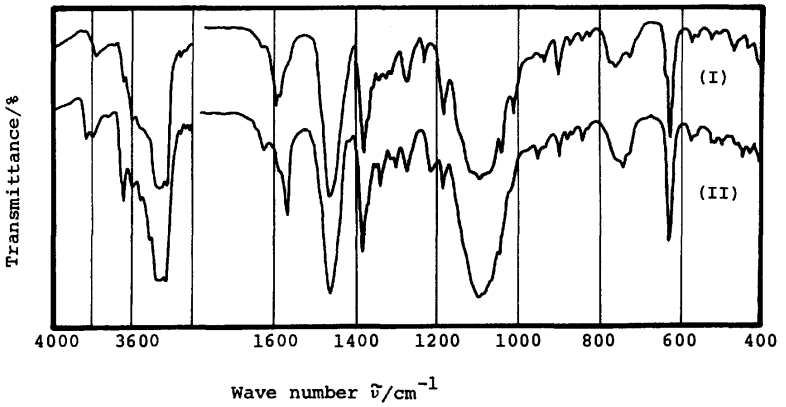

Fig. 7. Infrared spectra of *mer*-[Co(aepn)(dien)]$^{3+}$.

resemble each other. In $[Co(dien)_2]^{3+}$, Yoshikawa and Yamasaki[1] identified the absorption bands at 1610—1550 cm^{-1} as antisymmetric NH_2 bending vibrations and observed a larger splitting for the *mer*-isomer. In the case of $[Co(aepn)(dien)]^{3+}$, similar splitting was observed (I; 1585, 1595, 1625 cm^{-1}, II; 1570, 1585(sh), 1625 cm^{-1}). This observation confirmed that I and II are *mer*-type isomers.

Yoshikawa and Yamasaki investigated in detail the isomeric ratio of $[Co(dien)_2]^{3+}$[1] and $[Co(dema)(dien)]^{3+}$[2] using several synthetic pathways, and reported that the use of *mer*-$[CoCl_3(dien)]$ as a starting material gave the *mer*-isomer in an overwhelming yield. This agrees with the results obtained in the present paper. Thus, in the *mer*-$[CoCl_3(dien)] \rightarrow [Co(aepn)(dien)]^{3+}$ process, clearly no rearrangement of the configuration occurred. Therefore, the remaining three *fac*-isomers were not obtained through this synthetic pathway. The *fac*-$[CoCl_3(dien)]$ complex seems to be one of the most suitable starting materials for the *fac*-$[Co(aepn)(dien)]^{3+}$; unfortunately, this complex is not yet well known. The present author's attempts to obtain this complex were unsuccessful. Some synthetic attempts to obtain these *fac*-$[Co(aepn)(dien)]^{3+}$ were, therefore, carried out with the use of typical compounds as raw materials.

1) The oxidation of a mixture containing equivalent amounts of $CoCl_2 \cdot 6H_2O$, dien, and aepn with an air stream in the presence of active charcoal.

2) The stirring of a mixture containing equivalent amounts of $[CoCl(NH_3)_5]^{2+}$, dien, and aepn.

Both methods were carried out in aqueous solutions and gave large amounts of the by-products, $[Co(dien)_2]^{3+}$ and $[Co(aepn)_2]^{3+}$, and a small amount of $[Co(aepn)(dien)]^{3+}$. The $[Co(aepn)(dien)]^{3+}$ thus obtained was chromatographically identified as consisting of *mer*-isomers. The *fac*-isomers were never isolated or detected, however. For both synthetic pathways, further attempts were carried out in the nonaqueous solvent DMSO. The reaction, however, did not proceed, and $[Co(aepn)(dien)]^{3+}$ was not obtained. Therefore, no *fac*-$[Co(aepn)(dien)]^{3+}$ has yet been isolated, though there may be a possibility of formation *via* other pathways. However, in the case of the $[Co(triamine)_2]^{3+}$ complexes, it is known that the *mer*-isomer is obtained as the chief product. In particular, it has been observed that any attempts to prepare $[Co(dpt)_2]^{3+}$ gave only the *mer*-isomer.[3] These facts suggest that the probability of obtaining the *fac*-$[Co(aepn)(dien)]^{3+}$ isomers is low.

The CD spectrum of the I-(1) isomer has a small positive peak on the lower energy side of the first absorption band region and a main negative peak on the higher energy side. As has been mentioned before, Okiyama *et al.* determined the molecular structure of a similar *mer*-type complex, *mer*-$[Co(dien)_2]^{3+}$, by the X-ray analysis of the $(+)_{589}$ *mer*-$[Co(dien)_2]Br_3 \cdot 1.6H_2O$ crystal; the absolute configuration of this antipode, which showed a main negative peak in the first absorption band region (19500 cm^{-1} $\Delta\varepsilon$=+0.096 mol^{-1} dm^3 cm^{-1}, 21900 cm^{-1} $\Delta\varepsilon$=−0.181 mol^{-1} dm^3 cm^{-1}), was assigned to *trans*-λ-NH. In the present work, an obvious inversion was observed for the CD pattern between *mer-trans*-δ-NH-$[Co(dien)_2]^{3+}$ and *mer-trans*-δ-NH(*R*)-$[Co(aepn)(dien)]^{3+}$ (or *mer-trans*-λ-NH-$[Co(dien)_2]^{3+}$ and *mer-trans*-λ-NH(*S*)-$[Co(aepn)(dien)]^{3+}$). At first sight, *mer*-$[Co(dien)_2]^{3+}$ appears to have pseudo-planes of symmetry and two-fold axes of rotation in the octahedral situation. However, the possibility of a second source of asymmetry arises in this situation. Since the conformations of the two fused five-membered chelate rings must be δ and λ, the chiral contribution from the conformational effects may be cancelled out. The net chirality in the optically active geometry probably comes from the stereochemical relationship between the two N(secondary)–H bonds of two dien ligands. In contrast to this simple model, the chirality of *mer*-$[Co(aepn)(dien)]^{3+}$ may be complicated by the presence of the six-membered chelate ring of the aepn ligand; that is, the contributions coming from the asymmetric secondary nitrogen of aepn and from the remaining conformational effect must be applied. As has been mentioned above, the isomerism of *mer*-$[Co(aepn)(dien)]^{3+}$ is a new type. For example, in the case of the $[Co(triamine)_2]^{3+}$ complex, neither theoretical attempts nor empirical attempts to estimate these contributions were carried out. However, it will be possible to find, in the complexes containing quadridentate tetramine ligands, convenient models which possess this geometrical feature in common with the *mer*-$[Co(aepn)(dien)]^{3+}$. Among these models, *trans*-(*R*,*R*)-$[Co(3,2,3\text{-tet})XY]^{n+}$ (n=1, 2, 3: X, Y=unidentate ligands: 3,2,3-tet=4,7-diazadecane-1,10-diamine; Fig. 8) could be one of the complexes which would supply useful clues. Since the 3,2,3-tet moiety of this complex coincides with those of the aepn of *mer-trans*-δ-NH(*R*) (Fig. 2 (a), *mer*-I) and *mer-trans*-λ-NH(*R*)-$[Co(aepn)(dien)]^{3+}$ (Fig. 2 (c), mer-II), there are extensive similarities between the geometries of these species. Bosnich and Harrowfield[13] have studied in detail the spectra of *trans*-(*R*,*R*)-$[Co(3,2,3\text{-tet})XY]^{n+}$. In the case of X=Y=$NH_3$, a typical CoN_6 species, they found that *trans*-(*R*,*R*)-$[Co(3,2,3\text{-tet})(NH_3)_2]^{3+}$ had a main negative peak in the first absorption band region. From the structure shown in Fig. 8, it is clear that the chirality of the 3,2,3-tet complex arises exclusively from the contributions of the configurations of the asymmetric nitrogen atoms and the conformations of the chelate rings. Thus, the main negative peak can be expected to reflect these contributions exactly. The chirality of

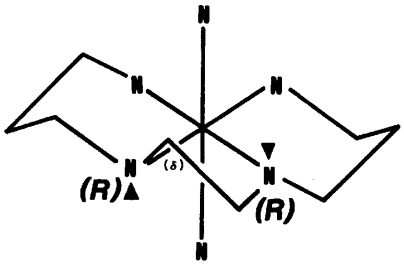

Fig. 8. Conformation of *trans*-(*R*,*R*)-$[Co(3,2,3\text{-tet})(NH_3)_2]^{3+}$.

mer-[Co(aepn)(dien)]$^{3+}$ came from the effects of the relationships between the two *trans*-NH bonds, the configuration of the asymmetric atom, and the conformation of the chelate rings, as has previously been described. In the first absorption band region, the main negative peak observed for *mer-trans-δ*-NH(*R*)-[Co(aepn)(dien)]$^{3+}$ suggests that the last two contributions may be superior to the first. It is clear that the inversion of the CD pattern in this region is attributable to differences between the magnitudes of these contributions. This finding can help us establish the relationships between the sign of the CD main peak in the first absorption band region and the situation of aepn. By the use of these relationships, the following structures of the remaining enantiomers can be assigned: II-(1); *trans-λ*-NH(*R*), and II-(2); *trans-δ*-NH(*S*).

In *mer*-[Co(dpt)$_2$]$^{3+}$, Yamada *et al.*[3] obtained a CD spectrum with an extraordinarily small value of $\Delta\varepsilon$ and predicted a decrease in the contribution from the two N-H bonds as a result of a flattering of the four six-membered rings. For *mer*-[Co(aepn)(dien)]$^{3+}$ also, such a decrease can be expected.

The author gratefully acknowledges the valuable discussions and encouragement to Professor M. Nakahara of Rikkyo (St. Paul's) University during the course of this work.

References

1) Y. Yoshikawa and K. Yamasaki, *Bull. Chem. Soc. Jpn.*, **45**, 179 (1972).

2) M. Kojima, M. Iwagami, Y. Yoshikawa, and J. Fujita, *Bull. Chem. Soc. Jpn.*, **50**, 3216 (1977).

3) S. Yamada, M. Umehara, M. Ishii, and M. Nakahara, *Nippon Kagaku Kaishi*, **1983**, 1733.

4) M. Kobayashi, F. Marumo, and Y. Saito, *Acta Crystallogr., Sect. B*, **28**, 470 (1972).

5) M. Konno, F. Marumo, and Y. Saito, *Acta Crystallogr., Sect. B*, **29**, 739 (1973).

6) K. Okiyama, S. Sato, and Y. Saito, *Acta Crystallogr., Sect. B*, **35**, 2389 (1979).

7) D. A. House, *Inorg. Nucl. Chem. Lett.*, **3**, 67 (1967).

8) By the use of a 0.20 mol dm^{-3} Na_2SO_4 solution (pH≈7) as an eluent, two bands were also eluted from the column of the Na^+ from. However, they isomerized to each other while being purified. When the elution was carried out with a 0.20 mol dm^{-3} Na_2SO_4+H_4SO_4 acidic solution (pH≈2), a mixture of the isomers was separated into two bands which behaved chromatographically like the I and II isomers. In an earlier paper (Ref. 12), the present author and his associates reported a separation into four layers. It seems clear that this earlier report overlooked this isomerization and so should be amended here.

9) The [Co(dien)$_2$]$^{3+}$ was prepared according to Method C described in Ref. 1 of this paper.

10) A paper to be submitted to *Bull. Chem. Soc. Jpn.*, will describe the preparation and isolation of the isomers in detail. Under these conditions, the [Co(aepn)$_2$]$^{3+}$ showed no separation. The absorption spectroscopic data of the mixture are as follows: 20900 cm^{-1} (log ε=1.95 mol^{-1} dm^3 cm^{-1}), 29000 cm^{-1} (log ε=2.08 mol^{-1} dm^3 cm^{-1}).

11) M. Kojima, H. Yamada, H. Ogino, and J. Fujita, *Bull. Chem. Soc. Jpn.*, **50**, 2325 (1977).

12) M. Ishii, S. Sato, Y. Saito, and M. Nakahara, *Chem. Lett.*, **1981**, 1613; *Bull. Chem. Soc. Jpn.*, **57**, 3094 (1984).

13) B. Bosnich and J. M. Harrowfield, *Inorg. Chem.*, **14**, 828 (1975).

Crystal Structure of $(-)^{CD}_{474}$ *mer*-{*N*-(2-Aminoethyl)-1,3-propanediamine}(diethylenetriamine)cobalt(III) Iodide Monohydrate, $(-)^{CD}_{474}$ *mer*-[Co(aepn)(dien)]$I_3 \cdot H_2O$

Minoru Ishii,* Shoichi Sato,† Yoshihiko Saito,†† and Masayoshi Nakahara
Department of Chemistry, College of Science, Rikkyo (St. Paul's) University, Nishi-ikebukuro, Toshima-ku, Tokyo 171
†*The Institute for Solid State Physics, The University of Tokyo, Roppongi 7, Minato-ku, Tokyo 106*
††*Department of Chemistry, Faculty of Science and Technology, Keio University, 3-14-1, Hiyoshi, Kohoku-ku, Yokohama 223*
(Received February 24, 1984)

The crystal structure of $(-)^{CD}_{474}$ *mer*-[Co{*N*-(2-aminoethyl)-1,3-propanediamine}(diethylenetriamine)]$I_3 \cdot H_2O$ has been determined by means of X-ray diffraction. The crystal is monoclinic, with a space group of $P2_1$, a=9.662 (2), b=14.602(2), c=8.201(3), β=112.87(4)°, and Z=2. The structure was solved by the Patterson-Fourier method and refined by the full-matrix least-squares method, which yielded an R value of 0.060 for the 2441 observed reflections. Each ligand molecule acts as a terdentate with meridional configurations. The absolute configuration of the coordinated asymmetric nitrogen atom in *N*-(2-aminoethyl)-1,3-propanediamine was determined to be *R*. The six-membered chelate ring in *N*-(2-aminoethyl)-1,3-propanediamine adopts a chair conformation, and the conformation of the five-membered chelate ring is δ. The conformations of the two five-membered chelate rings formed by diethylenetriamine are δ and λ, and the N(secondary)-H bond is oriented toward the six-membered chelate ring formed by *N*-(2-aminoethyl)-1,3-propanediamine.

Two linear triamines, *N*-(2-aminoethyl)-1,3-propanediamine ($NH_2CH_2CH_2CH_2NHCH_2CH_2NH_2$: abbreviated as aepn) and diethylenetriamine ($NH_2CH_2CH_2NHCH_2CH_2NH_2$; abbreviated as dien), can act as terdentate ligands and coordinate to the central metal ion in two topological modes. The cobalt(III) complex, $[Co(aepn)(dien)]^{3+}$, which contains three five-membered chelate rings and one six-membered ring, can exist in five geometrical isomers, as is shown in Fig. 1. The two *mer*-isomers differ in the orientation of the N(secondary)–H bond in the dien ligand. Further, the optical isomers arising from the alternative disposition of the N–H bond of the secondary nitrogen atom in aepn (*R*/*S*) can be expected for each of the two *mer*-geometries (Fig. 2).

Three *mer* type complexes, *mer*-$[Co(dien)_2]^{3+}$,[1] *mer*-[Co(dema)(dien)]$^{3+}$ (dema; *N*-menthylbis(2-aminoethyl)-amine),[2] and *mer*-$[Co(dpt)_2]^{3+}$ (dpt; bis(3-aminopropyl)amine),[3] have been prepared. The crystal structure of $(+)_{589}$*mer*-$[Co(dien)_2]Br_3 \cdot 1.6H_2O$ has previously been determined, and the absolute configuration of the complex ion has been identified as *trans*-λ-NH.[4]

Complexes with five-membered chelate rings have been extensively studied, but little is known concerning the complexes involving a six-membered chelate ring. Thus, it is of interest to study the stereochemistry

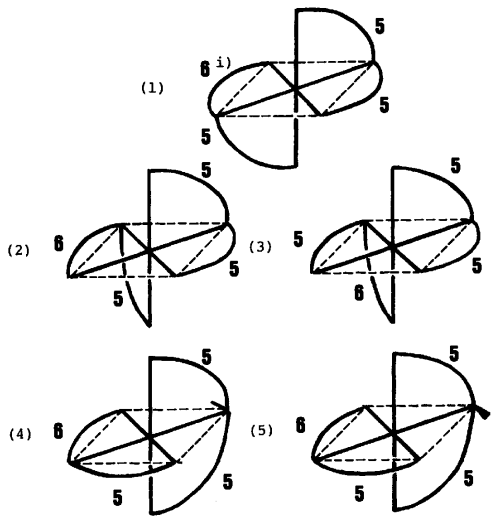

Fig. 1. Geometrical isomers of $[Co(aepn)(dien)]^{3+}$ (1): *sym-fac* type, (2),(3): *unsym-fac* type, (4),(5): *mer* type.
i) Numbers 5, 6 indicate the number of chelate ring members.

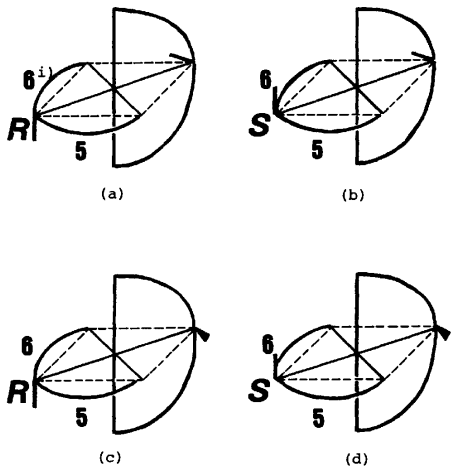

Fig. 2. Two types of *mer*-$[Co(aepn)(dien)]^{3+}$ and their antipodes (simplified).
mer-I type: (a) *trans*-δ-NH(*R*),[11] (b) *trans*-λ-NH(*S*)
mer-II type: (c) *trans*-λ-NH(*R*), (d) *trans*-δ-NH(*S*).
i) Numbers 5, 6 indicate the number of chelate ring members. ii) See Appendix.

of $[Co(aepn)(dien)]^{3+}$.

In this paper, the structure and the absolute configuration of $(-)^{CD}_{474}$ *mer*-{*N*-(2-aminoethyl)-1,3-propanediamine}(diethylenetriamine)cobalt(III) iodide monohydrate, $(-)^{CD}_{474}$ *mer*-[Co(aepn)(dien)]$I_3 \cdot H_2O$ are reported.

Experimental

The $[Co(aepn)(dien)]^{3+}$ complex was prepared by the method described in the literature.[5] Of the two fractions obtained by means of SP-Sephadex C-25 ion-exchange chromatography, the faster one was collected and resolved by this chromatography. The $(-)^{CD}_{474}$ isomer was converted into iodide in the anion-exchange region (I^- form, ϕ 1.0 cm×30 cm), and the effluent was evaporated to a few cm^3 under reduced pressure. Crystals were grown from an aqueous solution acidified with acetic acid, and elemental analyses gave:

Found: C, 15.87; H, 4.30; N, 12.54%. Calcd for $Co(C_9H_{28}N_6)I_3 \cdot H_2O$: C, 15.94; H, 4.46; N, 12.39%.

The crystals are orange-red, transparent hexagonal prisms. They are monoclinic. The observed systematic absences on Weissenberg photographs, *0, k, 0* for $k=2n$, indicated that the possible space group was $P2_1$ or $P2_1/m$. Since the crystal was optically active, the space group was uniquely determined to be $P2_1$.

Crystal data:

$(-)^{CD}_{474}$*mer*-[Co(aepn)(dien)]$I_3 \cdot H_2O$, $Co(C_9H_{28}N_6)I_3 \cdot H_2O$ $M_w=678.02$, monoclinic, $a=9.662(3)$, $b=14.602(2)$, $c=8.201(3)$ Å, $\beta=112.87(4)°$, $V=1065.9(4)$ Å^3, $Z=2$, $D_m=2.19$ ($D_c=2.11$) g cm^{-3}, μ for Mo $K\alpha$ ($\lambda=0.7107$ Å) $=51.10$ cm^{-1}, space group $P2_1$.

A crystal with dimensions of *ca.* 0.4×0.2×0.15 mm^3 was used for the intensity measurements. The intensities were collected on a PHILIPS 1100 four-circle diffractometer with graphite-monochromated Mo $K\alpha$ radiation up to $2\theta=70°$, the θ-2θ scan technique being employed. Independent 2441 reflections with $|F_o|<3\sigma(|F_o|)$ were used for the structure determination. The usual corrections were made for the Lorentz, polarization, and absorption factors, but no correction was applied for extinction. The structure was solved by the Patterson-Fourier method with a local version of UNICS.[6] The calculations were carried out on a FACOM M-160F computer at the Institute for Solid State Physics (The University of Tokyo) and on a HITAC 200H computer at the Computer Center of the University of Tokyo.

Determination and Refinement of the Structure

The positions of the I and Co atoms were deduced from three-dimensional Patterson maps, while the positions of all the non-hydrogen atoms were derived by the Fourier method. They were refined by the block-diagonal least-squares method with anisotropic thermal parameters. At the stage of $R=0.074$, eight hydrogen atoms among the twenty-eight hydrogen atoms (except for those of the water molecule) were found from a different synthesis. The positions of the remaining twenty hydrogen atoms were located theoretically. The final refinement was carried out using the full-matrix least-squares program LINUS[7] with anisotropic thermal parameters for non-hydrogen atoms and isotropic ones for hydrogen atoms. The final R and R_2 values were 0.060 and 0.073 respectively.[8]

The absolute structure was determined by the anomalous-scattering technique. Some $h\ k\ l$ and $h\ \bar{k}\ l$ pairs were examined on Weissenberg photographs recorded using Cu $K\alpha$ radiation. As is shown in Table 1, a comparison of the observed and calculated differences between $|F(hkl)|$ and $|F(h\bar{k}l)|$ indicates that the calculated values differ by more than 10%. The concordance in Table 1 indicates that the $(-)^{CD}_{474}$-isomer has the absolute configuration illustrated in Fig. 4. The enantiomeric structure was refined in the same way and converged at residuals $R=0.061$ and $R_2=0.074$. The application of the R-factor ratio test[9] showed that the latter can be rejected at the 0.05 significance level in favor of the former.

The final atomic parameters and thermal factors of non-hydrogen atoms and hydrogen atoms are given in Tables 2 and 3 respectively.[10]

Results and Discussion

A projection of the crystal structure along *b*, and

Table 1. Determination of the absolute configuration

$h\ k\ l$	$F_c(hkl)$	Observed	$F_c(\bar{h}kl)$
3 1 2	50.0	>	42.3
3 3 2	73.6	<	81.3
7 1 0	30.6	<	36.4
7 1 1	24.1	>	14.2
7 2 2	49.8	<	55.0

Table 2. Final atomic positional parameters and equivalent temperature factors for non-hydrogen atoms, with their estimated standard deviations in parentheses

Atom	x	y	z	U_{eq}(Å^2)[a]
I (1)	0.0580(1)	0.4155(2)	0.0360(2)	0.051(1)
I (2)	0.3290(1)	0.1805(1)	0.7830(2)	0.042(<1)
I (3)	0.3524(2)	0.8072(1)	0.5169(2)	0.043(<1)
Co	0.3023(2)	0.5000(0)	0.6612(2)	0.020(1)
N (1)	0.0990(11)	0.5180(8)	0.6464(17)	0.022(4)
N (2)	0.2614(12)	0.5689(7)	0.4356(16)	0.021(4)
N (3)	0.5101(11)	0.4856(7)	0.6693(17)	0.020(4)
N (4)	0.3519(12)	0.4238(8)	0.8782(16)	0.021(4)
N (5)	0.3470(14)	0.6158(7)	0.7993(18)	0.023(5)
N (6)	0.2187(13)	0.3891(7)	0.5167(16)	0.021(4)
C (1)	−0.0108(16)	0.4723(11)	0.4920(21)	0.042(6)
C (2)	0.0607(16)	0.3722(9)	0.4991(23)	0.044(6)
C (3)	0.0734(19)	0.6181(11)	0.6670(26)	0.054(7)
C (4)	0.2151(19)	0.6484(10)	0.8310(23)	0.050(7)
C (5)	0.3877(15)	0.5533(10)	0.3793(22)	0.042(6)
C (6)	0.5299(15)	0.5539(10)	0.5420(21)	0.040(6)
C (7)	0.6384(16)	0.4881(13)	0.8377(23)	0.050(7)
C (8)	0.6273(15)	0.4141(13)	0.9690(23)	0.054(7)
C (9)	0.5024(18)	0.4331(12)	1.0268(21)	0.047(6)
O (W)	0.0213(38)	0.6677(37)	0.1454(74)	0.222(35)

a) $U_{eq}=1/3(U_{11}+U_{22}+U_{33}+2U_{13}\cos\beta)$.

a perspective drawing of the complex cation are shown in Figs. 3 and 4 respectively. The two ligands coordinate to the central cobalt atom in *mer* positions by means of their six nitrogen atoms, thus forming a slightly distorted octahedral complex. The complex

Table 3. Final atomic positional parameters and equivalent temperature factors for hydrogen atoms, with their estimated standard deviations in parentheses

Atom	x	y	z	U_{eq}(Å^2)[a]
H1(N1)	0.084(0)	0.487(0)	0.747(0)	0.057(0)
H1(N2)	0.209(23)	0.651(16)	0.428(30)	0.067(64)
H2(N2)	0.165(0)	0.546(0)	0.342(0)	0.057(0)
H1(N3)	0.512(0)	0.419(0)	0.633(0)	0.057(0)
H1(N4)	0.260(0)	0.418(0)	0.907(0)	0.057(0)
H2(N4)	0.342(0)	0.359(0)	0.837(0)	0.057(0)
H1(N5)	0.433(0)	0.606(0)	0.912(0)	0.057(0)
H2(N5)	0.375(0)	0.664(0)	0.728(0)	0.057(0)
H1(N6)	0.220(0)	0.398(0)	0.394(0)	0.057(0)
H2(N6)	0.258(0)	0.320(0)	0.561(0)	0.057(0)
H1(C1)	−0.028(21)	0.536(15)	0.393(26)	0.056(53)
H2(C1)	−0.111(0)	0.468(0)	0.501(0)	0.057(0)
H1(C2)	0.004(0)	0.337(0)	0.388(0)	0.057(28)
H2(C2)	0.059(0)	0.337(0)	0.603(0)	0.057(0)
H1(C3)	0.068(0)	0.660(0)	0.564(0)	0.057(0)
H2(C3)	0.007(13)	0.651(9)	0.717(17)	0.011(28)
H1(C4)	0.230(0)	0.706(0)	0.844(0)	0.057(0)
H2(C4)	0.214(0)	0.620(0)	0.943(0)	0.057(0)
H1(C5)	0.375(0)	0.496(0)	0.312(0)	0.057(0)
H2(C5)	0.389(0)	0.606(0)	0.296(0)	0.057(0)
H1(C6)	0.516(28)	0.627(20)	0.553(31)	0.091(81)
H2(C6)	0.607(13)	0.520(9)	0.526(17)	0.010(28)
H1(C7)	0.745(22)	0.481(16)	0.842(26)	0.055(56)
H2(C7)	0.644(0)	0.550(0)	0.892(0)	0.057(0)
H1(C8)	0.724(0)	0.413(0)	1.075(0)	0.057(0)
H2(C8)	0.611(0)	0.353(0)	0.910(0)	0.057(0)
H1(C9)	0.504(0)	0.383(0)	1.132(0)	0.057(0)
H2(C9)	0.516(18)	0.506(14)	1.091(23)	0.047(0)

a) $U_{eq}=1/3(U_{11}+U_{22}+U_{33}+U_{13}\cos\beta)$.

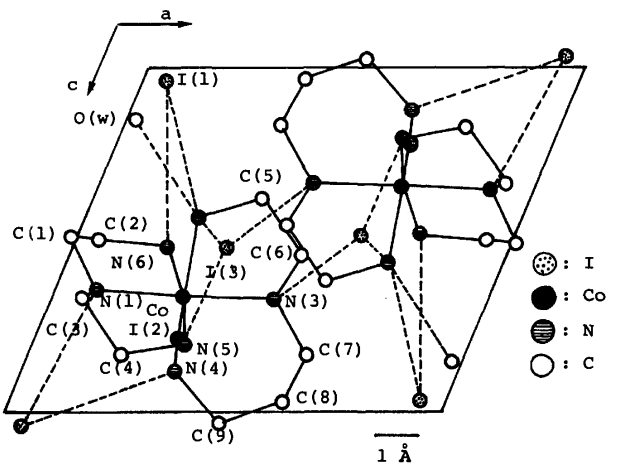

Fig. 3. A projection of the crystal structure along *b*.

cation, $(-)^{CD}_{474}$ *mer*-[Co(aepn)(dien)]$^{3+}$ corresponds to the *mer*-I type (Fig. 2 (a)). The absolute configuration of the asymmetric nitrogen atom (N(3)) was determined to be *R*.[11] The structure shown in Fig. 4 was assigned to *trans*-δ-NH(*R*) (Fig. 2 (a)).[12] The conformations of the two fused five-membered chelate rings in dien were δ and λ, in agreement with the observation for $(+)_{589}$ *mer*-[Co(dien)$_2$]Br$_3\cdot$1.6H$_2$O.[4] The conformation of the six-membered chelate ring formed by aepn was chair (Fig. 5), and the conformation of its five-membered chelate ring was δ.

The bond distances and angles in the complex ion are listed in Table 4, together their estimated standard deviations.

The Co-N(secondary) bond distance in dien (Co-N(1)) is significantly shorter than the Co-N(terminal) bond distances (Co-N(5), Co-N(6)). Such a trend was also observed for $(+)_{589}$ *mer*-[Co(dien)$_2$]Br$_3\cdot$1.6H$_2$O[4] and $(-)_{589}$*unsym-fac*-[Co(dien)$_2$][Co(CN)$_6$]$\cdot$2H$_2$O.[13] In contrast to this, the three Co-N distances (Co-N(2), Co-N(3), and Co-N(4)) in aepn are within 1.0σ of each other.

The N(terminal)-Co-N(terminal) angles in the five-membered chelate rings (N(1)-Co-N(6), N(1)-Co-N(5), and N(2)-Co-N(3)) are smaller than 90°, in agreement with the result obtained for similar complexes containing five-membered chelate rings.[14]

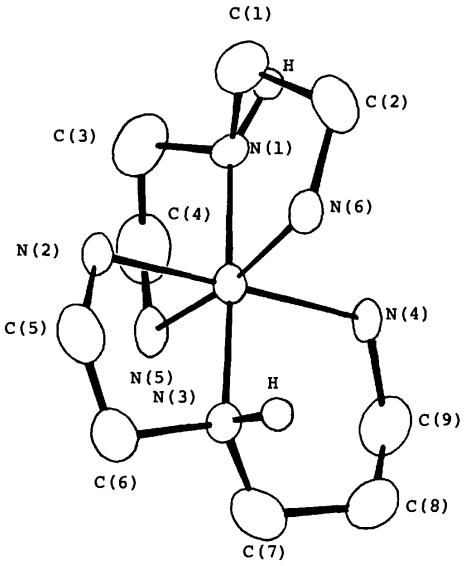

Fig. 4. A perspective drawing of the complex cation.

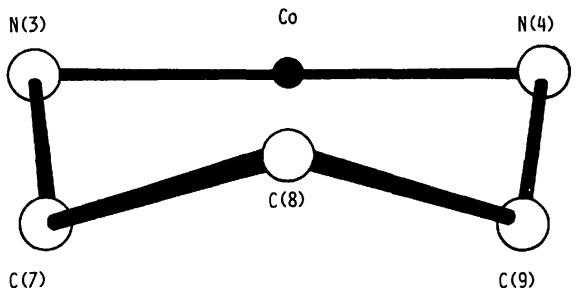

Fig. 5. Edge-on view of the chelate ring with respect to the plane formed by the Co and two N atoms.

TABLE 4. BOND DISTANCES AND ANGLES WITHIN THE COMPLEX CATION, *mer*-[Co(aepn)(dien)]$^{3+}$, WITH THEIR ESTIMATED STANDARD DEVIATIONS IN PARENTHESES

Bond distance	l/Å	Bond distance	l/Å
Co-N (1)	1.939 (12)	N (3) - C (7)	1.454 (17)
Co-N (2)	2.006 (13)	N (4) - C (9)	1.497 (17)
Co-N (3)	1.994 (12)	N (5) - C (4)	1.476 (25)
Co-N (4)	1.993 (12)	N (6) - C (2)	1.497 (21)
Co-N (5)	1.988 (11)		
Co-N (6)	1.984 (11)	C (1) - C (2)	1.607 (21)
		C (3) - C (4)	1.565 (21)
N (1) - C (1)	1.460 (17)	C (5) - C (6)	1.498 (18)
N (1) - C (3)	1.503 (20)	C (7) - C (8)	1.558 (28)
N (2) - C (5)	1.481 (23)	C (8) - C (9)	1.485 (27)
N (3) - C (6)	1.509 (22)		

Bond angle	ϕ/°	Bond angle	ϕ/°
N (1) - Co - N (2)	92.4 (5)	N (1) - Co - N (6)	84.6 (5)
N (1) - Co - N (3)	177.7 (5)	N (2) - Co - N (3)	85.3 (5)
N (1) - Co - N (4)	91.0 (5)	N (2) - Co - N (4)	175.2 (5)
N (1) - Co - N (5)	84.9 (5)	N (2) - Co - N (5)	91.1 (5)
N (2) - Co - N (6)	88.3 (5)		
N (3) - Co - N (4)	91.2 (5)	C (1) - N (1) - C (3)	116.5 (11)
N (3) - Co - N (5)	94.5 (5)	C (6) - N (3) - C (7)	110.5 (11)
N (3) - Co - N (6)	96.0 (5)		
N (4) - Co - N (5)	92.4 (5)	N (1) - C (1) - C (2)	103.1 (10)
N (4) - Co - N (6)	88.8 (5)	N (1) - C (3) - C (4)	104.1 (11)
N (5) - Co - N (6)	169.4 (5)	N (2) - C (5) - C (6)	107.6 (13)
		N (3) - C (6) - C (5)	107.1 (11)
Co - N (1) - C (1)	111.7 (10)	N (3) - C (7) - C (8)	112.2 (14)
Co - N (1) - C (3)	109.4 (9)	N (4) - C (9) - C (8)	112.1 (14)
Co - N (2) - C (5)	108.6 (9)	N (5) - C (4) - C (3)	106.5 (14)
Co - N (3) - C (6)	107.7 (8)	N (6) - C (2) - C (1)	105.2 (11)
Co - N (3) - C (7)	120.3 (10)		
Co - N (4) - C (9)	119.8 (9)	C (7) - C (8) - C (9)	112.0 (15)
Co - N (5) - C (4)	111.3 (10)		
Co - N (6) - C (2)	110.8 (10)		

In the six-membered ring, this angle (N(3)-Co-N(4)) is slightly greater than 90°. The Co-N-C angles (Co-N(3)-C(7), Co-N(4)-C(9)) are larger by 10% than the other bond angles in the chelate ring. The six-membered chelate ring is thus flattened like those in $[Co(tn)_3]^{3+}$.[15]

The N(terminal)-Co-N(terminal) angles in both ligands (N(5)-Co-N(6), N(2)-Co-N(4)) are obviously smaller than 180°, whereas the N(secondary)-Co-N(secondary) angle (N(1)-Co-N(3)) is nearly 180°. The three ligating nitrogen atoms of each ligand and the cobalt atom are nearly co-planar, and the two coordination planes are perpendicular. These observations suggest that the presence of the six-membered chelate ring does not introduce much distortion into the octahedral geometry of the complex cation and that any such distortion is relieved by the flexibility of the six-membered ring.

The relevant interatomic distances of less than 3.9 Å between complexes, along with the estimated standard deviations, are listed in Table 5. The bond length of I(1)-N(4) (3.55(2) Å) is clearly shorter than the sum of the ionic radii. This might lead to the hydrogen bond formation of N-H···I.

TABLE 5. RELEVANT INTERATOMIC DISTANCES OUTSIDE THE COMPLEX ION, *mer*-[Co(aepn)(dien)]$^{3+}$, WITH THEIR ESTIMATED STANDARD DEVIATIONS IN PARENTHESES

Key operations			
i) x, y, z		ii) x, y, $1/2+z$	
Distance	l/Å	Distance	l/Å
I (1) ^{I}-N (2)	3.82 (3)	I (3) ^{I}-N (2)	3.68 (7)
-N2H1	2.99 (3)	-N2H1	2.62 (6)
-N (6)	3.65 (6)	-N (5)	3.64 (2)
N6H1	2.75 (3)	-N5H2	2.67 (1)
I (2) ^{I}-N (4)	3.63 (6)	I (1) ^{II}-N (1)	3.68 (7)
-N4H2	2.63 (8)	-N1H1	3.22 (7)
-N (6)	3.65 (7)	-N (4)	3.55 (2)
-N6H2	2.63 (8)	-N4H1	2.55 (7)

Appendix

Remarks on Chirality Specification. The four isomers of *mer*-[Co(aepn)(dien)]$^{3+}$ shown in Fig. 2 can be specified easily by means of common chirality descriptors. Without any consideration of the conformations of the chelate rings, the chirality of these isomers can be said to arise from the dissymmetric disposition of the two coordinated NH groups and from the dissymmetry around the secondary nitrogen atom of aepn. If we employ the same descriptor as was used for *mer*-[Co(dien)$_2$]$^{3+}$,[4] they can be denoted by:

(a) *trans*-δ-NH(R), (b) *trans*-λ-NH(S), (c) *trans*-λ-NH(R), (d) *trans*-δ-NH(S),

where δ or λ refers to the non-oriented N-N and H-H lines defined by the two N-H groups under consideration and where R or S represents the absolute configuration of the asymmetric nitrogen atom of aepn. Recently, Damhus and Schäffer proposed a new reference system consisting of oriented lines.[16] When this new system is employed, the four isomers can be represented as follows:

(a) $\vec{\Lambda}(R)$, (b) $\vec{\Delta}(S)$, (c) $\vec{\Delta}(R)$, (d) $\vec{\Lambda}(S)$.

References

1) Y. Yoshikawa and K. Yamasaki, *Bull. Chem. Soc. Jpn.*, **45**, 179 (1972).
2) M. Kojima, M. Iwasaki, Y. Yoshikawa, and J. Fujita, *Bull. Chem. Soc. Jpn.*, **50**, 3216 (1977).
3) S. Yamada, M. Umehara, M. Ishii, and M. Nakahara, *Nippon Kagaku Kaishi*, **1983**, 1733.
4) K. Okiyama, S. Sato, and Y. Saito, *Acta Crystallogr., Sect. B*, **35**, 2389 (1979).
5) M. Ishii, S. Sato, Y. Saito, and M. Nakahara, *Chem. Lett.*, **1981**, 1613; M. Ishii, *Bull. Chem. Soc. Jpn.*, **57**, 3088 (1984).
6) T. Sakurai, UNICS, The Universal Crystallographic Computing System, Tokyo: The Crystallographic Society of Japan (1967).
7) P. Coppens and W. C. Hamilton, *Acta Crystallogr., Sect. A*, **26**, 71 (1970).
8) $R=\sum||F_o|-|F_c||/\sum|F_o|$, $R_2=\sum[w(|F_o|-|F_c|)^2/\sum w|F_o|^2]^{1/2}$.
9) W. C. Hamilton, *Acta Crystallogr.*, **18**, 502 (1965).
10) The complete F_o-F_c data are deposited as Document No. 8443 at the Office of the Editor of the Bulletin of the

Chemical Society of Japan.

11) In an earlier letter (Ref. 5), the symbol of the absolute configuration in aepn was incorrect. *R* in Ref. 5. should read *S*.

12) Remarks on the chirality specification may be found in the Appendix section in this paper.

13) M. Konno, F. Marumo, and Y. Saito, *Acta Crystallogr., Sect. B*, **29**, 739 (1973).

14) For example, Refs.4 and 13 in this paper; M. Kobayashi, F. Marumo, and Y. Saito, *Acta Crystallogr., Sect. B*, **28**, 470 (1972); S. Sato and Y. Saito, *ibid.*, **33**, 860 (1977); M. Mikami, R. Kuroda, and Y. Saito, *ibid.*, **33**, 1485 (1977); S. Sato and Y. Saito, *ibid.*, **34**, 3352 (1978).

15) T. Nomura, F. Marumo, and Y. Saito, *Bull. Chem. Soc. Jpn.*, **42**, 1016 (1969); R. Nagao, F. Marumo, and Y. Saito, *Acta Crystallogr., Sect. B*, **29**, 2438 (1973).

16) T. Damhus and C. Shäffer, *Inorg. Chem.*, **22**, 2406 (1983).

Formation of an *N,N*-Bidentate Chelate, Bis[4-(4-methyl-2-pyridylazo)resorcinol]nickel(II) Perchlorate, in Dioxane

Yoshihiro KUDO, Noboru YOSHIDA, Taira IMAMURA, and Masatoshi FUJIMOTO*
Department of Chemistry, Faculty of Science, Hokkaido University, Sapporo 060
(Received February 29, 1984)

The formation of a new *N,N*-bidentate complex of nickel(II) perchlorate with an *N,N,O*-terdentate ligand, 4-(4-methyl-2-pyridylazo)resorcinol (4-MePAR), was first detected in dioxane spectrophotometrically. The stability of the *N,N*-bidentate species in dioxane is strongly affected by the presence of a proton acceptor such as water, ethanol, imidazole, and Cl^-, which promote the coordination of the *ortho* phenolic oxygen in the ligand to form the *N,N,O*-terdentate complex. The new complex was isolated from dioxane solution and identified to be an *N,N*-bidentate complex salt, $[Ni(4\text{-mepar})_2](ClO_4)_2$, having two counter ions, ClO_4^-. A distorted-planar configuration of the complex was suggested on the basis of IR, X-ray photoelectron spectroscopic, and magnetic measurements.

o-(Pyridylazo)phenol compounds coordinate to metal ions to form *N,N,O*-terdentate complexes in aqueous media.[1,2] Kinetic studies on the reactions of 4-(2-pyridylazo)resorcinol (PAR)[3] and 1-(2-pyridylazo)-2-naphthol (β-PAN)[4] with nickel(II) ion in aqueous solution suggested the following reaction mechanism involving the formation of an *N,N*-bidentate complex (II) as an intermediate. However, the intermediate complex II presumed in the scheme 1 has not been detected so far.[5]

In the present study, the formation of the *N,N*-bidentate complex II of nickel(II) perchlorate with 4-(4-methyl-2-pyridylazo)resorcinol (4-MePAR) was first detected spectrophotometrically in an aprotic solvent, 1,4-dioxane. The stability of the *N,N*-bidentate complex strongly depends on the solvent basicity and/or the presence of a proton acceptor.

The intermediate bidentate complex II was first isolated as a perchlorate from dioxane solution and identified.

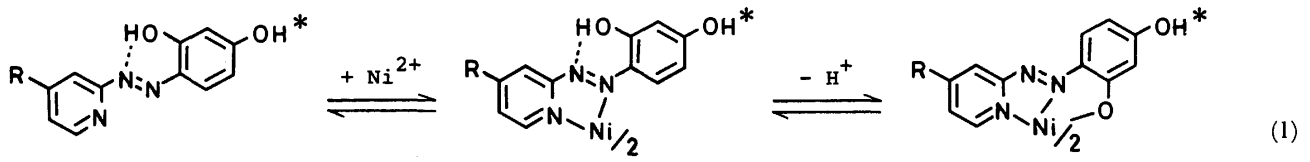

(1)

I LHH*† | II $[Ni(LHH^*)_2]^{2+}$ | III $[Ni(LH^*)_2]^0$

PAR: R=H; 4-MePAR: R=Me

Experimental

Materials. Deionized water was distilled. Reagent grade materials were used unless otherwise specified.

Nickel(II) perchlorate monohydrate was obtained by heating recrystallized hexahydrate at 90±5 °C for 5 h *in vacuo* and kept in a desiccator over P_2O_5. The nickel(II) content in the monohydrate was determined titrimetrically with EDTA. The concentrations of the solutions were calculated from the weighed amount.

The ligands, 4-MePAR,[6] 4-(2-pyridylazo)phenol (*p*-PAP),[7] and 5-dimethylamino-2-(2-pyridylazo)phenol (DAPAP),[8] were synthesized as described in the literature. The concentrations of the solutions were calculated from the weighed amount.

In order to remove peroxides, dioxane (Wako) was passed through a column of basic alumina, dried with sodium metal, and distilled under argon immediately before use.

Syntheses of the Nickel(II) Complexes. *1)* N,N,O-*Terdentate Complex*: $[Ni(LH^*)_2]^0$. The complex was prepared by mixing an aqueous solution of nickel(II) chloride (3.1 mmol) with that of 4-MePAR (3.9 mmol). The red-dish brown complex was identified to be $Ni(C_{12}H_{10}N_3O_2)_2$ by elemental analysis.

2) N,N-*Bidentate Complex*: $[Ni(LHH^*)_2](ClO_4)_2$. 4-MePAR (200 mg, 0.87 mmol) was dissolved in dioxane (*ca.* 200 cm^3) under argon atmosphere. To the solution $Ni(ClO_4)_2 \cdot H_2O$ (100 mg, 0.36 mmol) suspended in dioxane (*ca.* 100 cm^3) was slowly added. The mixture was stirred for several hours and allowed to stand overnight in the dark under argon atmosphere. The yellowish red precipitate was filtered, washed with dioxane, and dried for 2 d *in vacuo* over P_2O_5. Yield *ca.* 40%. Found: C, 40.01; H, 3.19; N, 11.49; Cl, 8.83%.[9] Calcd for $Ni(C_{12}H_{11}N_3O_2)_2(ClO_4)_2$: C, 40.26; H, 3.10; N, 11.74; Cl, 9.90%.

3) Other Nickel(II) Complexes. The 1:2 complex of nickel(II) with *p*-PAP, $[Ni(pap)_2]^0 \cdot H_2O$, was synthesized as reported in the literature.[7] The *N,N*-bidentate nickel(II) complex of DAPAP was prepared and purified by the same method as that for the synthesis of $[Ni(LHH^*)_2](ClO_4)_2$. The isolated complex was identified to be $Ni(C_{13}H_{14}N_4O)_2(ClO_4)_2 \cdot 2H_2O$ by elemental analysis.

Measurements. Since most of the reagents used in the study were moisture-sensitive, all measurements were performed under dry argon atmosphere. All sample solutions were prepared in a glove bag filled with dry argon.

Visible absorption spectra were measured at 25.0±0.3 °C with a Hitachi EPS-3T recording spectrophotometer.

The IR spectra were measured with a JASCO IR-G infrared spectrophotometer in the region 4000—400 cm^{-1} with use of

† The ligand is abbreviated as LHH*, where H and H* denote the protons of the *ortho* and the *para* hydroxyl group, respectively.

the KBr pellet technique. The KBr disk was carefully prepared under dry argon atmosphere. The influence of the moisture during the measurements was negligibly small.

X-Ray photoelectron spectra were obtained for powdered samples using an electron spectrometer Model VG ESCA 3. Mg *Kα* (1253.6 eV) X-ray radiation was used as the excitation source. The measurements were conducted at room temperature under a vacuum of *ca.* 10^{-6} Pa.

The magnetic susceptibilities of the nickel(II)-4-MePAR complexes were measured at room temperature using Gouy method. Diamagnetic corrections for the ligands were calculated from Pascal's constants; -32.0×10^{-6} c.g.s emu mol^{-1} was used as the correction for perchlorate ion.[10]

The ^1H NMR data for the dioxane solution of the new complex were not obtained owing to very low solubility.

The pH* of the aqueous dioxane solution was measured at 25 °C with a Hitachi-Horiba pH-meter Model F-7ss. The values of pC_H (=$-\log C_H$) were calculated by the following relationship between pH-meter readings (pH*) and the values of $\log U_H$: $pC_H=pH^*+\log U_H$.[11]

Results and Discussion

Spectral Changes in the Complex Formations of Nickel(II) Perchlorate with 4-MePAR. Figure 1(a) shows the spectral changes in the complex formation of nickel(II) perchlorate with 4-MePAR in 10%(v/v) dioxane–water at pH* 4.2. Upon addition of nickel(II) perchlorate to the solution of 4-MePAR, the absorption around 380 nm due to 4-MePAR decreased with the increase of a new absorption at 511 nm; a well-defined isosbestic point was observed at 465 nm, which indicates the presence of a simple equilibrium. Molar ratio method indicates the formation of a 1:2 nickel(II) complex. The feature of the final spectrum of the complex (Curve 5) is essentially the same as the absorption spectrum of the *N,N,O*-terdentate 1:2 complex of PAR in 10%(v/v) dioxane–water,[12] namely, the final spectrum is ascribed to the *N,N,O*-terdentate complex, $[Ni(LH^*)_2]^0$.

In neat dioxane, different spectral changes were observed. Figure 1(b) shows the spectral changes observed upon addition of nickel(II) perchlorate to the dioxane solution of 4-MePAR. The absorption around 380 nm due to the free ligand decreased with the increase of new absorption around 420 and 480 nm with a single isosbestic point at 399 nm (Curves 1→3) in the region of the low concentrations of nickel(II) perchlorate ($[Ni(II)]_t/[4\text{-MePAR}]_t\leqq0.3$). With further increase in the concentration of nickel(II) perchlorate, a new absorption peak appeared (λ_{max}=430 and 470 nm (sh)) with another set of isosbestic points at 400 and 471 nm (Curves 4→6). These spectral changes suggest the existence of two successive equilibria.

Molar ratio method indicated the formation of a 1:3 and a 1:2 nickel(II) complex in the first and the second step of the reaction, respectively.[13] The final spectrum of the 1:2 nickel(II) complex (Curve 6) clearly differs from the spectrum characteristic of the *N,N,O*-terdentate 1:2 complex (Curve 5 in Fig. 1(a)).

Electronic Spectra of the Isolated Nickel(II) Complexes in Dioxane. Figure 2 shows the electronic spectra in dioxane of the free ligand 4-MePAR, the isolated new yellowish red complex, $[Ni(C_{12}H_{11}N_3O_2)_2](ClO_4)_2$, and the terdentate complex, $[Ni(LH^*)_2]^0$.

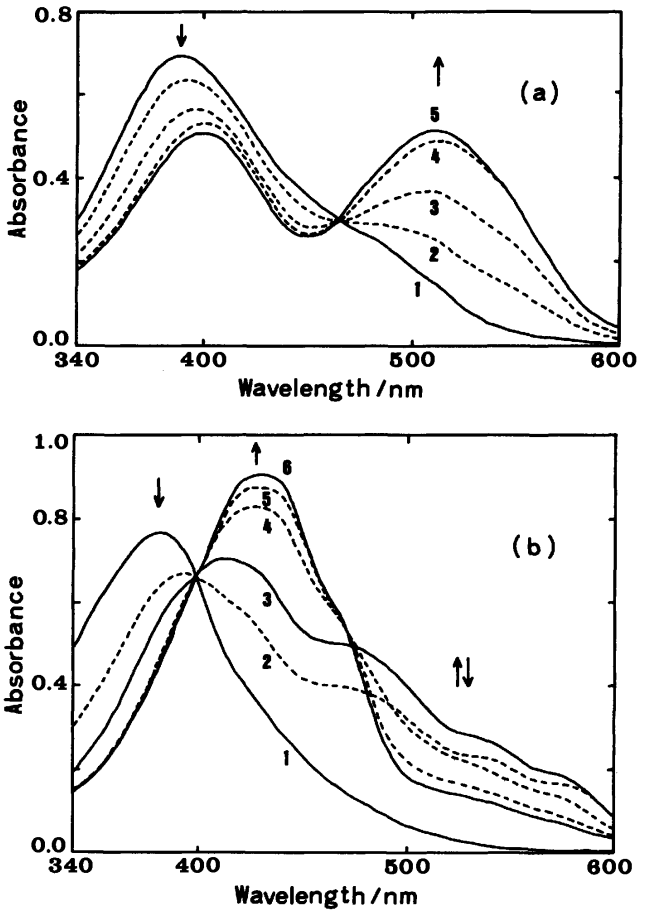

Fig. 1. (a) Spectral change upon addition of nickel(II) perchlorate to the 10% (v/v) dioxane–water solution of 4-MePAR at pH*=4.2, I=0.1 mol dm^{-3} ($NaClO_4$), and 25 °C.
$[4\text{-MePAR}]_t=3.67\times10^{-5}$ mol dm^{-3} ([ ]$_t$ denotes the total concentration). $[Ni(II)]_t$=0.00 (1), 0.48 (2), 0.95 (3), 3.17 (4), and 15.8×10^{-5} mol dm^{-3} (5).
(b) Spectral change upon addition of nickel(II) perchlorate to the dioxane solution of 4-MePAR at 25 °C.
$[4\text{-MePAR}]_t=3.65\times10^{-5}$ mol dm^{-3}. $[Ni(II)]_t$=0.00 (1), 0.41 (2), 1.03 (3), 1.64 (4), 1.97 (5), and 19.7×10^{-5} mol dm^{-3} (6).

The absorption spectrum of the free ligand has a single peak at 381 nm ($\varepsilon_{max}=2.10\times10^4$ mol^{-1} dm^3 cm^{-1}) (Curve 1). The spectra of the complexes show the large bathochromic shifts compared with the spectrum of the free ligand. The spectrum of the new complex with a single peak at 426 nm ($\varepsilon_{max}=3.90\times10^4$ mol^{-1} dm^3 cm^{-1}) and a shoulder around 470 nm ($\varepsilon_{sh}=3\times10^4$ mol^{-1} dm^3 cm^{-1}) (Curve 2) essentially coincides with that of the dioxane solution prepared by mixing a large excess of nickel(II) perchlorate with 4-MePAR (Curve 6 in Fig. 1(b)). The spectrum of the bis-terdentate complex, $[Ni(LH^*)_2]^0$, has two absorption bands at 400 ($\varepsilon_{max}=3.2\times10^4$) and 542 nm ($\varepsilon_{max}=3.2\times10^4$ mol^{-1} dm^3 cm^{-1}) in dioxane (Curve 3).

The feature of the absorption spectrum with two bands is characteristic of the coordination of the *ortho* phenolic oxygen in the ligand. The spectrum of the new complex is quite different from that of the *N,N,O*-

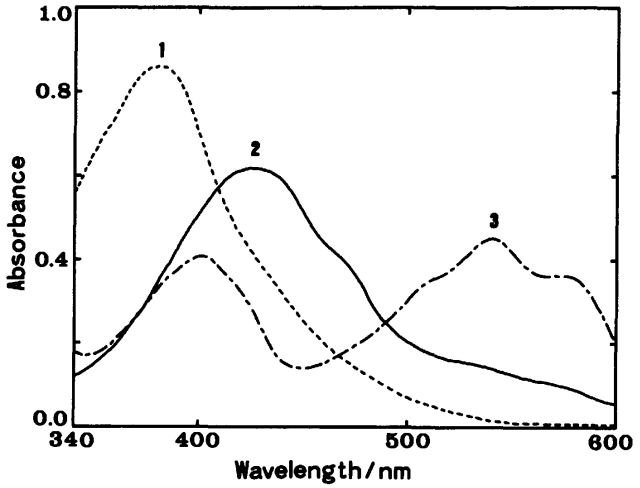

Fig. 2. Electronic spectra of the free ligand 4-MePAR and its nickel(II) complexes at 25 °C in neat dioxane. (1) 4-MePAR: $[LHH^*]_t = 4.09 \times 10^{-5}$ mol dm^{-3}; (2) the new complex: $[Ni(C_{12}H_{11}N_3O_2)_2(ClO_4)_2]_t = 1.57 \times 10^{-5}$ mol dm^{-3}; (3) the *N,N,O*-terdentate complex: $[Ni(LH^*)^0_2]_t = 1.3 \times 10^{-5}$ mol dm^{-3}.

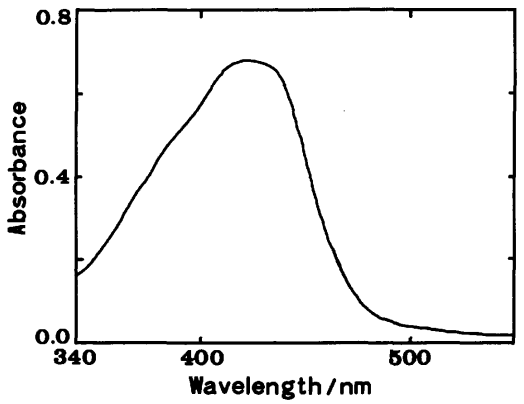

Fig. 3. Electronic spectrum of the *N,N*-bidentate chelate between nickel(II) perchlorate and *p*-PAP at 25 °C in dioxane.
$[Ni(II)]_t = 5.25 \times 10^{-5}$ mol dm^{-3}, $[p\text{-PAP}]_t = 3.63 \times 10^{-5}$ mol dm^{-3}.

terdentate complex, $[Ni(LH^*)_2]^0$. Furthermore, the spectrum of the new complex is similar to that of the *N,N*-bidentate 1:2 nickel(II) complex of *p*-PAP with no coordinating *o*-hydroxyl group (Fig. 3).

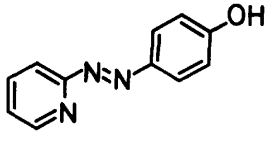

p-PAP

These observations indicate that the new complex has an *N,N*-bidentate structure with uncoordinated *ortho* phenolic oxygen. This conclusion is also supported by the elemental analysis; the isolated new complex is $[Ni(LHH^*)_2](ClO_4)_2$ having two perchlorate ions as counter ions.

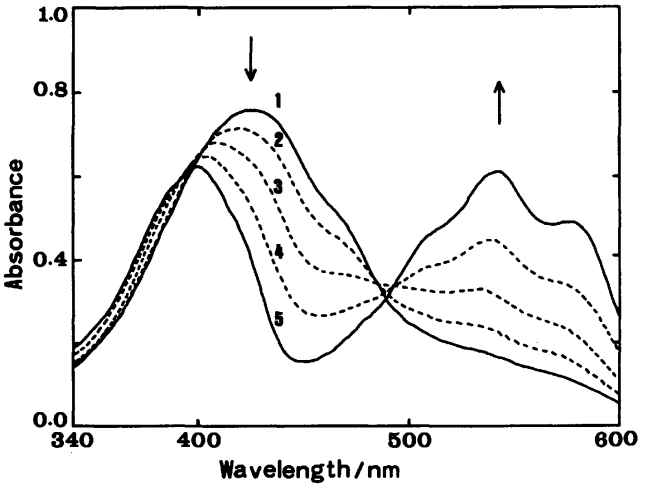

Fig. 4. Spectral change observed on addition of imidazole to the 1.52×10^{-5} mol dm^{-3} dioxane solution of the new complex at 25 °C.
$[Imidazole]_t = 0.00$ (1), 0.60 (2), 1.19 (3), 2.09 (4), and 7.46×10^{-5} mol dm^{-3}.

Reactions of Brønsted Bases with the New Bidentate Complex. The formation of the *N,N*-bidentate complex in dioxane was seriously influenced by the presence of a Brønsted base as a proton acceptor which would promote the release of the *ortho* phenolic proton and the subsequent formation of the *N,N,O*-terdentate complex.

Upon addition of a nitrogen base, imidazole, to the dioxane solution of the new complex, the yellow solution turned pink. Figure 4 shows the spectral change upon addition of imidazole to the solution of the new complex; two-step reactions were demonstrated by two sets of isosbestic points at 403 and 485, and 392 and 493 nm. The final spectrum essentially coincides with the spectrum of the dioxane solution of the *N,N,O*-terdentate complex, $[Ni(LH^*)_2]^0$, isolated from aqueous solution. This indicates that the observed spectral change results from the coordination of the *ortho* phenolic oxygen of the ligand; imidazole acts as a proton acceptor and not as a ligand.

The stoichiometry of the two-step reaction between the bidentate complex and imidazole, B, was found to be 1:1 for the first step and 1:2 for the overall reaction by molar ratio method. The feature of the spectral change is explained by the following reaction scheme,

$$[Ni(LHH^*)_2]^{2+} \xrightarrow[HB^+]{B} [Ni(LHH^*)(LH^*)]^+ \xrightarrow[HB^+]{B} [Ni(LH^*)_2]^0. \quad (2)$$

yellow orange pink

The same spectral change was observed upon addition of water or ethanol to the dioxane solution of the new complex. The addition of tetrabutylammonium chloride to the dioxane solution of the new complex also gave the similar spectral change. This result suggests a role as a proton acceptor of chloride ion.[14]

Liberation of ortho *Protons from the New Bidentate Complex in Aqueous Media.* In the solution pre-

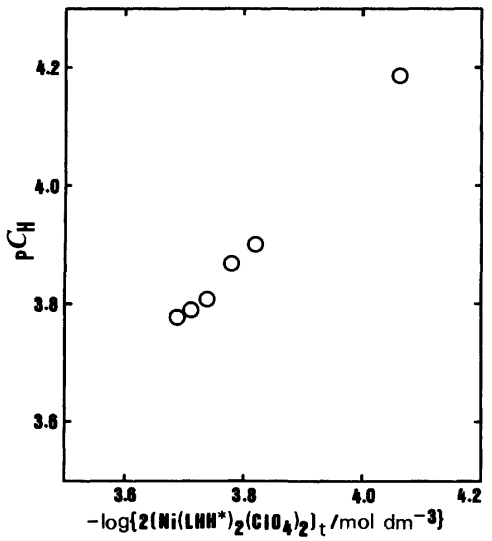

Fig. 5. Plot of pC_H *vs.* $-\log\{2[Ni(LHH^*)_2(ClO_4)_2]_t\}$ in 10%(v/v) dioxane-water at 25 °C.

pared by dissolving the new complex in 10%(v/v) dioxane-water the characteristic absorption peak at 426 nm of the new complex was not observed, instead, the two absorption bands around 400 and 511 nm were observed, which were ascribed to the *N,N,O*-terdentate complex, $[Ni(LH^*)_2]^0$. The pH* values of the solutions were lowered in accordance with the amount of the dissolved new complex. The plot of the values of pC_H against $-\log\{2[Ni(LHH^*)_2(ClO_4)_2]_t\}$ demonstrates the liberation of two protons from the new complex (Fig. 5). The liberation of protons should be owed to the *ortho* protons of the *N,N*-bidentate complex: $[Ni(LHH^*)_2]^{2+}+2H_2O\rightarrow[Ni(LH^*)_2]^0+2H_3O^+$, since the *para* protons of the terdentate complex, $[Ni(LH^*)_2]^0$, could not be dissociated under the experimental conditions.[15] In addition, the spectral and pH measurements in the similar experiments with the nickel(II) complex, isolated from dioxane, of DAPAP having no *p*-hydroxyl group gave the same results as those for the new bidentate complex, $[Ni(LHH^*)_2](ClO_4)_2$.

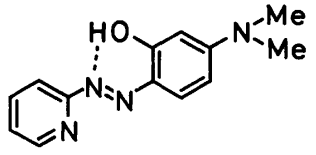

DAPAP

From these results, we concluded that the new yellowish red complex is the *N,N*-bidentate intermediate complex II proposed in the Scheme 1.

Possible Configuration of the Isolated New Complex. The IR spectrum of the new complex perchlorate, $[Ni(LHH^*)_2](ClO_4)_2$, shows a single strong broad band at 1060—1150 cm^{-1}, which corresponds to the $\nu_{Cl\text{-}O}$ of the free perchlorate ion, ClO_4^-. This indicates that the perchlorate anions do not coordinate to the central nickel(II) atom.[16]

The binding energy of Ni(II)($2p_{3/2}$) bonded to the same ligands under different geometries increases in general in the order of a square-planar (*ca.* 853—854 eV), a tetrahedral (*ca.* 853—854 eV), and an octahedral configuration (*ca.* 855 eV).[17]

Table 1. Core electron binding energies and magnetic moments of the free ligands and their nickel(II) complexes

Species	Binding energy[a]/eV			μ_{eff}[b]/BM
	N(1s)	O(1s)	Ni($2p_{3/2}$)	
LHH*	395[c]	528		
	398.3[c]	531.3		
$[Ni(LHH^*)_2](ClO_4)_2$	400.0[c]	—[d]	853	3.04
$[Ni(LH^*)_2]^0$	400.3[c]	528	856	3.08
		532.1		
p-PAP	399.2[c]	531.2		
$[Ni(pap)_2]^0\cdot H_2O$	399.6[c]	514.7	853	
		520.4		
$[NiCl_2(phen)_2]^0\cdot 4H_2O$[e]	398.3		854.1	
Bpy[f]	398.6			
$[NiCl_2(bpy)_2]^0$[e]	399.1		854.9	

a) All raw binding energies were corrected to hydrocarbon C(1s) value of 285.0 eV.[20] b) Measured at 290 K. c) Ref. 19. d) Unable to measure due to the strong O(1s) signal of the perchlorate ion. e) Ref. 17. f) Ref. 18.

The X-ray photoelectron spectral data of the free ligands and their nickel(II) complexes are summarized in Table 1 together with the data of magnetic moments. The increase in the binding energy of N(1s) of the ligand on the formation of the complexes, $[Ni(LH^*)_2]^0$,[19] $[Ni(pap)_2]^0\cdot H_2O$,[19] and $[NiCl_2(bpy)_2]^0$,[17] is due to the coordination of the nitrogen atoms to the nickel(II) atom.[20] A positive chemical shift in the N(1s) binding energy observed in the new complex suggests the coordination of the nitrogen atoms to nickel(II) in the complex, $[Ni(LHH^*)_2](ClO_4)_2$. The Ni(II)($2p_{3/2}$) binding energy of the new complex formulated as $[Ni(LHH^*)_2](ClO_4)_2$ is in good agreement with that of a four-coordinated complex, $[Ni(pap)_2]^0\cdot H_2O$, and is obviously lower than that of the typical octahedral complexes, $[Ni(LH^*)_2]^0$, $[NiCl_2(phen)_2]^0\cdot 4H_2O$,[17] and $[NiCl_2(bpy)_2]^0$.[17]

These X-ray photoelectron spectral data strongly suggest the four-coordinated *N,N*-bidentate structure for the complex, $[Ni(LHH^*)_2](ClO_4)_2$.

The magnetic moments, μ_{eff}, of four-coordinated nickel(II) complexes in general depend on its spin-state and ligand field symmetry.[21] The magnetic moment of $[Ni(LHH^*)_2](ClO_4)_2$ was found to be 3.04 BM at 290 K. This value suggests that the new complex, $[Ni(LHH^*)_2](ClO_4)_2$, has a distorted-planar structure.

The authors thank Professor Isamu Toyoshima and Dr. Katsumi Tanaka at the Research Institute for Catalysis for help in the measurements of X-ray photoelectron spectra. They also thank Professor Yoshio Matsunaga for the kindness in the measurements of magnetic susceptibilities.

References

1) W. J. Geary, G. Nickless, and F. H. Pollard, *Anal. Chim. Acta*, **26**, 575 (1962).

2) X-Ray crystallographic studies on the metal complexes of some *o*-(pyridylazo)phenol and/or *o*-(thiazolylazo)phenol compounds confirmed the *mer*-configuration of the complexes by the coordination of the *ortho* phenolic oxygen, one of the azo nitrogens, and the heterocyclic nitrogen atoms. See, S. Ooi, D. Carter, and Q. Fernando, *Chem. Commun.*, **1967**, 1301; M. Kurahashi, *Chem. Lett.*, **1974**, 63, 1271; *Bull. Chem. Soc. Jpn.*, **47**, 2045, 2067 (1974); **49**, 127, 872, 1419, 2927, 3053 (1976).

3) M. Fujimoto, 21st Ann. Meeting Coord. Chem., Nagoya, 1971, Abstracts, p. 87.

4) C. D. Hubbard and D. Pacheco A., *J. Inorg. Nucl. Chem.*, **39**, 1373 (1977).

5) The possibility of the formation of an *N,N*-bidentate complex between nickel(II) and PAR in an aprotic solvent, nitromethane, was pointed out by kinetic measurements. See, H. L. Fritz and J. H. Swinehart, *Inorg. Chem.*, **14**, 1935 (1975).

6) W. J. Geary and F. Bottomley, *Talanta*, **14**, 537 (1967).

7) R. G. Anderson and G. Nickless, *Anal. Chim. Acta*, **39**, 469 (1967).

8) T. M. Florence, D. A. Johnson, and Y. J. Farrar, *Anal. Chem.*, **41**, 1652 (1969).

9) The lower value of Cl content would be due to the interference of nickel(II) ion with the determination of Cl^-. However, the result of the elemental analysis clearly indicates the presence of two moles of ClO_4^- in the isolated bidentate complex.

10) A. Earnshaw, "Introduction to Magnetochemistry," Academic Press, London (1968), p. 4.

11) N. Yoshida and M. Fujimoto, *Bull. Chem. Soc. Jpn.*, **50**, 1328 (1977).

12) D. Nonova and B. Evtimova, *Anal. Chim. Acta*, **49**, 103 (1970).

13) The formation of a 1:3 nickel(II) complex of 4-MePAR will not be discussed here in detail.

14) The formation of the new complex was not observed also in the reactions of nickel(II) chloride, acetate, and nitrate with 4-MePAR in neat dioxane. These results indicate the role of the counter-ion, Cl^-, CH_3COO^-, and NO_3^-, as a proton acceptor in dioxane. However, perchlorate ion, ClO_4^-, does not act as a proton acceptor in dioxane.

15) The pK_{a1} and pK_{a2} values in 10%(v/v) dioxane-water for the dissociation of the two *p*-hydroxyl protons in the bis-terdentate complex, $[Ni(LH^*)_2]^0 \overset{pK_{a1}}{\rightleftharpoons} [Ni(LH^*)L]^- + H^+ \overset{pK_{a2}}{\rightleftharpoons} [NiL_2]^{2-} + 2H^+$, were determined by pH titration to be 5.82 and 7.09, respectively. See, H. Shimoda, N. Yoshida, and M. Fujimoto, presented at the 1980 Winter Meeting in Hokkaido of the Chemical Society of Japan and the Japan Society for Analytical Chemistry, Sapporo, February 1, 1980, Abstracts, p. 38.

16) B. J. Hathaway and A. E. Underhill, *J. Chem. Soc.*, **1961**, 3091; L. E. Moore, R. B. Gayhart, and W. E. Bull, *J. Inorg. Nucl. Chem.*, **26**, 896 (1964).

17) L. J. Matienzo, L. I. Yin, S. O. Grim, and W. E. Swartz, Jr., *Inorg. Chem.*, **12**, 2762 (1973).

18) P. A. Grutsch, M. V. Zeller, and T. P. Fehlner, *Inorg. Chem.*, **12**, 1431 (1973).

19) The observed N(1s) binding energy was obtained only as the average of the values of the binding energy of the pyridyl and azo nitrogen atoms.

20) C. A. Tolman, W. M. Riggs, W. J. Linn, C. M. King, and R. C. Wendt, *Inorg. Chem.*, **12**, 2770 (1973).

21) B. N. Figgis and J. Lewis, "The Magnetic Properties of Transition Metal Complexes," in "Progress in Inorganic Chemistry," ed by F. A. Cotton, Interscience Publishers, New York, N. Y. (1964), Vol. 6, p. 207.

 © 1984 The Chemical Society of Japan Bull. Chem. Soc. Jpn., 57, 3104—3110 (1984) [Vol. 57, No. 11

Preparation and Stereochemistry of Bis(ethylenediamine)-cobalt(III) Complexes with Selenium Donor Atom

Takumi KONNO,* Ken-ichi OKAMOTO, and Jinsai HIDAKA
Department of Chemistry, University of Tsukuba, Sakura, Ibaraki 305
(Received March 29, 1984)

Five optically active cobalt(III) complexes of [Co(bidentate-*N,Se*)(en)$_2$] type were prepared; here bidentate-*N,Se* denotes 2-aminoethaneselenolato (aes), 2-aminoethaneselenenato (aesee), 2-(methylseleno)ethylamine (mseea), 2-(ethylseleno)ethylamine (eseea), and 2-(benzylseleno)ethylamine (bseea). These complexes were characterized from their absorption, CD and ^{1}H NMR spectra. Of these complexes, the crystal structure of $(+)^{CD}_{500}$-[Co(mseea)(en)$_2$](ClO$_4$)$_3$ was determined by the X-ray diffraction method. The red plate crystal was orthorhombic, space group $P2_12_12_1$, a=12.220(15), b=19.224(7), c=8.977(11) Å, Z=4, and the final R value was 0.087. The coordinated selenium atom takes the (*R*) configuration for the *Λ* isomer. The absorption and CD spectra of the five complexes are discussed in comparison with those of the corresponding cobalt(III) complexes containing a coordinated sulfur atom.

A few cobalt(III) complexes with selenium-containing ligand have been investigated,[1-4] but little information concerning their spectrochemical and stereochemical properties has been reported up to now. It is favorable to compare the properties of cobalt(III) complexes containing a selenium donor atom with those of the corresponding complexes containing a sulfur donor atom, which have been extensively studied.[5-13]

This work is concerned with the preparation and stereochemistry of cobalt(III) complexes with a coordinated selenium atom. The cobalt(III) complex with 2-aminoethaneselenolato ($NH_2CH_2CH_2Se^-$), $[Co(aes)(en)_2]^{2+}$, was optically resolved, and the optically active cobalt(III) complexes with 2-aminoethaneselenenato ($NH_2CH_2CH_2SeO^-$), $(+)^{CD}_{500}\cdot(-)^{CD}_{360}$-[Co(aesee)(en)$_2$]$^{2+}$, 2-(methylseleno)ethylamine ($NH_2CH_2CH_2SeCH_3$), $(+)^{CD}_{500}$-[Co(mseea)(en)$_2$]$^{3+}$, 2-(ethylseleno) ethylamine ($NH_2CH_2CH_2SeC_2H_5$), $(+)^{CD}_{500}$-[Co(eseea)(en)$_2$]$^{3+}$, and 2-(benzylseleno)ethylamine ($NH_2CH_2CH_2SeCH_2C_6H_5$), $(+)^{CD}_{500}$-[Co(bseea)(en)$_2$]$^{3+}$, were derived from $(+)^{CD}_{500}$-[Co(aes)(en)$_2$]$^{2+}$.[14] The crystal structure of the selenoether complex, $(+)^{CD}_{500}$-[Co(mseea)(en)$_2$]$^{3+}$, was determined by X-ray diffraction and was compared to that of the corresponding thioether complex, [Co(mea)(en)$_2$]$^{3+}$ (mea=2-(methylthio)ethylamine).[9] This is the first example of the structural analysis of the cobalt(III) complex with a selenoether donor atom. The absorption and CD spectra of the present complexes are discussed in comparison with those of the corresponding [Co(bidentate-*N,S*)(en)$_2$] type complexes.[9-13]

Experimental

1) Preparation and Resolution of the Complexes. a) $(+)^{CD}_{500}$-(2-Aminoethaneselenolato)bis(ethylenediamine)cobalt(III) Perchlorate. $(+)^{CD}_{500}$-[Co(aes)(en)$_2$](ClO$_4$)$_2$: [Co(aes)(en)$_2$](NO$_3$)$_2$ was prepared by the method of Deutsch *et al.*[1] A solution containing 2.0 g of $K_2[Sb_2(d\text{-tart})_2]\cdot 3H_2O$ in 20 cm^3 of water was added with stirring to a solution containing 2.4 g of [Co(aes)(en)$_2$](NO$_3$)$_2$ in 80 cm^3 of water at 50 °C. The solution was stirred for 5 min, though fine dark brown crystals soon began to appear. The crystals were collected by filtration and it was found from a CD measurement that the crystals were the $(+)^{CD}_{500}$ diastereomer with a small amount of the $(-)^{CD}_{500}$ type. After the $(-)^{CD}_{500}$ diastereomer contamination was removed by grinding in a mortar several times with 10 cm^3 of an aqueous solution of NaClO$_4$ (1.5 mol dm^{-3}), the remaining $(+)^{CD}_{500}$ diastereomer was dissolved in an aqueous solution of NaClO$_4$. The solution was concentrated with a rotary evaporator until fine needle crystals of the selenolato complex appeared. After cooling in a refrigerator, crystals of $(+)^{CD}_{500}$-[Co(aes)(en)$_2$](ClO$_4$)$_2$ were collected by filtration, and washed with ethanol and ether. Found: C, 14.81; H, 4.32; N, 13.96%. Calcd for $(+)^{CD}_{500}$-[Co(aes)(en)$_2$](ClO$_4$)$_2$=$C_6H_{22}N_5O_8Cl_2SeCo$: C, 14.38; H, 4.42; N, 13.97%.

b) $(+)^{CD}_{500}\cdot(-)^{CD}_{360}$-(2-Aminoethaneselenenato)bis(ethylenediamine)cobalt(III) Perchlorate. $(+)^{CD}_{500}\cdot(-)^{CD}_{360}$-[Co(aesee)(en)$_2$](ClO$_4$)$_2$: A calculated amount of 0.31 cm^3 of 1% aqueous H_2O_2 was added dropwise to a solution containing 0.05 g of $(+)^{CD}_{500}$-[Co(aes)(en)$_2$](ClO$_4$)$_2$ in 1 cm^3 of water and the solution was stirred for 15 min. An orange-yellow precipitate was obtained from the reaction solution after the addition of 2-propanol. This complex was recrystallized from a small amount of water by adding ethanol. The selenenato complex obtained showed the identical absorption and CD spectra with those of the reaction solution, indicating that the $(+)^{CD}_{500}\cdot(-)^{CD}_{360}$ isomer was selectively formed. Found: C, 13.96; H, 4.04; N, 13.35%. Calcd for $(+)^{CD}_{500}\cdot(-)^{CD}_{360}$-[Co(aesee)(en)$_2$](ClO$_4$)$_2$=$C_6H_{22}N_5O_9Cl_2SeCo$: C, 13.93; H, 4.28; N, 13.54%.

c) $(+)^{CD}_{500}$-(2-(Methylseleno)ethylamine)bis(ethylenediamine)cobalt(III) Perchlorate. $(+)^{CD}_{500}$-[Co(mseea)(en)$_2$]ClO$_4$)$_3$: To a solution containing 0.05 g of $(+)^{CD}_{500}$-[Co(aes)(en)$_2$](ClO$_4$)$_2$ in 1 cm^3 of water was added 1 cm^3 of dimethyl sulfate. The mixture was allowed to stand in a refrigerator overnight and separated into two layers. The orange-red upper layer was poured onto a column of QAE-Sephadex A-25 (ClO$_4^-$ form, 2 cm×20 cm), and the column was eluted with water. The eluate was concentrated with a rotary evaporator until red crystals appeared. The resultant red complex was recrystallized from a small amount of water and obtained as fairly large plate crystals. A piece of a crystal was used in the X-ray diffraction study. Found: C, 13.89; H, 3.94; N, 11.39%. Calcd for $(+)^{CD}_{500}$-[Co(mseea)(en)$_2$](ClO$_4$)$_3$=$C_7H_{25}N_5O_{12}Cl_3SeCo$: C, 13.65; H, 4.09; N, 11.37%.

d) $(+)^{CD}_{500}$-(2-(Ethylseleno)ethylamine)bis(ethylenediamine)cobalt(III) Perchlorate. $(+)^{CD}_{500}$-[Co(eseea)(en)$_2$](ClO$_4$)$_3$: To a solution containing 0.05 g of $(+)^{CD}_{500}$-[Co(aes)(en)$_2$](ClO$_4$)$_2$ in 2 cm^3 of *N,N*-dimethylformamide was added 0.25 g of ethyl iodide. The mixture was allowed to stand in a refrigerator for two days, whereupon the color of the solution turned from dark brown to dark red. *N,N*-Dimethylformamide and unreacted ethyl iodide were extracted into ether and to the remaining dark red oil was added a small amount of water. This solution was poured onto a column of QAE-Sephadex

A-25 (ClO_4^- form, 2 cm×20 cm) and the column was eluted with water. The eluate was concentrated almost to dryness with a rotary evaporator and to this was added a small amount of ethanol. After cooling in a refrigerator, the resultant crystals were collected by filtration and washed with ethanol–ether (1:1) and ether. Found: C, 15.15; H, 4.19; N, 10.98%. Calcd for $(+)^{CD}_{500}$-[Co(eseea)(en)$_2$]$(ClO_4)_3$= $C_8H_{27}N_5O_{12}Cl_3SeCo$: C, 15.26; H, 4.32; N, 11.12%.

e) $(+)^{CD}_{500}$-(2-(Benzylseleno)ethylamine)bis(ethylenediamine)cobalt(III) Perchlorate. *$(+)^{CD}_{500}$-[Co(bseea)(en)$_2$]$(ClO_4)_3$*: This complex was prepared by a procedure similar to that used for $(+)^{CD}_{500}$-[Co(eseea)(en)$_2$]$(ClO_4)_3$ described in *d*), using benzyl chloride instead of ethyl iodide. Found: C, 21.57; H, 4.11; N, 9.88%. Calcd for $(+)^{CD}_{500}$-[Co(bseea)(en)$_2$]$(ClO_4)_3\cdot 1.5H_2O$= $C_{13}H_{29}N_5O_{12}Cl_3SeCo\cdot 1.5H_2O$: C, 21.73; H, 4.49; N 9.74%.

f) $(+)^{CD}_{500}$-(2-Aminoethanethiolato)bis(ethylenediamine)cobalt(III) Perchlorate. *$(+)^{CD}_{500}$-[Co(aet)(en)$_2$]$(ClO_4)_2$*: This complex was prepared by a procedure similar to that used for $(+)^{CD}_{500}$-[Co(aes)(en)$_2$]$(ClO_4)_2$ described in *a*). $(+)^{CD}_{500}$-[Co(aet)-(en)$_2$]$(ClO_4)_2$ showed the same CD pattern as that of *Λ*-[Co-(aet)(en)$_2$]$^{2+}$ reported by Yamanari *et al.*,[5] but the CD intensity of the former ($\Delta\varepsilon_{522}$=+1.37) are much higher than that of the latter ($\Delta\varepsilon_{522}$=+0.54). Found: C, 15.86; H, 4.90; N, 15.51%. Calcd for $(+)^{CD}_{500}$-[Co(aet)(en)$_2$]$(ClO_4)_2$=$C_6H_{22}N_5O_8SCl_2Co$: C, 15.86; H, 4.88; N, 15.42%.

g) $(+)^{CD}_{500}$·$(+)^{CD}_{360}$- and $(+)^{CD}_{500}$·$(-)^{CD}_{360}$-(2-Aminoethanesulfenato)-bis(ethylenediamine)cobalt(III) Perchlorate. *$(+)^{CD}_{500}$·$(+)^{CD}_{360}$- and $(+)^{CD}_{500}$·$(-)^{CD}_{360}$-[Co(aese)(en)$_2$]$(ClO_4)_2$*: A calculated amount of 1.24 cm^3 of 1% aqueous H_2O_2 was added dropwise to a solution containing 0.2 g of $(+)^{CD}_{500}$-[Co(aet)(en)$_2$]$(ClO_4)_2$ in 4 cm^3 of water and the mixture was stirred for 15 min. An orange precipitate was obtained from the reaction solution after adding a large amount of 2-propanol. This complex was dissolved in a small amount of water and then 2-propanol was added until fine orange crystals began to appear. After cooling in a refrigerator overnight, the crystals of $(+)^{CD}_{500}$·$(+)^{CD}_{360}$-[Co(aese)(en)$_2$]$(ClO_4)_2$ was collected by filtration. $(+)^{CD}_{500}$·$(-)^{CD}_{360}$-[Co(aese)(en)$_2$]$(ClO_4)_2$ was obtained from the filtrate by the addition of 2-propanol. These two isomers were recrystallized twice from water by adding 2-propanol. $(+)^{CD}_{500}$·$(+)^{CD}_{360}$ and $(+)^{CD}_{500}$·$(-)^{CD}_{360}$ aese isomers showed the same CD spectra as *Λ*-(*S*)- and *Λ*-(*R*)-[Co(aese)(en)$_2$]$^{2+}$, respectively, reported by Kita *et al.*[11] The formation ratio of the two isomers, *Λ*-(*S*) : *Λ*-(*R*), was about 1:3, which was evaluated from the CD spectra of the reaction solution. Found for $(+)^{CD}_{500}$·$(+)^{CD}_{360}$ isomer: C, 15.52; H, 4.52; N, 14.68%. Found for $(+)^{CD}_{500}$·$(-)^{CD}_{360}$ isomer: C, 15.45; H, 4.47; N, 14.77%. Calcd for $(+)^{CD}_{500}$·$(+)^{CD}_{360}$- and $(+)^{CD}_{500}$·$(-)^{CD}_{360}$-[Co(aese)(en)$_2$]$(ClO_4)_2$=C_6H_{22}-$N_5O_9SCl_2Co$: C, 15.32; H, 4.71; N, 14.89%.

h) $(+)^{CD}_{500}$-(2-(Methylthio, Ethylthio or Benzylthio)ethylamine)-bis(ethylenediamine)cobalt(III) Nitrate. *$(+)^{CD}_{500}$-[Co(mea, eea or bea)(en)$_2$]$(NO_3)_3$*: These thioether complexes were prepared by a procedure similar to those used for selenoether complexes described in *c*)—*e*), using $(+)^{CD}_{500}$-[Co(aet)(en)$_2$]-$(ClO_4)_2$ instead of $(+)^{CD}_{500}$-[Co(aes)(en)$_2$]$(ClO_4)_2$. The nitrate salts were obtained by the use of an anion exchange resin (QAE-Sephadex A-25, NO_3^- form). $(+)^{CD}_{500}$-[Co(mea or eea)-(en)$_2$]$(NO_3)_3$ showed the same CD spectra as *Λ*-(*R*)-[Co(mea or eea)(en)$_2$]$^{3+}$, reported by Yamanari *et al.*[5] Found for $(+)^{CD}_{500}$ mea complex: C, 18.68; H, 5.53; N, 24.45%. Calcd for $(+)^{CD}_{500}$-[Co(mea)(en)$_2$]$(NO_3)_3$=$C_7H_{25}N_8O_9SCo$: C, 18.42; H, 5.52; N, 24.55%. Found for $(+)^{CD}_{500}$ eea complex: C, 21.00; H 5.92; N, 22.97%. Calcd for $(+)^{CD}_{500}$-[Co(eea)(en)$_2$]$(NO_3)_3\cdot 0.25C_2H_5OH$= $C_8H_{27}N_8O_9SCo\cdot 0.25C_2H_5OH$: C, 21.19; H, 5.96; N, 23.25%. Found for $(+)^{CD}_{500}$ bea complex: C, 28.23; H, 5.66; N, 20.23%. Calcd for $(+)^{CD}_{500}$-[Co(bea)(en)$_2$]$(NO_3)_3\cdot H_2O$=$C_{13}H_{29}N_8O_9$-$SCo\cdot H_2O$: C, 28.37; H, 5.68; N, 20.36%.

2) General Data. The electronic absorption spectra were recorded with a JASCO UVIDEC-1 spectrophotometer, and the CD spectra with a JASCO J-20 spectropolarimeter. All measurements were carried out in an aqueous solution at room temperature. The ^{1}H NMR spectra were recorded in deuterium oxide on a JEOL JNM-FX-100 NMR spectrometer at probe temperature. Sodium 2,2-dimethyl-2-silapentane-5-sulfonate (DSS) was used as an internal reference. The calculations were carried out on a FACOM M-200 computer at University of Tsukuba.

3) X-Ray Characterization. The unit cell parameters and intensity data were measured on a Rigaku-denki four circle diffractometer (AFC-5) with a graphite-monochromatized Mo *Kα* radiation. The unit cell parameters were determined by least-squares refinement based on 24 reflections. The systematic absences led to the space group $P2_12_12_1$. Crystal data: $C_7H_{25}N_5O_{12}Cl_3SeCo$, *M.W.*=615.6, *a*=12.220 (15), *b*=19.224(7), *c*=8.977(11) Å, *V*=2108.9(11) Å^3, orthorhombic, space group $P2_12_12_1$, d_x=1.91 g cm^{-3}, d_c=1.92 g cm^{-3}, and *Z*=4.

The intensity data were collected by the ω–2θ scan technique up to 2θ=60° with a scan rate of 4° min^{-1}. The intensity data were converted to the F_o data in the usual manner. Absorption corrections were not applied. A total of 2176 independent reflections with $|F_o|>3\sigma(|F_o|)$ were considered as 'observed' and used for the structure analysis.

4) Determination of the Crystal Structure. The positions of the cobalt and selenium atoms were obtained from the three-dimensional Patterson function. The difference-Fourier maps based on the cobalt and selenium positions revealed all non-hydrogen atom. The structure was refined by a full-matrix least-squares refinement of the positional and anisotropic thermal parameters of all the non-hydrogen atoms (program RFINE by L. W. Finger, which was modified by H. Horiuchi, was used). The neutral atomic scattering factors for all the non-hydrogen atoms were taken from the literature.[15] The final residual values were *R*=0.090 and R_w=0.119, respectively. We attempted to determine the absolute configuration of the complex cation by an anomalous-scattering technique. When the refinements were carried out by use of a set of the atomic parameters containing the *Λ* configuration of the complex cation, the residual values converged to *R*=0.087 and R_w=0.114, respectively. On the contrary, the refinements in the enantiomeric atomic parameters (the *Δ* corfiguration) resulted in the residual values of *R*=0.095 and R_w=0.124, respectively. These facts suggest that the former is probably the correct choice, namely, the complex cation has the *Λ* configuration. This absolute configuration coincides with the result that $(+)^{CD}_{500}$-[Co-(mseea)(en)$_2$]$^{3+}$ is assigned to the *Λ* configuration based on the CD spectral behavior (*vide infra*).

The final positional parameters are listed in Table 1. List of structure factors (Table A), anisotropic thermal parameters (Table B), bond lengths and angles for perchlorate ion (Table C), and the projected figure of the crystal structure, which indicated distance in the range of 2.90—3.04 Å, are kept at the Chemical Society of Japan (Document No. 8445).

Results and Discussion

Structure of $(+)^{CD}_{500}$-[Co(mseea)(en)$_2$]$^{3+}$. The perspective drawing of the $(+)^{CD}_{500}$-[Co(mseea)(en)$_2$]$^{3+}$ ion is shown in Fig. 1. The bond lengths and angles are summarized in Table. 2. The coordination geometry around the cobalt atom is approximately octahedral. The selenium atom coordinates to the cobalt atom and the mseea ligand acts as a bidentate. The asymmetric selenium atom in $(+)^{CD}_{500}$-[Co(mseea)(en)$_2$]$^{3+}$, which has the *Λ* configuration, takes the (*R*) configuration. This result supports the prediction that a steric inter-

action occurs between the methyl group and the ethylenediamine chelate ring, N2-C4-C5-N3, if the asymmetric selenium donor atom takes the (*S*) configuration. The methyl group of this isomer takes the axial orientation, which causes the chelate ring of 2-(methylseleno)ethylamine, Se-C2-C3-N1, to have the gauche form with λ conformation (Fig. 1 and Table 3), though the methyl group is expected to take the equatorial orientation in general.[16,17] This fact seems to point out that the methyl group and the amino groups, N3 and N4, repel each other, if the methyl group takes the equatorial orientation. The ethylenediamine chelate ring, N4-C6-C7-N5, takes the reasonable gauche form with δ conformation (Fig. 1 and Table 3). The other ethylenediamine chelate ring, N2-C4-C5-N3, takes the unusual gauche form with λ conformation (Fig. 1 and Table 3).

The bond lengths and angles are similar to those for the [Co(L)(en)$_2$] type complexes, where L denotes selenium- or sulfur-containing ligand such as 2-aminoethaneselenolato,[1] 2-aminoethaneseleninato,[2] and 2-(methylthio)ethylamine.[9] The average Co-N

TABLE 1. POSITIONAL AND THERMAL PARAMETERS

Atom	*x*	*y*	*z*	B_{eq}/Å^2 [a]
Co	0.0383(2)	−0.1444(1)	0.3033(2)	3.02
Se	−0.1078(1)	−0.0720(1)	0.2191(3)	5.22
N1	0.0308(12)	−0.0951(7)	0.4976(16)	4.18
N2	−0.0741(10)	−0.2122(8)	0.3687(17)	3.77
N3	0.0402(12)	−0.1953(9)	0.1192(16)	4.90
N4	0.1552(10)	−0.0840(7)	0.2349(19)	4.60
N5	0.1569(10)	−0.2016(8)	0.3859(18)	4.11
C1	−0.0400(24)	0.0092(13)	0.1150(33)	8.69
C2	−0.1316(19)	−0.0357(13)	0.4196(26)	7.06
C3	−0.0253(20)	−0.0257(12)	0.4917(28)	6.69
C4	−0.1130(28)	−0.2463(22)	0.2291(44)	16.71
C5	−0.0166(23)	−0.2645(12)	0.1284(27)	7.43
C6	0.2663(14)	−0.1210(11)	0.2548(29)	6.42
C7	0.2664(14)	−0.1606(13)	0.3903(29)	6.95
CL1	0.3085(4)	−0.3489(3)	0.2018(5)	4.63
CL2	0.7182(5)	−0.4203(3)	0.1679(7)	5.74
CL3	0.5909(4)	−0.1714(3)	0.3222(7)	5.86
O11	0.3504(15)	−0.3295(9)	0.3385(20)	8.29[b]
O12	0.3859(26)	−0.3664(16)	0.1078(36)	16.08[b]
O13	0.2657(22)	−0.2884(14)	0.1209(31)	13.74[b]
O14	0.2218(33)	−0.3944(19)	0.2235(45)	21.41[b]
O21	0.8232(35)	−0.4252(23)	0.1180(49)	22.83[b]
O22	0.7268(21)	−0.4373(13)	0.3151(30)	13.04[b]
O23	0.6918(27)	−0.3592(18)	0.1146(40)	17.93[b]
O24	0.6404(30)	−0.4566(20)	0.1096(43)	20.41[b]
O31	0.6914(22)	−0.1624(13)	0.3681(30)	13.27[b]
O32	0.5252(24)	−0.1708(16)	0.4616(33)	14.55[b]
O33	0.5692(27)	−0.2453(20)	0.3186(38)	18.25[b]
O34	0.5343(38)	−0.1474(24)	0.2063(51)	25.84[b]

a) B_{eq} is the equivalent isotropic temperature factors defined by Hamilton.[19] b) Isotropic temperature factor.

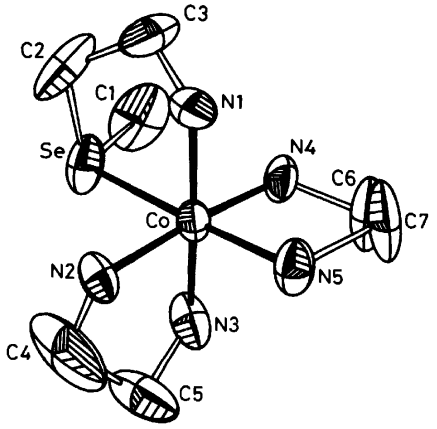

Fig. 1. A perspective drawing of Λ-(+)$_{500}^{CD}$-[Co(mseea)-(en)$_2$]$^{3+}$ with the numbering scheme of atoms.

TABLE 2. INTERMOLECULAR DISTANCES AND BOND ANGLES (WITH e.s.d.'s)

	(a) Bond distances (l/Å)		
Co-Se	2.386(3)	Co-N1	1.987(15)
Co-N2	1.983(14)	Co-N3	1.921(15)
Co-N4	1.940(14)	Co-N5	1.964(14)
Se-C1	1.999(26)	Se-C2	1.952(24)
N1-C3	1.501(27)	N2-C4	1.492(42)
N3-C5	1.503(29)	N4-C6	1.543(22)
N5-C7	1.554(23)	C2-C3	1.464(34)
C4-C5	1.525(45)	C6-C7	1.435(36)
	(b) Bond angles (ϕ/°)		
Se-Co-N1	88.0(4)	Se-Co-N2	87.7(4)
Se-Co-N3	91.9(5)	Se-Co-N4	95.8(4)
Se-Co-N5	176.2(5)	N1-Co-N2	91.2(6)
N1-Co-N3	177.1(6)	N1-Co-N4	91.5(7)
N1-Co-N5	88.2(6)	N2-Co-N3	85.9(7)
N2-Co-N4	175.6(6)	N2-Co-N5	91.7(6)
N3-Co-N4	91.4(7)	N3-Co-N5	91.8(7)
N4-Co-N5	84.9(6)	Co-Se-C1	107.1(8)
Co-Se-C2	91.6(7)	C1-Se-C2	102.3(11)
Co-N1-C3	114.4(13)	Co-N2-C4	105.1(17)
Co-N3-C5	113.5(13)	Co-N4-C6	109.6(11)
Co-N5-C7	111.1(12)	Se-N2-C3	108.7(16)
N1-C3-C2	107.8(18)	N2-C4-C5	110.6(25)
N3-C5-C4	100.8(21)	N4-C6-C7	110.1(16)
N5-C7-C6	104.3(16)		

TABLE 3. DISPLACEMENTS OF ATOMS FROM THE LEAST-SQUARES PLANE (d/Å)

2-(Methylseleno)ethylamine chelate ring

Plane 1, $0.66326X-0.67175Y-0.32990Z+2.45197=0$

Co 0.0000 Se −0.0000 N1 −0.0000 C1 1.9064
C2 −0.3179 C3 0.4590

Ethylenediamine chelate ring

Plane 2, $-0.71865X-0.59399Y-0.36156Z+2.96969=0$

Co 0.0000 N2 0.0000 N3 0.0000 C4 0.4060
C5 −0.3208

Plane 3, $0.04888X+0.51340Y-0.85676Z+0.88497=0$

Co −0.0001 N4 0.0001 N5 0.0001 C6 0.2782
C7 −0.3723

The *X*, *Y*, and *Z* coordinates in Å are referred to the crystallographic axes.

length is 1.959 Å and no significant trans effect is observed, as well as the cobalt(III) complexes with coordinated thioether sulfur atom.[9,18] The bond lengths of Co–Se, Se–Cl, and Se–C2 (2.386, 1.999, and 1.952 Å) are longer than the bond lengths of Co–S (2.267) and S–C (1.817 and 1.834 Å) in the corresponding [Co(mea)(en)$_2$]$^{3+}$,[9] and this results in a smaller bond angle of Co–Se–C2 (91.6°) that the angle of the corresponding Co–S–C (97.9°).[9] The other two bond angles around the selenium atom (Co–Se–Cl=107.1° and Cl–Se–C2=102.3°) are reasonable for the tetrahedral geometry in contrast to those around the sulfur atom in [Co(mea)(en)$_2$]$^{3+}$ (Co–S–C=114.2° and C–S–C=99.4°).[9] This fact seems to depend on the longer bond lengths of Se–Co and Se–Cl.

Absorption and CD Spectra. The electronic absorption and CD spectra of the selenolato complex, $(+)^{CD}_{500}$-[Co(aes)(en)$_2$]$^{2+}$, selenenato complex, $(+)^{CD}_{500}\cdot(-)^{CD}_{360}$-[Co(aesee)(en)$_2$]$^{2+}$, and selenoether complexes, $(+)^{CD}_{500}$-[Co(mseea)(en)$_2$]$^{3+}$, $(+)^{CD}_{500}$-[Co(eseea)(en)$_2$]$^{3+}$, and $(+)^{CD}_{500}$-[Co(bseea)(en)$_2$]$^{3+}$, are shown in Figs. 2—5, together with those of the corresponding [Co(bidentate-*N*,*S*)(en)$_2$] type complexes; the data are summarized in Tables 4 and 5. The absorption spectral behavior of the cobalt(III) complexes which belong to [Co(*N*)$_5$(*Se*)] type is quite similar to those of the corresponding [Co(*N*)$_5$(*S*)] type complexes (Figs. 2—6).[5,9-12] The intense absorption bands at around 32—36×10^3 cm^{-1} are assigned to the charge transfer ones due to the coordinated selenium atom, which correspond to the so-called sulfur-to-metal charge transfer band.[5,9-12] The charge transfer bands of the selenolato, selenenato and selenoether complexes commonly shift to a lower energy than those of the corresponding thiolato, sulfenato and thioether ones, respectively (Figs. 2—6).[5,9-12] Of these complexes, [Co(aesee)(en)$_2$]$^{2+}$ shows another intense band at 27.55×10^3 cm^{-1} (Fig. 3). This band corresponds well with the characteristic band (*ca.* 27.0×10^3 cm^{-1}) of the sulfenato complex, [Co(aese)(en)$_2$]$^{2+}$ (Fig. 3).[10-12] Therefore, the band at 27.55×10^3 cm^{-1} seems to be characteristic for the selenenato complex as well as for the sulfenato complex.

In the first absorption band region, [Co(aes)(en)$_2$]$^{2+}$ shows an explicit shoulder on the lower energy side of the major peak (*ca.* 16.6×10^3 cm^{-1}) as well as [Co(aet)(en)$_2$]$^{2+}$ (Fig. 2).[5] This kind of shoulder was also observed in the absorption spectra of the cobalt(III) complexes with thiolato-type ligand such as L-cysteinate[7,8] and D- or L-penicillaminate,[8,13] and

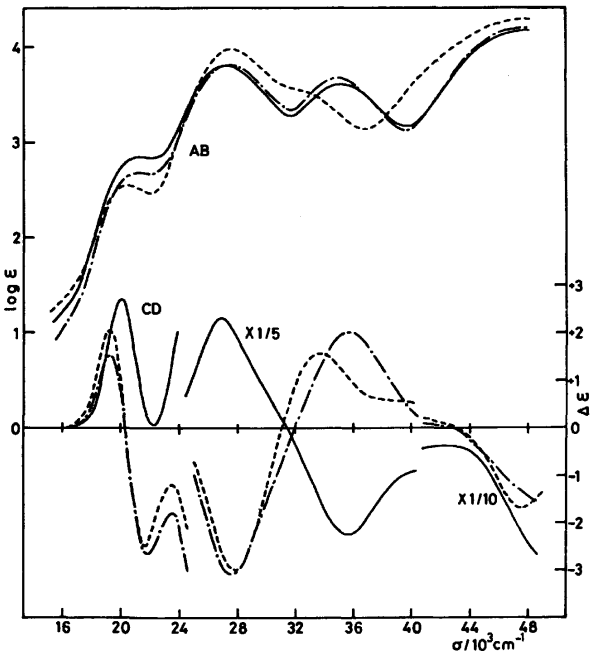

Fig. 3. Absorption and CD spectra of $(+)^{CD}_{500}\cdot(-)^{CD}_{360}$-[Co(aesee)(en)$_2$]$^{2+}$ (----), $(+)^{CD}_{500}\cdot(-)^{CD}_{360}$-[Co(aese)(en)$_2$]$^{2+}$ (—·—) and $(+)^{CD}_{500}\cdot(+)^{CD}_{360}$-[Co(aese)(en)$_2$]$^{2+}$ (——).

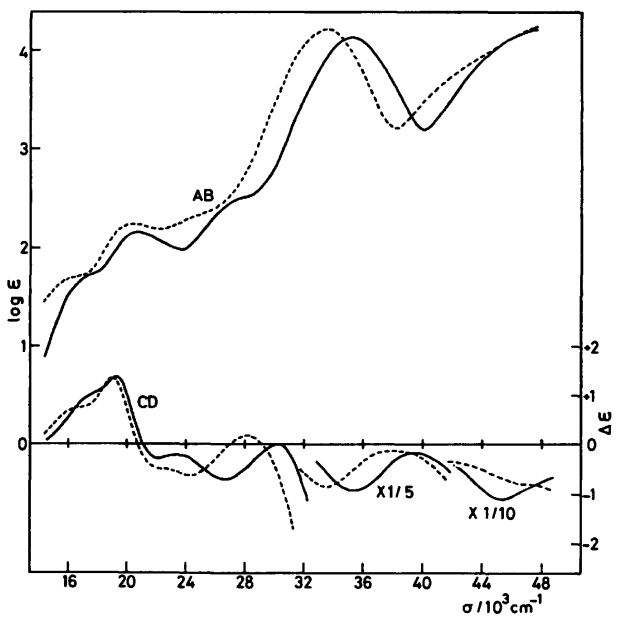

Fig. 2. Absorption and CD spectra of $(+)^{CD}_{500}$-[Co(aes)(en)$_2$]$^{2+}$ (----) and $(+)^{CD}_{500}$-[Co(aet)(en)$_2$]$^{2+}$ (——).

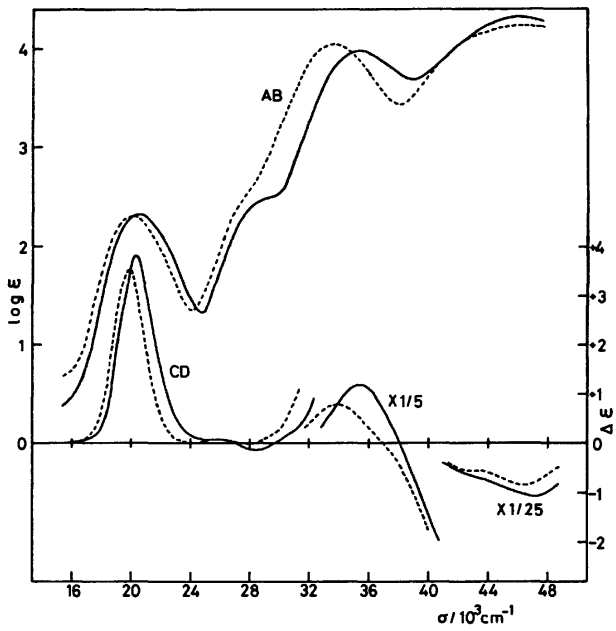

Fig. 4. Absorption and CD spectra of $(+)^{CD}_{500}$-[Co(mseea)(en)$_2$]$^{3+}$ (----) and $(+)^{CD}_{500}$-[Co(mea)(en)$_2$]$^{3+}$ (——).

accordingly, this band seems to be also characteristic for the selenolato coordination. The mseea, eseea and bseea complexes show a rather sharp first absorption band without a shoulder as the case of the corresponding thioether complexes (Figs. 4—6).[5,9]

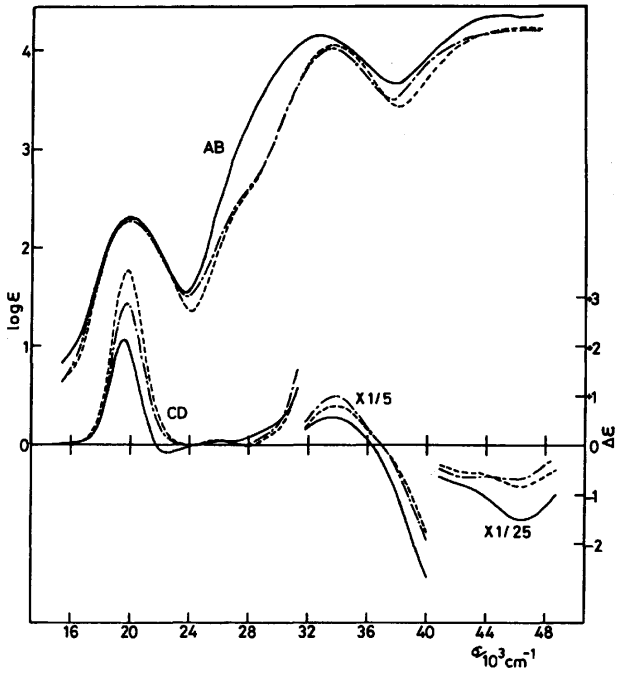

Fig. 5. Absorption and CD spectra of $(+)^{CD}_{500}$-[Co(mseea)-$(en)_2]^{3+}$ (----), $(+)^{CD}_{500}$-[Co(eseea)$(en)_2]^{3+}$ (———), and $(+)^{CD}_{500}$-[Co(bseea)$(en)_2]^{3+}$ (——).

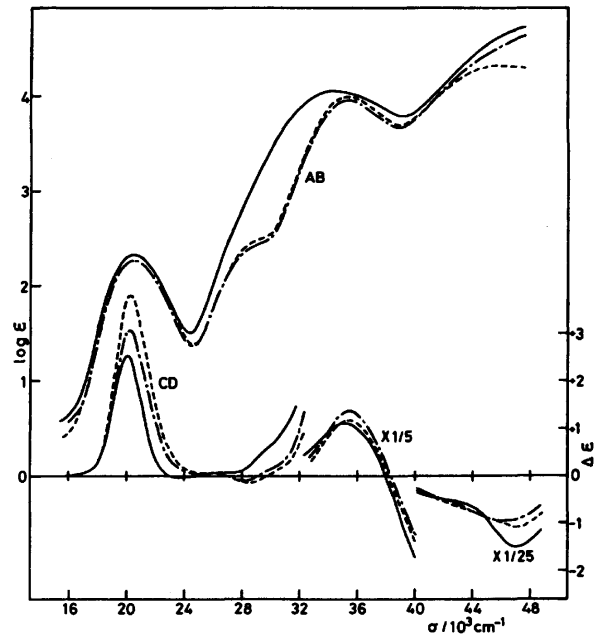

Fig. 6. Absorption and CD spectra of $(+)^{CD}_{500}$-[Co(mea)-$(en)_2]^{3+}$ (----), $(+)^{CD}_{500}$-[Co(eea)$(en)_2]^{3+}$ (———), and $(+)^{CD}_{500}$-[Co(bea)$(en)_2]^{3+}$ (——).

TABLE 4. ABSORPTION DATA OF [Co(bidentate-*N*,*Se* OR -*N*,*S*)$(en)_2$] TYPE COMPLEXES

Complex	First band	Second band	Charge transfer band
$(+)^{CD}_{500}$-[Co(aes)$(en)_2]^{2+}$	16.5 (1.71 sh)	24.7 (2.33 sh)	33.44 (4.22)
	20.35 (2.24)		
$(+)^{CD}_{500}\cdot(-)^{CD}_{360}$-[Co(aesee)$(en)_2]^{2+}$	20.45 (2.55)		27.55 (3.99)
			32.0 (3.55 sh)
			47.85 (4.30)
$(+)^{CD}_{500}$-[Co(mseea)$(en)_2]^{3+}$	20.00 (2.30)		33.56 (4.06)
			46.30 (4.24)
$(+)^{CD}_{500}$-[Co(eseea)$(en)_2]^{3+}$	19.96 (2.27)		33.44 (4.03)
			46.51 (4.22)
$(+)^{CD}_{500}$-[Co(bseea)$(en)_2]^{3+}$	19.92 (2.31)		32.57 (4.16)
			44.84 (4.36)
$(+)^{CD}_{500}$-[Co(aet)$(en)_2]^{2+}$	17.5 (1.72 sh)	28.2 (2.52 sh)	35.21 (4.13)
	20.66 (2.16)		48.78 (4.22)
$(+)^{CD}_{500}\cdot(-)^{CD}_{360}$-[Co(aese)$(en)_2]^{2+}$	21.12 (2.68)		27.32 (3.82)
			34.84 (3.68)
			49.26 (4.21)
$(+)^{CD}_{500}\cdot(+)^{CD}_{360}$-[Co(aese)$(en)_2]^{2+}$	21.12 (2.85)		26.99 (3.81)
			35.03 (3.61)
			49.26 (4.18)
$(+)^{CD}_{500}$-[Co(mea)$(en)_2]^{3+}$	20.47 (2.32)	29.3 (2.50 sh)	35.34 (3.99)
			45.66 (4.32)
$(+)^{CD}_{500}$-[Co(eea)$(en)_2]^{3+}$	20.45 (2.26)	29.4 (2.45 sh)	35.34 (3.95)
			48.90 (4.63)
$(+)^{CD}_{500}$-[Co(bea)$(en)_2]^{3+}$	20.45 (2.33)		34.31 (4.05)
			49.0 (4.75 sh)

Wave numbers and log ε values (in parentheses) are given in 10^3 cm^{-1} and mol^{-1} dm^3 cm^{-1}, respectively. Sh denotes a shoulder.

TABLE 5. CD DATA OF [Co(bidentate-*N*,*Se* OR -*N*,*S*)(en)$_2$] TYPE COMPLEXES

Complex	First band	Second band	Charge transfer band
$(+)^{CD}_{500}$-[Co(aes)(en)$_2$]$^{2+}$	16.6 (+0.75 sh)	24.45 (−0.61)	33.44 (−4.26)
	19.01 (+1.35)	28.17 (+0.18)	
	22.2 (−0.47 sh)		
$(+)^{CD}_{500}\cdot(-)^{CD}_{360}$-[Co(aesee)(en)$_2$]$^{2+}$	19.23 (+2.04)		27.78 (−15.04)
	22.12 (−2.25)		33.56 (+7.80)
			38.5 (+2.95 sh)
			47.62 (−16.9)
$(+)^{CD}_{500}$-[Co(mseea)(en)$_2$]$^{3+}$	19.80 (+3.55)	25.97 (+0.10)	33.90 (+3.98)
			46.3 (−20.8)
$(+)^{CD}_{500}$-[Co(eseea)(en)$_2$]$^{3+}$	19.76 (+2.87)	25.97 (+0.08)	33.90 (+5.05)
			45.7 (−16.8)
$(+)^{CD}_{500}$-[Co(bseea)(en)$_2$]$^{3+}$	19.61 (+2.15)	26.32 (+0.07)	33.56 (+2.85)
	22.47 (−0.15)		46.3 (−37.2)
$(+)^{CD}_{500}$-[Co(aet)(en)$_2$]$^{2+}$	17.5 (+1.00 sh)	26.67 (−0.71)	35.34 (−4.62)
	19.27 (+1.37)		45.5 (−11.1)
	22.08 (−0.29)		
$(+)^{CD}_{500}\cdot(-)^{CD}_{360}$-[Co(aese)(en)$_2$]$^{2+}$	19.27 (+1.53)		27.55 (−15.39)
	21.83 (−2.65)		35.59 (+10.24)
			41.7 (+0.64 sh)
			48.8 (−15.8)
$(+)^{CD}_{500}\cdot(+)^{CD}_{360}$-[Co(aese)(en)$_2$]$^{2+}$	19.96 (+2.72)		26.88 (+11.56)
			35.59 (−11.29)
			40.5 (−4.28 sh)
$(+)^{CD}_{500}$-[Co(mea)(en)$_2$]$^{3+}$	20.20 (+3.82)	28.41 (−0.15)	35.46 (+5.92)
			47.1 (−27.5)
$(+)^{CD}_{500}$-[Co(eea)(en)$_2$]$^{3+}$	20.20 (+3.08)	28.17 (−0.10)	35.46 (+6.90)
			45.9 (−23.1)
$(+)^{CD}_{500}$-[Co(bea)(en)$_2$]$^{3+}$	20.04 (+2.54)		35.09 (+5.47)
	23.53 (−0.02)		47.2 (−37.6)

Wave numbers and $\Delta\varepsilon$ values (in parentheses) are given in 10^3 cm^{-1} and mol^{-1} dm^3 cm^{-1}, respectively. Sh denotes a shoulder.

The aesee complex shows the first absorption band with a large molar absorption coefficient and it seems to be affected by the intense charge transfer band at 27.55×10^3 cm^{-1} (Fig. 3). The first absorption bands of the selenolato, selenenato, and selenoether complexes shift to a lower energy than those of the corresponding thiolato, sulfenato, and thioether complexes,[5,9-12] respectively (Figs. 2—6), indicating that the order of the ligand field strength is *S*>*Se*.

The *Δ* and *Λ* isomers are possible for [Co(aes)(en)$_2$]$^{2+}$. As shown in Fig. 2, the CD spectrum of $(+)^{CD}_{500}$-[Co(aes)(en)$_2$]$^{2+}$ agrees with that of *Λ*-$(+)^{CD}_{500}$-[Co(aet)(en)$_2$]$^{2+}$ in the whole region,[5] and then the $(+)^{CD}_{500}$ aes isomer is assignable to the *Λ* configuration. Taking the asymmetric selenium donor atom, (*R*) and (*S*), into consideration, four isomers, *Λ*-(*R*), *Λ*-(*S*), *Λ*-(*R*), and *Λ*-(*S*), are possible for each of [Co(aesee)(en)$_2$]$^{2+}$, [Co(mseea)(en)$_2$]$^{3+}$, [Co(eseea)(en)$_2$]$^{3+}$, and [Co(bseea)(en)$_2$]$^{3+}$. In contrast to the fact that two isomers, *Λ*-(*R*) and *Λ*-(*S*), were formed for [Co(aese)(en)$_2$]$^{2+}$ (*Λ*-(*R*):*Λ*-(*S*)=3:1), $(+)^{CD}_{500}\cdot(-)^{CD}_{360}$-[Co(aesee)(en)$_2$]$^{2+}$ was selectively formed by the stoichiometric oxidation reaction of *Λ*-$(+)^{CD}_{500}$-[Co(aes)(en)$_2$]$^{2+}$ with H_2O_2. The $(+)^{CD}_{500}\cdot(-)^{CD}_{360}$ aesee isomer shows quite similar CD spectrum to that of the *Λ*-(*R*) aese isomer (Fig. 3),[11] and then it is suggested that the $(+)^{CD}_{500}\cdot(-)^{CD}_{360}$ aesee isomer takes the *Λ*-(*R*) configuration. This stereoselectivity may suggest that there is an intramolecular hydrogen bond between the selenenato or sulfenato oxygen atom and the adjacent amino proton in *Λ*-(*R*)-[Co(aesee or aese)(en)$_2$]$^{2+}$ and the hydrogen bond stabilizes the *Λ*-(*R*) configuration. The hydrogen bond is more favorable for the *Λ*-(*R*) aesee isomer than for the *Λ*-(*R*) aese one, because the bond lengths of Co–Se and Se–O are longer than those of Co–S and S–O, respectively.[1,2] The $(+)^{CD}_{500}$ mseea, eseea and bseea isomers, which were derived from *Λ*-$(+)^{CD}_{500}$-[Co(aes)(en)$_2$]$^{2+}$, show a positive CD band (*ca.* 19.7×10^3 cm^{-1}) whose intensity decreases with the order of the mseea, eseea, and bseea isomers, though the bseea isomer shows a weak negative CD band at the higher energy side in the first absorption band region. A similar CD spectral behavior was observed for a series of the corresponding thioether isomers, $(+)^{CD}_{500}$ mea, eea, and bea (Fig. 6). Taking these facts and the assignments of the $(+)^{CD}_{500}$ mea and eea isomers[5] into consideration, the $(+)^{CD}_{500}$ mseea, eseea, bseea, and bea isomers are assigned to the *Λ* configuration. The ^{1}H NMR spectrum of the $(+)^{CD}_{500}$ mseea

isomer exhibits a single peak in the methyl protons region (2.26 ppm from DSS) and that of the $(+)_{500}^{CD}$ eseea isomer one set of triplet peaks (centered at 1.57 ppm). The $(+)_{500}^{CD}$ bseea isomer shows a single peak due to the aromatic protons (7.52 ppm). The ^1H NMR spectral behavior of the selenoether isomers is in line with that of the corresponding thioether isomers.[5,9] Molecular model constructions of the selenoether and thioether complexes reveal that the *Λ*-(*R*) configuration is preferable, because the *Se*- or *S*-alkyl group in the *Λ*-(*S*) configuration have a nonbonding interaction with the adjacent ethylenediamine chelate ring. Moreover, the X-ray structural analysis indicates that the $(+)_{500}^{CD}$ mseea isomer has the (*R*) configuration for the coordinated selenium atom when the isomer takes the *Λ* configuration. Based on these results, it is suggested that the $(+)_{500}^{CD}$ selenoether and thioether isomers take selectively the *Λ*-(*R*) configuration in solution.

In the charge transfer band region, the *Λ*-(*R*) selenoether and thioether isomers show one positive CD band, while *Λ*-[Co(aes)$(en)_2$]$^{2+}$, *Λ*-[Co(aet)$(en)_2$]$^{2+}$ and *Λ*-[Co(aesi-*N,S*)$(en)_2$]$^{2+}$ (aesi=2-aminoethanesulfinato),[2] which have no chirality due to the chalcogen donor atom, show a negative one (Figs. 2 and 4—6). This fact suggests that the CD band in this region is contributed by not only the configurational chirality due to the skew pair of chelate rings but also the chirality of the selenium or sulfur donor atom.

References

1) C. A. Stein, P. E. Ellis, Jr., R. C. Elder, and E. Deutsch, *Inorg. Chem.*, **15**, 1618 (1976).

2) K. Okamoto, T. Konno, M. Nomoto, H. Einaga, and J. Hidaka, *Bull. Chem. Soc. Jpn.*, **57**, 1494 (1984).

3) K. Nakajima, M. Kojima, and J. Fujita, *Chem. Lett.*, **1982**, 925.

4) L. Roecher, M. H. Dickman, D. L. Nosco, R. J. Doedens, and E. Deutsch, *Inorg. Chem.*, **22**, 2022 (1983).

5) K. Yamanari, J. Hidaka, and Y. Shimura, *Bull. Chem. Soc. Jpn.*, **50**, 2299 (1977).

6) R. H. Lane, F. A. Sedor, M. J. Gilroy, P. F. Eisenhardt, J. P. Bennett, Jr., R. X. Ewall, and L. E. Bennett, *Inorg. Chem.*, **16**, 93 (1977).

7) D. L. Herting, C. P. Sloan, A. W. Cabral, and J. H. Krueger, *Inorg. Chem.*, **17**, 1649 (1978).

8) H. C. Freeman, C. J. Moore, W. G. Jackson, and A. M. Sargeson, *Inorg. Chem.*, **17**, 3513 (1978).

9) R. C. Elder, G. J. Kennard, M. D. Payne, and E. Deutsch, *Inorg. Chem.*, **17**, 1296 (1978).

10) I. K. Adzamli, K. Libson, J. D. Lydon, R. C. Elder, and E. Deutsch, *Inorg. Chem.*, **18**, 303 (1979).

11) M. Kita, K. Yamanari, and Y. Shimura, *Bull. Chem. Soc. Jpn.*, **55**, 2873 (1982).

12) M. Kojima and J. Fujita, *Bull. Chem. Soc. Jpn.*, **56**, 139 (1983).

13) K. Wakayama, K. Okamoto, H. Einaga, and J. Hidaka, *Bull. Chem. Soc. Jpn.*, **56**, 1995 (1983).

14) T. Konno, K. Okamoto, and J. Hidaka, *Chem. Lett.*, **1982**, 535.

15) "International Tables for X-Ray Crystallography," The Kynoch Press, Birmingham, (1974), Vol. IV.

16) C. J. Hawkins, "Absolute Configuration of Metal Complexes," John-Wiley & Sons, Inc., New York, (1971).

17) T. Makino, S. Yano, and S. Yoshikawa, *Inorg. Chem.*, **18**, 1048 (1979).

18) K. Okamoto, M. Suzuki, H. Einaga, and J. Hidaka, *Bull. Chem. Soc. Jpn.*, **56**, 3513 (1983).

19) W. C. Hamilton, *Acta Crystallogr.*, **12**, 609 (1959).

 © 1984 The Chemical Society of Japan Bull. Chem. Soc. Jpn., 57, 3111—3116 (1984)

Preparation and Characterization of Cobalt(III) Complexes with *S,S*-Bridge *R,S*-Sexidentate-N_2,S_2,O_2 Type Ligands. Crystal Structure of $(+)^{CD}_{560}$-((2*R*,9*S*)-Diamino-3,3,8,8-tetramethyl-4,7-dithia-1,10-decanedioato)cobalt(III) Ion

Mikako KANESAKA, Ken-ichi OKAMOTO,* Masayo NOMOTO, and Jinsai HIDAKA
Department of Chemistry, University of Tsukuba, Sakura, Ibaraki 305
(Received April 12, 1984)

[Co(*R,S*-sexidentate-N_2,S_2,O_2)] and [Co(*R*-terdentate-*N,S,O*)(*S-terdentate-N,S,O*)] type complexes, including the title complex cation, [Co(*R,S*-ebp)]$^+$, were prepared and resolved. The crystal structure and absolute configuration of the $(+)^{CD}_{560}$-[Co(*R,S*-ebp)]$^+$ isomer were determined by X-ray diffraction. The complex cation has an [*S*] configuration. The *R,S*-ebp coordinates as a sexidentate, of which two sulfur donor atoms take selectively *R*(*S*). The absorption and CD spectra are discussed in comparison with those of the related complexes.

In a previous paper,[1] we reported the preparation, CD spectra, and stereochemistry of [Co(LL-sexidentate-N_2,S_2,O_2)] and [Co-(L-terdentate-*N,S,O*)$_2$] type complexes. Regarding the CD spectral analysis of these complexes, the CD contribution due to *S*(*C*) of the ligand was troublesome. This paper deals with the preparation and resolution of [Co(*R,S*-sexidentate-N_2,S_2,O_2)] type complex cations, [Co(OOCCH(NH_2)C(CH_3)$_2$S(CH_2)$_n$SC(CH_3)$_2$CH(NH_2)COO)]$^+$ (n=2, *R,S*-ebp; n=3, *R,S*-tbp; n=4, *R,S*-tetp),[2] and (*S*-methyl-*R*-penicillaminato)(*S*-methyl-*S*-penicillaminato)cobalt(III), [Co(*R*-smp)(*S*-smp)]$^+$, and with the X-ray crystal structure analysis of $(+)^{CD}_{560}$-[Co(*R,S*-ebp)]$^+$. The reaction of *cis*·*cis*·*cis*-(*R*-penicillaminato)(*S*-penicillaminato)cobaltate(III),[3] [Co(*R*-pen)(*S*-pen)]$^-$, with Br(CH_2)$_n$Br (n=2, 3, and 4) spanned with ethylene, trimethylene, or tetramethylene the thiolato type sulfur donor atoms of the *R*- and *S*-pen to give an *R,S*-ebp, *R,S*-tbp, or *R,S*-tetp complex. The reaction of *cis*·*cis*·*cis*-[Co(*R*-pen)(*S*-pen)]$^-$ with dimethyl sulfate gave *cis*·*cis*·*cis*-[Co(*R*-smp)(*S*-smp)]$^+$, and the oxidation reaction of a cobalt(II) ion with the *R*- and *S*-smp gave *cis*·*cis*·*cis*- and *trans*·*trans*·*trans*-[Co(*R*-smp)(*S*-smp)]$^+$. The *cis*·*cis*·*cis* isomers of the above complexes were resolved into their optical isomers, which can be designated as [*R*] and [*S*] based on the chiral arrangement of the coordinated atoms.[4]

Experimental

1) Preparation of the Ligand. *a)* *S*-Methylpenicillamine was prepared by a procedure similar to that used for *S*-benzylpenicillamine.[5] Found: C, 44.95; H, 8.20; N, 9.36%. Calcd for $C_6H_{13}NO_2S$: C, 44.14; H, 8.02; N, 8.58%.

2) Preparation and Resolution of Complexes. *b) [Co(*R,S*-ebp)]Br.* An excess (5 cm^3) of 1,2-dibromoethane was added to a solution containing 0.8 g of *cis*·*cis*·*cis*-K[Co(*R*-pen)(*S*-pen)]·2H_2O[3] in 14 cm^3 of dimethyl sulfoxide. The mixture was stirred at room temperature for a few minutes and allowed to stand for about 1 d. The color of the solution changed from green to dark-red, and then to a deep-red. Dimethyl sulfoxide and unreacted 1,2-dibromoethane were extracted with ether several times. To the remaining dark-red solution a small amount of water was added. This solution was then poured onto a column of SP-Sephadex C-25 (Na^+ form, 4.0 cm×25 cm). After the column had been swept with water, the adsorbed band was eluted with a 0.05 mol dm^{-3} aqueous solution of NaBr. Only one red-violet band was eluted and fractionated. It was found, from the absorption spectral measurements, that all the eluates contained only [Co(*R,S*-ebp)]$^+$. The eluates were combined and concentrated to a small volume with a rotary evaporator at a temperature below 25 °C. The deposited NaBr was filtered off. The filtrate was poured onto a column of Sephadex G-10 (3.0 cm×85 cm) and eluted with water. The eluate was concentrated to a small volume again and an appropriate amount of ethanol was added to the solution. The resulting red-violet crystals were collected by filtration, recrystallized from water by adding ethanol, and washed with ethanol and ether. Found: C, 27.21; H, 5.65; N, 5.28%. Calcd for [Co(*R,S*-ebp)]Br·4H_2O=$CoC_{12}H_{22}N_2O_4S_2Br$·4$H_2O$: C, 27.02; H, 5.65; N, 5.25%.

To a solution containing 86 mg of the racemic [Co(*R,S*-ebp)]Br·4H_2O and 32.4 mg of $(+)_{546}$-K[Co(edta)]·2H_2O[6] (edta; ethylenediaminetetraacetate) in a small amount of water were added 14 mg of silver acetate and 17 mg of silver perchlorate. After the mixture was stirred for 10 min, the precipitated silver bromide and potassium perchlorate were filtered off. After the filtrate had been concentrated to a small volume, the concentrated solution, to which was added a small amount of ethanol, was kept in a refrigerator for 5 d. The less-soluble diastereomer (violet needle crystals) was recrystallized from water by adding ethanol. A piece of a crystal was used for an X-ray diffraction study. By use of the anion exchange column (Br^- form), the diastereomer was converted into the bromide salt, $(+)^{CD}_{560}$-[Co(*R,S*-ebp)]Br. The $\Delta\varepsilon$ values were evaluated from the absorption spectral data.

*c) [Co(*R,S*-tbp)]Br.* The $(-)^{CD}_{560}$-[Co(*R,S*-tbp)]$^+$ complex was prepared and resolved by a procedure similar to that used for [Co(*R,S*-ebp)]Br described in *b)*, using 1,3-dibromopropane instead of 1,2-dibromoethane. Found for the *R,S*-tbp complex: C, 30.79; H, 5.48; N, 5.50%. Calcd for [Co(*R,S*-tbp)]Br·2H_2O=$CoC_{13}H_{24}N_4O_4S_2Br$·2$H_2O$: C, 30.54; H, 5.52; N, 5.28%. Found for the less-soluble diastereomer: C, 35.05; H, 4.95; N, 6.91%. Calcd for [Co(*R,S*-tbp)][Co(edta)]·2.5H_2O=$Co_2C_{23}H_{36}N_6O_{12}S_2$·2.5$H_2O$: C, 35.07; H, 5.25; N, 7.11%.

The bromide salt was obtained by the same procedure as in *b)* and the $\Delta\varepsilon$ values were also evaluated from the absorption spectral data.

*d) [Co(*R,S*-tetp)]Br.* The $(+)^{CD}_{560}$-[Co(*R,S*-tetp)]$^+$ complex was prepared and resolved by a procedure similar to that used for [Co(*R,S*-ebp)]Br as in *b)*, using 1,4-dibromobutane instead of 1,2-dibromoethane, and $(-)_{546}$-K[Co(edta)]·2H_2O as resolving agent. Found for the *R,S*-tetp complex: C, 32.55; H, 5.41; N, 5.41%. Calcd for [Co(*R,S*-tetp)]Br·

$1.5H_2O$=$CoC_{14}H_{26}N_2O_4S_2Br \cdot 1.5H_2O$: C, 32.56; H, 5.65; N, 5.42%. The bromide salt and the $\Delta\varepsilon$ values were obtained by the same procedure as in *b)*.

Here, it is noted that for the *S,S*-bridge complex, the [*S*]-$(+)_{560}^{CD}$ *R,S*-ebp isomer forms the less-soluble diastereomer with $(+)_{546}$-[Co(edta)]$^-$, whereas the [*R*]-$(-)_{560}^{CD}$ *R,S*-tbp isomer forms the less-soluble diastereomer with $(+)_{546}$-[Co(edta)]$^-$ and the [*S*]-$(+)_{560}^{CD}$ *R,S*-tetp isomer with $(-)_{546}$-[Co(edta)]$^-$.

*e) [Co(*R*-smp)(*S*-smp)]NO_3. Method 1.* This complex was prepared by a procedure similar to that used for [Co(*R*-smp)(dien)]$^+$ [7] and [Co(*S*-smp)$_2$]$^+$,[8] namely, *cis·cis·cis*-[Co(*R*-smp)(*S*-smp)]$^+$ was obtained by the reaction of the coordinated thiolato type donor atoms of *cis·cis·cis*-[Co(*R*-pen)(*S*-pen)]$^-$ [3] with dimethyl sulfate. It was confirmed using a cation exchange column chromatography (Dowex 50W-X8, 200—400 mesh, Na^+ form, 3.5 cm×20 cm) that no isomerization had taken place. Found: C, 29.60; H, 5.77; N, 8.60%. Calcd for [Co(*R*-smp)(*S*-smp)]$NO_3 \cdot 2.5H_2O$ =$CoC_{12}H_{24}N_3O_7S_2 \cdot 2.5H_2O$: C, 29.39; H, 5.96; N, 8.57%.

Method 2. The [Co(*R*-smp)(*S*-smp)]$^+$ complex was also prepared by a procedure similar to that used for [Co(L-met)$_2$]$^+$,[9] using *S*-methylpenicillamine instead of L-methionine. The reaction mixture was filtered to remove any insoluble material. The filtrate was allowed to stand at room temperature overnight and was then poured onto a column of Dowex 50W-X8 (200—400 mesh, Na^+ form, 3.5 cm×60 cm). After the column had been swept with water, the adsorbed band was eluted with a 0.1 mol dm^{-3} aqueous solution of NaCl. Three colored bands, dark-violet (F-1), reddish violet (F-2), and violet (F-3), were eluted in this order and were in the ratio of about F-1:F-2:F-3=1:5:3. From their absorption spectral measurements, it was found that F-1 and F-2 eluates contained *trans·trans·trans-* and *cis·cis·cis*-[Co(*R*-smp)(*S*-smp)]$^+$ isomers, respectively. The F-3 eluate showed the same spectrum as the *trans*(*S*)-[Co(*S*-smp)$_2$]$^+$ isomer,[8] but did not exhibit the optical activity, indicating it was a mixture of *trans*(*S*)-[Co(*S*-smp)$_2$]$^+$ and *trans*(*S*)-[Co(*R*-smp)$_2$]$^+$. Each of the F-1 and F-2 eluates was concentrated to a small volume with a rotary evaporator at a temperature of about 20 °C. The deposited NaCl was filtered off. As the amount of the earlier eluate (F-1) was very small, it could not be obtained as in crystal form. The absorption spectrum of the *trans·trans·trans*-[Co(*R*-smp)(*S*-smp)]$^+$ was measured with the solution and it is illustrated with an arbitrary scale in Fig. 3.

The F-2 eluate, which showed the same absorption spectrum as that in *Method 1*, was poured onto a column of SP-Sephadex C-25 (Na^+ form, 3.0 cm×90 cm). After the column had been swept with water, the adsorbed band was eluted with a 0.03 mol dm^{-3} aqueous solution of K_2[Sb$_2$(*d*-tart)$_2$]·$3H_2O$. After circulating the eluates in the same column two times, they separated into two reddish violet bands and fractionated. Each of the fractions was concentrated to a small volume with a rotary evaporator at a temperature of about 20 °C and the deposited K_2[Sb$_2$(*d*-tart)$_2$] was filtered off. The filtrate was converted into the bromide salt using a column of QAE-Sephadex A-25 (Br^- form) and the CD spectra were measured with its solutions. The earlier eluate contained $(-)_{560}^{CD}$-*cis·cis·cis*-[Co(*R*-smp)(*S*-smp)]$^+$ and the later contained $(+)_{560}^{CD}$ one. The $\Delta\varepsilon$ values were also evaluated from the absorption spectral data.

3) General Data. The electronic absorption spectra were recorded with JASCO UVIDEC-1 and UVIDEC-610 spectrophotometers and the CD spectra with a JASCO J-20 spectropolarimeter. All measurements were carried out in aqueous solutions at room temperature. The calculations were carried out on a FACOM M-200 computer at University of Tsukuba.

4) X-Ray Characterization. The unit cell parameters and intensity data for the single crystal (*ca.* 0.12×0.18×0.35 mm^3) were measured on a Rigaku-denki automated four circle diffractometer (AFC-5) with graphite-monochromatized Mo $K\alpha$ radiation. The unit cell parameters were determined by a least-squares refinement based on 38 reflections. The systematic absence led to the space group $P2_12_12_1$. Crystal data: $Co_2C_{22}H_{44}N_4O_{17}S_2$, *M.W.*=818.6, orthorhombic, space group $P2_12_12_1$, a=13.215(5), b=37.035(12), c=6.527(2) Å, V=3194.1(18) Å^3, D_m=1.72 g cm^{-3} (by the flotation), D_x=1.70 g cm^{-3}, Z=4, and μ(Mo $K\alpha$)=12.9 cm^{-1}.

Intensity data up to 2θ=60° were collected by the ω-2θ scan technique with a scan rate of 3° min^{-1}. During the course of the data collection, three reflections were monitored every 40 reflections. The intensity data were converted into F_o data in the usual manner. Absorption corrections were not applied. A total of 2322 independent reflections with $|F_o|>3\sigma(|F_o|)$ was observed and used for the structure analysis.

5) Determination of the Crystal Structure. The positions of two cobalt atoms were obtained from the three dimensional Patterson function. The difference Fourier maps, based on the cobalt positions, revealed all the non-hydrogen atoms. The structure was refined by a full-matrix least-squares refinement of the positional and anisotropic thermal parameters of all the non-hydrogen atoms (program RFINE by L. W. Finger was used). The neutral atomic scattering factors for all the non-hydrogen atoms were taken from the literature.[10] The final R value converged to 0.088. The absolute configuration could not be determined by the anomalous scattering technique, using Cu $K\alpha$ radiation, but it was determined on the basis of the known configuration of the $(+)_{546}$-[Co(edta)]$^-$.[6] The final atomic parameters with their estimated standard deviations are given in Table 1. A list of structure factors, anisotropic thermal parameters of non-hydrogen atoms, and the projected figure of the crystal structure, which indicated distance in the range of 2.63—3.02 Å, are kept at the Chemical Society of Japan as Document No. 8446.

Results and Discussion

Description of the Structure. The perspective drawings of the complex cation and anion are given in Figs. 1 and 2, respectively, together with their numbering scheme. The bond lengths and angles with their estimated standard deviations in the complex ions are listed in Table 2. The cobalt atom in the complex cation is surrounded by two *cis* sulfur, two *cis* oxygen, and two *cis* nitrogen atoms, and the *R,S*-ebp coordinates to cobalt atom as a sexidentate. The [Co(*R,S*-ebp)]$^+$ complex, was resolved into the optical isomers, which are designated as [*R*] and [*S*] configurations based on the chiral arrangement of the coordinated atoms.[4] The absolute configuration of the $(+)_{560}^{CD}$-[Co(*R,S*-ebp)]$^+$ isomer was determined to be the [*S*] configuration (Fig. 1) on the basis of the known configuration, Δ, of the $(+)_{546}$-[Co(edta)]$^-$ (Fig. 2).[6] Both of the chiral sulfur donor atoms take selectively the *R*(*S*)[4] configuration and the *S,S*-bridged five-membered chelate ring has a gauche form with the λ conformation (Fig. 1 and Table 3). The remaining chelate rings of the $(+)_{560}^{CD}$-[Co(*R,S*-ebp)]$^+$ isomer show similar conformations to those of the cobalt(III) complexes having the same framework as the penicillamine moiety.[3,11-13] The bond lengths and angles for the $(+)_{560}^{CD}$-[Co(*R,S*-ebp)]$^+$ isomer are quite similar to those

of the parent complex, *cis·cis·cis*-[Co(*R*-pen)(*S*-pen)]$^-$.[3] These facts suggest that the two sulfur atoms of the parent complex anion react with 1,2-dibromoethane to give an *S,S*-bridged five-membered ring without any strain. It is noted that the Co–S bond lengths of 2.199(7) and 2.221(8) Å for the $(+)^{CD}_{560}$ *R,S*-ebp isomer are significantly shorter than those of the thioether type complexes such as *trans*(*S*)-bis(*S*-methyl-L-cysteinato)cobalt(III)[11] and *trans*(*O*)-*N,N'*-ethylenebis(*S*-methyl-L-cysteinato)cobalt(III),[12] which have a similar framework to the penicillamine moiety of the *R,S*-ebp.

Table 1. Positional and thermal parameters ($\times 10^4$)

Atom	*x*	*y*	*z*	B_{eq}/Å^2 a)
Co1	2083(2)	2248(1)	439(5)	1.65
Co2	1272(2)	4203(1)	1689(5)	1.94
N1	1433(12)	1893(5)	2190(29)	1.90
N2	3126(14)	2325(5)	2469(28)	2.24
N3	2072(14)	3765(5)	1429(29)	2.12
N4	−43(15)	4003(5)	2558(32)	2.50
S1	1933(4)	4191(2)	4781(9)	2.13
S2	573(5)	4740(2)	2224(11)	2.70
O1	1206(11)	2599(4)	1551(24)	2.44
O2	−64(12)	2679(5)	3767(30)	4.11
O3	1047(10)	2086(4)	−1461(25)	2.05
O4	469(12)	1545(5)	−2461(28)	3.97
O5	2717(11)	2643(4)	−994(22)	2.57
O6	3569(12)	3152(5)	−277(31)	3.78
O7	2952(12)	1889(4)	−724(24)	2.28
O8	4510(13)	1649(4)	−368(30)	3.69
O9	2434(12)	4450(4)	506(27)	2.80
O10	4009(14)	4326(5)	−418(30)	3.93
O11	662(12)	4176(5)	−997(25)	2.87
O12	−850(14)	4127(6)	−2496(28)	4.58
C1	521(16)	2477(6)	2857(36)	1.81
C2	550(16)	2061(6)	3170(42)	2.07
C3	886(16)	1741(8)	−1179(43)	2.97
C4	1158(21)	1584(6)	898(36)	2.93
C5	3200(17)	2858(6)	218(39)	2.29
C6	3290(18)	2738(7)	2417(36)	2.81
C7	3818(20)	1872(6)	89(38)	2.68
C8	4093(17)	2155(6)	1725(41)	2.65
C9	2257(19)	1803(7)	3811(34)	3.03
C10	2726(17)	2162(7)	4444(35)	2.69
C11	1954(19)	4673(6)	5300(41)	3.07
C12	831(19)	4783(7)	4999(37)	3.21
C13	3219(18)	4254(7)	400(41)	2.46
C14	3127(17)	3920(7)	1752(41)	2.67
C15	3250(16)	4026(7)	4112(37)	2.73
C16	3416(17)	3679(6)	5379(44)	2.71
C17	4080(21)	4317(9)	4419(43)	4.63
C18	4639(17)	846(7)	930(45)	2.90
C19	−754(16)	4202(8)	1264(32)	2.33
C20	−813(17)	4620(8)	1791(49)	3.52
C21	−1400(20)	4667(7)	3800(41)	3.80
C22	−1165(19)	4851(7)	30(39)	3.38
O21	940(13)	3340(5)	4176(27)	3.85
O22	2080(17)	813(7)	3022(39)	8.07
O23	1052(15)	533(7)	−98(44)	8.28
O24	6738(16)	4048(6)	3036(40)	6.67
O25	6306(13)	1727(5)	1707(27)	3.46

a) B_{eq} is the equivalent isotropic temperature factors defined by Hamilton.[16]

The bond lengths and angles in the $(+)_{546}$-[Co(edta)]$^-$ isomer agree well with the data for [Co(sarmp)$(NH_3)_3$]·$(+)_{546}$-[Co(edta)] (sarmp; *N*-(2-carboxyethyl)-sarcosinate) (Table 2).[6] The crystal structure consists of the complex cations and anions, and water molecules. The several hydrogen bonds are recognized between the complex ions and/or water molecules (Fig. A).

Absorption and CD Spectra. The electronic absorption and CD spectra of the non-bridge complex, [Co(*R*-smp)(*S*-smp)]$^+$, and the S,S-bridge complexes, [Co(*R,S*-ebp)]$^+$, [Co(*R,S*-tbp)]$^+$, and [Co(*R,S*-tetp)]$^+$, are shown in Figs. 3 and 4, and their spectral data are summarized in Table 4. Two geometrical isomers, *cis·cis·cis* and *trans·trans·trans*, are possible for the non-bridge complex, [Co(*R*-smp)(*S*-smp)]$^+$. In the first absorption band region, the F-1 isomer exhibits well separated two absorption components, while the F-2 isomer exhibits a sharp band (Fig. 3 and Table 4). These absorption spectral patterns indicate that the F-1 isomer takes the *trans·trans·trans* configuration and the F-2 isomer takes the *cis·cis·cis* configuration.

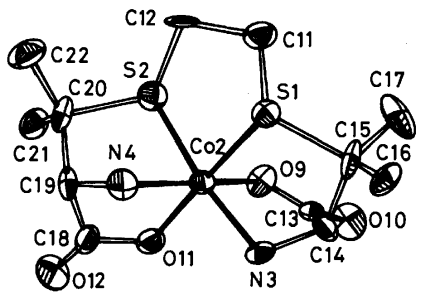

Fig. 1. A perspective drawing of [*S*]-$(+)^{CD}_{560}$-[Co(*R,S*-ebp)]$^+$ with the numbering scheme of atoms.

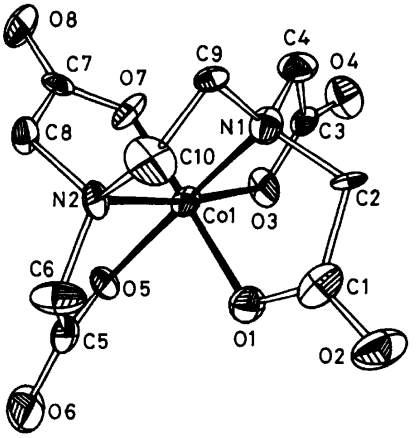

Fig. 2. A perspective drawing of Λ-$(+)_{546}$-[Co(edta)]$^-$ with the numbering scheme of atoms.

Furthermore, the maximum positions of their thioether charge transfer bands ($29.59\times10^3\,cm^{-1}$ for F-1 and $32.95\times10^3\,cm^{-1}$ for F-2) also support the geometries which *trans(S)* is for F-1 isomer and *cis(S)* for F-2 one. These absorption spectra agree well with those of $[Co(aeta)_2]^+$ and $[Co(aetp)_2]^+$ (aeta; (2-aminoethylthio)acetate and aetp; 3-(2-aminoethylthio)propionate).[14] All the *S,S*-bridge complexes exhibit similar absorption spectral patterns over the whole region to that of the *cis·cis·cis*-[Co(*R*-smp)(*S*-smp)]$^+$ isomer, indicating the same geometrical arrangements with respect to the coordinated atoms. The *R,S*-ebp, *R,S*-tbp, and *R,S*-tetp complexes exhibit a sharp first absorption band at *ca.* $19\times10^3\,cm^{-1}$, regardless of their *S,S*-bridged backborn rings (five-, six-, and seven-membered ones, respectively). On the contrary, the absorption maxima of the sulfur-to-metal charge tansfer bands are shifted to lower energy in the order of *R,S*-ebp>*R,S*-tbp>*R,S*-tetp≈non-bridge complex, as shown in Figs. 3 and 4, and Table 4. This order seems to run parallel to the rigidity of the *S,S*-bridged backborn rings.

The $(+)^{CD}_{560}$-[Co(*R,S*-tbp)]$^+$ and $(+)^{CD}_{560}$-[Co(*R,S*-tetp)]$^+$ isomers exhibit quite similar CD spectral patterns over the whole region to that of [*S*]-$(+)^{CD}_{560}$-[Co(*R,S*-ebp)]$^+$, accordingly, it is assigned that the $(+)^{CD}_{560}$ *R,S*-tbp and $(+)^{CD}_{560}$ *R,S*-tetp isomers also take an [*S*] configuration, respectively. Similarly, the $(+)^{CD}_{560}$-*cis·cis·cis*-[Co(*R*-smp)(*S*-smp)]$^+$ isomer can be tentatively assigned to an [*S*] configuration by comparing its CD spectrum with that of the [*S*]-$(+)^{CD}_{560}$-[Co(*R,S*-ebp)]$^+$ isomer, though a little difference from that of the *R,S*-ebp isomer is observed (Fig. 3).

In order to estimate the absolute configuration of

Table 2. Intermolecular distances and bond angles (with e.s.d.'s)

	(a) Bond distances (l/Å)			Co1-N2-C6	103.4(13)	Co1-N2-C8	108.8(14)
[Co(edta)]$^-$:				Co1-N2-C10	106.0(13)	Co1-O1-C1	115.7(14)
Co1-N1	1.942(18)	Co1-N2	1.932(18)	Co1-O3-C3	109.1(14)	Co1-O5-C5	112.6(14)
Co1-O1	1.886(15)	Co1-O3	1.943(15)	Co1-O7-C7	114.2(15)	O1-C1-C2	113.9(19)
Co1-O5	1.928(15)	Co1-O7	1.915(15)	O1-C1-O2	122.2(21)	O2-C1-C2	123.8(21)
N1-C2	1.47(3)	N1-C4	1.47(3)	N1-C2-C1	112.4(18)	O3-C3-O4	123.3(24)
N1-C9	1.55(3)	N2-C6	1.54(3)	O3-C3-C4	117.4(22)	O4-C3-C4	119.1(24)
N2-C8	1.51(3)	N2-C10	1.52(3)	N1-C4-C3	105.9(19)	O5-C5-O6	125.2(23)
O1-C1	1.32(3)	O2-C1	1.23(3)	O5-C5-C6	116.2(20)	O6-C5-C6	118.6(22)
O3-C3	1.31(3)	O4-C3	1.24(3)	N2-C6-C5	107.6(19)	O7-C7-O8	125.8(22)
O5-C5	1.29(3)	O6-C5	1.24(3)	O7-C7-C8	118.2(20)	O8-C7-C8	115.9(21)
O7-C7	1.26(3)	O8-C7	1.27(3)	N2-C8-C7	107.9(18)	N1-C9-C10	106.5(18)
C1-C2	1.56(3)	C3-C4	1.52(4)	N2-C10-C9	105.0(18)		
C5-C6	1.51(4)	C7-C8	1.54(4)	[Co(*R,S*-ebp)]$^+$:			
C9-C10	1.52(4)			S1-Co2-S2	92.2(3)	S1-Co2-N3	81.2(6)
[Co(*R,S*-ebp)]$^+$:				S1-Co2-N4	94.5(6)	S1-Co2-O9	93.5(6)
Co2-S1	2.199(7)	Co2-S2	2.221(8)	S1-Co2-O11	175.7(6)	S2-Co2-N3	170.9(6)
Co2-N3	1.944(18)	Co2-N4	1.972(20)	S2-Co2-N4	85.6(6)	S2-Co2-O9	88.3(5)
Co2-O9	1.945(16)	Co2-O11	1.933(16)	S2-Co2-O11	90.9(5)	N3-Co2-N4	101.0(7)
S1-C11	1.82(2)	S1-C15	1.89(2)	N3-Co2-O9	85.9(7)	N3-Co2-O11	96.0(8)
S2-C12	1.85(3)	S2-C20	1.91(2)	N4-Co2-O9	170.2(8)	N4-Co2-O11	82.7(8)
N3-C14	1.52(3)	N4-C19	1.46(3)	O9-Co2-O11	89.6(7)	Co2-S1-C11	99.0(9)
O9-C13	1.27(3)	O10-C13	1.20(3)	Co2-S1-C15	99.2(8)	Co2-S2-C12	98.9(8)
O11-C18	1.36(3)	O12-C18	1.21(3)	Co2-S2-C20	99.7(9)	Co2-N3-C14	99.9(13)
C11-C12	1.55(4)	C13-C14	1.52(4)	Co2-N4-C19	102.2(14)	Co2-O9-C13	113.5(15)
C14-C15	1.60(4)	C15-C16	1·54(4)	Co2-O11-C18	113.0(16)	S1-C11-C12	102.7(16)
C15-C17	1.55(4)	C18-C19	1.53(4)	S2-C12-C11	106.1(17)	O9-C13-O10	127.5(24)
C19-C20	1.59(4)	C20-C21	1.53(4)	O9-C13-C14	111.5(21)	O10-C13-C14	120.4(22)
C20-C22	1.51(4)			N3-C14-C13	107.4(19)	C13-C14-C15	110.5(21)
	(b) Bond angles (ϕ/°)			N3-C14-C15	108.6(18)	S1-C15-C14	102.0(14)
[Co(edta)]$^-$:				S1-C15-C16	106.0(15)	S1-C15-C17	113.3(18)
N1-Co1-N2	90.7(8)	N1-Co1-O1	88.2(7)	C14-C15-C16	109.0(21)	C14-C15-C17	111.5(20)
N1-Co1-O3	81.6(7)	N1-Co1-O5	172.5(7)	C16-C15-C17	114.1(20)	O11-C18-O12	120.6(24)
N1-Co1-O7	91.6(7)	N2-Co1-O1	94.2(7)	O11-C18-C19	111.1(21)	O21-C18-C19	128.0(21)
N2-Co1-O3	170.3(7)	N2-Co1-O5	84.9(7)	N4-C19-C18	105.3(19)	N4-C19-C20	113.4(19)
N2-Co1-O7	86.9(7)	O1-Co1-O3	91.5(7)	C18-C19-C20	109.4(22)	S2-C20-C19	102.2(15)
O1-Co1-O5	86.1(7)	O1-Co1-O7	178.8(7)	S2-C20-C21	109.4(19)	S2-C20-C22	106.1(18)
O3-Co1-O5	103.4(7)	O3-Co1-O7	87.4(7)	C19-C20-C21	108.7(21)	C19-C20-C22	113.8(23)
O5-Co1-O7	94.3(6)	Co1-N1-C2	108.8(13)	C21-C20-C22	115.6(21)		
Co1-N1-C4	107.4(14)	Co1-N1-C9	103.6(13)				

the sulfur donor atom in the present complexes, the ^1H and ^{13}C NMR spectra of the *S*,*S*-bridge complexes and *cis*·*cis*·*cis*-[Co(*R*-smp)(*S*-smp)]$^+$ isomer were measured. The ^{13}C NMR spectrum of the [*S*]-$(+)_{560}^{CD}$-[Co(*R*,*S*-ebp)]$^+$ isomer, which takes selectively $R(S)_D$,$R(S)_L$ configuration,[15] exhibits the eleven resonance lines for the twelve carbon atoms (Fig. 5). Similar ^{13}C NMR spectral behavior is observed for the [*R*]-

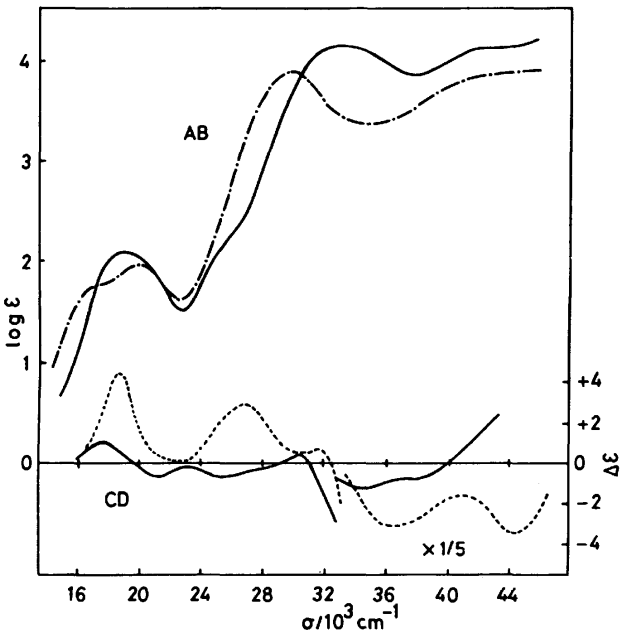

Fig. 3. Absorption and CD spectra of [Co(*R*-smp)(*S*-smp)]$^+$: *trans*·*trans*·*trans* (—·—) and $(+)_{560}^{CD}$-*cis*·*cis*·*cis* (——), together with CD spectrum of $(+)_{560}^{CD}$-[Co(*R*,*S*-ebp)]$^+$ (----).

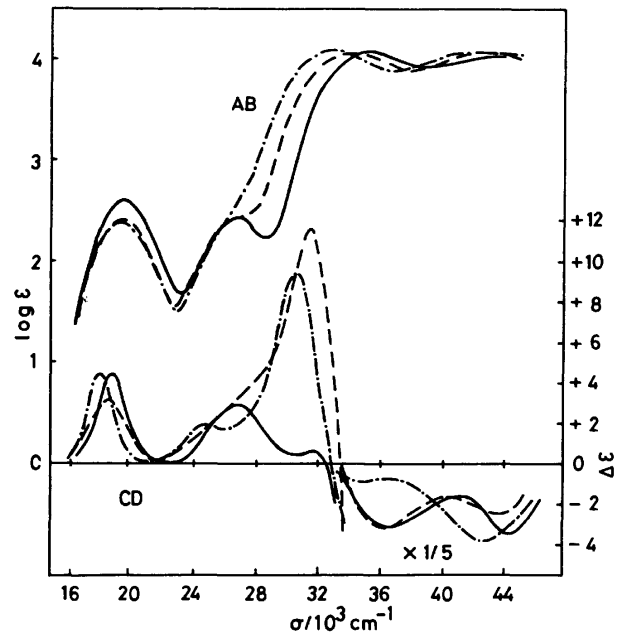

Fig. 4. Absorption and CD spectra of $(+)_{560}^{CD}$-[Co(*R*,*S*-ebp)]$^+$ (——), $(+)_{560}^{CD}$-[Co(*R*,*S*-tbp)]$^+$ (----), and $(+)_{560}^{CD}$-[Co(*R*,*S*-tetp)]$^+$ (—·—).

Table 3. Displacements of atoms from the least-squares plane (d/Å) for [Co(*R*,*S*-ebp)]$^+$ ion

Plane 1. *S*-*S* chelate ring (five-membered ring)
$-0.8256X-0.4444Y+0.3477Z+7.9228=0$
Co2 0.000 S1 0.000 S2 0.000
C11 −0.698 C12 0.278
Plane 2. *N*-*S* chelate ring
$-0.7766X-0.5401Y+0.3244Z+9.3553=0$
Co2 0.000 S1 0.000 N3 0.000
C14 −1.324 C15 −1.162 C16 −0.371
C17 −2.531
Plane 3. *N*-*S* chelate ring
$-0.3174X+0.0190Y-0.9481Z+1.2833=0$
Co2 0.000 S2 0.000 N4 0.000
C19 1.113 C20 0.842 C21 −0.152
C22 2.095
Plane 4. *N*-*O* chelate ring
$-0.3732X-0.1475Y-0.9159Z+3.9343=0$
Co2 0.001 N3 0.001 O9 0.000
O10 −0.157 C13 −0.217 C14 −0.797
Plane 5. *N*-*O* chelate ring
$0.3581X-0.9270Y-0.1116Z+13.9501=0$
Co2 0.000 N4 0.000 O11 0.000
O12 −0.440 C18 −0.415 C19 −0.925

Table 4. Absorption and CD spectral data of [Co(*R*,*S*-sexidentate-N_2,S_2,O_2)] and [Co(*R*-smp)(*S*-smp)]$^+$ complexes

Complex ion	Absorption maxima σ/10³ cm⁻¹ (log ε/ mol⁻¹ dm³ cm⁻¹)	CD extrema σ/10³ cm⁻¹ ($\Delta\varepsilon$/ mol⁻¹ dm³ cm⁻¹)
$(+)_{560}^{CD}$-[Co(*R*,*S*-ebp)]$^+$	19.23 (2.63)	18.52 (+4.51)
	26.67 (2.45)	26.67 (+3.06)
	35.09 (4.09)	31.75 (+0.68)
	44.44 (4.08)	36.36 (−16.2)
		44.44 (−18.0)
$(-)_{560}^{CD}$-[Co(*R*,*S*-tbp)]$^+$	19.31 (2.43)	18.35 (−3.17)
	26.7 (2.44 sh)	31.45 (−11.7)
	33.90 (4.08)	35.97 (+16.1)
	42.55 (4.08)	43.86 (+13.1)
$(+)_{560}^{CD}$-[Co(*R*,*S*-tetp)]$^+$	19.12 (2.39)	17.89 (+4.45)
	24.7 (1.96 sh)	24.69 (+1.95)
	32.79 (4.08)	30.53 (+9.60)
	42.02 (4.05)	34.97 (−4.71)
		42.74 (−19.2)
$(+)_{560}^{CD}$-*cis*·*cis*·*cis*-[Co(*R*-smp)(*S*-smp)]$^+$	18.94 (2.09)	17.92 (+1.00)
	25.4 (2.14 sh)	20.96 (−0.60)
	32.95 (4.14)	25.32 (−0.75)
	42.74 (4.18)	30.30 (+0.47)
		34.36 (−6.82)
		38.17 (−3.88)
		45.45 (+15.8)
trans·*trans*·*trans*-[Co(*R*-smp)(*S*-smp)]	16.7 (—— sh)	
	19.80 (——)	
	29.59 (——)	
	42.92 (——)	

Sh denotes a shoulder.

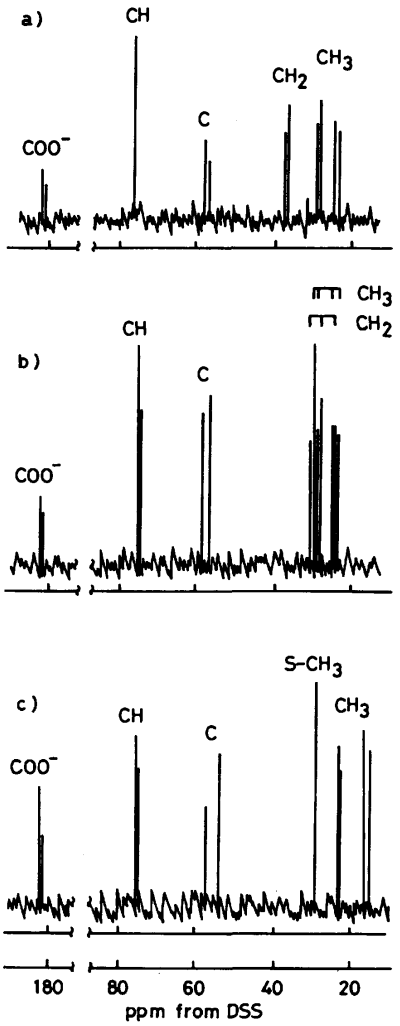

Fig. 5. ^{13}C NMR spectra of the complexes: (a) $(+)^{CD}_{580}$-[Co(*R*,*S*-ebp)]$^+$, (b) $(-)^{CD}_{580}$-[Co(*R*,*S*-tbp)]$^+$, and (c) $(-)^{CD}_{560}$-*cis*·*cis*·*cis*-[Co(*R*-smp)(*S*-smp)]$^+$.

$(-)^{CD}_{560}$-[Co(*R*,*S*-tbp)]$^+$ (thirteen lines for thirteen carbons) and [*R*]-$(-)^{CD}_{500}$-*cis*·*cis*·*cis*-[Co(*R*-smp)(*S*-smp)]$^+$ (eleven lines for twelve carbons) isomers, as shown in Fig. 5. Further, the ^{1}H NMR spectrum of the $(-)^{CD}_{560}$-*cis*·*cis*·*cis*-[Co(*R*-smp)(*S*-smp)]$^+$ isomer shows two sharp signals (2.27 and 2.03 ppm) due to the *S*-methyl protons. Stereomodel examination elucidates these results as follow; namely, the $S(S)_D$,$S(S)_L$ configuration is assigned for [*R*]-$(-)^{CD}_{560}$-[Co(*R*,*S*-tbp)]$^+$. The $R(S)_D$, $S(S)_L$ configuration is probable for the [*R*]-$(-)^{CD}_{560}$-*cis*·*cis*·*cis*-[Co(*R*-smp)(*S*-smp)]$^+$ isomer because of the steric interaction between the two *S*-methyl groups, though an $S(S)_D$,$S(S)_L$ configuration is also possible for the isomer. The CD spectrum of the $(+)^{CD}_{560}$-*cis*·*cis*-[Co(*R*-smp)(*S*-smp)]$^+$ isomer, which was assigned to the same [*S*] configuration as the $(+)^{CD}_{560}$ *R*,*S*-ebp isomer, differs partially from that of the latter, as mentioned above. A similar difference was observed between the CD spectra of the *trans*(*O*)-[Co(L-smp)$_2$]$^+$ and *trans*(*O*) *S*,*S*-bridge isomers, *trans*(*O*)-[Co(LL-sexidentate-N_2,S_2,O_2)].[1] Taking the results from the ^{1}H and ^{13}C NMR spectral behavior of the present isomers into consideration, it is possible to consider that the difference is related to the additional CD contribution due to the fixation of two sulfur donor atoms located in the *cis* position.

The authors wish to express thanks to Miss Hiroko Nishimoto for her aid in the experiment.

References

1) T. Konno, K. Okamoto, and J. Hidaka, *Bull. Chem. Soc. Jpn.*, **56**, 2631 (1983).
2) The abbreviations of the ligands are as follows: *R*,*S*-ebp=(2*R*,9*S*)-diamino-3,3,8,8-tetramethyl-4,7-dithia-1,10-decanedioate, *R*,*S*-tbp=(2*R*,10*S*)-diamino-3,3,9,9-tetramethyl-4,8-dithia-1,11-undecanedioate, and *R*,*S*-tetp=(2*R*,11*S*)-diamino-3,3,10,10-tetramethyl-4,9-dithia-1,12-dodecanedioate.
3) H. M. Helis, P. de Meester, and D. J. Hodgson, *J. Am. Chem., Soc.*, **99**, 3309 (1977). In this paper, the symbols, D and L, were used instead of *S* and *R*, respectively.
4) The symbols, [*R*] and [*S*], are denoted by the method of Chan *et al.*, (R. S. Chan, C. K. Ingold, and V. Prelog, *Angew, Chem, Int. Ed. Engl.*, **5**, 385 (1966)). The symbols, *R*(*S*) and *S*(*S*), are denoted the absolute configuration of the chiral sulfur atom.
5) R. Neher, M. Spillman, L. H. Werner, A. Wettstein, and K. Miescher, *Helv. Chim. Acta*, **29**, 1874 (1946).
6) K. Okamoto, T. Tsukihara, J. Hidaka, and Y. Shimura, *Bull. Chem. Soc. Jpn.*, **51**, 3534 (1978).
7) K. Wakayama, K. Okamoto, H. Einaga, and J. Hidaka, *Bull. Chem. Soc. Jpn.*, **56**, 1995 (1983).
8) K. Okamoto, K. Wakayama, H. Einaga, S. Yamada, and J. Hidaka, *Bull. Chem. Soc. Jpn.*, **56**, 165 (1983).
9) J. Hidaka, S. Yamada, and Y. Shimura, *Chem. Lett.*, **1974**, 1487.
10) "International Tables for X-Ray Crystallography," The Kynoch Press, Birmingham (1974), Vol. IV.
11) P. de Meester and D. J. Hodgson, *J. Chem. Soc., Dalton Trans.*, **1976**. 618.
12) K. Okamoto, T. Isago, M. Ohmasa, and J. Hidaka, *Bull. Chem. Soc. Jpn.*, **55**, 1077 (1982).
13) K. Okamoto, K. Wakayama, H. Einaga, M. Ohmasa, and J. Hidaka, *Bull. Chem. Soc. Jpn.*, **55**, 3473 (1982).
14) K. Yamanari, J. Hidaka, and Y. Shimura, *Bull. Chem. Soc. Jpn.*, **50**, 2451, 2643 (1977).
15) The subscripts, D and L, correspond to the absolute configurations, *S*(*C*) and *R*(*C*), of the penicillaminate moiety, respectively.
16) W. C. Hamilton, *Acta Crystallogr.*, **12**, 609 (1959).

 © 1984 The Chemical Society of Japan Bull. Chem. Soc. Jpn., 57, 3117—3121 (1984)

Dynamic NMR as a Nondestructive Method for the Determination of Rates of Dissociation. IX. Rates of Dissociative Reactions of the Coordinated Form of [*o*-(Diethylaminomethyl)-phenyl]halodimethyl(or diphenyl)stannanes[1,2]

Michinori Ōki* and Manabu Ohira
Department of Chemistry, Faculty of Science, The University of Tokyo, Bunkyo-ku, Tokyo 113
(Received April 11, 1984)

The coordinated form of [*o*-(diethylaminomethyl)phenyl]halodimethyl(or diphenyl)stannanes was found to exhibit dynamic behaviors in their ^{1}H NMR spectra. Examination of a series of halogen compounds by total line shape analysis of the diastereotopic methylene proton signals revealed that, at 10 °C, the rates of dissociation were 11.7, 22.9, 28.6, and 73.3 s^{-1} for fluoro, chloro, bromo, and iodo compounds, respectively: The results are in conformity with the expectation from the electronegativity of halogens. The relatively small differences in the activation parameters in the whole series may include contribution by solvation energies. The diphenyl compound exhibited fast exchange rates relative to the corresponding dimethyl compound. This was attributed to the steric factor rather than the $p\pi$-$d\pi$ interaction.

The ligand exchange is one of the fundamental reactions in coordination chemistry. The dissociative reactions are often found in the ligand exchange and have been the target of many investigations.[3] As to the methodology for the determination of the rates of exchange, not only classical chemical reactions but also the dynamic NMR technique played an important role, because the latter affords data which are too fast for the ordinary laboratory time scale. Among many others we can pick up following examples which dealt with the coordination chemistry of amine ligands by dynamic NMR in the literature.

After the pioneering work by Mole,[4] various groups of investigators studied the exchange reactions of trivalent aluminium-amine complexes.[5,6] This technique was extended to boron-amine[7] and gallium-amine[8] complexes. An amine-sulfur dioxide complex was also studied.[9] These classic literatures use excess of substrates, usually the base, to observe coalescence of complexed and uncomplexed signals. Thus it may be said that these techniques determine the rates of exchange, either dissociative or associative, in the presence of excess of other reagents than the solvent concerned.

Observation of the dissociative processes in the absence of foreign materials is important, since it affords information about the "intrinsic" dissociative nature of the complex concerned. This is, on one hand, possible by observing the spin-spin coupling between the central metal atom in a complex and the atom, which has non-zero nuclear spin, in the ligand because the coupling disappears on dissociation. This technique has been reviewed.[10] Although the most of ligands contain atoms, which have non-zero nuclear spin, such as hydrogen, the central atom is not necessarily NMR-active. Therefore, the observation of spin-spin couplings has limitation in this respect.

Since we have been able to show that dissociation rates of a type of ammonium salts could be followed by the dynamic NMR method,[11] we are interested in applying this method to the problem in coordination chemistry. The necessary conditions for detection by this procedure are that 1) the compound in question has a pair of diastereotopic NMR-active nuclei, 2) the diastereotopic nuclei exchange their sites by dissociation, and 3) preferably the ligand which dissociates is singular. Literature search revealed that there were some examples which are similar but not exactly the same with our topomerization technique. van Koten and associates found that spin-exchange between the diastereotopic methyl protons in the coordinated form of bromo[*o*-(dimethylaminomethyl)phenyl]methylphenylstannane (**1**) was observed by the dynamic NMR technique.[12] They further elaborated to show that a diastereomer of bromo[*o*-[1-(dimethylamino)ethyl]-phenyl]methylphenylstannane (**2**) isomerized to another slowly at a low temperature.[13] These phenomena can be explained by dissociation of the amine ligand followed by internal rotation, inversion of amine and religation (or alternatively the chiral center of tin racemizes after dissociation of the ligand). Corriu *et al.* reported the similar phenomenon in the corresponding silicon compounds (**3**),[14] although they postulated that coordinated and decoordinated forms were observed. We believe our explanation of dissociation-topomerization is more likely than the postulate by Corriu *et al.*

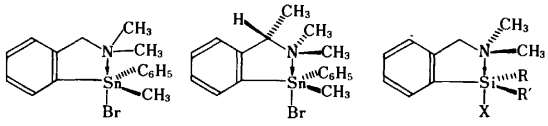

1 2 3

van Koten *et al.* extended their work further to more complicated tin compounds in which a 6-membered ring was formed by ligation.[15] Deeming and Rothwell were able to show dynamic nature of an amine ligand in a similar situation in palladium complexes, although they postulated that the mechanism of the exchange is different from that discussed here.[16]

The works cited above were possible because the metal atom was a chiral center. However, the diastereotopic nature does not require the presence of a chiral center. Therefore, by designing a proper molecule, we

should be able to observe topomerization by dissociation in a compound which has no chiral center. This will broaden the scope of the technique and is worthwhile to be tried. We designed bromo[*o*-(diethylaminomethyl)phenyl]dimethylstannane (**4**: R=CH_3, X=Br) because the methylene protons in the ethyl group should be diastereotopic when the amine coordinates but it topomerizes when the ligand dissociates, internal rotation takes place, the amine inverts, and then the ligand recoordinates (Scheme 1).

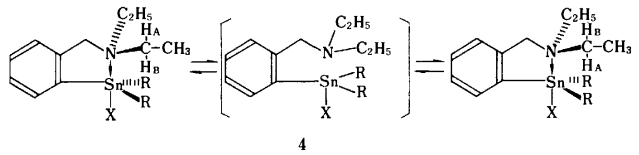

4

Scheme 1.

This paper reports successful observation of topomerization in **4** and discusses the effect of the substituents on the rates of topomerization.

Experimental

N,N-Diethylbenzylamine (**5**) was prepared by adding 20 g of diethylamine in 30 mL of acetone to 25.0 g of benzyl chloride and 30 g of potassium carbonate in 50 mL of water and 100 mL of acetone and heating the mixture for 5 h. The yield was 54%. Colorless oil, bp 60—62 °C/3.5 mmHg (lit,[17] bp 211—212 °C). ^{1}H NMR ($CDCl_3$, δ): 1.01 (6H, t, J=7 Hz), 2.49 (4H, q, J=7 Hz), 3.53 (2H, s), 7.1—7.4 (5H, br s).

Bromo[o-(diethylaminomethyl)phenyl]dimethylstannane (4: R=CH$_3$, X=Br). To a mixture of 20 mL of dry ether and 5 mL of 1.5 M butyllithium (1M=1 mol dm^{-3}) in hexane, 1.2 g (7.4 mmol) of *N,N*-diethylbenzylamine was added with stirring. The mixture was stirred at room temperature under a nitrogen atmosphere until the Gilman color test II[18] became negative. This required 7—10 d. The solution of *o*-lithio-*N,N*-diethylbenzylamine was added to a solution of 2.4 g (7.8 mmol) of dibromodimethylstannane in 20 mL of dry ether during the course of 1 h with stirring. The stirring was continued for further 3 h and the solvents were evaporated. The residue was taken up in benzene and evaporated. Recrystallization of the product from benzene-hexane gave 0.5 g (17%) of the desired compound, mp 145—146 °C. Found: C, 40.01; H, 6.00; N, 3.48; Br, 20.66%. Calcd for $C_{13}H_{22}$BrNSn: C, 39.94; H, 5.67; N, 3.58; Br, 20.44%. ^{1}H NMR ($CDCl_3$, δ): 0.92 (6H, s), 0.99 (6H, t, J=7 Hz), 2.65 (4H, q, J=7 Hz), 3.65 (2H, s), 6.9—7.4 (3H, m), 8.23 (1H, m). ^{1}H NMR (toluene-d_8, δ): 0.43 (6H, t, J=7 Hz), 0.73 (6H, s), 2.03 (4H, q, J=7 Hz), 3.03 (2H, s), 6.5—7.4 (3H, m), 8.62 (1H, m).

Chloro[o-(diethylaminomethyl)phenyl]dimethylstannane (4: R=CH$_3$, X=Cl), mp 150—151 °C, was similarly prepared in 30% yield. Found: C, 44.92; H, 6.65; N, 3.87; Cl, 10.70%. Calcd for $C_{13}H_{22}$ClNSn: C, 45.07; H, 6.40, N, 4.04; Cl, 10.23%. ^{1}H NMR ($CDCl_3$, δ): 0.80 (6H, s), 0.99 (6H, t, J=7 Hz), 2.64 (4H, q, J=7 Hz), 3.64 (2H, s), 6.9—7.5 (3H, m), 8.18 (1H, m).

Chloro[o-(diethylaminomethyl)phenyl]diphenylstannane (4: R=C$_6$H$_5$, X=Cl), mp 135—136 °C, was similarly prepared in 9% yield. Found: C, 58.49; H, 5.62; N, 3.10; Cl, 7.67%. Calcd for $C_{23}H_{26}$ClNSn: C, 58.70; H, 5.57; N, 2.98; Cl, 7.53%. ^{1}H NMR ($CDCl_3$, δ); 0.70 (6H, t, J=7 Hz), 2.24 (4H, q, J=7 Hz), 3.59 (2H, s), 7.1—7.9 (13H, m), 8.47 (1H, m).

Iodo[o-(diethylaminomethyl)phenyl]dimethylstannane (4: R=CH$_3$, X=I). To a solution of 0.30 g (0.87 mmol) of compound **4** (R=CH_3, X=Cl) in 20 mL of ethyl acetate was added 0.13 g (0.87 mmol) of sodium iodide in 20 mL of ethyl acetate. The precipitate of sodium chloride was filtered off and the filtrate was concentrated. The residue was purified by recrystallization from dichloromethane-pentane to give 0.34 g (90%) of the desired compound, mp 140—141 °C. Found: C, 35.60; H, 5.45; N, 3.16; I, 28.42%. Calcd for $C_{13}H_{22}$INSn: C, 35.66; H, 5.06; N, 3.20; I, 28.98%. ^{1}H NMR ($CDCl_3$, δ): 1.01 (6H, t, J=7 Hz), 1.12 (6H, s), 2.68 (4H, q, J=7 Hz), 3.68 (2H, s), 6.9—7.5 (3H, m), 8.32 (1H, m).

Fluoro[o-(diethylaminomethyl)phenyl]dimethylstannane (4: R=CH$_3$, X=F). A solution of 0.28 g of **4** (R=CH_3, X=I) in 20 mL of methanol was mixed with 0.10 g of potassium fluoride in 5 mL of water and the whole was refluxed for 3 h. The solvents were evaporated and the residue was taken up in benzene. The benzene solution was evaporated and the residue was recrystallized from ether-hexane to afford the desired compound, mp 74—77 °C, in 80% yield. Found: C, 47.10; H, 6.75; N, 4.28%. Calcd for $C_{13}H_{22}$FNSn: C, 47.31; H, 6.71; N, 4.24%. ^{1}H NMR ($CDCl_3$, δ): 0.62 (6H, d, J_{HF}=4.2 Hz), 1.00 (6H, t, J=7 Hz), 2.66 (4H, q, J=7 Hz), 3.64 (2H, s), 7.0—7.5 (3H, m), 7.99 (1H, m).

Dynamic NMR Measurement. The measurement was carried out on a JEOL FX-400 NMR spectrometer which operates at 400 MHz for protons. The samples were dissolved in chloroform-*d* to make up *ca.* 100 mmol/L solutions. The data were accumulated for 200 times. Temperature was calibrated by the chemical shift differences of methanol protons. The chemical shift differences of the AB protons and the coupling constants at *ca.* −50 °C are summarized in Table 1. J_{AX} and J_{BX} were constant at 7.2—7.3 Hz for all the compounds examined.

Total Line Shape Analysis and Kinetic Parameters. The line shapes were analyzed by computer simulation with the use of the modified Binsch program.[19] The spectra were analyzed as an AB part of an ABX_3 system. The coupling constants were constant throughout the temperature range examined but the chemical shift differences drifted as temperature changed but one case, compound **4** (R=CH_3, X=I). Thus for those which gave drifts in chemical shift differences, the chemical shift differences were checked at several temperatures where the rates of exchange were negligibly small. The chemical shift change was found to be linearly correlated with temperature and the following equations gave chemical shift differences at a given temperature. T_2 was estimated from the

4: R=C_6H_5, X=Cl

$$\Delta\nu_{AB} = -0.409T + 62.66 \quad (r=0.996)$$

4: R=CH_3, X=Cl

$$\Delta\nu_{AB} = -0.0336T + 25.37 \quad (r=0.999_5)$$

4: R=CH_3, X=F

$$\Delta\nu_{AB} = -0.0582T + 16.35 \quad (r=0.991_5)$$

4: R=CH_3, X=Br

$$\Delta\nu_{AB} = -0.0170T + 26.74 \quad (r=1.000)$$

Table 1. Chemical shift differences of the methylene protons in ethyl groups and coupling constants at *ca.* −50 °C at 400 MHz

R	X	$\Delta\nu_{AB}$/Hz	J_{AB}/Hz
CH_3	F	19.3	−13.7
CH_3	Cl	27.0	−13.7
CH_3	Br	27.6	−13.7
CH_3	I	27.8	−13.7
C_6H_5	Cl	82.8	−13.9

line widths of benzyl protons and was assumed to be constant at 0.16 s. The calculated spectra and the observed ones were matched by the visual method. The agreement of the both spectra were excellent. The following rate constants were obtained (k/s^{-1} and T/°C in parentheses are given). For **4** (R=C_6H_5, X=Cl), see Fig. 1.

4 (R=CH_3, X=F): 6.1 (5.1), 12.0 (10.5), 27.0 (16.2), 35.0 (18.1), 47.0 (20.7), 58.0 (22.6).
4 (R=CH_3, X=Cl): 7.0 (1.9), 11.5 (5.0), 22.0 (9.2), 42.0 (14.5), 75.0 (18.7), 98.0 (21.5), 120.0 (22.8).
4 (R=CH_3, X=Br): 7.5 (1.3), 16.0 (6.6), 25.0 (9.0), 33.0 (10.9), 45.0 (12.7), 62.0 (21.5), 118.0 (20.0).
4 (R=CH_3, X=I): 4.0 (−8.4), 8.0 (−4.5), 18.0 (0.7), 36.0 (5.1), 78.0 (10.5), 90.0 (11.3), 175.0 (16.2).

The rate constants thus obtained were put into the Eyring equation to obtain the activation parameters. The rate constants and free energies of activation at a given temperature were calculated with the use of these activation parameters.

Results and Discussion

The first point which we wish to raise is the steric effect in the synthesis of the compounds which was performed as is shown in Scheme 2. Although lithiation of *N,N*-dimethylbenzylamine with butyllithium

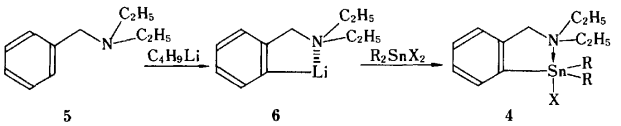

Scheme 2.

proceeded smoothly and the Gilman color test II became negataive after a day or so at room temperature,[20] the same lithiation of *N,N*-diethylbenzylamine (**5**) required 7—10 d to give the negative Gliman test II. We were not able to lithiate completely the ortho position of *N,N*-diisopropylbenzylamine. It seems that the steric effect in the coordinated form (**6**) which stabilizes the lithiated compound is severely affected by the bulkiness of the substituent on the nitrogen.

The ^{1}H NMR spectra of **4** at 60 or 90 MHz gave a simple A_2X_3 quartet for the methylene protons of the ethyl groups. This could mean either the rate of exchange was large on the NMR time scale or the chemical shift differences were too small to detect, although the exchange rate was small. A ^{1}H NMR spectrum at 60 MHz at −50 °C showed essentially no change from that at room temperature. Summing up this result and the data reported by van Koten *et al.*,[12] we concluded that the chemical shift differences of the AB protons were too small for a spectrometer operating at 60 MHz. Then we shifted to a spectrometer operating at 400 MHz.

The AB part of the spectrum of **4** (R=CH_3, X=Br) at 400 MHz showed a barely resolved signal at room temperature but it became a distinct AB part of the ABX_3 system when the spectrum was determined at lower temperatures. The other compounds showed the similar trend. Since the spectral change due to temperature for **4** (R=CH_3, X=Br) is given in a preliminary note,[2] the temperature dependent spectra of **4** (R=C_6H_5, X=Cl) are shown in Fig. 1 together with the calculated spectra. Activation parameters obtained from the rate constants and temperatures are summarized in Table 2 together with $\Delta G^{\ddagger}$'s and k's at 10 °C, which were obtained by calculation, for comparison. The correlation coefficients were very close to 1 and we may discuss the effect of substituents with the use of these data.

The first point we wish to discuss is that argument, saying that the results by van Koten *et al.*[12,13] and

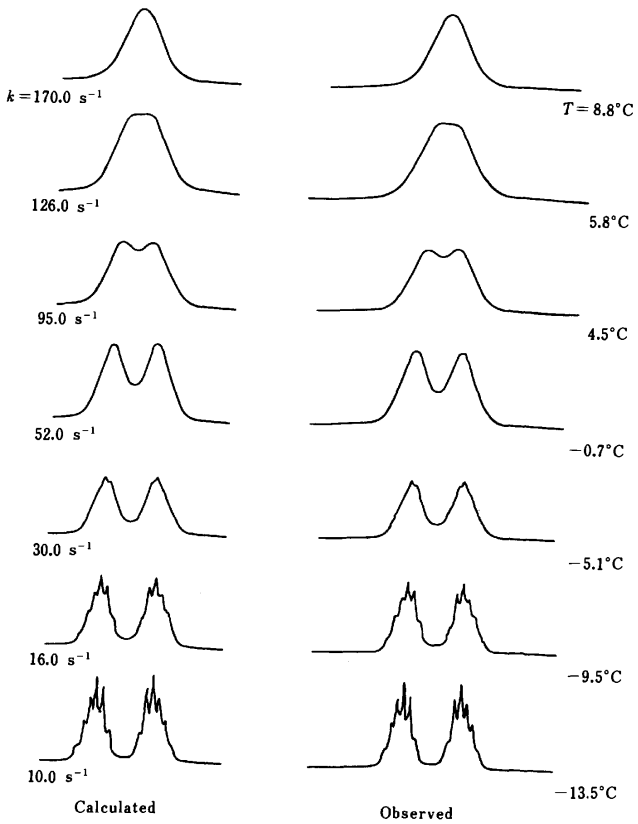

Fig. 1. Calculated and observed spectra of the AB part of ABX_3 patterns in **4** (R=C_6H_5, X=Cl) at various temperatures.

Table 2. Activation parameters for topomerization of **4** in chloroform-*d* and pertinent data

R	CH_3	CH_3	CH_3	CH_3	C_6H_5
X	F	Cl	Br	I	Cl
Correlation Coeff.	0.9994	0.9991	0.9990	0.9998	0.9991
$\Delta H^{\ddagger}$/kcal mol^{-1} [a]	21.0±0.7	21.1±0.8	23.4±0.9	22.8±0.3	18.2±0.7
$\Delta S^{\ddagger}$/e. u.	20.5±2.5	22.3±2.7	30.9±1.1	30.5±1.1	16.2±2.5
$\Delta G^{\ddagger}_{283}$/kcal mol^{-1}	15.2	14.8	14.7	14.1	13.7
k_{283}/s^{-1}	11.7	22.9	28.6	73.3	195

a) 1 cal=4.184 J

Corriu *et al.*[14] could be caused by the fluxional behavior of the complexes, can be denied by the present results. The X-ray crystallography of compound **1** was carried out and concluded that nitrogen and bromine occupy the apical positions.[21] Although electronegative groups favor to be in the apical positions in trigonal bipyramid complexes, this general trend cannot rule out the possibility that a configuration in which nitrogen or bromine occupies the basal position is present in solution. However, in our cases, if it were the fluxional behavior of the complexes, the coalescence of the AB proton signals could not have been observed for the following reasons. The AB protons at a site (that is either apical or basal) give their own chemical shifts but they are still diastereotopic in another site unless they dissociate and inversion of nitrogen takes place. Therefore, the fluxional behavior could explain the change in the chemical shift differences due to temperature but not the coalescence of the diastereotopic proton signals. Topomerization by dissociation is the process we observe.

The common feature of the activation parameters for compound **4** is that large positive entropies of activation are observed. The feature of the entropy of activation gives suggestions in diagnosing the rate-determining step of the observed topomerization processes. As stated earlier, there are four steps involved in the observation: Dissociation of the amine ligand, rotation about the NCH_2–phenyl bond, inversion of amine, and religation. Inversion of the amine is easily rejected, because the free energy of activation for the observed process is 14—15 kcal/mol at 283 K, whereas that for nitrogen inversion in dibenzylmethylamine is 6.6 kcal/mol at 132 K[22] and that for diethylmethylamine is 7.9 kcal/mol at 160 K.[23] Ruling out the NCH_2–phenyl rotation from being the possible rate-determining step is difficult: *o,o'*-disubstituted neopentylbenzenes are known to show a barrier to rotation about the C_{CH_2}–C_{Ar} bond of 13—15 kcal/mol[24] but the effect of removing one *o*-substituent is not known, in addition to the fact that the effect of the stannyl substituent on the barrier is unknown. However, it scarcely happens that the internal rotation of a molecule shows a large positive entropy of activation. Therefore, being a rate-determining step for the NCH_2–phenyl rotation is less likely. The third possibility, that the religation is the rate-determining step, can also be ruled out because we observe only the ligated form: We should have been able to observe the dissociated form, if the barrier to religation were high relative to that for dissociation of the ligand. Then the most probable rate-determining step for the observed topomerization is the dissociation of the ligand.

The same trend, a large positive entropy of activation, was also observed for the dissociation of anilinium ions.[11] The increase in the entropy in the transition state of a reaction seems to be a commonly observed feature when we go from an ionic ground state to a less ionic transition state. This has been attributed to the increase in the freedom of motion of solvent molecules.[25]

When we descend the periodic table from fluorine to chlorine, to bromine, and then to iodine, the free energy of activation at 10 °C decreases and consequently the rates of topomerization increase in this order. This is reasonable in the sense that a more electronegative halogen causes a stronger N–Sn bond than a less electronegative halogen. However, when we see the ΔH^*'s and ΔS^*'s which are obtained by division of the free energies of activation at various temperatures, we notice that things are not so simple as are expected from the electronegativity. As far as numericals concern, the fluoro compound gives a rather small enthalpy of activation and the bromo and iodo compounds give large enthalpies of activation. The increase in entropy seems to be large in the bromo and iodo compounds relative to the fluoro compound. Since the division of free energy of activation into enthalpy and entropy terms may include errors, we may not be able to get further into insight. However, it is tempting to consider that solvent molecules and/or the stages of the transition state play important roles in determining the activation parameters.

In view of the fact that topomerization by dissociation of an amine ligand in coordination compounds involves a large positive entropy of activation, it is dangerous to compare free energies at different temperatures. In our examples, the fluoro compound gave the smallest $\Delta\nu_{AB}$ (Table 1) among the compounds examined. This will necessarily make the coalescence temperature low. Since the free energy of activation calculated by the coalescence method is a function of T, the low temperature tends to give a small free energy of activation. The smallest free energy of activation in the fluoro compound in a series of silicon compounds[14] may have the origin in this area. Reexamination is awaited.

The data for **4** (R=C_6H_5, X=Cl) suggest that topomerization in this compound is much faster than others: The enthalpy of activation is definitely smaller and the increase in entropy in the transition state seems to be smaller than others. It may be possible to attribute the small ΔH^* to the decrease in acidity of the tin atom due to pπ-dπ interactions but out choice is the steric effect. Firstly, the d orbital which interacts with the 2p orbital of the phenyl group is 5d. This will make the overlap of the orbitals less effective. Secondly, the phenyl group is large. This will make the steric repulsion significant when the coordination bond is formed. The small entropy of activation seems to support the idea, together with the small enthalpy of activation. The steric interactions will make the Sn–N bond long, thus making the Sn–N bond less ionic. The latter factor should contribute to lessen the entropy of activation, because the freedom of motion of solvent molecules in the ground state will be large, relative to a strongly ionic case, if the ionic nature of a bond is weak.

Finally we wish to discuss the steric effects of the alkyl groups on the nitrogen atom. From the chemical shift differences of diastereotopic methyl protons in **1** and coalescence temperature (30 °C), the free energy of activation for topomerization of **1** is calculated as 15.4 kcal/mol. If we calculate the free energy of activation for topomerization of **4** (R=CH_3, X=Br) at the same

temperature, we obtain 14.0 kcal/mol which is much less than the value for **1**. One would argue on the basis of various factors, but we believe this is due to the steric effects (or entropic effects) of the ethyl group. One of the bases on which we postulate the steric effect is a preliminary study on the rates of topomerization of a compound in which one of the ethyl groups in **4** (R=CH_3, X=Br) is replaced by a methyl group. This compound gave free energy of activation of 15.2 kcal/mol at 33.5 °C by the coalescence method. Thus replacing the ethyl group by a small methyl group caused the raise of the activation energy.

So far we have discussed on the dissociation of amine ligands. Although this technique cannot be applied to phosphines and arsines due to their slow inversion rates, there is a possibility that this affords information on the dissociation of sulfur or oxygen ligands. Exchange of oxygen ligands in borane–ether complexes is reported,[26] by looking at the coalescence of ^{19}F signals due to $(CH_3)_2O \cdot BF_3$ and $(C_2H_5)_2O \cdot BF_3$. It might be possible to study the dissociation of their complexes without foreign materials by this technique. There is one point which should be kept in mind, however, when we apply the topomerization technique to the dissociation of oxygen or sulfur ligands. That is to distinguish dissociation from inversion. It is clear that the postulate by Brownstein that he observed inversion of pyramidal oxygen and sulfur[27] should be reexamined. We now plan to extend the technique to these areas.

We wish to thank Professor Haruo Seto and Mr. Kazuo Furihata of Institute of Applied Microbiology, The University of Tokyo, for their technical assistance in measuring the 400 MHz spectra. Our thanks are also due to the Ministry of Education, Science and Culture for a Grant in Aid for Scientific Research which supported this work.

References

1) Part VIII: M. Ōki and M. Ohira, *Bull. Chem. Soc. Jpn.*, **57**, 3025 (1984).
2) A preliminary note has been published: M. Ōki and M. Ohira, *Chem. Lett.*, **1982**, 1267.
3) F. Basolo and R. G. Pearson, "Mechanisms of Inorganic Reactions—A Study of Metal Complexes in Solution," John Wiley, New York (1967).
4) T. Mole, *Aust. J. Chem.*, **16**, 801 (1963).
5) C. A. Smith and M. G. H. Wallbridge, *J. Chem. Soc., A*, **1967**, 7.
6) a) Z. Buczkowski, A. Gryff-Keller, and P. Szczeciński, *Tetrahedron Lett.*, **1971**, 607; b) *Idem., Roczniki Chem.*, **46**, 195 (1972); *Chem. Abstr.*, **76**, 152777r (1972).
7) A. H. Cowley and J. L. Mills, *J. Am. Chem. Soc.*, **91**, 2911 (1969).
8) J. B. DeRoos and J. P. Oliver, *Inorg. Chem.*, **4**, 1741 (1965).
9) R. K. Harris and R. A. Spragg, *Org. Magn. Reson.*, **1**, 329 (1969).
10) J. P. Jensen and E. L. Muetterties, "Dynamic Molecular Process in Inorganic and Organometallic Compounds," in "Dynamic Nuclear Magnetic Resonance Spectroscopy," ed by L. M. Jackman and F. A. Cotton, Academic Press, New York (1975), pp. 253—316.
11) M. Ōki, Y. Yoshioka, H. Kihara, and N. Nakamura, *Chem. Lett.*, **1980**, 1625; M. Ōki, M. Ohira, Y. Yoshioka, T. Morita, H. Kihara, and N. Nakamura, *Bull. Chem. Soc. Jpn.*, **57**, 2224 (1984).
12) G. van Koten and J. B. Noltes, *J. Am. Chem. Soc.*, **98**, 5393 (1976).
13) G. van Koten, J. T. B. H. Jastrzebski, J. G. Noltes, W. M. G. F. Potenagel, J. Kroon, and A. L. Spek, *J. Am. Chem. Soc.*, **100**, 5021 (1978).
14) R. J. P. Corriu, J. Royo, and A. de Saxcè, *J. Chem. Soc., Chem. Commun.*, **1980**, 892.
15) G. van Koten, J. T. B. H. Jastrzebski, J. G. Noltes, G. V. Verhoeckx, A. L. Spek, and J. Kroon, *J. Chem. Soc., Dalton Trans.*, **1980**, 1352.
16) A. J. Deeming and I. P. Rothwell, *J. Chem. Soc., Dalton Trans.*, **1978**, 1497.
17) V. Meyer, *Ber.*, **10**, 309 (1877).
18) H. Gilman and J. Swiss, *J. Am. Chem. Soc.*, **62**, 1847 (1940).
19) G. Binsch, *Top. Stereochem.*, **3**, 97 (1968).
20) G. van Koten, C. A. Schaap, and J. G. Noltes, *J. Organomet. Chem.*, **99**, 157 (1975).
21) G. van Koten, J. G. Noltes, and A. L. Spek, *J. Organomet. Chem.*, **119**, 183 (1976).
22) C. H. Bushweller, J. W. O' Neil, and H. S. Bilofsky, *Tetrahedron*, **28**, 2697 (1972).
23) C. H. Bushweller, S. H. Fleischman, G. L. Grady, P. McGoff, C. D. Rithner, M. R. Whalon, J. G. Brennan, R. P. Marcantonio, and R. P. Domingue, *J. Am. Chem. Soc.*, **104**, 6224 (1982).
24) A. J. M. Reuvers, A. Sinnema, Th. J. Nieuwstad, F. van Rantwijk, and H. van Bekkum, *Tetrahedron*, **27**, 3713 (1971).
25) J. W. Moore and R. G. Pearson, "Kinetics and Mechnism," John Wiley, New York (1981), p. 256.
26) A. C. Rutenberg, A. A. Palko, and J. S. Drury, *J. Am. Chem. Soc.*, **85**, 2702 (1963).
27) S. Brownstein, *J. Am. Chem. Soc.*, **98**, 2663 (1976).

 © 1984 The Chemical Society of Japan Bull. Chem. Soc. Jpn., 57, 3122—3124 (1984) [Vol. 57, No. 11

Chemical Effects on the X-ray *K* Emission Spectra of Phosphorus in Organic Compounds

Seiji YASUDA
The Government Industrial Research Institute, Kyushu, Shuku-machi, Tosu-shi, Saga 841
(Received April 21, 1984)

Spectral changes in the P $K\alpha$ and P $K\beta$ X-ray emission lines of solid organic phosphorus compounds were measured with a two-crystal X-ray spectrometer. The P $K\alpha$ line shifted to higher energies with an increasing number of oxygen atoms attached directly to a phosphorus atom. Similar shifts were found in the P $K\alpha$ satellites, which were always 1.5—2.0 times larger than those of the parent $K\alpha$ line. There was no simple correlation for relating the P $K\beta_1$ shift to the phosphorus form. The P $K\beta$ profiles of organic phosphorus seemed to be characterized by the surrounding atoms or groups. The appearance of the $K\beta'$ band offered possible evidence for the existence of phosphorus–oxygen bonding in the samples.

It has been found that the chemical bonding forms of phosphorus affect the wavelenghts, spectral profiles and intensities of the phosphorus X-ray emission lines to a measurable degree.[1-5] These phenomena have received considerable attention from analytical chemists, since they can offer much direct information about phosphorus forms in unknown samples.[6,7] Most of the published work on the spectral changes in the P $K\alpha$ and P $K\beta$ lines has been concentrated on inorganic phosphorus compounds such as phosphides, phosphates and glasses.[8-11] However, so far as organic phosphorus is concerned, there is a lack of the experimental evidence for the chemical shifts and profile changes in the P K emission lines. Only a few measurements on the P $K\beta$ profile changes have been directed to the theoretical interpretation of the phosphorus–ligand bonding in certain organic coordination compounds.[12,13]

In a preceding paper,[14] more reliable data related to the chemical shifts of the sulfur $K\alpha$ and $K\beta$ lines from many organic compounds were shown together with certain regularities in their profile changes. The present paper deals in an analogous way with several solid organic phosphorus compounds. The observed spectral changes are discussed qualitatively with regard to phosphorus bonding forms.

Experimental

The P $K\alpha$ and P $K\beta$ spectra were automatically measured by a step-scanning method at regular intervals of 0.005° or 0.01° 2θ using a Rigaku SX X-ray fluorescence spectrometer equipped with a two-crystal spectrometer. Ge(111) ($2d$= 6.5327 Å) analyzer crystals and a flow proportional counter were used. The primary radiation used for exciting the spectrum was provided by a chromium X-ray tube operated at 50 KV, 35 mA. The 2θ positions of the P $K\alpha$, its satellite and P $K\beta$ lines were determined by averaging the goniometer settings at which the same intensity was measured on either side of the peak at the approximately 90% of the maximum intensity. The values of the chemical shifts of the P $K\alpha$ and P $K\alpha_4$ satellite were determined as an energy difference between a compound and red phosphorus and those of the P $K\beta_1$ were determined in relation to that of Li_3PO_4. At least three independent measurements were made for each compound. The experimental errors were estimated to be nearly 0.01 eV for the P $K\alpha$ shifts and 0.04 eV for the other shifts. Background corrections were made regarding the intensity measurements.

Organic phosphorus compounds used in this study were of the highest commercial grade available. Each sample was prepared by pressing a fine powder into an aluminium ring using a sample preparation kit. All compounds were confirmed by X-ray diffraction or IR analysis.

Results and Discussion

P K$\alpha_{1,2}$ *Spectrum.* The P $K\alpha_1$ and P $K\alpha_2$ emission lines appeared as an unresolved $K\alpha_{1,2}$ doublet under the present experimental conditions. By convention, this doublet is designated as P $K\alpha$ throughout this paper. The P $K\alpha$ width, at half-maximum intensity, was constant at about 1.78 eV in all compounds and red phosphorus. This suggests that the compounds used were not contaminated by significant amounts of phosphorus in a different bonding form. Table 1 lists the data of the P $K\alpha$ chemical shifts of organic phosphorus compounds and some inorganic phosphorus compounds chosen as a difference, together with their P $K\alpha_4$ and P $K\beta_1$ shifts to be discussed below.

TABLE 1. THE CHEMICAL SHIFTS OF THE PHOSPHORUS $K\alpha$ AND $K\beta$ LINES

Compound	Chemical shift/eV		
	$K\alpha$	$K\alpha_4$	$K\beta_1$
P	0	0	+2.36
Ph_3P	+0.02	+0.20	+0.91
Ph_3PO	+0.37	+0.76	+0.43
Ph(H)PO(OH)	+0.47	+0.83	−0.43
$PhPO(OH)_2$	+0.62	+1.03	+0.53
$PhPO(ONa)_2 \cdot xH_2O$	+0.66	+1.06	+0.05
$(PhO)_3PO$	+0.74	+1.16	−0.10
$PhOPO(OH)_2$	+0.78	+1.16	+0.55
$PhOPO(ONa)_2 \cdot xH_2O$	+0.78	+1.19	+0.55
$NO_2PhOPO(ONa)_2 \cdot 6H_2O$	+0.78	+1.19	+0.58
$C_{12}H_{25}OPO(ONa)_2$	+0.78	+1.19	+0.58
$NH_2CONH_2 \cdot H_3PO_4$	+0.78	+1.19	+0.58
$NaPH_2O_2 \cdot H_2O$	+0.46	+0.90	−0.43
$NaPHO_3$	+0.62	+1.03	−0.05
Na_2HPO_4	+0.81	+1.19	+0.24
Li_3PO_4	+0.81	+1.26	0

The P $K\alpha$ line of all compounds investigated here shifted to higher energies than that of red phosphorus. A relatively small shift of +0.02 eV was obtained for triphenylphosphine, Ph_3P. For triphenylphosphine oxide, Ph_3PO (in which one oxygen is attached directly to phosphorus) the P $K\alpha$ line moved +0.37 eV. A further positive shift was observed for phenylphosphinic acid, Ph(H)PO(OH), in which two oxygen atoms are bonded directly to phosphorus. The observed P $K\alpha$ shift of +0.47 eV for this acid agreed closely to that of sodium phosphinate. Phenyl phosphonic acid, $PhPO(OH)_2$, and its disodium salt (with three adjacent oxygen atoms) exhibited P $K\alpha$ shifts of +0.62 and +0.66 eV, respectively. These are almost comparable to that of sodium hydrogenphosphate. Except for triphenyl phosphate, $(PhO)_3PO$, with a P $K\alpha$ shift of +0.74 eV, the remaining organic phosphates gave a constant P $K\alpha$ shift of +0.78 eV. The data were slightly less than those for inorganic phosphates. More recently, Maekawa *et al.*[16] reported a significant difference in the P $K\alpha$ shifts among inorganic phosphates. However, such differences were not found in most organic phosphates of interest here.

From the above results, it is concluded that the P $K\alpha$ line of organic phosphorus compounds is successively shifted to higher energies with an increase in the number of oxygen atoms bonded directly to a phosphorus atom. Therefore, the data on the P $K\alpha$ shifts (listed in Table 1) can be expected to be utilized to analyze phosphorus forms in unknown organic samples.

P $K\alpha_{3,4}$ *Satellite Spectrum.* The P $K\alpha_{3,4}$ group of satellites was observed on the high-energy tails of the parent $K\alpha$ line. Figure 1 shows the spectral profiles of the P $K\alpha_{3,4}$ satellites for several compounds. In every case, three components $K\alpha_4$, $K\alpha_3$, and $K\alpha'$ could be resolved from the high-energy side, but the remaining components, $K\alpha_3'$ and $K\alpha''$, reported in the literature[17,18] were obscure. The intensity of the $K\alpha_4$ or $K\alpha_3$ satellite was approximately 4% of that of the parent $K\alpha$, whereas the $K\alpha'$ satellite was quite low in intensity, and sometimes even ambiguous. Spectral changes related to phosphorus bonding forms were observed in the relative intensities and energy positions of the resolved satellites. The intensity ratio, $K\alpha_4/K\alpha_3$, at each peak position increased slightly with an increasing number of oxygen atoms attached directly to the phosphorus. The ratio changed from nearly 0.57 in Ph_3P to 0.85 in Ph_3PO and to 0.90 in phosphates. A similar trend has been found in the sulfur $K\alpha_{3,4}$ satellites of organic sulfur compounds.[14]

The P $K\alpha_{3,4}$ satellites moved as a group with an almost constant offset of about 2.56 eV between $K\alpha_4$ and $K\alpha_3$ and of about 5.10 eV between $K\alpha_3$ and $K\alpha'$. Therefore, only the P $K\alpha_4$ shift of each compound relative to red phosphorus is shown in Table 1. The direction of the P $K\alpha_4$ shift was quite similar to that of the parent P $K\alpha$ line, while the data of the $K\alpha_4$ shifts were always 1.5—2.0 times larger than those of the P $K\alpha$ line. This result supports the general prediction[17] that the chemical shift of the $K\alpha$ satellites should be much more sensitive to the chemical-bonding forms of elements than is the parent $K\alpha$ line. However, more valuable information about the phosphorus forms than those from P $K\alpha$ shifts could not be obtained from the spectral changes in the P $K\alpha$ satellites.

P $K\beta$ *Spectrum.* The high-resolution P $K\beta$ spectra of organic phosphorus compounds revealed very complex band structures, composed of several strongly overlapping lines caused by transitions involving valence-band electrons.[9] In this study, some attempts were made to reveal possible regularities in the chemical shift of the $K\beta_1$ and in the P $K\beta$ profile changes. The most intense peak in each spectrum was noted to be $K\beta_1$ and additional low-energy bands were noted to be $K\beta_x$ and $K\beta'$. As shown in the last column of Table 1, the observed P $K\beta_1$ chemical shifts of organic phosphorus compounds relative to that of Li_3PO_4

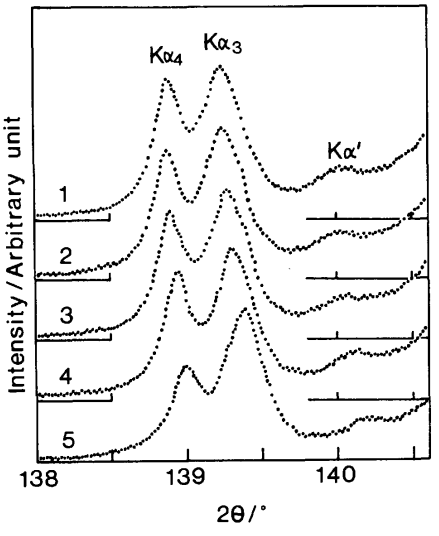

Fig. 1. Phosphorus $K\alpha_{3,4}$ satellite spectra.
1: $PhOPO(OH)_2$, 2: $PhPO(OH)_2$, 3: Ph(H)PO(OH), 4: Ph_3PO, 5: Ph_3P.

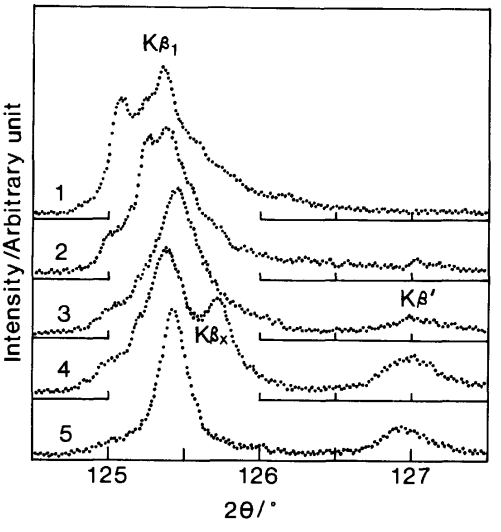

Fig. 2. Phosphorus $K\beta$ spectra.
1: Ph_3P, 2: Ph_3PO, 3: Ph(H)PO(OH), 4: $PhPO(OH)_2$, 5: $PhPO(ONa)_2 \cdot xH_2O$.

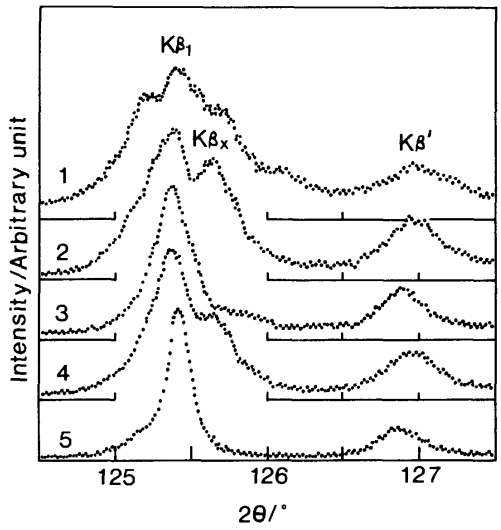

Fig. 3. Phosphorus $K\beta$ spectra.
1: $(PhO)_3PO$, 2: $PhOPO(OH)_2$, 3: $PhOPO(ONa)_2 \cdot xH_2O$, 4: $NH_2CONH_2 \cdot H_3PO_4$, 5: Li_3PO_4.

varied from −0.43 eV for Ph(H)PO(H) to +0.91 eV for Ph_3P. However, a simple correlation between the P $K\beta_1$ shifts and the chemical-bonding forms of phosphorus could not be found.

The P $K\beta$ profiles of organic phosphorus varied from compound to compound. Some of them are shown in Figs. 2 and 3. Each spectrum was normalized relative to the maximum intensity of $K\beta_1$. The $K\beta$ profiles of red phosphorus and inorganic phosphorus compounds tested here are almost identical to those reported by Fichter[9]; therefore, they are not shown. The first characteristic feature of the P $K\beta$ profile change was the occurrence of a low-energy band $K\beta'$ in the $K\beta$ spectra involving compounds with phosphorus–oxygen bonding. This band was observed at about 13.5—14.0 eV below $K\beta_1$ and its intensity increased slightly with an increasing number of oxygen atoms attached directly to the phosphorus. Consequently, it seems reasonable to assume that the appearance of the $K\beta'$ band can offer evidence for phosphorus–oxygen bonding. This feature was the only possible regularity obtained in the present study on the P $K\beta$ profile changes of organic phosphorus compounds. Such a feature is also supported by the fact that the $K\beta'$ band disappeared in the $K\beta$ spectra involving red phosphorus and Ph_3P. However, in the $K\beta$ spectrum of Ph_3PO with a phosphorus–oxygen bonding, the $K\beta'$ band became obscure and its $K\beta$ profile was rather closer to that of Ph_3P which exhibited a clearly resolved high-energy band at about 2.6 eV above $K\beta_1$.

The next interesting feature of the P $K\beta$ profile change was the behaviour of the low-energy band $K\beta_x$ adjacent to $K\beta_1$. For phenyl dihydrogenphosphate, $PhOPO(OH)_2$, and $PhPO(OH)_2$, the $K\beta_x$ band was clearly resolved at about 2.7 eV below $K\beta_1$. However, this band was no longer detectable in the $K\beta$ spectra from their disodium salts in which two hydrogen atoms in hydroxyl groups are substituted by two sodium atoms. These salts exhibited a relatively sharp $K\beta_1$ with a nearly symmetrical structure. Similar $K\beta$ profiles were obtained for the other disodium salts such as $NO_2PhOPO(ONa)_2 \cdot 6H_2O$ and $C_{12}H_{25}OPO(ONa)_2$. Such a behaviour of the $K\beta_x$ band suggests that this band may be associated with bonding between phosphorus and a hydroxyl group. This feature was supported by the appearance of a $K\beta_x$ band from urea phosphate, which involves three hydroxyl groups. However, in the $K\beta$ spectrum from Ph(H)PO(OH), which has one hydroxyl group attached to phosphorus, the $K\beta_x$ band was unclear or extremely weak. The high-energy subband $K\beta''$ has been frequently resolved from the $K\beta$ spectra of third-period elements[15] in certain compounds such as sulfites, sulfoxides and chlorates. However, the corresponding $K\beta''$ band was not discernible in the P $K\beta$ spectra of any of the compounds studied here.

The present study does not cover more extensive organic phosphorus compounds and, hence, there is a lack of data for certain forms of organic phosphorus. Consequently, a clear rule for relating the P $K\beta$ profile changes to various phosphorus forms could not be established. However, it seems possible to predict phosphorus forms of unknown samples by a comparison with the P $K\beta$ profiles shown in Figs. 2 and 3.

References

1) O. Lundquist, *Z. Phys.*, **102**, 768 (1936).
2) E. Schnell, *Monatsh. Chem.*, **94**, 703 (1963).
3) T. C. Yao and J. J. Holst, *Spectrochim. Acta, Part B*, **23B**, 19 (1967).
4) G. Wiech, *Z. Phys.*, **216**, 472 (1968).
5) Y. Takahashi, *Bull. Chem. Soc. Jpn.*, **45**, 4 (1972).
6) T. Handa, Y. Yoshioka, N. Soga, and M. Kunugi, *Yogyo Kyokai Shi*, **87**, 395 (1979).
7) H. Nishikawa and S. Minami, *Denki Kagaku*, **50**, 770 (1982).
8) K. Myers and G. Andermann, *J. Phys. Chem.*, **76**, 3975 (1972).
9) M. Fichter, *Spectrochim. Acta, Part B*, **30B**, 417 (1975).
10) G. Leonhardt, I. Topol, K. Unger, and A. Meisel, *Ann. Phys. (Leipzig)*, **28**, 245 (1972).
11) Y. Takahashi, *Bull. Chem. Soc. Jpn.*, **46**, 2039 (1973).
12) K. Myers and G. Andermann, *J. Phys. Chem.*, **77**, 280 (1973).
13) V. I. Nefedov, Y. V. Salyn, I. I. Moiseev, A. P. Sadovskii, A. S. Berenbljum, A. G. Knizhnik, and S. L. Mund, *Inorg. Chim. Acta*, **35**, L343 (1979).
14) S. Yasuda and H. Kakiyama, *Spectrochim. Acta, Part A*, **35A**, 485 (1979).
15) G. Karlsson and R. Manne, *Phys. Scr.*, **4**, 119 (1971).
16) T. Maekawa, M. Furukawa, and T. Yokokawa, *Bull. Chem. Soc. Jpn.*, **57**, 295 (1984).
17) F. A. Gianturco, *J. Phys. B*, **1**, 614 (1968).
18) H. Hartmann, L. Papula, and W. Strehl, *Thoer. Chim. Acta*, **21**, 261 (1971).

 © 1984 The Chemical Society of Japan Bull. Chem. Soc. Jpn., 57, 3125—3129 (1984)

Stability Constants of Some Bivalent Metal Chelates of 3-Aryl-2,4-pentanedione in 75% v/v 1,4-Dioxane-Water Medium

Yoshito WAKUI, Katsunori YANO, Yoshiharu NAKANO, Kousaburo OHASHI,* and Katsumi YAMAMOTO
Department of Chemistry, Faculty of Science, Ibaraki University, Mito 310
(Received April 19, 1984)

A new ligand, 3-(1-naphthyl)-2,4-pentanedione, was prepared. Concentration proton-dissociation constants of 3-aryl-2,4-pentanedione (aryl group; phenyl, 2,4-dinitrophenyl, and 1-naphthyl) and concentration stability constants of some bivalent metal chelates of 3-aryl-2,4-pentanedione were determined in a 75% v/v 1,4-dioxane-water medium containing 0.05 mol dm^{-3} sodium perchlorate by a pH-titrimetric method. The dissociation constant (pK_a) of 3-(2,4-dinitrophenyl)-2,4-pentanedione, 2,4-pentanedione, 3-phenyl-2,4-pentanedione, and 3-(1-naphthyl)-2,4-pentanedione were found to be 8.87, 10.93, 11.50, and 11.71, respectively. The order of acidity in 2,4-pentanedione was explained by the field effect of the aryl group. The stability constants of the bivalent metal chelates of these ligands were in accord with the Irving-Williams series. The stepwise stability constant of the chelate increased with an increasing pK_a value of 3-aryl-2,4-pentanedione. This result cannot be explained by the steric and solvation effect of an aryl substituent.

There have been a large number of articles describing the preparation of 2,4-pentanedione derivatives, their proton-dissociation[1,2] and partition[3,4] equilibrium constants, stability and partition equilibrium[5] constants of their metal chelates, and solvent extraction[6] of metal ions with 2,4-pentanedione derivatives. The investigations involving metal chelates of 3-substituted 2,4-pentanedione seem to be rare compared to those involving metal chelates of 1-substituted 2,4-pentanedione.

The effect of alkyl substituents at the 1-position of 2,4-pentanedione on the stability constant of a metal chelate has been studied.[1,2] An alkyl substituent lowers the acidity, and the stability constants of copper(II) chelates are generally smaller than expected on the basis of a pK_a–log β (overall stability constant) relationship.

Martin and Martin[7] studied the steric and solvation effect of an alkyl substituent at the 3-position of 2,4-pentanedione on the chelating tendency and found that there was no linear pK_a–log β relationship for bivalent metal chelates of 3-alkyl-2,4-pentanedione. They assert that the effect of an alkyl substituent at the 3-position on the chelating tendency is complicated, and that the solvation effect may be more important than the steric effect.[7]

When methylene-hydrogen of 2,4-pentanedione was substituted with an aryl group, the aromatic ring of an aryl group should adopt a conformation perpendicular to the 2,4-pentanedione ring, and all mesomeric effects of the aromatic ring shold be excluded. The authors' interest lies in clarifying the effect of the aryl group on the proton-dissociation constant and the stability constant of bivalent metal chelates of 3-aryl-2,4-pentanedione.

Experimental

Synthesis of 3-(1-Naphthyl)-2,4-pentanedione. A mixture of 1-naphthylacetonitrile (100 g, 0.60 mol) and ethyl acetate (60 cm^3) was added to a 1-butanol solution of butoxide (sodium metal 7.1 g +1-butanol 100 cm^3) while being stirred. After the reaction mixture was warmed to 80 °C, it was allowed to cool to room temperature while being stirred. The whole mixture became a gray cake. It was dissolved in water and acidified. The oily layer was extracted with ether and the ether was evaporated. A mixture of acetic acid, water, and sulfuric acid (520 cm^3 each) was added to the crude product. The resulting mixture was refluxed for 6 h. Black oil was extracted with ether and crude 1-naphthylacetone was obtained after the usual work-up. 40.5 g (32.4%), bp 115—120 °C /0.1 mm Hg. The 1-naphthylacetone was treated with a mixture of acetic anhydride (55.1 cm^3, 0.59 mol) and a BF_3–acetic acid complex (264 g) at 50 °C for 20 h. To the reaction mixture was added 1100 cm^3 of a sodium acetate solution (about 8%) and the resulting mixture was refluxed for 2 h. A crude product was extracted with ether, transferred to an aqueous sodium hydroxide solution (5%) and then the resultant alkaline solution was acidified with 5 mol dm^{-3} hydrochloric acid. Crude 3-(1-naphthyl)-2,4-pentanedione precipitated was recrystallized from ethanol: Yield 20.0 g (14.7%). It was further chromatographed (Wako gel C-200). mp 105.0—106.5 °C, IR (KBr): 3020, 2930, 1600 cm^{-1}; ^{1}H-NMR ($CDCl_3$, δ): 17.02 (s, 1H), 8.0—7.3 (m, 7H), 1.75 (s, 6H); MS: m/z 226 (parent), 211, 183, 165 (base), 43. Anal ($C_{15}H_{14}O_2$) C,H.

Since the ^{1}H-NMR spectrum showed intramolecular hydrogen-bonded *OH proton equivalent to about one proton* in $CDCl_3$, 3-(1-naphthyl)-2,4-pentanedione should adopt the enol form. The fact that two methyl ring are magnetically equivalent, suggests that an aromatic ring of substituent is perpendicular to the 2,4-pentanedionate ring and 2,4-pentanedione is in equilibrium between the tautomeric isomers at a more rapid rate than NMR time scale.

Materials. 3-(2,4-dinitrophenyl)-2,4-pentanedione was prepared by a method described in the reference,[8] and identified by its melting point, ^{1}H-NMR and IR spectra, and a chemical analysis of carbon, nitrogen, and hydrogen, Reagent-grade 3-phenyl-2,4-pentanedione (Tokyo Kasei Co., Ltd.) was used without purification. Reagent-grade 2,4-pentanedione (Wako Co., Ltd.) was distilled before use. Reagent-grade 1,4-dioxane (Kanto Co., Ltd.) was shaken with solid potassium hydroxide, refluxed with sodium metal for 10 h, and distilled. The distilled 1,4-dioxane was preserved in a nitrogen atmosphere. Sodium perchlorate was recrystallized from an aqueous solution and dissolved in redistilled and decarbonized water. The concentration of the sodium perchlorate solution was determined by the titration of the hydrogen ion concentration after an aliquot of the perchlorate solution was passed through a column of cation-exchange resin in the hydrogen from. The solutions of metal

perchlorate were prepared by converting the metal powder (Mitsuwa Co., Ltd.) to metal perchlorate. Their concentrations were determined by EDTA titration using appropriate indicators. The concentration of the perchloric acid in a metal perchlorate solution was determined by the method similar to that used for the determination of sodium perchlorate.

pH Measurement. The pH measurement was conducted using a Hitachi-Horiba model F-7 type pH meter. A Horiba glass-electrode type 1026-05T was used. A Horiba 2535A-06T type reference electrode, with a double-junction mantle with 3.33 mol dm^{-3} potassium chloride in water and 0.05 mol dm^{-3} sodium perchlorate in 75% v/v 1,4-dioxane-water as an internal solution, was used. The pH meter was standardized using buffer solutions (pH 4.01, 6.86, 10.02 at 25 °C). A fifty-cm^3 portion of 75% v/v 1,4-dioxane-water containing $(1.5—2.0)\times10^{-3}$ mol dm^{-3} metal ion, $(5.0—6.5)\times10^{-3}$ mol dm^{-3} ligand, 0.003 mol dm^{-3} perchloric acid, and 0.05 mol dm^{-3} sodium perchlorate was placed in a 100-cm^3 tall beaker shielded with copper plates and thermostated at 25±0.1 °C. The solution was titrated with 0.02 mol dm^{-3} sodium hydroxide solution containing 0.03 mol dm^{-3} sodium perchlorate. The solution was agitated continuously by passing pure nitrogen. The titration was started 2 h after the electrodes were thermostated in the solution. The response of the electrode was very slow in the 75% v/v 1,4-dioxane-water medium. It took less than 20 min to get a constant reading after each addition of titrant.

Calculation of the Results. A. personal computer (PC 8001 mk II (NEC Co., Ltd.)) was used for the calculatation of the results. N_{80}-basic was used as the language.

Results and Discussion

Determination of pK_a of 3-Aryl-2,4-pentanedione. The concentration of hydrogen ions (pH_c) in 1,4-dioxane-water could not be directly determined from the reading of the pH meter. A potentionmetric titration method modified by Ohtaki[9] was used to find the hydrogen ion concentration in a 75% v/v 1,4-dioxane-water medium. When the concentration of the bulk electrolyte was larger than that of the hydrogen ion concentration, the activity coefficient of the hydrogen ion became constant. The pH_c value can be calculated using the analytical hydrogen ion concentration. The pH_c values are related to the reading of the pH meter, pH_R, by

$$pH_c = pH_R + \Delta pH, \quad (1)$$

ΔpH depending on the concentration of 1,4-dioxane, the ionic strength, *etc.* The ΔpH value obtained using Gran's plot[10] was +0.13±0.04. The electrode worked well enough to obtain the proton-dissociation and stability constants. The concentration of deprotonated 3-aryl-2,4-pentanedione can be given by $a=h-[ClO_4^-]+[Na^+]-K_w h^{-1}$ where h and K_w are the hydrogen ion concentration and the ion product of water in 75% v/v 1,4-dioxane-water medium (3.45×10^{-19})[11] and the proton-dissociation constant can be represented by $K_a=ah/[HL]$. The ratio of $[HL]:[HL]_T$ can be represented as follows:

$$Z = \frac{(C_L - a)}{C_L},$$

where C_L represents the total concentration of 3-aryl-2,4-pentanedione. This ratio was calculated by the hydrogen ion concentration and the proton-dissociation constant as follows:

$$Z = \frac{10^{x+p}}{1+10^{x+p}},$$

where $x=\log h$, $p=\log K_a$ ($\equiv -pK_a$). Normalized curve Z is obtained as follows:

$$Z = \frac{10^x}{1+10^x}. \quad (3)$$

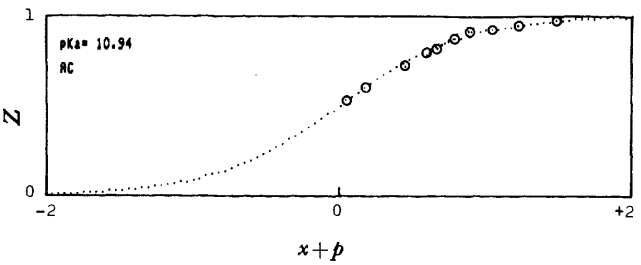

Fig. 1. Determination of pK_a value of 2,4-pentanedione by curve-fitting method (in 75% v/v 1,4-dioxane-water medium containing 0.05 mol dm^{-3} $NaClO_4$, 25 °C). (·····): Normalized curve, (⊙⊙): Experimental data.

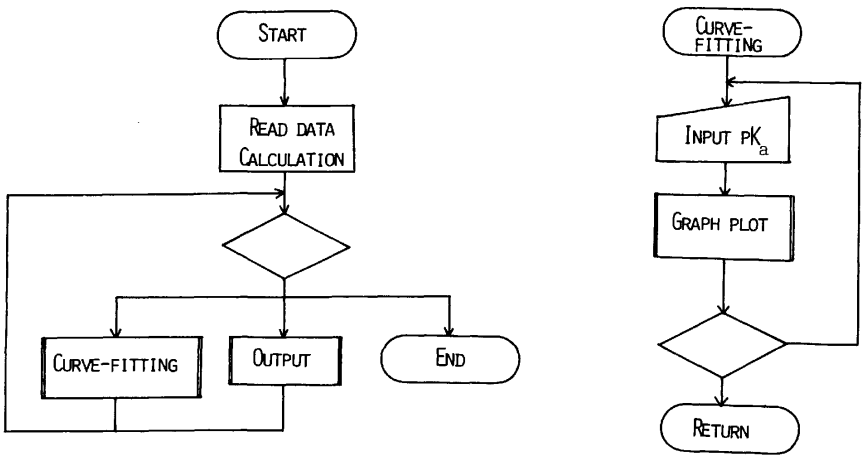

Fig. 2. Block flow chart of program used for dtermination of proton-dissociation constant of 3-aryl-2,4-pentanedione.

A plot of the experimental data Z ($=10^{x+p}/1+10^{x+p}$) was adjusted to coincide with a normalized curve Z until a best fit was obtained. Then, the x value coinciding with $X=0$, $p=-x$ was read. In this work, we attempted to determine the proton-dissociation constant using a program for curve-fitting.[12] The procedure for obtaining the best fit was performed on the display unit of a microcomputer. Fugure 1 shows plots of Z *vs.* $(x+p)$ and a normalized curve of $Z=10X/1+10X$. Thus, the pK_a value of 2,4-pentanedione was obtained to be 10.93±0.08 which is in good agreement with that obtained graphically. Figure 2 represents the block flow chart of the program used for the determination of the proton-dissociation constant of 3-aryl-2,4-pentanedione. The values of pK_a of 3-aryl-2,4-pentanedione are listed in Table 1.

Determination of the Stability Constant. The reaction of the chelate formation of bivalent metal ions with 3-aryl-2,4-pentanedione can be represented by Eqs. 4 and 5:

$$M + L \overset{K_1}{\rightleftharpoons} ML, \tag{4}$$

$$ML + L \overset{K_2}{\rightleftharpoons} ML_2, \tag{5}$$

where K_1 and K_2 represent the stepwise stability constants of 1:1 and 1:2 metal chelates. The average number of 3-aryl-2,4-pentanedione bound per metal ion, Z, is related with K_1 and K_2:

$$Z = \frac{K_1a + 2K_2a^2}{1+K_1a+K_2a}. \tag{6}$$

This formula is derived to

$$Z = \frac{p_2 10^{x+p_1} + 2(10^{x+p_1})^2}{1+p_2 10^{x+p_1} + (10^{x+p_1})^2}, \tag{7}$$

where notations are: $x=\log a$, $p_1=1/2 \log K_2$, $p_2=K_1 \cdot K_2^{-1/2}$. The normalized curve Z is represented as

$$Z = \frac{p_2 10^{X} + 2(10^{X})^2}{1+p_2 10^{X} + (10^{X})^2}. \tag{8}$$

In order to find the required parameters, experimental data Z should be moved along the X axis until the best fit is found. The $\log K_2$ values are then determined by reading $\log a$ at $X=0$. Again the curve-fitting

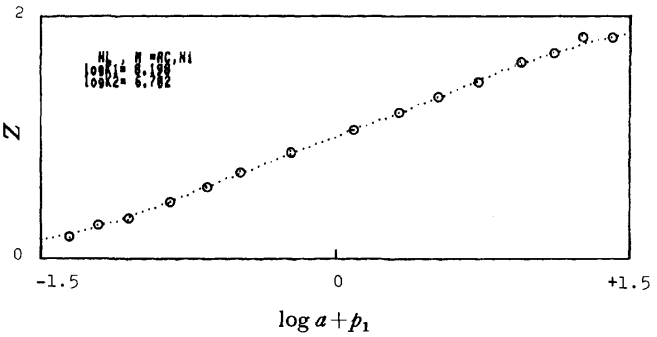

Fig. 3. Determination of concentration stability constant of nickel(II) chelate of 2,4-pentanedione by curve-fitting method (in 75% v/v 1,4-dioxane-water medium containing 0.05 mol dm^{-3} $NaClO_4$, 25 °C). (·····): Normarized curve, (⊙⊙): Experimental data.

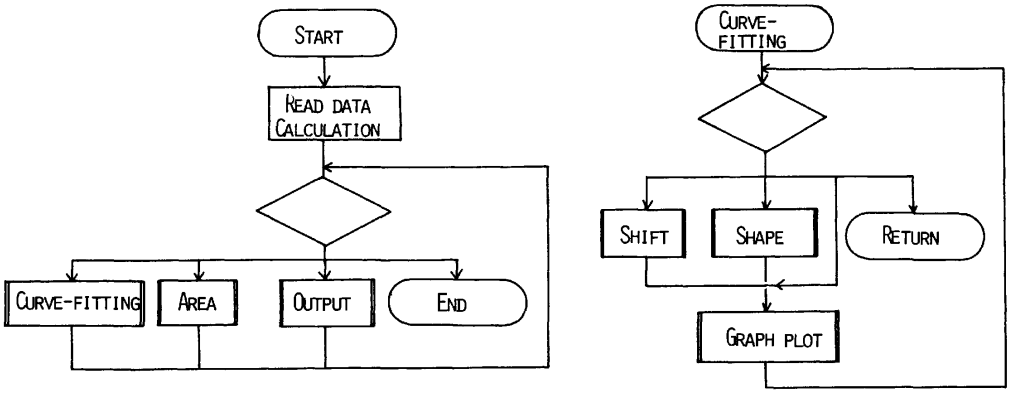

Fig. 4. Block flow chart of program used for determination of stability constant of bivalent metal chelates of 3-aryl-2,4-pentanedione.

Table 1. Concentration proton-dissociation constants and stability constants of some bivalent metal chelates of 3-aryl-2,4-pentanedione (in 75% v/v 1,4-dioxane-water medium, 25 °C)

3-aryl-2,4-pentanedione	pK_a	Co(II)		Ni(II)		Cu(II)		Zn(II)	
		$\log K_1$	$\log K_2$	$\log K_1$	$\log K_2$	$\log K_1$	$\log K_2$	$\log K_1$	$\log K_2$
2,4-pentanedione	10.93	7.8	6.6	8.2	6.7	10.5	9.1	7.6	7.0
3-(3,4-dinitrophenyl)-2,4-pentanedione	8.87	5.9	5.4	6.6	5.9	8.6	7.6	5.8	5.0
3-phenyl-2,4-pentanedione	11.50	7.4	6.8	8.1	7.0	10.5	9.4	7.2	6.7
3-(1-naphthyl)-2,4-pentanedione	11.71	7.7	7.1	8.7	7.8	10.9	9.7	7.5	6.7
(Error)	±0.08	±0.2						±0.4	

was performed on the display unit of a microcomputer. The plot of Z *vs.* log $a+p_1$ is shown in Fig. 3. The obtained values of K_1 and K_2 agreed with those obtained graphically. A block flow chart of the program for the determination of the stepwise stability constants, K_1 and K_2, is shown in Fig. 4.

The thermodynamic proton-dissociation constant (pK_a) of 2,4-pentanedione and stability constant of bivalent metal chelates of 2,4-pentanedione in 75% v/v 1,4-dioxane–water medium, which were obtained by van Uitert and his colaborators,[13] were larger than those obtained in this study. The difference in the results may be ascribed to a difference in experimental conditions. Since the keto-enol tautometric equilibrium of these 3-aryl-2,4-pentanedione in 75% v/v 1,4-dioxane–water is not known, the thermodynamic proton-dissociation and stability constants could not be determined. Manome and Saito[11] found that the pK_a value and the stability constant of the 1:1 bivalent metal chelates of 1,3-diphenyl-1,3-propanedione obtained under almost the same experimental conditions as ours were smaller than thermodynamic data obtained by van Uitert.[13]

The pK_a value of 3-aryl-2,4-pentanedione obtained in the present study increased in the following order: 3-(2,4-dinitrophenyl)-2,4-pentanedione<2,4-pentanedione<3-phenyl-2,4-pentanedione≲3-(1-naphthyl)-2,4-pentanedione. Since the aromatic ring of the substituent should adopt a conformation perpendicular to the 2,4-pentanedione ring, all the mesomeric effect of aryl group may be excluded for these 3-aryl-2,4-pentanedione.

The pK_a values of acetic acid, cyclohexyl acetic acid, and phenyl acetic acid were 4.75, 4.80, and 4.31, respectively.[14] Acidity of these acetic acid derivatives was explained in terms of the inductive effect or the field effect, that is, the interaction between the dipole of the substituent and dissociatable hydrogen through an intervening medium.[14] As mentioned above, there should be no mesomeric effect of 3-aryl group for 3-aryl-2,4-pentanedione. The pK_a value of 3-aryl-2,4-pentanedione and 2,4-pentanedione indicates the order opposit to the case of acetic acid derivatives. Consequently, the order of the acidity of 2,4-pentanedione and 3-aryl-2,4-pentanedione cannot be explained by the inductive effect of an aryl group. For 3-phenyl-2,4-pentanedione and 3-(1-naphthyl)-2,4-pentanedione, the field effect may be an important factor controlling the acidity rather than the inductive effect. Thus, phenyl and naphthyl groups which are rich in π-electrons would be considered to destabilize the conjugate base and decrease the acidity. In the case of 3-(2,4-dinitrophenyl)-2,4-pentanedione having π-electron-withdrawing nitro groups, benzene moiety of 2,4-dinitrophenyl ring may become electron defficient. The positively polarized benzene ring would interact with 2,4-pentanedione moiety. The interaction stabilizes the conjugate base to make the acidity greater than 2,4-pentanedione.

The stepwise stability constants of the 1:1 and 1:2 bivalent metal chelates are in accord with the Irving-Williams series.[15] The relationship between pK_a and

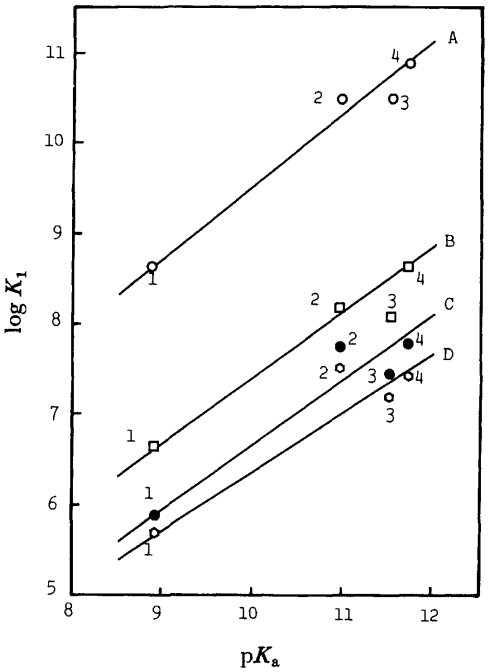

Fig. 5. Variation of log K_1 of bivalent metal chelates as a function of pK_a for 3-aryl-2,4-pentanedione. Metal ion: A, copper(II); B, nickel(II); C, cobalt(II); D, Zinc(II). 3-aryl-2,4-pentanedione: 1) 3-(2,4-dinitrophenyl)-2,4-pentanedione; 2) 2,4-pentanedione; 3) 3-phenyl-2,4-pentanedione; 4) 3-(1-naphthyl)-2,4-pentanedione.

log K_1 for 3-aryl-2,4-pentanedione is shown in Fig. 5, indicating that there is no linear relationship between pK_a and the stability constant, log K_1. However, the stability constant increased with increasing pK_a value of 3-aryl-2,4-pentanedione. Also, a similar result was obtained for the 1:2 metal chelates. The linear relationship between pK_a and the overall stability constant, log β, has been observed for the copper(II) chelates of 2,4-pentanedione derivatives (1,1,1-trifluro-2,4-pentanedione, 2,4-pentanedione, 1-phenyl-1,3-butanedione, and 3-methyl-2,4-pentanedione).[16]

Though the pK_a value of 3-phenyl-2,4-pentanedione was larger than that of 2,4-pentanedione by 0.6, the stability constants of these metal chelates of 3-phenyl-2,4-pentanedione were found to be smaller than those of 2,4-pentanedione or to be of the same magnitude.

The linear pK_a–log β relationship was not observed for copper(II) and other bivalent metal chelates of 3-alkyl-2,4-pentanedione,[3] as mentioned above. The hydrophobic character of the ligand was proposed as one reason for the above results. However, it may be very difficult to clearly explain the effect of a substituent at the 3-position of 2,4-pentanedione on the stability constant at the present stage.

3-(2,4-dinitrophenyl)-2,4-pentanedione can be a useful extractant for metal ions because of the complex formation of metal chelates in an acidic medium and the large hydrophobic character.

The authors wish to thank Dr. Toshitaka Terasaka for his kind and useful advice on data analysis using a

microcomputer.

References

1) M. Calvin and K. W. Wilson, *J. Am. Chem. Soc.*, **67**, 2003 (1945).
2) B. B. Martin and W. C. Fernelius, *J. Am. Chem. Soc.*, **81**, 2342 (1959).
3) H. Watarai and N. Suzuki, *Bull. Chem. Soc. Jpn.*, **53**, 1848 (1980).
4) T. Omori, T. Wakahayashi, S. Oki, and N. Suzuki, *J. Inorg. Nucl. Chem.*, **26**, 2265 (1964).
5) H. Awano, H. Watarai, and N. Suzuki, *J. Inorg. Nucl. Chem.*, **42**, 1516 (1980).
6) T. Sekine and N. Ihara, *Bull. Chem. Soc. Jpn.*, **44**, 2943 (1971).
7) D. F. Martin and B. B. Martin, *Inorg. Chem.*, **1**, 404 (1961).
8) S. S. Joshi and I. R. Gambhir, *J. Am. Chem. Soc.*, **78**, 2222 (1956).
9) H. Ohtaki, *Inorg. Chem.*, **6**, 808 (1967).
10) G. Gran, *Analyst*, **77**, 661 (1952).
11) A. Manome and K. Saito, *Bull. Chem. Soc. Jpn.*, **41**, 2419 (1968).
12) L. G. Sillén, *Acta Chem. Scand.*, **10**, 186 (1956).
13) LeGrand G. van Uitert, C. G. Hass, W. C. Fernelius, and B. E. Douglas, *J. Am. Chem. Soc.*, **75**, 451, 455, 458 (1954).
14) C. K. Ingold, "Structure and Mechanism in Organic Chemistry," 2nd ed, Cornell University (1970), p. 1110.
15) H. M. N. H. Irving and R. J. P. Williams, *J. Chem. Soc.*, **1953**, 3192.
16) M. Calvin and K. Wilson, *J. Am. Chem. Soc.*, **67**, 2003 (1945).

Solvent-extraction Behavior of Molybdenum(VI) with 1,5-Diphenylcarbazone and the Extraction-spectrophotometric Determination of Molybdenum(VI)

Kousaburo OHASHI,* Kiichiro NAGASHIMA, Rumiko SEITA, and Katsumi YAMAMOTO
Department of Chemistry, Faculty of Science, Ibaraki University, Mito 310
(Received May 7, 1984)

The solvent extraction of molybdenum(VI) with 1,5-diphenylcarbazone (Hdpco) into chloroform, benzene, or tributyl phosphate (tbp) was studied. The molar ratio of molybdenum(VI):1,5-diphenylcarbazone in the complex extracted into chloroform or benzene in the range from 1.0 mol dm^{-3} HNO_3 to pH 1.9 was found to be 1:2. The extracted complex was estimated to be $MoO_2(dpco)_2$. On the other hand, molybdenum(VI) may be extracted into tbp as a mixture of $MoO_2(dpco)_2$ and $MoO_2(dpco)(OH)(tbp)$. The extraction constants, K_{ex} ($=[MoO_2(dpco)_2]_o/[Mo(OH)_6][Hdpco]_o^2$), were determined to be 7.9×10^6 and 3.8×10^8 mol^{-2}dm^6 for chloroform and benzene respectively. A black complex formulated as $MoO_2(dpco)_2\cdot5H_2O$ was formed. Molybdenum(VI) can be determined over the range from 1.50 to 19.0 μg/10 cm^3 within a relative error of ±4%. The interference of diverse ions will be described.

Extraction-spectrophotometric determinations of molybdenum(VI) have been extensively investigated.[1] However, there have been few reports describing a detailed extraction behavior of molybdenum(VI) compared to those of other metal ions because of the diversity of molybdenum(VI) species in an aqueous solution. Molybdenum(VI) was extracted as $MoO_2(tta)_2$ and $HMoO_2(tta)_3$ with 4,4,4-trifluoro-1-(2-thienyl)-1,3-butanedione (tta) from 6.0 mol dm^{-3} hydrochloric acid and 0.05 mol dm^{-3} sulfuric acid solutions respectively.[2] In some cases, molybdenum(VI) is reduced by chelating extractants with a sulfur atom to give a molybdenum(V) complex.[3] Thus, the solvent extraction of molybdenum(VI) is characterized by varied extraction behavior.

1,5-diphenylcarbazone, which has a structure similar to that of 3-mercapto-1,5-diphenylformazan, reacts with a large number of metal ions to form intensively colored complexes. However, because of the poor extractability and instability of the molybdenum(VI)–dpco complex, dpco has not been employed as the extractant for molybdenum(VI). The unstable cadmium(II)- and manganese(II)–dpco complexes in benzene were stabilized by the addition of tbp.[4]

The present work describes the extraction behavior of molybdenum(VI) with Hdpco, the preparation of $MoO_2(dpco)_2$, and the determination of molybdenum(VI).

Experimental

Apparatus. A Hitachi 170-30-type atomic-absorption spectrophotometer was used for the determination of molybdenum(VI). A Hitachi 200-10-type automatic-recording absorption spectrophotometer was used to measure the absorption spectra of molybdenum(VI)–dpco complexes. The pH measurements were made by using a Hitachi-Horiba M-7-type pH meter.

Reagents. *Standard Molybdenum(VI) Solution*: A 0.10-mol dm^{-3} molybdenum(VI) solution was prepared by dissolving 2.419 g of sodium molybdate-water (1/2) (Kanto Co. Ltd.) in 100 cm^3 of a sodium hydroxide solution (pH 9). The working solutions were prepared by diluting the stock solution with redistilled water.

Standard Hdpco Solution: Hdpco (GR. grade, Tokyo Kasei Co., Ltd.) was purified by the method described in the literature.[5] A 1.00×10^{-2}-mol dm^{-3} Hdpco solution was prepared by dissolving 0.240 g of Hdpco in 100 cm^3 of an organic solvent.

Organic Solvent: Chloroform, benzene, and tbp of a reagent grade were purified by distillation and then saturated with redistilled water.

All the other reagents were of a guaranteed reagent quality.

Procedure for the Extraction. A 10-cm^3 portion of a 8.00×10^{-5} mol dm^{-3} molybdenum(VI) solution was placed in a 100-cm^3 separatory funnel. To the solution, 10 cm^3 of a given concentration of Hdpco in an organic solvent was added. The pH of the molybdenum(VI) solution was adjusted with nitric acid. The solutions were vigorously shaken for 60, 30, and 10 min for chloroform, tbp, and benzene respectively. After the phases had been allowed to separate, the pH of the aqueous phase was measured. The pH change was negligibly small during the extraction. The distribution ratio of molybdenum(VI) was determined by measuring the molybdenum(VI) in the aqueous phase .

Preparation of $MoO_2(dpco)_2\cdot5H_2O$. A 400-cm^3 portion of a 0.20-mol dm^{-3} molybdenum(VI) aqueous solution and a 400-cm^3 portion of a 1.0×10^{-2} mol dm^{-3} Hdpco in benzene were placed in a 1-dm^3 separatory funnel. The pH of the molybdenum(VI) solution was adjusted to 2.0 with nitric acid. The solutions were vigorously shaken for 30 min. After the separation, the benzene was distilled out quickly. Black crystals were recrystallized from benzene–heptane (yield, 0.6 g). Found: C, 49.80; N, 17.43; H, 4.20%. Calcd for $MoC_{26}N_8O_7H_{28}$: C, 49.69; N, 17.82; H, 4.49%.

Procedure for the Determination of Molybdenum(VI). A 10-cm^3 portion of a sample solution containing up to 19.0 μg was placed in a 100-cm^3 separatory funnel. To the solution, 10 cm^3 of 3.00×10^{-3} mol dm^{-3} Hdpco in benzene was then added. The pH of the solution was adjusted to 2.0 before placing the molybdenum(VI) solution in the separatory funnel. The solutions were vigorously shaken for 10 min. After the phase separation, the organic phase was transferred to a 10-mm cell. Within 30 min after the separation, the absorbances of the organic phases were measured at 545 nm against a reagent blank obtained in the same way.

Results and Discussion

Extraction of Molybdenum(VI) with Hdpco. Figure 1 represents the effect of the pH on the extraction of 8.00×10^{-5} mol dm^{-3} molybdenum(VI) with $(1-3)\times10^{-3}$ mol dm^{-3} Hdpco into chloroform. The optimum pH range is 2—3. The extractability decreased on both sides of the optimum pH range. Similar results were

obtained for benzene and tbp. For 8.00×10^{-5} mol dm^{-3} molybdenum(VI), the distribution curve of the Mo-$(OH)_6$ species[7] was very similar to these extraction—pH curves.

The proton-dissociation constant (pK_a) of Hdpco in an aqueous solution has been reported to be about 8.[8] Under these experimental conditions, all the species of Hdpco distributed in the aqueous phase should exist in a neutral form. The extraction—pH curve shown in Fig. 1 can not be explained by considering the equilibrium of the proton-dissociation of Hdpco in the aqueous phase. The results obtained indicates that a species of $Mo(OH)_6$ other than the molybdenum(VI) species such as $Mo(OH)_5(H_2O)^+$ and $Mo(OH)_5O^-$ is responsible for the extraction of molybdenum(VI) with Hdpco.

The number of molecules of Hdpco involved in the molybdenum(VI)-dpco complex extracted can be obtained from the slope of a plot of log D *vs.* log $[Hdpco]_0$. The result is shown in Fig. 2. The straight lines with the slope of 2.0 suggest that two molecules of Hdpco are involved in the extraction

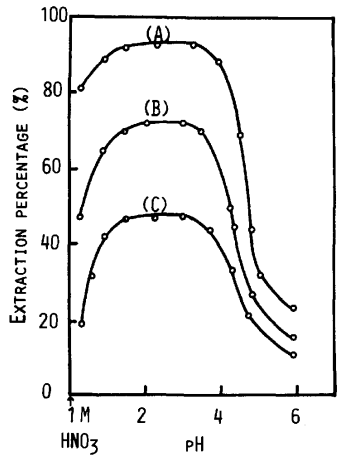

Fig. 1. Effect of pH on extraction of molybdenum(VI) with Hdpco into chloroform.
Mo^{VI}: 8.00×10^{-5} mol dm^{-3}. Hdpco: (A), 3.00×10^{-3} mol dm^{-3}; (B), 2.00×10^{-3} mol dm^{-3}; (C), 1.00×10^{-3} mol dm^{-3}.

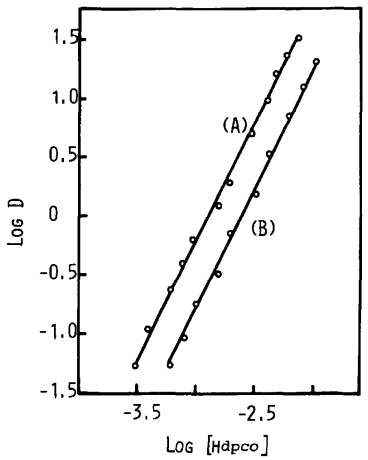

Fig. 2. Relationship between log D and log [Hdpco].
Mo^{VI}: 8.00×10^{-5} mol dm^{-3}. pH: (A) 1.9, (B) 1.0 mol dm^{-3} HNO_3. Organic solvent: chloroform.

of one molybdenum(VI) atom. Similarly, a straight line with a slope of 2.0 was also obtained for benzene. Thus, the ratio of molybdenum(VI):dpco in the molybdenum(VI)-dpco complex extracted into chloroform and benzene agreed with that of the isolated complex, $MoO_2(dpco)_2$. For tbp, on the other hand, the plots of log D *vs.* log [Hdpco] gave straight lines with a slope between 1.2 and 1.7 over the range from 1.0 mol dm^{-3} HNO_3 to pH 4.3 (Fig. 3). Molybdenum(VI) may be extracted with Hdpco into tbp as a mixture of $MoO_2(dpco)_2$ and $MoO_2(dpco)$-(OH)(tbp).

Absorption Spectra of Molybdenum(VI)-dpco Complex. The absorption maximum of isolated $MoO_2(dpco)_2$ appeared at 545 nm in chloroform, benzene, or tbp. However, the absorption spectra of the molybdenum-

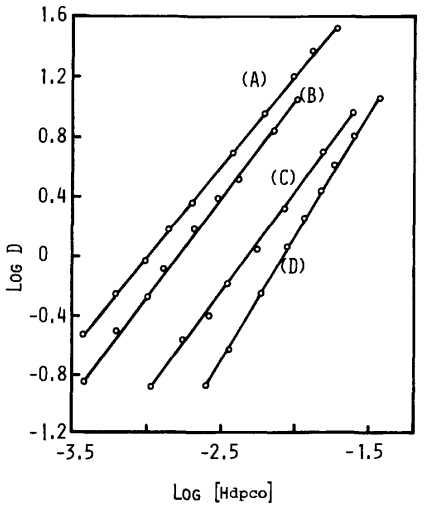

Fig. 3. Relationship between log D and log [Hdpco].
Mo^{VI}: 8.00×10^{-5} mol dm^{-3}. Organic solvent: tbp. pH: (A) 1.9, (B) 1.0, (C) 1.0 mol dm^{-3} HNO_3, (D) pH 4.3.

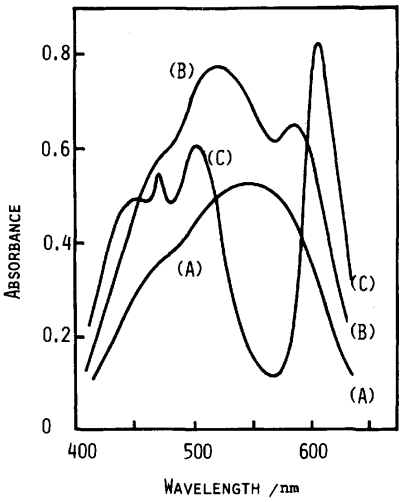

Fig. 4. Absorption spectra of extracted molybdenum(VI)-dpco complex.
Mo^{VI}: 4.00×10^{-5} mol dm^{-3}. HNO_3: 0.10 mol dm^{-3}; Organic solvent: chloroform. Hdpco: (A) 1.00×10^{-3} mol dm^{-3}; (B) 1.50×10^{-3} mol dm^{-3}; (C) 3.00×10^{-3} mol dm^{-3}.

(VI)-dpco complex extracted into chloroform depended on the (1—3)$\times10^{-3}$ mol dm^{-3} Hdpco concentration (Fig. 4) and also on the pH (Fig. 5). The absorption spectrum of the molybdenum(VI) dpco complex extracted with 2.00×10^{-3} mol dm^{-3} of Hdpco at pH 2.3 gave the three peaks at 470, 500, and 610 nm. The absorption maximum of the molybdenum(VI)-dpco complex extracted with 3.00×10^{-3} mol dm^{-3} of Hdpco into tbp (Fig. 6) and benzene appeared at *ca.* 545 nm. The absorption spectra of the extracted molybdenum-(VI)-dpco complex depended on the organic solvent used. The addition of an excess Hdpco to isolated

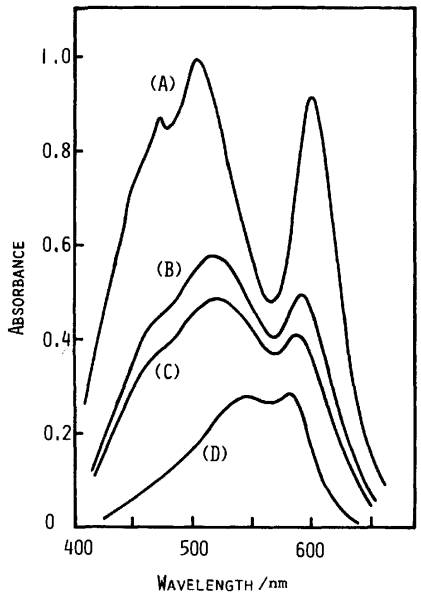

Fig. 5. Absorption spectra of extracted molybdenum (VI)-dpco complex.
Mo^{VI}: 4.00×10^{-5} mol dm^{-3}. Hdpco: 2.00×10^{-3} mol dm^{-3}; Organic solvent: chloroform. pH (A) 2.3; (B) 1.0 mol dm^{-3} HNO_3, (C) 4.5; (D) 5.0.

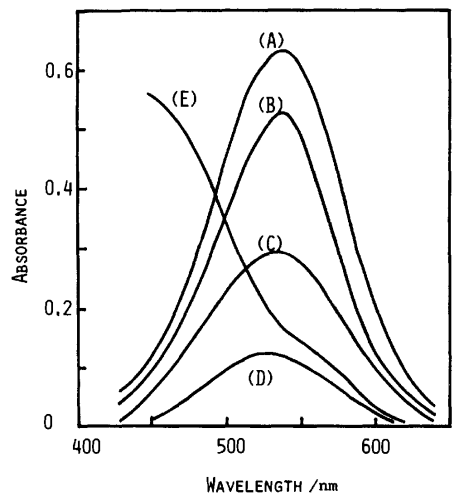

Fig. 6. Absorption spectra extracted molybdenum(VI)-dpco complex into tbp and 1.00×10^{-3} mol dm^{-3} Hdpco (E).
Mo^{VI}: 2.00×10^{-5} mol dm^{-3}. Hdpco: 3.00×10^{-3} mol dm^{-3}. pH: (A) 1.9; (B) 0.30 mol dm^{-3} HNO_3; (C) 1.0 mol dm^{-3} HNO_3; (D) 4.4.

$MoO_2(dpco)_2$ in chloroform, benzene, or tbp caused an absorption spectral change, giving spectra similar to those of the molybdenum(VI)-dpco complex extracted with 3.00×10^{-3} mol dm^{-3} of Hdpco. This abnormal absorption spectral behavior probably results from the reaction of the extracted $MoO_2(dpco)_2$ with free Hdpco in the organic phase. The structure and composition of the molybdenum(VI)-dpco complex extracted with a large excess of Hdpco were not ascertained.

In general, molybdenum(VI) complexes of organic ligands involve a *cis*-MoO_2^{2+} structure.[9,10] A *cis*-MoO_2^{2+} structure for $MoO_2(dpco)_2$ may be proposed in spite of the lack of any direct proof supporting a *cis*-structure.

Extraction Constant for the Extraction of $Mo(OH)_6$ with Hdpco. As has been mentioned above, $Mo(OH)_6$ would be a more reactive species toward Hdpco than $Mo(OH)_5(H_2O)^+$ and $Mo(OH)_5O^-$, which exist at pH 2.0. At the optimum pH of 1.9—2.5, molybdenum(VI) is present predominantly as $Mo(OH)_6$.[7] Therefore, the equation which best represents the extraction equilibrium at pH 2.0 is perhaps:

$$Mo(OH)_6 + 2Hdpco \overset{K_{ex}}{\rightleftharpoons} MoO_2(dpco)_2,$$

with the extraction constant:

$$K_{ex} = \frac{[MoO_2(dpco)_2]_o}{[Mo(OH)_6][Hdpco]_o^2},$$

where the subscript o refers to the organic phase. The values of K_{ex} for chloroform and benzene were determined to be 7.9×10^6 and 3.8×10^6 mol^{-2} dm^6, respectively at 20 °C. The value of K_{ex} for benzene was about 50 times that for chloroform. It was also found that the extractability of the molybdenum(VI)-dpco complex into chloroform was better than that into tbp, though the K_{ex} for tbp was not determined.

Back-extraction of Molybdenum(VI)-dpco Complex. The back-extraction of the molybdenum-(VI)-dpco complex extracted into chloroform, benzene, or tbp with aqueous solutions of various pHs was studied by the following procedure. Ten cm^3 of a molybdenum(VI)-dpco complex solution, which had

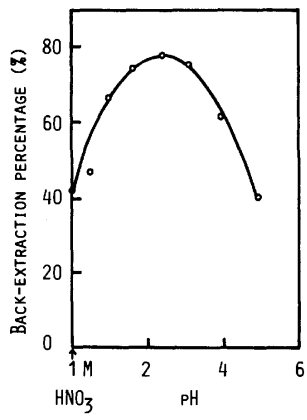

Fig. 7. Effect of pH on back-extraction of molybdenum-(VI)-dpco complex extracted into chloroform.
Mo^{VI}: 8.00×10^{-5} mol dm^{-3}. Hdpco: 2.00×10^{-3} mol dm^{-3}. pH values were adjusted by using nitric acid solution.

been prepared by shaking 8.00×10^{-5} mol dm^{-3} of molybdenum(VI) solution with 2.00×10^{-3} mol dm^{-3} of Hdpco in an organic solvent at pH 1.9, was shaken with 10-cm^3 portions of aqueous solutions of various pHs for 60 min. The results are shown in Fig. 7. The back-extraction–pH curve, was quite similar to that of the forward-extraction–pH curve, indicating that the extraction equilibrium is reversible. For benzene and tbp, similar results were obtained.

Infrared Spectrum of MoO_2(dpco)$_2$. The infrared spectrum of $MoO_2(dpco)_2$ was distinctly different from that of Hdpco. The free Hdpco showed the strong band assigned to the carbon–oxygen vibration at 1705 cm^{-1}. In the case of $MoO_2(dpco)_2$, the band of the carbon–oxygen vibration disappeared completely. The dpco in $MoO_2(dpco)_2$ must be present in the enol configuration. The infrared spectrum of $MoO_2(dpco)_2$ was quite similar to that of $Cr(dpco)(H_2O)_4^{2+}$.[11] The three weak bands at 620, 610, and 595 cm^{-1} for $Cr(dpco)(H_2O)_4^{2+}$ were ascribed to the vibrational chromium–oxygen band.[6] The two weak bands at 600 and 630 cm^{-1} for $MoO_2(dpco)_2$ may be assigned to the vibrational molybdenum–oxygen bands. The molybdenum(V) oxo complexes of 2-methyl-8-quinolinol, $(C_{10}H_8NO)_4Mo_2O_3$, $(C_{10}H_8NO)_2MoO(OH)$, and $(C_{10}H_8NO)_2Mo_2O_4$, showed vibrational molybdenum–oxygen bands at 932—945, 935—945, and 930—945 cm^{-1} respectively.[11] The strong broad band between 900 and 940 cm^{-1} for $MoO_2(dpco)_2$ may be assigned to the molybdenum–oxygen stretching.

Determination of Molybdenum(VI). Molybdenum(VI) was determined based on the foregoing procedure. The method obeyed Beer's law at molybdenum(VI) concentrations from 1.50 to 19.0 μg/10 cm^3, within a relative error of ±4%. The molar extinction coefficient was 5.1×10^4 dm^3 mol cm^{-1} at 545 nm. The effects of various metal ions on the determination of 9.6 μg/10 cm^3 molybdenum(VI) were also examined. The presence of such metal ions as cobalt(II), zinc(II), nickel(II), manganese(II), lead(II), and tungsten(VI) can be tolerated in amounts up to 2.5×10^2 μg/10 cm^3, within a relative error of ±5%. The presence of amounts of iron(III), tin(II), and zirconium(IV) equal to that of molybdenum(VI) can be tolerated below a relative error of 5%. The interference of 20 μg/10 cm^3 of copper(II) can be masked in the presence of 0.01 mol dm^{-3} of sodium hydrogensulfite. The present method was more sensitive than the thiocyanate method[12], the dithiol method[13], the oxinate method[14], and the flavon-3-ol-2′-sulfonate method[10], but less sensitive than the pyrogallol red method[15] and 3,4-dihydroxyazobenzene method.[16]

References

1) S. Balt and E. V. Dalen, *Anal. Chim. Acta*, **30**, 434 (1964).
2) K. De Anil and S. Chittarantan, *J. Inorg. Nucl. Chem.*, **31**, 2257 (1969).
3) A. B. Blake, F. A. Cotton, and J. S. Wood, *J. Am. Chem. Soc.*, **86**, 3024 (1964).
4) L. G. Gavrilova and Yu. A. Zolotov, *Zh. Anal. Khim.*, **25**, 1054 (1970).
5) P. Krumholz and E. Krumholz, *Monatsh. Chem.*, **70**, 431 (1937) (*Chem. Abstr.*, **32**, 1267 (1938)).
6) G. J. Willems and Th. Zeegers-Huyskens, *Ann. Soc. Chim. Polonorum*, **50**, 1973 (1976).
7) L. G. Sillén, *Chem. Listy*, **55**, 1021 (1964).
8) G. J. Willems and C. J. De Ranter, *Anal. Chim. Acta*, **68**, 111 (1974).
9) K. H. Tytlo and O. Glemser, *Adv. Inorg. Chem. Radiochem.*, **19**, 239 (1976).
10) K. Yamamoto, J. Hara, and K. Ohashi, *Anal. Chim. Acta*, **135**, 173 (1982).
11) R. Lozano, A. Doadrio, and A. L. Doadrio, *Polyhedron*, **1**, 163 (1982).
12) C. E. Crouthamel and C. E. Johnson, *Anal. Chem.*, **26**, 1284 (1954).
13) L. J. Clark and J. H. Axley, *Anal. Chem.*, **27**, 2000 (1955).
14) K. Motojima, *Bunseki Kagaku*, **11**, 47 (1962).
15) T. Takeuchi and Y. Shijo, *Bunseki Kagaku*, **15**, 473 (1966).
16) Y. Wakamatsu, *Bunseki Kagaku*, **29**, 472 (1980).

 © 1984 The Chemical Society of Japan Bull. Chem. Soc. Jpn., 57, 3134—3138 (1984) [Vol. 57, No. 11

Preparation, and Thermal and Electronic Properties of Double Complex Salts and Cyanide-bridged Complexes Containing Cationic Copper(II) Complexes and Hexacyanoferrate(II) Ion

Masatatsu SUZUKI and Akira UEHARA*

Department of Chemistry, Faculty of Science, Kanazawa University, Kanazawa 920

(Received May 26, 1984)

Reaction of copper(II) ion with hexacyanoferrate(II) ion, $[Fe(CN)_6]^{4-}$, in an aqueous solution containing such an amine as en (1,2-ethanediamine), tn (1,3-propanediamine), dien (bis(2-aminoethyl)amine), or dpt (bis(3-aminopropyl)amine), gave two types of complexes: Double complex salts, $[Cu(en \text{ or } tn)_2]_2[Fe(CN)_6]\cdot nH_2O$ (n=5—8), and cyanide-bridged complexes, $[(Cu(dien \text{ or } dpt))_2(NC)_2Fe(CN)_4]\cdot 4H_2O$. The infrared spectra of the complexes in the ν_{CN} region revealed that the complexes, $[(Cu(dien \text{ or } dpt))_2(NC)_2Fe(CN)_4]\cdot 4H_2O$, contain cyanide bridges, while in $[Cu(en \text{ or } tn)_2]_2[Fe(CN)_6]\cdot nH_2O$, no cyanide bridge is present. The thermal reactions of the complexes in the solid state were investigated by means of derivatography under dynamic conditions (D conditions). It was found that dehydration from $[Cu(en)_2]_2[Fe(CN)_6]\cdot nH_2O$ resulted in formation of cyanide bridge in the apical position of square planer $[Cu(en)_2]^{2+}$. For $[(Cu(dien \text{ or } dpt))_2(NC)_2Fe(CN)_4]\cdot 4H_2O$, dehydration resulted in the formation of additional cyanide bridges. All the complexes showed metal to metal (iron(II) to copper(II)) charge-transfer transitions (MMCT) in the near ultraviolet or visible region. The complexes, $[Cu(en \text{ or } tn)_2]_2[Fe(CN)_6]\cdot nH_2O$, exhibited the outer sphere iron(II) to copper(II) charge-transfer bands (OSMMCT) in the near ultra-violet region. $[(Cu(dien \text{ or } dpt))_2(NC)_2Fe(CN)_4]\cdot 4H_2O$ and the dehydrated complexes prepared by thermal reaction showed the inner-sphere iron(II) to copper(II) charge transfer bands (ISMMCT) in the visible region. A good correlation was observed between the energies of the MMCT and the d-d band maxima of copper(II) ions.

Reaction of various metal ions with $[Fe(CN)_6]^{4-}$ forms a series of Prussian Blue type complexes which have cyanide-bridged structure and are polymeric in nature.[1-4] It is also known that $[Fe(CN)_6]^{4-}$ forms cation-anion ion pair with various cationic complexes in solution and they tend to form so called double complex salts or cyanide-bridged complexes which consist of discrete structural units.[5-7] These complexes are of paticular interest in studying the electron-transfer phenomena in the solid state. Unfortunately, no well characterized complex has been known except for those containing cationic Ru^{III} complexes as counter part or counter ion.[5-7] Further studies are needed for advanced elucidation of the solid state electron transfer of metal complexes. In this study, we prepared new double complex salts and cyanide-bridged complexes containing cationic copper(II) complexes and hexacyanoferrate(II) anion, $[Cu(en \text{ or } tn)_2]_2[Fe(CN)_6]\cdot nH_2O$ (n=5—8) and $[(Cu(dien \text{ or } dpt))_2(NC)_2Fe(CN)_4]\cdot 4H_2O$, where en represents 1,2-ethanediamne, tn 1,3-propanediamine, dien bis(2-aminoethyl)amine, and dpt bis(3-aminopropyl)amine. Their structures and electronic properties were investigated by means of infrared and electronic spectroscopies.

Uehara *et al.* demonstrated that the thermal reaction of the double complex salts such as $[(Cr \text{ or } Co)(OH_2)(NH_3)_5][(Cr \text{ or } Co)(CN)_6]$ in the solid state afforded various types of the cyanide-bridged complexes.[8,9] The thermal cyanide-bridging reactions are highly dependent on the nature of the metal ions contained in the cationic and anionic moieties. It is well known that the stereochemistry of the copper(II) complexes is flexible with respect to the coordination number and geometry.[10] Therefore, the solid state thermal reaction of the present double complex salts and cyanide-bridged complexes containing copper(II) ions is also expected to form various types of cyanide-bridged complexes. The thermal cyanide-bridging reaction of the present complexes is also one of the subjects of this study.

Experimental

Preparation of Complexes. *$[Cu(en)_2]_2[Fe(CN)_6]\cdot nH_2O$ (**1a**) (n=5—8).* To a solution of 1 mmol of $K_4[Fe(CN)_6]\cdot 3H_2O$ in 20 cm^3 of water was added a solution containing 2 mmol of $Cu(NO_3)_2\cdot 6H_2O$ and 5 mmol of en in 20 cm^3 of water. To the resulting mixture was added 10 cm^3 of methanol with stirring. The solution was allowed to stand overnight to give violet crystals, which were collected by filtration, washed with cold water, and air-dried. The complex salt contained 5—8 mol of water depending on the experimental conditions. Found: C, 24.95; H, 6.33; N, 29.45%. Calcd for the penta hydrate $C_{14}H_{42}N_{14}O_5Cu_2Fe$ (MW 669.57): C, 25.11; H, 6.32; N, 29.29%.

*$[Cu(tn)_2]_2[Fe(CN)_6]\cdot 5H_2O$ (**2a**).* The complex was prepared in a similar way to that of **1a**. Dark blue crystals were collected by filtration, washed with cold water, and air-dried. Found: C, 29.98; H, 6.92; N, 27.13%. Calcd for $C_{18}H_{50}N_{14}O_5Cu_2Fe$ (MW 725.67): C, 29.79; H, 6.94; N, 27.03%.

*$[(Cu(dien))_2(NC)_2Fe(CN)_4]\cdot 4H_2O$ (**3a**).* To a solution of 1 mmol of $K_4[Fe(CN)_6]\cdot 3H_2O$ in 20 cm^3 of water was added a solution containing 2 mmol of $Cu(NO_3)_2\cdot 6H_2O$ and 2.5 mmol of dien in 20 cm^3 of water. After a few minutes dark green crystals began to appear. The crystals deposited were collected by filtration, washed with cold water, and air-dried. Found: C, 27.08; H, 5.57; N, 27.30%. Calcd for $C_{14}H_{34}N_{12}O_4Cu_2Fe$ (MW 617.48): C, 27.23; H, 5.50; N, 27.23%.

*$[(Cu(dpt))_2(NC)_2Fe(CN)_4]\cdot 4H_2O$ (**4a**).* The complex was prepared in a similar way to that of **3a**. Dark green crystals deposited from an aqueous solution turned blue upon drying in air. Found: C, 32.05; H, 6.02; N, 25.13%. Calcd for $C_{18}H_{42}N_{12}O_4Cu_2Fe$ (MW 673.59): C, 32.09; H, 6.29; N, 24.69%.

Dehydrated Complexes. The dehydrated complexes, **1b**, **3b**, and **4b**, were obtained by heating **1a**, **3a**, and **4a**, respectively, for a given period of time at constant temperature with thermobalance (*vide infra*). Since the dehydrated

complexes were hygroscopic more or less, the measurements were carried out as soon as possible after preparations.

Measurements. The thermal reactions of the complexes were traced under dynamic conditions (D conditions) by using MOM Type-OD-102 Derivatograph. The measurements were carried out under a constant flow of nitrogen gas at heating rate of 2 °C min^{-1}. The electronic spectra in solution and nujol mull were measured with a Jasco UVIDEC 505 UV/VIS recording digital spectrophotometer and those in powder on a Hitachi EPU-2A spectrophotometer. Infrared spectra were obtained by a KBr-disk method with a Jasco A-3 infrared spectrophotometer.

The electronic spectra of **1a**, **2a**, and **4a** in aqueous solution were measured by the addition of 0.1 mol equivalent (against Cu^{II} concentration) of the corresponding amine to suppress the formation of reddish brown colloidal suspension, which is probably $Cu_2[Fe(CN)_6]\cdot nH_2O$. The electronic spectrum of **3a** in an aqueous solution could not be obtained because of its low solubility.

Results and Discussion

Derivatography. The derivatograms of the en complex, **1a**, revealed that the complex contains 5—8 mol of water depending on the preparative conditions. The representative derivatogram of the pentahydrate complex is given in Fig. 1. The TG curve of the complex shows weight loss at 60—100 °C and then a clear plateau is obtained. This weight loss corresponds to evolution of water molecules. The dpt complex, **4a**, also shows a similar behavior to that of **1a**: Four moles of water are evolved at 30—100 °C and then a clear plateau appears. The appearance of the clear plateaus in the TG curves indicates that the dehydrated complexes of **1a** and **4a** are easily obtained by thermal reaction. For the dien complex, **3a**, the evolution of 4 mol of water is seen up to *ca.* 130 °C, immediately followed by a slow successive weight loss. Therefore, it seems difficult to obtain the dehydrated complex in pure state under dynamic conditions. Preliminary experiments, however, showed that the isothermal heating of the complex at 120 °C for 5 h gave considerably pure anhydrous complex, which was used for infrared and electronic spectral measurements. The complicated TG curve of the tn complex, **2a**, suggests that it is difficult to obtain the dehydrated complex. All the complexes decomposed in complicated manners after dehydration. Although the decomposition products could not be characterized, the compounds obtained by heating at 200 °C for 0.5 h still showed the strong ν_{CN} bands at 2080—2040 cm^{-1}, which are indicative of the presence of $[Fe(CN)_6]^{4-}$ moiety.[11] This implies that the decompositions occur in the Cu^{II} moieties, but not in $[Fe(CN)_6]^{4-}$ moiety.

It should be noted that the decompositions of

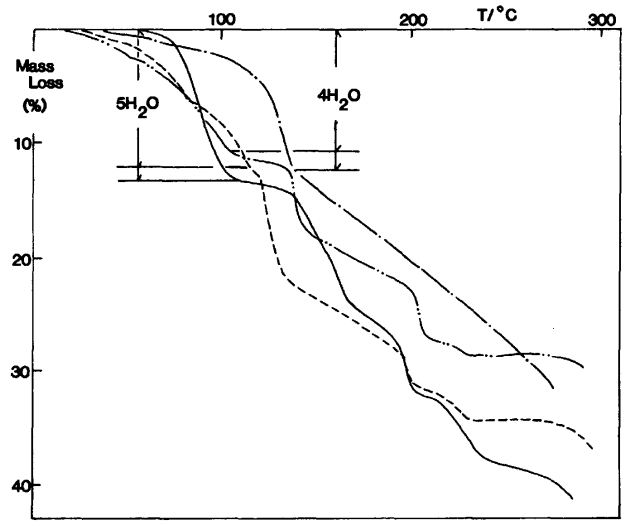

Fig. 1. Derivatograms of $[Cu(en)_2]_2[Fe(CN)_6]\cdot 5H_2O$ (**1a**) (——), $[Cu(tn)_2]_2[Fe(CN)_6]\cdot 5H_2O$ (**2a**) (----), $[(Cu(dien))_2(NC)_2Fe(CN)_4]\cdot 4H_2O$ (**3a**) (—·—), and $[(Cu(dpt))_2(NC)_2Fe(CN)_4]\cdot 4H_2O$ (**4a**) (—··—).

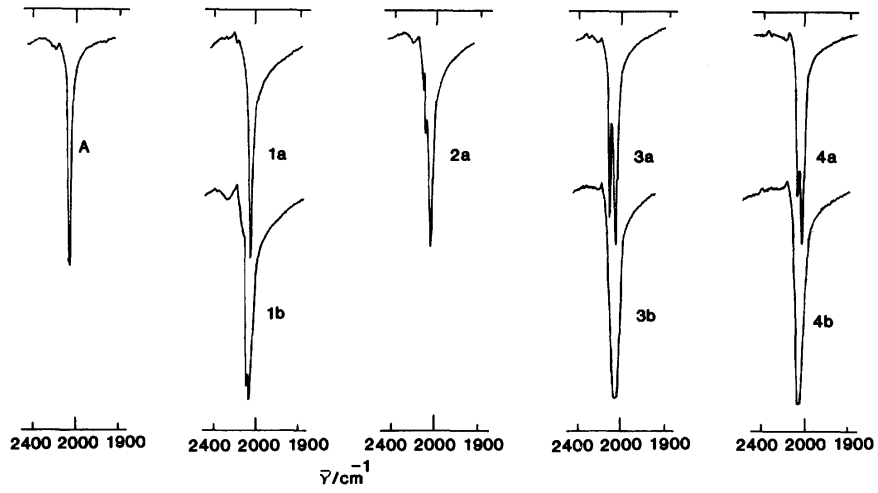

Fig. 2. Infrared spectra of $K_4[Fe(CN)_6]\cdot 3H_2O$ (**A**), $[Cu(en)_2]_2[Fe(CN)_6]\cdot 5H_2O$ (**1a**), dehydrated complex (**1b**) of **1a**, $[Cu(tn)_2]_2[Fe(CN)_6]\cdot 5H_2O$ (**2a**), $[(Cu(dien))_2(NC)_2Fe(CN)_4]\cdot 4H_2O$ (**3a**), dehydrated complex (**3b**) of **3a**, $[(Cu(dpt))_2(NC)_2Fe(CN)_4]\cdot 4H_2O$ (**4a**), and dehydrated complex (**4b**) of **4a**.

$[Cu(en)_2]^{2+}$ and $[Cu(tn)_2]^{2+}$ moieties began to take place at *ca.* 140 °C and 120 °C, respectively. $[Cu(en)_2]SO_4$ and $[Cu(tn)_2]SO_4$ have been shown to be stable up to 250 °C and 200 °C, respectively.[12] It is well known that the thermal stabilities of complexes are highly dependent on the counter ion.[12] Low stabilities of the present complexes may be attributable to an effect of the counter ion, $[Fe(CN)_6]^{4-}$, *i.e.*, it is likely that coordination ability of nitrogen atom of NC-Fe to copper(II) ion is strong enough to weaken the Cu-en and Cu-tn bonds (*vide infra*). This is in line with the fact that the complexes easily decomposed in an aqueous solution to form reddish brown colloidal suspension, which is probably $Cu_2[Fe(CN)_6]\cdot nH_2O$.

$[Cu(en\ or\ tn)_2]_2[Fe(CN)_6]\cdot nH_2O$. The infrared spectrum of $[Cu(en)_2]_2[Fe(CN)_6]\cdot 5H_2O$ is given in Fig. 2. The complex shows a strong ν_{CN} band at 2040 cm^{-1}, which is essentially identical to that of $K_4[Fe(CN)_6]\cdot 3H_2O$. This clearly indicates that no significant interaction is present between $[Cu(en)_2]^{2+}$ and $[Fe(CN)_6]^{4-}$ moieties, and the complex can be formulated as double complex salt, $[Cu(en)_2]_2[Fe(CN)_6]\cdot 5H_2O$. The electronic spectrum of the complex in the solid state exhibits a band at 18300 cm^{-1} and a shoulder at *ca.* 25000 cm^{-1} (Fig. 3). The former band is assigned to the d-d transitions of $[Cu(en)_2]^{2+}$ moiety. A shoulder at *ca.* 25000 cm^{-1} is not observed in the electronic spectra of the individual complexes, $[Cu(en)_2]^{2+}$ and $[Fe(CN)_6]^{4-}$. Therefore, this shoulder can be assigned to the outer sphere metal to meal (iron(II) to copper(II)) charge transfer transition (OSMMCT). The electronic spectrum in water (*ca.* 5×10^{-3} M. (1 M=1 mol dm^{-3})) exhibits two bands at 17800 cm^{-1} and 31200 cm^{-1} with a very small shoulder at *ca.* 24000 cm^{-1} (Fig. 3). The two bands are due to the d-d transitions of $[Cu(en)_2]^{2+}$ and $[Fe(CN)_6]^{4-}$, respectively. The very small shoulder at *ca.* 24000 cm^{-1} is assigned to OSMMCT. Such low intensity of the shoulder is ascribed to the low ion pair formation under the experimental conditions and to the low oscillator strength expected for the OSMMCT.[13]

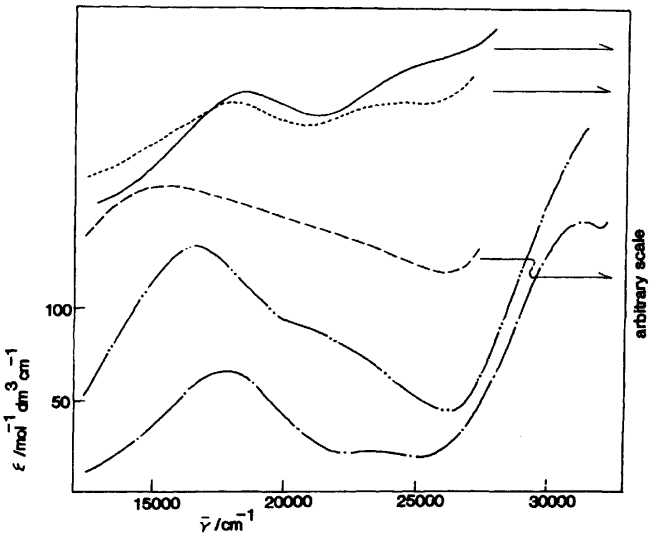

Fig. 3. Nujol mull spectra of $[Cu(en)_2]_2[Fe(CN)_6]\cdot 5H_2O$ (**1a**) (——), dehydrated complex (**1b**) of **1a** (·····), and $[Cu(tn)_2]_2[Fe(CN)_6]\cdot 5H_2O$ (**2a**) (----), and absorption spectra of $[Cu(en)_2]_2[Fe(CN)_6]\cdot 5H_2O$ (**1a**) (—·—) and $[Cu(tn)_2]_2[Fe(CN)_6]\cdot 5H_2O$ (**2a**) (—···—) in water.

As was mentioned before, 5 mol of water of **1a** is evolved at 60—100 °C in the solid state. During the dehydration process, the original violet complex turned blue. The dehydrated complex, **1b**, shows two ν_{CN} bands at 2065 cm^{-1} and 2040 cm^{-1} (main band) (Fig. 2). It is well known that if the M-CN group forms a M-CN-M′ type bridge, ν_{CN} shifts in a higher wave number region.[14] Thus in the dehydrated complex, Fe-CN-Cu type bridge is formed, *i.e.*, nitrogen atom of NC-Fe coordinates to the apical position of square planer $[Cu(en)_2]^{2+}$. At the present stage, however, it is not clear whether the cyanide bridges are formed in both of $[Cu(en)_2]^{2+}$ ions. A coordination to the apical position of square planer copper(II) complex has been known to be weak and termed as "semi-coordination".[15] A splitting of ν_{CN} band of the dehydrated complex, **1b**, (*ca.* 25 cm^{-1}) is much smaller than that of the dien complex, **3a**, (*ca.* 60 cm^{-1}). This smaller splitting of ν_{CN} band of **1b** may be interpreted in terms of a weaker coordination of nitrogen atom of NC-Fe to copper(II) ion (*vide infra*).

The dehydrated complex, **1b**, shows two bands at 17700 cm^{-1} and 23800 cm^{-1} in the solid state (Fig. 3). The former band is assigned to the d-d transitions of $[Cu(en)_2]^{2+}$ and the latter is ascribed to inner sphere MMCT (ISMMCT). The red shift of the d-d band maximum of Cu^{II} moiety in the dehydrated complex also supports a coordination of nitrogen atom of NC-Fe to the apical position of $[Cu(en)_2]^{2+}$. Hathaway *et al.* studied the electronic spectra of various $[Cu(en)_2]X_2$ type complexes (X=Cl^-, Br^-, NO_3^-, *etc.*).[16] The energies of the d-d band maxima of the complexes have been shown to be highly dependent on the degree of interaction between X and $[Cu(en)_2]^{2+}$ in the apical position. The energy of the band maximum of the hydrated complex, **1a**, is comparable to that of $[Cu(en)_2](NO_3)_2$, where NO_3^- ions weakly coordinate to the square planer $[Cu(en)_2]^{2+}$ in the apical position. Thus it is probable that in the hydrated complex, semi-coordination of water molecules to $[Cu(en)_2]^{2+}$ in the apical position is present. During the dehydration process, water molecules coordinated are removed and subsequently nitrogen atom of NC-Fe comes into the apical position of $[Cu(en)_2]^{2+}$. The observed red shift of the d-d band maximum of $[Cu(en)_2]^{2+}$ moiety upon semi-coordination of nitrogen atom of NC-Fe implies that the ligand field strength of nitrogen atom of NC-Fe is stronger than that of H_2O. A color change from violet to blue was also observed in the solid **1a** on standing it for several days at room temperature without weight loss. This fact suggests that the coordination ability of nitrogen atom of NC-Fe is stronger than that of H_2O.

The tn complex, **2a**, shows a strong ν_{CN} band at 2040 cm^{-1} with two small bands at 2150 and 2080 cm^{-1} (Fig. 2). The small bands may be ascribed not to cya-

nide bridge, but to lower symmetry of $[Fe(CN)_6]^{4-}$ moiety in the crystals. Therefore, we believe that no significant interaction between $[Cu(tn)_2]^{2+}$ and $[Fe(CN)_6]^{4-}$ moieties is present and the complex can be formulated as double complex salt, $[Cu(tn)_2]_2[Fe(CN)_6]\cdot 5H_2O$. The electronic spectrum of the complex in the solid state exhibits a very broad band in the visible region, which may be due to an overlapping of the d-d band of $[Cu(tn)_2]^{2+}$ and OSMMCT (Fig. 3). The position of the OSMMCT is not clear in this complex. On the other hand, the electronic spectrum in an aqueous solution shows the d-d band of $[Cu(tn)_2]^{2+}$ at 16700 cm^{-1} and a shoulder at *ca.* 22000 cm^{-1}, which is assigned to the OSMMCT.

[(Cu(dien or dpt))$_2$(NC)$_2$Fe(CN)$_4$]·4H$_2$O. The dien complex, **3a**, shows a splitting of ν_{CN} band at 2110 and 2050 cm^{-1} (main band), indicating the presence of cyanide bridge (Fig. 2). A possible structure of this complex is a discrete trinuclear Cu-NC-Fe-CN-Cu structure. The splitting of the ν_{CN} (60 cm^{-1}) is much larger than that of the dehydrated en complex, **1b**. Such a large difference in ν_{CN} splitting between **1b** and **3a** seems to be attributable to a strength of copper(II)-nitrogen bonding (Cu-NC-Fe), *i.e.*, the stronger the Cu-NC bonding, the larger the ν_{CN} splitting. In the case of the en complex, **1b**, nitrogen atom of NC-Fe binds to d_{z^2} orbital of square planar $[Cu(en)_2]^{2+}$ (out of plane bonding), whereas it is possible that in the dien complex, **3a**, nitrogen atom of NC-Fe binds to $d_{x^2-y^2}$ orbital (in plane bonding); the inplane bonding is much stronger than the out of plane bonding.

The complex shows the d-d band maximum of Cu^{II} moiety at 15900 cm^{-1} and the ISMMCT at 22000 cm^{-1} in the solid state (Fig. 4). In general, tridentate ligands such as dien and dpt tend to adopt a meridional form in copper(II) complexes.[17] Although a square planar structure having N_4 (dien and NC-Fe) donor set might be a plausible one, the energy of the d-d band maximum of the complex seems to be low for sqaure planar copper(II) complexes with N_4 (dien and NC-Fe) donor set, and this probably suggests that water molecules coordinate to copper(II) ion to form octahedral or five-coordinate structure. The dehydration from the complex caused a color change from green to blue. For the dehydrated complex, **3b**, the splitting of ν_{CN} disappears and the ν_{CN} band becomes broad (Fig. 2). In the dehydrated complex, two more coordination sites are available for the coordination of NC-Fe; therefore, it is likely that in the dehydrated complex, additional one or two cyanide bridges are formed and the strength of Cu-N (NC-Fe) bondings are not identical, resulting in an observed broadening of ν_{CN} band because of overlapping of various ν_{CN} bands. The complex may be polymeric. The d-d band of Cu^{II} moiety of the dehydrated complex becomes a shoulder and ISMMCT shifts to red (Fig. 4).

The dpt complex, **4a**, exhibits a splitting of ν_{CN} band (2090 and 2050 cm^{-1} (main band)) (Fig. 2). The splitting (*ca.* 40 cm^{-1}) is, however, smaller than that of the dien complex (*ca.* 60 cm^{-1}). This implies that the coordination of NC-Fe to Cu^{II} ion is weaker than that in the dien complex, **3a**, *i.e.*, cyanide bridge seems to occur in the apical position. The dpt complex is soluble in water, whereas the dien complex is insoluble at all. This remarkable difference in solubility may reflect a change in structure. This would be reconciled with the result derived from the above infrared spectra.

The bands at 15300 and 19400 cm^{-1} are ascribed to the d-d transitions of Cu^{II} moiety and the ISMMCT, respectively (Fig. 4). The fact that the dpt complex shows the d-d band in lower energy side than the dien complex is attributable to weaker ligand field strength of dpt than that of dien. In the dehydrated complex, **4b**, the splitting of ν_{CN} also disappears

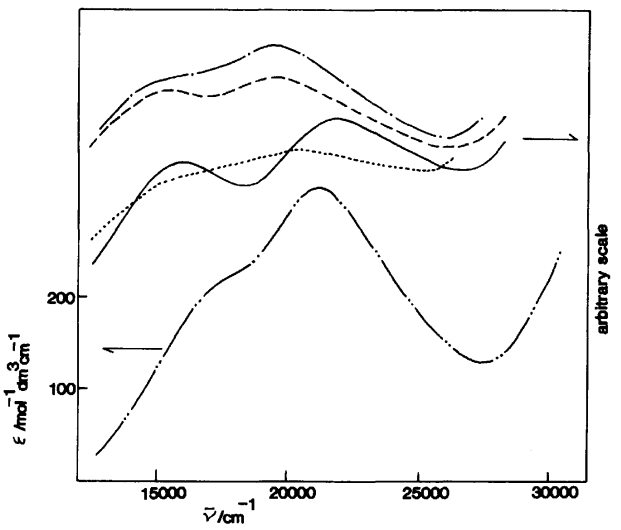

Fig. 4. Nujol mull spectra of $[(Cu(dien))_2(NC)_2Fe(CN)_6]\cdot 4H_2O$ (**3a**) (——), dehydrated complex (**3b**) of **3a** (·····), $[(Cu(dpt))_2(NC)_2Fe(CN)_4]\cdot 4H_2O$ (**4a**) (----), and dehydrated complex (**4b**) of **4a** (—·—), and absorption spectrum $[(Cu(dpt))_2(NC)_2Fe(CN)_4]\cdot 4H_2O$ (—···—) in water.

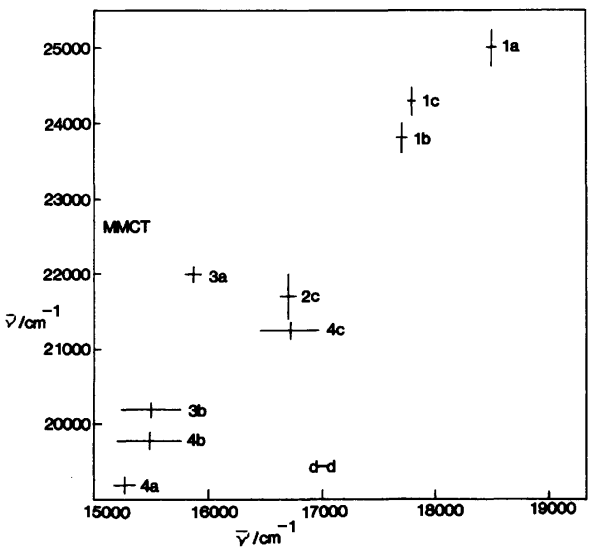

Fig. 5. Correlation between the energies of the d-d band maxima of Cu^{II} moieties and the energies of MMCT.

and the band becomes broad as well as that of the dien complex (Fig. 2). This broadening of ν_{CN} may be also due to the formation of additional cyanide bridges.

The electronic spectrum in an aqueous solution exhibits a strong band at 21300 cm^{-1} with a shoulder at *ca.* 17000 cm^{-1} (Fig. 4). The band at 21300 cm^{-1} is assigned to MMCT. This MMCT band is much more intense than those of the en and tn complexes. This is reasonably interpreted in terms of the presence of Cu-NC-Fe bridge in an aqueous solution as was found in the solid state.

Correlation between MMCT and d-d Transitions. Figure 5 shows a correlation between the energies of MMCT and the d-d band maxima of Cu^{II} moieties. A good correlation is observed. The MMCT of the presnt complexes are assigned to one-electron jump from the t_{2g} orbital of the low spin iron(II) to the $e_g(d_{x^2-y^2})$ orbital of copper(II) ion in octahedral symmetry.[2] Therefore, the energies of the MMCT depend on the energy difference between the $d_{x^2-y^2}$ orbital energy of Cu^{II} ion and t_{2g} orbital energy of Fe^{II} ion. Assuming that the t_{2g} orbital energies of Fe^{II} ions in the present complexes are almost constant, the energies of the MMCT are mainly dependent on the $d_{x^2-y^2}$ orbital energies of Cu^{II} ions; the higher the energy of the d-d band maximum of Cu^{II} moiety, the higher the $d_{x^2-y^2}$ orbital energy and the higher the energy of the MMCT.

Our thanks are due to Prof. R. Tsuchiya for his helpful discussions and encouragement throughout this study.

References

1) M. B. Robin, *Inorg. Chem.*, **1**, 337 (1962).
2) P. S. Braterman, *J. Chem. Soc., (A)*, **1966**, 1472.
3) H. E. Toma, *J. Inorg. Nucl. Chem.*, **38**, 431 (1976).
4) D. B. Brown and D. F. Shriver, *Inorg. Chem.*, **8**, 37 (1969).
5) H. E. Toma, *J. Chem. Soc., Dalton Trans.*, **1980**, 471.
6) J. C. Curtis and T. J. Meyer, *Inorg. Chem.*, **21**, 1562 (1982).
7) A. Vogler and J. Kisslinger, *J. Am. Chem. Soc.*, **104**, 2311 (1982).
8) R. Tsuchiya, S. Nakagawa, A. Uehara, and E. Kyuno, *Bull. Chem. Soc. Jpn.*, **46**, 169 (1973).
9) A. Uehara, S. Terabe, and R. Tsuchiya, *Inorg. Chem.*, **22**, 2864 (1983).
10) B. J. Hathaway and D. E. Billing, *Coord. Chem. Rev.*, **5**, 143 (1970).
11) D. F. Shriver, S. A. Shriver, and S. E. Anderson, *Inorg. Chem.*, **4**, 725 (1965).
12) W. W. Wendlandt and J. P. Smith, "The Thermal Properties of Transition Metal Ammine Complexes," Elsevier Pub. Co., Amsterdam (1967) pp. 132-143.
13) N. S. Hush, *Prog. Inorg. Chem.*, **8**, 391 (1967).
14) K. Nakamoto, "Infrared and Raman Spectra of Inorganic and Coordination Compounds," 3rd ed. Wiley-Interscience, New york (1978) pp. 259—267.
15) D. S. Brown, J. D. Lee, B. G. A. Melson, B. J. Hathaway, I. M. Procter, and A. A. G. Tomlinson, *J. Chem. Soc., Chem. Commum.* **1967**, 369.
16) I. M. Procter, B. J. Hathaway, and P. Nicholls, *J. Chem. Soc., (A)*, **1968**, 1678.
17) N. J. Ray, L. Hulett, R. Sheahan, and B. J. Hathaway, *J. Chem. Soc., Dalton Trans.*, **1981**, 1463.

Preparation and Characterization of $[CoX_2(edpp)_2]^+$(edpp=$NH_2CH_2CH_2P(C_6H_5)_2$, X=Cl^-, Br^-, I^-, NCO^-, NCS^-, N_3^-, NO_2^-) and $[CoX_2(en)(dppe)]^+$(en=$NH_2CH_2CH_2NH_2$, dppe=$(C_6H_5)_2PCH_2CH_2P(C_6H_5)_2$, X=$Cl^-$, Br^-, NCS^-). Crystal Structures of *trans*(NCS,NCS),*cis*(P,P)-$[Co(NCS)_2(edpp)_2]Br\cdot 3H_2O\cdot(CH_3)_2CO$ and *cis*-(NCS,NCS),*trans*(P,P)-$[Co(NCS)_2(edpp)_2]$-$Br\cdot CH_3OH$

Masamichi Atoh, Kazuo Kashiwabara, Haruko Ito,†
Tasuku Ito,† and Junnosuke Fujita*
Department of Chemistry, Faculty of Science, Nagoya University, Chikusa-ku, Nagoya 464
†*Division of Applied Molecular Science, Institute for Molecular Science, Okazaki 444*
(Received June 27, 1984)

Dianionocobalt(III) complexes of the $[CoX_2(edpp)_2]^+$-type (X=Cl^-, Br^-, I^-, NCO^-, NCS^-, N_3^-, NO_2^-) have been prepared, where edpp is (2-aminoethyl)diphenylphosphine. The corresponding $[CoX_2(en)(dppe)]^+$ complexes are rather unstable and have been obtained only for X=Cl^-, Br^-, and NCS^-, where en and dppe denote ethylenediamine and 1,2-bis(diphenylphosphino)ethane, respectively. Except for the NCS^- complex of edpp, only one geometrical isomer has been obtained for all the complexes. Two geometrical isomers of $[Co(NCS)_2(edpp)_2]^+$ have been isolated, and crystal structures of *trans*(NCS,NCS),*cis*(P,P)-$[Co(NCS)_2(edpp)_2]Br\cdot 3H_2O\cdot(CH_3)_2CO$ and *cis*(NCS,NCS),*trans*(P,P)-$[Co(NCS)_2(edpp)_2]Br\cdot CH_3OH$ have been determined by X-ray analyses. The NCS^- ions in these complexes coordinate to the cobalt(III) ion through their nitrogen atoms with nearly linear Co-N-C-S fragments. The Co-P distances in the isomers are similar to one another, but the average Co-NH_2 and Co-NCS distances in the *trans*(NCS,NCS) isomer (2.010 and 1.882 Å) are longer and shorter than those of the *cis*(NCS,NCS) isomer (1.970 and 1.960 Å), respectively. Absorption spectra of all the complexes in solution have been recorded and the results compared with those of related dianionocobalt(III) complexes.

In previous papers, we have reported the preparation[1] and molecular structure[2] of *trans*(Cl,Cl),*cis*(P,P)-$[CoCl_2(edpp)_2]^+$ (edpp=$NH_2CH_2CH_2P(C_6H_5)_2$). The complex will be a useful starting material for preparing various bis(edpp) complexes. For example, it easily reacts with chelate ligands such as acetylacetonate or oxalate ions to afford the $[Co(O-O)(edpp)_2]^{n+}$-type complexes.[1] This paper deals with the $[CoX_2(edpp)_2]$-type complexes obtained by reactions of the dichloro complex with various unidentate anions X^-. There are five possible geometrical isomers of $[CoX_2(edpp)_2]^+$. Except for the NCS^- complex, however, only one isomer has been obtained for all of the complexes. For the NCS^- complex, two geometrical isomers have been isolated and the crystals subjected to X-ray structure analysis in order to determine the geometrical configuration as well as the linkage isomerism of the NCS^- ligand. Some structurally related $[CoX_2(en)(dppe)]^+$ complexes (en=$NH_2CH_2CH_2NH_2$, dppe=$(C_6H_5)_2PCH_2CH_2P(C_6H_5)_2$) have been prepared. Absorption spectra of all the complexes have been recorded and the results compared with those of related diacidato cobalt(III) complexes.

Experimental

The edpp ligand was prepared by the literature method,[3] and handled under a nitrogen atmosphere until it formed cobalt(III) complexes. The dppe ligand was purchased from Strem Chemicals Inc. and used as received. Absorption spectra of the complexes were recorded on a Hitachi 323 spectrophotometer.

The starting complexes, *trans*(Cl,Cl)-$[CoCl_2(edpp)_2]ClO_4$, *trans*-$[CoCl_2(en)(dppe)]ClO_4\cdot H_2O$, *trans*-(P,N)-$[CoCO_3(edpp)_2]$-$Cl\cdot 3.5H_2O$, and $[CoCO_3(en)(dppe)]ClO_4$ were prepared by methods reported previously.[1]

trans*(Br,Br)-[CoBr$_2$(edpp)$_2$]Br·2H$_2$O*. To a methanol solution (20 cm³) of *trans*(P,N)-$[CoCO_3(edpp)_2]Cl\cdot 3.5H_2O$ (100 mg) was added 47% HBr (1.0 cm³) at 5 °C. The resulting brown solution turned green on heating at 60 °C, and then was cooled in an ice bath. On addition of a small amount of water yellow-green crystals were precipitated, collected, washed with water and diethyl ether, and air-dried. Yield: 65 mg(55%). Found: C, 42.12; H, 4.30; N, 3.45%. Calcd for $C_{28}H_{36}N_2Br_3CoO_2P_2$: C, 42.40; H, 4.57; N, 3.53%. The complex is soluble in methanol and CH_2Cl_2, but insoluble in water and diethyl ether.

[CoI$_2$(edpp)$_2$]I. A methanol solution (20 cm³) of *trans*(P,N)-$[CoCO_3(edpp)_2]Cl\cdot 3.5H_2O$ (100 mg) was degassed with nitrogen. To the solution was added colorless 57% HI (2.1 g) purified by passing a column of Dowex 1×8 (I^- form) dropwise at room temperature with stirring in an atmosphere of nitrogen. The color of the solution changed from red to brown, and a brown precipitate appeared. After 30 min the precipitate was filtered, washed with water and diethyl ether, and air-dried. Yield: 47 mg(35%). Found: C, 37.45; H, 3.99; N, 2.99%. Calcd for $C_{28}H_{32}N_2I_3CoP_2$: C, 37.44; H, 3.59; N, 3.12%.

cis*(NCS,NCS)-[Co(NCS)$_2$(edpp)$_2$]Cl·H$_2$O and* trans*(NCS,NCS)-[Co(NCS)$_2$(edpp)$_2$]Cl·1/2(NaCl)·H$_2$O*. A methanol solution (300 cm³) containing *trans*(Cl,Cl)-$[CoCl_2(edpp)_2]ClO_4$ (500 mg) and KNCS (200 mg) was stirred overnight at room temperature. The color of the solution slowly changed from green to dark red. The resulting solution was diluted with methanol (200 cm³) and water (1 dm³), and applied on a column (ϕ3 cm×10 cm) of SP-Sephadex C-25. The adsorbed product was eluted with 0.1 mol dm^{-3} NaCl in water–methanol (1:1), and the eluate was evaporated to half of its original volume at 35 °C under reduced pressure. The complex in the concentrate was extracted with CH_2Cl_2, and the extract was evaporated

to dryness under reduced pressure. The residue was dissolved in the minimum amount of benzene–methanol (3:1), and the solution was chromatographed by use of a column (ϕ3 cm×50 cm) of Sephadex LH-20 and an eluent, benzene–methanol (3:1). The column showed two separate bands, the first orange and the second red bands, the complexes in which were determined to have the *cis*(NCS,NCS) and *trans*-(NCS,NCS) structures, respectively, by X-ray structure analysis (*vide infra*). Each eluate of the two bands was evaporated to dryness under reduced pressure, and the complex was dissolved in a small amount of methanol. The solution was mixed with an aqueous NaCl solution and stored in a refrigerator to yield crystals of the chloride of the complex, which were filtered, washed with water, and air-dried. Yield: The *cis*(NCS,NCS) isomer=94 mg(19%), the *trans*(NCS,NCS) isomer=184 mg (35%). Found for the *cis*(NCS,NCS) isomer: C, 52.07; H, 4.67; N, 7.79%. Calcd for $C_{30}H_{34}N_4ClCoOP_2S_2$: C, 52.44; H, 4.98; N, 8.15%. Found for the *trans*(NCS,NCS) isomer: C, 50.21, H, 4.44; N, 7.64%. Calcd for $C_{30}H_{34}N_4Cl_{1.5}CoNa_{0.5}OP_2S_2$: C, 50.30; H, 4.78; N, 7.82%. These complexes are soluble in acetone, alcohols, and CH_2Cl_2, but insoluble in water and diethyl ether.

trans*(NCO,NCO)*-*[Co(NCO)$_2$(edpp)$_2$]Cl·3.5H$_2$O.* This complex was prepared by the same method as that for the NCS^- complex, using *trans*(Cl,Cl)-$[CoCl_2(edpp)_2]ClO_4$ (200 mg) and KNCO (80 mg). A very small orange band assignable to the *cis*(NCO,NCO) isomer was observed in column chromatography, but the complex could not be isolated. Yield: 41 mg(20%). Found: C, 51.37; H, 5.21; N, 7.72%. Calcd for $C_{30}H_{39}N_4ClCoO_{5.5}P_2$: C, 51.47; H, 5.61; N, 8.00%. The complex is purplish red in color, and its solubility is similar to that of the NCS^- complex chloride.

trans*(N$_3$,N$_3$)*-*[Co(N$_3$)$_2$(edpp)$_2$]Cl·NaCl.* A methanol solution (80 cm^3) containing *trans*(Cl,Cl)-$[CoCl_2(edpp)_2]ClO_4$ (100 mg) and NaN_3 (80 mg) was stirred at 50 °C for 1 h. The resulting greenish-brown solution was evaporated to dryness under reduced pressure, and the residue was mixed with water (100 cm^3) to yield a greenish-brown precipitate, which was collected and dissolved in a small amount of methanol. The solution was mixed with an aqueous NaCl solution and allowed to stand to yield a yellow-green crystalline precipitate, which was collected, washed with water and diethyl ether, and air-dried. In column chromatography of the product, no fraction indicative of other isomers was observed. Yield: 45 mg(45%). Found: C, 48.36; H, 4.78; N, 15.82%. Calcd for $C_{28}H_{32}N_8Cl_2CoNaP_2$: C, 48.36; H, 4.64; N, 16.11%. The complex is soluble in methanol and CH_2Cl_2, but insoluble in water and diethyl ether.

trans*(NO$_2$,NO$_2$)*-*[Co(NO$_2$)$_2$(edpp)$_2$]Cl·H$_2$O.* The complex in solution is photosensitive, and the following procedures should be carried out in the dark. A mixture of *trans*-(Cl,Cl)-$[CoCl_2(edpp)_2]ClO_4$ (300 mg) and $NaNO_2$ (160 mg) in methanol (220 cm^3) was stirred at 40 °C for 40 min to give a yellow solution. On further heating at 40 °C for 20 min the solution gave a yellow precipitate, and then Dowex 1×8 in the chloride form (1.0 g) was added to it. The mixture was stirred overnight at room temperature and filtered. The filtrate was diluted with water (1 dm^3), and the solution was applied on a column (ϕ3 cm×40 cm) of SP-Sephadex C-25. By elution with 0.05 mol dm^{-3} NaCl in methanol–water (1:4), a yellow, a very small yellow-orange, and a large brown bands were eluted separately. The eluate of the first yellow band was evaporated to a small volume under reduced pressure. The concentrate was mixed with NaCl and stored in a refrigerator to yield yellow crystals, which were filtered, washed with a small amount of cold water and diethyl ether, and air-dried. Yield: 18 mg (6.2%). Found: C, 50.59; H, 4.96; N, 8.17%. Calcd for $C_{28}H_{34}N_4ClCoO_5P_2$: C, 50.73; H, 5.17; N, 8.45%. The complex is soluble in water, methanol, and ethanol, but insoluble in diethyl ether.

The complex in the second yellow-orange band could not be isolated because of a small amount. The color of the last band became faint during the elution.

trans-*[CoBr$_2$(en)(dppe)]ClO$_4$.* To a methanol solution (15 cm^3) of $[CoCO_3(en)(dppe)]ClO_4$ (100 mg) was added dropwise 47% HBr at 20 °C. The resulting brown solution turned green on warming at 40 °C on a water bath. The green solution was further warmed at 45 °C for 2 min, and then $NaClO_4·H_2O$ (1 g) was added. After cooling to room temperature, the precipitated green crystals were filtered, washed with water, and air-dried. Yield: 44 mg(40%). Found: C, 44.06; H, 4.31; N, 3.56%. Calcd for $C_{28}H_{32}N_2Br_2ClCoO_4P_2$: C, 43.30; H, 4.15; N, 3.56%. The complex is soluble in methanol and CH_2Cl_2, but insoluble in water and diethyl ether.

trans-*[Co(NCS)$_2$(en)(dppe)]Cl·1.5H$_2$O.* This complex was prepared by a method similar to that for the $[Co(NCS)_2(edpp)_2]^+$ complex, using *trans*-$[CoCl_2(en)(dppe)]ClO_4·H_2O$ and KNCS. Yield: 23%. Found: C, 51.93; H, 4.86; N, 7.95%. Calcd for $C_{30}H_{35}N_4ClCoO_{1.5}P_2S_2$: C, 51.77; H, 5.07; N, 8.05%. The complex is red in color and its solubility is similar to that of *trans*(NCS,NCS)-$[Co(NCS)_2(edpp)_2]Cl·1/2(NaCl)·H_2O$. In column chromatography a trace of an orange complex assignable probably to the cis isomer was observed, but it could not be isolated.

Attempts to prepare the $[CoX_2(en)(dppe)]^+$-type complexes with other X^- ions such as I^-, NCO^-, N_3^-, or NO_2^- were all unsuccessful.

Table 1. Crystallographic data

	Complex 1[a]	Complex 2[b]
Formula	$CoBrC_{33}H_{44}N_4O_4P_2S_2$	$CoBrC_{31}H_{36}N_4OP_2S_2$
FW	825.64	745.55
Crystal system	Monoclinic	Triclinic
Space group	$P2_1/a$	$P\bar{1}$
a/Å	23.094(3)	13.158(2)
b/Å	17.513(3)	14.138(2)
c/Å	9.755(2)	9.723(1)
α/deg	90	104.99(1)
β/deg	105.23(1)	97.41(1)
γ/deg	90	103.6(2)
V/Å^3	3806(1)	1663.1(5)
Z	4	2
d_c/g cm^{-3}	1.44	1.49
d_m/g cm^{-3}	1.43[c]	1.46[d]
Crystal size/mm	0.40×0.32×0.16	0.16×0.24×0.48
μ/mm^{-1}	1.819	2.058
2θ range	2—55°	2—60°
No. of data	5342	6790
R	0.044	0.056
Rw[e]	0.060	0.051

a) Diffraction data at 168 K. Unit cell parameters at 292 K are $a=23.232(3)$, $b=17.621(3)$, $c=9.827(2)$ Å, $\beta=105.45(1)°$, $V=3877(1)$ Å^3. b) Diffraction data at 173 K. Unit cell parameters at 293 K are $a=13.194(2)$, $b=14.239(2)$, $c=9.808(1)$ Å, $\alpha=105.15(1)$, $\beta=97.27(1)$, $\gamma=103.66(2)°$, $V=1693.0(5)$ Å^3. c) At 298 K. d) At 293 K. e) The weight (ω) was taken as $\omega=[\sigma_c^2+(0.0151|F_o|)^2]^{-1}$, where σ_c denotes a standard deviation of F_o calculated from counting statistics.

X-Ray Analyses. For X-ray studies, the bromides of *trans*(NCS,NCS)- and *cis*(NCS,NCS)-$[Co(NCS)_2(edpp)_2]^+$ were prepared by methods similar to those for the corresponding chlorides, using KBr instead of NaCl. Single crystals of *trans*(NCS,NCS)-$[Co(NCS)_2(edpp)_2]Br \cdot 3H_2O \cdot (CH_3)_2CO$ (**1**) and *cis*(NCS,NCS)-$[Co(NCS)_2(edpp)_2]Br \cdot CH_3OH$ (**2**) were obtained by recrystallizing the respective bromides from methanol–acetone (1:1) and methanol–water (2:1) solutions, respectively.

Diffraction data were collected on a Rigaku AFC-5 four-

Table 2. Positional parameters for non-hydrogen atoms[a)]

trans(NCS,NCS),*cis*(P,P)-$[Co(NCS)_2(edpp)_2]Br \cdot 3H_2O \cdot (CH_3)_2CO$

Atom	x	y	z	B_{eq}/Å^2
Br	45195 (3)	11000 (3)	22604 (6)	2.7
Co	58282 (3)	15900 (4)	69470 (7)	1.4
P(1)	58333 (6)	18896 (7)	92163 (14)	1.6
P(2)	64714 (6)	24515 (8)	64230 (14)	1.7
S(1)	43044 (7)	32756 (9)	47579 (18)	3.2
S(2)	72927 (8)	−2625 (10)	84640 (19)	3.8
N(1)	51965 (18)	22639 (23)	61285 (43)	1.8
N(2)	64459 (18)	8866 (23)	76955 (43)	1.8
N(3)	52075 (19)	8041 (23)	70806 (45)	1.9
N(4)	57786 (19)	11535 (25)	50222 (43)	2.0
C(1)	48234 (23)	26622 (29)	55650 (54)	1.9
C(2)	67869 (23)	4222 (31)	79974 (51)	1.9
C(3)	54433 (25)	10433 (29)	96083 (56)	2.2
C(4)	49461 (25)	8869 (30)	83047 (61)	2.5
C(5)	62827 (24)	22852 (33)	45077 (53)	2.4
C(6)	62258 (26)	14290 (34)	43112 (56)	2.6
C(7)	65412 (23)	19535 (29)	105613 (50)	1.8
C(8)	67894 (24)	26663 (30)	109900 (54)	2.2
C(9)	73501 (26)	27238 (36)	119734 (61)	3.0
C(10)	76536 (26)	20588 (39)	125334 (61)	3.3
C(11)	74017 (27)	13546 (34)	121351 (59)	2.9
C(12)	68532 (25)	12973 (30)	111605 (54)	2.2
C(13)	54006 (22)	27026 (28)	95928 (53)	1.8
C(14)	53186 (23)	33623 (29)	87707 (54)	2.0
C(15)	49922 (26)	39630 (31)	90978 (61)	2.7
C(16)	47544 (24)	39206 (31)	102642 (61)	2.6
C(17)	48375 (25)	32745 (31)	110869 (57)	2.4
C(18)	51529 (23)	26677 (30)	107656 (53)	2.1
C(19)	63625 (23)	34633 (29)	66777 (56)	2.0
C(20)	59041 (22)	38716 (31)	57459 (57)	2.2
C(21)	58286 (25)	46350 (32)	59800 (65)	2.8
C(22)	61918 (28)	50013 (33)	71603 (72)	3.3
C(23)	66370 (28)	46054 (34)	80823 (67)	3.3
C(24)	67353 (25)	38397 (31)	78494 (58)	2.5
C(25)	72848 (23)	23277 (28)	70745 (53)	1.8
C(26)	76467 (24)	26215 (30)	62518 (59)	2.3
C(27)	82609 (26)	25920 (32)	67673 (64)	2.7
C(28)	85229 (24)	22926 (33)	80799 (65)	2.9
C(29)	81678 (25)	20151 (34)	88975 (60)	2.8
C(30)	75563 (24)	20290 (31)	83880 (55)	2.2
O(1)	70671 (18)	41646 (23)	44256 (42)	3.2
O(2)	90903 (18)	44892 (23)	50172 (39)	2.9
O(3)	65028 (21)	−7019 (28)	107638 (45)	4.5
O(4)	81923 (20)	45842 (26)	63161 (45)	3.9
C(31)	67839 (25)	46880 (33)	37436 (60)	2.6
C(32)	62678 (31)	45360 (43)	25318 (71)	4.4
C(33)	69433 (31)	55125 (35)	40649 (72)	3.8

cis(NCS,NCS),*trans*(P,P)-$[Co(NCS)_2(edpp)_2]Br \cdot CH_3OH$

Atom	x	y	z	B_{eq}/Å^2
Br(A)[b)]	49434 (4)	31649 (4)	64473 (5)	2.7
Br(B)[c)]	50281 (72)	19414 (77)	63560 (89)	5.4
Co	70130 (4)	26213 (4)	32526 (5)	1.4
S(1)	62816 (15)	2741 (11)	−13893 (14)	6.4
S(2)	103986 (9)	43694 (10)	29152 (13)	4.0
P(1)	60699 (7)	35292 (7)	22965 (9)	1.5
P(2)	78433 (7)	16019 (7)	41495 (9)	1.6
N(1)	67787 (20)	16244 (21)	13030 (28)	1.4
N(2)	83530 (23)	34570 (23)	30718 (29)	1.7
N(3)	71916 (24)	36679 (24)	51384 (31)	2.1
N(4)	56944 (23)	17825 (23)	35911 (31)	2.0
C(1)	65612 (32)	11075 (32)	2982 (48)	2.9
C(2)	91573 (30)	38436 (27)	30269 (35)	1.9
C(3)	60607 (29)	44989 (28)	39481 (37)	2.0
C(4)	70876 (31)	46815 (29)	50029 (38)	2.3
C(5)	66836 (30)	5810 (28)	40724 (41)	2.2
C(6)	58234 (31)	10893 (32)	44853 (42)	2.6
C(7)	47075 (26)	28438 (25)	13952 (35)	1.5
C(8)	44774 (30)	23742 (28)	−1020 (28)	2.1
C(9)	34418 (31)	18094 (30)	−8138 (41)	2.6
C(10)	26400 (32)	16900 (36)	−303 (48)	3.5
C(11)	28637 (32)	21407 (37)	14571 (47)	3.5
C(12)	38853 (30)	27179 (32)	21725 (39)	2.4
C(13)	66382 (26)	41801 (26)	10802 (35)	1.6
C(14)	73381 (30)	38185 (28)	2366 (37)	2.0
C(15)	77604 (30)	43439 (31)	−6692 (39)	2.2
C(16)	75042 (30)	52299 (30)	−7507 (39)	2.2
C(17)	68125 (32)	55742 (31)	511 (42)	2.6
C(18)	63703 (30)	50554 (29)	9697 (39)	2.1
C(19)	85884 (29)	21178 (28)	60113 (35)	1.9
C(20)	82645 (32)	17749 (32)	71461 (39)	2.6
C(21)	88861 (37)	21758 (35)	85165 (40)	3.2
C(22)	98214 (38)	29271 (37)	88062 (41)	3.6
C(23)	101549 (36)	32959 (36)	76952 (45)	3.5
C(24)	96326 (34)	28926 (32)	63133 (40)	2.8
C(25)	87546 (27)	10166 (27)	32088 (35)	1.7
C(26)	89960 (30)	1937 (30)	35603 (38)	2.2
C(27)	97637 (32)	−2085 (31)	29681 (41)	2.6
C(28)	102845 (31)	2024 (32)	20215 (42)	2.7
C(29)	100206 (31)	10075 (32)	16319 (40)	2.6
C(30)	92420 (30)	14021 (29)	22022 (38)	2.1
C(31)	19962 (48)	21886 (47)	53721 (63)	6.1
O(A)[d)]	25981 (31)	14784 (32)	49361 (54)	5.3
O(B)[e)]	18338 (115)	29634 (106)	47678 (150)	1.6

a) The values are multiplied by 10^5. The thermal parameters are given by the equivalent temperature factors.
b) Occupancy factor: 0.94. c) Occupancy factor: 0.06. d) Occupancy factor: 0.84. e) Occupancy factor: 0.16.

circle diffractometer with use of graphite-monochromatized Mo-$K\alpha$ radiation at 168K for complex **1** and at 173K for complex **2**. The low-temperature measurements were made with an attached Rigaku variable-temperature apparatus based on a cold nitrogen gas stream method. The procedures used for data collections as well as the methods used in the solution and refinement of the structure were standard and have been described previously.[4] The intensity data were corrected for Lorentz-polarization effects and for absorption. Non-hydrogen and hydrogen atoms were refined anisotropically and isotropically, respectively. Pertinent crystallographic data are summarized in Table 1. Tables 2 lists positional parameters for non-hydrogen atoms in complexes **1** and **2**. In complex **2** the bromide ion and the oxygen atom of methanol are disordered and located at two positions with occupancy factors (P) of $P_{Br(A)}$=0.94 and $P_{Br(B)}$=0.06, and $P_{O(A)}$=0.84 and $P_{O(B)}$=0.16, respectively. The F_o-F_c data, final thermal parameters, and hydrogen atomic coordinates are preserved by the Chemical Society of Japan (Document No. 8450).

All the calculations were carried out on a HITAC M-200H computer at the Computer Center of the Institute for Molecular Science with the Universal Computation Program System UNICS III.[5]

Results and Discussion

Structure of trans*(NCS,NCS)*,cis*(P,P)-[Co(NCS)$_2$(edpp)$_2$]Br·3H$_2$O·(CH$_3$)$_2$CO (1) and* cis*(NCS,NCS)*,trans*-(P,P)-[Co(NCS)$_2$(edpp)$_2$]Br·CH$_3$OH (2).* Figures 1 and 2 show stereoviews of the complex cations in **1** and **2**, respectively. The relevant bond lengths and bond angles based on the atomic numbering scheme in these figures are listed in Tables 3 and 4. All the cations have a distorted octahedral coordination with two P and four N atoms, the NCS^- ions coordinating to the cobalt(III) ion through their N atoms.

In complex 1 the complex cation has a *trans*(NCS, NCS),*cis*(P,P) configuration. The two edpp chelate rings adopt a skew (gauche) conformation of $\delta\delta$ or $\lambda\lambda$ chirality (racemic).[6] The same structure has been found for the bis(edpp) moiety of *trans*(Cl,Cl),*cis*(P,P)-[CoCl$_2$(edpp)$_2$][CoCl$_4$]$_{1/2}$,[2] (complex **3**). The orientation of phenyl groups on the P atoms in complex **1** is also very similar to that in complex **3**. The average Co–P distance of 2.270 Å in complex **1** is slightly longer than that in complex **3** (2.255 Å), whereas the average Co–NH_2 distance (2.010 Å) is slightly shorter than that in complex **3** (2.024 Å), although the differences may be less meaningful on the statistical ground. The average P–Co–P angle in complex **1** (103.3°) is also widened as has been seen in complex **3** (103.1°) to alleviate the overcrowding due to bulky substituents on the P atoms. Other structural parameters on the edpp chelate ligand are almost similar to those in complex **3**. The NCS^- ions are almost linear and coordinate to the cobalt(III) ion through their N atoms with a slightly bent structure, the Co–N–C angles ranging from 171.8—176.2°. The Co–NCS distances (1.881, 1.883 Å) are nearly the same as those reported for *trans*-[Co(NCS)$_2${P(OC$_2$H$_5$)$_3$}$_4$]$^+$ (1.838, 1.874 Å) and *trans*-[Co(NCS)$_2$(trien)]$^+$ (1.901, 1.884 Å; trien=triethylenetetramine).[8]

On the other hand, complex **2** has a *cis*(NCS,NCS), *trans*(P,P) structure. The formation of only *trans*(P,P) isomer in *cis*(NCS,NCS)-[Co(NCS)$_2$(edpp)$_2$]$^+$ is rather unusual, since complexes of the [Co(O–O)(edpp)$_2$]$^{n+}$ type, where O–O is a bidentate ligand such as an oxalate or acetylacetonate ion, form always the *trans*(P,N) isomer in the largest abundance among three possible isomers, *trans*(P,P), *trans*(P,N), and *trans*(N,N).[1] The Co–P distances (2.263, 2.275 Å) in complex **2** are nearly the same as those in complex **1** (2.272, 2.268 Å), despite the two trans-labilizing P donor atoms are in the trans positions to each other. On the other hand, the Co–NH_2 distances (1.976, 1.982 Å) are fairly shorter than those in complex **1** (2.003, 2.016 Å) and are nearly the same as those in cobalt(III) diamine complexes such

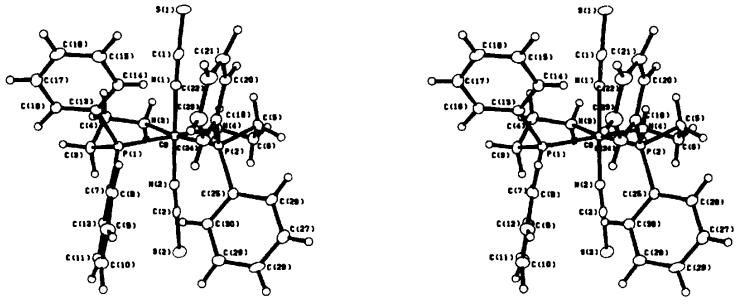

Fig. 1. ORTEP stereoview of *trans*(NCS,NCS),*cis*(P,P)-[Co(NCS)$_2$(edpp)$_2$]$^+$ in complex **1**.

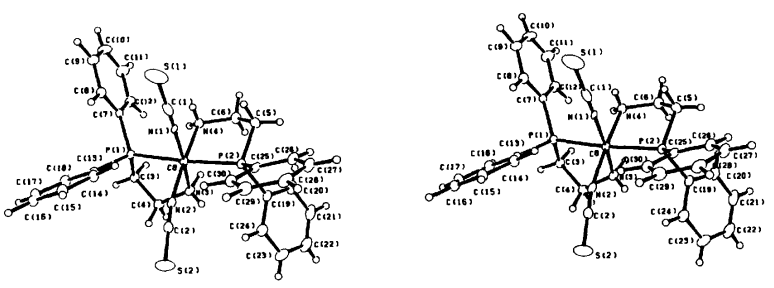

Fig. 2. ORTEP stereoview of *cis*(NCS, NCS), *trans*(P,P)-[Co(NCS)$_2$(edpp)$_2$]$^+$ in complex **2**.

Table 3. Selected bond lengths (Å) for *trans*-(NCS,NCS),*cis*(P,P)-[$Co(NCS)_2(edpp)_2$]Br·$3H_2O$·$(CH_3)_2CO$ (**1**) and *cis*(NCS,NCS),*trans*(P,P)-[$Co(NCS)_2(edpp)_2$]Br·CH_3OH (**2**)

	1	**2**
Co-P(1)	2.272(2)	2.263(3)
Co-P(2)	2.268(2)	2.275(3)
Co-N(1)	1.883(4)	1.984(3)
Co-N(2)	1.881(4)	1.935(5)
Co-N(3)	2.016(4)	1.982(3)
Co-N(4)	2.003(4)	1.976(5)
P(1)-C(3)	1.826(6)	1.825(4)
P(1)-C(7)	1.811(5)	1.805(4)
P(1)-C(13)	1.831(5)	1.809(4)
P(2)-C(5)	1.827(5)	1.816(6)
P(2)-C(19)	1.816(5)	1.815(3)
P(2)-C(25)	1.831(5)	1.821(4)
N(1)-C(1)	1.132(6)	1.015(5)
N(2)-C(2)	1.116(7)	1.083(5)
N(3)-C(4)	1.480(8)	1.508(6)
N(4)-C(6)	1.469(8)	1.492(6)
C(1)-S(1)	1.648(5)	1.690(4)
C(2)-S(2)	1.652(5)	1.658(5)
C(3)-C(4)	1.498(7)	1.512(5)
C(5)-C(6)	1.513(8)	1.520(7)

Table 4. Selected bond angles (ϕ/°) for *trans*-(NCS,NCS),*cis*(P,P)-[$Co(NCS)_2(edpp)_2$]Br·$3H_2O$·$(CH_3)_2CO$ (**1**) and *cis*(NCS,NCS), *trans*(P,P)-[$Co(NCS)_2(edpp)_2$]Br·CH_3OH (**2**)

	1	**2**
P(1)-Co-P(2)	103.3(1)	175.5(0)
P(1)-Co-N(1)	94.2(1)	90.4(1)
P(1)-Co-N(2)	87.9(1)	92.2(1)
P(1)-Co-N(3)	85.2(1)	85.7(1)
P(1)-Co-N(4)	170.4(1)	90.6(1)
P(2)-Co-N(1)	88.2(1)	87.3(1)
P(2)-Co-N(2)	92.8(1)	91.8(1)
P(2)-Co-N(3)	171.0(1)	96.5(1)
P(2)-Co-N(4)	85.5(1)	85.5(1)
N(1)-Co-N(2)	177.4(2)	94.0(2)
N(1)-Co-N(3)	88.3(2)	176.2(1)
N(1)-Co-N(4)	89.7(2)	89.3(2)
N(2)-Co-N(3)	90.4(2)	86.2(2)
N(2)-Co-N(4)	88.0(2)	175.7(1)
N(3)-Co-N(4)	86.2(2)	90.8(2)
Co-P(1)-C(3)	98.0(2)	100.3(2)
Co-P(1)-C(7)	119.5(2)	115.5(2)
Co-P(1)-C(13)	120.8(2)	117.8(1)
Co-P(2)-C(5)	97.5(2)	99.5(1)
Co-P(2)-C(19)	119.7(2)	117.2(1)
Co-P(2)-C(25)	121.1(2)	121.5(2)
Co-N(1)-C(1)	176.2(5)	172.9(3)
Co-N(2)-C(2)	171.8(4)	171.2(4)
Co-N(3)-C(4)	115.7(3)	114.1(2)
Co-N(4)-C(6)	116.3(3)	117.0(2)
N(1)-C(1)-S(1)	177.2(5)	176.3(4)
N(2)-C(2)-S(2)	179.3(5)	176.7(4)
N(3)-C(4)-C(3)	108.6(5)	108.6(3)
N(4)-C(6)-C(5)	108.3(5)	110.1(4)
C(3)-P(1)-C(7)	107.4(2)	108.7(2)
C(3)-P(1)-C(13)	105.3(3)	107.7(2)
C(7)-P(1)-C(13)	104.1(2)	106.3(2)
C(5)-P(2)-C(19)	106.9(3)	108.3(2)
C(5)-P(2)-C(19)	106.5(3)	107.3(2)
C(19)-P(2)-C(25)	103.6(2)	102.3(2)
P(1)-C(3)-C(4)	106.3(4)	106.9(3)
P(2)-C(5)-C(6)	106.1(4)	106.1(3)

as $[Co(en)_3]^{3+}$ (1.978 Å).[9] The elongation of Co-NH_2 distance in complex **1** is attributable to trans influence of the P atom.[2,10] The Co-NCS fragment is nearly linear geometry similar to those in complex **1**, but significant differences in bond distance are found between the two isomers. The average Co-N distance in complex **2** (1.960 Å) is longer than that in complex **1** (1.882 Å), whereas the average N-C distance in the former (1.049 Å) is shorter than that in the latter (1.124 Å). No significant difference is found for the C-S distance between complex **1** (1.650 Å) and complex **2** (1.674 Å). The octahedral angles around the cobalt(III) ion in complex **2** are not largely deviated from the right angle (85.3—96.5°). The two edpp chelate rings take δ and λ conformations, and the complex ion can be designated as a *lel·ob* isomer.

Complexes **1** and **2** include acetone and methanol, respectively as organic solvents of crystallization. Such inclusion of organic solvents in crystals has often been found in metal complexes containing bulky organic groups such as -PPh_2. Nonbonded distances in the crystals and stereoviews of the crystal structures are given in the supplementary materials (Document No. 8450).

Preparation and Absorption Spectra of the Complexes. The $[CoX_2(edpp)_2]^+$-type complexes (X=NCO^-, NCS^-, N_3^-, NO_2^-) were obtained by substitution reactions between *trans*(Cl,Cl)-$[CoCl_2(edpp)_2]^+$ and MX (M=Na or K) in methanol. The Br^- and I^- complexes were prepared by treating *trans*(P,N)-$[CoCO_3(edpp)_2]^+$ with HBr and HI, respectively, in order to avoid the contamination of mixed-halogeno complexes. The reaction for the I^- complex was carried out under an atmosphere of nitrogen to prevent oxidation of I^- to I_3^- which forms a quite insoluble salt with $[CoI_2(edpp)_2]^+$. For each complex only one isomer was obtained except for the NCS^- complex. It formed two isomers, *trans*-(NCS,NCS),*cis*(P,P)- and *cis*(NCS,NCS),*trans*(P,P)-isomers as described in the preceeding section. The formation ratio of the two isomers, trans:cis was *ca.* 2:1 under the given experimental conditions. Both isomers in ethanol are stable and do not isomerize even at a boiling point.

Attempts to prepare the corresponding $[CoX_2(en)(dppe)]^+$ complexes were made by procedures similar to those for $[CoX_2(edpp)_2]^+$, using *trans*-$[CoCl_2(en)(dppe)]^+$ and MX (M=Na or K, X=NCO^-, NCS^-, N_3^-, NO_2^-), and $[CoCO_3(en)(dppe)]^+$ and HX (X=Br, I). However, the complexes obtained are only those of Br^-

and NCS^-. No reaction took place between *trans*-$[CoCl_2(en)(dppe)]^+$ and KNCO at room temperature, reactions at higher temperatures or in the presence of large excess of KNCO causing reduction of cobalt(III) to cobalt(II). A dark-geen complex assignable to $[Co(N_3)_2(en)(dppe)]^+$ was yielded by a similar reaction with NaN_3, but the complex decomposed in the course of purification. In the case of the I^- complex, orange-yellow crystals were obtained from the reaction mixture. However, elemental analysis revealed the product to be the composition of $Co(dppe)_2I$. The reaction with $NaNO_2$ resulted in the formation of *trans*-$[Co(NO_2)_2(en)_2]^+$ and $[Co(NO)_2(dppe)]^+$.[11]

Figure 3 shows absorption spectra of $[CoX_2(edpp)_2]^+$ in methanol for X=Cl^- and Br^-, and in CH_2Cl_2 for X=I^-. Spectral data are given in Table 5. The near infrared spectra of the Cl^- and Br^- complexes were obtained in CH_2Cl_2 solutions. The structure of the Cl^- complex has been determined by X-ray analysis to have a *trans*-(Cl,Cl),*cis*(P,P) configuration.[2] Thus the Br^- complex which gives a spectrum similar to that of the Cl^- complex can be assigned to the *trans*(Br,Br),*cis*(P,P) isomer. The bands around 16000 cm^{-1} of these Cl^- and Br^- complexes are assigned to the split component (Ia) of the first d-d absorption band from a comparison with the spectrum of *trans*-$[CoCl_2(en)_2]^+$.[12] The I^- complex shows a broad spectrum with no peak except the band at 10200 cm^{-1} which can be assigned to the spin-forbidden d-d band described below, the spin-allowed, first d-d band being hidden by strong I^- to Co^{III} charge-transfer bands.[13] Thus the structure of this complex can not be assigned unequivocally from the spectrum. No good NMR spectrum of the complex was obtained because of its instability. The infrared spectrum somewhat differs from those of *trans*(X,X)-$[CoX_2(edpp)_2]X$ (X=Cl^-, Br^-). The structure of the I^- complex remains unknown at present.

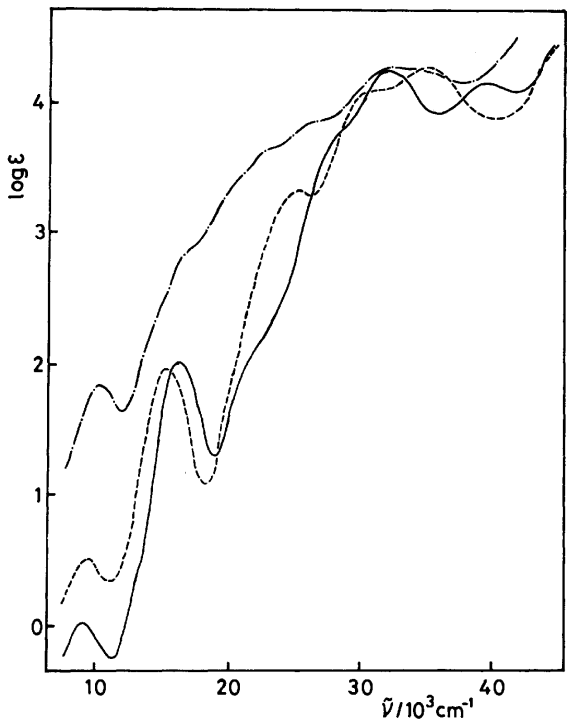

Fig. 3. Absorption spectra of *trans*(X,X)-$[CoX_2(edpp)_2]^+$: X=Cl^- (——), Br^- (----), and I^- (—·—).

All of the halogen complexes of edpp show a distinct band around 10000 cm^{-1}. The peak positions are not much different among the complexes, and the band intensities increase in the order of the Cl^-<Br^-<I^- complexes. These features are similar to those of the spin-forbidden d-d bands in the series of cobalt(III) halogeno complexes such as $[CoX(NH_3)_5]^{2+}$ (*ca.* 11000 cm^{-1})[14] or $[CoX(CN)_5]^{3-}$ (*ca.* 20000 cm^{-1}).[15] Thus the bands around 10000 cm^{-1} in the present halogeno complexes can be assigned to the spin-forbidden d-d band. The yellow-green $[CoBr_2(en)(dppe)]^+$ complex is assigned to the trans isomer, since the spectrum quite resembles that of *trans*-$[CoCl_2(en)(dppe)]^+$[1] as shown in Fig. 4. The corresponding X^- complexes of dppe and edpp show spectra similar to each other.

In Fig. 5 are compared absorption spectra of *trans*-(NCS,NCS),*cis*(P,P)- and *cis*(NCS,NCS),*trans*(P,P)-$[Co(NCS)_2(edpp)_2]^+$ and $[Co(NCS)_2(en)(dppe)]^+$ in methanol solutions. The spectrum of the dppe complex is very similar to that of the *trans*(NCS,NCS),*cis*-(P,P) isomer of the edpp complex, and the complex can be assigned to the trans isomer. The first d-d band of the *cis*(NCS,NCS),*trans*(P,P) isomer is observed as a shoulder absorption at *ca.* 20000 cm^{-1}. The shoulder

Table 5. Absorption spectral data of the complexes ($\tilde{\nu}/10^3$ cm^{-1} (log ε))

trans(Cl,Cl),*cis*(P,P)-$[CoCl_2(edpp)_2]^+$	8.8(0.13), 15.9(2.03), 21.5(2.1)*, 27.5(3.8)*, 31.5(4.27), 39.0(4.19)
trans-$[CoCl_2(en)(dppe)]^+$	16.5(2.13), 22.5(2.6)*, 28(3.6)*, 33.0(4.27), 39.0(4.44)
trans(Br,Br),*cis*(P,P)-$[CoBr_2(edpp)_2]^+$	9.3(0.50), 15.1(1.96), 24.9(3.34), 30(4.1)*, 34.5(4.30)
trans-$[CoBr_2(en)(dppe)]^+$	15.9(2.24), 24.5(3.2)*, 31(4.1)*, 35.0(4.35)
$[CoI_2(edpp)_2]^+$	10.2(1.84), 14(2.2)*, 16.5(2.8)*, 20(3.3)*, 22.5(3.6)*, 26.5(3.9)*, 32.5(4.26)
trans(NCS,NCS),*cis*(P,P)-$[Co(NCS)_2(edpp)_2]^+$	18.5(2.65), 27(3.9)*, 33.5(4.21)
trans-$[Co(NCS)_2(en)(dppe)]^+$	18.9(2.68), 27(3.7)*, 33.5(4.25)
cis(NCS,NCS),*trans*(P,P)-$[Co(NCS)_2(edpp)_2]^+$	20(3.0)*, 26.9(4.07), 33.1(4.15)
$[Co(NCO)_2(edpp)_2]^+$	18.4(2.35), 24(2.4)*, 30.8(4.33), 37(4.0)*
$[Co(N_3)_2(edpp)_2]^+$	15(2.0)*, 17.5(2.43), 27.5(4.09), 32.9(4.21)
$[Co(NO_2)_2(edpp)_2]^+$	22.5(2.9)*, 28.8(4.56)

* Shoulder absorption

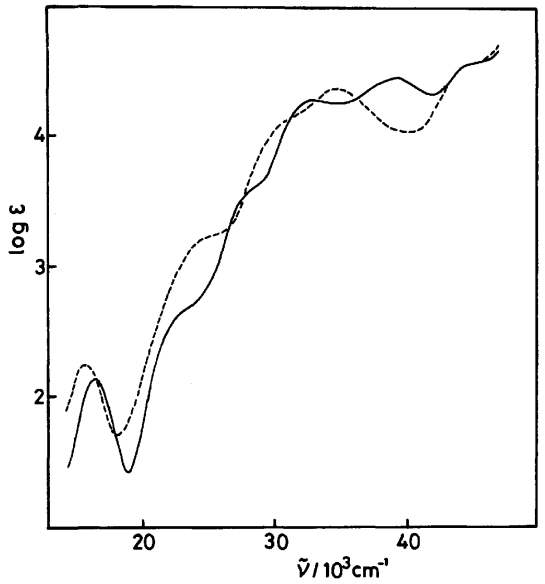

Fig. 4. Absorption spectra of *trans*-$[CoX_2(en)(dppe)]^+$: X=Cl^- (——), and Br^- (----).

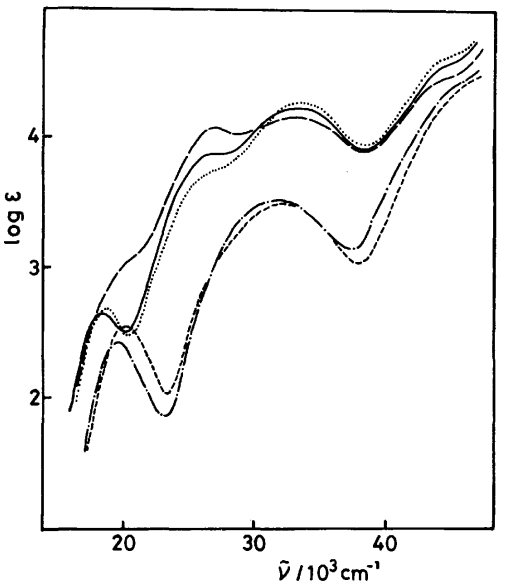

Fig. 5. Absorption spectra of bis(isothiocyanato) complexes: *trans*(NCS, NCS), *cis*(P,P)-$[Co(NCS)_2(edpp)_2]^+$ (——), *cis*(NCS, NCS), *trans*(P,P)-$[Co(NCS)_2(edpp)_2]^+$ (— —), *trans*-$[Co(NCS)_2(en)(dppe)]^+$ (……), *trans*-$[Co(NCS)_2(en)_2]^+$ (—·—), and *cis*-$[Co(NCS)_2(en)_2]^+$ (----).

lies in the high energy side and its intensity is fairly strong as compared with the first d-d band of the *trans*-(NCS,NCS),*cis*(P,P) isomer. A similar spectral difference has been reported between the first d-d bands of *cis*- and *trans*-$[Co(NCS)_2(en)_2]^+$ (cis isomer: 20400 cm^{-1}, log ε=2.54; trans isomer: 19700 cm^{-1}, log ε=2.44).[16] However, the difference in band intensity between the two isomers of the edpp complex is remarkable. The strong intensity of the cis isomer may be attributable to the *trans*(P,P) configuration involved in this isomer, since *trans*(P,P)-$[Co(C_2O_4)(edpp)_2]^+$ shows the first d-d

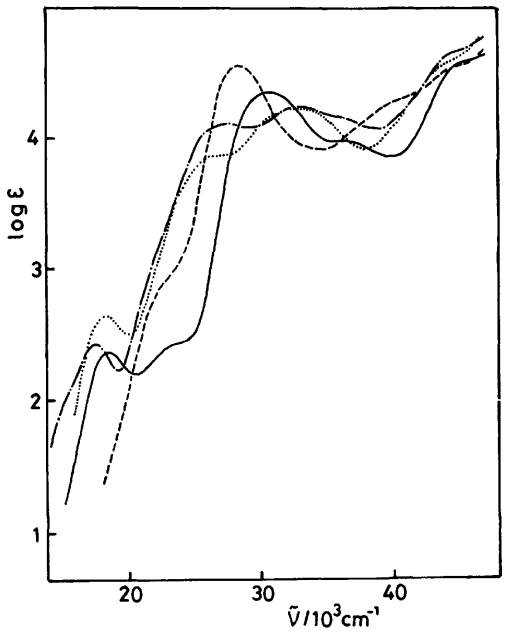

Fig. 6. Absorption spectra of $[CoX_2(edpp)_2]^+$: X= NCO^- (——), N_3^- (—·—), NO_2^- (----), and NCS^- (……).

band (20400 cm^{-1}, log ε=3.08) much stronger than that of the corresponding *trans*(P,N) isomer (20000 cm^{-1}, log ε=2.54).[1]

Figure 6 compares absorption spectra of $[CoX_2(edpp)_2]^+$ (X=NCO^-, N_3^-, and NO_2^-) in methanol solutions with that of *trans*(NCS,NCS),cis(P,P)-$[Co(NCS)_2(edpp)_2]^+$. At present, we can not assign geometrical structures of the complexes unequivocally on the basis of these spectra. In column chromatography using SP-Sephadex C-25 or Sephadex LH-20, however, any fractions of each of these complexes did not show optical activity, while *cis*(NCS,NCS),*trans*(P,P)-$[Co(NCS)_2(edpp)_2]^+$ was partially resolved by similar chromatography. Further, complexes of the $[CoX_2(edpp)_2]^+$ type seem to be more stable in the *trans*(X,X) isomer than the *cis*(X,X) one as exemplified by the formation ratio of the NCS^- complex. On the basis of these facts, all the complexes in Fig. 6 may be assigned to the *trans*(X,X) isomer. That the first d-d band of the N_3^- complex is at lower energy than that of the NCS^- complex is consistent with the ranking of N_3^- in the spectrochemical series.[17] The d-d band positions of the NCO^- and NO_2^- complexes clearly indicate the isocyanato and nitro coordination modes, respectively. The observed shoulder at *ca.* 24000 cm^{-1} in the NCO^- complex may be assigned to the second d-d band, although the energy separation between this shoulder and the first band is rather small. In general, the separation between the first and second d-d bands in cobalt(III) phosphine complexes has been reported to become small.[18] The intensities of d-d bands of the NCO^- and N_3^- complexes are not so strong as that of *cis*(NCS,NCS),*trans*(P,P)-$[Co(NCS)_2(edpp)_2]^+$. Thus the complexes will have the *trans*(X,X),*cis*(P,P) configuration. The NO_2^- complex shows the first absorp-

tion band with fairly strong intensity, and the spectral pattern in this band region resembles that of *cis*(NCS, NCS),*trans*(P,P)-[Co(NCS)$_2$(edpp)$_2$]$^+$, indicating the *trans*(NO$_2$,NO$_2$),*trans*(P,P) configuration. Examination of molecular models indicates that the NO_2^- ligands in the *trans*(NO$_2$,NO$_2$),*cis*(P,P) configuration cause a big hindrance with the phenyl groups, while such a hindrance is much reduced in the *trans*(NO$_2$, NO$_2$),*trans*(P,P) configuration. In fact, the [CoX$_2$(en)-(dppe)]$^+$- and [CoX$_2$(dpee)$_2$]$^+$-type complexes (dpee= *cis*-1,2-bis(diphenylphosphino)ethylene)[19], where the PPh$_2$ groups are in the cis positions, do not form stable complexes with NO_2^- ions.

For a given X$^-$ ligand, the first d-d band of *trans*-(X,X)-[CoX$_2$(edpp)$_2$]$^+$ is observed at slightly lower energy than that of *trans*(X,X)-[CoX$_2$(en)(dppe)]$^+$ (X= Cl$^-$, Br$^-$, NCS$^-$), and at similar energy to that of *trans*-(X,X)-[CoX$_2$(dpee)$_2$]$^+$ (X=Cl$^-$, Br$^-$, NCO$^-$, N$_3^-$).[19] The NCS$^-$ complex of dpee is reported to show the band at anomalously low energy (16800 cm^{-1}).[19] The corresponding *trans*(X,X)-[CoX$_2$(en)$_2$]$^+$ complex gives the first d-d band at the highest energy among these edpp, dppe, and dpee complexes.

In the ultraviolet region, the present phosphine complexes exhibit strong absorption bands due to charge-transfer transitions between the X$^-$, PPh$_2$, and NH$_2$ groups and cobalt(III). In order to assign properly these spectra, more spectral data will be needed.

The authors wish to thank the Ministry of Education for Scientific Research Grant-in-Aid No. 58470032.

References

1) M. Atoh, I. Kinoshita, K. Kashiwabara, and J. Fujita, *Bull. Chem. Soc. Jpn.*, **55**, 3179 (1982).

2) I. Kinoshita, Y. Yokota, K. Matsumoto, S. Ooi, K. Kashiwabara, and J. Fujita, *Bull. Chem. Soc. Jpn.*, **56**, 1067 (1983).

3) K. Issleib and D. Haferburg, *Z. Naturforsch., Teil B*, **20**, 916 (1965).

4) M. Sugimoto, J. Fujita, H. Ito, K. Toriumi, and T. Ito, *Inorg. Chem.*, **22**, 955 (1983).

5) T. Sakurai and K. Kobayashi, *Rikagaku Kenkyusho Hokoku*, **55**, 69 (1979).

6) In the crystal structure of hexafluorophosphate of *trans*(NCS,NCS),*cis*(P,P)-[Co(NCS)$_2$(edpp)$_2$]$^+$, two edpp chelate rings have been found to assume a $\delta\lambda$(meso) form. The X-ray crystal analysis (R=0.056) and elemental analysis are best fitted to the composition of [Co(NCS)$_2$(edpp)$_2$](PF$_6$)$_{1/3}$·F$_{2/3}$·(PF$_5$)$_{1/3}$·H$_2$O. M. Atoh, K. Kashiwabara, J. Fujita, T. Ito, and H. Ito, 31 st Symposium on Coordination Chemistry Japan (Sendai), 1981, Abstr. No. 3C14.

7) G. Albertin, G. Pelizzi, and E. Bordignon, *Inorg. Chem.*, **22**, 515 (1983).

8) Y. Kushi, M. Kuramoto, S. Utsuno, and H. Yoneda, *Bull. Chem. Soc. Jpn.*, **56**, 2742 (1983).

9) M. Iwata, K. Nakatsu, and Y. Saito, *Acta Crystallogr., Sect. B*, **33**, 1378 (1969).

10) a) I. Kinoshita, K. Kashiwabara, J. Fujita, K. Matsumoto, and S. Ooi, *Bull. Chem. Soc. Jpn.*, **54**, 2683 (1981); b) S. Ohba, Y. Saito, T. Ohishi, K. Kashiwabara, and J. Fujita, *Acta Crystallogr., Sect. C*, **39**, 49 (1983); c) T. Ohishi, K. Kashiwabara, H. Ito, T. Ito, and J. Fujita, *Bull. Chem. Soc. Jpn.*, **56**, 1551 (1983).

11) Inorg. Synth., **16**, 16 (1976).

12) M. Linhard and M. Weigel, *Z. Anorg. Allg. Chem.*, **271**, 101 (1952).

13) H. Yamatera, *Naturwissenschaften*, **44**, 632 (1957); *J. Inorg. Nucl. Chem.*, **15**, 50 (1960).

14) M. Linhard and M. Weigel, *Z. Phys. Chem., N, F.*, **11**, 308 (1957).

15) J. Fujita and Y. Shimura, *Bull. Chem. Soc. Jpn.*, **36**, 1281 (1963).

16) K. Yamasaki, J. Hidaka, and Y. Shimura, *Bull. Chem. Soc. Jpn.*, **50**, 2624 (1977).

17) Y. Shimura and R. Tsuchida, *Bull. Chem. Soc. Jpn.*, **29**, 311 (1956).

18) T. Ohishi, K. Kashiwabara, and J. Fujita, *Bull. Chem. Soc. Jpn.*, **56**, 3441 (1983).

19) V. M. Miskowski, J. L. Robbins, G. S. Hammond, and H. B. Gray, *J. Am. Chem. Soc.*, **98**, 2477 (1976).

Noncovalent Interactions in Metal Complexes. VIII.[1] Syntheses, Properties, and Stereoselectivities of Lanthanoid Complexes with 1-*l*-Menthyloxy-3-benzoylacetone

Michio NAKAMURA, Hisashi ŌKAWA,* Sigeo KIDA, and Seizo MISUMI†
Department of Chemistry, Faculty of Science, Kyushu University, 33, Hakozaki, Higashiku, Fukuoka 812
†*Department of Industrial Chemistry, Faculty of Engineering, Kyushu Sangyo University, Matsukadai 2-327, Higashi-ku, Fukuoka 813*
(Received May 21, 1984)

Lanthanoid complexes with 1-*l*-menthyloxy-3-benzoylacetone, [Ln(*l*-moba)$_3$(H$_2$O)$_n$] (Ln=La, Pr, Nd, Eu, Dy, Ho, Tm; n=0, 1, or 2), have been synthesized and characterized by elemental analyses, molecular weight determinations, and electronic, circular dichroism, and luminescence spectra. The molecular weight determinations suggest that the complexes are in a monomer-dimer equilibrium in nondonating solvents while they are monomeric in donating solvents. The complexes exhibit fairly intense circular dichroisms at the f-f band region, demonstrating the stereoselective formation of an enantiomer. The stereoselectivities have been discussed in terms of the intramolecular interligand CH/π-interaction operating between the phenyl and the menthyl groups of the ligands. [Eu(*l*-moba)$_3$(H$_2$O)] shows luminescence at the $^5D_0 \rightarrow {}^7F_1$ and $^5D_0 \rightarrow {}^7F_2$ transitions in benzene. Based on the concentration dependence of the luminescence, it is demonstrated that dimerization facilitates nonradiative relaxation and greatly reduces the quantum efficiency of luminescence.

Lanthanoid complexes with 1,3-diketones have been the subject of current studies because of the utility in NMR spectroscopy as shift reagents[2] and the interest in photoluminescence.[3,4] Recently much attention has been paid to the lanthanoid complexes with chiral 1,3-diketones in connection with the chirality recognition of enantiomers[5,6] and stereoselectivity of the complexes.[7] It is known, however, that the lanthanoid complexes with 1,3-diketones derived from *d*-camphor exhibit no optical activity in the f-f transition region.[8] This is probably due to the absence of the interligand interaction within a molecule because of the larger ionic radius of the lanthanoid ions.

In the previous paper of this series,[9] we reported that tris(1-*l*-menthyloxy-3-benzoylacetonato)M(III) complexes, [M(*l*-moba)$_3$] (M=Co, Cr, Mn) (Fig. 1), prefer a *cis*-Δ-configuration. The stereoselectivity was attributed to an intramolecular interligand CH/π-interaction between the *l*-menthyl and the phenyl residues of the ligand (Fig. 2). Similar stereoselectivities were also observed for tris(1-*l*-menthyloxy-3-acetylacetonato)M(III) [M(*l*-moac)$_3$] (M=Co, Cr)[10] and tris{1-*l*-methyloxy-3-(2-naphthoxyl)acetonato}M(III) [M(*l*-mona)$_3$] (M=Co, Cr, Mn).[11] It is particularly noteworthy that [Mn(*l*-moba)$_3$] and [Mn(*l*-mona)$_3$] are readily obtained as an optically active form without any effort to resolution, though tris(1,3-diketonato)manganese(III) complexes have been believed to be hardly resolved owing to the lability of manganese(III) for ligand substitution.[12] These findings prompted us to synthesize the lanthanoid complexes with *l*-moba$^-$ and study their property and stereochemistry to see the effect of the intramolecular interligand CH/π-interaction.

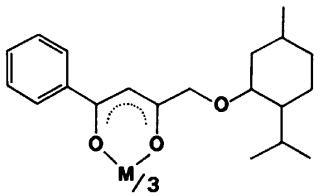

Fig. 1. Chemical structure of [M(*l*-moba)$_3$].

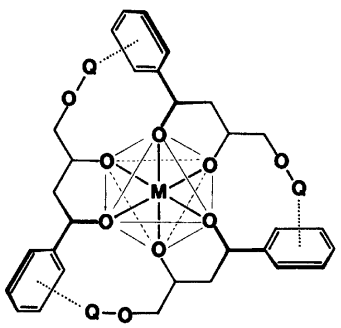

Fig. 2. Schematical representation of interligand CH/π-interaction supposed for [M(*l*-moba)$_3$] (Q=*l*-menthyl).

Experimental

Syntheses. Synthetic method of H(*l*-moba) was described in the preceding paper.[9] The lanthanoid complexes were obtained in a similar way. The procedure is exemplified by Eu^{III} complex. H(*l*-moba) (1.0 g) and NaOH (0.133 g) were dissolved in ethanol (10 cm^3). To this solution was added an ethanolic solution of EuCl$_3$·6H$_2$O (0.40 g), and the mixture was stirred for a few minutes and filtered. To the filtrate were added water (50 cm^3) and ether (100 cm^3), and the mixture was vigorously shaken. The ether layer was separated, shaken three times with water, and dried over sodium sulfate. On evaporating the solvent at room temperature, a yellow precipitate was obtained. It was collected and dried *in vacuo* over phosphorus pentaoxide.

Elemental analyses of the complexes thus prepared are given in Table 1.

Physical Measurements. Molecular weights were determined with a Hitachi Perkin-Elmer 115 Molecular Weight Apparatus in benzene and in ethanol. Electronic spectra were measured on a Shimadzu UV-visible Recording Spectrometer Model UV-240 in benzene. Circular dichroism spectra were recorded on a JASCO J-500C Spectropolarimeter in benzene. Luminescence spectra were recorded on a Hitachi Fluorescence Spectrophotometer in benzene with the excitation at 392.5 nm. The elemental analyses were carried out at

Table 1. Elemental analyses of complexes

Complex	Found (Calcd)/%		Color
	C	H	
La(*l*-moba)$_3$·H$_2$O	65.16(65.32)	7.78(7.58)	Cream yellow
Pr(*l*-moba)$_3$·H$_2$O	64.79(65.20)	7.63(7.57)	Greenish yellow
Nd(*l*-moba)$_3$·(H$_2$O)$_2$	64.13(63.97)	7.37(7.57)	Brick red
Eu(*l*-moba)$_3$·H$_2$O	64.08(64.56)	7.43(7.49)	Yellow
Dy(*l*-moba)$_3$	65.39(65.00)	7.79(7.54)	Cream yellow
Ho(*l*-moba)$_3$	64.78(64.85)	7.69(7.34)	Cream yellow
Tm(*l*-moba)$_3$	64.16(64.62)	7.71(7.32)	Cream yellow

the Service Center of Elemental Analysis, Kyushu University.

Results and Discussion

The lanthanoid(III) complexes of *l*-moba$^-$ were isolated as anhydrates, monohydrates, or dihydrate. The complexes of the first half of the lanthanoid series formed hydrates while the complexes of the latter half of the series formed anhydrates. This trend may be rationalized in terms of the lanthanoid contraction. That is, it is likely that in the complexes of the smaller metal ions the crowding of the hydrophobic residues of the ligand around the metal acts as an insulating sheath which interferes with the hydration, while such a steric effect is not so large as to hinder the hydration in the complexes with the large metal ions.

In donating solvents tris(1,3-diketonato) lanthanoid(III) complexes readily expand their coordination number from six to seven, eight, or nine by linking solvent molecules. In nondonating solvents, the complexes tend to dimerize (or polymerize) to achieve a higher coordination number than six by sharing the oxygen atoms of the ligand.[13] Hence, lanthanoid complexes with 1,3-diketones are in a monomer-dimer equilibrium in nondonating solvents.[6,7] In order to obtain an evidence for the equilibrium, molecular weights were determined in benzene over the concentration range 0.1—1.0 wt%. The results are shown in Fig. 3. Since each molecular weight increases with the increase of the concentration, the complexes evidently exist in a monomer-dimer equilibrium in benzene: 2[Ln(*l*-moba)$_3$]$\rightleftarrows$[Ln$_2$(*l*-moba)$_6$].[14]

As seen from Fig. 3, the dependency of molecular weight on concentration varies with the metal ions. The La^{III}, Pr^{III}, and Eu^{III} complexes show a large dependency on concentration, and almost all the molecules are dimerized at 1.0 wt%. It is likely that these complexes readily dimerize to achieve a higher coordination number owing to a relatively small interligand repulsion associated with the larger metal ions. Thus, the dimerization of these complexes is in line with their tendency to form hydrates. On the other hand, the molecular weights of the Dy^{III}, Ho^{III}, and Tm^{III} complexes show little dependency on concentration, and they are all monomeric in the concentration range examined. Since the size of the metal ion is relatively small, the bulky hydrophobic residues of the ligands

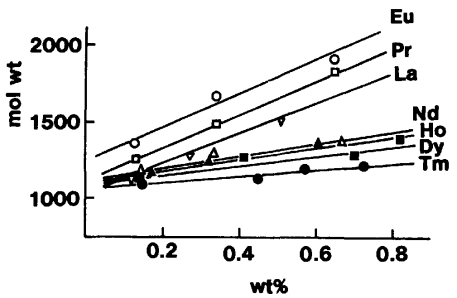

Fig. 3. Dependencies of molecular weights of the lanthanoid complexes on concentration in benzene: (▽): La, (□): Pr, (○): Eu, (△): Nd, (■): Dy, (▲): Ho, and (●): Tm complexes. The lines represent the trends of the molecular weight changes.

Table 2. Electronic and CD spectral data of complexes

Ln(III)	AB (ε)	CD ($\Delta\varepsilon\times10^3$)
Pr	444 (7.59)	445 (−3.71)
	472 (3.91)	471 (−1.93)
	485 (1.95)	486 (−1.56)
	580 (sh)	583 (−1.19)
Nd		528 (−2.87)
		532 (+2.16)
		537 (−1.96)
		541 (+0.98)
	571 (11.7)	568 (−3.04)
	587 (18.6)	577 (−3.27)
		585 (−3.51)
	682 (−)	680 (−0.61)
	736 (2.36)	730 (−0.91)
	742 (2.54)	740 (−0.61)
	753 (2.76)	755 (−0.61)
	784 (sh)	790 (−1.63)
	802 (4.12)	795 (+1.52)
Eu		464 (−0.93)
	525 (−)	524 (−1.48)
Dy	450 (−)	450 (+4.00)
		455 (−3.30)
Ho	468 (−)	463 (−4.17)
		467 (+1.69)
		473 (+1.36)
Tm	684 (2.61)	683 (−1.69)
	660 (0.41)	660 (−0.31)

would cover the metal center and interfere with the dimerization. The Nd^{III} complex showed a concentration-dependence of molecular weight similar to those of the Dy^{III} and Ho^{III} complexes, though Nd^{III} is rather similar to Pr^{III} and Eu^{III} in ionic size. It is likely that the Nd^{III} complex is of eight-coordination with two water molecules and thence exhibits a low tendency to dimerize.

In donating solvents tris(1,3-diketonato) lanthanoid-(III) complexes form solvent adducts to achieve a higher coordination number.[15] Such adducts formation would interfere with the dimerization of tris(1,3-diketonato)lanthanoid(III). Thus, we have measured the molecular weights of the *l*-moba complexes in ethanol, a donating solvent. The results indicate that the molecular weights are almost independent of concentration and fall in the range 1100—1200. It is obvious that the complexes forms adducts with one or two molecules of ethanol.

Difference spectral data of the complexes determined in benzene are given in Table 2. Each spectrum can be interpreted by means of free ionic terms. CD spectral data are also included in Table 2, and some of the spectra are shown in Figs. 4—6 as examples.

According to Richardson,[16] the interaction mechanisms between a metal ion and dissymmetric environment are classified into three: *i.e.*, (1) vicinal effect (chirality induced at the metal by the mere presence of asymmetric atom in the ligand), (2) conformational

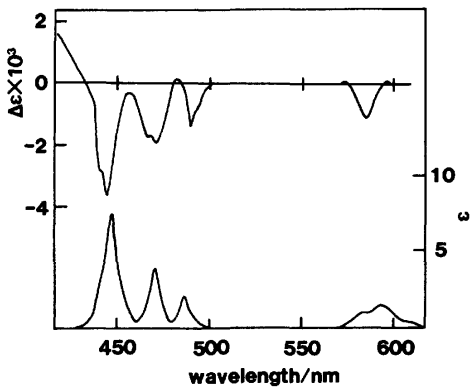

Fig. 4. Electronic and CD spectra of [Pr(*l*-moba)$_3$-(H_2O)] in benzene.

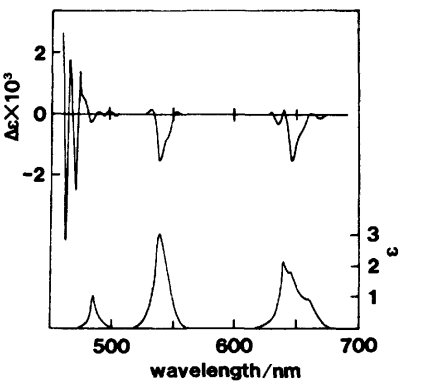

Fig. 5. Electronic and CD spectra of [Ho(*l*-moba)$_3$] in benzene.

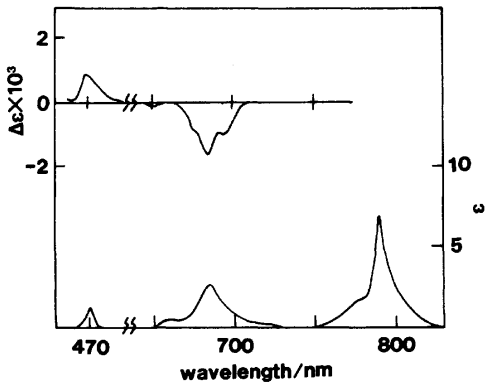

Fig. 6. Electronic and CD spectra of [Tm(*l*-moba)$_3$] in benzene.

effect (chilarity arising from the asymmetric atom in a chelate ring), and (3) the configurational effect (chirality due to an asymmetric disposition of chelate rings about the metal). In general, optical activity arising from the vicinal effect is at least one order of magnitude smaller than that from the conformational effect[17] and two orders of magnitude smaller than that from the configurational effect.[18]

In the present complexes the chiral group is out of the chelate ring and far apart from the metal ion. Hence, the optical activity induced at the f-f transition region by its vicinal effect would be supposed to be very small on this ground. However, the CD intensities observed for the present complexes are considerably high and comparable to those of the complexes with L-amino acidate ions.[19,20] This clearly indicates that the optical activities of the complexes are caused by the configurational effect. Therefore the present study has revealed that the interligand noncovalent interaction can bring about a stereoselectivity of lanthanoid complexes in spite of the lability of lanthanoid ions for ligand substitutions. In the cases of the Dy^{III}, Ho^{III}, and Tm^{III} complexes, the main species present in benzene is monomeric anhydrate at the concentration ($\approx 10^{-2}$M 1M=1 mol dm^{-3}) for the CD measurements. Thus, it is quite reasonable to assume that the interligand CH/π-interaction operating between the *l*-menthyl and phenyl residues of *l*-moba$^-$ (Fig. 2) causes the stereoselectivity producing the *cis*-Δ isomer, by analogy with the cases of the 3d-transition metal complexes with *l*-moba.[9,11]

On the other hand, the Pr^{III} and Eu^{III} complexes are substantially dimeric in benzene solution at the concentration for the CD measurements. Observations of considerably intense CD bands in the f-f transition region for these complexes indicate the existence of a stereoselectivity in the dimers. The stereoselectivities in the dimers can also be attributed to the interligand noncovalent interaction, though the detail of the interaction in the dimers is not clear at present because of the lack of crystallographic data.

It is expected that the stereoselectivity effected by the interligand noncovalent interactions also takes place in the solvent adducts of the *l*-moba complexes. We measured CD spectrum of [Dy(*l*-moba)3] as a representative example in ethanol and compared it

with the spectrum in benzene (Fig. 7). The CD spectrum in ethanol markedly differs from that of the monomeric [Dy(*l*-moba)$_3$] in benzene, implying the configurational change by the adduct formation. The considerably intense CD's in ethanol are indicative of a stereoselectivity in [Ln(*l*-moba)$_3$(EtOH)$_n$]. A similar stereoselectivity in the solvent adducts has been recognized for the lanthanoid complexes with the chiral 1,3-diketones derived from *d*-camphor.[4,15]

It is well known that Eu^{III} complexes with 1,3-diketones exhibit luminescence at the $^5D_0 \rightarrow {}^7F_1$ and $^5D_0 \rightarrow {}^7F_2$ transitions.[15,21-23] [Eu(*l*-moba)$_3$(H_2O)] also emits luminescence at 586 and 609 nm corresponding to the above transitions, respectively (Fig. 8). Interestingly, the intensity of the luminescence in benzene dramatically increases with the decrease of the concentration. Taking into account the monomer-dimer equilibrium of the complex, it is evident that the luminescence occurs only on the monomer. In relation to this, it should be noted that the Eu^{III} complexes with 1,3-diketones generally show only weak luminescence in nondonating solvents but its intensity is much enhanced on the addition of dimethyl sulfoxide to the solution.[15] Further, the adduct formations with "synergic agents" such as trioctylphosphine, tributyl phosphate, or dihexyl sulfoxide have been used to improve the quantum efficiency of luminescence[21]. Such enhancement of luminescence in these complexes can also be rationalized in terms of the shift of the monomer-dimer equilibrium to the monomeric species caused by the adduct formation with the solvent molecules or the synergic agents. It is generally accepted that the quantum efficiency of luminescence of lanthanoid complexes decreases when radiationless energy loss occurs in the excited state through the contact with other molecules, quenching impurities, or undesirable solvent molecules.[21] Therefore, the present results suggest that dimerization also facilitates nonradiative relaxation and thence greatly reduces the quantum efficiency of luminescence.

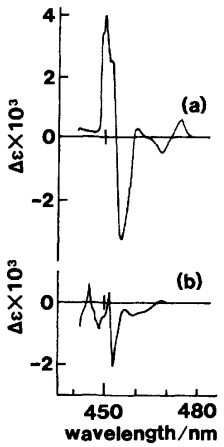

Fig. 7. CD spectra of [Dy(*l*-moba)$_3$]; (a) in benzene and (b) in ethanol.

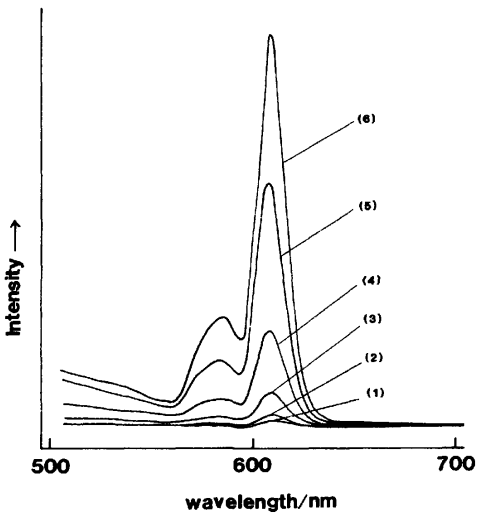

Fig. 8. Relative intensities of luminescence of [Eu(*l*-moba)$_3$(H_2O)] at various concentrations: (1): 3.681×10^{-2}, (2): 1.841×10^{-2}, (3): 1.104×10^{-2}, (4): 7.362×10^{-3}, (5): 3.681×10^{-3}, and (6): 1.472×10^{-3} M.

In conclusion the present study has shown that the interligand CH/π-interaction causes the stereoselectivity in the monomers, dimers, and solvent-adducts of the lanthanoid complexes. Further, it is suggested that the interligand CH/π-interaction forms an insulating sheath to protect the complexes from dimerization and solvation, especially in the cases of smaller lanthanoid ions and in dilute solutions.

The authors wish to thank to Dr. K. Yoshimura of Kyushu University for the measurements of luminescence spectra.

References

1) Part VII: Ref. 11.
2) A. F. Cockerill, G. L. O. Davis, R. C. Harden, and D. M. Rickman, *Chem. Rev.*, **73**, 553 (1973).
3) R. E. Siervers, "Nuclear Magnetic Resonances Shift Reagents," Academic Press, New York (1973).
4) H. G. Brittain, *J. Chem. Soc., Dalton Trans.*, **1983**, 1165, and references therein.
5) G. R. Sullivan, "Topics in Stereochemistry," ed by E. L. Eliel and N. L. Allinger, John Wiley & Sons Inc., New York (1978), Vol. 10, p. 287.
6) M. D. McCreary, D. W. Lewis, D. L. Wernick, and G. M. Whitesides *J. Am. Chem. Soc.*, **96**, 1038 (1974).
7) H. G. Brittain, *Coord. Chem. Rev.*, **48**, 243 (1983).
8) H. G. Brittain and F. S. Richardson, *J. Am. Chem. Soc.*, **98**, 5858 (1976).
9) H. Ōkawa, K. Ueda, and S. Kida, *Inorg. Chem.*, **21**, 1594 (1982).
10) M. Nakamura, H. Ōkawa, and S. Kida, *Chem. Lett.*, **1981**, 547.
11) M. Nakamura, H. Ōkawa, and S. Kida, *Inorg. Chim. Acta*, in press.
12) R. C. Fay, A. Y. Girgis, and U. Klabunde, *J. Am. Chem. Soc.*, **92**, 7056 (1970).
13) J. K. Przystal, W. G. Bos, and I. B. Liss, *J. Inorg. Nucl. Chem.* **33**, 679 (1971).
14) The possibility of forming oligomers higher than the dimer can not be ruled out. However, such oligomers must be much less than the dimer in the concentration range examined throughout this study.

15) H. G. Brittain, *Polyhedron*, **2**, 261 (1983).
16) F. A. Richardson, *Chem. Rev.*, **79**, 17 (1979).
17) T. Yasui, J. Hidaka, and Y. Shimura, *Bull. Chem. Soc. Jpn.*, **39**, 2417 (1966).
18) T. Yasui. J. Fujita, and Y. Shimura, *Bull. Chem. Soc. Jpn.*, **42**, 2081 (1969).
19) S. Misumi, S. Kida, T. Isobe, Y. Nishida, and H. Furuta, *Bull. Chem. Soc. Jpn.*, **42**, 3433 (1969).
20) S. Misumi, S. Kida, and T. Isobe, *Spectrochim. Acta*, **24A**, 271 (1966).
21) F. Halverson, J. S. Brinen, and J. R. Leo, *J. Chem. Phys.*, **40**, 2790 (1964).
22) H. G. Brittain, *J. Am. Chem. Soc.*, **101**, 1733 (1979).
23) H. G. Brittain, *Inorg, Chem.*, **19**, 640 (1980).

 © 1984 The Chemical Society of Japan Bull. Chem. Soc. Jpn., 57, 3152—3155 (1984)

Synthetic Photochemistry. XXVIII.[1] A Photochemical C_5-Homologation of 4-Isopropenyltoluene with Methyl 2,4-Dioxopentanoate to Isolaurene and a Formal Synthesis of Cuparene

Hitoshi TAKESHITA,* Akira MORI, and Satoshi NAKAMURA†

Research Institute of Industrial Science, 86, Kyushu University, Kasuga-koen, Kasuga, Fukuoka 816

†*Graduate School of Engineering Sciences, 39, Kyushu University, Kasuga-koen, Kasuga, Fukuoka 816*

(Received March 8, 1984)

Starting from the photocycloaddition of methyl 2,4-dioxopentanoate with 4-isopropenyltoluene, isolaurene was synthesized, and its further conversion to 5-cuparenone constituted the formal synthesis of cuparene. For the first time, the *proto*-(2+2)π cycloadduct, a β-keto cyclobutanol derivative, has been isolated from the product mixture.

Recently, we have extended the use of the photocycloadducts of methyl 2,4-dioxopentanoate (**1**) with olefins to a facile cyclopentane ring construction.[2] The method must be applicable to a synthesis of laurenoids or cuparenoids.

An advantage of using **1** as a photocycloaddend is a capability of reaction with conjugated olefins; with cyclopentadiene[2] and with cycloheptatriene,[3] it gave the (2+2)π cycloadducts in addition to the (2+4)π and/or (2+6)π cycloadducts. Even with an acyclic diene, isoprene, **1** smoothly produced the (2+2)π cycloadducts, from which sesquiterpenoids, geijerone and an elemene derivative,[4] and monoterpenoids, dehydroiridodial, and chrysomelidial,[5] have been synthesized. This constitutes a proper head-to-tail homologation of terpenoids with the C_5-unit. Based on this method, cuparenoids and migrated cuparenoids, many of which are physiologically active, can be constructed as shown in the following *retro*-synthetic scheme (Scheme 1).

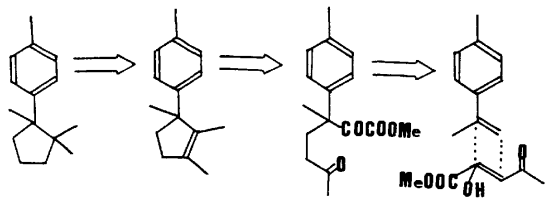

Scheme 1.

Since indene was photochemically reactive with **1**,[6] 4-isopropenyltoluene (**2**) should also be reactive enough to form the photoadduct (**3**) which could be just the proper starting material for the purpose.

When an ethyl acetate solution of **1** and **2** was internally irradiated by means of a high-pressure mercury lamp, formation of four photoproducts was recognized, as shown in Scheme 2. The major product (48% yield) was the desired (2+2)π cycloadduct (**3**). Its ^{1}H-NMR spectrum showed signals ascribable to the *p*-tolyl, acetyl, and methoxycarbonyl groups. Another compound (**4**, 10% yield) showed not only the NMR signals of acetyl and methoxycarbonyl groups, but those of a methine proton on the carbon bearing the methoxycarbonyl and hydroxyl groups and a terminal methylene group. Therefore, **4** must be an ene-reaction product.[7]

Another product (**5**), 0.2% yield, exhibited the $\nu_{C=O}$ band in the IR spectrum, and was converted into **3** under somewhat strong conditions. Therefore, **5** must be the *proto*-(2+2)π adduct. It is surprising that an intensive use of silica-gel column chromatography in the workup has not completed the *retro*-aldolization of such a strained aldol, **5**.

Although we have previously isolated the *proto*-(4+2)π[2] and (6+2)π[3] cycloadducts of **1** with conjugated olefins, this is the first example of an isolation of a *proto*-(2+2)π adduct.

From the less polar photoproduct mixture, 23% of a hydrocarbon (**6**) has been isolated; its NMR analysis determined the structure to be the ene-type dimer of **2**.

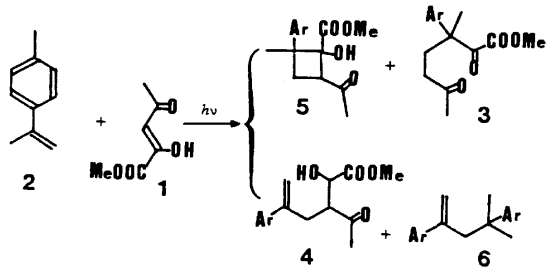

Scheme 2.

The formation of **3** from **2** can be regarded as a C_5 homologation of a monoterpene to sesquiterpenoid derivatives; subsequent transformations of **3**, in Scheme 3, may lead to a fundamental laurenoid skeleton. When **3** was treated with titanium(II) chloride,[5,8,9] generated *in situ* from titanium(IV) chloride and zinc dust, two *cis*-glycol derivatives (**7** and **8**) were formed in good yields. Both **7** and **8** formed the dioxolane derivatives (**9** and **10**) by treatment with 2,2-dimethoxypropane in the presence of pyridinium *p*-toluenesulfonate (PPTS) in benzene. Relative configurations of **7** and **9** *vs.* **8** and **10** were determined by the ^{1}H-NMR comparisons; the methoxyl signals of the ester groups of **7** and **9** appeared at δ=3.27 and 3.21, while those of **8** and **10** at 3.80 and 3.76, and the difference can be explained in terms of the anisotropic high-field shift due to the proximate aromatic ring in the formers. Therefore, the *p*-tolyl and the methoxycarbonyl groups of **7** and **9** are in *cis*-rela-

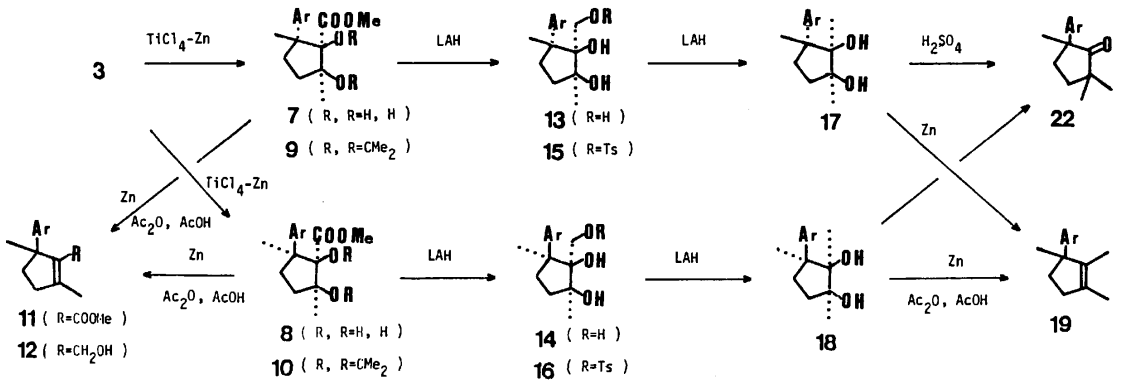

Scheme 3.

tionship.

The zinc-in-acetic acid reduction of both **7** and **8** afforded the same cyclopentene derivative (**11**), whose LAH (lithium aluminum hydride) reduction to an allyl alcohol (**12**) was unsatisfactory because of a low yield. Alternatively, **7** and **8** were at first reduced to the triols (**13** and **14**), and then their tosylates (**15** and **16**) were reduced again with LAH to the diols (**17** and **18**). The ^{1}H-NMR spectrum of **18** was identical with that of the osmium(VIII) oxide oxidation product of isolaurene, although the original workers[11] did not specify the stereochemistry.[11]

The reduction of **18** with zinc in acetic acid[12] gave a hydrocarbon (**19**) in 98% yield, whose reported NMR data in carbon tetrachloride was identical with isolaurene.[10] Consequently, an alternative synthesis of **19** has been completed.

On the other hand, the same treatment of **17** yielded **19** in a lower yield, 53%, together with the formation of two cyclopentadiene derivatives (**20** and **21**) in 33 and 6% yields. The structures of **20** and **21** were clarified by the NMR analysis; the formation of **20** from **17** in a substantial amount confirmed the assignment for the stereochemistry of the glycols, **7** and **8** (Scheme 4).

Following the conversion of **18** to 2,5,5-trimethyl-2-(*p*-tolyl)cyclopentanone (**22**),[10] **17** was also treated with methanolic sulfuric acid briefly; an exclusive product was the cyclopentanone (**22**) whose structure was firmly established by the NMR comparisons. In any case, the protic acid-induced rearrangement of **17** and **18** never furnished the cuparene skeleton. Probably, this comes from a preferential protonation to the C-3 hydroxyl groups over the C-2 hydroxyl group on steric grounds.

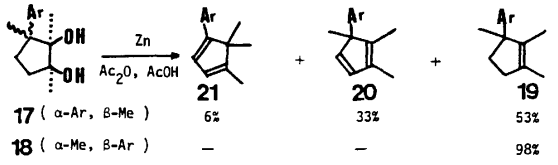

Scheme 4.

These results of the protic acid-catalyzed dehydration of **17** and **18** made us examine the Lewis acid-promoted reaction of an oxygenated isolaurene derivative. Indeed, when an epoxide (**23**) prepared from **19** and *m*-chloroperbenzoic acid (MCPBA) was treated with boron trifluoride etherate in benzene, a facile rearrangement occurred. The sole product formed was a cyclopentanone derivative (**24**) whose NMR data measured in carbon tetrachloride were identical with those of 2,3,3-trimethyl-2-(*p*-tolyl)cyclopentanone (5-cuparenone) already prepared by de Mayo and Suau.[13] As proposed in Scheme 5, the rearrangement of **23** to **24** involved migrations of the *p*-tolyl and the methyl groups *via* formation of the spirocyclic phenonium ion (**B**). Since cuparene[14] has been synthesized from **24**,[13] the present study constitutes another total synthesis of it.

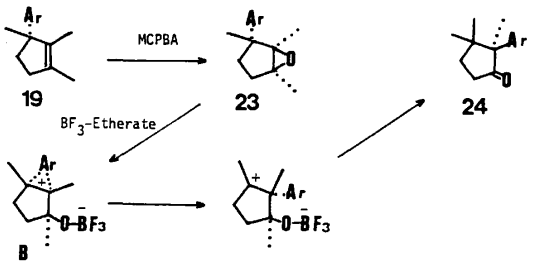

Scheme 5.

Experimental

The elemental analyses were performed by Miss M. Yamaguchi of This Institute. The NMR spectra were measured by an FX 100 Model spectrometer, JEOL, in $CDCl_3$ solutions unless otherwise specified, and the chemical shifts were expressed in δ units from the internal Me_4Si. The mass spectra were measured by an O1SG Model spectrometer, JEOL, and the IR spectra were taken either in solution (CCl_4 or $CHCl_3$) or as KBr disks, by an A 102 Model spectrometer, JASCO.

Photocycloaddition Reaction of 4-Isopropenyltoluene (2) with 1. An EtOAc solution (50 cm^3) of **2** (27.6 g) and **1** (9.2 g) was placed in an immersion well cooled with running water, and was internally irradiated with a 400-W high-pressure mercury lamp with an occasional check of the reaction with $FeCl_3$ coloration. After 25 h, the mixture was evaporated *in vacuo* at room temperature to remove the volatile material, and fractionated with benzene and aqueous Na_2CO_3. The organic layer containing the photoadducts was then dried on $MgSO_4$, and chromatographed on a silica-gel column; from the least polar fractions eluted with hexane was the hydrocarbon, **6**, 10.2 g (23%) [Found: M$^+$, 264.1857. Calcd for $C_{20}H_{24}$: M$^+$, 264.1875. δ=1.16 (6H, s), 2.24 (3H, s), 2.75 (2H, s), 4.70 (1H, dm, J=2 Hz), 5.09 (1H, d, J=2 Hz), and 6.8—7.2 (8H, m). δ(C)=20.8, 21.0, 28.8 (2C), 38.3, 49.6, 116.2, 125.9 (2C), 126.5 (2C), 128.7 (2C), 128.9 (2C), 134.8, 136.5, 140.8, 146.7, and 146.8. ν: 3200—2800, 1625, 1520, 900, 830, 817 cm^{-1}].

From the subsequent fractions eluted by hexane-EtOAc (9:1) gave a colorless oil, **3**, 8.0 g (48%). Cold finger distillation of a part of this sample yielded the analytical specimen, a colorless liquid [Found: C, 69.58; H, 7.36%. M^+, 276.1361. Calcd for $C_{16}H_{20}O_4$: C, 69.54; H, 7.30%; M^+, 276.1361. δ=1.57 (3H, s), 1.99 (3H, s), 2.0—2.3 (4H, m), 2.26 (3H, s), 3.50 (3H, s), and 7.07 (4H, s). δ(C)=20.8, 21.0, 29.6, 31.4, 38.3, 52.0, 52.8, 126.5 (2C), 129.5 (2C), 136.9, 137.0, 162.7, 197.3, and 207.1. ν: 1743, 1722 cm^{-1}].

Subsequently, the fractions from hexane-EtOAc (8:2) yielded a pale yellow oil, **4**, 1.7 g (10%) [Found: C, 69.47; H, 7.39%. M^+, 276.1358. δ=2.10 (3H, s), 2.34 (3H, s), 2.8—3.2 (4H, m, diminished to 3H by adding D_2O), 3.69 (3H, s), 4.21 (1H, d, J=3.2 Hz), 5.13 (1H, d, J=1.3 Hz), 5.53 (1H, d, J=1.3 Hz), and 6.8—7.3 (4H, m). δ(C)=21.1, 30.4, 33.8, 52.5, 53.0, 70.9, 115.0, 126.0 (2C), 129.3 (2C), 136.7, 137.7, 144.5, 173.8, and 210.9. ν: 3500, 1740, 1715 cm^{-1}]. An oily material obtained from more polar fractions was further purified by means of preparative thin-layer chromatography (PTLC) to yield a colorless oil, **5**, 29 mg (0.2%) [Found: M^+, 276.1367. Calcd for $C_{16}H_{20}O_4$: 276.1362. δ=1.44 (3H, s), 2.10 (3H, s), 2.0—2.4 (4H, m, diminished to 3H by adding D_2O), 2.31 (3H, s), 3.83 (3H, s), and 6.8—7.2 (4H, m). δ(C)=21.2, 24.8, 30.2, 31.5, 37.7, 39.7, 52.6, 62.3, 129.5 (2C), 129.8 (2C), 136.4, 173.3, and 208.7. ν: 3460, 1725, 1710 cm^{-1}].

Conversion of 5 to 3. A benzene solution (2 cm^3) of **5** (5 mg) and TsOH (1 mg) was refluxed for 1 h. PTLC of the reaction mixture afforded **3**, 3.5 mg (70%), whose identity with the authentic sample was confirmed by direct comparisons.

Reductive Cyclization of 3. Formation of 7 and 8. To an anhydrous tetrahydrofuran (THF, 60 cm^3) of $TiCl_4$ (650 mg), Zn (450 mg) and pyridine (240 mg) were added at 0 °C. The mixture, containing Ti(II) salt, was then cooled by ice-water, and a THF solution (20 cm^3) of **3** (631 mg) was added for 0.5 h at 0 °C with vigorous stirring. After 3 h, the mixture was poured into ice-water, and extracted with ether, and the ether extract was chromatographed on a silica-gel column with hexane-EtOAc (3:1) to give colorless crystals, mp 126—126.5 °C, **7**, 213 mg (34%) [Found: C, 69.29; H, 8.01%; M^+, 278.1509. Calcd for $C_{16}H_{22}O_4$: C, 69.04; H, 7.97%; M^+, 278.1520. δ=1.12 (3H, s), 1.50 (3H, s), 2.26 (3H, s), 2.4—2.8 (4H, m), 3.27 (3H, s), 3.4 (1H, br. s, disappeared by adding D_2O), 4.24 (1H, br. s, disappeared by adding D_2O), and 6.8—7.2 (4H, m). δ(C)=20.8, 25.5, 28.0, 32.9, 35.8, 51.8, 52.1, 80.3, 89.4, 124.9 (2C), 128.5 (2C), 135.0, 144.8, and 175.4. ν=3460, 1720, 1515, 1260 cm^{-1}], and a colorless oil, **8**, 219 mg (35%) [Found: M^+, 278.1520. δ=1.23 (3H, s), 1.37 (3H, s), 1.8—2.2 (3H, m), 2.28 (3H, s), 2.4—2.8 (2H, m), 3.48 (1H, br. s), 3.80 (3H, s), and 7.04 (4H, m). δ(C)=20.8, 25.4, 26.8, 34.6, 37.7, 52.3 (2C), 81.4, 88.6, 127.6 (2C), 128.4 (2C), 135.7, 141.7, and 174.1. ν: 3470, 1515, 1250 cm^{-1}].

Isopropylidenedioxy Derivative (9) from 7. To an anhydrous benzene solution (2 cm^3) of **7** (27.6 mg), 2,2-dimethoxypropane (2 cm^3) and PPTS (10 mg) were added at once, this mixture was kept at 15—25 °C for 8 h. It was then diluted with ether and washed with aqueous K_2CO_3 solution. PTLC of the organic extracts with hexane-EtOAc (4:1) yielded a colorless oil, 15 mg (55%), **9** [Found: M^+, 318.1839. Calcd for $C_{19}H_{26}O_4$: M^+ 318.1831. δ=1.38 (3H, s), δ=1.45 (3H, s), 1.50 (3H, s), 1.63 (3H, s), 1.8—2.9 (4H, m), 2.27 (3H, s), 3.21 (3H, s), and 7.03 (4H, s). δ(C)=21.0, 27.4, 27.6, 28.1, 28.4, 37.1, 39.6, 51.2, 54.5, 93.7, 100.0, 115.4, 125.3 (2C), 128.6 (2C), 135.2, 144.7, and 172.7. ν: 1750 cm^{-1}].

Isopropylidenedioxy Derivative (10) from 8. Similarly, **8** (52 mg) was converted to **10**, a colorless oil, 67.5 mg (74%) [Found: M^+, 318.1839. δ=1.28 (3H, s), 1.35 (6H, s), 1.58 (3H, s), 1.6—2.0 (4H, m), 2.29 (3H, s), 3.76 (3H, s), and 7.08 (4H, s). δ(C)=20.9, 24.9, 26.9, 27.2, 27.4, 34.7, 38.8, 51.6, 54.6, 93.4, 95.7, 109.8, 126.5 (2C), 128.6 (2C), 135.5, 141.5, and 171.8. ν: 1720 cm^{-1}].

Reduction of 7 with Zinc in Acetic Acid. To a mixed solution of Ac_2O (18 cm^3) and AcOH (9 cm^3) of **7** (142.5 mg), powdered Zn (3 g) was added in portions while refluxing for 6 h. The mixture was then evaporated *in vacuo* to remove the solvent, and the residue was poured into ice-water, and extracted with benzene. The extracts were purified by PTLC to give a colorless oil, 80 mg (64%), **11** [Found: M^+, 244.1463. Calcd for $C_{16}H_{20}O_2$: M^+, 244.1463. δ=1.61 (3H, s), 1.8—2.3 (4H, m), 2.14 (3H, s), 2.27 (3H, s), 3.50 (3H, s), and 7.0—7.1 (4H, m). δ(C)=16.9, 20.9, 25.0, 37.8, 42.5, 50.5, 53.8, 125.4 (2C), 128.7 (2C), 134.7, 135.1, 146.1, 155.1, and 166.3. ν: 1715, 1520, 1268 cm^{-1}].

Reduction of 8 with Zinc in Acetic Acid. Similarly, **8** (41 mg) was reduced with powdered Zn (670 mg) in Ac_2O (4 cm^3) and AcOH (2 cm^3) for 9.5 h to give a colorless oil, 35 mg (85%), which was identical with the sample of **12** obtained from the reduction of **7**.

LAH-Reduction of 11 to Give 12 An anhydrous ether solution (25 cm^3) of **11** (46.5 mg) was treated with LAH (22 mg) at 15—25 °C for 1.5 h. The mixture was then treated with EtOAc, and poured into ice-water, and extracted with ether. The PTLC of the extracts with hexane-EtOAc (3:1) gave a colorless oil, 2.4 mg (6%), **12** [Found: M^+, 216.1514. Calcd for $C_{15}H_{20}O$: M^+, 216.1514. δ=1.51 (3H, s), 1.83 (3H, s), 2.30 (3H, s), 3.83 (1H, d, J=12.5 Hz), 4.05 (1H, d, J=12.5 Hz), and 7.0—7.2 (4H, m). δ(C)=14.4, 20.9, 25.1, 36.1, 41.7, 53.9, 57.2, 125.9 (2C), 128.9 (2C), 135.2, 138.4, 141.1, and 146.1. ν: 3420, 1520 cm^{-1}].

LAH-Reduction of 7. Formation of 13. An anhydrous ether solution (30 cm^3) of **7** (188 mg) was treated with LAH (102 mg) at 15—25 °C for 0.5 h, and subsequently refluxed for 5 h. The mixture was then poured into ice-water and extracted with ether. Silica-gel column chromatography of the extracts yielded colorless needles, mp 126—127 °C, 168 mg (99%), **13** [Found: C, 72.09; H, 8.90; M^+, 250.1569. Calcd for $C_{15}H_{22}O_3$: C, 71.97; H, 8.86%; M^+, 250.1569. δ=1.12 (3H, s), 1.43 (3H, s), 1.8—2.4 (5H, m, diminished to 4H by adding D_2O), 2.29 (3H, s), 2.74 (1H, br. s, disappeared by adding D_2O), 3.33 (1H, d, J=12 Hz), 3.53 (1H, d, J=12 Hz), 3.84 (1H, br. s, disappeared by adding D_2O), and 7.0—7.2 (4H, m). δ(C)=20.8, 26.2, 26.7, 33.6, 38.0, 51.3, 64.7, 81.4, 83.3, 127.2 (2C), 129.0 (2C), 136.0, and 143.6. ν: 3500, 1360 cm^{-1}].

LAH-Reduction of 8. Formation of 14. Similarly, **8** (679 mg) was converted by the LAH reduction to colorless needles, mp 107—108 °C, 605 mg (99%), **14** [Found: C, 71.99; H, 8.98%; M^+, 250.1563. δ=1.35 (3H, s), 1.41 (3H, s), 2.0—2.3 (4H, m), 2.29 (3H, s), 3.00 (3H, br. s, disappeared by adding D_2O), 3.55 (1H, d, J=12 Hz), 3.70 (1H, d, J=12 Hz), and 6.8—7.2 (4H, m). δ(C)=20.7, 24.7, 25.4, 35.9, 38.7, 50.7, 63.1, 81.1, 81.2, 127.8 (2C), 128.5 (2C), 135.8, and 142.1. ν: 3450, 3300, 1510 cm^{-1}].

LAH-Reduction of a Monotosylate (15) Derived from 13. Preparation of 17. To a cold pyridine solution (5 cm^3) containing TsCl (380 mg), **13** (331 mg) was added and kept at 10—15 °C for 24 h. The mixture was then heated *in vacuo* to remove the volatile material, and the residue was washed with water, and extracted with $CHCl_3$. The extracts yielded colorless oily monotosylate, **15**, 528 mg (99%) [δ=1.18 (3H, s), 1.36 (3H, s), 1.6—2.3 (4H, m), 2.28 (3H, s), 2.41 (3H, s), 2.68 (1H, d, J=10 Hz), 2.83 (2H, br. s), 3.91 (1H, d, J=10 Hz), and 6.9—7.5 (8H, m). δ(C)=20.8, 21.6, 26.1, 26.5, 32.8, 38.1, 51.6, 72.0, 80.8, 81.8, 126.6 (2C), 127.8 (2C), 128.7 (2C), 129.6 (2C), 131.9, 135.6, 142.3, and 144.6. ν: 3500, 1360 cm^{-1}], on silica-gel column chromatography. Subsequently, **15** (145 mg) was dissolved in an anhydrous ether (10 cm^3), and was reduced with LAH (30 mg) in ether (25 cm^3) at 15—25 °C for 3 h. Then, the mixture was treated with EtOAc, poured into ice-water, and

extracted with ether. The extracts were chromatographed on a silica-gel column to give colorless needles, mp 91—92 °C, 81 mg (96%), **17** [Found: M^+, 234.1621. Calcd for $C_{15}H_{22}O_2$: M^+, 234.1620. δ=0.78 (3H, s), 1.21 (3H, s), 1.42 (3H, s), 1.8—2.1 (4H, m), 2.30 (3H, s), 2.6 (2H, br. s, disappeared by adding D_2O), and 7.0—7.2 (4H, m). δ(C)=21.0, 22.4, 25.5, 26.5, 31.9, 37.1, 51.7, 80.4, 82.5, 126.3 (2C), 128.6 (2C), 135.1, and 145.4. ν: 3600—3300, 1510 cm^{-1}].

Reduction of 14 to 18 via *Monotosylate (16).* Similarly, **14** (558 mg) was converted to a monotosylate (**16**), a colorless oil, 887 mg (99%) [δ=1.32 (3H, s), 1.41 (3H, s), 1.8—2.3 (4H, m), 2.27 (3H, s), 2.37 (3H, s), 2.62 (2H, br. s), 4.09 (1H, d, J=10 Hz), 4.23 (1H, d, J=10 Hz), and 7.0—7.5 (8H, m). δ(C)=20.8, 21.6, 24.2, 25.7, 36.7, 39.1, 50.8, 71.4, 80.6, 80.7, 126.6 (2C), 127.8 (2C), 128.6 (2C), 129.8 (2C), 132.4, 136.1, 140.8, and 144.9. ν: 3500, 1360 cm^{-1}]. Then, an anhydrous ether solution (30 cm^3) of **16** (465 mg) was reduced by LAH (95 mg) to a colorless oil, 268 mg (99%), **18** [Found: M^+, 234.1622. δ=1.12 (3H, s), 1.28 (3H, s), 1.34 (3H, s), 2.0—2.3 (4H, m), 2.30 (3H, s), 2.6 (2H, br. s, disappeared by adding D_2O), and 7.1—7.3 (4H, m). δ^{CCl_4}=1.08 (3H, s), 1.20 (3H, s), 1.29 (3H, s), 1.8—2.3 (4H, m), 2.30 (3H, s), and 7.0—7.1 (4H, m). δ(C)=19.4, 20.8, 25.6, 26.1, 33.9, 38.3, 51.4, 80.9, 82.4, 127.3 (2C), 128.9 (2C), 136.0, and 141.9. ν: 3450, 1515 cm^{-1}], of which the NMR taken in CCl_4 was in accord with that (lit, mp 114—116 °C) prepared by Irie *et al.*[10]

Reduction of 17 with Zinc in Acetic Acid. Formation of 19, 20, and 21. To a mixed solution of Ac_2O (12 cm^3) and AcOH (6 cm^3) of **17** (145 mg), powdered Zn (617 mg) was added in portions, and the mixture was refluxed for 3 h. It was then filtered, and the residue was washed with water, dil HCl, and ether. The filtrate was extracted with ether, and the combined organic layer was evaporated *in vacuo* to remove the volatile material. Then the residue was chromatographed on a silica-gel column. From the less polar fractions, a hydrocarbon, **19**, a colorless oil, 65 mg (53%) [Found: M^+, 200.1575. Calcd for $C_{15}H_{20}$: 200.1563. δ=1.37 (3H, s), 1.39 (3H, s), 1.71 (3H, s), 2.0—2.3 (4H, m), 2.30 (3H, s), and 7.07 (4H, s). δ^{CCl_4}=1.32 (3H, s), 1.35 (3H, s), 1.69 (3H, s), 1.8—2.3 (4H, m), 2.26 (3H, s), and 6.92 (4H, s). δ(C)=10.3, 14.3, 20.9, 34.3, 35.9, 41.6, 54.6, 126.1 (2C), 128.7 (2C), 131.8, 134.6, 137.5, and 146.2], was isolated, and was in accord with isolaurene in respects of the reported NMR.[10] From the more polar fractions, other hydrocarbons, **20**, 42 mg (33%) [Found: M^+, 198.1406. Calcd for $C_{15}H_{18}$: 198.1406. δ=1.44 (3H, s), 1.55 (3H, s), 1.85 (3H, s), 2.28 (3H, s), 6.10 (H, d, J=6.5 Hz), 6.28 (1H, d, J=6.5 Hz), and 6.9—7.05 (4H, m). ν: 2960, 2930, 1510, 815 cm^{-1}], and **21**, 7 mg (6%) [Found: M^+, 198.1392. δ=1.19 (6H, s), 1.87 (3H, d, J=2 Hz), 2.30 (3H, s), 5.94 (1H, quint, J=2 Hz), 6.53 (1H, d, J=2 Hz), and 7.05—7.35 (4H, m). δ(C)=12.4, 21.0, 22.5 (2C), 53.0, 123.3, 125.2, 125.8 (2C), 128.9 (2C), 133.6, 135.6, 145.1 and 155.5], were isolated.

Reduction of 18 with Zinc in Acetic Acid to 19. Similarly, **18** (231.5 mg) was refluxed with powdered Zn (980 mg) in Ac_2O (20 cm^3) and AcOH (10 cm^3) for 3 h. The mixture was then washed with water and with dil HCl, and extracted with ether. The ether extracts were heated *in vacuo* to remove the solvent, and the residue was chromatographed on a silica-gel column to give a colorless oil, **19**, 194 mg (98%) which was identical with the sample obtained from **17**.

Sulfuric Acid Treatment of 17. A methanolic H_2SO_4 solution (10%, 2 cm^3) of **17** (26.5 mg) was treated at 20—25 °C for 5 min. The mixture was then poured into water and extracted with benzene. The extracts were purified by PTLC to give **22**, 23.2 mg (95%) [Found: M^+, 216.1508. Calcd for $C_{15}H_{20}O$: M^+, 216.1514. δ=1.00 (3H, s), 1.14 (3H, s), 1.37 (3H, s), 1.6—2.3 (4H, m), 2.30 (3H, s), and 7.05—7.2 (4H, m). δ^{CCl_4}=0.94 (3H, s), 1.08 (3H. s), 1.29 (3H, s), 1.6—2.3 (4H, m), 2.28 (3H, s), and 6.95—7.1 (4H, m). δ(C)=20.9, 25.1, 25.5, 26.5, 34.7, 34.9, 45.5, 53.4, 126.3 (2C), 129.4 (2C), 136.2, 140.6, and 224.7. ν: 1735 cm^{-1}], which was identical with the product prepared by Irie *et al.* from **18**.[10]

Epoxidation of 19 to 23. A CH_2Cl_2 solution (25 cm^3) of **19** (200 mg) was mixed with MCPBA (90%, 345 mg), and kept at 15—25 °C for 24 h. After filtration of the resultant *m*-chlorobenzoic acid, the filtrate was washed with aqueous $NaHCO_3$, and chromatographed on a silica-gel column to give a colorless oil, 147 mg (68%), **23** [Found: M^+, 216.1512. Calcd for $C_{15}H_{20}O$: M^+, 216.1512. δ=1.12 (3H, s), 1.47 (3H, s), 1.49 (3H, s), 1.8—2.8 (4H, m), 2.32 (3H, s), and 7.0—7.1 (4H, m). δ(C)=11.7, 15.9, 20.2, 20.9, 31.8, 37.3, 48.5, 70.4, 72.7, 125.8 (2C), 129.0 (2C), 135.4, and 143.8. ν: 3150—2800, 1520, 1243, 815 cm^{-1}].

BF_3-Catalyzed Rearrangement of 23. Formation of 24. An anhydrous benzene solution (1 cm^3) of **23** (11.9 mg) was mixed with BF_3 etherate (0.05 cm^3), and kept at 20—25 °C for 5 min. The mixture was then poured into ice-water and extracted with $CHCl_3$. The extracts were chromatographed on a silica-gel column to give a colorless oil, 10.9 mg (92%), **24** [Found: M^+, 216.1512. Calcd for $C_{15}H_{20}O$: M^+, 216.1512. δ=0.67 (3H, s), 1.06 (3H, s), 1.32 (3H, s), 1.8—2.8 (4H, m), 2.30 (3H, s), and 6.95—7.1 (4H, m). δ^{CCl_4}=0.65 (3H, s), 1.04 (3H, s), 1.24 (3H, s), 1.8—2.8 (4H, m), 2.28 (3H, s), and 6.92 (4H, s). δ(C)=19.3, 20.9, 23.9, 26.5, 33.5, 36.0, 42.7, 59.9, 127.7 (2C), 128.4 (2C), 135.9, 137.9, and 222.1. ν: 3200—2800, 1742, 1510 cm^{-1}], which was in good agreement with the reported NMR data (in CCl_4) of de Mayo and Suau.[13]

The authors are grateful to the Ministry of Education, Science, and Culture for a Grant to H. T. (No. 57218019).

References.

1) Part. XXVII: H. Takeshita, S. Hatta, and T. Hatsui, *Bull. Chem. Soc. Jpn.*, **57**, 619 (1984).

2) H. Takeshita, A. Mori, and Y. Toyonaga, *Bull. Chem. Soc. Jpn.*, **48**, 307 (1975).

3) H. Takeshita, A. Mori, and S. Itô, *Bull. Chem. Soc. Jpn.*, **47**, 1767 (1974).

4) H. Takeshita, T. Hatsui, and T. Masuda, *Kyushu Daigaku Sogo Rikogaku Kenkyuka Hokoku*, **1**, 35 (1979).

5) H. Takeshita, T. Hatsui, N. Kato, T. Masuda, and H. Tagoshi, *Chem. Lett.*, **1982**, 1153.

6) H. Takeshita, A. Mori, and Y. Toyonaga, *Kyushu Daigaku Seisan Kagaku Kenkyusho Hokoku*, **64**, 25 (1976).

7) Occurrence of the ene-reaction in the photoreaction of **1** has already been reported. See H. Takeshita and K. Komiyama, *Kyushu Daigaku Seisan Kagaku Kenkyusho Hokoku*, **73**, 19 (1982).

8) T. Mukaiyama, N. Hayashi, and K. Narasaka, *Chem. Lett.*, **1973**, 291.

9) J. E. McMurry and M. P. Fleming, *J. Am. Chem. Soc.*, **96**, 4708 (1974).

10) T. Irie, T. Suzuki, Y. Yasunari, E. Kurosawa, and T. Masamune, *Tetrahedron*, **25**, 459 (1969).

11) Our results confirmed the *cis*-attack of OsO_4 to the double bond in regard of the *p*-tolyl group of **20**.

12) G. Goto, *Bull. Chem. Soc. Jpn.*, **50**, 186 (1977).

13) P. de Mayo and R. Suau, *J. Chem. Soc., Perkin Trans. I*, **1974**, 2559.

14) C. Enzell and H. Erdtman, *Tetrahedron*, **4**, 361 (1958); T. Nozoe and H. Takeshita, *Tetrahedron Lett.*, [23], 14 (1960).

The MCPBA-oxidation of 8*H*-Cyclohepta[*b*]thiophen-8-ones to Their 1,1-Dioxides and Further Ring-contracted Benzo[*b*]thiophene Derivatives

Hitoshi TAKESHITA,* Hideshi MOTOMURA,† and Hiroaki MAMETSUKA
Research Institute of Industrial Sciece, 86, Kyushu University, Kasuga-koen, Kasuga, Fukuoka 816
†*Graduate School of Engineering Sciences, 39, Kyushu University, Kasuga-koen, Kasuga, Fukuoka 816*
(Received May 4, 1984)

Upon MCPBA-oxidation, several 8*H*-cyclohepta[*b*]thiophen-8-ones yielded the 8*H*-cyclohepta[*b*]thiophen-8-one 1,1-dioxides and their epoxides. The latters were shown to be convertible to several ring-contracted derivatives, the benzo[*b*]thiophene 1,1-dioxides and/or their corresponding phenol and salicylaldehyde derivatives.

Recently, we have reported[1,2] a series of thermal rearrangement of functionalized 2-(allylthio)tropone derivatives. In connection with this, the thermolysis of the sulfonyl derivatives, *i.e.*, 2-(allylsulfonyl)tropones, should be of interest concerning potential precursors for α-keto sulfene intermediates. However, the sulfones have been shown to be stable around 110 °C, where the corresponding sulfinyl derivatives are reactive. Herein we wish to describe an unprecedent oxidative ring contraction to a variety of benzenoid derivatives from the isopropyltropone derivatives in the preparation of the 8*H*-cyclohepta[*b*]thiophen-8-one 1,1-dioxides.

In a hope to obtain thienotropone dioxide *via* a "*sulfono*"-Claisen rearrangement, 2-(2-chloro-2-propenylsulfonyl)tropone (**1**) was heated at 110 °C for 10 min, but no reaction occurred at all. However above 180 °C, a decomposition of the material gradually took place although no definite product could be isolated. Obviously, an alternative route must be the *m*-chloroperbenzoic acid (MCPBA)-oxidation of 2-methyl-8*H*-cyclohepta[*b*]thiophen-8-one (**2**).[1] In fact, oxidation in chloroform yielded two products (**3** and **4**); the NMR spectrum of the major product (**3**) indicated the retention of the seven-membered ring, and the IR spectrum showed absorptions due to the newly formed sulfonyl group. Therefore, it must be the expected product. However, the minor product (**4**), analyzing for $C_9H_8O_2S$ on the basis of the mass spectrum, was 2-methylbenzo[*b*]thiophene 1,1-dioxide, and the ^{1}H-[3] and ^{13}C-NMR[4] were in good agreement with the data already reported. A further MCPBA-oxidation of **3** under similar conditions gave **4**. This unexpected occurrence of a novel ring contraction prompted us to investigate the reaction in more detail.

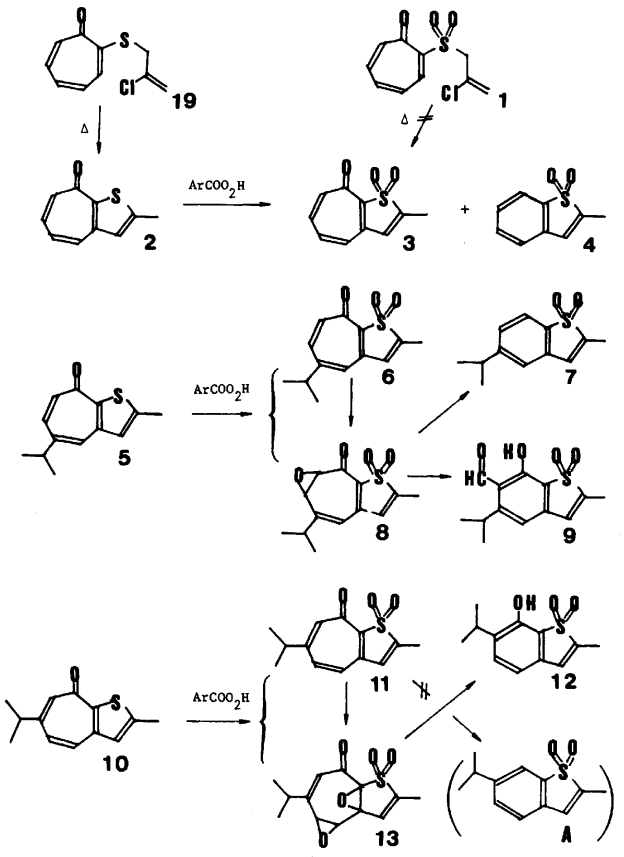

Scheme 1.

Accordingly, the oxidation of 5-isopropyl derivative (**5**)[1] was investigated. The four products identified were the corresponding isopropyl derivatives (**6** and **7**) of **3** and **4** together with two new products (**8** and **9**), which were isolated by preparative thin-layer chromatography (PTLC). One (**8**) of the minor products was assumed to be a further epoxidation product of **6** on the basis of its spontaneous conversion to **7** and **9**. Its extreme instability is not surprising because of a thiophene 1,1-dioxide structure. Nevertheless, the NMR spectrum of **8** showed a pair of *AB*-type signals at δ=3.71 and 4.08, of which the former was further spin-coupled to the other methine proton at δ=6.12, and showed a magnetically nonequvalent pair of doublet methyls, indicating a presence of sp^3-carbons in the vicinity of the isopropyl group. No other characterization was successful due to its rapid decomposition to **7** and **9**. The further MCPBA oxidation of **6** indicated a formation of **8** in substantial amount. Therefore, its structure is shown to be 6,7-epoxy-5-isopropyl-2-methyl-6,7-dihydro-8*H*-cyclohepta[*b*]thiophen-8-one 1,1-dioxide.

Another product, **9**, was 6-formyl-7-hydroxy-5-isopropyl-2-methylbenzo[*b*]thiophene 1,1-dioxide; the NMR spectrum exhibits only one phenyl proton as a singlet, and the isopropyl and thiophene 1,1-dioxide moieties still remained. In addition, there are characteristic signals at δ=10.36 and 12.58 ascribable to the

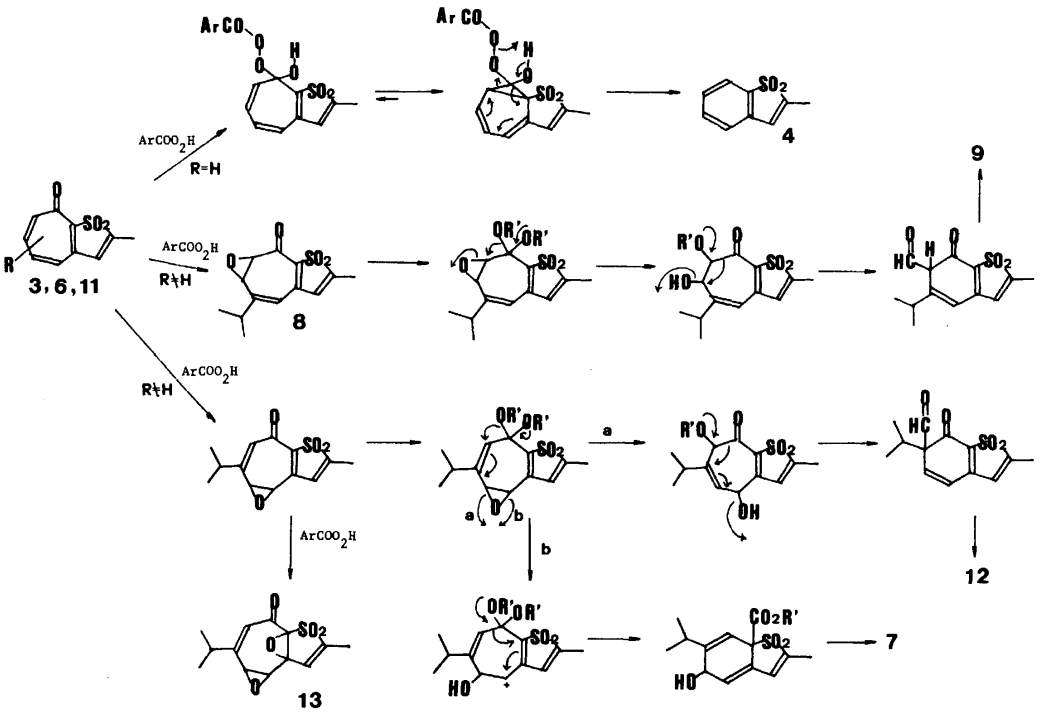

Scheme 2.

salicylaldehyde function. Since the chemical shift of the C-4 proton of the phenyl ring, δ=6.80, was higher than that of **7**, $\Delta\delta$=0.30, this should eliminate an alternative, 6-hydroxy-7-formyl structure.

On the other hand, the 6-isopropyl derivative (**10**)[1] gave the corresponding dioxide, 6-isopropyl-2-methyl-8*H*-cyclohepta[*b*]thiophen-8-one 1,1-dioxide (**11**), in good yield, but the ring-contracted 6-isopropyl-2-methylbenzo[*b*]thiophene 1,1-dioxide (**A**) was undetectable. Instead of this, a phenol (**12**) and an epoxide, 3a,8a:4,5-diepoxy-6-isopropyl-2-methyl-3a,4,5,8a-tetrahydro-8*H*-cyclohepta[*b*]thiophen-8-one 1,1-dioxide (**13**),[5] were obtained. The ^{1}H-NMR spectrum of **13** also showed the *AB*-signals due to epoxy methine protons and a nonequivalent pair of methyl doublets. The ^{13}C-NMR spectrum showed only five sp^2-carbons, and the mass spectrum indicated its composition to be $C_{13}H_{14}O_5S$. Moreover, **13**, unlike **8**, was relatively stable under the reaction conditions. Therefore, **13** could be formulated as shown.

The remaining product, **12**, was also identified from the NMR analysis to be 7-hydroxy-6-isopropyl-2-methylbenzo[*b*]thiophene 1,1-dioxide. Unlike **9**, **12** possesses the isopropyl group at C-6, and the α-formylcyclohexadienone as an intermediate could not be enolized to yield the salicylaldehyde derivative. Therefore, a mechanism for this eliminative rearrangement could be proposed as shown in Scheme 2.

It is not surprising that the substituent on the tropone ring determined the site of the reaction, and the subtle difference of such chemical properties leads to entirely different results. Another interesting feature is that, from the same type of precursors (the epoxycycloheptadienones), the formation of aromatic compounds at a different oxidation level, *i.e.*, benzene, phenol, and salicylaldehyde derivatives, occurred. Moreover, there must be two different mechanisms operative for the benzene formation; one is, operative in the parent tropone derivatives, the oxidative decarbonylation *via* the 7-acyldioxy-7-hydroxytropylidenes,[6] and the other is hydrolytic ring contraction of the epoxycycloheptadienones as verified in cases of the isopropyl derivatives.

To gain insight into the scope and limitations of this reaction, we have examined other heterocylic troponoids. 2-Methyl-8*H*-cyclohepta[*b*]furan-8-one (**14**)[7] resulted in a recovery of the starting **14**. On the other hand, the oxidation of 1,2-dimethyl-8*H*-cyclohepta[*b*]pyrrol-8-one (**15**)[8] should be of interest since it should at first be oxidized to an *N*-oxide, which resembles sulfonyl derivatives in respect to having a positive, formal charge on the C-2 substituent. An extensive decomposition occurred under thse conditions, and only a small amount of **15** was recovered. However, 3-chlorocyclohepta[*b*]thiopyran-9(4*H*)-one 1-oxide (**16**)[2] afforded 3-chloro-4*H*-benzo[*b*]thiopyran 1,1-dioxide (**17**) and 3-chlorocyclohepta[*b*]thiopyran-9(4*H*)-one 1,1-dioxide (**18**). From this, it seems to be characteristic for 2-sulfonyltropones. Indeed, when 2-(2-chloro-2-propenylthio) tropone (**19**) was oxidized with an excess of MCPBA, (2-chloro-2-propenylsulfonyl) benzene (**20**) was obtained as the by-product of **1** after a prolonged period.

Several examples on the ring contractions of troponoids or tropylidenes to benzene derivatives have been reported in the literature. Beside the well-known rearrangement of 2-halogeno- and 2-alkoxytropones to benzoic acid derivatives on base-treatment,[9] Mukai *et al.* have reported a thermolysis of tropone (**B**) to benzene (**C**) above 600 °C,[10] and Volpin *et al.*[11] have

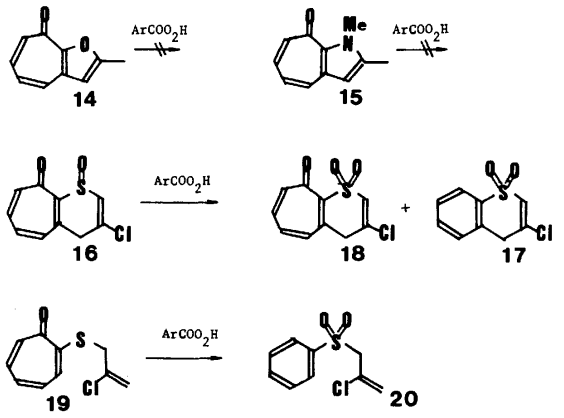

Scheme 3.

observed the formation of **C** in the hydrogen peroxide oxidation of the tropylium salt; probably, this would be a cheletropic fragmentation of tropyl hydroperoxide *via* the valence isomer, 7-hydroperoxybicyclo[4.1.0]-hepta-2,4-diene. A similar mode to this ring contraction to condensed benzenoid was also found in the MCPBA-oxidation of condensed polycyclic tropylium salt as well as the parent tropylium tetrafluoroborate.[12] However, no precedence has been known for the oxidative formation of benzenes from the tropones. In the concomitant formation of **C** and **B** from tropylidene during the sensitized photooxygenation, an intermediacy of **B** for **C** has been disproven by us.[13] Therefore, the present oxidation is the first example of that reaction.

Experimental

The mps were measured by a Yanagimoto Micro mp apparatus and not corrected. The elemental analyses were performed by Miss M. Yamaguchi and Miss S. Hirashima of this Institute. The high-resolution mass spactra were obtained with a JEOL OSIG Model spectrometer. The NMR spectra were taken with a JEOL FX 100 Model spectrometer in $CDCl_3$ solutions otherwise specified under the Fourier transform mode, and the chemical shifts expressed were δ unit from the internal Me_4Si. The IR spectra were measured either as KBr disk or CCl_4 solution with a Jasco IR 101 Model spectrophotometer.

Preparation of 2-(2-Chloro-2-propenylsulfonyl) tropone (1). A $CHCl_3$ solution (3 cm^3) of **19** (204 mg), prepared from 2-mercaptotropone and 2,3-dichloropropene,[1] was treated with MCPBA (534 mg) at 20 °C for 20 h. The mixture was then washed with aqueous $NaHCO_3$, and extracted with $CHCl_3$. The organic extracts were fractionated with silica-gel column to isolate **1**, 204 mg (87%), pale yellow needles, mp 79—80 °C [Found: C, 48.95; H, 3.48%. Calcd for $C_{10}H_9O_3SCl$: C, 49.08; H, 3.71%. δ=4.55 (2H, s), 5.48 (2H, s), 7.0—7.4 (4H, m), and 8.16 (1H, dd, J=8, 2 Hz). δ(C)= 63.3, 122.0, 128.9, 131.7, 136.1, 139.9, 140.8, 144.1, 146.2, and 182.3. ν: 1630, 1520, 1310, 1140, 900, and 790 cm^{-1}].

Attempted Thermolysis of 1. a) An *N,N*-dimethylformamide (DMF) solution (0.5 cm^3) of **1** (30 mg) was heated in a sealed NMR tube at 110 °C for 1 h. No appreciable change was detected.

b) A DMF solution (0.4 cm^3) of **1** (25 mg) was heated in a sealed NMR tube at 180 °C for 10 min. The NMR spectroscopy revealed an extensive decomposition to intractable material.

MCPBA-oxidation of 2-Methyl-8H-cyclohepta[b]thiophen-8-one (2).[1] A $CHCl_3$ solution (3 cm^3) of **2** (128 mg) was mixed with MCPBA (394 mg, 2.5 mol equiv) and kept at 15—25 °C for 48 h. The mixture was then washed with aqueous $NaHSO_3$ and $NaHCO_3$, and extracted with $CHCl_3$. PTLC of the extracts on silica gel gave **3**, 66 mg (44%), yellow needles, mp 192—193 °C [Found: C, 57.38; H, 3.95%. Calcd for $C_{10}H_8O_3S$: C, 57.68; H, 3.87%. δ=2.27 (3H, d, J=2 Hz), 6.62 (1H, q, J=2 Hz), and 6.9—7.4 (4H, m). δ(C)=9.5, 124.6, 132.2, 135.7, 140.0, 140.1, 140.9, 146.5(2C), and 177.3. m/z, 208 (M^+). ν: 1620, 1580, 1520, 1460, 1300, 1240, 1140, 860, and 800 cm^{-1}], **4**, colorless needles, mp 105—106 °C, 10 mg (8%) [δ=2.20 (3H, d, J=2 Hz), 6.74 (1H, q of quint, J=2, 1 Hz), and 7.2—7.7 (4H, m), δ(C)=9.1, 121.4, 124.2, 125.8, 129.2 131.6, 133.5, 136.4, and 140.9. ν: 1445, 1285, 1140, and 750 cm^{-1}].

Further Oxidation of 3 to 4. A $CDCl_3$ solution (0.3 cm^3) of **3** (16 mg) and MCPBA (34 mg, 2.1 mol equiv) was kept at 15—25 °C for 72 h. The NMR spectroscopy indicated the partial formation of **4**, 33%.

MCPBA-oxidation of 5-Isopropyl-2-methyl-8H-cyclohepta[b]-thiophen-8-one (5) to 6, 7, 8, and 9. A $CHCl_3$ solution (3 cm^3) of **5** (200 mg) was mixed with MCPBA (497 mg, 2.5 mol equiv) and kept at 15—20 °C for 72 h with stirring. After filtration of the resultant MCBA, the filtrate was chromatographed on a silica-gel column to give colorless needles, mp 53—54 °C, **7**, 3 mg (1.5%) [Found: M^+, 222.0712. Calcd for $C_{12}H_{14}O_2S$: M^+, 222.0715. δ=1.25 (6H, d, J=7 Hz), 2.21 (3H, d, J=2 Hz), 2.94 (1H, sept, J=7 Hz), 6.71 (1H, m), 7.10 (1H, d, J=1.5 Hz), 7.26 (1H, dd, J=8, 1.5 Hz), and 7.60 (1H, d, J=8 Hz). δ=9.2, 23.7 (2C), 34.5, 121.6, 122.6, 126.1, 127.4, 141.2, and 155.5. ν: 2975, 1295, 1145, and 825 cm^{-1}], and yellow needles, mp 196—197 °C, **6**, 124 mg (54%) [Found: C, 62.54; H, 5.68%. Calcd for $C_{13}H_{14}O_3S$: C, 62.38; H, 5.64%. δ=1.26 (6H, d, J=7 Hz), 2.28 (3H, d, J=2 Hz), 2.87 (1H, sept, J=7 Hz), 6.64 (1H, quint, J=2 Hz), 6.86 (1H, dd, J=2, 1.5 Hz), 7.08 (1H, dd, J=12, 1.5 Hz), and 7.22 (1H, dd, J= 12, 2 Hz). δ(C)=9.4, 22.5 (2C), 39.0, 125.7, 128.0, 137.7, 138.5, 140.8, 145.7, 146.2, 162.9, and 176.8. m/z, 250 (M^+). ν: 2980, 1620, 1560, 1300, 1140, and 870 cm^{-1}].

The combined filtrates were further purified by PTLC to give minor products, an unstable yellow oil, **8**, 13.6 mg (5.6%) [δ=1.27 (3H, d, J=7 Hz), 1.28 (3H, d, J=7 Hz), 2.22 (3H, d, J=2 Hz), 2.84 (1H, sept, J=7 Hz), 3.71 (1H, dd, J=4, 2 Hz), 4.08 (1H, d, J=4 Hz), 6.12 (1H, dd, J=2, 1 Hz), and 6.38 (1H, q, J=2 Hz)], and pale yellow needles, **9**, mp 166—167 °C, 9.7 mg (4%) [Found: M^+, 266.0591. Calcd for $C_{13}H_{14}O_4S$: M^+, 266.0608. δ=1.35 (6H, d, J=7 Hz), 2.24 (3H, d, J=2 Hz), 3.68 (1H, sept, J=7 Hz), 6.69 (1H, q, J=7 Hz), 6.80 (1H, s), 10.38 (1H, s), and 12.58 (1H, s). δ(C)=9.5, 22.4 (2C), 24.0, 113.0, 118.2, 124.5, 140.5, 146.6, 157.9, 161.4, and 216.7. ν: 2975, 1650, 1300, 1140, and 905 cm^{-1}].

Further MCPBA-oxidation of 6. A $CHCl_3$ solution (5 cm^3) of **6** (29 mg) was mixed with MCPBA (64 mg) and was kept at 15—25 °C for 72 h. The NMR spectral analysis of the mixture indicated the formation of **8**, 35%.

Spontaneous Conversion of 8 to 7, and 9. A neat liquid of **8** (10.7 mg) was kept in a glass vessel at 15—25 °C for 20 h. The resultant crystals thus formed were collected by filtration to give **9**, 4.2 mg (39%), and liquid chromatographic analysis of the filtrate, *ca.* 6 mg, indicated the composition of **7** and **9** as 53:47.

MCPBA-oxidation of 6-Isopropyl-2-methyl-8H-cyclohepta[b]-thiophen-8-one (10) to 11, 12, and 13. A $CHCl_3$ solution (3 cm^3) of **10** (206 mg) was mixed with MCPBA (523 mg, 2.5 mol eq) and kept at 15—20 °C for 72 h. After removal of MCBA by filtration, the filtrate was chromatographed on a silica-gel column to give yellow needles, **11**, mp 179—180 °C, 141 mg (60%) [Found: C, 62.10; H, 5.64%. δ=1.24 (6H, d, J= 7 Hz), 2.26 (3H, d, J=2 Hz), 2.78 (1H, sept, J=7 Hz), 6.68

(1H, q, J=2 Hz), 7.02 (1H, dd, J=11, 1 Hz), 7.12 (1H, dd, J=1.5, 1 Hz), and 7.22 (1H, dd, J=11, 1.5 Hz). δ(C)=9.5, 22.5 (2C), 38.7, 124.8, 131.0, 139.9, 140.2, 142.7 (2C), 146.2, 156.9, and 177.1. *m/z*, 250 (M^+). ν: 2970, 1615, 1580, 1305, 1140, and 880 cm^{-1}].

From more polar fractions, the minor products, yellow needles, **13**, mp 133—134 °C, 3 mg (1.2%) [Found: M^+, 282.0555. Calcd for $C_{13}H_{14}O_5S$: M^+, 282.0562, δ=1.20 (3H, d, J=7 Hz), 1.21 (3H, d, J=7 Hz), 2.09 (3H, d, J=2 Hz), 2.63 (1H, sept, J=7 Hz), 3.42 (1H, dd, J=4, 1 Hz), 3.90 (1H, d, J=4 Hz), 6.04 (1H, t, J=1 Hz), and 6.61 (1H, q, J=2 Hz). δ(C)=9.7, 20.9, 21.1, 37.5, 54.8, 55.1, 65.2, 124.9, 127.3, 147.1, 157.3, and 185.6. δ(C)C_6D_6=9.1, 20.5, 20.7, 36.8, 54.3 (2C or 3C), 63.8, 126.0, 147.6, 155.9, and 185.7. ν: 2980, 1165, 1325, 1295, and 1150 cm^{-1}], and colorless needles, **12**, mp 119—120 °C, 2.2 mg (1%) [Found: M^+, 238.0671. Calcd for $C_{12}H_{14}O_3S$: M^+, 238.0690. δ=1.24 (6H, d, J=7 Hz), 2.17 (3H, d, J=2 Hz), 3.22 (1H, sept, J=7 Hz), 6.67 (1H, q, J=7 Hz), 6.76 (1H, d, J=8 Hz), and 7.27 (1H, d, J=8 Hz). δ(C)=9.0, 22.6, 26.9, 116.9, 126.5, 130.5, 131.9, 133.2, 139.1, 140.2, and 149.5. ν: 3420, 2960, 1470, 1290, 1140, and 880 cm^{-1}], were isolated by further PTLC.

Further MCPBA-oxidation of 11. A $CHCl_3$ solution (5 cm^3) of **11** (132 mg) was mixed with MCPBA (287 mg) and was kept at 15—25 °C for 72 h. The HPLC analysis of the mixture revealed a formation of **12**, 21%, and **13**, 4%, together with the recovered **11**, 63%.

Attempted MCPBA-oxidation of 2-Methyl-8H-cyclohepta[b]furan-8-one (14). A $CDCl_3$ solution (2 cm^3) of **14** (52 mg) was mixed with MCPBA (147 mg, 2.0 mol equiv) and kept at 15—25 °C for 48 h. The NMR spectroscopy revealed no appreciable change.

Attempted MCPBA-oxidation of 1,2-Dimethyl-8H-cyclohepta-[b]pyrrol-8-one (15). A $CHCl_3$ solution (1 cm^3) of **15** (60 mg) and MCPBA (160 mg, 2.1 mol equiv) was kept at 15—25 °C for 24 h in an NMR tube. The ^{1}H-NMR spectrum of the mixture was complicated; the strongest signals were those of the starting compound, **15**. No further work was attempted.

MCPBA-oxidation of 3-Chloro-9-oxo-4H,9H-cyclohepta[b]-thiopyrane-1-oxide (16). A $CHCl_3$ solution (4 cm^3) of **16** (163 mg) and MCPBA (342 mg, 2.2 mol equiv) was kept at 15—20 °C for 72 h. The mixture was fractionated on a silica-gel column to give **17**, 8 mg (10%), colorless needles, mp 106—107 °C [Found: C, 50.43; H, 3.52%. Calcd for $C_9H_7O_2SCl$: C, 50.35; H, 3.29%. δ=4.53 (2H, d, J=2 Hz), 7.13 (1H, m), and 7.2—7.7 (4H, m). δ(C)=34.8, 121.7, 125.4, 129.0, 130.3, 130.5, 134.0, 137.3, and 140.6. *m/z*, 214 (M^+). ν: 1450, 1295, 1150, and 770 cm^{-1}], **18**, pale yellow fine needles, mp 130—132 °C (decomp), 39 mg (46%) [Found: C, 49.59; H, 2.98%. Calcd for $C_{10}H_7O_3SCl$: C, 49.49; H, 2.91%. $\delta^{(CD_3)_2CO}$=4.70 (2H, d, J=2 Hz), 7.0—7.6 (4H, m), and 7.36 (1H, t, J=2 Hz). δ(C)=34.8, 126.8, 131.9, 135.9, 138.7, 140.2, 146.0, 146.9, and 177.3. *m/z*, 242 and 244 (M^+). ν: 3100, 1615, 1580, 1310, 1140, and 800 cm^{-1}], and the recovered **16**, 85 mg (52%). On contact of **18** with water hydrolytic decomposition to an unidentifiable compound occurred.

Prolonged MCPBA-oxidation of 2-(2-Chloro-2-propenylsulfonyl)tropone (1). A $CHCl_3$ solution (2 cm^3) of **1** (106 mg) was kept at 15—20 °C for 95 h. The mixture was then washed with aqueous Na_2CO_3, and extracted with $CHCl_3$. The extracts were fractionated by PTLC to colorless needles, **20**, mp 45—46 °C, 9 mg (19%) [Found: C, 49.87; H, 4.15%. Calcd for $C_9H_9O_2SCl$: C, 49.88; H, 4.19%. δ=4.05 (2H, s), 5.34 (1H, d, J=1 Hz), 5.49(1H, d, J=1 Hz), and 7.4—8.0 (4H, m). δ(C)=64.6, 121.8, 128.5, 128.7, 129.1, 134.1, and 137.7. *m/z*, 216 and 218 (M^+)], and the recovered **1**, 50 mg (47%).

Alternative Preparation of 20. An EtOH solution (5 cm^3) of benzenethiol (119 mg) was mixed with 2,3-dichloropropene (106 mg) and refluxed for 2 h. The mixture containing **20** thus formed was then evaporated, dissolved in $CHCl_3$ (5 cm^3), and kept at 15—25 °C for 24 h with MCPBA (550 mg, 2.5 mol equiv). The colorless needles (20.7 mg, 97%) were identical with **20** in respects of mp, mass, and NMR spectra.

The authors are grateful to the Ministry of Education, Science and Culture for operating a Grant to H. M. (No. 58740235).

References

1) H. Takeshita, H. Mametsuka, and K. Uchida, *Heterocycles*, **20**, 1709 (1983).
2) H. Takeshita, H. Motomura, K. Uchida, and H. Mametsuka, *Heterocycles*, **22**, 467 (1984).
3) F. G. Bordwell, R. W. Hemwall, and D. A. Schexnayder, *J. Org. Chem.*, **33**, 3226 (1968).
4) P. Geneste, J.-L. Olive, S. N. Ung, M. El A. El Faghi, J. W. Easton, H. Beierbeck, and J. K. Saunders, *J. Org. Chem.*, **44**, 2887 (1979).
5) In connection with theoretical interest on possible homoconjugation, tropone epoxides have been prepared; H. Prinzbach, W. Seppelt, and H. Fritz, *Angew. Chem.*, **89**, 174 (1977).
6) The terms, tropylidene and tropyl, denote cycloheptatriene and cycloheptatrienyl.
7) H. Takeshita, K. Tajiri, and I. Kouno, *Heterocycles*, **6**, 1101 (1977).
8) H. Takeshita, A. Chisaka, and H. Mametsuka, *Bull. Chem. Soc. Jpn.*, **53**, 3373 (1980).
9) T. Nozoe, Y. Kitahara, K. Yamane, and K. Yamaki, *Proc. Jpn. Acad.*, **26** (8), 14 (1950); Y. Kitahara, *Sci. Repts, Tohoku Univ. Ser. I*, **39**, 250 (1955).
10) T. Mukai, T. Nakazawa, and T. Shishido, *Tetrahedron Lett.*, **1967**, 2465.

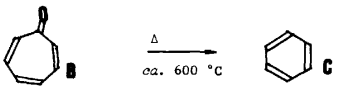

Scheme 4.

11) E. Volpin, D. N. Kursanov, and V. G. Dulova, *Tetrahedron*, **8**, 33 (1960).
12) K. Nakasuji, T. Nakamura, and I. Murata, *Tetrahedron Lett.*, **1978**, 1539.
13) H. Takeshita and A. Mori, *Heterocycles*, **11**, 319 (1978).

Electrochemical Reduction of Cyclic and Acyclic Sulfates

Tsutomu NONAKA,* Shuta KIHARA, Toshio FUCHIGAMI, and Manuel M. BAIZER*,†
Department of Electronic Chemistry, Graduate School at Nagatsuta, Tokyo Institute of Technology, 4259 Nagatsuta, Midori-ku, Yokohama 227
†*Department of Chemistry, University of California, Santa Barbara, California 93106, U.S.A.*
(Received April 11, 1984)

It was confirmed that cyclic and acyclic sulfates of diols and monoalcohols could be reduced at cathodes in nonaqueous solvents. The reduction products were greatly affected by the molecular structures of the sulfates. The reduction of the cyclic sulfates of 1,2-diols yielded the corresponding alkenes and disulfate dianions of the parent diols in high yields and current efficiencies were based on one-electron reduction. On the other hand, the cyclic sulfates of 1,3- and 1,4-diols were also reduced by one-electron transfer under similar conditions, but the cycloalkanes expected were not formed and the products were cyclic ethers along with acyclic alkane or unsaturated alcohol. The reduction of the cyclic sulfate of hydrated formaldehyde, which is regarded as a 1,1-diol, did not give any identified products except for a small amount of methane. Finally, acyclic dialkyl sulfates were reduced by one-electron transfer to give complicated mixtures consisting of monomeric alkanes and alkenes, dimeric alkanes, ethers, and/or alkyl metals. Based on the results obtained, the mechanism of reduction of sulfates (mainly cyclic sulfates of 1,2-diols) is discussed.

It is known that 1,2-diols themselves are electrochemically reduced only with great difficulty. However when the hydroxyl groups are derivatized to a good "leaving group" -OR, reduction leads to alkenes or alkanes. The diacetate of hydrobenzoin is reduced to bibenzyl in the presence of proton donors,[1] while the dioxalate also is reduced at a relatively low potential to give stilbene.[2] Highly aryl-substituted epoxides are reduced but selectivities for the corresponding alkenes are low.[3]

The above examples show that derivatives of only 1,2-diols involving di- or higher aryl-substituents can be reduced. This may suggest considerable difficulty in the reduction of derivatives of 1,2-diols which are not aryl-substituted. In fact, only one successful result had been reported prior to our previous report. Dey and Sullivan[4] found that propylene carbonate was reduced not directly but indirectly with electrogenerated lithium metal.

In previous works,[5,6] we showed the first example of the direct reduction of derivatives of 1,2-diols which are not aryl-substituted,[7] and the following points were established: (a) The sulfate was coulometrically reduced by one-electron transfer and (b) the yield of 2-butene formed did not exceed 50% based on the starting sulfate. Equation 1 was tentatively given as a stoichiometry for this reduction, postulating the elimination of radical anion $SO_4^{\cdot-}$ and its dimerization. This is distinguished by the one-electron transfer reduction, as contrasted to the four-[1] and two-electron[2-4] transfer reductions of other 1,2-diol derivatives.

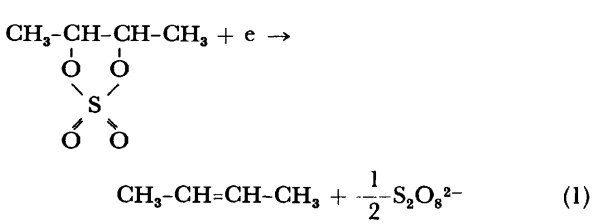

$$CH_3\text{-}CH=CH\text{-}CH_3 + \frac{1}{2}S_2O_8^{2-} \qquad (1)$$

More detailed examination of the reduction of sulfate of 2,3-butanediol and extension of the reduction to sulfates of other 1,1-, 1,2-, 1,3-, and 1,4-diols and of monoalcohols are reported here.

Results an Discussion

Reduction of the Cyclic Sulfate of 2,3-Butanediol. Stoichiometry: In order to establish the stoichiometry, the separation of products containing sulfur was attempted.

When the sulfate was reduced at a mercury cathode in Et_4NClO_4/DMF, very small amounts of precipitates, which decomposed in acid solutions, were formed. They were presumed to be a mercury salt of an oxyacid containing sulfur, *e.g.* Caro's acid,[9] from their properties.

If peroxodisulfate ions were formed according to Eq. 1, they would be present as the tetraethylammonium salt (soluble in DMF) and should be easily reduced to sulfate ions.[10] In fact, it was confirmed that ammonium peroxodisulfate was reduced consuming 2F (1F=96480C)/mole of charge at a less negative potential than the cyclic sulfate of 2,3-butanediol.

Peroxodisulfate ion can be regarded as equivalent to sulfate anion radical ($SO_4^{\cdot-}$) in some cases. Therefore, it was attempted to trap the anion radical in electrolyses in the presence of aniline[11] and styrene,[12] but the yield of 2-butene was not affected in both cases and also in the latter case neither styrene oxide nor polystyrene could not be detected.

A further investigation was made of products which are soluble in the catholyte and not volatile. After a complicated work-up procedure of the catholyte, the bis(tetrabutylammonium) salt of the acyclic disulfate dianion (**1**) of 2,3-butanediol was separated and derivatized to the dipotassium salt. The molecular structure of the dipotassium salt was confirmed by spectral and analytical data, and by the recovery of 2,3-butanediol and sulfuric acid after its hydrolysis. These results indicate Eq. 2 to be the most likely stoichiometry for the main reaction. The yield of **1** separated as the dipotassium salt was 42% according to Eq. 2; such a value lower than 100% seemed to be due to mainly to material loss in the complicated multi-step procedure for the separa-

tion. On the other hand, yields of 2-butene, which were tentatively reported to be lower (39—49%) than 50% according to Eq. 1 in the previous work,[5] can be re-evaluated as 78—99% according to Eq. 2.

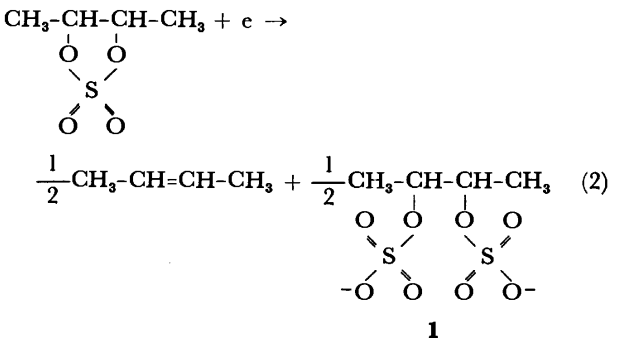

(2)

1

Reaction Mechanism: The initial steps of the reduction were investigated by voltammetric methods. As shown in Fig. 1, cyclic voltammetry indicated a totally irreversible process, since a more negative shift of reduction peak potentials at higher sweep rates and no oxidation peak were observed. The cyclic sulfate also gave a single polarographic wave ($E_{1/2}$ −1.86 V *vs.* Ag^+/Ag), the wave height of which was proportional to concentration and had a linear relationship to the square root of the mercury column height. The wave analysis of the polarograms gave a slope of *ca.* 160 mV. Since it has been confirmed that the cyclic sulfate undergoes one-electron reduction, the slope larger than 59 mV should indicate that the electron transfer step is also irreversible. Combining this result with that of cyclic voltammetry, a possible reaction route from the cyclic sulfate to a ring-opened anion radical (**3**) *via* another one (**2**) is shown in Scheme 1. This manner of ring-opening should be more favorable than others, in view of the higher electron negativity of oxygen than carbon and the strong electron-withdrawing power of the $-SO_2-$ part of **3**.

As the simplest route from **3** to the final products (2-butene and **1**), disproportionation (route A in Scheme 1) of **3** is conceptually proposed without either highly negative or positive experimental evidence. Since it is known that a radical with a leaving group at its β-position looses the latter as a radical and yields an olefin,[13] **3** may loose $SO_4^{\cdot-}$ to give 2-butene (route B). Although it has been confirmed by the electrolysis in the presence of $SO_4^{\cdot-}$ trapping reagents that the reaction does not involve any free $SO_4^{\cdot-}$ in the bulk of the catholyte, the formation of **1** by addition reaction of $SO_4^{\cdot-}$ to **3** or 2-butene in cathode interface can not be excluded in a case where the trapping reagents can

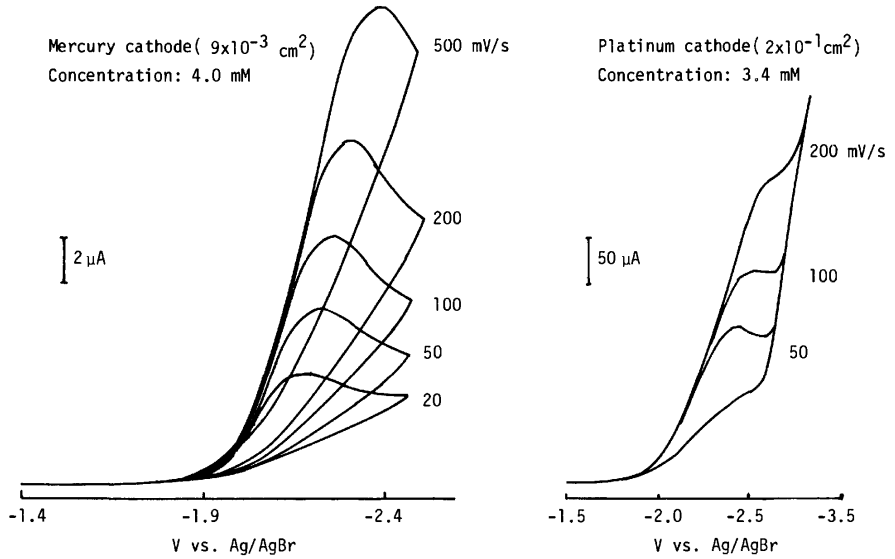

Fig. 1. Cyclic voltammograms of cyclic sulfate of 2,3-butanediol at various potential sweep rates in 0.2 M tetrabutylammonium perchlorate/DMF.

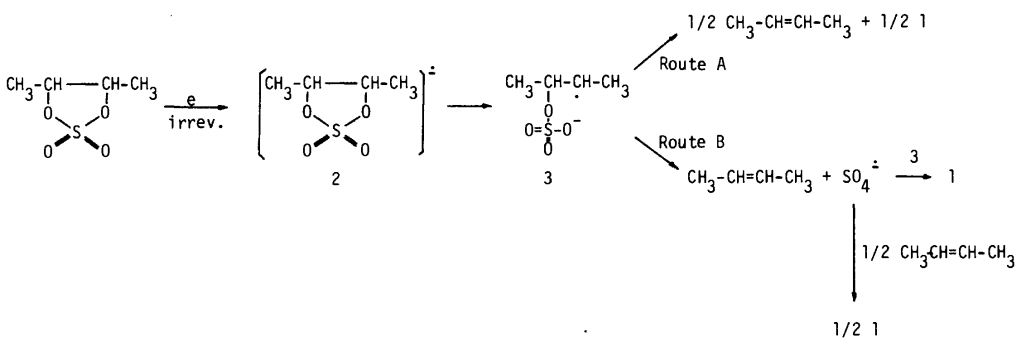

Scheme 1.

not enter the interface. However, it may be difficult to explain why $SO_4^{\cdot-}$, a strong oxidizing reagent, could not be reduced if it had been formed; a rationalization is possible if the rate of the addition reaction is very much higher than that of the reduction. In such a case, there should be no apparent difference between routes A and B, and at least they can not be distinguished by ordinary means. The reaction of $SO_4^{\cdot-}$ with mercury, if it occurred, should be considered separately from the main pathways.

Reduction of Cyclic Sulfates of 1,2-Diols Other Than 2,3-Butanediol. *i-E* Curves of the cyclic sulfate of four kinds of 1,2-diols including 2,3-butanediol were measured by a stationary method. As shown in Fig. 2, the reduction potential of the sulfates was apparently affected by steric hindrance of the diol molecules.

Table 1 shows results of controlled potential electrolyses of the sulfates at a mercury cathode in Et_4NClO_4/DMF. Yields and current efficiencies of the corresponding alkenes formed were estimated according to the stoichiometry of Eq. 2.

The cyclic sulfate of 1,2-ethanediol showed a unique phenomenon in the current-time relation during electrolysis. As shown in Fig. 3, the current decreased rapidly to the background level when the electrolysis was carried out at −1.3 V *vs.* Ag^+/Ag and only 0.6 F/mole of charge was passed. The current efficiency for ethene in this period was 22%. When the applied potential was reset now at −1.6 V, the current increased. Additional 0.3 F/mole of charge could be passed at this potential, till the current decreased again. The current efficiency in this period was 42%. The current could be increased again by resetting the potential at −1.8 V and 0.2 F/mole of charge was passed. The current efficiency was 44%. No more significant increase of the current was observed, when the potential was changed more cathodically after diminution of the current at −1.8 V. The overall current efficiency and total yield were 30 and 34%, respectively. No original sulfate remained unreacted. The above phenomenon is very intriguing but it seems difficult to explain; an attempted explanation is that electrogenerated species might initiate polymerization of the cyclic sulfate to form linear poly(1,2-ethanediol sulfate)s whose reduction

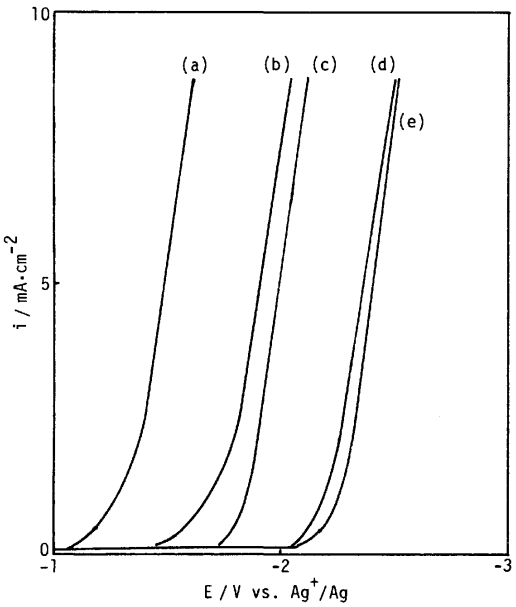

Fig. 2. *i-E* Curves of cyclic sulfates of 1,2-diols (0.04 M) at a mercury cathode.
Cyclic sulfates of 1,2-diols: (a) 1,2-ethanediol, (b) 2,3-butanediol, (c) 2,3-dimethyl-2,3-butanediol, (d) *trans*-1,2-cyclohexanediol, (e) background (0.4 M tetraethylammonium perchlorate/DMF).

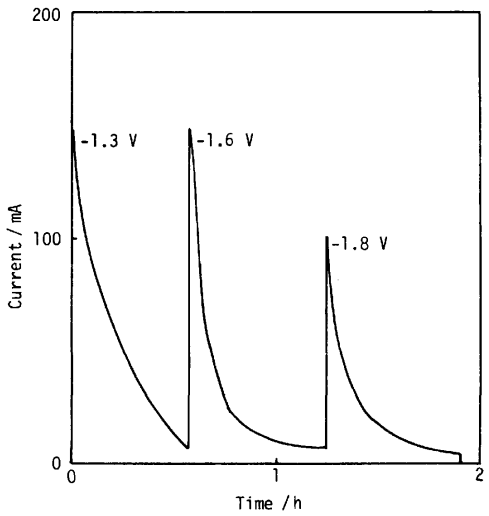

Fig. 3. Current-time relation in the electroreduction of the cyclic sulfate of 1,2-ethanediol at potentials changed stepwise.

Table 1. Results of electrolytic reduction of cyclic sulfates of 1,2-diols at a mercury cathode in tetraethylammonium perchlorate/DMF

Diol	Cathodic potential/ V *vs.* Ag^+/Ag	Charge passed[a] /F·mol	Alkene	
			Yield[b] /%	Current efficiency /%
1,2-Ethanediol	−1.3, −1.6, −1.8[c]	1.1	34	30
2,3-Butanediol	−1.7	1.0	78	78
2,3-Butanediol	−2.0	1.0	99	99
2,3-Dimethyl-2,3-butanediol	−1.9	1.1	66	60
trans-1,2-Cyclohexanediol	−2.4	2.3[d]	100	46

a) Corresponding to coulometric *n*-value. b) Estimated according to the stoichiometry of Eq. 2 in the text. c) Changed stepwise during the electrolysis (See Fig. 3.) d) Not coulometric.

potentials are more negative than that of the cyclic sulfate, depending on the degree of polymerization.

Beside the results given above, here, some informations about the reduction of the cyclic sulfate of 2,3-butanediol are supplemented. As shown in Table 1, a lower current efficiency and yield of 2-butene was obtained at a less negative potential at a mecury cathode; such a dependence of the efficiency and yield on the potential was not observed at a platinum cathode. This fact may suggest the occurrence of side reaction of **3** with a less negatively polarized mercury cathode. A gas chromatogram of the catholyte just after the electrolysis showed only a very small peak for 2-butanone(in addition to 2-butene), while the catholyte treated with aqueous sulfuric acid at 70 °C gave several small peaks which could not be identified. This result also suggests occurrence of side reactions.

The cyclic sulfate of 2,3-dimethyl-2,3-butanediol could be coulometrically reduced by one-electron transfer to give 2,3-dimethyl-2-butene in current efficiency and yield lower than those in the reduction of the sulfate of 2,3-butanediol. The tetrabutylammonium salt of the disulfate dianion of 2,3-dimethyl-2,3-butanediol could be separated pure from a catholyte consisting of Bu_4NClO_4 and acetonitrile.

The cyclic sulfate of *trans*-1,2-cyclohexanediol was reduced at such a negative potential(−2.4 V *vs.* Ag^+/Ag) that supporting electrolyte cation (Et_4N^+) was discharged; amalgam formation was observed indicating that indirect reduction with electrogenerated amalgam occurred simultaneously. The yield of cyclohexene was 100% when 2.3 F/mole of charge were passed.

Reduction of Cyclic Sulfates of Diols Other Than 1,2-Diols. The cyclic sulfate of hydrated formaldehyde, so-called methylene sulfate, can be regarded as the cyclic sulfate of a 1,1-diol and presents as an equilibrium mixture with the cyclic dimer.[14] As the sulfate decomposed exothermically in DMF, acetonitrile was used as a solvent for the electrolysis. The *i-E* curve of the sulfate is shown in Fig. 4, together with that of sulfates of other diols. As shown in Figs. 2 and 4, it is plain that the sulfate of 1,1-diol can be reduced at a considerably less negative potential than that required for any other diols, though different cathodes and/or solvents were used. The two-step reduction wave of the sulfate of the 1,1-diol may be due to the monomer/dimer equilibrium described above. The sulfate was reduced consuming coulometrically 1.0 F/mole of charge at −1.0 V *vs.* Ag^+/Ag corresponding to the first reduction wave at a mercury cathode in acetonitrile, but no product could be detected by gas-chromatographic analysis. When 0.9 F/mole of charge was coulometrically passed at a more negative potential (−1.8 V) corresponding to the second wave, small amounts (2% yield) of methane were formed. Using a platinum cathode, similar results were given. Because no ethene could be detected in any case, the generation of a carbene as an intermediate was not be verified.

The cyclic sulfate of 1,3-propanediol was reduced consuming 1 F/mole of charge at −1.9 V *vs.* Ag^+/Ag at mercury and platinum cathodes in DMF. The former cathode gave no gas-chromatographically detectable

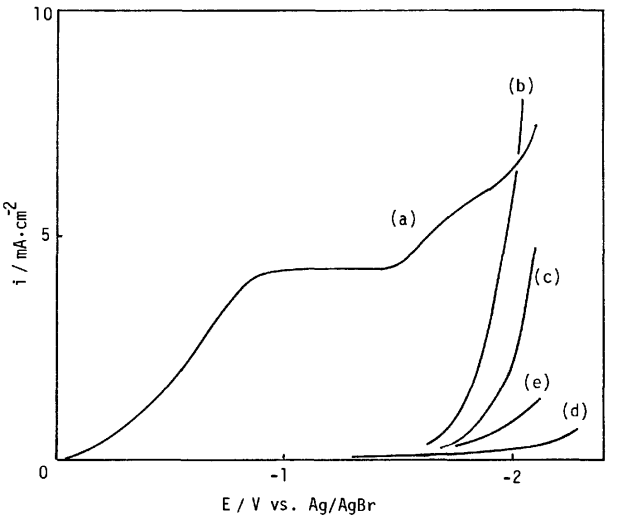

Fig. 4. *i-E* Curves of cyclic sulfates of 1,1-, 1,3-, and 1,4-diols.
(a) 0.1 M Cyclic sulfate of hydrated formaldehyde at a mercury cathode in 0.5 M tetrabutylammonium perchlorate/acetonitrile, (b) 0.1 M cyclic sulfate of 1,3-propanediol at a platinum cathode in 0.5 M tetrabutylammonium perchlorate/DMF, (c) 0.1 M cyclic sulfate of 1,4-butanediol at the same cathode in the same solution, (d) background for (a), (e) background for (b) and (c).

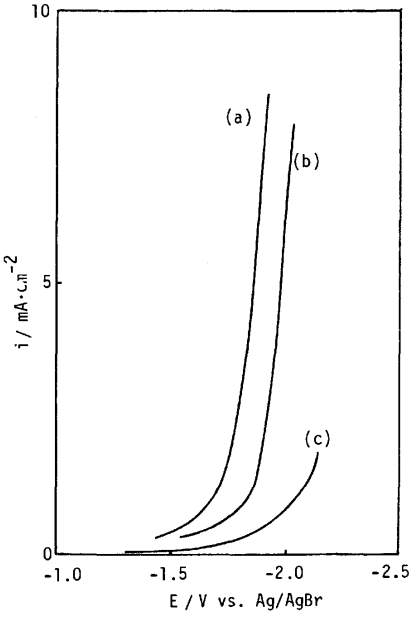

Fig. 5. *i-E* Curves of dialkyl sulfates (0.2 M) at a platinum cathode.
(a) Dimethyl sulfate, (b) diethyl sulfate, (c) background, 0.5 M tetrabutylammonium perchlorate/DMF.

product, while the latter gave allyl alcohol in 10% yield and one more product which had the same molecular weight as allyl alcohol but was not either propylene oxide or oxetane.

The reduction of the cyclic sulfate of 1,4-butanediol at a mercury cathode gave a result similar to that of 1,3-propanediol under the same conditions. Reduction at a platinum cathode resulted in the formation of

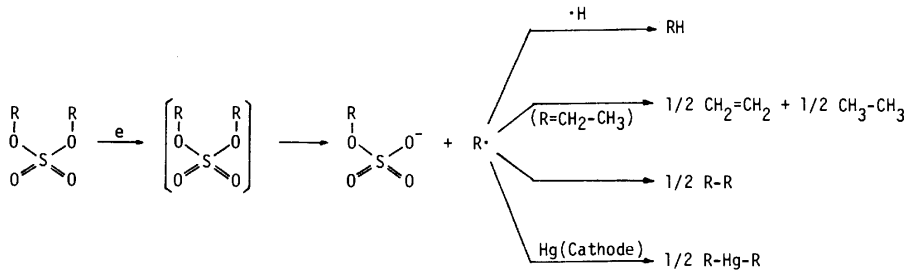

Scheme 2.

butane(16% yield) and THF(11%).

Although there have been some ambiguous points in the reduction of the cyclic sulfates of diols other than 1,2-diols, it is interesting to note that the manner of the reduction was quite different from that of 1,2-diols.

Reduction of Acyclic Sulfates of Monoalcohols. *i-E* curves of dialkyl sulfates are shown in Fig. 5. Dimethyl sulfate was reduced at a less negative potential than diethyl sulfate.

Dimethyl sulfate was completely reduced by about 1 F/mole at −1.9 V *vs.* Ag^+/Ag at a mercury cathode in DMF. The products detected were dimethyl ether and dimethylmercury. At a platinum cathode, methane(6% yield) was formed in addition to dimethyl ether(13%). Diethyl sulfate also was reduced by 1 F/mole at a mercury cathode to give diethyl ether in 38% yield, but the presence of diethylmercury was not checked. The reduction at a platinum cathode resulted in the formation of a variety of products: Diethyl ether (17% yield), ethanol(12%), ethane(37%), ethene(16%), and butane(trace). The formation of hydrocarbons and dialkylmercury in the reduction of dialkyl sulfates suggests the generation of alkyl radicals as intermediates, shown in Scheme 2. On the other hand, it seems difficult, just as in the reductions of the cyclic sulfates of diols other than 1,2-diols, to propose specific routes for the products containing oxygen from dialkyl sulfates; they may involve alkoxyl radicals, alkoxide anions and/or alkyl radicals.

Conclusions

This comparative study of the electrochemical reduction of a variety of types of organic sulfates leads to the following principal conclusions:

(a) All the sulfates used were reduced by one-electron transfer.

(b) The reduction products were greatly affected by the type of sulfates; cyclic/acyclic, diol/monoalcohol, and 1,1-/1,2-/1,3-/1,4-diols.

(c) Among the cyclic sulfates of diols, those of 1,2-diols were reduced in a unique manner to give the corresponding alkenes and 1,2-disulfate dianions.

Experimental

Voltammetry. Cyclic voltammograms were recorded at room temperature in 0.1—0.2 M† Bu_4NClO_4/DMF by using a potentiostat (Nikko Keisoku Co. Model MPGS-301), a function generator (Nikko Keisoku Co. Model NPS-2) and an X-Y recorder (Rikendenshi Co. Model F-3DH). Polarograms were measured using Yanaco Model P-1100. Working electrodes for the voltammetries were a platinum wire (diameter, 0.04 cm; length, 1.5 cm; area, 2×10^{-1} cm²), a hanging mercury electrode (drop weight, 1.1 mg; area, 9×10^{-3} cm²) and a dropping mercury electrode (drop weight at −2.10 V *vs.* Ag^+/Ag and 43.5 cm mercury column height, 1.3 mg; area, 1×10^{-2} cm²). Cathodic potentials were referred to a silver bromide electrode in 0.1 M Bu_4NClO_4/DMF. Three-electrode systems with large platinum counter electrodes were employed for all measurements.

Steady state *i-E* curves were measured by using the equipment and solutions similar to those used in the preparative electrolyses described below.

Preparative Electrolyses. An H-type divided cell, a potentiostat (Wenking Model ST-72 or Hokutodenko Model HA-105) and a coulometer (Hokutodenko Model HF-201) were used for electrolyses which were carried out at constant potentials at a mercury pool cathode (diameter, 4 cm; area, 12.5 cm² or diameter, 3 cm; area, 7.1 cm²) and a platinum plate cathode (3×4 cm; area, 12 cm²) at 20 °C. Catholytes were 50 cm³ of DMF or acetonitrile containing 0.4 M Et_4NClO_4 or 0.5 M Bu_4NClO_4 and 0.04—0.10 M starting sulfates.

Product Analyses. Gaseous products were introduced into a gas burette with a nitrogen stream and analyzed by gas chromatography (Porapak Q, 2 m, 40—100 °C). Products in the catholytes also were analyzed by gas chromatography (Porapak Q, 2 m, 100—200 °C for dimethyl ether, diethyl ether, THF, oxetane, propylene oxide, styrene oxide, ethanol and 2,3-butanediol; PEG 20M, 0.5 and 2 m, 30—150 °C for butane, 2-butene, 2-butanone, cyclohexene, 2,3-dimethyl-2-butene and allyl alcohol). Mass spectra were measured by a spectrometer (Jeol Model D-100) connected with gas chromatograph (Joel Model GJC-20K) or none.

The separation of salts of the acyclic disulfate dianion (**1**) of 2,3-butanediol from the catholytes and their identification were carried out by the following procedures: After the electrolysis of the cyclic sulfate of 2,3-butanediol, DMF was evaporated at 50 °C under reduced pressure from the catholyte containing tetrabutylammonium perchlorate; water was added to the residue. The perchlorate was removed from the resulting mixture by extraction with dichloromethane. The aqueous layer was evaporated to dryness under reduced pressure. The residual white solid, which was contaminated with water and DMF, seemed to consist mainly of the bis(tetrabutylammonium) salt of **1** (IR spectrum), but it could not be purified enough to confirm the molecular structure. Next, the separation from a catholyte containing acetonitrile instead of DMF was attempted in a different procedure. Acetonitrile was evaporated at room temperature under reduced pressure and then 30 cm³ of water and 9 cm³ of 0.5 M perchloric acid were added to the residue. The resulting mixture was extracted with two potions of 20 cm³ of dichlo-

† 1 M=1 mol dm^{-3}.

romethane to remove the tetrabutylammonium perchlorate. The aqueous layer was neutralized (pH 7.0) with potassium hydroxide solution and concentrated at room temperature under reduced pressure. The precipitated potassium perchlorate was removed from the solution by filtration. To the filtrate was added ethanol, and the precipitated potassium salt of **1** as white crystals was collected on a filter paper and washed repeatedly with ethanol. Yield, 42%; mp, 249.0—252.5 °C (dec); IR (KBr), 3010 (ν_{C-H}) and 1220—1290 cm^{-1} ($\nu_{S=O}$) MS (70 eV), *m/z* 88 (corresponding to the molecular weight of 3,4-dimethyldioxetane) and 72 (2,3-epoxybutane); ^{1}H-NMR (in D_2O), δ=1.37 (m, 6H) and 4.55 (m, 2H) (multiplet signals may be due to stereoisomers, *dl/meso*, of **1**); flame test, violet (potassium). Found: C, 14.82; H, 2.66; S, 18.80%. Calcd for $C_4H_8S_2O_8K_2$: C, 14.72; H, 2.47; S, 19.64%. Further confirmation of the structure was obtained by hydrolysis. 0.192 g (0.59 mole) of the potassium salt of **1** was heated for 6 h at 95 °C in 2 cm^3 of water containing three drops of 2 M hydrochloric acid. 2,3-Butanediol (45% yield) in the reaction mixture was detected by gas chromatography and barium sulfate (52% yield) was precipitated by addition of barium chloride solution.

A small amount of the bis(tetrabutylammonium) salt of the acyclic disulfate dianion of 2,3-dimethyl-2,3-butanediol also could be separated fairly pure from the corresponding catholyte of DMF. Mp, 94.5—95.0 °C; IR(KBr), 1110—1240 cm^{-1} ($\nu_{S=O}$). Found: C, 59.57; H, 11.24; N, 4.36; S, 9.02%. Calcd for $C_{38}H_{84}N_2S_2O_8$: C, 59.96; H, 11.12; N, 3.68; S, 8.42%.

Partial confirmation of the composition of the suspended pale gray particles formed in the electrolysis of the cyclic sulfate of 2,3-butanediol in DMF was made as follows: The particles were collected on a filter paper and washed with DMF and water. The fine powder thus obtained dissolved in dilute nitric acid generating gas. From the resulting nitric acid solution, black and yellow powders precipitated by adding to it aqueous solutions of sodium sulfide and potassium iodide, respectively. The former and the latter seemed to be probably HgS and β-HgI_2 which latter was slightly soluble in ether. The original powder also seemed to decompose in dilute sulfuric and hydrochloric acids and be transposed to finer white powders. The resulting acid solution did not oxidize iodide ions. The original powder was not organic as judged by the IR spectrum. The properties of the powder indicated that it was an inorganic mercury salt. Identification as $HgSO_4$ and $Hg(ClO_4)_2$ was excluded by comparison with authentic samples. From these results, the powder was presumed to be a mercury salt of an oxyacid containing sulfur, *e.g.* Caro's acid. No further structure determination of this powder was made, since, because of the very small quantity involved it should not be important in determining the main reaction paths.

Dimethylmercury was analyzed by mass spectroscopy combined with gas chromatography: MS (20 eV), *m/z* 234 (M^+), 232 (M^+), 231 (M^+), 230 (M^+), 229 (M^+), 219 (M^+-CH_3), 217 (M^+-CH_3), 216 (M^+-CH_3), 215 (M^+-CH_3), 214 (M^+-CH_3) and 213 (M^+-CH_3).

Materials. Chemicals, except for the cyclic sulfates, were commercially supplied from Tokyo Kasei Kogyo Co., Ltd., Aldrich Chemical Co. and Pfaltz & Bauer, Inc. The cyclic sulfates mentioned below, unless stated otherwise, were prepared by literature methods: The cyclic sulfates of 1,2-ethanediol,[15] 2,3-butanediol,[16] 2,3-dimethyl-2,3-butanediol,[17] *trans*-1,2-cyclohexanediol,[18] and hydrated formaldehyde.[19]

Cyclic Sulfate of 1,3-Propanediol: To a suspension of 42.6 g (0.56 mole) of 1,3-propanediol in 200 cm^3 of dichloromethane was dropwise added 72.6 g (0.62 mole) of thionyl chloride; the reaction mixture was reluxed for 1 h. The mixture was poured into 100 cm^3 of ice water and the organic layer was washed with 100 cm^3 of water and aqueous sodium hydrogencarbonate, and again with water. The organic layer was dried over anhydrous magnesium sulfate and evaporated under reduced pressure. By fractional distillation of the residual oil the cyclic sulfite of 1,3-propanediol was obtained. Yield, 71%; bp, 52—54 °C/ 8 Torr (1 Torr= 101×325/760 Pa); IR (liquid film), 1180 cm^{-1} ($\nu_{S=O}$). To a solution of 20.0 g (0.16 mole) of the cyclic sulfite in 150 cm^3 of acetic acid was added dropwise below 14 °C a solution of 20.0 g (0.13 mole) of potassium permanganate in 200 cm^3 of water. After the reaction mixture was stirred for 1 h at room temperature, 100 cm^3 of water was added and then a solution of sodium sulfite until the precipitating manganese dioxide disappeared. When the mixture was neutralized with sodium carbonate, considerable amounts of the cyclic sulfate of 1,3-propanediol precipitated as white solid. The mixture was thoroughly extracted with ether and the resulting ethereal solution after being washed with water was dried over anhydrous magnesium sulfate. The solution was evaporated and the recrystallization of the residual white solid from a mixture of ether and hexane afforded the pure sulfate of 1,3-propanediol as white needles. Yield, 20%; mp, 60.5—62.0 °C (lit,[20], 63 °C); IR(KBr), 1380 and 1190 cm^{-1} ($\nu_{S=O}$). Found: C, 26.11; H, 4.54; S, 23.25%. Calcd for $C_3H_6SO_4$: C, 26.01; H, 4.38; S, 23.21%.

Cyclic Sulfate of 1,4-Butanediol: Prepared by a procedure similar to that for the cyclic sulfate of 1,3-propanediol. The cyclic sulfite of 1,4-butanediol: Yield, 67%; bp, 71.0—72.0 °C/ 6 Torr (lit,[18], 90.5—91.0 °C/13 Torr); IR (liquid film), 1200 cm^{-1} ($\nu_{S=O}$). The cyclic sulfate of 1,4-butanediol (recrystallized from a mixture of benzene and hexane): Yield, 50% (based on the sulfite); mp, 41.5—43.0 °C (lit,[18] 44—45 °C); IR(KBr), 1360—1395 and 1195 cm^{-1} ($\nu_{S=O}$). Found: C, 31.41; H, 5.41; S, 20.81%. Calcd for $C_4H_8SO_4$: C, 31.57; H, 5.50; S, 21.07%.

We thank Mr. Kwangho Park, UCLA, for performing some of the analyses and Dr. Yoshio Saito, UCLA, for valuable suggestions. We are also grateful to the Solar Energy Research Institute (Subcontract XB-1-9039-1), U.S.A. and the Japanese Ministry of Education, Science, and Culture for making possible Nonaka's participation at an initial period of this study in U.S.A.

References

1) P. Martigny, M.-A. Michel, and J. Simonet, *J. Electroanal. Chem.*, **73**, 373 (1976).

2) D. W. Sopher and J. H. P. Utley, *J. Chem. Soc., Chem. Commun.*, **1981**, 134.

3) K. Boujlel and J. Simonet, *Electrochim. Acta*, **24**, 481 (1979).

4) A. N. Dey and B. P. Sullivan, *J. Electrochem. Soc.*, **117**, 222 (1970).

5) T. Nonaka and M. M. Baizer, *Electrochim. Acta*, **28**, 661 (1983).

6) M. M. Baizer, T. Nonaka, K. Park, Y. Saito, and K. Nobe, *J. Appl. Electrochem.*, **14**, 197 (1984).

7) Utley also found that the dioxalate of 2,3-butanediol was reduced under cyclic voltammetric condition, but no reduction product, except for carbon dioxide, was identified.[8]

8) J. H. P. Utley, Report to the Solar Energy Research Institute (U.S.A.). Also a private communication from J. H. P. Utley.

9) N. Tarugi, *Gazz. Chim. Ital.*, **33**, 127 (1903).

10) A. N. Frumkin and G. M. Florianovich, *Dokl. Akad. Nauk SSSR.*, **80**, 902 (1951); *Chem. Abstr.*, **49**, 1371g (1952); N.

V. Nikolaeva and A. A. Grosman, *Dokl. Akad. Nauk SSSR.*, **95**, 1013 (1954); *Chem. Abstr.*, **49**, 5166e (1955); P. Kivaro and H. A. Leitinen, *J. Am. Chem. Soc.*, **77**, 5206 (1955); I. M. Tordesilla and J. L. Saiz, *An. Quim.*, **66**, 513, 623 (1970); *Chem. Abstr.*, **74**, 37680a, 37681b (1971).

11) Y. Ogata, "Yukikagobutsu No Sanka To Kangen," Nankodo, Tokyo (1964), p. 243.

12) G. Koltzenburg, G. Behrens, and D. Schulte-Frohlinde, *J. Am. Chem. Soc.*, **104**, 7311 (1982).

13) W. A. Pryor, "Free Radicals," McGraw-Hill, New York (1972), p. 12.

14) W. Baker and F. B. Field, *J. Chem. Soc.*, **1932**, 86; A. Yanagase, N. Sugita, K. Kudo, and Y. Takezaki, *Nippon Kagaku Kaishi*, **1975**, 583.

15) J. Brucken and G. Glockner, *East Ger. Patent* 15024 (1958); *Chem Abstr.*, **54**, 3201i (1960).

16) H. K. Garner and H. J. Lucas, *J. Am. Chem. Soc.*, **72**, 5497 (1950).

17) W. Baker and B. F. Burrows, *J. Chem. Soc.*, **1961**, 2257.

18) J. Lichtenberger and J. Hincky, *Bull. Chim. Soc. Fr.*, **1961**, 1495.

19) W. Baker, *J. Chem. Soc.*, **1931**, 1765.

20) J. Lichtenberger and R. Lichtenberger, *Bull. Chim. Soc. Fr.*, **1948**, 1002.

 © 1984 The Chemical Society of Japan Bull. Chem. Soc. Jpn., 57, 3167—3172 (1984)

Studies on *N*-Glycopeptides. II. Separation of α- and β-Amide of *N*-(L-Aspartyl)-β-D-glucopyranosylamine Obtained *via* *N*-(Benzyloxycarbonyl)-L-aspartic Anhydride

Masahiro TAMURA, Hiroshi NISHIZAKI, Chiemi MIYAZAKI, and Hideo OKAI*
Department of Fermentation Technology, Faculty of Engineering, Hiroshima University, Shitami, Saijo-cho, Higashihiroshima 724
(Received April 28, 1984)

A mixture of *N*-(L-α-aspartyl)- and *N*-(L-β-aspartyl)-β-D-glucopyranosylamine was obtained by the condensation of *N*-(benzyloxycarbonyl)-L-aspartic anhydride with β-D-glucopyranosylamine. Attempts to separate the mixture by using cation-exchange chromatography, a copper(II) complex, and fractional recrystallization were carried out. These separations gave good yields of the desired β-amine.

In a previous paper, we reported the preparation of nine *N*-glycopeptides, obtained by the condensation of *N*-hydroxysuccinimide esters of aspartyltripeptides with three glycosylamines.[1] This active ester method realized a carbohydrate–peptide linkage formation reaction, which was scarce in the *N*-glycopeptide synthesis. However, another synthetic route is necessary in order to prepare more complex *N*-glycopeptides for which demand has been increasing. Preparations of aspartylpeptides *via* *N*-(benzyloxycarbonyl)-L-aspartic anhydride have also been reported. Hirata *et al.* condensed *N*-(benzyloxycarbonyl)-L-aspartic anhydride with a L-histidine benzyl ester, and separated the α- and β-isomer from the reaction mixture.[2] If an efficient separation of aspartyl α- and β-amide is established, this anhydride method can be applied to *N*-glycopeptide synthesis.

Jeanloz *et al.*, actually, prepared 2-acetamido-3,4,6-tri-*O*-acetyl-1-*N*-[*N*-(benzyloxycarbonyl)-L-β-aspartyl]-2-deoxy-β-D-glucopyranosylamine and some of their analogs by the condensation of *N*-(benzyloxycarbonyl)-L-aspartic anhydride with glycosylamines and the following fractional recrystallization or silica-gel column chromatography.[3] They however, carried out the condensation using fully *O*-protected glycosylamine, and so, the separation technique was limited. Moreover, de-*O*-acetylation at the final step requires an alkaline treatment which usually harms the aspartyl linkage. We have attempted to resolve this problem by condensing glycosylamine possessing unprotected hydroxyl groups. Futhermore, applying this idea to the synthesis of *N*-glycopeptide *via* *N*-(benzyloxycarbonyl)-L-aspartic anhydride should reap a greater variety of separations of the α- and β-aspartyl isomer than Jeanloz *et al.* has attempted. We prepared *N*-(L-α-aspartyl)cyclohexylamine, *N*-(L-β-aspartyl)cyclohexylamine, *N*-(L-α-aspartyl)-β-D-glucopyranosylamine, and *N*-(L-β-aspartyl)-β-D-glucopyranosylamine as models of carbohydrate-asparagine compounds. We then examined several separations by using cation-exchange resine chromatography, a copper (II) complex, and fractional recrystallization to find the most efficient ones.

Mixtures were prepared as shown in Schemes 1 and 2. *N*-(Benzyloxycarbonyl)-L-aspartic anhydride (**1**) was condensed with cyclohexylamine to give a mixture of **2a** and **2b**. This was hydrogenated in the presence of palladium black, and the desired mixture of **3a** and **3b** was obtained. *N*-(Benzyloxycarbonyl)-L-aspartic anhydride (**1**) was also condensed with β-D-glucopyranosylamine (**5**), which was prepared by the hydrogenation of β-D-glucopyranosyl azide[1] (**4**) in the presence of Adams' catalyst (PtO_2), to give a mixture of **6a** and **6b**. Hydrogenation of the mixture in the presence of palladium black gave the desired mixture of **7a** and **7b**.

It should be noted here that Kornguth *et al.* reported

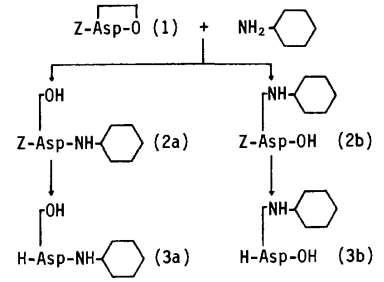

Scheme 1.

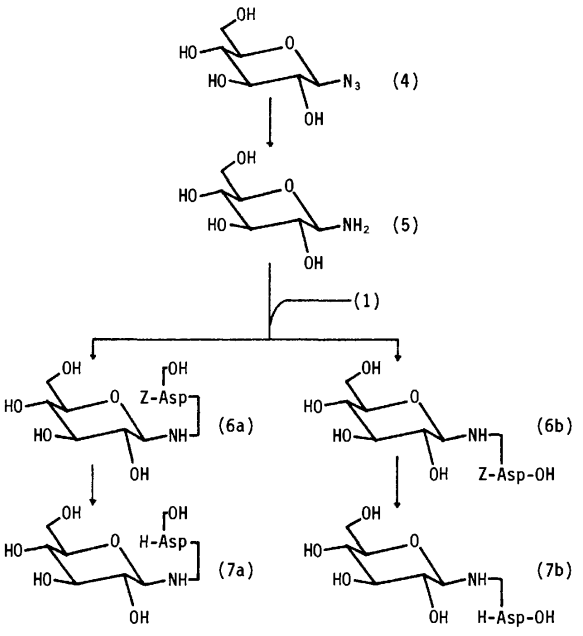

Scheme 2.

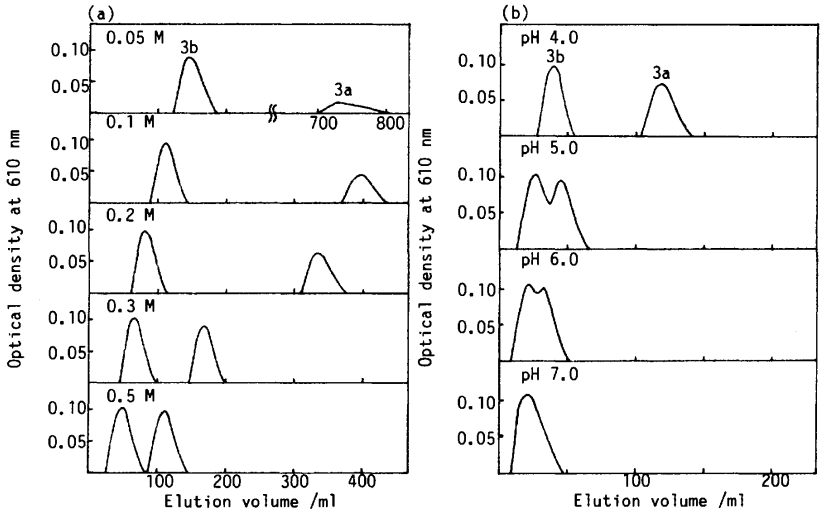

Fig. 1. Effect of salt concentration (a) and pH (b) in pyridinium acetate solvent system on separation of *N*-(L-α-aspartyl)cyclohexylamine (**3a**) and *N*-(L-β-aspartyl)cyclohexylamine (**3b**).

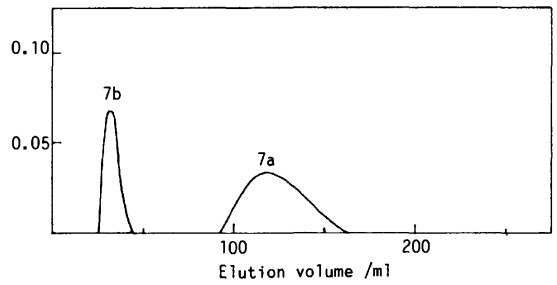

Fig. 2. Separation of *N*-(L-α-aspartyl)-β-D-glucopyranosylamine (**7a**) and *N*-(L-β-aspartyl)-β-D-glucopyranosylamine (**7b**) on a small column.
Amberlite CG-120 type II (pyridinium form, 1.2× 10 cm) Buffer solution ; 0.1 M pyridinium acetate (pH 4.0).

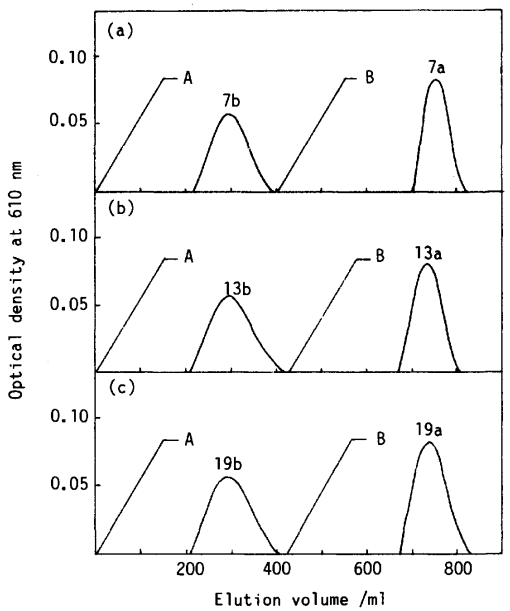

Fig. 3. Preparative separation of **7a** and **7b** (a), **13a** and **13b** (b), and **19a** and **19b** (c).
Amberlite CG-120 type I (pyridinium form, 2.8× 50 cm) Buffer solution ; A : 0.1 M pyridinium acetate (pH 4.0) B : 0.2 M pyridinium acetate (pH 4.0).

the separation of a mixture of ε-(L-α-glutamyl)-L-lysine and ε-(L-γ-glutamyl)-L-lysine using an amino-acid analyzer,[4] and Hirata *et al.* reported the separation of a mixture of L-α-aspartyl-L-histidine and L-β-aspartyl-L-histidine, or L-α-glutamyl-L-histidine and L-γ-glutamyl-L-histidine using a cation-exchange resin.[2] With this in mind, we first examined the separation of mixtures **3a** and **3b**, and **7a** and **7b** by cation-exchange resin chromatography. Preliminary experiments on a mixture of **3a** and **3b** were performed with a small column of Amberlite CG-120 using pyridinium acetate buffers at different pH and salt concentrations in order to find an optimal condition for the separation. The elution patterns of a mixture composed of **3a** and **3b** are indicated in Figs. 1-a and 1-b. 0.1 M† Pyridinium acetate (pH 4.0) separated the mixture most effectively. We then attempted to separate a mixture of **7a** and **7b** using the same solvent. As shown in Fig. 2, **7a** and **7b** were separated completely.

As a large-scale experiment we attempted to separate material composed of **7a** and **7b** into α- and β-amide with a large column (2.8×54 cm) of Amberlite CG-120, using 0.1 M pyridinium acetate (pH 4.0) as an eluent. After the first peak was eluted, the eluent was changed to 0.2 M pyridinium acetate (pH 4.0). Compounds **7a** and **7b** were separated completely (see Fig. 3-a) and provided high yields (250 mg and 120 mg, respectively).

We further prepared mixtures of α- and β-amide of β-D-galactopyranosylamine and α-D-mannopyranosylamine as shown in Schemes 3 and 4, and treated them using the same method as described for the separation of **7a** and **7b** in order to investigate the limit of separation using a cation-exchange resin. Both galactosyl (**13a** and **13b**) and mannosyl (**19a** and **19b**) derivatives were separated completely, as shown in Figs. 3-b and 3-c. From these results, the usefulness of the separation of

† 1M=1 mol dm^{-3}.

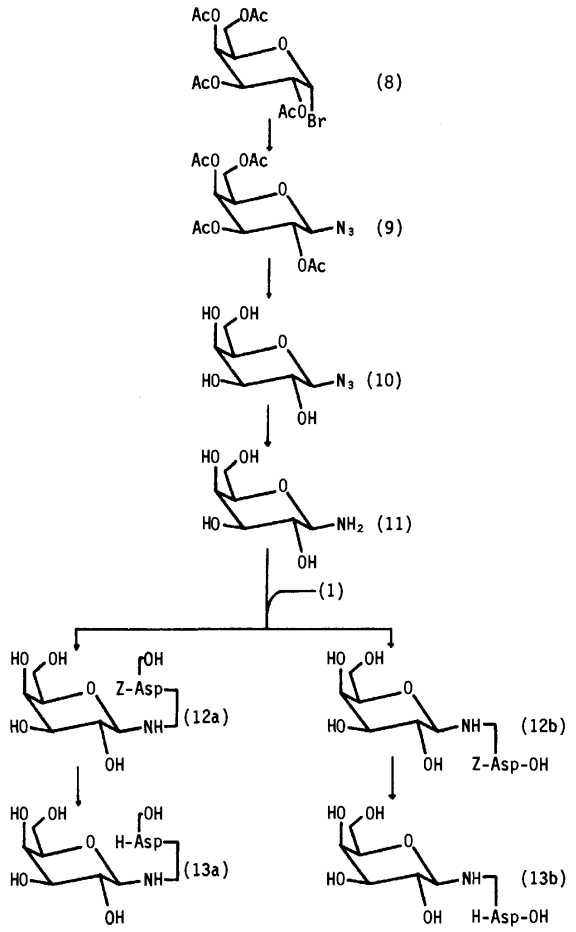

Scheme 3.

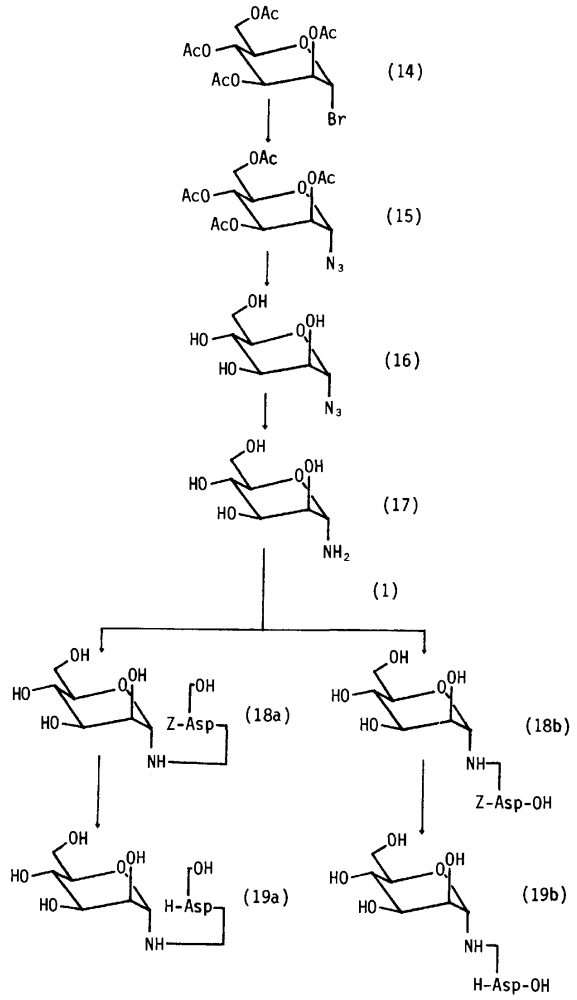

Scheme 4.

α- and β-amide of aspartyl residue from the reaction mixture (obtained by the condensation of *N*-(benzyloxycarbonyl)-L-aspartic anhydride with various glycosylamines) by the use of cation-exchange resin chromatography was proved.

We next applied a mixture of **7a** and **7b** to an amino acid analyzer. Compounds **7a** and **7b** were separated completely (see Fig. 4). The percentage of color yield of **7a** and **7b**, based on L-aspartic acid as 100%, were observed to be 89% and 162%, respectively. We used an amino acid analyzer to check the purity of the mixture after the following separations.

Secondly, we examined a separation using a copper (II) complex. By the addition of dicopper carbonate dihydroxide to **7a** and **7b**, 6-membered and 5-membered rings were formed, respectively. It is well-known that a 5-membered copper (II) complex is more stable than a 6-membered salt (see Fig. 5). We tried to separated **7a** and **7b** using the difference in their stabilities. The experiment was performed as shown in Scheme 5. The crystals (II) obtained were de-salted and apllied to an amino acid analyzer. We found that purification was as follows: **7a**:**7b**=9:91. The purification by the differential stability of copper (II) salts of **7a** and **7b** may be suitable in the preparation of *N*-glycopeptide.

Thirdly, we attempted to isolate **6b** from the mixture by fractional recrystallization. We prepared diastereomeric salts of **6a** and **6b** with cyclohexylamine and dicyclohexylamine, and these salts were recrystallized from methanol. The crystals obtained were hydrogenated, applied to an amino acid analyzer to confirm the purity of the mixture, and the results are listed in Table 1. We discovered an interesting and useful fact; the dicyclohexylammonium salt of **6b** is more soluble than

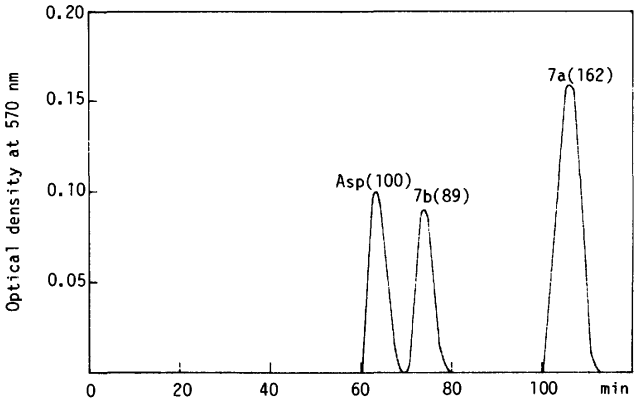

Fig. 4. Elution pattern of aspartic acid, *N*-(L-β-aspartyl) β-D-glucopyranosylamine (**7b**), and *N*-(L-α-aspartyl)-β-D-glucopyranosylamine (**7a**) by amino acid analyzer. Sample; 0.1 μmol/ml solution.

that of **6a**, whereas the cyclohexylammonium salt of **6b** is less soluble than that of **6a**. These facts were applied to separate a mixture of **6a** and **6b**. At the outset, we attempted to obtain **6b** by the repetitious recrystallization of a cyclohexylammonium salt as shown in Scheme 6, however, pure **6b** was obtained in a very low yield. Therefore, we used both a cyclohexylammonium salt and a dicylohexylammonium salt (shown in Scheme 7) to obtain a pure cyclohexylammonium salt of **6b** with a high yield.

We considered that fractional recrystallization has several merits, to wit; (a) fractional recrystallization is performed in organic solution, in which aspartyl residue is more stable than an acidic or basic solution of water, and (b) the resulting β-amide is suitable to elongate the peptide chain toward the C-terminal since fractional recrystallization is carried out using an *N*-protected aspartyl derivative.

We established separation techniques to obtain β-amide formed by the reaction of *N*-(benzyloxycarbonyl)-L-aspartic anhydride with glycosylamine. Each separation gave a good yield and compared favorably with that of Jeanloz *et al.* Additionally,and equally important, is the fact that this method goes to lesser extremes, yet is much more refined than the method of Nerberger *et al.* in which they condensed *N*-(benzyloxycarbonyl)-L-aspartic acid α-benzyl ester with 2-acetamido-3,4,6-tri-*O*-acetyl-2-deoxy-β-D-glucopyranosylamine in the presence of dicyclohexylcarbodimide.[5]

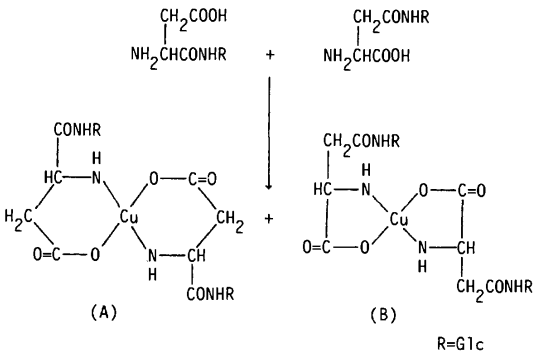

Fig. 5. Copper (II) complex of **7a** and **7b** (B).

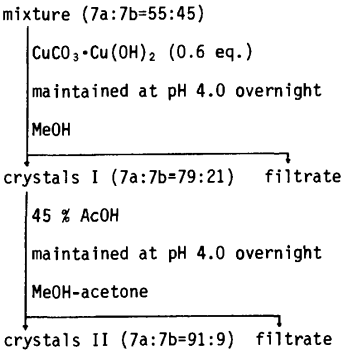

Scheme 5.

TABLE 1. RESULTS OF PRELIMINARY EXPERIMENTS OF FRACTIONAL RECRYSTALLIZATIONS BY THE USE OF ORGANIC BASES

Base	Yield of 1st crop*	Yield of 2nd crop**
Cyclohexylamine	79% (**6a** : **6b**=39 : 61)	12% (**6a** : **6b**=52 : 48)
Dicyclohexylamine	22% (**6a** : **6b**=100 : 0)	34% (**6a** : **6b**=0 : 100)

* 1st crop was crystallized by the aid of AcOEt–ether.
** 2nd crop was crystallized by the aid of petroleum ether.

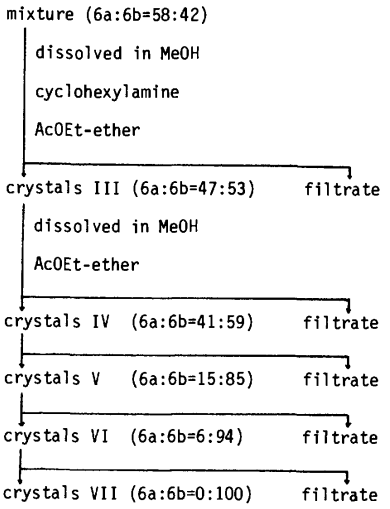

Scheme 6.

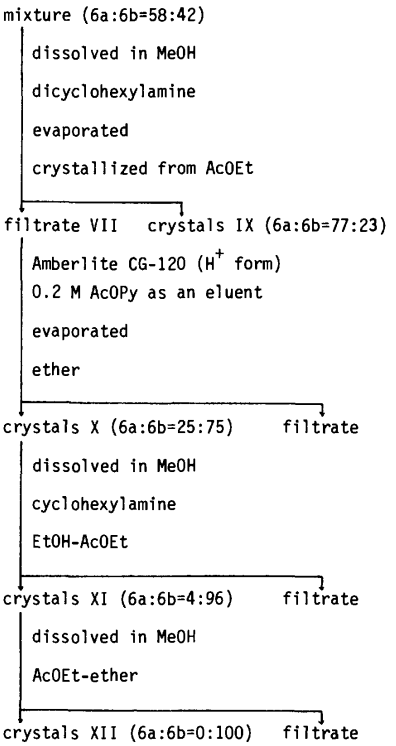

Scheme 7.

Experimental

All the melting points were uncorrected. The optical rotations were measured on a Union PM-101 Polarimeter. IR spectra were taken on a Jasco spectrophotometer Model IRA-1. Thin-layer chromatography was carried out on a Kieselgel G nach Stahl (Type 60) with 1-butanol–acetic acid–pyridine–water (4:1:1:2 v/v). Spots of material possessing a free amino group in a thin-layer plate were detected by ninhydrin, and those of the amino group-blocked material by spraying 25% HBr/AcOH and then ninhydrin. A quantitative analysis of the aspartyl derivatives was performed with a Hitachi Model KLA-5 amino acid analyzer. The amounts of color developed were determined using an Atago AG-4 Densitometer (slit 1×18 mm, 610 nm). Samples for elemental analysis were dried at 60 °C over phosphorus pentaoxide *in vacuo*.

Preparation of Mixtures. N-*(L-α-Aspartyl)- and* N-*(L-β-Aspartyl)cyclohexylamine (**3a** and **3b**)*: A solution of *N*-(benzyloxycarbonyl)-L-aspartic anhydride[6] (**1**) (1.25 g) in tetrahydrofuran (5 ml) was added to a solution of cyclohexylamine (0.7 ml) and triethylamine (0.56 ml) in tetrahydrofuran (5 ml) under vigorous stirring at room temperature overnight. The reaction mixture was evaporated to dryness and the residue was dissolved in ethyl acetate. The solution was washed with 4% sodium hydrogencarbonate and water, successively, dried over anhydrous sodium sulfate, and evaporated. A solid of **2a** and **2b** (1.40 g, 80%) was obtained by the aid of ether–petroleum ether.

The mixture of **2a** and **2b** (0.70 g) was dissolved in acetic acid (30 ml) and treated with hydrogen in the presence of palladium black. The filtrate from the catalyst was evaporated to dryness and a mixture of **3a** and **3b** was obtained after crystallization from ether; yield, 0.43 g.

Found: C, 56.00; H, 8.49; N, 13.01%. Calcd for $C_{10}H_{18}N_2O_3$: C, 56.05; H, 8.47; N, 13.08%.

N*[N-(Benzyloxycarbonyl)-L-α-aspartyl]- and* N-*[N-(Benzyloxycarbpnyl)-L-β-aspartyl]-β-D-glucopyranosylamine (**6a** and **6b**)*: To a solution of *β*-D-glucopyranosylamine[1] (**5**) (4.30 g), obtained by the hydrogenation of *β*-D-glucopyranosyl azide[1] (**4**), and triethylamine (3.36 ml) in water (20 ml), a solution of **1** (4.98 g) in tetrahydrofuran (20 ml) was added under vigorous stirring at room temperature. The stirring continued overnight. The reaction mixture was evaporated to dryness and the residue was dissolved in water (40 ml). The solution was adjusted to pH 4.0 by the addition of 2% hydrochloric acid and extracted with ethyl acetate (total 500 ml). The organic layer was dried over anhydrous sodium sulfate and evaporated. The residual oil was crystallized using ether; yield, 4.79 g (56%); R_f 0.79 (**6a**) and 0.72 (**6b**).

Found: C, 50.49; H, 5.66 N, 6.52%. Calcd for $C_{18}H_{24}N_2O_{10}$ C, 50.49; H, 5.65; N, 6.54%.

N-*(L-α-Aspartyl)- and* N-*(L-β-Aspartyl)-β-D-glucopyranosylamine (**7a** and **7b**)*: A mixture of **6a** and **6b** (1.28 g) was dissolved in methanol and hydrogenated in the presence of palladium black. After 4 h, the catalyst was filtered off and the filtrate was evaporated to dryness. A mixture of **7a** and **7b** was crystallized using ethanol; yield 0.58 g (66%); R_f 0.34.

Found: C, 40.14; H, 6.17; N, 9.52%. Calcd for $C_{10}H_{18}N_2O_8$: C, 40.18; H, 6.17; N, 9.52%.

*Tetra-O-acetyl-β-D-galactopyranosyl Azide (**9**)*: This compound was prepared by the method of W. Pfleiderer and B. Bühler.[7] The yield was 84% and the product had a mp of 92—93 °C; lit,[7] mp 96 °C. ν_{max}^{KBr} 1760 (OAc) and 2100 cm^{-1} (N_3).

Found: C, 45.00; H, 5.14; N, 11.22%

N-*(L-α-Aspartyl)- and* N-*(L-β-Aspartyl)-β-D-galactopyranosylamine (**13a** and **13b**)*: Compound (**9**) (7.46 g) was dissolved in methanol (20 ml) saturated with dry ammonia at 0 °C and was stored in a glass-stoppered bottle at room temperature overnight. The reaction mixture was then evaporated *in vacuo*. The residual oil was dissolved in methanol and hydrogenated in the presence of PtO_2. The filtrate from the catalyst was evaporated to dryness and the residue was solidified using ethanol; yield, 2.45 g.

This *β*-D-galactopyranosylamine (**11**) (4.30 g) and **1** (4.98 g) were treated as described for the preparation of a mixture of **6a** and **6b**, to give **12a** and **12b**; yield, 4.54 g (53%); R_f 0.82 (**12a**) and 0.74 (**12b**).

A mixture of **12a** and **12b** (1.28 g) was hydrogenated as described for the preparation of **7a** and **7b**; yield, 0.52 g (59%); R_f 0.38.

Found: C, 40.13; H, 6.19; N, 9.56%. Calcd for $C_{10}H_{18}N_2O_8$: C, 40.18; H, 6.27; N, 9.52%.

*Tetra-O-acetyl-α-D-mannopyranosyl Azide (**15**)*: This was prepared by the method of Paulsen *et al.*[8] The yield was 71% and the product had $[\alpha]_D^{20}$ +87° (*c* 1, chloroform): lit,[8] $[\alpha]_D^{20}$ +91° (*c* 1, dioxane), ν_{max}^{nujol} 1750 (OAx) and 2110 cm^{-1} (N_2).

Found: C, 45.12; H, 5.11; N, 11.21%.

N-*(L-α-Aspartyl)- and* N-*(L-β-Aspartyl)-α-D-mannopyranosylamine (**19a** and **19b**)*: **15** (7.46 g) was de-*O*-acetylated and hydrogenated as described for preparation of **11** to give **17**. **17** (4.30 g) and **1** (4.98 g) were treated as described for preparation of the mixture of **6a** and **6b**; yield, 4.88 g (57%); R_f 0.68 (**18a**) and 0.64 (**18b**).

A mixture of **18a** and **18b** (1.28 g) was hydrogenated as described for the preparation of **7a** and **7b**; yield, 0.51 g (58%); R_f 0.31.

Found: C, 40.22; H, 6.20; N, 9.50%. Calcd for $C_{10}H_{18}N_2O_8$: C, 40.18; H, 6.17; N, 9.52%.

*Separation of α- and β-Amide by Cation-exchange Resin Chromatography. Separation of **3a** and **3b** on a Small Column*: A column (1.2×10 cm) with Amberlite CG-120 (pyridinium form) was equilibrated by washing with pyridinium acetate (pH 4.0) of a definite salt concentration (0.05 M, 0.1 M, 0.2 M, 0.3 M, or 0.5 M) or 0.2 M pyridinium acetate of definite pH (4.0, 5.0, 6.0, or 7.0), and the mixture was applied to a column. The column was eluted with the same buffer at room temperature, and two ml fractions were collected at a flow rate of about 10 ml/h. Approximately 0.01 ml from each tube was spotted on a strip of filter paper. The strip was dried at 100 °C for 5 min, immersed in a 0.2% ninhydrin–acetone solution, and again heated. The degrees of coloration developed were determined by a densitometer. The resulting patterns are shown in Fig. 1.

*Separation of **7a** and **7b** on a Small Column*: A mixture of **7a** and **7b** (50 mg) was treated on a column of Amberlite CG-120 (pyridinium form) in same manner as the saparation of **3a** and **3b** using 0.1 M pyridinium acetate (pH 4.0). The resulting patterns are shown in Fig. 2.

*Preparative Separation of **7a** and **7b***: A mixture of **7a** and **7b** (500 mg) was applied to a large column (2.8×54 cm) of Amberlite CG-120 (pyridinium form) using 0.1 M pyridinium acetate (pH 4.0) as an eluent. For the elution of the slower peak, 0.2 M pyridinium acetate (pH 4.0) was used as an eluent. The elution patterns are shown in Fig. 3-a.

7a: Yield 256 mg (51%); mp 183—185 °C (decomp); $[\alpha]_D^{20}$ +13.5° (*c* 2, water). ν_{max}^{KBr} 3300 (broad OH and NH) and 1630 cm^{-1} (CONH).

Found: C, 40.90; H, 6.14; N, 9.51%. Calcd for $C_{10}H_{18}N_2O_8$: C, 40.81; H, 6.17; N, 9.52%.

7b: Yield, 120 mg (24%); mp 204 °C (decomp) $[\alpha]_D^{20}$ −5.5° (*c* 2, water). ν_{max}^{KBr} 3300 (broad OH and NH) and 1650 cm^{-1} (CONH).

Found: C, 40.87; H, 6.15; N, 9.49%. Calcd for $C_{10}H_{18}N_2O_8$: C, 40.81; H, 6.17; N, 9.52%.

Preparative Separation of 13a and 13b: A mixture of **13a** and **13b** (500 mg) was treated in same manner as has been described for the separation of **7a** and **7b**. The elution patterns are shown in Fig. 3-b.

13a: Yield, 211 mg (42%); mp 186—189 °C (decomp); $[\alpha]_D^{20}$ +16.5° (*c* 2, water). ν_{max}^{KBr} 3300 (broad OH and NH) and 1640 cm^{-1} (CONH).

Found: C, 40.84; H, 6.14; N, 9.55%. Calcd for $C_{10}H_{18}N_2O_8$: C, 40.81; H, 6.17; N, 9.52%.

13b: Yield, 163 mg (33%); mp 202—216 °C (decomp); $[\alpha]_D^{20}$ −6.0° (*c* 2, water). ν_{max}^{KBr} 3300 (broad OH and NH) and 1650 cm^{-1} (CONH).

Found: C, 40.81; H, 6.14; N, 9.51%. Calcd for $C_{10}H_{18}N_2O_8$: C, 40.81; H, 6.17; N, 9.52%.

Preparative Separation of 19a and 19b: A mixture of **19a** and **19b** (500 mg) was treated in the same manner as for the separation of **7a** and **7b**. The elution patterns are shown in Fig. 3-c.

19a: Yield, 158 mg (52%); mp 187—188 °C (decomp); $[\alpha]_D^{20}$ +16.5° (*c* 2, water). ν_{max}^{KBr} 3300 (broad OH and NH) and 1640 cm^{-1} (CONH).

Found: C, 40.79; H, 6.16; N, 9.54%. Calcd for $C_{10}H_{18}N_2O_8$: C, 40.81; H, 6.17; N, 9.52%.

19b: Yield, 119 mg (39%); mp 204—221 °C (decomp); $[\alpha]_D^{20}$ −4.0° (*c* 2, water). ν_{max}^{KBr} 3300 (broad OH and NH) and 1660 cm^{-1} (CONH).

Found: C, 40.85; H, 6.16; N, 9.50%. Calcd for $C_{10}H_{18}N_2O_8$: C, 40.81; H, 6.17; N, 9.52%.

Separation of α- and β-Amide by Copper (II) Complex. To a solution of **7a** and **7b** (**7a**:**7b**=55:45, 294 mg) in water (6 ml), dicopper carbonate dihydroxide (66 mg) was added. The solution was heated for 5 min and then 45% acetic acid was added. It was maintained at pH 4.0 onernight. Type-I crystals (139 mg, 43%) were obtained using methanol. A small amount of these were treated on a column of Amberlite CG-120 (H^+ form) (1.3×8.0 cm) with water and 0.2 M pyridinium acetate (pH 5.0) as an eluent. The eluting fraction was collected and evaporated to dryness. The residue was applied to an amino acid analyzer (**7a**:**7b**=36:64).

Type-I crystals were dissolved in hot water and 45% acetic acid was added to the solution. The mixture was maintained at pH 4.0 overnight. Type-II crystals (46 mg, 33%) were obtained using methanol-acetone. A small amount of these were treated on a column of Amberlite CG-120 (H^+ form) as described above (**7a**:**7b**=9:91).

Separation of α- and β-Amide by Fractional Recrystallization. Preliminary Experiments: To a solution of **6a** and **6b** (428 mg) in methanol (5 ml), cyclohexylamine or dicyclohexylamine (2 mmol each) was added. Crystals were obtained using ether (5 ml), and the filtrates were evaporated. Crystals were obtained using ether–petroleum ether as second crop. These crystals were dissolved in methanol, and hydrogenated in the presence of palladium black. Filtrates from the catalyst were evaporated and applied to an amino acid analyzer. The results are listed in Table 1.

Separation of 6a and 6b by the Use of Cyclohexylammonium Salt: A mixture of **6a** and **6b** (**6a**:**6b**=58:42, 428 mg) was dissolved in methanol (5 ml) and cyclohexylamine (0.23 ml) was added to the solution. Type-III crystals (295 mg, 56%) were obtained using ethyl acetate-ether. A small amount of these crystals were dissolved in methanol and hydrogenated in the presence of palladium black. The catalyst was filtered off the filtrate was evaporated. The residual oil was applied to an amino acid analyzer (**6a**:**6b**=47:53).

Type-III crystals were dissolved in methanol (5 ml) in methanol (5 ml) and type-IV crystals (210 mg, 71%) were obtained using ethyl acetate–ether. A small amount of these crystals were hydrogenated as described above, and applied to an amino acid analyzer (**6a**:**6b**=41:59).

Type-IV crystals were dissolved in methanol (5 ml) and type-V crystals (152 mg, 72%) were obtained using ethyl acetate–ether. A small amount of these crystals were hydrogenated and applied to an amino acid analyzer (**6a**:**6b**=15:85).

Type-V crystals were treated as described for the prepartion of type-IV crystals, and type-VI crystals (107 mg, 70%, **6a**:**6b**=6:94) was obtained.

Type-VI crystals were treated as described for the preparation of type-VI crystals, and type-VII crystals (75 mg, 70%, **6a**:**6b**=0:100) were obtained.

Separation of 6a and 6b by the Use of Both Cyclohexylammonium and Dicyclohexylammonium Salt: To a solution of **6a** and **6b** (428 mg, **6a**:**6b**=58:42) in methanol (5 ml), dicyclohexylamine (0.197 ml) was added. The mixture was evaporated to dryness and type-IX crystals (396 mg, 65%) were obtained by the recrystallization from hot ethyl acetate. A small amount of type-IX crystals were hydrogenated, applied to an amino acid analyzer (**6a**:**6b**=77:23).

A filtrate (VIII) was evaporated to dryness, and residual oil was dissolved in water (10 ml). The solution was treated on a column Amberlite CG-120 (H^+ form) using 0.2 M pyridinium acetate (pH 5.0) as an eluent. The eluting fractions was collected and evaporated to dryness. Type-X cryltals (123 mg, 29%) were obtained using ether. A small amount of type-X crystals were hydrogenated and applied to an amino acid analyzer (**6a**:**6b**=25:75).

Type-X crystals were dissolved in methanol (3 ml) and cyclohexylamine (0.05 ml) was added to the solution. The solution was evaporated to dryness and the residual oil was crystallized from ethanol–ethyl acetate to give type-XI crystals (120 mg, 79%). A small amount of type-XI crystals were hydrogenated and applied to an amino acid analyzer (**6a**:**6b**=4:96).

Type-XI crystals were dissolved in methanol (3 ml) and the solution was evaporated to dryness. Type-XII crystals (103 mg, 86%) were obtained using ethyl acetate–ether. A small amount of type-XII crystals were hydrogenated and applied to an amino acid analyzer (**6a**:**6b**=0:100).

References

1) M. Tamura and H. Okai, *Carbohydr. Res.*, in press.
2) M. Hirata, K. Noda, and N. Izumiya, *Bull. Chem. Soc. Jpn.*, **45**, 1790 (1972).
3) H. G. Garg and R. W. Jeanloz, *Carbohydr. Res.*, **23**, 437 (1972).
4) M. L. Kornguth, A. Neidle, and H. Waelsch, *Biochemistry*, **2**, 740 (1963).
5) G. S. Marks, R. D. Marshall, and A. Nerberger, *Biochem. J.*, **3**, 1596 (1964).
6) W. J. Le Quensne and G. T. Young, *J. Chem. Soc.*, **1952**, 24.
7) W. Pfleiderer and E. Bühler, *Chem. Ber.*, **99**, 3022 (1966).
8) H. Paulsen, Z. Györgydéak, and M. Friedmann, *Chem. Ber.*, **107**, 1568 (1974).

 © 1984 The Chemical Society of Japan Bull. Chem. Soc. Jpn., 57, 3173—3176 (1984)

Liquid Crystal Materials with Sulfur Atoms Incorporated in the Principal Structure 2. New Liquid Crystal Compounds; 2-Substituted-5-(*p*-substituted phenyl)-1,3-dithianes

Yuichiro HARAMOTO,* Koji AKAZAWA, and Hiroyoshi KAMOGAWA
Department of Applied Chemistry, Yamanashi University, Takeda 4, Kofu 400
(Received May 7, 1984)

2-Substituted-5-(*p*-substituted phenyl)-1,3-dithianes (**8**), new liquid crystals, were synthesized. The mesomorphic properties of these compounds were compared with those of the corresponding 2-(*p*-substituted phenyl)-5-alkyl-1,3-dithianes (**9**). The main difference found between these two liquid-crystal compounds was that some of **8** exhibited both monotropic nematic and smectic liquid-crystal phases but **9** exhibited only the monotropic nematic phase. This difference seems to originate in somewhat increased lateral interactions between molecules. Even for the three-ring compounds, many of them exhibited the monotropic liquid-crystal behavior. This should mean that these 1,3-dithiane compounds strongly tend to exhibit the monotropic liquid-crystal behavior.

In recent years, 2,5-disubstituted 1,3-dithianes and 1,3-oxathianes have been reported as new types of liquid-crystal materials.[1,2] Since these structures are quite novel as liquid crystals, we wish to report information on a further synthesis of 2-substituted-5-(*p*-substituted phenyl)-1,3-dithianes and to compare their liquid-crystal behavior with that of the 2-(*p*-substituted phenyl)-5-alkyl-1,3-dithianes previously reported.

Results and Discussion

2-Substituted-5-(*p*-substituted phenyl)-1,3-dithianes were synthesized *via* the following route.

In the synthesis of **2**, both esterification and etherification were done in one step. In step **2**→**3**, it was necessary to keep the reaction temperature at 190—200 °C for about 30 min under a reduced pressure (15 mmHg (1 mmHg=133.322 Pa)) for the complete evolution of carbon monoxide. This evolution of CO allowed us to check and control the progress of the reaction.

In step **4**→**5**, PBr_3 must be used for *p*-ethoxy compounds to prevent the cleavage of the ether bond, but in the case of *p*-methyl compounds $HBr-H_2SO_4$ could be used under conventional conditions. **8** was purified mostly by means of recrystallizations from hexane. Those compounds which could not be purified by recrystallization were purified first by column chromatography, then by recrystallization from hexane until only a single spot in TLC was obtained.

Thus synthesized **8**, were all colorless and odorless crystals or powders which were soluble in common organic solvents.

Absorption of C2 and C4, C6 carbons of the 1,3-dithiane ring in ^{13}C-NMR, as determined by ^1H-complete decoupling (COM), ^1H-off resonance decoupling (OFR), and ^1H-selective decoupling (SEL) procedures, are located at δ=47.46 and 37.06, respectively, for a 1,3-dithiane (R=C_2H_5O, R'=C_7H_{15}). According to Eliel, in the 1,3-dithiane substituted at the C2 carbon by the methyl group, the equatorial isomer absorbs at about 5 ppm lower field than the axial isomer does.[3] Since this compound exhibits liquidcrystal phases and any absorption does not exist between δ 47.46 and 63.39, it should be the pure equatorial isomer without contamination with the axial one.

Mesomorphic ranges of the synthesized 2-substituted-5-(*p*-substituted phenyl)-1,3-dithiane **8** and the corresponding 2-(*p*-substituted phenyl)-5-alkyl-1,3-dithiane **9** are given in Table 1.

Measurements of the mesomorphic ranges and the assignment of the mesophases were carried out by means of a micro melting-point apparatus equipped with polarizers. To decide on the type of smectic phase, a comparison was made of these smectic phases with the color photography found in the literature.[4]

The difference between **8** and **9** are : (1) Some of **8** exhibited smectic A, but **9** not at all and (2) **8** exhibited liquid-crystal phases down to temperatures lower than those corresponding to **9**.

Generally, the smectic phase appears by increasing the attractive side interactions between molecules. The difference in structure between **8** and **9** involves the position of the sulfur atoms. This difference seems to increase side interactions between **8**. That is, in **9**, S-atoms are located more closely to the benzene ring than in **8**, so that the steric effect which decreases lateral interactions seems to become more effective.

Since sulfur atoms are located more closely to the electron-withdrawing benzene ring in **9** than in **8**, this electron withdrawal might be responsible for the lower dipole moment and dispersion force of the C–S bond. In **8**, C–S bonds are more distant from the benzene ring than in the case of **9**, so that this diminishing effect may be very small. Therefore, lateral interactions in **9** should be smaller than those in **8**.

ΔH_{C-1} of the compound **8-5** and **8-6** are 4.97 kcal/mol (1 cal=4.184 J) and 5.90 kcal/mol, and ΔS_{C-1} of them are 15.0 cal/mol/K 17.6 cal/mol/K respectively. These values are somewhat smaller than those of other common liquid-crystal materials.[5]

Even in the three-ring compounds, many of them exhibit the monotropic liquid-crystal behavior. This fact indicates that the 1,3-dithiane compounds of the present study strongly tend to exhibit the monotropic liquid-crystal behavior.

Three-ring compounds having the 5-(*p*-ethoxyphenyl) group (**8-8**, **-10**, **-11**) have a stronger tendency to

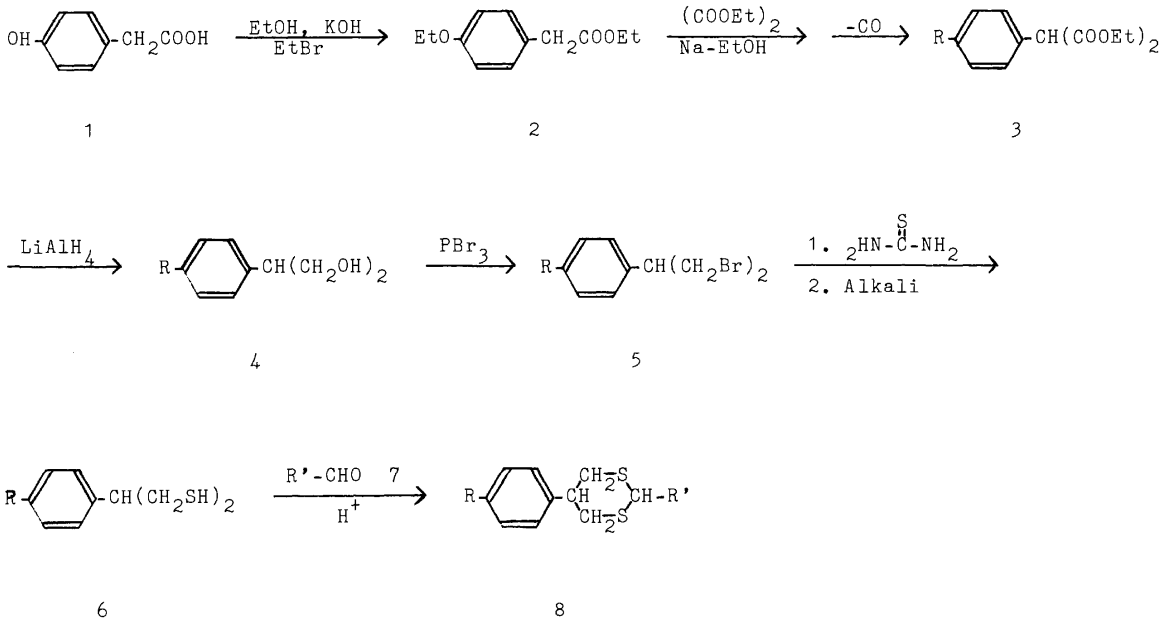

R: OC_2H_5, CH_3.
R′: C_2H_5, *n*-C_3H_7, *n*-C_5H_{11}, *n*-C_6H_{13}, *n*-C_7H_{15}, *n*-C_8H_{17}, $C_6H_4OC_2H_5$(*p*-), $C_6H_4OC_3H_7^n$(*p*-), $C_6H_4OC_4H_9^n$(*p*-), $C_6H_4OC_5H_{11}^n$(*p*-), $C_6H_4CH_3$(*p*-), C_6H_4CN(*p*-).

Fig. 1.

exhibit the enantiotropic liquid-crystal behavior than those having the 5-(*p*-methylphenyl) group (**8-13, -14, -15**). All of **8** which do not exhibit any liquid-crystal phases exhibited remarkable supercooling states. This property is common to both **8** and **9**.

Experimental

IR, ^{1}H-NMR, ^{13}C-NMR, and Mass spectra were obtained with a Hitachi 215 spectrophotometer, a JNM-PMX 60 spectrometer, a JNM FX 90Q FT-NMR spectrometer, and a Hitachi RMU-6 MG spectrometer, respectively. Elemental analyses were carried out with a Perkin-Elmer 250 instrument. Mesomorphic phases and the transition temperature were determined by means of both a Mitamura Riken micro melting-point apparatus equipped with polarizers and a differential scanning calorimeter. The rate of cooling was fixed to 1 °C/min.

Diethyl p-*Ethoxyphenylmalonate (3).* A conventional procedure was used for the syntheses of **3**.[6] Yield 60—70% Bp 160—163 °C/3—5 mmHg IR ($CHCl_3$) 2850—3000 (alkyl), 1740 (C=O), 1600 (Ar), 1260 (ether) cm^{-1}. ^{1}H-NMR ($CDCl_3$) δ=1.3 (q, 9H, CH_3), 3.9—4.5 (m, 6H, O-CH_2), 4.6 (s, 1H, CH), 6.8—7.6 (q, 4H, ArH).

Diethyl p-*Methylphenylmalonate (3′).* Yield 50—60% Bp 137—140 °C/5—8 mmHg IR ($CHCl_3$) 2850—3000 (alkyl), 1740 (C=O), 1600 (Ar) cm^{-1}. ^{1}H-NMR ($CDCl_3$) δ=1.25 (t, 6H, CH_2-CH_3), 2.3 (s, 3H, CH_3), 4.25 (q, 4H, O-CH_2), 4.6 (s, 1H, CH), 7.2 (s, 4H, ArH).

*2-(*p-*Ethoxyphenyl)-1,3-propanediol (4).* $LiAlH_4$-reduction of **3** in ether at 35 °C for 18 h provided **4**. Yields ranged from 90 to 95%. IR ($CHCl_3$) 3600 (OH), 2850—3000 (alkyl), 1605 (Ar), 1250 (ether) cm^{-1}. ^{1}H-NMR ($CDCl_3$) δ= 1.4 (t, 3H, CH_3), 2.5—4.3 (m, 9H, CH_2-O, CH, OH), 7.05 (q, 4H, ArH).

*2-(*p-*Methylphenyl)-1,3-propanediol (4′).* Yield 90%. IR ($CHCl_3$) 3600 (OH), 2850—3000 (alkyl), 1600 (Ar) cm^{-1}. ^{1}H-NMR ($CDCl_3$) δ=2.3 (s, 3H, CH_3), 2.5—4.0 (m, 7H, CH_2-O, OH), 7.2 (s, 4H, ArH).

*2-(*p-*Ethoxyphenyl)-1,3-dibromopropane (5).* To a solution of PBr_3 (0.03 mol), anhyd benzene (10 ml), and pyridine (0.8 g) cooled in an ice bath were added, dropwise, a solution of **4** (0.04 mol), anhyd benzene (10 ml), and pyridine (0.3 g) (30 min.). The solution was kept at 0—5 °C for 1 h, then at 30—40 °C for 15 h. The reaction mixture was poured into ice water (400 ml) and extracted twice with ether (400 ml). The extract was washed with cold water, dried over anhyd Na_2SO_4, and evaporated *in vacuo* at 30 °C.

Yield 53%. IR ($CHCl_3$) 2800—3000 (alkyl), 1600 (Ar), 1250 (ether) cm^{-1}. ^{1}H-NMR ($CDCl_3$) δ=1.4 (t, 3H, CH_3), 3.0—4.5 (m, 7H, CH_2-O, CH_2-Br, CH), 7.0 (q, 4H, ArH).

*2-(*p-*Methylphenyl)-1,3-dibromopropane (5′).* To a solution of 48% HBr (50g) and concd H_2SO_4 (15 g) cooled in an ice bath were added successively **4′** (0.1 mol) and concd H_2SO_4 (25g). The solution was kept at 95—100 °C for 18 h. The reaction mixture was then poured into water (200g). The mixture was stirred for a while and extracted twice with ether (each 400 ml). The extract was washed with cold 10% aq $NaHCO_3$, and concentrated on a rotary evaporator at 30 °C. The residue was distilled *in vacuo* to afford a transparent liquid in a 50% yield.

Bp 125—130 °C/1 mmHg. IR ($CHCl_3$) 2850-3000 (alkyl), 1600 (Ar) cm^{-1}. ^{1}H-NMR ($CDCl_3$) δ=2.3 (s, 3H, CH_3), 2.8—4.0 (m, 5H, CH_2, CH), 7.2 (s, 4H, ArH).

*2-(*p-*Ethoxyphenyl)-1,3-propanedithiol (6).* To a solution of thiourea (0.064 mol, 4.9 g) in triethylene glycol (8 ml) kept at 75 °C was added **5** (0.016 mol) under the nitrogen atmosphere followed by stirring at 75 °C for 18 h.

Tetraethylenepentamine (0.016 mol, 3.03 g) was then added, and the mixture was stirred at 75 °C for 2 h under the nitrogen atmosphere. The reaction mixture was poured into ice water (200 g) and extracted twice with ether (each 300 ml). The extract was dried over anhyd Na_2SO_4, and evaporated *in vacuo* at 30 °C.

Yield 55%. IR ($CHCl_3$) 2800—3000 (alkyl), 1600 (Ar), 1250 (ether) cm^{-1}. ^{1}H-NMR ($CDCl_3$) δ=1.0—1.7 (m, 5H, SH, CH_3), 2.9 (s, 4H, CH_2-S), 3.0—3.6 (m, 1H, CH), 4.05 (q, 2H,

Table 1. Transition temperature of compounds 8 and the corresponding 2-(*p*-ethoxyphenyl)-5-alkyl-1,3-dithianes

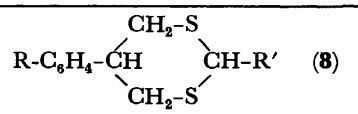

	R	R′	Transition temp /°C[a]
8-1	OC_2H_5	C_2H_5	C $\underset{21}{\overset{56}{\rightleftharpoons}}$ I
8-2	OC_2H_5	n-C_3H_7	C $\underset{28}{\overset{96}{\rightleftharpoons}}$ I
8-3	OC_2H_5	n-C_4H_9	C $\underset{22}{\overset{67}{\rightleftharpoons}}$ I
8-4	OC_2H_5	n-C_5H_{11}	C $\underset{48}{\overset{55}{\rightleftharpoons}}$ I
8-5	OC_2H_5	n-C_6H_{13}	C 58 I; 12 S_A $\underset{27}{\overset{}{\rightleftharpoons}}$ N 46
8-6	OC_2H_5	n-C_7H_{15}	C 63 I; 17 S_A $\underset{27}{\overset{}{\rightleftharpoons}}$ N 52
8-7	OC_2H_5	n-C_8H_{17}	C 66 I; 41 S_A $\underset{43}{\overset{}{\rightleftharpoons}}$ N 53
8-8	OC_2H_5	$C_6H_4OC_2H_5$(*p*-)	C $\underset{176}{\overset{176}{\rightleftharpoons}}$ N $\underset{195}{\overset{195}{\rightleftharpoons}}$ I
8-9	OC_2H_5	$C_6H_4OC_3H_7^n$(*p*-)	C 173 I; 167 N 173
8-10	OC_2H_5	$C_6H_4OC_4H_9^n$(*p*-)	C $\underset{148}{\overset{148}{\rightleftharpoons}}$ N $\underset{182}{\overset{182}{\rightleftharpoons}}$ I
8-11	OC_2H_5	$C_6H_4OC_5H_{11}^n$(*p*-)	C $\underset{126}{\overset{126}{\rightleftharpoons}}$ N $\underset{175}{\overset{175}{\rightleftharpoons}}$ I
8-12	OC_2H_5	$C_6H_4CH_3$	C 165 I; 132 N 165
8-13	CH_3	$C_6H_4OC_4H_9^n$(*p*-)	C 170 I; 110 N 156
8-14	CH_3	$C_6H_4OC_5H_{11}$(*p*-)	C 146 I; 121 N 142
8-15	CH_3	C_6H_4CN(*p*-)	C 180 I; 142 N 160

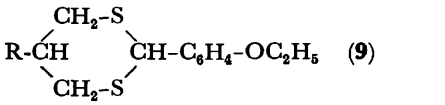

2-(*p*-Ethoxyphenyl)-5-alkyl-1,3-dithiane

	R	Transition temp /°C[a]
9-1[b]	n-C_4H_9	C $\underset{35}{\overset{75}{\rightleftharpoons}}$ I
9-2	n-C_5H_{11}	C $\underset{35}{\overset{57}{\rightleftharpoons}}$ I
9-3	n-C_6H_{13}	C 64 I; 32 N 43
9-4	n-C_7H_{15}	C 70 I; 49 N 57

a) C=crystal; N=nematic; I=isotropic; S=smectic. b) Cited from Ref. 2.

CH_2-O), 7.0 (q, 4H, ArH).

2-(p-Methylphenyl)-1,3-propanedithiol (6′). Yield 66% IR ($CHCl_3$) 2800—3000 (alkyl), 1600 (Ar) cm^{-1}. ^{1}H-NMR ($CDCl_3$) δ=0.9—1.5 (m, 2H, SH), 2.3 (s, 3H, CH_3), 2.5—3.7 (m, 5H, CH, CH_2-S), 7.1 (s, 4H, ArH).

2,5-Disubstituted 1,3-Dithianes (8). To a solution of **6** (0.004 mol) and aldehyde **7** (0.004 mol) in anhyd $CHCl_3$ (200 ml) cooled in an ice bath were added BF_3-$(C_2H_5)_2O$ (0.5 g) and Molecular Sieve (3A, 1/15; 3g). The mixture was stirred at 0—5 °C for 8 h and then at 20—25 °C for 18h. The solution was washed with 10% $NaHCO_3$ (400 ml), then with water (400 ml), dried over anhyd Na_2SO_4, and evaporated *in vacuo* at 40 °C. The crude product was purified by alumina column chromatography to collect the hexane-benzene=1:1 eluate.

Upon evaporation of the eluate *in vacuo*, the residue was purified by recrystallization from hexane.

2-Alkyl-5-(p-ethoxyphenyl)-1,3-dithianes. IR ($CHCl_3$) 2800—3000 (alkyl), 1600 (Ar), 1250 (ether) cm^{-1}. ^{1}H-NMR ($CDCl_3$) δ=0.7—2.0 (m, alkyl), 2.6—3.4 (m, 5H, CH_2-S, CH), 3.8—4.3 (m, 3H, CH_2-O, $\overset{S}{S}$>CH-), 7.0 (q, 4H, ArH).

2-Ethyl-5-(p-ethoxyphenyl)-1,3-dithiane (8-1): Yield, 28%. Found: C, 62.51; H, 7.915. Calcd for $C_{14}H_{20}S_2O$: C, 62.71; H, 7.51%. MS (*m/z*) 268 (M^+).

2-Propyl-5-(p-ethoxyphenyl)-1,3-dithiane (8-2): Yield 27%. Found: C, 63.56; H, 7.55%. Calcd for $C_{15}H_{22}S_2O$: C, 63.78; H, 7.85%. MS (*m/z*) 282 (M^+).

2-Butyl-5-(p-ethoxyphenyl)-1,3-dithiane (8-3): Yield, 17%. Found: C, 64.94; H, 8.15%. Calcd for $C_{16}H_{24}S_2O$: C, 64.82; H, 8.16%. MS (*m/z*) 296 (M^+).

2-Pentyl-5-(p-ethoxyphenyl)-1,3-dithiane (8-4): Yield, 16%. Found: C, 65.97; H, 8.70%. Calcd for $C_{17}H_{26}S_2O_1$: C, 65.76; H, 8.44. MS (*m/z*) 310 (M^+).

2-Hexyl-5-(p-ethoxyphenyl)-1,3-dithiane (8-5): Yield, 15%. Found: C, 66.75; H, 8.68. Calcd for $C_{18}H_{28}S_2O$: C, 66.61; H, 8.70%. MS (*m/z*) 338 (M^+). ^{13}C-NMR ($CDCl_3$) δ=47.46 (C2), 37.06 (C4, C6), 42.86 (C5).

2-Heptyl-5-(p-ethoxyphenyl)-1,3-dithiane (8-6): Yield, 15%. Found: C, 67.17; H, 8.96%. Calcd for $C_{19}H_{30}S_2O$: C, 67.40; H, 8.93%. MS (*m/z*) 338 (M^+). NMR ($CDCl_3$) δ=47.46 (C2), 37.06 (C4, C6), 42.86 (C5).

2-Octyl-5-(p-ethoxyphenyl)-1,3-dithiane (8-7): Yield, 21%. Found: C, 68.01; H, 9.17%. Calcd for $C_{20}H_{32}S_2O$: C, 68.13; H, 9.15%. MS (*m/z*) 352 (M^+).

2-(p-Alkoxyphenyl)-5-(p-ethoxyphenyl)-1,3-dithiane. IR ($CHCl_3$) 2800—3000 (alkyl), 1600 (Ar), 1250 (ether) cm^{-1}. ^{1}H-NMR ($CDCl_3$) δ=0.7—2.0 (m, -OH_2C-R), 2.8—3.5

(m, 5H, CH_2-S, CH), 4.0 (m, 4H, CH_2-O), 5.25 (s, 1H, $\overset{S}{S}$>CH-), 6.8—7.7 (m, 8H, ArH).

2,5-Bis(p-ethoxyphenyl)-1,3-dithiane (8-8): Yield, 28%. Found: C, 66.58 ;H, 6.71%. Calcd for $C_{20}H_{24}S_2O_2$: C, 66.63; H, 6.71%. MS (*m/z*) 360 (M^+).

2-(p-Propoxyphenyl)-5-(p-ethoxyphenyl)-1,3-dithiane (8-9): Yield, 47%. Found: C, 67.38; H, 7.16%. Calcd for $C_{21}H_{26}S_2O_2$: C, 67.34; H, 7.00%. MS (*m/z*) 374 (M^+).

2-(p-Butoxyphenyl)-5-(p-ethoxyphenyl)-1,3-dithiane (8-10): Yield, 39%. Found: C, 67.70; H, 7.29%. Calcd for $C_{22}H_{28}S_2O_2$: C, 68.00; H, 7.26%. MS (*m/z*) 388 (M^+).

2-(p-Pentyloxyphenyl)-5-(p-ethoxyphenyl)-1,3-dithiane (8-10): Yield, 31%. Found: C, 68.36; H, 7.81%. Calcd for $C_{23}H_{30}S_2O_2$: C, 68.61; H, 7.51%. MS (*m/z*) 402 (M^+).

2-(p-Methoxyphenyl)-5-(p-ethoxyphenyl)-1,3-dithiane (8-12): Yield, 38%. IR ($CHCl_3$) 2800—3000 (alkyl), 1605 (Ar), 1250 (ether) cm^{-1}. ^{1}H-NMR ($CDCl_3$) δ 1.45 (t, 3H, OCH_2-C<u>H</u>$_3$), 2.4 (s, 3H, CH_3), 2.7—3.5 (m, 5H, CH_2-S, CH), 4.05 (q, 2H, OCH_2), 5.25 (s, 1H, $\overset{S}{S}$>CH-), 6.8—7.7 (m, 8H, ArH). Found: C, 68.76; H, 7.02%. Calcd for $C_{19}H_{22}S_2O$: C, 69.05; H, 6.71%. MS (*m/z*) 330 (M^+).

2-(p-Alkoxyphenyl)-5-(p-methylphenyl)-1,3-dithiane. IR ($CHCl_3$) 2800—3000 (alkyl), 1600 (Ar), 1250 (ether) cm^{-1}. ^{1}H-NMR ($CDCl_3$) δ=0.7—2.0 (m, OCH_2-<u>R</u>), 2.3 (s, 3H, CH_3), 2.8—3.5 (m, 5H, CH_2-S, CH), 4.0 (t, 2H, CH_2-O), 5.25 (s, 1H, $\overset{S}{S}$>CH), 6.8—7.6 (m, 8H, ArH).

2-(p-Butoxyphenyl)-5-(p-methylphenyl)-1,3-dithiane (8-13): Yield, 42%. Found: C, 70.59; H, 7.28%. Calcd for $C_{21}H_{26}S_2O_1$: C, 70.36; H, 7.31%. MS (*m/z*) 358 (M^+).

2-(p-Pentyloxyphenyl)-5-(p-methylphenyl)-1,3-dithiane (8-14): Yield, 47%. Found: C, 70.67; H, 7.48%. Calcd for $C_{22}H_{28}S_2O$: C, 70.92; H, 7.58%. MS (*m/z*) 372 (M^+).

2-(p-Cyanophenyl)-5-(p-methylphenyl)-1,3-dithiane (8-15): Yield, 15%. IR ($CHCl_3$) 2800—3000 (alkyl), 2220 (CN), 1600 (Ar) cm^{-1}. ^{1}H-NMR ($CDCl_3$) δ=2.3 (s, 3H, CH_3), 2.5—3.5 (m, 5H, CH_2-S, CH), 5.25 (s, 1H, $\overset{S}{S}$>CH), 7.2 (s, 4H, Ar<u>H</u>-CH_3), 7.7 (s, 4H, Ar<u>H</u>-CN). Found: C, 69.02; H, 5.51; N, 4.53%. Calcd for $C_{18}H_{17}NS_2$: C, 69.41; H, 5.50; N, 4.50%. MS (*m/z*) 311 (M^+).

Reference

1) Y. Haramoto, H. Kamogawa, *J. Chem. Soc., Chem. Commun.*, **1983**, 75.

2) Y. Haramoto, A. Nobe, and H. Kamogawa, *Bull. Chem. Soc. Jpn.*, **57**, 1966 (1984).

3) E. L. Eliel, V. S. Rao, and F. G. Riddell, *J. Am. Chem. Soc.*, **98**, 3583 (1976).

4) D. Demus and L. Richter, "Textures of Liquid Crystals," Verlag Chemie, Weinheim, New York (1978).

5) G. W. Gray P. A. Winsor, "Liquid Crystals & Plastic Crystals," Wiley, New York (1974), Vol. 1, p. 254.

6) A. H. Blatt, *Org. Synth.*, Coll. Vol. II, 288 (1966).

Oxidation of Lipids. IX. Decomposition of Methyl Linoleate and Methyl Linolenate Hydroperoxides in Solution†

Yorihiro YAMAMOTO, Noriyuki SAEKI, Schunichi HAGA,
Etsuo NIKI,* and Yoshio KAMIYA
Department of Reaction Chemistry, Faculty of Engineering, University of Tokyo, Hongo, Tokyo 113
(Received May 7, 1984)

Decompositions of methyl linoleate hydroperoxide (LOOH) induced by di-*t*-butyl diperoxyoxalate and cobalt ions were investigated in benzene at 50 °C under vacuum to elucidate the degradation mechanism. The major products were dimer (LOOL), oxodiene, hydroxydiene and epoxyhydroxyene (and/or epoxyoxoene). It was suggested that these products were formed by the recombination of L· and LOO· radicals, β-scission of LO· radical, hydrogen abstraction of LO· radical, and intramolecular epoxidation of LOO· radical, respectively. The decomposition of methyl linolenate hydroperoxide (L'OOH) was also studied. The major products were dimer, oxotriene, hydroxytriene, and thiobarbituric acid reactive substances, which were suggested to be formed by the intramolecular cyclization of L'OO· radical.

Polyunsaturated fatty acids (PUFA), which are present as phosphoglyceride esters in biological membranes, are quite susceptible to oxidation.[1] The oxidation of PUFA gives peroxides as primary products,[2] and it is suggested that the formation of so-called "lipid peroxides" is associated with aging and the appearance of geriatric disorders such as heart attack, stroke, diabates, *etc.*[3-8] Therefore, it is very important to understand the formation and the decomposition of the lipid peroxide in the living system. The oxidation of PUFA and behavior of hydroperoxides derived from PUFA are also important subjects in food chemistry.[5,6]

The decomposition of peroxides is important since it can contribute to chain initiation of lipid peroxidation and xenogenous toxicity. It has been reported that the decomposition of linoleic acid hydroperoxide gave various products such as oxodiene,[9-16] epoxyhydroxyene,[10,12-14,16-18] epoxyoxoene,[10,14,16,17] trihydroxyene,[10,14] peroxide-bridged dimer,[14] carbon-carbon bridged dimer,[19] hydroxydiene,[12] oxodihydroxyene,[14] oxohydroxyene,[10,16] and hydroperoxyoxoene.[17] The distribution of products is dependent on experimental variables such as atmosphere, catalysts, absence and presence of hydrogen donors and reductants, and pH.

In this study, we undertook a simple system in order to elucidate the mechanism of homolytic decomposition of linoleate and linolenate hydroperoxides induced by radicals and metal ions in a homogeneous solution.

Experimental

Material. Methyl linoleate (LH) was obtained from Sigma Chemical Co. and used as received. Little peroxide was observed by HPLC analysis.[21,22] Methyl linoleate hydroperoxide (LOOH) was synthesized[22,23] from LH by the action of soybean lipoxygenase (Sigma Chem. Co.) and purified by passing through a silica-gel column using hexane and ether as eluent. It was found by HPLC analysis that the ratio of (9*Z*,11*E*)-13-hydroperoxy-9,11-octadecadienoic acid methyl ester to total peroxide was higher than 95%. LOOH was stored as a benzene solution below 0 °C. Under these conditions, the decomposition and isomerization[22] of LOOH were very slow.

Methyl linolenate(L'H) was obtained from Sigma Chemical Co. and purified by silica-gel column chromatography. Methyl linolenate hydroperoxide (L'OOH) was also prepared using soybean lipoxygenase. It was purified with a silica-gel column and stored as a benzene solution below 0 °C to avoid the decomposition and isomerization of hydroperoxide. More than 95% of hydroperoxide was found to be (9*Z*,11*E*, 15*Z*)-13-hydroperoxy-9,11,15-octadecatrienoic acid methyl ester by HPLC analysis.[24]

Di-*t*-butyl diperoxyoxalate (DBPO) was prepared by the reaction of oxalyl chloride and *t*-butyl hydroperoxide followed by recrystallization from pentane.[25] α-Methylstyrene (α-MS) was purified by the conventional method; washing with alkali and distillation. 2,6-Di-*t*-butyl-4-methylphenol (BMP) was recrystallized from methanol. Bis (acetylacetonato) cobalt (II) ($Co(acac)_2$) and benzene were those of the highest grade available.

Procedure. A 3 ml of benzene solution of LOOH was taken into a 30 ml Pyrex glass ampoule with additives, if necessary, such as DBPO and $Co(acac)_2$. The ampoule was degassed by freeze and thaw method and sealed by a Teflon valve (6VD type, Nupro Co.). Then the ampoule was put into a water bath kept at 50 °C for desired time. The reaction mixture was stirred vigorously.

After the reaction, the ampoule was cooled by liquid nitrogen, opened, and then warmed up to the room temperature. The reaction mixture was analyzed by TLC and HPLC. A portion of the reaction mixture was evacuated to remove the solvent on water aspiration, then hexane was added. UV absorbances of the hexane solution at 235 and 270 nm were measured to determine the conjugated diene and oxodiene; their extinction coefficients were taken from the literature[20,26] as 28000 and 20000 $M^{-1}\,cm^{-1}$, respectively.

Analytical Method. Merck Silica-Gel 60 plate and hexane/ether/acetic acid (60/40/1, by volume) eluent were used for the TLC analysis. Spots were visualized by iodine vapour. TLC/FID analyzer (IATRON model TH-10) was applied for quantitative measurement. HPLC analysis was described in the previous paper.[21] GPC spectra were measured on a Simadzu LC model 830 equipped with a UV detector, Shimadzu model UV 202. Shimadzu GPC columns, HSG 15 and 30, were used in series and eluent was tetrahydrofuran. The formation of α-methylstyrene oxide was determined by GLC. 2-Thiobarbituric acid reactive substances (TBARS) were measured by the conventional

† Presented at the Annual Meeting of the Chemical Society of Japan, August, 1983.

photometric method.[2] Molecular weight of a dimer was measured with a vapour pressure osmometer in benzene at 40 °C. ^{1}H NMR spectroscopy was performed on a Varian 360 spectrometer.

Results and Discussion

Table 1 shows the result of DBPO-induced decomposition of LOOH in 3 ml benzene *in vacuo* at 50 °C for 5 h. LOOH was thermally stable in benzene *in vacuo* at 50 °C (Run 1). However, LOOH was decomposed when incubated with DBPO (Run 2). The half life of DBPO is 23.1 min at 50 °C,[25] therefore more than 99% of DBPO decomposes in 5h at 50 °C. The amount of LOOH decomposed was almost twice as that of DBPO added, which is quite reasonable since DBPO produces 2 moles of *t*-butoxyl radical as discussed later in the text. Table 2 summarizes the result of cobalt-catalyzed decomposition of LOOH in 3 ml benzene *in vacuo* at

TABLE 1. DBPO-INDUCED DECOMPOSITION OF METHYL LINOLEATE HYDROPEROXIDE (LOOH) IN 3 ml BENZENE *in vacuo* AT 50 °C IN 5 h[a]

Run No	1	2[h]	3	4
Reactant				
LOOH	30.0	25.3	23.6	27.5
LH,[b] mmol			1.05	
α-MS,[c] mmol				0.32
DBPO[d]	0	9.4	9.4	17.9
Disappearance of LOOH and formation of products				
Δ LOOH	0	−17.2	−3.6	−24.3
Δ LOH[e]	0	0	0	0
Δ $(C=C)_2$	0	−5.9	9.5	−7.3
Δ Oxodiene	0	0.9	1.0	1.8
Dimer[f]	−	+++	+++++	++
5[f,g]	−	+++	−	+
α-MS oxide				6.6

a) Numbers show μmol in 3 ml. b) Methyl linoleate. c) α-Methylstyrene. d) Di-*t*-butyl diperoxyoxalate. e) Hydroxydiene. f) − and + show that the spot is negative and positive, respectively. The increased numbers of + indicate the relative increase of the formation. g) Assumed to be epoxide (see Text and Fig. 1). h) Ratios of dimer, LOOH, and **5** were 1.0/1.0/1.0 by TLC/FID.

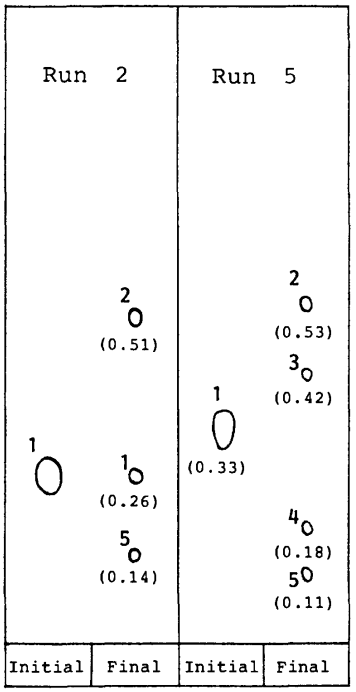

Fig. 1. Thin-layer chromatograms of initial and decomposed LOOH. Numbers in the parentheses are R_f values. Reaction conditions are described in Tables 1 and 2.
1: LOOH, **2**: Dimer (LOOL), **3**: Oxodiene (−C(O)−(CH=CH)$_2$−), **4**: Hydroxydiene (LOH), **5**: Epoxyhydroxyene and/or Epoxyoxoene.
L=$CH_3(CH_2)_4$−CH−(CH=CH)$_2$−$(CH_2)_7COOCH_3$.

TABLE 2. COBALT-CATALYZED DECOMPOSITION OF METHYL LINOLEATE HYDROPEROXIDE (LOOH) IN 3 ml BENZENE *in vacuo* AT 50 °C IN 5 h[a]

Run No	5[f]	6	7	8[g]	9
Reactant					
LOOH	24.4	21.8	24.3	24.4	23.3
LH, mmol		0.98			
BMP[b]			15.8		
α-MS, mmol					1.92
$Co(acac)_2$[c]	3.9	4.3	3.5	5.1	3.9
Disappearance of LOOH and formation of products					
Δ LOOH	−24.4	−21.8	−24.3	−24.4	−23.3
Δ LOH	4.1	7.2	7.9	3.7	5.1
Δ $(C=C)_2$	−7.2	0.2	−4.2	−13.2	
Δ Oxodiene	11.5	12.6	10.1	13.0	
Dimer[d]	+++	++++	−	±	++
5[d,e]	+++	−	±	±	+
α-MS oxide					5.8

a) Numbers show μmols in 3 ml. b) 2,6-Di-*t*-butyl-4-methylphenol. c) Bis(acetylacetonato) cobalt(II). d) Same as footnote. f) In Table 1. e) Assumed to be epoxide (see text and Fig. 1). f) Ratios of dimer, oxodiene + LOH, and **5** were 1.0/3.1/1.2 by TLC/FID. g) Under air.

50 °C for 2h. LOOH was decomposed completely in every run, which suggests that $Co(acac)_2$ decomposes LOOH catalytically.

Figure 1 shows the thin layer chromatograms of initial LOOH and decomposition products. As shown, chromatograms were clear. Thin layer chromatography of the reaction mixture was carried out with larger scale than that shown in Fig. 1, and each spot was collected, analyzed, and found as dimer, oxodiene, LOH, and unknown product **5** by the following results.

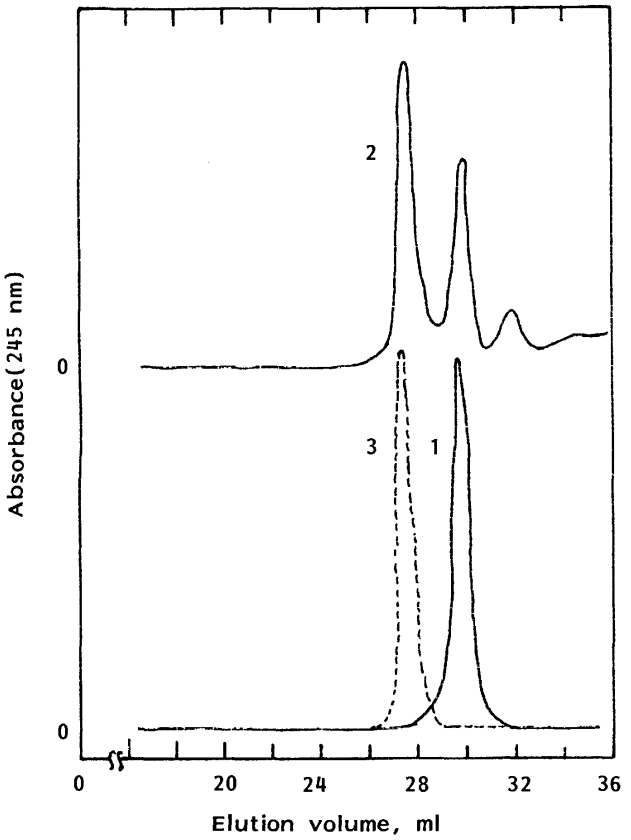

Fig. 2. Gel permeation chromatograms of initial LOOH-(**1**), reaction product of Run 2(**2**), and isolated dimer-(**3**).

2: Figure 2 shows the gel permeation chromatograms of initial LOOH (line 1), reaction mixture of Run 2 (line 2), and isolated **2** (dotted line 3). As shown, a new peak (elution volume=27.5 ml) was observed in the reaction mixture and **2** gave an identical chromatogram. The molecular weight of **2**, as measured with a vapour pressure osmometer, was 619±15. **2** has a strong absorption at 231.5 nm and its extinction coefficient was about 40000 $M^{-1}cm^{-1}$, suggesting that **2** has two conjugated dienes in a molecule. ^1H NMR spectra $\delta(CCl_4)$; 3.63 (s, 6H,$OC\underline{H}_3$), 4.1—4.5 (m, 2H, O-C-$\underline{H}$), 5.2—6.3 (m, 8H, $(C\underline{H}=C\underline{H})_2$) indicate that **2** is a peroxide-bridged dimer LOOL. The calculated molecular weight for LOOL is 619.

3: **3** has a strong characteristic UV absorption at 270 nm and R_f value(0.42) is between those of LOOH(0.33) and LH(0.83). By comparing with the previous results,[14,26] **3** was attributed to oxodiene, $-C(O)-(C=C)_2-$.

4: R_f value of **4** was identical with that of the products obtained by reduction of LOOH with triphenylphosphine. Therefore, **4** must be hydroxyoctadecadienoic acid methyl ester, LOH.

The decrease of LOOH and the formation of LOH shown in Tables 1 and 2 were measured by HPLC. The decrease of conjugated diene and the increase of oxodiene were determined by UV absorbance at 235 and 270 nm, respectively. The yields of dimer and **5** were estimated by the deepness of the color of the spot. The ratios of dimer, oxodiene, LOOH, LOH, and **5** were also measured by TLC/FID in Runs 2 and 5. In other Runs, LH and α-MS disturbed the TLC/FID analysis. α-Methylstyrene oxide was determined by glc.

As shown in Table 1 and Fig. 1, the major products of DBPO-induced decomposition of LOOH were dimer and the unknown compound **5**. The addition of methyl linoleate (LH) decreased **5** (Run 3), while it increased

Table 3. DBPO-induced and Cobalt-catalyzed decomposition of methyl linolenate hydroperoxide (L'OOH) in benzene *in vacuo* at 50 °C[a]

Run No	10	11	12	13	14	15	16[d]
Reactant							
L'OOH	13.2	26.4	26.4	13.2	13.2	13.2	13.2
LH, mmol			1.48		1.46		
BMP						37.2	
DBPO	0	23.3	21.9				
$Co(acac)_2$				3.0	3.0	3.0	3.0
Time, h	5	5	5	2	2	2	2
Disappearance of L'OOH and formation of products							
Δ L'OOH	0.7	−26.4	−5.2	−13.2	−13.2	−13.2	−13.2
Δ L'OH	0	0	0	2.2	1.3	4.0	0.6
Δ $(C=C)_2$	0	−4.1	24.7	−1.9	5.2		
Δ Oxotriene	0			4.8	7.1	7.5	Trace
TBARS[b]	0.2	11.0	7.3	4.5	6.4	2.8	2.6
Dimer[c]	−	++	+++++	++	+++	−	±

a) Numbers in μmol. b) Thiobarbituric acid reactive substances. c) Same as footnote f) in Table 1. d) Under air.

the dimer. The major products of cobalt-catalyzed decomposition of LOOH were dimer, oxodiene, hydroxydiene (LOH), and **5**. Oxodiene and LOH were not observed in the DBPO-induced decomposition of LOOH. The yield of dimer was increased by the addition of LH (Run 6) and decreased by the addition of BMP (Run 7). Furthermore, little dimer was observed in the decomposition of LOOH under air (Run 8). The yield of **5** decreased by the addition of LH and BMP, and by changing the atmosphere to air (Runs 6—8). Little TBARS was observed in the decomposition of LOOH.

Table 3 summarizes the results of DBPO-induced and cobalt-catalyzed decomposition of methyl linolenate (L'OOH) in benzene *in vacuo* at 50 °C. L'OOH was thermally stable in benzene *in vacuo* at 50 °C (Run 10). The DBPO-induced decomposition of L'OOH gave dimer and TBARS. In addition to them, hydroxytriene (L'OH) and oxotriene were produced in the cobalt catalyzed decomposition of L'OOH. The yield of dimer was increased by the addition of methyl linoleate (LH) (Runs 12 and 14) and decreased by the addition of BMP (Run 15) and by changing the atmosphere to air (Run 16).

The results and discussion described above suggest that the decompositions of LOOH and L'OOH proceed by the scheme shown below. DBPO decomposes to give *t*-butoxyl radical (*t*-BuO·) and carbon dioxide (Eq. 1).

$$\text{DBPO} \longrightarrow 2\,t\text{-BuO}\cdot + 2CO_2, \quad (1)$$

$$t\text{-BuO}\cdot + \text{LOOH} \longrightarrow t\text{-BuOH} + \text{LOO}\cdot, \quad (2)$$

$$\text{LOOH} + Co^{2+} \longrightarrow \text{LO}\cdot + OH^- + Co^{3+}, \quad (3)$$

$$\text{LOOH} + Co^{3+} \longrightarrow \text{LOO}\cdot + H^+ + Co^{2+}, \quad (4)$$

$$\text{LOO}\cdot \rightleftharpoons \text{L}\cdot + O_2, \quad (5)$$

$$\text{LOO}\cdot + \text{L}\cdot \longrightarrow \text{LOOL}, \quad (6)$$

$$2\text{LOO}\cdot \longrightarrow \text{LOH} + \text{Oxodiene} + O_2, \quad (7)$$

$$\text{LOO}\cdot \longrightarrow \mathbf{5}\ (\text{epoxyhydroxyene and/or epoxyoxoene}), \quad (8)$$

$$\text{LO}\cdot \xrightarrow{\text{LOOH, LH, BMP}} \text{LOH}, \quad (9)$$

$$\text{LO}\cdot \longrightarrow \text{Oxodiene}, \quad (10)$$

$$\text{L'OO}\cdot + \text{L'}\cdot \longrightarrow \text{L'OOL'}, \quad (11)$$

$$\text{L'O}\cdot \xrightarrow{\text{L'OOH, LH, BMP}} \text{L'OH}, \quad (12)$$

$$\text{L'O}\cdot \longrightarrow \text{Oxotriene}, \quad (13)$$

$$\text{L'OO}\cdot \longrightarrow \text{TBARS}, \quad (14)$$

t-Butoxyl radical abstracts hydrogen from LOOH to give peroxyl radical LOO·(Eq. 2). Equations 3 and 4 show the redox decomposition of LOOH by cobalt ions. Therefore, LOO·radical is a key intermediate in the DBPO-induced decomposition of LOOH. Under low concentration of oxygen, LOO·radical liberates oxygen and gives resonance-stabilized alkyl radical, L·(Eq. 5). The recombination of peroxyl radical and alkyl radical is quite fast and consequently dimer, LOOL, is formed (Eq. 6). The presence of oxygen must suppress the formation of dimer, since the bimolecular interaction of peroxyl radicals gives LOH and oxodiene (Eq. 7) rather than LOOL. Reaction 7 is not important under low concentration of oxygen.[21] In fact, the amounts of LOH and oxodiene were very small in Run 2.

Unknown product **5** is also produced from peroxyl radical (Eq. 8). The formation of α-methylstyrene oxide in the presence of α-methylstyrene (Runs 4 and 9) and the low R_f value of **5** suggest that **5** is an epoxide such as epoxyhydroxyene and/or epoxyoxoene produced by intramolecular epoxidation of LOO·radical as shown below.[27]

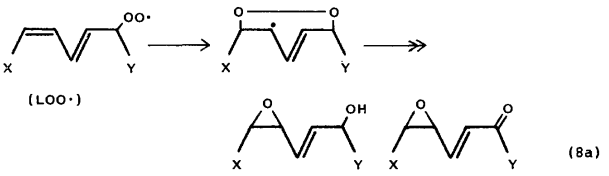

$X=(CH_2)_7COOCH_3$, $Y=(CH_2)_4CH_3$

In addition to peroxyl radical, alkoxyl radical, LO·, plays an important role in the redox decomposition of LOOH and gives LOH and oxodiene by hydrogen abstraction (Eq. 9) and β-scission (Eq. 10), respectively. BMP acts as an efficient hydrogen donor to oxygen radicals and increases LOH.

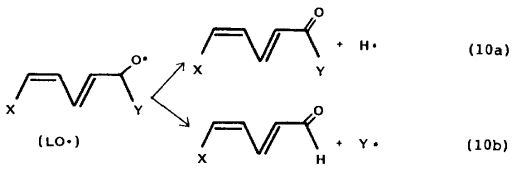

$X=(CH_2)_7COOCH_3$, $Y=(CH_2)_4CH_3$

The decomposition of L'OOH proceeds similarly as LOOH; peroxyl radical, L'OO·gives dimer (Eq. 11) and alkoxyl radical, L'O·gives hydroxytriene, L'OH, (Eq. 12) and oxotriene (Eq. 13). However, TBARS was produced instead of **5**, probably by intramolecular cyclization of peroxyl radical (Eq. 14a).[30-32]

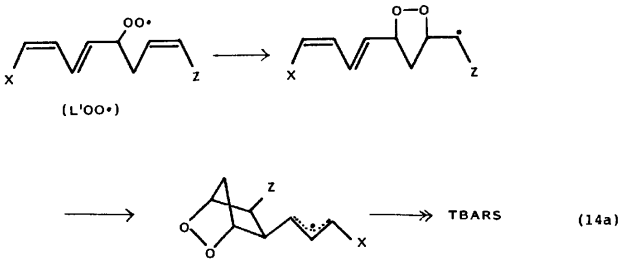

$X=(CH_2)_7COOCH_3$, $Z=CH_2CH_3$

In conclusion, the homolytic decomposition of linoleate hydroperoxide gave dimer, oxodiene, hydroxydiene, and epoxyhydroxyene (and/or epoxyoxoene) and that of linolenate hydroperoxide gave dimer, oxotriene, hydroxytriene, and TBARS.

References

1) "Free Radicals in Biology," ed by W. A. Pryor, Academic Press, New York (1976), Vol. I.

2) Y. Yamamoto, E. Niki, and Y. Kamiya, *Bull. Chem. Soc. Jpn.*, **55**, 1548 (1982) and references cited therein.
3) "Tocopherol, Oxygen and Biomembranes," ed by C. de Duve and O. Hayaishi, Elsevier, Amsterdam (1978).
4) "Free Radicals in Biology," ed by W. A. Pryor, Academic Press, New York (1980), Vol. IV.
5) "Autoxidation in Food and Biological Systems," ed by M. G. Simic and M. Karel, Plenum Press, New York (1980).
6) "Kasanka Shishitsu to Shikkan," ed by K. Yagi and Y. Goto, Igaku-Shoin, Tokyo (1981).
7) "Lipid Peroxides in Biology and Medicine," ed by K. Yagi, Academic Press, New York (1982).
8) "Free Radicals in Biology," ed by W. A. Pryor, Academic Press, New York (1982), Vol. V.
9) G. J. Garssen, J. F. G. Vliegenthart, and J. Boldingh, *Biochem. J.*, **122**, 327 (1971).
10) H. W. Gardner, R. Kleiman, and D. Weisleder, Lipids, **9**, 696 (1974).
11) J. Terao, T. Ogawa, and S. Matsushita, *Agric. Biol. Chem.*, **39**, 397 (1975).
12) M. Hamberg, *Lipids*, **10**, 87 (1975).
13) J. Verhagen, A. A. Bouman, J. F. G. Vliegenthart, and J. Boldingh, *Biochem. Biophys. Acta*, **486**, 114 (1977).
14) P. Schieberle, B. Tsoukalas, and W. Grosch, Z. Lebensm. *Unters. Forsch.*, **168**, 448 (1979).
15) E. N. Frankel, W. E. Neff, and E. Selke, *Lipids*, **16**, 279 (1981).
16) H. W. Gardner and P. A. Jursinic, *Biochim. Biophys. Acta*, **665**, 100 (1981).
17) H. W. Gardner, D. Weileder, and R. Kleiman, *Lipids*, **13**, 246 (1978).
18) G. J. Garssen, G. A. Veldink, J. F. G. Vliegenthart, and J. Boldingh, *Eur. J. Biochem.*, **62**, 33 (1979).
19) G. J. Garssen, J. F. G. Vliegenthart, and J. Boldingh, *Biochem. J.*, **130**, 435 (1972).
20) H. W. S. Chan and G. Levett, *Lipids*, **12**, 99 (1977).
21) Y. Yamamoto, E. Niki, and Y. Kamiya, *Lipids*, **17**, 870 (1982).
22) H. W. S. Chan, C. T. Costaras, F. A. A. Prescott, and P. A. T. Swoboda, *Biochim. Biophys. Acta*, **398**, 347 (1975).
23) M. O. Funk, R. Issac, and N. A. Porter, *Lipids*, **11**, 113 (1976).
24) H. W. S. Chan and G. Levett, *Lipids*, **12**, 837 (1977).
25) P. D. Bartlett, E. P. Benzing, and R. E. Pincock, *J. Am. Chem. Soc.*, **82**, 1762 (1960).
26) D. J. Sessa, H. W. Gardner, R. Kleiman, and D. Weisleder, *Lipids*, **12**, 613 (1977).
27) Formation of epoxide from polyunsaturated fatty acid hydroperoxide catalyzed by acid and hematin has been reported recently.[28,29]
28) T. A. Dix and L. J. Marnett, *J. Am. Chem. Soc.*, **105**, 7001 (1983).
29) H. W. Gardner, D. Weisleder, and E. C. Nelson, *J. Org. Chem.*, **49**, 508 (1984).
30) W. A. Pryor and J. P. Stanley, *J. Org. Chem.*, **40**, 3615 (1975).
31) N. A. Porter and M. O. Funk, *J. Org. Chem.*, **40**, 3614 (1975).
32) D. E. O'Connor, E. D. Mihelich, and M. C. Coleman, *J. Am. Chem. Soc.*, **103**, 223 (1981).

 © 1984 The Chemical Society of Japan Bull. Chem. Soc. Jpn., 57, 3182—3196 (1984) [Vol. 57, No. 11

Synthesis, and the Adjuvant and Tumor-Suppressive Activities of Quinonyl Muramyl Dipeptides[1)]

Shigeru KOBAYASHI,* Tsunehiko FUKUDA, Hidefumi YUKIMASA, Masahiko FUJINO, Ichiro AZUMA,† and Yuichi YAMAMURA††

Central Research Division, Takeda Chemical Industries, Ltd., Yodogawa-ku, Osaka 532
†*Institute of Immunological Science, Hokkaido University, Kita-ku, Sapporo 060*
††*Osaka University, Suita-shi, Osaka 565*

(Received May 10, 1984)

ω-(1,4-Benzoquinon-2-yl)alkanoic acids, 2-[10-(5,6-dimethoxy-3-methyl-1,4-benzoquinon-2-yl)decyl]-3-hydroxytetracosanoic acid, all-*trans*-5,9,13,17-tetramethyl-4,8,12,16-octadecatetraenoic acid, and stearic acid were coupled to the 6-*O*-position of the carbohydrate moiety of muramyl dipeptide alkyl esters, and 6-*O*-aminoacyl-muramyl dipeptide methyl esters. The aminoacyl residues used were Gly, Leu, Ahx, and Aud. New synthetic methods were developed for ω-(1,4-benzoquinon-2-yl)alkanoic acids such as 22-(5,6-dimethoxy-3-methyl-1,4-benzoquinon-2-yl)docosanoic acid, and the α-branched ω-(1,4-benzoquinone-2-yl) β-hydroxy acid, 2-[10-(5,6-dimethoxy-3-methyl-1,4-benzoquinon-2-yl)decyl]-3-hydroxytetracosanoic acid. The effects of the resulting quinonyl, multiprenylacetyl, and stearoylmuramyl dipetides on the induction of delayed-type hypersensitivity to ABA-Tyr in guinea pigs and the tumor(meth-A)-suppressive activity in syngeneic BALB/c female mice were measured. The results revealed that all these muramyl-dipeptide derivatives retained the adjuvant activity whereas the potent tumor-suppressive activity was observed only in quinonylmuramyl dipeptides, indicating that the 5,6-dimethoxy-3-methyl-1,4-benzoquinone ring is a requisite for the manifestation of the tumor-suppressive activity. The lipophilicity-hydrophilicity balance of the molecule was also important. Among the compounds tested, *N*-acetyl-6-*O*-[10-(5,6-dimethoxy-3-methyl-1,4-benzoquinon-2-yl)decanoyl]muramyl-L-valyl-D-isoglutamine methyl ester showed the most potent tumor-suppressive activity. This compound also showed tumor-regressive activity in guinea pigs, and hence is a good candidate for further studies.

The immunotherapy of cancer, especially with *Mycobacterium tubeculosus Bacillus Calmette-Guèrin* (BCG), originally incorporated into clinical studies by Mathé and his colleagues, was investigated in many centers.[2)] The observation that BCG has serious side effects has stimulated clinical trials of less toxic material such as the cell wall skelton of BCG and that of *Nocardia*;[3)] the potent immunological activity of these materials is well established.[4)] Consequently, the discovery that *N*-acetylmuramyl-L-alanyl-D-isoglutamine (MDP) is able to replace mycobacterial whole cells in Freund's complete adjuvant stimulated efforts to develop a new antitumor agent by modifying this immunoactive minimal component of the cell wall peptidoglycan.[5)] In 1980 McLaughlin *et al.* reported that some synthetic MDP analogues, when administered in combination with trehalose dimycolate (TDM) as oil-in-water emulsion, caused line-10 hepatocellular-carcinoma regression in strain 2 guinea pigs.[6)] It was postulated that the presence of TDM enabled the water-soluble MDP analogues to disperse efficiently in the organic phase, and hence facilitated their antitumor activity. In an earlier attempt, Yamamura *et al.* reported that the incorporation into the MDP molecule of mycolic acid, a lipophilic constituent of the mycobacterial cell wall, resulted in a weak, compared with BCG cell wall skeleton, but distinct manifestation of the antitumor activity as determined by Meth-A fibrosarcoma suppression in syngeneic BALB/c female mice.[7)] Later, Kusumoto *et al.* found that the Meth-A fibrosarcoma suppressive effect of the 6-*O*-mycoloyl derivatives of MDP was unaffected when mycolic acid was replaced by a synthetic mycolic acid-mimic α-branched β-hydroxy fatty acid with 48 carbon atoms.[8)] These findings suggest that the lipophilicity-hydrophilicity balance of the molecule may be required for antitumor activity and the application of an MDP derivative with more favorable characteristics for cancer immunotherapy is possible.

In our efforts to obtain an agent for cancer immunotherapy, we tried to incorporate immunologically active lipophilic carboxylic acids, such as quinonyl[9)] and multiprenylacetic acids,[10)] into the MDP molecule using 6-*O*-aminoacyl MDP intermediates, which provided an effective means for introducing these labile carboxylic acids.[11)] Most of the resulting compounds, especially those having a 10-(5,6-dimethoxy-3-methyl-1,4-benzoquinon-2-yl)decanoyl group, exhibited a favorable biological effect on the induction of delayed-type hypersensitivity to *N*-acetyl-3-(4-arsonophenylazo)-L-tyrosine (ABA-Tyr) in guinea pigs.[11)] The apparent tumor-suppressive effect of the methyl esters of these derivatives has also been established.[12)] In this paper, we describe further the synthesis and immunological activities of quinonyl muramyl dipeptide alkyl ester derivatives **1** and a new general procedure for the synthesis of quinonyl acids, including mycoloyl-type quinonyl acid, having a long hydrocarbon chain. [A mycoloyl-type quinonyl acid (quinonylmycolic acid in this paper) is an α-branched β-hydroxyalkanoic acid having a quinone ring at the ω-position (**25**).]

Chemistry. Six ω-(5,6-dimethoxy-3-methyl-1,4-benzoquinon-2-yl)alkanoic acids, QS-3, 6, 10, 16, 22, and 34 (**2**)[13)] and quinonylmycolic acid (**25**) were prepared. QS-3 (**2a**), 6 (**2b**), and 10 (**2c**) were prepared by the reported procedure.[14)] Since a convenient synthetic sequence of QS-16 (**2d**), 22 (**2e**), and 34 (**2f**) with long hydrocarbon chains has not been described, we developed a general synthetic method for those quinonyl acids (Scheme 1): ω-(3,4-dimethoxy-2-hydroxy-6-methylphenyl)alkanoic acid **3**[14)] was acetylated and then converted to the carbonyl chloride **4** by treatment with oxalyl dichloride. The chloride **4** was condensed

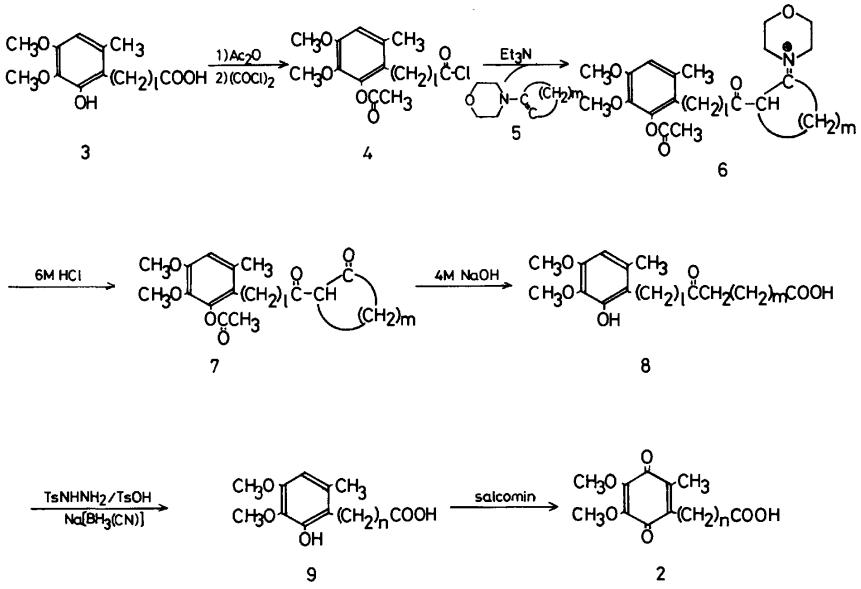

Scheme 1.

with an enamine **5**,[15] having an appropriate ring size, to give a condensation product **6**. After successive hydrolysis with 6 M HCl and 4 M NaOH, the carbonyl group of **8** was reduced with sodium cyanotrihydroborate in the presence of *p*-toluenesulfonohydrazide[16] to give **9**. When a 6-membered enamine (1-morpholinocyclohexene **5a**, m=4) and a 12-membered enamine (1-morpholinocyclododecene **5b**, m=10) are used, 6 and 12 carbon atoms can be extended, respectively [**3a**(1=9)→**9a**(n=15) and **3a**→**9b**(n=21)], in this conversion. By oxidation of **9a** with (*N*,*N*′-disalicylideneethylenediaminato)cobalt(II) (salcomin)[17] the target compound **2** was obtained. In this oxidation, potassium nitrosodisulfonate (Fremy's salt) used for the synthesis of quinonyl acids, such as QS-10 with a short hydrocarbon chain, could not be used for the synthesis of those with a long hydrocarbon chain because the yield was low or the reaction failed to proceed.[14] Compound **9b** (n=21), newly obtained by this procedure, was used as the starting material to synthesize **2f** (n=33). These findings demonstrate the accomplishment of a facile chain elongation of the alkyl side chain in quinonyl acids.

The synthesis of partially protected muramyl dipeptide alkyl esters **16** and their condensation with these carboxylic acids were carried out as outlined in Schemes 2 and 3: Secondary and tertiary alkyl ester analogues **13c** and **d** were prepared in a manner similar to the synthesis of the methyl ester analogue **13a**,[18] *i.e.* D-Glu was esterified at the γ-carboxyl group initially. After α-amino protection and amidation, either Boc-Val-ONB or *Z*-Val-ONB was coupled with α-amino-deprotected D-isoGln isopropyl and *t*-butyl ester to give **13c** and **d**, respectively (Scheme 2, Method A). Other Boc-Val-D-isoGln alkyl ester analogues (**13b**, **e**, and **f**) were prepared by esterification of Boc-Val-D-isoGln (**12**) with an appropriate alcohol; 6-chloro-1-(*p*-chlorophenylsulfonyloxy)benzotriazole (CCBT)[19]

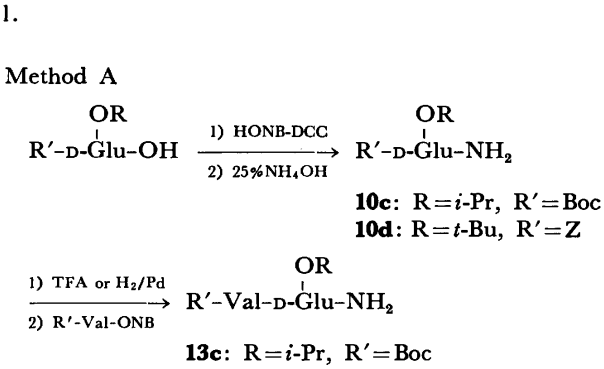

Scheme 2.

was used as a coupling agent. Dipeptide **12** was obtained by catalytic hydrogenolysis from Boc-Val-D-isoGln benzyl ester (**11**)[18] (Scheme 2, Method B).

Boc-Val-D-isoGln alkyl esters **13** thus obtained were deblocked by TFA and coupled with the 1-*O*-benzyl-4,6-*O*-benzylidene-*N*-acetyl-α-muramic acid HONB ester (**14**).[18] In the case of compound **13d**, the *Z* group was removed by hydrogenolysis. The 4,6-*O*-benzylidene group of the muramyl moiety of the resulting protected glycopeptide **15** was removed by treatment with hot 75% acetic acid to give the partially protected muramyl dipeptide alkyl esters **16**, to which were condensed the above-mentioned quinonyl acids **2** by DCC in a mixture of pyridine and DMF. The yield from this procedure of quinonyl acids having short

† 1 M=1 mol dm^{-3}.

TABLE 1. YIELDS AND PHYSICOCHEMICAL PROPERTIES OF INTERMEDIATE DIPEPTIDES **13**
Boc-Y-D-Glu(OR)-NH_2

Compd	Y	R	Method[a]	Yield %	Mp θ_m/°C	$[\alpha]_D$ (c 0.5) (Temp., Solvent)	Formula	Analysis Found(Calcd) C	H	N
13a[b]	Val	Me	A	84.3	117—119	+8.6° (23, EtOH)	$C_{16}H_{29}N_3O_6$	53.72 (53.46	8.10 8.13	11.44 11.69)
13b	Val	Et	B	43.9	128—129	+8.4° (23, DMF)	$C_{17}H_{31}N_3O_6$	54.71 (54.76	8.21 8.37	11.31 11.25)
13c	Val	*i*-Pr	A	79.6	144—145	+10.2° (23, DMF)	$C_{18}H_{33}N_3O_6$	55.73 (55.79	8.59 8.58	10.60 10.84)
13d[c]	Val	*t*-Bu	A	68.1	210—211	+19.1° (23, DMF)	$C_{22}H_{33}N_3O_6$	60.51 (60.67	7.56 7.64	9.60 9.65)
13e	Val	*n*-Hex	B	22.0	94— 95	+9.4° (23, DMF)	$C_{21}H_{39}N_3O_6 \cdot 1/2H_2O$	57.66 (57.51	8.92 9.19	9.96 9.58)
13f	Val	St	B	37.0	88— 89	+4.0° (23, DMF)	$C_{33}H_{63}N_3O_6$	66.26 (66.29	11.10 10.62	7.10 7:03)
13g	Ser(Bzl)	Me	A	71.2	103—104	+7.0° (22, EtOH)	$C_{21}H_{31}N_3O_7$	57.05 (57.65	7.15 7.14	9.55 9.61)
13h	Thr(Bzl)	Me	A	93.1	131—132	+7.0° (22, EtOH)	$C_{22}H_{33}N_3O_7$	58.71 (58.52	7.43 7.37	9.25 9.31)

a) See text. b) Compound **13a** was reported previously: Ref. 18. c) Boc is replaced by Z in this compound.

TABLE 2. YIELDS AND PHYSICOCHEMICAL PROPERTIES OF PROTECTED AND PARTIALLY PROTECTED MURAMYL DIPEPTIDES **15** AND **16**

Compd	Y	R	Yield %	Mp θ_m/°C	$[\alpha]_D$ (Temp)[a]	Formula	Analysis Found(Calcd) C	H	N
15a[b]	Val	Me	92.0	242 (d)	+86.1° (22)	$C_{36}H_{48}N_4O_{11} \cdot H_2O$	59.35 (59.16	6.80 6.90	7.70 7.68)
15b	Val	Et	74.3	>255	+98.4° (23)	$C_{37}H_{50}N_4O_{11}$	61.00 (61.14	6.97 6.93	7.65 7.71)
15c	Val	*i*-Pr	83.2	>255	+93.9° (23)	$C_{38}H_{52}N_4O_{11}$	61.89 (61.60	7.27 7.08	7.63 7.56)
15d	Val	*t*-Bu	75.3	186—188 (d)	+97.4° (23)	$C_{39}H_{54}N_4O_{11}$	62.20 (61.92	7.25 7.21	7.56 7.42)
15e	Val	*n*-Hex	76.2	>255	+93.4° (23)	$C_{41}H_{58}N_4O_{11}$	62.74 (62.79	7.33 7.47	7.23 7.16)
15f	Val	St	84.8	249 (d)	+67.5° (23)	$C_{53}H_{82}N_4O_{11} \cdot H_2O$	65.81 (65.67	8.66 8.76	5.90 5.78)
15g	Ser(Bzl)	Me	80.0	277—288	+92.0° (21)	$C_{41}H_{50}N_4O_{12}$	62.25 (62.26	6.35 6.37	7.15 7.09)
15h	Thr(Bzl)	Me	85.5	248	+92.0° (21)	$C_{42}H_{52}N_4O_{12}$	62.27 (62.67	6.44 6.51	7.20 6.96)
16a	Val	Me	73.0	242	+111.3° (23)	$C_{29}H_{44}N_4O_{11}$	55.59 (55.76	7.16 7.10	8.97 8.70)
16b	Val	Et	95.7	235	+110.5° (23)	$C_{30}H_{46}N_4O_{11}$	56.04 (56.41	7.22 7.26	8.61 8.77)
16c	Val	*i*-Pr	85.6	207—208	+111.2° (23)	$C_{31}H_{48}N_4O_{11} \cdot 1/2H_2O$	56.26 (56.26	7.46 7.31	8.43 8.46)
16d	Val	*t*-Bu	69.2	197—199	+110.3° (23)	$C_{32}H_{50}N_4O_{11} \cdot 1/2H_2O$	56.84 (56.84	7.55 7.60	8.19 8.27)
16e	Val	*n*-Hex	78.3	210—212	+101.6° (23)	$C_{34}H_{54}N_4O_{11} \cdot 1/2H_2O$	57.99 (58.02	7.91 7.88	7.95 7.96)
16f	Val	St	83.8	231 (d)	+85.1° (23)	$C_{46}H_{78}N_4O_{11} \cdot 1/2H_2O$	63.94 (64.01	9.19 9.11	6.47 6.49)
16g	Ser(Bzl)	Me	80.0	224—225	+99.2° (21)	$C_{34}H_{46}N_4O_{12}$	57.96 (58.10	6.51 6.60	8.22 7.97)
16h	Thr(Bzl)	Me	85.7	181—182	+102.4° (21)	$C_{35}H_{48}N_4O_{12} \cdot 1/2H_2O$	57.95 (57.91	6.66 6.81	7.65 7.72)

a) Solvent, DMF (c 0.5). b) Compound **15a** was reported previously: Ref. 18.

TABLE 3. YIELDS AND PHYSICOCHEMICAL PROPERTIES OF PROTECTED QUINONYL MURAMYL DIPEPTIDES **17**

Compd	R″	Y	R	Yield %	Mp θ_m/°C	$[\alpha]_D^{23}$ a) (Solvent)	Formula	Analysis Found(Calcd) C	H	N
17a	QS-10	Val	Me	75.8	172—175	+70.2° (MeOH) b)	$C_{48}H_{70}N_4O_{16}\cdot 1/2H_2O$	59.87 (59.55	6.99 7.39	6.14 5.79)
17b	QS-10	Val	Et	41.1	177	+66.7° ($CHCl_3$)	$C_{49}H_{72}N_4O_{16}\cdot 1/2H_2O$	59.73 (59.92	7.32 7.49	5.85 5.71)
17c	QS-10	Val	*i*-Pr	56.0	177—179	+69.0° (EtOH)	$C_{50}H_{74}N_4O_{16}$	60.89 (60.83	7.67 7.56	5.76 5.68)
17d	QS-10	Val	*t*-Bu	53.3	157	+65.6° (EtOH)	$C_{51}H_{76}N_4O_{16}$	61.16 (61.18	7.65 7.65	5.61 5.61)
17e	QS-10	Val	*n*-Hex	36.9	174—176	+46.9° ($CHCl_3$)	$C_{53}H_{80}N_4O_{16}$	61.75 (61.85	7.74 7.84	5.37 5.44)
17f	QS-10	Val	St	30.6	180	+38.4° ($CHCl_3$)	$C_{65}H_{104}N_4O_{16}\cdot H_2O$	64.22 (64.22	8.61 8.79	5.21 4.61)
17g	QS-3	Val	Me	37.6	189—190	+60.0° ($CHCl_3$)	$C_{41}H_{56}N_4O_{16}\cdot 1/2H_2O$	56.72 (56.60	6.66 6.61	6.47 6.44)
17i	QS-16	Val	Me	60.4	188—190	+59.2° (DMF)	$C_{54}H_{82}N_4O_{16}\cdot 1/2H_2O$	61.45 (61.63	7.93 7.95	5.51 5.33)
17j	QS-22	Val	Me	27.8	182—184	+52.8° (DMF)	$C_{60}H_{94}N_4O_{16}\cdot 1/2H_2O$	63.78 (63.41	8.93 8.42	5.42 4.93)
17k	QS-10	Ser(Bzl)	Me	72.3	162—165	+65.4° (EtOH) b)	$C_{53}H_{72}N_4O_{17}$	61.67 (61.37	7.15 7.00	5.13 5.40)
17l	QS-10	Thr(Bzl)	Me	74.9	143	+59.6° (EtOH) b)	$C_{54}H_{74}N_4O_{17}\cdot 1/2H_2O$	61.02 (61.17	7.05 7.13	5.40 5.29)
17m	St	Val	Me	31.2	214	+56.0° ($CHCl_3$) c)	$C_{47}H_{78}N_4O_{12}$	62.99 (63.35	8.74 8.82	6.35 6·29)

a) *c* 0.5. b) Temperature=21 °C. c) *c* 0.4; Temperature=24 °C.

alkyl chains (**2a**: n=2; **2c**: n=9) reached up to 70%. The yield of quinonyl acids with long alkyl chains (**2d**: n=15; **2e**: n=21) was 35 and 25%, respectively, and that of **2f** (n=33) was much lower. Stearic acid was also condensed to *N*-acetyl-1-*O*-benzyl-α-muramyl-L-valyl-D-isoglutamine methyl ester (**16a**) in a similar manner to obtain *N*-acetyl-6-*O*-stearoylmuramyl-L-valyl-D-isoglutamine methyl ester (**1o**) to evaluate the effect of the quinonyl moiety on biological activities.

Alternatively, the partially protected muramyl dipeptide alkyl esters **16** were condensed with the *p*-nitrophenyl ester of the quinonyl acids in the presence of HOBt and NEM in DMF at room temperature for 2 d. This procedure was also used for the condensation of benzyloxycarbonyl amino acids with the partially protected muramyl dipeptide **16a** to obtain compounds with a linking amino acid between a lipophilic carboxylic acid and muramyl dipeptide moiety[10] (Scheme 6, **16a**→**33**). The protected quinonyl muramyl dipeptide alkyl esters **17** were then hydrogenated in acetic acid or methanol with palladium black as a catalyst. The hydroquinonyl group was oxidized by $FeCl_3$ in methanol to the desired 6-*O*-quinonyl-*N*-acetylmuramyl-L-valyl-D-isoglutamine alkyl esters **1** (Scheme 3). Compound **1h** was obtained in a moderate yield directly by the coupling of quinonyl acid **2b** (n=5) with *N*-acetylmuramyl-L-valyl-D-isoglutamine methyl ester[18] using DCC as a condensing agent. Compounds **1m** and **n** having a Ser of Thr residue instead of the Val residue of **1a** were synthesized similarly with Boc-Ser(Bzl)-D-isoGln methyl ester (**11g**) or Boc-Thr(Bzl)-D-isoGln methyl ester (**11h**) as a starting material, respectively.

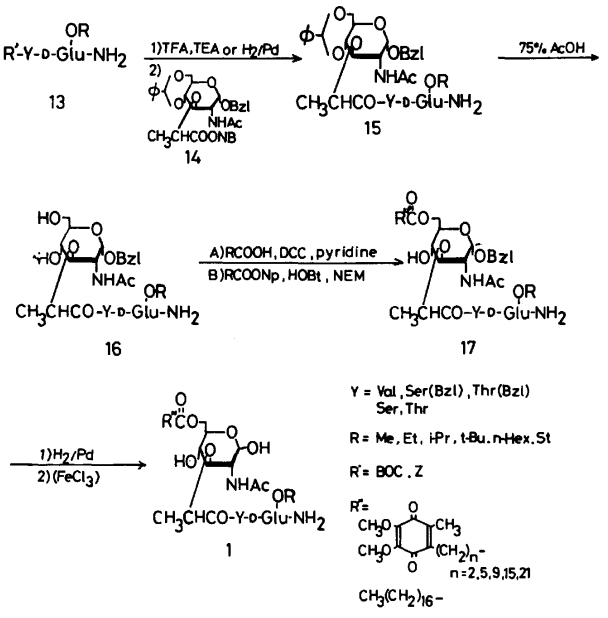

Scheme 3.

We also developed a novel general synthetic route for quinonylmycolic acid **25** with 10-(5,6-dimethoxy-3-methyl-1,4-benzoquinon-2-yl)decyl acetate (**18**)[14] as a starting material (Scheme 4). Compound **18** was hydrogenated and the hydroxyl groups of the resulting hydroquinone were methoxymethylated by methoxymethyl chloride in the presence of NaH and subsequent hydrolysis with 4M NaOH gave the protected quinonyl alcohol **19**. Compound **19** was oxidized with

dimethyl sulfoxide using pyridine-sulfur trioxide complex to the aldehyde **20**, which was then condensed with the ethyl 3-oxoalkanoate **21**[20] in the presence of acetic acid-piperidine to produce the condensation product **22**. Catalytic hydrogenation of the double bond of **22** and subsequent reduction with sodium borohydride afforded the protected quinonylmycolic acid ethyl ester **23**, which was then hydrolyzed with 3M NaOH to yield

TABLE 4. YIDLDS AND PHYSICOCHEMICAL PROPERTIES OF QUINONYL MURAMYL DIPEPTIDES **1**

Compd	R''	Y	R	Yield %	Mp θ_m/°C	$[\alpha]_D^{23}$ a) (Solvent)	Formula	Analysis Found (Calcd) C	H	N
1a	QS-10	Val	Me	73.0	188—189	+35.2° (EtOH) b)	$C_{41}H_{64}N_4O_{16}$	56.47 (56.67	7.42 7.42	6.43 6.45)
1b	QS-10	Val	Et	77.9	—	+33.0° (EtOH)	$C_{42}H_{66}N_4O_{16}\cdot H_2O$	55.67 (55.98	7.53 7.61	6.07 6.22)
1c	QS-10	Val	*i*-Pr	69.1	194—195	+35.4° (EtOH)	$C_{43}H_{68}N_4O_{16}$	57.39 (57.57	7.75 7.64	6.14 6.25)
1d	QS-10	Val	*t*-Bu	53.3	192—193	+35.6° (EtOH)	$C_{44}H_{70}N_4O_{15}$	57.73 (58.00	7.83 7.75	6.16 6.16)
1e	QS-10	Val	*n*-Hex	57.3	200—202	+39.2° (EtOH)	$C_{46}H_{74}N_4O_{16}\cdot H_2O$	57.59 (57.72	7.91 8.00	6.06 5.85)
1f	QS-10	Val	St	67.7	—	+20.3° ($CHCl_3$)	$C_{58}H_{100}N_4O_{16}\cdot 1/2H_2O$	62.23 (62.28	8.93 9.10	5.18 5.01)
1g	QS-3	Val	Me	67.1	167	+42.9° (EtOH)	$C_{34}H_{50}N_4O_{16}\cdot H_2O$	51.57 (51.76	6.63 6.65	7.12 7.10)
1h	QS-6	Val	Me	38.8	174 (d)	+43.8° (EtOH)	$C_{37}H_{56}N_4O_{16}\cdot 1/2H_2O$	53.95 (54.06	6.98 6.99	6.76 6.82)
1i	QS-16	Val	Me	67.6	193—195	+33.1° (EtOH)	$C_{47}H_{76}N_4O_{16}\cdot H_2O$	58.33 (58.13	8.14 8.10	5.81 5.78)
1j	Q-22	Val	Me	48.2	204	+28.6° (EtOH)	$C_{53}H_{88}N_4O_{16}\cdot H_2O$	60.42 (60.32	8.65 8.60	5.35 5.31)
1k	Qmy c)	Val	Me	33.0	—	+26.9° (EtOH)	$C_{65}H_{112}N_4O_{17}$	63.64 (63.90	9.32 9.42	4.59 4.34)
1l	Qmy c)	Ala	H	33.4	—	+21.2° (EtOH)	$C_{62}H_{106}N_4O_{17}\cdot 3H_2O$	60.25 (60.36	9.11 9.15	4.82 4.54)
1m	QS-10	Ser	Me	72.6	149—150	+39.2° (MeOH) d)	$C_{39}H_{60}N_4O_{17}$	54.81 (54.66	7.01 7.06	6.80 6.54)
1n	QS-10	Thr	Me	78.0	147—148	+37.2° (MeOH) b)	$C_{40}H_{62}N_4O_{17}$	55.38 (55.16	7.40 7.18	6.79 6.43)
1o	St	Val	Me	96.3	178—181 (d)	+34.9° (EtOH)	$C_{40}H_{72}N_4O_{12}\cdot H_2O$	57.31 (57.39	8.81 9.15	6.89 6.69)

a) *c* 0.5. b) Temperature=21 °C. c) Quinonylmycoloyl. d) Temperature=22 °C.

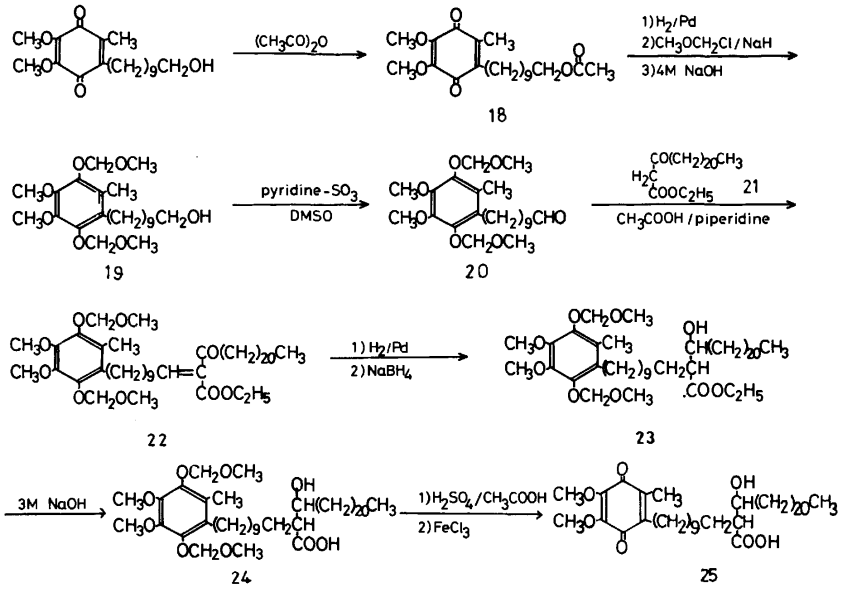

Scheme 4.

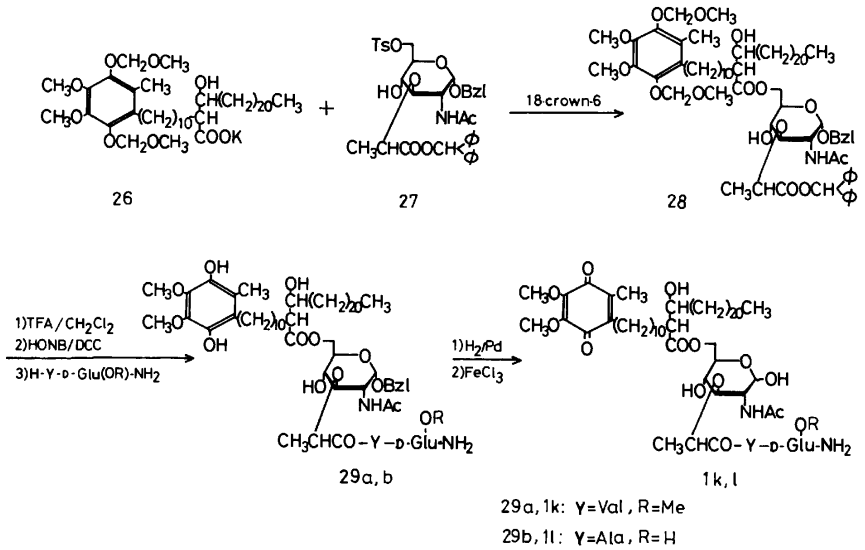

Scheme 5.

24. The protecting methoxymethyl group of **24** was then removed by heating at 100 °C for 10 min in a mixture of 2M H_2SO_4 and acetic acid. The resulting hydroquinone was reoxidized with $FeCl_3$ in dioxane to the desired quinonylmycolic acid **25**.

The synthesis of 6-*O*-quinonylmycoloylmuramyl dipeptides **1k** and **l** was carried out as shown in Scheme 5 as in the case for the synthesis of 6-*O*-mycoloylmuramyl dipeptides,[7] since the condensation of **25** with *N*-acetyl-1-*O*-benzyl-α-muramyl dipeptides by DCC in a mixture of pyridine and DMF did not proceed. Protected quinonylmycolic acid **24** was converted to the potassium salt **26**, which was then condensed with *N*-acetyl-1-*O*-benzyl-6-*O*-tosyl-α-muramic acid diphenylmethyl ester (**27**)[7] in the presence of 18-crown-6. The diphenylmethyl and methoxymethyl protecting groups of **28** were then removed by TFA. The resulting carboxylic acid was activated by the HONB-DCC method[21] and condensed *in situ* with the dipeptides to give the protected quinonylmycoloylmuramyl dipeptide **29**. The removal of the benzyl protecting group by catalytic hydrogenolysis and reoxidation of the hydroquinone ring by $FeCl_3$ produced target compound **1**.

The methyl ester with a linking amino acid between a lipophilic acid and the muramyl dipeptide moiety **33a—d** were prepared by acylating the corresponding 6-*O*-aminoacylmuramyl dipeptide methyl esters **31** with *p*-nitrophenyl ester of 10-(5,6-dimethoxy-3-methyl-1,4-benzoquinon-2-yl)decanoic acid (Scheme 6). *N*-Acetyl-6-*O*-(all-*trans*-5,9,13,17-tetramethyl-4,8,12,16-octadecatetraenoyl-L-leucyl)muramyl-L-valyl-D-isoglutamine methyl ester (**33e**) was also obtained in this procedure. The esters **33a** and **b** could also be obtained by treating the corresponding γ-carboxyl-free derivatives **32** with diazomethane in methanol as exemplified in Scheme 7. The γ-carboxyl-free derivatives **32** were obtained according to the procedure reported earlier.[11]

The purification of all these desired products **1** was carried out by column chromatography on silica

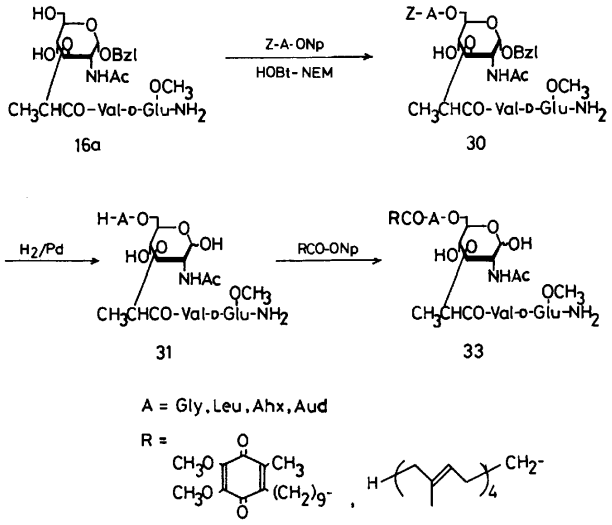

Scheme 6.

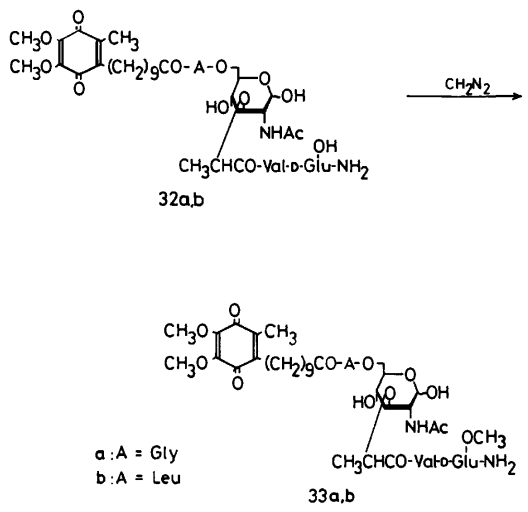

Scheme 7.

TABLE 5. YIELDS AND PHYSICOCHEMICAL PROPERTIES OF QUINONYL AND MULTIPRENYL MURAMYL DIPEPTIDES **33** AND THEIR INTERMEDIATES **30** AND **31**

Compd	R	A	Yield %	Mp θ_m/°C	$[\alpha]_D$ (c 0.5) (Temp., Solvent)	Formula	Analysis Found(Calcd) C	H	N
30a	—	Gly	59.1	189—190	+84.8° (21, DMF)	$C_{39}H_{53}N_5O_{14}$	57.35 (57.41	6.58 6.55	8.13 8.59)
30b	—	Leu	71.1	232—234	+72.2° (22, DMF)	$C_{43}H_{61}N_5O_{14}$	58.98 (59.23	7.19 7.05	8.10 8.03)
30c	—	Ahx	71.8	189—191	+78.6° (21, DMF)	$C_{43}H_{61}N_5O_{14}$	59.26 (59.23	7.10 7.05	8.25 8.03)
30d	—	Aud	68.2	177—179	+74.4° (22, DMF)	$C_{48}H_{71}N_5O_{14}$	61.22 (61.19	7.72 7.60	7.60 7.44)
31a	—	Gly	80.5	—	+36.8° (21, 95%EtOH)	$C_{24}H_{41}N_5O_{12}\cdot H_2O$	47.60 (47.28	7.13 7.11	11.55 11.49)
31b	—	Leu	82.6	105—108	+45.3° (23, DMF)	$C_{28}H_{49}N_5O_{12}\cdot CH_3COOH$	50.97 (50.91	7.73 7.55	10.00 9.90)
31c	—	Ahx	74.9	122—124	+39.6° (21, EtOH)	$C_{28}H_{49}N_5O_{12}\cdot 1/2H_2O$	51.46 (51.21	7.84 7.68	10.61 10.67)
31d	—	Aud	82.7	121—122	+41.5° (21, EtOH)	$C_{33}H_{59}N_5O_{12}\cdot H_2O$	53.78 (53.86	8.13 8.36	9.76 9.52)
32a	QS-10	Gly	77.1	175—177 (d)	+26.0° (22, 85%EtOH)	$C_{42}H_{65}N_5O_{17}\cdot 2H_2O$	53.36 (53.20	7.21 7.34	7.54 7.39)
32b	QS-10	Leu	46.7	103—106	+19.4° (22, EtOH)	$C_{46}H_{73}N_5O_{17}\cdot 3/2H_2O$	55.56 (55.52	7.43 7.70	6.93 7.04)
33a	QS-10	Gly	24.0	190—191	+23.0° (22, EtOH)	$C_{43}H_{67}N_5O_{17}\cdot H_2O$	54.69 (54.71	7.51 7.37	7.69 7.42)
33b	QS-10	Leu	40.7	193—195 (d)	+21.0° (23, EtOH)	$C_{47}H_{75}N_5O_{17}$	57.07 (57.48	7.78 7.70	7.15 7.13)
33c	QS-10	Ahx	48.7	176—177 (d)	+31.2° (21, EtOH)	$C_{47}H_{75}N_5O_{17}\cdot 1/2H_2O$	56.98 (56.95	7.72 7.73	6.91 7.07)
33d	QS-10	Aud	57.1	185—186 (d)	+32.6° (21, EtOH)	$C_{52}H_{85}N_5O_{17}$	59.06 (59.35	8.25 8.14	6.44 6.66)
33e	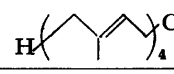	Leu	76.9	93— 97	+23.3° (23, EtOH)	$C_{50}H_{83}N_5O_{13}\cdot H_2O$	61.49 (61.26	8.70 8.74	7.16 7.15)

gel and Sephadex LH-20. The physicochemical properties of the intermediates and the desired MDP derivatives are shown in Tables 1—5.

Measurement of Adjuvant and Tumor Suppressive Activities. The adjuvant activity of the synthetic MDP derivatives **1** and **33** on the induction of delayed-type hypersensitivity to ABA-Tyr in guinea pigs was assayed by the following method.[12] Hartley guinea pigs each weighing 300—500 g were immunized in the footpads (all four) with a total of 50 μg of ABA-Tyr in Freund's incomplete adjuvant containing the synthetic MDP derivatives. Five animals were used per group. Control groups were immunized with ABA-Tyr alone in Freund's incomplete adjuvant (Control 1) or with Freund's incomplete adjuvant alone (Control 2). After 2 weeks, skin tests were performed with 50 or 100 μg of ABA-Tyr-bovine serum alubmin (ABA-BSA) prepared by the method of Tabachnick and Sobotka.[22] Skin reaction were measured 24 and 48 h after an intradermal injection of the test antigen. The results are shown as the average diameter (mm) ± the standard error (SE) of the skin reaction (induration) of five guinea pigs.

The evaluation of the suppressive activity on a transplantable tumor in syngeneic mice was carried out according to the procedure reported previously.[12] A mixture of tumor cells (Meth-A, 1×10^5 cells) and the synthetic MDP derivatives suspended in phosphate-buffered saline was inoculated intradermally into the flanks of BALB/c female mice. Tumor size at the site of the inoculation and survival rates were examined every week. The results were obtained 4 weeks after the fibrosarcoma inoculation. Animals with tumors less than 2 mm were considered to be tumor free; such mice were then rechallenged by Meth-A (1×10^5 cells) and observed for an additional 2 weeks to confirm the immunotherapeutic activity of the test materials.

Results and Discussion

Some lipid-soluble vitamins, such as retinol, α-tocopherol, and ubiquinones, are known to exert diverse immunological effects.[23] The metabolites of ubiquinones and their synthetic related compounds are also lipophilic and possess various biological characteristics of ubiquinones including the enhancement of humoral immune response.[24] It has been argued that, among a series of MDP derivatives, the lipophilicity or lipophilicity-hydrophilicity balance is a fundamental requirement for the expression of the antitumor activity.[8,25] It was reported that 6-*O*-mycoloyl-MDP exhibited a tumor-suppressive effect, but was unable to

enhance humoral antibody formation.[26] Therefore, the incorporation of lipophilic and immunologically active quinonyl acids, which enhance humoral immune response,[24] may produce some additional favorable effects in MDP. These were the considerations that led us to synthesize several quinonyl derivatives of MDP in the hope of creating an effective antitumor agent. We examined the adjuvant activity of the compounds on the induction of delayed-type hypersensitivity to ABA-Tyr in guinea pigs. The suppression test of a transplantable tumor in syngeneic mice was carried out on those compounds that exhibited potent adjuvant activity. In this study, the Ala residue in MDP was replaced mostly with the Val residue since *N*-acetylmuramyl-L-valyl-D-isoglutamine showed the most potent activity on inducing delayed-type hypersensitivity.[18] Some other lipophilic MDP analogues, such as **1o** and **33e**, were also synthesized and tested to evaluate the effect of the quinonyl group on the adjuvant and tumor-suppressive activities.

Compounds **1a—f** were synthesized and examined to assess the effect produced by varying the ester substituent at the γ-carboxyl group of the isoglutamine moiety. Ester functionality was varied in the sequence of methyl, ethyl, isopropyl, *t*-butyl, hexyl, and stearyl (octadecyl). As shown in Table 6 (Expt. 1), the adjuvant activity of all the ester derivatives were more potent than MDP; the isopropyl homologue **1c** showed maximum activity. Although an ester substituent bigger than the *t*-butyl group (**1d**) caused a slight decrease in activity, there was little variation in activity between each ester set. This indicates a reduced dependence of the adjuvant activity on steric factors and/or the lipophilicity of the ester substituents at the γ-carboxyl group of the isoglutamine moiety.

The extent of increase in the adjuvant activity was appreciably affected by the chain length in the quinonyl acid moiety (Table 6; Expt. 2). Among the normal alkyl groups investigated (**1a**, and **1g—j**), activity was optimal for the decanoyl derivative **1a** and decreased for the longer chain derivatives **1i** and **1j**. Decreasing activity was a function of chain length. Compounds with shorter chain length, **1g** and **1h**, also exhibited less potent adjuvant activity than **1a**. The lower activity of these compounds could be interpreted as a consequence of either an inadequate lipophilicity of the molecule or an inadequate spacial arrangement of the quinone ring and MDP moiety. In the quinonylmycoloyl series, the adjuvant activity of the methylated Val derivative **1k** is less potent than even MDP whereas the γ-carboxyl-free MDP derivative **1l** showed the most potent activity (Table 6; Expt. 2). This finding also indicates that excess lipophilicity of the molecule causes decreased adjuvant activity.

In the tumor-suppressive activity, as in the adjuvant activity, most of the ester homologues showed comparable potent activity whereas the chain length of the quinonyl acid moiety greatly affected the activity; thus some parallelism exists between the adjuvant and the tumor-suppressive activity (data not shown). Among the quinonyl muramyl dipeptide ester derivatives,

Table 6. Adjuvant activity of quinonyl MDP derivatives **1** on the induction of delayed-type hypersensitivity to ABA-Tyr in guinea pigs

Compd[a]	R	n	Skin reaction with ABA-Tyr	
			24 h	48 h
Expt. 1			(mm)	(mm)
1a	Me	9	23.8±1.0	19.9±0.9
1b	Et	9	24.1±0.5	19.0±0.6
1c	*i*-Pr	9	23.5±0.8	20.6±0.9
1d	*t*-Bu	9	21.9±0.8	19.1±1.4
1e	*n*-Hex	9	21.6±0.6	19.3±0.4
1f	St	9	20.1±0.8	19.8±1.1
MDP			20.7±0.5	18.1±0.4
Control 1 (ABA-Tyr+FIA[c])			3.0±1.0	0
Control 2 (FIA[c] alone)			0	0
Expt. 2				
1g	Me	2	18.6±0.5	16.4±1.4
1h	Me	5	18.9±0.7	15.1±0.7
1a	Me	9	18.3±1.0	17.8±0.6
1i	Me	15	17.4±0.6	17.1±0.5
1j	Me	21	17.9±0.8	13.8±1.0
1k	Me	Quinonylmycoloyl	16.6±1.0	15.1±0.7
1l[b]	H	Quinonylmycoloyl	17.1±0.5	19.1±0.8
MDP			16.4±0.3	16.6±0.9
Control 1 (ABA-Tyr+FIA[c])			5.8±0.7	0
Control 2 (FIA[c] alone)			0	0

a) Dose: 100 μg. b) In this compound the dipeptide moiety is Ala-D-isoGln. c) FIA: Freund's incomplete adjuvant.

methyl ester homologue **1a** showed the most potent activity when 5×10^5 Meth-A cells were used (Table 7). Therefore, compound **1a** was further modified and tested for adjuvant and tumor-suppressive activity. The compounds synthesized for this purpose were those in which the Val residue of **1a** was replaced with Ser (**1m**) and Thr (**1n**), and those having a linking amino acid between the quinonyl acid and muramyl-dipeptide moiety (**33**).

The effects of these synthetic MDP derivatives **1m**, **1n**, and **33** together with those of the most immunoadjuvant active analogues of MDP, *N*-acetylmuramyl-L-valyl-D-isoglutamine (**34**) and its methyl ester (**35**),[18] on the induction of delayed-type hypersensitivity to ABA-Tyr is shown in Table 8. The results for 6-*O*-stearoyl (**1o**) and 6-*O*-multiprenyl (**33e**) derivatives, and nonmethylated quinonyl MDP derivatives having Gly (**32a**) and Leu (**32b**) as the linking amino acids are also included for comparison. The effect on Meth-A suppression is shown in Table 9.

The 10-(5,6-dimethoxy-3-methyl-1,4-benzoquinon-2-yl)decanoyl group incorporated directly into the 6-*O*-position of the muramyl moiety (**1a**) maintained the adjuvant activity of the parent molecules **34** and **35**. Differences in activity among **1a**, **1m**, and **1n**, in which the Ala of MDP was replaced with Val, Ser, and Thr, reflect differences in activity observed among the corresponding parent MDP analogues, *i.e.*, *N*-acetylmuramyl-L-valyl, L-seryl, and L-threonyl-D-isoglutamine.[18] These derivatives also showed potent tumor-suppressive activity even though they were administered as a suspension in phosphate-buffered saline whereas mycoloyl-MDP was reported to be active when administered as an oil-in-water emulsion.[7] The activity developed by **1m** and **1n** was somewhat lower than that of **1a**. The potency of all three derivatives was in good accordance with that of their adjuvant activity when 5×10^5 Meth-A cells were used (Table 9, Expt. 1). A dose response was obtained for **1a** (Table 9, Expt. 2). The induction of systemic tumor immunity that suppressed tumor growth in mice was demonstrated by the reinoculation of 1×10^5 Meth-A cells. The adjuvant activity of stearoyl-MDP derivative **1o** diminished slightly and its apparent low tumor-suppressive activity indicated that not only lipophilicity but some other biological

TABLE 7. TUMOR-SUPPRESSIVE ACTIVITY OF QUINONYL MDP DERIVATIVES

Compd[b]	Primary suppression[a]	
	Meth-A (1×10^5)	Meth-A (5×10^5)
1a	10/10	6/10
1b	10/10	1/10
1c	10/10	2/10

a) Figures represent the ratio of tumor-free mice to surviving mice. b) Dose: 100 μg.

TABLE 8. ADJUVANT ACTIVITY OF MDP DERIVATIVES ON THE INDUCTION OF DELAYED-TYPE HYPERSENSITIVITY TO ABA-Tyr IN GUINEA PIGS

Compd	Skin reaction with ABA-Tyr (mm±SE)	
Expt. 1	24 h	48 h
1a	24.4±1.2	19.2±0.9
1m	23.8±0.6	19.1±0.4
1n	21.1±0.5	17.3±0.9
1o	22.5±0.6	18.4±0.4
34	23.6±0.8	19.4±0.7
35	24.1±0.8	19.7±0.4
Control 1	3.3±1.4	0
Control 2	0	0
Expt. 2		
33a	21.7±0.5	20.6±0.6
33b	21.3±0.7	19.7±0.9
33c	23.9±0.7	18.3±1.2
33d	22.2±0.5	15.5±1.2
33e	22.9±0.8	20.2±1.0
34	22.0±0.4	19.9±0.8
Control 1	3.0±1.2	0
Control 2	0	0

TABLE 9. TUMOR-SUPPRESSIVE ACTIVITY OF MDP DERIVATIVES

Compd.	Dose (μg)	Primary suppression[a]	Rechallenge[a,b]
Expt. 1			
1a	100	10/10 (6/10)[c]	5/10
1m	100	3/10 (4/10)[c]	2/3
1n	100	6/10 (0/10)[c]	6/6
34	100	0/10	—
35	100	0/9	—
Control	—	0/10 (0/10)[c]	—
Expt. 2			
1a	300	10/10	8/9
1a	100	4/10	3/3
Control	—	0/10	—
Expt. 3			
1a	100	6/10	ND
	20	2/10	ND
33a	100	8/10	ND
	20	0/10	—
33b	100	5/10	ND
	20	2/10	ND
Control	—	0/9	—
Expt. 4			
1a	100	8/10	ND
1o	100	2/9	ND
33a	100	1/10	ND
33b	100	4/10	ND
33c	100	2/10	ND
33d	100	2/10	ND
33e	100	2/8	ND
Control	—	0/10	—

a) Figures represent the ratio of tumor-free mice to surviving mice. b) ND=not determined. c) Meth-A: 5×10^5 cells.

activities rendered by quinonyl moiety, such as interaction with the cell surface membranes, are necessary for the development of tumor-suppressive activity.

Most of the quinonyl muramyl dipeptides with a linking amino acid between the quinonyl acid and the muramyl moiety (**33**) also exhibited adjuvant activity comparable to that of **34**. The lower activity of **33d**, with 11-aminoundecanoic acid as a linking unit, is compatible with the result obtained for nonmethylated quinonyl muramyl dipeptides with a long chain linking unit.[9] The tumor-suppressive activity of these quinonyl muramyl dipeptides **33** was also demonstrated (Table 9, Expt. 3). Compounds **33c** and **33d** are equipotent in tumor-suppressive activity in spite of the latter's diminished adjuvant activity. Among these quinonyl muramyl dipeptides with a linking amino acid, **33b** is almost as active as **1a**. The result for **33a** was variable. The retention of the adjuvant activity by the multiprenyl derivative **33e** showed that the quinonyl moiety is not a requisite for maintaining the induction activity for delayed-type hypersensitivity. The low activity in tumor suppression of **33e**, however, indicated the importance of the quinonyl moiety for the development of tumor suppression as observed in the case of stearoyl-MDP **1o**. Parent muramyl dipeptide analogues **34** and **35** did not cause any tumor-suppressive activity either.

From these results, we conclude that quinonyl muramyl dipeptide **1a** has the most potent adjuvant and tumor-suppressive activities. It is of particular interest that **1a**, when injected into the established tumor as an oil-in-water emulsion on day 2, 5, 8, and 15 after intradermal inoculation, caused complete regression of the line-10 hepatocellular carcinoma in strain 2 guinea pigs.[27] Metastasis was not observed. Although more extensive search to find an effective immunotherapeutic agent for cancer by modifying natural MDP is required, the potent adjuvant, tumor-suppressive, and tumor-regressive effects of **1a** make it a good candidate for further studies.

Experimental

Melting points were taken in open capillaries and are uncorrected. Optical rotations were determined with a Perkin Elmer model 141 polarimeter. ^{1}H NMR spectra were obtained on a Varian EM-390 spectrometer with tetramethylsilane as an internal standard. All chemicals and solvents were of reagent grade and were used without further purification. The reactions were monitored by TLC on Merck F_{254} silica gel pre-coated plates, which were generally developed with $CHCl_3$–acetone–EtOH (70:30:3, v/v) for compound **11**, $CHCl_3$–acetone–MeOH (10:3:2, v/v) for **1**, **15**, **16**, **17**, **30**, and **33**, AcOEt–pyridine–H_2O–AcOH (30:10:5:3, v/v) for **1**, **31**, and **33**, and *n*-BuOH–AcOH–AcOEt–H_2O (1:1:1:1, v/v) for **1** and **33**. Solution were concentrated in a rotary vacuum evaporator under reduced pressure at temperatures below 45 °C.

*10-(2-Acetoxy-3,4-dimethoxy-6-methylphenyl)decanoyl Chloride (**4a**).* A solution of 10-(3,4-dimethoxy-2-hydroxy-6-methylphenyl)decanoic acid (**3a**)[14] (12.6 g, 37.1 mmol) in Ac_2O (30 ml) was combined with concd H_2SO_4 (1 ml), and the mixture was stirred for 1.5 h at room temperature. Water (10 ml) was then added carefully and the stirring was continued for 2 h. After the removal of the solvent, the residue was dissolved in AcOEt (100 ml), and the solution was washed with 5% $NaHCO_3$. The aqueous layer was back-washed with AcOEt (100 ml). The extracts were combined, washed successively with 1M HCl and water, and dried ($NaSO_4$). The solvent was evaporated to give an oily acetyl compound (13.5 g, 95.6%) which was dissolved in benzene (20 ml). To this was added oxalyl dichloride (9.25 ml, 0.1 mol) dropwise at room temperature, then the mixture was stirred at 50 °C for 1 h. After the removal of the solvent, the residue was flushed with benzene, and dried (NaOH pellets): 13.0 g (91.8%) ^{1}H NMR ($CDCl_3$): δ=1.28—1.90 (14H, m), 2.25—2.73 (8H, m), 2.91 (2H, t), 3.85 (3H, s), 3.90 (3H, s), and 6.72 (1H, s).

*22-(3,4-Dimethoxy-2-hydroxy-6-methylphenyl)-13-oxodocosanoic Acid (**8b**).* A solution of **4a** (7.98 g, 20 mmol) in $CHCl_3$ (4 ml) was added dropwise to a mixture of 1-morpholinocyclododecene (**5b**)[28] (6.29 g, 24 mmol) and Et_3N (3.08 ml, 22 mmol) at 0 °C over a period of 30 min, and the reaction mixture was stirred at room temperature for 15 h. To this were added $CHCl_3$ (5 ml) and 6M HCl (10 ml); the mixture was heated under reflux for 5 h, cooled to room temperature, diluted with water (20 ml), and extracted with $CHCl_3$ (2×30 ml). The combined extracts were washed with water, and dried (Na_2SO_4). After the removal of the solvent, the residue was purified by column chromatography (6×11 cm) on silica gel using $CHCl_3$ as an eluant to give 2-[10-(2-acetoxy-3,4-dimethoxy-6-methylphenyl)decanoyl]cyclododecanone (**7b**): 8.63 g (79.2%). Then, a solution of compound **7b** in EtOH (8 ml) was added to hot 4M NaOH (7.8 ml) and the mixture was heated for 10 min under reflux, cooled to room temperature, acidified to pH 2 with 6M HCl, and extracted with AcOEt (30 ml). The extract was washed with water, dried (Na_2SO_4), and concentrated to give the residue, which was recrystallized from ether–petroleum ether: 6.12 g (74.4%). mp 63—64 °C. ^{1}H NMR ($CDCl_3$): δ=1.17—1.90 (32H, m), 2.22—2.78 (11H, m), 3.88 (3H, s), 3.92 (3H, s), and 6.40 (1H, s).

Found: C, 71.57; H, 10.17%. Calcd for $C_{31}H_{52}O_6$: C, 71.50; H, 10.07%.

*16-(3,4-Dimethoxy-2-hydroxy-6-methylphenyl)-7-oxohexadecanoic Acid (**8a**).* This compound was synthesized from **4a** and **5a** in a manner similar to that of **8b**: 35.9%. mp 55—57 °C.

Found: C, 68.64; H, 9.40%. Calcd for $C_{25}H_{40}O_6$: C, 68.77; H, 9.23%.

*34-(3,4-Dimethoxy-2-hydroxy-6-methylphenyl)-13-oxotetracontanoic Acid (**8c**).* This compound was synthesized from **4b**, which was derived from **3b** and **5b** in a manner similar to that of **8b**: 32.7%. mp 92—93 °C.

Found: C, 74.88; H, 11.29%. Calcd for $C_{43}H_{76}O_6$: C, 74.95; H, 11.12%.

*22-(3,4-Dimethoxy-2-hydroxy-6-methylphenyl)docosanoic Acid(**9b**).* Compound **8b** (5.21 g, 10 mmol), *p*-toluenesulfonohydrazide (2.33 g, 12.5 mmol) and cyclohexane (25 ml) were added to a solution of DMF–sulfolane (25 ml—25 ml) containing *p*-toluenesulfonic acid (250 mg) at 100 °C. After 5 min, Na[BH_3(CN)] (2.51 g, 41 mmol) was added. The mixture was stirred for 20 min at the same temperature and the solution was diluted with brine, and extracted with ether (2×100 ml). The extracts were combined, washed with water, 0.5M HCl and water successively, and dried (Na_2SO_4). After the removal of the solvent, the residue was recrystallized from a small amount of ether: 3.13 g (58.6%). mp 67—68 °C (lit,[14] mp 67—68 °C).

Found: C, 73.76; H, 10.78%. Calcd for $C_{31}H_{54}O_5$: C, 73.47; H, 10.74%.

*16-(3,4-Dimethoxy-2-hydroxy-6-methylphenyl)hexadecanoic Acid (**9a**).* This compound was synthesized from **8a** in a manner similar to that of **9b**: 57.4%. mp 45 °C.

Found: C, 71.13; H, 10.13%. Calcd for $C_{25}H_{42}O_5$: C, 71.05;

H, 10.02%.

*34-(3,4-Dimethoxy-2-hydroxy-6-methylphenyl)tetracontanoic Acid (**9c**).* This compound was synthesized from **8c** in a manner similar to that of **9b**: 70.6%. mp 93 °C.

Found: C, 76.73; H, 11.91%. Calcd for $C_{42}H_{78}O_5$: C, 76.50; H, 11.65%.

*22-(5,6-Dimethoxy-3-methyl-1,4-benzoquinon-2-yl)docosanoic Acid (**2e**).* A mixture of **9b** (2.0 g, 3.95 mmol) and (N,N'-disalicylideneethylenediaminato)cobalt(II) (salcomin 325 mg, 1 mmol) in DMF (10 ml) was stirred under oxygen at room temperature for 24 h. The solvent was evaporated and the residue was dissolved in AcOEt (50 ml). The insolubles were filtered and the filtrate was washed succesively with 0.5 M HCl and water, and dried (Na_2SO_4). After the removal of the solvent, the residue was purified on a column (4.5×11 cm) of silica gel using $CHCl_3$ as an eluent and then recrystallized from EtOH: 1.04 g (50.6%). mp 83—84 °C (lit,[14] mp 86—87 °C).

Found: C, 71.44; H, 10.18%. Calcd for $C_{31}H_{52}O_6$: C, 71.50; H, 10.07%.

*16-(5,6-Dimethoxy-3-methyl-1,4-benzoquinon-2-yl)hexadecanoic Acid (**2d**).* This compound was synthesized from **9a** in a manner similar to that of **2e**: 58.9%. mp 70—71 °C.

Found: C, 68.89; H, 9.30%. Calcd for $C_{25}H_{40}O_6$: C, 68.77; H, 9.23%.

*34-(5,6-Dimethoxy-3-methyl-1,4-benzoquinon-2-yl)tetracontanoic Acid (**2f**).* This compound was synthesized from **9c** in a manner similar to that of **2e**: 21.3%. mp 89—90 °C.

Found: C, 74.73; H, 11.09%. Calcd for $C_{43}H_{76}O_6$: C, 74.95; H, 11.12%.

N-(t-Butoxycarbonyl)-D-glutamic Acid γ-Isopropyl Ester DCHA Salt. Thionyl chloride (2 ml, 27 mmol) was added dropwise to isopropyl alcohol (40 ml) at −10 °C. To this was added D-glutamic acid (3.0 g, 20 mmol), and the mixture was stirred at room temperature for 3 days. After the insolubles were removed by filtration, ether (200 ml) was added to the filtrate to give D-glutamic acid γ-isopropyl ester HCl salt (1.6 g, 35.4%). Without further purification, the salt (1.5 g, 6.64 mmol) was dissolved in water (5 ml) and the resulting solution was combined with DMF solution (5 ml) of *O-t*-butyl *S*-(4,6-dimethyl-2-pyrimidinyl) thiocarbonate (1.91g, 7.97 mmol). Et_3N (1.84 ml) was then added at 4 °C, and the mixture was stirred at room temperature for 20 h, diluted with water (20 ml), and extracted with ether (2×30 ml). The pH of the aqueous layer was adjusted to 2 with 2M HCl under cooling and the mixture was extracted with AcOEt (50 ml). The AcOEt layer was washed with 1M HCl and water succesively, and dried (Na_2SO_4). After the removal of the solvent, the residue (1.90 g) was converted to DCHA salt in ether by adding DCHA (1.3 ml): 2.50 g (80.0%). mp 131 °C. $[\alpha]_D^{23}$ −7.1° (*c* 0.5, DMF).

Found: C, 63.57; H, 10.01; N, 6.08%. Calcd for $C_{25}H_{46}N_2O_6$: C, 63.80; H, 9.85; N, 5.95%.

*N-(t-Butoxycarbonyl)-D-isoglutamine Isopropyl Ester (**10c**).* *N*-(*t*-Butoxycarbonyl)-D-glutamic acid γ-isopropyl ester DCHA salt (704 mg, 1.5 mmol) was converted to free carboxylic acid by the usual method. The resulting oil and *N*-hydroxysuccinimide (207 mg, 1.8 mmol) were dissolved in CH_3CN (10 ml). To this was added DCC (371 mg, 1.8 mmol) at 4 °C, and the mixture was stirred at room temperature for 2 h. After the removal of the precipitates by filtration, 25% aqueous ammonia (0.6 ml) was added under cooling and the mixture was stirred at 4 °C for 30 min. The solvent was evaporated and the resulting crystals were washed with hot water: 375 mg (86.8%). mp 148—150 °C. $[\alpha]_D^{23}$ −3.2° (*c* 0.5, DMF).

Found: C, 54.60; H, 8.75; N, 9.63%. Calcd for $C_{13}H_{24}N_2O_5$: C, 54.15; H, 8.39; N, 9.72%.

*N-(Benzyloxycarbonyl)-D-isoglutamine t-Butyl Ester (**10d**).* This compound was synthesized in a similar manner to that described for 10c: 67.8%. mp 113 °C. $[\alpha]_D^{22}$ −2.5° (*c* 0.5, DMF).

Found: C, 61.13; H, 7.23; N, 8.36%. Calcd for $C_{17}H_{24}N_2O_5$: C, 60.70; H, 7.19; N, 8.33%.

*N-(t-Butoxycarbonyl)-L-valyl-D-isoglutamine (**12**).* *t*-Butoxycarbonyl-L-valyl-D-isoglutamine benzyl ester (**11**)[18] (7.50 g, 17.2 mmol) was hydrogenated in MeOH (150 ml) using palladium black as a catalyst at room temperature for 6 h. After the removal of the catalyst by filtration, the filtrate was concentrated to give the residue which was reprecipitated from AcOEt–petroleum ether: 6.00 g (quantitative). mp 89—90 °C. $[\alpha]_D^{23}$ +5.8° (*c* 0.5, DMF).

Found: C, 51.96; H, 8.10; N, 12.11%. Calcd for $C_{15}H_{27}N_3O_6$: C, 52.16; H, 7.88; N, 12.17%.

*N-(t-Butoxycarbonyl)-L-valyl-D-isoglutamine Isopropyl Ester (**13c**).* Compound **10c** (173 mg, 0.6 mmol) was treated with TFA (2 ml) at room temperature for 20 min. After the removal of TFA, the residual oil was washed with a mixture of ether and petroleum ether (1 : 1, v/v) by decantation. The resulting oil was then dissolved in CH_3CN (5 ml) together with *N*-(*t*-butoxycarbonyl)-L-valine HONB ester (277 mg, 0.6 mmol), Et_3N (0.1 ml) was added, and the mixture was stirred at room temperature for 15 h. After the usual work-up, the product was crystallized from petroleum ether: 185 mg (79.6%). The physicochemical data are given in Table 1.

*N-(Benzyloxycarbonyl)-L-valyl-D-isoglutamine t-Butyl Ester (**13d**).* Compound **10d** (202 mg, 0.6 mmol) was hydrogenated in MeOH (10 ml) with palladium black as a catalyst at room temperature for 3 h. After the removal of the catalyst by filtration, the fltrate was concentrated to dryness. The residue was dissolved in CH_3CN (10 ml) together with *N*-(benzyloxycarbonyl)-L-valine HONB ester (248 mg, 0.6 mmol), and the mixture was stirred at room temperature for 15 h. To this was added 5% citric acid solution, and the resulting crystals were collected by filtration and recrystallized from MeOH–AcOEt–petroleum ether: 178 mg (68.1%). The physicochemical data are given in Table 1.

*N-(t-Butoxycarbonyl)-L-valyl-D-isoglutamine Octadecyl Ester (**13f**).* Compound **12** (1.73 g, 5 mmol) was combined with Et_3N (0.84 ml, 6 mmol) in DMF (5 ml) at 4 °C, and to this was added 6-chloro-1-(*p*-chlorophenylsulfonyloxy) benzotriazole[19] (2.06 g, 6 mmol) with stirring. Soon after, the mixture became clear and stirring was continued at room temperature for 4 h. A solution of 1-octadecanol (4.05 g, 15 mmol) and Et_3N (0.7 ml) in CH_2Cl_2 (30 ml) was then added at 4 °C and the mixture was stirred at room temperature for additional 24 h. After the usual work-up, the residue was recrystallized from AcOEt–petroleum ether: 1.10 g (37.0%).

Compounds **13b** and **e** were prepared similarly from appropriate alcohols and **12**. The yields and physicochemical data are given in Table 1.

*N-(t-Butoxycarbonyl)-O-benzyl-L-seryl-D-isoglutamine Methyl Ester (**13g**).* *N*-(*t*-Butoxycarbonyl)-D-isoglutamine methyl ester[18] (0.65 g, 2.5 mmol) was treated with TFA (5 ml) at room temperature for 20 min. After the removal of TFA, the residue was triturated with ether. The resulting oily D-isoglutamine methyl ester trifluoroacetate was dried over NaOH pellets, dissolved in AcOEt (5 ml), and neutralized with Et_3N (0.35 ml) under cooling. A solution of *N*-(*t*-butoxycarbonyl)-*O*-benzyl-L-serine HONB ester (1.14 g, 2.5 mmol) in AcOEt (5 ml) was then added, and the mixture was stirred at room temperature for 16 h. After the usual work-up, the residue was recrystallized from AcOEt–ether: 776 mg (71.2%).

Compound **13h** was prepared in a similar manner. The yield and physicochemical data are given in Table 1.

*N-Acetyl-1-O-benzyl-4,6-O-benzylidene-α-muramyl-L-valy-D-isoglutamine t-Butyl Ester (**15d**).* Compound **13d** (160

mg; 0.38 mmol) was hydrogenated in MeOH (20 ml) with palladium black as a catalyst at room temperature for 2 h. After the removal of the catalyst by filtration, the filtrate was concentrated to give the residue which was dissolved in CH_3CN (10 ml) together with **14** (240 mg, 0.38 mmol). The mixture was left at room temperature for 15 h, then the resulting crystals were collected and recrystallized from CH_3CN–ether: 216 mg (75.3%). The physicochemical data are given in Table 2.

N-Acetyl-1-O-benzyl-4,6-O-benzylidene-α-muramyl-O-benzyl-L-seryl-D-isoglutamine Methyl Ester (15g). Dipeptide **11h** (0.44 g, 1 mmol) was treated with TFA (6 ml) at room temperature for 20 min. After the removal of TFA, the residue was triturated with a mixture of ether and petroleum ether (1:1, v/v). The resulting powder was filtered, dried over NaOH pellets, and dissolved in THF (4 ml). After neutralization with Et_3N (0.14 ml) under cooling, this was combined with a solution of *N*-acetyl-1-*O*-benzyl-4,6-*O*-benzylidene-α-muramic acid HONB ester (**14**) (0.63 g, 1 mmol) in THF (2 ml). The mixture was then stirred at room temperature for 16 h, and the gel was filtered and washed thoroughly with THF. The solid obtained was reprecipitated from EtOH–DMF: 0.55 g 80.0%.

Compounds **15a—c**, **e**, **f**, and **h** were prepared in a similar manner. The yields and physicochemical data of **15** are given in Table 2.

N-Acetyl-1-O-benzyl-α-muramyl-L-valyl-D-isoglutamine Methyl Ester (16a). *N*-Acetyl-1-*O*-benzyl-4,6-*O*-benzylidene-α-muramyl-L-valyl-D-isoglutamine methyl ester[18] (10.1 g, 14.4 mmol) in 75% acetic acid (200 ml) was heated in a boiling water bath for 20 min. After the removal of the solvent, the residue was flushed with water and then toluene, and reprecipitated from EtOH–ether: 0.84 g (73.0%).

Compound **16b—h** were prepared in a similar manner. The yields and physicochemical data of **16** are given in Table 2.

N-Acetyl-1-O-benzyl-6-O-[10-(5,6-dimethoxy-3-methyl-1,4-benzoquinon-2-yl)decanoyl]-α-muramyl-L-valyl-D-isoglutamine Methyl Ester (17a). *Method A.* Compound **16a** (1.25 g, 2 mmol) in DMF (10 ml) and 10-(5,6-dimethoxy-3-methyl-1,4-benzoquinon-2-yl)decanoic acid (0.85 g, 2.4 mmol) in dry pyridine (4 ml) was combined. To this was added DCC (0.83 g, 4 mmol) under cooling and the mixture was stirred at 4 °C for 6 d. After the usual work-up, the crude material was recrystallized from a mixture of MeOH and ether: 1.47 g (75.8%). *Method B.* Compound **16a** (0.25 g, 0.4 mmol) and 10-(5,6-dimethoxy-3-methyl-1,4-benzoquinon-2-yl)decanoic acid *p*-nitrophenyl ester (0.38 g, 0.8 mmol), HOBt (0.22 g, 1.6 mmol), and NEM (0.21 g, 1.6 mmol) were dissolved in DMF (2 ml) and the mixture was stirred at room temperature for 2 d. After the removal of the solvent, the residue was applied onto a silica-gel column which was eluted with $CHCl_3$–MeOH–AcOH (18:2:1, v/v) as an eluting solvent. The resulting **17a** was further purified by column chromatography of Sephadex LH-20 (1.5×90 cm) with EtOH as an eluent: 0.19 g (49.1%).

Compounds **17b—g**, **i**, and **j** were synthesized in a manner similar to that described in method B. Compounds **17k—m** were synthesized in a manner similar to that described in method A and purified as described in method B. The yields and physicochemical data of **17** are given in Table 3.

N-Acetyl-6-[10-(5,6-dimethoxy-3-methyl-1,4-benzoquinon-2-yl)decanoyl]muramyl-L-valyl-D-isoglutamine Methyl Ester (1a). Compound **17a** (192 mg, 0.2 mmol) was hydrogenated in MeOH (4 ml) with palladium black as a catalyst at room temperature for 4 h and the catalyst was removed. The methanol solution of the resulting hydroquinone was combined with an aqueous solution of $FeCl_3 \cdot 6H_2O$ (1 g), and the mixture was stirred at room temperature for 30 min. To this was added AcOEt (50 ml), and the AcOEt layer was washed with water (15 ml) and dried (Na_2SO_4). After the removal of the solvent, the crystalline residue was purified by column chromatography of Sephadex LH-20 (1.8×44 cm) with a mixture of EtOH and 0.1 M AcOH (3:2, v/v) as an eluent. Recrystallization from EtOH–ether–petroleum ether gave **1a**: 127 mg (73.0%).

Compounds **1b—g** and **i—m** were synthesized in a similar manner. The yields and physicochemical data of **1** are given in Table 4.

N-Acetyl-6-O-[6-(5,6-dimethoxy-3-methyl-1,4-benzoquinon-2-yl)hexanoyl]muramyl-L-valyl-D-isoglutamine Methyl Ester (1h). 6-(5,6-Dimethoxy-3-methyl-1,4-benzoquinon-2-yl)hexanoic acid (**2b**) (35.6 mg, 0.12 mmol) and *N*-acetylmuramyl-L-valyl-D-isoglutamine methyl ester[18] (53.3 mg, 0.1 mmol) were dissolved in a mixture of DMF and pyridine (0.4 ml each). To this was added DCC (41.2 mg, 0.2 mmol), and the solution was stirred at room temperature for 30 h. The precipitate formed was filtered and the filtrate was concentrated to give the residue which was purified by column chromatography on silica gel (15 g) using $CHCl_3$–MeOH–acetone (50:9:6, v/v) as an eluant. Recrystallization from EtOH–ether gave **1h**: 31.5 mg (38.8%). The physicochemical data are given in Tabel 4.

Ethyl 3-Oxotetracosanoate (21).[20] A solution of diethyl malonate (21.7 g, 0.12 mol) in EtOH (13 ml) was slowly added dropwise to a suspension of magnesium (4.1 g, 0.17 mol) in a mixture of EtOH (4 ml) and CCl_4 (0.2 ml), maintaining a vigorous reaction. Ether (50 ml) was then added, and the mixture was refluxed for 3 h. After the removal of the solvent, the residue was flushed with benzene to remove EtOH and the residue was dissolved in ether (60 ml). To this was added over a period of 30 min an ethereal solution (50 ml) of docosanoyl chloride (0.15 mol), and the mixture was stirred at 50 °C for 2 h and at room temperature for 15 h. After 1M H_2SO_4 (300 ml) was added carefully, the mixture was extracted with ether (300 ml). The organic layer was washed with water, dried (Na_2SO_4), and concentrated to give 2-ethoxycarbonyl-3-oxotetracosanoic acid ethyl ester (75.4 g, 93.5%). This was dissolved in DMSO (50 ml) containing *p*-toluenesulfonic acid (2.1 g) and the mixture was heated at 200—210 °C in an oil bath for 20 min. After the evolution of CO_2 gas had ceased, the mixture was allowed to cool to room temperature, diluted with water (500 ml), and extracted with ether (500 ml). The extract was washed with water, dried (Na_2SO_4), and concentrated to give the residue, which was purified by column chromatography on silica gel (700 g) using hexane–diisopropyl ether (9:1, v/v) as an eluting solvent: 27.9 g (45.2%).

Found: C, 76.31; H, 12.23%. Calcd for $C_{26}H_{50}O_3$: C, 76.04; H, 12.27%.

10-(5,6-Dimethoxy-3-methyl-1,4-benzoquinon-2-yl)decyl Acetate (18). A solution of 10-(5,6-dimethoxy-3-methyl-1,4-benzoquinon-2-yl)-1-decanol[14] (50.4 g, 0.15 mol) and pyridine (48.6 ml, 0.6 mol) in CH_2Cl_2 (250 ml) was combined with acetic anhydride (42.6 ml, 0.45 mol) at 4 °C, and the mixture was stirred at room temperature for 15 h. Water (50 ml) was then added and the mixture was stirred at room temperature for 30 min. After the removal of the solvent, AcOEt (300 ml), $NaHCO_3$ (60 g) and water (200 ml) were added to the residue, and the mixture was stirred at room temperature for additional 1 h. The organic layer was washed succesively with 1M HCl and water, and dried (Na_2SO_4). After the removal of the solvent, the residue was triturated with petroleum ether to give **18** as a crystal: 51.5 g (90.7%). mp 39—40 °C.

Found: C, 66.35; H, 8.53%. Calcd for $C_{21}H_{32}O_6$: C, 66.30; H, 8.48%.

10-(3,4-Dimethoxy-2,5-dimethoxymethyloxy-6-methylphenyl)-1-decanol (19). Compound **18** (30.3 g, 80 mmol) was

hydrogenated in DMF (300 ml) with 5% palladium on carbon as a catalyst at room temperature for 2 h and the catalyst was removed by filtration. To the filtrate was added NaH (7.04 g, 0.18 mol) under nitrogen. After being stirred for 30 min, the mixture was combined with methoxymethyl chloride (13.4 ml, 0.18 mol) at 4 °C, and the stirring was continued at room temperature for additional 15 h. The reaction mixture was then diluted with water (2 l) and extracted with ether (500 ml). The extract was concentrated to give an oil (40 g) which was dissolved in EtOH (200 ml) and treated with 4M NaOH (60 ml). The mixture was stirred at room temperature for 15 h, diluted with water (1 l), and extracted with ether (300 ml). The extract was washed with water, dried (Na_2SO_4), and concentrated to give a residue which was purified by column chromatography on silica gel (300 g) with $CHCl_3$–MeOH (50:1, v/v) as an eluting solvent: 27.4 g (80.3%).

Found: C, 63.24; H, 9.35%. Calcd for $C_{23}H_{40}O_7 \cdot 1/2H_2O$: C, 63.13; H, 9.45%.

*10-(3,4-Dimethoxy-2,5-dimethoxymethyloxy-6-methylphenyl)-decanal (**20**).* A solution of pyridine-sulfur trioxide complex (30.7 g, 0.19 mol) in DMSO (120 ml) was added dropwise to a solution of **19** (27.4 g, 64.2 mmol) and Et_3N (44.9 ml, 0.32 mol) in DMSO (60 ml) over a period of 1 h, and the mixture was stirred at room temperature for 1 h. The mixture was poured into ice-cold water (500 ml) and extracted with ether (500 ml). The extract was washed with water, dried (Na_2SO_4), and concentrated to give a residue which was purified by column chromatography on silica gel (300 g) with $CHCl_3$: 22.1 g (81.1%).

Found: C, 64.29; H, 9.07%. Calcd for $C_{23}H_{38}O_7$: C, 64.76; H, 8.98%.

*2-[10-[3,4-Dimethoxy-2,5-bis(dimethoxymethoxy)-6-methylphenyl]decylidene]-3-oxotetracosanoic Acid Ethyl Ester (**22**).* A solution of **21** (14.4 g, 35 mmol) and **20** (14.9 g, 35 mmol) in anhydrous benzene (40 ml) was combined with AcOH (0.35 ml) and piperidine (0.18 ml), and the mixture was heated under reflux to remove the water formed azeotropically. After the removal of the solvent, the residue was purified by column chromatography on silica gel (450 g) with $CHCl_3$–MeOH (9:1, v/v): 18.8 g (65.6%). ^1H NMR ($CDCl_3$): δ=0.88 (3H, t), 1.10—1.72 (57H, b), 2.20 (3H, s), 2.34—2.81 (4H, m), 3.59 (6H, s), 4.20 (2H, q), 5.03 (4H, s), 5.33—5.71 and 6.60—7.00 (1H, m).

Found: C, 71.18; H, 10.53%. Calcd for $C_{49}H_{89}O_9 \cdot 1/2H_2O$: C, 71.06; H, 10.46%.

*2-[10-[3,4-Dimethoxy-2,5-bis(dimethoxymethoxy)-6-methylphenyl]decyl]-3-hydroxytetracosanoic Acid Ethyl Ester (**23**).* Compound **22** (18.4 g, 22.5 mmol) was hydrogenated in a mixture of dioxane (200 ml) and EtOH (150 ml) with palladium black as a catalyst at room temperature for 8 h. The catalyst was removed by filtration and the filtrate was concentrated. The resulting residue was dissolved in a mixture of dioxane (120 ml) and MeOH (40 ml), and to this was added $NaBH_4$ (851 mg, 22.5 mmol) with stirring. After 30 min, the pH of the mixture was adjusted to 3 with 5% citric acid. The mixture was then diluted with water (200 ml) and extracted with AcOEt (200 ml). The extract was washed with water, dried (Na_2SO_4), and concentrated to give a crystalline residue which was recrystallized from MeOH: 16.9 g (91.2%). mp 42—44 °C.

Found: C, 71.75; H, 11.30%. Calcd for $C_{49}H_{90}O_9$: C, 71.48; H, 11.02%.

*2-[10-[3,4-Dimethoxy-2,5-bis(dimethoxymethoxy)-6-methylphenyl]decyl]-3-hydroxytetracosanoic Acid (**24**).* A solution of **23** (16.5 g, 20 mmol) in a mixture of EtOH (70 ml) and dioxane (50 ml) was combined with 3M NaOH (30 ml), and the mixture was heated under reflux for 2 h. After the solution was cooled to room temperature, the pH was adjusted to 3 with 10% citric acid. The mixture was diluted with water (300 ml) and extracted with AcOEt (150 ml). The extract was washed with water, dried (Na_2SO_4), and concentrated to give a residue which was purified by column chromatography on silica gel (200 g) with $CHCl_3$–MeOH (50:1, v/v): 14.3 g (89.9%). mp 60 °C. ^1H NMR ($CDCl_3$): δ=0.87 (3H, t), 1.07—1.80 (58H, broad s), 2.20 (3H, s), 2.34—2.82 (3H, m), 3.28—3.50 (1H, m), 3.59 (6H, s), and 5.00 (4H, s).

Found: C, 70.86; H, 11.01%. Calcd for $C_{47}H_{86}O_9$: C, 70.99; H, 10.90%.

*2-[10-(5,6-Dimethoxy-3-methyl-1,4-benzoquinon-2-yl)decyl]-3-hydroxytetracosanoic Acid (**25**).* A solution of **24** (1.59 g, 2 mmol) in hot AcOH (20 ml) was combined with 2M H_2SO_4 (2 ml), and the mixture was stirred at 100 °C for 10 min. After the removal of the solvent, the residue was dissolved in AcOEt (50 ml) and the solution was washed with water. The solvent was evaporated and the residue was dissolved in dioxane (30 ml). To this was added a solution of $FeCl_3 \cdot 6H_2O$ (2.70 g, 10 mmol) in water, and the mixture was stirred at room temperature for 1 h, diluted with water (100 ml), and extracted with AcOEt (50 ml). The extract was washed with water, dried (Na_2SO_4), and concentrated to give a residue which was crystallized from MeOH: 1.03 g (73.1%). mp 72—73 °C ^1H NMR ($CDCl_3$): δ=0.89 (3H, t), 1.10—1.67 (58H, broad s), 2.00 (3H, s), 2.30—2.61 (3H, m), 3.73—3.93 (1H, m), and 3.98 (6H, s).

Found: C, 73.01; H, 10.87%. Calcd for $C_{43}H_{76}O_7$: C, 73.25; H, 10.87%.

*N-Acetyl-1-O-benzyl-6-O-[2-[10-[3,4-dimethoxy-2,5-bis(dimethoxymethoxy)-6-methylphenyl]decyl]-3-hydroxytetracosanoyl]-α-muramic Acid Diphenylmethyl Ester (**28**).* A solution of **24** (3.18 g, 4 mmol) in $CHCl_3$ (30 ml) was made basic to phenolphthalein with a solution of 0.5 M KOH in MeOH (8.1 ml) and then the solvent was removed to give a waxy potassium salt **26**. This salt (833 mg, 1 mmol) was dissolved, together with *N*-acetyl-1-*O*-benzyl-6-*O*-(*p*-tolyluenesulfonyl)-α-muramic acid diphenylmethyl ester (**27**)[7] (703 mg, 1 mmol) and 18-crown-6 (60 mg, 0.23 mmol), in anhydrous toluene (40 ml). After being stirred at 80 °C for 4 h, the mixture was concentrated to give a residue which was purified by column chromatography on silica gel (30 g) with $CHCl_3$–MeOH (99:1, v/v): 1.05 g (79.1%).

Found: C, 69.47; H, 9.03; N, 1.10%. Calcd for $C_{78}H_{119}NO_{16} \cdot H_2O$: C, 69.66; H, 9.07; N, 1.04%.

*N-Acetyl-6-O-[2-[10-(5,6-dimethoxy-3-methyl-1,4-benzoquinon-2-yl)decyl]-3-hydroxytetracosanoyl]muramyl-L-valyl-D-isoglutamine Methyl Ester (**1k**).* A solution of **28** (1.0 g, 0.75 mmo) and anisole (1.1 ml) in CH_2Cl_2 (10 ml) was combined with TFA (10 ml) at 4 °C with stirring and the stirring was continued for additional 1 h. After the removal of the solvent, the residue was dissolved in ether (30 ml) and the solution was washed with water, dried (Na_2SO_4), and concentrated. The residue was purified by column chromatography on silica gel (20 g) with $CHCl_3$–acetone–MeOH (10:3:2, v/v) as an eluting solvent to give *N*-acetyl-1-*O*-benzyl-6-*O*-[2-[10-(2,5-dihydroxy-3,4-dimethoxy-6-methylphenyl)decyl-3-hydroxytetracosanoyl]-α-muramic acid (500 mg, 62.2%). This acid (214 mg, 0.2 mmol) was dissolved in THF (3 ml) together with L-valyl-D-isoglutamine methyl ester hydrochloride (65 mg, 0.27 mmol), Et_3N (38 μl, 0.27 mmol), and HONB (54 mg, 0.3 mmol). To this was added DCC under cooling, and the mixture was stirred at room temperature for 15 h. After the removal of the precipitate by filtration, the filtrate was concentrated and the residue was dissolved in AcOEt (30 ml). The solution was washed successively with 5% citric acid and water, dried (Na_2SO_4), and concentrated to give a residue which was purified by column chromatography on silica gel (5 g) with $CHCl_3$–MeOH (97:3, v/v) as an eluant. The resulting crystalline

protected glycopeptide **29a** (106 mg) was hydrogenated in a mixture of THF (2 ml) and AcOH (1 ml) with palladium black as a catalyst at room temperature for 3 h and the free glycopeptide obtained was dissolved in dioxane (10 ml). To this was added a solution of $FeCl_3 \cdot 6H_2O$ (270 mg, 1 mmol) in a small amount of water, and the mixture was stirred at room temperature for 3 min to oxidize the hydroquinone ring. After the removal of the solvent, the residue was dissolved in AcOEt (20 ml). The solution was washed with water, dried (Na_2SO_4), and concentrated to give a residue which was lyophilized from *t*-BuOH: 88 mg (33.0%). The physicochemical data are given in Table 4.

N-Acetyl-6-O-[2-[10(5,6-dimethoxy-3-methyl-1,4-benzoquinon-2-yl)decyl]-3-hydroxytetracosanoyl]muramyl-L-alanyl-D-isoglutamine (11) was synthesized in a manner similar to that of **1k**. The yield and physicochemical data are given in Table 4.

N-Acetyl-1-O-benzyl-6-O-(benzyloxycarbonyl-L-leucyl)-α-muramyl-L-valyl-D-isoglutamine Methyl Ester (30b). A mixture of **16a** (31.2 g, 5 mmol), benzyloxycarbonyl-L-leucine *p*-nitrophenyl ester (3.86 g, 10 mmol), HOBt (2.70 g, 20 mmol) and NEM (2.56 ml, 20 mmol) in DMF (50 ml) was stirred at room temperature for 60 h. After the removal of the solvent, the residue was purified by column chromatography of silica gel with $CHCl_3$–MeOH (19:1, v/v) as an eluent. Reprecipitation from MeOH–ether gave **30b**: 3.1 g (71.7%).

Compounds **30a**, **c**, and **d** were synthesized in a similar manner. The yields and physicochemical data are given in Table 5.

N-Acetyl-6-O-(L-leucyl)muramyl-L-valy-D-isoglutamine Methyl Ester (31b). Compound **30b** (0.3 g, 0.35 mmol) was hydrogenated in AcOH (10 ml) with palladium black as a catalyst at room temperature for 4 h, and the catalyst was removed by filtration. After the removal of the solvent, the residue was reprecipitated from a mixture of MeOH and ether: 0.19 g (82.6%).

Compounds **31a**, **c**, and **d** were synthesized in a similar manner. The yields and physicochemical data are given in Table 5.

N-Acetyl-6-O-[10-(5,6-dimethoxy-3-methyl-1,4-benzoquinon-2-yl)decanoyl-L-leucyl]muramyl-L-valyl-D-isoglutamine Methyl Ester (33b). *Method A.* A mixture of **31b** (51.8 mg, 0.08 mmol), 10-(5,6-dimethoxy-3-methyl-1,4-benzoquinon-2-yl)decanoic acid *p*-nitrophenyl ester (41.7 mg, 0.088 mmol), and NEM (0.012 ml, 0.09 mmol) in DMF (0.5 ml) was stirred at room temperature for 60 h. After the removal of the solvent, the residue was applied onto a silica-gel column (2× 12 cm) which was eluted with AcOEt–pyridine–H_2O–AcOH (130:10:5:3, v/v). The resulting crude **33b** was further purified by column chromatography of Sephdex LH-20 (1.5×90 cm) with EtOH–0.1 M AcOH (3:2, v/v) as an eluent and lyophilized from *t*-BuOH: 32 mg (40.7%). *Method B.* *N*-Acetyl-6-*O*-[10-(5,6-dimethoxy-3-methyl-1,4-benzoquinon-2-yl)decanoyl-L-leucyl]muramyl-L-valyl-D-isoglutamine[29] (32b, 20 mg) was dissolved in MeOH (0.3 ml). To this was added excess ethereal diazomethane solution dropwise under cooling and the mixture was stirred at 4 °C for 30 min. After the removal of the solvent, the residue was purified as described in method A: 13.8 mg (67.0%).

Compounds **33a**, **c**, and **d** were synthesized in a similar manner as described in method A, and compounds **33a** and **e** in method B. The yields and physicochemical data of **33** are given in Table 5.

We wish to thank Professor T. Shiba of Osaka University for discussions and Dr. J. Miller for reviewing the manuscript.

References

1) Part of this work was presented at the International Symposium on Immunomodulation by Microbial Products and Related Synthetic Compounds, Osaka, July 27—29, 1981: Proceedings, ed by Y. Yamamura, S. Kotani, I. Azuma, A. Koda, and T. Shiba, Excerpta Medica, Amsterdam (1982), pp. 159. Abbreviation used are those recommended by the IUPAC-IUB Commission on Biochemistry Nomenclature: *J. Biol. Chem.*, **247**, 977 (1972). Other abbreviations used are Ahx, 6-aminohexanoyl; Aud 11-aminoundecanoyl; HONB, *N*-hydroxy-5-norbornene-2,3-dicarboximide; HOBt, 1-hydroxybenzotriazole; DCC, dicyclohexylcarbodiimide; NEM, *N*-ethylmorpholine; DCHA, dicyclohexylamine; TFA, trifluoroacetic acid; *i*-Pr, isopropyl; *t*-Bu, *t*-butyl; *n*-Hex, hexyl; St. stearyl (octadecyl).

2) Review: R. W. Baldwin and M. V. Pimm, *Adv. Cancer Res.*, **28**, 91 (1978).

3) Y. Yamamura, T. Ogura, F. Hirao, K. Yasumoto, K. Sawamura, S. Hattori, Y. Hayata, S. Kishimoto, K. Yamada, H. Niitani, and T. Masaoka, *Cancer Treat. Rep.*, **65**, 707 (1981).

4) I. Kawase, M. Uemiya, T. Yoshimoto, T. Ogura, F. Hirao, and Y. Yamamura, *Cancer Res.*, **41**, 660 (1981).

5) F. Ellouz, A. Adam, R. Ciorbaru, and E. Lederer, *Biochem. Biophys. Res. Commun.*, **59**, 1317 (1974); S. Kotani, Y. Watanabe, F. Kinoshita, T. Shimono, I. Morisaki, T. Shiba, S. Kusumoto, Y. Tarumi, and K. Ikehana, *Biken J.*, **18**, 105 (1975); Review: P. Dukor, L. Tarcsay, and G. Baschang, *Ann. Rep. Med. Chem.*, **14**, 146 (1979); E. Lederer, *J. Med. Chem.*, **23**, 819 (1980).

6) C. A. McLaughlin, S. T. Schwartzman, B. L. Horner, G. H. Jones, J. G. Moffatt, J. J. Nestor, Jr., and D. Tegg, *Sciences*, **208**, 415 (1980).

7) Y. Yamamura, I. Azuma, K. Sugimura, M. Yamawaki, M. Uemiya, S. Kusumoto, S. Okada, and T. Shiba, *Proc. Jpn. Acad.*, **53**, 63 (1977); T. Shiba, S. Okada, S. Kusumoto, I. Azuma, and Y. Yamamura, *Bull. Chem. Soc. Jpn.*, **51**, 3307 (1978).

8) S. Kusumoto, M. Inage, T. Shiba, I. Azuma, and Y. Yamamura, *Tetrahedron Lett.*, **1978**, 4899.

9) T. Fukuda, S. Kobayashi, H. Yukimasa, I. Imada, M. Fujino, I. Azuma, and Y. Yamamura, *Chem. Pharm. Bull.*, **29**, 2215 (1981).

10) T. Fukuda, S. Kobayashi, H. Yukimasa, S. Terao, M. Fujino, T. Shiba, I. Saiki, I. Azuma, and Y. Yamamura, *Bull. Chem. Soc. Jpn.*, **54**, 3530 (1980).

11) S. Kobayashi, T. Fukuda, H. Yukimasa, I. Imada, M. Fujino, I. Azuma, and Y. Yamamura, *Bull. Chem. Soc. Jpn.*, **53**, 2917 (1980).

12) a) S. Kobayashi, T. Fukuda, I. Imada, M. Fujino, I. Azuma, and Y. Yamamura, *Chem. Pharm. Bull.*, **27**, 3139 (1979); b) I. Saiki, Y. Tanio, M. Yamawaki, M. Uemiya, S. Kobayashi, T. Fukuda, H. Yukimasa, and I. Azuma, *Infect. Immun.*, **31**, 114 (1981).

13) QS-n is an ω-(5,6-dimethoxy-3-methyl-1,4-benzoquinon-2-yl)alkanoic acid having a set of unbranched methylene groups of n number in the side chain: K. Okamoto, M. Kawada, M. Watanabe, S. Kobayashi, I. Imada, and H. Morimoto, *Biochem. Biophys. Acta*, **682**, 145 (1982).

14) K. Okamoto, M. Watanabe, M. Kawada, G. Goto, Y. Ashida, K. Oda, A. Yajima, I. Imada, and H. Morimoto, *Chem. Pharm. Bull.*, **30**, 2729 (1982).

15) S. Hünig, E. Lücke, and W. Brenninger, *Org. Synth.*, **41**, 65 (1961).

16) R. O. Hutchins, C. A. Milewski, and B. E. Maryanoff, *J. Am. Chem. Soc.*, **95**, 3662 (1973).

17) C. R. H. I. De Jonge, H. J. Hageman, G. Hoentjen, and W. J. Mijs, *Org. Synth.*, **57**, 78 (1977).

18) S. Kobayashi, T. Fukuda, H. Yukimasa, M. Fujino, I. Azuma, and Y. Yamamura, *Bull. Chem. Soc. Jpn.*, **53**, 2570 (1980).
19) M. Itoh, D. Hagiwara, and J. Notani, *Synthesis*, **1975**, 456.
20) Compound **21** was synthesized in a similar manner to that reported by B. Riegel and W. M. Lilienfeld: *J. Am. Chem. Soc.*, **67**, 1273 (1945).
21) M. Fujino, S. Kobayashi, M. Obayashi, T. Fukuda, S. Shinagawa, and O. Nishimura, *Chem. Pharm. Bull.*, **22**, 1857 (1974).
22) M. Tabachnick and H. Sobotka, *J. Biol. Chem.*, **234**, 1726 (1959).
23) I. Azuma, *Vitamins (Japan)*, **52**, 503 (1978).
24) I. Imada, M. Watanabe, and H. Morimoto, *Vitamins (Japan)*, **52**, 493 (1978).
25) S. Kusumoto, S. Okada, K. Yamamoto, and T. Shiba, *Bull. Chem. Soc. Jpn.*, **51**. 2122 (1978).
26) I. Azuma, K. Sugimura, M. Yamawaki, M. Uemiya, S. Kusumoto, S. Okada, T. Shiba, and Y. Yamamura, *Infect. Immun.*, **20**, 600 (1978).
27) Y. Tanio, H. Souma, Y. Tokushima, Y. Yamamura, and I. Azuma, *Gann*, **74**, 192 (1983).
28) $Bp_{0.1}$ 125 °C: compound **5b** was prepared in a similar manner to that of 1-morpholinocyclohexene (**5a**) described in Ref. 15.
29) Compound **32b** was prepared as reported for the synthesis of *N*-acetyl-6-*O*-[10-(5,6-dimethoxy-3-methyl-1,4-benzoquinon-2-yl)decanoyl-L-leucyl]muramyl-L-seryl-D-isoglutamine in Ref. 11.

 © 1984 The Chemical Society of Japan Bull. Chem. Soc. Jpn., 57, 3197—3202 (1984)

Structure-taste Relationships of Aspartyl Tripeptide Esters

Yasuo Ariyoshi

Central Research Laboratories, Ajinomoto Co., Inc., Suzuki-cho, Kawasaki-ku, Kawasaki 210

(Received May 18, 1984)

A series of twenty four analogues of L-α-Asp-Gly-Gly-OMe has been synthesized in relation to structural features of sweet peptides. The rule in the structure-taste relationships of dipeptides is held in the sweet aspartyl tripeptide esters. In order for the aspartyl tripeptide esters to be sweet, the second amino acid must have a D-configuration and a small, compact alkyl group (Me, Et, or *i*-Pr) at R^2. An L-configuration of the third amino acid is required for a potent sweet taste. It has been concluded that the small alkyl group at R^2 participates in binding with the receptor through a hydrophobic interaction and increases the sweetness potency.

A wide variety of structural features have been known in sweet-tasting compounds. Attempts to elucidate the structural features necessary to elicit a sweet taste have been made, and several molecular theories have been proposed to relate the various structural features[1].

Since the discovery[2] of a sweet taste in L-α-Asp-L-Phe-OMe, a large number of analogues have been synthesized in an attempt to elucidate structure-taste relationships, and to obtain more potent and stable sweet peptides. It has been demonstrated that the L-Asp moiety in the original L-α-Asp-L-Phe-OMe molecule is restricted to L-aspartic acid[2] or aminomalonic acid[3] but that considerable modification can be made to the L-Phe-OMe moiety. The L-Phe-OMe has been successfully replaced by alkyl- and arylamines,[4] D-and L-amino acid esters,[2,5] D-amino acid alkylamides,[6] D-amino acid derivatives,[7] and aminomalonic acid diesters.[8] The importance of the peptide bond has also been demonstrated, since any modification in its structure results in a complete loss of sweetness.[9]

The sweetness potency in L-α-aspartyl dipeptide analogues has been quantitatively analyzed in relation to structural, electronic, and hydrophobic parameters.[10] A possible sweet conformation of L-α-Asp-L-Phe-OMe has also been determined by an NMR study, a potential energy calculation,[11] and an examination of L-α-Asp-Δ^z-Phe-OMe.[12]

In a previous paper,[13] the tastes of aspartyl dipeptides were relationalized through Fischer projection formulas. In this paper, these formulas have been translated into the structure shown in Fig. 1.

The structural features of sweet aspartyl dipeptide esters have been successfully explained on the basis of the general structure (Ia),[13a] in which the carboxyl and amino groups serve as a proton acceptor and a proton donor, respectively, in the hydrogen bonding with the receptor. The small hydrophobic side chain (S) is considered to participate in the hydrophobic interaction

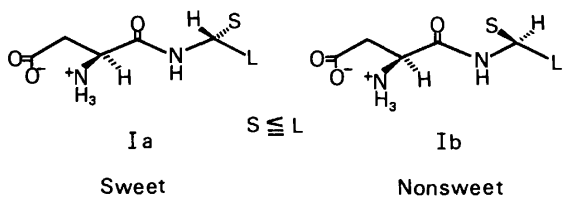

Fig. 1. General structure for sweet aspartyl dipeptide esters: S=small hydrophobic group (1—4 atoms); L=larger hydrophobic group (3—6 atoms).[13a]

with the receptor and to increase the sweetness potency. The larger hydrophobic group (L) seems to be associated with the conformation and hydrophilic-hydrophobic balance of the whole molecule. The hydrophilic-hydrophobic balance in a molecule is another important factor. Space-filling properties are also important, since the receptor site seems to be in the shape of a deep narrow cleft,[11] a pocket,[13b] or a hydrophobic tube[14] with the binding sites inside it.

In an attempt to extend the general structure (Ia) for sweet dipeptides to tripeptides, several aspartyl tripeptides have been synthesized and tested.[13b] The sweetness potencies were weak, 1—3 times sweeter than sucrose.

In order to confirm our previous conclusion on the roles of the S and L groups in the structure (Ia) and to extend the general structure (Ia) to tripeptides, various aspartyl tripeptide esters were synthesized, and several intensely-sweet tripeptides were obtained after an examination of the sweet structure (Ia) and a consideration of the hydrophilic-hydrophobic balance in a sweet molecule.

Synthesis

The protected dipeptides in Table 1 were prepared by the dicyclohexylcarbodiimide (DCC) method.[15] When the dipeptides (**1**, **3**, **5**) were obtained as oily residues, a *t*-butoxycarbonyl (Boc) group of these peptides was deprotected with hydrogen chloride in methanol and the resulting hydrochlorides (**2**, **4**, **6**) were crystallized. Compound **7** was left over from a previous experiment. The Boc group of the protected dipeptides in Table 1 was removed with *p*-toluenesulfonic acid monohydrate[16] in methanol, and the resulting dipeptide ester *p*-toluenesulfonates were used for the next step without further purification. The protected tripeptides in Table 2 were prepared by condensation of β-benzyl *N*-benzyloxycarbonyl-L-aspartate with the appropriate dipeptide ester using DCC. Compounds **42**—**44**, **47**—**49**, and **51** were prepared by the active ester method,[17] in which *N*-benzyloxycarbonyl-L-aspartic acid β-benzyl α-succinimido ester was coupled with the appropriate dipeptide ester. The desired tripeptide esters in Table 3 were obtained by deprotection of the benzyloxycarbonyl and benzyl groups from the protected tripeptides in Table 2 by hydrogenation over Pd/C.

Results and Discussion

In order to evaluate contributions of the side chains

Table 1. Protected dipeptides

No.	Compound[a]	Yield %	Mp θ/°C	Crystn solvent[b]	Appearance[c]	$[\alpha]_D$ Degree[d]	Temp °C
1	Boc-Gly-L-Ala-OMe[e]	89.7	Oil				
2	HCl·H-Gly-L-Ala-OMe[f]	86.4	158.5—159.5	M—E	P	−49.8	23
3	Boc-Gly-D-Ala-OMe[e]	67.3	Oil				
4	HCl·H-Gly-D-Ala-OMe	93.8	158.5—159.5	M—E	P	+50.4	23
5	Boc-Gly-L-Val-OMe[e]	97.8	Oil				
6	HCl·H-Gly-L-Val-OMe	75.5	139.5—140.5	M—E	N	−18.8	22
7	HCl·H-Gly-L-Leu-OMe	—	163—165	M—E	P	−32.0	23
8	Boc-D-Ala-L-Ala-OMe	75.4	65.5—66.5	EA—H	N	−3.2	25
9	Boc-D-Ala-D-Ala-OMe	80.9	109—110	EA—H	N	+60.8	25
10	Boc-D-Ala-L-Ala-OEt	68.4	81—82	H	Pr	−1.8	23
11	Boc-D-Ala-L-Val-OMe	61.1	101.5—102.5	EA—H	P	+15.5	25
12	Boc-D-Ala-L-Leu-OMe	66.4	82—83.5	EA—H	N	−2.2	25
13	Boc-D-Ala-L-Phe-OMe	73.8	97.5—98.5	EA—H	N	+24.9	25
14	Boc-D-Val-L-Ala-OMe	72.9	98—99	EA—H	N	−8.1	25
15	Boc-D-Val-D-Ala-OMe	65.3	141—142	EA—H	N	+52.3	25
16	Boc-D-Val-L-Val-OMe	77.3	109—110	EA—H	N	+3.6	25
17	Boc-D-Val-L-Leu-OMe	60.9	87—88	H	Pr	−7.7	16
18	Boc-D-Val-L-Phe-OMe	72.3	105.5—106.5	EA—H	N	+4.5	23
19	Boc-D-Leu-L-Ala-OMe[g]	66.1	85—86	H	Pr	+3.0	21
20	Boc-L-Ala-Gly-OMe[e]	79.8	Oil				
21	Boc-L-Ala-L-Ala-OMe[h]	77.0	109—110	EA—H	N	−61.2	25
22	Boc-L-Abu-L-Val-OMe	75.0	110—111	EA—H	N	−44.5	23
23	Boc-L-Ala-L-Val-OMe[i]	67.5	65—66	EA—H	N	−50.0	30
24	Boc-L-Val-L-Ala-OMe[j]	62.8	141—142	EA—H	N	−53.2	27
25	Boc-L-Val-D-Ala-OMe[k]	57.4	97—98	EA—H	N	+8.7	21
26	Boc-L-Val-L-Val-OMe[l]	64.2	167—168	EA—H	N	−44.2	29
27	Boc-L-Val-L-Leu-OMe[m]	67.1	133—134	EA—H	Pr	−51.9	21

a) Abbreviations follow the recommendations of the IUPAC-IUB Commision on Biochemical Nomenclature in *J. Biol. Chem.*, **247**, 977 (1972). All compounds were analyzed for C, H, and N (Compounds **2**, **4**, **6**, and **7** were analyzed for C, H, N, and Cl), and results were within ±0.3% of the theoretical values. Complete analytical data for all compounds have been deposited at the office of the Chemical Society of Japan (Document No. 8447). b) Crystallization solvent: M, Methanol; E, Ether; EA, Ethyl Acetate; H, Hexane. c) Appearance: P, plates; N, needles; Pr, Prisms. d) In methanol, $c=1.0\%$. e) Not analyzed. f) G. Weitzel, F.-U. Bauer, and K. Eisele, Hoppe-Seyler's *Z. Physiol. Chem.*, **357**, 187 (1976); mp 161—162 °C; $[\alpha]_{578}^{20}$ −30.0° (*c* 1, DMF). g) E. N. Shepel, S. Iordanov, I. D. Ryabova, A. I. Miroshnikov, V. T. Ivanov, and Y. Ovachinnikov, *Bioorg. Khim.*, **2**, 581 (1976); $[\alpha]_D$ +3.1° (*c* 0.13, MeOH). h) H. Kinoshita, K. Inomata, O. Miyano, and H. Kotake, *Bull. Chem. Soc. Jpn.*, **52**, 2619 (1979); mp 105—106 °C; $[\alpha]_D$ −63.6° (*c* 0.66, MeOH). i) See reference h); mp 63—64 °C; $[\alpha]_D$ −49.5° (*c* 0.31, MeOH). j) P. G. Katsoyannis, Y. Okada, and C. Zault, *Biochemistry*, **12**, 2516 (1973); mp 141—142 °C; $[\alpha]_D^{26}$ −52.9° (*c* 1, MeOH). k) D. E. Nitecki, B. Halpern, and J. Westley, *J. Org. Chem.*, **33**, 864 (1968); mp 91—92 °C; $[\alpha]_D^{25}$ +8.0° (*c* 1, MeOH). l) D. J. Shafer, *J. Chem. Soc., Perkin Trans. 1*, **1972**, 1452; mp 167—168 °C. m) See reference k); mp 126—128 °C, $[\alpha]_D$ −54.2 (*c* 1, MeOH).

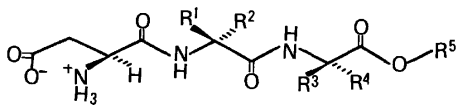

II

Fig. 2. L-α-Aspartyl tripeptide esters.

of each amino acid, the substituents R^1—R^5 of II were systematically modified. The results are summarized in Table 4. In the relationships between the sweet dipeptides (Ia) and tripeptides (II), S (a small hydrophobic group) of Ia corresponds to R^2 (a small alkyl group) of II, and L (a larger hydrophobic group) corresponds to $-CONHCR^3(R^4)COOR^5$. In systematic structural variation of the tripeptides (II), it was assumed that R^2 (a small alkyl group) in II was one of the groups responsible for sweetness, through a hydrophobic interaction with the receptor.

As reported previously,[13b] L-α-Asp-Gly-Gly-OMe (**76**), which is tasteless (Table 4), was selected as a standard of tripeptides because it has the simplest structure and a correlation with other tripeptides is easy.

As the first step, the contribution of the third amino acid to sweetness was evaluated. The introduction of a methyl group at R^4 of **76** gave a weakly sweet peptide (**52**). When the methyl group of **52** was introduced on the opposite side (R^3), the resulting peptide (**53**) was also weakly sweet. Replacement of the methyl group in

Table 2. Protected tripeptides, Z-L-Asp(OBzl)-X

No.	Compound[a] X	Yield %	TLC R_f[b]	Mp θ_m/°C	Crystn Solvent[c]	Appearance[d]	$[\alpha]_D$ Degree[e]	Temp °C
28	Gly-L-Ala-OMe[f]	89.3		Oil				
29	Gly-D-Ala-OMe[f]	89.3		Oil				
30	Gly-L-Val-OMe[f]	75.0		Oil				
31	Gly-L-Leu-OMe[f]	99.7		Oil				
32	D-Ala-L-Ala-OMe	68.6	0.81	145—146	EA—H	N	+3.3	22
33	D-Ala-D-Ala-OMe	52.6	0.73	141—142	EA—H	N	+27.7	22
34	D-Ala-L-Ala-OEt	58.6	0.80	139—140	EA	N	+4.2	22
35	D-Ala-L-Val-OMe	60.7	0.80	112—113	EA—H	N	+7.0	23
36	D-Ala-L-Leu-OMe	75.3	0.89	87—89	EA—H	N	−0.8	25
37	D-Ala-L-Phe-OMe	70.3	0.85	108—110	EA—H	A	+16.7	19
38	D-Val-L-Ala-OMe	67.0	0.86	168.5—169.5	EA	N	+4.7	22
39	D-Val-D-Ala-OMe	65.6	0.85	190—191	EA	N	+32.2	22
40	D-Val-L-Val-OMe	57.9	0.91	145—146 (125—126)[g]	EA—H	N	+11.2	19
41	D-Val-L-Leu-OMe	54.4	0.90	161.5—162.5	EA—H	N	+2.2	16
42	D-Val-L-Phe-OMe	67.8	0.90	203—205	D—EA	A	−28.8[h]	25
43	D-Leu-L-Ala-OMe	71.3	0.86	123—124	EA—H	N	+7.1	18
44	L-Ala-Gly-OMe	68.3	0.90	113.5—114.5	EA—H	N	−16.1	20
45	L-Ala-L-Ala-OMe	70.6	0.76	144—145 (114—115)[g]	EA—H	A	−26.0	19
46	L-Ala-L-Val-OMe	55.4	0.88	145—146	EA	N	−18.5	30
47	L-Abu-L-Val-OMe	71.3	0.89	149—150	EA	A	−17.7	18
48	L-Val-L-Ala-OMe	75.2	0.90	202—203	EA	N	−33.1	27
49	L-Val-D-Ala-OMe	89.0	0.95	164—165	EA	A	−10.0	18
50	L-Val-L-Val-OMe	63.9	0.92	145—146	EA	N	−24.6	29
51	L-Val-L-Leu-OMe	87.9	0.96	145—146	EA—H	N	−35.2	18

a) All compounds were analyzed for C, H, and N, and results were within ±0.3% of the theoretical values. Complete analytical data for all compounds have been deposited at the office of the Chemical Society of Japan (Document No. 8447). b) TLC: $CHCl_3$:MeOH:AcOH=45:4:1 (v/v), detected with I_2 vapor. c) Crystallization solvent: EA, Ethyl acetate; H, Hexane; D, *N*,*N*-Dimethylformamide. d) Appearance: N, Needles; A, Amorphous powder. e) In acetic acid, $c=1.0\%$. f) Not analyzed. g) Softened. h) In *N*,*N*-dimethylformamide, $c=0.5\%$.

52 by an isopropyl or an isobutyl group gave **54** and **55**, respectively, which were bitter. These results show that a modification of the third amino acid alone does not effect elicitation of sweetness.

Secondly, the contribution of the second amino acid to sweetness was evaluated. As mentioned above, it seems that a small alkyl group (Me, Et or *i*-Pr) at R^2 is required for sweetness. Therefore, in this experiment, a small alkyl group was introduced at R^2 so as to meet the sweet structure (Ia), in which S corresponds to R^2 of II in the configuration. As reported previously, replacement of a methyl group at R^2 of **76** gave **77**,[13b] which was 3 times sweeter than sucrose. Replacement of the methyl group by an ethyl or an isopropyl group gave **78** and **79**,[13b] which were sweet and tasteless, respectively. The ethyl ester analogue (**80**)[13b] of **79** was also tasteless. As described above, the modification of the second amino acid alone gave a similar result in the case of the modification of the third amino acid.

Thirdly, the combined contribution of the second and third amino acids was evaluated. In this experiment, a small alkyl group of the second amino acid was also introduced at R^2 by the reason mentioned above. Introduction of an alkyl group to the α-carbon of Gly in L-α-Asp-D-Ala-Gly-OMe (**77**) significantly increased the sweetness potency (**56—60**). The potent sweetness seems to result from an increased hydrophobicity as compared with **77**. The sweet taste changed to a bitter taste (**61**) with increasing hydrophobicity of the group (R^4). In the same way, when a small alkyl group was introduced to the α-carbon of Gly in L-α-Asp-D-Val-Gly-OMe (**79**), the resulting peptides (**62—65**) became intensely sweet. Compound **66** may be too hydrophobic to taste sweet. A substituent at R^2 is considered to be a small, compact alkyl group, such as Me, Et or *i*-Pr, from the previous work on the dipeptide sweeteners, especially in L-α-Asp-D-amino acid esters. A need for the small alkyl group (R^2) was confirmed by the fact that L-α-Asp-D-Leu-L-Ala-OMe (**67**) was not sweet but bitter. The *i*-Bu group in **67** seems to be too bulky to interact effectively at the sweet receptor site. These observations suggest that the hydrophilic-hydrophobic balance in a molecule and the space-filling properties are important. It is interesting that the sweetness potencies were significantly changed by altering the configuration of the third amino acid (**52** and **53**; **56** and **57**; **62** and **63**). The observation shows that the L-configuration of the third amino acid is

Table 3. Tripeptide esters, L-α-Asp-X

No.	Compound[a] X	Yield %	TLC R_f[b]	Mp θ_m/°C	Crystn Solvent[c]	Appearance[d]	$[\alpha]_D$ Degree[e]	Temp °C
52	Gly-L-Ala-OMe	57.3	0.12	162—163	W—A	N	−21.1	25
53	Gly-D-Ala-OMe	53.2	0.18	189—190 dec	W—A	N	+83.9	23
54	Gly-L-Val-OMe	40.1	0.25	167—168 (83)[f]	E—H	A	−9.2	20
55	Gly-L-Leu-OMe	64.6	0.21	84—85 dec	A—EA	A	−16.0	30
56	D-Ala-L-Ala-OMe	78.1	0.19	164—165	W—A	N	+16.9	25
57	D-Ala-D-Ala-OMe	87.2	0.16	182—183 dec	W—A	N	+112.9	30
58	D-Ala-L-Ala-OEt	62.2	0.19	166—167	W—A	N	+16.9	22
59	D-Ala-L-Val-OMe	63.3	0.24	182.5—183.5 dec	W	N	+22.7	30
60	D-Ala-L-Leu-OMe	65.3	0.38	189—190 dec	W—A	N	+16.5	26
61	D-Ala-L-Phe-OMe	73.6	0.29	181—182 dec	W—A	N	+40.1	24
62	D-Val-L-Ala-OMe	70.9	0.26	207—208 dec	W	N	+16.0	26
63	D-Val-D-Ala-OMe	66.7	0.24	221—222 dec	W—A	N	+94.7	22
64	D-Val-L-Val-OMe	62.1	0.30	202—203 dec	W	N	+15.7	22
65	D-Val-L-Leu-OMe	52.7	0.44	200—201	W	N	+9.9	23
66	D-Val-L-Phe-OMe	38.6	0.40	209—210	W	N	+16.2[g]	25
67	D-Leu-L-Ala-OMe	58.8	0.35	204—204.5 dec	W	N	+16.3	21
68	L-Ala-Gly-OMe	71.8	0.19	200—201 dec	W—A	N	−23	19
69	L-Ala-L-Ala-OMe	91.0	0.11	210—211 dec	W—A	A	−67.1	24
70	L-Ala-L-Val-OMe	59.2	0.34	185—186 dec	W	N	−53.9	29
71	L-Abu-L-Val-OMe	60.2	0.39	194—195 dec	W	N	−46.9	22
72	L-Val-L-Ala-OMe	74.7	0.32	210—211 dec	W	N	−58.5	25
73	L-Val-D-Ala-OMe	86.3	0.38	209—210 dec	W	N	+27.0	19
74	L-Val-L-Val-OMe	81.2	0.50	225.5—226.5 dec	W	N	−46.6	28
75	L-Val-L-Leu-OMe	72.6	0.38	222.5—223.6 dec	W	N	−36.0[g]	20

a) All compounds were analyzed for C, H, and N, and results were within ±0.3% of the theoretical values. Complete analytical data for all compounds have been deposited at the office of the Chemical Society of Japan (Document No. 8447). b) TLC: $CHCl_3$:MeOH:AcOH:H_2O=32:15:1:3 (v/v), detected with ninhydrin. c) Crystallization solvent: W, Water; A, Acetone. d) Appearance: N, Needles; A, Amorphous powder. e) In water, c=1.0%. f) Softened. g) In acetic acid, c=0.5%.

required for a potent sweet taste. The importance of the spacial orientation of the side chain may suggest another hydrophobic interaction at R^4 with the receptor site. The sweet receptor is considered to be a protein,[18] therefore, such an interaction appears to occur possibly at the receptor site.

Finally, in order to reconfirm the required configurations (R^2=small alkyl group; R^1=H) at the second amino acid, several tripeptides having opposite configurations at this chiral center were synthesized. All of the peptides (**68—75**) were essentially tasteless or bitter. Among them, however, compounds **71**, **73**, **74**, and **75** were bitter-sweet. The sweetness of these compounds did not come from contamination of their sweet isomers. Compound **74** was found by thin-layer chromatography (TLC) and high-performance liquid chromatography (HPLC) to be free from **64**. TLC analyses of **71**, **73**, and **75** showed no other compounds to be detectable. The weak sweet taste observed in compounds **71**, **73**, **74**, and **75** with all L-configurations may show that sweetness cannot necessarily be correlated with D-isomerism at the second amino acid. These four compounds, however, were essentially bitter. It is therefore concluded that the general structure (Ia) for sweet dipeptides is extended to that for sweet tripeptides (II), in which R^1 is H and R^2 is a small alkyl group. Exceptions that **71**, **73**, **74**, and **75** with the L-configuration at the second amino acid showed a weak sweet taste along with a bitter taste may be interpreted in terms of their conformations, in which a certain conformer may possibly fit the narrow receptor pocket.

Summary

A series of twenty four analogues of L-α-Asp-Gly-Gly-OMe (**76**) has been synthesized in relation to our previous conclusion that the small alkyl group (S) of the sweet dipeptides (Ia) increases the sweetness potency through a hydrophobic interaction with the receptor. It has been concluded that the small alkyl group at R^2 in the tripeptides (II) participates in binding with the receptor through the hydrophobic interaction and increases the sweetness potency. In order for the tripeptides to be sweet, the second amino acid must have the D-configuration and a small, compact alkyl group (Me, Et or *i*-Pr) at R^2. The L-configuration of the third amino acid is required for a potent sweet taste. This suggests another hydrophobic interaction at R^4. The rule in the general structure (Ia) for the sweet dipeptides is held in the sweet tripeptides (II). The sweetness potencies of the tripeptides obtained here, however, were lower than those of aspar-

Table 4. Taste of tripeptide esters (L-α-Asp-X)[a]

No.	X	R^1	R^2	R^3	R^4	R^5	Taste[b]
76	Gly-Gly-OMe	H	H	H	H	Me	0
52	Gly-L-Ala-OMe	H	H	H	Me	Me	2
53	Gly-D-Ala-OMe	H	H	Me	H	Me	1
54	Gly-L-Val-OMe	H	H	H	*i*-Pr	Me	—
55	Gly-L-Leu-OMe	H	H	H	*i*-Bu	Me	—
77	D-Ala-Gly-OMe	H	Me	H	H	Me	3
78	D-Abu-Gly-OMe	H	Et	H	H	Me	1
79	D-Val-Gly-OMe	H	*i*-Pr	H	H	Me	0
80	D-Val-Gly-OEt	H	*i*-Pr	H	H	Et	0
56	D-Ala-L-Ala-OMe	H	Me	H	Me	Me	50
57	D-Ala-D-Ala-OMe	H	Me	Me	H	Me	5
58	D-Ala-L-Ala-OEt	H	Me	H	Me	Et	15
59	D-Ala-L-Val-OMe	H	Me	H	*i*-Pr	Me	50
60	D-Ala-L-Leu-OMe	H	Me	H	*i*-Bu	Me	15
61	D-Ala-L-Phe-OMe	H	Me	H	Bzl	Me	—
62	D-Val-L-Ala-OMe	H	*i*-Pr	H	Me	Me	25
63	D-Val-D-Ala-OMe	H	*i*-Pr	Me	H	Me	4
64	D-Val-L-Val-OMe	H	*i*-Pr	H	*i*-Pr	Me	30
65	D-Val-L-Leu-OMe	H	*i*-Pr	H	*i*-Bu	Me	40
66	D-Val-L-Phe-OMe	H	*i*-Pr	H	Bzl	Me	—
67	D-Leu-L-Ala-OMe	H	*i*-Bu	H	Me	Me	—
68	L-Ala-Gly-OMe	Me	H	H	H	Me	0
69	L-Ala-L-Ala-OMe	Me	H	H	Me	Me	—
70	L-Ala-L-Val-OMe	Me	H	H	*i*-Pr	Me	0
71	L-Abu-L-Val-OMe	Et	H	H	*i*-Pr	Me	− (2)
72	L-Val-L-Ala-OMe	*i*-Pr	H	H	Me	Me	0
73	L-Val-D-Ala-OMe	*i*-Pr	H	Me	H	Me	− (1)
74	L-Val-L-Val-OMe	*i*-Pr	H	H	*i*-Pr	Me	− (4)
75	L-Val-L-Leu-OMe	*i*-Pr	H	H	*i*-Bu	Me	− (4)

a) For structures, see Figure 2. b) Times sucrose (weight basis, sucrose=1). 0=tasteless; −=bitter; −( )= bitter-sweet, the number in parentheses is sweetness value.

tyl dipeptides. This result suggests the importance of the hydrophilic-hydrophobic balance and space-filling properties (shape, size, length, and conformation) in a sweet peptide. The tripeptides are generally more hydrophilic than potent sweet dipeptides and the hydrophilic property will cause the decreased sweetness potency. The receptor site for sweet amino acids and peptides seems to be not a plane but the shape of a pocket[13b] or a similar one as mentioned before. With increasing length of a peptide, it becomes difficult to fit such a narrow site. The decreased binding of the sweet molecule to the receptor reduces the potency.

Experimental

All melting points were taken on a Yanagimoto capillary melting point apparatus Model MP-21 and are uncorrected. Optical rotations were measured on a JASCO DIP-140 digital polarimeter with a 10-cm cell at room temperature and a 1% concentration. TLC was performed on precoated silica gel $60F_{254}$ plates (E. Merck) and spots were detected with ninhydrin or I_2 vapor. All compounds were essentially homogeneous on TLC. HPLC was carried out on a Hitachi 635A instrument with a Unisil Q C-18 reverse-phase column (4 mm ×25 cm) eluting with 23% methanol in pH 3.5 NaH_2PO_4 buffer at a flow rate of 0.8 ml/min. Sweetness potency was not evaluated by the panel method due to quantities available. In general, a panel evaluation needs a large quantity of sample. The yield, after purification, of each sweet peptide (Table 3) was less than 0.5 g. The quantity of tripeptides obtained here was insufficient for the panel evaluation. Therefore, sweetness evaluation was carried out by the author by matching a threshold concentration of each compound with that of sucrose. Test solutions of the tripeptides were made up at several concentrations. A series of the solutions were tasted up and down. Thus, it was possible to reproducibly determine the concentration which matched a 0.6% aqueous solution of sucrose. In order to confirm the sweetness values, compounds **56**, and **62—65** were also evaluated by a well trained sensory panelist, and the potencies were in fair agreement with those listed in Table 4. Therefore, it has been considered that the sweetness potencies in Table 4 are reproducible and reliable enough to discuss the functions of a small hydrophobic group.

Materials: Boc-amino acids were purchased from Peptide Institute Inc., except for Boc-L-Abu (Kokusan Chemical Works Ltd.). Esters of Gly, D-Ala, L-Phe, and L-Val were synthesized in our laboratory. Z-L-Asp(OBzl)-OH and esters of L-Ala and L-Leu were purchased from Kokusan Chemical Works Ltd.

Boc-Dipeptide Esters (1, 3, 5, 8—27). A typical run (**11** in Table 1) was as follows: To an ice-cooled stirred solution of H-L-Val-OMe·HCl (2.77 g, 16.5 mmol) and triethylamine (Et_3N) (1.67 g, 16.5 mmol) in 40 ml of chloroform was added Boc-D-Ala-OH (2.84 g, 15 mmol), followed by DCC (3.09 g,

15 mmol). The resulting mixture was stirred in an ice-bath for 1 h and then kept standing overnight, after which a few drops of acetic acid were added to the reaction mixture. The mixture was then stirred for 15 min and filtered. The filtrate was washed successively with water, a 10% citric acid solution, a 5% sodium hydrogencarbonate solution and water and then concentrated under reduced pressure to give an oily product. The oil was crystallized from ethyl acetate–hexane to give 2.77 g (61.1%) of Boc-D-Ala-L-Val-OMe (**11**) as plates. Recrystallization was effected from the same solvent. The data are given in Table 1.

Protected Tripeptide Esters (28—51). a) The DCC Method. A typical run (**35** in Table 2) was as follows: To a solution of Boc-D-Ala-L-Val-OMe (**11**, 2.23 g, 7.38 mmol) in 20 ml of methanol was added *p*-toluenesulfonic acid monohydrate (TosOH·H_2O) (1.78 g, 9.4 mmol). The mixture was stirred at 30 °C for 5 h. The solvent was evaporated under reduced pressure at a bath temperature of 50 °C to give H-D-Ala-L-Val-OMe·TosOH as an oily residue. The residue was used for the next step without further purification. H-D-Ala-L-Val-OMe·TosOH thus obtained was dissolved in 40 ml of chloroform and neutralized with Et_3N (0.95 g, 9.4 mmol) in an ice-bath. To the stirred ice-cooled solution was added Z-L-Asp(OBzl)-OH (2.50 g, 7 mmol), followed by DCC (1.44 g, 7 mmol). The mixture was stirred while cooling for 1 h and at room temperature for 3 h and then kept standing overnight. A few drops of acetic acid were then added to the reaction mixture. The mixture was stirred at room temperature for 15 min and then filtered. The filtrate was washed successively with water, 1M HCl (twice), a 5% sodium hydrogencarbonate solution (twice) and water, and then concentrated under reduced pressure to leave an oily product. The oil was crystallized from ethyl acetate–hexane to give Z-L-Asp(OBzl)-D-Ala-L-Val-OMe (**35**) as needles. Recrystallization was carried out from the same solvent. The data are given in Table 2.

b) The active ester method. A typical run (**51** in Table 2) was as follows: DCC (3.10 g, 15 mmol) was added to an ice-cooled mixture of Z-L-Asp(OBzl)-OH (5.36 g, 15 mmol) and *N*-hydroxysuccinimide (2.07 g, 18 mmol) in 50 ml of chloroform with stirring. The mixture was stirred in an ice-bath for 1 h and at room temperature for 3 h and then kept standing overnight. A few drops of acetic acid were then added to the reaction mixture, which was stirred at room temperature for 15 min and filtered. The filtrate was washed successively with water, a 5% sodium hydrogencarbonate solution and water, and then concentrated under reduced pressure to leave an oily product, which turned to crystals upon standing. Recrystallization from ethyl acetate–hexane gave Z-L-Asp(OBzl)-ONSu as needles; yield, 4.75 g (69.7%); mp 83—84 °C; $[\alpha]_D^{24}$ −19.1° (*c* 1, ethyl acetate). To a solution of Boc-L-Val-L-Leu-OMe (**27**, 3.10 g, 9 mmol) in 20 ml of methanol was added TosOH·H_2O (2.05 g, 10.8 mmol). The mixture was stirred at 30 °C for 5 h. The solvent was evaporated under reduced pressure at a bath temperature of 50 °C to give H-L-Val-L-Leu-OMe·TosOH as an oily residue. The oil was dissolved in 40 ml of chloroform and cooled in an ice-bath. To this solution was added Et_3N (1.10 g, 10.8 mmol), followed by Z-L-Asp(OBzl)-ONSu (3.79 g, 8.34 mmol) with stirring. The mixture was stirred at room temperature for 3 h and then kept standing overnight. The reaction mixture was worked up as a) to give Z-L-Asp(OBzl)-L-Val-L-Leu-OMe (**51**) as crystals, which were recrystallized from ethyl acetate—hexane to give **51** as needles. Recrystallization was carried out from the same solvent. The data are given in Table 2.

Tripeptide Esters (52—75). A typical run (**59** in Table 3) was as follows: Z-L-Asp(OBzl)-D-Ala-L-Val-OMe (**35**, 1.85 g) was dissolved in a mixture of acetic acid (40 ml) and water (10 ml), and hydrogenated in the presence of 5% Pd/C (0.6 g) with stirring at atmospheric pressure and room temperature for 6 h. The reaction mixture was filtered and the filtrate was concentrated under reduced pressure to dryness. The residue was dissolved in water and the solvent was evaporated under reduced pressure to remove remaining acetic acid. The procedure was repeated three times. The crystalline residue, thus obtained, was recrystallized from water–acetone to give 0.76 g (63.3%) of L-α-Asp-D-Ala-L-Val-OMe·$2H_2O$ (**59**) as needles. Recrystallization from water afforded 0.26 g of pure **59** dihydrate as needles. The data are given in Table 3. In another experiment, the peptide (**59**) was recrystallized from water to give **59** monohydrate as needles; mp 160—161 °C.

The author wishes to thank Mr. T. Takemoto for HPLC analyses and Dr. S. Yamaguchi for sensory evaluation.

References

1) a) R. S. Shallenberger and T. E. Acree, *Nature*, **216**, 480 (1967); b) R. S. Shallenberger, T. E. Acree, and C. Y. Lee, *ibid*, **221**, 555 (1969); c) L. B. Kier, *J. Pharm. Sci.*, **61**, 1394 (1972).

2) R. H. Mazur, J. M. Schlatter, and A. H. Goldkamp, *J. Am. Chem. Soc.*, **91**, 2684 (1969).

3) a) M. T. Briggs and J. S. Morley, Brit. Patent, 1,299,265 (1972); b) M. Fujino, M. Wakimasu, K. Tanaka, H. Aoki, and N. Nakajima, *Naturwissenschaften*, **60**, 351 (1973).

4) R. H. Mazur, A. H. Goldkamp, P. A. James, and J. M. Schlatter, *J. Med. Chem.*, **13**, 1217 (1970).

5) a) R. H. Mazur, J. A. Leuter, K. A. Swiatek, and J. M. Schlatter, *J. Med. Chem.*, **16**, 1284 (1973); b) Y. Ariyoshi, N. Yasuda, and T. Yamatani, *Bull. Chem. Soc. Jpn.*, **47**, 326 (1974).

6) T. M. Brennan and M. E. Hendric, Eur. Pat. Appl. EP34386 (1982); *Chem. Abstr.*, **96**, 104780c (1982).

7) M. Miyoshi, K. Nunami, H. Sugano, and T. Fujii, *Bull. Chem. Soc. Jpn.*, **51**, 1433 (1978).

8) M. Fujino, M. Wakimasu, M. Mano, K. Tanaka, N. Nakajima, and H. Aoki, *Chem. Pharm. Bull.*, **24**, 1211 (1976).

9) S. A. MacDonald, C. G. Willson, M. Chorev, F. S. Vernacchia, and M. Goodman, *J. Med. Chem.*, **23**, 413 (1980).

10) a) A. van der Heijden, L. B. P. Brussel, and H. G. Peer, *Chemical Senses and Flavour*, **4**, 141 (1979); b) H. Iwamura, *J. Med. Chem.*, **24**, 572 (1981).

11) F. Lelj, T. Tancredi, P. A. Temussi, and C. Toniolo, *J. Am. Chem. Soc.*, **98**, 6669 (1976).

12) S. W. King and C. H. Stammer, *J. Org. Chem.*, **46**, 4780 (1981).

13) a) Y. Ariyoshi, *Agric. Biol. Chem.*, **40**, 983 (1976); b) Y. Ariyoshi, *ibid.*, **44**, 943 (1980).

14) H. Wieser, H. Jugel, and H.-D. Belitz, *Z. Lebensm. Unters.-Forsch.*, **164**, 277 (1977).

15) J. C. Sheehan and G. P. Hess, *J. Am. Chem. Soc.*, **77**, 1067 (1955).

16) J. Goodacre, R. J. Ponsford, and I. Stirling, *Tetrahedron Lett.*, **1975**, 3609.

17) G. W. Anderson, J. E. Zimmerman, and F. M. Callahan, *J. Am. Chem. Soc.*, **85**, 3039 (1963).

18) a) F. R. Dastri, D. V. Lopiekes, and S. Price, *Biochemistry*, **7**, 1160 (1968); b) Y. Hiji, *Nature*, **256**, 427 (1975).

Asymmetric Catalytic Hydrogenations of Chiral α-Keto Amides

Kaoru HARADA* and Toratane MUNEGUMI
Department of Chemistry, The University of Tsukuba, Sakura-mura, Niihari, Ibaraki 305
(Received May 21, 1984)

Asymmetric catalytic hydrogenations of chiral pyruvamides were carried out using palladium on charcoal (Pd-C) as a catalyst to give lactamides with the diastereoisomeric purities (d.p.) of up to 62%. It was found that there was a linear correlation between the d.p. and the dielectric constant of the solvents used in the hydrogenations of chiral pyruvamides. The results were explained by employing the chelation model and the adsorption of the phenyl group in the substrate molecule on the catalyst. The temperature effect on the d.p. of the product was also examined. The catalytic hydrogenations of chiral benzoylformamides were also performed to give low d.p. presumably, the chelation complexes of the substrates could not take a predominant conformation with the catalyst.

Several studies on the asymmetric catalytic hydrogenations of α-keto acid derivatives have been performed.[1-7] However, a few examples of the asymmetric catalytic hydrogenations of chiral α-keto amides have been reported.[1,7,8] Mitsui and Kanai carried out[1] the hydrogenations of *N*-[(*S*)-α-methylbenzyl]benzoylformamide in ethanol over palladium catalysts. Ojima *et al.* performed[7] the hydrogenations of pyruvamides employing an amino acid ester as the chiral source with palladium on charcoal. In the previous study,[8] we reported the stereochemistry in the catalytic hydrogenations of three pyruvamides whose chiral sources were (*S*)-α-methylbenzylamine, (*S*)-α-ethylbenzylamine, and (*S*)-α-(1-naphthyl)ethylamine. The steric courses in the catalytic hydrogenations could be explained by the formation of a five-membered substrate-catalyst complex-(chelation mechanism[8-17]). It was considered that the complexes were stabilized by the adsorption of the phenyl group in the chiral source, on the catalyst.[8]

In this paper, we wish to describe the stereochemistry on the catalytic hydrogenations of three types of chiral α-keto amides (**3**, **5**, and **10** as shown in Scheme 1—4) over palladium on charcoal using several solvents, in connection with the adsorption of phenyl group on the catalyst. We also would like to correct the analytical data reported in the previous paper,[8] by means of a more accurate analytical method.[17]

In the catalytic hydrogenations of substrates **5** and **10**, it was found that there was a linear correlation between the diastereoisomeric purities(d.p.) of the products and the dielectric constant of the solvents used.

Results and Discussion

Catalytic Hydrogenations of Benzoylformamides **3**. The substrates **3a—c** were prepared as shown in Scheme 1, and were hydrogenated over palladium on charcoal-(Pd-C) at 30 °C in several solvents. The d.p. of the products are listed in Table 1, along with optical purities(o.p.) of mandelic acid obtained through the hydrolyses of the products. The d.p. of the products were determined by the gas chromatographic separation of diastereomeric mandelamides.

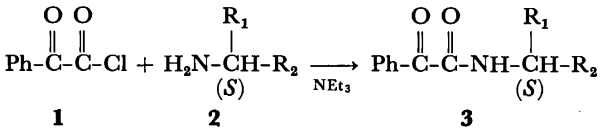

1 **2** **3**

2a: $R_1=CH_3$, $R_2=Ph$ **3a**: $R_1=CH_3$, $R_2=Ph$
2b: $R_1=C_2H_5$, $R_2=Ph$ **3b**: $R_1=C_2H_5$, $R_2=Ph$
2c: $R_1=CH_3$, $R_2=Naph$ **3c**: $R_1=CH_3$, $R_2=Naph$

Scheme 1.

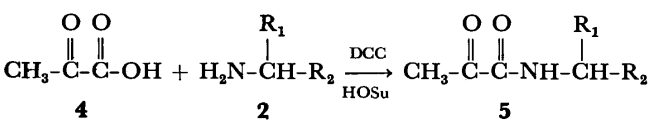

4 **2** **5**

2a: $R_1=CH_3$, $R_2=Ph(S)$ **5a**: $R_1=CH_3$, $R_2=Ph(S)$
2b': $R_1=C_2H_5$, $R_2=Ph(R)$ **5b**: $R_1=C_2H_5$, $R_2=Ph(R)$
2c: $R_1=CH_3$, $R_2=Naph(R)$ **5c**: $R_1=CH_3$, $R_2=Naph(R)$

Scheme 2.

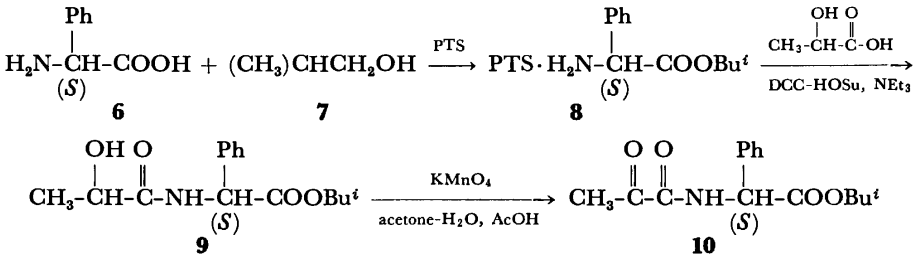

6 **7** **8** **9** **10**

PTS: *p*-toluenesulfonic acid. Bu^i: isobutyl.

Scheme 3.

All the hydrogenations of substrate **3a** gave (*R*)-mandelic acid (*S*)-amide [(*R*,*S*)-mandelamide] preferentially. And all the hydrogenations of substrate **3b** gave (*S*)-mandelic acid (*S*)-amide [(*S*,*S*)-mandelamide] preferentially. However, the d.p. of the products were too low (1.3—7.7%) to discuss the steric courses of the catalytic hydrogenations by using these experimental data(Table 1). The reason for the low d.p. could be caused by the adsorption of phenyl group, which attached to the carbonyl carbon, on the catalyst surface, and the adsorbed substrate-catalyst complex could not take a predominant conformation.

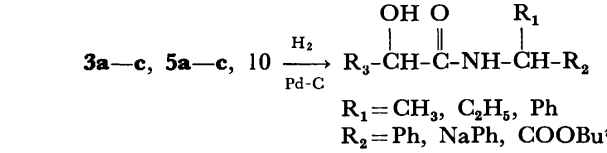

Scheme 4.

The catalytic hydrogenations of substrates **3a—b** were carried out in methanol at various temperatures. The temperature effect on d.p. of the products is shown in Table 2. The hydrogenations of substrate **3a** at low temperature mainly gave (*S*,*S*)-mandelamide slightly in excess. The hydrogenation of substrate **3b** at −10 °C

TABLE 1. CATALYTIC HYDROGENATIONS OF SUBSTRATES **3a—c**

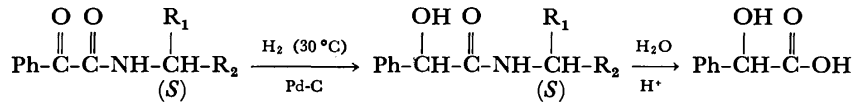

R_1	R_2	Config.[a]	Solvent	Yield/%	$[\alpha]_D^{20}$ [b]	O.p./%[c]	D.p./%[d]	Config.[e]
CH_3	Ph	*S*	MeOH	59[f] (84)[g]	−3.3	2.2	2.7	*R*
			EtOH	64 (99)	−1.7	1.1	1.3	*R*
			Pr^{i}OH	63 (94)	−1.6	1.1	2.2	*R*
			Bu^{t}OH	60 (100)	−2.2	1.4	2.8	*R*
			C_5H_{11}^{t}OH	67	−2.8	1.8		*R*
			Benzene	61	−1.4	0.9		*R*
C_2H_5	Ph	*S*	MeOH	61 (94)	+4.8	3.2	5.0	*S*
			EtOH	58 (100)	+4.9	3.2	5.4	*S*
			Pr^{i}OH	60 (100)	+4.2	2.8	7.7	*S*
			Bu^{t}OH	66 (98)	+3.7	2.4	7.1	*S*
			C_5H_{11}^{t}OH	59	+5.3	3.5		*S*
			Benzene	63	+8.0	5.3		*S*
			AcOEt	(100)			5.8	*S*
CH_3	Naph	*S*	EtOH	57	−3.9	2.5		*R*
			Benzene	58	0	0		

a) Configuration of the chiral amines. b) c 2.5, H_2O. c) Optical purity of mandelic acid obtained by the hydrolysis. d) Diastereoisomeric purity of mandelamide = $[(R,S)-(S,S)]/[(R,S)+(S,S)]\times 100$ or $[(S,S)-(R,S)]/[(R,S)+(S,S)]\times 100$. e) Configuration of the newly formed chiral center. f) Chemical yield of mandelic acid. g) Chemical yield of mandelamide determined by means of gas chromatography.

TABLE 2. TEMPERATURE EFFECT ON THE CATALYTIC HYDROGENATIONS OF SUBSTRATES **3a—b**

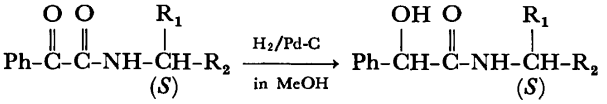

R_1	R_2	Config.[a]	Temp[b]/°C	Yield/%	D.p./%[c]	Config.[d]
CH_3	Ph	*S*	−30	100	≥0	*S*
			−10	100	3.4	*S*
			+10	100	4.5	*S*
			+30	84	2.7	*R*
			+50	82	1.3	*S*
C_2H_5	Ph	*S*	−30	100	7.3	*S*
			−10	100	9.8	*S*
			+10	100	7.0	*S*
			+30	94	5.0	*S*
			+50	82	0.8	*S*

a) Configuration of the chiral amines. b) Temperature of the reaction mixtures during the catalytic hydrogenations. c) Diastereoisomeric purity of mandelamide. d) Configuration of the newly formed chiral center.

TABLE 3. SOLVENT EFFECT ON THE CATALYTIC HYDROGENATIONS OF SUBSTRATES **5a—c**

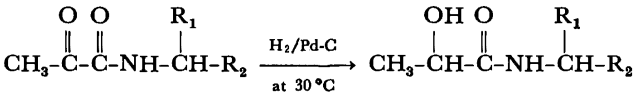

R_1	R_2	Confign.[a]	Solvent (ε)[b]	Yield/%	D.p./%[c]	Confign.[d]
CH_3	Ph	*S*	MeOH (32.7)	75	59	*S*
		S	EtOH (24.5)	79	55	*S*
		S	Pr^{i}OH (19.9)	72	53	*S*
		S	Bu^{t}OH (12.4)	79	52	*S*
		S	AcOEt (6.0)	72	37	*S*
		S	Benzene (2.0)	56	17	*R*
		S	DMF (36.7)	68	62	*S*
		S	H_2O-MeOH 7 : 3 (46.3)	100	21	*S*
C_2H_5	Ph	*R*	MeOH	76	54	*R*
		R	EtOH	71	46	*R*
		R	Pr^{i}OH	70	35	*R*
		R	Bu^{t}OH	61	29	*R*
		R	AcOEt	69	13	*R*
		R	DMF	71	53	*R*
CH_3	Naph	*R*	MeOH	30	48	*R*
		R	EtOH	18	35	*R*
		R	Pr^{i}OH	24	27	*R*
		R	AcOEt	28	31	*R*

a) Configuration of the chiral amines. b) Dielectric constant of the solvents. c) Diastereoisomeric purity. d) Configuration of the newly formed chiral center.

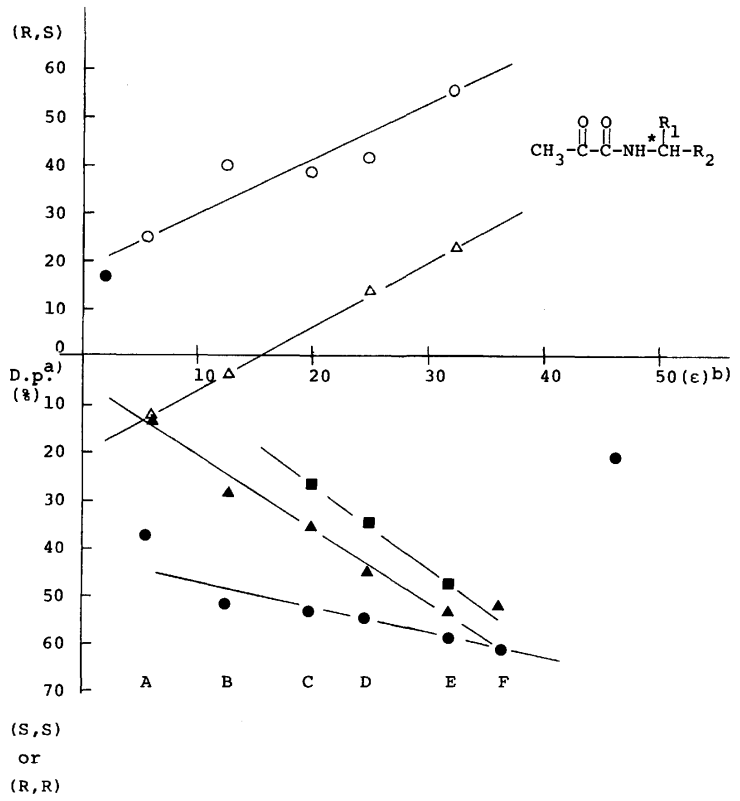

Fig. 1. Solvent effect on the hydrogenations of the substrates **5**, **10**. a) Diastereoisomeric purity of lactamide. b) Dielectric constant. ●: R_1=CH_3, R_2=Ph(S). ▲: R_1=C_2H_5, R_2=Ph(R). :■ R_1=CH_3, R_2=Naph(R). ○: R_1=Ph, R_2=COOBu^t(S). △: R_1=CH_3, R_2=COOBu^t(S). A: Ethyl acetate. B: 2-Methyl-2-propanol. C: 2-Propanol. D: Ethanol. E: Methanol. F: DMF.

gave (*S,S*)-mandelamide in up to 9.8%. However, detailed discussion could not be made on the temperature effect, because the d.p. of mandelamides were so low.

Catalytic Hydrogenations of Substrates 5a—c. This section describes the catalytic hydrogenations of three chiral pyruvamides **5a—c**. (*S*)-α-Methylbenzylamine, (*R*)-α-ethylbenzylamine, (*R*)-1-(1-naphthyl)-ethylamine were used as the chiral sources of pyruvamides.

The substrates were prepared by the coupling of pyruvic acid and the chiral amines with dicyclohexylcarbodiimide (DCC) in the presence of *N*-hydroxysuccinimide (HOSu) as shown in Scheme 2.

The results of the catalytic hydrogenations of substrates **5a—c** at 30 °C in several solvents are listed in Table 3. The d.p. of the products are plotted against the dielectric constants of the solvents used for the hydrogenation as shown in Fig. 1.

Substrate **5a** whose chiral moiety was (*S*)-α-methylbenzyl amine gave *N*-[(*S*)-lactoyl]-(*S*)-amide [(*S,S*)-lactamide] in excess. Substrate **5b** whose chiral moiety was (*R*)-α-ethylbenzylamine and substrate **5c** whose chiral moiety was (*R*)-1-(naphthyl)ethylamine, preferentially gave *N*-[(*R*)-lactoyl]-(*R*)-amide [(*R,R*)-lactamide]. The d.p. of the products in the hydrogenations of substrate **5a** were higher than the results in the hydrogenations of other substrates in all solvents, and the order of the d.p. was as follows: **5a**>**5b**>**5c**.

When *N,N*-dimethylformamide (DMF) was used as the solvent, the d.p. of (*S,S*)-lactamide reached to 62%. When benzene was used as the solvent, substrate **5a** gave (*R,S*)-lactamide in excess contrary to the results obtained with alcoholic solvents. Hydrogenation of substrate **5a** in MeOH–H_2O (7:3) gave (*S,S*)-lactamide with 21% d.p.

The linear correlation beween the dielectric constant of the solvents and the d.p. of the products was explained by using the chelation mechanism as shown in Fig. 2. The chelation mechanism involves a two step adsorption of the substrate during the catalytic hydrogenations. In the first step, the substrate molecule forms a five-membered chelated intermediate with the catalyst surface. In the second step, the resulting chelated intermediate is adsorbed on the catalyst from the less bulky side of the substrate and then hydrogenated. The *s-cis* conformation shown in Fig. 2 could be the first stage of the adsorption of the substrate (the chelated intermediate) in the chelation mechanism. The stereochemistry in the catalytic hydrogenation would be determined by the conformation of the first adsorption (the chelated intermediate). The *s-trans* conformation in Fig. 2 shows the mechanism involving one step adsorption on the catalyst. Since the d.p. of the hydrogenation of substrate **5a** was larger than those of **5b** and **5c**, the asymmetric induction would not be caused by the difference of bulkiness between H and alkyl(R_1) groups. Therefore, *s-trans* adsorption state which produces (*S,S*)-lactamide in excess would not affect largely on the asymmetric induction. The steric courses of these reactions could be interpreted by means of three *s-cis* (chelation) adsorption states (conformer A, B, and C)

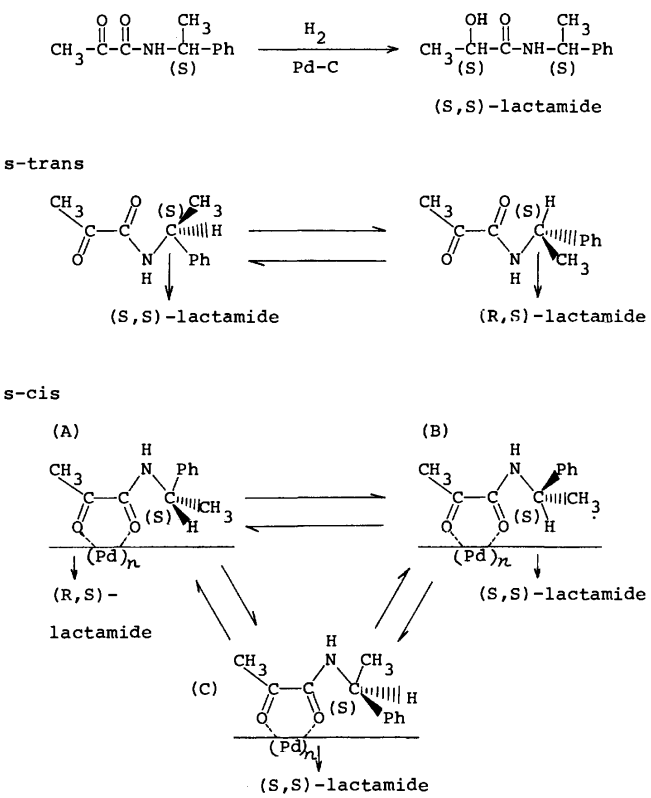

Fig. 2. Possible steric course in the catalytic hydrogenation of substrate **5a**.

in Fig. 2.

Conformer A produces (*R,S*)-lactamide and conformer B and C produces (*S,S*)-lactamide preferentially. Since the hydrogenations of substrate **5a** in the polar solvents gave (*S,S*)-lactamide, the substrate molecule would be hydrogenated mainly through conformer B and C. The decrease of d.p. of (*S,S*)-lactamide with the decrease of dielcectric constant of the solvents could be interpreted by the increase of the proportion of conformer A. In polar solvents, the substrate molecule would tend to take conformer B or C, because of the adsorption of the phenyl group on the catalyst or the phenyl group's escaping from the polar solvent. On the other hand, since the interaction between the phenyl group and the solvent would be stronger in less polar solvents than in polar solvents, the proportion of substrate molecule taking conformation A would increase. Therefore, d.p. of (*S,S*)-lactamide would increase with the increase of the dielectric constant of the solvent used.

The adsorption of the phenyl group on the catalyst could be confirmed by the result obtained by the hydrogenation of substrate **5a** using benzene as a solvent. The hydrogenation of substrate **5a** in benzene gave (*R,S*)-lactamide in excess (17% d.p.) contrary to the results in the hydrogenation in alcoholic solvents [(*S,S*)-lactamide in excess]. Since the phenyl group in the substrate molecule would interact with benzene, the substrate molecule would tend to take conformation A and then be hydrogenated to afford (*R,S*)-lactamide in excess.

The decrease of d.p. in the hydrogenation in

MeOH–H_2O (7:3), which is a very polar solvent system, could not be explained by means of the polarity of the solvent.

It was found that d.p. obtained by the hydrogenations in polar solvents were high (up to 62%) in spite of 1,4-asymmetric induction. These results suggested that the chelated intermediate (conformer B or C) were stable. If the two carbonyl groups were not fixed in *s-cis* conformation by the chelation to the catalyst, these high d.p. of the products would not be obtained.

The catalytic hydrogenations of substrates **5a—c** in methanol were carried out at various temperatures. The results of the hydrogenations are listed in Table 4. (*S,S*)-Lactamide was obtained in excess from substrate **5a** at all temperatures. (*R,R*)-Lactamide was obtained in excess from substrate **5b**. However, the temperature effect was rather low on the d.p. of the resulting (*S,S*)-lactamide or (*R,R*)-lactamide.

Catalytic hydrogenations of substrate ***10***. High d.p. in the catalytic hydrogenations of substrates **5a—c** were explained by the chelation of the two carbonyl groups and the adsorption of the phenyl group included in the chiral moiety, on the catalyst. The solvent effect of the catalytic hydrogenations of substrate **10** clarifies the adsorption of the phenyl group, on the catalyst.

Substrate **10** was prepared by oxidation of *N*-lactoyl-(*S*)-phenylglycine ester as shown in Scheme 3. The catalytic hydrogenations were carried out over palladium on charcoal in several solvents. The results of the hydrogenations are listed in Table 5. The hydrogenations of substrate **10** in all solvents gave *N*-[(*R*)-lactoyl]-(*S*)-phenylglycine ester [(*R,S*)-lactamide] in excess. The d.p. of the product [(*R,S*)-lactamide] increased with the increase of the dielectric constant of the solvents. Thus, there was a linear correlation between d.p. and the dielectric constant (Fig. 1).

In the previous paper[15] on the hydrogenations of *N*-pyruvoyl-(*S*)-amino acid esters, we have reported a similar relationship between d.p. and the dielectric

Table 4. Temperature effect on the catalytic hydrogenations of substrates **5a—c**

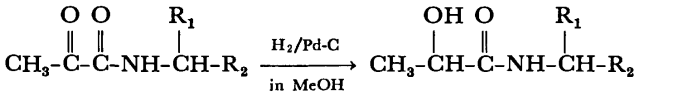

R_1	R_2	Confign.[a]	Temp/°C[b]	Yield/%	D.p./%[c]	Confign.[d]
CH_3	Ph	*S*	−30	72	61	*S*
		S	−10	79	53	*S*
		S	0	73	58	*S*
		S	+10	72	57	*S*
		S	+30	75	59	*S*
		S	+50	75	58	*S*
C_2H_5	Ph	*R*	−30	72	45	*R*
		R	−10	75	42	*R*
		R	+10	—	42	*R*
		R	+30	76	54	*R*
		R	+50	80	38	*R*
CH_3	Naph	*R*	−30	25	36	*R*
		R	+30	30	48	*R*

a) Configuration of the chiral amines. b) Temperature of the reaction mixtures during the catalytic hydrogenations. c) Diastereoisomeric purity of lactamide. d) Configuration of the newly formed chiral center.

Table 5. Catalytic hydrogenations of substrate **10**

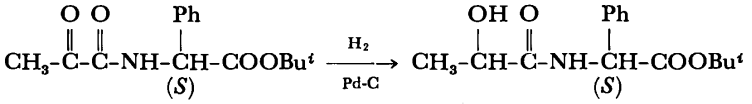

Confign.[a]	Solvent	Temp/°C[b]	Yield/%	D.p./%[c]	Confign.[d]
S	MeOH	+30	100	55	*R*
S	EtOH	+30	100	42	*R*
S	Pr^{i}OH	+30	83	39	*R*
S	Bu^{t}OH	+30	100	40	*R*
S	AcOEt	+30	98	25	*R*
S	MeOH	−10	88	42	*R*
S	MeOH	+10	—	49	*R*

a) Configuration of phenylglycine. b) Temperature of the reaction mixtures during the catalytic hydrogenations. c) Diastereoisomeric purity of lactamide. d) Configuration of the newly formed chiral center.

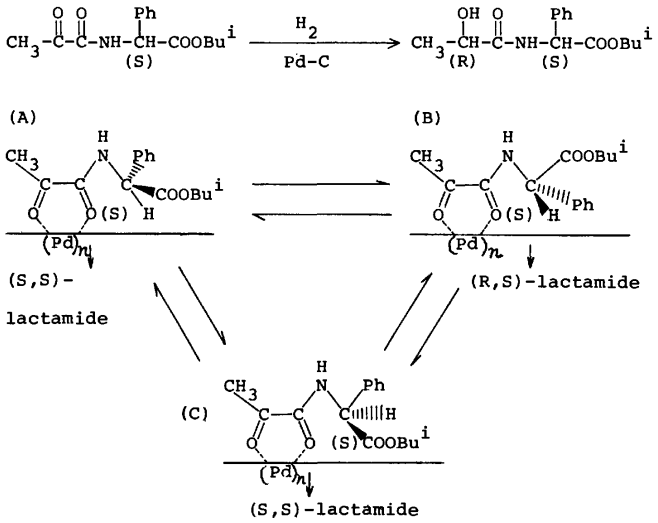

Fig. 3. Possible steric course in the catalytic hydrogenation od substrate **10**.

constant (Fig. 1). The substrates containing (*S*) 2-aminoalkanoic acid isobutyl ester as a chiral source, gave (*R,S*)-lactamide preferentially in polar solvents. And the d.p. of (*R,S*)-lactamide increase with the increase of the dielectric constant of the solvent. However, d.p. in the hydrogenations of substrate **10** were higher (up to 55%) than those in the hydrogenations[15] of other *N*-pyruvoyl-(*S*)-amino acid esters. These results were explained by the adsorption of the phenyl group on the catalyst (Fig. 3). In polar solvents, adsorption of the phenyl group of substrate **10** on the catalyst would be strong as well as substrate **5a**. The affinity between the phenyl group and the catalyst would be weaker with the decrease of the dielectric constant of the solvent. And the affinity between the COOBu^i and the catalyst would be stronger with the decrease of the dielectric constant of the solvents.[15] The proportion of conformer C (Fig. 3) of substrate **10** would increase in less polar solvents.

Therefore, d.p. of (*R,S*)-lactamide obtained from the hydrogenations of substrate **10** were smaller than those of (*S,S*)-lactamide obtained from the hydrogenations of substrate **5a**. (Substrate **5a** does not have an ester group in its chiral moiety.)

In other experiments, the catalytic hydrogenations of substrate **10** in methanol were also carried out at various temperatures. The temperature effect is shown in Table 5. (*R,S*)-Lactamide was preferentially obtained in all temperatures. However, the temperature effect was rather small on the d.p. of the resulting (*R,S*)-lactamide.

Experimental

All the melting points were uncorrected. Optical rotations were measured with a JASCO DIP-181 Digital Polarimeter. All the gas chromatographic analyses were carried out with a Hitachi 163 gas chromatograph, and the peaks on the chromatograms were integrated with a Hitachi 834-30 chromatoprocessor. NMR spectra were measured with a Hitachi R-24 High Resolution NMR spectrometer. IR spectra were measured with a Hitachi 260-50 infrared spectrometer.

Benzoylformyl Chloride[19,20] *1.* A mixture of benzoylformic acid (23.7 g, 158 mmol) and oxalyl chloride (80 g, 630 mmol) was refluxed for 6 h, and the extra oxalyl dichloride was distilled off. The residue was distilled under reduced pressure (68 °C/4 mm Hg (1 mm Hg=133.322 Pa)), and pale yellow liquid was obtained (14.8 g, 56%). IR, 1690 cm^{-1} (C=O), 1780 cm^{-1} (C=O).

Chiral Amines 2a—c. Chiral amine **2a** was purchased from Aldrich Chemical Company, Inc. $[\alpha]_D^{20}$ −39.0° (neat). Chiral amine 2b was obtained by the optical resolution[22] of racemic amine which was prepared by the method reported in the literture.[23] $[\alpha]_D^{20}$ −21.3° (*c* 1.53, benzene). Chiral amine 2c was purchased from Sigma Chemical Company. $[\alpha]_D^{25}$ −59.0° (*c* 1.0, ethanol).

(S)-Phenylglycine 6. $[\alpha]_D^{20}$ +155.6° (*c* 1.0, 1 mol dm^{-3} HCl).

N-[(S)-α-Methylbenzyl]benzoylformamide[1] *3a.* To a cooled dry benzne solution (200 ml) in which benzoylformyl chloride (7.30 g, 43.5 mmol) was dissolved, (*S*)-α-methylbenzylamine (5.27 g, 43.5 mmol) and triethylamine (4.41 g, 43.5 mol) were added dropwise. The reaction mixture was stirred for 2 h at 5—10 °C and 12 h at room temperature. After the reaction, the resulting white precipitate was filtered off and was washed with benzene. The benzene solution was extracted with three 150 ml portions of 1 mol dm^{-3} HCl, saturated $NaCO_3$ aqueous solution and brine respectively. The benzene layer was dried with $MgSO_4$. After drying agent was filtered off, the solution was evaporated *in vacuo*. The oil was purified with silica-gel flash chromatography[24] (eluent; ethyl acetate-hexane (1:9)). The fraction which contained the product were evaporated and the resulting crude white solid was recrystallized from chloroform-hexane. Yield, 7.41 g (67%). Mp, 111—112 °C (lit,[1] 110—111 °C). R_f= 0.28 (silica gel TLC; developing solvent, ethyl acetate-hexane (1:9)). $[\alpha]_D^{25}$ −106° (*c* 1.0, ethanol). NMR (CCl_4): δ=1.5 (3H, *J*=7 Hz), 5.0 (1H, m), 7.25 (9H, m), 8.25 (2H, m). Calcd for $C_{16}H_{15}NO_2$: 75.86; H, 5.96; N, 5.52%. Found: C, 75.86; H, 5.92; N, 5.49%.

N-[(S)-α-Ethylbenzyl]benzoylformamide 3b. To a cooled dry benzene solution (180 ml) in which benzoylformyl chloride (6.17 g, 36.8 mmol) was dissolved, (*S*)-α-ethylbenzylamine (4.98 g, 36.8 mmol) and triethylamine (3.72 g, 36.6 mmol) were added dropwise. The crude product was synthesized and purified by the similar manner in the preparation of 3a. Yield, 5.39 g (55%). Mp, 88.5—89.5 °C. R_f=0.28 (silica gel TLC; developing solvent, ethyl acetate-hexane (1:9)). $[\alpha]_D^{24}$ −107° (*c* 1.0, ethanol). NMR ($CDCl_3$): δ=0.9 (3H, t, *J*=7.5 Hz), 1.9 (2H, q, *J*=7.5 Hz), 4.9 (1H, m), 7.35 (9H, m), 8.3 (2H, m). Calcd for $C_{17}H_{17}NO_2$, C, 76.38; H, 6.41; N, 5.23%. Found: C, 76.31; H, 6.40; N, 5.30%.

N-[(S)-1-(1-Naphthyl)ethyl]benzoylformamide 3c. To a cooled dry benzene solution (30 ml) in which benzoylformyl chloride (1.00 g, 6.00 mmol) was dissolved, (*S*)-1-(1-naphthyl)ethylamine (1.02 g, 6.00 mmol) and triethylamine (0.60 g, 6.00 mmol) were added dropwise. After the reaction, usual treatment was carried out. An oily product was obtained. Yield, 0.92 g (51%). R_f=0.24 (ethyl acetate-hexane (9:1)). $[\alpha]_D^{23.5}$ +0.8° (*c* 1.0, ethanol). $[\alpha]_D^{22.5}$ −46.8° (*c* 1.0, benzene). NMR (CCl_4); δ=1.6 (3H, d, 7 Hz), 5.9 (1H, m), 7.9 (13H, br). Calcd for $C_{20}H_{17}NO_2$: C 79.18; H, 5.64; N, 4.61%. Found: C, 78.04; H, 5.70; N, 4.53%.

Pyruvamides 5a—c. Chiral pyruvamides **5a**—c were prepared by the same manner as shown in the literatures.[8,21]

(S)-Phenylglycine Isobutyl Ester p-Toluenesulfonate[10]. (*S*)-Phenylglycine (3.02 g, 20.0 mmol), *p*-toluenesulfonic acid monohydrate (4.19 g, 22.0 mmol), and isobutyl alcohol (20 ml), were mixed in benzene (80 ml). The mixture was

refluxed for 58 h, and the water formed during the esterification was distilled off by the azeotropic method. Crude white product obtained after evaporation of the reaction mixture was recrystallized from ethanol–ether. Yield, 7.95 g (89%). Mp, 180—181 °C. $[\alpha]_D^{25}$ +67.0° (*c* 1.04, ethanol). R_f=0.60 (1-buthanol–acetic acid–water (4:1:2)). Calcd for $C_{19}H_{25}NO_5S$: C, 60.13; H, 6.64; N, 3.69%. Found: C, 60.26; H, 6.68; N, 3.67%.

N-Pyruvoyl-(S)-phenylglycine Isobutyl Ester **10**. To a cooled ethyl acetate solution of **8** (2.26 g, 5.67 mmol), racemic lactic acid (0.50 g, 5.67 mmol), triethylamine (0.57 g, 5.6 mmol), and *N*-hydroxysuccinimide (0.8 g, 6.9 mmol), dicyclohexylcarbodiimide (1.3 g, 6.3 mmol) was added. After the usual treatment of the reaction product, a crude oily product was obtained. The oily product was purified with silica-gel column chromatography (eluent; ethyl acetate–benzene (1:1)). A white solid was obtained by the evaporation of the fraction containing the product. Yield, 1.34 g (85%). This white solid (1.00 g, 3.58 mmol) was dissolved in 30 ml of acetone. To this solution, water (10 ml), acetic acid (1 ml), and $KMnO_4$ (1.0 g) was added under cooling in an ice–water bath. The reaction was carried out for 4 h in an ice–water bath and for 20 h at room temperature. After the reaction was over, MnO_2 was filtered off and the solution was extracted with three 50 ml of portions of benzene. The benzene layer was dried with $MgSO_2$, and then evaporated to afford crude oily product. This was purified with silica-gel column chromatography (benzene–ethyl acetate (19:1)). Yield, 0.28 g (28%). Mp, 63—64 °C. NMR ($CDCl_3$): δ=0.81 (6H, d, J=6 Hz), 1.9 (1H, m), 2.45 (3H, s), 3.92 (2H, d, J=6Hz), 5.49 (1H, d, J=8 Hz), 7.35 (5H, s), 7.85 (1H, br). $[\alpha]_D^{24}$ +114° (*c* 1.1, ethanol). Calcd for $C_{15}H_{19}NO_4$: C, 64.96; H, 6.90; N, 5.05%. Found: C, 64.91; H, 6.91; N, 5.01%.

Hydrogenations of **3a—c** *and Hydrolyses of the Products.* Substrates **3a—c** (500 mg) were dissolved in 10 ml of solvents [methanol (MeOH), ethanol (EtOH), 2-propanol (Pr^iOH), 2-methyl-2-propanol (Bu^tOH), 2-methyl-2-butanol ($C_5H_{11}{}^tOH$), and benzen] and were hydrogenated over 5% palladium on charcoal (purchased from Nippon Engelhald) at 30 °C. After 8—10 h reaction, the catalyst was filtered off, and the reaction mixtures were evaporated *in vacuo* to afford oily products. To these oily products, 20 ml of 6 mol dm^{-3} HCl was added and the mixtures were refluxed for 6 h. After hydrolysis, the reaction mixture was extracted with three 30 ml portions of ether. The ether layer was dried with $MgSO_4$ and the ether layer was evaporated to white solids. Chemical yields were determined by the measurement of the weight of the white solids and the optical purities of mandelic acid were determined by the measurement of the optical rotation.

Hydrogenations of **3a—c** *and Derivatization of the Products for GC Separation.* Substrates **3a—c** (25 mg, 0.10 mmol) were dissolved in 3 ml of solvents [MeOH, EtOH, Pr^iOH, Bu^t, ethyl acetate (AcOEt)] and were hydrogenated over 5% palladium on charcoal at 30 °C. After 8—10 h reaction, the catalyst was filtered off, and the reaction mixtures were evaporated to dryness. The chemical yields of the products were determined by the GC analyses of the residues. A portion of the residue was derivatized to *O*-TFA lactamide by the manner as described in the literature.[18] D. p. was determined by the GC separation of the *O*-TFA derivatives of diastereomeric mandelamides with a chiral stationary phase (Chirasil-Val).[18,25]

Catalyic Hydrogenations of Substrates **5a—c**[9] *and* **10**. Substrates **5a—c** (20 mg, 0.1 mmol) were dissolved in 3 ml of solvents [MeOH, EtOH, Pr^iOH, Bu^tOH, AcOEt, benzene, and *N,N*-dimethylformamide (DMF)], and were hydrogenated at 30 °C over 5% palladium on charcoal (100 mg) for 12—48 h. After the catalyst was filtered off, the reaction mixtures were evaporated to dryness. Both chemical yields[21] and d.p.[18] of the resulting lactamides were determined by the similar manner in the hydrogenations of substrates **3a—c**.

References

1) S. Mitsui and A. Kanai, *Nippon Kagaku Zasshi*, **86**, 627 (1965).
2) S. Mitsui and A. Kanai, *Nippon Kagaku Zasshi*, **87**, 179 (1966).
3) S. Mitsui and Y. Imai, *Nippon Kagaku Zasshi*, **88**, 86 (1967).
4) T. Kamaishi and S. Mitsui, *Nippon Kagaku zasshi*, **86**, 623 (1965).
5) M. Kawana and S. Emoto, *Bull. Chem. Soc. Jpn.*, **41**, 259 (1968).
6) D. Vallentine, Jr. and J. W. Scott, *Synthesis*, 329 (1978).
7) I. Ojima, T. Tanaka, and T. Kogure, *Chem. Lett.*, **1981**, 823.
8) K. Harada, T. Munegumi, and S. Nomoto, *Tetrahedron Lett.*, **22**, 111 (1981).
9) K. Harada and K. Matsumoto, *J. Org. Chem.*, **32**, 1794 (1967).
10) K. Harada and T. Yoshida, *Bull. Chem. Soc. Jpn.*, **43**, 921 (1970).
11) K. Harada and K. Matsumoto, *Bull. Chem. Soc. Jpn.*, **44**, 1068 (1971).
12) K. Harada and T. Yoshida, *J. Org. Chem.*, **37**, 4366 (1972).
13) K. Harada and Y. Kataoka, *Chem. Lett.*, **1978**, 791.
14) K. Harada and M. Tamura, *Bull. Chem. Soc. Jpn.*, **52**, 1227 (1979).
15) K. Harada and T. Munegumi, *Bull. Chem. Soc. Jpn.*, **56**, 2774 (1983).
16) K. Harada and S. Shiono, *Bull. Chem. Soc. Jpn.*, **57**, 1040 (1984).
17) K. Harada and S. Shiono, *Bull. Chem. Soc. Jpn.*, **57**, 1367 (1984).
18) T. Munegumi and K. Harada, *J. Chromatogr.*, **291**, 354 (1984).
19) M. S. Kharasch and H. C. Brown, *J. Am. Chem. Soc.*, **64**, 399 (1942).
20) D. D. Tarnner and N. C. Das, *J. Org. Chem.*, **35**, 3972 (1970).
21) T. Munegumi and K. Harada, *Bull. Chem. Soc. Jpn.*, **56**, 298 (1983).
22) A. J. Little, T. M. Lean, and F. J. Wilson, *J. Chem. Soc.*, **1941**, 337.
23) A. W. Ingersoll, *Org. Synth.*, Coll. Vol. II, 503 (1943).
24) W. C. Still, M. Kahn, and A. Mitra, *J. Org. Chem.*, **43**, 2923 (1978).
25) H. Frank, G. J. Nicolson, and E. Bayer, *J. Chromatogr.*, **146**, 197 (1978).

Studies on Peptide Antibiotic "Gratisin"

Makoto TAMAKI
Department of Chemistry, Faculty of Science, Toho University, Miyama, Funabashi-shi, Chiba 274
(Received June 1, 1984)

According to a primary structure proposed for an antibiotic peptide, gratisin, four peptides containing respectively partial sequences, L-Phe-L-Pro-L-Tyr, D-Phe-L-Pro-L-Tyr, L-Phe-L-Pro-D-Tyr, and D-Phe-L-Pro-D-Tyr, were synthesized by a liquid phase method. Among them, *cyclo*(-L-Val-L-Orn-L-Leu-D-Phe-L-Pro-D-Tyr-)$_2$ showed the strongest activity against the Gram-positive microorganisms tested. The activity toward *Bacillus subtilis* was similar to that of gramicidin S. Therefore, it is quite possible that natural gratisin is identical to this peptide. To facilitate a further investigation of the structure-activity relationship, four additional analogs were prepared. The results of their antibiotic activities showed that an interchange of D-Phe residues with D-Tyr residues caused the decrease of activity, and that the hydroxyl group of D-Tyr residues had no important role in this activity. The peptides possessing partial sequences, D-Phe-D-Tyr-L-Pro and L-Pro-D-Phe-D-Phe, exhibited strong activity. These facts show that the positions of Pro residues are not restricted to 5 and 5′ for the exhibition of the activity. The CD spectra of these synthetic peptides in an aqueous solution reflected the partial sequences around Pro residues, which affect largely the conformation of these synthetic antibiotics. The temperature dependence of these CD spectra indicated that the conformation of biologically active peptides is more stable than those of less active peptides.

An antibiotic peptide, gratisin, showing activity toward *Bacillus subtilis* 720 was isolated from *Bacillus brevis* Y-33 by Silaev *et al.*[1] It is a cyclododecapeptide composed of two each of Val, Orn, Leu, Phe, Pro, and Tyr residues. From an analogy of the primary structure of gramicidin S (GS) produced by *Bacillus brevis* ATCC 9999, the primary structure of gratisin was proposed (as shown in Fig. 1).[2,3] However, the configuration of each amino acid residue has not yet been established.

In this paper, the synthesis of several gratisin peptides shown in Fig. 2[4] and the relationship between structure and antibiotic activity will be described.

In the first of a series of studies on gratisin, gratisin peptide **I** consisted of only L-amino acid residues and gratisin peptide **II**, which has a structure analogous to GS containing D-Phe residues at positions 4 and 4′, were synthesized and the antibiotic activities of these peptides were examined.[5,6] Peptide **II** showed an activity against the Gram-positive microorganisms tested, but was less potent than GS. On the other hand, peptide **I** showed little activity. To study configurations of amino acid residues following Pro residues, peptide **III** having a Phe-Pro-D-Tyr partial sequence and peptide **IV** having a D-Phe-Pro-D-Tyr partial sequence were synthesized.[7,8] Peptide **III** was almost inactive. On the other hand, peptide **IV** showed a marked activity against the Gram-positive microorganisms tested. Its activity against *Bacillus subtilis* was similar to that of GS and stronger than that of peptide **II**. Peptide **V** having a D-Tyr-Pro-D-Phe partial sequence and peptide **VI** having a D-Phe-Pro-D-Phe partial sequence were synthesized in order to investigate the role of the side chain of D-Phe residues at 4 and 4′, and D-Tyr residues at 6 and 6′. A Pro residue is frequently found in β-turns in naturally occuring proteins[9] and peptides[10–12], and is known to play an important role in stabilizing their conformations. To investigate the roles of Pro residues in gratisin, peptide **VII** having Pro residues at positions 6 and 6′, and peptide **VIII** having Pro residues at 4 and 4′ were synthesized.

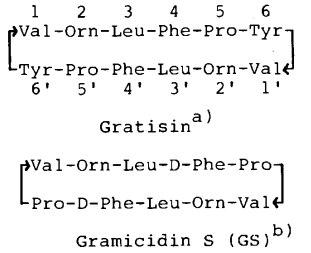

Fig. 1. Proposed structure of gratisin and structure of gramicidin S.
a) The configuration of each amino acid residue has not been established yet. b) Abbreviations with no prefix show L-amino acid residue.

I. cyclo(-Val-Orn-Leu-Phe-Pro-Tyr-)$_2$
II. cyclo(-Val-Orn-Leu-D-Phe-Pro-Tyr-)$_2$
III. cyclo(-Val-Orn-Leu-Phe-Pro-D-Tyr-)$_2$
IV. cyclo(-Val-Orn-Leu-D-Phe-Pro-D-Tyr-)$_2$
V. cyclo(-Val-Orn-Leu-D-Tyr-Pro-D-Phe-)$_2$
VI. cyclo(-Val-Orn-Leu-D-Phe-Pro-D-Phe-)$_2$
VII. cyclo(-Val-Orn-Leu-D-Phe-D-Tyr-Pro-)$_2$
VIII. cyclo(-Val-Orn-Leu-Pro-D-Phe-D-Phe-)$_2$

Fig. 2. Structure of synthesized peptides **I—VIII**.
Abbreviations with no prefix show L-amino acid residue.

Results and Discussion

Synthesis of Gratisin Peptides I—VIII. Each cyclododecapeptide **I—VIII** consists of two identical hexapeptide sequences (Fig. 2). Therefore, these peptides were synthesized according to the following three steps: 1) synthesis of hexapeptides by stepwise elongation; 2) synthesis of dodecapeptides by condensation between two of the fragment hexapeptides; 3) cyclization of the dodecapeptides by an azide or active-ester method. In the synthesis of these peptides, Pro residue was chosen as the C-terminal amino acid in order to avoid racemization in the fragment

condensation and the cyclization step. The benzyl (Bzl) group was used as the protector of the carboxyl groups. α-amino groups were protected by a *t*-butoxycarbonyl (Boc) group. The δ-amino group of Orn residue was protected by a benzyloxycarbonyl (Z), and the hydroxyl group of Tyr residue by a benzyl (Bzl) group or a 2,6-dichlorobenzyl ($BzlCl_2$) group. In the synthesis of gratisin peptides **I**—**VIII**, each Boc-hexapeptide benzyl ester was synthesized by stepwise elongation using dicyclohexylcarbodiimide (DCC) or 1-ethyl-3-(3-dimethylaminopropyl)carbodiimide (WSCD) and 1-hydroxybenzotriazole (HOBt) (Scheme 1). Throughout the synthesis of each Boc-hexapeptide benzyl ester, intermediates were purified by only washing with 5% citric acid and 5% Na_2CO_3. The purities of the intermediates were confirmed by thin-layer chromatography with several solvent systems. Finally, each Boc-hexapeptide benzyl ester was purified by silica-gel column chromatography followed by recrystallization. The homogeneity of each Boc-hexapeptide benzyl ester was confirmed by thin-layer chromatography, amino acid analysis and elemental analysis.

i) Synthesis of Gratisin Peptide I. Three different procedures were examined for the synthesis of gratisin peptide **I**. In the first trial, Pro residue was chosen as the C-terminal amino acid of the dodecapeptide, and cyclization was carried out by an azide method. However, the cyclization of H-[Tyr(Bzl)-Val-Orn(Z)-Leu-Phe-Pro-]$_2$-N_3, did not proceed under the usual conditions. In the pathway of the biosynthesis of GS and tyrocidine in *Bacillus brevis*, they are produced by cyclization of the linear decapeptide with a Leu residue at the C-terminal.[13,14] In the imitation of the biosynthesis, a Leu residue was chosen as the C-terminal residue and the cyclization was also tried using an azide method *via* H-[Phe-Pro-Tyr(Bzl)-Val-Orn(Z)-Leu-]$_2$-N_3. Though this trial was also unsuccessful, it afforded a ninhydrin-negative compound. In an amino acid analysis of the acid hydrolysate of this product, each value of Val, Orn, Phe, Pro, and Tyr was in good agreement with the value expected for the gratisin peptide, but the value obtained by Leu was one-half of the value. The results of amino acid and elemental analyses of this product can be explained by giving it the following tentative structure; *cyclo*[-Phe-Pro-Tyr-(Bzl)-Val-Orn(Z)-Leu-Phe-Pro-Tyr(Bzl)-Val-Orn(Z)-

$$\begin{array}{l} CH_2\text{-}CH(CH_3)_2 \\ | \\ NH\text{-}CH\text{-}NH\text{-}CO\text{-} \end{array}$$

].

The cyclization to give peptide **I** was finally achieved using an active-ester method, according to Scheme 2. The active ester (**Id'**) was prepared by the following procedure. The coupling of Boc-hexapeptide hydrazide (**Ib**) with H-Tyr(Bzl)-Val-Orn(Z)-Leu-Phe-Pro-OH derived from **Ic** was carried out by an azide method. The product was purified by Sephadex LH-20 gel filtration, which was very effective for the removal of the contaminating amine and acid components. The Boc-dodecapeptide (**Id**) was converted into the corresponding active ester by WSCD and *N*-hydroxysuccinimide (HOSu). The active ester (**Id'**) was deprotected with trifluoroacetic acid (TFA) in the presence of anisole and then subjected to cyclization at 60 °C for 3 h under high dilution in pyridine ($<3\times10^{-3}$ M 1 M=1 mol dm^{-3}) to minimize intermolecular reactions. The product was purified by chromatography on a silica-gel column followed by recrystallization. The yield of the cyclization was 29%. The removal of the protecting groups of cyclododecapeptide (**Ie**) by hydrogenolysis in methanol containing hydrogen chloride afforded peptide **I**.

In the synthesis of gratisin peptide **III**, cyclization *via* the azide, H-[D-Tyr($BzlCl_2$)-Val-Orn(Z)-Leu-Phe-Pro-]$_2$-N_3, did not proceed. Hence, cyclization was carried out using an active-ester method similar to that described in the synthesis of gratisin peptide **I**. The desired peptide was obtained at a yield of 60%.

Peptides **VII** and **VIII** were also synthesized in a similar manner. The yields of cyclization by an active-ester method were 62% (peptide **VII**) and 57% (**VIII**).

ii) Synthesis of Gratisin Peptide II. Peptide **II** was prepared according to Scheme 3. Boc-dodecapeptide benzyl ester (**IIc**) was obtained by the coupling of two hexapeptides (**IIa'** and **IIb**). The product was

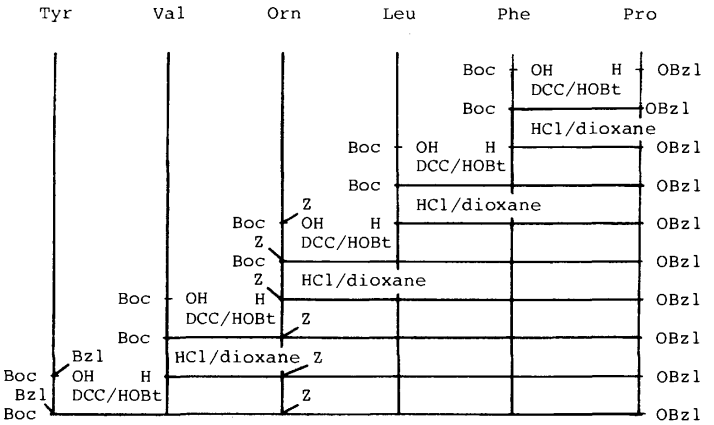

Scheme 1. Synthesis of Boc-Tyr(Bzl)-Val-Orn(Z)-Leu-Phe-Pro-OBzl (**Ia**).
* Each hexapeptide (**IIa**—**VIIIa**) was synthesized by a similar method.
WSCD was used the coupling reagent in synthesis of **IVa**—**VIIIa** instead of DCC.

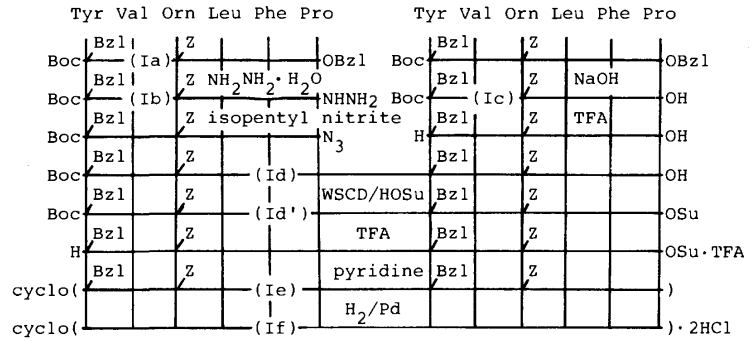

Scheme 2. Synthesis of *cyclo*(-Tyr-Val-Orn-Leu-Phe-Pro-)$_2$·2HCl (**If**).
* Gratisin peptides **III**, **VII**, and **VIII** were synthesized by a similar manner.

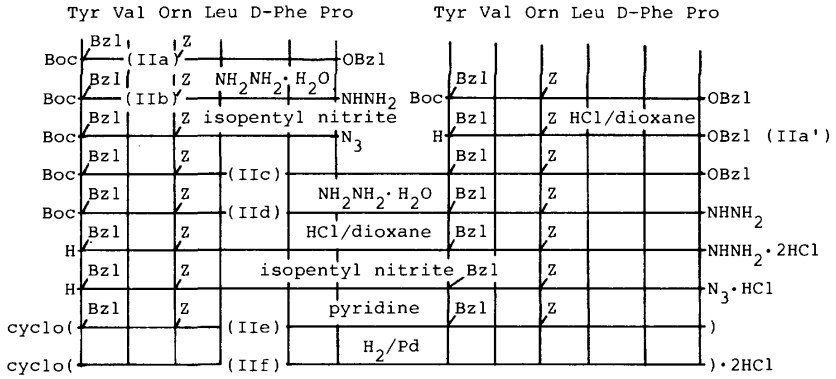

Scheme 3. Synthesis of *cyclo*(-Tyr-Val-Orn-Leu-D-Phe-Pro-)$_2$·2HCl (**IIf**).
* Gratisin peptides **IV**—**VI** were synthesized by a similar manner.

purified by Sephadex LH-20 gel filtration and silica-gel column chromatography. **IIc** was converted into hydrazide **IId**. Then, it was treated with 4M HCl/dioxane in the presence of anisole, and converted into an azide with isopentyl nitrite at −20 °C for 15 min. The azide could be cyclized under high dilution in pyridine at 0 °C for 3 d. The resulting product was purified by silica-gel column chromatography following recrystallization. The yield of cyclization was 43%. The removal of all masking groups by hydrogenolysis yielded peptide **II**.

Peptides **IV**—**VI** were synthesized by a method similar to that described for peptide **II**. The yields of cyclization by the azide method were 63 (peptide **IV**), 29 (**V**), and 41% (**VI**).

The homogeneity of peptides **I**—**VIII** was confirmed by means of thin-layer chromatography, electrophoresis, amino acid analysis and elemental analysis (Table 1 and 3). The molecular weight of the fully protected cyclic peptides were measured by a vapor-pressure osmometer and were in good agreement with the respective calculated values.

In the synthesis of peptides **I**—**IV**, cyclization was carried out by an azide method in the first trial. In the case of peptides **II** and **IV**, both having a D-Phe-Pro partial sequence, the cyclization proceeded satisfactorily. On the other hand, the cyclization of peptides **I** and **III**, both having a L-Phe-Pro partial sequence, did not proceed well by this method. The investigation of CPK molecular models of these four sequences elucidated that the β-methylene group

Table 1. Amino acid analysis of gratisin peptides **I**—**VIII**

	Val	Orn	Leu	Phe	Pro	Tyr
I.	1.04	1.04	1.06	1.02	0.94	0.91
II.	1.04	1.03	1.04	1.03	0.96	0.91
III.	1.07	1.03	1.01	0.94	0.94	0.94
IV.	1.03	1.09	1.02	0.92	0.95	0.90
V.	0.95	1.07	1.08	0.93	1.06	0.90
VI.	1.01	0.99	1.04	1.93	1.02	—
VII.	1.00	1.02	1.00	1.00	1.02	0.95
VIII.	1.00	0.99	1.03	1.99	0.99	—

of L-Phe residue preceding Pro residue collides with the δ-methylene group of the Pro residue if the L-Phe-Pro sequence take GS-like β-turn. On the other hand, the D-Phe-Pro sequence seems to favor the formation of β-turn. A similar tendency to β-turn formation was also reported for cyclic hexapeptides containing a D-Phe-Pro sequence by Kopple *et al.*[15], and on GS analogs and linear tetrapeptides with partial sequences related to the β-turn part of GS by Nagai *et al.*[16,17] The feasibility of the cyclization in the preparation of peptides **II** and **IV** by an azide method might result from such a β-turn preference in their primary structure containing a D-Phe-Pro sequence. The synthesis of peptides **I** and **III** was finally accomplished by an active-ester method. Under the conditions of this method, the degree of conformational freedom of the corresponding linear peptides

Table 2. Antibiotic activities of GS and synthetic peptides I—VIII[a]

Test organisms	GS	I	II	III	IV	V	VI	VII	VIII
Staph. aureus ATCC 6538P	1.6	>50	50	50	6.3	25	6.3	3.1	12.5
Strept. pyogenes N.Y. 5	1.6	>50	12.5	>100	3.1	12.5	6.3	6.3	6.3
Micrococcus flavus ATCC 10240	0.8	25	12.5	12.5	3.1	6.3	1.6	1.6	6.3
Corynebact. diphtheriae P.W. 8	0.8	25	3.1	100	3.1	6.3	1.6	1.6	3.1
Bac. subtilis ATCC 6633	3.1	>50	50	>100	3.1	25	6.3	3.1	3.1
E. coli NIHJ-JC2	>100	>50	>50	>100	>50	>50	>100	>100	>50
Proteus vulgaris OX 19	>100	>50	>50	>100	>50	>50	>100	>100	>50

a) Minimum inhibitory concentration in μg/ml: The minimum amount of the compounds necessary for the complete inhibition of the growth was determined by an agar dilution method with 10^6 organisms per milliter.

was enhanced as compared with that in an azide method, because the reaction was performed at a higher temperature. The increase of a chance collision between N- and C-terminals in the linear peptides might explain why cyclization by an active-ester method proceeded better than with an azide method.

Antibiotic Activity. The antibiotic activities of synthetic peptides **I—VIII** are shown in Table 2. Peptides **I—IV** have the amino acid sequence proposed by Silaev *et al.*, although the configurations of the amino acid residues preceding and following the Pro residue differ from each other. The extent of the activities of these pepides is influenced by the configuration of the amino acid residues. Peptide **I** and **III** having, respectively, L-Phe-Pro-L-Tyr and L-Phe-Pro-D-Tyr partial sequences showed little activity. Peptide II containing a D-Phe-Pro-L-Tyr partial sequence was active toward Gram-positive miroorganisms tested, but its activity against *Bacillus subtilis* was 1/16 of that of GS. On the other hand, peptide **IV** possessing a D-Phe-Pro-D-Tyr partial sequence was most active in peptides **I—IV**, and its activity against *Bacillus subtilis* was similar to that of GS. These results indicated that the presence of D-Phe residues at 4 and 4′ is important for activity, and D-residues at positions 6 and 6′ also contribute to activity. Although we have had no opportunity to directly compare our synthetic peptides with natural gratisin, it is quite possible that synthetic peptide **IV** possessing D-residues in positions 4, 4′, 6, and 6′ is identical with the natural antibiotic.

The activity of peptide **V** was 1/2—1/8 of that of peptide **IV**. This result points out the significance of the D-Phe residues at 4 and 4′ regarding activity. Similar results have been obtained for GS analogs.[18–20] For example, [D-Tyr$^{4,4'}$]-GS containing D-Tyr residues in place of D-Phe residues displayed only about 1/3 of the activity of GS.[18] On the other hand, peptide **VI** showed a similar activity to that of peptide **IV**. The result suggests that the hydroxyl groups of D-Tyr residues in the 6 and 6′ positions are not necessary for activity.

Peptide **VII** showed the highest activity among peptides **I—VIII**, and its activity against *Bacillus subtilis* was the same as that of GS. The activity of peptide **VIII** against *Bacillus subtilis* was also the same as that of GS, but the activity against other microorganisms was a little less compared to peptides **IV** and **VII**. It is an unexpected result that peptides **VII** and **VIII**, in which the Pro residues occupy positions different from 5 and 5′, showed a strong antibiotic activity, considering the restriction of the sequence in GS for its activity.[21] Supposing that the action mode of gratisin is the same as that of GS[22], this result suggests that the presence of additional amino acid residures, D-Tyr or D-Phe, in gratisin peptides make them more likely to adopt a conformation suitable for the antibiotic action regardless of the transfer of Pro residue, in comparison with rigidity of the structure of GS.

Secondary Structure-Activity Relationship. CD spectra of GS and synthetic peptides **I—VIII** (dihydrochloride) in aqueous solution are shown in Figs. 3 and 4. These spectra are classified into four groups according to their configuration around the Pro residue (Fig. 3). The spectrum of gratisin peptide **I** was characterized by a small negative band near 211 nm and a shoulder near 230 nm (Fig. 3-a), and resembles that of [L-Ala$^{4,4'}$]-GS.[16] The spectrum of peptide **II** showed double-minima in a similar region to that of GS, although its ellipticity was less (Fig. 3-b). Since peptide **II** has a D-Phe-Pro partial sequence similar to GS, these two peptides seem to adopt an analogous conformation to give similar CD spectra. A similar result was obtained by Takiguchi *et al.*[23] in a study on an analog of GS with a larger ring size. Their analog (*iso*-GS) involves two amide bonds between the carboxyl groups of Val residues and the δ-amino groups of Orn residues and, hence, the number of ring members of this analog is equal to that of peptide **II**. This analog showed an ORD spectrum similar to that of GS, but its trough was shallower than that of GS. The CD pattern of peptide **VII** is also similar to that of GS. (Fig. 3-b) and might result from the presence of a D-X-Pro-L-Y partial sequence in the peptide. The spectrum of peptide **III** showed negative bands near 199 nm and 230 nm, and a shoulder near 215 nm (Fig. 3-c). The CD spectrum of peptide **VIII** was characterized by a positive band at 217 nm and a shoulder near 205 nm, but was similar in shape to that of peptide **III**. The spectra of peptides **IV—VI** resembled each other and were characterized by negative bands near 200 nm and shoulders near 220 nm (Fig. 3-d). Some differences were found in ellipticities near 200 nm. However, no relationship between the depth of the trough in these CD spectra and antibiotic activity could be found.

Table 3. Yields, physical properties and analytical data of gratisin peptides **I**—**VIII**

	Yield %	Mp θ_m/°C	$[\alpha]_D^{25}$ (c 1, DMF)		Elemental analysis/%				R_f^1	R_f^2	R_f^3	R_f^4
						C	H	N				
Gratisin Peptide **I**												
a) Boc-Tyr(Bzl)-Val-Orn(Z)-Leu-Phe-Pro-OBzl	47	196—199	−27.7	$C_{66}H_{83}N_7O_{12}$	C:	67.96	7.17	8.41	0.94	0.67		
					F:	67.66	7.26	8.39				
b) Boc-Try(Bzl)-Val-Orn(Z)-Leu-Phe-Pro-$NHNH_2$	71	174—178	−27.4	$C_{59}H_{79}N_9O_{11}$	C:	64.99	7.30	11.56	0.69	0.62		
					F:	64.89	7.56	11.46				
c) Boc-Tyr(Bzl)-Val-Orn(Z)-Leu-Phe-Pro-OH	88	163—166	−23.2	$C_{59}H_{77}N_7O_{12}$ $\cdot 1/2H_2O$	C:	65.29	7.24	9.04	0.60	0.62		
					F:	65.24	7.38	9.22				
d) Boc-[Tyr(Bzl)-Val-Orn(Z)-Leu-Phe-Pro-]$_2$-OH	67	216—219 (dec.)	−32.0	$C_{113}H_{144}N_{14}O_{21}$ $\cdot 1/2H_2O$	C:	66.42	7.15	9.60	0.52	0.65		
					F:	66.42	7.39	10.04				
e) *cyclo*[-Tyr(Bzl)-Val-Orn(Z)-Leu-Phe-Pro-]$_2$	29	268—269 (dec.)	−47.5	$C_{108}H_{134}N_{14}O_{18}$ $\cdot H_2O$	C:	67.06	7.09	10.14	0.65	0.50		
					F:	66.77	7.02	10.14				
f) *cyclo*(-Tyr-Val-Orn-Leu-Phe-Pro-)$_2\cdot$2HCl	94	236—241 (dec.)	−78.0 (EtOH c 0.15)	$C_{78}H_{110}N_{14}O_{14}$ $\cdot 2HCl\cdot 7H_2O$	C:	56.20	7.62	11.77			0.78	0.81
					F:	56.00	7.47	12.24				
Gratisin Peptide **II**												
a) Boc-Tyr(Bzl)-Val-Orn(Z)-Leu-D-Phe-Pro-OBzl	64	205—207	−27.7	$C_{66}H_{83}N_7O_{12}$	C:	67.96	7.17	8.14	0.94	0.64		
					F:	67.68	7.36	7.93				
b) Boc-Tyr(Bzl)-Val-Orn(Z)-Leu-D-Phe-Pro-$NHNH_2$	100	180—182	−30.4	$C_{59}H_{79}N_9O_{11}$	C:	64.99	7.30	11.56	0.65	0.54		
					F:	64.57	7.58	11.68				
c) Boc-[Tyr(Bzl)-Val-Orn(Z)-Leu-D-Phe-Pro-]$_2$-OBzl	60	180—183	−42.8	$C_{120}H_{150}N_{14}O_{21}$	C:	67.84	7.12	9.23	0.93	0.64		
					F:	67.51	7.13	9.33				
d) Boc-[Tyr(Bzl)-Val-Orn(Z)-Leu-D-Phe-Pro-]$_2$-$NHNH_2$	94	153—157	−42.0	$C_{113}H_{146}N_{16}O_{20}$ $\cdot H_2O$	C:	65.68	7.22	10.84	0.77	0.60		
					F:	65.28	7.21	10.88				
e) *cyclo*[-Tyr(Bzl)-Val-Orn(Z)-Leu-D-Phe-Pro-]$_2$	43	169—173	−77.5 (c 0.2)	$C_{108}H_{134}N_{14}O_{18}$ $\cdot H_2O$	C:	67.06	7.09	10.14	0.72	0.60		
					F:	67.04	7.21	10.34				
f) *cyclo*(-Tyr-Val-Orn-Leu-D-Phe-Pro-)$_2\cdot$2HCl	90	267—269 (dec.)	−130.0 (EtOH c 0.15)	$C_{78}H_{110}N_{14}O_{14}$ $\cdot 2HCl\cdot 7H_2O$	C:	56.20	7.62	11.77			0.69	0.79
					F:	56.51	7.14	11.42				
Gratisin peptide **III**												
a) Boc-D-Tyr($BzlCl_2$)-Val-Orn(Z)-Leu-Phe-Pro-OBzl	63	170—173	−17.9	$C_{66}H_{81}N_7O_{12}Cl_2$ $\cdot H_2O$	C:	63.25	6.67	7.82	0.73	0.64		
					F:	63.31	6.58	7.81				
b) Boc-D-Tyr($BzlCl_2$)-Val-Orn(Z)-Leu-Phe-Pro-$NHNH_2$	97	138—142	−12.3	$C_{59}H_{77}N_9O_{11}Cl_2$ $\cdot 1/2H_2O$	C:	60.65	6.73	10.79	0.48	0.41		
					F:	60.89	6.41	10.67				
c) Boc-D-Tyr($BzlCl_2$)-Val-Orn(Z)-Leu-Phe-Pro-OH	99	146—150	−13.3	$C_{59}H_{75}N_7O_{12}Cl_2$ $\cdot H_2O$	C:	60.92	6.67	8.43	0.30	0.45		
					F:	61.34	6.58	7.82				
d) Boc-[D-Tyr($BzlCl_2$)-Val-Orn(Z)-Leu-Phe-Pro-]$_2$-OH	43	175—179	−12.9	$C_{113}H_{140}N_{14}O_{21}Cl_4$ $\cdot 2H_2O$	C:	61.46	6.57	8.88	0.28	0.40		
					F:	61.85	6.75	8.34				

Table 3. Continued.

		Yield %	Mp θ_m/°C	$[\alpha]_D^{25}$ (c 1, DMF)		Elemental analysis/%			R_f^1	R_f^2	R_f^3	R_f^4
							C	H	N				
e)	*cyclo*[-D-Tyr($BzlCl_2$)-Val-Orn(Z)-Leu-Phe-Pro-]$_2$	60	228—229	+0.9	$C_{108}H_{130}N_{14}O_{18}Cl_4$	C:	63.15	6.38	9.55	0.70	0.60		
						F:	62.79	6.22	9.55				
f)	*cyclo*(-D-Tyr-Val-Orn-Leu-Phe-Pro-)$_2$·2HCl	55	283—287 (dec.)	−44.5 (DMF c 0.25)	$C_{78}H_{110}N_{14}O_{14}$ ·2HCl·6H_2O	C:	56.81	7.58	11.89			0.69	0.79
						F:	57.00	7.39	11.64				
	Gratisin peptide **IV**												
a)	Boc-D-Tyr($BzlCl_2$)-Val-Orn(Z)-Leu-D-Phe-Pro-OBzl	41	172—176	−15.6	$C_{66}H_{81}N_7O_{12}Cl_2$	C:	64.17	6.67	7.94	0.66	0.59		
						F:	63.85	6.89	7.66				
b)	Boc-D-Tyr($BzlCl_2$)-Val-Orn(Z)-Leu-D-Phe-Pro-$NHNH_2$	95	144—148	−19.5	$C_{59}H_{77}N_9O_{11}Cl_2$ ·H_2O	C:	60.20	6.60	10.70	0.49	0.45		
						F:	60.20	6.82	10.09				
c)	Boc-[D-Tyr($BzlCl_2$)-Val-Orn(Z)-Leu-D-Phe-Pro-]$_2$-OBzl	64	199—201	−21.7	$C_{120}H_{146}N_{14}O_{21}Cl_4$	C:	63.70	6.50	8.68	0.70	0.60		
						F:	63.62	6.25	8.67				
d)	Boc-[D-Tyr($BzlCl_2$)-Val-Orn(Z)-Leu-D-Phe-Pro-]$_2$-$NHNH_2$	94	205—206	−27.1	$C_{113}H_{142}N_{16}O_{20}Cl_4$ ·2H_2O	C:	61.07	6.62	10.08	0.46	0.43		
						F:	61.13	6.72	9.58				
e)	*cyclo*[-D-Tyr($BzlCl_2$)-Val-Orn(Z)-Leu-D-Phe-Pro-]$_2$	63	273—276	−24.0 (c 0.2)	$C_{108}H_{130}N_{14}O_{18}Cl_4$	C:	63.15	6.38	9.55	0.65	0.59		
						F:	63.26	6.25	9.51				
f)	*cyclo*(-D-Tyr-Val-Orn-Leu-D-Phe-Pro-)$_2$·2HCl	90	246—249 (dec.)	−72.3 (EtOH c 0.2)	$C_{78}H_{110}N_{14}O_{14}$ ·2HCl·7H_2O	C:	56.20	7.62	11.77			0.66	0.75
						F:	56.43	7.64	11.18				
	Gratisin peptide **V**												
a)	Boc-D-Phe-Val-Orn(Z)-Leu-D-Tyr($BzlCl_2$)-Pro-OBzl	63	152—155	−20.7	$C_{66}H_{81}N_7O_{12}Cl_2$	C:	64.17	6.67	7.94	0.72	0.59		
						F:	63.86	6.75	7.77				
b)	Boc-D-Phe-Val-Orn(Z)-Leu-D-Tyr($BzlCl_2$)-Pro-$NHNH_2$	90	132—135	−28.0	$C_{59}H_{77}N_9O_{11}Cl_2$	C:	61.13	6.70	10.87	0.59	0.46		
						F:	60.79	6.68	10.58				
c)	Boc-[D-Phe-Val-Orn(Z)-Leu-D-Tyr($BzlCl_2$)-Pro-]$_2$-OBzl	56	195—196	−22.3	$C_{120}H_{146}N_{14}O_{21}Cl_4$	C:	63.70	6.50	8.68	0.83	0.59		
						F:	63.56	6.74	8.41				
d)	Boc-[D-Phe-Val-Orn(Z)-Leu-D-Tyr($BzlCl_2$)-Pro-]$_2$-$NHNH_2$	85	188—190	−27.6	$C_{113}H_{142}N_{16}O_{20}Cl_4$	C:	62.08	6.55	10.25	0.64	0.50		
						F:	62.05	6.79	9.96				
e)	*cyclo*[-D-Phe-Val-Orn(Z)-Leu-D-Tyr($BzlCl_2$)-Pro-]$_2$	29	256—257	−32.0	$C_{108}H_{130}N_{14}O_{18}Cl_4$	C:	63.15	6.38	9.55	0.80	0.59		
						F:	62.90	6.37	9.15				
f)	*cyclo*(-D-Phe-Val-Orn-Leu-D-Tyr-Pro-)$_2$·2HCl	95	234—237 (dec.)	−107.0 (EtOH c 0.2)	$C_{78}H_{110}N_{14}O_{14}$ ·2HCl·7H_2O	C:	56.20	7.62	11.77			0.73	0.72
						F:	56.29	7.44	11.12				
	Gratisin peptide **VI**												
a)	Boc-D-Phe-Val-Orn(Z)-Leu-D-Phe-Pro-OBzl	70	181—183	−20.3	$C_{59}H_{77}N_7O_{11}$	C:	66.83	7.32	9.25	0.70	0.58		
						F:	66.35	7.34	8.62				
b)	Boc-D-Phe-Val-Orn(Z)-Leu-D-Phe-Pro-$NHNH_2$	95	174—176	−26.7	$C_{52}H_{73}N_9O_{10}$	C:	63.46	7.48	12.81	0.49	0.40		
						F:	63.04	7.84	12.37				

Table 3. Continued.

		Yield %	Mp θ_m/°C	$[\alpha]_D^{25}$ (c 1, DMF)		Elemental analysis/%			R_f^1	R_f^2	R_f^3	R_f^4
							C	H	N				
c)	Boc-[D-Phe-Val-Orn(Z)-Leu-D-Phe-Pro-]$_2$-OBzl	51	216—219	−26.3	$C_{106}H_{138}N_{14}O_{19}$	C:	66.58	7.27	10.25	0.85	0.56		
						F:	66.36	7.44	10.06				
d)	Boc-[D-Phe-Val-Orn(Z)-Leu-D-Phe-Pro-]$_2$-NHNH$_2$	93	212—216	−24.6	$C_{99}H_{134}N_{16}O_{18}$ ·H_2O	C:	64.13	7.44	12.09	0.63	0.42		
						F:	64.12	7.41	11.98				
e)	*cyclo*[-D-Phe-Val-Orn(Z)-Leu-D-Phe-Pro-]$_2$	41	288—289 (dec.)	−37.3	$C_{94}H_{122}N_{14}O_{16}$	C:	66.25	7.22	11.51	0.63	0.56		
						F:	66:10	7.28	11.75				
f)	*cyclo*(-D-Phe-Val-Orn-Leu-D-Phe-Pro-)$_2$·2HCl	81	254—257 (dec.)	−90.8 (EtOH c 0.2)	$C_{78}H_{110}N_{14}O_{12}$ ·2HCl·6H_2O	C:	57.94	7.73	12.13			0.73	0.73
						F:	58.09	7.41	12.14				
	Gratisin peptide **VII**												
a)	Boc-Val-Orn(Z)-Leu-D-Phe-D-Tyr(BzlCl$_2$)-Pro-OBzl	63	111—115	−16.7	$C_{66}H_{81}N_7O_{12}Cl_2$ ·1/2H_2O	C:	63.70	6.64	7.88	0.88	0.54		
						F:	63.68	6.61	7.82				
b)	Boc-Val-Orn(Z)-Leu-D-Phe-D-Tyr(BzlCl$_2$)-Pro-NHNH$_2$	98	112—118	−16.9	$C_{59}H_{77}N_9O_{11}Cl_2$	C:	61.13	6.70	10.87	0.64	0.54		
						F:	60.92	7.01	10.98				
c)	Boc-Val-Orn(Z)-Leu-D-Phe-D-Tyr(BzlCl$_2$)-Pro-OH	92	135—139	−11.3	$C_{59}H_{75}N_7O_{12}Cl_2$	C:	61.88	6.60	8.56	0.50	0.50		
						F:	61.87	6.68	8.45				
d)	Boc-[Val-Orn(Z)-Leu-D-Phe-D-Tyr(BzlCl$_2$)-Pro-]$_2$-OH	20	145—148	−12.6 (c 0.5)	$C_{113}H_{140}N_{14}O_{21}Cl_4$ ·H_2O	C:	61.97	6.53	9.02	0.55	0.53		
						F:	61.58	6.53	9.39				
e)	*cyclo*[-Val-Orn(Z)-Leu-D-Phe-D-Tyr(BzlCl$_2$)-Pro-]$_2$	62	151—153	−16.6 (c 0.3)	$C_{108}H_{130}N_{14}O_{18}Cl_4$ ·H_2O	C:	62.72	6.24	9.48	0.70	0.58		
						F:	62.46	6.41	9.60				
f)	*cyclo*(-Val-Orn-Leu-D-Phe-D-Tyr-Pro-)$_2$·2HCl	83	231—235 (dec.)	−102.7 (EtOH c 0.2)	$C_{78}H_{110}N_{14}O_{14}$ ·2HCl·8H_2O	C:	55.60	7.65	11.64			0.68	0.78
						F:	55.36	7.14	11.54				
	Gratisin peptide **VIII**												
a)	Boc-D-Phe-D-Phe-Val-Orn(Z)-Leu-Pro-OBzl	52	207—208	−29.6	$C_{59}H_{77}N_7O_{11}$	C:	66.83	7.32	9.25	0.84	0.57		
						F:	66.67	7.43	9.26				
b)	Boc-D-Phe-D-Phe-Val-Orn(Z)-Leu-Pro-NHNH$_2$	85	174—176	−23.3	$C_{52}H_{73}N_9O_{10}$	C:	63.46	7.48	12.81	0.53	0.52		
						F:	63.21	7.45	12.65				
c)	Boc-D-Phe-D-Phe-Val-Orn(Z)-Leu-Pro-OH	75	156—162	−25.0	$C_{52}H_{71}N_7O_{11}$	C:	64.38	7.38	10.10	0.55	0.53		
						F:	64.16	7.48	10.20				
d)	Boc-[D-Phe-D-Phe-Val-Orn(Z)-Leu-Pro-]$_2$-OH	57	177—185	−18.6	$C_{99}H_{132}N_{14}O_{19}$ ·H_2O	C:	64.57	7.34	10.65	0.45	0.67		
						F:	64.11	7.17	10.64				
e)	*cyclo*[-D-Phe-D-Phe-Val-Orn(Z)-Leu-Pro-]$_2$	57	275—277 (dec.)	+55.5 (c 0.2)	$C_{94}H_{122}N_{14}O_{16}$ ·H_2O	C:	65.51	7.26	11.38	0.72	0.60		
						F:	65.28	7.19	11.25				
f)	*cyclo*(-D-Phe-D-Phe-Val-Orn-Leu-Pro-)$_2$·2HCl	78	258—260 (dec.)	−9.7 (EtOH c 0.2)	$C_{78}H_{110}N_{14}O_{12}$ ·2HCl·5H_2O	C:	58.55	7.69	12.26			0.66	0.81
						F:	58.90	7.21	11.85				

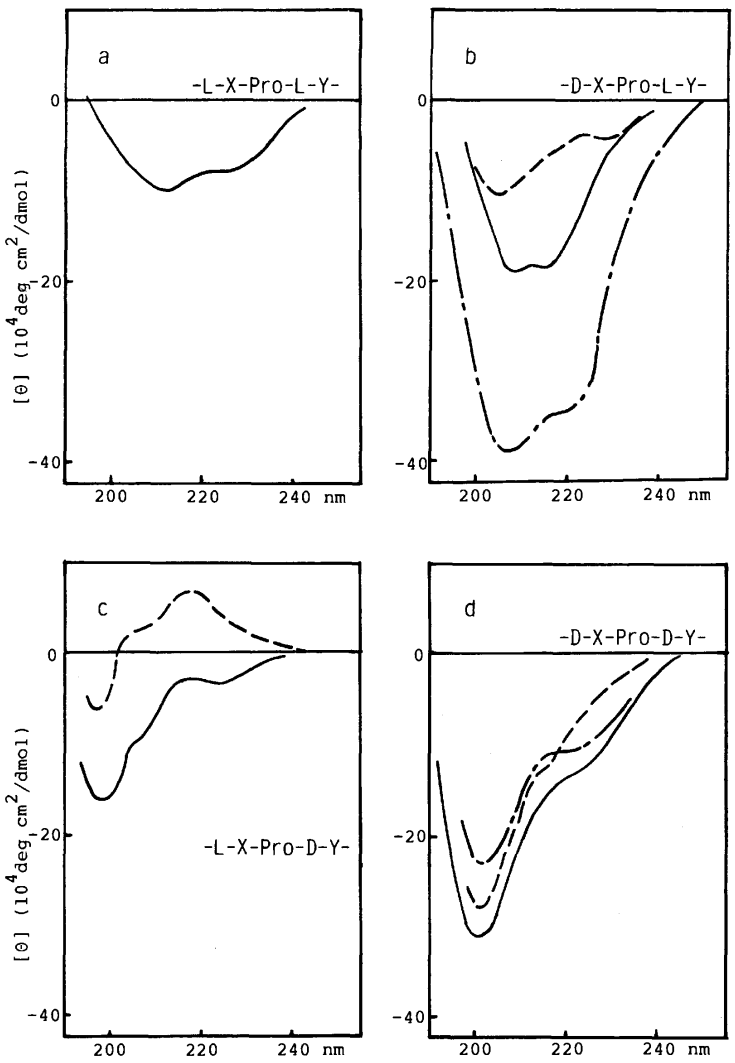

Fig. 3. CD spectra of GS and gratisin peptides **I**—**VIII** in aqueous solution. (a) **I**. *cyclo*(-Val-Orn-Leu-Phe-Pro-Tyr-)$_2$ ——; (b) **II**. *cyclo*(-Val-Orn-Leu-D-Phe-Pro-Tyr-)$_2$ ——, **VII**. *cyclo*(-Val-Orn-Leu-D-Phe-D-Tyr-Pro-)$_2$ ——, GS. *cyclo*(-Val-Orn-Leu-D-Phe-Pro-)$_2$ ——; (c) **III**. *cyclo*(-Val-Orn-Leu-Phe-Pro-D-Tyr-)$_2$ ——, **VIII**. *cyclo*(-Val-Orn-Leu-Pro-D-Phe-D-Phe-)$_2$ ——; (d) **IV**. *cyclo*(-Val-Orn-Leu-D-Phe-Pro-D-Tyr) ——, **V**. *cyclo*(-Val-Orn-Leu-D-Tyr-Pro-D-Phe-)$_2$ ——, **VI**. *cyclo*(-Val-Orn-Leu-D-Phe-Pro-D-Phe-)$_2$ ——.

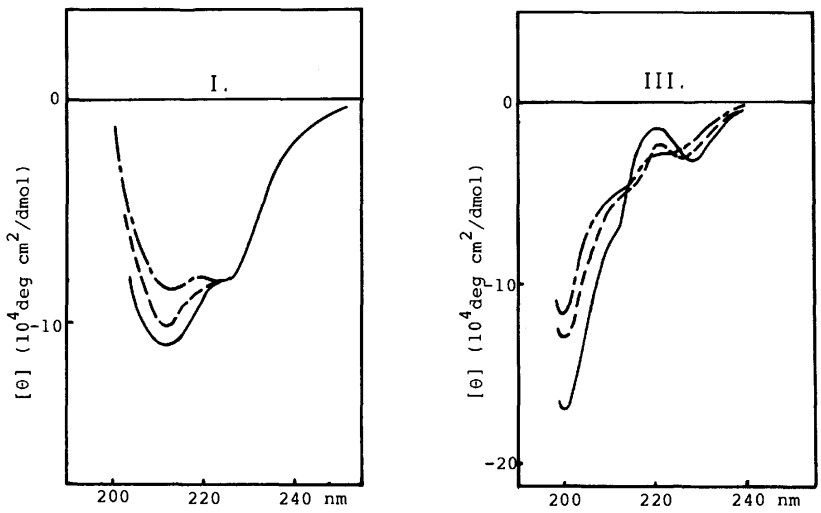

Fig. 4. CD spectra of gratisin peptides **I** and **III** at different temperature. 24 °C ——, 40 °C —— 60 °C —·—.

The shapes of CD spectra of active peptides **IV**, **VII**, **VIII**, and GS (Fig. 3) differ from each other, and no relationship between the pattern of the CD spectra in an aqueous solution and antibiotic activity could be found. These results indicate that these peptides have a different conformation in an aqueous solution. However, it is likely that when these peptides interact with a cell membrane of a target microorganisms, they adopt a GS-like conformation and exhibit antibiotic activities.

The CD spectroscopic study indicated that the partial sequence around a Pro residue is important for the conformation of these peptides. The significance of the sequence for conformation was similarly reported by Blout *et al.* on cyclic hexapeptides[24] and by Nagai *et al.* on linear tetrapeptides.[17]

The CD spectra of these synthetic peptides **I**—**VIII** in aqueous solutions were obtained at different temperatures (24, 40, and 60 °C) (Fig. 4). The CD spectra of peptides **II** and **IV**—**VIII** did not vary between 24 and 60 °C, indicating that the conformations of these peptides were stable within this temperature range. On the other hand, the ellipticities of peptides **I** and **III** decreased with a rise in temperature (Fig. 4). These results indicate that the conformations of peptides **I** and **III** with smaller activities are more labile than those of active peptides **II** and **IV**—**VIII**.

Experimental

All the melting points are uncorrected. CD spectra were obtained with a JASCO spectropolarimeter (model J-20 or J-500). The CD spectroscopy of gratisin peptides **I**—**VIII** was carried out using aqueous solutions of their dihydrochlorides. The molecular weights of the protected cyclododecapeptides were determined by a Hitachi-Perkin-Elmer vapor-pressure osmometer (model 115) using DMF as a solvent. Amino acid analyses were carried out using an ATTO MLC-703, after hydrolysis of the peptides in 6 M HCl at 110 °C for 24 h. Thin-layer chromatography was performed on Merck silica-gel F_{254} plates with the following solvent systems (v/v): R_f^1, $CHCl_3$–MeOH (9:1); R_f^2, $CHCl_3$–MeOH–AcOH (95:5:3); R_f^3, *n*-BuOH–AcOH–H_2O (4:1:1); R_f^4, *n*-BuOH–pyridine–AcOH–H_2O (4:1:1:2). Yields, physical properties and analytical data of peptides **I**—**VIII** and the intermediary products are summarized in Table 3. The yield of each benzyl ester of Boc-hexapeptide was calculated on the basis of the amount of Pro-OBzl used as a starting material.

*Boc-Tyr(Bzl)-Val-Orn(Z)-Leu-Phe-Pro-OBzl (**Ia**).* DCC (2.06 g, 10 mmol) was added to a solution of Boc-Phe (2.65 g, 10 mmol), HOBt (1.48 g, 11 mmol), Pro-OBzl·HCl (2.42 g, 10 mmol) and TEA (1.39 ml) in $CHCl_3$ (50 ml) at 0 °C. This solution was stirred for 2 h at 0 °C and overnight at room temperature. After the reaction mixture was concentrated *in vacuo*, AcOEt (20 ml) was added to the residue and insoluble substances were removed by filtration. The filtrate was then diluted with AcOEt (150 ml). The solution was washed successively with 5% citric acid, water, 5% Na_2CO_3 and water, and then dried over sodium sulfate. After removal of the drying agent, the solvent was evaporated *in vacuo*. The residue was dissolved in 4 M HCl/dioxane (20 ml) containing anisole (0.5 ml) at 0 °C. After stirring for 30 min at room temperature, the solution was concentrated *in vacuo*. The residue was dissolved in $CHCl_3$ (30 ml). The solution was washed with 10% Na_2CO_3 and water under cooling with an ice bath. To this solution were added Boc-Leu (2.4 g, 10 mmol), HOBt (1.48 g, 11 mmol) and DCC (2.06 g, 10 mmol) at 0 °C. The same procedure as described above was repeated for this reaction mixture. Further, Boc-Orn(Z), Boc-Val, and Boc-Tyr(Bzl) were successively coupled by the same method. All reactions were followed by TLC on a silica-gel plate. The crude protected hexapeptide obtained from the final reaction mixture was purified by chromatography on a silica-gel column (1.2×60 cm) using a solvent system of $CHCl_3$–MeOH (50:1). The fractions containing the desired product were combined and concentrated. The product was reprecipitated from AcOEt–ether; overall yield, 5.49 g (47% from Pro-OBzl).

Compounds **IIa**—**VIIIa** were prepared in a similar manner. In the synthesis of **IVa**—**VIIIa**, WSCD·HCl was used instead of DCC as the coupling reagent.

*Boc-Tyr(Bzl)-Val-Orn(Z)-Leu-Phe-Pro-NHNH$_2$ (**Ib**).* A solution of **Ia** (2.3 g, 2.1 mmol) and hydrazine hydrate (2 ml) in DMF (15 ml) was allowed to stand for 5 d at room temperature. The solution was concentrated, and then water was added to the residue. The resulting solid product was collected by filtration; yield, 1.5 g (71%).

Compounds **IIb**—**VIIIb** were prepared in a similar manner.

*Boc-Tyr(Bzl)-Val-Orn(Z)-Leu-Phe-Pro-OH (**Ic**).* In a solution of **Ia** (1.75 g, 1.5 mmol) in MeOH (24 ml) and dioxane (12 ml), 2 M NaOH (1.5 ml) was added. The solution was then stirred for 12 h at room temperature. After the addition of water (10 ml), the solution was concentrated *in vacuo* at a low temperature, and then water (50 ml) was added to the residue. The resulting solid product was collected by filtration, washed with water and dried. The product was recrystallized from MeOH–ether; yield 1.43 g (88%).

Compounds **IIIc**, **VIIc**, and **VIIIc** were prepared in a similar manner.

*Boc-[Tyr(Bzl)-Val-Orn(Z)-Leu-Phe-Pro-]$_2$-OH (**Id**).* Compound **Ic** (0.86 g, 0.8 mmol) was dissolved in TFA (15 ml) containing anisole (0.5 ml) at 0 °C. After stirring at room temperature for 30 min, the solution was concentrated *in vacuo*. Ether (50 ml) was added to the residue, and the resulting solid, H-Tyr(Bzl)-Val-Orn(Z)-Leu-Phe-Pro-OH·TFA, was collected by filtration. To a solution of **Ib** (0.87 g, 0.8 mmol) in DMF (10 ml) were added 4.4 M HCl/dioxane (0.54 ml, 2.4 mmol) and isopentyl nitrite (0.12 ml, 0.9 mmol) at −40 °C. After stirring at −20 °C for 20 min, TEA (0.34 ml, 2.4 mmol) was added at −40 °C. This mixture was combined with a solution of the total amount of H-Tyr(Bzl)-Val-Orn(Z)-Leu-Phe-Pro-OH·TFA prepared above and NMM (0.09 ml) in DMF (10 ml). The mixture was stirred at 0 °C for 3 d and concentrated. A solution 10% citric acid (50 ml) was added to the residue and the resulting product was collected by filtration, washed with water and dried. The product was purified by gel filtration on a Sephadex LH-20 column (2.5×120 cm) using DMF as a solvent. The fractions containing the desired product were then combined and concentrated. The product was recrystallized from hot EtOH; yield 1.1 g (67%).

Compounds **IIId**, **VIId**, and **VIIId** were prepared in a similar manner. In the removal of the Boc group of compounds **VIIc** and **VIIIc**, 4 M HCl/dioxane was used instead of TFA.

cyclo[-*Tyr(Bzl)-Val-Orn(Z)-Leu-Phe-Pro-*]$_2$ (**Ie**). *Active-Ester Method.* To a solution of **Id** (300 mg, 0.14 mmol) in DMF (10 ml) was added HOSu (32 mg, 0.28 mmol) and WSCD·HCl (53 mg, 0.28 mmol) at 0 °C, and then the mixture was stirred for 7 h at room temperature. The solvent was evaporated and then water was added to the residue. The resulting solid product was collected by filtra-

tion, washed with water and dried. It was dissolved in TFA (5 ml) containing a few drops of anisole at 0 °C. The mixture was stirred for 30 min at room temperature and then concentrated. The residue, trifluoroacetate of dodecapeptide active ester, was triturated with ether, collected by filtration and dissolved in DMF (10 ml). The solution was added, dropwise, to pyridine (150 ml) at 60 °C. After stirring for 3 h at 60 °C and overnight at room temperature, the solvent was evaporated, and then water was added to the residue. The resulting solid product was collected by filtration, washed with water and dried. The crude product was purified by chromatography on a silica-gel column (1.2×30 cm) using a solvent system of $CHCl_3$–MeOH (50:1). The fractions containing the desired product were combined and concentrated. The product was recrystallized from EtOH–ether; yield, 83 mg (29%).

Compounds **IIIe**, **VIIe**, and **VIIIe** were prepared in a similar manner.

A Trial by an Azide Method. The cyclization of H-[Phe-Pro-Tyr(Bzl)-Val-Orn(Z)-Leu-]$_2$-$NHNH_2$ with an azide method was attempted by a procedure (described later) used in the preparation of compound **IIe**. In the purification of the product by column chromatography on silica-gel, a small amount of ninhydrin negative substance was isolated. The analytical results of the product are as follows: amino acid ratios in acid hydrolyzate; Phe 1.10, Pro 0.96, Tyr 0.86, Val 1.01, Orn 1.01, Leu 0.56. Elemental analysis: C, 66.61; H, 7.10; N, 10.81%. These results are not in agreement with the values expected for the desired product, *cyclo*[-Phe-Pro-Tyr(Bzl)-Val-Orn(Z)-Leu-]$_2$, but coincide with the following value calculated for the tentative urea-type structure described earlier: amino acid ratios; Phe 1, Pro 1, Tyr 1, Val 1, Orn 1, Leu 0.5. Calcd for $C_{108}H_{135}N_{15}O_{18}\cdot H_2O$: C, 66.54; H, 7.08; N, 10.77%.

cyclo*(-Tyr-Val-Orn-Leu-Phe-Pro-)$_2$·2HCl (If).* Compound **Ie** (50 mg, 0.026 mmol) was dissolved in a mixture of 90% MeOH (30 ml), dioxane (5 ml), and 1 M HCl (0.1 ml). It was hydrogenated in the presence of palladium black for 15 h at room temperature. After removal of the catalyst, the filtrate was concentrated *in vacuo*. The product was recrystallized from EtOH-ether; yield, 38 mg (94%).

Gratisin peptides, **IIIf**, **VIIf**, and **VIIIf** were prepared in a similar manner.

Boc-[Tyr(Bzl)-Val-Orn(Z)-Leu-D-Phe-Pro-]$_2$-OBzl (IIc). Compound **IIa** (1.17 g, 1 mmol) was dissolved in 4 M HCl/dioxane (20 ml) containing anisole (0.5 ml) at 0 °C. After stirring at room temperature for 30 min, the solution was concentrated *in vacuo*. Ether (50 ml) was added to the residue, and the resulting solid, H-Tyr(Bzl)-Val-Orn(Z)-Leu-D-Phe-Pro-OBzl·HCl, was collected by filtration. To a solution of **IIb** (1.1 g, 1 mmol) in DMF (10 ml) were added 8.83 M HCl/dioxane (0.34 ml) and isopentyl nitrite (0.15 ml, 1 mmol) at −40 °C. After stirring at −20 °C for 15 min, the solution was cooled again to −40 °C and neutralized with TEA (0.42 ml, 3 mmol). This solution was combined with a chilled solution of H-Tyr(Bzl)-Val-Orn(*Z*)-Leu-D-Phe-Pro-OBzl·HCl mentioned above and NMM (0.11 ml, 1 mmol) in DMF (10 ml). The reaction mixture was stirred at 0 °C for 3 d, and then concentrated. The residue was dissolved in AcOEt (150 ml), and the solution was washed with 5% citric acid, water, 5% Na_2CO_3 and water, and dried over sodium sulfate. After concentrating the solution, the residue was purified by gel filtration on a Sephadex LH-20 column (2.5×120 cm) using DMF as solvent, and the fractions containing the desired product were combined and concentrated. Further purification was performed by chromatography on a silica-gel column (1.2×30 cm) using a solvent system of $CHCl_3$–MeOH (50:1), following by recrystallization from hot EtOH; yield, 1.23 g (60%).

Compounds **IVc**, **Vc**, and **VIc** were prepared in a similar manner. But the gel filtration on a Sephadex LH-20 column was not required for purification.

Boc-[Tyr(Bzl)-Val-Orn(Z)-Leu-D-Phe-Pro-]$_2$-$NHNH_2$ (IId). Compound **IIc** (1.1 g, 0.5 mmol) was treated with hydrazine hydrate (1.5 ml) as described for the preparation of **Ib**. The product was purified by gel filtration as described in the preparation of **Id**; yield, 0.96 g (94%).

Compound **IVd**, **Vd**, and **VId** were prepared in a similar manner.

cyclo*[-Tyr(Bzl)-Val-Orn(Z)-Leu-D-Phe-Pro-]$_2$ (IIe).* Compound **IId** (500 mg, 0.24 mmol) was dissolved in 4 M HCl/dioxane (15 ml) containing anisole (0.5 ml). The mixture was stirred for 40 min at room temperature and then concentrated *in vacuo*. The residue was triturated with ether and collected by filtration. To a solution of the hydrochloride of the dodecapeptide hydrazide in DMF (10 ml) was added 8.8 M HCl/dioxane (0.09 ml) and isopentyl nitrite (0.036 ml, 0.27 mmol) at −40 °C. After 15 min, the mixture was poured, dropwise, into pyridine (200 ml) at 0 °C. After stirring for 3 d at 0 °C, the solution was concentrated. Addition of water to the residue afforded a precipitate, which was filtrated and washed with water. Purification was performed by chromatography on a silica-gel coulmn (1.2×30 cm) using a solvent system of $CHCl_3$–MeOH (50:1), followed by recrystallized from hot EtOH; yield 198 mg (43%).

Compounds **IVe**, **Ve**, and **VIe** were prepared in a similar manner. In removal for Boc group of compounds **IVd** and **Vd**, TFA was used instead of 4 M HCl/dioxane.

cyclo*(-Tyr-Val-Orn-Leu-D-Phe-Pro-)$_2$·2HCl (IIf).* Compound **IIe** (100 mg, 0.052 mmol) was dissolved in 90% MeOH (20 ml), and then 1 M HCl (0.15 ml) was added to the solution. The mixture was hydrogenated in the presence of palladium black for 15 h. After removing the catalyst, the filtrate was concentrated *in vacuo*. The product was purified by gel filtration on a Sephadex LH-20 column (1×150 cm) using EtOH as solvent, and by reprecipitation from EtOH–ether; yield, 72 mg (90%).

Compounds **IVf**, **Vf**, and **VIf** were prepared in a similar manner. But, in this case, the gel-filtration purification procedure was not required.

Cellulose Plate Electrophoresis. Electrophoresis of the products was carried out with a cellulose (Avicel) plate and with a solvent system of HCOOH–AcOH–MeOH–H_2O (1:3:6:10 v/v, pH 1.3) for 2 h at 500 V/20 cm. Each of the peptides **I**—**VIII** revealed a single spot, the mobility being the same as that of GS.

The author wishs to express his sincere thanks to Professor Ichiro Muramatsu, Rikkyo University, for his kind guidance throughout this work, and to Professor Michiaki Takimoto, Toho University, for his encouragement. He is also grateful to Associate Professor Shosuke Sofuku, Rikkyo University, for his helpful discussions. He is indebted to the members of the Research Laboratories of Toyo Jozo Co. for their elemental analyses and microbiological assays and to Professor Yasutomo Sugimura, Toho University, for performing amino acid analyses.

References

1) G. G. Zharikova, S. P. Myaskovskaya, and A. B. Silaev, *Vestn. Mosk. Univ., Biol. Pochovoved.*, **27**, 110 (1972).

2) S. P. Myaskovskaya, G. G. Zharikova, and A. B. Silaev, *Vestn. Mosk. Univ., Biol. Pochovoved.*, **28**, 123 (1973).

3) G. G. Zharikova, A. P. Zarubina, D. M. Kherat, S. P. Myaskovskaya, and V. N. Maksimov, *Antibiotiki IKh*

Produtsenty., **1975**, 163.

4) Amino acid residues with no prefix are of L-configuration unless otherwise noted. The abbreviations for amino acids and peptides are in accordance with the rules of IUPAC-IUB Commission of Biochemical Nomenclature. Abbreviations used are as follows: Boc, *t*-butoxycarbonyl; Z, benzyloxycarbonyl; OBzl, benzyloxy; Bzl, benzyl; $BzlCl_2$, 2,6-dichlorobenzyl; DCC, dicyclohexylcarbodiimide; WSCD, 1-ethyl-3-(3-dimethylaminopropyl)carbodiimide; HOBt, 1-hydroxybenzotriazole; HOSu, *N*-hydroxysuccinimide; TFA, trifluoroacetic acid; TEA, triethylamine; NMM, *N*-methylmorpholine; DMF, *N,N*-dimethylformamide.

5) M. Tamaki, M. Takimoto, S. Sofuku, and I. Muramatsu, *J. Antibiotics.*, **34**, 1227 (1981).

6) M. Tamaki, M. Takimoto, S. Sofuku, and I. Muramatsu, "Peptide Chemistry 1980" ed by K. Okawa, Protein Research Foundation, Osaka (1981), p. 203.

7) M. Tamaki, M. Takimoto, S. Sofuku, and I. Muramatsu, *J. Antibiotics.*, **36**, 751 (1983).

8) M. Tamaki, M. Takimoto, S. Sofuku, and I. Muramatsu, "Peptide Chemistry 1982" ed by S. Sakakibara, Protein Research Foundation, Osaka (1983), p. 111.

9) P. Y. Chou and G. D. Fasman, *J. Mol. Biol.*, **115**, 135 (1977).

10) M. Kuo and W. A. Gibbons, *Biochemistry.*, **18**, 5855 (1979).

11) D. W. Urry and R. Walter, *Pro. Nat. Acad. Sci. U.S.A.*, **68**, 956 (1971).

12) I. L. Karle, J. Karle, T. Wieland, W. Burgermeister, H. Faulstich, and B. Witkop, *Pro. Nat. Acad. Sci. U.S.A.*, **70**, 1836 (1973).

13) S. G. Laland, Φ. Frφyshov, C. Gilhuus-Moe, and T. L. Zimmer, *Nature (New Biology).*, **239**, 43 (1972).

14) F. Lipmann, *ACC. Chem. Res.*, **6**, 361 (1973).

15) K. D. Kopple, A. Go, T. J. Schamper, and C. S. Wilcox, *J. Am. Chem. Soc.*, **95**, 6090 (1973).

16) M. Kawai and U. Nagai, *Biopolymers.*, **17**, 1549 (1978).

17) K. Sato, M. Kawai, and U. Nagai, *Bull. Chem. Soc. Jpn.*, **56**, 1527 (1983).

18) H. Yonezawa, K. Okamoto, M. Kaneda, N. Tominaga, and N. Izumiya, "Peptide Chemistry 1982" ed by S. Sakakibara, Protein Research Foundation, Osaka (1983), p. 283.

19) R. Nagai, M. Waki, M. Kondo, H. Aoyagi, T. Kato, S. Makisumi, and N. Izumiya, *Bull. Chem. Soc. Jpn.*, **40**, 963 (1967).

20) S. Ando, H. Aoyagi, M. Waki, T. Kato, and N. Izumiya, "Peptide Chemistry 1981" ed by T. Shioiri, Protein Research Foundation, Osaka (1982), p. 85.

21) K. Sato and U. Nagai, "Peptide Chemistry 1980" ed by K. Okawa, Protein Research Foundation, Osaka (1981), p. 193.

22) S. N. Semenov, E. I. Mel'nik, L. G. Snezhikova, A. I. Miroshikov, and V. T. Ivanov, *Bioorg. Khim.*, **3**, 1055 (1977).

23) H. Takiguchi and N. Izumiya, *Bull. Chem. Soc. Jpn.*, **47**, 221 (1974).

24) L. M. Gierasch, C. M. Deber, V. Madison, C. Niu, and E. R. Blout, *Biochemistry.*, **20**, 4730 (1981).

 © 1984 The Chemical Society of Japan Bull. Chem. Soc. Jpn., 57, 3221—3233 (1984)

Diene-transmissive Diels-Alder Cycloaddition Reaction of Bis(silyloxy) Cross-conjugated Trienes

Otohiko Tsuge,* Eiji Wada, Shuji Kanemasa, and Hirohiko Sakoh
Research Institute of Industrial Science, and Department of Molecular Science and Technology, Interdisciplinary Graduate School of Engineering Sciences Kyushu University, Kasugakoen, Kasuga 816
(Received June 18, 1984)

Multiple Diels-Alder reaction of bis(silyloxy) cross-conjugated trienes is presented. Two trienes, 3-benzylidene- and 3-(methoxymethylene)-2,4-bis(trimethylsilyloxy)-1,4-pentadiene, undergo two sequential Diels-Alder cycloadditions with a variety of dienophiles forming hydronaphthalene rings. Some characteristics of this reaction have been discussed in terms of stereo-, regio-, and chemoselectivity. It is proposed that this process is referred to as "diene-transmissive Diels-Alder reaction".

There have been reported numerous processes by which ring systems can be prepared. Although each has the characteristic advantages, one of the most reliable processes is the Diels-Alder cycloaddition that generally proceeds in a highly diastereoselective manner.[1] Recently a process that produces more than one ring in a single reaction has been often requested in elaborating complex natural products. Attracting is the use of the Diels-Alder reaction as a part of ring construction steps. Some examples are known for the multiple sequence of the Diels-Alder cycloaddition and called Domino,[2] Timed,[3] and Tandem Diels-Alder reaction.[4,5] However, their applications in organic synthesis are rare.

We have found a new process of multiple sequence of the Diels-Alder reaction. The process, referred to as "diene-transmissive Diels-Alder reaction",[6] involves two sequential cycloadditions of cross-conjugated triene: A part of the triene **A** undergoes the first cycloaddition to a dienophile (A=B) forming a six-membered ring **B** with an endocyclic double bond which serves as a part of diene for the following reaction. The second cycloaddition gives a bis-cycloadduct **C**. The cross-conjugated triene **A** of our choice carries two silyloxy moieties (X=OTMS, TMS: trimethylsilyl) as diene-activating and directing substituents.

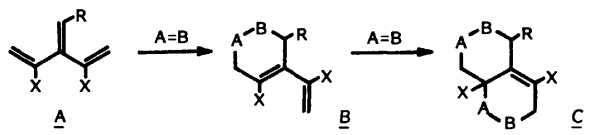

A B C

The present paper describes the full detail of our investigation on the diene-transmissive Diels-Alder reactions of bis(silyloxy) cross-conjugated trienes, a part of which has been already reported as preliminary communications.[6-8]

Results and Discussion

Synthesis of Bis(silyloxy) Cross-conjugated Trienes. Blomquist[9] and Bailey[10] have reported the first examples of diene-transmissive Diels-Alder reaction using the parent cross-conjugated triene, 3-methylene-1,4-pentadiene. However, this elegant ring formation has long discouraged its application in organic synthesis because of tough handling, ready polymerization, low reactivity as a diene, and difficult structural modification of the triene. Our bis (silyloxy) cross-conjugated trienes can be synthesized in two steps from readily available 2,4-pentanedione, and a variety of substituents may be introduced from aldehydes.

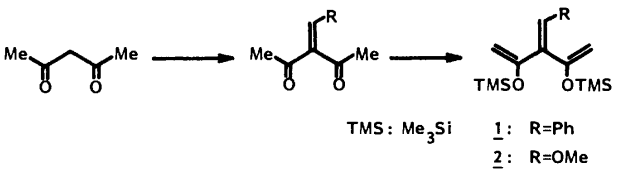

Scheme 1.

Scheme 1 illustrates the synthesis of trienes, 3-benzylidene- **1** and 3-(methoxymethylene)-2,4-bis(trimethyl silyloxy)-1,4-pentadiene **2**. The condensation products of 2,4-pentanedione with benzaldehyde and trimethyl orthoformate were silylated with chlorotrimethylsilane giving **1** and **2**. The use of 1,8-diazabicyclo-[5.4.0]undec-7-ene in dichloromethane[11] for **1** and of triethylamine together with a catalytic amount of zinc chloride in benzene[12] for **2** gave the best results.

The trienes **1** and **2** are stable enough to be purified by a vacuum distillation and chromatographed over silica gel if carefully handled.[13] In the absence of moisture, they may be stored for a long time without decomposition and polymerization.[14] Such thermal stability of **1** and **2** is a great advantage over the parent triene.

Cycloadditions to Acetylenic Dienophiles. The reaction of **1** with dimethyl acetylenedicarboxylate **3a** (five equiv) under reflux in benzene gave a desilylated bis-adduct **5a** after the usual work-up with methanol (Scheme 2 and Table 1). As shown in Scheme 2, the first Diels-Alder reaction between **1** and **3a** forms a mono-cycloadduct **D** that bears a diene functionality activated by two silyloxy moieties. The second reaction occurs smoothly affording a bis-cycloadduct **E**. Aromatization of the secondarily formed ring induces the elimination of trimethylsilanol leading to **4a**. On work-up with methanol, **4a** is desilylated into **5a**. As the diene function in **D** is highly activated by two silyloxy substituents, the second cycloaddition is even more accelerated than the first, only a trace of mono-adduct **6a** being formed.

The diene-transmissive Diels-Alder reaction of **1** with an unsymmetrical acetylene provides another advan-

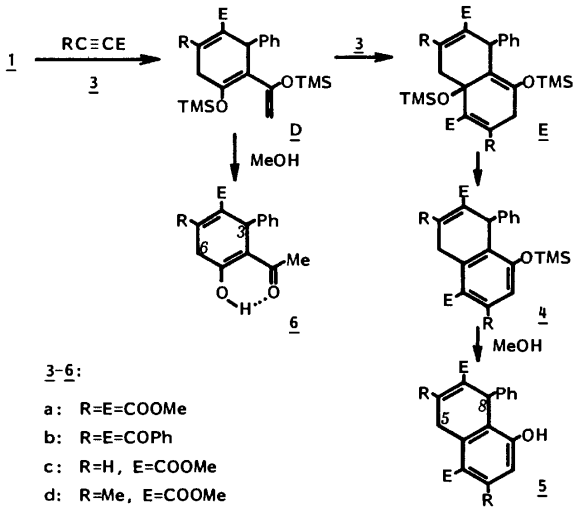

Scheme 2.

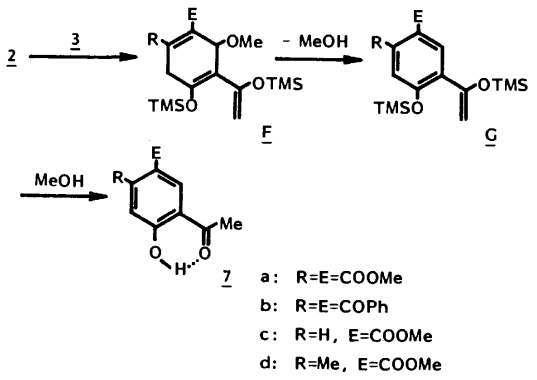

Scheme 3.

tage. The reaction with methyl propiolate **3c** gave bis-cycloadducts **4c** and **5c** besides a poor yield of mono-adduct **6c**, meaning that both the first and second cycloadditions proceeded in a highly regioselective manner. That is, the silyloxy groups in **1** serve not only as diene-activating substituents but also as directing ones.

Dibenzoylacetylene **3b** and methyl 2-butynoate **3d** failed in the formation either mono- or bis-adducts.

The other triene **2** was found much more reactive than **1**. It reacts with **3a** and **3b** even at room temperature, however the only products were mono-adducts **7a** and **7b** (Scheme 3 and Table 1). The exclusive formation of mono-adduct **7** from a reactive triene **2** remarkably contrasts with the predominant formation of bis-adduct **5** from a rather sluggish triene **1**. This is because of the ready elimination of methanol from the initially formed mono-cycloadduct **F**. ^{1}H-NMR spectral analysis of the reactions indicated that the methanol elimination occurred even at room temperature.

The triene **2** is a well designed conjugation system. Since it carries three alkoxyl groups, any two in a 1,3-relationship, both the first and second cycloadditions are highly accelerated and also regioselective. In addition, the methoxyl group is eliminated after the cycloaddition is complete, adding an unsaturation to the cycloadduct.

The reactions with **3c** and **3d**, under harder reaction conditions, provided regioselective mono-adducts **7c** and **7d**, respectively.

Cycloadditions to Cyclic Olefinic Dienophiles. To investigate the stereochemical aspect of diene-transmissive Diels-Alder reaction the cycloadditions with cyclic olefinic dienophiles were carried out.

The reaction of **1** with excess of *N*-methylmaleimide **8a** under reflux in benzene and the work-up with methanol gave a bis-adduct **10a** together with low yields of two isomeric mono-adducts **11a** and **12a** (Scheme 4 and Table 2). The minor products were assigned as the 3a,4-*cis*- **11a** and 3a,4-*trans*-hydroisoindolinedione **12a**, respectively, on the basis of the spectral data, especially of the coupling constants between 3a-H and 4-H (**11a**: 6.0 Hz; **12a**: 2.0 Hz) as well as the chemical shifts of *N*-Me (**11a**: δ 2.38; **12a**: δ 3.00). The cis and trans mono-adducts correspond to the products derived through an endo and an exo approach of dienophile **8a** across the trans diene part of **1**, respectively.[15] In the present paper, therefore, the compound of type **11a** is to be called an endo adduct and **12a** an exo adduct.

Stereochemistry of the bis-adduct **10a** has been determined at two stages, the first Diels-Alder reaction (from **1** to the mono-cycloadduct) and the second reaction (the path to the second cycloadduct). Main path of the first cycloaddition should be endoselective since **11a** was only isolated in the reaction of **1** with **8a** at room temperature (Table 2). The ^{1}H-NMR spectrum con-

Table 1. Reactions of **1** and **2** with acetylenic dienophiles **3**

Triene	Acetylene (equiv)	Reaction Conditions			Product (yield/%)[a]	
		Solvent	Temp	Time/h	Bis-adduct	Mono-adduct
1	**3a** (5.0)	Benzene	Reflux	72	**5a** (51)	+
1	**3c** (3.0)	Toluene	110—5 °C[b]	140	**5c** (37)	+
1	**3c** (11.0)	Benzene	Reflux	168	**4c** (37), **5c** (10)	**6c** (2)
2	**3a** (2.0)	Benzene	r.t.	24	—	**7a** (57)
2	**3b** (2.0)	Benzene	r.t.	24	—	**7b** (47)
2	**3c** (2.0)	Benzene	Reflux	48	—	**7c** (35)
2	**3d** (2.0)	Toluene	Reflux	48	—	**7d** (8)

a) Isolated yields based on the trienes. The sign + (or −) means that adducts were (or were not) detected by ^{1}H-NMR spectroscopy. b) In a sealed tube.

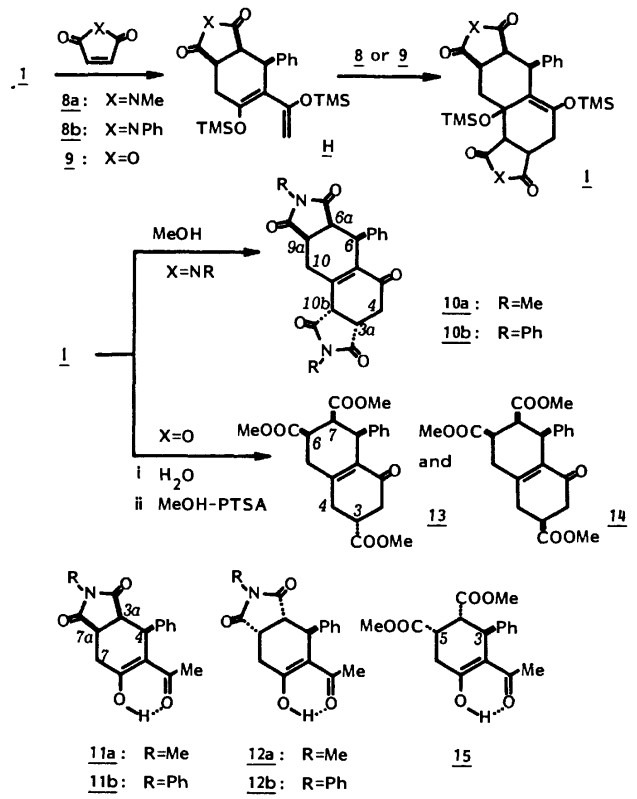

Scheme 4.

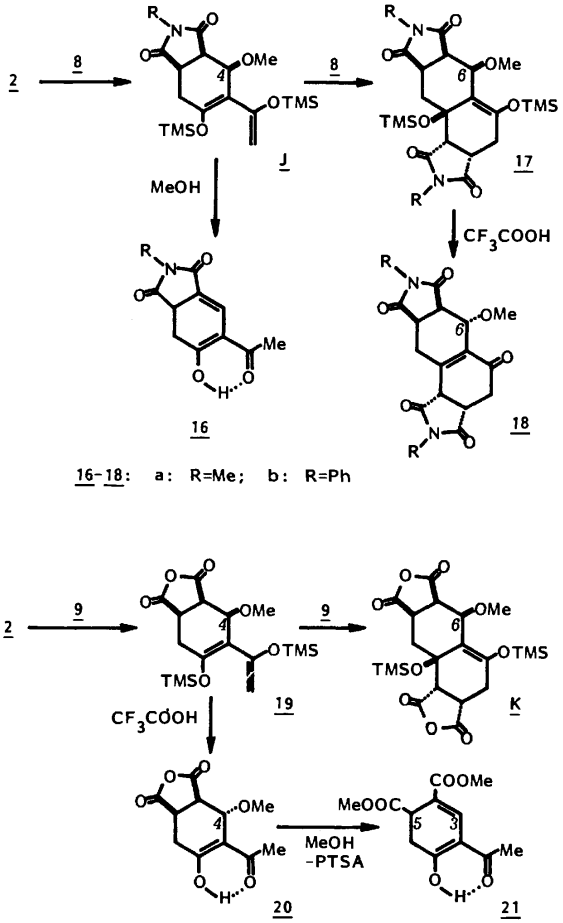

Scheme 5.

firmed cis configuration at the 6- and 6a-positions of **10a** (J_{6-6a}=6.0 Hz; *N*-Me: δ 2.33). Although the stereochemistry at the 3a- and 10b-junctions could not be determined only on the basis of the spectral data, it was tentatively assigned according to the probable reaction pathway shown in Scheme 4. The first cycloaddition of **1** to **8a** is highly endoselective leading to an endo mono-cycloadduct **H** (X=NMe). The second molecule of **8a** approaches across the diene conjugation of **H** in an endo fashion from the less hindered side (the opposite side of the fused maleimide ring and the phenyl) forming a stereoselective skeleton of bis-cycloadduct **I** (X=NMe). When treated with methanol, desilylation occurs to give a fused cyclohexenone ring **10a**.

Similar results were given in the reaction of **1** with *N*-phenylmaleimide **8b** as shown in Scheme 4 and Table 2.

Maleic anhydride **9** was found much more reactive than the maleimides. Triene **1** reacted with two equivalents of **9** under reflux in benzene forming **I** (X=O) as a major product, which was found composed of two isomers of bis-cycloadducts. The followed esterification with methanol in the presence of *p*-toluenesulfonic acid gave two isomeric decarboxylated bis-adducts **13** and **14** besides a small amount of exo mono-adduct **15**. Even with less than one equivalent of **9** at room temperature, **I** was only obtained in a good yield. It is surprising that the second cycloaddition of **9** has shown such a low stereoselectivity. The reason has not been clarified yet.

One of the four expected ester groups in the esterified bis-adducts was missing. It was eliminated during the hydrolysis of two anhydride rings in **I** (X=O). On the basis of the ^{1}H-NMR spectrum which showed no methylene multiplets upfield of δ 2.0,[16] it was confirmed that the lost carboxyl group had been at the 4-position. Among four positions (3-, 4-, 6-, and 7-positions), a carbanion that is expected to form on decarboxylation would be best stabilized at the 4-position.

The activated cross-conjugated triene **2** readily reacts with **8** and **9** under mild reaction conditions in a highly chemoselective manner. Type of products is dependent upon the amount of dienophile as well as the reaction conditions as shown in Scheme 5 and Table 2.

The reaction of **2** with an equivalent of **8a** in benzene at room temperature was followed by the work-up with methanol giving only a mono-adduct **16a** in a good yield. As **16a** was accompanied with the elimination of methanol, stereoselectivity in the first cycloaddition leading to a mono-cycloadduct **J** is not clear. With two equivalents of **8a** under reflux in benzene, a stereoselective bis-cycloadduct **17a** was isolated as the single product. Desilylation readily took place giving a bis-adduct **18a** when **17a** was treated with a catalytic amount of trifluoroacetic acid in benzene. Interesting is that the configuration at the 6-position of **17a** was inverted at the acid-catalyzed desilylation stage, probably through an elimination-addition mechanism.

As the structure of **17a** could not be determined only on the basis of spectral data, it was tentatively assigned by the following discussion: Molecular model inspection indicates that the most stable conformation for **J** is an envelope type in which a bulky substituent **R'** (=OMe) occupies an axial position in order to minimize the steric repulsion to the 3-carbonyl and the protruding silyloxy groups (Fig. 1). Although both sides of diene in the exo mono-cycloadduct exo-**J** as well as the upper side of the endo one endo-**J** are sterically hindered for the approach of **8a**, an endo approach from the bottom side of diene in endo-**J** looks quite easy. This approach must be the reaction leading to the stereoselective bis-cycloadduct **17a**. Thus, **17a** was assigned as a bis-cycloadduct formed via the endo mono-cycloadduct endo-**J**. On the other hand, the stereochemistry at the 6- and 6a-positions of **18a** was easily determined as trans on the basis of small J_{6-6a} (4.0 Hz) since this ring has an envelope conformation with an axial 6-methoxyl substituent.

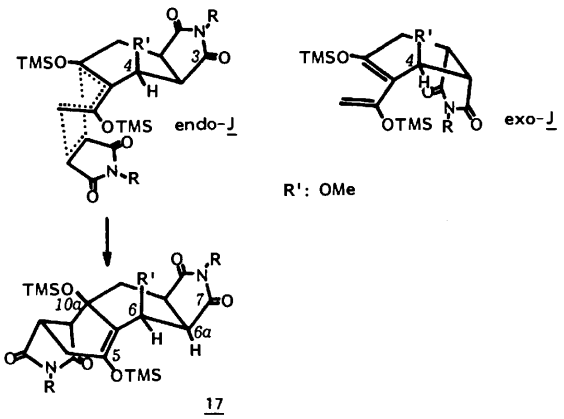

Fig. 1. Possible configuration and conformation for mono-cycloadduct **J**, and stereochemistry for second cycloaddition.

Similarly the stereoselective mono- **16b** and bis-adducts **17b** and **18b** were selectively formed in the reactions with *N*-phenylmaleimide **8b**. The stage of desilylation of **17b** into **18b** was also accompanied with the inversion of methoxyl moiety.

The reaction of **2** with an equivalent of maleic anhydride **9** was so rapid as to be completed in 10 min at room temperature forming a quantitative yield of endo mono-cycloadduct **19**. Treatment of **19** with trifluoroacetic acid in benzene provided a desilylated mono-adduct **20** while the usual work-up with methanol gave a mixture of two isomeric half esters. Esterification of **20** with methanol in the presence of *p*-toluenesulfonic acid led to a methanol eliminated mono-adduct **21** that was also obtained directly from **19** under the same conditions. Although the quantitative formation of a bis-cycloadduct **K** was confirmed in the reaction between **2** and two equivalents of **9**, neither its purification nor the conversion into isolable derivatives was successful.

To be emphasized are given as follows: 1) The first cycloaddition of both **1** and **2** is highly endoselective and the second reaction selectively takes place with an endo approach of dienophiles from the less hindered side of diene moiety. 2) The double cycloaddition sequence of **2** is highly chemoselective. Either the mono- or bis-cycloadduct is selectively formed depending upon the amount of dienophiles. 3) The elimination of methanol in the reactions of **2** adds an unsaturation to the products.

Cycloadditions to Acyclic Olefinic Dienophiles. Compared with such highly reactive dienophiles as **3**, **8**, and **9**, acyclic olefinic dienophiles show a low reactivity toward the trienes **1** and **2**. The first cycloaddition slowly proceeds with a poor stereoselec-

Table 2. Reactions of **1** and **2** with cyclic olefinic dienophiles **8** and **9**

Triene	Olefin (equiv)	Reaction Conditions[a]		Product (yield/%)[b]	
		Temp	Time/h	Bis-adduct	Mono-adduct
1	**8a** (2.3)	r.t.	48		**11a** (23)
1	**8a** (3.0)	Reflux	72	**10a** (60)	**11a** (2), **12a** (3)
1	**8b** (2.0)	r.t.	120	**10b** (13)	**11b** (26)
1	**8b** (3.0)	Reflux	48	**10b** (80)	**11b** (3), **12b** (6)
1	**9** (2.0)	Reflux	48	**13** (57), **14** (22)	**15** (7)
1	**9** (2.0)	Reflux	48	**I** (82)[c]	—
1	**9** (0.75)	r.t.	72	**I** (63)[d]	—
2	**8a** (1.0)	r.t.	24	—	**16a** (64)
2	**8a** (2.0)	Reflux	24	**17a** (63)	—
2	**8b** (1.0)	50 °C	20	—	**16b** (73)
2	**8b** (2.0)	Reflux	20	**17b** (62)[e]	—
2	**9** (1.0)	r.t.[f]	0.2	—	**19** (100)[g]
2	**9** (1.0)	r.t.[f]	0.2	—	**21** (56)
2	**9** (2.0)	r.t.	4	**K** (100)[h]	

a) All the reactions were carried out in dry benzene. b) Isolated yields based on the trienes. c) Isomer ratio= 2.5 : 1. d) Isomer ratio=3 : 1. e) Together with an unidentified bis-adduct (9%). f) Without solvent. g) Determined by ^{1}H-NMR spectroscopy. h) Determined by ^{1}H-NMR spectroscopy. Its isolation failed.

tivity, a mixture of endo and exo mono-cycloadducts being formed in a comparable ratio. Regardless of the stereochemistry of mono-cycloadduct, the second cycloaddition is extremely slow probably because the initially formed six-membered ring takes a half-chair conformation which is hardly favored for the approach of the second molecule of dienophile. Therefore, the major products in the diene-transmissive Diels-Alder reactions with acyclic olefinic dienophiles are mono-adducts.

The reaction of **1** with dimethyl maleate **22** (large excess) gave an exo mono-adduct **15** that was identical with the minor product in the reaction of **1** with **9** (Scheme 6 and Table 3). On the other hand, with dimethyl fumarate **23a** under the same reaction conditions, an exo- **24a** and an endo mono-adduct **25a** were obtained together with a mixture of two isomeric bis-adducts **26**. In this case also the exo adduct **24a** was the major product. When the same reaction was carried out under harder conditions (under reflux in toluene), the yield of **26** increased up to 88% and those of both **24a** and **25a** decreased. These results indicate that two isomers of bis-adducts **26** carry different stereochemistry in the initially formed ring, and further indicate that both the endo and exo mono-cycloadducts **L** can undergo the second cycloaddition with a comparable easiness.

The most stable conformation for the six-membered rings of **15**, **24a**, and **25a** is a half-chair type.[17] Molecular model inspection shows that the bulky phenyl substituent at the 3-position occupies an axial position to avoid the steric hindrance to the adjacent acetyl moiety. Consequently an axial substituent at the 5-position, which is in a 1,3-relationship to the phenyl, faces closely to the phenyl plane and therefore is magnetically shielded. Thus the isomer with a shielded ester group (COOMe: δ 3.32) was assigned to **24a**, and then the other **25a**.

Two conformers of the exemplified compound **14** are illustrated in Fig. 2. It is clear that not the adjacent but the next ester is most intensely shielded when it is sitting cis to the axial phenyl. The following six compounds give good examples for the chemical shifts of a variety of ester methyls and the coupling constants J_{3-4} of cyclohexene ring systems of related compounds. These values agree with the ones estimated on the axial-phenyl conformation model.

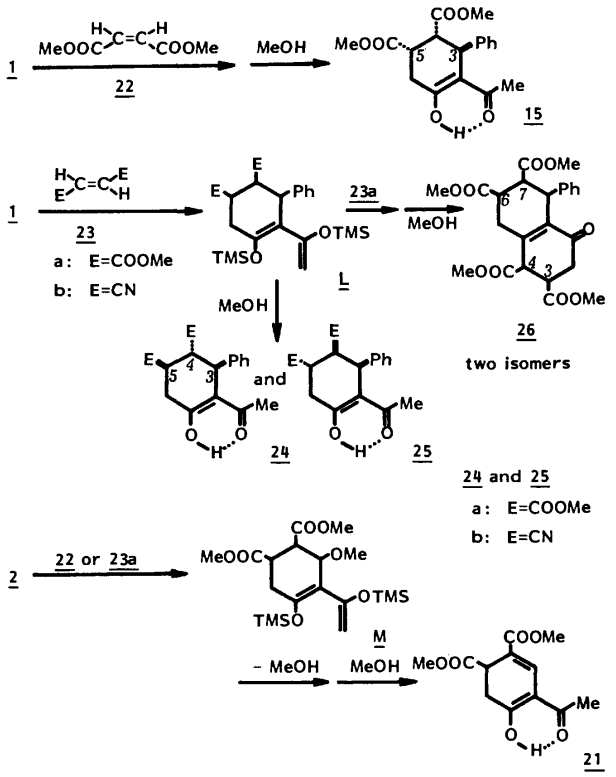

Scheme 6.

Table 3. Reactions of **1** and **2** with acyclic dienophiles **22**, **23**, and **27**

Triene	Olefin (equiv)	Reaction Conditions			Product (yield/%)[a]	
		Solvent	Temp	Time/h	Bis-adduct	Mono-adduct
1	**22** (6.3)	Benzene	Reflux	7 d		**15** (45)
1	**23a** (3.0)	Benzene	Reflux	7 d	**26** (25)[b]	**24a** (55), **25a** (11)
1	**23a** (2.2)	Toluene	Reflux	7 d	**26** (88)[b]	**24a** (10), **25a** (2)
1	**23b** (3.0)	Toluene	Reflux	7 d		**24b** (10)[c], **15b** (55)
2	**22** (1.0)	Benzene	Reflux	48		**21** (42)
2	**22** (3.0)	Benzene	Reflux	72		**M** (100)[d]
2	**23a** (1.0)	Benzene	Reflux	48		**21** (82)
1	**27a** (20)	Benzene	Reflux	6 d		**28a** (48), **29a** (20)
1	**27b** (20)	Benzene	Reflux	5 d		**28b** (70), **29b** (22)
1	**27c** (e)	**27c**	Reflux	58		**28c** (54), **29c** (18)
1	**27c** (e)	Benzene	110 °C[f]	5 d	**30** (38)[b]	**28c** (27), **29c** (6)
2	**27a** (5.0)	Benzene	Reflux	48		**31a** (60)
2	**27b** (3.0)	Benzene	Reflux	48		**31b** (66)
2	**27c** (5.0)	Benzene	75 °C	48		**31c** (73)

a) Isolated yields based on the trienes. b) Mixtures of two isomers. c) Determined by ^{1}H-NMR. d) The structure was assigned as exo mono-cycloadduct on the basis of ^{1}H-NMR spectrum. e) The dienophile was also used as the solvent. f) In a sealed tube.

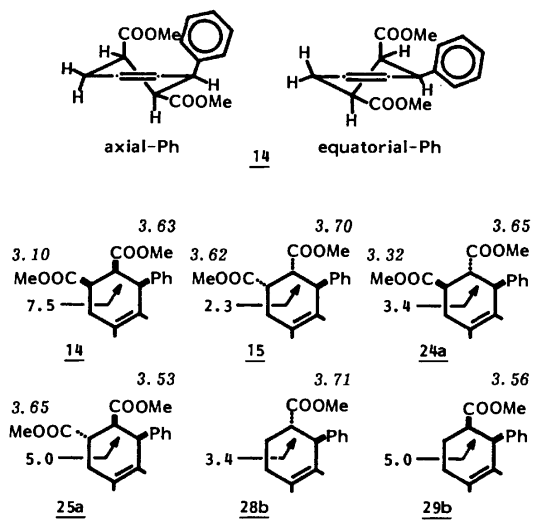

Fig. 2. Two half-chair conformations for **14**, and chemical shifts (δ ppm) of ester methyls and coupling constants (Hz) between 3-H and 4-H of related cyclohexene ring systems.

Fumaronitrile **23b** also reacted with **1** under reflux in toluene giving a mixture of two isomeric mono-adducts **24b** and **25b**, but in this case the endo adduct **25b** was the major product.

The same methanol-eliminated mono-adduct **21** was yielded both in the reaction of **2** with the fumarate **22** and in that with the maleate **23a**. As have been shown in Scheme 5, this compound **21** is also obtainable from **2** and maleic anhydride **9**. In the prolonged reaction with excess of **22**, a quantitative formation of exo mono-cycloadduct **M** was confirmed by ^{1}H-NMR spectroscopy, no trace of either bis-adduct or endo mono-adduct being formed. These results indicate that the reaction of activated triene **2** with **22** takes place in a highly chemoselective (selective mono-cycloadduct formation) and exoselective manner, and that the methanol elimination occurs only after the desilylation. When the cycloadduct **M** was treated with methanol, **21** was obtained in a good yield.

Both trienes **1** and **2** reacted with unsymmetrical olefinic dienophiles such as methyl vinyl ketone **27a**, methyl acrylate **27b**, and acrylonitrile **27c** in a highly regioselective manner, but its stereoselectivity was low. So far as these reactions were carried out around 80 °C, only the mono-adducts were afforded.

Even with large excess of **27**, the reactions of **1** under reflux in benzene or in a dienophile itself (**27c**) gave only the mono-adducts as mixtures of exo **28** and endo isomers **29** (Scheme 7 and Table 3). In all cases, the exo isomers were the major products. Their structures were based on the chemical shifts of substituents at the 4-position as well as the coupling constants between 3-H and 4-H. When the reaction with **27c** was carried out under harder conditions (at 110 °C in a shield tube for 5 d), a mixture of two isomeric bis-adducts **30** was obtained in a fair yield. They are the isomers which have different configurations in the initially formed six-membered ring.

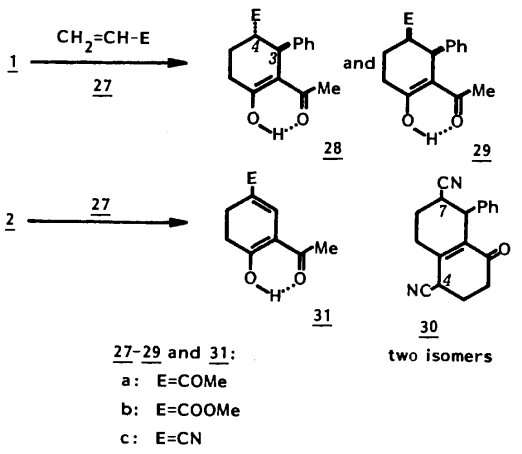

Scheme 7.

In the similar reactions of **2** with **27**, the only obtained products were the regioselective mono-adducts **31**. These products were also accompanied with methanol elimination, the stereochemical selectivity of mono-cycloadduct formation being ambiguous.

Experimental

General. Melting points were determined on a Yanagimoto micro melting point apparatus and uncorrected. IR spectra were taken with a JASCO IRA-1 or a JASCO A-102 spectrometer. ^{1}H-NMR spectra were recorded on a Hitachi R-40 or a JEOL FX-100 instrument and ^{13}C-NMR spectra were obtained on a JEOL FX-100 spectrometer at 25.05 MHz. Chemical shifts are expressed in parts per million downfield from tetramethylsilane. Mass spectra were measured with a JEOL JMS-01SG-2 spectrometer at 75 eV of ionization energy. Elementary analyses were performed on a Hitachi 026 CHN analyzer. Thin-layer chromatography (TLC) was accomplished on 0.2 mm precoated plates of silica gel 60 F-254 (Merck) or on 0.2 mm precoated plates of aluminum oxide 60 F-254 type E (Merck). Visualization was with ultraviolet light (254 and 365 nm) and iodine. Wakogel C200 and C300 (Wako) were used for preparative column chromatography. Preparative high performance liquid chromatography (HPLC) was carried out on a Kusano KHLC-201 apparatus with a UV-detector Uvilog-III using a column (22×300 mm) packed with silica gel (Wakogel LC-50H). Micro vacuum distillation was performed with a Sibata GTO-250R Kugelrohr distilling apparatus. Solvents were evaporated with a Tokyo Rikakikai rotary evaporator type V at about 50 °C unless otherwise stated.

Benzene and toluene were purified by the distillation of the predried commercial solvents and stored on sodium wire. Dichloromethane was dried on calcium chloride and then distilled on calcium hydride.

Materials. 3-Benzylidene-[18] and 3-(methoxymethylene)-2,4-pentanedione[19] were prepared by the condensations of 2,4-pentanedione with benzaldehyde in the presence of piperidine and with trimethyl orthoformate in the presence of acetic anhydride, respectively. Dibenzoylacetylene **3b**[20] was synthesized from the bromination and dehydrobromination procedure of *trans*-1,2-dibenzoyl-ethene. Methyl propiolate **3c**[21] and 2-butynoate **3d** were obtained by the esterification of the corresponding acids with methanol in the presence of *p*-toluenesulfonic acid. Propynoic acid was commercially available and 2-butynoic acid[22] was prepared by the reaction of propyne with butyllithium and then with carbon dioxide.

As for the following reagents, the ones of commercial grade were purified by distillation or crystallization: Triethylamine: distilled on potassium hydroxide and stored on the same agent; 1,8-diazabicyclo[5.4.0]undec-7-ene (DBU): distilled and stored on molecular sieves 5A; zinc chloride: crystallized from anhydrous dioxane and dried over phosphorus pentaoxide under vacuum; dimethyl acetylenedicarboxylate **3a**, methyl vinyl ketone **27a**, methyl acrylate **27b**, and acrylonitrile **27c**: distilled; maleic anhydride **9**: distilled under vacuum and stored in a bottle with a tightly-fitting stopper. The other reagents were all commercially available and no further purification was needed.

3-Benzylidene-2,4-bis(trimethylsilyloxy)-1,4-pentadiene **1**. To a mixture of 3-benzylidene-2,4-pentanedione (9.41 g, 0.1 mol) and DBU (15.22 g, 0.1 mol) in dry dichloromethane (25 ml) was added chlorotrimethylsilane (13.9 ml, 0.11 mol) at room temperature. The mixture was heated at 40 °C under dry atmosphere for 20 h and then all the volatile materials were removed *in vacuo*. The residue was triturated with dry hexane (100 ml) and the hexane separated from the insoluble DBU·HCl was concentrated *in vacuo* to give 15.05 g (91%) of crude **1**. This crude triene **1** was purified by a column chromatography over silica gel (Wako C200) using a mixture of benzene–hexane (1:9) as an eluent affording pure **1** (9.45 g, 57%) as a colorless liquid: bp 115 °C (107 Pa) (bulb-to-bulb); IR (neat) 1625, 1595 (C=C), 1245, and 830 cm^{-1} (TMS); ^{1}H-NMR (CCl_4) δ=0.17, 0.27 (each 9H, s, TMS), 4.17, 4.38 (each 1H, d, J=1.0 Hz, 1- and/or 5-CH_2), 4.35, 4.69 (each 1H, dd, J=1.0 and 0.6 Hz, 1- and/or 5-CH_2), 6.72 (1H, t, J=0.6 Hz, phC<u>H</u>=), and 7.00—7.46 (5H, m, ArH); ^{13}C-NMR (CCl_4) δ=0.00, 0.10 (each q, TMS), 94.83, 95.95 (each t, 1- and 5-C), 153.06, and 155.30 (each s, 2- and 4-C); MS m/z (rel. intensity) 332 (M^+; base peak), 241 (M^+−92, 25) and 73 (TMS^+, 79).

Found: C, 64.74; H, 8.60%; M^+, 332. Calcd for $C_{18}H_{28}O_2Si_2$: C, 65.00; H, 8.49%; M, 332.

Another procedure for **1** was briefly presented in the preceding communication.[6]

3-(Methoxymethylene)-2,4-bis(trimethylsilyloxy)-1,4-pentadiene **2**. A mixture of dry zinc chloride (0.57 g) and triethylamine (31.17 g, 0.31 mol) was vigorously stirred at room temperature for 1 h and mixed with a solution of 3-(methoxymethylene)-2,4-pentanedione (9.95 g, 0.07 mol) and chlorotrimethylsilane (35.5 ml, 0.28 mol) in dry benzene (50 ml). The resultant mixture was heated at 40 °C for 24 h and cooled to room temperature. The salt precipitated was filtered off and the filtrate was concentrated *in vacuo* to afford a yellow residue. Vacuum distillation of the residue gave 16.44 g (82%) of triene **2** as colorless liquid: bp 72 °C (240 pa); IR (neat) 1685—1600 (C=C), 1250, and 840 cm^{-1} (TMS); ^{1}H-NMR ($CDCl_3$) δ=0.18, 0.23 (each 9H, s, TMS), 3.65 (3H, s, OMe), 4.13, 4.26, 4.40, 4.49 (each 1H, s, =CH_2), and 6.40 (1H, s, C<u>H</u>OMe); ^{13}C-NMR ($CDCl_3$) δ=0.15, 0.24 (each q, TMS), 60.47 (q, OMe), 91.52, 97.27 (each t, =CH_2), 117.34 (s, 3-C), 145.38 (d, C<u>H</u>OMe), 150.92, and 153.79 (each s, 2- and 4-C); MS m/z 286 (M^+), 271 (M^+−15, base peak), 147, 63, and 45.

Found: m/z 286.1435. Calcd for $C_{13}H_{26}O_3Si_2$: M, 286.1420.

Cycloaddition of **1** *to* **3a** *Leading to* **5a**. A mixture of freshly distilled **1** (0.64 g, 1.92 mmol) and **3a** (1.37 g, 9.6 mmol) in dry benzene (5 ml) was refluxed under nitrogen for 72 h, the benzene was evaporated *in vacuo*, and the residue was treated with methanol (10 ml) at room temperature overnight. The methanol was completely removed off *in vacuo* to give a viscous oil which was then chromatographed over silica gel using chloroform–hexane (1:1) as an eluent. Crude **5a** (0.438 g, 51%) was purified by crystallization from ether–hexane.

5a: Colorless prisms; mp 171—173 °C; IR (KBr) 3360 (OH), 1725, 1715, 1665 (C=O), 1590, 1280, and 1245 cm^{-1}; ^{1}H-NMR ($CDCl_3$) δ=3.64 (1H, dd, J_{5-8}=2.8 and J_{gem}=21.8 Hz, one of 5-CH_2), 3.64, 3.74, 3.76, 3.89 (each 3H, s, COOMe), 3.95 (1H, dd, J_{5-8}=4.0 and J_{gem}=21.8 Hz, the other of 5-CH_2), 5.30 (1H, dd, 8-H), and 7.04—7.16 (6H, m, ArH and 2-H); ^{13}C-NMR ($CDCl_3$) δ=29.12 (t, 5-C), 42.08 (d, 8-C), 52.55, 52.80 (each q, COO<u>Me</u>), 114.78 (d, 2-C), 153.99 (s, 1-C), 166.27, 167.74, 168.15, and 169.43 (each s, <u>C</u>OOMe); MS m/z (rel. intensity) 454 (M^+, 10), 423 (M^+−31, 39), 422 (M^+−32, 75), 363 (79), 345 (base peak), 313 (11), 304 (16), and 189 (10).

Found: C, 63.15; H, 4.98%; M^+, 454. Calcd for $C_{24}H_{22}O_9$: C, 63.43; H, 4.88%; M, 454.

Cycloaddition of **1** *to* **3c** *Leading to* **4c**, **5c**, *and* **6c**. A mixture of **1** (0.685 g, 2.06 mmol) and **3c** (2.0 g, 23.8 mmol), both freshly distilled, in dry benzene (3 ml) was refluxed under nitrogen for 168 h. When all the volatile materials were removed off *in vacuo* and the residue was treated with methanol (10 ml), colorless solid of **4c** (0.313 g, 37%) was precipitated. The methanol filtrate was stirred at room temperature overnight and then evaporated *in vacuo*. The viscous oil obtained was chromatographed over silica gel with chloroform–hexane (1:1) to give **5c** (0.07 g, 10%) and **6c** (0.01 g, 2%). Repeated chromatography provided a pure sample of **4c**; **5c** was purified by crystallization from ether–hexane to give colorless prisms; **6c** was distilled on a micro distillation apparatus.

4c: Colorless solid; mp 143—145 °C; IR (KBr) 1720, 1700 (C=O), 1250, 875, and 840 cm^{-1} (TMS); ^{1}H-NMR ($CDCl_3$) δ=0.13 (9H, s, TMS), 3.67, 3.83 (each 3H, s, COOMe), 4.09 (1H, dt, J_{5-6}=J_{5-8}=3.3 and J_{gem}=22.5 Hz, one of 5-CH_2), 4.15 (1H, ddd, J_{5-6}=5.2, J_{5-8}=2.6, and J_{gem}=22.5 Hz, the other of 5-CH_2), 5.30 (1H, dd, 8-H), 6.62 (1H, d, J_{2-3}=8.5 Hz, 2-H), 7.00—7.30 (6H, m, ArH and 6-H), and 7.76 (1H, d, 3-H); ^{13}C-NMR ($CDCl_3$) δ=0.00 (q, TMS), 30.41 (t, 5-C), 39.69 (d, 8-C), 51.25 (q, COO<u>Me</u>), 115.43 (d, 2-C), 120.77 (s, 4-C), 135.80 (d, 6-C), 156.34 (s, 1-C), 166.03, and 167.14 (each s, <u>C</u>OOMe); MS m/z (rel. intensity) 411 (M^++1, 30), 410 (M^+, base peak), 379 (15), 378 (13), 351 (16), 334 (17), 333 (68), 301 (43), and 73 (40).

Found: C, 67.41; H, 6.44%; M^+, 410. Calcd for $C_{23}H_{26}O_5Si$: C, 67.29; H, 6.38%; M, 410.

5c: Colorless prisms (from ether–hexane); mp 179—181 °C; IR (KBr) 3230 (OH), 1720—1660 (C=O), 1575, 1250, and 1225 cm^{-1}; ^{1}H-NMR ($CDCl_3$) δ=3.67, 3.84 (each 3H, s, COOMe), 4.08 (1H, dt, J_{5-6}=J_{5-8}=3.2 and J_{gem}=23.0 Hz, one of 5-CH_2), 4.15 (1H, ddd, J_{5-6}=5.2, J_{5-8}=2.6, and J_{gem}=23.0 Hz, the other of 5-CH_2), 5.41 (1H, dd, 8-H), 6.60 (1H, d, J_{2-3}=8.5 Hz, 2-H), 7.00—7.34 (6H, m, ArH and 6-H), and 7.76 (1H, d, 3-H); ^{13}C-NMR ($CDCl_3$) δ=30.65 (t, 5-C), 39.39 (d, 8-C), 51.78 (q, COO<u>Me</u>), 113.31 (d, 2-C), 120.30 (s, 4-C), 136.85 (d, 6-C), 157.04 (s, 1-C), 166.85, and 167.73 (each s, <u>C</u>OOMe); MS m/z (rel. intensity) 339 (M^++1, 19), 338 (M^+, 83), 307 (M^+−31, 23), 306 (M^+−32, 20), 279 (21), 278 (32), 261 (64), 260 (31), 247 (64), 229 (base peak), 191 (25), 189 (41) and 115 (21).

Found: C, 70.93; H, 5.39%; M^+, 338. Calcd for $C_{20}H_{18}O_5$: C, 70.99; H, 5.36%; M, 338.

6c: Colorless viscous liquid; bp 120 °C (200 Pa) (bulb-to-bulb); IR (neat) 3400 (OH), 1720, 1660 (C=O), 1600, and 1245 cm^{-1}; ^{1}H-NMR ($CDCl_3$) δ=2.05 (3H, s, COMe), 3.27 (1H, ddd, J_{6-3}=3.0, J_{6-5}=4.8, and J_{gem}=22.0 Hz, one of 6-CH_2), 3.37 (1H, ddd, J_{6-5}=3.2, J_{6-3}=3.7, J_{gem}=22.0 Hz, the other of 6-CH_2), 3.68 (3H, s, COOMe), 4.83 (1H, dd, 3-H), 6.83 (1H, dd, 5-H), 7.10-7.24 (5H, br. s, ArH), and 15.96 (1H, br. s, OH); ^{13}C-NMR ($CDCl_3$) δ=25.60 (t, 6-C), 32.58 (1, CO<u>Me</u>), 41.80 (d, 3-C), 51.72 (q, COO<u>Me</u>), 109.56 (s, 2-C), 165.68 (s, <u>C</u>OOMe), 177.89 (s, <u>C</u>OMe), and 199.20 (s, 1-CO); MS m/z (rel. intensity) 273 (M^++1, 17), 272 (M^+, base peak), 254 (M^+−18, 34), 222 (22), 213 (31), 197 (29), 195 (34), 129 (40), and 128 (17).

Found: C, 70.45; H, 6.08%; M^+, 272. Calcd for $C_{16}H_{16}O_4$: C,

70.57; H, 5.92%; M, 272.

Cycloaddition of 2 to 3a Leading to 7a. A solution of **2** (0.85 g, 3.0 mmol) and **3a** (0.843 g, 6.0 mmol), both freshly distilled, in dry benzene (4 ml) was stirred at room temperature under nitrogen for 24 h. After evaporation of all the volatile materials, the residue was treated with methanol (10 ml) at room temperature overnight. The methanol was completely evaporated *in vacuo* to give a residue which was then chromatographed over silica gel using chloroform–ethyl acetate (3:1) as an eluent. Colorless needles (from aqueous methanol) of **7a** (0.425 g, 57%) were obtained:

7a: Colorless needles from aqueous methanol; mp 77 °C; IR (KBr) 1720 and 1645 cm^{-1} (C=O); ^1H—NMR ($CDCl_3$) δ= 2.67 (3H, s, MeCO), 3.87, 3.90 (each 3H, s, COOMe), 7.02 (1H, s, 6-H), 8.27 (1H, s, 3-H), and 12.50 (1H, s, OH); MS *m/z* 252 (M^+), 237 (M^+-15), and 221 (M^+-31, base peak).

Found: C, 56.93; H, 4.87%; M^+, 252. Calcd for $C_{12}H_{12}O_6$: C, 57.14; H, 4.80%; M, 252.

Cycloaddition of 2 to 3b Leading to 7b. Similar reaction between **2** (0.547 g, 1.9 mmol) and **3b** (0.447 g, 1.9 mmol) in 3 ml of benzene under the conditions shown in Table 1 gave 0.31 g (47%) of **7b** which was precipitated on the work-up with methanol.

7b: Colorless leaflets from dichloromethane–methanol; mp 189-190 °C; IR (KBr) 1670—1640 cm^{-1} (C=O); ^1H-NMR ($CDCl_3$) δ=2.60 (3H, s, COMe), 7.07 (1H, s, 6-H), 7.20—7.70 (10H, m, ArH), 8.02 (1H, s, 3-H), and 12.60 (1H, s, OH); MS *m/z* 344 (M^+) and 267 (M^+-77, base peak).

Found: C, 76.47; H, 4.75%; M^+, 344. Calcd for $C_{22}H_{16}O_4$: C, 76.73; H, 4.68%; M, 344.

Cycloaddition of 2 to 3c Leading to 7c. Similar reaction starting from **2** (0.573 g, 2.0 mmol) and **3c** (0.336 g, 4.0 mmol) under the conditions shown in Table 1 gave 0.134 g (35%) of **7c**, after a chromatography over silica gel with chloroform.

7c: Colorless needles from aqueous methanol; mp 99—99.5 °C; IR (KBr) 1720 cm^{-1} (C=O); ^1H-NMR ($CDCl_3$) δ=2.68 (3H, s, COMe), 3.90 (3H, s, COOMe), 6.96 (1H, d, J_{6-5}=9.0 Hz, 6-H), 8.06 (1H, dd, J=9.0 and 2.0 Hz, 5-H), 8.42 (1H, d, J= 2.0 Hz, 3-H), and 12.60 (1H, s, OH); MS *m/z* 194 (M^+) and 179 (M^+-15, base peak).

Found: C, 62.09; H, 5.14%; M^+, 194. Calcd for $C_{10}H_{10}O_4$: C, 61.85; H, 5.19%, M, 194.

Cycloaddition of 2 to 3d Leading to 7d. Similar reaction between **2** (0.886 g, 3.1 mmol) and **3d** (0.607 g, 6.2 mmol) under the conditions of Table 1 gave 0.045 g (8%) of **7d**, after a chromatography over silica gel with chloroform.

7d: Colorless needles from aqueous methanol; mp 70 °C; IR (KBr) 1720 and 1635 cm^{-1} (C=O); ^1H-NMR ($CDCl_3$) δ=2.60 (3H, s, 5-Me), 2.64 (3H, s, COMe), 3.87 (3H, s, COOMe), 6.77 (1H, s, 6-H), 8.36 (1H, s, 3-H), and 12.42 (1H, s, OH); MS *m/z* 208 (M^+) and 193 (M^+-15, base peak).

Found: 63.17; H, 5.99%; M^+, 208. Calcd for $C_{11}H_{10}O_4$: C, 63.45; H, 5.81%; M, 208.

Cycloaddition of 1 to 8a Leading to 10a, 11a, and 12a. A solution of **1** (0.43 g, 1.29 mmol) and **8a** (0.333 g, 3.0 mmol) in dry benzene (1.5 ml) was stirred at room temperature under nitrogen for 48 h. The benzene was evaporated *in vacuo* and the residue was treated with methanol (10 ml) at room temperature overnight. The methanol was removed *in vacuo* to afford a viscous residue, it was treated with water, extracted with chloroform, the chloroform was dried over magnesium sulfate, and finally evaporated *in vacuo*. Trituration of the viscous oil obtained with ether–hexane gave 0.089 g (23%) of **11a**.

11a: Colorless prisms from ether–hexane; mp 163—165 °C; IR (KBr) 1775, 1700 (C=O), and 1610 cm^{-1}; ^1H-NMR ($CDCl_3$) δ=2.04 (3H, s, COMe), 2.38 (3H, s, NMe), 2.80 (1H, dd, J_{gem}=21.0 and J_{7-7a}=12.5 Hz, one of 7-CH_2), 3.00—3.45 (3H, m, the other of 7-CH_2, 3a-, and 7a-H), 4.38 (1H, d, J_{4-3a}=6.0 Hz, 4-H), and 6.80—7.30 (5H, m, ArH); ^{13}C-NMR ($CDCl_3$) δ=24.07 (7-C), 24.54 (NMe), 27.53 (COMe), 37.05, 41.33 (3a- and 7a-C), 46.15 (4-C), 108.38 (5-C), 127.99, 128.40, 128.69, 137.20, 176.84 (CON-), 178.01 (CON-), 182.71 (COMe), and 197.03 (6-C); MS *m/z* (rel. intensity) 299 (M^+, 27), 281 (25), 256 (19), 131 (22), 126 (30), 115 (26), and 77 (22).

Found: C, 68.37; H, 5.80; N, 4.63%; M^+, 299. Calcd for $C_{17}H_{17}NO_4$: C, 68.21; H, 5.73; N, 4.68%; M, 299.

A solution of **1** (0.475 g, 1.43 mmol) and **8a** (0.477 g, 4.29 mmol) in dry benzene (5 ml) was refluxed under nitrogen for 72 h. The benzene was evaporated *in vacuo* to give a residue which solidified on treatment with methanol (15 ml). This colorless solid of **10a** (0.21 g) was collected on a filter and washed with another 5 ml of methanol. The combined methanol filtrate was stirred at room temperature overnight, evaporated *in vacuo*, and the residue obtained was chromatographed over silica gel. The fraction with chloroform–hexane (2:1) gave 0.055 g of mixture between **11a** (2%) and **12a** (3%), from which only **12a** was isolated by crystallization from ether–hexane. The fraction with chloroform–ethyl acetate 19:1 afforded 0.14 g of **10a**. Total amount of **10a** was 0.35 g (60%).

10a: Colorless prisms from benzene–hexane; mp 213—215 °C; IR (KBr) 1760, 1675 (C=O), and 1420 cm^{-1}; ^1H-NMR ($CDCl_3$) δ=2.33 (3H, s, NMe), 2.53 (1H, dd, J_{gem}=17.0 and J_{10-9a}=9.0 Hz, one of 10-CH_2), 2.95 (1H, dd, J_{gem}=17.0 and J_{10-9a}=4.5 Hz, the other of 10-CH_2), 3.04 (3H, s, NMe), 3.20—3.75 (5H, m, 4-CH_2, 3a-, 6a-, and 9a-H), 3.92 (1H, d, J_{10b-3a}=8.0 Hz, 10b-H), 4.70 (1H, dd, J_{6-6a}=6.0 and J_{6-9a}=2.0 Hz, 6-H), and 6.70—7.22 (5H, m, ArH); ^{13}C-NMR ($CDCl_3$) δ=23.90 (t, 10-C), 25.36, 25.48 (each q, NMe), 34.64 (t, 4-C), 36.99, 38.34 (each d, 3a-, 6a-, and 9a-C), 44.09 (d, 10b-C), 44.50 (d, 6-C), 127.75 (d), 128.46 (d), 135.80 (s), 136.27 (s), 146.13 (s), 174.37, 176.66, 178.59 (each s, CON-), and 190.98 (s, 5-CO); MS *m/z* (rel. intensity) 393 (M^++1, 33), 392 (M^+, base peak), 374 (59), 289 (35), 280 (29), 203 (25), 178 (28), 167 (22), 165 (28), and 115 (25).

Found: C, 67.59; H, 5.25; N, 7.14%; M^+, 392. Calcd for $C_{22}H_{20}N_2O_5$: C, 67.33; H, 5.14; N, 7.14%; M, 392.

12a: Colorless solid from ether–hexane; mp 126—128 °C; IR (KBr) 3420 (OH) and 1690 cm^{-1} (C=O); ^1H-NMR ($CDCl_3$) δ=2.11 (3H, s, COMe), 2.54 (1H, dd, J_{gem}=19.5 and J_{7-7a}= 9.0 Hz, one of 7-CH_2), 2.76 (1H, dd, J_{gem}=19.5 and J_{7-7a}=2.3 Hz, the other of 7-CH_2), 3.00 (3H, s, NMe), 3.19 (1H, dt, J_{7a-7}=J_{7a-3a}=9.0 and J_{7a-7}=2.3 Hz, 7a-H), 3.60 (1H, dd, J_{3a-7a}=9.0 and J_{3a-4}=2.0 Hz, 3a-H), 4.68 (1H, d, J_{4-3a}=2.0 Hz, 4-H), and 7.04—7.43 (5H, m, ArH); MS *m/z* (rel. intensity) 300 (M^++1, 17), 299 (M^+, 87), 281 (base peak), 170 (32), 142 (28), and 126 (42).

Found: C, 68.37; H, 5.79; N, 4.80%; M^+, 299. Calcd for $C_{17}H_{17}NO_4$: C, 68.21; H, 5.73; N, 4.68%; M, 299.

Cycloaddition of 1 to 8b Leading to 10b, 11b, and 12b. A solution of **1** (0.665 g, 2.0 mmol) and **8b** (0.692 g, 4.0 mmol) in 6 ml of dry benzene was stirred at room temperature under nitrogen for 120 h. The benzene was evaporated *in vacuo* and the residue was treated with methanol (15 ml) overnight to precipitate 0.18 g (26%) of **11b** which was collected and washed with another portion (5 ml) of methanol. The combined methanol filtrate was evaporated *in vacuo* and the viscous oil obtained was triturated with ether to give 0.135 g (13%) of **10b**.

10b: Colorless solid from chloroform–hexane; mp 278—280 °C; IR (KBr) 1770, 1700 (C=O), 1585, 1375, and 1175 cm^{-1}; ^1H-NMR ($CDCl_3$) δ=2.63 (1H, dd, J_{gem}=16.5 and J_{10-9a}=9.0 Hz, one of 10-CH_2), 3.05 (1H, dd, J_{gem}=16.5 and J_{10-9a}=5.5 Hz, the other of 10-CH_2), 3.20—3.85 (5H, m, 4-CH_2, 3a-, 6a-, and 9a-H), 3.96 (1H, d, J_{10b-3a}=8.0 Hz, 10b-H), 4.86 (1H, d, J_{6-6a}=6.5 Hz, 6-H), and 6.37—7.60 (15H, m, ArH); MS *m/z* 516 (M^+).

Found: C, 74.13; H, 4.82; N, 5.32%; M+, 516. Calcd for $C_{32}H_{24}N_2O_5$: C, 74.40; H, 4.68; N, 5.42%; M, 516.

11b: Colorless needles from ether-hexane; mp 188—190 °C; IR (KBr) 1770, 1700 (C=O), 1600, 1380, 740, and 695 cm^{-1}; ^{1}H-NMR ($CDCl_3$) δ=2.05 (3H, s, COMe), 2.88 (1H, m, one of 7-CH_2), 3.20—3.62 (3H, m, the other of 7-CH_2, 3a-, and 7a-H), 4.48 (1H, m, 4-H), 6.40—7.32 (10H, m, ArH), and 16.02 (1H, s, OH); ^{13}C-NMR ($CDCl_3$) δ=24.72 (q, COMe), 27.53 (t, 7-C), 37.28, 41.57 (each d, 3a- and 7a-C), 45.62 (d, 4-C), 108.73 (s, 5-C), 126.23 (d), 128.11 (d), 128.69 (d), 128.93 (d), 129.10 (d), 131.10 (s), 137.56 (s), 175.66, 177.18 (each s, CON-), 182.00 (s, COMe), and 197.62 (s, 6-C); MS *m/z* (rel. intensity) 362 (M^++1, 26), 361 (M^+, base peak), 343 (57), 318 (47), 199 (27), 188 (48), 131 (32), 91 (29), and 77 (23).

Found: C, 72.94; H, 5.56; N, 3.87%; M+, 361. Calcd for $C_{22}H_{19}NO_4$: C, 73.11; H, 5.30; N, 3.88%; M, 361.

A mixture of **1** (0.345 g, 1.04 mmol) and **8b** (0.519 g, 3.0 mmol) in dry benzene (6 ml) was refluxed under nitrogen for 48 h. The benzene was removed off *in vacuo*, the residue was treated with methanol (15 ml) at room temperature for 5 h, the methanol was completely evaporated *in vacuo*, and finally the viscous oil obtained was chromatographed over silica gel. The fraction with chloroform gave 0.042 g of mixtrure of **11b** (3%) and **12b** (6%), from which only **12b** was isolated by crystallization from chloroform-hexane. Continued elution with chloroform-ethyl acetate (9:1) afforded 0.43 g (80%) of **10b**.

12b: Colorless prisms from ether-hexane; mp 204—206 °C; IR (KBr) 3400 (OH), 1700 (C=O), and 1380 cm^{-1}; ^{1}H-NMR ($CDCl_3$) δ=2.13 (3H, s, COMe), 2.60 (1H, dd, J_{gem}=16.5 and J_{7-7a}=8.5 Hz, one of 7-CH_2), 2.84 (1H, dd, J_{gem}=16.5 and J_{7-7a}=2.0 Hz, the other of 7-CH_2), 3.34 (1H, ddd, J_{7a-7}=8.5, J_{7a-7}=2.0, and J_{7a-3a}=9.0 Hz, 7a-H), 3.82 (1H, dd, J_{3a-7a}=9.0 and J_{3a-4}=2.0 Hz, 3a-H), 4.77 (1H, d, J_{4-3a}=2.0 Hz, 4-H), 7.00—7.56 (10H, m, ArH), and 15.86 (1H, s, OH); ^{13}C-NMR ($CDCl_3$) δ=22.54 (COMe), 33.35 (7-C), 38.28, 39.99 (3a- and 7a-C), 46.26 (4-C), 107.09 (5-C), 126.28, 126.64, 127.28, 128.87, 129.22, 131.57, 139.79, 177.36 (CON-), 188.40 (COMe), and 191.87 (6-C); MS *m/z* 361 (M^+).

Found: C, 73.07; H, 5.33; N, 3.80%; M+, 361. Calcd for $C_{22}H_{19}NO_4$: C, 73.11; H, 5.30; N, 3.88%; M, 361.

Cycloaddition of ***1*** *to* ***9*** *Leading to* ***1(X=O)***, ***13***, ***14***, *and* ***15***. A solution of **1** (0.267 g, 0.83 mmol) and **9** (0.174 g, 1.77 mmol) in dry benzene (5 ml) was refluxed under nitrogen for 48 h. The benzene was evaporated off *in vacuo* and the residue was heated under reflux in methanol (60 ml) in the presence of *p*-toluenesulfonic acid (0.2 g) for 24 h. The methanol was removed off *in vacuo*, the residue was treated with water, extracted with ether, the ether was dried over magnesium sulfate, and finally evaporated *in vacuo* to give a viscous oil. This oil was chromatographed over silica gel using chloroform-hexane (1:2) as an eluent. The first fraction gave 0.02 g (7%) of **15** and the second 0.263 g of mixture between **13** (57%) and **14** (22%) which were separated by repeated chromatography over silica gel with ether-hexane (1:1) and crystallization.

13: Colorless needles from hexane; mp 141—143 °C; IR (KBr) 1720, 1650 (C=O), 1430, 1200, 1170, and 1000 cm^{-1}; ^{1}H-NMR ($CDCl_3$) δ=2.25—3.85 (9H, m, CH_2 and CH), 3.10, 3.62, 3.70 (each 3H, s, COOMe), 4.13 (1H, br. d, J_{8-7}=7.5 Hz, 8-H), and 6.80—7.30 (5H, m, ArH); ^{13}C-NMR ($CDCl_3$) δ= 30.65 (t), 33.47 (t), 38.46, 39.51, 40.51, 42.27, 46.09, 51.02 (q), 52.13 (q), 126.35 (d), 127.34 (d), 127.93 (d), 132.62 (s), 140.61 (s), 155.58 (s), 171.90 (s), 172.67 (s), 173.25 (s), and 193.86 (s); MS *m/z* (rel. intensity) 401 (M^++1, 25), 400 (M^+, base peak), 341 (17), 340 (34), 281 (52), 249 (29), and 221 (47).

Found: C, 65.75; H, 6.08%; M+, 400. Calcd for $C_{22}H_{24}O_7$: C, 65.99; H, 6.04%; M, 400.

14: Colorless solid from hexane; mp 114—116 °C; IR (KBr) 1740, 1725, 1660 (C=O), 1440, 1200, and 1040 cm^{-1}; ^{1}H-NMR ($CDCl_3$) δ=2.35—3.50 (9H, m, CH_2 and CH), 3.15, 3.59, 3.75 (each 3H, s, COOMe), 4.14 (1H, br. d, J_{8-7}=7.0 Hz, 8-H), and 6.90—7.30 (5H, m, ArH); MS *m/z* (rel. intensity) 401 (M^++1, 45), 400 (M^+, base peak), 369 (27), 340 (33), 309 (66), 281 (78), 277 (25), 249 (59), and 221 (91).

Found: C, 65.95; H, 6.15%; M+, 400. Calcd for $C_{22}H_{24}O_7$: C, 65.99; H, 6.04%; M, 400.

15: Colorless prisms from ether-hexane; mp 153—155 °C; IR (KBr) 1720 (C=O), 1600, and 1250—1200 cm^{-1}; ^{1}H-NMR ($CDCl_3$) δ=1.90 (3H, s, COMe), 2.48—2.97 (2H, m, one of 6-CH_2 and 5-H), 3.06 (1H, dd, J_{gem}=20.0 and J_{6-5}=12.6 Hz, the other of 6-CH_2), 3.37 (1H, dd, J_{4-3}=2.3 and J_{4-5}= 3.2 Hz, 4-H), 3.62, 3.70 (each 3H, s, COOMe), 4.50 (1H, d, J_{3-4}=2.3 Hz, 3-H), 7.10—7.40 (5H, m, ArH), and 15.95 (1H, s, OH); ^{13}C-NMR ($CDCl_3$) δ=25.42 (q, COMe), 29.36 (t, 6-C), 34.64, 42.33 (each d, 4- and 5-C), 48.50 (d, 3-C), 52.08, 52.37 (each q, COOMe), 106.27 (s, 2-C), 127.34 (d), 127.75 (d), 128.98 (d), 142.55 (s), 171.67, 172.61 (each s, COOMe), 179.95 (s, COMe), and 200.90 (s, 1-C); MS *m/z* (rel. intensity) 332 (M^+, 5), 301 (M^+—31, 3), 213 (21), 115 (26), 59 (20), and 43 (base peak).

Found: C, 65.19; H, 6.12%; M+ 332. Calcd for $C_{18}H_{20}O_6$: C, 65.05; H, 6.07%; M, 332.

A solution of **1** (0.37 g, 1.11 mmol) and **9** (0.226 g, 2.3 mmol) in dry benzene (5 ml) was refluxed under nitrogen for 48 h. The residue obtained by evaporation of the benzene *in vacuo* was triturated with benzene-hexane (1:9) to give 0.48 g (82%) of **I** (X=O) as colorless solid. The product **I** was found to contain two isomers (2.5:1) on the basis of ^{1}H-NMR spectrum (δ_{TMS}: the major isomer: 0.00 and 0.26; the minor isomer: −0.30 and 0.27). The bis-cyclo-adduct mixture **I** (X=O) (0.265 g, 0.5 mmol) was heated in water (30 ml) under reflux for 24 h. The water was evaporated to dryness *in vacuo* and the residue was washed with benzene to give 0.17 g (95%) of tricarboxylic acid. This acid (0.155 g, 0.43 mmol) was heated under reflux in methanol (100 ml) in the presence of *p*-toluenesulfonic acid (0.15 g) for 48 h. The methanol was evaporated *in vacuo*, the residue was treated with water, extracted with ether, the ether was washed with aqueous sodium hydrogencarbonate, dried over magnesium sulfate, and evaporated *in vacuo*. The residue was chromatographed over silica gel using ether-hexane (1:1) as an eluent to give 0.088 g (51%) of **13** and 0.033 g (19%) of **14**.

Similarly, **1** (0.70 g, 2.1 mmol) and **9** (0.149 g, 1.52 mmol) were stirred in dry benzene (2 ml) at room temperature under nitrogen for 72 h. The reaction mixture was added to a large quantity of hexane to precipitate colorless solid of **I** (0.25 g, 63%) which was composed of two isomers (3:1).

Cycloaddition of ***2*** *to an Equivalent of* ***8a*** *Leading to* ***16a***. A mixture of **1** (0.662 g, 2.3 mmol) and **8a** (0.257 g, 2.3 mmol) in 1 ml of dry benzene was stirred at room temperature under nitrogen for 24 h. After evaporation of the solvent *in vacuo*, the residue was treated with methanol (15 ml) at room temperature overnight to precipitate 0.278 g of **16a**. The methanol separated from the solid was evaporated completely *in vacuo* and the viscous oil obtained was chromatographed over silica gel with hexane-ethyl acetate (3:1) to give 0.048 g of **16a**. Total amount of **16a** was 0.326 g (64%).

16a: Colorless needles from aqueous methanol; mp 186 °C; IR (KBr) 1755, 1685 (C=O), and 1640-1580 cm^{-1}; ^{1}H-NMR ($CDCl_3$) δ=2.28 (3H, s, COMe), 2.54 (1H, dd, J_{gem}=17.0 and J_{7-7a}=15.0 Hz, one of 7-CH_2), 3.02 (1H, dd, J_{gem}=17.0 and J_{7-7a}=7.0 Hz, the other of 7-CH_2), 3.05 (3H, s, NMe), 3.60 (1H, ddd, J_{7a-7}=15.0, 7.0, and J_{7a-4}=2.5 Hz, 7a-H), 7.32 (1H, d, J_{4-7a}=2.5 Hz, 4-H), and 15.94 (1H, s, OH); ^{13}C-NMR ($CDCl_3$) δ=20.35 (q, COMe), 24.77 (q, NMe), 35.18 (t, 7-C),

38.12 (d, 7a-C), 108.01 (s, 5-C), 119.77 (s, 3a-C), 127.07 (d, 4-C), 167.83, 174.89 (each s, CON-), 186.07 (s, COMe), and 199.19 (s, 6-C); MS *m/z* 221 (M^+, base peak).

Found: C, 59.77; H, 4.93; N, 6.26%; M^+, 221. Calcd for $C_{11}H_{11}NO_4$: C, 59.73; H, 5.01; N, 6.33%; M, 221.

Cycloaddition of **2** *to two Equivalents of* **8a** *Leading to* **17a** *and* **18a**. Triene **2** (0.989 g, 3.5 mmol) and **8a** (0.767 g, 7.0 mmol) were heated under reflux in dry benzene (3 ml) under nitrogen for 24 h. After cooled to room temperature, the solution was treated with 10 ml of hexane at room temperature for 0.5 h to precipitate 1.104 g (63%) of **17a**. To a solution of **17a** (0.204 g, 0.4 mmol) in 2.5 ml of dry benzene was added a drop of trifluoroacetic acid, and immediately colorless solid of **18a** was precipitated (0.125 g, 90%).

17a: Colorless solid; mp 185—187 °C; IR (KBr) 1775, 1700 (C=O), 1250, and 880 cm^{-1} (TMS); ^{1}H-NMR ($CDCl_3$) δ=0.15, 0.21 (each 9H, s, TMS), 2.26—3.65 (8H, m, CH_2 and CH), 2.88, 2,96 (each 3H, s, NMe), 3.09 (3H, s, OMe), and 4.70 (1H, d, J_{6-6a}=3.6 Hz, 6-H); ^{13}C-NMR ($CDCl_3$) δ=0.17, 2.17 (each q, TMS), 24.66, 24.95 (each q, NMe), 29.59, 33.35 (each t, 4- and 10-C), 36.17, 39.04, 44.50, 54.01 (each d, 3a-, 6a-, 9a-, and 10b-C), 55.72 (q, OMe), 71.10 (d, 6-C), 73.86 (s, 10a-C), 113,84 (s, 5a-C), 152.35 (s, 5-C), 175.72, 177.13, 179.01, and 180.47 (each s, CON-); MS *m/z* 508 (M^+), 493 (M^+-15), and 73 (base peak).

Found: C, 54.37; H, 7.14; N, 5.37%; M^+ 508. Calcd for $C_{23}H_{36}N_2O_7Si_2$: C, 54.30; H, 7.13; N, 5.51%; M, 508.

18a: Colorless prisms; mp 180—182 °C; IR (KBr) 1780 and 1720—1640 cm^{-1} (C=O); ^{1}H-NMR ($CDCl_3$) δ=2.50—3.90 (8H, m, CH_2 and CH), 2.97, 3.00 (each 3H, s, NMe), 3.05 (3H, s, OMe), and 5.00 (1H, d, J_{6-6a}=4.0 Hz, 6-H); ^{13}C-NMR ($CDCl_3$) δ=24.83, 25.42 (each q, NMe), 26.42, 34.05 (each t, 4- and 10-C), 36.64, 37.57, 43.97, 45.91 (each d, 3a-, 6a-, 9a-, and 10b-C), 57.54 (q, OMe), 68.46 (d, 6-C), 135.15 (s, 5a-C), 153.00 (s, 10a-C), 173.72, 175.83, 176.71, 178.83 (each s, CON-), and 191.04 (s, 5-CO), MS *m/z* 346 (M^+), 331, 316 (base peak), and 314 (M^+-32).

Found: C, 58.94; H, 5.19; N, 8.47%; M^+, 346. Calcd for $C_{17}H_{18}N_2O_6$: C, 58.96; H, 5.24; N, 8.09%; M, 346.

Cycloaddition of **2** to an Equivalent of **8b** *Leading to* **16b**. A solution of **2** (0.741 g, 2.6 mmol) and **8b** (0.448 g, 2.6 mmol) in dry benzene (2 ml) was stirred at room temperature under nitrogen for 20 h and the benzene was evaporated *in vacuo*. When the residue was treated with methanol (15 ml), colorless solid of **16b** (0.536 g, 73%) was immediately separated.

16b: Colorless leaflets from dichloromethane-methanol; mp 227 °C; IR (KBr) 1765 and 1710—1610 cm^{-1} (C=O); ^{1}H-NMR ($CDCl_3$) δ=2.25 (3H, s, COMe), 2.64 (1H, dd, J_{gem}=16.2 and J_{7-7a}=14.4 Hz, one of 7-CH_2), 3.07 (1H, dd, J_{gem}=16.2 and J_{7-7a}=7.1 Hz, the other of 7-CH_2), 3.73 (1H, ddd, J_{7a-7}=14.4, 7.1, and J_{7a-4}=2.4 Hz, 7a-H), 7.22 (1H, d, J_{4-7a}=2.4 Hz, 4-H), 7.20—7.50 (5H, m, ArH), and 16.00 (1H, s, OH); MS *m/z* 283 (M^+) and 136 (base peak).

Found: C, 67.83; H, 4.54; N, 5.05%; M^+, 283. Calcd for $C_{16}H_{13}NO_4$: C, 67.84; H, 4.63; N, 4.94%; M, 283.

Cycloaddition of **2** *to two Equivalents of* **8b** *Leading to* **17b** *and* **18b**. Triene **2** (0.515 g, 1.8 mmol) and **8b** (0.623 g, 3.6 mmol) in dry benzene (2 ml) was heated at 50 °C under nitrogen for 20 h. After cooled to room temperature, the reaction mixture was triturated with 6 ml of hexane to separate colorless precipitation of **17b** (0.704 g, 62%). To a solution of **17b** (0.19 g, 0.3 mmol) in 2.5 ml of dry benzene was added a drop of trifluoroacetic acid. The mixture was stirred at room temperature for 15 min and treated with hexane to precipitate 0.125 g (89%) of **18b**.

17b: Colorless solid; mp 188—190 °C; IR (KBr) 1775, 1705 (C=O), 1250, and 845 cm^{-1} (TMS); ^{1}H-NMR ($CDCl_3$) δ=0.19, 0.25 (each 9H, s, TMS), 2.48—3.80 (8H, m, CH_2 and CH), 3.20 (3H, s, OMe), 4.91 (1H, d, J_{6-6a}=3.5 Hz, 6—H), and 7.00—7.52 (10H, m, ArH); ^{13}C-NMR ($CDCl_3$) δ=1.00, 2.23 (each q, TMS), 29.77, 33.35 (each t, 4- and 10-C), 36.46, 39.16, 44.91, 54.01 (each d, 3a-, 6a-, 9a, and 10b-C), 55.95 (q, OMe), 71.74 (d, 6-C), 74.03 (s, 10a-C), 113.66 (s, 5a-C), 126.23, 126.64, 128.34, 128.98, 129.28, 131.51, 132.27, 152.76 (s, 5-C), 174.89, 176.30, 178.01, and 179.48 (each s, CON-); MS *m/z* 632 (M^+), 617 (M^+-15), and 73 (base peak).

Found: C, 62.64; H, 6.37; N, 4.65%; M^+, 632. Calcd for $C_{33}H_{40}N_2O_7Si_2$: C, 62.63; H, 6.37; N, 4.43%; M, 632.

18b: Colorless prisms; mp 148—150 °C; IR (KBr) 1775 and 1720—1660 cm^{-1} (C=O); ^{1}H-NMR ($CDCl_3$) δ=2.45—3.92 (8H, m, CH_2 and CH), 3.12 (3H, s, OMe), 5.10 (1H, d, J_{6-6a}=4.0 Hz, 6-H), and 7.10—7.60 (10H, m, ArH); ^{13}C-NMR ($CDCl_3$) δ=26.36, 34.23 (each t, 4- and 10-C), 36.34, 37.93, 44,03, 45.85 (each d, 3a-, 6a-, 9a-, and 10b-C), 57.65 (q, OMe), 68.75 (d, 6-C), 126.05, 126.52, 128.22, 128.63, 129.10, 129.22, 131.10, 131.92, 134.97 (s, 5a-C), 152.76 (s, 10a-C), 172.67, 175.01, 175.48, 178.07 (each s, CON-), and 190.86 (s, 5-CO); MS *m/z* 438 (M^+-32).

Found: C, 68.45; H, 4.61; N, 6.05%. Calcd for $C_{27}H_{22}N_2O_6$: C, 68.93; H, 4.71; N, 5.95%.

Cycloaddition of **2** *to an Equivalent of* **9** *Leading to* **19**, **20**, *and* **21**. A mixture of **2** (0.904 g, 3.2 mmol) and **9** (0.309 g, 3.2 mmol) was allowed to stand at room temperature for 10 min. ^{1}H-NMR measurement of this mixture showed that **19** was formed in a quantitative yield. It was isolated as unstable liquid by vacuum distillation on a micro distillation apparatus (0.469 g, 39%). To the mixture of each equivalent of **2** and **9** was added a drop of trifluoroacetic acid, and then hexane to precipitate colorless solid of **20**.

19: Yellow liquid; bp 180 °C (133 Pa) (bulb-to-bulb); IR (neat) 1860, 1785 (C=O), 1250, and 850 cm^{-1} (TMS); ^{1}H-NMR ($CDCl_3$) δ=0.24 (18H, s, TMS), 2.48 (1H, dd, J_{gem}=16.5 and J_{7-7a}=10.0 Hz, one of 7-CH_2), 2.85 (1H, dd, J_{gem}=16.5 and J_{7-7a}=7.5 Hz, the other of 7-CH_2), 3.12 (1H, dd, J_{3a-4}=3.5 and J_{3a-7a}=10.0 Hz, 3a-H), 3.17 (3H, s, OMe), 3.47 (1H, dt, J_{7a-7}=7.5, 10.0 and J_{7a-3a}=10.0 Hz, 7a-H), 4.37, 4.63 (each 1H, d, J_{gem}=1.0 Hz, =CH_2), and 4.65 (1H, d, J_{4-3a}=3.5 Hz, 4-H); ^{13}C-NMR ($CDCl_3$) δ=0.59, 0.94 (each s, TMS), 28.42 (t, 7-C), 37.28, 47.26 (each d, 3a- and 7a-C), 55.83 (q, OMe), 73.27 (d, 4-C), 93.82 (t, =CH_2), 114.60 (s, 5-C), 151.36 (s, 6-C), 171.02, and 173.90 (each s, COO-); MS *m/z* 384 (M^+), 369 (M^+-15), and 73 (base peak).

20: Colorless needles from chloroform; mp 117—118 °C; IR (KBr) 1850, 1770 (C=O), and 1600 cm^{-1}; ^{1}H-NMR ($CDCl_3$) δ=2.20 (3H, s, COMe), 2.54 (1H, dd, J_{gem}=16.5 and J_{7-7a}=9.0 Hz, one of 7-CH_2), 2.96 (1H, dd, J_{gem}=16.5 and J_{7-7a}=8.0 Hz, the other of 7-CH_2), 3.14 (3H, s, OMe), 3.26 (1H, dd, J_{3a-4}=3.0 and J_{3a-7a}=11.0 Hz, 3a-H), 3.55 (1H, m, 7a-H), 4.70 (1H, d, J_{4-3a}=3.0 Hz, 4-H), and 15.80 (1H, s, OH); ^{13}C-NMR ($CDCl_3$) δ=20.20 (q, COMe), 32.53 (t, 7-C), 35.53, 47.14 (each d, 3a- and 7a-C), 55.31 (q, OMe), 73.45 (d, 4-C), 105.27 (s, 5-C), 170.55, 173.01 (each s, COO-), 185.17 (s, COMe), and 195.91 (s, 6-C); MS *m/z* 240 (M^+), 209 (M^+-31), and 43 (base peak).

Found: C, 55.27; H, 5.03%; M^+, 240. Calcd for $C_{11}H_{12}O_6$: C, 55.00; H, 5.04%; M, 240.

Crude **19**, which had been prepared from **2** (0.749 g, 2.6 mmol) and **9** (0.256 g, 2.6 mmol), was heated under reflux in methanol (50 ml) in the presence of *p*-toluenesulfonic acid (0.1 g) for 24 h. The methanol was evaporated *in vacuo* and the residue was dissolved in ether. The ether was washed with aqueous sodium hydrogencarbonate (5%), dried over magnesium sulfate, and then evaporated *in vacuo* to give viscous oil which was chromatographed over silica gel using chloroform–ethyl acetate (9:1). Colorless solid of **21** was obtained (0.371 g, 56%).

21: Colorless needles from hexane; mp 92—92.5 °C; IR

(KBr) 1725, 1690 (C=O), and 1610 cm^{-1}; ^{1}H-NMR ($CDCl_3$) δ=2.14 (3H, s, COMe), 2.71 (1H, dd, J_{gem}=17.5 and J_{6-5}=7.0 Hz, one of 6-CH_2), 2.94 (1H, dd, J_{gem}=17.5 and J_{6-5}=3.2 Hz, the other of 6-CH_2), 3.64, 3.77 (each 3H, s, COOMe), 3.94 (1H, dd, J_{5-6}=7.0 and 3.2 Hz, 5-H), 7.54 (1H, s, 3-H), and 15.94 (1H, s, OH); ^{13}C-NMR ($CDCl_3$) δ=19.96, 37.22, 38.40, 51.96, 52.49, 107.13, 117.48, 134.56, 166.20, 172.37, 184.76, and 198.14; MS *m/z* 254 (M^+) and 195 (M^+−59, base peak).

Found: C, 56.59; H, 5.51%; M^+, 254. Calcd for $C_{12}H_{14}O_6$: C, 56.69; H, 5.55%; M, 254.

Cycloaddition of 2 to two Equivalents of 9 Leading to K. The reaction of **2** (0.10 g, 0.3 mmol) with **9** (0.068 g, 0.6 mmol) in benzene-d_6 (3 ml) was followed by ^{1}H-NMR spectroscopy. After 4 h at room temperature, both the starting materials were consumed and the following signals were observed: δ=0.06, 0.11 (each 9H, s, TMS), 2.10—3.50 (8H, m, CH_2 and CH), 3.00 (3H, s, OMe), and 4.75 (1H, d, J_{6-6a}=3.5 Hz, 6-H).

Cycloaddition of 1 to 22 Leading to 15. A solution of **1** (0.53 g, 1.59 mmol) and **22** (1.44 g, 10.0 mmol) in dry benzene (5 ml) was refluxed under nitrogen for 7 d. The usual work-up with methanol as described above and the followed column chromatography over silica gel gave 0.25 g (45%) of **15**.

Cycloaddition of 1 to 23a Leading to 24a, 25a, and 26. A solution of **1** (0.365 g, 1.1 mmol) and **23a** (0.476 g, 3.3 mmol) in dry benzene (5 ml) was refluxed under nitrogen for 7 d. After evaporation of all the volatile materials *in vacuo*, the residue was treated with methanol (10 ml) at room temperature overnight. The methanol was evaporated off *in vacuo* and the viscous oil obtained was chromatographed over silica gel. The fraction eluted with chloroform-hexane (1:1) afforded a mixture (0.24 g, 65%) of **24a** and **25a**. The ratio was determined by ^{1}H-NMR spectroscopy (**24a**: 55%; **25a**: 11%). They were separated into each isomer by a preparative thin-layer chromatography (silica gel) using chloroform as an eluent and purified by crystallization. The fraction with chloroform gave 0.13 g (25%) of **26**.

24a: Colorless prisms from ether-hexane; mp 83—84 °C; IR (KBr) 3400 (OH), 1725 (C=O), 1600, and 1240 cm^{-1}; ^{1}H-NMR ($CDCl_3$) δ=1.77 (3H, s, COMe), 2.50—3.32 (4H, m, 6-CH_2, 4-, and 5-H), 3.32, 3.65 (each 3H, s, COOMe), 4.32 (1H, m, 3-H), and 7.00—7.40 (5H, m, ArH); ^{13}C-NMR ($CDCl_3$) δ=26.01 (s, COMe), 30.88 (t, 6-C), 39.10, 42.86 (each d, 4- and 5-C), 50.49 (d, 3-C), 51.96, 52.31 (each s, COOMe), 107.79 (s, 2-C), 127.05, 127.81, 128.09, 142.55 (s), 172.31, 173.19 (each s, COOMe), 179.30 (s, COMe), and 200.56 (s, 1-C); MS *m/z* 332 (M^+), 257, 195, 115, and 43 (base peak).

Found: C, 65.14; H, 6.09%; M^+, 332. Calcd for $C_{18}H_{20}O_6$: C, 65.05; H, 6.07%; M, 332.

25a: Colorless prisms from ether-hexane; mp 153—155 °C; IR (KBr) 3400 (OH), 1725 (C=O), 1600, and 1230 cm^{-1}; ^{1}H-NMR ($CDCl_3$) δ=1.90 (3H, s, COMe), 2.58 (1H, dd, J_{gem}=18.5 and J_{6-5}=11.3 Hz, one of 6-CH_2), 2.70—3.40 (3H, m, the other of 6-CH_2, 4-, and 5-H), 3.53, 3.65 (each 3H, s, COOMe), 4.31 (1H, d, J_{3-4}=5.0 Hz, 3-H), and 7.10-7.35 (5H, m, ArH); MS *m/z* (rel. intensity) 332 (M^+, 20), 314 (21), 301 (26), 289 (62), 257 (45), 213 (26), 195 (25), and 43 (base peak).

Found: C, 64.88; H, 6.21%; M^+, 332. Calcd for $C_{18}H_{20}O_6$: C, 65.05; H, 6.07%; M, 332.

26: Colorless liquid as a mixture of two isomeric bis-adducts (the isomer ratio was about 6—7:1). The spectral data for the major product are given as follows: ^{1}H-NMR ($CDCl_3$) δ=2.40—4.00 (8H, m, CH_2 and CH), 3.32, 3.57, 3.67, 3.83 (each 3H, s, COOMe), 4.26 (1H, br. d, J_{8-7}=5.5 Hz, 8-H), and 6.80—7.30 (5H, m, ArH); ^{13}C-NMR ($CDCl_3$) δ= 31.00, 37.13 (each t, 2- and 5-C), 39.67, 41.42, 42.35, 48.68 (each d, 3-, 4-, 6-, and 7-C), 49.61 (d, 8-C), 52.00, 52.53, 52.87 (each q, COOMe), 126.55, 127.53, 128.31, 134.50, 141.90, 149.40 (s, 4a-C), 170.99, 172.06, 172.70, 173.33 (each s, COOMe), and 192.48 (s, 1-CO); MS *m/z* 459 (M^+).

Found: C, 63.66; H, 5.78%; M^+, 459. Calcd for $C_{24}H_{26}O_9$: C, 63.87; H, 5.72%; M, 459.

Similar reaction of **1** (1.57 g, 4.72 mmol) with **23a** (2.16 g, 15.0 mmol) under reflux in dry toluene (10 ml) for 7 d and the same work-up as mentioned gave a mixture of **24a** (10%) and **25a** (2%), and **26** (88%).

Cycloaddition of 1 to 23b Leading to 24b and 25b. Triene **1** (0.75 g, 2.25 mmol) and **23b** (0.527 g, 6.75 mmol) in toluene (6 ml) were allowed to react under the conditions shown in Table 3. The usual work-up with methanol and the followed chromatography over silica gel with chloroform afforded a mixture (0.386 g, 64%) of **24b** and **25b**. The isomer ratio was found be 2:11 (**24b**: 10%; **25b**: 55%). Only the major product **25b** was isolated as colorless solid which solidified when the above mixture was treated with methanol.

25b: Colorless needles from methanol; mp 210—211.5 °C; IR (KBr) 3400 (OH), 2250 (CN), and 1590 cm^{-1}; ^{1}H-NMR ($CDCl_3$) δ=1.76 (3H, s, COMe), 2.80—3.00 (4H, m, 6-CH_2, 4-, and 5-H), 4.33 (1H, d, J_{3-4}=8.5 Hz, 3-H), and 7.10—7.44 (5H, m, ArH); MS *m/z* (rel. intensity) 267 (M^++1, 12), 266 (M^+, 40), 248 (61), 221 (26), 195 (21), 170 (28), 168 (36), 167 (26), 155 (27), 145 (28), 117 (27), 81 (24), and 43 (base peak).

Found: 71.88; H, 5.20; N, 10.28%; M^+, 266. Calcd for $C_{16}H_{14}N_2O_2$: C, 72.16; H, 5.30; N, 10.52%, M, 266.

Cycloaddition of 2 to 22 Leading to M and 21. A mixture of **2** (0.779 g, 2.7 mmol) and **22** (0.392 g, 2.7 mmol) in dry benzene (3 ml) was heated under reflux under nitrogen for 48 h. The benzene was evaporated *in vacuo*, the residue was treated with methanol (15 ml) at room temperature overnight, and the methanol was removed off *in vacuo*. Viscous oil obtained was chromatographed over silica gel using chloroform-ethyl acetate (9:1) to give 0.293 g (42%) of **21** which was identical with a product given in the reaction of **2** with maleic anhydride **9**.

Similar reaction of **2** with three equivalents of **22** was carried out under reflux in dry benzene for 72 h. After all the volatile materials were removed off *in vacuo*, the residue was submitted for ^{1}H-NMR measurement. The spectrum showed the quantitative formation of exo mono-cycloadduct M: ^{1}H-NMR ($CDCl_3$) δ=0.18, 0.23 (each 9H, s, TMS), 2.20—3.50 (4H, m, 6-CH_2, 4-, and 5-H), 3.37 (3H, s, OMe), 3.60, 3.69 (each 3H, s, COOMe), 4.40, 4.60 (each 1H, s, =CH_2), and 4.48 (1H, d, J_{3-4}=2.8 Hz, 3-H).

Cycloaddition of 2 to 23a Leading to 21. Similar reaction starting from **2** (0.461 g, 1.6 mmol) and **23a** (0.234 g, 1.6 mmol) under the conditions shown in Table 3 and the same work-up as mentioned above gave 0.336 g (82%) of **21**.

Cycloaddition of 1 to 27a Leading to 28a and 29a. Triene **1** (0.92 g, 2.72 mmol) and **27a** (5 ml, large excess) in dry benzene (3 ml) were refluxed under nitrogen for 6 d. After all the volatile materials were evaporated *in vacuo*, the residue was treated with methanol (20 ml) at room temperature overnight. The methanol was removed off *in vacuo* and the residue was chromatographed over silica gel using chloroform-hexane (1:1) to give 0.34 g (48%) of **28a** and then 0.14 g (20%) of **29a**.

28a: Colorless prisms from hexane; mp 31—32 °C; IR (KBr) 3400 (OH), 1700 (C=O), and 1598 cm^{-1}; ^{1}H-NMR ($CDCl_3$) δ=1.75—2.00 (2H, m, 5-CH_2), 1.85, 2.15 (each 3H, s. COMe), 2.42 (2H, m, 6-CH_2), 2.74 (1H, dt, J_{4-5}=5.2 and J_{4-3}=4.0 Hz, 4-H), 4.31 (1H, d, J_{3-4}=4.0 Hz, 3-H), and 7.00—7.40 (5H, m, ArH); ^{13}C-NMR ($CDCl_3$) δ=19.55 (t, 5-C), 25.71 (q, COMe), 28.24 (t, 6-C), 28.36 (q, COMe), 40.92 (d, 4-C), 55.31 (d, 3-C), 108.14 (s, 2-C), 126.70, 127.69, 128,69, 144.48, 180.47 (s, 2-COMe), 200.90 (s, 4-COMe), and 208.47 (1-CO); MS *m/z* (rel. intensity) 258 (M^+, 16), 215 (49), 197 (33), 173 (21), 155 (31), and 43 (base peak).

Found: C, 74.62; H, 6.97%; M+, 258. Calcd for $C_{16}H_{18}O_3$: C, 74.39; H, 7.02%; M, 258.

29a: Colorless grains from hexane; mp 81—82 °C; IR (KBr) 3400 (OH), 1700 (C=O), and 1590 cm^{-1}; ^{1}H-NMR ($CDCl_3$) δ=1.80—2.30 (2H, m, 5-CH_2), 1.85, 1.88 (each 3H, s, COMe), 2.55 (2H, m, 6-CH_2), 2.83 (1H, ddd, J_{4-5}=4.0, 12.1, and J_{4-3}=4.9 Hz, 4-H), 4.26 (1H, d, J_{3-4}=4.9 Hz, 3-H), 6.90—7.36 (5H, m, ArH); ^{13}C-NMR ($CDCl_3$) δ=17.79 (t, 5-C), 25.36, 28.83 (each q, COMe), 29.82 (t, 6-C), 42.74 (d, 4-C), 52.66 (d, 3-C), 109.73 (s, 2-C), 127.34 (d), 128.46 (d), 128.93 (d), 139.73 (s), 180.59 (s, 2-COMe), 200.79 (s, 4-COMe), and 209.65 (s, 1-CO); MS *m/z* (rel. intensity) 259 (M^++1, 48),258 (M^+, base peak), 215 (63), 197 (41), 187 (23), 173 (23), 155 (27), 131 (22), and 43 (61).

Found: C, 74.39; H, 7.01%; M+, 258. Calcd for $C_{16}H_{18}O_3$: C, 74.39; H, 7.02%; M, 258.

Cycloaddition of 1 to 27b Leading to 28b and 29b. Similar reaction of **1** (0.376 g, 1.13 mmol) with **27b** (2 ml) in benzene (6 ml) followed by the work-up with methanol afforded the crude product which was then chromatographed over silica gel. The fraction eluted with chloroform-hexane (3:7) gave 0.11 g of **28b** and the continued fraction 0.15 g of mixture between **28b** and **29b** (**28b**: 35%; **29b**: 13%). The fraction with chloroform-hexane (1:1) provided 0.028 g of **29b**. Total amount of **28b** was 0.22 g (70%) and that of **29b** was 0.068 g (22%).

28b: Pale yellow liquid by repeated column chromatography; IR (neat) 3400 (OH), 1720 (C=O), and 1595 cm^{-1}; ^{1}H-NMR ($CDCl_3$) δ=1.60—2.10 (2H, m, 5-CH_2), 1.88 (3H, s, COMe), 2.30—2.60 (2H, m, 6-CH_2), 2.76 (1H, dt, J_{4-5}= 4.5 and J_{4-3}=3.4 Hz, 4-H), 3.71 (3H, s, COOMe), 4.40 (1H, d, J_{3-4}=3.4 Hz, 3-H), and 7.00—7.40 (5H, m, ArH); ^{13}C-NMR ($CDCl_3$) δ=18.85 (t, 5-C), 25.60 (q, COMe), 27.95 (t, 6-C), 41.92 (d, 4-C), 47.03 (d, 3-C), 52.08 (q, COOMe), 107.68 (s, s, 2-C), 126.87 (d), 127.81 (d), 128.75 (d), 143.96 (s), 173.66 (s, COOMe), 180.94 (s, COMe), and 201.08 (s, 1-CO); MS *m/z* 274 (M^+), 231, and 196.

Found: C, 70.19; H, 6.67%; M+, 274. Calcd for $C_{16}H_{18}O_4$: C, 70.05; H, 6.61%; M, 274.

29b: Colorless prisms from ether-hexane; mp 93—95 °C; IR (KBr) 3400 (OH), 1730 (C=O), 1600, 1400, and 1220 cm^{-1}; ^{1}H-NMR ($CDCl_3$) δ=1.70—3.04 (5H, m, 5-, 6-CH_2, and 4-H), 1.89 (3H, s, COMe), 3.56 (3H, s, COOMe), 4.29 (1H, d, J_{3-4}=5.0 Hz, 3-H), and 6.90-7.35 (5H, m, ArH); MS *m/z* (rel. intensity) 275 (M^++1, 18), 274 (M^+, base peak), 231 (58), 197 (37), 155 (20), 145 (21), and 42 (53).

Found: C, 69.93; H, 6.87%; M+ 274. Calcd for $C_{16}H_{18}O_4$: C, 70.05; H, 6.61%; M, 274.

Cycloaddition of 1 to 27c Leading to 28c and 29c. Triene **1** (0.65 g, 1.95 mmol) was heated under reflux in freshly distilled **27c** (5 ml) under nitrogen for 58 h. The crude product obtained by the usual work-up with methanol was chromatographed over silica gel. The fraction eluted with chloroform-hexane (2:1) afforded 0.084 g of **28c**, and then 0.21 g of **28c** and **29c** (3.3:1). The other fraction with chloroform gave 0.045 g of **29c**. Total amount of **28c** was 0.245 g (54%) and that of **29c** was 0.094 g (18%).

28: Colorless prisms from ether-hexane; mp 153—155 °C; IR (KBr) 3400 (OH), 2230 (CN), 1590, 1410, 1240, and 960 cm^{-1}; ^{1}H-NMR ($CDCl_3$) δ=1.60-2.10 (2H, m, 5-CH_2), 1.88 (3H, s, COMe), 2.48 (1H, dt, J_{gem}=19.0 and J_{6-5}=4.5 Hz, one of 6-CH_2), 2.86 (1H, dt, J_{gem}=19.0 and J_{6-5}=9.0 Hz, the other of 6-CH_2), 3.00 (1H, dt, J_{4-5}=4.1 and J_{4-3}=2.7 Hz, 4-H), 4.20 (1H, d, J_{3-4}=2.7 Hz, 3-H), and 7.00—7.44 (5H, m, ArH); ^{13}C-NMR ($CDCl_3$) δ=18.85 (t, 5-C), 25.42 (t, 6-C), 27.30 (q, COMe), 33.17 (d, 4-C), 43.44 (d, 3-C), 105.97 (s, 2-C), 120.59 (s, CN), 127.89, 129.10, 141.25, 180.18 (s, COMe), and 201.03 (s, 1-CO); MS *m/z* (rel. intensity) 241 (M^+, 28), 214 (26), 196 (23), 187 (22), 155 (37), 145 (35), 115 (29), 77 (26), and 44 (base peak).

Found: C, 74.88; H, 6.34; N, 5.84%; M+, 241. Calcd for $C_{15}H_{15}NO_2$: C, 74.66; H, 6.27; N, 5.81%; M, 241.

29c: Colorless prisms from ether-hexane; mp 144—146 °C; IR (KBr) 3400 (OH), 2220 (CN), 1600, 1410, 1240, and 940 cm^{-1}; ^{1}H-NMR ($CDCl_3$) δ=1.86 (3H, s, COMe), 1.94 (2H, m, 5-CH_2), 2.59 (2H, dd, J_{6-5}=6.1 and 7.1 Hz, 6-CH_2), 3.10 (1H, m, 4-H), 4.09 (1H, d, J_{3-4}=4.9 Hz, 3-H), and 7.10—7.50 (5H, m, ArH); ^{13}C-NMR ($CDCl_3$) δ=18.85 (t, 5-C), 25.48 (t, 6-C), 29.30 (q, COMe), 32.25 (d, 4-C), 41.63 (d, 3-C), 108.03 (s, 2-C), 119.77 (s, CN), 128.16, 128.63, 129.34, 138.09, 179.18 (s, COMe), and 200.85 (s, 1-CO); MS *m/z* (rel. intensity) 241 (M^+, 35), 214 (22), 187 (21), 155 (33), 145 (32), and 77 (23).

Found: C, 74.68; H, 6.31; N, 5.83%; M+, 241. Calcd for $C_{15}H_{15}NO_2$: C, 74.66; H, 6.27; N, 5.81%; M, 241.

Similar reaction of **1** (0.769 g, 2.3 mmol) with **27c** (3.1 ml, 46 mmol) was carried out in a sealed tube (At 110 °C for 5 d in 6 ml of dry benzene). The usual work-up with methanol gave viscous oil which was purified by chromatography over silica gel. The fraction eluted with hexane-ethyl acetate (4:1) afforded 0.116 g of **28c** and 0.065 g of mixture between **28c** and **29c** (1:1). The continued elution with hexane-ethyl acetate (2:1) gave 0.243 g of **30**. Total amounts were as follows: **28c**: 0.149 g (27%); **29c**: 0.033 g (6%); **30**: 0.243 g (38%). The bis-adduct **30** was found to be a mixture of two isomers whose ^{1}H-NMR spectrum was given as shown below: ^{1}H-NMR ($CDCl_3$) δ=1.68—2.10 (2H, m, CH_2), 2.10—3.10 (7H, m, CH_2 and CH), 3.44—3.80 (1H, m, CHCN), 4.37 (1H, br. CHPh), and 6.80—7.44 (5H, m, ArH).

Cycloaddition of 2 to 27a Leading to 31a. A solution of **2** (0.856 g, 3.0 mmol) and freshly distilled **27a** (1.2 ml, 15 mmol) was heated under reflux in dry benzene (3 ml) under nitrogen for 48 h. The usual work-up with methanol gave the crude product. It was chromatographed over silica gel using hexane-chloroform (3:1) to give 0.325 g (60%) of **31a**.

31a: Colorless prisms from ether-hexane; mp 42—44 °C; IR (KBr) 1680—1540 cm^{-1} (C=O); ^{1}H-NMR ($CDCl_3$) δ=2.28, 2.36 (each 3H, s, COMe), 2.50—2.70 (4H, m, CH_2), 7.32 (1H, br. s, 3-H), and 16.23 (1H, s, OH); ^{13}C-NMR ($CDCl_3$) δ=20.14 (t, CH_2), 20.31, 24.95 (each q, COMe), 34.05 (t, CH_2), 107.56 (s), 129.81 (s), 133.27 (d, 3-C), 185.40 (s, 2-COMe), 196.50 (s, 4-COMe), and 199.91 (s, 1-C); MS *m/z* 180 (M^+), 137 (M^+−43), and 43 (base peak).

Found: C, 66.91; H, 6.79%; M+, 180. Calcd for $C_{10}H_{12}O_3$: C, 66.65; H, 6.71%; ,M, 180.

Cycloaddition of 2 to 27b Leading to 31b. Similar procedure starting from **2** (0.81 g, 2.8 mmol) and **27b** (0.73 g, 8.4 mmol) and the followed column chromatography over silica gel using chloroform gave 0.367 g (66%) of **31b**. The reaction conditions were listed in Table 3.

31b: Colorless needles from aqueous methanol; mp 60 °C; IR (KBr) 1700 and 1640—1580 cm^{-1} (C=O); ^{1}H-NMR ($CDCl_3$) δ=2.23 (3H, s, COMe), 2.40—2.80 (4H, m, CH_2), 3.75 (3H, s, COOMe), 7.40 (1H, br. s, 3-H), and 16.07 (1H, s, OH); ^{13}C-NMR ($CDCl_3$) δ=20.20 (q, COMe), 21.37, 34.35 (each t, CH_2), 51.72 (q, COOMe), 107.73 (s), 120.00 (s), 132.74 (d, 3-C), 167.14 (s, COOMe), 184.64 (s, COMe), and 199.79 (s, 1-CO); MS *m/z* 196 (M^+), 181 (M^+−15), and 43 (base peak).

Found: C, 61.07; H, 6.23%; M+, 196. Calcd for $C_{10}H_{12}O_4$: C, 61.22; H, 6.16%; M, 196.

Cycloaddition of 2 to 27c Leading to 31c. The same procedure using **2** (0.765 g, 2.7 mmol) and **27c** (0.88 ml, 13.5 mmol) and the followed column chromatography over silica gel using dichloromethane gave 0.316 g (73%) of **31c**. The reaction conditions were shown in Table 3.

31c: Colorless prisms from dichloromethane-hexane; mp 108—109 °C; IR (KBr) 2200 (CN) and 1680—1500 cm^{-1}

(C=O); ^{1}H-NMR ($CDCl_3$) δ=2.20 (3H, s, COMe), 2.60 (4H, m, CH_2), 7.04 (1H, s, 3-H), and 16.03 (1H, s, OH); ^{13}C-NMR ($CDCl_3$) δ=20.14 (q, COMe), 23.78, 33.58 (each t, CH_2), 107.73 (s, 2-C), 111.96 (s), 119. 65 (s, CN), 137.67 (d, 3-C), 184.70 (s, COMe), and 198.03 (s, 1-CO); MS *m/z* 163 (M^+, bask peak).

Found: C, 66.38; H, 5.65; N, 8.43%; M^+, 163. Calcd for $C_9H_9NO_2$: C, 66.25; H, 5.56; N, 8.58%; M, 163.

The present work was partially supported by a Grant-in-Aid for Scientific Research No.58750694 from the Ministry of Education, Science and Culture to E. W.

References

1) As recent reviews on the Diels-Alder reaction: W. Oppolzer, *Angew. Chem. Int. Ed. Engl.*, **16**, 10 (1977); W. Oppolzer, *Synthesis*, **1978**, 793; G. Brieger and J. N. Bennett, *Chem. Rev.*, **80**, 63 (1980); T. Wagner-Jauregg, *Synthesis*, **1980**, 165; J. Sauer and R. Sustmann, *Angew. Chem., Int. Ed. Engl.*, **19**, 779 (1980); S. Danishefsky, *Acc. Chem. Res.*, **14**, 400 (1981); M. Petrzilka and J. I. Grayson, *Synthesis*, **1981**, 753; D. L. Boger, *Tetrahedron*, **39**, 2869 (1983).

2) L. A. Paquett and M. J. Wyvratt, *J. Am. Chem. Soc.*, **96**, 4671 (1974); D. McNeil, B. R. Vogt, J. J. Sudol, S. Theodoropulos, and E. Hedaya, *ibid.*, **96**, 4673 (1974); D. J. Cram and G. R. Knox, *ibid.*, **83**, 2204 (1971); D. J. Cram, C. S. Montgomery, and G. R. Knox, *ibid.*, **88**, 515 (1966); M. A. Battiste, L. A. Kapicak, M. Mathew, and G. J. Palenik, *J. Chem. Soc., Chem. Commun.*, **1977**, 1536.

3) G. A. Kraus and J. Tashner, *J. Am. Chem. Soc.*, **102**, 1974 (1980).

4) B. M. Trost and M. Shimizu, *J. Am. Chem. Soc.*, **104**, 4299 (1982).

5) At the 49th Annual Meeting of the Chemical Society of Japan, Tokyo, April, 1984, two tandem reaction systems have been presented: 1,2-dibenzylidenecyclobutane by T. Minami, Y. Taniguchi, and I. Hirao (Abstr. No. 3F06) and 2-dimethylaminomethyl-3-trimethylsilylmethyl-1,3-butadiene by K. Otaka, A. Hosomi, and H. Sakurai (Abstr. No. 1Z28).

6) O. Tsuge, E. Wada, and S. Kanemasa, *Chem. Lett.*, **1983**, 239.

7) O. Tsuge, E. Wada, and S. Kanemasa, *Chem. Lett.*, **1983**, 1525.

8) O. Tsuge, S. Kanemasa, H. Sakoh, and E. Wada, *Chem. Lett.*, **1984**, 273.

9) A. T. Blomquist and J. A. Verdol, *J. Am. Chem. Soc.*, **77**, 81 (1955).

10) W. J. Bailey and J. Economy, *J. Am. Chem. Soc.*, **77**, 1133 (1955); W. J. Bailey, C. H. Cunov, and L. Nicholas, *ibid.*, **77**, 2787 (1955).

11) Y. Taniguchi, J. Inanaga, and M. Yamaguchi, *Bull. Chem. Soc. Jpn.*, **54**, 3229 (1981).

12) S. Danishefsky and T. Kitahara, *J. Am. Chem. Soc.*, **96**, 7807 (1974).

13) Both **1** and **2** can be purified by a chromatography over silica gel (Wako gel C200) using hexane-benzene mixture (9:1), but with poor recovery (30—50%).

14) The trienes can be stored in a freezer under nitrogen in the presence of hydroquinone. The polymerization inhibitor is needed only for **1**. No detectable decomposition has been observed at least in one month under the above conditions. Prior to their use, they are purified by a vacuum distillation on a bulb-to-bulb distillation apparatus.

15) It is known that a trans diene undergoes the Diels-Alder reaction much faster than a cis diene (J. Sauer, *Angew. Chem., Int. Ed. Engl.*, **6**, 16 (1967) and references cited therein).

16) If **14** were carrying an ester group at the 4-position instead of 3-position, the methylene protons at the 3-position should have appeared upfield of δ 2.0 as complex signals.

17) E. L. Eliel, N. L. Allinger, S. J. Angyal, and G. A. Morrison, "Conformational Analysis," Interscience Publishers, a division of John Wiley and Sons, Inc., New York, London, Sydney (1965), p. 109—111.

18) M. Yamashita, Y. Watanabe, T. Mitsudo, and Y. Takegami, *Tetrahedron Lett.*, **1975**, 1867.

19) L. Crombie, D. E. Games, and A. W. G. James, *J. Chem. Soc., Perkin Trans. 1*, **1979**, 464.

20) R. E. Lutz and W. R. Smithey, Jr., *J. Org. Chem.*, **16**, 51 (1951).

21) E. H. Ingold, *J. Chem. Soc.*, **1925**, 1199.

22) L. Brandsma and H. D. Verkruijsse, "Synthesis of Acetylenes, Allenes and Cumulenes," in "Studies in Organic Chemistry," Elsevier Scientific Publishing Company, Amsterdam, Oxford, New York (1981), Vol. 8, p. 59.

 © 1984 The Chemical Society of Japan Bull. Chem. Soc. Jpn., 57, 3234—3241 (1984) [Vol. 57, No. 11

Cross Diene-transmissive Diels-Alder Cycloaddition Reaction of Bis(silyloxy) Cross-conjugated Trienes

Otohiko TSUGE,* Shuji KANEMASA, Hirohiko SAKOH, and Eiji WADA
Research Institute of Industrial Science, and Department of Molecular Science and Technology, Interdisciplinary Graduate School of Engineering Sciences, Kyushu University, Kasugakoen, Kasuga 816
(Received June 18, 1984)

Cross type of diene-transmissive Diels-Alder cycloaddition has been demonstrated by using two bis-silyloxy cross-conjugated trienes. The first cycloaddition stage of cross reaction, which has to be highly selective in the formation of mono-cycloadducts, has been performed by the reactions of an activated triene with cyclic olefins or those of trienes with acyclic olefins. The secod cycloadditions with a variety of dienophiles provide cross types of bis-adducts. The characteristics of these cross reactios are discussed.

The diene-transmissive Diels-Alder reaction is a process that involves two sequential Diels-Alder cycloadditions of cross-conjugated triene.[1] Of great value as a synthetic tool is the cross type of diene-transmissive Diels-Alder reaction in which each different dienophile participates in each stage of cycloadditions leading to the formation of cross bis-cycloadduct (**A**→**B**→**C**). Success of the cross reaction mainly depends upon the chemoselective formation of mono-cycloadduct **B**. This selectivity may be conveniently called "monoselectivity" in the present paper.

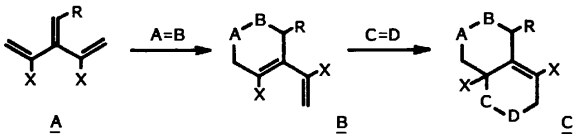

A B C

The preceding paper has dealt with the diene-transmissive Diels-Alder reaction of bis (silyloxy) cross-conjugated trienes, 3-(methoxymethylene)- **1** and 3-benzylidene-2,4-bis(trimethylsilyloxy)-1,4-pentadiene **2**.[1] The reaction of **1** with an equivalent of cyclic olefinic dienophiles was highly monoselective, while with two equivalents the bis-cycloadducts were exclusively formed. On the other hand, the reaction of either **1** or **2** with acyclic olefinic dienophiles below 80 °C was also monoselective even if excess of dienophiles was used.

Therefore, the cross type of diene-transmissive Diels-Alder reaction may be achieved through the following two possible approaches: The first method involves the initial formation of the mono-cycloadducts between **1** and cyclic olefinic dienophiles and the followed second cycloaddition with appropriate dienophiles. The second method is initiated by the initial cycloaddition of either **1** or **2** with acyclic olefinic dienophiles and followed by the second cycloaddition with highly reactive dienophiles.

Results and Discussion

The most promising cross process of diene-transmissive Diels-Alder reaction may be achieved by use of the activated triene **1**. When an equivalent of **1** is used, the cycloadduct to cyclic olefinic dienophiles is highly monoselective forming endo mono-cycloadducts. The endo approach of the second molecule of dienophiles from the less hindered side easily occurs giving stereoselective bis-cycloadducts when another equivalent of dienophiles is added.[1]

Each equivalent of **1** and *N*-phenylmaleimide **3a** in benzene was allowed to react at room temperature for 20 h during which time the endo mono-cycloadduct **D** was formed. After the addition of dimethyl acetylenedicarboxylate **4a** (1.5 equivalent) as the second dienophile, the reaction was continued under reflux for an additional 20 h. The usual desilylating work-up with methanol gave a cross bis-adduct **5aa** (Scheme 1 and Table 1). It was assigned that the initially formed ring of **5aa** had trans configuration on the basis of the coupling constant between 3a-H and 4-H (J_{3a-4}=3.0 Hz) This means that the stereochemistry at the 4-position of mono-cycloadduct **D** was inverted. Such inversion, which must have occurred at or later the desilylation stage, has been generally observed in the reactions of **1** with cyclic olefinic dienophiles.[1]

Similar reaction of **1** with *N*-methylmaleimide **3b** and then with **4a** or that of **1** with **3b** and then with dibenzoylacetylene **4b**, under the reaction conditions shown in Table 1, gave the cross bis-adduct **5ba** or **5bb**, respectively.

When maleic anhydride **3c** was used as the first dienophile, the cycloaddition was completed in 2 h at room temperature. The second cycloaddition with **4a** was followed under reflux in benzene for 24 h. Esterification of the reaction mixture with methanol in the presence of *p*-toluenesulfonic acid gave two isomeric cross bis-adducts **6ca** and **7ca**. Their ratio is not so important because **6ca** gradually changes into **7ca** when heated or treated with methanol in the presence of *p*-toluenesulfonic acid. The structures were confirmed on the basis of the coupling constant between 1-H and 2-H (**6ca**: 6.0 Hz; **7ca**: 3.0 Hz).

^{1}H-NMR analysis of the reaction of isolated mono-cycloadduct **D** (X=O) with **4a** showed the formation of aromatized cross bis-adducts **F** and **G** (R=E=COOMe) whose isolation failed. Their ratio was found to change depending upon the reaction temperature and time: Only **F** (after 24 h at room temperature), a mixture of **F** and **G** (4:3, after 24 h under reflux in benzene), and only **G** (after a week at room temperature or after 3 d under reflux in benzene) were formed, indicating that the endo bis-cycloadduct **F** and the exo one **G** are kinetically and thermodynamically controlled products, respectively.

Thus, in the cross cycloadditions of **1** with cyclic

olefinic dienophiles and then with acetylenic ones, the first stage is an endoselective cycloaddition leading to **D**. The acetylenes approach from the less hindered side, opposite to the 4-MeO and fused maleimide ring, forming the stereoselective cross bis-cycloadducts **E** which are immediately aromatized by the elimination of a silanol. The inversion of 4-MeO substituent starts giving more stable isomers probably through an elimination-addition mechanism. In the cases of maleimides, only the inverted bis-adducts **5** were isolated, and in the case of maleic anhydride, a mixture of bis-adducts **6** and **7** was yielded.

Similar reaction of **1** with **3c** and then with **4b**, under similar reaction conditions (Table 1), gave an exo cross bis-adduct **7cb** together with a methanol-eliminated bis-adduct **8cb**, no trace of endo bis-adduct **6cb** being obtained.

As the diene moiety of mono-cycloadduct **D** carries two silyloxy substituents in a 1,3-relationship, the second cycloaddition to unsymmetrically substituted dienophiles should be regioselective.[2] As expected, the reaction of **1** with **3c** and then with methyl propiolate **4c** gave a regioselective methanol-eliminated cross bis-adduct **8cc**, but in a low yield.

Olefinic dienophiles can be employed as well in the second cycloaddition. Thus, the endo mono-cycloadduct **D** (X=O), which had been formed in the initial cycloaddition of **1** to **3c**, was allowed to react with **3b** and the reaction mixture was treated with trifluoroacetic acid. The only product isolated in 38% yield was a stereoselective cross bis-adduct **9** which was accompanied with the inversion at the 6-position. Although the configuration at the points of fusion (the 3a and 10b positions) was not clear only on the basis of the spectral data, it was tentatively assigned as shown in Scheme 2 according to the most likely approach of **3b**. The second olefinic dienophile **3b** must have approached to **D** in an endo fashion from the opposite side to the 4-MeO and the fused maleimide ring, giving a stereoselective bis-cycloadduct **H**.

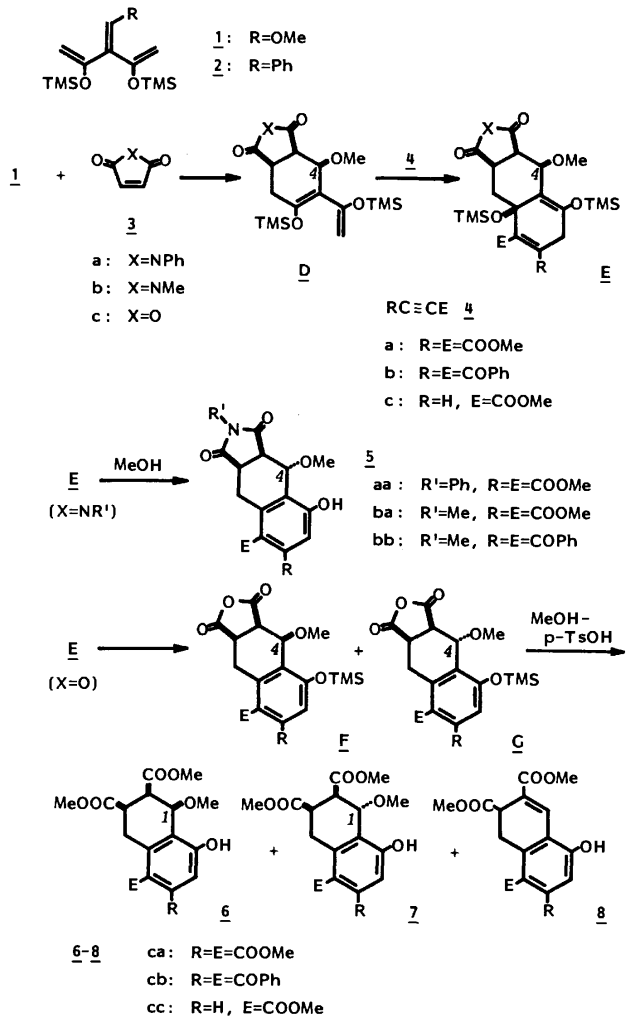

Scheme 1.

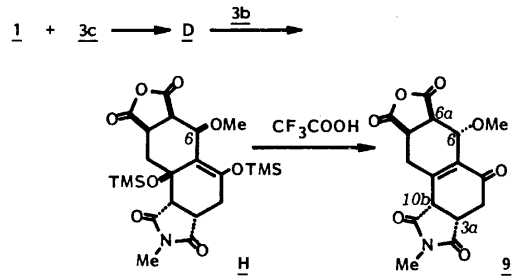

Scheme 2.

Table 1. Cross cycloadditions of **1** to cyclic olefins **3** and then acetylenes **4**

Olefin (equiv)	Acetylene (equiv)	Reaction Conditions[a] 1st Reaction	2nd Reaction	Product (yield/%)[b]
3a (1.0)	**4a** (1.5)	24 h at r.t.	20 h under Reflux	**5aa** (49)
3b (1.0)	**4a** (1.5)	24 h at r.t.	20 h under Reflux	**5ba** (41)
3b (1.0)	**4b** (1.0)	24 h at r.t.	36 h under Reflux	**5bb** (47)
3c (1.0)	**4a** (1.4)	2 h at r.t.	24 h under Reflux	**6ca** (14), **7ca** (19)
3c (1.0)	**4b** (1.0)	2 h at r.t.	24 h at r.t.	**7cb** (33)[c], **8cb** (6)
3c (1.0)	**4c** (2.0)	2 h at r.t.	48 h under Reflux	**8cc** (15)

a) All the reactions were carried out in dry benzene. The first and second reactions were performed in the same flask. When **3c** was used as the first dienophile, esterification procedure was followed after the second cycloaddition was complete (under reflux in methanol for 24 h in the presence of *p*-toluenesulfonic acid). b) All isolated yields based on **1**. c) A part of **7cb** was isolated as a silylated derivative **G** (R=E=COPh).

As the cross bis-cycloadducts and also their derivatives formed in the cross reactions of **1** with two different cyclic olefinic dienophiles were found all quite labile, the cross reactions with such combinations were not further investigated.

As described in the preceding paper,[1] both trienes **1** and **2** react with acyclic olefinic dienophiles affording only the mixture of endo and exo mono-cycloadducts, even when excess of the dienophiles is used. But, the prolonged reactions at higher temperature produce poor yields of bis-cycloadducts, indicating that the cross type of diene-transmissive Diels-Alder reaction may be achieved by reacting the triene **1** or **2** with acyclic olefins as the first dienophiles and then with highly reactive second dienophiles.

The triene **1** reacted with excess of methyl acrylate **10a** under reflux in benzene for 48 h. It was found from the separate experiment that two isomeric mono-cycloadducts **I** (isomer ratio=1:2)[3] were formed in good yields in this reaction mixture. After the solvent and the excess dienophile **10a** were completely removed, the residue was allowed to react further with the second dienophile **4a** under the conditions shown in Table 2. The work-up with methanol gave two isomeric cross bis-adducts **11aa** and **12aa** (Scheme 3). Again in this case, the isomer ratio is not important because they are interconvertible each other.

Similar cross reactions were performed by using **10a** or acrylonitrile **10b** as the first dienophile and **4a** or **4b** as the second. Results obtained are listed in Table 2.

In the cross cycloaddition of triene **1**, the use of unsymmetric dienophiles does not make any trouble since the both stage of double Diels-Alder reactions are highly regioselective. Disadvantage is that mono-cycloadducts to acyclic olefins take a half-chair conformation which disturbs the approach of the second dienophiles.[4] This sluggish second cycloaddition is often accompanied with some side reactions. One of them is the Michael reaction. In the reaction of mono-cycloadduct **I** (E=CN) with **4a**, a considerable amount of Michael adduct was obtained.[5]

Heating the triene **2** in large excess of **10a** for a long time (5 d at 80 °C) produces endo- **K** and exo mono-cycloadduct **L** in 22 and 70% yields, respectively.[6] When this mixture was allowed to react with **4a**, two isomeric cross bis-adducts **13** (endo, 10%) and **14** (exo, 36%) were yielded besides the mono-adducts **15** (6%, endo:exo=1:3). This result indicates that the endo mono-cycloadduct **K** cycloadds to **4a** as slowly as the exo one **L** does.

In the cross type of diene-transmissive Diels-Alder reactions using acyclic olefins, the second dienophiles are required to be highly reactive. Although the use of cyclic olefins as the second reagent led to the formation of rather unstable cross bis-adducts such as **9**, their high reactivity is still attracting.

The regioselective mono-cycloadduct **I** formed in the reaction of **1** with **10a** was allowed to react with an equivalent of **3b** under reflux in benzene for 24 h. The

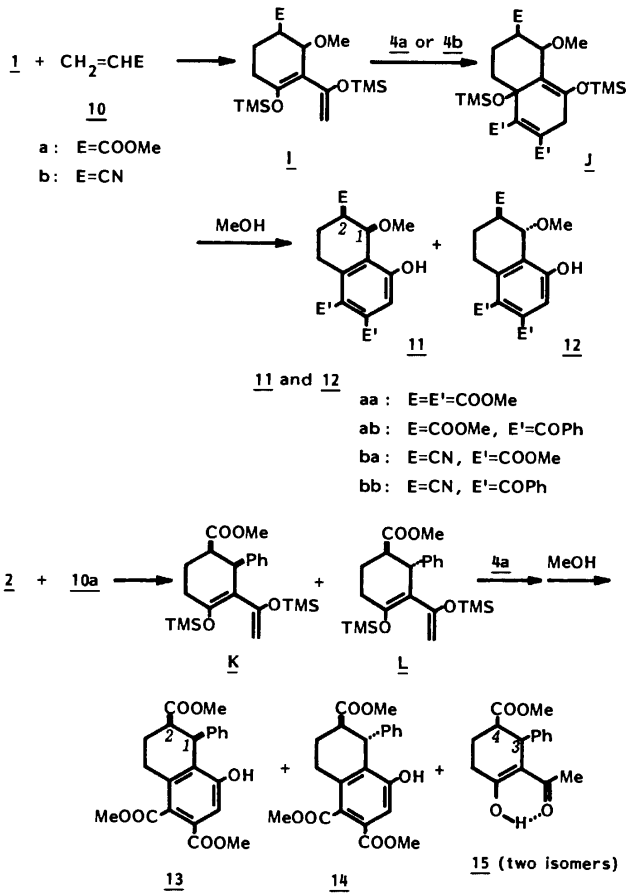

Scheme 3.

Table 2. Cross cycloadditions of **1** and **2** to acyclic olefins **10** and then acetylenes **4**

Triene	Olefin (equiv)	Acetylene (equiv)	Reaction Conditions[a] 1st Reaction	Reaction Conditions[a] 2nd Reaction	Product (yield/%)[b]
1	**10a** (3.0)	**4a** (1.1)	48 h at 80 °C	48 h under Reflux	**11aa** (21), **12aa** (8)
1	**10a** (3.0)	**4b** (1.0)	48 h at 80 °C	48 h under Reflux	**11ab** (15), **12ab** (21)
1	**10b** (5.0)	**4a** (2.0)	48 h at 75 °C	48 h under Reflux	**11ba** (23), **12ba** (12)
1	**10b** (5.0)	**4b** (1.0)	48 h at 75 °C	48 h under Reflux	**11bb** (28), **12bb** (10)
2	**10a** (20.0)	**4a** (1.1)	120 h at 80 °C	48 h under Reflux	**13** (10)[c], **14** (36)[c]

a) After the first cycloadditions in dry benzene was complete, the solvent and excess dienophiles **10** were completely removed off. To the residue were added dry benzene and acetylenes **4**, and the mixture was allowed to react under the shown conditions. b) All isolated yields based on the trienes. c) Separation was unsuccessful. Accompanied with the formation of mono-adduct **15** (endo : exo = 1 : 3, in 6% yield).

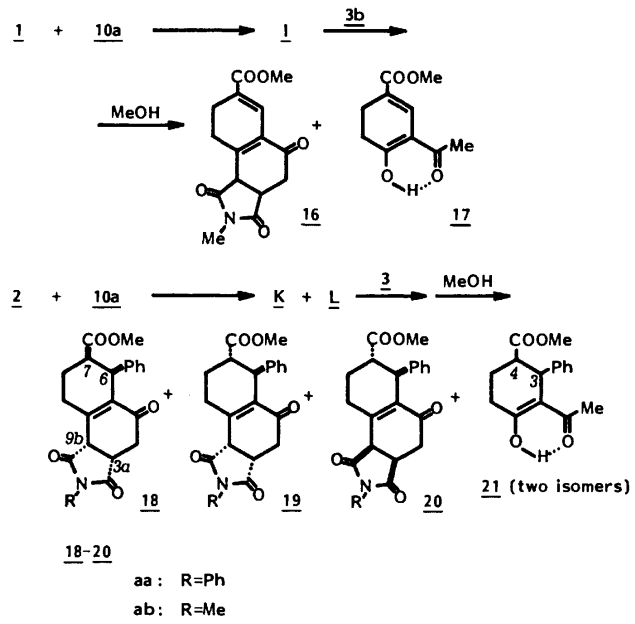

Scheme 4.

usual work-up with methanol gave a cross bis-adduct **16** (25%) together with the mono-adduct **17** (28%) which was derived from unreacted **I** (Scheme 4). There are no ambiguities on the stereochemistry of **16** since methanol elimination as well as desilylation has occured. Due to the instability, it failed to purify **16**.

Similar cross reactions were investigated by using triene **2**. When a mixture of **K** (endo) and **L** (exo) (**K**:**L**=22:70) was reacted with an equivalent of **3a** under reflux in benzene for 48 h, three kinds of cross bis-adducts **18aa**, **19aa**, and **20aa** were formed in 49% yield (**18aa**:**19aa**:**20aa**=2:14:3) besides a small amount of isomeric mono-adducts **21** (11%, endo:exo=1:5). Only the major product **19a** was isolated in pure form from a mixture of the other two. The structural assignment was based on the coupling constants between 6-H and 7-H as well as the stereochemical aspect of the reaction paths.[7]

The endo/exo ratio in the mono-cycloadducts (**K**:**L**=22:70) was found quite different from that in the products. The ratio of all the products from **K** to those from **L** was 7:53. This is probably because all of the cross bis-adducts **18aa**—**20aa** are labile. Actually they were partly decomposed when chromatographed over silica gel or heated in methanol. Under the same conditions, the second cycloaddition with **3b** recovered relatively large amount of the mono-cycloadducts **K** and **L** in the forms of **21** (38%, endo:exo=1:3) together with three cross bis-adducts **18ab**, **19ab**, and **20ab** (26%, **18ab**:**19ab**:**20ab**=1:4:2). The isomer ratios of unreacted mono-cycloadducts (endo/exo ratios of **21**) are about the same to the ratio between **K** and **L**, meaning that there is little difference of reactivity between the exo- **K** and endo mono-cycloadduct **L** in the cycloadditions to such cyclic olefins.

Experimental

General and Materials. Melting points were determined on a Yanagimoto micro melting point apparatus and uncorrected. IR spectra were taken with a JASCO IRA-1 or a JASCO A-102 spectrometer. ^{1}H-NMR spectra were recorded on a Hitachi R-40 or a JEOL FX-100 instrument and ^{13}C-NMR spectra were obtained on a JEOL FX-100 spectrometer at 25.05 MHz. Chemical shifts are expressed in parts per million downfield from tetramethylsilane. Mass spectra were measured with a JEOL JMS-01SG-2 spectrometer at 75 eV of ionization energy. Elementary analyses were performed on a Hitachi 026 CHN analyzer. Thin-layer chromatography (TLC) was accomplished on 0.2 mm precoated plates of silica gel 60 F-254 (Merck) or on 0.2 mm precoated plates of aluminum oxide 60 F-254 type E (Merck). Visualization was made with ultraviolet light (254 and 365 nm) or iodine. Wako gel C200 and C300 (Wako) were used for preparative column chromatography. Preparative high performance liquid chromatography (HPLC) was carried out on a Kusano KHLC-201 apparatus with a UV-detector Uvilog-III using a column (22×300 mm) packed with silica gel (Wako gel LC-50H). Micro vacuum distillation was performed with a Sibata GTO-250R Kugelrohr distilling apparatus in a glass tube oven. When this apparatus was used, boiling points were expressed with the oven temperature. Solvents were evaporated with a Tokyo Rikakikai rotary evaporator type V at about 50 °C unless otherwise stated.

Benzene was purified by the distillation from sodium and stored on sodium wire. Both trienes, 3-(methoxymethylene)-**1** and 3-benzylidene-2,4-bis(trimethylsilyloxy)-1,4-pentadiene **2**, were prepared by the silylation of 3-(methoxymethylene)- and 3-benzylidene-2,4-pentanedione with chlorotrimethylsilane, respectively, as shown in the preceding paper.[1] The commercial materials of maleic anhydride **3c**, dimethyl acetylenedicarboxylate **4a**, methyl acrylate **10a**, and acrylonitrile **10b** were purified by distillation. The commercial grades of *N*-phenyl- **3a** and *N*-methylmaleimide **3b** were used without further purification. Dibenzoylacetylene **4b** was synthesized from 1,2-dibenzoylethene.[8] Methyl propiolate **4c** was obtained by the esterification of the commercial propiolic acid in the presence of *p*-toluenesulfonic acid.[9]

Cycloaddition of 1 to 3a and then 4a Leading to 5aa. A solution of freshly distilled **1** (0.773 g, 2.7 mmol) and **3a** (0.425 g, 2.5 mmol) in dry benzene (3 ml) was stirred at room temperature under nitrogen for 24 h. After **4a** (0.523 g, 3.7 mmol) was added, the resulting mixture was heated under reflux for 20 h. All the volatile materials were evaporated *in vacuo* and the residue obtained was stirred in methanol (10 ml) overnight. Evaporation of the methanol *in vacuo* left the residue which was then chromatographed over silica gel using chloroform–ethyl acetate (5:1) to give 0.524 g (49%) of **5aa**. The analytical sample of **5aa** was available through the repeated chromatography since its purification by crystallization was unsuccessful.

5aa: Colorless leaflets; mp 230 °C; IR (KBr) 3400 (OH); 1775, 1720, and 1685 cm^{-1} (C=O); ^{1}H-NMR (CDCl$_3$+DMSO-d_6) δ=2.70—3.90 (4H, m, 9-CH$_2$, 3a-, and 9a-H), 3.11 (3H, s, OMe), 3.81, 3.82 (each 3H, s, COOMe), 5.40 (1H, d, J_{4-3a}= 3.0 Hz, 4-H), and 7.10—7.56 (7H, m, ArH, 6-H, and OH); ^{13}C-NMR (CDCl$_3$+DMSO-d_6) δ=23.01, 35.75, 44.09, 50.96, 54.84, 68.10, 113.31, 123.47, 124.49, 125.34, 126.87, 127.40, 128.46, 130.98, 135.27, 154.58, 164.56, 167.03, 173.95, and 177.01; MS *m/z* 439 (M$^+$), 408 (M$^+$−31), and 228 (base peak).

Found: C, 62.78; H, 4.70; N, 3.67%; M$^+$, 439. Calcd for $C_{23}H_{21}NO_8$: C, 62.87; H, 4.82; N, 3.19%; M, 439.

Cycloaddition of 1 to 3b and then 4a Leading to 5ba. A solution of freshly distilled **1** (0.455 g, 1.6 mmol) and **3b** (0.161 g, 1.4 mmol) in dry benzene (2 ml) was stirred at room temperature under nitrogen for 24 h. After **4a** (0.309 g, 2.2 mmol) was added, the mixture was heated under reflux for 20 h. All the volatile materials were evaporated *in vacuo* and the residue was stirred in methanol (10 ml) overnight. Evapo-

ration of the methanol *in vacuo* left viscous oil which was then chromatographed over silica gel using chloroform–ethyl acetate (3:1) to give 0.266 g (41%) of **5ba**. It was purified by repeated chromatography.

5ba: Colorless solid; mp 248 °C; IR (KBr) 3420 (OH), 1785, 1725, and 1670 cm^{-1} (C=C); ^1H NMR (DMSO-d_6) σ=2.60—3.20 (4H, m, 9-CH_2, 3a-, and 9a-H), 2.88 (3H, s, NMe), 3.00 (3H, s, OMe), 3.80 (6H, s, COOMe), 5.23 (1H, d, J_{4-3a}=3.0 Hz, 4-H), 7.28 (1H, s, 6-H), and 8.24 (1H, s, OH); ^{13}C-NMR (DMSO-d_6) δ=24.32, 36.84, 44.98, 52.34, 52.58, 55.85, 68.90 (d, 4-C), 114.32 (d, 6-C), 124.46 (s), 129.72 (s), 136.73 (s), 155.74 (s, 5-C), 165.78, 168.02 (each s, COOMe), 176.01 and 179.18 (each s, 1- and 3-CO); MS *m/z* 377 (M^+), 346 (M^+−31), and 228 (base peak).

Found: C, 57.01; H, 4.92; N, 3.81%; M^+, 377. Calcd for $C_{18}H_{19}NO_8$: C, 57.29; H, 5.07; N, 3.71%; M, 377.

Cycloaddition of 1 to 3b and then 4b Leading to 5bb. A solution of fresh **1** (0.521 g, 1.8 mmol) and **3b** (0.202 g, 1.8 mmol) in dry benzene (3 ml) was stirred at room temperature under nitrogen for 24 h. To this solution was added **4b** (0.426 g, 1.8 mmol) and the mixture was refluxed under nitrogen for 36 h. All the volatile materials were removed off *in vacuo* and the residue was stirred in methanol (10 ml) at room temperature overnight. The methanol was completely evaporated *in vacuo* to afford viscous oil which was chromatographed over silica gel with chloroform–ethyl acetate (4:1). Analytical sample of **5bb** (0.402 g, 47%) was obtained by repeated chromatography.

5bb: Colorless solid; mp 160—162 °C; IR (KBr) 3400 (OH), 1775, and 1705—1650 cm^{-1} (C=O); ^1H-NMR (DMSO-d_6) δ=2.64—3.40 (4H, m, 9-CH_2, 3a-, and 9a-H), 2.84 (3H, s, NMe), 3.10 (3H, s, OMe), 5.34 (1H, d, J_{4-3a}=3.5 Hz, 4-H), 7.00 (1H, s, 6-H), 7.32—7.80 (10H, m, ArH), and 10.58 (1H, s, OH); ^{13}C-NMR (DMSO-d_6) δ=24.31 (q, NMe), 24.83 (t, 9-C), 36.99, 45.09 (each d, 3a- and 9a-C), 55.95 (q, OMe), 69.04 (d, 4-C), 115.43 (d, 6-C), 124.82 (s), 128.16 (d), 128.40 (d), 128.63 (s), 129.57 (s), 130.28 (d), 136.33 (d), 137.27 (s), 137.91(s), 138.79 (s), 155.05 (s, 5-C), 176.01, 179.06 (each s, 1- and 3-CO), 195.27, and 196.56 (each s, COPh); MS *m/z* 469 (M^+), 437 (M^+−32), and 105 (base peak).

Found: C, 71.45; H, 4.89; N, 3.04%; M^+, 469. Calcd for $C_{28}H_{23}NO_6$: C, 71.63; H, 4.94; N, 2.98%; M, 469.

Cycloaddition of 1 to 3c and then 4a Leading to 6ca and 7ca. A solution of freshly distilled **1** (0.579 g, 2.0 mmol) and **3c** (0.18 g, 1.8 mmol) in dry benzene (2 ml) was stirred at room temperature under nitrogen for 2 h. To this solution was added **4a** (0.391 g, 2.8 mmol) and the mixture was heated under reflux for 24 h. After all the volatile materials were evaporated *in vacuo*, the residue was refluxed in methanol (50 ml) in the presence of *p*-toluenesulfonic acid (0.1 g) for 24 h. The residue obtained after evaporation of the methanol *in vacuo* was dissolved in chloroform (30 ml), the chloroform solution was washed with 5% aqueous sodium hydrogen carbonate, dried over magnesium sulfate, and evaporated *in vacuo* to give viscous oil which was found to contain **6ca** and **7ca** in a ratio of 2:3 by ^1H-NMR spectroscopy. The oil was separated into **6ca** (0.1 g, 13%) and **7ca** (0.146 g, 19%) by column chromatography over silica gel using chloroform–ethyl acetate (4:1).

6ca: Colorless solid from chromatography; mp 129—130 °C; IR (KBr) 3280 (OH) and 1720 cm^{-1} (C=O); ^1H-MNR ($CDCl_3$) δ=2.85—3.92 (4H, m, 4-CH_2, 2-, and 3-H), 3.64 (3H, s, OMe), 3.67, 3.72, 3.83, 3.87 (each 3H, s, COOMe), 4.90 (1H, d, J_{1-2}=6.0 Hz, 1-H), 7.23 (1H, s, 7-H), and 8,78 (1H, s, OH); ^{13}C-NMR ($CDCl_3$) δ=25.48, 39.45, 41.68, 51.96, 52.43, 56.95, 79.43, 116.36, 122.76, 126.40, 129.22, 134.33, 157.46, 165.91, 169.43, 169.61, and 172.20; Ms *m/z* 410 (M^+), 378 (M^+−32), and 287 (base peak).

Found: C, 55.33; H, 5.37%; M^+, 410. Calcd for $C_{19}H_{22}O_{10}$: C, 55.61; H, 5.40%; M, 410.

7ca: Colorless leaflets from aqueous methanol; mp 173—174 °C; IR (KBr) 3410 (OH) and 1720 cm-$^{-1}$ C=O)); ^1H-NMR ($CDCl_3$) δ=2.90—3.96 (4H, m, 4-CH_2, 2-, and 3-H), 3.48 (3H, s, OMe), 3.60, 3.74, 3.80, 3.88 (each 3H, s, COOMe), 5.08 (1H, d, J_{1-2}=3.0 Hz, 1-H), 7.19 (1H, s, 7-H), and 7.53 (1H, br. s, OH); ^{13}C-NMR ($CDCl_3$) δ=25.07 (t, 4-C), 36.34, 43.03 (each d, 2- and 3-C), 52.25, 52.60 (each q, COOMe), 72.21 (d, 1-C), 114.49 (d, 7-C), 125.17 (s), 126.99 (s), 129.34 (s), 134.92 (s), 156.41 (s, 8-C), 166.15, 169.43, 170.84, and 173.55 (each s, COOMe); MS *m/z* 410 (M^+), 378 (M^+−32), and 287 (base peak).

Found: C, 55.82 H, 5.40%; M^+, 410. Calcd for $C_{19}H_{22}O_{10}$: C, 55.61; H, 5.40%; M, 410.

Methanol Elimination of 7ca into 8ca. When **7ca** (0.14 g, 0.34 mmol) was heated under reflux in toluene (10 ml) for 48 h and then cooled to room temperature, colorless solid of **8ca** (0.088 g, 68%) was precipitated. It was washed with ether to give pure sample of **8ca**.

8ca: Colorless solid; mp 222—224 °C; IR (KBr) 3460 (OH) and 1710 cm^{-1} (C=O); ^1H-NMR ($CDCl_3$+DMSO-d_6) δ=2.90 (1H, dd, J_{gem}=16.8 and J_{vic}=8.0 Hz, one of CH_2), 3.28 (1H, dd, J_{gem}=16.8 and J_{vic}=3.5 Hz, the other of CH_2), 3.60—3.90 (1H, m, CHCOOMe), 3.56, 3.79, 3.82 (each 3H, s, COOMe), 7.25 (1H, s, ArH), and 7.90 (1H, s, =CH); ^{13}C-NMR ($CDCl_3$+DMSO-d_6) δ=28.06 (t, CH_6), 37.28 (q, OMe), 51.84, 51.96, 52.13, 52.43 (each q, COOMe), 115.01 (d), 122.12 (s), 124.35 (s), 126.87 (s), 130.46 (s), 130.57 (s), 133.74 (s), 155.74 (s), 165.62, 165.91, 167.97, and 171.73 (each s, COOMe); MS *m/z* 378 (M^+).

Found: C, 57.26; H, 4.82%; M^+, 378. Calcd for $C_{18}H_{18}O_9$: C, 57.14; H, 4.80%; M, 378.

Cycloaddition of 1 to 3c and then 4b Leading to G (R=E=COPh), 7cb, and 8cb. A solution of fresh **1** (0.545 g, 1.9 mmol) and **3c** (0.187 g, 1.9 mmol) in dry benzene (2 ml) was stirred at room temperature under nitrogen for 2 h. After **4b** (0.446 g, 1.9 mmol) was added, the resultant mixture was continued to stir at the same temperature under nitrogen for additional 24 h. All the volatile materials were evaporated *in vacuo* and the residue was treated with methanol (10 ml) to precipitate 0.274 g (27%) of **G** (R=E=COPh). It was collected on a filter and washed with a small amount of methanol (20 ml). To the filtrate was added 80 ml of methanol and this solution was refluxed in the presence of *p*-toluenesulfonic acid (0.1 g) for 24 h. The same work-up as mentioned above gave viscous oil which was chromatographed over silica gel using chloroform–ethyl acetate (4:1) to afford a mixture of **7cb** and **8cb** (0.102 g, 11%, 1:1). Repeated chromatography gave pure **8cb**, but **7cb** was always contaminated with a trace of **8cb**.

G (R=E=COPh): Colorless solid; mp 199—200 °C; IR (KBr) 1860, 1780, 1650 (C=O), 1250, and 845 cm^{-1} (TMS); ^1H-NMR ($CDCl_3$) δ=0.32 (9H, s, TMS), 2.90—3.36 (4H, m, 9-CH_2, 3a-, and 9a-H), 3.20 (3H, s, OMe), 5.38 (1H, d, J_{4-3a}= 3.2 Hz, 4-H), 6.93 (1H, s, 6-H), and 7.24—7.72 (10H, m, ArH); MS *m/z* 528 (M^+), 429 (base peak), and 105.

Found: C, 68.24; H, 5.36%; M^+, 528. Calcd for $C_{30}H_{28}O_7Si$: C, 68.16; H, 5.34%; M, 528.

7cb: Colorless solid; IR (KBr) 3200 (OH), 1730, 1710, and 1640 cm^{-1} (C=O); ^1H-NMR ($CDCl_3$+DMSO-d_6) δ= 2.60—3.80 (4H, m, 4-CH_2, 2-, and 3-H), 3.56 (6H, s, COOMe), 3.67 (3H, s, OMe), 5.10 (1H, d, J_{1-2}=3.0 Hz, 1-H), 6.96 (1H, s, 7-H), and 9.80 (1H, br. s, OH); MS *m/z* 470 (M^+), 411 (M^+−59, base peak), 105, and 77.

8cb: Colorless solid; mp 142—145 °C; IR (KBr) 3100 (OH), 1705, and 1640 cm^{-1} (C=O); ^1H-NMR ($CDCl_3$+ DMSO-d_6) δ=2.82 (1H, dd, J_{gem}=17.0 and J_{vic}=7.5 Hz, one of CH_2), 3.06 (1H, dd, J_{gem}=17.0 and J_{vic}=3.3 Hz, the other of CH_2), 3.67—3.90 (1H, m, CH), 3.41, 3.78 (each 3H,

s, COOMe), 7.00 (1H, s, ArH), 7.20—7.72 (10H, m, ArH), and 7.99 (1H, s, =CH); MS *m/z* 470 (M^+), 411 (M^+-59, base peak), and 105.

Found: C, 70.94; H, 4.79%; M^+, 470. Calcd for $C_{28}H_{22}O_7$: C, 71.48; H, 4.71%; M, 470.

Methanol elimination of **7cb** into **8cb** was achieved as follows: The comound **7cb** (0.125 g, 0.25 mmol) was heated under reflux in toluene for 24 h. Colorless solid which was precipitated on cooling was collected on a filter and washed with ether to give pure **8cb** (0.096 g, 0.204 mmol, 82%).

Cycloaddition of 1 to 3c and then 4c Leading to 8cc. Triene **1** (0.845 g, 2.9 mmol) was treated with **3c** (0.289 g, 2.9 mmol) and then **4c** (0.496 g, 5.8 mmol) in dry benzene (3 ml) under the conditions shown in Table 1. The benzene was removed off *in vacuo*, the residue was refluxed in methanol (50 ml) in the presence of *p*-toluenesulfonic acid (0.1 g), and the methanol was evaporated *in vacuo*. The residue was treated in the usual way as mentioned above and chromatographed over silica gel using chloroform–ethyl acetate (5:1) to give 0.14 g (15%) of **8cc**. It was purified by repeated column chromatography.

8cc: Colorless solid; mp 182—183 °C, IR (KBr) 3340 (OH), 1720, 1700, and 1675 cm^{-1} (C=O); ^{1}H-NMR (DMSO-d_6) δ= 2.92—4.20 (3H, m, CH_2 and CH), 3.50, 3.73, 3.77 (each 3H, s, COOMe), 6.80, 7.70 (each 1H, d, J_{vic}=9.0 Hz, ArH), 7.86 (1H, s, =CH), and 10.92 (1H, s, OH); ^{13}C-NMR (DMSO-d_6) δ=28.06 (t, CH_2), 37.16 (d, CH), 51.67, 51.84, 52.02 (each q, COOMe), 113.60 (d), 119.18 (s), 119.42 (s), 124.64 (s), 131.10 (d), 133.74 (d), 138.67 (s), 158.11 (s), 166.09, 166.32, and 172.49 (each s, COOMe); MS *m/z* 320 (M^+), 261 (M^+-59), and 229 (base peak).

Found: C, 59.85; H, 4.82%; M^+, 320. Calcd for $C_{16}H_{16}O_7$: C, 60.00; H, 5.03; M, 320.

Cycloaddition of 1 to 3c and then 3b Leading to 9. Triene **1** (0.587 g, 2.0 mmol) and **3c** (0.201 g, 2.0 mmol) were stirred in dry benzene (2 ml) at room temperature under nitrogen for 2 h. To this solution was added **3b** (0.228 g, 2.0 mmol) and the mixture was refluxed for 20 h, cooled to room temperature, treated with a few drops of trifluoroacetic acid, and then triturated with hexane. Colorless precipitate of **9** (0.257 g, 38%) was collected on a filter and washed with ether-hexane.

9: Colorless solid; mp 186—188 °C; IR (KBr) 1885, 1780, and 1720—1640 cm^{-1} (C=O); ^{1}H-NMR ($CDCl_3$+DMSO-d_6) δ=2.70—4.10 (8H, m, 4-, 10-CH_2, 3a-, 6a-, 9a-, and 10b-H), 2.95 (3H, s, NMe), 3.07 (3H, s, OMe), and 4.92 (1H, d, J_{6-6a}=3.7 Hz, 6-H); ^{13}C-NMR (DMSO-d_6) δ=24.19, 32.82, 35.29, 36.17, 42.74, 45.62, 55.95 (OMe), 66.93 (6-C), 131.98 (5a-C), 151.53 (10a-C), 169.67, 172.72, 172.84, 176.01 (COO- and CON-), and 190.51 (5-CO); MS *m/z* 333 (M^+), 301 (M^+-32), and 230 (base peak).

This compound **9** was too unstable to provide an analytically pure sample by chromatography or crystallization. No satisfied analytical data were available.

Cycloaddition of 1 to 10a and then 4a Leading to 11aa and 12aa. A solution of freshly distilled **1** (0.877 g, 3.1 mmol) and **10a** (0.81 ml, 9.2 mmol) in dry benzene (3 ml) was heated at 80 °C under nitrogen for 48 h. The solvent and excess of **10a** were all evaporated completely *in vacuo* and the residue was dissolved in another 3 ml of dry benzene containing **4a** (0.435 g, 3.4 mmol). This solution was refluxed for 48 h. The usual work-up with methanol and column chromatography over silica gel with hexane–ethyl acetate (2:1) gave 0.228 g (21%) of **11aa**. Continued elution with the same solvent afforded 0.086 g (8%) of **12aa**.

11aa: Colorless prisms from benzene–hexane; mp 116—116.5 °C; IR (KBr) 3370 (OH) and 1715 cm^{-1} (C=O) ^{1}H-NMR ($CDCl_3$) δ=1.80—2.30, 2.64—2.88 (each 2H, m, 3- and 4-CH_2), 3.08 (1H, ddd, J_{2-3}=4.0, 10.8, and J_{2-1}=9.0 Hz, 2-H), 3.28 (3H, s, OMe), 3.78, 3.87, 3.89 (each 3H, s, COOMe), 5.36 (1H, d, J_{1-2}=9.0 Hz, 1-H), 7.28 (1H, s, 7-H), and 8.21 (1H, s, OH); ^{13}C-NMR ($CDCl_3$) δ=24.07, 25.60 (each t, 3- and 4-C), 42.33 (d, 2-C), 52.31, 52.55 (each q, COOMe and OMe), 75.80 (d, 1-C), 115.48 (d, 7-C), 124.00 (s), 126.46 (s), 129.45 (s), 136.85, 157.28 (s, 8-C), 166.03, 169.49, and 173.55 (each s, COOMe); MS *m/z* 352 (M^+) and 320 (M^+-32).

Found: C, 58.06; H, 5.81%; M^+, 352. Calcd for $C_{17}H_{20}O_8$: C, 57.95; H, 5.72%; M, 352.

12aa: Colorless needles from aqueous acetone; mp 185—186 °C; IR (KBr) 3260 (OH) and 1710 cm^{-1} (C=O); ^{1}H-NMR ($CDCl_3$) δ=1.92—2.24 (2H, m, 3- or 4-CH_2), 2.40—3.04 (3H, m, 3- or 4-CH_2 and 2-H), 3.42 (3H, s, OMe), 3.74, 3.84, 3.87 (each 3H, s, COOMe), 5.04 (1H, d, J_{1-2}=4.5 Hz, 1-H), 7.24 (1H, s, 7-H), and 7.37 (1H, s, OH); ^{13}C-NMR ($CDCl_3$) δ=17.58, 24.98 (each t, 3- and 4-C), 43.47 (d, 2-C), 51.34, 51.99, 52.46, 58.27 (each q, COOMe and OMe), 70.13 (d, 1-C), 112.75 (d, 7-C), 125.26 (s), 127.25 (s), 128.31 (s), 135.94 (s), 156.43 (s, 8-C), 165.65, 168.46, and 172.58 (each s, COOMe); MS *m/z* 352 (M^+) and 320 (M^+-32).

Found: C, 58.07; H, 5.84%; M^+, 352. Calcd for $C_{17}H_{20}O_8$: C, 57.95; H, 5.72%; M, 352.

Cycloaddition of 1 to 10a and then 4b Leading to 11ab and 12ab. Under the same conditions as shown above (see Table 1), triene **1** (1.249 g, 4.4 mmol) was allowed to react with **10a** (1.2 ml, 13.1 mmol) and then **4b** (1.021 g, 4.4 mmol). The crude product was chromatographed over silica gel using hexane–ethyl acetate (1:1) to give 0.295 g (15%) of **11ab** and then 0.415 g (21%) of **12ab**.

11ab: Colorless prisms from dichloromethane–hexane; mp 133—135 °C; IR (KBr) 3300 (OH), 1725, 1655 (C=O), and 1580 cm^{-1}; ^{1}H-NMR ($CDCl_3$) δ=1.80—2.20, 2.50—2.74 (each 2H, m, 3- and 4-CH_2), 3.10 (1H, ddd, J_{2-3}=4.0, 10.8, and J_{2-1}=9.0 Hz, 2-H), 3.34 (3H, s, OMe), 3.76 (3H, s, COOMe), 5.44 (1H, d, J_{1-2}=9.0 Hz, 1-H), 6.97 (1H, s, 7-H), 7.20—7.80 (10H, m, ArH), and 8.32 (1H, s, OH); ^{13}C-NMR ($CDCl_3$) δ= 24.25, 26.18 (each t, 3- and 4-C), 42.45 (d, 2-C), 52.25, 52.96 (each q, COOMe and OMe), 75.91 (d, 1-C), 116.25 (d, 7-C), 123.17, 128.11, 128.98, 129.99, 131.86, 132.86, 133.09, 136.68, 137.67, 137.91, 138.56, 156.67 (s, 8-C), 173.61 (s, COOMe), 195.56, and 198.09 (each s, COPh); MS *m/z* 444 (M^+) and 412 (M^+-32).

Found: C, 72.78; H, 5.42%; M^+, 444. Calcd for $C_{27}H_{24}O_6$: C, 72.96; H, 5.44%; M, 444. **12ab**: Colorless prisms from aqueous acetone; mp 194—195.5 °C; IR (KBr) 3440 (OH), 1715, 1655 (C=O), and 1580 cm^{-1}; ^{1}H-NMR ($CDCl_3$) δ=1.80—3.04 (5H, m, 3-, 4-CH_2, and 2-H), 3.50 (3H, s, OMe), 3.72 (3H, s, COOMe), 5.07 (1H, d, J_{1-2}=4.5 Hz, 1-H), 6.90 (1H, s, 7-H), and 7.20—7.80 (11H, m, ArH and OH); ^{13}C-NMR (DMSO-d_6) δ=17.79, 25.71 (each t, 3- and 4-C), 43.62 (d, 2-C), 51.31, 58.53 (each q, COOMe and OMe), 70.57 (d, 1-C), 114.19 (d, 7-C), 126.58, 128.52, 129.57, 130.69, 132.92, 136.56, 137.27, 137.67, 155.70 (s, 8-C), 172.61 (s, COOMe), 195.32, and 197.27 (each s, COPh); MS *m/z* 412 (M^+-32).

Found: C, 72.96; H, 5.44%. Calcd for $C_{27}H_{24}O_6$: C, 72.90; H, 5.45%.

Cycloaddition of 1 to 10b and then 4a Leading to 11ba and 12ba. Triene **1** (1.306 g, 4.6 mmol) and **10b** (1.5 ml, 22.8 mmol) were heated at 75 °C in dry benzene (3 ml) under nitrogen for 48 h. All the volatile materials were completely evaporated off *in vacuo* and the residue was allowed to react with **4a** (1.296 g, 9.1 mmol) in benzene (3 ml) under reflux for 48 h. After the reaction mixture was subjected to the usual work-up with methanol, it was chromatographed over silica gel with hexane–ethyl acetate (2:1) to give 0.336 g (23%) of **11ba** and 0.175 g (12%) of **12ba**.

11ba: Colorless prisms from benzene–hexane; mp 163—164 °C; IR (KBr) 3400 (OH), 2240 (CN), and 1700 cm^{-1} (C=O); ^{1}H-NMR ($CDCl_3$) δ=1.80—2.40, 2.70-3.00 (each 2H, m, 3-

and 4-CH_2) 3.24 (1H, ddd, J_{2-3}=4.0, 6.5, and J_{2-1}=5.5 Hz, 2-H), 3.46 (3H, s, OMe), 3.85, 3.88 (each 3H, s, COOMe), 4.91 (1H, d, J_{1-2}=5.5 Hz, 1-H), 7.24 (1H, s, 7-H), and 7.50 (1H, s, OH); ^{13}C-NMR (DMSO-d_6) δ=18.32, 22.37 (each t, 3- and 4-C), 27.01 (d, 2-C), 52.19, 52.60, 57.54 (each q, COOMe and OMe), 70.28 (d, 1-C), 113.13 (d, 7-C), 119.71 (s, CN), 124.70 (s), 124.94 (s), 129.22 (s), 134.86 (s), 157.46 (s, 8-C), 165.73, and 168.26 (each s, COOMe); MS *m/z* 319 (M^+) and 287 (M^+−32).

Found: C, 60.09; H, 5.41; N, 4.65%; M^+, 319. Calcd for $C_{16}H_{17}NO_6$: C, 60.18; H, 5.37; N, 4.39%; M, 319.

12ba: Colorless needles from aqueous acetone; mp 158—159 °C; IR (KBr) 3300 (OH), 2250 (CN), and 1720 cm^{-1} (C=O); ^{1}H-NMR ($CDCl_3$) δ=1.80—3.40 (5H, m, 3-, 4-CH_2, and 2-H), 3.68 (3H, s, OMe), 3.84, 3.87 (each 3H, s, COOMe), 4.82 (1H, d, J_{1-2}=4.5 Hz, 1-H), 7.23 (1H, s, 7-H), and 7.87 (1H, s, OH); ^{13}C-NMR ($CDCl_3$) δ=21.61, 24.01 (each t, 3- and 4-C), 30.24 (d, 2-C), 52.66, 58.18 (each q, COOMe and OMe), 73.45 (d, 1-C), 115.43 (d, 7-C), 118.83 (s, CN), 123.94, 129.57, 134.68, 156.70 (s, 8-C), 165.97, and 169.43 (each s, COOMe); MS *m/z* 319 (M^+) and 287 (M^+−32).

Found: C, 59.90; H, 5.34; N, 4.49%; M^+, 319. Calcd for $C_{16}H_{17}NO_6$: C, 60.18; H, 5.37; N, 4.39%; M, 319.

Cycloaddition of ***1*** *to* ***10b*** *and then* ***4b*** *Leading to* ***11bb*** *and* ***12bb***. The same procedure as described above (see Table 1) starting from **1** (1.13 g, 3.9 mmol), **10b** (1.3 ml, 19.7 mmol), and **4b** (0.924 g, 3.9 mmol) gave 0.458 g (28%) of **11bb** and 0.168 g (10%) of **12bb**. The latter was purified by repeated chromatography.

11bb: Colorless needles from ethyl acetate-hexane; mp 220 °C; IR 3300 (OH), 2240 (CN), 1665, 1645 (C=O), and 1585 cm^{-1}; ^{1}H-NMR ($CDCl_3$) δ=1.80—2.36, 2.60—2.80 (each 2H, m, 3- and 4-CH_2), 3.22 (1H, ddd, J_{2-3}=3.5, 8.5, and J_{2-1}=6.5 Hz, 2-H), 3.54 (3H, s, OMe), 5.04 (1H, d, J_{1-2}=6.5 Hz, 1-H), 6.96 (1H, s, 7-H), and 7.20—7.76 (11H, m, ArH and OH) ^{13}C-NMR (DMSO-d_6) δ=18.55, 23.01 (each t, 3- and 4-C), 27.12 (d, 2-C), 57.65 (q, OMe), 70.57 (d, 1-C), 114.54 (d, 7-C), 119.89 (s, CN), 124.05 (s), 128.52 (d), 128.69, 129.69, 130.51 (s), 133.09 (d), 135.39 (s), 136.59 (s), 137.73 (s), 137.85 (s), 156.70 (s, 8-C), 195.32, and 197.09 (each s, COPh); MS *m/z* 411 (M^+), 379 (M^+−32), and 105 (base peak).

Found: C, 75.65; H, 5.12; N, 3.65%; M^+, 411. Calcd for $C_{26}H_{21}NO_4$: C, 75.90; H, 5.14; N, 3.40%; M, 411.

12bb: Colorless solid; mp 186—189 °C; IR (KBr) 3280 (OH); 2240 (CN); 1660, 1635 (C=O), and 1580 cm^{-1}; ^{1}H-NMR ($CDCl_3$) δ=1.70—3.00 (4H, m, 3- and 4-CH_2), 3.10—3.40 (1H, m, 2-H), 3.69 (3H, s, MeO), 4.86 (1H, d, J_{1-2}=4.5 Hz, 1-H), 6.90 (1H, s, 7-H), 7.10—7.90 (10H, m, ArH), and 8.28 (1H, s, OH); ^{13}C-NMR ($CDCl_3$+DMSO-d_6) δ=20.02, 24.95 (each t, 3- and 4-C), 30.71 (d, 2-C), 59.42 (q, OMe), 69.10 (d, 1-C), 114.19 (d, 7-C), 120.06 (s, CN), 124.41 (s), 127.58, 127.81, 128.22, 129.22, 130.57, 132.22, 132.45, 134.56, 136.27, 137.32, 137.56, 155.63 (s, 8-C), 195.03, and 197.27 (each s, COPh); MS *m/z* 379 (M^+−32) and 105 (base peak).

Found: C, 75.41; H, 5.18; N, 3.52%. Calcd for $C_{26}H_{21}NO_4$: C, 75.90; H, 5.14; N, 3.40%.

Cycloaddition of ***2*** *to* ***10a*** *and then* ***4a*** *Leading to* ***13*** *and* ***14***. A solution of **2** (0.895 g, 2.7 mmol), **10a** (4.9 ml, 54 mmol), and a catalytic amount of 1,4-benzenediol in dry benzene (10 ml) was refluxed under nitrogen for 5 d. All the volatile materials were completely evaporated *in vacuo* and the residue was dissolved in dry benzene (3 ml) containing **4a** (0.421 g, 3.0 mmol). This solution was refluxed under nitrogen for 48 h and the benzene was evaporated *in vacuo*. The residue was treated with methanol (20 ml) at room temperature overnight and the methanol was removed off. The viscous oil obtained was chromatographed over silica gel. The fraction eluted with hexane-ethyl acetate (4:1) afforded 0.045 g (6%) of **15**. The continued elution with hexane-ethyl acetate (2:1) gave a mixture of **13** and **14** (0.496 g, 46%). Both column chromatography over silica gel and high performance liquid chromatography were not effective for the separation of **13** and **14**.

13+14: Colorless solid (**13**:**14**=2:7, mp 77—83 °C); IR (KBr) 3400 (OH) and 1720 cm^{-1} (C=O); ^{1}H-NMR ($CDCl_3$) δ=1.80—2.20 (2H, m, CH_2), 2.60—3.00 (3H, m, CH_2 and CH), 3.53, 3,62, 3.76, 3.84, 3.92 (9H, each s, COOMe), 4.75 (1H, br. d, 1-H), 6.40 (1H, s, OH), and 6.80-7.32 (5H, m, ArH); MS *m/z* 398 (M^+).

Cycloaddition of ***1*** *to* ***10a*** *and then* ***3b*** *Leading to* ***16***. Triene **1** (0.94 g, 3.3 mmol) and fresh **10a** (0.89 ml, 9.9 mmol) were heated under reflux in dry benzene (3 ml) under nitrogen for 48 h. All the volatile materials were evaporated off *in vacuo* and the residue was then heated together with **3b** (0.401 g, 3.6 mmol) in dry benzene (3 ml) under reflux for 24 h. The usual work-up of the reaction mixture with methanol gave viscous oil of crude product. It was chromatographed over silica gel using hexane-ethyl acetate (4:1) to afford 0.182 g (28%) of **17**. The continued elution with hexane-ethyl acetate (1:1) gave 0.233 g (25%) of **16** (mp 45—55 °C). During the purification of **16** by column chromatography under the same conditions, only one third of the charged amount was recovered and the purity of **16** was not so improved (mp 55—60 °C). Some spectral data of **16** are given below.

16: ^{1}H-NMR ($CDCl_3$) δ=2.40—3.20 (6H, m, CH_2), 3.00 (3H, s, NMe), 3.40—3.92 (2H, m, CH), 3.76 (3H, s, COOMe), and 7.44 (1H, br. s, 6-H); ^{13}C-NMR ($CDCl_3$) δ=20.49, 25.42, 27.24, 33.70, 37.46, 44.68, 51.90, 127.52, 128.93, 130.98, 150.59, 166.97, 173.72, 176.77, and 190.46; MS *m/z* 289 (M^+) and 274 (M^+−15).

Cycloaddition of ***2*** *to* ***10a*** *and then* ***3a*** *Leading to* ***18aa, 19aa, and 20aa***. A solution of **2** (0.895 g, 2.7 mmol), fresh **10a** (4.8 ml, 54 mmol), and 1,4-benzenediol (trace) in dry benzene (10 ml) was refluxed under nitrogen for 5 d. All the volatile materials were evaporated *in vacuo* and the residue was dissolved in another 3 ml of benzene containing **3a** (0.513 g, 3.0 mmol). The resulting solution was again refluxed for 48 h. The mixture was subjected to the usual work-up with methanol and then the column chromatography over silica gel. The fraction eluted with hexane-ethyl acetate (4:1) afforded **21** (0.082 g, 11%, endo:exo=1:5). The continued elution with hexane-ethyl acetate (1:1) gave 0.156 g (13%, 2:3) of a mixture of **18aa** and **20aa**, and then 0.413 g (36%) of **19aa**. The separation of **18aa** and **20aa** was unsuccessful (^{1}H-NMR ($CDCl_3$) δ=1.60—3.92 (9H, m, CH_2 and CH), 3.52 (3×0.4H, s, COOMe of **18aa**), 3.57 (3×0.6H, s, COOMe of **20aa**), 4.52 (1×0.6H, br. s, 6-H of **20aa**), 4.56 (1×0.4H, d, J_{6-7}=6.0 Hz, 6-H of **18aa**), and 6.80—7.60 (10H, m, ArH)).

19aa: Colorless solid from HPLC; mp 80—83 °C; IR (KBr) 1775, 1720, and 1670 cm^{-1} (C=O); ^{1}H-NMR ($CDCl_3$) δ=1.70—3.84 (9H, m, CH_2 and CH), 3.67 (3H, s, COOMe), 4.45 (1H, br. s, 6-H), and 6.88-7.60 (10H, m, ArH); MS *m/z* 429 (M^+, base peak).

Found: M^+, *m/z* 429.1583. Calcd for $C_{26}H_{23}NO_5$: M, 429.1576.

Cycloaddition of ***2*** *to* ***10a*** *and then* ***3b*** *Leading to* ***18ab, 19ab, and 20ab***. Similar procedures using **2** (0.479 g, 1.4 mmol), **10a** (2.6 ml, 28 mmol), and a trace of 1,4-benzenediol in dry benzene (the first reaction: under reflux for 5 d; the second reaction: under reflux for 48 h) gave viscous oil of crude product. It was chromatographed over silica gel using hexane-ethyl acetate as an eluent to afford 0.15 g (38%) of **21** (endo:exo=1:3). The continued elution with hexane-ethyl acetate (1:1) gave a mixture of **18ab**, **19ab**, and **20ab** (0.138 g, 26%, **18ab**:**19ab**:**20ab**=1:4:2). The separation

of these isomers by column chromatography over silica gel was unsuccessful. Pure **18ab** and **19ab** were obtained through HPLC using dichloromethane-ethyl acetate (2:1) as an eluent.

18ab: Colorless solid from HPLC; mp 225—228 °C; IR (KBr) 1775, 1735, 1700, and 1675 cm^{-1} (C=O); ^{1}H-NMR ($CDCl_3$) δ=1.60—2.04 (2H, m, CH_2), 2.10—3.82 (7H, m, CH_2 and CH), 3.00 (3H, s, NMe), 3.52 (3H, s, COOMe), 4.52 (1H, d, J_{6-7}=5.5 Hz, 6-H), and 6.80—7.36 (5H, m, ArH); MS *m/z* 367 (M^+, base peak).

19ab: Colorless plates from ether-hexane; mp 82—85 °C; IR (KBr) 1775 and 1720—1665 cm^{-1} (C=O); ^{1}H-NMR ($CDCl_3$) δ=1.60—3.60 (9H, m, CH_2 and CH), 3.05 (3H, s, NMe), 3.65 (3H, s, COOMe), 4.41 (1H, br. s, 6-H), and 6.84—7.36 (5H, m, ArH), MS *m/z* 367 (M^+).

Found: M^+, *m/z* 367.1413. Calcd for $C_{21}H_{21}NO_5$: M, 367.1418.

Some characteristic signals of crude **20ab** in the ^{1}H-NMR spectrum in $CDCl_3$ are given as follows: δ=3.00 (3H, s, NMe), 3.60 (3H, s, COOMe), and 4.44 (1H, br. s, 6-H).

The present work was partially supported by a Grant-in-Aid for Scientific Research No. 58750694 from the Ministry of Education, Science and Culture to E. W.

References

1) O. Tsuge, E. Wada, S. Kanemasa, and H. Sakoh, *Bull. Chem. Soc. Jpn.*, **57**, 3221 (1984).

2) S. Danishefsky, T. Kitahara, C. F. Yan, and J. Morris, *J. Am. Chem. Soc.* , **101**, 6996 (1979).

3) After the reaction of **1** with **10a** was complete (reflux in dry benzene for 48 h), all the volatile materials were evaporated *in vacuo* and the residue was subjected to ^{1}H-NMR measurement. The spectrum was very clean and showed that only two isomeric mono-cycloadducts were formed in quantitative yields (isomer ratio was 1:2). the major isomer: δ=0.16, 0.22 (each 9H, s, TMS), 3.36 (3H, s, OMe), and 3.66 (3H, s, COOMe); the minor isomer: δ= 0.18, 0.24 (each 9H, s, TMS), 3.36 (3H, s, OMe), and 3.72 (3H, s, COOMe).

4) According to the molecular model inspection, the approach of the second dienophile across the diene part of mono-cycloadduct is sterically hindered, on both sides, when the cycloadduct has a half-chair conformation. On each side, there are each two repulsive axial substituents in this conformation, disturbing the approach of dienophile.

5) A mixture of two Michael adducts of mono-cycloadduct to **4a** was obtained in 22% yield. The Michael addition of enol silyl ethers is known: K. Yamamoto, S. Suzuki, and J. Tsuji, *Chem. Lett.* , **1978**, 649.

6) When the reaction mixture was treated with methanol at this stage, the endo and exo mono-adducts were isolated in 22 and 70% yields, respectively (see Ref. 1).

7) The configuration of the initially formed six-membered rings was determined on the basis of the coupling constants J_{6-7}. The stereochemistry of fused maleimide rings was based on the stereochemical characteristics of diene-transmissive Diels-Alder cycloaddition.

8) R. E. Lutz and W. R. Smithey, Jr., *J. Org. Chem.* , **16**, 51 (1951).

9) E. H. Ingold, *J. Chem. Soc.*, **1925**, 1199.

Reformatsky Type Reaction with New Aluminium Reagents Containing Al-Sn or Al-Pb Linkage[1)]

Seijiro MATSUBARA, Noriyuki TSUBONIWA, Yoshitomi MORIZAWA, Koichiro OSHIMA,* and Hitosi NOZAKI
Department of Industrial Chemistry, Faculty of Engineering Kyoto University, Yoshida, Kyoto 606
(Received June 28, 1984)

Treatment of α-bromo carbonyl compounds with the reagent prepared from *n*-Bu_3SnLi and Et_2AlCl or from $SnCl_2$ and Et_2AlCl affords enolates which react with ketone or aldehyde to give β-hydroxy carbonyl compounds in good to excellent yields. The reactions proceed similarly with the reagents which are generated from R_3PbLi (R=Ph, *n*-Bu) and Et_2AlCl. Catalysis by the added $Pd(PPh_3)_4$ complex promotes the reduction effectively and improves the yields of the desired adducts. The regio- and stereoselectivities are disclosed.

Cross aldol condensation is one of the most versatile method of making a carbon–carbon bond. The old procedures, however, have some drawbacks of accompanying self aldol condensation and retro-aldol reaction, which provide undesired by-products.[2)] During the past decade, numerous efforts have been made to overcome these shortages.[3)] Among many metal enolates such as Li,[2)] Mg,[2)] Zn,[2)] Ti,[4a)] B,[4b)] Al,[4c,4d,4e)] Si,[4f)] and Sn,[4g)] having been explored, aluminium enolate is suitable for trapping the initially formed aldol adducts as stable chelates.[4c)] Previously reported[4c)] aldol reaction is based on the generation of the regiospecific aluminium enolate by the coupled attack of Et_2AlCl and Zn on the α-halo carbonyl compounds. Here we wish to describe another effective method for the regioselective formation of aluminium enolates which are sufficiently reactive to attack carbonyl components under mild conditions.

A novel reagent which is believed to have an aluminium-tin single bond[5)] is produced by treatment of *n*-Bu_3SnLi[6)] with an equimolar amount of Et_2AlCl. The aluminium atom should behave as a Lewis acid center, which will coordinate the carbonyl oxygen and will give rise to *n*-Bu_3Sn anion acting as a potent reductant (Scheme 1). In fact, treatment of an α-bromo carbonyl compound with this reagent gave an enolate which reacted with a ketone or aldehyde to afford a β-hydroxy carbonyl compound in good yield after aqueous work-up. The success is ascribed to the strong affinity of tin for bromine[7)] as well as that of aluminium for oxygen. Actually, treatment of a mixture of α-bromoacetophenone and benzaldehyde with *n*-Bu_3SnLi alone gave a small amount of β-hydroxy ketone (<5%) in addition to 1,3-diphenyl-2,3-epoxy-1-propanone (33% yield), a Darzens type product.[8)] The latter compound was produced exclusively in 63% yield in the reaction of *n*-Bu_3SnLi–Me_3Al combination instead of *n*-Bu_3SnLi–Et_2AlCl. Strong basicity of the Sn^- anion accompanying Li^+ ion explains the observed results (Scheme 2).

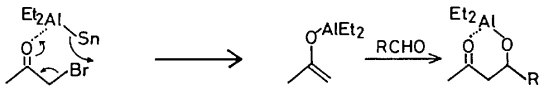

Scheme 1.

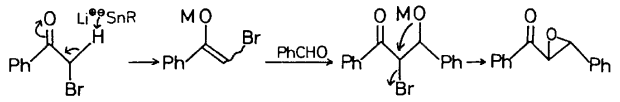

Scheme 2.

As shown in Table 1, the *n*-Bu_3SnLi–Et_2AlCl reagent can be applied equally well to the Reformatsky reaction[9–11)] of α-bromo esters. Reactions of methyl γ-bromocrotonate shown in Scheme 3 gave the α-adducts exclusively in contrast to the normal Reformatsky reactions producing mixtures of α-adducts and γ-adducts in roughly 7:3 ratios.[12)] This high regioselectivity is a characteristic of the aluminium dienolate.[4c,4e)]

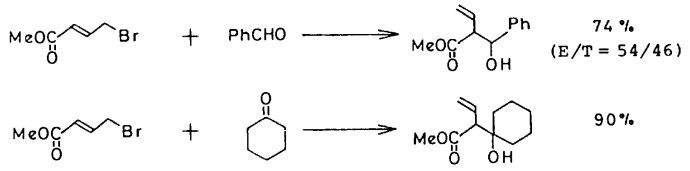

Scheme 3.

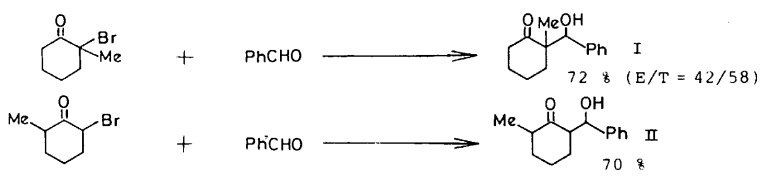

Scheme 4.

Table 1. Reformatsky type reaction with n-Bu_3SnLi-Et_2AlCl system

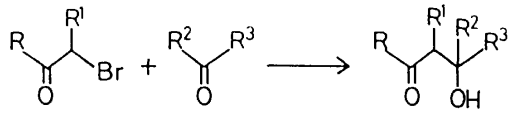

Run	R	R^1	R^2	R^3	Additive	Yield/%	E/T
1	Ph	H	Ph	H	—	92[a]	—
2	Ph	H	$-(CH_2)_5-$		—	76[a]	—
3	Ph	H	n-C_8H_{17}	H	—	79	—
4	Ph	H	Ph	H	—	54[a,c]	—
5	Ph	H	Ph	H	$Pd(PPh_3)_4$[b]	70[a,c]	—
6	Ph	H	Me	H	—	53[c]	—
7	Ph	H	Me	H	$Pd(PPh_3)_4$[b]	77[c]	—
8	EtO	H	Ph	H	—	58[a]	—
9	EtO	H	$-(CH_2)_5-$		—	87[a]	—
10	EtO	H	Ph	H	—	54[c]	—
11	EtO	H	Ph	H	$Pd(PPh_3)_4$[b]	75[c]	—
12	$-(CH_2)_5-$		Ph	H	—	69[a]	25/75[d]
13	$-(CH_2)_5-$		Ph	H	$Pd(PPh_3)_4$[b]	75[a]	26/74[d]
14	n-C_6H_{13}	H	Ph	H	—	81	—
15	n-C_6H_{13}	H	$-(CH_2)_5-$		—	54	—
16	n-C_6H_{13}	H	$-(CH_2)_5-$		$Pd(PPh_3)_4$[b]	85	—
17	Et	Me	Ph	H	—	61[e]	50/50[f]

a) These compounds gave satisfactory specra data. See Ref. 4c. b) A catalytic amount of $Pd(PPh_3)_4$ (5 mol%) was added. c) No 1,4-adduct was detected among the reaction mixture. d) The ratio of the stereoisomers (erythro and threo) was determined by an absorption due to the benzylic proton. See Ref. 4 g. e) This compound was identical with the authentic sample. See Ref. 4f. f) Determined by nmr analysis. See Ref. 4f.

Table 2. Reformatsky type reactions with $SnCl_2$-Et_2AlCl system

Run	Bromo ketone or bromo ester	Ketone or aldehyde	Additive	Products	Yield/%
1	$PhCOCH_2Br$	PhCHO	—	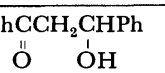	70
2	$PhCOCH_2Br$	PhCHO	$Pd(PPh_3)_4$[a]	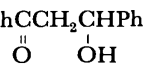	91
3	Ethyl bromoacetate	Cyclohexanone	$Pd(PPh_3)_4$[a]	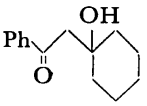	89
4	Ethyl bromoacetate	PhCHO	$Pd(PPh_3)_4$[a]	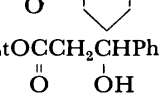	88
5	Ethyl bromoacetate	Cyclohexanone	$Pd(PPh_3)_4$[a]	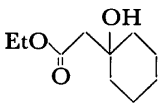	61
6	2-Bromocyclohexanone	PhCHO	$Pd(PPh_3)_4$[a]	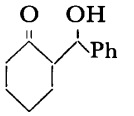	95 (31/69)[b]
7	*Methyl γ-bromo*-crotonate	PhCHO	—[c]	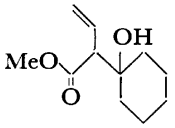	80 (41/59)[d]

a) A catalytic amount of $Pd(PPh_3)_4$ (5 mol%) was added. b) The ratio of the stereo isomers (erythro and threo) was determined by an absorption due to the benzylic proton. See Ref. 4g. c) Palladium catalyst was not effective. d) Erythro/threo ratio was determined by an absorption due to the methoxyl proton. See Ref. 4c.

TABLE 3. REFORMATSKY TYPE REACTIONS WITH R_3PbLi-Et_2AlCl SYSTEM

Run	Bromo ketone or bromo ester	Ketone or aldehyde	Reagent	Products	Yield/%
1	$PhCOCH_2Br$	PhCHO	A	$PhCCH_2CHPh$ (O, OH)	86
2	$PhCOCH_2Br$	PhCHO	B	$PhCCH_2CHPh$ (O, OH)	78
3	$PhCOCH_2Br$	Cyclohexanone	A	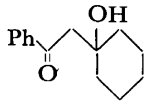	61
4	$PhCOCH_2Br$	Cinnamaldehyde	B[a]	$PhCCH_2-CH-CH=CHPh$ (O, OH)	84
5	2-Bromocyclohexanone	PhCHO	A	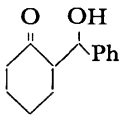	77 (28/72)[b]
6	Methyl γ-bromo-crotonate	Cyclohexanone	A[a]	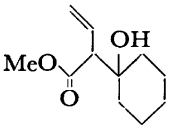	74
7	Methyl γ-bromo-crotonate	Cyclohexanone	A	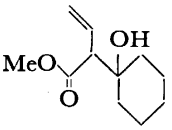	56

Reagent A: n-Bu_3PbLi-Et_2AlCl; Reagent B: Ph_3PbLi-Et_2AlCl. a) A catalytic amount of $Pd(PPh_3)_4$ (5 mol%) was added. b) The ratio of the stereo isomers (erythro and threo) was determined by an absorption due to the benzylic proton. See Ref. 4g.

The regioselectivity of the reaction was demonstrated by the following two examples (Scheme 4). Treatment of a mixture of 2-bromo-2-methylcyclohexanone[13] and benzaldehyde with n-Bu_3Sn-$AlEt_2$ gave the expected β-hydroxy ketone I.[4a] Meanwhile, the reaction of 2-bromo-6-methylcyclohexanone[14] provided the regioisomer II[4a] exclusively. Each product I or II was obtained as a single product without any contamination of the opposite regioisomer. Since the starting bromides are prepared with high regioselectivity, the present method provided us with a simple route to the β-hydroxy ketones I and II.

It should be noted that these reactions proceeded more effectively in the presence of a catalytic amount of $Pd(PPh_3)_4$ (Run 5, 7, 11, 13, and 16). For instance, the yield of the adduct of α-bromoacetophenone and cinnamaldehyde was increased from 54% to 75% in the presence of a catalytic amount of $Pd(PPh_3)_4$.[15] We may safely assume that Pd(0) facilitates the reduction of bromo ketone[16] to the aluminium enolate.

The addition of a hexane solution of Et_2AlCl to a suspension of anhydrous $SnCl_2$ in dichloromethane gave a dark red homogeneous solution.[17] The reagent thus prepared also was found to be effective for the Reformatsky type reaction (Table 2). The stereochemistry of the adducts and the regiochemistry of these reactions are similar to those with n-Bu_3SnLi-Et_2AlCl reagent (Run 6, 7).

The use of $PhMe_2SiLi$[18] and Ph_3GeLi[19] instead of n-Bu_3SnLi resulted in a formation of only a small amount of desired β-hydroxy ketone in addition to unidentified products. The combination of R_3PbLi-Et_2AlCl[20] (R=n-Bu, Ph), however, proved to be as effective as n-Bu_3SnLi-Et_2AlCl system (Table 3). The stereochemical outcomes were almost same as those with n-Bu_3SnLi-Et_2AlCl system.

Experimental

The IR spectra were determined on a Shimadzu IR-27-G spectrometer, the mass spectra on a Hitachi M-80 machine, and the NMR spectra on a Varian EM-390 spectrometer. The chemical shifts are given in δ, with TMS as an internal standard. The analyses were carried out by the staff at the Elemental Analyses Center of Kyoto University. Tetrahydrofuran was freshly distilled from sodium benzophenone ketyl. Purification of products were performed by column chromatography on silica gel (Wakogel C-100) or preparative thin-layer chromatography (TLC). Analytical GLPC was performed with a Yanagimoto GCG-550-F and a Shimadzu GC-4CPT.

Preparation of β-Hydroxy Carbonyl Compounds with the Reagent Prepared from n-*Bu₃SnLi–Et₂AlCl.* A hexane solution of butyllithium (1.6 M†, 3.8 ml, 6.0 mmol) was added to a suspension of anhydrous tin(II) chloride (0.38 g, 2.0 mmol) in THF (4 ml) at 0 °C. After being stirred for 20 min, the reaction mixture was treated with a hexane solution of diethylaluminum chloride (1.0 M, 2.0 ml, 2.0 mmol) at 0 °C. After the resulting mixture was stirred for another 20 min, a mixture of α-bromo carbonyl compound (1.0 mmol) and ketone or aldehyde (1.0 mmol) in THF (3 ml) was added [$Pd(PPh_3)_4$ (58 mg, 0.05 mmol) was added successively, if necessary] and the whole was stirred for 30 min. The reaction mixture was poured into 1M hydrochloric acid (20 ml) and

† 1 M=1 mol dm^{-3}.

extracted with ether. The combined organic layers were washed with brine, dried over anhydrous sodium sulfate, and concentrated. The crude product was purified by silica-gel column chromatography (hexane–ethyl acetate, 2:1).

3-Hydroxy-1-phenyl-1-undecanone: Mp 41.5 °C (pentane); IR (nujol) 3500, 1672, 1205 cm^{-1} NMR (CCl_4): δ=0.90 (t, J=6 Hz, 3H), 1.05—1.70 (m, 14H), 2.80—3.20 (m, 3H), 3.85—4.25 (m, 1H), 7.20—7.60 (m, 3H), 7.75—8.00 (m, 2H); MS m/z (%): 244 (30; M^+-18), 220 (34), 120 (35) 105 (100); Found: C, 77.75; H, 10.22%. Calcd for $C_{17}H_{26}O_2$: C, 77.82; H, 9.99%.

(E)-3-Hydroxy-1-phenyl-4-hexen-1-one: Bp 80 °C (bath temp, 1 Torr††); IR (neat): 3350, 2875, 1700, 1660, 1428 cm^{-1}; NMR (CCl_4) δ=1.68 (d, J=5.7 Hz, 3H), 2.80 (bs, 1H), 3.02 (d, J=6.0 Hz, 2H), 4.40—4.70 (m, 1H), 5.36—5.90 (m, 2H), 7.2—7.65 (m, 3H), 7.75—8.05 (m, 2H); MS m/z (%) 172 (2, M^+-18), 120 (30), 105 (100), 77 (52); Found: C, 75.60; H, 7.50%. Calcd for $C_{12}H_{14}O_2$: C, 75.76; H, 7.42%.

Ethyl (E)-3-Hydroxy-5-phenyl-4-pentenoate: Bp 75 °C (bath temp, 1 Torr); IR (neat): 3400, 1705, 1150, 1020, 960 cm^{-1}; NMR (CCl_4): δ=1.25 (t, J=7.5 Hz, 3H), 2.50 (d, J=6 Hz, 2H), 2.90 (bs, 1H), 4.10 (q, J=7.5 Hz, 2H), 4.35—4.75 (m, 1H), 6.33 (d,d, J=6.7 Hz, 15.3 Hz, 1H), 6.90—7.40 (m, 6H); MS m/z (%): 220 (19, M^+), 202 (25), 174 (15), 129 (71), 104 (100), 91 (19); Found: C, 71.04, H, 7.50%. Calcd for $C_{13}H_{16}O_3$: C, 70.89, H, 7.32%. Saponification and dehydration gave 5-phenylpentadienoic acid, which was identical with an authentic sample.[21]

1-Hydroxy-1-phenyl-3-nonanone: Bp 104 °C (bath temp, 0.7 Torr); IR (neat): 3400, 2899, 1679, 1443 cm^{-1}; NMR (CCl_4): δ=0.90 (t, J=6 Hz, 3H), 1.05—1.70 (m, 8H), 2.35 (t, J=6.6 Hz, 2H), 2.60 (d, J=6 Hz, 1H), 2.63 (d, J=7.5 Hz, 1H), 3.15—3.45 (m, 1H), 4.8—5.1 (m, 1H), 6.95—7.30 (m, 5H); MS m/z (%): 234 (0.5, M^+), 216 (3.8), 146 (69), 131 (100), 77 (13), 58 (26); Found: C, 77.05, H, 9.60%. Calcd for $C_{15}H_{22}O_2$: C, 76.88, H, 9.46%.

1-(1-Hydroxycyclohexyl)-2-octanone: Bp 58 °C (bath temp, 1 Torr); IR (neat): 3455, 1690, 1400, 970 cm^{-1}; NMR (CCl_4): δ=0.90 (t, J=6 Hz, 3H), 1.0—2.0 (m, 18H), 2.30 (t, J=6.6, 2H), 2.40 (s, 2H), 3.30 (bs, 1H); MS m/z (%): 226 (15, M^+), 208 (35), 156 (8), 113 (100), 99 (51); Found: C, 74.38, H, 11.87%. Calcd for $C_{14}H_{26}O_2$: C, 74.29, H, 11.58%.

Methyl 2-(1-Hydroxycyclohexyl)-3-butenoate: Bp 51 °C (bath temp, 0.7 Torr); IR (neat): 3450, 1700, 1620, 1155, 985, 905 cm^{-1}; NMR (CCl_4): δ=0.80—1.90 (m, 10H), 2.82 (bs, 1H), 2.91 (t, J=9 Hz, 1H), 3.67 (s, 3H), 5.07 (d,d, J=16.5, 1.5 Hz, 1H), 5.13 (d,d, J=7.5, 1.5 Hz, 1H), 5.90 (d,d,d, J=16.5, 7.5, 1.5 Hz, 1H); MS m/z (%): 198 (0.76, M^+), 183 (2.5), 155 (10), 100 (100), 99 (92), 81 (36), 69 (17), 68 (29); Found: C, 77.05, H, 9.60%. Calcd for $C_{11}H_{18}O_3$: C, 76.88, H, 9.46%.

Preparation of β-Hydroxy Carbonyl Compounds with the Reagent Prepared from $SnCl_2$–Et_2AlCl. A hexane solution of diethylaluminum chloride (1.0 M, 2.0 ml, 2.0 mmol) was added to a suspension of anhydrous tin (II) chloride (0.38 g, 2.0 mmol) in CH_2Cl_2 (5 ml) at 0 °C. The solution turned to red immediately. After being stirred for 20 min, a mixture of α-bromo carbonyl compound (1.0 mmol) and ketone or aldehyde (1.0 mmol) in CH_2Cl_2 (3 ml) was added [$Pd(PPh_3)_4$ (58 mg, 0.05 mmol) was added at the same time, if necessary] and the whole was stirred for 1 h. The reaction mixture was poured into 1M hydrochloric acid (30 ml) and extracted with ether. The combined organic layers were washed with brine, dried over anhydrous sodium sulfate, and concentrated. The crude product was purified by silica-gel column chromatgraphy (hexane–ethyl acetate, 2:1).

Preparation of β-Hydroxy Carbonyl Compounds with the Reagent Prepared from R_3PbLi–Et_2AlCl. A hexane solution of butyllitium (1.6 M, 3.8 ml, 6.0 mmol) or an ether solution of phenyllilitum (2.7 M, 2.2 ml, 6.0 mmol) was added to a suspension of a lead (II) chloride (0.56 g, 2.0 mmol) in THF (4 ml) at 0 °C. After being stirred for 20 min, the whole was cooled to −20 °C, and a hexane solution of diethylaluminum chloride (1.0 M, 2.0 ml, 2.0 mmol) was added at the same temperature. After the resulting mixture was stirred for another 20 min, a mixture of α-bromo carbonyl compound (1.0 mmol) and ketone or aldehyde (1.0 mmol) in THF (3 ml) was added [$Pd(PPh_3)_4$ (58 mg, 0.05 mmol) was added at this time, if necessary] and the whole was warmed up to 0 °C and stirred for 30 min. The reaction mixture was poured into 1 M hydrochloric acid and extracted with ether. The combined organic layers were washed with brine, dried over anhydrous sodium sulfate, and concentrated. The residual liquid was submitted to silica-gel column chromatgraphy with hexane–ethyl acetate=2:1 as an eluent.

Darzens Type Reactions with n-Bu_3SnLi–Me_3Al System. A hexane solution of trimethylaluminium (1.0 M, 2.0 ml, 2.0 mmol) was added to a solution of *n*-Bu_3SnLi prepared from *n*-BuLi (6.0 mmol) and $SnCl_2$ (0.38 g, 2.0 mmol) as described above, in THF (3.0 ml) at 0 °C. After stirring for 2 h, a mixture of α-bromoacetophenone (0.20 g, 1.0 mmol) and benzaldehyde (0.11 g, 1.0 mmol) in THF (2.0 ml) was added at 0 °C and the resulting mixture was stirred for another 20 min. The reaction mixture was poured into 1 M hydrochloric acid (30 min) and extracted with ether. The combined organic layers washed with brine, dried and concentrated. Purification by preparative TLC on silica-gel (hexane-ethyl acetate, 5:1) gave 1,3-diphenyl-2,3-epoxy-1-propanone in 63% yield.

1,3-Diphenyl-2,3-epoxy-1-propanone: Mp 88.5 °C (CH_2Cl_2/penthane); IR (CCl_4): 3000, 1680, 1590, 1500, 1210, 1000, 890 cm^{-1}; NMR (CCl_4): δ=3.90—4.05 (m, 2H) 6.90—7.60 (m, 3H), 7.27 (s, 5H), 7.80-8.10 (m, 2H); MS m/z (%): 224 (12.4, M^+), 165 (9), 105 (100), 91 (23), 77 (64), 65 (16), 51 (31); Found C, 79.87, H, 5.30. Calcd for $C_{15}H_{12}O_2$: C, 80.34, H, 5.39%.

Financial support by the Ministry of Education, Science and Culture, Japanese Government (Grant-in Aid for Special Project Reserch 58110005) is acknowledged. We also thank Toyo Stauffer Chemical Company for a gift of Et_2AlCl.

References

1) Preliminary report, N. Tsuboniwa, S. Matsubara, Y. Morizawa, K. Oshima, and H. Nozaki, *Tetrahedron Lett.*, **24**, 2569 (1984).

2) For a general discussion, see H. O. House, "Modern Synthetic Reactions", 2nd ed. W. A. Benjamin, Inc., Menlo Park (1972), pp 629—732, and K. Narasaka, *Yuki Gosei Kagaku Kyokai Shi*, **37**, 307 (1979).

3) For recent synthetic methods of aldol synthesis, see, R. W. Stevens and T. Mukaiyama, *Chem. Lett.*, **1983**, 1799; N. Iwasawa and T. Mukaiyama, *Chem. Lett.*, **1983**, 297; Y. Yamamoto and K. Maruyama, *J. Am. Chem. Soc.*, **104**, 2323 (1982); E. Nakamura and I. Kuwajima, *Tetrahedron Lett.*, **24**, 3343, 3347 (1983); H. Urabe and I. Kuwajima, *ibid*, **24**, 5001 (1983).

4) a) T. Mukaiyama, K. Banno, and K. Narasaka, *J. Am. Chem. Soc.*, **96**, 7503 (1974); b) D. A. Evans, *Aldrichimica Acta*, **15**, 23 (1982); S. Masamune and W. Choy, *ibid*, **15**, 47 (1982); c) K. Maruoka, S. Hashimoto, Y. Kitagawa, H. Yamamoto, and H. Nozaki, *J. Am. Chem. Soc.*, **99**, 7705 (1977); *Bull. Chem. Soc. Jpn.*, **53**, 3301 (1980); d) A. Itoh, S. Ozawa, K. Oshima, and H. Nozaki, *Bull. Chem. Soc. Jpn.*, **54**, 274 (1981); e) H. Nozaki, K. Oshima, K. Takai, and S. Ozawa, *Chem. Lett.*, **1979**, 379; J. Tsuji, T. Yamada, M. Kaito, and T. Mandai, *Tetrahedron Lett.*, **1979**, 2257; f) R. Noyori, I. Nishida, and J.

†† 1 Torr≈133.322 Pa.

Sakata, *J. Am. Chem. Soc.*, **105**, 1598 (1983); g) Y. Yamamoto, H. Yatagai, and K. Maruyama, *J. Chem. Soc., Chem. Commun.*, **1981**, 162; S. Shenvi and J. K. Stille, *Tetrahedron Lett.*, **23**, 627 (1982); T. Mukaiyama, J. Kato, and M. Yamaguchi, *Chem. Lett.*, **1982**, 1291; K. Kobayashi, M. Kawanisi, T. Hitomi, and S. Kojima, *Chem. Lett.*, **1983**, 851.

5) For another reaction using this reagent, J. Hibino, S. Matsubara, Y. Morizawa, K. Oshima, and H. Nozaki, *Tetrahedron Lett*, **25**, 2151 (1984).

6) C. Tamborski, F. E. Ford, and E. J. Soloski, *J. Org. Chem.*, **28**, 237 (1963); W. C. Still, *J. Am. Chem. Soc.*, **99**, 4836 (1977); **100**, 1481 (1978); W. Kitching, H. A. Olszowg, and K. Harvey, *J. Org. Chem.*, **47**, 1893 (1982).

7) The affinity of tin to bromine is well documented and used for the oxidation of alcohols. See below. K. Saigo, A. Morikawa, and T. Mukaiyama, *Bull. Chem. Soc. Jpn.*, **49**, 1656 (1976); Y. Ueno and M. Okawara, *Tetrahedron Lett.*, **1976**, 4597; T. Ogawa and M. Matsui, *J. Am. Chem. Soc.*, **98**, 1629 (1976).

8) T. Mukaiyama, T. Haga, and N. Iwasawa, *Chem. Lett.*, **1982**, 1601.

9) The classical Reformatsky reaction, see, R. L. Shriner, *Org. React.*, **1**, 1 (1942); M. W. Rathke, *ibid.*, **22**, 423 (1975).

10) For recent development, see: J. G. A. Luiten, *Chem. and Ind. (London)*, **1972**, 103; d) M. W. Rathke and A. Lindert, *J. Org. Chem.*, **35**, 3966 (1970); e) J. F. Ruppert and J. D. White, *ibid.*, **39**, 269 (1974); f) R. D. Rieke and S. J. Uhm, *Synthesis*, **1975**, 452.

11) For Reformatsky type reactions using tin reagent, see: T. Harada and T. Mukaiyama, *Chem. Lett.*, **1982**, 161, 467; J. Kato and T. Mukaiyama, *ibid.*, **1983**, 1727.

12) E. R. H. Jozes, D. G. O' Suliivan, and M. C. Whiting, *J. Chem. Soc.*, **1949**, 1415.

13) E. W. Gurbisch, Jr., *J. Org. Chem.*, **30**, 2109 (1965).

14) P. L. Stotter and K. A. Hill, *J. Org. Chem.*, **38**, 2576 (1973).

15) H. Urata, H. Suzuki, Y. Moro-oka, and T. Ikawa, *J. Organomet. Chem.*, **234**, 367 (1982); M. Kosugi, T. Ohya, and T. Migita, *Bull. Chem. Soc. Jpn.*, **56**, 3539 (1983).

16) J. P. Collman and L. S. Hegedus, "Principles and Applications of Organotransition Metal Chemistry", University Science Books, Mill Valley (1980), pp. 190—191.

17) The authors are greatly indebted to Prof. Kenji Itoh, Toyohashi University of Technology, for his valuable suggestions to try this reaction.

18) H. Hayami, M. Sato, S. Kanemoto, Y. Morizawa, K. Oshima, and H. Nozaki, *J. Am. Chem. Soc.*, **105**, 4491 (1983) and references cited therein.

19) H. Oda, Y. Morizawa, K. Oshima and H. Nozaki, *Tetrahedron Lett.*, in press; H. Gilman and C. W. Gerow, *J. Am. Chem. Soc.*, **77**, 4675 (1955).

20) H. Gilman, L. Summers, and R. W. Lupper, *J. Org. Chem.*, **17**, 630 (1952).

21) M. W. Rathke, *J. Am. Chem. Soc.*, **92**, 3222 (1970); W. R. Dunnanvant and C. R. Hauser, *J. Org. Chem.*, **25**, 503 (1960).

 © 1984 The Chemical Society of Japan Bull. Chem. Soc. Jpn., 57, 3247—3252 (1984)

Electroluminescent Properties of *n*-GaAs in Peroxodisulfate Solutions. Transient Behavior and Carrier Concentration Effect on Emission Spectra

Kohei UOSAKI* and Hideaki KITA

Department of Chemistry, Faculty of Science, Hokkaido University, Sapporo 060

(Received April 12, 1984)

Electroluminescence (EL) due to band-to-band transition was observed for *n*-GaAs in solutions containing peroxodisulfate ions. Digital simulation shows that the observed transient current and EL intensity stimulated by negative potential pulses can be explained by assuming that the surface concentration of $S_2O_8^{2-}$ was zero during potential pulses and that the EL intensity was proportional to the surface concentration of SO_4^{-} (generated by the one-electron reduction of $S_2O_8^{2-}$). Surface composition change seems to be the main reason for the relation between the potential and EL intensity. A hydrogen evolution reaction reduces the EL efficiency at relatively negative potentials. Although the potential and time had no observed effect on the shape of the EL spectra, the carrier concentration affected the peak position and the full width at half maximum (FWHM) of the EL spectra. For greater carrier concentrations, the wavelength of the EL peak became shorter and the FWHM became larger. These results agree with those reported regarding solid-state luminescence and can be explained by the filling of the conduction band states by electrons (Burnstein-Moss shift).

The luminescent properties of semiconductors in solutions have proved to be useful in understanding the mechanism of electrochemical reactions at semiconductor electrodes.[1-10] Photoluminescence (PL) measurements are often used to determine the quantum efficiency of photoelectrochemical reactions[11-13] and electroluminescence (EL) measurements are used to probe the intermediates of reactions and the surface states of semiconductors.[14-18]

Gallium arsenide (GaAs) has been one of the most frequently studied semiconductors and its luminescent properties at p/n and semiconductor/metal junctions have become well known.[19-25] The luminescent properties of GaAs in solution, however, have been studied less. Recently, Hobson and Ellis thoroughly studied the photoluminescent properties of *n*-GaAs in a solution containing Te^{2-}/Te_2^{2-}.[26] Only a few reports are available involving the electroluminescence properties of GaAs.[27-30]

In this paper, we describe the transient behavior of the current and the EL intensity of *n*-GaAs electrodes in solutions containing $S_2O_8^{2-}$ and the effect of carrier concentration on the EL spectra.

Experimental

Materials. Four types of *n* -GaAs single crystals with different carrier concentrations were used in the present study. Their properties are summarized in Table 1. Ohmic contacts to the crystals were obtained using an In-Ga alloy. The procedure for mounting the electrodes was similar to one reported before.[31] The electrode surface was etched in HNO_3-HCl (1:1) before each experiment. Reagent-grade NaOH and $K_2S_2O_8$, and water purified using a Milli-Q water purification system (Millipore Corp.) were used to prepare electrolyte solutions.

Electrochemical and Luminescent Measurements. The potential of the electrode was controlled with a potentiostat (Hokuto Denko, HA-301) with respect to an Ag/AgCl reference electrode. A large Pt foil, which surrounded a GaAs working electrode, was used as a counter electrode. The EL intensity was monitored with a photomultiplier (Hamamatsu TV Co. Ltd., R406) having a response similar to S-1. A programmable function generator (Hokuto Denko, HB-105) and a wave-memory unit (NF Electronic Co. Ltd., WM-811 with an 8-bit resolution) were used to study the transient behavior of the EL intensity and current. Both the function generator and the wave-memory unit were controlled by a personal computer (Nippon Electronic Co. Ltd., PC-8801) *via* a GP-IB interface and a PIO interface with TTL signals, respectively. After each measurement, data were transferred to the computer and, to improve the signal-to-noise ratio, the data were averaged 2—64 times. The averaged data were then transferred to and stored on a floppy disc. The time sequence for the transient behavior measurements is shown in Fig. 1(a).

Time-resolved EL spectra were obtained by pulsing the potential between −0.5 V and −3.65 V, following the time sequence shown in Fig. 1(b). In this case, the computer was used to provide potential pulses *via* a 12-bit D/A convertor, to collect the photomultiplier (PMT) response which was amplified by a fast-response amplifier (NF Electronic Co. Ltd., LI-75A, 1 MHz, gain=100) *via* a 12-bit D/A convertor every 10 msec and to control a monochromator (Ritsu Oyo Kogaku Co. Ltd., MC-20N, having a grating with 1200 grooves/mm blazed at 0.75 μm). After the EL intensity was measured and averaged at one wavelength, the monochromator was driven to make measurements at a new wavelength. After all the measurements were completed, the EL data were trans-

TABLE 1. PROPERTIES OF *n*-GaAs SINGLE CRYSTALS

Sample	Face	Dopant	Donor density/cm^{-3}	Specific Resistance/$\Omega \cdot cm$	Mobility/$cm^2 \cdot V^{-1} \cdot s^{-1}$
1	(100)	Si	0.84×10^{18}	0.0033	2235
2	(100)	Si	2.6×10^{18}	0.0015	1656
3	(100)	Si	$4.2-8.0 \times 10^{18}$	0.0007—0.0008	1171—1882
4	(100)	Te	0.96×10^{18}	0.0024	2712

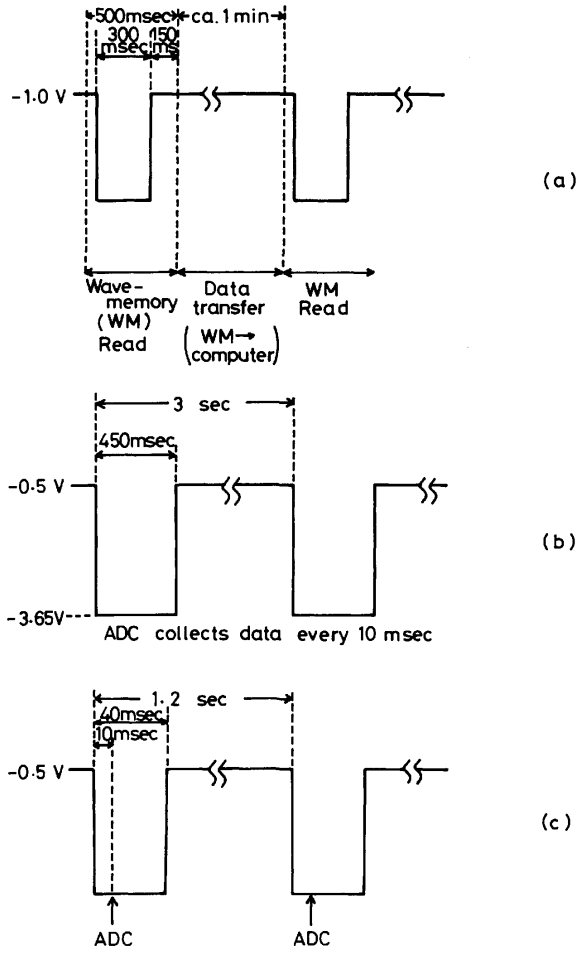

Fig. 1. Time sequence for the measurements of (a) transient behavior, (b) time resolved EL spectra, and (c) potential dependence of EL spectra.

ferred to and stored on a floppy disc.

Similar arrangements were employed to study the potential dependence of the EL spectra. The time sequence for this type measurement is shown in Fig. 1(c). The potential was pulsed between −0.5 V and a given potential. The resulting PMT response was observed at a given wavelength 10 msec after the potential step, amplified by the LI-75A amplifier, monitored by a 12-bit A/D convertor and stored in the computer. After measurements at a given potential were completed, measurements at new potentials were carried out. Measurements were repeated at 2.5 or 5 nm intervals. After all the measurements were completed, the EL data were transferred to and stored on a floppy disc.

Digital simulation was carried out using the computer and calculated results were plotted on an X-Y plotter (RY 11Z, Rika Denki Co. Ltd.).

Results

The Transient behavior and Potential Dependence of Current and EL Intensity. Typical EL-i-t relations of *n*-GaAs (sample No.4) in a solution containing 5 M NaOH (1 M=1 mol dm^{-3}) and 0.10 M $K_2S_2O_8$ for potential pulses of 300 msec are shown in Fig. 2. The electrode potential was kept at −1.0 V for about 1 min before each potential pulse. As the pulse was made more negative, the maximum EL intensity became

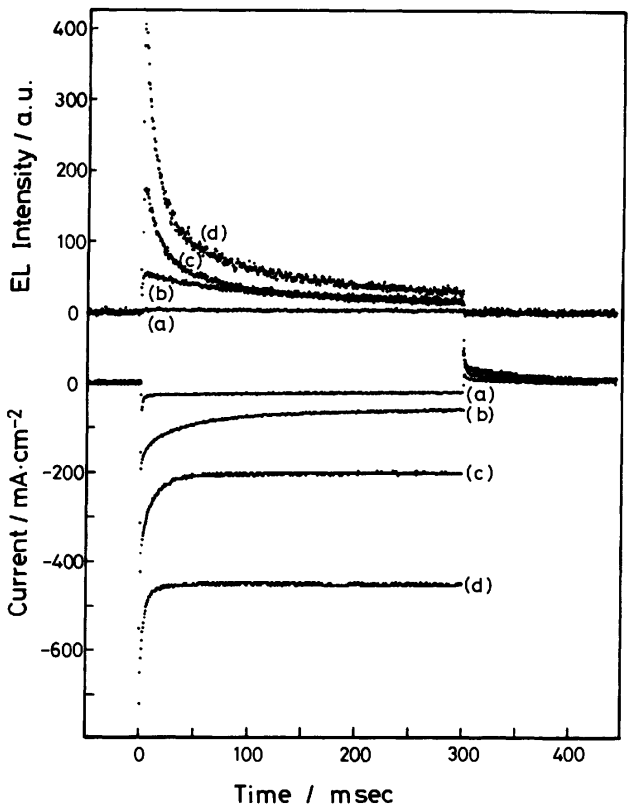

Fig. 2. EL-i-t relations of *n*-GaAs (Te doped, 0.96×10^{18} cm^{-3}) in a solution containing 5 M NaOH and 0.10 M $K_2S_2O_8$ for potential pulses from −1.0 V (1 min) to a given potential (300 msec). (a): −1.5 V, (b): −2.0 V, (c): −2.5 V, (d): −3.0 V.

greater and the maximum cathodic current became larger. The potential dependence of the EL intensity is, in general, not so simple. The EL intensity and the current at 50, 100, 200, and 295 msec after the cathodic potential pulse was applied are plotted against the pulsed potential (Fig. 3). The EL intensity was made to increase by applying a more negative cathodic pulse, until *ca.* −1.9—−2.0 V. However, it decreased between −2.0 and −2.2 V and then increased again.

EL Spectra. The EL Spectra of *n*-GaAs (sample No.4) in a solution containing 5 M NaOH and 0.15 M $K_2S_2O_8$ at 10, 30, 50, and 70 msec after a potential was pulsed from −0.5 V to −3.65 V are shown in Fig. 4(a). The EL peak appeared at 855 nm (1.45 eV), which is in good agreement with the band-gap energy of GaAs.[32] There seems to be no spectral change within this time domain, which is clearly seen in Fig. 4(b) where the EL spectra are normalized to the peak intensity of each spectrum.

To study the potential dependence of the EL spectra, only data 10 msec after the pulses were applied were obtained for four GaAs samples, since there was no spectral change during the potential pulse. Typical EL spectra are shown in Fig. 5(a). Normalized spectra are shown in Fig. 5(b). No potential effect on EL spectra was observed in any of the four samples.

The relation of carrier concentration on the EL spectra was also studied. Since no time or potential depen-

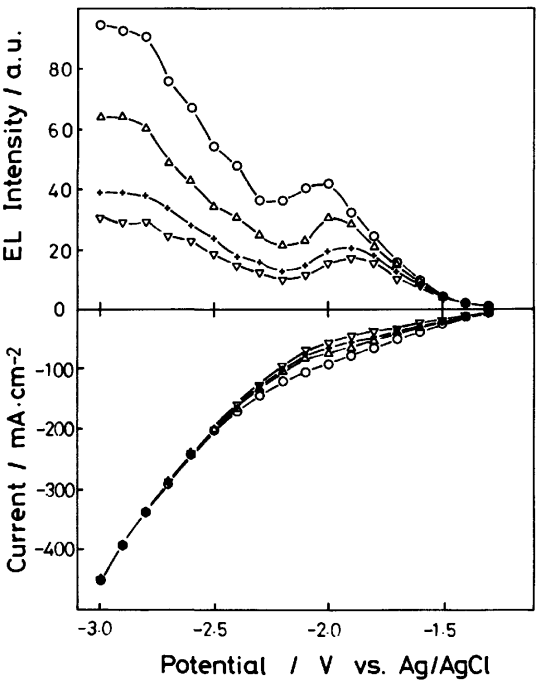

Fig. 3. Pulsed potential dependence of EL intensity and current at 50 (○), 100 (△), 200 (+), and 295 (▽) msec after potential was stepped from −1.0 V. Other experimental conditions are as same as those of Fig. 2.

dencies were observed, only the normalized EL spectra obtained 10 msec after the potential was pulsed from −0.5 V to −3.5 V are shown in Fig. 6. For higher carrier concentrations, the peak energy increased and the FWHM of the EL spectra became larger. It was rather difficult to study the effect of carrier concentration on EL intensity quantitatively because the surface area of the electrodes and the alignment varied from experiment to experiment. The effect of a dopant on spectral shape was negligible, as far as a comparison between Si and Te was concerned.

Although Pettinger *et al.* reported that sub-band emission is much stronger than band-edge emission for *n*-GaAs,[27] we observed only small, if any, sub-band emission. Because of the poor sensitivity of the PMT employed in this study at wavelengths longer than 1000 nm, it is not possible to quantitatively compare the intensity of the band-edge emission to that of the sub-band emission.

Discussion

It is well known that the EL of *n*-type semiconductors in solutions containing $S_2O_8^{2-}$ is predominanly caused by the following reactions[6]

$$S_2O_8^{2-} + e_c^- \longrightarrow SO_4^{\cdot-} + SO_4^{2-}, \quad (1)$$

$$SO_4^{\cdot-} \longrightarrow SO_4^{2-} + p_v^+. \quad (2)$$

Thus, $S_2O_8^{2-}$ is first reduced by electrons of the conduction band, e_c^-, producing $SO_4^{\cdot-}$ which is a strong oxidant to be able to inject holes into the valence band of semiconductors, p_v^+. A part of p_v^+ recombine radiatively

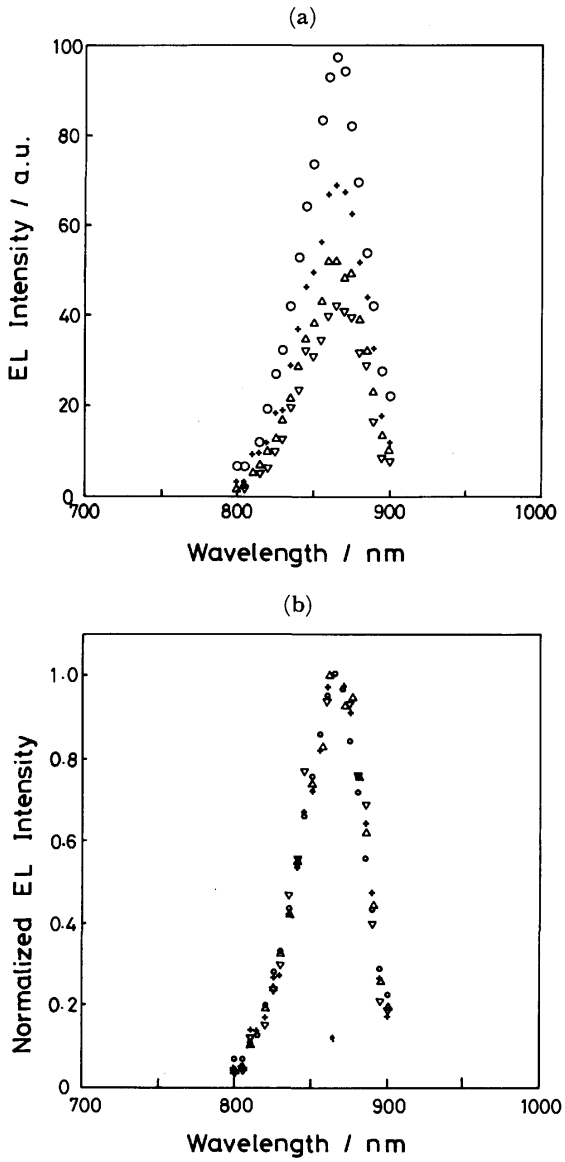

Fig. 4. EL spectra (a) and normalized EL spectra (b) of *n*-GaAs (Te doped, 0.96×10^{18} cm^{-3}) in a solution containing 5 M NaOH and 0.15 M $K_2S_2O_8$ at 10 (○), 30 (+), 50 (△), and 70 (▽) msec after potential was pulsed from −0.5 V to −3.65 V.

with e_c^- either directly or *via* intermediate levels such as surface states, lattice defects or impurity states. The former process generates edge emission and the latter sub-band emission. As mentioned before, the energy of the major peak in the EL spectra of GaAs in this study coincides with the energy gap of GaAs, suggesting that the band-to-band transition is the dominant process in the generation of EL.

The transient behaviors of the EL of *n*-ZnO and of ZnS were studied by Yamase and Gerischer[5] and by Fan *et al.*[7], respectively, but that of *n*-GaAs is not available. The potential dependence of the transient behavior of EL and current is more clearly seen by studying the transient behavior of EL efficiency, which is the ratio of the EL intensity to current, as shown in Fig. 7. The S/N ratio at relatively positive potentials was low because of

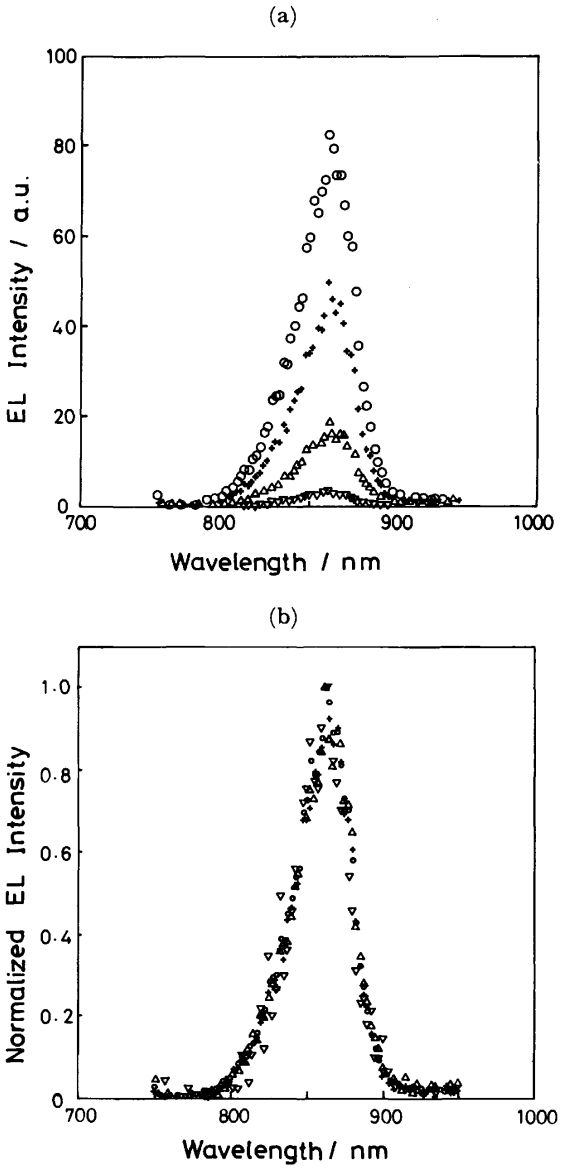

Fig. 5. EL spectra (a) and normalized EL spectra (b) of n-GaAs (Si doped, 0.84×10^{18} cm^{-3}) in a solution containing 5 M NaOH and 0.15 M $K_2S_2O_8$ at 10 msec after potential was pulsed from -0.5 V to -2.5 V (∇), -3.0 ($\triangle$), -3.5 (+), and -4.0 (O) V.

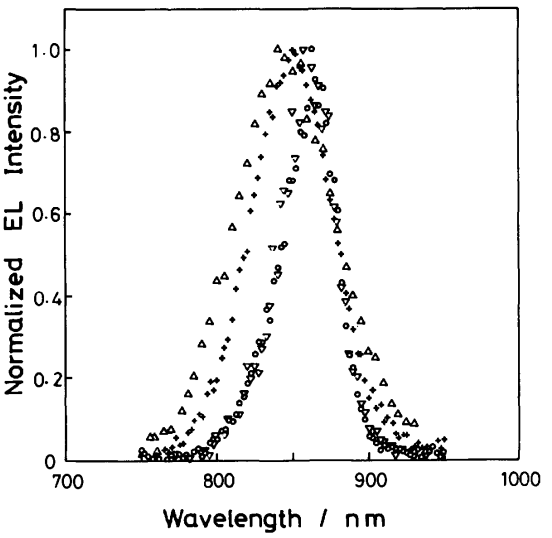

Fig. 6. Normalized EL spectra of n-GaAs in a solution containing 5 M NaOH and 0.15 M $K_2S_2O_8$ at 10 msec after potential was pulsed from -0.5 V to -3.5 V. O: Si doped; 0.84×10^{18} cm^{-3}, +: Si doped; 2.6×10^{18} cm^{-3}, $\triangle$: Si doped; $4.2-8.0\times10^{18}$ cm^{-3}, ∇: Te doped; 0.96×10^{18} cm^{-3}.

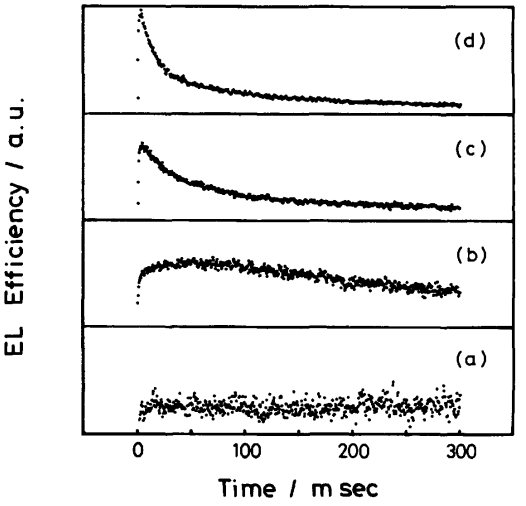

Fig. 7. Transient behavior of EL efficiency calculated from the data in Fig. 2.

the small values of EL intensity and current. It is, however, clear that while the efficiency was almost constant at -1.5 V, it gradually increased and then decreased with time at -2.0 V. A similar trend was observed at more negative potentials but the time to reach the maximum intensity was smaller at more negative potentials. The EL efficiency-potential relations for different time domains are shown in Fig. 8. There is a clear maximum in each relation around -2.2 V. Similar results were reported for n-GaAs in solutions containing several hole-injecting species,[30] for n-InP in dilute nitric acid[10] and for ZnO in a solution containing $S_2O_8^{2-}$.[5] Two reasons should be considered. One is the depletion of $S_2O_8^{2-}$ near the electrode surface and the other is a change in surface characteristics. At the beginning of the potential pulse, no $SO_4^{\cdot-}$ exists and, therefore, no EL is observed. $SO_4^{\cdot-}$ is generated by the reaction (1) and the EL intensity increases. However, $S_2O_8^{2-}$ is depleted at the surface and eventually $SO_4^{\cdot-}$ also decreases. Thus, the EL intensity decreases. This can be formulated, semiquantitatively, by assuming that the surface concentration of $S_2O_8^{2-}$ is zero during the potential pulse, *i.e.*, the rate of reaction (1) is controlled by diffusion of $S_2O_8^{2-}$, and EL intensity is proportional to $SO_4^{\cdot-}$ concentration. The surface concentration of $SO_4^{\cdot-}$, c_s, is given by solving

$$\frac{dc_s}{dt} = \frac{\sqrt{D}c^*}{\sqrt{\pi t}} - k_1 c_s, \tag{3}$$

where D and c^* are the diffusion coefficient and bulk concentration of $S_2O_8^{2-}$, respectively, k_1 is the rate constant for reaction (2) and t is the time after potential is

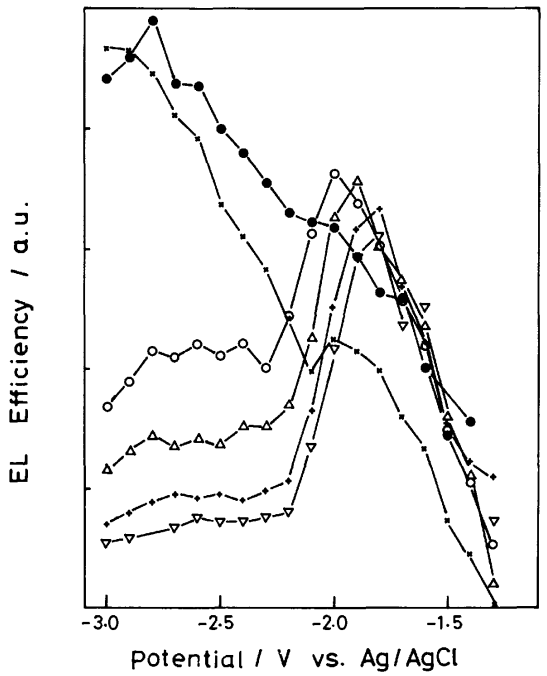

Fig. 8. Pulsed potential dependence of EL efficiency at 1 (▲), 10 (×), 50 (○), 100 (△), 200 (+), and 295 (▽) msec after potential was stepped from −1.0 V. Other experimental conditions are as same as those of Fig. 2.

pulsed. The EL intensity, I_{EL}, is given by

$$I_{EL} = \eta k_1 c_s, \tag{4}$$

where η is the EL efficiency. η should be determined by surface characteristics. To see if this simple model could explain the EL-t relations, Eq. 3 was solved using a digital-simulation technique. Figure 9(a) shows k_1c_s, which is proportional to I_{EL} if η is assumed to be constant, and $\frac{\sqrt{D}c^*}{\sqrt{\pi t}}+k_1c_s$, which is proportional to the current due to reduction of both $S_2O_8^{2-}$ and $SO_4^{\cdot-}$, against time for several values of k_1. The time dependence of the relative EL efficiency, *i.e.*, $k_1c_s/(\frac{\sqrt{D}c^*}{\sqrt{\pi t}}+k_1c_s)$, is shown in Fig. 9(b). The results in Fig. 9 prove that EL-i-t and EL efficiency-t relations can be explained by just considering a simple concentration profile change as a function of time. Of course, a hydrogen evolution reaction becomes a dominant process when $S_2O_8^{2-}$ is depleted, particularly at relatively negative potentials and its contribution to the EL efficiency should be taken into account in a more thorough examination.

Although the time dependence of the EL can be explained by just considering the depletion of $S_2O_8^{2-}$ (as shown above), the potential dependence of EL intensity and EL efficiency needs other explanations. When the potential was made more negative, band bending and the concentration of electrons in the conduction band near the surface became greater. Since the radiation recombination of electrons in the conduction band and holes in the valence band is more effective at a higher concentration of electrons in the conduction band and holes in the valence band,[21] the EL efficiency should be higher at more negative potentials. The EL-V and EL efficiency-V relations show that this is not so. Around −2.0 V, the EL starts to decrease after applying a more negative potential.

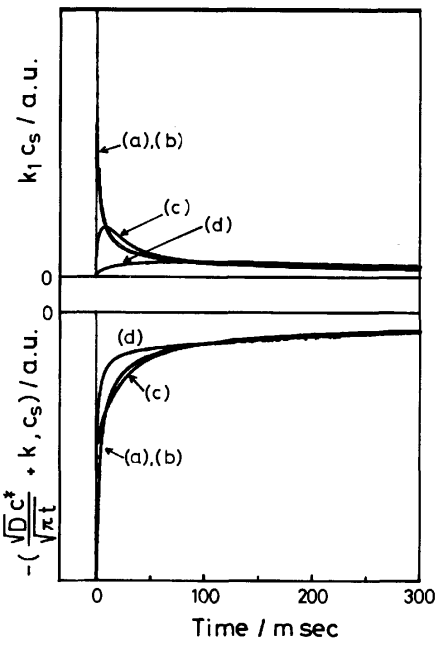

Fig. 9(a). Time dependence of $\left(-\frac{\sqrt{D}c^*}{\sqrt{\pi t}}+k_1c_s\right)$ which is propotional to current and k_1c_s which is propotional to EL intensity.
$D=10^{-5}$ cm^2 s^{-1}. $c^*=10^{-3}$ M. $k_1=10000$ s^{-1} (a), 1000 s^{-1} (b), 100 s^{-1} (c), and 10 s^{-1} (d).

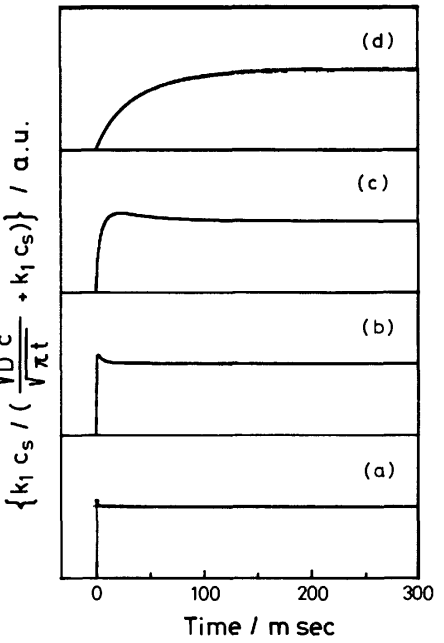

Fig. 9(b). Time dependence of $\left\{k_1c_s/\left(\frac{\sqrt{D}c^*}{\sqrt{\pi t}}+k_1c_s\right)\right\}$ which is propotional to EL efficiency. Parameters for the calulation are as same as those of Fig. 9(a).

Decker *et al.* proposed that a compositional change in the semiconductor surface, which was suggested for GaAs by Gerischer and Mattes,[33] causes the EL quenching for GaAs in solutions containing various redox agents.[30] Thus, the present GaAs was also covered with an oxide layer at −1.0 V and the potential pulse to −2.1—−2.2 V introduced unsaturated surface states (dangling bonds) which acted as recombination centers and reduced radiation recombination. Thus, η in Eq. 4 first increases with a more negative polarization due to a larger band bending while the surface characteristics remain constant. However, η starts to decrease beyond *ca.* −2.0 V because of the introduction of the recombination centers. When the potential is pulsed in this region, a change in the surface composition is initiated. Since composition change needs some time, EL intensity (efficiency) is high even at this potential region just after the pulse is applied. When the potential becomes much more negative (*e.g.* −2.3 V), the surface states are restabilized by hydride formation and η, *i.e.*, EL intensity, again increases, although the EL efficiency measured later than 50 msec after the potential pulse is applied does not increase even at these potentials, because the hydrogen evolution reaction becomes dominant.

Although Bard *et al.* reported that the EL spectral shape of ZnS was affected by current (*i.e.*, potential) and time,[7] no such effect was observed in our experiment. This difference is reasonably understood since only the potential dependence on the band-edge emission spectra was investigated in the present study, while the EL observed at ZnS was the sub-band emission. There could be some effect in the sub-band emission region even in the present arrangement, but it was not detected clearly enough to be analysed.

The carrier concentration dependence of the cathode- and photo-luminescent spectra of GaAs have been measured using p/n and Schottky junctions, but no report on EL in a solution is available. The results in Fig. 6, *i.e.*, a blue shift of the peak energy and a widening of the peak at highly doped GaAs, are, however, in good agreement with the results reported for solid-state luminescence[22] and can be explained by the filling of the conduction band sates by electrons (Burnstein-Moss shift).[34] These results again confirm that the EL spectra obtained are due to band-edge emission and suggest that the EL study at a semiconductor/solution interface conveniently provides information on band-edge energy.

The present work was partialy supported by a Grant-in-Aid for Scientific Research, Ministry of Education, Science and Culture. We gratefully acknowledge stimulating discussions with Prof. A. B. Ellis and Dr. W. S. Hobson of the University of Wisconsin at Medison where the preliminary part of this work was carried out by one of us (K.U.) supported by the Japan/U.S. Cooperative Program on Solar Energy Conversion by Photosynthesis. We are also grateful to Prof. A. B. Ellis and Dr. W. S. Hobson for donating several semiconductors.

References

1) H. Gobrecht, M. Schaldach, F. Hein, and W. Paatsch, *Electrochim. Acta*, **13**, 1279 (1968).
2) R. Memming and G. Schwandt, *Electrochim. Acta*, **13**, 1299 (1968).
3) K. H. Beckmann and R. Memming, *J. Electrochem. Soc.*, **116**, 368 (1968).
4) B. Pettinger, H. R. Schöppel, T. Yokoyama, and H. Gerischer, *Ber. Bunsenges. Phys. Chem.*, **78**, 1024 (1974).
5) T. Yamase and H. Gerischer, *Ber Bunsenges. Phys. Chem.*, **87**, 349 (1983).
6) R. W. Noufi, P. A. Kohl. S. N. Frank, and A. J. Bard, *J. Electrochem. Soc.*, **125**, 246 (1978).
7) F.-R. Fan, P. Leempoel, and A. J. Bard, *J. Electrochem. Soc.*, **130**, 1866 (1983).
8) H. H. Streckert, B. R. Karas, D. J. Morano, and A. B. Ellis, *J. Phys. Chem.*, **84**, 3232 (1980).
9) H. H. Streckert, J. Tong, and A. B. Ellis, *J. Amer. Chem. Soc.*, **104**, 581 (1982).
10) E. Aharon-Shalon and A. Heller, *J. Phys. Chem.*, **87**, 4913 (1983)
11) B. R. Karas, D. J. Morano, D. K. Bilich, and A. B. Ellis, *J. Electrochem. Soc.*, **127**, 1144 (1980).
12) H. H. Streckert, J. Tong, M. K. Carpenter, and A. B. Ellis, *J. Electrochem. Soc.*, **129**, 772 (1982).
13) A. Fujishima, Y. Maeda, S. Suzuki, and K. Honda, *Chem. Lett.*, **1982**, 179.
14) Y. Nakato, A. Tsumura, and H. Tsubomura, *Chem. Phys. Lett.*, **85**, 387 (1982).
15) Y. Nakato, A. Tsumura, and H. Tsubomura, *J. Phys. Chem.*, **87**, 2402 (1983).
16) H. Morisaki and K. Yazawa, *Appl. Phys. Lett.*, **33**, 1013 (1979).
17) H. Morisaki, H. Kitada, and K. Yazawa, *Jpn. J. Appl. Phys.*, **19**, 679 (1980).
18) M. A. Butler and D. S. Ginley, *Appl. Phys. Lett.*, **36**, 845 (1980).
19) E. W. Williams, *Phys. Rev.*, **168**, 922 (1968).
20) U. Langmann, *Applied Phys.*, **1**, 219 (1973).
21) H. C. Casey, Jr. and R. Z. Bachrach, *J. Appl. Phys.*, **44**, 2795 (1973).
22) H. C. Casey, Jr. and R. H. Kaiser, *J. Electrochem. Soc.*, **114**, 149 (1967).
23) J. C. Sarace, R. H. Kaiser, J. M. Whelan, and R. C. C. Leite, *Phys. Rev.*, **137**, A623 (1965).
24) P. D. Southgate, *J. Phys. Chem. Solids*, **31**, 55 (1970).
25) A. Bahraman and W. G. Oldham, *Solid State Electronic*, **15**, 907 (1972).
26) W. S. Hobson and A. B. Ellis, *J. Appl. Phys.*, **54**, 5956 (1983).
27) B. Pettinger, H. R. Schöppel, and H. Gerischer, *Ber. Bunsenges. Phys. Chem.*, **80**, 849 (1976).
28) D. J. Benard and P. Handler, *Surf. Sci.*, **40**, 141 (1973).
29) H. Gerischer, N. Müller, and O. Haas, *J. Electroanal. Chem.*, **119**, 41 (1981).
30) F. Decker, B. Pettinger, and H. Gerischer, *J. Electrochem. Soc.*, **130**, 1336 (1983).
31) K. Uosaki and H. Kita, *J. Electrochem. Soc.*, **128**, 2153 (1981).
32) J. S. Blakemore, *J. Appl. Phys.*, **53**, R123 (1982).
33) H. Gerischer and I. Mattes, *Z. Phys. Chem. N. F.*, **49**, 112 (1966).
34) S. Bendapudi and D. N. Bose, *Appl. Phys. Lett.*, **42**, 287 (1983).

 © 1984 The Chemical Society of Japan Bull. Chem. Soc. Jpn., 57, 3253—3257 (1984)

Enhanced Circular Dichroism and Phase Separation of Azobenzene-Containing Chiral Bilayer[1)]

Naotoshi NAKASHIMA, Kozo MORIMITSU, and Toyoki KUNITAKE*
Department of Organic Synthesis, Faculty of Engineering, Kyushu University, Fukuoka 812
(Received May 30, 1984)

An azobenzene-containing chiral amphiphile showed a drastic enhancement of circular dichroism (CD) due to formation of the rigid bilayer assembly. The drastic CD change was caused by phase transition of the matrix bilayer in the case of mixed bilayers with dihexadecyldimethylammonium bromide, but was caused by phase transition of the chiral component in the case of the single component bilayer. Both CD and absorption spectra of the azobenzene-containing chiral bilayer were used for detecting phase separation of mixed membranes. It was pointed out that the CD technique is widely applicable to phase separation studies.

We have shown that synthetic amphiphiles undergo spontaneous formation of bilayers in water.[2,3)] Double-chain ammonium salts are typical examples. In these cases, introduction of the amino acid residue often gives rise to well-developed bilayer assemblies.[4—6)] The amino acid-derived chiral bilayer was found to display very peculiar circular dichroism when the aromatic chromophore was present.[7)] The same is true with bilayers of single-chain amphiphiles, as briefly described.[8)]

Phase separation is one of the most fundamental characteristics of bilayers. The bilayer of the biomembrane is composed of various lipid constituents and their distribution plays critical roles in the control of the physiological function. Detection of the phase separation in the biomembrane has been conducted by calorimetry,[9,10)] the spin probe technique,[11,12)] freeze-fracture electron microscopy,[13)] and recently, by neutron small-angle scattering.[14,15)] In the synthetic system, the spectral shift of the azobenzene chromophore was shown to be especially useful for its detection,[16)] and this technique has been applied to examinations of the interaction of the surface receptor[17)] and of the cluster formation of the reacting species in the catalytic hydrolysis.[18)] The excimer formation of the benzene chromophore was also useful for this purpose.[19)]

In the present paper, we wish to demonstrate that circular dichroism is a convenient technique for studying phase separation. The large CD enhancement of the chiral bilayer arises from the interaction of spatially fixed chromophores in the gel state and is not observed for fluid (non-interacting) chiral components.[7,8)] Therefore, the CD enhancement can be associated with the cluster formation (in the rigid bilayer matrix). The probe amphiphile used in this study is C_6-L-Ala-Azo-$C_{10}N^+$, and the matrix membrane is $2C_{16}N^+2C_1$. Since this bilayer-forming amphiphile is chiral and contains the azobenzene chromophore, both of CD and absorption spectra are used for detecting phase separation. A comparison of the two spectral methods is discussed.

Experimental

Materials. *p*-(*p*-Hydroxyphenylazo)benzoic acid was prepared by the procedure of Cohen and McGilbery,[20)] mp 246→264 °C (dec) (The arrow indicate the liquid-crystalline range), lit,[20)] mp 268 °C.

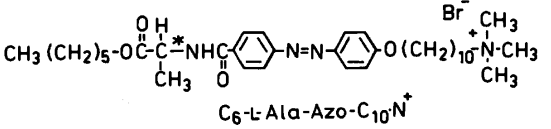

C_6-L-Ala-Azo-$C_{10}N^+$

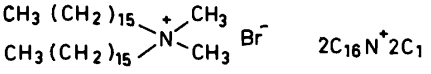

$2C_{16}N^+2C_1$

The benzoic acid was allowed to react with 1,10-dibromodecane to give *p*-[*p*-(10-bromodecyloxy)phenylazo]-benzoic acid in 54% yield after recrystallization from acetic acid/ethyl acetate, mp 195→225 °C. The Williamson product (1 g, 2.2 mmol) and 0.5 g of Na_2CO_3 were added to 10 cm^3 of $SOCl_2$. After the mixture was refluxed for 2 h, excess $SOCl_2$ was removed, and the red-brown residue was condensed with 0.7 g (2.2 mmol) of hexyl-L-alaninate *p*-toluenesulfonate in dry tetrahydrofuran(THF) to give 0.4 g (30% yield) of hexyl *N*-[*p*-[*p*-(10-bromodecyloxy)phenylazo]-benzoyl] alaninate, mp 100—103 °C. Quaternization of this product with trimethylamine in THF produced C_6-L-Ala-Azo-$C_{10}N^+$ in 46% yield, mp room temp→117 °C. The final product was identified by IR and NMR spectroscopies and by elemental analyses. Found: C, 61.2; H, 8.30; N, 8.00%. Calcd for $C_{35}H_{55}N_4O_4Br \cdot H_2O$: C, 61.39; H, 8.24; N, 8.18%.

Preparation of $2C_{16}N^+2C_1$ was described elsewhere.[21,22)]

Measurement. Electron microscopy was performed with a Hitachi H-500 instrument as described before.[2,3)] Differential scanning calorimetry(DSC) was carried out for 20-mmol·dm^{-3} samples with a Daini-Seikosha SSC/560 instrument. The temperature was raised from 0 °C at a rate of 2 °C/min. The details have been described.[22)]

For spectral measurements of single-component bilayers, 5—10 mg of C_6-L-Ala-Azo-$C_{10}N^+$ were dissolved in $CHCl_3$, thin films of the amphiphile obtained by solvent removal were added with distilled water, and the mixture was sonicated for 30 s (Bransonic Cell Disruptor 185) to obtain clear dispersions (5×10^{-4} M, 1 M=1 mol dm^{-3}) and used for spectral measurements after aging for 30 min in ice water.

Aqueous samples of mixed bilayers were similarly prepared from C_6-L-Ala-Azo-$C_{10}N^+$ (5.0×10^{-4} M) and $2C_{16}N^+2C_1$ (5.0×10^{-3} M). The solutions were aged for 10 min at 60 °C and spectral measurements were made after slowly cooling to given temperatures and aging for 20 min. The spectral measurement was subsequently done in the heating process in similar manners.

The absorption and circular dichroism spectra were obtained on a Hitachi 220A spectrophotometer and a JASCO J-40AS spectropolarimeter, respectively. They were equipped with cell holders. The path length of the cell was 1 mm.

Results and Discussion

Electron Microscopy and DSC Study. We have shown that many azobenzene-containing, single-chain amphiphiles form bilayer aggregates.[23] Figure 1 is an electron micrograph of aqueous bilayer of C_6-L-Ala-Azo-$C_{10}N^+$. It is clear that the layered aggregate is formed. The DSC measurement indicates that the aqueous bilayer possess the crystal-to-liquid crystal phase transition at 57 °C (transition range, 40—65 °C) with the enthalpy change of 19.2 kJ/mol.

Absorption and CD Spectra. The absorption spectrum of C_6-L-Ala-Azo-$C_{10}N^+$ possesses maxima at 358 and 234 nm in ethanol and at 359 and 238 nm in the aqueous hexadecyltrimethylammonium bromide (CTAB, 10 mM) micelle, and does not vary with temperature. In contrast, small temperature dependence was found for the aqueous bilayer: λ_{max} are located at 351 and 252 nm at low temperatures and absorption intensities decrease upon raising temperature (Fig. 2a). These reversible spectral changes are apparently related to the phase transition of the bilayer.

The CD spectrum of the amphiphile has the following characteristics: $[\theta]_{355}=+2{,}000$ (maximum) in ethanol, and $[\theta]_{360}=+3{,}000$ (maximum) in CTAB micelle. It is enormously intensified in water as shown in Fig. 2b. At low temperatures, $[\theta]$ is 5.0×10^5 deg·cm^2 dmol^{-1} at 365 nm (maximum) and is -2.9×10^5 at 332 nm (minimum). The spectral intensity decreases drastically at high temperatures (50—70 °C) with sign reversal: $[\theta]_{366}=-1.0\times10^4$ and $[\theta]_{330}=+8.0\times10^3$. The CD enhancement due to temperature reaches fifty fold in magnitude.

The absorption near 350 nm is associated with the transition moment along the long axis of the azobenzene moiety.[24] Therefore, the shape of the low-temperature CD spectrum in this region is indicative of strong exciton coupling among the electric transition moments.[25] The 250-nm absorption corresponds to the transition moment along the short axis of azobenzene. The CD enhancement in this region is smaller by an order of magnitude compared with that in the 350-nm region: $[\theta]_{267}=-50{,}000$ and $[\theta]_{250}=-18{,}000$. However, these values are still greater than those in ethanol (no bilayer formed) or those at high temperatures. The exciton coupling is also apparent.

Figure 3 is obtained by plotting $[\theta]_{365}$ against temperature. The $[\theta]_{365}$ value remains constant at 10—35 °C and drastically decreases at 45—50 °C. As mentioned in the previous section (DSC data), the phase transition of the C_6-L-Ala-Azo-$C_{10}N^+$ bilayer starts at 45 °C and the DSC peak is located at 57 °C. Therefore, the CD enhancement is lost almost completely at the temperature region where the chain melting starts. Virtually the same change is observed in the heating cycle, and hysteresis is essentially absent. It must be noted, however, that the CD in-

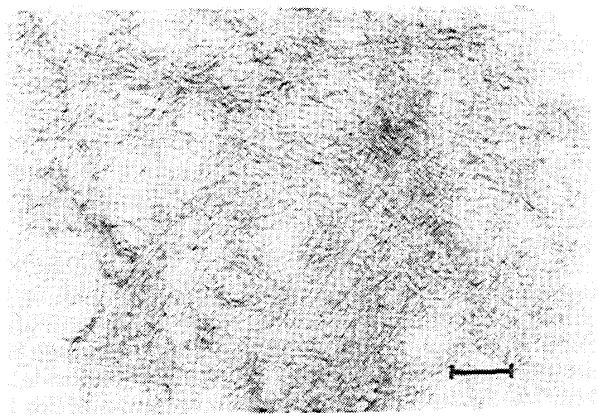

Fig. 1. Electron micrograph of C_6-L-Ala-Azo-$C_{10}N^+$ stained by uranyl acetate, 10 mM; initial magnification, × 40,000, scale bar indicates, 1000 Å.

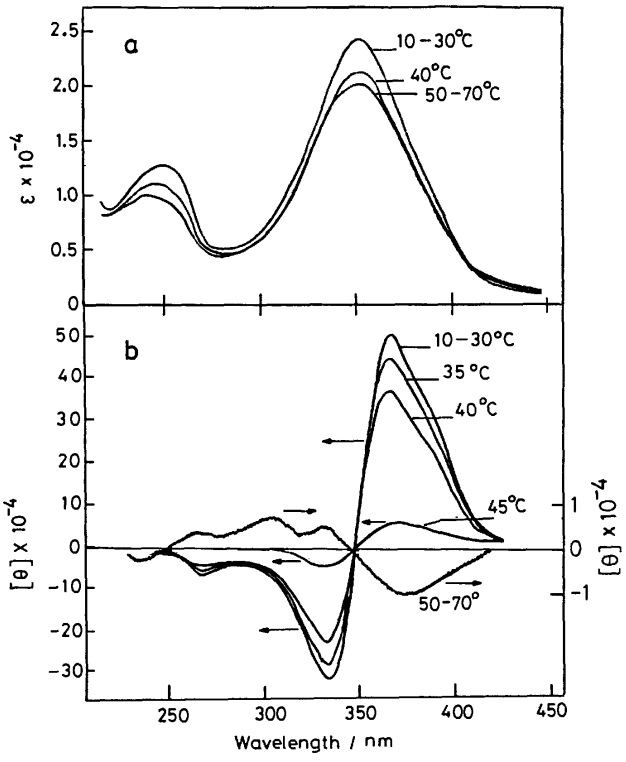

Fig. 2. Temperature dependence of absorption (a) and CD (b) spectra. C_6-L-Ala-Azo-$C_{10}N^+$, 5×10^{-4} M, heating cycle.

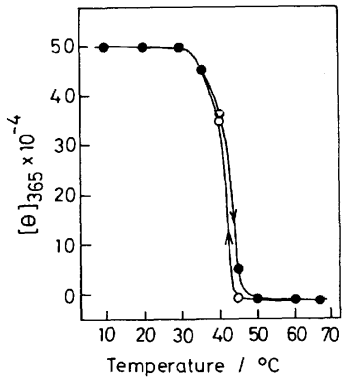

Fig. 3. Temperature dependence of CD intensity. ○: cooling cycle, ●: heating cycle C_6-L-Ala-Azo-$C_{10}N^+$, 5×10^{-4} M.

tensity of the liquid-crystalline bilayer is larger than that of the isolated molecule in ethanol or in CTAB micelle.

These results (exciton coupling and temperature dependence) are essentially the same as those described briefly for bilayers of a biphenyl-containing single-chain amphiphile (C_{12}–Bph–L-Ala–C_2N^+)[8] and a benzene-containing double-chain amphiphile ($2C_{12}$–L-Glu–ph–C_4N^+).[7]

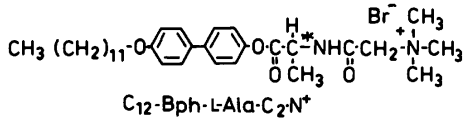

C_{12}-Bph-L-Ala-C_2N^+

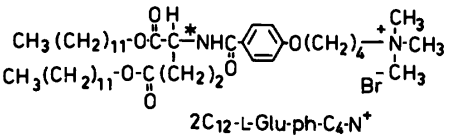

$2C_{12}$-L-Glu-ph-C_4N^+

Spectral Changes of Mixed Bilayer. Table 1 summarizes the $[\theta]_{365}$ values of mixed bilayers of C_6–L-Ala–Azo–$C_{10}N^+$ and $2C_{16}N^+2C_1$ at 10 °C. The $[\theta]_{365}$ value decreases with decreasing molar ratios of the chiral component. The CD enhancement is observed, when the molar ratio is not smaller than 1/10.

The enhancement is totally lost with the molar ratios of less than 1/20. As discussed above, the CD enhancement is produced by the exciton coupling of the fixed azobenzene chromophores. Therefore, the CD enhancement in the two-component bilayer indicates the presence of the cluster of the chiral amphiphile. The data of Table 1 suggest that the cluster is only partially formed at the molar ratio of 1/10, and this molar ratio was used in the subsequent experiments.

Table 1. Influence of the composition of a mixed bilayer on CD intensity[a]

$[C_6$–L-Ala–Azo–$C_{10}N^+]/[2C_{16}N^+2C_1]$	$[\theta]_{365}\times10^{-4}$
chiral component only	50
1/2	40
1/5	21
1/10	14
1/20	*ca.* 0.1
1/30	*ca.* 0.1

a) $[C_6$–L-Ala–Azo–$C_{10}N^+]=5\times10^{-4}$ M (constant), 10 °C

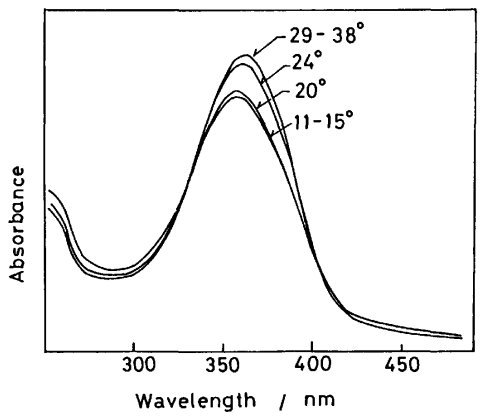

Fig. 4. Temperature dependence of absorption spectra of mixed bilayers. C_6–L-Ala–Azo–$C_{10}N^+$, 5×10^{-4} M, $2C_{16}N^+2C_1$, 5×10^{-3} M, cooling process.

A mixed (1:10) bilayer of C_6–L-Ala–Azo–$C_{10}N^+$ and $2C_{16}N^+2C_1$ was subjected to aging at 60 °C, and absorption and CD spectra were measured in the cooling and, subsequently, heating processes. The absorption spectra in the cooling process are displayed in Fig. 4. Although the overall spectral change is not remarkable, its temperature dependence is more clearly seen in Fig. 5 by plotting the maximum absorbance (A_{max}) and the location of λ_{max} against temperature. Both of A_{max} and λ_{max} change critically at 20—25 °C. Virtually the same temperature dependence was observed in the heating process. The CD spectral shape of the mixed bilayer is the same as those illustrated in Fig. 2b, however, its temperature dependence is different. In the cooling process, the enhanced CD is not observed from 60 °C to 26 °C, and the enhancement starts at *ca.* 22 °C. The temperature dependence of $[\theta]_{365}$ of the mixed bilayer in this process is illustrated in Fig. 6, together with that in the heating process (from 10 °C). The $[\theta]_{365}$ value drastically changes at *ca.* 25 °C in both processes, and this critical temperature agrees with those in absorption spectra (Fig. 5). The hysteresis is small in this system as well.

The 1:10 mixed bilayer gives an DSC peak at 28 °C. This T_c value is almost identical with that of the single-component bilayer of $2C_{16}N^+2C_1$.[22] The DSC peak corresponding to the bilayer of C_6–L-Ala–Azo–$C_{10}N^+$ (57 °C) was not detected. Apparently the two components exist as separate clusters in the rigid bilayer matrix of $2C_{16}N^+2C_1$, but the chiral component cannot form separate domains in the fluid $2C_{16}N^+2C_1$ matrix.

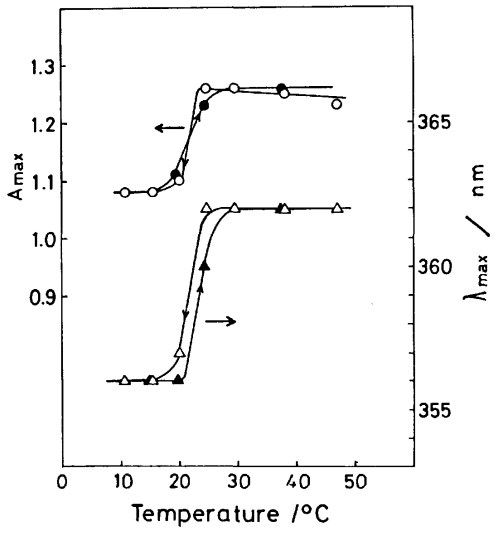

Fig. 5. Plots of A_{max} and λ_{max} against temperatures. C_6–L-Ala–Azo–$C_{10}N^+$, 5×10^{-4} M, $2C_{16}N^+2C_1$, 5×10^{-3} M, ○: cooling process, ●: heating process.

Phase Separation and CD Enhancement. The DSC behavior of the mixed bilayer is consistent with the spectral data. The CD enhancement is not observed at 30—40 °C where DSC data suggest dispersion of C_6-L-Ala-Azo-$C_{10}N^+$ molecules in the fluid $2C_{16}N^+2C_1$ bilayer. The bilayer cluster of the chiral amphiphile would have produced enhanced CD at these temperatures (see Fig. 2b). The phase separation occurs at 22—26 °C where the $2C_{16}N^+2C_1$ bilayer undergoes the liquid crystal-to-crystal phase transition. The domain of the C_6-L-Ala-Azo-$C_{10}N^+$ bilayer is in the crystalline state at these temperatures, and therefore, enhanced CD results. It is noteworthy that the drastic CD change is caused by *phase transition of the matrix bilayer* in the case of the mixed bilayer, but that it is caused by *phase transition of the chiral component* in the single-component bilayer system. It is possible, therefore that mixed bilayers are selected in such a way that large CD changes occur at desired temperatures. These situations are illustrated schematically in Fig. 7.

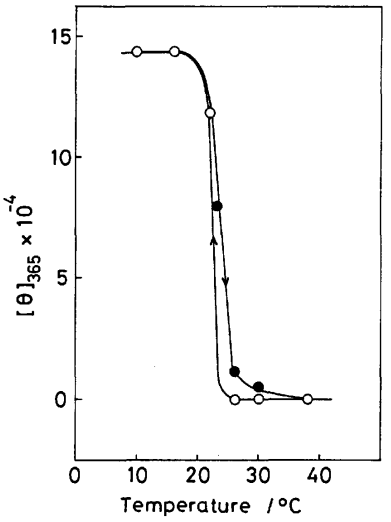

Fig. 6. Temperature dependence of $[\theta]_{365}$ of the mixed bilayer.
C_6-L-Ala-Azo-$C_{10}N^+$, 5×10^{-4} M, $2C_{16}N^+2C_1$, 5×10^{-3} M, ○: cooling process, ●: heating process.

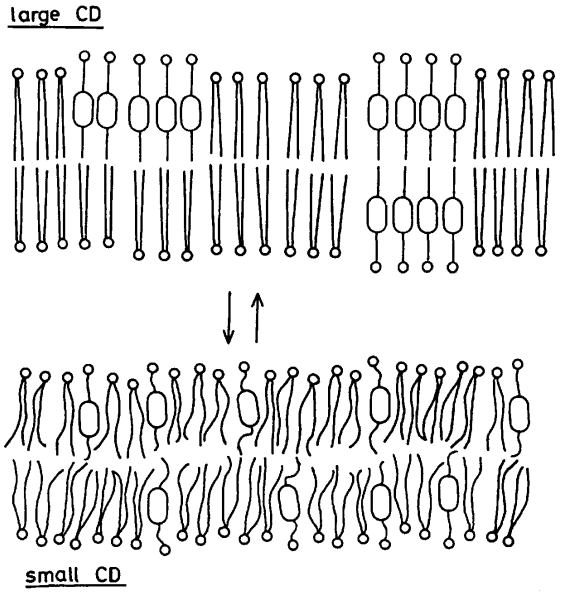

Fig. 7. Schematic illustration of the phase separation.

It was reported from these laboratories that azobenzene-containing bilayers give rise to varied spectral characteristics depending on membrane physical states and chemical structures of the component.[23] For instance, C_{12}-Azo-$C_{10}N^+$ possesses λ_{max} at 330 nm as bilayer clusters and λ_{max} at 355 nm as an isolated chromophore. This spectral shift has been used to detect phase separation. The azobenzene amphiphile used in this study unfortunately displays only a very small difference in absorption spectra, which is not sensitive enough to probe phase separation. Instead, much enhanced CD spectra of the rigid chiral bilayer are a powerful tool for phase separation studies.

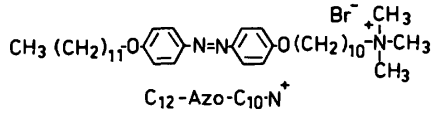

C_{12}-Azo-$C_{10}N^+$

Conclusion

An azobenzene-containing, chiral amphiphile exhibited remarkable CD enhancements due to formation of rigid bilayers. This phenomenon was used to study the phase separation behavior in mixed bilayers. Phase separation of synthetic bilayers has been examined by the DSC technique,[18,19] absorption spectroscopy,[16] and excimer formation.[19] The CD technique becomes the fourth methods. The present CD results are consistent with those of the absorption spectrum of the azobenzene chromophore in that phase separation is induced by the liquid crystal-to-crystal phase transition of the matrix bilayer. The spectral shift of chromophores is usually not large enough to made detection of phase separation possible. In contrast, the CD enhancement is observed for many chiral bilayers which possess aromatic chromophores. This indicates that the CD technique is widely applicable to phase separation studies.

We are grateful to Professor K. Yamafuji for the use of a spectropolarimeter.

References

1) Contribution No. 733 from Department of Organic Synthesis.
2) T. Kunitake and Y. Okahata, *J. Am. Chem. Soc.*, **99**, 3860 (1977).
3) T. Kunitake, Y. Okahata, M. Shimomura, S. Yasunami, and K. Takarabe, *J. Am. Chem. Soc.*, **103**, 5401 (1981).
4) T. Kunitake, N. Nakashima, S. Hayashida, and K. Yonemori, *Chem. Lett.*, **1979**, 1413.
5) Y. Murakami, A. Nakano, and K. Fukuya, *J. Am. Chem. Soc.*, **102**, 4253 (1980).

6) Y. Murakami, A. Nakano, and H. Ikeda, *J. Org. Chem.*, **47**, 2137 (1983).
7) T. Kunitake, N. Nakashima, M. Shimomura, Y. Okahata, K. Kano, and T. Ogawa, *J. Am. Chem. Soc.*, **102**, 6642 (1980).
8) T. Kunitake, N. Nakashima, and K. Morimitsu, *Chem. Lett.*, **1980**, 1347.
9) S. Mabrey and J. M. Sturtevant, *Proc. Natl. Acad. Sci. U.S. A.*, **73**, 3862 (1976).
10) D. Chapman, J. Urbina, and K. M. Keough, *J. Biol. Chem.*, **249**, 2512 (1974).
11) E. J. Shimshick and H. M. McConnell, *Biochem.*, **12**, 2351 (1973).
12) T. Ito and S. Ohnishi, *Biochim. Biophys. Acta.*, **363**, 351 (1974).
13) E. Sackmann, *Ber. Bunsenges. Phy., Chem.*, **82**, 891(1978).
14) W. Knoll, J. Haas, H. B. Stuhrmann, H. H. Fuldner, H. Vogel, and E. Sackmann, *J. Appl. Cryst.*, **14**, 191 (1981).
15) Y. Toyoshima, T. Takeda, K. Akabori, and S. Komura, *Physica*, **120B**, 440 (1983).
16) M. Shimomura and T. Kunitake, *Chem. Lett.*, **1981**, 1001.
17) M. Shimomura and T. Kunitake, *J. Am. Chem. Soc.*, **104**, 1757 (1982).
18) T. Kunitake, H. Ihara, and Y. Okahata, *J. Am. Chem. Soc.*, **105**, 6070 (1983).
19) T. Kunitake, S. Tawaki, and N. Nakashima, *Bull. Chem. Soc. Jpn.*, **56**, 3235 (1983).
20) P. P. Cohen and R. W. McGilvery, *J. Biol. Chem.*, **166**, 261 (1946).
21) T. Kunitake, Y. Okahata, K. Tamaki, F. Kumamaru, and M. Takayanagi, *Chem. Lett.*, **1977**, 387.
22) Y. Okahata, R. Ando, and T. Kunitake, *Ber. Bunsenges. Phys. Chem.*, **85**, 789 (1981).
23) M. Shimomura, R. Ando, and T. Kunitake, *Ber. Bunsenges. Phys. Chem.*, **87**, 1134 (1983).
24) H. Nakahara and K. Fukuda, *J. Colloid Interface Sci.*, **93**, 530 (1983).
25) A. S. Davydov, "Theory of Molecular Excitons," M. Kasha, M. Oppenheimer, Jr., Trans, McGraw Hill, New York, 1962.

The Specific Heat Capacities of D-Glucose and D-Xylose in Water-Ethanol System

Fumio KAWAIZUMI,* Nobuo SASAKI, Yasushi OHTSUKA,
Hiroyasu NOMURA, and Yutaka MIYAHARA
Department of Chemical Engineering, School of Engineering, Nagoya University, Chikusa-ku, Nagoya 464
(Received June 5, 1984)

Using an isoperibol twin calorimeter the specific heat capacities of solutions of D-glucose and D-xylose dissolved in water-ethanol mixtures (10, 20, 30, and 50 wt% of ethanol) have been measured at temperature close to 30 °C and the apparent molar heat capacity of te solutes ϕ_{C_p} has been calculated. Dependence of ϕ_{C_p} upon solute concentration varied markedly with the solvent composition but the variation was similar for both solutes. The infinite dilution values of $\phi_{C_p}^{\circ}$ *i.e.* $C_{p,2}^{\infty}$ are higher for D-glucose than for D-xylose at any compositions of the solvent system. The $C_{p,2}^{\infty}$ decreased first noticeably with the amount of ethanol in the solvent, reaching a minimum value at approximately 20 wt% of ethanol, then it increased. Values of the parameter $\Delta C_{p,2}^{\infty}=C_{p,2}^{\infty}-C_{p,2}^{*}$, where $C_{p,2}^{*}$ is the specific heat capacity of the solute in the solid state, are negative in 10, 20, and 30 wt% of ethanol, while it is positive in 50 wt%. The values of $\Delta C_{p,2}^{\infty}$ have been discussed in its connection with the degree of structuring of the solvents.

To date we have measured the specific heat capacity, C_p, of aqueous solutions of hexose (D-fructose, D-galactose, D-glucose, and D-mannose,[1] pentose (D-xylose, D-arabinose, D-ribose, and L-arabinose),[2] as well as several kinds of commercial samples of dextran[3] which is an anhydroglucose polymer. The solute-solvent interaction between these saccharide molecules and solvent water has been discussed on the basis of the partial molar heat capacity at infinite dilution, $C_{p,2}^{\infty}$, calculated from our experimental results.

As a continuation of the above-mentioned measurements we will describe in this paper the results of determination of the specific heat capacities of solutions of D-glucose and D-xylose in the mixed solvent consisting of water and ethanol (10, 20, 30, and 50 wt% of ethanol).

Addition of ethanol to the aqueous solution of saccharides will result in the precipitation of saccharides. This phenomenon can be considered as a result of removal of hydrated water by the added ethanol. In fact, compressibility measurements[4,5] have shown that in pure water the partial specific compressibility, $\bar{\kappa}_2^{\circ}$, of D-glucose and dextran is negative, showing the hydration of these solutes, but that the $\bar{\kappa}_2^{\circ}$ increases with increasing content of ethanol and it becomes a constant positive value in the solvents containing more than 20 wt% of ethanol. In such solvents water molecules preferentially hydrated to saccharides are completely removed by the action of ethanol, then the values of $\bar{\kappa}_2^{\circ}$ correspond to the compressibility of the solutes themselves. Measurements of specific heat capacity and those of compressibility are complementary in elucidating the solute-solvent interaction. The former results seem to give more direct information on the structural change of solvent caused by the addition of solutes.[1-3]

Experimental

Materials. Commercially available guaranteed grade D-glucose and D-xylose were dried in an electric vacuum oven and used without further purification. The ethanol used for preparation of the mixed solvents was obtained by drying by anhydrous $CaSO_4$ and then distilling the guaranteed pure-grade reagents.

Calibration of the Calorimeter and Measurements. Specific heat capacities of solutions were determined using an isoperibol twin calorimeter of dry-shield type. Details concerning this calorimeter and procedures of measurements have been reported earlier.[1] However, the manipuration has been modified slightly. Preliminary experiment of this work demonstrated that introduction of 100 g each of solution to be examined and a reference liquid into each Dewar vessel does not give a successful result. This is due to the large variation of density with the composition of the water-ethanol mixture. The difference in the volume of two liquids leads immediately to the difference in the surface area not immersed in liquids in the two Dewar vessels. To reduce the relative magnitude of the heat leak through the inner surface of the vessels, we have increased the amount of sample solution and reference liquid in each Dewar vessel to 150 g. Following the

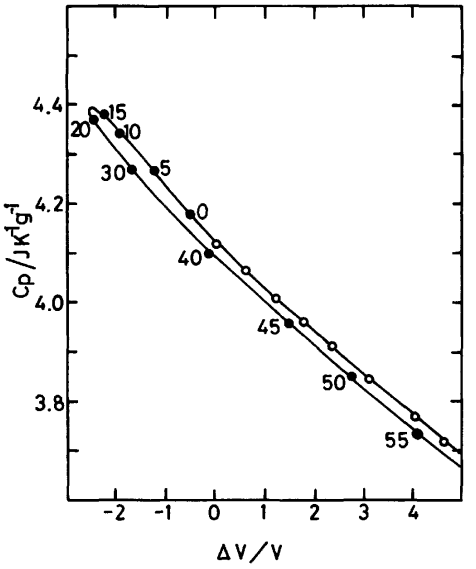

Fig. 1. Calibration curve of the twin calorimeter using 150 g of aqueous solutions of sodium chloride and of ethanol. ΔV is the change of potential of the thermistor bridge during 5 min. ○: sodium chloride, ●: ethanol.
The rotational rate of the stirring system is at 450 min.$^{-1}$ The numeral in the figure refers to the weight per cent of ethanol in the solvent.

procedures described in our early work,[1] we have carried out calibration of the calorimeter using aqueous solutions of ethanol and sodium chloride, whose specific heat capacities are given in the literature.[6] Results of calibration are illustrated schematically in Fig. 1. In principle, the calibration based on the C_p data of aqueous solutions of ethanol and sodium chloride should give an identical curve. This is not the case in Fig. 1. It may be noted here, however, that the calibration using 100 g of sample and reference liquids led to much larger differences between the two sets of calibration than those shown in Fig. 1. Increase of the rotational rate of the stirrer from 450 to 600 min^{-1} resulted in a minor effect on the general features illustrated in Fig. 1.

Dissolution of D-glucose and D-xylose in the solvent system concerned in this work always results in the lowering of the C_p value of the solutions. We, therefore, used the upper curve for the measurements in 10 wt% of ethanol, while the lower calibration curve was adopted for the determination of C_p in 20, 30, and 50 wt% of ethanol. Measurement was not done in 40 wt% of ethanol, for in this mixed solvent the potential difference ΔV to be detected is very small (see, Fig. 1) and desired precision of the measurement could not be attained. On the other hand, measurements in ethanol-rich solvents are also difficult owing to the limited solubility of the solutes D-glucose and D-xylose.

Measurements of C_p have been done at six to eight different concentrations of solute at temperature close to 30 °C and the infinite dilution values of the partial molar heat capacity $C_{p,2}^{\infty}$ have been determined.

Table 1. Specific heat capacity and apparent molar heat capacity of D-glucose in water–ethanol system as functions of molality m

wt% of EtOH	m / mol·kg^{-1}	C_p / J·g^{-1}K^{-1}	ϕ_{C_p} / J·mol^{-1}K^{-1}
10	0	4.342	—
	0.5001	4.077	205
	0.6501	4.017	224
	0.8003	3.961	238
	1.000	3.890	250
	1.200	3.837	258
	1.300	3.810	277
	1.500	3.767	295
20	0	4.371	—
	0.5001	4.090	175
	0.6499	4.021	186
	0.8000	3.964	205
	1.001	3.897	228
	1.200	3.831	240
	1.351	3.792	254
	1.500	3.758	269
30	0	4.271	—
	0.4000	4.074	242
	0.6002	3.989	249
	0.8000	3.910	253
	1.000	3.832	251
	1.119	3.788	251
	1.201	3.765	257
50	0	3.848	—
	0.1001	3.820	408
	0.2000	3.785	367
	0.2541	3.764	347
	0.3000	3.743	324
	0.3302	3.732	321
	0.3603	3.721	318
	0.4001	3.707	315
	0.5030	3.655	275

Results and Discussion

C_p Data and Determination of $C_{p,2}^{\infty}$. In view of the paucity of the C_p data of solutions in general, and especially in mixed solvent system, presentation of our experimental results in an original numerical form seems worthy. All the C_p values determined in this study are summarized in Tables 1 and 2. From these data the apparent molar heat capacity of solute, ϕ_{C_p}, at solute concentration of molality m was calculated using the equation,

$$\phi_{C_p} = \frac{1}{m}[(1000 + mM_2)C_p - 1000C_{p,1}], \quad (1)$$

where $C_{p,1}$ is the specific heat capacity of the solvent system and M_2 is the molar mass of the solute. The values of ϕ_{C_p} at infinite dilution, $\phi_{C_p}^{\circ} = C_{p,2}^{\infty}$, were deter-

Table 2. Specific heat capacity and apparent molar heat capacity of D-xylose in water–ethanol system as functions of molality m

wt% of EtOH	m / mol·kg^{-1}	C_p / J·g^{-1}K^{-1}	ϕ_{C_p} / J·mol^{-1}K^{-1}
10	0	4.342	—
	0.2000	4.229	70
	0.5000	4.100	132
	0.7000	4.005	120
	1.000	3.926	173
	1.300	3.826	178
	1.500	3.775	189
20	0	4.371	—
	0.1999	4.265	110
	0.5995	4.072	113
	0.7992	3.993	127
	0.9925	3.940	157
	1.200	3.865	159
	1.400	3.833	191
30	0	4.271	—
	0.2000	4.178	162
	0.4000	4.081	138
	0.6000	3.983	118
	0.8000	3.899	120
	1.000	3.816	118
	1.200	3.733	112
50	0	3.848	—
	0.1000	3.827	365
	0.2000	3.791	284
	0.2700	3.765	258
	0.3300	3.738	228
	0.4000	3.708	207
	0.5000	3.664	182

mined from the least-squares fitting of the experimental data.[1,2]

Concentration Dependence of ϕ_{Cp}. The coefficient related with concentration dependence of ϕ_{Cp} of a nonelectrolyte has significances physically similar to the first order parameter, B_c, of the following expression used in the case of ϕ_{Cp} of electrolytic solutes:

$$\phi_{C_p} = C^{\infty}_{p,2} + A_c m^{1/2} + B_c m, \quad (2)$$

where A_c is a parameter derived from the Debye-Hückel theory. In numerous papers describing the determination of C_p and ϕ_{Cp} of solutions which have hitherto been published, those making reference to the concentration dependence of ϕ_{Cp} are rather few in number.[7-10] The concentration dependence coefficient of ϕ_{Cp} should not be treated as a mere adjustable parameter to reproduce the experimental results. More attention must be paid to this coefficient, as it can serve as a clue in elucidating the nature of solute-solute-solvent interactions. Unfortunately, no theoretical prediction of this coefficient has been put forth. Experiments have shown that it is positive or negative, depending on the circumstances. The values of the coefficients listed in Table 3 are those obtained as first-order coefficients of the function $\phi_{Cp}(m)$ with respect to the molality m. The purpose of this work is chiefly the determination of $C^{\infty}_{p,2}$ rather than that of the concentration dependence of ϕ_{Cp}. Although the values shown in Table 3 are not so precise as to deserve a detailed discussion of these values, the general trend of the concentration dependence of ϕ_{Cp} in the aqueous mixed solvent system is clearly seen in Table 3; solute concentration dependence of ϕ_{Cp} varies remarkably with the solvent system but the variation is qualitatively the same for D-glucose and D-xylose. Table 3 suggests that with variation of the media surrounding the solute, the degree of solute-solute-solvent interactions varies in a similar fashion for D-glucose and D-xylose dissolved in the water-ethanol mixture.

Table 3. Concentration dependence coefficient of ϕ_{C_p} of D-glucose and D-xylose in water-ethanol system

wt% of EtOH	D-glucose	D-xylose
0	26±7	−1±2
10	86±4	66±9
20	91±2	89±11
30	12±3	−24±5
50	−284±16	−346±24

$C^{\infty}_{p,2}$ and $\Delta C^{\infty}_{p,2}$. The values of $\phi_{Cp}{}^{\circ}=C^{\infty}_{p,2}$ determined in this work and those in pure water obtained in our previous work,[1,2] are presented in Table 4. It is noteworthy in Table 4 that the $C^{\infty}_{p,2}$'s of D-glucose are always higher than those of D-xylose in any compositions of the solvent system, showing the positive contribution of $C^{\infty}_{p,2}$ (-CH(OH)-) in water-ethanol system. Variation of $C^{\infty}_{p,2}$ with the content of ethanol in the solvent given in Table 4 is more easily understood by the aid of Fig. 2. Here again similar variation can be observed for both solutes and the minimum appears at about 20 wt% of ethanol. This behavior differs

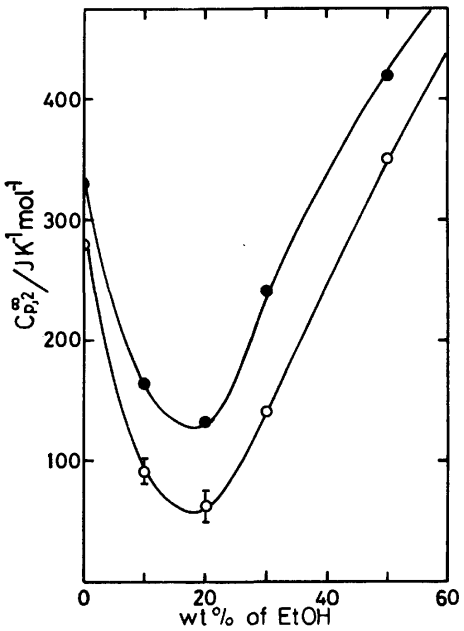

Fig. 2. Variation of $C_{p,2}$ with the ethanol content in the solvent system. ●: D-glucose, ○: D-xylose.

Table 4. Limiting partial molar heat capacities $C^{\infty}_{p,2}$ and increment $\Delta C^{\infty}_{p,2}(=C^{\infty}_{p,2}-C^{*}_{p,2})$ for D-glucose and D-xylose in water-ethanol system

wt% of EtOH	D-glucose		D-xylose	
	$C^{\infty}_{p,2}$ / J K^{-1} mol^{-1}	$\Delta C^{\infty}_{p,2}$ / J K^{-1} mol^{-1}	$C^{\infty}_{p,2}$ / J K^{-1} mol^{-1}	$\Delta C^{\infty}_{p,2}$ / J K^{-1} mol^{-1}
0	331±7[a]	107[a]	281±2[b]	97[b]
10	164±5	−60	92±11	−92
20	132±3	−92	63±13	−121
30	241±3	17	141±5	−43
50	419±6	195	350±10	166

$C^{*}_{p,2}=224\pm3$ J K^{-1} mol^{-1} for D-glucose[a]
$=184$ J K^{-1} mol^{-1} for D-xylose[b]
a) Ref. 1. b) Ref. 2.

significantly from the case of the partial specific compressibility $\bar{\kappa}_2^\circ$ which, as stated in the introductory part of this paper, takes a constant positive value at above 20 wt% of ethanol.[4,5] In this connection it is remembered that in water the $\bar{\kappa}_2^\circ$ gave the hydration number of saccharides which is not proportional to the number of monomer unit contained in the saccharides, whereas the $\Delta C_{p,2}^\infty$, a quantity which will be mentioned immediately below, increases linearly with the molecular dimension from mono- to trisacharides.[1] According to the Kirkwood-Buff solution theory[11] the isothermal compressibility of a binary solution is describable in terms of the pair correlation function. On the other hand, an extended treatment of the Kirkwood-Buff theory[12] has proved that the specific heat capacity of pure liquids at constant volume contains contributions from three- and four-particle distribution function. Differences in adiabatic and isothermal compressibility, or heat capacity at constant pressure and at constant volume are essentially indifferent in the present consideration. Hence, it seems reasonable to consider that the $\bar{\kappa}_2^\circ$ reflects predominantly the interaction in the vicinity of solute molecules, while the partial molar heat capacity is concerned with the long range molecular interaction in solutions and is pertinent to the discussion of the structural change of the solvent system.

Ben-Naim[13] proposed a theory to analyse the relation between ϕ_{C_p} of non-polar gases and the equilibrium species in the two-state model of water. However, his theory was unsuccessful even to predict the definite sign of the quantity ϕ_{C_p}. As before,[1-3] we prefer to use the quantity $\Delta C_{p,2}^\infty$ in discussing the structural change of the solvent system. The $\Delta C_{p,2}^\infty$ is defined as

$$\Delta C_{p,2}^\infty = C_{p,2}^\infty - C_{p,2}^*, \tag{3}$$

where $C_{p,2}^*$ in the specific heat capacity of the pure solute. In water we have classified the "structure-forming" and "structure-breaking" effects of solute according to the sign of the $\Delta C_{p,2}^\infty$. With the same criteria as in water, D-glucose and D-xylose are working as structure-breaking solutes in solvents containing 10, 20, and 30 wt% of ethanol, while they are structure-forming solutes in water and 50 wt% (presumably also at 40 wt%, see Fig. 2) of ethanol. This conclusion is simple but is not persuasive. Rather, the following interpretation seems more plausible; the structure of solvent is different for each solvent system and we are observing a structuring of the respective solvent systems through the parameter $\Delta C_{p,2}^\infty$. Consequently, the positive value of $\Delta C_{p,2}^\infty$ at 50 wt% of ethanol does not correspond straightfowardly to the structure promotion by the added solutes D-glucose or D-xylose, but it shows that the promoted structure exists even before addition of the solutes. The promoted structure in the water-ethanol system is expected, for example, from viscosity data of this mixture which shows the very high peak at *ca.* 45 wt% of ethanol. Values of the concentration dependence of ϕ_{C_p} in water-ethanol system as shown in Table 3 may also be related to the structure promotion in this aqueous mixed solvent.

Combination of the results of $\bar{\kappa}_2^\circ$ and $C_{p,2}^\infty$ leads to the following conclusion; addition of ethanol in the aqueous solutions of D-glucose and D-xylose gives rise to the removal of preferentially hydrated water molecules and at the same time the structuring of the solvent system as a whole decreases. With increasing ethanol content in the solvent, the structure promotion in water-ethanol system becomes progressively predominant up to certain ethanol content. Owing to this process the minimum appears and $\Delta C_{p,2}^\infty$ again takes a positive value at 50 wt% of ethanol.

The authors wish to express their thanks to Mr. Ko-hei Itano for his efforts in carrying out supplementary measurements.

References

1) F. Kawaizumi, N. Nishio, H. Nomura, and Y. Miyahara, *J. Chem. Thermodyn.*, **13**, 89 (1981).
2) F. Kawaizumi, S. Kushida, and Y. Miyahara, *Bull. Chem. Soc. Jpn.*, **54**, 2282 (1981).
3) F. Kawaizumi, N, Nishio, H. Nomura, and Y. Miyahara, *Polym. J.*, **13**, 209 (1981).
4) H. Shiio, T. Ogawa, and H. Yoshihashi, *J. Am. Chem. Soc.*, **77**, 4980 (1955).
5) H. Nomura, M. Onoda, and Y. Miyahara, *Polym. J.*, **14**, 249 (1982).
6) For aqueous solutions of sodium chloride, P. Picker, P.-A. Leduc, P. R. Philip, and J. E. Desnoyers, *J. Chem. Thermodyn.*, **3**, 631 (1971). For aqueous solutions of ethanol, Landolt-Börnstein, "Zahlenwerte und Funktionen aus Naturwissenschaften und Technik" Springer, Berlin (1977) Neue Serie, VI 1b.
7) P. R. Philip and J. E. Desnoyers, *J. Solution Chem.*, **1**, 353 (1972).
8) C. Jolicoeur and J. Boileau, *J. Solution Chem.*, **3**, 889 (1974).
9) P.-A. Leduc, J.-L. Fortier, and J. E. Desnoyers, *J. Phys. Chem.*, **78**, 1217 (1974).
10) C. Jolicoeur and G. Lacroix, *Can. J. Chem.*, **54**, 624 (1976).
11) J. G. Kirkwood and F. P. Buff, *J. Chem. Phys.*, **19**, 774 (1951).
12) F. P. Buff and R. Brout, *J. Chem. Phys.*, **23**, 458 (1955).
13) Ben-Naim, *Trans. Faraday Soc.*, **66**, 2749 (1970).

Peierls Structure of $(H_3O)_{0.33}Li_{0.8}[Pt(mnt)_2]\cdot 1.67H_2O$

Akiko KOBAYASHI,* Takehiko MORI, Yukiyoshi SASAKI, Hayao KOBAYASHI,†
M. M. AHMAD,†† and A. E. UNDERHILL††

Department of Chemistry, Faculty of Science, The University of Tokyo, Hongo, Tokyo 113
†*Department of Chemistry, Faculty of Science, Toho University, Funabashi, Chiba 274*
††*Department of Chemistry, University College of North Wales, Bangor, Gwynedd LL57 2UW, U.K.*

(Received June 9, 1984)

The crystal structure determination of the title compound (abbreviated as α-LiPt(mnt) has been performed at room temperature and 153 K. The $[Pt(mnt)_2]^{n-}$ (mnt=1,2-dicyano-1,2-ethylenedithiolato, $C_4N_2S_2^{2-}$) anions stack face-to-face along the c-axis with Pt···Pt distance of 3.6 Å. The room temperature structure and the average structure of the 153 K superstructure are almost the same. The room temperature conductivity of α-LiPt(mnt) is about 200 S cm^{-1}, and the compound undergoes a metal-insulator transition (Peierls transition) at 220 K. In α-LiPt(mnt) the conduction pathway is through the ligand-centered π-system which is composed of predominantly S $3p_z$ orbitals. Oscillation photographs about the c-axis show strong satellite spots on the layerlines of $(0.41+n)c^*$ and $(0.59+n)c^*$ (n=0, ±1, ±2, ···). The content of Li cation reveals that these satellite spots can be described as $2k_F$ spots. The regular appearance of characteristic satellite reflections indicates that α-LiPt(mnt) has a sinusoidally modulated lattice. The wave vector of the lattice modulation wave is $\mathbf{k}=0.15\mathbf{b}^*+0.59\mathbf{c}^*$ and the amplitude of the lattice modulation wave is $0.045\,\boldsymbol{a}/a+0.13\boldsymbol{b}/b+0.060\boldsymbol{c}/c$ Å. The overlap integrals along face-to-face stacking directions are much larger than the interstack overlap integrals and the resulting large anisotropy indicates that α-LiPt(mnt) is a one-dimensional metal.

The crystal structures, syntheses and electrical conduction properties of 1,2-dithiolene complexes have been extensively studied.[1-3] Recently a new type one-dimensional partially oxidized $[M(mnt)_2]^{n-}$ (M= Ni, Pd, Pt; mnt=1,2-dicyano-1,2-ethylenedithiolato, $C_4N_2S_2^{2-}$) complex has been reported.[4,5] Metallic behavior has been found for crystals of $(H_3O)_{0.33}Li_{0.8}[Pt(mnt)_2]\cdot 1.67H_2O$, which is abbreviated as α-LiPt(mnt).[4-6]† Its room temperature conductivity, 200 S cm^{-1} is as large as that of $K_2[Pt(CN)_4]\cdot Br_{0.3}\cdot 3.2H_2O$ (KCP(Br)). Although the $[Pt(mnt)_2]^{n-}$ anions stack face-to-face with a Pt···Pt distance of 3.639 Å, the partially oxidized 1,2-dithiolene complexes have a conduction pathway based on the ligand-centered π-system (predominantly sulfur $3p_z$ orbitals). This is in contrast to the high conductivity of inorganic one-dimensional metals containing tetracyano-platinate and bis(oxalato)platinate anions which arises from a partially occupied Pt $5dz^2$ electron energy band.

α-LiPt(mnt) undergoes a metal-insulator transition at about 220 K.[4] The static magnetic susceptibility of α-LiPt(mnt) has been measured from 2—300 K by J. R. Cooper *et al.*[6] Above 150 K, the conduction electron paramagnetism $X_p=X_s-C/T$ gradually develops. It shows a sharp knee at 220 K corresponding to metal-semiconductor phase transition.

In this paper we report the crystal structures of α-LiPt(mnt) at room temperature and at 153 K. The 153 K superstructure corresponds to a so-called Peierls structure.

Experimental

Crystal Preparation, Data Collection, and Structure Solution. Slow aerial oxidation of a 50% aqueous acetone solution of $H_2[Pt(mnt)_2]$ and LiCl gave $Li_xH_y[Pt(mnt)_2]\cdot nH_2O$ as a black microcrystalline product containing small shining black needle crystals (α-LiPt(mnt))[7] and plate crystals (β-LiPt(mnt)).[8] The needle crystals were used in this experiment. Details concerning crystal characteristics and X-ray diffraction methodology are shown in Table 1. Intensities were measured on a Rigaku automated four-circle diffractometer with Mo $K\alpha$ radiation at room temperature and at 153 K. Graphite-monochromatized Mo $K\alpha$ radiation (0.71073 Å) was used for data collection. Intensities were collected by using a $\omega-2\theta$ scan technique. The scan width was determined for each reflection according to the formula $w=(A+B\tan\theta)°$. Three standard reflections monitored every 50

Table 1. Crystal and refinement data for α-LiPt(mnt)

	At room temperature	At 153 K
Formula weight	517.52	517.52
a/Å	15.596(4)	15.564(4)
b/Å	6.410(3)	6.320(3)
c/Å	3.639(2)	5.597(1)
α/°	100.52(9)	99.35(2)
β/°	90.75(5)	90.54(2)
γ/°	96.28(6)	96.25(3)
V/Å^3	355.3(2)	346.9(1)
Space group	$P\bar{1}$	$P\bar{1}$
Z	1	1
d_{calc}/g·cm^{-3}	2.418	2.418
Crystal dimension/mm^3	0.04×0.25×0.38	0.031×0.2×0.35
μ/cm^{-1}	112.12	112.12
$2\theta_{max}$/°	60	60
Number of independent reflections $\|F_o\|>3\sigma(\|F_o\|)$	1686	2015
Parameters	96	96
R_w	0.065	0.068
Standard reflections	3	3
Scan	$2\theta-\omega$	$2\theta-\omega$
$A+B\tan\theta$	$1.2+0.6\tan\theta$	$1.24+0.5\tan\theta$
Scan speed 2θ/°	2°/min	4°/min
Background/sec	10	5

† This compound was initially reported to be $Li_x[Pt(mnt)_2]\cdot 2H_2O$ (where $x\approx 0.8$) but has recently been shown to contain protons in the lattice.[7]

(at room temperature) and every 100 (at 153 K) measurements, and their intensities remained essentially constant during the data collection. The data was corrected for Lorentz and polarization. The crystal was covered with epoxy resin for measurements at room temperature and was sealed in a glass capillary for measurements at 153 K. At 153 K, the relatively weak satellite reflections were observed, but these were not included in the analyses of the average structure. The structure was solved by the heavy-atom method and refined to $R=0.065$ and $R=0.068$, $w=1/[\sigma^2+0.01|F_o|^2]$ for $|F_o|\geqq 15$, $w=0.2$ for $|F_o|<15$ using 1686 and 2015 independent reflections for which $I>3\sigma(I)$ at room temperature and at 153 K, respectively. Absorption corrections were performed in both cases, but did not result in much improvement of the room temperature structure because the crystal used for the data collection was twinned.

The c*-axis projection of the structure of α-LiPt(mnt) is shown in Fig. 1. Atomic parameters are shown in Table 2. The thermal parameters and F_o-F_c tables are kept at the office of this Bulletin as Document No. 8451.

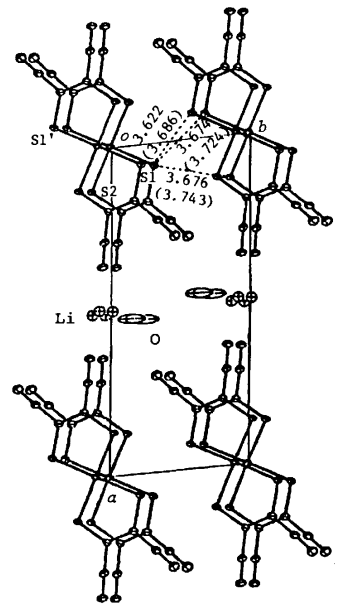

Fig. 1. The c*-axis projection of the average structure of α-LiPt(mnt) at 153 K. The intermolecular distances in parentheses are those at room temperature.

Table 2. Atomic parameters (×10000)

	X	Y	Z	B/Å²
a) At room temperature				
Pt	0	0	0	2.8(0)
S_1	708(2)	3322(5)	1946(10)	3.7(1)
S_2	1276(2)	−1377(5)	−865(10)	3.7(1)
C_1	1765(7)	2854(17)	1685(34)	3.1(3)
C_2	2012(7)	881(18)	459(37)	3.5(3)
C_3	2416(7)	4586(18)	2854(38)	3.8(4)
C_4	2925(7)	626(18)	200(42)	4.3(4)
N_1	2958(7)	5913(18)	3796(39)	6.0(4)
N_2	3633(6)	475(17)	29(42)	6.2(4)
O	4753(7)	7614(33)	4695(91)	23.4(13)
Li*	499(4)	18(11)	88(15)	3.9(10)
b) At 153 K				
Pt	0	0	0	1.6(0)
S_1	700(2)	3335(5)	1981(10)	2.1(1)
S_2	1284(2)	−1371(5)	−846(10)	2.0(1)
C_1	1761(8)	2845(22)	1727(36)	2.0(3)
C_2	2003(8)	852(19)	431(33)	1.7(3)
C_3	2407(8)	4617(23)	2940(40)	2.4(3)
C_4	2910(9)	627(22)	271(42)	2.4(3)
N_1	2963(9)	6015(22)	3919(43)	3.5(4)
N_2	3644(8)	514(21)	102(43)	3.2(3)
O	4742(13)	8007(52)	4076(101)	14.6(15)
Li*	496(6)	19(15)	66(22)	3.4(13)

* The occupancy probability is 0.40.

Results and Discussions

The Room Temperature Structure and the Average Structure of the 153 K Superstructure. The crystal structures of α-LiPt(mnt) at both temperatures are almost the same. The planar $[Pt(mnt)_2]^{n-}$ anions stack face-to-face along the c-axis with an eclipsed configuration to form a columnar stacked structure. The interplanar distance between the $[Pt(mnt)_2]^{n-}$ anions are 3.592 and 3.537 Å, and the Pt···Pt distances are 3.639 and 3.597 Å, at room temperature and at 153 K respectively. In α-LiPt(mnt), all the inter-anion distances within the stack are equal. This is different from the structures found for the similar $[Pt(mnt)_2]$ complexes $Rb[Pt(mnt)_2]\cdot 2H_2O$[9] and β-LiPt(mnt),[8] both of which possess dimeric structures. In $Rb[Pt(mnt)_2]\cdot 2H_2O$ the interplanar spacing within the dimer is 3.356 Å and between dimers 3.512 Å. In β-LiPt(mnt) the interplanar spacing within the dimer is 3.346 Å and between dimers 3.631 Å and 3.643 Å. In both compounds the anions are arranged along the column in a fully eclipsed configuration, which is a characteristic of $M_x[Pt(mnt)_2]$ compounds containing small cations. Mono-anion salts with bulky organic cations often pos-

Table 3. Comparison of bond lengths (l/Å) and angles (φ/°) in $[Pt(mnt)_2]^{n-}$ anions

	α-LiPt(mnt) (R. T.)	α-LiPt(mnt) (153 K)
Pt-S	2.271(2)	2.267(3)
S-C	1.722(8)	1.705(10)
C-C (inner ring)	1.360(16)	1.365(18)
C-C	1.436(11)	1.433(14)
C-N	1.123(11)	1.115(16)
SPtS α	90.4(1)	90.3(1)
PtSC β	102.2(3)	102.0(4)
SCC γ	122.8(6)	122.8(7)
SCC δ	118.3(6)	118.3(7)
CCC ε	119.0(7)	118.9(8)
CCN φ	117.9(8)	177.5(11)

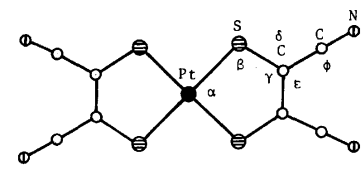

sess columnar stacks containing anion dimers with a staggered configuration.[10] The $[Pt(mnt)_2]^{n-}$ anion is almost planar with average bond lengths (in Å) Pt–S 2.271(2), 2.267(3), S–C 1.722(8), 1.705(10), and C–C 1.360(16), 1.365(18), at room temperature and at 153 K, respectively. The bond lengths and angles are compared in Table 3.

In $Rb_{1.67}[Pt(C_2O_4)_2]\cdot 1.5H_2O$,[11] intermolecular distances are much shortened by the formation of the Pt···Pt bonds. The Pt···Pt distances are modulated by the Peierls distortion and the molecular plane is concave in order to reduce the steric hindrance with the ligands of the neighbouring molecules. Terminal oxygen atoms of the ligands are deviated 0.4—0.5 Å from the plane. However, in α-LiPt(mnt) the molecule is almost planar both at room temperature and at 153 K probably because of the large intermolecular separation. The equations of the best planes and the perpendicular distances from these planes are deposited and kept at the office of this Bulletin.

Intermolecular short contacts are also shown in Fig 1. The transverse interatomic distances between the S atoms are considerably shortened in the low temperature. Close S···S contacts of less than 3.8 Å are shown in Table 4. The short interatomic distances between the S atoms on adjacent molecules in adjacent stacks are 3.686, 3.724, and 3.743 Å at room temperature and 3.622, 3.674, and 3.676 Å at 153 K. Close S···S contacts in the transverse direction of the Pt chain have been also found in α-LiPt(mnt) and $Rb[Pt(mnt)_2]\cdot 2H_2O$. There are two Li sites in the unit cell. The Li ions are disordered and the occupancy probability of the Li site is 40%. The Li ions are six-coordinated and Li···N(O) distances vary from 1.94 to 2.69 Å at room temperature and 2.06 to 2.54 Å at 153 K. There are two oxygen atoms and $0.8Li^+$ cations in the unit cell. They are located in-between the $[Pt(mnt)_2]$ anions along the a-axis. As mentioned before, the results of the chemical analysis of α-LiPt(mnt) have shown that the unit cell should contain 0.33 H_3O^+ but the crystal structure analyses could not distinguish the sites of H_3O^+ from those of H_2O. Table 5 lists short interatomic distances of less than 3.0 Å within the coordination spheres around the Li cation and the oxygen atom of the water molecule (or hydroxonium ion).

Measurements of satellite reflections by oscillation photographs. We examined temperature dependence of intensities of X-ray reflections within the temperature range between 90 K and 300 K. An oscillation photograph around the c-axis shows that the strong satellite spots appear on the layer lines of $(0.41+n)c^*$, or $(0.59+n)c^*$ ($n=0, \pm1, \cdots$) (Fig. 2). The cation content revealed that these satellite spots can be described as $2k_F$ spots.[7] The satellite reflections show that α-LiPt(mnt) has a sinusoidally modulated lattice. Figure 3 shows the temperature dependence of intensities of the satellite spots ($\xi\ \eta\ \zeta$). The intensities of satellite reflections, (−13, −2.85, −0.41), (6, 3.85, 0.41), and (13, 2.15, 0.59)

TABLE 4. THE SHORT INTERATOMIC DISTANCES (l/Å) BETWEEN S ATOMS LESS THAN 3.8 Å

	At room temperature	At 153 K
$S_1\cdots S_1$[a]	3.639(8)	3.597(7)
$S_1\cdots S_2$[b]	3.743(5)	3.676(5)
$S_1\cdots S_1$[c]	3.686(7)	3.622(7)
$S_1\cdots S_2$[d]	3.724(7)	3.674(7)

Symmetry codes

a) $x,\ y,\ 1+z$
b) $x,\ 1+y,\ z$
c) $-x,\ 1-y,\ -z$
d) $-x,\ 1-y,\ 1-z$

TABLE 5. SHORT INTERATOMIC DISTANCES (l/Å) WITHIN THE COORDINATION SPHERES TO 3.0 Å AROUND THE Li CATIONS AND OXYGEN ATOMS OF WATER MOLECULES

	At room temperature	At 153 K
Li···Li[a]	0.65(10)	0.52(16)
Li···O[b]	1.94(6)	2.06(8)
Li···N_2[c]	2.17(7)	2.09(10)
Li···N_2[a]	2.25(7)	2.28(10)
Li···O[d]	2.34(7)	2.00(10)
Li···O[e]	2.53(6)	2.22(10)
Li···O[f]	2.69(7)	2.54(8)
O···N_1[c]	2.88(2)	2.91(3)
O···O[g]	(>3.0)	2.54(6)

Symmetry code

a) $1-x,\ -y,\ -z$
b) $1-x,\ 1-y,\ 1-z$
c) $x,\ y,\ z$
d) $x,\ -1+y,\ z$
e) $x,\ -1+y,\ -1+z$
f) $1-x,\ 1-y,\ -z$
g) $1-x,\ 2-y,\ 1-z$

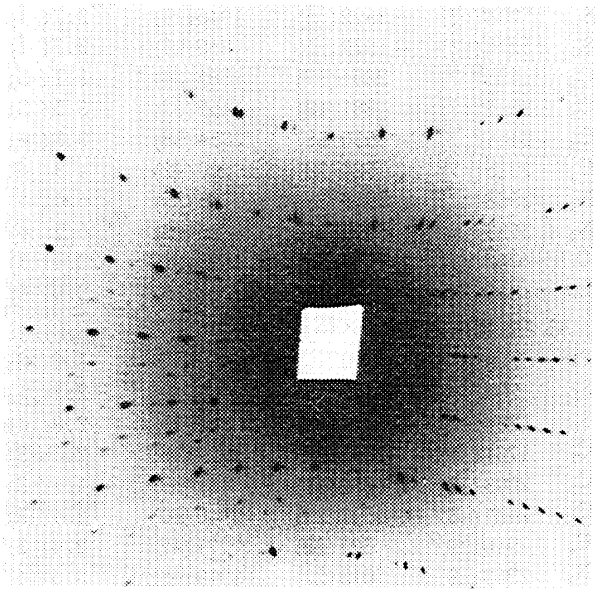

Fig. 2. An oscillation photograph around the c-axis at 153 K. Strong satellite spots appear on the layer lines of $(0.41\pm n)$ c* or $(0.59\pm n)c^*$ ($n=0,1,\cdots$).

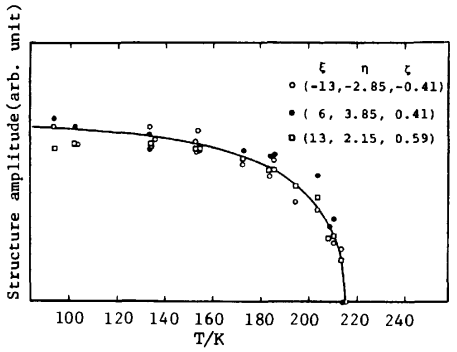

Fig. 3. Temperature dependence of the intensities of satellite reflections between the temperature range of 90 K–300 K.

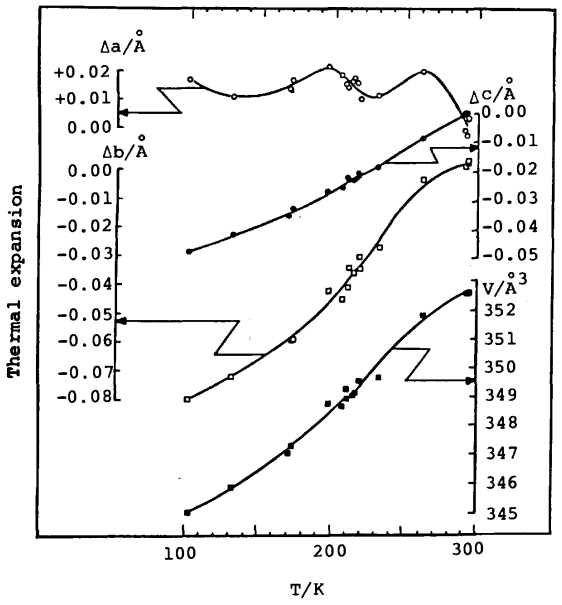

Fig. 4. Temperature dependence of the cell parameters.

were measured under the same conditions as the main reflections. The intensities are roughly proportional to $\sqrt{T-T_c}$ (T_c=213 K).

Temperature Dependence of the Cell Parameters. The temperature dependence of the cell parameters are shown in Fig. 4. The cell constants b and c are shortened by 8 and 5% within the temperature range between 300 K and 90 K and a is expanded by up to 2%.

It is worth noticing that the contraction of the transverse direction b, is larger than the change in a and c. The stack of the $[Pt(mnt)_2]$ complexes is parallel to the c axis. The large contraction of b indicates that the S···S interaction in the transverse direction of complexes are strengthened in the low temperature.

The Analysis of the Modulation wave in the Peierls Structure. As is well-known, the one-dimensional metallic state is not stable at low temperature. The system tends to be distorted periodically in order to gain electronic energy. The lattice instability brings about the superstructure and characteristic X-ray diffuse scatterings appear below transition temperature (T_c). The lattice-modulation wave with the wave number of $2k_F$ develops below T_c.

When the lattice is sinusoidally modulated, the position of the j-th atom of the n-th cell, $\mathbf{r}_{jn}$, is given by $\mathbf{r}_{jn}=\mathbf{R}_n+\mathbf{d}_j+\mathbf{P}\sin(2\boldsymbol{k}_F\cdot\mathbf{R}_n)$, where $\mathbf{R}_n$ is the lattice vector of the n-th lattice point of the average structure, $\mathbf{P}$ is an amplitude of the modulation wave, and $\boldsymbol{k}_F$ is the wave vector of the modulation wave. The intensity formula of X-ray diffraction by the crystal with sinusoidal modulation waves whose fundamental lattice contains only one molecule, is as follows

$$I(\xi\eta\zeta) = |F(\xi\eta\zeta)|^2, \tag{1}$$

$$F(\xi\eta\zeta) = \sum_{n_1}\sum_{n_2}\sum_{n_3} F_o(\xi\eta\zeta)\exp[2\pi i(\xi n_1+\eta n_2+\zeta n_3)] \times \exp[2\pi i(p_1\xi+p_2\eta+p_3\zeta)] \times \sin 2\pi(\phi_1 n_1+\phi_2 n_2+\phi_3 n_3), \tag{2}$$

where scattering vector $\mathbf{s}=2\pi(\xi\boldsymbol{a}^*+\eta\boldsymbol{b}^*+\zeta\boldsymbol{c}^*)$, $2\boldsymbol{k}_F=2\pi(\phi_1\boldsymbol{a}^*+\phi_2\boldsymbol{b}^*+\phi_3\boldsymbol{c}^*)$, and $F_o(\xi\ \eta\ \zeta)$ is the scattering amplitude of the averaged structure without modulation wave. $I(\xi\ \eta\ \zeta)$ can be written as follows by the use of Bessel functions which satisfy the equation $\exp[x/2-(t-t^{-1})]=\sum_{n=-\infty}^{\infty} J_n(x)t^n$. Intensities of main reflections and satellite reflections $I(\xi\ \eta\ \zeta)$ can be written

$$I(\xi\eta\zeta) \propto |F_o(hkl)|^2 J_o^2[2\pi(p_1h+p_2k+p_3l)]\cdots\cdots(hkl) \tag{3}$$

$$\propto |F(h+m\phi_1, k+m\phi_2, l+m\phi_3)|^2 \times J_m^2\{2\pi[p_1(h+m\phi_1)+p_2(k+m\phi_2)+p_3(l+m\phi_3)]\}\cdots\cdots(h+m\phi_1, k+m\phi_2, l+m\phi_3). \tag{4}$$

The intensities of the m-th satellite spots are proportional to the square of the m-th Bessel functions. In the case of $2\pi(\phi_1\boldsymbol{a}^*+\phi_2\boldsymbol{b}^*+\phi_3\boldsymbol{c}^*)=2\boldsymbol{k}_F$ the first satellite reflections are called $2k_F$ spots and the second satellite reflections appear at the $(h+4\pi\phi_1,\ k+4\pi\phi_2,\ l+4\pi\phi_3)$ in the reciprocal space. Since the amplitude of the periodical lattice modulation wave is small, $2\pi(p_1\xi+p_2\eta+p_3\zeta)(=x)$ is much less than 1.0 and $J_o(x)^2 \gg J_1(x)^2 \gg J_2(x)^2 \gg \cdots$. Therefore the intensities of the higher order satellite reflections are much smaller than those of the 1-st order satellite reflections. In facts, 2-nd order reflections can be scarecely seen on the Weissenberg photographs. When $x \ll 1$, $J_1(x)\simeq(1/2)x$ and the intensity formula becomes very simple.

If the periodical lattice distortion wave of α-LiPt(mnt) can be described in terms of the simple sinusoidal wave, A, defined by the following equation,

$$A = \sum_{\xi\eta\zeta}(|F_{obs}(\xi\eta\zeta)| - kS(\xi\eta\zeta)|F_{calc}(\xi\eta\zeta)|\times 2\pi(p_1\xi+p_2\eta+p_3\zeta)/2)^2$$

must be minimized. $F_{obsd}(\xi\ \eta\ \zeta)$ is an observed structure amplitude of the first order satellite reflection. $F_{calcd}(\xi\ \eta\ \zeta)$ is a structure amplitude calculated from the atomic parameters of the average structure and $S(\xi\ \eta\ \zeta)(=\mathrm{sign}(p_1\xi+p_2\eta+p_3\zeta))$ was easily determined by the examination of the intensity distribution of the 1337 satellite reflections. The conditions for the data collection were the same as those used in

determining the average structure at 153 K.

Figure 5 shows the examples of the intensity distributions of the observed structure amplitude of $|F(h+\phi_1, k+\phi_2, l+\phi_3)|$. The distribution of the $|F(\xi\ \eta\ \zeta)|$ is divided into two regions where the values of the $|F(\xi\ \eta\ \zeta)|$ are not zero. The position of this boundary changes according to ζ and forms a plane in the three dimensional reciprocal space. The intensities of satellite reflections are proportional to $|J_1(x)|^2$. When x is constant, $2\pi(p_1\xi+p_2\eta+p_3\zeta)(=x)$ represents one plane and intensities of satellite reflections are zero at the points of the reciprocal space where $(p_1\xi+p_2\eta+p_3\zeta)=0$. The intensities become stronger according to the departure from this plane. The sign of the satellite reflection is changed on this plane. Thus $S(\xi\ \eta\ \zeta)$ values in one region are determined +1 and those in the other region are −1. On the whole the intensity of satellite reflection becomes weaker, when $(\xi\ \eta\ \zeta)$ departs from the origin of the reciprocal space. p_1, p_2, and p_3 are determined by the minimization of A. From $\partial A/\partial p_1=0$, $\partial A/\partial p_2=0$, $\partial A/\partial p_3=0$, we obtain

$$\sum_{\xi\eta\zeta}(|F_o|-\pi kS|F_c|(p_1\xi+p_2\eta+p_3\zeta))\xi = 0,$$
$$\sum_{\xi\eta\zeta}(|F_o|-\pi kS|F_c|(p_1\xi+p_2\eta+p_3\zeta))\eta = 0,$$
$$\sum_{\xi\eta\zeta}(|F_o|-\pi kS|F_c|(p_1\xi+p_2\eta+p_3\zeta))\zeta = 0. \quad (5)$$

We used the scale factor k obtained in the structure determination of the averaged structure at 153 K. Based on the 1337 satellite reflections, p_1, p_2, and p_3 were determined as 0.045 Å, 0.137 Å, and 0.060 Å. The phase parameters (ϕ_1, ϕ_2, ϕ_3) were determined from the positions where the satellite reflections have maximum intensities in the reciprocal space. The four-circle diffractometer was scanned varying the indices of the reflections at intervals of 0.01 around the main reflections in order to gain the diffraction maxima of the satellite reflections. The diffraction maxima corresponding to Eqs. 3 and 4 represent main and satellite reflections which appear regularly at intervals of $|\phi_1 a^*+\phi_2 b^*+\phi_3 c^*|$. The measurement of the coordinates of the reflections in the reciprocal space gave $\phi_1=0.0$, $\phi_2=0.15$, $\phi_3=0.59$. The reliability factor R of 1337 satellite reflections was 0.18. Considering that R was calculated on the basis of the considerably weak satellite reflections, this result is satisfactory. The modulation wave of α-LiPt(mnt) is shown in Fig. 6. The amplitude of the modulation wave of α-LiPt(mnt) is 0.14 Å, which is similar to those of $Rb_{1.67}[Pt(C_2O_4)_2]\cdot 1.5H_2O$ (Rb-OP)[11] and $K_{1.81}[Pt(C_2O_4)_2]\cdot 2H_2O$ (γ-K-OP).[12] Comparison of the struc-

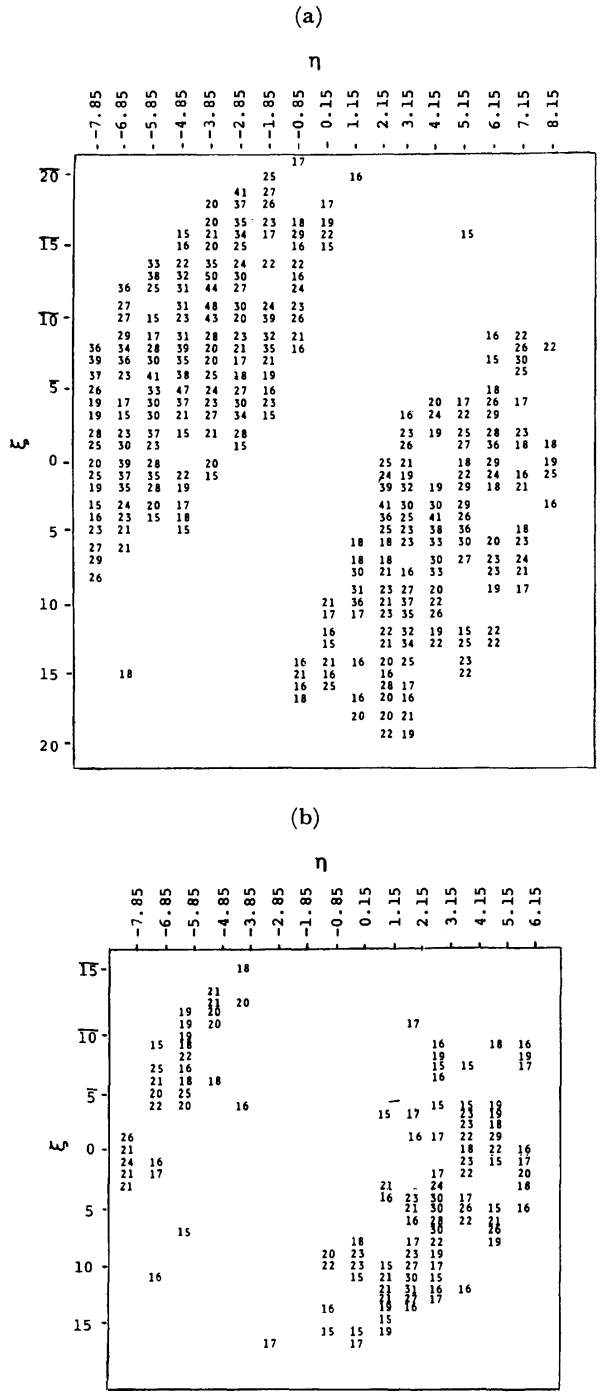

Fig. 5. Examples of the intensity distributions of the observed structure amplitudes of the satellite reflections, $|F(h+\phi_1, k+\phi_2, l+\phi_3)|$. The distribution of the $|F(\xi\eta\zeta)|$ is divided into two regions where the values of the $|F(\xi\eta\zeta)|$ are not zero. a): $\zeta=0.59$, b): $\zeta=2.59$.

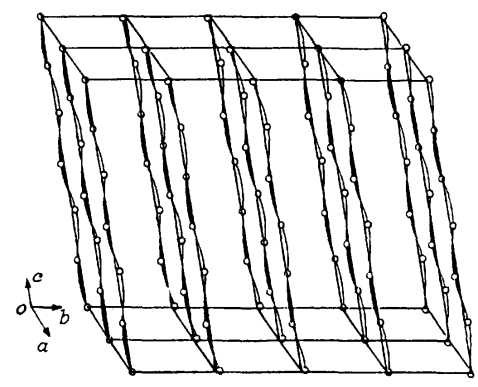

Fig. 6. Schematic drawing of the modulation wave of α-LiPt(mnt).

Table 6. Comparison of the superstructures of Pt complexes

	α-LiPt(mnt)	Rb-OP[11]	γ-K-OP[12]	KCP(Br)[13]
Chemical formula	$(H_3O)_{0.33}Li_{0.8}[Pt(mnt)_2]\cdot 1.67H_2O$	$Rb_{1.67}[Pt(C_2O_4)_2]\cdot 1.5H_2O$	$K_{1.81}[Pt(C_2O_4)_2]\cdot 2H_2O$	$K_2[Pt(CN)_4]Br_{0.3}\cdot 3H_2O$
Crystal System	Triclinic	Triclinic	Triclinic	Tetragonal
Pt···Pt Distance	3.597/Å	2.72, 2.83, 3.02/Å	2.84, 2.87/Å	2.89/Å
Modulation Wave	Transverse and Longitudinal	Longitudinal and Transverse	Transverse and Longitudinal	Longitudinal
Amplitude	0.14/Å(153 K) (0.045, 0.137, 0.060)/Å	0.17/Å(300 K)	0.17/Å(300 K) (0.20, −0.08, 0.11)/Å	0.02/Å(T<100 K)
Period	$2.38\times R_{Pt\cdots Pt}$(8.56/Å)	$6\times R_{Pt\cdots Pt}$(17.1/Å)	$10.5\times R_{Pt\cdots Pt}$(30.0/Å)	$6.5\times R_{Pt\cdots Pt}$(18.8/Å)
Order of the Chain Distortion	Complete Superstructure	Complete Sixfold Superstructure	Complete Supeestructure	Incomplete (Fluctuation of the Lattice Distortion)

Table 7. List of semiempirical parameters[14-16] (energy in eV)

		ζ	ε/eV			ε	ε/eV
C	2s	1.625	−21.4	N	2s	1.925	−26.0
	2p	1.625	−11.4		2p	1.925	−13.4
S	3s	2.122	−20.0	Pt	5d	*	−12.59
	3p	1.827	−11.0		6s	2.554	−9.077
	3d	1.5	−8.0		6p	2.554	−5.475

* double-ζ
$\chi = 0.6334\chi_1(6.013) + 0.5513\chi_2(2.696)$

Table 8. Intermolecular overlap integrals between the b_{3g} LUMO of the neutral molecules $[Pt(mnt)_2]^0$

S(**c**)*	-0.2365×10^{-1}
S(**b**)	-1.1189×10^{-2}
S(**b**+**c**)	0.3961×10^{-4}
S(**b**−**c**)	≈0

* S(m**b**+n**c**) indicates the overlap integral between the molecules located at (0, 0, 0) and (0, m**b**, n**c**).

tural data of the superstructures of platinum complexes is shown in Table 6. It may be of interest that in one-dimensional platinum complexes the lattice distortion wave gives rise to a periodical variation of the charge density along the Pt chains. The phase of the periodical distortion wave is considered to be governed by the interchain Coulomb coupling and the Pt chains are anti-phase ordered so as to minimize the Coulomb energy.[11] In α-LiPt (mnt), anti-phase ordering does not hold, perhaps due to the fairly strong transverse S···S interactions.

MO Calculation. We calculated the intermolecular overlap integrals(S) between LUMO of the neutral $Pt(mnt)_2$ molecule, obtained by means of the extended Hückel method. The molecule was idealized to have D_{2h} symmetry. The overlap integrals were calculated from Slater type orbitals. The semiempirical parameters are listed in Table 7. The overlap integrals along the face-to-face stacking direction are much larger than the interstack overlap integrals. The LUMO of the neutral $[Pt(mnt)_2]^0$ is b_{3g}, which agrees with the results of Schrauzer[17] and Yamatera.[18] Further the LUMO is consistent with the change of the bond distances obtained by the structure determination of $Ni(mnt)_2^{2-}$ and $Ni(mnt)_2^{1-}$.[10] The overlap integral of dz^2 orbital in the platinum chain in α-LiPt(mnt) is one-tenth of those of one-dimensional platinum complexes of tetracyanates or bisoxalates because of the large Pt··· Pt distance in α-LiPt(mnt). On the other hand, the intrastack overlap integrals of S atoms are the same order as those of the dz^2 orbitals of tetracyanoplatinates or bis(oxalato)platinates. The intermolecular overlap integrals between the b_{3g} LUMO of the neutral molecules were calculated and the values obtained are shown in Table 8. The overlap integrals along face-to-face stacking S(**c**) (intrastack) is much larger than the interstack overlap integrals S(***b***) or S(***b***+**c**), S(***b***−**c**). The large anisotropy indicates this compound is a one-dimensional metal. The value of S(**c**) indicates that the band width may be about 0.5 eV. Magnetic susceptibility measurements by J. R. Cooper show the conduction electron bandwidth ($4t_{//}$) in a tight binding model is 0.66 eV. This value is about a factor of 2.5 larger than that determined from the plasma frequency (0.26 eV).[6] The plasma frequency of this compound is much smaller than that observed for the usual platinum complexes of tetracyanates or bisoxalates.

Role of the Interchain Transverse S···S Contacts. The electrical conductivity of one-dimensional platinum complexes such as tetracyanoplatinates and bis(oxalato)platinates is strongly dependent on the periodicity of the Pt chain. Similar correlation between the electrical properties and the periodicity of the Pt chains can be also seen in $[Pt(mnt)_2]$ complexes. α-LiPt(mnt) is metallic at room temperature and at 213 K(T_c) a metal-insulator transition is observed. Since the $[Pt(mnt)_2]^{n-}$ are stacked regularly above T_c, the band is partially (59%) filled and one-dimensional metallic properties are observed. In $Rb[Pt(mnt)_2]\cdot 2H_2O$,[9] the band is half filled, which is consistent with the dimer structure and the semiconducting resistivity (≈10^5 Ωcm). In the case of β-LiPt(mnt)[8] the band is 1/4 (or 3/4) filled and the Peierls distortion produces a fourfold structure with a band gap at the Fermi level resulting in semiconducting properties which agree with the temperature dependence of its conductivity (≈10^{-3} Scm^{-1}). Though $M_x[Pt-$

$(mnt)_2$] has one-dimensional stacks of the platinum complexes, it cannot be regarded as typical one-dimensional system. In a one-dimensional system, the relationship between the band gap (2Δ) and the metal-insulator transition temperature (T_c) formed for the system without fluctuations, $2\Delta/T_c=3.73$, cannot be applied because the $2k_F$ lattice distortion does not develop until the temperature is lowered to as low as $T \lesssim T_c/3$ (hence $2\Delta/T_c \gtrsim 10$). In α-LiPt(mnt), $2\Delta/T_c$ is 3.95, which is close to the value derived from the mean field theory 3.73. The reason for the depression of the fluctuations of the lattice distortion wave lies in the characteristic interchain transverse contacts due to S atoms. Thus, despite of the one-dimensional nature of the electronic structure, α-LiPt(mnt) does not behave as one-dimensional system in the presence of the lattice distortion mode.

This work was supported by the Grant-in-Aid for special Research Projection "The Properties of Molecular Assembly" (No. 58218008), from the Ministry of Education, Science and Culture.

References

1) J. S. Miller and A. J. Epstein, *Prog. Inorg.Chem.*, **20**, 1 (1976).

2) J. S. Miller and A. J. Epstein, *J. Coord. Chem.*, **8**, 191 (1979).

3) J. W. Bray, H. R. Hart, J., L. V. Interrante, I. S. Jacobs, J. S. Kasper, P. A. Piacente, and G. D. Watkins, *Phys. Rev. B*, **16**, 1359 (1977).

4) A. E. Underhill and M. M. Ahmad, *J. Chem. Soc., Chem. Commun.*, **1981**, 67; M. M. Ahmad and A. E. Underhill, *J. Chem. Soc., Dalton Trans.*, **1982**, 1065; M. M. Ahmad, D. J. Turner, A. E. Underhill, C. S. Jacobsen, K. Mortensen, and K. Carneiro, *Phys. Rev. B*, **29**, 4796 (1984).

5) A. Kobayashi, Y. Sasaki, H. Kobayashi, A. E. Underhill, and M. M. Ahmad, *J. Chem. Soc., Chem. Commun.*, **1982**, 390.

6) J. R. Cooper, M. Miljak, M. M. Ahmad, and A. E. Underhill, *J. de Physique*, **44**, 1391 (1984).

7) A. E. Underhill and P. E. Clemenson, to be published. Recent investigation of average charge on the anion by treating the compound with an excess of iodine and back titrating the iodine with sodium thiosulphate, showed that the average charge on the anion appears to be 1.15. Further pH titrations on solutions of the salt revealed that there are approximately 0.33 protons per platinum in two different samples. Elemental analysis of Li was performed and the contents of Li was obtained as 0.75 with the aid of atomic emission spectrometry. On the other hand, we observed $2k_F$ satellite spots to appear on the layer lines of $(0.41\pm n)c^*$, or $(0.59\pm n)c^*$ (n=0,1,..) on the oscillation photograph around the c-axis. From the X-ray experiment total charge of the anion is supposed to be 0.82 or 1.18. The value of 1.18 is good agreement with the value of 1.15 obtained from the chemical analysis. Therefore the chemical formula of α-LiPt(mnt) is considered to be $(H_3O)_{0.33}Li_{0.8}[Pt(mnt)_2]\cdot 1.67H_2O$.

8) A. Kobayashi, Y. Sasaki, H. Kobayashi, A. E. Underhill, and M. M. Ahmad, *Chem. Lett.*, **1984**, 305.

9) M. M. Ahmad, D. J. Turner, A. E. Underhill, A. Kobayashi, Y. Sasaki, and H. Kobayashi, *J. Chem. Soc., Dalton, Trans.*, in press.

10) A. Kobayashi and Y. Sasaki, *Bull. Chem. Soc. Jpn.*, **50**, 2650 (1977).

11) A. Kobayashi, Y. Sasaki, and H. Kobayashi, *Bull. Chem. Soc. Jpn.*, **52**, 3682 (1979).

12) H. Kobayashi, I. Shirotani, A. Kobayashi, and Y. Sasaki, *Solid State Commun.*, **23**, 409 (1977); "Extended Linear Chain Compounds, Vol. 2," ed by J. S. Miller, Plenum Press, New York and London (1982).

On the basis of the intensity formula and the properties of Bessel funtions $J_m^2(X)=1$, some simple relations between Bessel functions and the relative intensities of the main and satellite reflections are derived. In the case of $K_{1.81}[Pt(C_2O_4)_2]\cdot 2H_2O$ we obtained the amplitude of the modulation wave using these simple relations. Satellite reflections were recorded on equi-inclination Weissenberg photographs and visually estimated.

13) J. W. Lynn, M. Iizumi, and G. Shirane, *Phys. Rev. B*, **12**, 1154 (1975).

14) R. S. Somnerville and R. Hoffman, *J. Am. Chem. Soc.*, **98**, 7240 (1976).

15) E. Clementi and D. J. Raimondi, *J. Chem. Phys.*, **38**, 2686 (1963).

16) H. Basch and H. B. Gray, *Theor. Chim. Acta*, **4**, 367 (1966).

17) G. N. Schrauzer and V. P. Mayweg, *J. Am. Chem. Soc.*, **87**, 3585 (1965).

18) M. Sano, H. Adachi, and H. Yamatera, *Bull. Chem. Soc. Jpn.*, **54**, 2636 (1981).

 © 1984 The Chemical Society of Japan Bull. Chem. Soc. Jpn., 57, 3269—3273 (1984)

The Molecular Structure of Trimethylamine-Borane as Studied from Gas Electron Diffraction and Spectroscopic Data

Kinya IIJIMA, Nobuhiro ADACHI, and Shuzo SHIBATA*
Department of Chemistry, Faculty of Science, Shizuoka University, Oya, Shizuoka 422
(Received June 18, 1984)

The molecular structure of trimethylamine-borane $(CH_3)_3N \cdot BH_3$ has been determined from gas electron-diffraction data with spectroscopic data. The molecular parameter values and their uncertainties are r_g(B-H)= 1.261±0.006 Å, r_g(N-B)=1.656±0.002 Å, r_g(C-N)=1.485±0.001 Å, r_g(C-H)=1.108±0.002 Å, ∠HBH=112.8±0.4°, and ∠CNC=109.2±0.2°. The potential barrier around the N-B bond has been estimated to be larger than 5 kcal mol^{-1} (1 cal=4.183 J). The isotope effects on the B-D bond distance and the DBD angle have also been estimated to be −0.006 Å and 0.4°, respectively, in r_a^0 parameters.

Trimethylamine-borane $(CH_3)_3N \cdot BH_3$ is one of stable molecular complexes, and the gaseous molecular structure has been determined from microwave spectroscopic data by two research groups.[1,2] The N-B distances obtained from both studies, 1.609 and 1.638 Å, are considerably different from each other. On the other hand the N-B distances in $(CH_3)_3N \cdot BX_3$ (where X is F, Cl, Br, and I), on which we have studied by electron diffraction,[3] fall into the range of 1.65—1.67 Å. The N-B distances of $(CH_3)_3N \cdot BH_3$ obtained by MW spectra are out of this range, though it appears to be difficult to determine precisely the molecular parameters of this compound from MW data because only one rotational constant is available for one isotope species and the center of mass in this compound locates close to the nitrogen atom.

The acceptor power of borane for trimethylamine or pyridine has been discussed in relation with heat of formation,[4,5] dipole moment,[6] chemical shift of NMR spectra,[7] and displacement reaction.[8] We have also reported that on complex formation the changes of molecular structure of the donor and the acceptor molecules have some relation with the acceptor power of boron trihalides.[3] In order to discuss the acceptor power of borane in this point of view, it is necessary to know the precise values of molecular parameters of $(CH_3)_3N \cdot BH_3$. We undertook thus the structure analysis by a gas electron-diffraction method in combination with microwave spectroscopic data.

Experimental

The sample of trimethylamine-borane was purified by sublimation in vacuum. Electron diffraction photographs were taken by the use of an r^3-sector on Kodak Electron-Image plates at camera distances of 293.30 and 143.60 mm. The sample is highly volatile and a nozzle was heated at 346 K to introduce the vaporized sample to vacuum from a warmed sample holder. An accelerating voltage was 40 kV and the wavelength was determined from the diffraction patterns of thallium(I) chloride.[9] The exposure times were about 135 and 280 s for the long and short camera distance photographs, respectively, with an electron-beam current of 0.8 μA. The pressure in the diffraction chamber was 5×10^{-6} Torr (1 Torr=133.322 Pa) during the experiment. Three plates and four plates were selected for the long and short camera distance photographs, respectively, and their optical densities were measured at 0.4 mm intervals by the use of a digital microphotometer. The electron diffraction unit and the digital microphotometer used in the present study have been described elsewhere.[10]

Analysis and Results

Molecular Intensity and Radial Distribution. The scattering intensities in the range of s=2.8—16.5 Å^{-1} were obtained from the long camera-distance plates and those in the range of s=10.1—33.3 Å^{-1} from the short camera-distance plates. They were leveled by using theoretical backgrounds, and the intensities for each camera distance were averaged. The elastic and inelastic scattering factors were taken from the tables prepared by Schäfer *et al.*[11] and by Cromer and Mann,[12] respectively. The inelastic scattering factor for the hydrogen atom was taken from the table by Tavard *et al.*[13] The experimental background curve was drawn smoothly,[14] and the experimental molecular intensities obtained are shown in Fig. 1. Figure 2 shows the experimental radial distribution function calculated from the experimental molecular intensities. The molecular model of $(CH_3)_3N \cdot BH_3$ and the numbering of the atoms are shown in Fig. 3.

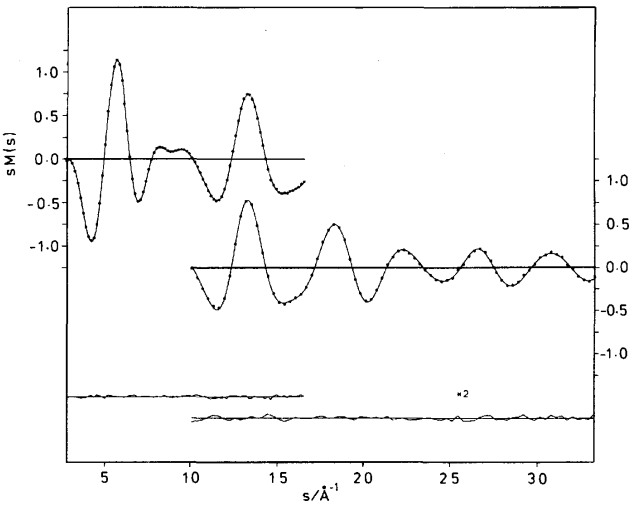

Fig. 1. Molecular intensities for trimethylamine-borane. The two upper curves are long and short camera-distance data. Dots represent observed intensities, solid curves calculated intensities, and the lower curves are their residuals.

Vibrational Amplitude and Shrinkage Correction. Root-mean-square amplitudes of the atomic pairs in $(CH_3)_3N \cdot BH_3$ with the staggered form were calculated by using the Urey-Bradley force field for related molecules,[3] which was changed slighly so as to obtain better agreement with the observed mean amplitudes. The force constants are listed in Table 1, and the calculated mean amplitudes and the shrinkage corrections, $r_a - r_\alpha$,[15] are listed in Table 2.

The height of the rotational barrier around the N-B bond, V_3, was estimated to be about 10 kcal mol^{-1} from the force constant of Y by the relation $V_3=(2/9)Y$. The lower limit was calculated to be 5 kcal mol^{-1} from the lower limit of the Y value which was estimated from the error of the observed mean amplitude of the *gauche* $C_2 \cdots H_1$ atomic pair, because the Y value has the main contribution to the mean amplitude of that atomic pair.[16]

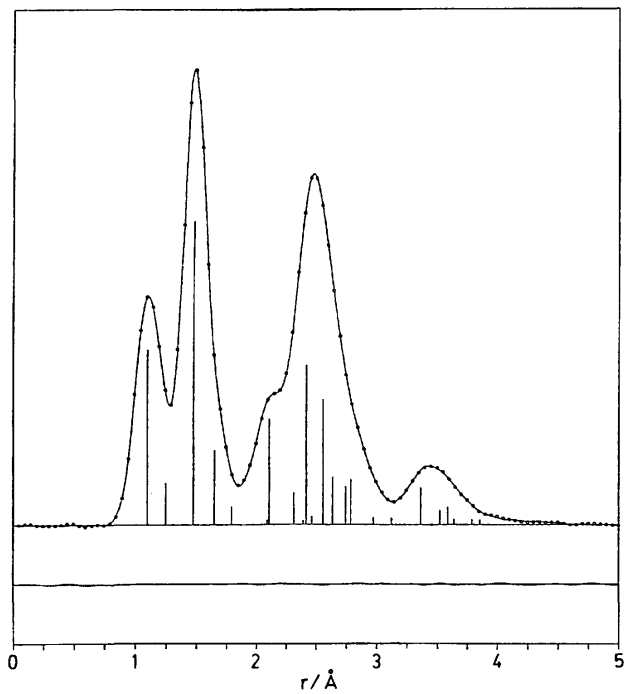

Fig. 2. Radial distribution for trimethylamine–borane. Dot represents the experimental one, the solid curve the calculated one, and the difference is shown below. The vertical bars represent bond distances and the scattering powers.

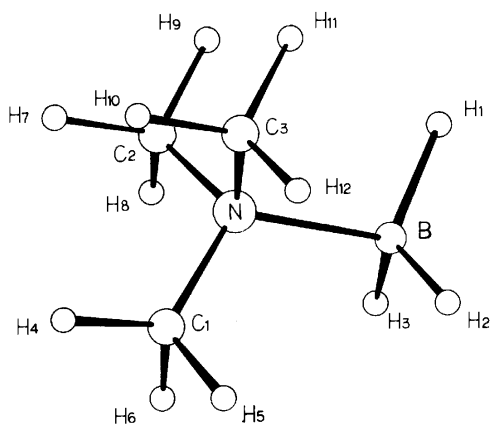

Fig. 3. Numbering of atoms in trimethylamine–borane.

Analysis of Electron Diffraction Intensities and Rotational Constant. At first the molecular parameters of $(CH_3)_3N \cdot BH_3$ were determined by the least-squares analysis of the molecular intensities. Here it was assumed that the molecule has the C_{3v} symmetry in a staggered form, and the methyl and the borane groups also have the C_{3v} symmetry. The geometrical parameters and the root-mean-square amplitudes listed in Tables 3 and 4 were refined. The mean amplitudes of the other atomic pairs and the shrinkage corrections were fixed to the calculated values listed in Table 2. The asymmetry parameters, κ, for the B-H, N-B, C-N, and C-H bonds were estimated to be 21, 4.7, 2.1, and 12×10^{-6} Å, respectively, by the diatomic approximation[17] and were fixed throughout the analysis. Those for the other atomic pairs were ignored.

Table 1. Urey-Bradley force field for $(CH_3)_3N \cdot BH_3$

K(N-B)	1.0	H(HCH)	0.4
K(B-H)	4.0	H(NCH)	0.3
K(C-N)	2.0	F(H(B)H)	0.1
K(C-H)	4.7	F(N(B)H)	0.3
Y(C-N)	0.14	F(CC)	0.3
Y(N-B)	0.33	F(CB)	0.15
H(HBH)	0.2	F(H(C)H)	0.1
H(NBH)	0.3	F(N(C)H)	0.5
H(CNC)	0.3	p	−0.05
H(CNB)	0.25		

The torsional force constant, Y, and the internal tension of the methyl carbon, p, are in 10^{-18} N m, while the others are in 10^2 N m^{-1}.

Table 2. Root-mean-square amplitudes and shrinkage corrections for $(CH_3)_3N \cdot BH_3$ (in 10^{-4} Å)

Atomic pair	l	$r_a - r_\alpha$	Atomic pair	l	$r_a - r_\alpha$
B-H_1	809	170	N-C	541	13
B-N	659	8	N$\cdots$$H_4$	1040	121
B$\cdots$$C_1$	915	−12	$C_1\cdots C_2$	792	−4
B$\cdots$$H_4$	1127	61	C_1-H_4	774	247
B$\cdots$$H_5$	1785	−7	$C_1\cdots H_7$	1673	9
$H_1\cdots H_2$	1354	200	$C_1\cdots H_8$	1669	10
$H_1\cdots$N	1144	78	$C_1\cdots H_9$	1051	70
$H_1\cdots C_1$	1149	44	$H_4\cdots H_5$	1264	353
$H_1\cdots C_2$	1676	−8	$H_4\cdots H_7$	2470	−33
$H_1\cdots H_4$	1457	77	$H_4\cdots H_8$	2594	−72
$H_1\cdots H_5$	1805	56	$H_4\cdots H_9$	1780	76
$H_1\cdots H_7$	1859	48	$H_5\cdots H_8$	1775	76
$H_1\cdots H_8$	2532	−67	$H_5\cdots H_9$	1369	103
$H_1\cdots H_9$	2500	−58	$H_5\cdots H_{12}$	2461	−30

The numbering of the atoms is shown in Fig. 3. The mean amplitudes and shrinkage corrections were calculated for the same temperature (346 K) as in the experiment.

The r_α parameters for bonds obtained by the analysis of electron diffraction data were transformed to r_α^0 parameters at 0 K by the relation $r_\alpha^0 = r_\alpha + K_T - K_0 - 3/2\, a(l_T^2 - l_0^2)$,[15] and the angle parameters were assumed to be equal to those at 0 K. The rotational constant, B_α^0, which was calculated from these r_α^0 parameters was 0.15065(68) cm^{-1}. The rotational constant observed for the normal species was 0.1506482 cm^{-1},[2] and the value corrected for the vibrational effect, B_z,[18] was 0.150629 (19) cm^{-1}, as listed in Table 5. The uncertainty in the correction was tentatively assumed to be 100%. Although the B_α^0 value from the electron diffraction data was in agreement with the observed one, B_z, within the limits of error, the joint analysis of electron diffraction data and rotational constant was performed. The relative weight for the observed rotational constant in the least-squares calculation was estimated to be 1×10^7 in such a way that 2.6 times the standard deviation of the rotational constant obtained from the least-squares calculation is nearly equal to the uncertainty in B_z. The r_α^0 parameters and the mean amplitudes obtained from the joint analysis are listed in Tables 3 and 4, respectively, with their errors. The random errors were 2.6 times as large as the errors estimated by the least-squares calculations. The systematic errors were estimated from the errors in both the measurements of camera distance (0.03%) and wavelength (0.08%). The best-fit molecular intensities and the theoretical radial distribution function are shown in Figs. 1 and 2, respectively. The experimental intensities, the experimental smooth backgrounds, and the correlation matrix for the molecular parameters are deposited as Document No. 8452 at the Office of the Editor of the Bulletin of the Chemical Society of Japan. The least-squares calculations were carried out on a HITAC M-200H computer in the Computer Center of the University of Tokyo.

Table 6 lists the observed rotational constants of the isotope species[2] and the corresponding ones calculated by the use of the r_α^0 parameters in Table 3. The

Table 3. Molecular parameters obtained from least-squares analysis for $(CH_3)_3N \cdot BH_3$

	r_α [a]	r_g [b]	r_α^0 [c]	r_g [d]
B-H/Å	1.239 (6)	1.260	1.243 (6)	1.261
N-B/Å	1.652 (3)	1.656	1.651 (2)	1.656
C-N/Å	1.482 (1)	1.485	1.482 (1)	1.485
C-H/Å	1.078 (2)	1.108	1.088 (2)	1.108
H···(B)···H/Å	2.071 (14)	2.100	2.078 (13)	2.100
C···C/Å	2.419 (3)	2.421	2.419 (3)	2.421
∠NCH/°	109.2 (2)		109.0 (2)	
∠HBH/° [e]	113.5 (6)	112.9	113.4 (4)	112.8
∠CNC/° [e]	109.4 (2)	109.2	109.4 (2)	109.2

Limits of error are in parentheses. Parameters r_α, r_α^0, and r_g are defined in Ref. 15. a) Results from electron diffraction data. b) r_g parameters transformed from r_α parameters. The limits of error are equal to those in the r_α parameters. c) Results from the joint analysis of electron diffraction data and rotational constant. d) r_g parameters transformed from r_α^0 parameters. The limits of error are equal to those in the r_α^0 parameters. e) Dependent parameters.

Table 4. Root-mean-square amplitudes for $(CH_3)_3N \cdot BH_3$

	l_{obsd}/Å [a]	l_{calcd}/Å [b]
N-C_1	0.057 (1)	0.054
C_1-H_4	0.076 (2)	0.077
C_1···C_2	0.080 (3)	0.079
N-B	0.072 (3)	0.066
B···C_1	0.091 (5)	0.092
B-H_1	0.077 (7)	0.081
N···H_4	0.104 (2)	0.104
C_2···H_1	0.168 (12)	0.168

a) Results obtained from the joint analysis of electron diffraction data and rotational constant. b) Values calculated from the force constants in Table 1.

Table 5. Observed and calculated rotational constants of $(CH_3)_3N \cdot BH_3$

B_o/cm^{-1} [a]	0.1506482 (2)
B_z/cm^{-1} [b]	0.150629 (19)
B_α^0/cm^{-1} [c]	0.15065 (68)
B_{av}/cm^{-1} [d]	0.150630 (20)

a) Observed rotational constant for the ground vibrational state. Ref. 2. b) Rotational constant corrected for the vibrational effect. c) Rotational constant calculated from the parameters obtained by the analysis of electron diffraction data. d) Best-fit rotational constant obtained from the joint analysis.

Table 6. Rotational constants of isotope species of $(CH_3)_3N \cdot BH_3$

	B_o/cm^{-1} [a]	B_z/cm^{-1} [b]	B_α^0/cm^{-1} [c]	$(B_z - B_\alpha^0)/10^{-5}$ cm^{-1}
$(CH_3)_3{}^{15}N \cdot {}^{11}BH_3$	0.150662	0.15064	0.15063 (15)	1
$(CH_3)_3{}^{14}N \cdot {}^{10}BH_3$	0.154367	0.15434	0.15438 (15)	−4
$(CH_3)_3{}^{15}N \cdot {}^{10}BH_3$	0.154381	0.15437	0.15438 (15)	−1
$(CH_3)_3{}^{14}N \cdot {}^{11}BD_3$	0.134857	0.13484	0.13453 (10)	31
$(CH_3)_3{}^{15}N \cdot {}^{11}BD_3$	0.134862	0.13485	0.13452 (10)	33
$(CH_3)_3{}^{14}N \cdot {}^{10}BD_3$	0.137540	0.13753	0.13723 (10)	30
$(CH_3)_3{}^{15}N \cdot {}^{10}BD_3$	0.137548	0.13754	0.13722 (10)	32

a) Observed rotational constants, Ref. 2. b) Rotational constants corrected for the vibrational effect. c) Rotational constants calculated from the r_α^0 parameters in Table 3. The correlations between the parameters were taken into consideration in calculating the errors.

Table 7. Comparison of molecular parameters

	r(N-B)/Å	r(B-X)/Å	r(C-N)/Å	∠XBX/°	∠CNC/°
$(CH_3)_3N\cdot BH_3$[a]	1.656 (2)	1.261 (6)	1.485 (1)	112.8 (4)	109.2 (2)
$(CH_3)_3N\cdot BF_3$[b]	1.674 (4)	1.374 (2)	1.485 (2)	112.6 (3)	109.2 (4)
$(CH_3)_3N\cdot BCl_3$[b]	1.652 (9)	1.836 (2)	1.497 (3)	110.9 (2)	108.1 (3)
$(CH_3)_3N\cdot BBr_3$[b]	1.663 (13)	2.001 (3)	1.500 (5)	110.3 (3)	107.8 (5)
$(CH_3)_3N\cdot BI_3$[b]	1.663 (13)	2.245 (4)	1.497 (5)	108.6 (4)	106.0 (8)
$(CH_3)_3N$[c]			1.461 (2)		110.6 (6)
B_2H_6[d]		1.196 $\binom{+8}{-6}$		120.2 (18)	

The values represent r_g parameters.
a) Present study. b) Ref. 3. c) Ref. 22. d) The B-H bond and the HBH angle represent the B-H_t and the H_tBH_t in Ref. 23.

calculated rotational constants of the species with deuterium are significantly different from the observed ones, while those of the other species are in good agreement with the observed ones. These differences may indicate isotope effects on the B-D bond and the DBD angle. However, they cannot be estimated only from the rotational constant of $(CH_3)_3N\cdot BD_3$. The isotope effect on the B-D bond was thus estimated by the diatomic approximation and Δr_a^0 (=r_a^0(B-D)−r_a^0(B-H)) was assumed to be equal to Δr_g^0 (=r_g^0(B-D)−r_g^0(B-H)), because the force field used is not so reliable to calculate the precise perpendicular amplitude of the B-H bond, as described later. Thus, Δr_g^0 was obtained from $(3/2)a[l_0(\text{B-D})^2-l_0(\text{B-H})^2]$,[19] where a is Morse constant and was assumed to be 2.0 Å^{-1}. The mean amplitudes of the B-D and the B-H bonds at 0 K were calculated from the relation of $l_0^2=h/8\pi^2\mu c\nu$,[20] where h is Planck constant, μ is reduced mass, c is light velocity, and ν is the wave number for B-D (1656 cm^{-1}) or B-H (2267 cm^{-1}) bond stretching.[21] The isotope effect on the B-D bond distance was −0.006 Å. Then the isotope effect on the DBD angle was estimated so as to give the best agreement of the calculated rotational constant of $(CH_3)_3{}^{14}N\cdot{}^{11}BD_3$ with the observed one, and resulted in the value (=∠DBD−∠HBH) of 0.4±0.1°, where 100% uncertainty was assumed for the isotope correction to the B-D bond.

Discussion

The N-B bond distance of $(CH_3)_3N\cdot BH_3$, 1.656± 0.002 Å, is nearly equal to those of trimethylamine-boron trihalides, which were also determined by an electron-diffraction method,[3] as listed in Table 7. On the complex formation the B-H and the C-N bond distances of the complex increase by 4.4 and 1.6%, respectively, and the HBH and the CNC angles of the complex decrease by 6.1 and 1.1%, respectively, comparing the molecular parameters of $(CH_3)_3N\cdot BH_3$ with those of its component molecules,[22,23] in which BH_3 refers to the terminal part of diborane. These relative changes of the molecular parameters are nearly equal to the corresponding ones in $(CH_3)_3N\cdot BF_3$.[3] This seems to show that the acceptor power of borane is similar to that of boron trifluoride in accord with the result from the measurement of the enthalpy change.[5]

The rotational barrier around the N-B bond of this complex is higher than 5 kcal mol^{-1} and it seems to be larger than the barrier of a methyl group.[24] We deduced the V_3 value from the Y value, which was adjusted so that the calculated mean amplitude of the *gauche* $C_2\cdots H_1$ atomic pair agree with the observed one. Force constants for angle deformation, H(CNB) and H(NBH), also contributed to the mean amplitude of the *gauche* $C_2\cdots H_1$ pair. In the present study the H(CNB) was reasonably estimated from the observed mean amplitude of the C···B pair, but the H(NBH) could not be optimized. Therefore the deduced value of V_3 is not a reasonable one. However it should be noticed that the configuration around the nitrogen atom of this complex is nearly regular tetrahedral, but the observed mean amplitude of the C···B pair, 0.091± 0.005 Å, is considerably larger than that of the C···C pair, 0.080±0.003 Å. This fact shows that the BH_3 group vibrates more than the CH_3 group. Thus the mobility of the borane group seems to hinder the rotation around the N-B bond and increase the barrier height.

The isotope effects were found on the B-D bond distance and the DBD angle and they were estimated to be −0.006 Å and 0.4°, respectively, though the isotope effect on the B-D bond distance depends on the assumption of the diatomic approximation with the anharmonic constant of 2.0 Å^{-1}. The isotope effect on the C-D bond distance in CD_4 and that on the N-D bond distance in ND_3 have been estimated to be both −0.004 Å.[25,26] The isotope effect on the B-D bond distance of $(CH_3)_3N\cdot BD_3$ is comparable with them while the isotope effect on the DBD angle differs from that on the DND angle of ND_3, in which the DND angle is nearly equal to the HNH angle of NH_3.[26] It seems that in ND_3 the DND angle remains unchanged in spite of the shortening of the N-D distance because of the strong repulsion between the lone paired electrons of the N atom and the paired electrons of the N-D bond.

References

1) J. R. Durig, Y. S. Li, and J. D. Odom, *J. Mol. Struct.*, **16**, 443 (1973).
2) P. Cassoux, R. L. Kuczkowski, P. S. Bryan, and R. C. Taylor, *Inorg. Chem.*, **14**, 126 (1975).
3) K. Iijima and S. Shibata, *Bull. Chem. Soc. Jpn.*, **52**, 711 (1979); **53**, 1908 (1980); **56**, 1891 (1983).

4) H. C. Brown and R. R. Holmes, *J. Am. Chem. Soc.*, **78**, 2173 (1956).
5) W. A. G. Graham and F. G. A. Stone, *J. Inorg. Nucl. Chem.*, **3**, 164 (1956).
6) C. M. Bax, A. R. Katritzky, and L. E. Sutton, *J. Chem. Soc.*, **1958**, 1258.
7) J. M. Miller and M. Onyszchuk, *Can. J. Chem.*, **42**, 1518 (1964).
8) J. M. Miller and M. Onyszchuk, *Can. J. Chem.*, **41**, 2898 (1963).
9) W. Witt, *Z. Naturforsch., Teil A*, **19**, 1363 (1964).
10) S. Shibata, K. Iijima, R. Tani, and I. Nakamura, *Rep. Fac. Sci. Shizuoka Univ.*, **9**, 33 (1974).
11) L. Schäfer, A. C. Yates, and R. A. Bonham, *J. Chem. Phys.*, **55**, 3055 (1971).
12) D. T. Cromer and J. B. Mann, *J. Chem. Phys.*, **47**, 1892 (1967); D. T. Cromer, *ibid.*, **50**, 4857 (1969).
13) C. Tavard, D. Nicolas, and M. Rouault, *J. Chim. Phys.*, **64**, 540 (1967).
14) J. Karle and I. L. Karle, *J. Chem. Phys.*, **18**, 957 (1950).
15) For the definitions of various distances, see K. Kuchitsu and S. J. Cyvin, "Molecular Structures and Vibrations," ed by S. J. Cyvin, Elsevier, Amsterdam (1972), Chap. 12.
16) Y. Morino and E. Hirota, *J. Chem. Phys.*, **28**, 185 (1958).
17) K. Kuchitsu, *Bull. Chem. Soc. Jpn.*, **40**, 505 (1967).
18) M. Toyama, T. Oka, and Y. Morino, *J. Mol. Spectrosc.*, **13**, 193 (1964).
19) L. S. Bartell, *J. Chem. Phys.*, **38**, 1827 (1963).
20) R. W. James, *Physik Z.*, **33**, 737 (1932).
21) W. Sawodny and J. Goubeau, *Z. Phys. Chem.*, **44**, 227 (1965).
22) B. Beagley and A. R. Medwid, *J. Mol. Struct.*, **38**, 229 (1977).
23) L. S. Bartell and B. L. Carroll, *J. Chem Phys.*, **42**, 1135 (1965).
24) W. G. Fateley and F. A. Miller, *Spectrochim. Acta*, **18**, 977 (1962).
25) L. S. Bartell, K. Kuchitsu, and R. J. deNeui, *J. Chem. Phys.*, **35**, 1211 (1961).
26) K. Kuchitsu, J. P. Guillory, and L. S. Bartell, *J. Chem. Phys.*, **49**, 2488 (1968).

Phosphorylation of Nucleosides with Sodium *cyclo*-Triphosphate

Mitsutomo TSUHAKO,* Mayumi FUJIMOTO, Shigeru OHASHI,†
Hiroyuki NARIAI,†† and Itaru MOTOOKA††
Kobe Women's College of Pharmacy, Kitamachi, Motoyama, Higashinada-ku, Kobe 658
†*Department of Chemistry, Faculty of Science, Kyushu University 33, Hakozaki, Higashi-ku, Fukuoka 812*
††*Department of Chemistry, Faculty of General Education, Kobe University, Tsurukabuto, Nada-ku, Kobe 657*
(Received January 12, 1984)

Phosphorylation of nucleosides with sodium *cyclo*-triphosphate (P_{3m}) was studied under various conditions (mixing ratio of P_{3m} to nucleoside, pH, reaction temperature and time). 1) Adenosine, cytidine, guanosine, and uridine were easily phosphorylated by P_{3m} to form selectively nucleoside 2′-monophosphates, 3′-monophosphates, and 2′,3′-cyclic monophosphates. On the other hand, 2′-deoxyadenosine, 3′-deoxyadenosine, 2′-deoxycytidine, and thymidine could not be phosphorylated by P_{3m}. 2) The phosphorylation of adenosine, cytidine, guanosine, and uridine varied strongly, depending on the reaction conditions; mixing ratio, pH, reaction temperature and time. Under conditions of a high mixing ratio of P_{3m} to nucleoside (5:1—10:1), high pH (12—14), high temperature (70—100 °C) for a short time (1—2 d) or low temperature (room temperature) for a long time (70—150 d), nucleoside 2′- and 3′-monophosphate could be obtained in high yield (about 50—100%). 3) At the initial stage of the phosphorylation reactions of adenosine, cytidine, and guanosine with P_{3m}, nucleoside 2′,3′-cyclic monophosphates were formed, though a small amount (about 1—3%), but in the course of the reaction for a long time, they were hydrolyzed to nucleoside 2′- and 3′-monophosphates. 4) 2′-deoxyadenosine, 3′-deoxyadenosine, 2′-deoxycytidine, and thymidine could not be phosphorylated by P_{3m}. This means that the presence of hydroxyl groups at the 2′- and 3′-positions of the ribose was necessary for the phosphorylation of nucleosides with P_{3m}. 5) Phosphorylation of nucleosides with short-chain phosphates (ortho-, pyro-, and triphosphate) could not be observed at all. 6) The mechanism of formation of nucleoside 2′-monophosphates, 3′-monophosphates, and 2′,3′-cyclic monophosphates in the phosphorylation of nucleosides with P_{3m} was discussed.

Nowadays, as phosphorylating agents for nucleosides and related organic compounds are usually used phosphoryl chloride, polyphosphoric acid[1-4] and various organic phosphorus compounds.[5-8] However, the phosphorylation of nucleosides with such reagents is generally a tedious operation. Feldmann[9] has reported that sodium *cyclo*-triphosphate(P_{3m}) reacted with alcohol or sugar in an alkaline solution to form its monophosphate or triphosphate derivatives. Also, Schwartz[10] and Saffhill[11] have reported that, by the phosphorylation of nucleosides with condensed phosphates, nucleosie 2′-, 3′-, and 5′-monophosphates were obtained. However, their formation conditions and the reaction mechanism are scarcely known at present. The present authors[12] have already reported that inosine was easily phosphorylated by P_{3m} at 2′- and 3′-positions of the ribose to form selectively inosine 2′-monophosphate(2′-IMP) and 3′-monophosphate(3′-IMP). Accordingly, in the present study adenosine, 2′- and 3′- deoxyadenosine, cytidine, 2′-deoxycytidine, guanosine, uridine, and thymidine were phosphorylated with P_{3m} under various experimental conditions, and the reaction products as well as the reaction mechanism were investigated.

Experimental

1) Phosphorylation of Adenosine with cyclo-*Triphosphate.* With 50 cm^3 of 0.2 mol dm^{-3} aqueous sodium *cyclo*-triphosphate(P_{3m}) solution were mixed 50 cm^3 of adenosine solutions of various concentrations ranging from 0.02 to 0.04 mol dm^{-3}, and each mixed solution (molar ratio P_{3m}: adenosine=5:1—10:1) was adjusted to the prescribed pH value (14, 12, 10, 7, and 2) by use of sodium hydroxide or hydrochloric acid solution and was allowed to react at 100 °C, 70 °C, and room temperature. Because the pH of the mixed solution decreased with the progress of the reaction, the pH of the solution was kept always at the prescribed value using sodium hydroxide solution.

2) Phosphorylation of Cytydine with cyclo-*Triphosphate.* With 50 cm^3 of 0.5 mol dm^{-3} aqueous P_{3m} solution were mixed 50 cm^3 of aqueous cytidine solution of various concentrations ranging from 0.1 to 0.5 mol dm^{-3}, and each mixture (P_{3m}: cytidine=1:1—5:1) was allowed to react at pH 14—2, at room temperature and 70 °C.

3) Phosphorylation of Guanosine with cyclo-*Triphosphate.* With 50 cm^3 of 0.2 mol dm^{-3} aqueous P_{3m} solution was mixed 50 cm^3 of 0.04 mol dm^{-3} guanosine solution and the mixture (P_{3m}: guanosine=5:1) was allowed to react, similarly to the experiments of adenosine and cytidine series.

4) Phosphorylation of Uridine with cyclo-*Triphosphate.* With 50 cm^3 of 0.05—0.5 mol dm^{-3} aqueous P_{3m} solutions was mixed 50 cm^3 of 0.05 mol dm^{-3} aqueous uridine solution, and each mixed solution (P_{3m}:uridine=1:1—10:1) was allowed to react at pH 12 and 70 °C.

5) Phosphorylation of Thymidine with cyclo-*Triphosphate.* With 50 cm^3 of 0.2 mol dm^{-3} aqueous P_{3m} solution was mixed 50 cm^3 of 0.04 mol dm^{-3} aqueous thymidine solution, and the mixed solution (P_{3m}: thymidine=5:1) was allowed to react at pH 12—14 and 70 °C.

6) Phosphorylation of 2′- or 3′-Deoxyadenosine with cyclo-*Triphosphate.* With 50 cm^3 of 0.2 mol dm^{-3} aqueous P_{3m} solution was mixed 50 cm^3 of 0.04 mol dm^{-3} aqueous solution of 2′- or 3′-deoxyadenosine, the mixture was adjusted to pH 12 with 6 mol dm^{-3} sodium hydroxide solution and was allowed to react at 70 °C.

7) Phosphorylation of 2′-Deoxycytidine with cyclo-*Triphosphate.* With 50 cm^3 of 0.5 mol dm^{-3} aqueous P_{3m} solution was mixed 50 cm^3 of 0.1 mol dm^{-3} aqueous 2′-deoxycytidine solution, and the mixture was allowed to react at pH 12 and 70 °C.

8) Phosphorylation of Nucleosides with Ortho-, Pyro-, or Triphosphate. With 50 cm^3 of 0.2 mol dm^{-3} aqueous solution of a short-chain sodium ortho-, pyro-, or triphosphate was mixed 50 cm^3 of 0.04 mol dm^{-3} aqueous solutions of adenosine, cytidine, guanosine, uridine and thymidine, and each mixture was allowed to react at pH 12 and 70 °C, similarly to the phosphorylation of nucleosides with P_{3m}.

Chemicals. Sodium *cyclo*-triphosphate hexahydrate, $Na_3P_3O_9 \cdot 6H_2O$, was prepared by the procedure described in the previous paper[13] and recrystallized five times from an aqueous solution. Guaranteed grade adenosine, 2'- and 3'-deoxyadenosine, cytidine, 2'-deoxycytidine, guanosine, uridine, and thymidine from Sigma Chemical Company were used without purification.

Anion-exchange Chromatography. A column of 1.5X64 cm packed with an anion-exchange resin Dowex 1X2 (formate form) of 200—400 mesh was employed. The eluent used in the experiments of adenosine series was 0.3 mol dm^{-3} formic acid solution, pH being about 2.1. The sample solution (1 cm^3) was injected into a column, and the eluate was fractionated in 10-g fractions with a fraction collector of the weight type. Adenosine, adenosine 2'-monophosphate (2'-AMP), adenosine 3'-monophosphate(3'-AMP), and 2', 3'-cyclic monophosphate(2', 3'-cAMP) were determined by means of spectrophotometry at 260 nm.

In experiments of cytidine series, a mixture of 0.05 mol dm^{-3} formic acid with equal volume of 0.01 mol dm^{-3} sodium formate solution was used as the eluent. The pH of the mixed solution was about 3.0. The absorbance was measured at 279 nm.

In experiments of guanosine series, an equal volume mixture of 1 mol dm^{-3} formic acid and 0.15 mol dm^{-3} sodium formate solution was used as the eluent. The pH of the mixed solution was about 2.7. The absorbance was measured at 255 nm.

The eluent used in experiments of uridine and thymidine series was an equal volume mixture of 1 mol dm^{-3} formic acid and 0.1 mol dm^{-3} sodium formate solution. The pH of the mixed solution was about 2.5. The absorbance was measured at 260 and 267 nm in experiments of uridine and thymidine series, respectively.

High Performance Liquid Chromatography (HPLC).[12] HPLC was carried out by use of a Shimadzu LC-3A, under the following conditions: packing material Lichromosorb H_2N (5 μm, E. Merck), column size 250X4.6 mm I.D., pressure 70 kg/cm^2, column temperature 40 °C, eluent 0.015 mol dm^{-3} ammonium dihydrogen orthophosphate, flow rate 1.0 cm^3/min.

Thin-layer Chromatography (TLC). Plates used were DC-Alufolin cellulose F_{254} and DC-Fertigplatten cellulose F (E. Merck). As the developer was used a mixture solution consisting of saturated ammonium sulfate, 1 mol dm^{-3} ammonium acetate solution, and 2-propanol, in the ratio of 80:18:12.

Results and Discussion

Phosphorylation of Adenosine with P_{3m}. With 50 cm^3 of 0.2 mol dm^{-3} aqueous P_{3m} solution was mixed 50 cm^3 of 0.02 mol dm^{-3} aqueous adenosine solution (P_{3m}:adenosine=10:1) and the mixture was allowed to react at pH 12 and 70 °C. The pH of the mixture decreased gradually and reached to about 7.5 after 1 d. This fact suggests that P_{3m} reacted with water or adenosine to form linear phosphates or their derivatives. As an example, results of anion-exchange chromatography of the reaction products are shown in Fig. 1. As can be seen from Fig. 1, after 1 d peaks corresponding to adenosine 2'-monophosphate(2'-AMP), adenosine 3'-monophosphate(3'-AMP), and adenosine 2', 3'-cyclic monophosphate(2', 3'-cAMP) were observed at about 700, 1070, and 1200 cm^3 of the effluent, respectively. Reaction products of adenosine with P_{3m} were only 2'-AMP, 3'-AMP, and 2', 3'-cAMP. On the other hand, the peak of adenosine appeared at 70 cm^3 of the effluent. The products obtained in the reaction were identified to be 2'-AMP, 3'-AMP, and 2', 3'-cAMP, by comparing their data of anion-exchange chromatography, HPLC, and TLC with those of the authentic samples, as well as by chemical analysis of the reaction products. Also, it is found that the amounts of 2'-AMP and 3'-AMP increase with the reaction time.

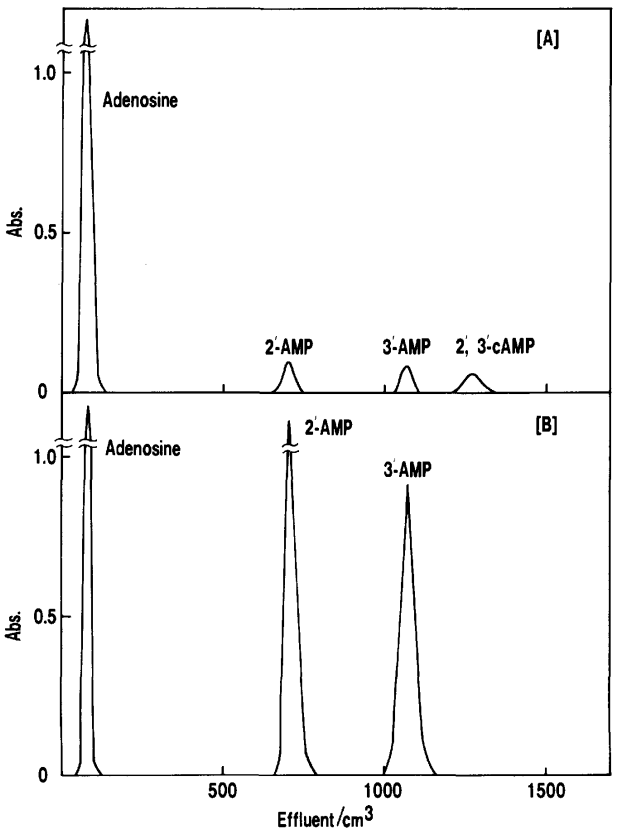

Fig. 1. Elution patterns for the reaction products of P_{3m} with adenosine at 70 °C and pH 12.
P_{3m}: Adenosine=10:1, (A): After 1 d, (B): After 17 d.

In Fig. 2, the amounts of 2'-AMP, 3'-AMP, and 2', 3'-cAMP, formed by the reaction of P_{3m} with adenosine (mixing ratio=10:1) at pH 12 and 70 °C, are plotted as a function of time. With the progress of the reaction, amounts of 2'-AMP and 3'-AMP increased gradually to maximum values, about 37 and 45% after 17—25 d respectively, and then decreased slowly. On the contrary, the amount of 2',3'-cAMP was largest (about 3%) after 1 d, and decreased rapidly with the reaction time, and finally became entirely zero after 8 d. On the other hand, with the increase of 2'-AMP and 3'-AMP formation, the starting material(adenosine) decreased.

Further, after a long reaction time (more than 30 d) the amounts of decomposition products of adenosine, 2′-AMP, and 3′-AMP increased gradually.

Figure 3 shows the change of the amounts of 2′-AMP and 3′-AMP in the reaction of P_{3m} with adenosine under conditions of mixing ratio 5:1, pH 12, and room temperature. The decrease in the mixing ratio as well as the lowering of the reaction temperature caused to decrease extremely the formation rate and the yields of products. Further, formation of 2′,3′-cAMP observed at the initial stage of the reaction, was so little that it was omitted in Fig. 3.

The amounts of 2′-AMP, 3′-AMP, and 2′, 3′-cAMP obtained by the phosphorylation of adenosine with P_{3m} under various conditions are summarized in Table 1. As can be seen, the phosphorylation of adenosine with P_{3m} could not proceed at pH 7 or less, namely in neutral or acidic medium. The larger the ratio of P_{3m} to adenosine, the higher the pH and the higher the reaction temperature are, the larger are the amounts of 2′-AMP and 3′-AMP formed.

The phosphorylation of 2′-deoxyadenosine, 3′-deoxyadenosine, and adenine (purine base of adenosine) with P_{3m} were also investigated under conditions similar to those for the phosphorylation of adenosine with P_{3m}. However, these compounds could not be phosphorylated at all. Results of the phosphorylation of 2′- and 3′-deoxyadenosine are also shown in Table 1 for reference.

Based on above-described results, 2′-AMP and 3′-AMP could be selectively obtained by the phosphorylation of adenosine with P_{3m} under conditions of high mixing ratio (P_{3m}:adenosine=5:1—10:1), high pH (pH 10—14), and high temperature (70—100 °C). Also, 2′, 3′-cAMP was formed in a short period (1—3 d) after the reaction, but it was easily decomposed with time and thus its amount was so little as about 3% at the highest. Based on the fact that 2′,3′-cAMP is easily hydrolyzed under the present experimental conditions to form 2′-AMP and 3′-AMP, 2′, 3′-cAMP formed at the initial stage of the reaction is considered to be hydrolyzed.

From the above results, the optimum conditions for the phosphorylation of adenosine with P_{3m} are found to be mixing ratio 10:1, pH 12, and 70 °C. Further, the fact that 2′- and 3′-deoxyadenosine cannot be phosphorylated at all with P_{3m} may suggest that the presence of hydroxyl groups at both 2′- and 3′-positions of the

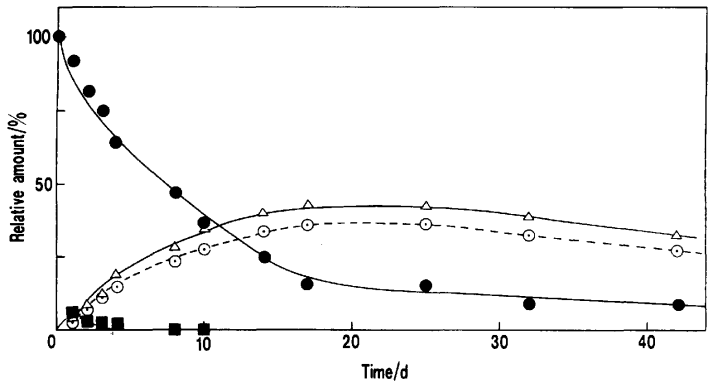

Fig. 2. Change of the amounts of 2′-AMP, 3′-AMP, 2′,3′-cAMP, and adenosine in the reaction of adenosine with P_{3m}.
P_{3m}: adenosine=10:1, pH 12, 70 °C.
--⊙--; 2′-AMP, —△—; 3′-AMP, —■—; 2′,3′-cAMP, —●—; adenosine.

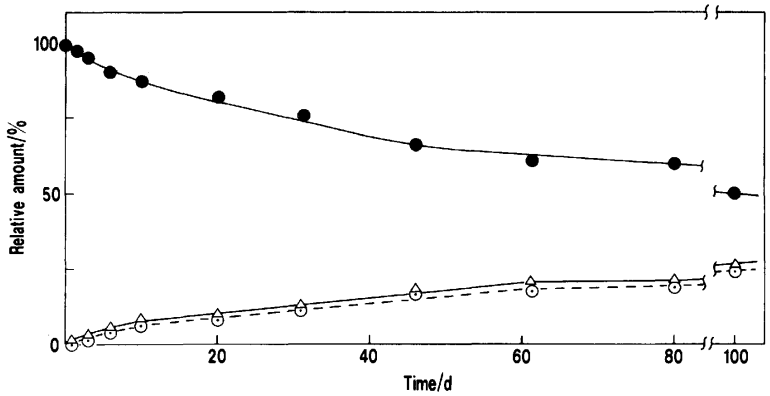

Fig. 3. Change of the amounts of 2′-AMP, 3′-AMP, and adenosine in the reaction of adenosine with P_{3m}.
P_{3m}: adenosine=5:1, pH 12, room temp.
--⊙--; 2′-AMP, —△—; 3′-AMP, —●—; adenosine.

Table 1. Phosphorylation of adenosine, 2′-deoxyadenosine, and 3′-deoxyadenosine with P_{3m}

Reaction conditions				Yield/%		
Mixing ratio	pH	Temp/°C	Time/d	2′-AMP	3′-AMP	2′,3′-cAMP
P_{3m}: Adenosine						
5 : 1	14	70	1	10	11	0
	12	100	1	13	17	0
	12	70	4	6	7	1
			21	29	36	0
	12	room	20	9	9	0.6
			100	24	26	0
	10	70	20	7	9	0.4
			64	13	17	0
	7	70	35	0	0	0
	2	70	35	0	0	0
10 : 1	12	70	1	2	3	3
			17	37	45	0
P_{3m}: 2′-Deoxyadenosine						
5 : 1	12	70		—	0	—
P_{3m}: 3′-Deoxyadenosine						
5 : 1	12	70		0	—	—

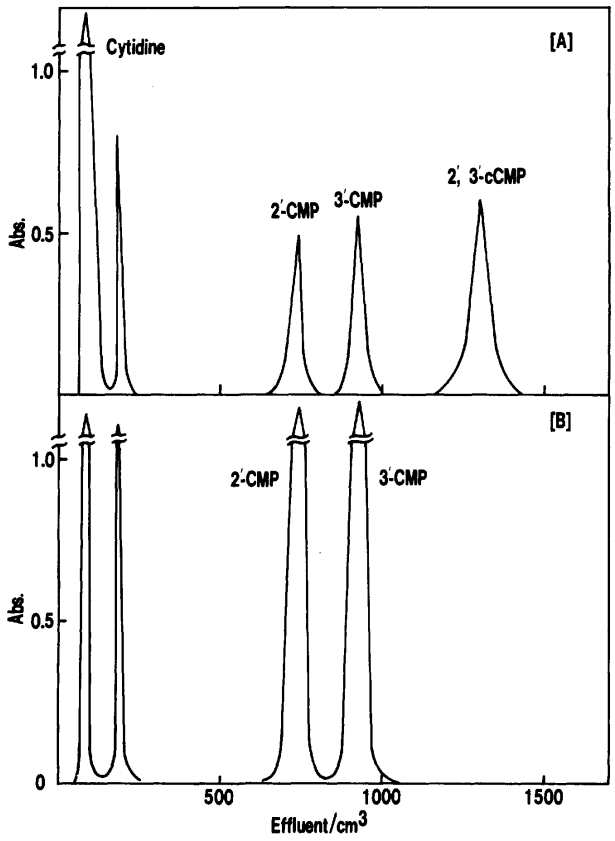

Fig. 4. Elution patterns for the reaction products of P_{3m} with cytidine at 70 °C and pH 12.
P_{3m}: Cytidine=1 : 1, (A): After 3 d, (B): After 9 d.

ribose is required for the phosphorylation of nucleosides with P_{3m}.

Phosphorylation of Cytidine with P_{3m}. In Fig. 4 are shown the results of anion-exchange chromatography of the reaction products in the phosphorylation of cytidine with P_{3m}. Peaks corresponding to cytidine 2′-monophosphate(2′-CMP), cytidine 3′-monophosphate(3′-CMP), and cytidine 2′,3′-cyclic monophosphate(2′,3′-cCMP) appeared at about 740, 930, and 1300 cm^3 of the effluent, respectively. These products were identified by comparing their data of anion-exchange chromatography, HPLC, and TLC with those of the authentic samples. The peak of cytidine appeared also at about 80 cm^3 of the effluent. Further, a large peak (about 180 cm^3) appeared between those of cytidine and 2′-CMP was proved to correspond to the decomposition product of cytidine by the experiment, in which cytidine alone was treated at pH 12 and 70 °C. As the decomposition product is, however, not identified yet and is beyond the purpose of the present study, it is not described here.

The reaction products of the phosphorylation of cytidine with P_{3m} were only 2′-CMP, 3′-CMP, and 2′, 3′-cCMP. In the reaction for a long time, 2′-CMP and 3′-CMP were formed markedly.

Yields of 2′-CMP, 3′-CMP, and 2′, 3′-cCMP in the phosphorylation of cytidine or 2′-deoxycytidine with P_{3m} are summarized in Table 2. At pH 14 and 70 °C, cytidine was phosphorylated with P_{3m} in a short time (10—24 hr), namely about 55% of the starting material (cytidine) was phosphorylated after 1 d. With the elapse of the reaction time, however, 2′-CMP and 3′-CMP once formed were hydrolyzed, and as the result, the amounts of them decreased rapidly. At the same reaction temperature, the phosphorylation of cytidine with P_{3m} became slower with the decrease of pH, and the phosphorylation did not proceed under acidic conditions. 2′, 3′-cCMP was easily formed at the initial stage of the reaction, but with the elapse of reaction time, 2′, 3′-cCMP was hydrolyzed to form 2′-CMP and 3′-CMP. 2′,3′-cCMP was well formed at pH 12 and room temperature (about 4.2%).

Table 2. Phosphorylation of cytidine and 2′-deoxycytidine with P_{3m}

Reaction conditions				Yield/%		
Mixing ratio	pH	Temp/°C	Time/d	2′-CMP	3′-CMP	2′,3′-cCMP
P_{3m}: Cytidine						
1 : 1	14	70	0.3	16	24	0.6
			0.9	22	32	0
			3	7	5	0
	12	70	3	1	2	2.6
			14	17	24	0
			21	17	23	0
	12	room	4	8	11	4.2
			65	35	45	0.2
	10	70	5	1	2	1.3
			16	4	7	0
	7	70	7	0.4	0.6	0.2
			26	0.4	1.6	0
	2	70	14	0	0	0
5 : 1	12	70	3	4	6	2
			7	24	35	0
P_{3m}: 2′-Deoxycytidine						
5 : 1	12	70		—	0	—

At pH 12 and room temperature after a long time(65 d), about 80% of cytidine was phosphorylated to form about 35 and 45% of 2′-CMP and 3′-CMP, respectively. As can be seen from Table 2, at such a high pH as 14 and at high temperature (70 °C), 2′-CMP and 3′-CMP once formed were easily hydrolyzed.

The optimum conditions for the phosphorylation of cytidine with P_{3m} are either at pH 12 and room temperature for a long time (65—70 d) or at pH 14 and 70 °C for a short time (12—24 h). Cytidine, differing from adenosine series, was found to be phosphorylated even at pH 7, though small in amount. On the other hand, the phosphorylation of 2′-deoxycytidine with P_{3m} could not be observed at all, similarly to the cases of 2′-deoxyadenosine and 3′-deoxyadenosine. For the phosphorylation of cytidine, the presence of hydroxyl groups at both 2′- and 3′-positions of the ribose was also suggested to be necessary. The basis of this conclusion will be discussed later in detail.

Phosphorylation of Guanosine with P_{3m}. An example of the results of anion-exchange chromatography of the reaction products obtained in the phosphorylation of guanosine with P_{3m} is shown in Fig. 5-(A). Guanosine was easily phosphorylated with P_{3m} to form chiefly guanosine 2′-monophosphate(2′-GMP) and guanosine 3′-monophosphate (3′-GMP). Also in the phosphorylation of guanosine, the formation of guanosine 2′, 3′-cyclic monophosphate(2′,3′-cGMP), though small in amount, was observed at the initial stage of the reaction. Amounts of 2′-GMP and 3′-GMP obtained under various conditions are summarized in Table 3. The optimum conditions for the phosphorylation of guanosine with P_{3m} are found to be the mixing ratio 5:1, pH 12, room temperature, and long reaction period (70 d).

Phosphorylation of Uridine with P_{3m}. Figure 6 shows the results of HPLC of the reaction products in the phosphorylation of uridine with P_{3m}. Comparing the data with those of the authentic samples, the main reaction products were uridine 2′-monophosphate (2′-UMP) and uridine 3′-monophosphate(3′-UMP).

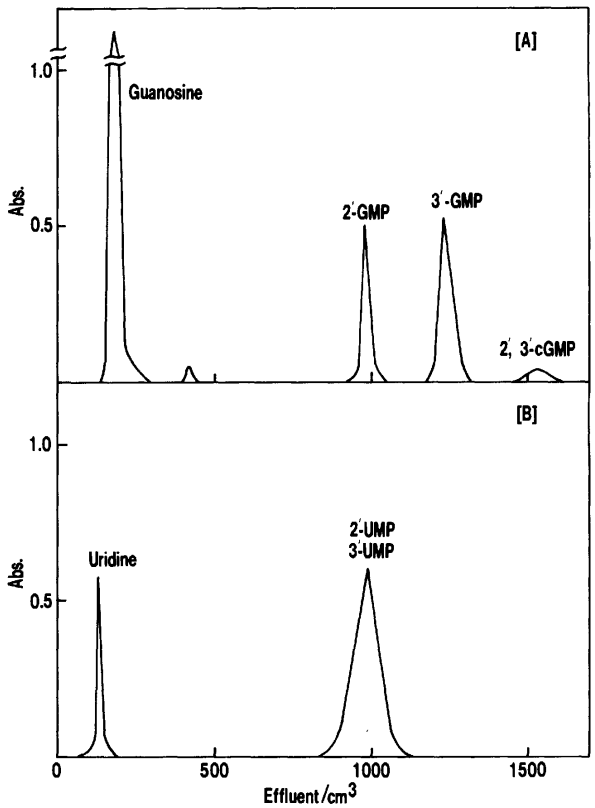

Fig. 5. Elution patterns for the reaction products of P_{3m} with guanosine or uridine at 70 °C and pH 12.
(A); P_{3m}: Guanosine=5 : 1, after 14 d.
(B); P_{3m}: Uridine=10 : 1, after 4 d.

Table 3. Phosphorylation of guanosine with P_{3m}

Reaction conditions				Yield/%		
Mixing ratio	pH	Temp/°C	Time/d	2′-GMP	3′-GMP	2′,3′-cGMP
P_{3m}: Guanosine						
5 : 1	12	70	25	21	23	2.0
	12	Room	2	3	4	3.2
			70	39	44	0
	10	70	25	9	11	0
	7	70	34	0	0	0
	2	70	30	0	0	0

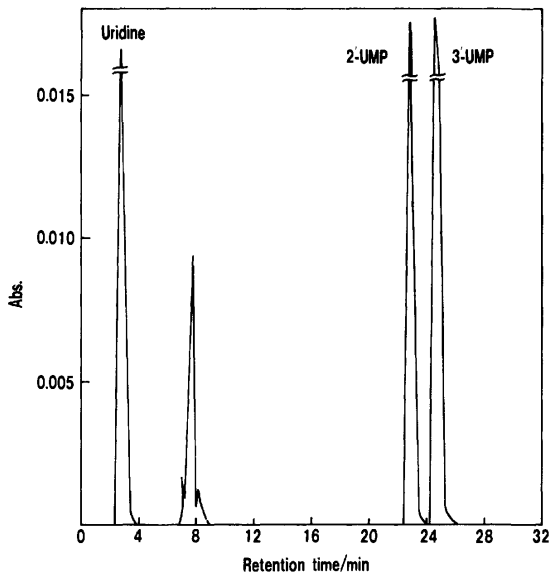

Fig. 6. Elution profile of the reaction products of P_{3m} with uridine at 70 °C and pH 12.
P_{3m}: Uridine=10 : 1, after 49 d.

Three small peaks, appeared between those of the starting material (uridine) and 2′-UMP, were proved to be those of decomposition products of uridine, based on the experiment carried out with uridine alone under the same conditions (pH 12 and 70 °C). On the other hand, 2′-UMP and 3′-UMP was not separated by anion-exchange chromatography under the above-described conditions, as shown in Fig. 5-(B). Further, the formation of 2′, 3′-cUMP could not be ascertained by means of HPLC and anion-exchange chromatography. It is not clear yet whether 2′, 3′-cUMP was not formed originally or 2′, 3′-cUMP once formed at the initial stage of the reaction, being very unstable, was easily hydrolyzed. It may be reasonable, however, to consider that the latter is more probable, similarly to the case of adenosine, cytidine, and guanosine series.

In Table 4 are shown the results of phosphorylation of uridine with P_{3m} under various conditions. Under the conditions of P_{3m}:uridine=10:1, pH 12, and room temperature, uridine is phosphorylated with P_{3m} completely (100%) after 140 d. Thus, the starting material (uridine), 2′-UMP, and 3′-UMP were not hydrolyzed at all at room temperature.

Phosphorylation of Thymidine with P_{3m}.[14] Thymidine, one of 2′-deoxynucleosides, was not phosphorylated at all under above-described conditions. This fact may be explained similarly to the above-described cases of 2′- and 3′-deoxyadenosine and 2′-deoxycytidine. The reasons will be discussed later in detail.

Table 4. Phosphorylation of uridine with P_{3m}

Reaction conditions				Yield/%
Mixing ratio	pH	Temp/°C	Time/d	2′(3′)-UMP
P_{3m}: Uridine				
1 : 1	12	70	36	29
	12	room	35	12
	2	70	35	0
5 : 1	12	70	10	78
	10	70	10	23
	7	70	12	7
10 : 1	12	70	4	84
	12	room	7	32
			140	100

Phosphorylation of Nucleosides with Ortho-, Pyro-, and Triphosphate. The phosphorylation of nucleosides with short-chain phosphates such as ortho-(P_1), pyro-(P_2), and triphosphate(P_3) was also investigated under similar experimental conditions to those with P_{3m}, but the phosphorylation of nucleosides with short-chain phosphates was not observed at all.

Mechanism of Phosphorylation of Nucleosides with P_{3m}. The mechanism of the phosphorylation of adenosine, cytidine, guanosine, and uridine with P_{3m} is summarized in Fig. 7. First, a hydrogen bond is formed between the hydroxyl group at the 2′- or 3′-position of ribose of nucleoside and an oxygen atom of P_{3m}. Then, by the attack of the corresponding oxygen atom of the hydroxyl group at 3′- or 2′-position upon a phosphorus atom of P_{3m}, the ring of P_{3m} is opened to give an intermediate product, a triphosphate derivative of nucleoside. This triphosphate derivative, however, is immediately hydrolyzed to give nucleoside 2′- or 3′-monophosphate and P_2. On the other hand, the mechanism of formation of nucleoside 2′,3′-cyclic monophosphate may be as follows: As shown in Fig. 7, the intermediate, nucleoside 2′- or 3′- triphosphate formed first by the reaction of nucleoside with P_{3m}, is attacked by the hydroxyl group at 3′- or 2′- position, to give 2′,3′-cyclic monophosphate and P_2. Nucleoside 2′,3′-cyclic monophosphate thus formed is hydrolyzed to give 2′- and

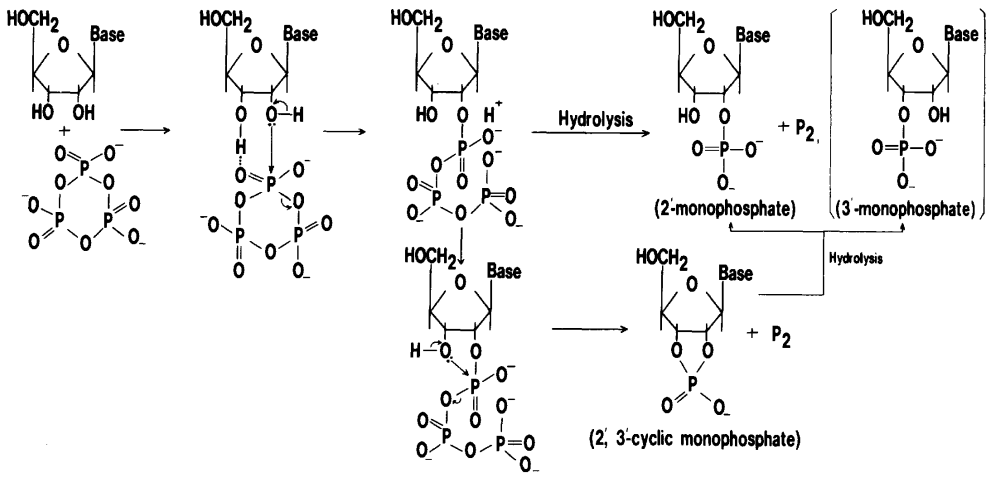

Fig. 7. Mechanism of phosphorylation of nucleosides with P_{3m}.

3'-monophosphate.

As can be seen from above-mentioned experimental results, nucleoside 2'- and 3'-monophosphates, formed by the phosphorylation of adenosine, cytidine, guanosine or uridine with P_{3m}, are nearly equal in amount. This means that the probability to form a hydrogen bond between the hydroxyl group at 2'- or 3'-position of the ribose and an oxygen atom of P_{3m} are practically equal. Further, based on the fact that 2'-deoxyadenosine, 3'-deoxyadenosine, 2'-deoxycytidine, and thymidine cannot be phosphorylated with P_{3m} at all, the presence of hydroxyl groups at both 2'- and 3'-positions of the ribose is suggested to be indispensable for the phosphorylation. In this connection, formation of the above-mentioned hydrogen bond between the hydroxyl group at 2'- or 3'- position and an oxygen atom of P_{3m} is considered to be really possible in aqueous solution, because the bond length of P=O in crystalline sodium *cyclo*-triphosphate is 1.48 Å,[9] while that of C–C bond at 2'- and 3'-positions of ribose in nucleoside is 1.53 Å.[15]

References

1) R. H. Hall and H. G. Khorana, *J. Amer. Chem. Soc.*, **77**, 1871 (1955).

2) A. W. Schwartz and C. Ponnamperuma, *Nature*, **218**, 443 (1968).

3) J. Hulshof and C. Ponnamperuma, *Origins of Life*, **7**, 197 (1976).

4) M. Yoshikawa, T. Kato, and T. Takenishi, *Tetrahedron Lett.*, **1967**, 5065.

5) M. Ikehara, T. Ueda, and E. Otsuka, "Kakusan Yuki Kagaku," Kagaku Dojin (1979), p. 85.

6) M. Ikehara, "Tanpakushitsu Kakusan Khoso," **6**, 615 (1961).

7) D. W. Hutchinson, in E. Haslam (Editor), "Comprehensive Organic Chemistry," Pergamon Press, New York (1979), Vol. 5, p. 123.

8) V. M. Clark, G. W. Kirby, and A. Todd, *J. Chem. Soc.*, **1957**, 1497.

9) W. Feldmann, *Chem. Ber.*, **100**, 3850 (1967).

10) A. W. Schwartz, *Chem. Comm.*, **1969**, 1393.

11) R. Soffhill, *J. Org. Chem.*, **35**, 2881 (1970).

12) M. Tsuhako, M. Fujimoto, and S. Ohashi, *Chem. Lett.*, **1981**, 849.

13) M. Tsuhako, N. Fujita, A. Nakahama, T. Matsuo, M. Kobayashi, and S. Ohashi, *Bull. Chem. Soc. Jpn.*, **53**, 1968 (1980).

14) M. J. Bishop, R. Lohrmann, and L. E. Orgel, *Nature*, **237**, 162 (1972).

15) J. Feder, in M. Grayson and E. J. Griffith (Editors), "Topics in Phosphorus Chemistry," John Wiley and Sons, New York (1983), Vol. 11, p. 1.

 © 1984 The Chemical Society of Japan Bull. Chem. Soc. Jpn., 57, 3281—3285 (1984)

Potassium-ion Exchange on α-Hafnium Phosphate

Isao TOMITA,* Masaru BANJU,† Katsumi NOGUCHI,† and Toshihiro NAKAMURA†

Tokyo University of Fisheries, Konan, Minato-ku, Tokyo 108

†*Department of Industrial Chemistry, Faculty of Engineering, Meiji University, Higashi-Mita, Tama-ku, Kawasaki 214*

(Received April 16, 1984)

Forward and backward pH titration curves were measured for potassium-ion exchange on crystalline α-hafnium phosphate which had been prepared by the direct-precipitation method. Exchange in each direction proceeded in two steps, and the hysteresis was observed in the region of smaller loadings of the potassium ions. Exchange in the ternary H^+–Li^+–K^+ system was also preliminarily investigated, the selectivity of the potassium and lithium ions was what would be expected from the results of the binary hydrogen ion-alkali metal ion systems.

Lithium-ion-exchange behavior on crystalline α-hafnium bis(hydrogenphosphate) monohydrate, $Hf(HPO_4)_2 \cdot H_2O$, was reported in a previous paper[1], where this compound was considered not to form as many exchanged phases as α-zirconium phosphate because of the single-step lithium-ion exchange.

In contrast to the lithium-ion exchange, the potassium-ion exchange proceeds step-by-step as is the case for α-zirconium phosphate, but considerable difference is observed in the forward and backward titrations. Detailed experiments were thus carried out for K^+- and H^+-ion exchange, as well as for ternary-ion exchange (H^+–Li^+–K^+), and will be reported in this paper. The α-hafnium phosphate employed here had been synthesized by the direct-precipitation method. Comparison between the ion exchangers prepared by the reflux method and by the direct-precipitation method was also made.

Experimental

Ion-exchangers. Alberti and Torracca[2] prepared α-zirconium phosphate by the direct-precipitation method. Hasegawa and Kuwayama,[3] and Inoue and Yamada[4] have further developed methods for α-zirconium phosphate. There has been no data for the direct precipitation of α-hafnium phosphate, but a method similar to α-zirconium phosphate preparation can be expected to be useful. For the preparation of α-hafnium phosphate, the methods adopted by the above-mentioned authors were applied to the hafnium compound with some modifications. Hafnium tetrachloride was dissolved in hydrofluoric acid. To this we then added phosphoric acid, the concentrations of the resulting solutions were 0.13 mol·dm^{-3} in Hf^{IV}, 0.76 mol·dm^{-3} in HF, and 2.5 mol·dm^{-3} in H_3PO_4. The solution was transferred into a polyethylene bottle and placed in a water bath kept at 56 °C; then prehumidified air was passed through for more than 100 h. The crystalline precipitates thus formed were centrifuged and washed with deionized water until the pH of the supernatant solution became 4.5. The product was stored over silica gel, and characterization was made by means of X-ray powder diffractometry and thermal analysis (TG, DTA).

The potassium form of α-hafnium phosphate was prepared from α-hafnium phosphate by the batch method in the presence of 0.033 mol·dm^{-3} KCl and 0.067 mol·dm^{-3} KOH. The potassium salt employed in the backward titration was a monohydrate of the dipotassium salt of α-hafnium phosphate.

Ion-exchange Experiment. This experiment was carried out by the batch method. In the binary K^+–H^+ forward experiment, mixed solutions of 0.1 mol·dm^{-3} KCl and 0.1 mol·dm^{-3} KOH at variable mixing ratios were used to give solutions with differing pH values, while the K^+ ion concentration was kept constant. A weighed amount (150 mg) of α-hafnium phosphate was placed in contact with each of the above-mentioned solutions (15 cm^3) in a stoppered Erlenmeyer flask, and the mixture was shaken for 5 d at 25 °C. After equilibration, the solution was centrifuged, and the supernatant was subjected to pH measurement, as well as to the determination of potassium by means of gravimetry with sodium tetraphenylborate.[5] The analytical data for potassium were used for the calculation of the K^+ ionic fraction ($\overline{XK}$) of the exchanger. The solid phase was analyzed by means of X-ray powder diffractomety with a Shimadzu X-ray diffractometer, XD-3A. The samples were either in a slightly wet state before mesurement or in a completely dry state after having been placed over silica gel. Thermogravimetry and differential thermal analysis were carried out with a Shimadzu thermal analyzer, DT-30.

In the backward titration, a 180-mg portion of potassium salt was taken, the amount being equivalent to 150 mg of α-hafnium phosphate. Fifteen-cm^3 portions of the mixed solutions of 0.1 mol·dm^{-3} KCl and 0.1 mol·dm^{-3} HCl at variable mixing ratios were placed in contact with the potassium form for 5d at 25 °C.

In the case of the ternary H^+–Li^+–K^+ system, a 150-mg portion of α-hafnium phosphate was equilibrated with mixed solutions of 0.1 mol·dm^{-3} LiCl, 0.1 mol·dm^{-3} LiOH, 0.1 mol·dm^{-3} KCl, and 0.1 mol·dm^{-3} KOH at 25 °C. The equilibration time was 5 d. The lithium in the supernatant was determined by means of flame photometry with a Hitachi atomic absorption spectrophotometer, 170-50A.

Results and Discussion

Synthesis of α-Hafnium Phosphate by the Direct-precipitation Method. The X-ray powder diffraction data of the α-hafnium phosphate prepared by the direct-precipitation method are given in Table 1, together with those obtained for that prepared by the reflux method.[6] A very good agreement is seen between the *d*-spacings measured for both specimens. The relative intensities of some diffraction lines differ considerably, however; especially, the reflection from the (002) plane is very strong in the specimen obtained by the direct-precipitation method as compared to that obtained by the reflux method, in which the reflection from the (112) plane is the most intense. The results of TG and DTA are shown for both specimens in Fig. 1. The dehydration of 1 mol

of water takes place at about 170 °C in both cases, but the sample prepared by the direct-precipitation method is dehydrated very slowly until it has released 1 mol of water up to 550 °C. The finely powdered specimen gave the same result.

Forward K^+–H^+ Ion Exchange. The pH-titration curve for K^+ ion exchange is shown in Fig. 2. The forward exchange, where H^+ ions of α-hafnium phosphate were replaced by K^+ ions, proceeded in two steps. The first plateau, in the Region I at a pH value of around 2.7, corresponds to the existence of two phases, namely, α-hafnium phosphate and monopotassium salt. Slightly before a half exchange, the pH values increased rather abruptly and attained the second plateau at a pH value of around 7.3. The second plateau is very flat and corresponds to the stage where the mono- and dipotassium salts coexist. The titration curve is completed at approximately the theoretical exchange capacity of 5.15 meq·g^{-1} α-hafnium phosphate. This dibasic feature of the curve has not been observed in the case of Li^+ ion exchange on α-hafnium phosphate.[1]

Table 1. X-ray powder patterns of α-hafnium phosphate

Reflux[a]		Direct Precipitation		*hkl*[b]
d/Å	I/I_0	*d*/Å	I/I_0	
7.55	65	7.56	100	002
4.44	54	4.44	16	110
4.40	30	4.40	8	012
4.19	14	4.20	6	$11\bar{2}$, $20\bar{2}$
3.78	9	3.79	11	004
3.54	100	3.55	48	112
3.51	52	3.51	25	$20\bar{4}$
3.21	20	3.21	12	202
3.07	6	3.07	5	014
2.64	20	2.64	15	020
2.63	31	2.62	13	114
2.61	35	2.61	11	$20\bar{6}$
2.40	21	2.40	15	204

a) α-Hafnium phosphate prepared by refluxing in 12 mol·dm^{-3} H_3PO_4 for 245 h. b) The *hkl* indices are tentatively assigned by referring to the powder data of α-zirconium phosphate (JCPDS 22-1022, 1971), with small modifications.

The X-ray powder patterns of the exchanger at every stage of the forward exchange were measured in the wet and dry states of the sample and are represented in Figs. 3 and 4 respectively. In the case of the exchanger in the wet state, the diffraction line from the (002) plane(d=7.6 Å) decreased in intensity as the K^+-ion exchange proceeded, and the line at 8.1 Å appeared. This indicates the formation of the monohydrate of monopotassium salt. At the ionic fraction ($\overline{XK}$) of 0.44, the 7.6 Å peak appears to have increased again, but this is due to the overlapping of the reflection because the anhydride of monopotassium salt has almost the same d value, as will be described later. On the further progress of the K^+-ion exchange, the second plateau of the titration curve started, and the dipotassium salt with the interlayer distance of 10.8 Å soon appeared. This means that the trihydrate of dipotassium salt formed after the half exchange. Figure 4 shows the powder patterns which have been measured on the exchangers dried over silica gel. A considerable variation of the patterns with the drying conditions of the samples can be seen. Thus, the monohydrate of monopotassium salt loses 1 mol of water on standing over silica gel at room temperature, and it gives anhydride with the interlayer distance of 7.6 Å. Similarly, the trihydrate of dipotas-

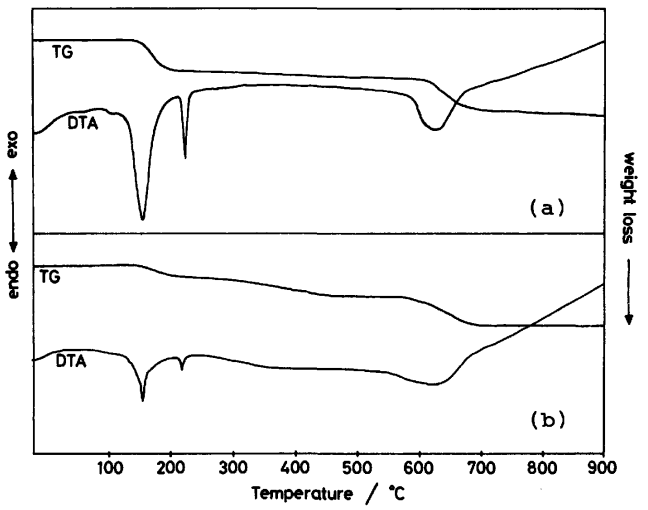

Fig. 1. TG and DTA curves of α-hafnium phosphate prepared by the reflux method and the direct precipitation method. (a): reflux method, (b): direct precipitation method

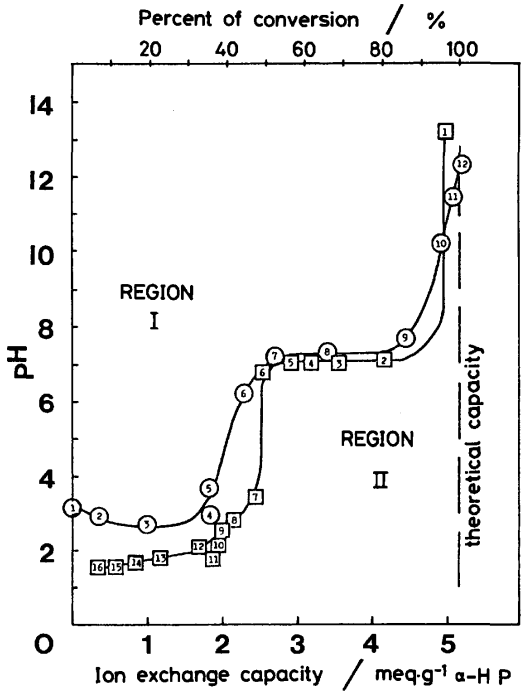

Fig. 2. The forward and backward pH titration curves for K^+ ion exchange on α-hafnium phosphate.
○: Forward, □: Backward.
α-HP stands for α-hafnium phosphate.

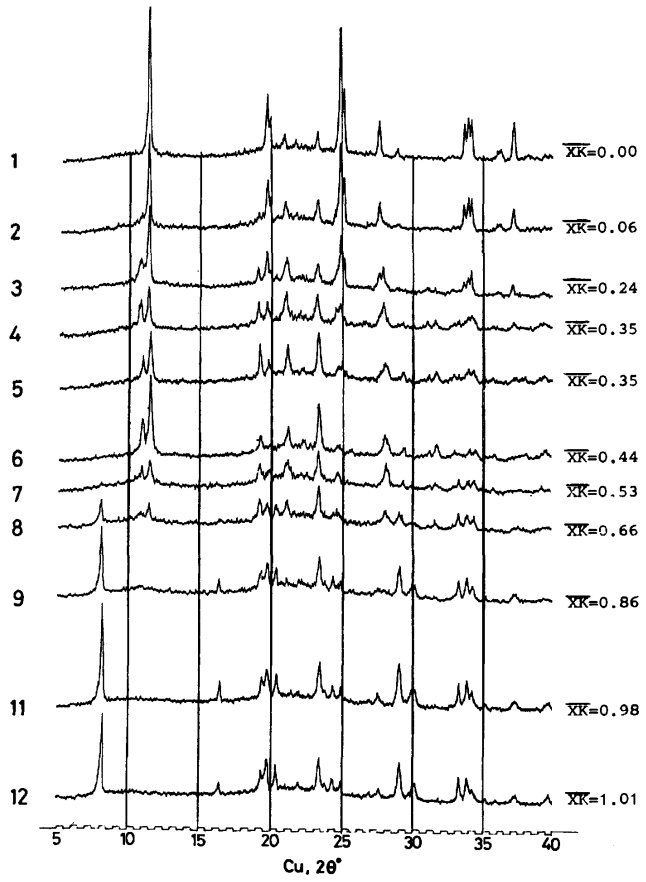

Fig. 3. The X-ray powder patterns of wet exchanged forms of α-hafnium phosphate at several stages of forward exchange.
$\overline{XK}$ denotes the potassium ionic fraction. The numbers 1 to 12 indicate the corresponding points in the titration curve in Fig. 2.

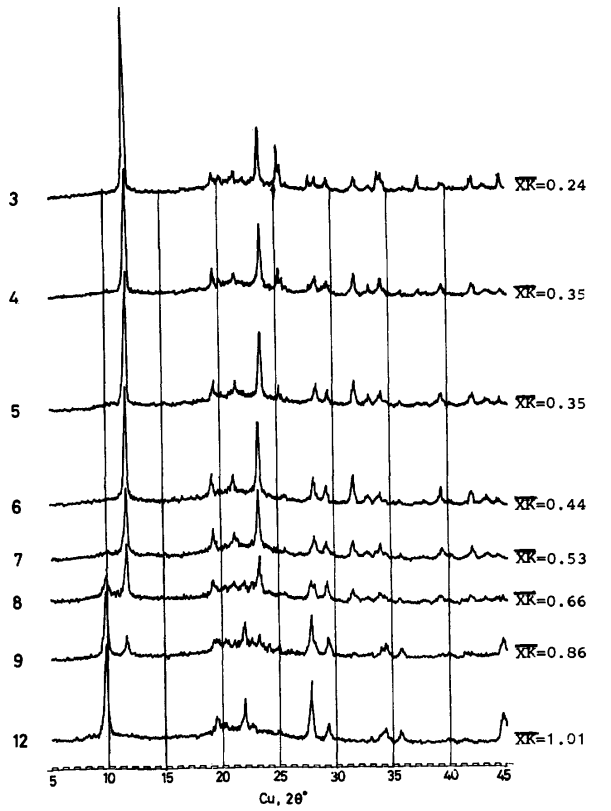

Fig. 4. The X-ray powder patterns of dry exchanged forms of α-hafnium phosphate at several stages of forward exchange. The numbers 3 to 12 indicate the corresponding points in Fig. 2.

sium salt is converted into monohydrate with the interlayer distance of 9.2 Å. The water content has been confirmed by thermogravimetry. The above results may be summarized as follows:

$$\underset{(7.6\,\text{Å})}{Hf(HPO_4)_2\cdot H_2O} \longrightarrow$$

$$\begin{array}{ccc} Hf(KPO_4)(HPO_4)\cdot H_2O & \longrightarrow & Hf(KPO_4)_2\cdot 3H_2O \\ (8.1\,\text{Å}) & & (10.8\,\text{Å}) \\ \downarrow & & \downarrow \\ Hf(KPO_4)(HPO_4) & & Hf(KPO_4)_2\cdot H_2O \\ (7.6\,\text{Å}) & & (9.2\,\text{Å}) \end{array}$$

Backward K^+–H^+-ion Exchange. The pH titration curve of the backward process is given in Fig. 2. A two-step ion exchange is clearly observed. The plateau at a pH value of around 7.0 corresponds to the coexistence of the dipotassium salt and the monopotassium salt. The forward and backward curves practically coincide in this region (Region II in the figure), indicating that the process is reversible, not only in the ion-exchange reaction, but also in the structural change of the exchanger. An abrupt change in the pH at the half exchange shows the existence of a single monopotassium salt phase. This has been confirmed by the X-ray powder data which will be shown below. As the exchange progressed, the deviation of the backward curve from the forward one became remarkable. This kind of hysteresis can often be observed in alkali-metal ion exchange on α-zirconium phosphate; it suggests that the formation of the dihydrogen form does not always result in a α-type crystal. It is further noted that a small fraction of the K^+ ions could not be released with 0.1 mol·dm^{-3} HCl within 5d.

The X-ray powder patterns of the exchanger at every stage of the backward exchange in wet and dry states are given in Figs. 5 and 6 respectively. The starting exchanger has an interlayer distance of the monohydrate of dipotassium salt of 9.2 Å instead of the 10.8 Å of the trihydrate, because it was necessary to weigh the exchanger in the dry state. As may be seen in Fig. 5, up to $\overline{XK}$=0.57 the 9.2 Å peak disappeared, and the reflection lines from the monopotassium salt appeared. At about a half exchange, two reflections at 2θ=11° amd 11.6° corresponding to the monohydrate (d=8.1 Å) and the anhydride (d=7.6 Å) of monopotassium salt, were observed. The relative intensities of the two peaks depended on how wet the X-rayed specimens were. As K^+ ions in the exchanger were replaced by H^+ ions, however, the position of the lowest-angle reflection remained essentially unchanged, suggesting that the 8.1 Å peak still predominated even if the monopotas-

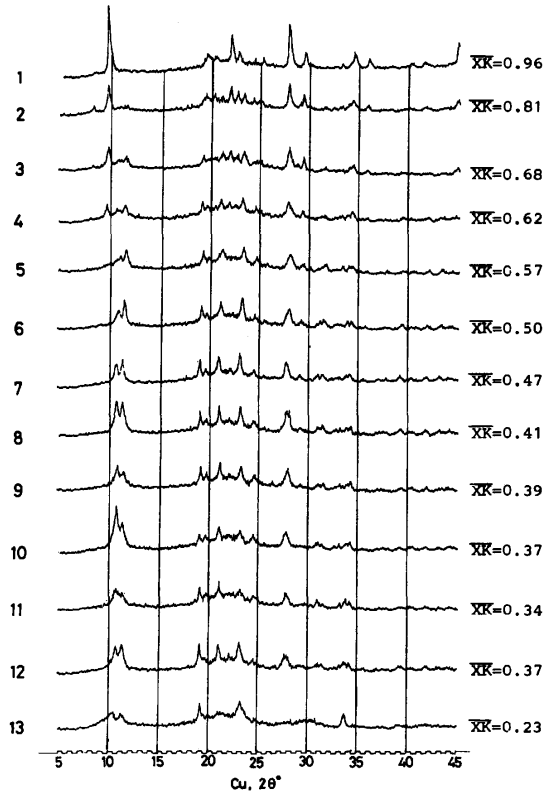

Fig. 5. The X-ray powder patterns of wet exchanged forms of hafnium potassium phosphate at several stages of backward exchange. The numbers 1 to 13 indicate the corresponding points in Fig. 2.

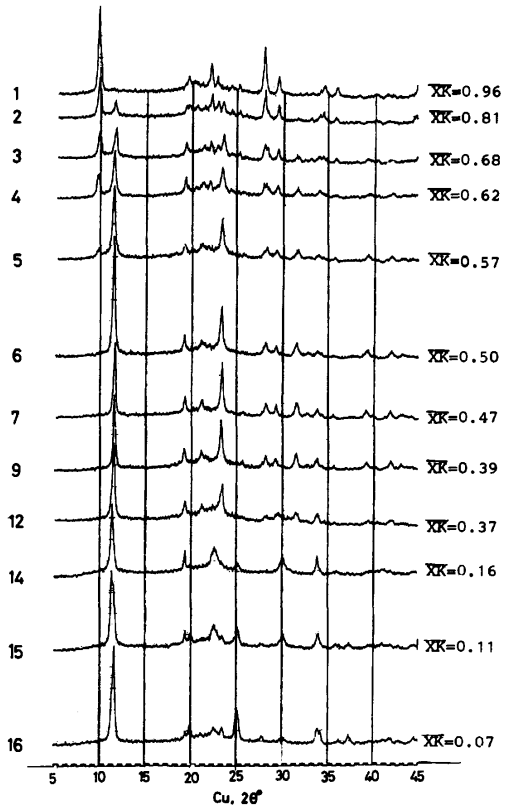

Fig. 6. The X-ray powder patterns of dry exchanged forms of hafnium potassium phosphate at several stages of backward exchange. The numbers 1 to 16 indicate the corresponding points in Fig. 2.

sium salt was converted into the dihydrogen form. This fact correlates with the deviation of the forward and the backward curves from each other; it can be considered that, in the backward process, the solid-solution formation takes place, that is H^+ ions are incorporated with the monopotassium form without any esssential change in the crystal structure. In α-zirconium phosphate, it is known that a wider range of the solid-solution formation is observed as the degree of crystallinity becomes poorer. The same trend may be thought to be found in α-hafnium phosphate. The complete desorption of K^+ ions was not possible under the experimental conditions used, but it was confirmed that some portion of the exchanger was converted into α-hafnium phosphate. In this case, the diffraction line around $2\theta=25°$ ($d=3.5$ Å) is useful in identifying α-hafnium phosphate, because the line at $2\theta=11.6°$ ($d=7.6$ Å) overlapped with that of the anhydride of monopotassium salt. In the same way, the monopotassium-salt phase can be differentiated from α-hafnium phosphate for the forward process (Fig. 3). The backward exchange can be shown as follows:

$$\begin{array}{ccccc} \underset{(10.8\,\text{Å})}{Hf(KPO_4)_2\cdot 3H_2O} & \longrightarrow & \underset{(8.1\,\text{Å})}{Hf(KPO_4)(HPO_4)\cdot H_2O} & \longrightarrow & \left\{\begin{array}{l} \underset{(8.1\,\text{Å})}{Hf(HPO_4)_2\cdot xH_2O} \\ \\ \underset{(7.6\,\text{Å})}{Hf(HPO_4)_2\cdot H_2O} \end{array}\right. \\ \downarrow & & \downarrow & & \\ \underset{(9.2\,\text{Å})}{Hf(KPO_4)_2\cdot H_2O} & & \underset{(7.6\,\text{Å})}{Hf(KPO_4)(HPO_4)} & & \end{array}$$

Ternary H^+–Li^+–K^+ Ion Exchange. Figure 7 shows the titration curve for Li^+–H^+ and K^+–H^+ binary ion exchange on α-hafnium phosphate in the forward direction obtained by the present authors. From the selectivity point of view, it is clear that the exchanger prefers K^+ ions to Li^+ ions up to an ion-exchange capacity of around 2 meq $M^+\cdot g^{-1}$ α-hafnium phosphate, where M^+ denotes the Li^+ or K^+ ion. Above this capacity, the selectivity is reversed until the completion of the exchange. However, this argument has to be examined experimentally, because, in the ternary H^+–Li^+–K^+ system, some new solid phases including Li^+ and K^+ ions might be formed, and this might affect the selectivity of two ions. On the other hand, if no such new solid phases are formed, the selectivity should follow those obtained in the binary systems. Figure 8 gives the variation in the alkali-metal-ion uptake with the pH. Thus, up to an ion-exchange capacity of about 2 meq $\cdot g^{-1}$ exchanger, K^+ ions were preferably taken up, whereas Li^+ ion remained in the equilibrating

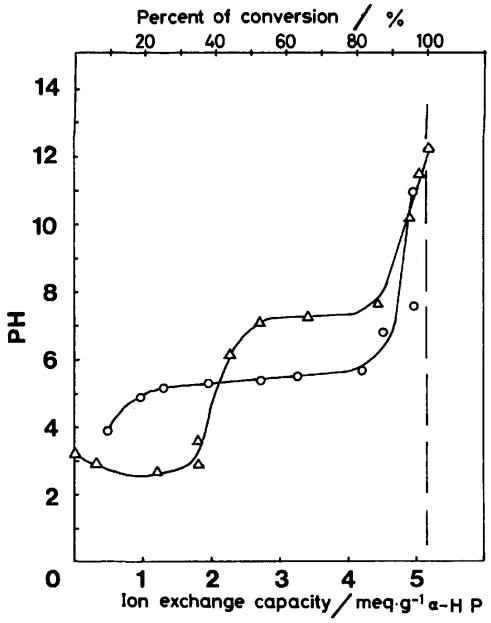

Fig. 7. The pH titration curves for binary H^+–Li^+ and H^+–K^+ forward exchange on α-hafnium phosphate.
△: K^+, ○: Li^+.
α-HP stands for α-hafnium phosphate.

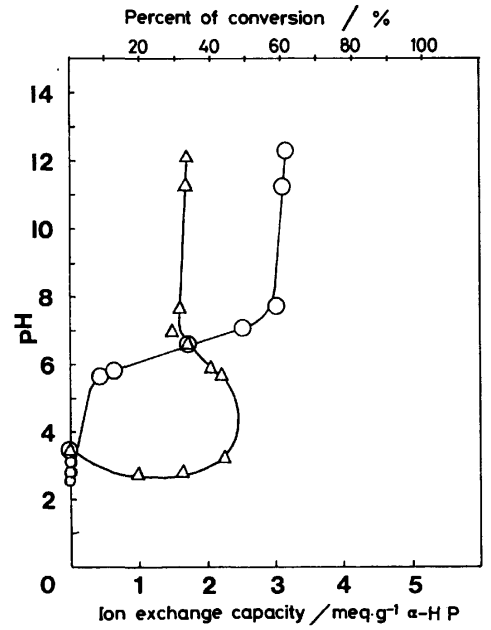

Fig. 8. K^+ and Li^+ uptake curves for ternary H^+–Li^+–K^+ exchange on α-hafnium phosphate.

△: K^+, ○: Li^+.
α-HP stands for α-hafnium phosphate.

solution. Above this point, *i.e*, above $\overline{XK}$=0.43, the Li^+-ion uptake started and the pH value of the solution rose steeply. The lithium-ion uptake proceeded as not

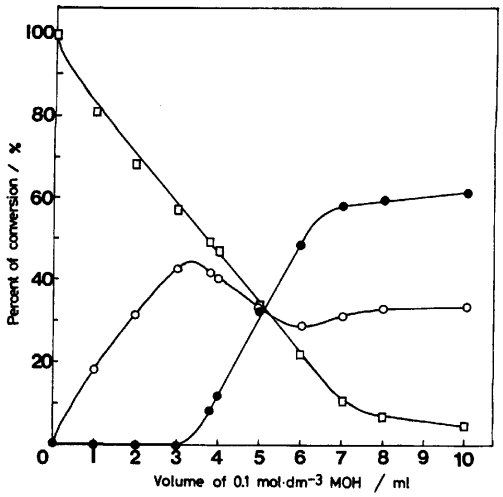

Fig. 9. Distribution of H^+, Li^+, and K^+ ions on α-hafnium phosphate at different hydroxide concentrations.
□: H^+, ●: Li^+, ○: K^+.

only H^+ ions but also K^+ ions were replaced by Li^+ ions. The pH-titration curve thus behaved differently from that for the binary system after the half exchange, but the selectivity sequence of the K^+ and Li^+ ions is almost exactly the one expected from the binary systems. Figure 9 represents the distribution of H^+, Li^+, and K^+ ions on α-hafnium phosphate at varying hydroxide concentrations. Thermogravimetry showed that the final product of the titration was dehydrated over the range of 120—400 °C. Its chemical composition was $Hf(K_{0.67}Li_{1.23}H_{0.10})(PO_4)_2 \cdot 1.17H_2O$. However, the X-ray patterns showed that the reflections were rather broad and that the crystallinity had deteriorated. The sample in the wet state had one broad line at 2θ=11° (d=8 Å), whereas that in the dry state had two lines, at about 11° and 10.3° (d=8.6 Å). The formation of a phase having a larger interlayer distance than that in the wet state can not be the consequence of dehydration. There is some possibility that an amorphous form was converted into the crystalline form during storage and drying, but no definite assignment to the known phase is possible at present.

References

1) I. Tomita, K. Magami, H. Watanabe, K. Suzuki, and T. Nakamura, *Bull. Chem. Soc. Jpn.*, **56**, 3183 (1983).
2) G. Alberti and E. Torracca, *J. Inorg. Nucl. Chem.*, **30**, 317 (1968).
3) Y. Hasegawa and M. Kuwayama, *Bull. Chem. Soc. Jpn.*, **51**, 3485 (1978).
4) Y. Inoue and Y. Yamada, *Bull. Chem. Soc. Jpn.*, **52**, 3528 (1979).
5) K. Ueno, M. Saito, and K. Tamaoku, *Bunseki Kagaku*, **18**, 81 (1969).
6) I. Tomita and K. Suzuki, unpublished data.

Steam Reforming of Hydrocarbons and Water Gas Shift Reaction Through a Wall of Stabilized Zirconia Used as Hydrogen Separator

Kiyoshi Otsuka,* Seiichiro Yokoyama, and Akira Morikawa
Department of Chemical Engineering, Tokyo Institute of Technology, Ookayama, Meguro-ku, Tokyo 152
(Received October 28, 1983)

Steam reforming of CH_4 and C_2H_4 or water gas shift reaction was allowed to occur through a wall of stabilized zirconia acting as hydrogen separator. The reactions proceed *via* transport of oxygen ions in the zirconia lattice from cathode to anode of the wall, accompanying an electron transfer in the reverse direction through the outer lead wire. Hydrogen without CO_2, CO, or hydrocarbons can be obtained directly by each reaction at the cathode side. The rate of hydrogen production increases exponentially with a rise in applied potentials *via* chromel-constantan thermocouples. The presence of reducing gas such as CO, CH_4, or H_2 at the anode side will decrease considerably the applied potential required to produce hydrogen at the same rate. A tentative reaction mechanism is proposed on the basis of kinetic information of the reaction.

Steam reforming or partial oxidation of hydrocarbons is at present the most efficient and economical process for hydrogen manufacture. The product gas, often called synthesis gas, is converted to high-content hydrogen through water gas shift reaction with simultaneous production of carbon dioxide. Removal of carbon dioxide, carbon monoxide, and hydrocarbons from make-gas is indispensable for getting high-purity hydrogen, which will inevitably raise the hydrogen cost. Under these circumstances, it is desired that high-purity hydrogen should be obtained directly by steam reforming of hydrocarbons or by water gas shift reaction without any removal processes for carbon dioxide, unreacted hydrocarbons, and carbon monoxide. We describe in this report a simple method to obtain pure hydrogen without carbon dioxide, carbon monoxide, or hydrocarbons by running water gas shift reaction or steam reforming of methane and ethylene with the aid of stabilized zirconia. The calcia-stabilized and yttria-stabilized zirconia used in this work are well known as solid electrolytes in which conduction is due almost entirely to oxygen ion transport in a lattice with anion vacancies.[1)]

The basic concept of the method will be explained by Fig. 1. At the anode, CH_4, C_2H_4, and CO are oxidized by oxygen ion as follows:

$$\text{Anode:}\quad CH_4 + 4O^{2-} \rightarrow CO_2 + 2H_2O + 8e^-, \quad (1)$$

$$C_2H_4 + 6O^{2-} \rightarrow 2CO_2 + 2H_2O + 12e^-, \quad (2)$$

$$CO + O^{2-} \rightarrow CO_2 + 2e^-. \quad (3)$$

The electrode works not only as an accepter of electrons liberated but also as a catalyst for the reaction. The electrons are transported through the lead wire connecting both the electrodes of anode and cathode. At the cathode, water vapor is reduced by the electrons transported from the anode, producing only hydrogen:

$$\text{Cathode:}\quad H_2O + 2e^- \rightarrow H_2 + O^{2-}. \quad (4)$$

The overall reactions can be written as follows:

From Eqs. 1 and 4,

$$CH_4 + 2H_2O \rightarrow CO_2 + 4H_2. \quad (5)$$

From Eqs. 2 and 4,

$$C_2H_4 + 4H_2O \rightarrow 2CO_2 + 6H_2. \quad (6)$$

From Eqs. 3 and 4,

$$CO + H_2O \rightarrow CO_2 + H_2. \quad (7)$$

Equations 5 and 6 represent steam reforming of methane and ethylene, respectively. Equation 7 is water gas shift reaction. By the method described above, we can get pure hydrogen directly by steam reforming of hydrocarbons or water gas shift reaction without any separation processes for CO_2, CO, and hydrocarbons.

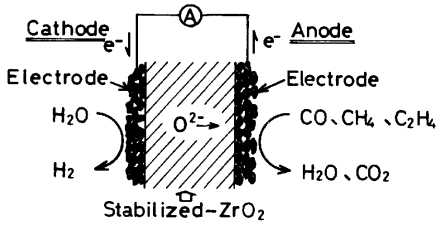

Fig. 1. Schematic model of reactions proceeding through the wall of stabilized zirconia.

Experimental

The calcia-stabilized zirconia (CSZ) and yttria-stabilized zirconia (YSZ) used were obtained from Nippon Kagaku Togyo Company. The contents of CaO and Y_2O_3 were 11 and 8 mol%, respectively. The geometry of the reactor used is illustrated in Fig. 2. The outer diameter of the zirconia tube was 21 mm and its thickness was 2.5 mm. The length of the tube was 300 mm. The outer diameter of the reactor was 30 mm. The electrodes were affixed on to the zirconia tube by wetting the tube with a suspension of powders of metal oxide in acetone followed by evaporation of the acetone. The metallic electrodes were prepared by decomposition or reduction of the oxides at 873 K in a flow of helium or hydrogen before use. The apparatus employed was a glassmade flow reactor system operated at atomospheric pressure. The reaction temperatures were 873—1273 K. Water vapor (usually 2.7 kPa) carried by helium was fed into the reactor. The feed rate of water vapor was usually 23 μmol min^{-1}. Pure H_2, CH_4, CO, and C_2H_4 were used as anode gases usually without dilution. The flow rate of anode gas was 0.22—2.2 mmol min^{-1}.

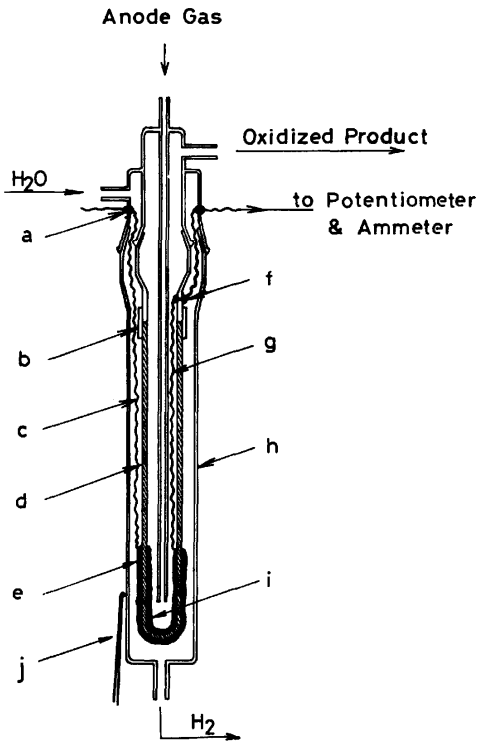

Fig. 2. The geometry of reactor; a and f: silicone seals, b: silicone rubber, c and g: lead wires, d: CSZ or YSZ, e: electrode (cathode), i: electrode (anode), h: quartz glass, j: thermocouple.

Results and Discussion

Electrode Material. Table 1 shows the efficiency of electrode materials for either the cathode or anode of CSZ. The reactivity test on electrode materials was carried out by using aged silver (Ag*), which had been used for reaction at 973 K for more than 20 h, on one side of the electrodes. The geometric area of the zirconia surface coated with Ag* was 80.1 cm^2. The areas of the electrode materials tested were 52.8 cm^2. Hydrogen was used as a test anode gas. For every electrode pair given in Table 1, hydrogen was produced according to the theory described above. This was confirmed by the fact that the amount of hydrogen produced at the cathode side (analyzed by gas chromatography) corresponded well to those calculated from currents measured with the ampere meter A in Fig. 1. Moreover, the reaction ceased and resumed in correspondence to disconnecting and connecting the lead wires for both the electrodes, respectively.

The results in Table 1 indicate that Ag, Ni, Pt, Pd, and In_2O_3-SnO_2 are all good electrodes as far as the efficiency of hydrogen formation is concerned. However, Ni, Pt, Pd, and In_2O_3-SnO_2 could not be attached firmly to the zirconia tube by the method described in the experimental section. In contrast, the silver electrode may be ascribed to a solid contact of silver particles on the zirconia surface.

The high efficiency of hydrogen production for the fresh silver pair (Ag-Ag) decreased considerably after 20 h reaction at 973 K (Ag*-Ag*) probably because of the sintering of silver particles during the reaction. After 20 h, however, the electrode pair Ag*-Ag* showed a reproducible activity when the reaction had been run below 973 K. Hence, the following studies were carried out with the electrode pair of Ag*(cathode)-Ag*(anode).

Table 1. Comparison of efficiencies of electrode materials on CSZ at 973 K

Electrode material		Rate of H_2 formation at cathode/μmol min^{-1}
Cathode	Anode	
Ag	Ag	2.62
Ag	Ag*	1.88
Ag*	Ag*	0.68
In_2O_3-SnO_2	Ag*	0.15
Ni	Ag*	1.34
Pt	Ag*	1.22
Pd	Ag*	1.11
Ag*	In_2O_3-SnO_2	1.12
Ag*	Ni	1.59
Ag*	$PrCoO_3$	0.81
Ag*	Pt	0.75
Ag*	Pd	0.75

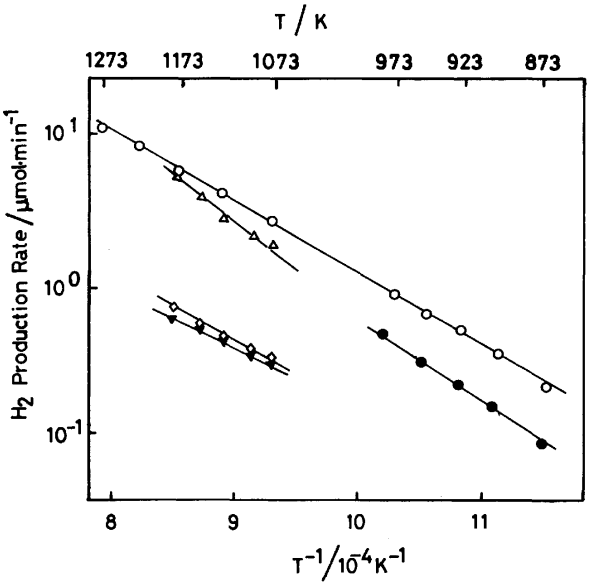

Fig. 3. The rates of hydrogen formation as functions of temperature for different anode gases. The flow rate of anode gas was 0.63 mmol min^{-1}. Anode gas; ○: H_2(using YSZ), ●: H_2(using CSZ), △: C_2H_4(YSZ), ◇: CO(YSZ), ▼: CH_4(YSZ).

Comparison of Efficiencies of Anode Gases for YSZ and CSZ. The effect of anode gases on the rate of hydrogen formation was examined for both YSZ and CSZ. Rates of hydrogen production using different reducing gases on the anode side are plotted in Fig. 3. as a function of reaction temperature. The results in Fig. 3 show that there are large differences among the efficiencies of the anode gases for the production of hydrogen in both the cases of YSZ or CSZ used. The apparent activation energies calcu-

lated from the slopes in Fig. 3 are 79 (YSZ; anode gas, H_2), 94 (YSZ; C_2H_4), 77 (YSZ; CO), and 70 kJ mol^{-1} (YSZ; CH_4). The activation energy for CSZ with H_2 as anode gas (closed circles) is 80 kJ mol^{-1} which is very close to that for the YSZ–H_2 system (open circles). Moreover, there are not so much differences between the rates for YSZ (open circles) and for CSZ (closed circles); the ratio of the rates is less than 2.6.

Effect of Applied Potential from Thermocouples. The maximum rate of hydrogen formation observed in this work (Fig. 3; YSZ at 1273 K with anode gas of H_2) is 10.8 μmol min^{-1} corresponding to a current density of 0.72 mA cm^{-2}. This value is far too low for the application of the method to practical use. Therefore, in order to enhance the rate of hydrogen formation, we attempted to apply an electric potential between both the electrodes. Electric energy was supplied on the Seebeck effect from the heat stored in the furnace of reactor *via* 30 pairs of chromel-constantan thermocouples connected in series. Figure 4 shows a sharp increase in the rate of hydrogen formation as a function of effective applied potentials from the thermocouples. The rate increases exponentially with a rise in the applied potential for all the cases using different anode gases. Although the efficiency of thermoelectric generation of electricity is still low,[2,3] the method can easily be applied and utilization of waste heat from chemical plants may be feasible. Whatever the primary energy source of electricity may be or whatever the method for final conversion of energy into electricity may be, the results of Fig. 4 suggest that the applied potential required to yield the same rate of hydrogen formation is caused to decrease when a reducing gas is present at the anode side of the stabilized zirconia, as compared with the value in the case of helium as anode gas (the arrows in Fig. 4 indicate an example of differences in the potentials required). From a viewpoint of electrochemical decomposition of water vapor, the results are taken to indicate that the reducing gas would favorably reduce the consumption of electric power.

Although the efficiency of hydrogen production is still far low for practical use, we have been able to demonstrate that the method proposed in this work can be used for the production of pure hydrogen. Higher temperatures, higher pressures of steam and anode gas, greater electric applied potentials, thinner thicknesses of stabilized zirconia, and higher surface areas of zirconia and electrodes, must improve the efficiency remarkably.

Effects of Concentrations of Gases at Anode and Cathode. Effects of concentrations of anode gases are shown in Fig. 5. The conversion of water to hydrogen depends strongly on the concentration of anode gas irrespective of the presence or absence of electric potential applied. On the other hand, the rate of water decomposition does not depend on the concentration of water vapor (cathode gas) as shown in Fig. 6. The conversion of anode gases is in the range 0.02—0.92% depending on reaction conditions as seen from Figs. 5 and 6. The conversion of water vapor to hydrogen does not depend much on the flow rate of anode gas in the range between 2.2 and 0.22 mmol min^{-1}. Thus, the conversion of pure hydrogen as anode gas increases from 0.26 to 2.4% when the flow rate of anode gas has been decreased from 2.2 to 0.22 mmol min^{-1}.

The rate of hydrogen formation, *viz.*, the current during reaction, increases exponentially with a rise in the applied potential (Fig. 4). If the diffusion of oxygen ion is the rate determining step, Ohm's law should be observed. Hence, the results in Fig. 4 suggest that the rate determining step is of electrochemical reaction. The results that the conversion of water vapor depends on the kind of anode gas (Fig. 3)

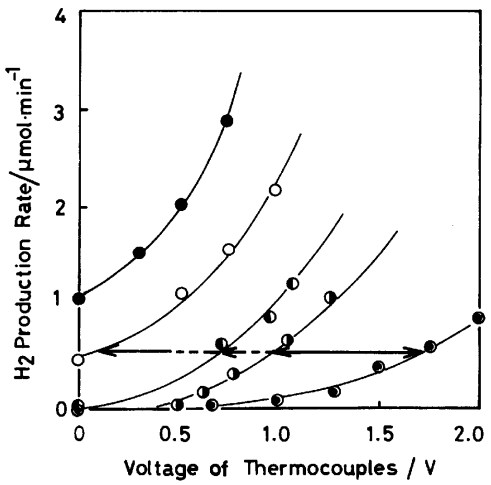

Fig. 4. Rate of hydrogen formation as functions of applied potential from thermocouples using different anode gases. The reactions were carried out at 973 K. The flow rate of anode gas was 0.63 mmol min^{-1}. Anode gas; ●: H_2(using YSZ), ○: H_2(CSZ), ◐: CO(CSZ), ◑: CH_4(CSZ), ⊙: He(CSZ).

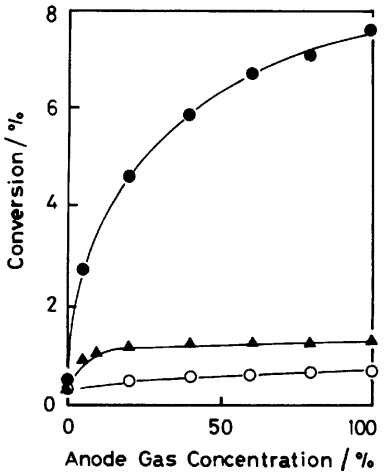

Fig. 5. Effect of the concentration of anode gas on the conversion of water vapor. The reaction at 973 K using CSZ. Anode gases were diluted with He. The flow rate of the gas mixture of He and anode gas was 50 ml min^{-1}. Anode gas; ●: H_2(with applied potential, E=1.0 V), ▲: CO(E=1.0 V), ○: H_2(without applied potential).

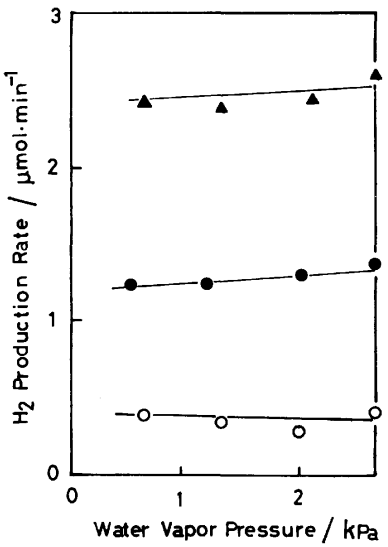

Fig. 6. Effect of the pressure of water vapor at cathode on the rate of water decomposition. The reaction at 973 K using CSZ. Flow rate of anode gas was 2.2 mmol min^{-1}. Anode gas and the value of applied potential; ▲: H_2(with applied potential, $E=1.0$ V), ●: CO($E=1.2$ V), ○: H_2($E=0$ V).

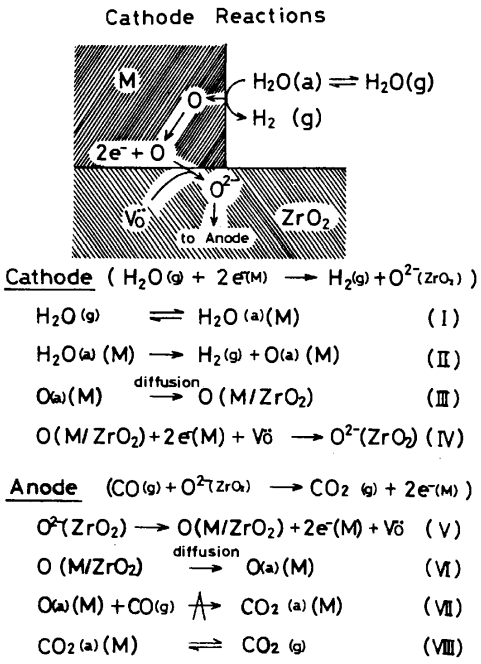

Fig. 7. The reaction mechanism.

and on the concentration of anode gas (Fig. 5), suggest that the rate determining step is the oxidation process of anode gas by oxygen at the surface of silver electrode. The oxygen is transported from the cathode through the stabilized zirconia. The ion conductivity of oxygen in YSZ is 9 to 11 times as high as that in CSZ in the temperature range between 873 K and 973 K.[4] However, the rate of hydrogen formation on YSZ is no more than 2.6 times that on CSZ (Fig. 3). This obsevation together with the results in Figs. 3, 4, and 5 excludes the possibility that the diffusion of the oxygen ion is the rate determining step under the reaction condition in this work. The diffusion may become the rate determining step when the rate of overall reaction has been increased remarkably.

The reaction mechanism which we have in mind is shown in Fig. 7. At the cathode side, the oxygen atom formed through decomposition of the adsorbed water (Eq. II) on silver electrode (M) diffuses through the surface or bulk of the electrode (Eq. III). The oxygen atom is transfered into the stabilized zirconia through the reaction with anion vacancies (Vö) and electrons which have been supplied from the anode *via* the outer circuit (Eq. IV). The reactions of Eqs. V to VIII occur at the anode side. Equations V and VI are the reverse reactions of Eqs. IV and III, respectively. Equation VII is the reaction when carbon monoxide is used as anode gas. Similar reactions can be considered when hydrogen, ethylene, or methane instead of carbon monoxide is used. The oxidation of anode gas by the adsorbed oxygen atom (Eq. VII) is assumed to be the rate determining step. The applied potential between the anode and cathode would increase the activity of oxygen at the anode, thus enhancing the rate of hydrogen production exponentially (Fig. 4). Further studies are needed to confirm the mechanism proposed in Fig. 7.

In conclusion, the method examined in this work can be used in principle for the production of pure hydrogen. However, much more improvement in the efficiency of hydrogen production is needed for practical application of the method.

References

1) E. C. Subbarao, "Solid Electrolytes and Their Applications," Plenum Press, New York (1980), P. 40.
2) T. Mukaibo, M. Aoki, and Y. Sekine, "Energy," Iwanami, Tokyo (1976), p. 113.
3) M. Ali Kettani, "Direct Energy Conversion," Addison-Weseley, New York (1970), p. 146.
4) Nippon Kagaku Togyo Company, Catalog No. 581 (1980).

Synergistic Effect of Alcohol-Benzene Mixtures for Coal Extraction

Masashi IINO* and Minoru MATSUDA
Chemical Research Institute of Non-Aqueous Solutions, Tohoku University, Katahira, Sendai 980
(Received February 25, 1984)

Coals were extracted with alcohol-benzene mixtures at room temperature. For coals of high oxygen content, Yallourn and Taiheiyo coals, the extraction yields for the mixtures were much greater than those for alcohols and benzene alone. This synergistic effect was more marked for less bulky alcohols: The order was methanol>ethanol>isopropyl alcohol>*t*-butyl alcohol. The degree of swelling and the apparent density of the coals in alcohols were measured. The results show that smaller alcohols may permeate into pores of the coals more extensively and cause greater swelling than larger alcohols. It is reasonable to consider that this swelling of the coals then facilitates the extraction with benzene or alcohol-benzene mixtures, which are better solvents in solubility for coal molecules than alcohols. For Shin-yubari coal having low oxygen content, no such a synergistic effect was observed, probably due to the lower degree of swelling of this coal.

Solvent extraction at room temperature, which causes no chemical change of coals, provides useful knowledge about coal structure through the studies on extraction mechanism and the characterization of extracts, even though extraction yields are usually low. It is also connected with coal liquefaction, which includes a step of coal dissolution with a suitable solvent under pyrolysis conditions. Many studies on solvent extraction have been reported[1] and attempts have been made to explain the extraction mechanism.

Dryden[2] has extensively studied solvent extraction; he used about 30 British coals and many organic solvents at or above room temperature. His conclusion concerning extraction yield is that a good solvent contains a nitrogen atom or an oxygen one (less efficient than nitrogen) possessing an unshared pair of electrons. He has also found that the quantity of imbibition of solvents used, which correlates to the swelling degree of coals in the solvents, is related to extract yields.

Marzec and coworkers[3] have presented a model for extraction of coal: Coal consists of a macromolecular network and extractable substances filling the pores of a network; the donor-acceptor interactions proposed by Gutmann[4] are responsible for binding together the network and the extractable substances. According to their model, solvent extraction is a substitution reaction in which extractable substances are replaced by a solvent molecule through donor-acceptor interaction of solvent and network or solvent and extractable substances.

Another approach to the extraction mechanism is a theoretical one from thermodynamics, namely, a correlation between the solubility parameter, δ, and the coal extractability or the solubility of coal-derived matter.[5] This theory states that a solvent having a δ value like that of the coal used will give the highest extraction yield. Hombach[6] has reported a result which may demonstrate the theory by using mixtures of solvents having different δ values. δ also has been found to be related to the swelling of coals.[5b,7]

However, there are some examples[8,9] indicating insufficient extraction which means that considerable amount of substances soluble in the solvent still exists in coal after the extraction. For example, the carbon disulfide-soluble part of pyridine extract is 4% based on coal, but the yield in a direct extraction of the same coal with carbon disulfide is only 0.2%.[8] Similarly, 13% is the chloroform-soluble part of the pyridine extract, but only 2.4% is the chloroform extraction yield.[9] Insufficient permeation into coals may be responsible for this result.

A mixed solvent is considered to be a powerful means in the elucidation of such a complex extraction mechanism, especially when this shows a large synergistic effect. We have reported[10] that the carbon disulfide-pyridine mixture shows a very large synergistic effect for extractions of bituminous coals. For Shin-yubari coal, the extraction yields for 1 h at room temperature are 0.9, 3.0, and 28.7% for carbon disulfide, pyridine, and their 1 : 1 mixture, respectively. The mechanism for this extraction is not clear at present. In this study we will report the mechanism of the extractions with alcohol-benzene mixtures. Alcohol-benzene mixtures are well known to show synergistic effects for coal extractions[11] and are often used to obtain wax and other coal-derived materials from brown coals.[12]

Experimental

Materials. Yallourn, Taiheiyo, and Shin-yubari coals, stored in water, were dried in air, ground, and sieved to <60 mesh. The coals were further dried at 107 °C under nitrogen atmosphere to constant weight (usually 1—2 h). The proximate and ultimate analyses (daf) are shown in Table 1.

All the solvents for extraction studies were reagent-grade (>98%) and were used without purification.

General Solvent Extraction Procedure of Coals. 4 g of coal sample was extracted with 100 ml of a solvent or a solvent mixture with stirring using a magnetic stirrer in an Erlenmeyer flask for 1 h at room temperature. After separation by centrifugation and filtration, the solvent was removed from the solution by a rotatory evaporater. The extract and the residue were dried *in vacuo* at 80 °C to constant weight. Extraction yield (daf) were determined from Eq. 1 and ash % is the value on dry-base. The yields were reproduced within ±10% for repeated runs.

Table 1. Ultimate and proximate analyses of coals

Coal	Proximate analysis (wt%)				Ultimate analysis (wt/%, daf)				
	Moisture	VM[a]	FC[b]	Ash	C	H	N	S	O[c]
Yallourn	14.3	47.3	37.6	0.8	66.1	5.3	0.6	0.3	27.7
Taiheiyo	4.4	49.2	34.1	12.3	75.4	7.0	1.2	0.3	16.1
Shin-yubari	0.9	38.0	54.1	7.0	86.7	6.2	1.7	0.3	5.1

a) Volatile matter. b) Fixed carbon. c) Difference.

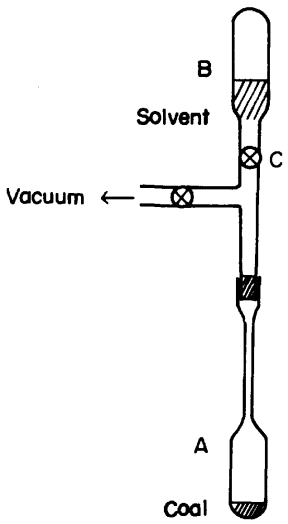

Fig. 1. The apparatus for apparent density measurement.

$$\text{Extraction yield (\%)} = \frac{\text{extract (g)} \times 100}{(1-\text{ash(\%)}/100) \times \text{coal feed (g)}} \quad (1)$$

For the extraction with alcohols, benzene, and their mixtures the recoveries of extracts+residues are always nearly or below 100%, indicating negligible inclusions of solvents in extracts and residues.

Relative Swelling Degree Measurement of Coals. The method reported by Hombach[6] was used. 600 mg of ground coal sample (<170 mesh) was placed in a cylindrical glass tube (d=10 mm, l=170 mm). 1.5 ml of solvent was added and the tube was immersed in a thermostat regulated at 30 °C, occasionally shaking the mixture to remove the gas which evolved. The height of the coal powder layer was measured after 1 and 24 h, respectively. The relative swelling degree for a solvent was estimated from the ratio of the height for a solvent to that for hexane as a standard and was reproduced within ±10% for repeated runs. The measurements at a time longer than 24 h showed no significant change. This rather simple method enables the relative swelling degree of a coal immersed in a solvent to be estimated easily.

Apparent Specific Gravity Measurement of Coals. 10 g of coal sample was charged into a glass ampoule, A, with a glass tube of 4 mm i.d. in Fig. 1. After evacuation for 3 h at room temperature the solvent in a tube, B, which was connected with a needle valve, C, was introduced into the ampoule, A, and the ampoule was immersed in a water bath regulated at 30 °C for 20 h. Then the position of the meniscus of the solvent was marked. The quantity of the solvent introduced was measured gravimetrically. The volume, V, of the coal-solvent mixture was determined by replacing it with distilled water, measuring the volume of water from its weight and specific gravity. A temperature of 30 °C was used, since t-butyl alcohol has freezing point higher than 25 °C. The apparent density was determined from Eq. 2 and was reproduced within ±5% for repeated runs.

$$\text{Apparent density (g/ml)} = \frac{\text{coal feed (g)}}{V\ \text{(ml)} - \text{volume of the solvent (ml)}} \quad (2)$$

Results

Extraction with Alcohol-Benzene Mixtures at Room Temperature. Figure 2 shows the effect of solvent composition of methanol-benzene mixture on extraction yields. For Yallourn and Taiheiyo coals, the yields for the mixture are higher than those for methanol and benzene alone. No such synergistic effect was observed for Shin-yubari coal.

Table 2 shows the effect of the structure of the alcohols on the extraction yields for Yallourn and Taiheiyo coals. The yields increase in the order of methanol>ethanol>isopropyl alcohol>t-butyl alcohol for the cases of the alcohol alone and of the mixture with benzene. The degree of the synergistic effect was estimated from the ratio of the yield for the mixtures to the sum of those for the alcohol and benzene alone; this is listed in the parentheses of the third and fifth columns in Table 2. These values also increase with decreasing the bulkiness of the alcohols used here.

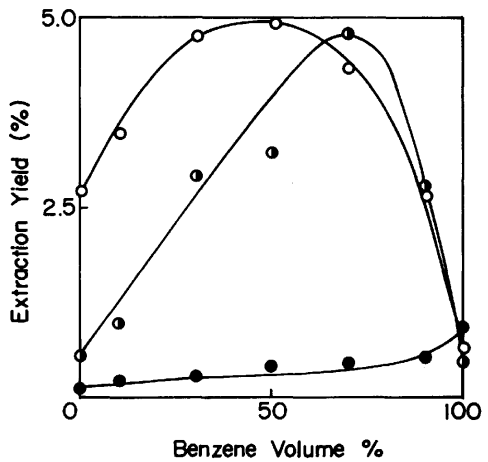

Fig. 2. Effect of solvent composition on the extraction with methanol-benzene mixture.
○: Yallourn coal, ◑: Taiheiyo coal, ●: Shinyubari coal.

Table 2. Extraction with alcohols, hexane, and their mixtures with benzene[a]

Solvent	Extraction yield/%			
	Yallourn		Taiheiyo	
	Single[b]	Mixture[c]	Single[b]	Mixture[c]
Methanol	2.6_5	4.6_5 (1.40)[d]	0.6_0	3.4_0 (3.10)[d]
Ethanol[e]	2.6_0	4.4_0 (1.35)[d]	0.4_0	2.1_5 (2.40)[d]
Isopropyl alcohol	1.9_5	3.5_0 (1.30)[d]	0.3_0	1.1_5 (1.45)[d]
t-Butyl alcohol	0.6_5	1.4_5 (1.20)[d]	0.2_0	0.9_0 (1.30)[d]
Hexane	0.4_5	0.4_0 (0.35)[d]	0.1_0	0.3_5 (0.60)[d]
Benzene	0.7_0	—	0.5_0	—

a) 4.0 g of coal (−60 mesh) in 100 ml of the solvent for 1 h at room temperature. b) The solvent in the first column was used. c) 1:1 mixture by volume with benzene was used. d) The ratio of the yield for the mixture to the sum of those for the alcohol (or hexane) and benzene alone. e) 95% ethanol.

Table 3. Relative swelling degrees of yallourn, taiheiyo, and shin-yubari coals[a] in alcohols, hexane, and benzene at 30 °C

Solvent	Yallourn		Taiheiyo		Shin-yubari	
	1 h	24 h	1 h	24 h	1 h	24 h
Methanol	1.3_5	1.4_0	1.2_5	1.2_5	1.0_5	1.0_0
Ethanol[b]	1.3_5	1.4_5	1.3_0	1.3_0	1.0_5	1.0_0
Isopropyl alcohol	1.3_0	1.4_0	1.2_5	1.2_5	—[c]	1.0_0
t-Butyl alcohol	1.0_0	1.0_0	1.1_5	1.2_0	—[c]	0.9_0
Hexane[d]	(1.0)	(1.0)	(1.0)	(1.0)	(1.0)	(1.0)
Benzene	1.0_0	1.1_0	1.1_5	1.1_5	1.0_5	1.1_0

a) −170 mesh. b) 95% alcohol. c) Insufficient sedimentation. d) A standard solvent.

The extract from Taiheiyo coal with 1:1 methanol–benzene mixture is soluble in benzene and almost insoluble in methanol. Its carbon and hydrogen % (daf), 81.0 and 10.4%, are higher than those for the raw coal, indicating that a hydrocarbon-like extract was obtained. The extraction yields increase with decreasing particle size, namely 0.3_0, 0.5_5, 1.4_0, and 3.3_5% for 9—16, 16—60, 60—100, and 100—170 mesh, respectively, probably due to the increase of the surface area of the coal. The extraction for 3 h gave a little higher yield (5%) than that for 1 h, in the extraction with 1:1 methanol–benzene mixture.

Shin-yubari coal showed no synergistic effect for other alcohols than methanol.

Relative Swelling Degrees and Apparent Densities in Alcohols. Table 3 shows that relative swelling degrees in alcohols were in the order of ethanol> methanol≃isopropyl alcohol>*t*-butyl alcohol≃benzene≃hexane for Yallourn and Taiheiyo coals, and benzene>methanol≃ethanol≃isopropyl alcohol≃ hexane>*t*-butyl alcohol for Shin-yubari coal. Here hexane is known to be inert for swelling of coals. It is clear from Table 3 that alcohols induce a swelling of Yallourn and Taiheiyo coals, but not for Shin-yubari coal, and that this swelling is generally more marked for less bulky alcohols.

Apparent densities measured at 30 °C are summarized in Table 4. This apparent density is considered to reflect the extent of permeation of a solvent into coal; greater density may correspond to greater permeation of a solvent. Table 4 shows that the order of the densities among the alcohols is the same as that of the extraction yields for Yallourn and Taiheiyo coals (Table 2). Namely, smaller alcohols have greater permeation and extraction yield than larger alcohols. Table 4 also shows that apparent densities for Taiheiyo coal were greater than those for Shin-yubari coal in all solvents measured. Toda, Yoshida, Honda, and Hatami[13] have obtained a similar result in their extensive studies on pore structures of various coals that Taiheiyo coal (*C*%, 77.8%) has greater apparent densities than Yubari coal (*C*%, 86.2%) both for methanol and hexane solvents. They discussed these results from the viewpoints of the true densities of the coals and the permeation of the solvents into the coals.

Table 4. Apparent densities of taiheiyo and shin-yubari coals in alcohols and hexane at 30 °C

Solvent	Density (g/cm³)	
	Taiheiyo[a]	Shin-yubari[a]
Methanol	1.425	1.321
Ethanol[b]	1.390	1.305
Isopropyl alcohol	1.348	1.275
t-Butyl alcohol	1.322	1.253
Hexane	1.369	1.313

a) −60 mesh. b) 95% alcohol.

Extraction with Various Methanol-organic Solvent Mixtures. Various methanol-organic solvent

Table 5. Extraction with various organic solvents and their mixtures with methanol[a)]

Solvent	Extraction yield/%					
	Yallourn		Taiheiyo		Shin-yubari	
	Single[b)]	Mixture[c)]	Single[b)]	Mixture[c)]	Single[b)]	Mixture[c)]
Carbon tetrachloride	0.2 (98) [d)]	4.5 (102) [d)]	0.5 (98) [d)]	2.5 (100) [d)]	0.2 (101) [d)]	0.3 (101) [d)]
Benzene	0.7 (98) [d)]	4.7 (97) [d)]	0.5 (99) [d)]	3.4 (101) [d)]	0.9 (100) [d)]	0.4 (100) [d)]
Carbon disulfide	1.9 (100) [d)]	5.3 (98) [d)]	1.0 (98) [d)]	7.0 (100) [d)]	0.7 (101) [d)]	3.5 (101) [d)]
Tetrahydrofuran	5.7 (101) [d)]	6.6 (100) [d)]	3.1 (98) [d)]	4.4 (102) [d)]	0.9 (101) [d)]	0.4 (101) [d)]
Pyridine	7.3 (105) [d)]	6.8 (102) [d)]	6.4 (110) [d)]	4.4 (104) [d)]	3.0 (101) [d)]	0.7 (101) [d)]

a) 4.0 g of coal (−60 mesh) in 100 ml of the solvent for 1 h at room temperature. b) The solvent in the first column was used. c) 1:1 mixture by volume with methanol was used. d) [(extract+residue) (g)/coal feed (g)] × 100.

mixtures were examined. The results are summarized in Table 5, together with the result for methanol-benzene mixture. For Yallourn and Taiheiyo coals, methanol mixtures with carbon tetrachloride, benzene, carbon disulfide, and tetrahydrofuran gave higher extraction yields than these organic solvents alone. For Shin-yubari coal, carbon disulfide and pyridine gave higher and lower yields for the mixture with methanol, respectively.

Discussion

Synergistic Effect of Alcohol-Benzene Mixtures. Figure 2 and Table 2 show that the synergistic effect for alcohol-benzene mixtures was observed for Yallourn and Taiheiyo coals; this was more marked for less bulky alcohols. Tables 3 and 4 show that smaller alcohols may permeate into pores of a coal more extensively and may cause greater swelling than larger alcohols. It is not unreasonable to consider that this swelling, in turn, may facilitate an extraction with another solvents.[14)] The solubility test for the extracts of Taiheiyo coal with methanol-benzene mixture indicates that benzene has a greater solubility than alcohols. Swelling with alcohols may facilitate extraction with benzene or alcohol-benzene mixtures. In the case of Yallourn coal, an extracting solvent may be alcohol-benzene mixtures, not benzene alone, since 15% of the extract was not soluble in benzene nor methanol. Swelling has been suggested by Dryden[2)] to be an important factor for extraction. Pajak and Marzec[15)] have also reported that the extraction yields with solvents of low extraction power, for example, benzene and diethyl ether, increased when a coal (*C*% 80.7%) was pre-swollen with methanol, tetrahydrofuran, dimethyl formamide, or pyridine.

For Shin-yubari coal, on the other hand, neither swelling by alcohols nor any synergistic effect were observed. This may be attributed to low content of hydroxyl groups, which is deduced from the IR spectrum and from the oxygen content of Shin-yubari coal. Nelson, Mahajan, and Walker[16)] have found that methanol-induced swelling increases linearly with the oxygen content of coals, due to an increased affinity of coal molecules for methanol.

Patel and coworkers[17)] have reported that the solubility of solvent-refined coal and solvent-refined lignite in benzene or chloroform increased from 50—60 to 80—100% upon either acetylation or silylation and this can be explained by the disruption of the intermolecular hydrogen bond in coal. The similar increase of benzene or chloroform extract yield has been reported by Liotta and coworkers[18)] in alkylation of coal which proceeds under mild conditions; this is again ascribed to the reduction of intermolecular associations in coals. In our case, hydrogen bonding between coal molecules in Yallourn and Taiheiyo coals may be broken by hydrogen bonding with the permeating alcohols and the swelling of coal may thus be induced.

Although the extraction yields in our experiments are low, the mechanism proposed here may apply to other solvent systems and may be one example where bulkiness of solvents plays an important role in extraction.

Extraction with Various Methanol-organic Solvent Mixtures. Table 5 shows that the recovery of extract+residue considerably exceeds 100% in extractions of Yallourn and Taiheiyo coals with methanol-pyridine mixture. Collins and coworkers[19)] have reported that pyridine and ethylenediamine were retained in both the extract and residue even after washing with benzene. In our case the solvent may be retained in the extract and residue. Other solvents in Table 5 than pyridine showed nearly 100% recovery. The increased yields for the methanol mixtures with carbon tetrachloride in Yallourn and Taiheiyo coals may be caused by the same mechanism as in the case of the mixture with benzene. On the other hand, decreased yields in the case of pyridine for Shin-yubari coal may be caused by its hydrogen bonding with methanol. Dryden[2)] has reported that ethylenediamine loses its high extractability when it contains water, since it forms hydrogen bonds with the nitrogen atoms of ethylenediamine.

Carbon disulfide seems to be different from other solvents listed in Table 5, in that its mixture with methanol is effective for all the coals in Table 5. We have found and reported that carbon disulfide–pyridine mixture is a very efficient solvent for Shin-yubari coal: It gives about 40% extraction yield at room temperature.[10)]

References

1) J. R. Pullen, "Solvent Extraction of Coal," IEA Coal Research, London (1981), Chap. 2.
2) I. G. C. Dryden, *Fuel*, **30**, 39, 145, 217 (1951).
3) A. Marzec, M. Juzwa, K. Betlej, and M. Sobkowlak, *Fuel Proc. Technol.* **2**, 35 (1979).
4) V. Gutmann, *Electrochimica Acta*, **21**, 659 (1976).
5) a) D. W. Van Krevelen, *Fuel*, **44**, 229 (1965); b) N. Y. Kirov, J. M. O'Shea, and G. D. Sergeant, *Fuel*, **46**, 415 (1967); c) J. M. Angelovich, G. R. Paster, and H. F. Silver, *Ind. Eng. Chem. Process Des. Develop.*, **9**, 106 (1970).
6) H-P. Hombach, *Fuel*, **59**, 465 (1980).
7) a) Y. Sanada and H. Honda, *Fuel*, *45*, 295, 451 (1966); b) V. L. Weinberg and R. A. Yen, *Fuel*, **59**, 287 (1980).
8) H. L. Retcofsky and R. A. Friedel, *Fuel*, **50**, 113 (1971).
9) T. Toshii and F. Yoshimura, *Fuel*, **50**, 113 (1971).
10) M. Iino and M. Matsuda, *Fuel*, **62**, 744 (1983).
11) For example, A. Wielopolski and I. Witt, *Koks, Smola, Gaz*, **22**, 47 (1977); *Chem. Abstr.*, **87**, 138440w (1977).
12) For example, I. I. Lishtvan and A. A. Terentev, *Khim. Tverd. Topl.*, 74 (1975); *Chem. Abstr.*, **84**, 138183c (1976).
13) Y. Toda, Y. Yoshida, H. Honda, and M. Hatami, *J. Fuel Soc. Japan.* **47**, 880 (1968); Our densities are 5—10% higher than the values reported for similar coal in this reference. This may be due to smaller particle size (−60 mesh for our case *vs.* 28—60 mesh for their case), the lower evacuation temperature (room temperature *vs.* 100—110 °C), and the higher measurement temperature (30 °C *vs.* 25 °C) in our experiments.
14) It is not clear why methanol has smaller swelling, but greater extraction yields than ethanol, as shown in Tables 2 and 3. One tentative explanation is that strong interaction between methanol and the surface of the coals, which is suggested by Franklin, makes the pore volume inside the coal increase and facilitates the extraction; R. E. Franklin, *Trans. Faraday Soc.*, **45**, 274 (1949).
15) J. Pajak and A. Marzec, *Fuel*, **62**, 979 (1983).
16) J. R. Nelson, O. P. Mahajan, and P. L. Walker Jr., *Fuel*, **59**, 831 (1980)
17) K. M. Patel, V. I. Stenberg, R. J. Baltisberger, N. F. Woolsey, and K. J. Klabunde, *Fuel*, **59**, 449 (1980).
18) R. Liotta, K. Rose, and E. Hippo, *J. Org. Chem.*, **46**, 277 (1981).
19) C. J. Collins, E. W. Hagaman, R. M. Jones, and V. F. Raaen, *Fuel*, **60**, 359 (1981).

 © 1984 The Chemical Society of Japan Bull. Chem. Soc. Jpn., 57, 3295—3299 (1984)

Unstable Excimer Formation in *cis*-1,2-Di(2-naphthyl)cyclobutane

Shinzaburo ITO,* Masahide YAMAMOTO, and Yasunori NISHIJIMA
Department of Polymer Chemistry, Faculty of Engineering, Kyoto University, Sakyo-ku, Kyoto 606
(Received May 10, 1984)

An unstable intramolecular excimer which is formed in an excited state of *cis*-1,2-di(2-naphthyl)cyclobutane is investigated. The excimer formation-rate constants and dissociation-rate constants in fluid solutions at low temperatures were determined by picosecond time-resolving measurements. The formation processes are interpreted in relation to the bending motion of the cyclobutane ring. Photophysical characteristics of unstable excimers are shown in this system.

Intramolecular excimer formation has been investigated in a number of compounds having two or more aromatic chromophores in a molecule. Since Hirayama's noted work for various diphenylalkanes, it has been confirmed that the most favorable geometry for a stable excimer is a symmetrical sandwich-like parallel arrangement of aromatic planes at a distance of 0.3—0.4 nm. This is easily achieved for a compound in which two chromophores along the alkane chain are separated by three carbon atoms.[1] This result was also confirmed for naphthalene derivatives.[2,3]

But, the existence of an unstable excimer, besides the stable excimer, was found in poly(*N*-vinylcarbazole).[4,5] It has been reported that the unstable excimer, which is often called a second excimer, comes from a partially overlapping structure of two aromatic rings. Much attention has been paid to the unstable excimers since their photophysical behavior is closely related to the relaxation processes of excitation energy in polymer systems. Recently, unstable excimer formation was reported in a few bichromophoric model compounds.[6,7] Studies on such compounds are useful in clarifying the geometry and conformation of the unstable excimer due to the well defined molecular structure and simple relaxation process.[8]

In the present work, we report on a new kind of unstable excimer formed in the compound *cis*-1,2-di(2-naphthyl)cyclobutane. Its detailed photophysical characteristics and excimer formation mechanisms are elucidated by means of photostationary and time-resolving measurements. This information will be important for interpreting the excited-state kinetics in more complex polymer systems.

Experimental

Materials. *cis*-1,2-Di(2-naphthyl)cyclobutane (DNCB) was prepared by the photodimerization of 2-vinylnaphthalene in a benzene solution.[9] The products were fractionated by column chromatography on silica gel with hexane–dichloromethane (7:1) as the eluent. The obtained DNCB was recrystallized from methanol solution prior to use: mp 95—97 °C; NMR (CCl_4) δ=2.5—2.7 (2H, m), 4.1—4.3 (1H, m), and 6.8—7.6 (7H, m). 2-Ethylnaphthalene (Aldrich Chemical Co.) was used as a monomeric model compound. Spectrograde hexane (Nakarai Chemicals Ltd.) was used as a solvent without further purification.

Measurements. All spectroscopic measurements were carried out in hexane solutions degassed by repeated freeze-thaw cycles at *ca.* 10^{-3} Pa. The concentrations were adjusted to 10^{-4} mol dm^{-3}, at which intermolecular excimer formation was negligible. Fluorescence spectra were measured with a Shimadzu RF-502 spectrofluorophotometer whose spectral response was calibrated according to a standard tungsten lamp. The quantum yields of fluorescence were determined relative to that of quinine sulfate in 0.5 mol dm^{-3} sulfuric acid.[10] The decay curves of fluorescence were measured by a single photon counting technique (Ortec Inc., 9200 nanosecond fluorescence spectrometer). For the measurements of the rise and decay curves in the picosecond time region, the 4th harmonic (266 nm, 20 ps) of a passively mode-locked Nd^{3+}:YAG laser was used as an exciting light source. The emission was detected by a Hamamatsu Photonics streak camera (C979) and digitized by a TV camera/microcomputer system (C1000).[11,12] Suitable combinations of optical filters were used in order to isolate the monomer fluorescence and the excimer fluorescence.

Results

The absorption spectra of DNCB and 2-ethylnaphthalene are very similar, although a slight red shift of 1.5—2 nm is observed for DNCB. Such a red shift has been reported for a similar compound, *cis*-1,2-diphenylcyclopentane,[13] and observed for compounds in which plural naphthyl groups are closely linked intramolecularly, *e.g.*, poly(2-vinylnaphthalene).

The fluorescence spectra of DNCB in hexane at various temperatures are shown in Fig. 1. The spectra clearly show broad excimer emission at 400 nm in the low-temperature range, but the excimer emission is not observed either at room temperature or at 77 K in a rigid glass solvent. The fluorescence excitation spectra for the excimer emission band and for the monomer emission band at a wavelength of about 330 nm agree well with the absorption spectrum. Quantum yields of the monomer and excimer emission are shown in Fig. 2, together with the monomer emission quantum yields of 2-ethylnaphthalene. The quantum yields of excimer emission (Φ_D) have the largest value at an extremely low temperature, −95 °C, which is the freezing point of the solvent. As the temperature increases, Φ_D decreases monotonously, and the quantum yields of monomer emission (Φ_M) increase slightly because of the dissociation of excimer. A further increase of temperature rapidly quenches both of the monomer and excimer fluorescence. The total emission quantum yields of DNCB show much smaller values than those of 2-ethylnaphthalene in the high-temperature region, shown in Fig. 2. These results show that DNCB is able

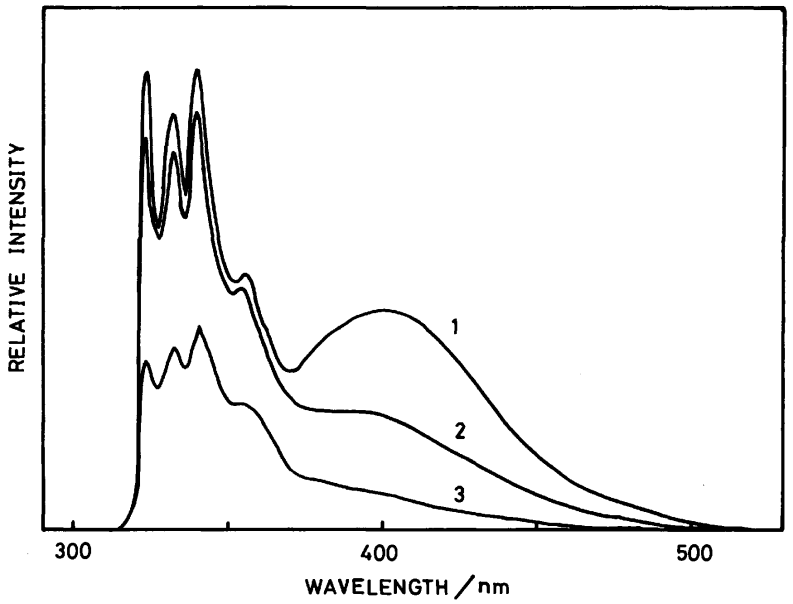

Fig. 1. Fluorescence spectra of DNCB in hexane. 1: −80 °C, 2: −50 °C, and 3: −20 °C.

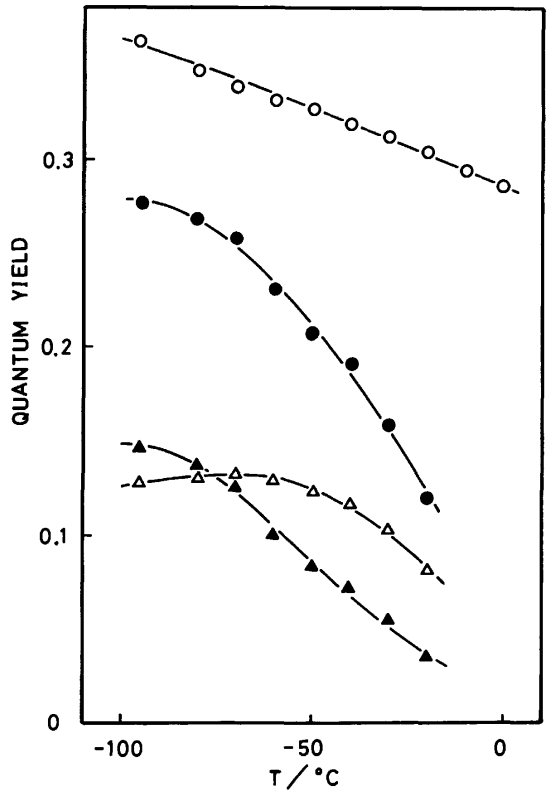

Fig. 2. Fluorescence quantum yields of monomer emission (△), excimer emission (▲) and total emission (●) of DNCB, and quantum yields of monomer emission of 2-ethylnaphthalene (○).

to form an intramolecular excimer by a dynamic process after photoexcitation. The formation process can be achieved by a little conformational change whose rate is very fast even at low temperatures. Since the formed excimer state is not stable, it dissociates to the monomer state or deactivates to the ground state radiationlessly, with increasing temperature.

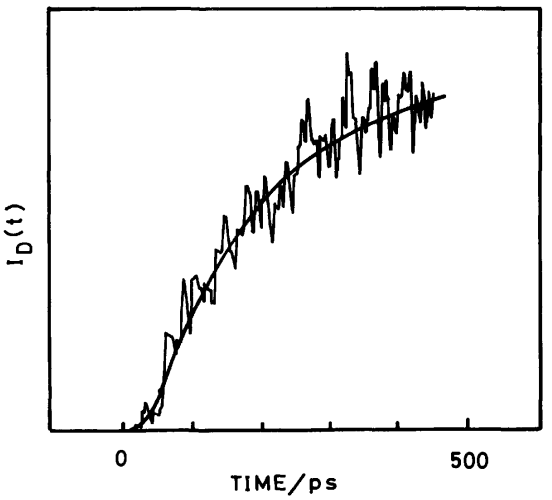

Fig. 3. Rise curve of excimer fluorescence of DNCB at −37°C.
The solid line shows the curve simulated by the function of $I_D(t) = \exp(-t/63\text{ ns}) - \exp(-t/0.16\text{ ns})$.

The dynamic process of excimer formation is well confirmed by time-resolved measurements for monomer and excimer fluorescence. Figure 3 shows a rise curve of excimer emission of DNCB in the picosecond time region. The measurements were carried out at various temperatures and the rise-time constants were determined by a simulation method. The decay-time constants were also obtained by the single photon counting technique in the nanosecond region. For the monomer fluorescence, the decay curve should be given as a double exponential decay function, but it could not be confirmed by the picosecond time-resolving measurements because of the weak signal intensities. Decay times for the monomer emission in the nanosecond region are the same as those of excimer emission in the observed temperature range. This fact shows that the

association and dissociation rate constants of the excimer are fairly large compared with the other rate constants. Thus, the dynamic equilibrium between the excited monomer state and the excimer state is achieved before deactivation to the ground state. The observed rise- and decay- time constants are summarized in Fig. 4.

Discussion

The naphthyl groups of DNCB come face to face with each other without a deformation of the aromatic rings, as shown in Fig. 5. The pair of naphthyl groups can be expected to form an intramolecular excimer since the aromatic rings can achieve an arrangement similar to the sandwich-type conformation. However, the interaction between two naphthyl groups in the ground state is too weak to make a dimeric complex which would give a different absorption spectrum from an isolated naphthalene unit.[14] Furthermore, the monomer fluorescence spectrum of DNCB is similar to that of 2-ethylnaphthalene. From these facts, it can be concluded that the excited state immediately after photoexcitation is the monomer state and the intramolecular excimer is formed from this excited state by some dynamic processes accompanied by conformational changes of the cyclobutane ring.

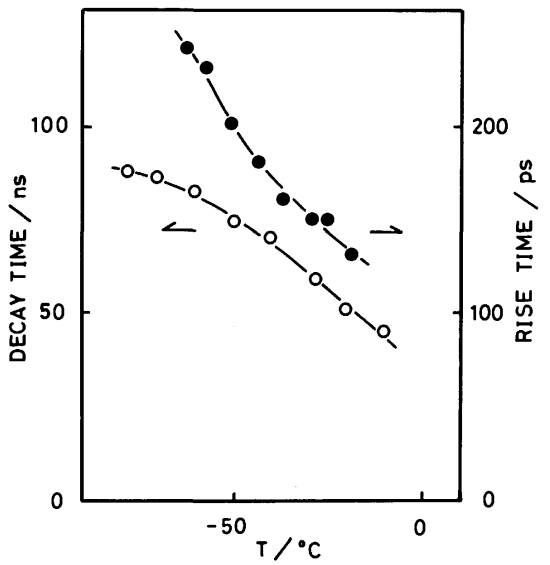

Fig. 4. Temperature dependence of rise and decay time constants.

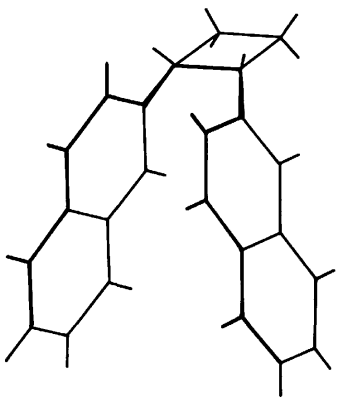

Fig. 5. Schematic molecular structure of DNCB at the planar conformation of cyclobutane ring.

We can obtain the excimer-formation rate constant by time-resolving measurements. The kinetic scheme of this system, and the notation of rate parameters are written as follows.

$$\begin{aligned}
&M + h\nu \longrightarrow M^* \\
&M^* \longrightarrow M + h\nu_1 && k_{01}^f \\
&M^* \longrightarrow M && k_{01}^n \\
&M^* \longrightarrow D^* && k_{21} \\
&D^* \longrightarrow M^* && k_{12} \\
&D^* \longrightarrow M + h\nu_2 && k_{02}^f \\
&D^* \longrightarrow M && k_{02}^n
\end{aligned}$$

where M and M* represent the naphthyl group in the ground state and the excited state, respectively, and D* is the intramolecular excimer. In the present system, the dynamic equilibrium conditions[15] are satisfied: k_{21}, $k_{12} \gg k_{01}$, k_{02}, where $k_{01}=k_{01}^f+k_{01}^n$, and $k_{02}=k_{02}^f+k_{02}^n$. The rate constants, k_{01} and k_{02}, for the naphthyl groups have previously been reported to be of the order of $10^7\ s^{-1}$.[16] Judging from the fast rise times of excimer emission and its slow decay, the rate constants k_{21} and k_{12} are larger than k_{01} and k_{02} by a factor of at least 100. Under dynamic equilibrium conditions, the following equations are used.

$$\lambda_2 = k_{21} + k_{12}$$
$$\Phi_M = k_{01}^f k_{12}/\lambda_1\lambda_2$$

where λ_1 and λ_2 are the decay time constant and rise time constant, respectively, in the excimer response function,

$$I_D(t) = \exp(-\lambda_1 t) - \exp(-\lambda_2 t).$$

The value of k_{01}^f was determined by measurements of the fluorescence quantum yield and lifetime for 2-ethylnaphthalene in the same temperature range: $k_{01}^f=4.2-4.4\times10^8\ s^{-1}$. From the data, λ_1, λ_2, Φ_M, and k_{01}^f, the excimer formation and dissociation rate constants, k_{21} and k_{12} can be determined. Errors in this calculation come mainly from the simulated values of λ_2, and these are of the order of several per cent. The Arrhenius plots of thus-obtained k_{21} and k_{12} are shown in Fig. 6. From the slopes of these plots, the activation energy of the excimer formation process, E_{21} was found to be 5.0 kJ/mol, and that of the dissociation process, E_{12} was 8.4 kJ/mol (with an error of about ±0.5 kJ/mol). Then, the formation- and dissociation-rate constants are expressed by,

$$k_{21} = 5.1\times10^{10}\exp(-5.0\times10^3/RT)$$
$$k_{12} = 1.6\times10^{11}\exp(-8.4\times10^3/RT)$$

where R is the gas constant. The enthalpy change for the excimer formation in DNCB is given as the difference between E_{21} and E_{12}: $\Delta H=-3.4$ kJ/mol. This value is much smaller than the reported ΔH value

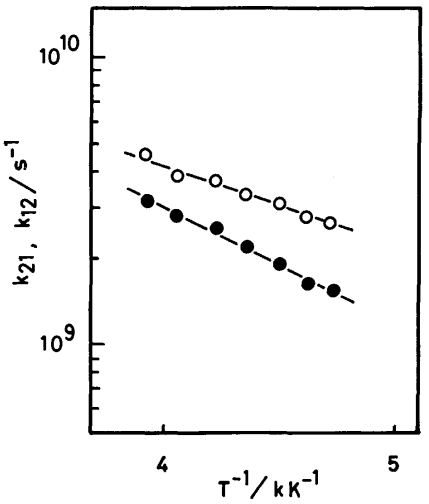

Fig. 6. Arrhenius plots of k_{21}(○) and k_{12}(●).

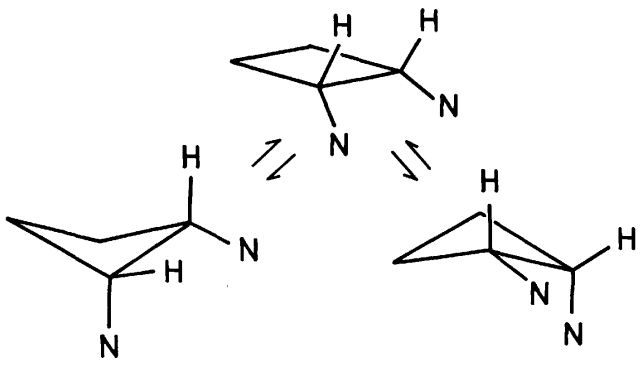

Fig. 7. Bending motion of cyclobutane ring. N: 2-Naphthyl.

for the stable excimer of 2-ethylnaphthalene: −18 kJ/mol.[3,17] Thus, the intramolecular excimer of DNCB has a very weak binding energy and exists only in the low-temperature region in contrast to the stable excimers formed in various dinaphthylalkanes.[16]

The excimer formation and dissociation processes seem to correspond with the bending motion of the cyclobutane ring between puckered forms, as shown in Fig. 7. Two naphthalene rings of DNCB can take an overlapped arrangement at the planar form of cyclobutane ring as shown in Fig. 5, which is attained in the course of the bending motion. The planar conformation has been said to be in a little higher energy state, *ca.* 6.2 kJ/mol than the puckered forms studied by Raman spectroscopy.[18] The overlapping arrangement at the planar form of the cyclobutane ring is not a parallel-sandwich arrangement with respect to the naphthyl groups. Assuming the angle, N-C-H, to be 110°, and the distances, C(aliphatic)-C(aliphatic)=0.155 nm, C(aliphatic)-C(aromatic)=0.152 nm, and C(aromatic)-C(aromatic)=0.139 nm, the planes of naphthalene rings come face to face with each other at an angle, *ca.* 50°. This means their C(aliphatic)-C(aromatic) in-plane axes are inclined at an angle *ca.* 50°, and the distance between the two naphthalene rings is estimated to be 0.28 nm and 0.67 nm for the nearest and farthest aromatic

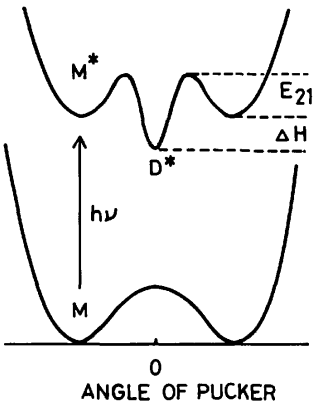

Fig. 8. Schematic potential energy diagram of DNCB.

carbon atoms, respectively. The instability of the excimer state is due to this structural restriction which prevents the naphthalene rings from forming the stable parallel sandwich conformation at the distance of 0.3—0.4 nm. The transition rate of the two puckered forms has been assumed to be considerably fast because of the low barrier energy for the ring inversion. In the present work, it is clear that the rate of bending motion is in the order of 10^9 s^{-1}, thus the conformational lifetime of a puckered form is less than a few hundred picoseconds.

According to the above discussion, the schematic potential energy diagram is illustrated in Fig. 8. The photophysical properties of this unstable excimer are noted: 1) small enthalpy gain for the formation process, 2) large dissociation rate to the excited monomer state even in low temperatures, 3) increase of radiationless dissipation to the ground state at high temperatures. Similar properties have been observed for the unsymmetrical naphthalene excimers formed in 1-(1-naphthyl)-3-(2-naphthyl)propane, whose binding energy was found to be 8.8 kJ/mol.[19] These characteristics seem to be common to the unstable intramolecular excimers. It has often been reported that unstable excimers give somewhat blue shifted fluorescence spectra compared with the stable excimer. But, DNCB shows the same excimer emission band as the stable excimer in spite of its instability. The wavelength of excimer fluorescence should be determined by the difference between the excited state electronic energy and the ground state energy of the excimer geometry. If the ground state energy becomes higher than that of the stable excimer, it is possible that the unstable excimer shows longer wavelength emission than that of the stable excimer. In the present case, the cyclobutane ring at the planar conformation forces the naphthyl groups to have a higher energy geometry both in the ground state and in the excimer state. Therefore, the emission band of excimers seems to be unsuitable as a measure of instability.

The authors wish to express their gratitude to Professor Keitaro Yoshihara and Associate Professor Nobuaki Nakashima, Institute for Molecular Science, for their kind co-operation in picosecond time-resolving mea-

surements. This work has partially been supported by the Fuji Xerox Academic Research Found.

References

1) F. Hirayama, *J. Chem. Phys.*, **42**, 3163 (1965).
2) E. A. Chandross and C. J. Dempster, *J. Am. Chem. Soc.*, **92**, 3586 (1970).
3) S. Ito, M. Yamamoto, and Y. Nishijima, *Rep. Prog. Polym. Phys. Jpn.*, **22**, 453 (1979).
4) G. E. Johnson, *J. Chem. Phys.*, **62**, 4697 (1975).
5) A. Itaya, K. Okamoto, and S. Kusabayashi, *Bull. Chem. Soc. Jpn.*, **49**, 2082 (1976).
6) F. C. De Schryver, J. Vandendriessche, S. Toppet, K. Demeyer, and N. Boens, *Macromolecules*, **15**, 406 (1982).
7) H. Itagaki, N. Obukata, A. Okamoto, K. Horie, and I. Mita, *J. Am. Chem. Soc.*, **104**, 4469 (1982).
8) F. Evers, K. Kobs, R. Memming, and D. R. Terrell, *J. Am. Chem. Soc.*, **105**, 5988 (1983).
9) T. Asanuma, M. Yamamoto, and Y. Nishijima, to be published.
10) W. H. Melhuish, *J. Phys. Chem.*, **65**, 229 (1961).
11) M. Sumitani, N. Nakashima, K. Yoshihara, and S. Nagakura, *Chem. Phys. Lett.*, **51**, 183 (1977).
12) N. Nakashima, A. Namiki, and K. Yoshihara, *J. Photochem.*, **9**, 230 (1978).
13) D. J. Cram, N. L. Allinger, and H. Steinberg, *J. Am. Chem. Soc.*, **76**, 6132 (1954).
14) M. Irie, T. Kamijo, M. Aikawa, T. Takemura, K. Hayashi, and H. Baba, *J. Phys. Chem.*, **81**, 1571 (1977).
15) J. B. Birks, "Photophysics of Aromatic Molecules," Wiley-Interscience, London (1970), Chap. 7.
16) S. Ito, M. Yamamoto, and Y. Nishijima, *Bull. Chem. Soc. Jpn.*, **54**, 35 (1981).
17) B. K. Selinger (*Aust. J. Chem.*, **19**, 825 (1966)) reported the enthalpy change for 2-methylnaphthalene in ethanol: −21 kJ/mol.
18) R. M. Moriarty, "Topics in Stereochemistry," ed by E. L. Eliel and N. L. Allinger, Interscience, New York (1974), Vol. 8, p. 271.
19) S. Ito, M. Yamamoto, and Y. Nishijima, *Polym. Preprints, Jpn.*, **30**, 131 (1981). E. A. Chandross *et al.* (Ref. 2) reported some spectroscopic data for the 1-(1-naphthyl)-3-(2-naphthyl)propane.

 © 1984 The Chemical Society of Japan Bull. Chem. Soc. Jpn., 57, 3300—3306 (1984) [Vol. 57, No. 11

Polarized Raman and Phosphorescence Spectra of [$^1H_4$]- and [$^2H_4$]Pyrimidines

Masayuki UMEMOTO,† Taketora OGATA,†† Hiroko SHIMADA,†† and Ryoichi SHIMADA*
†*Yamaguchi Prefectural Environmental Pollution Research Center, Hiruta, Asada, Yamaguchi 753*
††*Department of Chemistry, Faculty of Science, Fukuoka University, Nanakuma, Jonan-ku, Fukuoka 814*
Department of Chemistry, Faculty of Science, Kyushu University, 33, Hakozaki, Higashi-ku, Fukuoka 812
(Received June 21, 1984)

Assignments of the out-of-plane normal vibrations of [$^1H_4$]- and [$^2H_4$]pyrimidines were reexamined through studies of the polarized Raman, time-resolved phosphorescence and polarized dark sublevel phosphorescence spectra. The vibrational analyses of the phosphorescence spectra based on their polarization behavior indicate that the appearance of the strong 0-0 and totally symmetric vibronic bands in the dark sublevel phosphorescence spectra is attributed to the distortion of the molecular structure along the b_1 normal coordinates in the lowest triplet state.

The phosphorescence spectrum of pyrimidine has been studied by many workers and the emitting triplet state of this molecule was assigned to $^3B_1$ (n, π^*).[1-4] Nishi *et al.*[5] observed the phosphorescence spectrum at 4.2 K and pointed out that the 0-0 and totally symmetric vibronic bands arise from the T_z (B_2) and T_y (A_1) sublevels of the lowest triplet state, while the out-of-plane vibronic bands arise, very likely, from the dark T_x (A_2) sublevel, where the x and z axes were taken as the direction normal to the molecular plane and the C_2 axis, respectively. Chan and Sharnoff[6] determined the ordering of the sublevels of the lowest triplet state in pyrimidine to be T_x, T_y, and T_z using the microwave optical double-resonance technique. Burland and Schmidt[7] investigated the dynamic behavior of the pyrimidine molecule in the lowest triplet state using the microwave-induced delayed phosphorescence technique and pointed out that the populating rate for the T_x sublevel was unexpectedly high. Recently, Inoue and Lim[8] observed the zero-field electron paramagnetic resonance transitions among the sublevels of the lowest triplet state of pyrimidine in a benzene host crystal at 1.6 K by the optical detection of the resonance transitions and suggested that the unusually high T_x population is associated with the pseudo-Jahn-Teller distortions of the potential surfaces in the $^3A_1$ (π, π^*) and $^3B_2$ (π, π^*) states perturbed by a close-lying $^3A_2$ (n, π^*) state.

In this paper, the vibrational analyses of the phosphorescence spectra of [$^1H_4$]- and [$^2H_4$]pyrimidines will be reexamined through the studies of the polarized T_x sublevel phosphorescence spectra in benzene host crystals and the polarized Raman spectra in single crystals. The molecular structure in the lowest triplet state will be also discussed.

Experimental

Chemicals. [$^1H_4$]Pyrimidine, obtained from Nakarai Chemicals, was purified by repeated distillation under reduced pressure. [$^2H_4$]Pyrimidine, which was kindly supplied by Professor Lionel Goodman of Rutgers University, was purified by vacuum distillation. Methylcyclohexane and benzene of Dotite Spectrosol Grade were used without further purification.

Optical Measurements. The time-resolved phosphorescence spectra and the phosphorescence lifetimes of [$^1H_4$]- and [$^2H_4$]pyrimidines were studied in methylcyclohexane and benzene matrices at various temperatures between 4.2 and 1.4 K. Liquid helium in the Dewar vessel, where the sample was held, was pumped out with a rotary pump of 1000 L min^{-1} displacement, and the sample was kept at desired temperatures by controlling the speed of evacuation of helium gas with a valve placed between the pump and the Dewar vessel. The temperature of the sample was determined by measuring the vapor pressure of helium in the top of the Dewar vessel. The short-lifetime phosphorescence was observed in the following way. The sample was excited for 10 ms. Two ms after the excitation ceased, the phosphorescence was sampled for 10 ms. The long-lifetime phosphorescence was observed at exciting, waiting, and sampling times of 200, 200, and 200 ms, respectively.

The polarized long-lifetime phosphorescence spectra were observed in a benzene host crystal at 1.4 K. The single-crystal specimen was obtained as follows. Single crystals of benzene doped with [$^1H_4$]- and [$^2H_4$]pyrimidines, were made by the Bridgman method at low temperature. Well grown single crystals examined under polarized light were cut about 2 mm in thickness along a cleavage plane with a razor blade in a cold room kept at −15 °C and suspended in an inner Dewar vessel precooled to −30 °C. Liquid nitrogen was poured into an outer Dewar vessel and the Dewar vessels were allowed to stand for about 10 h. Then, after pouring liquid helium very gradually into the inner Dewar vessel, the samples were examined again under polarized light. Only the crystals which were not cracked were used for the measurement of the polarized spectrum. Since we had no crystallographic knowledge about the cleavage plane cut out from the benzene single crystal, the polarized phosphorescence spectrum was observed with a rotatable polarizer whose orientation was set in such a way that the intensity of the 0-0 band of the long-lifetime phosphorescence spectrum became the strongest and the rotation of the polarizer by 90° gave the weakest intensity. The spectra observed at the former and latter orientations of the polarizer are drawn with solid and dotted lines (referred to as A and B spectra, respectively). The optical and electronic arrangements used for the measurements of the time-resolved phosphorescence spectrum, the polarized phosphorescence spectrum and the phosphorescence lifetimes are exactly the same as those described previously.[9,10]

The polarized Raman spectra of [$^1H_4$]- and [$^2H_4$]pyrimidine single crystals were observed at −30 °C in the crystal orientation where the Raman bands observed at 395 cm^{-1} for [$^1H_4$]-pyrimidine and at 365 cm^{-1} for [$^2H_4$]pyrimidine showed drastic change of polarization behavior by rotating the polarizer under the same way as described previously.[11]

The Raman spectrum polarized parallel to the crystal growth direction is referred to as // spectrum and the spectrum polarized perpendicular to as ⊥ spectrum.

Results and discussion

Out-of-plane Normal Vibrations. Although the normal vibrations of [$^1H_4$]- and [$^2H_4$]pyrimidines have been studied by many workers,[12-15] the assignments given for the normal vibrations, especially for the out-of-plane vibrations, do not agree with each other. Therefore, the out-of-plane vibrations were reexamined by studing the polarized Raman spectrum and normal coordinate calculations. The normal coordinate calculation for the out-of-plane vibrations was carried out with a valence force field and the ϕ-type torsional coordinate using the same method as described previously.[16] Values of the force constants are given in Table 1, where the notations Q, q, P, p, and t are the same as those given by Whiffen.[17] Calculated vibrational frequencies and modes for [$^1H_4$]- and [$^2H_4$]pyrimidines are listed in Tables 2 and 3, respectively.

The polarized Raman spectra of [$^1H_4$]- and [$^2H_4$]-pyrimidines are shown in Fig. 1. As can be seen in this figure, the non-totally symmetric Raman bands, which are depolarized in molten phase, are classified into three types (I, II, and III) based on their polarization behavior. In the first type, the intensity of the ⊥ band is stronger than that of the // band. In the second type, the intensity of the // band is stronger than that of the ⊥ band, and in the third type the intensity of the ⊥ band is much stronger than that of the // band. A comparison of the polarization behavior of the Raman bands with the band contours of the corresponding infrared bands observed in a vapor phase[12] indicates that the type-I and-II Raman bands should be assigned to vibrations belonging to b_2 and b_1 symmetry species, respectively. Hence, the type-III Raman bands are assigned to a_2 species.

TABLE 1. FORCE CONSTANTS FOR OUT-OF-PLANE VIBRATIONS

$Q_{C'-N}$	0.17
Q_{C-N}	0.18
Q_{C-C}	0.20
q^o	−0.06
q^m	0.03
$P_{H'}$	0.31
P_H	0.34
p^o	0.07
$p^m_{H,H'}$	−0.05
$p^m_{H,H}$	−0.07
p^p	0.02
$t^o_{C'-N,H'}$	−0.04
$t^o_{C-N,H}$	−0.02
$t^o_{C-C,H}$	−0.02

[in aNmrad^{-2}(=mdyn Å/rad^2)units]

C′ is the carbon atom placed between the two N atoms.
H′ is the hydrogen atom bonded to the C′ atom.

The Raman bands of [$^1H_4$]pyrimidine observed at 345, 725, 775, and 982 cm^{-1} showed type-II polarization behavior and, thus, these were assigned to the ν_{16b}, ν_{11}, ν_4, and ν_{17b} vibrations of b_1 species, respectively. The vibrational modes were determined based on the normal coordinate calculation and also through the analysis of the phosphorescence spectrum. The bands observed at 395 and 1004 cm^{-1} showed type-III polarization and, thus, they were assigned to the ν_{16a} and ν_{17a} vibrations of a_2 species, respectively. The Raman bands of [$^2H_4$]pyrimidine observed at 300, 553, 675, 720, and 850 cm^{-1} showed type-II polarization behavior and the bands at 365 and 807 cm^{-1} showed type-III polarization. Thus, the former were assigned to the ν_{16b}, ν_{11}, ν_{10b}, ν_4, and ν_{17b} vibrations and the latter to the ν_{16a} and ν_{17a} vibrations, respectively. The ν_{10b} vibration of [$^1H_4$]pyrimidine could not be identified in the polarized Raman spectrum. The out-of-plane normal vibrations thus assigned are given in Tables 2 and 3, together with those given by previous workers.[12-15] Our assignments explain well the observed polarization behavior of the phosphorescence spectra (described later).

Phosphorescence Spectrum. The temperature dependence of the relative intensities of the ν_{17b}, ν_{11}, and ν_{16b} bands with respect to the 0-0 band in the long-lifetime phosphorescence and that of the lifetime of the long-lifetime phosphorescence observed in methylcyclohexane are shown in Figs. 2 and 3, respectively. As can be seen in these figures, the relative intensity and the lifetime became almost

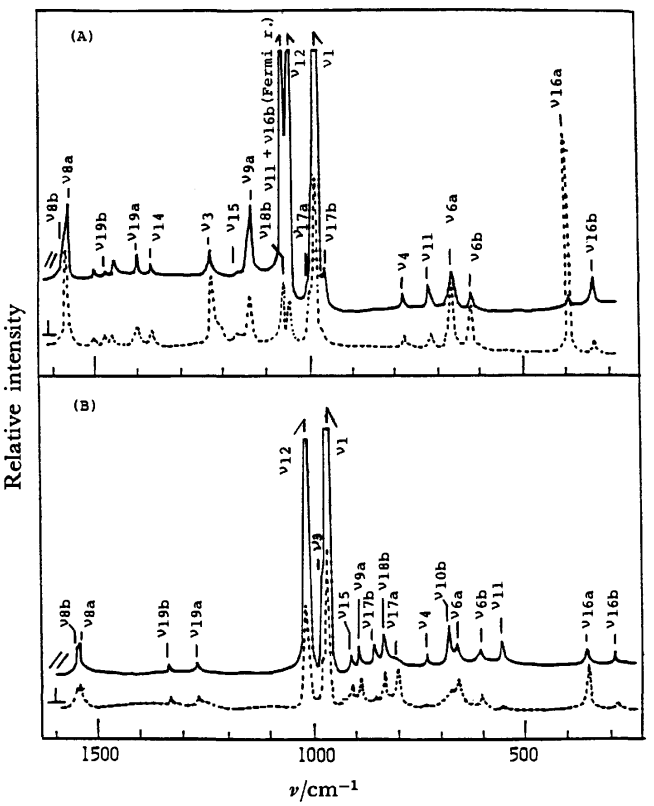

Fig. 1. Polarized Raman spectra of [$^1H_4$]-(A) and [$^2H_4$]pyrimidine (B) single crystals.

Table 2. Out-of-plane vibrations of [$^1H_4$]pyrimidine

Sym. Spec.	Mode	Sbrana[12]	Foglizzo[13]	Milani[14]-Nejad	Bokobza[15]-Sebagh	This work			
						Raman	Calcd	Phosphorescence in Mc[b]	in Bz[b]
		$\tilde{\nu}$/cm^{-1}	$\tilde{\nu}$/cm^{-1}	$\tilde{\nu}$/cm^{-1}	$\tilde{\nu}$/cm^{-1}	$\tilde{\nu}$/cm^{-1}	$\tilde{\nu}$/cm^{-1}	$\tilde{\nu}$/cm^{-1}	$\tilde{\nu}$/cm^{-1}
a_2	ν_{17a}	870			927	1004	994	1005	1002
	ν_{16a}	394	393	398.5	398	395	395	392	405
b_1	ν_{17b}[a]	993	981	980	980	982	993	962	969
	ν_{10b}	719	829	721	955		861	804	820
	ν_{11}	804	720	811	810	725	723	716	732
	ν_4	709	717	708	720	775	770		
	ν_{16b}	344	344	344	346	345	354	339	349

a) Previous workers[12–15] gave ν_5 mode for this vibration. b) Mc=methylcyclohexane, Bz=benzene.

Table 3. Out-of-plane vibrations of [$^2H_4$]pyrimidine

Sym. spec.	Mode	Sbrana[12]	Milani[14]-Nejad	This work			
				Raman	Calcd	Phosphorescence in Mc	in Bz
		$\tilde{\nu}$/cm^{-1}	$\tilde{\nu}$/cm^{-1}	$\tilde{\nu}$/cm^{-1}	$\tilde{\nu}$/cm^{-1}	$\tilde{\nu}$/cm^{-1}	$\tilde{\nu}$/cm^{-1}
a_2	ν_{17a}		801	807	818	800	811
	ν_{16a}		369	365	360	374	371
b_1	ν_{17b}[a]	848	820	850	857	833	840
	ν_{10b}	552	561	675	662	669	675
	ν_{11}	669	669	553	545	556	560
	ν_4		553	720	714		716
	ν_{16b}	304	304	300	303		

a) Previous workers[12,14] gave ν_5 mode for this vibration.

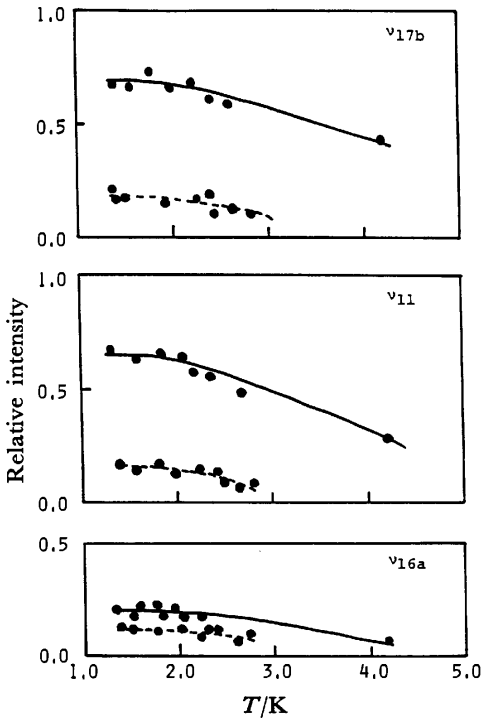

Fig. 2. Temperature dependence of the relative intensities of the ν_{17b}, ν_{11}, and ν_{16a} bands to the 0-0 band in the long-lifetime phosphorescences of [$^1H_4$]-(——) and [$^2H_4$]pyrimidins (----).

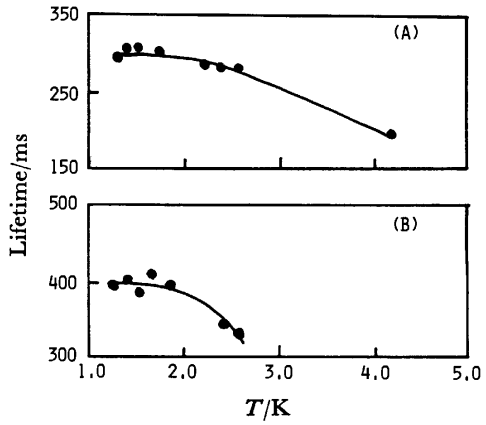

Fig. 3. Temperature dependence of the lifetimes of the long-lifetime phosphorescences of [$^1H_4$]-(A) and [$^2H_4$]pyrimidines (B).

constant at temperatures below 2 K. This indicates that the spin lattice relaxation, involving the dark T_x sublevel of the lowest triplet state, hardly takes place at temperatures below 2 K within the lifetime of the T_x sublevel. Thus, one can conclude that the long-lifetime phosphorescence observed at 1.4 K arises directly from the T_x sublevel.

The lifetimes of the lowest triplet sublevels at 1.4 K are given in Table 4, together with the values measured by Burland and Schmidt.[7] The lifetime of the T_x sub-

Table 4. Phosphorescence lifetimes of [$^1H_4$]- and [$^2H_4$]pyrimidines

	[$^1H_4$]Pyrimidine			[$^2H_4$]Pyrimidine		
	Burland[7] (1.2 K)	This work (1.4 K)		Burland[7] (1.2 K)	This work (1.4 K)	
	in Bz	in Bz	in Mc	in Bz	in Bz	in Mc
T_x	324	330	310	465	440	400
T_y	16.6			17.8		
		15	13		20	15
T_z	11.8			13.0		

(in ms units)

level is so long compared with those of the T_y and T_z sublevels that the long-lifetime phosphorescence spectrum can easily be separated out from the short-lifetime T_y and T_z spectra. While the T_z sublevel spectrum could not be separated from the T_y spectrum under our experimental technique due to very close lifetimes of these two sublevels.

The time-resolved phosphorescence spectra of [$^1H_4$]- and [$^2H_4$]pyrimidines observed in methylcyclohexane matrix at 1.4 K are shown in Figs. 4 and 5, respectively. Intensity ratio of the 0-0 bands of the "long-" and "short-" lifetime spectra extrapolated at t=0 ms, that is, when the excitation light was cut off, was determined to be about 1/100. The

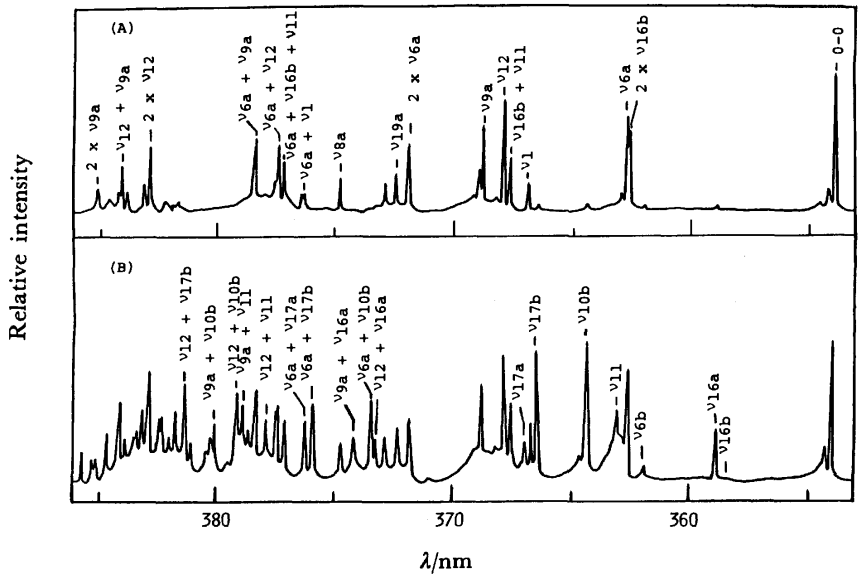

Fig. 4. Short (A) and long (B) lifetime phosphorescence spectra of [$^1H_4$]pyrimidine in methylcyclohexane at 1.4 K.

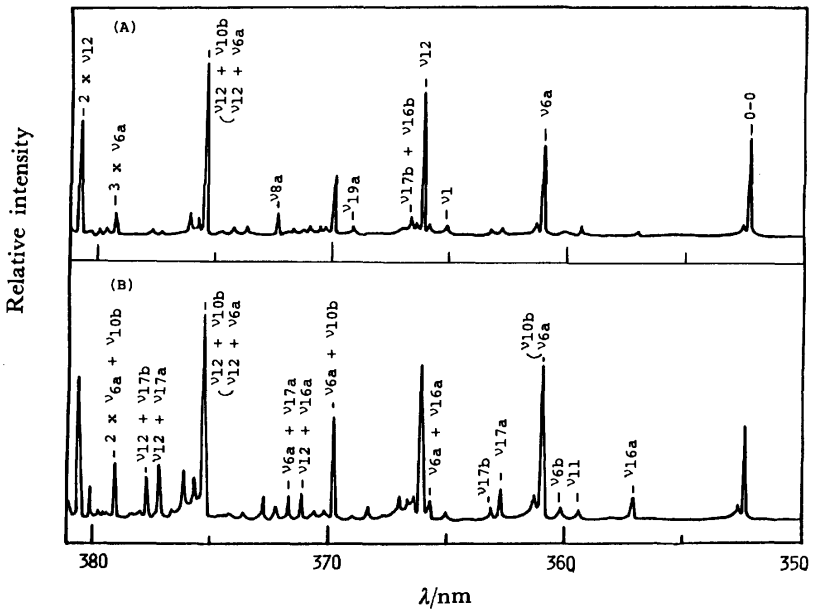

Fig. 5. Short (A) and long (B) lifetime phosphorescence spectra of [$^2H_4$]pyrimidine in methylcyclohexane at 1.4 K.

spectra shown in Figs. 4 and 5 were drawn after the observed intensities of the 0-0 bands in both the spectra were normalized to unity. Vibrational analysis made on the appreciably intense bands in the short-lifetime phosphorescence spectrum was the same as that given by Nishi *et al.*[5] and Hochstrasser and Marzzacco[18] for the phosphorescence spectrum observed at 4.2 K. Although the long-lifetime phosphorescence gave essentially the same spectral structure as that of the short-lifetime phosphorescence, the most characteristic feature of the long-lifetime spectrum was a remarkable increase of the relative intensities of some vibronic bands with respect to the 0-0 band.

The short-and long-lifetime phosphorescence spectra observed in a benzene matrix at 1.4 K showed essentially the same spectral structure as those observed in methylcyclohexane. The polarized long-lifetime phosphorescence spectra of [$^1H_4$]- and [$^2H_4$]-pyrimidines doped in a benzene host single crystal are given in Figs. 6 and 7, respectively. The bands in the polarized phosphorescence spectrum can be classified into two types. In the first type, the intensity of the A spectrum is stronger than that of the B spectrum while in the second type the intensity relation is *vice versa*. Based on the polarization behavior of the bands, vibrational analyses of the phosphorescence spectra of [$^1H_4$]- and [$^2H_4$]pyrimidines were carried out.

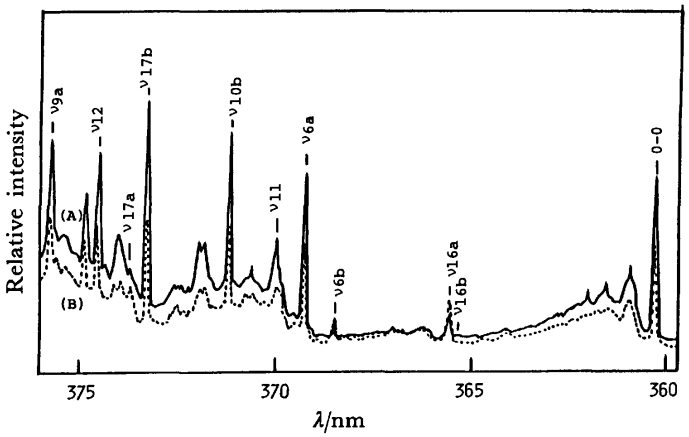

Fig. 6. Polarized long-lifetime phosphorescence spectrum of [$^1H_4$]pyrimidine in benzene host crystal at 1.4 K. A and B are referred to the paper.

[$^1H_4$]Pyrimidine: The phosphorescence bands separated by 392, 618, 716, 804, 962, 1005, 1465, 1484, 1533, 1646, 1795, 1861, 1876, 1940, and 2030 cm^{-1} from the 0-0 band are much intensified relative to the 0-0 band in the long-lifetime spectrum compared with the short-lifetime spectrum. Among them the 392, 618, 1005, 1465, and 1533 cm^{-1} bands showed the second-type polarization behavior in the polarized long-lifetime phosphorescence spectrum, while the other showed the first-type polarization. By referring the polarized Raman spectrum and the normal coordinate calculation, 392, 618, 716, 804, 962, and 1005 cm^{-1} bands were assigned to the ν_{16a}, ν_{6b}, ν_{11}, ν_{10b}, ν_{17b}, and ν_{17a} vibrations, respectively. Hence, it is concluded that the intensified bands showing the first-type polarization behavior can be assigned to the b_1 vibronic bands, while those showing the second-type polarization to the a_2 or b_2 bands. The other intensified bands were assigned to combination bands involving these out-of-plane vibrations based on their polarization behaviors. Generally, the H wagging vibrations are the most effective for the vibronic coupling between (n, π^*) and (π, π^*) states and thus the H wagging vibrations are expected to be observed with fairly strong intensity in the dark sublevel phosphorescence spectrum. Therefore, intensified bands in the dark T_x sublevel phosphorescence spectrum could be assigned to the H wagging vibrations. Our assignment given for the modes of the out-of-plane vibrations were made based on this point.

[$^2H_4$]Pyrimidine: The phosphorescence bands separated by 374, 556, 608, 669, 800, 833, 1029, 1323, 1421, 1465, 1720, and 1857 cm^{-1} from the 0-0 band in methylcyclohexane are intensified relative to the 0-0 band in the long-lifetime spectrum. Among them the 374, 608, 800, 1029, 1421, 1465, and 1857 cm^{-1} bands showed the second-type polarization behavior in the polarized phosphorescence spectrum and the

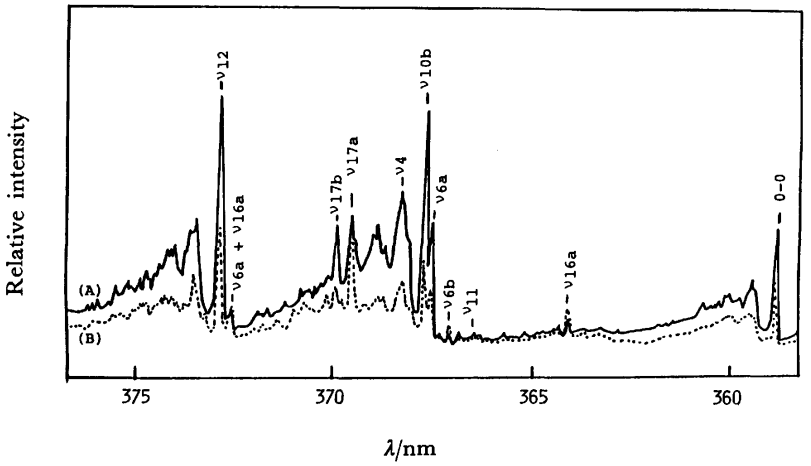

Fig. 7. Polarized long-lifetime phosphorescence spectrum of [$^2H_4$]pyrimidine in benzene host crystal at 1.4 K.

others showed the first-type polarization. The 374, 608, and 800 cm^{-1} bands were assigned to the ν_{16a}, ν_{6b}, and ν_{17a} vibrations, respectively, and the 556, 669, and 833 cm^{-1} bands to the ν_{11}, ν_{10b}, and ν_{17b} vibrations, respectively, by referring Table 3. As in the case of [$^1H_4$]pyrimidine, the first-type polarization behavior in the phosphorescence spectrum is attributed to the b_1 vibronic bands and the second type to the a_2 or b_2 bands. It should be noted that the 0-0 and totally symmetric vibronic bands showed the first type, that is, b_1 polarization behavior in the long-lifetime phosphorescence spectra of [$^1H_4$]- and [$^2H_4$]pyrimidines as can be seen in Figs. 6 and 7. Detailed vibrational analyses are given in Figs. 4 and 5.

Molecular Structure in the Lowest Triplet State. It is quite impossible that the a_1 and b_1, and also a_2 and b_2 vibronic bands show the same polarization behavior, respectively, so far as the molecular geometry of pyrimidine keeps the point group C_{2v} in the lowest triplet state even if the pyrimidine molecules take any orientations in a benzene host crystal. We will now discuss the orientation of the pyrimidine molecule in a benzene host single crystal. Hong and Robinson[19] observed two spectral origins in the phosphorescence of pyrazine in a benzene host crystal, where one is much stronger than the other, and suggested that most of the pyrazine molecules preferentially occupy the substitutional site of the host crystal with a certain fixed orientation. Since the molecular structure of pyrimidine is similar to that of pyrazine and the phosphorescence spectrum in a benzene host crystal shows single origin and distinct polarization behavior as can be seen in Figs. 6 and 7, it is believed that almost all pyrimidine molecules are oriented in a single way in a benzene host crystal. If the pyrimidine molecule, which belongs to the point group C_{2v}, deforms along the normal coordinates of a_2 symmetry species, the molecular symmetry reduces to the point group C_2 and thus a_1 and a_2 symmetry species go into a species, and b_1 and b_2 species into b species. On the other hand, if the molecule deforms along the b_1 normal coordinates the molecular symmetry reduces to the point group C_s, where the plane perpendicular to the original molecular plane and involving the z axis is the symmetry plane. In this case, a_1 and b_1 symmetry species go over into a′ species, and a_2 and b_2 species into a″ species. Thus the symmetrically forbidden transition in the C_{2v} molecular geometry becomes allowed if the molecular structure deforms to the point group C_2 or C_s.

The transitions from the T_x sublevel in the lowest triplet state to the totally symmetric vibrational levels in the ground state are strictly forbidden when the molecule has the C_{2v} geometry, while the transitions become allowed with z-polarization when the molecule deforms along the a_2 normal coordinates. In this case, the transitions from the T_x sublevel to the b_1 and b_2 vibrational levels of the ground state have x- and/or y-polarization, while transitions to the a_1 and a_2 levels have z-polarization. On the other hand, if the molecule deforms along the b_1 normal coordinates, the transitions from the T_x sublevel to the a_1 and b_1 vibrational levels have y-polarization, while the transitions from the T_x sublevel to the a_2 and b_2 levels have x- and/or z-polarization. These polarization behaviors are illustrated in Fig. 8.

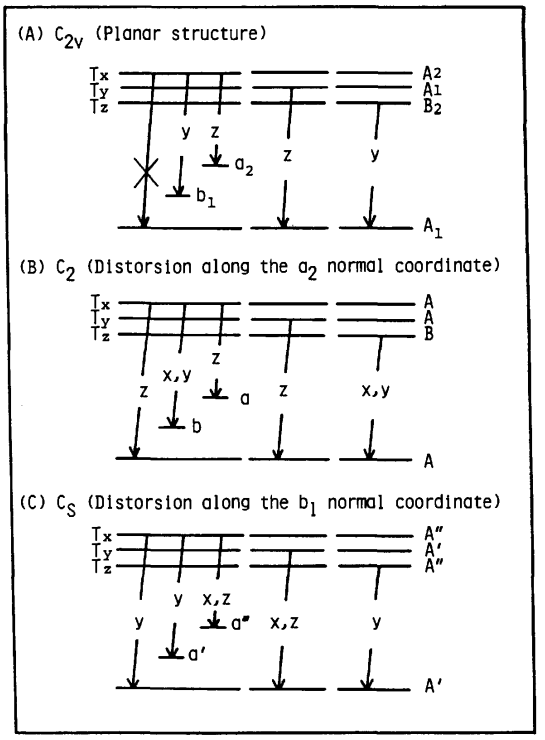

Fig. 8. Polarization directions of the phosphorescence bands emitted from each sublevels of the lowest triplet state in C_{2v} molecular geometry (A), in C_2 geometry (B), and in C_s geometry (C).

Since the 0-0 and totally symmetric vibronic bands show the same polarization behavior as that of the b_1 vibronic bands, as described above, one can understand that the direction of the transition moments of the 0-0 and totally symmetric vibronic bands coincide with that of the b_1 vibronic bands. Thus, one could conclude that the appearance of the 0-0 and totally symmetric bands in the long-lifetime phosphorescence spectrum is responsible for the molecular distortion along the b_1 normal coordinates in the lowest triplet state. This conclusion was supported by the fact that the b_2 and a_2 vibronic bands showed the same polarization behavior in the polarized long-lifetime phosphorescence spectrum, as described above.

We would like to express our thanks to Mr. Shoji Kizuki for his great help in the experiment. The present work was partially supported by a Grant-in-Aid for Scientific Research from the Ministry of Education, Science and Culture (No. 57470013).

References

1) R. Shimada, *Spectrochim. Acta*, **17**, 30 (1961).
2) V. G. Krishna and L. Goodman, *J. Am. Chem. Soc.*, **83**, 2042 (1961).
3) L. Goodman and R. W. Harrell, *J. Chem. Phys.*, **30**, 1131 (1959).
4) V. G. Krishna and L. Goodman, *J. Chem. Phys.*, **36**, 2217 (1962).
5) N. Nishi, R. Shimada, and Y. Kanda, *Bull. Chem. Soc.*

Jpn., **43**, 41 (1970).
6) Y. Chan and M. Sharnoff, *J. Lumin*, **3**, 155 (1970).
7) D. M. Burland and J. Schmidt, *Mol. Phys.*, **22**, 19 (1971).
8) A. Inoue and E. C. Lim, *Chem. Phys. Lett*, **62**, 250 (1979).
9) Y. Urabe, T. Watanabe, Y. Ishibashi, H. Shimada, and R. Shimada, *Mem. Fac. Sci. Kyushu Univ. Ser. C*, **13**, 1 (1981).
10) T. Watanabe, H. Shimada, and R. Shimada, *Bull. Chem. Soc. Jpn.*, **55**, 2564 (1982).
11) Y. Ishibashi, F. Arakawa, H. Shimada, and R. Shimada, *Bull. Chem. Soc. Jpn.*, **56**, 1327 (1983).
12) G. Sbrana, G. Adembri, and S. Califano, *Spectrochim. Acta*, **22**, 1831 (1966).
13) R. Foglizzo and A. Novak, *J. Chim. Phys.*, **64**, 1484 (1967).
14) F. Milani-Nejad and H. D. Stidham, *Spectrochim. Acta, Part A*, **31**, 1433 (1975).
15) L. Bokobza-Sebagh and J. Zarenbowitch, *Spectrochim. Acta, Part A*, **32**, 797 (1976).
16) Y. Ishibashi, R. Shimada, and H. Shimada, *Bull. Chem. Soc. Jpn.*, **55**, 2765 (1982).
17) D. H. Whiffen, *Philos. Trans. R. Soc. London, Ser A*, **248**, 131 (1955).
18) R. M. Hochstrasser and C. J. Marzzacco, *J. Mol. Spectrosc.*, **42**, 75 (1972).
19) H. K. Hong and G. W. Robinson, *J. Mol. Spectrosc.*, **42**, 75 (1972).

Synthesis and Characterization of Iron(III) Complexes with Unsymmetrical Quadridentate Schiff Bases, and Spin Equilibrium Behavior in Solution[1)]

Naohide MATSUMOTO,* Kazuhiro KIMOTO, Akira OHYOSHI, and Yonezo MAEDA†
Department of Industrial Chemistry, Faculty of Engineering, Kumamoto University, Kurokami 2-39-1, Kumamoto 860
†*Department of Chemistry, Faculty of Science, Kyushu University, Hakozaki, Higashi-ku, Fukuoka 812*
(Received March 23, 1984)

Several iron(III) complexes with planar unsymmetrical quadridentate Schiff bases composed of 1:1:1 condensation products of acetylacetone, ethylenediamine, and each of salicylaldehyde and *o*-hydroxyacetophenone have been prepared and characterized, where the Schiff bases are abbreviated as [H_2salacen] and [H_2hapacen], respectively. The effective magnetic moment of [FeCl(hapacen)] increases gradually from 3.46 BM at 80 K to 5.31 BM at 301 K, and was interpreted by a spin-spin interaction model based on a binuclear structure with an antiferromagnetic interaction parameter of $J=-10$ cm^{-1} ($S_1=S_2=5/2$), while the magnetic moment for [FeCl(salacen)] is 5.86 BM at 80 K and 5.96 BM at 302 K, indicating that the complex is a monomeric species of high-spin type. The bis(imidazole)iron(III) complexes [Fe(im)$_2$(salacen)]$BPh_4\cdot CH_3OH$ and [Fe(im)$_2$-(hapacen)]$BPh_4\cdot 2CH_3OH$ showed a striking thermochromic behavior in various organic solvents, changing from dark red to green with decrease of the temperature. The complexes are essentially of low-spin type in solids, where im and BPh_4 denote imidazole and tetraphenylborate, respectively. Electronic, ^{1}H NMR (Evans method), and ESR spectra confirmed that the thermochromism is caused by spin-equilibrium between high-spin($S=5/2$) and low-spin($S=1/2$) states of iron(III).

Several iron(III) complexes such as tris(dialkyldithiocarbamato)iron(III) and iron(III) complexes with hexadentate Schiff bases or porphyrin derivatives have been known as examples of cross-over complexes in solids.[2)] Spin-equilibrium behavior attributable to high-spin($S=5/2$)$\rightleftharpoons$low-spin($S=1/2$) of iron(III) in solution has been observed in iron(III) hemoproteins such as methemoglobin and cytochrome peroxidase,[3)] and synthetic iron(III) complexes with hexadentate Schiff bases.[4)] In order to develop a model complex for the spin-equilibrium behavior of natural products, it is desirable to study iron(III) complexes with planar quadridentate ligands exhibiting spin-equilibrium in solution.

Nishida *et al.*[5)] investigated the magnetic properties of the iron(III) complexes [Fe(im)$_2$(sal$_2$en)]BPh_4 and [Fe(im)$_2$(ac$_2$en)]BPh_4 with ligand structures of **1** and **3** of Fig. 1, and elucidated that the complexes [Fe(im)$_2$-(sal$_2$en)]BPh_4 and [Fe(im)$_2$(ac$_2$en)]BPh_4 are of high-spin and low-spin type in solids, respectively. When the discussion is limited to bis(imidazole)iron(III) complexes with similar types of ligand systems, a complex with a ligand field strength intermediate between those of **1** and **3** is expected to be a candidate for a spin cross-over complex. The in-plane ligand field strength can be estimated by the positions of d-d band maxima of the corresponding copper(II) complexes, where the d-d band maxima of the copper(II) complexes are given in parentheses in Fig. 1.[6)] The position of the d-d band maximum of the unsymmetrical quadridentate copper(II) complex of **2** is intermediate between those of **1** and **3**, as would be predicted by the ligand structures. Based on the criterion described above, the ligands **4** and **5**,

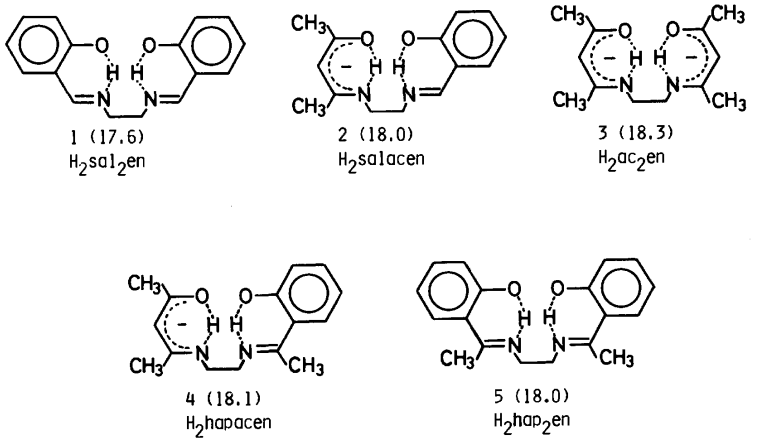

Fig. 1. Structures of [H_2sal$_2$en] (**1**), [H_2salacen] (**2**), [H_2ac$_2$en] (**3**), [H_2hapacen] (**4**), and [H_2hap$_2$en] (**5**). The positions of d-d band maxima of the corresponding copper(II) complexes are given in parentheses (10^3 cm^{-1}).

in addition to the ligand **2**, were selected, where the structures of the ligands, along with the positions of d-d band maxima of the corresponding copper(II) complexes in parentheses, are shown in Fig. 1.

In this study, bis(imidazole)iron(III) complexes with ligands **2**, **4**, **5** along with their chloro iron(III) complexes, were prepared and characterized by elemental analyses, melting points, magnetic susceptibilities, and ESR spectra. The bis(imidazole)iron(III) complexes with unsymmetrical quadridentate ligands (**2**, **4**) showing a striking thermochromism in solution were investigated by electronic, ESR, and ^{1}H NMR (Evans method)[7] spectra.

Experimental

Physical Measurements. Melting points were measured on a Yanagimoto melting points apparatus and are uncorrected. Elemental analyses were performed by Mr. Shinichi Miyazaki at the Technical Service Center of Kumamoto University. Thermogravimetric analysis (TGA) was carried out on a Shimadzu TGC-20 type microthermobalance at a heating rate of 5 °C min^{-1}, using *ca.* 10 mg of a sample for each run. Magnetic moments for the bis(imidazole)iron(III) complexes in dichloromethane were obtained by using the Evans ^{1}H NMR technique at ambient temperature (28 °C),[7] a JEOL MH 100 spectrometer being used at 100 MHz. Electronic spectra in Nujol mull were recorded on a Shimadzu spectrophotometer UV 200, while electronic spectra in solution at room temperature and *ca.* 200 K were recorded on a Hitachi recording spectrophotometer 323, where a jacketed, insulated quartz cell was used, and the temperature was monitored by a YEW Type 2572 digital thermometer. Variable temperature spectra were obtained on a Hitachi 340 spectrophotometer, where the temperature of a sample solution was thermostated within ±0.1 °C by use of a temperature controlled circulating bath, Neslab RTE-8, and measured immediately before and after each spectral measurement with a copper-constantan thermocouple and a digital thermometer, Takeda TR-2121.[8] ESR spectra were measured at ambient temperature and liquid nitrogen temperature on a JEOL JES-FEAX (X-band), using Mn^{2+} doped in MgO as reference. Magnetic susceptibilities on polycrystalline samples were determined by the Faraday method, using an electrobalance Type 2002 (Cahn Instrument) with an electromagnet (8000 G) operated at 20 A. The temperature was controlled over 78—300 K by using a digital temperature controller, Model 3700 (Scientific Instrument). $HgCo(NCS)_4$ was used as a calibration substance. The effective magnetic moment was calculated by the formula of $\mu_{eff}=2.828\sqrt{\chi_A T}$, where χ_A is a molar susceptibility after diamanetic correction.

Synthesis. Ligands. Unsymmetrical quadridentate Schiff base ligands (**2**, **4**) were prepared by the demetallation reaction of the corresponding copper(II) complexes with gaseous hydrogen sulfide in dichloromethane solution, according to the method reported earlier,[9] and identified by the ^{1}H NMR spectra. Symmetrical quadridentate Schiff base **5** was prepared by the method of literature.[10]

Chloroiron(III) Complexes. The preparative methods of the chloroiron(III) complexes [FeCl(salacen)], [FeCl(hapacen)], and [FeCl(hap$_2$en)] are similar, so that only the synthesis of [FeCl(salacen)] is described in detail. To a solution of [H_2salacen] (10 mmol) in 50 cm^3 of absolute methanol was added a solution of anhydrous iron(III) chloride (10 mmol) in 50 cm^3 of absolute methanol. To this mixture, triethylamine (20 mmol) was added. The resulting solution was stirred at 60 °C for 1 h and allowed to stand for several hours at room temperature. The black crystals which separated were filtered, washed with absolute methanol and diethyl ether, and dried *in vacuo*.

Bis(imidazole)iron(III) Complexes. The preparative methods of the bis(imidazole)iron(III) complexes [Fe(im)$_2$(salacen)]BPh_4, [Fe(im)$_2$(hapacen)]BPh_4, and [Fe(im)$_2$(hap$_2$en)]BPh_4 are similar, and only the synthesis of [Fe(im)$_2$(salacen)]BPh_4 is exemplified in detail. The mixture of [FeCl(salacen)] (2 mmol) and imidazole (4 mmol) in 150 cm^3 of absolute methanol was stirred at 60 °C for 20 min, and the solution was filtered while hot. The filtrate was added to a solution of sodium tetraphenylborate (30 mmol) in 10 cm^3 of absolute methanol, and the resulting red solution was allowed to stand overnight to precipitate green crystals. The green needle crystals were filtered, washed with a small amount of absolute methanol and diethyl ether, and dried *in vacuo*. They were recrystallized from a mixture of dichloromethane and absolute methanol.

Results and Discussion

Analytical data and melting points are given in Table 1. As indicated by the elemental analyses, the bis(imidazole) iron(III) complexes tend to crystallize as solvates. The number of solvent molecule of crystallization was evaluated by thermogravimetric analysis (TGA), where the weight losses estimated by the elemental analyses were observed.

Magnetic Properties in Solids. Chloroiron(III) Complexes. The value of the effective magnetic moment of [FeCl(salacen)] is 5.86 BM at 80 K and 5.96 BM at 302 K, indicating that the complex is a mononuclear species with a high-spin state of iron(III). On the other hand, the effective magnetic moment of [FeCl(hapacen)] increases gradually from 3.46 BM at 80 K to 5.31 BM at 302 K (see Fig. 2). Magnetic susceptibility data for [FeCl(hapacen)] were analyzed with

TABLE 1. ELEMENTAL ANALYTICAL DATA AND MELTING POINTS[a]

Compound	C (%)	H (%)	N (%)	Mp θ_m/°C
[FeCl(salacen)]	49.69 (50.11)	4.82 (4.81)	8.19 (8.35)	213
[FeCl(hapacen)]	51.49 (51.53)	5.27 (5.09)	7.82 (8.01)	244
[FeCl(hap$_2$en)]	54.41 (54.64)	4.86 (5.31)	6.97 (6.91)	>290
[Fe(im)$_2$(salacen)]$BPh_4\cdot CH_3OH$	68.77 (68.63)	6.00 (6.14)	10.69 (10.67)	125
[Fe(im)$_2$(hapacen)]$BPh_4\cdot 2CH_3OH$	67.33 (67.72)	6.26 (6.53)	9.94 (10.08)	118
[Fe(im)$_2$(hap$_2$en)]$BPh_4\cdot 2CH_3OH$	68.81 (69.06)	6.09 (6.26)	9.82 (9.66)	131

a) Calcd values are in parentheses.

a spin-spin interaction model based on the spin Hamiltonian $-2JS_1 \cdot S_2$ ($S_1=S_2=5/2$). The susceptibility per iron atom of a binuclear species is given in Eq. 1.[11]

$$\chi_A = Ng^2\beta^2[55+30\exp(10x)+14\exp(18x)+5\exp(24x)+\exp(28x)]/kT[11+9\exp(10x)+7\exp(18x)+5\exp(24x)+3\exp(28x)+\exp(30x)] \quad (x=-J/kT) \quad (1)$$

Assuming an isotropic g value of 2.00, the J value obtained by the best-fit of the susceptibility data to Eq. 1 is $-10\ cm^{-1}$.[12] Figure 2 shows the experimental effective magnetic moments and the theoretical curve with the bast-fit value of J. The J value of $-10\ cm^{-1}$ is comparable to the J values of chloro(*N*,*N*-disalicylideneethylenediaminato)iron(III) ([FeCl(sal$_2$en)]) and analogous complexes.[13] Figure 3 shows a proposed structure of [FeCl(hapacen)], based on the structure of [FeCl(sal$_2$en)].[13]

Bis(imidazole)iron(III) Complexes. The effective magnetic moments for [Fe(im)$_2$(salacen)]BPh$_4$·CH$_3$OH and [Fe(im)$_2$(hapacen)]BPh$_4$·2CH$_3$OH are 3.02 and 3.20 BM at 301 K, respectively, indicating that the complexes are essentially of low-spin type in the solid state. ESR spectra for [Fe(im)$_2$(salacen)]BPh$_4$·CH$_3$OH and [Fe(im)$_2$hapacen]BPh$_4$·2CH$_3$OH in the solid state showed a single signal at *ca.* g=2.1 at 298 K, and the signal split into three components at liquid nitrogen temperature, which is characteristic of low-spin iron(III) complexes.[14] Experimental anisotropic g values are listed in Table 2. The nature of the ground state Kramers doublet of the ^{2}T of pseudo-octahedral iron(III) complexes can be elucidated by using the anisotropic g values. In this calculation, the spin-orbit coupling interaction and the crystal field distortion are considered. The eigenfunctions of a $(t_2)^1$ configuration may be written as

$$\Psi_i^+ = A_i|1^+> + B_i|\zeta_1^-> + C_i|-1^+>$$
$$\Psi_i^- = A_i|-1^-> - B_i|\zeta_1^+> + C_i|+1^->,$$

where $|1>=-(d_{xz}+id_{yz})/\sqrt{2}$, $|-1>=(d_{xz}-id_{yz})\cdot\sqrt{2}$, $|\zeta_1>=id_{xy}$, i=1, 2, 3, and the superscripts + and − mean the α-spin and β-spin wave functions. The Kramers doublet will be split by the magnetic field interaction $\mathbf{H}=\beta(k\mathbf{l}+2\hat{s})\mathbf{H}$, where k, the orbital reduction factor, is fixed at 0.9 in this calculation. The g values for the ground state level may be given as[14]

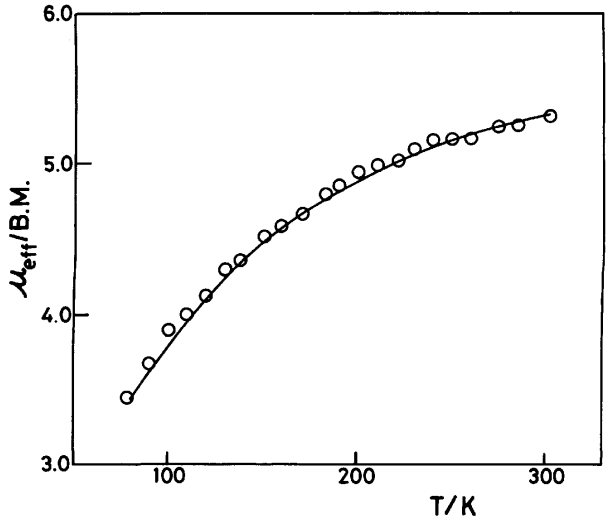

Fig. 2. Temperature dependence of the effective magnetic moment for [FeCl(hapacen)] (o), where the solid line represents theoretical curve of Eq 1 with the parameters of J=10 cm^{-1} and g=2.00.

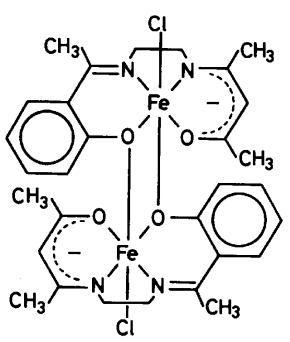

Fig. 3. A proposed structure for [FeCl(hapacen)].

Table 2. ESR parameters and occupied orbital of unpaired electron for [Fe(im)$_2$(salacen)]BPh$_4$·CH$_3$OH (**1**) and [Fe(im)$_2$(hapacen)]BPh$_4$·2CH$_3$OH (**2**)

	(**1**)	(**2**)
g_x	2.349	2.322
g_y	2.138	2.155
g_z	1.938	1.931
A_1	0.104	0.105
B_1	0.995	0.993
C_1	−0.036	−0.028
unpaired electron orbital	d_{xy}	d_{xy}

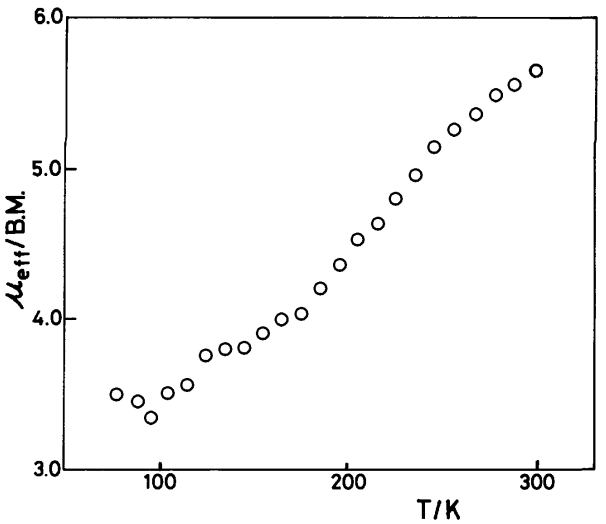

Fig. 4. Temperature dependence of the effective magnetic moment for [Fe(im)$_2$(hap$_2$en)] BPh$_4$·2CH$_3$OH (○).

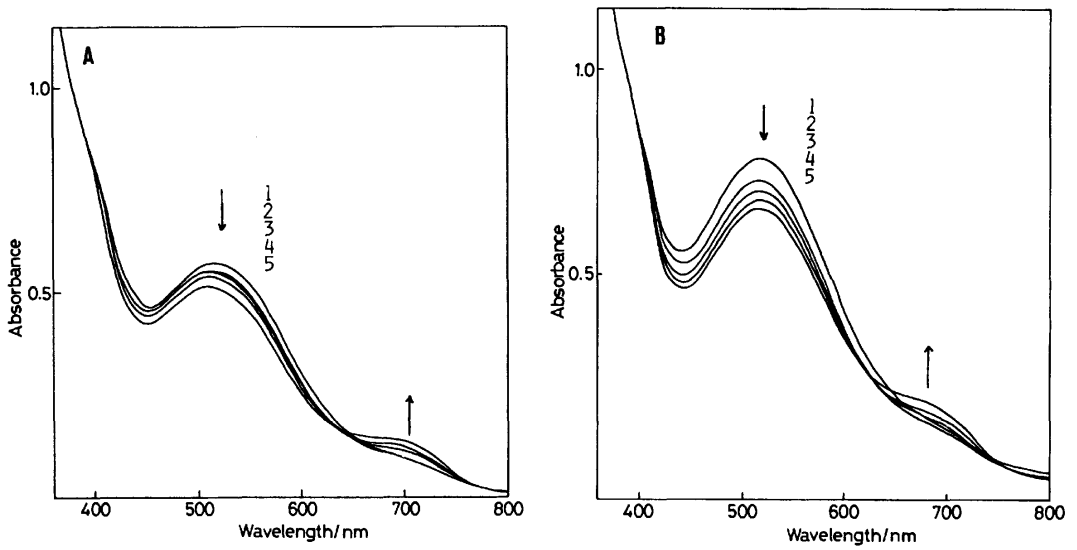

Fig. 5. Absorption spectra of [Fe(im)$_2$(salacen)] $BPh_4 \cdot CH_3OH$ (**A**) (3.098×10^{-4} mol dm^{-3}) and [Fe(im)$_2$(hapacen)]$BPh_4 \cdot 2CH_3OH$ (**B**) (2.735×10^{-4} mol dm^{-3}) in dichloromethane solution at various temperatures (301 (**1**), 288 (**2**), 273 (**3**), 263 (**4**), 251 (**5**) K).

$$g_z = 2[A^2 - B^2 + C^2 + k(A^2 - C^2)]$$
$$g_x = 2[B^2 - 2AC + \sqrt{2}kB(A - C)]$$
$$g_y = 2[B^2 + 2AC + \sqrt{2}kB(A + C)]$$
$$A^2 + B^2 + C^2 = 1$$

The values of A, B, and C are selected to solve the above equations by using the experimental anisotropic g values. Since the signs of the observed g values are not determined experimentally, the values of A, B, and C are not obtained unequivocally, so that it is necessary to try many assignments to solve the equations. The reasonable solutions[14] are selected and listed in Table 2. As shown in Table 2, the ground state Kramers doublet consists mainly of the state wherein the unpaired electron remains in the d_{xy} orbital, because the B value is nearly equal to 1.

Figure 4 shows the temperature dependence of the magnetic moment of [Fe(im)$_2$(hap$_2$en)]$BPh_4 \cdot 2CH_3OH$ in the solid state. The value of the effective magnetic moment increases gradually from 3.50 BM at 78 K to 5.64 BM at 298 K. This behavior is attributable to a spin-equilibrium between high-spin an low-spin states of iron(III).

Thermochromic Behavior in Solution. Green needle crystals of [Fe(im)$_2$(salacen)]$BPh_4 \cdot CH_3OH$ and [Fe(im)$_2$(hapacen)]$BPh_4 \cdot 2CH_3OH$ are dissolved in various organic solvents such as acetone, dichloromethane, chloroform, *N,N*-dimethylformamide, and acetonitrile, to change their colors to dark red at room temperature. At *ca.* 200 K (Dry Ice/acetone bath), the color changes from dark red to green, showing a striking thermochromic behavior. It should be noted that such a thermochroism was not observed for the symmetrical complexes [Fe(im)$_2$(sal$_2$en)]BPh_4 and [Fe(im)$_2$(hap$_2$en)]$BPh_4 \cdot 2CH_3OH$. Temperature dependence of the electronic spectra of [Fe(im)$_2$(salacen)]$BPh_4 \cdot CH_3OH$ and [Fe(im)$_2$(hapacen)]-

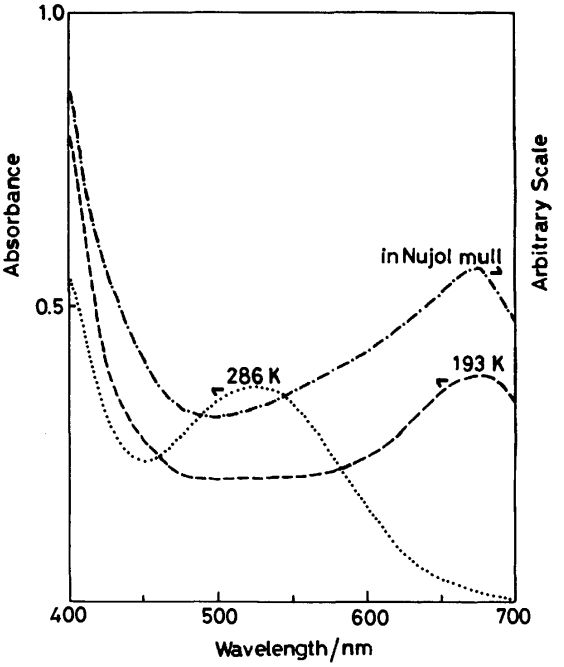

Fig. 6. Electronic absorption spectra of [Fe(im)$_2$(hapacen)]$\cdot 2CH_3OH$ in dichloromethane at 286 and 193 K, along with the spectrum in Nujol mull.

$BPh_4 \cdot 2CH_3OH$ in dichloromethane over the temperature range of *ca.* 300—250 K is shown in Fig. 5. The spectrum of [Fe(im)$_2$(hapacen)]$BPh_4 \cdot 2CH_3OH$ in dichloromethane at 286 and 193 K, along with the spectrum in Nujol mull at room temperature is shown in Fig. 6. As shown in Fig. 5 and 6, the spectrum of [Fe(im)$_2$(hapacen)]$BPh_4 \cdot 2CH_3OH$ at 300 K exhibits an absorption band at 520 nm with an extinction coefficient on the order of *ca.* 2500 mol^{-1} dm^3 cm^{-1}. With a lowering of the temperature, this band decreases its intensity and a new band

appears at 680 nm. The electronic spectrum of [Fe(im)$_2$(hapacen)]BPh$_4$·2CH$_3$OH at 193 K in dichloromethane resembles that in Nujol mull at room temperature, where the complex is confirmed to be a low-spin type in the solid state on the basis of the magnetic moment and the ESR spectrum, as described earlier. Therefore the lower energy band around 680 nm is due to a low-spin species. The magnetic moments for [Fe(im)$_2$(salacen)]BPh$_4$·CH$_3$OH and [Fe(im)$_2$(hapacen)]BPh$_4$·2CH$_3$OH in dichloromethane at 301 K were estimated by the Evans ^{1}H NMR method to be 5.45 and 5.60 BM, respectively, which lie in the range expected for high-spin iron(III) complexes, so that the higher energy band around 520 nm is due to a high-spin species.

The authors wish to express their thanks to Dr. Tasuku Ito of the Institute for Molecular Science and Mr. Toshiaki Kanao of Kumamoto University, for the measurements of the variable temperature electronic spectra.

References

1) A part of this work has been already reported: N. Matsumoto, K. Kimoto, K. Nishida, A. Ohyoshi, and Y. Maeda, *Chem. Lett.*, **1984**, 479.

2) F. A. Cotton, *Coord. Chem. Rev.*, **8**, 184 (1972); R. Rickard, C. E. Johnson, H. A. O. Hill, *J. Chem. Phys.*, **48**, 523 (1968).

3) T. Iizuka, "Kinzoku Ion No Seibutsu-katusei," "Kagaku Zokan," ed by Y. Kiya, H. Tanaka, and A. Nakahara, Kagaku Dozin, Kyoto (1982), Vol. 95, pp. 5—19, and references therein.

4) M. F. Tweedle and L. J. Wilson, *J. Am. Chem. Soc.*, **98**, 4824 (1975); R. A. Binstead, J. K. Beattie, T. G. Dewey, and D. H. Turner, *J. Am. Chem. Soc.*, **102**, 6442 (1980); T. Ito, M. Sugimoto, K. Toriumi, H. Nakayama, W. Mori, and M. Sekizaki, *Chem. Lett.*, **1983**, 121; R. H. Petty, E. V. Dose, M. F. Tweedle, and L. J. Wilson, *Inorg. Chem.*, **17**, 1064 (1978).

5) Y. Nishida, S. Oshio, and S. Kida, *Chem. Lett.*, **1975**, 79; Y. Nishida, S. Oshio, and S. Kida, *Bull. Chem. Soc. Jpn.*, **50**, 119 (1977).

6) N. Matsumoto, M. Asakawa, H. Nogami, M. Higuchi, and A. Ohyoshi, *J. Chem. Soc., Dalton Trans.*, in press.

7) D. F. Evans, *J. Chem. Soc.*, 2003 (1959).

8) M. Sugimoto, M. Nonoyama, T. Ito, and J. Fujita, *Inorg. Chem.*, **22**, 950 (1983).

9) H. A. Kusuka, M. F. Farona, P. Pappas, and S. Potterton, *J. Coord. Chem.*, **1**, 259 (1971); P. N. Howells, J. W. Kenney, J. H. Nelson, and R. A. Henry, *Inorg. Chem.*, **15**, 124 (1976); N. Matsumoto, M. Asakawa, H. Nogami, and A. Ohyoshi, *Inorg. Chim. Acta*, in press.

10) Y. Nakao, N. Nonagase, and A. Nakahara, *Bull. Chem. Soc. Jpn.*, **42**, 452 (1969).

11) Y. Muto and K. Kato, "*Chelate Kagaku (2)*," ed by K. Ueno, Nankoudo, Tokyo (1976), pp. 389—496.

12) M. Mikuriya, H. Okawa, and S. Kida, *Bull. Chem. Soc. Jpn.*, **54**, 2943 (1981).

13) M. Gerloch, J. Lewis, F. E. Mabbs, and A. Richards, *J. Chem. Soc. (A)*, **1968**, 112.

14) H. Ohshio, Y. Maeda, and Y. Takashima, *Inorg. Chem.*, **22**, 2684 (1983); Y. Maeda, N. Tsutsumi, and Y. Takashima, *Inorg. Chem.*, **23**, 2440 (1984); M. S. Haddad, M. W. Lynch, W. D. Federer, and D. N. Hendrickson, *Inorg. Chem.*, **20**, 123 (1981).

Ozonization of Triphenylmethane Dyes

Masaki MATSUI,* Hideki NAKABAYASHI, Katsuyoshi SHIBATA, and Yoshimi TAKASE
Department of Industrial Chemistry, Faculty of Engineering, Gifu University, Yanagido, Gifu 501-11
(Received November 21, 1983)

The reaction of Malachite Green (MG, **1a**), a model compound of triphenylmethane dye, with ozone proceeded *via* two paths. The first path involved an ozone attack at the dimethylamino moiety to give a *N*-formylmethylamino derivative **4a**. The second path produced 4-(dimethylamino)benzophenone (**2a**) and *p*-(dimethylamino)phenol (**6**). Other ozonized products, **3a** and **5a** were also detected. The following is a discussion of the ozonization mechanism.

The reactions of dyes with ozone have been studied from the point of dye-wastewater treatment. Currently, such reactions are being looked at in terms of the decrease in the chemical oxygen demand (COD) and decolorization.[1] However, the ozonization mechanism has scarcely been touched. In this respect, the ozonization reactions of pyrazolone,[2] azo,[3-6] indigoid,[7] and diphenylmethane[8] dyes have been reported.

Reactions involving triphenylmethane dyes have been discussed regarding photo-fading. The photoreaction of MG in water was reported to give 4-(dimethylamino)benzophenone, the carbinol base of MG, and *p*-(dimethylamino)phenol.[9] The photoreactions of Crystal Violet (CV) have been reported to give *p*-(dimethylamino)phenol, 4,4′-bis(dimethylamino)benzophenone, the leuco and demethylated derivatives of CV, *etc.*[10-12]

The ozonization reaction of MG, a model compound of the triphenylmethane dye, is discussed.

Experimental

General. Ozone was generated by a Nihon ozon 0-1-2 type ozonizor. IR, NMR, and mass spectra were recorded on a Hitachi EPI-S2 spectrometer, a Hitachi R-24 spectrometer, and a Hitachi M-52 spectrometer, respectively. Melting points were measured with a Yanagimoto micro-melting-point apparatus. Gas chromatography was performed using Shimadzu 3AH and 4C-PF gas chromatographs. Purity of the materials used was confirmed by gas chromatography.

Materials. The materials which were used are shown in Figure 1. **1a** (MG, Nakarai Chemicals, Ltd.) was recrystallized from benzene-ethanol; ^{1}H ($CDCl_3$) δ=3.35 (12H, s) and 6.8—7.9 (13H, m). **1b** was synthesized as described in the literature;[13] ^{1}H NMR ($CDCl_3$), δ=2.88 (12H, s), 3.53 (3H, s), and 6.5—7.1 (12H, m). **1c** was also synthesized as described in the literature;[13] ^{1}H NMR ($CDCl_3$) δ=3.00 (12H, s) and 7.0—8.0 (12H, m). **1d** (CV, Nakarai Chemicals, Ltd.) was recrystallized from water; ^{1}H NMR ($CDCl_3$) δ=3.28 (18H, s) and 6.9—7.4 (12H, dd). Dimethylaminobenzophenones **2a—c** were synthesized as described in the literature,[14] and recrystallized from ethanol. 4-(Dimethylamino)benzophenone (**2a**); mp 87.5—89.0 °C (lit 89.5—90.5 °C).[14] 4-Dimethylamino-4′-methoxybenzophenone (**2b**); mp 131.4 °C (lit 133 °C).[15] 3-Nitro-4′-(dimethylamino)benzophenone (**2c**); mp 173.6 °C (lit 173 °C).[15] 4,4′-Bis(dimethylamino)benzophenone (**2d**) was synthesized by the oxidation of Auramine 0;[16] mp; 171.0—172.3 °C (lit 172—174 °C).[17] *N*-Formylmethylaminobenzophenones **3a—d** were synthesized by the oxidation of the corresponding *p*-(dimethylamino)benzophenones **2a—d** with Collins reagent[18] and purified by column chromatography (silica gel, acetone). 4-(*N*-Formylmethylamino)benzophenone (**3a**); mp 188.5 °C; ^{1}H NMR ($CDCl_3$) δ=3.42 (3H, s), 7.3—8.0 (9H, m), and 8.75 (1H, s); MS (20 eV) *m/z* (rel intensity) 239 (M^+; 26), 238 (1), 162 (26), 134 (24), 105 (44), and 77 (100); IR (KBr disk) 1600 cm^{-1} (C=O). 4-(*N*-Formylmethylamino)-4′-methoxybenzophenone (**3b**); mp 132.8 °C; ^{1}H NMR ($CDCl_3$) δ=3.35 (3H, s), 3.38 (3H, s), 6.9—7.9 (8H, m), and 8.63 (1H, s); MS (20 eV) *m/z* (rel intensity) 269 (M^+; 37), 268 (1), 162 (20), 135 (100), and 107 (17); IR (KBr disk) 1600 cm^{-1} (C=O). 3-Nitro-4′-(*N*-formylmethylamino)benzophenone (**3c**); mp 145.4 °C; ^{1}H NMR ($CDCl_3$) δ=3.38 (3H, s), 7.2—8.6 (8H, m), and 8.73 (1H, s); MS (20 eV) *m/z* (rel intensity) 284 (M^+; 30), 162 (26), 150 (9), 134 (100), and 122 (4); IR (KBr disk) 1605 (C=O), 1530, and 1320 cm^{-1} (NO_2). 4-(Dimethylamino)-4′-(*N*-formylmethylamino)benzophenone (**3d**); mp 170.1 °C; ^{1}H MNR ($CDCl_3$) δ=3.08 (3H, s), 3.40 (6H, s), 7.3—7.9 (8H, m), and 8.63 (1H, s); MS (20 eV) *m/z* (rel intensity) 282 (M^+; 63), 281 (13), 267 (54), 162 (4), 148 (100), 134 (33), and 120 (8); IR (KBr disk) 1600 cm^{-1}

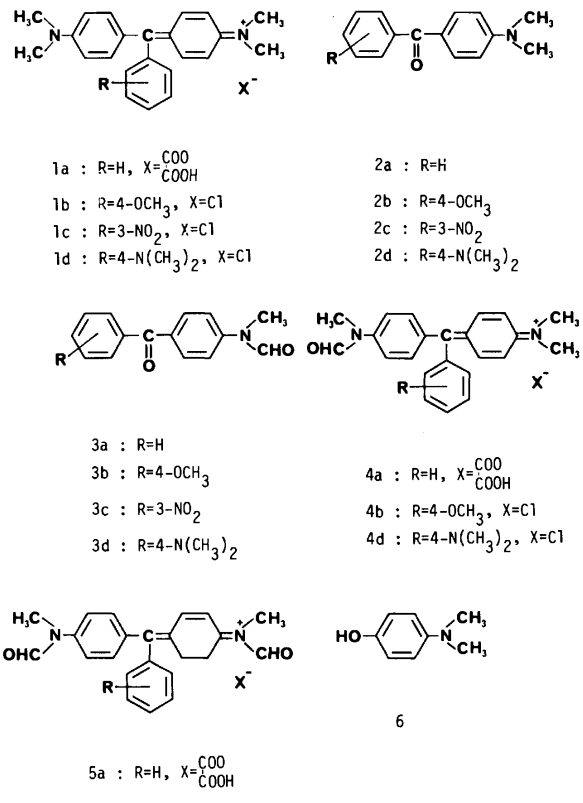

Fig. 1. Materials.

(C=O). **4a** was synthesized by the oxidation of **1a** with Collins reagent and purified by column chromatography (silica gel, acetone); ^{1}H NMR ($CDCl_3$) δ=2.90 (3H, s), 3.25 (6H, s), 7.0—7.6 (13H, m), and 8.42 (1H, s); MS (20 eV) *m/z* (rel intensity) 344 (100), 343 (10), 267 (60), and 210 (50). **4b** was isolated by the ozonization of **1b** and purified by column chromatography (silica gel, methanol:acetone=1:3); ^{1}H NMR ($CDCl_3$) δ=2.93 (6H, s), 3.38 (3H, s), 3.78 (3H, s), 6.7—7.4 (12H, m), and 8.40 (1H, s); MS (20 eV) *m/z* (rel intensity) 374 (100), 373 (17), 267 (15), and 240 (46). **4d** was synthesized by the oxidation of **1d** with Collins reagent; ^{1}H NMR ($CDCl_3$) δ=2.98 (12H, s), 3.05 (3H, s), 6.6—7.1 (12H, m), and 8.41 (1H, s); MS (20 eV) *m/z* (rel intensity) 387 (35), 386 (15), 267 (50), 253 (100), 134 (25), and 120 (60). **5a** was synthesized by a further oxidation of **1a** with Collins reagent; ^{1}H NMR ($CDCl_3$) δ=3.20 (6H, s), 7.0—7.5 (13H, m), and 8.30 (2H, s); MS (20 eV) *m/z* (rel intensity) 358 (3), 357 (10), 224 (6), 134 (22), and 77 (100). *p*-(Dimethylamino)phenol (**6**) was synthesized as described in the literature;[9] mp 74.1 °C (lit 74—76 °C).[19] The mass spectra of **4a**, **4b**, **4d**, and **5a** were recorded as the leuco derivatives.

Ozonization. The method of ozonization was the same as that described in a previous paper.[8] Ozonization was carried out with an ozone-oxygen mixture (ozone: 9.0 mg min^{-1}, oxygen: 200 cm^3 min^{-1}) on 0.136 mmol of substrate in 10 ml of solvent. Excess ozone was determined by iodometric titration. The ozonization products were analyzed using gas chromatography and identified by comparing their mass spectra with those of authentic samples. Yields were determined by comparisons with standard solutions of known compounds by GLC using 2% Silicone OV-1, 2% FFAP, and Chromosorb 101 columns.

Results and Discussion

When MG (**1a**) was ozonized, 4-(dimethylamino)benzophenone (**2a**), 4-(*N*-formylmethylamino)benzophenone (**3a**), *N*-formylmethylamino derivative **4a**, *N,N'*-diformylmethylamino derivative **5a**, and *p*-(dimethylamino)phenol (**6**) were detected. The result is shown in Table 1. In each case, a trace amount of **5a** was detected. Since no significant difference between the distribution of the products found in methanol and that found in dichloromethane was observed (runs 1 and 2), the possibility that a reaction of **1a** with the peroxides formed through the ozonization of methanol yielded the products was excluded. The reaction of **1a** with ozone proceeds *via* two paths. The first path produces **4a** *via* an ozone attack at the dimethylamino moiety of **1a**. The second path produces **2a** and **6** *via* an ozone attack at the carbon adjacent to the triphenylmethyl carbon of **1a**. **2a**, and **4a** are further ozonized to give **3a**, **5a**, and **6**. The ratio of the ozone attack on each position was calculated from the yields of **4a** and **2a**. The results are also shown in Table 1. The ratio N/C decreased with increasing temperature (runs 1, 3, and 4), since the reactivity of **2a** with ozone increases with decreasing temperature. Yields of the products decreased as the ratio of water in methanol increased (runs 4, 5, 6, 7, and 8). Ozone decomposes easily in water to give an hydroxyl radical which is a strong oxidizing agent.[20] The products detected by the ozonization of **1a**, however, were not obtained in the reaction of **1a** with Fenton's reagent, which generates a hydroxyl radical. The ratio of ozone(consumed)/**1a**(reacted) increased as the ratio of water in methanol became greater (runs 4, 5, 6, 7, and 8). From these results, it was found that the added water played only a role involving the acceleration of the decomposition of ozone to give a hydroxyl radical. Then, yields of the ozonization products decreased.

The substituent effect on the ozonization of **1a** is shown in Table 2. When **1c** was ozonized, ketone **2c** and *p*-(dimethylamino)phenol (**6**) were predominantly produced. On the other hand, ozonization of **1d** preferentially afforded *N*-formylmethylamino derivative **4d**. When **1a** and **1b** were ozonized, the ketones, the *N*-formylmethylamino derivative, and *p*-(dimethylamino)phenol were detected, respectively. The ratio N/C changed drastically and was in the order **1c**< **1a**<**1b**<**1d**, which consists with that of electron-donative ability of the substituent. This result suggests that an electrophilic ozone attack takes place on the dimethylamino nitrogen.

The probable ozonization mechanism of the dimethylamino moiety of **1a** is proposed in Scheme 1, by reference to the ozonization mechanism of aromatic

Table 1. Ozonization of **1a**[a]

Run	Temp °C	Solvent	Ozone consumed 10^{-4} mol	**1a** reacted 10^{-4} mol	Yield[b]/% **2a**	**3a**	**4a**	**6**	Ozone (consumed)/**1a** (reacted)	N/C[c] attack
1	−78	CH_3OH	0.40	0.34	7	1	47	10	1.2	6.7
2	−78	CH_2Cl_2	0.58	0.36	5	2	41	8	1.6	8.2
3	−20	CH_3OH	0.40	0.32	9	1	54	11	1.3	6.0
4	0	CH_3OH	0.34	0.31	18	trace	45	18	1.1	2.5
5	0	$CH_3OH:H_2O=3:1$	1.14	0.41	8	3	19	12	2.8	2.4
6	0	$CH_3OH:H_2O=1:1$	2.07	0.52	3	trace	8	5	4.0	2.7
7	0	$CH_3OH:H_2O=1:3$	2.78	0.59	3	trace	5	4	4.7	1.7
8	0	H_2O	3.89	0.73	1	trace	0	3	5.3	0

a) Ozonization was carried out with an ozone-oxygen mixture (ozone: 0.016 mmol s^{-1}, oxygen: 3.3 cm^3 s^{-1}) on 0.136 mmol of **1a** in 10 ml of solvent. b) Yield was based on **1a** reacted. c) The value of ratio N/C attack was based on **4a**/**2a**.

TABLE 2. SUBSTITUENT EFFECT ON THE OZONIZATION OF TRIPHENYLMETHANE DYE[a)]

Run	Substrate	Ozone consumed / 10^{-4} mol	Substrate reacted / 10^{-4} mol	Yield[b)]/% 2	3	4	6	Ozone (consumed) / Substrate (reacted)	N/C[c)] attack
1	**1c**	0.44	0.42	26	0	0	23	1.1	0
2	**1a**	0.40	0.34	7	1	47	10	1.2	6.7
3	**1b**	0.41	0.32	1	3	60	4	1.3	60
4	**1d**	0.30	0.18	trace	trace	72	5	1.7	∞

a) Ozonization was carried out with an ozone-oxygen mixture (ozone: 0.016 mmol s^{-1}, oxygen: 3.3 cm^3 s^{-1}) on 0.136 mmol of substrate in 10 ml of methanol at 0 °C. b) Yield was based on the substrate reacted. c) The value of ratio N/C attack was based on **4**/**2**.

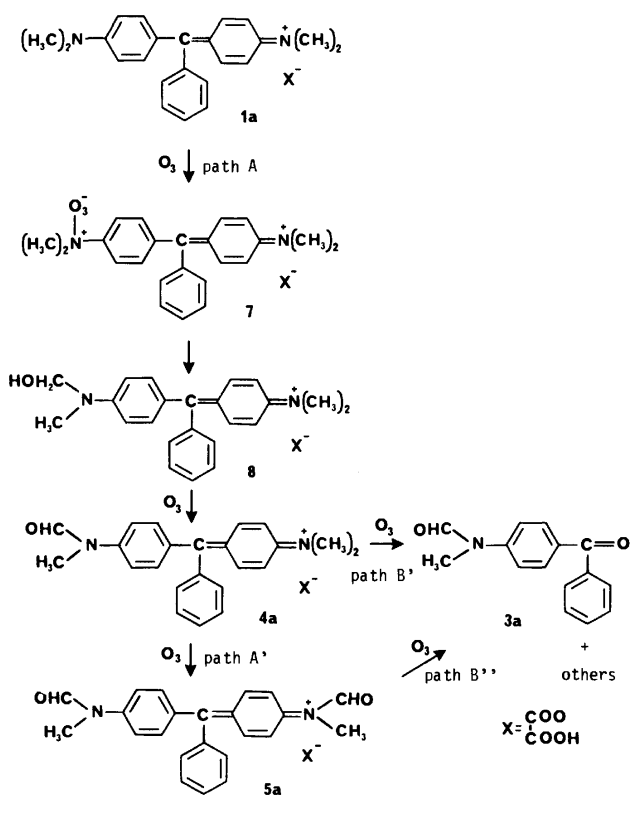

Scheme 1.

tertiary-amines.[21,22)] Ozone electrophilically attacks the dimethylamino nitrogen to give **1a**-ozone adduct **7**, which is converted into *N*-hydroxymethyl-*N*-methylamino derivative **8** [path A]. Since the value of the ratio ozone(consumed)/substrate(reacted) of **1d**, whose dimethylamino moiety is preferentially attacked by ozone was 1.7 (Table 2, run 4), it was concluded that the *N*-hydroxymethyl-*N*-methylamino derivative **8** is further ozonized to give the *N*-formylmethylamino derivative **4a**. Some radical process in which an oxygen molecule takes part may be involved. The *N*-formylmethylamino derivative **4a** is further ozonized to give either *N*,*N*'-diformylmethylamino derivative **5a** [path A'] or the ketone **3a** and *p*-(dimethylamino)phenol (**6**) [path B']. The *N*,*N*'-diformylmethylamino derivative **5a** is further ozonized to give the ketone **3a** [path B"].

A mechanism for the ozone attack on the skeleton of **1a** is proposed in Scheme 2. Except for the primary ozonides of α,β-unsaturated carbonyl compounds, certain allylic compounds, and certain substituted cinnamic esters, primary ozonides decompose into the corresponding carbonyl oxides and carbonyl compounds.[23)] In Scheme 2, carbons C1 and C2 are considerably more negative than carbon C3, due to the mesomeric effect produced by the dimethylamino groups. When ozone electrophilically attacks C1 and C2, a primary ozonide **9** is formed [path B]. The direction of the cleavage of the primary ozonide **9** follows two possible paths. The primary ozonide **9** can cleave to carbonyl oxide **10** and ketone **11** [path C]. The carbonyl oxide **10** reacts with water to give 4-(dimethylamino)benzophenone (**2a**) and hydrogen peroxide (**13**) *via* hydroperoxide **12**. The ketone **11** can be converted into *p*-(dimethylamino)phenol (**6**) at the injection room of the gas chromatograph during analysis.

In contrast, the primary ozonide **9** can decompose to 4-(dimethylamino)benzophenone (**2a**) and carbonyl oxide **14**, which reacts with water to give *p*-(dimethylamino)phenol (**6**) and oxalic acid (**16**) *via* hydroperoxide **15** [path D].

In fact, the presence of a small amount of water (*ca.* 0.2%) was confirmed by gas chromatography. In order to differentiate path C from path D, the following experiments were carried out. If the primary ozonide **9** had cleaved by path C, hydrogen peroxide (**13**), which is formed from the hydroperoxide **12**, should have been detected. Unfortunately, it was impossible to differentiate the hydrogen peroxide (**13**) from the peroxides formed by the ozonization of methanol which was used as a solvent. On the other hand, if the primary ozonide **9** had cleaved by path D, the phenolic proton of *p*-(dimethylamino)phenol would have come from the water. The relative yield of *p*-(dimethylamino)phenol-*d* for *p*-(dimethylamino)phenol produced by the ozonization of **1a** in the presence of heavy water is shown in Fig. 2. For a greater ratio of heavy water, the relative yield of *p*-(dimethylamino)phenol-*d* also increased. However, this result does not sufficiently prove that the primary ozonide **9** cleaves mainly by path D. Since even in the presence of *ca.* 70 molar equivalents of heavy

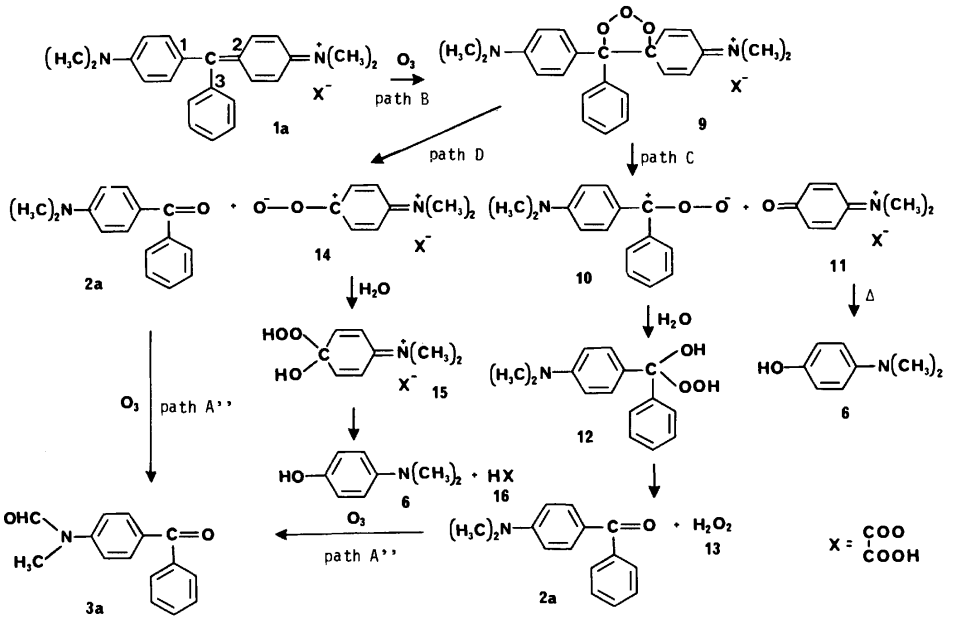

Scheme 2.

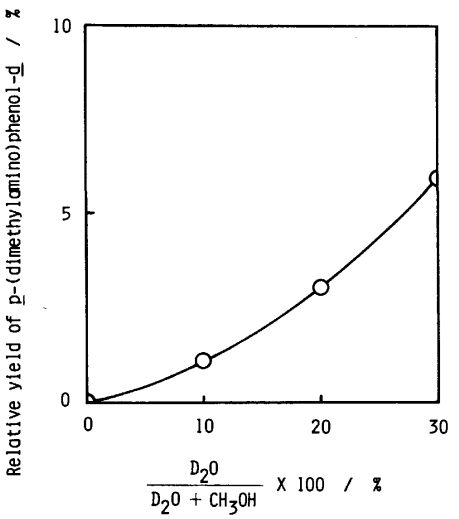

Fig. 2. Relative yield of *p*-(dimethylamino)phenol-*d* in the ozonization of **1a**.

water (30%), only 6% of *p*-(dimethylamino)phenol-*d* was observed. It was thus concluded that the primary ozonide **9** mainly cleave by way of path C and to a lesser extent by way of path D. The result is consistent with the general rule that a primary ozonide cleaves to a carbonyl oxide whose carbocation is more liable to be stabilized by the mesomeric effect.[24] 4-(Dimethylamino)benzophenone (**2a**) was further ozonized to give 4-(*N*-formylmethylamino)benzophenone (**3a**) [path A"].

The authors are grateful to Professor Teijiro Kitao, Associate Professor Masaru Matsuoka, and Dr. Hiroyuki Nakazumi of the University of Osaka Prefecture for useful discussion.

References

1) E. H. Snider and J. J. Porter, *American Dyestuff Reporter*, **64** (8), 36 (1974).
2) D. P. Harnish, H. J. Osborn, and B. W. Rossiter, *J. Org. Chem.*, **34**, 1687 (1969).
3) Y. Onari, *Nippon Kagaku Kaishi*, **1978**, 1570.
4) K. Ishizaki, K. Sakata, N. Shinriki, and A. Ikehata, *Nippon Kagaku Kaishi*, **1979**, 1124.
5) M. Matsui, K. Kobayashi, K. Shibata, and Y. Takase, *J. Soc. Dyers Colour.*, **97**, 210 (1981).
6) M. Matsui, H. Miyazaki, K. Kobayashi, K. Shibata, and Y. Takase, *Sen'i Gakkai Shi*, **37**, T-381 (1981).
7) M. Matsui, M. Morita, K. Shibata, and Y. Takase, *Nippon Kagaku Kaishi*, **1982**, 1268.
8) M. Matsui, H. Nakabayashi, K. Shibata, and Y. Takase, *Sen'i Gakkai Shi*, **39**, T-133 (1983).
9) J. J. Porter and S. B. Spears Jr., *Textile Chemist and Colorist*, **2**, 191 (1970).
10) C. M. Desai and B. K. Vaidga, *J. Indian Chem. Soc.*, **31**, 261 (1954).
11) N. Kuramoto and T. Kitao, *Dyes and Pigments*. **3**, 49 (1982).
12) R. Nakamura and M. Hida, *Sen'i Gakkai Shi*, **38**, T-183 (1982).
13) E. Votocek and J. Jelinek, *Ber.*, **40**, 406 (1907).
14) C. D. Hurd and C. N. Webb, *Org. Synth., Coll. Vol.* **I**, 217 (1956).
15) R. C. Shar, R. K. Deshpanda, and J. S. Chaubal, *Journal of the Chemical Society of London*, **1932**, 642.
16) W. Fehrmann, *Ber.*, **20**, 2844 (1887).
17) W. Michler, *Ber.*, **9**, 716 (1876).
18) J. C. Collins, W. W. Hess, and F. J. Frank, *Tetrahedron Lett.*, **1968**, 3363.
19) H. V. Pechmann, *Ber.*, **32**, 3681 (1899).
20) M. Teramoto, S. Imamura, N. Yanagi, and H. Teranishi, *J. Chem. Ind. Jpn.*, **14**, 383 (1981).
21) G. H. Kerr and O. Meth-Cohn, *J. Chem. Soc., (C)*, **1971**, 1369.
22) P. Kolsaker and B. Teige, "Ozone Reactions with Organic Compounds," in "Advanced in Chemistry Series,"

ed by R. F. Gould, American Chemical Society, Washington (1972), Vol. 112, Chap. 8, pp 101—113.
23) P. S. Bailey, "Ozonation in Organic Chemistry," Academic Press, Inc., New York (1978), Vol. 1, Chap. 3, pp 9—13.
24) S. Fliszár and M. Granger, *J. Am. Chem. Soc.*, **91**, 3330 (1969).

The Synthesis of Partially-protected 2′-Deoxyribonucleotide Dimers by the Selective Phosphorylation of Stannylated Nucleosides[1)]

Masajiro KAWANA,* and Hiroyoshi KUZUHARA
Riken (The Institute of Physical and Chemical Research), Wako-shi, Saitama 351-01
(Received June 30, 1984)

A new method for the synthesis of the title compounds is described. The activation of the hydroxyl moieties of 5′-*O*-dimethoxytrityl and 3′,5′-*unprotected* 2′-deoxyribonucleosides, which were appropriately protected on their base residues, was done with bis(tributyltin) oxide in separate flasks. The resulting stannylated nucleosides were coupled with 2-chlorophenyl phosphorodichloridate to form the dimers with 3′→5′ internucleotide linkages in yields of more than 71%, along with the corresponding 3′→3′ isomers in yields of less than 10%. The method of Cashion *et al.* was also evaluated, in which up-to-date protecting groups were employed.

The formation of internucleotide linkages by the coupling of two nucleoside components which have minimum protecting groups on their hydroxyl functions is, in principle, very attractive for the rapid synthesis of the nucleotide dimers that have been useful for the preparation of oligonucleotides of defined length and sequence.[2a,b)] Cashion *et al.*[3)] have reported on such method. Thus, 3′→5′ linked 2′-deoxyribonucleotide dimers were synthesized in a one-pot procedure by phosphorylation of 5′-*O*-methoxytritylated nucleosides with 4-chlorophenyl phosphorodi-1,2,4-triazolidate, followed by condensation with 3′-terminal units of 3′,5′-*unprotected* nucleosides: The starting nucleosides were appropriately protected on their base residues. A phosphomonotriazolide intermediate produced in this reaction was activated by the addition of a large amount of 1-methyimidazole. Later, Agarwal *et al.*[4)] reported that triethylammonium benzenesulfonate was also effective for this activation. Even though the 5′-(primary hydroxyl) group of the incoming nucleoside in this coupling reaction is more reactive than its 3′-(secondary hydroxyl) one, there is the possibility that an undesired isomeric dimer with a 3′→3′ internucleotide linkage is produced.

We wish to report herein the evaluation of Cashion's method using up-to-date protecting groups for the synthesis of oligodeoxynucleotides, and our alternative approach to the dimers by the activation of hydroxyl functions with bis(tributyltin) oxide. Recently, metal-mediated phosphorylation by activating the hydroxyl groups in nucleosides has been shown to be useful for the synthesis of deoxyribonucleotides.[5)] The reaction proceeded smoothly without the activation of a phosphotriester intermediate. It is well known that organic tin compounds have been used effectively for the selective activation of hydroxyl groups in ribofuranosides[6)] and glycopyranosides.[7)]

Results and Discussion

We first examined the synthetic reaction of the partially-protected thymidylyl(3′→5′)thymidine (**4a**) (Scheme 1). A mixture of 1 mol equiv of 5′-*O*-dimethoxytritylthymidine (**1a**) and 0.6 mol equiv of bis(tributyltin) oxide in benzene was refluxed for 15 min with an azeotropic removal of water; a clear solution was obtained and no decomposition of the starting nucleoside was observed. Similarly, a mixture of 1.5 mol equiv of thymidine (**2a**) and 0.9 mol equiv of bis(tributyltin) oxide in benzene containing a small amount of *N*,*N*-dimethylformamide (DMF) was treated for 30 min. The stannylated derivative prepared in the first solution was then phosphorylated with 1.4 mol equiv of 2-chlorophenyl phosphorodichloridate at room temperature. The reaction was completed within 15 min, as judged by its TLC analysis; we could detect no formation of a 3′→3′ dimer at this step. To this solution was added the second solution containing the incoming nucleoside. The coupling reaction was over

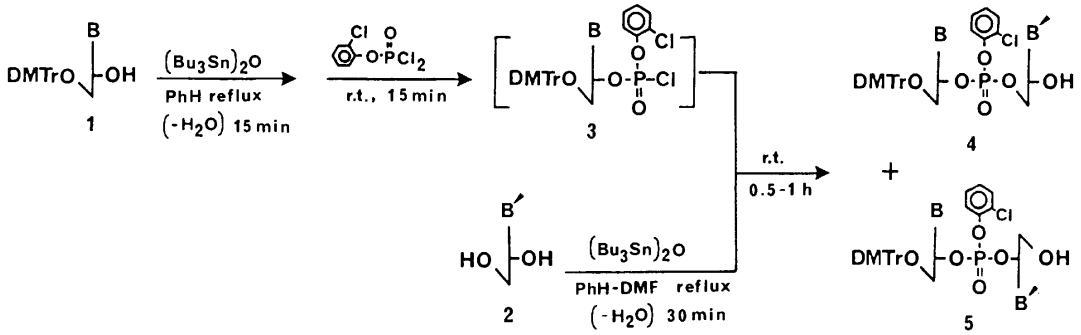

BB′=TT (**a** series), CT, AT, TC, AC, or TA.
T=thymin-1-yl; C=4-*N*-benzoylcytosin-1-yl; A=6-*N*-benzoyladenin-9-yl; DMTr=4,4′-dimethoxytrityl.

Scheme 1.

at room temperature in 30 min. Evaporation of the benzene followed by chromatography gave **4a** in a 94% yield (93% purity), while the 3′→3′ dimer (**5a**) was formed in a yield of less than 3%. These yields were not appreciably changed, when the amount of the tin compound required for the activation of **2a** was increased to 1.5 mol equiv, which was enough to derivatize its 3′ and 5′-hydroxyl groups into their stannylated functions (Table 2, the second line).

On the other hand, according to the slightly modified procedure of Cashion *et al.* using the same protecting groups as ours, **4a** was prepared in a 73% yield, while a large amount (15%) of **5a** was also isolated. The ^{1}H NMR spectrum of **4a** prepared by this procedure was identical with that from ours except difference in the intensity of signals between two diastereoisomers due to the chirality of the phosphorous triester. The 3′→5′ dimer could easily be distinguished from its 3′→3′ isomer by means of their TLC and ^{1}H NMR spectroscopic analyses (Tables 2 and 3). These analyses also showed that **4a** from our procedure contained a very small amount (less than 3 mol%) of an unidentified tin compound,[8] which could not be excluded without loss of the desired dimer. However, it seemed that this contamination did not interfere with further reaction.[9]

Table 1. The yields(%) of the partially-protected nucleotide dimers

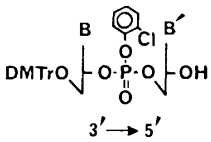

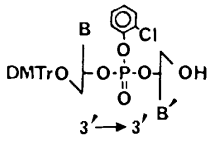

BB′ [a]	Tin method[b] 3′→5′	Tin method[b] 3′→3′	Triazolide method[b] 3′→5′	Triazolide method[b] 3′→3′
TT	94	<3	73 (92) [c]	15
CT	81	6	59	9
AT	76	<3	59	12
TC	77	7	57 (90) [c]	20
AC	71	10	50	16
TA	75	<3	66 (90) [c]	7

a) T=thymin-1-yl; C=4-*N*-benzoylcytosin-1-yl; A=6-*N*-benzoyladenin-9-yl; DMTr=4,4′dimethoxytrityl. b) The dimers were obtained as foams, which were dried at room temperature over diphosphorus pentaoxide *in vacuo* for 4 h; the purity of the 3′→5′ dimers was grater than 90%, as judged by their ^{1}H NMR spectroscopic assay. c) The value in the parentheses is the original data of Cashion *et al.* (Ref. 3) with the following protecting groups: 4-Chlorophenyl for the phosphate; 4-methoxytrityl for the 5′-hydroxyl group; anisoyl for the cytosine residue; benzoyl for the adenine residue. No data for the corresponding 3′→3′ isomers are described in their paper.

Our method was successfully applied to the synthesis of five partially-protected dinucleotides of d(CT), d(AT), d(TC), d(AC), and d(TA) in yields of more than 71%. Both results from the procedure of Cashion *et al.* and ours are summarized in Table 1. The formation of a relatively large amount of the 3′→3′ dimers was observed in the former procedure. Originally, they have used the 4-chlorophenyl protecting group for the phosphate moiety, instead of the present 2-chlorophenyl group, and have obtained the partially-protected 3′→5′ dimers of d(TT), d(TC), d(TA), and d(AG) in about 90% yields (Table 1). It is considered that subtle changes in the protecting groups at the 5′-position and the base residue (from the original nucleoside to the present one) did not exert an important effect upon the reactivity of the coupling reaction, since the changed moieties are located far from the reaction center. Therefore, it seemed likely that the 2-chlorophenyl group was not suitable for the original procedure, presumably because of its steric reason.

Our method with bis(tributyltin) oxide has improved not only regarding yields of the desired 3′→5′ dimers, but also regarding selectivity of the coupling reaction with the 3′,5′-unprotected nucleosides as far as the six dimers are concerned. However, the synthetic reactions for ten other possible dimers still have problems to be solved. There are mainly due to the lower reactivity of the phosphorochloridate intermediates (**3**) with incoming stannylated nucleosides.

Table 2. The synthesis of the partially-protected nucleotide dimers with $(Bu_3Sn)_2O$

BB′ [a]	5′-Protected component mmol (equiv)	$(Bu_3Sn)_2O$[b] mmol (equiv)	2-Cl-Phenyl phosphorodichloridate mmol (equiv)	3,5′-Unprotected component mmol (equiv)	$(Bu_3Sn)_2O$[c] mmol (equiv)	DMF[d] ml	Yield/% (R_f value)[e] 3′→5′	Yield/% (R_f value)[e] 3′→3′
TT	0.7 (1.0)	0.42 (1.2)	0.98 (1.4)	1.05 (1.5)	0.63 (1.8)	1	94 (0.46)	<3 (0.56)
TT	0.7 (1.0)	0.7 (2.0)	0.98 (1.4)	1.05 (1.5)	1.05 (3.0)	0	92	<3
CT	0.5 (1.0)	0.3 (1.2)	0.7 (1.4)	0.75 (1.5)	0.75 (3.0)	1	81 (0.54)	6 (0.63)
AT	0.5 (1.0)	0.5 (2.0)	0.7 (1.4)	0.75 (1.5)	0.75 (3.0)	1	76 (0.51)	<3 (0.59)
TC	0.5 (1.0)	0.3 (1.2)	0.6 (1.2)	0.70 (1.4)	0.53 (2.1)	1.5	73 (0.51)	10 (0.65)
TC	0.5 (1.0)	0.3 (1.2)	0.7 (1.4)	0.75 (1.5)	0.45 (1.8)	2	77	7
AC	0.5 (1.0)	0.5 (2.0)	0.7 (1.4)	0.75 (1.5)	0.75 (3.0)	1.5	71 (0.54)	10 (0.68)
TA	0.5 (1.0)	0.3 (1.2)	0.7 (1.4)	0.75 (1.5)	0.75 (3.0)	1.5	75 (0.45)	<3 (0.64)

a) For the abbreviations and protecting groups of the dimers, see the footnote in the Table 1. b) Used for the 5′-protected component. c) Used for the 3′,5′-unprotected component. d) See the Experimental section. e) TLC on silica gel with chloroform-methanol (9:1). Broad spots due to the diastereoisomers were observed.

Experimental

The ^{1}H NMR spectra were recorded on a JEOL JNM-GX 400 spectrometer, with tetramethylsilane as the internal standard. Merck silica gel GF_{254} was used for TLC, and the compounds were detected by heating after spraying them with a methanol-sulfuric acid-4-methoxybenzaldehyde mixture (85:15:5, v/v) or 5% ethanolic solution of molybdophosphoric acid. Merck silica gel 60 (0.063—0.29 mm) was utilized for column chromatography.

The protected nucleosides were prepared according to known procedures.[10] Bis(tributyltin) oxide and 1-methylimidazole, as well as 4-chlorophenyl phosphorodichloridate and 1*H*-1,2,4-triazole, were purchased from Tokyokasei Co., Ltd. (Tokyo, Japan) and Dojindo Lab. (Kumamoto, Japan), respectively.

The General Procedure for the Synthesis of Partially-protected 2'-Deoxyribonucleotide Dimers. Some of the results and reaction conditions are described in Tables 1 and 2, while the ^{1}H NMR spectral data are summarized in Table 3.

(A) The Method with Bis(tributyltin) Oxide. A mixture of 5'-*O*-(4,4'-dimethoxytrityl)nucleoside (0.5 mmol) and bis(tributyltin) oxide (0.3—0.5 mmol) in benzene (20 ml) was refluxed at 110 °C (bath temperature) for 15 min with azeotropic removal of water by means of a Dean-Stark apparatus. The resulting solution was concentrated to *ca.* 5 ml (solution A). Similarly, a mixture of 3',5'-unprotected nucleoside (0.75 mmol) and bis(tributyltin) oxide (0.45—0.75 mmol) in benzene (20 ml) and dry DMF (1—2 ml) was refluxed at 110 °C (bath temperature) for 30 min with a water trap. The resulting solution was concentrated to *ca.* 5 ml (solution B). To solution A was added a solution of 2-chlorophenyl phosphorodichloridate[11] (0.6—0.7 mmol) in dry benzene (1 ml) at room temperature under an atmosphere of dry nitrogen. The solution was stirred for *ca.* 15 min. Solution B was then added at room temperature, and the mixture was stirred for 0.5—1 h. Dry pyridine (0.2 ml) was added, and the benzene was then removed at room temperature *in vacuo*. The residue was chromatographed on a silica-gel (65 ml) column made up in benzene-ethyl acetate-pyridine (20:20:1). The tin compounds were first eluted successively with the same solvent system (150 ml) and benzene-ethyl acetate-methanol (20:20:1, 130 ml), and the dimers were then eluted with the latter solvent system (5:5:0.8—5:5:1). Under these conditions for the chromatography, the isolated 3'→5' dimers of d(AT) and d(AC) were still contaminated with a small amount of the starting 3',5'-unprotected nucleosides. The thymidine in the former was removed by washing a chloroform solution of the dimer with 0.5 M† phosphate buffer (KH_2PO_4-K_2HPO_4, pH 5.0), and 4-*N*-benzoyl-2'-deoxycytidine in the latter was taken off by means of rechromatography on a silica-gel (20 ml) column with chloroform-methanol (95:5).

(B) The Slightly Modified Method of Cashion *et al.*[3] The nucleosides used in this procedure had been dried by means of azeotropic distillation with dry pyridine.

To a solution of 1*H*-1,2,4-triazole (2.8 mmol, 4 equiv) and triethylamine (2.8 mmol, 4 equiv) in dry pyridine (4 ml) there was added 2-chlorophenyl phosphorodichloridate (0.84 mmol, 1.2 equiv) at room temperature with stirring under an atmosphere of dry nitrogen. After 3 min, 1-methylimidazole (11.2 mmol, 16 equiv) was added, and the stirring was continued for another 5 min. To this mixture was added a solution of 5'-*O*-(4,4'-dimethoxytrityl)nucleoside (0.7 mmol, 1 equiv) in dry pyridine (2.5 ml) at room temperature. After the mixture had been stirred for 30 min, a solution of the 3',5'-unprotected nucleoside (1.4 mmol, 2 equiv) in dry pyridine (3 ml) was added. In the case of the deoxycytidine derivative, a mixture of dry pyridine (3 ml) and dry DMF (2 ml) was used. The mixture was stirred at room temperature for 4—5 h, quenched with 50% aqueous pyridine, and diluted with chloroform (100 ml). The mixture was washed, successively, with 0.5M phosphate buffer (KH_2PO_4-K_2HPO_4, pH 5.0, 30 ml×2) and brine (30 ml), dried over magnesium sulfate, and concentrated. The pyridine was removed below 45 °C *in vacuo* by co-evaporation with toluene. The residue was chromatographed on a silica-gel (100 ml) column with chloroform-methanol (97:3→9:1) to give the dimers.

† 1 M=1 mol dm^{-3}.

Table 3. The ^{1}H NMR spectral data (δ) of the partially-protected nucleotide dimers[a]

BB' [b]	3'→5' Dimer		3'→3' Dimer	
	$H_{1',1''}$(2H)	$H_{3'}$(1H)[c]	$H_{1',1''}$(2H)	$H_{3',3''}$(2H)[c]
TT	6.31(t)	5.27(br. t)	6.25(q)	5.31(br. s)
	6.44(m)	5.35(br. t)	6.47(m)	
CT	6.30(m)	5.27(br. t)	6.21(t)	5.3 (m)
		5.33(br. t)	6.26(t)	5.4 (br. s)
			6.31(t)	
AT	6.23(t)	5.50(br. q)	6.21(q)	5.35(br. q)
	6.27(t)		6.52(q)	5.47(br. q)
	6.47(m)			
TC	6.26(q)	5.33(br. t)	6.23(q)	5.33(br. s)
	6.40(m)	5.27(br. t)	6.45(m)	
AC	6.27(t)	5.48(br. t)	6.17(q)	5.36(br. s)
	6.52(q)		6.55(q)	5.46(br. q)
TA	6.47(m)	5.24(br. t)	6.45(m)	5.31(br. t)
		5.31(br. t)		5.49(br. t)

a) Measured in $CDCl_3$. The clear signals were not obtained because of the presence of the diastereoisomers. b) For the abbreviations and protecting groups of the dimers, see the footnote in the Table 1. c) Deshielded by the phosphate moiety.

We wish to thank Dr. Tomoya Ogawa for his encouragement during the course of this work, Dr. Jun Uzawa and Mrs. Tamiko Chijimatsu for the ^{1}H NMR measurements, and Mr. Yoshitaka Ichikawa for his helpful discussions. We are also indepted to Messrs. Shinji Kubota, Kenji Masuda, Tomoshi Yamamoto, and Takuya Ogawa, and Misses Kazuko Miyata and Fuki Nakamura for their experimental help.

References

1) A part of this work was presented at the 49th National Meeting of the Chemical Society of Japan, Tokyo, April, 1984, Abstr. No. 3V15.

2) a) For the synthesis of 2'-deoxyribonucleotides, see R. L. Letsinger and V. Mahadevan, *J. Am. Chem. Soc.*, **87**, 3526 (1965); R. L. Letsinger and K. K. Ogilvie, *ibid.*, **91**, 3350 (1969); J. B. Chattopadhyaya and C. B. Reese, *Nucleic Acids Res.*, **8**, 2039 (1980); M. Sekine, K. Hamaoki, and T. Hata, *Bull. Chem. Soc. Jpn.*, **54**, 3815 (1981); b) For ribonucleotides, see S. S. Jones, B. Rayner, C. B. Reese, A. Ubasawa, and M.

Ubasawa, *Tetrahedron*, **36**, 3075 (1980); G. Kumar, L. Celewicz, and S. Chádek, *J. Org. Chem.*, **47**, 634 (1982); E Ohtsuka, A. Yamane, and M. Ikehara, *Chem. Phar. Bull.*, **31**, 1534 (1983); E. Ohtsuka, M. Ohkubo, A. Yamane, and M. Ikehara, *ibid.*, **31**, 1910 (1983).

3) P. Cashion, K. Porter, T. Cadger, G. Sathe, T. Tranquilla, H. Notman, and E. Jay, *Tetrahedron Lett.*, **1976**, 3769.

4) K. L. Agarwal and F. Riftina, *Nucleic Acids Res.*, **5**, 2809 (1978).

5) Y. Hayakawa, Y. Aso, M. Uchiyama, and R. Noyori, *Tetrahedron Lett.*, **1983**, 1165.

6) I. D. Jenkins, J. P. H. Verheyden, and J. G. Moffatt, *J. Am. Chem. Soc.*, **93**, 4323 (1971); D. Wagner, J. P. H. Verheyden, and J. G. Moffatt, *J. Org. Chem.*, **39**, 24 (1974); I. Hirao, K. Itoh, N. Sakairi, Y. Araki, and Y. Ishido, *Carbohydr. Res.*, **109**, 181 (1982).

7) T. Ogawa and M. Matsui, *Carbohydr. Res.*, **56**, Cl (1977); *idem.*, *Tetrahedron*, **37**, 2363 (1981).

8) The signal due to the methyl group of this tin compound appeared at δ 0.92 as a triplet (J=7.3 Hz). This compound was also visualized on a TLC plate by treating it with the ethanolic solution of molybdophosphoric acid.

9) We have succeeded in the conversion of **4a** into a 2-chlophenyl ester of thymidylyl(3′→5′)-3′-*O*-benzoylthymidine (78% yield from **1a**) in a one-pot procedure by the conventional benzoylation followed by detritylation without isolation of any intermediates starting from **1a** and **2a**.

10) H. Schaller, G. Weimann, B. Lerch, and H. G. Khorana, *J. Am. Chem. Soc.*, **85**, 3821 (1963); G. S. Ti, B. L. Gaffney, and R. A. Jones, *ibid.*, **104**, 1316 (1982).

11) This reagent which had been repeatedly exposed to moisture colored the reaction mixture in red for an instant. Such occasion gave unsatisfactory results.

© 1984 The Chemical Society of Japan

NOTES

Bull. Chem. Soc. Jpn. 57, 3321—3322 (1984)

Pressure Effect on Conformational Equilibria of 1,2-Dichloroethane and 1,2-Dibromoethane by Means of Raman Spectroscopy

Hiroyasu NOMURA,* Kenji MURASAWA, Nobuyuki ITO,† Fumisato IIDA,† and Yasuo UDAGAWA†

Department of Chemical Engineering, School of Engineering, Nagoya University, Chikusa-ku, Nagoya 464

†*Institute for Molecular Science, Myodaiji-cho, Okazaki 444*

(Received December 3, 1983)

Synopsis. The conformational equilibria of 1,2-dichloroethane and 1,2-dibromoethane have been investigated through a study of the pressure and temperature dependences of these materials in pure liquid states. The volume changes estimated here under a trans-gauche transformation of 1,2-dichloroethane and 1,2-dibromoethane are -2.7 ± 0.4 and -5.2 ± 0.5 cm³/mol, respectively.

Many compounds, as mixtures of conformers, have vibrational modes characteristic to each conformer. Measurements of the quantitative intensity of certain vibrations as a function of the variation in pressure and temperature provided volume and enthalpy differences between the conformers.

In the present work, the enthalpy and volume differences between the trans and gauche conformers of 1,2-dichloroethane and 1,2-dibromoethane in a neat liquid state were determined by means of Raman spectroscopy. The trans conformer of 1,2-dichloroethane and 1,2-dibromoethane has one Raman-active C–X (X= halogene) stretching vibration (A_g species) at 754 cm^{-1} and 658 cm^{-1}, respectively. The gauche form exhibited two bands which were assigned to the symmetric and antisymmetric stretching vibrations, respectively (655 cm^{-1} and 678 cm^{-1} for 1,2-dichloroethane and 522 cm^{-1} and 588 cm^{-1} for 1,2-dibromoethane).[1,2]

The Raman spectra under high pressure were recorded using a Laser Raman Spectrometer consisting of an argon-ion laser (NEC, GLG 3200, 2W) and a Spec 1403 double monochromater. The high-pressure Raman cell used is shown in Fig. 1. This high-pressure optical cell with three quartz glass windows (10× 10 mmϕ) is made of stainless steel, SUS 630 (Hitachi PSL stainless steel). The cell is similar to that used by Taniguchi *et al.*[3] Sample liquids were inserted directly into the cell and compressed hydrostatically by a piston (Hand pump. UP-21, Rikenkiki Co., Ltd.) connected to a intensifier (Model 15770-1, manufactured by Haskel Co., Ltd.). The pressure was measured using a Heise precision Bourdon-type guage (Heise Guage, Model CM, manufactured by Dresser Co., Ltd.). This guage works well up to 7.0×10^8 Pa, with a scale graduated to 5×10^5 Pa. The measurements involving pressure effects were carried out at room temperature (about 298 K) for 1,2-dichloroethane, but at 323 K for 1,2-dibromoethane since 1,2-dibromoethane solidifies at about 7×10^7 Pa at room temperature. The spectra were recorded at intervals of about 2.5×10^7 Pa. The temperature dependence of the Raman spectra was also measured at atmospheric pressure. Temperatures ranged from 292 to 363 K. A variable-temperature cell of the Harney-Miller type was used. The spectra were recorded three to five times at each temperature and pressure. The integrated intensities of each band were determined by weighting five Xerox copies of the spectral charts.

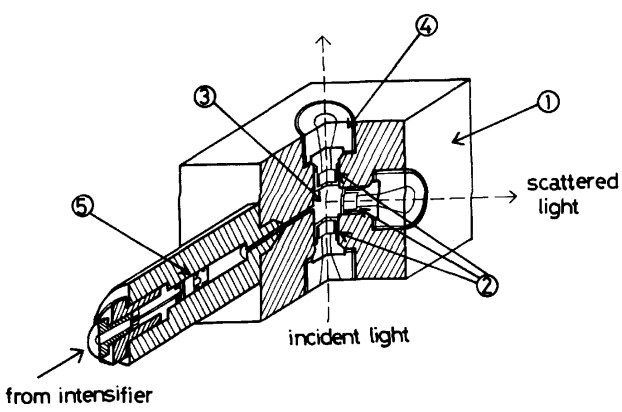

Fig. 1. High pressure optical cell.
1: Pressure bomb, 2: Quartz glass winodw, 3: Sample room, 4: Plug, 5: Piston.

The ratios of the sum of the integrated intensities of the two C–X stretching bands of the gauche form (I_g) to the intensity of the C–X stretching band of the trans form (I_t) were obtained as a function of temperature and pressure.

The enthalpy and volume differences between the two conformers can be estimated by the following equations.

$$\Delta H = -8.31 \times \left(\frac{\partial \ln [I_g/I_t]}{\partial \ln [1/T]}\right)_P \quad \text{[J/mol]} \qquad (1)$$

$$\Delta V = -8.21 \times 10^6 T\left(\frac{\partial \ln [I_g/I_t]}{\partial P}\right)_T \quad \text{[cm³/mol].} \qquad (2)$$

Figure 2 shows $\ln[I_g/I_t]$ *vs.* P plot for 1,2-dichloroethane. The open circles indicate the paralell components and the solid ones are those for the perpendicular components, using 90° scattering and linearly polarized light. As is seen in Fig. 2, a linear relationship was obtained within the experimental error and the slopes for different polarization components coincide with each other. The volume changes obtained here for the trans-gauche transformation of 1,2-dichloroethane and 1,2-dibromoethane are -2.7 ± 0.4 and -5.2 ± 0.5 cm³/mol, respectively. The enthalpy differences of 1,2-dichloroethane and 1,2-dibromoethane are 0.0 and 3.6 ± 0.6 kJ/mol, respectively and are in good agreement with those reported previously.[4–6]

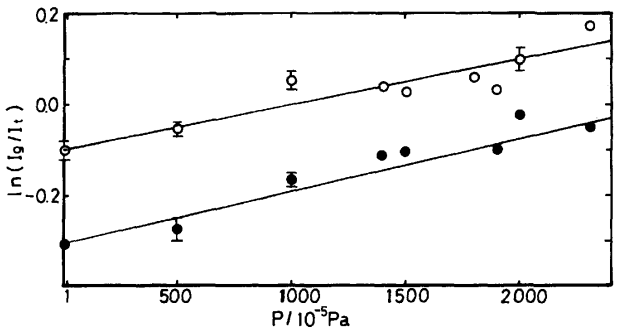

Fig. 2. Relationship between the logarithmic ratio of the integrated intensities of C–Cl stretching bands of *gauche-* and *trans-* 1,2-dichloroethane against the pressure at room temperature.
○: Parallel scattered light, ●: polarized scattered light.

If we assume that $V=M/d$, where d is the bulk density of liquid, the volume change ratios, $\Delta V/V$'s are $-3.4\pm0.5\%$ for 1,2-dichloroethane and $-6.0\pm0.6\%$ for 1,2-dibromoethane. The value of 1,2-dibromoethane is in good agreement with that obtained by ultrasonic work,[7] but that of 1,2-dichloroethane is about a half of the one obtained by their method.[8] At this stage, the discrepancy can not be interpreted.

Devaure and Lascombe,[9] starting from a thermodynamical consideration, derived the following equation for the relation between the enthalpy and volume differences of the conformational equilibria in liquids.

$$\Delta H_{liq} - \Delta H_{gas} = RT^2\left(\frac{\partial f}{\partial T}\right)_\rho + \Delta V_{liq}\frac{\alpha}{\beta}T \qquad (3)$$

where α and β are the expansion coefficient and isothermal compressibility, respectively and f is $\ln[K/K_0]$, in which K is the equilibrium constant in liquid state and K_0 in gaseous state. They claimed that the first term in Eq. 3 is negligible, as predicted by Pratt-Chandler's theory.[10]

The enthalpy differences of the trans-gauche transformation of 1,2-dichloroethane and 1,2-dibromoethane in a gaseous state, ΔH_{gas}, have been found to be 5.10 and 6.94 kJ/mol (on the average),[4-6] respectively. We can estimate the left hand side of Eq. 3, $\Delta=\Delta H_{liq}-\Delta H_{gas}$, to be -5.10 and -3.34 kJ/mol for 1,2-dichloroethane and 1,2-dibromoethane, respectively. The second term of the right hand side of Eq. 3 can also be calculated, from data on thermal-expansion coefficients[11] and isothermal compressibilities (where isothermal compressibility was calculated from the data of adiabatic compressibility,[12] β_s, heat capacity,[13] C_p, and molar volume, V using the equation of $\beta=\beta_s+\frac{TV\alpha^2}{C_p}$). The values of $\Delta V_{liq}\frac{\alpha}{\beta}T$ were -1.15 and -2.12 kJ/mol for 1,2-dichloroethane and 1,2-dibromoethane, respectively. Comparing the values of Δ with $\Delta V_{liq}\frac{\alpha}{\beta}T$, the first term in the right hand side of Eq. 3 can not be neglected in comparison with the second term, at least in this case, even if taking into account of the experimental errors.

The authors should like to express their appreciation to Prof. Y. Taniguchi of Ritsumeikan University for advices in designing the high pressure optical cell.

References

1) S. Mizushima, T. Shimanouchi, I. Harada, Y. Abe, and H. Takeuchi, *Can. J. Phys.*, **53**, 2085 (1975).
2) K. Tanabe, J. Hiraishi, and T. Tamura, *J. Mol. Struct.*, **33**, 19 (1976).
3) Y.Taniguchi, K. Yukimoto, K. Suzuki, Y. Okahara, and T. Kunitake, "Studies in Physical and Theoretical Chemistry, Vol. 27 Ions and Molecules in Solution," ed by N. Tanaka, H. Ohtaki, and R. Tamamushi, Elsevier Pub. (1983), p. 457.
4) N. Sheppard, *Adv. Spectros.*, **1**, 288 (1959).
5) Yu. A. Pentin, and V. M. Tatevskii, *Dokl. Akad. Nauk. SSSR*, **108**, 290 (1956).
6) M. V. Volenshtein, "High Polymer vol. 17, Configurational Statistics of Polymeric Chains," Interscience, New York, (1965).
7) W. Seki, P-K Choi, and K. Takagi, *Chem. Phys. Lett.*, **98**, 518 (1983).
8) K. Takagi, P-K Choi, and W. Seki, *J. Chem. Phys.*, **79**, 964 (1983).
9) J. Devaure and J. Lascombe, *Nouveau J. Chim.*, **3**, 579 (1979).
10) L. R. Pratt, C. S. Hsu, and D. Chandler, *J. Chem. Phys.*, **69**, 4202 (1975).
11) R. F. Brunell and V. Bibber, "International Critical Table," Vol. 3 McGraw-Hill, New York (1928).
12) R. T. Lagemann, D. R. McMilian, Jr., and W. E. Woolf, *J. Chem. Phys.*, **17**, 369 (1949).
13) K. S. Pitzer, *J. Am. Chem. Soc.*, **62**, 331 (1940).

Hydrogenation of 3-Ethoxy-1-propene Catalyzed by Supported Nickel Catalysts

Hiromi MATSUHASHI and Hideshi HATTORI*
Department of Chemistry, Faculty of Science, Hokkaido University Sapporo 060
(Received March 15, 1984)

Synopsis Nickel catalysts supported on different kinds of metal oxides were prepared to search for active catalysts for 3-ethoxy-1-propene hydrogenation. Ni/ThO_2 and Ni/SiO_2–Al_2O_3 catalysts exhibited high activity and selectivity for 1-ethoxypropane, while Ni/MgO, Ni/CaO, and Ni/La_2O_3 catalysts preferentially catalyzed double bond migration to 1-ethoxy-1-propene which undergo hydrogenation with difficulty.

In contrast to extensive studies of hydrogenation of olefins, less attention has been given to hydrogenation of unsaturated compounds containing hetero atoms. We have reported that for the hydrogenation of unsaturated compounds containing nitrogen the activities of nickel catalysts varied considerably with the type of support and the support acted as one function in bifunctional catalysis.[1)]

For unsaturated compounds containing oxygen, hydrogenation of allyl alcohols has been studied with heterogeneous catalysts to some extent.[2)] However, hydrogenation of allyl ethers has been studied only with Raney Ni[3)] and NiB.[4)] The present study was undertaken to understand more about hydrogenation of allyl ethers on supported Ni catalysts. Ten kinds of metal oxides were selected as supports for Ni, and used for hydrogenation of 3-ethoxy-1-propene. It was found that the Ni catalysts supported on ThO_2 and SiO_2–Al_2O_3 were highly active and selective.

Supported Ni catalysts were prepared by an impregnation method. The metal oxides used as support, and their surface areas, were MgO (84 m^2/g), CaO (16 m^2/g), La_2O_3 (43 m^2/g), ThO_2 (42 m^2/g), ZrO_2 (65 m^2/g), TiO_2 (85 m^2/g), Al_2O_3 (227 m^2/g), SiO_2 (333 m^2/g), and SiO_2–Al_2O_3 (278 m^2/g). Prior to impregnation, there metal oxides were calcined at 773 K in air for 6 h. The metal oxides were suspended in aqueous nickel nitrate, and the water was evaporated to dryness over a water bath. The nickel nitrate on the metal oxides was then decomposed at 773 K in air for 3 h. Prior to the reaction, the catalysts were reduced with hydrogen at 773 K. The Ni content was 9.1—9.2 wt% for all catalysts except Ni/Al_2O_3. The Ni/Al_2O_3 contained 10 wt% Ni.

A greaseless closed recirculation reactor was used for carrying out the reaction. A mixture of 1.3 kPa 3-ethoxy-1-propene and 2.6 kPa hydrogen was allowed to react with *ca.* 100 mg of catalyst (24—32 mesh grain) at 273 K or 323 K. The products were analyzed by GLC. Identification was by NMR for separately collected products.

The amount of hydrogen adsorbed on catalysts was measured volumetrically at 273 K. The saturated amounts of hydrogen were calculated by applying the adsorption isotherm to the Langumuir equation for dissociative adsorption.

Time dependences of the composition in the reaction are shown in Fig. 1 for Ni/Al_2O_3 and in Fig. 2 for Ni/ThO_2 and Ni/SiO_2–Al_2O_3. Over Ni/Al_2O_3, 3-ethoxy-1-propene underwent both hydrogenation to 1-ethoxypropane and double bond migration to (*E*)- and (*Z*)-1-ethoxy-1-propene when the reaction was carried out at 273 K. 3-Ethoxy-1-propene disappeared after 240 min. As the reaction temperature was raised to 323 K, 1-ethoxy-1-propene underwent appreciable hydrogenation. This feature of the time dependence was commonly observed for all catalysts except for Ni/SiO_2–Al_2O_3, though the relative rate of hydrogenation to that of double bond migration varied with the type of catalyst. For instance, over Ni/La_2O_3, the double bond migration was very fast as compared with hydrogenation. Over Ni/ThO_2, hydrogenation was

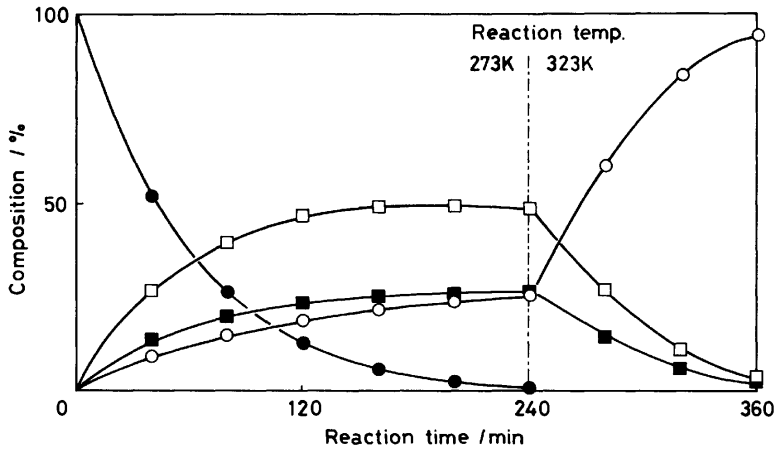

Fig. 1. Time dependence of the composition in the hydrogenation of 3-ethoxy-1-propene over Ni/Al_2O_3.
○: 1-Ethoxypropane, ●: 3-Ethoxy-1-propene, □: (*Z*)-1-Ethyoxy-1-propene, ■: (*E*)-1-Ethyoxy-1-propene.

Table 1. Hydrogenation of 3-ethoxy-1-propene over supported Ni catalysts

Catal.	Weight /mg	Conv. of reactant/%	Composition of products/%				Amount of H_2 adsorption /$\times 10^{-5}$ mol g^{-1}
			3-ethoxy-1-propene	(*Z*)-1-ethoxy-1-propene	(*E*)-1-ethoxy-1-propene	1-ethoxy-propane	
Ni/ThO_2	104	100	0.0	0.0	0.0	100	0.9
Ni/La_2O_3	105	100	0.0	74.8	12.3	12.9	0.6
Ni/CaO	107	100	0.0	87.4	4.2	8.4	0.1
Ni/MgO	97	100	0.0	99.3	0.7	0.0	0.0
Ni/SiO_2–Al_2O_3	102	100	0.0	0.0	0.0	100	4.0
Ni/TiO_2	105	9.4	90.6	0.9	0.0	8.5	0.8
Ni/ZrO_2	100	3.0	97.0	0.0	0.0	3.0	0.2
Ni/Al_2O_3	109	62.8	37.2	34.1	16.9	11.8	—
Ni/SiO_2	100	15.2	84.8	1.9	4.0	9.3	12.8

Reaction temperature; 273 K; reaction time; 60 min.

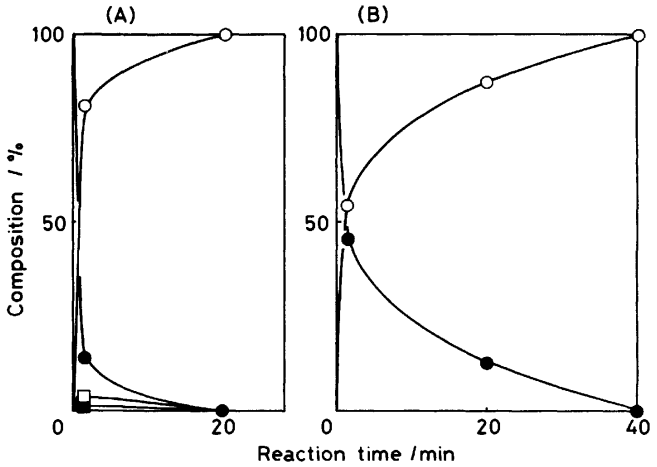

Fig. 2. Time dependences of the composition in the hydrogenation of 3-ethyoxy-1-propene over Ni/ThO_2 (A) and Ni/SiO_2–Al_2O_3 (B).
○: 1-Ethyoxypropane, ●: Ethyoxy-1-propene, □: (*Z*)-1-Ethyoxy-1-propene, ■: (*E*)-1-Ethyoxy-1-propene.

complete in 20 min, and the amount of 1-ethoxy-1-propene formed was very small as shown in Fig. 2(A). The characteristic feature with Ni/SiO_2–Al_2O_3 is seen in Fig. 2(B); double bond migration to 1-ethoxy-1-propene did not occur.

The composition of the products after 60 min when reactions were carried out at 273 K over *ca.* 100 mg of catalyst samples are summarized in Table 1. Other products such as ethanol and propane were not detected. The amounts of hydrogen adsorbed are also included. The Ni/ThO_2 and Ni/SiO_2–Al_2O_3 exhibited high activity; giving 100% hydrogenated product in 60 min. In particular, the Ni/ThO_2 gave 100% hydrogenated product even in 20 min. The hydrogenation activities were low for the catalysts other than Ni/ThO_2 and Ni/SiO_2–Al_2O_3. With Ni/MgO, Ni/CaO, and Ni/La_2O_3, large amounts of 1-ethoxy-1-propene resulted from the double bond migration. 1-Ethoxy-1-propene undergoes hydrogenation at a much slower rate than 3-ethoxy-1-propene does. To obtain a faster hydrogenation rate, catalysts are desirable that do not catalyze the double bond migration of 3-ethoxy-1-propene. The low hydrogenation activities of Ni/MgO, Ni/CaO, and Ni/La_2O_3 are considered to be due to the high activity of the supports for double bond migration.[5]

The active catalysts, Ni/ThO_2 and Ni/SiO_2–Al_2O_3, adsorbed relatively large amount of hydrogen. Although Ni/SiO_2 adsorbed large amounts of hydrogen but showed low activity, a capability of adsorption of a large amount of hydrogen may be required for a catalyst to be active for hydrogenation.

References

1) H. Hattori, H. Imai, and K. Tanabe, *Appl. Catal.*, **4**, 87 (1982).
2) For example; Y. Izumi, *Proc. Jpn. Acad.*, **53**, 38 (1977).
3) V. B. Mikhant'ev, H. Priebs, and L. M. Bulgakva, Deposited Doc., VINITI 95—77, 7 (1977).
4) T. W. Russell and R. C. Hoy, *J. Org. Chem.*, **36**, 2016 (1971).
5) H. Matsuhashi and H. Hattori, *J. Catal.*, **85**, 457 (1984).

Heats of Solution of Bolaform Electrolytes in Water. II. Polymethylenebis(trimethylammonium) Dibromides

Kunio TAMAKI* and Rie FURUYA
Department of Chemistry, Yokohama City University, Kanazawa-ku, Yokohama 236
(Received May 21, 1984)

Synopsis. The heats of solution of polymethylenebis(trimethylammonium) dibromides $[(CH_3)_3N(CH_2)_nN(CH_3)_3]Br_2$ (n=3—6, 8, 10, and 12) and alkyltrimethylammonium bromides $C_nH_{2n+1}N(CH_3)_3Br$ (n=2—6) in water were measured at 15, 25, and 35 °C. The hydrophobic character of the polymethylene groups was compared with that of alkyl groups on the basis of the changes in the heat capacity for dissolution, which were obtained from the relation between the heats of solution and the temperature.

In a previous paper,[1] the heats of solution for two series of bolaform electrolytes, polymethylenediammonium dichlorides and disodium polymethylene disulfates, in water were reported, and hydrophobic character of polymethylene groups in bolaform electrolytes was compared with that of alkyl groups for corresponding monovalent electrolytes, alkylammonium chlorides and sodium alkyl sulfates, respectively. The present paper is the extension of the previous work, and the heats of solution for a series of polymethylenebis(trimethylammonium) dibromides ($[(CH_3)_3N(CH_2)_nN(CH_3)_3]Br_2$, which will be abbreviated as, MeC_nMe) and for comparison for a series of alkyltrimethylammonium bromides ($C_nH_{2n+1}N(CH_3)_3Br$, which will be abbreviated as, C_nMe) in water will be reported. The changes in the heat capacity for dissolution in water, $\Delta C_p°$, for MeC_nMe and C_nMe were obtained from the relation between the heats of solution and the temperature, and the hydrophobic character of the polymethylene groups in MeC_nMe was compared with that of the alkyl group in C_nMe.

Experimental

Materials. MeC_nMe were prepared by the reactions of the α,ω-dibromoalkane with an excess of trimethylamine in ethanol.[3] The salts, except for $MeC_{12}Me$, were purified several times by recrystallization from ethanol. $MeC_{12}Me$ was recrystallized from an ethyl acetate–ethanol solution. C_nMe were prepared by the reactions of alkyl bromides with an excess of trimethylamine in ethanol. The salts were recrystallized several times from ethanol. All the salts were dried *in vacuo* at room temperature for several days, and were analyzed for bromide ion by argentometric titration. All the salts were found to have a purity greater than 99.6%. Water was triply distilled.

Calorimetry. The heats of solution were measured by a method similar to that described in previous papers.[1,2]

Results and Discussion

Heat-of-solution measurements have been carried out over the concentration range of 8×10^{-4}—3×10^{-3} mol dm^{-3}. In this concentration range, any dependence of the heats of solution on the concentration is within the limit of experimental error, so the average of three or more measurements was taken as the heats of solution at infinite dilution, $\Delta H_s°$. The $\Delta H_s°$ values of MeC_nMe and C_nMe are listed in Table 1. The $\Delta H_s°$ values were used to calculate the changes in the heat capacity, $\Delta C_p°$, in going from the pure compounds to an aqueous solution at infinite dilution:

$$\Delta C_p° = d\Delta H_s°/dT,$$

where T is the temperature. The magnitude and sign of $\Delta C_p°$ can be taken as relative measure of the solute-solvent interaction.[4-6] The $\Delta C_p°$ values of simple salts indicate negative values, whereas the $\Delta C_p°$ values of hydrophobic solutes indicate positive values.

Table 1. Heats of solution and heat-capacity change

n	$\Delta H_s°$/kJ mol^{-1}			$\Delta C_p°$/J K^{-1} mol^{-1}
	15 °C	25 °C	35 °C	25 °C
	$C_nH_{2n+1}N(CH_3)_3Br$			
2	17.11	17.15	16.95	0
3	9.43	10.12	10.77	67
4	9.65	10.54	11.49	92
5	18.44	20.47	22.40	198
6	11.06	13.59	16.31	262
	$[(CH_3)_3N(CH_2)_nN(CH_3)_3]Br_2$			
3	21.70	19.97	18.47	−162
4	25.84	24.87	24.00	−92
5	27.05	26.77	26.76	−14
6	31.01	31.56	32.07	53
8	27.14	28.94	30.58	172
10	24.87	27.91	30.80	297
12	38.04	42.15	46.69	433

The $\Delta C_p°$ values obtained at 25 °C are listed in Table 1. As may be seen in Table 1, for the MeC_nMe series, MeC_3Me, MeC_4Me, and MeC_5Me show the negative $\Delta C_p°$ values. Therefore, the electrostrictive hydration due to the charge-bearing groups $-N(CH_3)_3^+$ may interfere with the interaction of the hydrophobic $-(CH_2)_n-$ group of the lower homologs with water. In the case of MeC_6Me and larger MeC_nMe homologs, the $\Delta C_p°$ values become positive and they increase with an increase in the chain length. They are classified as hydrophobic structure-makers.

With the C_nMe series, the $\Delta C_p°$ value for tetramethylammonium bromide ($(CH_3)_4NBr$, abbreviated as C_1Me in this paper) was reported to be −42 J K^{-1} mol^{-1} by Sarma, Mohanty, and Ahluwalia[7] and −47 J K^{-1} mol^{-1} by Arnett and Campion.[4] Table 1 indicates that the $\Delta H_s°$ values of C_2Me are virtually independent of the temperature, for which electro-

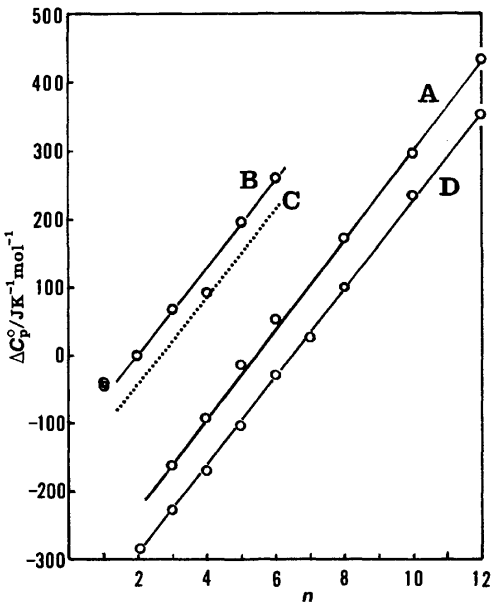

Fig. 1. Plot of ΔC_p° against n. A: $[(CH_3)_3N(CH_2)_n$-$N(CH_3)_3]Br_2$, B: $C_nH_{2n+1}N(CH_3)_3Br$, C: $-(CH_2)_n$-$N(CH_3)_3Br$, D: $[H_3N(CH_2)_nNH_3]Cl_2$.

strictive and hydrophobic hydration balance each other. In the case of C_3Me and higher homologs, the ΔC_p° values become positive, and they are hydrophobic structure-makers.

The ΔC_p° values are plotted against the number of carbon atoms, n, in the polymethylene or alkyl group for MeC_nMe and C_nMe in Fig. 1. If we take one-half the ΔC_p° values for MeC_nMe, the ΔC_p° values for a series of $-(CH_2)_nN(CH_3)_3Br$ can be estimated. The ΔC_p° *vs.* n relation thus obtained is plotted as a dotted line in Fig. 1. It is found that for the same number of n, the ΔC_p° values for $-(CH_2)_nN(CH_3)_3Br$ are lower than those for C_nMe. With the same ΔC_p° values, the difference in n between the two ΔC_p°-*vs.*-n lines for C_nMe and $-(CH_2)_nN(CH_3)_3Br$ corresponds to about 0.8. Therefore, the hydrophobic character of the polymethylene chain in MeC_nMe is considerably diminished below that of alkyl chain in monovalent C_nMe salts with the same number of n.

In Fig. 1, a plot of the ΔC_p° values against n for polymethylenediammonium dichlorides reported in a previous paper[1] is also included. For the same number of n, the ΔC_p° values for MeC_nMe are larger by about 75 J K^{-1} mol^{-1} than those for polymethylenediammonium dichlorides. This may be mainly attributed to the hydrophobic effect of the methyl groups attached to the two terminal nitrogen atoms, because the difference in ΔC_p° values due to the variation in halide ions for the same cations is very small.[6]

References

1) K. Tamaki and K. Irie, *Bull. Chem. Soc. Jpn.*, **56**, 2831 (1983).
2) K. Tamaki, Y. Ōhara, M. Inabe, T. Mori, and F. Numata, *Bull. Chem. Soc. Jpn.*, **56**, 1930 (1983).
3) T. L. Broadwater and D. F. Evans, *J. Phys. Chem.*, **73**, 3985 (1969).
4) E. M. Arnett and J. J. Campion, *J. Am. Chem. Soc.*, **92**, 7097 (1970).
5) B. Chawla and J. C. Ahluwalia, *J. Solution Chem.*, **4**, 383 (1975).
6) K. Tamaki, S. Yoshikawa, and M. Kushida, *Bull. Chem. Soc. Jpn.*, **48**, 3018 (1975).
7) T. S. Sarma, R. K. Mohanty, and J. C. Ahluwalia, *Trans. Faraday Soc.*, **65**, 2333 (1969).

Internal Rotation of Tetraphenylethylene Dianion as Studied by H-1 and C-13 NMR

Masaru MORIKAWA, Hideki MATSUI, Akihiro YOSHINO, Kensuke TAKAHASHI,* and Goh MIYAJIMA†
Department of Industrial Chemistry, Nagoya Institute of Technology, Gokiso-cho, Showa-ku, Nagoya 466
†*Naka Works, Hitachi Ltd., Ichige-cho 882, Katsuta-shi, Ibaraki 312*
(Received May 25, 1984)

Synopsis. The line-shape analyses of the ^{1}H NMR spectra of the title anion have been made by means of a program of DNMR3. The thermodynamical parameters thus obtained are discussed in terms of counterions and other additives.

The ^{1}H NMR spectra of the title dianion has been reported previously.[1] A pictorial description of the dianion studied is shown in Scheme 1. As shown in the scheme, two internal rotations, A and B, exist in the carbanion. This study aims to obtain the thermodynamical parameters of these internal rotations. Our preliminary results have previously been reported.[2]

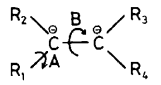

$R_1=R_2=R_3=R_4=C_6H_5$

Scheme 1.

Experimental

The strarting material (Tetraphenylethylene) was a commercial one and was used without further purification except for degassing by repetitive melting and freezing in a vacuum. The procedures for preparing the carbanion were the same as those previously reported.[1]

The H-1 and C-13 NMR measurements were carried out on a Hitachi R-20B spectrometer at 60 MHz and on a Hitachi R-900 FT spectrometer at 22.6 MHz. The sample concentration was about 1.0 mol dm^{-3} in the case of the potassium salt in THF-d_8. The H-1 and C-13 chemical shifts were evaluated with the high-field solvent peaks of THF-d_7 and -d_8 used as internal references. They were taken to be 1.75 and 25.2 ppm respectively with respect to TMS.

The temperature-dependent H-1 NMR spectra were analyzed by using the program of DNMR3 (QCPE No. 165).[3] In the original program, the maximum dimension of the B submatrices has been fixed at 48 and the maximum line number, at 136. For the analysis of the present material, it was necessary to expand them to 100 and 210 respectively. The calculations were carried out by a HITAC-8400 computer system installed in this Institute.

Results and Discussion

H-1 and C-13 NMR Spectra. The spectra of the title dianion have been observed at temperatures from 31.5 to −90 °C, with potassium as counterions in THF-d_8. The C_o signals in the temperature-dependent C-13 NMR spectra have decreased in height at −50 °C, been broadened at −60 °C, and clearly split into doublets at −74 °C. The H-1 NMR spectra of the carbanion were analyzed by the LAOCN3 program.[4] The coupling constants and the chemical shifts thus obtained are tabulated in Table 1. The H-1 and C-13 chemical-shift differences at low temperatures are about δ 1.35 and 0.07 for the H_o and H_m, and δ 2.3 and 1.2 for the C_o and C_m, respectively. The comparatively large difference in chemical shift between two H_o peaks can be explained by the ring-current effect of the phenyl groups.[5]

Line-shape Analyses. The temperature-dependent H-1 and C-13 NMR spectra were measured by using the same sample sealed in a 5-mm O.D. tube. Therefore, the C-13 NMR spectra were not suitable for the line-shape analyses because of their low signal-to-noise ratio. However, the proton-decoupled C-13 spectra were so simple that a rough estimate of the two-site exchange problem using a computer program, CLATUX[6] was possible, giving the activation energy of about 34 kJ mol^{-1}. The H-1 NMR line-shape analyses, however, could give a more exact activation energy. The rate constants for the two-site-five-spin exchange problem are given in Table 2 for various temperatures. The calculated and corresponding observed spectra are given in Fig. 1 for three typical temperatures. From the values in Table 2, the thermodynamical parameters tabulated in Table 3 are obtained. The values are compared with those

Table 1. H-1 and C-13 NMR data of tetraphenylethylene dianion potassium salt in THF-d_8

H-1 Data at 31.5 °C[a]		H-1 Data for DNMR3	C-13 Data at −74 °C	
H_o:	418.83 Hz	459.4 Hz 378.2	C_o:	118.11 ppm 115.86
H_m:	387.72	389.7 385.7	C_m:	129.03 127.86
H_p:	334.62	334.6	C_p:	106.38
J_{om}:	8.58	8.6	C_i:	147.77
J_{op}:	1.12	1.2	C_α:	95.95
J_{mp}:	6.69	6.7		

a) The values are obtained with an RMS error of 0.18 Hz and with standard errors of 0.03 Hz.

Table 2. Rate constants (k) of the phenyl rotation in tetraphenylethylene dianion potassium salt in THF-d_8

Temp/K	k/s^{-1}
254.8	3460±70
243.6	1840±40
232.7	800±30
230.4	680±30
225.0	320±10
214.9	118± 5
204.7	40± 2

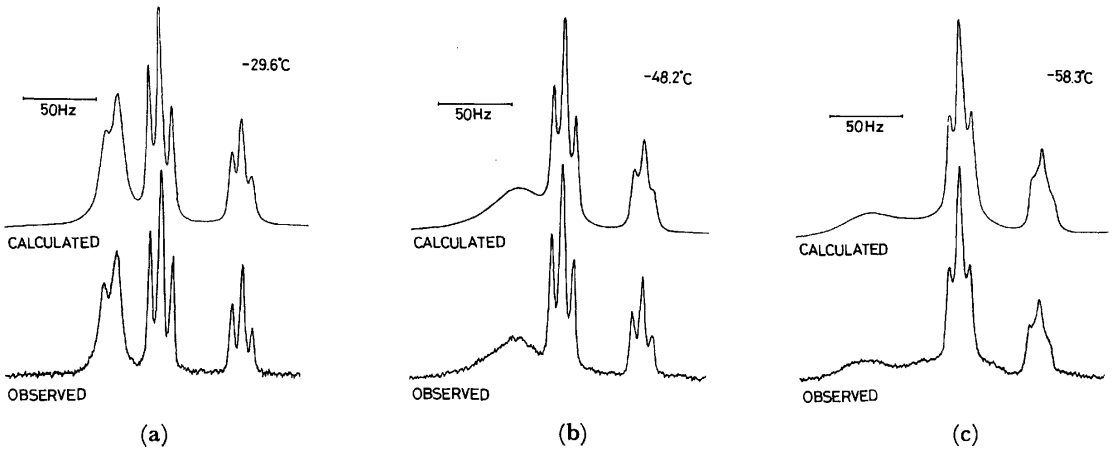

(a) (b) (c)

Fig. 1. Calculated (upper) and Observed (lower) H-1 NMR spectra of tetrapehnylethylene dianion potassium salt in THF-d_8 at 60 MHz; (a) at −29.6 °C; (b) at −48.2 °C; (c) at −58.3 °C.

Table 3. Thermodynamical parameters for the hindered rotation of the phenyl groups of tetraphenylethylene dianion potassium salt in THF-d_8

E_a/kJ mol^{-1}	ln A	ΔH^*/kJ mol^{-1}	ΔS^*/J K^{-1} mol^{-1}
39.8±1.5	27.1±0.8	37.9±1.5	−25.7±6.6

reported for the phenylmethanide and diphenylmethanide ions.[7-12] The activation energy observed in this study is the smallest value reported thus far. This may be attributed to the fact that the carbanion is sterically inhibited from having the planar structure rather than to its resonance stabilization in the ground state.

Effects of Counterions and Other Additives. The coalescence temperatures of the H_o in the carbanion are affected by the counterions. Several attempts were made to obtain the exact thermodynamical parameters. However, the solubilities of the lithium and sodium salts are too small for us to obtain good line-shaped spectra in THF at low temperatures. Therefore, the line-shaped analyses described above are possible only for the potassium salt. The coalescence temperatures are estimated to be about −40, −55, and −60 °C for the K^+, Na^+, and Li^+ counterions respectively. The temperatures decrease with a decrease in the metal radius and with an increasing proximity of the metal to the active carbon site. The coalescence temperatures can be used to estimate the changes in the free energy of activation for the rotation A in the carbanions using the following equation:

$$\Delta G_c^{\ddagger}=aT_c[9.972+\log(T_c/\Delta\nu_{ab})],$$

where T_c, $\Delta\nu_{ab}$, and a are the coalescence temperature, the chemical-shift difference of two exchanging sites, and a constant of 19.14 J mol^{-1} respectively.[13] In the case of the sodium salt, the $\Delta G_c^{\ddagger}$ value is 43.7 kJ mol^{-1} when the values of T_c and $\Delta\nu_{ab}$ are adopted as *ca.* 218 K and 67 Hz. This value is reasonable as compared with that obtained for the potassium salt (43.9 kJ mol^{-1} at 233.2 K). Hexamethylphosphoric triamide (HMPA) was used to check the effect of other additives, because it has a high dielectric constant. The effect of HMPA caused a rise in the coalescence temperature by about 5 K in the potassium and sodium salts. Therefore, the effect appears as an increase in the activation energy of the rotation A. This is consistent with that observed for diphenylmethanide ions by Olah and Watkins.[12]

References

1) K. Takahashi, Y. Inoue, and R. Asami, *Org. Magn. Reson.*, **3**, 349 (1971).
2) U. Urata, M. Morikawa, A. Yoshino, K. Takahashi, and G. Miyajima, Preprint, presented at the 42nd National Meeting of the Chemical Society of Japan, Sendai, Sept. **1980**, 4E07.
3) D. A. Kleier and G. Binsch, *J. Magn. Reson.*, **3**, 146 (1970).
4) A. A. Bothner-By and S. M. Castellano, "Computer Programs for Chemistry," ed by D. F. Detar, Vol. **1**, W. A. Benjamin, New York (1968), p. 10.
5) K. Takahashi, M. Takaki, and R. Asami, *J. Phys. Chem.*, **75**, 1062 (1971).
6) G. Binsch, *Topics in Stereochem.*, **3**, 97 (1968).
7) V. R. Sandel, S. V. McKinley, and H. H. Freedman, *J. Am. Chem. Soc.*, **90**, 495 (1969).
8) S. Brownstein and D. J. Worsfold, *Can. J. Chem.*, **50**, 1246 (1972).
9) G. Fraenkel, J. G. Russell, and Y. H. Chen, *J. Am. Chem. Soc.*, **95**, 3208 (1973).
10) C. H. Bushweller, J. S. Sturges, M. Cipullo, S. Hoogasian, M. W. Gabeiel, and S. Bank, *Tetrahedron Lett.*, **1978**, 1359.
11) G. Fraenkel and J. M. Geckle, *J. Am. Chem. Soc.*, **102**, 2869 (1980).
12) G. A. Olah and M. I. Watkins, *Proc. Natl. Acad. Sci. U.S.A.*, **77**, 703 (1980).
13) J. Sandström, "Dynamic NMR Spectroscopy", Academic Press, London (1982), p. 96.

Vibrational Distributions of CO^+ (A) Produced from the Charge-transfer Reactions of Ne^+ and He^+ with OCS at Thermal Energy

Hiroshi Sekiya,* Masaharu Tsuji, and Yukio Nishimura
Research Institute of Industrial Science, and Department of Molecular Science and Technology, Graduate School of Engineering Sciences, Kyushu University, Kasuga-shi, Fukuoka 816
(Received June 15, 1984)

Synopsis. The Ne^++OCS and He^++OCS charge-transfer reactions have been studied by emission spectroscopy in a flowing afterglow. The relative vibrational populations of $CO^+(A^2\Pi)$ were determined by observing the $CO^+(A^2\Pi-X^2\Sigma^+)$ emission system produced from the above reactions. The populations decrease approximately exponentially with the vibrational quantum number.

Optical spectroscopic studies on the thermal-energy charge-transfer (CT) reactions between Ne^+ and small molecules are limited,[1,2] although those on the reactions between He^+ and small molecules have been made extensively.[3,4] Previously we have reported on the $CO^+(A^2\Pi-X^2\Sigma^+)$ emission produced from the Ne^++OCS CT reaction in a flowing afterglow.[1] The $CO^+(A\text{-}X)$ emission arises also from the He^++OCS CT reaction.[5] In order to understand the overall CT process, it is important to determine the internal energy state distribution of the products resulting from the thermal-energy CT reactions between rare gas ions and small molecules. In this Note we describe the vibrational distribution of $CO^+(A)$ produced from the Ne^++OCS reaction in comparison with that produced from the He^++OCS reaction. To our knowledge, this is the first report on the vibrational distribution of a product resulting from the Ne^+ CT reaction.

Experimental

The flowing afterglow apparatus is essentially identical to that described previously.[1] Active species of Ne and He were generated in a 2450 MHz microwave discharge. The Ne and He pressures ranged from 80 to 87 Pa (1 Pa=7.5×10^{-3} Torr). Emission spectra were observed on a Nippon Jarrell Ash 1-m monochromator equipped with either a HTV R376 or a HTV R585 photomultiplier. The relative sensitivity of the detection system was calibrated by a halogen lamp.

Results and Discussion

The $CO^+(A\text{-}X)$ emission system was observed in both Ne and He afterglows together with numerous emission systems which have been reported in the earlier papers.[1,5] The $CO^+(A\text{-}X)$ emission systems observed in the above two afterglows arise from the following CT reactions, respectively:

$$Ne^+ + OCS \longrightarrow CO^+(A) + S + Ne,$$
$$CO^+(A) \longrightarrow CO^+(X) + h\nu. \quad (1)$$
$$He^+ + OCS \longrightarrow CO^+(A) + S + He,$$
$$CO^+(A) \longrightarrow CO^+(X) + h\nu. \quad (2)$$

The recombination energies of $Ne^+(^2P_{1/2,3/2})$ are 21.66 and 21.56 eV, while that of the ground-state $He^+(^2S)$ is 24.58 eV.[6] Meanwhile, the calculated minimum energy required for the formation of $CO^+(A)$ from OCS is 19.73 eV, which is obtained on the assumption that sulfur atoms are formed in the ground ^3P state.[7] In Fig. 1 is shown a typical emission spectrum of the $CO^+(A\text{-}X)$ in the He afterglow, where a pulsed modulation system[5,8] was employed to eliminate the emissions due to the $He(2^3S)$+OCS Penning ionization. The $CO^+(B\text{-}A)$ emission has been observed in the $He(2^3S)$+CO Penning ionization.[9] However, no $CO^+(B\text{-}A)$ emission could be identified in the He^++OCS reaction, although weak $CO^+(B\text{-}X)$ emission could be identified.[5] Accordingly, the contribution of the $CO^+(B\text{-}A)$ cascade to the production of $CO^+(A)$ is very small in the He^++OCS reaction. The identified vibrational levels of $CO^+(A)$ range from $v'=0$ to $v'=5$ in the Ne^++OCS reaction[1] and from $v'=0$ to $v'=11$ in the He^+ +OCS reaction. In the Ne^++OCS reaction, as a partner of $CO^+(A)$ for $v'=0$—4, sulfur atoms in the ^3P and ^1D states are energetically possible, while sulfur atoms only in the ^3P state are energetically possible as a partner of $CO^+(A)$ for $v'=5$. On the other hand, in the He^++OCS reaction sulfur atoms in the ^3P, ^1D, and ^1S states are energetically accessible as a partner of $CO^+(A)$ for $v'=0$—11.

The relative vibrational populations were obtained from the emission spectra by means of a procedure reported in the previous paper.[8] The contribution of the vibrational relaxation of $CO^+(A)$ has been examined in the He pressures ranging from 80 to 800 Pa: Little difference has been found between the vibrational populations observed at 80 Pa and those extrapolated to zero He pressure. In the Ne^++OCS reaction, no pressure dependence of the vibrational populations of $CO^+(A)$ could be examined owing to the low intensity of the $CO^+(A\text{-}X)$ emission. We regarded the vibrational distribution of $CO^+(A)$ measured at 80 Pa as an approximate initial distribution in both Ne^++OCS and He^++OCS reactions. The relative vibrational populations of $CO^+(A)$, N_v, thus obtained are shown in Fig. 2. It should be

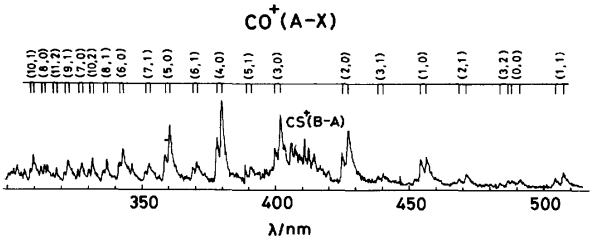

Fig. 1. A typical emission spectrum resulting from the He^++OCS CT reaction in a He afterglow.

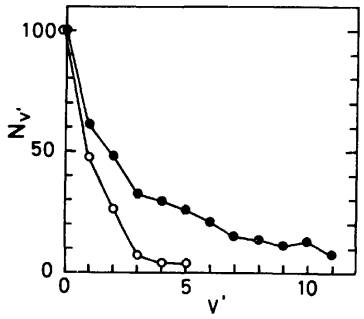

Fig. 2. Relative vibrational distribution of CO^+ (**A**). ○: Produced from the Ne^++OCS reaction, ●: Produced from the He^++OCS reaction.

noted that $N_{v'}$ decreases approximately exponentially with v' not only in the He^++OCS reaction but also in the Ne^++OCS reaction. Assuming a Boltzmann distribution for the vibrational levels, the effective vibrational temperatures are estimated to be 3400±400 K and 10100±1000 K for the Ne^++OCS and He^++OCS reactions, respectively. No photoelectron spectroscopic experiment has been reported on the excited electronic states of OCS^+ lying above 20 eV, which would be optically inaccessible states. The precursor states leading to the $CO^+(A)$ state in the Ne^++OCS and He^++OCS reactions would be optically forbidden multiple-electron-transition states of OCS^+ lying above 20 eV, which have been identified by Carnovale *et al.*[9] through electron-ion coincidence.

References

1) H. Sekiya, M. Tsuji, and Y. Nishimura, *Chem. Phys. Lett.*, **100**, 494 (1983).
2) R. Marx, G. Mauclaire, T. R. Govers, M. Gérard, S. Fenistein, and M. Derai, *J. Chim. Phys.*, **76**, 417 (1979).
3) R. Marx, "Kinetics of Ion-Molecule Reactions," ed by P. Ausloos, Plenum Press, New York (1979), p. 103.
4) M. Tsuji and Y. Nishimura, *Bunko Kenkyu*, **32**, 77 (1983), and references therein.
5) M. Tsuji, M. Matsuo, and Y. Nishimura, *Int. J. Mass Spectrom. Ion. Phys.*, **34**, 273 (1980).
6) C. E. Moore, "Atomic Enery Levels," National Bureau of Standards Circular 467, 1949.
7) P. H. Krupenie, National Bureau of Standards Ref. Data Ser., Natl. Bur. Stand., 5 (1966).
8) M. Endoh, M. Tsuji, and Y. Nishimura, *J. Chem. Phys.*, **79**, 5368 (1983).
9) F. Carnovale, A. P. Hitchcock, J. P. D. Cook, and C. E. Brion, *Chem. Phys.*, **66**, 249 (1982).

Photoinduced Potential Changes across Poly(vinyl chloride)/Crown Ether Membranes. Membrane Potential in the Presence of Alkaline Earth Metal Cations

Jun-ichi ANZAI, Hiroshi SASAKI, Akihiko UENO, and Tetsuo OSA*
Pharmaceutical Institute, Tohoku University, Aobayama, Sendai 980
(Received June 15, 1984)

Synopsis. The potential change across poly(vinyl chloride)/crown ether membrane was induced by photoirradiation in the presence of alkaline earth metal cations. The photoresponse of the membrane potential depended markedly on the kind and concentration of the cation species, the magnitude of the potential shift lying in the order of $Mg^{2+}>Ca^{2+}\approx Sr^{2+}>Ba^{2+}$.

We[1-3] and Shinkai *et al.*[4-8] have reported independently that the cation binding and transporting properties of azobenzene-modified crown ethers are successfully regulated by photoirradiation. Recently, we have found that the potential across the poly(vinyl chloride) (PVC)/4,4′-bis[3,4-(1,4,7,10,13-pentaoxatridecane-1,13-diyl)benzyloxycarbonyl]azobenzene (**1**) membrane changes reversibly upon alternate UV and visible light irradiation in the presence of alkali metal chloride.[9-11] The photoresponse of the membrane potential has been explicated based on the surface potential changes originating from the enhanced uptake of the alkali metal cation onto the membrane surface by photogenerated *cis*-**1**. The purpose of this note is to describe a different aspect in the photoresponse of the potential across PVC/**1** membrane with alkaline earth metal chloride.

Experimental

Materials. PVC (molecular weight of *ca.* 70000) was purchased from Wako Pure Chemical Industry Ltd. and used without further purification. Dibutyl phthalate (DBP), tetrahydrofuran (THF), and alkaline earth metal chloride are of extra pure reagent grade. The synthetic procedure and analytical data of **1** were reported previously.[2,3]

Membrane Preparation. PVC/**1** membrane of *ca.* 0.1 mm thickness was prepared by pouring the mixture of 235 mg of PVC, 0.54 ml of DBP, 1.3 mg of **1**, and 20 ml of THF onto a flat Petri dish (9.2 cm diameter) and allowing the solvent to evaporate.

Membrane Potential Measurement. All measurements were conducted at 25 °C. The composition of the electrochemical cell for the membrane potential measurements was as follows; Hg, Hg_2Cl_2(s)|KCl(sat.)|0.1 mol dm^{-3} $(CH_3)_4NCl$| electrolyte solution (c_1)|PVC/**1** membrane| electrolyte solution (c_2)|0.1 mol dm^{-3} $(CH_3)_4NCl$|KCl(sat.)|Hg_2Cl_2(s), Hg. The electrode in the c_1 compartment was earthed. Photoirradiation was carried out with 500 W xenon lamp with cut-off filters Toshiba UV D-35 and Corning 3-74 to isolate UV ($320\,nm<\lambda<400\,nm$) and visible ($\lambda>410\,nm$) light, respectively.

Results and Discussion

In the previous papers[9-11] we have reported that the membrane potential across PVC/**1** membrane interposed between two alkali metal chloride solutions changes upon photoirradiation. The magnitude and sign of the photoinduced potential shift, $\Delta(\Delta\Phi)$, were dependent on the kind and concentration of the cations, **1** content in the membrane, and the direction from which the membrane was irradiated. The photoresponsive behavior of the membrane potential was explained based on the surface potential change of the membrane, which was caused by the charge density change of the membrane surface through the photoinduced variation in the binding ability of **1** for alkali metal cations. The photoresponse was presumed to arise from the formation of sandwich-type complexes in which *cis*-**1** trapps a cation by its two crown-ether moieties.

Figure 1 illustrates the photoresponse of the membrane potential in the presense of $MgCl_2$. After a steady state potential difference, $\Delta\Phi$, had been reached under dark conditions, a negative shift of the potential was induced upon UV irradiation from the c_2 compartment

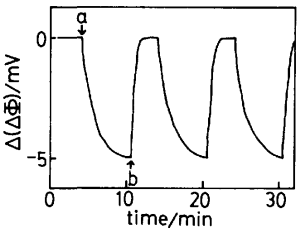

Fig. 1. Photoresponse of the membrane potential upon alternate UV (a) and visible (b) light irradiation. c_1; $[MgCl_2]=1\times10^{-3}$ mol dm^{-3}. c_2; $[MgCl_2]=5\times10^{-1}$ mol dm^{-3}.

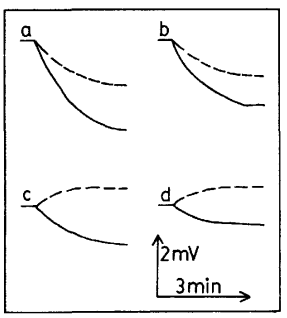

Fig. 2. Effect of the ionic concentration on the photoresponse in the presence of $MgCl_2$. Photoirradiation was conducted from c_1 (----) and c_2 (——) compartment sides. c_1; $[MgCl_2]=1\times10^{-2}$ (a), 1×10^{-1} (b), 5×10^{-1} (c), 1 (d) mol dm^{-3}. c_2; $[MgCl_2]=$ 1 mol dm^{-3}.

side. About 6 min sufficed to attain a steady state potential under UV light and the initial potential was recovered rapidly by switching the UV light to the visible one. The on-off cycle of the membrane potential was fairly reversible.

The effect of the ionic concentration on the photoresponse of the potential was examined by irradiating the membrane from the direction c_1 or c_2 compartment side. When the membrane was irradiated by UV light from the direction of c_2 compartment, the negative shift of the potential was always induced. The $\Delta(\Delta\Phi)$ values related closely to the ionic concentration in c_1 compartment. Larger $\Delta(\Delta\Phi)$ values were obtained in the case that the concentration gradient between the two solutions was increased. Even when the concentration gradient was zero ($c_1=c_2=1$ mol dm^{-3}), the potential shift was observed. On the other hand, the photoresponse was not simple when the membrane surface facing the compartment with a lower electrolyte concentration (c_1) was exposed to UV light. Under the conditions that the concentration gradient between the two electrolyte solutions was large, the membrane potential shifted to the negative direction (Figs. 2-a and 2-b). On the contrary, the positive shift of the potential was observed when the concentration gradient was small (Fig. 2-c). In the case of $c_1=c_2=1$ mol dm^{-3} (Fig. 2-d), the $\Delta(\Delta\Phi)$ value was equal in magnitude but opposite in sign to that obtained by irradiating from the c_2 side. This photoresponsive behavior was much the same as that observed for alkali metal cations.[9-11] We can explained the phenomena similarly to the case of alkali metal cations, that is, (i) the membrane potential changes are resulting from the fact that the charge density of the membrane surface (*i.e.*, surface potential) is perturbed by the photoinduced change in the binding ability of **1** for cations, (ii) the magnitude of the charge density changes of the membrane surface is determined by both factors of *trans*-**1**/*cis*-**1** ratio at the membrane surface and the ionic concentration in the solution, (iii) the

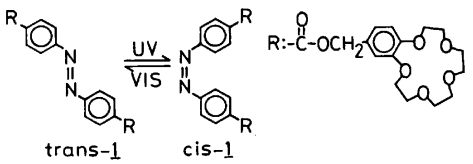

trans-**1**/*cis*-**1** ratio at one surface of the membrane is different from that of the opposite surface under UV light. The third argument can be the reason why the membrane potential changed even when no concentration gradient existed between the two solutions.

Figure 3 shows the photoresponse for $MgCl_2$, $CaCl_2$, $SrCl_2$, and $BaCl_2$. In the high c_2/c_1 regions, the larger $\Delta(\Delta\Phi)$ values were obtained for all salts. The magnitude of the $\Delta(\Delta\Phi)$ values lies in the order of $MgCl_2>CaCl_2\approx SrCl_2>BaCl_2$. This dependence of $\Delta(\Delta\Phi)$ values on the kind of cation species does not coincide with the order expected from the fitness between each cation and *cis*-**1**; the diameters of Mg^{2+}

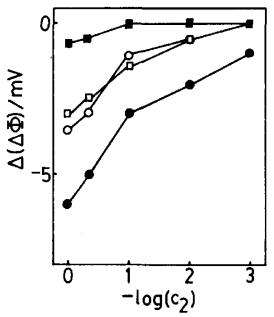

Fig. 3. Effect of the ionic concentration on the potential shift.
c_1; [Metal chloride]$=1\times10^{-3}$ mol dm^{-3}.
■; $BaCl_2$, □; $SrCl_2$, ○; $CaCl_2$, ●; $MgCl_2$.

and Ca^{2+} (1.22 Å and 1.98 Å, respectively) seem too small to form the sandwich-type complex, but the size of Ba^{2+} is appropriate (2.70 Å).[12] The data are incompatible with those obtained for alkali metal cations, where larger $\Delta(\Delta\Phi)$ values were observed for K^+ and Rb^+ which have suitable ionic sizes to form stable sandwich-type complexes with *cis*-**1**. Considering from these facts, any other factors, though not clear in the present stage, may participate in determining the binding ability of **1** for alkaline earth metal cations at the membrane/solution interface.

Thus, it became obvious that the potential across the PVC/**1** membrane interposed between two aqueous alkaline earth metal chloride changed upon photoirradiation in the different manner from that for alkali metal chloride although the factors governing the binding ability of **1** for alkaline earth metal cations at the membrane/solution interface remain equivocal.

References

1) A. Ueno and T. Osa, *Yuki Gosei Kagaku*, **38**, 207 (1980).
2) J. Anzai, A. Ueno, H. Sasaki, K. Shimokawa, and T. Osa, *Makromol. Chem., Rapid Commun.*, **4**, 731 (1983).
3) J. Anzai, H. Sasaki, K. Shimokawa, A. Ueno, and T. Osa, *Nippon Kagaku Kaishi*, **1984**, 338.
4) S. Shinkai, T. Ogawa, T. Nakaji, Y. Kusano, and O. Manabe, *Tetrahedron Lett.*, **1979**, 4569.
5) S. Shinkai, T. Ogawa, Y. Kusano, and O. Manabe, *Chem. Lett.*, **1980**, 283.
6) S. Shinkai, T. Nakaji, T. Ogawa, K. Shigematsu, and O. Manabe, *J. Am. Chem. Soc.*, **103**, 111 (1981).
7) S. Shinkai, H. Kinda, and O. Manabe, *J. Am. Chem. Soc.*, **104**, 2933 (1982).
8) A. Kumano, O. Niwa, T. Kajiyama, M. Takayanagi, K. Kano, and S. Shinkai, *Chem. Lett.*, **1983**, 1327.
9) J. Anzai, H. Sasaki, A. Ueno, and T. Osa, *J. Chem. Soc., Chem. Commun*, **1983**, 1045.
10) J. Anzai, H. Sasaki, A. Ueno, and T. Osa, *Chem. Lett.*, **1984**, 1205.
11) J. Anzai, H. Sasaki, A. Ueno, and T. Osa, *J. Chem. Soc., Perkin 2*, in press.
12) J. O. Bockris and A. K. N. Reddy, "Modern Electrochemistry," Plenum/Rosetta Ed., (1976).

Deprotection of 4-Methoxybenzyloxycarbonyl Group with *p*-Toluenesulfonic Acid in Acetonitrile. Application to a Large-scale Preparation of 7-[D-2-Amino-2-(4-hydroxyphenyl)acetamido]cephalosporanic Acid

Hirotada YAMADA,* Hisao TOBIKI, Norihiko TANNO, Hiroyuki SUZUKI, Kiyokazu JIMPO, Shinji UEDA, and Takenari NAKAGOME

Takarazuka Research Center, Pharmaceuticals Research Laboratory, Sumitomo Chemical Co., Ltd., 3-1-98, Kasugade-naka, Konohana-ku, Osaka 554

(Received January 5, 1984)

Synopsis. The 4-methoxybenzyloxycarbonyl group of 7-[D-2-(4-hydroxyphenyl)-2-(4-methoxybenzyloxycarbonylamino)acetamido]cephalosporanic acid was effectively removed with *p*-toluenesulfonic acid in acetonitrile. The mechanism of the deprotection is discussed and the role of acetonitrile can reasonably be explained in terms of the Ritter reaction.

In a previous report[1] of our screening study, we reported that the 4-methoxybenzyloxycarbonyl group [Z(OMe)] of 7-[D-2-(4-hydroxyphenyl)-2-(4-methoxybenzyloxycarbonylamino)actamido]cephalosporanic acid (**1**) could be successfuly removed by trifluoroacetic acid without adverse effect on the compound. Trifluoroacetic acid is conveniently used in laboratory synthesis, but its use for a large-scale preparation is undesirable because of its irritation on mucous membrane.

We now report a practical deprotection of the Z(OMe) group of **1** which has given a solution to this problem. The deprotection is accomplished by treatment of **1** with *p*-toluenesulfonic acid or methanesulfonic acid in

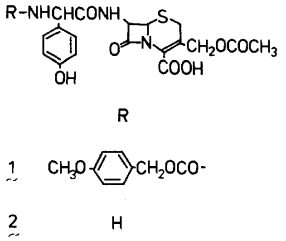

Table 1. Conditions for removal of Z(OMe) group and ratios of **1** and **2**

Sulfonic acid[a] (molar ratio)	Solvent[a] System & composition		Temperature °C	Reaction Time/min	Molar ratio/% **1**	Molar ratio/% **2**
PTS (2 equiv)	MeCN-ACT		10	60	32	68
		9 : 1[b]	20	30	5	95
				60	0	100
		4 : 1		60	3	97
		1 : 1			19	81
	MeCN-Dioxane	9 : 1	20	60	2	98
		4 : 1			7	93
		1 : 1			36	64
	MeCN-H_2O	4 : 1	20	60	100	0
	ACT	—	25	60	39	61
	Dioxane	—			84	16
	EtOH	—			96	4
	DMF	—			100	0
PTS (1 equiv)	MeCN-ACT	9 : 1	20	30	61	39
				60	48	52
MSA (2 equiv)				60	23	77

a) Abbreviations: PTS, *p*-toluenesulfonic acid monohydrate; MSA, methanesulfonic acid; ACT, acetone; DMF, *N*,*N*-dimethylformamide. b) By volume.

acetonitrile. The deprotection extremely depended on the nature of solvents tested and acetonitrile was found to be the most effective solvent (Table 1). Removal of the Z(OMe) group of **1** was completed within 60 min by using two equivalents of *p*-toluenesulfonic acid at 20—25 °C in acetonitrile–acetone (9:1, v/v). Addition of acetone or dioxane to acetonitrile in a small ratio was useful for preventing deposits from separating out of reaction mixtures as the removal reaction proceeded, but their addition in increased ratios slowed down the reaction. The reaction was also slowed down when smaller amounts of *p*-toluenesulfonic acid or lower reaction temperatures were used. Addition of excess water to acetonitrile interfered with the deprotection. Methanesulfonic acid also removed the Z(OMe) group, but a slightly longer reaction time was required than for the use of *p*-toluenesulfonic acid.

The role of acetonitrile was made clear as follows: A treatment of *N*-Z(OMe)-*p*-hydroxyphenylglycine (**3a**) with *p*-toluenesulfonic acid in acetonitrile gave *N*-(4-methoxybenzyl)acetamide (**4a**) in 49% yield as well as *p*-hydroxyphenylglycine *p*-toluenesulfonic acid salt in 93% recovery. This result suggests that the Ritter reaction occurs in this deprotection. Chauvette *et al.*[2] reported that a Boc group was effectively removed in acetonitrile by treatment with *p*-toluenesulfonic acid. But the mechanism was not cleared. A treatment of *N*-Boc-*p*-hydroxyphenylglycine (**3b**) under similar conditions also gave the corresponding acetamide **4b** in 51% yield. In both cases, the role of acetonitrile can reasonably be explained on the basis of the mechanism shown in Scheme 1, although the yields of **4a** and **4b** were not quantitative.

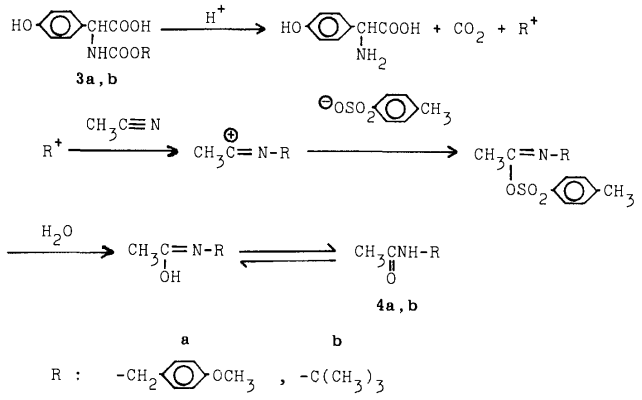

Scheme 1.

This deprotection has successfully been applied to a several-hundred-gram scale preparation of cefpiramide,[3] a new broad-spectrum cephalosporin with antipseudomonal activity.

Although acetonitrile has not been a common solvent in peptide synthesis, this procedure using acetonitrile may be recommended for efficient deprotection of a Z(OMe) or a Boc group.

Experimental

Melting points were determined in open capillary tubes with a Thomas-Hoover Uni-Melt apparatus and are uncorrected. ^{1}H NMR spectra were recorded on a JEOL FX-90Q (90 MHz) spectrometer with TMS used as internal standard; all chemical shifts are reported in δ values. Separation and quantitative analysis were performed with a high performance liquid chromatograph (Model No. ALC/GPL 204, Japan Waters, Ltd.) equipped with a LiChrosorb RP-8 column (10 μm particle size, 30 cm by 4 mm).

Removal of a Z(OMe) Group of 7-[D-2-(4-Hydroxyphenyl)-2-(4-methoxybenzyloxycarbonylamino)acetamido]cephalosporanic Acid (1). A mixture of compound **1**[1] (0.5 g), solvent (5 ml), and *p*-toluenesulfonic acid or methanesulfonic acid was stirred under the conditions given in Table 1. A part of the reaction mixture was sampled and analyzed by HPLC. The mobile phase used was a mixture of 0.01 M (1M=1 mol dm^{-3}) phosphate buffer (pH 6.8) and MeOH (6:4 by volume). The ratios of **1** and **2** in Table 1 were determined from each peak area corrected for the UV sensitivity of each compound.

Removal of a Z(OMe) Group of D-2-(4-Hydroxyphenyl)-2-(4-methoxybenzyloxycarbonylamino)acetic Acid (3a). To a solution of **3a** (1.0 g, 3 mmol) in MeCN (40 ml) was added a solution of *p*-toluenesulfonic acid monohydrate (1.15 g, 6 mmol) in MeCN (15 ml). The mixture was stirred at room temperature for 3.5 h. The *p*-hydroxyphenylglycine *p*-tolenesulfonic acid salt precipitated was collected by filtration, washed with MeCN (10 ml) and dried *in vacuo*: yield 0.95 g (93%); mp 222—223 °C (dec.) (lit,[6] 229 °C).

The combined filtrate and washings were concentrated *in vacuo*. To the residue was added a solution of sodium bicarbonate (0.507 g) in water (15 ml) and the mixture was extracted successively three times with diethyl ether (15 ml) and twice with ethyl acetate (15 ml). The extracts were combined, dried over $MgSO_4$, and the solvent removed *in vacuo*, leaving a yellow solid. It was chromatographed on a thin layer (Merck; pre-coated TLC plate Silica Gel $60F_{254}$, 20×20 cm, of layer thickness 0.50 mm) with EtOAc to give *N*-(4-methoxybenzyl)acetamide (0.195 g, 36.0%): mp 95—96 °C (lit,[4] 95—97 °C). The content of this compound in the reaction mixture was 0.27 g (49%) as determined by an HPLC analysis using a mobile phase consisting of 0.01 M phosphate buffer (pH 6.8) and MeOH (1:1 by volume).

A similar treatment of D-*N*-Boc-*p*-hydroxyphenylglycine (**3b**) with *p*-toluenesulfonic acid in acetonitrile gave *N*-(*t*-butyl)acetamide in 51% yield, which was identified by elemental analysis and by comparison of its melting point and ^{1}H NMR spectrum with those of an authentic sample.[5]

The authors wish to thank Dr. Masataka Fukumura for his useful suggestions on this report. The authors also wish to thank Mr. Kenzo Hosotani for his excellent technical assistance in the synthesis.

References

1) H. Yamada, K. Jimpo, H. Tobiki, T. Komatsu, H. Noguchi, K. Irie, and T. Nakagome, *J. Antibiot.*, **36**, 522 (1983).

2) R. R. Chauvette, P. A. Pennington, C. W. Ryan, R. D. G. Cooper, F. L. Jose, I. G. Wright, E. M. Van Heyningen, and G. W. Huffman, *J. Org. Chem.*, **36**, 1259 (1971).

3) H. Yamada, H. Tobiki, K. Jimpo, T. Komatsu, T. Okuda, H. Noguchi, and T. Nakagome, *J. Antibiot.*, **36**, 543 (1983).

4) K. Shirakawa and H. Kawasaki, *Yakugaku Zasshi*, **71**, 1213 (1951); *Chem. Abstr.*, **46**, 5544e (1952).

5) J. J. Ritter and P. P. Minieri, *J. Am. Chem. Soc.*, **70**, 4045 (1948).

6) T. Shirai, Y. Tashiro, and S. Aoki, *Japan Kokai*, **75**, 111033; *Chem. Abstr.*, **85**, 5373p.

Synthesis of 2,4-Di(*p*-formyl)-α-truxillic Acid by Crystal Engineering

Fusae NAKANISHI,* Michiko ISHII, and Hachiro NAKANISHI
Research Institute for Polymers and Textiles 1-1-4 Yatabe-Higashi, Tsukuba, Ibaraki 305
(Received February 21, 1984)

Synopsis. *p*-Formycinnamic acid, which usually crystallizes in either the β-form or γ-form of packing, was converted into its diethyl acetal. The introduction of such bulky groups onto a benzene ring successfully provided us with the α-form of packing, from which the desired photodimer, 2,4-di(*p*-formyl)-α-truxillic acid (*c*-2, *t*-4-bis(*p*-formylphenyl)-*r*-1,*t*-3-cyclobutanedicarboxylic acid) was obtained with a yield of 85—90%.

We have previously reported[1] the preparation of 3,4-di(*p*-formyl)-β-truxilic acid (*t*-3, *t*-4-bis(*p*-formylphenyl)-*r*-1, *c*-2-cyclobutanedicarboxylic acid) from *p*-formylcinnamic acid (*p*-FCA)crystals using irradiated light. Two polymorphic forms of *p*-FCA were found, each depending on recrystallization conditions: β-form; photo-reactive and γ-form; photostable. Attempted recrystallization using various kinds of solvents did not provide for the formation of α-form crystals, the photodimerization of which gives us 2,4-di(*p*-formyl)-α-truxillic acid **3** (*c*-2, *t*-4-bis(*p*-formylphenyl)-*r*-1-, *t*-3-cyclobutanedicarboxylic acid). The synthesis of **3** is of considerable interest since it might be converted into the same compound as the photodimer of diethyl 3,3′-(*p*-phenylene)diacrylate and the crystal structure and the photoreactivity of this dimer might provide us with crucial information on the mechanism of the four-center type photopolymerization,[2] *i.e.*, a kind of crystal transition reaction from the monomer to the polymer.

This report is concerned with the successful formation of **3** by crystal engineering. The data on the crystal structure of cinnamic acid derivatives suggest that the introduction of a bulky group onto a benzene ring of cinnamic acid may lead to the formation of α-form crystals since the steric hindrance of a bulky group avoids the β-type packing. We have chosen a diethyl acetal group as an example of such a bulky group since it is easy to introduce and to retrieve.

First, preparation of **1** of *p*-FCA was attempted by the usual method, using various kinds of acids. The results are shown in Table 1. In the presence of a strong acid, such as conc. sulfuric acid, *p*-FCA was almost converted into **1**. However, the crystals of the diethyl acetal derivative, thus obtained, were unstable and were readily hydrolyzed by moisture in the air. Presumably the crystals were contaminated with acid residues. Even an attempted neutralization of the reaction mixture by washing was not effective in the interior of the crystals and an attempted improvement of the yield was unsuccessful. By means of acetic acid catalysis, the acetal formed was stable to moisture, but *p*-FCA still remained in a considerable amount and, moreover, separation of the acetal from the reaction mixture was rather difficult. Therefore, the following method was carried out in order to improve the preparation. After exposure to hydrogen chloride gas, acidified β-form crystals of *p*-FCA were suspended in ethanol at 15 °C. The UV spectrum of these suspended crystals gradually changed. The maximum of the UV absorption gradually shifted from 295 nm (*p*-FCA) to 276 nm. The crystals obtained at this stage were colorless with a mp of 142 °C, and were identified as **1** of *p*-FCA on the basis of elemental analysis and spectroscopic data (IR, UV, and NMR). This simple reaction proceeded under mild conditions, and side reactions, such as esterification, were not observed and quite pure **1** was obtained. It should be noted that the photostable γ-form of crystalline *p*-FCA was not converted into the acetal under the same conditions. These results suggest that the reaction was controlled by the crystal structure, that is, a topochemical reaction. The crystal structure of β-form of *p*-FCA[3] showed that formyl groups were exposed on the well-developed crystal face. Though we can not establish the mechanism of this reaction in detail because of lack of the data on the crystal structure of γ-form of *p*-FCA, it seems that the reaction proceeds from a well-developed crystal face through an attack by an ethanol molecule, in a mechanism similar to that proposed for the solid-gas reaction of carboxylic acid with ammonia.[4] The diethyl acetal crystals were found to be photoreactive. The absorption peak of the UV spectrum of irradiated diethyl acetal crystals in ethanol deceased gradually to a small peak with λ_{max} around 269 nm. At this stage, no absorption peak ascribed to double bonds was observed in the IR spectrum of irradiated crystals. In the NMR spectrum of irradiated crystals in DMSO-d_6, double bonds peaks disappeared and new peaks appeared at δ 3.7—4.6. The proton ratio of each peak in the NMR spectrum (benzene : methine : methylene and new peaks :

TABLE 1. PREPARATION OF ETHYL ACETAL OF *p*-FORMYLCINNAMIC ACID (*p*-FCA)

Reactants	Acid	Reaction conditions	Yield/%
Acidified EtOH+*p*-FCA	Conc H_2SO_4	Reflux	Not isolated
	HCl Gas	Reflux	Mixture of *p*-FCA and diethyl acetal
	CH_3COOH	Reflux	
	HCl	Reflux	45
EtOH+Acidified *p*-FCA	HCl Gas	15 °C	88
Acidified EtOH+*p*-FCA	HCl Gas	15 °C	76

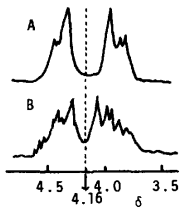

Fig. 1. Cyclobutane ring proton signals of (A) 3,4-di (*p*-formyl)-*β*-truxillic acid and (B) 2,4-di(*p*-formyl)-*α*-truxillic acid.

methyl) was found to be 8:2:12:12. New peaks (4 protons) were assingned as cyclobutane ring protons, based on a comparison with the reported data on cyclobutane rings.[5] These facts suggest that dimer **2** was formed by cycloaddition of **1**. In order to hydrolyze to a formyl derivative, diethyl acetal groups of the dimer **2** were treated with hydrochloric acid. Formation of dimer **3** was supported by elemental analysis, IR and NMR spectra. The configuration of the cyclobutane ring of **3** was determined by comparing the shape and the mid-point of symmetrical spin patterns of the cyclobutane rings in the NMR spectrum with those of reported cyclobutane rings. According to the report by Ben-Efraim *et al.*,[5] mid-points of cyclobutane ring proton patterns of *α*-truxillic acid, *β*-truxinic acid and *μ*-truxinic acid (*t*-3, *c*-4-diphenyl-*r*-1, *t*-2-cyclobutanedicarboxylic acid) have the same position. As shown in Fig. 1, the cyclobutane ring patterns of **3**, (B), were mirror-symmetrical but the shape was different from those of 3,4-di(*p*-formyl)-*β*-truxinic acid,[1] (A). The mid-points of both spin patterns were the same value (4.16). These facts suggest that **3** was either *α*-truxillic acid or a *μ*-truxinic acid-type dimer. The cyclobutane ring patterns of **3** are similar to those of *α*-truxillic acid.[5] Based on these facts, it was certain that product **3** was an *α*-truxillic acid-type dimer. The over-all reaction is shown in Scheme 1. This is the first preparation of *α*-truxillic acid carrying formyl groups on benzene rings.

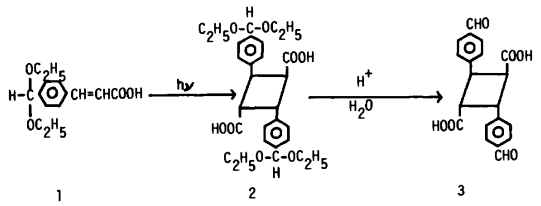

Scheme 1.

Experimental

p-FCA was prepared according to Wiely.[6] It crystallized into two different modifications, depending on the crystallization solvent. *β*-Form crystals were obtained from ethanol and *γ*-form from acetone. Both forms have the same melting point, 249 °C, but they have different X-ray diffraction patterns.

Preparation of Diethyl Acetal of p-*Formylcinnamic Acid.* *β*-Form crystals of *p*-FCA (2 g) were exposed to anhydrous hydrogen chloride gas for 30 min and the crystals were acidified. They were suspended in ethanol (30 ml) while stirring at 15 °C. At this temperature, 10% of the *p*-FCA crystals were dissolved in the ethanol. In order to determine the progress of reaction, the UV spectrum of the suspended crystals was occasionally measured while in the ethanol. When the absorption peak of the crystals ceased to shift, the crystals were collected by filtration. Some of diehyl acetal of *p*-FCA was further obtained by the evaporation of the mother liquor. The combined yield was 2.5 g. Found: C, 67.02; H, 6.93%. Calcd for $C_{14}H_{18}O_4$: C, 67.18; H, 7.25%. Mp 142 °C (from ethanol-hexane); UV_{max} (EtOH) 276 nm; ^1H NMR (DMSO-d_6); δ=1.2 (6H, t, $-CH_3$) 3.3—3.7 (4H, q, $-CH_2-$), 5.5 (1H, s, -CH), 6.4—7.9 (2H, d, -CH=CH-), 7.3—7.8 (4H, m, aromatic proton).

Photodimerization of Diethyl Acetal of p-*FCA in the Crystalline State.* Diethyl acetal crystals (100 mg) of *p*-FCA were suspended in hexane (100 ml) and irradiated with a 500 W xenon lamp at 15—20 °C. After 6 h diethyl acetal of *p*-FCA was changed to the dimer in the yield of 85—90%. Mp 230—232 °C; ^1H NMR (DMSO-d_6); δ=1.15 (12H, t, $-CH_3$), 3.3—3.7 (8H, q, $-CH_2-$), 5.5 (2H, s, -CH), 3.7—4.6 (4H, m, cyclobutane proton), 7.3 (8H, m, aromatic proton).

Dimer **2** (100 mg) was suspended in dil HCl (50 ml) for a few hours while stirring. By this treatment dimer **3** was obtained. Mp 273—275 °C (from ethanol-water); UV_{max} (EtOH) 264 nm; Found: C, 68.17; H, 4.68%. Calcd for $C_{20}H_{16}O_6$: C, 68.18; H, 4.58%. ^1H NMR (DMSO-d_6); δ=3.7—4.6 (4H, m, cyclobutane proton), 7.4—8.0 (8H, m, aromatic proton), 10.0 (2H, s, -CHO).

References

1) F. Nakanishi, H. Nakanishi, T. Tsuchiya, and M. Hasegawa, *Bull. Chem. Soc. Jpn.*, **49**, 3096 (1976).
2) F. Suzuki, Y. Suzuki, H. Nakanishi, and M, Hasegawa, *J. Polym. Sci.*, A-1, **7**, 2391 (1969).
3) H. Nakanishi, Unpublished data.
4) R. S. Miller, D. Y. Curtin, and I. C. Paul, *J. Am. Chem. Soc.*, **96**, 6329 (1974).
5) D. A. Ben-Efraim and B. S. Green, *Tetrahedron*, **30**, 2357 (1974).
6) R. H. Wiley and P. H. Hobson, *J. Am. Chem. Soc.*, **71**, 2429 (1949).

Reactions of Azoxybenzene with Dichlorocarbene in the Phase-transfer-catalyzed System

Shizen SEKIGUCHI,* and Tomohisa FUJIU
Department of Synthetic Chemistry, Faculty of Engineering, Gunma University, Ten-jin cho, Kiryu, Gunma 376
(Received March 8, 1984)

Synopsis. Azoxybenzene (**1**) reacted with dichlorocarbene (**2**) at 40 °C in the presence of a phase-transfer catalyst (18-crown-6 or tributylamine) in a binary solvent ($CHCl_3$–aqueous KOH), giving 2,2,3,3-tetrachloro-1-phenylaziridine (**4**), azobenzene (**5**), and 2-hydroxy-1-phenylbenzimidazole.

The phase-transfer technique has been regarded as a useful tool in improving the preparative processes and syntheses used in laboratories. Although the reactions of dihalocarbenes with olefins,[1-3] amides,[4] imines,[5] alcohols[6] and adamantane[7] have already been studied, only a few studies involving the addition of dichlorocarbenes to -N(O)=N- (azoxy) bonds have been published.

Seyferth and his coworkers have reported the reaction of azoxybenzene (**1**) with dichlorocarbene (**2**) in benzene, in which phenyl(bromodichloromethyl)mercury ($PhHgCCl_2Br$) was used as a source reagent of **2**. They found that 1,1-dichloro-*N*-phenylmethanimine (**3**, yield 3%), 2,2,3,3-tetrachloro-1-phenylaziridine (**4**, yield 12%) and azobenzene (**5**, yield 6%) were formed (Eq. 1).[8]

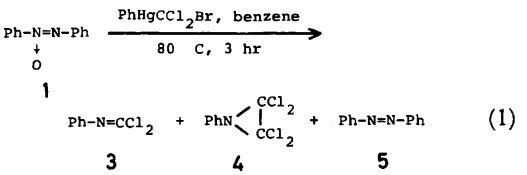

(1)

We have also carried out a reaction of **1** with **2** in the presence of 18-crown-6 or tributylamine as a phase-transfer catalyst (PTC) under the phase-transfer-catalyzed conditions (50% aqueous KOH–$CHCl_3$), in which the different products, except for **4** and **5**, were formed (Eq. 2). The results are indicated in Table 1.

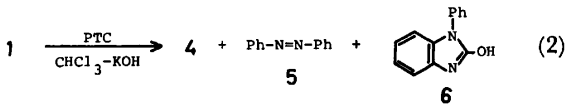

(2)

Azobenzene (**5**) is probably formed *via* the following path (Eq. 3).[9,10] In such polar solvents as chloroform

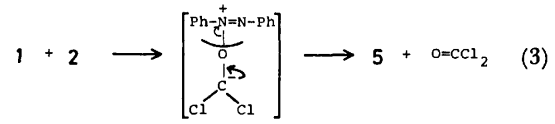

(3)

the intermediate shown in the bracket (Eq. 3) might reasonably be considered to intervene with the electrophilic character of **2**.

Further, in order to elucidate the formation path of **4** and **6**, a reaction of **5** with **2** under the same conditions described in Table 1 (PTC tributylamine; temp 40 °C; time 4 h) was carried out, in which **4** and **6** were formed in 31.0 and 15.5% yields (based on **5** consumed), respectively. These results would indicate that **4** and **6** are formed *via* the following path (Eq. 4).[11]

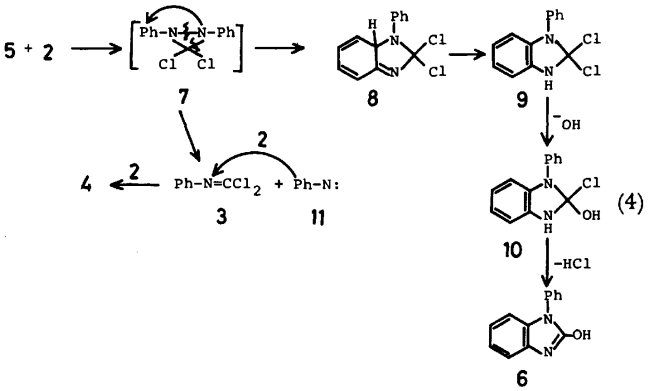

(4)

It is not clear, at present, whether the N-N bond fission in **7** is heterolytic or homolytic. The intermediacy of **7**, however, is reasonable from considering the formation of **4** and **6**.[11,12] As is shown in Eq. 3, the abstraction of an oxygen atom by **2** is interesting and such a reductive function of **2** would be excepted to attract attention.

TABLE 1. REACTION OF AZOXYBENZENE WITH DICHLOROCARBENE IN THE PRESENCE OF PHASE TRANSFER CATALYSTS

1 mmol	$CHCl_3$ mmol	aq KOH (50%) mmol	Temp °C	Time h	Product/%[a] 4	5	6	Conv. %
					18-Crown-6[b]			
30.0	419	446	40	10	36.8	3.0	1.7	35.0
					Tributylamine[c]			
			40	4	42.0	5.3	8.5	37.6
			10	24	32.2	6.1	4.2	37.1

a) Based on the azoxybenzene consumed. b) 18-Crown-6 0.76 mmol. c) Tributylamine 0.76 mmol.

Experimental

General Comments. The products were identified using NMR and MS spectrometers, UV and IR spectrophotometers, and elemental analyses. All the capillary melting points were uncorrected.

Preparation of Azoxybenzene (1). Following a method described in the literature,[12] **1** was prepared from nitrobenzene, diarsenic trioxide, and sodium hydroxide (yield 65%): mp 34—35 °C (35.5—36.6 °C).[12]

Reaction of Azoxybenzene (1) with Dichlorocarbene (2) for Isolation of the Products. The preparative procedure was as follows: A solution of 5.95 g (30.0 mmol) of **1**, 0.204 g (0.76 mmol) of 18-crown-6, and 50.0 g (446 mmol) of aqueous KOH (50%) was added to an Erlenmeyer flask with a reflux condenser and a thermometer placed on a heating plate. The flask was covered with aluminium foil in order to shield it from light.

After the chloroform layer was filtered and concentrated, by aqueous H_2SO_4 (5N) and extracted with chloroform. Then, the extract was dried overnight over anhydrous $MgSO_4$. After the chloroform layer was filtered and concentrated, the residue was processed by column chromatography (silica gel [Wako gel C-200]-benzene).

In addition, **4** was seperated from unreacted **1**, **5**, and **6**, using a column [silica gel-ligroin (bp 80—100 °C)], and purified by reduced distillation [bp 70—72 °C/2.66 Pa[8]].

The ligroin fraction containing unreacted **1**, **5**, and **6** was processed by column chromatography [firstly, silica gel-benzene-ligroin (4:1 v/v), and secondly, silica gel-benzene-acetone (9:1 v/v)] giving the **6** fraction. It was concentrated and the residue was recrystallized from acetone, giving pure **6**.

After the residual ligroin fraction was concentrated, the residue was subjected to fractional crystallization from methanol, giving pure **1** (mp 35—36 °C) and **5** (mp 67.5—68 °C).

2,2,3,3-Tetrachloro-1-phenylaziridine (4); bp 70—72 °C/2.66 Pa (70—72 °C/Pa).[8]

2-Hydroxy-1-phenylbenzimidazole (6); mp 210 °C; M^+ 210; NMR (DMSO-d_6) δ=11.1 (1H, s, broad, OH and NH), 7.7 (5H, s, 1-phenyl), and 7.2—7.5 (4H, m, phenyl); IR (KBr) 3400, 3100, 1750—1660, 1600, 1450, 760, 740, and 690 cm^{-1}; Anal. ($C_{13}H_{10}N_2O$) C. H. N. The chemical shift at δ=11.1 and the absorption band at 1750—1660 cm^{-1} clearly indicate that there are two tautomers (**6** and 2-oxo-1-phenyl-2,3-dihydrobenzimidazole).

Reaction of Azobenzene (5) with Dichlorocarbene (2) for Isolation of the Products. The preparative procedure was the same as that involved in the reaction of **1** with **2**.

Determination of Products. After the reaction was completed, the mixture was neutralized with aqueous H_2SO_4 (5M (1M=1 mol dm^{-3})) to pH 6—7 and extracted with two 200 ml portions of chloroform. Then, the chloroform layer was dried over anhydrous $MgSO_4$.

After the chloroform layer was filtered and the filtrate was concentrated, the residue was diluted exactly to 50 ml with a mixed solvent [methanol-chloroform (7:3 v/v)]. A 5-ml portion of the solution was analyzed by HPLC under the following conditions to determine **6**: Column JASCO SC-02L (silica gel) 0.46ϕ×25 cm, flow rate 1.0 ml/min, wave length 290 nm, solvent methanol-H_2O (6:4 v/v), internal standard biphenyl.

The residual 45-ml solution was concentrated and subjected to column chromatography [silica gel (Wako gel C-200)-benzene] to remove residual tarry matter.

After the eluent was concentrated, it was diluted to 20 ml with a mixed solvent [methanol-chloroform (7:3 v/v)]. The solution was subjected to GLC (HITACHI 164) to determine **4**, unreacted **1**, and **5**. The operating conditions were as follows: column (0.5ϕ×100 cm) Celite 545 impregnated with SE-30 (silicone) (10 wt%), column temperature 120 °C (for **4**) and 250 °C (for **1** and **5**), flow rate 20 (for **4**) and 10 ml/min (for **1** and **5**), carrier gas He; internal standard azobenzene (**5**) (for **4**) and benzyl benzoate (for **1** and **5**).

References

1) C. M. Starks, *J. Am. Chem. Soc.*, **93**, 195 (1971).
2) M. Makosza and M. Wawrzyniewicz, *Tetrahedron Lett.*, 4659 (**1969**).
3) S. Kwon, Y. Nishimura, M. Ikeda, and Y. Tamura, *Synthesis*, 249 (**1976**).
4) T. Saraie, T. Ishiguro, K. Kawashima, and K. Morita, *Tetrahedron Lett.*, 2121 (**1973**).
5) M. Makosza and A. Kacprowicz, *Roxz. Chem.*, **48**, 2929 (1974).
6) I. Tabushi, Z. Yoshida, and N. Takahashi, *J. Am. Chem. Soc.*, **93**, 1820 (1971).
7) I. Tabushi, Z. Yoshida, and N. Takahashi, *J. Am. Chem. Soc.*, **92**, 6670 (1970).
8) D. Seyferth, W. Tronich, and H.-m. Shin, *J. Org. Chem.*, **39**, 158 (1974).
9) E. E. Schweizer and G. J. O'Neill, *J. Org. Chem.*, **28**, 2460 (1963).
10) R. Oda, M. Mieno, and Y. Hayashi, *Tetrahedron Lett.*, 2363 (**1967**).
11) T. Sasaki, S. Eguchi, and T. Ogawa, *Heterocycles*, **3**, 193 (1975).
12) J. S. Buch and W. S. Ide, *Org. Synth.*, Coll. Vol. **II**, 57 (1948).

Preparatively Useful Method for the Synthesis of Diels-Alder Adducts between Furan and Methyl Acrylate

Hiyoshizo KOTSUKI,* Kazuhiko ASAO, and Hiroyuki OHNISHI
Department of Chemistry, Faculty of Science, Kochi University, Akebono-cho, Kochi 780
(Received March 15, 1984)

Synopsis. The Diels-Alder adducts of furan with methyl acrylate were successfully prepared by two methods on a preparative scale. The $BF_3 \cdot OEt_2$-catalyzed reaction of furan with methyl acrylate gave a 7:3 mixture of endo and exo adducts in 75.7% yield. When acryloyl chloride was used as a dienophile, after esterification with methanol, a 3:7 mixture of the same adducts was obtained in 76.5% overall yield.

The 7-oxabicyclo[2.2.1]heptyl system has been widely employed as a source of important intermediates in natural product syntheses.[1] The most straightforward approach to the construction of the 7-oxabicyclo[2.2.1]heptyl system takes advantage of the Diels-Alder reaction between furan and a suitable dienophile. However, the Diels-Alder reaction of furan with conventional dienophiles is usually sluggish because of the aromatic character of the furan ring (resonance energy *ca.* 25 kcal/mol).[2]

Previously, we have demonstrated the solution to this problem by the application of high-pressure technique.[3] Recently, however, it has been reported that some Lewis acid catalysts could provide an alternative approach to realize these Diels-Alder reactions.[4] These results prompt us to report our preliminary finding for a convenient preparation of Diels-Alder adducts between furan and methyl acrylate in preparatively useful amounts.

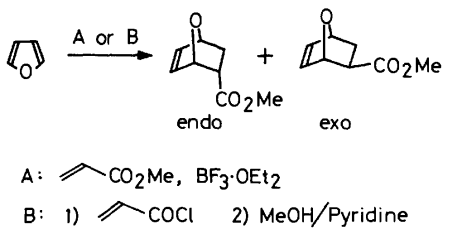

Firstly, the Lewis acid-catalyzed method is described. Among several Lewis acids, $BF_3 \cdot OEt_2$ was found to be a most effective catalyst for this reaction (Table 1). Thus, when the mixture of freshly distilled furan and methyl acrylate was catalyzed with 0.1 equiv of $BF_3 \cdot OEt_2$ *without solvent* at 5 °C for 10 h under nitrogen atmosphere , the desired endo and exo Diels-Alder adducts were obtained in 75.7% combined yields *with high endo selectivity* (endo:exo=7:3). For instance, the reported yield of the adducts is 55% using ZnI_2 as catalyst[4b] or 62% at 15 kbar pressure[3b] (endo:exo= 1:2 for the former or 6:4 for the latter). So the newly developed method considerably improves both the yield and the endo selectivity as the result of the kinetically controlled reaction.[5] Other Lewis acids such as $AlCl_3$, $SnCl_4$, and $ZnCl_2$ gave only resinous products and with other dienophiles such as methyl vinyl ketone, acrylonitrile, and dimethyl maleate either the reaction was not catalyzed or polymerization was predominant. Reaction with 2-methylfuran gave adducts in low yield and 2,5-dimethylfuran gave no adducts.

An alternative procedure is the use of a strongly reactive dienophile of acryloyl chloride. It has been known that acryloyl chloride reacts with furan in high yield.[6] However, the detailed experimental procedure has not been published. We found the reaction was greatly improved by addition of propylene oxide as a hydrogen chloride scavenger. Thus, the reaction of furan with acryloyl chloride in the presence of a few drops of propylene oxide gave adducts in high yield by ^1H NMR measurement. Esterification of the product with absolute methanol followed by purification gave the endo and exo adducts in 76.5% overall yield *in high exo selectivity* (endo:exo= 3:7), in contrast to the former case. This is probably due to the thermodynamic stability of the exo adduct. The reaction with 2-methylfuran gave the known Michael adduct[6,7] and 2,5-dimethylfuran gave no adducts.

By these two methods Diels-Alder adducts of furan with methyl acrylate have become available in large quantity. Both endo and exo stereoisomers are readily separable by column chromatography; for the preparation of the endo-isomer the first procedure is preferred and the second one is convenient for the exo-isomer.

TABLE 1. DIELS-ALDER REACTION OF FURAN WITH METHYL ACRYLATE

Catalyst	Solvent	Temp °C	Time h	Yield %	endo/exo ratio
—[a]	CH_2Cl_2	27	4	62[b]	6 : 4
ZnI_2[c]	—	40	48	55	1 : 2
$Cu(BF_4)_2$–HQ[d]	—	RT	2 weeks	33	ND[e]
$BF_3 \cdot OEt_2$[f]	—	5	10	75.7	7 : 3
$BF_3 \cdot OEt_2$[f]	CCl_4	5	14	41	7 : 3
$TiCl_4$[f]	CCl_4[g]	−20[g]	8	50	7 : 3

a) Ref. 3b. b) At 15 kbar pressure. c) Ref. 4b. d) Ref. 4c. e) Not described. f) 0.1 equiv based on methyl acrylate. g) Without solvent or at 0 °C only polymerization has occurred.

Experimental

^{1}H NMR spectra were obtained on a JEOL MH-100 spectrometer and the IR spectra were recorded on a JASCO IRA-1. All reactions were carried out in the presence of a catalytic amount of hydroquinone (HQ) under N_2 atmosphere. Furan and methyl acrylate were freshly distilled prior to use. $BF_3 \cdot OEt_2$ was fractionally distilled from CaH_2. Acryloyl chloride was prepared from acrylic acid according to the literature[8] and was freshly distilled prior to use. Column chromatography was performed with Wakogel C-200. Merck's precoated silica-gel 60 F-254 plates (0.25 mm) were used for monitoring the reactions.

Evaporation of the excess reagents or solvents was performed *in vacuo* below 35 °C. All the products were identified by comparing their spectral data with those of authentic samples.

Methyl 7-Oxabicyclo[2.2.1]hept-5-ene-2-carboxylate. *A) With $BF_3 \cdot OEt_2$ Catalyst:* To a mixture of furan (24 g; 0.353 mol) and methyl acrylate (10 g; 0.116 mol) 1.5 ml of $BF_3 \cdot OEt_2$ was added *via* syringe at −20 °C with stirring. Thereafter, the reaction was allowed to proceed in the refrigerator (<5 °C) for 10 h. During the reaction, the solution color changed to pale yellow and a small amount of brown deposit formed. After evaporation of the excess reagents, the residue was poured into CH_2Cl_2 and washed successively with water, satd $NaHCO_3$, and satd NaCl, dried over $MgSO_4$, and concentrated. Purification of the oily product (14 g) by silica-gel column chromatography gave 9.86 g (55.1%) of endo-adduct and 3.69 g (20.6%) of exo-one. With hexane–AcOEt the endo-isomer was obtained from earlier fractions.

B) With Acryloyl Chloride: A mixture of furan (21.6 g; 0.32 mol), acryloyl chloride (10.2 g; 0.113 mol), and 3—4 drops of propylene oxide was stirred in the dark at room temperature for 48 h. After evaporation of the excess reagents, 15.6 g of the product was obtained as a dark yellow oil. The product was esterified conventionally with abs. MeOH (10 ml) using 3 equiv of pyridine at room temperature for 36 h and then quenched with ice-water. The excess MeOH was removed and the aqueous phase was extracted with AcOEt. The combined extracts were washed successively with water, 2M HCl (1 M=1 mol dm^{-3}), satd $NaHCO_3$, and satd NaCl, dried over $MgSO_4$, and concentrated. The yellowish product (14.16 g) was purified as above to afford 3.72 g (21.4%) of endo-adduct and 9.42 g (54.1%) of exo-one.

3-(5-Methyl-2-furyl)propanoyl Chloride. A mixture of 2-methylfuran (3 g; 37 mmol), acryloyl chloride (3 g; 33 mmol), and 2—3 drops of propylene oxide was stirred at room temperature for 24 h. Evaporation of the excess reagents gave an almost pure product (4.64 g; 81.5%), bp 95—100 °C/15 mmHg (lit,[7] 99 °C/15 mmHg; 1 mmHg=133.322 Pa).

The present work was partially supported by a Grant-in-Aid for Scientific Research from the Ministry of Education (No. 5874025).

References

1) See, for recent examples A. Zamoiski, A. Banoszek, and G. Grynkiewicz, *Adv. Carbohyd. Chem. Biochem.*, **40**, 74—80 (1982); R. R. Schmidt, C. Beitzke, and A. K. Forrest, *J. Chem. Soc., Chem. Commun.*, **1982**, 909; A. B. Holmes, C. L. D. Jennings-White, and D. A. Kendrick, *ibid.*, **1983**, 415; P. A. Grieco, R. E. Zelle, R. Lis, and J. Finn, *J. Am. Chem. Soc.*, **105**, 1403 (1983); T. Kitahara, K. Tanida, and K. Mori, *Agr. Biol. Chem.*, **47**, 581 (1983); L. A. Van Royen, R. Mijngheer, and P. J. De Clercq, *Tetrahedron Lett.*, **24**, 3145 (1983); M. M. Campbell, A. D. Kaye, and M. Sainsbury, *ibid.*, **24**, 4745 (1983).

2) R. M. Acheson, "An Introduction to the Chemistry of Heterocyclic Compounds," 3rd Ed, Wiley, New York (1976), p. 124.

3) a) H. Kotsuki and H. Nishizawa, *Heterocycles*, **16**, 1287 (1981); b) H. Kotsuki, H. Nishizawa, M. Ochi, and K. Matsuoka, *Bull. Chem. Soc. Jpn.*, **55**, 496 (1982).

4) a) E. Vieira and P. Vogel, *Helv. Chim. Acta*, **65**, 1700 (1982) and the references cited therein; b) F. Brion, *Tetrahedron Lett.*, **23**, 5299 (1982); c) J. A. Moore and E. M. Partain, III, *J. Org. Chem.*, **48**, 1105 (1983); d) E. Vieira and P. Vogel, *Helv. Chim. Acta*, **66**, 1865 (1983).

5) I. Fleming, "Frontier Orbitals and Organic Chemical Reactions," Wiley, New York (1976), p. 161.

6) T. A. Eggelte, H. de Koning, and H. O. Huisman, *Heterocycles*, **4**, 19 (1976).

7) V. G. Glukhovtsev and S. V. Zakharova, *Izv. Akad. Nauk SSSR, Ser. Khim.*, **1965**, 751 and 1096; *Chem. Abstr.*, **63**, 2944e and 8291e (1965).

8) C. E. Rehberg, M. B. Dixon, and C. H. Fisher, *J. Am. Chem. Soc.*, **67**, 208 (1945).

Preparation of Tetraalkylammonium *N*-Chloro-*p*-toluenesulfonamides and Their Application to Imination of Phosphorus Compounds and Sulfides

Tamotsu YAMAMOTO,* Daisaburo YOSHIDA, Jun HOJYO, and Hiranari TERAUCHI
Department of Industrial Chemistry, Faculty of Engineering, Kanto Gakuin University, Mutsuura, Kanazawa-ku, Yokohama 236
(Received April 5, 1984)

Synopsis. Tetraalkylammonium *N*-chloro-*p*-toluenesulfonamides were prepared from chloramine T and tetraalkylammonium chlorides as a substance corresponding to anhydrous chloramine T, and found to give rise to the effective tosylimination of phosphorus compounds and diaryl sulfides.

Chloramine T (sodium *N*-chloro-*p*-toluenesulfonamide **1**) is a useful reagent for tosylimination but commercially available as its trihydrate. In general the tosylimination is effectively accomplished using the trihydrate in water or alcohol containing water. With triphenyl phosphine, however, the trihydrate gives a phosphonium salt [$(Ph_3P^+\text{-}NHTs)_2NTs^{2-}$] in stead of the phosphine imide, while the anhydrous **1** gives the latter product.[1]

$$Ph_3P + \mathbf{1}(H_2O)_0 \longrightarrow Ph_3P{=}NTs$$

$$Ph_3P + \mathbf{1}(H_2O)_3 \longrightarrow (Ph_3P^+\text{-}NHTs)_2NTs^{2-}$$

$$Ts = p\text{-}CH_3C_6H_4SO_2$$

Furthermore, with the special sulfides, such as 2-haloethyl phenyl sulfides, the tosylimination using the anhydrous **1** has been known to give better result than that using the trihydrate.[2]

On the other hand, recently Sharpless *et al.* have developed a new use of the anhydrous chloramine T, allylic amination of olefins.[3]

As described above, the anhydrous chloramine T is very interesting. However, it is explosive and is not easily available. On the basis of the fact that most quaternary ammonium salts are anhydrous, we tried to prepare tetraalkylammonium *N*-chloro-*p*-toluenesulfonamides (**2**) and to apply to imination of phosphorus compounds and sulfides.

Results and Discussion

Preparation of Tetraalkylammonium N-Chloro-p-toluenesulfonamides (2). Initially tetrabutylammonium *N*-chloro-*p*-toluenesulfonamide (**2a**) was prepared by the ion-exchange reaction of chloramine T trihydrate with tetrabutylammonium halides (chloride and bromide) in water. For obtaining well crystallizable **2a**, the use of tetrabutylammonium chloride and an excess amount of **1** to the ammonium salt are required.

Similarly other tetraalkylammonium *N*-chloro-*p*-toluenesulfonamides (**2b—2e**) were prepared from the corresponding tetraalkylammonium chlorides and chloramine T trihydrate.

$$\mathbf{1}(H_2O)_3 + \underset{\mathbf{3}}{R^1{}_3R^2N^+X^-} \longrightarrow \underset{\mathbf{2}}{R^1{}_3R^2N^+N(Cl)\text{-}Ts^-}$$

X=Cl, Br

Although these ammonium salts **2** were obtained in solid state, the purification by recrystallization was unsuccessful. The structures of **2** were confirmed by IR and NMR spectra and determination of active chlorine. The results are given in Table 1.

To know the thermal stability of **2** their decomposition temperatures were measured by a thermal differential analyzer. As shown in Table 1, the compounds **2** have such high decomposition temperatures, but they gradually decompose even at room temperature and so the storing in a freezer is recommended.

Tosylimination of Phosphorus Compounds and Tosylimination of Phosphorus Compounds and Sulfides Using 2a. The reaction of **2a** with triphenylphosphine (**4a**) in dichloromethane was carried out at room temperature for 5 h to give *N*-(*p*-tolylsulfonyl)-*P,P,P*-triphenylphosphine imide (**5a**) in a 96% yield. This shows that **2a** can be used as an alternate to the anhydrous chloramine T. Similarly the reactions of **2a** with tributyl (**4b**) and triphenyl phosphites (**4c**) gave the corresponding phosphorimidates, (**5b**)[4] and (**5c**), in 91 and 96% yields, respectively.

$$\underset{\mathbf{4}}{R_3P} + \mathbf{2a} \xrightarrow{CH_2Cl_2} R_3P{=}NTs + n\text{-}Bu_4N^+Cl^-$$

5a: R=Ph, **b**: R=*n*-BuO, **c**: R=PhO

Table 1. Preparation of **2**[a]

	3		**2**				
	R^1	R^2	Mp θ_m/°C	Y/%[b]	Cl/%[c]	NMR($CDCl_3$): δ	T_d/°C[d]
a	*n*-C_4H_9	*n*-C_4H_9	74—76	99	7.85 (7.93)	1.00(bt 12H J=5 Hz), 1—2(m 16H) 2.36(s 3H), 3.20(bt 8H J=6 Hz), 7.24(d 2H J=8 Hz), 7.73 (d 2H J=8 Hz)	156
b	CH_3	*n*-$C_{12}H_{25}$	100—101	86	8.18 (8.18)	0.89(bt 3H J=5 Hz), 1—2(m 20H), 2.36(s 3H), 3.33(s 9H), 3.45(m 2H), 7.24(d 2H J=8 Hz), 7.73(d 2H J=8 Hz)	132
c	CH_3	*n*-$C_{16}H_{33}$	98—99	94	7.08 (7.25)	0.88(bt 3H J=5 Hz), 1—2(m 28H), 2.36(s 3H), 3.33(s 9H), 3.40(m 2H), 7.24(d 2H J=8 Hz), 7.73(d 2H J=8 Hz)	162
d	CH_3	*n*-$C_{18}H_{37}$	107—108	85	6.64 (6.85)	0.87(bt 3H J=5 Hz), 1—2(m 32H), 2.36(s 3H), 3.33(s 9H), 3.38(m 2H), 7.24(d 2H J=8 Hz), 7.73(d 2H J=8 Hz)	163
e	CH_3	$C_6H_5CH_2$	oil	83	9.92 (9.99)	2.36(s 3H), 3.15(s 9H), 4.71(s 2H), 7.24(d 2H J=8 Hz), 7.73(d 2H J=8 Hz), 7.3—7.7(bs 5H)	122

a) The molar ratios of reactants (**1**/**3**) were taken as follows: **1**/**3a**, **1**/**3b**, and **1**/**3e**=1.2, **1**/**3c**=1.6, and **1**/**3d**=1.8. b) The yields are based on **3**. c) Active chlorine content (parentheses show the calcd values). d) Decomposition temperature.

TABLE 2. *S*-TOSYLIMINATION OF SULFIDES **6** USING **2a** IN DICHLOROMETHANE

	6		Temp	Time	7		Method[a]
	R^1	R^2	°C	h	Mp θ_m/°C	Y/%	
a	$-(CH_2)_4-$		35—40	5	132—134	61	A
					(134—135)[b]	88	B
b	$C_6H_5CH_2$	$C_6H_5CH_2$	35—40	5	191—192	63	A
					(193)[c]	59	B
c	C_6H_5	C_6H_5	35—40	5	108—110	93	A
					(108—110)[b]	6	B
d	$4\text{-}CH_3C_6H_4$	$4\text{-}CH_3C_6H_4$	35—40	5	151—152	89	A
					(152—155)[d]	58	B
e	$4\text{-}ClC_6H_4$	$4\text{-}ClC_6H_4$	35—40	5	123—124	93	A
						22	B
						53	C
f	$4\text{-}CH_3C_6H_4$	$4\text{-}NO_2C_6H_4$	35—40	5	131—132	90	A
						0	B
						42	C
g	C_6H_5	$BrCH_2CH_2$	35—40	5	98—99	84	A
					(98—98.5)[e]	47[f]	B
						62[f]	D

a) A, B, C and D show the methods using **2a**, $1(H_2O)_3$ (in MeOH, 40 °C, 5 h), $1(H_2O)_3$ (presence of AcOH in MeOH, 40 °C, 5 h), and $1(H_2O)_0$ (in absolute EtOH), respectively. b) D. S. Tarbell *et al.*, *J. Am. Chem. Soc.*, **63**, 2939 (1941). c) F. G. Mann *et al.*, *J. Chem. Soc.*, **121**, 1052 (1922). d) I. W. J. Still, *et al.*, *Synthesis*, **1978**, 540. e) T. Yamamoto *et al.*, *Chem. Lett.*, **1975**, 581. f) From Ref. 2.

For the reactions of **2a** with sulfides (**6**), seven kinds of sulfides listed in Table 2 were chosen. The reactions were carried out at 35—40 °C for 5 h, the resulting mixture worked up in common way. The results together with those obtained in the reactions using chloramine T trihydrate in methanol with or without acetic acid, are given in Table 2. The yields of sulfilimines (**7**) using **2a** are almost independent of their structures.

$$\underset{\mathbf{6}}{R^1SR^2} + \mathbf{2a} \xrightarrow{CH_2Cl_2} R^1S(R^2)=NTs + n\text{-}Bu_4N^+Cl^- \quad \mathbf{7}$$

This is contrasted with hydrated chloramine T, the reactions of which with diaryl sulfides give the corresponding sulfilimines only in low yields. In addition the *S*-imination of 2-bromoethyl phenyl sulfide (**6g**) with **2a**, is more effective than that with anhydrous **1**.[5] The *S*-imination of diaryl sulfides using **2a** may be more effective than that using trihydrated **1** in the presence of acetic acid.[6] Such an effective tosylimination by **2a** may be brought *via* radical mechnism in which more active species (radical) than *N*-chloro-*p*-toluenesulfonamide[6] is included, since **2a** decolors the violet of *N,N*-diphenyl-*N'*-picryl hydrazyl and in the presence of H·donor (hydroquinone) does not give rise to the tosylimination of diaryl sulfides.

Experimental

All melting points are not corrected. The ^{1}H-NMR spectra were measured with a JEOL JNM-PMX60 spectrometer using TMS as the internal standard. The mass spectra were obtained on a JEOL JMS-D300 mass spectrometer with an ionizing potential of 70 ev. The decomposition temperatures were obtained with a Rigaku Denki E-1 thermal differential analyzer.

Preparation of Tetraalkylammonium N-*Chloro*-p-*toluenesulfonamides* (**2**). *General Procedure*: To a stirred solution of 12—18 mmol of **1** $(H_2O)_3$ in 20 ml of water was dropped 10 mmol of tetraalkylammonium chloride in 20 ml of water below 5 °C. After stirring below 5 °C for 5 h, the resulting mixture was extracted with CH_2Cl_2 and dried over anhydrous sodium sulfate. The dried solution was evaporated to dryness under vacuum to give **2**.

Tosylimination of Phosphorus Compounds Using **2a**. To a stirred solution of 3.3 mmol of **2a** in 15 ml of CH_2Cl_2 was added a solution of 3.0 mmol of phosphorus compound **4** in 15 ml of CH_2Cl_2. After the solution was stirred at 35—40 °C for 5 h, the resulting solution was washed with water and dried over anhydrous sodium sulfate. The dried solution was evaporated to dryness and the residue obtained was triturated or washed with ether. **5a**: Yield 96%; mp 186—188 °C (from EtOH)(187 °C);[1] IR (KBr): 1140 cm^{-1} (P=N). **5b**: Yield 91%; oil (after several washing with ether). IR (NaCl): 1310 and 1130 (SO_2), 1150 (P→N), and 1020 cm^{-1} (P-O-C), NMR ($CDCl_3$): δ=0.89 (t, 9H J=5 Hz), 1.0—1.9 (m 12H), 2.35 (s 3H), 4.05 (m 6H), 7.21 (d 2H J=8 Hz), and 7.79 (d 2H J=8 Hz). MS *m/z* (%): 419 (M^+ 11), 364 (28), 363 ($M^+-C_4H_8$ 90), and 251 (100). **5c**: Yield 96%; oil (after several washing with ether). IR (NaCl): 1270 and 1140 (SO_2), 1180 (P-O-C), and 1160 cm^{-1} (P=N). NMR ($CDCl_3$): δ=2.21 (s 3H), 7.06 (d 2H J=8 Hz), 7.64 (d 2H J=8 Hz), and 7.21 (broad s 15H). MS *m/z* (%): 479 (M^+ 19), 386 ($M^+-C_6H_5O$ 90), 385 ($M^+-C_6H_6O$ 95), and 325 (100).

Tosylimination of Sulfides. General Procedure: To a stirred solution of 3.3 mmol of **2a** in 15 ml of CH_2Cl_2 was added a solution of 3.0 mmol of sulfide **6** in 15 ml of CH_2Cl_2. After the solution was stirred at 35—40 °C for 5 h, the resulting solution was washed with water and dried over anhydrous sodium sulfate. The dried solution was evaporated to dryness and the residue obtained was triturated with ether. **7e**: Yield 93%; mp 123—124 °C (from MeOH). IR (KBr): 1290 and 1135 (SO_2), and 968 cm^{-1} (S=N). NMR ($CDCl_3$): δ=2.37 (s 3H), 7.24 (d 2H J=8 Hz), 7.2—7.7 (m 8H), and 7.73 (d 2H J=8 Hz). Found: C, 53.45; H, 3.56; N, 3.56%. Calcd for $C_{19}H_{15}Cl_2NO_2S_2$: C, 53.77; H, 3.57; N, 3.30%. **7f**: Yield 90%; mp 131—132 °C (from MeOH). IR (KBr): 1520 and 1342 (NO_2), 1298 and 1140 (SO_2), and 960 cm^{-1} (S=N), NMR ($CDCl_3$): δ=2.37 (s 6H), 7.13 (d 2H J=8 Hz), 7.24 (d 2H J=8 Hz), 7.52 (d 2H J=8 Hz), 7.69 (d 2H J=9 Hz), 7.78 (d 2H J=8 Hz), and 8.22 (d 2H J=9 Hz). Found: C, 57.78; H, 4.36; N, 6.66%. Calcd for $C_{20}H_{18}N_2O_4S_2$: C, 57.95; H, 4.39; N, 6.76%.

References

1) P. G. Mann and E. J. Chaplin, *J. Chem. Soc.*, **1937**, 527.
2) T. Yamamoto, M. Kakimoto, and M. Okawara, *Bull. Chem. Soc. Jpn.*, **52**, 841 (1979).
3) K. B. Sharpless, T. Hori, L. K. Truesdale, and C. O. Dietrich, *J. Am. Chem. Soc.*, **98**, 269 (1976).
4) A. V. Kirsanov and V. L. Shevchenko [*Zhur. Obshchei Khim.*, **24**, 1980 (1954)] obtained **5b** as oil from *P,P,P*-trichloro-*N*-(*p*-tolylsulfonyl)phosphine imide and butoxide.
5) T. Yamamoto and M. Okawara, *Chem. Lett.*, **1975**, 581.
6) K. Tsujihara, N. Furukawa, K. Oae, and S. Oae, *Bull. Chem. Soc. Jpn.*, **42**, 2631 (1969).

Photoreaction of *S*-Butyl 3-Methoxy-2-butenethioate. Competitive 1,5-Methyl Migration and *O*-Demethylation

Tadashi HASEGAWA,* Kazuhiko IWASAKI, and Nobutoshi YOSHIHARA
Department of Chemistry, Tokyo Gakugei University, Nukuikitamachi, Koganeishi, Tokyo 184
(Received April 12, 1984)

Synopsis. Irradiation of *S*-butyl (*Z*)-3-methoxy-2-butenethioate (**1Z**) gave the 1,5-methyl migration product **2** and the *O*-demethylation product **3**. The photo-1,5-methyl migration occured competitively with the *O*-demethylation from the π, π^* excited triplet state of **1Z**. The migration product **2** underwent the secondary photoreaction to **3** in a nondegassed benzene solution.

Recently we reported the photoreaction of *S*-alkyl 3-oxobutanethioates to the corresponding disulfides.[1] The photoreaction occurred only from the keto form though the 3-oxobutanethioates exhibit keto-enol tautomerism. Irradiation of a model compound for the enol form, *S*-butyl (*Z*)-3-methoxy-2-butenethioate (**1Z**), under nitrogen gave no disulfides but an *O*-demethylated product. Although the photoreactions of enol esters have been well studied,[2] those of enol ethers have received only little attention.[3] We investigated the further details of the enol ether **1Z** and found thst **1Z** underwent the unusual 1,5-methly migration competing with the *O*-demethylation. The migration was followed by the secondary photoreaction in the presence of dissolved oxygen. In this paper we will descrive these results of the photoreaction of **1Z**.

Irradiation of a degassed benzene solution of **1Z** in a sealed Pyrex tube with a 450 W high-pressure mercury lamp gave 4-butylthio-4-methoxy-3-butene-2-one (**2**) and *S*-butyl 3-oxobutanethioate (**3**) in 65 and 25% yield, respectively.[4] The structure of **2** was elucidated by spectral data and by elemental analysis. The IR spectrum of **2** showed the characteristic absorption of α,β-unsaturated carbonyl at 1680 cm^{-1}. The ^1H NMR spectrum of **2** showed two singlets at δ 2.28 and 3.64, attributable to the acetyl and the methoxyl group, respectively. The peak at δ 3.64 underwent large upfield shift in benzene-d_6 and was observed at δ 2.94. The ^1H NMR spectra of α,β-unsatulated compounds undrego large chaneges when these substances are dissolved in aromatic solvents.[5] The solvent effect of **2** can be explained in terms of the diamagnetic anisotropy of the aromatic nucleus in the intermolecular complex between the α,β-unsatulated carbonyl compounds and the aromatic solvent. The ^{13}C NMR spectrum of **2** showed a doublet at δ 99.3 and singlets at δ 169.9 and 187.8 attributable to α-, β-, and carbonyl carbon, respectively. These results supported the structure of **2**.

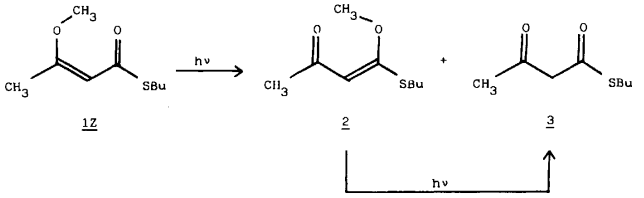

The photochemical reaction of **1Z** was pursured by quantitative analysis of the products and the starting material. The time-conversion curves are given in Figs 1 and 2. Since no quantitative measurement was taken of the intensity of the light for irradiation and absorption of the light by the enol form of the product 3-oxobutanethioate **3**, only the relative reactivity will be discussed here. Figure 1 shows that both the compound **2** and **3** were formed even at low conversion percentage of **1Z**. The figure also shows that the amount of **2** and **3** were nearly constant after the staring material had completly disappaered. Therefore, the migration from **1Z** to **2** competes with the demethylation to **3**. The formation of both **2** and **3** from **1Z** were efficiently and equally quenched with 1,3-pentadiene and sensitized with *p*-methoxy acetophenone, so that both **2** and **3** formations take place from the same triplet state of **1Z**.

The ratio of photoproduct **2** to **3** was strongly affected by the irradiation conditions. Figure 2 shows that compound **2** converts to compound **3** by prolonged

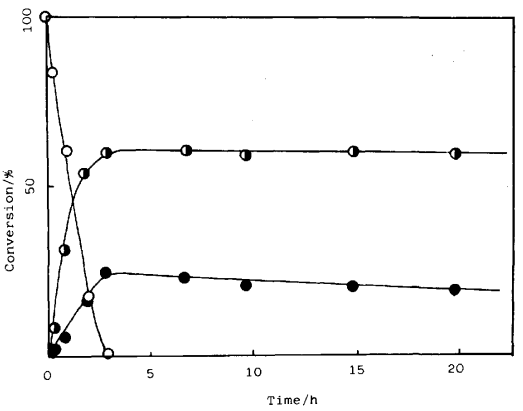

Fig. 1. Time-conversion curves for the photochemical reaction of **1Z** in degassed benzene-d_6
—○—: 1Z, —◑—: 2, —●—: 3.

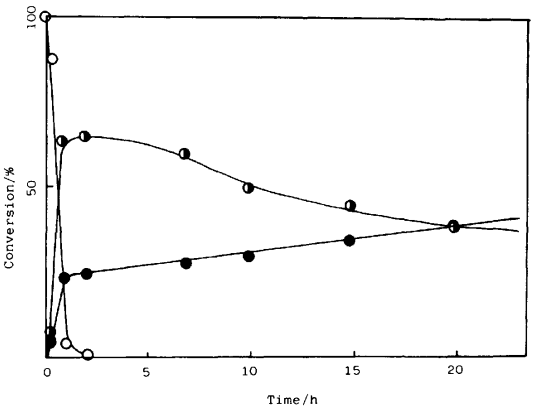

Fig. 2. Time-conversion curves for the photochemical reaction of **1Z** in nondegassed benzene-d_6
—○—: 1Z, —◑—: 2, —●—: 3.

iradiation in a nondegassed benzene solution. Dissolved oxyen might causes the transformation of **2** to **3**. The Figure also shows that the rate of disappearance of the starting compound **1Z** is enhanced in the nondegased benzene. Ethyl bromide also accelerated the photoreaction of **1Z** and the secondary photoreaction of **2**. The compounds containing heavy atoms enhance the rate of π,π^* S→T* intersystem crossing, and no heavy-atom enhancement of the rate of intersystem crossing takes place in the n,π^* excited state of ketones.[6] The external heavy atom effects on photoreactions of **1Z** and **2** suggest both the primary and the secondary photoreaction proceed from the π,π^* excited triplet state. Dissolved oxygen in solution probably operates through the catalysed intersystem crossing.[7]

The formation of **3** can be explained in terms of homolytic carbonoxygen bond cleavage from the π,π^* excited triplet state of **1Z**. Biphenyl could be detected by GLC analysis of a reaction mixture of a degassed benzene solution of **1Z**. This result supports the above mechanism for the formation of **3**. The formation of the methyl migration product **2** may be explained in terms of either the concerted 1,5-sigmatropic reaction or the nonconcerted radical rearrangement. Although the 1,5-sigmatropic reactions with inversion at the migration center are photochemically allowed,[8] the reactions in general do not take place from the $^3\pi,\pi^*$ states.[9] Therefore, the nonconcerted radicalrearrangement seems to be probable for the mechanism of the 1,5-methyl migration of **1Z**.

Irradiation of a benzene solution of the *E*-isomer 1E gave the *O*-demethylated product **3** in 58% yield.[10] No methyl migration products could be detected. Abcence of the methyl migration products in photolysis of the *E*-isomer seems to be explained in terms of the principle of least motion.[11] The distance separating the methoxyl and the carbonyl group should be larger in the *E*-isomer than in the *Z*-isomer. Therefore, the 1,5-methyl migration occurs easily in the case of the *Z*-isomer. The cage radical pair from the *E*-isomer seems to diffuse to free radicals.

Experimental

The IR spectra were recorded on a JASCO A-3 spectrometer. The UV spectra were taken on a JASCO HUN-790 spectrometer. The ^{1}H and the ^{13}C NMR spectra were measued on a JEOL FX-90Q spectrometer using TMS as an internal standard. Irradiation was carried out with an Ushio 450 W high-pressure mercury lamp.

Chemicals. The butenethioate **1Z** and **1E** were prepared by treatment of the 3-oxobutanethioate **3** with diazomethane in the usual way.[12] The *E*- and *Z*-configuration were deduced by ^{1}H NMR spectroscopic data.[13]

S-Butyl (E)-3-Methoxy-2-butenethioate (1E): Mp 44.6—45 °C; IR (KBr) 1430, 1510, 1660 cm^{-1}; UV λ_{max}^{EtOH} 293 nm (ε 6360); ^{1}H NMR ($CDCl_3$) δ=0.91 (3H, t, CH_3), 1.1—1.8 (4H, m, CH_2), 2.14 (3H, s, CH_3), 2.82 (2H, t, SCH_2), 3.83 (3H, s, OCH_3), 5.68 (1H, s, olefinic); ^{13}C NMR ($CDCl_3$) δ= 13.6 (q), 22.0 (t), 28.3 (t), 30.5 (q), 31.7 (t), 58.2 (q), 97.7 (d), 173.8 (s), 194.3 (s); Found: C, 57.23; H, 8.64%. Calcd for $C_9H_{16}O_2S$: C, 57.41; H, 8.65%.

S-Buthyl (Z)-3-Methoxy-2-butenethioate (1Z): Mp 41.5—42 °C; IR (KBr) 1380, 1600, 1660 cm^{-1}; UV λ_{max}^{EtOH} 273 nm (ε 6960); ^{1}H NMR ($CDCl_3$) δ=0.91 (3H, t, CH_3), 1.1—1.8 (4H, m, CH_2), 2.01 (3H, s, CH_3), 2.86 (2H, t, SCH_2), 3.85 (3H, s, OCH_3), 5.24 (1H, s, olefinic); ^{13}C NMR ($CDCl_3$) δ= 13.7 (q), 18.7 (q), 22.1 (t), 28.0 (t), 32.0 (t), 56.2 (q), 105.1 (d), 165.1 (s), 186.1 (s); Found: C, 57.24; H, 8.60%. Calcd for $C_9H_{16}O_2S$: C, 57.41; 8.65%.

Preparative Irradiation of 1Z. A solution of **1Z** (300 mg, 1.60 mmol) in benzene (5 cm^3) was placed in a 15×150 mm Pyrex culture tube. The solution was degassed by three freeze-pump-thaw cycles, sealed and irradiated for 2 h with a high-pressure mercury lamp. After removal of the solvent, the residual oil was chromatographed on silica gel. Elution with benzene–ethyl acetate (4:1) gave **2** (195 mg, 65%) and **3** (70 mg, 25%). **2**: bp 220 °C/10 Torr (1 Torr≈ 133.322 Pa); IR (neat) 1680 cm^{-1}; UV λ_{max}^{EtOH} 263 nm (ε 5360); ^{1}H NMR ($CDCl_3$) δ=0.92 (3H, t, CH_3), *ca.* 1.2—1.8 (4H, m, CH_2), 2.28 (3H, s, CH_3CO), 2.88 (2H, t, SCH_2), 3.64 (3H, s, OCH_3), 5.39 (1H, s, olefinic); ^{1}H NMR (C_6D_6) δ=0.81 (3H, t, CH_3), *ca.* 1.1—1.7 (4H, m, CH_2), 2.28 (3H, s, CH_3CO), 2.88 (3H, s, OCH_3), 2.94 (2H, t, SCH_2), 5.26 (1H, s, olefinic); ^{13}C NMR ($CDCl_3$) δ=13.7 (q), 19.7 (q), 22.1 (t), 28.4 (t), 32.2 (t), 55.4 (q), 99.3 (d), 169.9 (s), 187.8 (s); Found: C, 57.51; H, 8.61%. Calcd for $C_9H_{16}O_2S$: C, 57.41; H, 8.56%.

Preparative Iradiation of 1E. A solution of **1E** (12 mg, 0.65 mmol) in benzene (5 cm^3) was irradiated for 10 h with a high-pressure mercury lamp. The usual work-up gave the unreacted **1E** (62 mg) and **3** (32 mg, 58%).

Quantitative Analysis of Photoreaction of 1Z. A degassed/nondegassed benzene-d_6 solution of **1Z** (0.30 mol/L) in a sealed NMR tube was irradiated. The amounts of **1Z**, **2**, and **3** were determined by ^{1}H NMR spectroscopy.

References

1) T. Hasegawa, T. Shimizu, K. Iwasaki, and S. Oguchi, *Bull. Chem. Soc. Jpn.*, **56**, 1869 (1983).
2) M. Gorodetsky and Y. Mazur, *Tetrahedron*, **22**, 3607 (1966) and the references cited therein.
3) Y. Izawa and Y. Ogata, *J. Org. Chem.*, **35**, 3192, (1970).
4) We could not obtain the migration product **2** when a dilute benzene solution of **1Z** was irradiated under nitrogen. Ref. 1.
5) J. V. Hatton and R. E. Richards, *Mol. Phys.*, **5**, 153 (1962); C. J. Timmons, *J. Chem. Soc., Chem. Commun.*, **1965**, 576.
6) P. J. Wagner, *J. Chem. Phys.*, **45**, 2335 (1966).
7) J. A. Bartrop and J. D. Coyle, "Excited States in Organic Chemistry," John Wiley & Sons, New York (1978) p.116.
8) R. B. Woodward and R. Hoffmann, "The Conservation of Orbital Symmetry," Academic Press Inc. (1970) p. 118.
9) N. J. Turo, "Modern Molecular Photochemistry," Benjamin/Cummings Publishing Co., Menlo Park (1978) p. 485.
10) Under degassed conditions the photoreaction did not take place.
11) O. S. Tee, *J. Am. Chem. Soc.*, **91**, 7144 (1969).
12) V. Pechmann, *Chem. Ber.*, **28**, 1627 (1895).
13) M. Akino, I. Hori, and H. Midorikawa, *Sci. Pap. Inst. Phys. Chem. Res.*, **62**, 127 (1968).

Reaction of Allene with Water Catalyzed by Palladium(0) in the Presence of Carbon Dioxide

Yoshio INOUE,* Yukihiro OHTSUKA, and Harukichi HASHIMOTO
Department of Applied Chemistry, Faculty of Engineering, Tohoko University, Aoba Aramaki Sendai 980
(Received April 14, 1984)

Synopsis. A novel reaction involving allene and water took place using palladium(0)-triphenylphosphine as a catalyst in the presence of carbon dioxide to yield 3-methyl-2-methylene-3-buten-1-ol, selectively. A related reaction of allene with methanol or ethanol was found to occur without carbon dioxide.

It has been reported that the dimerization of allene by palladium catalysts involves the incorporation of nucleophiles. The reaction produces functionalized 2,3-dialkyl-1,3-butadiene derivatives. The nucleophiles used so far has been carboxylic acids,[1] amines,[2] and active methylene compounds.[2] Triethylsilane also adds to allene to form triethylallylsilane.[2] In connection with the reaction of 1,3-diene with water,[3] we have studied the reaction of allene with water in the presence of palladium(0) catalysts and have found that a novel reaction took place under a carbon dioxide (CO_2) atmosphere to yield 3-methyl-2-methylene-3-buten-1-ol (**1**). The effect of CO_2 on the reaction of 1,3-butadiene with water has also been reported.[4] The related reaction of allene with alcohols, such as methanol and ethanol, was found to occur in the absence of CO_2. In this paper we describe the scope of the reaction.

Results and Discussion

It is possible to react allene with water in the presence of $Pd(dba)_2$–triphenylphosphine [dba=dibenzylideneacetone] (the catalyst) under a certain pressure of CO_2 to give 3-methyl-2-methylene-3-buten-1-ol (**1**). Allene oligomers were also formed in small amounts as by-products. Without CO_2 the reaction was very sluggish and gave only a trace amount of **1**.

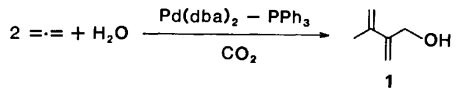

1

Results are shown in Table 1. Generally ethers, such as tetrahydrofuran (THF) and 1,4-dioxane, were suitable as the solvent for the formation of **1**, except diethyl ether. Among them, THF was the best with respect to yield and selectivity toward **1**. Employment of a large excess of water (water/allene=10) did not give rise to **1**.

A reaction temperature of 80—90 °C and a reaction time of 1 h were the most suitable conditions. Longer reaction times caused a decrease in the yield, indicating that the product underwent further reaction.

The effect of the molar ratio $PPh_3/Pd(dba)_2$ on the reaction was investigated. The best result was obtained at a P/Pd ratio of 3 with 63% yield and 93% selectivity toward **1** at 80 °C in THF. A further addition of phosphine (P/Pd=4) led to a pronounced reduction of **1** (yield only 5%). When a molar ratio P/Pd=1 was used, a solvent-insoluble allene-polymer was formed at the expense of **1** (yield of **1**, 25%). The IR spectrum of the allene-polymer showed peaks at 1630, 1420, and 890 cm^{-1} indicating its structure as $[-CH_2C(=CH_2)-]_n$.[5]

The effect of diphosphines of the structure $Ph_2P(CH_2)_nPPh_2$ (n=1, 2, 3, 4, 6, 10, 12) was also examined under standard reaction conditions (diphosphine/Pd=1, THF, 80 °C, 1 h). Generally, these diphosphines retarded the formation rate of **1** (yield< 23%), especially with n=2 and 3, the reaction stopped. These observations may be explained by the chelating

Table 1. Reaction of allene with water[a]

Solvent	PPh_3/Pd	Reaction		Yield of **1**[b]/%	Selectivity[c] %
		Temp/°C	Time/h		
Acetone	2	80	0.5	10	71
		80	1	26	74
		80	2	21	62
		80	4	16	71
THF	2	60	1	13	71
		80	1	58	93
		100	1	57	87
		120	1	42	90
	3	60	1	12	98
		80	1	63	93
		90	1	61	93
		100	1	35	97
1,4-Dioxane	2	80	1	40	67
Diethyl ether	2	80	1	6	75
Diglyme[d]	2	80	1	44	59
Acetonitrile	2	80	1	10	50
t-Butyl alcohol	2	80	1	10	50

a) Allene (1.0 g, 24.9 mmol) in most cases. $Pd(dba)_2$(0.5 mmol), H_2O(50 mmol), solvent(10 cm^3), CO_2(10 atm). b) Based on allene charged. c) Apparent selectivity based on the area ratio in the glc chart. d) $(CH_3OCH_2CH_2)_2O$.

effect of the diphosphine ligands. They occupy coordination sites of the metal and prevent allene from occupying sufficient coordination sites for the reaction.

The introduction of CO_2 changes the acidity of the medium. Thus, further studies examined the effects of acids and bases. The addition of an acid such as $BF_3 \cdot OEt_2$ (10 equiv with respect to Pd) or trifluoroacetic acid (1.5 equiv) inhibited the formation of alcohol **1**. The formation of **1** was also inhibited by $NaHCO_3$ (2 equiv with respect to Pd) or NaOH (10 equiv). Interestingly, the catalytic activity was restored by the introduction of CO_2 in the case of $NaHCO_3$. The effect of CO_2 was characteristic.

Apparently hydrogen in the water was incorporated into the C_6 moiety of dienol **1**. ^1H NMR analysis clearly showed that a deuterium migrated into the methyl group of product **1** obtained from the experiment employing D_2O. However the reaction mechanism

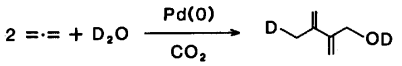

cannot be easily delineated by this observation alone, because such an incorporation of hydrogen may occur *via* a variety of mechanisms including the bis(σ-allyl)palladium intermediate.[2] At present we hesitate to propose a conclusive mechanism.

Unlike the allene–water reaction, the related reaction of allene with alcohol took place in the absence of CO_2. The product was 4-alkoxy-2-methyl-3-methylene-1-butene (**2**). The results are summarized in Table 2. The introduction of CO_2 led to a decreased formation of **2**,

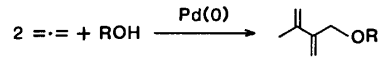

2a R=Me
b R=Et

contrary to the case of water. The reaction was markedly effected by the molecular weight of the alcohol employed. Thus, methanol gave rise to a higher yield of **2a**, whereas 1-butanol gave this product only in trace amounts. Since there is only a little difference in the acidity constant among the alcohols used, steric factors may be responsible for such an effect.

Table 2. Reaction of allene with alcohol[a]

Alcohol cm³		Solvent cm³	Yield[b] %	Selectivity[c] %
MeOH	10	—	**2a** 9	100
	5	THF 5	40	96
	5	C_6H_6 5	29	100
	5	THF 5	11[d]	100
	5	THF 5	1[e]	26
	5	THF 5	25[f]	94
EtOH	5	THF 5	**2b** 16	84
n-BuOH	5	THF 5	trace	—

a) Allene(1.0 g, 24.9 mmol) in most cases. $Pd(dba)_2$ (0.5 mmol), PPh_3(1.0 mmol); 100 °C, 2 h. b) Based on allene charged. c) Apparent selectivity based on the area ratio in the glc chart. d) Under CO_2 pressure (10 atm). e) CH_3ONa(5.0 mmol) was added. f) Under CO_2 pressure(10 atm) in the presence of CH_3ONa(5.0 mmol).

Experimental

Reaction of Allene with Water. Typically, allene (1.0 g, 24.9 mol) was allowed to react with H_2O (50 mmol) in THF (10 cm³) in the presence of $Pd(dba)_2$ (0.5 mmol) and PPh_3 (1.0 mmol) at 80 °C for 1 h under CO_2 pressure (10 atm) in an autoclave. After the reaction, the mixture was filtered to remove allene polymers, if any. The filtrate was analyzed by glc; Silicone GE SE-52, 90 °C.

Isolation of 3-Methyl-2-methylene-3-buten-1-ol (1). The products of several experiments were combined. The solvent (THF) was removed by distillation under a reduced pressure at room temperature. The residue was subjected to flash-distillation under reduced pressure. The distillate consisted of organic and water layers. Glc analysis showed that the organic layer contained dienol **1** with a purity of ≈93% (area ratio). This organic sample yielded the following data: IR (neat) 3300, 1600, 1440, 1380, 1040, and 890 cm^{-1}. ^1H NMR ($CDCl_3$) δ=1.62 (s, 1H), 1.94 (s, 3H), 4.36 (s, 2H), 5.08 (m, 2H), and 5.23 (m, 2H). ^{13}C NMR ($CDCl_3$) δ=21.05 (q), 63.88 (t), 112.52 (t), 112.66 (t), 140.78 (s), and 145.60 (s). MS (20 V) *m/z* 98 (M^+), 79, 69, and 55.

Reaction of Allene with Deuterium Oxide. This reaction was carried out in a manner similar to that described for the reaction of water with allene (1.0 g, 24.9 mmol), $Pd(dba)_2$ (0.5 mmol), PPh_3 (1.0 mmol), and D_2O (0.9 cm³) in THF (10 cm³) under CO_2 pressure (10 atm) at 80 °C for 1 h. Isolation by flash-distillation gave 0.27 g (22%) of the deuterated dienol in 95% purity. ^1H NMR analysis revealed that the incorporation of deuterium was exclusively on the methyl carbon, δ=1.95 (br. s, ≈2H).

Reaction of Allene with Methanol and Ethanol. The reaction was performed in a manner similar to that described above for the corresponding reaction of water employing allene (1.0 g, 24.9 mmol), $Pd(dba)_2$ (0.5 mmol), PPh_3 (1.0 mmol), and methanol (or ethanol) (5 cm³) in THF (5 cm³) at 100 °C for 2 h. The product analysis was carried out by glc.

Isolation of 4-Methoxy-2-methyl-3-methylene-1-butene (2a) and 4-Ethoxy-2-methyl-3-methylene-1-butene (2b). Most of the THF was removed by distillation under reduced pressure. The flash-distillation of the residue gave a mixture of **2a** and methanol (or **2b** and ethanol). A pure product was obtained by preparative glc. **2a**: IR (CCl_4) 1595, 1085, and 890 cm^{-1}. ^1H NMR ($CDCl_3$) δ=1.90 (s, 3H), 3.31 (s, 3H), 4.10 (s, 2H), 5.00 and 5.10 (m, 2H), and 5.20 (s, 2H). MS (20 V) *m/z* 112 (M^+), 97, 82, 79, and 67. **2b**: IR (CCl_4) 1590, 1090, and 890 cm^{-1}. ^1H NMR ($CDCl_3$) δ=1.21 (t, 3H), 1.92 (s, 3H), 3.50 (q, 2H), 4.16 (s, 2H), 5.00 and 5.10 (m, 2H), and 5.22 (s, 2H).

References

1) G. D. Shier, *J. Organomet. Chem.*, **10**, 15 (1967).
2) D. R. Coulson, *J. Org. Chem.*, **38**, 1483 (1973).
3) Y. Inoue, M. Sato, M. Satake, and H. Hashimoto, *Bull. Chem. Soc. Jpn.*, **56**, 637 (1983).
4) K. E. Atkins, W. E. Walker, and R. M. Manyik, *J. Chem. Soc., Chem. Commun.*, **1971**, 330.
5) S. Otsuka, K. Mori, and F. Imaizumi, *J. Am. Chem. Soc.*, **87**, 3017 (1965).

Efficient Preparation of 3-Alkyl(or Aryl)thio-1(or 2)-propenyl *p*-Tolyl Sulfones

Katsuyuki OGURA,* Teruyuki IIHAMA, Kazumasa TAKAHASHI, and Hirotada IIDA
Department of Synthetic Chemistry, Faculty of Engineering, Chiba University, Yayoicho 1-33, Chiba 260
(Received April 27, 1984)

Synopsis. Synthetic routes from 3-chloro-1-propenyl *p*-tolyl sulfone to 3-(*p*-tolylthio)-1(or 2)-propenyl *p*-tolyl sulfone, 3-isopropylthio-1(or 2)-propenyl *p*-tolyl sulfone, and 3-methylthio-2-propenyl *p*-tolyl sulfone were exploited.

In connection with 1,3-bis(methylthio)-2-propenyllithium, an synthetic equivalent of 2-formylethenyl carbanion,[1] our attention was focused on the utilization of 3-alkyl(or aryl)thio-1(or 2)-propenyl *p*-tolyl sulfone (**1** or **2**) as a new type of synthetic reagent.[2] Since these compounds (**1** and **2**) were unknown in the literature,[3] an effective method for the preparation of **1** and **2** first had to be secured in order to accomplish organic syntheses utilizing them. Hence, we chose (*E*)-3-chloro-1-propenyl *p*-tolyl sulfone (**3**)[4] as a starting material.

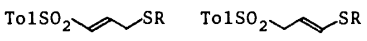

1 **2**

a: R = Tol b: R = i-Pr c: R = CH_3

[Tol = p-tolyl]

In the reaction of **3** with a thiolate anion, displacement of chlorine atom by alkyl(or aryl)thio group and the Michael-type addition of a thiol (**4**) to the C–C double bond of **3** are anticipated to take place. Furthermore, migration of the C–C double bond of the displacement product (**1**) must be taken into consideration.[5,6] As is apparent from Table 1, the ratio of the products depended on the employed solvent and reaction time. In the reaction of **3** with **4a** and K_2CO_3 in DMF or CH_3CN, the displacement product (**1a**) was predominantly formed at the first stage, but the proportion of **2a** increased as the reaction proceeded. In contrast, the employment of THF as a solvent afforded **1a** in 90% yield even after a prolonged reaction time. This is probably because the solubility of K_2CO_3 in THF is too low to catalyze the migration of the C–C double in **1a**.

Compared with **4a**, **4b** produced a significant amount of the Michael-type adduct (**5b**) as shown in Table 1. Especially, the yield of **5b** was 70% in the reaction conducted in THF. Scheme 2 shows the whole

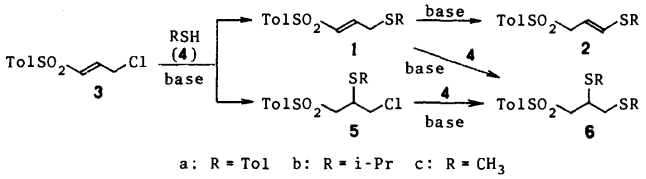

a: R = Tol b: R = i-Pr c: R = CH_3

Scheme 1.

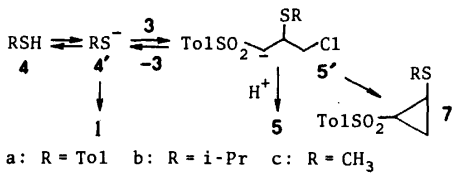

a: R = Tol b: R = i-Pr c: R = CH_3

Scheme 2.

sequence for the conversion of **3** to **1** and **5**, where a thiolate anion (**4'**) is in equilibrium with **4** and **4'** reacts reversibly with **3** to form the carbanion (**5'**) of **5**. The reaction of **3** with lithium 2-propanethiolate in THF resulted in the exclusive formation of a cyclopropane derivative (**7b**) through an intramolecular cyclization of the intermediary carbanion (**5'b**). This fact suggests that the displacement reaction leading to **1** is relatively slow and **5'** is indeed produced under the present reaction conditions. Since **4b** is a relatively weak acid, the most part of the employed **4b** might remain unchanged to serve as a proton source. The insolubility of K_2CO_3 in THF seems to increase the population of **4b** to cause the rapid protonation of **5'b** resulting in the predominant formation of **5b**. We tried to facilitate the displacement reaction by utilizing of 3-iodo-1-propenyl *p*-tolyl sulfone (**8**). The starting material (**8**) was easily obtained on treatment of **3** with KI in refluxing acetone. In fact, when **8** was subjected to the reaction with **4b** (1.0 mol-equiv) and $NaHCO_3$ (1.0 mol-equiv) in DMF at room temperature, **1b** was cleanly produced in 82% yield.

In the reaction of **3** with **4c**, a commercially available 15% aqueous solution of sodium methanethiolate could be used as a source of methanethiolate

Table 1. Reaction of **3** with a thiol (**4**) and K_2CO_3[a]

R (equiv)	K_2CO_3[b]	Solvent	Time	Yield/%			
				1[c]	2(Z : E)[d]	5	6
Tol (2.0)	2.0	DMF	5 min[e]	77	—	7	—
Tol (2.0)	4.0	DMF	30 min	—	92 (43 : 57)	—	7
Tol (2.0)	2.0	CH_3CN	30 min	93	—	—	—
Tol (2.0)	2.0	CH_3CN	10 h	—	99 (63 : 37)	—	—
Tol (2.0)	2.0	THF	24 h	90	—	—	—
i-Pr (1.0)	2.0	DMF	20 min	50	10 (60 : 40)	29	—
i-Pr (1.0)	1.5	DMF	72 h	—	64 (54 : 46)	29	—
i-Pr (1.0)	1.2	CH_3CN	48 h	—	38 (63 : 37)	45	2
i-Pr (1.0)	2.0	THF	48 h	9	12 (60 : 40)	70	—

a) At room temperature. b) Mol-equiv to **3**. c) (*E*)-isomer. d) The value in the parenthesis is the ratio of the (*Z*)- and (*E*)-geometrical isomers (by ^1H NMR analysis). e) **3** was recovered in 15% yield.

anion to give **2c** as the only isolable product, but its yield was relatively low (72% in DMF, 38% in CH_3CN, and 46% in methanol). Hence, the Schneider's method[7] was applied to the preparation of **1c** or **2c**. Thus, a 1:10 mixture of **3** and dimethyl sulfide was stirred at room temperature for 4 d, but no reaction occurred. In contrast, the addition of KI (3 equiv) accelerated the reaction to form a 42:58 mixture of **1c** and **2c**. The complete conversion of this mixture to **2c** was readily achieved by treatment with K_2CO_3 in CH_3CN at room temperature. The overall yield of **2c** from **3** was 92%.

Experimental

Reaction of **3** with p-*Toluenethiol* (**4a**). *A Typical Procedure.* To a solution of **4a** (126 mg: 1.01 mmol) in CH_3CN (10 ml) were added K_2CO_3 (137 mg: 1.01 mmol) and **3**[4] (231 mg: 1.00 mmol), and the resulting mixture was stirred at room temperature for 10 h under an atmosphere of nitrogen. Then, saturated aqueous NH_4Cl (30 ml) was added and the mixture was extracted with CH_2Cl_2 (3× 40 ml). The extracts were combined, washed with water, and dried (Na_2SO_4). After evaporating the solvent, the residual yellow solid was subjected to column chromatography on silica gel [hexane–benzene(2:1)] to give 3-(*p*-tolylthio)-2-propenyl *p*-tolyl sulfone (**2a**) (317 mg; 99% yield) as a mixture of two geometrical isomers (*Z*:*E*=63:37). The (*Z*)-isomer was obtained in a pure form by recrystallization from EtOH. (*Z*)-**2a**: colorless crystals; mp 78—79 °C; IR (KBr) 1605, 1595, 1290, 1124 cm^{-1}; ^1H NMR ($CDCl_3$) δ=2.29 (3H, s), 2.42 (3H, s), 4.01 (2H, d, *J*=8 Hz), 5.69 (1H, dt, *J*=10, 8 Hz), 6.45 (1H, d, *J*=10 Hz), 7.00 (4H, s), 7.30 (2H, d, *J*=8 Hz), 7.80 (2H, d, *J*=8 Hz). Anal. ($C_{17}H_{18}O_2S_2$) C, H. The (*E*)-isomer of **2a** was isolated by recrystallization of a mixture of two geometrical isomers (*Z*:*E*=43:57) given in the reaction of **3** with **4a** in DMF. (*E*)-**2a**: colorless crystals; mp 109—110 °C (from EtOH); IR (KBr) 1603, 1598, 1302, 1129 cm^{-1}; ^1H NMR ($CDCl_3$) δ= 2.33 (3H, s), 2.46 (3H, s), 3.78 (2H, d, *J*=7.4 Hz), 5.54 (1H, dt, *J*=15.5, 7.4 Hz), 6.18 (1H, d, *J*=15.5 Hz), 7.0—7.45 (6H, m), 7.72 (2H, d, *J*=7.5 Hz). Anal.($C_{17}H_{18}O_2S_2$) C, H.

1a: colorless crystals; mp 77—78 °C (from EtOH); ^1H NMR ($CDCl_3$) δ=2.25 (3H, s), 2.44 (3H, s), 3.51 (2H, d, *J*=7 Hz), 6.14 (1H, d, *J*=15 Hz), 6.88 (1H, dt, *J*=15, 7 Hz), 6.97 (2H, d, *J*=7 Hz), 7.14 (2H, d, *J*=7 Hz), 7.31 (2H, d, *J*=7.2 Hz), 7.60 (2H, d, *J*=7.2 Hz). Anal.($C_{17}H_{18}O_2S_2$) C, H. **1b**: colorless crystals; mp 36—38 °C; ^1H NMR ($CDCl_3$) δ=1.24 (6H, d, *J*=6.5 Hz), 2.45 (3H, s), 2.72 (1H, septet, *J*=6.5 Hz), 3.23 (2H, d, *J*=6 Hz), 6.35 (1H, d, *J*=14.4 Hz), 6.77 (1H, dt, *J*= 14.4, 6 Hz), 7.30 (2H, d, *J*=8 Hz), and 7.70 (2H, d, *J*=8 Hz). Anal.($C_{13}H_{18}O_2S_2$) C, H. (*E*)-**2b**: colorless crystals; mp 75.5—76.5 °C; ^1H NMR ($CDCl_3$) δ=1.20 (6H, d, *J*=7.2 Hz), 2.40 (3H, s), 3.05 (1H, septet, *J*=7.2 Hz), 3.77 (2H, d, *J*=7.2 Hz), 5.49 (1H, dt, *J*=16.2, 7.2 Hz), 6.09 (1H, d, *J*=16.2 Hz), 7.35 (2H, d, *J*=8.5 Hz), 7.72 (2H, d, *J*=8.5 Hz). Anal.($C_{13}H_{18}O_2S_2$) C, H. (*Z*)-**2b**: colorless crystals; mp 60.5—61.5 °C; ^1H NMR ($CDCl_3$) δ=1.17 (6H, d, *J*=7.0 Hz), 2.44 (3H, s), 2.75 (1H, septet, *J*=7 Hz), 3.80 (2H, d, *J*=7.2 Hz), 5.69 (1H, dt, *J*=11, 7.2 Hz), 6.30 (1H, d, *J*=11 Hz), 7.29 (2H, d, *J*= 7.8 Hz), 7.75 (2H, d, *J*=7.8 Hz). Anal.($C_{13}H_{18}O_2S_2$) C, H.

Reaction of **3** *with Lithium 2-Propanethiolate.* To a solution of 2-propanethiol (421 mg: 5.52 mmol) in THF (5 ml), was added a 1.5 mol/l hexane solution (3.9 ml) of butyllithium (6.0 mmol) under ice-cooling, and the resulting mixture was stirred at room temperature for 1 h. After the addition of **3** (1.28 g: 5.53 mmol), the mixture was further stirred under ice-cooling for 2 h. The aqueous workup and column chromatography on silica gel [benzene–hexane (1:1)] gave **7** (834 mg: 56%) as colorless crystals: mp 58 °C (from benzene–hexane); ^1H NMR ($CDCl_3$) δ=1.20 (3H, d, *J*=6.6 Hz), 1.23 (3H, d, *J*=6.6 Hz), 1.45—1.85 (2H, m), 2.45 (3H, s), 2.40—3.05 (4H, m), 7.29 (2H, d, *J*=7.8 Hz), 7.71 (2H, d, *J*=7.8 Hz). Anal.($C_{13}H_{18}O_2S_2$) C, H.

Preparation of (E)-*1b via 3-Iodo-1-propenyl* p-*Tolyl Sulfone* (*8*). A mixture of **3** (932 mg: 4.04 mmol) and KI (2.01 g: 12.1 mmol) in acetone (30 ml) was refluxed for 3 h. The aqueous workup gave crude **8** as a pale yellow solid. After a mixture of 2-propanethiol (91 mg: 1.2 mmol) and $NaHCO_3$ (103 mg: 1.22 mmol) in DMF (10 ml) was stirred at room temperature for 30 min, the crude **8** (382 mg: 1.18 mmol) was added and the resulting mixture was further stirred at room temperature for 12 h under an atmosphere of nitrogen. The usual workup followed by column chromatography gave 263 mg (82% yield) of **1b** as colorless crystals.

Reaction of **3** *with Sodium Methanethiolate.* To a solution of **3** (387 mg: 1.68 mmol) in DMF (10 ml), was added a 15% aqueous solution (1.73 g: 4.13 mmol) of sodium methanethiolate (Tokyo Kasei Inc.) under an atmosphere of nitrogen, and the resulting mixture was stirred at room temperature for 3 h. The aqueous workup and the subsequent separation by column chromatography on silica gel [hexane–benzene (1:2)] to afford **2c** (290 mg: 71% yield) as a mixture of two geometrical isomers (*Z*:*E*=27:73). Rechromatography of this mixture and recrystallization gave pure (*Z*)-**2c** and pure (*E*)-**2c**. (*E*)-**2c**: colorless crystals; mp 79—80 °C (from ethanol); ^1H NMR ($CDCl_3$) δ=2.23 (3H, s), 2.46 (3H, s), 3.77 (2H, d, *J*=7.5 Hz), 5.35 (1H, dt, *J*=16, 7.5 Hz), 6.13 (1H, d, *J*=16 Hz), 7.35 (2H, d, *J*=8.5 Hz), and 7.73 (2H, d, *J*=8.5 Hz). Anal.($C_{11}H_{14}O_2S_2$) C, H. (*Z*)-**2c**: a colorless oil; ^1H NMR ($CDCl_3$) δ=2.12 (3H, s), 2.44 (3H, s), 3.94 (2H, d, *J*=7.5 Hz), 5.54 (1H, dt, *J*=7.5 Hz), 6.25 (1H, d, *J*=9 Hz), 7.29 (2H, d, *J*=8.5 Hz), 7.72 (2H, d, *J*=8.5 Hz). Anal.($C_{11}H_{14}O_2S_2$) C, H.

Reaction of **3** *with Dimethyl Sulfide* A mixture of dimethyl sulfide (41.8 g: 0.25 mol), **3** (15.4 g: 0.067 mol), and KI (33.7 g: 0.020 mol) was stirred at room temperature for 7 d. After the addition of water (100 ml), the resulting mixture was extracted with CH_2Cl_2 (3×80 ml). The extracts were combined, washed with saturated aqueous $NaHSO_3$, dried (Na_2SO_4), and evaporated. The residue was dissolved in CH_3CN (50 ml) and K_2CO_3 (929 mg: 6.70 mmol) was added. The mixture was stirred at room temperature for 1 d and water (100 ml) was added. The usual workup followed by column chromatography gave **2c** (14.94 g: 92% yield) (*Z*:*E*=28:72).

References

1) E. J. Corey and R. Noyori, *Tetrahedron Lett.*, **1970**, 311; E. J. Corey, B. W. Erickson, and R. Noyori, *J. Am. Chem. Soc.*, **93**, 1724 (1971).

2) K. Ogura, T. Iihama, K. Takahashi, and H. Iida, *Tetrahedron Lett.*, **25**, 2671 (1984).

3) To our best knowledge, there has been the only report that relates with this type of compound: A. H. Raper and E. Rothstein. *J. Chem. Soc.*, **1963**, 2463.

4) K. Ogura, N. Shibuya, and H. Iida, *Tetrahedron Lett.*, **22**, 1519 (1981); K. Ogura, N. Shibuya, K. Takahashi, and H. Iida, *Bull. Chem. Soc. Jpn.*, **57**, 1092 (1984).

5) D. S. Tarbell and W. E. Lovett, *J. Am. Chem. Soc.*, **78**, 2259 (1956).

6) D. E. O'Connor and W. I. Lyness, *J. Am. Chem. Soc.*, **86**, 3840 (1964); C. D. Broaddus, *ibid.*, **88**, 3865 (1966) and **90**, 5504 (1968).

7) A. J. H. Labuschagne, J. S. Malherbe, C. J. Meyer, and D. F. Schneider, *Tetrahedron Lett.*, **1976**, 3571; *idem.*, *J. Chem. Soc.*, **1978**, 955.

Alkoxylation of Ferrocene by Photolysis of Haloferrocenes in Aqueous Alcohols

Katsuyoshi SHIBATA,* Yoshiyuki SAITO, Masaki MATSUI, and Yoshimi TAKASE
Department of Industrial Chemistry, Faculty of Engineering, Gifu University, Yanagido, Gifu 501-11
(Received May 4, 1984)

Synopsis. The UV irradiation of haloferrocenes in aqueous alcohols resulted in an alcoholysis with the formation of the corresponding alkoxyferrocenes accompanied by the formation of ferrocence. The order of the reactivities of haloferrocenes was I>Br>Cl.

Considerable attention has been directed to the realm of photosubstitution of aromatic compounds.[1] However, photosubstitution of ferrocene derivatives has not been extensively studied.[2] In this paper, we report the photolysis of haloferrocenes in aqueous alcohols. The photochemical substitution of halogens with alkoxyl groups occurred.

The irradiation of an aqueous methanol solution of bromoferrocene in the presence of sodium carbonate afforded methoxyferrocene(60%) and ferrocene(8%). Similarly, iodo- and chloroferrocenes produced methoxyferrocene. Photolysis of these haloferrocenes in other alcohols also gave mixtures of the corresponding alkoxyferrocenes and ferrocene.

The photoreactions are generalized in Scheme 1. The results are summarized in Table 1. The reactivities of halogens are I>Br>Cl for both photosubstitution and photoreduction.

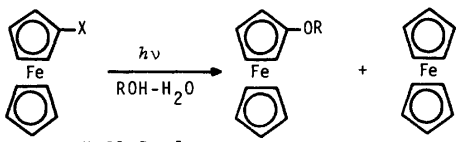

Scheme 1.

TABLE 1. PHOTOCHEMICAL REACTIONS OF HALOFERROCENES WITH ALCOHOLS

FcX[a] X	ROH[b] R	Time of irradn/h[c]	Conversion/%	Yield/%[d] FcOR	Yield/%[d] FcH
Cl	Me	10	69	46	5
	i-Pr	10	40	20	8
Br	Me	1.5	87	60	8
	Et	1.5	75	37	10
	n-Pr	1.5	59	14	13
	i-Pr	1.5	64	21	15
	t-Bu	1.5	45	8	18
I	Me	1.0	93	47	25
	i-Pr	1.0	74	18	28

a) [FcX] = 1.8 mmol dm^{-3}. b) The solutions contained 10% of water and 10 mmol dm^{-3} of Na_2CO_3. c) High pressure Hg arc lamp with a Pyrex filter. d) Yields were determined by GLC and based on unrecovered haloferrocene.

The nucleophilic substitution of ferrocene derivatives takes place with difficulty, and few cases have been reported.[3] The alkoxyferrocenes, other than methoxyferrocene, have not been synthesized. This type of reaction affords a new route for the introduction of alkoxyl groups into the ferrocene ring: The reactivity of chloroferrocene is too small. The reaction of iodoferrocene gave a considerable amount of ferrocene. Consequently, bromoferrocene is adequate for the synthesis of alkoxyferrocenes.

Experimental

The melting points were measured with a Mettler FR-2 melting point apparatus and are uncorrected. IR spectra were obtained with a JASCO A-302 spectrometer. ^{1}H NMR spectra were taken with a Hitachi R-22 apparatus an chemical shifts are given in ppm from TMS internal standard. GLC analysis were carried out by means of a Shimadzu 4C-PF apparatus. Mass spectra were obtained using a Hitachi M-52 mass spectrometer at 20 eV.

Materials. Bromo- and iodoferrocenes were synthesized by the reaction of *N*-halosuccinimides with ferrocenylmercury(II) chloride.[4] Bromoferrocene; mp 31.5—32 °C (lit,[4] 30—31 °C). Iodoferrocene; mp 46—47 °C (lit,[4] 45.5—46 °C). Chloroferrocene was prepared by refluxing iodoferrocene with copper(I) chloride in pyridine.[5] mp 57—57.5 °C (lit,[5] 56—56.5 °C).

Irradiation of Haloferrocenes. A solution of haloferrocene(1.8 mmol dm^{-3}) in alcohol-water(9:1 v/v, 200 cm^3) in the presence of sodium carbonate(5 mmol dm^{-3}) was irradiated in a Pyrex vessel with a 300 W high pressure Hg arc lamp (Eikosha) externally at room temperature. The reaction mixture was extracted with benzene, and resultant benzene solution was washed with water and dried (Na_2SO_4). After removal of the solvent, products were isolated by means of preparative TLC (Merck Silica Gel 60 PF_{254}-hexane).

Methoxyferrocene: Mp 40—41 °C (lit,[4] 39—40.5 °C). Found: M$^+$ 216.

Ethoxyferrocene: An orange oily substance. IR (neat) 3120, 2995, 1108, 1025, 1003, 816, 688 (Fc ring), 2950, 1476, 1382, 1251, and 1065 cm^{-1} (EtO); ^{1}H NMR ($CDCl_3$) δ=1.32 (t, 3H), 3.81 (q, 2H), 3.75—3.95 (m, 2H), 4.0—4.15 (m, 2H) and 4.16 (s, 5H); MS *m/z* (rel intensity) 230 (M$^+$, 100), 202 (76), 172 (33), and 121 (33). Found: C, 62.38; H, 6.01. Calcd for $C_{12}H_{14}OFe$: C, 62.64; H, 6.13.

Propoxyferrocene: An orange oily substance; IR (neat) 3105, 2970, 1104, 1000, 815, 682 (Fc ring), 2940, 2880, 1472, 1387, 1250, and 1060 cm^{-1} (*n*-PrO); ^{1}H NMR ($CDCl_3$) δ=1.00 (t, 3H), 1.73 (sex, 2H), 3.76 (t, 2H), 3.86 (s, 2H), 4.10 (s, 2H), and 4.20 (s, 5H); MS *m/z* (rel intensity) 244 (M$^+$, 59), 202 (75), 172 (18), and 121 (100). Found: C, 63.62; H, 6.45. Calcd for $C_{13}H_{16}OFe$: C, 63.96; H, 6.61.

Isopropoxyferrocene: An orange oily substance; IR (neat) 3120, 3000, 1003, 819, 629 (Fc ring), 2955, 2870, 1388, 1378, 1255, 1122, 1045, and 918 cm^{-1} (*i*-PrO); ^{1}H NMR ($CDCl_3$) δ=1.28 (d, 6H), 3.8—4.0 (m, 2H), 4.0—4.2 (m, 3H), and 4.19 (s, 5H); MS *m/z* (rel intensity) 244 (M$^+$, 100), 202 (76), 172 (33), and 121 (33). Found:

C, 63.57; H, 6.48. Calcd for $C_{13}H_{16}OFe$: C, 63.96; H, 6.61.

t-Butoxyferrocene: mp 68—68.5 °C; IR (KBr) 3110, 2995, 1110, 1012, 802 (Fc ring), 2950, 2880, 1460, 1373, 1365, 1246, and 1055 cm^{-1} (*t*-BuO); ^1H NMR ($CDCl_3$) δ=1.13 (s, 9H), 3.8—4.0 (m, 2H), and 4.05—4.3 (m, 7H), MS *m/z* (rel intensity) 258 (M^+, 100), 202 (98), 172 (50), and 121 (33). Found: C, 65.01; H, 7.07. Calcd for $C_{14}H_{18}OFe$: C, 65.14; H, 7.03.

References

1) J. Cornelisse and E. Havinga, *Chem. Rev.*, **75**, 353 (1975).

2) Y. Hoshi, T. Akiyama, and A. Sugimori, *Tetrahedron Lett.*, **1970**, 1485; T. Akiyama, Y. Hoshi, S. Goto, and A. Sugimori, *Bull. Chem. Soc. Jpn.*, **46**, 1851 (1973); T. Akiyama, A. Sugimori, and H. Herman, *ibid.*, **46**, 1855 (1973).

3) C. Baker and W. H. Horspool, *J. Chem. Soc., Perkin Trans. 1*, **1979**, 1862, 2294, 2298.

4) R. W. Fish and M. Rosenblum, *J. Org. Chem.*, **30**, 1253 (1965).

5) M. Sato, T. Ito, I. Motoyama, K. Watanabe, and K. Hata, *Bull. Chem. Soc. Jpn.*, **42**, 1976 (1969).

A Synthesis of *dl*-Pumiliotoxin-C

Kyo Abe,* Teruhisa Tsugoshi, and Nobuo Nakamura
Department of Chemistry, Osaka City University, 3-3-138 Sugimoto-cho, Sumiyoshi-ku, Osaka 558
(Received May 5, 1984)

Synopsis. Reductive aminocyclization of trans-2-(3-oxohexyl)-3-methyl-1-cyclohexanone (**4**) with sodium cyanotrihydroborate and ammonium bromide gave *dl*-pumiliotoxin-C (**5**) and its stereochemical isomer (**6**) in a ratio of 48:52.

Recently, we have reported of reductive aminocyclization of 2,6-alkanediones with sodium cyanotrihydroborate and ammonium bromide to afford *cis*-6-alkyl-2-methylpiperidine as a sole product.[1]

This experimental fact stimulated us to synthesize **5**, a minor component of the frog Dendrobates pumilio,[2] although many chemists have already reported on its synthesis.[3–6]

This paper reports of experimental results and discussion of our synthesis of **5**.

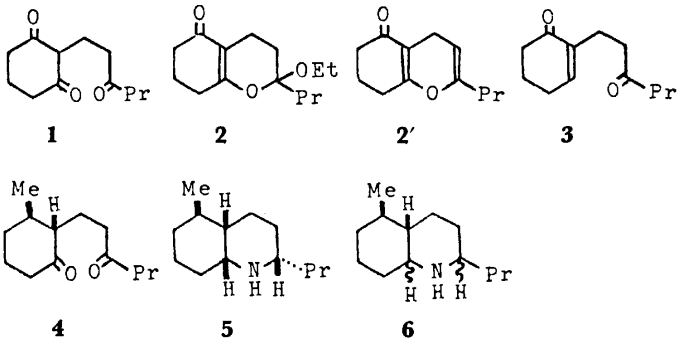

Results and Discussion

For reductive aminocyclization, *trans*-2-(3-oxohexyl)-3-methyl-1-cyclohexanone (**4**) was prepared from 1,3-cyclohexanedione in 4 steps: In the first step, 1,3-cyclohexanedione was alkylated with 1-chloro-3-hexanone under alkaline conditions to afford 2-(3-oxohexyl)-1,3-cyclohexanedione (**1**) in 40% yield. **1** was refluxed in ethanol and benzene with a catalytic amount of *p*-toluenesulfonic acid to give 2-ethoxy-2-propyl-7,8-dihydro-5(6*H*)-chromanone (**2**) quantitatively. The structure of **2** was confirmed from the following two experimental facts: even when **2** was treated with an excess amount of lithium aluminum hydride, 2-(3-oxohexyl)-2-cyclohexen-1-one (**3**) as a sole product was given in 80% yield; **2** was easily converted to 2-propyl-5,6,7,8-tetrahydro-4*H*-chromen-5-one (**2′**) on distillation. The enone **3** was treated with lithium dimethylcuprate(**I**) in dry ether to give **4** in 90% yield. The stereochemical correlation between the methyl and 3-oxohexyl groups must be trans configuration. Thus **4** was treated with sodium cyanotrihydroborate and ammonium bromide in dry methanol at room temperature for 4 d and worked up to give a basic yellow oil in 88% crude yield. A GLC analysis showed that the basic oil consisted of two components in a ratio of 48:52 at R_t's 4.5 and 4.8 min, respectively. The first peak was identical with an authentic sample of **5** as revealed by the co-injection method. They were separated by means of preparative GLC using a glass column packed with 5% Silicone OV-1. Each of them was converted to its hydrochloride. The salt of the first peak component was identical with an authentic sample of *dl*-pumiliotoxin-C hydrochloride as revealed by comparison of their melting points and ^{13}C NMR spectra. The hydrochloride of the second one had the same chemical formula as the hydrochloride of **5** as a result of elemental analysis and melted at 246—250 °C. These facts suggest that the second one **6** seems to be a stereochemical isomer of **5**. But we could not determine its stereochemistry.

Experimental

All melting and boiling points are uncorrected. ^1H and ^{13}C NMR spectra were measured with a JEOL PS-100 and a JEOL FX-100, respectively, using tetramethylsilane as internal standard.

2-(3-Oxohexyl)-1,3-cyclohexanedione (1). Into 30 ml of aqueous solution of potassium hydroxide (8.4 g, 0.15 mol) was dissolved solid 1,3-cyclohexanedione (10.8 g, 0.15 mol). Then a solution of 1-chloro-3-hexanone (20.3 g, 0.15 mol) in methanol (75 ml) was added into it. The reaction mixture was stirred for 24 h at room temperature and then concentrated to one fifth volume. It was made alkaline with aqueous solution of potassium hydroxide and then extracted with ether several times. The aqueous layer was acidified with hydrochloric acid and then extracted with ether (30 ml×5). The ethereal extract was washed with brine and dried over anhydrous sodium sulfate. After removal of the solvent, the residue became crystalline, which was recrystallized from hexane to give **1** (7.5 g, 40% yield): mp 87—88 °C; IR (CCl_4) 3150, 1680, and 1600 cm^{-1}; UV (EtOH) 263 nm (1.5×10^4); MS 210 (M^+); ^1H NMR ($CDCl_3$) δ=0.93 (t, J=7 Hz, 3H), 1.42—2.20 (m, 5H), 2.20—2.60 (m, 8H), and 2.60—2.81 (m, 2H): Found C, 68.54; H, 8.63. Calcd for $C_{12}H_{18}O_3$: C, 68.56; H, 8.72.

2-Ethoxy-2-propyl-7,8-dihydro-5(6H)-chromanone (2). A mixture of **1** (4 g, 19 mmol), a catalytic amount of *p*-toluenesulfonic acid, ethanol (60 ml), and benzene (180 ml) was slowly refluxed in a Dean-Stark apparatus to remove deposited water azeotropically. It was washed with 10% aque-

ous solution of sodium hydroxide three times and with brine, and dried over anhydrous sodium sulfate. After removal of the solvent, the residue obtained was used for the next step without further purification. When it was distilled under reduced pressure, it decomposed to 2-propyl-5,6,7,8-tetrahydro-4*H*-chromen-5-one (**2'**): Crude yield 4.5 g, quantitative; IR (neat) 1700, 1650, 1620, 1380, 1220, 1180, and 1130 cm^{-1}; ^1H NMR ($CDCl_3$) δ=0.95 (t, J=7 Hz, 3H), 1.10 (t, J=7.5 Hz, 3H), 1.2—1.7 (m, 4H), 1.7—2.1 (m, 4H0, 2.25 (t, J=7 Hz, 6H), and 3.45 (q, J=7.5 Hz, 2H).

2-Propyl-5,6,7,8-tetrahydro-4H-chromen-5-one (2'). ^1H NMR ($CDCl_3$) δ=0.93 (t, J=7 Hz, 3H), 1.50 (sex, J=7 Hz, 2H), 1.90 (t, J=7 Hz, 2H), 2.88 (t, J=7 Hz, 4H), and 4.70 (t, J=4.5 Hz, 1H).

2-(3-*Oxohexyl*)-2-*cyclohexen*-1-*one* (**3**). To a stirred suspension of lithium aluminum hydride (0.83 g, 0.02 mol) in dry ether (50 ml) was added dropwise a solution of **2** (2.38 g, 0.01 mol) in dry ether (50 ml). The mixture was stirred for 3 h at room temperature and then treated carefully with water. The white solid formed was filtered through Celite and washed successively with ether. The filtrate was washed with brine. After removal of the solvent, the residue was distilled under reduced pressure to give **3** (15.6 g, 80% yield): bp 81—90 °C (0.01 mmHg) (1 mmHg=133.322 Pa); IR (neat) 1700, 1660, 1610, 1440, 1410, 1370, 1250, 1170, 1130, 1100, 1080, 1000, and 900 cm^{-1}; ^1H NMR ($CDCl_3$) δ= 0.9 (t, J=7.5 Hz, 3H), 1.55 (t, J=4.5 Hz, 2H), 2.00 (m, 2H), 2.15—2.60 (m, 1H), and 6.70 (t, J=4.5 Hz, 1H); MS 119 (M^+). Found: C, 74.19; H, 9.14. Calcd for $C_{12}H_{18}O_2$: C, 73.76; H, 9.35.

2-(3-Oxohexyl)-3-methyl-1-cyclohexanone (4). To a suspension of copper(I) iodide (5.73 g, 0.03 mol) in dry ether (100 ml) was added an ethereal solution of methyllithium (0.06 mol) at −15 °C in an argon atmosphere. When the mixture became transparent, a solution of **3** (3.88 g, 0.02 mol) in dry ether (60 ml) was added at −15 °C. The reaction mixture was stirred for 30 min and then treated with aqueous solution of ammonium chloride. The ethereal layer was washed with brine and dried over anhydrous sodium sulfate. After removal of the solvent, the residue was distilled under reduced pressure to give **4** (3.8 g, 91% yield): bp 85—89 °C (0.03 mmHg); IR (neat) 1720, 1700, 1450, 1400, 1370, 1130, and 1040 cm^{-1}. ^1H NMR ($CDCl_3$) δ=9.25 (t, 7.5 Hz, 3H), 1.33 (d, J=7.5 Hz, 3H), 1.20—2.00 (m, 9H), and 2.20—2.70 (m, 7H). Found: C, 74.04; H, 10.53. Calcd for $C_{13}H_{22}O_2$: C, 74.24; H, 10.54.

Reductive Aminocyclization of 4 to dl-*Pumiliotoxin-C (5) and its Stereochemical Isomer (6).* To a suspension of **4** (2.38 g, 0.023 mol) and ammonium bromide (2.22 g, 0.023 mol) in dry methanol (30 ml) was added all at once sodium cyanotrihydroborate (0.71 g, 0.012 mol). The reaction mixture was stirred at room temperature for 4 d. Then it was acidified with conc. hydrochloric acid (pH 3) and stirred for additional 30 min. After evaporation of solvent from the reaction mixture under reduced pressure, the residue was washed with ether several times and then dissolved in water. The aqueous solution was extracted with ether by using an eternal extactor. The extracted ethereal solution was dried over anhydrous sodium sulfate and condensed to give a yellow oil (crude 2.93 g, 88% yield), which was offered for preparative GLC.

Preparative GLC of the Basic Yellow Oil. The GLC was carried out with a AEROGRAPH Model 920 (glass column, 5 mm×3 M, packed with 5% Silicone OV-1 on 80—100 mesh Chomosorb W, oven temp, 145 °C; injection temp, 160 °C). Two peaks appeared at R_t's 4.5 and 4.8 min in a ratio of 48:52, respectively. The first peak was identical with an authentic sample of **5**. The preparative GLC was carried out under the same conditions. The first component was converted to its hydrochloride in a usual manner: mp 230 °C [lit,[6] 232 °C]; ^{13}C NMR ($CDCl_3$) δ=13.19, 19.83, 20.63, 23.19, 25.29, 27.28, 29.15, 34.18, 34.69, 58.04, and 60.10. The second component also was converted to its hydrochloride, which was recrystallized from ethyl acetate and isopropyl alcohol (5:1): mp 246—250 °C (white needle); ^{13}C NMR ($CDCl_3$) δ=13.33, 18.28, 24.09, 25.29, 28.02, 29.89, 34.92, 36.56, 44.42, 58.12, and 61.70; Found: C, 67.26; H, 11.38, N, 5.94. Calcd for $C_{13}H_{26}ClN$: C, 67.39; H, 11.23; N, 6.05.

The authors wish to thank Drs. Toshiro Ibuka and Takashi Tokuyama for their offer of the precious sample of *dl*-pumiliotoxin-C, and also Mr Jun'ichi Goda for conducting the elemental analysis.

References

1) K. Abe, H. Okumura, T. Tsugoshi, and N. Nakamura, *Synthesis*, **1984**, 597.

2) J. W. Daly, T. Tokuyama, G. Habermehl, I. L. Karle, and B. Witkop, *Justus Liebigs Ann. Chem.*, **729**, 198 (1969).

3) G. Habermehl, H. Andres, K. Miyahara, B. Witkop, and J. W. Daly, *Justus Liebigs Ann. Chem.*, **1976**, 1577.

4) T. Ibuka, N. Masaki, I. Saji, K. Tanaka, and Y. Inubushi, *Chem. Pharm. Bull.*, **23**, 2779 (1975).

5) L. E. Overman and P. J. Jessup, *Tetrahedron Lett.*, **1977**, 1253.

6) W. Oppolzer and E. Flaskamp, *Helv. Chim. Acta.*, **60**, 205 (1977).

One-pot Synthesis of Alkyl Aryl Trithiocarbonates from Benzenethiols, Alkyl Halides, and Carbon Disulfide with a Phase-transfer Catalyst

Akira SUGAWARA,* Masami SHIRAHATA, Seiki SATO, and Ryu SATO†
Department of Industrial Chemistry, Tsuruoka Technical College, Tsuruoka, Yamagata 997
†*Department of Resource Chemistry, Faculty of Engineering, Iwate University, Ueda, Morioka, Iwate 020*

(Received May 17, 1984)

Synopsis. Various alkyl aryl trithiocarbonates may readily be synthesized in good yield at low temperatures such as 20 °C by allowing trioctylmethylammonium chloride (phase-transfer catalyst) to catalyze reaction of benzenethiols and alkyl halides with carbon disulfide.

Much attention has been focused on the synthesis of trithiocarbonates, which are very important intermediates for the preparation of insecticides and oil additives.[1] Some procedures for the synthesis of trithiocarbonates have been developed which employ reactions of sodium trithiocarbonates with alkyl halides,[2] thiophosgene with benzenethiols,[3] aryl chlorodithioformates with alkanethiols,[4] and lithio-2-alkyl thio-1,3-dithiolanes with alkyl halides.[5] Wepplo and Wright[6] synthesized alkyl cyanoalkyl trithiocarbonates *via* reaction of alkanethiols and haloalkanenitriles with carbon disulfide in the presence of tetrabutylammonium sulfate, but they were unable to obtain alkyl aryl trithiocarbonates.[6] These known procedures are not preferrable with respect to various points such as synthetic convenience, intractability of reagents and substrates, and availability of starting materials. In the course of our investigations on the chemistry of organosulfur compounds,[7] we have studied on the development of a new synthetic method for alkyl aryl trithiocarbonates. Here we wish to report of a convenient one-pot synthesis of trithiocarbonates from benzenethiols, carbon disulfide, and alkyl halides in the presence of a phase-transfer catalyst such as trioctylmethylammonium chlorid (TOMAC), the reaction sequence being summarized by Eqs. 1 and 2. Results obtained for the reaction of benzenethiol and carbon disulfide with methyl iodide are listed in Table 1. It should be noted that only a trace of trithiocarbonate is obtained in the absence of phase-transfer catalyst (run 5), whereas in the presence of 0.3 mmol TOMAC the desired trithiocarbonate **2a** is formed in a yield of 64% (run 6). Thus, a remarkable accelerating effect of TOMAC is found for this reaction. Moreover, a higher yield of trithiocarbonate **2a** is obtained with decreasing temperature (runs 3 and 4). This phenomenon is not unexpected since the intermediate, anion **1**, may be considered to be unstable at higher temperatures.

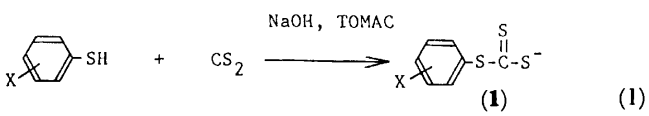

(1)

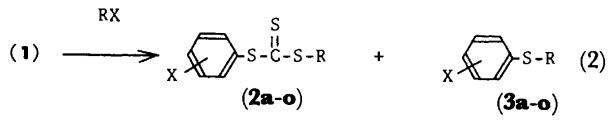

(2)

Table 1. Reaction of benzenethiol, CS_2, and methyl iodide in the presence of trioctylmethylammonium chloride (TOMAC)

Run[a]	React. Temp/°C	React. Time/h	TOMAC /mmol	Yield of product/%[b] **2a**	Yield of product/%[b] **3a**
1	r.t.	3	1.0	63	32
2	r.t.	3	1.0[c]	50	34
3	0	3	1.0	68	15
4	40	3	1.0	46	39
5	r.t.	3	0	trace	84
6	r.t.	3	0.3	64	26
7	r.t.	3	3.0	51	44

a) Benzenethiol, 10 mmol; methyl iodide, 10 mmol; NaOH, 10 mmol; CS_2, 20 mmol. b) Isolated yield based on benzenethiol. c) Tetrabutylammonium bromide was used as catalyst.

Many alkyl aryl trithiocarbonates **2a—o** were syn-

Table 2. Synthesis of alkyl aryl trithiocarbonates **2b—2o**

Run[a]	Thiol X-C_6H_4-SH/X	Alkyl halide	Yield of product/%[b] **2**	Yield of product/%[b] **3**
1	H	$C_6H_5CH_2Br$	65 **2b**	25 **3b**
2	H	C_2H_5I	57 **2c**	32 **3c**
3	H	C_2H_5Br	40 **2c**	29 **3c**
4	H	*n*-C_3H_7I	56 **2d**	41 **3d**
5	H	*n*-C_3H_7Br	29 **2d**	18 **3d**
6	H	$(CH_3)_2CHI$[c]	39 **2e**	16 **3e**
7	H	*n*-C_4H_9Br[c]	41 **2f**	38 **3f**
8	H	*n*-$C_5H_{11}Br$	39 **2g**	51 **3g**
9	H	*i*-$C_5H_{11}Br$	38 **2h**	40 **3h**
10	H	*n*-$C_6H_{13}Br$	39 **2i**	48 **3i**
11	H	*n*-$C_8H_{17}Br$	40 **2j**	48 **3j**
12	4-CH_3	CH_3I	72 **2k**	22 **3k**
13	2-CH_3	CH_3I	61 **2l**	22 **3l**
14	3-CH_3	CH_3I	51 **2m**	37 **3m**
15	4-Cl	CH_3I	24 **2n**	44 **3n**
16	4-CH_3	$C_6H_5CH_2I$	85 **2o**	10 **3o**

a) Thiol, 10 mmol; alkyl halide, 10 mmol; CS_2, 20 mmol; NaOH, 10 mmol; TOMAC, 0.3 mmol; react, time, 3 h; react. temp., r.t. b) Isolated yield based on thiols. c) React. time, 24 h.

thesized *via* the reaction of benzenethiols with alkyl halides and carbon disulfide in the presence of TOMAC. As shown in Table 2, methyl 4-methylphenyl trithiocarbonate **2k** and benzyl 4-methylphenyl trithiocarbonate **2o** were obtained especially in high yields, 72 (run 12) and 85% (run 16), respectively. Trithiocarbonates bearing an electron-withdrawing group such as chlorine, however, were formed in low yield by this procedure (run 15). A plausible pathway for this reaction may comprise a nucleophilic attack of the thiolate anion moiety of intermediate **1** on the carbon atom of alkyl halides in the presence of TOMAC, as shown in Eqs. 1 and 2. The above results demonstrate that the catalytic approach utilized in this study may be of significant value for the preparation of alkyl aryl trithiocarbonates.

Experimental

IR spectra were obtained on a JASCO IR-G spectrophotometer. NMR spectra were measured with a Hitachi R-20B spectrophotometer (60 MHz) in $CDCl_3$ using TMS as internal standerd.

General Procedure. Carbon disulfide (20 mmol) and TOMAC (0.3 mmol) were added to a solution of benzenethiol (10 mmol) in aq NaOH (10 mmol) and after 2 h stirring at room temperature, alkyl halide (10 mmol) in benzene (10 ml) was added and stirring was continued for 3 h at room temperature. After completion of reaction the benzene layer was dried on sodium sulfate and then concentrated by evaporation of benzene under vacuum. Alkyl aryl trithiocarbonates **2a—o** and alkyl aryl sulfides **3a—o** were obtained by vacuum distillation and column chromatography on silica-gel (Wako Gel C-300) using hexane-chloroform (9:1) as eluent.

*Physical Properties of **2a—o**.* *Methyl Phenyl Trithiocarbonate (**2a**)*: Bp 142—6 °C (2 mmHg) (1 mmHg=133.322 Pa); IR 1048 and 1076 cm^{-1}; NMR ($CDCl_3$) δ=2.46 (S, 3H) and 7.39 (s, 5H). Found: C, 48.13; H,4.26. Calcd for $C_8H_8S_3$: C, 47.96; H, 4.03.

*Benzyl Phenyl Trithiocarbonate (**2b**)*: Bp 130—2 °C (2 mmHg); IR 1048 and 1062 cm^{-1}; NMR ($CDCl_3$) δ=4.46 (s, 2H) and 7.0—7.3 (m, 10H). Found: C, 60.52; H, 4.12. Calcd for $C_{14}H_{12}S_3$; C, 60.83; H, 4.38.

*Ethyl Phenyl Trithiocarbonate (**2c**)*: Bp 144—7 °C (2 mmHg); IR 1056 and 1072 cm^{-1}; NMR ($CDCl_3$) δ=1.12 (t, 3H), 3.12 (t, 2H), and 7.3—7.5 (m, 5H). Found: C, 51.14; H, 4.73. Calcd for $C_9H_{10}S_3$: C, 50.43; H, 4.70.

*Phenyl Propyl Trithiocarbonate (**2d**)*: Bp 145—9 °C (2 mmHg); IR 1037 and 1065 cm^{-1}; NMR ($CDCl_3$) δ=0.83 (t, 3H), 1.2—1.9 (m, 2H), 3.13 (t, 2H), and 7.0—7.5 (m, 5H). Found: C, 52.74; H, 5.52. Calcd for $C_{10}H_{12}S_3$: C, 52.59; H, 5.30.

*Isopropyl Phenyl Trithiocarbonate (**2e**)*: Bp 130—2 °C (2 mmHg); IR 1042 and 1062 cm^{-1}; NMR ($CDCl_3$) δ=1.22 (d, 6H), 4.00 (m, 1H), and 7.2—7.4 (m, 5H). Found: C, 52.73; H, 5.56. Calcd for $C_{10}H_{12}S_3$: C, 52.59; H, 5.30.

*Butyl Phenyl Trithiocarbonate (**2f**)*: Oil; IR 1060 and 1040 cm^{-1}, NMR ($CDCl_3$) δ=0.90 (t, 3H), 1.4—1.8 (m, 4H), 3.21 (t, 2H), and 7.45 (s, 5H). Found: C, 54.96; H, 5.96. Calcd for $C_{11}H_{14}S_3$: C, 54.55; H, 5.79.

*Pentyl Phenyl Trithiocarbonate (**2g**)*: Oil; IR 1060 and 1040 cm^{-1}; NMR ($CDCl_3$) δ=0.90 (t, 3H), 1.3—1.5 (m, 6H) and 7.48 (s, 5H). Found: C, 56.67; H, 6.20. Calcd for $C_{12}H_{16}S_3$: C, 56.25; H, 6.25.

*Isopentyl Phenyl Trithiocarbonate (**2h**)*: Oil; IR 1056 and 1045 cm^{-1}; NMR ($CDCl_3$) δ=0.92 (d, 6H), 1.4—1.7 (m, 3H), 3.22 (t, 2H), and 7.47 (s, 5H). Found; C, 56.61; H, 6.34. Calcd for $C_{12}H_{16}S_3$: C, 56.25; H, 6.25.

*Hexyl Phenyl Trithiocarbonate (**2i**)*: Oil; IR 1062 and 1040 cm^{-1}; NMR ($CDCl_3$) δ=0.88 (t, 3H), 1.25—1.6 (m, 8H), 3.21 (t, 2H), and 7.48 (s, 5H). Found: C, 58.04; H, 6.71. Calcd for $C_{15}H_{22}S_3$: C, 57.78; H, 6.67.

*Octyl Phenyl Trithiocarbonate (**2j**)*: Oil; IR 1063 and 1045 cm^{-1}; NMR ($CDCl_3$) δ=0.88 (t, 3H), 1.25—1.6 (m, 10H), 3.20 (t, 2H), and 7.45 (s, 5H). Found: C, 60.68; H, 7.36. Calcd for $C_{15}H_{22}S_3$: C, 60.40; H, 7.38.

*Methyl 4-Methylphenyl Trithiocarbonate (**2k**)*: Bp 152—157 °C (2 mmHg); IR 1048 and 1074 cm^{-1}; NMR ($CDCl_3$) δ=2.29 (s, 3H), 2.42 (s, 3H), and 7.2—7.4 (m, 4H). Found: C, 50.86; H, 4.65. Calcd for $C_9H_{10}S_3$: C, 50.43; H, 4.70.

*Methyl 2-Methylphenyl Trithiocarbonate (**2l**)*: Mp 49.2—49.5 °C; IR 1048 cm^{-1}; NMR ($CDCl_3$) δ=2.42 (s, 3H), 2.58 (s, 3H), and 7.4—7.3 (t, 4H). Found: C, 50.63; H, 4.73. Calcd for $C_9H_{10}S_3$: C, 50.43; H, 4.70.

*Methyl 3-Methylphenyl Trithiocarbonate (**2m**)*: Oil; IR 1072 and 1044 cm^{-1}; NMR ($CDCl_3$) δ=2.36 (s, 3H), 2.52 (s, 3H), and 7.3-7.2 (d, 4H). Found: C, 49.90; H, 4.83. Calcd for $C_9H_{10}S_3$: C, 50.43; H, 4.70.

*4-Chlorophenyl Methyl Trithiocarbonate (**2n**)*: Bp 152—159 °C (4 mmHg); IR 1050 and 1078 cm^{-1}; NMR ($CDCl_3$) δ=2.60 (s, 3H) and 7.43 (s, 4H). Found: C, 40.27; H, 3.15. Calcd for $C_8H_7S_3Cl$: C, 40.93; H, 3.01.

*Benzyl 4-Methylphenyl Trithiocarbonate (**2o**)*: Oil; IR 1040 and 1065 cm^{-1}; NMR ($CDCl_3$) δ=2.34 (s, 3H), 4.40 (s, 2H) and 7.17—7.46 (m, 9H). Found: C, 62.06; H, 4.84. Calcd for $C_{15}H_{14}S_3$: C, 62.02; H, 4.87.

References

1) J. T. Bashour, U. S. Patent, 2676129 (1954); *Chem. Abstr.*, **48**, 8472i (1954); 2731487 (1956); *Chem. Abstr.*, **50**, 15583h (1956); H. J. Renner, G. Schneider, and J. Weissflog, Ger. (East), 15431 (1958), *Chem. Abstr.*, **54**, 2650f (1960); E. S. Blake, U. S. Patent, 2396487 (1946); *Chem. Abstr.*, **40**, 2974 (1946).

2) F. Runge, Z. El-Hewehi, H. J. Renner, and E. Taeger, *J. Prakt. Chem.*, **4**, 284 (1960).

3) F. Runge, and Z. El-Hewehi, *J. Prakt. Chem.*, **10**, 268 (1959); M. Zbirovsky and V. Ettel, *Chem. Listy*, **51**, 2094 (1957); *Chem. Abstr.*, **52**, 6318 (1958).

4) H. C. Godt, Jr. and A. E. Wann, *J. Org. Chem.*, **26**, 4047 (1961).

5) S. Tanimoto, T. Oida, H. Ikehira, and M. Okano, *Bull. Chem. Soc. Jpn.*, **55**, 1977 (1982).

6) P. J. Wepplo and D. P. Wright, Jr., Ger. Often., 2937334 (1980); *Chem. Abstr.*, **93**, 149828d (1980).

7) R. Sato, T. Goto, Y. Takikawa, and S. Takizawa, *Synthesis*, **1980**, 615; R. Sato, T. Etchu, Y. Takikawa, S. Takizawa and M. Saito, *ibid.* **1983**, 44; R. Sato, S. Chiba, Y. Takikawa, S. Takizawa, and M. Saito, *Chem. Lett.*, **1983**, 535; R. Sato, N. Saito, and M. Satio, *ibid.*, **1983**, 1063; R. Sato, N. Saito, Y. Takikawa, S. Takizawa, and M. Saito, *Synthesis*, **1983**, 1045.

Oxidation Products of β-Methyl-substituted δ-Lactones Using Benzeneseleninic Anhydride and Selenium Dioxide

Takanao MATSUI,* Shuji TAHARA, and Mitsuru NAKAYAMA†
Faculty of Engineering, Miyazaki University, Miyazaki 880
†*Faculty of Science, Hiroshima University, Hiroshima 730*
(Received May 31, 1984)

Synopsis. When 9,9-ethylenedioxy-6-methoxycarbonyl-5-methyl-2-oxabicyclo[4.4.0]decan-3-one was treated with benzeneseleninic anhydride and selenium dioxide, the former yielded preferentially the 4,5-dehydrogenated compound (**2**) together with small amounts of the 5-formyl compound (**3**) and the contraction product (**4**) of the δ-lactone ring, while the latter produced solely **2** in a poor yield.

Utility of benzeneseleninic anhydride (BSA) as an oxidizing reagent has been growing in organic synthesis concerning the preparation of aldehydes and ketones from alcohols and benzylic hydrocarbons.[1] More recently, Barton *et al.* have reported that δ-lactones such as 4-oxa-5α-cholestan-3-one reacted with BSA to form the α,β-unsaturated lactones,[2] but there has been relatively few utilization of BSA as dehydrogenating reagent for lactones and lactams. In addition to the examples, we also wish to report the pretty preparation of 9,9-ethylenedioxy-6-methoxycarbonyl-5-methyl-2-oxabicyclo[4.4.0]dec-4-en-3-one (**2**)[3] from its 4,5-dihydro compound (**1**) by the use of BSA and the investigation of the oxidation products from cyclic lactones (**1**, **2**, and **5**) with BSA and SeO_2.

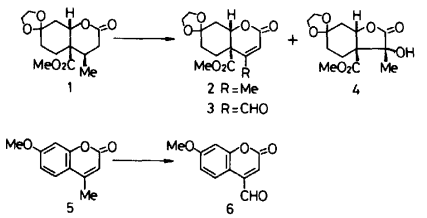

Scheme 1.

Oxidation reaction of **1** with 1.3 molar equivalent of BSA in chlorobenzene at 80—85 °C for 42 h under N_2 afforded the dehydrogenated compound **2** in 70% yield along with small amounts of the aldehyde **3** and contraction product, 4,4-ethylenedioxy-9-hydroxy-1-methoxycarbonyl-9-methyl-7-oxabicyclo[4.3.0]nonan-8-one (**4**) (Run 2). This method represented better yield of **2** and one-step preparation of α,β-unsaturated δ-lactone in comparison with the previous result due to oxidation-fragmentation of the phenylseleno derivative of **1**.[3] Some results obtained from the reactions which were carried out under a range of the reaction conditions as discussed below are shown in Table 1. The longer reaction time, 95—96 h at 82—90 °C (Run 4, 5) seemed to afford improvement of the yield of **2**, but when performed with more than 1.3 molar equivalent of BSA and refluxing conditions the yield of **2** became somewhat lower (Run 10). Attempts to effect a progressive preparation of **3** from **1** or **2** by utilizing BSA under various reaction conditions were unsuccessful, suggesting little participation of BSA itself in the formation of **3**. In contrast with BSA, using SeO_2 to the oxidation of **1** and **2** under refluxing conditions afforded **2** in *ca.* 17% yield (Run 15) and **3** in *ca.* 26% yield (Run 13), respectively. These results noted that the methyl group on C-5 of **2** was considerably oxidizable with SeO_2. Furthermore, a similar allylic oxidation reaction of an α,β-unsaturated δ-lactone moiety such as 7-methoxy-4-methylcoumarin (**5**) in hot chlorobenzene containing SeO_2 gave an excellent yield (89%) of its 4-formyl compound **6**. All the products **2**, **3**, **4**, and **6** gave satisfactory spectroscopic data and elemental analyses. In addition, the molecular of **4** was established unambiguously by an X-ray crystal structure analysis of its acetate (Fig 1).[5]

A pathway for the formation of **2** and **4** from **1** by the use of BSA can be explained on the basis of that for BSA oxidation proposed by Barton *et al.* (Scheme 2).[2,6] On the other hand, the case of **3** is considered that it was likely produced by further oxidation of **2** with some selenoxide species such as an analog of SeO_2 which would be allowed in the course of the oxidation reaction in the presence of BSA.

Thus, the use of BSA seems to be an effective way in view of the simple handling procedure in order to obtain α,β-unsaturated δ-lactones from its saturated lactones. It was also found that BSA is not convenient

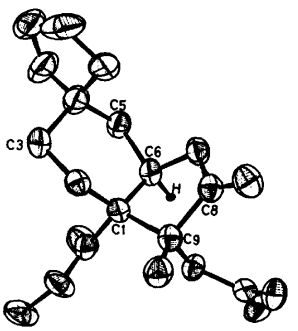

Fig. 1. ORTEP drawing of the molecular structure of acetate of **4**.[4]

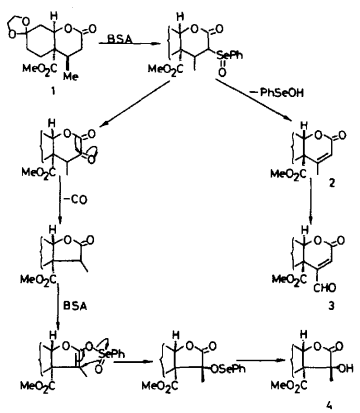

Scheme 2.

Table 1. Yields of 2 and 3[a]

Run	Compd	BSA or SeO_2[b]	Reaction temp/°C and time/h	Yield[c]/%	
				2	3
1[d]	1	1.30 BSA	65—67 40	17	None
2	1	1.30 BSA	80—85 42	70	Trace
3	1	1.29 BSA	90—95 42	69	Trace
4	1	1.30 BSA	82—88 95	75	Trace
5	1	1.30 BSA	78—90 96	78	Trace
6[d]	1	0.51 BSA	83—88 44	26	None
7[d]	1	0.86 BSA	82—87 42	41	None
8[d]	1	1.13 BSA	84—88 42	50	Trace
9	1	1.31 BSA	Reflux 20	41	6
10	1	2.50 BSA	Reflux 20	33	7
11[d]	2	1.28 BSA	Reflux 20		7
12[d]	2	2.50 BSA	Reflux 20		5
13[d]	2	1.25 SeO_2	Reflux 20		26
14[d]	1	2.50 SeO_2	Reflux 20	9	None
15[d]	1	1.20 SeO_2	Reflux 20	17	None

a) The reactions were carried out in chlorobenzene except those of Run 13 and 15 in *o*-xylene. b) Molar ratio of BSA or SeO_2 to the starting material. c) Determined by column chromatographic separation. d) These reactions, Run 1, 6—8, and 11—15 gave recovery of the starting material in 59, 51, 35, 44, 26, 68, 53, and 51%, respectively.

for the oxidation of allylic methyl group in comparison with SeO_2.

Experimental

IR and NMR spectra were measured in $CHCl_3$ and $CDCl_3$, respectively. Chemical shifts are given in δ values (ppm) downfield from the internal TMS reference. The X-ray diffraction data were obtained on an Enraf-Nonius CAD-4 automated four-circle diffractometer with a SDP program package.

General Procedure for the Oxidation of δ-Lactones Using BSA. A mixture of starting material and BSA in dry chlorobenzene was stirred under N_2. After removal of the solvent *in vacuo*, the residue was separated and purified by chromatographic work-up on silica gel with a mixture of benzene and ethyl acetate. **2**: Colorless plates, mp 105—107 °C (ethyl acetate–hexane); IR: 1735, 1720, and 1645 (weak) cm^{-1}; ^{1}H-NMR: 1.4—1.8 and 2.0—2.2 (6H, m, 3X-CH_2-), 2.07 (3H, s, C_5-CH_3), 3.76 (3H, s, -CO_2CH_3), 3.96 (4H, s, ethylenedioxy group), 5.04 (1H, dd, J=6 and 10 Hz, C_1-H), and 5.96 (1H, s, C_4-H); ^{13}C-NMR: 19.9 (q, C_5-CH_3), 26.9, 31.5, and 37.2 (each t, C_7, C_8, and C_{10}), 49.8 (s, C_6), 53.2 (q, -$CO_2\underline{C}H_3$), 64.6 (t, ethylenedioxy group), 77.6 (d, C_1), 107.1 (s, C_9), 120.0 (d, C_4), 155.2 (s, C_5), 162.7 (s, C_3), and 171.9 (s, -$\underline{C}O_2CH_3$); MS: *m/z* 282 (M^+); Found: C, 59.79; H, 6.51%. Calcd for $C_{14}H_{18}O_6$: C, 59.56; H, 6.43%. **3**: Colorless needles, mp 144—145.5 °C (ethyl acetate–hexane); IR: 2850, 2750 (weak), 1740, 1720, and 1620 (weak) cm^{-1}; ^{1}H-NMR: 1.3—1.6, 1.9—2.3, and 2.4—2.7 (6H, m, 3X-CH_2-), 3.75 (3H, s, -CO_2CH_3), 3.98 (4H, s, ethylenedioxy group), 5.04 (1H, dd, J=6 and 8 Hz, C_1-H), 6.76 (1H, s, C_4-H), and 9.73 (1H, s, -CHO); ^{13}C-NMR: 26.0, 31.1, and 37.2 (each t, C_7, C_8, and C_{10}), 47.3 (s, C_6), 53.4 (q, -$CO_2\underline{C}H_3$), 64.9 (t, ethylenedioxy group), 79.4 (d, C_1), 106.8 C_9), 134.0 (d, C_4), 150.0 (s, C_5), 161.9 (s, C_3), 171.0 (s, -$\underline{C}O_2CH_3$), and 191.3 (d, -CHO); MS: *m/z* 296 (M^+); Found: C, 56.93; H, 5.55%. Calcd for $C_{14}H_{16}O_7$: C, 56.75; H, 5.44%. **4**: Colorless plates, mp 183.5—185.5 °C (ethyl acetate–hexane); IR: 3600, 1780, and 1740 cm^{-1}; ^{1}H-NMR: 1.5—2.3 (6H, m, 3X-CH_2-), 1.50 (3H, s, C_9-CH_3), 3.21 (1H, s, OH), 3.78 (3H, s, -CO_2CH_3), 3.92 (4H, s, ethylenedioxy group), and 5.20 (1H, t, J=4 Hz, C_6-H); ^{13}C-NMR: 17.7 (q, C_9-CH_3), 25.2, 30.8, and 33.9 (each t, C_2, C_3, and C_5), 52.5 (q, -$CO_2\underline{C}H_3$), 55.2 (s, C_1), 64.2 and 64.7 (each t, ethylenedioxy group), 77.5 (d, C_6), 78.6 (s, C_9), 106.3 (s, C_4), 170.5 (s, -$\underline{C}O_2CH_3$), and 174.8 (s, C_8); MS: *m/z* 286 (M^+); Found: C, 54.61; H, 6.35%. Calcd for $C_{13}H_{18}O_7$: C, 54.55; H, 6.29%. This compound was obtained in less than 10% yield. Acetate of 4: Colorless plates, mp 129—130.5 °C (ethyl acetate–hexane); IR: 1790, 1750, and 1740 cm^{-1}, ^{1}H-NMR: 1.5—2.3 (6H, m, 3X-CH_2-), 1.66 (3H, s, C_9-CH_3), 2.00 (3H, s,-$OCOCH_3$), 3.79 (3H, s, -CO_2CH_3), 3.92 (4H, s, ethylenedioxy group), and 5.15 (1H, t, J=4 Hz, C_6-H); MS: *m/z* 328 (M^+); Found: C, 54.96; H, 5.85%. Calcd for $C_{15}H_{20}O_8$: C, 54.87; H, 6.14%.

4-Formyl-7-methoxycoumarin (6). A mixture of **5** (480 mg, 2.53 mmol), SeO_2 (400 mg, 3.60 mmol; purified by sublimation method) in dry chlorobenzene (70 ml) was refluxed for 20 h under N_2. After the usual work-up, the crude solid was chromatographed on silica gel using dichloromethane as the eluent to afford 460 mg of **6**; yellow needles, mp 204—206 °C recrystd from dichloromethane (lit,[7] mp 195 °C). IR: 2850, 2750 (weak), 1750 sh, 1720, and 1615 cm^{-1}; ^{1}H-NMR: 3.89 (3H, s, -OCH_3), 6.76 (1H, s, C_3-H), 6.91 (1H, d, J=3 Hz, C_8-H), 7.02 (1H, dd, J=3 and 8 Hz, C_6-H), 8.54 (1H, d, J=8 Hz, C_5-H), and 10.14 (1H, s, -CHO), MS: *m/z* 204 (M^+); Found: C, 64.92; H, 3.90%. Calcd for $C_{11}H_8O_4$: C, 64.70; H, 3.95%.

The authors appreciate to the Research Center for Material Analysis in Miyazaki University for the NMR and MS measurements and the X-ray crystallographic analyses.

References

1) R. Okazaki and K-T. Kang, *Yuki Gosei Kagaku Kyokai Shi*, **38**, 1223 (1980) and references cited therein.

2) D. H. R. Barton, R. A. H. F. Hui, S. V. Ley, and D. J. Williams, *J. Chem. Soc., Perkin Trans. 1*, **1982**, 1919.

3) Compound **2** has been synthesized in 49% yield by α-phenylselenenylation of **1** with lithium diisopropylamide and benzeneselenenyl chloride, followed by oxidation of the phenylseleno derivative with H_2O_2; J. D. White, T. Matsui, and J. A. Thomas, *J. Org. Chem.*, **46**, 3376 (1981).

4) C. K. Johnson, ORTEP. Oak Ridge National Laboratory Report ORNL-3794 (1965).

5) The complete Fo and Fc data are deposited at the Office of the Editor of the Bulletin of the Chemical Society of Japan (Document No. 8453).

6) D. H. R. Barton, D, J. Lester, and S. V. Ley, *J. Chem. Soc., Chem. Commun.*, **1978**, 130.

7) A. Schiavello and E. Cingolani, *Gazz. Chim. Ital.*, **81**, 717 (1951); *Chem. Abstr.*, **46**, 6126 (1952).

Deoximation of Oxime *O*-Acetates, Oximes, and Oxime Ethers by Nonacarbonyldiiron or Pentacarbonyliron. An Electronic Effect for the N-O Bond Cleavage[1)]

Makoto NITTA,* Ichiro SASAKI, Hiroyuki MIYANO, and Tomoshige KOBAYASHI
Department of Chemistry, School of Science and Engineering, Waseda University, Shinjuku-ku, Tokyo 160
(Received June 5, 1984)

Synopsis. The reaction of $[Fe_2(CO)_9]$ or $[Fe(CO)_5]$ with oxime *O*-acetates, oximes, and oxime ethers under photoirradiation or thermal conditions undergoes deoximation to give the corresponding ketones. The oxime *O*-acetate was found to be the most reactive class of these compounds. A proposed mechanism involves an initial complexation of the $[Fe(CO)_4]$ species to the nitrogen atom of the oxime group, and the subsequent N-O bond cleavage to give an imido complex. Then the imido complex could collapse to the corresponding ketone via an imine intermediate in protic media.

Previous works in this series have included the papers involving a system which formally contains a C=N-O group.[2,3)] The reaction of substituted 2-isoxazolines with $[Fe_2(CO)_9]$ or $[Fe(CO)_5]$ in methanol under thermal conditions or photoirradiation has been shown to undergo the N-O and C_4-C_5 bond cleavages to give two fragments of aldehydes and the complexed nitrenes, which could collapse to ketones in protic media.[2,4)] Under similar reaction conditions, substituted isoxazoles could undergo a reductive cleavage of the N-O bond to give β-amino enones in good yields.[3)] Although the transformation of oximes to the corresponding ketones has been accomplished thermally by $[Fe(CO)_5]$-$BF_3 \cdot OEt_2$[5)] or $[Fe(CO)_5]$[6)] in anhydrous solvent, the role of $BF_3 \cdot OEt_2$ or the electronic factor controlling the N-O bond cleavage is ambiguous.

In this paper we report on the deoximation of oxime *O*-acetates **1a—d**, oximes **2a—d**, and oxime ethers **3a,c** by $[Fe_2(CO)_9]$ or $[Fe(CO)_5]$ in methanol under thermal conditions or photoirradiation, and suggest that the greater pertinence of the N-O bond cleavage for the oxime *O*-acetates may lead to the corresponding ketones **4a—d**. The reaction conditions and the yields of the products are summarized in Table 1.

Thermal reaction of oxime O-acetates **1a—d** with $[Fe_2(CO)_9]$ in methanol at 60 °C for 1 h afforded the corresponding ketones **4a—d** in good yields (Table 1, entries 1—4). Similarly, photoirradiation of **1a—d** with $[Fe(CO)_5]$ in methanol at the ambient temperature afforded the ketones and the remainder being unreacted starting materials (entries 5—8). On the other hand, thermal reaction of oximes **2a—d** (entries 9—12) or oxime ether **3a** (entry 17) with $[Fe_2(CO)_9]$ proceeded slowly and afforded the corresponding ketones, along with the unreacted starting materials. Furthermore, photoreaction of **2a—d** (entries 13—16) or **3c** (entry 18) with $[Fe(CO)_5]$ also proceeded very slowly as compared to the cases of **1a—d** (5—8). The oximes of conjugated ketones (entries 13 and 14) seem to be less reactive than those of nonconjugated ketones (entries 15 and 16). Regarding the reaction time and the yields of the

TABLE 1. DEOXIMATION OF OXIME *O*-ACETATES **1**, OXIMES **2**, AND OXIME ETHERS **3**

Entry	Compound	Reaction conditions[a)]	Reaction time/h	Product[b)]	
				Ketone **4**	Recovery
1	**1a**	A	1	94	0
2	**1b**	A	1	87	0
3	**1c**	A	1	91	0
4	**1d**	A	1	82	0
5	**1a**	B	22	82	10
6	**1b**	B	22	53	23
7	**1c**	B	16	76	11
8	**1d**	B	18	53	27
9	**2a**	A	1	32	64
10	**2b**	A	4	30	51
11	**2c**	A	1	67	19
12	**2d**	A	1	60	24
13	**2a**	B	60	65	26
14	**2b**	B	48	28	61
15	**2c**	B	22	89	0
16	**2d**	B	48	81	0
17	**3a**	A	4	15	80
18	**3c**	B	24	65	6

a) A: A molar equivalent quantity of $[Fe_2(CO)_9]$ was used, being heated at 60 °C. B: 2 Molar equivalent quantity of $[Fe(CO)_5]$ was used, being photoirradiated. b) Isolated yield based on the starting material used. c) Isolated yield of the unreacted starting material.

ketones, the oxime *O*-acetates are very labile as compared to the oximes or oxime ethers under both the thermal and photoirradiation conditions. Therefore, the deoximation of oxime *O*-acetates by $[Fe_2(CO)_9]$ under thermal conditions appears most promising.

The present reactions are best explained by the mechanism shown in Scheme 1. Free or solvated $[Fe(CO)_4]$ species have been generally assumed to be the reactive common intermediate in the photolysis[7] or thermolysis ($\geq$80 °C) of $[Fe(CO)_5]$ and thermolysis ($\geq$20 °C) of $[Fe_2(CO)_9]$.[8] Therefore, thermally or photochemically generated $[Fe(CO)_4]$ species could be a reasonable intermediate in the present deoximation reactions.[2,3] The initial step could be a complexation to give **5**. The subsequent N–O bond cleavage could give imido complex **6**.[2] In methanol, the nitrogen moiety of **6** could be reduced by iron moiety,[2,4] and the subsequent protonation could give an imine such as **7**,[6] which could collapse to the ketones by stray water or under workup conditions.

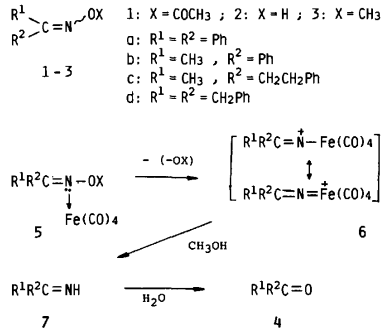

Scheme 1.

2-Isoxazoline is a cyclic ether of oximes, and it undergoes facil N–O and C-4–C-5 bond cleavages to give an aldehyde and a complexed nitrene intermediate which collapses to the corresponding ketone.[2] However, the reactions of oximes **2a-d** as well as oxime ethers **3a,c** are not completed after prolonged heating or photoirradiation (Table 1). Regarding the rigid *N*-complexed C=N–O group (formal hetero-analogue of an allylic anion) of **8** (R=Phenyl or Alkyl), the delocalization of π-d electron from the iron to the π^* orbital of the C=N–O group was suggested to weaken the N–O bond.[2]

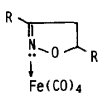

8 R = Ph or Alkyl

This electronic effect allowing a facile N–O bond cleavage seems to be reduced by a free rotation across the N–O bond in the cases of oximes and oxime ethers as well as oxime *O*-acetates. The higher reactivity of oxime *O*-acetate as compared to oximes or oxime ethers could be ascribed to the large leaving ability of the OAc group as compared to the OH or OR group.

The reductive[9] or oxidative[10] transformation of oximes to the corresponding ketones has been accomplished. The reductive deoximation of oxime *O*-acetates has also been accomplished by chromium(II) acetate.[11] The present reaction of oxime *O*-acetates could also serve as a convenient method for the deoximation reaction.

Experimental

$[Fe(CO)_5]$ (Strem Chemical Inc.) is a commercial sample. $[Fe_2(CO)_9]$ was prepared by the standard method.[12] All of the reactions were carried out under a dry nitrogen atmosphere. The photoirradiation was carried out using Rayonet Photoreactor fitted with RPR-350 lamps through a Pyrex filter. The oximes and oxime O-acetates were prepared by the standard method. The oxime ethers were prepared by a phase transfer method.[13]

General Procedure for the Deoximation of Oxime O-Acetates 1a—d, Oximes 2a—d, and Oxime Ether 3a with $[Fe_2(CO)_9]$ under Thermal Conditions. A solution of **1a—d**, **2a—d**, or **3a** (1 mmol) and $[Fe_2(CO)_9]$ (437 mg, 1 mmol) in 10 cm^3 of anhydrous methanol was heated at 60 °C for an adequate period. After removal of the methanol, the residue was dissolved in 30 cm^3 of a benzene–hexane mixture (2/1) and filtered through Celite to remove insodluble materials. Then the filtrate was concentrated and the resulting residue was separated by TLC on silica gel using benzene as the eluent to give the corresponding ketones and unreacted starting materials. The results are summarized in Table 1.

General Procedure for the Deoximation of Oxime O-Acetates 1a—d, Oximes 2a—d, and Oxime Ether 3c with $[Fe(CO)_5]$ under Photoirradiation. A solution of **1a—d**, **2a—d**, or **3c** (1 mmol) and $[Fe(CO)_5]$ (392 mg, 2 mmol) in 10 cm^3 of anhydrous methanol was irradiated for an adequate period. After the methanol was evaporated, the residue was dissolved in 30 cm^3 of a benzene–hexane mixture (2/1). Then the solution was filtered through Celite to remove insoluble materials. After evaporating the filtrate the resulting residue was separated by TLC on silica gel using benzene as the eluent to give the corresponding ketones and unreacted starting materials. The results are summarized in Table 1.

References

1) This paper was presented at the National Meeting of Chemical Society of Japan, April 1983.
2) M. Nitta and T. Kobayashi, *Chem. Lett.*, **1983**, 51; M. Nitta and T. Kobayashi, *J. Chem. Soc., Perkin Trans. I*, **1984**, 2103.
3) M. Nitta and T. Kobayashi, *Tetrahedron Lett.*, **23**, 3925 (1982).
4) M. Nitta and T. Kobayashi, *Bull. Chem. Soc. Jpn.*, **57**, 1035 (1984).
5) H. Alper and J. T. Edward, *J. Org. Chem.*, **32**, 3938 (1968).
6) A. Dondoni and J. Turner, *Chem. Commun.*, **1975**, 761.
7) M. Poliakoff and J. Turner, *J. Chem. Soc., Dalton Trans.*, **1974**, 210, 2276.
8) R. C. Kerber, "*The Chemistry of Iron*," ed by F. W. Crevels and I. Fishler, Academic Press, New York, 1981, p 1.
9) D. P. Curran, J. F. Brill, and D. M. Rakiewicz, *J. Org. Chem.*, **49**, 1654 (1984); and the references cited therein.
10) G. A. Olah, J. Welch, and M. Henninger, *Synthesis*, **1977**, 308; G. A. Olah, J. Welch, G. K. Suruya Parakash, and Tse-Lok Ho, *Synthesis*, **1976**, 808; G. A. Olah, and Tse-Lok Ho, *Synthesis*, **1976**, 610; and the references cited in these papers.
11) E. J. Corey and J. E. Richman, *J. Am. Chem. Soc.*, **92**, 5276 (1970).
12) R. B. King, *Org. Synth.*, Academic Press, **1965**, vol. 1, p 93.
13) H. Shinozaki, N. Yoshida, and M. Tajima, *Chem. Lett.*, **1980**, 869.

The Reductive Amination of Carbonyl Compounds Using Sodium Hydrogentelluride as a Reducing Reagent

Masakazu YAMASHITA,* Mamoru KADOKURA,† and Rikisaku SUEMITSU
Department of Applied Chemistry, Doshisha University, Kamikyo-ku, Kyoto 602
(Received July 11, 1984)

Synopsis. Carbonyl compounds were aminated to secondary amines in moderate yields under mild conditions using sodium hydrogentelluride as a reducing reagent.

Sodium hydrogentelluride (NaTeH, **1**) has been known as a useful reducing reagent and has been used for the reduction of *vic*-dibromo compounds,[1] α,β-unsaturated carbonyl compounds,[2] nitro compounds,[3] α,β-epoxy ketones,[4] *gem*-dibromocyclopropanes,[5] and α-halo carbonyl compounds.[6]

In this paper, we wish to report that **1** is also useful for the reductive amination of carbonyl compounds to secondary amines (Eq. 1).[7]

$$\begin{matrix} R^1 \\ R^2 \end{matrix}\!\!>\!C{=}O + R^3NH_2 \xrightarrow[\text{EtOH, r.t.}]{1} \begin{matrix} R^1 \\ R^2 \end{matrix}\!\!>\!CH\text{-}NHR^3 \qquad (1)$$

For example, benzaldehyde (2 mmol) and butylamine (2 mmol) were added to an ethanolic solution of **1** prepared *in situ* from tellurium and $NaBH_4$, and the mixture wes stirred at room temperature for 20 h. The usual subsequent work-up gave *N*-butylbenzylamine in an 88% yield. The results are summarized in Table 1. As can be seen from Table 1, aliphatic amines afforded the products in good yields, although the yields of the products derived from aniline were rather low. However, when two equivalents of aniline were used, the yield of the corresponding amine was improved (Run 2). In these cases, unreacted aniline and carbonyl compounds were recovered, and no by-product was formed. When glutaraldehyde was treated with amines, *N*-substituted piperidines were obtained as the sole reaction product (Table 2). When 2,5-hexanedione was used, the yield of the pyrrolidine derivative was less than 10%.

Generally, Schiff bases are considered as intermediate of the reductive amination reaction of carbonyl compounds,[7] therefore, in this reaction, the base is also assumed to be formed as an intermediate. In fact, *N*-benzylideneaniline, a representative Schiff base, was reduced by **1** to *N*-benzylaniline in a 70% yield under same reaction conditions.

The good yields of the products, the ease of the reaction procedure, the mildness of the reaction conditions, and the absence of any side reaction make it possible to utilize this reaction for the one-pot synthesis of secondary amines.

Experimental

General. The nuclear magnetic resonance (^1H NMR) spectra were recorded on Hitachi R-600 FT-NMR spectrometer (60 MHz), using Me_4Si as the internal standard. The mass spectra were recorded on a Hitachi RM-50 GC-MS spectrometer. The infrared spectra (IR) were recorded on a Hitachi 260-10 infrared spectrometer. Thin-layer chromatography was performed on Merck Silica Gel.

Materials. The tellurium powder and $NaBH_4$ were purchased from Nakarai Chemicals in an extra pure grade and were used without further purification. The ethanol was distilled and stored over 3A molecular sieves. The *N*-benzylideneaniline was synthesized according to the method in the literature.[8] The glutaraldehyde was available as a 25 wt% solution in water and was used without distillation. All the other compounds in this report were commercial products and were used without further purification.

General Procedure for Reductive Amination. Finely divided tellurium powder (0.65 g, 5 mmol) and $NaBH_4$ (0.45 g, 11 mmol) were placed in a two-necked flask containing a

Table 1. Reductive amination of carbonyl compounds

Run	Carbonyl compound	Amine	Product	Yield/%[a]
1	Benzaldehyde	Aniline	*N*-Benzylaniline	41
2	Benzaldehyde	Aniline[b]	*N*-Benzylaniline	73
3	Benzaldehyde	*p*-Toluidine	*N*-Benzyl-*p*-toluidine	49
4	Benzaldehyde	*p*-Anisidine	*N*-Benzyl-*p*-anisidine	58
5	Benzaldehyde	Cyclohexylamine	*N*-Cyclohexylbenzylamine	80
6	Benzaldehyde	Butylamine	*N*-Butylbenzylamine	88
7	*p*-Tolualdehyde	Aniline	*N*-Phenyl-4-methylbenzylamine	20
8	*p*-Anisaldehyde	Aniline	*N*-Phenyl-4-methoxybenzylamine	44
9	Butyraldehyde	Aniline	*N*-Butylaniline	24
10	Butyraldehyde	Benzylamine	*N*-Butylbenzylamine	96
11	Cyclohexanone	Aniline	*N*-Cyclohexylaniline	6
12	Cyclohexanone	Butylamine	*N*-Butylcyclohexylamine	94
13	Acetone	Benzylamine	*N*-Isopropylbenzylamine	80

a) Isolated yield based on starting carbonyl compounds. b) Two equivalents of aniline were used.

† Present address: Department of Hydrocarbon Chemistry, Kyoto University.

Table 2. Reductive amination of glutaraldehyde

Run	Amine	Product	Yield/%[a)]
1	Aniline	*N*-Phenylpiperidine	34
2	Benzylamine	*N*-Benzylpiperidine	86
3	Butylamine	*N*-Butylpiperidine	54

a) Isolated yield based on starting carbonyl compounds.

Teflon-covered stirring bar. The system was then evacuated and filled with argon. Dry ethanol (25 ml) was injected by means of a syringe, and the suspension was heated at 45 °C until a purple solution was formed. The evolution of hydrogen occurred in this period. This solution was cooled to −20 °C, and then 1 ml of acetic acid in 4 ml of ethanol was injected.[9)]

To a solution of NaTeH, prepared *in situ* as above, a carbonyl compound (2 mmol) and an amine (2 mmol) were added at −20 °C. The resulting mixture was stirred for 20 h at room temperature. The tellurium thus precipitated was filtered, and the filtrate was concentrated *in vacuo*. The residue was dissolved in 20 ml of ethyl acetate and acidified with 3 mol dm^{-3} hydrochloric acid. The combined aqueous layer was made basic with NaOH and extracted with two 30-ml portions of ethyl acetate. The extract was dried over anhydrous Na_2SO_4, concentrated, and purified by TLC (elution with hexane and ethyl acetate). The products were identified by a comparison of their NMR, IR, and mass spectra with those of authentic samples.

References

1) K. Ramasamy, S. K. Kalyanasundaram, and P. Shanmugam, *Synthesis*, **1978**, 311.
2) a) K. Ramasamy, S. K. Kalyanasundaram, and P. Shanmugam, *Synthesis*, **1978**, 545; b) M. Yamashita, Y. Kato, and R. Suemitsu, *Chem. Lett.*, **1980**, 847.
3) A. Osuka, H. Shimizu, and H. Suzuki, *Chem. Lett.*, **1983**, 1373.
4) A. Osuka, K. Takaoka, and H. Suzuki, *Chem. Lett.*, **1984**, 271.
5) A. Osuka, K. Takechi, and H. Suzuki, *Bull. Chem. Soc. Jpn.*, **57**, 303 (1984).
6) A. Osuka and H. Suzuki, *Chem. Lett.*, **1983**, 119.
7) W. S. Emerson, *Organic Reactions*, **4**, 174 (1948).
8) L. A. Bigelow and H. Eatough, *Organic Syntheses*, Coll. Vol. **I**, (1941), p. 80.
9) D. H. R. Barton and S. W. McCombie, *J. Chem Soc., Perkin I*, **1975**, 1574.

O- and *C*-Perfluoroalkylations of Phenol System with (Perfluoroalkyl)phenyliodonium Triflates

Teruo UMEMOTO,* and Osamu MIYANO
Sagami Chemical Research Center, Nishi-Ohnuma 4-4-1, Sagamihara, Kanagawa 229
(Received March 23, 1984)

Synopsis. The reaction of FITS reagents with the phenols bearing bulky substituents at *C*-positions yielded *O*- and *C*-perfluoroalkylation products whose ratios were dependent on the steric bulkiness of the substituents or the perfluoroalkyl groups and the reaction temperature.

It is well known that both *O*- and *C*-alkylations occur when phenoxide anions are allowed to react with electrophilic agents such as alkyl halides.[1] However, similar alkylations utilizing perfluoroalkyl halides have never been reported. This may be because the perfluoroalkyl halides would not be effective electrophilic reagents, since the perfluoroalkyl (Rf) group has an extraordinary high electronegativity (3.45).[2]

In 1977, Shreeve and Kitazume reported that phenol reacted with bis(trifluoromethyl)bis(trifluoromethoxy)-sulfurane to give trifluoromethoxybenzene.[3] They, however, proposed a mechanism involving the intramolecular displacement of the phenolic hydroxyl group with the trifluoromethoxyl group *via* an electrocyclic process. Accordingly, their reaction may not be the electrophilic perfluoroalkylation of phenol. Such perfluoroalkylations would be realized only when very efficient electrophilic perfluoroalkylating agents have been developed.

In recent years,[4] we have developed an effective perfluoroalkylating agents, *i.e.* (perfluoroalkyl)phenyliodonium triflates (FITS reagents). In the previous paper,[5] it was demonstrated that the FITS reagent reacts with phenol at its aromatic ring to afford perfluoroalkylphenols. In the present paper, it is shown that both *C*- and *O*-alkylations take place when alkylphenols are allowed to react with FITS reagents.

Results and Discussion

Phenol reacted with FITS-2 or 3*i* in acetonitrile in the presence of pyridine at room temperature to produce a mixture of *C*-Rf phenols without occurrence of *O*-perfluoroalkylation (Eq. 1). The use of FITS-3*i* diminished the formation of the *o*-isomer, suggesting

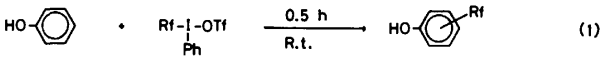

(1)

FITS-2 (Rf = C_2F_5) 53% (o-/p- = 1)
FITS-3i (Rf = i-C_3F_7) 51% (o-/p- = 0.67)

TABLE 1. *O*/*C*-PERFLUOROALKYLATIONS OF **1** WITH FITS-3*i* OR -3

Run	FITS	Solvent	Temp/°C	Yield/% 2	3	1 (Recovered)	Ratio 2/3
1	-3*i*	CH_2Cl_2	−78→R.t.[a]	11	48	24	0.23
2	-3*i*	CH_3CN	R.t.	26	24	22	1.1
3	-3*i*	CH_2Cl_2	R.t.	27	21	30	1.3
4	-3*i*	CH_2Cl_2	Reflux	28	17	29	1.6
5	-3*i*	CH_3CN	Reflux	30	14	26	2.1
6	-3*i*	$ClCH_2CH_2Cl$	Reflux	31	15	34	2.1
7	-3	CH_2Cl_2	R.t.	9	41	23	0.22
8	-3	$ClCH_2CH_2Cl$	Reflux	14	29	31	0.48

a) Addition of FITS was carried out at −78 °C and the reaction mixture was gradually warmed to room temperature overnight.

that steric repulsion between the bulky perfluoroisopropyl and the hydroxyl groups influenced the proportions of the products formed.

When 4-*t*-butylphenol **1** having a bulky substituent at the *p*-position was allowed to react with FITS-3*i* or

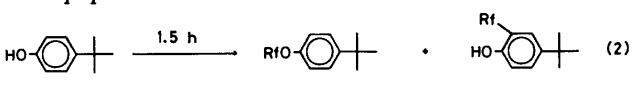

(2)

1 FITS-3i 2a (Rf = i-C_3F_7) 3a
FITS-3 2b (Rf = n-C_3F_7) 3b

-3, *O*-perfluoroalkylation was found to take place in addition to *C*-perfluoroalkylation. The reaction was carried out under several conditions and the results are shown in Table 1. The formation of the *O*-isomer **2a** exceeded that of *C*-isomer **3a** in the reaction of FITS-3*i* at room temperature, while the proportion of the *O*-isomer **2b** by FITS-3 was very low (Run 2 or 3, and 7). It may be attributed to the lesser bulk of the perfluoropropyl group of FITS-3 compared with that of the perfluoroisopropyl group of FITS-3*i*. The ratios of *O*/*C*-Rf phenols were also dependent on the reaction temperature. In the case of FITS-3*i*, **3a** was produced as a major component at low temperature, whereas elevated temperature gave predominantly **2a**. However, the amount of **2b** formed by FITS-3 was less than half of that of **3b** even at the elevated temperature (Run 8). On the other hand, the change in polarity of solvents brought about no significant difference in the ratios of **2**/**3**. From the above results, the appearance of *O*-perfluoroalkylation in the case of the phenol **1** would be mainly ascribed to the steric factor between the bulky substituent at an aromatic ring of **1** and the other bulky FITS reagents.

As expected, 3,5-di-*t*-butylphenol **4** where the *C*-positions are more hindered by two bulky substituents provided the higher proportion of *O*-perfluoroalkylation, but the *O*/*C* ratios were little affected by change in the reaction temperature (Eq. 3, Table 2).

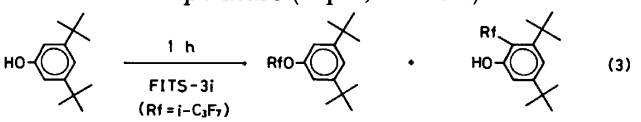

(3)

4 5 6

Furthermore, 2,4,6-tri-*t*-butylphenol **7** where all the reactive *C*- and *O*-positions are blocked gave three *C*-Rf compounds **9**—**11** and a small amount of *O*-Rf

TABLE 2. *O*/*C*-PERFLUOROALKYLATIONS OF **4** WITH FITS-3*i*

Run	Solvent	Temp	Yield/% 5	6	4 (Recovered)	Ratio 5/6
1	CH_2Cl_2	R.t.	50	15	10	3.3
2	$ClCH_2CH_2Cl$	Reflux	56	16	18	3.5

phenol **8** (Eq. 4). The reaction proceeded smoothly at room temperature with change of color. Addition of FITS-3 to a solution of **7** in dichloromethane in the presence of an equivalent amount of pyridine produced a blue color, which soon faded. No color developed in the reactions with phenol, **1**, and **4**. From this fact, it appears that the reaction mechanism of the hindered phenol **7** with FITS is different from that of phenol, **1**, and **4**. The appearance of the color may suggest that the reaction of **7** proceeds *via* a radical cation generated by a one electron transfer from **7** to FITS. It is reasonable that **9** and **10** are formed through cyclohexadienone **12** and **11** with loss of *t*-butyl groups, respectively. The former **12** was not isolated.

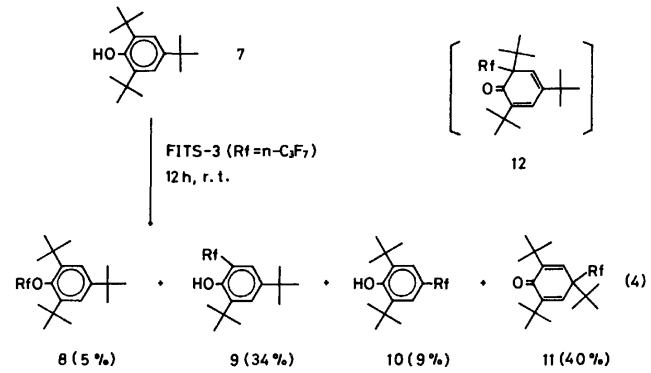

Experimental

NMR spectra were measured in $CDCl_3$ and ^{19}F chemical shifts were given in ppm upfield from $CFCl_3$ as an internal standard. A gas chromatograph with a column of 20% Apiezon grease L on Uniport B or 2% Silicone OV-1 on Chromosorb WAW DMCS was used for analysis of the products. All the reactions were done under argon atmosphere. FITS-2, -3, and -3*i* were prepared by the method described in our first paper.[4] Reaction solvents were purified and dried by the usual methods.

Reaction of Phenol with FITS-2 or -3i. *Typical Procedure*: Into a solution of 376 mg (4 mmol) of phenol and 162 μl (2 mmol) of pyridine in 8 ml of acetonitrile, 944 mg (2 mmol) of FITS-2 was added in several portions at room temperature. The mixture was stirred for 0.5 h at room temperature. After evaporation of the solvent, the residue was column chromatographed on silica gel using dichloromethane as an eluent to give 120 mg (28%) of the *o*-isomer and 107 mg (25%) of the *p*-isomer. The *m*-isomer could not be isolated. The gas chromatography showed the corresponding small peak. *o*-C_2F_5-phenol: Slightly yellow oil. NMR: δ=5.68 (1H, bs, OH), 6.91—7.52 (4H, m). ^{19}F NMR: 85.0 (3F, s), 112.0 (2F, s). *p*-C_2F_5-phenol: Colorless crystals, mp 94—96 °C. NMR: δ=5.09 (1H, s, OH), 6.88 (2H, d, *J*=8.6 Hz), 7.44 (2H, d, *J*=8.6 Hz). ^{19}F NMR: 85.35 (3F, s), 114.3 (2F, bs). IR (KBr): 3280 (OH) cm^{-1}. MS: 212 (M^+). Found: C, 45.14; H, 2.46%. Calcd for $C_8H_5F_5O$: C, 45.30; H, 2.38%. *o-i*-C_3F_7-phenol: Slightly yellow oil. NMR: δ=5.73 (1H, bd, OH, *J*=14 Hz), 6.87—7.44 (4H, m). ^{19}F NMR: 75.32 (6F, d, *J*=7 Hz), 179.0 (1F, m). IR (neat): 3650 (OH), 3450 (OH) cm^{-1}. MS: 262 (M^+). *p-i*-C_3F_7-phenol: Slightly yellow crystals, mp 75—79 °C. NMR: δ=5.25 (1H, bs, OH), 6.88 (2H, d, *J*=8.6 Hz), 7.44 (2H, bd, *J*=8.6 Hz). ^{19}F NMR: 76.62 (6F, d, *J*=8 Hz), 182.2 (1F, heptet, *J*=8 Hz). IR (KBr): 3300 (OH) cm^{-1}. MS: 262 (M^+). Found: C, 41.18; H, 1.94%. Calcd for $C_9H_5F_7O$: C, 41.24; H, 1.92%.

Reaction of 1 or 4 with FITS-3i or -3. *Typical Procedure*: Into a solution of 206 mg (1 mmol) of **4** and 89 μl (1 mmol) of pyridine in 10 ml of dichloromethane, 522 mg (1 mmol) of FITS-3*i* was added in several portions at the temperature shown in Table 2. The mixture was stirred for 1 h at that temperature. Yields were determined by GC. The results are shown in Tables 1 and 2. For the isolation of the products, a similar post-treatment as described above was carried out. **2a**: Colorless oil. NMR: δ=1.31 (9H, s), 7.06 (2H, d, *J*=9.0 Hz), 7.33 (2H, d, *J*=9.0 Hz). ^{19}F NMR: 79.04 (6F, d, *J*=3.4 Hz), 135.6 (1F, m). MS: 318 (M^+). Found: C, 48.94; H, 4.12%. Calcd for $C_{13}H_{13}F_7O$: C, 49.06; H, 4.09%. **3a**: Colorless oil. NMR: δ=1.28 (9H, s), 5.57 (1H, d, OH, *J*=14 Hz), 6.84 (1H, dd, *J*=9.1, 1.0 Hz), 7.39 (1H, dd, *J*=9.1, 2.4 Hz), 7.38 (1H, m). ^{19}F NMR: 75.36 (6F, d, *J*=7.0 Hz), 178.9 (1F, m). IR (neat): 3660 (OH) cm^{-1} MS: 318 (M^+). Found: C, 48.92; H, 4.22%. Calcd for $C_{13}H_{13}F_7O$: C, 49.06; H, 4.09%. **2b**: Colorless oil. NMR: δ=1.31 (9H, s), 7.08 (1H, d, *J*=9.0 Hz), 7.36 (1H, d, *J*=9.0 Hz). ^{19}F NMR: 81.72 (3F, t, *J*=5.0 Hz), 83.92 (2F, m, OCF_2), 129.9 (2F, t, *J*=2.0 Hz). MS: 318 (M^+). **3b**: Colorless oil. NMR: δ= 1.29 (9H, s), 5.45 (1H, t, OH, *J*=5.0 Hz), 6.87 (1H, d, *J*=8.7 Hz), 7.33 (1H, d, *J*=2.2 Hz), 7.43 (1H, dd, *J*=8.7, 2.2 Hz). ^{19}F NMR: 70.02 (3F, t, *J*=10.0 Hz), 98.79 (2F, m, OCF_2), 127.0 (2F, s). IR (neat): 3660 (OH), 3500 (OH) cm^{-1}. MS: 318 (M^+). Found: C, 48.87; H, 4.19%. Calcd for $C_{13}H_{13}F_7O$: C, 49.06; H, 4.09%. **5**: Colorless oil. NMR: δ=1.31 (18H, s), 7.02 (2H, m), 7.34 (1H, d, *J*=1.6 Hz). ^{19}F NMR: 78.87 (6F, d, *J*=3 Hz), 134.7 (1F, m). MS: 374 (M^+). Found: C, 54.72; H, 5.47%. Calcd for $C_{17}H_{21}F_7O$: C, 54.55; H, 5.61%. **6**: Slightly yellow crystals, mp 118—120 °C. NMR: δ=1.30 (9H, s), 1.44 (9H, d, *J*=4.0 Hz), 5.08 (1H, bs, OH), 6.69 (1H, t, *J*=2.0 Hz), 7.37 (1H, d, *J*=2.0 Hz). ^{19}F NMR: 71.88 (6F, d, *J*=2.2 Hz), 164.8 (1F, m). IR (KBr): 3475 (OH) cm^{-1}. MS: 374 (M^+). Found: C, 54.98; H, 5.69%. Calcd for $C_{17}H_{21}F_7O$: C, 54.55; H, 5.61%.

Reaction of 7 with FITS-3. Phenol **7** (535 mg, 2 mmol) was treated with 1.04 g (2 mmol) of FITS-3 and 178 μl (2 mmol) of pyridine in 8 ml of dichloromethane at room temperature in a similar manner as described above. After stirring for 12 h at room temperature, a similar post-treatment as above gave **8**, **9**, **10**, and **11** in 5, 34, 9, and 40% isolated yields, respectively. **8**: Colorless oil. NMR: δ=1.30 (9H, s), 1.36 (18H, s), 7.26 (2H, bs). ^{19}F NMR: 77.72 (2F, q, OCF_2 *J*=10.0 Hz), 81.74 (3F, t, *J*=10.0 Hz), 126.3 (2F, s). **9**: Slightly yellow oil. NMR: δ=1.29 (9H, s), 1.41 (9H, s), 582 (1H, t, OH, *J*=10.0 Hz), 7.18 (1H, m), 7.49 (1H, bd, *J*=2.0 Hz). ^{19}F NMR: 80.60 (3F, t, *J*=10.0 Hz), 108.1 (2F, dq, *J*=10.0, 10.0 Hz), 126.9 (2F, s). IR (neat): 3700 (OH) cm^{-1}. MS: 374 (M^+). Found: C, 54.50; H, 5.80%. Calcd for $C_{17}H_{21}F_7O$: C, 54.55; H, 5.61%. **10**: Colorless crystals, mp 58—60 °C. NMR: δ=1.44 (18H, s), 5.54 (1H, s, OH), 7.33 (1H, s). ^{19}F NMR: 80.56 (3F, t, *J*=10.0 Hz), 110.8 (2F, q, *J*=10.0 Hz), 126.8 (2F, s). IR (KBr): 3670 (OH) cm^{-1}. MS: 374 (M^+). Found: C, 54.56; H, 5.66%. Calcd for $C_{17}H_{21}F_7O$: C, 54.55; H, 5.61%. **11**: Pale yellow oil. NMR: δ=1.07 (9H, m), 1.25 (18H, s), 6.62 (2H, t, *J*=1.5 Hz). ^{19}F NMR: 80.25 (3F, t, *J*=13 Hz), 109.9 (2F, m), 121.1 (2F, bs). IR (neat): 1670 (C=O) 1645 (C=C), cm^{-1}. MS: 430 (M^+).

References

1) Gompper, *Angew. Chem. Int. Ed. Engl.*, **3**, 560 (1964) and references cited therein.

2) J. E. Huheey, *J. Phys. Chem.*, **69**, 3284 (1965).

3) T. Kitazume and J. M. Shreeve, *J. Am., Chem. Soc.*, **99**, 4194 (1977).

4) T. Umemoto, Y. Kuriu, H. Shuyama, O. Miyano, and S. Nakayama, *J. Fluorine Chem.*, **20**, 695 (1982); T. Umemoto, *Yuki Gosei Kagaku Kyokai Shi*, **41**, 251 (1983); T. Umemoto, *Tetrahedron Lett.*, **25**, 81 (1984) and references cited therein.

5) T. Umemoto, Y. Kuriu, and H. Shuyama, *Chem. Lett.*, **1981**, 1663.

Adsorption Effects of Highly Polarizable Organic Compounds on Electrode Kinetics

Osamu IKEDA,* Ken-ichi WATANABE, Yasuhiko TANIGUCHI, and Hideo TAMURA
Department of Applied Chemistry, Faculty of Engineering, Osaka University, 2-1 Yamadaoka, Suita, Osaka 565
(Received January 17, 1984)

Adsorption effects of ureas and thioureas on electrode kinetics were studied by using the electrode reactions of $Zn^{2+}/Zn(Hg)$ and Eu^{3+}/Eu^{2+}. The standard rate constant for $Zn^{2+}/Zn(Hg)$ is controlled by the inner-layer permittivity. The effect of this permittivity has been explained in terms of the solvent reorganization energy. The effect of the adsorbates on the electrode kinetics of Eu^{3+}/Eu^{2+} cannot be explained in terms of the inner-layer permittivity. These two results suggest different locations for the formation of the activated complex: Inside the adsorption layer for Zn^{2+} and just outside layer for Eu^{3+}.

Various factors governing electrode kinetics have been reviewed with respect to the electroreduction of inorganic cations in the presence of organic adsorbates.[1,2] In general, organic adsorbates lower the electroreduction rate, but some adsorbates increase the rate; especially markedly thiourea accelerates the reduction of In^{3+},[3] H_3O,[4] and Zn^{2+} and Bi^{3+}.[2] No satisfactory explanation, however, has yet been given to this accelerating action of thiourea. Recently, Sykut *et al.*[5] found that the acceleration of the electroreduction of Zn^{2+} and Bi^{3+} requires both that the capacity of adsorbate solution should be larger than that of base electrolyte solution and that lone pair electrons should be present in the adsorbate, and they termed this cooperative action the "cap-pair" effect. This effect is speculated to be correlated intimately to a larger permittivity of the surface adsorption layer. Then, this effect was studied more precisely by using highly polarizable organic compounds: thiourea (TU), 1,1-dimethylthiourea (DMTU), tetramethylthiourea (TMTU), urea (U), 1,1-dimethylurea (DMU), and tetramethylurea (TMU). The electrode reactions of $Zn^{2+}/Zn(Hg)$ and Eu^{3+}/Eu^{2+} were chosen as representative of reactions of deposition and simple charge-transfer types, respectively.

Experimental

Most of the organic compounds used as adsorbates were of high-purity reagent grade, but they were further purified by double distillation (TMU) or double recrystallization from methanol (DMU) or distilled water (U, TU, TMTU, and DMTU). Only DMTU was synthesized by reaction of dimethylcyanamide with thiourea.[6]

Since the double-layer parameters for the adsorbates have been obtained mainly in 0.5 M NaF solution (1 M=1 mol dm^{-3}), the electrode reaction of $Zn^{2+}/Zn(Hg)$ was studied in 0.5 M NaF solutions containing 1.0×10^{-3} M of Zn^{2+} and an adsorbate at various concentrations. On the other hand, the electroreduction of Eu^{3+} was carried out in 0.5 M aqueous $NaClO_4$ containing 0.93×10^{-3} M of Eu^{3+} and an adsorbate at different concentrations, because Eu^{3+} formes a precipitate of EuF_3 in the aqueous NaF solution. In this case, the double-layer parameters for the adsorbates are assumed not to differ from those in 0.5 M NaF.

Polarographic measurements were carried out with a three-electrode system consisting a polarograph (Yanaco, P-8 Polarograph) equipped with a dropping mercury electrode at 25 °C, and the instantaneous current at the end of drop life was recorded. The drop time was mechanically adjusted to 3.5 s, and the flow rate of mercury was 3.03 mg s^{-1}. The apparent standard rate constant k_s^{app} for $Zn^{2+}/Zn(Hg)$ with the standard electrode potential −1.003 V *vs.* SCE[7] was evaluated according to the analytical procedure for quasi-reversible systems.[8,9] When the concentration of thioureas (TU, DMTU, and TMTU) exceeds the level corresponding to surface coverage about 0.3, the systems yield reversible current-potential curves. For such systems, only the standard rate constant at full coverage was evaluated by the faraday impedance method.[10] On the other hand, k_s^{app} for Eu^{3+}/Eu^{2+} with the standard potential −0.600 V *vs.* SCE[11] was evaluated according to the equation for irreversible systems.[8]

Results and Discussion

Adsorption Behavior of Adsorbates. According to adsorption behavior the adsorbates used in the present study can be classified into two groups, ureas (U,[12] DMU,[13] and TMU[14]) and thioureas (TU,[15,16] DMTU,[13] and TMTU[17]). The orientation common to the ureas at the mercury/aqueous solution interface is the positioning of the C=O bond nearly parallel to the electrode surface. The fit to the Langmuir isotherm observed for U and DMTU indicates the absence of interaction between adsorbed molecules. However, only TMU, which shows a fit to the Frumkin isotherm, exhibits a small positive interaction parameter, which means an attractive interaction between adsorbed molecules around the potentials where the reductions of Zn^{2+} and Eu^{3+} take place.

On the other hand, the orientation common to the thioureas is the positioning of the C=S bond fully vertical to the electrode surface. A repulsive interaction between adsorbed molecules is indicated by the positive values of the second virial coefficient for TU[16] and the negative values of the interaction parameters for DMTU and TMTU.

Effects of Adsorbates on Electrode Kinetics of $Zn^{2+}/Zn(Hg)$. Figure 1 shows the variation of the apparent standard rate constant k_s^{app} due to adsorption of the ureas and thioureas. Only with TMU, a remarkable lowering in the reduction rate was

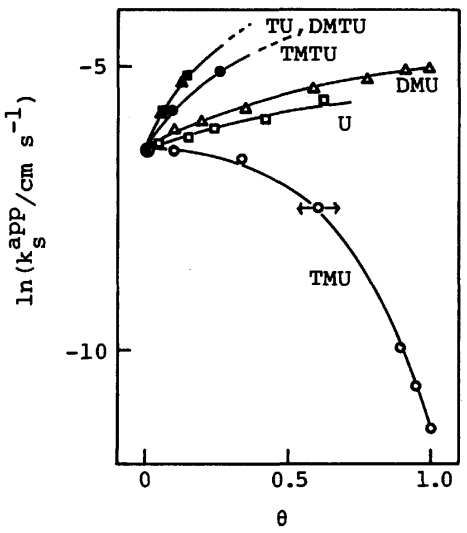

Fig. 1. Variation of ln k_s^{app} for Zn^{2+}/Zn(Hg) with suraface coverage at various adsorbates. Adsorbates: TU (thiourea, ■), DMTU (1,1-dimethylthiourea, ▲), TMTU (tetramethylthiourea, ●), U (urea, □), DMU (1,1-dimethylurea, △), and TMU (tetramethylurea, ○). Arrows representing a speculated coverage for TMU are due to a mixed adsorption consisting of similar two orientations differed in the occupied srera.[17]

observed, but U and DMU accelerated the reaction slightly with an increase in the coverage. The thioureas showed a strong accelerating action even at lower coverages. Since the rate constants at higher coverages could not be evaluated owing to a change into a reversible system, the standard rate constant at the full coverage was estimated by the faraday impedance method[10] only with TMTU and DMTU. The results are summarized in Table 1 together with various double-layer parameters at the full coverage, the values of which are estimated at each apparent half-wave potential $E_{1/2}$, because the rate constants were evaluated around this potential and the plot of these rate constants against potential was then extrapolated to the standard electrode potential to obtain k_s^{app}.

The results relating to the potential drop across the diffuse double layer $\Delta_S^2\phi$ suggest that the reduction rate is not controlled by the Frumkin effect.[18] The effect of adsorbate's dipole charges located at the solution side upon the surface concentration of reacting ion, which is to be considered for the reduction of Eu^{3+} in the subsequent section, is not operative either for the reduction of Zn^{2+}. The electrode process of Zn^{2+}/Zn(Hg) seems to proceed in the adsorption layer. However, it is found that the ϕ_1 potential ($\Delta_1^M\phi$) in the adsorption layer[19] cannot explain the large change in ln k_s^{app} with adsorbates, in analogy with the ϕ_2 potential ($\Delta_2^M\phi$) at the Helmholtz plane. One of interfacial properties susceptible to a large change with adsorbates is the permittivity of the adsorption layer or the inner-layer permittivity ε_1, as can be seen from Table 1. Then, the effect of this permittivity on the rate constant was examined more precisely. For a thin adsorption layer with lower permittivity than that in the solution bulk, Afanas'ev and Damaskin[20] treated the above effect as the work involved in transferring a reacting ion from the solution bulk into the structured surface layer. But, we have treated this effect simply as the work for the activation of Zn^{2+} in the adsorption layer.

When the interaction between reactant and electrode is negligibly weak and the activation free energy is mainly controlled by the solvent reorganization energy, the Marcus theory[21,22] predicts the following simplified relation for the standard rate constant:

$$\ln k_s^{app} = \text{const} - \lambda_o/4kT, \quad (1)$$

where λ_o is a quantity relating to the solvent reorganization energy and represented by

$$\lambda_o = (ne)^2(1/2a - 1/4R)(1/\varepsilon_o - 1/\varepsilon_s), \quad (2)$$

where ne is the charge transferred, a the radius of the reacting ion, R the distance between the center of reacting ion and the electrode surface, and ε_o and ε_s are the optical and static permittivities of medium, respectively. If a and R can be assumed to be constant for the same reaction, one may obtain the following equation related to the permittivity of the medium:

$$\ln k_s^{app} = \text{const} - (1/4kT)(ne)^2(1/2a - 1/4R)(1/\varepsilon_o - 1/\varepsilon_s). \quad (3)$$

TABLE 1. KINETIC DATA FOR Zn^{2+}/Zn(Hg) AND DOUBLE-LAYER PARAMETERS AT SATURATION WITH VARIOUS ADSORBATES[a]

Adsorbate	C_{org}^f	$E_{1/2}$	α^{app}	$k_s^{app}\times10^{3}$ [b]	$\Delta_S^2\phi$	K_1^i	d_1	$\varepsilon_1\times10^{11}$	$P_1\times10^{30}$
	M	V *vs.* SCE		cm s^{-1}	mV	μF cm^{-2}	nm	F m^{-1}	C m
TMTU	0.05	−1.013	0.27	20	−33	16.7	0.71	11.9	−14.7
DMTU	0.1	−1.015	0.30	45	−30	21.0	0.71	14.9	−15.2
TMU	0.5	−1.282	0.24	0.011	−55	8.8	0.62	5.4	6.1
DMU	2.0	−1.013	0.30	5.6	−48	15.1	0.60	9.2	1.7
H_2O	—	−1.024	0.28	1.5	−58	21.3	0.31	6.6	—

a) C_{org}^f and α^{app} mean the concentration corresponding to full coverage and the apparent transfer coefficient, respectively. $\Delta_S^2\phi$, K_1^i, d_1, ε_1, and P_1 are the potential drop across the diffuse layer, the integral inner-layer capacity, the thickness of the inner layer, the permittivity of the inner layer, and the dipole moment of an adsorbed molecule at saturation with the adsorbate, respectively. The double-layer parameters are estimated at each half-wave potential $E_{1/2}$. A positive (negative) value of P_1 corresponds to an orientation having the positive (negative) end of dipole directing toward the electrode surface. b) The values for TMTU and DMTU were evaluated from the data obtained by the faraday impedance method, while those for TMU, DMU, and H_2O by d.c. polarography.

One can assume the surface layer formed by adsorbates to be the medium for the electroreduction of Zn^{2+}. In general, the permittivity of the surface adsorption layer on the electrode is quite different from that of the bulk.[23] When electrode processes occur in this surface adsorption layer, therefore, we have to use the permittivity of this layer. This permittivity of the surface layer or the inner-layer permittivity at saturation with an adsorbate, ε_1, can be estimated from the integral inner-layer capacity $K_1^i(=\varepsilon_1/d_1)$ and the thickness of the inner layer, d_1. The definition of K_1^i is

$$K_1^i = \sigma/(\Delta_2^M\phi_\sigma - \Delta_2^M\phi_{\sigma=0}), \quad (4)$$

where σ is the surface charge density on the electrode, and $\Delta_2^M\phi_\sigma$ and $\Delta_2^M\phi_{\sigma=0}$ are the potential drops across the inner layer at an arbitrary charge density and at the zero charge density, respectively. When the reorientation of adsorbate is not so significant, Eq. 4 can be approximated to[24]

$$1/K_1^i = 1/K_1^{i(\text{ion})} - 1/K_1^{i(\text{dipole})}. \quad (5)$$

Since the first term of the right hand side of Eq. 5 is due to the free charges on the electrode and is affected by the electronic polarizability of the adsorbate, and the second term is due to the dipole orientation, Eq. 5 can be reduced to

$$1/\varepsilon_1 = 1/\varepsilon_o - 1/\varepsilon_s, \quad (6)$$

which means that one may obtain $(1/\varepsilon_o - 1/\varepsilon_s)$ from $1/\varepsilon_1$ which can be estimated from the integral inner-layer capacity. The contribution of ε_s to the inner-layer permittivity has been considered to be minor,[23] which in fact is the case with TMTU.[17]

A plot of $\ln k_s^{app}$ against $1/\varepsilon_1$ is shown in Fig. 2. In this figure, no points for U and TU are included for the lack of ε_1 in the literature, and the point for H_2O refers to the surface layer covered with water molecules only, *i.e.*, the surface layer corresponding to the base 0.5M NaF solution containing no adsorbates.

The plot in Fig. 2 shows a linear relation, which verifies the validity of Eq. 3. However, the slope gives R=1.1 nm on the assumption of $a=R$. This value is rather too large, because R is expected to be 0.3—0.4 nm by taking into account the water layer thickness (0.31 nm) and the ionic radius of Zn^{2+} (0.074—0.088 nm).

Several reasons will be given for the unexpected value of R: (i) neglect of the work, U_i, for transferring reactants from the solution bulk to the discharge site; (ii) no distinction between two layers with different permittivities; (iii) neglect of the thickness of the adsorption layer, d_1; (iv) probable change in a and R during the electrode process. Kharkats[25] discussed effects of two layers with different permittivities and d_1 on the solvent reorganization energy E_s and U_i, and represented E_s and U_i as functions of a, R, d_1, and permittivity.

In the calculation of E_s and U_i, the static permittivity for the adsorption layer is assumed to be 10 times the optical one, and the optical and static permittivities for the water layer adjacent to the adsorption layer are taken as 6.3×10^{-11} and 70×10^{-11} Fm^{-1}, respectively. When the energies controlling the electrode process are concentrated on E_s and U_i, $\ln k_s^{app}$ can be given by

$$\ln k_s^{app} = \text{const} - (E_s+U_i)^2/4E_skT. \quad (7)$$

Figure 3 shows the plot of $\ln k_s^{app}$ for $Zn^{2+}/Zn(Hg)$ against $(E_s+U_i)^2/E_s$, for which 0.4 nm is chosen for a and R so that the experimental slope may agree with the

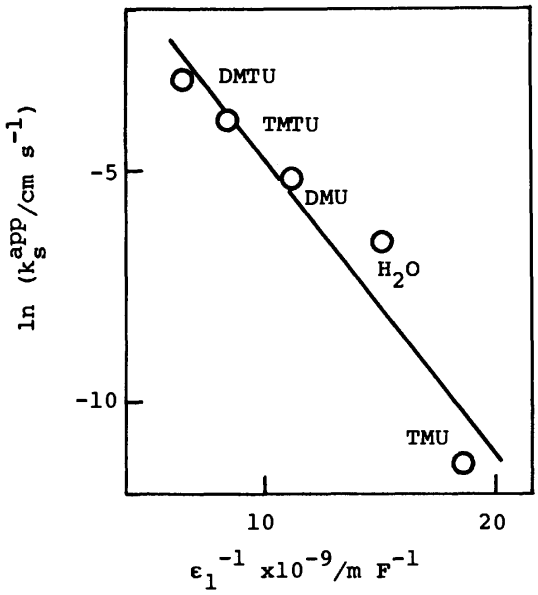

Fig. 2. Plot of $\ln k_s^{app}$ for $Zn^{2+}/Zn(Hg)$ against ε_1^{-1} at saturation with various adsorbates.

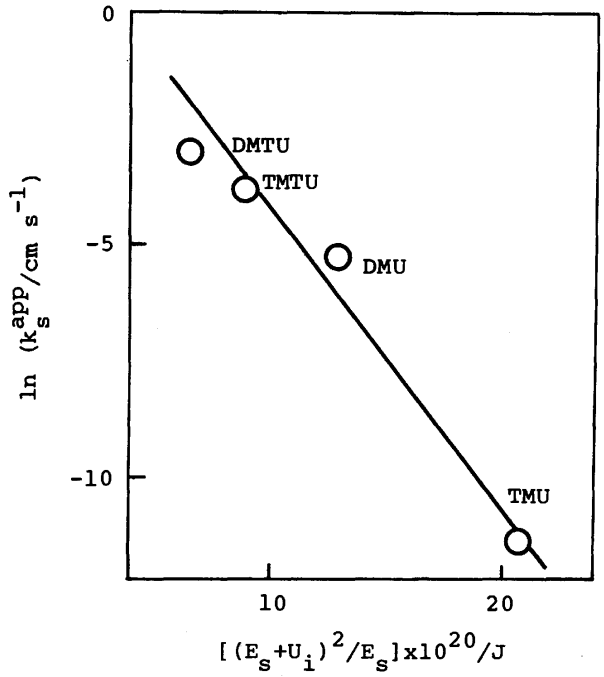

Fig. 3. Plot of $\ln k_s^{app}$ for $Zn^{2+}/Zn(Hg)$ against $(E_s+U_i)^2/E_s$ at saturation with various adsorbates.

TABLE 2. KINETIC DATA FOR Eu^{3+}/Eu^{2+} AND DOUBLE-LAYER PARAMETERS AT $E_{1/2}$[a)]

Adsorbate	C_{org}	$E_{1/2}$	α^{app}	$k_s^{app}\times10^{5}$[b)]	θ	$\Delta_S^2\phi$	K_1^i	d_1	$\varepsilon_1\times10^{11}$	$P_1\times10^{30}$
	M	V *vs.* SCE		cm s^{-1}		mV	$\mu F\,cm^{-2}$	nm	$F\,m^{-1}$	C m
H_2O	—	−0.665	0.33	26	1	−31	25.5	0.31	7.9	—
TMU	0.005	−0.661	0.33	26	0.27	−29				
	0.01	−0.663	0.33	28	0.52	−29				
	0.05	−0.676	0.35	22	0.78	−33				
	0.1	−0.690	0.51	15	0.89	−35				
	0.2	−0.696	0.52	14	1	−37	12.5	0.61	7.6	8.1
TMTU	0.001	−0.741	0.46	0.93	0.60	−21				
	0.005	−0.807	0.48	0.065	0.86	−19				
	0.01	−0.840	0.42	0.062	0.94	−20				
	0.05	−0.910	0.32	0.055	1	−27	17.0	0.71	12.1	−15.4

a) C_{org} and θ represent the concentration and surface coverage of adsorbate, respectively. The meanings of the other notations are the same as those in Table 1. b) All the values were evaluated from data obtained by d.c. polarography.

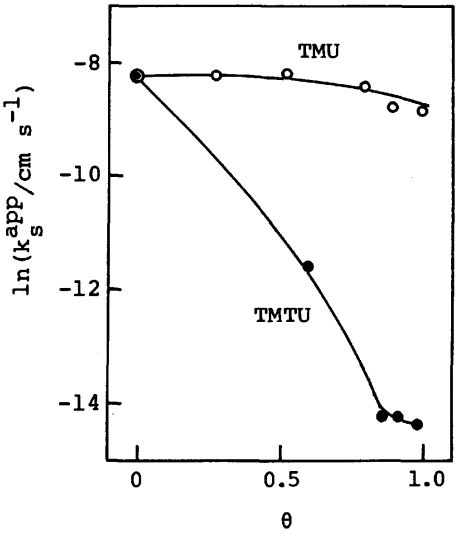

Fig. 4. Variation of ln k_s^{app} for Eu^{3+}/Eu^{2+} with surface coverage at TMU and TMTU.

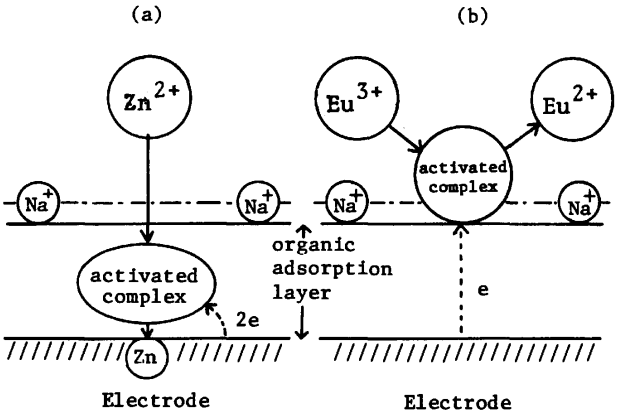

Fig. 5. Reaction paths elucidated for the reductions of (a) Zn^{2+} and (b) Eu^{3+}.

theoretical one ($1/4kT$). The above value $a=R=0.4$nm is in fair agreement with the expected value of 0.3—0.4nm. However, the point for H_2O is excluded from the plot in Fig. 3, because $(E_s+U_i)^2/E_s$ calculated for H_2O was an unreasonable value. Probably, the discharge site would be located just outside the water adsorption layer, and the selected values might be different from those for the bulk water.

Effects of Adsorbates on Electrode Kinetics of Eu^{3+}/Eu^{2+}. Figure 4 shows the variation of ln k_s^{app} for Eu^{3+}/Eu^{2+} with the adsorption of TMU and TMTU. The kinetic data and double-layer parameters at each $E_{1/2}$ are summarized in Table 2. The effect of TMU and TMTU on the reduction rate of Eu^{3+} is in quite a contrast to that on the reduction rate of Zn^{2+}; TMTU increases the reduction rate of Zn^{2+} but lowers the rate of Eu^{3+} significantly. The nearly constant values of ln k_s^{app} at higher coverages suggest a tunneling transition[26] through the adsorption layer to the strongly hydrated Eu^{3+} ion.[27] The estimate of ln [k_s^{app} (TMU)/k_s^{app} (TMTU)] on the basis of the tunneling transition,[28] however, is 0.6, which is rather a small value as compared with the experimental value of 5.6. The Frumkin correction for the surface concentration of Eu^{3+} cannot explain the above experimental value, either. As a matter of course, the permittivity effect predicts an opposite result to the experimental one. It is most likely that the adsorbate's dipole charges located at the solution side affect the surface concentration of Eu^{3+}, because such charges are positive for TMTU and negative for TMU as can be seen from the value, P_1, of dipole moment of an adsorbed molecule in Table 2.

Reaction Paths. A comparison of the two types of electrode reactions has led us to assign the reaction paths shown in Fig. 5 to the reductions of Zn^{2+} and Eu^{3+}. In Fig. 5, the locations where the activated complex is formed are different: (a) Inside the adsorption layer for Zn^{2+} and (b) just outside the layer for Eu^{3+}.

The hydration structure of Zn^{2+} in 0.5M aqueous NaF solution is considered to be $[ZnF(H_2O)_3]^+$.[29] We could detect no clear complex formation of Zn^{2+} with the ureas or thioureas used as adsorbates, because no change was caused in the UV-visible spectrum for the 1.0×10^{-3}M Zn^{2+}+0.5M NaF solution by addition of the adsorbates. This result does not deny the possibility that the complex is formed during the transfer of Zn^{2+} into the surface adsorption layer. When thioureas formes a strong complex with a reacting ion such as Cu^{2+} or Cd^{2+}, however, it is well known that the

reduction rate of these ions is caused to decrease.[2] These results suggest that any complexation of Zn^{2+} occurs with the thioureas or ureas neither in the solution bulk nor in the adsorption layer.

The characteristics of the UV-visible spectrum for the case of Eu^{3+} are similar to those for Zn^{2+}. Since water molecule also is a ligand, we believe that Eu^{3+} in a dilute aqueous solution of any one of the thioureas and ureas will form no complex with them.

References

1) J. Lipkowski and Z. Galus, *J. Electroanal. Chem. Interfacial Electrochem.*, **61**, 11 (1975).

2) B. B. Damaskin and B. N. Afanas'ev, *Elektrokhimiya*, **13**, 1099 (1977).

3) A. A. Kazsrov and M. A. Loshkarev, *Elektrokhimiya*, **3**, 681 (1967).

4) K. Meures and L. Gierst, *Collect. Czech. Chem. Commun.*, **36**, 389 (1971).

5) K. Sykut, G. Dalmata, B. Nowicka, and J. Saba, *J. Electroanal. Chem. Interfacial Electrochem.*, **90**, 299 (1978).

6) S. Birtell, F. H. S. Curd, J. A. Hendry, and F. L. Rose, *J. Chem. Soc.*, **1948**, 1645.

7) L. Briel, *Gazz. Chim. Ital.*, **64**, 261 (1934).

8) I. Luzic, *J. Electroanal. Chem. Interfacial Electrochem.*, **49**, 407 (1974).

9) R. Tamamushi and N. Tanaka, *Z. Phys. Chem. (Frankfurt am Main)*, **39**, 117 (1963).

10) L. Gierst and P. Cornelissen, *Collect. Czech. Chem. Commun.*, **25**, 3004 (1970).

11) M. Sluyters-Rehbach, J. S. M. C. Breukel, and J. H. Sluyters, *J. Electroanal. Chem. Interfacial Electrochem.*, **19**, 85 (1968).

12) R. Parsons, R. Peat, and R. M. Reeves, *J. Electroanal. Chem. Interfacial Electrochem.*, **62**, 151 (1975).

13) O. Ikeda, to be published.

14) O. Ikeda, H. Jimbo, and H. Tamura, *J. Electroanal. Chem. Interfacial Electrochem.*, **137**, 127 (1983).

15) F. W. Schapink, M. Oudeman, K. W. Lew, and J. N. Helle, *Trans. Faraday Soc.*, **56**, 415 (1960).

16) R. Parsons, *Proc. R. Soc. London, Ser. A*, **261**, 79 (1961).

17) O. Ikeda, H. Jimbo, and H. Tamura, *Bull. Chem. Soc. Jpn.*, **56**, 855 (1983).

18) A. N. Frumkin, *Z. Phys. Chem. (Leipzig)*, **164 A**, 121 (1933).

19) A. N. Frumkin, *Dokl. Akad. Nauk SSSR*, **85**, 373 (1952).

20) B. N. Afanas'ev and B. B. Damaskin, *Elektrokhimiya*, **11**, 1556 (1975).

21) R. A. Marcus, *J. Chem. Phys.*, **24**, 966 (1956).

22) R. A. Marcus, "Special Topics in Electrochemistry," ed by P. A. Rock, Elsevier, New York (1977), p. 161.

23) L. I. Krishtalik, *Elektrokhimiya*, **13**, 1890 (1977).

24) S. Trasatti, *J. Electroanal. Chem. Interfacial Electrochem.*, **91**, 293 (1978).

25) Yu. I. Kharkats, *Elektrokhimiya*, **15**, 246 (1979).

26) J. Lipkowski. E. Kosińska, M. Goledzinowski, J. Nieniewska, and Z. Galus, *J. Electroanal. Chem. Interfacial Electrochem.*, **98**, 91 (1979).

27) C. W. De. Kreuk, M. Sluyters-Rehbach, and J. H. Sluyters, *J. Electroanal. Chem. Interfacial Electrochem.*, **28**, 391 (1970).

28) O. Ikeda, K. Tsuura, and H. Tamura, *Bull. Chem. Soc. Jpn.*, **54**, 661 (1981).

29) S. Varvicka and J. Koryta, *Collect, Gzech. Chem. Commun.*, **32**, 2346 (1967).

Interactions of Excited Lithium Atom with Molecular Hydrogen. II. Properties of Wave Functions in the Potential Crossing Region

Kimiko MIZUTANI,* Takakazu YANO,† Atsushi SEKIGUCHI,†† Kazuko HAYASHI,††† and Shiro MATSUMOTO
Department of Chemistry, College of Science and Engineering, Aoyama Gakuin University, Chitosedai, Setagaya-ku, Tokyo 157
(Received January 31, 1984)

To elucidate the electronic mechanism of the quenching of electronically excited Li atoms by H_2 molecules, CASSCF calculations were made regarding the Li-H_2 system with various geometries. Special attention was payed to the electronic structure of the system in the crossing, or pseudocrossing, region of the potential energy surfaces. Simple CASSCF functions do not have a satisfactory spacial symmetry when the upper and the lower states are almost degenerate in energy, and need to be refined by the addition of a nonorthogonal CI. In the crossing region, electron density maps have shown that the Li atom is bonded more strongly to the nearer H atom than to the farther H atom in the ground state, whereas the opposite is the case for an excited state. Such properties of the wave function lead naturally to a picture of a nonadiabatic process occurring in the crossing region. The pseudocrossing of the first excited and the ground state potential energy surfaces has also been found for all geometries midway between the C_{2v} and $C_{\infty v}$ symmetries.

In a previous report,[1] we have shown that for the Li-H_2 system, the lowest $^2A_1$ and $^2B_2$ potential energy surfaces cross in a line located in an energetically accessible region. This has been determined as being the critical region where the nonadiabatic transition between an excited state and the ground state occurs with fair probability. However, the C_{2v} geometry seems to be too restrictive to describe the whole nonadiabatic process occurring in the system. It has thus become desired that the calculation be extended to more general geometries. Extensive calculations for the Li-H_2 system have been reported by P. J. A. Ruttink and J. H. van Lenthe,[2] and A. F. Wagner and A. C. Wahl[3] using large basis functions. Quite recently, Hobza and Schleyer[4] have reported calculations on the ground state of a Li-H_2 complex with MP2/6—311G (2d, 2p). These calculations, however, do not include any description concerning nonadiabatic transitions.

We report, in this paper, the results of further calculations using more general geometries[5] in order to search for other channels of the nonadiabatic transitions. The properties of the electronic wave function with regard to the geometries around the critical region were studied in some detail. The low-lying potential energy surfaces with a $C_{\infty v}$ geometry did not come close to each other. However pseudocrossing regions did exist for geometries intermediate between the C_{2v} and $C_{\infty v}$ symmetries, although they were located at somewhat higher energies. The MCSCF wave function, including insufficient CSF's, showed inappropriate properties in the critical region. The defect could be corrected by including an additional nonorthogonal configuration interaction.[11c] However, an examination of the crude wave functions led to a new schematic view of the nonadiabatic process. Meyer *et al.*[6] recently reported results of studies on the Na-H_2 system which were conducted for a similar reason as the one reported here. Our results for Li-H_2 parallel theirs in many respects.

Method of Calculation

Geometric parameters were taken as shown in Fig. 1. The bases were minimal STO-3G[7] functions, the electronic wave functions were computed with a CASSCF method,[8] and all orbitals other than the core orbital (1a′) were included in the active space. Computational details and notations are the same as those previously described.[1] The convergence of the MCSCF calculations was judged by the sum: $\sum_p \sum_{q(\neq p)} \langle \phi^p | \hat{R} | \phi^q \rangle^2$, as well as by the steadiness of the energy expectation values. In the above sum, ϕ^p denotes the p-th orbital function just computed, and $\hat{R}$ is the coupling operator.[1] Summations are taken over all the different pairs of orbitals. The value of the sum is denoted as the "residue" below, which should vanish at complete self-consistency. Iterations were continued until the residue value fell below 10^{-20} (hartree)^2. Good convergence was essential for assuring the quality of the wave functions. In one instance, a wave function with a residue value of 10^{-14} (hartree)^2 gave density maps that were quite different from those obtained from a wave function well converged to a residue value of less than 10^{-20} (hartree)^2.

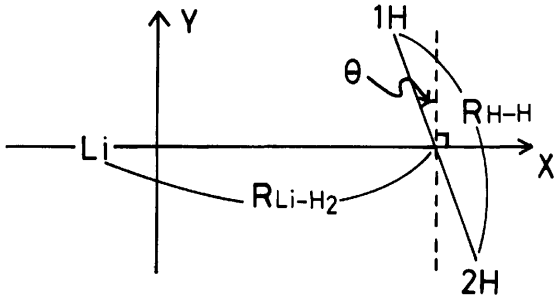

Fig. 1. Geometrical parameters for the Li-H_2 system.

†Present address: Citizen Watch Co., Tokorozawa, Saitama, 359.

††Present address: Anelva Corporation, Fuchu, Tokyo, 183.

†††Present address: Aoyama Gakuin High School, Shibuya-ku, Tokyo 150.

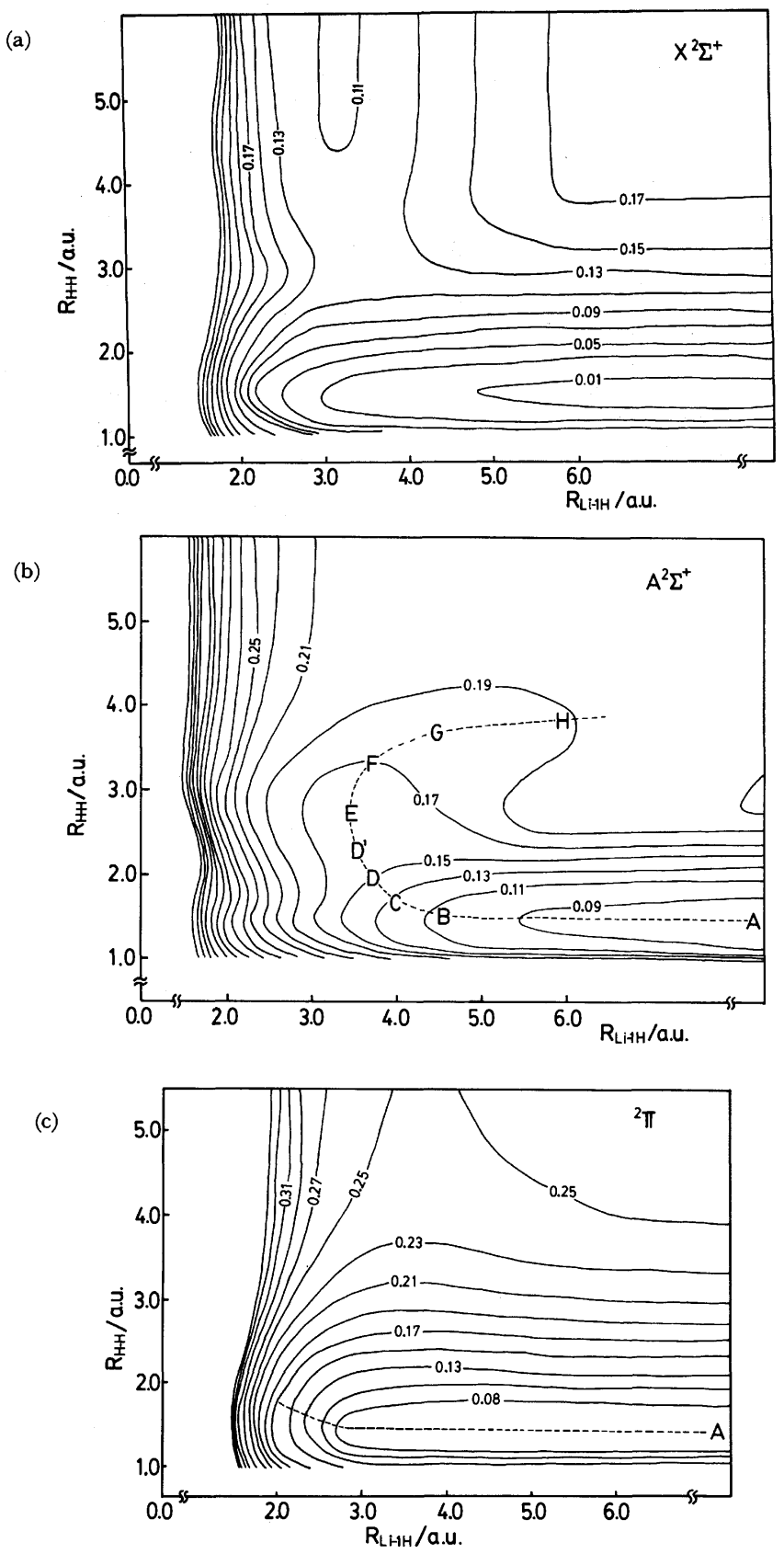

Fig. 2. Two-dimensional potential energy surfaces for the collinear geometry $\theta=90°$; (a) X $^2\Sigma^+$, (b) A $^2\Sigma^+$, and (c) $^2\Pi$. Energies are given in hartrees minus −8.47 on each curve (dashed line is the minimum energy reaction path on the A$^2\Sigma^+$ surface and on the $^2\Pi$ surface, A, B, ···, H are several selected points on the curve).

Results and Discussion

Potential Energy Surfaces in $C_{\infty v}$ Geometry. Figure 2(a) shows the ground state potential energy surface. Figures 2(b) and 2(c) are the two excited state potential energy surfaces leading to a ground hydrogen and to the $2\,^2P$ lithium atom computed with $C_{\infty v}$ symmetry. It can be seen that neither of the excited potential energy surfaces come close to the ground state surface, unlike in the case with a C_{2v} geometry.[1] The minimum energy path, starting from isolated H_2 ($X\,^1\Sigma_g$) and Li ($2\,^2P$) is shown by a dashed line on each excited state surface. The energy differences between the ground and the excited states along these lines are shown in Fig. 3. It seems, therefore, that a $C_{\infty v}$ geometry is far less favored for the quenching process of a $2\,^2P$ Li atom than the C_{2v} geometry,at least at moderate temperatures.

Potential Energy Surfaces for θ=45°. The ground and the first excited state potential energy surfaces for the arrangement θ=45° are shown in Fig. 4. Both states belong to the A′ representation of the C_s point group, and cannot intersect with each other. However, the surfaces come close together in the region shown by short dashed lines in Fig. 4. Figure 5 shows a cross section of the potential surfaces parallel to the ordinate. The potential curves display features of pseudocrossing. It is tempting, therefore, to speculate that nonadiabatic transitions may occur around these geometries, although their energies are somewhat higher than in the C_{2v} case.

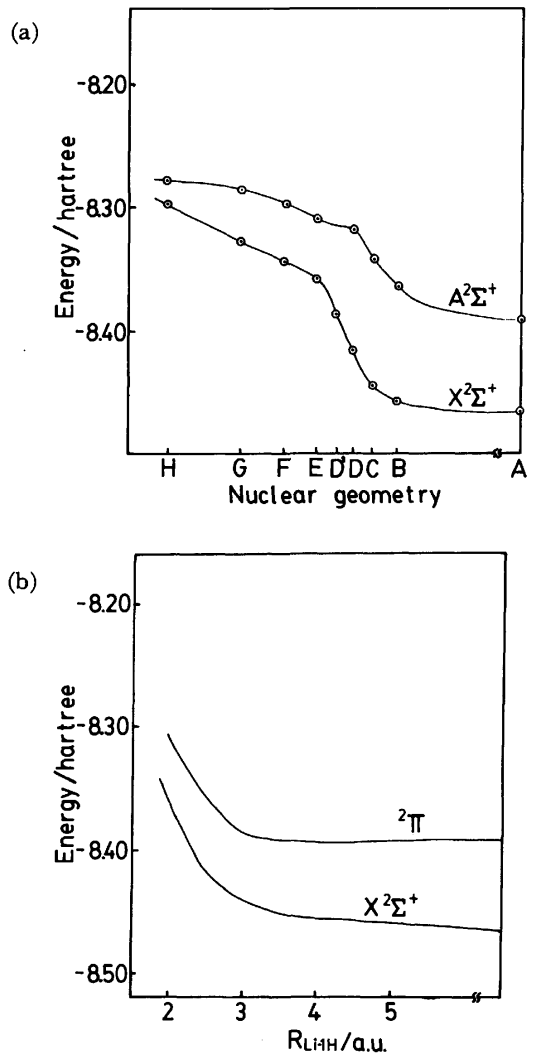

Fig. 3. Energies along the minimum energy path in Fig. 2(b) and 2(c), respectively; (a) $X\,^2\Sigma^+$, $A\,^2\Sigma^+$, and (b) $X\,^2\Sigma^+$, $^2\Pi$. Nuclear geometries A, B, ···, H in Fig. 3(a) correspond to those in Fig. 2(b).

Properties of Potential Energy Surfaces Near the Critical Region of C_{2v} Potential Crossing. It is important to examine the wave function of the system for all the variations of nuclear geometry in the critical region in order to obtain a picture of the nonadiabatic process and to have an estimate of its occurrence probability. Even for the present simplest system, there are three degrees of freedom of the nuclei, and this is a nontrivial task. As an attempt, we selected "normal coordinates" around a geometrical point which seemed to be characteristic of the crossing (or pseudocrossing) region. The central point may be appropriately assigned to the lowest point (hereafter called "point P") on the intersection line of $^2B_2$ and $^2A_1$ surfaces (Figs. 2 and 3 of Ref. 1). By transforming the coordinate system ($R_{\text{Li-H}_2}$, $R_{\text{H-H}}$) to a mass-weighted system ($(m_{\text{Li}}\, m_{\text{H}_2}/(m_{\text{Li}}+m_{\text{H}_2}))^{1/2}\, R_{\text{Li-H}_2}$, $(m_{\text{H}}/2)^{1/2}\, R_{\text{H-H}}$), and by drawing a tangent and a normal at point P to the potential contour line passing through P, we obtained a type of normal coordinate system (Fig. 6). We had, of course, two different coordinate systems depending on which of the potential surfaces we utilized. In practice, the two sets of directions turned out to be not very different, and we took the one constructed on the $^2B_2$ surface, as we expected the process to be occurring from the excited state. Calculations with a larger basis sets[9] revealed the same feature. We shall call the normal direction as the reaction coordinate and the tangential direction as the direction of C_{2v} vibration, for convenience. Another vibrational degree of freedom is an antisymmetric stretching mode (b_2) analogous to that of a stable isosceles triangular molecule. It coincides to the first order with a θ-deformation (*i.e.* rotation by θ (Fig.1) of the H_2 molecule about its center while the center and the inter-hydrogen distance are fixed). Thus, we have taken the angle θ as the third parameter describing the nuclear geometry for visual simplicity and for later conveniences of discussing rotational perturbation separately. The normal vibration of the C_{2v} symmetry plays a role which becomes important only for more quantitative calculations of transition probabilities. Thus, we defer its inclusion until the results of more quantitative calculations are discussed. Figure 7 shows potential energy curves for a θ-deformation at point P,[10] and at several points along the reaction coordinate. The potential curve at P consists virtually of two quasiparabolas crossing at P and symmetrically placed

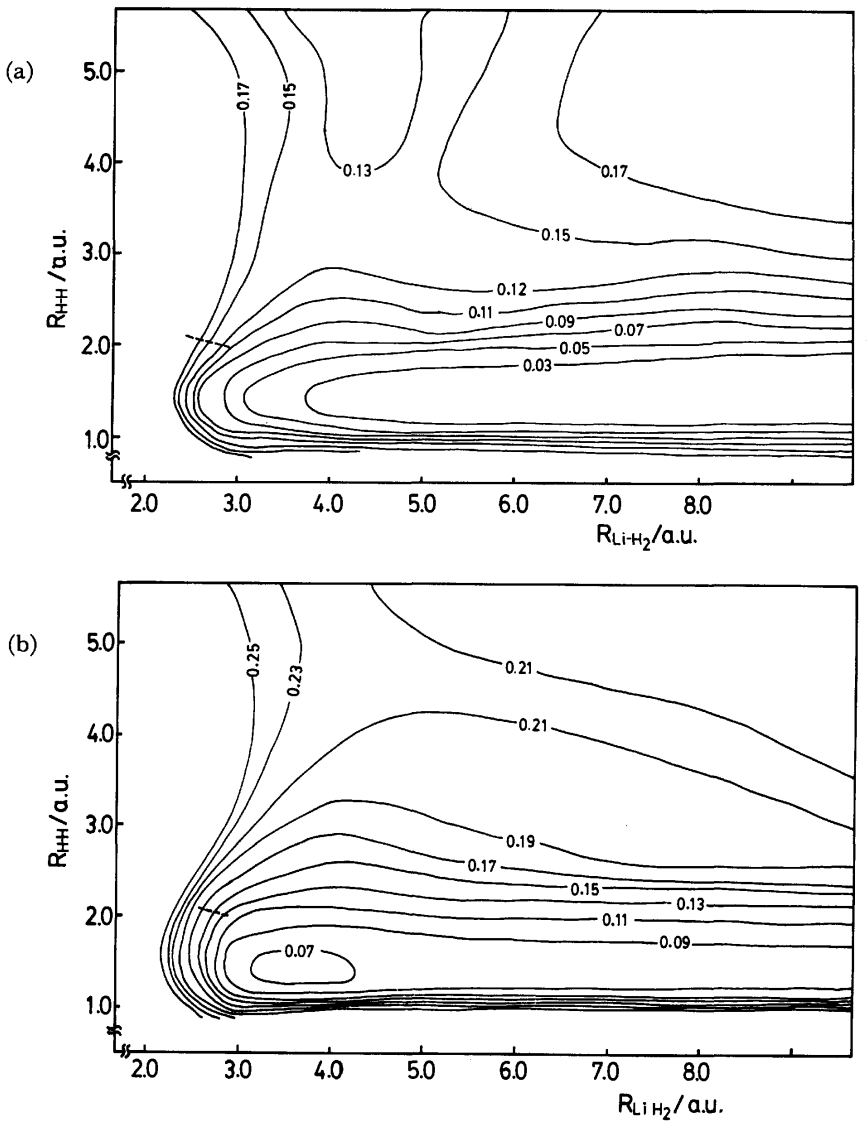

Fig. 4. Potential energy surfaces for C_s geometry $\theta=45°$; (a) lowest $^2A'$ and (b) 2nd. $^2A'$. Energies are given in hartrees minus −8.47 on each curve.

with respect to the ordinate. The points of energy minima lie only slightly lower than P, but they are distinctly displaced from the ordinate. The ground state potential energy curves at points on the reaction coordinate other than P have similar minima, while each of their excited counterparts has a single minimum at $\theta=0°$. It will be noticed that while the ground state potential energy curves at Q''' and R''' have cusps at $\theta=0°$, other ground state curves passing through points more distant from P look smooth at $\theta=0°$. This fact is related to with the quality of our MCSCF wave functions and will be discussed in the next section.

Singularity of MCSCF Wave Functions in a Critical Region. The electron density maps of the 3a′ natural orbitals of the two (nearly)[10] degenerate MCSCF wave functions at point P were obtained by CASSCF calculations and are shown in Fig. 8. As may be apparent from the figures, these two wave functions are in themselves neither symmetric nor antisymmetric with respect to the xz-plane, but are mutually symmetric with respect to this plane, in contradiction to group theoretical requirements. The mirror image relationship is also seen in the 1a′ core orbitals of both wave functions (Tables 1 and 2). A similar dissymmetry of the wave functions is observed when the ground state potential energy curves display cusps, as shown in Fig. 7. In separate CASSCF calculations we obtained MCSCF wave functions while constraining the orbitals to belong to irreducible representations of the C_{2v} point group. The energies of the resulting two wave functions ($^2A_1$ and $^2B_2$) again agreed to 10^{-9} hartree, but were somewhat higher than those without the symmetry constraints on the orbitals. These phenomena have resulted from the near degeneracy of the 3a′ and 4a′ orbitals[11c] and/or the imperfectness of the CSF's involved in the calculation. They may be of the same sort as the doublet instability[11] found for

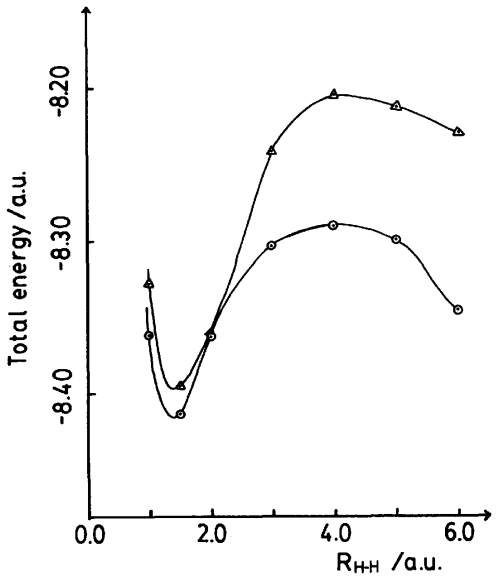

Fig. 5. A cross section of the potential energy surfaces of Fig. 4 cut by a plane perpendicular to the sheet and parallel to and apart by 3.0 bohr from ordinate. ⊙: lowest $^2A'$, ▲: 2nd. $^2A'$.

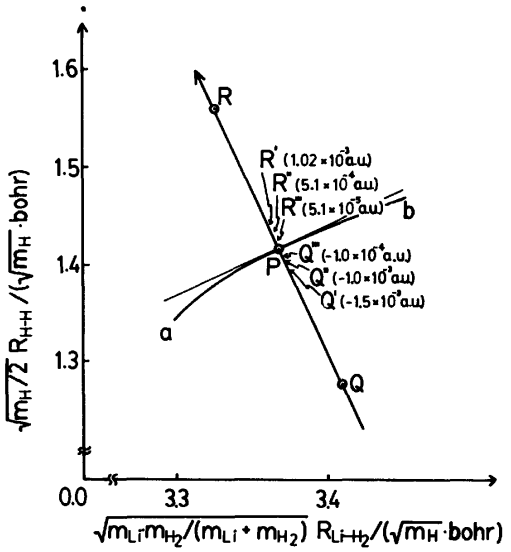

Fig. 6. Normal coordinate system at the lowest point P of the crossing seam of the lowest $^2A_1$ and $^2B_2$ surfaces, displayed in mass weighted scale. *aPb* is the energy contour line through P and *QPR* corresponds to the reaction coordinate on the $^2B_2$ surface. The figures beside letters *R'*, *R''*, *etc.* are the distances from point P.

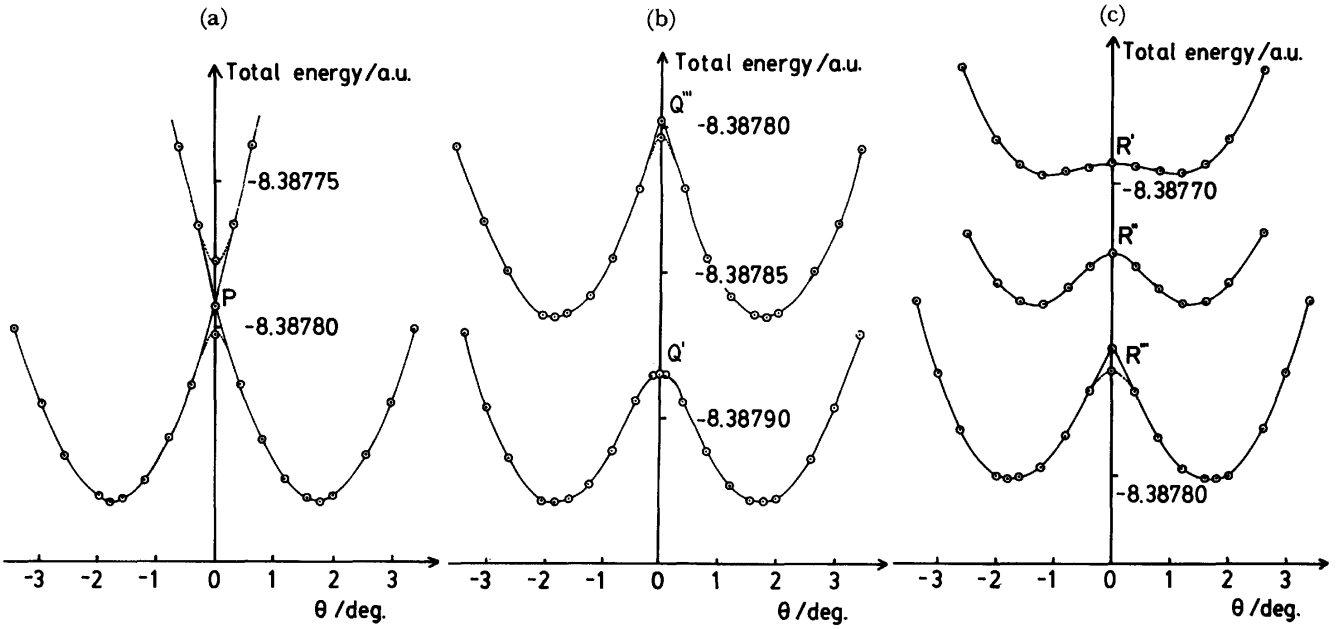

Fig. 7. Total energy *versus* C_s deformation angle from C_{2v} geometry passing: (a) *P*, (b) *Q'*, and *Q'''*, and (c) *R'*, *R''*, *R'''*. The locations of *P*, *Q'*, *Q'''*, *R'*, *R''*, and *R'''*, are shown in Fig. 6. In (b) and (c), only the lower state curves are shown. As to the dashed curves see text.

some stable molecules. Thus, MCSCF wave functions composed of only limited CSF's should be handled with care near geometries where potential crossing occurs, though those functions are quite good in other regions as will be shown below. One remedy is to perform an additional nonorthogonal CI[11c] between the wave functions. Thus, at P two wave functions are obtained, each belonging to one of the irreducible representations of the symmetry point group. The results of this treatment are shown in Fig. 9 and by dashed lines in Fig. 7(a). The energy displacements were of the order of 10^{-6} hartree at point P. Thus, the two curves crossing at P separate out into two smooth pseudocrossing curves. The same smoothing out of the potential curves passing through *Q'''* and *R'''* is shown in Fig. 7 as dashed lines. It will be noted, from the figure, that though the singularity is marked, qualitatively, it is relatively insignificant, quantitatively. Energy shifts resulting from the additional nonorthogonal CI are only remarkable (though the actual values are quite small) near the degenerate point, and do not alter the gross appearance of the MCSCF potential surfaces. The insignificance of the additional CI outside the critical region is seen from the data shown in Table 3.

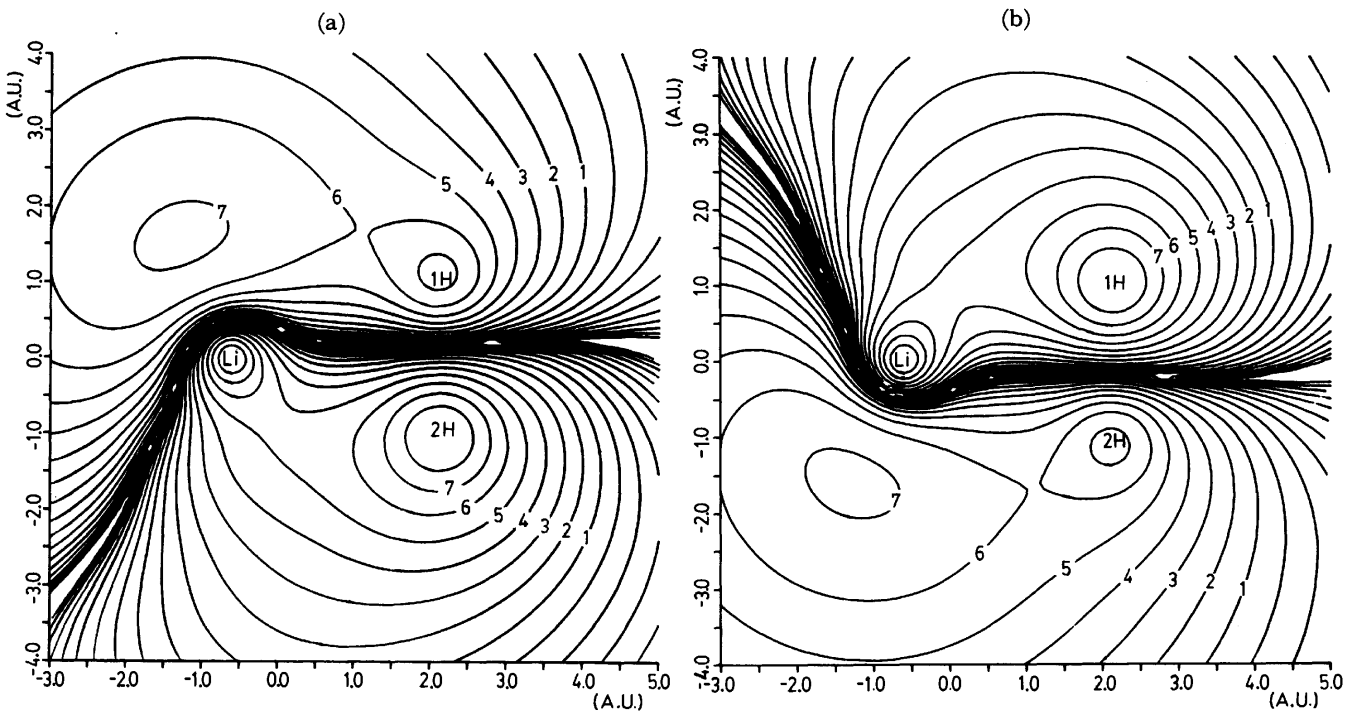

Fig. 8. Contour plots of 3a′ natural orbital electron density of simple MCSCF functions at P; each of (a) and (b) displays either one of the mutually symmetric pair functions degenerate at P. They correspond two states shown by the two curves in Fig. 7(a). The numbers 1, 2, ···, and 7 beside the contours indicate electron density of 3.5565×10^{-4}, 6.3246×10^{-4}, 1.1247×10^{-3}, 2.000×10^{-3}, 3.5565×10^{-3}, 6.3246×10^{-3}, 1.1247×10^{-2} electrons/bohr^3, respectively.

Table 1. Natural orbitals of one of the wave functions degenerate at point P

Basis	MO	$\phi_{1a'}$	$\phi_{2a'}$	$\phi_{3a'}$	$\phi_{4a'}$
Li	1s	0.9956	−0.1087	−0.1069	0.0567
Li	2s	0.0216	0.0931	0.6076	−0.3182
Li	$2p_x$	−0.0036	0.1039	−0.2871	0.1676
Li	$2p_y$	0.0022	0.0076	−0.6304	0.3310
1H	1s	0.0030	0.5329	−0.3180	−0.9401
2H	1s	0.0022	0.5111	0.1835	1.0163

Table 2. Natural orbitals of the other wave function of the degenerate states at point P

Basis	MO	$\phi_{1a'}$	$\phi_{2a'}$	$\phi_{3a'}$	$\phi_{4a'}$
Li	1s	0.9956	−0.1087	−0.1069	0.0567
Li	2s	0.0216	0.0931	0.6076	−0.3182
Li	$2p_x$	−0.0036	0.1039	−0.2871	0.1676
Li	$2p_y$	−0.0022	−0.0076	0.6304	−0.3310
1H	1s	0.0022	0.5111	0.1835	1.0163
2H	1s	0.0030	0.5329	−0.3180	−0.9401

Full CI calculations are also feasible with the small basis set used here. Preliminary results of the full CI calculation[12] closely parallel those of the above CI-corrected functions.

Bond Exchange View of the Nonadiabatic Transition. The "primitive MCSCF function" shown in Figs. 7(a) and 8 have certain defects. They are, however, illustrative of an important property of the adiabatic function near the crossing. The electronic wave function should belong to one of the representations of the C_{2v} point group when the nuclear arrangement has that symmetry. It is more properly described as a linear combination of two mutually symmetric components having the features shown in Fig. 8, rather than by a single one of them. As the nuclear geometry is deformed by a very small angle θ[13] from a precise isosceles structure, one of the components rapidly reveals its predominance, as is be apparent from the small separation of the dashed lines from the solid lines in Fig. 7(a). For example, when θ is slightly positive, the electronic structure is characterized by a 3a′ natural orbital closely resembling that in Fig. 8(a). The 3a′ orbital bonds Li more strongly to the nearer 1H than to the farther 2H, and forces the geometry farther to the potential minima at a positive θ value. The feature of the corresponding excited state in this situation is characterized by the 3a′ natural orbital essentially of the form of Fig. 8(b). In this state, the distant 2H atom is more strongly bonded to the Li than the nearer 1H. In this sense, the nonadiabatic transition near point P may be viewed as a bond-type change, which occurs smoothly. It is noted that the potential curves in Fig. 7(a) (and more schematically in Fig. 10) are similar to those used to schematize a bimolecular replacement reaction.[14]

A rapid change in the mixing coefficients of the wave functions of the type represented in Fig. 8(a) and those in Fig. 8(b) as we pass through $\theta=0°$ means there is a strong dependence of the wave function on the nuclear geometry. That is a condition[15] which is necessary for the electronic transitions caused by nuclear motion. More specifically, we can view each single state of Fig. 7(a) as a kind of diabatic state[16] appropriate to describing the nonadiabatic transition at P (or its

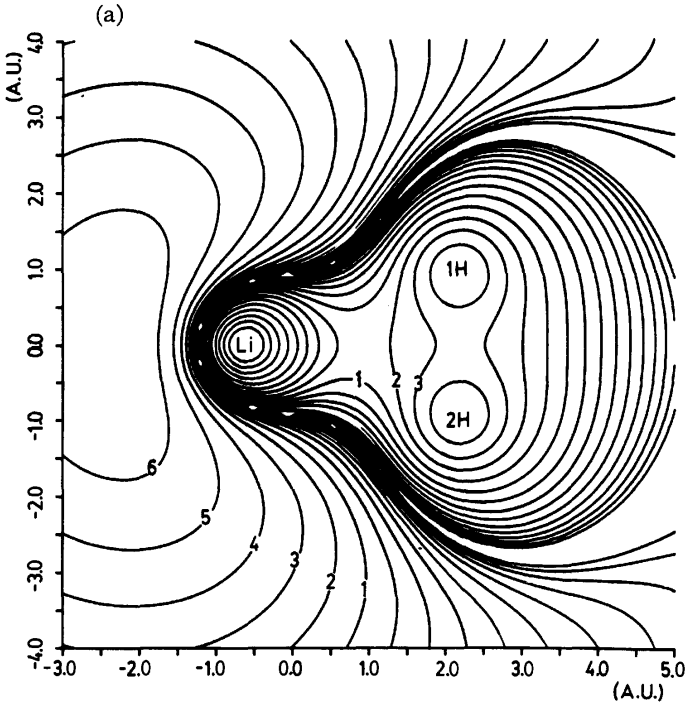

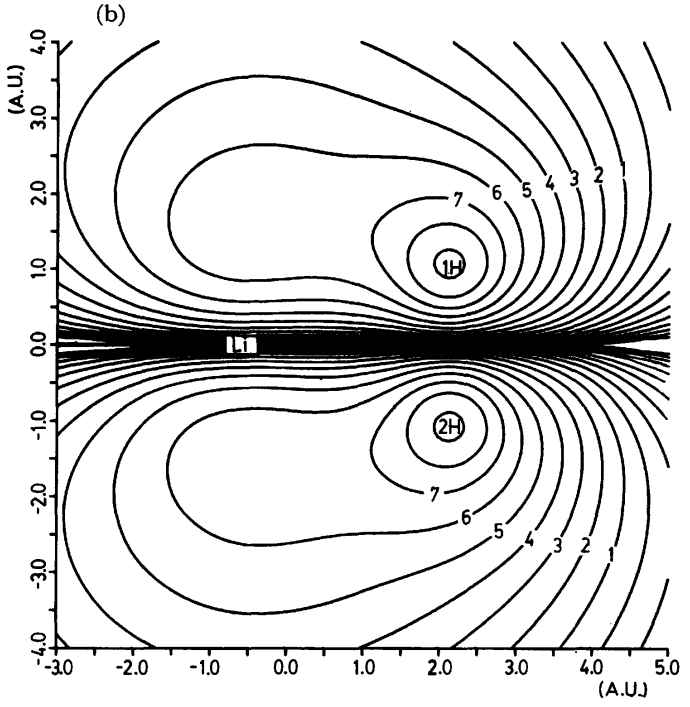

Fig. 9. Contour plots of 3a′ natural orbital electron density of wave functions at P, corrected by an additional CI; (a) upper state and (b) lower state. Figures besides contours have the same meaning as in Fig. 8.

Table 3. Energy difference and energy shifts after an additional nonorthogonal CI

$E_2^0-E_1^{0a)}$	$<1.0\times10^{-10}$	7.4×10^{-5}	7.9×10^{-3}	4.3×10^{-2}
$\lvert\Delta E_1\rvert$	5.8×10^{-6}	1.6×10^{-7}	8.5×10^{-10}	$<1.0\times10^{-15}$
$\lvert\Delta E_2\rvert$	7.6×10^{-6}	1.3×10^{-7}	3.5×10^{-9}	$<1.0\times10^{-15}$

a) Energy difference between the excited $^2A'$ state and the ground $^2A'$ state before an additional CI. Energy unit is hartree.

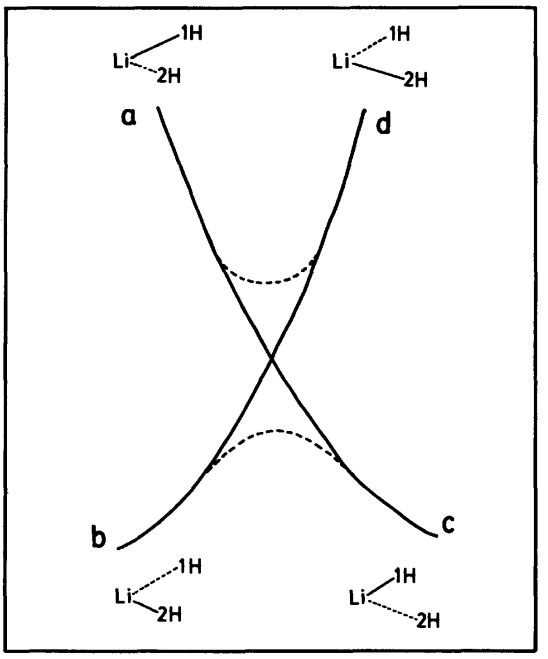

Fig. 10. Schematic representation of potential curves in the pseudocrossing region.

neighborhood) caused by a θ vibration.[11c] Thus as θ changes from a negative to a positive value with a finite velocity, there is a finite probability that the state of the system will follow the diabatic curve from *a* to *c* rather than the adiabatic curve (dashed line) from *a* to *d* (Fig. 10). In other words, there is a finite probability that the system changes from a state in which a more distant atom pair is bonded to a state of the inverse bonding mode.

The presence of cusps in the potential curve at $\theta=0°$ (Fig. 7) is related to the singularity of the density map at $\theta=0°$. The density maps of the 3a′ natural orbitals for points Q', R', and R'', where virtually no cusps are discernible, have a C_{2v} symmetry, while those for points Q''' and R''' have more or less similar abnormal features found at P. We made careful calculations at numerous points along the reaction coordinate and found that the change from the normal behaivor at points far from P to the abnormal one near P was, in reality, continuous. Moreover, the same series of converging functions were obtained irrespective of the starting 0-th approximation of the wave function. Thus, it seems that the singularity seen in the wave function obtained at P and its neighborhood was not the result of pathological progressions of iterations, but the result of an inappropriate form of wave function, as noted above.

Figure 11 shows the potential energy contour maps, thus computed, on the QR-θ plane. Figure 12 is a wide view comprising θ values up to 90°. It shoud be noticed that the shallow channels located at both sides of the reaction coordinate in Fig. 11 are quite immaterial in the gross potential surface (Fig. 12). The depth of the channels was only of the order of

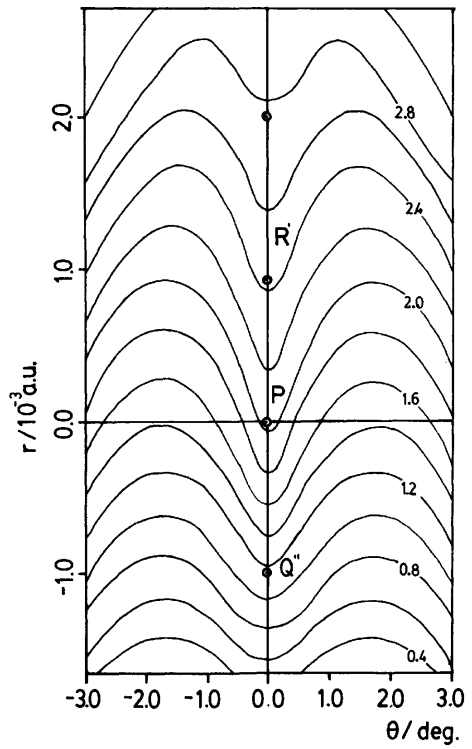

Fig. 11. Contour plots of the potential energy surface of the lowest $^2A'$ state near point P for C_s deformation (finer view). Abscisa: angle of deformation from C_{2v}. Ordinate: reaction coordinate. Figures beside curves indicate the values (E_{total}+8.3880 hartrees)/(10^{-4} hartree).

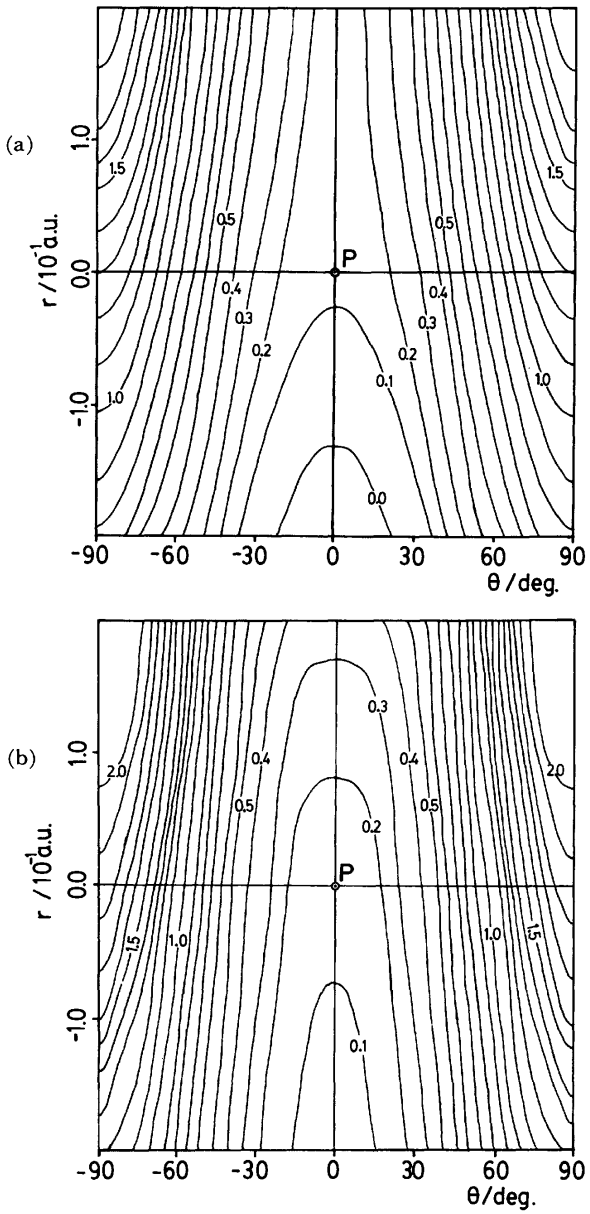

Fig. 12. Contour plots of the potential energy surfaces of the two lowest $^2A'$ states for C_s deformation from C_{2v}. (wider view). Abscisa: deformation angle from C_{2v}. Ordinate: reaction coordinate. (a) lowest $^2A'$ and (b) 2nd. $^2A'$. Figures beside curves indicate the values (E_{total}+8.4000 hartree)/(10^{-1} hartree).

50 cal/mol in this calculation. It may be neglected compared to thermal energy in the usual quenching experiments. The steep ascent of the potential surface to the θ direction implies the energetic disadvantages of a transition through a skewd geometry, as described at the beginning of this discussion. It is interesting that even for linear arrangement of the nuclei, the 3a' natural orbital shows similar bond exchange features as found above for the nearly C_{2v} geometry. Figure 13 shows electron density maps at point F of Fig. 2, and is compared with features shown in Figs. 8 and 9. The whole view of the first and second potential energy surfaces displayed with R_{LiH_2} and θ as parameters may be sketched roughly as in Fig. 14. They touch conically near point P in this dimension.

Conclusions

Potential energy surfaces of a system consisting of an $X^1\Sigma_g^+H_2$ and a Li atom in either 2^2S or 2^2P state come close or even cross, aside from collinear arrangement, for almost all inclination angles of the H_2 axis relative to the direction joining the components. Quenching of the excited Li atom by the H_2 molecule is expected to occur along any of the paths passing through these crossing regions. Among these paths, the ones having an isosceles or nearly isosceles geometry seem to be energetically most favorable. CASSCF wave functions,in which all the orbitals other than the core are included as active states, are almost as good as the full CI wave functions for every nuclear geometry in describing the finer electron density profiles as well as the energetic behavior of the system, except for small cririca regions where crossing or pseudocrossing occur. In the latter regions it is necessary to perform an additional nonorthogonal configuration interaction, or full CI if possible. Energetic corrections are quite small in these regions. The primary wave functions, themselves, reveal characteristic electronic properties of the system in the crossing region. Around the pseudocrossing point, ground state potential curves for

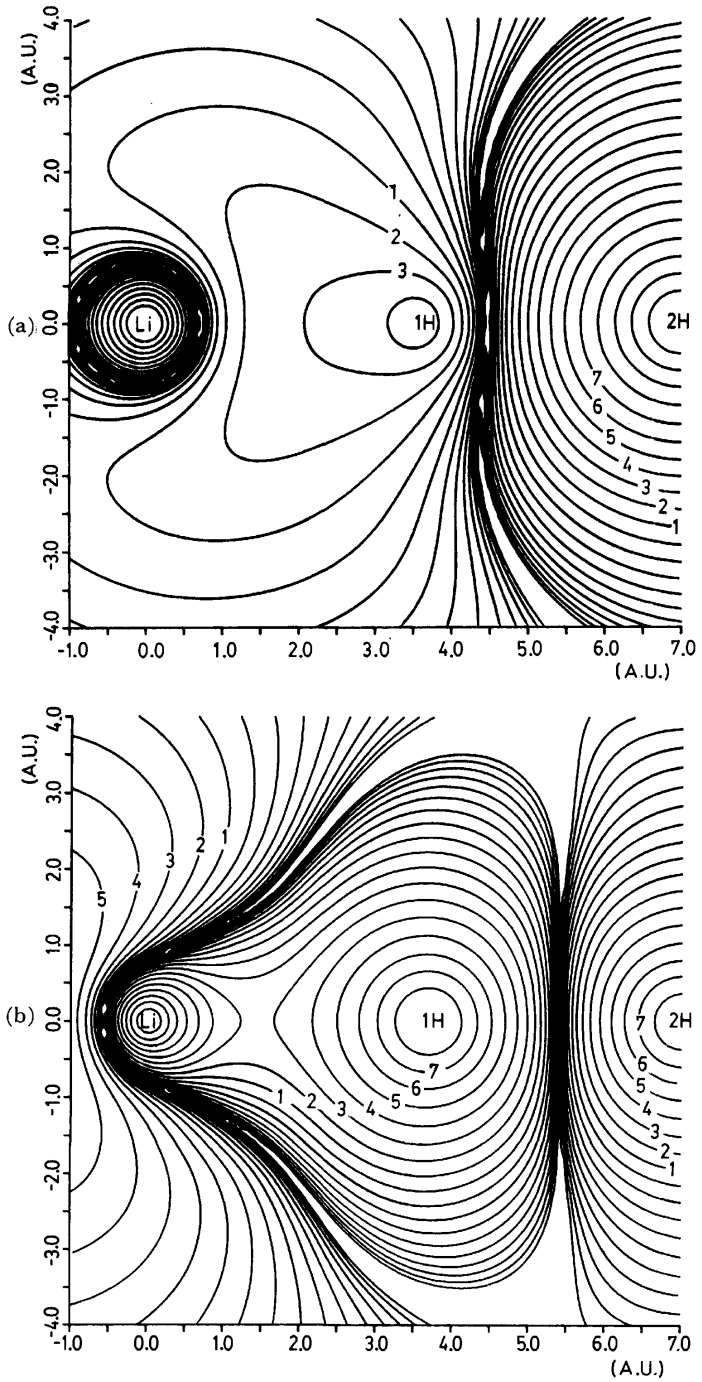

Fig. 13. Contour plots of 3a′ natural orbital electron density map for collinear geometry θ=90°, $R_{Li\text{-}H_2}$= 3.7 bohr, $R_{H\text{-}H}$=3.3 bohr. (a) lowest $^2\Sigma^+$ and (b) 2nd. $^2\Sigma^+$. Figures beside curves have the same meaning as in Fig. 8.

a θ-deformation from the C_{2v} geometry have shallow but distinct minima located at a few degrees on both sides. The whole potential curves may be viewed as resulting from a resonance splitting of the two crude "diabatic" curves, each describing one of the two modes of bonding. In this connection, electron density maps reveal features of bond type alternation upon nonadiabatic transitions induced by the b_2 vibration of the complex. These features resemble the mechanism of a bimolecular exchange reaction.

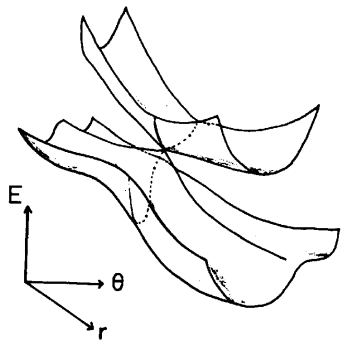

Fig. 14. Schematic view of the $1^2A'$ and the $2^2A'$ adiabatic potential energy surfaces in θ and r dimensions near the conical touch points.

We thank Professor Keiji Morokuma and Dr. Shigeki Kato of the Institute for Molecular Science for their helpfull suggestions, discussions and encouragement. Calculations were carried out at the Computer Center of the IMS, Okazaki National Research Institutes, at the Computer Center of the University of Tokyo, and at the Aoyama Gakuin University Computer Center. Thanks are due to Mr. Toyama for his help in these calculations. The present work was partially supported by a Grant-in-Aid for Scientific research No. 57740248 from the Ministry of Education, Science and Culture.

References

1) K. Mizutani, Y. Kuribara, K. Hayashi, and S. Matsumoto, *Bull. Chem. Soc. Jpn.*, **52**, 2184 (1979).

2) P. J. A. Ruttink and J. H. van Lenthe, *Theor. Chim. Acta.*, **44**, 97 (1977).

3) A. F. Wagner, A. C. Wahl, A. M. Karo anfd R. Krejci, *J. Chem. Phys.*, **69**, 3756 (1978).

4) P. Hobza and P. R. Schleyer, *Chem. Phys. Lett.*, **105**, 630 (1984).

5) Part of the results was presented by K. Hayashi, K. Mizutani, and S. Matsumoto at the 41st. National Meeting of the Chemical Society of Japan, Osaka, April 1980, Abstr. P. 170.

6) P. Botschwina, W. Meyer, I. V. Hertel, and W. Reiland, *J. Chem. Phys.*, **75**, 5438 (1981).

7) W. J. Hehre, R. F. Stewart and J. A. Pople, *J. Chem. Phys.*, **51**, 2657 (1969).

8) B. O. Roos, P. R. Taylor and P. E. M. Siegbahn, *Chem. Phys.*, **48**, 157 (1980); P. E. M. Siegbahn, J. Almlof, A. Heiberg and B. O. Roos, *J. Chem. Phys.*, **74**, 2384 (1981).

9) Given at Molecular Structure Symposium, October 1981, Kyoto, Japan, Abstr. No. 2M02 and will be published separated paper.

10) At point P, the energies of $^2A_1$ and $^2B_2$ states almost coincide (to 10^{-10} hartree in this case). However, after an additional CI (see below), it is no more a point of potential surface intersection. Actually, it was a point somewhat displaced toward point R in Fig. 6 after the nonorthogonal CI.

11) a) J. Paldus and J. Cizek, *Chem. Phys. Lett.*, **3**, 1 (1969); J. Paldus and J. Cizek, *J. Chem. Phys.* **52**, 2919 (1970); b) A.

Toyota and T. Nakajima, *Bull. Chem. Soc. Jpn.*, **50**, 97 (1977); c) C. F. Jackels and E. R. Davidson, *J. Chem. Phys.*, **64**, 2908 (1976).

12) Given at the 49th National Meeting of the Chemical Society of Japan, Tokyo, April 1984, Abstr. p. 38.

13) Calculations showed that only an order of 5×10^{-2} degree deformation was sufficient.

14) S. G. Christov, "Lecture Notes in Chemistry, 18, Collision Theory and Statistical Theory of Chemical Reactions," Springer-Verlag, Berlin, 1980, p. 19.

15) T. F. O'Malley, "Advances in Atomic and Molecular Physics Vol. 7" Academic Press, New York, 1971, p. 227; E. E. Nikitin and L. Zulicke, "Lecture Notes in Chemistry, 8, Theory of Chemical Elementary Processes," Springer-Verlag, Berlin, 1978, p. 20.

16) T. F. O'Malley, "Advances in Atomic and Molecular Physics Vol. 7," Academic Press, New York, 1971, p. 223; R. Cimiraglia and M. Persico, *Mol. Phys.*, **38**, 1707 (1979).

NQR of the 1 : 2 Molecular Complex of 1,4-Diazabicyclo[2.2.2]-octane with Chloroform

Hisao NEGITA, Toshinori SUZUKI, Tsuneo KUBO, Michio MAEKAWA, Shinei GIMA, and Tsutomu OKUDA*

Department of Chemistry, Faculty of Science, Hiroshima University, Naka-ku, Hiroshima 730

(Received March 5, 1984)

The ^{14}N and ^{35}Cl NQR and ^{14}N spin-lattice relaxation have been studied at various temperatures on the 1:2 molecular complex of 1,4-diazabicyclo[2.2.2]octane (DABCO) with $CHCl_3$. Two transitions have been observed near 123 K and 138 K. In the lowest temperature phase a minimum in the T_1 was observed and attributed to the axial reorientation of DABCO molecules. The activation energy for this motion was determined to be 12.1 ± 1.2 kJ mol^{-1}. The electron population is discussed for the DABCO complexes with $CHCl_3$ and $CDCl_3$ using the Townes-Dailey treatment.

DABCO has been known to form a molecular complex with chloroform by charge transfer from the former to the latter. The crystal structure of this complex has not been determined as yet. DABCO itself is well known as a plastic crystal and its motions have been studied in detail by NMR and NQR.[1,2] Since DABCO is globular, its motion in the complex will offer information about intermolecular interactions and, consequently, a clue to the molecular structure. Lucus and Guibé have already measured ^{14}N and ^{35}Cl NQR of this complex.[3] They reported the average ^{14}N NQR frequency and three ^{35}Cl NQR lines at liquid nitrogen temperature. We observed the temperature dependence of the ^{14}N and ^{35}Cl NQR lines and the ^{14}N spin-lattice relaxation times of the complex in order to examine the molecular motions and intermolecular interactions.

Experimental

The molecular complex was prepared by adding chloroform to DABCO purified by sublimation in an evacuated vessel and then cooling the mixture gently below 250 K. ^{14}N NQR measurements were carried out using a pulsed NQR spectrometer.[4] On the other hand, ^{35}Cl NQR spectra were observed using a superregenerative spectrometer. The temperature was measured by the use of a copper-constantan thermocouple. The frequency was checked by means of a frequency counter.

Results and Discussion

Temperature Dependence of ^{14}N and ^{35}Cl NQR Lines.

TABLE 1. ^{14}N NQR PARAMETERS IN DABCO COMPLEXES AT LIQUID NITROGEN TEMPERATURE

Complex	ν_-/kHz[a]	ν_+/kHz[a]	η/%	(e^2Qq/h)/kHz
$C_6H_{12}N_2 \cdot 2CHCl_3$	3551.0		0	4734.7
	3545.8	3583.9	1.603	4753.1
	3532.7	3567.5	1.470	4730.9
	3528.9	3562.2	1.409	4734.7
$C_6H_{12}N_2 \cdot 2CDCl_3$	3553.1		0	4737.5
	3551.1	3587.6	1.534	4759.1
	3535.9	3571.9	1.519	4738.5
	3532.8	3564.5	1.340	4731.5

a) Experimental error is within ±0.1 kHz.

Tables 1 and 2 show the NQR frequencies for the DABCO complexes at liquid nitrogen temperature. Seven ^{14}N and eleven ^{35}Cl resonance lines were observed for the complex of DABCO with $CHCl_3$ whereas seven ^{14}N and ten ^{35}Cl resonance lines were observed for the complex of DABCO with $CDCl_3$.

In the complex of DABCO with $CHCl_3$, the average frequency of four ^{14}N NQR lines (except three ν_+ lines) is 3.5396 MHz and agrees well with the value of 3.5397 MHz reported by Lucus and Guibé.[3] For ^{35}Cl NQR lines, frequencies of three among eleven resonance lines coincide approximately with the three frequencies, 37.666, 37.853, and 37.955 MHz, reported by Lucus and Guibé.[3] It is not possible at present to interpret the discrepancy in the number of ^{35}Cl resonance lines between the present study and Ref. 3.

Figure 1 shows the temperature dependence of ^{14}N NQR frequencies in the $CHCl_3$ complex. Seven resonance lines at liquid nitrogen temperature are denoted as (a), (b), (c), ···, and (g) as shown in Fig. 1. (a) and (b) as well as (e) and (f) approached each other with increasing temperature and coincided at about 123 K. The intensity of (d) was about twice as strong as those of the rest at liquid nitrogen temperature. As the temperature was raised, (d) became weak from 115 K and faded out near 123 K. Therefore, the seven resonance lines reduced to four near 123 K. These lines disappeared at 138 K but one broad line 50 kHz wide appeared just above this temperature as shown by the solid line in Fig. 1. As the temperature was raised, the

TABLE 2. ^{35}Cl NQR FREQUENCIES OF DABCO COMPLEXES AT LIQUID NITROGEN TEMPERATURE

Complex	ν/MHz[a]		
$C_6H_{12}N_2 \cdot 2CHCl_3$	37.122	37.360	37.402
	37.491	37.642	37.728[b]
	37.818	37.831	37.917
	37.932	38.059	
$C_6H_{12}N_2 \cdot 2CDCl_3$	37.135	37.368	37.412
	37.498	37.648	37.737[c]
	37.833[b]	37.923	37.942
	38.059		

a) Experimental error is within ±0.005 MHz. b) Double intensity line. c) Doublet.

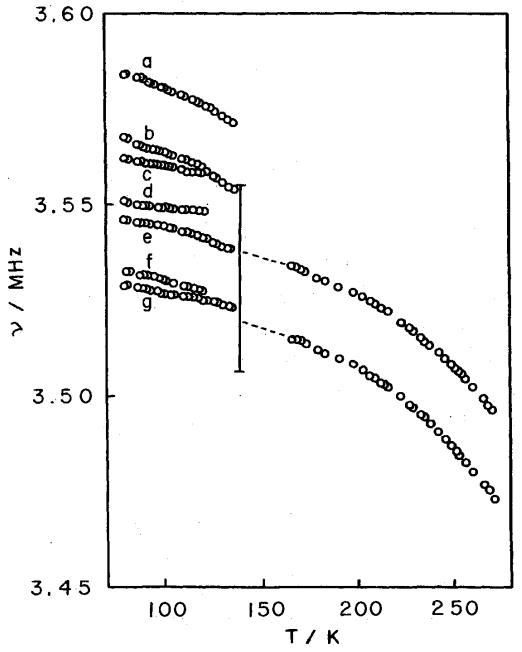

Fig. 1. Temperature dependence of ^{14}N NQR frequencies in $C_6H_{12}N_2 \cdot 2CHCl_3$.

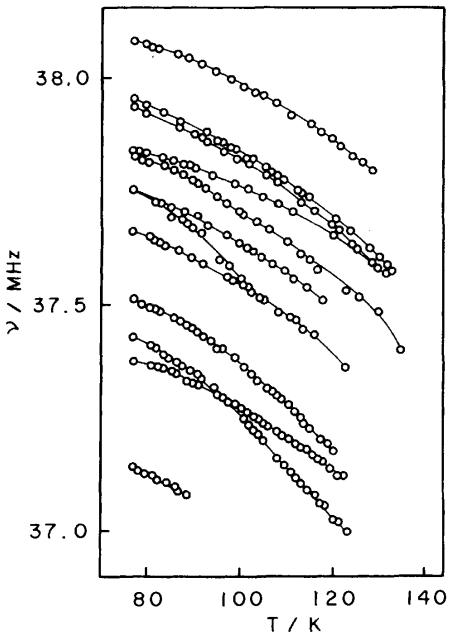

Fig. 2. Temperature dependence of ^{35}Cl NQR frequencies in $C_6H_{12}N_2 \cdot 2CHCl_3$.

linewidth decreased gradually and near 165 K the broad line split into two components. Since it was impossible to determine the resonance frequency with accuracy over the temperature range from 138 K to 165 K, the resonance lines are shown by the dotted lines in Fig. 1.

On the other hand, the temperature dependence of ^{35}Cl NQR frequencies in the $CHCl_3$ complex is shown in Fig. 2. Eleven resonance lines were observed at liquid nitrogen temperature, indicating that there are at least four $CHCl_3$ molecules in this complex. By analogy with ^{14}N resonance lines, the number of ^{35}Cl resonance lines decreased to half near 123 K and faded out

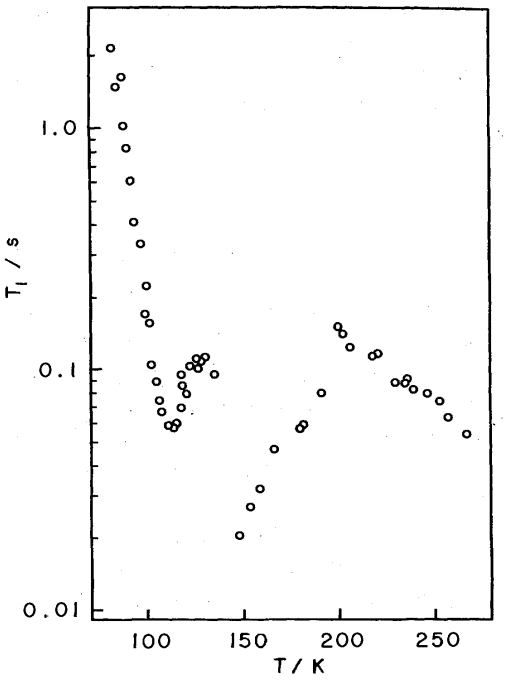

Fig. 3. Temperature dependence of ^{14}N spin-lattice relaxation times in $C_6H_{12}N_2 \cdot 2CHCl_3$. The spin-lattice relaxation times were measured for the (e) line between 80 K and 138 K and for the higher resonance line above 138 K.

near 138 K. However, no ^{35}Cl resonance lines appeared above 138 K up to the melting point (*ca.* 273 K).

^{14}N Spin-Lattice Relaxation Time. Figure 3 shows the temperature dependence of ^{14}N spin-lattice relaxation time in the complex of DABCO with $CHCl_3$. In the temperature range from 80 K to 123 K, the most remarkable feature is the appearance of the T_1 minimum at about 115 K. This process can be attributed to the reorientation of the DABCO molecule about its three-fold axis. The activation energy for this motion was calculated. In this case, the dominant relaxation mechanism can be regarded as magnetic dipole-dipole interaction between ^{14}N and nearby protons. Then, the relaxation time is given by the following equation:[1]

$$1/T_1 = C\tau/(1+\omega_Q^2\tau^2), \quad (1)$$

where C is a constant related to the intrinsic nature of the molecular motion. τ is the correlation time of the motion, and ω_Q is the resonance angular frequency. Assuming that the Arrhenius' relation for the correlation time, the following equation holds:

$$\tau = \tau_0 \exp(E_a/RT), \quad (2)$$

where τ_0 is the inverse frequency factor and E_a is the activation energy for the motion. E_a was calculated to be 12.1±1.2 kJ mol^{-1} for this motion from Eqs. 1 and 2 and the observed T_1 values. In the case of DABCO itself, the activation energy about the N-N axis was found to be 34.2±1.3 kJ mol^{-1} by Zussman *et al.*[1] This

value is nearly three times as large as that of the present complex. This finding suggests that the packing of the molecules is somewhat loose in the complex because the DABCO molecule lies between two bulky chloroform molecules.

At T_1 minimum, $\omega_Q\tau=1$ and the following equation holds:[1]

$$T_1^{min} = (8/81)(\omega_Q r_{NH}^6/\gamma_N^2\gamma_H^2\hbar^2), \quad (3)$$

where r_{NH} is the N-H distance in DABCO. γ_N and γ_H are the gyromagnetic ratio of nitrogen and hydrogen, respectively. Assuming that the structure of DABCO in the complex is the same as that in the pure DABCO crystal,[1] the value of T_1 minimum was calculated to be 60 ms. This is in good agreement with the observed value, 63 ms.

Bond Nature. In the case of the ^{14}N resonance, a pair of resonance lines, ν_- and ν_+, are observed and their frequencies are expressed as follow:

$$\nu_\pm = (e^2Qq/4h)(3\pm\eta), \quad (4)$$

where e^2Qq/h and η are the quadrupole coupling constant and the asymmetry parameter, respectively. In the complex of DABCO with $CHCl_3$, two ^{14}N resonance lines at temperatures above 138 K were found to be one pair of ν_- and ν_+ by measuring their Zeeman effect. Below 138 K the small intensity and small spacing of the multiple resonance lines make the measurement of the Zeeman effect unavailable. However, the temperature dependence of the ^{14}N and ^{35}Cl resonance frequencies makes their assignment to resonance lines possible. Since there are at least four crystallographically nonequivalent $CHCl_3$ molecules at liquid nitrogen temperature as described above, four nonequivalent nitrogen atoms should exist: There are seven ^{14}N resonance lines consisting of three pairs of ν_- and ν_+ and one single line. Between 123 K and 138 K, there are four ^{14}N and six ^{35}Cl resonance lines, indicating the presence of two nonequivalent nitrogen and chloroform. Since (b) and (f) lines coincided to (a) and (e) lines, respectively, at the first transition point as shown in Fig. 1, (a) and (e), (b) and (f), and (c) and (g) are paired. The asymmetry parameters and quadrupole coupling constants obtained by this pairing are listed in Table 1.

^{14}N resonance lines of the complex of DABCO with $CDCl_3$ are also listed in Table 1 together with the asymmetry parameters and quadrupole coupling constants evaluated by the same pairing as that of the $CHCl_3$ complex. The ^{14}N resonance frequencies of the $CDCl_3$ complex shift to the higher frequency region than those of the complex with $CHCl_3$ in the same manner as the ^{35}Cl resonance frequencies. In both complexes the nitrogen atoms are considered to form sp^3 hybrid orbitals. Three hybrid orbitals form N-C sigma bonds and the rest is a lone pair nonbonding orbital. Therefore, the quadrupole coupling constant is given by,[6]

$$e^2Qq/h = (3/4)(m-n)e^2Qq_0/h, \quad (5)$$

where m and n are the electron population in the lone pair and sigma bond orbitals, respectively, and e^2Qq_0/h is the quadrupole coupling constant by a 2p electron of nitrogen and is assumed to be 11.3 MHz.[7] From Eq. 5 and the average coupling constant, the value of $(m-n)$ is computed to be 0.5599 and 0.5595 for the $CHCl_3$ and $CDCl_3$ complexes, respectively. This indicates that the electron population in the lone pair nonbonding orbital in the $CDCl_3$ is larger by 0.0004 than those in the $CHCl_3$ if the frequency difference is taken to arise only from hydrogen bonding formation.

References

1) A. Zussman and S. Alexander, *J. Chem. Phys.*, **48**, 3534 (1968).
2) P. J. Haigh and L. Guibé, *C. R. Acad. Sci.*, **261**, 2328 (1965).
3) A. D. Lucus and L. Guibé, *Mol. Phys.*, **19**, 88 (1979).
4) H. Negita, T. Kubo, M. Maekawa, A. Ueda, and T. Okuda, *Bull. Chem. Soc. Jpn.*, **52**, 1881 (1979).
5) G. W. Smith, *J. Chem. Phys.*, **43**, 4325 (1965).
6) R. A. Marino, *Adv. Nucl. Quadrupole Reson.*, **1**, 391 (1974).
7) R. Ikeda, S. Noda, D. Nakamura, and M. Kubo, *J. Magn. Reson.*, **5**, 54 (1971).

Behavior of Benzo-18-crown-6 Complexes with Alkali Metal Ions in Various Nonaqueous Solvents

Yasuyuki TAKEDA,* Yoshihiko OHYAGI, and Sadatoshi AKABORI†
Department of Chemistry, Faculty of Science, Chiba University, Yayoi-chō, Chiba 260
†*Department of Chemistry, Toho University, Funabashi, Chiba 274*
(Received March 13, 1984)

The formation constants for 1 : 1 complexes of benzo-18-crown-6 (B18C6) with alkali metal ions and the solubility of B18C6 in various solvents were determined at 25 °C by conductometry and spectrophotometry, respectively. In general, the selectivity of B18C6 for alkali metal ions is governed primarily by the size relationship between cations and the B18C6 cavity. For a given alkali metal ion, the solvation ability of the solvent plays the most important role in determining stability sequences of the B18C6 complex in the solvents. Transfer activity coefficients of B18C6-alkali metal ion complexes were calculated. The transfer activity coefficient of the B18C6 complex from methanol to aprotic solvents somewhat varies with alkali metal ions in the B18C6 cavity. The magnitudes of the transfer activity coefficients of the B18C6 complex from acetonitrile and propylene carbonate to DMF and DMSO are determined mainly by the relative strength of the solvation ability of the former group and the latter group for the alkali metal ion in the B18C6 cavity. In methanol, due to the hydrogen bonds between ether oxygen atoms of B18C6 and methanol, the B18C6 complex is more strongly solvated than the corresponding alkali metal ion, compared to the case of the aprotic solvents.

In a previous paper,[1] various factors, which affect stabilities of 18-crown-6 (18C6) and dibenzo-18-crown-6 (DB18C6) complexes with alkali metal ions in several protic and aprotic solvents, were systematically investigated from a thermodynamic point of view. These factors are (1) the relative sizes of the alkali metal ions and the crown ether cavity, (2) the solvation ability of a solvent for the alkali metal ions, (3) the electron density of the crown ether cavity, and (4) the ligand-ring flexibility.

The behavior of 18C6 and DB18C6 complexes with alkali metal ions in a variety of solvents was studied by conductometry.[1-3] In each case of propylene carbonate[3] and *N,N*-dimethylformamide (DMF),[1] the mobilities of 18C6 complexes with alkali metal ions (Na^+, K^+, Rb^+, Cs^+) were nearly equal. Although the sizes of the 18C6-K^+ complex and $(n\text{-}C_4H_9)_4N^+$ are almost identical, the 18C6 complex in H_2O and CH_3OH does not enforce the hydrogen-bonded structure around the complexed ion as $(n\text{-}C_4H_9)_4N^+$ does.[2] It was proved from Walden products that the behavior of the 18C6-K^+ complex regarding transport phenomena is much the same in protic and aprotic solvents, as is the DB18C6-K^+ complex.[2] In order to obtain information about solute-solvent interactions with regard to 18C6[4,5] and DB18C6[6] complexes with univalent metal ions dissolved in various solvents, transfer activity coefficients of the complexes were determined. The solvation properties of the complexes are discussed in detail.

The structure of benzo-18-crown-6 (B18C6) is intermediate between 18C6 and DB18C6. In analytical chemistry, B18C6 is widely used as a moiety of bis(crown ether)s,[7] a pendant of polymers,[8] and colorimetric extraction-reagents[9] in order to achieve high selectivity for a given metal ion. Only a few thermodynamic studies have, however, been reported on B18C6 complexes with metal ions in solutions.[10-12]

In the present work, formation constants for 1:1 complexes of B18C6 with alkali metal ions and the solubility of B18C6 in protic and aprotic solvents were determined at 25°C by conductometry and spectrophotometry, respectively. The transfer activity coefficients of the B18C6 complexes with alkali metal ions were calculated from these data and values found in the literature regarding the transfer activity coefficients of alkali metal ions. The stabilities and solvation behavior of the B18C6 complexes in solutions are discussed.

Experimental

Materials. Benzo-18-crown-6 was prepared according to Pedersen.[13] The product was recrystallized three times from heptane and dried at 40 °C in a vacuum oven before use. Its purity was checked by melting point, elemental analysis, NMR, and conductometry.

Extremely pure sodium, potassium, rubidium, and caesium chlorides were obtained from Merck Japan Ltd., and were used without further purification. Rubidium and caesium perchlorates were prepared by adding a little excess of perchloric acid to aqueous solutions of rubidium and caesium chlorides, respectively. Sodium and potassium perchlorates were purchased from Merck Japan Ltd. All the perchlorates were recrystallized four times from distilled water and, prior to use, dried at 150 °C in a vacuum oven.

The method of purification of acetonitrile,[2] propylene carbonate,[3] methanol,[14] DMF,[1] and dimethyl sulfoxide (DMSO)[2] was previously described. For these five solvents, the middle 70% of the distillate was used. The conductivities of these final products of acetonitrile, propylene carbonate, methanol, DMF, and DMSO were less than 3×10^{-7}, 6×10^{-8}, 2×10^{-7}, 3×10^{-7}, and 7×10^{-8} $\Omega^{-1}cm^{-1}$, respectively.

Alkali metal chlorides were employed for the methanol system and alkali metal perchlorates for the other solvent systems.

Apparatus and Procedure. The conductance measurements were made on a Fuso conductivity apparatus,

model 362A, in a water bath thermostated at 25±0.005°C. Three cells were used with cell constants of 0.059705, 0.093939, and 0.097761 cm^{-1}. The experimental procedure to obtain formation constants of B18C6 complexes with alkali metal ions was almost the same as that described in a previous paper.[3]

Solubilities of B18C6. Solubilities of B18C6 in acetonitrile (275nm), propylene carbonate (275nm), methanol (225nm), DMF (278nm), and DMSO (276nm) were determined spectrophotometrically at 25±0.02°C. They are 2.8×10^{-1}, 2.4, 2.9, 3.0, and 2.8M (1 M=1 mol dm^{-3}) for acetonitrile, propylene carbonate, methanol, DMF, and DMSO, respectively.

Results and Discussion

The procedure for obtaining formation constants (K_{ML^+}) of B18C6 complexes with alkali metal ions was the same as that described in a previous work,[3] where $K_{ML^+}=[ML^+]/[M^+][L]$. M^+ and L designate an alkali metal ion and a crown ether, respectively. In the present study, it is assumed that the association between a cation and an anion is negligible under the highly dilute experimental conditions (total concentration of an alkali metal ion$\approx5\times10^{-4}$ M) and that B18C6 forms a 1:1 complex with an alkali metal ion. Since the B18C6 concentration was kept below 2.5×10^{-3}M during the experiments, corrections for viscosity changes were neglected. The log K_{ML^+} values are listed in Table 1, together with the literature values.

The molar conductivity (Λ) *vs.* $[L]_t/[M]_t$ plots for propylene carbonate and DMF systems at 25°C are illustrated in Figs. 1 and 2, where $[L]_t$ and $[M]_t$ denote total concentrations of B18C6 and the alkali metal ion, respectively. Since the Λ *vs.* $[L]_t/[M]_t$ curves for the other solvent systems are similar, they have been omitted. Every plot of Λ *vs.* $[L]_t/[M]_t$, except for the $NaClO_4$–DMSO system, shows a decrease in Λ with an increase in the B18C6 concentration. This indicates that the alkali metal ion complexed by B18C6 is less mobile than the corresponding free alkali metal ion. For the $NaClO_4$–DMSO system, the change in Λ was so small in spite of an increase in the B18C6 concentration that the complex-formation constant could not be determined conductometrically. It can be seen from Fig. 1 that, in the cases of Na^+, K^+, and Rb^+, the slope of each curve changes sharply at $[L]_t/[M]_t=1$. The same

TABLE 1. Log (K_{ML^+}/$mol^{-1}dm^3$) VALUES AT 25°C AND CRYSTAL IONIC RADII OF ALKALI METALS (Å)

		Na^+	K^+	Rb^+	Cs^+
Crystal ionic radius[15]		0.95	1.33	1.48	1.69
AN[a]	18C6	4.5[6]	5.7[6] 5.7[2]	—	>4[16]
	B18C6	4.9	5.3	4.4	3.8
	DB18C6	4.8[6] 5.0[17] 5.0[18]	4.8[6] 4.7[17] 4.8[18] 4.7[2]	3.7[17]	3.5[6] 3.5[17]
PC[b]	18C6	5.6[3] 5.2[6]	6.2[3] 6.3[6]	5.3[3]	4.4[3] 4.5[6] 4.2[16]
	B18C6	5.3	5.4	4.5	3.6
	DB18C6	5.2[6]	5.1[6]	3.9[6]	3.3[6]
CH_3OH	18C6	4.3[19] 4.3[20,21]	6.1[19] 6.0[20] 6.0[2] 6.1[21]	5.3[20]	4.6[19] 4.7[20]
	B18C6	4.5 4.0[10] 4.35[11]	5.7 5.2[10] 5.05[11]	5.1 4.6[10]	4.1 3.6[10]
	DB18C6	4.3[19] 4.4[6] 4.5[22]	5.0[19] 5.0[6] 5.1[22] 4.6[17] 4.6[18] 5.0[2]	4.2[6]	3.5[19]
DMF	18C6	2.4[1]	4.3[1]	3.9[1]	3.6[1] 3.9[16]
	B18C6	2.5	3.6	3.2	2.8
	DB18C6	2.4[6] 2.8[23]	2.8[6]	2.1[6]	1.5[16]
DMSO	18C6	1.4[6]	3.2[6] 3.2[2]	—	3.0[16]
	B18C6	—	2.8	2.6	2.4
	DB18C6	1.9[6]	2.4[6] 2.5[24] 2.5[2]	1.9[6]	1.3[16]

a) Acetonitrile. b) Propylene carbonate.

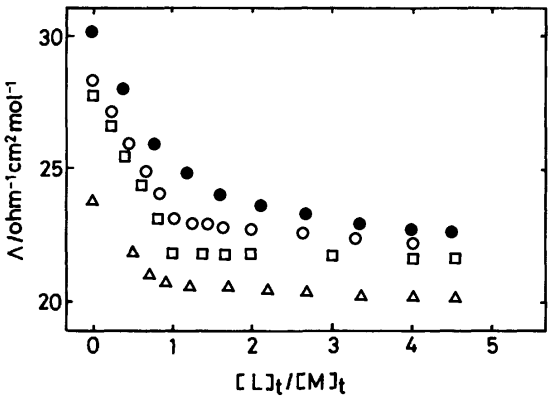

Fig. 1. Λ *vs.* $[L]_t/[M]_t$ curves for B18C6-alkali metal perchlorate systems in propylene carbonate at 25 °C.
△: Na^+, □: K^+, ○: Rb^+, ●: Cs^+, $[M]_t=5\times10^{-4}$ M.

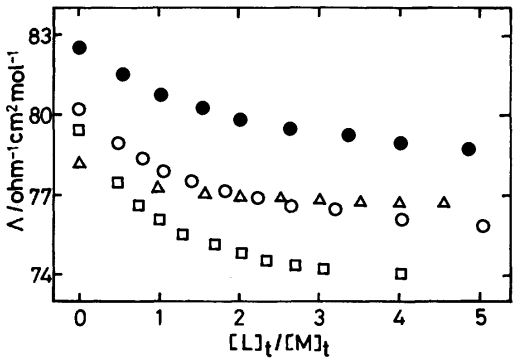

Fig. 2. Λ *vs.* $[L]_t/[M]_t$ curves for B18C6-alkali metal perchlorate systems in DMF at 25 °C.
△: Na^+, □: K^+, ○: Rb^+, ●: Cs^+, $[M]_t=5\times10^{-4}$ M.

tendency was observed for the Na^+-, K^+- acetonitrile, and the Na^+-, K^+-, Rb^+-methanol systems. For the other systems, no such clear breaking point was observed. These data indicate that the following three factors play an important role in causing the clear breaking point. (1) Benzo-18-crown-6 forms a stable complex with an alkali metal ion (log $K_{ML^+}\geqq4.5$). (2) The difference in mobility between the B18C6-alkali metal ion complex and the corresponding free alkali metal ion is large. (3) A higher-order B18C6 complex such as a 1:2 sandwich complex of an alkali metal ion with B18C6 is not formed.

Stability Constants. It can be seen from Table 1 that the log K_{ML^+}-value sequences of B18C6 complexes with K^+, Rb^+, and Cs^+ for the same solvent are $K^+>Rb^+>Cs^+$. This indicates that the selectivity tendency of B18C6 (18C6 cavity radius: 1.34—1.43 Å[20]) agrees well with the size-fit concept. Among all the B18C6 complexes with alkali metal ions (Na^+, K^+, Rb^+, Cs^+), the log K_{ML^+} value of the Na^+-B18C6 complex is the second largest for acetonitrile and propylene carbonate, the third largest for methanol, and the smallest for DMF and DMSO. This reflects the fact that in every one of these solvents Na^+ is the most strongly solvated of all the alkali metal ions (Na^+, K^+, Rb^+, Cs^+), and that the differences in the free energies of the solvation of Na^+ and K^+, Na^+ and Rb^+, and Na^+ and Cs^+ are much smaller for acetonitrile and propylene carbonate than for the other solvents.[1] A similar tendency to that described above was observed for the stabilities of 18C6 and DB18C6 complexes with alkali metal ions in various solvents.[1]

Since an aliphatic ether oxygen atom is more basic than an aromatic ether oxygen atom, the interaction of an alkali metal ion with the former is stronger than that with the latter. Benzo-18-crown-6 and DB18C6 have two and four aromatic ether oxygen atoms, respectively. Thus, it can be expected that the stabilities of the complexes of these three crown ethers with the same alkali metal ion in a given solvent decrease in the order 18C6>B18C6>DB18C6. The data in Table 1 are in good accord with this expectation except for the Na^+-acetonitrile, methanol, DMF, and DMSO systems. For propylene carbonate, however, the difference in the log K_{ML^+} values of Na^+ between 18C6 and B18C6 (0.4), and that between B18C6 and DB18C6 (0.1) are both small compared to the other alkali metal ions (K^+, Rb^+, Cs^+). Since Na^+ is smaller than the 18C6 cavity and has the greatest charge density of all the alkali metal ions (Na^+, K^+, Rb^+, Cs^+), Na^+ held in the cavity may attract the donor oxygen atoms of the crown ether much more strongly than the other alkali metal ions. It follows from this that the complexation reaction of Na^+ with a flexible crown ether causes the largest ligand-ring conformational change among all the alkali metal ions. Consequently, the more flexible is a crown ether, the more destabilized is the Na^+ complex with the crown ether on account of entropy contribution. It thus appears from Table 1 that the stability sequences of Na^+ complexes with 18C6, B18C6, and DB18C6 for the same solvent largely depend on competition between the ligand-ring flexibility and the electron density of the crown ether cavity.

For acetonitrile and propylene carbonate, the log K_{ML^+} value of Na^+ with DB18C6 is the largest; while, those with B18C6 and 18C6 are the second largest. For methanol, the log K_{ML^+} values of Na^+ with DB18C6, B18C6, and 18C6 are the second largest, the second smallest, and the smallest, respectively. For DMF and DMSO, the log K_{ML^+} value of Na^+ with DB18C6 is the second largest; while, those with B18C6 and 18C6 are the smallest. For the same solvent, the difference in the log K_{ML^+} values of the same crown ether between Na^+ and the other alkali metal ion, which forms a more stable complex with the crown ether compared to Na^+, increases in the order DB18C6<B18C6<18C6; that between Na^+ and the other alkali metal ion, which forms a less stable complex with the crown ether compared to Na^+, decreases in the order DB18C6>B18C6>18C6. These results indicate that, on moving from DB18C6 to 18C6, the Na^+ complex is much more destabilized than the other alkali metal ion complexes on account of entropy contribution because the ligand-ring flexibility increases in the order DB18C6<B18C6<18C6.

Solvation-ability sequences of the solvents for the same alkali metal ion are as follows:

Na^+: PC < AN < CH_3OH ≪ DMF < DMSO,
K^+ : CH_3OH < PC < AN ≪ DMF < DMSO,
Rb^+: CH_3OH < PC ≦ AN ≪ DMF ≦ DMSO,
Cs^+ : CH_3OH < PC ≦ AN ≪ DMF < DMSO.[1]

Log K_{ML^+}-value sequences of the B18C6 complex with the same alkali metal ion for the solvents are as follows:

Na^+: PC > AN > CH_3OH ≫ DMF,
K^+ : CH_3OH > PC ≧ AN ≫ DMF > DMSO,
Rb^+: CH_3OH > PC ≧ AN ≫ DMF > DMSO,
Cs^+ : CH_3OH > AN > PC ≫ DMF > DMSO,

where PC and AN denote propylene carbonate and acetonitrile respectively (Table 1). This shows that, for the same alkali metal ion, the log K_{ML^+}-value sequences of B18C6 for the solvents are completely the reverse of the solvation-ability sequences of the solvents except for the log K_{ML^+}-value sequence of Cs^+ for acetonitrile and propylene carbonate. For the solvents used in this work, there exists a very large difference in the solvation ability for the same alkali metal ion between the group of methanol, propylene carbonate, and acetonitrile, and that of DMF and DMSO,[1] and also a large difference in the log K_{ML^+} values of B18C6 about the same alkali metal ion. From the above discussion, it can be concluded that, for the same alkali metal ion, the solvation ability of a solvent plays the most important role in determining the stability sequences of the B18C6 complex for the solvents. A similar conclusion to that mentioned above was obtained for 18C6 and DB18C6.[1]

Transfer Activity Coefficient. The transfer activity coefficient ($\log {}^{s_1}\gamma^{s_2}(ML^+)$) of a B18C6-alkali metal ion complex between the solvent S_1 and the solvent S_2 is calculated by Eq. 1.

$$\log {}^{s_1}\gamma^{s_2}(ML^+) = (\log K_{ML^+})_{s_1} - (\log K_{ML^+})_{s_2} + \log {}^{s_1}\gamma^{s_2}(L) + \log {}^{s_1}\gamma^{s_2}(M^+) \quad (1)$$

These values are listed in Table 2.

It is noted that, although ether oxygen atoms of B18C6 form hydrogen bonds with methanol, the solubility of B18C6 for methanol is approximately equal to those for the aprotic solvents other than acetonitrile. The $\log {}^{CH_3OH}\gamma^s(L)$ value of B18C6 is much larger than the corresponding $\log {}^{CH_3OH}\gamma^s(L)$ value of DB18C6, indicating that B18C6 is much more soluble in methanol than in the aprotic solvents, as compared to DB18C6. This is ascribed to the fact that, since DB18C6 has one more benzo group than B18C6, enforcement of a hydrogen-bonded structure of methanol for the hydrophobic benzo group more decreases the solubility of DB18C6 in methanol than that of B18C6. From Table 2, when s=PC, DMF, and DMSO, $\log {}^{CH_3OH}\gamma^s$(B18C6)−$\log {}^{CH_3OH}\gamma^s$(DB18C6) is of the order of 1, whereas, only for acetonitrile, that is of the order of 2.

In general, in the case of B18C6, $\log {}^{CH_3OH}\gamma^s(ML^+)$ values for the same aprotic solvent of K^+ and Rb^+ are nearly equal to each other; however, they are somewhat different from those of Na^+ and Cs^+. These results reflect the following fact. The sizes of K^+ and Rb^+ are nearly identical with that of the B18C6 cavity; Cs^+ is larger than the B18C6 cavity. Since Na^+ is smaller than the B18C6 cavity, it shifts up and down in the direction perpendicular to the plane of oxygen atoms of B18C6. Thus, the surface charge of K^+ and Rb^+ held in the B18C6 cavity is more effectively screened by the B18C6 from surrounding solvent molecules than that of Na^+ and Cs^+. Consequently, both B18C6 complexes with K^+ and Rb^+ exhibit apparently similar chemical nature; however, the Na^+ and the Cs^+ complexes show somewhat different chemical nature from the others.

From $\log {}^{CH_3OH}\gamma^s(ML^+)$ values in Table 2, solvation-ability sequences of the solvents for the same B18C6-alkali metal ion complex are as follows:

Na^+-B18C6: AN < PC < CH_3OH < DMF,
K^+-B18C6 : AN < PC < CH_3OH < DMSO < DMF,
Rb^+-B18C6: AN < PC < CH_3OH < DMSO < DMF,
Cs^+-B18C6 : AN < CH_3OH ≈ PC ≪ DMF < DMSO.

For the aprotic solvents, the solvation ability of DMF and DMSO for the same B18C6-alkali metal ion

Table 2. Transfer activity coefficients at 25 °C

$\log {}^{CH_3OH}\gamma^s(M^+)$[6]		s=AN[a]		s=PC[b]		s=DMF		s=DMSO	
	Na^+	0.9		1.5_4		−3.1		−3.9	
	K^+	−0.4		-0.1_6		−3.5		−3.9	
	Rb^+	−0.6		-0.4_8		−3.6		−3.7	
	Cs^+	−0.8		-0.6_6		−3.3		−3.9	
		B18C6	DB18C6[6]	B18C6	DB18C6[6]	B18C6	DB18C6[6]	B18C6	DB18C6[6]
$\log {}^{CH_3OH}\gamma^s(L)$		1.0	-1.6_5	0.082	-1.0_6	−0.015	-1.6_0	0.015	-1.5_4
$\log {}^{CH_3OH}\gamma^s(ML^+)$									
	Na^+	1.5	−1.3	0.8	−0.3	−1.1	−3.1	—	−2.9
	K^+	1.0	−1.9	0.2	-1.3_5	−1.4	—	−1.0	−2.9
	Rb^+	1.1	−1.8	0.2	-1.2_2	−1.7	—	−1.2	—
	Cs^+	0.5	−2.5	−0.08	-1.4_8	−2.0	−2.9	−2.2	−3.1

a) Acetonitrile. b) Propylene carbonate.

complex is relatively larger than that of AN and PC; similarly, that of DMF and DMSO with respect to the same alkali metal ion is much greater than that of PC and AN. When s_1=AN and PC and s_2=DMF and DMSO, $\log^{s_1}\gamma^{s_2}(M^+\text{-B18C6})$ is much smaller than $\log^{s_1}\gamma^{s_2}$(B18C6). This indicates that, in DMF and DMSO, a B18C6-alkali metal ion complex much more strongly undergoes solvation than a free B18C6, in comparison with the cases of AN and PC. From the above data, it can be concluded that there is an appreciable interaction between the alkali metal ion held in the B18C6 cavity and solvent molecules, and, furthermore, that, when s_1=AN and PC and s_2=DMF and DMSO, the magnitude of the $\log^{s_1}\gamma^{s_2}(ML^+)$ value is determined mainly by the relative strength of solvation ability of s_1 and s_2 for the alkali metal ion in the B18C6 cavity. $\text{Log}^{PC}\gamma^{AN}(ML^+)-\log^{PC}\gamma^{AN}(L)$ values of B18C6 for Na^+, K^+, and Cs^+ are negative, and that for Rb^+ is nearly equal to zero. Although an alkali metal ion is more strongly solvated in acetonitrile than in propylene carbonate, the reverse is true for a B18C6-alkali metal ion complex. This may be attributed to the fact that B18C6 itself is comparatively more soluble in propylene carbonate than in acetonitrile ($\log^{PC}\gamma^{AN}$(B18C6)=0.93).

The solvation ability of methanol for K^+, Rb^+, and Cs^+ is the lowest of all the solvents used in this work; however, that for the B18C6 complexes with K^+, Rb^+, and Cs^+ is the third largest. $\text{Log}^{CH_3OH}\gamma^s(ML^+)-\log^{CH_3OH}\gamma^s(M^+)$ values for B18C6 are positive except the Na^+-PC system. These results reflect the fact that, in methanol, on account of hydrogen bonds between ether oxygen atoms of B18C6 and methanol molecules, a B18C6-alkali metal ion complex is more strongly solvated than the corresponding alkali metal ion, compared to the case of the aprotic solvent.

Values of $\log^{CH_3OH}\gamma^s(M^+\text{-B18C6})-\log^{CH_3OH}\gamma^s(M^+\text{-DB18C6})$ are 2.8—3.0, 1.1—1.6, 0.9—2.0, and 0.9—1.9 for s=AN, PC, DMF, and DMSO, respectively (Table 2). Generally, these values are nearly equal to the corresponding values of $\log^{CH_3OH}\gamma^s$(B18C6)$-\log^{CH_3OH}\gamma^s$(DB18C6). Since s is an aprotic solvent, this may be largely due to the entropy effect[4] caused by the enforcement of a hydrogen-bonded structure of methanol for the benzo group, as is mentioned above.

The authors thank Mr. Takaya Yusa of this laboratory for his experimental assistance in conductance measurements.

References

1) Y. Takeda, *Bull. Chem. Soc. Jpn.*, **54**, 3133 (1981).
2) Y. Takeda, *Bull. Chem. Soc. Jpn.*, **56**, 866 (1983).
3) Y. Takeda, H. Yano, M. Ishibashi, and H. Isozumi, *Bull. Chem. Soc. Jpn.*, **53**, 72 (1980).
4) M. K. Chantooni, Jr. and I. M. Kolthoff, *Proc. Natl. Acad. Sci. U.S.A.*, **78**, 7245 (1981).
5) M. H. Abraham and H. C. Ling, *Tetrahedron Lett.*, **23**, 469 (1982).
6) I. M. Kolthoff and M. K. Chantooni, Jr., *Anal. Chem.*, **52**, 1039 (1980).
7) K. Kimura, H. Tamura, and T. Shono, *J. Electroanal. Chem.*, **105**, 335 (1979).
8) K. Kimura, M. Nakajima, and T. Shono, *Anal.Lett.*, **13**, 741 (1980).
9) H. Nakamura, M. Takagi, and K. Ueno, *Anal. Chem.*, **52**, 1668 (1980).
10) G. Ercolani, L. Mandolini, and B. Masci, *J. Am. Chem. Soc.*, **103**, 7484 (1981).
11) D. E. Fenton, D. Parkin, and R. F. Newton, *J. Chem. Soc., Perkin Trans. 1*, **1981**, 449.
12) R. Ungaro, B. El Haj, and J. Smid, *J. Am. Chem. Soc.*, **98**, 5198 (1976).
13) C. J. Pedersen, *J. Am. Chem. Soc.*, **89**, 7017 (1967).
14) Y. Takeda and H. Yano, *Bull. Chem. Soc. Jpn.*, **53**, 1720 (1980).
15) L. Pauling, "The Nature of the Chemical Bond," 3rd ed, Cornell Univ. Press (1960).
16) E. Mei, A. I. Popov, and J. L. Dye, *J. Phys. Chem.*, **81**, 1677 (1977).
17) A. Hofmanova, J. Koryta, M. Brezina, and M. Mittal, *Inorg. Chim. Acta*, **28**, 73 (1978).
18) D. F. Evans, S. L. Wellington, J. A. Nadis, and E. L. Cussler, *J. Solution Chem.*, **1**, 499 (1972).
19) H. K. Frensdorff, *J. Am. Chem. Soc.*, **93**, 600 (1971).
20) J. D. Lamb, R. M. Izatt, C. S. Swain, and J. J. Christensen, *J. Am. Chem. Soc.*, **102**, 475 (1980).
21) G. Michaux and J. Reisse, *J. Am. Chem. Soc.*, **104**, 6895 (1982).
22) P. U. Früh and W. Simon, "Protides of the Biological Fluids-20th Colloquium," ed by H. Peeters, Pergamon Press, New York (1978).
23) E. Shchori, J. Jagur-Grodzinski, Z. Luz, and M. Schporer, *J. Am. Chem. Soc.*, **93**, 7133 (1971).
24) D. P. Nelson, Ph. D. Thesis, Brigham Young University, Provo, Utah, 1971.

A Study of the Charge-Discharge Characteristics of the Lithium-Polyacetylene Battery by Means of the FFT Impedance Measurement

Tetsuya OSAKA* and Takashi KITAI
Department of Applied Chemistry, School of Science and Engineering, Waseda University, Okubo, Shinjuku-ku, Tokyo 160
(Received March 13, 1984)

The charge-discharge characteristics of the anion-doped lithium-polyacetylene [$(CH)_x$] battery was investigated by means of the FFT impedance method, by which the impedance-frequency dispersion could be measured by very high speed. The charging and self-discharging of the Li-$(CH)_x$ battery were represented by the Randles-type equivalent circuit, added with the corrective term concerned with surface roughness. These processes and their doping states of the $(CH)_x$ film were readily detected by the variation in the resistive component, *Rr*, in the equivalent circuit. The *Rr* value of the self-discharge process was clearly correlated to the open-circuit voltage, *Voc*, regardless of the charging current; furthermore, it was strongly indicated that the self-discharge process is mainly caused by the dopant diffusion from the interface into the interior part of $(CH)_x$ films. For the discharging process, another mechanism, closely concerned with dopant diffusion, was suggested by the impedance results.

The electrochemical doping-undoping method in polyacetylene has been of much interest when applied for lightweight rechargeable batteries.[1,2] The MacDiarmid group[1] indicated the high potential on rechargeable battery by using 6% ClO_4^- doped polyacetylene as a cathode-active material. Moreover, they[2] summarized some characteristics of the lithium-polyacetylene battery in which 7% doped polyacetylene was used as the cathode. The electrochemical doping-undoping processes of polyacetylene have already been studied by FFT impedance measurement[3] and the basic doping-undoping process could readily be analysed by means of the resistive component measured by the FFT impedance measurement at a high speed. In this paper, we wish to report the charge-discharge and self-discharge characteristics of the ClO_4^- doped lithium-polyacetylene battery as established by means of electrochemical measurements, especially by the FFT impedance method.[4]

Experimental

The *cis*-polyacetylene films 0.1 mm thick (weight density, 0.44 g cm^{-3}) were prepared by the Sirakawa method.[5] The cell construction, composed of 8 mmϕ *cis*-$(CH)_x$ working and Li counter electrodes attached to platinum plates, without any reference electrode, is shown schematically in Fig. 1. The volume of the cell was 0.283 cm^3. The polyacetylene working and lithium counter electrodes were fixed by the use of stainless steel SUS 304 fittings with O-rings for sealing. One mol dm^{-3} $LiClO_4$ electrolyte and propylene carbonate (PC) were purified and handled in the usual method.[6] The Li-*p*-$(CH)_x$ battery was galvanostatically charged or discharged using the step-by-step or the consecutive method. The doping level of the $(CH)_x$ film was calculated according to Eq. 1; one percent of the doping level for the film corresponded to 278 mC. The doping was carried out conveniently until the 6% level was reached by referring the Refs. 1 and 2 in order to avoid the irreversible oxidation of the $(CH)_x$ film. The cell impedance was measured from 0.001 to 2.5 kHz by means of the on-line FFT impedance meter constructed by the authors' laboratory.[4] All the experiments were carried out in a dry and inert Ar gas atmosphere.

Results and Discussion

Open-circuit Voltage, Voc, *on Charging-Discharging Process of ClO_4^- Doped Li-$(CH)_x$ Battery.* The relations between the open-circuit voltage, *Voc*, and the doping level, *y*, for the step-by-step charging-discharging process of lithium/1 mol dm^{-3} $LiClO_4$ in the propylene carbonate/$(CH)_x$ battery have already been reported by several workers.[1,2] The basic charging process for the ClO_4^- anion doping into the $(CH)_x$ film is represented by:

$$(CH)_x + xyClO_4^- \longrightarrow [CH^{y+}(ClO_4^-)_y]_x + xye. \quad (1)$$

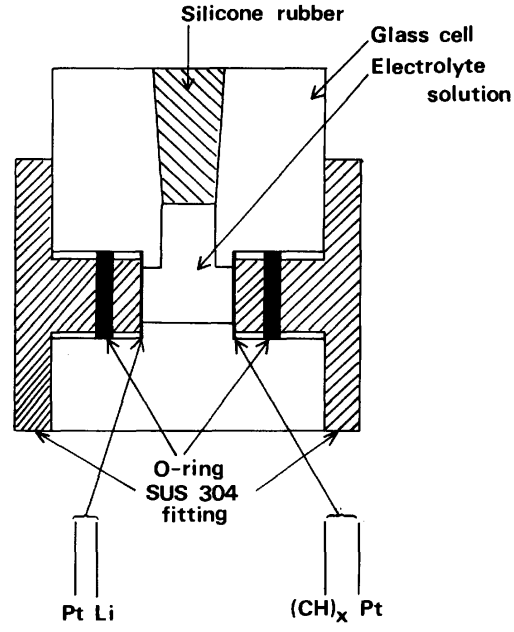

Fig. 1. Schematic cell construction of Li/1 mol dm^{-3} in PC/$(CH)_x$.

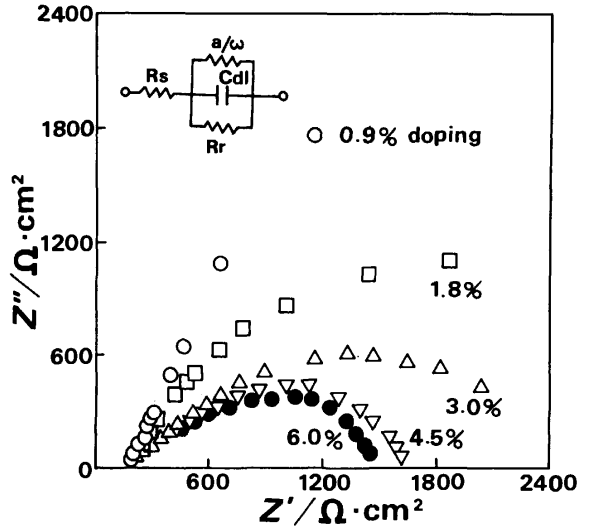

Fig. 2. Cell-impedance representation of charging process for Li-$(CH)_x$ battery step-by-step-charged at 0.5 mA cm^{-2}, where the cell impedance was measured after 24h at each doping level.

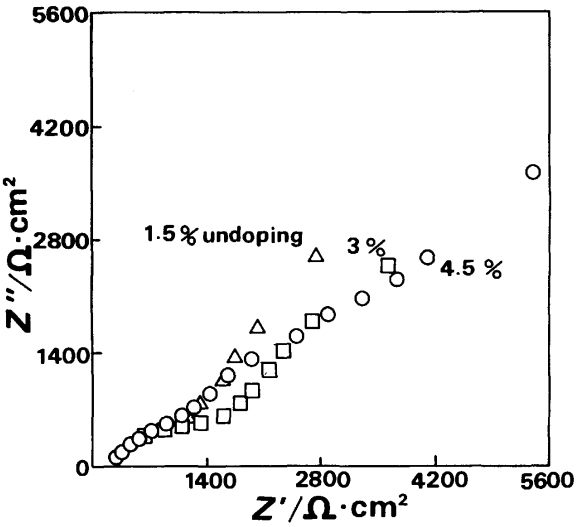

Fig. 3. Cell-impedance representation of the 6% ClO_4^- doped Li-$(CH)_x$ battery for discharging process at 0.5 mA cm^{-2}, where the cell impedance was measured after 24h at each undoping level.

The reduction of Li^+ to metallic Li occurs simultaneously:

$$Li^+ + e \longrightarrow Li. \quad (2)$$

In our experiments, results identical to those in the previous papers[1,2] were obtained. In particular, the *Voc* decrease after charging and the *Voc* increase after discharging were clearly observed. For example, for the charging process, the *Voc*-charged values after 2h were always higher than those after 24h, while for the discharging process, the reverse was true. By considering the previously reported finding[2,3] that a quick charging process causes a nonequivalent concentration gradient of the doped ion in the $(CH)_x$ film for the depth profile, the above results can be interpreted by the facts that most of the ClO_4^- dopant exists near the surface region of the $(CH)_x$ film just after the charging process and, furthermore, that the dopant at the surface diffuses into the film interior with the passage of time. Thus, the *Voc* value is controlled by the dopant concentration at the surface. On the other hand in the discharging process, an immediate discharge produces a decrease in the dopant concentration at the surface region, but the passage of time after discharging process causes a increase in diffusion from the interior to the exterior parts of films.

Impedance Measurement of Charging-Discharging Process using Li-$(CH)_x$ Battery. The impedance-frequency dispersions for the Li-$(CH)_x$ at various charging levels were measured by the FFT impedance method. The cell-impedance representation for the battery galvanostatically charged step by step at 0.5 mA cm^{-2} is shown in Fig. 2. The cell-impedance measurement was done after 24h at each doping level. The cell-impedance representation becomes an inclined semicircle, like the behavior of the polyacetylene film itself.[3] Since two electrode reactions, (1) and (2), in the charging process occur simultaneously at the anode and the cathode respectively, the cell impedance should represent the whole reaction of the Li-$(CH)_x$ battery. However, the cell impedance can be regarded as mainly due to the polyacetylene electrode reaction (1), because the impedance due to the lithium-electrode reaction can almost be ignored because its value is lower than that due to the polyacetylene reaction (*i.e.*, the former reaction rate is faster than the latter). In practice, the semicircle impedance plots are somewhat distorted as compared with those of the $(CH)_x$ film itself,[3] so the influence of the Li-electrode reaction on the cell-impedance behavior may be somewhat contained. The Randles-type equivalent circuit shown in the insert of Fig. 2, which has already been discussed in a previous paper,[3] is applied to the frequency-dispersion behavior showing a semicircle. The components, *Rs*, *Rr*, *Cdl* and $a\ \omega^{-1}$ (ω: angular frequency), are the solution resistance, the resistive component due to the electrode reaction and the film conductivity, the double-layer capacitance, and the corrective term concerned with the surface roughness. The polyacetylene film surface may be porous, for it is composed of fibril units, so that the term concerned with surface roughness should be assumed, and the *Cdl* value becomes the total value of each pore's double-layer capacitance. In these components, the *Rr* value, which corresponds to the semicircle's diameter of impedance behavior, greatly reflects the change in the charging or doping level. Therefore, the charging process of the Li-$(CH)_x$ battery can be pursued and discussed in terms of the variation in the *Rr* value as well as that of the $(CH)_x$ film itself. The resistive component, *Rr*, arises mainly from the two factors of the partial oxidation (or doping) reaction and of the film resistivity itself; it

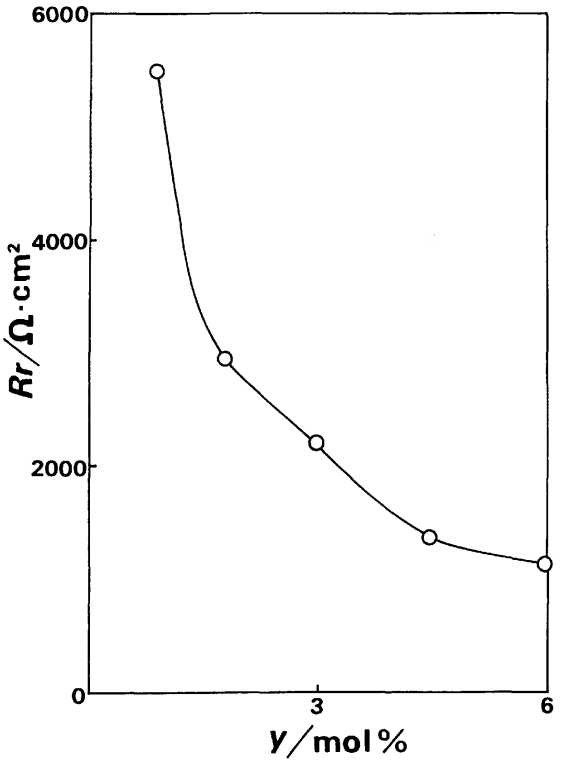

Fig. 4. Relation between resistive component, *Rr*, in the equivalent circuit and doping level, *y*, of the Li-$(CH)_x$ battery step-by-step-charged at 0.5 mA cm^{-2}, where the data were calculated from those in Fig. 2 at each doping level.

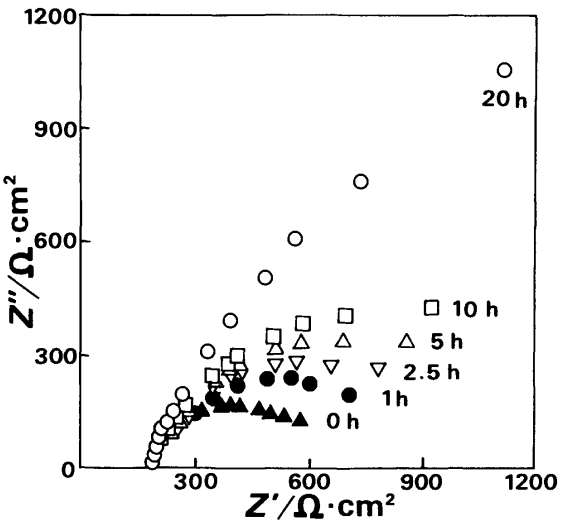

Fig. 5. Cell-impedance representation for self-discharge of Li-$(CH)_x$ battery after consecutive-charged at 0.1 mA cm^{-2}, up to the 6% ClO_4^- doping level.

greatly reflects the dopant concentration not of the whole amount of the charge, but of the amount at the surface region of the $(CH)_x$ film, as is discussed in our previous paper.[3)]

Figure 3 shows the cell-impedance representation for the discharging process of the Li-$(CH)_x$ battery at 0.5 mA cm^{-2} on various undoping levels from the 6% ClO_4^- doped polyacetylene. Each plot was also measured 24 h after the end of discharge. In the discharging process, there was observed to be no difference in cell-impedance behavior between measurements immediately after and 24 h later. Furthermore, the frequency-dispersion behavior of cell impedance is almost independent of the undoping level, as may be seen in Fig. 3. The cell-impedance behavior in the discharging process displays two regions of semicircles at higher frequencies and a linear line at lower frequencies. The linear region is usually concerned with the diffusion process, so the dopant diffusion at the interface is considered to be greatly concerned with and to control the discharging process of the Li-$(CH)_x$ battery.

Figure 4 shows a typical variation in the *Rr* value as a function of the doping level, *y*, on a step-by-step-charging process at 0.5 mA cm^{-2}, which is derived from the data in Fig. 2. The results indicate a good correlation between *Rr* and *y*; namely, the *Rr* value decreases with the increase in the doping level, *y*. The *Rr* decrease tends to change sharply at the initial doping stage.

Impedance of Self-discharge for the Li-$(CH)_x$ Battery after Consecutive Charging up to the 6% ClO_4^- Doping Level. Since the self-discharge phenomenon was observed after charging the ClO_4^- doped Li-$(CH)_x$ battery, the time dependence of impedance for the battery after it had been charged up to the 6% doping level was examined in order to clarify this phenomenon.

Figure 5 shows the cell-impedance representation of the self-discharge of the Li-$(CH)_x$ battery after it has been charged at 0.1 mA cm^{-2} up to the 6% ClO_4^- doping level. The frequency dispersion of the impedance loci becomes a semicircle, just as in Fig. 2. Similar the cell-impedance behavior was also observed in the cases of the 0.2 and 0.5 mA cm^{-2} charging currents. The *Rr* value in the equivalent circuit, corresponding to the semicircle's diameter in the cell-impedance representation, increases with the passage of time. These results can be explained by the fact that the dopant diffuses from the exterior into the interior parts of the $(CH)_x$ film with the increase in time, as well as by the *Voc* results previously discussed.

Figure 6 presents the time dependence of the resistive component, *Rr*, and the open-circuit voltage, *Voc*, for the self-discharge of the Li-$(CH)_x$ battery after it has been charged up to the 6% ClO_4^- doping level. The *Rr* value shown in Fig. 6a increases with an increases in the time after the charging process, finally reaching the maximum constant value of *ca.* 3500 Ωcm^2. The time required to reach the maximum constant value, *tm*, becomes longer with the increase in the charging-current value. This indicates that the dopant diffusion into the $(CH)_x$ film occurs until it reaches a dopant-concentration equivalent to the 6% doping level, whose state is established after the *tm* value, and also that the lower charging-current value produces the more uniform doping state. The behavior of the *Voc* value

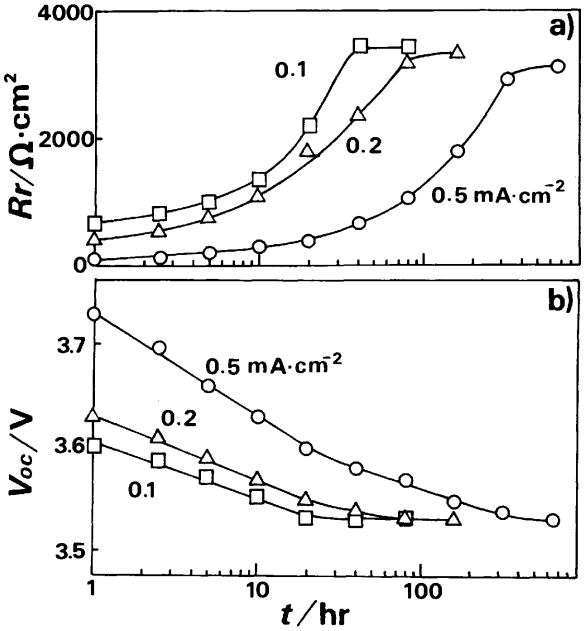

Fig. 6. Time dependence of resistive component, *Rr*, and open-circuit voltage, *Voc*, for self-discharge of Li-$(CH)_x$ after consecutive-charged at various current densities up to the 6.0% ClO_4^- doping level.

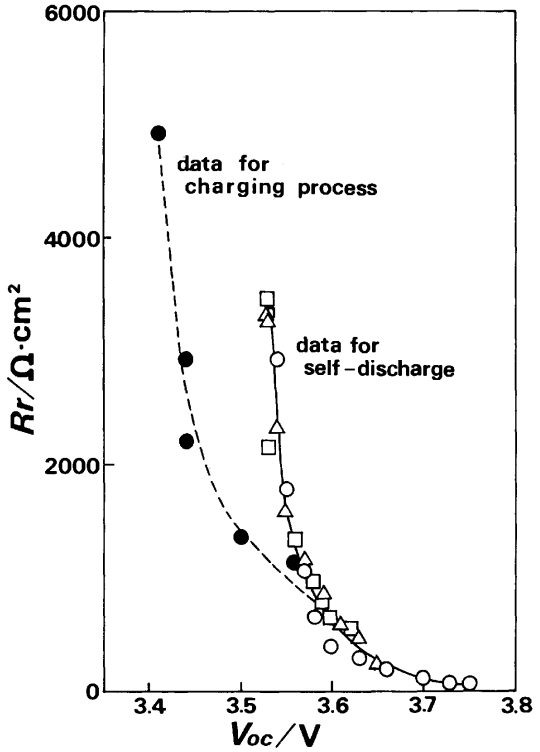

Fig. 7. Relation between resistive component, *Rr*, and open-circuit voltage, *Voc*, for self-discharge after consecutive-charged up to the 6.0% ClO_4^- doping level (*cf.*, Fig. 6), and for step-by-step-charging process (*cf.*, Fig. 2).
○: 6.0% doped at 0.5 mA cm^{-2}, △: 0.2 mA cm^{-2}, □: 0.1 mA cm^{-2}, ●: 0.9—6.0% stepwise-doped at 0.5 mA cm^{-2}.

shown in Fig. 6b displays almost the same trend as that of the *Rr* value in Fig. 6a; that is, the *Voc* value gradually decreases with the passage of time, finally reaching the almost constant value of 3.53 V. The higher charging current makes the *tm'* (the time required to reach a constant *Voc*) longer at the same 6% doping level. The time, *tm*, in the *Rr-t* relation corresponds nearly to the time, *tm'*, in the *Voc-t* relation. The *Voc* value is entirely almost determined by the dopant concentration at the $(CH)_x$ surface[1,2], thus, it may be concluded from the dependence of *tm* or *tm'* on the charging current that the higher charging current produces the higher dopant-concentration gradient for the depth profile, and, furthermore, that the doping states in the $(CH)_x$ film can be evaluated sensitively from the *Rr*-value behavior.

Since the correlation between *Rr* and *Voc* can be presumed from the data in Fig. 6, the relation between *Rr* and *Voc* obtained by the time dependence of *Rr* and *Voc* after charging up to the 6% doping is obtained as shown in Fig. 7. In Fig. 7, there are two kinds of data for the self-discharge process after consecutive charging up to the 6% ClO_4^- doping level, calculated from the data in Fig. 6, and for the step-by-step-charging process from the 0.9 to the 6% doping level, calculated from the data in Fig. 2. For the self-discharge process, there clearly appears a correlation between *Rr* and *Voc*, regardless of the charging current. The *Voc* for the self-discharge process becomes close to the equivalent value of *ca.* 3.5 V for the 6% doping level regardless of the charging current. The *Voc* value higher than 3.5 V clearly means that the doped-ion-concentration gradient occurs at the surface. For the step-by-step charging, the same *Rr* value as that for the self-discharge process correlates with the lower *Voc* value, and the final *Voc* value at the 6% doping level shows the equivalent value of *ca.* 3.5 V, so that the slow step-by-step charging is suitable for uniform doping with no occurrence of the higher dopant-concentration gradient producing the self-discharge. Finally, the *Rr* value after the charging process not only reflects closely the doping states of the $(CH)_x$ film, but can also be used to investigate the self-discharge conditions of the Li-$(CH)_x$ battery.

Conclusion

Charge-discharge and self-discharge characteristics of the ClO_4^- anion-doped lithium-polyacetylene battery were studied by means of the FFT impedance measurement. The impedance-frequency dispersion for charging and self-discharging of the battery was basically interpreted by the Randles-type equivalent circuit. The conditions of the charged battery and the self-discharge were strongly correlated to the resistive component, *Rr*, in the equivalent circuit. The discharging process was observed to behave differently from the charging process. In conclusion, the nonequivalent states of the doped-ion-concentration gradient of the polyacetylene film were readily checked by the *Rr* component, and the large self-discharge

phenomenon was produced by the nonequivalent states of the doped ions.

The authors would like to thank Mr. Yoshimitsu Sawada, Showa Denko Co., Ltd., for providing the polyacetylene samples and for his valuable discussion.

References

1) P. J. Nigrey, D. MacInnes Jr., D. P.Nairns, and A. G. MacDiarmid, *J. Electrochem. Soc.*, **128**, 1651 (1981).
2) K. Kaneto, M. Maxfield, D. P. Nairns, and A. G. MacDiarmid, *J. Chem. Soc., Faraday Trans.*, **78**, 3417 (1982).
3) T. Osaka and T. Kitai, *Bull. Chem. Soc. Jpn.*, **57**, 759 (1984).
4) T. Osaka and K. Naoi, *Bull. Chem. Soc. Jpn.*, **55**, 36 (1982).
5) Y. Ito, H. Shirakawa, and S. Ikeda, *J. Polym. Sci.*, **12**, 11 (1974).
6) Y. Matsuda, *Denki Kagaku*, **48**,665 (1980).

The Excited-state Absorption and Phosphorescence of Rhodium(III) Compounds at Room Temperature

Takeshi OHNO* and Shunji KATO
Chemistry Department, College of General Education, Osaka University, Toyonaka, Osaka 560
(Received March 21, 1984)

The excited states of rhodium(III) compounds including $[Rh(4,7\text{-diphenyl-}1,10\text{-phenanthroline})_3]^{3+}$ ($[Rh(dp\text{-}phen)_3]^{3+}$), $[Rh(1,10\text{-phenanthroline})_3]^{3+}$ ($[Rh(phen)_3]^{3+}$), $[RhCl_2(dp\text{-}phen)_2]^+$, and $[RhCl_2(phen)_2]^+$, have been investigated by means of emission spectroscopy and laser photolysis spectroscopy. The transient species with the lifetime of 0.055—72 μs are identified as the triplet (π-π^*) excited state of the ligand for $[Rh(dp\text{-}phen)_3]^{3+}$ and $[Rh(phen)_3]^{3+}$ and as the triplet ligand-field excited states for $[RhCl_2(dp\text{-}phen)_2]^+$ and $[RhCl_2(phen)_2]^+$. The molar absorption coefficients of the excited states are 9600 $M^{-1}cm^{-1}$ at 550 nm for $[Rh(dp\text{-}phen)_3]^{3+}$, 2750 $M^{-1}cm^{-1}$ at 560 nm for $[RhCl_2(dp\text{-}phen)_2]^+$, 2300 $M^{-1}cm^{-1}$ at 510 nm for $[Rh(phen)_3]^{3+}$, and 1600 $M^{-1}cm^{-1}$ at 550 nm for $[RhCl_2(phen)_2]^+$. The lifetime of the ligand-field excited state of $[RhCl_2(phen)_2]^+$ (700 ns in acetonitrile) decreases to 55 ns in water.

It has been found that the phosphorescent states of metal complexes containing 2,2′-bipyridine* or 1,10-phenanthroline* as ligands have unusual long lifetimes enabling them to undergo bimolecular electron-transfer reactions. The luminescence or the excited-state absorption (ESA) has been utilized to investigate the photochemical reactions of ruthenium(II),[1] chromium(III),[2,3] and rhodium(III) compounds.[4-6] The lifetime and the quenching reaction of the excited state can be derived from the luminescence measurement. Meanwhile, the formation of the excited state can be determined from the measurement of ESA using the molar-absorption coefficient. Provided that the molar-absorption coefficient of the reaction product is also available, one can estimate the efficiency of the product formation in the quenching of the excited state. However, only a few studies of the elementary reactions of excited-metal complexes have been done, since the molar-absorption coefficients of metal complexes are unknown except for the phosphorescent states of $[Ru(bpy)_3]^{2+}$,[7] $[Cr(bpy)_3]^{3+}$,[3] and $[Cr(4,7\text{-diphenyl-}1,10\text{-phenanthroline}^*)_3]^{3+}$.[3] As for rhodium(III), ESA are known only for $[RhBr_2(bpy)_2]^+$[8] and $[RhCl(NH_3)_5]^{2+}$.[9] We will report here the ESA of four rhodium(III) compounds, ···$[Rh(dp\text{-}phen)_3]^{3+}$, $[RhCl_2(dp\text{-}phen)_2]^+$, $[Rh(phen)_3]^{3+}$, and $[RhCl_2(phen)_2]^+$, which are known to be photoactive.[4,5,10] The molar-absorption coefficients of ESA are also determined for the dp-phen complexes which can be efficiently excited by the second harmonics of a ruby laser (347 nm). The phosphorescences of the rhodium(III) compounds at room temperature are also described for purposes of comparison. The solvent dependence of the lifetimes of the ligand-field excited states at room temperature is discussed in connection with the photo-substitution reaction.

Experimental

Apparatus. An NEC SLG-2018 Q-switched ruby laser capable of providing up to 0.17 J per flash at 347 nm was used. The details of the laser apparatus and the monitoring device have been described elsewhere.[3,11] Transient changes in the absorption and decay of luminescence were fed into a Iwatsu 8123 Storagescope, followed by computer analysis using a NEC PC8001 MKII microcomputer. A Hitachi 323 Spectrophotometer and a Hitachi MPF-2A Spectrofluorophotometer were used for the measurements of the absorption and the luminescence spectra, respectively.

Materials. $[Rh(phen)_3]Cl_3\cdot 3H_2O$ was prepared by the method of Harris and McKenzie.[12] $[RhCl_2(phen)_2]Cl\cdot 3H_2O$ was prepared by a catalytic method in the literature,[13] which was applied to the preparation of $[Rh(dp\text{-}phen)_3](ClO_4)_3\cdot 4H_2O$ and $[RhCl_2(dp\text{-}phen)_2]Cl\cdot 3H_2O$. The crude sample were purified by recrystallization; $[Rh(phen)_3]Cl_3\cdot 3H_2O$ and $[RhCl_2(phen)_2]Cl\cdot 3H_2O$ from the aqueous solution, $[Rh(dp\text{-}phen)_3](ClO_4)_3\cdot 4H_2O$ from the ethanol solution (Found; C, 58.79; H, 3.45; N, 5.72. Calcd for $C_{72}H_{56}N_6Cl_3O_{16}Rh$: C, 58.81; H, 3.84; N, 5.72%), and $[RhCl_2(dp\text{-}phen)_2]Cl\cdot 3H_2O$ from the acetonitrile solution (Found: C, 61.40; H, 4.06; N, 5.98. Calcd for $C_{48}H_{38}N_4Cl_3O_3$: C,62.12; H, 4.13; N, 6.04%). Free ligands of dp-phen and phen of analytical grade were used without further purification. Acetonitrile (AN), methanol, and ethanol of G. R. grade were used as supplied by Wako Pure Chemical Co. Water was purified by passing it through a Millipore deionizer and filter. The test solution were deaerated by purging for 15—20 min with nitrogen.

Measurements. All the measurements were done at 13±2 °C, unless otherwise noted. The molar absorption coefficients of the excited states were obtained on the assumption that all the molecules in the 10—40 μM (1 M=1 mol dm^{-3}) of $[Rh(dp\text{-}phen)_3]^{3+}$ or $[RhCl_2(dp\text{-}phen)_2]^+$ were excited to the phosphorescent state by one shot of the laser. The complete excitation of the compounds to the phosphorescent state was ascertained by a constant production of the transient absorption, accompanied by an attenuation of the laser intensity.

The decay of ESA was monitored at 500 nm for $[Rh(phen)_3]^{3+}$ and at 560 nm for $[RhCl_2(phen)_2]^+$, $[Rh(dp\text{-}phen)_3]^{3+}$, and $[RhCl_2(dp\text{-}phen)_2]^+$. The decay of the phosphorescence was monitored using an interference filter with the maximum transparency at 510 nm for $[Rh(dp\text{-}phen)_3]^{3+}$, at 597 nm for $[Rh(phen)_3]^{3+}$, or at 669 nm for $[RhCl_2(dp\text{-}phen)_2]^+$ and $[RhCl_2(phen)_2]^+$.

Results

$[Rh(dp\text{-}phen)_3]^{3+}$. The title compound exhibited

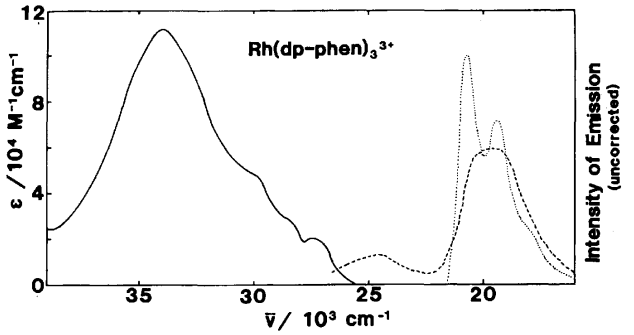

Fig. 1. Absorption and emission spectra of [Rh(dp-phen)$_3$]$^{3+}$.
The full line; the absorption of the 50% AN aqueous solution, the broken line; the emission of the 50% AN aqueous solution (11.4 μM), and the dotted line; the emission of the ethanol-methanol (4:1 by volume) solution (40 μM) at 77 K.

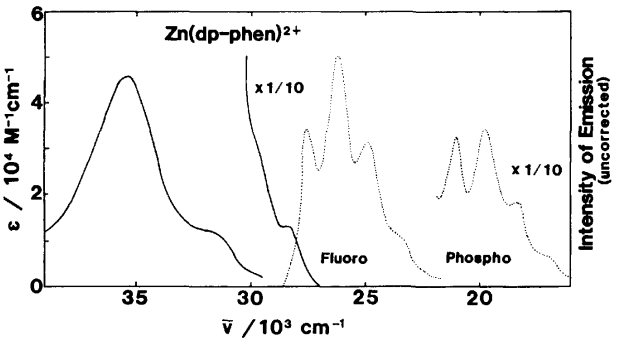

Fig. 2. Absorption and emission spectra of [Zn(dp-phen)]$^{2+}$.
The full line; the absorption of sample containing $Zn(NO_3)_2$ of $(1—5)\times10^{-4}$ M and dp-phen of $(0.2—2)\times10^{-4}$ M in AN-water (1:1) and the dotted line; the emission of the sample containing $Zn(NO_3)_2$ of 2×10^{-4} M and dp-phen of 10^{-4} M in methanol-water (4:1) at 77 K.

almost the same absorption spectrum as the dp-phen coordinated to the zinc(II) ion**, as is shown in Figs. 1 and 2, which is essentially ascribed to the π-π^* transitions of the ligand. The weak band of the free dp-phen at 28800 cm^{-1} (ε=440 M^{-1}cm^{-1}) is strengthened in Zn(dp-phen)$^{2+}$ and [Rh(dp-phen)$_3$]$^{3+}$ by three to thirteen times. As the luminescence spectra in Figs. 1 and 2 show, the coordination of dp-phen to the rhodium(III) ion enormously strengthens the π-π^* phosphorescence, which is shifted to a lower energy with the same fine structure as the phosphorescence of [Zn(dp-phen)]$^{2+}$. While a rise in the temperature weakens the phosphorescence of [Rh(dp-phen)$_3$]$^{3+}$, a phosphorescence with a lifetime of 72 μs and a quantum yield of -10^{-4} is still observed at room temperature. The phosphorescent state of $^3(\pi$-$\pi^*)$ was observed as an absorption by means of laser-photolysis spectroscopy at room temperature. The laser excitation of [Rh(dp-phen)$_3$]$^{3+}$ of 11 μM gives rise to an transient absorption, as is shown in Fig. 3. This transient absorption has the same lifetime (63 μs) as the phosphorescence, so it may be concluded that it is due to the triplet π-π^* state ($^3(\pi$-$\pi^*)$). The molar-absorption coefficient of the $^3(\pi$-$\pi^*)$ is obtained as 9600 M^{-1}cm^{-1} at 550 nm on the condition that the [Rh(dp-phen)$_3$]$^{3+}$ of 11 μM are completely excited to $^3(\pi$-$\pi^*)$ by one shot of the laser, as Fig. 4 shows. The wide ESA of $^3(\pi$-$\pi^*)$ compared to that of the excited free dp-phen indicates the appearance of a new transition. The lifetime of $^3(\pi$-$\pi^*)$ increased by 25% with the increase in the water content in the solvent.

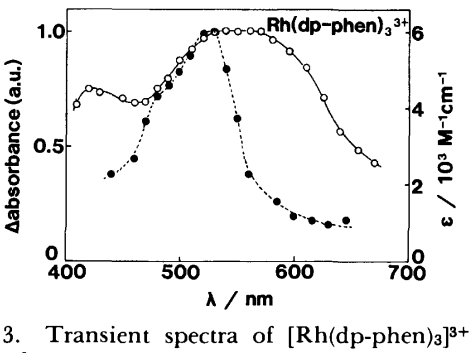

Fig. 3. Transient spectra of [Rh(dp-phen)$_3$]$^{3+}$ and dp-phen.
The full line; [Rh(dp-phen)$_3$]$^{3+}$ of 11.4 μM in AN-water (1:1) and the broken line; dp-phen of 1.21 mM in AN.

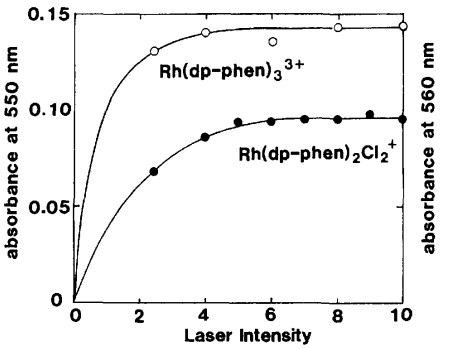

Fig. 4. Dependence of the transient absorbance on the laser intensity.
The open circle; [Rh(dp-phen)$_3$]$^{3+}$ of 11.4 μM in AN-water (1:1) (the left ordinate) and the closed circle; [RhCl$_2$(dp-phen)$_2$]$^+$ of 40 μM in AN (the right ordinate).

[RhCl$_2$(dp-phen)$_2$]$^+$. The pale yellow AN solution of [RhCl$_2$(dp-phen)$_2$]$^+$ emits a weak and broad phosphorescense with a maximum at 690 nm at room temperature (Fig. 5); this can presumably be assigned to the ligand-field phosphorescence ($^3T_1\rightarrow{}^1A_1$)***. It resembles the low-temperature emission of [RhCl$_2$(phen)$_2$]$^+$, with a maximum at 704 nm.[14,15] The lifetime of [RhCl$_2$(dp-phen)$_2$]$^+$ is 1.1 μs at room temperature in AN several hundred times as long as those of [RhX$_2$(NH$_3$)$_4$]$^+$ (X=Cl$^-$ and Br$^-$) in water.[5]

The excited state of $^3T_1$ was also detected by means of laser-photolysis spectroscopy. The transient absorption of the AN solution (Fig. 6) is identified as $^3T_1$ because its lifetime (1.0 μs) is close to that of the phosphorescence. The molar absorption coefficient was obtained as 2750 M^{-1}cm^{-1} at 560 nm from the complete conversion to $^3T_1$, which is ascertained by

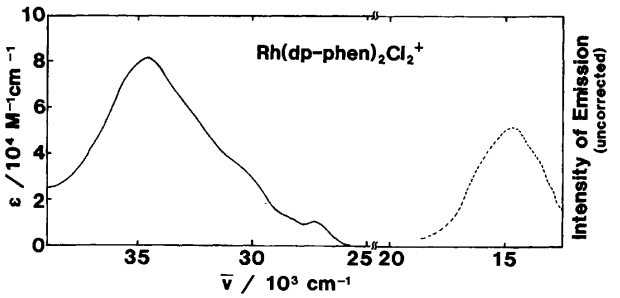

Fig. 5. Absorption spectrum (solid line) and emission spectrum (broken line) of $[RhCl_2(dp\text{-}phen)_2]^+$ in AN.

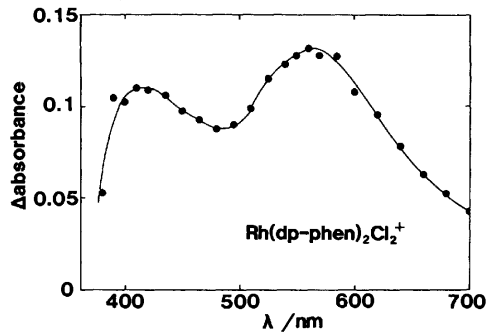

Fig. 6. Transient absorption spectra of $[RhCl_2(dp\text{-}phen)_2]^+$ (50 μM) in AN.

the saturation of the transient absorbance with an attenuation of the laser intensity, as is shown in Fig. 4. The lifetime of $^3T_1$ becomes shorter with the water content in the solvent; the lifetime of 1.02 μs in the AN solution decreases to 340 ns in the 50% AN aqueous solution and to 127 ns in the 20% AN aqueous solution.

$[Rh(phen)_3]^{3+}$. The coordination of phen to the rhodium(III) ion strengthens the lowest transition of free phen by thirteen times, which is symmetry forbidden.[16] On excitation with the second harmonics of the ruby laser, a transient species with an absorption maximum at 510 nm was observed in an alcoholic solvent at room temperature, as well as they at 77 K, as is shown in Fig. 7. Since the transient absorption has as long a lifetime as the phosphorescence (48 ms) from $^3(\pi\text{-}\pi^*)$ at 480 nm,[15] the transient absorption is ascribed to $^3(\pi\text{-}\pi^*)$. The molar-absorption coefficient of the ESA in water was obtained as 2300 $M^{-1}cm^{-1}$ from the complete conversion to the excited state. The lifetime of the $^3(\pi\text{-}\pi^*)$, as monitored by the ESA, decreased at room temperature to 60 ns in methanol, 85 ns in AN–water (4:1), and 440 ns in water. Correspondingly, the $\pi\text{-}\pi^*$ phosphorescence was replaced by a broad emission with the maximum at 580 nm, which has been assigned by Bolleta[17] to the phosphorescence from $^3T_1$. The same lifetime of the phosphorescence from $^3T_1$ as the ESA of $^3(\pi\text{-}\pi^*)$ supports the idea that the thermal activation from $^3(\pi\text{-}\pi^*)$ to $^3T_1$ is responsible for the broad phosphorescence at room temperature.[17] The $^3(\pi\text{-}\pi^*)$ in water has the longest lifetime, in contrast to the triplet ligand-field excited states of $[RhCl_2(dp\text{-}phen)_2]^+$ and $[RhCl_2(phen)_2]^+$, which have the shortest

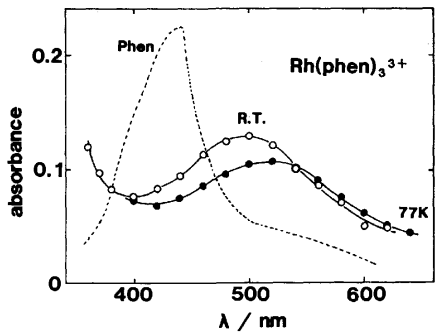

Fig. 7. Transient absorption spectra of $[Rh(dp\text{-}phen)_3]^{3+}$ and free phen.
The open circle; $[Rh(dp\text{-}phen)_3]^{3+}$ of 100 μM in water, the closed circle; $[Rh(dp\text{-}phen)_3]^{3+}$ of 100 μM in ethanol-methanol (4:1) at 77 K, the solid line; phen of 0.04 M in AN.

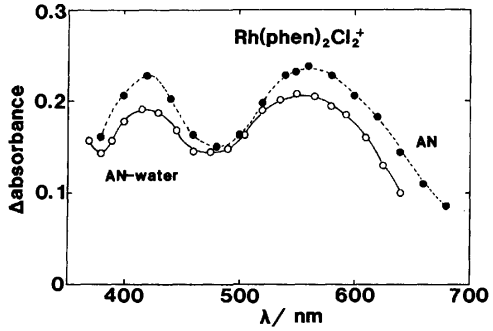

Fig. 8. Transient absorption spectra of $[RhCl_2(phen)_2]^+$ (200 μM) in AN–water (1:1) (open circle) and AN (closed circle).

lifetime in water (*vide infra*). It should be noted that the ESA of $[Rh(phen)_3]^{3+}$ disagrees with that of free phen, with the maximum at 440 nm.

$[RhCl_2(phen)_2]^+$. The lowest excited state of $[RhCl_2(phen)_2]^+$ is $^3T_1$ of the ligand-field excitation, which emits a broad phosphorescence at 77 K.[14,15] The weak phosphorescnce with the lifetime of 680 ns in the AN solution was observed at room temperature, too. The ESA of $^3T_1$ with the molar absorption coefficient of 1600 $M^{-1}cm^{-1}$ at 550 nm is also observed by means of laser photolysis spectroscopy as Fig. 8 shows; it is independent of the solvent. The lifetime of the ESA in the AN solution (700 ns) agrees with that of the ligand field phosphorescence and becomes as short as to 200 ns in the 50% AN aqueous solution and 55 ns in the aqueous solution.

Discussion

The $^3(\pi\text{-}\pi^*)$ of $[Rh(dp\text{-}phen)_3]^{3+}$ and $[Rh(phen)_3]^{3+}$ have some different characters from those of the ligand-field excited states of $[RhCl_2(dp\text{-}phen)_2]^+$ and $[RhCl_2(phen)_2]^+$. The $^3(\pi\text{-}\pi^*)$ of $[Rh(dp\text{-}phen)_3]^{3+}$ has a longer lifetime and a larger molar absorption than the $^3T_1$ of the $[RhCl_2(dp\text{-}phen)_2]^+$. The longest phosphorescent lifetime of $[Rh(dp\text{-}phen)_3]^{3+}$ can be explained as follows. The $^3(\pi\text{-}\pi^*)$ of $[Rh(dp\text{-}phen)_3]^{3+}$

is localized in the large ligand of dp-phen so that the spin-orbit interaction due to the rhodium(III) ion is not effective on the internal conversion ($^3(\pi\text{-}\pi^*) \rightarrow {}^1A_1$). The much shorter lifetimes of the ligand-field triplet-excited states in the aqueous solution may be closely related to the aquation reaction of $[RhCl_2(phen)_2]^+$.[5,18] It can be explained in terms of a competition between the phosphorescence and the aquation that $[RhCl_2(phen)_2]^+$, with less photoactivity (ϕ=0.01),[10] has a longer lifetime (55 ns) than that (1 ns)[5] of *cis*-$[RhBr_2(NH_3)_4]^+$ in the aqueous solution, which undergoes a photoaquation reaction with the quantum yield of 0.3.

The $^3T_1$ of $[RhCl_2(dp\text{-}phen)_2]^+$ and $[RhCl_2(phen)_2]^+$ have large molar-absorption coefficients (2750 $M^{-1}cm^{-1}$ and 1600 $M^{-1}cm^{-1}$, respectively), which can be explained not by the parity-forbidden ligand-field transition, but by a charge-transfer transition ($\pi \rightarrow d_\pi$). As for $[Rh(dp\text{-}phen)_3]^{3+}$, the wide absorption of $^3(\pi\text{-}\pi^*)$ with the absorption coefficient of 9600 $M^{-1}cm^{-1}$ indicates the appearance of a charge-transfer transition ($d_\pi \rightarrow \pi^*$) in addition to the ($\pi\text{-}\pi^*$) transition of the excited free ligand. Such an appearance of the charge-transfer transition ($\pi \rightarrow d_\pi$) in the ESA also has been proposed in the cases of excited doublet states of chromium(III) compounds.[3] By using these large molar-absorption coefficients, one can estimate the formation of the excited state on photoexcitation. The formation of the excited state is indispensable to an estimation of the efficiency of product formation in the quenching process of the excited rhodium(III) compound, which has been qualitatively studied by several workers.[4,19] Both $^3(\pi\text{-}\pi^*)$ and $^3T_1$ of the rhodium(III) compounds studied are subjected to electron-transfer quenching by some aromatic amines. The efficiencies of product formation in the quenching are calculated to be more than 0.1 by using these absorption coefficients. The details of the electron transfer quenching will be reported elsewhere.

References

* The following abbreviations will be used; 2,2′-bipyridine: bpy; 1,10-phenanthroline: phen; and 4,7-diphenyl-1,10-phenanthroline: dp-phen.

** The enhancement of the lowest band of dp-phen on its coodination confirmed the formation of $Zn(dp\text{-}phen)^{2+}$ in dilute solutions of $Zn(NO_3)_3$ and free dp-phen.

*** The rhodium(III) compounds studied do not belong to the Oh group, but the electronic states are denoted by the irreducible representations of the Oh group for the sake of convenience.

sake.

1) C. R. Bock, T. J. Meyer, and D. G. Whitten, *J. Am. Chem. Soc.*, **97**, 2909 (1974).

2) R. Ballardini, G. Varani, M. T. Indelli, F. Scandola, and V. Balzani, *J. Am. Chem. Soc.*, **100**, 7219 (1978).

3) T. Ohno and S. Kato, *Bull. Chem. Soc. Jpn.*, **57**, 1528 (1984).

4) R. Ballardine, G. Varani, and V. Balzani, *J. Am. Chem. Soc.*, **102**, 1719 (1980).

5) D. A. Sexton, L. H. Skibsted, D. Madge, and P. C. Ford, *J. Phys. Chem.*, **86**, 1758 (1982).

6) P. C. Ford, *Coord. Chem.Rev.*, **44**, 61 (1982).

7) U. Lachish, P. P. Infelta, and M. Grätzel, *Chem. Phys. Lett.*, **62**, 317 (1979).

8) T. Kobayashi and Y. Ohashi, *Chem. Phys. Lett.*, **86**, 289 (1982).

9) A. W. Adamson, *Pure and Applied Chem.*, **51**, 313 (1979).

10) J. A. Broomhead and W. Grumley, *Chem. Commun.*, **1968**, 1211; M. M. Muir and W-L. Huang, *Inorg. Chem.*, **12**, 1831 (1973).

11) T. Ohno, S. Kato, and N. N. Lichtin, *Bull. Chem. Soc. Jpn.*, **55**, 2753 (1982).

12) C. M. Harris and E. D. McKenzie, *J. Inorg. Nuclear Chem.*, **25**, 171 (1963).

13) P. M. Gidney, R. D. Gillard, and B. T. Heaton, *J. Chem. Soc., Dalton Trans.*, **1972**, 2621.

14) J. N. Demas and G. A. Crosby, *J. Am. Chem. Soc.*, **92**, 7262 (1970).

15) M. K. DeArmond and J. E. Hill, *J. Chem. Phys.*, **54**, 2247 53 (1971).

16) H. Groper and F. Dorr, *Z. Electrochem.*, **67**, 46 (1963).

17) F. Bolleta, A. Rossi, F. Barigelletti, S. Dellonte, and V. Balzani, *Gazz. Chim. Ital.*, **111**, 155 (1981).

18) N. A. P. Kane-Maguire, W. S. Crippen, and P. K. Miller, *Inorg. Chem.*, **22**, 3831 (1983).

19) M. Kirch, J. M. Lehn, and J. P. Sauvage, Helv. Chim. Acta, 62, 1345 (1979); M. T. Indelli, R. Ballardini, and F. Scandola, *J. Phys. Chem.*, to be published.

Preferred Orientation of Particles in Reflection-type Powder Diffractometry. Preferred Orientations in Benzamide and α-2-Pyrazinecarboxamide Powders

Kazuaki NAKATA,* Hiroshi SUGIHARA, Shinya MORI,
Hiroshi YAMAGUCHI,† and Yoshito TAKAKI
Department of Physics, Osaka Kyoiku University, Tennoji-ku, Osaka 543
†*Department of Earth Science (Mineralogy), Osaka Kyoiku University, Tennoji-ku, Osaka 543*
(Received March 28, 1984)

An improved method for the determination of the orientation distribution function of a powder consisting of preferentially oriented plate-like and needle-like particles was reported. Using this method, the coarse and fine powders of benzamide and α-2-pyrazinecarboxamide were investigated. It was found that the domains (a domain is defined as a collection of particles having the same preferred orientation plane or axis) of preferentially oriented particles exhibit two distinct changes when undergoing grinding of the powder. One change involves a decrease and the other an increase in volume, indicating that the particles in the domain showing the former change transform into those in the domain showing the latter change following grinding. The increase in volume of the domain can be well explained in relation to the existence of molecular layers connected to each other by weak van der Waals force in the crystal.

Takaki and Yamaguchi[1] reported a process for the determination of an orientation distribution function for preferentially oriented plate-like particles by the usual reflection-type powder diffractometry. The orientation distribution function, $N(\alpha)$, is defined in such a way that the fractional number of plate-like particles whose normals are contained in a solid angle $d\Omega$ at an angle α to the direction normal to the sample-holder is given by $N(\alpha)d\Omega$. They showed that $N(\alpha)$ can be obtained from the distribution function $\rho(\alpha)$

$$\rho(\alpha) = K \cdot N(\alpha) = I_{pre}(\alpha)/I_{ran}(\alpha), \quad (1)$$

where K is a constant, $I_{pre}(\alpha)$ is the intensity for an hkl reflection from preferentially oriented particles, $I_{ran}(\alpha)$ is that from randomly oriented particles and α is an angle between an hkl plane and the plane of preferred orientation.

As for the analytical approximation to the mean distribution function $N(\alpha)$, Uda and Sasa[2-5] and Toraya and Marumo[6] have shown in their studies on preferred orientation in inorganic powder samples that a Gaussian-type function

$$N(\alpha) = C_0 + C_1 \exp(-P\alpha^2) \text{ and } C_0 + C_1 = 1 \quad (2)$$

gives an excellent approximation to the distribution of oriented plate-like particles. The first term is a constant which is responsible for the random orientation of particles in a powder, the second term is a mean distribution function for preferentially oriented particles and P represents the degree of preferred orientation. On the other hand, Yamaguchi *et al.*[7] have shown that a Cauchy-type function

$$N(\alpha) = C_0 + C_1\{1/[1+P\alpha^2] + 1/[1+P(\pi-\alpha)^2]\} \quad (3)$$

gives a good approximation to the distribution function in γ_{II}-Li_2ZnSiO_4 and *p*-iodobenzamide powder samples.

We have found that the above function is unsuitable to express the distribution for very poorly oriented plate-like particles since, for a very small value of P, the value of $N(\alpha)$ at $\alpha=0$ is smaller than that at $\alpha=\pi/2$. Therefore, we will use the following revised distribution function

$$N(\alpha) = C_0 + C_1/[1+P\alpha^2], \quad (4)$$

where the first and the second terms express contributions from randomly oriented and preferentially oriented particles, respectively.

Then, using distribution functions of the above Gaussian (2) and Cauchy (4) types, we reexamined the preferred orientations in several inorganic and organic substances of which X-ray powder-diffraction data or observed orientation-distribution curves have been given.[3-12] The results indicate that, as has already been reported,[6] the Gaussian-type function is superior to the Cauchy-type function in representing the distribution of plate-like particles for exceedingly oriented powders,[3,4,6] while the Cauchy-type function gives a good approximation for all the other poorly oriented powder samples.

Similar to the case of plate-like particles, the distribution of preferentially oriented needle-like particles may be obtained from the distribution function

$$\rho(\beta) = K \cdot N(\beta) = I_{pre}(\beta)/I_{ran}(\beta), \quad (5)$$

where β is the acute angle between the axis normal to an hkl plane and that of preferred orientation. Function $N(\beta)$ can then be obtained[6] in the form

$$N(\beta) = C_0 + C_1'/[1+P'(\pi/2-\beta)^2]. \quad (6)$$

The preferred orientation of needle-like particles in an *m*-iodobenzoic acid powder sample has been well explained using expression (6).

Recently, Yamaguchi *et al.*[8] and Kurisu *et al.*[9] have

extended the above treatment to include domains with different preferred orientations, where a domain is defined as a collection of particles having the same preferred orientation plane or axis. The orientation distribution functions given by them are:

$$N(\alpha) = C_0 + \sum C_n/[1+P_n\alpha_n^2], \quad (7a)$$

for plate-like particles and

$$N(\beta) = C_0 + \sum C_n'/[1+P_n'(\pi/2-\beta_n)^2], \quad (7b)$$

for needle-like particles. Here $N(\alpha)\equiv N(\alpha_1, \alpha_2, \cdots, \alpha_n, \cdots, \alpha_m)$ and $N(\beta)\equiv N(\beta_1, \beta_2, \cdots, \beta_n, \cdots, \beta_m)$, where m is the number of preferred orientation planes (or axes), α_n is the acute angle between an hkl reflection plane and the nth plane of preferred orientation and β_n is the acute angle between the axis normal to an hkl reflection plane and the nth axis of preferred orientation.

Here, we have extended the above treatment to include the case where domains with plate-like and needle-like particles coexist in a powder. The distribution function is then given by

$$N(\alpha, \beta) = C_0 + \sum C_n/[1+P_n\alpha_n^2] + \sum C_m'/[1+P_m'(\pi/2-\beta_m)^2], \quad (8)$$

where the second and the third terms give contributions from plate-like and needle-like particles, respectively.

The relative volumes of domains in a powder sample are obtained from the following expressions:[9]

$$V_0 = 4\pi C_0 \int_0^{\pi/2} \sin\alpha d\alpha = 4\pi C_0, \quad (9)$$

$$V_n = 4\pi C_n \int_0^{\pi/2} \{1/[1+P_n\alpha_n^2]\} \sin\alpha d\alpha, \quad (10a)$$

for plate-like particles and

$$V_m = 4\pi C_m' \int_0^{\pi/2} \{1/[1+P_m'(\pi/2-\beta_m)^2]\} \sin\beta d\beta, \quad (10b)$$

for needle-like particles, where V_0, V_n, and V_m are normalized in such a way that

$$V_0 + \sum V_n + \sum V_m = 1.$$

In this paper we apply the above treatment to coarse and fine powders of benzamide[13] and α-2-pyrazinecarboxamide[14] and examine the change in the preferred orientation of particles following a grinding of the powder.

Experimental

Powder samples were prepared by grinding an aggregate of each crystal in an agate mortar. X-Ray powder diffraction patterns were taken with an X-ray powder diffractometer (Rigaku-Denki, D-2F) with Cu$K\alpha$ radiation using a divergence slit of 1° and a scanning speed of 1° (2θ/min). Each powder sample was packed in a standard specimen holder without any special treatment and was pressed gently to make a flat surface at constant pressure. Diffraction-intensity measurements were made by cutting out the background-subtracted peak areas from each trace and weighing.

Intensities, I_{ran}, were calculated from the following expression:

$$I_{ran} = m \cdot Lp \cdot F_o^2, \quad (11)$$

where F_o's are observed or calculated structure factors, m is multiplicity and Lp is Lorentz-polarization factor. Low-angle reflections (2θ<13°) were not used for least-squares calculations since the intensities of these reflections were

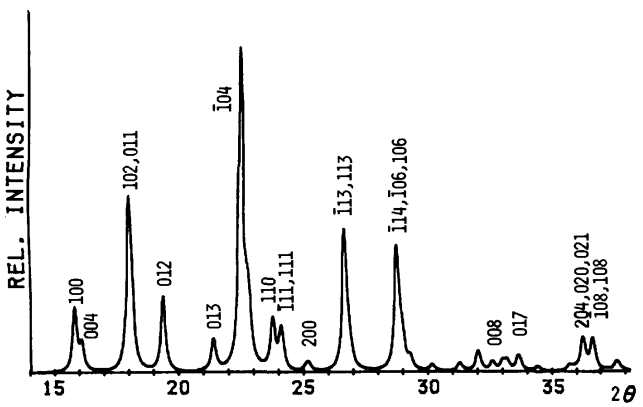

Fig. 1. Calculated powder intensity pattern for randomly oriented particles of benzamide.

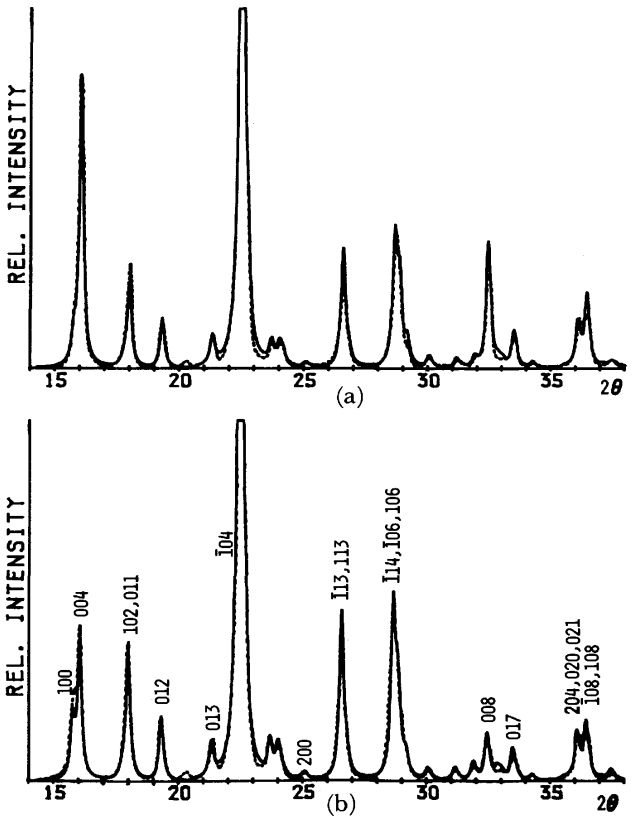

Fig. 2. Observed (dotted line) and calculated (full line) powder intensity patterns for benzamide. (a) Coarse powder. (b) Fine powder.

TABLE 1. PREFERRED ORIENTATION PARAMETERS FOR BENZAMIDE POWDER SAMPLES. E.S.D.'S ARE GIVEN IN PARENTHESES.

	C_0[a]	C_1[a]	P_1	C_2[a]	P_2	V_0[b]	V_1[b]	V_2[b]	R[c]	R_0[d]
Orientation plane		(001)		($\bar{1}$04)						
Coarse powder	0.00(1)	0.92(3)	18(1)	0.08(1)	12(5)	0.02	0.88	0.10	0.06	0.60
Fine powder	0.02(1)	0.70(5)	6.4(5)	0.28(2)	4.7(4)	0.09	0.61	0.30	0.05	0.44

a) Parameters C_j's are so normalized that $C_0+C_1+C_2=1$. b) V_0, V_1, and V_2 are relative volumes of domains. c) $R=\sum|I_{pre}-I_{ran}\cdot N(\alpha)|/\sum I_{pre}$. d) R_0 is the initial value of R.

seriously affected by the size of the divergence-slit.

Powder-intensity profiles were calculated from the following expression:

$$y_i = \sum\left[\frac{2}{3}I_nL(2\theta_i, 2\theta_{n1}) + \frac{1}{3}I_nL(2\theta_i, 2\theta_{n2})\right] \quad (12)$$

where y_i is the intensity at a given point $2\theta_i$ in a profile.

The summation is taken over all possible contributing reflections at $2\theta=2\theta_i$; I_n is the intensity for the nth reflection from preferentially oriented particles; $L(2\theta_i, 2\theta_{n1})$ and $L(2\theta_i, 2\theta_{n2})$ are line shape functions for Cu $K\alpha_1$ and Cu $K\alpha_2$, respectively, and are represented by a Cauchy function with the half width of the diffraction peak, H_n. The angular dependence of H_n is represented by

$$H_n^2 = U\cdot\tan^2\theta_n + V\cdot\tan\theta_n + W \quad (13)$$

where U, V, W are constants.

Results and Discussion

Benzamide. Figure 1 shows the intensity pattern for randomly oriented particles calculated from observed F_o's for 42 reflections.[13] X-Ray intensity patterns taken at two different stages of grinding are shown in Fig. 2. Comparing Figs. 1 with 2(a), one can see that the intensities of both the 004 and 008 reflections are prominently enhanced in Fig. 2(a), indicating that the 001 plane is a plane of preferred orientation.

To obtain the distribution function $\rho(\alpha)$, we selected 23 reflections from diffraction peaks in each of the two powder patterns; seven reflections, 012, 013, $\bar{1}$04, 110, 200, 008, 017, with single peaks, five pairs of reflections (100, 004), (102, 011), ($\bar{1}$11, 111), ($\bar{1}$13, 113), ($\bar{1}$08, 108), and two triad reflections ($\bar{1}$14, $\bar{1}$06, 106), (204, 020, 021) with overlapped peaks.

Preferred orientation parameters of $N(\alpha)$ for the 001 preferred orientation plane for the two powder samples were determined by a least-squares technique using a modified program based on one written by Kurisu *et al.*[9] At this stage, we calculated the intensity pattern using the above preferred-orientation parameters and found that the observed intensity for the $\bar{1}$04 reflection was still remarkably strong (especially in the fine powder) as compared with the corresponding intensity in Fig. 1, suggesting that the $\bar{1}$04 plane is another plane of preferred orientation. The final preferred orientation parameters obtained from the above two preferred orientation planes are listed in Table 1. Calculated intensity patterns are shown in Fig. 2.

In Fig. 2, one finds that the calculated intensity patterns are in good agreement with the observed patterns for both the coarse and fine powders. As seen in Table 1, the value of P_1 for the 001 preferred orientation plane decreases from 18 (coarse powder) to 6.4 (fine powder). Similarly, the value of P_2 for the $\bar{1}$04 plane decreases from 12 to 4.7.

The relative volume of V_1 decreases from 0.88 to 0.61, while that of V_2 increases significantly from 0.10 to 0.30. This suggests that a considerable part of the particles in the domain of V_1 change with grinding into those having the $\bar{1}$04 preferred-orientation plane. The existence of this preferred-orientation plane can well be explained from the fact that molecular layers parallel to ($\bar{1}$04) in the crystal are connected with each other by weak van der Waals force.[13]

A microscopic examination revealed that the majority of particles in the coarse powder were thin plates. Comparing the above result, one may say that these plates would probably be those with (001) well developed.

α-2-Pyrazinecarboxamide. Takaki *et al.*[14] have reported that crystals obtained from crystal growth are colorless needles elongated along the c axis and sometimes laths with (010) well developed. A microscopic observation of a coarse powder showed many typical needles. Therefore, it is very interesting to examine the change in the preferred-orientation parameters for needle-like particles following the grinding of the powder.

A total of 16 reflections were used for obtaining preferred-orientation parameters. There included four reflections, 310, 410, $\bar{4}$01, 320, with single peaks, three pairs of reflections, (210, 400), (600, 510), ($\bar{2}$10, 001), and a hexad of reflections (201, 610, $\bar{1}$11, $\bar{2}$11, 220, 011) with overlapped peaks.

Preferred-orientation parameters for coarse and fine powders were obtained by introducing two kinds of domains with preferentially oriented particles; one was the domain with the c preferred orientation axis and the other was that with the 100 preferred orientation plane. Final parameters are listed in Table 2. Figure 3(a) shows the intensity pattern for randomly oriented particles calculated from observed F_o's for 53 reflections.[14] The observed and calculated intensity patterns for the fine powder are shown in Fig. 3(b).

As seen in Table 2, all P values decreased upon grinding. The relative volume of the domain with the c preferred orientation axis decreased from 0.58 (coarse powder) to 0.42 (fine powder), indicating that many of

TABLE 2. PREFERRED ORIENTATION PARAMETERS FOR α-2-PYRAZINECARBOXAMIDE POWDER SAMPLES

	C_0	C_1'	P_1'	C_2	P_2	V_0	V_1	V_2	R	R_0
Orientation axis or plane		c-axis			(100)					
Coarse powder	0.05(1)	0.30(1)	7(1)	0.65(3)	22(2)	0.19	0.58	0.23	0.06	0.69
Fine powder	0.06(1)	0.28(1)	2.5(7)	0.66(8)	4.1(7)	0.16	0.42	0.42	0.08	0.47

TABLE 3. PREFERRED ORIENTATION PARAMETERS OBTAINED BY USE OF THE GAUSSIAN-TYPE FUNCTION FOR FINE POWDER SAMPLES OF BENZAMIDE AND α-2-PYRAZINECARBOXAMIDE

	C_0	C_1 C_1'	P_1 P_1'	C_2	P_2	V_0	V_1	V_2	R	R_0
Benzamide	0.12(1)	0.61(5)	3.0(2)	0.27(1)	3.1(3)	0.46	0.38	0.16	0.06	0.44
α-2-pyrazine-carboxamide	0.20(1)	0.22(1)	2.4(11)	0.58(9)	1.9(2)	0.43	0.26	0.31	0.10	0.47

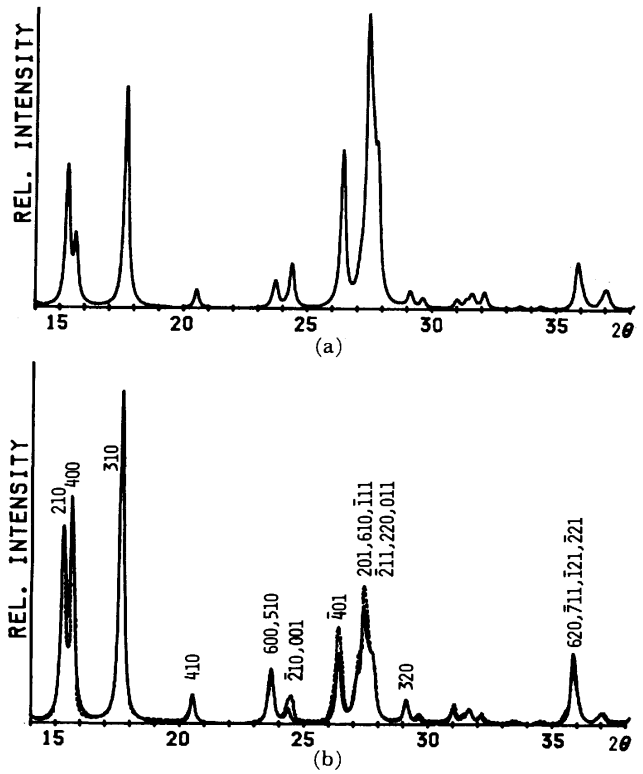

Fig. 3. Powder intensity patterns for α-2-pyrazine-carboxamide.
(a) Calculated intensity pattern for randomly oriented particles. (b) Observed (dotted line) and calculated (full line) intensity patterns for the fine powder.

the needle-like particles obtained from crystal growth retained their shape unchanged, although they diminished in size upon grinding. On the other hand, the domain with the 100 preferred orientation plane increased noticeably in volume from 0.23 to 0.42. The above results may suggest that particles in domains V_0 and V_1 change into those having the 100 preferred orientation plane upon grinding. The existence of the 100 preferred orientation plane can be well explained in terms of the layer structure of the crystal.[14]

Concluding Remarks

In Table 3, we give preferred orientation parameters obtained by use of the Gaussian-type function for the above fine-powder samples. Comparing the parameters in Tables 1 and 2 with those in Table 3, one may find that the R values for both benzamide and α-2-pyrazinecarboxamide fine powders are smaller than the corresponding values in Table 3, showing that in this case also a Cauchy-type function gives a good approximation for representing distribution function of preferentially oriented particles. It is to be noted that significant discrepancies can be found in the values of C_0 for two types of distribution functions, owing to the characteristic features of the Cauchy and Gaussian functions.

References

1) Y. Takaki and H. Yamaguchi, *Yogyo Kyokai Shi*, **90**, 34 (1982).
2) M. Uda, *Z. Anorg. Allg. Chem.*, **350**, 105 (1967).
3) Y. Sasa and M. Uda, *J. Solid State Chem.*, **18**, 63 (1976).
4) Y. Sasa and M. Uda, *Yogyo Kyokai Shi* (in Japanese), **88**, 316 (1980).
5) M. Uda and Y. Sasa, *J. Solid State Chem.*, **46**, 121 (1983).
6) H. Toraya and F. Marumo, *Miner. Journ.*, **10**, 211 (1981).
7) H. Yamaguchi, K. Nakata, A. Kurisu, Y. Takaki and K. Akatsuka, *Mem. Osaka Kyoiku Univ. Ser. III*, **30**, 185 (1982).
8) H. Yamaguchi, K. Akatsuka, A. Kurisu, Y. Takaki, and M. Setoguchi, Annual Meeting of Mineralogical Society of Japan, Tsukuba, June 1982, Abstr., No. 36.
9) A. Kurisu, K. Nakata, H. Yamaguchi, and Y. Takaki, *Mem. Osaka Kyoiku Univ. Ser. III* (in Japanese), **31**, 83 (1983).
10) P. M. DE WOLFF and W. H. SAS, *Acta Cryst.*, **A25**, 206 (1969).
11) P. J. DE COURVILLE, D. TCHOUBAR, and C. TCHOUBAR, *J. Appl. Cryst.*, **12**, 332 (1979).
12) A. Plançon, *J. Appl. Cryst.*, **13**, 524 (1980).
13) C. C. F. Blake and R. W. H. Small, *Acta Cryst.*, **B28**, 2201 (1972).
14) Y. Takaki, Y. Sasada, and T. Watanabé, *Acta Cryst.*, **13**, 693 (1960).

 © 1984 The Chemical Society of Japan Bull. Chem. Soc. Jpn., 57, 3399—3402 (1984)

Determination of the Vapor Pressures of Lithium Iodide and Potassium Chloride by Molecular Beam Surface Ionization

Hiroyuki KAWANO* and Tsutomu KENPŌ

Department of Chemistry, Faculty of Science, Ehime University, 2-5, Bunkyō-chō, Matsuyama 790

(Received March 30, 1984)

Combined techniques of molecular beam effusion from a Knudsen cell and of positive surface ionization on a heated polycrystalline rhenium filament were employed to determine the vapor pressures P (in atm) of LiI and KCl as a function of cell temperature T (in K), thereby yielding the equations:

$$\log_{10} P(\mathrm{LiI}) = (7.498 \pm 0.046) - (9254 \pm 30)/T \text{ for } 583—717 \text{ K},$$

$$\log_{10} P(\mathrm{KCl}) = (7.210 \pm 0.058) - (11135 \pm 45)/T \text{ for } 687—877 \text{ K}.$$

The present data on the pressure and on both entropy and enthalpy of sublimation are compared with others in literature.

In the research fields of thermochemistry and molecular beam chemistry, it is one of the important problems to know the accurate value of vapor pressure at a given temperature. From this point of view, we have been trying to determine the vapor pressures of alkali-metal halides after having developed a technique of molecular beam surface ionization, and we have already published some of the results thus obtained with CsF and CsCl[1] and with LiCl and NaBr.[2] In this paper we describe the experimental results obtained with LiI and KCl.

Experimental

In the same manner as in the previous works,[1,2] a molecular beam of an alkali-metal halide (MX) effusing from a Knudsen cell heated to a temperature (T) was directed onto a polycrystalline rhenium filament (F) kept at a high temperature (T_F) in the residual gas pressue of about 3×10^{-5} Pa. The total ion current ($I^+(M^+)$) of an alkali-metal ion (M^+) emitted from F was measured as a function of T or T_F. The samples of LiI and KCl used in this work were obtained from Aldrich Chem. Co., Inc. and Wako Pure Chem. Ind., Ltd., respectively.

Results and Discussion

In order to find a filament temperature suitable for producing M^+ from MX under study, $I^+(M^+)$ was measured as a function of T_F while the Knudsen cell was kept at a constant temperature such as T=766, 761, 686, or 627 K for LiI or as T=877, 874, or 763 K for KCl. Two examples of the results thus obtained are illustrated in Fig. 1. The reason why the two are quite different in emission pattern may be explained reasonably[3] by our previous theory[4] that the degrees of both dissociation of MX and ionization of M depend upon the effective work function for positive surface ionization. As may be seen in Fig. 1, $I^+(Li^+)$ and $I^+(K^+)$ are virtually constant at 3.10 ± 0.08 and 13.1 ± 0.4 nA in the ranges $T_F\simeq1280$—1390 and $\gtrsim1050$ K, respectively. These results indicate that the ionization efficiencies of LiI and KCl incident upon F are virtually unity in the respective ranges. Consequently, F was kept at a constant temperature in either of the above ranges, and $I^+(M^+)$ was measured as a function of T. The vapor pressure is given by[1]

$$P(\mathrm{MX}) = 0.0144\, S_C^{-1}[M(\mathrm{MX})\, T]^{1/2}\, I^+(\mathrm{M}^+), \quad (1)$$

where $P(\mathrm{MX})$ and $I^+(M^+)$ are expressed in atm and ampere, respectively, and $M(\mathrm{MX})$ is the molecular weight of MX. The values of the effusing slit area S_C were 1.13×10^{-2} and 1.46×10^{-2} cm^2 in the experiments with LiI and KCl, respectively.

The data on $P(\mathrm{MX})$ determined in this work are summarized in Table 1, and they are illustrated in Figs. 2 and 3, leading to a general expression:

$$\log_{10} P(\mathrm{MX}) = A - B/T. \quad (2)$$

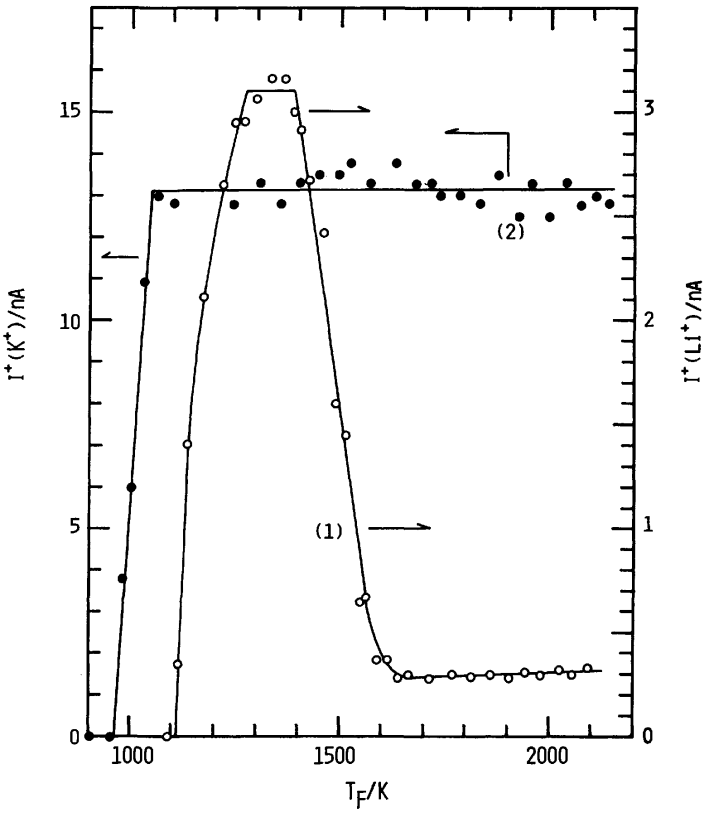

Fig. 1. Dependence of the total ion current ($I^+(M^+)$) upon the filament temperature (T_F) at a constant cell-temperature (T).
(1): Li^+ from LiI at T=686 K, (2): K^+ from KCl at T=874 K.

TABLE 1. VAPOR PRESSURES DETERMINED IN THIS WORK

Sample	T_F/K	T/K	P(MX)/atm	T_F/K	T/K	P(MX)/atm
LiI	1309	717	3.73×10^{-6}	1299	706	2.47×10^{-6}
		701	1.95×10^{-6}		688	1.11×10^{-6}
		681	8.43×10^{-7}		674	5.81×10^{-7}
		669	4.86×10^{-7}		662	3.36×10^{-7}
		650	1.76×10^{-7}		640	1.09×10^{-7}
		634	8.08×10^{-8}		621	4.07×10^{-8}
		611	2.27×10^{-8}		603	1.40×10^{-8}
		596	9.13×10^{-9}		583	4.17×10^{-9}
KCl	2113	877	3.15×10^{-6}	1588	874	3.19×10^{-6}
		860	1.64×10^{-6}		855	1.58×10^{-6}
		841	8.49×10^{-7}		836	7.72×10^{-7}
		818	3.58×10^{-7}		824	4.83×10^{-7}
		796	1.60×10^{-7}		804	2.36×10^{-7}
		777	7.30×10^{-8}		786	1.08×10^{-7}
		753	2.64×10^{-8}		764	4.20×10^{-8}
		738	1.28×10^{-8}		742	1.69×10^{-8}
		723	6.35×10^{-9}		729	8.32×10^{-9}
		704	2.36×10^{-9}		715	4.22×10^{-9}
		687	1.11×10^{-9}		692	1.26×10^{-9}
	1193	866	2.38×10^{-6}	1193	765	4.66×10^{-8}
		847	1.23×10^{-6}		744	1.80×10^{-8}
		827	6.22×10^{-7}		729	8.88×10^{-9}
		807	2.75×10^{-7}		714	4.01×10^{-9}
		787	1.21×10^{-7}		696	1.68×10^{-9}

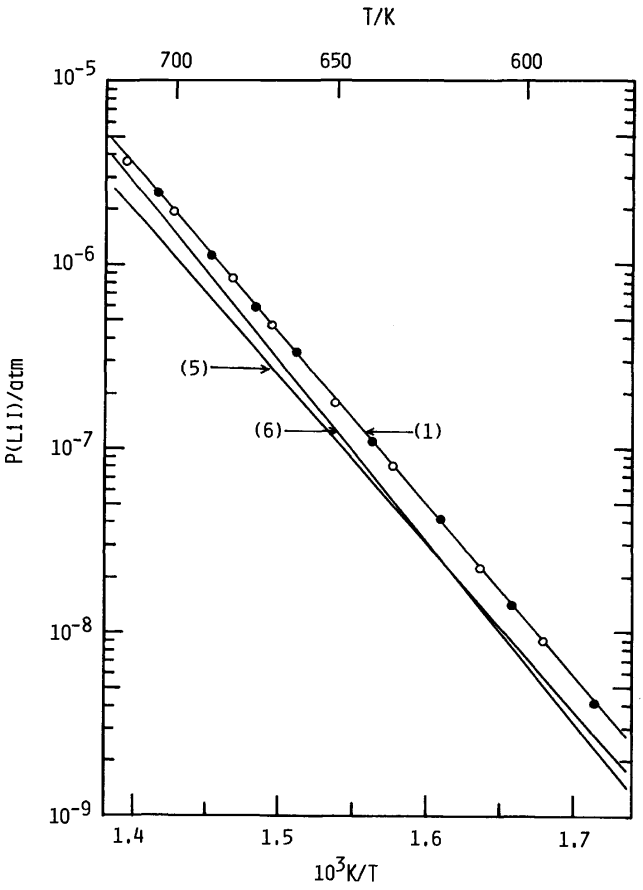

Fig. 2. Temperature dependence of the vapor pressure of LiI.
(1): This work at T_F=1309 K (open circle) or 1299 K (solid circle), (5): Ref. 5, (6): Ref. 6.

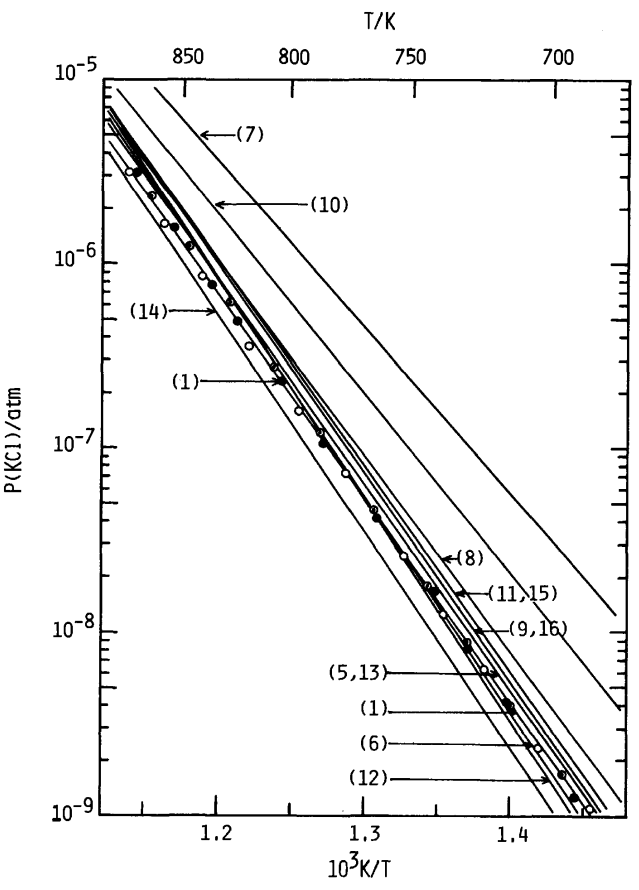

Fig. 3. Temperature dependence of the vapor pressure of KCl.
(1): This work at T_F=2113 K (open circle), 1588 K (solid circle), or 1193 K (double circle), (5, 13): Refs. 5 and 13, (6): Ref. 6, (7): Ref. 7, (8): Ref. 8, (9, 16): Refs. 9 and 16, (10): Refs. 10, (11, 15): Refs. 11 and 15, (12): Ref. 12, (14): Ref. 14.

TABLE 2. SUMMARY OF THE EXPERIMENTAL DATA OBTAINED BY THE PRESENT AND OTHER WORKERS

Sample	T_R / K	$\bar{T}$ / K	A	B / K	P(MX)/μatm 600 K	700 K	800 K	$\Delta S(\bar{T})$ / cal* mol^{-1} K^{-1}	$\Delta S(300)$ / cal mol^{-1} K^{-1}	$\Delta H(\bar{T})$ / kcal mol^{-1}	$\Delta H(300)$ / kcal mol^{-1}	Ref.
LiI	500–700	600	7.000±0.057	9081±33	0.00733	1.06	—	32.0±0.3	35.3±0.3	41.6±0.2	43.0±0.2	5
	574–697	636	8.094±0.156	9752±98	0.00693	1.45	—	37.0±0.7	40.5±0.8	44.6±0.4	46.2±0.5	6
	596–717	657	7.486±0.093	9247±61	0.0119	1.89	—	34.3±0.4	37.9±0.5	42.3±0.3	44.0±0.3	(a)
	583–706	645	7.513±0.040	9263±26	0.0119	1.91	—	34.4±0.2	37.9±0.2	42.4±0.1	44.0±0.1	(b)
	583–717	650	7.498±0.046	9254±30	0.0119	1.90	—	34.3±0.2	37.9±0.2	42.3±0.1	44.0±0.1	(A)
KCl	600–900	750	7.360±0.047	11207±34	—	0.00224	0.225	33.7±0.2	37.8±0.2	51.3±0.2	53.3±0.2	5
	693–989	841	7.936±0.089	11682±98	—	0.00177	0.216	36.3±0.4	41.0±0.5	53.4±0.4	55.9±0.5	6
	821–1407	1114	5.389	9027	—	0.0311	1.27	24.7	30.6	41.3	45.0	7
	853–955	904	6.837±0.035	10685±45	—	0.00374	0.303	31.3±0.2	36.3±0.2	48.9±0.2	51.6±0.2	8
	819–945	882	7.574	11324	—	0.00249	0.262	34.7	39.5	51.8	54.4	9
	818–1118	968	6.016	9788	—	0.0108	0.604	27.5	32.8	44.8	47.8	10
	859–1024	942	7.318±0.040	11116±37	—	0.00274	0.265	33.5±0.2	38.7±0.2	50.9±0.2	53.8±0.2	11
	899–935	917	8.289±0.329	11981±409	—	0.00149	0.206	37.9±1.5	43.0±1.7	54.8±1.9	57.6±2.0	12
	847–936	892	7.352±0.067	11207±109	—	0.00220	0.220	33.6±0.3	38.6±0.4	51.3±0.5	54.0±0.5	13
	898–959	929	7.695±0.170	11658±281	—	0.00110	0.133	35.2±0.8	40.3±0.9	53.3±1.3	56.2±1.4	14
	624–945	785	7.395±0.053	11154±56	—	0.00289	0.283	33.8±0.2	38.2±0.3	51.0±0.3	53.2±0.3	15
	711–870	791	7.570	11310	—	0.00259	0.271	34.6	39.1	51.7	54.0	16
	687–877	782	6.976±0.071	10966±54	—	0.00204	0.186	31.9±0.3	36.3±0.4	50.2±0.2	52.4±0.3	(c)
	692–874	783	7.337±0.065	11234±50	—	0.00194	0.197	33.6±0.3	37.9±0.3	51.4±0.2	53.6±0.2	(d)
	696–866	781	7.376±0.050	11249±39	—	0.00202	0.206	33.8±0.2	38.1±0.3	51.5±0.2	53.6±0.2	(e)
	687–877	782	7.210±0.058	11135±45	—	0.00201	0.196	33.0±0.3	37.3±0.3	50.9±0.2	53.1±0.2	(B)

*1 cal=4.184 J.

The values of A and B determined by the present and other workers are summarized in Table 2. The entropy and enthalpy changes due to sublimation at the mean temperature ($\bar{T}$) in the range (T_R) covered in each measurement and also those at 300 K were evaluated from Eqs. 3—6, respectively, in order to compare the latter with literature values at the same temperature (see Table 2).

$$\Delta S(\bar{T}) = 4.575\,A \text{ cal mol}^{-1}\text{ K}^{-1}, \quad (3)$$

$$\Delta H(\bar{T}) = 4.575\times10^{-3}\,B \text{ kcal mol}^{-1}, \quad (4)$$

$$\Delta S(300) = \Delta S(\bar{T}) + \int_{300}^{\bar{T}}\left[\frac{C_p(c)-C_p(g)}{T}\right]dT \simeq \Delta S(\bar{T}) + aR[\ln\bar{T}-\ln 300], \quad (5)$$

$$\Delta H(300) = \Delta H(\bar{T}) + \int_{300}^{\bar{T}}[C_p(c)-C_p(g)]dT \simeq \Delta H(\bar{T}) + aR[\bar{T}-300]. \quad (6)$$

Here, 1 cal is equal to 4.184 J, and $C_p(c)$ and $C_p(g)$ are the specific heats of MX at crystalline and gaseous states at 1 atm, respectively. On the basis of data on the heats,[5] the values of a in the ranges 300—650 and 300—850 K may be taken as 2.35 and 2.28 for LiI and KCl, respectively.

The values of T_F in the present works indicated as (a)—(e) in the last column in Table 2 were 1309, 1299, 2113, 1588, and 1193 K, respectively. The present works (A) and (B) indicate the mean values of those (a) and (b) and those (c)—(e), respectively.

To the best of our knowledge, it is from Refs. 5 and 6 alone that the data on P(LiI) below a melting point (719 K) are available today. As may be seen in Fig. 2 and Table 2, the data on P(LiI) do not agree well with each other among the three, suggesting the necessity of further measurements by many workers using various experimental methods. Both Fig. 3 and Table 2 show that the values of P(KCl) measured in this work are very close to those in Refs. 5, 6, and 13, and also suggest that the data in Refs. 7 and 10 are very poor in reliability probably because of systematic errors.

References

1) H. Kawano, T. Kenpō, and Y. Hidaka, *Bull. Chem. Soc. Jpn.*, **57**, 581 (1984).

2) H. Kawano and T. Kenpō, *Bull. Chem. Soc. Jpn.*, **57**, 1415 (1984).

3) H. Kawano and T. Kenpō, *J. Chem. Phys.*, **81**, 1248 (1984).

4) H. Kawano, Y. Hidaka, and M. Suga, *Bull. Chem. Soc. Jpn.*, **54**, 1675 (1981).

5) D. R. Stull and H. Prophet, "JANAF Thermochemical Tables," 2nd ed, Natl. Bur. Stand., Washington (1971).

6) M. S. Chandrasekharaiah, "Volatilities of Refractory Inorganic Compounds" in "The Characterization of High-Temperature Vapors," ed by J. L. Margrave, John Wiley & Sons, London (1967), Appendix B, pp. 495—507.

7) G. G. Schlessinger, "Vapor Pressures, Critical Temperatures and Critical Pressures of Inorganic Compounds" in "Handbook of Chemistry and Physics," 52nd ed, ed by R. C. Weast, The Chemical Rubber Co., Cleaveland (1971—1972), pp. D-171—D-180.

8) K. Niwa, *J. Fac. Sci. Hokkaido Imp. Univ., Ser. III*, **2**, 201 (1938).

9) A. C. P. Pugh and R. F. Barrow, *Trans. Faraday Soc.*, **54**, 671 (1958).

10) H.-H. Emons, W. Horlbeck, and D. Kiessling, *Z. Chem.*, **21**, 416 (1981).

11) W. D. Treadwell and W. Werner, *Helv. Chim. Acta*, **36**, 1436 (1953).
12) J. E. Mayer and I. H. Wintner, *J. Chem. Phys.*, **6**, 301 (1938).
13) V. Deitz, *J. Chem. Phys.*, **4**, 575 (1936).
14) M. J. Copley and V. Deitz, *Rev. Sci. Instr.*, **8**, 314 (1937).
15) B. H. Zimm and J. E. Mayer, *J. Chem. Phys.*, **12**, 362 (1944).
16) R. S. Bradley and P. Volans, *Proc. Roy. Soc.*, **A 217**, 508 (1953).

Pulse Radiolysis of Cycloserine in Aqueous Solutions. One-Electron Oxidation by OH Radicals

Masako TANAKA,* Hiroshi SAKUMA,† Osamu KOHANAWA,†† Seijun FUKAYA,††† and Meiseki KATAYAMA
Department of Atomic Science and Nuclear Engineering, Faculty of Engineering, Hokkaido University, Sapporo 060
(Received May 23, 1984)

The reaction of (*R*)-4-amino-3-isoxazolidinone (cycloserine) with OH radicals was studied in aqueous solutions by optical pulse radiolysis at pHs 6.5—12. It was concluded, from a comparison of the transient spectra with those obtained in a reaction with N_3 radicals, that OH radicals attacked at the dissociated peptide group, $-N^-CO-$, and an oxidized radical, $-\dot{N}CO-$, was produced through one-electron oxidation. From a kinetic analysis, the reaction was considered to have proceeded by two steps: The first step was the formation of OH adducts, where the rate constant, k(OH+cycloserine), was 8×10^9 mol^{-1} dm^3 s^{-1} for the zwitterion form of cycloserine at pH 6.5 and 1.2×10^{10} mol^{-1} dm^3 s^{-1} for anion form at pHs 8—10. The second step was the formation of oxidized radicals at a rate of $3—4\times10^6$ s^{-1}. These radicals decayed with a second-order rate, suggesting a radical-radical recombination. D-Serine was detected as the major product.

The hydroxyl (OH) radical is one of the most reactive species generated in irradiated water. A number of investigations have been carried out on its reaction with peptides in aqueous solutions, and it has been established that the abstraction of hydrogen from the carbon adjacent to the peptiede nitrogen is the major reaction for linear peptides as well as cyclic dipeptides.[1-6] For the series of five-membered cyclic compounds containing one peptide linkage, such as pyrrolidinone derivatives, the reaction of OH radicals is known to be essentially the same as that on linear peptides.[7] Cycloserine, 4-amino-3-isoxazolidinone (I), which is one of the broad-spectrum antibiotics and is known as an effective inhibitor of transaminase enzyme systems, has a cyclic structure containing one peptide linkage. The sturcture of cycloserine in aqueous solution is a zwitterion as described in (I), the pK values of which are 4.4 and 7.4, respectively.[8] Therefore, it is

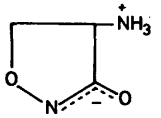

Cycloserine (I)

expected that this compound has a high reactivity toward OH radicals and that the OH radicals will attack the dissociated pepetide groups at around biological pHs. In this work we investigated the site of attack of OH radicals and the reaction mechanism of intermediates by studying the transient spectra and kinetics with pH dependence of them.

Experimental

The 45 MeV linac of Hokkaido University, producing 10 ns pulses of 45 MeV electrons, was used for the optical pulse radiolysis experiments. The dose per pulse was 80—100 Gy, which was measured by the KCNS method. The optical detection system was basically the same as that designed by Hunt and Thomas.[9] The light from a high-pressure mercury lamp (HB-50101, Ushio) was chopped by a rotating chopper at 25 Hz and focused at an irradiation cell of which the optical path length was 2 cm. The absorption signals, after passing through a monochromator, were detected by a photomultiplier (R928, Hamamatsu TV), then followed on a transient digitizer (DM901, Iwatsu) and recorded on an X-Y recorder. The range of wavelengths examined was 270 to 350 nm.

The (*R*)-cycloserine was supplied by Aldrich. NaN_3 and other reagents were supplied by Wako Junyaku. All reagents were used without further purification. Solutions were prepared by using triply distilled water the day before the experiment and kept in a refrigirator. The pH values of the solutions were adjusted by adding sodium hydroxide and were determined with a pH meter (pH501, Yokogawa). Solutions were saturated with N_2O gas (1 atm, (N_2O)= 2.5×10^{-2} mol dm^{-3}) just before irradiation in order to prevent the reaction by e_{aq}^-, in which N_2O converts them into OH radicals.

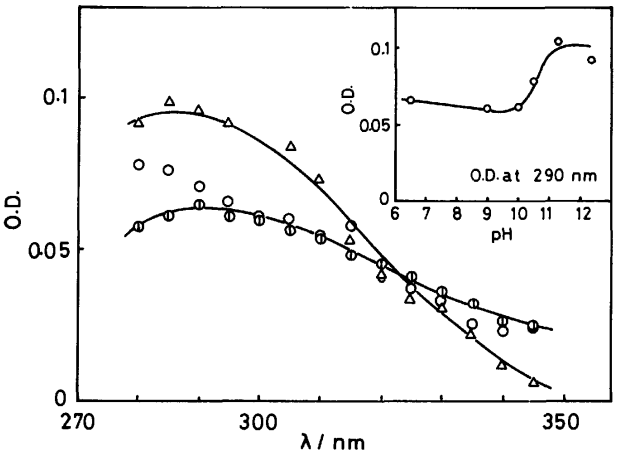

Fig. 1. The transient spectra produced on pulse radiolysis of 10^{-3} mol dm^{-3} cycloserine in presence of N_2O at pH 6.5 (○), 9.0 (◐), and 12.4 (△). The insert shows the pH dependence of the absorbance at 290 nm.

† Present addresses: Research and Development Center, Ebara Infilco, Co. Ltd., Fujisawa, Fujisawa 251.

†† Present addresses: Kobe Shipyard & Engine Works, Mitsubishi Heavy Industries, Ltd., Hyogo-ku, Kobe 652.

††† Present addresses: Victor Company of Japan, Kanagawa-ku, Yokohama 221.

The radiolytic yield of serine, which was the major product, was determined as follows. A solution of 10^{-3} mol dm^{-3} cycloserine (saturated with N_2O) was irradiated by the γ rays of ^{60}Co for 10 min at a dose rate of 3×10^{3} Gy/h. The total absorption dose corresponded to a 10% conversion. Then, the solution was dried in a vacuum and the residue was dissolved in a buffer solution and passed through a conventional automatic aminoacid analyzer (JLC-6AH, JEOL). Upon elution with a buffer solution (pH 3.2), serine and 3-(aminooxy)alanine (which was produced by the hydrolysis of cycloserine in an acidic buffer solution) were separated. Cycloserine was separated by the buffer solution of pH 7.3. The evaluations of G(serine) and G(−cycloserine) were made after the correction for 3-(aminooxy)alanine. The optical isomerism of serine was examined by IR spectra using KBr discs of the residues. In this case, the N_2O saturated solutions of 2×10^{-2} mol dm^{-3} were γ-irradiated for 10 h at a dose rate of 3×10^{3} Gy/h and dried. The irradiation time was chosen so that most of the cyclsoerine could be decomposed.

Results

Transient Absorption Spectra. The absorption spectra were obtained 1.25 μs after a pulse for solutions containing 1.0×10^{-3} mol dm^{-3} cycloserine with various pH values from 6.5 to 12 and are presented in Fig. 1. The spectra, except the one at pH 6.5, have a broad maximum at 290 nm. The band maximum was not observed in the spectrum at pH 6.5. The insert in Fig. 1 shows the change of absorbance at 290 nm with pH. The increase in absorbance was observed above pH 10. The spectra shown in Fig. 1 were compared with those obtained in a reaction with N_3 radicals. The concentration of the N_3^- ion added was 10^{-2} mol dm^{-3}, and the spectra were obtained 10 μs after a pulse in order to avoid the contribution of the absorption due to the remaining N_3 radicals. Transient spectra are shown in Fig. 2. All the spectra at pH 6.5 to 12 showed broad absorption maxima at around 290 nm and were very similar to the spectra shown in Fig. 1. However, as shown in the insert of Fig. 2, the absorbance at 290 nm

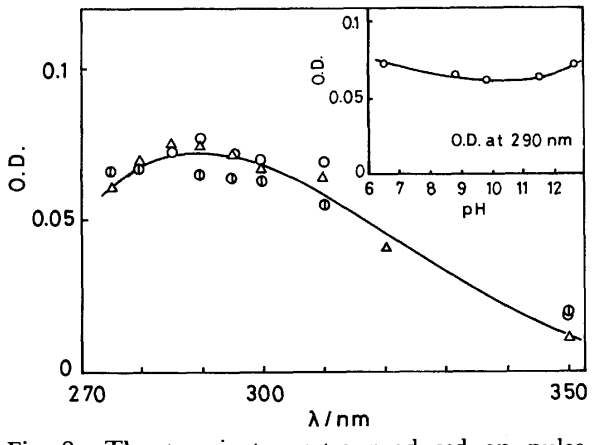

Fig. 2. The transient spectra produced on pulse radiolysis of 10^{-3} mol dm^{-3} cycloserine with 10^{-2} mol dm^{-3} NaN_3 in presence of N_2O at pH 6.5 (○), 9.0 (⦶), 12.4 (△). The insert shows the pH dependence of absorbance at 290 nm.

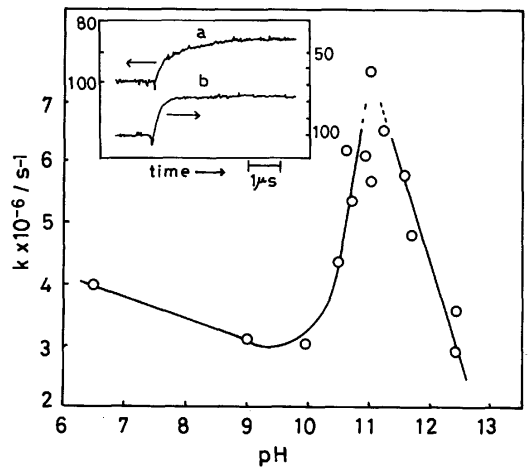

Fig. 3. The pH dependence of rate of formation of the intermediates measured at 290 nm on pulse radiolysis of 10^{-3} mol dm^{-3} cycloserine. The insert shows the example of signal traces at pH 9.9 (a) and 11.3 (b). The ordinates indicate the transmission, %.

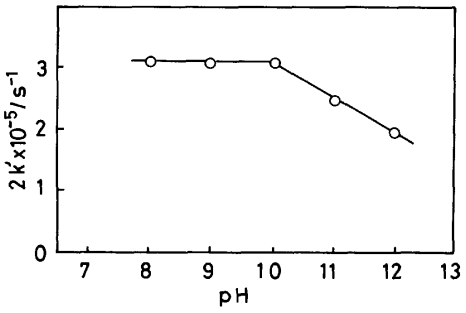

Fig. 4. The pH dependence of the decay rate measured in absorbance on pulse radiolysis of 10^{-3} mol dm^{-3} cycloserine. The true second-order decay rate, $2k$, is related with $2k'$ as follws: $2k=2k'\varepsilon_{290}l$, where ε_{290} is the molar extinction coeffident of intermediate at 290 nm and l is the optical path length.

did not change within the whole pH range examined.

Kinetics of the Formation and Decay of Intermediates. The rates of formation of transient species, shown in Fig. 1, were determined from the growth of the absorption signals at 290 nm for solutions of various pHs. The results are shown in Fig. 3. The insert presents a typical example of the signal traces of growth after pulse. The first-order rate constants are $3-4\times10^{6}$ s^{-1} between neutral and pH 10, increased between pH 10 and 11 and decreased above pH 11. It appeared that the base-catalyzed reaction, or deprotonation, occurred between pH 10 and 11.

The absorbance at 290 nm decayed by second-order kinetics. The pH dependence of the relative decay rates is shown in Fig. 4. The rates decreased above pH 10. The intermediates observed in the reaction of N_3 radicals also decayed by a similar second-order rate.

Determination of k(OH+cycloserine). The reaction rates of OH radicals with cycloserine were determined for solutions of various pHs by using the KCNS method.[10,11] The concentrations of cycloserine and KCNS used were 0.5 to 1.0×10^{-3} mol dm^{-3} and

1.0×10^{-3} mol dm^{-3}, respectively. The absorption due to the $(CNS)_2^-$ radical ions was measured at 475 nm. As the observed rates of growth of $(CNS)_2^-$ did not show simple first-order kinetics, the rate constants were evaluated by fitting the theoretical kinetic expressions to observed data. When the solution contained both cycloserine and CNS^-, the following competitive reactions occurred:

$$OH + CNS^- \xrightarrow{k_1} CNS + OH^-, \quad (1)$$

$$CNS + CNS^- \xrightarrow{k_2} (CNS)_2^-, \quad (2)$$

$$OH + \text{cycloserine} \xrightarrow{k_c} \text{product}, \quad (3)$$

where k_1, k_2, and k_c are the rate constants in these reactions. The time dependence of the concentration of $(CNS)_2^-$ after pulse is given by the following equation, which is derived from the competitive reaction mechanism involving Reactions 1, 2, and 3,

$$\{(CNS)_2^-\}_t = \frac{k_1'k_2'(OH)_0}{k_2'-(k_c'+k_1')}\left\{-\frac{e^{-(k_c'+k_1')t}}{k_c'+k_1'}+\frac{e^{-k_2't}}{k_2'} + \frac{k_2'-(k_c'+k_1')}{k_2'(k_c'+k_1')}\right\}, \quad (4)$$

where $k_1'=k_1(CNS^-)$, $k_2'=k_2(CNS^-)$, and $k_c'=k_c$(cycloserine), and $(OH)_0$ is the initial concentration of OH radicals which was estimated from the maximum absorbance at 475 nm reached after pulse in the solution without cycloserine. The values of k_1 and k_2 were determined by fitting Eq. 4 with $k_c'=0$ to the observed traces of the build-up signal in the solution containing only CNS^- ions. These values are $k_1=1.0\times10^{10}$ mol^{-1}dm^{3}s^{-1} and $k_2=6\times10^9$ mol^{-1}dm^{3}s^{-1}, respectively, which agreed well with reported values.[12] The values of the k_c's are determined by fitting Eq. 4 to the observed traces of growth in solutions containing CNS^- and cycloserine with various pHs. The results are listed in Table 1. The data of pH 12 was estimated by assuming the $k_1=1.0\times10^9$ mol^{-1}dm^{3}s^{-1}.[10] The rates obtained at pHs 8 to 11 are $1.2-1.3\times10^{10}$ mol^{-1}dm^{3}s^{-1}, and did not show the increase between 10 and 11 as observed in the formation rates in Fig. 3. The slightly slow rate obtained at pH 6.5 is reasonable because the net charge is zero at this pH.

Detection of Serine. The radiolytic yield of serine, G(serine), was determined to be 2.5 at pH 6.5—10, and 1.0 at pH 11. The yield of the decrease of cycloserine, G(−cycloserine), was also determined to be approximately 10.0 at pH<10. The IR spectra of the dried residues of the irradiated solution in which cycloserine mostly decomposed showed that the main product was D-serine.

Table 1. The rate constants of the reaction of OH radicals with cycloserine ($\times10^{10}$ mol^{-1}dm^{3}s^{-1})

pH	k_1	k_2	k_c
6.5	1.0	0.65	0.8
9.0	1.0	0.65	1.2
10.0	1.2	0.65	1.3
11.3	1.2	0.65	1.2
12.5	0.1		0.13*

* This value was calculated by the comparison of absorbances at 475 nm in the experiment for only CNS^- with that for CNS^-+cycloserine, assuming $k_1=1.0\times10^9$ mol^{-1}dm^{3}s^{-1} as calculated by Simic and coworkers.[1-3]

Discussion

Upon the irradiation of solutions containing N_3^- ions, N_3 radicals are known to be produced from a reaction of OH radicals with the N_3^- ions,[13] as follows:

$$N_3^- + OH \rightleftharpoons N_3 + OH^-, \quad k(N_3^- + OH) = 1.2\times10^{10}\ \text{mol}^{-1}\ \text{dm}^3\ \text{s}^{-1}. \quad (5)$$

It is also known that the reaction of N_3 radicals is exclusively one-electron oxidation and it is inert toward aliphatic H atoms, whereas the typical reaction of OH radicals is radical addition or H-atom abstraction. The intermediate, which is produced through one-electron oxidation of the isoxazolidinone ring by N_3 radicals, should be the isoxazolidinone radical (II) as described in Reaction 6.

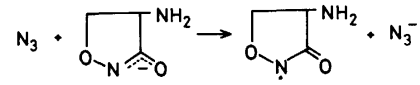

(6)

(II)

Under our experimental conditions, the production of N_3 radicals was completed within a pulse. The contribution of the absorption due to the N_3 radical (absorption maximum is 270 nm) to the transient spectra was negligible 10 μs after the pulse. Thus, the species responsible for the absorption band shown in Fig. 2 was the oxidized radical (II). Since the transient spectra at pH 8 to 10 shown in Fig. 1, where cycloserine exists as anion, are very similar to those in Fig. 2, we attributed the absorption band in Fig. 1 to the oxidized radical (II). Therefore, the site of attack of OH radicals was the dissociated peptide group, $-N^-CO-$, and the radicals were produced through one-electron oxidation by OH radicals. The spectrum at pH 6.5 was slightly different from others. Taking into account the slow k(OH+cycloserine), this would be induced by the lowered selectivity of OH radicals to the peptide group owing to the protonated amino groups, producing different species.

The absorbance at 290 nm in Fig. 1 and the rate of formation in Fig. 3 increased at the same pH range, pH 10—11, in the reaction of OH radicals, whereas these changes were not observed in the reaction with N_3 radicals. These results suggest that the change in the site of attack of OH radicals occur within this pH range. Since this pH range corresponds to the pK of the OH radical, $OH \rightleftharpoons O^- + H^+$, p$K$=11.9,[14] H-atom abstraction by O^- is expected to occur. As shown in Fig. 4, the rate of radical recombination was also found to decrease at this pH range, which suggested the formation of radical anions as intermediates in this pH region. There is one

possibility that the amino groups were attacked by O^- or OH radicals, producing the anion radicals, since dehydrogenation of N-H bonds by these radicals in aliphatic amines on γ-radiolysis[15] and in simple aminoacids on pulse radiolysis[16] in alkaline solutions has been reported. Taking into account the increase in the rate-of-formation of the intermediates, it is also conceivable that the dehydrogenation by OH or O^- radicals occurred on the carbon adjacent to the amino group. In this case, the amino groups may be prompted to deprotonate and the intermediates of anion form could be produced. It is known that the peptide hydrogen adjacent to a radical carbon can dissociate upon pulse radiolysis of the derivatives of 2,5-piperazindione, in which the pK value of the radical is 9.6.[3] The result that pH dependence was observed in the rates-of-formation of the oxidized radical, as shown in Fig. 3, whereas the values of k(OH+cycloserine) were independent of pH, as shown in Table 1, implies that the oxidized radicals observed in Fig. 1 were not formed immediately as the result of the attack of OH radicals, but were formed from a precursor, OH adducts of cycloserine, and therefore k(OH+cycloserine) represents the rate of the formation of OH adduct. This implication is supported by the fact that the rate-of-formation of the oxidized radicals did not change significantly in 10^{-2} mol dm^{-3} solutions.

As the oxidized radicals decayed by second-order kinetics, the reaction mechanism of these species was considered to be predominantly through radical-radical recombination. Probably, two oxazolidinone rings become linked through N atoms to lead to the formation of a hydrazine-type bond. This was assumed from the analogy with the previous report that the oxidation of *N*-acyl-*O*-alkylhydroxylamine, RCONHOR$^-$, resulted in the formation of a hydrazine-type compound through N-N coupling.[17]

In this experiment, the value of G(OH) was the sum of $G(e_{aq}^-)$ and the original G(OH), that is, 5.6. If the OH radicals react with cycloserine quantitatively and the decomposition of one hydrazine-type intermediate produce two serine molecules, G(serine) and G(−cycloserine) will be equal to G(OH). However, the radiolytic yield of serine was roughly a half of G(OH) and G(−cycloserine) was higher than G(OH). Thus, the one molecule of serine would be formed through the deomposition of one dimerized intermediate, and some additional cycloserine molecules would react secondarily with the entity which remained after the elimination of serine from the dimerized species.

On the basis of the above considereation, the whole reaction scheme of the radiolysis of the cycloserine anion by OH radicals can be described according to reactions (7) and (8) at a pH range from 8 to around 10:

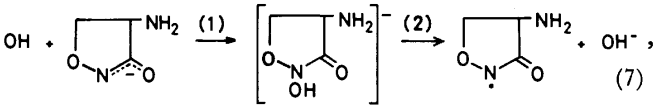

(7)

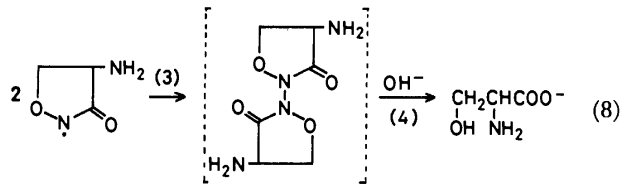

(8)

The rate constants of step (1) and (2) were 1.2×10^{10} mol^{-1}dm^{3}s^{-1} and $3-4\times10^6$s^{-1}, respectively. The second-order rate constant of step (3), $2k$, is equal to the products of the apparent rate constant, $2k'$, the molar extinction coefficinent of the oxidized radical (II) at 290 nm, ε_{290}, and the optical path length of the cell. The value of $2k'$ was 3×10^5s^{-1}, as shown in Fig. 4. The value of ε_{290} was roughly estimated to be 630 mol^{-1}dm^{3}cm^{-1} by using the absorbance of the oxidized radical in the reaction of N_3 radicals observed in Fig. 2 and the initial concentration of OH radicals which was estimated to be 5.6×10^{-5} mol dm^{-3} in the pulse of 100 Gy. The resulting rate constant of step (3) was $2k=3.8\times10^8$ mol^{-1}dm^{3}s^{-1} at pH range of 8 to 10.

It is considered that complex processes, such as the attack of OH or O^- radicals on multiple sites, may be occurring at a pH above or around 11.

The authors wish to thank Dr. Takeaki Enoto and Messers. Hiroaki Tanida and Koichi Sato for the help in operating the linac, and Miss Yumiko Misu for the analysis of aminoacids.

References

1) M. Simic, P. Neta, and E. Hayon, *J. Am. Chem. Soc.*, **92**, 4763 (1970).

2) M. Simic and E. Hayon, *Radiat. Res.*, **48**, 244 (1971).

3) E. Hayon and M. Simic, *J. Am. Chem. Soc.*, **93**, 6781 (1971).

4) R. Livingston, D. G. Doherty, and H. Zedes, *J. Am. Chem. Soc.*, **97**, 3198 (1975).

5) D. G. Doherty, R. Livingston, and H. Zedes, *J. Am. Chem. Soc.*, **98**, 7717 (1976).

6) A. Joshi, S. Rustgi, H. Moss, and P. Riesz, *Int. J. Radiat. Biol.*, **33**, 205 (1978).

7) H. Taniguchi and Y. Kirino, *J. Am. Chem. Soc.*, **99**, 3625 (1977).

8) a) F. A. Kuehl, F. J. Wolf, N. R. Trenner, R. L. Peck, E. Howe, B. D. Hunnewell, G. Downing, E. Newstead, R. P. Buhs, I. Putter, R. Ormond, J. E. Lyons, L. Chaiet, and K. Folkers, *J. Am. Chem. Soc.*, **77**, 2344 (1955).
b) P. H. Hidy, E. B. Hodge, V. V. Young, R. L. Harned, G. A. Brewer, W. F. Phillips, W. F. Runge, H. E. Stavely, A. Pohland, H. Boaz, and H. R. Sullivan, *J. Am. Chem. Soc.*, **77**, 2345 (1955).

9) J. W. Hunt and J. K. Thomas, *Radiat. Res.*, **32**, 149 (1967).

10) G. E. Adams, J. W. Boag, J. Current, and B. D. Michael, in "Pulse Radiolysis," M. Ebert, J. P. Keene, A. J. Swallow, and J. H. Baxendale, Ed., Academic Press, New York, N. Y., 1965, p. 133.

11) J. H. Baxendale, P. L. T. Bevan, and D. A. Scott, *Trans. Faraday Soc.*, **64**, 2389 (1968).

12) D. H. Ellison, G. A. Salmon, and F. Wilkinson, *Proc. Roy. Soc.*, **A328**, 23 (1972).
13) E. Hayon,and M. Simic, *J. Am. Chem. Soc.*, **92**, 7486 (1970).
14) J. Rabani and M. S. Matheson, *J. Am, Chem. Soc.*, **86**, 3175, (1964).
15) G. G. Jayson, G. Scholes, and J. J. Weiss, *J. Chem. Soc.*, **1955**, 2594.
16) P. Neta, M. Simic, and E. Hayon, *J. Phys. Chem.*, **74**, 1214 (1970).
17) J. H. Cooley, M. W. Mosher, and M. A. Khan, *J. Am. Chem. Soc.*, **90**, 1876 (1968).

 © 1984 The Chemical Society of Japan Bull. Chem. Soc. Jpn., 57, 3408—3412 (1984) [Vol. 57, No. 12

Mercury- and Cadmium-photosensitized Reactions of γ-Butyrolactone

Shunzo YAMAMOTO,* Shuzo MATSUDA, Chihiro OZAKI, Hiroshi TAKAHOSO, and Norio NISHIMURA
Department of Chemistry, Faculty of Science, Okayama University, 3-1-1, Tsushima-naka, Okayama 700
(Received May 1, 1984)

The mercury- and cadmium-photosensitized reactions of γ-butyrolactone have been compared. The products obtained in the two photosensitizations were quite different. The gaseous products from the mercury-photosensitized reaction were carbon dioxide, cyclopropane, and propylene, while the products obtained in the cadmium-photosensitized reaction were carbon monoxide and ethylene. This difference suggests that the decomposition of γ-butyrolactone takes place through different intermediates in the two reactions. Possible mechanisms are discussed.

Numerous studies of chemical reactions induced by excited atoms have been published. Cadmium-photosensitized reactions have often been compared with mercury-photosensitized reactions to obtain information about the detailed mechanism of the reaction. It is generally accepted that these reactions are the same by nature, and that a difference in quantum yields of products can be explained by the difference in their excitation energies.

We studied the mercury- and cadmiun-photosensitized reactions of γ-butyrolactone and found quite different products in these reactions. In a previous short communication,[1] we reported briefly the results of these studies. The present paper will report the details of the reactions.

Experimental

The mercury-photosensitized reaction was studied at 125 °C in a cylindrical quartz cell, 4cm in diameter and 10 cm long, fitted with plane quartz windows. A spiral quartz mercury discharge lamp filled with 670Pa Ar was used. The 184.9nm resonance line was filtered out by a Vycor filter. Light intensity absorbed by mercury atoms at 253.7nm was determined by ethylene actinometry.[2]

The cadmium-photosensitized reaction was studied at 300°C in a cylindrical Pyrex cell, 2cm in diameter and 20cm long. A U-shaped cadmium discharge lamp made of Pyrex, filled with 670Pa Ar, was used. Absorbed light intensity at 326.1nm was determined by *cis*-2-butene actinometry.[3]

Product analysis was done by fractionation at −196 and −60°C, and measurement with gas burette and gas chromatography, using a 12m column of VZ-7 (Gasukuro Kogyo Co., LTD) at 0°C.

γ-butyrolactone (Tokyo Kasei Ind., E.P. grade) was purified by trap-to-trap distillation. Liquid butyrolactone was injected into the cell by a microsyringe, and was fully degassed by many careful freeze-pump cycles. *cis*-2-Butene (Nihon Tokushu Gasu K. K., pure-grade) and N_2O (Nihon Sanso K. K., pure-grade) were used as supplied.

Results and Discussion

The Mercury-photosensitized Reaction. Since the vapor pressure of butyrolactone is low at room temperature, it is necessary to elevate the reaction temperature in order to obtain sufficient vapor pressure. The thermal decomposition of butyrolactone at 125°C was found to be negligible.

The major products were carbon dioxide, cyclopropane, and propylene, while carbon monoxide and hydrogen were minor products. These major products were also observed by Simonatis and Pitts[4] and Krull and Arnold,[5] in mercury-photosensitized reaction of γ-butyrolactone. These products are also those which originate from the triplet manifold of lactone in the direct photolysis.[4] This is reasonable, because sensitization by $Hg(^3P_1)$ is expected to give triplet lactone due to spin conservation.

Yields of Carbon dioxide, cyclopropane, and propylene increased linearly with reaction time and light intensity. This shows that carbon dioxide, cyclopropane, and propylene are primary products. Quantum yields of product formation are shown in Fig. 1 as a function of lactone pressure; the quantum yield of carbon dioxide is independent of lactone pressure, while that of cyclopropane increases and that of propylene decreases with increasing lactone pressure. The quantum yield of carbon dioxide was only 0.25, even at the lowest pressure examined. This suggests that most of the triplet lactone formed undergoes the other reactions. As no products volatile at −60°C were obtained except for carbon dioxide, cyclopropane, and propylene, the isomerization to succinaldehyde which was obtained in the direct photolysis of γ-butyrolactone[4] and the process that the triplet lactone loses its excitation energy without forming any products seem to be important.

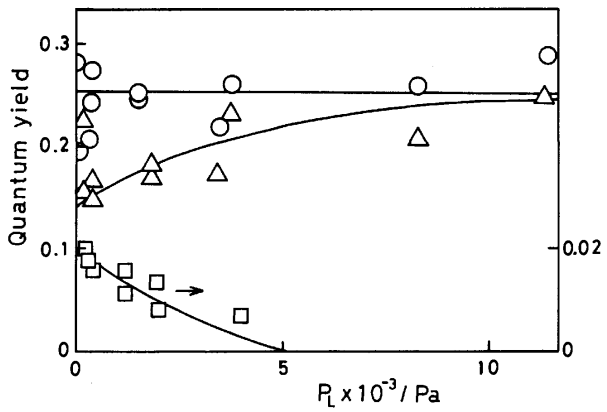

Fig. 1. Pressure dependence of quantum yields of CO_2 (○), cyclopropane (△), and propylene (□) in the mercury-photosensitized reaction of γ-butyrolactone.

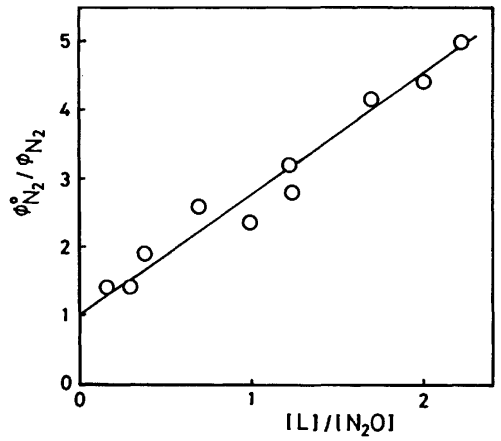

Fig. 2. Competitive quenching plots for lactone.

The quenching cross-section for lactone was obtained from competitive rates of the mercury-photosensitized reactions of lactone and N_2O. Figure 2 shows the competitive quenching plots for lactone. Yields of nitrogen from N_2O are expressed by the expression;

$$\frac{\phi^\circ_{N_2}}{\phi_{N_2}} = 1 + \beta\frac{[L]}{[N_2O]}, \tag{1}$$

where $\phi^\circ_{N_2}$ and ϕ_{N_2} are quantum yields in the absence and in the presence of lactone. The best straight line was obtained by the method of least squares. The quenching cross-section for lactone can be calculated by the following equation;[6]

$$\frac{\sigma^2_L}{\sigma^2_{N_2O}} = \beta\left(\frac{1+M_{Hg}/M_{N_2O}}{1+M_{Hg}/M_L}\right)^{-1/2}, \tag{2}$$

where $\sigma^2_{N_2O}$ is the cross-section for N_2O and we used the value of 18.0 Å^2. The value of 41 Å^2 for lactone was obtained and it can be compared with that for acetone (53 Å^2) and for acetoaldehyde (41 Å^2). In the presence of N_2O, the observed decrease in the quantum yield of cyclopropane agreeds with that expected from competitive quenching within the limits of experimental error.

The following set of reactions is proposed to explain our results:

$$Hg + h\nu\ (253.7\,nm) \longrightarrow Hg(^3P_1), \tag{3}$$

$$Hg(^3P_1) + L \longrightarrow Hg + {}^3L, \tag{4}$$

$${}^3L \longrightarrow CO_2 + C_3H_6^*, \tag{5}$$

$${}^3L \longrightarrow \text{other reactions}, \tag{6}$$

$$C_3H_6^* \longrightarrow CH_3CH{=}CH_2, \tag{7}$$

$$C_3H_6^* + L \longrightarrow \text{cyclo-}C_3H_6 + L. \tag{8}$$

Here, ^3L denotes triplet lactone and $C_3H_6^*$ is a "hot" cyclopropane intermediate. From this mechanism the quantum yields of products should be given by

$$\phi_{CO_2} = \frac{k_5}{k_5+k_6}, \tag{9}$$

$$\phi_{CH_2CH=CH_2} = \frac{k_5}{k_5+k_6}\frac{k_7}{k_7+k_8[L]}, \tag{10}$$

$$\phi_{\text{cyclo-}C_3H_6} = \frac{k_5}{k_5+k_6}\frac{k_8[L]}{k_7+k_8[L]}. \tag{11}$$

These equations explain the observed pressure dependence of the quantum yields.

The Reaction, L→cyclo-C_3H_6+CO_2, is endothermic by about 29 kJ mol^{-1}.[4] Since the excitation energy of $Hg(^3P_1)$ is 469 kJ mol^{-1}, the energy to be distributed among the products is greater than 440 kJ mol^{-1}. This value is almost the same as that estimated for the average energy transferred to the cyclobutanone molecule from the $Hg(^3P_1)$ atom.[7] Photosensitized reaction of cyclobutanone has been reported to yield vibrationally excited cyclopropane and carbon monoxide, and the former is known to isomerize to propylene. In this case a propylene/cyclopropane ratio of 0.58 at about 1330 Pa was obtained. As is shown in Fig. 1, however, propylene was only about one-fifteenth of the cyclopropane at the same pressure. In order to explain this difference, it is suggested that if triplet carbon dioxide (with an energy of about 356 kJ mol^{-1} [18]) is formed in Reaction 5, the energ content of cyclopropane would be greatly reduced, making the isomerization impossible. If the reaction, $^3L \rightarrow {}^3CO_2$+cyclo-C_3H_6 (5′), is added to the mechanism, the following relation can be derived.

$$\frac{\phi_{\text{cyclo-}C_3H_6}}{\phi_{CH_2CH=CH_2}} = \frac{k_{5'}}{k_5} + \left(1+\frac{k_{5'}}{k_5}\right)\frac{k_8}{k_7}[L] \tag{12}$$

From the intercept of the straight line shown in Fig. 3, a value of $k_{5'}/k_5$ of about 12 is obtained. Thus the reaction which produces excited carbon dioxide, is the main process. Simonaitis and Pitts also pointed out the possibility of the formation of triplet carbon dioxide in the direct photolysis of γ-butyrolactone at 210 to 260 nm.[4] A value of 3.45×10^{-4} Pa^{-1} for k_8/k_7 ratio is also obtaine from the intercept and the slope of the straight line. This gives the value of k_7 as 2.75×10^8 s^{-1} by adopting 9.5×10^4 s^{-1} as the kinetic collision frequency at 1 Pa and by assuming unit collisional deactivation efficiency for lactone. The excess energy of energized cyclopropane can be estimated by the equation given by Rabinovitch and Diesen:[9]

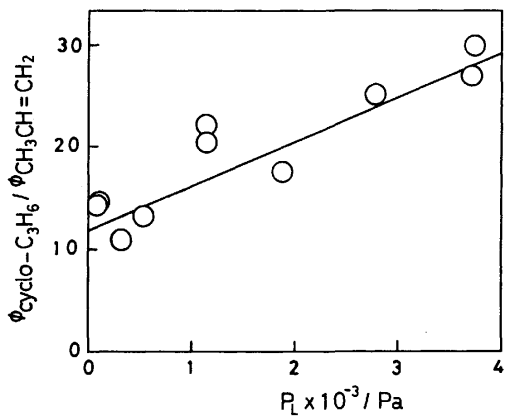

Fig. 3. Plots of $\phi_{\text{cyclo-}C_3H_6}/\phi_{CH_3CH=CH_2}$ against lactone pressure.

TABLE 1. COMPARISON OF EXCESS ENERGY OF CYCLOPROPANE

Compounds	Reactions	E / kJ mol^{-1}
γ-butyrolactone	Hg($^3P_1$)photosensitization	339
cyclobutanone	Hg($^3P_1$)photosensitization[a]	314±21
1-pyrazoline	direct photolysis(312.6 nm)[b]	314
tetrahydrofuran	direct photolysis(197.3 and 194.2 nm)[c]	331

a) Ref. 7. b) P. Cadman, H. M. Meunier, and A. P. Trotman-Dickenson, *J. Am. Chem. Soc.*, **91**, 7640 (1969). c) B. C. Roquitte, *J. Am. Chem. Soc,*. **91**, 7664 (1969).

$$k_7 = A'\left[\frac{E-E_0+a^+E_z^+}{E+aE_z}\right]^{s-1}. \quad (13)$$

Using experimental value of k_7 and substituting $A'=10^{15.80}s^{-1}$, E_0=262.4 kJ mol^{-1}, E_z=205.2 kJ mol^{-1}, E_z^+=179.1 kJ mol^{-1}, s=21, and a and a' which were obtained by being extrapolated from those given in Ref. (10), the value of E was found to be 339 kJ mol^{-1}. This corresponds to about 83% of the total energy (440 kJ mol^{-1}) to be distributed among the products. A comparison of the excess energy of cyclopropane in different systems is given in Table 1. As is shown in Table 1, the value of E in the present system is in fair agreement with those in other system, showing our result is reasonable.

The Cadmium-photosensitized Reaction. In the cadmium-photosensitized reaction, it is necessary to raise the reaction temperature to get a sufficient vapor pressure of cadmium. The thermal decomposition at 300 °C was found to give a small amount of carbon dioxide and cyclopropane, but not to give carbon monoxide and ethylene. The main products in the cadmium-photosensitized reaction were carbon monoxide and ethylene, quite different from those in the mercury-photosensitized reaction. To make sure that the difference between the two reactions is not owing to the difference in temperature, we examined the two reactions at the same temperature (235 °C), and obtained the same results as those obtained under the conditions mentioned above. If the triplet state of lactone lies at about 439 kJ/mol above the ground state, as Simonatitis and Pitts estimated,[11] it can not be formed by reaction of Cd($^3P_1$) which has energy of only 367 kJ mol^{-1}. This probably accounts for the difference between the mercury- and cadmium-photosensitized reactions of lactone. In the presence of a large pressure of nitrogen, oxetane was also observed.

Yields of carbon monoxide and ethylene increased linearly with reaction time, showing that those are primary products. The quantum yields of carbon monoxide and ethylene are shown in Fig. 4 as a function of lactone pressure. The yield of ethylene decreases a little more rapidly than that of carbon monoxide with increasing pressure.

When *cis*-2-butene was added to lactone, the quantum yields of the decomposition products decreased as the quantum yield of *trans*-2-butene formation increases. From the slope of the reciprocal plot of the quantum yield of *trans*-2-butene *vs.* the lactone/*cis*-2-butene ratio (Fig. 5), the quenching efficiency of lactone relative to that of *cis*-2-butene was estimated to be 0.92±0.10. This value is close to those for ethylene (1.03±0.09[12]), propylene (1.18±0.04[12]), and cyclopentanone (0.8±0.2[13]). Figure 6 shows the effect of *cis*-2-butene on the yields of carbon monoxide and ethylene. Solid line shows the relative quantum yields calculated using the relative quenching efficiency of lactone obtained above. As Fig. 6 shows, the decrease in the quantum yields of carbon monoxide and ethylene observed in the presence of *cis*-2-butene can be explained by competitive quenching of triplet lactone alone; *i.e.* the nature of the decomposition was not affected.

In order to explain the experimental results, the following set of reactions is proposed:

$$Cd(^1S_0) + h\nu\ (326.1\ nm) \longrightarrow Cd(^3P_1), \quad (14)$$

$$Cd(^3P_1) + L \longrightarrow CdL^*, \quad (15)$$

$$CdL^* \longrightarrow \cdot COCH_2CH_2CH_2O\text{-}Cd\cdot, \quad (16)$$

$$CdL^* \longrightarrow \text{other reactions}, \quad (17)$$

$$CdL^* + L \longrightarrow Cd + 2L, \quad (18)$$

$$\cdot COCH_2CH_2CH_2O\text{-}Cd\cdot \longrightarrow CO + \cdot CH_2CH_2CH_2O\text{-}Cd\cdot, \quad (19)$$

$$\cdot CH_2CH_2CH_2O\text{-}Cd\cdot \longrightarrow CH_2{=}CH_2 + CH_2O + Cd, \quad (20)$$

$$\cdot CH_2CH_2CH_2O\text{-}Cd\cdot + M \longrightarrow \underline{CH_2CH_2CH_2O} + Cd + M. \quad (21)$$

Here, CdL* stands for a transient complex between the excited cadmium atom and a lactone molecule, which is tentatively proposed to explain the difference between the mercury- and cadmium-photosensitized reactions of lactone. Formation of a similar complex between excited cadmium and saturated alcohols and ethers was suggested previously.[14] Formation of an O-Cd bond in Reactions 17 and 20 was assumed, because the excitation energy of Cd($^3P_1$) alone is not enough to produce biradicals $\cdot COCH_2CH_2CH_2O\cdot$ and $\cdot CH_2CH_2CH_2O\cdot$, as is shown in Table 2.

From this mechanism the following relation can be derived:

$$\frac{\phi_{CO}}{\phi_{C_2H_4}} = 1 + \frac{k_{21}}{k_{20}}[M]. \quad (23)$$

A plot of $\phi_{CO}/\phi_{C_2H_4}$ *vs.* lactone pressure is presented in Fig. 7, from which $k_{21}/k_{20}=1.3\times10^{-5}$ Pa^{-1}. The low value implies a relativly short lifetime for the biradical, $\cdot CH_2CH_2CH_2O\text{-}Cd\cdot$.

From the proposed mechanism, it is expected that the yield of oxetane should increases with increasing lactone pressure. We obtained only small amounts of oxetane in the pure lactone, and found that the yield was independent of lactone pressure. In the presence of a large pressure of nitrogen, however, we obtained

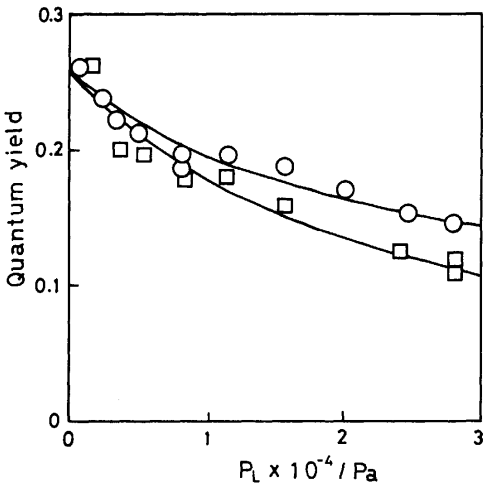

Fig. 4. Pressure dependence of quantum yields of CO (○) and ethylene (□) in the cadmium-photosensitized reaction of γ-butyrolactone.

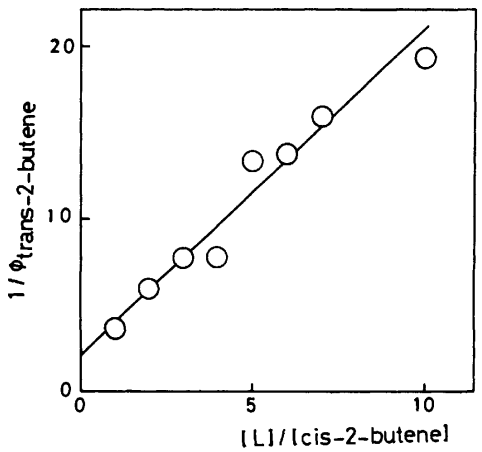

Fig. 5. Plots of the reciplocal of the quantum yield of *tran*-2-butene against the lactone/*cis*-2-butene pressure ratio.

a considerably more oxetane and found that the yield increased with increasing nitrogen pressure. These findings suggest that the biradical produced in Reaction 20 may react with lactone, limiting the yields of oxetane in the pure lactone.

In general, excitation of an ester molecule can be followed by any of three possible bond cleavages (processes I, II, and III); I and II would be indistinguishable for the usual experimental conditions, since radical decomposition (RCO_2 and R'OCO) would be very rapid.[15]

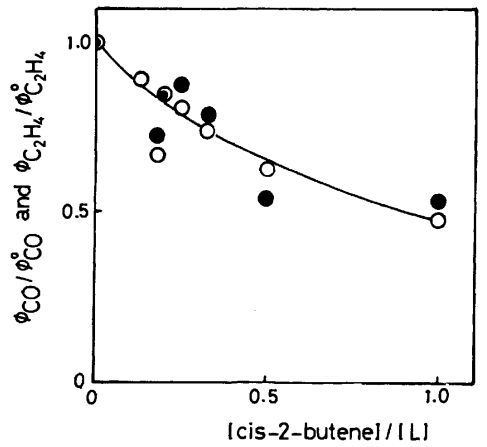

Fig. 6. Quantum yields of CO (○) and ethylene (●) in the cadmium-photosensitized reaction of γ-butyrolactone in the presence of *cis*-2-butene.

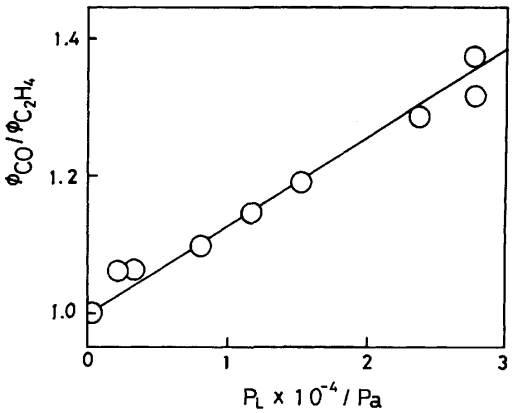

Fig. 7. Plots of $\phi_{CO}/\phi_{C_2H_4}$ against lactone pressure.

RCOOR' + $h\nu$

$\longrightarrow$ RCO_2 + R' ($\longrightarrow$ R + CO_2 + R'), I

$\longrightarrow$ R + CO_2R' ($\longrightarrow$ R + CO_2 + R'), II

$\longrightarrow$ RCO + OR' ($\longrightarrow$ R + CO + OR'). III

Mercury-photosensitized reaction of lactone seems to proceed by process I and/or II, while cadmium-photosensitized reaction seems to proceed by process III. The bond dissociation energies of some bonds in lactone were estimated by thermochemical data given by Benson:[16]

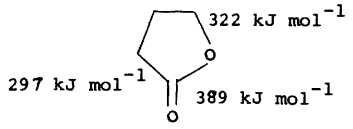

TABLE 2. ENTHALPY CHANGES FOR SOME REACTIONS BETWEEN γ-BUTYROLACTONE AND $Cd(^3P_1)$[a]

Reaction		ΔH / kJ mol^{-1}
$CH_2CH_2CH_2OCO+Cd(^3P_1)$	$\rightarrow \cdot COCH_2CH_2CH_2O\cdot+Cd$	22.2
	$\rightarrow \cdot COCH_2CH_2CH_2O\text{-}Cd\cdot$	−350.3
	$\rightarrow CO+\cdot CH_2CH_2CH_2O\cdot+Cd$	56.9
	$\rightarrow CO+\cdot CH_2CH_2CH_2O\text{-}Cd.$	−315.6

a) We used the value of 372.5kJ mol^{-1} for the bond energy of Cd-O. J. C. Bailar, H. J. EMeteus, Sir Ronald Nyholm, and A. F. Trotman-Dickenson, "Comprehensive Inorganic Chemistry," Vol. III, Pergamon Press, Oxford (1973).

It is easy to understand the mercury-photosensitized reaction of lactone, since the excitation energy of $Hg(^3P_1)$ is sufficiently large. Although the excitation energy of $Cd(^3P_1)$ is smaller than the bond energy of CO–O, the CO–O bond must break at first to produce carbon monoxide. Therefore, we assumed formation of an O–Cd bond in Reaction 16.

References

1) S. Yamamoto, S. Matsuda, C. Ozaki, and N. Nishimura, *Chem. Lett.*, **1981**, 1233.
2) B. deB. Darwent, *J. Chem. Phys.*, **20**, 1673 (1952).
3) S. Tsunashima and S. Sato, *Bull. Chem. Soc. Jpn.*, **41**, 284 (1968).
4) R. Simonaitis and J. N. Pitts, Jr., *J. Phys. Chem.*, **75**, 2733 (1971).
5) I. S. Krull and D. R. Arnold, *Tetrahedron Lett.*, **1969**, 1247.
6) R. J. Cvetanovic, "Mercury Photosensitized Reactions," Progress in Reaction Kinetics, Vol. 2, ed by G. Porter, The Macmillan Co., New York, 1964, p. 39.
7) D. C. Montague and F. S. Rowland, *J. Am. Chem. Soc.*, **91**, 7230 (1969).
8) M. A. A. Clyne and B. A. Thrush, *Proc. Roy. Soc., Ser. A.* **269**, 404 (1962).
9) B. S. Rabinovitch and R. W. Diesen, *J. Chem. Phys.*, **30**, 735 (1959).
10) D. W. Setser and B. S. Rabinovitch, *Can. J. Chem.*, **40**, 1425 (1962).
11) R. Simonaitis and J. N. Pitts, Jr., *J. Am. Chem. Soc.*, **90**, 1389 (1968).
12) S. Tsunashima, S. Satoh, and S. Sato, *Bull. Chem. Soc. Jpn.*, **42**, 329 (1969).
13) S. Tsunashima, O. Ohsawa, C. Takahashi, and S. Sato, *Bull. Chem. Soc. Jpn.*, **46**, 83 (1973).
14) S. Yamamoto, K. Tanaka, and S. Sato, *Bull. Chem. Soc. Jpn.*, **48**, 2172 (1975).
15) J. G. Calvert and J. N. Pitts, Jr., "Photochemistry," Wiley, New York, N. Y. 1966. p. 434.
16) S. W. Benson and H. E. O'Neal, "Kinetic Data on Gas Phase Unimolecular Reactions," NSRDS-NBS 21 U. S. 1970.

 © 1984 The Chemical Society of Japan Bull. Chem. Soc. Jpn., 57, 3413—3418 (1984)

Colloid Chemical Studies on the Aggregation of Phospholipid Vesicles with Metal Cations

Kunio FURUSAWA,* Hiroyuki KAKOKI, and Hideo MATSUMURA†
The University of Tsukuba, Department of Chemistry, Sakura-Mura, Ibaraki 305
†*Electrotechnical Laboratory, Sakura-Mura, Ibaraki 305*
(Received May 22, 1984)

Aggregation behavior of phosphatidylethanolamine (PE) and Phosphatidylserine (PS) vesicles that have resulted with various metal cations, has been studied to determine their adsorption characteristics. The critical flocculation concentration of these cations for both vesicles was determined by two techniques, *i.e.*, by the kinetic method in which the rate of flocculation was measured turbidimetrically, and by the traditional static method. The results have been analysed by the usual stability concept in the colloid chemistry, and these analyses revealed that there are two mechanisms in the vesicle aggregation. One is the charge neutralization of the polar groups on the vesicle surface, which is induced by the adsorption of multivalent cations (Th^{4+}, La^{3+}), and the other is the interparticle binding (or the interparticle bridging) caused by the divalent cations (Ca^{2+}, Mg^{2+}).

The importance of the interaction of metal cations with natural membranes has been pointed out by many authors in connection with ion permeability through membranes,[1] membrane stability[2-4] and ion adsorption on the membranes,[5] *etc.* In order to obtain some insight into the mechanism of ionic interaction with biological membranes, several authors have investigated the surface potential of monolayers[6,7] made of phospholipids in various ionic environments. Bangham *et al.*[8] observed the different effects of various divalent cations on the surface potential of acidic phospholipid monolayers. Mclaughlin *et al.*[9] obtained the association constants of various divalent cations by measuring the conductance of phosphatidylserine membranes. Barton[10] determined the degree of divalent cation association with phosphatidylserine membranes by measuring the electrophoretic mobility of phospholipid vesicles.

Only a few colloid chemical studies on the aggregation of phospholipid vesicles have been reported. It has generally been observed that acidic phospholipid vesicles, such as phosphatidylserine and phosphatidylethanolamine vesicles, are very sensitive to multivalent cations;[11,12] the addition of relatively small amounts of cations can cause them to aggregate. In this study, the aggregation behavior of phosphatidylethanolamine and phosphatidylserine vesicles have been studied using various metal cations as coagulants and the experimental results have been analysed by the stability concept in the colloid chemistry.[13]

The concentration of the counter ions required to aggregate the colloidal dispersion is called the critical flocculation concentration(CFC) or flocculation value (C_{CFC}). The CFC depends on a number of factors, such as the nature of colloid particles, the surface charge, the double layer thickness of the particles, and the valence and nature of the counter ions. The procedures for measuring the CFC can be divided into (1) the kinetic method and (2) the static method. In the kinetic method, the initial rate of aggregation is measured turbidimetrically as a function of the concentration of the coagulation agent at which further increase of the coagulant produces no further speeding up of the aggregation process. For a better understanding of colloid stability, measurements in the period immediately after mixing were indispensable because these results are more suitable to interpretation in terms of the particle-particle interaction than those obtained by the static method.

In the static method, a row of glass tubes including the colloidal suspension is prepared, increasing amounts of the coagulant are added and the CFC is determined after waiting a few hours. This method has the drawback that the stability criterion is somewhat arbitrary, but the advantage is that, if properly done, a time scale can be used to attain adsorption equilibrium between the colloidal particles and the coagulation agent. The turbidimetric titration technique can be regarded as a static method, if the titrants are added slowly to attain the adsorption equilibrium.

In this work, two types of measurement on the CFC of the phospholipid vesicles have been undertaken, and the resulting data have been analysed systematically. From these analyses, it appeared that these two techniques give independently important knowledge on the interaction of metal cations with phospholipid membrane.

Experimental

Materials. Bovine brain phosphatidylethanolamine (PE) and phosphatidylserine(PS) were used as the phospholipids which were purchased from Sigma Chemical Co., Ltd (U. S. A.). Other reagents used were of an analytical grade. All the solutions of these materials were made with deionized and doubly distilled water.

Vesicle Preparation. PE and PS vesicles were prepared by the sonication method at 4°C without using any buffer to reduce the spurious effects of the included buffer ions.[14] After the removal of the undispersed materials by the centrifugation (26000g, 1h), the dispersion was filtered through a membrane filter (0.1 μm pore size).

Turbidimetric Titration. Turbidimetric titration was carried out at 25°C under a nitrogen atmosphere using a Hirama automatic recording titrator (Tokyo Japan). The

transmittance (or turbidity) of the vesicle dispersion (30 ml, $1-8\times10^{-2}$ g/dl) was measured at the wavelength of 517 nm. The titrant solution (0.01—0.3 mol dm^{-3} salt solution) was added very slowly (0.01 ml/min) to the vesicle dispersion to attain the adsorption equilibrium between the vesicle surface and the titrant ions. As the titration proceeds, the dispersion begins to become turbid, and the transmittance reaches a minimum at a certain titrant volume (V_{min}) from which we have calculated the CFC on each condition.[12]

Measurements of Aggregation Rate. A Union stopped-flow spectrophotometer (Tokyo, Japan) with a 1 cm path length cell was used in the measurements. In this apparatus, the liquids to be mixed are contained in two syringes. By using a pressure actuator, equal volumes (1.5 ml) of each solution are reproducibly mixed within a very short time (10 ms). The turbidity of the mixture can be recorded on an attached recorder and the initial slope of the optical density (A) *vs.* time (t) curves can be measured. The CFC-value can be determined by plotting the logarithm of the reciprocal slope (log dt/dA) against log c, where c is the coagulant concentration. The measurements are carried out at room temperature and at a wavelength of 517 nm.

Electrophoresis. The electrophoretic mobilities of large vesicles were determined at various pH values in an aqueous solution at 25 °C. The measurements were performed in a Rank brother micro-electrophoretic apparatus (MK-2) using a rectangular glass cell.

Adsorption Experiments. Ten ml of vesicle dispersion (0.05 g/dl) were mixed with the various salt solutions containing different ion concentrations and left standing for one night at 25 °C. Only the vesicle particles were separated from the medium by ultrafiltration (Millipore PTGC) and the concentration of metal cations remaining in the filtrate as well as in the initial solution was measured analytically by means of the Inductively Coupled Argon Plasma Method (Jarrell-Ash 975). From the difference in the concentration before and after the adsorption process, the amounts of adsorption per unit of the vesicle weight (Ap) were calculated.

Membrane Potential Measurements. Monolayers of phospholipids were prepared by spreading chloroform–methanol (3:1) solution of phospholipid on the surface of subphase solution at the neutral pH in 80 ml Teflon trough. After a concentrated salt solution containing the metal cations was added to the subphase solution, the subphase solution was stirred for more than 30 min with a glass-sealed needle (5 mm length) by means of a magnetic stirrer. Thereafter, the surface potentials of the monolayer were measured as a function of salt concentration with a vibrating electrode against an Ag–AgCl reference electrode. All the monolayers used in these experiments have a packing density of 1/60(molecule/Å).

Results and Discussion

Static Method. In Fig. 1, some typical turbidimetric titration curves of PS vesicles with an added $ThCl_4$ aqueous solution are shown as a result of changing the vesicle concentration (C_p). As the titration proceeds, the vesicle dispersion begins to become turbid and the transmittance reaches a minimum at a certain titrant volume (V_{min}), from which we can calculate the CFC for each condition by connecting for the total volume of the sample solution and the added titrant. The V_{min} (or CFC)-value is much dependent on the C_p and the plot of the V_{min} (or CFC) against the C_p shows a straight line passing through the origin as shown in Fig. 2. This indicates that PS vesicles are quantitatively coagulated with Th^{4+} ions. We previously found that phosphatidylcholine (PC) vesicles are also coagulated quantitatively with trimethylammonium glycol-chitosan iodide (TAGC) and concluded that the vesicle coagulation with TAGC is based on a new salt-linkage formation between the phosphate group of PC and the trimethylammonium group in TAGC.[15] From the colloid chemical aspect, this phenomena can be explained as follows: The negative charge on the vesicle particle is neutralized by the adsorption of Th^{4+} ions, and the vesicle particles with zero-charge start to coagulate by the London-Vander Waals attraction forces.[13] In Fig. 2, a relation between the CFC and the C_p of PE vesicles is also plotted. A comparison of these two curves, reveals that the CFC for PS vesicles is always higher than the value of PE vesicles at a constant C_p. This difference will be based on the molecular structure of these phospholipids; the PS molecule has two species of the acidic polar groups (carboxyl and phosphate groups), and the PE molecule has only one group (phosphate group). Therefore, to complete the charge neutralization of the PS molecule, twice the number of cations will be necessary compared to

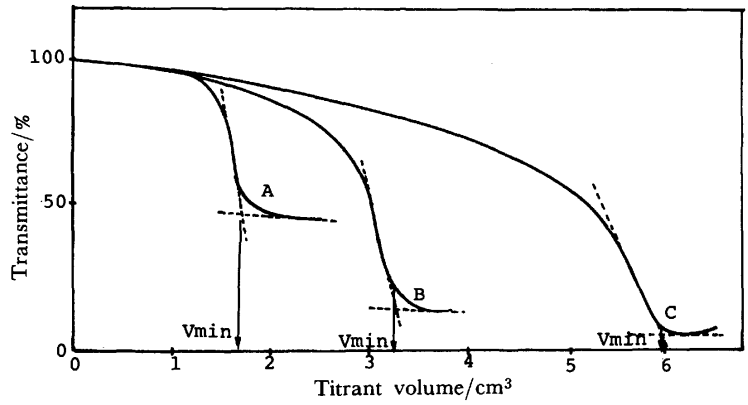

Fig. 1. Typical turbidimetric titration curves of PS vesicles with $ThCl_4$ solution. A: C_p=0.014 g/dl, B: C_p=0.0423 g/dl, C: C_p=0.0750 g/dl.

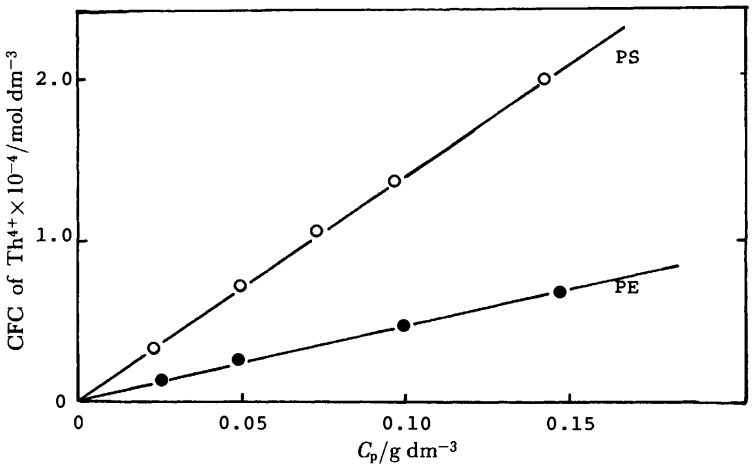

Fig. 2. Relations between the CFC of $ThCl_4$ and the C_p of PS and PE vesicles (pH 4.0).

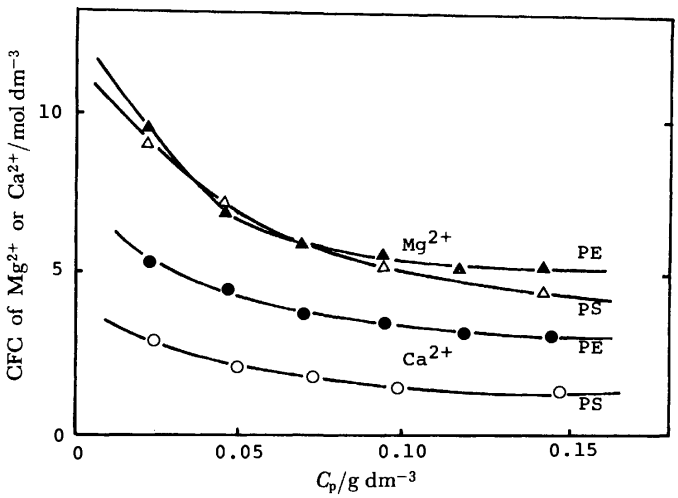

Fig. 3. Relations between the CFC of divalent cations and the C_p of PS and PE vesicles (pH 4.0).

the PE molecule. The tendency of Fig. 2 accords approximately with this assumption, and indicates again that the vesicle coagulation in these systems will be based on the charge neutralization of polar groups on the vesicle surface.

In Fig. 3, the relations between the CFC of divalent cations and the C_p of PE and PS vesicles are plotted. In contrast to Fig. 2, all the curves are decreasing with increasing the C_p. It means that a vesicle suspension with a high C_p can be coagulated by a lower salt solution than the suspension with a low C_p. Furthermore, the relation between the CFC-values of PE and PS vesicles is the reverse of the relation in Fig. 2. These results will oblige us to adopt a different coagulation mechanism from one in Fig. 2. The new mechanism will be an interparticle binding (or an interparticle bridging) caused by the addition of a divalent cation. Existense of the new mechanism is also confirmed by observation of the vesicle aggregates formed by the addition of the various metal cations, *i.e.*, the aggregates formed by Th^{4+} are compact and relatively small flock, while the aggregates formed by Ca^{2+} are large and loose in structure. The existence of two such aggregation mechanisms will be based on the different binding affinity of the added metal cations. Figure 4 shows the initial slope of adsorption isotherms of various metal cations to PE vesicles. The

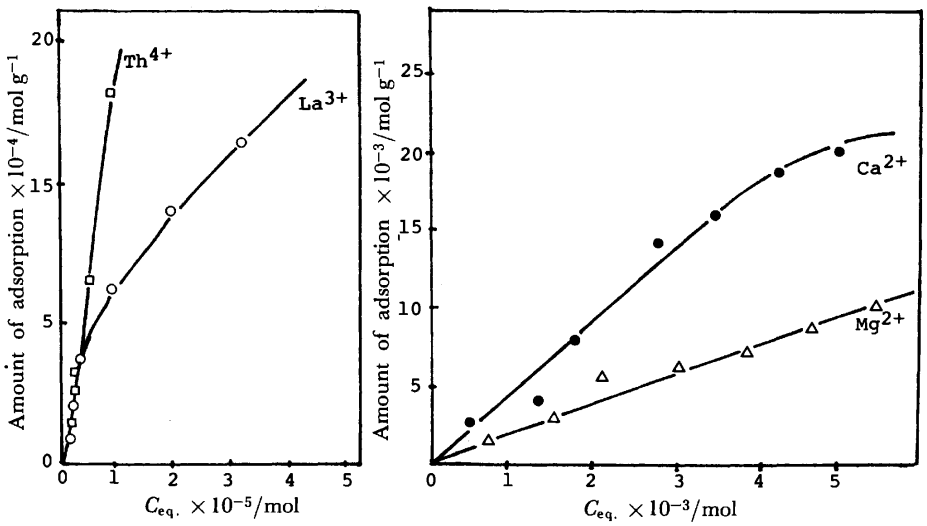

Fig. 4. Initial slope of adsorption isotherms of various metal cations to PE vesicles.

affinity is much dependent on the valence of the cation and especially Th^{4+} and La^{3+} ions show high affinities. From a comparison of Fig. 4 with Fig. 2(or Fig. 3), it is apparent that Th^{4+} or La^{3+} ion with a high adsorption affinity causes the vesicle aggregation due to the charge neutralization, and Ca^{2+} or Mg^{2+} ion with a moderate affinity brings to the aggregation based on the interparticle bridging. In the latter mechanism, the aggregation efficiency will increase by increasing the particle concentration, which is the same tendency with the result found in Fig. 3. Furthermore, this analysis explains reasonably the difference of coagulation behavior of Ca^{2+} and Mg^{2+} ions (see Fig. 3), *i.e.*, Ca^{2+} will make a bridge in higher efficiency than Mg^{2+} by its high adsorption affinity and such a tendency will appear definitely on PS vesicles with two acidic groups. Thus, Ca^{2+} ion has a lower CFC than Mg^{2+} ion, especially for PS vesicles.

Kinetic Method. Figure 5 shows some typical curves of optical density (A) *vs.* time (t), obtained by adding $CaCl_2$ aq solution to PE vesicles. In this figure, the salt concentrations indicated are the final concentrations after mixing by the stopped-flow method. It is clear from these curves that the initial portions are sufficiently linear in agreement with theoretical expectations.[16] The deviation from linearity is due to the non validity of the assumption that the scattering from aggregates is the same as that from spherical particles of the same total weight. By increasing the salt concentrations, the initial slope increases until finally a maximum region is attained where the coagulation rate becomes independent over the wide range of salt concentrations. The CFC is easily determined by plotting the logarithm of the reciprocal slope at the initial time (log dt/dA) which is proportional to the theoretical stability ratio,[13] against log c, where c is the coagulant concentration. In Fig. 6, the plots of log dt/dA *vs.* log c are given for PE and PS vesicles using $CaCl_2$ as the coagulant. The curves obtained are not of the forms predicted by the simple stability theory. They are linearly decreasing in the slow coagulation range and, after staying at a minimum value, they increase again in the high concentration region of $CaCl_2$. Each inflection point in the slow coagulation range is nearly equal to the CFC obtained from the turbidimetric titration.

The occurrence of the minimum stability ratio can be explained in terms of the interparticle bridging of Ca^{2+} ion, because the particle coagulation due to the bridging is a bimolecular process, the rate must be proportional to the product, $\theta(1-\theta)$, of the fraction of covered (θ) and uncovered ($1-\theta$) with adsorbed Ca^{2+} ions.[17] As may be seen in Fig. 6, the experimental points for both vesicles lie within experimental error on a parabola, corroborating the bimolecular coagulation,[18] *i.e.*, the rapid coagulation rate in the middle concentration region, changes again to the slow rate to lose the fraction of uncovered particle. The difference in

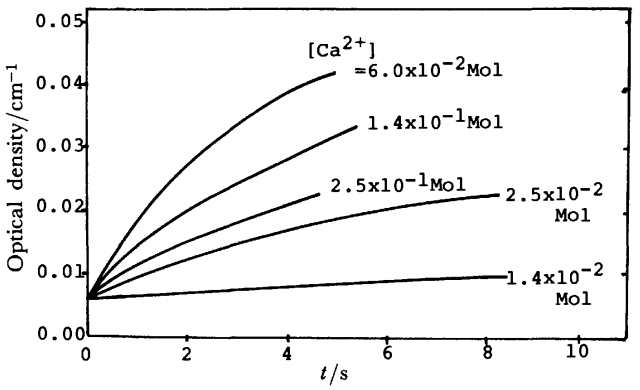

Fig. 5. Optical density (A) *vs.* mixing time curves for PE vesicles.

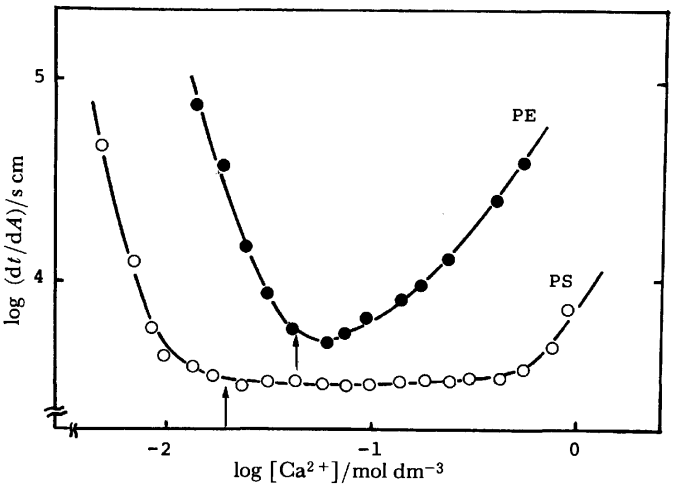

Fig. 6. Plots of logdt/dA *vs.* log[Ca^{2+}] for PE and PS vesicles (pH 4.0)

the stability curves of PE and PS vesicles in Fig. 6, may be explained by the different adsorption capacities of Ca^{2+} for both vesicles. In other words, the number of adsorption sites on PS vesicles is more than the site on PE vesicles. This is testified by the measurements of membrane potential for PE and PS monolayers. Figure 7 shows the membrane potential change (ΔV) of both monolayers with respect to the $CaCl_2$ concentration. Increasing the $CaCl_2$ concentration induces a gradual increase in ΔV and above 5×10^{-2} mol, the ΔV attains respective plateaus which will be proportional to the number of adsorption sites of Ca^{2+}. As may be seen from Fig. 7, the number of sites on the PS membrane is about double number of sites on the PE monolayer, which is an essential reason why PE and PS vesicles would take different aggregation behavior. Further, the detailed analysis between the experimental points of stability and the theoretical curve, will be discussed in the next paper of this series.

In Fig. 8, the stability curves for PE and PS vesicles using $LaCl_3$ are given. The curves of stability, especially for PS vesicles, have a form predicted from the simple stability theory,[19] *i.e.*, it is linear in the slow coagulation range and becomes parallel to the abscissa in the rapid coagulation range. However, the stabil-

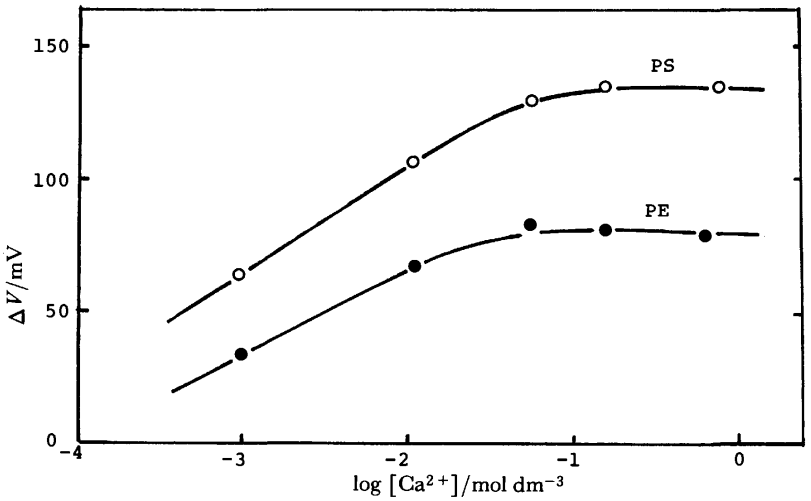

Fig. 7. Membrane potential change (ΔV) of PS and PE monolayers with $CaCl_2$ concentrations (pH 6—pH 8, 25°C).

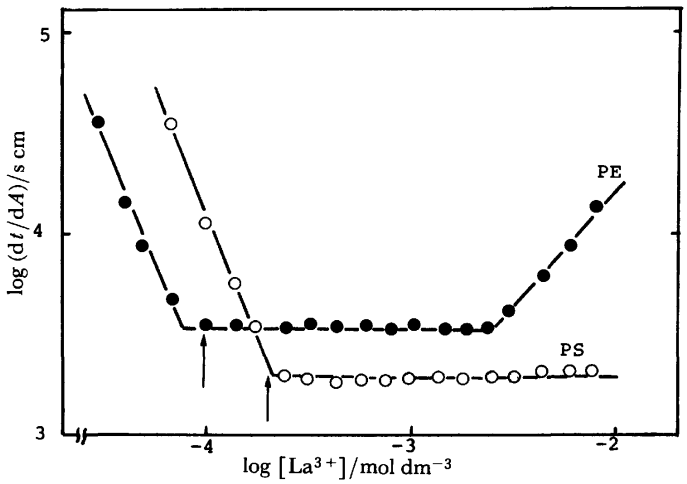

Fig. 8. Plots of log dt/dA *vs.* log[La^{3+}] for PE and PS vesicles (pH 4.0).

ity curve for PE vesicles has a slightly different form from the curve for PS vesicles, and is scarcely increased again in the high concentration region of the salt. As the vesicle coagulation with $LaCl_3$ is based on charge neutralization of polar groups on the surface, this difference between PE and PS vesicles in Fig. 8, must be explained in terms of electrostatic interaction between the particles. Figure 9 shows of zeta-potential *vs.* log molar concentration of $LaCl_3$ for PE and PS vesicles. As the concentration of $LaCl_3$ increases, the zeta-potential gradually decreases with the different slope in PE and PS vesicles; PS vesicles kept slightly negative values until the concentration of 1×10^{-2}mol $LaCl_3$, while, PE vesicles approach to zero and finally become to positive zeta-potential at the same $LaCl_3$ concentration. These electrophoretic results for PE vesicles suggest that the stability behavior in Fig. 8 is due to the reversal of vesicle charge. On the other hand, PS vesicles hardly reverse their electric sign and continue a low stability value over the wide range of $LaCl_3$ concentrations.

In conclusion, it may be said that the usual coagulation technique in the colloid chemistry is the best suitable for studying the properties of the membrane surface, and this gives important knowledge on the conformation and functionality of the polar head groups on the surface of the membrane.

References

1) S. G. McLaughlin, G. Szabo, G. Eisenman, and S. M.

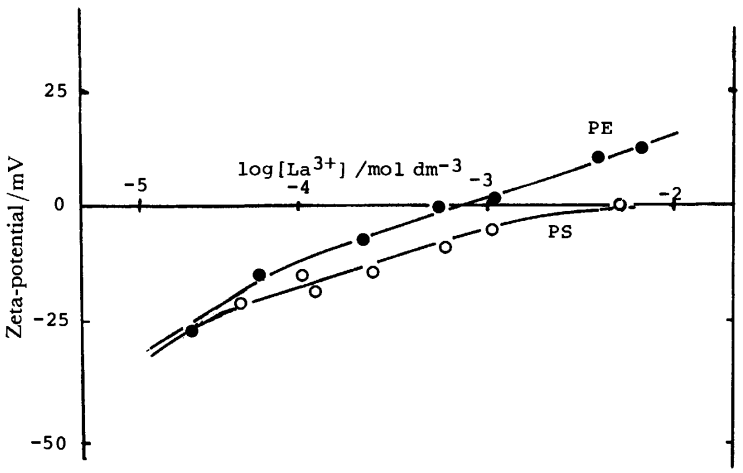

Fig. 9. Zeta-potential *vs.* log[La^{3+}] curves of PE and PS vesicles (pH 4.0, 25°C).

Ciani, *Proc. Natl. Acad. Sci. (U. S. A.)*, **67**, 1268 (1970).
2) V. A. Parsegian, *Trans. Faraday Soc.*, **62**, 848 (1966).
3) D. Gingell, *J. Theor. Biol.*, **17**, 451 (1967).
4) H. Trauble and H. Eibl, *Proc. Natl. Acad. Sci. (U. S. A.)*, **71**, 214 (1974).
5) D. H. Haynes, *J. Membrane Biol.*, **17**, 341 (1974).
6) S. Ohki and R. Sauve, *Biochim. Biophys. Acta*, **449**, 451 (1976).
7) C. Colacicco, *Chem. Phys. Lipid*, **10**, 66 (1973).
8) A. D. Bangham and D. Papahadjopoulos, *Biochim. Biophys. Acta*, **126**, 181 (1966).
9) S. G. McLaughlin, G. Szabo, and G. Eisenman, *J. Gen. Physiol.*, **58**, 667 (1973).
10) P. G. Barton, *J. Biol. Chem.*, **243**, 3884 (1968).
11) K. Furusawa, H. Kakoki, and T. Takei, *Nippon Kagaku Kaishi*, **1984**, 992.
12) S. Fujii, E. Kokufuta, and K. Furusawa, *Chem. Lett.* **1978**, 555.
13) E. J. W. Verwey and J. Th. G. Overbeek, "Theory of the Stability of Lyophobic Colloids," Elsevier, Amsterdam (1948).
14) K. Furusawa, N. Onda, E. Kokufuta, S. Fujii, and T. Takei, *Nippon Kagaku Kaishi*, **1980**, 506.
15) S.Fujii, E. Kokufuta, and K. Furusawa, *Chem. Lett.* **1978**, 1049.
16) A. Troelstra and H. R. Kruyt, *Kolloid-Z.*, **101**, 182 (1946).
17) V. K. Lamer and T. W. Healy, *Rev. Pure Appl. Chem.*, **13**, 112 (1963).
18) G. J. Fleer and J. Lyklema, *J. Colloid Interface Sci.*, **55**, 228 (1976).
19) H. Reerink and J. Th. G. Overbeek, *Disc. Faraday Soc.*, **18**, 74 (1954).

The Dispersion Stability of Colloidal Particles in Dioxane-Water Mixtures

Kazuhiko KANDORI,* Kijiro KON-NO, and Ayao KITAHARA
Department of Industrial Chemistry, Institute of Surface and Colloid Chemistry, Science University of Tokyo, Kagurazaka 1-3, Shinjuku-ku, Tokyo 162
(Received May 24, 1984)

The dispersion stability of titanium dioxide particles and two kinds of iron(III) oxide particles in dioxane-water mixtures was studied as a function of the dielectric constant(ε=2.2—78). The sedimentation of dispersions, the adsorption of sodium 1,2-bis(2-ethylhexyloxycarbonyl)ethanesulfonate (Aerosol OT or AOT) on the particles, and the zeta potential were measured. In the absence of AOT, the dispersions of all the particles were rapidly flocculated over all of the region of the dielectric constant, and little effect of the dielectric constant on the dispersibility was observed. In the presence of AOT, however, the dispersions of all the kinds of particles used were stabilized at both the lower(ε=2.2) and higher(ε=60—78) regions of the dielectric constant by the adsorption of AOT on the particles. However, the flocculation was accelerated for all kinds of particles, and AOT molecules were not at all, or scarcely, adsorbed on the particles in the middle region of the dielectric constant(ε=10—50). This behavior of the dispersibility corresponded with the results of the dynamic light scattering of the AOT solution, which reveal the aggregation of AOT molecules at various dielectric constants. The zeta potential changed from a positive sign to a negative sign with the increase in the dielectric constant, and the isoelectric dielectric point (IED), which means a zero value of the zeta potential, appeared. The order of the values of IED among the three kinds of particles agrees with the order of the isoelectric points(IEP) of the particles. This result can, therefore, be explained by the concept of the acid-base interaction between a particle and a solvent in dioxane-water mixtures.

The theory of the stability of colloidal dispersions in water based on the DLVO theory[1] has been extended to that in nonpolar organic media, and many data on the stability in nonpolar organic media have been accumulated for spherical particles, such as titanium dioxide.[2-7] On the other hand, the dispersion stability of pigments in polar organic media, (*e.g.*, magnetic paints) has recently drawn much attention. The dispersibility of the needle-like particles of iron oxide is very important for magnetic paints. The present authors have previously studied the stability of dispersions of magnetic and nonmagnetic iron(III) oxides and carbon-black particles in 2-butanone as a polar organic medium.[8-11] However, it is difficult to explain the dispersion stability of colloidal particles in several polar organic media, because there are some differences in the characteristics, *i.e.*, the dielectric constant, the solubility parameter, the viscosity, the density, and so on. Lyklema *et al.* have investigated the properties of the electric double layer of the silver iodide particles in a water-ethylene glycol mixture by means of the parameter of the dielectric constant.[12-14] In their study, the dielectric constant, however, was only varied between 38 and 78, and the dispersion stability in the region of low dielectric constants, especially in nonpolar organic media, was not discussed.

In this paper, the dispersions of two kinds of needle-like particles of Fe_2O_3-A, B and the spherical particle of TiO_2 for comparison in dioxane-water mixtures were used in order to discuss the effect of AOT as a dispersant. The dielectric constant of dioxane-water mixtures has been reported by Fuoss *et al.*[15] Systems of dioxane-water mixtures have various advantages; for example, water and dioxane mix in all proportions, so that it is possible to connect the aqueous and nonaqueous (nonpolar) systems.

Experimental

Materials. Two kinds of needle-like iron(III) oxides, A and B, and spherical titanium dioxide (Ishihara Sangyo Co., NR, rutile-type) were used. The two kinds of iron(III) oxides A and B, were prepared according to the references.[16-18] The properties of these three samples are shown in Table 1. They were purified by washing with solvents[8-11] and stored in a desiccator before use.

The dioxane used as a solvent was purified and dried from the GR-grade sample as usual and finally treated with Molecular Sieve 4A to remove any trace of water. The deionized water was distilled in Pyrex glass. The conductivity of the water used was less than 1×10^{-6}mho·cm^{-1}. The AOT used as a dispersant was purified according to an extraction method using a mixture of solvents.[19]

Preparation of Dispersions. The dispersions in media of

TABLE 1. PROPERTIES OF THREE KINDS OF PARTICLES

Sample	Class	Shape	Specific surface area (m^2/g)	Axis length or diameter (Å)	Density (g/cm^3)
Fe_2O_3-A	α-Fe_2O_3	Needle	108	1610×142	3.9
Fe_2O_3-B	α-Fe_2O_3	Needle	10.3	6770×765	3.9
TiO_2	Rutile	Spherical	3.1	2330	4.2

various dielectric constants were prepared under ultrasonic irradiation at 20 kHz 150 W for 5 min. The particle concentration was 0.2 wt%. The dielectric constant of the dispersion medium was changed by changing the mixing ratio of dioxane and water.[15]

Estimation of Dispersion Stability. The stability of a dispersion was estimated by means of the sedimentation experiment described in previous papers;[8-11] *i.e.*, the sedimentation velocity is the gradient of the time profiles of the sharp boundary between supernatant and sediment.

Measurement of Adsorption of AOT and Zeta Potential. The amount of adsorption was determined from the measurement of the equilibrium concentrations of AOT in the supernatant with an ultraviolet spectrometer (UV-200S, Shimadzu Co.).[11]

The zeta potential was measured by microelectrophoresis with the laser Zee TM Model 500 (PEN KEM Co.).[8-11]

Measurement of Dynamic Light Scattering. Dust and other extraneous matter were excluded from the solvents through a millipore filter (pore size=0.2 μm). The scattered light of each sample solution was measured in a cell which had been rinsed repeatedly with dust-free ethanol. The hydrodynamic radius of a micelle (r_h) was calculated from Einstein-Stokes' equation ($r_h=kT/6\pi\eta D$). The diffusion coefficients (D) for various dielectric constant solutions of AOT were measured by means of a dynamic light-scattering instrument at 30±0.1 °C. The wave length of the Ar laser used was 4880 Å.

Calculation of Potential Energy

The potential energy between particles at various dielectric constants was calculated according to the following equations in order to evaluate the dispersibility of three kinds of particles. The needle-like particles (A and B of Fe_2O_3) used in this study were assumed to be cylindrical, and parallel interaction was considered only for the cylindrical particles, because it is clear that parallel interaction is more predominant than head-tail interaction between the cylindrical particles.[9,20]

Three kinds of potential energies of the interaction between a pair of particles were considered; steric repulsion between adsorbed layers (V_R^{en}), electrostatic double-layer repulsion (V_R^{el}), and van der Waals attraction (V_A^L or V_A^δ). They are expressed in the following equations (1)—(6).

For Needlelike Particles: *i)* Steric repulsion between adsorbed layers: Here, Ottewill-Walker's equation was utilized:[21]

$$V_R^{en} = \frac{2kTC_v^2}{v_1\rho_2^2}\cdot(\psi_1-\kappa_1)\cdot V, \tag{1}$$

where V is the total volume of the overlapping zone of the adsorbed layer; C_v, the concentration of AOT in the adsorbed layer; v_1, the molecular volume of a solvent; ρ_2, the density of AOT, and ψ_1 and κ_1 the entropic and enthalpic parameters of mixing proposed by Flory.

ii) Electrostatic double-layer repulsion:[9,20]

$$V_R^{el} = \frac{\varepsilon\sqrt{h\kappa}\Psi_0^2}{2\pi}\left[\frac{2}{3}\left(\frac{1}{\exp(\kappa H+1)+1}-\frac{1}{\exp(\kappa H)+1}\right)\times(1+3\kappa H)+2\left\{\left(\frac{1}{\exp(\kappa H)+1}-\frac{1}{\exp(\kappa H+1)+1}\right)\kappa H+\frac{1}{\exp(\kappa H)+1}\right\}+1.142\exp(-\kappa H)-2\exp(-\kappa H-1)\right], \tag{2}$$

where h is the radius of the cylinder of a needlelike particle, H is the shortest distance between the particle surface, and κ is the reciprocal Debye length, expressed as follows:

$$\kappa = \sqrt{\frac{8\pi n\bar{Z}^2e^2}{\varepsilon kT}}. \tag{2}'$$

Equation (2), introduced under an assumption of $\kappa h>1$ in the previous paper,[9] was assumed to be useful for the system of the dielectric constant at ε=2.2 ($\kappa h<1$). This assumption is permissible because the contribution of this repulsion is comparatively small in nonpolar organic media.[20]

iii) Van der Waals attraction:[1]

$$V_A^L = -\frac{A}{48\pi}\left\{\frac{1}{(H/2)^2}+\frac{1}{(H/2+h)^2}-\frac{2}{(H/2+h/2)^2}\right\}, \tag{3}$$

where A is the Hamaker constant of the oxide in dioxane–water mixtures. Here, the effect of the adsorbed layer was neglected.

For the Spherical Particle (TiO_2): *i)* Steric repulsion between adsorbed layers:[21]

$$V_R^{en} = \frac{4\pi kTC_v^2}{3v_1^2\rho_2^2}\cdot(\psi_1-\kappa_1)\cdot\left(\delta-\frac{H}{2}\right)^2\cdot\left(3a+2\delta+\frac{H}{2}\right), \tag{4}$$

where H is the shortest distance between the particle surfaces, a, the radius of a particle, and δ, the thickness of an adsorbed layer.

ii) Electrostatic double-layer repulsion:[22]

$$V_R^{el} = \frac{\varepsilon a\zeta^2}{2}\ln\{1+\exp(-\kappa H)\}, \tag{5-1}$$

$$V_R^{el} = \frac{\varepsilon a^2\zeta^2}{2a+H}\exp(-\kappa H), \tag{5-2}$$

where ζ is the zeta potential. Eq. (5-1) and Eq. (5-2) were used for the dispersion systems of ε=10—78 and ε=2.2 respectively.

iii) Van der Waals attraction: Here Vold's equation was used, considering the effect of the adsorbed layer:[23]

$$V_A^\delta = -\frac{1}{12}\left\{(\sqrt{A_{22}}-\sqrt{A_{33}})^2\frac{a+\delta}{H}+(\sqrt{A_{33}}-\sqrt{A_{11}})^2\frac{a}{H+2\delta}+4a(\sqrt{A_{22}}-\sqrt{A_{33}})(\sqrt{A_{33}}-\sqrt{A_{11}})\frac{a+\delta}{(H+\delta)(2a+\delta)}\right\}, \tag{6}$$

where A_{11}, A_{22}, and A_{33} are the Hamaker constants of the TiO_2, a solvent, and the AOT adsorbed respectively.

Results

Effect of AOT on the Stability. In order to examine the effect of the AOT concentration on the dispersibility and the zeta potential, measurements of the sedimentation and zeta potential were carried out in dioxane (ε=2.2) and water (ε=78) systems for the three kinds of particles. The dependence of the sedimentation velocity and the zeta potential on the AOT concentration for Fe_2O_3-A is shown as an example in Figs. 1(a) and (b). The dispersion stability of both systems is markedly improved by the addition of a small amount of AOT. Similar results were also observed for the Fe_2O_3-B and TiO_2 particles.

The zeta potential showed a maximum in the curves for the dioxane system at the AOT concentration of 3mM (1M=1 moldm^{-3}), which approximately coincides with the concentration at which the dispersion stability was attained. On the other hand, it suddenly increased to a constant value upon the addition of a small amount of AOT to the water system.

Effect of Dielectric Constant on the Dispersibility. In order to examine the effect of the dielectric constant on the dispersibility and the zeta potential, measurements of the sedimentation and the zeta potential were carried out for various dielectric constants for the three kinds of particles. Here, the systems were examined in both the absence and presence of 20mM AOT. The dependence of the sedimentation velocity and the zeta potential on the dielectric constant is shown as the series of (a) and (b) in Figs. 2, 3, and 4.

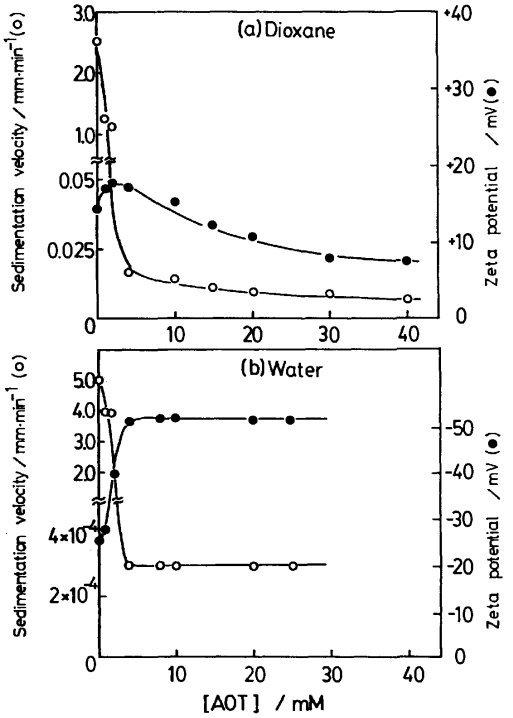

Fig. 1. Plots of the sedimentation velocity and zeta potential *vs.* AOT concentration of Fe_2O_3-A particles for dioxane system(a) and water system(b).

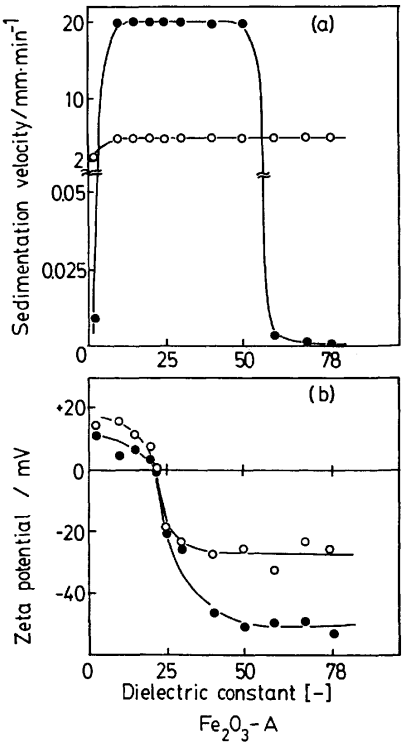

Fig. 2. Change of the sedimentation velocity(a) and zeta potential(b) as a function of the dielectric constant for Fe_2O_3-A particle.
O: In the absence of AOT, ●: In the presence of AOT.

The effect of AOT on the stability of the dispersion is remarkable; the sedimentation velocity is very low in the regions of the lower (at ε=2.2) and higher dielectric

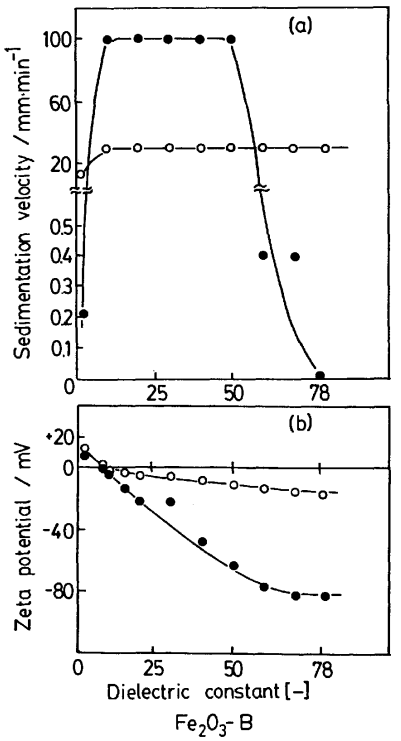

Fig. 3. Change of the sedimentation velocity(a) and zeta potential(b) as a function of the dielectric constant for Fe_2O_3-B particle.
O: In the absence of AOT, ●: In the presence of AOT.

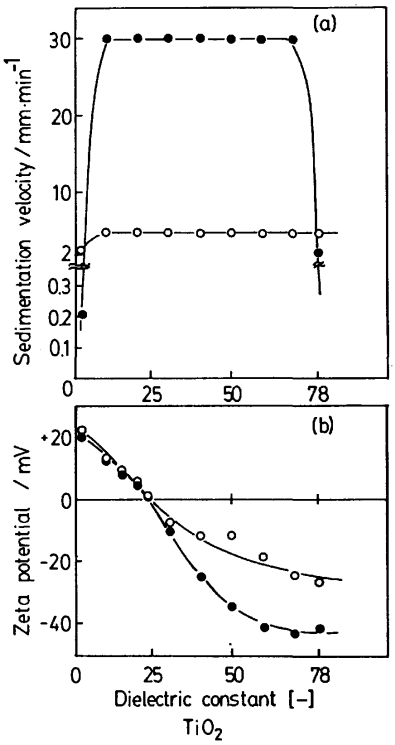

Fig. 4. Change of the sedimentation velocity(a) and zeta potential(b) as a function of the dielectric constant for TiO_2 particle.
○: In the absence of AOT, ●: In the presence of AOT.

constants (at ε=60—78), but it suddenly increases in the middle region of the dielectric constants (at ε=10—50). This characteristic flocculation of particles in the presence of AOT had previously been observed for carbon-black particles in polar organic media (2-butanone; ε=15.45).[20] On the other hand, in the absence of AOT, the sedimentation velocity is approximately constant, showing the occurrence of considerable flocculation over all of the regions of dielectric constants for the three kinds of particles.

Figures 2, 3, and 4 show that the value of the zeta potential is inverted from a positive sign to a negative sign with the increase in the dielectric constant and that it converges to the zeta potential of the water system for all of the particles. The absolute value of the zeta potential in the presence of AOT is larger than that in the absence of AOT above the isoelectric dielectric point (abbreviated as IED). The order of the magnitude of IED is as follows:

$$Fe_2O_3\text{-B}\ (8) \ll Fe_2O_3\text{-A}\ (22) < TiO_2\ (24). \qquad (A)$$

The figures in brackets show the IED. It is noticeable that the zeta potentials are approximately equal in the neighborhood of the IED for the systems in both the presence and absence of AOT. This result corresponds with the results of the adsorption experiment, which will be shown in Fig. 5.

Effect of Dielectric Constant on Adsorbability of AOT. The adsorption isotherms of AOT for the Fe_2O_3-A particle at various dielectric constants are shown in

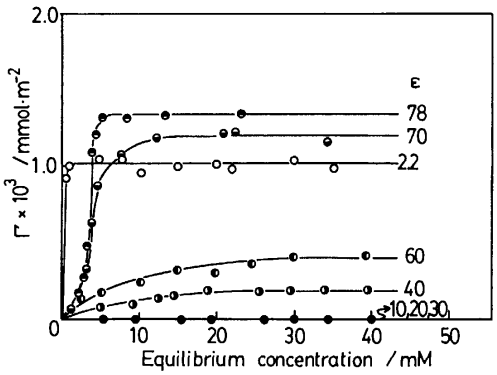

Fig. 5. The adsorption isotherms of AOT for Fe_2O_3-A particle at the various dielectric constants.

TABLE 2. THE DIFFUSION COEFFICIENT (D) MEASURED BY A DYNAMIC LIGHT-SCATTERING METHOD AND THE RESULTING HYDRODYNAMIC DIAMETER (d_h) OF MICELLES AT THE VARIOUS DIELECTRIC CONSTANTS

ε (—)	η (cP)	n (—)	$D\times10^6$ (cm²/s)	d_h (Å)
2.2	1.087	1.4221	1.83	22.0
10	1.445	1.4060	—	—
20	1.672	1.3926	4.08	6.4
30	1.673	1.3807	5.11	5.2
40	1.538	1.3696	2.06	13.8
50	1.339	1.3595	2.10	15.4
60	1.139	1.3493	2.04	18.8
70	0.945	1.3392	1.62	28.4
78	0.894	1.3300	1.65	29.8

Fig. 5. It is characteristic that AOT molecules are not adsorbed in the region of ε=10—30. Furthermore, in the region of ε=40—60, the adsorption isotherms are of the Langmuirian type, but their initial slopes are low and the saturation values of adsorption (Γ_m) are smaller than that of ε=2.2. On the other hand, in the region of ε=70—78, the adsorption isotherms are S-shaped, but the saturation values are higher, belonging to Type I in the Gile-MacEwan-Nakhwa-Smith classification.[24] Hence, in the region of ε=70—78, the most probable orientation of the first layer is with the nonpolar group outside, while the second layer is adsorbed by interchain cohesion with nonpolar groups and ionic groups outside. This observation agrees with the dispersibility of the particles and the zeta potential as shown in Figs. 2, 3, and 4. The amount of AOT adsorbed on Fe_2O_3-B and TiO_2 could not be measured by the ultraviolet method because of their low specific surface areas.

Effect of Dielectric Constant on Micelle Formation. The diffusion coefficient (D) and the hydrodynamic diameter of micelles (d_h) at various dielectric constants, as obtained by the dynamic light-scattering method, are listed in Table 2. As may be seen in Table 2, the values of d_h at ε=2.2, 70, and 78 are 22, 28.4, and 29.8Å respectively. Hence, it can be considered that AOT molecules form the reversed micelles at ε=2.2 and ordinary micelles at ε=70 and 78, because the length of a AOT molecule is approximately 15Å.

On the other hand, the diffusion coefficient (D)

TABLE 3. NUMERICAL VALUES OF Γ_m, C_v, v_1 AND δ USED FOR EQS.(1) AND (4)

ε (−)	$\Gamma_m \times 10^3$ (mmol/m²)	C_v (g/cm³)	v_1 (cm³)	δ (Å)
2.2	1.02	0.302	1.46×10^{-22}	15
10	0	0	1.26×10^{-22}	0
20	0	0	1.09×10^{-22}	0
30	0	0	9.40×10^{-23}	0
40	0.19	0.056	8.00×10^{-23}	15
60	0.41	0.122	5.40×10^{-23}	15
70	1.20	0.178	4.20×10^{-23}	30
78	1.35	0.200	3.00×10^{-23}	30

could not be measured at ε=10, and the values of d_h are very small at ε=20 and 30. These facts suggest that AOT molecules do not form micelles, but exist as monomers. The values of d_h are 13.8—18.8Å in the region of ε=40—60. This suggests that a small part of the AOT molecules associates as dimers or trimers. This change in the aggregation of AOT with the dielectric constant agrees with the results of Elworthy *et al.* for lecithin[25] and Kitahara *et al.* for AOT.[26]

Potential Energies of the Three Kinds of Particles. The dispersibility of the three kinds of particles at various dielectric constants in the presence of 20mM of AOT could be evaluated quantitatively from the magnitude of the total potential energy by the use of Eqs. (1)—(6).

The numerical values used for each equation were as follows: In Eqs. (1) and (4), $\psi_1-\kappa_1=0.1$,[27] a=1165Å and ρ_2=1.0g/cm³,[28] while C_v was calculated from the following equation for each particle: $C_v=\Gamma_m/\delta\cdot S_o$, where δ is the thickness of the adsorbed surfactant molecules and S_o is the specific surface area of each particle. Γ_m, C_v, v_1, are δ are listed in Table 3. The amount of AOT adsorbed for Fe_2O_3-B and TiO_2 could not be measured, but it was assumed that the values of Γ_m for the two particles were equal to that for the Fe_2O_3-A particle. In Eqs. (2) and (5), ζ and κ are listed in Table 4. Here, κ was calculated for each particle from Eq. (2)′ with the ion concentration (n) obtained from the electric conductivity (k). The values of k and κa and κh are also listed in Table 4. Here, Walden's law was adopted for the system of the solvent mixture.[14] In Eqs. (3) and (6), the Hamaker constants were as follows. The values of A, 4.6×10^{-20}J, in Eq. (3) for the Fe_2O_3 particle were calculated from the following equation: $A=(\sqrt{A_{11}}-\sqrt{A_{22}})^2$. $A_{11}=22.6\times10^{-20}$J for the TiO_2 particle,[29] $A_{22}=5.9\times10^{-20}$J for the solvent[29] (the values of water and dioxane are equal), and $A_{33}=2.5\times10^{-20}$J for the adsorbed layer.[27]

The results of the calculation for the three kinds of particles are shown in Figs. 6, 7, and 8 as the respective potential energy curves respectively. The dispersibility of the three kinds of particles and the effect of the dielectric constant can be discussed quantitatively on the basis of these results.

Discussion

Effect of AOT on the Dispersibility in Dioxane and Water System. As may be seen in Fig. 1(a) and (b), the dispersion stability of the dioxane and water systems is markedly improved by the addition of a small amount of AOT (4—5mM). This concentration is of the same order as the critical micellar concentrations of AOT in dioxane and water, which are 5mM and 5.5 mM respectively.[30] Furthermore, at these concentrations of AOT, the adsorption reaches saturation for both systems, as is shown in Fig. 5. This correspondence illustrates the effect of AOT molecules adsorbed on the Fe_2O_3-A particles in both systems.

The appearance of the maximum of the zeta potential in the dioxane system (in the nonpolar system), as is seen in Fig. 1(a), may be explained as follows. At a lower concentration of AOT, the counter ions of the AOT molecules (Na^+) are preferentially adsorbed on the particle, thus increasing the positive change of the zeta potential, followed by the adsorption of the negative ion ($-SO_3^-$), which decreases the zeta potential as the concentration of AOT increases.[31]

Effect of AOT on the Dispersibility of Three Kinds of Oxides at Various Dielectric Constants. As may be seen from the series of (a) in Figs. 2, 3, and 4, the effect of AOT is remarkable for all the particles. This fact is correlated with the adsorbability and micelle formation of AOT molecules, as may be seen in Fig. 5

TABLE 4. THE RESULTS OF ζ- POTENTIAL AND κ FOR THE THREE KINDS OF PARTICLES OBTAINED FROM THE ELECTRIC- CONDUCTIVITY METHOD AT VARIOUS DIELECTRIC CONSTANTS (20mM AOT system)

ε	ζ-potential(mV)			k	κ	Fe_2O_3-A	Fe_2O_3-B	TiO_2
	Fe_2O_3-A	Fe_2O_3-B	TiO_2	(mho·cm⁻¹)	(cm⁻¹)	κh* (−)	κh* (−)	κa** (−)
2.2	+10.8	+9.8	+20.3	0.05×10^{-6}	1.63×10^{5}	0.12	0.62	1.90
10	+4.1	−3.7	+9.3	59.8×10^{-6}	2.90×10^{6}	2.06	11.1	33.7
20	+4.1	−20.4	+4.5	2.87×10^{-4}	4.83×10^{6}	3.43	18.5	56.3
30	−25.8	−21.0	−10.4	4.26×10^{-4}	4.83×10^{6}	3.43	18.5	56.3
40	−47.0	−48.3	−25.1	5.31×10^{-4}	4.46×10^{6}	3.17	17.1	52.0
50	−51.1	−62.6	−34.8	6.30×10^{-4}	4.05×10^{6}	2.88	15.5	47.2
60	−49.4	−77.8	−41.4	7.60×10^{-4}	3.75×10^{6}	2.66	14.3	43.7
70	−48.0	−82.5	−43.8	9.20×10^{-1}	3.47×10^{6}	2.46	13.3	40.4
78	−52.0	−83.6	−41.4	1.090	3.31×10^{6}	2.35	12.7	38.6

*h: Fe_2O_3-A=71×10^{-8}cm, Fe_2O_3-B=382.5×10^{-8}cm. **a: TiO_2=1165×10^{-8}cm.

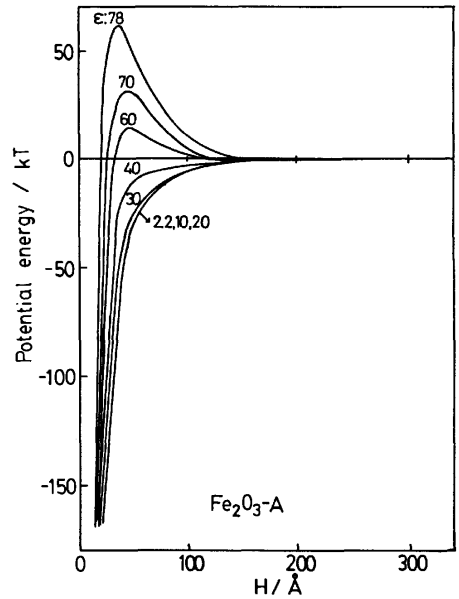

Fig. 6. Potential energy curves for Fe_2O_3-A particle.

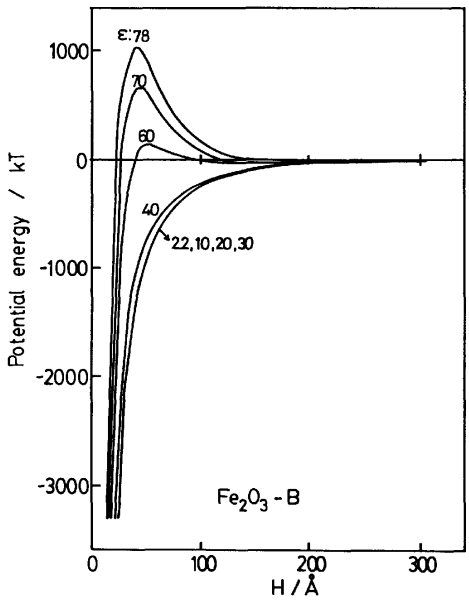

Fig. 7. Potential energy curves for Fe_2O_3-B particle.

and Table 2.

The flocculation of particles in the middle region of the dielectric constants in the presence of AOT is considered to be due to the following reasons. AOT molecules are not at all (at ε=10—30) or only a little (at ε=40, 60) adsorbed on the particle surface (Fig. 5). Hence, the particles can not be stabilized by the steric repulsion of the adsorbed layer of AOT. Therefore, the counter ion (Na^+) works as an indifferent ion in the middle region of the dielectric constant and the electric double layer is compressed.[20] This fact can be seen from κ in Table 4. Therefore, the particles can not be stabilized by the electric double-layer repulsion, either.

As may be seen in Figs. 6, 7, and 8, the potential curves for the three kinds of particles are very similar. That is, in the lower region of the dielectric constants (ε=2.2—40), the potential energy is attractive for all

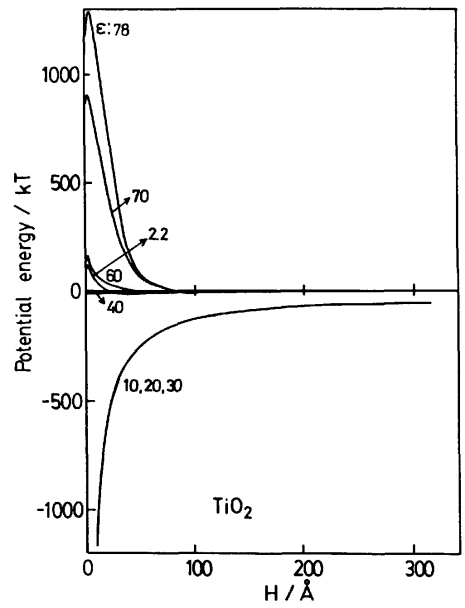

Fig. 8. Potential energy curves for TiO_2 particle.

distances, and the maxima of the potential curves do not appear except at ε=2.2 for the TiO_2 system. On the other hand, in the region of higher dielectric constants (ε=60—78), the maxima of the potential energy (V_{max}) appear in the potential curves. Moreover, the V_{max} increases with the increase in the dielectric constant. These results agree with the results of the dispersion stability of the three kinds of particles, as may be seen in Figs. 2, 3, and 4, except that ε=2.2 for A and B particles of Fe_2O_3. Furthermore, these results also agree with the results of the adsorbability and micelle formation of AOT molecules, shown in Fig. 5 and Table 2, except for ε=2.2. The exception at ε=2.2 is due to the use of Eq. (2) for cylindrical particles at ε=2.2, though $\kappa h<1$, as is shown in Table 4.

Concept of IED. The appearance of IED as seen in Figs. 2, 3, and 4 would be considered on the basis of the concept of acid-base interaction between a particle surface and a solvent as follows. The surface charge is caused by the acid-base interaction between a particle surface and a solvent expressed as Eq. (7):[22]

$$SH_2^+ + OH^- \overset{(a)}{\rightleftharpoons} SH + H_2O \overset{(b)}{\rightleftharpoons} S^- + H_3OH^+, \quad (7)$$

where SH is the surface of a particle and H_2O is either a solvent itself or the water contained in a solvent. If a particle surface is more basic than a solvent, reaction(a) occurs to make the surface positive. In the opposite case, reaction(b) occurs to make the surface negative.

In the region of lower dielectric constants (lower than IED), reaction(a) will occur to make the zeta potential positive, because dioxane is a weakly basic solvent.[32,33] With the increase in the concentration of water, reaction(a) will shift to reaction(b) to make the zeta potential negative, because water is a strongly basic solvent.[34] Hence, the appearance of the IED for all of the particles is considered to result from the shift of

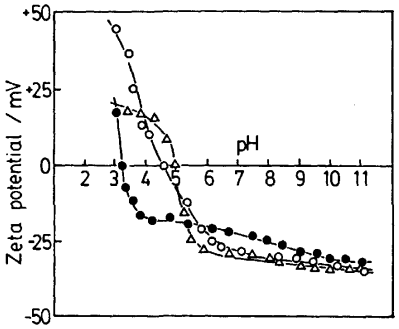

Fig. 9. Change of the zeta potential with pH of the dispersion medium at 20°C.
○: Fe_2O_3-A, ●: Fe_2O_3-B, ▲: TiO_2.

the reaction from (a) to (b).

Comparison of IED for Three Kinds of Particles. The result of (A) expressing the difference of IED can be explained by the following discussion using the above idea of acid-base interaction. The isoelectric points (IEP) of the three kinds of particles were also measured in order to evaluate the acidity or basicity of each particle. This experiment was done by the measure of the zeta potential under the change in the pH of a dispersion medium by the use of aqueous solutions of 10^{-3}M NaOH and 10^{-3}M HCl. The effect of the ionic strength on the zeta potential was neglected in order to see the zeta potential quantitatively.

The changes in the zeta potential with the pH for the three kinds of particles are shown in Fig. 9. The order of the magnitude of the IEP in Fig. 9 is as follows:

$$Fe_2O_3\text{-B}\ (3.2) < Fe_2O_3\text{-A}\ (4.5) < TiO_2\ (5.0), \qquad (B)$$

IEP can be explained by the concept of an acid-base interaction between a particle and a solvent containing the potential-determining ions (H^+, OH^-).[35] The surface of the Fe_2O_3-B particle is more acidic than that of the Fe_2O_3-A particle. Moreover, the surfaces of Fe_2O_3-A and B are more acidic than TiO_2 particle. This differences is probably due to the conditions of the preparation of the particles and the treatment of the particles.[36,37]

The order of the magnitude of result (A) agrees very well with result (B). Therefore, the order of IED can be explained by the concept of acid-base interaction between a particle surface and a solvent.

The authors wish to express their thanks to Dr. Kenji Kubota and Professor Yasunori Tominaga, Department of physics, Faculty of Science, Ochanomizu Women's University, for measuring the dynamic light scattering.

References

1) E. J. W. Verwey and J. Th. G. Overbeek, "Theory of Stability of Lyophobic Colloids," Elsevier, Amsterdam (1948).
2) J. L. van der Minne and P. H. J. Hermanie, *J. Colloid Sci.*, **7**, 600 (1952).
3) H. Koelmans and J. Th. G. Overbeek, *Discuss. Faraday Soc.*, **18**, 52, (1954).
4) J. L. van der Minne and P. H. J. Hermanie, *J. Colloid Sci.*, **8**, 38 (1953).
5) D. N. L. McGown and G. D. Parfitt, *Kolloid Z. Z. Polym.*, **220**, 56 (1967).
6) J. Briant and B. Bernelin, *Rev. Inst. France Petrole*, **16**, 1767 (1961).
7) D. N. L. McGown and G. D. Parfitt, *J. Colloid Interface Sci.*, **20**, 650 (1965); *Discuss. Faraday Soc.*, **42**, 225 (1966).
8) K. Kandori, A. Kitahara, and K. Kon-no, *Bull. Chem. Soc. Jpn.*, **56**, 1581 (1983).
9) K. Kandori, K. Kon-no, and A. Kitahara, *Nippon Kagaku Kaishi*, **7**, 963 (1983).
10) K. Kandori, A. Kitahara, and K. Kon-no, *J. Colloid Interface Sci.*, **99**, 455 (1984).
11) K. Kandori, A. Kazama, K. Kon-no, and A. Kitahara, *Nippon Kagaku Kaishi*, **11**, 1562 (1983).
12) J. N. de Wit and J. Lyklema, *J. Electroanal. Chem. Interfacial Electrochem.*, **41**, 259 (1973).
13) J. Lyklema and J. N. de Wit, *J. Electroanal. Chem.*, **65**, 443 (1975).
14) J. Lyklema and J. N. de Wit, *Colloid & Polymer Sci.*, **256**, 1110 (1978).
15) C. A. Kraus and R. M. Fuoss, *J. Am. Chem. Soc.*, **55**, 21 (1933).
16) M. Kiyama, *Funtai Oyobi Funmatsu Yakin*, **23**, 177 (1976).
17) M. Camras, U. S. Patent 2694656 (1954).
18) M. Camras, Kokai Tokkyo Koho, 26-7776 (1951).
19) A. Kitahara and K. Kon-no, *J. Phys. Chem.*, **70**, 3394 (1966).
20) K. Kandori, A. Kazama, K. Kon-no, and A. Kitahara, *Bull. Chem. Soc. Jpn.*, **57**, 1777 (1984).
21) R. H. Ottewill and T. Walker, *Kolloid Z. Z. Polym.*, **227**, 108 (1967).
22) J. Lyklema, *Adv. Colloid Interface Sci.*, **2**, 65 (1968).
23) M. J. Vold, *J. Colloid Sci.*, **16**, 1 (1961).
24) C. H. Giles, T. H. McEwan, S. N. Nakhwa, and D. Smith, *J. Chem. Soc.*, 3973 (1960); F. Z. Saleeb, *Kolloid Z. Z. Polym.*, **239**, 602 (1968).
25) P. H. Elworthy and D. S. McIntosh, *Kolloid Z. Z. Polym.*, **195**, 27 (1964).
26) A. Kitahara, T. Kobayashi, and T. Tachibana, *J. Phys. Chem.*, **66**, 363 (1962).
27) D. H. Napper, *Trans. Faraday Soc.*, **64**, 1701 (1968).
28) M. Gobe, K. Kon-no, K. Kandori, and A. Kitahara, *J. Colloid Interface Sci.*, **93**, 293 (1983).
29) B. Vincent, *J. Colloid Interface Sci.*, **42**, 270 (1973).
30) H. B. Klevens, *J. Am. Oil Chem. Soc.*, **30**, 74 (1954).
31) A. Kitahara, M.Amano, S. Kawasaki, and K. Kon-no, *Colloid & Polymer Sci.*, **255**, 1118 (1977).
32) P. Sorensen, *J. Paint Technology*, **47**, 31 (1975).
33) S. Tanaka and T. Satoh, *Shikizai Kyokaishi*, **56**, 753 (1983).
34) E. J. Verwey, *Rec. Trav. Chim.*, **60**, 625 (1941).
35) K. Tamaribuchi and M. L. Smith, *J. Colloid Interface Sci.*, **22**, 404 (1966).
36) R. H. Ottewill, and J. M. Tiffany, *J. Oil Colour Chemist Assos.*, **50**, 844 (1967).
37) T. W. Hearly, A. P. Herring, and D. W. Fuestenau, *J. Colloid Interface Sci.*, **21**, 435 (1966).

Stability Constants of Scandium Complexes. II. Dicarboxylate Complexes Species

Hisako Itoh, Yukihiro Ikegami, and Yasuo Suzuki*
Department of Industrial Chemistry, Faculty of Engineering, Meiji University, Higashi-mita, Tama-ku, Kawasaki 214
(Received April 14, 1984)

The stability constants of scandium complexes with malonate, maleate, itaconate, glutarate, adipate, and succinate ligands were determined titrimetrically at 25.0 °C and at an ionic strength of 0.1. The chelate effect was negligible for the stability of the scandium complexes with the dicarboxylate ligands studied in contrast with the lanthanoid complexes. The complex formation of scandium might be explained by an electrostatic ionic bond similar to ones exhibited in the lighter rare-earth complexes, due to linear relationships between the stability constants and the ionic potential Z^2/r.

Scandium has been known for almost one hundred years, although its chemistry, particularly its coordination chemistry, has been little studied. In 1970, a review[1] was given on its coordination chemistry. The lack of attention has probably been due to the difficulty, until recently, of obtaining a pure source, though the metal and the oxide are now commercially available in high purity.

In our previous paper,[2] stability constants of scandium complexes with some monobasic acids were reported and compared with those of the lanthanoid complexes. The constants of the scandium complexes were appreciably greater than those of the corresponding lanthanoid complexes, as expected from the smaller ionic radius. The scandium complexes were thought to be similar to the lighter rare-earth complexes with regard to coordinating characteristics and to the degree of cationic hydration. In this study, the stability constants of scandium complexes with some dicarboxylic acids were determined titrimetrically and compared with those of the lanthanoid complexes.

Experimental

Reagents and Apparatus. A scandium nitrate solution was prepared as described previously.[2] Stock solutions of dicarboxylic acids were prepared using analytical reagents and were standardized by potentiometric titration with a standard solution of sodium hydroxide. The pH-measuring system consisted of an Orion model 701A digital pH/mV meter, an Orion 91-01 glass electrode and a Beckman 39400 reference electrode. The instrument is capable of measuring the pH of a solution with an accuracy of 0.001 unit.

Procedure and Calculations. To determine the stability constants, solutions containing a ligand acid, scandium nitrate and potassium nitrate were titrated with standard sodium hydroxide. The solutions were stirred continuously and the temperature was maintained at 25.0 °C during the titrations. Sufficient time was allowed between successive additions of the base in order to obtain constant pH readings. The titrations were continued until precipitation occurred. The constants were calculated by the Bjerrum method.[3] The values of $\bar{n}$ and [A] calculated by the following equations were taken at or near $\bar{n}$=0.5 and 1.5,

$$[A] = \frac{(2-a)A_t - [H] + [OH]}{2[H]^2/K_{a1}K_{a2} + [H]/K_{a2}}$$

$$\bar{n} = \frac{A_t - ([H]^2/K_{a1}K_{a2} + [H]/K_{a2} + 1)[A]}{M_t},$$

where [A] is the concentration of free ligand acid, $\bar{n}$ is the ligand number, A_t and M_t are the total concentration of the ligand acid and scandium metal, respectively, K_{a1} and K_{a2} are the first and second dissociation constants of the acid, respectively, and a is the mole number of the sodium hydroxide added to one mole of the ligand acid. The acid-dissociation constants were determined in a similar way to the stability constants, as described above.

Results and Discussion

Depending on the basicity and the content of hydroxyl and iminodicarboxyl groups, organic ligands exhibit different stabilities and different numbers of binding sites. When only carboxyl and hydroxyl groups are present, the ligands are usually bidentate, tridentate and, in some cases, monodentate. Monobasic acids, including those containing hydroxyl groups, form complexes of the type ScL^{2+}, dibasic acids form ScL'^{+}, while the formation of the acid ion $ScHL''^{+}$ is characteristic of tribasic acids.

The acid-dissociation constants obtained are listed in Table 1. The experimental data for the titrations of the stability constants are shown as plots of $\bar{n}$ *vs.* log[A]

Table 1. Dissociation constants of dicarboxylic acids

Acid	pK_{a1}	pK_{a2}
Malonic acid	2.69	5.48
Maleic scid	1.84	5.83
Itaconic acid	3.68	5.23
Glutaric acid	4.19	5.09
Adipic acid	4.29	5.09
Succinic acid	4.00	5.29

Table 2. Stability constants of scandium complexes

Acid	log K_1		log K_2	
	This work	Previous work	This work	Previous work
Malonic acid	6.78	5.87[4]	5.12	4.25[4]
Maleic acid	5.98	5.34[5]	4.27	
Itaconic acid	4.77		4.00	
Glutaric acid	5.21	4.82[6]	3.70	
Adipic acid	5.25		3.50	
Succinic acid	5.55		3.88	

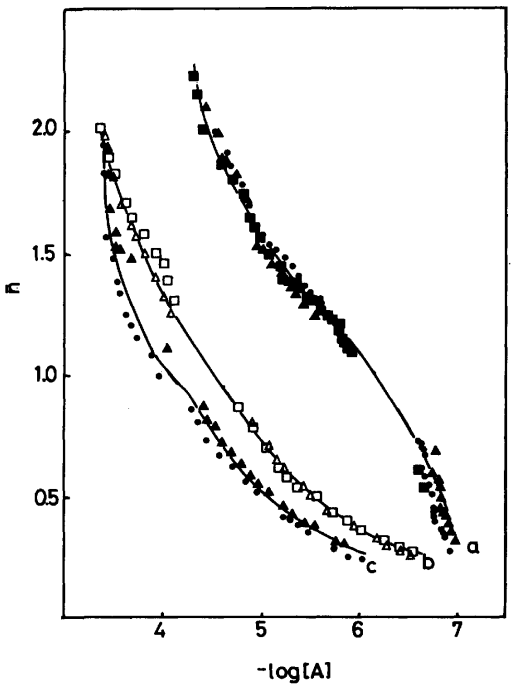

Fig. 1. Formation curves of scandium complexes. I.
a: Malonate, b: Succinate, c: Glutarate.

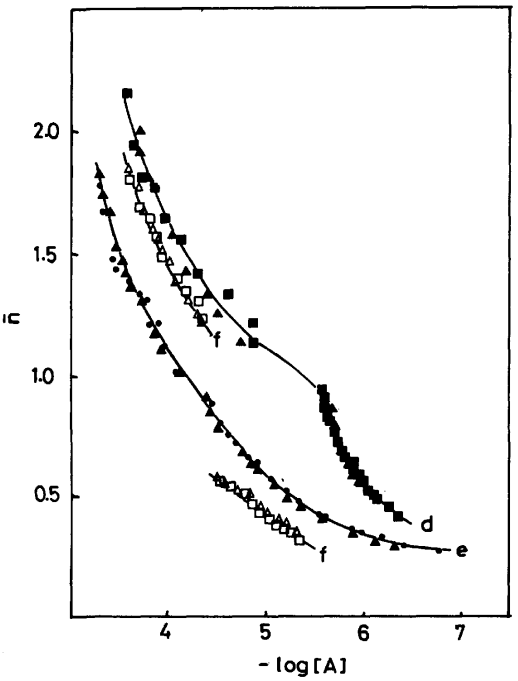

Fig. 2. Formation curves of scandium complexes. II.
d: Maleate, e: Adipate, f: Itaconate.

in Figs. 1 and 2. In the [A]-region investigated, the first and second complexes were formed and no evidence for the formation of higher complexes was found. Acid complexes were formed for the itaconato complexes, as can be seen from the formation curves and from the stability constants[4] of the lanthanoid-itaconato complexes.

The stability constants obtained are listed in Table 2, together with previously reported values.[5-7] The

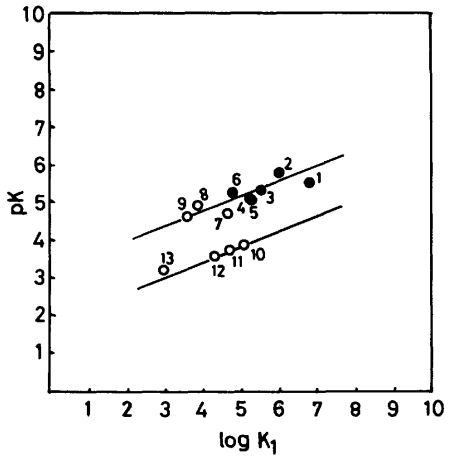

Fig. 3. Relation between the values of log K_1 and the pK_1 (of the monobasic ligands) or pK_2 (of the dibasic ligands).
1: Malonate, 2: Maleate, 3: Succinate, 4: Glutarate, 5: Adipate, 6: Itaconate, 7: Isobutyrate, 8: Propionate, 9: Acetate, 10: α-Hydoxyisobutyrate, 11: Glycolate, 12: D-Gluconate, 13: Mandelate.

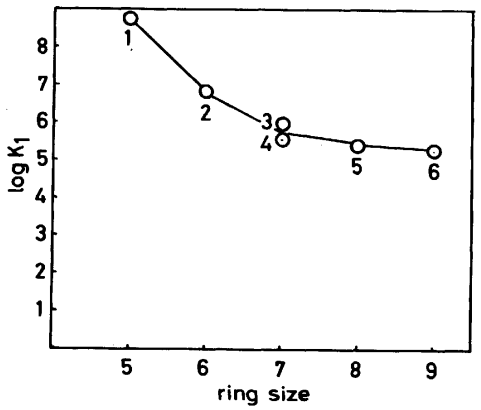

Fig. 4. Relation between stability constants and ring size.
1: Oxalate, 2: Malonate, 3: Maleate, 4: Succinate, 5: Glutarate, 6: Adipate.

values of log K_1 for scandium complexes of some mono- and dicarboxylate ligands are plotted as a function of pK_{a1} for the monocarboxylates and pK_{a2} for the dicarboxylates in Fig. 3. The plots of mono- and dicarboxylate ligands are located on the same straight line, indicating that the chelate effect would be negligible for the scandium complexes and that the hydroxyl groups play an important role in the formation of scandium complexes. The difference of log K_1 of two lines is approximately 3.5, corresponding to a hydrogen-bond energy of about 21 kJ mol^{-1}. The greater stability of ligands containing OH groups compared with those without OH groups would contribute to the intermolecular hydrogen bond between the OH groups and the carboxylate oxygen of the former ligands.

The relationship between the stability constants and ring size is shown in Fig. 4. The stability constant of an oxalato complex (having a five-membered ring)

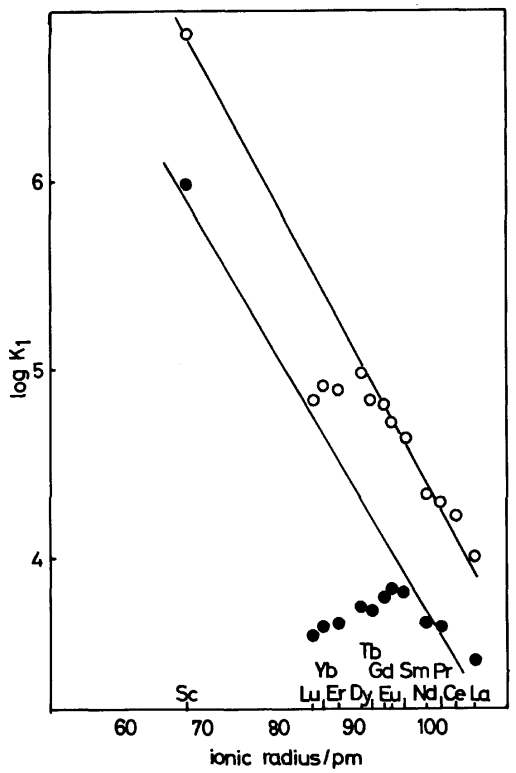

Fig. 5. Relation between stability constants and ionic radius.
○: Malonate, ●: Maleate.

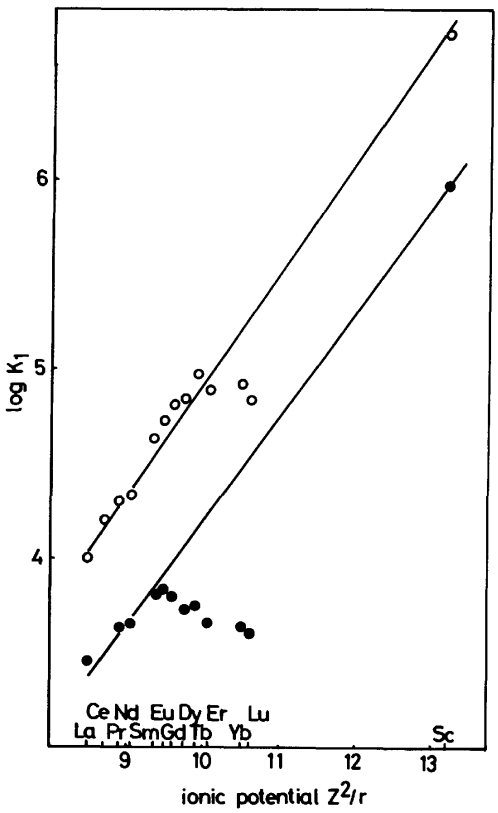

Fig. 6. Relation between stability constants and ionic potential (Z^2/r).
○: Malonate, ●: Maleate.

gives the greatest values (decreasing with increasing ring size). The greater stability of the malonato complex compared to the maleato, glutarato and adipato complexes indicates that the malonato complex forms six-membered rings while the maleato, glutarato, and adipato complexes have seven-, eight-, and nine-membered rings, respectively.

The relation between the stability constant (log K_1) of the scandium and lanthanoid complexes and the ionic radius are shown in Fig. 5. As well as the monobasic acids described before,[2] the stability constants of the scandium complexes with malonic and maleic acids are on the extrapolated lines of the lighter rare-earth complexes rather than those of the heavier rare earths. In the case of the itaconato, glutarato, adipato and succinato complexes, such relationships were not obtained due to a lack of the values for the corresponding lanthanoid complexes.

When a bond between metal and a ligand is purely ionic, the bond strength increases linearly with increasing ionic potential Z^2/r (Z: ionic charge, r: ionic radius), according to Born's equation. The relationships between the stability constants of the rare-earth complexes and the ionic potential are shown in Fig. 6. The linearity was obtained for the scandium and lighter rare-earth complexes, but not for the heavier rare-earth complexes.

Since there is a regular decrease in the crystal radii of rare-earth metal ions, simple electrostatic theory predicts a direct relationship betweeen the atomic number of the rare-earth ion and the stability constants. In nearly all complexes which have been studied, this relationship was precisely found for the values of log K_1 for complexes of the lighter rare earths. This simple relationship was, however, not generally found when the heavier rare-earth ions were considered. The trends in the stability constants for the heavier rare-earth elements can be divided qualitatively into three types. The first group contains those ligands for which there is a regular increase in the values of the stability constants. This does not imply that these ligands follow the simple electrostatic model, since the slope of a plot of log K_1 *vs.* r is usually not the same as for the lighter rare earths. Ligands for which this trend is observed are glycolic, α-hydroxyisobutyric, and mandelic acids. The only obvious similarity among these ligands is that each has at least one OH group. The ligands in the second classification form complexes for which the stability constants of the heavier rare earths have nearly the same values from gadolinium to lutetium. These ligands are acetic, propionic and isobutyric acids. The third group contains dicarboxyllic acids, such as malonic and maleic acids. The stability-constant values for the complexes of these ligands increase with the first elements beyond gadolinium and then show a slight decrease to lutetium. The position of scandium with respect to the relationship between the stability constant and ionic radius is of interest.

The studies with lanthanoid perchlorates and oxygen donor ligands have shown that the coordination number varies with ionic size (values from six to twelve being reported).[8-14] In view of the smaller size of the scandium ion compared with any of the trivalent lanthanoid ions, scandium exhibits a maximum coordination number of six on the low end of the range observed for the heavier rare earths.

The complex formation of scandium with any of the three types of ligands might be explained by an electrostatic ionic bond similar to ones exhibited in the lighter rare-earth complexes, although the coordination number of scandium differs from the lighter rare earths. Other factors besides the purely electrostatic bond might be incorporated in the complex formation of the heavier rare earths.

References

1) G. A. Melson and R. W. Stotz, *Coord. Chem. Rev.*, **7**, 133 (1971).

2) H. Itoh, N. Itoh, and Y. Suzuki, *Bull. Chem. Soc. Jpn.*, **57**, 716 (1984).

3) J. Bejerrum, "Metal Ammine Formation in Aqueous Solution," P. Haase and Son, Copenhagen (1957).

4) H. Schurmans, H. Thun, F. Verbeek, and W. Vanderleen, *J. Elelctroanal. Chem.*, **38**, 209 (1972).

5) I. Grenthe, G. Gordhammar, and E. Rundcrantz, *Acta Chem. Scand.*, **23**, 93 (1969).

6) I. M. Korenman and N. V. Zaglyadimova, *Zhur. Neorg. Khim.*, **18**, 2774 (1973).

7) E. I. Chubakova and N. A. Skorik, *Russ. J. Inorg. Chem.*, **18**, 1446 (1973).

8) V. N. Krishnamurthy and S. Sonndararajan, *J. Inorg. Nucl. Chem.*, **29**, 517 (1967).

9) F. N. Krishnamurthy and S. Sonndararajan, *Can. J. Chem.*, **45**, 189 (1967).

10) F. Kutek, *Collect. Czech. Chem. Commun.*, **33**, 1341 (1968).

11) J. O. Edwards, R. J. Goetsch, and J. A. Stritar, *Inorg. Chim. Acta*, **1**, 360 (1967).

12) T. Moeller and G. Vincentini, *J. Inorg. Nucl. Chem.*, **27**, 1477 (1965).

13) D. M. Mehs and S. K. Madan, *J. Inorg. Nucl. Chem.*, **30**, 3017 (1968).

14) R. D. Shannon and C. T. Prewitt, *Acta Crystallogr. Sect. B.*, **25**, 925 (1969).

Studies of the Metal Complexes of Cyclohexane Derivatives. VIII.[1] Preparation and Properties of Platinum(II) and Cobalt(III) Complexes Containing (1*R*,2*S*,3*S*)- or (1*S*,2*R*,3*R*)-3-Methyl-1,2-cyclohexanediamine

Reiko SAITO* and Yoshinori KIDANI†

Aichi Junior College of Nursing, Kamishidami, Moriyama-ku, Nagoya 463

†*Faculty of Pharmaceutical Siences, Nagoya City University, Tanabe-dori, Mizuho-ku, Nagoya 467*

(Received May 23, 1984)

(1*RS*,2*SR*,3*SR*)-3-Methyl-1,2-cyclohexanediamine (3m-chxn), a methyl derivative of *cis*-1,2-cyclohexanediamine, was prepared and optically resolved. The absolute configurations of the enantiomers obtained were assigned on the basis of the Cotton effect of the *trans*-dichlorobis(diamine) complexes, each containing active 3m-chxn. The complexes of the $[Pt(NH_3)_2L]^{2+}$, $[Pt(en)L]^{2+}$, and $[CoL_3]^{3+}$ types (en=1,2-ethanediamine, L=*R,S,S*- or *S,R,R*-3m-chxn) were also synthesized and characterized on the basis of their absorption, CD, and ^{13}C NMR spectra. It has been found that the chelate rings adopted by *R,S,S*- and *S,R,R*-3m-chxn predominantly take the δ and λ conformations respectively, because of the preferred equatorial orientation of the C_2–C_3 bond of the cyclohexane ring. The four diastereomers of $[Co(R,S,S\text{-3m-chxn})_3]^{3+}$ were chromatographically isolated and assigned to *fac*-$\Lambda(lel_3)$, *mer*-$\Lambda(lel_3)$, *fac*-$\Delta(ob_3)$, and *mer*-$\Delta(ob_3)$.

There have been many studies of the correlation between the conformations of the 1,2-diamine chelate ring and the steric structures of the ligands, but they have almost all been on the effects by the substituents attached to the diamine chelate ring.[2,3] The influences on complex formation of the substituents bonded to the carbon atom outside the chelate ring have not been so widely studied. Recently we ourselves have reported the properties of the complex containing (1*R*,2*S*)-1-aminomethyl-2-methylcyclohexylamine (*R,S*-2m-amcha).[1] The methyl group of this ligand, that is in the β-position to one of the donor atoms, strongly affects the conformation of the chelate ring. The conformation in which the C_1–C_2 bond of the cyclohexane ring is equatorially oriented with respect to the chelate ring is much more favorable than the other one which requires the methyl group to occupy a position over the chelate ring. In this study, we have prepared some Pt^{II} and Co^{III} complexes of (1*R*,2*S*,3*S*)- or (1*S*,2*R*,3*R*)-3-methyl-1,2-cyclohexanediamine (*R,S,S*- or *S,R,R*-3m-chxn). The methyl group is presumed to be situated in an equatorial position in the chair conformation of the cyclohexane ring. Its steric influence on the conformational preference in complex formation is considered to be similar to that of *R,S*-2m-amcha. Another concern of this paper is to obtain experimental data about the properties of the complexes of *cis*-1,2-cyclohexanediamine (*cis*-chxn) derivatives. Little investigatory work has been done on the Pt^{II} and Co^{III} complexes of this series of diamines compared with the *trans*-chxn derivatives.[4–6]

Experimental

Preparation and Resolution of the Ligands. *C*-3-Methyl-4-ene-*r*-1,*c*-2-cyclohexenedicarboxylic acid was prepared according to the procedure in the literature.[7] The reduction of the product with hydrogen in the presence of the rhodium catalyst gave the saturated dicarboxylic acid. A Schmidt reaction[8] of the reduced diacid yielded (1*RS*,2*SR*,3*SR*)-3-methyl-1,2-cyclohexanediamine. Optical resolution was performed using (2*R*,3*R*)-di-*O*-benzoyltartaric acid. From the less soluble diastereomeric salt ($[\alpha]_D=-76°$ (*c* 1.1, CH_3OH)), (+)-3m-chxn·2HCl was isolated. Found: C, 41.77; H, 8.96; N, 13.66%. Calcd for $C_7H_{18}N_2Cl_2$: C, 41.80; H, 9.02; N, 13.93%. $[\alpha]_D=2.9°$ (*c* 10, H_2O). In spite of its low $[\alpha]_D$ value, it is considered to be optically pure and is assigned to (1*R*,2*S*,3*S*)-3m-chxn·2HCl on the basis of the CD spectrum of *trans*-$[CoCl_2((+)\text{-3m-chxn})_2]^+$.[9] The decomposition of the more soluble diastereomeric salt ($[\alpha]_D=-96°$ (*c* 0.43, H_2O)) gave (−)-3m-chxn·2HCl, assignable to (1*S*,2*R*,3*R*). Found: C, 41.60; H, 9.21; N, 13.76%. Calcd for $C_7H_{18}N_2Cl_2$: C, 41.80; H, 9.02; N, 13.93%. $[\alpha]_D=-2.9°$ (*c* 10, H_2O).

Preparation of Complexes. *$[Pt(NH_3)_2L]Cl_2$ and $[Pt(en)L]Cl_2$(en=1,2-ethanediamine, L=*R,S,S- *or* S,R,R-*3m-chxn)*: $[Pt(NH_3)_2L]Cl_2$ and $[Pt(en)L]Cl_2$ were prepared by the reaction of $[PtCl_2L]$ with an aqueous ammonia and an en solution respectively in a manner similar to the procedure in the literature.[10,11] Found: $[Pt(NH_3)_2(R,S,S,\text{-3m-chxn})]Cl_2$, C, 19.26; H, 5.01; N, 12.71%, $[Pt(NH_3)_2(S,R,R\text{-3m-chxn})]Cl_2$, C, 19.02; H, 5.08; N, 12.65%. Calcd for $[Pt(NH_3)_2L]Cl_2\cdot 0.5H_2O=C_7H_{22}N_4Cl_2Pt\cdot 0.5H_2O$: C, 19.23; H, 5.30; N, 12.81%. Found: $[Pt(en)(R,S,S\text{-3m-chxn})]Cl_2$, C, 23.41; H, 5.23; N, 12.41%, $[Pt(en)(S,R,R\text{-3m-chxn})]Cl_2$, C, 23.62; H, 5.30; N, 12.45%. Calcd for $[Pt(en)L]Cl_2=C_9H_{24}N_4Cl_2Pt$: C, 23.79; H, 5.32; N, 12.33%.

trans-*$[CoCl_2L_2]ClO_4$*: An attempt to synthesize these complexes from $CoCl_2\cdot 6H_2O$ and the respective active diamine by the usual air oxidation was unsuccessful. Therefore, they were prepared by a method similar to that used for *trans*-$[CoCl_2(trans\text{-chxn})_2]^+$, using $[CoCO_3(NH_3)_4]NO_3\cdot 0.5H_2O$ as the starting material.[12] The resulting product seemed to be a mixture of *cis*- and *trans*-dichlorobis (diamine) complexes. The expected complexes were obtained by refluxing a methanol solution of a mixture by a method described in the literature.[13] Found: *trans*-$[CoCl_2(R,S,S\text{-3m-chxn})_2]ClO_4$, C, 34.01; H, 6.71; N, 11.13%, *trans*-$[CoCl_2(S,R,R\text{-3m-chxn})_2]ClO_4$, C, 34.39; H, 6.66; N, 11.31%. Calcd for $[CoCl_2L_2]ClO_4\cdot 0.5H_2O=C_{14}H_{32}N_4O_4Cl_3Co\cdot 0.5H_2O$: C, 33.99; H, 6.72; N, 11.32%.

Four Isomers of [Co(R,S,S-*3m-chxn)$_3$]Cl_3*: These complexes

were synthesized in a manner similar to that described previously.[1] The resulting product prepared from *trans*-$[CoCl_2py_4]Cl$ (1.3mmol) and *R,S,S*-3m-chxn (6.5mmol), was adsorbed on SP-Sephadex C-25. This resin was loaded on the top of an SP-Sephadex C-25 column (2.7cm×95cm) and eluted with a 0.2mol/dm³ Na_2SO_4 solution. The four bands which appeared, were named B'-1, B'-2, B-3, and B-4 in the order of elution. The B'-1 and B'-2 bands overlapped each other and contained only a small amount of the complexes. After six chromatographic runs, the combined fractions of B'-1 and B'-2 were evaporated to afford an orange solid. This solid was then chromatographed again using an SP-Sephadex C-25 column (2.7cm×95cm) with a 0.15mol/dm³ Na_3PO_4 solution. Two bands well-separated appeared, they were called B-1 and B-2 in the order of elution. The B-1, B-2, B-3, and B-4 complexes were obtained as chlorides by a procedure similar to that described in a previous report.[1] Yields: B-1; *ca.* 30mg, B-2; *ca.* 60mg, B-3; *ca.* 1300mg, B-4; *ca.* 1600mg. They were dissolved in a small amount of water and recrystallized by adding a 6mol/dm³ hydrochloric acid solution. The B-1, B-2, B-3, and B-4 complexes were obtained as red orange needles, a red orange crystalline powder, an orange crystalline powder, and orange needles respectively. Found: B-1, C, 42.56; H, 8.36; N, 14.11%, B-2, C, 42.28; H, 8.25; N, 14.13%. Calcd for $[CoL_3]Cl_3\cdot 0.5H_2O\cdot HCl=C_{21}H_{48}N_6Cl_3Co\cdot 0.5H_2O\cdot HCl$: C, 42.36; H, 8.46; N, 14.11%. Found: B-3, C, 41.13; H, 9.11; N, 13.86%. Calcd for $[CoL_3]Cl_3\cdot 3.5H_2O=C_{21}H_{48}N_6Cl_3Co\cdot 3.5H_2O$: C, 41.15; H, 9.04; N, 13.71%. Found: B-4, C, 41.88; H, 9.00; N, 14.17%. Calcd for $[CoL_3]Cl_3\cdot 3H_2O=C_{21}H_{48}N_6Cl_3Co\cdot 3H_2O$: C, 41.76; H, 9.01; N, 13.91%.

Measurements: A JASCO J-40 spectropolarimeter and a Shimadzu UV-210-A spectrometer were used to measure the CD and absorption spectra respectively. The optical rotation at 589nm were measured with a JASCO DIP-4 polarimeter. The ^{13}C NMR spectra were recorded on a JEOL JNM-FX-100 spectrometer, with D_2O as a solvent. The chemical shifts were measured with dioxane (δ 67.70ppm) as the internal reference.

Results and Discussion

Conformation of the Chelate Ring of the Pt^{II} Complexes. A representative ^{13}C NMR spectrum of the Pt^{II} complexes prepared in this study is shown in Fig. 1, while the numerical data are given in Table 1. The peak at around 32ppm was assigned to the C_3 carbon by the aid of the off-resonance proton-decoupling technique. The signal at around 27ppm is attributable to the resonance of the C_6 carbon, because it is expected to appear in a lower field than those of the C_4 and C_5 carbons. In the *R,S,S*- or *S,R,R*-3m-chxn Pt^{II} complexes, the C_3 carbon exhibited $^3J_{Pt-C}$ values of 37—38Hz. They were smaller than that of [Pt(bpy)(*trans*-chxn)]$^{2+}$ (52Hz)(bpy=2,2'-bipyridine),[5] whose chelate ring takes a rigid conformation, and also smaller than the two-folded $^3J_{Pt-C}$ values of [Pt(NH₃)₂(*cis*-chxn)]$^{2+}$ and [Pt(en)(*cis*-chxn)]$^{2+}$[14] (25—26Hz)(Table 1). In the *cis*-chxn complex, the two λ and δ conformations are feasibly interconvertible, with a simultaneous inversion of the cyclohexane ring. The $^3J_{Pt-C_3}$ values for the present complexes were found to be almost identical with those of [Pt(bpy)(pn)]$^{2+}$ (38Hz)(pn=1,2-propanediamine)[5] and [Pt(bpy)(2m-amcha)]$^{2+}$ (34Hz).[1] On the other hand, no satellite peaks due to the coupling with ^{195}Pt and the C_6 carbon were observed.

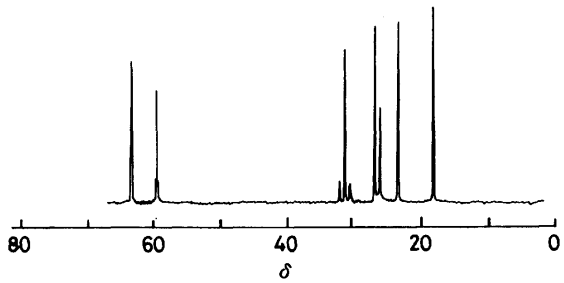

Fig. 1. ^{13}C NMR spectrum of [Pt(NH₃)₂(*S,R,R*-3m-chxn)]$^{2+}$.

The *R,S,S*- and *S,R,R*-3m-chxn ligands are assumed to have the same configuration as that of the *c*-3-methyl-*r*-1,*c*-2-cyclohexanedicarboxylic acid used for the preparation.[7] The possible conformations of *S,R,R*-3m-chxn are shown in Fig. 2. The cyclohexane ring of the ligand is presumed to exist predominantly

TABLE 1. ^{13}C NMR CHEMICAL SHIFTS[a] AND COUPLING CONSTANTS[b] FOR *R,S,S*- OR *S,R,R*-3m-chxn Pt^{II} COMPLEXES

Complex	^{13}C Resonance								
	C_2	C_1	C_3	C_6	C_4, C_5		CH_3	en	
$[Pt(NH_3)_2(R,S,S\text{-3m-chxn})]Cl_2$	63.56	59.80 (9)	31.68 (37.8)	27.10	26.37	23.64	18.43		
$[Pt(NH_3)_2(S,R,R\text{-3m-chxn})]Cl_2$	63.56	59.80 (10)	31.69 (37.8)	27.10	26.42	23.64	18.34		
$[Pt(en)(R,S,S\text{-3m-chxn})]Cl_2$	63.07	59.32 (12)	31.73 (36.6)	27.10	26.42	23.64	18.43	48.01	47.86
$[Pt(en)(S,R,R\text{-3m-chxn})]Cl_2$	63.07	59.32 (12)	31.73 (36.6)	27.05	26.42	23.64	18.43	48.01	47.86
$[Pt(NH_3)_2(cis\text{-chxn})]Cl_2$[14]	58.78[c]		27.01[d] (25.7)		21.40[e]				
$[Pt(en)(cis\text{-chxn})]Cl_2$[14]	58.07[c] (8)		27.03[d] (25.0)		21.40[e]			47.94	

a) Carbon chemical shifts in ppm from external TMS measured *vs.* internal dioxane. b) Coupling constants ($J_{^{195}Pt-C}$) are found in parentheses in Hz. c) Assignable to C_1 and C_2 carbon. d) Assignable to C_3 and C_6 carbon. e) Assignable to C_4 and C_5 carbon.

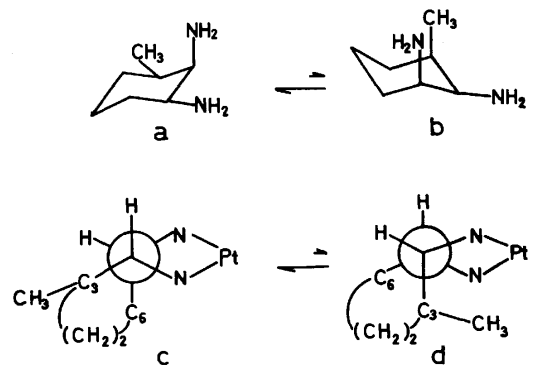

Fig. 2. Conformations of the *S,R,R*-3m-chxn and the chelate rings of the *S,R,R*-3m-chxn complex.
a, b: The conformational pair of *S,R,R*-3m-chxn, c, d: λ and δ conformations of *S,R,R*-3m-chxn complex.

in the conformation shown in Fig. 2, a, because the preference for the diequatorial-axial conformation (a) over the diaxial-equatorial conformation (b) seems very reasonable. The λ and δ conformations of the *S,R,R*-3m-chxn complex are also shown in Fig. 2. If the cyclohexane is assumed to take the more stable conformation (Fig. 2, a), then the chelate ring is seen necessarily to exist in the λ conformation (c). The δ conformation (d), in which the cyclohexane ring is assumed to adopt an unstable conformation (b), is disadvantageous. In addition, the steric hindrance caused by the methyl group located above the chelate ring may destabilize the δ conformation. This unfavorable steric effect attributable to the methyl group seemed to be similar to that of the higher-energy conformer of the *R,S*-2m-amcha complex.[1] The empirical result that no $^3J_{Pt\text{-}C_6}$ was detected indicates

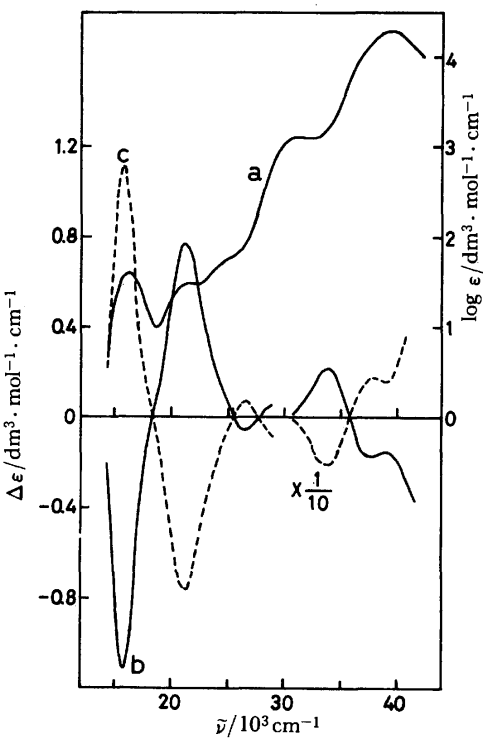

Fig. 3. Electronic (a) and CD (b, c) spectra.
—: *trans*-$[CoCl_2(R,S,S\text{-3m-chxn})_2]^+$, --: *trans*-$[CoCl_2(S,R,R\text{-3m-chxn})_2]^+$.

that the distribution of the less favorable conformer in the $\lambda \rightleftharpoons \delta$ equilibrium is very small. The smaller ^3J values for the present complexes should be ascribed to the unsymmetrical structure distorted from the idealized gauche form illustrated in Fig. 2, as has been described by Yano *et al.*[15] Therefore, it is concluded that the chelate ring of *S,R,R*-3m-chxn complexes

Table 2. Electronic and CD spectral data of Co^{III} complexes

Complex	Electronic		CD	
	$\tilde{\nu}/10^3\,cm^{-1}$	($\log\varepsilon$)	$\tilde{\nu}/10^3\,cm^{-1}$	($\Delta\varepsilon$)
trans-$[CoCl_2(R,S,S\text{-3m-chxn})_2]^+$	16.2	(1.60)	15.8	(−1.12)
	21.6	(1.49)	21.2	(+0.78)
	25.3	(1.79)	26.5	(−0.06)
	31.3	(3.12)	33.9	(+2.24)
	39.2	(4.29)	37.7	(−1.8)
trans-$[CoCl_2(S,R,R\text{-3m-chxn})_2]^+$	16.2	(1.60)	15.8	(+1.11)
	21.6	(1.50)	21.2	(−0.76)
	25.3	(1.79)	26.5	(+0.07)
	31.3	(3.10)	33.9	(−2.19)
	39.2	(4.26)	37.7	(+1.8)
fac-$\Lambda(lel_3)$-$[Co(R,S,S\text{-3m-chxn})_3]^{3+}$	20.8	(1.99)	19.8	(+3.03)
			23.0	(−0.07)
	28.7	(1.98)	27.5	(+0.35)
	45.5	(4.27)	42.3	(−33.8)
mer-$\Lambda(lel_3)$-$[Co(R,S,S\text{-3m-chxn})_3]^{3+}$	20.8	(2.02)	19.8	(+3.20)
	28.7	(2.01)	27.1	(+0.28)
	45.5	(4.26)	42.2	(−34.0)
fac-$\Delta(ob_3)$-$[Co(R,S,S\text{-3m-chxn})_3]^{3+}$	20.5	(2.17)	20.4	(−5.96)
	28.3	(2.19)	28.2	(+0.50)
	45.5	(4.31)	44.6	(+18.4)
mer-$\Delta(ob_3)$-$[Co(R,S,S\text{-3m-chxn})_3]^{3+}$	20.6	(2.14)	20.5	(−5.13)
	28.5	(2.14)	28.2	(+0.42)
	45.5	(4.30)	44.2	(+18.1)

preferrentially adopts the λ conformation, with the C_2–C_3 bond equatorially oriented.

Absolute Configulation of the Ligands. It has been established that the CD spectra of the *trans*-[$CoCl_2$(1,2-diamine)$_2$]$^+$ complexes, were 1,2-diamine=C-substituted optically active 1,2-diamine, were mainly due to the conformational effect.[16–18] In order to assign the configurations of the resolved (+)- and (−)-3m-chxn ligands, we synthesized the two enantiomers, *trans*-[$CoCl_2$((+)-3m-chxn)$_2$]$^+$ and *trans*-[$CoCl_2$((−)-3m-chxn)$_2$]$^+$. The electronic and CD spectra are shown in Fig. 3, while the numerical results are given in Table 2. The CD signs of *trans*-[$CoCl_2$((−)-3m-chxn)$_2$]$^+$ were observed to be positive in the I_a (16200 cm^{-1}) region and negative in the I_b (21600cm^{-1})

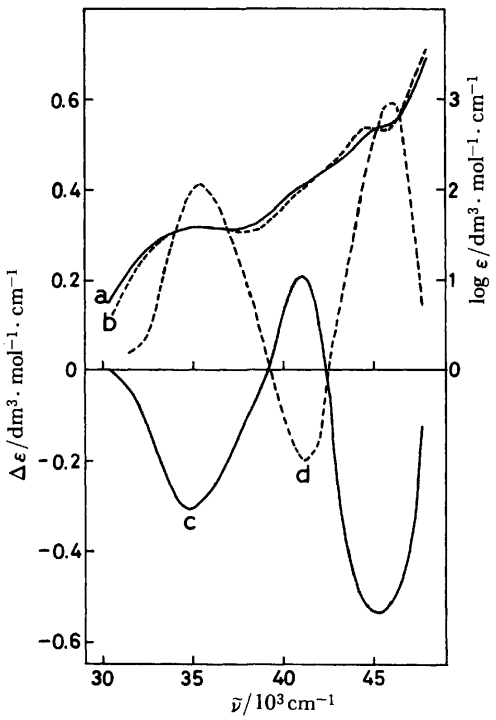

Fig. 4. Electronic (a, b) and CD (c, d) spectra.
—: [$Pt(NH_3)_2$(*R*,*S*,*S*-3m-chxn)]$^{2+}$, --: [Pt(en)(*S*,*R*,*R*-3m-chxn)]$^{2+}$.

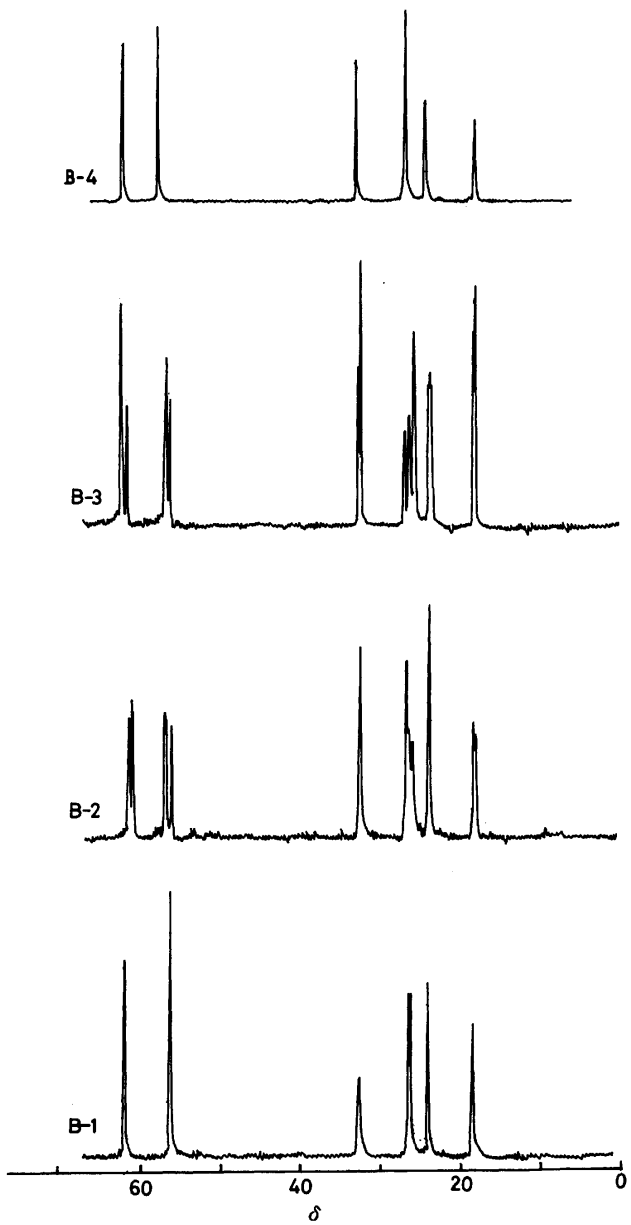

Fig. 5. ^{13}C NMR spectra of the B-1, B-2, B-3, and B-4 isomers of [Co(*R*,*S*,*S*-3m-chxn)$_3$]$^{3+}$.

Table 3. Electronic and CD spectral data of Pt^{II} complexes

Complex	Electronic		CD	
	$\tilde{\nu}/10^3 cm^{-1}$	($\log \varepsilon$)	$\tilde{\nu}/10^3 cm^{-1}$	($\Delta\varepsilon$)
[$Pt(NH_3)_2$(*R*,*S*,*S*-3m-chxn)]$^{2+}$	35.4	(1.59)	34.9	(−0.31)
	41 sh[a]	(2.0)	41.0	(+0.21)
	45.0	(2.66)	45.1	(−0.54)
[$Pt(NH_3)_2$(*S*,*R*,*R*-3m-chxn)]$^{2+}$	35.4	(1.58)	34.9	(+0.30)
	41 sh	(2.0)	41.0	(−0.23)
	45.0	(2.65)	45.1	(+0.53)
[Pt(en)(*R*,*S*,*S*-3m-chxn)]$^{2+}$	35.5	(1.59)	35.4	(−0.40)
	41 sh	(2.0)	41.2	(+0.18)
	44.6	(2.66)	46.1	(−0.54)
[Pt(en)(*S*,*R*,*R*-3m-chxn)]$^{2+}$	35.5	(1.60)	35.4	(+0.41)
	41 sh	(2.0)	41.2	(−0.20)
	44.6	(2.68)	46.1	(+0.59)

a) Shoulder.

region. Accordingly, this complex was supposed to have the λ conformation, like the *trans*-$[CoCl_2(R\text{-pn})_2]^+$ complex.[17,18] Since the λ conformation is much more favorable for the *S,R,R*-3m-chxn complex than for the *R,S,S*-3m-chxn complex (Fig. 2), the configuration of the (−)-diamine is identified as (1*S*,2*R*,3*R*). The other (+)-ligand is naturally deduced to have the (1*R*,2*S*,3*S*) configuration.

The CD Spectra of the Pt^{II} *Complexes.* The present complexes have two asymmetric carbons, with the *S,R*- or *R,S*- configuration,in their chelate ring, in contrast to the well-studied complexes, which have one *R(S)* or two *R,R(S,S)* chiral carbon(s) in the diamine ring. The electronic and CD spectra of $[Pt(NH_3)_2(R,S,S\text{-3m-chxn})]^{2+}$ and $[Pt(en)(S,R,R\text{-3m-chxn})]^{2+}$ are shown in Fig. 4. The three main bands (Table 3) observed at around 3500, 4100, and 4500 cm^{-1} were tentatively assigned to the $^1A_{1g}\rightarrow{}^3E_g$, $^1A_{1g}\rightarrow{}^1A_{2g}$, and $^1A_{1g}\rightarrow{}^1E_g$ transitions respectively.[4,19,20] According to the assignment by Nakayama *et al.*, however, the last band possibly includes a weak band due to the $^1A_{1g}\rightarrow{}^1B_{1g}$ transition.[21] The Cotton effects of the $^1A_{1g}\rightarrow{}^3E_g$ and $^1A_{1g}\rightarrow{}^1E_g$ transitions of the C-substituted diamine complexes with the *R*-configuration and the λ conformation have been known to be positive. Both the signs and the CD strengths of the ^1E_g and ^3E_g bands in $[Pt(NH_3)_2(S,R,R\text{-3m-chxn})]^{2+}$ and $[Pt(en)(S,R,R,\text{-3m-chxn})]^{2+}$ were similar to those in *R*-pn analogs.[4] These results indicate that, in the above transitions, the contribution to the Cotton effects imposed by the asymmetric α-carbons is small. On the basis of the signs of these bands, two series of Pt^{II} complexes, both containing *S,R,R*- and *R,S,S*-3m-chxn, were found to have λ and δ conformations respectively, as concluded from the CD spectra of the *trans*-$[CoCl_2L_2]^+$ complexes.

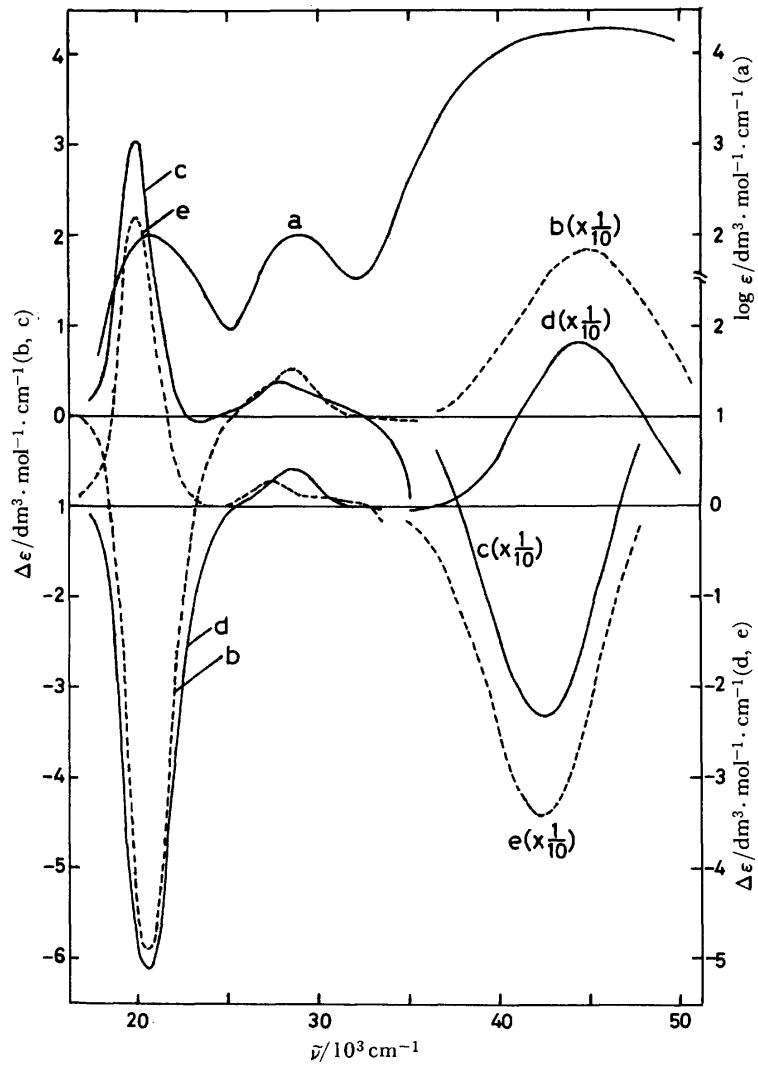

Fig. 6. Electronic spectrum of B-4 (a) and CD spectra of B-1, B-2, B-3, and B-4 (b, d, e, c).
a: *fac*-$\Lambda(lel_3)$-$[Co(R,S,S\text{-3m-chxn})_3]^{3+}$ (B-4), b: *fac*-$\Lambda(ob_3)$-$[Co(R,S,S\text{-3m-chxn})_3]^{3+}$ (B-1), c: *fac*-$\Lambda(lel_3)$-$[Co(R,S,S\text{-3m-chxn})_3]^{3+}$ (B-4), d: *mer*-$\Lambda(ob_3)$-$[Co\text{-}(R,S,S\text{-3m-chxn})_3]^{3+}$ (B-2), e: *mer*-$\Lambda(lel_3)$-$[Co(R,S,S\text{-3m-chxn})_3]^{3+}$ (B-3).

*The Isomers of [Co(*R,S,S-*3m-chxn)$_3$]$^{3+}$.* The [Co(*R,S,S*-3m-chxn)$_3$]$^{3+}$ is expected to contain four isomers. The complexes named B-3 and B-4 were isolated by SP-Sephadex C-25 chromatography, using a Na_2SO_4 solution as an eluent. The isomers named B-1 and B-2, obtained in much lower yields, were not separated from each other with the same eluent.

Figure 5 shows their ^{13}C NMR spectra. Since seven and six signals were observed for the B-1 and B-4 complexes respectively, both complexes were assigned to the *fac*-isomers (C_3-symmetry). Both the B-2 and B-3 complexes were assignable to the *mer*-isomers (C_1-symmetry) because of the inequality of each carbon in their spectra. The resonances for the methine carbon of the *lel* chelate ring in the analogous diamine complexes have been reported to appear in a lower field than those of the *ob* chelate ring.[22,23] The C_1 and C_2 signals of the B-3 isomer appeared at a slightly lower field than those of the B-2 isomer. Similar downfield shifts at the corresponding methine carbons of the B-4 complex were observed compared to the B-3 complex. From these results, in combination with the relative yield, the B-1, B-2, B-3, and B-4 complexes can be assigned to *fac*-(*ob*$_3$), *mer*-(*ob*$_3$), *mer*-(*lel*$_3$), and *fac*-(*lel*$_3$) respectively.

Sakakibara *et al.*[24] reported that the relative rate of the elution of $[CoN_6]^{3+}$-type-complex isomers was influenced by both the interaction between SP-Sephadex and the complex cation and that between the complex cation and the eluent anions, and presented an empirical rule for the elution order of the above type of complexes. However, the present *lel*$_3$ complexes did not follow this rule, being eluted extraordinarily slowly with a Na_3PO_4 solution. This may be caused by the considerably stronger interactions between the complex and SP-Sephadex resulting from the bulky ligand.

The absorption and CD spectra of these complexes are shown in Fig. 6, while the spectral data are summarized in Table 2. The CD spectra of the B-3 and B-4 complexes showed a positive peak in the first-absorption-band region, while those of the B-1 and B-2 complexes showed a very strong negative peak in the same region. Applying the empirical rule on the relationship between the absolute configuration of the tris diamine complex and the CD sign of the first absotption band[25,26] to these complexes, it is concluded that the B-1 and B-2 complexes have the *Δ* configuration, while the B-3 and B-4 have the *Λ* configuration. Since the chelate ring of the *R,S,S*-3m-chxn is restricted to the *δ* conformation, we have assigned the B-1, B-2, B-3, and B-4 complexes to *fac*-*Δ*(*ob*$_3$), *mer*-*Δ*(*ob*$_3$), *mer*-*Λ*(*lel*$_3$), and *fac*-*Λ*(*lel*$_3$) respectively.

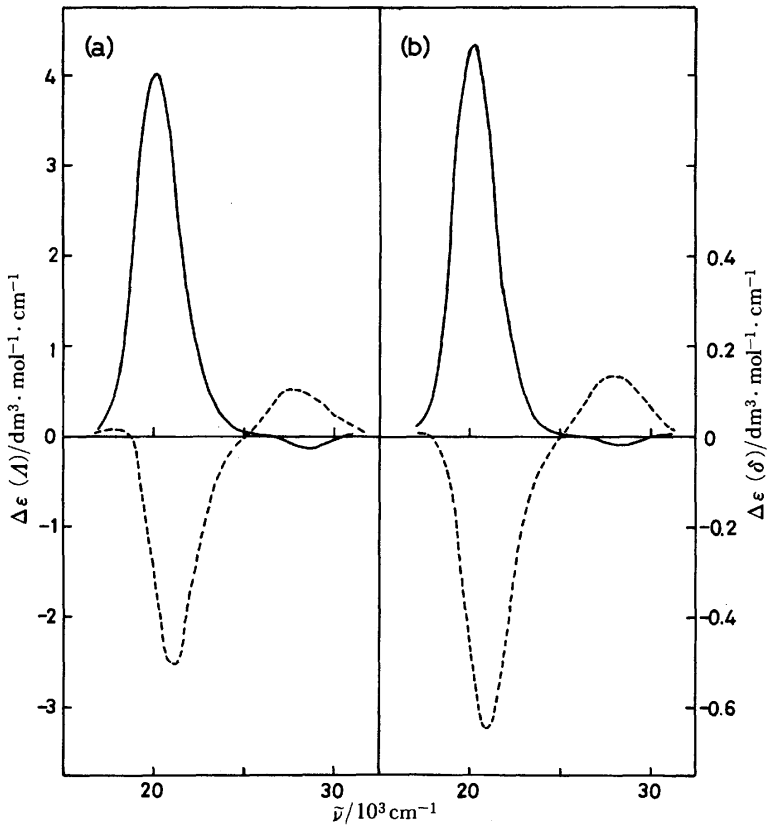

Fig. 7. Configurational effect of CD (*Δ* ε (*Λ*)) (—) and vicinal effect of CD (*Δ* ε (*δ*)) (--) of [Co(*R,S,S*-3m-chxn)$_3$]$^{3+}$.
a—: Calculated *Δ* ε (*Λ*)=1/2{*mer*-*Λ*(*lel*$_3$)−*mer*-*Δ*(*ob*$_3$)}, --: Calculated *Δ* ε (*δ*)=1/6{*mer*-*Λ*(*lel*$_3$)+*mer*-*Δ*(*ob*$_3$)}, b—: Calculated *Δ* ε (*Λ*)=1/2{*fac*-*Λ*(*lel*$_3$)−*fac*-*Δ*(*ob*$_3$)}, --: Calculated *Δ* ε (*δ*)=1/6{*fac*-*Λ*(*lel*$_3$)+*fac*-*Δ*(*ob*$_3$)}.

As is shown in Fig. 7, the configurational and vicinal CD curves derived from the *fac*-isomers resembled the respective curves from the *mer*-isomers. The CD strengths of the vicinal effect of the *tris*(*R,S,S*-3m-chxn) complexes were very similar to those of $[Co(R\text{-pn})_3]^{3+}$,[26-29] and $[Co(R\text{-chxn})_3]^{3+}$.[29] The *R,S,S*-3m-chxn complexes, as well as other related complexes involving cyclohexane rings in their structure, such as $[Co(R\text{-chxn})_3]^{3+}$,[29] $[Co(cis\text{-chxn})_3]^{3+}$,[30,31] and $[Co(R,S\text{-2m-amcha})_3]^{3+}$,[1] showed quite a large configurational effect.

We wish to thank the Instrument Center, Institute for Molecular Science, for the use of a NMR spectrometer (JEOL JNM-FX-100). We are also grateful to Misses Shizuko Iwauchi and Toshiko Naito of the Analytical Center of the Nagoya City University for their elemental analyses.

References

1) Part VII of this series: R. Saito and Y. Kidani, *Bull. Chem. Soc. Jpn.*, **56**, 449 (1983).
2) E. F. Corey and J. C. Bailar, *J. Am. Chem. Soc.*, **81**, 2620 (1959).
3) M. Kojima and J. Fujita, *Bull. Chem. Soc. Jpn.*, **54**, 2691 (1981).
4) H. Ito, J. Fujita, and K. Saito, *Bull. Chem. Soc. Jpn.*, **40**, 2584 (1967).
5) L. E. Erickson, J. E. Sarneski, and N. Reilley, *Inorg. Chem.*, **14**, 3007 (1975).
6) S. E. Harnung, B. S. Sørensen, I. Creaser, H. Maegaard, U. Pfenninger, and C. E. Schäffer, *Inorg. Chem.*, **15**, 2123 (1976).
7) J. F. Bussert, K. W. Greenlee, J. M. Derfer, and C. E. Boord, *J. Am. Chem. Soc.*, **78**, 6076 (1956).
8) N. W. Werner and J. Casanova, Jr., *Org. Synth.* **V**, 273 (1973).
9) For details, see the later section.
10) T. G. Appleton and J. R. Hall, *Inorg. Chem.*, **9**, 1800 (1970).
11) K. Matsumoto, S. Ooi, M. Sakuma, and H. Kuroya, *Bull. Chem. Soc. Jpn.*, **49**, 2129 (1976).
12) R. G. Asperger and C. F. Liu, *Inorg. Chem.*, **4**, 1492 (1965).
13) R. S. Treptow, *Inorg. Chem.*, **5**, 1593 (1966).
14) R. Saito and Y. Kidani, unpublished results.
15) S. Yano, T. Tukuda, M. Saburi, and S. Yoshikawa, *Inorg. Chem.*, **17**, 2520 (1978).
16) C. J. Hawkins, L. Larsen, and I. Olsen, *Acta Chem. Scand.*, **19**, 1915 (1965).
17) B. Bosnich and J. M. Harrowfield, *J. Am. Chem. Soc.*, **94**, 3425 (1972).
18) S. Yano, M. Saburi, S. Yoshikawa, and J. Fujita, *Bull. Chem. Soc. Jpn.*, **49**, 101 (1976).
19) E. A. Sullivan, *Can. J. Chem.*, **57**, 67 (1979).
20) C. J. Hawkins and J. Martin, *Inorg. Chem.*, **21**, 1074 (1982).
21) K. Nakayama, T. Komorita, and Y. Shimura, *Bull. Chem. Soc. Jpn.*, **57**, 1336 (1984).
22) M. Kojima and K. Yamasaki, *Bull. Chem. Soc. Jpn.*, **48**, 1093 (1975).
23) S. Bagger and O. Band, *Acta Chem. Scand.*, **30**, 765 (1976).
24) K. Sakakibara, Y. Yoshikawa, and H. Yamatera, *Bull. Chem. Soc. Jpn.*, **52**, 2725 (1979).
25) J. H. Dunlop, R. D. Gillard, and G. Wilkinson, *J. Chem. Soc.*, **1964**, 3160.
26) A. J. McCaffery, S. F. Mason, and B. J. Norman, *Chem. Commun.*, **1965**, 49.
27) K. Ogino, K. Murano, and J. Fujita, *Inorg. Nucl. Chem. Lett.* **4**, 351 (1968).
28) S. F. Mason, *J. Chem. Soc. (A)*, **1971**, 667.
29) M. Kunimatsu, H. Kanno, M. Kojima, K. Kashiwabara, and J. Fujita, *Bull. Chem. Soc. Jpn.*, **53**, 1571 (1980).
30) K. Ooba, J. Kojima, and J. Fujita, 36th National Meeting of the Chemical Society of Japan, Tokyo, April, 1977, Abst. No. 2D39.
31) H. Toftlund and T. Laier, *Acta Chem. Scand., A.* **31**, 651 (1977).

 © 1984 The Chemical Society of Japan Bull. Chem. Soc. Jpn., 57, 3437—3442 (1984)

Studies of the Hydrous Tin(IV) Oxide Ion-exchanger. III. Affinity for Cations and Some Applications

Yasushi INOUE* and Hiromichi YAMAZAKI
Department of Nuclear Engineering, Faculty of Engineering, Tohoku University, Aramaki, Sendai 980
(Received June 5, 1984)

The distribution coefficients of hydrous tin(IV) oxide for various cations were measured. The affinity series for alkali-metal ions and alkaline-earth-metal ions were $Li^+ \gg Na^+ > K^+ > Rb^+ \geqq Cs^+$ and $Mg^{2+} > Ca^{2+} > Sr^{2+} \approx Ba^{2+}$ respectively; the values decreased in the order of the increasing crystal radii of the cations. For transition-metal ions, which showed a markedly high affinity, the distribution coefficients had a strong correlation with the hydrolysis constants of the cations and the stability constants of their acetato complexes. Based on these findings, the transition-metal ions are considered to be adsorbed on the exchanger by a bond partially covalent in character, rather than by a pure ionic bond. By using NH_4Cl and $HClO_4$ solutions as eluants, nearly quantitative separations of Cs-Na-Li and Cs-Na-Sr were effected with a relatively small column. The applicability of the exchanger to the group separation of actinoids from long-lived fission products was also suggested.

Through a comprehensive study aimed at preparing a hydrous tin(IV) oxide ion-exchanger, the best conditions for synthesizing the exchanger were established; they have been reported previously. The method has the merits of simplicity and good reproducibility. The exchanger in the H^+ form prepared by this method has a composition of $SnO_2 \cdot 2.18H_2O$ and an ion-exchange capacity of 1.18 mmol Na^+ g^{-1} (at pH 11.3). The adsorption of cations on this material was confirmed to occur by means of an ion-exchange reaction, as shown by the fact that the equivalent amount of the hydrogen ion was released by the uptake of a definite amount of alkali-metal or alkaline-earth-metal ions. The material is an amphoteric ion-exchanger possessing at least two kinds of weakly dissociable ion-exchange sites. Other important properties of the exchanger, such as stability against various chemicals, stability during storage, dependence of the water content on the ionic composition, and physical properties, were also investigated, as has been described in the foregoing reports.[1]

The affinity of the exchanger for various cations is important in understanding the characteristic of the exchanger. There have, however, been only a few reports on the selectivity of the hydrous tin(IV) oxide. Fuller and Donaldson reported this selectivity series: $Cu(II) > Zn(II) > Co(II) \geqq Fe(II) > Ni(II) > Mn(II)$ and attempted the column separation of these transition-metal ions.[2] However, such data for deducing the ion-exchange mechanism are conspicuously lacking at the present time.

The purpose of the present investigation is to understand the cation-exchange reaction of the exchanger through the examination of the distribution coefficients of various cations as a function of the pH, and to show the applicability of the exchanger to the selective separation of actinoids in high-level radioactive waste and to the chromatographic separation of alkali-metal and alkaline-earth-metal ions.

Experimental

Reagents and Apparatus. The hydrogen-ion and sodium-ion forms of the hydrous tin(IV) oxide were prepared by the procedure recommended previously.[1] The exchanger in the Na^+ form was then converted to the NH_4^+ form by means of the column method; a solution of 0.3% NH_3 aq and 0.1 mol dm^{-3} NH_4Cl (pH 10.4) was passed through a column containing the Na^+-form exchanger until no sodium ion was detected in the effluent. The composition of the exchangers thus prepared is shown in Table 1. All the reagents used were of the highest-purity grade obtained from Wako Pure Chemical Industries, Ltd., or E. Merck AG. A well-type NaI (Tl) scintillation counter (Fuji Denki Model NHS-2) was used for the measurement of the γ-radioactivity. All the other apparatuses were the same as described previously.[1]

Distribution Coefficients. The distribution coefficient, K_d, was determined in the following way unless otherwise noted.

A 0.50-g portion of the exchanger in the desired ionic form was placed in contact, in a thermostatted water bath at 25 °C, with 20 cm^3 of a suitable solution containing 1×10^{-4} mol dm^{-3} of the cation in question until the concentration of the cation in the supernatant solution became constant (about 3 to 14 d). The pH and the concentration of the cation in the solution were then measured. The K_d value was calculated by

TABLE 1. COMPOSITION OF THE EXCHANGERS

Ionic form	M^+ content	Water content[1]	Composition (molar ratio)		
	mmol/g M^+form	wt%	SnO_2	M_2O	H_2O
H^+	—	20.51	1	—	2.16
Na^+	1.22	16.81	1	0.116	1.77
NH_4^+	0.86	20.24	1	0.081	1.66

1): Calculated from weight loss when 0.50 g of exchanger was calcinated at 850 °C.

means of the following equation:

$$K_d = \frac{C_i - C_f}{C_f} \cdot \frac{V}{m} \ (\mathrm{cm^3\ g^{-1}}),$$

where C_i and C_f are, respectively, the initial and the final concentration in the solution; V, the volume of the solution in cm^3, and m, the weight of the exchanger in g.

The metal ions were added as their chlorides, except Fe^{3+}, Cr^{3+}, Th^{4+}, and UO_2^{2+}, for which the corresponding nitrates were used. The pH was adjusted by using a desired combination of 0.3 moldm^{-3} $NaClO_4$, and 0.3 moldm^{-3} $HClO_4$ or 0.3 moldm^{-3} NaOH (ionic strength, 0.09). The analyses of Cs, Sr, Ba, Mn, Fe, Co, Cu, Zn, Sc, Y, La, Ce, Eu, Np, and Am were carried out radiometrically using ^{137}Cs, ^{85}Sr, ^{133}Ba, ^{54}Mn, ^{59}Fe, ^{60}Co, ^{64}Cu, ^{65}Zn, ^{46}Sc, ^{88}Y, ^{140}La, ^{144}Ce, ^{152}Eu, ^{239}Np, and ^{241}Am respectively as tracers. Their radioactive purity was confirmed by means of gamma-ray spectrometry. The ^{239}Np tracer was prepared by milking from ^{243}Am by the method of Sill.[3] The oxidation state of neptunium at the tracer concentration was adjusted by the method of Inoue and Tochiyama.[4] The Th^{4+} and UO_2^{2+} were analyzed spectrophotometrically using arsenazo III[5] and 2-(5-bromo-2-pyridylazo)-5-(diethylamimo)phenol[6] respectively as coloring reagents, while the concentration of the other cations were determined by means of atomic-absorption spectrophotometry.

Column Operation. To 2g of the exchanger in the NH_4^+ form was added a suitable amount of the solution used for converting the exchanger to the NH_4^+ form, and the slurry was poured into a glass column, 0.6cm in inside diameter. The column thus prepared had a height of 4.5cm. A solution containing 10 mequivdm^{-3} of the desired cation was passed through the column at a flow rate of 0.1 $cm^3 min^{-1}$.

Results and Discussion

Distribution Coefficients. Figure 1 shows the K_d values for Co^{2+} as a function of the loading at a nearly constant pH value (2.03—2.07). The K_d values were nearly constant lower than 4×10^{-5} mequivg^{-1}, wherefrom they decreased with an increase in the loading of the exchanger.

The cation-exchange reaction between A^+ and M^{n+} is expressed as:

$$n\overline{A}^+ + M^{n+} = \overline{M}^{n+} + nA^+, \quad (1)$$

for which the equilibrium constant, K, can be written as:

$$K = \frac{\bar{a}_M a_A^n}{\bar{a}_A^n a_M} = \frac{\bar{\gamma}_M[\overline{M}]\gamma_A^n[A]^n}{\gamma_M[M]\bar{\gamma}_A^n[\overline{A}]^n}. \quad (2)$$

In Eq. 2, a bar refers to the exchanger phase; a denotes the activity; [ ], the concentration, and γ, the activity coefficient. For the sake of simplicity, the charge in the cations is omitted in this expression. The distribution coefficient of M^{n+} is expressed as:

$$K_d = [\overline{M}]/[M] \ (\mathrm{cm^3\ g^{-1}}). \quad (3)$$

When the amount of M^{n+} uptaken is extremely small as compared with that of A^+ in the exchanger, $\bar{a}_A$ and $\bar{\gamma}_M$ are regarded as constant. Moreover, γ_M/γ_A^n is also constant if the ionic strength of the solution is kept constant. Under such conditions, the following equation holds:

$$\log K_d = \text{const.} - n \log [A], \quad (4)$$

which implies that a plot of log K_d *vs.* log [A] should be linear with a slope of $-n$.

The pH-dependency of the K_d values for Co^{2+}, Sr^{2+}, and Y^{3+} is shown in Fig. 2 for varying concentration of the cations in the solutions. The linear relation between log K_d and pH was observed as predicted from Eq. 4. The slopes of the straight lines, however, depended on the concentration and approached n only when the concentration became extremely dilute: For Co^{2+} and Sr^{2+}, $\leqq10^{-7}$ moldm^{-3}; for Y^{3+}, the tracer concentration. This strong dependency of the K_d values on the concentration of the cations may be ascribed to the limited amount of the cation-exchange sites in the

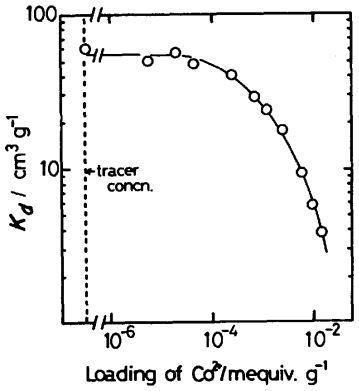

Fig. 1. Dependency of the distribution coefficient of Co^{2+} on loading.
Conditions; Ionic strength: 0.09 ($HClO_4$-$NaClO_4$), Temperature: 25°C, pH: 2.03—2.07.

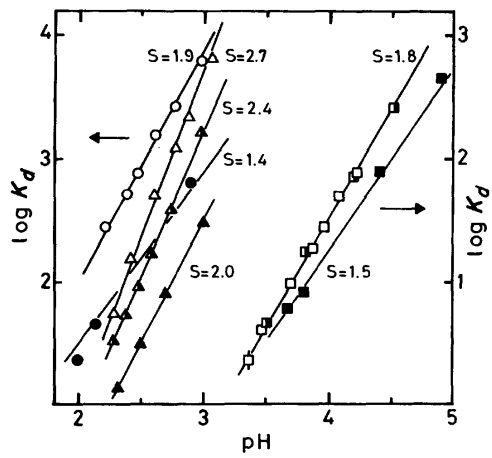

Fig. 2. Effect of the concentration of cations on their distribution coefficients.
Initial concentration of cation/mol dm^{-3}, Sr^{2+}; ■: 1×10^{-4}, ◨: 1×10^{-7}, □: 1×10^{-10}, Co^{2+}; ●: 1×10^{-4}, ○: 1×10^{-7}, Y^{3+}; ▲: 1×10^{-4}, ◭: 1×10^{-7}, △: 1×10^{-10}. S: Slope.

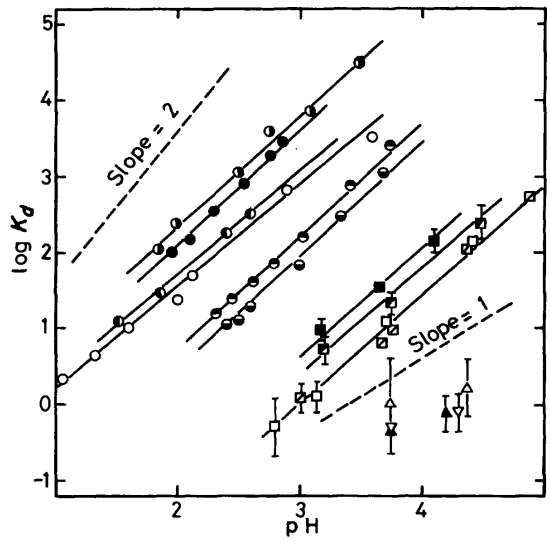

Fig. 3. Log K_d for some metal ions as a function of pH.
Conditions; Ionic strength: 0.09 ($HClO_4$-$NaClO_4$-NaOH), Temperature: 25°C.
Slope; ◑: Cu^{2+} 1.4, ●: UO_2^{2+} 1.5, ◐: Zn^{2+} 1.4, ○: Co^{2+} 1.4, ◒: Mn^{2+} 1.5, ◒: Ni^{2+} 1.5, ■: Mg^{2+} 1.5, ◩: Ca^{2+} 1.5, □: Sr^{2+} 1.5, ◰: Ba^{2+} 1.5, △: Li^+ —, ▲: Na^+ —, ▽: Cs^+ —.

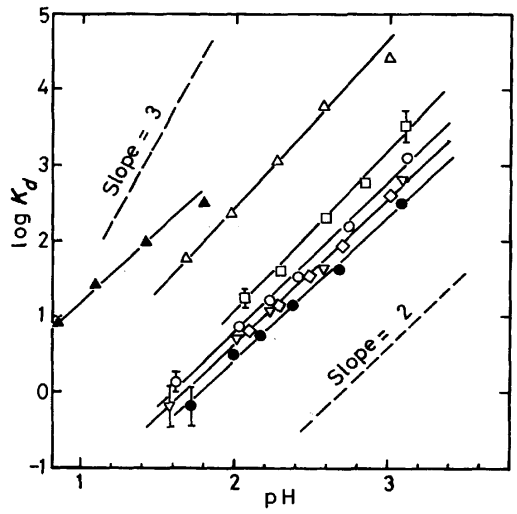

Fig. 4. Log K_d for some metal ions as a function of pH.
Conditions; Ionic strength: 0.09 ($HClO_4$-$NaClO_4$), Temperature: 25°C.
Slope; ▲: Fe^{3+} 2.0, △: Sc^{3+} 2.3, □: Cr^{3+} 2.2, ○: Eu^{3+} 2.1, ◇: Y^{3+} 2.1, ▽: Ce^{3+} 2.1, ●: La^{3+} 2.0.

pH region adopted in the present experiment, since the isoelectric point of the exchanger is around pH 4, as has been reported previously.[1] Because of this observation, it is preferable to use a concentration lower than 10^{-7} mol dm^{-3} in making a strict comparison of the selectivity of the exchanger between various cations. The lack of the sensitivity of the analytical methods for some cations, however, makes this very difficult. As the next best way, the distribution coefficients for various cations were compared at the lowest possible concentration and the constant initial concentration of the cations in solution, 1×10^{-4} mol dm^{-3}.

Figure 3 shows the pH-dependency of the K_d values for uni- and bivalent cations. Based on the selectivity, these cations can be grouped into three classes: transition metal>alkaline earth metal>alkali metal, in the same manner as ion-exchange resin. However, the order of selectivity for the alkaline-earth-metal ions, $Mg^{2+}>Ca^{2+}>Sr^{2+}\approx Ba^{2+}$, is the exact reverse of what would be expected from the ion-hydration theory, which claims that the strength of the electrostatic interaction between a hydrated cation and a fixed anionic group determines the ion-exchange selectivity of the strongly acidic resin; in fact, the selectivity coefficients for ions with the same charge increase with a decrease in the hydrated ionic radius. The selectivity series for transition-metal ions was $Cu^{2+}\geqq UO_2^{2+}>Zn^{2+}\geqq Co^{2+}>Mn^{2+}\geqq Ni^{2+}$. Figure 4 shows the results for tervalent transition-metal ions. When these results are compared with those for bivalent transition-metal ions, the affinity of these ions is not so great as would be expected from their charge. These affinity series, together with those for alkaline-earth-metal ions, show that the selectivity is higher for metal ions of a smaller crystalline radius than for those of a larger one; this cannot be explained by the ion-hydration theory. The slopes of the straight lines were smaller than the expected n, which is predicted from Eq. 4, as is shown in Figs. 3 and 4.

Since the amount of alkali-metal ions uptaken was very small in an acidic medium, a comparison of the affinity for these ions cannot be made by the use of the hydrogen-ion form. Thus, the ion-exchange reactions between Na^+ and the other alkali-metal ions were examined in an alkaline medium, as is shown in Fig. 5. This figure indicates that linear relationships with a slope of −1 held between the log K_d for alkali metal ions and the logarithm of the concentration of Na^+ in the solution; this agrees well with Eq. 4. This agreement appears unreasonable, however, because the decrease in the concentration of Na^+ from 0.1 mol dm^{-3} to 0.01 mol dm^{-3} will increase the activity coefficient of the cations and decrease the concentration of Na^+ in the exchanger. The change in log γ_M/γ_{Na}, however, is estimated to be smaller than 0.02 from the Debye-Hückel equation. The decrease in Na^+ in the exchanger was analyzed and found to be smaller than 0.04 mmol g^{-1}. Consequently, the present experimental conditions satisfy the assumptions made for deducing Eq. 4. Figure 5 also indicates that the order of the selectivity is: $Li^+\gg K^+>Rb^+\geqq Cs^+$. The distribution coefficients for Li^+, Na^+, and Cs^+ on the exchanger in NH_4^+ form were measured by the column method described in the experimental section; the results are presented in Table 2, along with the experimental conditions. The order of the selectivity, $Li^+\gg Na^+>Cs^+$, like that observed in Fig. 5, is the reverse of what would be expected from the ion-hydration theory.

Thus, the ion-exchange reaction may be brought

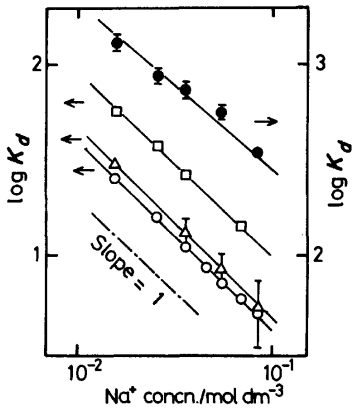

Fig. 5. Log K_d for alkali metal ions as a function of Na^+ concentration.
Conditions; Exchanger: 0.50 g (Na^+ form), Solution: 20 cm^3, pH: 10.5—10.9, Temperature: 25 °C.
Metal ion; ●: Li^+, □: K^+, △: Rb^+, ○: Cs^+.

TABLE 2. DISTRIBUTION COEFFICIENT OF NH_4^+-FORM EXCHANGER FOR ALKALI- METAL IONS(COLUMN METHOD)

	Loading	Eluant	Elution rate	K_d
	mequiv		cm^3/min	cm^3/g
Li^+	0.020			40±0.5
		5×10^{-2} mol dm^{-3}	0.07	
Na^+	0.020		≀	9.8±0.3
		NH_4Cl	0.12	
Cs^+	0.020			4.2±0.2

Column: 0.6 cmφ×4.5 cm(NH_4^+ form, 100—200 mesh, 2 g).

about by an electrostatic interaction between an unhydrated cation and the negatively charged site in the exchanger, similar to a weakly acidic resin, such as the carboxylic-acid and phosphonic-acid types. Such interaction would be closely related to the ionic potential of the cations. Figure 6 shows the correlation between log K_d at pH 3 and the ionic potential. Here, the ionic radii used were those obtained by using crystals in which the ion has the coordination number of 6,[7] while the log K_d values which could not be obtained by the experiment were those estimated from the extrapolation of the linear log K_d *vs.* pH plot. The correlation coefficient (R) is 0.76. At pH 2 and 4, the R values were 0.65 and 0.83 respectively. Therefore, as a whole, the affinity of the exchanger for various cations is associated with the electrostatic interaction between an unhydrated cation and the anionic site in the exchanger. However, the selectivity series for transition-metal ions deviates markedly from this relation; these ions have high K_d values, even in such an acidic medium as when a negligible amount of the representative element is adsorbed. This finding compels us to consider that factors other than the electrostatic force may play an important part in deciding the selectivity of the exchanger. In order to know such factors, the K_d values for metal ions at pH 3 were compared with their first hydrolysis constants[8] (Fig. 7) and the first stability constants of their acetato

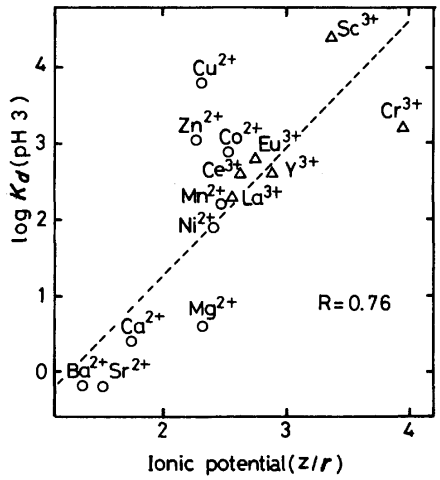

Fig. 6. Relation between logK_d and ionic potential of cation.
Ionic potential=z/r; z: Charge of cation, r: Ionic radius (coordination number (6)).[7]
R: Correlation coefficient.

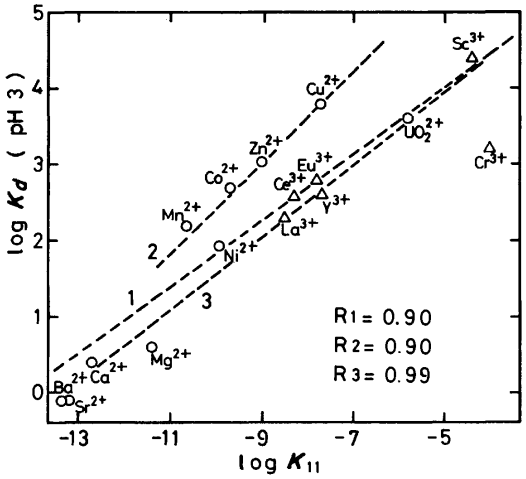

Fig. 7. Relation between logK_d and first hydrolysis constant of cation.
K_{11}: First hydrolysis constant.[8] R: Correlation coefficient.

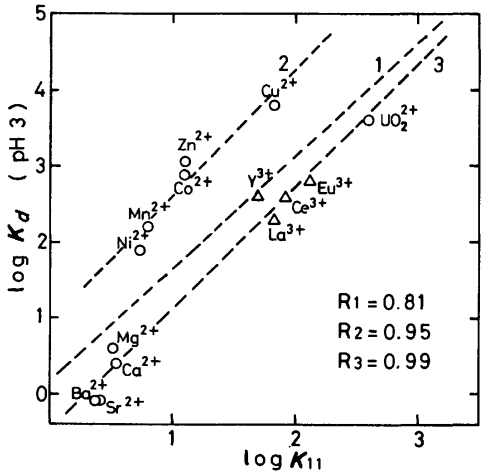

Fig. 8. Relation between log K_d and stability constant of $ML^{(n-1)+}$(L^-: CH_3COO^-).
K_{11}: Stability constant; equilibrium quotient at 25 °C and ionic strength 1.0.[9] R: Correlation coefficient.

complexes[9] (Fig. 8). As can be seen from Fig. 7, the K_d values have a strong correlation with the hydrolysis constant (R_1=0.90). Also, the softness of metal ions as Lewis acid affects the correlation: metal ions with characteristics between hard and soft acids, Cu^{2+}, Zn^{2+}, Co^{2+}, Ni^{2+}, and Mn^{2+}, show larger K_d values than on hard acids, such as uranyl(VI), lanthanoid, and alkaline-earth-metal ions. When metal ions are divided into two such groups, the K_d values can be more closely related to the hydrolysis constants and the first stability constants of acetato complexes (R_2, R_3). Consequently, we can conclude that the formation of a covalent bond between the anionic sites in the exchanger and metal ions plays a part in determining the selectivity of the exchanger, along with the remote coulombic interaction.

The Separation of Actinoids from Fission Products. As the K_d values for UO_2^{2+} are considerably higher than those for other transition-metal ions, it is considered possible to use the exchanger for separating actinoids from fission products in radioactive liquid waste. For this purpose, it is necessary to examine the selectivity for actinoids in a concentrated nitrate medium. Figure 9 shows the pH-dependency of the K_d values for Th^{4+}, UO_2^{2+}, NpO_2^+, NpO_2^{2+}, and Am^{3+} in a 1 mol dm^{-3} nitrate medium at 50 °C. Tracer concentrations of neptunium and americium were used, whereas the concentrations of Th^{4+} and UO_2^{2+} were 9.5×10^{-5} mol dm^{-3} and 1.1×10^{-5} mol dm^{-3} respectively, because of the limited sensitivity of the analytical method used for the present experiment. If we consider the dependency of the K_d values on the concentration (Figs. 1 and 2), the K_d values for these last two elements will be higher than those in Fig. 9 when their concentrations are at a tracer level. Thus, the difference in affinity between Th^{4+} and other actinoid ions is much greater than that shown in Fig. 9. For the same reason, the U(VI) ion shows an affinity higher than that indicated in the figure. The Np(V) ion showed a K_d value higher than 10^4 cm^3 g^{-1} at pH 3 where the uptake of alkali-metal ions was negligibly small. The Np(VI) ion also showed a high affinity, similar to that of the U(VI) ion, but it did not differ so markedly from the Np(V) ion as would be expected from the difference in charge. The high affinities for uranyl and neptunyl species cannot be explained only in terms of the electrostatic interaction between the ions and the anionic sites in the exchanger; it must also be ascribed to the formation of a bond with a partially covalent character, as has been mentiond before. On the other hand, Am^{3+} and Eu^{3+} exhibited almost the same affinity as the Np(VI) ion. Similar to Sr^{2+}, Co^{2+}, or Y^{3+} in a tracer concentration, the slopes of the straight lines of the log K_d *vs.* pH plot were found to be +1 and +2 for the Np(V) and Np(VI) ions respectively. For the Np(VI) ion, the plot deviated from linearity above pH 2.6. This deviation is probably due to a hydrolysis of the ions. The slope of this plot for Am^{3+} and Eu^{3+} was not 3, but about 2, despite the tracer concentration. Korotkin

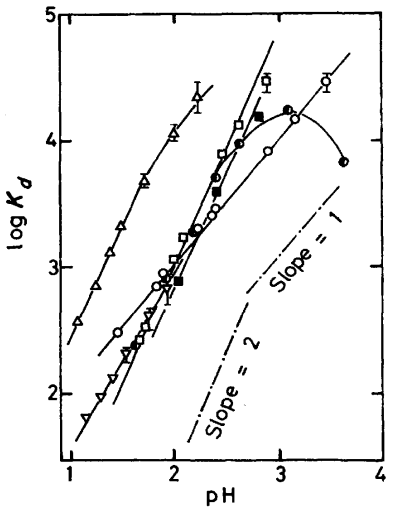

Fig. 9. Log K_d for some actinoid ions as a function of pH.
Conditions; Exchanger: 0.25 g, Solution: 20 cm^3, Ionic strength: 1.0 (HNO_3-NH_4NO_3), Temperature: 50 °C.
Concentration of cation; △: Th(IV) 9.5×10^{-5} mol dm^{-3}, ▽: U(VI) 1.1×10^{-5} mol dm^{-3}, ○: Np(V) tracer, ◐: Np(VI) tracer in 4×10^{-3} mol dm^{-3} $KMnO_4$, □: Am(III) tracer, ■: Eu(III) tracer.

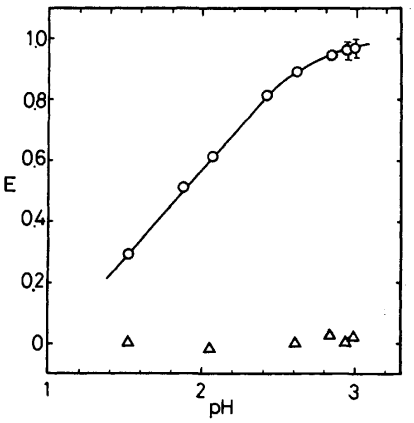

Fig. 10. Separation of UO_2^{2+}-Sr^{2+} by hydrous SnO_2 (Batch method).
Conditions; Exchanger: 0.25 g, Solution: 20 cm^3, Ionic strength: 1.0 (HNO_3-NH_4NO_3), Temperature: 50 °C.
Initial concentration; ○: UO_2^{2+} 1.1×10^{-3} mol dm^{-3} △: Sr^{3+} 1.0×10^{-3} mol dm^{-3}.

$$E\equiv \frac{C_{initial}-C_{final}}{C_{final}} \text{ or } \frac{a_{initial}-a_{final}}{a_{final}};\quad C=\mu g\,U/cm^3,$$

a=cpm/cm^3.

reported, in his study of the hydrolysis of Am(III) at concentrations lower than 10^{-6} mol dm^{-3}, that Am(III) exists as $Am(NO_3)^{2+}$ in a 0.1 mol dm^{-3} nitrate solution.[10] Based on this view, it may be considered that the nitro complexation is responsible for the behavior of Am^{3+} and Eu^{3+} similar to that of a double-charged cation such as NpO_2^{2+}.

As has been mentiond above, the exchanger exhibits a high selectivity for actinoids in a 1 mol dm^{-3} nitrate

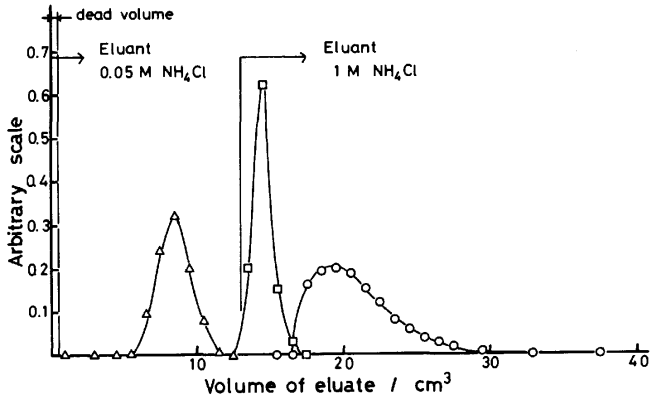

Fig. 11. Separation of Cs^+-Na^+-Li^+ by NH_4^+-form exchanger.
Column: 0.6 cmϕ×4.5 cm (100—200 mesh, 2.0 g), Elution rate: 5—6 $cm^3 h^{-1}$, Loading: 0.020 mequiv of each cation, Cation; △: Cs^+, □: Na^+, ○: Li^+.

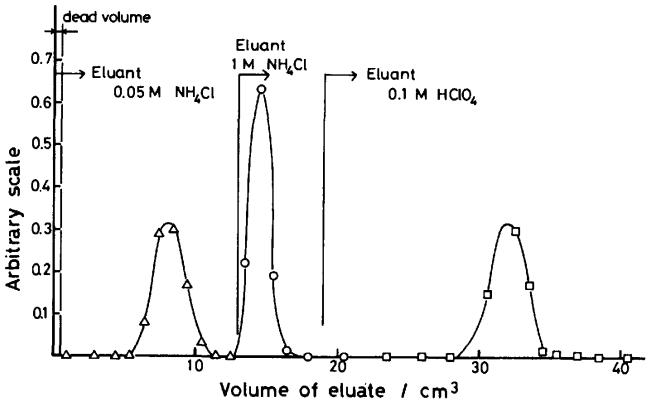

Fig. 12. Separation of Cs^+-Na^+-Sr^{2+} by NH_4^+-form exchanger.
Conditions are the same as those in Fig. 11.
Cation; △: Cs^+, ○: Na^+, □: Sr^{2+}.

medium, regardless of their oxidation states. Hence, actinoids may be selectively separated from such long-lived fission-products as ^{137}Cs and ^{90}Sr. The uptake of UO_2^{2+} and Sr^{2+}, both of 10^{-3} mol dm^{-3}, was measured in a 1 mol dm^{-3} nitrate medium at varying pH values, as is shown in Fig. 10. This figure shows that UO_2^{2+} could be separated nearly quantitatively from Sr^{2+} by a single-batch-operation at pH 2.8. As the exchanger exhibits a higher affinity for Sr^{2+} than for Cs^+, the quantitative separation of UO_2^{2+} will be much easier from Cs^+ than from Sr^{2+}. These facts suggest the applicability of the exchanger for separating actinoids from ^{137}Cs and ^{90}Sr, which are the major constituents of fission products in aged, high-level liquid wastes.

Separation of Li-Na-Cs and Na-Cs-Sr. In order to confirm the applicability of the exchanger to chromatographic separation, attempts were made to separate Li^+, Na^+, Cs^+, and Sr^{2+} by using the exchanger in a salt form which exhibits different affinities for these ions. The results are presented in Fig. 11. In this experiment, the exchanger in the NH_4^+ form was used. Cs^+ was quantitatively eluted with a 0.05 mol dm^{-3} NH_4Cl solution, while Na^+ and Li^+ were eluted with a 1 mol dm^{-3} NH_4Cl solution, in that order. The yield of the sodium ion was 99% at the eluate volume where Li^+ elution commenced. Lithium ions, however, showed a heavy tailing, which indicates that the neutral solution of ammonium salt was less effective. Figure 12 shows the separation of Na^+, Cs^+, and Sr^{2+}. After Cs^+ and Na^+ had been eluted with the NH_4Cl solution in a manner similar to that shown in Fig. 11, a 0.1 mol dm^{-3} $HClO_4$ solution was passed through, and then the Sr^{2+} was quantitatively eluted with 21 cm^3 of this eluant.

References

1) Y. Inoue and H. Yamazaki, *Bull. Chem. Soc. Jpn.*, **55**, 3782 (1982); **57**, 1534 (1984).
2) J. D. Donaldson and M. J. Fuller, *J. Inorg. Nucl. Chem.*, **30**, 1083, 2841 (1968); **32**, 1703 (1970).
3) C. W. Sill, *Anal. Chem.*, **38**, 802 (1966).
4) Y. Inoue and O. Tochiyama, *J. Inorg. Nucl. Chem.*, **39**, 1443 (1977).
5) H. Onishi, *Analyst*, **12**, 1153 (1963).
6) D. A. Johnson and T. M. Florence, *Anal. Chim. Acta*, **53**, 73 (1971); *Talanta*, **22**, 253 (1975).
7) R. D. Shannon and C. T. Prewitt, *Acta Crystallogr., Sect. A*, **25**, 925 (1969); *ibid.*, **32**, 751 (1976).
8) C. F. Baes, Jr., and R. E. Mesmer, "The Hydrolysis of Cations," John Wiley and Sons, Inc., New York (1976).
9) A. E. Martell and R. M. Smith, "Critical Stability Constants, Volume 3: Other Organic Ligands," Plenum Press, New York (1977), p. 3.
10) Yu. S. Korotkin, *Radiokhimiya*, **15**, 766 (1973).

Preparation, Stereochemistry, and Kinetics of Isomerization and Racemization of Acetylacetonato Complexes of Chromium(III) Containing 2,2′-Bipyridine *N,N′*-Dioxide or Its 3,3′-Dimethyl Derivative

Hideaki KANNO,* Shunji UTSUNO, and Junnosuke FUJITA†

Department of Chemistry, Faculty of Science, Shizuoka University, Oya, Shizuoka 422

†*Department of Chemistry, Faculty of Science, Nagoya University, Chikusa-ku, Nagoya 464*

(Received June 25, 1984)

New acetylacetonato (acac) chromium(III) complexes of the type, $[Cr(acac)_{3-n}L_n]^{n+}$ (n=1 and 2), where L denotes a seven-membered chelate ligand, 2,2′-bipyridine *N,N′*-dioxide (bpdo) or 3,3′-dimethyl-2,2′-bipyridine *N,N′*-dioxide (*rac*- or *R*-mbdo), were prepared. Optically active $[Cr(acac)_2(R\text{-mbdo})]^+$ and $[Cr(acac)(R\text{-mbdo})_2]^{2+}$ yielded only one isomer and were assigned to $\Delta(\lambda)(lel)$ and $\Delta(\lambda\lambda)(lel_2)$, respectively, on the basis of the circular dichroism spectra and molecular models. The $[Cr(acac)(mbdo)_2]^{2+}$ complex prepared from *rac*-mbdo formed two racemates of diastereomers, $lel_2(\Delta(\lambda\lambda), \Lambda(\delta\delta))$ and $lel\cdot ob$ $(\Delta(\lambda\delta), \Lambda(\delta\lambda))$, whereas $[Cr(acac)_2(bpdo)]^+$ formed only $lel(\Delta(\lambda), \Lambda(\delta))$ isomer which was resolved by column chromatography. Both *rac*- and $(-)_{589}$-$[Cr(acac)(bpdo)_2](ClO_4)_2\cdot H_2O$ resolved by a chemical method were found to crystallize in lel_2 isomer, but isomerize to the isomer in aqueous solution with the rate of 3.31×10^{-3} s^{-1} at 295.2 K, the rate constant for racemization ($\Delta \rightleftarrows \Lambda$) being 1.08×10^{-4} s^{-1} at 295.2 K. An intramolecular conformational inversion of the bpdo chelate ring for the isomerization and an intramolecular twist mechanism for the racemization were proposed.

In a metal complex, 2,2′-bipyridine *N,N′*-dioxide (bpdo) forms a skew seven-membered chelate ring of which conformation can exist in a pair of enantiomers, δ and λ (Fig. 1).[1] For a tris-bpdo complex, there are four possible racemic pairs of diastereomers (conformational isomers), $lel_3(\Delta(\lambda\lambda\lambda), \Lambda(\delta\delta\delta))$, $lel_2\cdot ob(\Delta(\lambda\lambda\delta), \Lambda(\delta\delta\lambda))$, $lel\cdot ob_2(\Delta(\lambda\delta\delta), \Lambda(\delta\lambda\lambda))$, and $ob_3(\Delta(\delta\delta\delta), \Lambda(\lambda\lambda\lambda))$, and the diastereomerism is analogous to that in $[M(en)_3]^{n+}$ (en=ethlyenediamine).[2] However, it was found that tris-type chromium(III) complexes with bpdo[3] and its derivative, 3,3′-dimethyl-2,2′-bipyridine *N,N′*-dioxide (mbdo)[4] give one and three diastereomers, respectively, and that $[Cr(bpdo)_3]^{3+}$ racemizes spontaneously in aqueous solution.[3] These results indicate that the bpdo chelate ring is flexible and changes its conformation ($\delta \rightleftarrows \lambda$) very easily. On the other hand, the mbdo chelate ring can not change its conformation because of the steric hindrance due to the methyl groups.[4]

This paper describes the preparation and stereochemistry of chromium(III) complexes of the type, $[Cr(acac)_{3-n}L_n]^{n+}$ (n=1, 2; L=bpdo, mbdo). Since the acac chelate ring is assumed to be planar, $[Cr(acac)_2L]^+$ and $[Cr(acac)L_2]^{2+}$ (L=bpdo or mbdo) have two $[lel(\Delta(\lambda), \Lambda(\delta))$ and $ob(\Delta(\delta), \Lambda(\lambda))]$ and three $[lel_2(\Delta(\lambda\lambda), \Lambda(\delta\delta))$, $lel\cdot ob(\Delta(\lambda\delta), \Lambda(\delta\lambda))$, and $ob_2(\Delta(\delta\delta), \Lambda(\lambda\lambda))]$ possible racemic pairs of diastereomers, respectively. In a preliminary paper, we have reported that the $[Cr(acac)(bpdo)_2]^{2+}$ complex isomerizes and racemizes spontaneously in aqueous solution at room temperature.[5] Kinetic studies for these reactions will be also described in detail in this paper.

Experimental

Since the new complexes are photosensitive causing hydrolysis, the following experiments were carried out in the dark.

Preparation and Resolution of $[Cr(acac)_2(bpdo)]^+$ and $[Cr(acac)_2(mbdo)]^+$. The complexes were prepared from $[Cr(acac)_3]$ and bpdo or mbdo according to a method similar to that for $[Cr(acac)_2(phen)]^+$ (phen=1,10-phenanthroline).[6] $[Cr(acac)_3]$ (4.0 g, 11.5 mmol) was added to 90% ethanol (400 cm^3) containing bpdo·H_2O[7] (2.4 g, 11.6 mmol) or racemic mbdo[4] (2.5 g, 11.6 mmol). The solution was adjusted to pH *ca.* 2 with hydrochloric acid and kept at 80 °C with stirring for 2d. The resulting solution was evaporated to a small volume under reduced pressure. The residue was diluted with water (500 cm^3) and the solution was applied on a column (ϕ3.0×50 cm) of SP-Sephadex C-25. The adsorbed species were eluted with a 0.8 mol/dm^3 NaCl solution to give three separate bands. The second green and the last green bands were found to contain bis-bpdo (or bis-mbdo) and tris-bpdo (or tris-mbdo) complexes, respectively. The first violet eluate was collected and mixed with $NaClO_4$ to give violet crystals, which were filtered, washed with a small amount of cold water, and recrystallized from warm water. Yield: bpdo-complex, 3.4g (54%); mbdo-complex, 1.6g (25%). Found for the bpdo complex: C, 44.67; H, 4.00; N, 5.26%. Calcd for $[Cr(acac)_2(bpdo)]ClO_4=C_{20}H_{22}N_2O_{10}ClCr$: C, 44.66; H, 4.12; N, 5.21%. Found for the mbdo complex: C, 46.69; H, 4.62; N, 4.94%. Calcd for $[Cr(acac)_2(mbdo)]ClO_4=C_{22}H_{26}N_2O_{10}ClCr$: C, 46.69; H, 4.63; N, 4.95%. Each of the bpdo and mbdo complexes gave only one racemic pair of diastereomers, no indication for the formation of the other isomer being detected on column chromatograms.

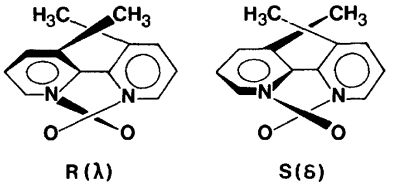

Fig. 1. A pair of enantiomers of mbdo.

The bpdo complex was resolved by DEAE-Sephadex A-25 column chromatography. The perchlorate of the complex (0.08g) was dissolved in water and the solution was applied on a column (ϕ3.8×140cm) of DEAE-Sephadex A-25 in the $[Sb_2(d\text{-tartrato})_2]^{2-}$ form.[8] The complex was eluted with

water, but only one band was observed on the column. However the front and rear fractions of the band showed positive and negative rotations at 546nm, respectively. Each of these fractions was collected separately and chromatographed repeatedly until no further increase in specific rotations at 546nm was observed. Each of the optically pure isomers was isolated as the perchlorate. The $(+)_{546}$- and $(-)_{546}$-isomers showed the following molar rotations in aqueous solutions: $[M]_{546}=+5750°$, $[M]_{546}=-5780°$. Found: C, 43.80; H, 3.94; N, 5.07%. Calcd for $(+)_{546}$-$[Cr(acac)_2(bpdo)]ClO_4\cdot 0.5H_2O=C_{20}H_{23}N_2O_{10.5}ClCr$: C, 43.93; H, 4.24; N, 5.12%.

The resolution of the mbdo complex was not achieved by the same chromatographic method. The optically pure mbdo complex was obtained from optically active mbdo[4] and $[Cr(acac)_3]$.

Preparation of $(+)_{546}$-*[Cr(acac)*$_2$*(R-mbdo)]*$^+$. The complex was obtained by the same method as that for the racemic complex using *R*-mbdo.[4] The perchlorate of the complex was obtained as violet crystals. Found: C, 46.62; H, 4.60; N, 4.75%. Calcd for $(+)_{546}$-$[Cr(acac)_2(R\text{-mbdo})]ClO_4=C_{22}H_{26}N_2O_{10}ClCr$: C, 46.69; H, 4.63; N, 4.95%.

Preparations of [Cr(acac)(bpdo)$_2$*]*$^{2+}$ *and [Cr(acac)(mbdo)*$_2$*]*$^{2+}$. The complexes were prepared by a method similar to that for the above bis-acac complexes using $[Cr(acac)_3]$ (4.0g, 11.5mmol) and bpdo·H_2O (4.8g, 23.3mmol) or racemic mbdo (5.2g, 24.0mmol). The complexes were obtained from the second green band on an SP-Sephadex column chromatograph (ϕ3.0×50cm, 0.8mol/dm^3 NaCl) and isolated as the perchlorate. Yield: bpdo-complex, 2.5g (29%); mbdo-complex, 2.8g (30%). Found for the bpdo complex: C, 40.51; H, 2.91; N, 7.24%. Calcd for $[Cr(acac)(bpdo)_2](ClO_4)_2\cdot H_2O=C_{25}H_{25}N_4O_{15}Cl_2Cr$: C, 40.33; H, 3.39; N, 7.53%. Found for the mbdo complex: C, 42.38; H, 4.35; N, 6.80%. Calcd for $[Cr(acac)(mbdo)_2](ClO_4)_2\cdot 2H_2O=C_{29}H_{35}N_4O_{16}Cl_2Cr$: C, 42.56; H, 4.31; N, 6.85%. For $[Cr(acac)(bpdo)_2]^{2+}$, attempts to separate possible diastereomers were all unsuccessful by column chromatography because of rapid isomerization of the complex (*vide post*). The $[Cr(acac)(mbdo)_2]^{2+}$ complex obtained from racemic mbdo was found to consist of two racemic pairs of diastereomers.[5]

Separation of Diastereomers of [Cr(acac)(mbdo)$_2$*]*$^{2+}$. The $[Cr(acac)(mbdo)_2]^{2+}$ complex (0.05g) was loaded on a column (ϕ2.2×130cm) of SP-Sephadex and eluted with a 0.1mol/dm^3 Na_2SO_4 solution. The column gave two bands, I and II in the order of elution. Each eluate was collected, diluted with water, and applied again on a small column (ϕ2.2×3cm) of SP-Sephadex. The adsorbed complex was eluted with a 1 mol/dm^3 NaCl solution. The eluate was collected and mixed with $NaClO_4$ to give crystals which were recrystallized from warm water. Found for isomer I: C, 42.53; H, 4.46; N, 6.77%. Calcd for $[Cr(acac)(mbdo)_2](ClO_4)_2\cdot 2H_2O=C_{29}H_{35}N_4O_{16}Cl_2Cr$: C, 42.56; H, 4.31; N, 6.85%. Found for isomer II: C, 43.50; H, 3.90; N, 6.77%. Calcd for $[Cr(acac)(mbdo)_2](ClO_4)_2\cdot H_2O=C_{29}H_{33}N_4O_{15}Cl_2Cr$: C, 43.51; H, 4.16; N, 7.00%. The formation ratio, I:II, was about 1:1.

Preparation of $(-)_{589}$-*[Cr(acac)(R-mbdo)*$_2$*]*$^{2+}$. The complex was prepared by the same method as that for the racemic complex using *R*-mbdo and isolated as the perchlorate. Found: C, 43.48; H, 3.96; N, 6.81%. Calcd for $(-)_{589}$-$[Cr(acac)(R\text{-mbdo})_2](ClO_4)_2\cdot H_2O=C_{29}H_{33}N_4O_{15}Cl_2Cr$: C, 43.51; H, 4.16; N, 7.00%. The absorption spectrum of this complex coincides with that of isomer II. The complex corresponding to isomer I was not formed.

Resolution of [Cr(acac)(bpdo)$_2$*]*$^{2+}$. The resolution was achieved by use of the perchlorate of the complex and potassium $(+)_{589}$-tartratoantimonate(III). The resolving agent (0.9g, 1.3mmol) was added to a hot aqueous solution (70°C, 50 cm^3) of the complex (1g, 1.3mmol). The mixture was cooled in an ice bath with stirring to give white precipitate of $KClO_4$. The precipitate was filtered off and methanol (150 cm^3) was added to the filtrate. The resulting solution was cooled in a refrigerator to give green crystals, which were collected, washed with 80% methanol and then methanol, and air-dried. An aqueous solution of these crystals showed a negative rotation at 589nm but lost gradually the activity. Yield: 1.1g. Found: C, 33.63; H, 2.98; N, 4.58%. Calcd for $(-)_{589}$-$[Cr(acac)(bpdo)_2][Sb_2(d\text{-tartrato})_2]\cdot 6H_2O=C_{33}H_{39}N_4O_{24}CrSb_2$: C, 33.84; H, 3.36; N, 4.78%. The crystals were dissolved in a small amount of ice-cold water, and immediately $NaClO_4$ was added to the solution with stirring. Green crystals which resulted were collected, washed with ice-cold water and then ethanol, and air-dried. The complex showed a negative rotation at 589nm in aqueous solution but rapidly lost the activity. Found: C, 40.41; H, 2.94; N, 7.36%. Calcd for $(-)_{589}$-$[Cr(acac)(bpdo)_2](ClO_4)_2\cdot H_2O=C_{25}H_{25}N_4O_{15}Cl_2Cr$: C, 40.33; H, 3.39; N, 7.53%.

Kinetic Runs. All kinetic experiments were carried out in the dark. Both racemic and $(-)_{589}$-$[Cr(acac)(bpdo)_2](ClO_4)_2\cdot H_2O$ in aqueous solutions show a rapid absorption spectral change. The change of absorbance at 620nm was continuously recorded in the temperature range of 15.8—34.6°C on a Shimadzu MPS-50L spectrophotometer with a cell jacket to maintain the temperature constant within ±0.3°C. The pH and ionic strengths of the solutions were adjusted with an aqueous solution of NaCl-HCl. The complex concentrations were in the range of 1.8—2.8mmol/dm^3. The rate of change obeyed the first order kinetic law and the observed rate constant (k_{obsd}) is expressed as follows: $k_{obsd}=-\ln[(A_t-A_\infty)/(A_0-A_\infty)]/t$ where A's are absorbances at the time denoted by suffixes.

A decrease in optical activity at 589nm of $(-)_{589}$-$[Cr(acac)(bpdo)_2](ClO_4)_2\cdot H_2O$ in aqueous solution was observed by similar procedures as described above using a Union PM-101 desital polarimeter. The temperature and the complex concentrations were in the range of 17.2—35.0°C and 1.4—2.5mmol/dm^3, respectively. The complex lost the optical activity in two steps with different rates, the first rapid and the subsequent slow steps (*vide post*).[5] In the latter step, the rate of decrease obeyed the first order kinetic law and the observed rate constant (k_{obsd}) is also expressed by the above equation where A's are degrees of optical rotation.

All kinetic data were treated by a least-squares method and all estimated errors are standard deviations.

Measurements. Absorption and circular dichroism (CD) spectra were recorded on a Shimadzu MPS-50L spectrophotometer and a Jasco J-40 spectropolarimeter, respectively. Optical rotations were measured with a Union PM-101 desital polarimeter.

Results and Discussion

Preparation and Characterization of the Complexes. Four new complexes, $[Cr(acac)_{3-n}L_n]^{n+}$ (n=1 and 2; L= bpdo or mbdo) were prepared from $[Cr(acac)_3]$ and the dioxide ligand in 90% ethanol by a method similar to

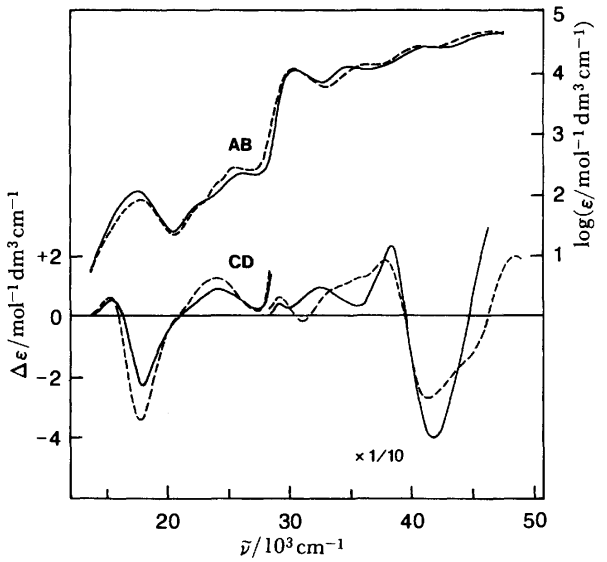

Fig. 2. Absorption (AB) and CD spectra of $(+)_{546}$-$[Cr(acac)_2(R\text{-mbdo})]^+$ (——) and $(+)_{546}$-$[Cr(acac)_2(bpdo)]^+$ (-----) in water.

that for $[Cr(acac)_2(phen)]^+$.[6] Each of the complexes was purified by SP-Sephadex column chromatography and isolated as the perchlorate. The complexes in aqueous solutions are stable in the dark, but undergo gradual hydrolysis in the light.

Both $[Cr(acac)_2L]^+$ complexes of bpdo and racemic mbdo form only one racemic pair of diastereomers of two possible ones, *lel* and *ob*. No indication for the formation of the other isomer was found by column chromatography. The optical resolution of the bpdo complex was achieved by DEAE-Sephadex A-25 ($[Sb_2(d\text{-tartrato})_2]^{2-}$ form) column chromatography with water as an eluent, although repeated chromatography was necessary to obtain the optically pure isomers. On the other hand, the mbdo complex was hardly resolved by the same chromatographic method. Hence the optically pure mbdo complex was prepared from optically active *R*-mbdo.[4] The obtained *R*-mbdo complex gave also only one isomer and its absorption spectrum coincides with that of the racemate prepared from racemic mbdo. The active bpdo and mbdo complexes are optically stable in aqueous solution.

Figure 2 shows the absorption and CD spectra of $(+)_{546}$-$[Cr(acac)_2(R\text{-mbdo})]^+$ and $(+)_{546}$-$[Cr(acac)_2(bpdo)]^+$. The spectral data are given in Table 1. Both absorption spectra are nearly the same over the whole region. The bands at 17530cm^{-1} and 17670cm^{-1} for the mbdo and bpdo complexes, respectively, can be assigned to the first absorption band ($^4T_{2g}\leftarrow{}^4A_{2g}$). The band at *ca.* 26000cm^{-1} for each complex shows a clear shoulder on the low energy side and the band shape is similar to that of $[Cr(acac)_3]$, which was assigned to the $\pi^*\leftarrow\pi$ or $\pi^*\leftarrow n$ transition of acac$^-$.[9,10] The position of the second band ($^4T_{1g}\leftarrow{}^4A_{2g}$) is uncertain because of overlapping with this band. In the ultraviolet region, the complexes exhibit a strong band at 30300cm^{-1} which was also found in $[Cr(acac)_3]$ and assigned to involve both the $\pi^*\leftarrow\pi$ transition of acac$^-$ and the charge transfer (acac$^-$ to metal) transition.[9,10] In the higher energy region, the complexes show three strong bands characteristic of the chelated dioxide ligands.[3,4]

The CD spectra of the two $(+)_{546}$-isomers show a similar pattern over the whole region. This suggests that the isomers have the same absolute configuration including chirality of the skew dioxide chelate ring. The CD patterns in the region of the first absorption band are very similar to those of $(-)_{589}$-$[Cr(acac)_3]$,[11] $(-)_{546}$-$[Cr(acac)_2en]^+$,[10] and $(+)_{589}$-$[Cr(acac)_2tn]^+$ (tn= trimethylenediamine),[12] all of which were reported to have the *Δ* configuration. Thus both $(+)_{546}$-isomers of the dioxide complexes can be assigned to the *Δ* configuration. In the ultraviolet region, the isomers do not show clear exciton CD bands due to two acac$^-$ ligands in the region of 30000 to 35000cm^{-1}.[10-12]

As stated previously, *R*-mbdo forms a *λ* skew chelate ring in a complex.[4] Thus $(+)_{546}$-$[Cr(acac)_2(R\text{-mbdo})]^+$ can be assigned to the *Δ*(*λ*)(*lel*) isomer. The $(+)_{546}$-isomer of the bpdo complex which shows a CD spectrum very similar to that of the *R*-mbdo complex can be assigned to the same isomer. Thus both bpdo and *R*-mbdo complexes form only a *lel* isomer stereoselectively. The $[Cr(en)_2(bpdo)]^{3+}$[3] and $[Co(en)_2L]^{3+}$ complexes (L=2,2′-diaminobiphenyl[13,14] and its 6,6′-dimethyl derivative;[13] these ligands form a skew seven-membered chelate ring similar to the dioxide) give also only a *lel* isomer. On the other hand, bis-(2,2′-bipyridine) and bis(1,10-phenanthroline) chromium(III) complexes containing bpdo or mbdo give only an *ob* isomer.[15] Examination with molecular models indicates that the difference in selectivity seems to come from steric conditions among the ligands.

Although $[Cr(acac)(rac\text{-mbdo})_2]^{2+}$ has three possible racemic pairs of diastereomers, lel_2, *lel*·*ob*, and ob_2, the complex yielded two racemic pairs of diastereomers, isomer I and II. The formation ratio of the isomers, I:II was about 1: 1. On the other hand, the optically active $[Cr(acac)(R\text{-mbdo})_2]^{2+}$ complex prepared from *R*-mbdo gave only one isomer of two possible ones, *Δ*(*λλ*)(lel_2) and *Λ*(*λλ*)(ob_2), and its absorption spectrum coincides with that of isomer II. Since molecular models show that the ob_2 isomer has an extremely crowded structure, the *R*-mbdo complex can be assigned to the *Δ*(*λλ*)(lel_2) isomer. Therefore isomer I and II can be assigned to have the *lel*·*ob* and lel_2 structures, respectively. Attempts to resolve both isomers, I and II, were all unsuccessful. Isomer I and II are stable and the active *R*-mbdo complex is optically stable in aqueous solutions.

Figure 3 shows the absorption spectra of the two isomers of $[Cr(acac)(rac\text{-mbdo})_2]^{2+}$ and the CD spectrum of $(-)_{589}$-$[Cr(acac)(R\text{-mbdo})_2]^{2+}$. The spectral data are given in Table 1. The absorption spectra of the two isomers fairly differ from each other in the visible region, while those in the ultraviolet region are similar. The absorption bands at 17390cm^{-1} with a shoulder

TABLE 1. ABSORPTION AND CD SPECTRAL DATA

Complex	Absorption	CD
	$\tilde{\nu}/10^3\,cm^{-1}$ (log ε)	$\tilde{\nu}/10^3\,cm^{-1}$ ($\Delta\varepsilon$)
$(+)_{546}$-[Cr(acac)$_2$(*R*-mbdo)]$^+$	17.53(2.03)	15.50(+0.52)
	23.0 (1.9)sh	17.86(−2.30)
	25.6 (2.3)sh	24.57(+0.87)
	26.18(2.33)	28.99(+4.37)
	30.33(4.03)	32.47(+9.98)
	34.54(4.08)	38.46(+23.7)
	40.90(4.39)	42.02(−39.9)
	46.0 (4.6)sh	
$(+)_{546}$-[Cr(acac)$_2$(bpdo)]$^+$	17.67(1.91)	15.24(+0.59)
	23.0 (1.9)sh	17.78(−3.43)
	25.38(2.43)	23.92(+1.27)
	29.8 (4.0)sh	29.24(+6.09)
	30.30(4.03)	31.06(−1.96)
	37.0 (4.1)sh	35.3 (+12)sh
	40.73(4.40)	37.88(+18.5)
	45.87(4.60)	41.32(−26.9)
		44.0 (−16)sh
		48.31(+20.0)
lel·ob-[Cr(acac)(*R*-mbdo)(*S*-mbdo)]$^{2+}$	16.5 (1.7)sh	
	17.39(1.71)	
	22.8 (1.8)sh	
	24.3 (2.0)sh	
	25.25(2.05)	
	29.5 (3.6)sh	
	30.03(3.63)	
	30.40(3.63)	
	34.60(4.24)	
	40.82(4.53)	
	45.5 (4.7)sh	
$(-)_{589}$-*lel*$_2$-[Cr(acac)(*R*-mbdo)$_2$]$^{2+}$	16.18(1.87)	15.85(+2.08)
	17.0 (1.8)sh	18.25(−0.35)
	22.42(1.91)	21.69(+0.67)
	25.8 (2.0)sh	28.25(−0.35)
	29.9 (3.6)sh	30.40(+6.05)
	30.40(3.65)	34.72(−20.3)
	30.77(3.65)	39.22(−33.6)
	34.72(4.19)	41.5 (−15)sh
	40.82(4.55)	47.06(+88.8)
	45.45(4.74)	
$(-)_{589}$-[Cr(acac)(bpdo)$_2$]$^{2+}$[a]	16.34(1.82)	16.75(+2.25)[b]
	17.24(1.81)	17.92(+2.43)
	22.73(1.91)	23.15(−0.41)
	24.0 (2.0)sh	29.5 (−5.5)sh
	25.32(2.07)	30.77(−8.34)
	30.40(3.71)	37.0 (−26)sh
	35.84(4.24)	38.76(−35.7)
	40.65(4.58)	42.74(+58.0)
	45.87(4.75)	

a) These data correspond to the spectra of an equilibrium mixture of *lel*$_2$ and *lel·ob* isomers (see text).
b) The $\Delta\varepsilon$ values were extrapolated to time zero. sh: Shoulder.

(16500cm^{-1}) and at 16180cm^{-1} with a shoulder (17000 cm^{-1}) for isomer I and II, respectively, can be assigned to the first absorption band ($^4T_{2g}\leftarrow{}^4A_{2g}$). The band of isomer II (*lel*$_2$) is more intense than that of isomer I (*lel·ob*). The *lel*$_3$ isomer of [Cr(mbdo)$_3$]$^{3+}$ also shows the most intense and the narrowest first absorption band among those of the three isomers, *lel*$_3$, *lel*$_2$*·ob*, and *lel·ob*$_2$.[4]

Figure 4 compares the absorption and CD spectra of a series of [Cr(acac)$_{3-n}$(*R*-mbdo)$_n$]$^{n+}$ (n=0—3). The first absorption band shifts to lower wavenumbers by replacing acac with mbdo. The intensities of bands in the region from 23000 to 50000 cm^{-1} are related to the number of dioxide and acac ligands. The CD spectra in the region of the first absorption band show a gradual change with an increasing number of n in [Cr(acac)$_{3-n}$(*R*-mbdo)$_n$]$^{n+}$, indicating the same absolute configuration. The $(-)_{589}$-[Cr(acac)$_3$][11] and [Cr(*R*-mbdo)$_3$]$^{3+}$[4] complexes have been assigned to the Δ and $\Delta(\lambda\lambda\lambda)$(*lel*$_3$) configurations, respectively. Thus our preceding assignments of $\Delta(\lambda)$(*lel*) and $\Delta(\lambda\lambda)$(*lel*$_2$), respectively, for [Cr(acac)$_2$(*R*-mbdo)]$^+$ and [Cr(acac)(*R*-

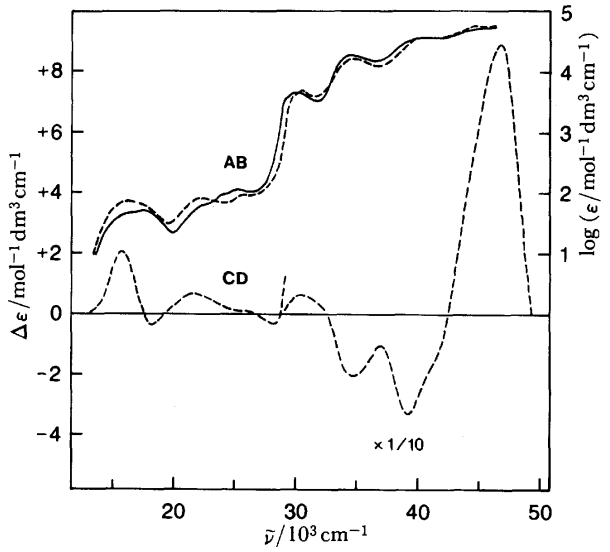

Fig. 3. Absorption (AB) spectrum of $[Cr(acac)(R\text{-mbdo})(S\text{-mbdo})]^{2+}$ (isomer I) (——), and absorption and CD spectra of $(-)_{589}$-$[Cr(acac)_2(R\text{-mbdo})_2]^{2+}$ (isomer II) (-----) in water.

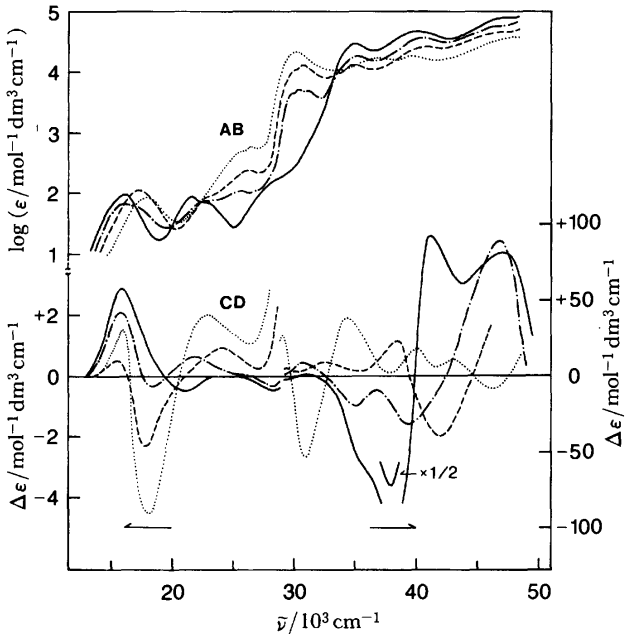

Fig. 4. Absorption (AB) and CD spectra of a series of Δ-$[Cr(acac)_{3-n}(R\text{-}mbdo)_n]^{n+}$ complexes in water; $(-)_{589}$-$[Cr(R\text{-mbdo})_3]^{3+}$ (——), $(-)_{589}$-$[Cr(acac)(R\text{-mbdo})_2]^{2+}$ (-·-·-), $(+)_{546}$-$[Cr(acac)_2(R\text{-mbdo})]^{+}$ (-----), and $(-)_{589}$-$[Cr(acac)_3]$ in ethanol (·····).[11]

mbdo)$_2$]$^{2+}$ are consistent with these CD spectra. The CD strength of the negative component in $[Cr(acac)_3]$ is gradually reduced by replacing acac with *R*-mbdo, $[Cr(R\text{-mbdo})_3]^{3+}$ showing only positive CD band. A similar CD change occurring with replacement of a seven-membered chelate ligand is observed in CD spectra of a series of $[Co(en)_x(tn)_y(tmd)_z]^{3+}$ $(x+y+z=3)$, where tmd denotes tetramethylenediamine which forms a seven-membered chelate ring upon coordination.[16]

The $[Cr(acac)(bpdo)_2]^{2+}$ complex has three possible racemic pairs of diastereomers as well as the corresponding *rac*-mbdo complex. However, attempts to separate such isomers were all unsuccessful by column chromatography because of rapid isomerization of the complex (*vide post*).[5] The optically active complex which was obtained by the chemical method with $K_2[Sb_2(d\text{-tartrato})_2]$ loses gradually its activity in aqueous solution at room temperature.

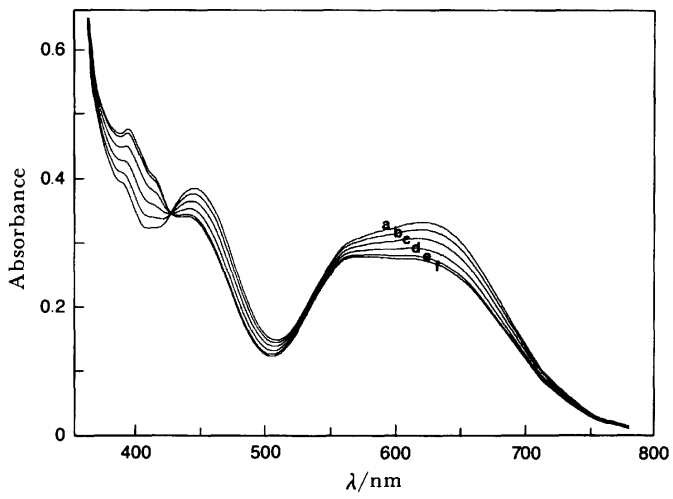

Fig. 5. Absorption spectral change of $[Cr(acac)(bpdo)_2]$-$(ClO_4)_2\cdot H_2O$ in water (pH 7) at 18.0 °C. Reaction time (min): a, 1; b, 3; c, 6; d, 12; e, 24; f, ∞.

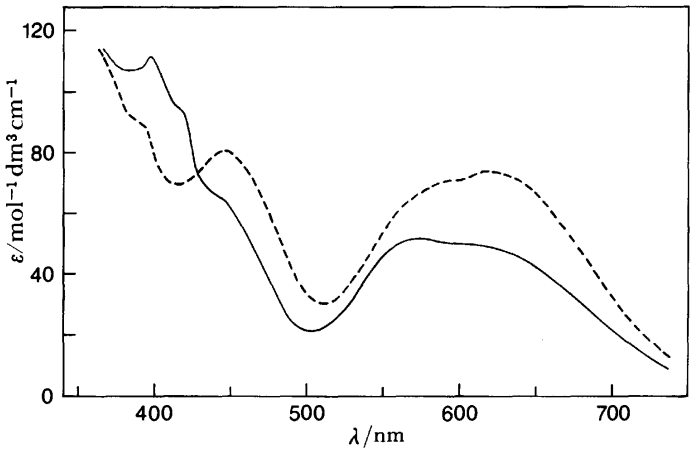

Fig. 6. Absorption spectra of two diastereomers of $[Cr(acac)(rac\text{-mbdo})_2]^{2+}$ in the visible region in water; isomer I(*lel·ob*) (——) and isomer II(lel_2) (-----).

Both racemic and $(-)_{589}$-$[Cr(acac)(bpdo)_2](ClO_4)_2$-$H_2O$ in aqueous solution show a rapid absorption spectral change with an isosbestic point at 427 nm as Fig. 5 shows. The complexes are not hydrolyzed during the change of spectra, since any hydrolyzed product was not detected in the resulting solutions by column chromatography. The species corresponding to absorption spectra a and f in Fig. 5 can be assigned by comparing these spectra with those of the isomers of $[Cr(acac)(rac\text{-mbdo})_2]^{2+}$ in Fig. 6. Spectrum a quite resembles that of the lel_2 isomer of the mbdo complex, and spectrum f seems to be an intermediate one between

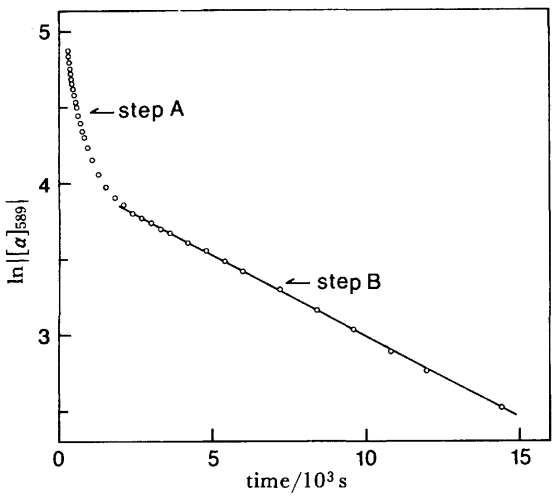

Fig. 7. Decrease in optical rotation of $(-)_{589}$-[Cr(acac)(bpdo)$_2$](ClO$_4$)$_2$·H$_2$O with time in water (pH 7) at 22.0 °C.

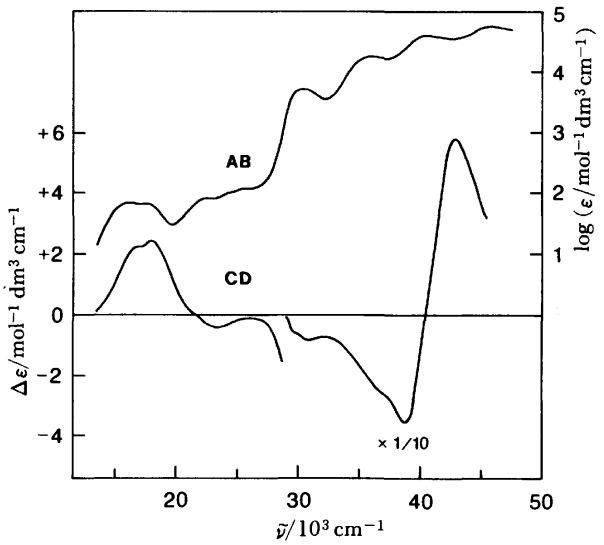

Fig. 8. Absorption (AB) and CD spectra of $(-)_{589}$-[Cr(acac)(bpdo)$_2$]$^{2+}$ in water. These were recorded after an equilibrium of *lel*$_2$ ⇌ *lel·ob* had been reached, and the CD spectrum was corrected for racemization (see text).

those of the two isomers (*lel*$_2$ and *lel·ob*). Thus the spectral change should be caused by isomerization of the complex, *lel*$_2$ ⇌ *lel·ob*. The bpdo chelate ring was shown to be flexible and change its conformation, $\delta \rightleftharpoons \lambda$, very easily.[2,3] Molecular models indicate that the *lel*$_2$ isomer seems to isomerize easily to the *lel·ob* one and *vice versa*, but the *ob*$_2$ isomer will be never formed because of its crowded structure.

As shown in Fig. 7, an aqueous solution of $(-)_{589}$-[Cr(acac)(bpdo)$_2$](ClO$_4$)$_2$·H$_2$O loses the optical activity in two steps with different rates, the first rapid (step A) and the subsequent slow (step B) steps.[5] In step A, the decrease in optical activity accompanies the absorption spectral change, while no spectral change is observed in step B. These results suggest that step A involves the isomerization reaction between the diastereomers, *lel*$_2$ ⇌ *lel·ob*, and step B the racemization reaction between the enantiomers, $\Delta \rightleftharpoons \Lambda$, of the complex.

Figure 8 shows the absorption spectrum of $(-)_{589}$-[Cr(acac)(bpdo)$_2$]$^{2+}$ in aqueous solution at 31 °C at 20 min after dissolution, when no more change in the absorption spectrum was observed. After the equilibrium was reached, the CD spectrum changed with time by step B (the racemization, $\Delta \rightleftharpoons \Lambda$), thus it was extrapolated to time zero by using the k_{obsd}(racemization) value (*vide post*). The corrected CD spectrum is also shown in Fig. 8. The spectral data are given in Table 1. The absorption spectrum in the ultraviolet region is also an intermediate one between those of the *lel*$_2$ and *lel·ob* isomers of [Cr(acac)(mbdo)$_2$]$^{2+}$. The first absorption band gives two components at 16340 and 17240 cm^{-1}. Corresponding to these components, the complex shows two positive CD bands and can be assigned to the Δ configuration. Thus it is concluded that $(-)_{589}$-[Cr(acac)(bpdo)$_2$](ClO$_4$)$_2$·H$_2$O crystallizes in the $\Delta(\lambda\lambda)$-(*lel*$_2$) structure and isomerizes in aqueous solution to the $\Delta(\lambda\delta)$(*lel·ob*) structure in step A.

Kinetics of Isomerization and Racemization of [Cr(acac)(bpdo)$_2$]$^{2+}$. The kinetic experiments were carried out in the dark so as to avoid photoinduced reactions.

The rate of the isomerization of [Cr(acac)(bpdo)$_2$]$^{2+}$, *lel*$_2$ ⇌ *lel·ob*, was followed by monitoring the absorption spectral change at 620 nm with time (in step A) in aqueous solution under the conditions described in Experimental part. The rate of spectral change obeyed the first order kinetic law for at least four half-lives and the rate constant (k_{obsd}) was obtained from the slope of $\log(A_t - A_\infty)$ *vs.* time where A's are absorbances at 620 nm. The rate for the $(-)_{589}$-isomer agreed with that for the racemate within the experimental error. The values of k_{obsd} are given in Table 2. Arrhenius treatment of $\log(k_{obsd})$ *vs.* T^{-1} yielded an activation energy of (77.3±1.2) kJ mol^{-1}) and Eyring treatment of $\log(k_{obsd}/T)$ *vs.* T^{-1} gave an activation enthalpy of (74.9±1.1) kJ mol^{-1} and an activation entropy of (−38.5±3.7) JK^{-1}mol^{-1}. The rate was independent of concentrations of H$^+$ and the free ligands. Hence it is suggested that the isomerization proceeds by an intramolecular mechanism. The small negative activation entropy value seems to reflect such a mechanism. This is consistent with the preceding conclusion that the isomeri-

Table 2. Rate constants for the isomerization of [Cr(acac)(bpdo)$_2$](ClO$_4$)$_2$·H$_2$O in aqueous solutions (I=0.1[a])

t/°C	$k_{obsd}\times10^3$/s^{-1}	t/°C	$k_{obsd}\times10^3$/s^{-1}
15.8	1.69±0.01[b]	22.0[f]	3.30±0.03
18.0[c]	2.14±0.02	22.1[c]	3.31±0.02
22.0	3.31±0.02	27.4[c]	5.64±0.07
22.0[d]	3.31±0.02	34.6	12.2±0.2
22.0[e]	3.30±0.03		

a) Ionic strength adjusted with NaCl. b) Errors are standard deviations estimated by least squares. c) For $(-)_{589}$-isomer. d) In 0.1 mol/dm^3 HCl. e) In 0.05 mol/dm^3 bpdo. f) In 0.02 mol/dm^3 Hacac.

TABLE 3. RATE CONSTANTS FOR THE RACEMIZATION OF $(-)_{589}$-$[Cr(acac)(bpdo)_2](ClO_4)_2 \cdot H_2O$ IN AQUEOUS SOLUTIONS (I=0.1[a])

t/°C	$k_{obsd}\times10^4$/s^{-1}	t/°C	$k_{obsd}\times10^4$/s^{-1}
17.2	0.621±0.006[b]	28.4[d]	2.22±0.01
22.0	1.08±0.01	28.4[e]	2.21±0.02
25.0	1.51±0.02	30.0	2.64±0.02
28.1[c]	2.20±0.02	35.0	4.76±0.03
28.2	2.20±0.01		

a) Ionic strength adjusted with NaCl. b) Errors are standard deviations estimated by least squares. c) In 0.1 mol/dm^3 HCl. d) In 0.05 mol/dm^3 bpdo. e) In 0.02 mol/dm^3 Hacac.

zation occurs by the conformational inversion ($\lambda \rightleftharpoons \delta$) of the bpdo chelate ring in the $\Delta(\lambda\lambda)(lel_2)$ isomer to afford the $\Delta(\lambda\delta)(lel\cdot ob)$ isomer. The difference in free energy between the lel_2 and $lel\cdot ob$ isomers of the complex is small in aqueous solution because of the almost equal formation ratio between the two isomers of $[Cr(acac)(rac\text{-mbdo})_2]^{2+}$.

For $(-)_{589}$-$[Cr(acac)(bpdo)_2](ClO_4)_2 \cdot H_2O$ in aqueous solution, the rate of decrease in optical activity was followed under the conditions described in experimental part. As Fig. 7 shows, the rate in step B obeyed the first order kinetic law for at least three half-lives and the rate constant (k_{obsd}) was obtained from the slope of $\log|\alpha_t|$ *vs.* time where α is degrees of optical rotation at 589 nm. The values of k_{obsd} are given in Table 3. The estimated values of activation energy, enthalpy, and entropy are (84.8±1.2) kJ mol^{-1}, (82.4±1.2) kJ mol^{-1}, and (−41.7±3.9) J K^{-1} mol^{-1}, respectively. The rate was independent of concentrations of H^+ and the free ligands. Thus the racemization ($\Delta \rightleftharpoons \Lambda$) will also proceed by an intramolecular mechanism. In a previous paper,[3] the rate of racemization of $[Cr(bpdo)_3]^{3+}$ in aqueous solution was found to be 1.40×10^{-4} s^{-1} at 26.9 °C with an activation energy and entropy of 81.3 kJ mol^{-1} and −49 J K^{-1} mol^{-1}, respectively, and the racemization was suggested to proceed *via* an intramolecular twist mechanism from a comparison of these kinetic parameters with those of other complexes such as $[Cr(phen)_3]^{3+}$,[17] for which the same mechanism was proposed. The rate constant and the activation parameters of $[Cr(acac)(bpdo)_2]^{2+}$ are very similar to those of $[Cr(bpdo)_3]^{3+}$, and the racemization will also proceed *via* a twist mechanism. The small negative activation entropy value seems to be consistent with such an intramolecular twist mechanism.

Tables 2 and 3 show that the rate of racemization ($\Delta \rightleftharpoons \Lambda$) is 30 times slower than that of the isomerization ($\delta \rightleftharpoons \lambda$); the complex in aqueous solution isomerizes from the lel_2 isomer to the $lel\cdot ob$ one prior to the racemization. Several different twist mechanisms have been proposed for the intramolecular racemization of a tris(chelate)-type complex.[18] However, it is difficult to determine which mechanism is the most probable for the racemization of the present complex.

This work was supported by a Grant-in-Aid for Scientific Research No. 574228 from the Ministry of Education, Science and Culture.

References

1) P. G. Simpson, A. Vinciguerra, and J. V. Quagliano, *Inorg. Chem.*, **2**, 282 (1963); A. Vinciguerra, P. G. Simpson, Y. Kakiuti, and J. V. Quagliano, *ibid.*, **2**, 286 (1963); A. R. Al-Karaghouli, R. O. Day, and J. S. Wood, *ibid.*, **17**, 3702 (1978).
2) E. J. Corey and J. C. Bailar, Jr., *J. Am. Chem. Soc.*, **81**, 2620 (1959).
3) H. Kanno, K. Kashiwabara, and J. Fujita, *Bull. Chem. Soc. Jpn.*, **52**, 761 (1979).
4) H. Kanno, K. Kashiwabara, and J. Fujita, *Bull. Chem. Soc. Jpn.*, **52**, 1408 (1979).
5) H. Kanno, T. Shimotori, S. Utsuno, and J. Fujita, *Chem. Lett.*, **1983**, 939.
6) D. Banerjea, J. Roy, and S. Sarkar, *Indian J. Chem.*, **8**, 372 (1970).
7) I. Murase, *Nippon Kagaku Zasshi*, **77**, 682 (1956).
8) R. D. Gilliard and P. R. Mitchell, *Trans. Met. Chem.*, **1**, 223 (1976).
9) I. Hanazaki, F. Hanazaki, and S. Nagakura, *J. Chem. Phys.*, **50**, 265, 276 (1969).
10) S. Kaizaki, J. Hidaka, and Y. Shimura, *Inorg. Chem.*, **12**, 135 (1973).
11) S. F. Mason, R. D. Peacock, and T. Prosperi, *J. Chem. Soc., Dalton Trans.*, **1977**, 702.
12) M. Nakano, S. Kawaguchi, and H. Kawaguchi, *Bull. Chem. Soc. Jpn.*, **52**, 2897 (1979).
13) W. T. Jordan, C-Y. Lin, and B. E. Douglas, *J. Coord. Chem.*, **3**, 1 (1973).
14) T. Tanimura, H. Ito, J. Fujita, K. Saito, S. Hirai, and K. Yamasaki, *J. Coord. Chem.*, **3**, 161 (1973).
15) H. Kanno, K. Kashiwabara, and J. Fujita, *Bull. Chem. Soc. Jpn.*, **53**, 2881 (1980).
16) M. Kojima, H. Yamada, H. Ogino, and J. Fujita, *Bull. Chem. Soc. Jpn.*, **50**, 2325 (1977).
17) N. A. P. Kane-Maguire and S. A. Edwards, *J. Inorg. Nucl. Chem.*, **38**, 1037 (1976); G. A. Lawrance and D. R. Stranks, *Inorg. Chem.*, **16**, 929 (1977).
18) See for example: F. Basolo and R. G. Pearson, "Mechanisms of Inorganic Reactions," (2nd Ed.), John Wiley & Sons (1967); N. Serpone and D. G. Bickley, "Inorganic Reaction Mechanisms Part II," in "Progress in Inorganic Chemistry," ed by J. O.b Edwards, Interscience (1972), Vol. 17, p. 391.

Oxygen-plasma Treatment of Packing Materials for Gas Chromatography. The Incorporation of Oxygen into the Hydrocarbon Liquid Phase and the Formation of Crosslinked Products on the Support Surface

Yukio YAMAMOTO,* Seiji OKA, and Koichiro HAYASHI
The Institute of Scientific and Industrial Research, Osaka University, 8-1 Mihogaoka, Ibaraki, Osaka 567
(Received June 27, 1984)

The oxygen-plasma treatment of column packings for gas chromatography was examined with diatomaceous earth coated with several kinds of stationary liquid phases from the point of view of the modification of their chromatographic properties. A remarkable effect on the gas chromatograms of polar compounds was observed for the packings with nonpolar liquids, such as squalane and Apiezon L. The elimination of tailing and the improvement of the resolution by the plasma treatment were attributed to the incorporation of oxygen into the hydrocarbon liquids and the formation of crosslinked products covering the adsorptive support surface. These results were compared with the previous data on argon-plasma treatment.

Recently, we have examined the argon-plasma treatment of packing materials for gas chromatography.[1-3] It was found that the plasma treatment is effective for reducing the tailing of chromatographic peaks on several kinds of packings, such as squalane, Apiezon L, Silicone DC, and dioctyl phthalate on diatomaceous earth. The effect has been attributed to the formation of an inert coating on the adsorptive support surface. Because the distributed liquid of packings is thin and has a large surface area exposed to plasma, plasma treatment provides an effective means of modifying the chromatographic properties of the packings.

In the present study, the oxygen-plasma treatment of packings was undertaken in order to investigate its effect on gas chromatograms and the reactions in the stationary liquid phase caused by the oxidizing plasma. The results are compared with our previous data on the argon-plasma treatment.

Experimental

The column packings (60/80 mesh) were obtained from Wako Pure Chemical Industry. The apparatus and experimental details of the plasma treatment were described previously.[2] The oxygen-plasma treatment was carried out at a pressure of 0.1 Torr (13 Pa) by means of a radiofrequency generator operated at 13.56 MHz and with an output of 50 W. The gas-chromatographic test of the treated packing was also carried out as has been described previously; the packing was packed into a 1m×3mm i.d. stainless tube, and the nitrogen flow rate was 30 ml/min.

The molecular-weight distribution of the liquid extracted from the plasma-treated squalane on Chromosorb W was measured by means of a gel-permeation chromatograph (Toyo Soda HLC-801) in tetrahydrofuran (THF). A differential refractometer and two 2-ft columns, TSK-Gel G2000H8 and G4000H8, connected in series, were used for the measurement. The IR spectrum of the extracted liquid was recorded on a Hitachi Model 295 spectrometer using NaCl plates.

Results

A remarkable effect was observed on the gas chromatograms of polar compounds when the packings with nonpolar liquids, such as squalane and Apiezon L, were treated with the oxygen plasma. Figure 1 shows the gas chromatograms of alcohols and aromatic ketones on Chromosorb W (non-acid washed (NAW))

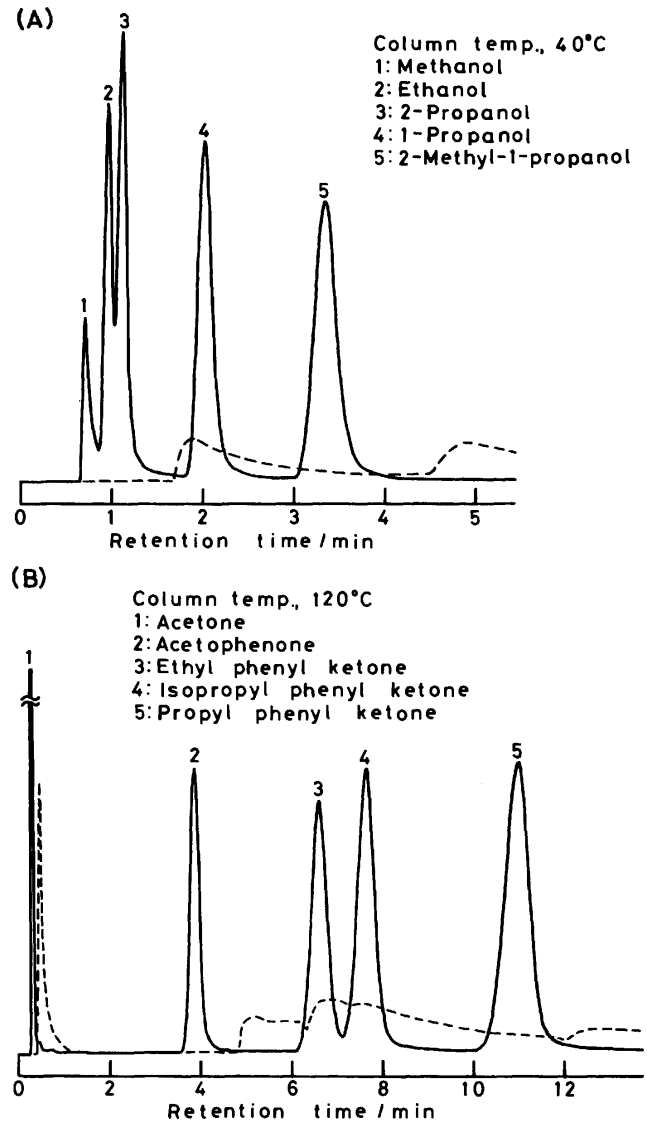

Fig. 1. Gas chromatograms on Chromosorb W (NAW) coated with 5% squalane: solid line, 10 min plasma treated; dotted line, untreated.

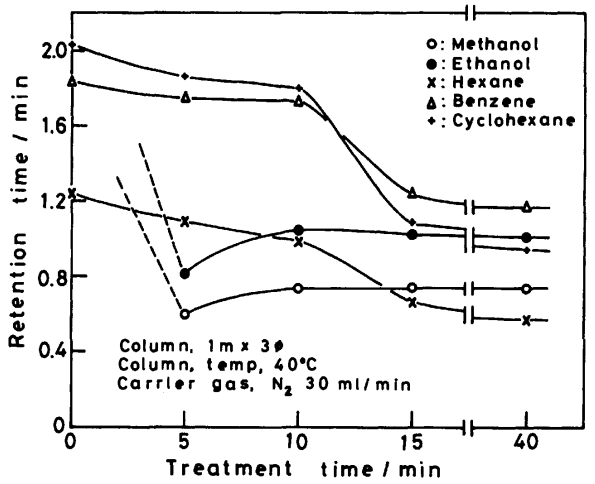

Fig. 2. Change in retention time by plasma treatment.

coated with 5% squalane before (dotted line) and after (solid line) the plasma treatment for 10min. Sharp and well-separated peaks are obtained on the plasma-treated packing, whereas the peaks are very broad, with extensive tailing, on the untreated packing. The best peak separation was attained at the treatment time of 10min. The changes in the retention times of several alcohols and hydrocarbons by the plasma treatment are compared in Fig. 2. The retention times of methanol and ethanol are significantly decreased during the first 5min and then slightly increased during the next 5min. On the other hand, the retention times of hexane, benzene, and cyclohexane slowly decreased with the increase in the treatment time. The effect of the plasma treatment was similar for 5% Apiezon L on Shimalite (NAW), as is illustrated in Fig. 3. By the plasma treatment, the retention time of ethanol is decreased much more than those of hexane and benzene, and the tailing of its peak is effectively reduced. Symmetrical and separated peaks are also obtained for the aromatic ketones on the plasma-treated packing.

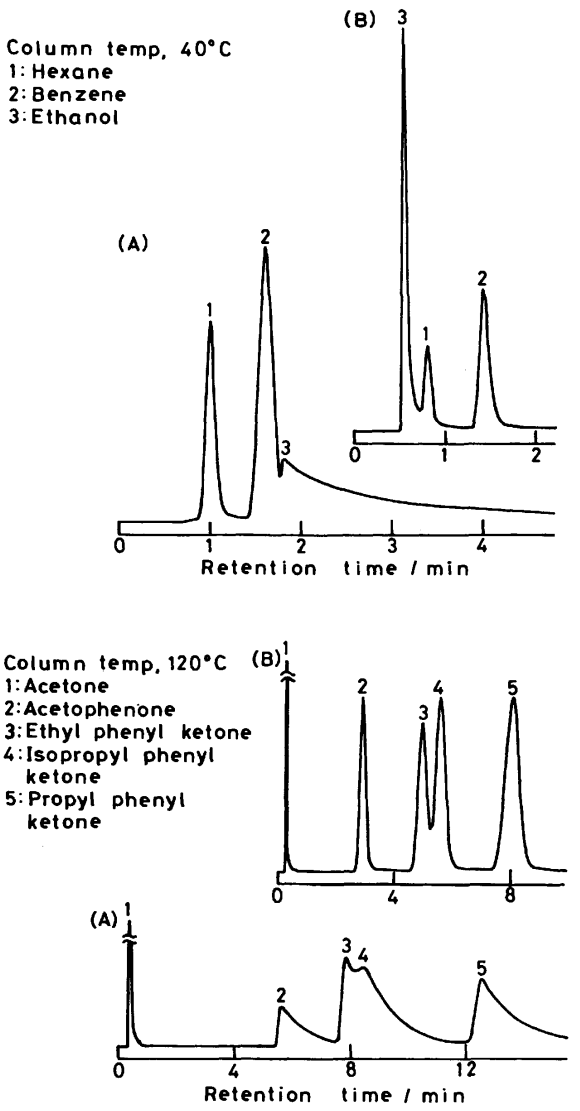

Fig. 3. Gas chromatograms on Shimalite (NAW) coated with 5% Apiezon L: (A) untreated; (B) 10min plasma treated.

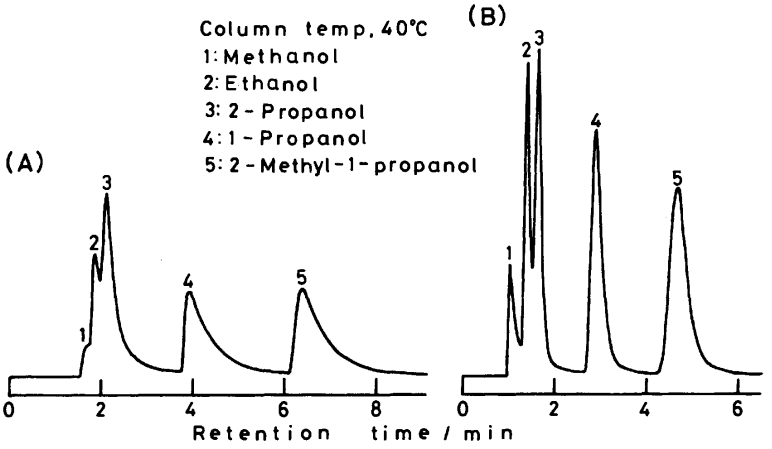

Fig. 4. Gas chromatograms on Chromosorb W (NAW) coated with 10% dioctyl phthalate: (A) untreated; (B) 10min plasma treated.

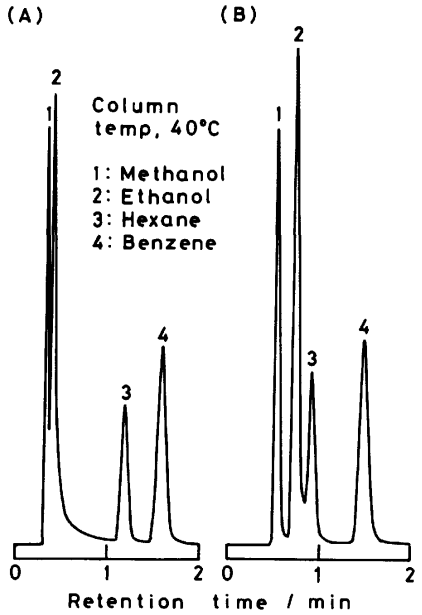

Fig. 5. Gas chromatograms on Chromosorb W (AW-DMCS) coated with 5% squalane: (A) untreated; (B) 10 min plasma treated.

Figure 4 shows the effect of the plasma treatment of Chromosorb W (NAW) coated with 10% dioctyl phthalate on the gas chromatogram of alcohols. Although the effect is less significant than those for the packings described above, the plasma treatment is effective for reducing the tailing. When packings coated with Silicone DC and polyethylene glycol were treated with the oxygen plasma for 10 min, only a slight decrease in retention time was observed, but there was no appreciable improvement in the resolution.

The oxygen-plasma treatment was also examined with acid-washed and dimethyldichlorosilane-treated (AW-DMCS) Chromosorb W coated with 5% squalane; the results are shown in Fig. 5. It can be seen that, by the plasma treatment, the retention times of methanol and ethanol are increased and the tailing of their peaks is eliminated. On the contrary, the retention times of hexane and benzene are decreased by the plasma treatment.

With a packing consisting of 5% squalane and Chromosorb W (NAW), experiments to elucidate the reactions caused by the oxygen-plasma treatment were carried out. After the plasma treatment, the distributed liquid was extracted from the packing with THF by using a Soxhlet extractor and refluxing for 5 h. The extract was submitted to gel-permeation chromatography. The molecular-weight distributions at different treatment times are shown in Fig. 6. These are normalized to the peak height at 28.5 counts corresponding to squalane itself. It is evident that the distributed liquid is polymerized during the plasma treatment. The yields of the higher-molecular-weight products increase with the increase in the treatment time. On the other hand, the formation of the polymerized products is limited in the case of the argon-

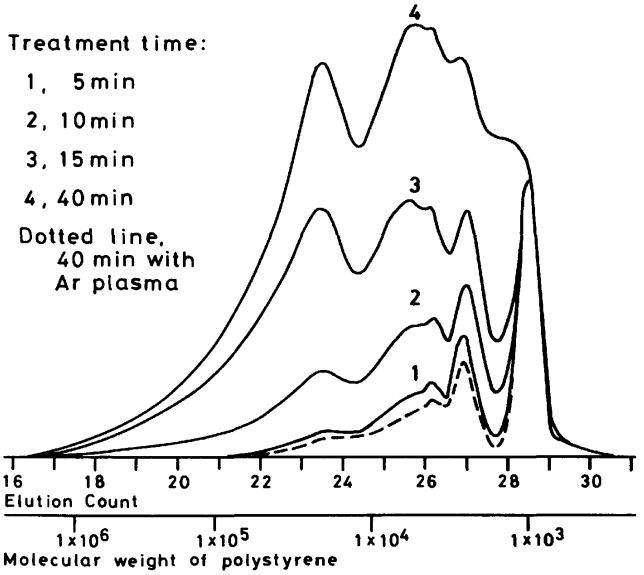

Fig. 6. Molecular weight distribution curves for liquids extracted from plasma treated packings (Chromosorb W (NAW) coated with 5% squalane).

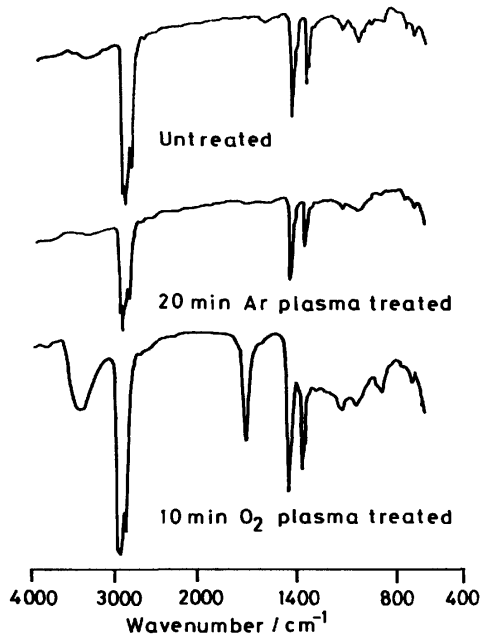

Fig. 7. IR spectra of the liquids extracted from packings (Chromosorb W (NAW) coated with 5% squalane).

plasma treatment, even at the longest treatment time examined, 40 min (dotted line).

The IR spectrum of the extracted liquid, which was measured after evaporating the THF from the extract, is shown in Fig. 7, together with those of the liquids extracted from the untreated and argon-plasma-treated packings. The IR spectrum for the oxygen-plasma treated packing shows the presence of carbonyl and hydroxyl groups, whereas there is no appreciable difference in the spectra between the untreated and argon-plasma-treated packings.

The support recovered from the packing by extract-

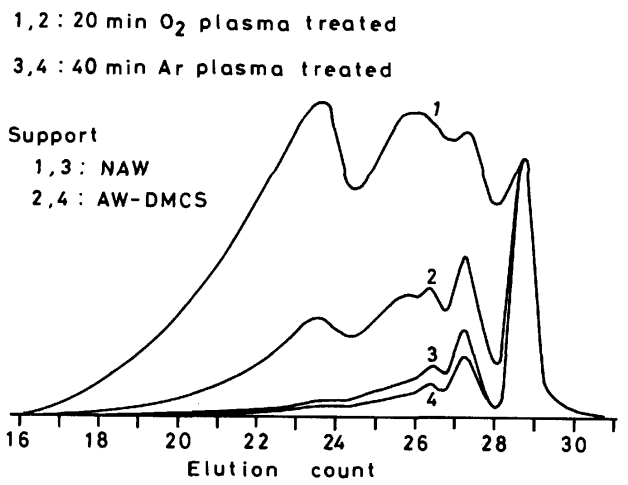

Fig. 8. Comparison of molecular weight distributions of extracted liquids for NAW and AW-DMCS supports.

ing the distributed liquid was dried under vacuum and then weighed to determine the weight loss of the packing due to the extraction. The weight loss decreased with the increase in the treatment time, much as in the case of the argon-plasma treatment,[2] indicating the formation of products not extracted with THF. The yield of such insoluble products, based on the distributed liquid, was 34.5% at a treatment time of 20min, which is comparable to that in the argon-plasma treatment, 31.7%.

For the sake of comparison, the molecular-weight distribution of the extracted liquid was measured for the packing with the AW-DMCS support. The formation of the soluble polymer depends on the support, as is shown in Fig. 8; that is, it is more pronounced on the NAW support in both the oxygen and argon-plasma treatments. Furthermore, the yields of the insoluble products remaining on the AW-DMCS support at the plasma-treatment time of 20min were 26.5 and 18.8% for the oxygen and argon-plasma treatments respectively. These yields are smaller than those on the NAW support.

Discussion

When a hydrocarbon substrate such as polyethylene is exposed to an oxygen plasma, the incorporation of oxygen and crosslinking are known to occur on the substrate surface.[4,5] Similar reactions are considered to occur in the hydrocarbon-liquid phase of the packing when it is treated with the oxygen plasma. The results for the packing with squalane demonstrate the incorporation of oxygen in the form of carbonyl and hydroxyl and the crosslinking to yield the high-molecular-weight products.

The formation of an inert coating on the support surface is considered to play an important role in the elimination of the tailing of chromatographic peaks, much as in the case of the argon-plasma treatment.[1-3] The yields of both the types of polymerized products, those extractable and unextractable with THF, on the NAW support were higher than those on the AW-DMCS support in the oxygen and argon-plasma treatments. Therefore, it seems likely that their formation is promoted by the NAW support surface and that the highly crosslinked products effectively cover it. It is also believed that the increase in the polarity of the liquid phase by the incorporation of oxygen reduces the adsorption of solutes on the support surface because of the increased interaction of the liquid with the support surface. Thus, the remarkable decrease in the retention times of the alcohols and aromatic ketones and the elimination of their tailing (Figs. 1 and 2) are attributable to the reduction of the support adsorptivity toward the solutes.

Another effect of the increase in the polarity of the distributed liquid is an increase in the retention times of the alcohols, resulting in a higher peak separation. This was observed for the packing with the NAW support during the second 5min of treatment (Fig. 2) and also for the packing with the AW-DMCS support (Fig. 5).

The formation of the soluble polymerized products was much more pronounced in the oxygen-plasma treatment than in the argon-plasma treatment. This can be explained by the reactions of oxygen with radical species inhibiting the crosslinking and/or initiating oxidative decomposition of the polymerized products.

This work was supported in part by the Shimadzu Co.

References

1) Y. Yamamoto, S. Oka, and K. Hayashi, *Chem. Lett.*, **1981**, 221.
2) Y. Yamamoto, S. Oka, and K. Hayashi, *Bull. Chem. Soc. Jpn.*, **55**, 441 (1982).
3) S. Oka, Y. Yamamoto, and K. Hayashi, *Bull. Chem. Soc. Jpn.*, **55**, 3496 (1982).
4) M. Hudis, "Techniques and Applications of Plasma Chemistry," ed by J. T. Hollahan and A. T. Bell, Wiley-Interscience, New York, N. Y. (1974), p. 113.
5) H. Yasuda, *J. Macromol. Sci., Chem.*, **A10**, 383 (1976).

Quantum Chemical Consideration of Substituent Effects on Tautomeric Properties of 2-Pyridones–2-Pyridinols

Masayuki KUZUYA,* Akihiro NOGUCHI, and Takachiyo OKUDA
Gifu Pharmaceutical Uuiversity, 6-1, Mitahora-higashi 5-Chome, Gifu 502
(Received January 5, 1984)

The tautomeric properties of 2-pyridones–2-pyridinols exerted by the substituent effect were discussed on the basis of quantum chemical quantities deduced from molecular orbital (MO) calculations. A substituent at the 6-position has the greatest stabilizing effect. The magnitude of this effect was greater on the 2-pyridinol form than the 2-pyridone form, irrespective of the nature of the substituent. This led to a large predominance of the 2-pyridinol form on the 6-polar-substituted derivatives to such an extent that it was observed by conventional UV measurements at ambient temperature. In the 6-methyl derivative, the 2-pyridinol form was not observed by a similar measurement due to the weak substituent effect. The association ability is still an important factor in determining tautomeric equilibrium in a solution, resulting in a strong lability to the molecular environment. The substituent effects on the stabilities of both tautomers were shown to be correlated with the N-atomic charges and ring structural modifications of the tautomers.

2-Pyridone–2-pyridinol (**1**) has been one of the basic tools in a number of studies on tautomeric equilibria, the properties of which are of interest regarding the structure-reactivity relationship and is of potential biological significance for understanding mutation due to base mispairing and enzymic reactions related to the bifunctional catalysis.[1,2] Thus, the study of 2-pyridone (**1**) has been attracting many investigators from more than one area.

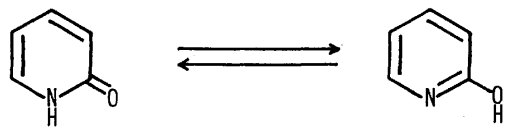

1a **1b**

Scheme 1.

It has now become well established that **1** exists very largely in the 2-pyridone tautomeric form (**1a**) in solution[1] and in the solid state,[3] but that there is no significant difference in the fundamental stabilities of the tautomers in the gas phase (ΔH=1.3±10 kJ mol^{-1}).[2] It was also been shown that self-association and/or solvation significantly affect tautomeric equilibria.[2,4]

A number of quantum chemical studies on the energetics of the tautomeric properties for **1** have already been published, but those studies have led to various diverse results regarding the energetics of tautomeric equilibria.[5] This may be mainly due to the differences in the method of calculation and the molecular geometric parameters employed. Recently, *ab initio* studies with extended basis sets, including full geometry optimization, were reported and the calculated tautomeric energy difference was shown to be in good agreement with experimental values related to the gas phase.[5k,5l,5m] The details of the substituent effects on the tautomeric properties of **1**, however, have yet been fully elucidated.

We felt it would be important and useful to investigate the substituent effect in order to achieve a full understanding of the factors which influence tautomeric equilibria. In fact, several derivatives of **1** which bear a polar substituent at the 6-position are known to favor the 2-pyridinol form over the 2-pyridone form,[1,6] and the substituent effects have been ascribed to the electron-withdrawing property.

Molecular orbital calculations are particularly useful for such studies since they can provide much information about less-abundant tautomeric species. It is now apparent that nonempirical *ab initio* calculations with extended basis sets must be used to achieve a high accuracy regarding the energetics of tautomeric equilibria.[5k,5l,5m] A large amount of computational time, however, is neccessary for such calculations for a large molecule. Thus, we systematically performed molecular orbital calculations supported by the CNDO/2 and MINDO/3 methods on various substituted 2-pyridones. We believe that the semiempirical method can provide a sufficient fundamental insight into the substituent effects on the relative stability and electronic structure of each tautomeric form.

In this paper, we present the special features disclosed by the calculations and discussed the substituent effects with the quantum chemical quantities derived from such calculations.

In order to obtain experimental data to support the calculated quantities, the IR spectra of several methyl derivatives of 2-pyridones were also measured in a CCl_4 solution.

Experimental

2-Pyridone was commercially available. The preparation of other substituted 2-pyridones is described in the literature.[7]

The infrared spectra were recorded with a JASCO 403G infrared spectrophotometer. The solvent of carbon tetrachloride (spectroscopic grade) was dried over molecular sieves. Solute concentrations were 5×10^{-4} M† (20mm NaCl cells). The cell was heated with a heat gun (PLAJET PJ-206,

†1M=1 mol dm^{-3}.

Ishizaki-Denki Co. Ltd.) to above 60°C. Then, heating was discontinued and the spectra in the 3200—3800cm^{-1} region were measured at *ca.* 50°C. The temperature, measured by a digital thermometer with a thermocouple directly fixed to the cell, was constant during the measurement. The intensities were determined to be given by $\log_{10}(T_0/T)$, where T_0 and T are the apparent intensities of the incident and transmitted radiation at the maximum wave number, respectively.

Calculations

All calculations were carried out on a FACOM M-382 computer at the Computation Center of Nagoya University. The CNDO/2,[8] MINDO/3,[9] MNDO,[10] and MNDOC[11] calculations were performed with the original standard parametrizations, respectively. Geometrical parameters were taken from the results of X-ray crystallographic studies on 2-pyridone[12] and 6-bromo-2-pyridinol[13] for the CNDO/2 and the MINDO/3 calculations with a fixed geometry. Standard bond lengths and bond angles[14] were used as the geometrical parameters of the substituents. The MINDO/3 calculation, with full geometry optimization, was carried out on the structures within C_s symmetry by the RPI/MINDO/3 which contains a convergence-forcing procedure.[15]

Results and Discussion

The molecular-orbital calculations were carried out for a set of 2-pyridones and 2-pyridinols substituted at various positions with methyl, cyano, and methoxy groups.

The computed results by the CNDO/2 method (with a fixed geometry) did not afford satisfactory substituent effects for the relative stability of the two tautomeric forms of the 6-substituted derivatives, which is experimentally known to favor the pyridinol form.[1,6] In contrast, the MINDO/3 method did afford satisfactory results for the substituent effect on the 6-position (*vide infra*). The introduction of substituents can also be expected to alter the ring geometries of both tautomeric forms. Thus, to obtain more precise information on the nature of substituent effects on tautomeric properties, MINDO/3 calculations (with full geometry optimization) were carried out. Details of the results, thus obtained, are presented and discussed in the following subsections.

Energetic Features. The heat-of-formation values (H_f) of a parent compound (**1**) were calculated to be −142.9 and −127.3 kJmol^{-1} for the pyridone form and the pyridinol form, respectively. The calculated energy difference between the two tautomeric forms (15.6kJmol^{-1}) was somewhat greater than the experimental value (1.3±10 kJmol^{-1}).[2]

However, the calculated relative energies (ΔH_f) compared to that of a parent compound (**1**) are a measure of the net substituent effect and are presented in Table 1.

The relative energies, thus obtained, clearly indicate that the 6-substituted derivatives in each tautomeric form are the most stable among the ones bearing the same substituent irrespective of the nature of the substituent. This fact might be rationalized in terms of the *ortho*-position relative to the nitrogen atom, which has a greater electron-accepting property. Thus, the 6-substituent has the greatest interaction with the ring system. Also, the greater stabilizing effect of the 6-substituents on the 2-pyridinol form than on the 2-pyridone form was also shown. This can be understood from the larger C_6–N double-bond character of the former as compared with that of the latter.

As for the effect of the substituent at the 5-position, the 5-methoxy substituent is as effective as 6-polar substituents in a shift of the tautomeric equilibria leading to the predominance of the 2-pyridinol form.

The 5- and 6-chloro derivatives have been shown by IR spectra to favor the 2-pyridinol form over the 2-pyridone form, compared with the 3- and 4-chloro derivatives.[6d] A similar effect of the ortho substituent

Table 1. Substituent effects on the heat of formation (H_f) of 2-pyridones and 2-pyridinols calculated by MINDO 3 with geometry optimization

Substituent	ΔH_f[a]/kJ mol^{-1}		$\Delta\Delta H_f$[b]/kJ mol^{-1}
	2-Pyridones	2-Pyridinols	
3-Me	−24.2	−26.6	−2.4
4-Me	−25.8	−25.1	0.7
5-Me	−29.6	−29.4	0.2
6-Me	−45.4	−48.6	−3.2
3-, 4-Me	−32.6	−33.8	−1.2
5-, 6-Me	−63.2	−67.9	−4.7
3-CN	78.5	73.6	−4.9
4-CN	88.1	87.2	−0.9
5-CN	79.6	78.3	−1.3
6-CN	61.2	52.9	−8.3
3-OMe	−173.5	−174.1	−0.6
4-OMe	−215.2	−211.9	3.3
5-OMe	−176.2	−186.3	−10.1
6-OMe	−227.6	−235.8	−8.2

a) H_f (substituted)−H_f (parent). b) ΔH_f (2-pyridinols)−ΔH_f (2-pyridones).

to the nitrogen atom has also been shown for 4-pyridones.[6c] Due to the similarity of the net electronic-substituent effect between the methoxy group and the halogen atom (σ-inductive and π-donative), the calculated substituent effects of the methoxy derivatives on the relative stabilities between the two tautomeric forms seem to be in accord with the experimental evidence.

The methyl-substituent effect on the relative energetics of the tautomers has been calculated to be not so strong. In fact, it is the 2-pyridone form that is observed in the UV spectral measurement of these derivatives in a nonpolar solvent. However, some supportive experimental data for such an effect were obtained by IR spectral measurements of several methyl derivatives in a CCl_4 solution (5×10^{-4} M) at *ca.* 50 °C, although, in the solutions, these derivatives exist largely as the self-associated 2-pyridone form and the intensities of the nonassociated species are fairly weak. The observed intensity ratio (I_{OH}/I_{NH}) of the O–H and N–H stretching bands (around 3580 and 3410cm , respectively) of the nonassociated species were 0.08, 0.06, 0.14, 0.10, and 0.19 for unsubstituted-, 4-methyl-, 5-methyl-, 6-methyl-, and 5,6-dimethyl-2-pyridones, respectively. Although the absorption coefficient for the same type of vibration may vary from one molecule to another, the difference in the observed intensity ratio could qualitatively represent the greater stabilization of the corresponding 2-pyridinol form in that order.

Electronic Features. It is known that the introduction of electron-donating substituents at the 2- and 4-positions of pyridine, especially at the 2-position, renders a stabilizing effect. Such effects were ascribed to be the consequence of an increase in the N-atomic electron densities.[16]

Thus, the redistributions of atomic electron densities, resulting from the introduction of substituents, were examined. The differential electron densities of substituted 2-pyridones and 2-pyridinols relative to parent compounds are shown in Fig. 1.

An interesting point regarding Fig. 1 is that the largest increments of electron density on the nitrogen atom were shown on each tautomeric form of the 6-substituted derivatives regardless of the nature of the substituent. This is atributable to the lower core potential (large electronegativity) of the nitrogen atom and the ortho-position against the nitrogen atom. On the other hand, the substituents at the 3-, 4-, 5-positions in both tautomeric forms are primarily explained in terms of the general electronic effects for an aromatic system, that is, the *ortho-* and *para*-orientation for electron-donating substituents and the *meta*-orientation for electron withdrawing substituents. As a result, the 4-cyano and 3- and 5-methoxy substituents lead to the smallest electron densities on the nitrogen atom.

The relationship between the relative N-atomic electron densities (ΔQ_N) and the relative energies (ΔH_f) was examined for each substituent (Fig. 2).

It is clear from Fig. 2 that the increments of the electron densities on the nitrogen atom are in parallel to the trend of the relative total energy gain.[17] The magnitude of this increment was greater for the 2-pyridinol form in the case of methyl and methoxy derivatives. However, the nature of the electron density on the nitrogen atom differs from each other between the tautomeric forms, and also between the substituents. Based on an analysis which divided the electron charge increments into the σ- and π-electron character, the contribution of the σ-electron was found to be greater in methyl derivatives, while in the methoxy and cyano derivatives some greater contributions of the π-electron were found. These differences in the contribution of the σ- and π-electron may cause some deviations from

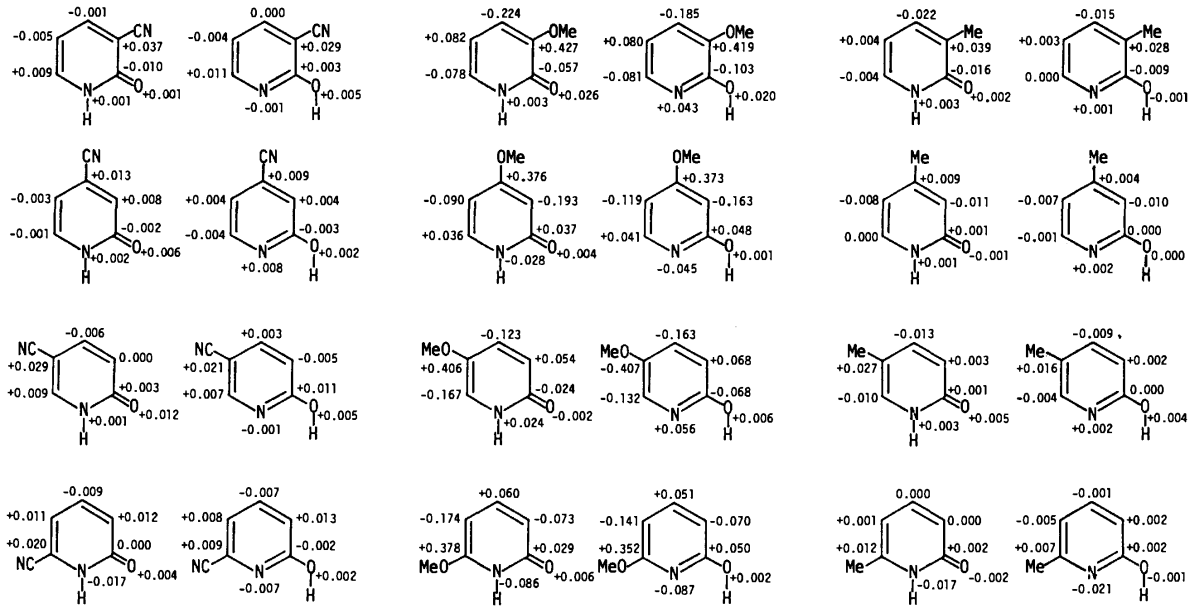

Fig. 1. Differential atomic electron densities of 2-pyridone and 2-pyridinol forms relative to those of the parent compounds.

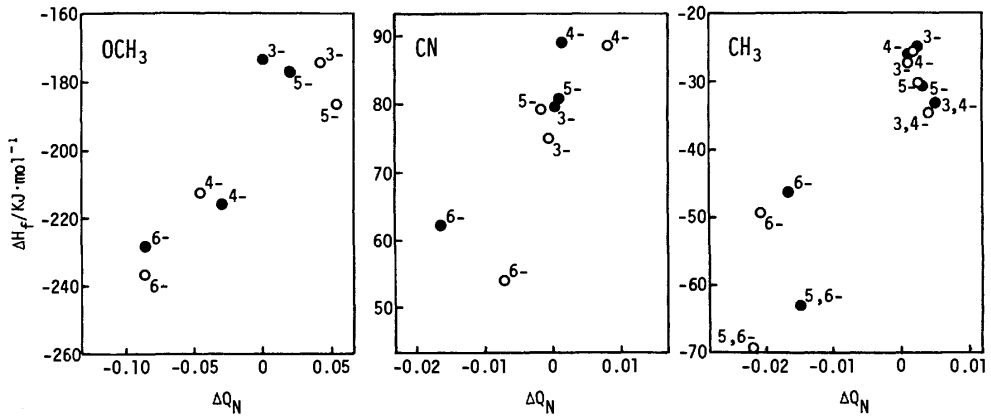

Fig. 2. Plots of the differential heat of formation (ΔH_f) *vs.* the differential N-atomic electron density (ΔQ_N) exerted by substituents. Filled and open symbols represent 2-pyridone and 2-pyridinol forms, respectively.

Table 2. Calculated bond lengths of 2-pyridones[a)]

Substituent	N-H	C_2-O	N-C_2	C_2-C_3	C_3-C_4	C_4-C_5	C_5-C_6	C_6-N
H	1.030	1.218	1.399	1.467	1.369	1.439	1.373	1.364
3-Me	1.031	1.218	1.398	1.489	1.386	1.435	1.372	1.362
4-Me	1.030	1.218	1.397	1.465	1.388	1.459	1.372	1.362
5-Me	1.033	1.217	1.398	1.464	1.368	1.460	1.390	1.363
6-Me	1.033	1.218	1.400	1.464	1.369	1.435	1.391	1.379
3-, 4-Me	1.031	1.219	1.394	1.489	1.408	1.459	1.370	1.359
5-, 6-Me	1.034	1.217	1.398	1.460	1.366	1.457	1.411	1.377
3-CN	1.031	1.216	1.399	1.485	1.387	1.435	1.374	1.361
4-CN	1.030	1.217	1.397	1.467	1.385	1.458	1.372	1.362
5-CN	1.031	1.215	1.402	1.464	1.368	1.458	1.392	1.358
6-CN	1.032	1.217	1.400	1.464	1.367	1.439	1.388	1.379
3-OMe	1.031	1.219	1.387	1.502	1.377	1.446	1.364	1.374
4-OMe	1.030	1.217	1.407	1.455	1.389	1.456	1.373	1.359
5-OMe	1.031	1.220	1.385	1.467	1.368	1.453	1.384	1.375
6-OMe	1.033	1.215	1.414	1.457	1.373	1.429	1.395	1.371

a) Bond lengths are given in Å.

Table 3. Calculated bond lengths of 2-pyridinols[a)]

Substituent	O-H	C_2-O	N-C_2	C_2-C_3	C_3-C_4	C_4-C_5	C_5-C_6	C_6-N
H	0.952	1.321	1.341	1.424	1.400	1.410	1.402	1.334
3-Me	0.951	1.321	1.338	1.446	1.417	1.407	1.400	1.333
4-Me	0.951	1.322	1.340	1.424	1.420	1.427	1.400	1.333
5-Me	0.951	1.320	1.340	1.421	1.397	1.429	1.421	1.328
6-Me	0.951	1.322	1.338	1.422	1.399	1.407	1.420	1.346
3-, 4-Me	0.952	1.323	1.337	1.443	1.444	1.427	1.398	1.330
5-, 6-Me	0.951	1.320	1.336	1.420	1.398	1.426	1.443	1.342
3-CN	0.952	1.318	1.339	1.443	1.418	1.407	1.403	1.333
4-CN	0.952	1.321	1.339	1.424	1.418	1.427	1.400	1.334
5-CN	0.952	1.318	1.341	1.423	1.398	1.428	1.422	1.329
6-CN	0.951	1.320	1.338	1.425	1.398	1.410	1.416	1.346
3-OMe	0.952	1.328	1.326	1.453	1.406	1.418	1.391	1.342
4-OMe	0.952	1.319	1.341	1.423	1.415	1.431	1.398	1.336
5-OMe	0.951	1.326	1.340	1.417	1.404	1.419	1.423	1.331
6-OMe	0.951	1.317	1.335	1.423	1.400	1.407	1.419	1.342

a) Bond lengths are given in Å.

the correlations in cyano and methoxy derivatives in Fig. 2.

Structural Features. The experimental geometries of 2-pyridones and 2-pyridinols have been reported for 2-pyridone,[3,12)] 5-chloro-2-pyridone,[18)] 6-chloro-2-pyridinol,[12,19)] and 6-bromo-2-pyridinol[13)] by the X-ray crystal structure analyses. The optimized geometries derived by the MINDO/3 method show good agreement with experimental facts. The optimized geometric parameters for the ring part of 2-pyridinol were nearly identical with the result for pyridine by the same method.[20)]

The computed bond lengths of the various substituted 2-pyridones and 2-pyridinols obtained by the MINDO/3 method with geometry optimization are summarized in Tables 2 and 3, respectively.

The ring structural perturbation due to an introduction of the substituents can be understood, on the whole, by an increase in bond lengths, including that of the atom attached to the substituent by about 2.0 pm. Also, the O–H bond lengths are nearly constant and variations in the C–O and C–N bond lengths are small. They seemed not to be associated with the tautomeric properties.

Here, it may be interesting to inspect the substituent effects, combining the structural features with the electronic effects described in a previous subsection. The geometric perturbations indicated that the C_3–C_4 bond length had a greater effect on the stabilities of the 2-pyridone and 2-pyridinol forms than the other bond length, considering that the energy gains by the geometrical optimizations in the 3-, or 4-substituted derivatives were greater than those in 5-, or 6-substitution. But, when a comparison between the energy gains in the two forms was made, it was found that the lengthening of the C_5–C_6 bond had an effect on stabilizing the 2-pyridinol form more than the 2-pyridone form (Table 1) (*vide supra*).

As a result of the C_5–C_6 bond lengthening, some parts of the electron density forming the C_5–C_6 bond must be transferred to the rest of the molecule. Among those, the nitrogen atom would naturally gain the greater part of the electron, resulting in the increment in the N-atomic electron densities.

Self-association. The hydrogen-bonded dimeric structure of 2-pyridones is well known from crystallographic[3,12,18] and thermodynamic studies.[21] The dimeric structure of the 2-pyridinol form with a centrosymmetry is also known through X-ray studies of 6-halo-2-pyridinols.[13,19] Thermodynamic parameters, such as the association constant, have been studied for 6-chloro-2-pyridinol[4] and results indicate that the association energies of the 2-pyridinol form are relatively smaller than those for the 2-pyridone form. The importance of self-association in the tautomeric equilibria of 2-pyridones (**1**) has also been stressed by P. Beak *et al.*[2,4] and O. Bensaude *et al.*,[22] and the mechanism by which the tautomerism occurs is widely accepted to be through the dimer. Although the OH proton in the pyridinol form is more acidic than the NH-proton in the pyridone form, based on both charge densities and bond-order terms, the relevant site for the self-association in the pyridone form is more sterically favorable over that in pyridinol form. The net effect of this may be that the pyridone-pyridone dimer is more feasible. Accordingly, the larger association energies of the 2-pyridone form result in a shift in the tautomeric equilibria of **1**, leading to the predominance of the 2-pyridone form (**1a**).

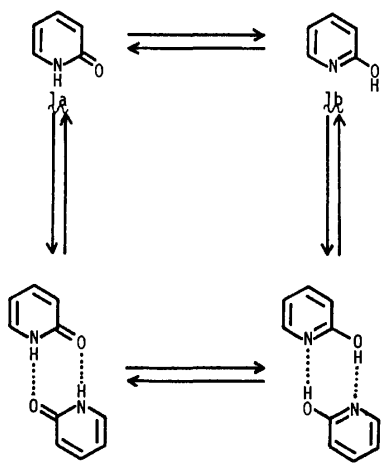

Scheme 2.

Thus, the substituent effect on the association energy of each tautomeric form is considered to be directly related to tautomeric equilibria. However, there is very little experimental or theoretical in formation available on this matter.

The defects of the MINDO/3 and MNDO methods for the evaluation of intermolecular interactions, particularly in the case of hydrogen-bonding interactions, have already been pointed out.[23,24] In fact, attempts to reproduce the self-association energies of the 2-pyridone (**1a**) and 2-pyridinol (**1b**) form by the MINDO/3 method (employing geometries based on the crystalline structures) resulted in the destabilization of 53.1 kJ mol^{-1} in the former and 74.4 kJ mol^{-1} in the latter.

Furthermore, in calculations related to the optimization of intermolecular distances, including those of NH and OH, energy minima were found at unrealistic interatomic distance between the nitrogen and the oxygen: 4.87 Å in 2-pyridone and 7.80 Å in 2-pyridinol, respectively.[25]

Although there are also documented failures of the CNDO/2 scheme's ability to acount correctly for hydrogen bonding or nonbonded interaction,[26] for certain limited structures set on specific association orientations, one can evaluate the relative energetics by the CNDO/2 method.

In fact, it has been reported that the CNDO/2 method has given the correct self-association energy values for formamide[27] and for several other cases of intermolecular systems such as those involving large contribution due to electrostatic interactions.[28]

Recently, Inuzuka *et al.* have reported the self-association energy of 2-pyridone supported by the CNDO/2 method with a geometry optimization, but without referring to the interrelation to the tautomerism.[29] The reported self-association energy was 147.7 KJ mol^{-1}. They deduced a corrected value of 68.2 kJ mol^{-1}, based on comparisons with several organic compounds. This was compatible with the experimental value (65.3 kJ mol^{-1}) obtained by the NMR technique.[29]

We have also evaluated the self-association energies

of various substituted 2-pyridone forms and 2-pyridinol forms on the dimeric structure experimentally determined by X-ray analyses[13,18] (Table 4).

In the present calculations, the self-association energy of the 2-pyridone form (**1a**) was 71.6 kJ mol^{-1}, which is in fairly satisfactory agreement with the above-mentioned experimental value (65.3 kJ mol^{-1}).[30] This value was greater than that of the 2-pyridinol form (**1b**) by 7.6 kJ mol^{-1}, proving a qualitative validity of this method.

However, when comparisons are made of the values between the 2-pyridone form and the 2-pyridinol form of such derivatives (as shown in Table 4), those of the former value were all greater than those of the latter by about 2.9—10.5 kJ mol^{-1}. This was even true for the case of the derivatives which exist very largely in the 2-pyridinol form (to such an extent as can be observed in conventional UV measurements). Therefore, the association ability seems not to be closely related to the tautomerism of the derivatives bearing a polar substituent at the 6-position, although the tautomerism is well known to occur *via* the dimer. On the other hand, parent and methylated derivatives exist largely in the 2-pyridone form due to the greater association energies compared to the tautomeric-energy differences.

Table 4. Dimerization energies calculated by the CNDO /2 method

Substituent	E_{dim}/kJ mol^{-1}	
	2-Pyridones	2-Pyridinols
H	71.7	64.1
3-Me	69.0	64.0
4-Me	74.7	64.9
5-Me	71.1	64.1
6-Me	74.4	64.8
3-CN	73.1	62.5
4-CN	72.7	63.1
5-CN	72.2	62.2
6-CN	70.2	61.8
3-OMe	70.3	62.9
4-OMe	74.2	66.4
5-OMe	70.7	62.5
6-OMe	69.6	66.4

Conclusion

It is often observed that the substituent effect on stability and reactivity can not be easily predicted and interpreted in a simple manner since the factors at play (steric, inductive, conjugative and others) may act in opposing ways. Nevertheless, the present studies considerably enhanced our understanding of the nature of the substituent effect on the tautomeric properties of 2-pyridone–2-pyridinol.

The conclusion reached from the present studies may be represented as follows: From calculations, the substituent at the 6-position have been shown to exert the strongest influence on the relative energetics of the tautomers, irrespective of the nature of the substituents. The introduction of polar substituents at this position stabilized the 2-pyridinol form much more than the 2-pyridone form. This effect is well correlated by N-atomic electron densities and ring structural modifications of the tautomers.

Thus, in this type of derivative, the association ability is not an important factor in controlling the tautomeric euilibria in solution, unlike unsubstituted 2-pyridone, although the association energies have been shown to vary with such substituents.

The introductin of a 6-alkyl substituent, such as a methyl group, also similarly resulted in a greater stabilization of the 2-pyridinol form than of the 2-pyridone form. However, due to the small difference in such a relative energetic of the tautomers, the 2-pyridinol forms were not observed by conventional UV spectral measurements, and the association abilities still play an important role in determining the tautomeric equilibria in solution. The tautomerism of these derivatives, therefore, can be considered to be more susceptible to their environmental conditions than that of unsubstituted 2-pyridone.

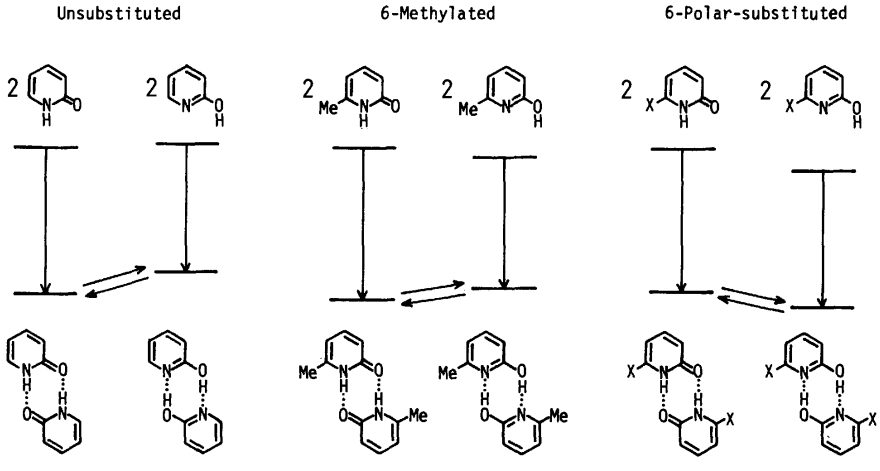

Fig. 3. Qualitative representations for 6-substituent effect on the relative stability of the two tautomers. 6-Polar substituent, **X**, denotes strong electron-withdrawing and donating substituents.

A comparison of the qualitative energy diagrams in the interrelation of the tautomer and dimer forms in solution is illustrated in Fig. 3.

References

1) A. R. Katritzky, and J. M. Lagowski, "Adv. Heterocycl. Chem.," Academic Press, New York (1963), Vol. 1, pp. 312—338; J. Elguero, C. Marzin, A. R. Katritzky, and P. Linda, "Adv. Heterocycl. Chem., Suppl. 1," Academic Press, New York, (1976), pp. 1—655.

2) P. Beak, F. S. Fry, Jr., J. Lee, and F. Steele, *J. Am. Chem. Soc.*, **98**, 171 (1976); P. Beak, *Acc. Chem. Res.*, **10**, pp. 186—192 (1977).

3) B. R. Penfold, *Acta Crystallogr.*, **6**, 591 (1953).

4) P. Beak, J. B. Covington, and J. M. White, *J. Org. Chem.*, **45**, 1347 (1980); P. Beak, J. B. Covington, J. M. White, and J. M. Zeigler, *ibid.*, **45**, 1354 (1980).

5) a) H. J. Gold, *J. Am. Chem. Soc.*, **90**, 3402 (1968); b) L. Paoloni, M. L. Tosato, and M. Cignitti, *Theor. Chim. Acta*, **14**, 221 (1969); c) N. Bodor, M. J. S. Dewar, and A. J. Harget, *J. Am. Chem. Soc.*, **92**, 2929 (1970); d) J. Kuthan and M. Ichova, *Collect. Czech. Chem. Commun.*, **36**, 1413 (1971); e) H. G. Benson and J. N. Murrell, *J. Chem. Soc., Faraday Trans. 2*, **68**, 129 (1972); f) M. Berndt, J. S. Kwiatkowski, J. Budzinski, and B. Szczodrowska, *Chem. Phys. Lett.*, **19**, 246 (1973); g) M. L. Tosato, M. Cignitti, and L. Paoloni, *Gazz. Chim. Ital*, **105**, 385 (1975); h) M. Cignitti and L. Paoloni, *ibid.*, **108**, 491 (1978); i) R. Czerminski, B. Lesyng, and A. Pohorille, *Int. J. Quantum Chem.*, **16**, 1141 (1979); j) C. Krebs, H. J. Hofmann, H. J. Kohler, and C. Weiss, *Chem. Phys. Lett.*, **69**, 537 (1980); k) M. J. Scanlan, I. H. Hiller, and R. H. Davis, *J. Chem. Soc., Chem. Commun.*, **1982**, 685; l) H. B. Schlegel, P. Gund, and E. M. Fluder, *J. Am. Chem. Soc.*, **104**, 5347 (1982); m) M. J. Scanlan, J. H. Hiller, and A. A. MacDowell, *J. Am. Chem. Soc.*, **105**, 3569 (1983); n) For the thorough review, see M. Kuzuya, A. Noguchi, H. Ohno, and T. Okuda, *Ann. Proc. Gifu Pharm. Univ.*, **33**, 16 (1984).

6) a) L. N. Jakhontov, D. M. Krasnokutskaya, E. M. Peresleni, J. N. Sheinker, and M. V. Rubtsov, *Tetrahedron*, **22**, 3233 (1966); b) A. R. Katritzky, F. D. Popp, and J. D. Rowe, *J. Chem. Soc., Perkin Trans. 2*, **1966**, 562; c) A. R. Katritzky, J. D. Rowe, and S. K. Roy, *ibid.*, **1967**, 758; d) G. Simchen, *Chem. Ber.*, **103**, 398 (1970); e) E. Spinner and G. B. Yeoh, *J. Chem. Soc,. Perkin Trans. 2*, **1971**, 279, 289, 296.

7) R. Adams and A. W. Schrecker, *J. Am. Chem. Soc.*, **71**, 1186, (1949); G. P. Gisby, S. E. Royall, and P. G. Sammes, *J. Chem. Soc., Perkin Trans. 1*, **1982**, 169.

8) J. A. Pople and G. A. Segal, *J. Chem. Phys.*, **44**, 3289 (1966).

9) R. C. Bingham, M. J. S. Dewar, and D. H. Lo, *J. Am. Chem. Soc.*, **97**, 1285 (1975); *QCPE*, **11**, 309 (1976).

10) M. J. S. Dewar and W. Thiel, *J. Am. Chem. Soc.*, **99**, 4899, 4907 (1977); *QCPE*, **13**, 428 (1981).

11) W. Thiel, *J. Am. Chem. Soc.*, **103**, 1413, 1420 (1981); *QCPE*, **14**, 438 (1982).

12) J. Almlof, A. Kvick, and I. Olovsson, *Acta Crystallogr., Sect. B*, **27**, 1201 (1971).

13) A. Kvick, *Acta Crystallogr., Sect. B*, **32**, 220 (1976).

14) K. J. Miller, J. F. Pycior, and K. Moschner, *QCPE*, **13**, 431 (1981).

15) J. A. Pople, and D. L. Beveridge, "Approximate Molecular Orbital Theory," McGraw-Hill, New York, (1970), p. 111.

16) J. E. Del Bene, *J. Am. Chem. Soc.*, **101**, 6184 (1979).

17) Quite irrespective of the tautomeric properties, both *N*-methyl-2-pyridone and *O*-methyl-2-pyridinol were also examined and shown to be of the much lower relative N-atomic densities and the much less relative total energy gaines as compared to those of the other mono-methyl derivatives having reinforced this relationship.

18) A. Kvick and S. S. Booles, *Acta Crystallogr., Sect. B*, **28**, 3405 (1972).

19) A. Kvick and I. Olovsson, *Arkiv. Kemi.*, **30**, 71 (1968).

20) R. C. Bingham, M. J. S. Dewar, and D. H. Lo, *J. Am. Chem. Soc.*, **97**, 1302 (1975).

21) M. H. Krackov, C. M. Lee, and H. G. Mautner, *J. Am. Chem. Soc.*, **87**, 892 (1965); G. G. Hammes and H. O. Spivey, *ibid.*, **88**, 1621 (1966); G. G. Hammes and A. C. Park, *ibid.*, **91**, 956 (1969); G. G. Hammes and P. J. Lillford, *ibid.*, **92**, 7578 (1970); K. A. Engdahl and P. Ahlberg, *J. Chem. Res. (S)*, **1977**, 340.

22) O. Bensaude and J. E. Dubois, *C. R. Acad. Sci., Ser. C*, **285**, 503 (1977); O. Bensaude, M. Dreyfus, G. Dodin, and J. E. Dubois, *J. Am. Chem. Soc.*, **99**, 4438 (1977); O. Bensaude, M. Chevrier, and J. E. Dubois, *ibid.*, **100**, 7055 (1978).

23) T. J. Zielinski, D. L. Breen, and R. Rein, *J. Am. Chem. Soc.*, **100**, 6266 (1978); G. Klopman, P. Andreozzi, A. J. Hopfinger, O. Kikuchi, and M. J. S. Dewar, *ibid.*, **100**, 6268 (1978).

24) M. J. S. Dewar and G. P. Ford, *J. Am. Chem. Soc.*, **101**, 5558 (1979).

25) With expectation of the satisfactory reproduction by the reparametrized MNDO method, *i.e.* the MNDOC method[11] with explicit inclusion of electron correlation, the evaluations of the hydrogen bonding dimer of formic acid were also tested with this method, but no stabilization was gained.

26) For recent references see, for example, A. R. Gregory and M. N. Paddon-Row, *J. Am. Chem. Soc.*, **98**, 7521 (1976); A. R. Gregory and M. Przybylska, *ibid.*, **100**, 943 (1978); K. B. Lipkowitz, *ibid.*, **100**, 7535 (1978).

27) A. Pullmann and H. Berthod, *Theor. Chim. Acta*, **10**, 461 (1968).

28) P. Schuster, in "The Hydrogen Bond," ed by P. Schuster, G. Zundel, and C. Sandorfy, North-Holland Publishing Company (1976), pp. 25—163.

29) K. Inuzuka and A. Fujimoto, *Bull. Chem. Soc. Jpn.*, **55**, 2537 (1982).

30) Such a good agreement on using experimental geometries in the CNDO/2 calculation is well known.

 © 1984 The Chemical Society of Japan Bull. Chem. Soc. Jpn., 57, 3461—3465 (1984)

Effects and Role of the Substituents upon 2-Pyridone-catalyzed Mutarotation of 2,3,4,6-Tetra-*O*-methyl-D-glucose

Masayuki KUZUYA,* Akihiro NOGUCHI, and Takachiyo OKUDA
Gifu Pharmaceutical Uuiversity, 6-1, Mitahora-higashi 5-Chome, Gifu 502
(Received January 13, 1984)

We have studied the catalytic activities of various substituted 2-pyridones on the mutarotation of 2,3,4,6-tetra-*O*-methyl-D-glucose (TMG). The results in an acetone solution at 37 °C showed that an introduction of the polar substituents into the 5- or 6-position, regardless of the nature of the substituents, retarded the relative rate of the mutarotation as compared to a parent compound, while that of alkyl substituents accelerated such rates. Further striking rate enhancements were observed in 5,6-dimethyl-substituted derivatives. Based on experimental results, we concluded that the 2-pyridones which can act as an effective catalyst are such that the 2-pyridone tautomeric form predominantly exists in solution due to its greater association ability and that the 2-pyridinol tautomeric form is energetically more stable for a lower activation energy of the double-proton transfer process in the 2-pyridone-TMG complex.

In a previous paper,[1] we described the influence on the tautomeric properties of 2-pyridones–2-pyridinols exerted by the introduction of substituents on the basis of the quantum mechanical quantities obtained from semiempirical molecular orbital calculations.

The importance of simultaneous two-proton transfers in a bifunctional catalysis is well known in relation to the enzymatic catalysis, and many related systems have been studied along these lines.[2] Among those is the classical 2-pyridone-catalyzed mutarotation of 2,3,4,6-tetra-*O*-methyl-D-glucose (TMG), which is of continued interest and is still under active investigations because of its high catalytic activity. Its very high catalytic efficiency can not be explained by the concerted general acid-base concept, since 2-pyridone is a relatively weak acid and base. Also, the reported rationalization of the catalytic functions are somewhat controversial. This indicates that a delicate balance of many blends of the effects can affect catalytic activities, and that the phenomenon can not be explained in a simple manner.

Tautomeric properties are considered to be of particular importance related to the efficiency of bifunctional catalytic activities, yet full details of the relationship to the tautomeric properties have not yet been understood. Part of our efforts in this area have involved an attempt to explore the substituent effects on the rate of the 2-pyridone-catalyzed mutarotation of TMG.

We report here on the interesting features of such effects and discuss the relations to the tautomeric properties. We also discuss the mechanism on the mutarotations with the aid of quantum mechanical quantities reported in a previous paper.[1]

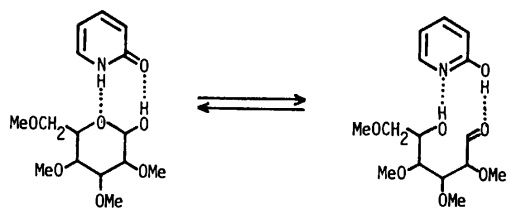

Scheme 1.

Experimental

^{1}H-NMR spectra were obtained on a Hitachi R-20 spectrometer (60 MHz), in $CDCl_3$ with tetramethylsilane (TMS) as an internal standard. All chemical shifts are in parts per million (δ) from TMS. IR spectra were taken on KBr disks with a JASCO A-102 spectrophotometer and were calibrated against polystyrene. UV spectra were measured in cyclohexane with a Hitachi 323 spectrophotometer. Mass spectra were obtained at 70 eV with a JEOL JMS-D300 spectrometer. Elemental analyses were carried out by the Microanalytical Laboratory, Gifu Pharmaceutical University. All melting points are uncorrected.

2-Pyridone (**1**) and 6-chloro-2-pyridinol (**17**) were commercially available. 3-Methyl- (**2**), 4-methy- (**3**), 5-methyl- (**4**), 6-methyl- (**5**), and 4,6-dimethyl-2-pyridone (**7**) were prepared by diazotization of the corresponding substituted 2-pyridinamine, respectively.[3] 3,5-Dimethyl-2-pyridone (**6**) was prepared from 3,5-lutidine *N*-oxide according to the method of Bain and Saxtone.[4] 4,5,6-Trimethyl-2-pyridone (**9**),[5] 5-bromo-3-methyl-2-pyridone (**13**),[6] 3-methyl-5-nitro-2-pyridone (**14**),[7] 2,3-dihydro-4-methylfuro[2,3-*b*]pyridin-6-ol (**15**),[8] and 6-methoxy-2-pyridinol (**16**)[9] were prepared according to reported procedures. 2,3,4,6-Tetra-*O*-methyl-D-glucose (TMG) was prepared according to a method found in the literature.[10] All compounds used for the present study gave satisfactory spectral properties and elemental analyses.

Preparation of 2-Pyridones (10, 11, and 12). General Procedure: To polyphosphoric acid (125 g) were added the β-ketonitrile (0.05 mol)[11,12] and the ketone (0.05—1.10 mol). The mixture was stirred at 70 °C for 1.5 h, then at 100—120 °C for 1.5 h. The dark mixture was then added to crushed ice (*ca.* 1 Kg) while stirring. Then, ether (500 ml) was added. The resulting mixture was stirred for 30 min. The aqueous layer was neutralized with solid sodium hydrogencarbonate. The precipitated solid was collected and recrystallized from ethanol to give the 2-pyridones.

3,4,5,6-Tetramethyl-2-pyridone (10): Colorless plates, mp 255—256 °C. Found: C, 71.27; H, 8.80; N, 9.04%. Calcd for $C_9H_{13}NO$: C, 71.49; H, 8.67; N, 9.26%. ^{1}H-NMR: δ=1.98 (s, 3H, 3-Me), 2.11 (s, 6H, 4-Me and 5-Me), 2.32 (s, 3H, 6-Me), 13.0 (br, s, 1H, NH); IR: 3200—2200 (br, NH), 1630 cm^{-1} (C=O); UV: 237 (ε 6600), 304 nm (ε 6500); EIMS: *m/z* (% of base) 151 (M^+, 100), 123 (20), 122 (75), 108 (35).

3,5,6-Trimethyl-4-phenyl-2-pyridone (11): Colorless plates, mp

216—217 °C. Found: C,78.98; H, 7.21; N, 6.64%. Calcd for $C_{14}H_{15}NO$: C, 78.84; H, 7.08; N, 6.56%. ^{1}H-NMR: δ= 1.67 (s, 3H, 3-Me), 1.85 (s, 3H, 5-Me), 2.35 (s, 3H, 6-Me), 13.2 (s, 1H, NH); IR 3200—2400 (br, NH), 1640cm^{-1} (C=O); EIMS: *m/z* (% of base) 213 (M^+, 62), 212 (100), 194 (17), 184 (11), and 167 (13).

*3-Methyl-4-phenyl-2*H*-cyclopenta[*b*]pyridin-2-one (12)*: Colorless needles, mp 213—215 °C. Found: C, 79.94; H, 7.76; N, 6.13%. Calcd for $C_{15}H_{15}NO$: C, 79.97; H, 6.71; N, 6.22%. ^{1}H-NMR: δ=1.98 (s, 3H, 3-Me), 2.02 (br, m, 2H, CH_2), 2.46 (br, t, J=6Hz, 2H, CH_2), 2.97 (br, t, J=9Hz, 2H, CH_2), 7.05—7.63 (m, 5H, Ar), 13.35 (br s, 1H, NH); IR: 3200—2200 (br, NH), 1630cm^{-1} (C=O); UV: 228 (ε 14800), 319nm (ε 5600); EIMS: *m/z* (% of base) 225 (M^+, 57), 224 (100), 216 (15), 196 (7).

Rate Measurements. The solvents of acetone and benzene (Extra-pure grade, Wako-pure Chemicals, Ltd.) were purified by distillation before use. The rate of mutarotation was followed using a JASCO DIP-4 digital polarimeter. The rate measurements were carried out according to the method of Smith and Hearn.[13] The pseudo first-order rate constants for the mutarotation were calculated by a least-squares method.

Infrared Spectral Measurements for Intensities of the Monomeric NH Stretching Bands (log I_o/I*).* The solvent of carbon tetrachloride (spectroscopic grade) was dried over molecular sieves. Measurements were made with a JASCO DS-403G Infrared Grating spectrophotometer using a 20mm NaCl cell. The infrared spectra (3600—3200cm^{-1}) were recorded with solvent compensation using a five-fold-scale expansion in transmittance at room temperature.

Results and Discussion

For the substituent effects of 2-pyridones on the mutarotation of TMG, only the study of each of its four monomethyl-substituted 2-pyridones in the 3-, 4-, 5- or 6-position and electron-withdrawing groups in the 5-position has been reported as far as we are aware.[13] It has been shown that the electron-withdrawing groups in the 5-position retarded the rate of mutarotation and that the active catalyst was in the 2-pyridone form. The tautomeric properties are considered to be an important factor in determining the reaction rate. All the 2-pyridones examined, however, were those known to exist largely in the 2-pyridone form in a polar solvent.

Substituent Effect of 2-Pyridone on the Catalytic Activity. We have studied the substituent effects on the rate of the mutarotation of TMG in acetone using various substituted 2-pyridones including compounds (**15**—**17**) whose tautomeric equilibria are experimentally known to favor the 2-pyridinol form in solution.[14] Acetone was chosen as a solvent because of the high solubility of the substituted 2-pyridones.

The rate-constants obtained at 37 °C are listed in Table 1.

Table 1 shows that the catalytic activities of 2-pyridones are not amenable to a simple rationalization and discloses several interesting features. The derivatives (**13**—**17**) which possess a polar substituent at the 5- or 6-position regardless of the electron-withdrawing or -donating substituents showed much less catalytic activity compared to that of the parent compound; the compounds bearing a rather strong electron-withdrawing group at the 5-position (**13**, **14**), which favor the 2-pyridone form over the 2-pyridinol form,[14] and the ones bearing a polar substituent (-OMe and -Cl) at the 6-position (**15**—**17**), which exist very largely in the 2-pyridinol form,[14] are both poor catalysts.

Hence, it appears that the catalytic activity of 2-pyridones on the mutarotation of TMG is not simply related to the apparent abundance of either of the tautomeric forms.

In contrast, the alkylated derivatives (**2**—**12**) were shown to display higher catalytic activities than the parent compound (**1**). Among them, the 6-methyl substituent seems to exert the strongest influence on the rate acceleration.[15] Further striking rate enhancements were observed in derivatives bearing methyl substituents at both the 5- and 6-positions (**8**—**10**).

It is known that each of 2-pyridones and TMG undergoes self-association by hydrogen bonding in nonpolar solvents[16] and that the tautomerisms occur *via* a dynamic process involving double proton transfers in self-association forms.[17] However, the initial stage of the 2-pyridone-catalyzed mutarotations of TMG must involve the formation of a hydrogen-bonded complex between 2-pyridone and TMG. Therefore, the association ability should closely be related to the catalytic activity of the 2-pyridones.

The self-association abilities can be regarded as an experimental criteria for the 2-pyridone-TMG association ability. Such abilities of several methyl derivatives were measured by IR spectra based upon the intensity of the NH stretching band (around 3400cm^{-1}) of the monomeric species as log (I_o/I).

The relative catalytic activities (k_r) in Table 1 were plotted against log (I_o/I), and are shown in Fig 1.

It can be seen from Fig. 1 that the abundance of the monomeric form in a series of 6-methy derivatives (**5** and **7**—**10**) is obviously small. This fact is also consistent with the greater self-association ability of these derivatives deduced from the CNDO/2 calculations previously reported.[1] Although the data, thus measured, are not of high accuracy due to experimental limitations, the relative catalytic activities (k_r) of **1**—**7** were shown to be considerably well correlated with log (I_o/I), as indicated in Fig. 1. Thus, it seems reasonable, to a first approximation, to consider that the catalytic activity of the 2-pyridone is proportional to its association ability.

However, the large deviation of 5,6-dimethyl derivatives (**8**—**10**) from the line strongly indicated that other factors could contribute to the higher catalytic activities of this series.

Concerning a Pronounced Effect of 5,6-Dimethyl Substitutions. In view of the observations that the association abilities of the 6-methyl (**5**) and (**7**), and

Table 1. Pseudo first- order rate constants for mutarotation of TMG catalyzed by substituted 2-pyridones at 37 °C[a)]

2-Pyridones catalyst	Substituent				$k_{obsd}/10^{-3}$ min^{-1}	r[b)]	k_r[c)]
	R_3	R_4	R_5	R_6			
1	H	H	H	H	4.16	0.9896	1.000
2	Me	H	H	H	4.25	0.9984	1.022
3	H	Me	H	H	7.45	0.9981	1.791
4	H	H	Me	H	6.56	0.9976	1.577
5	H	H	H	Me	8.55	0.9965	2.055
6	Me	H	Me	H	6.35	0.9982	1.526
7	H	Me	H	Me	9.67	0.9805	2.325
8	H	H	Me	Me	14.12	0.9973	3.394
9	H	Me	Me	Me	21.24	0.9861	5.106
10	Me	Me	Me	Me	20.45	0.9991	4.916
11	Me	Ph	Me	Me	24.25	0.9977	5.829
12	Me	Ph	$-(CH_2)_3-$		10.01	0.9968	2.406
13	Me	H	Br	H	2.32	0.9921	0.558
14	Me	H	NO_2	H	0.93	0.9903	0.224
15	H	Me	$-CH_2CH_2O-$		3.74	0.9978	0.899
16	H	H	H	OMe	0.92	0.9733	0.221
17	H	H	H	Cl	1.41	0.9879	0.339

a) [TMG]=0.09 M and [2-pyridones]=0.005 M. (1 M=1 mol dm^{-3}) b) Correlation coefficient. c) $k_{obsd}/k_{obsd(parent)}$

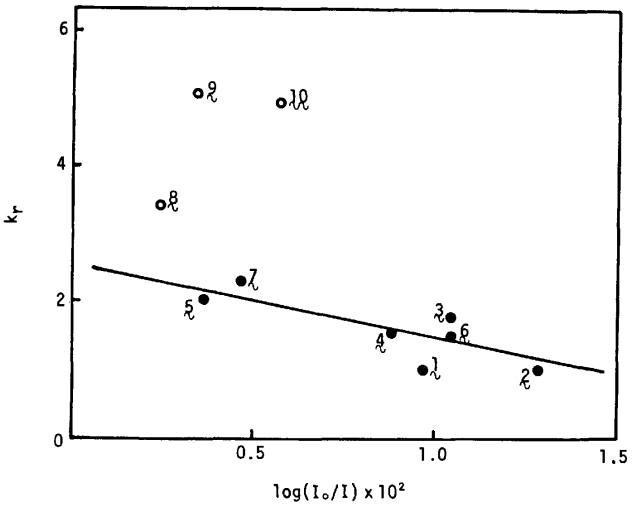

Fig. 1. Plot of the relative catalytic activities (k_r) *vs.* the intensities of the monomeric NH stretching band ($\log(I_0/I)$).
The straight line obtained by a least squares method of **1**—**7** may be expressed as $Y(k_r)=-1.2131\,X(\log(I_0/I))+2.6677$ and the correlation coefficient (r) was obtained as $r=-0.8126$.

5,6-dimethyl derivatives (**8**—**10**) are more or less the same (Fig. 1), such abilities do not account for the striking rate enhancement of a series of 5,6-dimethyl derivatives (**8**—**12**).

The 6-methyl substituent has been shown to render the effect in nature similar to the polar substituents on the relative energetic between the two tautomers (*i.e.* the greater stabilization of 2-pyridinol form), but to a much lesser extent and, to make the tautomeric equilibria labile to the molecular environment. It has also been shown that this propensity was further strengthened by 5,6-dimethyl substitutions.[1)] The origin of these particular substituent effects can be interpreted as due to bond lengthenings at the C_5–C_6 bond, which apparently weaken the diene character to lead to the more 2-pyridinol-like ring structure.

The ring structural difference between the two tautomeric forms should also be related to the kinetics of the tautomerization. Such may be inversely proportional to each other based on the principle of least nuclear motion,[18)] and the derivatives, which require less structural variations during the tautomerization, may be of small activation energies.

Thus, the further acceleration of the rate of the mutarotation catalyzed by 2-pyridones is ascribed to the tautomeric properties, since such reactions proceed with the tautomerization of 2-pyridones.

Inversely, the extremely large predominance to either of the two tautomeric forms induced by an introduction of polar substituents would lead to a retardation of the dynamic process involving the double proton transfers. This rationalization is consistent with the fact that 2-pyridones bearing 6-polar substituents were poor catalysts (*vide supra*), and no further rate enhancement of the mutarotation was observed in the cyclopenta-derivative (**12**) as compared to that of the other derivatives bearing two methyl groups at both 5- and 6-positions, since the C_5–C_6 bond in **12** is no longer lengthened due to the absence of the buttressing effects of the methyl group on each other.

Reactions in Benzene. We have measured the rate of the TMG-mutarotations on several methyl derivatives (**1**, **5**, and **8**) in benzene at various temperatures (10 °C—38 °C) because of the greater tendency for the enhancement of the association in a nonpolar solvent. The pseudo first-order kinetics (k_{obsd}) are summarized in Table 2 along with the correlation coefficient (r) of the least-squares treatment at each temperature.

Table 2 clearly indicated that a considerable rate

Table 2. Temperature-dependent rate constant for mutarotation of TMG catalyzed by substituted 2-pyridones in benzene[a)]

2-Pyridones catalyst	Temp/°C	k_{obsd}/ 10^{-3} min^{-1}	r[b)]
1	10.0	3.947	0.9966
	18.0	9.857	0.9940
	26.0	21.588	0.9984
	38.0	57.995	0.9966
5	10.0	4.817	0.9970
	18.0	13.054	0.9978
	27.0	27.141	0.9958
	36.5	56.956	0.9971
8	10.5	9.339	0.9979
	18.0	17.876	0.9989
	28.5	52.438	0.9975
	37.0	96.927	0.9987

a) [TMG]=0.09 M and [2-pyridones]=0.002 M. b) Correlation coefficient.

enhancement was observed in a benzene solution as compared to those in acetone at the same temperature. The solvent effect of acetone upon the lower rate can be rationalized in terms of the lower concentration of the 2-pyridone–TMG complex and a higher activation energy of the double proton-transfer process by the greater solvation in such a complex.

Conclusions

On the basis of the results and discussion described above, we deduced the sequences for the mutarotation of TMG catalyzed by 2-pyridones as shown in Scheme 2 for a parent compound (**1**) as an example.

In Scheme 2, the ring-opening processes, ***a*** and ***a'***, include the breaking of the σ-bond in TMG and are considered to require the largest activation energy, and to be important in determining the rate of mutarotation. Of these, process ***a*** is apparently important due to the greater association ability of the pyridone form and the activation energy is considered to be dependent on the relative energetics of **18** and **19**.

It can be concluded, therefore, that for the 2-pyridones to be effective catalysts, the 2-pyridone form predominantly exists in solution due to a greater self-association ability (for higher concentration of the complex (**18**)), and the 2-pyridinol tautomeric form is intrinsically more stable (for a lower activation energy of process ***a***). The tautomeric properties of 6-methyl derivatives, especially 5,6-dimethyl and 4,5,6-trimethyl derivatives, meet the above mentioned requirements[1)]

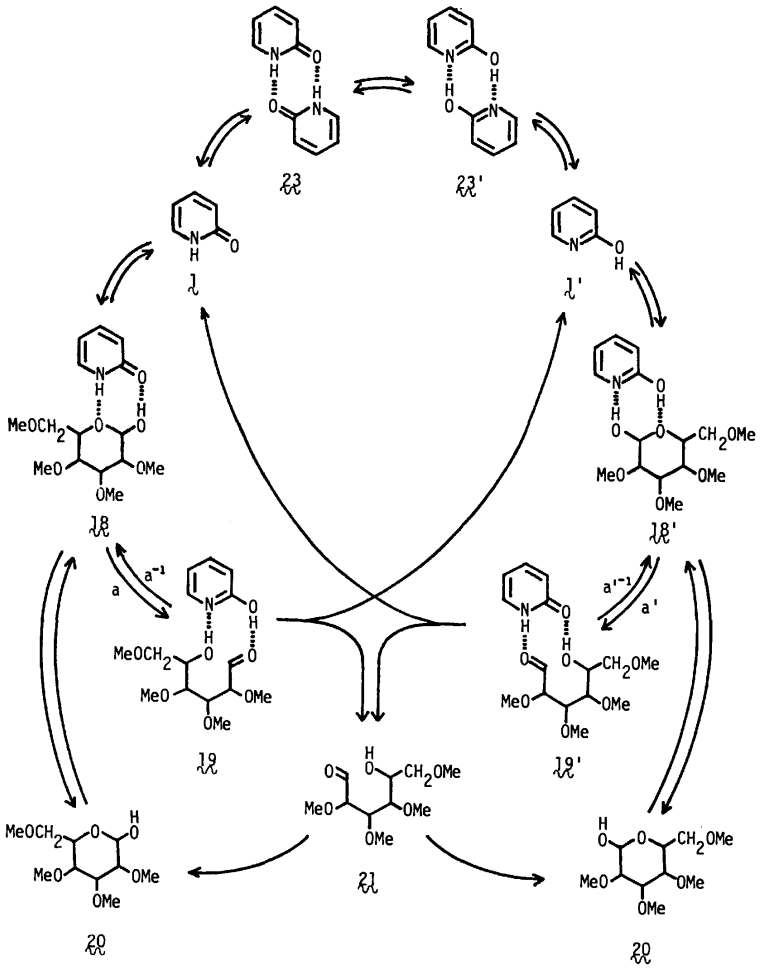

Scheme 2.

and, indeed, these derivatives were all effective catalysts.

References

1) M. Kuzuya, A. Noguchi, and T. Okuda, *Bull. Chem. Soc. Jpn.*, **57**, 3454 (1984).

2) a) W. P. Jencks, *Chem. Rev.*, **72**, 705 (1972); b) C. G. Swain and J. F. Brown, Jr., *J. Am. Chem. Soc.*, **74**, 2534, 2538 (1952); c) G. G. Hammes, *Nature*, **204**, 342 (1964); d) P. R. Rony, *J. Am. Chem. Soc.*, **91**, 6090 (1969); e) P. R. Rony and R. O. Neff, *J. Am. Chem. Soc.*, **95**, 2896 (1973); f) H. M. Niemeyer and P. Ahlberg, *J. Chem. Soc., Chem. Commun.*, **1974**, 799; g) H. M. Niemeyer, O. Goscinski and P. Ahlberg, *Tetrahedron*, **31**, 1699 (1975); h) O. Bensande, M. Chevrier, and J. E. Dubois, *J. Am. Chem. Soc.*, **101**, 2423 (1979).

3) W. Herz and D. R. K. Murty, *J. Org. Chem.*, **26**, 122 (1961).

4) B. M. Bain and J. E. Saxton, *J. Chem. Soc.*, **1961**, 5216.

5) V. Prelog, A. Komzak, and E. Moor, *Helv. Chim. Acta*, **25**, 1654 (1942).

6) D. J. Cook, R. E. Bowen, P. Sorter, and E. Daniels, *J. Org. Chem.*, **26**, 4949 (1961).

7) P. J. Bringnell, A. R. Katritzky, and H. O. Tarhan, *J. Chem. Soc., Perkin Trans. 2*, **1968**, 1477.

8) J. R. Stevens, R. H. Beutel, and E. Chamberlin, *J. Am. Chem. Soc.*, **64**, 1093 (1942).

9) A. R. Katritzky, F. D. Popp, and J. D. Rowe, *J. Chem. Soc., Perkin Trans. 2*, **1966**, 562.

10) E. S. West and R. F. Holden, *Org. Synth.* Coll. Vol. 3, **1955**, 800.

11) E. Mohr, *J. Prac. Chem.*, **90**, 198 (1914).

12) J. B. Dorsh and S. M. McElvain, *J. Am. Chem. Soc.*, **54**, 2960 (1932).

13) W. T. Smith, Jr. and T. L. Hearn, *Bioorg. Chem.*, **2**, 39 (1972).

14) P. Beak, F. S. Fry, Jr., J. Lee, and F. Steele, *J. Am. Chem. Soc.*, **98**, 171 (1976); P. Beak, *Acc. Chem. Res.*, **10**, 186 (1977); P. Beak, J. B. Covington, and J. M. White, *J. Org. Chem.*, **45**, 1347 (1980); O. Bensaude, M. Chevrier, J. Guillerez, and J. E. Dubois, *J. Am. Chem. Soc.*, **102**, 401 (1980); A. R. Katritzky, F. D. Popp, and J. D. Rowe, *J. Chem. Soc. (B)*, **1966**, 562; A. R. Katritzky, J. D. Rowe, and S. K. Roy, *J. Chem. Soc. (B)*, **1967**, 758; G. Simchen, *Chem. Ber*, **103**, 398 (1970); E. Spinner, and G. B. Yeoh, *J. Chem. Soc. (B)*, **1971**, 279, 289, 296.

15) It should be noted that the rate acceleration in the 6-methyl derivative is in sharp contrast to the reported result where the relative rate was slightly suppressed.[13] We have repeatedly measured the rate on this derivative, but obtained the consistent data as described.

16) K. Engdahl and P. Ahlberg, *J. Chem. Res. (s)*, **1977**, 340.

17) O. Bensande and J. E. Dubois, *C. R. Acad. Sc. Paris, Ser. C*, **285**, 503 (1977); O. Bensande, M. Chevrier, and J. E. Dubois, *J. Am. Chem. Soc.*, **100**, 7055 (1978).

18) J. Hine, *J. Org. Chem.*,**31**, 1236 (1966).

Synthetic Studies on the Ochtodane Type Terpenes I. Stereoselective Construction of the Ochtodane Skeleton from Myrcene

Yukio MASAKI,* Kinji HASHIMOTO, Kazuhiko SAKUMA, and Kenji KAJI
Gifu Pharmaceutical University, 5-6-1 Mitahora Higashi, Gifu 502
(Received May 4, 1984)

The ochtodane skeleton, the Carbon framework of 1,1-dimethyl-3-ethylcyclohexane (**1**) was constructed highly stereoselectively by the acid-catalyzed ($SnCl_4$ or CF_3CO_2H) cyclization of the terminally functionalized myrcene derivatives, the benzenesulfenyl chloride adduct (**7**), the terminal β-hydroxy sulfide (**8**) derived from **7**, and myrcene 6,7-epoxide (**10**). The stereoselectivity of the 3-exo-double bond in **1** formed concomitantly in the cyclization reaction was found to depend remarkably upon the reaction temperature and the 85—94% of *E*-stereoselectivity was attained at −78 °C. By the method, the ochtodane derivatives with the sulfur- or oxygen-functional groups on the C(6)-position were obtained. Synthetic applications of the ochtodane type compounds (**12**) and (**19**) to the aldehyde component (**4**) of the pheromone of the male boll weevils and to an ochtodane type terpene (**26**) isolated from the red alga *Ochtodes crockeri*, are reported.

In 1975 novel dihalogenated dimethylhexahydrobenzofurans including chondrocole A (**2**) were isolated by Moore from Hawaiian red alga *Chondrococcus hornemanni*.[1a] Recently, Fenical and coworkers have found a variety of polyhalogenated and/or oxygenated cyclic monoterpenes possessing the ring system of 1,1-dimethyl-3-ethylcyclohexane (**1**) in red seaweeds (Rhodophyta) of the genera *Chondrococcus* and *Ochtodes* (Rhizophyllidaceae),[1b] and they suggested the name "ochtodane" for the skeleton (**1**). They also reported that some of the ochtodane type monoterpenes appear to function as herbivore feeding deterrents in the marine environment and that a certain polyhalogenated compound of this class shows strong anti-bacterial activity. Interestingly, the less functionalized compounds (*Z*-**3**) and (*E*- and *Z*-**4**) with the carbon skeleton (**1**) already have been isolated and recognized by Tumlinson and coworkers in 1969 as the sex attractant and aggregating pheromonal components of the insect boll weevils *Anthonomus grandis* Boheman.[2a] These terpenes have been suggested to be biosynthesized from myrcene (**5**) directly or *via* the corresponding oxygenated or halogenated precursors in organisms.[1a,3] In the context, a unique sesquiterpene pleraplysillin-1 (**6**) isolated from a marine sponge *Pleraplysilla spinifera* may be classified as the higher homologue of the ochtodane type terpenes.[4]

Because of the practical interest in the agricultural purpose for extermination of noxious insects, a lot of synthetic efforts have focused on the pheromonal components (**3**) and (**4**).[2,5,6a] The biogenetic type cyclization of acyclic 1,5-dienes affording terpenoid-carbocycles was pioneered by Eschenmoser[7a] and by Stork,[7b] and has been extensively studied on not only the non-functionalized but also functionalized polyolefins.[7] In addition to the nonbiogenetic type synthetic route consisting of the two-carbons homologation of 3,3-dimethylcyclohexanone which in general appears non or less stereoselective concerning the geometry of the exocyclic double bond in (**3**) and (**4**),[2b,5] several routes utilizing the biogenetic type cyclization of acyclic monoterpenes including myrcene (**5**) have been reported: Acid-catalyzed cyclization of γ-geraniol,[6a] tricarbonyl myrcene iron,[6b] and 3,10-dihydromyrcene;[6c] and brominative cyclization of myrcene (**5**) using 2,4,4,6-tetrabromo-2,5-cyclohexadien-1-one.[6d] None of these precedents, however, has offered satisfactory stereoselectivities and requisite functionalizations for synthesis

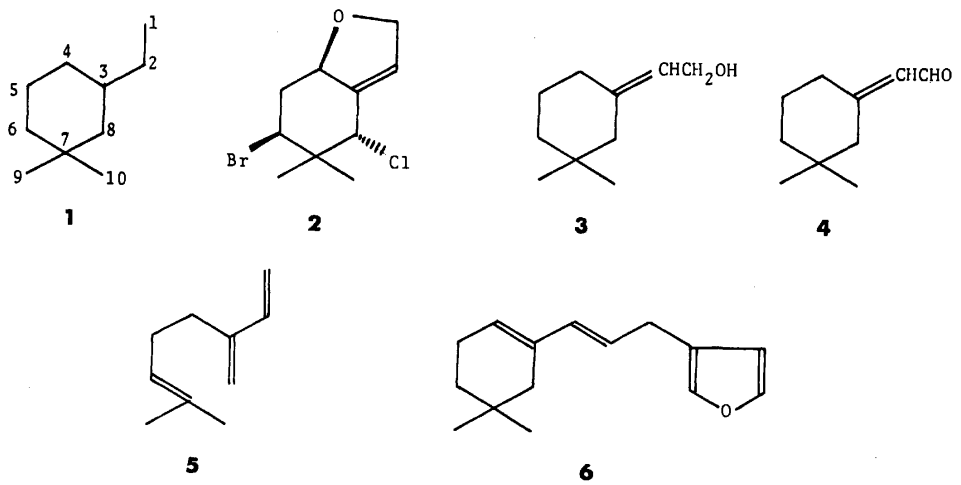

Chart 1.

of the highly functionalized ochtodane type terpenes. Here we disclose new biogenetic type and stereoselective cyclizations of myrcene (**5**) *via* the benzenesulfenyl chloride (PhSCl) adduct (**7**) or the epoxide (**10**) effectively affording the functionalized ochtodanes (**11—15, 17**) which are expected to be the promising intermediates for a variety of ochtodane type terpenes.[8]

Results and Discussion

In a general consideration concerning the possible acid- catalyzed cyclization of myrcene (**5**), the generated terminal tertiary cation (**i**) would cyclize to give the ochtodane type skeleton (**1**) and the other tertiary cation (**ii**), if generated, would form the cyclobutane framework (**iii**) found in glandisol which has been recognized to be the major pheromonal constituent of male boll weevils.[2] Wolinsky has examined the cyclization reaction of γ-geraniol (**iv**) and methyl γ-geranate (**v**) under acidic conditions and reported exclusive formation of the cyclohexane framework (**1**) so far.[6a] We also investigated in the preliminary experiments acid-catalyzed reactions of myrcene (**5**) itself under several conditions involving CF_3CO_2H (CH_2Cl_2/−20°C), $SnCl_4$ (CH_2Cl_2/0°C), 90% HCO_2H (reflux), and polyphosphoric acid (130°C), but the reactions produced complicated and intractable mixtures in all cases examined. Then we turned our attention to the examination of cyclization reaction of the terminally functionalized myrcene derivatives.

1) Acid-catalyzed Cyclization of Terminally Sulfur-substituted Myrcene Derivatives (Scheme 1). Mustafaeva reported that methyl geranate (**vi**) gave the cyclized product (**viii**) on treatment with PhSCl in the presence of $AgSbF_6$ in nitromethane by way of the *in situ* formed terminal adduct (**vii**)[9a] and Weiler also found that the PhSCl-adduct (**x**) of methyl 7-methyl-3-oxo-7-octenoate (**ix**) cyclized to give a cyclohexane derivative (**xi**) by refluxing with silica gel in CH_2Cl_2.[9b] Also we have observed the acid-catalyzed cyclization of terminally sulfur-functionalized geraniol and nerol derivatives (**xii, xiii**) affording the cyclohexane derivatives (**xiv, xv**).[10] Findings in the literatures[9] and our observations[10] prompted us to investigate the behaviors of the terminally sulfur-functionalized myrcene derivatives in the acid-catalyzed cyclization conditions.

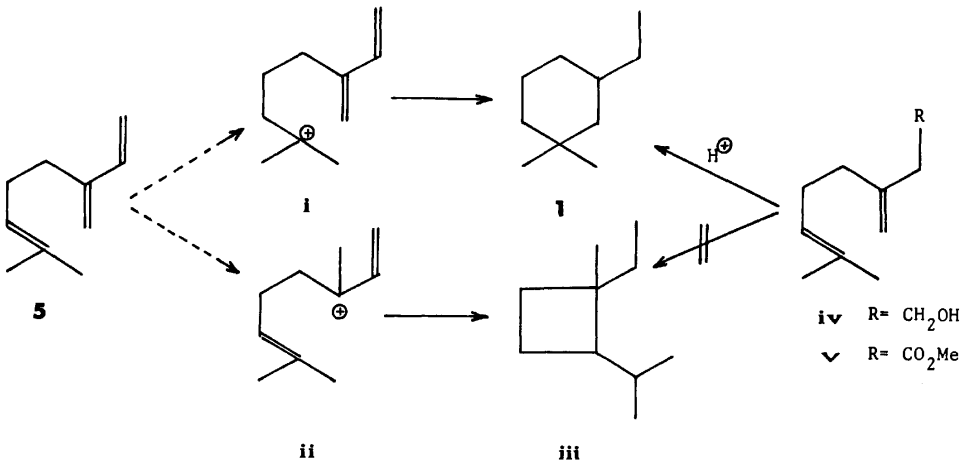

Chart 2.

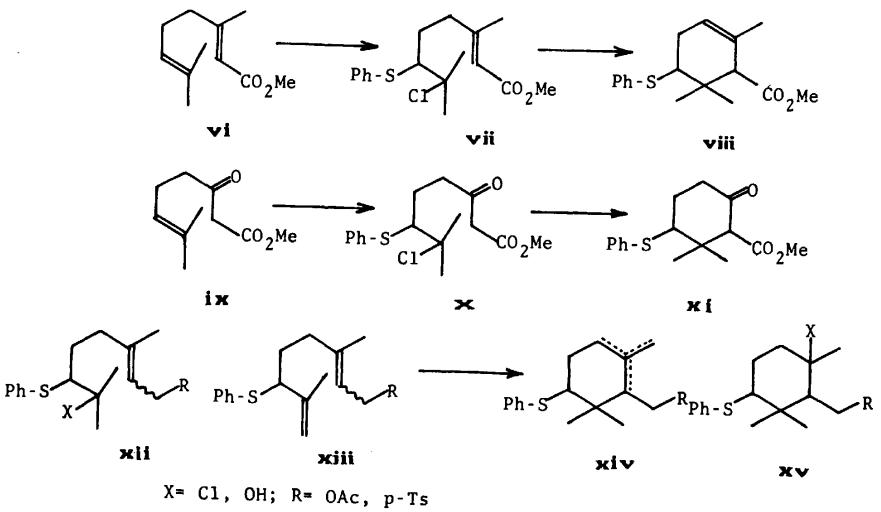

Chart 3.

The substrates, PhSCl-adduct (**7**), β-hydroxy sulfide (**8**), and terminal methallylic sulfide (**9**) was prepared from myrcene (**5**) by the method recently developed[11] for the terminal functionalzation of acyclic isoprenoids.

The crude adduct (**7**) was treated with 0.2equiv of $SnCl_4$ in CH_2Cl_2 at −20°C to produce expectingly the cyclized products (**11**) whose ^{1}H-NMR exhibited mainly sharp singlets at δ 0.69 and 1.16 assignable to the gem-dimethyl groups on the cyclohexane ring and a set of a doublet and a triplet respectively at δ 3.95 and 5.31 with the identical coupling constant (8.0Hz) assignable to the primary allylic chloride functionality. The crude product, without further purification, was converted to the corresponding acetate (**12**) by treatment with an excess amount of AcONa in *N,N*-dimethylformamide (DMF) at 60°C for 16h. Purification of the product by column chromatography on silica gel gave a stereoisomeric mixture of acetates (*E*-**12**) and (*Z*-**12**) in 58% overall yield from **5**. ^{1}H-NMR showed signals for one of the geminal methyl groups on the cyclohexane ring at δ 0.92 at a overlaped singlet and for the other one at δ 1.14 and 1.18 as the separate singlets in a ratio 75:25, the peaks which proved to be the diagnostic peaks representing the isomeric ratio. All of the other signals in ^{1}H-NMR, the molecular ion peak at *m/z* 304 in the mass spectrum, and the IR band at 1720cm^{-1} supported the structure of the acetate (**12**). The stereoisomeric ratio was finally determined by ^{1}H-NMR analysis of the aldehyde (**4**) derived from the acetate (**12**) by a sequence of reactions, *vide infra*. After alkaline hydrolysis of the acetate (**12**), desulfurization of the alcohol (**13**) obtained with Li in liquid NH_3 gave the sulfur-free alcohol (**3**) in 65% overall yield from **12**. Oxidation of the alcohol (**3**) with active MnO_2[12] led in 85% yield to the stereoisomeric mixture of α,β-unsaturated aldehydes (**4**), which are the components of the male boll weevil pheromone.[2] The *E/Z*-ratio of the aldehyde (**4**) was determined as 75:25 on the basis of its ^{1}H-NMR analysis: The diagnostic isolated allylic C(8)-methylene protons of each component were clearly observed as a couple of singlets at δ 2.05 (major) and 2.47 (minor) which had been assigned to that of the *E*- and *Z*-component respectively.[2,6a] On the detailed examination of the cyclization conditions, it was found that the stereoselectivity of the concomitant formation of the double bond in the present cyclization reaction is dependent upon the reaction temperature. Thus, cyclization of the adduct (**7**) using $SnCl_4$ (0.2equiv) at 0°C gave the *E/Z*-mixture of the acetate (**12**) in a ratio 59:41 after the subsequent acetoxylation of the crude chloride (**11**), and at −78°C yielded the *E/Z*-ratio of 85:15 contrastingly.

The cyclization reaction was investigated also on the β-hydroxy sulfide (**8**). On treatment of **8** with an excess amount of CF_3CO_2H in CH_2Cl_2 at −20°C, the cyclized trifluoroaceate (**14**) (62%) was obtained, whose isomeric ratio was tentatively estimated as 77:23 on the basis of ^{1}H-NMR analysis: The diagnostic signals of singlets indicating the isomeric ratio appeared at δ 1.16 (major) and 1.20 (minor) assignable to the one of the gem-dimethyl groups on the cyclohexane ring. The ratio was also verified by derivatization of **14** to the aldehyde (**4**) *via* hydrolysis of **14** leading to the alcohol (**13**). The analogous tendency of dependence of the stereoselectivity on the reaction temperature as described for the cyclization of the adduct (**7**) was observed and cyclization of **8** using CF_3CO_2H at 0°C gave a poor *E/Z*-ratio 64:36 of the trifluoroacetate (**14**). On the other hand, treatment of **8** with concd H_2SO_4 in Et_2O at room temperature afforded in this case a high yield (80%) of the regioisomeric cyclized diene mixture (**15**) in a ratio of 60:40 analyzed from its ^{1}H-NMR. The structure of **15** was confirmed by conversion to the regioisomeric mixture of the carboxylic ester

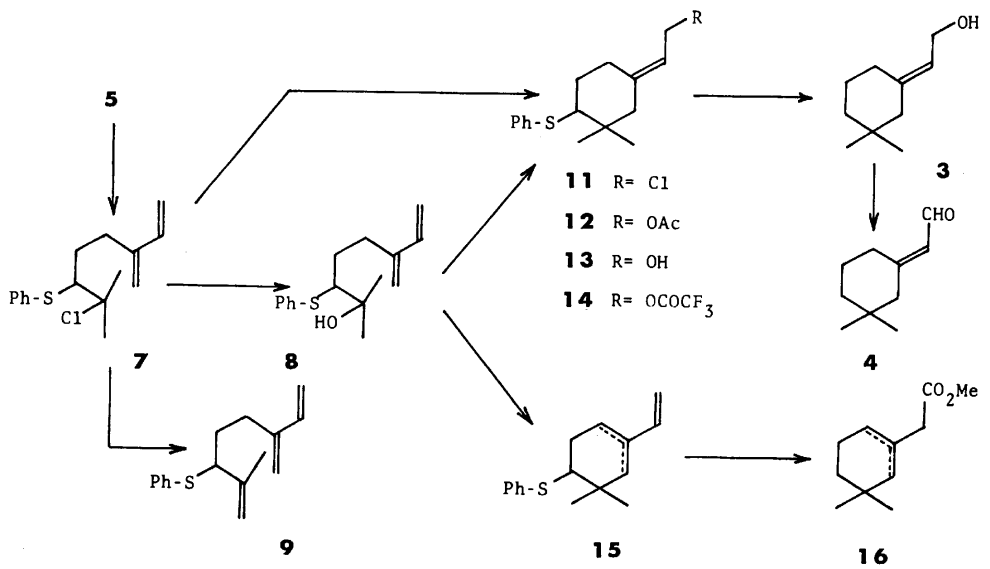

Scheme 1.

Table 1. Acid-catalyzed cyclization of the terminally sulfur-functionalized myrcene derivatives (**7**) and (**8**)

Substrate	Acid (mole equiv)	Reaction Conditions Solvent,	Temp	Time	Product (Ratio)	yield %	*E/Z*-ratio
7[a]	$SnCl_4$ (0.2)	CH_2Cl_2,	0°C,	30 min	**12**[b]	56	59:41
		CH_2Cl_2,	−20°C,	30 min	**12**[b]	58	75:25
		CH_2Cl_2,	−78°C,	30 min	**12**[b]	48	85:15
	$TiCl_4$ (0.3)	CH_2Cl_2,	−20°C,	30 min	**12**[b]	28	77:23
	CF_3CO_2H (excess)	CH_2Cl_2,	−20°C,	80 min	**11**+**14** (*ca.* 1:1)	55	—
8	$SnCl_4$ (1.0)	CH_2Cl_2,	0°C,	30 min	**12**[b]	54	50:50
	CF_3CO_2H (excess)	CH_2Cl_2,	0°C,	40 min	**14**	64	67:34
		CH_2Cl_2,	−20°C,	70 min	**14**	63	76:24
	H_2SO_4 (excess)	Et_2O,	15°C,	4 h	**15**	80	—

a) The crude adduct was used. b) The primary product (**11**) was not isolated and directly led to **12**.

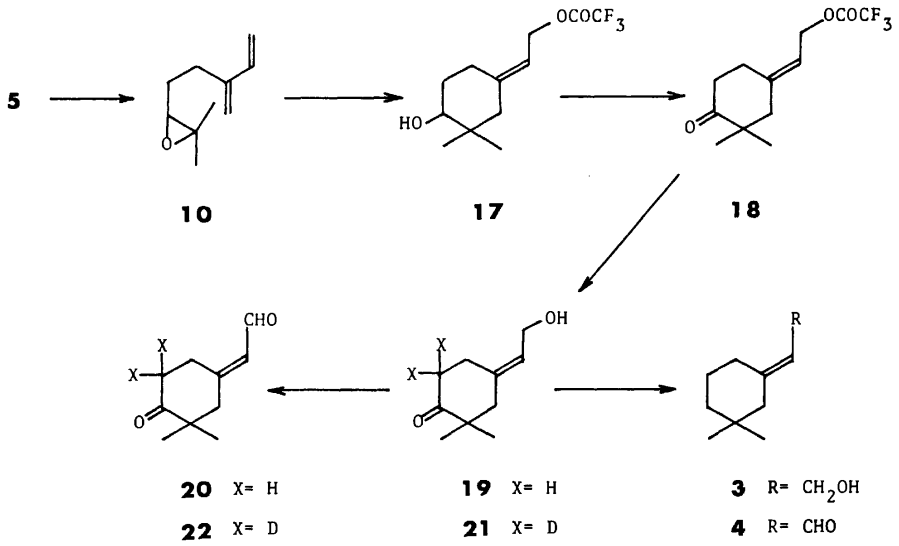

Scheme 2.

(**16**), which have been reported by Wolinsky,[6a] by a sequence of reactions involving hydroboration, desulfurization, Jones oxidation, and then esterification.

On the substrate terminal methallylic sulfide (**9**), unfortunately, all the several attempted conditions (1.0equiv $SnCl_4/CH_2Cl_2/0$—15°C/1 h; excess H_2SO_4/Et_2O/15°C/2 h; excess CF_3CO_2H/CH_2Cl_2/15°C/1 h) were not effective for the expected cyclization and gave recovery of the starting material. Results of the cyclization reactions examined on the PhSCl-myrcene adduct (**7**) and the β-hydroxy sulfide (**8**) are summarized in Table 1.

II) Cyclization of Myrcene 6,7-Epoxide (Scheme 2). The terminal epoxide functionality has been utilized in the carbocyclization of acyclic polyisoprenoids as much more general and efficient initiator.[7d] To our knowledge, however, the acid-catalyzed carbocyclization of myrcene 6,7-epoxide (**10**) has never been precedented in the literature. In order to construct the functionalized ochtodane skeleton, cyclization of **10** appeared to be one of the attractive candidates. Thus, the epoxide (**10**) was stirred with an excess amount of CF_3CO_2H in CH_2Cl_2 at −20°C. The structural analysis of the product (**17**) obtained in 54% yield revealed that the desirable cyclization was realized. All the data including the IR band at 3400 and 1780 cm^{-1}, M^+ peak at *m/z* 266 in the mass spectrum, and ^{1}H-NMR signals for the gem-dimethyl groups at δ 0.81 and 0.91, the primary allylic trifluoroacetate system at δ 4.77 (2H, d) and 5.28 (1H, t), and the secondary hydroxyl functionality at δ 1.89 (OH) and 3.40 (1H, ABXq) fully supported the structure (**17**) although the stereoisomeric ratio could not be estimated. Oxidation of the alcohol (**17**) with pyridinium chlorochromate (PCC) afforded the ketone (**18**) in 87% yield. In ^{1}H-NMR the ketone (**18**) exhibited sharp singlets at δ 1.04 and 1.07 in a ratio of intensity 87:13 which was supposed to represent the *E/Z*-stereoisomeric ratio of **18**. Exact determination of the ratio was perfomed by the ^{1}H-NMR analysis of the keto aldehyde (**20**) and its dideuterated derivative (**22**) as described below. The compound (**18**) was subjected to alkaline hydrolysis to lead to the keto alcohol (**19**) (92%) which was oxidized to the keto aldehyde (**20**) in 78% yield with active MnO_2. Also in this compound, separate singlets were observed at δ 1.10 and 1.13 in a ratio 87:13 of intensity in ^{1}H-NMR. Correspondence of the ratio to the stereochemistry of the bouble bond in **20** was clearly attained by the ^{1}H-NMR analysis of the 5,5-dideuterio keto aldehyde (**22**) derived by the deuterium

Table 2. Cyclization of myrcene 6, 7-epoxide (**10**) using CF_3CO_2H[a)]

Reaction Temp (°C)	Product	Yield/%	*E*/*Z*-ratio
−5	**17**	53	83:17
−20	**17**	54	87:13
−78	**17**	43	94:6

a) The reaction was carried out in CH_2Cl_2 for 30 min by using 5.0 equiv of CF_3CO_2H.

exchange reaction[13)] of the keto alcohol (**19**) in MeOD with Na followed by oxidation of the 5,5-dideuterio keto alcohol (**21**) with active MnO_2. Generally, the γ-*cis*-methylene protons of α,β-unsaturated aldehydes and esters are known to appear in lower ^{1}H-NMR chemical shifts than the corresponding γ-*trans*-methylene protons by the paramagnetic deshielding effect of the spatially proximate carbonyl group.[2,6a,14)] Thus, the major pair of 2H-signals at δ 2.48 and 3.09 proved to be assigned to the C(8)- and C(4)-methylenes of the *E*-component (*E*-**22**) and the minor pair of 2H-signals at δ 2.67 and 2.86 to the C(4)- and C(8)-methylenes of the *Z*-component (*Z*-**22**), and therefore, the *E*/*Z*-ratio of **22** was determined clearly as 87:13, which was well consisted with the estimation on the trifluoroacetoxy ketone (**18**). The identical *E*/*Z*-ratio was indicated by ^{1}H-NMR analysis of the aldehyde (**4**) derived from the keto alcohol (**19**) *via* deoxygenation[15)] of the corresponding tosylhydrazone with $NaBH_4$ providing the allylic alcohol (**3**). The stereoselectivity in this cyclization also proved to be dependent upon the reaction temperature. As shown in Table 2, the lower temperature resulted in the formation of the *E*-component (*E*-**17**) in higher proportion.

We propose that the higher *E*-stereoselectivity in the trisubstituted double bond formation at the lower temperature in these cyclizations ascribes to the preferential tandem cyclization of the cation (**A**) with the *s*-*trans*-1,3-diene system and concerted formation of the exo-double bond to the reaction of the other cation (**B**) bearing the *s*-*cis*-1,3-diene system.

III) Synthesis of an Oxygenated Ochtodane Type Terpene, (±)-(2Z)-2,4-Ochtodadiene-1,6-diol (26) (Scheme 3). A simple and successful application of the functionalized ochtodanes (**12**) and (**19**) obtained was achieved in the stereoselective synthesis of a diol component (**26**) isolated from the red alga *Ochtodes crockeri*.[1b)] Oxidation of the 6-phenylthio derivative (**12**) (*E*:*Z*=85:15) with 30% H_2O_2 in AcOH followed by heating the intermediate sulfoxide in xylene gave the diene acetate (**23**) in 79% yield from **12**. The structure of the compound (**23**) was supported by the spectral analysis: The M^+ ion was observed at *m*/*z* 194 in the mass spectrum, and the signals of the newly formed C(4)-allylic methylene at δ 2.78 (major (*E*-**23**)) and 2.70 (minor (*Z*-**23**)) as broad singlets and of the C(5)- and C(6)-olefinic protons at δ 5.40—5.60 were detected in ^{1}H-NMR. On treatment of the diene (**23**) with an

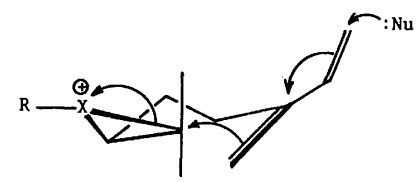

A

B

R= Ph, X= S
or
R= H, X= O

Chart 4.

equimolar amount of *m*-chloroperbenzoic acid in CH_2Cl_2 at −20°C, a selective epoxidation proceeded to lead in 59% yield the 5,6-epoxide (**24**), ^{1}H-NMR of which indicated that the allylic acetate system remained intact. Although the *E*- and *Z*-component of **24** were separable by column chromatography on silica gel, the tedious separation of the stereoisomers turned out to be not necessary for the synthesis of the target compound (**26**) because a unexpected kinetic stereoselection in the base promoted epoxide opening reaction of the epoxy alcohol (**25**) was observed. Thus, after alkaline hydrolysis of **24** (*E*:*Z*=15:85), the resulted epoxy alcohol (**25**) was treated with 2.5 equiv of lithium diisopropylamide (LDA) in THF at −78—−20°C for 2 h to furnish the desired diol (**26**) as the single stereoisomer in 73% yield and a small amount of recovery (less than 10%) of the starting epoxy alcohol which was substantially enriched in the *E*-isomr.[16)] The dienediol (**26**) obtained was identified with the natural one[1b)] by spectral comparisons.

The dienediol (**26**) was also synthesized alternatively from the keto alcohol (**19**) *via* a tandem procedure of selenylation and elimination of selenenic acid.[17)] Selenylation of **19** was carried out with LDA and diphenyl diselenide to give the seleno keto alcohol (**27**) (70%). Reduction of **27** with $LiAlH_4$ afforded in 84% yield the selenodiol (**28**), which was treated with $NaIO_4$ in aqueous MeOH at room temperature providing the diol (**26**) in 61% yield.

In conclusion, we established a facile stereoselective method providing the ochtodane skeleton with the functional group on the C(6)-position. The compounds obtained are claimed to be the promising

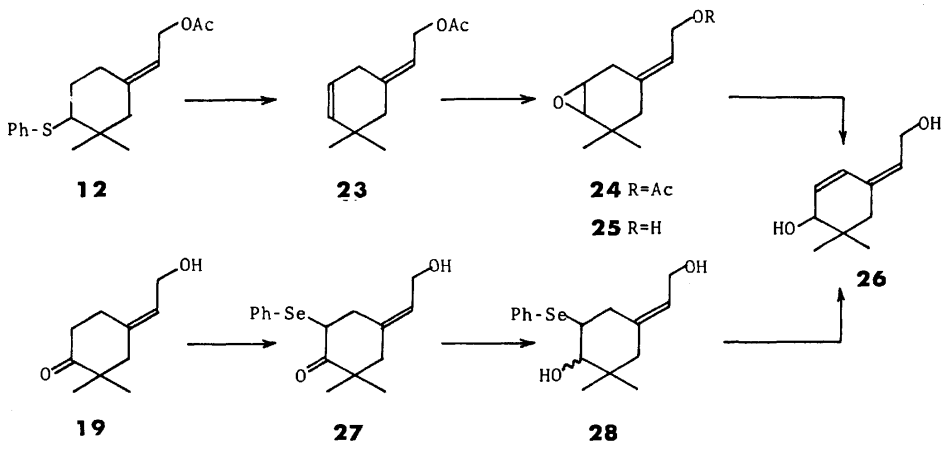

Scheme 3.

intermediates for the synthesis of a variety of natural ochtodane type terpenes including pleraplysillin-1 (**6**),[4] a unique sesquiterpene which is recognized synthetically as the homologated ochtodane at the C(1)-position with furfuryl moiety. A successful application of the ochtodane derivative (**3**) obtained in this work to the synthesis of the sesquiterpene (**6**) will be reported in the following paper.[18]

Experimental

General. IR spectra were taken on a JASCO IRA-1 spectrometer in $CHCl_3$ solution and the absorption bands (ν_{max}) are reported in cm^{-1}. Mass spectra (MS) were obtained on a JMS-D300 instrument at an ionizing potential of 70eV and peaks are reported in *m/z* values with relative intensities (%) in parenthesis. ^{1}H-NMR spectra were recorded on a Hitachi R-20B spectrometer (60MHz) in CCl_4 solution, unless otherwise noted, with tetramethylsilane (TMS) as an internal standard and chemical shifts are reported in δ (ppm) relative to TMS and coupling constants (*J*) in hertz (Hz). All the solvents used in reactions were freshly distilled to remove moisture. Reactions were carried out usually under nitrogen unless otherwise noted. Reaction mixtures were usually worked up as follows: A mixture was extracted with Et_2O, washed with water or saturated brine and saturated aqueous $NaHCO_3$, if necessary, dried over anhydrous $MgSO_4$, concentrated *in vacuo* using a rotary evaporator at water aspirator pressure below room temperature, to give a crude product which was purified by column chromatography. Silica gel (Wakogel B-5F) and Wakogel C-200 were employed respectively for analytical thin-layer (TLC) and column chromatography using hexane-Et_2O solvent system.

Materials. Myrcene (**5**) was purchased from Tokyo Kasei (TCI). Benzenesulfenyl chloride (PhSCl) was freshly prepared according to the literature.[19] Myrcene 6,7-epoxide (**10**) was obtained by the reported method.[20] The terminal methallylic sulfide (**9**) was prepared according to our reported method.[11] The β-hydroxy sulfide, 2-methyl-6-methylene-3-phenylthio-7-octen-2-ol (**8**) was prepared as follows: To a solution of myrcene (**5**) (680mg, 5.0mmol) in CH_2Cl_2 (10ml) was added dropwise a solution of PhSCl (725mg, 5.0mmol) in CH_2Cl_2 (3.0ml) at −20°C. After being stirred for 10min, the mixture was concentrated *in vacuo* to give the crude adduct (**7**) (1.4g).[11] The adduct was dissolved in aq CH_3CN ($CH_3CN:H_2O$=5:1)(20ml) and stirred at room temperature for 20h.[11a] The mixture was worked up by the usual manner to give **8** (720mg, 55) as oil. Date for **8** follow: IR 3400, 1595, 1590; MS 262 (M^+, 71), 204 (43), 137 (40), 136 (100), 135 (74), 123 (93), 110 (57); NMR 1.16, 1.23 (each 3H, $(C\underline{H}_3)_2C(OH)$, 2.31 (1H, s, OH), 2.98 (1H, dd, *J*=11.0 and 3.0, CH(SPh)), 4.80—5.30 (4H, m, $2X=CH_2$), 6.03—6.54 (1H, dd, *J*=18.0 and 11.0, $C\underline{H}=CH_2$). The compound **8** was also obtained alternatively as follows: The crude adduct (**7**) prepared from **5** (5mmol) was stirred with AcONa (1.23g, 15mmol) in AcOH (20ml) at 20°C for 1h. Usual work-up of the mixture gave the corresponding acetate of the β-hydroxy sulfide (**8**) (990mg, 65%),[11b] which was hydrolyzed in EtOH (15ml) with 3% NaOH (15ml) at room temperature for 2h to give **8** (690 mg, 81%).

Acid-catalyzed Cyclization of the Terminally Sulfur-Functionalized Myrcence Derivatives (7) and (8). Cyclization of the Benzenesulfenyl Chloride-Myrcene Adduct (7) Catalyzed by $SnCl_4$. To a solution of the adduct (**7**) prepared from myrcene (**5**) (550mg, 4.0mmol) and PhSCl (600mg, 4.1mmol) in CH_2Cl_2 (12ml) at −20°C, was added dropwise over 5 min a solution of $SnCl_4$ (100μl, 0.85mmol) in CH_2Cl_2 (2.0ml) at −20°C. After being stirred for 30min at −20°C, the mixture was diluted with CH_2Cl_2, washed with successively with saturated $NaHCO_3$ and water, dried, and concentrated to give the crude 1-chloro-6-phenylthio-2-ochtodene (**11**) (1.09g) as oil: MS 282 ($(M+2)^+$, 30), 280 (M^+, 72), 245 (75), 170 (33), 135 (63), 110 (100); NMR 0.96 (3H, s, one of the CH_3 of $C(7)(CH_3)_2$),
1.16 (major) and 1.19 (minor) (overall 3H, singlets (75:25), the other one of $C(7)(CH_3)_2$), 3.95 (2H, d, *J*=8.0, $=CHC\underline{H}_2Cl$), 5.31 (1H, bt, *J*=8.0, $=C\underline{H}CH_2Cl$). The crude chloride (**11**), without further purification, was warmed with AcONa (550mg, 6.7mmol) in DMF (12ml) at 60°C for 16h. The reaction mixture was worked up by the usual manner to leave an oily product (1.02g). Purification of the product by column chromatography afforded the oily acetate, 1-acetoxy-6-phenylthio-2-ochtodene (**12**) (705mg, 58% from **5**). Data for **12** follow: IR 1720, 1580; MS 304 (M^+, 7), 244 (30), 135 (100), 134 (66); NMR 0.92 (3H, s, one of the CH_3 of $C(7)(CH_3)_2$), 1.14 (major) and 1.18 (minor) (overall 3H, singlets (75:25), the other one of $C(7)(CH_3)_2$), 1.95 (3H, s, CH_3CO_2), 2.83—3.10 (1H, dd, *J*=10.0 and 4.5, CH(SPh)), 4.46 (2H, d, *J*=7.5, $=CHC\underline{H}_2OAc$), 5.21 (1H, bt, *J*=7.5, $=C\underline{H}CH_2OAc$); Found: C, 70.75; H, 7.83%. Calcd for $C_{18}H_{24}O_2S$: C, 71.10; H, 7.95%. Cyclizations of **7** at 0°C and −78°C were

examined and the results are listed in Table 1.

Cyclization of 7 Catalyzed by $TiCl_4$. Cyclization of **7** was carried out at −20 °C in CH_2Cl_2 using 0.3 equiv of $TiCl_4$ by the same procedure as described above and the crude product was directly converted into the acetate (**12**) (28%, *E*:*Z*=77:23).

Cyclization of 7 Using CF_3CO_2H. A solution of the crude adduct (**7**) (140 mg) in CH_2Cl_2 (0.5 ml) was added dropwise over 5 min at −20 °C into a mixture of CH_2Cl_2 (3.0 ml) and CF_3CO_2H (0.5 ml, 6.5 mmol). After being stirred for 80 min, the mixture was poured into water and the product was extracted with CH_2Cl_2, washed successively with saturated $NaHCO_3$ and brine, dried, and concentrated. The crude product (137 mg) was purified by column chromatography to give the chloride (**11**) (35 mg, 25%) as the less polar fraction and the trifluoroacetate, 6-phenylthio-1-trifluoroacetoxy-2-ochtodene (**14**) (45 mg, 25%) as the more polar one, spectral data of which follow: IR 1780, 1660, 1580; MS 358 (M^+, 37), 248 (26), 135 (100), 134 (41); NMR 0.93 (3H, s, one of the CH_3 of $C(7)(CH_3)_2$), 1.16 (major) and 1.20 (minor) (overall 3H, s, the other one of $C(7)(CH_3)_2$), 2.87—3.10 (1H, dd, *J*=10.0 and 4.0, CH(SPh)), 4.77 (2H, d, *J*=7.5, $=CHCH_2OTfa$), 5.32 (1H, bt, *J*=7.5, $=CHCH_2OTfa$).

Acid-catalyzed Cyclization of the β-Hydroxy Sulfide (8) Using $SnCl_4$. To an ice-cold solution of **8** (260 mg, 1.0 mmol) in CH_2Cl_2 (5.0 ml), $SnCl_4$ (110 μl, 1.0 mmol) was added dropwise. Stirring was continued for 30 min at the temperature and the reaction was quenched by addition of water. The mixture was extracted with Et_2O and worked up by the usual manner providing the crude chloride (**11**) which was converted into the corresponding acetate (**12**) (164 mg, 54%). The *E*:*Z*-ratio (*ca.* 50:50) was determined by ^{1}H-NMR analysis of the diagnostic methyl signal at δ 1.14 and 1.18.

Cyclization of 8 Using CF_3CO_2H. To an ice-cold solution of **8** (130 mg, 0.5 mmol) in CH_2Cl_2 (10 ml), CF_3CO_2H (4.0 ml) was added dropwise over 25 min and stirring was continued for 15 min at 0 °C. The mixture was poured into water and the product was extracted with CH_2Cl_2. The organic layer was worked up by the usual manner to give the trifluoroacetate (**14**) (114 mg, 64%) as oil. The *E*:*Z*-ratio was determined as 64:36 by ^{1}H-NMR analysis of the diagnostic methyl signal at δ 1.16 and 1.20. Results of the reaction of **8** with CF_3CO_2H at −20 °C in CH_2Cl_2 are listed in Table 1.

Cyclization of 8 Using H_2SO_4. To a solution of **8** (2.62 g, 10 mmol) in Et_2O (110 ml) was added dropwise over 10 min a mixture of concd H_2SO_4 (3.7 ml) and Et_2O (25 ml) at room temperature and the mixture was stirred for 4 h. The usual work-up of the mixture followed by the isolation of the product afforded the isomeric mixture of diene (**15**) (1.95 g, 80%) as oil. Data for **15** follow: MS 244 (M^+, 56), 164 (45), 136 (59), 135 (100), 134 (95), 119 (57); NMR 1.02 and 1.16 (major pair of singlets of 60 intensity), 1.10 and 1.27 (minor pair of singlets of 40 intensity) (overall 6H, $C(CH_3)_2$), 3.00—3.23 (1H, dd, *J*=9.0 and 5.5, CH(SPh)), 4.75—5.65 (3H, m, $C(1)H_2$ and C(4)H or C(8)H), 6.02—6.50 (1H, dd, *J*=18.0 and 11.0, C(2)H); Found: C, 78.36; H, 8.41%. Calcd for $C_{16}H_{20}S$: C, 78.63; H, 8.25%.

6-Phenylthio-2-ochtoden-1-ol (13): A mixture of the acetate (**12**) (360 mg, 1.18 mmol), EtOH (5.0 ml), and 3% NaOH (5.0 ml) was stirred for 20 h at room temperature. After evaporation of EtOH, the residue was worked up by the usual manner to give a crude product (310 mg), which was purified by column chromatography yielding the alcohol (**13**) (276 mg, 89%) as oil. Data for **13** follow: IR 3320, 1660, 1580; MS 262 (M^+, 28), 244 (15), 152 (22), 135 (100), 134 (72); NMR 0.92 (3H, s, one of the CH_3 of $C(7)(CH_3)_2$), 1.14 (major) and 1.18 (minor) (overall 3H, s, the other one of $C(7)(CH_3)_2$), 1.62 (1H, s, OH), 2.00 (2H, s, $C(8)H_2$), 2.84—3.10 (1H, dd, *J*=10.5 and 4.5, CH(SPh)), 4.01 (2H, d, *J*=7.0, $=CHCH_2OH$), 5.28 (1H, bt, *J*=7.0, $=CHCH_2OH$); Found: C, 72.98; H, 8.45%. Calcd for $C_{16}H_{22}OS$: C, 73.23; H, 8.45%.

2-Ochtoden-1-ol (3): A solution of the alcohol (**13**) (102 mg, 0.4 mmol) in THF (0.5 ml) was added dropwise into a chilled (−78 °C) blue solution of Li (50 mg, 7 mgatm) in liq. NH_3 (*ca.* 10 ml) and the mixture was stirred for 30 min at the temperature. Then, reaction was quenched by introduction of gaseous butadiene followed by addition of MeOH (1.0 ml) to destroy the excess Li and the cold bath was removed to evaporate NH_3. The residue was worked up by the usual manner and the crude product was purified by column chromatography to give the alcohol (**3**) (44 mg, 73%) as oil. Data for **3** follow: IR 3400, 1660; MS 154 (M^+, 16%), 136 (58), 121 (45), 95 (57), 93 (100); NMR 0.87 (6H, s, $C(CH_3)_2$), 1.85 (major) and 1.92 (minor) (overall 2H, s, $C(8)H_2$), 2.43 (1H, s, OH), 3.97 (minor) and 4.02 (major) (overall 2H, d, *J*=7.0, $=CHCH_2OH$), 5.24 (1H, d, *J*=7.0, $=CHCH_2OH$).

2-Ochtoden-1-al (4): The aldehyde (**4**) was obtained in 85% yield from the alcohol (**3**) by oxidation with active MnO_2 in pentane according to the literature.[2] Data for **4** follow: IR 1680, 1640; NMR 0.93 (major) and 0.97 (minor) (overall 6H, s, $C(CH_3)_2$), 2.05 (major) and 2.47 (minor) (overall 2H, s, $C(8)H_2$), 2.65 (2H, bt, *J*=6.0, $C(4)H_2$), 5.67 (major) and 5.81 (minor) (overall 1H, d, *J*=8.5, $=CHCHO$), 9.88 (minor) and 9.93 (major) (overall 1H, d, *J*=8.5, $=CHCHO$).

Transformation of the Diene Mixture (15) to the Regioisomeric Mixture of Esters (16). To an ice-cold solution of **15** (245 mg, 1.0 mmol) in THF (5.0 ml), a 1/3 M (1 M=1 mol dm^{-3}) solution of BH_3–THF (3.0 ml) was added dropwise over 30 min and the mixture was stirred for 30 min at 0 °C. To the mixture was added dropwise 3 M NaOH (0.8 ml) and 30% H_2O_2 (0.8 ml) at 0 °C successively. After being stirred for 2 h at room temperature, the mixture was worked up to give the dihydro alcohol, 6-phenylthio-3-ochtoden-1-ol (140 mg, 62%) with a recovery of **15** (36 mg). Data for the dihydro alcohol follow: IR 3560, 3400, 1580; MS 262 (M^+, 61), 153 (100), 136 (70); NMR 0.98, 1.07 (major pair of singlets) and 1.03, 1.20 (minor pair of singlets) (overall 6H, $C(CH_3)_2$), 2.50 (1H, s, OH), 2.90—3.20 (1H, m, CH(SPh)), 3.53 (2H, t, *J*=7.0, CH_2OH), 5.20 (minor singlet of C(8)-olefinic H) and 5.34 (major broad singlet of C(4)-olefinic H); Found: C, 73.18; H, 8.57%. Calcd for $C_{16}H_{22}OS$: C, 73.23; H, 8.45%. The 6-phenylthio alcohol obtained was desulfurized to 3-ochtoden-1-ol in 81% yield by the same procedure described for **3**. Data for the alcohol follow: MS 154 (M^+, 96), 139 (99), 121 (98), 109 (100), 107 (70); NMR 0.89 (major) and 0.95 (minor) (overall 6H, s, $C(CH_3)_2$), 2.57 (1H, s, OH), 3.53 (2H, t, *J*=7.0, CH_2OH), 5.15 (minor singlet of C(8)-olefinic H) and 5.39 (major broad singlet of C(4)-olefinic H). The alcohol (55 mg, 0.35 mmol) was dissolved in acetone (3.5 ml) and 15 drops of the Jones reagent prepared from CrO_3 (14 g), H_2O (100 ml), and concd H_2SO_4 (12 ml), was added to the ice-cold solution. The mixture was stirred for 2.5 h at 0 °C and then for 1 h at room temperature. Usual work-up of the mixture gave the crude carboxylic acid (55 mg) which was esterified with an ethereal solution of CH_2N_2 by the usual manner. Purification of the crude product by column chromatography provided the ester,

methyl 3-ochtoden-1-oate (**16**) (40mg, 62%). Spectral data of the ester were consistent with those reported by Wolinsky:[6a] IR 1740; NMR 0.91 (major) and 0.96 (minor) (overall 6H, s, $C(CH_3)_2$), 2.92 (2H, s, $=CCH_2CO_2$), 3.65 (3H, s, CO_2CH_3), 5.27 (minor singlet of C(8)-olefinic H) and 5.52 (major broad singlet of C(4)-olefinic H).

Cyclization of Myrcene 6,7-Epoxide (10). A solution of the epoxide (**10**) (300mg, 2.0mmol) in CH_2Cl_2 (1.0ml) was added dropwise into a mixture of CF_3CO_2H (0.8ml, 10mmol) and CH_2Cl_2 (8.0ml) at −20°C. The mixture was stirred for 20min at −20°C and then poured into water. Extraction of the mixture with CH_2Cl_2 followed by the usual work-up gave a crude product (427mg), which was purified by column chromatography to yield the hydroxy ester, 6-hydroxy-2-ochtodene-1-yl trifluoroacetate (**17**) (284mg, 54%). Data for **17** follow: IR 3400, 1780, 1660; MS 266 (M^+, 7), 248 (44), 152 (92), 135 (100), 134 (98), 119 (96); NMR 0.81, 0.91 (each 3H, s, $C(CH_3)_2$), 1.89 (1H, s, OH), 3.40 (1H, dd, J=8.0 and 4.0, $C\underline{H}(OH)$), 4.79 (2H, d, J=7.5, $=CHC\underline{H}_2OTfa$), 5.28 (1H, bt, J=7.5, $=C\underline{H}CH_2OTfa$); Found: C, 54.28; H, 6.53%. Calcd for $C_{12}H_{17}O_3F_3$: C, 54.13; H, 6.44%. Cyclization of **10** at −5°C and at −78°C was examined and the results are listed in Table 2, in which the E:Z-ratio was determined by ^{1}H-NMR analysis of the corresponding ketone (**18**) derived from **17**, *vide infra*.

6-Oxo-2-ochtoden-1-yl Trifluoroacetate (18): A solution of the alcohol (**17**) (80mg, 0.3mmol) in CH_2Cl_2 (0.5ml) was added dropwise into a solution of pyridinium chlorochromate (97mg) in CH_2Cl_2 (1.0ml) at room temperature and stirring was continued for 2h. To the mixture, Et_2O (5.0ml) was added and the insoluble materials were removed by filtration. The filtrate was concentrated and the residue was chromatographed to give the ketone (**18**) (69mg, 87%). Data for **18** follow: IR 1780, 1705; NMR 1.04 (major) and 1.07 (minor) (overall 6H, $C(CH_3)_2$), 2.33 (2H, s, $C(8)H_2$), 2.30—2.85 (4H, m, $COCH_2CH_2C=$), 4.89 (2H, d, J=7.5, $=CHC\underline{H}_2OTfa$), 5.53 (1H, bt, J=7.5, $=C\underline{H}CH_2OTfa$); Found: C, 54.82; H, 5.95%. Calcd for $C_{12}H_{15}O_3F_3$: C, 54.55; H, 5.72%.

1-Hydroxy-2-ochtoden-6-one (19): The trifluoroacetate (**18**) was hydrolyzed by treatment with a mixture of EtOH and 3% NaOH (1:1) at room temperature for 10min to give the oily keto alcohol (**19**) in 92% yield. Data for **19** follow: IR 3550, 3400, 1695; MS 168 (M^+, 15), 150 (100), 135 (17), 123 (32), 107 (72); NMR 1.03 (6H, s, $C(CH_3)_2$), 2.26 (2H, s, $C(8)H_2$), 2.35—2.80 (4H, m, $COCH_2CH_2C=$), 2.96 (1h, s, OH), 4.09 (2H, d, J=7.0, $=CHC\underline{H}_2OH$), 5.49 (1H, bt, J=7.0, $=C\underline{H}CH_2OH$); Found: C, 71.54; H, 9.85%. Calcd for $C_{10}H_{16}O_2$: C, 71.39; H, 9.59%.

5,5-Dideuterio-1-hydroxy-2-ochtoden-6-one (21): A solution of the keto alcohol (**19**) (30mg, 0.2mmol) in MeOD (0.5ml) was added into a solution of NaOMe in MeOD, prepared from Na (3mg) and MeOD (0.5ml), at room temperature and the mixture was stirred for 20h. After addition of D_2O (1.0ml), the mixture was extracted with Et_2O and worked up by the usual manner to give the 5,5-dideuterio keto alcohol (**21**) (21mg). Data for **21** follow: IR 3480, 1690; MS 170 (M^+, 15), 152 (100), 137 (26), 125 (40), 109 (98); NMR 1.03 (6H, s, $C(CH_3)_2$), 2.25 (2H, s, $C(8)H_2$), 2.50 (2H, s, $C(4)H_2$), 2.58 (1H, s, OH), 4.09 (2H, d, J=7.0, $=CHC\underline{H}_2OH$), 5.49 (1H, bt, J=7.0, $=C\underline{H}CH_2OH$).

6-Oxo-2-ochtodene-1-al (20): Active MnO_2 (1.0g) was added at 0°C into a stirred solution of the keto alcohol (**19**) (30mg, 0.2mmol) in $CHCl_3$ (10ml) and stirring was continued for 30min at the temperature. The mixture was filtered and the filtrate was purified by column chromatography to give the keto aldehyde (**20**) (28mg, 94%) as oil. Data for **20** follow: IR 1690, 1660; NMR 1.10 (major) and 1.13 (minor) (overall 6H, s, $C(CH_3)_2$), 2.39—2.70 (2H, m, $COC\underline{H}_2CH_2C=$), 2.48 (2H, d, J=2.0, $C(8)H_2$), 2.85—3.26 (2H, m, $C(4)H_2$), 5.89 (1H, dt, J=7.5 and 2.0, $=C\underline{H}CHO$), 9.93 (1H, d, J=7.5, $=CHC\underline{H}O$).

5,5-Dideuterio-6-oxo-2-ochtodene-1-al (22): The dideuterio keto aldehyde (**22**) was prepared from the dideuterio keto alcohol (**21**) by the same procedure described for **20**. Data for **22** follow: IR 1690, 1660; MS 168 (M^+, 56), 139 (97), 125 (100); NMR 1.10 (major) and 1.13 (minor) (overall 6H, s, $C(CH_3)_2$), 2.48 (major doublet (J=2.0)) and 2.67 (minor broad singlet) (overall 2H, $C(8)H_2$), 2.89 (minor) and 3.09 (major) (overall 2H, s, $C(4)H_2$), 5.89 (1H, dt, J=7.5 and 2.0, $=C\underline{H}CHO$), 9.93 (1H, d, J=7.5, $=CHC\underline{H}O$).

Deoxygenation of the Keto Alcohol (19) Providing the Alcohol (3). A mixture of the keto alcohol (**19**) (72mg, 0.4mmol) and *p*-toluenesulfonyl hydrazide (80mg, 0.4mmol) in MeOH (5.0ml) was heated under reflux for 4h. After cooling and addition of MeOH (4.0ml), $NaBH_4$ (325mg, 8.5mmol) was added portions to the mixture at 0°C, and the mixture was heated under reflux for 2h. The reaction mixture was concentrated and the residue was worked up by the usual manner to give a crude product (68mg). Purification of the product by column chromatography yielded the alcohol (**3**) (43mg, 65%). The alcohol exhibited identical spectra with those obtained from **13**.

Synthesis of (±)-(2Z)-2,4-Ochtodadiene-1,6-diol (26) Starting from the 6-Phenylthio Acetate (12). 1-Acetoxy-2,5-ochtodadiene (**23**): A mixture of the acetate (**12** E:Z=85:15) (1.3g, 4.3mmol), AcOH (15ml), and 30% H_2O_2 (460μl) was stirred for 20h at room temperature. The reaction mixture was poured into water and the mixture was extracted with CH_2Cl_2. The organic layer was worked up by the usual manner to give the crude sulfoxide (1.37g), which was, without further purification, heated under reflux with $NaHCO_3$ (720mg, 8.5mmol) in xylene (40ml) for 4h. The reaction mixture was diluted with Et_2O and worked up by the usual manner to give the oily diene acetate (**23**) (655mg, 79%). Data for **23** follow: IR 1725; MS 194 (M^+, 2), 134 (72), 119 (100); NMR 0.94 (major) and 0.98 (minor) (overall 6H, s, $C(CH_3)_2$), 1.95 (3H, s, CH_3CO_2), 2.08 (major) and 2.20 (minor) (overall 2H, s, $C(8)H_2$), 2.70 (minor) and 2.78 (major) (overall 2H, bs, $C(4)H_2$), 4.53 (2H, d, J=7.5, $=CHC\underline{H}_2OAc$), 5.33 (1H, bt, J=7.5, $=C\underline{H}CH_2OAc$), 5.40—5.60 (2H, m, CH=CH).

1-Acetoxy-5,6-epoxy-2-ochtodene (24): A solution of *m*-chloroperbenzoic acid (net 80%) (305mg, 1.4mmol) in CH_2Cl_2 (4.0ml) was added dropwise into a cold (−20°C) mixture of the diene acetate (**23** E:Z=85:15) (230mg, 1.2mmol) and $NaHCO_3$ (100mg, 1.2mmol) in CH_2Cl_2 (12ml) and the mixture was stirred for 3h at −20°C and then for 3.5h at 0°C. The reaction mixture was diluted with CH_2Cl_2 and worked up by the usual manner to give a crude product (260mg), which was purified by column chromatography to afford the oily epoxide (**24**) (135mg, 59%) with a small amount of the isomeric 1-acetoxy-2,3-epoxy-5-ochtodene (28mg). By careful column chromatography of the epoxide (**24**) on silica gel, the E- and Z-component were separable. The less polar and minor E-**24**: NMR ($CDCl_3$) 0.96, 1.12 (each 3H, s, $C(CH_3)_2$), 1.98 (2H, bs, $C(8)H_2$), 2.04 (3H, s, CH_3CO_2), 2.60 (2H, bd, J=3.0, $C(4)H_2$), 2.80 (1H, d, J=4.0, C(6)H), 3.23 (1H, m,

C(7)H), 4.54 (2H, d, J=7.0, =CHC$\underline{H}_2$OAc), 5.45 (1H, bt, J=7.0, =C$\underline{H}$CH$_2$OAc). The more polar and major *Z*-**24**: NMR ($CDCl_3$) 0.93, 1.10 (each 3H, s, C(CH_3)$_2$), 2.04 (3H, s, CH_3CO_2), 1.59, 2.25 (each 1H, d, J=13.0, C(8)H$_2$), 2.68 (2H, bs, C(4)H$_2$), 2.83 (1H, d, J=4.0, C(6)H), 3.23 (1H, br, C(5)H), 4.55 (2H, d, J=7.5, =CHC$\underline{H}_2$OAc), 5.28 (1H, bt, J=7.5, =C$\underline{H}$CH$_2$OAc); IR 1720; MS 210 (M^+, 2), 156 (76), 150 (100), 139 (91), 135 (92).

5,6-Epoxy-2-ochtoden-1-ol (25): A mixture of the epoxy acetate (**24**) (105mg) and 3% NaOH (4.0ml) in EtOH (4.0ml) was stirred for 1.5h at room temperature and the mixture was worked up by the usual manner to give the epoxy alcohol (**25**) (77mg, 92%). (*Z*)-**25**: IR 3560, 3400; MS 150 ($(M-18)^+$, 16), 135 (47), 121 (100), 107 (81); NMR ($CDCl_3$) 0.92, 1.06 (each 3H, s, C(CH_3)$_2$), 1.60, 2.21 (each 1H, d, J=14.0, C(8)H$_2$), 2.50 (1H, s, OH), 2.63 (2H, bs, C(4)H$_2$), 2.83 (1H, d, J=4.0, C(6)H), 3.21 (1H, m, C(5)H), 4.10 (2H, d, J=7.0, =CHC$\underline{H}_2$OH), 5.33 (1H, bt, J=7.0, =C$\underline{H}$CH$_2$OH). (*E*)-**25**: NMR ($CDCl_3$) 0.95, 1.10 (each 3H, s, C(CH_3)$_2$), 1.92 (2H, s, C(8)H$_2$), 2.42 (1H, s, OH), 2.54 (2H, bd, J=3.0, C(4)H$_2$), 2.78 (1H, d, J=4.0, C(6)H), 3.23 (1H, m, C(5)H), 4.08 (2H, d, J=7.0, =CHC$\underline{H}_2$OH), 5.48 (1H, bt, J=7.0, =C$\underline{H}$CH$_2$OH).

(±)-(2Z)-2,4-Ochtodadiene-1,6-diol (26): To a solution of lithium diisopropylamide (LDA) in THF, prepared from diisopropylamine (110μl), 1.6M solution of *n*-BuLi-hexane (0.53ml) in THF (1.5ml) at −20°C, was added dropwise a solution of the epoxy alcohol (**25** *E*:*Z*=15:85) (50mg, 0.3mmol) in THF (0.5ml) at −78°C under argon. The mixture was stirred for 40min under gradual warming up to −20°C, and then for 1h at −20°C. Reaction was quenched by addition of water and the mixture was worked up by the usual manner. Purification of the crude product by column chromatography afforded the oily diene diol (**26**) (38mg, 73%) with a small amount of recovery of starting material (**25**) (8mg) which proved to change in the *E*:*Z*-proportion to the ratio *E*:*Z*=70:30 from ^{1}H-NMR analysis. Spectral data of **26** obtained were consistent with those reported for the natural one:[1b] IR 3500, 3300, 1650, 1600; MS 168 (M^+, 15), 150 (45), 135 (68), 107 (100); NMR ($CDCl_3$) 0.87, 0.97 (each 3H, s, C(CH_3)$_2$), 1.73 (2H, s, 2×OH), 2.13 (2H, s, C(8)H$_2$), 3.95 (2H, d, J=3.0, C$\underline{H}$(OH)), 4.25 (2H, d, J=7.0, =CHC$\underline{H}_2$OH), 5.47 (1H, bt, J=7.0, =C$\underline{H}$CH$_2$OH), 5.75 (1H, dd, J=10.0 and 3.0, C(5)H), 6.43 (1H, d, J=10.0, C(4)H).

*Synthesis of **26** Starting from the Keto Alcohol (**19**). 1-Hydroxy-5-Phenylseleno-2-ochtoden-6-one (**27**)*: To a solution of LDA in THF, prepared from diisopropylamine (170μl) and 1.6M solution of *n*-BuLi-hexane (0.75ml) in THF (1.5ml), was added dropwise a solution of the keto alcohol (**19**) (84mg, 0.5mmol) in THF (0.5ml) at −78°C under argon and the mixture was stirred for 15min at −78°C and then for 45min at −20°C. After warming up of the mixture to 0°C, a solution of diphenyl diselenide (156mg, 0.5mmol) in THF (0.5ml) was added rapidly into the mixture. Stirring was continued for 1h at room temperature and the mixture was poured into water. The mixture was extracted with Et_2O and worked up by the usual manner to give a crude product (229mg). Purification of the product by column chromatography afforded the oily seleno keto alcohol (**27**) (89mg, 70%) and a recovery of the strating material **19** (18mg). Data for **27** follow: IR 3560, 3400, 1690, 1580; MS 324 (M^+, 28), 167 (100), 149 (65); NMR 1.08, 1.16 (each 3H, s, C(CH_3)$_2$), 2.30 (1H, s, OH), 2.10—3.20 (4H, m, C(4)H$_2$ and C(8)H$_2$), 3.97 (2H, d, J=7.0, =CHC$\underline{H}_2$-OH), 3.90—4.15 (1H, m, CH(SePh)), 5.52 (1H, bt, J=7.0, =C$\underline{H}$CH$_2$OH); Found: C, 59.32; H, 6.37%. Calcd for $C_{16}H_{20}O_2Se$: C, 59.44; H, 6.24%.

5-Phenylseleno-2-ochtodene-1,6-diol (28): A solution of the seleno keto alcohol (**27**) (90mg, 0.3mmol) in Et_2O (2.0ml) was added dropwise into a chilled auspension of $LiAlH_4$ (22mg, 0.6mmol) in Et_2O (1.0ml) at −20°C and the mixture was stirred for 2h at −20°C and then for 1h at room temperature. Reaction was quenched by addition of wet Et_2O and the mixture was decanted to remove inorganic substances. The organic layer was worked up by the usual manner. Purification of the product by column chromatography provide the oily seleno diol (**28**) (76mg, 84%) as a diastereoisomeric mixture. Data for **28** follow: IR 3560, 3450, 1660, 1580; NMR 0.78, 0.80, 0.98, 1.02 (each 3/2H, s, C(CH_3)$_2$), 1.30—3.80 (8H, m, 2×OH, C$\underline{H}$(OH), CH(SePh), C(4)H$_2$, and C(8)H$_2$), 4.02 (2H, bd, J=7.0, =CHC$\underline{H}_2$OH), 5.30 (1H, bt, J=7.0, =C$\underline{H}$CH$_2$OH).

(±)-(2Z)-2,4-Ochtodadiene-1,6-diol (26): To a solution of the seleno diol (**28**) (50mg, 0.15mmol) in MeOH (2.0ml) and water (0.75ml) was added $NaIO_4$ (65mg, 0.3mmol) in portions at 0°C. The mixture was stirred for 15min at 0°C and then for 7h at room temperature. After addition of 5% $NaHCO_3$ (5.0ml), the mixture was extracted with CH_2Cl_2 and worked up by the usual manner. Purification of the product by column chromatography gave the oily diene diol (**26**) (16mg, 61%), which showed identical apectral data with those obtained from **25**.

We thank Professor W. Fenical and Dr. V. Paul, Scripps Institution of Oceanography, University of California, for providing the spectral data of natural both stereoisomers of 2,4-ochtodadien-1,6-diol (**26**).

References

1) a) B. J. Burreson, F. X. Woolard, and R. E. Moore, *Chem. Lett.*, **1975**, 1111; b) O. J. McConnell and W. Fenical, *J. Org. Chem.*, **43**, 4238 (1978); V.J. Paul, O. J. McConnell, and W. Fenical, *ibid.*, **45**, 3401 (1980).

2) a) J. H. Tumlinson, D. D. Hardee, R. C. Gueldner, C. Thompson, P. A. Hedin, and J. P. Minyard, *Science*, **166**, 1010 (1969); b) J. H. Tumlinson, D. D. Hardee, R. C. Gueldner, C. Thompson, P. A. Hedin, and J. P. Minyard, *J. Org. Chem.*, **36**, 2616 (1971).

3) J. H. Tumlinson, D. D. Hardee, R. C. Gueldner, C. Thompson, P. A. Hedin, and J. P. Minyard, "Chemicals Controlling Insect Behavior," ed by M. Broza, Academic Press, New York, (1970).

4) G. Cimino, S. De Stefano, L. Minale, and E. Trivellone, *Tetrahedron*, **28**, 4761 (1972).

5) J. H. Babler and M. J. Coghlan, *Synth. Commun.*, **6**, 469 (1976) and references cited therein.

6) a) R. H. Bedoukian and J. Wolinsky, *J. Org. Chem.*, **40**, 2154 (1975); b) A. J. Pearson, *Aust. J. Chem.*, **29**, 1841 (1976); c) K. Tanaka and Y. Matsubara, *Nippon Kagaku Kaishi*, **1977**, 922; d) K. Yoshihara and Y. Hirose, *Bull. Chem. Soc. Jpn.*, **51**, 653 (1978).

7) a) A. Eschemoser, L. Ruzicka, O. Jeger, and D. Arigoni, *Helv. Chim. Acta*, **38**, 1890 (1955); b) G. Stork and A. W. Burgstahler, *J. Am. Chem. Soc.*, **77**, 5068 (1955); c) For excellent reviews see: W. S. Johnson, *Acc. Chem. Res.*, **1**, 1 (1968); E. E. van Tamelen, *ibid.*, **1**, 111 (1968); T. Kato and Y.

Kitahara, *J. Synth. Org. Chem. (Japan)*, **28**, 559 (1970); d) For recent advances in biomimetic terpene synthesis see: T. Kato, H. Takayanagi, T. Suzuki, and T. Uyehara, *Tetrahedron Lett.*, **1978**, 1201; A. Murai, A. Abiko, K. Kato, and T. Masamune, *Chem. Lett.*, **1981**, 1125; T. Kametani, H. Kurobe, and H. Nemoto, *J. Chem. Soc., Perkin Trans. I*, **1981**, 756; M. Nishizawa, H. Takenaka, H. Nishide, and Y. Hayashi, *Tetrahedron Lett.*, **24**, 2581 (1983); S. Hashimoto, A. Itoh, Y. Kitagawa, H. Yamamoto, and H. Nozaki, *J. Am. Chem. Soc.*, **99**, 4192 (1977); d) For the energetic studies on nonenzymic cyclization of poly-1,5-olefin terminal epoxides see: E. E. van Tamelen and J. R. Hwu, *J. Am. Chem. Soc.*, **105**, 2490 (1983); E. E. van Tamelen and D. R. James. *ibid.*, **99**, 950 (1977) and references cited therein.

8) For our preliminary communication see: Y. Masaki, K. Hashimoto, K. Sakuma, and K. Kaji, *Tetrahedron Lett.*, **23**, 1481 (1982).

9) a) M. T. Mustafaeva, M. Z. Krumer, V. A. Smit, A. V. Semenovskii, and V. F. Kucherov, *Izv. Akad. Nauk SSSR, Ser. Khim.*, **1972**, 2632 (*Chem. Abstr.*, **78**, 84551b (1973)); M. T. Mustafaeva, V. A. Smit, and V. F. Kucherov, *ibid.*, **1973**, 1349 (*Chem. Abstr.*, **79**, 105431a (1973)); b) M. Alderdice and L. Weiler, *Can. J. Chem.*, **59**, 2239 (1981).

10) Y. MasaKi, K. Hashimoto, K. Sakuma, and K. Kaji, "25th Symposium on the Chemistry of Terpenes, Essential oils and Aromatics," Chemical Society of Japan, Yamaguchi (1981), p. 212.

11) a) Y. Masaki, K. Hashimoto, and K. Kaji, *Tetrahedron Lett.*, **1978**, 4539; *Tetrahedron*, in press; b) Y. Masaki, K. Hashimoto, K. Sakuma, and K. Kaji, *J. Chem. Soc., Chem. Commun.*, **1979**, 855; *J. Chem. Soc., Perkin Trans. I*, **1984**, 1289.

12) It is familiar that oxidation of allylic alcohols with active MnO_2 generally gives α,β-unsaturated aldehydes or ketones without the geometric isomerization of the double bond: A. J. Fatiadi, *Synthesis*, **1976**, 65.

13) J. M. Watson, A. R. Tanner, and R. M. Roberts, *J. Org. Chem.*, **37**, 3743 (1972).

14) S. D. Levine, R. E. Adams, R. Chen, M. L. Cotter, A. F. Hirsch, V. V. Kane, R. M. Kanojia, C. Shaw, M. P. Wachter, E. Chin, R. Huettemann, P. Ostrowski, J. L. Mateos, L. Noriega, A. Guzman, A. Mijarez, and L. Tovar, *J. Am. Chem. Soc.*, **101**, 3404 (1979); K. C. Nicolaou, D. A. Claremon, and W. E. Barnette, *ibid.*, **102**, 6611 (1980).

15) L. Caglioti, *Tetrahedron*, **22**, 487 (1966).

16) For the hydroxyl group-assisted regioselective opening of epoxides, see: D. J. Morgans, Jr., K. B. Sharpless, and S. G. Traynor, *J. Am. Chem. Soc.*, **103**, 462 (1981).

17) H. J. Reich, J. M. Renga, and I. L. Reich, *J. Am. Chem. Soc.*, **97**, 5434 (1975).

18) Y. Masaki, K. Hashimoto, Y. Serizawa, and K. Kaji, *Bull. Chem. Soc. Jpn.*, **57**, 3476 (1984).

19) W. H. Mueller and P. E. Butler, *J. Am. Chem. Soc.*, **90**, 2075 (1968).

20) M. Matsumoto and K. Kondo, *J. Org. Chem.*, **40**, 2259 (1975).

Synthetic Studies on the Ochtodane Type Terpenes II.[1] Synthesis of Pleraplysillin-1

Yukio MASAKI,* Kinji HASHIMOTO, Yuzuru SERIZAWA, and Kenji KAJI
Gifu Pharmaceutical University, 5-6-1 Mitahora Higashi, Gifu 502
(Received May 4, 1984)

A furyl sesquiterpene pleraplysillin-1 (**1**), which possesses the ochtodane skeleton (**2**) in the molecule, was synthesized regio- and stereoselectively starting from the ochtodane type monoterpene (**5**). Two approaches were investigated: One is the route by way of the benzenesulfenyl chloride addition to a sesquiterpene (**9**) or (**13**) which involve the whole carbon framework of **1** and the exocyclic *E*- or *Z*-double bond, and the other involves the regioselective formation of the endocyclic double bond of the ochtodane synthon (**15**) utilizing the hydroxyl-assisted epoxide opening reaction followed by homologation with the 3-furylmethyl moiety. In both of the routes the geometry of the exocyclic double bond of the ochtodane synthon played an important role in the regioselective formation of the endocyclic double bond in **1**.

The explosive growth of marine natural product chemistry during the last decade has given rise to the discovery of a vast array of compounds which have polyhalogenated and/or oxygenated, and unique carbon frameworks never found in the terrestrial organisms.[2] In 1972, a furyl sesquiterpene pleraplysillin-1 (**1**) was isolated from a marine sponge, *Pleraplysilla spinifera*, by Cimino and coworkers.[3] The terpene (**1**) possesses a unique carbon skeleton which is postulated to arise by enzymic carbocyclization involving a lateral methyl group of the presumed farnesyl precursor and the terminal oxidation forming the furan portion. The structural elucidation of **1** has been done by spectral analyses of itself and the hydrogenated product.[3] Recently, two groups, Moore *et al.*[4a] and Fenical *et al.*,[4b] have isolated variously functionalized monoterpenes with the 3,3-dimethyl-1-ethylcyclohexane carbon skeleton (**2**), which was suggested to name "ochtodane."

The carbon framework of pleraplysillin-1 (**1**) is analyzed retro-synthetically as the assembly of an ochtodane (**3**) and 3-furylmethyl (**4**) derivatives. In the preceding paper, we have introduced a facile method for the stereoselective construction of the ochtodane skeleton (**2**) starting from myrcene.[1] Here we report the first regio- and stereoselective synthesis of the sesquiterpene (**1**).[5] The major synthetic efforts focused on the regio- and stereoselective construction of the conjugated diene system in the molecule (**1**). We have investigated two approaches. One of them involves the benzenesulfenyl chloride addition to the trisubstituted and exocyclic C(7)-olefin in the sesquiterpene (**9**) or (**13**) which contain the whole carbons of **1**, followed by formation of the requisite conjugated diene system. The other involves the regioselective formation of the requisite endocyclic C(3)-olefin of the ochtodane moiety followed by the homologation with 3-furylmethyl synthon and latent formation of the other acyclic C(6)-olefinic portion of the conjugated diene system. By the latter method the successful synthesis of **1** was achieved.

1) Approach by Way of the Benzenesulfenyl Chloride Addition (Scheme 1). In order to obtain the sesquiterpene (**9**), the key compound for the olefinic elaboration aiming at the requisite conjugated diene system, the ochtodane type compound with the sulfur-containing auxiliary activator for C–C bond formation at the C(1)-position was prepared from the (*E*)-alcohol (**5**) which was obtained highly stereoselectively by the reported method.[1] Thus, bromination of **5** with PBr_3 followed by treatment of the bromide (**6**) with *p*-Tol-SO_2Na in DMF afforded the crystaline sulfone (**7**), which was purified by recrystallization to remove the (*Z*)-isomer arising from the (*Z*)-alcohol which existed in the starting alcohol (**5**) as impurity.[1] The carbon–carbon bond formation between the allylic sulfone (**7**) and 3-furylmethyl bromide (**4** Y=Br) was performed smoothly in 76% yield with *n*-BuLi in THF at −78—

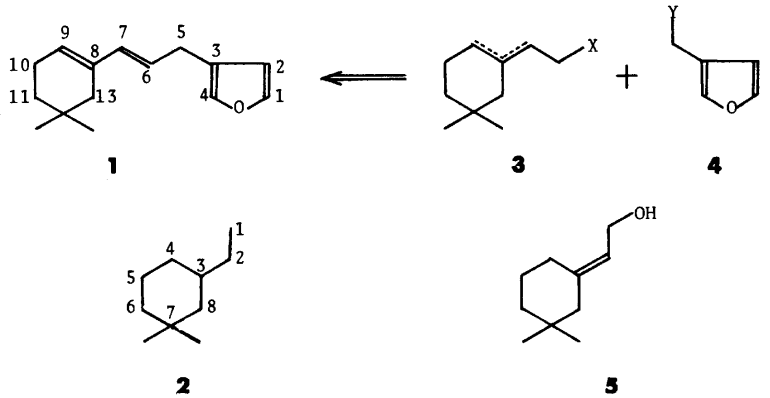

1 **3** **4**

2 **5**

Chart 1.

0°C providing the sesquiterpenoid (**8**). Reductive desulfurization of this compound leading to the sulfur-free compound (**9**) was carried out by the Birch reduction with Li in liq. NH_3 in 74% yield. Treatment of the furyl terpene (**9**), which possesses the pure exocyclic *E*-double bond, with an equimolar amount of PhSCl in CH_2Cl_2 at −78°C for 10 min followed by evaporation of the solvent at room temperature gave the regioisomeric mixture of allylic sulfides (**10**) (79%) instead of the expected adduct (**i**). The structure and regioisomeric proportion were determined by spectral analysis: Mass spectrum showed the M^+ ion at 326, and ^{1}H-NMR exhibited signals for the olefinic protons at δ 4.85 as the major singlet and 5.23 as the minor broad singlet in a ratio 77:23 and those of the geminal dimethyl groups at δ 0.65, 0.86, and at δ 0.80, 0.92 in the same ratio of intensity. The major component was assigned to the undesirable isomer (**10b**) on the basis of the shape of the signal at δ 4.85 for the isolated C(13)-olefinic proton in ^{1}H-NMR. The allylic sulfide (**10**) obtained was converted into the final conjugated diene (**11**) in 83% yield by the sequential treatment of **10** with 30% H_2O_2 in AcOH followed by heating the corresponding sulfoxide in refluxing toluene. Comparison of ^{1}H-NMR of the resultant diene (**11**) with the reported data of natural pleraplysillin-1 (**1**)[3] indicated that the product contains the desired **1** (**11a**) in a minor proportion (*ca.* 23%) and the regioisomer (**11b**) as the major component (*ca.* 77%). Characteristic signals of these regioisomers **1** and **11b** were detected at δ 0.92 (s) and 0.97 (s) assignable respectively to the geminal methyl groups of **1** and **11b**, at δ 1.68 (s) to the C(13)-methylene of **1**, and at δ 5.30 (s) to the C(13)-olefinic proton of **11b**.

Although the stereo-electronic mechanisms in the dehydrochlorination of the intermediary adduct (**i**) or the episulfonium ion (**ii**) are not clear, the stereochemistry of the exocyclic C(7)-double bond of **9** seemed to affect the regioselectivity in the formation of the allylic sulfide (**10**). Thus, we tried the same procedure on the (*Z*)-olefin (**13**) (*E*:*Z*=20:80), which was prepared from the (*E*)-olefin (**9**) (*E*:*Z*=85:15) *via* the epoxide (**12**) according to the method for geometric inversion of olefins developed by Vedejs.[6] Addition of PhSCl to the (*Z*)-olefin (**13**) gave the anticipated result that the product contained the desired allylic sulfide (**10a**) as the major component (60%) and the undesirable one (**10b**) as the minor (40%). The identical product ratio (**1**:**11b**=60:40) was observed in the final diene (**11**) derived analogously. The above results implied that the desired natural **1** would be obtained in less than *ca.* 77% regioselectivity concerning the C(8)-double bond so far as use of this sequence of procedures even if the pure (*Z*)-olefin (**13**) would be used. Attempted separation of each component of the regioisomers of allylic sulfides (**10**) and the final diene (**11**) was unsuccessful. So, we searched for the more regio- and stereoselective route.

II) Approach by Way of the Regioselective Epoxide-ring Opening (Scheme 2). Considering the above results, we investigated another route in which the endocyclic double bond in the ochtodane moiety of **1** is formed regioselectively in the early stage of the synthesis. Application of the regioselective epoxide-ring opening method developed by Sharpless[7] to the β,γ-epoxy alcohol (**14**) prepared from (*E*)-alcohol (**5**) seemed to be the method of choice for this purpose.

Epoxidation of the alcohol (**5**) with *m*-chloroperbenzoic acid providing the epoxide (**14**) (91%) and subsequent treatment of **14** with 1.2 equiv of $Ti(OPr^i)_4$ in CH_2Cl_2 at 15°C for 20 h afforded regioselectively the enediol (**15**) in 77% yield. ^{1}H-NMR spectrum of the product showed a little contamination of the undesirable regioisomer which would be ascribed to the

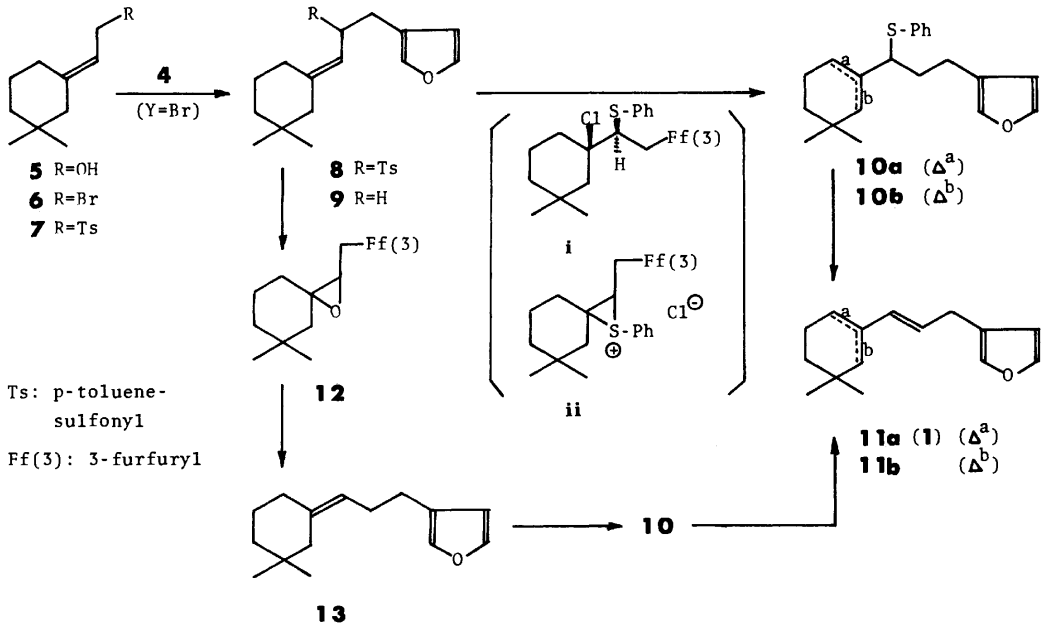

Scheme 1.

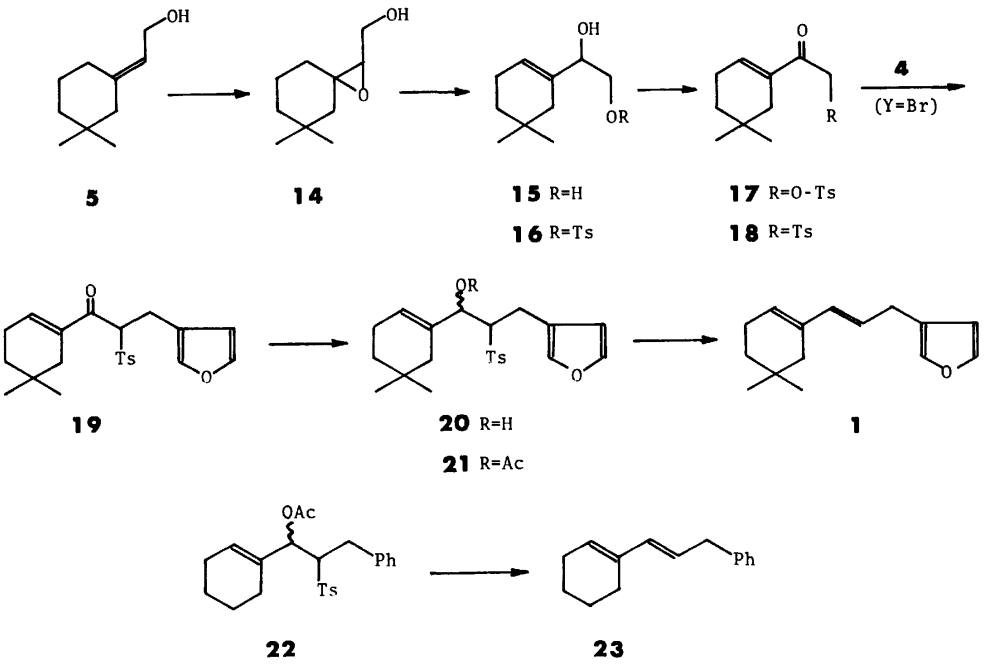

Scheme 2.

presence of the (*Z*)-isomer (*ca.* 6%) in the starting material (**5**),[1] and to the undesirable olefination which might take place slightly in the epoxide-ring opening reaction (**14**→**15**). Selective tosylation of the primary alcohol in **15** was carried out on treatment of **15** with 1.3 equiv of *p*-TsCl in pyridine to give the mono tosylate (**16**) in 76% yield. Oxidation of the allylic alcohol (**16**) with active MnO_2 gave the keto tosylate (**17**) which was converted to the crystalline keto sulfone (**18**) (70% overall yield from **16**) by treatment with *p*-Tol-SO_2Na in DMF. Purification of the compound **18** by recrystallization removed the undesirable olefinic regioisomer with 3(8)-double bond and furnished the regiochemically homogeneous sulfone (**18**) (mp 111—113°C). The structure of **18** was characterized by spectral and elemental analyses: Signals for the two allylic methylene at δ 1.96 (bs, C(8)-methylene) and 2.10—2.50 (m, C(5)-methylene) and for the C(4)-olefinic proton at δ 6.95 as broad singlet appeared in ^{1}H-NMR. The carbon-carbon bond formation between **18** and 3-furylmethyl bromide (**4** Y=Br) proceeded smoothly in the presence of 1.2 equiv of NaH DMF-THF (1:1) at 15°C to give the crystalline sulfone (**19**) (mp 136—140°C) in high (92%) yield. Attention was focused on the next step for the stereoselective formation of the other C(6)-olefinic bond of the conjugated diene system in **1**. Kocienski reported that treatment either of *erythro*- or *threo*-β-acetoxy sulfones with sodium amalgam (Na-Hg) effected reductive elimination to afford exclusively (*E*)-olefins.[8] We tried to apply this condition to our system. Reduction of the keto sulfone (**19**) with $NaBH_4$ in EtOH at 0°C afforded the crystalline alcohol (**20**), which was, without further separation of the diastereoisomers, acetylated to give the β-acetoxy sulfone (**21**) in nearly quantitative yield. Unfortunately, application of Kociensky's condition using 5% Na-Hg with MeOH in AcOEt at −20°C to **21** resulted in the preponderant formation of the methanolysis product (**20**) with a small amount of the conjugated diene (**1**) (7%) which proved to be contaminated with the undesirable (6*Z*)-olefinic isomer to some extent (*ca.* 20%) in high performance liquid chromatography (HPLC) using 5% $AgNO_3$-imprgnated silica gel (see the experimental section) and ^{1}H-NMR analyses. The desired reductive elimination producing **1**, in turn, was accomplished by treatment of **21** with Na and EtOH in THF at −78°C (modified Bouvault-Blanc conditions)[9] in 65% yield. Analyses by HPLC and ^{1}H-NMR proved the product containing *ca.* 11% of the (6*Z*)-isomer. This stereoselectivity observed in the reductive elimination was constant regardless of the stereochemistry of the β-acetoxy sulfone (**21**) because the stereochemically pure **21** prepared from the recrystallized β-hydroxy sulfone (**20**), although not characterized stereochemically, afforded the diene (**1**) with the identical isomeric ratio (**1**:(6*Z*)-isomer=89:11). The analogous results were obtained in the model compound (**22**). Thus, the compound **22** which possesses the same functionality as **21**, produced the conjugated diene (**23**) of the ratio *E*:*Z*=86:14. The desired diene (**1**) was separated by careful column chromatography on 5% $AgNO_3$-impregnated silica gel and identified with natural pleraplysilin-1 (**1**) by spectral comparison.[3]

Experimental

General. IR spectra were recorded on a JASCO IRA-1 spectrometer in $CHCl_3$ solution and the absorption bands (ν_{max}) are reported in cm^{-1}. Mass spectra (MS) were taken on a

JMS-D300 instrument at an ionizing potential of 70 eV and peaks are given in *m/z* values with relative intensities (%) in parenthesis. ^{1}H-NMR spectra were run on a Hitachi R-20B spectrometer (60 MHz)in CCl_4 solution, unless otherwise noted, with tetramethylsilane (TMS) as an internal standard and chemical shifts are reported in δ (ppm) relative to TMS and coupling constants (J) in hertz (Hz). The numbering of pleraplysillin-1 (**1**) was adopted in the description of the synthetic intermediates with sesquiterpene skeleton in ^{1}H-NMR data. All the solvents used in reactions were freshly distilled to remove moisture. Reactions were carried out under nitrogen unless otherwise noted. Reaction mixtures were usually worked up as follows: A mixture was extracted with Et_2O or CH_2Cl_2, washed with water or saturated brine and saturated $NaHCO_3$, if necessary, dried over anhydrous $MgSO_4$, concentrated *in vacuo* below room temperature to give a crude product which was purified by column chromatography. Silica gel (Wakogel B-5F) and Wokogel C-200 were employed respectively for analytical thin-layer (TLC) and column chromatography using hexane–Et_2O solvent system as eluent. High performance liquid chromatography (HPLC) was carried out by using a column (4.0 mm×25cm) packed with 5% $AgNO_3$-impregnated silica gel, which was prepared by drying the slurry of LiChrosorb Si 60 (MERCK) (10 g) and $AgNO_3$ (0.5 g) in water (40 ml) at 100—110 °C for 20 h, and by elution with hexane.

Materials. The starting material in the present synthesis, (*E*)-2-ochtodene-1-ol (**5**) was prepared in 85—94% of *E*-stereoselectivity from myrcene *via* the benzensulfenyl chloride adduct or the 6,7-epoxide according to the method described in the preceding parer.[1]

Synthetic Approach to Pleraplysillin-1 (1) by Way of the Benzenesulfenyl Chloride Addition. (E)-1-(p-Tolylsulfonyl) 2-ochtodene (7): PBr_3 (95 μl, 1.0 mmol) was added dropwise into an ice-cold solution of the alcohol (**5**) (376 mg, 2.4 mmol) in Et_2O (4.0 ml) and the mixture was stirred for 30 min at 0 °C and then kept in refrigerator 16 h. The mixture was diluted with Et_2O, washed successively with saturated $NaHCO_3$ and brine, dried, and concentrated to give the crude oily bromide (**6**) (420 mg, 80%): NMR 0.90 (6H, s, $C(CH_3)_2$), 1.20—1.90 (4H, m, $C(5)H_2C(6)H_2$), 1.93 (2H, s, $C(8)H_2$), 2.22 (2H, bt, J=5.5, $C(4)H_2$), 3.98 (2H, d, J=9.0, $=CHC\underline{H}_2Br$), 5.48 (1H, bt. J=9.0, $=CHC\underline{H}_2Br$). To a solution of the bromide in DMF (4.5 ml) was added in portions sodium *p*-toluenesulfinate (*p*-TsNa) (690 mg, 3.8 mmol) at room temperature and the mixture was stirred for 16 h. The reaction mixture was worked up by the usual manner to give a crude product (540 mg), which was purified by column chromatography providing the crystalline sulfone (**7**) (480 mg, 87%). Recrystallization from Et_2O–hexane gave pure (*E*)-sulfone (**7**), mp 65—66 °C. Data for **7** follow: IR 1650, 1595; MS 292 (M^+, 2), 157 (8), 137 (100), 136 (44), 121 (18); NMR ($CDCl_3$) 0.80 (6H, s, $C(CH_3)_2$), 1.20—1.40 (4H, br, $C(4)H_2$), 1.85 (2H, s, $C(8)H_2$), 2.43 (3H, s, CH_3Ph), 3.82 (2H, d, J=8.5, $=CC\underline{H}_2Ts$), 5.02 (1H, bt, J=8.5, $=C\underline{H}$-$C\underline{H}_2Ts$), 7.27—7.81 (4H, A_2B_2q, J=9.0, arom-H); Found: C, 69.75; H, 8.38%. Calcd for $C_{17}H_{24}O_2S$: C, 69.83; H, 8.27%.

(E)-3-[3-(3-Furyl)-2-(p-tolylsulfonyl)-propylidene]-1,1-dimethylcyclohexane (8): 1.6 M (1M=1 mol dm^{-3}) solution of *n*-BuLi–hexane (0.75 ml) was added dropwise over 5 min into a solution of the sulfone (**7**) (290 mg, 1.0 mmol) and hexamethylphosphoric triamide (HMPA) (250 μl) in THF (2.5 ml) at −78 °C under argon. After stirring the mixture for 20 min at the temperature, a solution of 3-furylmethyl bromide (**4** Y=Br) (170 mg, 1.1 mmol), freshly prepared from 3-furylmethanol, in THF (0.5 ml) was added into the mixture. The mixture was stirred for 1.5 h under gradual warming up to 0 °C and worked up by the usual manner to give a crude product (380 mg). Purification by column chromatography afforded the oily coupled sulfone (**8**) (282 mg, 76%). Data for **8** follow: NMR 0.63, 0.72 (each 3H, s, $C(CH_3)_2$), 1.73 (2H, s, $C(13)H_2$), 2.40 (3H, s, CH_3Ph), 2.59 (1H, dd, J=14.5 and 11.5, one of $C(5)H_2$), 3.28 (1H, dd, J=14.5 and 3.0, the other one of $C(5)H_2$), 3.92 (1H, m, J=11.5, 10.0, and 3.0, CH(Ts)), 4.78 (1H, d, J=10.0, C(7)H), 6.18, 7.15, 7.20 (each 1H, s, C(2)H, C(1)H, and C(4)H), 7.15—7.72 (4H, A_2B_2q, J=8.5, arom-H (Ts)); Found: C, 71.08; H, 7.51%. Calcd for $C_{22}H_{28}O_3S$: C, 70.94; H, 7.58%.

(E)-3-[3-(3-Furyl)propylidene]-1,1-dimethylcyclohexane (9): To a chilled blue solution of Li (70 mg, 10 mg atm) in liq. NH_3 (*ca.* 10 ml) was added dropwise a solution of the sulfone (**8**) (270 mg, 0.7 mmol) in THF (1.0 ml) at −78 °C under argon. Stirring was continued for 40 min at the temperature and then reaction was quenched by introduction of gaseous butadiene followed by addition of MeOH (1.0 ml). After the cold bath was removed to evaporate NH_3, the residue was extracted with Et_2O, washed with water, dried, and concentrated to give a crude oil (135 mg). Purification of the product by column chromatography yielded the sesquiterpene (**9**) (100 mg, 74%) as oil: NMR 0.82 (6H, s, $C(CH_3)_2$), 1.20—1.60 (4H, m, $C(10)H_2C(11)H_2$), 1.79 (2H, s, $C(13)H_2$), 1.85—2.50 (6H, m, $C(5)H_2C(6)H_2$ and $C(9)H_2$), 4.97 (1H, bt, J=6.0, C(7)H), 6.15, 7.08, 7.21 (each 1H, s, C(2)H, C(1)H and C(4)H).

Reaction of the (E)-Furyl Sesquiterpene (9) with Benzenesulfenyl Chloride (PhSCl). A solution of PhSCl (75 mg, 0.5 mmol) in CH_2Cl_2 (0.5 ml) was added dropwise into a cold mixture of the terpene (**9**) (110 mg, 0.5 mmol) in CH_2Cl_2 (3.0 ml) at −78 °C and the mixture was stirred for 10 min at the temperature. Evaporation of the solvent at room temperature gave a crude product (170 mg). Purification by column chromatography afforded the oily sulfide, 1-[3-(3-furyl)-1-(phenylthio)propyl]-5,5-dimethylcyclohexene and -3,3-dimethylcyclohexene (**10**) (130 mg, 79%). Data for **10** follow: IR 1580; MS 326 (M^+, 9), 217 (100), 135 (42); NMR 0.65, 0.86 (major pair of singlets of 77% intensity) and 0.80, 0.92 (minor pair of singlets of 23% intensity) (overall 6H, $C(CH_3)_2$), 3.25—3.65 (1H, m, CH(SPh)), 4.85 (major singlet assignable to C(13)H of **10b**) and 5.23 (minor broad singlet to C(9)H of **10a**) (overall 1H), 6.14 (1H, s, C(2)H), 7.00—7.35 (7H, m, arom-H); Found: C, 77.43; H, 7.89%. Calcd for $C_{21}H_{26}OS$: C, 77.27; H, 8.03%.

Oxidative Elimination of the Thiophenol from the Sulfide (10) Providing the Diene, (E)-1-[3-(3-Furyl)-1-propenyl]-5,5-dimethyl and 3,3-dimethylcyclohexene (11). A mixture of the sulfide (**10**) (100 mg, 0.3 mmol), 30% H_2O_2 (40 μl), and AcOH (2.0 ml stirred for 16 h at room temperature. The mixture was diluted with Et_2O, washed successively with water, saturated $NaHCO_3$, and brine, dried, and concentrated to give the crude sulfoxide (105 mg), which was, without further purification, heated with $NaHCO_3$ (50 mg) in toluene (6.0 ml) under reflux for 3 h. The mixture was worked up by the usual manner and purification of the product by column chromatography gave the oily diene (**11**) (55 mg, 83%). Data for **11** follow: IR 1560, 1500; MS 216 (M^+, 100), 201 (25), 160 (31), 135 (18), 107 (18); NMR 0.92 (minor) and 0.97 (major) (overall 6H, s (23:77), $C(CH_3)_2$), 1.20—2.20 (6H, m, $C(10)H_2C(11)H_2$ and $C(9)H_2$ or $C(13)H_2$), 3.16 (2H, d, J=6.0, $C(5)H_2$), 5.20—5.95 (3H, m, 3 =CH containing C(13)H of **11b** as singlet), 6.15, 7.10, 7.23

(each 1H, s, C(2)H, C(1)H, and C(4)H).

Olefinic Inversion of the (E)-Furyl terpene (9) via the Epoxide (12) Providing the (Z)-Furyl Terpene (13) by the Vedejs' Method.[8] *m*-Chloroperbenzoic acid (MCPBA) (net 80%) (202 mg, 0.9 mmol) was added in portions into a solution of the (*E*)-furyl terpene (**9** *E*:*Z*=85:15) (186 mg, 0.8 mmol), prepared from the alcohol (**5** *E*:*Z*=85:15) by the same procedure described above without recrystallization of the sulfone (**7**), in CH_2Cl_2 (10 ml) at 0 °C. The mixture was diluted with CH_2Cl_2, washed successively with 3% NaOH and water, dried, and concentrated to give a crude product (190 mg). Purification by column chromatography gave the epoxide (**12**) (152 mg, 76%) as oil: NMR 0.86, 0.95 (each 3H, s, $C(CH_3)_2$), 1.51—1.90 (10 H, m), 2.35—2.70 (3H, m, C(5)H_2 and C(7)H), 6.18, 7.13, 7.23 (each 1H, s, C(2)H, C(1)H, and C(4)H). To a solution of $LiP(Ph)_2$ in THF, prepared from $ClP(Ph)_2$ (120 mg, 0.5 mmol) and Li (7 mg, 1.0 mg atm) in THF (1.5 ml) under ultrasonic irradiation at 15 °C for 2 h, was added dropwise a solution of the epoxide (**12**) (100 mg, 0.4 mmol) in THF (0.5 ml) at room temperature under argon. After stirring the mixture for 1 h, MeI (50 μl) was added into the mixture at room temperature. Stirring was continued for 45 min and the mixture was worked up by the usual manner. Purification of the product by column chromatography provided the inverted olefin (**13**) (58 mg, 65%) as oil: NMR 0.82 (minor) and 0.86 (major) (overall 6H, s (20:80), $C(CH_3)_2$), 1.20—1.70 (4H, m, C(10)H_2C(11)H_2), 1.79 (minor) and 1.87 (major) (overall 2H, s, C(13)H_2), 1.80—2.50 (6H, m, C(5)H_2C(6)H_2 and C(9)H_2), 4.97 (minor) and 5.12 (major) (overall 1H, bt, *J*=6.0, C(7)H), 6.15, 7.08, 7.21 (each 1H, s, C(2)H, C(1)H, and C(4)H).

Synthesis of Pleraplysillin-1 (1) from (Z)-Furyl Sesquiterpene (13). The PhSCl addition of the (*Z*)-olefin (**13** *E*:*Z*=20:80) was carried out by the identical conditions described for the (*E*)-olefin (**9**) to give the allylic sulfide (**10**) in 77% yield. ^{1}H-NMR analysis indicated the isomeric ratio of **10** to be **10a**:**10b**=60:40 as follows: NMR 0.65, 0.86 (minor pair of singlets 40% intensity) and 0.80, 0.92 (major pair of singlets of 60% intensity) (overall 6H, $C(CH_3)_2$), 4.85 (minor singlet assignable to C(13)H of **10b**) and 5.23 (major broad singlet assignable to C(9)H of **10a**) (overall 1H, 40:60). Oxidative elimination of thiophenol from the sulfide (**10**) obtained was achieved analogously by oxidation with H_2O_2 in AcOH followed by heating in toluene as described above for **10** (**10a**:**10b**=23:77). The diene, thus obtained in 80% yield, contained desired pleraplysillin-1 (**1**) as the major component: IR 1560, 1500; MS 216 (M^+, 100), 201 (20), 160 (32), 135 (21), 107 (28); NMR 0.92 (major) and 0.97 (minor) (overall 6H, s (60:40), $C(CH_3)_2$), 1.34 (major triplet assignable to C(11)H_2 of **1**), 1.85 (major singlet assignable to C(13)H_2), 3.15 (2H, d, *J*=6.0, C(5)H_2), 5.20—6.10 (3H, m, 3 =CH), 6.15, 7.10, 7.23 (each 1H, s, C(2)H, C(1)H, and C(4)H). The major signals in ^{1}H-NMR were identical with those observed for the pure **1** synthesized by the alternative route, *vide infra*. The diene obtained showed a single peak in HPLC analysis and all the efforts for separation of each regioisomer were unsuccessful.

Synthetic Approach to Pleraplysillin-1 (1) by Way of Regioselective Epoxide-Ring Opening of the β,γ-Epoxy Alcohol (14). *2,3-Epoxyochtodane-1-ol (14)*: A solution of MCPBA net 80%) (920 mg, 4.3 mmol) in CH_2Cl_2 (10 ml) was added dropwise into an ice-cold solution of the alcohol (**5**) (600 mg, 3.9 mmol) in CH_2Cl_2 (20 ml) and the mixture was stirred for 45 min at 0 °C. The mixture was worked up analogously as described for **12** gave the epoxide (**14**) (605 mg, 91%): NMR 0.93, 0.98 (each 3H, s, $C(CH_3)_2$), 1.15—1.90 (8H, br), 2.77 (1H, t, *J*=6.0, C(O)HCH_2OH), 3.64 (2H, d, *J*=6.0, C(O)HCH_2OH), 3.92 (1H, bs, OH).

3-Ochtodene-1,2-diol (15): The epoxide-ring opening was achieved according to the procedure developed by Sharpless.[7] To a solution of the epoxy alcohol (**14**) (650 mg, 3.8 mmol) in CH_2Cl_2 (20 ml) was added dropwise a solution of $Ti(OPr^i)_4$ (1.3 g, 4.5 mmol) in CH_2Cl_2 (5.0 ml) at 0 °C. The mixture was stirred for 30 min at 0 °C and then for 15 h at room temperature. After evaporation of the solvent *in vacuo*, Et_2O (20 ml) and 5% H_2SO_4 (15 ml) was added to the residue and the mixture was stirred for 30 min at room temperature. The reaction mixture was worked up by the usual manner to give a crude product (630 mg), which was purified by column chromatography to afford the diol (**15**) (500 mg, 77%) as oil: IR 3520, 3380; NMR 0.88 (major) and 0.97 (minor) (overall 6H, s (94:6), $C(CH_3)_2$), 1.31 (2H, t, *J*=6.5, C(6)H_2), 1.73 (2H, s, C(8)H_2), 1.85—2.20 (2H, m, C(5)H_2), 3.35—4.10 (2H, m, C(OH)HCH_2OH), 3.85—4.13 (1H, m, C(OH)HCH_2OH), 4.46 (2H, bs, 2×OH), 5.40 (minor) and 5.65 (major) (overall 1H, bs (94:6), =CH).

2-Hydroxy-3-ochtodene-1-yl Tosylate (16): A mixture of the diol (**15**) (430 mg, 2.5 mmol) and *p*-TsCl (570 mg, 3.0 mmol) in pyridine (8.0 ml) was stirred for 16 h at room temperature. The reaction mixture was extracted with Et_2O, washed successively with 3% HCl, 5% $NaHCO_3$, and brine, dried, and concentrated to give a crude product (770 mg). Purification of the product by column chromatography afforded the mono tosylate (**16**) (620 mg, 76%) as oil: NMR 0.82 (major) and 0.91 (minor) (overall 6H, s, $C(CH_3)_2$), 1.23 (2H, t, *J*=7.0, C(6)H_2), 1.62 (2H, bs, C(8)H_2), 1.77—2.20 (2H, m, C(5)H_2), 2.39 (3H, s, CH_3Ph), 3.07 (1H, s, OH), 3.75—4.25 (3H, m, C(OH)HCH_2OTs), 5.38 (minor) and 5.60 (major) (overall 1H, bs, =CH), 7.20—7.80 (4H, A_2B_2q, *J*=8.5, arom-H).

2-Oxo-3-ochtodene-1-yl Tosylate (17): Active MnO_2 (2.5 g) was added into a solution of the alcohol (**16**) (440 mg, 1.3 mmol) in CH_2Cl_2 (20 ml) at room temperature and the mixture was stirred for 3.5 h. The reaction mixture was filtered and the filtrate was purified by column chromatography to give the keto tosylate (**17**) (390 mg, 89%) as oil: IR 1650, 1620, 1590; NMR 0.85 (major) and 1.02 (minor) (overall 6H, s, $C(CH_3)_2$), 1.30 (2H, t, *J*=6.5, C(6)H_2), 1.90 (2H, bs, C(8)H_2), 2.00—2.40 (2H, m, C(5)H_2), 2.40 (3H, s, CH_3Ph), 4.88 (2H, C(O)CH_2OTs), 6.46 (minor) and 6.77 (major) (overall 1H, bs, =CH), 7.20—7.83 (4H, A_2B_2q, *J*=8.5, arom-H).

1-Tosyl-3-ochtodene-2-one (18): A mixture of the keto tosylate (**17**) (370 mg, 1.15 mmol) and *p*-TsNa (574 mg, 2.2 mmol) in DMF (8.0 ml) was stirred for 16 h at room temperature. The reaction mixture was worked up by the usual manner to give a crude product (345 mg). Purification by column chromatography gave the crystalline keto sulfone (**18**) (286 mg, 82%). Recrystallization from Et_2O–hexane yielded the pure regio isomer (**18**), mp 110—113 °C. Data for **18** follow: IR 1650, 1625, 1595; NMR ($CDCl_3$) 0.89 (6H, s, $C(CH_3)_2$), 1.34 (2H, t, *J*=6.5, C(6)H_2), 1.96 (2H, bs, C(8)H_2), 2.10—2.50 (2H, m, C(5)H_2), 2.45 (3H, s, CH_3Ph), 4.44 (2H, s, C(O)CH_2Ts), 6.95 (1H, bs, =CH), 7.25—7.83 (4H, A_2B_2q, *J*=8.5, arom-H); Found: C, 66.53; H, 7.29%. Calcd for $C_{17}H_{22}O_3S$: C, 66.64; H, 7.24%.

1-[3-(3-Furyl)-2-tosylpropionyl]-5,5-dimethylcyclohexene (19): A solution of the keto sulfone (**18**) (140 mg, 0.45 mmol) in THF (0.5 ml) was added into an ice-cold mixture of NaH (13 mg, 0.55 mmol), THF (1.5 ml), and DMF (2.0 ml) and stirring was continued for 10 min at 0 °C. Then, a solution of 3-

furylmethyl bromide (**4** Y=Br) (82 mg, 0.5 mmol) in THF (0.5 ml) was added into the mixture at room temperature. The mixture was stirred for 16 h at room temperature and worked up by the usual manner. Purification of the crude product (172 mg) by column chromatography afforded the crystalline coupled keto sulfone (**19**) (164 mg, 92%), mp 136—140 °C (Et_2O-hexane). Data for **19** follow: IR 1650, 1630, 1600; NMR ($CDCl_3$) 0.77, 0.82 (each 3H, s, $C(CH_3)_2$), 1.25 (2H, t, J=6.5, $C(11)H_2$), 1.88 (2H, bs, $C(13)H_2$), 2.00—2.30 (2H, m, $C(10)H_2$), 2.42 (3H, s, CH_3Ph), 3.11, 3.12 (each 1H, d, J=8.5 and 6.0, C(Ts)HC$\underline{H}_2$-furyl), 4.93 (1H, dd, J=8.5 and 6.0, C(Ts)$\underline{H}CH_2$-furyl), 6.08 (1H, s, C(2)H), 6.73 (1H), bs, C(9)H), 7.07, 7.22 (each 1H, s, C(1)H and C(4)H), 7.20—7.72 (4H, A_2B_2q, J=8.5, arom-H); Found: C, 68.30; H, 6.86%. Calcd for $C_{22}H_{26}O_4S$: C, 68.37; H, 6.78%.

*3-(3-Furyl)-1-(5,5-dimethyl-1-hexenyl)-2-tosyl-1-propanol (**20**)*: $NaBH_4$ (24 mg, 0.63 mmol) was added in portions into a solution of the keto sulfone (**19**) (124 mg, 0.32 mmol) in EtOH (5.0 ml) at 0 °C and stirring was continued for 30 min at 0 °C. Extraction of the mixture with Et_2O followed by the usual work-up gave the crystalline hydroxy sulfone (**20**) (125 mg, 100%), mp 130—135 °C (Et_2O-hexane). Data for 20 follow: IR 3440, 1590; MS 388 (M^+, 2), 307 (19), 233 (85), 215 (100), 165 (47); NMR 0.79, 0.82 (each 3H, s, $C(CH_3)_2$), 1.15 (2H, t, J=6.5, $C(11)H_2$), 1.69 (1H, bs, $C(13)H_2$), 1.90—2.20 (2H, m, $C(10)H_2$), 2.42 (3H, s, CH_3Ph), 2.78, 2.85 (each 1H, d, J=6.0 and 5.0, C(Ts)HC$\underline{H}_2$-furyl), 3.15—3.57 (1H, m, C(OH)HC(Ts)$\underline{H}CH_2$-furyl), 4.00 (1H, d, J=4.0, OH), 4.32 (1H, dd, J=7.5 and 4.0, C(OH)$\underline{H}$C(Ts)H), 5.70 (1H, bs, C(9)H), 6.07, 7.06, 7.20 (each 1H, s, C(2)H, C(1)H, and C(4)H), 7.15—7.75 (4H, A_2B_2q, J=8.5, arom-H); Found: C, 68.04; H, 7.24%. Calcd for $C_{22}H_{28}O_4S$: C, 68.01; H, 7.26%.

*1-[1-Acetoxy-3-(3-furyl)-2-tosylpropyl]-5,5-dimethylcyclohexene (**21**)*: A mixture of the alcohol (**20**) (100 mg, 0.26 mmol), Ac_2O (0.5 ml), and pyridine (0.5 ml) was stirred for 16 h at room temperature. The reaction mixture was worked up by the usual manner to give the acetoxy sulfone (**21**) (105 mg, 95%) as oil. Data for **21** follow: IR 1740, 1595; MS 370 [$(M-60)^+$, 2], 275 (7), 232 (12), 215 (100); NMR 0.79, 0.83 (each 3H, s, $C(CH_3)_2$), 1.25 (2H, t, J=6.5, $C(11)H_2$), 1.55 (2H, bs, $C(13)H_2$), 1.67 (3H, s, CH_3CO_2), 1.83—2.20 (2H, m, $C(10)H_2$), 2.42 (3H, s, CH_3Ph), 2.76, 2.90 (each 1H, d, J=6.0 and 5.5, C(Ts)HC$\underline{H}_2$-furyl), 3.10—3.60 (1H, m, C(OAc)HC(Ts)$\underline{H}CH_2$-furyl), 5.36 (1H, d, J=8.0, C(OAc)$\underline{H}$C(Ts)H), 5.65 (1H, bs, C(9)H), 6.24, 7.17, 7.23 (each 1H, s, C(2)H, C(1)H, and C(4)H), 7.20—7.72 (4H, A_2B_2q, J=8.5, arom-H).

*Synthesis of Pleraplysillin-1 (1) by Reductive Elimination of the Acetoxy Sulfone (**21**). Method A Using Sodium Amalgam.*[8] 5% Na-Hg (2.0 g) was added at once into a cold solution of the acetoxy sulfone (**21**) (150 mg, 0.35 mmol) in a mixed solvent of MeOH (1.5 ml) and AcOEt (0.7 ml) at −20 °C and stirred was continued for 2.5 h at the temperature. The mixture was worked up by the usual manner. Purification of the product by column chromatography gave mainly the hydroxy sulfone (**20**) (96 mg, 71%) and a small amount of the sulfur-free diene (**1**) (5 mg, 7%), which appeared homogeneous in the ordinary TLC but proved to contain two compounds in a ratio *ca.* 80:20 by HPLC analysis using 5% $AgNO_3$-impregnated silica gel. The major less polar component was identified with pleraplysillin-1 (**1**) by coinjection of pure **1** prepared by the alternative conditions (Method B), *vide infra*. Spectral data for the diene were almost identical with those of pure **1** obtained by the modified Bouvault-Blanc conditions (Method B) except for the ratio (*ca.* 80:20) of intensity of the doublet signals at δ 3.15 and 3.26 (J=6.5 Hz) respectively assignable to the $C(5)H_2$ of **1** and the corresponding (6*Z*)-isomer in ^{1}H-NMR.

Method B Utilizing the Modified Bouvalut-Blanc Conditions.[9] Pieces of Na (70 mg, 3.0 mgatm) were added into a cold solution of the acetoxy sulfone (**21**) (150 mg, 0.35 mmol) and EtOH (0.3 ml) in THF (2.0 ml) at −78 °C and the mixture was stirred for 1 h at the temperature. The mixture was extracted with hexane, washed with water, dried, and concentrated. Purification of the product by column chromatography gave the diene (**1**) (49 mg, 65%) as oil. Spectral properties of the diene were consistent with those of the isolated pure **1**, described below, except for the appearance of minor doublet (*ca.* 11%) at 3.26 assignable to the $C(5)H_2$ of the corresponding (6*Z*)-isomer of **1** in ^{1}H-NMR. HPLC analysis also showed that the product contains a minor amount (*ca.* 11%) of the isomer as the more polar component. Careful column chromatography of the diene on 5% $AgNO_3$-impregnated silica gel by elution with hexane gave pure pleraplysillin-1 (**1**). Spectral data for the synthetic compound were consistent with those reported for the natural **1**:[3] IR 1560, 1500, 1445, 1425, 1380, 1360, 1050, 1010, 960, 865; MS 216 (M^+, 100), 201 (25), 160 (40), 145 (30), 135 (27), 131 (37), 118 (29), 107 (37), 91 (50), 81 (49); NMR 0.92 (6H, s, $C(CH_3)_2$), 1.34 (2H, t, J=6.0, $C(11)H_2$), 1.85 (2H, s, $C(13)H_2$), 2.00—2.25 (2H, m, $C(10)H_2$), 3.15 (2H, d, J=6.5, $C(5)H_2$), 5.20—5.70 (2H, m C(6)H and C(9)H), 6.03 (1H, d, J=15.0, C(7)H), 6.15, 7.10, 7.23 (each 1H, s, C(2)H, C(1)H, and C(4)H).

*Synthesis of the Model Compound, 1-(1-Acetoxy-3-phenyl-2-tosylpropyl)cyclohexene (**22**).* 1.6 M solution of *n*-BuLi-hexane (3.1 ml) was added dropwise into a solution of phenethyl *p*-tolyl sulfone (1.17 g, 4.5 mmol), prepared from phenethyl bromide, in THF (8.0 ml) at −78 °C under argon. After stirring of the mixture for 30 min at −78 °C, a solution of 1-cyclohexenecarbaldehyde (550 mg, 5.0 mmol), prepared from cyclohexanone *p*-tosylhydrazone,[10] in THF (1.0 ml) was added into the mixture. The mixture was stirred for 30 min at the temperature and worked up by the usual manner. Product isolation gave 1-(1-cyclohexenyl)-3-phenyl-2-tosyl-1-propanol (1.42 g, 85%) as a diasteroisomeric mixture: NMR 0.85—1.50 (6H, br, $C\underline{H}_2C\underline{H}_2C\underline{H}_2CH$=), 1.65—2.10 (2H, br, $C\underline{H}_2CH$=), 2.41 (3H, s, CH_3Ph), 2.40—3.60 (3H, m, C(OH)HC(Ts)$\underline{H}C\underline{H}_2Ph$), 4.03 (1H, s, OH), 3.92 (major doublet (J=15.0)) and 4.30 (minor doublet (J=12.0)) (overall 1H, C(OH)$\underline{H}$C(Ts)H), 5.62 (major) and 5.86 (minor) (overall 1H, bs, =C$\underline{H}CH_2$), 6.80—7.87 (9H, m, arom-H). Careful column chromatography of the diasteroisomeric mixture gave one of the stereoisomer as a TLC-homogeneous oil: IR 3450, 1595; MS 370 (M^+, 3), 352 (4), 260 (31), 214 (81), 197 (98), 196 (100); NMR showed almost identical spectrum with that of the stereoisomeic mixture except for absence of the minor doublet at δ 4.30 and of the minor broad singlet at δ 5.86. The hydroxy sulfone (diastereoisomeric mixture) was acetylated analogously as described for **20** to give the crystalline acetoxy sulfone (**22**) in 88% yield as a diastereoisomeric mixture. Data for **22** follow: IR 1740, 1590; NMR 1.10—1.55 (6H, br, $C\underline{H}_2C\underline{H}_2C\underline{H}_2CH$=), 1.66 (major) and 1.92 (minor) (overall 3H, s, CH_3CO_2), 1.70—2.05 (2H, br, $C\underline{H}_2CH$=), 2.38 (3H, s, CH_3Ph), 2.40—3.80 (3H, m, C(OAc)HC(Ts)$\underline{H}C\underline{H}_2$-Ph), 5.33 (1H, d, J=8.0, C(OAc)$\underline{H}$C(Ts)H), 5.40 (minor) and 5.60 (major) (overall 1H, bs, C$\underline{H}CH_2$), 7.09 (5H, s, arom-H (Ph)), 7.15—7.73 (4H, A_2B_2q, J=8.5, arom-H (Ts)). From the

purified stereoisomer of hydroxysulfone was obtained the stereochemically pure one of acetoxy sulfone (**22**); mp 81—83 °C (Et_2O–hexane). Spectral properties were identical with the corresponding diastereoisomeric mixture except for absence of the minor singlet at δ 1.92 and broad singlet at δ 5.40 in ^{1}H-NMR. Found: C, 69.72; H, 6.93%. Calcd for $C_{24}H_{28}O_4S$: C, 69.88; H, 6.84%.

*Reductive Elimination of the Acetoxy Sulfone (**22**) Providing the Diene, 1-(3-Phenyl-1-propenyl)cyclohexene (**23**).* Treatment of the acetoxy sulfone (**22**) with Na and EtOH in THF by the same procedure (Method B) as described for **21** gave the diene (**23**) in 76% yield as oil. HPLC analysis of the diene (**23**) obtained either from the diastereoisomeric mixture of **22** or from the stereochemically pure **22** showed the identical chromatogram of a mixture of the geometric isomers (86:14) concerning the disubstituted olefinic bond. Data for **23** follow: IR 1600, 1490, 1445, 1430; MS 198 (M^+, 100), 169 (24), 155 (34), 141 (34), 129 (45), 117 (33), 107 (63), 91 (90), 97 (84); NMR 1.40—1.77 (4H, br, CH_2CH_2), 1.88—2.27 (4H, br, 2×=CHC<u>H</u>$_2$), 3.35 (major) and 3.54 (minor) (overall 2H, d (*E*:*Z*=86:14) *J*=6.0, CHC<u>H</u>$_2$Ph), 5.21—5.70 (2H, m, 2×=C<u>H</u>CH_2), 5.94 (1H, d, *J*=15.0, =CC<u>H</u>=CHCH$_2$Ph).

References

1) The preceding paper: Y. Masaki, K. Hashimoto, K. Sakuma, and K. Kaji, *Bull. Chem. Soc. Jpn.*, **57**, 3466 (1983). The preliminary communicaton for the preceding paper: *Tetrahedron Lett.*, **23**, 1481 (1982).

2) For recent and excellent reviews concerning marine natural product chemistry see: D. J. Faulkner, *Tetrahedron*, **33**, 1421 (1977); D. J. Faulkner and W. H. Fenical (ed), "Marine Natural Products Chemisty," Plenum Press, New York (1977).

3) G. Cimino, S. De Stefano, L. Minale, and E. Trivellone, *Tetrahedron*, **28**, 4761 (1972).

4) a) B. J. Burreson, F. X. Woolard, and R. E. Moore, *Chem, Lett.*, **1975**, 1111; b) O. J. McConnell and W. Fenical, *J. Org. Chem.* **43**, 4238 (1978); V. J. Paul, O. J. McConnell, and W. Fenical, *ibid.*, **45**, 3401 (1980).

5) Preliminary communication: Y. Masaki, K. Hashimoto, Y. Serizawa, and K. Kaji, *Chem. Lett.*, **1982**, 1879.

6) E. Vedejs and P. L. Fuchs, *J. Am. Chem. Soc.*, **95**, 822 (1973).

7) D. J. Morgans, Jr., K. B. Sharpless, and S. G. Traynor, *J. Am. Chem. Soc.*, **103**, 462 (1981).

8) P. J. Kocienski, B. Lythgoe, and S. Ruston, *J. Chem. Soc., Perkin. 1*, **1978**, 829.

9) K. Sato, O. Miyamoto, S. Inoue, T. Yamamoto, and Y. Hirasawa, *J. Chem. Soc., Chem. Commun.*, **1982**, 153.

10) P. C. Traas, H. Boelens, and H. J. Takken, *Tetrahedron Lett.*, **1976**, 2287.

 © 1984 The Chemical Society of Japan Bull. Chem. Soc. Jpn., 57, 3483—3487 (1984)

Cycloaddition Reactions of Azepines and Diazepines with Conjugated Double Bonds Possessing Electron-Withdrawing Groups

Katsuhiro SAITO,* Shigenori IIDA, and Toshio MUKAI†
*Department of Chemistry, Nagoya Institute of Technology, Gokiso-cho, Showa-ku, Nagoya 466
†Department of Chemistry, Faculty of Science, Tohoku University, Aoba, Aramaki, Sendai 980
(Received April 5, 1984)

Cycloadditions of 1-ethoxycarbonyl-1*H*-azepine with 5-methoxycarbonyl-2-pyrone gave [4+2] and [4+6] type adducts and a benzazepine derivative, while the reaction of the azepine derivative with 3-methoxycarbonyl-2-pyrone afforded only a [4+2] type adduct. Similarly, an addition of 1-ethoxycarbonyl-1*H*-1,2-diazepine with 5-methoxycarbonyl-2-pyrone gave a benzodiazepine derivative. Reactions of the azepine and the diazepine derivatives with tetrachlorocyclopentadienone dimethyl acetal afforded [4+2] type adducts.

Azepine and diazepine derivatives are known to be nonplaner compounds and to behave as olefinic compounds rather than aromatic materials.[1-4] The addition reactions of azepines and diazepines have received considerable attention from the viewpoint of a synthetic utility and an elucidation of the chemical reactivity. Azepines and diazepines are known to give [4+2] type adducts when allowed to react with dienophiles and afford [4+2] and [4+6] type adducts in reactions with enophiles.[2]

As a part of our research effort concerning the addition reactions of the heterocyclic compounds,[3] we have studied the cycloaddition reactions of azepine and diazepine derivatives with 2-pyrone derivatives and cyclopentadiene derivatives. We wish to report the results of these reactions.

Results

1-Ethoxycarbonyl-1*H*-azepine (**1a**) was allowed to react with 5-methoxycarbonyl-2-pyrone (**3**) in benzene at 80 °C for 57 h to give adducts **6** and **7** in yields of 25 and 20%, respectively. The same reaction under more drastic conditions (in toluene, 140 °C for 10 d) afforded the benzazepine derivative **8** and the [6+6] type dimer **9**[4] of **1a** in 5 and 36% yields, respectively. The reaction of 1-methoxycarbonyl-1*H*-azepine (**1b**) with 3-methoxycarbonyl-2-pyrone (**4**) at 80 °C for 68 h afforded adduct **10** and the [6+4] type dimer **11**[5] of **1b** in yields of 5 and 11%, respectively. The reaction of 1-ethoxycarbonyl-1*H*-1,2-diazepine (**2**) and **3** in benzene at 80 °C for 10 d gave no adduct but the reaction at 110 °C in toluene for 10 d gave a benzodiazepine derivative **12** in 12% yield. The reaction of **2** with **4** gave no adduct. Under conditions analogous to the above, **1** and **2** were allowed to react with 2-pyrone (**5**), but no adduct was obtained.

Upon heating in xylene at 140 °C for 50 min adduct **6** gave the benzazepine derivative **8** in 5% yield, which was obtained in better yield (17%) by a reaction of **6** with o-chloranil in anisole at 140 °C for 45 min. After heating, adduct 7 underwent a retro-Diels-Alder reaction to yield **1a** and **3**. The adduct **10** gave a resinous material upon heating, which was not further characterized.

The reaction of **1a** with tetrachlorocyclopentadienone dimethyl acetal (**13**) at 100 °C for 5 h afforded adduct **14** as crystalline material of mp 68—70 °C in yield of 48%.[5] The diazepine derivative **2** was also allowed to react with **13** at 100 °C for 15 h to give the adduct **15** in 39% yield. Under conditions analogous to the above **1** and **2** were allowed to react with cyclopentadienone diethyl acetal, however, no adduct was obtained. All attempts to hydrolyze the acetal components of **14** and **15** to the corresponding ketones and to substitute the chlorine atoms with hydrogen atoms were unsuccessful.

Elemental analyses and/or the molecular ion peaks in the mass spectra revealed that products **6**, **7**, and **10** are the 1:1 adducts of **1a** and **3**, and **1b** and **4**, respectively. The existence of lactone rings in these products is shown by the IR spectra (**6**; 1780, **7**; 1760, and **10**; 1775 cm^{-1}). The structures of the [4+2] type adducts **6** and **10** were determined on the basis of NMR spectral properties, employing the double- and triple-resonance technique. The small coupling constants between the bridgehead protons (**6**; $J_{1,2}$=3.0, $J_{2,3}$=$J_{7,8}$=4.3, and $J_{8,9}$=2.3 Hz, **10**; $J_{1,2}$=2.2 and $J_{2,3}$=$J_{7,8}$=4.0 Hz) indicate the endo structures of **6** and **10**.[6] These structures were further substantiated by the similarity of their NMR spectra to those of the [4+2] type adduct **14**.[5]

The IR absorption due to the urethane group of **7** appears at 1705 cm^{-1}, indicating that this urethane group is not conjugated with any unsaturated group. The [6+6] type dimer **9** also shows an absorption due to the urethane group at almost the same wave length (1700 cm^{-1}) in its IR spectrum.[4] The structure of **7** was determined mainly on the basis of NMR spectral properties and was confirmed by a comparison of its NMR spectrum to that of an analogous compound **16**.[7]

The signals due to the bridgehead protons, H_2 and H_7 (5.06—5.43 ppm) of **7** were observed at rather low field. The same tendency was observed with the [6+6] type dimer **9** (4.95 ppm)[4] substantiating the structure of 7. Each signal due to H_1, H_8, and the protons of ethoxycarbonyl group appears as a pair of signals at a slightly different chemical shift in the NMR spectrum at room temperature. At 70 °C, these three pairs coalesced to three independent signals. This phenom-

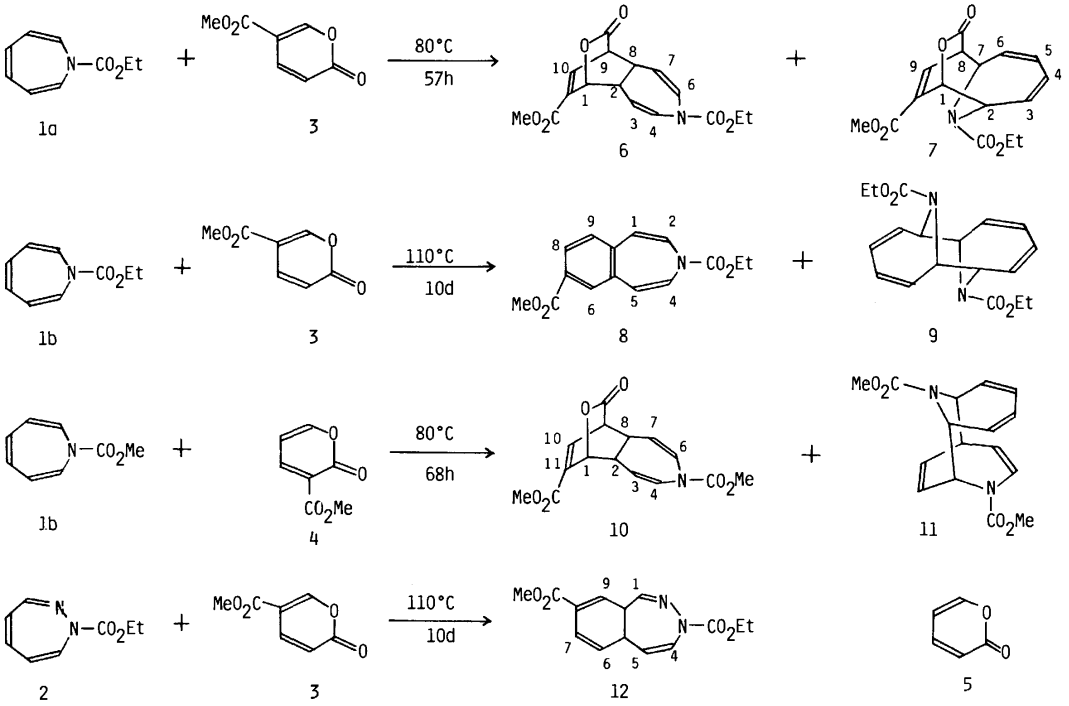

Fig. 1

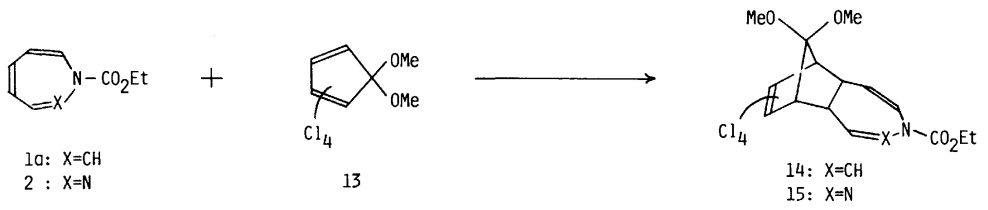

Fig. 2.

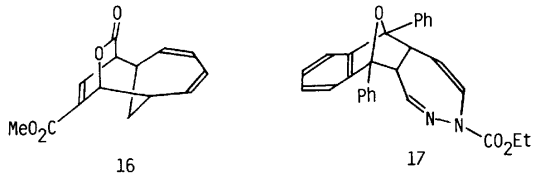

Fig. 3.

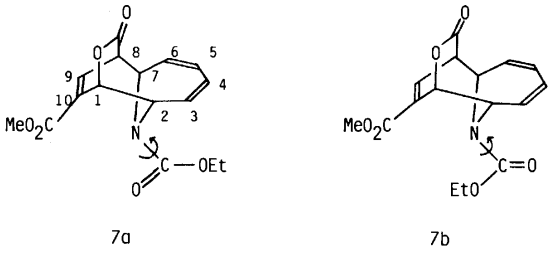

Fig. 4.

enon can be explained in terms of the existence of two rotamers (**7a** and **7b**) resulting from the rotation of the ethoxycarbonyl group as shown in Fig. 4.[3b,3d,8]

Elemental analyses and the molecular-ion peaks in the mass spectra indicate that **8** and **12** are the products of decarboxylations of the 1:1 adducts of **3** with **1a** and **2**, respectively. The UV spectra reveal that these products are the azepine and the diazepine derivatives.[9] The structure of **8** was determined on the basis of the NMR spectrum as well as the independent synthesis of **8** by the thermolysis of **6**. The NMR signals due to the protons on the seven-membered ring appear as two pairs of signals with slight differencies in chemical shift, showing **8** to be an almost symmetric compound.

In the NMR spectrum of **12**, the chemical shifts of H_1 (7.31 ppm), H_4 (6.47 ppm), and H_5 (5.55 ppm) closely resemble those of the corresponding protons (7.31, 6.22, and 5.67 ppm) of **2**, suggesting the presence of the 3*H*-2,3-benzodiazepine skeleton. The position of the methoxycarbonyl group on the benzene ring was determined by the appearance of the NOE between H_5 and H_6, and H_1 and H_9 with 15 and 17%, respectively.

The structure of **14** was confirmed by a comparison of the physical properties with values found in the literature.[5] The Structure of **15** was elucidated on the basis of its NMR spectrum and was confirmed by a comparison of its NMR spectrum to that of an analogous compound **17**.[3]

Discussion

Though the yields of the products mentioned above

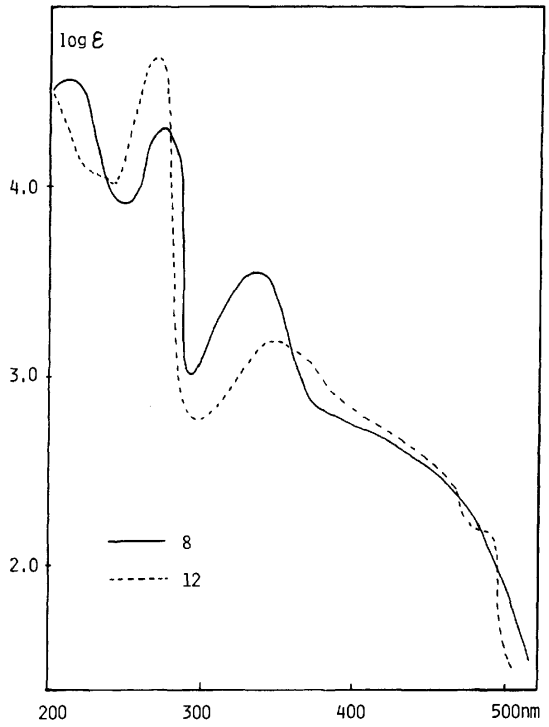

UV Spectra of 8 and 12 in Cyclohexane
Fig. 5.

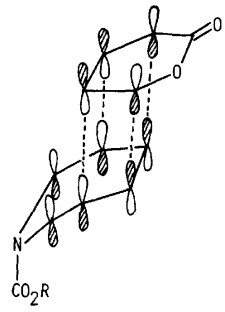

18
Fig. 6.

are not high, it is significant that 2-pyrone derivatives reacted with azepine and diazepine derivatives since it has been previously reported by Anastassiou *et al.* that 2-pyrone is inert toward heterocyclic compounds such as **1** and **2**.[10] The experimental results obtained in our laboratory seem to suggest that the introduction of electron-withdrawing groups such as the methoxycarbonyl group increased the reactivity of the 2-pyrones with azepine and diazepine derivatives. This phenomenon can be rationalized by visualizing the reaction as an inverse electron-demanding Diels-Alder reaction in which the HOMO of the heterocyclic compounds interact with the LUMO of the 2-pyrones.[2c,11] In such cases, a lowering of the LUMO of the 2-pyrones or an elevation of the HOMO of the heterocyclic compounds are thought to promote the interaction of the transition state which allows the chemical reaction to proceed. Thus, the introduction of a methoxycarbouyl group,

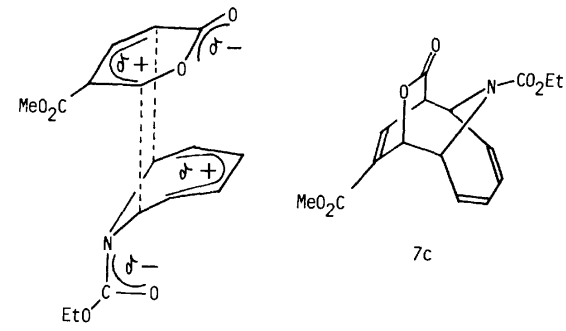

19

7c

Fig. 7.

which is known to lower the orbital energies of the system,[2c,12] is thought to be responsible for the success of the reaction.

The steric repulsion between the heterocyclic compounds and the methoxycarbonyl group at the reaction site of **4** may explain the lower yield of the reaction with **4** than with **3**. The endo mode of the reactions to form **6** and **10** is explained by the secondary orbital interaction in the transition state of **18**.

The preferential formation of **7**, and not **7c**, can be rationalized by the dipole-dipole interaction between the reactants in the transition state **19** as shown in Fig. 7.[2c,3c,13] The formation of **8** is a result of the decarboxylation reaction of **6** as shown by the experiment mentioned above. The benzodiazepine derivative **12** is also thought to be obtained through the decarboxylation reaction of the 1:1 adduct of **2** and **3**, corresponding to **6**.

The inactivity of cyclopentadienone diethyl acetal and the activity of **13** in the reactions with **1** and **2** can be explained by the following argument. Cyclopentadienone diethyl acetal contains an electron-rich conjugated double bond which is not suitable as an enophile in the inverse electron-demanding Diels-Alder reaction previously described.[2c] In fact, **13**, has an electron-defficient conjugated double bond substituted by chlorine atoms.

Experimental

All the reactions were carried out under a nitrogen stream. All melting and boiling points were uncorrected. NMR spectra were measured with a Varian HA-100 or Hitachi R-20B spectrometer with deuteriochloroform or carbon tetrachloride as solvents and tetramethylsilane as an internal standard. The IR spectra were measured in carbon tetrachloride solutions or potassium bromide disks and the UV spectra were measured in cyclohexane solutions. The mass spectra were measured with a Hitachi RMU 6D spectrometer at 70eV.

Reaction of **1a** *with* **3** *at 80°C.* A mixture of **1a** (1.52g, 9.2mmol) and **3** (7.10g, 46mmol) in benzene (20ml) was kept at 80°C for 57h. After evaporation of the solvent on a rotary evaporator, colorless crystals of recovered **3** were collected by filtration (4.67g, 66%). The filtrate was chromatographed on silica gel to give a red oil **1a** (120mg, 8%, pet ether-benzene 4:1 as an eluent), crystals **3** (1.19g, 17%, pet ether-benzene

1:1 as an eluent), a colorless viscous oil **6** (820mg, 25%, pet ether-benzene 1:2 as an eluent), and colorless crystals **7** (610 mg, 20%, ether as an eluent). The oil **6** and the crystals **7** were further purified by repeated chromatography on silica gel using benzene as an eluent and recrystallization from ethanol, respectively. **6**: Found: C, 60.19; H, 5.43; N, 4.14%. Calcd for $C_{16}H_{17}O_6N$: C, 60.18; H, 5.37; N, 4.39%. Ms *m/z* (rel intensity) 319 (M^+, 1), 165 (100), 127 (20), and 92 (54). IR (oil) 3050, 2950, 1780, and 1735cm^{-1}. NMR (CCl_4) δ=1.31 (t, CH_3, J=7.0Hz), 3.11 (ddd, H_8), 3.30 (ddd, H_2), 3.62 (dd, H_9), 3.70 (s, OCH_3), 4.20 (q, CH_2, J=7.0Hz), 4.77 (dd, H_3 or H_7), 4.82 (dd, H_7 or H_3), 5.46 (dd, H_1), 6.81 (d, 2H, H_4 and H_6), and 7.10 (dd, H_{10}). Coupling constants in Hz, $J_{1,2}$=3.0, $J_{2,8}$=8.1, $J_{2,3}$=$J_{7,8}$=4.3, $J_{3,4}$=$J_{6,7}$=11.3, $J_{8,9}$=2.3, $J_{9,10}$=6.0, and $J_{10,1}$=2.3. **7**: mp 97.5—100°C. Found: C, 60.14; H, 5.29; N, 4.11%. Calcd for $C_{16}H_{17}O_6N$: C, 60.18; H, 5.37; N, 4.39%. MS *m/z* (rel intensity) 319 (M^+, 1), 165 (100), 137 (14), and 92 (46). IR (KBr) 3030, 2950, 1760, and 1705cm^{-1}. NMR ($CDCl_3$) δ=1.20 and 1.28 (t,CH_3, J=7.0Hz), 3.79 and 3.82 (dd, H_8), 3.83 (s, OCH_3), 4.06 (q, CH_2, J=7.0Hz), 5.06—5.43 (m, 2H, H_2 and H_7), 5.54 and 5.62 (dd, H_1), 6.07 (bs, 4H, H_3-H_6), and 7.23 (dd, H_9). Coupling constants in Hz, $J_{1,2}$=4.8, $J_{1,9}$=1.4, $J_{2,3}$=4.7, $J_{7,8}$=4.0, and $J_{8,9}$=6.9.

Reaction of ***1a*** *with* ***3*** *at 110°C.* A mixture of **1a** (4.13g, 25mmol) and 3 (4.50g, 29mmol) in toluene (50ml) were kept at 110°C for 10d. After evaporation of the solvent on a rotary evaporator, the residue was chromatographed on silica gel to afford a red oil of recovered **1a** (420mg, 10%, pet ether-ether 1:1 as an eluent), red crystals **8** (300mg, 5%, pet ether-ether 4:6 as an eluent), and colorless crystals **9** (1.46g, 35%, pet ether-ether 3:7 as an eluent). Recrystallization of **8** from ethanol gave pure crystals, mp 82—84°C. Found: C, 65.61; H, 5.33; N, 5.10%. Calcd for $C_{15}H_{15}O_4N$: C, 65.92; H, 5.33; N, 5.13%. MS *m/z* (rel intensity) 273 (M^+, 83), 201 (39), 200 (100), 173 (22), 142 (16), and 115 (9). IR (KBr) 3030, 2960, and 1720cm^{-1}. NMR (CCl_4) δ=1.30 (t, CH_3, J=7.0Hz), 3.78 (s, OCH_3), 4.17 (q, CH_2, J=7.0Hz), 5.14 (d, H_1 or H_5), 5.19 (H_5 or H_1), 6.09 (d, H_2 or H_4), 6.15 (d, H_4 or H_2), 6.57 (d, H_9), 7.20 (d, H_6), and 7.48 (dd, H_8). Coupling constants in Hz, $J_{1,2}$=$J_{4,5}$=10.3, $J_{6,8}$=1.8, and $J_{8,9}$=8.0.

Reaction of ***1b*** *with* ***4***. A mixture of **1b** (900mg, 6.0 mmol) and **4** (4.62g, 30.0mmol) in benzene (10ml) was kept at 80°C for 68h. After evaporation of the solvent on a rotary evaporator, the residue was chromatographed on silica gel to yield a red oil of recovered **1b** (300mg, 33%, benzene-ether 19:1 as an eluent) and a colorless resinous oil (220mg, benzene-ether 9:1 as an eluent), which was thin-layer chromatographed on alumina using pet ether-ether 1:4 as a developing solvent to give colorless crystals **11** (100 mg, 11%, R_f=0.7) and a colorless resinous oil **10** (95mg, 5%, R_f=0.6). The oil **10** was unstable toward distillation (0.05Torr, bath temperature 135°C) and was purified by repeated thin-layer chromatography on alumina using pet ether-ether 1:4 as a developing solvent; however, an analytically pure sample could not be obtained. MS *m/z* (rel intensity) 305 (M^+, 1), 151 (100), 123 (6), and 92 (46). IR (oil) 3030, 2980, 1775, and 1740cm^{-1}. NMR (CCl_4) δ=3.33 (m, 2H, H_2 and H_8), 3.80 (s, OCH_3), 3.90 (s. OCH_3), 4.67 (m, 2H, H_3 and H_7), 5.00 (ddd, H_1), 6.36 (dd, H_{11}), 6.70 (dd, H_{10}), and 6.82 (d, H_4 and H_6). Coupling constatnts in Hz, $J_{1,2}$=2.2, $J_{1,10}$=2.0, $J_{1,11}$=4.7, $J_{2,3}$=$J_{7,8}$=4.0, $J_{3,4}$=$J_{6,7}$=10.0, and $J_{10,11}$=8.0.

Reaction of ***2*** *with* ***3***. A mixture of 2 (245mg, 1.5mmol) and **3** (350mg, 2.3mmol) in toluene (10ml) was kept at 110°C for 10d. After evaporation of the solvent on a rotary evaporator, the residue was chromatographed on silica gel to afford orange crystals **12** (48mg, 12%, pet ether-ether 1:2 as an eluent), which were purified by recrystallization from ethanol. However, an analytically pure sample was not obtained because of a tendency to decompose to a resinous material. **12**: MS *m/z* (rel intensity) 274 (M^+, 100), 243 (12), 215 (34), 202 (96), 174 (28), 144 (42), and 116 (26). IR (KBr), 3030, 2960, 1730, and 1710cm^{-1}. NMR (CCl_4) δ=1.34 (t, CH_3, J=7.0Hz), 3.84 (s, OCH_3), 4.22 (q, CH_2), 5.55 (d, H_5), 6.47 (d, H_4), 6.86 (d, H_6), 7.31 (s, H_1), 7.61 (d, H_9), and 7.77 (dd, H_7). Coupling constants in Hz, $J_{4,5}$=9.0, $J_{6,7}$=8.0, $J_{7,9}$=1.8.

Thermal Reaction of ***6***. A solution of **6** (55mg, 0.17mmol) in xylene (2ml) was kept at 140°C for 50min. After evaporation of the solvent on a rotary evaporator, the residue was thin-layer chromatographed on silica gel using pet ether-ether 1:1 as a developing solvent to give **8** (2mg, 4%, R_f=0.7) and the recovered **6** (27mg, 49%, R_f=0.5).

Reaction of ***6*** *with o-Chloranil.* A mixture of **6** (81mg, 0.25mmol) and *o*-chloranil (69mg, 0.28mmol) in anisole (5ml) was kept at 140°C for 45min. The reaction mixture was chromatographed on alumina to yield an oil (150mg) using ether as an eluent. The oil was thin-layer chromatographed on silica gel using pet ether-ether 1:1 as a developing solvent to give **8** (12mg, 17%, R_f=0.7).

Reaction of ***2*** *with* ***13***. A mixture of **2** (1.00g, 6.0mmol) and **13** (3.20g, 12.1mmol) in benzene (3ml) was kept at 100°C for 15h in a sealed ampoule. The reaction mixture was chromatographed on silica gel to give recovered **13** (2.46g, 77%, benzene as an eluent) and colorless crystals **15** (1.03g, 39%, benzene-ether 1:1 as an eluent), which were recrystallized from ether to give pure **15**; mp 77—77.5°C. Found: C, 41.84; H, 3.64; N, 6.38%. Calcd for $C_{15}H_{16}O_4N_2Cl_4$: C, 41.88; H, 3.75; N, 6.51%. MS *m/z* (rel intensity) 430 (M^+, 1) and 165 (100). IR (KBr) 3030, 2970, and 1720cm^{-1}. NMR ($CDCl_3$) δ=1.35 (t, CH_3, J=7.0Hz), 3.48 (m, 2H, H_2 and H_8), 3.53 (s, OCH_3), 3.60 (s, OCH_3), 4.23 (q, CH_2, J=7.0Hz), 4.95 (m, H_7), 6.93 (d, H_3), and 7.15 (d, H_6). Coupling constants, $J_{2,3}$=1.5, $J_{6,7}$=10.0, and $J_{7,8}$=2.5.

The authors are indebted to Professor Sho Ito of Tohoku University for his fruitfull suggestions.

References

1) I. C. Paul, S. M. Johnson, L. A. Paquette, J. H. Barrett, and R. J. Halusca, *J. Am. Chem. Soc.*, **90**, 5023 (1968); L. A. Paquette, "*Nonbenzenoid Aromatics*," Academic Press, p. 250 (1969).

2) a) W. S. Marphy and K. P. Raman, *Tetrahedron Lett.*, **21**, 319 (1980); b) U. Gockel, U. Hartmansgruber, A. Steigel, and J. Sauer, *ibid.*, **21**, 319 (1980); c) K. Harano, M. Yasuda, T. Ban, and K. Kanematsu, *J. Org. Chem.*, **45**, 4455 (1980).

3) a) S. Iida, T. Mukai, and K. Saito, *Heterocycles*, **11**, 401 (1978); b) K. Saito and K. Takahashi, *ibid.*, **12**, 263 (1979); c) K. Saito, S. Iida, and T. Mukai, *ibid.*, **19**, 1197 (1982); d) K. Saito, H. Kojima, T. Okudaira, and K. Takahashi, *Bull. Chem. Soc. Jpn.*, **56**, 175 (1983).

4) A. L. Johnson and H. E. Simons, *J. Am. Chem. Soc.*, **88**, 2591 (1966) and **89**, 3191 (1967); L. A. Paquette and J. H. Barrett, *ibid.*, **88**, 2590 (1966); L. A. Paquette and J. E. Kuhla, *ibid.*, **91**, 3616 (1969).

5) T. Imagawa, N. Sueda, and M. Kawanishi, *Tetrahedron*,

30, 2227 (1974).

6) L. A. Paquette, J. E. Kuhla, J. H. Barrett, and L. M. Leighter, *J. Org. Chem.*, **34**, 2888 (1969).

7) T. Sasaki, K. Kanematsu, Y. Yukimoto, and T. Hiramatsu, *J. Am. Chem. Soc.*, **96**, 2536 (1974).

8) T. Sato, Y. Fukazawa, Y. Fujise, and S. Ito, *Heterocycles*, **7**, 807 (1977).

9) G. Kaupp, J. Parreten, R. Reute, and H. Prinzbach, *Chem. Ber.*, **103**, 2288 (1970); M. Hirota, *Chem. Lett.*, **1976**, 519.

10) A. G. Anastassiou, E. Reichmanis, S. J. Girgenti, and M. Schaefer-Ridder, *J. Org. Chem.*, **43**, 315 (1978).

11) R. Hoffmann and R. B. Woodward, *Angew. Chem.*, **81**, 797 (1969).

12) R. Sustmann, *Tetrahedron Lett.*, **1971**, 2717 and 2721.

13) D. W. Jones, *J. C. S. Perkin I*, **1977**, 980.

Oxidative Coupling of 1-(2,6-Dichlorobenzoyl)pyrroles and -pyrazoles and Alkyl Acrylates by Palladium(II) Acetate

Toshio ITAHARA,* Kazukuni KAWASAKI, and Fumio OUSETO
Institute of Chemistry, College of Liberal Arts, Kagoshima University, Korimoto, Kagoshima 890
(Received April 21, 1984)

Treatments of 1-(2,6-dichlorobenzoyl)-, 3-acetyl-1-(2,6-dichlorobenzoyl)-, 1-(2,6-dichlorobenzoyl)-2-formyl-, and 1-(phenylsulfonyl)pyrroles with palladium acetate and alkyl acrylates gave the corresponding α-alkenyl-substituted pyrroles in good yields, while the reaction of 1-(2,6-dichlorobenzoyl)-2,5-dimethylpyrrole gave small amounts of β-alkenyl-substituted pyrroles. Under similar conditions, 1-(2,6-dichlorobenzoyl)pyrazole and 1-(2,6-dichlorobenzoyl)-3,5-dimethylpyrazole reacted with palladium acetate and alkyl acrylates to give the corresponding 4-alkenyl-substituted pyrazoles. The reaction of 1-(2,6-dichlorobenzoyl)-4-methylpyrazole gave 5-alkenyl-substituted pyrazole.

Palladium(II) salts-assisted alkenylation of arenes is a useful method for the direct synthesis of aromatic-substitued olefins.[1] Fujiwara *et al.* reported the alkenylation of heteroarenes with palladium acetate and olefins.[2,3] We reported that 2,6-dichlorobenzoyl group was an effective protecting substituent for the alkenylation of 1-acylindoles[4] and the arylation of 1-acylpyrroles with arenes.[5] Pyrrolyl-, pyrazolyl-, and imidazolyl-acrylic acids and their esters are important precursors for the synthesis of physiologically active compounds. These observations led us to examine reactions of 1-(2,6-dichlorobenzoyl)pyrroles, -pyrazoles, and -imidazoles with palladium acetate and alkyl acrylates. The treatment of 1-(2,6-dichlorobenzoyl)pyrroles with palladium acetate and alkyl acrylates gave alkyl 3-(2-pyrrolyl)acrylates in high yields. The reaction of 1-(phenylsulfonyl)pyrrole (**10**) also gave alkenyl-substituted pyrroles. Furthermore, 1-(2,6-dichlorobenzoyl)pyrazoles reacted with palladium acetate and alkyl acrylates to give alkyl 3-(4-pyrazolyl)acrylates, while an attempted oxidative coupling of 1-(2,6-dichlorobenzoyl)imidazoles and methyl acrylate failed under our experimental conditions.

Results and Discussion

Although it was reported that the treatment of 1-methylpyrrole with styrene in the presence of palladium acetate gave small amounts of 2- and 3-styryl-1-methylpyrroles,[2] the reaction of 1-methyl- and 1-benzoylpyrroles with palladium acetate and methyl acrylate in acetic acid at reflux temperature gave complex

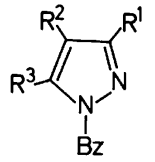

	R^1	R^2	R^3
13	H	H	H
14a	H	MeOCOCH=CH	H
14b	H	EtOCOCH=CH	H
15	Me	H	Me
16a	Me	MeOCOCH=CH	Me
16b	Me	EtOCOCH=CH	Me
17	H	Me	H
18a	H	Me	MeOCOCH=CH

Bz = 2,6-$Cl_2C_6H_3CO$

Fig. 2

	R	R^1	R^2	R^3	R^4
1	2,6-$Cl_2C_6H_3CO$	H	H	H	H
2a	2,6-$Cl_2C_6H_3CO$	MeOCOCH=CH	H	H	H
2b	2,6-$Cl_2C_6H_3CO$	EtOCOCH=CH	H	H	H
3a	2,6-$Cl_2C_6H_3CO$	MeOCOCH=CH	H	H	MeOCOCH=CH
3b	2,6-$Cl_2C_6H_3CO$	EtOCOCH=CH	H	H	EtOCOCH=CH
4	2,6-$Cl_2C_6H_3CO$	H	Me	MeCO	Me
5a	2,6-$Cl_2C_6H_3CO$	MeOCOCH=CH	Me	MeCO	Me
5b	2,6-$Cl_2C_6H_3CO$	EtOCOCH=CH	Me	MeCO	Me
6	2,6-$Cl_2C_6H_3CO$	H	H	H	OHC
7a	2,6-$Cl_2C_6H_3CO$	MeOCOCH=CH	H	H	OHC
7b	2,6-$Cl_2C_6H_3CO$	EtOCOCH=CH	H	H	OHC
8	2,6-$Cl_2C_6H_3CO$	Me	H	H	Me
9a	2,6-$Cl_2C_6H_3CO$	Me	MeOCOCH=CH	H	Me
9b	2,6-$Cl_2C_6H_3CO$	Me	EtOCOCH=CH	H	Me
10	$C_6H_5SO_2$	H	H	H	H
11b	$C_6H_5SO_2$	EtOCOCH=CH	H	H	H
12b	$C_6H_5SO_2$	EtOCOCH=CH	H	H	EtOCOCH=CH

Fig. 1

Table 1. Alkenylation of 1-(2,6-dichlorobenzoyl)- and 1-(phenylsulfonyl)pyrroles and of 1-(2,6-dichlorobenzoyl)pyrazoles with palladium acetate and alkyl acrylates[a)]

Substrate	CH_2=CHCOOR R	Reaction time h	Conversion %	Products Yield/%[b)]
1	Me	7	75	**2a**: 80; **3a**: 24
1	Et	18	81	**2b**: 76; **3b**: 25
2a	Me	18	67	**3a**: 71
4	Me	7	80	**5a**: 91
4	Et	18	97	**5b**: 85
6	Me	7	34	**7a**: 87
6	Et	14	44	**7b**: 66
8	Me	18	45	**9a**: 30
8	Et	18	45	**9b**: 26
10	Et	7	65	**11b**: 58; **12b**: 30
13	Me	7	29	**14a**: 93
13	Et	7	27	**14b**: 91
15	Me	7	15	**16a**: 61
15	Et	7	14	**16b**: 64
17	Me	7	14	**18a**: 59

a) The reaction was performed by heating an acetic acid solution (40 ml) of substrate (1 mmol), $Pd(OAc)_2$ (1 mmol), and alkyl acrylate (3 mmol) in air at reflux temperature. b) Yield based on the substrate consumed.

reaction mixtures. On the other hand, the treatment of 1-(2,6-dichlorobenzoyl)pyrrole (**1**) with methyl acrylate gave the expected coupling products (**2a**) and (**3a**) in almost quantitative yields based on palladium acetate used. Furthermore, the reaction of **2a** with methyl acrylate and palladium acetate gave **3a**, suggesting that **2a** is the intermediate in the formation of **3a** from **1**. The treatment of **1** with ethyl acrylate also gave the coupling products (**2b**) and (**3b**).

Substituent effects on the oxidative coupling of the pyrroles and alkyl acrylates were further investigated. The treatment of 3-acetyl-1-(2,6-dichlorobenzoyl)-2,4-dimethylpyrrole (**4**) with methyl acrylate and ethyl acrylate gave (**5a**) and (**5b**), respectively. Under similar conditions, 1-(2,6-dichlorobenzoyl)-2-formylpyrrole (**6**) gave (**7a**) and (**7b**), when treated with methyl acrylate and ethyl acrylate, respectively. The fact that the formyl group was transferred intact through the oxidation with palladium acetate was already reported in the case of dimerization[6)] and alkenylation with methyl acrylate[7)] of furfural and of 2-formylthiophenes. When the substrate was 2,5-disubstituted pyrrole such as 1-(2,6-dichlorobenzoyl)-2,5-dimethylpyrrole (**8**) β-alkenyl substituted products were obtained; the treatment of **8** with methyl acrylate and ethyl acrylate in the presence of palladium acetate gave (**9a**) and (**9b**), respectively, although the yields of **9a** and **9b** were not good.

Recently we reported the oxidative coupling of 1-(phenylsulfonyl)indole and olefins bearing electron-withdrawing groups by palladium acetate.[8)] Since the acylation of 1-(phenylsulfonyl)pyrrole (**10**) with acyl halides and Lewis acids has been reported,[9)] we carried out experiments on the oxidative coupling of **10** and ethyl acrylate. The reaction gave the expected coupling products (**11b**) and (**12b**).

In an effort to elucidate the scope of the oxidative coupling of aromatic heterocyles containing nitrogen atom and alkyl acrylates, the reactions of 1-(2,6-dichlorobenzoyl)pyrazoles and -imidazoles were investigated. The treatment of 1-(2,6-dichlorobenzoyl)pyrazole (**13**) with methyl acrylate and ethyl acrylate in the presence of palladium acetate gave 4-alkenyl-substituted pyrazoles (**14a**) and (**14b**), respectively. Similarly 1-(2,6-dichlorobenzoyl)-3,5-dimethylpyrazole (**15**) reacted with methyl acrylate and ethyl acrylate giving (**16a**) and (**16b**), respectively. On the other hand, the treatment of 1-(2,6-dichlorobenzoyl)-4-methylpyrazole (**17**) with methyl acrylate and palladium acetate gave a 5-alkenyl-substituted pyrazole (**18a**). These results are summarized in Table 1. However, no reaction occurred when the substrate was 1-(2,6-dichlorobenzoyl)-1*H*-indazole (**19**). The attempted oxidative coupling of the imidazoles such as 1-(2,6-dichlorobenzoyl)imidazole (**20**), 1-(2,6-dichlorobenzoyl)-2-methylimidazole (**21**), and 1-(2,6-dichlorobenzoyl)-2-phenyl-imidazole (**22**) and methyl acrylate failed either under our reaction conditions.

The structures of **1**—**22** except for the known compound (**10**)[10)] were determined on the basis of elemental analyses and spectral data. Furthermore, proton NMR spectra showed that all the coupling products have the E stereochemistry.

Table 1 shows an interesting fact that the presence of two methyl groups at the 3- and 5-positions of **15** decreased the conversions and yields of the alkenylation at the 4-position of the pyrazole, although methyl group is an electron-donating substituent. This fact may be interepreted in terms of steric effects. In order to elucidate the steric effects on the alkenylation with methyl acrylate, carboxylation reactions with carbon monoxide of methylbenzenes were also undertaken.

The treatment of *p*-xylene (**25**) under carbon mon-

oxide gave 2,5-dimethylbenzoic acid (**26**) and with methyl acrylate gave methyl 2,5-dimethylcinnamate (**27**). Hydrolysis of **27** gave 2,5-dimethylcinnamic acid (**28**), providing an evidence for the structure of **27**. Mesityrene (**29**) and pentamethylbenzene (**31**) also reacted with carbon monoxide to give 2,4,6-trimethylbenzoic acid (**30**) and pentamethylbenzoic acid (**32**), respectively. However, the reactions of **29** and **31** with methyl acrylate gave complex reaction mixtures under our reaction conditions, and no alkenyl-substituted benzenes such as methyl 2,4,6-trimethylcinnamate and methyl pentamethylcinnamate were obtained, although the oxidative coupling of **29** with styrene had been reported to proceed.[11]

The previous studies concerning the oxidative coupling of arenes and olefins[1] and the carboxylation of arenes with carbon monoxide[12,13] showed that the both reactions proceeded *via* the same intermediate, arylpalladium complex (**23**), as shown in Scheme 1. Therefore, the above results suggest that the formation of the intermediate **24** from **23** is affected by the steric effects of the two methyl groups at 2- and 6-positions of the benzene nucleus or at 3- and 5-positions of **15**, since Watanabe *et al.*[11] have reported that there is a steric hindrance in the transition state involving the palladium–carbon σ-bond on the coupling of styrene and alkylbenzene such as toluene, **25**, and **29**.

Palladium acetate-catalyzed reactions of **1** and **13** with methyl acrylate were carried out using AgOAc,[1] $Cu(OAc)_2$,[1] $Na_2S_2O_8$,[13] and $NaNO_2$[14] as re-oxidants. These results are summarized in Table 2.

It is known that the treatment of 1-substituted pyrazoles and 1-substituted pyrroles with butyllithium gives 1-substituted 5-lithiopyrazoles[15] and 1-substituted α-lithiopyrroles,[16] respectively. On the other hand, it was found that palladium acetate preferentially attacked the 4-position of the pyrazole nucleus, although the palladation of pyrroles occured at α-position of the pyrrole nucleus. The difference between lithiation and palladation of 1-substituted pyrazoles is of interest from the view point of synthetic chemistry utilizing metals.

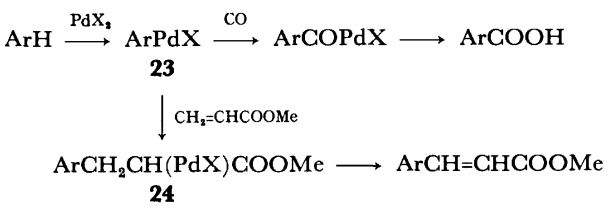

Scheme 1

Experimental

General. All the melting points are uncorrected. The elemental analyses were performed by the Analytical Center of Kyoto University. The infrared spectra were recorded with a JASCO IRA-1 spectrometer. The proton magnetic resonance spectra were recorded with a JEOL PMX60A spectrometer, using Me_4Si as the internal reference.

*Preparation of the Starting 1-(2,6-Dichlorobenzoyl)-Substituted Aromatic Heterocycles (**1**), (**4**), (**6**), (**8**), (**13**), (**15**), (**17**), (**19**), (**20**), (**21**), and (**22**).* To a stirred solution of 1*H*-aromatic heterocycle and sodium hydride in *N*,*N*-dimethylformamide (DMF), 2,6-dichlorobenzoyl chloride was added dropwise under nitrogen at 0 °C. Then the mixture was stirred at room temperature for 16 h and poured into an excess of ice-cooled water to give 1-(2,6-dichlorobenzoyl)-substituted aromatic heterocycle as a crystalline product, which was collected by suction and recrystallized from ether–hexane. These results are summarized in Table 3. The spectral and analytical data are given below.

*1-(2,6-Dichlorobenzoyl)pyrrole (**1**)*: Mp 121.5—122.5 °C; IR (Nujol) 1710 cm^{-1}; NMR ($CDCl_3$) δ=6.29 (t, 2H, J=3 Hz), 6.8—7.4 (broad, 2H), 7.33 (s, 3H). Found: C, 55.06; H, 2.91; N, 5.83%. Calcd for $C_{11}H_7NOCl_2$: C, 55.03; H, 2.94; N, 5.83%.

*3-Acetyl-1-(2,6-dichlorobenzoyl)-2,4-dimethylpyrrole (**4**)*: Mp 127.5—128.5 °C; IR (Nujol) 1720, 1675 cm^{-1}; NMR ($CDCl_3$) δ=2.11 (s, 3H), 2.44 (s, 3H), 2.80 (s, broad, 3H), 6.20 (s, broad, 1H), 7.30 (s, 3H); Mass: *m/z* (rel. intensity) 311 (12), 309 (19), 175 (61), 173 (100). Found: C, 57.94; H, 4.26; N, 4.43%. Calcd for $C_{15}H_{13}NO_2Cl_2$: C, 58.08; H, 4.22; N, 4.52%.

*1-(2,6-Dichlorobenzoyl)-2-formylpyrrole (**6**)*: Mp 125—126 °C; IR (Nujol) 1720, 1660 cm^{-1}; NMR ($CDCl_3$) δ=6.23 (t, 1H, J=3.5 Hz), 6.63—6.78 (m, 1H), 7.13—7.30 (m, 1H), 7.31 (s, 3H), 10.30 (s, 1H). Found: C, 53.56; H, 2.69; N, 5.21%. Calcd for $C_{12}H_7NO_2Cl_2$: C, 53.76; H, 2.63; N, 5.22%.

*1-(2,6-Dichlorobenzoyl)-2,5-dimethylpyrrole (**8**)*: Mp 102.5—104.0 °C; IR (Nujol) 1690 cm^{-1}; NMR ($CDCl_3$) δ=2.10 (s, broad, 6H), 6.83 (s, 2H), 7.30 (s, 3H); Mass: *m/z* (rel. intensity) 269 (16), 267 (25), 175 (64), 173 (100). Found: C, 58.19; H, 3.99; N,

Table 2. Palladium acetate-catalyzed alkenylation of **1** and of **13** with methyl acrylate and re-oxidants[a]

Substrate	Re-oxidant (mmol)	Products Yield/%[b]; Yield/%[c] (Conversion/%)
1	AgOAc (2)	**2a**: 534; 68(78), **3a**: 446; 29(78)
1	$Cu(OAc)_2$ (1)	**2a**: 444; 54(83), **3a**: 480; 29(83)
1	$Na_2S_2O_8$ (1)	**2a**: 586; 64(91), **3a**: 470; 26(91)
1	$NaNO_2$ (2)	**2a**: 386; 42(92), **3a**: 353; 19(92)
13	AgOAc (2)	**14a**: 93; 78(12)
13	$Cu(OAc)_2$ (1)	**14a**: 91; 88(11)
13	$Na_2S_2O_8$ (1)	**14a**: 98; 65(15)
13	$NaNO_2$ (1)	**14a**: 89; 71(13)

a) Reaction conditions used in all experiments: substrate (1 mmol), $Pd(OAc)_2$ (0.1 mmol), methyl acrylate (3 mmol), re-oxidant, acetic acid (40 ml), at reflux temperature in air, 16 h reaction. b) Yield based on $Pd(OAc)_2$ used. c) Yield based on the substrate consumed.

TABLE 3. SYNTHESIS OF 1-(2,6-DICHLOROBENZOYL)-SUBSTITUTED AROMATIC HETEROCYCLES FROM 1*H*-AROMATIC HETEROCYCLES

1*H*-Aromatic heterocycles (mmol)	NaH (mmol)	2,6-$Cl_2C_6H_3COCl$ (mmol)	DMF (ml)	Products (mmol; Yield/%[a])
Pyrrole (48)	48	48	200	**1** (37 mmol; 76%)
3-Acetyl-2,4-dimethylpyrrole (29)	29	29	150	**4** (23 mmol; 78%)
2-Formylpyrrole (52)	52	48	200	**6** (37 mmol; 71%)
2,5-Dimethylpyrrole (53)	53	48	200	**8** (10 mmol; 19%)
Pyrazole (59)	59	48	200	**13** (47 mmol; 79%)
3,5-Dimethylpyrazole (37)	37	37	150	**15** (29 mmol; 78%)
4-Methylpyrazole (18.3)	18.3	18.3	100	**17** (15 mmol; 81%)
Indazole (16.9)	16.9	14.6	100	**19** (15 mmol; 89%)
Imidazole (50)	50	48	200	**20** (28 mmol; 56%)
2-Methylimidazole (59.8)	58.8	47.8	200	**21** (36 mmol; 61%)
2-Phenylimidazole (31)	31	30.1	150	**22** (19 mmol; 62%)

a. Yields based on the 1H-aromatic heterocycles used.

5.05%. Calcd for $C_{13}H_{11}NOCl_2$: C, 58.23; H, 4.14; N, 5.22%.

*1-(2,6-Dichlorobenzoyl)pyrazole (**13**)*: Mp 118.5—119.5 °C; IR (Nujol) 1730 cm^{-1}; NMR ($CDCl_3$) δ=6.46 (d.d, 1H, J= 1 Hz, J=3 Hz), 7.29 (s, 3H), 7.66 (d, 1H, J=1 Hz), 8.30 (d, 1H, J=3 Hz), Found: C, 50.09; H, 2.41; N, 11.74%. Calcd for $C_{10}H_6N_2OCl_2$: C, 49.82; H, 2.51; N, 11.62%.

*1-(2,6-Dichlorobenzoyl)-3,5-dimethylpyrazole (**15**)*: Mp 169.5—170.0 °C; IR (Nujol) 1710—1700 (broad) cm^{-1}; NMR ($CDCl_3$) 2.14 (s, 3H), 2.68 (s, broad, 3H), 6.05 (s, broad, 1H), 7.33 (s, 3H). Found: C, 53.49; H, 3.65; N, 10.37%. Calcd for $C_{12}H_{10}N_2OCl_2$: C, 53.55; H, 3.75; N, 10.41%.

*1-(2,6-Dichlorobenzoyl)-4-methylpyrazole (**17**)*: Mp 165—166 °C; IR (Nujol) 1715—1700 (broad) cm^{-1}; NMR ($CDCl_3$) δ= 2.14 (d, 3H, J=1 Hz), 7.35 (s, 3H), 7.52 (s, 1H), 8.09 (q, 1H, J= 1 Hz). Found: C, 51.97; H, 3.09; N, 11.27%. Calcd for $C_{11}H_8N_2OCl_2$: C, 51.79; H, 3.16; N, 10.98%.

*1-(2,6-Dichlorobenzoyl)indazole (**19**)*: Mp 151.5—152.5 °C; IR (Nujol) 1690 cm^{-1}; NMR($CDCl_3$) δ=7.32 (s, 3H), 7.2—7.8 (m, 3H), 8.07 (s, 1H), 8.55 (broad, d, 1H, J=8 Hz). Found: C, 57.81; H, 2.67; N, 9.61%. Calcd for $C_{14}H_8N_2OCl_2$: C, 57.76; H, 2.77; N, 9.62%.

*1-(2,6-Dichlorobenzoyl)imidazole (**20**)*: Mp 60.5—61.5 °C; IR (KBr) 1730 cm^{-1}; NMR ($CDCl_3$) δ=7.06—7.20 (broad, 1H), 7.3—7.5 (broad, 4H), 7.76—7.9 (broad, 1H). Found: C, 49.73; H, 2.43; N, 11.65%. Calcd for $C_{10}H_6N_2OCl_2$: C, 49.82; H, 2.51; N, 11.62%.

*1-(2,6-Dichlorobenzoyl)-2-methylimidazole (**21**)*: Mp 120.5—121.0 °C; IR (Nujol) 1730 cm^{-1}; NMR ($CDCl_3$) δ=2.68 (s, 3H), 6.64—6.90 (m, 2H), 7.32(s, 3H). Found: C, 51.51; H, 3.32; N, 10.99%. Calcd for $C_{11}H_8N_2OCl_2$: C, 51.79; H, 3.16; N, 10.98%.

*1-(2,6-Dichlorobenzoyl)-2-phenylimidazole (**22**)*: Mp 102.5—104.0 °C; IR (Nujol) 1710 cm^{-1}; NMR ($CDCl_3$) δ=7.10—7.63 (m, 10H). Found: C, 60.39; H, 3.10; N, 8.73%. Calcd for $C_{16}H_{10}N_2OCl_2$: C, 60.59; H, 3.18; N, 8.83%.

*1-(Phenylsulfonyl)pyrrole (**10**).* To a stirred solution of pyrrole (149 mmol) and sodium hydride (149 mmol) in *N,N*-dimethylformamide (200 ml), benzenesulfonyl chloride (149 mmol) was added dropwise under nitrogen at 0 °C. Then the mixture was stirred at room temperature for 3 h and poured into an excess of ice-cooled water to give **10** (80.5 mmol; 54% yield based on pyrrole used): Mp 88—89 °C (lit,[8] 89.0—89.5 °C).

*General Procedure for the Stoichiometric Alkenylation of Pyrroles (**1**), (**2a**), (**4**), (**6**), (**8**), and (**10**), and Pyrazoles (**13**), (**15**), and (**17**) with palladium Acetate and Alkyl Acrylates.* A solution of the pyrroles or the pyrazoles (1 mmol), alkyl acrylates (3 mmol), and palladium acetate (1 mmol) in acetic acid (40 ml) was heated at reflux temperature in air. The reaction mixture was evaporated to give a brown residue which was then chromatographed on a silica-gel plate, developed by benzene or chloroform, to give alkyl 3-(2-pyrrolyl)- or 3-(4-pyrazolyl)acrylates. The results are summarized in Table 1. The spectral and analytical data are given below.

*Methyl (E)-3-[1-(2,6-Dichlorobenzoyl)-2-pyrrolyl]acrylate (**2a**)*: Mp 110.5—111.5 °C; IR (Nujol) 1720, 1700, 1630 cm^{-1}; NMR ($CDCl_3$) δ=3.79 (s, 3H), 6.23 (t, 1H, J=3.5 Hz), 6.27 (d, 1H, J=16 Hz), 6.5—6.9 (m, 2H), 7.35 (s, 3H), 8.45 (d, broad, 1H, J=16 Hz); Mass: *m/z* (rel. intensity) 325 (13), 323 (19), 175 (65), 173 (100). Found: C, 55.62; H, 3.46; N, 4.56%. Calcd for $C_{15}H_{11}NO_3Cl_2$: C, 55.58; H, 3.42; N, 4.32%.

*(E)-Ethyl 3-[1-(2,6-Dichlorobenzoyl)pyrrol-2-yl]acrylate (**2b**)*: Mp 133—134 °C; IR (Nujol) 1710, 1705, 1620 cm^{-1}; NMR ($CDCl_3$) δ=1.31 (t, 3H, J=7 Hz), 4.22 (q, 2H, J=7 Hz), 6.23 (t, 1H, J=3.5 Hz), 6.26 (d, 1H, J=16 Hz), 6.5—6.9 (m, 2H), 7.34 (s, 3H), 8.4 (d, broad, 1H, J=16 Hz); Mass: *m/z* (rel. intensity) 339 (7), 337 (11), 175 (65), 173 (100). Found: C, 56.74; H, 3.93; N, 4.19%. Calcd for $C_{16}H_{13}NO_3Cl_2$: C, 56.82; H, 3.87; N, 4.14%.

*Dimethyl (E,E)-3,3'-[1-(2,6-Dichlorobenzoyl)pyrrole-2,5-diyl]diacrylate (**3a**)*: Mp 166—168 °C; IR (Nujol) 1710 (broad), 1615 cm^{-1}; NMR ($CDCl_3$) δ=3.67 (s, 6H), 6.08 (d, 2H, J= 16 Hz), 6.63 (s, 2H), 7.30 (s, 3H), 7.50 (d, 2H, J=16 Hz). Mass: *m/z* (rel. intensity) 409 (8), 407 (12), 175 (65), 173 (100). Found: C, 56.15; H, 3.65; N, 3.42%. Calcd for $C_{19}H_{15}NO_5Cl_2$: C, 55.90; H, 3.70; N, 3.43%.

*Diethyl (E,E)-3,3'-[1-(2,6-Dichlorobenzoyl)pyrrole-2,5-diyl]diacrylate (**3b**)*: Mp 153—154 °C; IR (Nujol) 1710 (broad), 1615 cm^{-1}; NMR ($CDCl_3$) δ=1.28 (t, 6H, J=7 Hz), 4.14 (q, 4H, J=7 Hz), 6.13 (d, 2H, J=16 Hz), 6.68 (s, 2H), 7.37 (s, 3H), 7.53 (d, 2H, J=16 Hz); Mass: 437 (5), 435 (7), 175 (63), 173 (100). Found: C, 58.07; H, 4.47; N, 3.41%. Calcd for $C_{21}H_{19}NO_5Cl_2$: C, 57.81; H, 4.39; N, 3.21%.

*Methyl (E)-3-[4-Acetyl-1-(2,6-dichlorobenzoyl)-3,5-dimethyl-2-pyrrolyl]acrylate (**5a**)*: Mp 121—123 °C; IR (Nujol) 1720, 1660 1625 cm^{-1}; NMR ($CDCl_3$) δ=2.21 (s, 3H), 2.48 (s, 3H), 2.53 (s, 3H), 3.65 (s, 3H), 5.68 (d, 1H, J=16 Hz), 7.18 (d, 1H, J= 16 Hz), 7.30 (s, 3H); Mass: *m/z* (rel. intensity) 395 (9), 393 (14), 175 (63), 173 (100). Found: C, 57.59; H, 4.63; 3.70%. Calcd for $C_{19}H_{17}NO_4Cl_2$: C, 57.88; H, 4.35; N, 3.55%.

*Ethyl (E)-3-[4-Acetyl-1-(2,6-dichlorobenzoyl)-3,5-dimethyl-2-pyrrolyl]acrylate (**5b**)*: Mp 114—116 °C; IR (Nujol) 1710 (broad),

1660, 1625 cm^{-1}; NMR ($CDCl_3$) δ=1.26 (t, 3H, J=7 Hz), 2.22 (s, 3H), 2.50 (s, 3H), 2.56 (s, 3H), 4.12 (q, 2H, J=7 Hz), 5.68 (d, 1H, J=16 Hz), 7.16 (d, 1H, J=16 Hz), 7.33 (s, 3H); Mass: m/z (rel. intensity) 409 (8), 407 (13), 175 (63), 173 (100). Found: C, 58.65; H, 4.71; N, 3.20%. Calcd for $C_{20}H_{19}NO_4Cl_2$: C, 58.84; H, 4.69; N, 3.43%.

*Methyl (E)-3-[1-(2,6-Dichlorobenzoyl)-5-formyl-2-pyrrolyl]acrylate (**7a**)*: Mp 182.0—183.5 °C; IR (Nujol) 1720, 1705, 1675, 1630 cm^{-1}; NMR ($CDCl_3$) δ=3.70 (s, 3H), 6.19 (d, 1H, J=16 Hz), 6.65 (d, 1H, J=3.5 Hz), 7.10—7.55 (m, 2H), 7.33 (s, 3H), 9.72 (s, 1H); Mass: m/z (rel. intensity) 353 (4), 351 (6), 175 (62), 173 (100). Found: C, 54.67; H, 3.06; N, 4.12%. Calcd for $C_{16}H_{11}NO_4Cl_2$: C, 54.41; H, 3.14; N, 3.97%.

*Ethyl (E)-3-[1-(2,6-Dichlorobenzoyl)-5-formyl-2-pyrrolyl]acrylate (**7b**)*: Mp 145—147 °C; IR (Nujol) 1710 (broad), 1675, 1630 cm^{-1}; NMR ($CDCl_3$) δ=1.26 (t, 3H, J=7 Hz), 4.13 (q, 2H, J=7 Hz), 6.20 (d, 1H, J=16 Hz), 6.63 (d, 1H, J=3.5 Hz), 7.06—7.53 (m, 2H), 7.33 (s, 3H), 9.73(s, 1H); Mass: m/z (rel. intensity) 367 (4), 365 (6), 175 (64), 173 (100). Found: C, 55.56; H, 3.50; N, 3.89%. Calcd for $C_{17}H_{13}NO_4Cl_2$: C, 55.61; H, 3.57; N, 3.81%.

*Methyl (E)-3-[1-(2,6-Dichlorobenzoyl)-2,5-dimethyl-3-pyrrolyl]acrylate (**9a**)*: Mp 117—118 °C; IR (Nujol) 1725, 1700, 1635 cm^{-1}; NMR ($CDCl_3$) δ=2.07 (s, broad, 3H), 2.26 (s, broad, 3H), 3.76 (s, 3H), 6.05 (d, 1H, J=16 Hz), 6.14 (s, 1H), 7.33 (s, 3H), 7.60 (d, 1H, J=16 Hz); Mass: m/z (rel. intensity) 353 (11), 351 (17), 175 (65), 173 (100). Found: C, 58.14; H, 4.43; N, 3.96%. Calcd for $C_{17}H_{15}NO_3Cl_2$: C, 57.92; H, 4.29; N, 3.98%.

*Ethyl (E)-3-[1-(2,6-Dichlorobenzoyl)-2,5-dimethyl-3-pyrrolyl]acrylate (**9b**)*: Mp 126.5—127.5 °C; IR (Nujol) 1715, 1635 cm^{-1}; NMR ($CDCl_3$) δ=1.30 (t, 3H, J=7 Hz), 2.07 (s, broad, 3H), 2.25 (s, broad, 3H), 4.23 (q, 2H, J=7 Hz), 6.05 (d, 1H, J=16 Hz), 6.14 (s, 1H), 7.35 (s, 3H), 7.58 (d, 1H, J=16 Hz); Mass: m/z (rel. intensity) 367 (12), 365 (17), 175 (65), 173 (100). Found: C, 58.77; H, 4.73; N, 3.76%. Calcd for $C_{18}H_{17}NO_3Cl_2$: C, 59.03; H, 4.68; N, 3.82%.

*Ethyl (E)-3-[1-(Phenylsulfonyl)-2-pyrrolyl]acrylate (**11b**)*: Mp 78—79 °C; IR (Nujol) 1705, 1625, 1370, 1185 (broad) cm^{-1}; NMR ($CDCl_3$) δ=1.32 (t, 3H, J=7 Hz), 4.24 (q, 2H, J=7 Hz), 6.12 (d, 1H, J=16 Hz), 6.35 (t, 1H, J=3.5 Hz), 6.4—6.8 (m, 1H), 7.2—7.9 (m, 6H), 8.07 (d, 1H, J=16 Hz); Mass: m/z (rel. intensity) 305 (33), 141 (25), 136 (26), 119 (47), 77 (100). Found: C, 58.90; H, 4.83; N, 4.59%. Calcd for $C_{15}H_{15}NO_4S$: C, 59.00; H, 4.95; N, 4.89%.

*Diethyl (E,E)-3,3'-[1-(Phenylsulfonyl)pyrrole-2,5-diyl]diacrylate (**12b**)*: Mp 85—86 °C; IR (Nujol) 1705, 1620, 1380, 1370, 1175 (broad) cm^{-1}; NMR ($CDCl_3$) δ=1.32 (t, 6H, J=7 Hz), 4.25 (q, 4H, J=7 Hz), 6.16 (d, 2H, J=16 Hz), 6.64 (s, 2H), 7.2—8.0 (m, 5H), 8.24 (d, 2H, J=16 Hz); Mass: m/z (rel. intensity) 404 (25), 403 (100), 262 (63). Found: C, 59.54; H, 5.25; N, 3.56%. Calcd for $C_{20}H_{21}NO_6S$: C, 59.57; H, 5.25; N, 3.47%.

*Methyl (E)-3-[1-(2,6-Dichlorobenzoyl)-4-pyrazolyl]acrylate (**14a**)*: Mp 164—166 °C; IR (Nujol) 1730, 1700, 1660 cm^{-1}; NMR ($CDCl_3$) δ=3.75 (s, 3H), 6.27 (d, 1H, J=16 Hz), 7.32 (s, 3H), 7.52 (d, 1H, J=16 Hz), 7.82 (s, 1H), 8.42 (s, 1H); Mass: m/z (rel. intensity) 326 (6), 324 (8), 291 (10), 289 (28), 175 (66), 173 (100). Found: C, 51.85; H, 2.91; N, 8.56%. Calcd for $C_{14}H_{10}N_2O_3Cl_2$: C, 51.72; H, 3.10; N, 8.62%.

*Ethyl (E)-3-[1-(2,6-Dichlorobenzoyl)-4-pyrazolyl]acrylate (**14b**)*: Mp 133—134 °C; IR (KBr) 1725, 1695, 1660, 1620 cm^{-1}; NMR ($CDCl_3$) δ=1.33 (t, 3H, J=7 Hz), 4.27 (q, 2H, J=7 Hz), 6.32 (d, 1H, J=16 Hz), 7.38 (s, 3H), 7.58 (d, 1H, J=16 Hz), 7.89 (s, 1H), 8.49 (s, 1H); Mass: m/z (rel. intensity) 340 (6), 338 (9), 305 (11), 303 (32), 175 (63), 173 (100). Found: C, 53.32; H, 3.49; N, 8.14%. Calcd for $C_{15}H_{12}N_2O_3Cl_2$: C, 53.12; H, 3.57; N, 8.26%.

*Methyl (E)-3-[1-(2,6-Dichlorobenzoyl)-3,5-dimethyl-4-pyrazolyl]acrylate (**16a**)*: Mp 176—178 °C; IR (KBr) 1725, 1705, 1660, 1620 cm^{-1}; NMR ($CDCl_3$) δ=2.28 (s, 3H), 2.80 (s, 3H), 3.79 (s, 3H), 6.20 (d, 1H, J=16 Hz), 7.32 (s, 3H), 7.62 (d, 1H, J=16 Hz); Mass: m/z (rel. intensity) 354 (7), 352 (10), 319 (17), 317 (49), 175 (65), 173 (100). Found: C, 54.33; H, 3.89; N, 7.80%. Calcd for $C_{16}H_{14}N_2O_3Cl_2$: C, 54.40; H, 4.00; N, 7.93%.

*Ethyl (E)-3-[1-(2,6-Dichlorobenzoyl)-3,5-dimethyl-4-pyrazolyl]acrylate (**16b**)*: Mp 161—163 °C; IR (KBr) 1725, 1710, 1660, 1620 cm^{-1}; NMR ($CDCl_3$) δ=1.32 (t, 3H, J=7 Hz), 2.27 (s, 3H), 2.81 (s, 3H), 4.27 (q, 2H, J=7 Hz), 6.21 (d, 1H, J=16 Hz), 7.33 (s, 3H), 7.62 (d, 1H, J=16 Hz); Mass: m/z (rel. intensity) 368 (10), 366 (14), 333 (25), 331 (69), 175 (65), 173 (100). Found: C, 55.77; H, 4.37; N, 7.52%. Calcd for $C_{17}H_{16}N_2O_3Cl_2$: C, 55.60; H, 4.39; N, 7.63%.

*Methyl (E)-3-[2-(2,6-Dichlorobenzoyl)-4-methyl-2H-pyrazol-3-yl]acrylate (**18a**)*: Mp 161—162 °C; IR (Nujol) 1730—1710 (broad), 1660 cm^{-1}; NMR($CDCl_3$) δ=2.24 (s,3H), 3.83 (s, 3H), 6.30 (d, 1H, J=16 Hz), 7.33 (s, 3H), 7.52 (s, 1H), 8.40 (d, 1H, J=16 Hz); Mass: m/z (rel. intensity) 340 (10), 338 (14), 305 (9), 303(25), 175 (64), 173 (100); High-resolution Mass: m/z 338.0206 (M^+). Found: C, 52.62; H, 3.46; N, 8.21%. Calcd for $C_{15}H_{12}N_2O_3Cl_2$: C, 53.12; H, 3.57; N, 8.26%.

*Palladium Acetate-catalyzed Alkenylation of **1** and of **13** with Methyl Acrylate.* A solution of **1** or **13** (1 mmol), methyl acrylate (3 mmol), re-oxidants (listed in Table 2), and palladium acetate (0.1 mmol) in acetic acid (40 ml) was heated at reflux temperature in air for 16 h. The reaction mixture was evaporated to give a brown residue which was chromatographed on a silica-gel plate, developed by benzene or chloroform, to give alkenyl-substituted pyrroles (**2a**) and (**3a**) and pyrazole (**14a**). The results are summarized in Table 2.

Carboxylation of Methylbenzenes with Carbon Monoxide and Palladium Acetate. Carbon monoxide was bubbled through the stirred solution of methylbenzenes (10 mmol) in acetic acid (40 ml) containing palladium acetate (1 mmol) at reflux temperature for 7 h. The reaction mixture was evaporated and chromatorgaphed on a silica-gel column with benzene/ether to give methylbenzoic acids: 2,5-dimethylbenzoic acid (**26**) (0.16 mmol, 16% yield based on palladium acetate used); 2,4,6-trimethylbenzoic acid (**30**) (0.43 mmol, 43% yield); pentamethylbenzoic acid (**32**) (0.21 mmol, 21% yield): Mp 207—210 °C (lit,[17] 211 °C); IR (Nujol) 3300—2300, 1700 cm^{-1}; NMR ($CDCl_3$) δ=2.19 (s, broad, 9H), 2.27 (s, broad, 6H), 10.0 (s, broad, 1H). The structures of **26** and **30** were confirmed by comparing the IR spectra with those of the commercially available samples.

*Methyl (E)-2,5-Dimethylcinnamate (**27**).* A solution of *p*-xylene (**25**) (10 mmol), methyl acrylate (3 mmol), and palladium acetate (1 mmol) in acetic acid (40 ml) was stirred at reflux temperature in air for 7 h. The mixture was evaporated to give a brown residue which was chromatographed on a silica-gel plate, developed by a mixture of hexane and ether (1:1) to give **27** (0.50 mmol, 50% yield based on palladium acetate used): Bp 100 °C/10 Torr. (1 Torr=133.322 Pa); IR (Nujol) 1745, 1725, 1640 cm^{-1}; NMR($CDCl_3$) δ=2.32 (s, 3H), 2.36 (s, 3H), 3.78 (s, 3H), 6.29 (d, 1H, J=16 Hz), 7.00—7.35 (m, 3H), 3H), 7.91 (d, 1H, J=16 Hz). Found: C, 75.53; H, 7.63%. Calcd for $C_{12}H_{14}O_2$: C, 75.76; H, 7.42%.

(E)-2,5-Dimethylcinnamic Acid (28). A solution of **27** (1.85 mmol) and sodium hydroxide (52.5 mmol) in a mixture of methanol (50 ml) and water (50 ml) was heated at reflux temperature in air for 7 h. The mixture was poured into an excess of ice-cooled water and neutralized with dilute hydrochloric acid to give **28** as a crystalline product (1.70 mmol, 92% yield): Mp 130—132°C; IR (Nujol) 1690, 1620, 1610 cm^{-1}; NMR ($CDCl_3$) δ=2.32 (s, 3H), 2.39 (s, 3H), 6.32 (d, 1H, J=16 Hz), 7.06 (s, broad, 2H), 7.35 (s, broad, 1H), 8.03 (d, 1H, J=16 Hz), 10.14 (s, broad, 1H). Found: C, 74.97; H, 6.86%. Calcd for $C_{11}H_{12}O_2$: C, 74.72; H, 6.87%.

The authors wish to thank Professors Tsunao Hase and Tsutomu Sakakibara of Kagoshima University for their support throughout the study, and Dr. Tetsuo Iwagawa for his mass-spectrometric analyses.

References

1) For a review; I. Moritani and Y. Fujiwara, *Synthesis*, **1973**, 524.
2) R. Asano, I. Moritani, Y. Fujiwara, and S. Teranishi, *Bull. Chem. Soc. Jpn.*, **46**, 663 (1973).
3) Y. Fujiwara, O. Maruyama, M. Yoshidomi, and H. Taniguchi, *J. Org. Chem.*, **46**, 851 (1981).
4) T. Itahara, M. Ikeda, and T. Sakakibara, *J. Chem. Soc., Perkin Trans. 1*, **1983**, 1361.
5) T. Itahara, *J. Chem. Soc., Chem. Commun.*, **1981**, 254.
6) T. Itahara, M. Hashimoto, and H. Yumisashi, *Synthesis*, **1984**, 255.
7) T. Itahara and F. Ouseto, *Synthesis*, **1984**, 488.
8) T. Itahara, K. Kawasaki, and F. Ouseto, *Synthesis*, **1984**, 236.
9) R. X. Xu, H. J. Anderson, N. J. Gogan, C. E. Loader, and R. McDonald, *Tetrahedron Lett.*, **1981**, 4899; J. Rokach, P. Hamel, and M. Kakushima, *Tetrahedron Lett.*, **1981**, 4901.
10) E. P. papadopoulos and N. F. Haider, *Tetrahedron Lett.*, **1968**, 1721.
11) M. Watanabe, M. Yamamura, I. Moritani, Y. Fujiwara, and A. Sonoda, *Bull. Chem. Soc. Jpn.*, **47**, 1035 (1974).
12) P. M. Henry, *Tetrahedron Lett.*, **1968**, 2285; Ger. Pat. Dos 2340592; Y. Fujiwara, T. Kawauchi, and H. Taniguchi, *J. Chem. Soc., Chem. Commun.*, **1980**, 220; Y. Fujiwara, I. Kawata, H. Sugimoto, and H. Taniguchi, *J. Organomet. Chem.*, **256**, C35 (1983).
13) T. Itahara, *Chem. Ind. (London)* **1982**, 599.
14) T. Tisue and W. J. Downs, *J. Chem. Soc., Chem. Commun.*, **1969**, 410; P. M. Henry, *J. Org. Chem.*, **36**, 1886 (1971); R. O. C. Norman, W. J. E. Parr, and C. B. Thomas, *J. Chem. Soc., Perkin Trans. 1*, **1974**, 369.
15) P. W. Alley and D. A. Shirley, *J. Am. Chem. Soc.*, **80**, 6271, (1958); R. Huttel and M. E. Schön, *Justus Liebigs Ann. Chem.*, **625**, 55 (1959); D. E. Butler and S. M. Alexander, *J. Org. Chem.*, **37**, 215 (1972).
16) D. A. Shirley, B. H. Gross, and P. A. Roussel, *J. Org. Chem.*, **20**, 225 (1955); D. J. Chadwick and C. Willbe, *J. Chem. Soc., Perkin Trans. 1*, **1977**, 887; D. J. Chadwick and I. A. Cliffe, *J. Chem. Soc., Perkin Trans. 1*, **1979**, 2845; D. J. Chadwick and S. T. Hodgson, *J. Chem. Soc., Perkin Trans. 1*, **1982**, 1833.
17) O. Jacobson, *Ber.*, **19**, 1214 (1886).

 © 1984 The Chemical Society of Japan Bull. Chem. Soc. Jpn., 57, 3494—3506 (1984) [Vol. 57, No. 12

Syntheses and Physical Properties of Several Polyphenylenes Containing Mixed Linkages[1)]

Yasuhiro FUJIOKA
Kyoto Pharmaceutical University, Misasagi-nakauchi-cho, Yamashina-ku, Kyoto 607
(Received May 12, 1984)

Fourteen macrocyclic polyphenylenes, including the following ten new compounds, were synthesized by intra- or intermolecular homo-coupling of di-Grignard compound and by cross-coupling of two kinds of di-Grignard compounds with copper(II) chloride: *m,m,o,p,o*-pentaphenylene; *o,o,p,o,o,p*-, *m,o,p,m,o,p*-, *o,p,o,p,o,p*-, *m,o,p,o,p,o*-, *m,o,m,o,m,o*-, and *m,m,m,o,m,o*-hexaphenylene; *m,o,p,p,o,m,p*-, and *m,m,m,m,p,o,p*-heptaphenylene; and *m,o,o,m,o,o,m,o,o,m,o,o*-dodecaphenylene. ^{1}H NMR spectra of the polyphenylenes, compared with those of open-chain analogues, provide valuable information on the nonplanar spacial relationship of constituting phenylene rings. UV spectra of the compounds containing *p*-phenylene ring(s) suggest that the lack or decrease in intensity of K-band above *ca.* 260 nm or a marked shift of that band provides useful conformational information. Empirical Hückel molecular orbital calculations of longest-wavelength absorption bands of twelve polyphenylenes were also carried out. The calculations furnish additional bases for their conformational aspects deduced from their spectral data and Dreiding stereomodels. IR spectra indicate that lack of intense band(s) near 700 cm^{-1} may generally be regarded as a piece of plausible evidence for the macrocyclic structure containing no *m*-phenylene ring. Stabilities of the polyphenylenes to electron bombardment are also discussed.

In our previous studies[2)] a series of closely related linear and branched polyphenyls was synthesized and the relationship was discussed between the number and arrangement of benzene rings and physical properties including IR, UV, and ^{1}H NMR spectral characteristics. In addition, empirical Hückel molecular orbital (HMO) calculations were performed of longest-wavelength absorption bands of forty-two linear polyphenyls. The results indicated that the common parameters (cos θ and β) used might successfully apply to linear polyphenyls. In connection with these works on polyphenyls, I was much interested in studying syntheses of macrocyclic polyphenylenes in which both terminal rings of polyphenyls are linked to each other so that the rotation of pivot bonds is restricted significantly because of their rigid geometry.

Previously, syntheses and properties of several polyphenylenes have been reported by Rapson *et al.*[3)] and Wittig *et al.*[4)] for the *o*-series and by Staab *et al.*[5)] for the *m*-series from the viewpoint of transannular π-electronic interactions in macrocyclic systems. Recently, some of their heterocyclic analogues have also been prepared by Kauffmann.[6)] In addition, Vögtle *et al.*[7)] have synthesized helical compounds which are clamped by methylenes or other bridges at the ends of a linear polyphenyl chain. Nevertheless, only a few polyphenylenes consisting of mixed phenylene linkages have so far been reported.[8)]

The present study was undertaken to synthesize hitherto unknown polyphenylenes consisting of all of three or two kinds of phenylene linkages, and to investigate their spectral characteristics attributable to their macrocyclic structures. Their IR, UV, ^{1}H NMR, and mass (MS) spectra have been measured. By comparing data with those of open-chain analogues, restricted rotation of pivot bonds caused by the rigid geometry, π-electronic interactions, and other conformational problems have been discussed. Further, HMO calculations of longest-wavelength absorption bands of polyphenylenes have been performed to obtain additional valuable information about their conformational aspects.

Results and Discussion

Syntheses. The earlier reactions used for the preparation of polyphenylenes are based mainly on the following reactions: 1) Homo-coupling of di-Grignard compounds with copper(II) or cobalt(II) chloride,[3a,5)] 2) homo-coupling of dilithium aromatics with transition metal halides,[4,9)] and 3) Ullmann homo-coupling of appropriate diiodo compounds.[8b,10)] In the present work, reaction 1 has been adopted because of the facile preparation of the starting and intermediate materials, as well as of the facile isolation of polyphenylenes from several by-products. Thus eleven polyphenylenes (**1**—**11**) (Chart 1), including nine hitherto unknown compounds, were synthesized by the intra- or intermolecular homo-coupling of di-Grignard compound or by cross-coupling of two kinds of di-Grignard compounds, with copper(II) chloride.

The key intermediate dibromo compounds were prepared as follows: First, the following six intermediate dinitroterphenyls were prepared by the Ullmann cross-coupling of *o*- or *m*-diiodobenzene (**15** or **16**) and 2-chloro- or 3-iodonitrobenzene (**17** or **18**), and of 4-iodo-2′- or 4-iodo-3′-nitrobiphenyl (**19** or **20**) and **17** or **18**: 3,3″-dinitro-*o*-(**21a**), 2,2″-dinitro-*m*-(**22a**), and 3,3″-dinitro-*m*-terphenyl (**23a**), and 2,2″-(**24a**), 2,3″-(**25a**), and 3,3″-dinitro-*p*-terphenyl (**26a**). The dinitro compounds (**21a**—**26a**) thus obtained were reduced to the corresponding diamino compounds (**21b**—**26b**) with activated iron in hot benzene, and then converted into dibromoterphenyls (**21c**—**26c**) by the Sandmeyer

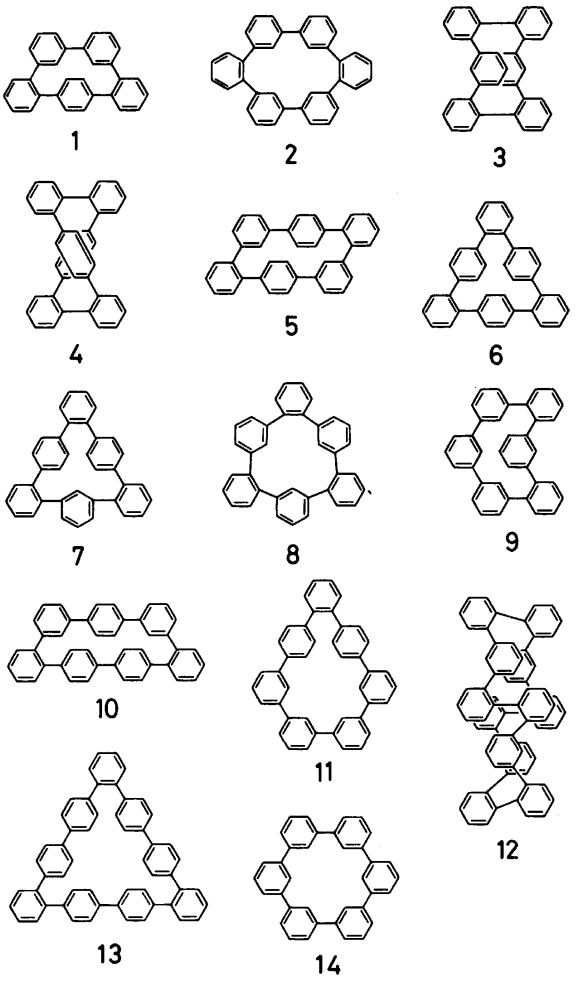

Chart 1.

reaction. Similarly, the dinitroquinquephenyls (2,2″-bis(3-nitrophenyl)-*p*-(**27a**) and 4,4″-bis(3-nitrophenyl)-*o*-terphenyl (**28a**)), obtained by the Ullmann cross-coupling of **18** and 2,2″-diiodo-*p*-(**24d**) or 4,4″-diiodo-*o*-terphenyl, were converted into the dibromo compounds (**27c** and **28c**) *via* the corresponding diamines (**27b** and **28b**). Analogously, 2,2‴-dibromo-*p*-quaterphenyl (**29c**) and 3,3′-dibromobiphenyl (**30c**) were prepared by the Sandmeyer reaction of the corresponding diamines, whereas only 4,4″-dibromo-*o*-terphenyl (**31c**) was obtained by direct bromination of *o*-terphenyl.

For the synthesis of polyphenylene **1**, three methods have primarily been applied (Scheme 1). Thus, the intramolecular homo-coupling of the di-Grignard compound derived from **27c** with anhydrous copper(II) chloride in a tetrahydrofuran (THF)–benzene (1 : 1, v/v) mixture (method A), gave macrocyclic pentaphenylene

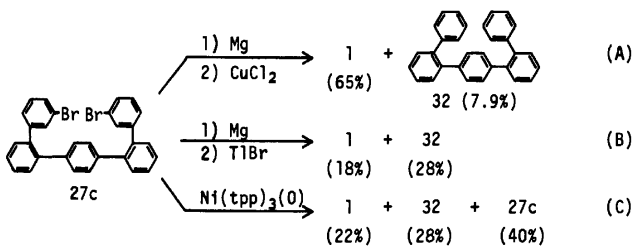

Scheme 1.

(**1**) in a fairly good yield (65%) with its open-chain analogue (2,2″-diphenyl-*p*-terphenyl (**32**), 7.9%). The coupling of the same di-Grignard compound with thallium(I) bromide (method B)[11] and that of **27c** with tris(triphenylphosphine)nickel(0)[12] (method C) afforded **1** only in low yields (18 and 22%, respectively), with predominant formation of **32** accompanied.

On the basis of these results, method A was adopted for the preparation of the remaining ten polyphenylenes (**2**—**11**). Thus, each of **2**—**5** was prepared by the intermolecular homo-coupling reaction of the di-Grignard compound derived from each of dibromides (**21c**, **22c**, **24c**, and **25c**) with anhydrous copper(II) chloride according to the reaction

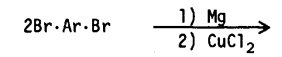

while each of **6**—**11** was obtained by the intermolecular cross-coupling of two kinds of di-Grignard compounds derived from each of dibromides (**21c**—**24c**, **26c**, and **28c**—**31c**) according to the reaction

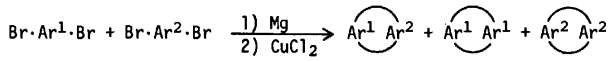

The yields of desired polyphenylenes and of other macrocyclic compounds, obtained as by-products, are given in Table 1.

The polyphenylenes **1**—**14**, thus prepared, gave satisfactory analytical results and spectral (IR and MS) data consistent with their proposed structures. Of these polyphenylenes, alternative syntheses of four species have been reported earlier by other workers (**2**,[8c] **3**,[8b] **13**,[8a] and **14**[5b]). The melting points and spectral data of these compounds except **2**[13] are practically consistent with those of previous authors.

In contrast to the yield of **1** (65%), those of the intermolecular homo-coupling products **2**—**5** were rather low (14—16%). Furthermore, the yields of the intermolecular cross-coupling products, except that of **6** (16%), were low (2.3—5.1%) as expected, presumably due to the competitive homo-coupling of each of the reactants and to more or less hindered conformations of the polyphenylenes. Indeed, in the preparations of **6**—**9** and **11**, one or two reasonable homo-coupled

Table 1. Syntheses of polyphenylenes

Reactants	Polyphenylene (Yield/%)	Other polyphenylenes (Yield/%)
27c	**1** (65)	—
21c	**2** (16)	—
22c	**3** (14)	**12** (1.3)
24c	**4** (13)	—
25c	**5** (14)	—
24c+**31c**	**6** (16)	**13** (4.5)
22c+**31c**	**7** (4.5)	**3** (6.5), **13** (2.6)
21c+**22c**	**8** (2.3)	**2** (3.3), **3** (4.4)
22c+**23c**	**9** (3.3)	**3** (4.9), **14** (4.1)
26c+**29c**	**10** (5.0)	—
28c+**30c**	**11** (5.1)	**14** (2.9)

polyphenylenes (**2**, **3**, **13**, and **14**) were isolated in yields of 2.6—6.5%. Beside these, macrocyclic dodecaphenylene (**12**), a tetramer of the reactant, was obtained. In spite of the low yields of the polyphenylenes, most of them were isolated rather with ease from a complex mixture of by-products[14] because of their sparing solubilities and distinguishable crystal forms.

Most of the polyphenylenes melt at much higher temperatures than the open-chain analogues,[15] and the rise in their melting points may be ascribed to the rigid geometry caused by their endless macrocyclic structures.

In the preparations of **3** and **8**, formation of two atropisomers were expected. However, only one compound in each, presumably having a centro-symmetrical conformation on the basis of spectral data to be described later, was isolated. Although the polyphenylene **4** would be a racemate, no identification of antipodes by resolution was attempted.

Physical Properties. *IR Spectra*: The IR spectra of the polyphenylenes **1**—**14** were measured by the KBr-disk method. All the polyphenylenes commonly give the following absorptions: A group of prominent bands due to C–H out-of-plane deformation vibrations in the 675—920 cm^{-1} region; intense bands due to C–C out-of-plane deformation vibrations in the fairly narrow region of 685—715 cm^{-1} (except for **4**, **6**, and **13**); medium bands due to C–C in-plane deformation vibrations near 1000 cm^{-1}; and weak bands due to C–H in-plane deformation vibrations in the 975—1350 cm^{-1} region. In addition, groups of medium bands due to C–C stretching vibrations and weak bands due to aromatic C–H stretching vibrations in the 1350—1600 and 3000—3100 cm^{-1} regions, respectively, are observed.

It has already been known that the prominent bands in the 675—920 cm^{-1} region of the linear polyphenyls are correlated closely to the substitution patterns of the benzene rings comprising each of the compounds.[2,16] A precise examination of the characteristic bands of the polyphenylenes in the same region, has proved that the assignments of the bands generalized for the polyphenyls may also apply to the macrocyclic polyphenylenes. Thus, the prominent bands of the polyphenylenes in the 675—920 cm^{-1} region correspond to the kinds of phenylene rings constituting each of the polyphenylenes as shown in Table 2.

Of the spectra of the fourteen polyphenylenes, those of **1**—**3**, **5**, **7**—**12**, and **14**, which contain *m*-phenylene ring(s), show without exception the strong C–C out-of-plane deformation vibration bands due to *m*-phenylene ring in the narrow range of 704—713 cm^{-1}, whereas those of remaining **4**, **6**, and **13**, which have no *m*-phenylene ring, do not show any analogous intense bands. Concerning these bands of polyphenyls, Stewart and Hellmann[16a] have pointed out that the strong bands due to the C–C out-of-plane bending vibrations near 700 cm^{-1} are characteristic of phenyl and *m*-phenylene rings, whereas the bands corresponding to the *o*- and *p*-phenylene rings are forbidden in IR. The above results, therefore, suggest that the lack of intense bands near 700 cm^{-1} with macrocyclic polyphenylenes may generally be regarded as a piece of plausible evidence for the macrocyclic structure containing no *m*-phenylene ring.

^1H NMR Spectra: The ^1H NMR spectra of the polyphenylenes **1**—**13** were measured at 200 and 80 MHz in $CDCl_3$ solution, and the chemical shifts from tetramethylsilane are summarized in Table 3.

The isolated *m*-phenylene proton signals of **1**, **5**, and **10** (δ=6.61—6.63, 6.23—6.26, and 6.50—6.53, respectively) are observed at much higher fields (by *ca.* 1.18, 1.56, and 1.29 ppm) than that of *m*-terphenyl (δ=7.78—7.83, m).[2e] The remarkable high-field shifts may reflect the anisotropic effects caused by the *p*-phenylene ring on which the isolated *m*-phenylene protons are located. On the other hand, the *p*-phenylene proton signals are found at higher field in **1** (0.43 ppm) and at much higher field in **5** (0.70 ppm) than that of *p*-terphenyl (δ=7.68, s),[2a,e] owing to the anisotropic effect of the inclined *m*-phenylene rings in **1** and **5** and an additional effect of the parallel *p*-phenylene rings in **5**. The analogous high-field shifts of the *p*-phenylene proton signals of **10** can also be explained in terms of the anisotropic effect similar to that described above. The foregoing considerations are fully substantiated by inspection of the Dreiding stereomodels.

The two *p*-phenylene rings of **4** are forced to face-to-face arrangement,[17] analogously to the *m*-phenylene rings of **3**.[8b] The *p*-phenylene proton signals (δ=6.68 and 6.90) of **4** are remarkably shifted toward high field (by *ca.* 1.00 and 0.78 ppm) relative to that of *p*-terphenyl (δ=7.68). This corresponds to the behavior of phenylene protons observed in [2.2]paracyclophane,[18] 4,4‴-dimethylene-*o*-quaterphenylophane,[7a] and a cyclic pyrazole analogue of **4**,[17b] and the marked high-field shift of **4** undoubtedly reflects the anisotropic effect of the faced *p*-phenylene rings. Analogous but more significant high-field shifts over 1 ppm are also observed in the *m*-phenylene proton signals of **3**. Furthermore, the spectrum of **3** is superimposable with that of the compound prepared alternatively by Wittig *et al.*[8b] Therefore, the macrocycle **3** obtained in the present work is evidently a "crosslike" conformer[8b] in the two possible atropisomers.

In the spectrum of **6**, consisting of two equivalent singlets (δ=6.97 and 7.41), the low-field one is assigned to the protons of the three *o*-phenylene rings by comparison with the *o*-phenylene proton signal of *o*-terphenyl (δ=7.41, s)[2a,e] and of **13** (δ=7.40—7.50), and therefore the high-field one is assignable to those of the three *p*-phenylene rings without any contradiction. The high-field shifts (by 0.71 and 0.20 ppm) of the singlet (δ=6.97), relative to the signal of the *p*-phenylene protons of *p*-terphenyl (δ=7.68) and that of the phenyl protons of *o*-terphenyl (δ=7.17),[2a,e] may be

TABLE 2. POSITIONS AND TENTATIVE ASSIGNMENTS OF THE CHARACTERISTIC BANDS IN THE IR SPECTRA (675—920 cm^{-1}) OF POLYPHENYLENES[a)]

1		2		3		4		5		6		7		8		9		10		11		12		13		14	
691 w	γ_{C-C}	708 s	γ_{C-C}	705 s	γ_{C-C}	679 w		708 s	γ_{C-C}	674 m		705 s	γ_{C-C}	707 sh,s	γ_{C-C}	704 s	γ_{C-C}	678 m		678 w		680 w		733 m		703 s	γ_{C-C}
704 m		725 m		707 s		699 w		713 sh,m		751 s	$\gamma_{C-H}(o)$	715 w		712 s		713 s		691 m		702 s		707 s		746 m	$\gamma_{C-H}(o)$	723 m	
709 m		761 s	$\gamma_{C-H}(o)$	707 s		744 sh,m		719 w		756 s		736 m	$\gamma_{C-H}(o)$	751 sh,s		721 w		706 m	γ_{C-C}	707 s		721 w		756 s		776 s	
741 sh,m		766 sh,s		714 w		751 s		736 m		770 w		756 s		756 s	$\gamma_{C-H}(o)$	752 s		733 m		734 w		746 sh,s		764 sh,m		813 s	$\gamma_{C-H}(m)$
751 s	$\gamma_{C-H}(o)$	781 sh,m		744 s		756 s		743 s	$\gamma_{C-H}(o)$	826 sh,m		806 m	$\gamma_{C-H}(m)$	836 s		757 s	$\gamma_{C-H}(o)$	753 s	$\gamma_{C-H}(o)$	763 sh,s		751 s	$\gamma_{C-H}(o)$	822 s		892 s	$\gamma_{C-H}(m)$
756 s		788 s	$\gamma_{C-H}(m)$	750 s		744 sh,m		757 s		834 s	$\gamma_{C-H}(p)$	823 w	$\gamma_{C-H}(p)$	839 sh,s	$\gamma_{C-H}(p)$	769 m		758 sh,s		769 s	$\gamma_{C-H}(o)$	764 sh,m	$\gamma_{C-H}(o)$	839 w	$\gamma_{C-H}(p)$	917 w	
767 m		806 w		759 s	$\gamma_{C-H}(o)$	751 s		765 s		838 s		836 s		847 m		787 m		792 s	$\gamma_{C-H}(m)$	774 sh,m		776 m		853 w			
794 w		826 w		763 sh,m		756 s	$\gamma_{C-H}(o)$	796 sh,s		7		873 w		905 m	$\gamma_{C-H}(m)$	803 m	$\gamma_{C-H}(m)$	797 sh,s		784 m		802 m	$\gamma_{C-H}(m)$	13		14	
801 m	$\gamma_{C-H}(m)$	875 m		778 w		770 w		799 s	$\gamma_{C-H}(m)$	705 s	γ_{C-C}	912 m	$\gamma_{C-H}(m)$	6		815 w		822 s		791 s		821 w		733 m		703 s	γ_{C-C}
809 w		883 m	$\gamma_{C-H}(m)$	805 s	$\gamma_{C-H}(m)$	826 sh,m		804 s		715 w		8		766 sh,s		873 w		826 s	$\gamma_{C-H}(p)$	792 sh,s		879 w		746 m		723 m	
839 m	$\gamma_{C-H}(p)$	3		872 m		834 s	$\gamma_{C-H}(p)$	808 sh,w		736 m	$\gamma_{C-H}(o)$	707 sh,s	γ_{C-C}	797 m	$\gamma_{C-H}(m)$	895 m	$\gamma_{C-H}(m)$	838 m		799 m		910 m	$\gamma_{C-H}(m)$	756 s	$\gamma_{C-H}(o)$	776 s	$\gamma_{C-H}(m)$
848 m		708 s	γ_{C-C}	882 w		838 s		836 s		756 s		712 s		805 m		907 w		843 w		807 m		14		764 sh,m		813 s	
869 w		725 m		885 w		7		839 sh,s	$\gamma_{C-H}(p)$	770 w		751 sh,s	$\gamma_{C-H}(o)$	875 w		10		874 w		807 m		703 s	γ_{C-C}	776 m		892 s	$\gamma_{C-H}(m)$
900 m	$\gamma_{C-H}(m)$	761 s	$\gamma_{C-H}(o)$	899 m	$\gamma_{C-H}(m)$	705 s	γ_{C-C}	847 m		826 sh,m		756 s		900 m	$\gamma_{C-H}(m)$	678 m		902 m	$\gamma_{C-H}(m)$	11		723 m		802 m	$\gamma_{C-H}(m)$	917 w	
916 m		766 sh,s		906 w		715 w		873 w		834 s	$\gamma_{C-H}(p)$	736 m	$\gamma_{C-H}(o)$	907 sh,m		691 m	γ_{C-C}	11		678 w		776 s		821 w			
2		781 sh,m		4		712 s	γ_{C-C}	905 m	$\gamma_{C-H}(m)$	838 s		756 s		9		706 m		702 s	γ_{C-C}	813 s	$\gamma_{C-H}(m)$	879 w					
788 s	$\gamma_{C-H}(m)$	751 sh,s		679 w		751 sh,s		912 m	$\gamma_{C-H}(m)$	7		806 m	$\gamma_{C-H}(m)$	10		733 m	$\gamma_{C-H}(o)$	707 s		892 s	$\gamma_{C-H}(m)$	910 m	$\gamma_{C-H}(m)$				
806 w		756 s	$\gamma_{C-H}(o)$	699 w		756 s	$\gamma_{C-H}(o)$	6		705 s	γ_{C-C}	823 w	$\gamma_{C-H}(p)$	678 m		753 s		734 w		917 w		13					
826 w		4		744 sh,m		8		674 m		715 w		836 s		691 m	γ_{C-C}	758 sh,s		763 sh,s	$\gamma_{C-H}(o)$			733 m					
875 m		679 w		751 s		707 sh,s	γ_{C-C}	751 s	$\gamma_{C-H}(o)$	736 m	$\gamma_{C-H}(o)$	872 w		706 m		792 s	$\gamma_{C-H}(m)$	769 s				746 m	$\gamma_{C-H}(o)$				
883 m	$\gamma_{C-H}(m)$	699 w				712 s		756 s		756 s		890 w	$\gamma_{C-H}(m)$	733 m	$\gamma_{C-H}(o)$	797 sh,s		774 sh,m				756 s	$\gamma_{C-H}(o)$				
3		744 sh,m				751 sh,s	$\gamma_{C-H}(o)$	753 s	$\gamma_{C-H}(o)$	758 sh,s		901 w		822 s		826 s	$\gamma_{C-H}(p)$	784 m				764 sh,m					
705 s	γ_{C-C}	751 s				756 s		792 s	$\gamma_{C-H}(m)$	797 sh,s	$\gamma_{C-H}(m)$	8		838 m		791 s						822 s	$\gamma_{C-H}(p)$				
707 s								797 sh,s		822 s		707 sh,s	γ_{C-C}	843 w		792 sh,s	$\gamma_{C-H}(m)$					839 w					
714 w								822 s		826 s	$\gamma_{C-H}(p)$	712 s		874 w		799 m						853 w					
744 s								826 s		838 m		751 sh,s	$\gamma_{C-H}(o)$	902 m	$\gamma_{C-H}(m)$	807 m											
750 s								838 m		843 w		756 s															
759 s	$\gamma_{C-H}(o)$							843 w		874 w																	
763 sh,m								874 w		902 m	$\gamma_{C-H}(m)$																
778 w								902 m	$\gamma_{C-H}(m)$																		
805 s	$\gamma_{C-H}(m)$																										
872 m																											
882 w																											
885 w																											
899 m	$\gamma_{C-H}(m)$																										
906 w																											

a) v, very; s, strong; m, medium; w, weak; sh, shoulder. γ_{C-C} and γ_{C-H} refer to the vibrations which are primarily the out-of-plane C-C and out-of-plane C-H bending motions, respectively. *o*, *m*, and *p* in parentheses refer to *ortho*-, *meta*-, and *para*-substituted rings, respectively.

ascribed to the mutual anisotropic effect of *p*-phenylene rings situated oppositely.

Furthermore, in the case of **7**, one of *m*-phenylene analogues of **6**, the isolated proton signal (δ=6.40—6.42) and the *p*-phenylene proton signals (δ=6.68 and 6.73, and 6.95 and 7.15) are observed in the high-field regions as compared with that of *m*-terphenyl (δ=7.78—7.83) and with those of *p*-terphenyl (δ=7.68) and **6** (δ=6.97), respectively. The significant high-field shifts reasonably reflect the conformation in which the *m*-phenylene ring is situated oppositely to two angular *p*-phenylene rings.

Finally, in the spectra of **2**, **8**, **9**, and **11**, a comparison of the characteristic features in phenylene proton signals with those of open-chain analogues[2)] is in full support of the validity of the conformational considerations developed based on the Dreiding stereomodels.

The foregoing results suggest that the prominent

Table 3. ^{1}H NMR spectral data for polyphenylenes (**1**—**13**) in $CDCl_3$[a)]

Compound	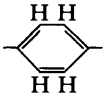	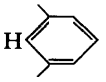	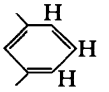	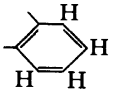
1	7.25 (4H, s)	6.61—6.63 (2H, apparent t, J=1.8 Hz)	7.21—7.77 (14H, m)	
2	———	7.15—7.31 (16H, m)		7.40—7.53 (8H, m, AA'BB'-type)
3	———	5.98—6.00 (2H, apparent t, J=1.7 Hz)	6.42—6.66 (6H, m)	7.19—7.56 (16H, m)
4	6.68 and 6.90 (8H, qd, J=8.1 and 2.0 Hz)	———	———	7.37—7.57 (16H, m)
5	6.98 (8H, s)	6.23—6.26 (2H, m)	7.24—7.66 (14H, m)	
6	6.97 (12H, s)	———	———	7.41 (12H, s)
7	6.68 and 6.73 (4H, qd, J=8.0 and 1.7 Hz) 6.95 and 7.15 (4H, qd, J=7.8 and 1.7 Hz)	6.40—6.42 (1H, m)	7.15—7.52 (15H, m)	
8	———	6.63—6.66 (3H, m)	7.22—7.25 (9H, m)	7.29—7.39 (12H, m, AA'BB'-type)
9	———	6.47—6.49 (1H, m, m-C_6H_4·m-$C_6\underline{H}$·m-C_6H_4)	6.75—6.91 (3H, m, o-C_6H_4·m-$C_6\underline{H}_3$·o-C_6H_4)	
		7.91—7.94 (1H, m, o-C_6H_4·m-$C_6\underline{H}$·o-C_6H_4)	7.30—7.68 (19H, m, o-$C_6\underline{H}_4$ and m-$C_6\underline{H}_4$·m-$C_6\underline{H}_3$·m-$C_6\underline{H}_4$)	
10	7.07 (4H, s, p-C_6H_4) 7.05 and 7.40 (8H, q, J=8.6 Hz, p-C_6H_4·p-C_6H_4)	6.50—6.53 (2H, m)	7.36—7.71 (14H, m)	
11	7.23 and 7.53 (8H, q, J=8.5 Hz)	7.90—7.92 (2H, m, m-$C_6\underline{H}$·(m-C_6H_4)$_2$·m-$C_6\underline{H}$) 8.04—8.06 (2H, m, m-C_6H_4·(m-$C_6\underline{H}$)$_2$·m-C_6H_4)	7.47—7.78 (16H, m)	
12	———		5.71—7.54 (48H, m)	
13	7.15 and 7.49 (24H, q, J=8.4 Hz)	———	———	7.40—7.50 (12H, m)

a) δ (ppm) from the internal standard TMS.

high-field shift found for the phenylene proton signals of macrocyclic polyphenylenes, as compared with those of open-chain analogues, may reflect the anisotropic effect of the neighboring phenylene rings, which, originating from the rigid geometry of the macrocyclic structures, may result in a restricted rotation of pivot bonds and an overcrowded conformation. Consequently, the ^{1}H NMR spectra of macrocyclic polyphenylenes, when compared with those of open-chain analogues, may provide useful information for the nonplanar spacial relationship of constituting phenylene rings in solution.

UV Spectra: The UV spectra of the polyphenylenes **1**—**14** were measured in cyclohexane solution. The absorption curves are shown in Figs. 1—6. The absorption maxima above 220 nm for **3**, **13**, and **14** coincide within 3 nm with those of other workers.[5b,8a,b)] All of the polyphenylenes, similarly to the open-chain analogues,[2,19)] display the E-band in the fairly narrow region of 190—210 nm and the K-band in the broad region of 230—320 nm with high intensity.

Previous studies on the UV spectra of the polyphenyls[2)] have indicated that a twist of the pivot bond in the conjugated system influences the interaction of π-electrons across the pivot bond as well as the conjugation of the system, and that the arrangement of the p-phenylene unit(s) in the molecule, even in the presence of o- or m-phenylene units, has a tendency to maintain the coplanarity of the benzene rings. In the case of the polyphenylenes, their overcrowded spacial relationship due to the rigid geometry may cause an enhanced restricted rotation of the pivot bonds, and consequently affects inevitably the spectral feature of K-band.

The spectrum of **1**, containing one *p*-phenylene ring, displays none of bands near 280 nm, which have been found characteristic of the *p*-phenylene unit in the spectrum of the open-chain analogue (**32**: 242 and 280 nm),[2a] but rather intense K-bands (237 and 256 (sh), ε=53700 and 36600), which are related closely to the K-bands of the open-chain compound (ϕommoϕ:[20] 237 and 252 (sh), 74100 and 45400) containing no *p*-phenylene rings.[2b,g] The lack of K-band near 280 nm provides conclusive evidence for the conformation, in which *o*- and *p*-phenylene rings should be highly twisted to one another owing to the steric repulsion of both the isolated hydrogen atoms (*m*-phenylene rings) and the π-electron cloud (*p*-phenylene ring) (Fig. 1). An analogous lack of K-band was also observed in the case of **7** (Fig. 2).

Similarly, an analogous spacial situation of *p*-phenylene ring may result in decrease of π-π interaction across the pivot bonds. Indeed, the spectrum of **5** (246 and 264 (sh)) shows a remarkable hypsochromic shift of the characteristic band for *p*-linkage, compared with those of the corresponding open-chain analogues (ϕmpoϕ: 250 and 275 (sh);[2a] ϕmopmϕ: 249 and 276 (sh)[2f]) (Fig. 3). Also, the spectrum of **6**, which has an alternate arrangement of *o*- and *p*-phenylene rings, has a K-band (276 (sh), 13500) similar in loca-

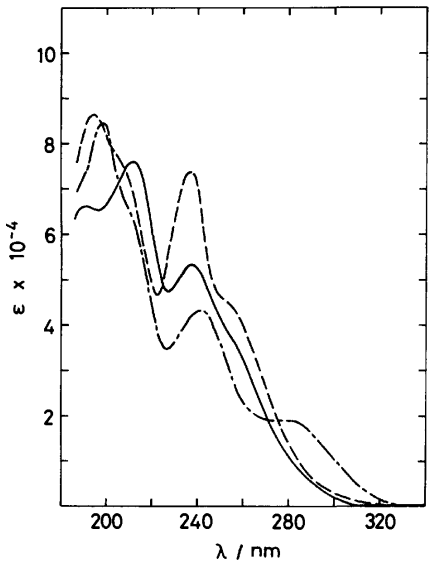

Fig. 1. UV spectra of pentaphenylene and open-chain analogues.
——: *m,m,o,p,o*-Pentaphenylene (**1**), ———: ϕommoϕ, ——·——: ϕopoϕ (**32**).

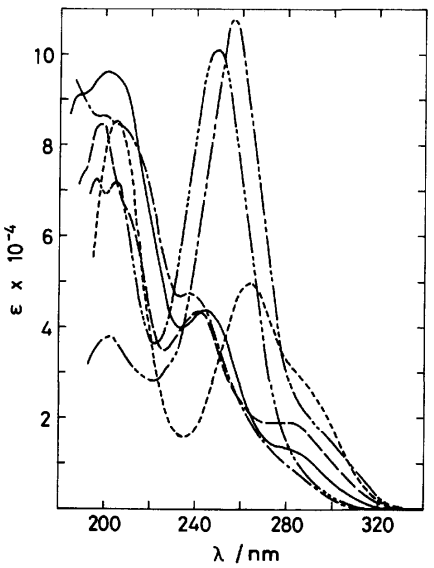

Fig. 2. UV spectra of hexa- and heptaphenylene and open-chain analogues.
——: *o,p,o,p,o,p*-Hexaphenylene (**6**), ——·——: *m,o,p,o,p,o*-hexaphenylene (**7**), ——: *m,m,m,m,p,o,p*-heptaphenylene (**11**), ———: ϕopoϕ (**32**), ------: ϕpopϕ, ——·——: *m*-sexiphenyl.

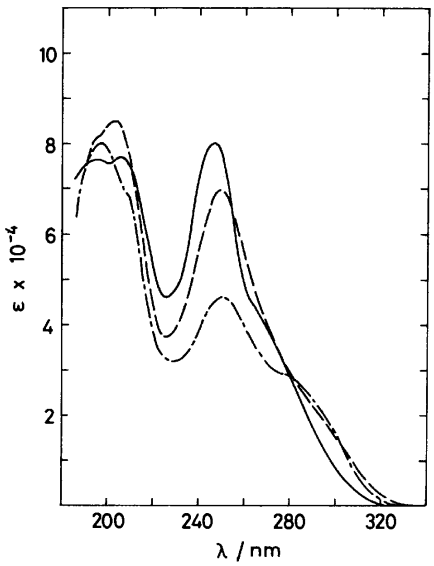

Fig. 3. UV spectra of hexaphenylene and open-chain analogues.
——: *m,o,p,m,o,p*-Hexaphenylene (**5**), ———: ϕmopmϕ, ——·——: ϕmpoϕ.

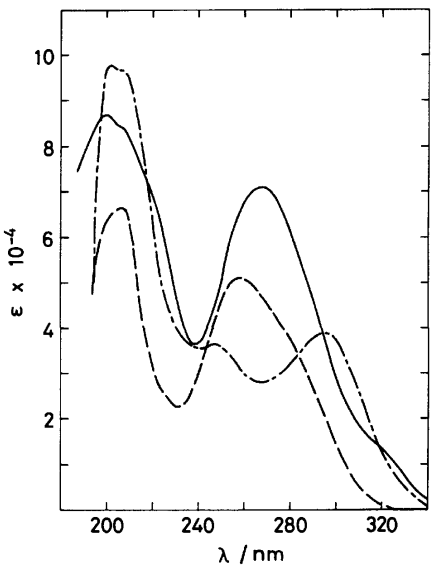

Fig. 4. UV spectra of heptaphenylene and open-chain analogues.
——: *m,o,p,p,o,m,p*-Heptaphenylene (**10**), ———: ϕmpmϕ, ——·——: ϕoppoϕ.

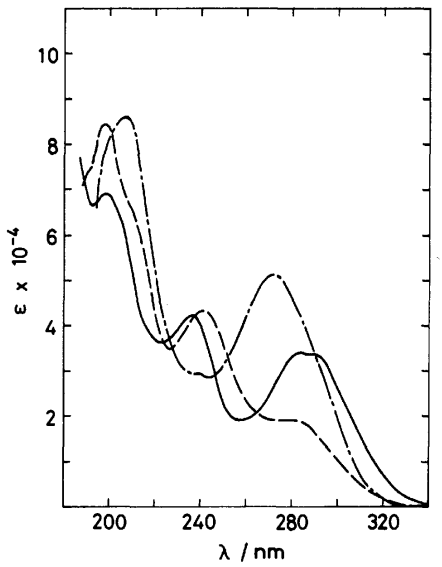

Fig. 5. UV spectra of hexaphenylene and open-chain analogues.
———: *o,o,p,o,o,p*-Hexaphenylene (**4**), — — —: *φopoφ* (**32**), —·—·—: *φpoopφ*.

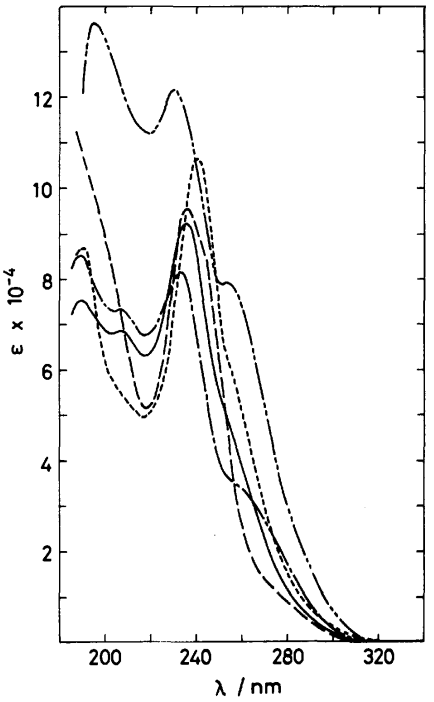

Fig. 6. UV spectra of hexa- and dodecaphenylene.
———: *m,m,o,m,m,o*-Hexaphenylene (**2**), — — —: *m,o,o,m,o,o*-hexaphenylene (**3**), —·—·—: *m,o,m,o,-m,o*-hexaphenylene (**8**),------: *m,m,m,o,m,o*-hexaphenylene (**9**),—··—: *m,o,o,m,o,o,m,o,o,m,o,o*-dodecaphenylene (**12**).

tion to, but much weaker in intensity than, those of the open-chain reference compounds (*cf.* **32**: 280, 18500; *φpopφ*: 284 (sh), 30600).[2a] In the case of **11**, beside an analogous decrease in intensity of K-bands near 280nm, a significant K-band (256 and 284 (infl), 107700 and 24100) similar to that of *m*-sexiphenyl (249, 101700)[2g] is reasonably observed (Fig. 2). The marked shift or decrease in intensity of the K-band near 280 nm surely reflects the reduced π-π interaction across the pivot bonds of *p*-phenylene ring because of an enhanced twisting of the bonds. In the spectrum of **10**, however, the weak shoulder (312, 16800) found at rather a long wavelength as compared with those of the reference compound (*φoppoφ*: 297, 38900),[2a] seems to be associated with the reduced twisting of *o*-phenylene linkages, caused by the relaxation of steric repulsion of the molecule, in contrast to the cases of **1** and **5** (Fig. 4).

On the other hand, in the spectrum of **4** (236, 286, and 288 (sh); 42300, 34000, and 33600), which has parallel *p*-phenylene rings, longer-wavelength bands are observed at rather red in comparison with those of the open-chain analogues (*cf.* **32**: 242 and 280, 43200 and 18500;[2a] *φpoopφ*: 240 (sh) and 272, 28100 and 51200[2b,g]). The marked shift corresponds to the behavior of [2.2]paracyclophane and other strained compounds[17a] and can be explained on the basis of transannular π-electronic interaction of the two chromophores lying face-to-face (Fig. 5).

The spectra of **2**, **3**, **8**, **9**, and **12**, all of which consist of *o*- and *m*-phenylene rings without any *p*-phenylene rings, show similar characteristic K-bands (near 235 and near 250 (sh)) related closely to those of the reference open-chain analogues (*cf.* *φommoφ*: 237 and 252 (sh); *φmoomφ*: 236 and 245;[2b] *φomooφ*: 232 and 250 (sh);[2f] *φmomφ*: 237 and 249 (sh); *φomoφ*: 234 and 250 (sh);[2a] *φmmomφ*: 239 and 250 (sh)).[2f] From these observations it may be deducible that the restricted rotation of pivot bonds caused by the macroring formation of such open-chain analogues will give no appreciable influence on the spectral feature of K-band (Fig. 6).

The foregoing results on the spectra of polyphenylenes containing *p*-phenylene ring(s) suggest the following aspect: The lack or decrease in intensity of K-band above *ca.* 260nm, or a marked shift of the band, reflects the enhanced restricted rotation of the pivot bonds of *p*-phenylene ring(s), and consequently provides useful conformational information. The proposed conformations of the polyphenylenes based on the UV spectral data have been confirmed to agree qualitatively with those obtained from the ^{1}H NMR spectral data.

HMO Calculations: Previously HMO calculations of longest-wavelength absorption bands of forty-two linear polyphenyls up to octiphenyls were performed by assuming dihedral angles of pivot bonds to be as follows: 50° for the phenyl—*o*- and *o*-—*o*-phenylene linkages, 35° for the *o*-—*p*- and *m*-—*o*-phenylene linkages, and 20° for the other linkages.[2a,c,d] Resonance integrals (π-π) were used with the values of cos θ of these dihedral angles. The results indicated that the parameters (cos θ and β) used successfully applied to many such linear polyphenyls.

In the present study, two sets of HMO calculations (A and B) of longest-wavelength absorption bands of

TABLE 4. CALCULATED AND OBSERVED LONGEST- WAVELENGTH ABSORPTION BANDS OF POLYPHENYLENES (**1—11** AND **14**)

Compound	Calcd trans. energy β[a]		Absorption band			Presumed dihedral angle of the pivot bond for B[b]
			Calcd		Obsd	
	A	B	A λ_{max}/nm	B λ_{max}/nm	λ_{max}/nm	
1	−1.1654	−1.3026	287	257	256 sh	m(60)m(40)o(50)p(50)o(40)m
2	−1.2538	−1.3416	267	250	248 sh	m(55)m(40)o(40)m(55)m(40)o(40)m
3	−1.2592	−1.3874	266	241	242 sh	m(50)o(55)o(50)m(50)o(55)o(50)m
4	−1.1260	−1.1856	298	283	288 sh	o(45)o(45)p(45)o(45)o(45)p(45)o
5	−1.1386	−1.2544	294	267	264 sh	m(40)o(45)p(45)m(40)o(45)p(45)m
6	−1.1918	−1.2268	281	273	276 sh	o(40)p(40)o(75)p(75)o(40)p(40)o
7	−1.1309	−1.4061	296	238	237	m(70)o(70)p(40)o(70)p(40)o(70)m
8	−1.2682	−1.3072	264	256	254 sh	m(40)o(40)m(40)o(40)m(40)o(40)m
9	−1.2532	−1.3234	267	253	252 sh	m(35)m(35)m(35)o(50)m(50)o(35)m
10	−1.0894	−1.0778	308	311	312 sh	m(30)o(30)p(30)p(30)m(30)o(20)p(20)m
11	−1.1322	−1.1728	296	286	284 infl	m(30)m(30)m(30)m(35)p(35)o(35)p(35)m
14	−1.2698	−1.3416	264	250	247	m(35)m(35)m(35)m(35)m(35)m(35)m

a) For β, −3.70 eV was used as a mean value calculated from the absorption bands of biphenyl and the first four *p*-polyphenyls (Refs. 2a, 2c, and 2d). b) m, o, and p refer to *m*-, *o*-, and *p*-phenylene rings. The figures in parentheses refer to the dihedral angle of the pivot bond. Both terminal phenylene rings are duplicated.

the polyphenylenes were carried out by assuming the dihedral angles of the pivot bonds as those 1) previously used for the linear polyphenyls (for A) and 2) obtained by an apparent inspection of the Dreiding stereomodels (for B). The results obtained are summarized in Table 4.

The calculated and observed longest wavelengths of the polyphenylenes show a poor agreement for the values by calculation A, except in the cases of **6** and **10**, but a fairly good agreement within 5 nm for those by calculation B. Evidently the above poor agreement is due to unsuitable parameters (cos θ) derived from the impractically small dihedral angles of the pivot bonds instead of relatively large ones caused by the rigid geometry of macrocyclic structure. The above favorable agreement presumably justifies the estimates of their dihedral angles, and supports the proposed conformations of the polyphenylenes based on the UV and ^{1}H NMR spectral data.

The foregoing results indicate that prediction of the longest-wavelength absorption bands of the polyphenylenes by HMO calculations is possible with a fairly good precision by use of the dihedral angles of the pivot bonds as estimated by inspection of the Dreiding stereomodels. The calculations gave also additional bases for their conformational aspects deduced from their spectral data and stereomodels.

MS Spectra: Only a few studies have been reported on MS spectra of polyphenylenes and related polyphenyls consisting of three or more benzene rings.[2e,5e,21] The MS spectra of the polyphenylenes **1—13** containing mixed linkages and of **14** were measured at 70 eV. The spectral data are briefed in Tables 5 and 6.

All of the spectra commonly display the molecular ion (M^+) as the most abundant ion. As fragment ions, $(M-Hy)^+$ and $(M-CxHy)^+$ are found in appreciable amounts. The spectra show also considerable amounts of doubly charged ions M^{2+}, $(M-Hy)^{2+}$, and $(M-CxHy)^{2+}$ together with small amounts of corresponding triply charged ions.

An inspection of each spectrum discloses the following facts: Firstly, the second most abundant ion is M^{2+} or $(M-1)^+$. Secondly, the amount of singly to triply charged molecular ions (including isotope ions) of **1—13**, each of which contains one or more *o*-phenylene rings, seems to be low in comparison with that of **14**, which consists of only *m*-phenylene rings. Furthermore, the values $(M^{2+}+M^{3+})/M^+$ of **1—13** increase approximately with increasing number of phenylene rings. The highest value of **14** obviously correlates to the absence of *o*-phenylene ring, which markedly reduces the stability of molecular ions as a result of lowered resonance stabilization. Thirdly, the value of $(M-Hy)^+/(M-Hy)^{2+}$ is rather high in the spectra of **1** and **11** and slightly high in those of **5—7**.

Previous electron-impact studies have shown that stabilities of *o*-polyphenylenes are less than those of *m*-polyphenylenes,[5e] and that those of polyphenyls decrease in the order of *p*->*m*->*o*-series.[2e,21] These results lead to a conclusion that the stabilities to electron bombardment of polyphenylenes containing *o*-phenylene rings, regardless of the presence of *m*- or *p*-phenylene ring(s), are substantially less than those of *m*-polyphenylenes.

Experimental

Melting points were determined with a Mettler FP-51 apparatus, except for those above 300 °C, which were determined with a Shimadzu DSC-30M differential scanning calorimeter. UV spectra were measured on a Shimadzu UV-360 spectrophotometer, IR spectra on a Leitz III-G spectrophotometer, and ^{1}H NMR spectra on Varian XL-200 (200 MHz) and CFT-20 (80 MHz) spectrometers with tetramethylsilane as an internal standard. MS spectra were recorded on a Hitachi RMU-6MG mass spectrometer. HMO

TABLE 5. MOLECULAR IONS OF POLYPHENYLENES (**1**—**14**)

Compound	M^+		M^{2+}		M^{3+}		Sum	$M^{2+}+M^{3+}$
	Irel[a]	$\%\Sigma$[b]	*Irel*	$\%\Sigma$	*Irel*	$\%\Sigma$	$\%\Sigma$	M^+
1	100.0	25.2	5.1	1.3	0.1	0.03	26.5	0.05
2	100.0	41.6	5.9	2.4	0.1	0.04	44.0	0.06
3	100.0	36.9	7.4	2.7	0.1	0.04	39.6	0.07
4	100.0	32.7	6.2	2.0	0.1	0.03	34.7	0.06
5	100.0	33.5	6.5	2.2	0.1	0.03	35.7	0.07
6	100.0	29.7	3.2	1.0	0.1	0.03	30.7	0.03
7	100.0	31.5	6.0	1.9	0.1	0.03	33.4	0.06
8	100.0	36.2	4.9	1.8	0.1	0.04	38.0	0.05
9	100.0	41.9	5.0	2.1	0.1	0.04	44.0	0.05
14	100.0	47.8	29.0	13.9	1.2	0.57	62.3	0.30
10	100.0	39.4	15.5	6.1	0.2	0.08	45.6	0.16
11	100.0	33.2	16.7	5.5	0.7	0.23	38.9	0.17
13	100.0	38.0	24.0	9.1	1.3	0.49	47.6	0.25
12	100.0	24.3	21.4	5.2	3.9	0.95	30.5	0.25

a) *Irel*: Relative intensity. b) $\%\Sigma$: Percentage of total ionization.

TABLE 6. PRINCIPAL FRAGMENT IONS OF POLYPHENYLENES (**1**—**14**)

Compound	$(M-1)^+$		$(M-Hy)^+$[a]	$(M-Hy)^{2+}$[a]	$(M-CxHy)^+$[b]	$(M-Cx'Hy)^+$[c]
	Irel	$\%\Sigma$	$\%\Sigma$	$\%\Sigma$	$\%\Sigma$	$\%\Sigma$
1	25.4	4.6	18.2	11.3	16.6	1.5
2	4.2	1.2	4.4	5.3	12.3	3.8
3	5.8	1.4	4.6	4.8	13.6	5.3
4	4.5	1.0	3.9	5.6	11.9	4.9
5	7.8	1.8	6.7	6.4	14.0	3.0
6	11.3	2.2	9.0	5.7	17.4	4.1
7	12.6	2.7	7.8	5.5	17.3	5.1
8	5.4	1.3	4.8	4.8	12.9	5.7
9	2.8	0.9	4.4	5.5	11.3	4.7
14	2.4	0.8	3.6	5.2	5.5	2.7
10	8.9	2.2	4.6	5.4	8.5	2.7
11	28.5	6.0	11.2	6.1	9.2	4.4
13	8.6	1.8	3.8	5.0	5.7	0.7
12	9.4	1.0	1.7	1.9	4.5	0.9

a)—c) The generic ions $(M-Hy)^+$, *etc.* refer to the sums of fragment ions corresponding to the loss of one to ten H atoms, to the loss of one to six carbon units, and to the loss of seven to twelve carbon units, respectively, from the molecular ions.

calculations were carried out on a Hewlett-Packard HP-85 personal computer with a 16K RAM attached.[22]

Commercially available *o*- (**15**) and *m*-diiodobenzene (**16**) and *o*-chloro- (**17**) and *m*-iodonitrobenzene (**18**) were purified before use. 4-Iodo-2′- (**19**) and 4-iodo-3′-nitrobiphenyl (**20**), 2,2‴-diamino-*p*-quaterphenyl,[2d] and 3,3′-diaminobiphenyl[2f] were prepared by the methods previously reported.

2,2″-Diiodo-*p*-terphenyl (**24d**) was prepared from the corresponding diamine (**24b**, described below) by a method similar to that of Cade and Pilbeam.[23] Colorless needles from ethanol: Mp 158.9°C; yield 50%. Found: C, 44.84; H, 2.42%. Calcd for $C_{18}H_{12}I_2$: C, 44.84; H, 2.51%.

4,4″-Dibromo-*o*-terphenyl (**31c**) was prepared by direct bromination[8a] of commercially available *o*-terphenyl. Colorless plates from ethanol: Mp 170.5°C (lit,[8a] 170°C); yield 61%. (Found: C, 55.55; H, 2.93%).

Preparation of Dinitropolyphenyls (21a—28a). Procedure A: A solution of two kinds of iodides in dimethylformamide (DMF) was brought to reflux. Copper powder was added in three portions at intervals of 2h with stirring, and the mixture was refluxed for an additional 16h. The hot reaction mixture was filtered, and the solid material was washed several times with hot DMF and benzene. The filtrates were combined and then cooled, and the resulting solid was removed by filtration.[24] After removal of the solvents *in vacuo*, the residue (after distillation *in vacuo* for the preparation of **23a**)[24] was subjected to a chromatography on alumina using a cyclohexane-benzene (3:7, v/v) mixture (C-B(3:7)) and benzene, or benzene as the eluents.[24]

3,3″-Dinitro-o-terphenyl (21a): A solution of **15** (26.4g) and **18** (159g) in DMF (600ml) was treated with copper powder (254g). The eluate with a C-B (3:7) mixture gave **21a** as pale yellow prisms from ethanol: Mp 142.0°C; yield 10.3g (40%). Found: C, 67.73; H, 3.65; N, 8.93%. Calcd for $C_{18}H_{12}N_2O_4$: C, 67.50; H, 3.78; N, 8.75%.

3,3″-Dinitro-m-terphenyl (23a): A solution of **16** (66.0g) and **18** (399g) in DMF (1300ml) was treated with copper powder (572g). A double crystallization of the eluate from benzene provided **23a** as pale yellow needles: Mp 142.1°C; 23.6g (37%). Found: C, 67.77; H, 4.08; N, 8.88%.

Procedure B: A mixture of two kinds of halides in a reaction tube (ϕ 4.5×20cm) was heated in an oil bath at 205—220°C (225—235°C for the preparation of **26a—28a**), copper powder was added in portions with stirring over a 2-h period, and then the mixture was heated at 215—230°C (230—240°C for the preparation of **26a—28a**) for an additional hour. After

cooling, the reaction product was extracted with hot benzene and then the solvent was distilled off. The remaining was distilled *in vacuo* to separate a distillate (bp 100—210 °C/667 Pa, 161—220 °C/667 Pa, 80—205 °C/933 Pa, and 150—240 °C/400 Pa in the preparation of **22a**, **24a**, **25a**, and **26a—28a**, respectively)[26] from a tarry or soild residue. The residue was recrystallized or chromatographed on alumina with benzene (C-B(1:1) in the preparation of **26a**).

2,2″-Dinitro-m-*terphenyl (22a)*: A mixture of **16** (8.25 g) and **17** (39.4 g) was treated with copper powder (95.3 g). Repeated crystallizations of the residue from benzene and then from ethanol afforded **22a** as pale yellow needles: Mp 163.4 °C; 2.5 g (31%). Found: C, 67.41; H, 3.93; N, 8.64%. Calcd for $C_{18}H_{12}N_2O_4$: C, 67.50; H, 3.78; N, 8.75%.

2,2″-Dinitro-p-*terphenyl (24a)*: A mixture of **19** (16.3 g) and **17** (39.4 g) was heated with copper powder (95.3 g). The eluate gave **24a** as pale yellow cubes from benzene: Mp 235.5 °C (lit,[27] 228—230.5 °C); 10.0 g (62%). (Found: C, 67.69; H, 4.02; N, 8.70%).

2,3″-Dinitro-p-*terphenyl (25a)*: A mixture of **20** (16.3 g) and **17** (39.4 g) was treated with copper powder (95.3 g). The eluate provided **25a** as pale yellow needles from benzene: Mp 145.4 °C; 4.9 g (31%). Found: C, 67.47; H, 3.75; N, 8.88%.

3,3″-Dinitro-p-*terphenyl (26a)*: A mixture of **20** (16.3 g) and **18** (49.8 g) was heated with copper powder (79.4 g). Several crystallizations of the eluate from benzene afforded **26a** as yellow needles: Mp 211.3 °C; 4.4 g (27%). Found: C, 67.78; H, 3.88; N, 8.90%.

2,2″-Bis(3-nitrophenyl)-p-*terphenyl (27a)*: A mixture of **24d** (9.64 g) and **18** (49.8 g) was treated with copper powder (76.3 g). Recrystallization of the eluate from benzene gave **27a** as pale yellow prisms: Mp 240.1 °C; 3.8 g (40%). Found: C, 76.52; H, 4.15; N, 5.97%. Calcd for $C_{30}H_{20}N_2O_4$: C, 76.26; H, 4.27; N, 5.93%.

4,4″-Bis(3-nitrophenyl)-o-*terphenyl (28a)*: A mixture of 4,4″-diiodo-*o*-terphenyl[2e] (12.1 g) and **18** (49.8 g) was treated with copper powder (79.4 g). Recrystallization of the eluate from benzene afforded **28a** as yellow needles: Mp 228.0 °C; 2.7 g (23%). Found: C, 76.42; H, 4.12; N, 5.68%.

Preparation of Diaminopolyphenyls (21b—28b). A solution of each of the dinitro compounds (**21a—26a**: 16.0 g, **27a** and **28a**: 14.2 g) in hot benzene (800—1200 ml) was treated with activated iron by a method similar to that of Hazlet and Dornfeld.[28] After filtration, hydrobromic acid (about 47%) was added in portions to the filtrate with stirring, and then the precipitate formed was collected, washed with benzene and small amount of water, and dried; yield 96—98%. A portion of the salt was treated in the usual manner with aqueous alkali into the free base, which crystallized from ethanol or benzene.

3,3″-Diamino-o-*terphenyl (21b)*: Brown oil. **21b**·2HBr: White powder. Found: C, 51.33; H, 4.22; N, 6.73%. Calcd for $C_{18}H_{18}Br_2N_2$: C, 51.21; H, 4.30; N, 6.64%.

2,2″-Diamino-m-*terphenyl (22b)*: Colorless prisms; mp 120.9 °C. Found: C, 83.12; H, 6.22; N, 10.54%. Calcd for $C_{18}H_{16}N_2$: C, 83.04; H, 6.19; N, 10.76%.

3,3″-Diamino-m-*terphenyl (23b)*: Colorless oil. Found: C, 83.23; H, 5.96; N, 10.70%.

2,2″-Diamino-p-*terphenyl (24b)*: Colorless needles; mp 212.0 °C (lit,[27] 204.5—205.5 °C). (Found: C, 82.99; H, 6.10; N, 10.86%).

2,3″-Diamino-p-*terphenyl (25b)*: Colorless needles; mp 180.0 °C. Found: C, 82.76; H, 6.08; N, 10.82%.

3,3″-Diamino-p-*terphenyl (26b)*: Colorless needles; mp 196.6 °C. Found: C, 83.24; H, 6.40; N, 10.66%.

2,2″-Bis(3-aminophenyl)-p-*terphenyl (27b)*: Colorless prisms; mp 229.1 °C. Found: C, 87.27; H, 5.64; N, 6.61%. Calcd for $C_{30}H_{24}N_2$: C, 87.35; H, 5.86; N, 6.79%.

4,4″-Bis(3-aminophenyl)-o-*terphenyl (28b)*: Colorless plates; mp 210.4 °C. Found: C, 87.64; H, 5.89; N, 6.70%.

Preparation of Dibromopolyphenyls (21c—30c). A suspension of bishydrobromide of each of the diamino compounds (50 mmol) in 47% hydrobromic acid (100 ml) and water (150 ml) was bis-diazotized with sodium nitrite (7.3 g, 106 mmol) in water (20 ml) at 0—5 °C with stirring for 2 h. The cold suspension of bis(diazonium) salt formed was added in portions to a solution of freshly prepared copper(I) bromide (15.8 g, 110 mmol) in 47% hydrobromic acid (70 ml) with stirring, and the mixture was heated slowly up to *ca.* 80 °C and then cooled. The benzene extract was washed successively with water, sodium thiosulfate solution, sodium hydroxide solution, and water. After removal of the solvent, the residue was chromatographed on alumina with cyclohexane and/or C-B (9:1, 4:1, and 1:1) mixtures as the eluent to give dibromo compounds.

3,3″-Dibromo-o-*terphenyl (21c)*: Colorless needles from ethanol; mp 90.9 °C; yield 42%. Found: C, 55.87; H, 3.01%. Calcd for $C_{18}H_{12}Br_2$: C, 55.71; H, 3.12%.

2,2″-Dibromo-m-*terphenyl (22c)*: Colorless cubes from benzene; mp 76.3 °C; 64%. Found: C, 55.88; H, 3.28%.

3,3″-Dibromo-m-*terphenyl (23c)*: Colorless oil (lit,[5c] colorless viscous oil); 47%. (Found: C, 55.95; H, 3.04%).

2,2″-Dibromo-p-*terphenyl (24c)*: Colorless needles from ethanol; mp 137.4 °C; 58%. Found: C, 55.92; H, 3.14%.

2,3″-Dibromo-p-*terphenyl (25c)*: Colorless plates from ethanol; mp 114.9 °C; 63%. Found: C, 55.98; H, 2.94%.

3,3″-Dibromo-p-*terphenyl (26c)*: Colorless plates from benzene; mp 149.8 °C; 45%. Found: C, 55.83; H, 2.99%.

2,2″-Bis(3-bromophenyl)-p-*terphenyl (27c)*: Colorless prisms from benzene-cyclohexane; mp 190.1 °C; 64%. Found: C, 66.94; H, 3.67%. Calcd for $C_{30}H_{20}Br_2$: C, 66.69; H, 3.73%.

4,4″-Bis(3-bromophenyl)-o-*terphenyl (28c)*: Colorless needles from ethanol-benzene; mp 142.3 °C; 53%. Found: C, 66.89; H, 3.76%.

2,2‴-Dibromo-p-*quaterphenyl (29c)*: Colorless needles from benzene-ethanol; mp 174.8 °C; 30%. Found: C, 61.86; H, 3.32%. Calcd for $C_{24}H_{16}Br_2$: C, 62.10; H, 3.47%.

3,3′-Dibromobiphenyl (30c): Colorless needles from ethanol; mp 54.6 °C (lit,[5c] 53 °C); 55%. (Found: C, 46.31; H, 2.59%).

Preparation of m,m,o,p,o-*Pentaphenylene (1). Procedure A*: A solution of di-Grignard compound was prepared from **27c** (2.70 g, 5.9 mmol), magnesium turnings (0.25 g, 10 mmol), and a THF-benzene (1:1, v/v) mixture (T-B(1:1)) (40 ml) under nitrogen in the usual manner. To the Grignard reagent thus prepared, after dilution with T-B (1:1) (60 ml), anhydrous copper(II) chloride (1.74 g, 13 mmol) was added. The mixture was refluxed with stirring for 4 h and then hydrolyzed with ammonium chloride (2 g) and concentrated hydrochloric acid (4 ml) in water (40 ml). The product was extracted with benzene. The organic layer was separated, washed with water, and then dried. After removal of the solvent, the residue was chromatographed on alumina with C-B (9:1) to give 2,2″-diphenyl-*p*-terphenyl (**32**) as colorless needles from ethanol: Mp 185.7 °C (lit,[2a] 185.8 °C); yield 151 mg (7.9%). Subsequent elutions with C-B (9:1), C-B

(4:1), and C-B (3:1) provided **1**.

1: Colorless cubes from hexane; mp 188.6°C; yield 1233 mg (65%); UV λ_{max} (ε) 190 (66300), 211 (76900), 237 (53700), and 256 nm (sh) (36600). Found: C, 94.97; H, 5.29%; M^+, 380. Calcd for $C_{30}H_{20}$: C, 94.70; H, 5.30%; M^+, 380.

Procedure B: A mixture of the di-Grignard reagent, prepared from **27c** (540 mg, 1.0 mmol) and magnesium turnings (50 mg, 2 mmol) in T-B (1:1) (20 ml), and thallium(I) bromide (569 mg, 2.0 mmol) was stirred and refluxed under nitrogen for 5 h, and then hydrolyzed with dilute hydrochloric acid.[11] The benzene extract of the product was worked up as described for procedure A to afford **32** (105 mg, 28%) and **1** (68 mg, 18%).

Procedure C: A solution of tris(triphenylphosphine)nickel(0) [Ni(tpp)$_3$] was prepared from bis(triphenylphosphine)nickel(II) dichloride[29] (635 mg, 1.0 mmol), triphenylphosphine (524 mg, 2.0 mmol), and zinc powder (66 mg, 1.0 mmol) in dry, O_2-free DMF (5 ml) under nitrogen at 50°C for 1 h, by a method similar to that of Kende *et al.*[12] To the red-brown slurry of Ni(tpp)$_3$ thus prepared, **27c** (540 mg, 1.0 mmol) in dry, O_2-free DMF (2 ml) was added and the reaction mixture was stirred under nitrogen at 50°C for 24 h. It was then cooled, poured into 2% hydrochloric acid (20 ml), extracted into benzene, and washed well with water, and the solvent was distilled off. The products were analyzed by quantitative GLPC, using *p*-terphenyl as an internal standard calibrated against the pure samples, to give **32** (28%), **1** (22%), and starting material **27c** (40%).

Preparation of m,m,o,m,m,o-*Hexaphenylene (2)*. To the solution of di-Grignard compound prepared from **21c** (3.88 g, 10 mmol) and magnesium turnings (0.49 g, 20 mmol) in THF (20 ml), after dilution with THF (80 ml), anhydrous copper(II) chloride (3.40 g, 25 mmol) was added. The mixture was worked up as described for **1**. The benzene extract was chromatographed on alumina, with cyclohexane and then with C-B (9:1) as the eluents, to provide **2** and a bromosexiphenyl: Colorless needles from benzene-ethanol; mp 150.0°C; 39 mg. Found: C, 80.52; H, 4.61%; M^+, 537. Calcd for $C_{36}H_{25}Br$: C, 80.45; H, 4.69%; M^+, 537.

2: Colorless prisms from benzene-ethanol; mp 292.0°C; 363 mg (16%); UV λ_{max} (ε) 188 (75500), 207 (68600), 236 (92800), and 248 nm (sh) (58700). Found: C, 94.86; H, 5.45%; M^+, 456. Calcd for $C_{36}H_{24}$: C, 94.70; H, 5.30%; M^+, 456.

Preparation of m,o,o,m,o,o-*Hexaphenylene (3)*. The Grignard reagent prepared from **22c** (9.70 g), magnesium turnings (1.22 g), and THF (50 ml), after dilution with THF (200 ml) followed by addition of anhydrous copper(II) chloride (8.60 g), was treated as described for the preparation of **1**. The benzene extract was dissolved in benzene and then allowed to stand overnight to separate out colorless, transparent plates and an amorphous precipitate. The plates and liquid part containing the amorphous precipitate were separated by decantation. Recrystallization of the former from benzene gave **3** (425 mg). The latter together with filtrates, after removal of the solvent, was chromatographed on alumina with C-B (4:1) to afford an additional **3** (650 mg) and *m,o,o,m,o,o,m,o,o,m,o,o*-dodecaphenylene (**12**).

3: Colorless plates from benzene; mp 403°C (lit,[8b] 382°C); 799 mg (14%); UV λ_{max} (ε) 235 (95700) and 242 nm (sh) (87300) (lit,[8b] λ_{max} (log ε) 235 (4.98)). (Found: C, 94.62; H, 5.28%; M^+, 456).

12: Colorless needles from benzene; mp 444°C; 73 mg (1.3%); UV λ_{max} (ε) 195 (136400), 230 (121600), and 252 nm (sh) (79200). Found: C, 94.78; H, 5.25%; M^+, 912. Calcd for $C_{72}H_{48}$: C, 94.70; H, 5.30%; M^+, 912.

Preparation of o,o,p,o,o,p-*Hexaphenylene (4)*. The Grignard reagent prepared from **24c** (9.70 g) and magnesium turnings (1.22 g) in T-B (1:1) (80 ml),[30] after dilution with T-B (1:1) (120 ml) followed by addition of anhydrous copper(II) chloride (8.60 g), was worked up as described for **1**. The benzene extract was dissolved in benzene, and then allowed to stand overnight. The precipitate formed was collected and recrystallized from benzene to afford **4** (540 mg). The filtrates, after removal of the solvent, were subjected to a chromatography on alumina with C-B (4:1) to give *p*-terphenyl (**33**) (105 mg). Subsequent elutions with C-B (4:1) and C-B (2:1) provided an additional **4** (230 mg).

4: Colorless cubes from benzene; mp 446°C; 770 mg (14%); UV λ_{max} (ε) 198 (69300), 203 (sh) (66000), 236 (42300), 284 (34000), and 288 nm (sh) (33600). Found: C, 94.98; H, 5.13%; M^+, 456. Calcd for $C_{36}H_{24}$: C, 94.70; H, 5.30%; M^+, 456.

Preparation of m,o,p,m,o,p-*Hexaphenylene (5)*. The Grignard reagent prepared from **25c** (7.76 g) and magnesium turnings (0.98 g) in T-B (2:1) (90 ml), after dilution with T-B (2:1) (110 ml), was treated with anhydrous copper(II) chloride (6.80 g) as described for **1**. The benzene extract was chromatographed on alumina with C-B (4:1). The repeated fractional crystallizations of the eluate from hexane-benzene afforded **33** (125 mg) and **5**.

5: Colorless needles from hexane-benzene; mp 292.2°C; 630 mg (14%); UV λ_{max} (ε) 195 (76800), 206 (77800), 246 (80300), and 264 nm (sh) (43600). Found: C, 94.63; H, 5.04%; M^+, 456. Calcd for $C_{36}H_{24}$: C, 94.70; H, 5.30%; M^+, 456.

Preparation of o,p,o,p,o,p-*Hexaphenylene (6)*. To a mixture of two kinds of di-Grignard reagents prepared from **24c** (3.88 g, 10 mmol) and **31c** (19.41 g, 50 mmol), magnesium turnings (2.92 g, 120 mmol), and T-B (2:1) (150 ml), after dilution with T-B (1:2) (150 ml), anhydrous copper(II) chloride (20.4 g, 150 mmol) was added. The mixture was refluxed with stirring for 5 h, and hydrolyzed with a mixture of ammonium chloride (24 g), concentrated hydrochloric acid (48 ml), and water (480 ml), and then the precipitate formed was filtered. The benzene extract of the filtrate was washed with water and then dried. The precipitate was extracted with hot benzene. The combined benzene extract, after removal of the solvent, was treated with 800 ml of hot C-B (4:1) to be separated into soluble and insoluble parts. The benzene solution of the latter was allowed to stand for 2 d to separate out colorless, transparent cubes and an amorphous precipitate. The cubes were separated by decantation followed by several crystallizations from benzene to give *o,p,p,o,p,p,o,p,p*-nonaphenylene (**13**) (350 mg). The former was subjected to a chromatography on alumina with C-B (4:1) and C-B (2:1) to provide **6** and an additional **13** (163 mg).

6: Colorless needles from hexane; mp 312°C; 734 mg (16%); UV λ_{max} (ε) 188 (sh) (91500), 200 (96500), 245 (43700), and 276 nm (sh) (13500). Found: C, 94.95; H, 5.11%; M^+, 456. Calcd for $C_{36}H_{24}$: C, 94.70; H, 5.30%; M^+, 456.

13: Colorless cubes from benzene; mp 488°C (lit,[8a] 492°C); 513 mg (4.5%); UV λ_{max} (ε) 203 (133500), 279 (89100), and 320 nm (sh) (21900) (lit,[8a] 282.5 nm (82300) in $CHCl_3$). (Found: C, 94.69; H, 5.23%; M^+, 684).

Preparation of m,o,p,o,p,o-*Hexaphenylene (7)*. To a solution of two kinds of di-Grignard compounds prepared from **22c** (3.88 g) and **31c** (19.41 g), magnesium turnings (2.92 g), and T-B (1:1) (150 ml), after dilution with T-B (1:1) (150 ml), anhydrous copper(II) chloride (20.4 g) was added,

and then the mixture was worked up as described for **6**. The benzene extract, after removal of the solvent, was treated with hot C-B (4:1) (1000ml) to be separated into soluble and insoluble parts. Several crystallizations of the latter from benzene afforded **13** (180mg). The former was chromatographed on alumina with C-B (4:1) and C-B (1:1) to give two fractions. The repeated fractional crystallizations of the first from C-B (1:1) afforded **3** (148mg, 6.5%) and **7**. The second, upon recrystallization from benzene, provided an additional **13** (116mg; total yield 2.6%).

7: Colorless cubes from benzene; mp 308°C; 205mg (4.5%); UV λ_{max} (ε) 198 (86600), 205 (sh) (84900), and 237nm (46600). Found: C, 94.67; H, 5.28%; M^+, 456. Calcd for $C_{36}H_{24}$: C, 94.70; H, 5.30%; M^+, 456.

Preparation of m,o,m,o,m,o-*Hexaphenylene (8).* A mixture of two kinds of di-Grignard reagents prepared from **21c** (3.88g) and **22c** (3.88g), magnesium turnings (980mg), and T-B (2:1) (75ml), after dilution with T-B (2:1) (75ml), was terated with anhydrous copper(II) chloride (6.88g) as described for **6**. The benzene extract was chromatographed on alumina with C-B (9:1) and C-B (5:1) to give **3** (100mg, 4.4%), **2** (75mg, 3.3%), and **8**.

8: Colorless needles from hexane; mp 270.8°C; 105mg (2.3%); UV λ_{max} (ε) 189 (85600), 207 (73200), 233 (81800), and 254nm (sh) (36000). Found: C, 94.80; H, 5.35%; M^+, 456. Calcd for $C_{36}H_{24}$: C, 94.70; H, 5.30%; M^+, 456.

Preparation of m,m,m,o,m,o-*Hexaphenylene (9).* A mixture of two kinds of di-Grignard reagents prepared from **22c** (5.82g), **23c** (3.88g), and magnesium turnings (1.22g) in T-B (1:1) (60ml), after dilution with T-B (1:1) (80ml) followed by addition of anhydrous copper(II) chloride (8.60g), was worked up as described for **6**. After hydrolysis of the reaction mixture, the precipitate formed was filtered off. Recrystallization of the precipitate from xylene gave *m*-hexaphenylene (**14**). The benzene extract of the filtrate, after removal of the solvent, was chromatographed on alumina with C-B (4:1) and C-B (1:1). The repeated fractional crystallizations of the eluate from benzene-hexane provided **9** and **3** (168mg, 4.9%).

9: Colorless prisms from hexane; mp 315°C; 150mg (3.3%); UV λ_{max} (ε) 190 (87500), 240 (107300), and 252nm (sh) (65700). Found: C, 94.82; H, 5.40%; M^+, 456. Calcd for $C_{36}H_{24}$: C, 94.70; H, 5.30%; M^+, 456.

14: Colorless needles from xylene; mp 505°C (lit,[5b] 507—508°C); 94mg (4.1%); UV λ_{max} (ε) 191 (99800), 198 (sh) (88100), and 247nm (118900) (lit,[5b] 251 (119000) in THF). (Found: C, 94.42; H, 5.59%; M^+, 456).

Preparation of m,o,p,p,o,m,p-*Heptaphenylene (10).* A mixture of two kinds of di-Grignard reagents prepared from **26c** (3.88g), **29c** (4.64g), and magnesium turnings (980mg) in T-B (1:1) (150ml), after dilution with T-B (1:1) (150ml), was treated with anhydrous copper(II) chloride (6.88g) as described for the preparation of **6**. The soluble part of the benzene extract in C-B (4:1) (500ml) was chromatographed on alumina with C-B(4:1) and C-B (1:1) to afford **10**.

10: Colorless needles from benzene; mp 341°C; 266mg (5.0%); UV λ_{max} (ε) 198 (87200), 205 (sh) (84600), 267 (71400), and 312nm (sh) (16800). Found: C, 94.59; H, 5.47%; M^+, 532. Calcd for $C_{42}H_{28}$: C, 94.70; H, 5.30%; M^+, 532.

Preparation of m,m,m,m,p,o,p-*Heptaphenylene (11).* To a solution of two kinds of di-Grignard compounds prepared from **28c** (5.4g), **30c** (15.6g), and magnesium turnings (2.93g) in T-B (2:1) (200ml), after dilution with T-B (2:1) (200ml), anhydrous copper(II) chloride (20.6g) was added, and then the mixture was worked up as described for **6**. The reaction mixture was treated with benzene to be separated into soluble and insoluble parts. Recrystallization of the latter from xylene gave **14** (185mg). The former was subjected to a chromatography on alumina progressively with C-B (4:1) and with C-B (1:1) to provide an additional **14** (38mg, total yield 2.9%) and **11**, respectively.

11: Colorless needles from benzene; mp 378°C; 273mg (5.1%); UV λ_{max} (ε) 202 (38700), 256 (107700), and 284nm (infl) (24100). Found: C, 94.68; H, 5.41%; M^+, 532. Calcd for $C_{42}H_{28}$: C, 94.70; H, 5.30%; M^+, 532.

The author wishes to thank Professor Aritsune Kaji of Kyoto University for his valuable discussions and suggestions. Thanks are due to Nippon Shinyaku Co., Ltd. and Mr. Yasuhiro Fujiwara of this university for the measurements of ^1H NMR spectra.

References

1) This paper forms Part XIII of "Studies of Polyphenyls and Polyphenylenes." The preceding paper, Part XII: Y. Fujioka, S. Ozasa, K. Sato, and E. Ibuki, *Chem. Pharm. Bull.*, in press.

2) a) S. Ozasa, N. Hatada, Y. Fujioka, and E. Ibuki, *Bull. Chem. Soc. Jpn.*, **53**, 2610 (1980); b) E. Ibuki, S. Ozasa, Y. Fujioka, and H. Kitamura, *Chem. Pharm. Bull.*, **28**, 1468 (1980); c) S. Ozasa, Y. Fujioka, M. Fujiwara, and E. Ibuki, *ibid.*, **28**, 3210 (1980); d) S. Ozasa, Y. Fujioka, M. Tsukada, and E. Ibuki, *ibid.*, **29**, 344 (1981); e) S. Ozasa, Y. Fujioka, M. Okada, H. Izumi, and E. Ibuki, *ibid.*, **29**, 370 (1981); f) E. Ibuki, S. Ozasa, Y. Fujioka, M. Okada, and Y. Yanagihara, *ibid.*, **30**, 2369 (1982); g) *cf.* E. Ibuki, S. Ozasa, and K. Murai, *Bull. Chem. Soc. Jpn.*, **48**, 1868 (1975).

3) a) W. S. Rapson, R. G. Shuttleworth, and J. N. van Niekerk, *J. Chem. Soc.*, **1943**, 326; b) W. S. Rapson, H. M. Schwartz, and E. T. Stewart, *ibid.*, **1944**, 73.

4) a) G. Wittig and G. Lehmann, *Chem. Ber.*, **90**, 875 (1957); b) G. Wittig and G. Klar, *Justus Liebigs Ann. Chem.*, **704**, 91 (1967); c) G. Wittig and K. -D. Rumpler, *ibid.*, **751**, 1 (1971).

5) a) H. A. Staab and F. Binnig, *Tetrahedron Lett.*, **1964**, 319; b) H. A. Staab and F. Binnig, *Chem. Ber.*, **100**, 293 (1967); c) H. Bräunling, F. Binnig, and H. A. Staab, *ibid.*, **100**, 880 (1967); d) H. A. Staab and F. Binnig, *ibid.*, **100**, 889 (1967); e) H. A. Staab and C. Wünsche, *ibid.*, **101**, 887 (1968); f) H. Irngartinger, L. Leiserowitz, and G. M. J. Schmidt, *ibid.*, **103**, 1132 (1970).

6) T. Kauffmann, *Angew. Chem., Int. Ed. Engl.*, **18**, 1 (1979).

7) a) F. Vögtle, M. Atzmuller, W. Wehner, and J. Grütze, *Angew. Chem.*, **89**, 338 (1977); b) F. Vögtle and E. Hammerschmidt, *Angew. Chem., Int. Ed. Engl.*, **17**, 268 (1978).

8) a) H. Meyer and H. A. Staab, *Justus Liebigs Ann. Chem.*, **724**, 30 (1969); b) G. Wittig, S. Fischer, and G. Reiff, *ibid.*, **1973**, 495; c) H. Meyer, Dissertation, University of Heidelberg, Heidelberg, Germany, 1969.

9) G. Wittig and F. Bickelhaupt, *Chem. Ber.*, **91**, 883 (1958).

10) H. A. Staab, H. Bräunling, and K. Schneider, *Chem. Ber.*, **101**, 879 (1968).

11) A. Mckillop, L. F. Elsom, and E. C. Taylor, *J. Am. Chem. Soc.*, **90**, 2423 (1968).
12) A. S. Kende, L. S. Liebeskind, and D. M. Braitsch, *Tetrahedron Lett.*, **1975**, 3375.
13) Precise published data for **2** have not yet been found.
14) By the techniques of gas chromatography and mass spectrometry, it was proved that the by-products consisted of polyphenyls, their mono- and dihalo derivatives originating from the starting di-Grignard reagents, and higher coupling products of these.
15) The melting point (446 °C) of **4**, for example, can be compared with that of the open-chain analogues (2,2′-di(4-biphenylyl)biphenyl: mp 191—192.5 °C (Ref. 2b); 2,4′-di(2-biphenylyl)biphenyl: mp 154.9 °C (Ref. 2f)).
16) a) J. E. Stewart and M. Hellmann, *J. Res. Natl. Bur. Stand.*, **60**, 125 (1958); b) L. J. Bellamy, "The Infrared Spectra of Complex Molecules," 3rd ed, Chapman and Hall Ltd., London (1975), pp. 72—96; c) J. Dale, *Acta Chem. Scand.*, **11**, 640 (1957); d) R. C. Doss and P. W. Solomon, *J. Org. Chem.*, **29**, 1567 (1964); e) S. Sandroni and F. Geiss, *Fresenius' Z. Anal. Chem.*, **220**, 321 (1966).
17) a) D. J. Cram and H. Steinberg, *J. Am. Chem. Soc.*, **73**, 5691 (1951); b) T. Kauffmann and H. Lexy, *Angew. Chem., Int. Ed. Engl.*, **17**, 755 (1978).
18) J. S. Waugh and R. W. Fessenden, *J. Am. Chem. Soc.*, **79**, 846 (1957); D. J. Cram, C. K. Dalton, and G. R. Knox, *ibid.*, **85**, 1088 (1963); H. Hopf, *Angew. Chem.*, **84**, 471 (1972).
19) J. Dale, *Acta Chem. Scand.*, **11**, 650 (1957); H. Suzuki, *Bull. Chem. Soc. Jpn.*, **32**, 1340 (1959).
20) ϕ, o, m, and p refer to phenyl and *o*-, *m*-, and *p*-phenylene rings, respectively.
21) E. J. Gallegos, *J. Phys. Chem.*, **71**, 1647 (1967).
22) The program used was the one presented by Tominaga: N. Tominaga, *Kagaku No Ryoiki*, **36**, 724 (1982).
23) J. A. Cade and A. Pilbeam, *Chem. Ind. (London)*, **1959**, 1578.
24) Recrystallization of the solid and the eluate with benzene or the distillate (bp 150—240 °C/400 Pa) provided 3,3′-dinitrobiphenyl as by-product: Mp 204.6 °C (lit, 202 °C: Ref. 25); yield 60 and 52% in the preparation of **21a** and **23a**, respectively.
25) E. Ibuki, S. Ozasa, and H. Kitamura, *Nippon Kagaku Zasshi*, **92**, 361 (1971).
26) Recrystallization of the distillate gave 2,2′-(mp 125.1 °C (lit, 122.5—124.5 °C: Ref. 2g)) and 3,3′-dinitrobiphenyl as by-products in the preparation of **22a**, **24a**, and **25a**, and **26a—28a**, respectively (yield: 44—54%).
27) L. H. Klemm, W. O. Johnson, and A. Weisert, *J. Heterocycl. Chem.*, **8**, 763 (1971).
28) S. E. Hazlet and C. A. Dornfeld, *J. Am. Chem. Soc.*, **66**, 1781 (1944).
29) E. Ibuki, S. Ozasa, Y. Fujioka, M. Okada, and K. Terada, *Bull. Chem. Soc. Jpn.*, **53**, 821 (1980).
30) The preparation of the di-Grignard reagent required a 5 h refluxing with a small amount of iodine added.

Preparation and ESR Studies of New Stable Tocopheroxyl Model Radicals

Kazuo MUKAI,* Kimiko TAKAMATSU, and Kazuhiko ISHIZU
Department of Chemistry, Faculty of Science, Ehime University, Matsuyama 790
(Received May 24, 1984)

New tocopherol (vitamin E) model compounds (tocopherol **1**; 7-*t*-butyl-2,2-dimethyl-6-chromanol, tocopherol **2**; 7-*t*-butyl-2,2,5-trimethyl-6-chromanol, and tocopherol **3**; 5,7-diisopropyl-2,2-dimethyl-6-chromanol) have been synthesized by condensation of 2-methyl-3-buten-2-ol to the corresponding alkylhydroquinone. Electron spin resonance measurements were performed for the tocopheroxyl radicals obtained from the above tocopherol model compounds by oxidizing the phenol precursors with PbO_2 in toluene. The proton hyperfine coupling constants and g_{iso}-values were determined. The tocopheroxyl radicals **2** and **3** having large alkyl substituents at both ortho positions (C-5 and C-7) are fairly stable, and the radical stability, as measured by the intensities of the ESR signals, increases in the order tocopheroxyl **1**<α-tocopheroxyl model<tocopheroxyl **2**<tocopheroxyl **3**. The result suggests that the *in vitro* antioxidant activities of tocopherols **2** and **3** are higher than that of α-tocopherol model.

It has been well recognized that tocopherols (vitamin E) function as natural antioxidants, particularly in biomembranes by protecting unsaturated lipids from peroxidation.[1-3] The ESR study of the tocopheroxyl radicals obtained by the oxidation of tocopherols is of biological interest since they are involved in vitamin E reactions. Therefore, recently, some workers have reported the ESR spectra of α-, β-, γ-, and δ-tocopheroxyl radicals and their model compounds, and determined the proton hyperfine splittings exactly.[4-10]

Generally, in these tocopheroxyl radicals, replacement of ortho methyl groups at C-5 and C-7 positions with protons lowers the concentration of the tocopheroxyl radicals in solution, as well as the longevity of the radicals. The approximate order of stability, as measured by the intensities of the ESR signals, was: α-, β-, γ-, and δ-tocopheroxyl.[8] The above relative stabilities of the tocopheroxyl radicals correlate well with their biological activities[11] which yield: α->β->γ->δ-tocopherol, and with *in vitro* tests of their relative reactivities toward peroxide radical[12] and singlet oxygen[13] which yield the same order. Further, α-tocopherol and α-tocopherol model, where the isoprenoid side chain is replaced by a methyl group, have similar *in vitro* antioxidant activity,[12] although the latter compound generally shows little or no vitamin E activity *in vivo*.[14,15] These findings suggest that the presence of methyl groups at C-5 and C-7 positions in tocopherols and their model compounds is of great importance to their antioxidant action.

In the present work, in order to obtain further information on such antioxidant action, we have prepared three kinds of new tocopherol model compounds (tocopherol **1**; 7-*t*-butyl-2,2-dimethyl-6-chromanol, tocopherol **2**; 7-*t*-butyl-2,2,5-trimethyl-6-chromanol, and tocopherol **3**; 5,7-diisopropyl-2,2-dimethyl-6-chromanol) (see Fig. 1), and have succeeded in measuring well-resolved ESR spectra of tocopheroxyl-type radicals obtained by the PbO_2 oxidation of the above tocopherol model compounds in toluene at room temperature. The proton hyperfine coupling constants and g_{iso}-values were correctly determined for each radical. From the results, the electronic structure of the tocopheroxyl radicals has been discussed. Especially, the tocopheroxyls **2** and **3** having large alkyl groups at both ortho positions (C-5 and C-7) showed higher radical stability than that of α-tocopheroxyl model, as measured by the ESR intensity change. The result suggests that tocopherols **2** and **3** have higher *in vitro* antioxidant activity than that of α-tocopherol model.

Experimental

Measurements. The ESR measurements were carried out using a JES-FE-2XG spectrometer equipped with a Takeda-Riken microwave frequency counter. The g-values were measured relative to the value of Li-TCNQ powder, calibrated with $(KSO_3)_2NO$ (g=2.0054).[16] All the ESR spectra have been measured in a sealed, degassed system. In all the cases, we made careful measurements of the decay of the ESR signal intensity for the tocopheroxyl radicals obtained by oxidizing the toluene solution of tocopherol precursors (1.0 ml, 5.0×10^{-3} M (1 M=1 mol dm^{-3})) with PbO_2 (0.7 g).

Preparation of Specimens. 2-*t*-Butyl-6-methylhydroquinone (mp 98.5—100.5 °C) (lit, 97—98 °C)[17] and 2,6-diisopropylhydroquinone (mp 108.5—110.0 °C) (lit, 105.5—106.0 °C)[17]

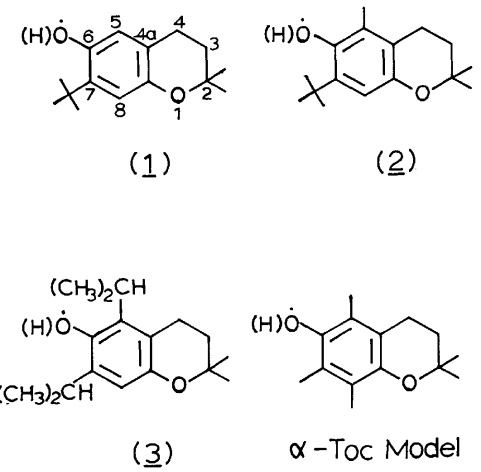

Fig. 1. Molecular structures of tocopherols and tocopheroxyls (**1**, **2**, **3**, and α-model), and the atomic numbering system.

were prepared from 2-*t*-butyl-6-methylphenol and 2,6-diisopropylphenol respectively by the standard procedure, as reported for the syntheses of the 2,3-, 2,5-, and 2,6-dimethylhydroquinone.[18]

2,2,5,7,8-Pentamethyl-6-chromanol (α-tocopherol model) and 2,2-dimethyl-6-chromanol (tocol model) were prepared according to the method of Nilsson *et al.*[19] Tocopherols **1**, **2**, and **3** were synthesized by condensation of 2-methyl-3-buten-2-ol to the corresponding alkylhydroquinone, according to a procedure similar to that used by Nilsson *et al.* to prepare α-, β-, γ-, and δ- tocopherol models.[19] Tocopherol **1** was also prepared by the reaction of 2,2-dimethyl-6-chromanol (tocol model) with isobutene in benzene in the presence of H_2SO_4.[20]

7-t-Butyl-2,2,5-trimethyl-6-chromanol (Tocopherol 2). 2-*t*-Butyl-6-methylhydroquinone (4.0 g, 22 mmol) was dissolved in formic acid (99%) (50 ml) and THF (tetrahydrofuran) (5 ml), and the solution was heated to reflux. A THF (2 ml) solution of 2-methyl-3-buten-2-ol (1.9 g, 22 mmol) was added dropwise slowly during 1 h, and the refluxing was continued for an additional 3 h with stirring. The reaction mixture was poured onto crushed ice (150 g), and extracted with diethyl ether (5×25 ml). Petroleum ether (bp 40—50 °C) (25 ml) was added to the combined diethyl ether extracts and the mixture was washed with water (5×25 ml). After removal of the solvent, the residue was dissolved in methanol (75 ml), 1 ml of concd HCl was added, and the solution was refluxed for 20 min to hydrolyze formate of **2** produced. The methanol was then evaporated, and the residue was taken up in diethyl ether (100 ml), washed with $NaHCO_3$ solution and with water, and the solution was dried over anhydrous sodium sulfate. The solvent was evaporated, and the residual oil was extracted three times with hot petroleum ether (bp 50—60 °C) (3×100 ml). After removal of the solvent, the oily solids obtained were recrystallized twice from benzene, giving white crystals (1.5 g). Mp 145.0—147.0 °C. Found: C, 77.39; H, 9.93%. Calcd for $C_{16}H_{24}O_2$: C, 77.38; H, 9.74%. UV spectrum (ethanol) λ_{max}=292 nm, log ε=3.55. NMR spectrum δ=1.29 ppm (6H, s, 2-CH_3), 1.37 (9H, s, 7-*t*-Bu), 1.77 (2H, t, 3-CH_2, *J*=6.7 Hz), 2.10 (3H, s, 5-CH_3), 2.60 (2H, t, 4-CH_2, *J*=6.7 Hz), 4.27 (1H, s, 6-OH), 6.54 (1H, s, 8-H); δ in $CDCl_3$ with TMS as an internal standard.

5,7-Diisopropyl-2,2-dimethyl-6-chromanol (Tocopherol 3). Tocopherol **3** was prepared from 2,6-diisopropylhydroquinone (4.0 g, 21 mmol) and 2-methyl-3-buten-2-ol (1.8 g, 21 mmol) in 50 ml of formic acid (99%) and 7 ml of THF, following a method similar to that used with tocopherol **2**. After hydrolysis of the formate of **3** and diethyl ether extraction, the diethyl ether was evaporated and the crude product was extracted several times with petroleum ether to remove the unreacted 2,6-diisopropylhydroquinone. After removal of the petroleum ether, a viscous oil remained. The residue was twice chromatographed on 50 g of silica gel with benzene as the eluting agent. The subsequent removal of the benzene from **3** solution left a slightly brownish oil; this was dissolved in diethyl ether (5 ml) and heated at 60 °C for 2 h under a vacuum (5×10^{-3} Torr (1 Torr≈133.322 Pa)) in order to completely remove the benzene solvent included in the crystal. Viscous oil (2.2 g). Found: C, 77.67; H, 10.26%. Calcd for $C_{17}H_{26}O_2$: C, 77.82; H, 9.99%. UV spectrum (ethanol) λ_{max}=295 nm, log ε=3.57. NMR spectrum δ=1.20 (6H, d, 5- or 7-$CH(CH_3)_2$, *J*=7.0 Hz), 1.28 (6H, s, 2-CH_3), 1.34 (6H, d, 5- or 7-$CH(CH_3)_2$, *J*=7.0 Hz), 1.73 (2H, t, 3-CH_2, *J*=6.6 Hz), 2.68 (2H, t, 4-CH_2 *J*=6.6 Hz), 2.64—3.46 (2H, m, 5- and 7-$CH(CH_3)_2$), 4.28 (1H, s, 6-OH), 6.48 (1H, s, 8-H); δ in $CDCl_3$ with TMS as an internal standard).

7-t-Butyl-2,2-dimethyl-6-chromanol (Tocopherol 1). Method A: To 1.0 g (5.6 mmol) of 2,2-dimethyl-6-chromanol (tocol model) in 13 ml of benzene, 5 drops of concd H_2SO_4 were added, and isobutene (6.0 g, 0.107 mol) was introduced for 3 h under stirring at 50 °C.[20] The reaction mixture was washed with water, and dried over anhydrous sodium sulfate. After removal of the benzene, the solids remained were recrystallized first from ligroin (bp 75—90 °C), and then from ethanol, giving white crystals (0.3 g). Mp 184.0—185.0 °C. Found: C, 76.70; H, 9.49%. Calcd for $C_{15}H_{22}O_2$: C, 76.88; H, 9.46%. UV spectrum (ethanol) λ_{max}=226 nm, log ε=3.63, λ_{sh}=230 nm, log ε=3.59, λ_{max}=298 nm, log ε=3.65. NMR spectrum δ=1.25 (6H, s, 2-CH_3), 1.29 (9H, s, 7-*t*-Bu), 1.74 (2H, t, 3-CH_2, *J*=6.7 Hz), 2.65 (2H, t,4-CH_2, *J*=6.7 Hz), 4.48 (1H, s, 6-OH), 6.38 (1H, s, 5- or 8-H), 6.70 (1H, s, 5- or 8-H); δ in $CDCl_3$ with TMS as an internal standard.

7-t-Butyl-2,2-dimethyl-6-chromanol (Tocopherol 1). Method B: Tocopherol **1** was prepared from 2-*t*-butylhydroquinone (3.7 g, 22 mmol) and 2-methyl-3-buten-2-ol (1.9 g, 22 mmol) in 50 ml of formic acid (99%) and 7 ml of THF, following a method similar to that used with **2**. The product was extracted and the formates were hydrolyzed as before. The oily residue obtained was chromatographed on 50 g of silica-gel with ether–petroleum ether (1:5) as the eluting agent. After removal of the solvent, the oily crystals remained were washed with petroleum ether, and recrystallized from ligroin, giving white crystals (0.5 g). Mp 183.0—185.0 °C. The ultraviolet and NMR spectra of the compound were shown to be identical with the material prepared by method A.

Results and Discussion

As has been described in our previous paper, the oxidation product of the α-, β-, γ-, δ-tocopherols, tocol and their model compounds with PbO_2 in toluene gives well-resolved hyperfine patterns, and the spectra were assigned to the primary tocopheroxyl-type radicals formed from the parent tocopherols by abstraction of a phenolic hydrogen atom.[8]

The tocopherol **1** was similarly oxidized with PbO_2 in toluene under vacuum. The ESR spectrum of this solution at room temperature is shown in Fig. 2a. The spectrum can be reconstracted with three groups of 1, 2 and 1 equivalent protons, showing three different hyperfine couplings 5.91, 1.22, and 1.04 G (1 G=10^{-4} T), respectively. These couplings will be assigned to a ring proton at C-5 (a_5^H=5.91 G), two equivalently interacting methylene protons at C-4 ($a_4^{CH_2}$=1.22 G), and a ring proton at C-8 (a_8^H=1.04 G), taking the analysis of α-, β-, γ-, and δ-tocopheroxyls into account. No interaction was observed for the methylene protons at C-3 and the *t*-butyl protons at C-7.

Similarly, the toluene solution ESR spectrum of the tocopheroxyl **2** radical has been measured (see Fig. 2b). The spectrum at 20 °C can be easily analyzed, giving three different hyperfine couplings, $a_5^{CH_3}$= 6.05 G, $a_4^{CH_2}$=1.55 G, and a_8^H=0.72 G.

The ESR spectrum of the tocopheroxyl **3** measured at 20°C is given in Fig. 2c. The spectrum can be reconstructed with four groups of 1, 2, 1, and 1 equivalent protons, showing four different hyperfine splittings (2.72, 1.39, 0.75, and 0.65 G), respectively. The assignment of the hyperfine splittings has been performed by a comparison of experimentally obtained hyperfine couplings with reported ones for α-, β-, γ-, and δ-tocopheroxyls[8] and 2,6-diisopropyl-4-methoxyphenoxyl radical.[17] The tentative assignments are as follows: a_7^{CH}=2.72 G, $a_4^{CH_2}$=1.39 G, a_8^{H}=0.75 G, and a_5^{CH}=0.65 G.

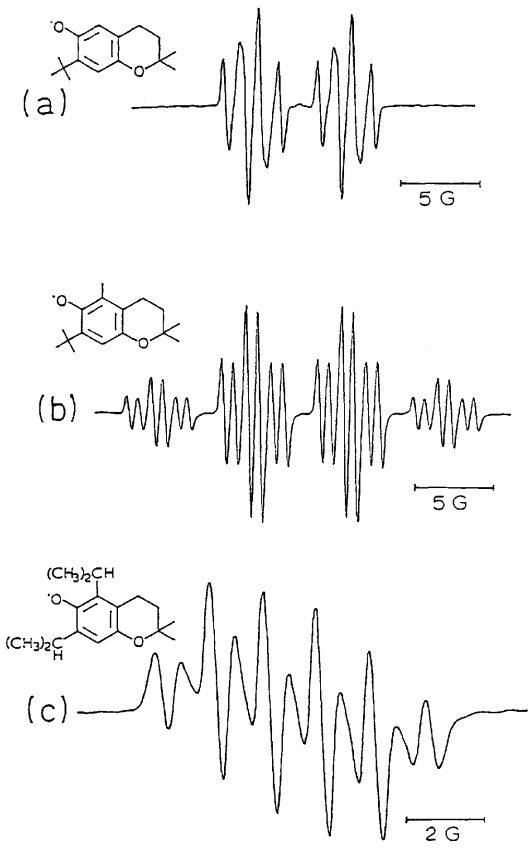

Fig. 2. ESR spectra of (a) tocopheroxyl **1**, (b) tocopheroxyl **2**, and (c) tocopheroxyl **3** in toluene at 20°C.

All the hyperfine couplings and g_{iso}-values obtained for these new tocopheroxyl model radicals are summarized in Table 1, together with those of α-tocopheroxyl model.[7]

The experimental values of spin densities (ρ_i^π) were estimated using the relations, $a_i^H=27\rho_i^\pi$, $a_i^{CH_3}=27\rho_i^\pi$, and $a_4^{CH_2}=54\cos^2 30°\times\rho_{4a}^\pi$, as performed for α-, β-, γ-, and δ-tocopheroxyl radicals.[7,8] All the experimental spin densities (ρ_i^π) calculated from the ESR hyperfine couplings are summarized in Table 1.

As is clear from the results listed in Table 1, unpaired spin density at C-5 position is similar to each other in these tocopheroxyl radicals. On the other hand, unpaired spin densities at C-8 position in **1**, **2**, and **3** are 8% higher, 25% lower, and 22% lower than that at C-8 position in α-tocopheroxyl model, respectively. Similarly, the unpaired spin densities at C-4a position are different each other in these tocopheroxyls. The result suggests that alkyl-substitution effect is considerable for the unpaired spin density at meta carbon atoms (C-4a and C-8 positions) with small negative spin densities. However, it is not clear at present how the above differences in the electronic structure of these tocopheroxyls relate to the antioxidant activity of tocopherols.

In order to obtain the information on the radical stability of these tocopheroxyls, radical decay measurements were performed on tocopheroxyls **1**, **2**, **3**, and α-tocopheroxyl model in toluene. Shown in Fig. 3 are typical plots of the ESR signal intensity as a function of time for the tocopheroxyls at 20°C. As it is clear from the results shown in Fig. 3, the order of stability, as measured by the intensities of the ESR signals, was tocopheroxyl **3**, **2**, and α-tocopheroxyl model. Especially, tocopheroxyl **3** is very stable and the ESR signal

Table 1. Hyperfine couplings (a_i^H) (in gauss), g_{iso}-values, and spin densities (ρ_i^π) of the tocopheroxyl radicals derived from tocopherol model compounds in toluene at 20°C

Tocopheroxyls		5	7	8	4	g_{iso}-values
		H	$C(CH_3)_3$	H	CH_2	
1	a_i^H	5.91[a]	—	1.04	1.22	2.00477[c]
	ρ_i^π	0.2189	—	−0.0385	−0.0301[b]	
		CH_3	$C(CH_3)_3$	H	CH_2	
2	a_i^H	6.05	—	0.72	1.55	2.00477
	ρ_i^π	0.2241	—	−0.0267	−0.0383	
		$CH(CH_3)_2$	$CH(CH_3)_2$	H	CH_2	
3	a_i^H	0.65	2.72	0.75	1.39	2.00472
	ρ_i^π	—	—	−0.0278	−0.0343	
		CH_3	CH_3	CH_3	CH_2	
α-Toc Model	a_i^H	5.94[d]	4.51	0.96	1.46	2.00471
	ρ_i^π	0.2200	0.1670	−0.0356	−0.0360	

a) Experimental errors ±0.04 G. 1 G=10^{-4} T. b) Spin densities at C-4a. c) Experimental errors ±0.00005. d) From Ref. 8.

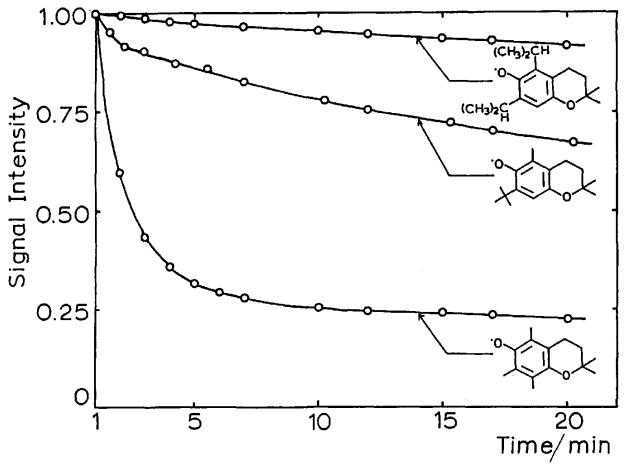

Fig. 3. Plots of the ESR signal intensity of tocopheroxyl **2**, tocopheroxyl **3**, and α-tocopheroxyl model at 20°C as a function of time.

intensity decreased to about half of the initial intensity after 20 h, because **3** has large isopropyl groups at both C-5 and C-7 positions. On the other hand, tocopheroxyl **1** has no alkyl substituent at C-5 position which is the most reactive site of the tocopheroxyl, and thus showed fast radical decay.

As described in a previous section, the relative radical stability of α-, β-, γ-, and δ-tocopheroxyls[8] is in agreement with *in vivo* and *in vitro* tests of their relative antioxidant activities which yield: α->β->γ->δ-tocopherol.[3,11-13] The result of the present radical decay measurement shows that tocopheroxyls **2** and **3** are more stable than α-tocopheroxyl. Therefore, we can expect that tocopherols **2** and **3** have higher antioxidant activity than α-tocopherol. Measurements of *in vitro* antioxidant activity of these tocopherols are now in progress.

We are very grateful to Professor Kenji Fukuzawa for his valuable discussions and suggestions. We also wish to thank Mr. Nobuyuki Kuwano and Miss Chie Morimoto for their help in the preparation of tocopherol **1**.

References

1) P. Schudel, H. Mayer, and O. Isler, "The Vitamins," 2nd ed, ed by W. H. Sebrell, Jr. and R. S. Harris, Academic Press, New York (1972), Vol. 5, pp. 168—218.
2) M. L. Scott, The Fat-Soluble Vitamins ed by H. F. DeLuca, Plenum Press, New York (1978), pp. 133—210.
3) K. Fukuzawa, A. Tokumura, S. Ouchi, and H. Tsukatani, *Lipids*, **17**, 511 (1982).
4) D. H. Kohl, J. R. Wright, and M. Weissman, *Biochim. Biophys. Acta*, **180**, 536 (1969).
5) W. Boguth and H. Niemann, *Biochim. Biophys. Acta*, **248**, 121 (1971).
6) T. Ozawa, A. Hanaki, S. Matsumoto, and M. Matsuo, *Biochim. Biophys. Acta*, **531**, 72 (1978).
7) K. Mukai, N. Tsuzuki, K. Ishizu, S. Ouchi, and K. Fukuzawa, *Chem. Phys. Lipids*, **29**, 129 (1981).
8) K. Mukai, N. Tsuzuki, S. Ouchi, and K. Fukuzawa, *Chem. Phys. Lipids*, **30**, 337 (1982).
9) M. Matsuo and S. Matsumoto, *Lipids*, **18**, 81 (1983).
10) J. Tsuchiya, E. Niki, and Y. Kamiya, *Bull. Chem. Soc. Jpn.*, **56**, 229 (1983).
11) B. Century and M. K. Horwitt, *Fed. Proc. Am. Soc. Exp. Biol.*, **24**, 906 (1965).
12) G. W. Burton and K. U. Ingold, *J. Am. Chem. Soc.*, **103**, 6472 (1981).
13) G. W. Grams and K. Eskins, *Biochemistry*, **11**, 606 (1972).
14) W. A. Skinner, R. M. Parkhurst, J. Scholler, P. Alaupovic, Q. E. Crider, and K. Schwarz, *J. Med. Chem.*, **10**, 657 (1967).
15) W. A. Skinner and R. M. Parkhurst, *Lipids*, **5**, 184 (1970).
16) J. J. Windle and A. K. Wiersma, *J. Chem. Phys.*, **39**, 1139 (1963).
17) J. Petranek and J. Pilar, *Collect. Czech. Chem. Commun.*, **35**, 830 (1970).
18) J. L. G. Nilsson, H. Sievertsson, and H. Selander, *Acta Pharm. Suecica*, **5**, 215 (1968).
19) J. L. G. Nilsson, H. Sievertsson, and H. Selander, *Acta Chem. Scand.*, **22**, 3160 (1968).
20) G. H. Stillson, D. W. Sawyer, and C. K. Hunt, *J. Am. Chem. Soc.*, **67**, 303 (1945).

Copper(II)-Poly(L-histidine) as an Enzyme Model for L-Ascorbate Oxidase

Jun-ichi UEDA and Akira HANAKI*
National Institute of Radiological Sciences, 4-9-1 Anagawa, Chiba 260
(Received June 13, 1984)

The autoxidation catalyzed by copper(II)-poly(L-histidine) was studied by a rapid-mixing spectrophotometric method. The reaction obeys Michaelis-Menten kinetics. The double reciprocal plots of the velocity against the concentrations, *i.e.* the Lineweaver-Burk plots, of ascorbate and of oxygen gave a straight line. A kinetic analysis of the Lineweaver-Burk plot of the reaction reveals that the autoxidation of ascorbate by Cu(II)-PLH proceeds a so-called Ping-Pong mechanism. Copper(II) ion associates with PLH. The rate of ascorbate autoxidation appeared to depend on the concentration of copper(II) ion in the PLH phase, which is designated as the average binding number. The copper(II) ion concentrated in the PLH phase is highly reactive and is likely to be perturbed by the addition of inert electrolytes. The labile copper(II) ion, which is concentrated in the polymer phase, may be the catalytically active species.

The copper-catalyzed autoxidation of ascorbate has been widely studied as a model of the enzyme reaction.[1,2] The catalytic activity of copper(II) ion is substantially dependent on the nature of the ligand and the coordination environment around the metal ion. Chloride ion was found to induce an increase in the catalytic activity of the copper(II) ion,[3] while ethylenediaminetetraacetic acid[4] or 1,10-phenanthroline[5] inhibited the oxidation. Of much interest is that the copper(II) complex of poly(L-histidine) (Cu(II)-PLH) shows a higher catalytic activity than copper(II) ions in their aqua or amino acidato complexes.[6] On the other hand, other cationic poly(amino acid)s, such as poly(L-lysine) and poly(L-arginine), exhibited little effect on the acceleration of the reaction.[4] The specific effect of PLH on the reaction, which is abolished in the presence of moderate concentration of inert electrolyte, is interpreted by the electrostatic effect of the polyelectrolyte on the concentration of the substrate involved in the close vicinity of the bound copper(II) ion.[6]

We consider that PLH participates not only in the concentration of the substrate by the electrostatic effect in the vicinity of the catalytically active site, but also in the modification of catalytic activity of copper(II) ion by the Cu(II)-PLH interaction. The purpose of this study is to examine how the reaction mechanism of autoxidation and the catalytic activity of copper(II) ions are altered in the presence of PLH.

Experimental

Materials. PLH was a product of Sigma Chemical Co. (lot 98c-5026, degree of polymerization 58, approximate molecular weight based on viscosity measurement 8000). The polymer dissolved in 0.01 mol dm^{-3} acetic acid was dialyzed against doubly distilled water and then lyophylized. L-Ascorbic acid, copper(II) perchlorate, and acetic acid were reagent grade chemicals, which were commercially available, and used without further purification. A stock solution of copper(II) perchlorate dissolved in doubly distilled water was standardized by the conventional complexometric titration with EDTA. The copper(II) solution was diluted by acetate buffer to an appropriate concentration. The ascorbic acid solution was freshly prepared just before kinetic runs.

Kinetic Procedure. The oxidation of ascorbate was conducted at 25 °C in a quartz flow-cell by using a rapid-mixing technique with a Union MX-7 mixing apparatus. Routinely, the reaction was carried out in 0.02 mol dm^{-3} acetate buffer and under 100% oxygen. The solutions of copper(II) ion and ascorbate were saturated with pure oxygen or nitrogen-oxygen mixture by bubbling prior to the kinetic run. The concentration of oxygen dissolved in the medium was determined electrometrically with a Beckman Fieldlab oxygen analyzer, which had been calibrated against air-saturated water. The reaction was started by mixing rapidly both the reactants. After the start of the reaction, the decrease of ascorbate concentration was recorded spectrophotometrically at 260nm with a Union 401 spectrophotometer. In the kinetic experiment, initial rates were determined at pH 3.6, 4.0, and 4.4 by a graphical method. The pH value of the solution was measured on a TOA DENPA HM-5A pH meter.

Equilibrium Dialysis. Equilibrium dialysis was performed according to the method of Yamaoka *et al.*[7] A 4ml plastic dialysis cell which was seperated to two chambers by a Visking cellulose membrane was used. In one chamber(A) was contained 2ml of copper(II) solution containing various amounts of PLH, and in another (B) 2ml of copper(II) solution. The initial concentrations of copper(II) in both chambers are set to be equal. The dialysis cell was shaken at room temperature for 18h to reach an equilibrium and then the concentration of copper(II) in the chamber(B) was determined by atomic absorption spectrophotometry with a HITACHI 170-70 Zeeman spectrometer. Since copper(II) adsorbed on the cellulose membrane is very small, total amount of copper(II) in the cell is considered to be constant. If PLH has an ability to bind with copper(II) ion, the copper(II) ion in the chamber (B) diffuses across the chamber (A). Then, the concentration of copper(II) increases in the chamber (A), in which both free and PLH-bound copper(II) ions are contained. Under the equilibrium condition, the concentration of free copper(II) ion, $[Cu^{2+}]$, is equal in both chambers. The difference of the copper(II) concentration between the initial and equilibrated states corresponds to the quantity of the PLH-bound copper(II). The equation describing those relations is shown in Eq. 1.

$$[Cu^{2+}]_{bound} = \{[Cu^{2+}]_o - [Cu^{2+}]\} \times \{(V_1+V_2)/V_1\}, \quad (1)$$

where $[Cu^{2+}]_{bound}$ and $[Cu^{2+}]_o$ represent the concentration of

PLH-bound copper(II) ion in the chamber(A) and the initial concentration of copper(II) ion, and V_1 and V_2 are the volumes of the solutions in the chambers(A) and (B), respectively. The concentration of bound copper(II) ion in the polymer phase constructing by PLH, which is usually termed as the average binding number, $\bar{\nu}$, is given by Eq. 2.

$$\bar{\nu} = [Cu^{2+}]_{bound}/[PLH]_{total} \quad (2)$$

Results

1) Effect of PLH. The copper-catalyzed autoxidation of ascorbate was enhanced by the addition of PLH. In Table 1 is summarized the rate of oxidation at various concentrations of ascorbate. Obviously, the rate was observed to increase at least fivefold by the addition of 5 mg dm^{-3} PLH over the range of 0.5—10×10^{-5} mol dm^{-3} ascorbate. The reaction obeys the Michaelis-Menten mechanism. In the absence of PLH, the rate increased linearly with an increase of the ascorbate concentration.

The catalytic activity of copper(II) ion depends closely on the concentration of PLH added. Though PLH itself does not possess the catalytic activity, it enhances the autoxidation of ascorbate probably by complexing with copper(II) ion. When the rate is plotted against the amounts of PLH added, the rate profile displays a bell-shaped curve with the maximum varied depending on the pH of the medium. Some examples are shown in Fig. 1, where the total concentration of copper(II) ion is fixed at constant.

2) Effect of pH. The rate of the autoxidation varied depending on pH as shown in Fig. 2. The rate of oxidation catalyzed by free copper(II) ion increased with pH throughout the range measured, whereas the Cu(II)-PLH-catalyzed oxidation showed a different behavior. The pH-rate profile displayed a bell-shaped curve with a maximum at pH 4.3.

3) Effect of Varying Concentrations of Ascorbate. In the copper-catalyzed autoxidation, the double reciprocal plot of the rate against the ascorbate concentration, *i.e.* Lineweaver-Burk plot, gives a straight line. The

TABLE 1. RATE OF ASCORBATE OXIDATION IN THE PRESENCE AND ABSENCE OF PLH

[Ascorbate]	V_{Cu}	$V_{Cu\text{-}PLH}$	$V_{Cu\text{-}PLH}$
10^{-5}mol dm^{-3}	10^{-6}mol dm^{-3} min^{-1}	10^{-6}mol dm^{-3} min^{-1}	V_{Cu}
0.5	0.3	4.5	15
1.0	0.5	7.3	15
2.5	1.4	13	9
5.0	2.4	18	8
10	5.0	24	5

$[Cu^{2+}]_o$=6.0×10^{-6}mol dm^{-3}, [PLH]=5 mg dm^{-3}, pH 4.0 (0.02 mol dm^{-3} acetate buffer).

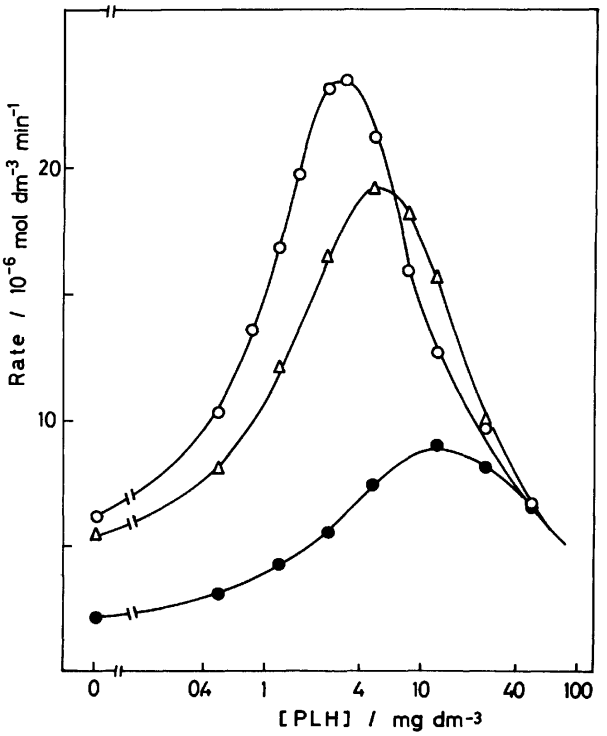

Fig. 1. Plot of the oxidation rate against PLH concentration.
$[Cu^{2+}]_o$=6.0×10^{-6} mol dm^{-3}, [Ascorbate]=5.0×10^{-5} mol dm^{-3}, pH=3.6(●), 4.0(△), and 4.4(○).

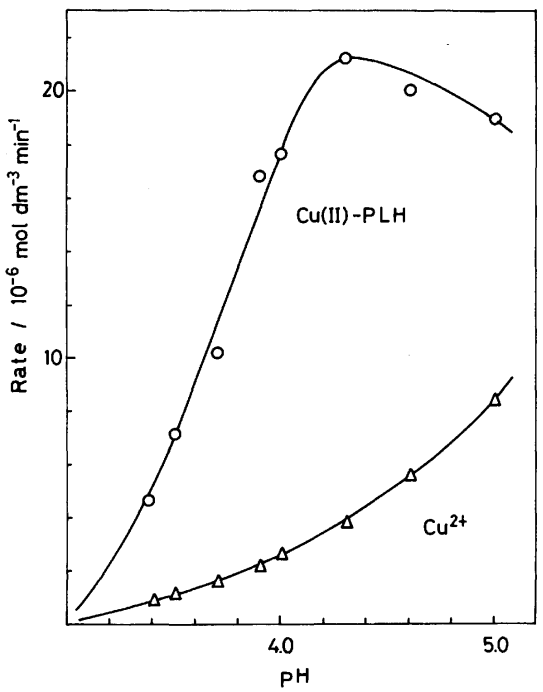

Fig. 2. pH profile of oxidation rate.
$[Cu^{2+}]_o$=6.0×10^{-6} mol dm^{-3}, [PLH]=5 mg dm^{-3}, [Ascorbate]=5.0×10^{-5} mol dm^{-3}.

families of straight lines of those double reciprocal plots obtained by changing the concentrations of oxygen intersect at a point on the abscissa as shown in Fig. 3A. The intercepts at the ordinate and at the abscissa correspond respectively to the reciprocals of the apparent maximal velocity, V'_{max}, and of the half saturation concentration of ascorbate, $K_{0.5}$, for the reaction. The value of V'_{max} and $K_{0.5}$ at 5×10^{-5} mol dm^{-3} ascorbic acid are shown in Table 2. On the other hand, in the Cu(II)-PLH-catalyzed oxidation, the double reciprocal plot of the rate against the ascorbate concentration at a fixed oxygen concentration gives straight line as shown in Fig. 3B. A series of the double reciprocal plots for the various concentrations of oxygen appears to be parallel. V'_{max} and $K_{0.5}$ at 5×10^{-5} mol dm^{-3} ascorbic acid are given in Table 2.

4) Effect of Varying Concentrations of Oxygen. Both the rates of the copper(II)- and Cu(II)-PLH-

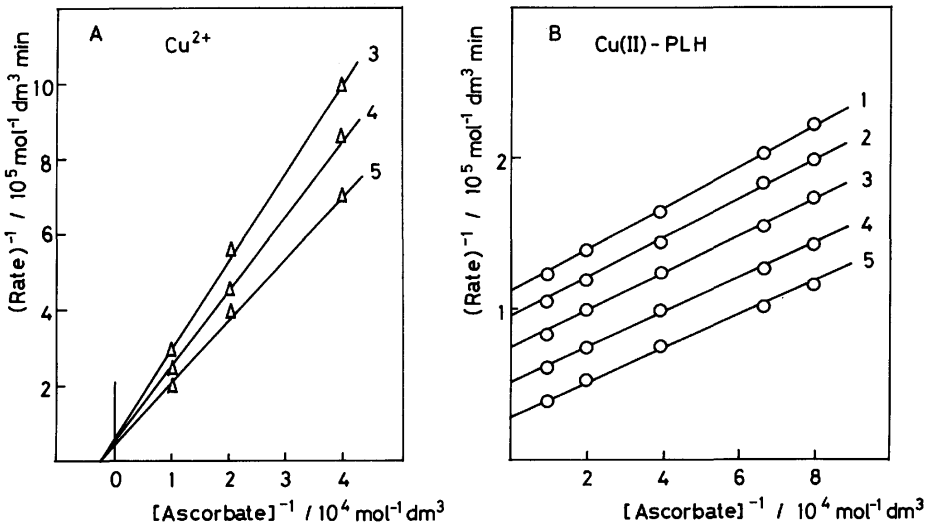

Fig. 3. Double reciprocal plot of the rate against the concentration of ascorbate.
$[Cu^{2+}]_0=6.0\times10^{-6}$ mol dm^{-3}, [PLH]=5 mg dm^{-3}, [O_2]=(1) 0.27, (2) 0.43, (3) 0.55, (4) 0.87, and (5) 1.34×10^{-3} mol dm^{-3}, pH 4.0.

TABLE 2. KINETIC PARAMETER FOR Cu(II)-PLH- AND COPPER(II)-CATALYZED OXIDATION

Substrate	$K_{0.5}/10^{-4}$mol dm^{-3}		$V'_{max}/10^{-5}$mol dm^{-3} min^{-1}	
	Cu(II)-PLH	Cu^{2+}	Cu(II)-PLH	Cu^{2+}
Ascorbate	0.3	3.3	3.0	2.0
Oxygen	12.0	5.3	3.2	0.4

[Ascorbate]=5×10^{-5} mol dm^{-3}, [Oxygen]=1.3×10^{-3} mol dm^{-3}, $[Cu^{2+}]=6\times10^{-6}$ mol dm^{-3}, [PLH]=5 mg dm^{-3}, pH 4.0 (0.02 mol dm^{-3} acetate buffer).

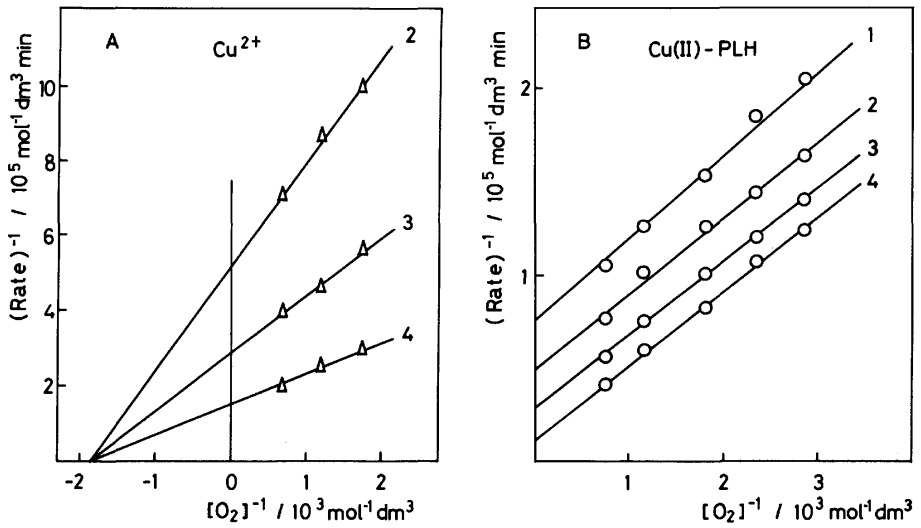

Fig. 4. Double reciprocal plot of the rate against the concentration of oxygen.
$[Cu^{2+}]_0=6.0\times10^{-6}$ mol dm^{-3}, [PLH]=5 mg dm^{-3}, [Ascorbate]=(1) 1.5, (2) 2.5, (3) 5.0, and (4) 10×10^{-4} mol dm^{-3}, pH 4.0.

catalyzed oxidation depended on the concentration of oxygen. In the copper(II)-catalyzed autoxidation, the families of the double reciprocal plots obtained by changing the concentrations of ascorbate intersect at a point on the abscissa as shown in Fig. 4A. The value of V'_{max} and $K_{0.5}$ at 1.3×10^{-3} mol dm^{-3} oxygen are shown in Table 2. In the Cu(II)-PLH-catalyzed reaction, a series of the double reciprocal plots for the various concentrations of ascorbate appears to be parallel as shown in Fig. 4B. V'_{max} and $K_{0.5}$ at 1.3×10^{-3} mol dm^{-3} oxygen are shown in Table 2. The presence of parallel Lineweaver-Burk plots for various concentrations of another reactant indicates a possibility that the reaction proceeds by a Ping-Pong mechanism[8] as discussed later.

5) Effect of Anion. Inert electrolyte such as acetate ion modified the catalytic activity. The effect of anion at various concentrations on the rate is shown in Fig. 5. The effect of anion is shown to vary depending on the concentration of PLH-bound copper(II) and pH. At pH 4.4, the addition of increasing amounts of acetate ion brings a rapid reduction in the rate at 1.1 mmol Cu/g PLH, while a slow reduction at 0.97 mmol Cu/g PLH. These results indicate that the highly active Cu(II)-PLH complex which contains more than 1.0 mmol Cu/g PLH is apt to undergo strucural perturbation by inert electrolyte. At pH 4.0, such distinct effect by anion was not shown.

Discussion

1) Reaction Mechanism. The presence of PLH enhances remarkably the catalytic activity of copper(II) ion and alters the mechanism of the reaction. In the copper(II)-catalyzed autoxidation, a series of the Lineweaver-Burk plots for the various concentrations of ascorbate or oxygen intersect on the abscissa as shown in Figs. 3A and 4A. In the autoxidation catalyzed by Cu(II)-PLH, on the contrary, a series of the Lineweaver-Burk plots was parallel. Parallel Lineweaver-Burk plots observed for various concentrations of another reactant, which are obtained in the reaction by several oxidase such as ascorbate oxidase,[9] are explained by the Ping-Pong mechanism. In the Ping-Pong mechanism, the oxidation of the substrate by the catalyst (Eq. 3) and the reoxidation of the catalyst (Eq. 4) proceed alternatively.

$$S + Cu(II)^* \underset{k_{-1}}{\overset{k_1}{\rightleftharpoons}} Cu(II)^*\text{-}S \xrightarrow{k_2} Cu(I)^* + P, \quad (3)$$

$$Cu(I)^* + O_2 \xrightarrow{k_3} Cu(II)^* + O_2^-, \quad (4)$$

where Cu(II)* and Cu(I)* stand for the oxidized and reduced forms of the catalyst, respectively. S and P stand for the substrate and the product, respectively. The values of k are rate constants. O_2^- produced is probably either dismuted to O_2 and H_2O_2 or reduced to H_2O_2. The mechanism for Cu(II)-PLH-catalyzed oxidation resembles kinetically that of the enzyme reaction.

The steady state rate equation for this mechanism is

$$V_{max}/v = 1 + K_{0.5}/[S] + k_2/k_3 \times 1/[O_2], \quad (5)$$

where $K_{0.5}$ represents the Michaelis constant, *i.e.* the half saturation concentration of ascorbate, of Eq. 3. From the plot of $1/v$, where v represents the apparent maximal velocity of ascorbate oxidation at various oxygen concentrations, against $1/[O_2]$, it is possible to obtain the true maximal velocity (V_{max}) at infinite concentrations of ascorbate and oxygen; V_{max} was obtained as 1.7×10^{-4} mol dm^{-3}min^{-1}.

2) Cu(II)-PLH Binding and the Catalytic Activity. Cu(II)-PLH appears to be an excellent reaction model

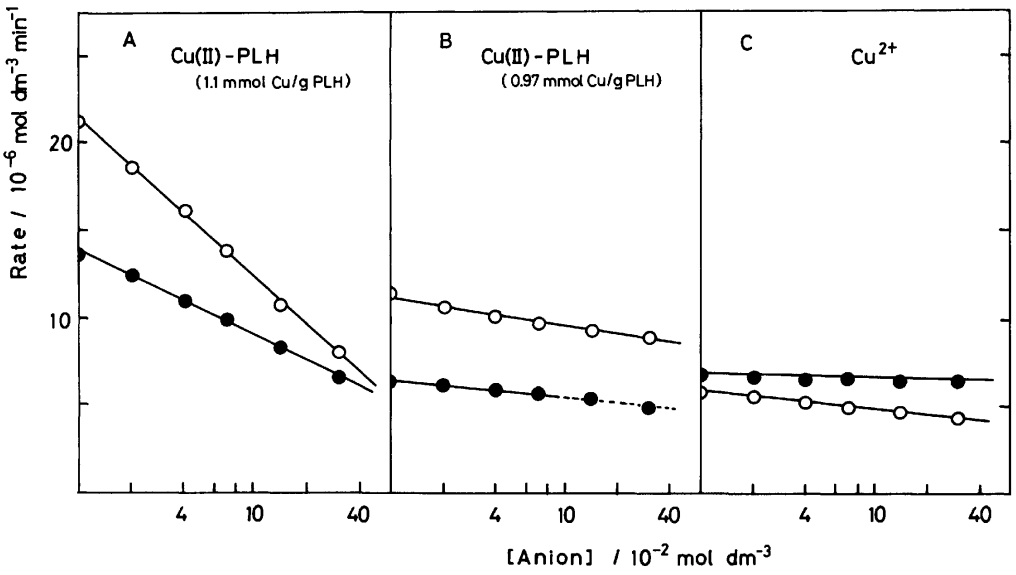

Fig. 5. Effects of various concentrations of anion on the oxidation rate.
$[Cu^{2+}]_0=6.0\times10^{-6}$ mol dm^{-3}, [Ascorbate]$=7.0\times10^{-5}$mol dm^{-3}, anion=AcO$^-$(○) and ClO_4^-(●), [PLH]= (A) 2 mg dm^{-3}, (B) 8 mg dm^{-3}, and (C) 0 mg dm^{-3}, pH 4.4.

TABLE 3. RELATION OF OXIDATION RATE AND CONCENTRATION OF PLH-BOUND Copper(II)

[PLH]	pH 4.0				pH 4.4			
	V	$\bar{\nu}$	bound-Cu	free-Cu	V	$\bar{\nu}$	bound-Cu	free-Cu
mg dm^{-3}	10^{-6}mol dm^{-3}min^{-1}	mmol g^{-1}	%	%	10^{-6}mol dm^{-3} min^{-1}	mmol g^{-1}	%	%
0	5.2	0	0	100	6.4	0	0	100
0.5	8.1	0.96	5	95	10.3	1.13	5	95
1.2	12.2	0.89	10	90	16.8	1.11	12	88
2.4	16.5	0.82	18	82	23.1	1.09	24	76
4.8	19.2	0.74	32	68	21.2	1.04	45	55
8.0	18.2	0.64	47	53	15.8	0.97	70	30
12	15.6	0.53	58	42	12.5	0.84	92	8
24	10.0	0.33	72	28	8.6	0.46	100	0
48	6.6	0.21	92	0	6.6	0.23	100	0

for ascorbate oxidase. The binding of copper(II) ion to PLH, which is confirmed by the equilibrium dialysis experiment, seems necessary for the enhancement of the reaction. PLH is shown to bind copper(II) ion at low pH, starting at pH 3, with a maximum binding constant at pH 5.[10] The catalytically inactive poly-(amino acid)s do not associate with copper(II) ion. Therefore, the catalytic activity is expected to be related to the amount of the PLH-bound copper(II) ion, which locates in the polymer phase and is evaluated by the average binding number ($\bar{\nu}$) given by Eq. 2.

The quantity of PLH-bound copper(II), $[Cu^{2+}]_{bound}$, was obtainable from the equilibrium dialysis experiment under the same experimental conditions. The values of $\bar{\nu}$ under the same conditions as the kinetic run are shown in Table 3 along with the rate observed. In the Cu(II)-PLH system, both PLH-bound and free copper(II) ion always exist in the medium and both possess the catalytic activity. Then, the observed rate of the oxidation, V_{obsd}, may be expressed as the sum of the rates due to PLH-bound copper(II) ion, $V_{bound\,Cu}$ and due to free copper(II) ion, V_{Cu}.

$$V_{obsd} = V_{bound\,Cu} + V_{Cu}. \quad (6)$$

Since the value of V_{Cu} is linearly proportional to the concentration of free copper(II) ion, which had been examined by a separate experiment. V_{Cu} can be estimated in each kinetic run. Accordingly, the rate of oxidation by Cu(II)-PLH, $V_{bound\,Cu}$, is obtainable by Eq. 6. Under the experimental conditions, the total concentration of copper(II) ion is kept at constant. But, since the amounts of PLH are variable, the concentration of copper(II) ion in the polymer phase, which corresponds to $\bar{\nu}$, is variable. Therefore, the rate per the PLH-bound copper(II) ion, which is designated as k_{sp}, should be expressed by $V_{bound\,Cu}/[Cu^{2+}]_{bound}$. We tried to obtain a correlation between k_{sp} and $\bar{\nu}$. If PLH acts merely as chelating agent for copper(II) ion, k_{sp} is expected to be a constant irrespective of the variation of $\bar{\nu}$. However, as shown in Fig. 6, the plots of k_{sp} against $\bar{\nu}$ at pH 4.0 and 4.4 indicate that the specific rate, k_{sp}, increases with $\bar{\nu}$, but not proportional to $\bar{\nu}$. As shown above, the binding number of copper(II) ion per PLH corresponds to the concentration of copper(II) ion located in the polymer matrix of PLH. Ascorbate is also suggested to be concentrated in the polymer phase.[6] Then, the encounter of the copper(II) ion in PLH phase with ascorbate anion may increase with an increase of $\bar{\nu}$. Under the conditions at $\bar{\nu}<1.0$ mmol Cu(II)/g PLH, k_{sp} is larger at pH 4.0 than at pH 4.4. This may be explained by the pH dependence of the ligand exchange rate between copper(II) ion and PLH. A ^{1}H NMR study of the Cu(II)-PLH interaction indicates that the ligand exchange of copper(II) ion in the PLH matrix occurs rapidly under weakly acidic conditions, reducing with increase of pH over pH 3.5.[11] It is suggested that the Cu(II)-PLH binding is rather labile at pH 4.0 and rather tight at pH 4.4. Hence, labile copper(II) ion in PLH phase is assumed

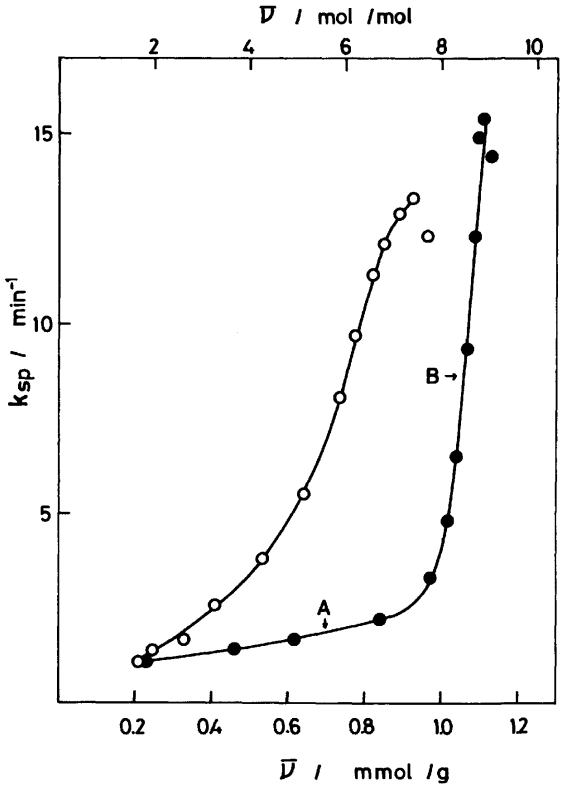

Fig. 6. Relation of Cu(II)-PLH binding and catalytic activity.
pH=4.0(○) and 4.4(●).

to be catalytically active. Of much interest is that the plot at pH 4.4 appears to be composed of two phases, which can be distinguished clearly and is designated A and B, respectively. k_{sp} begins to increase drastically from $\bar{\nu}$=1.0 mmol Cu/g PLH. Provided that the apparent molecular weight of the PLH used is 8000, 1.0 mmol Cu/g PLH corresponds to 8 mol Cu/mol PLH. The PLH used can bind maximally with 9 molar copper(II) at pH 4.4. The mode of interaction of copper(II) ion with PLH also changes dramatically from $\bar{\nu}$=1.0 mmol Cu/g PLH, which is deduced from the effect of electrolytes on the rate of oxidation. As shown in Fig. 5, at $\bar{\nu}$=1.1 mmol Cu/g PLH, where the bound copper(II) ion is in the phase (B), the rate decreased rapidly by the addition of acetate anion. In the phase (A) where $\bar{\nu}$ is 0.97 mmol Cu/g PLH, on the contrary, the rate decreased a little by the addition of the electrolyte. The copper(II) ion in the phase (B) interacts very weakly with PLH, being easily perturbed by electrolyte as compared with the copper(II) ion in the phase (A). These findings support that the bound copper(II) ion which is labile in the matrix of PLH, is a highly catalytic active species.

In conclusion, we suggest that specific effect of PLH on the ascorbate oxidation is not only the concentration of the copper(II) ion and/or ascorbate in the matrix of PLH, but also the formation of a labile and catalytically active copper(II) ion.

References

1) a) A. E. Martell and M. M. Taqui Khan, "Inorganic Biochemistry," Vol. 2, ed by G. I. Eichorn, Elsevier, Amsterdam, (1973), p. 654; b) H. Gampp and A. D. Zuberbuhler, "Metal Ions in Biological System," Vol. 12, ed by H. Sigel, M. Dekker, Inc., New York, (1981), p. 133.

2) Ref. 1a, p. 208.

3) R. F. Jameson and N. J. Blackburn, *J. Chem. Soc., Dalton Trans.*, **1982**, 9.

4) I. Pecht and M. Amber, *Nature*, **207**, 1386 (1965).

5) A. Hanaki, *Chem. Pharm. Bull.*, **17**, 1964 (1969).

6) I. Pecht, A. Levitzki, and M. Amber, *J. Am. Chem. Soc.*, **89**, 1587 (1967).

7) T. Masujima and K. Yamaoka, *Biopolymers*, **19**, 477 (1980).

8) I. E. Segal, "Enzyme Kinetics," John Wiley & Sons, Inc., New York, (1975), p. 505.

9) T. Nakamura, N. Makino, and Y. Ogura, *J. Biochem.*, **64**, 189 (1968).

10) A. Levitzki, I. Pecht, and A. Berger, *J. Am. Chem. Soc.*, **94**, 6844 (1972).

11) R. E. Wasylishen and J. S. Cohen, *J. Am. Chem. Soc.*, **99**, 2480 (1977).

 © 1984 The Chemical Society of Japan Bull. Chem. Soc. Jpn., 57, 3517—3522 (1984)

The *in situ*-Generated Nickel(0)-catalyzed Homo-coupling of Alkenyl Halides with Zinc Powder. A Specific Outcome in Stereochemistry

Kentaro TAKAGI,* Harutaka MIMURA,† and Saburo INOKAWA†

College of Liberal Arts and Science, Okayama University, Tsushima, Okayama 700

†*Department of Chemistry, Faculty of Science, Okayama University, Tsushima, Okayama 700*

(Received June 13, 1984)

The catalytic activity of nickel(0) generated *in situ* from nickel(II) salt was examined in a dehalogenative coupling of alkenyl halides with zinc powder. The reaction of alkenyl bromides took place provided that potassium iodide was present to assist the reduction of nickel(II) with zinc powder, and also to convert the alkenyl bromides to the corresponding alkenyl iodides. A speculative view concerning the disproportionation step is advanced in an attempt to explain the unique stereochemistry observed.

It is well known that a variety of transition-metal complexes react readily with such organic halides as aryl halides and alkenyl halides to afford dehalogenative coupling products, biaryls, and conjugated alkadienes.[1] The excellent reactivities of nickel(0) complexes to the Ullmann-type coupling have previously been proved, but the synthetic usefulness of the nickel-assisted reaction has been limited since stoichiometric amounts of unstable complexes are required to perform the reaction.[2] Recently, however, a catalytic procedure has been devised in which the dehalogenative coupling of aryl halides proceeds by the utilization of chemical reducing agents like zinc powder or electrochemically in the presence of a small amount of a stable nickel(II)-phosphine complex as a catalyst.[3]

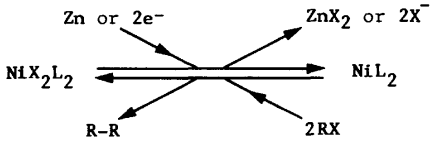

L=PPh_3,[3] PR_3,[5] none[4]

R=Aryl, Alkenyl, Heteroaromatic

In a previous paper, we reported that a simple, phosphine-free nickel(II) compound like nickel(II) chloride or bromide is more effective for the dehalogenative coupling of aryl halides with zinc powder than the nickel(II)-phosphine complex.[4] In this paper, the simple nickel(II) catalyst is applied to a dehalogenative coupling of alkenyl halides with zinc powder hoping thus to achieve a convenient method of synthesizing conjugated dienes from alkenyl halides, but also to obtain insight into the mechanism of this kind of coupling reaction through the product analysis.[6]

Results and Discussion

Reaction Conditions. The reaction of 2-bromo-1,1-diphenylethene (**1**) with zinc powder in the presence of nickel(II) salt was examined under various conditions (Eq. 1). The results are listed in Table 1. It is noteworthy that the coupling product, 1,1,4,4-tetraphen-

$$\underset{\mathbf{1}}{2\,Ph_2C{=}CHBr} + Zn \xrightarrow{NiX_2} \underset{\mathbf{2}}{Ph_2C{=}CH{-}CH{=}CPh_2} + ZnX_2 \quad (1)$$

TABLE 1. NICKEL(0)-CATALYZED HOMO-COUPLING OF **1**[a]

Run	Nickel(II)[b]	Additive		Solvent	Time	**2**[c]
	Ni/**1**[d]	KI/**1**[d]	TMTU/**1**[d]		h	%
1	0.4	2.0	0	HMPA	4	96
2	0.4	2.0	0	NMP	4	94
3	0.4	2.0	0	TMU	4	90
4	0.4	2.0	0	DMF[e]	4	0
5	0.4	2.0	0	THF[f]	4	4
6	0.4	2.0	0	Toluene	4	0
7[g]	0.4	2.0	0	HMPA	7	99
8[h]	0.4	2.0	0	HMPA	10	72
9	0.4	0	0	HMPA	4	0
10	0.04	2.0	0	HMPA	3	97
11	0.04	0.4	0	HMPA	12	18
12	0.04	2.0	0.04	HMPA	1	89
13	0.04	0.4	0.04	HMPA	12	85

a) In the presence of 0.25 mmol of **1** and 0.25 mmol of Zn in 0.5 cm^3 of the solvent at 40 °C under nitrogen. b) Crystalline $NiCl_2$ (0.10 mmol) or 0.17 mol dm^{-3}-DMF solution of $NiBr_2$ (0.01 mmol) was used. c) Yields based on using **1** were determined by GLC using internal standards. d) Molar ratio. e) *N,N*-Dimethylformamide. f) Tetrahydrofuran. g) Run at 20 °C. h) Run using 0.15 mmol of Zn.

yl-1,3-butadiene (**2**), was obtained only in the runs where potassium iodide was present in the reaction mixture (Runs 1 and 9). This fact probably suggests that the metallic nickel generated *in situ* acted as an active catalyst, since the presence of potassium iodide is critical to reduce a nickel(II) salt with zinc powder under the conditions examined.[4] Thus, in the presence of catalytic amounts (0.04—0.4 molar equivalents to **1**) of nickel(II) salt and potassium iodide (2.0 molar equivalents to **1**), the coupling reaction proceeded smoothly using a stoichiometric amount of or a little more (0.6—1.0 molar equivalents to **1**) of zinc powder in such a solvent as hexamethylphosphoric triamide (HMPA), *N*-methyl-2-pyrrolidone (NMP) or 1,1,3,3-tetramethylurea (TMU) under mild conditions (20—40 °C) to afford **2** in a high yield. Thiourea (TU) or 1,1,3,3-tetramethylthiourea (TMTU), which assists the reduction of nickel(II) salt with zinc powder in the same manner as potassium iodide,[7] accelerated the reaction (Runs 1 and 11—13 and Table 2).

The results from various alkenyl halides are listed in Table 2. All the alkenyl bromides and iodides examined gave coupling products in fair to excellent yields, whereas alkenyl chlorides gave such products in extremely poor yields (Runs 16 and 17). No substitution pattern (α-, or β-substitution, α,β-, or β,β'-disubstitution, or functional group) significantly influenced the total reactivities. Unfortunately, the coupling products from β-substituted alkenyl halides always consisted of geometrical isomers (Runs 22—29). However, the major products were the desired ones, which were, in certain cases, obtained in geometrically pure forms from such mixtures after a simple procedure of purification (Runs 25, 26, and 28).[8]

Although readily available alkenyl bromides were the substrates of choice in most experiments, they might not afford coupling products directly. That is, under the present conditions, alkenyl bromides are known to react readily with iodide ions to yield the corresponding alkenyl iodides,[9] and, in fact, interrupted experiments showed that alkenyl bromides turned rapidly to alkenyl iodides (Run 35 in Table 3), and subsequently to coupling products at diminished rates (Runs 34 and 1). Furthermore, the reactions of alkenyl iodides did not necessarily need the presence of potsssium iodide in the reaction mixture if TU or TMTU was present in the place of potassium iodide (Runs 39 and 43).

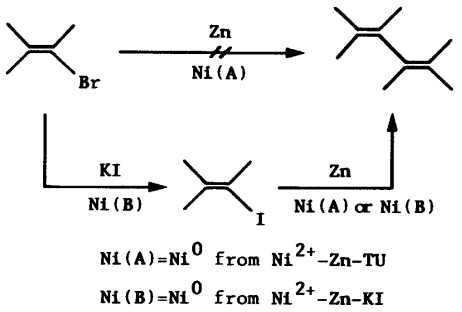

TABLE 2. NICKEL(0)-CATALYZED HOMO-COUPLING OF ALKENYL HALIDES[a]

Run	R^1	R^2	R^3	X	Temp °C	Time h	Alkadiene[b] %	Composition[b] (*E*,*E*)/(*E*,*Z*)/(*Z*,*Z*)
14	Ph	Ph	H	I	40	1.5	(96)	
15	Ph	Ph	H	Br	40	7	78	
16	CH_3	CH_3	H	Br	40	9	74	
17	CH_3	CH_3	H	Cl	40	24	(7)	
18[c]	$-(CH_2)_5-$		H	Br	40	5	72	
19[c]	H	$-(CH_2)_5-$		Br	40	6	40	
20[d]	H	$-(CH_2)_6-$		Br	50	2	80	
21[d]	H	H	CH_3	Br	50	1.5	(38)	
22	CH_3	H	H	Br	50	0.5	(64)	0/6/94
23	Ph	H	H	Br	40	2	(76)	4/30/66
24	H	Ph	H	Br	40	1	(78)	90/10/0
25	H	*p*-$CH_3C_6H_4$	H	Br	40	7	57	
26	H	*p*-ClC_6H_4	H	Br	40	4	48	
27	CH_3O_2C	H	H	Br	25	1.5	(90)	12/19/69
28	CH_3O_2C	H	H	Br	40	5	79	
29	CH_3O_2C	H	H	I	25	2	(90)	7/19/64
30	H	*p*-ClC_6H_4	H	Br	40			71/29/0
31	H	Ph	H	Br	40			78/22/0
32	H	*p*-$CH_3C_6H_4$	H	Br	40			82/18/0
33	Ph	H	H	Br	40			7/34/59

a) In the presence of 0.25 mmol of alkenyl halide in 0.5 cm^3 of HMPA (Runs 14, 17, 21—24, 27, and 29—33) or 1.0—10 mmol of alkenyl halide in 2—20 cm^3 of HMPA (Runs 15, 16, 18—20, 25, 26, and 28) under nitrogen. The molar ratios of the components were as follows: RX/$NiCl_2$/Zn/KI=1.0/0.4/1.0/2.0 (Runs 15—27 and 29), RX/$NiBr_2$/Zn/KI=1.0/0.04/1.0/2.0 (Runs 14 and 30—33), or RX/$NiBr_2$/Zn/KI=1.0/0.02/0.5/2.5 (Run 28). b) Isolated yields after purification. Yields in parentheses and compositions of isomers were determined by GLC using internal standards. c) Run with TMTU (molar ratio of TMTU/Ni=0.1). d) Run with TU (molar ratio of TU/Ni=0.1).

TABLE 3. COMPARISON OF REACTIVITIES OF ALKENYL BROMIDES WITH THOSE OF ALKENYL IODIDES IN NICKEL (0)-CATALYZED HOMO-COUPLING[a]

Run	R^1	R^2	X	Additive: KI	Additive: TMTU or TU	Time / h	Alkadiene[b] / %
1	Ph	Ph	Br	+	−	4	96
34	Ph	Ph	Br	+	−	1.5	28[c]
35	Ph	Ph	Br	+	−	0.5	1[d]
36	Ph	Ph	Br	−	+	4	1[e]
9	Ph	Ph	Br	−	−	4	0
12	Ph	Ph	Br	+	+	1	89
37	Ph	Ph	I	+	−	3.5	90
38	Ph	Ph	I	+	+	1.5	79
39	Ph	Ph	I	−	+	3.5	77
40	Ph	Ph	I	−	−	4	2[f]
27	CH_3O_2C	H	Br	+	−	1.5	90[g]
41	CH_3O_2C	H	Br	−	+	1.5	11[g]
42	CH_3O_2C	H	Br	−	−	1.5	0
43	CH_3O_2C	H	I	−	+	2	78[g]

a) In the presence of 0.25 mmol of alkenyl halide in 0.5 cm^3 of HMPA at 40 °C (Runs 34—42) or at 25 °C (Run 43) under nitrogen. The molar ratios of the components were as follows: RX/$NiCl_2$/Zn/KI(when used)/TMTU(Runs 36, 38, and 39) or TU(Runs 41 and 43)=1.0/0.4/1.0/2.0/0.04. b) Yields were determined by GLC using internal standards. c) The conversion was 96%. The yield of 2-iodo-1,1-diphenylethene was 62%. d) The conversion was 78%. The yield of 2-iodo-1,1-diphenylethene was 76%. e) The conversion was 6%. f) The conversion was 3%. g) Mixture of geometrical isomers.

This result is in marked contrast with that of the reaction of alkenyl bromides, where potassium iodide could not be replaced by TU or TMTU (Runs 36 and 41). These facts probably suggest that alkenyl iodides are reactive toward the coupling reaction, while alkenyl bromides are essentially not reactive under the conditions examined.

Stereochemistry. As is shown in Table 2, the reaction took place with some isomerization at the double bond. Although the low stereoselectivity considerably restricted the synthetic utility, the unique stereochemistry observed obviously ruled out the random scrambling of the configuration at sp^2-carbon; one of the two double bonds in a produced diene invariably retained the original geometry at the double bond except for the methyl 3-haloacrylates. For example, (*Z*)-1-bromopropene afforded (*Z,Z*)-2,4-hexadiene mainly, plus (*E,Z*)-isomer as a minor product, but little of the (*E,E*)-isomer (Run 22). It is apparent that the extent of concomitant isomerization ((*E,Z*)/(*E,E*) from (*E*)-alkenyl halide or (*E,Z*)/(*Z,Z*) from (*Z*)-alkenyl halide) was affected by both the steric and electronic effects of substituents bonded to the β positions. Then, the reaction of *p*-substituted β-bromostyrene was undertaken in order to examine the electronic effect on the composition of geometrical isomers exactly. Since the (*E,Z*)-isomer tended to isomerize to the (*E,E*)-isomer under the present reaction conditions, the composition at zero conversion had been determined (see Experimental). The results clearly showed that the extent of the concomitant isomerization increased with the increase in the electron-withdrawing ability of the substituents (Runs 30—32).

Reaction Path. For a nickel(0) or palladium(0)-assisted dehalogenative coupling of aryl halides or alkenyl halides, sequential steps of oxidative addition (Eq. 2), disproportionation (Eq. 3), and reductive elimination (Eq. 4) had been proposed as a reaction path:[4,10,11]

$$\mathrm{Ni(0)} + \mathrm{RX} \rightleftharpoons \mathrm{R\text{-}Ni\text{-}X}, \quad (2)$$

$$\mathrm{R\text{-}Ni\text{-}X} \longrightarrow 1/2\ \mathrm{R\text{-}Ni\text{-}R} + 1/2\ \mathrm{NiX_2}, \quad (3)$$

$$\mathrm{R\text{-}Ni\text{-}R} \longrightarrow 1/2\ \mathrm{R\text{-}R} + 1/2\ \mathrm{Ni(0)}. \quad (4)$$

Each step is well-known and is frequently encountered in organotransition-metal chemistry. In our reaction, RX represents alkenyl iodides, and the nickel(II) generated in Eq. 3 may react further with excess zinc powder in the presence of potassium iodide, TU, or TMTU to regenerate the nickel(0) to ensure the catalytic cycle (Eq. 5). Some comments can be

$$\mathrm{NiX_2} + \mathrm{Zn} \xrightarrow{\text{KI or TU}} \mathrm{Ni(0)} + \mathrm{ZnX_2} \quad (5)$$

made based on the obtained results.

The observed difference in reactivities between alkenyl bromides and alkenyl iodides may partly come from the difference in the bridging efficiencies of the halogen atoms. It is known that an iodide ligand can bridge two metal species far more effectively than a bromide ligand.[12] Therefore, an iodide ligand in an oxidative adduct (**3**) may bring two nickel atoms close to (**4**), and such an association should be favorable for the succeeding disproportionation.

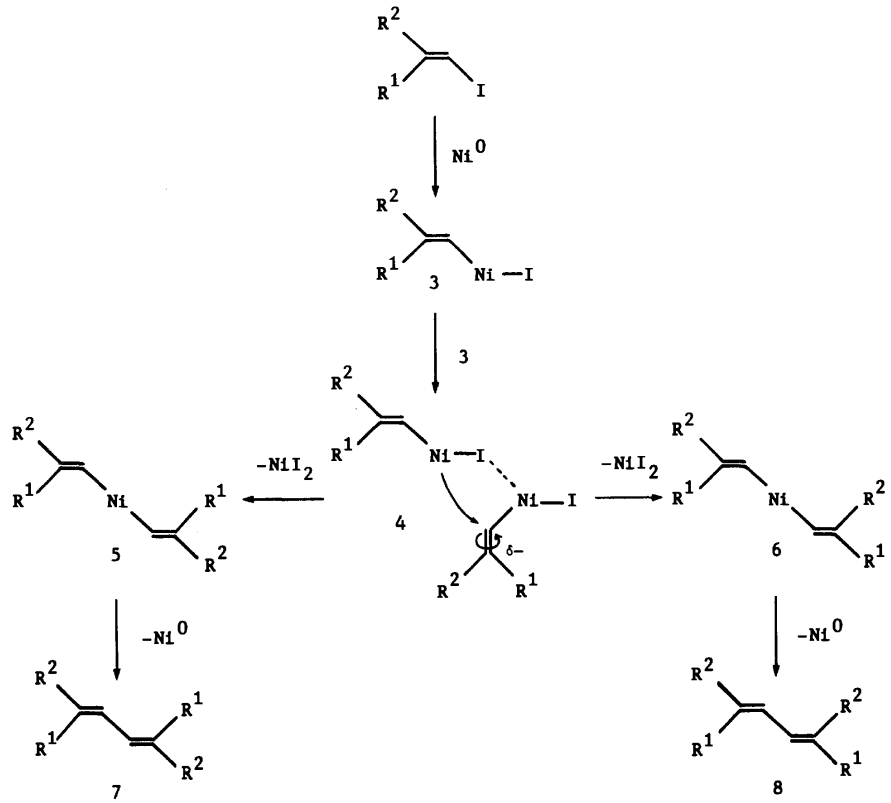

It has been established that the oxidative addition of alkenyl halides to low-valent transition-metal complexes proceeds with a retention of the configuration of the alkenyl groups,[13] and it is also believed that reductive elimination proceeds with the retention of the configuration of alkenyl ligands.[14] Therefore, the observed specific geometrical isomerization possibly took place at a stage of disproportionation; the double-bond character of the transferred alkenyl ligand might be partly released at the same stage, and, consequently, two kinds of dialkenylnickel complexes (**5** and **6**) may be produced from **3**. Another observation, that electron-withdrawing groups attached to the double bond tended to increase the ratio of isomerized diene (**8**), possibly suggests that an anionic character appeared synchronously on the transferred alkenyl ligand as the weakening of the double bond progressed.[15] Further investigations are, however, necessary to clarify the mechanistic details of this disproportionation step.

Experimental

All the reagents were used directly as obtained commercially, unless otherwise noted. The solvents were distilled and were dried over Molecular Sieve (3A). The 2-bromo-1,1-diphenylethene,[17] 2-iodo-1,1-diphenylethene,[18] 1-bromo-2-methyl-1-propene,[19] 1-bromo-1-cycloheptene,[20] 1-bromo-1-cyclooctene,[20] 1-bromomethylenecyclohexane,[21] (*E*)-β-bromostyrene (*Z*/*E*<1/99),[22] (*Z*)-β-bromostyrene (*Z*/*E*=98/2),[23] (*E*)-*p*-methyl-β-bromostyrene (*Z*/*E*<1/99),[24] (*E*)-*p*-chloro-β-bromostyrene (*Z*/*E*<1/99),[24] methyl (*Z*)-3-bromoacrylate (*Z*/*E*>99/1),[25] and methyl (*Z*)-3-iodoacrylate (*Z*/*E*>99/1),[25] were prepared according to the procedures in the literature. A Hitachi 160 gas chromatograph was used for the GLC analysis. The peak areas were determined with a Shimadzu Chromatopac 1A. The ^{1}H NMR spectra were obtained on a JOEL PMX 60 spectrometer, using Me_4Si as the internal standard. The IR spectra were recorded on a Hitachi 260-10 spectrometer. Photoisomerizations were carried out using a Rayonet Photochemical Reactor (Soutbern New England Ultraviolet Company).

General Procedure for Homo-coupling. Preparation of 1,1,4,4-Tetraphenyl-1,3-butadiene: A mixture of 2-bromo-1,1-diphenylethene (260 mg, 1.0 mmol), nickel(II) chloride (52 mg, 0.40 mmol), zinc powder (65 mg, 1.0 mmol), potassium iodide (332 mg, 2.0 mmol), and HMPA (2 cm^3) was evacuated, flushed with nitrogen, and kept at 40 °C with stirring for 7 h. To the mixture, dilute hydrochloric acid (1 mol dm^{-3}, 6 cm^3) was then added and the organic materials were extracted with a mixture of ether (10 cm^3) and chloroform (4 cm^3), washed with two portions of aqueous sodium chloride (4 cm^3), and dried over anhydrous magnesium sulfate. The subsequent evaporation of the solvents gave a pale yellow solid, which was triturated with a small amount of hexane to leave 143 mg of 1,1,4,4-tetraphenyl-1,3-butadiene (78%). Both the NMR and IR spectra were consistent with those of an authentic sample. Mp 193—196 °C (lit,[26] 207—210 °C). Found: C, 94.00; H, 6.07%. Calcd for $C_{28}H_{22}$: C, 93.81; H, 6.19%.

2,5-Dimethyl-2,4-hexadiene: Mp 13—15 °C (lit,[27] 14.5 °C). Found: C, 86.68; H, 12.67%. Calcd for 0.9935 C_8H_{14}: C, 86.62; H, 12.73%.

1,1'-(1,2-Ethanediylidene)biscyclohexane: Mp 42—44 °C (lit,[28] 45—47 °C). Found: C, 88.47; H, 11.60%. Calcd for $C_{14}H_{22}$: C, 88.35; H, 11.65%.

1,1'-Bi(1-cycloheptenyl): Bp 110—113 °C/1.5 mmHg (1 mmHg=133.322 Pa) (lit,[29] 133 °C/10 mmHg). Found: C,

88.57; H, 11.56%. Calcd for $C_{14}H_{22}$: C, 88.35; H, 11.65%.

1,1'-Bi(1-cyclooctenyl): Mp 38 °C (lit,[30] 43 °C). Found: C, 87.73; H, 11.93%. Calcd for $C_{16}H_{26}$: C, 88.00; H, 12.00%.

Preparation of (E,E)-1,4-Bis(4-methylphenyl)-1,3-butadiene: A mixture of (*E*)-*p*-methyl-β-bromostyrene (493 mg, 2.5 mmol), nickel(II) chloride (130 mg, 1.0 mmol), zinc powder (163 mg, 2.5 mmol), potassium iodide (880 mg, 5.0 mmol), and HMPA (2.5 cm^3) was kept at 40 °C for 6 h with stirring under nitrogen. Subsequent treatment similar to that described above gave 290 mg of 1,4-bis(4-methylphenyl)-1,3-butadiene (1:5 mixture of (*E,Z*)- and (*E,E*)-isomers). Recrystallization from ethanol gave 168 mg of pure (*E,E*)-diene (57%). The absence of (*E,Z*)-diene was ascertained by means of GLC. The NMR spectrum was consistent with the previously reported one.[31] Mp 210—211 °C (lit,[32] 198 °C). IR (KBr) 994, 852, and 796 cm^{-1}. Found: C, 92.88; H, 7.45%. Calcd for $C_{14}H_{10}$: C, 92.26; H, 7.74%.

(E,E)-1,4-Bis(4-chlorophenyl)-1,3-butadiene:[33] Mp 214—215 °C. IR (KBr) 1093, 997, 855, and 801 cm^{-1}. ^1H NMR (THF-d_8) δ=6.2—7.1 (m, 4H, olefinic H), and 7.4 (s, 8H, aromatic H). Found: C, 69.89; H, 4.63%. Calcd for $C_{16}H_{12}Cl_2$: C, 69.84; H, 4.40%.

Dimethyl (Z,Z)-2,4-Hexadienedioate: Mp 70.5—72 °C (lit,[34] 73 °C). Found: C, 56.42; H, 5.87%. Calcd for $C_8H_{10}O_4$: C, 56.47; H, 5.92%.

Composition of Geometrical Isomers at Zero Conversion. The Reaction of (E)-p-Methyl-β-bromostyrene: A mixture of (*E*)-*p*-methyl-β-bromostyrene (49 mg, 0.25 mmol), nickel(II) bromide (0.059 cm^3 of 0.17 mol dm^{-3}-DMF solution, 0.01 mmol), potassium iodide (83 mg, 0.50 mmol), zinc powder (16 mg, 0.25 mmol), and HMPA (0.5 cm^3) was heated at 40 °C for 20 min. To the mixture, ether (8 cm^3) and dibenzyl ether (10 mg, internal standard) were then added. GLC analysis of the mixture showed that 0.9% of (*E,Z*)-diene and 4.5% of (*E,E*)-diene were produced. (Authentic samples of (*E,Z*)-dienes were prepared following the previously reported methods.[31,35]) In a similar mixture which had been heated for 35 min or 45 min, 3% or 5% of (*E,Z*)-diene and 16% or 28% of (*E,E*)-diene were produced. From the plot of the molar ratio of the two isomers *vs.* the total yield ((*E,Z*)/(*E,E*):yield=4.8:5.4%, 5.1:19%, 5.4:33%), the molar ratio of the two isomers at 0% was estimated to be 4.6.

References

1) See, *e.g.*, J. March, "Advanced Organic Chemistry: Reactions, Mechanisms, and Structure," 2nd ed, McGraw-Hill, New York (1977), pp. 408 and 606; P. W. Jolly, "Nickel Catalyzed Coupling of Organic Halides and Related Reactions," in "Comprehensive Organometallic Chemistry," ed by G. Wilkinson, Pergamon Press, Oxford (1982), Vol. 8, p. 723.

2) M. F. Semmelhack, P. M. Helquist, and L. D. Jones, *J. Am. Chem. Soc.*, **93**, 5909 (1971); M. F. Semmelhack, P. M. Helquist, and J. D. Gorzynski, *ibid.*, **94**, 9234 (1972); M. F. Semmelhack, P. Helquist, L. D. Jones, L. Keller, L. Mendelson, L. S. Ryono, J. G. Smith, and R. D. Stauff, *ibid.*, **103**, 6460 (1981).

3) A. S. Kende, L. S. Liebeskind, and D. M. Braitsch, *Tetrahedron Lett.*, **1975**, 3375; M. Zembayashi, K. Tamao, J. Yoshida, and M. Kumada, *ibid.*, **1977**, 4089; P. W. Jennings, D. G. Pillsbury, J. L. Hall, and V. T. Brice, *J. Org. Chem.*, **41**, 719 (1976); M. Mori, Y. Hashimoto, and Y. Ban, *Tetrahedron Lett.*, **21**, 631 (1980).

4) K. Takagi, N. Hayama, and S. Inokawa, *Chem. Lett.*, **1979**, 917; *Bull. Chem. Soc. Jpn.*, **53**, 3691 (1980).

5) K. Takagi, N. Hayama, and K. Sasaki, *Bull. Chem. Soc. Jpn.*, **57**, 1887 (1984).

6) For a preliminary communication on a portion of this work, see K. Takagi and N. Hayama, *Chem. Lett.*, **1983**, 637.

7) G. P. Chiusoli and L. Cassar, *Angew. Chem. Int. Ed. Engl.*, **6**, 124 (1967).

8) Certain σ-donor ligands seem likely to improve the stereoselectivity. See Ref. 5 and P. Caubere, *Angew. Chem. Int. Ed. Engl.*, **22**, 599 (1983).

9) This reaction proceeds with a retention of the configuration; K. Takagi, N. Hayama, and S. Inokawa, *Chem. Lett.*, **1978**, 435; T. T. Tsou and J. K. Kochi, *J. Org. Chem.*, **45**, 1930 (1980).

10) G. W. Parshall, *J. Am. Chem. Soc.*, **96**, 2360 (1974); F. R. S. Clark, R. O. C. Norman, and C. B. Thomas, *J. Chem. Soc., Perkin Trans. 1*, **1975**, 121; H. Matsumoto, S. Inaba, and R. D. Rieke, *J. Org. Chem.*, **48**, 840 (1983).

11) T. T. Tsou and J. K. Kochi, *J. Am. Chem. Soc.*, **101**, 7547 (1979).

12) F. Basolo and R. G. Pearson, "Mechanisms of Inorganic Reactions," 2nd ed, John Wiley and Sons, New York (1967), p. 495.

13) J. K. Stille, "Principles of Transition Metal Chemistry," in "Modern Synthetic Methods," ed by R. Scheffold, Otto Salle Verlag, Frankfurt am Main (1983), Vol. 3, p. 10.

14) Ref 13, p. 22; M. K. Loar and J. K. Stille, *J. Am. Chem. Soc.*, **103**, 4174 (1981); J. W. Labadie and J. K. Stille, *ibid.*, **105**, 6129 (1983).

15) The negative charge might arise from a nucleophilic attack of a neighboring nickel on the π* orbital of the transferred alkenyl group. Thus, structure **9** may be attributable to a canonical form of the transient intermediate. A similar structure had been proposed in organocopper chemistry to explain a stereoselective substitution.[16]

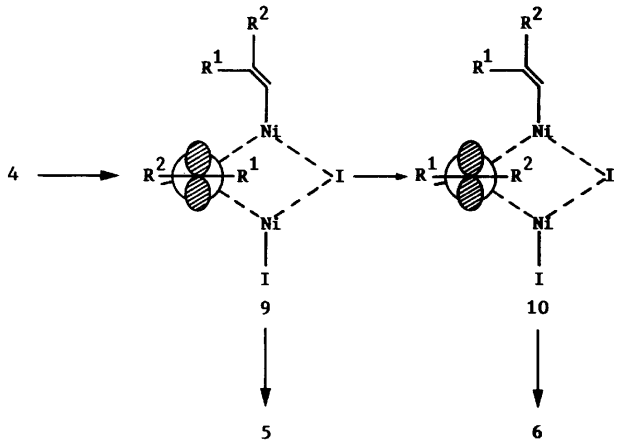

16) J. Klein and R. Levene, *J. Am. Chem. Soc.*, **94**, 2520 (1972); See also D. Dodd, M. D. Johnson, B. S. Meeks, D. M. Titchmarsh, K. N. Van Duong, and A. Gaudemer, *J. Chem. Soc., Perkin Trans. 2*, **1976**, 1261.

17) P. Lipp, *Ber.*, **56**, 567 (1923).

18) K. Takagi, N. Hayama, and T. Okamoto, *Chem. Lett.*, **1978**, 191.

19) H. A. Dieck and R. F. Heck, *J. Am. Chem. Soc.*, **96**, 1133 (1974).

20) K. Schank and B. Eistert, *Ber.*, **99**, 1414 (1966).
21) J. Wolinsky and K. L. Erickson, *J. Org. Chem.*, **30**, 2208 (1965).
22) L. J. Dolby, C. Wilkins, and T. G. Frey, *J. Org. Chem.*, **31**, 1114 (1966).
23) S. J. Cristol and W. P. Norris, *J. Am. Chem. Soc.*, **75**, 2645 (1953).
24) M. K. Loar and J. K. Stille, *J. Am. Chem. Soc.*, **103**, 4180 (1981).
25) A. N. Kurtz, W. E. Billups, R. B. Greenlee, H. F. Hamil, and W. T. Pace, *J. Org. Chem.*, **30**, 3141 (1965).
26) C. D. Hurd and C. N. Webb, *J. Am. Chem. Soc.*, **49**, 546 (1927).
27) C. Prevost, *Compt. Rend.*, **184**, 1460 (1927).
28) I. T. Harrison, B. Lythgoe, and S. Trippett, *J. Chem. Soc.*, **1955**, 4016.
29) W. J. Ball and S. R. Landor, *J. Chem. Soc.*, **1962**, 2298.
30) D. S. Greidinger and D. Grinsburg, *J. Org. Chem.*, **22**, 1406 (1957).
31) T. V. Singh, G. P. Pandey, and K. N. Mehrotra, *Indian J. Chem.*, **18**, 8 (1979).
32) V. V. R. Rao, C. V. Kumar, and D. Devaprabhakara, *J. Organomet. Chem.*, **179**, C7 (1979).
33) E. K. Fields (Standard Oil Co.), U. S. Patent 4, 174, 447 (1979); *Chem. Abstr.*, **92**, P110636u (1980).
34) J. A. Elvidge, R. P. Linstead, P. Sims, and B. A. Orkin, *J. Chem. Soc.*, **1950**, 2235.
35) G. Zweifel, N. L. Polston, and C. C. Whitney, *J. Am. Chem. Soc.*, **90**, 6244 (1968).

Convenient Syntheses of Vitamin K and Coenzyme Q by the Coupling of Grignard Reagents with Allylic Phosphate

Shuki ARAKI, Takashi SATO, Hiroyuki MIYAGAWA, and Yasuo BUTSUGAN*
Department of Synthetic Chemistry, Nagoya Institute of Technology, Gokiso-cho, Showa-ku, Nagoya 466
(Received July 6, 1984)

Convenient syntheses of vitamin K and coenzyme Q are described. Grignard coupling of polyprenyl diethyl phosphates with 1,4-dimethoxy-3-methyl-2-naphthylmagnesium bromide gave high yields of the polyprenylated hydroquinone dimethyl ethers regioselectively with the preservation of the stereochemistry. The precursors of coenzyme Q were similarly obtained by the coupling of 2,3,4,5-tetramethoxy-6-methylphenylmagnesium bromide and the polyprenyl phosphates. The synthesized (polyprenyl)hydroquinone dimethyl ethers are known to be oxidized to the biologically active quinones.

Regio- and stereoselective carbon–carbon bond formation at either the α- or γ-position of an allylic system is a fundamental subject in synthetic organic chemistry. A number of methods with satisfactory selectivity have been developed, some of which involve the coupling of allylic species and organometallics.[1] Recently we have reported that phosphate esters of primary allylic alcohols such as geraniol and nerol allylate a variety of Grignard reagents at the α-position with the preservation of the stereochemistry of the allylic double bond.[2] As an application of this coupling reaction, the syntheses of the biologically active quinones, vitamin K and coenzyme Q, are described in the present paper.

Vitamin K and coenzyme Q are composed of a polyprenyl chain and a naphthoquinone or a benzoquinone nucleus.[3] The synthetic methods of these quinones hitherto reported can be classified into four groups in regard to the fashion of the coupling between the nucleus and the side chain: (a) Friedel-Crafts type coupling,[4] (b) reaction of π-allylnickel complex with halohydroquinone,[5] (c) Lewis acid catalyzed coupling of (polyprenyl)stannane with quinone,[6] and (d) reaction of aryl Grignard reagent or arylcuprate(I) with polyprenyl halide.[7] The method reported in this paper is a modification of the last group, which involves the reaction of polyprenyl phosphates with the Grignard reagents of hydroquinone dimethyl ethers. The coupling proceeded regioselectively in excellent yields without loss of the stereochemistry.

Results and Discussion

To a stirred solution of 1,4-dimethoxy-3-methyl-2-naphthylmagnesium bromide (**1**) in tetrahydrofuran (THF) was added prenyl diethyl phosphate (**2a**) and the mixture was stirred overnight at room temperature. After hydrolysis and vacuum distillation, the coupling product, 1,4-dimethoxy-3-methyl-2-prenylnaphthalene (**3a**), was isolated in high yield (93%) (Table 1). As expected,[2] the coupling occurred exclusively at the α-position of the prenyl phosphate (**2a**), and the formation of the γ-attack product [1,4-dimethoxy-3-methyl-2-(1,1-dimethyl-2-propenyl)naphthalene] was not observed by glc and ^{1}H NMR analyses. In a similar way, geranyl (**2b**) and neryl diethyl phosphates (**2c**) gave the respective coupling products (**3b** and **3c**) in 80 and 86% yields, respectively. Glc showed that no *E*-*Z* isomerization occurred during the coupling. Snyder reported[7a] that the reaction of the Grignard reagent (**1**) and geranyl and neryl bromides gave **3b** and **3c**, however the yield of the *Z*-isomer (**3c**) was relatively lower (62%) than that of the *E*-isomer (**3b**) (92%). The present coupling using allylic phosphates did not show such suppression of the yield even in the reaction of the neryl phosphate (**2c**). (2*E*)- and (2*Z*)-Farnesyl derivatives were also obtained regioselectively with the preservation of the stereochemistry of the farnesyl group (confirmed by HPLC). The precursor (**3f**) of vitamin K_1 was similarly prepared from phytyl diethyl phosphate (**2f**) in 87% yield. The synthesized (polyprenyl)hydroquinone dimethyl ethers (**3a—f**) are known[7a,7c] to be demethylatively oxidized by silver(II) oxide or cerium(IV) diammonium nitrate to the respective vitamin K_2 (**4a—e**) and vitamin K_1 (**4f**).

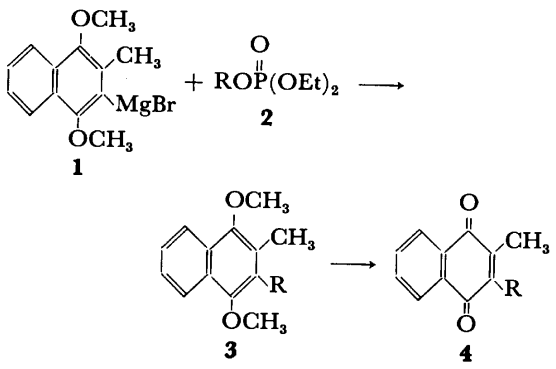

TABLE 1. YIELDS AND STEREOCHEMISTRY OF 1,4-DIMETHOXY-2-METHYL-3-POLYPRENYLNAPHTHALENES (**3a—f**)

R	Yield/%	Stereochemistry at Δ^2 (*E*/*Z*)
Prenyl (**3a**)	93	—
Geranyl (**3b**)	80	10/0[a]
Neryl (**3c**)	86	0/10[a]
(2*E*)-Farnesyl (**3d**)	76	10/0[b]
(2*Z*)-Farnesyl (**3e**)	87	2/8[b,c]
Phytyl (**3f**)	87	10/0[d]

a) Determined by glc. b) Determined by HPLC. c) Due to (2*E*)-farnesol mixed in the (2*Z*)-farnesol used (*E*/*Z*=2/8). d) Determined by ^{1}H NMR (200 MHz).

The precursors (**6a—e**) of coenzyme Q were analogously prepared from 2,3,4,5-tetramethoxy-6-methylphenylmagnesium bromide (**5**) and polyprenyl diethyl phosphates (**2a—e**). The yields are listed in Table 2. Again, no detectable amounts of γ-coupling nor *E-Z* isomerization were observed. The dimethyl ethers (**6a—e**) can be demethylatively oxidized to coenzyme Q (**7a—e**).[7a,7c]

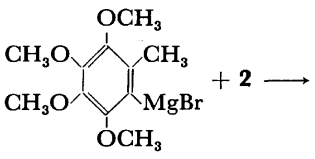

5

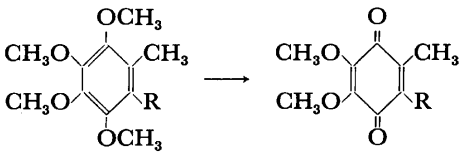

6 **7**

In summary, several examples of vitamin K and coenzyme Q precursors bearing a polyprenyl chain of different length and stereochemistry were synthesized. The advantages of the present method are (1) regioselectivity is very high and the isomerization of the allylic double bond is negligible, (2) the yields are excellent, (3) reaction conditions are mild, and (4) experimental operations are simple. Therefore, this method provides a convenient route for the syntheses of vitamin K and coenzyme Q.

Experimental

General. Infrared spectra were recorded on a JASCO IRA-1 spectrophotometer. ^{1}H NMR spectra were determined with a Hitachi R-24A (60 MHz) spectrometer, or with a Varian XL-200 (200 MHz) spectrometer in CCl_4 or $CDCl_3$. Chemical shifts (δ) are recorded in ppm downfield from Me_4Si. Mass spectra were measured on a Hitachi M-52 mass spectrometer, operating with an ionization energy of 20 eV. HPLC analysis was performed by using a JASCO TRI ROTAR-II with a silica-gel column (Fine Sil 20, 4.6 mm× 25 cm) eluting with hexane–chloroform (100 : 1). Glc analysis was done on a Yanaco G1800 gas chromatograph, equipped with a column packed with Apiezon Grease L on Uniport B. Elemental analysis was performed at the Elemental Analysis Center of Kyoto University. Polyprenyl diethyl phosphates (**2a—f**) were prepared from polyprenyl alcohols and diethyl phosphorochloridate according to the method for the corresponding diphenyl phosphates.[8] (2*Z*)-Farnesol (2*Z*/2*E*=8/2) was prepared by the diisobutylaluminum hydride reduction of ethyl (2*Z*)-farnesoate (2*Z*/2*E*=8/2) which was obtained by the fractional distillation of a mixture of the (2*Z*)- and (2*E*)-isomers (2*Z*/2*E*=2/8) synthesized by the Wittig-Horner reaction of geranylacetone.[9]

Grignard Coupling of 1,4-Dimethoxy-3-methyl-2-naphthylmagnesium Bromide (1) with Polyprenyl Diethyl Phosphates (2a—f). The following preparation of **3a** is a representative. The Grignard reagent, 1,4-dimethoxy-3-methyl-2-naphthylmagnesium bromide (**1**), was prepared in a conventional manner using tetrahydrofuran (THF) as a solvent. To a stirred solution of **1** (2.28 mmol) in 3 ml of THF was added a solution of prenyl diethyl phosphate (**2a**) (297 mg, 1.34 mmol) in 3 ml of THF at 0 °C. The reaction mixture was stirred overnight at room temperature and then quenched by the addition of water. The product was extracted with ether and the extracts were dried over anhydrous sodium sulfate and then concentrated. The residue was distilled (Kugelrohr) to give 1,4-dimethoxy-2-methylnaphthalene [bp 130 °C/5 Torr (1 Torr≈133.322 Pa), 177 mg] and **3a** (bp 150 °C/5 Torr, 335 mg, 93%). Higher analogs of the polyprenylated compounds (**3b—f**) were similarly prepared and purified by column chromatography on silica-gel (benzene–ether gradient).

Table 2. Yields and stereochemistry of 1,2,3,4-tetramethoxy-5-methyl-6-polyprenylbenzenes (**6a—e**)

R	Yield/%	Stereochemistry at Δ^2 (*E*/*Z*)
Prenyl (**6a**)	85	—
Geranyl (**6b**)	82	10/0[a]
Neryl (**6c**)	84	0/10[a]
(2*E*)-Farnesyl (**6d**)	70	10/0[b]
(2*Z*)-Farnesyl (**6e**)	75	2/8[b,c]

a) Determined by glc. b) Determined by ^{1}H NMR (200 MHz). c) Due to (2*E*)-farnesol mixed in the (2*Z*)-farnesol used (*E*/*Z*=2/8).

1,4-Dimethoxy-2-methyl-3-prenylnaphthalene (3a):[7c] IR (neat) 2950, 1594, 1452, 1355, 1266, 1195, 1065, 1018, 975, 775, and 712 cm^{-1}: ^{1}H NMR (CCl_4) 7.16—8.01 (m, 4H, aromatic), 5.07 (t, *J*=6 Hz, 1H, olefin), 3.81 (s, 3H, OCH_3), 3.78 (s, 3H, CH_3), 3.47 (d, *J*=6 Hz, 2H, CH_2), 2.33 (s, 3H, CH_3), 1.81 (s, 3H, CH_3), 1.70 (s, 3H, CH_3); Mass *m*/*z* 270 (M^+).

1,4-Dimethoxy-2-methyl-3-geranylnaphthalene (3b):[7a] IR (neat) 2950, 1590, 1450, 1355, 1265, 1190, 1060, 830, and 770 cm^{-1}; ^{1}H NMR (CCl_4) 7.16—8.05 (m, 4H, aromatic), 4.81—5.24 (m, 2H, olefin), 3.75 (s, 3H, OCH_3), 3.44 (d, *J*=6 Hz, 2H, CH_2), 2.26 (s, 3H, CH_3), 1.94 (m, 4H, CH_2×2), 1.75 (s, 3H, CH_3), 1.56 (s, 3H, CH_3), 1.50 (s, 3H, CH_3); Mass *m*/*z* 338 (M^+).

1,4-Dimethoxy-2-methyl-3-nerylnaphthalene (3c):[7a] IR (neat) 2950, 1600, 1460, 1360, 1270, 1200, 1070, 830, and 780 cm^{-1}; ^{1}H NMR (CCl_4) 7.12—8.04 (m, 4H, aromatic), 4.86—5.22 (m, 2H, olefin), 3.73 (s×2, 6H, OCH_3), 3.43 (d, *J*=7 Hz, 2H, CH_2), 2.26 (s, 3H, CH_3), 2.17 (m, 4H, CH_2×2), 1.58—1.71 (m, 9H, CH_3×3); Mass *m*/*z* 338 (M^+).

1,4-Dimethoxy-2-methyl-3-[(2E)-farnesyl]naphthalene (3d): IR (neat) 2945, 1592, 1456, 1355, 1268, 1066, and 770 cm^{-1}; ^{1}H NMR ($CDCl_3$) 8.10 (m, 2H, aromatic), 7.50 (m, 2H, aromatic), 5.11 (m, 3H, olefin), 3.89 (s, 3H, OCH_3), 3.87 (s, 3H, OCH_3), 3.59 (d, *J*=6 Hz, 2H, CH_2), 2.39 (s, 3H, CH_3), 2.06 (m, 8H, CH_2×4), 1.84 (s, 3H, CH_3), 1.66 (s, 3H, CH_3), 1.60 (s, 6H, CH_3×2); Mass *m*/*z* 406 (M^+). Found: C, 82.44; H, 9.17%. Calcd for $C_{28}H_{38}O_2$: C, 82.71; H, 9.42%.

1,4-Dimethoxy-2-methyl-3-[(2Z)-farnesyl]naphthalene (3e): IR (neat) 2950, 1596, 1456, 1356, 1269, 1068, and 774 cm^{-1}; ^{1}H NMR ($CDCl_3$) 8.10 (m, 2H, aromatic), 7.50 (m, 2H, aromatic), 5.27 (m, 1H, olefin), 5.16 (m, 2H, olefin), 3.88 (s, 3H, OCH_3), 3.86 (s, 3H, OCH_3), 3.59 (d, *J*=6 Hz, 2H, CH_2), 2.40 (s, 3H, CH_3), 2.35—1.90 (m, 8H, CH_2×4), 1.73 (m, 3H, CH_3), 1.70 (s, 3H, CH_3), 1.68 (s, 3H, CH_3), 1.63 (s, 3H, CH_3); Mass *m*/*z* 406 (M^+). Found: C, 82.63; H, 9.52%. Calcd for $C_{28}H_{38}O_2$:

C, 82.71; H, 9.42%.

*1,4-Dimethoxy-2-methyl-3-phytylnaphthalene (**3f**)*: IR (neat) 2940, 1592, 1455, 1355, 1265, 1192, 1098, 1065, 1014, 970, and 770 cm^{-1}; ^1H NMR (CCl_4) 7.03—8.01 (m, 4H, aromatic), 5.03 (t, J=6 Hz, 1H, olefin), 3.81 (s, 3H, OCH_3), 3.78 (s, 3H, OCH_3), 3.41 (d, J=6 Hz, 2H, CH_2), 2.25 (s, 3H, CH_3), 2.20—1.50 (m, 5H, CH_2 and CHX3), 1.73 (s, 3H, CH_3), 1.12 (br, 16H, CH_2X8), 0.81 (d, J=7 Hz, 12H, CH_3X4); Mass m/z 480 (M^+). Found: C, 82.30; H, 11.17%. Calcd for $C_{33}H_{52}O_2$: C, 82.44; H, 10.90%.

Precursors (**6a—e**) of coenzyme Q were analogously obtained by the Grignard reactions of 2,3,4,5-tetramethoxy-6-methylphenylmagnesium bromide and the polyprenyl phosphates (**2a—e**), and characterized by IR, ^1H NMR, and Mass spectra.

*1,2,3,4-Tetramethoxy-5-methyl-6-prenylbenzene (**6a**)*: IR (neat) 2950, 1468, 1408, 1355, 1260, 1196,, 1100, 1070, 1042, and 980 cm^{-1}; ^1H NMR (CCl_4) 4.96 (t, J=6 Hz, 1H, olefin), 3.82 (s, 6H, OCH_3X2), 3.73 (s, 6H, OCH_3X2), 3.22 (d, J=6 Hz, 2H, CH_2), 2.09 (s, 3H, CH_3), 1.75 (s, 3H, CH_3), 1.67 (s, 3H, CH_3); Mass m/z 280 (M^+). Found: C, 68.05; H, 8.78%. Cacld for $C_{16}H_{24}O_4$: C, 68.54; H, 8.63%.

*1,2,3,4-Tetramethoxy-5-methyl-6-geranylbenzene (**6b**)*:[7c] IR (neat) 2950, 1470, 1410, 1350, 1260, 1200, 1100, 1040, and 980 cm^{-1}; ^1H NMR (CCl_4) 4.79—5.09 (m, 2H, olefin), 3.76 (s, 6H, OCH_3X2), 3.67 (s, 6H, OCH_3X2), 3.21 (d, J=7 Hz, 2H, CH_2), 2.11 (s, 3H, CH_3), 1.92 (m, 4H, CH_2X2), 1.68 (s, 3H, CH_3), 1.57 (s, 3H, CH_3), 1.51 (s, 3H, CH_3); Mass m/z 338 (M^+).

*1,2,3,4-Tetramethoxy-5-methyl-6-nerylbenzene (**6c**)*: IR (neat) 2950, 1470, 1410, 1350, 1260, 1200, 1100, 1040, and 980 cm^{-1}; ^1H NMR (CCl_4) 4.78—5.16 (m, 2H, olefin), 3.76 (s, 6H, OCH_3X2), 3.67 (s, 6H, OCH_3X2), 3.17 (d, J=7 Hz, 2H, CH_2), 2.10 (m, 4H, CH_2X2), 2.02 (s, 3H, CH_2), 1.62 (m, 9H, CH_3X3); Mass m/z 338 (M^+). Found: C, 72.09; H, 9.26%. Calcd for $C_{21}H_{32}O_4$: C, 72.38; H, 9.26%.

*1,2,3,4-Tetramethoxy-5-methyl-6-[(2E)-farnesyl]benzene (**6d**)*: IR (neat) 2950, 1465, 1408, 1355, 1108, 1042, and 980 cm^{-1}; ^1H NMR ($CDCl_3$) 5.08 (m, 3H, olefin), 3.92 (s, 6H, OCH_3X2), 3.80 (s, 6H, OCH_3X2), 3.33 (d, J=7 Hz, 2H, CH_2), 2.17 (s, 3H, CH_3), 2.04 (m, 8H, CH_2X4), 1.78 (s, 3H, CH_3), 1.67 (s, 3H, CH_3), 1.59 (s, 3H, CH_3); Mass m/z 406 (M^+). Found: C, 74.87; H, 9.72%. Calcd for $C_{26}H_{40}O_4$: C, 74.96; H, 9.68%.

*1,2,3,4-Tetramethoxy-5-methyl-6-[(2Z)-farnesyl]benzene (**6e**)*: IR (neat) 2930, 1465, 1406, 1352, 1103, 1041, and 978 cm^{-1}: ^1H NMR ($CDCl_3$) 5.24 (m, 1H, olefin), 5.07 (m, 2H, olefin), 3.92 (s, 6H, OCH_3X2), 3.80 (s, 6H, OCH_3), 3.36 (d, J=7 Hz, 2H, CH_2), 2.40—1.90 (m, 4H, CH_2X2), 2.16 (s, 3H, CH_3), 1.70 (s, 6H, CH_3X2), 1.66 (s, 3H, CH_3), 1.63 (s, 3H, CH_3); Mass m/z 406 (M^+). Found: C, 75.14; H, 9.74%. Calcd for $C_{26}H_{40}O_4$: C, 74.96; H, 9.68%.

We are grateful to Kuraray Co., Ltd., for a generous gift of some starting compounds. This work was supported by a Grant-in-Aid for Scientific Research (No. 58550562) from the Ministry of Education, Science, and Culture of Japan.

References

1) R. M. Magid, *Tetrahedron*, **36**, 1901 (1980); E. Negishi, "Organometallics in Organic Synthesis," Wiley-Interscience, New York (1980); R. Noyori, "Transition Metal Organometallics in Organic Synthesis," ed by H. Alper, Academic Press, New York (1976).

2) S. Araki, T. Sato, and Y. Butsugan, *J. Chem. Soc., Chem. Commun.*, **1982**, 285.

3) R. A. Morton, ed "Biochemistry of Quinones," Academic Press, New York (1965); R. H. Thompson, "Naturally Occurring Quinones," Academic Press, New York, (1971).

4) L. F. Fieser, *J. Am. Chem. Soc.*, **61**, 3467 (1939); C. H. Shunk, B. O. Linn, E. L. Wong, P. E. Witteich, F. M. Robinson, and K. Folkners, *ibid.*, **80**, 4753 (1958); for a recent review, S. Yamada, T. Takeshita, and J. Tanaka, *Yuki Gosei Kagaku Kyokai Shi*, **40**, 268 (1982).

5) S. Inoue, R. Yamagami, and K. Saito, *Bull. Chem. Soc. Jpn.*, **47**, 3098 (1974); K. Saito, S. Inoue, and R. Yamaguchi, *J. Org. Chem.*, **37**, 1889 (1972); L. S. Hugedus, E. L. Waterman, and J. Catline, *J. Am. Chem. Soc.*, **94**, 7155 (1972); K. Sato, S. Inoue, and K. Saito, *J. Chem. Soc., Perkin Trans. 1*, **1973**, 2289.

6) Y. Naruta, *J. Org. Chem.*, **45**, 4097 (1980); *J. Am. Chem. Soc.*, **102**, 3774 (1980); K. Maruyama and Y. Naruta, *J. Org. Chem.*, **43**, 3796 (1978); Y. Naruta and K. Maruyama, *Chem. Lett.*, **1979**, 881, 885.

7) a) C. D. Snyder and H. Rapoport, *J. Am. Chem. Soc.*, **96**, 8046 (1974); b) R. W. Raynolds, M. J. Manning, and J. S. Swenton, *J. Chem. Soc., Chem. Commun.*, **1977**, 499; c) L. Syper, K. Kloc, and J. Młochowski, *Tetrahedron*, **36**, 123 (1980); d) Y. Fujita, M. Ishiguro, T. Onishi, and T. Nishida, *Synthesis*, **1981**, 469.

8) J. A. Miller and H. C. S. Wood, *J. Chem. Soc.,C*, **1968**, 1837.

9) Y. Butsugan, M. Murai, and T. Matsuura, *Nippon Kagaku Kaishi*, **89**, 431 (1968).

7-Diazo-7*H*-benz[*de*]anthracene and 7*H*-Benz[*de*]anthracen-7-ylidene

Akira IZUOKA, Shigeru MURATA, and Hiizu IWAMURA*
Department of Applied Molecular Science, The Institute for Molecular Science, Myodaiji, Okazaki 444
(Received April 14, 1984)

7-Diazo-7*H*-benz[*de*]anthracene has been prepared by the HgO oxidation of the corresponding hydrazone in ether. The yellow-green diazo compound in a 2-methyltetrahydrofuran matrix has been photolyzed with a high-pressure mercury lamp in an ESR cavity at 14 K. From the *X*, *Y*, and *Z* transitions due to the unoriented triplet species, the zero-field splitting parameters of 7*H*-benz[*de*]anthracen-7-ylidene have been determined: $|D|=0.2662$ and $|E|=0.0175\,cm^{-1}$. A temperature dependence experiment showed linear signal intensities *vs.* $1/T$ plots, indicating that the carbene is in the ground triplet state. The zero-field splitting parameters have been theoretically calculated by assuming the dipolar interaction of the electron spins one on the n-orbital at the 7-position and the other delocalized on the Hückel π-framework.

High-spin organic molecules are of recent interest as a model for organic ferromagnets.[1] Special attention has been devoted to antiaromatic annulenes[2] and polyradicals.[3] Our approach to the subject is characterized by the construction of polycarbenes by taking advantage of triplet diphenylcarbene as an appropriate building block.[4] Thus the nonet ground state of a tetracarbene, *m*-phenylenebis((diphenylmethylen-3-yl)methylene), has been generated and characterized by ESR spectroscopy.[5] In order to develop magnetic organic materials of interest, there remain several difficulties to overcome. The increase of the spin multiplicity and the thermal stability of the polycarbenes is one of the few important factors. As a part of these efforts, we have scrutinized several new carbenes to be used as a unit. In this paper, we report the preparation of the diazo compound and generation of the triplet carbene derived from 7*H*-benz[*de*]-anthracen-7-one. The ESR spectra of the carbene have also been fully analyzed.

Results and Discussion

Preparation of 7-Diazo-7H-benz[de]anthracene. The diazo compound was prepared by typical mercury(II) oxide oxidation of the corresponding hydrazone which in turn was obtained by sluggish reaction of 7*H*-benz[*de*]-anthracen-7-one with hydrazine hydrate. The yellow-green diazo compound crystallized in fine prisms. A characteristic IR band was observed at $2030\,cm^{-1}$. UV absorptions due to the π-π^* and n-π^* transitions were observed at 407 (log ε=4.14), 425 (4.10) and 600 nm (2.42), respectively. The 400 MHz ^{1}H NMR spectrum exhibited first-order multiplets (Fig. 1) which were analyzed by the standard decoupling technique. The upfield shifts of the hydrogens peri to the diazo group are noted. The corresponding hydrogens of the precursor ketone appear in the lowest field.

Photochemical Generation and ESR Characterization of 7H-Benz[de]anthracen-7-ylidene. 7-Diazo-7*H*-benz-[*de*]anthracene in 2-methyltetrahydrofuran matrices was irradiated with a high-pressure mercury lamp in an ESR cavity at 14K. The resulting ESR spectrum obtained at 9.332GHz is reproduced in Fig. 2. The signals are typical fine structure patterns for unoriented triplet species. Signals at 420.9, 485.5, and 617.5 mT are assigned to a set of the high-field *X*, *Y*, and *Z* transitions from which the zero-field splitting parameters were obtained as $|D|=0.2662$ and $|E|=0.0175\,cm^{-1}$ by solving Eqs:[6a]

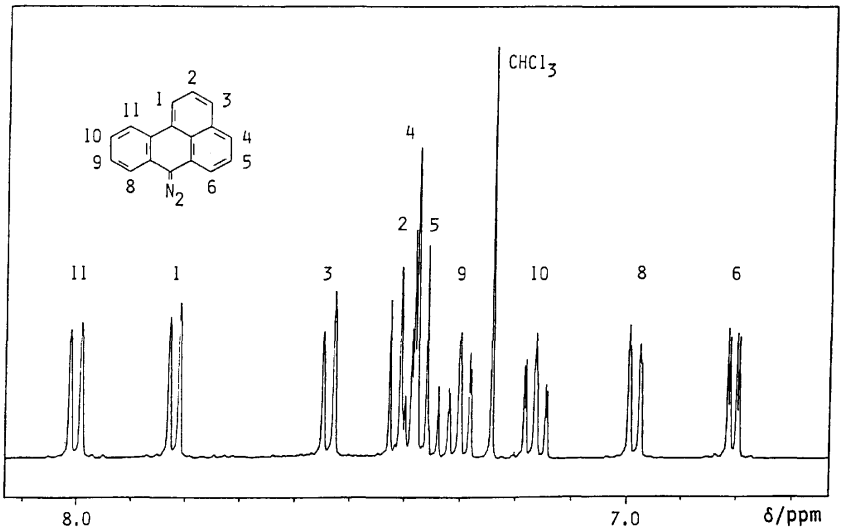

Fig. 1. ^{1}H NMR spectrum (400 MHz) of 7-diazo-7*H*-benz[*de*]anthracene.

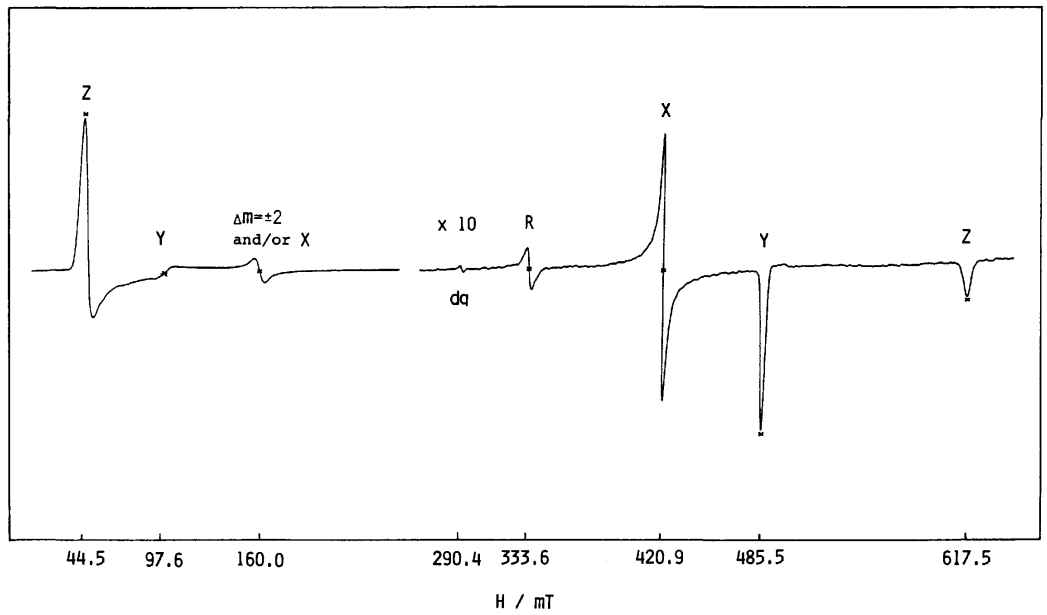

Fig. 2. ESR spectrum (9.332 GHz) obtained by photolysis of 7-diazo-7H-benz[de]-anthracene in 2-methyltetrahydrofuran glass at 14 K.

$$(g\beta H_X)^2 = (g_e/g_{XX})^2[(g\beta H_0 \pm D \mp E)(g\beta H_0 \mp 2E)]$$
$$(g\beta H_Y)^2 = (g_e/g_{YY})^2[(g\beta H_0 \pm D \pm E)(g\beta H_0 \pm 2E)] \quad (1)$$
$$(g\beta H_Z)^2 = (g_e/g_{ZZ})^2[(g\beta H_0 \pm D)^2 \mp E^2].$$

The corresponding low-field X, Y, and Z transitions were calculated from these zero-field parameters using Eqs. 1 to give the resonance fields 157.4, 93.5, and 44.5 mT, respectively. These values agree reasonably well with the observed low-field transitions as shown in Fig. 2. The resonance at 160 mT which was assigned to the X transition may contain the signal due to $\Delta m = \pm 2$ transition. Other signals at 290.4 and 333.6 mT are assigned to the double quantum transition of the carbene and a normal resonance due to fortuitous doublet species, respectively.

The D values of typical diarylcarbenes are in the range 0.41—0.37 cm^{-1}. With the exception of di(9-anthryl)methylene (D=0.113 cm^{-1} at 4 K),[6b] the D parameter of 7H-benz[de]anthracen-7-ylidene obtained in this study is the smallest ever reported, showing extensive delocalization of the odd electron in the π-framework of the molecule.

The temperature dependence of the ESR signal intensity of the low-field Z transition in the range 15—77 K obeyed the Curie-Weiss linear plot (Fig. 3). The triplet carbene is concluded not to be thermally populated from the ground state singlet. In 2-methyltetrahydrofuran matrices, the ESR signals started to disappear at 85 K. In powdered crystals which gave birth to 7H-benz[de]anthracen-7-ylidene on irradiation ($|D|$=0.2608 and $|E|$=0.0181 cm^{-1}), it was stable up until 205 K. The thermal stability of the carbene due to delocalization of the odd electron in the π-orbital was not so satisfactory as it was expected.

Calculation of the Zero-field Splitting Parameters. The zero-field splitting parameters D and E have been calculated theoretically by the point dipole approximation; only the two-center Coulomb term in the single configuration approximation was considered. The sites of the point electron spins were empirically fixed according to the method of Hutton and Roth[7] for the reason of simplicity and empirical reproducibility. Thus the electron spin in the π-orbitals was simulated by two point spins in the π-

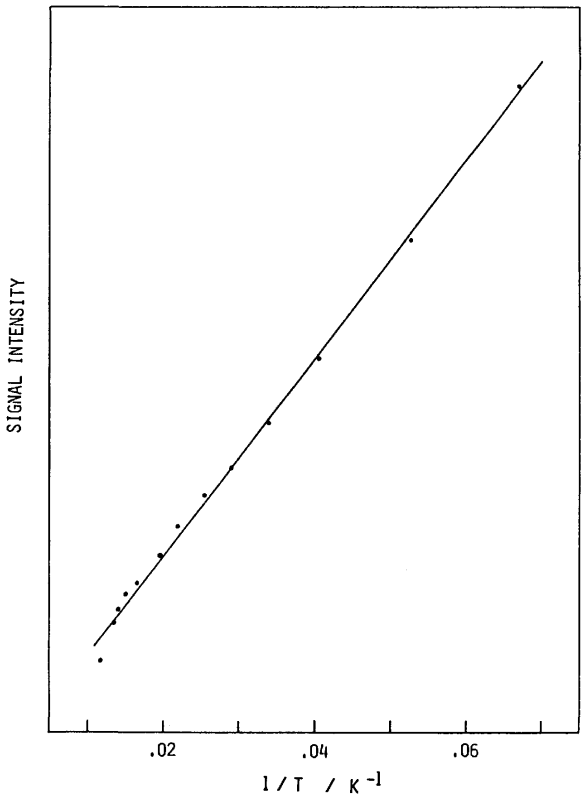

Fig. 3. Plots of signal intensity of the lowfield Z line of 7H-benz[de]anthracen-7-ylidene *vs.* $1/T$.

lobes located 0.821 Å above and below and molecular plane, each with a half of the spin density on the atom. The σ-electron spin was assumed to be localized on the divalent carbon and expressed by two point spins in the sp^2-orbital placed at ±0.876 Å from the carbon atom with the spin density of 0.7 in the negative lobe and 0.3 in the positive lobe.[7] The molecular geometry used in the calculation was constructed by the C-C bond distance of 1.40 Å and the bond angles of 120°.

Since the spin-orbit coupling of the two electrons is considered not to contribute to the zero-field parameters in carbenes containing only first-row atoms,[8] only the dipolar spin-spin interaction was taken into consideration. The spin-spin Hamiltonian is described by Eq. 2:

$$H_{ss} = S\mathbf{D}S, \tag{2}$$

where S is the total spin operator and $\mathbf{D}$ is the dipolar coupling tensor, the elements of which are obtained by the summation of the interactions of each σ spin with each π spin. When the matrix is diagonalized, the zero-field splitting parameters D and E are calculated as Eqs. 3:

$$D = -\frac{3}{2}Z, \qquad E = -\frac{1}{2}(X-Y), \tag{3}$$

where $-X$, $-Y$, and $-Z$ are the components of the diagonalized matrix.

As in the calculation by Hutton and Roth,[7] it was assumed that the π spin density distribution was equal to that in the corresponding radical 7*H*-benz[*de*]anthracen-7-yl. We obtained the spin densities of the radical by the McLachlan method with the use of the zero-order spin densities derived from the Hückel molecular orbital (HMO) theory; the usual HMO parameters α_o and β_o were employed in all the carbon atoms and C-C bonds, respectively.

Table 1. The π spin densities of 7*H*-benz[*de*]anthracen-7-yl used for calculation of the π spin distribution in 7*H*-benz[*de*]anthracen-7-ylidene

Atom	Spin density	Atom	Spin density
1	0.1456	7	0.3567
2	−0.0512	7a	−0.0478
3	0.1502	8	0.0901
3a	−0.0459	9	−0.0362
3b	0.0149	10	0.0798
4	0.2385	11	−0.0370
5	−0.0745	11a	0.0792
6	0.2441	11b	−0.0433
6a	−0.0632		

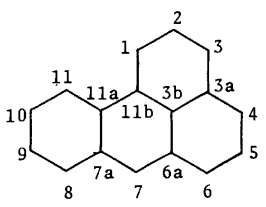

The π spin density distribution calculated by the above method is shown in Table 1. The spin density is found to be delocalized mostly in the naphthalene moiety. With the use of the values in Table 1, the dipolar interaction matrix $\mathbf{D}$ was calculated and diagonalized.[9] The zero-field splitting parameters were obtained according to Eqs. 3: D=0.2486 and E=0.0130 cm^{-1}. The agreement with the experimental values is commendable.

The spin delocalization in the π system and consequent low density at C-7 (0.357) account for the low D value. The spin distribution in the naphthalene ring of 7*H*-benz[*de*]anthracen-7-ylidene carries an interesting implication as regards the magnetic interaction between the molecules in crystal packing. It is usually the case for organic molecules in the crystal field to have the intermolecular distances governed by the van der Waals interaction. At these distances (~4 Å), the exchange interaction between the electron spins on the neighboring molecules tends to be negative. The more stable Coulomb interaction under these conditions is the α spins of one molecule facing the β spins of the other. Therefore, if the molecules of 7*H*-benz[*de*]anthracen-7-ylidene take the superimposable stacking has the crystals, the different spins (α and β) will develop between the two neighboring triplet molecules and the intermolecular interaction should become antiferromagnetic. On the other hand, if the parallel stacking has the phase shift or inversion as shown in Fig. 4, the α *vs.* β relationship holds in the overlapping naphthalene moieties with the high σ and π spin densities at the 7-position having the same sign of spins. The interaction could now become ferromagnetic. Thus the crystal structure of these and other aromatic diazo compounds is of interest and under current study in these laboratories.

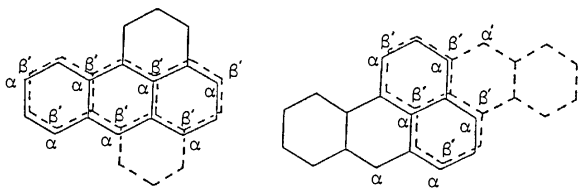

Fig. 4. Some molecular stacking models for potentially ferromagnetic molecular interaction.

Experimental

7H-Benz[de]anthracen-7-one Hydrazone. A mixture of 7*H*-benz[*de*]anthracen-7-one (2.00 g, 8.70 mmol), zinc chloride (3.60 g, 26.5 mmol) and 30 cm^3 of hydrazine hydrate in 60 cm^3 of ethylene glycol was refluxed with stirring for 12 h, poured into 200 cm^3 of water, and extracted with dichloromethane. The organic layer was washed with water, dried over anhydrous sodium sulfate, and concentrated under reduced pressure. The residue was chromatographed on alumina and eluted with dichloromethane. Recrystallization from hexane gave 1.16 g (55%) of yellow microcrystalline needles; mp 126—127 °C; IR (KBr) 1630 (C=N), 3180, 3320

(NH_2) cm^{-1}; ^1H NMR ($CDCl_3$) δ=7.41 (t, J=7.0 Hz, 1H), 7.44 (t, J=7.0 Hz, 1H), 7.62 (dd, J=7.3, 8.2 Hz, 1H), 7.63 (dd, J=7.3, 8.2 Hz, 1H), 7.82 (d, J=8.2 Hz, 1H), 7.88 (d, J=8.2 Hz, 1H), 8.08 (d, J=7.0 Hz, 1H), 8.17 (d, J=7.0 Hz, 1H), 8.22 (d, J=7.3 Hz, 1H) and 8.41 (d, J=7.3 Hz, 1H).

Found: C, 83.88; H, 4.87; N, 11.41%. Calcd for $C_{17}H_{12}N_2$: C, 83.58; H, 4.95; N, 11.47%.

7-Diazo-7H-benz[de]anthracene. Yellow mercury(II) oxide (1.8 g, 8.3 mmol), anhydrous sodium sulfate (2.0 g) and five drops of a freshly prepared saturated solution of potassium hydroxide in absolute ethanol were added to a solution of 0.20 g (0.82 mmol) of 7*H*-benz[*de*]anthracen-7-one hydrazone in 20 cm^3 of dry tetrahydrofuran at room temperature. The mixture was stirred for 1.5 h in the dark. Inorganic salts were removed by filtration and the solution was concentrated under reduced pressure at room temperature to give 0.2 g (quantitative yield) of yellow-green powder. The product was already spectroscopically pure. The analytical sample was prepared by recrystallization from ether; mp 98—100 °C (decomp); IR (KBr) 2030 cm^{-1}; UV (ether) 269 (log ε 4.53), 285 (4.37), 327 (3.93), 407 (4.14), 425 (4.10), and 600 nm (2.42); ^1H NMR ($CDCl_3$) δ=6.81 (d, J=6.7 Hz, 1H), 6.97 (d, J=7.9 Hz, 1H), 7.16 (dd, J=7.6, 8.3 Hz, 1H), 7.30 (dd, J=7.9, 8.3 Hz, 1H), 7.36 (dd, J=6.7, 8.8 Hz, 1H), 7.39 (d, J=8.8 Hz, 1H), 7.41 (dd, J=7.3, 8.2 Hz, 1H), 7.54 (d, J=8.2 Hz, 1H), 7.82 (d, J=7.3 Hz, 1H), and 8.00 (d, J=7.6 Hz, 1H).

Found: C, 84.22; H, 4.45; N, 11.58%. Calcd for $C_{17}H_{10}N_2$: C, 84.27; H, 4.16; N, 11.57%.

Spectral Measurements. IR spectra were recorded on a JASCO IR-810 spectrometer. NMR spectra were obtained on a JNM GX-400 spectrometer (400 MHz for ^1H) using tetramethylsilane as an internal standard. UV spectra were measured on a HITACHI 340 spectrometer.

ESR spectra were measured on a Varian E-112 spectrometer (X-band microwave unit, 100 kHz field modulation) equipped with an Air Products LTD-3-110 liquid helium transfer system. The diazo compound (*ca.* 2 mg) was dissolved in 2-methyltetrahydrofuran (0.5 cm^3) and the solution was degassed in a quartz cell by three freeze-thaw cycles. The sample was rapidly cooled in a pre-cooled ESR cavity and irradiated with a high-pressure mercury lamp (500 W) at 14 K. The signals due to the triplet carbene appeared immediately after the start of irradiation. The resonance magnetic field values of the signals were measured with the aid of a Varian E500 NMR gauss meter. The dependence of the signal intensities on temperatures was measured by the use of a temperature controlling accessory. The low-field Z line (at 44.5 mT at 14 K) was scanned repeatedly at several temperatures and the peak heights were plotted against $1/T$. In a separate run, the diazo compound (5 mg) was mixed with 7*H*-benz[*de*]anthracen-7-one (100 mg) in a mortar with a pestle made of agate, and the mixture was placed in a quartz sample tube (5 mm o.d.) 2 cm in height from the bottom. The sample was irradiated in an ESR cavity to obtain the spectrum of the triplet species.

Theoretical Calculations. Calculations were carried out on a Hitachi M-200H computer, using the program named "Huckel Molecular Orbirtal Calculation" programmed by Dr. H. Kihara and filed in the Program Library of the Computer Center of the Institute for Molecular Science. The McLachlan correction parameter λ was set at 1.2 in the program.

We wish to thank Dr. T. Sugawara of these laboratories for his helpful comments during this work. A collaboration of Prof. R. D. McKelvey in the preliminary preparation of the hydrazone is acknowledged.

References

1) In the chemistry briefing made to the White House Office of Science and Technology Policy, the G. C. Pimentel Committee to Survey Opportunities in the Chemical Sciences put chemical reactivity as one of the priority areas. As an example of the fundamental questions to be answered in the chemical reactivity studies, the possibility of organic ferromagnetic compounds is mentioned (Chemical and Engineering News, January 2, 1984, pp. 8—39).

2) R. Breslow, B. Jaun, R. Q. Kluttz, and C.-Z. Xia, *Tetrahedron*, **38**, 863 (1982).

3) A. A. Ovchinnikov, *Dokl. Akad. Nauk SSSR*, **236**, 928 (1977); A. L. Buchachenko, *ibid.*, **244**, 1146 (1979).

4) K. Itoh, *Chem. Phys. Lett.*, **1**, 235 (1967); N. Mataga, *Theor. Chim. Acta*, **10**, 372 (1968); K. Itoh, *Pure Appl. Chem.*, **50**, 1251 (1978). H. Iwamura, *Kagaku no Ryoiki*, **37**, 146 (1983); K. Itoh, *ibid.*, **37**, 152 (1983).

5) Y. Teki, T. Takui, K. Itoh, H. Iwamura, and K. Kobayashi, *J. Am. Chem. Soc.*, **105**, 3722 (1983).

6) a) E. Wasserman, L. C. Snyder, and W. A. Yager, *J. Chem. Phys.*, **41**, 1763 (1964); b) E. Wasserman, V. J. Kuck, W. A. Yager, R. S. Hutton, F. D. Greene, V. P. Abegg, and W. M. Weinshenker, *J. Am. Chem. Soc.*, **93**, 6335 (1971).

7) R. S. Hutton and H. D. Roth, *J. Am. Chem. Soc.*, **104**, 7395 (1982). These approximations were first employed to assign the spin density distributions obtained for fluorenylidene by the ENDOR method.[8] Later the empirical values were modified by Hutton and Roth to reproduce the zero-field splitting parameters of methylene. The latter values were used in this study. Since the triplet carbene discussed here is considered to have a smaller bond angle at the divalent carbon owing to the constraint of the ring, a new set of parameters should have been introduced to obtain better agreement with the experimental D and E values.

8) See for example: C. A. Hutchison, Jr. and G. A. Pearson, *J. Chem. Phys.*, **47**, 520 (1967).

9) In the concrete, the dipolar interaction matrix in Eq. 2 for 7*H*-benz[*de*]anthracen-7-ylidene was given by Eq.:

$$\boldsymbol{D} = \frac{(g\beta)^2}{2}\begin{bmatrix} \frac{r^2-3x^2}{r^5} & \frac{-3xy}{r^5} & \frac{-3xz}{r^5} \\ \frac{-3xy}{r^5} & \frac{r^2-3y^2}{r^5} & \frac{-3yz}{r^5} \\ \frac{-3xz}{r^5} & \frac{-3yz}{r^5} & \frac{r^2-3z^2}{r^5} \end{bmatrix}$$

$$= \begin{bmatrix} -0.0699 & 0.0 & -0.0029 \\ 0.0 & -0.0958 & 0.0 \\ -0.0029 & 0.0 & 0.1657 \end{bmatrix}$$

The calculation was made on the assumption that the molecular plane makes the xz plane and the origin of the coordinates is at the atom 7 (*i.e.* divalent carbon). The off-

diagonal elements in the above matrix are so small that, after diagonalization, the values of the diagonal elements are little changed.

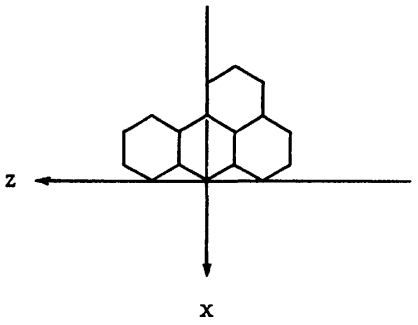

The coordinate systm given here was arbitrarily taken for convenience of calculations and different from the principal axes *X*, *Y*, and *Z* of the carbene molecule. Conventionally used **H** was employed in a unit of mT throughout this paper to represent magnetic fux density **B**.

The Mechanism and Stereochemistry of Asymmetric Transformation *via* Chiral Oxazolines

Saizo SHIBATA,* Hajime MATSUSHITA, Hajime KANEKO, Masao NOGUCHI, Takao SAKURAI,† Masahiko SABURI,† and Sadao YOSHIKAWA†

Central Research Institute, The Japan Tobacco and Salt Public Corporation, 6-2 Umegaoka, Midori-ku, Yokohama, Kanagawa 227

†*Department of Synthetic Chemistry, Faculty of Engineering, The University of Tokyo, Hongo, Bunkyo-ku, Tokyo 113*

(Received June 9, 1984)

The stereoselectivity of asymmetric transformation of 2-substituted alkanoic acids *via* oxazolines was clarified by measuring the isomeric ratio of ^{13}C-labeled lithio oxazolines by ^{13}C NMR. The mechanism of the process was discussed from substituent effects of the oxazoline ring and solvent effects on the transformation.

Theoretically, asymmetric transformation of racemic compounds into a single optically active form is one of the best methods to obtain chiral substances.[1,2] However, suitable substances for the transformation have been practically limited to optically labile compounds such as atropisomers.[3]

In a previous paper,[4] we reported the asymmetric transformation of optically stable alkanoic acids into optically active form *via* chiral oxazolines. In the transformation, optically active alkanoic acids were obtained by metalation of oxazolines with butyllithium followed by quenching the lithio oxazolines by addition of water, and subsequent hydrolysis (Scheme 1). In this paper the mechanism and stereochemistry of the process will be discussed.

Oxazolines **1**, **2**, and ^{13}C-labeled **1**, **2** (**1***, **2***) were prepared according to the methods described previously,[4] and the epimers (**1a**, **1b**, **1a***, **1b***, **2a**, **2b**, **2a***, **2b***) were separated by silica-gel chromatography. Each epimer was submitted to the transformation separately. Deuterium oxide was used instead of water to quench the carbanions to assure the quantitative formation of carbanions (**I** and **II**). Thus, **1** and **2** were converted to the deuterated epimers (**1-d** and **2-d**) as shown in Scheme 2. The extent of asymmetric induction through the metallation and protonation process was monitored by GLPC analysis. The isomeric ratios of the intermediate lithio oxazolines were measured by ^{13}C NMR.

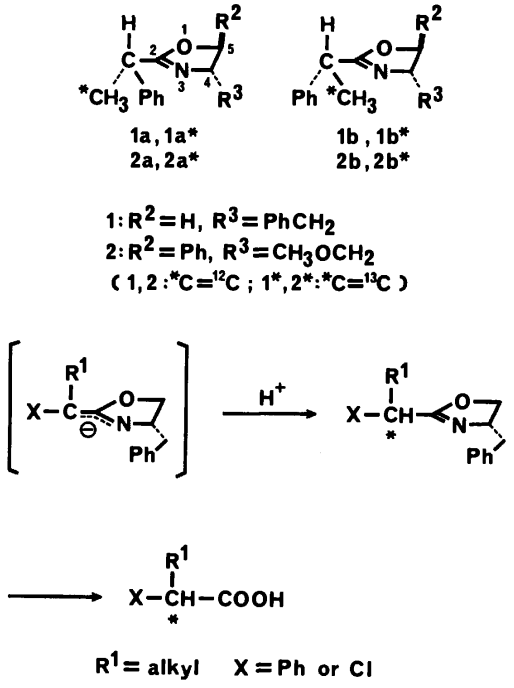

Scheme 1.

Experimental

IR spectra were measured with a JASCO A-3 spectrometer, mass spectra were recorded with a Hitachi M-80 mass spectrometer, optical rotations were measured with a JASCO Digital Automatic Polarimeter Model DIP-181. ^1H NMR spectra were obtained with a JNM-PS-100 spectrometer (100 MHz), and chemical shifts are expressed in δ downfield from TMS as an internal standard. ^{13}C NMR spectra were obtained with a JNM-FX-100 (25 MHz), and chemical shifts are reported in δ values relative to the β-THF signal which we defined as δ 25.0. GLPC analysis was carried out on a Shimadzu Gas Chromatograph GC-4CM equipped with a hydrogen flame ionization detector (column: OV-1 0.3 mm×50 m).

(4S)-2-(1-Phenylethyl)-4-benzyl-2-oxazoline (1a and 1b). A mixture of two epimers (**1a** and **1b**) was prepared from (4*S*)-(−)-2,4-dibenzyl-2-oxazoline and iodomethane according to the method described previously.[4] The two epimers were separated by silica-gel chromatography [silica gel 60 prepacked column (Merck), 40% ether–hexane].

1a: ^1H NMR ($CDCl_3$) δ=1.54 (3H, d, J=7 Hz, $\underline{CH_3}CH$),

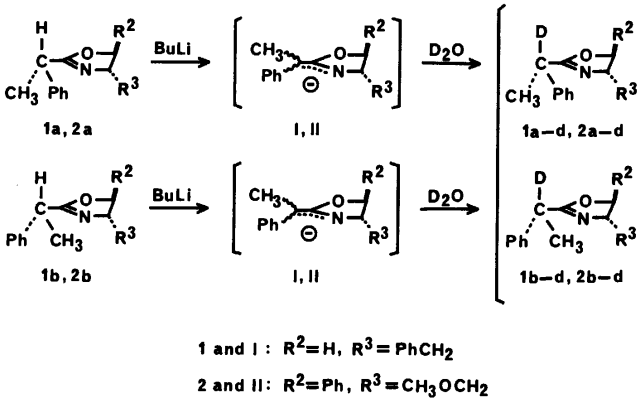

Scheme 2.

2.66 (1H, dd, J=14 and 8Hz, PhC$\underline{H}_2$), 3.11 (1H, dd, J=14 and 5Hz, PhC$\underline{H}_2$), 3.71 (1H, q, J=7Hz, $CH_3C\underline{H}$, 3.9—4.6 (3H, m), and 7.2—7.5 (10H, m).

1b: ^{1}H NMR ($CDCl_3$) δ=1.52 (3H, d, J=7Hz, C$\underline{H}_3$CH), 2.66 (1H, dd, J=14 and 8Hz, PhC$\underline{H}_2$), 3.13 (1H, dd, J=14 and 5Hz, PhC$\underline{H}_2$), 3.72 (1H, q, J=7Hz, $CH_3C\underline{H}$), 3.9—4.6 (3H, m) and 7.1—7.5 (10H, m).

Absolute Configuration of 1a and 1b. To determine the absolute configuration at C-2 *exo* methine of **1a** and **1b**, the mixture of **1a** and **1b** (**1a**:**1b**=10:90, 133mg) was hydrolyzed in 3M sulfuric acid (1M=1 mol dm^{-3}). The configuration of the resulting 2-phenylpropionic acid [yield 88%; $[\alpha]_D^{25}$ −54.8° (c 1.6, $CHCl_3$) o.p. 72%] was the *R*-configuration.[5]

(4S)-2-(1-Phenyl[2-^{13}C]ethyl)-4-benzyl-2-oxazoline (1a and 1b*).* A mixture of ^{13}C-enriched **1a** and **1b** (**1a*** and **1b***) was prepared using *ca.* 50% enriched [^{13}C]-iodomethane by the method described previously.[4] The two epimers were separated by silica-gel chromatography as described above.

(4S,5S)-2-(1-Phenylethyl)-4-methoxymethyl-5-phenyl-2-oxazoline (2a and 2b). A mixture of two epimers (**2a** and **2b**) was prepared according to the method described by Meyers *et al.*[6] The two epimers were separated by silica-gel chromatography [C.I.G. prepacked column (Kusano Kagakukikai Co.), 1% ethanol-hexane].

2a: ^{1}H NMR ($CDCl_3$) δ=1.62 (3H, d, J=7Hz, C$\underline{H}_3$CH), 3.40 (3H, s, C$\underline{H}_3$O), 3.6 (2H, m) 3.87 (1H, q, J=7Hz, $CH_3C\underline{H}$), 4.1 (1H, m), 5.28 (1H, d, J=6Hz, PhC$\underline{H}$O), and 7.1—7.5 (10H, m).

2b: ^{1}H NMR ($CDCl_3$) δ=1.60 (3H, d, J=7Hz, C$\underline{H}_3$CH), 3.40 (3H, s, C$\underline{H}_3$O), 3.6 (2H, m), 3.87 (1H, q, J=7Hz, $CH_3C\underline{H}$), 4.1 (1H, m), 5.25 (1H, d, J=6Hz, PhC$\underline{H}$O), and 7.1—7.5 (10H, m).

Absolute Configuration of 2a and 2b. To determine the absolute configuration at C-2 *exo* methine of **2a** and **2b**, the mixture of **2a** and **2b** (6:94, 148mg) was hydrolyzed in 6M sulfuric acid. The configuration of the resulting 2-phenylpropionic acid [yield 85%; $[\alpha]_D^{34}$ −53.8° (c 1.6, $CHCl_3$) o.p. 70%] was the *R*-configuration.[5]

(4S,5S)-2-(1-Phenyl[2-^{13}C]ethyl)-4-methoxymethyl-5-phenyl-2-oxazoline (2a and 2b*).* A mixture of ^{13}C-enriched **2a** and **2b** (**2a*** and **2b***) was prepared using *ca.* 90% enriched [^{13}C]-iodomethane by the method described previously.[6]

TABLE 1. ASYMMETRIC TRANSFORMATION OF 1 IN THF

Post metalation period[a]/min	5		45		300	
1a:**1b**	**1a-d**:**1b-d**	*D*/%	**1a-d**:**1b-d**	*D*/%	**1a-d**:**1b-d**	*D*/%
98: 2	82:18	96	83:17	97	83:17	95
49:51	71:29	93	71:29	93	68:32	94
4:96	63:37	91	62:38	95	62:38	95

a) Samples were metalated at −78°C and stirred for the intervals indicated at −78°C.

TABLE 2. ASYMMETRIC TRANSFORMATION OF 1 IN 25% HMPA-THF

1a:**1b**	**1a-d**:**1b-d**	*D*/%[a]
98: 2	39:61	94
49:51	41:59	91
4:96	41:59	94

a) Post metalation period was 45 min.

The two epimers were separated by silica-gel chromatography as described above.

Asymmetric Transformation of 1 in Tetrahydrofuran. The three mixtures of **1a** and **1b** [13.3mg (0.05mmol); **1a**:**1b**= 98:2, 49:51, 4:96] were prepared, and each mixture was dissolved in 1ml of dry tetrahydrofuran under nitrogen atmosphere. Each solution thus prepared was cooled to −78 °C, and a solution of butyllithium (0.16ml, 0.2mmol) in hexane was added dropwise to the solution under stirring at −78°C.[7] The reaction mixture was stirred for a given period (5, 45, and 300min; the post metalation period) at −78 °C, and then 1ml of 25% deuterium oxide-tetrahydrofuran solution was added and allowed to warm to room temperature. The mixture was extracted with ether, and the organic layer was washed with brine, dried over sodium sulfate, and concentrated under reduced pressure. The ratio of deuterated epimers (**1a-d** and **1b-d**) in this residue was determined by GLPC (170°C), and deuterium incorporation was detected by Mass and ^{1}H NMR spectra. The results are shown in Table 1.

Asymmetric Transformation of 1 in 25% Hexamethlphosphoric Triamide-Tetrahydrofuran. The three mixtures of **1a** and **1b** [13.3mg (0.05mmol); **1a**:**1b**=98:2, 49:51, 4:96] were prepared, and each mixture was dissolved in 1ml of dry 25% hexamethylphosphoric triamide-tetrahydrofuran under nitrogen atmosphere. The samples were treated as the method described for the asymmetric transformaiton of **1** in tetrahydrofuran, and in these reactions the post metalation period was 45min. The results are shown in Table 2.

^{13}C NMR Measurements of Lithio Oxazolines of ^{13}C-Labeled 1. Five mixtures of ^{13}C-labeled epimers of **1** (**1a***:**1b***= 99:1, 74:26, 49:51, 26:74, 3:97) were prepared. Each mixture (26.6mg, 0.1mmol) was dissolved in 0.2ml of dry tetrahydrofuran under nitrogen atmosphere, and 0.17ml of butyllithium in hexane (1.2M, 0.2mmol) was added to the solution with stirring at −78°C.[7] The ^{13}C NMR spectrum of each solution was recorded at −78°C under quantitative conditions,[8,9] and showed a major peak at δ 16.1 (lithio oxazoline **IA***) and a minor peak at δ 18.1 (lithio oxazoline **IB***). After the measurment of the spectrum, 0.2ml of 25% deuterium oxide-tertrahydrofuran solution was added to the sample at −78°C. The ratio of the deuterated epimers (**1a***-**d** and **1b***-**d**) in the resulting mixture was determined by GLPC analysis as described before. The results are shown in Table 3.

^{13}C NMR Measurements of Lithio Oxazolines of ^{13}C-Labeled 2. Five mixtures of ^{13}C-labeled epimers of **2** (**2a***:**2b***= 95:5, 73:27, 54:46, 30:70, 2:98) were prepared. Each mixture (14.8mg, 0.05mol) was dissolved in 0.3ml of dry tetrahydrofuran under nitrogen atmosphere, and 0.071ml of butyllithium in hexane (1.4M, 0.1mmol) was added to the solution with stirring at −78°C.[7] The ^{13}C NMR spectrum of each solution was recorded as described above, and showed two peaks at δ 15.8 (lithio oxazoline **IIA***) and δ 18.0 (lithio

TABLE 3. ASYMMETRIC TRANSFOMATION OF 1* IN THF

1a*:**1b***	**IA***(δ16.1):**IB***(δ18.1)	**1a***-**d**:**1b***-**d**
99: 1	94: 6	85:15
74:26	83:17	80:20
49:51	73:27	73:27
26:74	66:34	69:31
3:97	55:45	62:38

oxazoline **IIB***). After the measurment of the spectrum, 0.1 ml of 25% deuterium oxide–tetrahydrofuran was added to the sample at −78°C. The ratio of the deuterated epimers (**2a*-d** and **2b*-d**) in the resulting mixture was determined by GLPC analysis as described before. The results are shown in Table 4.

(4R,5R)-2-(1-Phenylethyl)-4-methyl-5-phenyl-2-oxazoline (4). (4*R*,5*R*)-2-Benzyl-4-methyl-5-phenyl-2-oxazoline was prepared from (−)-norpseudoephedrine and ethyl 2-phenylacetimidate by the method described previously.[4] The obtained oxazoline was alkylated by iodomethane according to the method described by Meyers *et al.* to give **4**:[6] IR (neat 1670cm^{-1}; ^{1}H NMR ($CDCl_3$) δ=1.35 (3H, d), 1.60 (3h, d), 3.8 (2H, m), 4.77 (1H, d), and 6.8—7.5 (10H, m); MS (70eV) *m/z* (rel intensity) 265 (M^+; 2), 160 (19), 159 (86), 144 (23), 106 (5), 105 (100), and 77 (16).

(4R,5S)-2-(1-Phenylethyl)-4-methyl-5-phenyl-2-oxazoline (5). (4*R*,5*S*)-2-Benzyl-4-methyl-5-phenyl-2-oxazoline was prepared from (+)-norephedrine, and this oxazoline was alkylated to give **5** by the same method as described above: IR (neat) 1670cm^{-1}; ^{1}H NMR ($CDCl_3$) δ=0.74 (3H, d), 1.59 (3H, d), 3.8 (1H, m), 4.3 (1H, m), 5.37 (1H, d), and 6.8—7.4 (10H, m); *m/z* (rel intensity) 265 (M^+; 4), 160 (28), 159 (79), 144 (34), 105 (100), 79 (28), and 77 (33).

Hydrolysis of 4 and 5 before and after the Asymmetric Transformation. **4** and **5** were hydrolyzed before and after the asymmetric transformation as described previously to give chiral 2-phenylpropionic acid,[4] and the results are shown in Table 5.

Results and Discussion

Asymmetric Transformation of 1. After the asymmetric transformation of **1** in tetrahydrofuran, **1a** (98%) gave a deuterated mixture of **1a-d** and **1b-d** in a ratio of 8:2, and **1b** (96%) gave it in a ratio of 6:4 as shown in Table 1. In this transformation the configuration at C-2 *exo* methine of **1a** was retained *ca.* 80%, whereas in the case of **1b** inversion of the configuration predominated over retention of the configuration. This difference is not due to insufficient deprotonation from **1a** or **1b** because deuterium incorporation was above 90% in both cases. The post metalation period (stirring period of the reaction mixture after the addition of butyllithium) was varied in the range of 5min, 45min, and 300min to examine the effect on the transformation. As shown in Table 1, ratios of the resulting epimers were practically independent on the post metalation period.

To clarify solvent effects, the transformation was performed in 25% hexamethylphosphoric triamide–tetrahydrofuran solution. The results are shown in Table 2. In this case, both **1a** (98%) and **1b** (96%) gave **1a-d** and **1b-d** in a ratio of 4:6 with deuterium incorporation above 90% in contrast with the results obtained in tetrahydrofuran.

These results indicate that the ratio of intermediate lithio oxazolines fomed in 25% hexamethylphosphoric triamide–tetrahydrofuran solution did not depend on that of **1a** and **1b**. On the other hand the ratio of the lithio oxazolines formed in tetrahydrofuran solution depended on that of starting epimers, and once they were formed the ratio did not change under the experimental conditions.

^{13}C NMR Measurment of Intermediate Lithio Oxazolines. This asymmetric transformation consists of the formation of lithio carbanions and successive protonation to them. To elucidate the mechanism of the process in tetrahydrofuran, the ratio of the lithio oxazolines was measured by ^{13}C NMR. In order to facilitate the ^{13}C NMR measurement, ^{13}C-enriched oxazolines (**1a*** and **1b***) were synthesized. The mixtures of **1a*** and **1b*** were prepared in various epimeric ratios and dissolved in tetrahydrofuran. Yellow solutions of lithio oxazolines were obtained by adding butyllithium. Two signals due to ^{13}C-enriched methyl carbon were observed at δ 16.1 (**IA***) and δ 18.1 (**IB***). After integration of these two signals (Table 3), the lithio oxazolines were quenched by deuterium oxide. ^{1}H NMR spectra showed that deuterium was incorporated to the *exo* methine carbon, α to the oxazoline ring. The ratios of the resulting deuterated **1a*-d** and **1b*-d** are summarized in Table 3.

The relationships between the ratio of **1a***:**1b*** and that of lithio oxazolines (**IA***:**IB***), and the ratio of lithio oxazolines and that of **1a*-d**:**1b*-d** are shown in Figs. 1 and 2, respectively.

Previously, the stereochemistry of the lithio carban-

Table 4. Asymmetric transformation of **2*** in THF

2a*:2b*	**IIA***(δ15.8):**IIB***(δ18.0)	**2a*-d:2b*-d**
95: 5	91: 9	76:24
73:27	76:24	70:30
54:46	67:33	66:34
30:70	54:46	60:40
2:98	37:63	53:47

Table 5. Hydrolysis of **4** and **5** before and after the asymmetric transformation

	Before the transformation				After the transformation			
	Yield %	$[\alpha]_D$[a]	O.p.[b] %	Config.	Yield %	$[\alpha]_D$[a]	O.p.[b] %	Config.
4	80	+0.7°	1	*S*	60	−13°	17	*R*
5	75	+1.5°	2	*S*	65	−26°	34	*R*

a) The concentrations at which the rotations were taken were *ca.* 2g/100ml in chloroform. b) Optical purities were based upon the highest literature values available: Ref. 5b; $[\alpha]_D^{25}$ +76.3° (*c* 1.6, $CHCl_3$).

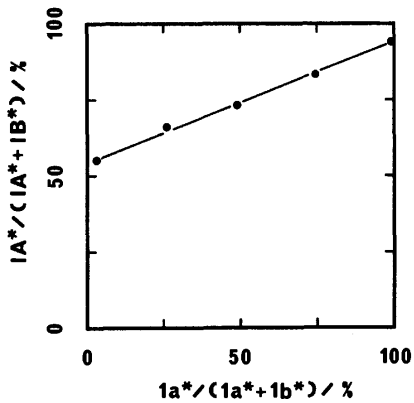

Fig. 1. Relationship between the ratio of **1a***:**1b*** and the lithio oxazoline ratio.

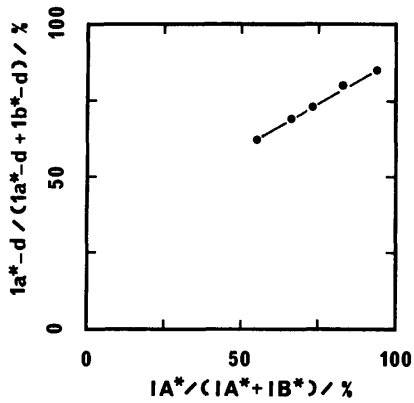

Fig. 2. Relationship between the lithio oxazoline ratio and the ratio of **1a*-d**:**1b*-d**.

ions of (4*S*,5*S*)-2-[2-^{13}C]ethyl-4-methoxymethyl-5-phenyl-2-oxazoline (**3***) were established by Meyers *et al.*[9] and Newcomb *et al.*[10] Therefore, (4*S*,5*S*)-2-(1-phenyl[2-^{13}C]ethyl)-4-methoxymethyl-5-phenyl-2-oxazoline (**2***), which has an analogous structure to **3*** and also to **1***, was prepared and treated in the same manner as described for **1*** to clarify the stereochemistry of the intermediate lithio oxazolines. Two signals due to ^{13}C-enriched methyl carbon of the lithio oxazoline were observed at δ 15.8 (**IIA***) and δ 18.0 (**IIB***). The results for the stereoselective transformation are summarized in Table 4, Fig. 3, and Fig. 4.

Stereochemistry of Intermediate Lithio Oxazolines. In the case of **1*** and **2***, ^{1}H NMR spectra showed that deuterium was incorporated to the *exo* methine carbon, α to the oxazoline ring. Two signals due to ^{13}C-enriched methyl carbon were observed for **1*** and **2***, respectively, in ^{13}C NMR spectra. These spectral data indicate that intermediate lithio oxazolines (**I**, **II**) exist as mixtures of *E*- and *Z*-isomers.

The relationship between the structure of lithio oxazoline of **3*** and the chemical shift of its ^{13}C-enriched methyl carbon was established by Meyers *et al.*[9] and Newcomb *et al.*[10] They assinged, in tetrahydrofuran solutions, a high field peak to **IIIA*** and a low field one to **IIIB***, respectively (Fig. 5).

According to the above structual assignment, in the

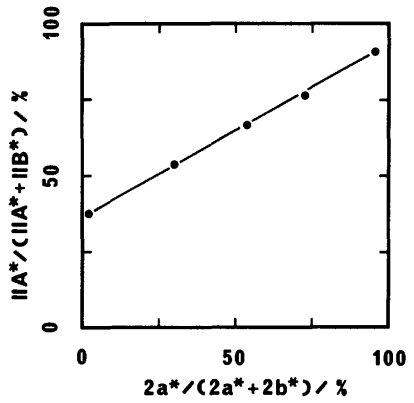

Fig. 3. Relationship between the ratio of **2a***:**2b*** and the lithio oxazoline ratio.

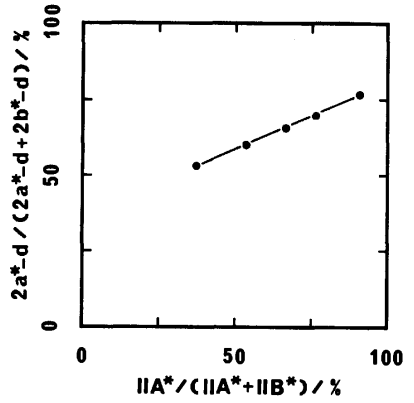

Fig. 4. Relationship between the lithio oxazoline ratio and the ratio of **2a*-d**:**2b*-d**.

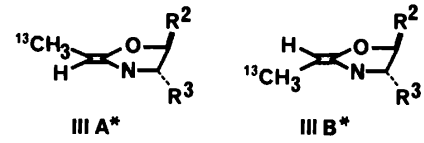

R^2=Ph, R^3=CH_3OCH_2

Fig. 5.

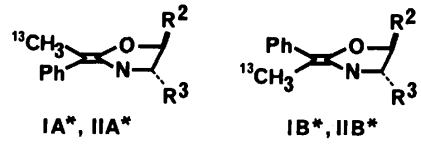

I*: R^2=H, R^3=$PhCH_2$

II*: R^2=Ph, R^3=CH_3OCH_2

Fig. 6.

TABLE 6. CHEMICAL SHIFTS ASSIGNMENTS OF I*—III*

	ppm		ppm
IA*	16.1	**IB***	18.1
IIA*	15.8	**IIB***	18.0
IIIA*	10.9[a]	**IIIB***	11.7[a]

a) Ref. 9.

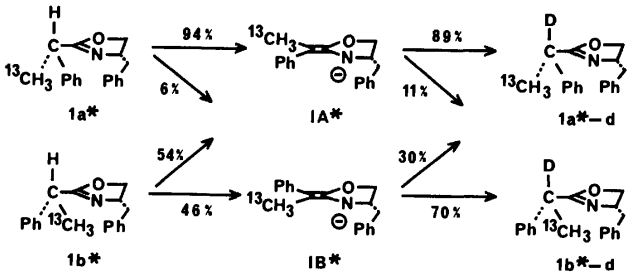

Scheme 3.

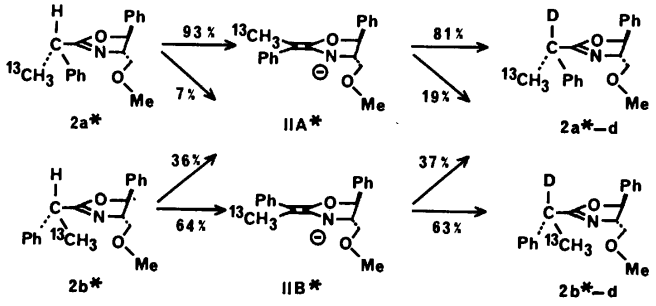

Scheme 4.

case of **1*** and **2***, lithio oxazolines **IA***, **IB***, **IIA***, and **IIB*** are assigned to the structures illustrated in Fig. 6 from their chemical shifts. Chemical sifts of ^{13}C-enriched methyl signals of **I***—**III*** are summarized in Table 6.

Stereoselectivity of Asymmetric Transformation. The selectivities of the formation of the lithio oxazolines from **1*** and **2***, and that of deuterated epimers from the lithio oxazolines were calculated from the slopes of the straight lines in Figs. 1—4. Since the structures of lithio oxazolines were assigned as described above, the selectivities of the asymmetric transformation are illustrated in Schemes 3 and 4.

In the case of **1***, retention of the stereochemistry of **1a*** was explained by the selective formation of **IA*** from **1a*** and that of **1a*-d** from **IA***. Inversion of the stereochemstry of **1b*** was accounted for by the preferential formation of **IA*** from **1b*** and by the partial formation of **1a*-d** from **IB***. **2*** also showed the same trend of stereoselectivity to **1***. However in the case of **2***, the stereoselectivity of deuterium incorporation was slightly lower than that of **1***. This fact can be explained by the steric effect of substituents at oxazoline ring of **2*** which has a phenyl group on the oppsite side of a methoxymethyl group. The deuterium approach from the top side of the ring may be interfered to some extent by the phenyl group.

In both cases of **1*** and **2***, deuterium was incorporated from the top side of the oxazoline ring, and this stereoselectivity is seemed to be determined by steric effects at 4 position of the oxazoline ring. To elucidate the steric effects of substituents at 4 and 5 positions, asymmetric transformation of oxazolines **4** and **5** was examined. Configurations of the acids ob-

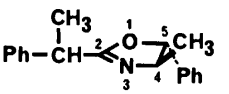

4

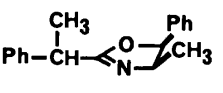

5

tained by hydrolysis of **4** and **5** after the asymmetric transformation were both *R*-configuration as shown in Table 5. Because the configuration of the resulting acids was not affected by the C-5 configuration, steric effects of a 5 positioned substituent was accounted to be smaller than that of a 4 positioned substituent.

From above results, at first deuterium is considered to approach stereoselectively to the nitrogen of the oxazoline ring, and in this approach the selectivity would be substantially affected by the 4 positioned substituents.

This stereoselective deuterium approach and the subsequent stereoselective deuterium transfer to the α carbon would result in the deuterium incorporation to the oxazoline anions (**I** and **II**) from the top side of the ring. This stereoselective process is well correspond to that observed in the asymmetric transformation of carbonyl compounds *via* enamines.[11]

References

1) H. B. Kagan and J. C. Fiaud, "Topics in Stereochemistry," ed by E. L. Eliel and N. L. Allinger, John Wiley & Sons, New York (1978), Vol. 10, p. 229.

2) H. Matsushita, M. Noguchi, M. Saburi, and S. Yoshikawa, *Bull. Chem. Soc. Jpn.*, **48**, 3715 (1975).

3) M. M. Harris, "Progres in Stereochemistry," ed by W. Klyne and P. B. D. Mare, Butterworths Scientific Publications, London (1958), Vol. 2, p. 157.

4) S. Shibata, H. Matsushita, H. Kaneko, M. Noguchi, M. Saburi, and S. Yoshikawa, *Bull. Chem. Soc. Jpn.*, **55**, 3546 (1982).

5) a) K. S. Y. Lau, R. W. Fries, J. K. Stille, *J. Am. Chem. Soc.*, **96**, 4983 (1974); b) S. P. Bakshi and E. E. Turner, *J. Chem. Soc.*, **1961**, 171.

6) A. I. Meyers, G. Knaus, K. Kamata, and M. E. Ford, *J. Am. Chem. Soc.*, **98**, 567 (1976).

7) Large excess amounts of butyllithium were used to exclude insufficient deprotonation from the oxazolines.

8) To assure quantitative conditions, the spin-lattice relaxation time (T_1) determination was performed for the β methyl carbon in **2a** and **2b** at −78°C using the standard inversion recovery techniques. The relaxation times of the β methyl carbon for both **2a** and **2b** were almost identical and equal to 0.25s. The ^{13}C NMR measurement was carried out using gated decoupling to suppress the Overhauser effect (NOE) [a delay time (τ)>5T_1].

9) A. I. Meyers, E. S. Snyder, and J. J. H. Ackerman, *J. Am. Chem. Soc.*, **100**, 8186 (1978).

10) M. A. Hoobler, D. E. Bergbreiter, and M. Newcomb, *J. Am. Chem. Soc.*, **100**, 8182 (1978).

11) H. Matsushita, Y. Tsujino, M. Noguchi, and S. Yoshikawa, *Bull. Chem. Soc. Jpn.*, **51**, 201 (1978).

Syntheses of 23-Dialkylamino-23-deoxydemycinosyltylosins and Conformational Study of Mycaminosyl Tylonolide by Nuclear Overhauser Difference Spectroscopy

Shuichi SAKAMOTO, Tsutomu TSUCHIYA,* Toshiaki MIYAKE, Akihiro TANAKA, and Sumio UMEZAWA

Institute of Bioorganic Chemistry, 1614 Ida, Nakahara-ku, Kawasaki 211

(Received July 6, 1984)

23-Dialkylamino-23-deoxydemycinosyltylosins have been prepared by treating 23-deoxy-23-iododemycinosyltylosin (**2**) with a series of amines including dimethylamine, diethylamine, and piperidine. 14(23)-Unsaturated derivatives, 23-deoxy-14(23)-enomycaminosyl tylonolide (**17**) and 23-deoxy-14(23)-enodemycinosyltylosin (**4**) have also been prepared. The conformation of mycaminosyl tylonolide dissolved in chloroform-*d* was determined by nuclear Overhauser difference spectroscopy, revealing that the two three-member groups of H(10), Me(22), and H(14) and of H(11), H(13), and H(15) stood, respectively, in a line in this order.

Demycinosyltylosin (DMT), which cannot be prepared practically by acidic hydrolysis of tylosin on account of the preferential removal of mycarose moiety from tylosin, was isolated from a culture of a blocked mutant[1] of tylosin-producing strain, *Streptomyces fradiae*. Okamoto *et al.*[2] also prepared the same compound in large amounts by fermentation of a blocked mutant (YO-9010) of *Streptomyces fradiae* NRRL 2702. Tatsuta *et al.*[3] synthesized the compound in the course of the total synthesis of tylosin. The compound has a reactive primary hydroxyl group at C-23, and this stimulated us to prepare derivatives having functional groups other than the hydroxyl at the C-23.

Recently we prepared 23-dialkylamino derivatives[4] of mycaminosyl tylonolide (MT) and 4′-deoxymycaminosyl tylonolide[5] (DT) by converting their hydroxyls at C-23 to dialkylamino groups *via* the corresponding iodo derivatives and found that the dialkylamino derivatives showed strong antibacterial activities against Gram-negative bacteria. Since DMT (**1**) includes MT-mycarose (1″→4′) structure, the C-23-dialkylamino derivatives of **1** were expected to have similar antibacterial activities as well.

Results and Discussion

Treatment of DMT (**1**) with iodine and triphenylphosphine according to Matsubara *et al.*[6] but changing the solvent to pyridine,[7] without protection of the formyl group, gave readily 23-deoxy-23-iododemycinosyltylosin (**2**). The structure was confirmed by the ^{1}H-NMR spectrum. Treatment of the iodo derivative (**2**) with dimethylamine in hot acetonitrile according to Tanaka *et al.*[4] gave the 23-deoxy-23-dimethylamino derivative (**3**) in a short period in high yield (83%) with slight 14(23)-ene product (**4**) accompanied. If, in this reaction, excess dimethylamine was used, proportion of **4** increased. In a similar fashion, other 23-deoxy-23-dialkylamino derivatives of **1** were prepared from **2** and a series of dialkylamines, namely, diethylamine, *N*-methyl-2-hydroxyethylamine, pyrrolidine, piperidine, hexahydroazepine, and octahydroazocine (giving **9**—**14**, respectively). Reaction conditions and analytical data of these products are shown in Table 1.

4″-*O*-Acetyl derivative (**7**) of **3** was next prepared. Treatment of **3** with acetic anhydride in acetonitrile in the presence of sodium hydrogencarbonate at room temperature gave almost quantitatively the 2′-*O*-acetyl derivative (**5**), which was then acetylated with acetic anhydride in pyridine under conditions to avoid the acetylation of HO-3. After a week at 0°C, 2′,4″-di-*O*-acetyl derivative (**6**) was obtained in a moderate yield (52%) with the starting material (**5**) and 2′,3,4″-tri-*O*-acetyl compound (**8**). Compound **8** was prepared, in a separate experiment, by per-*O*-acetylation of **3** (see Experimental). Heating **6** in methanol selectively cleaved the 2′-*O*-acetyl group to give the 4″-*O*-acetyl derivative (**7**) in high yield. Possibly, the selective deacetylation at C-2′ may be due to the presence of the dimethylamino group at C-3′ which attracts a proton

TABLE 1. REACTION PERIODS, YIELDS FROM **2**, OPTICAL ROTATIONS AND ELEMENTAL ANALYSIS OF COMPOUNDS **3** AND **9**—**14**

Compound formed	Reaction period (min)	Yield %	$[\alpha]_D^{22}$ (c 1, $CHCl_3$)	Formula	C Calcd	C Found	H Calcd	H Found	N Calcd	N Found
3	60	83	−26°	$C_{40}H_{70}N_2O_{12}\cdot 1/2H_2O$	61.78	61.82	8.88	8.60	3.60	3.79
9	200	61	−23°	$C_{42}H_{72}N_2O_{12}$	63.32	63.00	9.05	8.85	3.52	3.57
10	150	79	−19°	$C_{41}H_{70}N_2O_{13}\cdot H_2O$	60.29	60.24	8.82	8.50	3.43	3.47
11	60	49	−24°	$C_{42}H_{70}N_2O_{12}\cdot H_2O$	62.07	62.38	8.87	8.53	3.45	3.73
12	75	76	−17°	$C_{43}H_{72}N_2O_{12}\cdot H_2O$	62.47	62.62	8.96	8.70	3.39	3.04
13	60	62	−14°	$C_{44}H_{74}N_2O_{12}\cdot H_2O$	62.86	62.87	9.05	8.72	3.33	3.19
14	60	60	−15°	$C_{45}H_{76}N_2O_{12}\cdot H_2O$	63.23	63.12	9.13	9.30	3.28	3.27

from a methanol molecule to form an ion pair as depicted in I, followed by attack of the MeO^- upon the acetyl carbon as shown in Formula 1.

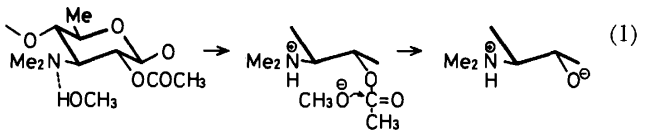

(1)

I

^{1}H-NMR Spectral Studies. Chemical structures of **2**, **3**, **5**, **6**, **7**, and **8** were confirmed by their ^{1}H-NMR spectra. The proton chemical shifts of these compounds, MT, and DMT (**1**) are shown in Table 2, and the spectrum of MT, in Fig. 1. In MT and DMT, no substantial differences in shift values between the corresponding protons of both compounds were observed, although slight differences being observed in H-1′, 2′, 3′, 4′, and *N*-methyls at C-3′. In the 23-iodo compound (**2**), pronounced up-field shifts of methylene protons at C-23 were observed, in comparison to **1**, and moderate shift changes in H-13, 14, and 15, all of these hydrogen atoms locating in the vicinity of C-23. In the 23-dimethylamino derivative (**3**), pronounced up-field shifts of the methylene protons at C-23 were observed, in comparison to the iodo derivative (**2**), and moderate to slight shift changes in H-10, 13, 14, and 15. These

TABLE 2. PROTON CHEMICAL SHIFT DATA[a] OF MT, DMT(**1**), **2**, **3**, **4**, **5**, **6**, **7**, AND **8** (in $CDCl_3$ at 50°[b] for MT and DMT, and 24° for other compounds)

H-atom	MT	DMT(1)	2	3	5	6	7	8	4
2a	1.97 d	1.95	1.93	1.94	1.91	1.91	1.94	1.97	
2b	2.50 dd	2.51	2.53	2.52	2.49	2.48	2.51	2.59	
3	3.87 d[c]	3.85[c]	3.84[c]	3.84[c]	3.82[c]	3.82[c]	3.84[c]	5.12	3.85 d[c]
4	≈1.64 m	≈1.64	≈1.64						
5	3.75 ddd	≈3.74	3.72	3.72 **	3.61	3.62 **	3.72	3.45	3.75
6	2.23 m[d]	2.20[d]	2.18[d]						
7a	1.48 d	1.49	1.50	≈1.5		≈1.5			
7b	≈1.64 m	≈1.64	≈1.64						
8	2.68 m[d] *	2.64	≈2.62	≈2.6 *	≈2.52	≈2.52 *	≈2.57	2.58	
10	6.27 d	6.29 *	6.33 *	6.25	6.27	6.27	6.24	6.27	6.32 d
11	7.30 d	7.31	7.33	7.36	7.36	7.34	7.37	7.43	7.21 d
13	5.88 d[c]	5.86[c] **	5.71[c] *	5.76[c]	5.76[c]	5.74[c]	5.76[c]	5.82	6.20 s
14	2.88 ddd	≈2.91 m **	2.81 dq *	≈2.87 m	≈2.86	≈2.84	≈2.85	≈2.87 m	
15	4.98 dt	4.97 **	4.86 **	4.75	4.74	4.77	4.75	4.63	5.38 t
16a	≈1.68 m	≈1.65	≈1.68						≈1.76
16b	1.86 m	≈1.88							≈1.90
17	0.95 t	0.95	0.96	0.93	0.94	0.94	0.94	0.92	0.99
18	1.01 d	1.00	1.01	1.01 *	0.93	0.92 *	1.01	0.97	0.98
19a	2.36 dd	2.39							
19b	2.91 dd *	≈2.85				≈2.87	≈2.85		
20	9.69 s	9.68	9.69	9.69	9.67 d[e]	9.68[e]	9.68 s	9.61 d[e]	9.74 s
21	1.22 d	1.21	1.23	1.22	1.22	1.22	1.20	1.23	1.20
22	1.83 d[e]	1.83[e]	1.83[e]	1.83[e]	1.83[e]	1.82[e]	1.83[e]	1.83[e]	1.86[e]
23a	≈3.73	≈3.74 ***	3.10 dd ***	2.29	2.29	2.31	2.28	2.29	5.09 s
23b		***	3.27 ***	2.53 dd *	2.47	2.47	2.46	2.46	5.33 s
C(23)NMe$_2$				2.19 s	2.19	2.19	2.19	2.19	
1′	4.30 d *	4.23	4.22	4.22 *	4.27	4.29 *	4.22	4.25	4.25
2′	3.49 dd *	3.54	3.54	3.54 ***	5.01	5.01 ***	3.52	5.01	3.57
3′	2.43 t *	2.47		≈2.47 ***	2.69	2.71 ***	≈2.45	2.70	
4′	3.09 t **	3.21—3.33	3.2—3.33	3.2—3.33 **	3.29	3.29	≈3.28	3.23—3.25	
5′	3.31 m *			*	3.24	3.26	≈3.28		
6′	1.28 d	1.26[f]	1.25[f]	1.24[f]	1.26[f]	1.26	1.24	1.26[f]	1.27
C(3′)NMe$_2$	2.55 s *	2.49	2.50	2.49 **	2.39	2.42 **	2.52	2.41	2.50
1″		5.06 d	5.08	5.08	5.07	5.06	5.07	5.07	5.09
2″a		1.76 dd	1.76	1.77	1.77 *	1.84	1.85	1.85	1.77
2″b		2.03 d	2.03	2.02	2.03 *	1.98 *	2.02	1.99	2.04
C(3″)Me		1.33 s *	1.24	1.24	1.23 **	1.11	1.13	1.13	1.24
4″		≈2.91			≈2.90 ***	4.60 d	4.62	4.61	
5″		4.07 dq	4.06	4.06 *	4.01 ***	4.29 **	4.46	4.53	4.08 m
6″		1.29 d	1.30	1.30	1.29 **	1.13	1.14	1.14	1.30
3-OAc								2.11	
2′-OAc					2.08 s	2.06		2.07	
4″-OAc						2.14 s	2.16	2.16	

a) After the shift values (δ), multiplicity of the signals is cited, that is omitted if the multiplicity is the same with that of the left-handed compound. Asterisk, *, **, and *** mean that the $\Delta\delta$ between the figures of the right and the left are 0.04—0.09, 0.1—0.2, and >0.2ppm, respectively, except for **4** and **8**. b) Signals of MT and DMT were not sharp at 24°. c) Slightly broadened, d) Broadened, e) $J \leq 1$ Hz, f) Signal height is 60—70% of that of H-6″.

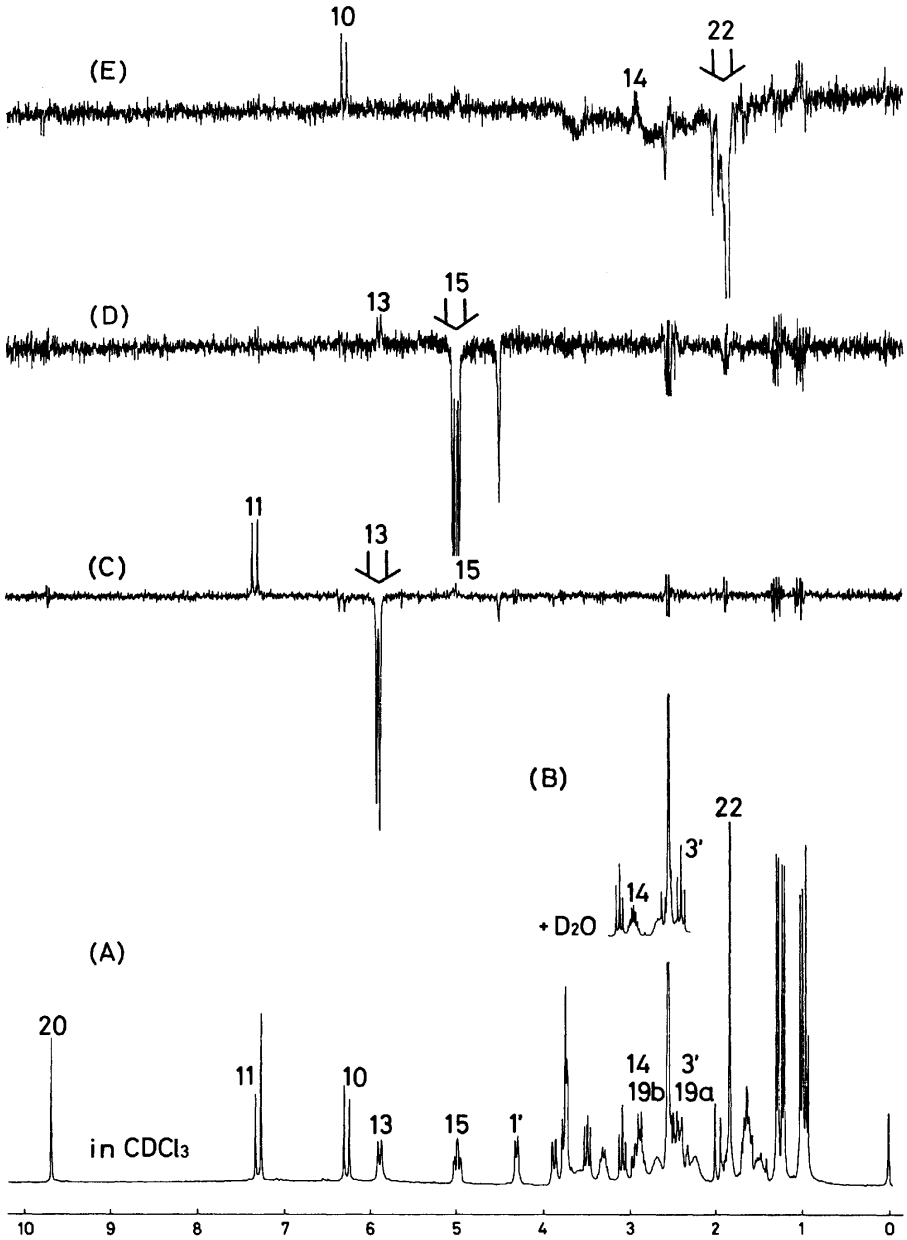

Fig. 1. ^{1}H-NMR spectra of MT. (A) Normal spectrum, (B) measured after addition of D_2O followed by standing for 5d with occasional shaking (indicating that H-19a, b were deuterated), (C–E) NOE difference spectrum; arrows mean the positions irradiated.

results indicate that functional group changes occur at the C-23. The momo-*O*-acetyl derivative (**5**) of **3** showed pronounced down-field shift of H-2′, and moderate shift changes of *N*-methyls at C-3′, H-4′, and 5′, in comparison to the corresponding chemical shifts of **3**, indicating that HO-2′ was acetylated. The di-*O*-acetyl derivative (**6**) showed pronounced down-field shifts of H-2′ and 4″ in comparison to the corresponding shifts of **3**, indicating that HO-4″ (and not HO-3) was acetylated in addition to HO-2′. Selective deacetylation of **6** gave monoacetyl derivative (**7**), that showed up-field shift of H-2′, indicating that 2′-*O*-acetyl group was removed. It is worthy to mention that *O*-acetyl methyl protons at C-2′, 3, and 4″ resonated invariably at δ 2.08, 2.11, and 2.16, respectively in the four compounds (**5**, **6**, **7**, **8**) usable for diagnosis of the acetyl positions.

Decoupling results obtained in MT are shown in Table 3, with the general coupling constants relating to **2**, **3**, **5**, **6**, **7**, **8**, MT, and DMT. As was cited in the Table, substantially the same J values were observed in the corresponding protons in all compounds described above, with slight exceptions, and the values showed good accordance with those of rosaramicin reported.[8]

Some stereochemical problems between the range of C-10 and C-15 are next described. The large coupling constants of $J_{10,11}$ in the compounds described above indicate that H-10 and 11 are in trans relationship, as repeatedly reported in similar compounds. However, ^{1}H-NMR spectral study in a solution describing the

TABLE 3. DECOUPLING DATA OF MT (UNLESS OTHERWISE STATED) AND COUPLING CONSTANTS RELATING TO MT, DMT(**1**), **2**, **3**, **5**, **6**, **7**, AND **8**

Position to be irradiated (δ)	Observed[a]	A	B	$J_{A,B}$(Hz)
2.50 (H-2b, partly H-3′)	2a→s, 3→s, 2′→incomplete t,	2a,	2b	17
	4′→change	2a,	3	0
		2b,	3	10—10.5
3.87 (H-3)	2b→d (*J* 17), 2a→no change	3,	4	≈1
		4,	5	9.3—10.5
2.23 (H-6)	5→no change,	5,	6	0
	7a→change, 7b→change,	6,	19a	4.5
	19a, 19b→ABq	6,	19b	10
		19a,	19b	≈17
1.48 (H-7a)	6 and 8→not clear	6,	7a	10.5
		6,	7b	
2.68 (H-8)	7a→dd (*J* 10, 15), 7b→change,	7a,	7b	15
	21→s	7a,	8	5
		7b,	8	≈12
1.22 (H-21)	8→simplified	8,	21	6.5
1.21 (H-21) DMT	8→simplified			
7.30 (H-11)	10→s	10,	11	15.5—16
5.88 (H-13)	14→dq, 22→s	13,	22	≈1
2.90 (H-14,19b)	6→slight change, 13→s,	13,	14	10.5
	15→dd (*J* 3, 10), 19a→br. s,	14,	23a	4.5 (for **3**, **5**, **6**)
	23a,b→br. s,	14,	23b	10 (for **3**, **5**, **6**)
		23a,	23b	12 (for **3**, **5**, **6**)
		14,	15	9.5
3.74 (H-5, 23a,b)	6→change, 14→t (*J* 9.5)			
1.61 (H-4, 7b,16a)	3→no change, 8→change	15,	16a	9.5
	15→change, 17→change,	15,	16b	3
	18→s	16a,b,	17	6—7.5
1.68 (H-16a)	5→incomplete s, 15→d (*J* 9),	18,	4	6—7
	17→slight change, 18→incomplete s			
4.98 (H-15)	16a→q, 16b→q, 14→change			
1.86 (H-16b)	15→t (*J* 9.5), 17→d			
3.09 (H-4′)	3′→d (*J* 10)	1′,	2′	7.5
3.27 (H-4′, 5′) DMT	6′→s, 3′→not clear	2′,	3′	10—10.5
		3′,	4′	10
		4′,	5′	9.3
		5′,	6′	6—6.3
5.06 (H-1″) DMT	2″a→d (*J* 15)	1″,	2″a	3.5—4
1.76 (H-2″a) DMT	1″→s, 2″b→s	1″,	2″b	0
2.91 (H-4″) DMT	5″→q	2″a,	2″b	14—15
4.07 (H-5″) DMT	6″→s	4″,	5″	9.5—10
		5″,	6″	6.3—6.5

a) The figures after the arrow mean the multiplicity after irradiation.

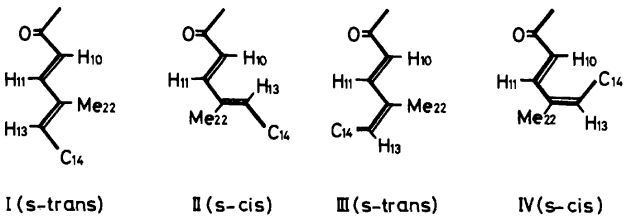

Chart 1.

spacial situation related to H-11, Me-22, and H-13 has not been reported yet. Theoretically, the following four structures (I, II, III, and IV) should be considered. Omura *et al.*[9] reported, by the X-ray crystallographic study of protylonolide, that Me-22 and H-13 are trans, and that Me-22 and H-11 are also trans. From the former result, structures III and IV should be abandoned. However, in the latter relationship, possibility of structure II should be considered, because, in a solution, rotational energy around the axis of C(11)—C(12), is thought to be not so high as to prevent the debate. To clarify the problem, nuclear Overhauser effects (NOE) between some important hydrogen atoms were measured using the NOE difference spectroscopy[10] (Fig. 1). Irradiation at δ 1.83 (Me-22) of MT caused pronounced positive enhancement (≈15%) of each of the resonances of H-10* and 14, but not other resonances including H-11* and 13. On this experiment, if strongly irradiated, slight enhancement of H-15 was observed. This may be caused by the simultaneous irradiation of H-16b (δ ≈1.86) as well as

*Resonances at δ 6.3 and 7.3, both appeared as a doublet, were assigned to H-10 and 11, respectively. These assignments will be reasonable from the point of view of mesomeric effect[11a] and the comparison of the chemical shifts of the corresponding protons of, for example, mycinamicins,[12] which have a similar α,β,γ,δ-unsaturated carbonyl fragments lacking the methyl group at C-12.

Me-22, and H-15 may be enhanced through space or through bond interaction. Irradiation of H-11 and H-13 also caused pronounced positive enhancements (20—22%) of H-13 and H-11, respectively, with small signal increase (5—6%) of H-15 in the latter case. Irradiation of H-15 also caused enhancement (≈5%) of H-13. In conclusion, these results show that Me-22 is located in close proximity with both H-10 and 14, that is, between H-10 and 14, and H-13 is located be-

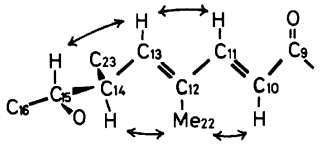

Chart 2.

tween H-11 and 15, as depicted above. The conclusion clearly supported the structure of I having *s*-trans[13] structure, and also confirmed the absolute configuration at C-15 to be *R*.

The structure of **4** was confirmed by the ^{1}H-NMR spectrum (Table 2). In the spectrum, H-13 appeared as a singlet suggesting the absence of H-14. Resonances of methylene protons at C-23, which appeared at $\delta \approx 3.7$ in MT, appeared as two singlets at δ 5.09 and 5.33. The chemical shifts and zero coupling suggest[11b] the presence of a terminal double bond.

To confirm the structure of **4** further, 23-deoxy-14(23)-enomycaminosyl tylonolide (**17**), a simpler analog, was prepared starting from 23-bromo-23-deoxymycaminosyl tylonolide diethyl acetal[7] (**15**) with silver fluoride *via* the corresponding 14(23)-ene compound (**16**). The ^{1}H-NMR spectra of the macrolactone portions of **17** and **4** showed good accordance.

Antibacterial spectra (Table 4) of the new derivatives showed that introduction of a dialkylamino group at C-23 of DMT (**1**) gave activities, comparable to that of parent DMT. Among the compounds, the 4″-*O*-acetyl derivative (**7**), 23-deoxy-23-piperidino and hexahydroazepine-1-yl derivatives (**12**, **13**) were most active against both Gram-positive and-negative bacteria.

Experimental

General. Optical rotations were measured with a Perkin-Elmer 241 polarimeter. Thin-layer chromatography (TLC) was carried out on Kieselgel 60 F-254 (E. Merck) silica

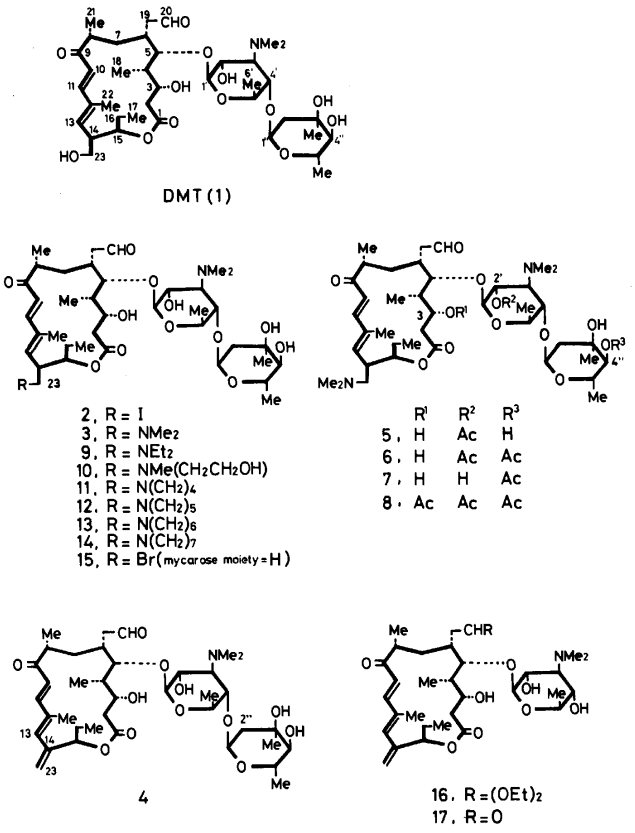

Chart 3.

gel with detection by spraying with sulfuric acid, followed by slight heating. Column chromatography was performed on Wakogel C-200, or Kieselgel 60, 230—400 mesh (E. Merck). UV spectrum was recorded with a Hitachi 200-10 spectrometer. ^{1}H-NMR spectra were recorded at 90 MHz with a Varian EM-390 spectrometer, or at 250 MHz in the FT mode with a Bruker WM 250 spectrometer at 24°C unless otherwise stated.

23-Deoxy-23-iododemycinosyltylosin (2). A mixture of crude demycinosyltylosin (**1**, 1.06 g) obtained from a culture, triphenylphosphine (0.93 g), and iodine (0.4 g) in dry pyridine (52 ml) was stirred under nitrogen at 0°C for 3.5 h. After addition of 0.1 M aqueous sodium thiosulfate (3 ml) to decompose the excess iodine, the mixture was evaporated. The chloroform solution of the residue was washed with saturated aqueous sodium hydrogencarbonate, saturated aqueous sodium sulfate, dried (Na_2SO_4), and evaporated. Silica-gel column chromatography of the residue with chloroform–methanol–28% aqueous ammonia (50:1:0.1) as the eluant gave a solid of **2**, 930 mg. It showed, on TLC with chloroform–methanol–28% aqueous ammonia (10:1:0.1), a single

Table 4. Minimal inhibitory concentrations (μg/ml) of the products

	3	7	9	10	11	12	13	14	DMT
Staph. aureus 209P	0.78	0.78	0.78	1.56	1.56	0.78	0.78	0.78	0.78
Sarcina lutea PCI 1001	0.39	<0.2	<0.2	<0.2	<0.2	<0.2	<0.2	<0.2	<0.2
B. subtilis B-558	0.39	0.78	0.78	0.78	0.78	0.39	0.39	0.78	0.78
E. coli NIHJ	3.12	6.25	6.25	6.25	6.25	6.25	6.25	6.25	6.25
Kl. pneumoniae PCI 602	6.25	3.12	6.25	6.25	6.25	3.12	3.12	3.12	6.25
Sh. dysenteriae JS 11910	6.25	3.12	6.25	1.56	1.56	1.56	1.56	3.12	1.56
Sal. enteritidis 1891	3.12	6.25	6.25	3.12	6.25	3.12	3.12	3.12	6.25

spot of R_f 0.47 (*cf* **1**, 0.32), $[\alpha]_D^{22}$+4° (*c* 1, chloroform). ^{1}H-NMR ($CDCl_3$): $J_{14,23a}$ 9, $J_{14,23b}$≈3, $J_{23a,23b}$ 10 Hz. Irradiation of H-14 collapsed the signals of H-15, H-23a, 23b, and H-13 to double doublets, a doublet, a doublet, and a singlet, respectively. Irradiation at δ 3.3 (H-23b), or of H-13 collapsed the signals of H-14 to a quartet, and double triplets, respectively. Irradiation of H-1″ collapsed the double doublets of H-2″a to a doublet.

Found: C, 52.76; H, 7.05; N, 1.36; I, 14.52%. Calcd for $C_{38}H_{62}INO_{12}\cdot H_2O$: C, 52.47; H, 7.36; N, 1.61; I, 14.61%.

23-Deoxy-23-dimethylaminodemycinosyltylosin (3) and 23-Deoxy-14(23)-enodemycinosyltylosin (4). A solution of **2** (750mg) and dimethylamine (0.88ml of 5M solution in acetonitrile (1M=1 moldm^{-3}); 5mol equivalents for **2**) in acetonitrile (15ml) was heated at 80°C for 30min. The same amount of dimethylamine was added, and the reaction was continued for further 30min. On TLC with chloroform–methanol–28% aqueous ammonia (10:1:0.1), the solution showed spots of R_f 0.35 (**3**) and 0.47 (slight, **4**, the R_f value being the same with that of **2**). Evaporation gave a residue, which was extracted with chloroform. The organic layer was washed with saturated aqueous sodium hydrogencarbonate and saturated aqueous sodium sulfate, dried (Na_2SO_4), and evaporated to give a solid (718mg). Purification by silica-gel column chromatography with chloroform–methanol–28% aqueous ammonia (40:1:0.1) gave solids of **3**, 564mg (83%) and **4**, 71mg (11%).

Compound **4**: $[\alpha]_D^{20}$+11° (*c* 1, chloroform); ^{1}H-NMR ($CDCl_3$): $J_{2b,3}$ 10, $J_{4,5}$ 7, $J_{10,11}$ 16, $J_{13,22}$ 1, $J_{15,16a}$=$J_{15,16b}$ ≈6.5, $J_{23a,23b}$ 0, $J_{1',2'}$ 7.5, $J_{2',3'}$ 10, $J_{1'',2''a}$ 3.7, $J_{1'',2''b}$ 0, $J_{2''a,2''b}$ 15 Hz.

Irradiation at δ 1.83 (H-16a,b) collapsed the triplet of H-15 and H-17 to a singlet, respectively. Irradiation of H-13 collapsed the small doublet of H-22 to a singlet. Irradiation of H-1″ collapsed the double doublets of H-2″a to a doublet.

Found: C, 59.74; H, 7.91; N, 1.78%. Calcd for $C_{38}H_{61}NO_{12}\cdot H_2CO_3$: C, 59.62; H, 8.03; N, 1.78%.

2′-O-Acetyl-23-deoxy-23-dimethylaminodemycinosyltylosin (5). To a solution of **3** (564mg) in acetonitrile (11ml) were added acetic anhydride (0.37ml) and powdered sodium hydrogencarbonate (0.6g) and the mixture was stirred at room temperature for 4h. Evaporation gave a residue, which was treated with ice-cold aqueous half-saturated sodium hydrogencarbonate under stirring for 30min. Extraction of the mixture with chloroform, washing the organic layer with a saturated aqueous sodium sulfate, drying over sodium sulfate, and evaporation gave a solid of **5**, 568mg (95%), $[\alpha]_D^{20}$−37° (*c* 1, chloroform).

Found: C, 62.05; H, 8.58; N, 3.36%. Calcd for $C_{42}H_{70}N_2O_{13}$; C, 62.22; H, 8.64; H, 3.46%.

2′,4″-Di-O-acetyl-23-deoxy-23-dimethylaminodemycinosyltylosin (6). A mixture of **5** (43.6mg) and acetic anhydride (8.2μl) in pyridine (0.22ml) was kept at 0°C for 7d. After addition of water (0.05ml), followed by standing for a few min, the mixture was poured into saturated aqueous sodium hydrogencarbonate (2ml). Extraction of the mixture with chloroform, washing the organic layer with saturated aqueous sodium hydrogencarbonate and then saturated aqueous sodium sulfate, drying over sodium sulfate, and evaporation gave a residue. Silica-gel column chromatography of the residue with toluene–acetone (2:1) as the developer gave **6**, 24mg (52%) and a mixture of **5** recovered and tri-*O*-acetyl compound, 19.7mg. **6**: $[\alpha]_D^{20}$−47° (*c* 1, chloroform).

Found: C, 61.68; H, 8.38; N, 3.12%. Calcd for $C_{44}H_{72}N_2O_{14}$: C, 61.97; H, 8.45; N, 3.29%.

4″-O-Acetyl-23-deoxy-23-dimethylaminodemycinosyltylosin (7). A solution of **6** (24mg) in methanol (0.24ml) was heated at 60°C overnight. Evaporation gave a solid, that was chromatographed on a silica-gel column with chloroform–methanol–28% aqueous ammonia (50:1:0.1) to give a solid of **7**, 20.9mg (91.5%), $[\alpha]_D^{22}$−28° (*c* 1, chloroform).

Found: C, 60.56; H, 8.17; N, 3.26%. Calcd for $C_{42}H_{70}N_2O_{13}\cdot 1/2H_2CO_3$: C, 60.64; H, 8.44; N, 3.33%.

2′,3,4″-Tri-O-acetyl-23-deoxy-23-dimethylaminodemycinosyltylosin (8). A mixture of **3** (21mg) and acetic anhydride (42μl) in pyridine (0.1ml) was kept at 0°C for 2d. After addition of water (20μl) the solution was concentrated. The chloroform solution of the residue was treated as usual to give, after chromatography, a solid of **8**, 15mg (63%), $[\alpha]_D^{20}$−35° (*c* 1, chloroform).

^{1}H-NMR ($CDCl_3$): Irradiation of H-2b collapsed the doublet of H-2a and the broad doublet of H-3 to a singlet, respectively. Irradiation at δ 1.80 (H-2″a) collapsed the doublet of H-1″ to a singlet.

Found: C, 60.95; H, 8.07; N, 3.06%. Calcd for $C_{46}H_{74}N_2O_{15}\cdot 1/2H_2O$: C, 61.13; H, 8.31; N, 3.10%.

Preparation of 9, 10, 11, 12, 13, and 14. To a solution of **2** (≈100mg) in acetonitrile (2ml) was added the corresponding amine (5 equivalents for **2**), that is, diethylamine (for the preparation of **9**), *N*-methyl-2-hydroxyethylamine (for **10**), pyrrolidine (for **11**), piperidine (for **12**), hexahydroazepine (for **13**), and octahydroazocine (for **14**), and the solution was heated at 80°C for the period cited in Table 1. Work-up as described for **3** gave the desired 23-dialkylamino derivatives.

^{1}H-NMR spectra of **9**, **10**, **11**, **12**, **13**, and **14** in $CDCl_3$. Compound **9**: H-23a signals did not appear near δ 2.3, and were hardly discernible by overlapping by other signals. Some other signals were: δ 4.75 (1H, dt, H-15), 5.76 (1H, d, H-13), 6.25 (1H, d, H-10).

Compound **10**: δ 1.83 (1H, d, H-22), 2.24 (3H, s, NMe), 4.76 (1H, dt, H-15), 5.74 (1H, d, H-13), 6.28 (1H, d, H-10).

Compound **11**: δ 2.54 (1H, dd, *J* 4.5 and 12Hz, H-23b), 2.63 (1H, dd, *J* 10 and 12Hz, H-23a), 4.77 (1H, dt, H-15), 5.80 (1H, d, H-13), 6.26 (1H, d, H-10).

Compound **12**: δ 4.75 (H-15), 5.76 (H-13), 6.26 (H-10).

Compound **13**: δ ≈2.57 (H-23a) 2.66 (1H, dd, *J* 4.5 and 12Hz, H-23b), 4.77 (H-15), 5.79 (H-13), 6.26 (H-10).

Compound **14**: δ 4.75 (H-15), 5.81 (H-13), 6.26 (H-10).

23-Deoxy-14(23)-enomycaminosyl Tylonolide Diethyl Acetal (16). To a solution of **15**[7] (55mg) in pyridine (0.55ml) was added silver fluoride (30mg) and the mixture was stirred at room temperature overnight. The solution showed, on TLC with chloroform–methanol (6:1), a single spot having the same R_f value with that of **15**. Concentration gave a residue, which was extracted with dichloromethane. Evaporation with several additions of toluene gave a solid, which was purified by column chromatography with chloroform–methanol (6:1) to give a solid, 47.1mg (96%), $[\alpha]_D^{25}$+19° (*c* 1, chloroform) ^{1}H-NMR ($CDCl_3$): δ 1.90 (3H, d, H-22), 2.55 (6H, s, NMe_2), 4.35 (1H, d, $J_{1',2'}$ 7.5Hz, H-1′), 5.12 (1H, s, H-23a), 5.35 (1H, s, H-23b), ≈5.3 (1H, H-15), 6.22 (1H, s, H-13), 6.42 (1H, d, $J_{10,11}$ 16Hz, H-10), 7.22 (1H, d, H-11).

Found: C, 64.24; H, 8.93; N, 2.13%. Calcd for $C_{35}H_{59}NO_{10}$: C, 64.29; H, 9.10; N, 2.14%.

23-Deoxy-14(23)enomycaminosyl Tylonolide (17). A solution of **16** (30mg) in a mixture of acetonitrile (0.6ml) and 0.1M aqueous hydrochloric acid (0.92ml) was kept at

room temperature for 1 h. The solution showed, on TLC with chloroform–methanol (6:1), a spot at R_f 0.23 (*cf* **16**: R_f 0.32). Neutralization with sodium hydrogencarbonate followed by usual work-up gave a solid, which was purified by column chromatography with chloroform–methanol–28% aqueous ammonia (13:1:0.1) to give a solid, 21.4 mg (88%), $[\alpha]_D^{25}$+59° (*c* 1, chloroform), λ_{max}^{MeOH} 292 (ε 23000). This value was in good agreement with the calculated value (293) by Woodward generalization[14], treating the unsaturated ketone as an acylic system.

^{1}H-NMR ($CDCl_3$): δ 1.90 (3H, d, H-22), 2.53 (6H, s, NMe_2), 4.33 (1H, d, $J_{1',2'}$ 7.5 Hz), 5.13 (1H, s, H-23a), 5.37 (1H, s, H-23b), 6.26 (1H, s, H-13), 6.38 (1H, d, $J_{10,11}$ 16 Hz, H-16), 7.28 (1H, d, H-11), 9.88 (1H, s, H-20).

Found: C, 64.49; H, 8.68; N, 2.34%. Calcd for $C_{31}H_{49}NO_9$: C, 64.23; H, 8.52; N, 2.42%.

We are grateful to Professor Hamao Umezawa of Institute of Microbial Chemistry for the support and encouragements thoroughout the studies. Starting material, demycinosyltylosin was kindly supplied by Dr. Tomio Takeuchi of the Institute. We are also grateful to Dr. Masa Hamada of the Institute for bioassay, to Mrs. Yukiko Otsuka, and Miss Ikuko Inoue of our Institute for measurements of the ^{1}H-NMR spectra, to Mr. Saburo Nakada of Keio University for elemental analysis, and to Miss Sachiko Yanagida for preparation of the manuscript.

References

1) R. H. Baltz and E. T. Seno, *Antimicrob. Agents Chemother.*, **20**, (4), 214, 1981.

2) R. Okamoto, K. Kiyoshima, M. Yamamoto, K. Takada, T. Ohnuki, T. Ishikura, H. Naganawa, K. Tatsuta, T. Takeuchi, and H. Umezawa, *J. Antibiot.*, **35**, 921 (1982).

3) K. Tatsuta, Y. Amemiya, Y. Kanemura, H. Takahashi, and M. Kinoshita, *Tetrahedron Lett.*, **23**, 3375 (1982).

4) A. Tanaka, T. Tsuchiya, Y. Okada, S. Umezawa, M. Hamada, and H. Umezawa, *J. Antibiot.*, **35**, 113 (1982).

5) A. Tanaka, T. Tsuchiya, S. Umezawa, and H. Umezawa, *J. Antibiot.*, **34**, 1374 (1981).

6) H. Matsubara, K. Miyano, A. Nakagawa, and S. Omura, *Chem. Pharm. Bull.*, **30**, 97 (1982).

7) A. Tanaka, T. Tsuchiya, S. Umezawa, M. Hamada, and H. Umezawa, *J. Antibiot.*, **34**, 1377 (1981).

8) M. S. Puar, *J. Antibiot.*, **34**, 602 (1981).

9) S. Omura, H. Matsubara, A. Nakagawa, A. Furusaki, and T. Matsumoto, *J. Antibiot.*, **33**, 915 (1980).

10) For example see: L. D. Hall and J. K. M. Sanders, *J. Chem. Soc., Chem. Commun.*, **1980**, 368.

11) a) L. H. Jackman and S. Sternell, "Application of nuclear magnetic resonance spectroscopy in organic chemistry," 2nd edition, Pergamon Press, Oxford, (1969), p. 70; b) p. 278.

12) M. Hayashi, H. Ohara, M. Ohno, H. Sakakibara, S. Satoi, K. Harada, and M. Suzuki, *J. Antibiot.*, **34**, 1075 (1981).

13) For example see: E. L. Eliel, "Stereochemistry of carbon compounds," McGraw-Hill Book Co. Inc. (1962), p. 331.

14) J. B. Hendrickson, D. J. Cram, G. S. Hammond, "Organic Chemistry," McGraw-Hill, Inc. (1970), p. 246.

Photoelectron Angular Distribution for Jahn-Teller Split Bands of Some Molecules in VUV Photoelectron Spectroscopy

Haruo SHIROMARU and Shunji KATSUMATA*
Physical Chemistry Laboratory, Institute of Applied Electricity, Hokkaido University, Sapporo 060
(Received June 28, 1984)

Measurements of photoelectron angular distribution were carried out with NeI and HeI resonance lines for Jahn-Teller split bands of methane, ethane, cyclopropane, neopentane, tetramethylsilane, carbon tetrachloride, and ammonia. The variation of an asymmetry parameter β across the band is presented. Significant β variations across the Jahn-Teller split bands due to the 1^2T_2 states of $C(CH_3)_4^+$ and CCl_4^+ could not be explained in terms of photoelectron energy dependence of β. These abnormal variations will be discussed on the basis of characteristics of the degenerate molecular orbitals split by the Jahn-Teller effect.

Ejection of an electron from a fully occupied degenerate orbital in a molecule induces an orbitally degenerate doublet state of the corresponding ion. The degeneracy of such a state can be removed by a spin-orbit coupling and/or the Jahn-Teller (J-T) effect. The Jahn-Teller effect means that a molecule in a degenerate electronic state is unstable toward distortions that lower the molecular symmetry, thereby removing the electronic degeneracy. The J-T split bands in molecular photoelectron spectroscopy are well known and we can see some typical examples in fundamental molecules as summarized by Rabalais.[1] Interestingly two evidences called the static and dynamic Jahn-Teller effects are distinguished for convenience. The static Jahn-Teller effect means that the distorted molecule has a permanent distortion that lowers its symmetry and that the interaction between the electronic and vibrational motions may be very small. The dynamic Jahn-Teller effect refers to the coupling of the electronic and vibrational motions. The difference between these Jahn-Teller effects should be discriminated by analyzing the appearance of the J-T active vibrational modes and the magnitude of the J-T energy splitting.

On the other hand, measurement of photoelectron angular distribution gives important and valuable information on the electronic structure of a molecule and on the coupling between electronic and vibrational motions. The former information gives correlation between the nature (σ or π types) of ionized molecular orbital and the value of β, an asymmetry parameter,[2-10] and has so far been used to confirm the orbital assignments of photoelectron (PE) spectra for many large molecules by several workers.[11-25] The latter information mainly associated with shape resonances has demonstrated several aspects of photoionization processes.[26-29] Photoelectron vibrational structures obtained with line sources such as NeI and HeI resonance lines are typically well represented by the Franck-Condon (F-C) factors between vibrational wavefunctions of the ground and ionic states, and generally give the same photoelectron angular distribution. Deviations are the exception and are usually attributed to many-electron interactions with an intermediate and autoionizing state. However shape resonances which lead to the temporary trapping of photoelectrons by a centrifugal barrier enhance the coupling between electronic and nuclear motions and the effects are large in both vibrational intensities and angular distributions. Therefore, when there is no autoionization process in the vicinity of shape resonances, the effects of shape resonance on PE bands induce non-Franck-Condon vibrational intensity distribution and the vibration-dependent angular distribution. Experimental confirmation of non-F-C intensity distribution was reported for the 5σ levels of CO[26] and for the $3\sigma_g$ level of N_2.[28] Experimental confirmation of the v-dependent angular distribution has also been reported for N_2,[27,30,31,33,35-38] CO,[29,34-37,39] O_2[31,35,37] and CO_2.[32,35,36,40] Most measurements of vibrationally resolved angular distributions have been restricted to the single HeI wavelength,[30-36] so that energy-dependence effects could not be confirmed.

In relation to the dependence of β on vibrational structures, it is of interest to know how β values for J-T split bands depend on geometrical distortions of individual components of the final state. Photoelectron angular distribution measurements have been so far reported for J-T split bands of some molecules.[11,12,18,19,41] Carlson and White reported for the first time that the HeI β values of components for each of J-T split bands in halomethanes are essentially equal to one another.[11] Leng and Nyberg pointed out that this fact is also true in cases of cyclopropane and allene.[18,19] Sell and Kuppermann have found the monotonic change of β across band II in SF_6[41] but concluded that the β variation is typical of general photoelectron energy dependence.[7]

Focusing on the problem about the β variation across the J-T split band, we carefully measured photoelectron angular distributions for various J-T split bands of several molecules.

Experimental

The photoelectron angular distribution of free molecules for unpolarized radiation is given by

$$J(\theta) \propto 1 + \frac{1}{2}\beta\left(\frac{3}{2}\sin^2\theta - 1\right), \quad (1)$$

where $J(\theta)$ is the photoelectron intensity, θ is the angle between the incoming photons and the outgoing photoelectrons, and β is the asymmetry parameter ranging between -1 and 2. Therefore, the β values of individual bands were calculated from PE spectral data obtained at two angles of 90° and 135° with the following expression derived from Eq. 1

$$\beta = 8(R-1)/(R+2) \quad (2)$$

where $R=J\,(90°)/J\,(135°)$.

Measurements of photoelectron angular distribution were carried out with a photoelectron spectrometer (VG Scientific Ltd., model ADES-400), as previously described elsewhere.[24] The PE spectrometer was connected to a microcomputer (NEC COMPO BS/80) system, in order to automatically control a scan voltage, a sample pressure and rotation of a turn table putting an analyzer. The PE spectra obtained were stored temporarily in a multichannel scaler (16bits×4K channels) and preserved in a floppy disk for calculating β values later. The multichannel scaler and controllers were home-made. Each β value of the spectral data was evaluated with Eq. 2 after subtracting the background and correcting the energy shift between the data obtained at 90° and 135°.

Since the β values obtained by an angular-dispersive PE spectrometer often contain a systematic error because of the various experimental problems, the systematic error must always be assessed in order to determine the most accurate values. Therefore we measured the β values for the PE bands of Ar, Xe, N_2, O_2, and CO_2 as a check on a calibration before and after measurements of samples in question. For these calibration gases, plots of our experimental raw β values against the corresponding ones taken from Ref. 36 exhibit a linear relationship in the range between -1 and 2, as shown in Fig. 1. Therefore all β values presented in this work were corrected by using such linear relationship. Furtheremore, standard deviations of the β values were found to be less than 0.03 under our experimental conditions. Energy resolutions used here were about 55 and 120meV in a full width at half maximum of the peak ($^2P_{3/2}$) of Ar.

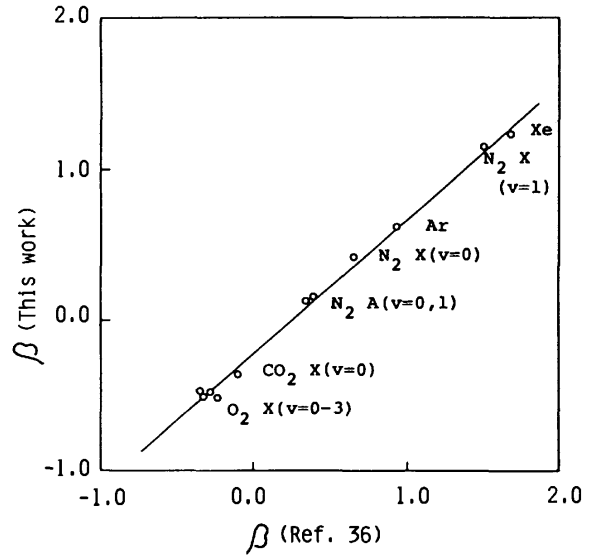

Fig. 1. Plot of our experimental raw β values of PE bands for calibration gases against those taken from Ref. 36.

The samples used here are methane, ethane, cyclopropane, neopentane, tetramethylsilane, carbon tetrachloride and ammonia. Methane and ethane were purchased from Gascro Kogyo K. K., neopentane and tetramethylsilane from Tokyo Kasei K. K., and cyclopropane from Takachiho Kagaku Cogyo K. K. All gaseous chemicals were about 99.5% pure. Ammonia was dehydrated by use of the drying agent of CaO, and the others were used without further purification.

Results

Plots of β values against ionization energies are shown in Figs. 2—8 for the PE spectra of the molecules mentioned above, together with the HeI spectra obtained at θ=90°. Each value of β is the mean value for eleven channels' and the error bar indicates the standard deviation. The experimental NeI and HeI β values for various bands are summarized in Table 1, together with assignments of the ionic states and the available data.

The PE spectrum of methane (Fig. 2) consists of three components of the 1^2T_2 state split by the J-T effect.[42] The HeI β value for each of the components is found to be almost the same. On the other hand, the NeI β values decreases monotonically above 15eV. However, considering the vicinity to the threshold and the background of slow electrons, this variation of the NeI β value cannot be verified definitely. Our NeI and HeI β values are slightly larger than those of Carlson *et al.*[43] and Marr and Holmes.[44] However, it may be concluded that no significant variation of the HeI β across the J-T split band was observed in agreement with the result of Carlson *et al.*[43]

The PE spectrum of ethane (Fig. 3) consists of the 1^2E_g, 1^2A_{1g}, and 1^2E_u ionic states.[42] There are three band maxima in the 11.5—14.5eV region which were assigned to the 1^2E_g and 1^2A_{1g} states although the order of their states has been controversial. To our knowledge, no data of β values for these bands have ever been published. It has been expected that the order of the 1^2A_g and 1^2E_g states might be determined from photoelectron angular distribution measurements. However, the order could not be identified clearly since, as can be seen from Fig. 3, no definite difference among β values for these maxima was observed at both NeI and HeI radiations. Nevertheless it may be concluded that there is no variation of β across the J-T split band of the 1^2E_g state. The PE band assigned to the 1^2E_u state in the region of 14.5 to 16.5eV exhibits two maxima due to the J-T splitting. The HeI β variation across the band seems to slightly decrease toward higher ionization energy (*ca.* 0.05/eV) while the NeI β variation is steep but it is not certain owing to the vicinity to the threshold.

The PE spectrum of neopentane (Fig. 4) in the 10-17eV region consists of four bands due to ionization from the $4t_2$, $1t_1$, 1e, and $3t_2$ orbital.[42] All these bands display the J-T splittings as discussed by Jonas *et al.*[12] Concerning the β variation across each of the

TABLE 1. EXPERIMENTAL ASYMMETRY PARAMETERS FOR JAHN-TELLER SPLIT BANDS OF VARIOUS MOLECULES

Molecule	Ionic State[a]	I_v/eV[a]	NeI photon[b]		HeI photon[b]	
			E_e/eV	β	E_e/eV	β
CH_4		13.6[c]	3.25	0.59	7.62	0.72
$[T_d]$	1^2T_2	14.5	2.35	0.57	6.72	0.71 (0.6)[d]
		15.2	1.65	0.44	6.02	0.74
C_2H_6	1^2E_g	11.99	4.86	0.14	9.23	0.22
$[D_{3d}]$		12.70	4.15	0.10	8.52	0.21
	1^2A_g	13.5	3.35	0.11	7.72	0.21
	1^2E_u	15.15	1.70	0.36	6.07	0.57
		15.9	0.95	0.16	5.32	0.54
C_3H_6	$1^2E'$	10.60	6.25	(0.35)[e]	10.62	0.42 (0.60)[e]
$[D_{3h}]$		11.30	5.55	(0.40)	9.92	0.33 (0.50)
	$1^2E''$	13.0	3.85	(0.28)	8.22	0.23 (0.43)
$C(CH_3)_4$		10.90	5.95	0.29	10.32	0.27
$[T_d]$	1^2T_2	11.41	5.44	0.33	9.81	0.34 (0.7)[d]
		11.9	4.95	0.27	9.32	0.42
		12.55	4.30	−0.12	8.67	0.36
	1^2T_1	12.9	3.95	−0.15	8.32	0.37 (0.7)
		13.2	3.65	—	8.02	—
	1^2E	13.93			7.29	0.71 (0.9)
		14.3			6.92	0.72
		15.24			5.98	0.56
	2^2T_2	15.6			5.62	0.52 (0.9)
		15.9			5.32	—
$Si(CH_3)_4$		10.29[f]	6.56	−0.02	10.93	0.33
$[T_d]$	1^2T_2	10.62	6.23	−0.06	10.60	0.33 (0.4)[d]
		10.9	5.95	−0.08	10.32	0.34
	1^2T_1	12.7	4.15	−0.02	8.52	0.39 (0.4)
		12.9	3.95	—	8.32	—
	2^2T_2	13.8			7.42	—
		14.1			7.12	0.59 (0.6)
	1^2A_1	14.5			6.72	—
	1^2E	15.6			5.62	0.64 (0.8)
CCl_4	1^2T_1	11.69[g]	5.16	(0.28)[h]	9.53	0.42 (0.54)[h]
$[T_d]$		12.44	4.41		8.78	0.71
	1^2T_2	12.65	4.20	(0.65)	8.57	0.79 (0.74)
		12.78	4.07		8.44	0.82
	1^2E	13.37	3.48	(0.50)	7.85	0.57 (0.55)
		13.50	3.35		7.72	0.57
	2^2T_2	16.58			4.64	0.00 (0.00)
NH_3	$1^2A'$	10.85			10.37	1.18 (0.82)[i]
$[C_{3v}]$	$1^2E'$	15.8			5.42	0.47 (0.21)
		16.5			4.72	0.44

a) Taken from Ref. 42 unless other comments are made. I_v indicates the ionization energy for each peak in the band. b) E_e is the photoelectron kinetic energy. NeI and HeI photon energies are 16.85 and 21.22 eV, respectively. c) Ref. 48. d) Ref. 43. e) Ref. 19. f) Ref. 12. g) Ref. 49. h) Ref. 45. i) Ref. 35.

four bands, significant variations were observed for the first and fourth bands but no variations for the second and third bands, as can be seen in Fig. 4. The HeI β variation across the first band (1^2T_2) (Fig. 5) was found to increase monotonically toward higher ionization energy (*ca.* 0.15/eV). This variation seems to be also realized even in the NeI β variation. In Fig. 4, NeI β plots for the first and second components for the 1^2T_2 band split by the J-T effect increase gradually, but that for the third component decreases suddenly by the overlap effect of the small β value of the second band (1^2T_1). The HeI β variation across the fourth band (2^2T_2) is seen to decrease in contrast with that for the first band. The NeI β variation across the 2^2T_2 band is uncertain as well as that of the third band (1^2E) owing to the vicinity of the threshold and the background of slow electrons. Our HeI β values obtained here are considerably small in comparison with those of Jonas *et al.*[12] It may be concluded that the first and fourth bands show the significant β variations.

Figure 6 shows the PE spectrum of $Si(CH_3)_4$ and NeI and HeI β plots for PE bands in the region of 10 to 16eV. The HeI β values are in good agreement with those reported by Jonas *et al.*[12] This molecule is interesting by virtue of the similarity to $C(CH_3)_4$. Concerning the variation of β across the first band due

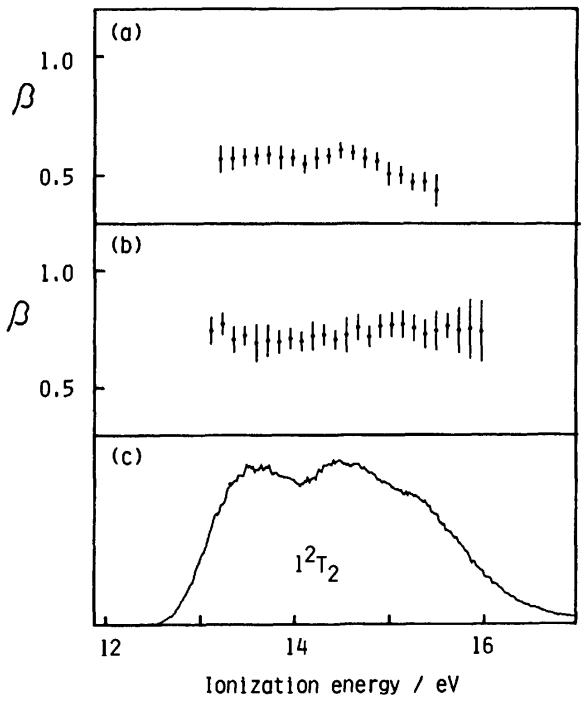

Fig. 2. Plots of β values of methane obtained with (a) NeI and (b) HeI photons and (c) HeI PE spectrum at θ=90°.

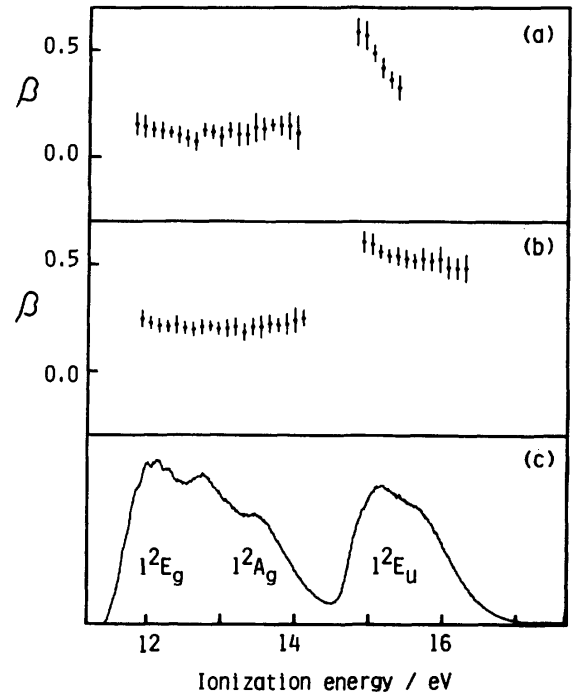

Fig. 3. Plots of β values of ethane obtained with (a) NeI and (b) HeI photons and (c) HeI PE spectrum at θ=90°.

to the 1^2T_2 state, the HeI β plot shows no variation but the NeI β plot a significant variation. Variations of β for the other bands were uncertain because the PE bands are heavily overlapped with each other.

Carbon tetrachloride has the same valence electronic structure as neopentane. Orbital assignments of the PE spectra (Figs. 7A and 7B) are well known and the first

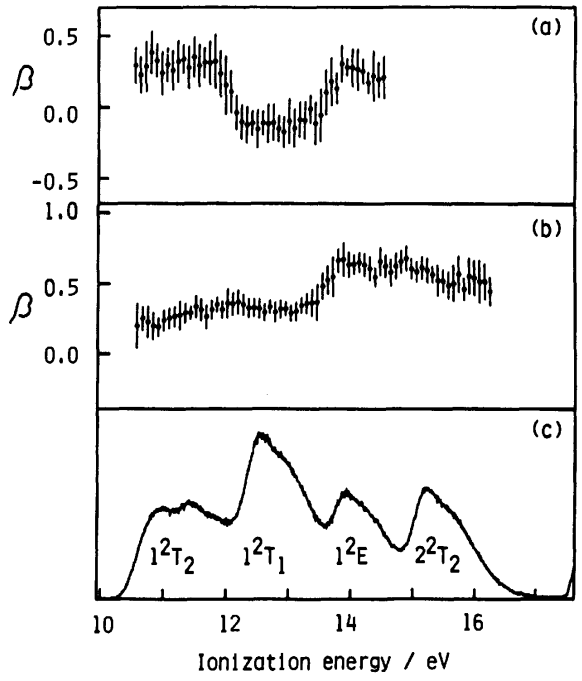

Fig. 4. Plots of β values of neopentane obtained with (a) NeI and (b) HeI photons and (c) HeI PE spectrum at θ=90°.

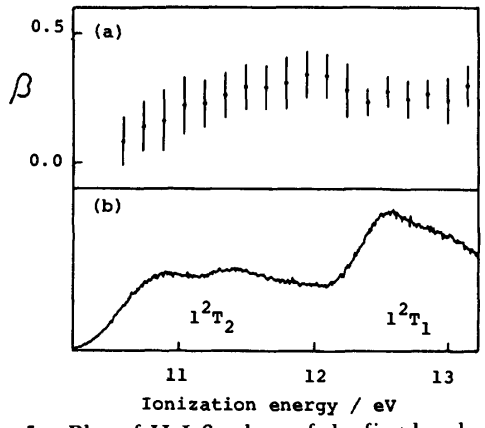

Fig. 5. Plot of HeI β values of the first band of neopentane and HeI PE spectrum obtained at θ=90°.

four bands are assigned to the 1^2T_1, 1^2T_2, 1^2E, and 2^2T_2 states, respectively.[42] The second (1^2T_2) and third (1^2E) bands show the J-T splittings. The HeI β values for these four bands have so far been reported by Carlson and White[11] and Carlson *et al.*[45] who have not taken account of β variation across each of the bands. Our HeI β values for the four bands are in good agreement with those of Carlson *et al.*[45] It is found from Figs. 7A and 7B that the β variations exist definitely for the 1^2T_2 and 2^2T_2 bands but no significant variation for the other bands. Carbon dioxide and argon shown in Figs. 7A and 7B, respectively, were used as an internal standard to check and correct energy shifts between the spectra obtained at 90° and 135°. The correction was performed by making the β values for the peak of the the internal standard flat.

For the PE spectrum of ammonia, the second band assigned to the $1^2E'$ ionic state exhibits the J-T splitting

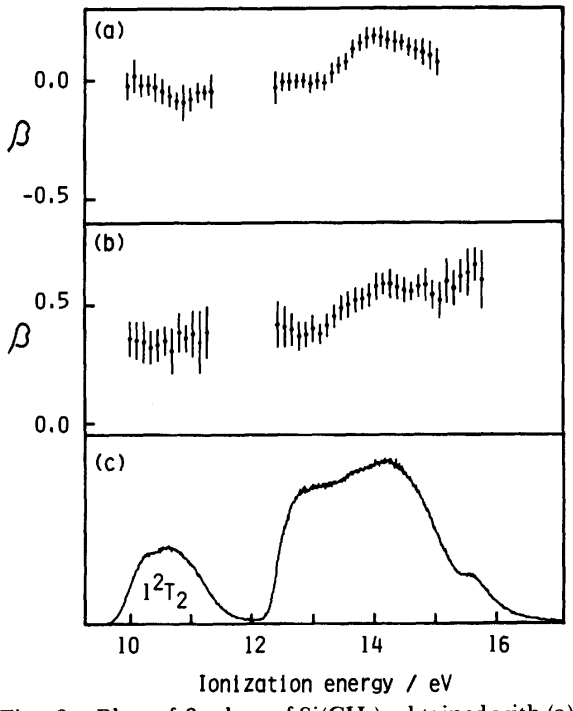

Fig. 6. Plots of β values of $Si(CH_3)_4$ obtained with (a) NeI and (b) HeI photons and (c) HeI PE spectrum at θ=90°.

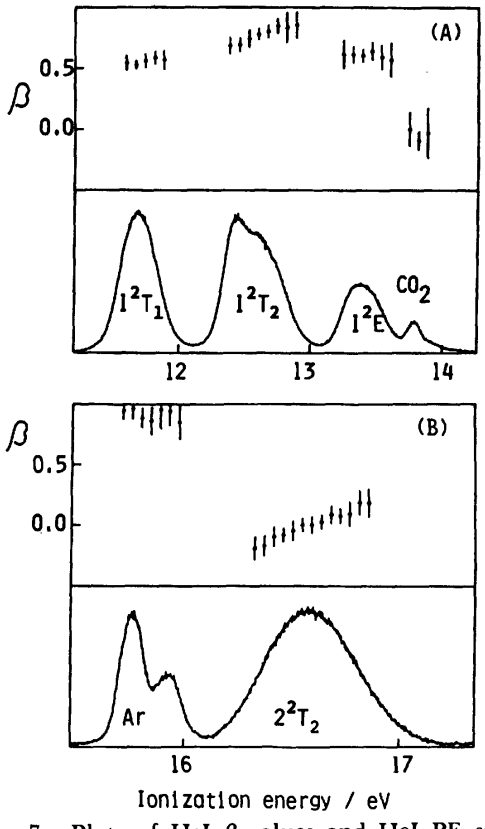

Fig. 7. Plots of HeI β values and HeI PE spectra obtained at θ=90° for (A) the first three bands of CCl_4 and (B) the fourth band of CCl_4.

of about 0.7eV.[42] The HeI β variation across the band is flat as shown in Fig. 8A. Our HeI β values obtained here are higher by about 0.3 than those of Hancock and Samson.[35]

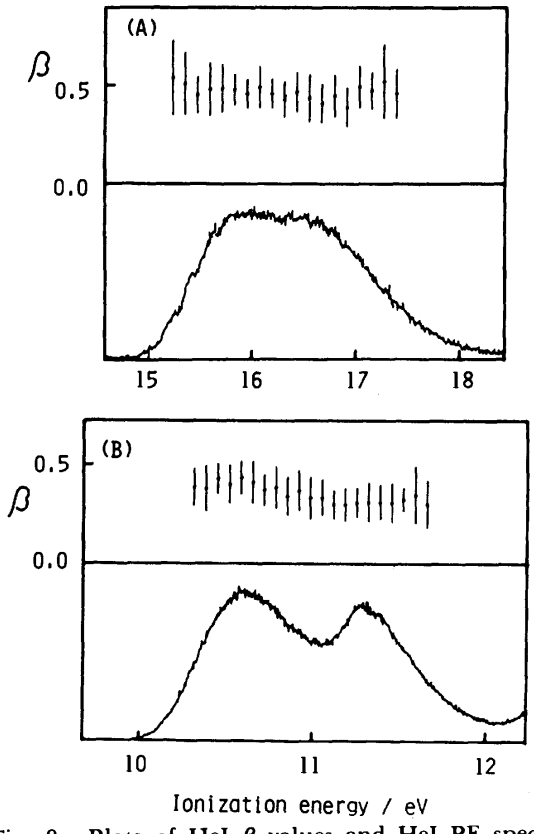

Fig. 8. Plots of HeI β values and HeI PE spectra obtained at θ=90° for (A) the second band of ammonia and (B) the first band of cyclopropane.

For the PE spectrum of cyclopropane (Fig. 8B), the first band ($1^2E'$) having two peaks shows the relatively large splitting (0.7eV) by the J-T effect.[42] Leng and Nyberg[19] have reported a significant variation of β across the band. We also confirmed the same variation although our HeI β values obtained here are slightly lower than those of Leng and Nyberg, as listed in Table 1.

Discussion

The asymmetry parameter basically depends on two factors; the kinetic energy of the photoelectron and the nature of the molecular orbital from which the photoelectron is ejected. When considering variation of β across a band, it must be checked whether the variation is analogous to the photoelectron energy dependence. The energy dependence of β for various bands is shown in Fig. 9 by using the experimental NeI and HeI β values. Here, the energy dependence was assumed to be linear in the region of NeI to HeI photon energies. This assumption seems to be valid from the fact that the energy separation between the two photon energies is relatively small. For example, the energy dependence of β obtained with synchrotron radiation[45] is nearly linear for each of the four bands of CCl_4, as shown in Fig. 9. Consequently it may be noted from Fig. 9 that the energy dependence of β for

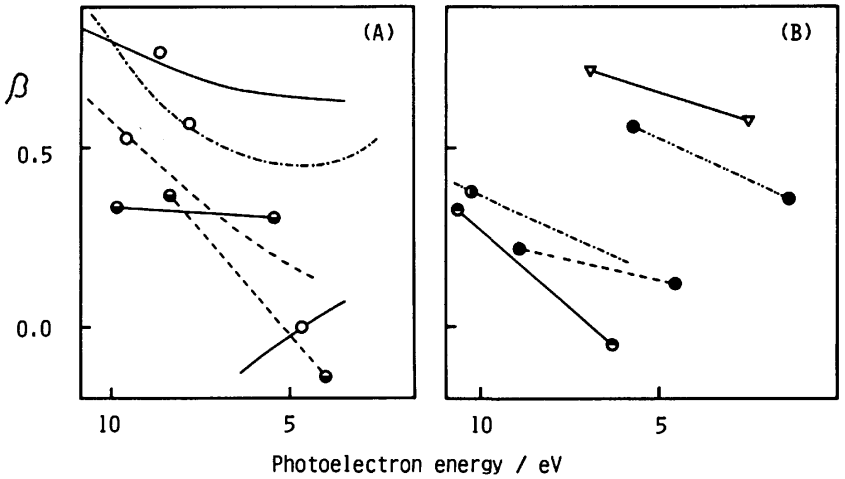

Fig. 9. Photoelectron energy dependence of β in the region of NeI and HeI photons for (A) CCl_4 (○) and neopentane (◒); $^2T_2$ (——), $^2T_1$ (----), and ^2E (-·-·-), and (B) 1^2T_2 (—▽—) of methane, $1^2E'$ (-·-◑-·-) of cyclopropane 1^2E_{1g} (--●--) and 1^2E_{1u} (-··-●-··-) of ethane, and 1^2T_2 (—◒—) of TMS.

each of the bands discussed in this work decreases commonly toward lower photoelectron energy, except for that of the 2^2T_2 band of CCl_4.

Figure 10 shows the degree of variation of HeI β with the J-T splitting for each of the J-T split bands in question. Then, it is found that the trend of β variations for the 1^2T_2 band of CCl_4 and the 1^2T_2 band of $C(CH_3)_4$ is certainly different from the energy dependence of β as shown in Fig. 9. The β variations for the other bands are very small or similar to the tendency of the energy dependence. The variations of β across the vibrational envelopes of π bands for various unsaturated hydrocarbons[2,7,8] and across the J-T split bands of some molecules[11,19,41] have been so far reported. Most of the β variations were interpreted in terms of the photoelectron energy dependence. In this sense, β variations for the 1^2T_2 bands of CCl_4 and $C(CH_3)_4$ cannot be explained in terms of the energy dependence. Here we tried to consider the abnormal β variation on the basis of characteristics of the ionized molecular orbitals.

The asymmetry parameter for an atom is given as a function of the quantum number (l) of an orbital angular momentum of an ionized orbital,[46] and it may be generally recognized that the larger the value of l is, the lower the β value. For molecular orbitals (MOs), the value of l is usually a poor quantum number. An MO (ψ_j) is expanded in terms of the spherical harmonics $Y_{lm}(\theta,\phi)$,[13,47]

$$\Psi_j(r,\theta,\phi) = \sum_{l=0}^{\infty}\sum_{m=-l}^{l} C_{lm}(r)Y_{lm}(\theta,\phi), \quad (3)$$

$$C_{lm}(r) = \iint Y^*_{lm}(\theta,\phi)\Psi_j(r,\theta,\phi)\sin\theta\,d\theta\,d\phi, \quad (4)$$

where $C_{lm}(r)$ is the expansion coefficient, depending on the character of the MO and on a position of the origin of the one-center expansion. If the molecule has a center of symmetry, it is reasonable to select the center as the origin. The most probable value of l is that one corresponding to the maximum value of $|C_{lm}|^2$ integrated over r. We abbreviate $|C_{lm}|^2$ to C^2_{lm} hereafter. The C^2_{lm} value for each component of the degenerate MO in the ionic state is the same but the values for the individual MOs lifted by the J-T effect should be different from each other. A significant variation of β across the J-T split band should be attributed to the value of l or the value of C^2_{lm} for the corresponding MO.

In this sense, we calculated the values of C^2_{lm} integrated over r to determine the most probable values

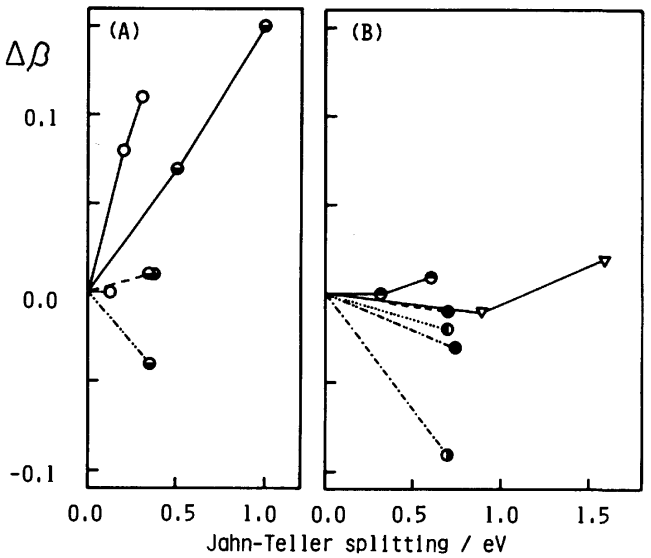

Fig. 10. Degree of β variations against Jahn-Teller splittings for (A) 1^2T_2 (—○—) and ^2E (····○····) of CCl_4^+ and 1^2T_2 (—◒—), 1^2T_1 (--◒--), ^2E (---◒---), and 2^2T_2 (-··-◒-··-) of $C(CH_3)_4^+$, and (B) 1^2T_2 (—▽—) of methane, 1^2T_2 (—◒—) of TMS, $1^2E'$ (-·-◑-·-) of cyclopropane, $1^2E'$ (····◐····) of ammonia, and 1^2E_{1g} (--●--) and 1^2E_{1u} (-··-●-··-) of ethane.

Table 2. The largest two values of C_{lm}^2 for MO of the individual components in the J-T split 1^2T_2 state of $CH_4^{+a)}$

MO level[b]	Td		Type I		Type I′		Type IV	
/eV	l=1	l=2	l=1	l=2	l=1	l=2	l=1	l=2
I_1 13.6	0.892	0.077	0.870	0.094	0.870	0.089	0.876	0.090
I_2 14.5	0.892	0.077	0.896	0.071	0.896	0.071	0.885	0.080
I_3 15.2	0.892	0.077	0.908	0.064	0.901	0.070	0.908	0.060

a) Concerning Types I, I′, and IV, see text. b) The values are the experimental ionization energies.

Table 3. The values of C_{lm}^2 for MOs of individual components in various J-T split states of CCl_4^+

Ionic state	MO level[a] /eV		Theoretical values of C_{lm}^2				
			l=1	l=2	l=3	l=4	l=5
1^2T_1	I_1				0.590	0.212	
	I_2	11.69			0.610	0.203	
	I_3				0.617	0.203	
1^2T_2	I_1	12.44	0.267	0.208	0.071	0.260	
	I_2	12.65	0.272	0.188	0.065	0.273	
	I_3	12.78	0.277	0.177	0.058	0.288	
1^2E	I_1	13.37		0.589		0.107	0.199
	I_2	13.50		0.597		0.094	0.202
2^2T_2	I_1		0.477	0.252	0.103		
	I_2	16.58	0.469	0.261	0.106		
	I_3		0.468	0.272	0.108		

a) The values are the experimental ionization energies.

of l for the MOs corresponding to the J-T split components in the $^2T_2$ state of CH_4^+. The values of l and m used for this expansion were from 0 to 6 and 0 to 4, respectively. The normalized condition was completely satisfied within these limitations of l and m. The calculated results are listed in Table 2. We used the MOs obtained in Types I, I′, and IV described in Ref. 48 as the J-T distorted geometries of CH_4^+. It is found from Table 2 that the most probable l value for each of the MOs is 1. Concerning the values of C_{lm}^2 for l=1, those of the degenerate MOs (Td) are equal to one another whereas each of the split MOs' is not the same and increases with increase of the ionization energy. The variation of β may be attributed to this slight variation of C_{lm}^2 (about 0.03).

The calculation of the MO expansion for CCl_4^+ was also carried out. The molecular orbitals obtained in Type I were used for CCl_4^+.[50] The calculated results are listed in Table 3. The normalized condition was almost completely (90%) satisfied. It is found that the most probable l values for the 1^2T_1, 1^2E, and 2^2T_2 states are 3, 2, and 1, respectively. However, the most probable value for the second state (1^2T_2) cannot be determined because the C_{lm}^2 values for l=1, 2, and 4 are close to one another. The difference of the C_{lm}^2 values among the J-T split MOs in the individual ionic states is commonly slight (0.03) as shown in Table 3. If experimental β values can be estimated on the basis of the weighted average on the theoretical β values for the quantum numbers (ls) obtained from the one-center expansion method, it may be noted that the more the number of ls inducing significant variations of the C_{lm}^2 values is, the larger the variation of β. Considering that the abnormal variation of β appears only in the second PE band of CCl_4, the interpretation in terms of the variation of the C_{lm}^2 value seems to be consistent with the experimental results.

As another approarch, we calculated radial distributions ($4\pi r^2\psi^2$) of the degenerate MOs of neutral molecules to predict the β variations in the approximation of Koopmans' theorem. This is to compare distribution patterns of the MOs for the bands showing β variations with those of the MOs for the bands showing no β variation. This comparison is more useful for the intramolecular bands than the intermolecular bands. Figure 11 shows the radial distributions of the degenerate orbitals for CH_4, NH_3, and $C(CH_3)_4$, the centers of the molecules being taken at C and N atoms. The β variations for the 1^2T_2 state of CH_4^+ and for the $1^2E'$ state of NH_3^+ are very small although the magnitude of the J-T splittings are considerably large. The β variations for the 1^2T_1 and 1^2E states for $C(CH_3)_4^+$ are also very small. The radial distributions for these states exhibit the pattern which consists of a single peak. On the other hand, the β variation for the 1^2T_2 state of $C(CH_3)_4^+$ is abnormal, and the radial distribution for this state shows the pattern which consists of two peaks. This pattern is quite different from those for the $^2T_1$ and ^2E states of this molecule. The radial distribution pattern for the 2^2T_2 state, which consists of one shoulder and one peak, is closer to that for the 1^2T_2 rather than those for the $^2T_1$ and ^2E states although the variation of β for the 2^2T_2 band is not so remarkable.

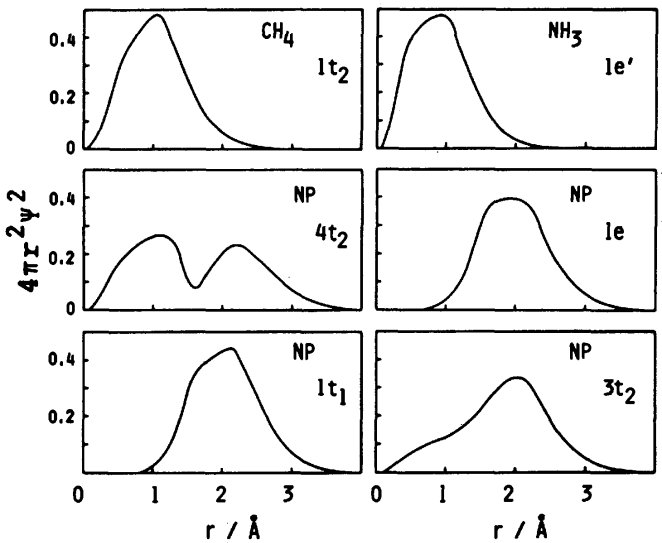

Fig. 11. Radial distributions of various MOs for methane, ammonia and neopentane (NP).

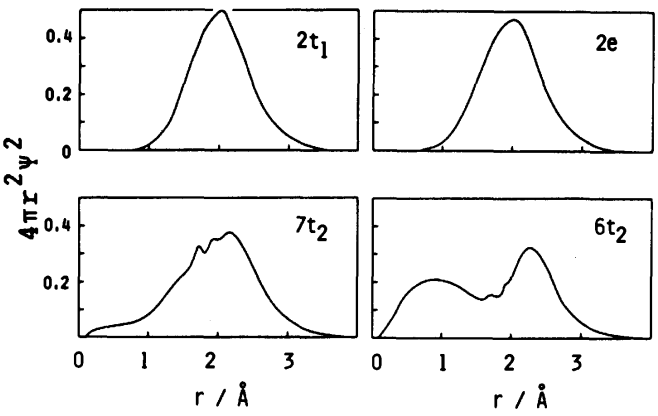

Fig. 12. Radial distributions of various MOs for CCl_4.

Concerning the radial distributions in CCl_4 shown in Fig. 12, the distribution patterns for the 1^2T_2 and 2^2T_2 states in CCl_4^+ are very similar to those for the 2^2T_2 and 1^2T_2 states in $C(CH_3)_4^+$, respectively. For CCl_4, the β variation for the 1^2T_2 state is abnormal. The β variation for the 2^2T_2 state shows the change of about 0.7 per 1 eV (Fig. 7B) which is quite large in comparison with the energy dependence of β (about 0.06 per 1 eV).[44]

In addition to the above considerations, we suggest that the effects of the shape resonance and the vibronic interaction on the β variation across the J-T split band should be investigated for these molecules.

The *ab initio* SCF MO calculations and the calculations of the one-center expansion of the MOs and the radial distributions of the MOs were carried out at the Hokkaido University Computing Center. The *ab initio* SCF MO calculations were performed with IMS version of GAUSSIAN 70 using 4-31 G basis set.

References

1) J. W. Rabalais, "Principles of Ultraviolet Photoelectron Spectroscopy," John Wiley and Sons, New York (1977).
2) R. M. White, T. A. Carlson, and D. P. Spears, *J. Electron Spectrosc. Relat. Phenom.*, **3**, 59 (1974).
3) T. Kobayashi, *Phys. Lett. A*, **69**, 105 (1978).
4) T. Kobayashi, *Phys. Lett. A*, **70**, 292 (1979).
5) J. A. Sell, D. M. Mintz, and A. Kuppermann, *Chem. Phys. Lett.*, **58**, 601 (1978).
6) J. A. Sell and A. Kuppermann, *J. Chem. Phys.*, **71**, 4703 (1979).
7) D. M. Mintz and A. Kuppermann, *J. Chem. Phys.*, **71**, 3499 (1979).
8) M. H. Kibel, M. K. Livett, and G. L. Nyberg, *J. Electron Spectrosc. Relat. Phenom.*, **15**, 275 (1979).
9) J. Kreile and A. Schweig, *Chem. Phys. Lett.*, **69**, 71 (1980).
10) D. Mehaffy, P. R. Keller, J. W. Taylor, T. A. Carlson, M. O. Krause, F. A. Grimm, and J. D. Allen Jr., *J. Electron Spectrosc. Relat. Phenom.*, **26**, 213 (1982).
11) T. A. Carlson and R. M. White, *Faraday Discuss. Chem. Soc.*, **54**, 285 (1972).
12) A. Jonas, G. K. Schweitzer, F. A. Grimm, and T. A. Carlson, *J. Electron Spectrosc. Relat. Phenom.*, **1**, 29 (1972/73).
13) T. A. Carlson and C. P. Anderson, *Chem. Phys. Lett.*, **10**, 561 (1971).
14) T. Kobayashi and S. Nagakura, *J. Electron Spectrosc. Relat. Phenom.*, **7**, 187 (1975).
15) C. Utsunomiya, T. Kobayashi, and S. Nagakura, *Bull. Chem. Soc. Jpn.*, **51**, 3482 (1978).
16) C. Utsunomiya, T. Kobayashi, and S. Nagakura, *Bull. Chem. Soc. Jpn.*, **53**, 1216 (1980).
17) T. Kobayashi, T. Kubota, K. Ezumi, and C. Utsunomiya, *Bull. Chem. Soc. Jpn.*, **55**, 3915 (1982).
18) F. J. Leng and G. L. Nyberg, *J. Chem. Soc., Faraday Trans. II*, **73**, 1719 (1977)
19) F. J. Leng and G. L. Nyberg, *J. Electron Spectrosc. Relat. Phenom.*, **11**, 293 (1977).
20) F. Carnovale, M. H. Kibel, G. L. Nyberg, and J. B. Peel, *J. Electron Spectrosc. Relat. Phenom.*, **25**, 171 (1982).
21) J. A. Sell and A. Kuppermann, *Chem. Phys.*, **33**, 367, 379 (1978).
22) J. A. Sell and A. Kuppermann, *Chem. Phys. Lett.*, **61**, 355 (1979).
23) S. Katsumata, H. Shiromaru, K. Mitani, S. Iwata, and K. Kimura, *Chem. Phys.*, **69**, 423 (1982).
24) S. Katsumata, H. Shiromaru, and T. Kimura, *Bull. Chem. Soc. Jpn.*, **57**, 1784 (1984).
25) M. N. Piancastelli, P. R. Keller, J. W. Taylor, F. A. Grimm, and T. A. Carlson, *J. Am. Chem. Soc.*, **105**, 4235 (1983).
26) R. Stockbauer, B. E. Cole, D. L. Ederer, J. B. West, A. C. Parr, and J. L. Dehmer, *Phys. Rev. Lett.*, **43**, 757 (1979).
27) J. L. Dehmer, D. Dill, and S. Wallace, *Phys. Rev. Lett.*, **43**, 1005 (1979).
28) J. B. West, A. C. Parr, B. E. Cole, D. L. Ederer, R. Stockbauer, and J. L. Dehmer, *J. Phys. B*, **13**, L105 (1980).
29) B. E. Cole, D. L. Ederer, R. Stockbauer, K. Codling, A. C. Parr, J. B. West, E. D. Poliakoff, and J. L. Dehmer, *J. Chem. Phys.*, **72**, 6308 (1980).
30) T. A. Carlson and A. E. Jonas, *J. Chem. Phys.*, **55**, 4913 (1971).
31) T. A. Carlson, *Chem. Phys. Lett.*, **9**, 23 (1971)

32) T. A. Carlson and G. E. McGuire, *J. Electron Spectrosc. Relat. Phenom.*, **1**, 209 (1972/73).
33) D. M. Mintz and A. Kuppermann, *J. Chem. Phys.*, **69**, 3953 (1978).
34) J. A. Sell, A. Kuppermann, and D. M. Mintz, *J. Electron Spectrosc. Relat. Phenom.*, **16**, 127 (1979).
35) W. H. Hancock and J. A. R. Samson, *J. Electron Spectrosc. Relat. Phenom.*, **9**, 211 (1976).
36) J. Kreile and A. Schweig, *J. Electron Spectrosc. Relat. Phenom.*, **20**, 191 (1980).
37) R. M. Holmes and G. V. Marr, *J. Phys. B*, **13**, 945 (1980).
38) T. A. Carlson, M. O. Krause, D. Mehaffy, J. W. Taylor, F. A. Grimm, and J. D. Allen, *J. Chem. Phys.*, **73**, 6056 (1980).
39) J. A. Stephens, D. Dill, and J. L. Dehmer, *J. Phys. B*, **14**, 3911 (1981).
40) J. R. Swanson, D. Dill, and J. L. Dehmer, *J. Phys. B*, **14**, L207 (1981).
41) J. A. Sell and A. Kuppermann, *Chem. Phys.*, **33**, 379 (1978).
42) K. Kimura, S. Katsumata, Y. Achiba, T. Yamazaki, and S. Iwata, "Handbook of HeI photoelectron spectra of fundamental organic molecules," Japan Scientific Society, Tokyo (1981).
43) T. A. Carlson, G. E. McGuire, A. E. Jonas, K. C. Cheng, C. P. Anderson, C. C. Lu, and B. P. Pullen, "Electron Spectroscopy," ed by D. A. Shirley, North-Holland Publishing, Amsterdam (1972).
44) G. V. Marr and R. M. Holmes, *J. Phys. B*, **13**, 939 (1980).
45) T. A. Carlson, M. O. Krause, F. A. Grimm, P. Keller, and J. W. Taylor, *J. Chem. Phys.*, **77**, 5340 (1982).
46) J. Cooper and R. N. Zare, *J. Chem. Phys.*, **48**, 942 (1968).
47) J. W. Rabalais, T. P. Debies, J. L. Berkosky, J-T. J. Huang, and F. O. Ellison, *J. Chem. Phys.*, **61**, 529 (1974).
48) H. Shiromaru, K. Takeshita, and S. Katsumata, *Chem. Lett.*, **1984**, 721.
49) A. W. Potts, H. J. Lempka, D. G. Streets, and W. C. Price, *Phil. Trans. R. Soc. London, Ser. A*, **268**, 59 (1970).
50) H. Shiromaru, K. Takeshita, and S. Katsumata, to be published.

Molecular Structure of [2]Paracyclo[2](2,5)furanophane†

Fumio HAMA,†† Yasushi KAI, Noritake YASUOKA,††† and Nobutami KASAI*
Department of Applied Chemistry, Faculty of Engineering, Osaka University, Yamadaoka, Suita, Osaka 565
(Received June 30,1984)

The molecular structures of [2]paracyclo[2](2,5)furanophane (**1**) at 20 °C and −150 °C have been determined by means of X-ray diffraction. The crystal is tetragonal, with a=15.996(1), c=8.374(1)Å (at 20 °C), and a=15.823(3), c=8.330(3)Å (at −150 °C), space group $P\bar{4}2_1c$, and Z=8. The structures were solved by the direct method, and refined anisotropically by the block-diagonal least-squares procedure: R=0.069 and 0.075 for the structures at 20 °C and −150 °C, respectively. The furan ring has an envelope form, and the benzene ring boat-shape.

Many multi-layered paracyclofuranophanes have been synthesized by Misumi and his co-workers[1] in order to investigate the trans-annular π-electron interaction between benzene and heteroaromatic rings. They observed the ring inversion phenomena of furan rings in double-, triple-, and quadruple-layered paracyclofuranophanes by variable temperature NMR spectroscopy. The flipping of furan ring in triple- and quadruple-layered paracyclofuranophanes were found to be easier than that in double-layered one. On the other hand, no ring inversion of the thiophene ring was observed in the multi-layered paracyclothiophenophanes.

In a series of structural studies on layered cyclophanes, the molecular sturctures of double- and triple-layered paracycloheterophane containing furan and thiophene rings have been determined by means of X-ray diffraction in order to obtain structural informations about the ring inversion. The molecular structures of triple-layered paracyclofuranophane (**3**) and dimethyl triple-layered paracyclothiopheneophane (**4**) have been reported.[2] This paper deals with the molecular structure of double-layered paracyclofuranophane (**1**) ([2]paracyclo[2](2,5)furanophane) at 20 °C and −150 °C, temperatures above and below the coalescence (−39 °C) of NMR signals of aromatic protons of benzene ring faced to the furan ring.[1]

The structure analysis of double-layered paracyclothiophenophane ([2]paracyclo[2](2,5)thiophenophane) was also tried; however, due to the reason mentioned later the intensity data collection has been discontinued.

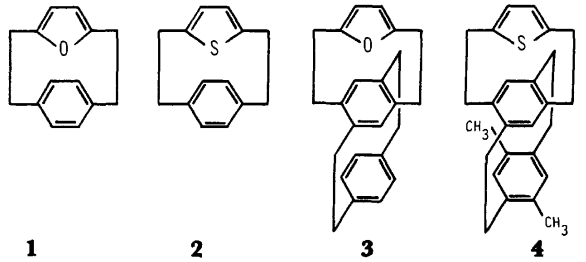

1 **2** **3** **4**

1: [2]Paracyclo[2](2,5)furanophane
2: [2]Paracyclo[2](2,5)thiophenophane
3: Triple-layered paracyclofuranophane
4: Dimethyl triple-layered paracyclothiophenophane

Experimental

[2]Paracyclo[2](2,5)furanophane (1). Crystals of double-layered paracyclofuranophane are colorless tetragonal prisms. Preliminary oscillation and Weissenberg photographs showed that the crystal belongs to the tetragonal system, and the systematic absence of reflections (hhl; l=2n+1 and $h00$; h=2n+1) determined the space group as $P\bar{4}2_1c$.

For the measurements of the unit-cell dimensions and integrated intensities, a Rigaku automated, four-circle diffractometer was used. A crystal with approximate dimensions of 0.2×0.2×0.2mm was selected for the X-ray work. The unit-cell parameters were precisely determied by the least-squares fit of 2θ values of high angle reflections.

Crystal Data. $C_{14}H_{14}O$, M 198.3, tetragonal, space group $P\bar{4}2_1c$, (20 °C) a=15.996(1), c=8.374(1)Å, V=2142.5(4)Å^3, Z=8, D_m=1.23 g cm^{-3}, D_c=1.229 g cm^{-3}, μ(Cu$K\alpha$)=5.97 cm^{-1}; (−150 °C) a=15.823(3), c=8.330(3)Å, V=2085.4(10)Å^3, Z=8, D_c=1.263 g cm^{-3}, μ(Mo$K\alpha$)=0.84 cm^{-1}.

Intensity measurements were carried out by the θ−2θ scan technique at a 2θ scan rate of 4 ° min^{-1}. For the room temperature (20 °C) experiment nickel-filtered Cu$K\alpha$ radiation was used. The scan width was $\Delta 2\theta=(2.0+0.3\tan\theta)°$. The backgrounds were counted for 7.5 s at both ends of a scan. For the low temperature experiment the crystal was kept at −150 °C with the liquid nitrogen gas flow method. Graphite monochromatized Mo$K\alpha$ radiation was used. The scan width was $\Delta 2\theta=(2.0+0.7\tan\theta)°$. The backgrounds were counted for 5 s. The scans were repeated up to three times when the structure factor magnitude $|F_o|$ was less than $3\sigma(F_o)$, where $\sigma(F_o)$ is the standard deviation estimated from the counting statistics. Totals of 922 (at 20 °C; Cu$K\alpha$, $2\theta \leqq 120°$) and 1728 (at −150 °C; Mo$K\alpha$, $2\theta \leqq 60°$) reflections were collected, among which 106 and 267 reflections less than $3\sigma(F_o)$ were considered as unobserved. No intensity decrease of standard reflections was observed during the experiment. Corrections for the usual Lorentz and polarization effects were carried out, but no absorption correction was made [μ(Cu$K\alpha$)=5.97 and μ(Mo$K\alpha$)=0.84 cm^{-1}].

[2]Paracyclo[2](2,5)thiophenophane (2). *Crystal Data.* $C_{14}H_{14}S$, M 214.3, tetragonal, space group $P4_2nm$, $P\bar{4}n2$, or $P4_2/mnm$, a=7.762, c=9.159Å, V=551.9Å^3, Z=2, D_m=1.27 g cm^{-3}, D_c=1.29 g cm^{-3}.

The systematic absence of reflections showed the space group to be $P4_2nm$ (No. 102), $P\bar{4}n2$ (No. 118), or $P4_2/mnm$ (No. 136). Since two molecules are contained per unit-cell, the molecular symmetry in the crystal should be mm for the

† Structural Chemistry of Layered Cyclophanes. X.

†† Present address: Research Laboratory, Kanzaki Paper Mfg. Co. Ltd., Jokoji-motomachi, Amagasaki 680.

††† Present address: Institute for Protein Research, Osaka University, Yamadaoka, Suita, Osaka 565.

space group $P4_2nm$, 222 or $\bar{4}$ for $P\bar{4}n2$, or mmm for $P4_2/mnm$. However, the possible highest symmetry of the present molecule is m, the crystal may include some disordered structure. For this reason the further X-ray experiment was given up.

Structure Solution and Refinement

The room temperautre structure was first solved by the direct method (*MULTAN* 74).[3] 18 peaks on the E map, synthesized with the set of phases with the highest figure of merit, gave an approximate structure of the molecule, but three peaks among them were later excluded as spurious. The refinement was carried out by the block-diagonal least-squares procedure with unit weight (*HBLS* V).[4] Six cycles of isotropic refinement gave the R index of 0.123. After an anisotropic refinement of non-hydrogen atoms (4 cycles, R=0.105) hydrogen atoms located on their calculated positions with isotropic temperature factors were included in the refinement. The final R value was 0.069 for the observed reflections. Atomic paramters are given in Table 1.*

The refinement of the low temperature structure started from the positional paramters for the 15 non-hydrogen atoms determined with the room temperature data: the isotropic temperature factor of B=2.0 Å^2 being assumed for each atom. Successive anisotropic refinement (four cycles) gave the R value of 0.105. Hydrogen atoms were located at the calculated positions and refined isotropically. The weighting scheme used was $w=\{\sigma^2(F_o)+a|F_o|+b|F_o|^2\}^{-1}$ for $|F_o|>0$ and w=c for $|F_o|=0$. The final R value was 0.076 (R_w=0.078) with a=−0.0893, b=0.0018, and c=0. The final atomic parameters with equivalent temperature facors are given in Table 1.*

The atomic scattering factors for non-hydrogen atoms were taken from International Tables for X-ray Crystallography, Vol. IV[5] and those for hydrogen atoms from Stewart, Davidson, and Simpson.[6] Computations were done on an ACOS 700S computer at the Crystallographic Research Center, Institute for Protein Reserach, Osaka University.

Results and Discussion

Molecular Structure. A perspective view of the molecular structure of double-layered paracyclofuranophane at −150 °C is drawn (ORTEP II)[7] in Fig. 1, with the atomic labelling. The molecular structure projected onto the plane defined by the C(10), C(11), C(13), and C(14) atoms is shown in Fig. 2(a), that onto the plane formed by the C(1), C(2), C(7), and C(8) in Fig. 2(b), and that along the plane made by the C(10), C(11), C(13), and C(14) in Fig. 2(c). Interatomic bond distances and bond angles at −150 °C are also given in Fig. 2 with estimated standard deviations, together with the parameters to describe the out-of-plane deformation of the benzene ring. No essential difference has been observed between the structures at 20 °C and −150 °C; therefore, the discussion will be limited hereafter on the low temperature structure otherwise stated.

The coincidence of structural parameters of chemically equivalent parts of the molecule is good: the molecule has an approximate mirror symmetry. The furan ring takes an envelope form with the oxygen atom away from the benzene ring: the dihedral angle between the planes made by the O, C(3), and C(6) atoms and the C(3), C(4), C(5), and C(6) being 3.3°. This is similar to the corresponding angle in the triple-layered paracyclofuranophane[3.8°].

Two CH_2–CH_2 bridge bonds also have a similar structure as those in the triple-layered paracyclophane: C–C distances being 1.589(6) and 1.582(6) Å, and the torsion angles around the C–C bond 34.8 and 30.3°. The C(1)–C(2)–C(3) and C(6)–C(7)–C(8) angles are 113.4(3) and 114.6(3)°, respectively, which are larger than the C(2)–C(1)–C(12) [108.3(3)°] and C(7)–C(8)–C(9) [108.3(3)°] angles.

The benzene ring adopts a symmetrical boat form as in the case of many other cyclophanes. The C(9) and C(12) atoms deviate from the plane defined by the C(10), C(11), C(13), and C(14) atoms by 13.8 and 14.2°, respectively. The C(1)–C(12) vector makes an anlge of 15.6° to the plane made by the C(11), C(12), and C(13), and the corresponding angle of the C(8)–C(9) vector is 15.1°. The C(1)–C(12)–C(13) and C(8)–C(9)–C(14) angles [117.8(3) and 117.7(3)°, respectively] are smaller than the C(1)–C(12)–C(11) and C(8)–C(9)–C(10) [122.3(4) and 122.0(4)°, respectively], which are also smaller than the corresponding angles in the triple-layered paracyclofuranophane. These facts may be explained by the fact that the C(1) and C(8) atoms are shifted back to the C(13) and C(14) atoms, respectively, so that the nonbonded atomic interactions between the furan and benzene rings is minimized.

Table 2 summarizes the structural parameters to

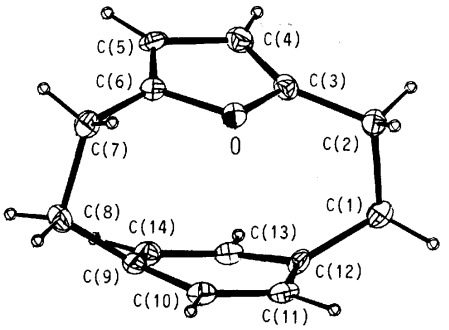

Fig. 1. A perspective view (*ORTEP* drawing)[7] of the double-layered paracyclofuranophane molecule (−150°C) with the atom labelling.
Non-hydrogen atoms are represented by thermal ellipsoids with 50% probability level, hydrogen atoms as spheres with B=0.5 Å^2.

*Tables of observed and calculated structure factors and anisotropic temperature factors of both structures 20 °C and −150 °C are kept at the Chemical Society of Japan, Document No. 8433.

Table 1. Final atomic positional parameters of [2]paracyclo[2](2,5)furanophane with eatimated standard deviations in parentheses

Room temperature structure(20°C)

a) Non-hydrogen atoms

Atom	x	y	z	B_{eq}[8]/Å^2
O	0.2627(3)	0.9515(2)	0.8712(5)	3.7
C(1)	0.2378(5)	0.9342(4)	0.4905(8)	5.1
C(2)	0.2804(4)	0.8773(4)	0.6214(9)	5.0
C(3)	0.3187(4)	0.9254(4)	0.7557(8)	3.9
C(4)	0.3938(4)	0.9580(4)	0.7890(8)	4.6
C(5)	0.3845(4)	1.0097(4)	0.9293(8)	5.0
C(6)	0.3038(4)	1.0055(4)	0.9732(7)	4.0
C(7)	0.2476(5)	1.0485(4)	1.0895(8)	5.0
C(8)	0.1958(4)	1.1245(4)	1.0158(9)	5.2
C(9)	0.1790(4)	1.1075(4)	0.8451(8)	4.4
C(10)	0.1161(4)	1.0513(4)	0.7978(9)	4.9
C(11)	0.1265(4)	1.0035(5)	0.6610(7)	4.5
C(12)	0.2001(4)	1.0089(4)	0.5698(7)	4.4
C(13)	0.2518(4)	1.0792(4)	0.5981(8)	4.9
C(14)	0.2399(4)	1.1274(4)	0.7347(9)	4.5

b) Hydrogen atoms

Atom	x	y	z	B/Å^2
H(1A)	0.191(4)	0.897(4)	0.420(7)	4.3(16)
H(1B)	0.281(5)	0.952(4)	0.405(9)	6.6(21)
H(2A)	0.326(4)	0.846(4)	0.568(8)	5.3(18)
H(2B)	0.235(5)	0.840(4)	0.671(8)	5.9(19)
H(4)	0.441(4)	0.955(4)	0.726(8)	4.2(16)
H(5)	0.425(4)	1.045(4)	0.987(8)	5.0(18)
H(7A)	0.288(5)	1.065(4)	1.189(8)	5.9(20)
H(7B)	0.209(5)	1.015(5)	1.149(8)	7.6(23)
H(8A)	0.233(5)	1.174(5)	1.022(10)	7.0(22)
H(8B)	0.150(4)	1.131(4)	1.087(7)	4.7(17)
H(10)	0.070(5)	1.040(5)	0.873(8)	6.2(21)
H(11)	0.088(4)	0.956(4)	0.627(7)	4.0(16)
H(13)	0.300(4)	1.092(4)	0.518(8)	4.3(17)
H(14)	0.286(4)	1.173(4)	0.753(8)	3.3(15)

Low temperature structure(−150°C)

a) Non-hydrogen atoms

Atom	x	y	z	B_{eq}[8]/Å^2
O	0.26235(16)	0.95118(16)	0.8727(3)	1.20
C(1)	0.2371(3)	0.9356(3)	0.4887(5)	1.67
C(2)	0.2797(3)	0.8765(3)	0.6201(5)	1.47
C(3)	0.3184(3)	0.9246(3)	0.7568(5)	1.39
C(4)	0.3962(3)	0.9572(3)	0.7888(5)	1.57
C(5)	0.3866(3)	1.0102(3)	0.9297(5)	1.48
C(6)	0.3045(3)	1.0055(3)	0.9742(5)	1.36
C(7)	0.2483(3)	1.0490(3)	1.0945(5)	1.55
C(8)	0.1960(3)	1.1259(3)	1.0246(5)	1.65
C(9)	0.1782(3)	1.1087(3)	0.8496(5)	1.37
C(10)	0.1144(3)	1.0535(3)	0.8006(5)	1.45
C(11)	0.1250(3)	1.0053(3)	0.6631(5)	1.50
C(12)	0.1989(3)	1.0110(3)	0.5732(5)	1.36
C(13)	0.2513(3)	1.0817(3)	0.6005(5)	1.41
C(14)	0.2413(3)	1.1299(3)	0.7377(5)	1.53

b) Hydrogen atoms

Atom	x	y	z	B/Å^2
H(1A)	0.192(4)	0.901(4)	0.428(6)	1.3(12)
H(1B)	0.280(4)	0.949(4)	0.423(6)	0.9(11)
H(2A)	0.323(3)	0.845(4)	0.565(6)	0.7(11)
H(2B)	0.235(4)	0.838(4)	0.664(6)	1.5(12)
H(4)	0.446(4)	0.950(4)	0.734(6)	1.1(11)
H(5)	0.431(4)	1.041(3)	0.978(6)	1.0(12)
H(7A)	0.281(4)	1.063(4)	1.178(6)	1.4(12)
H(7B)	0.208(4)	1.006(4)	1.135(6)	1.5(12)
H(8A)	0.230(4)	1.175(4)	1.046(6)	0.8(11)
H(8B)	0.150(4)	1.134(4)	1.092(6)	0.8(11)
H(10)	0.062(3)	1.046(3)	0.873(6)	0.8(11)
H(11)	0.079(4)	0.960(4)	0.633(6)	0.9(11)
H(13)	0.301(4)	1.089(4)	0.537(6)	0.9(11)
H(14)	0.284(4)	1.177(4)	0.771(7)	1.5(12)

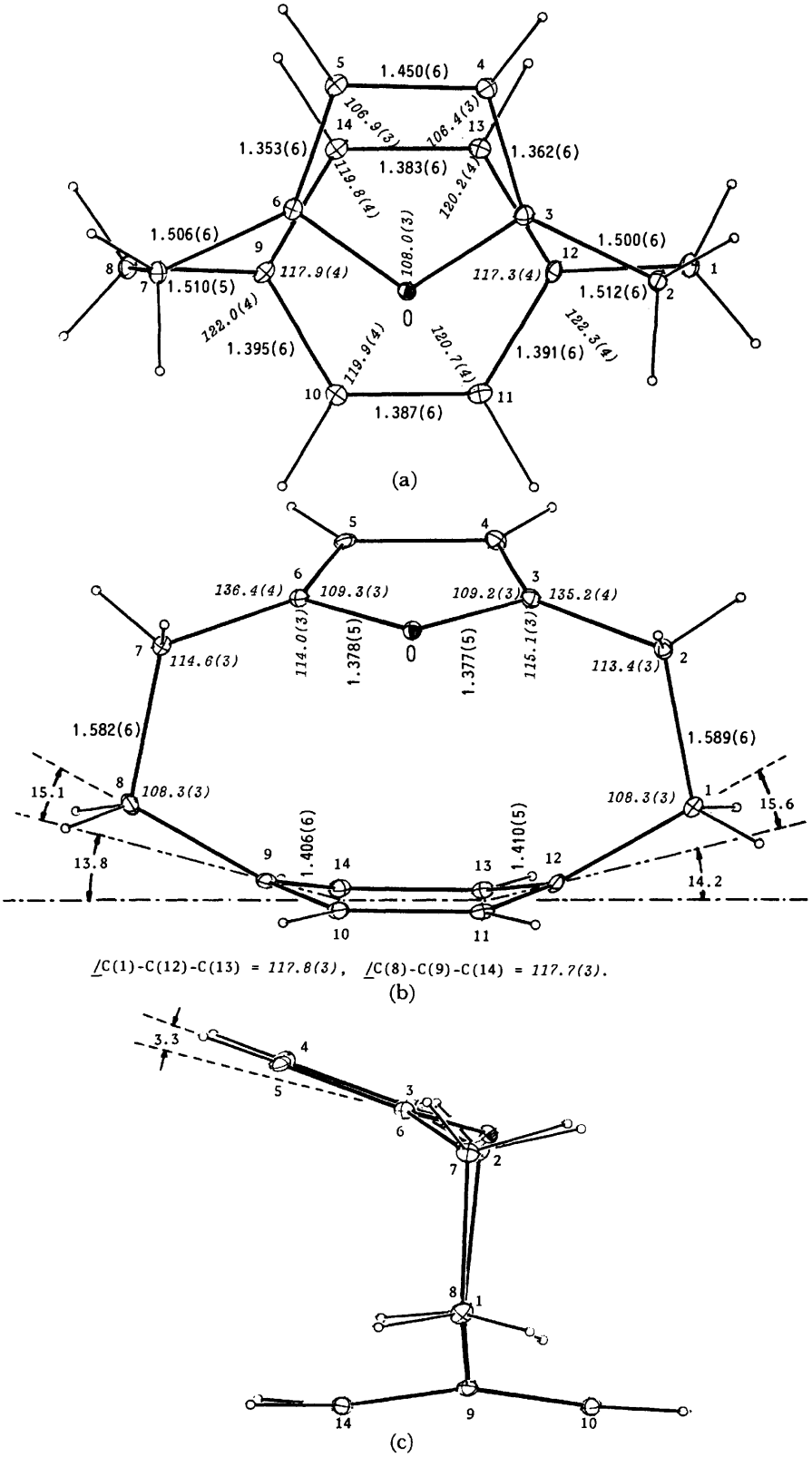

Fig. 2. Molecular structure (*ORTEP* drawing)[7] with bond distances, bond angles and other structural parameters at −150°C. Estimated standard deviations in parentheses.

(a) Projection onto the plane defined by the C(10), C(11), C(13), and C(14) atoms.

(b) Projection onto the plane defined by the C(1), C(2), C(7), and C(8) atoms. Structural parameters given in Fig. 2(a) are omitted.

(C) Projection along the plane defined by the C(10), C(11), C(13), and C(14) atoms.

Table 2. Comparison of some structural parameters of double- and triple- layered paracyclofuranophanes (F-X and F-D-X) and dimethyl triple- layered paracyclothiophenophane(T-D-D)

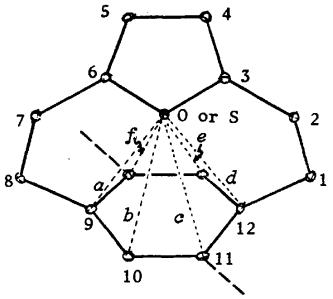

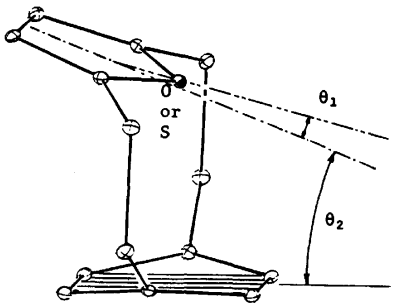

	Dihedral angle (ϕ/°)		Intramolecular atomic contact (l/Å)					
	θ_1	θ_2	*a*	*b*	*c*	*d*	*e*	*f*
					(O····C)			
F-X[a] (**1**) (−150°C)	3.3	20.6	2.833(5)	2.909(5)	2.916(5)	2.851(5)	3.072(4)	3.062(4)
(20°C)	3.4	20.9	2.840(7)	2.902(8)	2.921(7)	2.866(7)	3.070(7)	3.058(7)
F-D-X[b,c] (**3**) (20°C)	3.8	18.6	2.860	2.927	3.054	2.820	3.012	3.174
					(S····C)			
T-D-D[b] (**4**) (20°C)	8.3	6.8	3.123(3)	3.044(3)	3.196(3)	3.124(3)	3.438(3)	3.597(3)

a: present study; b: reference 2; c: average of three independent molecules

show the out-of-plane deformation of heteroaromatic ring (θ_1), relative position of the heteroaromatic ring to the benzene ring next to it(θ_2), and nonbonded distances between the heteroatom and benzene carbon atoms (*a* to *f*) in double- and triple-layered paracyclofuranophane and triple-layered paracyclothiophenophane molecules.

The marked difference between the molecular structures of double- and triple-layered paracyclofuranophanes is that *c* and *f* distances in the triple-layered one are much longer than those in the double-layered one. On the other hand, *a*, *b*, *d*, and *e* distances in these two molecules have respectively similar values. This feature is due to the structural difference of the benzene ring next to the furan ring in these molecules; boat form in the double-layered one and twisted form in the triple-layered one. This is probably the most important structural factor to lower the energy barrier of the ring inversion of the furan in triple- and quadruple-layered paracyclofuranophane compared with the double-layered one.

Crystal Structure. Figure 3 shows the crystal structure of double-layered paracyclofuranophane. Molecules are loosely packed in the crystal. Only one or two intermolecular atomic contacts are less than 3.8 Å: the closest one being C(5)(x,y,z)····C(4) (−0.5+y, 0.5+x, 0.5+z)[3.727(9)(20°C) and 3.667(6)Å (−150°C)].

The authors wish to express their deep thanks to Professor Soichi Misumi and co-workers, Institute for Scientific and Industrial Research, Osaka University for crystals and helpfull discussions.

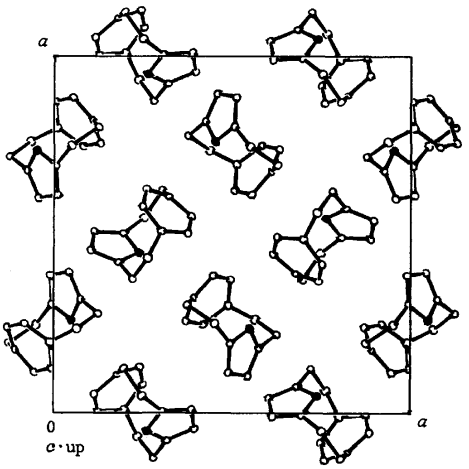

Fig. 3. Crystal structure viewed down along the c axis (*ORTEP* drawing).[7]
Carbon and oxygen atoms are respectively represented by white and black ellipsoids. Hydrogen atoms omitted.

References

1) T. Otsubo, S. Mizogami, N. Osaka, Y. Sakata, and S. Misumi, *Bull. Chem. Soc. Jpn.*, **50**, 1841 (1977).
2) Y. Kai, T. Watanabe, N. Yasuoka, and N. Kasai, *Acta Crystallogr., Sect. B*, **36**, 2276 (1980).
3) P. Main, M. M. Woolfson, L. Lessinger, G. Germain, and J. P. Declercq, *MULTAN* 74, "A System of Computer Programs for the Automatic Solution of Crystal Structures from X-ray Diffraction Data," Univs. of York, England and Louvain, Belgium (1974).
4) T. Ashida, *HBLS* V, "The Universal Crystallographic Computing System-Osaka," The Computation Center, Osaka Univ. (1973), p. 55.
5) International Tables for X-Ray Crystallography, Vol. IV, Kynoch Press, Birmingham (1974), p. 71.
6) R. F. Stewart, E. R. Davidson, and W. T. Simpson, *J. Chem. Phys.*, **42**, 3175 (1965).
7) C. K. Johnson, *ORTEP* II, Report ORNL-5138, Oak Ridge National Laboratory, Tennessee (1976).
8) W. C. Hamilton, *Acta Crystallogr.*, **12**, 609 (1959).

Coexistence of Hydrogen Atom Transfer Reactions through and not through Triplet Ion Pair between *p*-Chloranil and Durene

Harumichi KOBASHI,* Masa-aki FUNABASHI, Tomoyuki KONDO, Toshifumi MORITA, Tadashi OKADA,† and Noboru MATAGA†

Department of Chemistry, Faculty of Engineering, Gunma University, Kiryu, Gunma 376

†*Department of Chemistry, Faculty of Engineering Science, Osaka University, Toyonaka, Osaka 560*

(Received, July 13, 1984)

Mechanisms of hydrogen atom abstraction reactions by triplet state *p*-chloranil (^{3}CA) from durene (DH) were studied by picosecond and nanosecond laser photolysis and transient photoconductivity measurements. ^{3}CA was quenched by DH through diffusional encounter to form a triplet ion pair (IP) between CA and DH, *p*-chloranil semiquinone radical (CAH·), and 2,4,5-trimethylbenzyl radical (D·). Ionic dissociation of IP was observed in 1,2-dichloroethane (DCE) as well as in acetonitrile. However, no transient species was observed by direct excitation of a charge-transfer (CT) band of the electron donor-acceptor (EDA) complex between CA and DH. The H-atom transfer leading to production of CAH· was found to proceed through two distinct mechanisms; H-atom transfer *via* IP (Mechanism I) and a more rapid transfer competing with IP formation (Mechanism II). The quantum yields of CAH· produced by Mechanisms I and II and the first-order rate constants for proton transfer, ionic dissociation, and intersystem crossing competing with one another in the IP state were estimated to be (0.1 and 0.2) and (2, 5, and 13)$\times 10^6$ s^{-1}, respectively, in DCE at room temperature.

In the case of the photochemical hydrogen abstraction reaction of triplet ketones or quinones, two different and noteworthy mechanisms have been reported. One is the two-step mechanism of electron transfer followed by proton transfer *via* ion-pair (IP) state (Mechanism I). This is the case of triplet benzophenone and several amines in high-polarity solvents[1] as well as the case of the excited singlet pyrene–aromatic amines.[2] Another is the rapid H-atom transfer in nonrelaxed encounter complex competing with IP formation (Mechanism II) as observed in the system of triplet state 2,6-diphenyl-*p*-benzoquinone and aromatic amines.[3] Since most of the triplet state quinones are strong electron and hydrogen acceptors, it is not easy to determine which mechanism is predominant in their H abstraction reactions. Very careful examinations based on direct observation of short-lived transient species are neccesary to elucidate the reaction mechanism.

In the course of our investigations concerning photo-reduction of ^{3}CA by several electron and hydrogen donors,[4] we observed in the CA–DH system that CAH· radicals were produced simultaneously with the formation of IP between CA and DH and also grew up concomitantly with the decay of IP. We have examined the mechanism of this reaction mainly in DCE solution by means of picosecond (ps) and nanosecond (ns) laser photolysis and transient absorption measurements as well as transient photoconductivity studies in the ns time region. Results show coexistence of Mechanisms I and II.

Experimental

Transient absorption spectra in the ps and ns region were measured using a mode-locked ruby laser system (λ 347 nm, FWHM ≈30 ps, energy ≈10 mJ)[5] at 25 °C and a conventional ns ruby laser system[4] at 20±1 °C unless otherwise stated. Photolysis at 502 as well as 532 nm was also performed by using a flash-lamp pumped dye laser (dye: Green-4 of Phase-R Co., pulse width ≈250 ns, energy ≈110 mJ)[6] and a ps Nd^{3+}: YAG laser system,[7] respectively. Transient photocurrents were measured using the same type of quartz cuvette with two Ni- or Pt-plate electrodes as utilized previously.[8] The DC voltage (90—540 V) was supplied between the electrodes from a bank of dry batteries. The output signal across a 50 Ω load resister was fed into a 200 MHz oscilloscope (Iwatsu, SS-6200) through AC coupling. The ground state absorption spectra were recorded on a Hitachi Model 200 spectrophotometer. All solutions were carefully degassed by freeze-pump-thaw cycles.

p-Chloranil (CA: tetrachloro-*p*-benzoquinone) was purified by the same method as described elsewhere.[4a] The GR grade durene (DH: 1,2,4,5-tetramethylbenzene) was recrystallized twice from cyclohexane and sublimed *in vacuo*. Solvents: 1,2-dichloroethane, acetonitrile, and ethyl acetate were purified by the usual methods.

Results and Discussion

EDA Complex Formation in the Ground State. The DCE solutions of CA (0.001—0.002 mol dm^{-3}) and DH (0.075—0.40 mol dm^{-3}) showed a CT band (λ_{max} 480 nm; ε 2650±100 dm^3 mol^{-1} cm^{-1}) due to the EDA complex (CA···DH) with the formation constant K=0.89±0.03 dm^3 mol^{-1} (at 20 °C) which was determined using the Benesi-Hildebrand method. The thermodynamic quantities, ΔH (−18.1±1.2 kJ mol^{-1}) and ΔS (−63±4 J mol^{-1} K^{-1}), were obtained by the measurement of the temperature dependence of K in the range 4—57 °C. These values are comparable with those for the same complex in carbon tetrachloride reported previously.[9] The absorption spectra of the complex and uncomplexed CA involved in the DCE solution are illustrated in Fig. 1.

Picosecond and Nanosecond Laser Photolysis. The laser photolysis at 502 as well as 532 nm, where exclusive-

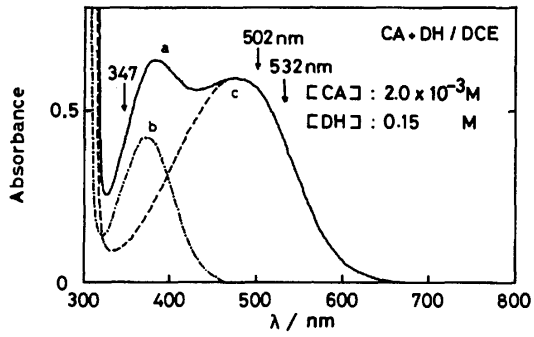

Fig. 1. Ground state absorption spectra of the CA (2.0×10^{-3} mol dm^{-3}) and DH (0.15 mol dm^{-3}) system in DCE at 18°C. (a): observed spectrum, (b): spectrum of uncomplexed CA (1.76×10^{-3} mol dm^{-3}) present in the solution, (c): spectrum of the EDA complex alone obtained by (a)—(b).
Wavelengths of lasers used for excitation are indicated by arrows.

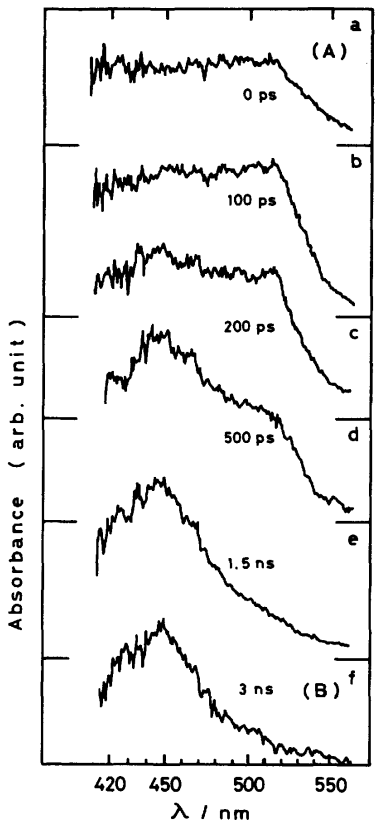

Fig. 2. Time-resolved absorption spectra obtained by the picosecond laser photolysis for the CA and DH system in DCE:
[CA]=3.0×10^{-3} mol dm^{-3}, [DH]=0.20 mol dm^{-3}.
The absorbance is not corrected for shot-to-shot variations of the exciting-pulse intensity.

ly the CT band was excited (indicated by arrows in Fig. 1), did not give any transient absorption over the time range from picosecond to several microseconds. No permanent change of the ground state absorption spectrum was recognized after several laser shots. These findings suggest that the S_1 state of the complex decays so rapidly through internal conversion that its detection is not possible even by means of the ps laser photo-

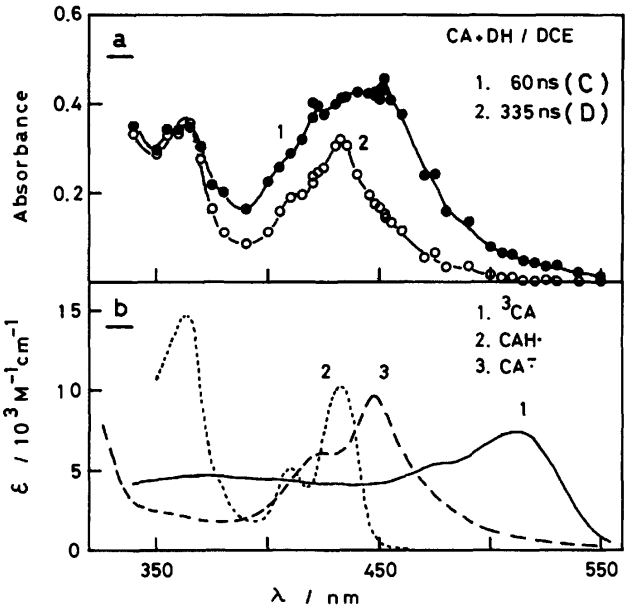

Fig. 3. a) Transient absorption spectra obtained by the nanosecond flash photolysis for the CA-DH-DCE system.
[CA]=3.0×10^{-3} mol dm^{-3}, [DH]=0.20 mol dm^{-3}; (1) 60 ns and (2) 335 ns after the beginning of laser oscillation.
b) Reference absorption spectra.
(1): ^{3}CA in DCE, (2): CAH· in DCE, (3): CA$^-$ in acetonitrile.

lysis method. Some discussions will be given later concerning this result.

In the following we show results of the photolysis at 347 nm where excitation of uncomplexed CA is possible. Figure 2 presents time-resolved absorption spectra for the solution containing CA (3.0×10^{-3} mol dm^{-3}) and DH (0.20 mol dm^{-3}) observed by the ps ruby laser photolysis. Figure 3a shows transient absorption spectra measured by the ns flash photolysis and Fig. 3b gives reference spectra of ^{3}CA,[4a] CAH·,[4b] and *p*-chloranil radical anion (CA$^-$).[10]

The absorption band around 510 nm in the spectrum observed at 0 ps (Fig. 2a) resembles that of ^{3}CA. After reaching the maximum intensity, the absorbance around 510 nm decreases while a new band around 450 nm grows up. The latter absorption band is similar to that of CA$^-$. The spectra observed at several delay times from 100 ps to 1.5 ns could be reproduced by the superposition of the spectra at 0 ps (**A**) and 3 ns (**B**), which has been performed by a microcomputer using the least-square method. An example for the spectrum at 500 ps is given in Fig. 4, where the agreement between the calculated spectrum (b(1)) composed of **A** and **B** and the observed one (a) is satisfactory. The time dependence of each component obtained by such procedure is indicated in Fig. 5. The decay time of **A** and the rise time of **B** are estimated respectively to be about 0.7 and 0.6 ns, being in agreement with each other. This indicates that the species responsible for the spectrum **B** is produced from the transient which

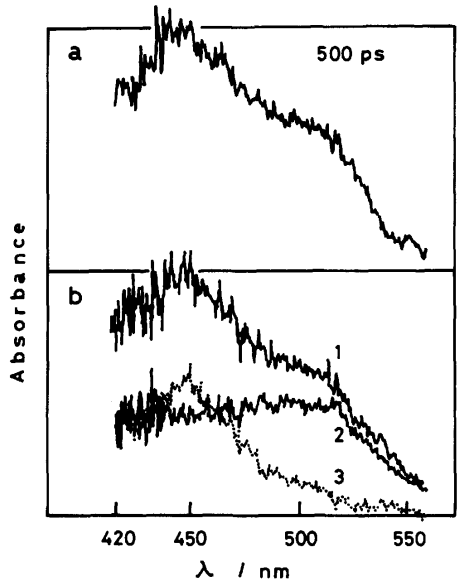

Fig. 4. Comparison of the spectrum observed at 500 ps with the spectrum obtained by superposition of **A** and **B**.
a): observed spectrum, b): (1) calculated spectrum (**A**+**B**), (2) component spectrum **A**, (3) component specturm **B**.

shows the spectrum **A**.

As can be seen from Fig. 3, no absorption band around 510nm corresponding to **A** was observed by the ns laser photolysis since the transient species responsible for **A** was quenched by DH of high concentration (0.20 moldm^{-3}) very rapidly. The spectrum (**C**) observed immediately after excitation by the ns pulse (Fig. 3a(1)) is quite similar, in the 420—500nm region, to the spectrum **B**. Therefore, it is plausible that **C** is substantially the same as **B**. Comparison of **C** with **B** in the wavelength region less than 420nm was not possible because of the absence of observed band in the case of **B** owing to the low intensity of the ps probe pulse.

The spectrum **C** is replaced completely by the spectrum (**D**) with definite absorption maxima at 435 and 365nm and a shoulder around 448nm at the delay time of 335ns. The decay profile of the absorbance at 448nm is shown in Fig. 6, which indicates the existence of two components. Since the long-lived component did not show decay in 100ns domain, we subtracted its absorbance (D_∞) from the observed total absorbance D. A straight line (b) obtained by plotting log (D—D_∞) against time yields the decay time (τ_d) of 49±2ns at 20°C of the transient species responsible for the band at 448nm. The τ_d values were independent on [CA] in the (0.81—3.65)×10^{-3}moldm^{-3} range, [DH] in the 0.05—0.20 moldm^{-3} range, and on monitoring wavelength in the 448—480nm region, within experimental accuracy.

Assignment of Transient Spectra and Reaction Mechanism. Since no transient absorption was observed by direct excitation of the EDA complex, only free CA present

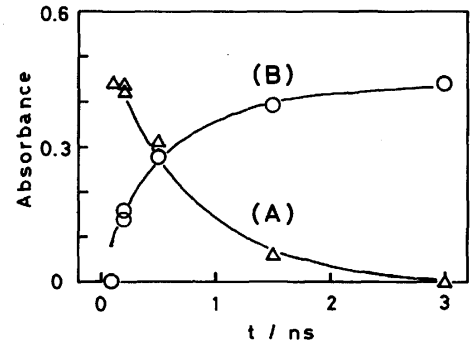

Fig. 5. Time dependence of absorbances of specturm **A** at 510nm (△) and spectrum **B** at 448nm (○). Absorbances are corrected for variations of the laser intensity.

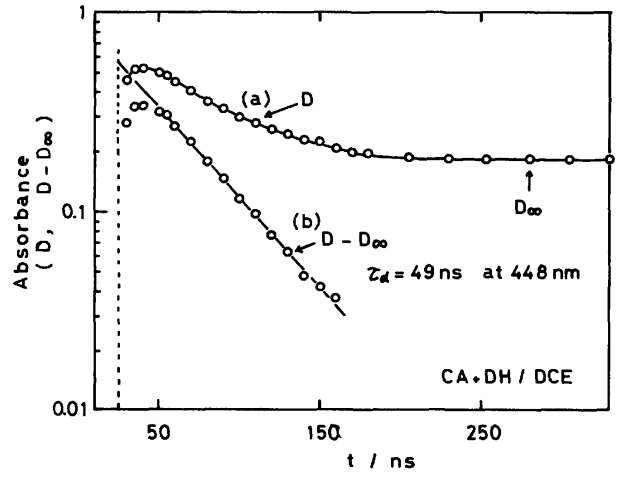

Fig. 6. Semi-logarithmic plots of absorbance at 448nm *vs.* time in the CA-DH-DCE system. (a): log D *vs.* t, (b): log (D-D$_\infty$) *vs.* t.

in the solution seems to contribute to the appearance of **A**. Excited CA is known to cause rapid intersystem crossing (ISC, $k_{ISC} \approx 3\times10^{10}s^{-1}$, $\Phi_{ISC}=1$) from S_1 to T_1 in acetonitrile.[11] We have also confirmed that ISC is also rapid ($>3\times10^{10}s^{-1}$) in the DCE solution of CA (0.003 moldm^{-3})-diphenylamine (0.1 moldm^{-3}) system in a separate experiment performed by means of the Nd^{3+}: YAG laser photolysis.[12] Therefore, the spectrum **A** can be assigned to that of ^{3}CA.[13]

As shown in Fig. 3b, CA$^{\cdot-}$ shows a strong band with maximum at 448nm where CAH· shows only a negligibly weak absorption. Therefore, the absorption band at 448nm in **B**, **C**, and **D** can be attributed to CA$^{\cdot-}$. Figure 5 shows that CA$^{\cdot-}$ in question is produced in the course of the collisional quenching of ^{3}CA by DH, since ^{3}CA is quenched by DH with nearly diffusion-controlled rate.[14] However, the transient species showing the 448nm absorption in **C** (*i.e.*, **B**) is not free CA$^{\cdot-}$ because its decay obeys the first-order kinetics (Fig. 6b). Accordingly, this absorption band at 448nm can be assigned to CA$^{\cdot-}$ of the triplet ion pair ^{3}(CA$^{\cdot-}$··· DH$^+$). The spin state should be assigned to the triplet state because the observed species with a fairly long life was produced from the triplet state precursor while no

CT singlet state $^1(CA^{\overline{\cdot}}\cdots DH^+)$, which should be produced by the direct excitation of the CT band, was observed. That no absorption band due to the counter ion DH^+ was detected is probably due to its low intensity in the visible region.[15] The ion-pair formation may be rationalized also from the following estimations concerning the free energy change ΔG of the reaction $^3CA+DH\rightarrow{}^3(CA_s^{\overline{\cdot}}\cdots DH_s^+)$ or $^3(CA^{\overline{\cdot}}\cdots DH^+)_s$, where $^3(CA_s^{\overline{\cdot}}\cdots DH_s^+)$ represents the solvent-separated ion pair and $^3(CA^{\overline{\cdot}}\cdots DH^+)_s$ refers to the contact ion pair or the triplet exciplex with nearly complete CT character. The quenching of ^3CA is not attributable to the T-T energy transfer, $^3CA+DH\rightarrow CA+{}^3DH$, in view of the fact that the energy of ^3CA above the ground state ($E_T(^3CA)\approx 2.13$ eV[16]) is much lower than that of ^3DH ($E_T(^3DH)=3.37$ eV).[17] The ΔG values of the ion-pair formation in DCE are estimated approximately to be -0.43 eV for $^3(CA_s^{\overline{\cdot}}\cdots DH_s^+)$ by the equation:[18]

$$\Delta G(CA_s^{\overline{\cdot}}\cdots DH_s^+) = E(DH/DH^+) - E(CA^{\overline{\cdot}}/CA) - E_T(^3CA) - e^2/\varepsilon R + (e^2/2)(1/R_+ + 1/R_-)(1/\varepsilon - 1/37.5), \quad (1)$$

and -0.73 eV for $^3(CA^{\overline{\cdot}}\cdots DH^+)_s$ by[19]

$$\Delta G(CA^{\overline{\cdot}}\cdots DH^+)_s = E(DH/DH^+) - E(CA^{\overline{\cdot}}/CA) - E_T(^3CA) + 0.32 - 0.7[f(\varepsilon) - 0.5f(n^2)] \quad (2)$$

in eV unit, where $E(DH/DH^+)$ and $E(CA^{\overline{\cdot}}/CA)$ are the polarographic oxidation potential of DH (1.59 V)[20] and the reduction potential of CA (0.01 V)[21] respectively, ε and n are the dielectric constant and refractive index of solvent respectively, $f(x)=2(x-1)/(2x+1)$, and other symbols and parameter values are the same as used in the references. Since both values of ΔG are negatively large, the electron transfer would occur to form the ion pairs. Contact and solvent-separated ion pairs have been discriminated in some EDA systems.[1c,3b,22,23] However, the discrimination between them was not possible for the present system in DCE solution. Therefore, we use throughout this paper the term "triplet ion pair (IP)," without discrimination between contact and solvent-separated ion pairs, for the species exhibiting the 448 nm band in the spectrum **C** (and **B**) with the lifetime of 49 ns.

The spectra **C** and **D** in Fig. 3a appear at first glance to resemble the reference spectra of $CA^{\overline{\cdot}}$ and CAH· respectively but close inspection makes clear the differences between them. The ratio of 435 to 448 nm absorbance in **C** is significantly higher than the corresponding ratio in the reference spectrum of $CA^{\overline{\cdot}}$ and additionally **C** involves the band at 365 nm which is characteristic of CAH·. In the spectrum **D**, the intensity ratio of 365 to 435 nm band is small compared with that of CAH· and the shoulder around 448 nm which is characteristic of $CA^{\overline{\cdot}}$ is observed. It is, therefore, suggested that both spectra **C** and **D** involve the absorption bands of the two species CAH· and $CA^{\overline{\cdot}}$. The decomposition of the spectrum into CAH· and $CA^{\overline{\cdot}}$ was then performed very carefully and the result is given in Fig. 7. The procedure for decomposition was made by normalizing the reference spectrum of $CA^{\overline{\cdot}}$ to the observed one at 448 nm and then subtracting the former from the latter. The obtained spectrum (Fig. 7a (3)) agrees with the spectrum of CAH·. A small difference between the spectrum of $CA^{\overline{\cdot}}$ and the observed one (**C**) in the wavelength region longer than 448 nm seems attributable to a small difference in the spectra between IP and free $CA^{\overline{\cdot}}$. The spectrum **D** can be reproduced quite well by superposing spectra of CAH· and $CA^{\overline{\cdot}}$ (Fig. 7b). Since, as is shown in Fig. 8, the 448 nm absorbance in **D** shows the second order decay, this absorption band may be assigned to free $CA^{\overline{\cdot}}$. From the results of the analysis indicated in Fig. 7, it can be concluded that CAH· radicals are rapidly produced in part competitively with IP formation and further increase in accordance with decrease of IP.

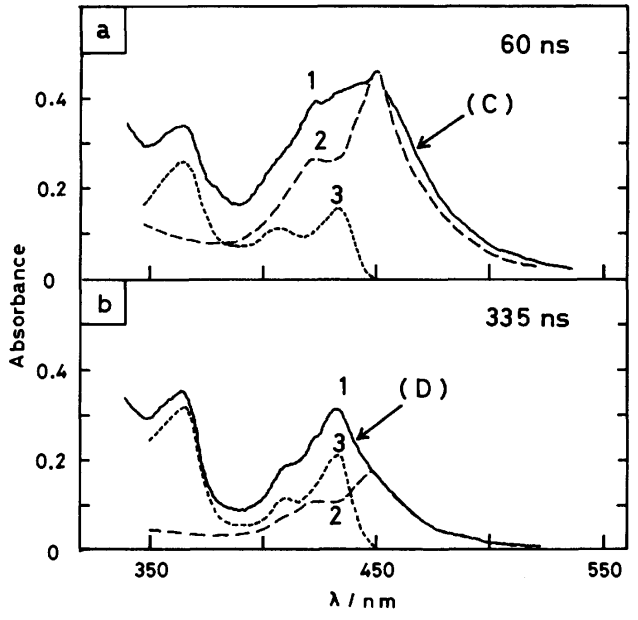

Fig. 7. Spectrum decomposition for the spectra in Fig. 3a observed at 60 ns (a) and at 335 ns (b); (1) observed spectrum, (2) spectrum of $CA^{\overline{\cdot}}$ component (3) (1)—(2).

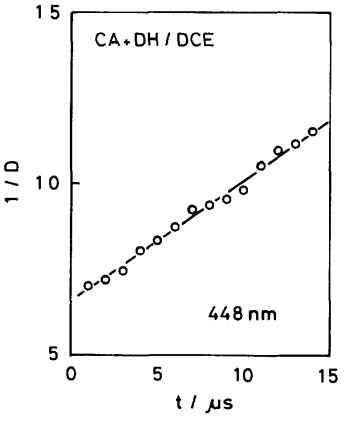

Fig. 8. A second-order decay plot for the spectrum **D** at 448 nm.

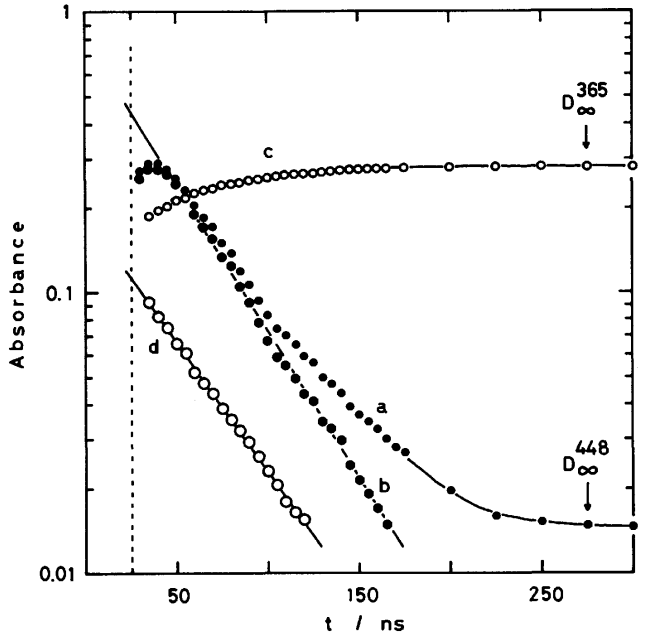

Fig. 9. Time dependence of 365 and 448 nm absorbances observed in ethyl acetate solution of CA (0.0011 mol dm^{-3}) and DH (0.20 mol dm^{-3}):
(a) log D *vs.* t and (b) log $(D-D_\infty)$ *vs.* t measured at 448 nm, (c) log D *vs.* t and (d) log $(D_\infty-D)$ *vs.* t measured at 365 nm.

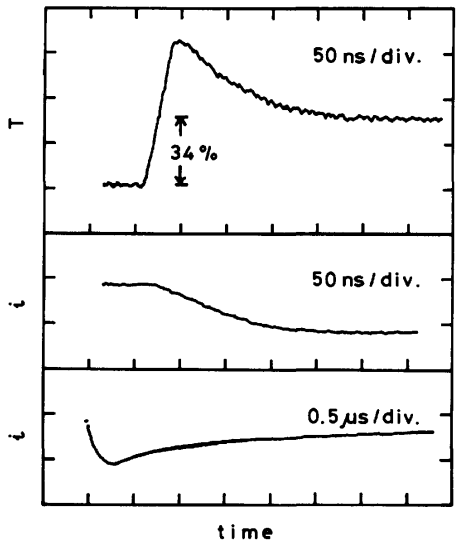

Fig. 10. Oscilloscope traces for transient absorption (T: transmittance) monitored at 448 nm (a) and transient photocurrents ($i\approx0.1$ mA/div), (b) and (c), in DCE solution:
[CA]=0.0025 mol dm^{-3}, [DH]=0.20 mol dm^{-3}.

Therefore, it is confirmed that the H-atom transfer in problem proceeds through both Mechanisms I and II.

Although in DCE solution the slow rise of CAH· was established on the basis of the result of spectrum decomposition, the rise was observed directly by monitoring the characteristic absorption band of CAH· at 365 or 435 nm in other less polar solvents. Figure 9 shows time dependence of 365 nm absorbance, D^{365}, (line c) together with that of 448 nm absorbance, D^{448}, (line a) observed in ethyl acetate solution. The line b is the plot of $D^{448}-D_\infty^{448}$ against t yielding the decay time (τ_d) of IP. The line d is the plot of $D_\infty^{365}-D^{365}$, yielding the rise time (τ_r) of CAH·. Here, D_∞^{448} and D_∞^{365} are the absorbances in the plateau region observed at 448 and 365 nm, respectively. It is clear that CAH· grows up concomitantly with decay of IP because τ_r value (51 ns) agrees with τ_d value (47 ns) within experimental accuracy.

The formation of free ions as noted in the discussion of the spectrum **D** was examined by transient photoconductivity measurement. Figure 10 demonstrates the oscillograms of photocurrent together with the temporal behavior of transient absorption. The rise time (50±3 ns from 5 runs) of the photocurrent was in good agreement with the decay time of IP and the decay of the current followed exactly the second-order kinetics. It is therefore confirmed that the ionic dissociation producing free CA^- occurs subsequent to the IP formation.

In addition to these measurements, we have observed a fairly sharp absorption band around 330 nm simultaneously with the bands of CAH·. This observation suggests strongly the pair production of CAH· and 2,4,5-trimethylbenzyl radical (D·), because D· has a sharp band at 330 nm.[24]

From the above described results, the deactivation processes of ^{3}CA by the interaction with DH may be schematically represented as follows:

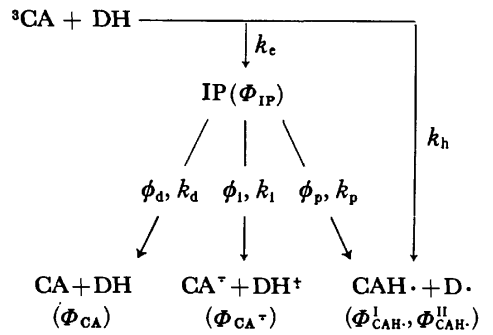

(3)

Here, the letters Φ, ϕ, and k represent the quantum yield of transient species from ^{3}CA, the fractional efficiency of each reaction from IP, and the rate constant of each reaction process, respectively. The subscripts e, h, p, i, and d refer in turn to the processes of electron transfer, hydrogen transfer, proton transfer, ionic dissociation, and degradation through ISC of IP returning back to the ground state. $\Phi^I_{CAH\cdot}$ and $\Phi^{II}_{CAH\cdot}$ denote the quantum yields of CAH· formation by the mechanism I and II, respectively. Estimation for these values measured in DCE solution will be given in the later section.

No Transient Formation by Direct Excitation of the EDA Complex. We examine here the mechanism for the result that direct photoexcitation into the CT band of the complex affords no transient absorption. The energy levels of locally excited (LE) singlet ^{1}(CA*···

DH) and triplet ^{3}(CA*···DH) states may be approximately the same as those of ^{1}CA*+DH and ^{3}CA*+DH states which lie in 2.63[25] and 2.31 eV[16] above the CA+DH state, respectively. The energies of CT singlet ^{1}($CA^{\cdot-}$···DH^+) and triplet ^{3}($CA^{\cdot-}$···DH^+) states may be given approximately as 1.7 and 1.3 eV, respectively, from the position of onset of the CT band and from the energy of ^{3}($CA^{\cdot-}$···D^+)$_s$ state estimated by using Eq. 2. Since the energy gap between zero-order ^{1}CT and ^{1}LE states is large, their mixing will be small. This condition results in small splitting betwecn ^{1}CT and ^{3}CT states. In practice, ^{1}($CA^{\cdot-}$···DH^+) and ^{3}($CA^{\cdot-}$···DH^+) states will lie closer to each other than the expectation from the above estimation owing to the intra-complex as well as stabilization induced by solvent reorientation in ^{1}($CA^{\cdot-}$···DH^+). In any way, these ^{1}($CA^{\cdot-}$···DH^+) and ^{3}($CA^{\cdot-}$···DH^+) states will be the lowest excited singlet and triplet states, respectively, and ^{3}(CA*···DH) state will locate higher than ^{1}($CA^{\cdot-}$···DH^+) state.

The fact that no transient formation was observed in the case of direct excitation of EDA complex means that ISC does not take place effectively in the complex from the ^{1}CT state to the ^{3}CT state. This is also supported by the fact that no CT phosphorescence could be observed at low temperature. ISC between the CT states is forbidden since the matrix element of spin-orbit interaction, $<^1\mathrm{CT}|H_{SO}|^3\mathrm{CT}>$ which governs the ISC rate, becomes null in the usual one-electron approximation. Therefore, ISC may be unfavorable to take place competing with the allowed internal conversion from the ^{1}CT state to the ground state. Since no LE state lies between the ^{1}CT and ^{3}CT states, the conclusion inferred above is in harmony with the selection rule proposed by Lim *et al.* for the systems of tetracyanoethylene-methylated benzenes and 1,2,4,5-tetracyanobenzene-methylated benzenes.[26] The internal conversion would be so rapid that no transient species was observed even by the present ps time resolution. Similar results of ps laser photolysis studies have been reported also for the duroquinone-triethylamine,[27a] porphyrin-quinone,[27b] and pyrene-pyromellitic dianhydride[27c] systems.

Yields of IP, CAH·, and $CA^{\cdot-}$ and Rate Constants for Decay Processes of IP. Estimation of Φ_{IP}, $\Phi^{II}_{CAH\cdot}$, k_e, *and* k_h: Since the triplet yield of CA has been known to be unity,[4a,11b] Φ_{IP} can be estimated from Fig. 5 using Eq. 4:

$$\Phi_{IP} = \frac{D_{IP}(3)/\varepsilon_{IP}}{D_{3CA}(0)/\varepsilon_{3CA}}, \quad (4)$$

where $D_{IP}(3)$ is the 448 nm absorbance due to IP at 3 ns, D_{3CA} (0) is the 510 nm absorbance of ^{3}CA at 0 ps, ε_{IP} is the molar absorption coefficient of IP at 448 nm (9.0×10^3 $dm^3mol^{-1}cm^{-1}$)[28] and ε_{3CA} is that of ^{3}CA in DCE at 510 nm, $(7.3\pm0.3)\times10^3$ $dm^3mol^{-1}cm^{-1}$.[29] The Φ_{IP} value obtained is 0.81 within the error of about 10%. $\Phi^{II}_{CAH\cdot}$ value is obtained to be 0.19 by the relation $\Phi^{II}_{CAH\cdot}=1-\Phi_{IP}$ according to (3). By using the quenching rate constant of ^{3}CA by DH measured at 15 °C,[14] approximate values of second-order rate constants, k_e and k_h, are estimated to be 2.5×10^9 $dm^3mol^{-1}s^{-1}$ and 0.6×10^9 $dm^3mol^{-1}s^{-1}$, respectively.

Determination of $\Phi^{total}_{CAH\cdot}$, $\Phi_{CA^{\cdot-}}$, $\Phi^{I}_{CAH\cdot}$ *and* Φ_{CA}: For the pupose of obtaining the total yields of CAH· ($\Phi^{total}_{CAH\cdot}\equiv\Phi^{I}_{CAH\cdot}+\Phi^{II}_{CAH\cdot}$) and $\Phi_{CA^{\cdot-}}$ values, the ns laser photolysis was carried out, under the same laser intensity, for solutions of CA in the presence and absence of DH. The absorbances at 347 nm of the solutions were adjusted equal to each other. The solutions containing CA alone were used as references for the yield of ^{3}CA. Then, $\Phi^{total}_{CAH\cdot}$ and $\Phi_{CA^{\cdot-}}$ can be expressed by Eqs. 5 and 6 respectively using transient absorbances measured at 300 ns after the laser excitation.

$$\Phi^{total}_{CAH\cdot} = \frac{D_{CAH\cdot}/\varepsilon_{CAH\cdot}}{D^{calc}_{3CA}/\varepsilon_{3CA}}, \quad (5)$$

$$\Phi_{CA^{\cdot-}} = \frac{D_{CA^{\cdot-}}/\varepsilon_{CA^{\cdot-}}}{D^{calc}_{3CA}/\varepsilon_{3CA}}, \quad (6)$$

where $D_{CAH\cdot}$ and $D_{CA^{\cdot-}}$ are the absorbances of CAH· at 435 nm and $CA^{\cdot-}$ at 448 nm after the spectrum decomposition, respectively, and $D^{calc}_{3CA}\equiv D_{3CA}\cdot D^0_{CA}/(D^0_{CA}+D^0_C)$ is the calculated absorbance of ^{3}CA which should be produced in the mixed solution of CA and DH immediately after the excitation. D_{3CA} is the 510 nm absorbance of ^{3}CA observed in the reference solution of CA. D^0_{CA} and D^0_C are the 347 nm absorbances of uncomplexed CA and complex CA···DH respectively and hence $D^0_{CA}/(D^0_{CA}+D^0_C)$ means the fraction of absorbance due to free CA present in the mixed solution to the total absorbance at 347 nm. $\varepsilon_{CAH\cdot}$ is the molar absorption coefficient of CAH· in DCE (1.0×10^4 $dm^3mol^{-1}cm^{-1}$ at 435 nm)[30] and $\varepsilon_{CA^{\cdot-}}$ is that of $CA^{\cdot-}$ (9.0×10^3 $dm^3mol^{-1}cm^{-1}$ at 448 nm).[28b,31] Table 1 shows results obtained. Although rather large error (about 20%) was presumed for each Φ value, the agreement among several measurements for each pair of solutions was good (within 10%). Both values of $\Phi^{total}_{CAH\cdot}$ and $\Phi_{CA^{\cdot-}}$ are independent on [CA] as well as [DH]. $\Phi^{I}_{CAH\cdot}$ was evaluated to be 0.10 by using the relation $\Phi^{I}_{CAH\cdot}=\Phi^{total}_{CAH\cdot}-\Phi^{II}_{CAH\cdot}$ with the value of $\Phi^{II}_{CAH\cdot}=0.19$. The Φ_{CA} value was calculated to be 0.52 by $\Phi_{CA}=1-\Phi^{total}_{CAH\cdot}-\Phi_{CA^{\cdot-}}$. If the quenching of ^{3}CA yielding no transient species is competing with IP formation in

TABLE 1. YIELDS OF CAH· AND $CA^{\cdot-}$ IN DCE AT 20 °C

[CA] /10^{-3}mol dm^{-3}	[DH] /10^{-1}mol dm^{-3}	$\Phi^{total}_{CAH\cdot}$	$\Phi_{CA^{\cdot-}}$
2.0	0.1	0.29	0.18
2.0	1.0	0.29	0.17
2.0	1.5	0.28	0.19
2.0	2.0	0.28	0.21
2.0	2.5	0.29	0.21
2.5	1.0	0.29	0.20
2.0	1.0	0.30	0.19
1.5	1.0	0.28	0.19
		av. 0.29	0.19

the encounter complex, Φ_{CA} must satisfy the relation $\Phi_{CA}=1-\Phi_{IP}-\Phi^{II}_{CAH\cdot}<1-\Phi_{IP}=0.19$. This relation contradicts the experimental result ($\Phi_{CA}=0.52$), so that the deactivation to the ground state competing with IP formation may be neglected in (3).

Determination of ϕ_p, ϕ_i, ϕ_d, k_p, k_i, *and* k_d: Using the Φ values together with the τ_d value the efficiencies (ϕ) for decay channels of IP and the first-order rate constants (k) for the corresponding processes could be estimated as follows:

$$\begin{aligned} \phi_p &= 0.1_2, \; k_p = 2\times10^6\ s^{-1}, \\ \phi_i &= 0.2_3, \; k_i = 5\times10^6\ s^{-1}, \\ \phi_d &= 0.6_5, \; k_d = 13\times10^6\ s^{-1}. \end{aligned} \tag{7}$$

On the other hand, from the time dependence of absorbances obtained by the ns laser photolysis alone, we could also estimate $\phi_p=0.1_4$ by Eq. 8,

$$\phi_p = \frac{\{D_{CAH\cdot}(300)-D_{CAH\cdot}(50)\}/\varepsilon_{CAH\cdot}}{D_{448}(50)/\varepsilon_{IP}} \tag{8}$$

assuming that D_{448} (50), the 448nm absorbance observed at 50ns, is due to IP. In Eq. 8, $D_{CAH\cdot}$ (50) and $D_{CAH\cdot}$ (300) are the absorbances of CAH· at 435nm (after the spectrum decomposition) measured at 50 and 300ns, respectively, and $\varepsilon_{CAH\cdot}$ and ε_{IP} are the same as in Eqs. 5 and 6.

For the purpose of comparison we present here briefly some results obtained in the CA-diphenylamine (DPA)-DCE system.[12] We have found the triplet IP, $^3(CA^{\overline{\cdot}}\cdots DPA^+)$, with a lifetime of *ca.* 8ns, $k_i\approx1\times10^7\ s^{-1}$, and $k_d\approx1.1\times10^8\ s^{-1}$, whereas no proton transfer in $^3(CA^{\overline{\cdot}}\cdots DPA^+)$ has been detected. The k_p value given in Eq. 7 is much less than the corresponding values for benzophenone (BP)-*N*,*N*-dimethylaniline (DMA) system ($k_p=2.0\times10^9 s^{-1}$ in acetonitrile)[1] and pyrene (P)-primary or secondary aromatic amine system (*e.g.*, ($k_p=5\times10^9 s^{-1}$ for P-DPA system in toluene).[2] Although the number of data of k_p value in Mechanism I is still scarce for any detailed discussion, these data appear to indicate that the rate of proton transfer in IP decreases with increase of the free energy change of this reaction.[32] In Eq. 7, the k_i value is larger than the k_p value by a factor of about 2.5. However, the rate of ionic dissociation in DCE is much slower than that in acetonitrile, where the photocurrent has been found to reach its maximum intensity immediately after the pulsing (Fig. 11). Therefore, the slow dissociation in DCE

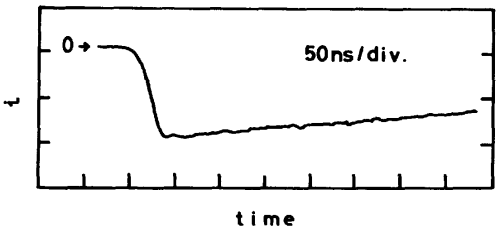

Fig. 11. Transient photocurrent measured in acetonitrile.

may be largely dependent on a fairly strong binding by Coulomb force between the ions in IP, which does not contradict the fact that both k_i values for $^3(CA^{\overline{\cdot}}\cdots DH^+)$ and $^3(CA^{\overline{\cdot}}\cdots DPA^+)$ are close to each other. It is known that the ionic dissociation to free ions occurs from solvent-separated ion pair (SSIP)[22] while the proton transfer takes place from contact ion pair (CIP).[1] From the fact that the rise time of photocurrent is equal to the decay time of IP, it may be inferred that IP observed here in DCE comprises both CIP and SSIP in equilibrium with each other. It is often used that because of spin-forbidden nature a back electron-transfer in triplet IP leading to the ground state cannot compete with ionic dissociation. However, in DCE of moderately polar solvent the back electron-transfer (k_d) can take place effectively rather than the ionic dissociation (k_i). Similar observation about the competition between k_d and k_i processes has been reported for various quinone-aromatic amine systems.[33] Moreover, the k_d value ($\approx1.1\times10^8 s^{-1}$) for $^3(CA^{\overline{\cdot}}\cdots DPA^+)$ obtained by us in DCE agrees well with $k_d=1.1\times10^8\ s^{-1}$ obtained by a different procedure in benzene-benzonitrile mixture.[3c] The k_d value in $^3(CA^{\overline{\cdot}}\cdots DH^+)$ is of one order of magnitude smaller than that in $^3(CA^{\overline{\cdot}}\cdots DPA^+)$. This tendency is parallel to the linear relation between log k_d and the energy level of IP above the ground state,[33] since the energy of $^3(CA^{\overline{\cdot}}\cdots DPA^+)$ is estimated by Eq. 2 to be lower by 0.81eV than that of $^3(CA^{\overline{\cdot}}\cdots DH^+)$. Hence, it seems to indicate that ISC of IP obeys the energy gap law of radiationless transition.

Competition of Mechanisms I and II. Finally we consider the mechanism of competition of I and II. A key point determining the mechanism must be involved in a collision complex between ^{3}CA and DH. Since in the present case DH approaches by diffusion to ^{3}CA from random directions, the collision complex with various donor-acceptor configurations might be produced. It may be true that an electron transfer occurs depending principally on the separation distance but not so severely on the mutual orientation between donor and acceptor. On the other hand, H-atom transfer will depend strongly on the local disposition of the transfer sites in the collision complex. Therefore, difference in conformations of the collision complexes seems to reflect the difference in the mechanisms of H-atom transfer. In the present case, it is supposed that a large part (about 80%) of the collision complexes can take conformations favorable to cause the electron transfer followed by immediate relaxation to the IP state; *e.g.*, a conformation with face to face approach between the donor and the acceptor. The other collision complexes of about 20% would take some special conformations favorable to undergo the rapid H-atom transfer; *e.g.*, a conformation with the transfer sites very close to each other like a hydrogen bonding bridge between O-atom of the acceptor and H-atom of methyl groups on the donor. Such a rapid H-atom transfer in the collision complex has been suggested for the dynamic quench-

ing in the hydrogen bonding interaction systems such as 2-naphthol-pyridine-cyclohexane system[34] as well as the quenching of triplet quinones by aromatic amines.[3] Recently, very fast H-atom transfer by a two-step mechanism of electron transfer followed by proton transfer has been verified both in EDA systems[1,2] and in hydrogen bonding interaction systems.[18,35] Taking these facts into account, it seems that the rapid H-atom transfer observed here also proceeds through the mechanism by transitory electron transfer preceding proton transfer.[36] Therefore, it may be interpreted that the first event of the quenching is an electron transfer from DH to ^{3}CA and succesively, in the collision complex, a rapid proton transfer and relaxation to the IP state compete with each other. The net H-atom transfer by Mechanism I occurs relatively slowly depending on the rate of proton transfer in IP. This suggests that a fairly high potential barrier is necessary to take a conformation favorable for causing the proton transfer from the relaxed state IP. A detailed study of the temperature dependence of this process will be published in a separate paper.

References

1) a) K. S. Peters, S. C. Freilich, and C. G. Schaeffer, *J. Am. Chem. Soc.*, **102**, 5701 (1980); b) C. C. Shaefer and K. S. Peters, *J. Am. Chem. Soc.*, **102**, 7566(1980); c) J. D. Simon and K. S. Peters, *J. Am. Chem. Soc.*, **103**, 6403 (1981).

2) a) T. Okada, N. Tashita, and N. Mataga, *Chem. Phys. Lett.*, **75**, 220 (1980); b) T. Okada, I. Karaki, and N. Mataga, *J. Am. Chem. Soc.*, **104**, 7191 (1982).

3) a) V. A. Kuzmin, A. P. Darmanyan, and P. P. Levin, *Chem. Phys. Lett.*, **63**, 509 (1979); b) P. P. Levin, A. P. Darmanyan, V. A. Kuzmin, A. Z. Yankelvich, and V. M. Kuznets, *Bull. Acad. Sci. USSR, Div. Chem. Sci.*, **29**, 1919 (1980); c) P. P. Levin and T. A. Kokrashvili, *Bull. Acad. Sci. USSR, Div. Chem. Sci.*, **30**, 971 (1981).

4) a) H. Kobashi, H. Gyoda, and T. Morita, *Bull. Chem. Soc. Jpn.*, **50**, 1731 (1977); b) H. Kobashi, T. Nagumo, and T. Morita, *Chem. Phys. Lett.*, **57**, 369 (1978); c) H. Kobashi, Y. Tomioka, and T. Morita, *Bull. Chem. Soc. Jpn.*, **52**, 1568 (1979); d) H. Kobashi, E. Sunoh, and T. Morita, *Symposium on Photochemistry*, Tokyo, December **1979**, Abstr. No.BIII-210; *Chem. Abstr.*, **93**, 45538t (1980).

5) T. Okada, M. Migita, N. Mataga, Y. Sakata, and S. Misumi, *J. Am. Chem. Soc.*, **103**, 4715 (1981).

6) H. Shioyama, H. Masuhara, and N. Mataga, *Chem. Phys. Lett.*, **88**, 161 (1982).

7) H. Masuhara, N. Ikeda, M. Miyasaka, and N. Mataga, *J. Spectrosc. Soc. Jpn.*, **31**, 19 (1982).

8) Y. Taniguchi, Y. Nishina, and Mataga, *Bull. Chem. Soc. Jpn.*, **45**, 764 (1972).

9) G. Briegleb, "Elektron-Donor-Acceptor-Komplexe," Springer-Verlag, Berlin (1962).

10) J. J. Andre and G. Weil, *Mol. Phys.*, **15**, 97 (1968).

11) a) E. F. Hilinski, S. V. Milton, and P. M. Rentzepis, *J. Am. Chem. Soc.*, **105**, 5193 (1983); b) R. Gschwind and E. Haselbach, *Helv. Chim. Acta*, **62**, 941 (1979).

12) Details will be published elsewhere.

13) The spectrum **A** appears slightly diffuse compared with the reference spectrum of ^{3}CA. Although there may be a possibility that the diffuseness is due to contribution of a broad Sn—S_1 absorption of CA,[11] its contribution seems here to be minor even if present.

14) The quenching rate constant k_q was measured by us to be 3.1×10^9 dm^{3}mol^{-1}s^{-1} at 15°C in the low concentration range (0.001—0.0075 mol dm^{-3}) of the quencher DH.

15) K. Schested, J. Holcman, and E. J. Hart, *J. Phys. Chem.*, **81**, 1363 (1977).

16) N. A. Shcheglova, D. N. Shigoline, G. G. Yakobson, and L. Sh. Tushishvili, *Zh. Fiz. Khim.*, **43**, 1984 (1969).

17) H. Sponer and Y. Kanda, *J. Chem. Phys.*, **40**, 778 (1964).

18) a) N. Ikeda, T. Okada, and N. Mataga, *Bull. Chem. Soc. Jpn.*, **54**, 1025 (1981); b) A. Weller and K. Zachariasse, "Molecular Luminescence," ed by E. C. Lim, Benjamin, New York (1969) p. 895.

19) a) H. Beens and A. Weller, "Organic Molecular Photophysics," Vol. 2, ed. by J. B. Birks, John Wiley, London (1975) p. 159. b) Y. Taniguchi, Y. Nishina, and N. Mataga, *Bull. Chem. Soc. Jpn.*, **43**, 764 (1972). c) J. Schroeder and F. Wilkinson *J. Chem. Soc., Faraday Trans. 2*, **75**, 896 (1979).

20) N. L. Weinberg and H. R. Weinberg, *Chem. Rev.*, **68**, 449 (1968). The value of 1.29 V *vs.* Ag | 0.1 N Ag$^+$ electrode listed in the reference must be corrected by +0.3 V for comparison with the other value *vs.* SCE.

21) M. E. Peover, *J. Chem. Soc.*, **1962**, 4540.

22) Y. Hirata, Y. Kanda, and N. Mataga, *J. Phys. Chem.*, **87**, 1659 (1983).

23) J. D. Simon and K. S. Peters, *J. Am. Chem. Soc.*, **105**, 4875 (1983).

24) K. Schested, H. Corfitzen, H. C. Christensen, and E. J. Hart, *J. Phys. Chem.*, **79**, 310 (1975).

25) H. P. Trommosdorf, P. Sahy, and J. Kahane-Paillous, *Spectrochim. Acta, PartA*, **26**, 1135 (1970).

26) B. T. Lim, S. Okajima, A. K. Chandra, and E. C. Lim, *Chem. Phys. Lett.*, **79**, 22 (1981).

27) a) H. Ootani, T. Kobayashi, K. Suzuki, and S. Nagakura, *Symposium on Molecular Structure*, Fukuoka, October **1980**, Abstr. No.4D23; b) N. Mataga, A. Karen, T. Okada, S. Nishitani, N. Kurata, Y. Sakata, and S. Misumi, *J. Am. Chem. Soc.*, **106**, 2442 (1984); c) H. Shioyama and N. Mataga, to be published.

28) An ε_{IP} value may be approximated by the molar absorption coefficient of CA$^-$ (ε_{CA^-}). The ε_{CA^-} values reported previously are: a) 9.7×10^3 dm^{3}mol^{-1}cm^{-1} in acetonitrile at 448 nm,[10] b) 9.0×10^3 dm^{3}mol^{-1}cm^{-1} in acetone at 450 nm (Y. Iida, *Bull. Chem. Soc. Jpn.*, **43**, 2772 (1970)), and c) 7.7×10^3 dm^{3}mol^{-1}cm^{-1} in ethanol at 454.5 nm (N. Sakai, I. Shirotani, and S. Minomura, *Bull. Chem. Soc. Jpn.*, **44**, 675 (1971)). The ε_{CA^-} values fairly depend on solvent properties such as protic or aprotic solvent or solvent polarity. As the ε_{IP} value, we here employed the ε_{CA^-} value in acetone which is aprotic solvent with a dielectric constant (21.5) rather close to that of aprotic DCE (10.7).

29) This value which was estimated again by the same method as used in Ref. 4a is in good agreement with the previously reported value: $(7.2\pm1.3)\times10^3$ dm^{3}mol^{-1}cm^{-1}.[4a]

30) This $\varepsilon_{CAH\cdot}$ value in DCE was determined by comparison with the known value: 7.7×10^3 dm^{-1}cm^{-1} (S. K. Wong, L. Fabes, W. J. Green, and J. K. S. Wan, *J. Chem. Soc. Faraday Trans. 1*, **68**, 211 (1972)) in 1,4-dioxane at 435 nm as a reference, assuming that the integrated intensity of CAH· absorption around 435 nm is independent on solvent.

31) Since the spectrum of $CA^{\cdot-}$ in CH_3CN was used as a reference of free $CA^{\cdot-}$ in the spectrum decomposition (Fig. 7), the value of $\varepsilon_{CA^{\cdot-}}$ in CH_3CN might be also employed. However, the use of it did not alter the results in Table 1.

32) For example, the energy separations (E_R) between the ground CA+DH and radical pair states in the CA-DH and BP-DMA systems are estimated nearly equal, because the H-atom transfer sites of both systems, >C=O and $-CH_3$, are very similar to each other. If the entropy changes for proton transfer in contact ion-pair (CIP) states, $(CA^{\cdot-}\cdots DH^+)_s$ and $(BP^{\cdot-}\cdots DMA^+)_s$, leading to the formation of neutral radicals are approximately equal, the free energy change (ΔG) accompaning this reaction depends on the energy of CIP above the gorund state (E_{CIP}). The E_{CIP} values for $(CA^{\cdot-}\cdots DH^+)_s$ in DCE and $(BP^{\cdot-}\cdots DMA^+)_s$ in CH_3CN are estimated to be 134 and 305 kJmol^{-1}, respectively, and hence ΔG value is larger for the CA-DH system than for the BP-DMA system. It has been measured that the energy of radical pair state produced in BP-aniline system in ethanol is 188 kJmol^{-1} above the ground state (L. J. Rothberg, J. D. Simon, M. Bernstein, and K. S. Peters, *J. Am. Chem. Soc.*, **105**, 3464 (1983)). Assuming that this value is approximately equal to the E_R value since the bond energies of C-H and N-H are also approximately equal to each other, the proton transfer from CIP is endothermic for the CA-DH system and exothermic for the BP-DMA system. The marked difference in k_p values for the two systems may be attributed to these conditions.

33) P. P. Levin, T. A. Kokrashvili, and V. A. Kuzmin, *Bull. Acad. Sci. USSR, Div. Chem. Sci.*, **31**, 466 (1982).

34) S. Yamamoto, K.Kikuchi, and H. Kokubun, *J. Photochem.*, **7**, 177 (1977).

35) M. M. Martin, N. Ikeda, T. Okada, and N. Mataga, *J. Phys. Chem.*, **86**, 4148 (1982).

36) N. Mataga and M. Ottolenghi, "Molecular Association," Vol. 2, ed by R. Foster, Academic Press, London (1979) p. 1.

Structural Study of Germanate Glasses by ^{119}Sn Mössbauer Spectroscopy

Tetsuaki NISHIDA,* Motomi KATADA,† and Yoshimasa TAKASHIMA
Department of Chemistry, Faculty of Science, Kyushu University 33, Hakozaki, Higashi-ku, Fukuoka 812
†*Department of Chemistry, Faculty of Science, Tokyo Metropolitan University, Fukasawa, Setagaya-ku, Tokyo 158*
(Received April 7, 1984)

Mössbauer study of potassium germanate glasses containing a small amount of Sn^{4+} has been performed to know the relationship between the abnormal composition dependence of physical properties, so-called germanate anomaly, and the local structural change of the glasses. Distinct increases in isomer shift and linewidth and a distinct decrease in quadrupole splitting are observed when the concentration of alkali oxide exceeds about 16 mol%. These changes are ascribed to the formation of nonbridging oxygen atoms in GeO_4 units. This is also supported by a drastic decrease in a parameter of intermolecular force constant obtained from the temperature dependence of Mössbauer absorption area. The composition dependence of the parameter is well consistent with that of glass transition temperature (T_g) of the same samples. Transformation of GeO_4 tetrahedra into GeO_6 octahedra is also confirmed by increases in the parameter of intermolecular force constant and in T_g in the alkali content region lower than 16 mol%. The role of Sn^{4+} is concluded to be a network modifier which is present at an interstitial site of three-dimensional network composed of GeO_4 and GeO_6 units.

Abnormal change in the physical properties of germanate glasses, so-called germanate anomaly, was first reported by Ivanov and Evstroviev.[1] They found maxima in the density- and refractive index-composition curves at the alkali oxide concentration of 10—15 mol%. Similar results were also obtained by Murthy and Ip,[2] and by Murthy and Scroggie[3] in germanate and aluminogermanate glasses, respectively. The germanate anomaly was also observed on viscosity[4] and glass transition temperature,[4,5] and in these physical properties-composition curves, the maxima were observed at the alkali contents of about 17[4] and 15—16[5] mol%, respectively. The decreases in viscosity and glass transition temperature at the alkali content region higher than the critical concentration (17 and 15—16 mol%) were tentatively attributed to the formation of nonbridging oxygen (NBO), because the decreases were thought to be due to the decrease in the cohesiveness of the glasses,[4] and to the depolymerization of the glass network.[5]

Structural study of germanate glasses was first carried out by Murthy and Kirby,[6] and a change in the coordination number of germanium(IV) from 4 to 6 was concluded from a red shift of IR absorption band due to Ge–O–Ge stretching vibration. Fraction of GeO_6 units was first estimated by Sakka *et al.*[7] based on the difference in the IR peak position of the Ge–O–Ge stretching vibration between hexagonal GeO_2 composed of GeO_4 units (875 cm^{-1}) and tetragonal GeO_2 composed of GeO_6 units (700 cm^{-1}). As the result, a maximum fraction of GeO_6 units (28%) was observed at a composition of about 15—20 mol% alkali oxide. The same idea as that in the IR study[7] was applied to X-ray diffraction study[8] and a maximum fraction of GeO_6 units (10—35%) was obtained at a composition region of 20—30 mol% alkali oxide. EXAFS study was also utilized by Sakka *et al.*[9] to know the fraction of GeO_6 units in germanate glasses, and a maximum was observed at an alkali oxide concentration of 15—16 mol%. Raman study by Verweij and Buster[10] revealed the presence of NBO in germanate glasses, in which stretching vibration band due to $Ge-O^-$ was observed at 850—880 cm^{-1}. The Raman study led to a conclusion that the fraction of GeO_6 units increases in the alkali content region ranging from 0 to 18 mol% and then decreases in the region from 18 to 33 mol% with the formation of NBO in GeO_4 units. Smets and Lommen[11] estimated the fraction of NBO in germanate and silicate glasses using X-ray photoelectron spectroscopy (XPS), and the formation of NBO was concluded to start at an alkali oxide concentration of 18 mol% in the case of germanate glasses.

Mössbauer spectroscopy of ^{57}Fe has been successfully used by the present authors for the structural studies of borate,[12–17] borosilicate,[18–19] phosphate,[20,21] and borophosphate[22] glasses to estimate the formation of NBO[12–14,18–22] and, furthermore, the fraction of NBO.[13,14,19] Mössbauer spectroscopy has also been used to examine the steric configuration of halide ions[15,16] in borate glasses as well as a chemical effect of $^{10}B(n,\alpha)^7Li$ nuclear reaction.[17] Kinetic study of the crystallization of borosilicate glasses has also been performed by means of Mössbauer spectroscopy.[23,24] Mössbauer spectroscopy of ^{119}Sn has been utilized to know the structures of borate[25–28] and silicate[25,29,30] glasses. The studies clarified that most Sn^{4+} species are present in octahedral environment and also that stannous ions in borate[27,28] and silicate[30] glasses play a role of network modifier when the SnO content is not so high. It is also noteworthy that the formation of NBO in borate glasses is observed in an alkali content region $\geq$20 mol%, which is consistent with our previous results[12–14,17] obtained from ^{57}Fe Mössbauer studies. These Mössbauer results are reproduced in a review article[31] by Müller-Warmuth and Eckert together with the NMR results of several kinds of glasses.

The present study was carried out to elucidate the local structure of germanate glasses, because most results on the structure and physical properties of the

glasses obtained so far are contradictory and also the germanate anomaly is assumed to be closely correlated with the presence of NBO.

Experimental

All glass samples, denoted by a formula $x\mathrm{K_2O}\cdot(100-x)\mathrm{GeO_2}\cdot 2\mathrm{SnO_2}$, were prepared by fusing mixtures of weighed quantities of guaranteed reagent grade $\mathrm{K_2CO_3}$, $\mathrm{GeO_2}$, and $\mathrm{SnO_2}$ at 1200 °C for 2h in an electric muffle furnace. The $\mathrm{K_2O}$ content, x, was changed from 10 to 30 at 5 intervals. Transparent and colorless glasses were prepared by quenching the melts in platinum crucibles with cold water. All the glass samples prepared in this way were confirmed to be amorphous by X-ray diffraction. Mössbauer measurements were performed by a constant acceleration method at various temperatures using a source of $\mathrm{Ca^{119m}SnO_3}$. Barium stannate ($\mathrm{BaSnO_3}$) was used as a reference for isomer shift. The velocity of spectrometer was calibrated with a metallic iron enriched with $^{57}\mathrm{Fe}$. All the Mössbauer spectra were fitted to Lorenzian lineshapes by computer calculations. DTA measurements of the glasses (10mg) were performed with a heating rate of 5 °C $\mathrm{min^{-1}}$ ranging from room temperature to 700 °C.

Results and Discussion

Mössbauer spectra for the germanate glasses containing tin proved to consist apparently of a single absorption peak, as shown in Fig. 1. The isomer shift suggests that tin is present as tetravalent ionic species ($\mathrm{Sn^{4+}}$) with octahedral symmetry[32] because the value is close to, and also smaller than zero velocity. Each

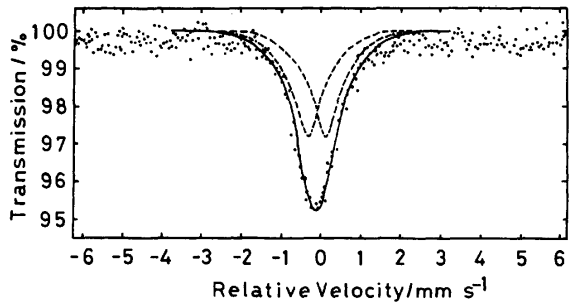

Fig. 1. Mössbauer spectrum of $10\mathrm{K_2O}\cdot 90\mathrm{GeO_2}\cdot 2\mathrm{SnO_2}$ glass.

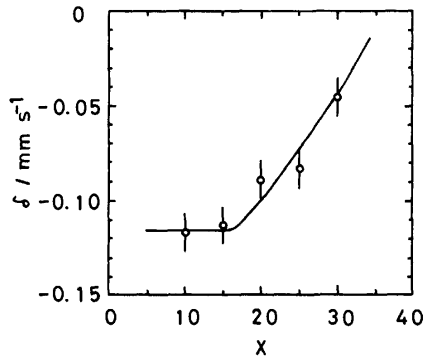

Fig. 2. Variation of the isomer shift of $\mathrm{Sn^{4+}}$ with $\mathrm{K_2O}$ content.

Mössbauer spectrum was analyzed into a kind of doublet, as shown by broken lines in Fig. 1, and also as a single peak shown by a solid line. The doublet analysis was performed because it was expected that some information on the electric field gradient at tin nucleus or symmetry around $\mathrm{Sn^{4+}}$, if present, could be obtained from the quadrupole splitting. The change in the isomer shift of the $\mathrm{Sn^{4+}}$ absorption peak is shown in Fig. 2 as a function of the $\mathrm{K_2O}$ content. (Each isomer shift value plotted in Fig. 2 is also consistent with the corresponding value obtained from a single peak analysis, within the experimental error.) It is seen from Fig. 2 that the isomer shift of $\mathrm{Sn^{4+}}$ increases almost linearly in the alkali content region higher than $x=$ 16—17. The increase in the isomer shift means the increased s-electron density at tin nucleus.[32] This is consistent with our previous results obtained in the case of borate[12] and borosilicate[18] glasses containing iron, where a continuous decrease in the isomer shift of $\mathrm{Fe^{3+}}$ was attributed to an increased s-electron density at the iron nucleus owing to the formation of NBO. (The decrease in the isomer shifts of $\mathrm{Fe^{2+}}$ and $\mathrm{Fe^{3+}}$ corresponds to the increase in the s-electron density at the iron nucleus because the radius of iron nucleus at the excited state is smaller than that at the ground state). The increase in the isomer shift of $\mathrm{Sn^{4+}}$, *i.e.*, the increase in the s-electron density at tin nucleus, is then assumed to be related in anyway with the formation of NBO in germanate glasses. In the case of $\mathrm{Sn^{4+}}$ the increase in isomer shift is known to be related to the increase in covalency.[27,32] The increase in the covalency with the formation of NBO is also observed in the case of borate glasses[28,28] containing $\mathrm{Sn^{2+}}$, although the apparent phenomenon is contrary to the present result. Mössbauer measurements at lower temperatures also gave a result similar to that shown in Fig. 2, and the individual isomer shift values slightly increased as a whole because of the reduced second order Doppler effect (*ca.* 0.04—0.05 $\mathrm{mm\,s^{-1}}$ in the temperature range from 78 to 298K). The second order Doppler effect shifts the peak position in the direction of negative velocity, in proportion to the vibration frequency of solid or measuring temperature.[33] The increase in the isomer shift of $\mathrm{Sn^{4+}}$ shown in Fig. 2 is therefore concluded to be due not to the second order Doppler shift, but to the increased s-electron density at tin nucleus and the increased covalency in the chemical bond between tin and oxygen, as described above.

Change in the quadrupole splitting of $\mathrm{Sn^{4+}}$ is shown in Fig. 3. The quadrupole splitting decreases linearly with alkali oxide content in the alkali content region higher than $x\simeq 17$. This is compatible with the result of isomer shift shown in Fig. 2. The decrease in the quadrupole splitting of $\mathrm{Sn^{4+}}$ suggests the increase in the symmetry around tin nucleus because the contribution of valence electrons (q_{val}) to the electric field gradient is negligible in the case of $\mathrm{Sn^{4+}}$ with an electron configuration of $4d^{10}$. This is also the case for

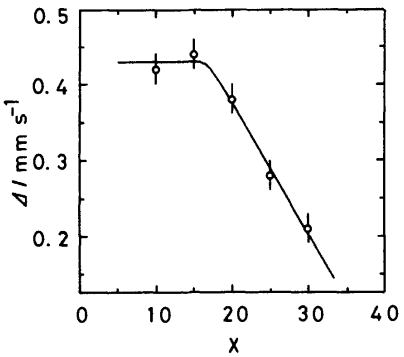

Fig. 3. Variation of the quadrupole splitting of Sn^{4+} with K_2O content.

Fe^{3+} with the $3d^5$ configuration, where a decrease in quadrupole splitting due to the formation of NBO has been observed in borate,[12] borosilicate,[18] phosphate,[20] and borophosphate[22] glasses. The continuous decrease in the quadrupole splitting shown in Fig. 3 is therefore ascribed to the increased symmetry around Sn^{4+} surrounded by six oxygen atoms, owing to the formation of NBO.

Change in the linewidth (FWHM) of the double peak is shown in Fig. 4. In general linewidths of absorption lines for amorphous materials are known to be greater than those for the corresponding crystalline materials. The linewidth ranges from 0.8 to 1.44 $mm\,s^{-1}$ in the case of Sn^{4+} in glasses.[25,26,29,34] The present result is also consistent with those results. The most remarkable feature of Fig. 4 is that the linewidth shows a drastic increase in the alkali content region higher than x=17—18, suggesting an increased irregularity of the steric configuration of glass forming atoms such as oxygen and germanium. This is a quite reverse phenomenon as compared with the earlier results of borate[12] or borosilicate[18] glasses containing Fe^{3+} ions where a continuous decrease in linewidth was observed with the formation of NBO. This will probably be explained by the difference in the structural roles of Fe^{3+} and Sn^{4+}, *i.e.*, the former ion plays a role of network former at the substitutional site of B and Si constituting BO_4 and SiO_4 tetrahedral units, respectively, and the latter is assumed to be present as a network modifier with octahedral symmetry at interstitial sites in a three-dimensional network composed of GeO_4 and GeO_6 units. In contrast with the well-studied role of iron in glasses, the role of tin has not been well understood and the results so far published are contradictory each other.[31] Dannheim *et al.*[30] suggested that both Sn^{4+} and Sn^{2+} in silicate glasses occupy the position of network modifier when the alkali concentration is not so high. This is consistent with the present result. In view of the distinct changes in the isomer shift (Fig. 2) and quadrupole splitting (Fig. 3), from which a formation of NBO could be deduced, the increase in the linewidth of Sn^{4+} is ascribed to the increased disorder brought about by the formation of NBO at the neighboring site of Sn^{4+}.

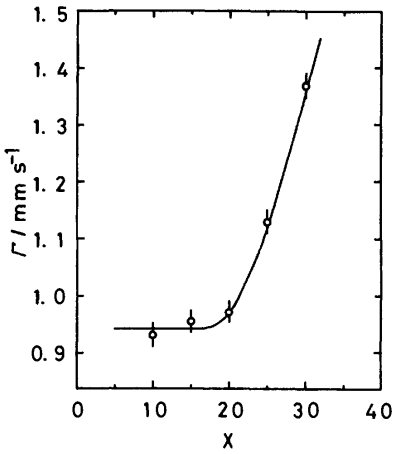

Fig. 4. Variation of the linewidth of Sn^{4+} with K_2O content.

Lattice dynamic study was then performed to confirm the conclusion obtained from the results of isomer shift, quadrupole splitting, and linewidth because it was expected that lattice vibration would be changed with the formation of NBO, *i.e.*, with the depolymerization of three-dimensional network. The correlation between the lattice vibration and the Mössbauer recoil-free fraction f has already been reported by using a Debye approximation.[32,33] In the high temperature limit

$$f = \exp(-6E_R T/k\theta^2), \tag{1}$$

where E_R and k are recoil energy and Boltzmann constant, respectively, and θ is the Debye temperature denoted as $k\theta=h\nu_{max}$ where h is Planck constant and ν_{max} is the maximum lattice vibration frequency. The correlation between E_R and Mössbauer transition energy E (23.9keV in the present study) is given by

$$E_R = E^2/2Mc^2, \tag{2}$$

where M is the mass of Mössbauer nucleus and c is the velocity of light. Combining the two equations, we obtain

$$f = \exp(-3E^2T/Mc^2k\theta^2). \tag{3}$$

Equation 3 is further modificated by differentiating the natural logarithm of f with T:

$$\theta^2M = \frac{3E^2}{kc^2}\left(\frac{-\mathrm{d}\ln f}{\mathrm{d}T}\right)^{-1}. \tag{4}$$

Matsubara *et al.*[34] showed the proportionality of θ^2M to the intermolecular force constant α and termed θ^2M "parameter of intermolecular force constant." They also showed the relationship between θ^2M and the degree of polymerization in a number of organotin compounds. As the result, the parameter was proved to be very useful for the determination of the degree of polymerization and molecular association. In the present study $\mathrm{d}\ln A/\mathrm{d}T$ was utilized instead of $\mathrm{d}\ln f/\mathrm{d}T$ because the latter can be approximated by the former

when a very thin sample is measured and the absorption area (A) is not saturated. In Fig. 5 the individual absorption areas are normalized by the area at 78K. It is seen from Fig. 5 that there is a linear relationship between $\ln A$ and T. Therefore θ^2M is obtained by dividing $3E^2/kc^2$, *i.e.*, 2.13×10^4 in the case of 23.9keV ^{119}Sn, with the slope of the individual straight line. The values of θ^2M are plotted in Fig. 6, together with the Debye temperature calculated by substituting the formula weight in M. Considering the Mössbauer and Raman study by Herber *et al.*,[35] where M is consistent with the molecular weight of organotin compound, the Debye temperatures shown in Fig. 6 are assumed to be rather reasonable ones. The values of θ^2M (All the values in the present paper must be multiplicated by a factor of 10^6) are reported to be about unity for monomer and to be 1.3 and 1.7 for one- and two- dimensional polymers, respectively.[34] It is also reported that the θ^2M values are 2.1 and 3.2 for two three-dimensional polymer compounds.[34] These are the values reported for the organotin compounds in which the chemical bonds between tin and the neighboring atoms are essentially covalent. The parameter (θ^2M) for ionic compound can also be obtained if the Debye temperature or the recoil-free fraction at different temperatures is known. The values of θ^2M calculated for the representative ionic compounds $BaSnO_3$[36] and SnO_2[37] are 22.4 and 8.9 (amorphous) —14.8 (crystalline), respectively, being larger than those for the covalent compounds. From the difference in the Debye temperature of SnO_2,[37] θ^2M is expected to be larger for the crystalline material than for the corresponding amorphous material. Comparing the magnitude of θ^2M obtained in the present study with those for the covalent and ionic compounds described above, the chemical bond between Sn^{4+} and oxygen seems to be essentially ionic. It is generally known that the chemical bonds between network modifier and the neighboring atoms, *i.e.*, oxygen in the case of oxide glasses, are essentially ionic. The present result therefore leads to a conclusion that the role of Sn^{4+} in germanate glasses is a network modifier which is present at an interstitial site of three-dimensional network composed of GeO_4 and GeO_6 units. It is expected that the intermolecular force for a Mössbauer nucleus at an interstitial site becomes less intense than that at a substitutional site. In fact, the θ^2M values obtained in the present study (6.2—8.7) are smaller than that for the amorphous SnO_2 (8.9). The role of Sn^{4+} in germanate glasses is therefore concluded to be similar to that of alkali metal ions like Na^+ and K^+.

Another important feature of Fig. 6 is the distinct composition dependence of θ^2M (and also θ) with a maximum at the K_2O concentration of about x=16. The increase in θ^2M with increasing alkali content of the germanate glasses is reasonably explained by an increase in the number of bridging oxygen atoms owing to the formation of GeO_6 units instead of GeO_4

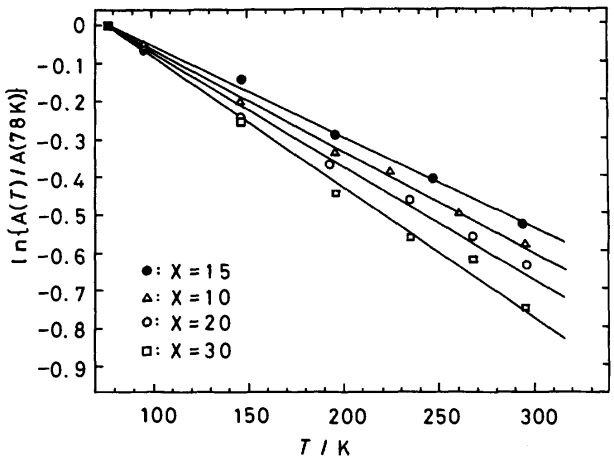

Fig. 5. Plots of the absorption area against temperature.

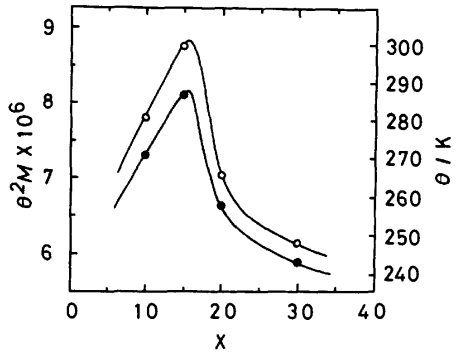

Fig. 6. Variations of the parameter of intermolecular force constant (○) and the Debye temperature (●) with K_2O content.

units. The decrease in θ^2M at the alkali content region higher than x=16 is well explained by the formation of NBO which is expected to bring about a drastic decrease in the intermolecular force because of the destruction of network structure. The structural change will result in some physical properties such as glass transition temperature (T_g) and viscosity. Figure 7 shows the result of DTA measurement, which is well consistent with the result of θ^2M. A maximum is observed at almost the same alkali concentration as does that in the θ^2M plot. It is interesting to note that the decrease in T_g is not so rapid as that of θ^2M at the higher alkali content region. This may be due to the different characteristics of the two methods, *i.e.*, T_g corresponds to the mean transition energy for the glass matrix, while θ^2M is closely concerned with the local vibrational energy in the neighborhood of ^{119}Sn. It is therefore, concluded that the parameter of intermolecular force constant, as well as the Mössbauer parameters like isomer shift and quadrupole splitting, is exceedingly sensitive to the structural change of glasses.

All the experimental results obtained in the present study are as follows. In potassium germanate glasses of which the alkali oxide contents are lower than about 16mol%, the increase of the alkali contents results in the increase in the fraction of GeO_6 units. In the alkali

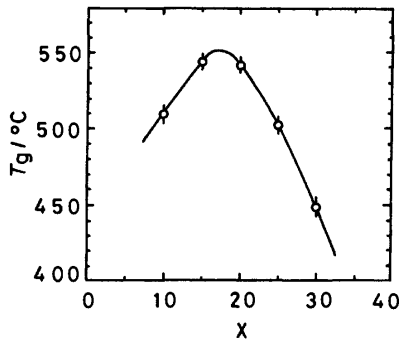

Fig. 7. Variation of the glass transition temperature with K_2O content.

content region higher than about 16mol% the increase in the alkali contents results in the formation of NBO in GeO_4 units in competition with the formation of GeO_6 units, and the former reaction will be predominant with increasing alkali contents. Stannic ion would be present at a site similar to that of K^+, *i.e.*, at an interstitial site in the network composed of GeO_4 and GeO_6 units, as a network modifier with octahedral symmetry.

The authors are indebted to Prof. Sumio Sakka of Kyoto university for his useful suggestion on the structure of germanate glasses. They are also grateful to Prof. Hirotoshi Sano of Tokyo Metropolitan University for his useful discussion.

References

1) A. O. Ivanov and K. S. Yestropovb, *Dokl. Akad. Nauk SSSR*, **145**, 797 (1962).
2) M. K. Murthy and J. Ip, *Nature*, **201**, 285 (1964).
3) M. K. Murthy and B. Scroggie, *Phys. Chem. Glasses*, **6**, 162 (1965).
4) J. E. Shelby, *J. Am. Ceram. Soc.*, **57**, 436 (1974).
5) J. E. Shelby, *J. Appl. Phys.*, **46**, 193 (1975).
6) M. K. Murthy and E. M. Kirby, *Phys. Chem. Glasses*, **5**, 144 (1964).
7) S. Sakka, K. Kamiya, and T. Mizuno, *Res. Rep. Fac. Eng., Mie Univ.*, **2**, 73 (1977).
8) K. Kamiya and S. Sakka, *Phys. Chem. Glasses*, **20**, 60 (1979).
9) S. Sakka, K. Kamiya, and M. Hayashi, *Bull. Inst. Chem. Res., Kyoto Univ.*, **59**, 172 (1981).
10) H. Verweij and J. H. J. M. Buster, *J. Non-Cryst. Solids*, **34**, 81 (1979).
11) B. M. J. Smets and T. P. A. Lommen, *J. Non-Cryst. Solids*, **46**, 21 (1981).
12) T. Nishida and Y. Takashima, *J. Non-Cryst. Solids*, **37**, 37 (1980).
13) T. Nishida, T. Shiotsuki, and Y. Takashima, *J. Non-Cryst. Solids*, **41**, 161 (1980).
14) T. Nishida, T. Hirai, and Y. Takashima, *J. Non-Cryst. Solids*, **43**, 221 (1981).
15) T. Nishida, N. Kai, and Y. Takashima, *Phys. Chem. Glasses*, **22**, 107 (1981).
16) T. Nishida, T. Nonaka, T. Isobe, and Y. Takashima, *Phys. Chem. Glasses*, **24**, 88 (1983).
17) T. Nishida, T. Hirai, and Y. Takashima, *Radiochem. Radioanal. Lett.*, **53**, 153 (1982).
18) T. Nishida, T. Hirai, and Y. Takashima, *Phys. Chem. Glasses*, **22**, 94 (1981).
19) T. Nishida, T. Hirai, and Y. Takashima, *Bull. Chem. Soc. Jpn.*, **54**, 3735 (1981).
20) T. Nishida, T. Shiotsuki, and Y. Takashima, *J. Non-Cryst. Solids*, **43**, 115 (1981).
21) T. Nishida, T. Shiotsuki, and Y. Takashima, *J. Non-Cryst. Solids*, **43**, 123 (1981).
22) T. Nishida, Y. Miyamoto, and Y. Takashima, *Bull. Chem. Soc. Jpn.*, **56**, 439 (1983).
23) T. Nishida, T. Hirai, and Y. Takashima, *Phys. Chem. Glasses*, **24**, 113 (1983).
24) T. Nishida, T. Hirai, and Y. Takashima, *Mem. Fac. Sci., Kyushu Univ., Ser. C*, **14**, 91 (1983).
25) K. P. Mitrofanov and T. A. Sidorov, *Sov. Phys.-Solid State*, **9**, 693 (1967).
26) N. A. Eissa, E. E. Shaisha, and A. L. Hussiun, *J. Non-Cryst. Solids*, **16**, 206 (1974).
27) A. Paul, J. D. Donaldson, M. T. Donoghue, and M. J. K. Thomas, *Phys. Chem. Glasses*, **18**, 125 (1977).
28) A. Lechtenbohmer, B. D. Mosel, W. Müller-Warmuth, and H. Dutz, *Glastechn. Ber.*, **55**, 161 (1982).
29) G. M. Bartenev, S. M. Brekhovskikh, A. Z. Varisov, L. M. Landa, and A. D. Tsyganov, *Sov. Phys.-Solid State*, **12**, 972 (1970).
30) H. Dannheim, H. J. Oel, and G. Tomandl, *Glastechn. Ber.*, **49**, 170 (1976).
31) W. Müller-Warmuth and H. Eckert, *Phys. Rep.*, **88**, 91 (1982).
32) P. A. Flinn, "Tin Isomer Shifts," in "Mössbauer Isomer Shift," ed by G. K. Shenoy and F. E. Wagner, North-Holland Publ. Co., Amsterdam, New York (1978), Chap. 9a.
33) N. N. Greenwood and T. C. Gibb, "Mössbauer Spectroscopy," Chapman and Hall Ltd., London (1971), Chaps. 1 and 3.
34) S. Matsubara, M. Katada, K. Sato, I. Motoyama, and H. Sano, *J. Phys. (Paris), Colloq. C2*, **40**, 363 (1979).
35) R. H. Herber, M. F. Leahy, and Y. Hazony, *J. Chem. Phys.*, **60**, 5070 (1974).
36) H. Sano and R. H. Herber, *J. Inorg. Nucl. Chem.*, **30**, 409, (1968).
37) G. S. Collins, T. Kachnowski, N. Benczer-Koller, and M. Pasternak, *Phys. Rev. B*, **19**, 1369 (1979).

 © 1984 The Chemical Society of Japan Bull. Chem. Soc. Jpn., 57, 3571—3573 (1984)

Determination of Trace Amounts of Copper as the Complex with Bathocuproinedisulfonate after Enrichment in the Thin Layer of Anion-exchange Resin

Masaaki OHTA and Kunio OHZEKI*

Department of Chemistry, Faculty of Science, Hokkaido University, Sapporo 060

(Received May 21, 1984)

A simple and selective method for the determination of trace amounts of copper is developed. The method is based on the concentration of copper as the complex with bathocuproinedisulfonate (BCS) with the use of finely divided anion-exchange resin, collection of the resin on a membrane filter as the disk of thin layer, and determination of the colored complex in the resin phase by densitometry. The copper(I)-BCS complex in sample volumes ranging from 50—200 cm^3 was effectively concentrated by factors ranging from 2500—10000. The method was applied to tap water. Copper at ppb ($\mu g\ dm^{-3}$) level was successfully determined.

As well known, cuproine and its derivatives are highly selective color-developing reagents for copper.[1] Among them, bathocuproinedisulfonate has been used for the direct determination of copper in the aqueous solutions.[2]

Fugimoto *et al.*[3] studied the resin spot test of copper and reported that copper(I) bathocuproinedisulfonate was extremely strongly fixed on the beads of anion-exchange resin. The idea of resin spot test was further extended to ion-exchanger colorimetry,[4] in which the resin phase absorbance was measured directly in a 1-mm cell. Nigo *et al.*[5] applied the method to the trace determination of copper as the porphyrin complex. The method of combined use of finely divided anion- and cation-exchange resins was also reported.[6,7] The colored species collected in the thin layer of mixed resins were determined spectrophotometrically[6] or densitometrically.[7]

In the present paper, the extraction of trace amounts of copper as bathocuproinedisulfonate is studied by the use of finely divided anion-exchange resin. The determination is carried out by using densitometer and the results are compared with those obtained by the combined use of anion- and cation-exchange resins.

Experimental

Reagents. Hydrochloric acid used was of super special grade (SSG reagent, Wako). All other chemicals used were of analytical reagent grade. A stock copper(II) solution (1000 $\mu g\ Cu\ cm^{-3}$) was prepared by dissolving copper(II) sulfate pentahydrate in deionized water containing hydrochloric acid (pH *ca.* 1). The working solution (10 $\mu g\ Cu\ cm^{-3}$) was prepared by appropriate dilution. The reagents, 2,9-dimethyl-4,7-diphenyl-1,10-phenanthroline (Bathocuproine, abbreviated as BC) and disodium salt of 2,9-dimethyl-1,10-phenanthrolyl-4,7-dibenzene-*p,p'*-disulfonic acid (Bathocuproinedisulfonic acid, disodium salt, abbreviated as BCS) were obtained from Dojindo Lab., and used without further purification. A 1 $mmol\ dm^{-3}$ ethanolic solution of BC and 0.67 $mmol\ dm^{-3}$ aqueous solution of BCS were prepared. The purity of BCS, which was estimated from absorbance-mole ratio (BCS/Cu) plots, was 78%. An aqueous 10% W/V solution of hydroxylammonium chloride and 30% W/V sodium acetate solution were purified by extracting the impurity due to copper ion as the BC complex into chloroform.

Ion-exchange Resin Suspension. The macroreticular type ion exchangers, Amberlyst 15 and A-27 (Rhom and Haas Co.) were used in RSO_3H and $RN(CH_3)_3Cl$ forms, respectively. The cation-exchange resin suspension (CRS) and the anion-exchange resin suspension (ARS) were prepared according to the reported method,[8] that is, the wet resin was crashed in the slurry and sieved through 3G3 glass filter. The ion-exchange capacities of CRS and ARS were determined by the conductometric titration with standard solutions of sodium hydroxide and silver nitrate. The capacities of CRS and ARS were found to be 6.72 $\mu eq\ cm^{-3}$ and 5.11 $\mu eq\ cm^{-3}$, respectively. When 2 cm^3 of CRS was mixed with 3 cm^3 of ARS, both resins were almost completely coagulated and quantitatively collected on a filter paper.

Apparatus. The densitometer used was a Shimadzu Chromatoscanner CS-920 equipped with linearizer. A Shimadzu UV-visible recording spectrophotometer, type UV-240, was used for measuring absorption spectra. A Toyo KG-25 filter holder was used. The filters used were TM-1 (0.65 μm pore size, 47 mm in diameter, Toyo) or No. 5B filter paper. Micropipets were used.

General Procedure. A 50-cm^3 aliquot of sample solution containing less than 1 μg of copper was placed in a 100-cm^3 beaker. A 1-cm^3 portion of 10% hydroxylammonium chloride, 0.5 cm^3 of 0.67 $mmol\ dm^{-3}$ BCS, and 1 cm^3 of 30% sodium acetate solution were added successively. The pH of final solution was about 6. The solution was stirred by means of a magnetic stirrer for 2 min and then 1.0 cm^3 of ARS was added. The mixture was further stirred for 10 min. The anion-exchange resin was then collected by filtration with suction on a membrane filter (TM-1). The copper(I)-BCS complex was thus concentrated in a disk of the thin layer with 17 mm in diameter and about 0.1 mm in thickness. The wet membrane filter was placed on a white plastic plate fixed on a scanning board in the densitometer. The absorbance was measured with or without linearizer at 485 nm by scanning the light beam in a range of 24 mm wide and 30 mm long. In the case of the mixed resin method, the combination of 2.0 cm^3 CRS and 3.0 cm^3 ARS was used and the mixed resins were collected on a filter paper of No. 5B.

Results and Discussion

Copper(I)-BCS Complex in the Resin Phase. A

trace amount of copper was quantitatively extracted to the resin phase when the amount of BCS was in excess of the stoichiometric value (Fig. 1). A constant coloration was obtained at pH above 3. Figure 2 shows the absorption spectrum of the complex in the resin phase. Although there is a general similarity between the absorption spectra of the complex in the solution and in the resin phase, but a small shift of the maximum wavelength was observed from 480 nm in the solution to 485 nm in the resin phase. The coloration was stable for at least 2 h, when the resin thin layer was kept wet with water.

The maximum fixable amounts of copper(I)-BCS complex and BCS on the resin in 1.0 cm^3 of ARS were found to be 0.16 μmol and 0.57 μmol, respectively. These values were much smaller than the total exchange capacity (5.11 μeq) of the resin. The bulky ions might be fixed only on the surface of the resin particles. Since the recovery of the complex corresponding to 0.5 μg of copper was quantitative in the presence of 10 μmol of BCS, it was indicated that the copper(I)-BCS complex was much more strongly fixed on the resin than the reagent.

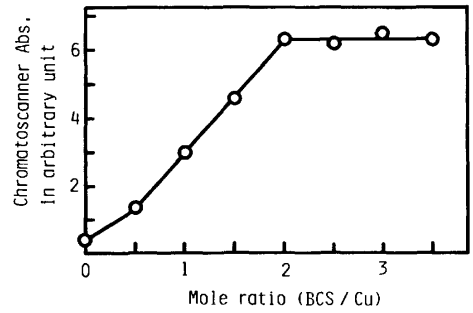

Fig. 1. Effect of BCS amount on the fixation of copper as the BCS complex to the anion-exchange resin.
Copper: 1.0 μg, sample volume: 50 cm^3, pH: 6, ARS: 1.0 cm^3 (5.11 μeq).

Effect of Sample Volume. The effect of sample volume was examined by the use of 1.0 cm^3 of ARS. A 1.0-μg portion of copper was effectively recovered from different sample volumes ranging from 50—200 cm^3. The rate of filtration was about 10 $cm^3 min^{-1}$. The volume of resin phase was estimated to be about 0.02 cm^3, and so the concentration factors were in the range of 2500—10000.

Effect of Foreign Ions. The effect of foreign ions on the determination of copper(II) was examined (Table 1). Except for iron(III), other cations and anions studied did not affect the determination of copper. Iron(III) gave a positive error, which was due to the formation of colored hydroxide. The interference by

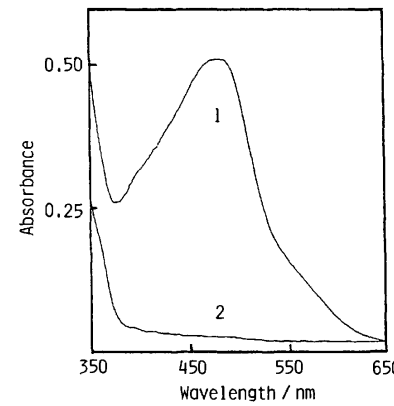

Fig. 2. Absorption spectra of copper(I)-BCS complex and reagents in the resin phase.
1: Spectrum of copper(I)-BCS complex in the resin thin layer obtained from 50 cm^3 solution (pH 6) containing 2.0 μg of copper, 1 cm^3 of 10% hydroxylammonium chloride, 0.3 μmol BCS, 1 cm^3 of 30% sodium acetate, and 1.0 cm^3 ARS.
2: Spectrum of resin thin layer obtained from 50 cm^3 solution without addition of copper(II). Other components were the same as in Curve 1.
Reference: resin thin layer obtained from 50 cm^3 solution containing 1.0 cm^3 of ARS.

Table 1. Effect of foreign ions on the determination of copper[a)]

Cation	Added(μg)	Error[b)](%)	Anion	Added(mg)	Error[b)](%)
K	40	−1.5	F^-	19	−0.1
Mg	40	0.8	Cl^-	4	−1.2
Ca	40	−2.3	Br^-	4	2.3
Ba	40	−1.4	I^-	4	4.5
Cr^{III}	40	1.9	NO_3^-	4	0.9
Mn^{II}	40	−0.6	CO_3^{2-}	4	1.2
Fe^{III}	40	71.9	SO_4^{2-}	4	4.1
Fe^{III}	4	1.9	PO_4^{3-}	4	−2.8
Fe^{III}	40[c)]	1.5	NaCl[d)]	Added(mol)	Error[b)](%)
Co^{II}	40	3.3			
Ni^{II}	40	2.4	NaCl	0.05	2.3
Zn^{II}	40	3.7	NaCl	0.10	2.4
Cd^{II}	40	2.9	NaCl	0.15	4.8
Al^{III}	40	−1.1	NaCl	0.20	2.1
Pb^{II}	40	−2.5			

a) Copper taken: 0.4 μg, sample volume: 50 cm^3 b) Calculated using % Relative Error=$(A_2-A_1)/(A_1-A_0)$, where A refers to the Chromatoscanner absorbance and the subscripts 0, 1, and 2 refer to blank thin layer and thin layers without and with the foreign ion, respectively. c) A 2-cm^3 portion of 0.5 mol dm^{-3} sodium fluoride was added. d) Sodium chloride solution was previously purified by extracting impurity copper as the BC complex into chloroform.

TABLE 2. COMPARISON OF SINGLE RESIN METHOD WITH MIXED RESIN METHOD

	Single resin method	Mixed resin method	
Resin	Amberlyst A-27	Amberlyst A-27	Amberlyst 15
Capacity of resin suspension	5.11 μeg cm^{-3}	5.11 μeg cm^{-3}	6.72 μeg cm^{-3}
Amount of resin suspension	1.0 cm^3	3.0 cm^3	2.0 cm^3
Filter	Membrane filter[a]	Filter paper[b]	
Filtration rate	10 cm^3 min^{-1}	10 cm^3 min^{-1}	
Volume of resin thin layer	0.02 cm^3	0.07 cm^3	
Concentration factor[c]	2500	700	
Calibration curve[d]	$Y=6.60X+0.39$	$Y=2.93X+3.21$	
Relative standard deviation[e]	1.4% ($n=7$)	1.7% ($n=4$)	
Standard deviation of blank value	0.02 ($n=6$)	0.06 ($n=6$)	
Limit of detection[c]	0.18 μg copper dm^{-3}	1.2 μg copper dm^{-3}	

a) Pore size: 0.65 μm, diameter: 47 mm. b) No. 5B. c) Sample amount: 50 cm^3 d) X: amount of copper in μg, Y: Chromatoscanner absorbance in arbitrary unit. The intercept at $X=0$ is the blank value including resin matrix. e) Amount of copper: 0.4 μg.

TABLE 3. DETERMINATION OF TOTAL COPPER IN TAP WATER

Sample amount (cm^3)	Copper(II) added (μg)	Single resin Method		Mixed resin method	
		Copper(II) found (μg)	Concn. in tap water (μg dm^{-3})	Copper(II) found (μg)	Concn. in tap water (μg dm^{-3})
100	0.00	0.30	3.0	0.29	2.9
75	0.00	0.21	2.8	0.26	3.5
75	0.10	0.33	3.1	0.35	3.4
50	0.00	0.12	2.4	0.16	3.3
50	0.10	0.22	2.4	0.24	2.8
50	0.20	0.35	3.0	0.34	2.8
			2.78±0.33[a]		3.12±0.33[a]

a) 95% confidence limits

iron was eliminated by the addition of sodium fluoride. It was found that the copper(I)-BCS complex was quantitatively recovered even in the presence of 4 mol dm^{-3} sodium chloride.

Calibration Curve. The calibration curves obtained by the single resin method and the mixed resin method showed good linearity when the linearizer was applied. The slope of calibration curve obtained by the single resin method was about two times greater than that obtained by the mixed resin method. The results were summarized in Table 2, in which the limit of detection of copper was calculated as three times the standard deviation of the blank value.[9]

Determination of Total Copper in Tap Water. The single resin method and the mixed resin method were applied to the determination of total copper in the tap water supplied to our laboratory from a well in the University campus. After running the water for more than 20 min, the sample water was taken and acidified to pH 1. The results were summarized in Table 3. No significant difference was found between the variables (F-test) as well as between the mean values (t-test).

Comparison of the Methods. Generally, the concentration factor and thus the sensitivity of the single resin method is superior to those of the mixed resin method. However, as the mixed resins coagulate tightly with each other, the resulting thin layer is much more sturdy than that obtained by a single resin method. Therefore, it is possible to immerse the thin layer of mixed resins in the solution for making additional coloration, as successfully indicated in the determination of hexacyanoferrate(III) as Turnbull's Blue[10] and cobalt as the thiocyanate complex.[11]

References

1) O. G. Koch and G. A. Koch-Dedic, "Handbuch der Spurenanalyse," 2. Auflage, Springer-Verlag, p. 666 (1974).
2) D. Blair and H. Diehl, *Talanta*, **7**, 163 (1961).
3) T. Takahashi, T. Imamura, and M. Fujimoto, *Mikrochim. Acta* (Wien) 1973, 69.
4) K. Yoshimura, H. Waki, and S. Ohashi, *Kagaku no Ryoiki*, **31**, 67 (1977).
5) K. Yoshimura, S. Nigo, and T. Tarutani, *Talanta*, **29**, 173 (1982).
6) K. Ohzeki, T. Sakuma, and T. Kambara, *Bull. Chem. Soc. Jpn.*, **53**, 2878 (1980).
7) K. Ohzeki, Y. Satoh, Y. Kawamura, and T. Kambara, *Bull. Chem. Soc. Jpn.*, **56**, 2618 (1983).
8) M. Abe, K. Ohzeki, and T. Kambara, *Bull. Chem. Soc. Jpn.*, **51**, 1090 (1978).
9) G. L. Long and J. D. Winefordner, *Anal. Chem.*, **55**, 713 (1983).
10) K. Suzuki, G-D. Park, K. Ohzeki, and T. Kambara, *Bull. Chem. Soc. Jpn.*, **55**, 3335 (1982).
11) K. Suzuki, K. Ohzeki, and T. Kambara, *Bull. Chem. Soc. Jpn.*, **56**, 2624 (1983).

 © 1984 The Chemical Society of Japan Bull. Chem. Soc. Jpn., 57, 3574—3579 (1984) [Vol. 57, No. 12

Preparation and Spectroscopic Studies of the Stereoisomers of $[Co(acac)_2(R^1R^2NCH_2CH_2NR^3R^4$ or *o*-Phenylenediamine)]$^+$ (R^1—R^4= H, CH_3, or C_6H_5; acac=2,4-Pentanedionate ion) and Isomer Distribution at Equilibrium

Yue OUYANG,† Masaaki KOJIMA, and Junnosuke FUJITA*
Department of Chemistry, Faculty of Science, Nagoya University, Chikusa-ku, Nagoya 464
(Received July 11, 1984)

A series of complexes of the type, $[Co(acac)_2L]^+$, where acac=2,4-pentanedionate ion and L denotes $R^1R^2NCH_2CH_2NR^3R^4$ (R^1—R^4=H or CH_3), *N*-phenylethylenediamine, *N*,*N*′-diphenylethylenediamine, and *o*-phenylenediamine were prepared and the isomers separated. The absorption spectra and the distributions of the isomers at equilibrium were determined and the results are discussed.

York *et al.*[1] reported that the *N*,*N*,*N*′,*N*′-tetramethylethylenediamine (Me_4en) ligand in $[Co(acac)_2(Me_4en)]^+$ (acac=2,4-pentanedionate ion) has a very low ligand field strength comparable to that of the oxygen donors of acac. Akamatsu and Shimura[2] showed that the ligand field strength of the tertiary amine end of *N*,*N*-dimethylethylenediamine (*N*,*N*-Me_2en) is weaker than those of oxalato and carbonato ligands. Thus the ligand field strength of ethylenediamine (en) is considerably reduced by the introduction of methyl groups on the nitrogen. In this paper, we report the preparation of $[Co(acac)_2(R^1R^2NCH_2CH_2NR^3R^4)]^+$ (R^1—R^4=H or CH_3), the separation of the isomers, the distributions of the isomers at equilibrium, and the absorption spectra of the isomers. Very recently Ito[3] reported the absorption spectra of bis(acac)-cobalt(III) complexes with *N*-methylated ethylenediamine, however, the complexes were not separated into the isomers.

A cobalt(III) complex with an *N*-phenyl-substituted ethylenediamine ligand will be less stable than the corresponding en complex for both steric and electronic reasons.[4] The two acac ligands seem to stabilize the *N*-phenyl-substituted amine-cobalt(III) system; we have obtained $[Co(acac)_2$(Ph-en, *N*,*N*′-Ph_2en, or opd)$]^+$ (Ph-en=*N*-phenylethylenediamine, *N*,*N*′-Ph_2en=*N*,*N*′-diphenylethylenediamine, opd=*o*-phenylenediamine).

Experimental

Λ(R),Δ(S)-[Co(acac)$_2$(Me-en)]ClO$_4$·0.5H$_2$O and Λ(S),Δ(R)-[Co(acac)$_2$(Me-en)]ClO$_4$(Me-en=N-*Methylethylenediamine).* To a solution of $[Co(acac)_3]$ (3.0 g, 8.4 mmol) in methanol (300 cm^3) were added Me-en (0.69 g, 9.3 mmol) and active charcoal (0.5 g). The mixture was stirred for 30 min and then filtered. The purple filtrate was diluted with water (3 dm^3), and applied on a column (ϕ4.5 cm×20 cm) of SP-Sephadex C-25. By elution with 0.05 mol dm^{-3} NaCl, a purple and a red band developed in this order. The eluate containing the purple band was collected and evaporated to a small volume. To the concentrate sodium perchlorate was added to yield purple crystals, which were recrystallized from water (50 °C). Yield: 1.5 g. The crystals were a mixture of the two racemic pairs of diastereomers, and they were separated by a column chromatographic method. About 0.3 g of the mixture was dissolved in a small amount of water and the solution was applied on a column (ϕ2.2 cm×50 cm) of SE-Toyopearl[5] HW-40 (fine; eluent: 0.05 mol dm^{-3} NaCl). A recycling-chromatographic technique was employed. After three times of recycling, the column showed two purple bands, M-I (*Λ*(*R*), *Δ*(*S*)) and M-II (*Λ*(*S*), *Δ*(*R*)), in the order of elution with the ratio of 1:3. From each eluate the perchlorate of the diastereomer was obtained by the same method as that described above. Anal. (*Λ*(*R*), *Δ*(*S*), $C_{13}H_{25}N_2ClCoO_{8.5}$) C, H, N. Anal. (*Λ*(*S*), *Δ*(*R*), $C_{13}H_{24}N_2ClCoO_8$) C, H, N.

(−)$_{589}$-Λ(S)- and (−)$_{589}$-Λ(R)-[Co(acac)$_2$(Me-en)]ClO$_4$. A suspension of *Λ*(*S*), *Δ*(*R*)-$[Co(acac)_2(Me\text{-}en)]ClO_4$ (0.866 g, 2.0 mmol) and Dowex 1×8 (Cl^- form, *ca.* 3 g) in 30 cm^3 of water was stirred for 20 min, filtered, and the exchanger washed with water (5 cm^3×2). To the combined filtrate and washings was added a hot (*ca.* 70 °C) solution containing sodium di-*O*-benzoyl-*d*-tartrate (0.402 g, 1.0 mmol) and di-*O*-benzoyl-*d*-tartaric acid monohydrate (0.376 g, 1.0 mmol) in 100 cm^3 of water. The mixture was allowed to stand overnight at room temperature and recrystallized from hot water (70 cm^3). Yield: 0.30 g. The diastereomer was dissolved in water and applied on a column (ϕ2 cm×5 cm) of SP-Sephadex C-25. The column was washed with water, and the complex (*Λ*(*S*)-isomer) was eluted with 0.2 mol dm^{-3} NaCl. The complex was isolated as the perchlorate and recrystallized in the same way as for the racemate. Yield: 80 mg. Anal. ($C_{13}H_{24}N_2ClCoO_8$) C, H, N.

The *Λ*(*S*)-isomer (60 mg) was epimerized in 0.1 mol dm^{-3} NaOH (20 cm^3, pH *ca.* 13) at room temperature. After 1 h, the reaction mixture was applied on a column (ϕ2.2 cm×50 cm) of SE-Toyopearl HW-40 (fine). By elution with 0.05 mol dm^{-3} NaCl, two purple bands developed. From the eluate containing the faster-moving band the perchlorate of the *Λ*(*R*)-isomer was obtained as described for the racemate. Yield: 20 mg. Anal. ($C_{13}H_{24}N_2ClCoO_8$) C, H, N. The *Λ*(*S*)-isomer was recovered from the slower-moving band.

[Co(acac)$_2$(N,N-Me$_2$en)]ClO$_4$. This complex was prepared by a method analogous to that described for the corresponding Me-en complexes. Column chromatography on SP-Sephadex C-25 (eluent: 0.05 mol dm^{-3} NaCl) showed two purple bands. From the eluate containing the faster-moving band the complex was isolated as the perchlorate by the same method as for the Me-en complex, and recrystallized from chloroform by the addition of diethyl ether. Yield: 60%.

†Pressent address: Department of Chemistry, Unversity of Hainan, Hainan Island, Kwantung Province, People's Republic of China.

Anal. ($C_{14}H_{26}N_2ClCoO_8$) C, H, N. The slower-moving band seemed to contain $[Co(acac)(N,N\text{-}Me_2en)_2]^{2+}$ but this complex was not isolated.

Λ(RR),Δ(SS)- and Λ(SR),Δ(RS)-[Co(acac)$_2$(N,N′-Me$_2$en)]ClO$_4$, and Λ(SS),Δ(RR)-[Co(acac)$_2$(N,N′-Me$_2$en)]ClO$_4$·H$_2$O (N,N′-Me$_2$*en*=N,N′-*Dimethylethylenediamine).* These complexes were prepared in the same way as that for the Me-en complexes in a 48% yield and separated into the three racemic pairs of diastereomers, *Λ(RR),Δ(SS)*, *Λ(SR),Δ(RS)*, and *Λ(SS), Δ(RR)* in the ratio of 5:1:3 by the same chromatographic method as used for the Me-en complex. Anal. (*Λ(RR), Δ(SS)*, and *Λ(SR), Δ(RS)*, $C_{14}H_{26}N_2ClCoO_8$) C, H, N. Anal. (*Λ(SS), Δ(RR)*, $C_{14}H_{28}N_2ClCoO_9$) C, H, N.

Λ(R),Δ(S)- and Λ(S), Δ(R)-[Co(acac)$_2$(Me$_3$en)]ClO$_4$(Me$_3$en=N,N,N′-*Trimethylethylenediamine).* These complexes were prepared by the same method as that described for the Me-en complexes in a total yield of 78%. The two racemic pairs of diastereomers, *Λ(R), Δ(S)* and *Λ(S), Δ(R)* were obtained as the perchlorate salts in the ratio 10:1 from the mixture of the isomers. Anal. (*Λ(R), Δ(S)*, and *Λ(S), Δ(R)*, $C_{15}H_{28}N_2ClCoO_8$) C, H, N.

[Co(acac)$_2$(Me$_4$en)]ClO$_4$. This complex was prepared analogous to the Me-en complex. Column chromatography of the reaction mixture on SP-Sephadex C-25 (eluent: 0.05 mol dm^{-3} NaCl) developed three bands; brown, pink, and green in the order of elution. From the green eluate the complex was isolated as the perchlorate. Yield: 20%. Anal. ($C_{16}H_{30}N_2ClCoO_8$) C, H, N. York *et al.*[1] prepared this complex by the reaction of *trans*-Na[Co(NO$_2$)$_2$(acac)$_2$] with Me$_4$en in the presence of active charcoal.

Λ(R),Δ(S)- and Λ(S),Δ(R)-[Co(acac)$_2$(Ph-en)]ClO$_4$. To a solution of [Co(acac)$_3$] (3 g, 8.4 mmol) in methanol (100 cm^3) were added a solution of Ph-en (1.27 g, 9.3 mmol) in methanol (50 cm^3), active charcoal (0.5 g), and acetic acid (2 cm^3). The mixture was stirred for 3 h and then filtered. The filtrate diluted with water (3 dm^3) was applied on a column of SP-Sephadex C-25 by the same procedure as for the Me-en complex to give a single band. From the purple eluate the complex was isolated as the perchlorate. Yield: 75%. By fractional crystallization from chloroform, the complex was separated into the two racemic pairs of diastereomers, *Λ(S), Δ(R)* and *Λ(R), Δ(S)*. The *Λ(S), Δ(R)*-pair is less soluble and the more soluble *Λ(R), Δ(S)*-pair was obtained from the mother liquor by the addition of diethyl ether, the ratio of the former to the latter being *ca.* 1:7. Both pairs were recrystallized from acetonitrile by the addition of diethyl ether. Found for the *Λ(S), Δ(R)*-pair: C, 43.49; H, 5.72; N, 5.58%. Found for the *Λ(R), Δ(S)*-pair: C, 43.74; H, 5.28; N, 5.69%. Calcd for $C_{18}H_{26}N_2ClCoO_8$: C, 43.87; H, 5.32; N, 5.68%. The complexes were converted into the more soluble chlorides by means of Dowex 1×8 (Cl^- form) before the determination of the isomer distribution.

Λ(RR),Δ(SS)-[Co(acac)$_2$(N,N′-Ph$_2$en)]ClO$_4$·0.5H$_2$O. This complex was prepared analogous to the Ph-en complexes except that the reaction mixture was stirred for a longer time (60 h). Column chromatography on SP-Sephadex C-25 (eluent: 0.05 mol dm^{-3} NaCl) resulted in three bands, green, violet, and red in the order of elution. From the green band, the complex was isolated as the perchlorate in the same way as for the Me-en complexes. Yield: 85%. When the preparation was carried out without the addition of acetic acid, the reaction proceeded slowly; about half of the starting complex remained unreacted after 60 h. The complex isolated was the *Λ(RR), Δ(SS)*-pair as confirmed by the ^{1}H NMR spectrum (*vide infra*). Anal. ($C_{24}H_{30}N_2ClCoO_8$) C, H, N. No fraction indicative of other isomers was obtained in column chromatography. The violet and the red band do not contain the desired complex.

[Co(acac)$_2$(opd)]ClO$_4$. To a solution of [Co(acac)$_3$] (1 g, 2.8 mmol) in methanol (50 cm^3) was added active charcoal (0.5 g). The mixture was deoxygenated with nitrogen, and then mixed with a deoxygenated solution of opd (0.33 g, 3.1 mmol) in methanol (20 cm^3). The mixture was stirred for 1 h and filtered. The purple filtrate was diluted with 0.01 mol dm^{-3} HCl (1 dm^3) and applied on a column (ϕ4.5 cm×30 cm) of SP-Sephadex C-25. By elution with 0.05 mol dm^{-3} NaCl-0.01 mol dm^{-3} HCl, two bands, purplish red and violet appeared in this order. The eluate containing the purplish red band was collected and evaporated to a small volume, and to the concentrate was added an excess of $NaClO_4$ to yield the perchlorate of the complex. It was recrystallized from 0.02 mol dm^{-3} $HClO_4$ (50 °C). Yield: 35%. Anal. ($C_{16}H_{22}N_2ClCoO_8$) C, H, N. This complex is unstable in neutral or alkaline solution.

Isomer Distribution at Equilibrium. A racemic pair of diastereomers of Me-en, *N,N′*-Me$_2$en, or Me$_3$en complex (*ca.* 1 mg) was epimerized in 0.1 mol dm^{-3} Na_3PO_4 (pH 12.1, 2 cm^3) at 25 °C. Portions (0.2 cm^3) of the reaction mixture were withdrawn at timed intervals, neutralized with dilute acetic acid, and chromatographed (sample volume: 4×10^{-3} cm^3) on a JASCO FINE SIL C_{18} column (ϕ4.6 mm×30 cm) with 0.01 mol dm^{-3} sodium 1-heptanesulfonate in 97.5% MeOH–2.5% H_2O as the eluent (flow rate: 0.5 cm^3 min^{-1}). The chromatographic procedures were carried out with a JASCO TRI ROTAR HPLC system, and the complexes were detected by a JASCO UVIDEC 100-IV spectrophotometric detector at 240 nm. The areas of the bands on the chromatograms were determined by weighing paper cutouts matching the bands. The experiments were carried out until the mixture attained equilibrium and no change in the elution curve was observed.

The isomer distribution of the Ph-en complex was determined by a ^{1}H NMR method. The chloride of the *Λ(S), Δ(R)* (or *Λ(R), Δ(S)*) pair (*ca.* 0.2 g) was dissolved in 0.1 mol dm^{-3} Na_3PO_4 (20 cm^3, pH 12.1) at 25 °C. Portions (4 cm^3) of the reaction mixture were withdrawn every 2 h and mixed with a solution of $NaClO_4$ (*ca.* 2 mol dm^{-3}) in 0.1 mol dm^{-3} $HClO_4$. The perchlorate of the complex which precipitated was collected by filtration, air dried, and the ^{1}H NMR spectrum was measured in CD_3CN. The distribution of the isomers was determined by measuring the intensities of the methine proton signals of the acac chelate rings (*vide infra*).

Measurements. Absorption and circular dichroism (CD) spectra were recorded on a Hitachi 323 spectrophotometer and a JASCO J-40CS spectropolarimeter, respectively. ^{1}H NMR spectra were measured with a JEOL PMX-60 spectrometer. Optical rotations at 589 nm were measured with a JASCO DIP-4 polarimeter.

Results and Discussion

Preparation and Characterization of the Isomers. All the complexes, $[Co(acac)_2(diamine)]^+$ were prepared from [Co(acac)$_3$] and the diamine ligand in methanol in the presence of active charcoal. The opd complex was prepared under a nitrogen atmosphere.

By the preparations of the Ph-en and *N,N'*-Ph_2en complexes, acetic acid was added to promote the reaction (Experimental). The two acac ligands seem to stabilize the *N*-phenyl-substituted amine–cobalt(III) system. A cobalt(III) complex with an *N*-phenyl-substituted amine ligand is usually unstable and difficult to prepare. For example, although the preparation of $[Co(opd)_3]^{3+}$ has been reported,[6] we could not repeat the results in spite of many attempts. Redox reaction between the phenyl group and the cobalt(III) ion seems to be related to the instability. All the complexes prepared in the present study were purified by column chromatography on SP-Sephadex C-25, and isolated as the perchlorates. The complexes containing a chiral nitrogen atom were separated into the racemic pairs of diastereomers by SE-Toyopearl column chromatography. It has been found that this exchanger is more effective than SP-Sephadex in the separation of diastereomers of uni- and dipositive cobalt(III) complexes.[7,8] However, the separation of the pairs *Λ*(*R*), *Δ*(*S*) and *Λ*(*S*), *Δ*(*R*) of $[Co(acac)_2(Ph\text{-}en)]^+$ was not achieved by the chromatographic method, but by fractional crystallization of their perchlorates. The *Λ*(*S*), *Δ*(*R*)-$[Co(acac)_2(Me\text{-}en)]^+$ pair was resolved by the chemical method with hydrogen di-*O*-benzoyl-*d*-tartrate. The *Λ*(*S*)-isomer formed the less soluble diastereomeric salt which was converted into the perchlorate. The *Λ*(*S*)-isomer was epimerized to give a mixture of the *Λ*(*S*)- and *Λ*(*R*)-isomers which were separated by column chromatography on SE-Toyopearl.

The structures of the isomers were assigned on the basis of the ^1H NMR and CD spectra. Four isomers, *Λ*(*R*), *Λ*(*S*), *Δ*(*R*), and *Δ*(*S*) are possible for $[Co(acac)_2(Me\text{-}en)]^+$ (Fig. 1). In the *Δ*(*R*) and *Λ*(*S*) configurations, the *N*-methyl group is placed over one of the two acac chelate rings and the methyl protons will be shielded by the acac ring. Thus, pair M-I (Experimental) which shows a doublet assignable to the *N*-methyl protons at a higher magnetic field (1.80, Table 1) is assigned to the racemic pair of diastereomers, *Δ*(*R*) and *Λ*(*S*). The structures of the complexes with *N,N'*-Me_2en and Me_3en were assigned in the same way (Table 1). Examination of molecular models indicates that in *Λ*(*S*)- and *Λ*(*R*)-$[Co(acac)_2(Ph\text{-}en)]^+$, the phenyl group strongly shields the methine proton of one of the two acac chelate rings. The resonance at δ 4.88 of the more soluble racemic pair can safely be attributed to the shielded methine proton, and thus the pair is assigned to the racemic pair of diastereomers, *Δ*(*S*) and *Λ*(*R*). The *N,N'*-Ph_2en complex which shows a singlet (2H, 4.86 ppm) attributable to the shielded methine protons is assigned to the racemic pair of the *Δ*(*SS*) and *Λ*(*RR*) isomers.

The absolute configurations, *Λ* or *Δ*, of the optically active Me-en complexes were assigned on the basis of the CD spectra (Fig. 2). In general, the optical activity of a metal complex is explained as a superposition of the configurational and the vicinal effects, the former being usually larger than the latter.[9,10] The two isomers in Fig. 2 show a similar CD pattern and exhibit a main positive CD band in the region of the first absorption band. Thus both isomers are assigned to the *Λ* configuration. Half the sum of the two CD spectra should give the *Λ* configurational effect. In fact, the calculated CD curve is quite similar to the reported CD spectrum of *Λ*-$[Co(acac)_2(en)]^+$[11] where no vicinal effect exists. This result shows that the additivity between the two effects holds for the two isomers, and confirms the above assignments.

Absorption Spectra. The absorption data for the complexes are listed in Table 2, and the representative spectra are shown in Figs. 3 and 4. All the complexes show the first absorption band, $^1A_{1g} \rightarrow {}^1T_{1g}$ (O_h) in the

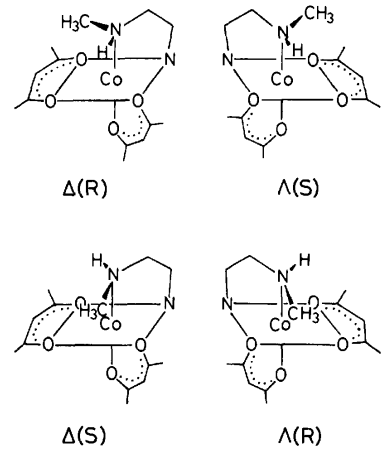

Fig. 1. The four isomers of $[Co(acac)_2(Me\text{-}en)]^+$.

TABLE 1. ^1H NMR DATA FOR $[Co(acac)_2L]^+$ AND THE DISTRIBUTIONS OF THE ISOMERS AT EQUILIBRIUM (25 °C)

L	Assignment	^1H NMR (*N*-methyl or acac methine signal, δ)	Relative Abundance, %
Me-en	*Λ*(*R*), *Δ*(*S*)	2.10d[a]	55
	Λ(*S*), *Δ*(*R*)	1.80d[a]	45
N,N'-Me_2en	*Λ*(*RR*), *Δ*(*SS*)	2.02d[a]	52
	Λ(*SS*), *Δ*(*RR*)	1.77d[a]	30
	Λ(*SR*), *Δ*(*RS*)	1.78d, 2.06d[a]	18
Me_3en	*Λ*(*R*), *Δ*(*S*)	1.87s, 2.02d, 2.07s[a]	64
	Λ(*S*), *Δ*(*R*)	1.73d, 1.78s, 2.07s[a]	36
Ph-en	*Λ*(*R*), *Δ*(*S*)	4.88s, 5.52s[b]	*ca.* 60
	Λ(*S*), *Δ*(*R*)	5.53s, 5.63s[c]	*ca.* 40
N,N'-Ph_2en	*Λ*(*RR*), *Δ*(*SS*)	4.86s[b]	*ca.* 100

a) The chloride in D_2O. b) The perchlorate in $CDCl_3$. c) The perchlorate in CD_3CN.

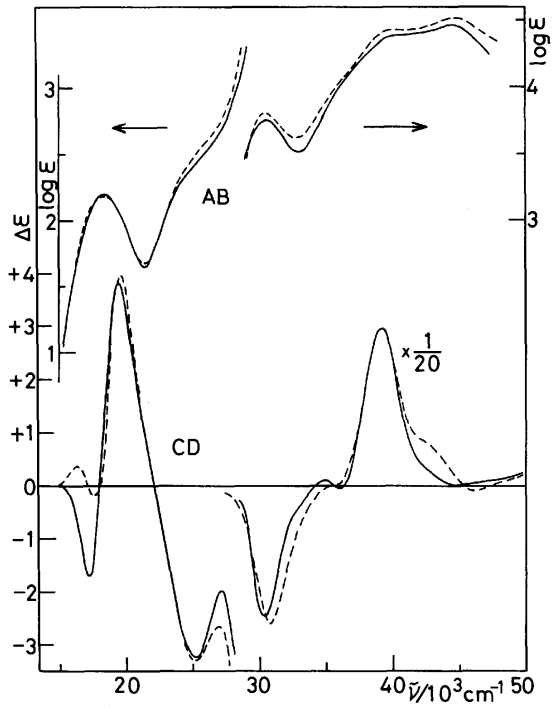

Fig. 2. Absorption and CD spectra of (−)$_{589}$-Λ(R)-(——) and (−)$_{589}$-Λ(S)-[Co(acac)$_2$(Me-en)]ClO$_4$(----) in water.

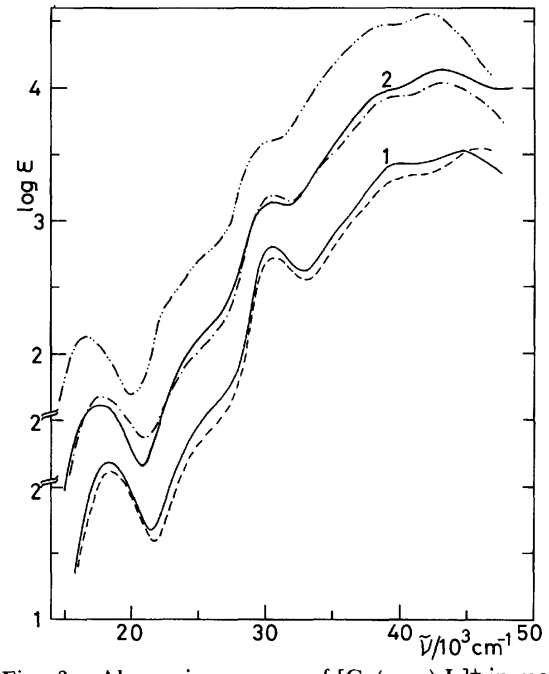

Fig. 3. Absorption spectra of [Co(acac)$_2$L]$^+$ in methanol. L=en (----), Me-en (Λ(S),Δ(R)-pair, ——1), N,N-Me$_2$en (-·-·-), Me$_3$en (Λ(S),Δ(R)-pair, ——2), and Me$_4$en (-···-).

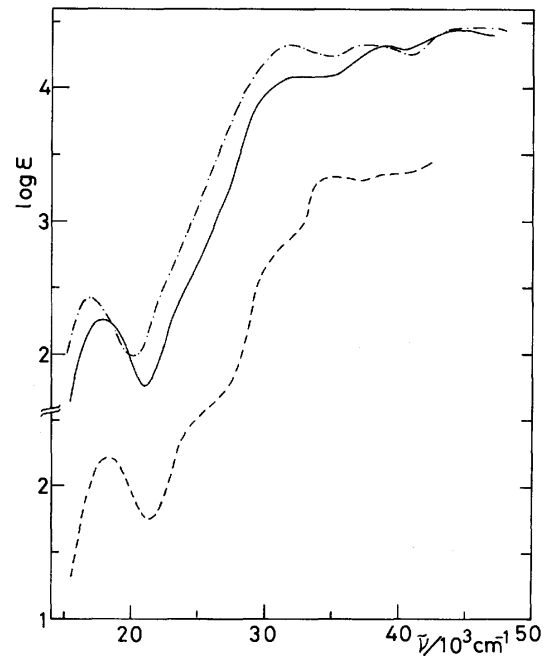

Fig. 4. Absorption spectra of [Co(acac)$_2$L]$^+$ in methanol. L=Ph-en (Λ(S),Δ(R)-pair, ——), N,N'-Ph$_2$en (-·-·-), and opd (---).

region of 16600 to 18300 cm^{-1}. Most of the spectra show a weak shoulder around 25000 cm^{-1}. The corresponding en complex shows a shoulder at *ca.* 24000 cm^{-1} and the transition has been assigned by Boucher to the second d-d absorption band, $^1A_{1g}\rightarrow{}^1T_{2g}$ (O_h)[11]. As seen in Fig. 5 the first absorption band shifts to lower energy as the number of the substituents (CH_3 or C_6H_5) on the nitrogen atom increases. York *et al.*[1] pointed out that the Me$_4$en ligand in [Co(acac)$_2$(Me$_4$en)]$^+$ has a ligand field strength comparable to that of the oxygen donors of acac; the complex shows the first absorption band (16640 cm^{-1}) at nearly the same position as that of [Co(acac)$_3$] (16750 cm^{-1}). The low ligand field strength of the Me$_4$en ligand was ascribed to the steric repulsions which occur in the complex.[1] The [Co(acac)$_2$(N,N-Me$_2$en)]$^+$ complex exhibits the first absorption band at lower energy than those of any of the isomers of the corresponding N,N'-Me$_2$en complex. When the methyl group attached to the nitrogen atom is replaced by a phenyl group, the d-d absorption band shifts to lower energy. Thus the ligand field strengths of the diamines studied here decrease in the order of en>Me-en>N,N'-Me$_2$en>N,N-Me$_2$en~Ph-en>Me$_3$en>N,N'-Ph$_2$en>Me$_4$en. The first absorption band of the opd complex (18250 cm^{-1}) is at nearly the same position as those of the Me-en complexes (18250 and 18300 cm^{-1}, respectively). Except for the Me$_3$en complex, the isomer in which the substituent attached to the nitrogen atom is placed over an acac chelate ring exhibits the first absorption band at lower energy than the other isomers.

The complexes containing an N-methyl-substituted ethylenediamine show a band assignable to a Co^{III}-to-acac d$\pi\rightarrow\pi^*$ transition[12] at 30600—30300 cm^{-1}. For the en complex the corresponding transition occurs at 30700 cm^{-1}. The position shifts slightly to lower energy with an increasing number of methyl groups. On the other hand, the positions of a shoulder (38500—39500 cm^{-1}) which is assigned to another d$\pi\rightarrow\pi^*$ transition,[12] and the $\pi\rightarrow\pi^*$ transition of acac[12]

Table 2. Absorption spectral data for $[Co(acac)_2L]^+$ in methanol and CD spectral data of the Me-en isomers in water

L	Configuration	$\tilde{\nu}_{max}/10^3\,cm^{-1}(\log\varepsilon)$, $\tilde{\nu}_{ext}/10^3\,cm^{-1}(\Delta\varepsilon)$
en		18.45(2.20) 30.70(3.82) 40.0(4.26)[a] 46.00(4.64)
Me-en	$\Lambda(R)$	18.30(2.19) 30.60(3.75) 39.5(4.45)[a] 44.40(4.58)
	CD:	17.30(−1.72) 19.57(+3.82) 25.12(−3.23) 30.49(−49) 35.00(+2.1) 36.10(−1.0) 39.20(+60)
	$\Delta(S)$	18.25(2.18) 30.60(3.76) 39.5(4.42)[a] 44.40(4.55)
	CD:	16.39(+0.39) 17.70(−0.23) 19.70(+3.98) 25.19(−3.28) 30.77(−52) 39.22(+59) 42.60(+15)[a] 46.30(−2.0)
N,N-Me_2en		17.80(2.16) 30.50(3.68) 39.5(4.42)[a] 43.40(4.52)
N,N'-Me_2en	$\Lambda(RR)$, $\Delta(SS)$	18.05(2.17) 30.50(3.71) 39.5(4.45)[a] 43.70(4.54)
	$\Lambda(SS)$, $\Delta(RR)$	17.90(2.14) 30.50(3.69) 39.5(4.41)[a] 43.80(4.52)
	$\Lambda(SR)$, $\Delta(RS)$	17.95(2.16) 30.50(3.68) 39.5(4.46)[a] 43.75(4.58)
Me_3en	$\Lambda(R)$, $\Delta(S)$	17.30(2.15) 30.45(3.65) 39.0(4.51)[a] 43.30(4.65)
	$\Lambda(S)$, $\Delta(R)$	17.35(2.11) 30.45(3.63) 39.0(4.47)[a] 43.00(4.63)
Me_4en		16.60(2.12) 30.30(3.59) 38.5(4.45)[a] 42.40(4.54)
Ph-en	$\Lambda(R)$, $\Delta(S)$	17.80(2.32) 32.30(4.11) 39.40(4.36) 44.60(4.51)
	$\Lambda(S)$, $\Delta(R)$	17.90(2.26) 32.25(4.08) 39.10(4.32) 44.40(4.45)
N,N'-Ph_2en	$\Lambda(RR)$, $\Delta(SS)$	16.95(2.42) 31.85(4.32) 37.90(4.33) 44.40(4.45)
opd		18.25(2.20) 25.0(2.50)[a] 31.0(3.78)[a] 35.10(4.32) 39.40(4.34)

a) Shoulder.

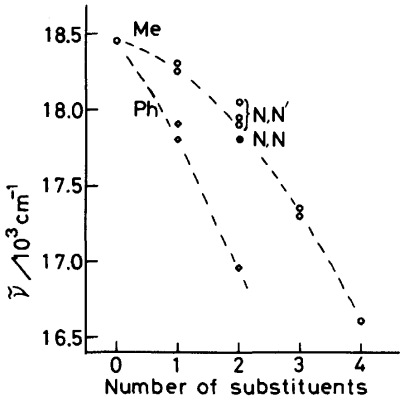

Fig. 5. Correlation between the positions of the first absorption band of $[Co(acac)_2(R^1R^2NCH_2CH_2NR^3R^4)]^+$ (R^1—R^4=H, CH_3, or C_6H_5) and the number of substituents on the nitrogen atoms.

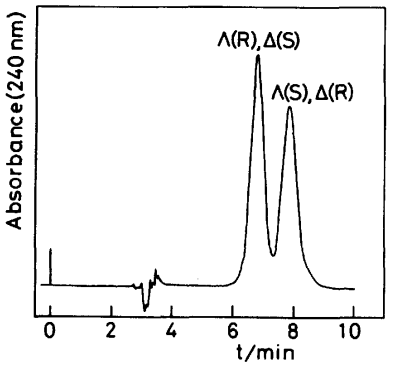

Fig. 6. Elution curve of $[Co(acac)_2(Me\text{-}en)]^+$ equilibrated at pH 12.1 and 25 °C. Chromatographic conditions: column, JASCO FINE SIL C_{18} (ϕ4.6 mm×30 cm); eluent, 0.01 mol dm^{-3} sodium 1-heptanesulfonate in 97.5% MeOH-2.5% H_2O; flow rate, 1 cm^3 min^{-1}; sample volume, 4×10^{-3} cm^{-3} containing *ca.* 4×10^{-9} mol complex.

(42400—44400 cm^{-1}) shift to lower energy to a larger extent as the number of the *N*-methyl groups increases.

Equilibrium Isomer Distribution. The isomers of Me-en, *N,N'*-Me_2en, and Me_3en complexes were equilibrated at pH 12.1 and 25 °C, and the distributions were analyzed by the reversed-phase high performance liquid chromatographic technique.[13] This method has the great advantages of short elution time and micro quantities of samples.[8,14] All the complexes attained equilibrium within one day. Figure 6 shows an example of the Me-en complex and the results are given in Table 1. No decomposition product was observed in column chromatography. The runs starting from any isomer gave the same result within the experimental error (*ca.* ±3%). In general, the more crowded or strained isomer of a metal complex exhibits the d-d absorption bands at lower energy and the abundance is smaller than that of the other isomer.[15] There is, however, no clear relationship between the distribution of the isomers and positions of the absorption bands (Tables 1 and 2).

It was difficult to separate the isomers of the Ph-en complex by HPLC technique, and thus the isomer distribution was determined by the ^1H NMR method. The epimerization was accompanied by a slight decomposition of the complex to cobalt(II), which resulted in a broadening of the ^1H NMR signals. Thus, it was necessary to isolate the cobalt(III) complex after the reaction in order to obtain a well-resolved spectrum. The complex attained equilibrium in 5h at pH 12.1 and 25 °C. The rate of epimerization seems to be similar to those of the *N*-methyl-substituted diamine complexes. A detailed account of kinetic studies will be reported subsequently.

References

1) R. J. York, W. D. Bonds, Jr., B. P. Cotsoradis, and R. D. Archer, *Inorg. Chem.*, **8**, 789 (1969).

2) K. Akamatsu and Y. Shimura, *Bull. Chem. Soc. Jpn.*, **51**, 2586 (1978).
3) K. Ito, *Inorg. Chem.*, **22**, 2872 (1983).
4) M. Zehnder and H. Löliger, *Helv. Chim. Acta*, **63**, 754 (1980).
5) M. Fujita, Y. Yoshikawa, and H. Yamatera, *Chem. Lett.*, **1982**, 437.
6) W. Malitzkii, *J. Chim. Ukraine*, **1**, 374 (1925); *Chem. Abst.*, **20**, 2627 (1926).
7) K. Nakabayashi, K. Doi, M. Kojima, and J. Fujita, *Bull. Chem. Soc. Jpn.*, **57**, 989 (1984).
8) K. Nakajima, M. Kojima, M. Fujita, and J. Fujita, *J. Chromatogr.*, **301**, 241 (1984).
9) B. E. Douglas, *Inorg. Chem.*, **4**, 1813 (1965); C. T. Liu and B. E. Douglas, *ibid.*, **3**, 1356 (1964).
10) K. Ogino, K. Murano, and J. Fujita, *Inorg. Nucl. Chem. Lett.*, **4**, 351 (1965).
11) L. J. Boucher, *Inorg. Chem.*, **9**, 1202 (1970).
12) I. Hanazaki, F. Hanazaki, and S. Nagakura, *J. Chem. Phys.*, **50**, 265 (1969); D. W. Barnum, *J. Inorg. Nucl. Chem.*, **22**, 183 (1961).
13) For example, D. A. Buckingham, C. R. Clark, M. M. Deva, and R. F. Tasker, *Inorg. Chem.*, **22**, 2754 (1983).
14) Y. Yoshikawa, M. Kojima, M. Fujita, M. Iida, and H. Yamatera, *Chem. Lett.*, **1974**, 1163.
15) S. E. Harnung, B. S. Sϕrensen, I. Creaser, H. Maegaard, U. Phenninger, and C. E. Schaffer, *Inorg. Chem.*, **15**, 2123 (1976); M. Kunimatsu, H. Kanno, M. Kojima, K. Kashiwabara, and J. Fujita, *Bull. Chem. Soc. Jpn.*, **53**, 1571 (1980).

Steric and Electronic Effects of Unidentate Tertiary Phosphine Ligands on Chemical and Absorption Spectral Properties of Their Mixed Cobalt(III) Complexes with Acetylacetonate Ions

Katsuaki KATOH, Hirofumi SUGIURA, Kazuo KASHIWABARA, and Junnosuke FUJITA*
Department of Chemistry, Faculty of Science, Nagoya University, Chikusa-ku, Nagoya 464
(Received July 14, 1984)

A large number of new unidentate tertiary phosphine-cobalt(III) complexes containing acetylacetonate ions were prepared. The complexes are grouped into four types; (A) *cis*- and *trans*-$[Co(acac)_2(PR_nPh_{3-n})_2]^+$, (B) *trans*-$[Co(acac)_2(H_2O)(PR_nPh_{3-n})]^+$, (C) *trans*-$[Co(acac)_2(L)(PMe_2Ph)]^{n+}$, and (D) *trans*-(P,P)-$[Co(acac)(CN)_2(PR_nPh_{3-n})_2]$ (acac: acetylacetonate ion, R: CH_3(Me), C_2H_5(Et), *n*-C_3H_7(Pr), *i*-C_3H_7(Pr^i), *n*-C_4H_9(Bu), *i*-C_4H_9(Bu^i), *c*-C_6H_{11} (Cy), Ph: C_6H_5, L: NH_3, CH_3NH_2, C_5H_5N(py), NCS^-). The complexes of type A form cis and trans isomers in a different ratio depending upon the bulkiness and basicity of a phosphine ligand, and the ratios for the complexes with R=Me and Et were examined in some detail. The trans isomers of type A show a strong absorption band in the d-d transition region, which is assumed to involve charge transfer transitions between the cobalt(III) ion and a phosphine ligand, while the cis isomers exhibit the first d-d band split into two components with medium intensity. The complexes of type B show a distinct peak of the first d-d band, the energy shifts of which were discussed in terms of the bulkiness and basicity of phosphine ligands. The complexes of types C and D were prepared to compare the chemical and absorption spectral properties with those of complexes of types A and B.

It is well known that changing substituents on a phosphorus donor atom has a marked influence on physical and chemical properties of metal phosphine complexes.[1] To our knowledge, however, little work has been reported on Co^{III} complexes probably because of the lack of suitable complexes. In a previous paper,[2] we reported that a series of unidentate phosphine ligands, $P(CH_3)_n(C_6H_5)_{3-n}$ (n=1,2,3) forms mixed Co^{III} complexes of the type, $[Co(acac)_2(phosphine)_2]^+$ (acac= acetylacetonate ion). The complexes yielded cis and/or trans isomers depending on the kind of phosphines, and large differences in electronic spectra were observed among the complexes. In order to examine more thoroughly such chemical and spectroscopic properties of Co^{III}-phosphine complexes, we have prepared a large number of Co^{III} complexes containing many kinds of unidentate phosphine ligands. The phosphines used in this study are PR_nPh_{3-n}(***P***) (R= CH_3(Me), C_2H_5(Et), *n*-C_3H_7(Pr), *i*-C_3H_7(Pr^i), *n*-C_4H_9(Bu), *i*-C_4H_9(Bu^i), *c*-C_6H_{11}(Cy), Ph=C_6H_5), and the new (55) and known (10)[2] complexes examined are grouped into the following four types; *cis*- and/or *trans*-$[Co(acac)_2(\boldsymbol{P})_2]^+$(26 complexes), *trans*-$[Co(acac)_2(H_2O)(\boldsymbol{P})]^+$ (18 complexes), *trans*-$[Co(acac)_2(L)(PMe_2Ph)]^{n+}$ (4 complexes with L=NH_3, CH_3NH_2, C_5H_5N(py), or NCS^-), and *trans*(P,P)-$[Co(acac)(CN)_2(\boldsymbol{P})_2]$ (17 complexes).

Experimental

The phosphine ligands were prepared according to the literature methods,[3] and handled under an atmosphere of nitrogen until they formed Co^{III} complexes. Absorption and ^1H NMR spectra were recorded on a Hitachi 323 spectrophotometer, and a Jeol JNM-PMX 60 spectrometer, respectively.

Preparation of Complexes. *1) cis-$[Co(acac)_2(PR_nPh_{3-n})_2]^+$ and trans-$[Co(acac)_2(H_2O)(PR_nPh_{3-n})]^+$ (R=Et, Pr, Bu; n=1, 2, 3).* These complexes were prepared by two methods a) and b). a) A mixture of $[Co(acac)_3]$[4] (2mmol), the phosphine ligand (4mmol), and active charcoal (*ca.* 0.1g) in ethanol-acetic acid (10:1, 60cm^3) was stirred at room temperature for 10h, and then filtered. The filtrate was diluted with water-methanol (2:1, 3dm^3), and the solution was applied on a small column (ϕ2.7cm×3cm) of SP-Sephadex C-25. The Sephadex charged with the product was placed on the top of a column (ϕ2.7cm×130cm) of SP-Sephadex C-25. By elution with 0.02mol/dm^3 NaCl the band separated into two bands. The fraction of the first band, the color of which changing from blue-violet to green during the elution, was collected and concentrated to a small volume under reduced pressure. To the concentrate was added $NaPF_6$ (or $NaClO_4$). The resulting green precipitate was filtered and dissolved in the minimum amount of methanol-water (5:1). The solution was filtered and allowed to stand at room temperature. Green crystals of *trans*-$[Co(acac)_2(H_2O)(PR_nPh_{3-n})]PF_6$ (or ClO_4) were slowly deposited with evaporation of the solvent, filtered, and air dried. From the second red-brown band were obtained red-brown crystals of *cis*-$[Co(acac)_2(PR_nPh_{3-n})_2]PF_6$ (or ClO_4) by the same procedure as that for the first band. In cases of the PPr_3 and PPr_2Ph complexes, *cis*-$[Co(acac)_2(\boldsymbol{P})_2]^+$ was eluted faster than *trans*-$[Co(acac)_2(H_2O)(\boldsymbol{P})]^+$ was. The combined yield of *trans*-$[Co(acac)_2(H_2O)(PR_nPh_{3-n})]^+$ and *cis*-$[Co(acac)_2(PR_nPh_{3-n})_2]^+$ was 30—60%, and the ratio of the former to the latter increased as the number of phenyl groups of the phosphine ligand increases.

b) $[Co(acac)_2(H_2O)_2]$[5] (2mmol) and the phosphine ligand (4.1mmol) were dissolved in a mixture of ethanol (80cm^3) and acetic acid (1cm^3), and then PbO_2 (2.1mmol) was added to the solution. The mixture was stirred for 2h, and then active charcoal (*ca.* 0.1g) was added. Stirring was continued for 10h. The resulting solution was filtered, and the filtrate was diluted with water-methanol (2:1, 2dm^3). The solution was subjected to column chromatography and the complexes were isolated by the same way as that described in a). The yield was 60—80% and better than that by method a). In particular, the yields of the $PRPh_2$ complexes increased markedly.

2) trans-*[Co(acac)$_2$(H$_2$O)(PR$_n$Ph$_{3-n}$)]$^+$ (PR$_n$Ph$_{3-n}$=PPh$_3$, PPr^{i}Ph$_2$, PPr$^i_2$Ph, PBu^{i}Ph$_2$, PBu$^i_2$Ph, PBu$^i_3$, and PCy$_3$).* These complexes were prepared by a method similar to method b). [Co(acac)$_2$(H$_2$O)$_2$] (2 mmol) and the phosphine ligand (2 mmol) were dissolved in a mixture of ethanol (60 cm^3) and acetic acid (1 cm^3). To the solution was added PbO_2 (2.1 mmol), and the mixture was stirred for 2 h, and then filtered. The filtrate was diluted with water (1 dm^3), and the solution was applied on a column (ϕ3 cm×30 cm) of SP-Sephadex C-25. The column was eluted with 0.05 mol/dm^3 NaCl, and a green fraction was collected. To the fraction was added $NaPF_6$ or $NaClO_4$ until a precipitate appears, and then the solution was allowed to stand at room temperature. Green crystals of *trans*-[Co(acac)$_2$(H$_2$O)(PR$_n$Ph$_{3-n}$)]PF$_6$ or ClO$_4$ were filtered, washed with a small amount of cold water, and air dried. The yield was 50—80%. The complexes decompose slowly in aqueous solution. No *cis*-[Co(acac)$_2$(PR$_n$Ph$_{3-n}$)$_2$]$^+$ was formed even though the reaction was carried out in the presence of two molar quantity of the phosphine and active charcoal.

3) trans-*[Co(acac)$_2$(PR$_n$Ph$_{3-n}$)$_2$]$^+$ (R=Et, Pr, Bu; n=0, 1, 2, 3) and* trans-*[Co(acac)$_2$(PRPh$_2$)$_2$]$^+$ (R=Pr^i, Bu^i).* These complexes can be prepared by two methods a) and b). a) An ethanol solution (30 cm^3) containing *trans*-[Co(acac)$_2$(H$_2$O)(PR$_n$Ph$_{3-n}$)]PF$_6$ or ClO$_4$ (0.3 mmol) and the phosphine ligand (1 mmol) was stirred for 30 min. To the resulting solution was added hexane until a red-brown precipitate was no longer formed. The precipitate was filtered and recrystallized from dichloromethane by adding hexane. The yield was *ca.* 80%.

b) [Co(acac)$_2$(H$_2$O)$_2$] (2 mmol) and the phosphine ligand (4 mmol) were dissolved in a mixture of ethanol (40 cm^3) and acetic acid (1 cm^3) with stirring, and then PbO_2 (2.1 mmol) was added. After stirring for 2 h the mixture was filtered, and excess $NaPF_6$ or $NaClO_4$ was added to the filtrate. The resulting precipitate was filtered and recrystallized from dichloromethane by adding hexane. The yield was *ca.* 80%. The bis(phosphine) complexes of PBu$^i_3$, PBu$^i_2$Ph, and PPr$^i_2$Ph seem to be formed in solution since the solution is intensely colored, but the complexes could not be isolated. The bis(PCy$_3$) complex seems to be very unstable, since a green ethanol solution of *trans*-[Co(acac)$_2$(H$_2$O)(PCy$_3$)]$^+$ turns intense red-brown on addition of excess PCy$_3$, but rapidly changes to a pale pink solution indicating the reduction of Co^{III} to Co^{II}.

4) trans-*[Co(acac)$_2$(L)(PMe$_2$Ph)]$^{n+}$ (L=NH$_3$, CH$_3$NH$_2$, py, NCS$^-$).* A methanol solution (20 cm^3) containing [Co(acac)$_2$(H$_2$O)(PMe$_2$Ph)]PF$_6$[2] (0.5 mmol) and ligand L (5 mmol) was stirred for 30 min at room temperature, and then water (10 cm^3) was added. The solution was allowed to stand at room temperature. The crystals which were slowly deposited with evaporation of the solvent were filtered and recrystallized from ethanol by adding an aqueous solution of ligand L. Yields: 40% (NH_3), 50% (CH_3NH_2), 75% (py), and 90% (NCS^-).

5) trans*(P,P)-[Co(acac)(CN)$_2$(PR$_n$Ph$_{3-n}$)$_2$] (R=Et, Pr, Bu, Bu^i; n=1, 2, 3. R=Pr^i; n=1).* These complexes were prepared by a method similar to that for the corresponding PMePh$_2$ complex.[2] A mixture of K[Co(acac)$_2$(CN)$_2$] (2 mmol) and the phosphine ligand (4 mmol) in ethanol (60 cm^3) was stirred at 30—40 °C for 10 h for the complexes of R=Et, Pr, and Bu, and at 40—50 °C for 24 h for the complexes of R=Bu^i and Pr^i. The resulting orange yellow solution was evaporated to dryness under reduced pressure, and the residue was extracted with a small amount of chloroform. The extract was chromatographed by use of an alumina column (ϕ3 cm×5 cm)

TABLE 1. ANALYTICAL AND SPECTRAL DATA OF [Co(acac)$_2$(*P*)$_2$]$^+$

Complex	C(%) Found(Calcd)	H(%) Found(Calcd)	Absorption $\tilde{\nu}_{max}/10^3$cm^{-1}(logε)	Solvent	^{1}H NMR acac =CH-	acac -CH$_3$	Solvent
cis-[Co(acac)$_2$(PEt$_3$)$_2$]PF$_6$	41.33(41.39)	6.65(6.95)	18.2(2.39), 21.3(2.4)^{sh}	a	5.52	1.80, 2.21	c
cis-[Co(acac)$_2$(PPr$_3$)$_2$]PF$_6$	46.34(46.54)	7.73(7.81)	18.2(2.39), 21.3(2.4)^{sh}	a	5.60	1.81, 2.19	c
cis-[Co(acac)$_2$(PBu$_3$)$_2$]ClO$_4$	53.42(53.65)	9.11(9.00)	18.1(2.41), 21.2(2.4)^{sh}	a	5.56	1.79, 2.18	c
cis-[Co(acac)$_2$(PEt$_2$Ph)$_2$]PF$_6$	49.45(49.06)	6.05(6.04)	18.0(2.41), 20.5(2.5)^{sh}	a	5.57	1.90, 2.16	c
cis-[Co(acac)$_2$(PPr$_2$Ph)$_2$]PF$_6$	51.63(51.65)	6.65(6.63)	18.1(2.41), 20.5(2.5)^{sh}	a	5.57	1.90, 2.16	c
cis-[Co(acac)$_2$(PBu$_2$Ph)$_2$]PF$_6$	53.38(53.90)	7.09(7.14)	18.0(2.43), 20.5(2.5)^{sh}	a	5.61	1.90, 2.17	c
cis-[Co(acac)$_2$(PMePh$_2$)$_2$]PF$_6$	54.14(53.88)	5.03(5.02)	18(2.6)^{sh}, 20.0(2.7)^{sh}	a	5.17	1.74, 1.94	c
cis-[Co(acac)$_2$(PEtPh$_2$)$_2$]PF$_6$	55.22(54.95)	5.28(5.34)	17.2(2.60)	a	5.29	1.71, 1.95	c
cis-[Co(acac)$_2$(PPrPh$_2$)$_2$]PF$_6$	56.02(55.95)	5.76(5.63)	17.2(2.61)	a	5.38	1.72, 1.93	c
cis-[Co(acac)$_2$(PBuPh$_2$)$_2$]PF$_6$	56.89(56.89)	5.93(5.91)	17.2(2.60)	a	5.46	1.76, 1.94	c
trans-[Co(acac)$_2$(PEt$_3$)$_2$]PF$_6$	41.66(41.39)	6.86(6.95)	23.1(4.06)	b	5.47	1.97	c
trans-[Co(acac)$_2$(PPr$_3$)$_2$]PF$_6$	46.55(46.54)	8.06(7.81)	23.0(4.09)	b	5.44	1.98	d
trans-[Co(acac)$_2$(PBu$_3$)$_2$]PF$_6$	50.54(50.62)	8.84(8.50)	23.0(4.10)	b	5.49	1.97	c
trans-[Co(acac)$_2$(PEt$_2$Ph)$_2$]PF$_6$	49.33(49.06)	5.90(6.04)	22.1(4.15)	b	5.15	1.64	c
trans-[Co(acac)$_2$(PPr$_2$Ph)$_2$]PF$_6$	51.84(51.65)	6.60(6.63)	22.0(4.19)	b	5.10	1.64	d
trans-[Co(acac)$_2$(PBu$_2$Ph)$_2$]ClO$_4$	56.24(56.96)	7.45(7.55)	22.0(4.18)	b	5.13	1.66	c
trans-[Co(acac)$_2$(PEtPh$_2$)$_2$]ClO$_4$·1/2H$_2$O	57.48(57.46)	5.71(5.71)	20.9(4.17)	b	e	e	
trans-[Co(acac)$_2$(PPrPh$_2$)$_2$]PF$_6$	56.22(55.95)	5.56(5.63)	20.8(4.19)	b	4.70	1.48	d
trans-[Co(acac)$_2$(PBuPh$_2$)$_2$]ClO$_4$	60.23(59.97)	6.71(6.23)	20.8(4.16)	b	4.77	1.50	c
trans-[Co(acac)$_2$(PBu^{i}Ph$_2$)$_2$]PF$_6$	56.61(56.89)	5.89(5.91)	20.5(4.09)^f	b	4.99	1.51	d
trans-[Co(acac)$_2$(PPr^{i}Ph$_2$)$_2$]PF$_6$	55.82(55.95)	5.09(5.63)	19.8(3.97)^f	b	4.99	1.50	d
trans-[Co(acac)$_2$(PPh$_3$)$_2$]PF$_6$	59.81(59.62)	4.68(4.79)	19.0(4.06)^g	b	4.53	1.49	d

a: CH_3OH, b: CH_2Cl_2, c: CD_3Cl, d; CD_2Cl_2. e: No clear peak was observed because of low solubility. f: The spectrum showed a slight change with time. g: The spectrum showed a slight change with time even in the presence of a large excess of PPh_3. For the data of *cis*-[Co(acac)$_2$(PMe$_3$)$_2$]PF$_6$, *cis*-[Co(acac)$_2$(PMe$_2$Ph)$_2$]PF$_6$, *trans*-[Co(acac)$_2$(PMe$_2$Ph)$_2$]PF$_6$, and *trans*-[Co(acac)$_2$(PMePh$_2$)$_2$]PF$_6$, see Ref. 2).

TABLE 2. ANALYTICAL AND SPECTRAL DATA OF *trans*-[Co(acac)$_2$(L)(***P***)]$^{n+}$

Complex	C(%) Found(Calcd)	H(%) Found(Calcd)	N(%) Found(Calcd)	Absorption $\tilde{\nu}_{max}/10^3cm^{-1}(log\varepsilon)$	Solvent	^{1}H NMR acac =CH-	acac -CH$_3$	Solvent
[Co(acac)$_2$(H$_2$O)(PEt$_3$)]PF$_6$·1/2H$_2$O	34.86(35.11)	5.71(5.53)		17.5(2.46)	a	5.75	2.12	c
[Co(acac)$_2$(H$_2$O)(PPr$_3$)]PF$_6$	39.55(39.32)	5.92(6.43)		17.5(2.46)	a	5.75	2.12	c
[Co(acac)$_2$(H$_2$O)(PBu$_3$)]PF$_6$	42.43(42.45)	6.87(6.96)		17.5(2.45)	a	5.78	2.12	c
[Co(acac)$_2$(H$_2$O)(PBu$_3^i$)]PF$_6$·H$_2$O	41.20(41.26)	7.19(7.08)		17.2(2.38)	a	5.59	1.97	c
[Co(acac)$_2$(H$_2$O)(PCy$_3$)]ClO$_4$	51.16(51.34)	7.53(7.54)		16.3(2.29)[e]	b	5.73	2.07	c
[Co(acac)$_2$(H$_2$O)(PEt$_2$Ph)]PF$_6$·1/2H$_2$O	40.20(40.35)	5.24(5.42)		17.1(2.47)	a	5.57	1.99	c
[Co(acac)$_2$(H$_2$O)(PPr$_2$Ph)]PF$_6$	43.30(43.01)	5.77(5.74)		17.1(2.48)	a	5.56	2.00	c
[Co(acac)$_2$(H$_2$O)(PBu$_2$Ph)]PF$_6$	44.80(44.87)	6.11(6.12)		17.0(2.47)	a	5.56	1.99	c
[Co(acac)$_2$(H$_2$O)(PBu$_2^i$Ph)]PF$_6$	44.66(44.87)	5.92(6.16)		16.8(2.44)	a	5.59	1.97	c
[Co(acac)$_2$(H$_2$O)(PPr$_2^i$Ph)]PF$_6$·H$_2$O	41.52(41.78)	5.97(5.90)		16.3(2.34)	a	5.54	2.02	c
[Co(acac)$_2$(H$_2$O)(PEtPh$_2$)]ClO$_4$	48.73(48.95)	5.17(5.31)		16.4(2.46)	a	5.42	1.94	c
[Co(acac)$_2$(H$_2$O)(PPrPh$_2$)]PF$_6$	46.99(46.31)	5.55(5.13)		16.4(2.44)	a	5.43	1.93	c
[Co(acac)$_2$(H$_2$O)(PBuPh$_2$)]PF$_6$	46.87(47.14)	5.44(5.33)		16.4(2.44)	a	5.46	1.94	c
[Co(acac)$_2$(H$_2$O)(PBu^{i}Ph$_2$)]ClO$_4$	50.67(50.62)	5.61(5.72)		16.3(2.40)	a	5.53	1.93	c
[Co(acac)$_2$(H$_2$O)(PPr^{i}Ph$_2$)]PF$_6$	46.52(46.31)	5.17(5.13)		16.2(2.38)	a	5.53	1.95	c
[Co(acac)$_2$(H$_2$O)(PPh$_3$)]ClO$_4$	52.99(52.80)	4.83(4.91)		15.5(2.38)[e]	b	5.35	1.93	c
[Co(acac)$_2$(NH$_3$)(PMe$_2$Ph)]PF$_6$	38.82(38.79)	5.15(4.52)	2.47(2.51)	18.6(2.36)	b	5.32	1.95	d
[Co(acac)$_2$(CH$_3$NH$_2$)(PMe$_2$Ph)]PF$_6$	39.80(39.94)	5.31(5.29)	2.38(2.45)	18.8(2.41)	b	5.31	1.94	d
[Co(acac)$_2$(C$_5$H$_5$N)(PMe$_2$Ph)]PF$_6$	44.77(44.60)	4.92(4.88)	2.27(2.26)	18.9(2.44)	b	5.12	1.87	d
[Co(acac)$_2$(NCS)(PMe$_2$Ph)]·H$_2$O	48.53(48.41)	5.75(5.77)	3.19(2.97)	18.0(2.53)	b	5.25	1.94	d

a: CH_3OH, b: CH_2Cl_2, c: CD_3OD, d: CD_3Cl. e: The spectrum showed a slight change with time. For the data of *trans*-[Co(acac)$_2$(H$_2$O)(PMe$_2$Ph)]PF$_6$·1/2H$_2$O and *trans*-[Co(acac)$_2$(H$_2$O)(PMePh$_2$)]PF$_6$, see Ref. 2).

TABLE 3. ANALYTICAL AND SPECTRAL DATA OF *trans*(P,P)-[Co(acac)(CN)$_2$(***P***)$_2$]

Complex	C(%) Found(Calcd)	H(%) Found(Calcd)	N(%) Found(Calcd)	Absorption $\tilde{\nu}_{max}/10^3cm^{-1}(log\varepsilon)$	Solvent	^{1}H NMR acac =CH-	acac -CH$_3$	Solvent
[Co(acac)(CN)$_2$(PEt$_3$)$_2$]	50.09(50.11)	8.33(8.41)	6.05(6.15)	24.4(3.35)	a	5.27	1.89	b
[Co(acac)(CN)$_2$(PPr$_3$)$_2$]	56.54(56.60)	9.27(9.31)	5.25(5.28)	24.4(3.36)	a	5.28	1.88	b
[Co(acac)(CN)$_2$(PBu$_3$)$_2$]	60.23(60.57)	9.60(10.00)	4.37(4.56)	24.4(3.38)	a	5.27	1.80	b
[Co(acac)(CN)$_2$(PBu$_3^i$)$_2$]·1/2H$_2$O	59.55(59.70)	10.12(10.02)	4.74(4.49)	23.8(3.35)	a	5.30	1.91	b
[Co(acac)(CN)$_2$(PEt$_2$Ph)$_2$]	60.05(59.78)	6.55(6.88)	5.24(5.16)	23.3(3.53)	a	4.71	1.13	b
[Co(acac)(CN)$_2$(PPr$_2$Ph)$_2$]	62.23(62.20)	7.74(7.58)	4.51(4.68)	23.3(3.54)	a	4.69	1.10	b
[Co(acac)(CN)$_2$(PBu$_2$Ph)$_2$]	64.34(64.21)	8.15(8.16)	4.30(4.28)	23.3(3.55)	a	4.66	1.10	b
[Co(acac)(CN)$_2$(PBu$_2^i$Ph)$_2$]·H$_2$O	62.69(62.49)	8.11(8.24)	4.43(4.16)	23.0(3.46)	a	4.53	0.97	b
[Co(acac)(CN)$_2$(PEtPh$_2$)$_2$]	66.03(65.83)	5.59(5.84)	4.10(4.39)	21.9(3.53)	a	4.67	0.98	b
[Co(acac)(CN)$_2$(PPrPh$_2$)$_2$]	65.22(64.91)	6.16(6.33)	3.89(4.09)	21.9(3.57)	a	4.67	0.99	b
[Co(acac)(CN)$_2$(PBuPh$_2$)$_2$]·1/2H$_2$O	66.37(66.57)	6.46(6.59)	3.91(3.95)	20.8(3.58)	a	4.67	0.98	b
[Co(acac)(CN)$_2$(PBu^{i}Ph$_2$)$_2$]·1/2H$_2$O	66.45(66.57)	6.54(6.59)	3.78(3.98)	21.8(3.57)	a	4.60	0.93	b
[Co(acac)(CN)$_2$(PPr^{i}Ph$_2$)$_2$]·1/2H$_2$O	65.82(65.78)	5.75(6.27)	4.05(4.15)	21.2(3.42)	a	4.51	0.77	b

a: CH_3OH, b: $CDCl_3$. For the data of *trans*(P,P)-[Co(acac)(CN)$_2$(PMe$_3$)$_2$], *trans*(P,P)-[Co(acac)(CN)$_2$(PMe$_2$Ph)$_2$], *trans*(P,P)-[Co(acac)(CN)$_2$(PMePh$_2$)$_2$], and *trans*(P,P)-[Co(acac)(CN)$_2$(PPh$_3$)$_2$], see Ref. 2).

and a mixture of hexane and ethanol (1:10). The eluate was concentrated to a small volume, and the concentrate was rechromatographed by use of a column (ϕ3 cm×60 cm) of SP-Sephadex LH-20 and a mixture of hexane and ethanol (5:1). The orange yellow eluate was evaporated to a small volume, and then water was added until a precipitate began to appear. The crystals which were deposited on standing at room temperature were filtered and air-dried. Yields: 45—70% (R=Et, Pr), 20—50% (R=Bu), 10% (R=Pr^i, Bu^i). The yield tends to decrease with the increasing bulkiness of R and the increasing number of phenyl groups of the ligand.

Analytical data of the new complexes are given in Tables 1—3.

Isomer Distribution of [Co(acac)$_2$(PR$_n$Ph$_{3-n}$)$_2$]$^+$ (R=Me, Et; n=0, 1, 2, 3) at Equilibrium. a) A mixture of *cis*- or *trans*-[Co(acac)$_2$(PR$_n$Ph$_{3-n}$)$_2$]PF$_6$ (*ca.* 0.1 mmol), the corresponding phosphine ligand (*ca.* 0.01 mmol), and a small amount of active charcoal in ethanol-dichloromethane (1:1, 20 cm^3) was stirred at 20±0.5 °C for 24 h. The mixture was filtered, and the filtrate was evaporated to dryness under reduced pressure. The residue was stored in a vacuum dessicator overnight for complete elimination of the solvent and moisture. The sample thus obtained was dissolved in CD_2Cl_2, and the ^{1}H NMR spectrum was recorded. The formation ratio of the cis to trans isomers was determined from the intensity ratio of methine signals of acac in these isomers.

b) [Co(acac)$_2$(H$_2$O)$_2$] (2 mmol) and the phosphine ligand (4.5 mmol) were dissolved in a mixture of ethanol (60 cm^3) and acetic acid (1 cm^3), and then PbO_2 (2.1 mmol) was added. The mixture was stirred for 2 h, and then active charcoal (*ca.* 0.1 g) was added. The whole was kept at 20±0.5 °C with stirring for 24 h. The resulting mixture was filtered, and the filtrate was chromatographed by the same method as that described in 1) method b) in order to separate the two isomers. The trans isomer completely changed into *trans*-[Co(acac)$_2$(H$_2$O)(PR$_n$-Ph$_{3-n}$)]$^+$ during the elution. The abundance of the complex

in each fraction was determined by measuring the optical density. The values of formation ratio of the *cis*-bis(phosphine) complex to the *trans*-(aqua)(phosphine) complex thus obtained were almost the same as those determined by the above ^1H NMR method.

Results and Discussion

Preparation and Chemical Properties of the Complexes. In a previous paper,[2] we reported that trimethylphosphine and its phenyl analogs, PMe_nPh_{3-n} (n=1, 2, 3) react with [Co(acac)$_3$] in ethanol in the presence of active charcoal to yield $[Co(acac)_2(PMe_nPh_{3-n})_2]^+$, but the reaction with bulky PPh_3 does not take place under similar conditions. Bulky alkylphosphines such as PBu^i_3, PPr^i_2Ph, and PCy_3 used in this study do not react with [Co(acac)$_3$] either. Thus reactivity of unidentate phosphine ligands toward [Co(acac)$_3$] seems to depend on their bulkiness. In this study, however, we have prepared such bulky phosphine complexes of the $[Co(acac)_2(\boldsymbol{P})_2]^+$ type in good yields by oxidizing a mixture of $[Co(acac)_2(H_2O)_2]$ and the phosphine ligand in ethanol with PbO_2. The less bulky phosphine complexes can also be prepared by this method in good yield.

The new preparative method affords only the trans isomer of $[Co(acac)_2(\boldsymbol{P})_2]^+$ when active charcoal is not added to the reaction mixture. In the presence of active charcoal, however, both trans and cis isomers are formed if the complex can exist in the cis isomer. The structure of the complex can be easily assigned from NMR and absorption spectra as reported for the PMe_nPh_{3-n} complexes.[2] The cis isomers, the formation of which was confirmed by column chromatography, are those with PR_nPh_{3-n} (R=Me, Et, Pr, Bu; n= 1, 2, 3). For the most bulky PCy_3 ligand, only *trans*-$[Co(acac)_2(H_2O)(PCy_3)]^+$ is isolated, no bis(PCy_3) complex being formed under the given experimental conditions (see Experimental). The Co^{III}–P bond would lengthen and weaken with increasing bulkiness of the phosphine ligand. The bulkiness of phosphine ligands can be estimated in terms of the cone angle(θ°) defined by Tolman.[1] In a series of $[Co(DH)_2(Cl)(\boldsymbol{P})]$ ($\boldsymbol{P}$=PBu_3, PPh_3, PCy_3; DH=dimethylglyoximate ion), the Co^{III}–P bond lengthens in the order of the PBu_3(2.271 Å)[6] <PPh_3(2.327 Å)[7] <PCy_3(2.369 Å)[8] complexes, with the increasing cone angle of the phosphine ligands, PBu_3(132°)<PPh_3(145°)<PCy_3(170°).

Both trans and cis isomers of $[Co(acac)_2(PR_nPh_{3-n})_2]^+$ (R=Me, n=2; R=Et, Pr, Bu, n=1, 2, 3) isomerize to each other in ethanol in the presence of active charcoal, and the isomerization attains equilibrium fairly rapidly. Distributions of the two isomers at 25 °C were examined for the complexes with R=Me and Et. The proportions (%) of the trans isomers are plotted against the cone angles (θ°) of phosphine ligands in Fig. 1. With the increasing cone angle, the proportion of the trans isomer increases, and almost linear relationships are seen among the complexes with PR_nPh_{3-n} (n=2,3) and among those with PR_nPh_{3-n} (n=0, 1). The smallest PMe_3 complex affords only the cis isomer, while the largest PPh_3 complex only the trans one. The $PMePh_2$ and PEt_2Ph ligands have the same cone angle (136°), but form the trans isomer in a remarkably different proportion. The difference might come from the difference in electronic effect of the phosphine ligands. According to the parameter($\sum\chi i/cm^{-1}$) given by Tolman[1] for the electronic effect of phosphines, PEt_2Ph (7.9) is more basic than $PMePh_2$ (11.2). Thus it is seen that when two kinds of phosphine ligands have a similar steric effect, the complex with the more basic phosphine ligand yields the cis isomer in a larger amount. Cotton *et al.*[9] reported a tendency to isomerize to the trans isomer in $[Mo(CO)_4(PR_3)_2]$ (R=Me, Et, Bu) with an increasing bulkiness of PR_3. Ounapu *et al.*[10] observed also a similar trend in $[W(CO)_4(PRPh_2)_2]$ (R=Me, Et, Pr^i, Bu^t, Ph); the value of the trans/cis ratio increases with an increase in bulkiness of R.

All of *trans*-$[Co(acac)_2(PR_nPh_{3-n})_2]^+$ rapidly hydrolyze when dissolved in ethanol (not anhydrous) to afford *trans*-$[Co(acac)_2(H_2O)(PR_nPh_{3-n})]^+$. The hydrolysis is depressed by addition of the free phosphine ligand, and hence the complex in solution will exist in the following equilibrium;

$$\textit{trans}\text{-}[Co(acac)_2(PR_nPh_{3-n})_2]^+ \underset{PR_nPh_{3-n}}{\overset{H_2O}{\rightleftharpoons}} \textit{trans}\text{-}[Co(acac)_2(H_2O)(PR_nPh_{3-n})]^+$$

The rapid hydrolysis can be attributed to a strong trans effect of PR_nPh_{3-n}. Similar solvolyses were reported for *trans*-$[Co(acac)_2(NO_2)_2]^-$ in water[11] and *trans*-[Co(acac)$_2$(CN)(py)] in dimethyl sulfoxide(DMSO),[12] which rapidly yield *trans*-$[Co(acac)_2(NO_2)(H_2O)]$ and *trans*-[Co(acac)$_2$(CN)(DMSO)], respectively. The resulting *trans*-$[Co(acac)_2(H_2O)(PR_nPh_{3-n})]^+$ complexes are stable to further hydrolysis, although those with bulky PCy_3, PPr^i_2Ph and PPh_3 decompose slowly to

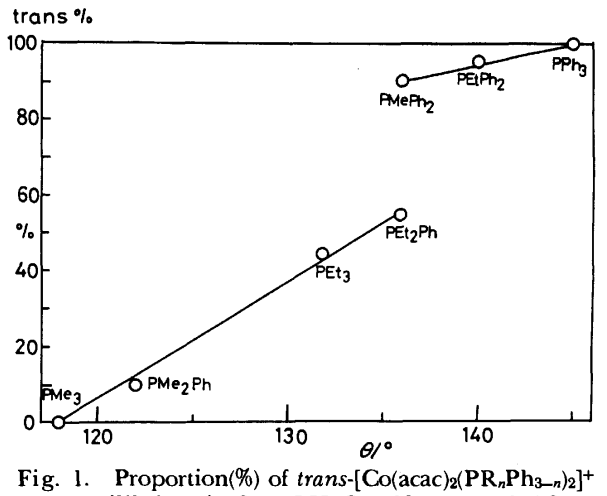

Fig. 1. Proportion(%) of *trans*-$[Co(acac)_2(PR_nPh_{3-n})_2]^+$ at equilibrium in C_2H_5OH–CH_2Cl_2 (1:1) at 25 °C *vs.* Tolman's cone angle (θ°) of the phosphine ligand.

give Co^{II} species. The aqua ligand in *trans*-$[Co(acac)_2(H_2O)(PR_nPh_{3-n})]^+$ is readily replaced by various bases (L) to afford *trans*-$[Co(acac)_2(L)(PR_nPh_{3-n})]^{n+}$. We have isolated complexes of this type for PMe_2Ph and L=NH_3, CH_3NH_2, py, or NCS^-. All of these complexes immediately lose L to give original *trans*-$[Co(acac)_2(H_2O)(PMe_2Ph)]^+$ when dissolved in methanol or ethanol (not anhydrous). This is in marked contrast to the inertness of *trans*-$[Co(acac)_2(NO_2)(NH_3$ or py$)]$ in solvolysis.[13] The trans effects of cyanide and phosphine ligands should be much greater than that of NO_2^-.[14] When $PMePh_2$ for L is added to a methanol solution of *trans*-$[Co(acac)_2(H_2O)(PMe_2Ph)]^+$, a disproportionation reaction takes place to yield *trans*-$[Co(acac)_2(PMe_2Ph)_2]^+$ and *trans*-$[Co(acac)_2(PMePh_2)_2]^+$ in addition to *trans*-$[Co(acac)_2(PMe_2Ph)(PMePh_2)]^+$. The reaction of CN^- with $[Co(acac)_2(H_2O)(PMe_2Ph)]^+$ affords *cis*-$[Co(acac)_2(CN)(PMe_2Ph)]$, no trans isomer being formed. Since CN^- has strong ability of trans influence as a phosphine and is much smaller in size, the complex would be greatly stabilized in the cis isomer.

The $[Co(acac)(CN)_2(PR_nPh_{3-n})_2]$-type complexes have been prepared from *cis*-$[Co(acac)_2(CN)_2]^-$ and PR_nPh_{3-n} by a method similar to that for the corresponding PMe_nPh_{3-n} complexes.[2] All the complexes yield only the trans (P,P) isomer of three possible geometrical isomers. The assignment of the trans (P,P) isomer can be made easily from NMR spectra as reported for the PMe_nPh_{3-n} complexes.[2] The stereoselective formation of the trans (P,P) isomer over various kinds of phosphines might result from stronger trans influence of CN^- than that of a phosphine ligand. Furthermore, the steric effect of bulky phosphine ligands would facilitate formation of the trans (P,P) isomer. The yield of the complex decreases with increasing bulkiness of phosphines, and extremely bulky phosphines such as PPr_2^iPh and PCy_3 do not react with *cis*-$[Co(acac)_2(CN)_2]^-$. All the complexes obtained are stable in methanol or ethanol, and show no solvolysis in contrast to trans-$[Co(acac)_2(PR_nPh_{3-n})_2]^+$ stated previously. The reason for this remains unknown. Since the *trans*-$[Co(CN)_4(PMe_nPh_{3-n})_2]^-$ (n=0, 1, 2) complexes are also inert to solvolysis,[2] strong and soft cyanide ions in such trans (P,P) complexes might play an important role in strengthening the Co^{III}–P bond.

^1H NMR Spectra. In Tables 1—3 are listed data of the methine and methyl signals of acac in ^1H NMR spectra of the complexes. General features in chemical shift of these signals are similar to those reported for the complexes of PMe_nPh_{3-n}.[2] For *trans*-$[Co(acac)_2(PR_nPh_{3-n})_2]^+$ the methine signal of acac shows a remarkable high field shift as the number of phenyl groups on the phosphorus atom increases. The methyl signal also shows the same high field shift, but the extent of shift is not so large as that of the methine signal. As suggested in our previous papers,[2,15] the high field shift of these protons can be attributed to a shielding effect by the ring current of phenyl groups of the phosphine ligand located over the acac ring. No such remarkable high field shifts are observed for *cis*-$[Co(acac)_2(PR_nPh_{3-n})_2]^+$ (n=1, 2). In a previous paper, we examined the crowded structure of *cis*-$[Co(acac)_2(PMe_2Ph)_2]^+$ with molecular models, and suggested a structure where the methyl proton (s) of PMe_2Ph is placed over the acac ring. This structure is supported by the fact that the chemical shift of the methine proton is very similar to that in *cis*-$[Co(acac)_2(PMe_3)_2]^+$. A similar structure can be assigned to other PR_2Ph complexes of this type (R= Et, Pr, Bu), since all methine proton signals of these complexes and *cis*-$[Co(acac)_2(PR_3)_2]^+$ (R=Et, Pr, Bu) are observed at nearly the same position. The methine signals of *cis*-$[Co(acac)_2(PRPh_2)_2]^+$ shift to a high field compared with those of the PR_3 and PR_2Ph complexes, but the magnitudes of shift are much smaller than those observed in the corresponding trans isomers. Thus the $PRPh_2$ complexes would also have a structure similar to that of the PR_2Ph complexes; the R group is located over the acac ring.

In contrast to *trans*-$[Co(acac)_2(PR_nPh_{3-n})_2]^+$ (n= 0, 1, 2), *trans*-$[Co(acac)_2(H_2O)(PR_nPh_{3-n})]^+$ (n=0, 1, 2) show a very small high field shift in the methine signals, although both types of complex are similar and have the phosphine ligand at the apical site to the plane formed by two acac ligands. In these aqua complexes, the two acac chelate rings might not be planar, but bent toward the small aqua ligand to release the crowding with the bulky phosphine ligand as have been observed for *trans*-$[Co(DH)_2(Cl)(\boldsymbol{P})]$ ($\boldsymbol{P}$= PBu_3[6], PPh_3[7], PCy_3[8]). Accordingly, the methine proton would not be effectively shielded by the phenyl group to give a very small high field shift. The same explanation can be offered for the small high field shift of the methine signals in *trans*-$[Co(acac)_2(L)(PMe_2Ph)]^{n+}$ (L=NH_3, CH_3NH_2,py, NCS^-). Both methine and methyl signals of *trans*(P,P)-$[Co(acac)(CN)_2(PR_nPh_{3-n})_2]$ (n=0, 1, 2) are observed at a remarkably high field compared with those of the corresponding PR_3 complexes. The magnitudes of shift, in particular those in the PR_2Ph complexes are even larger than those observed in *trans*-$[Co(acac)_2(PR_nPh_{3-n})_2]^+$ (n=0, 1, 2). As stated previously, these dicyano complexes are quite stable to solvolysis, and hence the Co^{III}–P bonds would be stronger and shorter than those in *trans*-$[Co(acac)_2(PR_nPh_{3-n})_2]^+$ which rapidly undergo solvolysis. The large high field shift might be caused by such strong coordination of the PR_nPh_{3-n} (n=0, 1, 2) ligands at the apical position.

Absorption Spectra. In Fig. 2 are shown absorption spectra of PPr_nPh_{3-n} complexes of the types, *trans*- and *cis*-$[Co(acac)_2(\boldsymbol{P})_2]^+$, *trans*-$[Co(acac)_2(H_2O)(\boldsymbol{P})]^+$, and *trans*(P,P)-$[Co(acac)(CN)_2(\boldsymbol{P})_2]$. The spectral patterns remain almost unchanged by changing the kind of alkyl groups. Tables 1—3 list the data of absorption bands observed in the low energy region.

All of *trans*-$[Co(acac)_2(PR_nPh_{3-n})_2]^+$ show a very

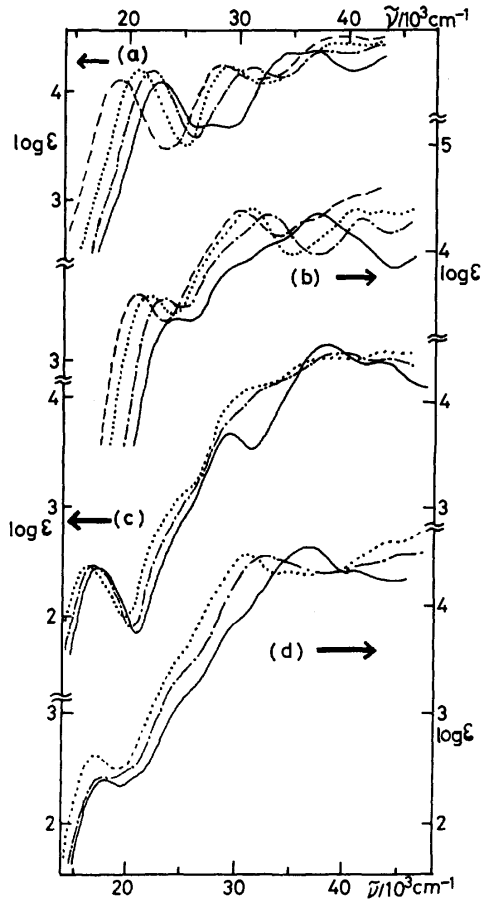

Fig. 2. Absorption spectra of a) *trans*-$[Co(acac)_2(\boldsymbol{P})_2]^+$ b) *trans*(P,P)-$[Co(acac)(CN)_2(\boldsymbol{P})_2]$, c) *trans*-$[Co(acac)_2(H_2O)(\boldsymbol{P})]^+$, d) *cis*-$[Co(acac)_2(\boldsymbol{P})_2]^+$ where denote PPr_3 (——), PPr_2Ph (-·-·-), $PPrPh_2$ (·····), and PPh_3 (----).

strong band in the 19000—23000 cm^{-1} region. Because of the strong intensity, these bands may be assigned to a charge transfer transition. However, no such low energy, strong bands are observed in the phosphine complexes of other types studied here. The bands shift largely to the low energy side as the number of phenyl groups in PR_nPh_{3-n} increases. The first absorption band of the complexes is almost hidden by this strong band, but the shoulders in the lowest energy region observed in the PR_3 and PR_2Ph complexes can be assigned to a part of the first absorption band. The spectra of a series of *trans*-$[Co(acac)_2(CH_3NH_2)_n(PMe_2Ph)_{2-n}]^+$ (n=0, 1, 2) given in Fig. 3 show more clearly that *trans*-$[Co(acac)_2(PR_nPh_{3-n})_2]^+$ has the first absorption band on the low energy side of the strong band. Neither *cis*-$[Co(acac)_2(PR_nPh_{3-n})_2]^+$ nor *trans*-$[Co(acac)_2(H_2O)(PR_nPh_{3-n})]^+$ exhibit such a strong band in the low energy region. The complexes show a band of medium intensity in this region, which can be assigned to the first absorption band from a comparison with the spectra shown in Fig. 3 and those of *cis*-$[Co(acac)_2(CN)_n(PMe_3)_{2-n}]^{(1-n)+}$ (n=0, 1, 2).[2] The *trans*-(P,P)-$[Co(acac)(CN)_2(PR_nPh_{3-n})_2]$ complexes give a fairly strong band in the 21000—24000 cm^{-1} region.

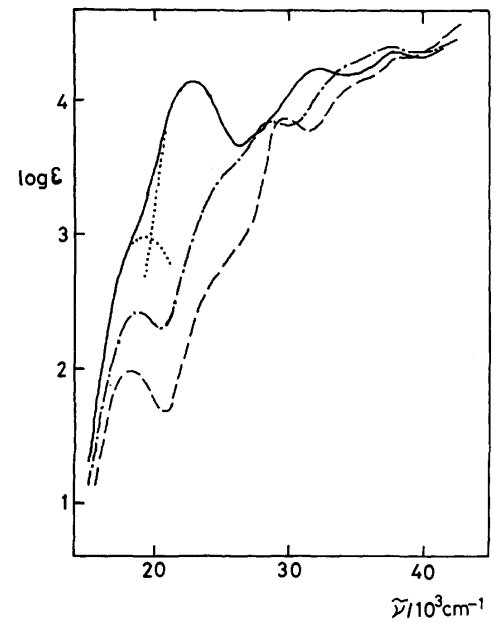

Fig. 3. Absorption spectra of *trans*-$[Co(acac)_2(PMe_2Ph)_2]^+$ (——), *trans*-$[Co(acac)_2(CH_3NH_2)(PMe_2Ph)]^+$ (-·-·-), and *trans*-$[Co(acac)_2(CH_3NH_2)_2]^+$ (-----).

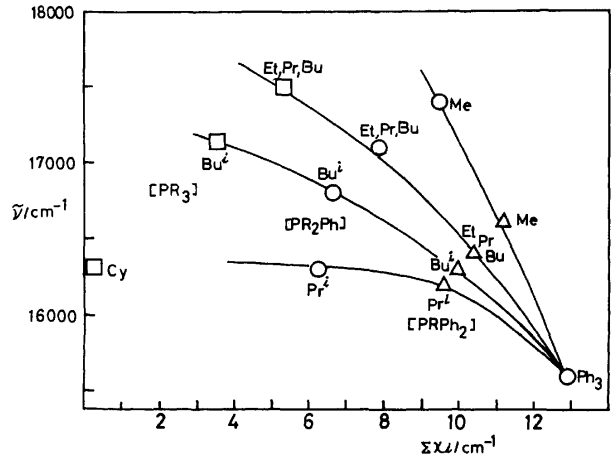

Fig. 4. Plots of the first absorption band(cm^{-1}) of *trans*-$[Co(acac)_2(H_2O)(\boldsymbol{P})]^+$ *vs.* Tolman's substituent additivity value, $\sum\chi i(cm^{-1})$ of the phosphine ligand.

These bands may be assigned to the first absorption band, since the $Ph_2PCH_2CH_2PPh_2$ and $Ph_2PCH_2CH_2CH_2PPh_2$ complexes of the *cis*-[Co(acac)(CN)$_2$(diphosphine)] type also show a similar band in this region with a little smaller intensity of $\log\varepsilon$=3.03 and 3.12, respectively. It has been reported that the first absorption band of *trans*(P,P)-phosphine complexes is always stronger than that of the corresponding cis(P,P) isomers.[2] The same relation is seen between the first absorption bands of *trans*- and *cis*-$[Co(acac)_2(PR_nPh_{3-n})_2]^+$ shown in Fig. 2a and 2d. In the higher energy region, all of the complexes show complicated spectra, and no clear assignment can be made at present.

In Fig. 4 are plotted the absorption maxima of the first bands of *trans*-$[Co(acac)_2(H_2O)(PR_nPh_{3-n})]^+$ *vs.* Tolman's parameters, $\sum\chi i$ (electronic effect) for the

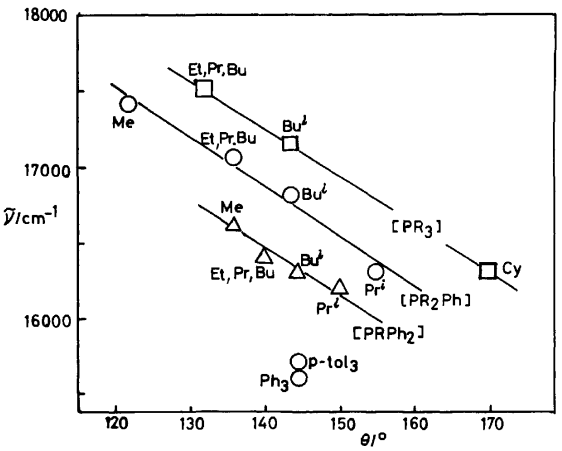

Fig. 5. Plots of the first absorption band(cm^{-1}) of *trans*-[Co(acac)$_2$(H$_2$O)(***P***)]$^+$ *vs.* Tolman's cone angle (θ°) of the phosphine ligand.

phosphine ligands. In general, the absorption maxima shift to high energy with decreasing the value of $\sum\chi i$ (increasing basicity). However, the extent of shift depends clearly on the kind of R on PR$_n$Ph$_{3-n}$; the more bulky the R group becomes, the smaller the extent of shift arises. The PCy$_3$ ligand is much more basic than PPr$^i_2$Ph, but the former is more bulky (Tolman's cone angle: 170°) than the latter (155°), and consequently the complexes of these two phosphines show the first absorption band at nearly the same position. Of the phosphines, four PBu^i_nPh$_{3-n}$ (n=0, 1, 2, 3) have a similar cone angle (*ca.* 145°). Hence the line connecting the points of these phosphines in Fig. 4 would show the electronic effect of phosphines with a constant cone angle (*ca.* 145°) on the first absorption bands of *trans*-[Co(acac)$_2$(H$_2$O)(PR$_n$Ph$_{3-n}$)]$^+$. The complexes with a less bulky phosphine and those with a more bulky one than PB^i_nPh$_{3-n}$ give the first absorption band at higher and lower energy, respectively, than values on the line, when the phosphine has the same $\sum\chi i$ value as that of PBu^i_nPh$_{3-n}$.

Figure 5 shows a plot of the first absorption maxima *vs.* Tolman's cone angles(θ°) (steric effect) for phosphine ligands in the same *trans*-[Co(acac)$_2$(H$_2$O)-(PR$_n$Ph$_{3-n}$)]$^+$ complexes. Good linear relations are seen between the absorption maxima and each group of phosphines, PR$_3$, PR$_2$Ph, and PRPh$_2$, *i.e.*, for each group of phosphines, the absorption maxima shift linearly to lower energy with an increase in cone angle of the phosphine ligand. As stated previously, four PBu^i_nPh$_{3-n}$ have a similar cone angle. The energy difference in absorption maxima of these phosphine complexes should come from the difference in basicity of the phosphines. Thus Figs. 4 and 5 clearly demonstrate that the ligand field strength of phosphines to the Co^{III} ion is dependent not only on the basicity but also on the bulkiness strongly. Similar dependence is seen for the lowest energy bands of the *trans*(P,P)-[Co(acac)(CN)$_2$(PR$_n$Ph$_{3-n}$)$_2$] complexes.

The authors wish to thank the Ministry of Education for Scientific Research Grant-in-Aid No. 58470032.

References

1) C. A. Tolman, *Chem. Rev.*, **77**, 313 (1977).
2) K. Kashiwabara, K. Katoh, T. Ohishi, J. Fujita, and M. Shibata, *Bull. Chem. Soc. Jpn.*, **55**, 149 (1982).
3) L. Maier, "Organic Phosphorus Compounds," ed by L. Maier and G. M. Kosolapott, Wiley, New York (1972), Vol. 1, p. 1.
4) *Inorg. Synth.*, **5**, 188 (1957).
5) *Inorg. Synth.*, **11**, 83 (1968).
6) N. Bresciani-Pahor, M. Calligaris, and L. Randaccio, *Inorg. Chim. Acta*, **39**, 173 (1980).
7) S. Brückner and L. Randaccio, *J. Chem. Soc., Dalton*, **1974**, 1017.
8) N. Bresciani-Pahor, M. Calligaris, L. Randaccio, and L. G. Marzilli, *Inorg. Chim. Acta*, **32**, 181 (1979).
9) F. A. Cotton, D. J. Darensbourg, S. Klein, and B. W. S. Kolthammer, *Inorg. Chem.*, **21**, 2661 (1982).
10) L. M. Ounapu, J. A. Mosbo, J. M. Risley, and B. N. Storhoff, *J. Organomet. Chem.*, **194**, 337 (1980).
11) B. P. Cotosoradis and R. D. Archer, *Inorg. Chem.*, **6**, 800 (1967); **4**, 1584 (1965).
12) L. J. Boucher, C. G. Coe, and D. R. Herrington, *Inorg. Chim. Acta*, **11**, 123 (1974).
13) L. J. Boucher and J. C. Bailar, Jr., *J. Inorg. Nucl. Chem.*, **27**, 1093 (1965).
14) F. Basolo and R. G. Pearson, "Mechanisms of Inorganic Reactions," John Wiley and Sons, New York (1967).
15) K. Kashiwabara, I. Kinoshita, T. Ito, and J. Fujita, *Bull. Chem. Soc. Jpn.*, **54**, 725 (1981).

Optical and ESR Studies on the Micellar Formation with Surfactant Cu(II)-Porphyrin

Kunihiko TAJIMA,* Yuji ISHIKAWA, Kazuo MUKAI, Kazuhiko ISHIZU, and Hiromu SAKURAI†

Department of Chemistry, Faculty of Science, Ehime University, Matsuyama 790

†Faculty of Pharmaceutical Sciences, University of Tokushima, Tokushima 770

(Received December 24, 1983)

Synopsis. A new surface-active porphyrin, 1-dodecyl-4-(10,15,20-triphenyl-5-porphinyl)pyridinium bromide, and its copper complex (Cu(II)DPyTPP) were synthesized. In toluene, chloroform and ethanol, a typical ESR hyperfine structure (hfs) ascribable to monomeric Cu(II) porphyrin was observed. In ethanol containing a buffer of pH=7.4, a reversible formation of the micellar colloid which is strongly dependent on the water/ethanol mixing ratio, was confirmed based on mearsurements of ESR line broadening and the splitting of the Soret band.

As a simple model for naturally occuring Hemeproteins, micellar vesicles which contain surface-active porphyrins have already been reported.[1,2] Yamamura synthesized Cu(II)-4,4′,4″,4‴-(5,10,15,20-porphyneteayl)-tetrakis{1-octadecylpyridinium}tetraiodide, whose ESR spectra revealed a broadened ESR line width, related to strong paramagnetic interactions between the metal active sites in the reversed micellar visicles.[3] On the other hand, Katagi *et al,* found that the Soret band (426nm) of magnesium porphyrins showed a red shift when it was incorporated into liposome vesicles.[4] A concomitant decrease of the absorption intensity was also observed.

To our present knowledge, there have been a few investigations of the Cu(II) porphyrin systems incorporated in the micellar vesicles, in which the ESR and optical spectrographic data were combined in order to understand the physicochemical properties of the metallo-porphyrins systems. We now report on the preparation of a new surface active porphyrin copper complex, Cu(II)DPyTPP, which bears both the hydrophilic pyridinium group and the hydrophobic alkyl group (Fig. 1). At a critical value in the water-ethanol mixing ratio, a reversible formation of micelles was clearly demonstrated based on measurements of the line broadening of the ESR hfs and the anomalous splitting in the Soret band of the Cu(II)-DPyTPP complex.

Experimental

Preparation: $DPyTPPH_2$ was prepared by the N-alkylation of the free base, $PyTPPH_2$, which was obtained from the usual mixed aldehyde method.[5] The N-alkylation of $PyTPPH_2$ was carried out in a refluxing DMF[6] in the presence of a 50-fold excess of dodecyl bromide; yield 70 (%).

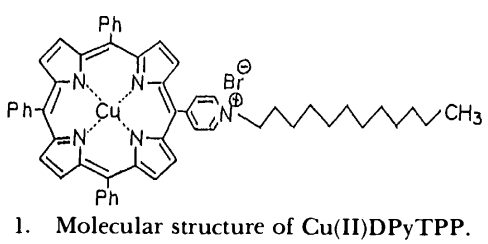

Fig. 1. Molecular structure of Cu(II)DPyTPP.

Found (%): C, 76.37; H, 6.29; N, 8.10; Br, 9.24. Calcd (%) for $C_{55}H_{54}N_5Br$: C, 76.38; H, 6.41; N, 8.03; Br, 9.34. Cu(II)-DPyTPP was prepared by the ordinary method; the 40% excess of dry $CuBr_2$ and $DPyTPPH_2$ were treated in refluxing ethanol for 1 hour under a nitrogen atomsphere.

Found (%): C, 70.84; H, 5.86; N, 7.76; Br, 8.82. Calcd (%) for $C_{55}H_{52}N_5BrCu$: C, 71.13; H, 5.87; N, 7.54; Br, 8.69.

Measurments: ESR measurments were carried out while changing the solvent mixing ratio, r=water/ethanol, 0/10 to 9/1. The final concentration of the copper complex kept in 2×10^{-5}M (1M=1 mol dm^{-3}), and the pH was adjusted to 7.4 with 2×10^{-3}M Tris-Cl. ESR spectra at 77K were recorded with a JEOL-FE-2XG X-band spectrometer with a 100KHz modulation. The magnetic field was calibrated by the splitting of Mn(II) in MgO (A_{3-4}=8.69mT) and the g-values were standardized using Li-TCNQ (g=2.00252) as a reference. The optical spectra were recorded with a JASCO UVDEC-1 spectrometer at room temperature. All the measurements were performed at the Advanced Instrumental Center for Chemical Analysis, Ehime University.

Results and Discussion

The optical spectrum of Cu(II)DPyTPP measured in ethanol was identical with that reported previously (Soret band λ_{max}=426nm, $\varepsilon=2.31\times10^5$, α-band; λ_{max}=548nm, $\varepsilon=22\times10^3$, β-band; λ_{max}=578nm, $\varepsilon=3\times10^3$).[7] When the buffer solution was added to the ethanol solution, the intensity of the Soret band decreased depending on the solvent composition, but no significant shift of λ_{max} was observed in both the Soret band and α-band until r=4/6, as shown in Fig. 2. When the r-value became about 7/3, a drastic spectral change was observed involving an abrupt decrease of the Soret band and a splitting of the Soret band into two different absorption maxima, (λ_{max}=440nm, $\varepsilon=4.96\times10^4$ and λ_{max}=392nm, $\varepsilon=2.6\times10^4$) (Fig. 2). A concomitant red shift was also noted in the α-band from 540nm to 553nm. With higher r-values than 7/3, the sparated maxima in the Soret band began to merge into a single peak with an increased ε-value and the α-band blue shifted, (Fig. 2). The observed trend in the visible absorption spectra is consistent with a spectral change reported for a surfactant Mg(II) porphyrin incorporated into liposome vesicles.[4] The formation of micelles with our surfactant Cu(II)porphyrin, therefore, was suggested. In order to understand the mechanism of this surfactant porphyrin in detail, studies were made with the aid of ESR spectrometry. As shown in Fig. 3-a, a well resolved hfs of the monomeric Cu(II)DPyTPP was ovserved in ethanol. The observed ESR parameters were actually identical with those measured in toluene and chloroform, ($g_{//}$=2.196, $g_{\perp}$=2.067, $A_{\perp}=203.8\times10^{-4}$cm^{-1}).[8] When a buffer solution was added to the ethanol, a slight decrease in the ESR line intensity ascribed to the ligand N hyperfine was ob-

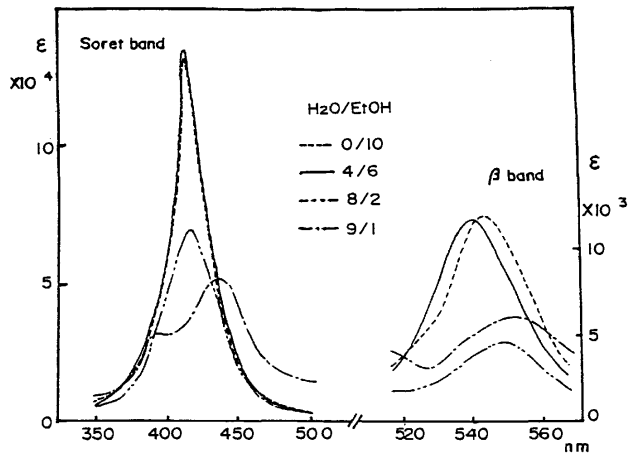

Fig. 2. Absorption spectra of Cu(II)DPyTPP (2×10^{-5} M), with various mixing ratio of ethanol and water, where the pH was adjusted to 7.4 by Tris-Cl (2×10^{-3}M).

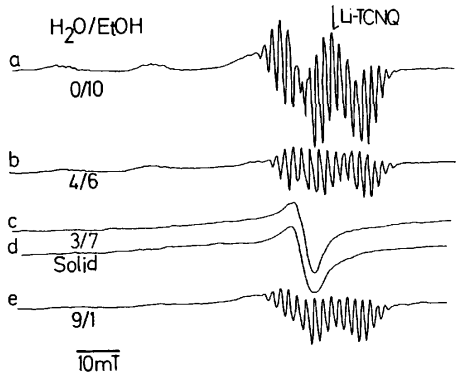

Fig. 3. ESR spectra of Cu(II)DPyTPP (2×10^{-5}M) at 77K, with various mixing ratio of ethanol and water, where the pH adjusted to 7.4 by Tris-Cl (2×10^{-3}M).

served. However, the mangitude of the hfs for both copper and the ligand N atoms showed no significant changes unitil $r=4/6$, as shown in Fig. 3-b. An abrupt decrease in the net ESR line intensity and anomalous line broadening occures at the r-value 7/3, where hyperfine splittings for ligand N and copper atoms were smeared out except for the hfs due to the g-anisotropy. It is notewothy that the ESR line shape of Fig. 3-c was analogous to that measuerd for a powdered Cu(II)DPyTPP complex, Fig. 3-d. A similar line broadening due to a clustering of the copper tetra-alyl porphyrin has been described for copper complexes involving the surfactant active porphyrins upon the micellar formation.[3] The central copper ions interact magnetically in such a way as to smear out the copper nuclear hyperfine interaction. The ESR spectra of the dimer Cu(II) obtained from the proto-porphyrin derivatives have already been reported, and the internuclear distance between the copper ions were found to lie in a range from 3.5 to 4 Å.[9] Many trials were made to detect the formation of the triplet species in the ESR spectra. In the persent case, however, positive evidence for the dimer formation was hardly obtained everywhere. With a further addition of the buffer solution, 9/1, the ESR signal again revealed a well resolved hfs due to the monomeric Cu(II) and ligand N was clearly detected as shown in Fig. 3-e, ($g_{//}=2.202$, $g_{\perp}=2.064$, $A_{//}=195\times10^{-4}\,cm^{-1}$). In comparision with the values measured in a weak polar solvent, such as chloroform and toluene, the observed $g_{//}$-value was slightly higher and the $A_{//}$-value was, conversely, reduced. On the bases of the observation of the optical and ESR spectra, some important notions on micelle formation with a surfactant metallo-porphyrin can be deduced. For lower contents of water (0/10 to 4/6) the spectroscopic data suggest that a relatively small intermolecular interaction exists between each chromophore. The decrease in the magnitude of the ESR line intensity and the disappearance of the ligand N hyperfine observed in the medium water content, 4/6 to 7/3, might be attributed to an electron spin-spin interaction among the metal sites, which can be accessible together by the hydrophobic interaction between the long alkyl chains. The splittings of the Soret band supported the evidence that the metalloporphyrin actually formed the micellar vesicles. For r-values greater than 9/1, the reappearance of a well resolved ESR hfs and the collapes of the splittings in the Soret band were observed. These findings suggest that a molecular rearrangement on metalloporphyrin array occurs in the micell vesicles, in which the interaction between the active sites is reduced. Such a rearrangement of metallo-porphyrin is probably due to the hydration of the metal chrmophore, where the hydration would be greatly accelerated by the hydrophilic pyridinium group involved in the surfactant porphyrin. In this situation, the solvation of the water molecule causes a distortion of the copper porphyrin, as judged from the trend in the observed ESR parameter. This trend indicates that the $g_{//}$-value shows a slight increase while the $A_{//}$- value is reduced.[10] The results herein may provide not only a model for metalloporphyrin containing proteins but also a useful tool for understanding the orientation of the metalloporphyrin moiety in proteins.

References

1) M. Calvin, *Acc. Chem. Res.*, **11**, 369 (1978).
2) T. Matsuo, K. Itoh, K. Takuma, K. Hashimoto, and T. Nagamura, *Chem. Lett.*, **1980**, 1009.
3) T. Yamamura, *Chem. Lett.*, **1977**, 773.
4) Y. Katagi, T. Yamamura, T. Saito, and Y. Sasaki, *Chem. Lett.*, **1982**, 417.
5) A. D. Adler, E. R. Longo, and W. Shergalis, *J. Am. Chem. Soc.*, **86**, 3145 (1964).
6) Y. Okuno, W. E. Ford, and M. Calvin, *Synthesis*, 537 (1980).
7) M. Goutman, *J. Mol. Spectroscopy*, **6**, 138 (1961).
8) J. M. Assour, *J. Chem. Phys.*, **43**, 2477 (1965).
9) P. D. W. Boyd, T. D. Smith, J. H. Price, and J. R. Pilbrow, *J. Chem. Phys.*, **56**, 1253 (1972).
10) K. Miyoshi, H. Tanaka, E. Kimura, S. Tsuboyama, S. Murata, H. Shimizu, and K. Ishizu, *Inorg. Chim. Acta.*, **78**, 23 (1983).

Ab Initio Gradient Calculation of the Molecular Structures of Dimethyl Ether and Dimethyl Sulfide

Akira TSUBOYAMA, Kouichi TAKESHITA, Shigehiro KONAKA, and Masao KIMURA*
Department of Chemistry, Faculty of Science, Hokkaido University, Sapporo 060
(Received June 28, 1984)

Synopsis. The molecular structures and torsional potentials of $(CH_3)_2O$ and $(CH_3)_2S$ have been calculated by the *ab initio* gradient method using a MIDI-4 basis set augumented with polarization functions. The calculations have confirmed that the molecules take the staggered-staggered conformation with C_{2v} symmetry.

According to microwave spectroscopic studies, dimethyl ether[1] and dimethyl sulfide[2] molecules have C_{2v} symmetry in the equilibrium state and each methyl group is staggered against the opposite C–O or C–S bond. However, there remains a possibility of a near staggered-staggered conformation with C_2 symmetry. Actually, the torsional angle, τ, for dimethyl ether was calculated to be 4° from the r_s-structure (as for the definition of τ, see Fig. 1), although Blukis *et al.* ascribed it to the zero-point torsional effect because such a small separation of the two potential minima requires an unreasonably high and sharp potential hump between them.[1] Recently Tamagawa *et al.*[3] have studied the structure of dimethyl ether by a joint analysis of the electron-diffraction and microwave spectroscopic data and determined τ to be 2(11)°. The possibility of C_2 symmetry has thus not been excluded.

Lombardi *et al.* performed a conformational analysis of dimethyl ether based on a model where the barrier to internal rotation was assumed to arise only as a result of exchange interactions among electrons on nonbonded atoms and lone-pair electrons on the oxygen.[4] According to their calculation, the torsional potential of dimethyl ether has two separate minima at $\tau=\pm17.5°$ and the height of the barrier between them is 0.52 kcal/mol.† It may be noted that their exchange perturbation theory was successfully applied to the calculation of the rotational barriers of more than thirty molecules.[5]

A recent electron-diffraction study[6] has revealed that the di-*t*-butyl sulfide molecule takes only one stable conformation of C_2 symmetry with the *t*-butyl groups rotated by 12(8)° from the staggered conformation. Although no question has so far been raised on the molecular symmetry of dimethyl sulfide, it is worthwhile to investigate it theoretically in connection with dimethyl ether and di-*t*-butyl sulfide.

A number of *ab initio* MO calculations have been reported for dimethyl ether and dimethyl sulfide. The barriers to internal rotation have been studied with the STO-3G basis set,[7,8] but the possibility of a near staggered-staggered conformation has not been examined. The bond lengths and angles of dimethyl ether for the staggered model have been calculated by several authors,[9–11] but no *ab initio* calculation has been reported for the structural parameters of dimethyl sulfide. The purpose of the present work is to study the torsional potentials and structures of these molecules by *ab initio* calculations using Pulay's gradient method.[12] The JAMOL3 program[13] and the MIDI-4 basis set,[14] augumented with d polarization functions for the C, O, and S atoms, were used for the SCF-LCAO-MO calculations, while geometry optimizations were performed with the GRAMOL program[15] by assuming C_2 symmetry. Optimizations were repeated until the largest atomic forces were of the order of 2×10^{-2} mdyn.††

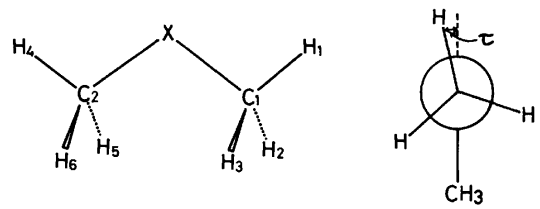

Fig. 1. Numbering of atoms and definition of the torsional angle, τ. X represents O or S.

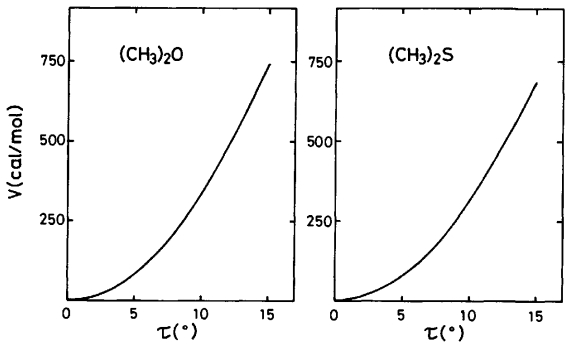

Fig. 2. Torsional potentials for dimethylether and dimethylsulfide.

The calculated torsional potentials are displayed in Fig. 2. The minima of the potentials are at $\tau=0$. The calculated potentials cover only a limited range of τ-values, but they fit well into a simple analytical expression for the torsional potentials with threefold symmetry, *i.e.*, $V_3(1-\cos3\tau)$. The values of the potential barrier, V_3, were thus estimated to be 2.5 and 2.3 kcal/mol for dimethyl ether and dimethyl sulfide respectively. The experimental values of V_3 are 2.72[1] and 2.70 kcal/mol[16] for dimethyl ether and 2.1 kcal/mol[2] for dimethyl sulfide. The present calculations give potential barriers close to the experimental data.

The calculated geometrical parameters are compared with the observed ones in Table 1. The agreement between the calculated and experimental geometries is

†1 cal/mol=4.184 J/mol.

††1 mdyn=10^{-8} N.

TABLE 1. STRUCTURAL PARAMETERS FOR DIMETHYL ETHER AND DIMETHYL SULFIDE[a]

	$(CH_3)_2O$			$(CH_3)_2S$		
	r_e[b]	r_s[c]	r_{av}[d]	r_e[b]	r_s[e]	r_{av}[f]
r(C-X)/Å	1.389	1.410(3)	1.413(1)	1.817	1.802(2)	1.805(2)
r(C-H_1)Å	1.089	1.091(7)	1.108(2)[g]	1.092	1.091(5)[g]	1.104(3)[g]
r(C-H_2)/Å	1.097	1.100(5)		1.093		
∠CXC/°	114.1	111.7(3)	111.8(2)	99.5	98.9(2)	99.05(4)
∠XCH_1/°	107.6	107.2(6)		107.3		
∠XCH_2/°	111.5	110.8(3)		110.9		
∠H_1CH_2/°	108.8	109.5(6)	109.2(2)[h]	108.9	109.6(3)[h]	109.3(5)[h]
∠H_2CH_3/°	108.5	108.7(5)		109.8		
θ[i]/°	2.6	2.5(7)	3.6(17)	2.4	2.45(25)	2.35[j]
E[k]/a.u.[l]	−153.8834			−475.8927		

a) The numbers in parentheses represent the limits of error attached to the last significant digits. See Fig. 1 for atomic numbering. b) Equilibrium structures calculated in the present study. c) r_s-structure from Ref. 1. d) Zero-point average structure from Ref. 3. e) r_s-structure from Ref. 2. f) Zero-point average structure from Ref. 17. g) Average C-H distance. h) Average HCH angle. i) θ is the tilt angle of the methyl groups, which is defined as the angle between the C-X bond and a line perpendicular to the H_3 plane. j) Assumed value. k) Total energy. l) 1 a.u.=4.359814×10^{-18} J.

reasonable. The present calculations demonstrate that both dimethyl ether and dimethyl sulfide molecules take the staggered conformation with C_{2v} symmetry in the equilibrium state. Computations were performed on a HITAC M-200H of the Institute for Molecular Science.

References

1) U. Blukis, P. H. Kasai, and R. J. Myers, *J. Chem. Phys.*, **38**, 2753 (1963).

2) L. Pierce and M. Hayashi, *J. Chem. Phys.*, **35**, 479 (1961).

3) K. Tamagawa, M. Takemura, S. Konaka, and M. Kimura, *J. Mol. Struct.*, in press.

4) E. Lombardi, G. Tarantini, L. Pirola, and P. Torsellini, *J. Chem. Phys.*, **64**, 5229 (1976).

5) E. Lombardi, G. Tarantini, L. Pirola, L. Jansen, and R. Ritter, *J. Chem. Phys.*, **61**, 894 (1974).

6) A. Tsuboyama, S. Konaka, and M. Kimura, *J. Mol. Struct.*, in press.

7) F. F. Roelandt, D. F. van de Vondel, and G. P. van der Kelen, *J. Mol. Struct. THEOCHEM*, **76**, 187 (1981).

8) M.-H. Whangbo and S. Wolfe, *Can. J. Chem.*, **55**, 2778 (1977).

9) C. E. Blom, L. P. Otto, and C. Altona, *Mol. Phys.*, **32**, 1137 (1976).

10) J. O. Williams, J. N. Scarsdale, and L. Schäfer, *J. Mol. Struct.*, **76**, 11 (1981).

11) J. E. Boggs, M. Altman, F. R. Cordell, and Y. Dai, *J. Mol. Struct.*, **94**, 373 (1983).

12) P. Pulay, *Mol. Phys.*, **17**, 197 (1969); *Theor. Chim. Acta*, **50**, 299 (1979).

13) H. Kashiwagi, T. Takada, E. Miyoshi, and S. Obara, Program JAMOL3 from the Program Library, the Hokkaido University Computing Center, Sapporo, Japan. See, *e.g.*, K. Ohno, "Horizons of Quantum Chemistry," ed by K. Fukui and B. Pullman, Reidel, Dordrecht (1979), p. 245.

14) H. Tatewaki and S. Huzinaga, *J. Comput. Chem.*, **1**, 205 (1980).

15) K. Takeshita and F. Sasaki, Program GRAMOL from the Program Library, the Hokkaido University Computing Center, Sapporo, Japan.

16) P. Groner and J. R. Durig, *J. Chem. Phys.*, **66**, 1856 (1977).

17) T. Iijima, S. Tsuchiya, and M. Kimura, *Bull. Chem. Soc. Jpn.*, **50**, 2564 (1977).

Vibronic-Level Dependence of the Radiative Decay Rate in Pyrazine and Pyrimidine Vapors: Re-examination under High Spectral Resolution

Osamu SEKIGUCHI, Nobuhiro OHTA, and Hiroaki BABA*

Division of Chemistry, Research Institute of Applied Electricity, Hokkaido University, Sapporo 060

(Received July 16, 1984)

Synopsis. The radiative decay rate constants (k_F) for vibronic levels in S_1 of pyrazine and pyrimidine were derived by using the quantum yields measured under the conditions of SVL excitation. The vibronic level dependence of k_F in pyrazine can be explained by the Herzberg-Teller theory.

Pyrazine and pyrimidine are prototypes of intermediate-case molecules and their fluorescence emissions consist of two components, fast and slow fluorescence, in the vapor phase at low pressure. The vibronic coupling through the ν_{10a} vibration in the S_1 state of pyrazine was studied by Yamazaki *et al.*[1,2] From quantum yields and lifetimes measured for the fast fluorescence, they derived the radiative decay rate constants for individual vibronic levels, and compared these experimental decay constants with theoretical ones obtained on the basis of the Herzberg-Teller theory. They concluded that the theory overestimates the rate constants for levels involving the ν_{10a} vibration. However, their quantum yields were obtained with the spectral resolution ($\approx 20\,cm^{-1}$) insufficient for exciting single vibronic levels (SVL) separately,[1] while their lifetimes were obtained with significantly higher resolution.[2] We have newly measured the SVL fluorescence quantum yields for pyrazine and pyrimidine in the vapor phase with narrow-band excitation ($\approx 0.5\,cm^{-1}$) and re-examined the magnitude of the vibronic coupling in pyrazine. In this study we are solely concerned with the fast fluorescence; hereafter it will be simply called fluorescence.

Experimental

The apparatus and the method for optical measurements were the same as described previously;[3,4] the exciting laser pulse has a bandwidth of $\approx 0.5\,cm^{-1}$. The sample vapors were at moderately high pressures (17.0 mTorr† pyrazine +12.2 Torr SF_6, and 156 mTorr pyrimidine+36 Torr SF_6), where the slow component is quenched completely and the fast is free from collision.[3] Since the excitation spectra were obtained by monitoring a part of the total fluorescence intensity, a correction was made so that the ratio of the actually monitored intensity to the total might be constant for all the bands studied.

Results and Discussion

Figure 1 shows absorption and fluorescence-excitation spectra for pyrazine. Owing to the high resolution, vibronic bands (*e.g.*, $10a_0^1$ and $6a_0^1 16b_1^1$) are well separated from one another and even their band contours are discernible to a certain extent. The relative fluorescence quantum yield for each SVL was obtained by comparing the integrated intensity of the band, related to the SVL, in the excitation spectrum with that of the corresponding absorption band. In either case the contribution of the underlying continuum due to the overlapping of the other bands was subtracted from the integrated intensity.

The SVL fluorescence quantum yields (Φ_F) of pyr-

†1 Torr≈133.322 Pa.

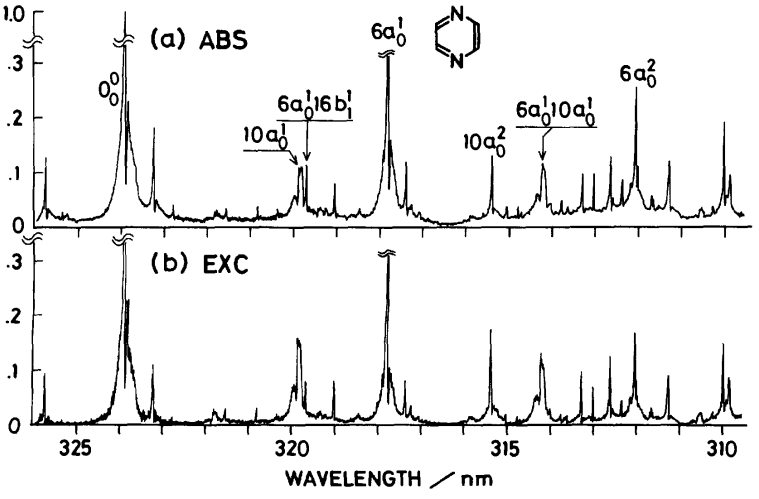

Fig. 1. Absorption spectrum (a) and fluorescence excitation spectrum (b) for pyrazine. In each spectrum, the peak height of the 0_0^0 band is normalized to unity. The peak heights of the $6a_0^1$ band in the absorption and excitation spectra are 0.74 and 0.50, respectively. The excitation spectrum has been corrected for the variation of the exciting laser intensity, but in this spectrum the correction described in the text has not been made.

TABLE 1. QUANTUM YIELDS, LIFETIMES AND RADIATIVE RATE CONSTANTS

	Level	Φ_F	τ_F[b]	k_F^{exp}[c]	k_F^{theor}[d]
		10^{-4}	ns	$10^6 s^{-1}$	$10^6 s^{-1}$
Pyrazine	0^0	1.4[a]	0.12	1.2	1.2
	$10a^1$	3.3	0.15	2.2	2.0
	$6a^1$	1.5	0.11	1.4	1.2
	$10a^2$	3.4	0.16	2.2	2.8
	$6a^110a^1$	3.3	0.13	2.5	2.0
	$6a^2$	2.0	0.11	1.9	1.2
Pyrimidine	0^0	39[a]	2.8	1.4	
	$6a^1$	18	2.0	0.90	
	$6b^2$	14	1.9	0.74	
	1^1	9.6	1.6	0.60	
	12^1	15	1.9	0.79	
	$6a^2$	9.7	1.3	0.75	
	$6a^112^1$	9.1	1.4	0.65	
	12^2	7.8	1.4	0.56	
	$6a^212^1$	9.1	1.4	0.65	

a) The absolute Φ_F value for the 0^0 level was determined by reference to the data in Ref. 3. b) The lifetimes for pyrazine were taken from Ref. 2, and those for pyrimidine were newly measured in this study with an excitation bandwidth of $\approx 0.5\,cm^{-1}$. c) Experimentally obtained k_F. d) Theoretically obtained k_F; the relative values of k_F originally obtained from the theory were placed on an absolute scale by fitting $k_F^{theor}(0^0)$ to $k_F^{exp}(0^0)$.

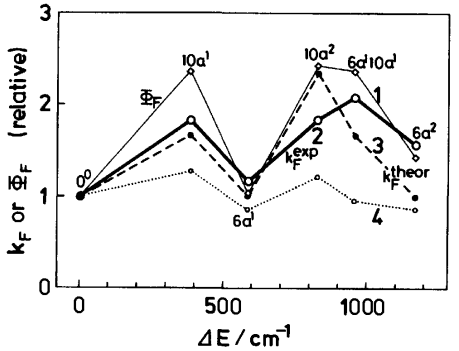

Fig. 2. Relative values for Φ_F and k_F plotted against ΔE for pyrazine: (1) Φ_F; (2) k_F^{exp}; (3) k_F^{theor}; (4) k_F, obtained in a low resolution experiment. Values in (1)—(3) were obtained in this study and those in (4) were taken from Ref. 2.

azine are given in Table 1, and a plot of Φ_F against the excess vibrational energy (ΔE) is shown in Fig. 2 by a lean solid line. The values of Φ_F for the levels involving $10a^j$ (Φ_F^j) are significantly larger than that for the 0^0 level (Φ_F^0), *i.e.*, $\Phi_F^j/\Phi_F^0 \gtrsim 2$ for $j \geq 1$. The ν_{10a} (b_{1g}) vibration can induce vibronic coupling between $S_1(^1B_{3u})$ and $S_2(^1B_{2u})$. Since the transition from S_0 to S_2 has a much larger oscillator strength, levels involving $10a^j$ will show larger radiative decay rate constants (k_F), and hence larger Φ_F values, than do the other vibronic levels. It is to be noted, however, that large Φ_F values may result not only from large k_F values but also from small total decay constants, as pointed out by Yamazaki *et al.*[2]

The values of k_F were obtained by combining the values of Φ_F measured in the present study with the lifetimes (τ_F) reported by Yamazaki *et al.*[2] (Table 1). As is shown in Fig. 2 with a thick solid line, the resulting k_F values vary with ΔE more widely than those obtained from the low resolution study[2] (shown by a dotted line). The values of k_F, like those of Φ_F, are obviously large for the levels involving $10a^j$, *i.e.*, $k_F^j/k_F^0 \gtrsim 2$ for $j \geq 1$. This is a direct manifestation of the vibronic coupling through the ν_{10a} vibration.

We treat the vibronic-level dependence of k_F in pyrazine by means of the Herzberg-Teller theory[5] assuming the harmonic oscillator approximation for the ν_{10a} vibration. Although ν_{10a} is known to be anharmonic,[6] the anharmonicity is not large enough to produce a significant effect on the following discussion.[1] The radiative decay rate constant for the $10a^j$ level relative to that for the zero-point level is given by[1]

$$\frac{k_F^j}{k_F^0} = \frac{1+(\zeta/u)(2j+1)}{1+\zeta/u}, \qquad (1)$$

where j is the quantum number of ν_{10a}, ζ the intensity ratio of the $10a_0^1$ absorption band to the 0_0^0, and u is a numerical factor equal to 0.346 in this case. Yamazaki *et al.*[1] derived $\zeta=0.23$ for pyrazine from a high resolution spectrum. We obtained $\zeta=0.18$ by excluding the underlying continuum, although 0.23 was obtained by including it. The value of k_F calculated theoretically by using $\zeta=0.18$ is plotted against ΔE, with the result shown in Fig. 2 by a broken line (see also Table 1). It is seen that with respect to k_F the present experimental result agrees fairly well with what is predicted by the simple Herzberg-Teller theory.

For pyrimidine, the experimental k_F value, obtained in the same manner as k_F of pyrazine, was found to decrease roughly monotonically up to $\Delta E \approx 2500\,cm^{-1}$ (Table 1), as in the case of the low resolution study, indicating that the vibronic levels in S_1 pyrimidine are not appreciably perturbed by vibronic coupling.

References

1) I. Yamazaki, M. Fujita, and H. Baba, *Chem. Phys.*, **57**, 431 (1981).
2) I. Yamazaki, T. Murao, and K. Yoshihara, *Chem. Phys. Lett.*, **87**, 384 (1982).
3) H. Baba, N. Ohta, O. Sekiguchi, M. Fujita, and K. Uchida, *J. Phys. Chem.*, **87**, 943 (1983).
4) H. Baba, M. Fujita, N. Ohta, and Y. Shindo, *J. Spectrosc. Soc. Jpn.*, **29**, 387 (1980).
5) A. C. Albrecht, *J. Chem. Phys.*, **33**, 156 (1960).
6) D. L. Narva and D. S. McClure, *Chem. Phys.*, **11**, 151 (1975).

Solvent Extraction of Copper(II) with 2-(*o*-Hydroxyphenyl)benzothiazole

Kenji SHIMIZU and Akiko FURUHASHI*
Department of Chemistry, Aoyama Gakuin University, 1626 Ono, Atsugi 243-01
(Received January 10, 1984)

Synopsis. Equilibrium and kinetic aspects of the solvent extraction of Cu(II) with 2-(*o*-hydroxyphenyl)benzothiazole have been carried out using a water–chloroform system. The complex extracted into chloroform was greenish-brown in color and the absorbance at 490.0 nm obeyed Beer's law up to 2×10^{-4} mol/dm^3. The complex was 1:2 (Cu^{2+}:ligand) type and the over-all stability constant, β_2, was 1.3×10^{17} at an ionic strength of 0.3. The extraction constant, K_{ex}, was 2.5×10^{-8}. The extraction kinetics were first order with Cu(II) ions and the reagent anions. The rate constant for the reaction was found to be 5.0×10^{9} mol^{-1} min^{-1}.

Solvent extraction (liquid-liquid extraction) of metal chelate complexes has been used as a separation method for a long time. For extraction of metal ions, it is preferable that the chelating reagent used has a high distribution coefficient (K_{DR}) and pH dependence in the system chosen. Thus, dithizone,[1] 8-quinolinol, cupferron and others have been used widely.[2] In this study, extraction of copper(II) with 2-(*o*-hydroxyphenyl)benzothiazole was investigated. It could have been expected that this reagent would be effective for extraction of certain metal ions because of its high molecular weight and low solubility in water. The reagent forms complex compounds with certain metal ions such as Co(II), Pb(II), and Ni(II).[3] However, there is no report of solvent extraction being attempted with this reagent. On the other hand, its luminescence properties have been studied.[4] In this paper, equilibrium and kinetic studies with this reagent of copper(II) in a water–chloroform system are reported.

Experimental

Reagents. 2-(*o*-hydroxyphenyl)benzothiazole(HPBT) was obtained from INC Pharmaceuticals Inc. All reagents for this study were of reagent grade from Wako Chemical Co. Ltd.

Instrumentation. The atomic absorption spectra were obtained using a Nippon Jarrel Ash AA-1 Mark-II Atomic Absorption Spectrophotometer by the use of air and acetylene flame. The electronic spectra were obtained with a Shimazu UV-240 Spectrophotometer.

All equilibrium extraction were performed by agitating the samples in 25 dm^3 vials for 30 min (120 strokes/min) at 25±1 °C. After agitation, the solutions were allowed to stand for 10 min before further operations were carried out.†

The kinetic study was carried out in the same manner as the equilibrium investigation, and only the agitating time was changed.

Measurement of Reagent Distribution Constant (K_{DR}). Equal volumes (6 dm^3) of 0.1 mol/dm^3 solution of HPBT in chloroform and the appropriate buffer solution were shaken and the aqueous phase was pipetted into a glass tube and centrifuged. The pH was adjusted to the first measured pH. Then 4.5 dm^3 each of the aqueous phase and chloroform were shaken together. The absorbance of the organic phase at 334.7 nm was measured. The distribution ratio D was obtained by the $D=(\varepsilon C_o-A_f)/A_f$, where ε is the molar absorptivity, C_o is original concentration of HPBT in chloroform and A_f is final absorbance of the chloroform layer.

Distribution Measurement of Copper(II). A 5-dm^3 chloroform solution of HPBT (0.01—0.03 mol/dm^3) and an equal volume of a buffer solution (pH, 1—13) containing Cu(II) ion*1 of 2×10^{-4} mol/dm^3 were agitated. The copper content in the chloroform layer was determined by atomic absorption spectra using the 324.8-nm line.

The absorption spectra of the chloroform layer were determined over the range 350—700 nm. At 490.0 nm the absorbance obeyed Beer's law up to 2×10^{-4} mol/dm^3 of Cu(II). Consequently, the determination of copper extracted into chloroform was carried out by the spectrophotometric method.

The extractability (E%) and distribution ratio (D) are obtained by the equations $E\%=A_2/A_1\times100$ and $D=E/(100-E)$, where A_1, is the copper concentration in the initial aqueous phase and A_2 is the copper concentration in the chloroform at extraction equilibrium.

Measurement of Distribution Coefficient of Copper Complex (K_{DC}). 5 dm^3 each of 2×10^{-1} mol/dm^3 of HPBT solution in chloroform and 2×10^{-3} mol/dm^3 of copper ion*2 in buffer solution (pH=9.0) were agitated. Then 4.5 dm^3 each of the aqueous layer and chloroform were shaken and the absorbance of the chloroform layer was measured at 490.0 nm. K_{DC} can be obtained as the equation $K_{DC}=A_1/A_2$, where A_1 and A_2 are absorbance of the chloroform layers first and second extracted, respectively.

Results and Discussion

The theoretical basis for the determination of the several constants will not be discussed here in detail. They are not special and a number of references are available.[5–7]

Distribution of Reagent. Experimental results were shown in Fig. 1. The constants for HPBT are tabulated in Table 1.

Extraction of Copper. Extractability of copper changes according to pH as was showm in Fig. 2. The plots of log D against pH (fixed concentration of HPBT) or log [HPBT] (fixed pH) showed linear relations and their slopes were all 2. The results indicate the extracted complex has 1:2 (Cu^{2+}:HPBT) composition.[8] The results for the complex were summarized in Table 2. The over-all stability constant (β_2) is smaller than that of the 8-quinolinol complex (23.4)[9] although the molecular weight of HPBT is larger and pK_{a2} is higher as compared with the respective values for 8-quinolinol. It can be presumed that HPBT forms a six-membered chelate ring with the metal ion but 8-quinolinol forms a five-membered chelate ring. Free rotation of the hydroxyphenyl group and the bonding distance with copper(II) may influence the result.

Kinetic of Extraction of Copper(II) Ion. The reaction with the metal ion was taken to obey a first order reaction by analogy with other work.[10] The

†The condition was investigated previously.

*1, *2, Copper (II) acetate was used. The results when copper (II) nitrate was used did not change.

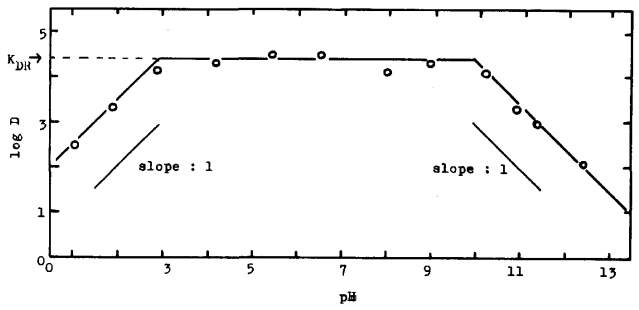

Fig. 1. Distribution ratio change of HPBT with pH in water-chloroform system.

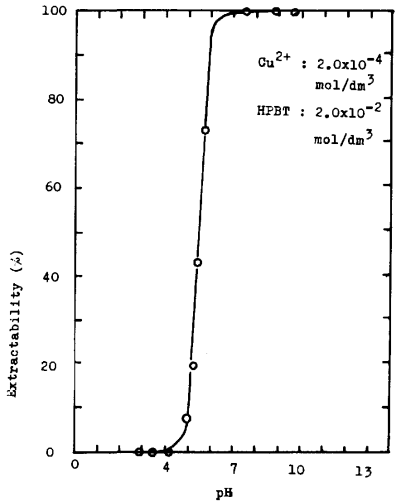

Fig. 2. Extractability change of Cu^{2+} with HPBT with pH.

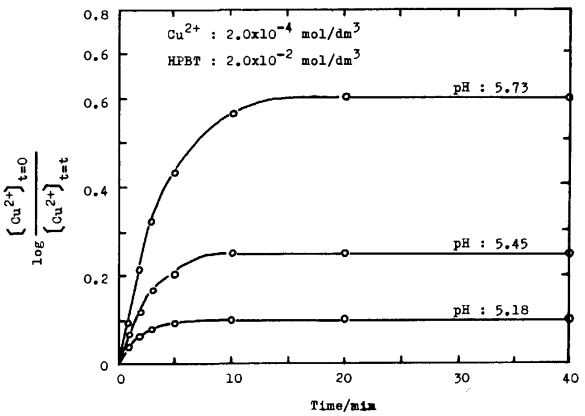

Fig. 3. Relationship between $\log[Cu^{2+}]_{t=0}/[Cu^{2+}]_{t=t}$ and extraction time.

reaction rate should be given by

$$-d[Cu^{2+}]/dt = k[Cu^{2+}][PBT^-] \quad (1)$$

for the slowest reaction $Cu^{2+}+PBT^- \rightarrow [Cu\cdot PBT]^+$. For this reaction, the rate constant, k, is presented. An equation

$$\log(\log[Cu^{2+}]_{t=0}/[Cu^{2+}]_{t=t}) = \log(kK_{a2}/2.303K_{DR}) + \log[HPBT]_o + pH + \log t$$

can be obtained by substituting $K_{a2}=[H^+][PBT^-]/[HPBT]$ and $K_{DR}=[HPBT]_{org}/[HPBT]_w$ into the Eq. 1 and integration. The plots of $\log(\log[Cu^{2+}]_{t=0}/[Cu^{2+}]_{t=t})$ *vs.* pH and $\log[HPBT]_0$ showed linear relations with all slopes equal to unity, indicating that the rate-determining step was controlled by the formation of the 1 : 1 complex. The initial slopes were changed in the plots of $\log[Cu^{2+}]_{t=0}/[Cu^{2+}]_{t=t}$ *vs.* time as were shown in Fig. 3. The kinetic data are shown in Table 3. From this the rate constant, k, can be calculated by the relation $k=k'\times K_{DR}/K_{a2}$, where k'=slope$\times$2.303$[H^+]$/ $[HPBT]_0$.

The value of k thus obtained was 5.0×10^9 mol^{-1} min^{-1}. The value is relatively large compared with the case of the extraction of Co^{2+} and Ni^{2+} with dithizone. It is assumed that this is due to the Jahn-Teller effect. Namely, water molecules on the z axis are liberated easily.[7] For Co^{2+} extraction with HPBT, we obtained $k=4.2\times10^5$ mol^{-1} min^{-1}.

Table 1. Distribution and dissociation constants of HPBT

$\log K_{DR}$*1	$pH_{1/2}$*2	pK_{a1}	$pH_{1/2}$*2	pK_{a2}
4.4	−1.6	2.8	14.5	10.1

*1, $K_{DR}=[HPBT]_o/[HPBT]_w$, *2, At these points, log D=O

Table 2. Extraction and stability constants of Cu(II) complex

$pH_{1/2}$*1	K_{DC}	K_{ex}	β_2
5.5	2.0×10^4	2.5×10^{-8}	1.3×10^{17}

*1, 50% of Cu^{2+} is extracted into chloroform from water.

Table 3. Kinetic data for extraction of Cu(II)

$[HPBT]_0$	$[H^+]$	slope	k'
2.0×10^{-2}	6.61×10^{-6}	2.07×10^{-2}	1.58×10^{-5}
2.0×10^{-2}	3.55×10^{-6}	3.91×10^{-2}	1.60×10^{-5}
2.0×10^{-2}	1.86×10^{-6}	10.6×10^{-2}	2.27×10^{-5}
1.4×10^{-2}	6.61×10^{-6}	1.19×10^{-2}	1.29×10^{-5}
1.4×10^{-2}	3.55×10^{-6}	3.15×10^{-2}	1.84×10^{-5}
1.4×10^{-2}	1.86×10^{-6}	5.05×10^{-2}	1.55×10^{-5}
1.0×10^{-2}	6.61×10^{-6}	0.90×10^{-2}	1.37×10^{-5}
1.0×10^{-2}	3.55×10^{-6}	1.70×10^{-2}	1.39×10^{-5}
1.0×10^{-2}	1.86×10^{-6}	3.11×10^{-2}	1.33×10^{-5}
			Av. 1.58×10^{-5}

The authors would like to express their appreciation to professor K. Kimura of Aoyama Gakuin University.

References

1) H. Irving, S. J. H. Cooke, S. C. Woodger, and R. J. P. Williams, *J. Chem. Soc., Dalton Trans*, **1949**, 1841.
2) N. P. Komar, and I. G. Perkov, *J. Anal. Chem. USSR*, **19**, 19-2, 145 (1964).
3) R. G. Charles, and H. Freiser, *Anal. Chim. Acta*, **11**, 1 (1954).
4) R. Nakagaki, T. Kobayashi, and S. Nagakura, *Bull. Chem. Soc. Jpn.*, **51**, 1671 (1978).
5) T. Sekine, and Y. Hasegawa, "Solvent Extraction Chemistry, Fundamentals and Applications," Decker, New York (1977).
6) Y. A. Zotorov, Translated by M. Tanaka, T. Nakasuka, I. Kojima, "Kireto Kagobutsu no Chyushutsu," Baifukan, Tokyo (1974).
7) M. Tanaka, "Yobai Chyushutsu no Kagaku," Kyoritsu Shuppan, Tokyo (1979).
8) P. Stenson, *Acta Chim. Scand.*, **23**, 1514 (1969).
9) L. G. Sillen, and A. E. Martell, "Stability Constants of Metalion Complexes," The Chemical Society (1964), p. 597.
10) B. E. McClellan, and H. Freiser, *Anal. Chem.*, **36**, (12) 2262 (1964).

The Phosphorus-31 Nuclear Magnetic Resonance Spectra of Bis(acetylacetonato)cobalt(III) Complexes Containing Bidentate Diphosphines

Yoshio KOIKE, Toshio TAKAYAMA, and Masatoshi WATABE*,†
Department of Chemistry, Kanagawa University, Yokohama 221
†*General Education Department, Kogakuin University, Hachioji 192*
(Received April 26, 1984)

Synopsis. The phosphorus-31 nuclear magnetic resonance spectra of $[Co(acac)_2(P\text{-}P)]^+$(P-P=diphosphine ligand) of the Werner type were measured, and the coordination chemical shifts were compared with those of complexes studied before. The coordination chemical shifts of the five-membered chelate ring were twice as much as those of the six-membered ring.

The nuclear magnetic resonance spectoroscopy of phosphines in coordination compounds is an area of considerable potential interest and a great deal of ^{31}P NMR data of transition metal phosphine complexes have been reported. However, all the metals dealt with thus far have been soft, such as the Pt, Rh, Hg, and Ag atoms and Ni, Mn, Co, Cr, Mo, and W in their lower-valence states.[1,2] Though recently several cobalt(III) phosphine complexes of the Werner type have been prepared, no ^{31}P-NMR data of these complexes have been reported.[3] The paper deals with the ^{31}P NMR spectra of bis(acetylacetonato)cobalt(III) complexes with a bidentate diphosphine. Some complexes were newly prepared.

Experimental

The diphosphine ligands and their abbreviations are as follows;

(a) $Ph_2PCH_2CH_2PPh_2$ (dppe)
(b) $Ph_2PCH(CH_3)CH_2PPh_2$ (mdppe)
(c) $Ph_2PCH_2CH_2CH_2PPh_2$ (dppp)
(d) $Ph_2PCH(CH_3)CH_2CH_2PPh_2$ (mdppp)
(e) $Ph_2PCH{=}CHPPh_2$ (dpp)

The dppe, dppp, and dpp ligands were prepared by the method of Hewertson and Watson,[4] while the mdppe and mdppp ligands were prepared by the method of Fryzuk.[5] All the complexes were prepared by a method similar to that of Kashiwabara *et al.*[3] from tris(acetylacetonato)cobalt(III) and the corresponding diphosphine. The analytical data of the new complexes are as follows; Calcd for $[Co(acac)_2mdppe]BF_4 \cdot H_2O$ C, 57.39; H, 5.47; N, 0.00%. Found: C, 57.21; H, 5.08; N, 0.02%. The ^{31}P NMR spectra were obtained in the Fourier transform mode with a Varian FT-80A spectrometer. The chemical shifts at 32.206 MHz were determined by the use of a 4 kHz range and a 16 K memory and were measured with respect to an external 85% H_3PO_4. The pulse width was 15 μs, and the pulse delay, 4s. About 200 mg of the complex was dissolved in 1.5 cm^3 of $CDCl_3$ in a 10 mm tube, and the spectra were accumulated 1000 times for free ligands and 15000 times for the complexes at 37 °C.

Results and Discussion

The ^{31}P NMR spectra of the ligands are shown in Fig. 1 (upper). Symmetrical ligands have one peak (ligands (a), (c), (e)), while unsymmetrical ones have more than one peak (ligands (b), (d)). The chemical shifts of the ligands can reasonably be predicted from the group contributions in terms of the α, β, and γ substituent effects at the α, β, and γ positions (P_α-C_β-C_γ-C_δ; P=phosphorus, C=carbon). The effect of substituting a methyl group for a hydrogen atom at C_β is deshielding, while an upfield shift is observed when a methyl group replaces a hydrogen atom at C_γ. The splitting of the two peeks for Ligand (b) is due to the ^{31}P-^{31}P coupling (24.6 Hz).

The ^{31}P NMR spectra of bis(acetylacetonato)cobalt(III) complexes with a bidentate diphosphine are shown in Fig. 1 (lower). The chemical shift data are listed in Table 1. When the saturated 5-membered chelate ligands (a) and (b) coordinate to the cobalt(III) ion, the coordination chemical shifts, $\Delta(=\delta(\text{coordinated}) - \delta(\text{free}))$, are about 56—62 ppm for Ligands (a) and (b), whereas the values for the saturated 6-membered chelate ligands (c) and (d) are 26—28 ppm, much smaller than those for Ligands (a), (b). Several authors have found a trend of ^{31}P NMR chemical shifts in relation to the chelate effect of diphosphins in organometallic complexes. The coordination chemical shifts always show a low-field shift for four-, five-, and six-membered

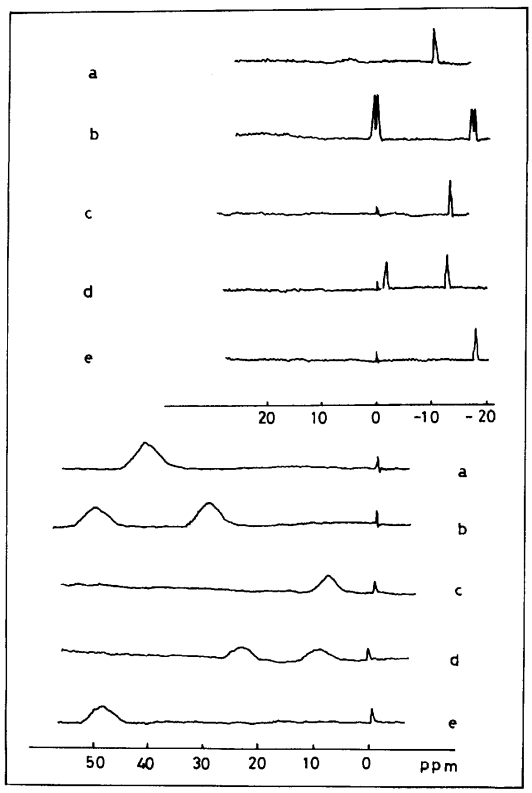

Fig. 1. ^{31}P NMR spectra of ligands(upper) and the complexes(lower).

TABLE 1. ^{31}P CHEMICAL SHIFTS OF THE FREE LIGANDS AND THEIR COMPLEXES

Ligand	Free	Complex	Δ
(a) $Ph_2PCH_2CH_2PPh_2$	−12.42	49.68	62.10
(b) $Ph_2PCH(CH_3)CH_2PPh_2$	−20.80	36.02	56.82
	0.93	60.24	59.31
(c) $Ph_2PCH_2CH_2CH_2PPh_2$	−17.17	9.32	26.49
(d) $Ph_2PCH(CH_3)CH_2CH_2PPh_2$	−16.77	9.33	26.10
	−2.64	24.84	27.48
(e) $Ph_2PCH=CHPPh_2$	−19.87	57.13	77.00

*δ ppm from H_3PO_4. $\Delta=\delta_{complex}-\delta_{free}$.

diphosphine chelate-ring complexes,[1,2] the Δ values of five-membered chelate rings are about two or three times as much as those of six-membered chelate rings. For example, the values of Δ for $[Pt(CH_3)_2dppe]$ and $[Pt(CH_3)_2dppp]$ are 67.7 and 20.5 ppm respectively. As is shown in Table 1, the coordination chemical shifts of the five-membered chelate rings obtained are twice as large as those of the six-membered chelate rings.

The coordination chemical shift of $[Co(acac)_2dpp]$ is 77 ppm, the largest of all the complexes studied here. It shoud be compared with the datum that the Δ value of +120 ppm for $[CpV(CO)_2(dpp)]$ (Cp=cyclopentadienyl) is slightly larger than that of +112 ppm for $[CpV(CO)_2(dppe)]$.[6]

Organometallic phosphine complexes have been reported to show relatively sharp signals, with couplings of the phosphorus atom to other nuclei of spin 1/2, while all the peaks studied here show broadening (half-width, *ca.* 100 Hz). Though the complexes containing the (b) and (d) ligands must have diastereomers, it is of no use to ascertain their geometries because the broad peaks were obtained. Several possible origins may be considered the broadening of the ^{31}P NMR peaks of cobalt(III) complexes: (a) a configurational change between Δ and Λ (b) a coupling between cobalt-59 and phosphorus atom, and (c) the paramagnetic effect. The (a) factor can easily be eliminated because $[Co(acac)_2(S\text{-}mdppe)]$ could be resolved to Δ and Λ isomers with Sephadex A-25 chromatography. No datum has been reported concerning any coupling between the cobalt-59 and phosphorus-31 atoms. The paramagnetic effect may broaden the ^{31}P signals, this parhaps because of cobalt(II) ion yielded by the following redox reaction.

$$2Co^{3+} + \gtrdot P + H_2O \longrightarrow 2Co^{2+} + \gtrdot P{=}O + 2H^+$$

However the ^1H NMR spectra of these complexes show sharp signals for all complexes. We can not explain this broadening well.

References

1) a) J. F. Nixon and A. Pidcock, "Phosphorus-31 NMR Spectra of Coordination Compounds. Annual Review of NMR Spectroscopy," Vol. 12, Academic Press (1969); b) P. S. Pregosin and R. W. Kunz, "^{31}P and ^{13}C NMR of Transition Metal Phosphine Complexes," Springer-Verlag, Berlin (1979).
2) P. E. Garrou, *Chem. Rev.*, **81**, 229 (1981).
3) K. Kashiwabara, I. Kinoshita, T. Ito, and J. Fujita, *Bull. Chem. Soc. Jpn.*, **54**, 725 (1981).
4) W. Hewertson and H. Watson, *J. Chem. Soc.*, 1962, 1490.
5) M. D. Fryzuk and D. B. Bosnich, *J. Am. Chem. Soc.*, **100**, 5491 (1978).
6) H. C. Bechthold and D. Reder, *J. Organomet. Chem.*, **172**, 331, (1979).

A Facile Method for Activation of Carboxylic Acids

Shizuaki MURATA

Department of Chemistry, College of General Education, Nagoya University, Chikusa-ku, Nagoya 464

(Received March 13, 1984)

Synopsis. 1,1′-Oxalyldiimidazole, -1,2,4-triazole, and -1,2,3,4-tetrazole were prepared *in situ* from oxalyl dichloride and corresponding 1*H*-azoles. The 1,1′-oxalyldiazoles converted carboxylic acids and their salts into 1-acylazoles.

1-Acylazoles have been widely used as activated acyl species.[1] It was reported in a previous paper that 1,1′-oxalyldiimidazole[2] is a suitable reagent for the preparation of 1-acylimidazoles.[3] There remained, however, two problems worthy of further investigation; *i.e.* the isolation of the 1-acylazoles and the application to a variety of 1-acylazoles. In the present paper, these problems are examined and an effective method for the preparation of various 1-acylazoles is described.

1,1′-Oxalyldiimidazole (**1**) was reported to be prepared by the reaction of 1*H*-imidazole and oxalyl dichloride in the presence of a tertiary amine.[3] This procedure was found to also be applicable for the synthesis of other 1,1′-oxalyldiazoles. 1,1′-Oxalyldi-1,2,4-triazole (**2**) and -1,2,3,4-tetrazole (**3**) were formed in a reaction involving the corresponding 1*H*-azole and oxalyl dichloride in the presence of *N,N*-diisopropylethylamine at 0—30°C. *N,N*-Dicyclohexylmethylamine and 2,6-di-*t*-butylpyridine, as well as the 1*H*-azoles themselves, could be used for the hydrogen chloride acceptor. The resulting mixtures involving **2** and **3** were used in a follow-up reaction to prepare 1-acylazoles.

Now, the reaction of **2** or **3** with a carboxylic acid, such as linoleic acid (C 18, Δ=2), linolenic acid (C 18, Δ=3), and arachidonic acid (C 20, Δ=4), in chloroform proceeded with CO and CO_2 evolution to give the corresponding 1-acyl-1,2,4-triazole (**5**) or -1,2,3,4-tetrazole (**6**) in high yields. In DMF, **2** and **3** converted the lithium and sodium salts of those fatty acids into **5** and **6**. The isolation and purification of produced 1-linoleoylimidazole (**4a**), -1,2,4-triazole (**5a**), and -1,2,3,4-tetrazole (**6a**) were performed successfully by extraction with a light petroleum followed by distillation.

1-Linoleoylimidazole (**4a**) was converted into methyl linoleate (**7a**) by its treatment with methanol in the presence of potassium *t*-butoxide. It is known that the condensation of 1-acylimidazole **4** with an alcohol requires a basic catalyst.[1] Since the reaction of **5a** or **6a** with methanol proceeded smoothly in the absence of a basic catalyst, it may be concluded that **5** and **6** are more reactive than **4**. 1-Linolenoylimidazole (**4b**) and 1-arachidonoyltetrazole (**6c**) were converted into the methyl esters **7b** and **7c** by the same treatment. The results are summerized in Table 1.

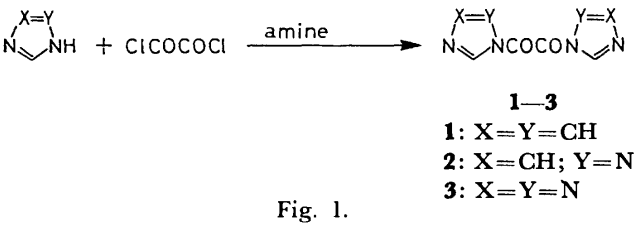

1—3

1: X=Y=CH
2: X=CH; Y=N
3: X=Y=N

Fig. 1.

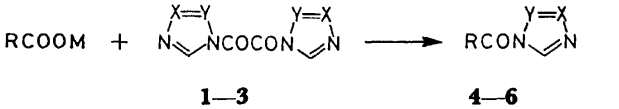

1—3 **4—6**

4: X=Y=CH
5: X=CH; Y=N
6: X=Y=N

Fig. 2.

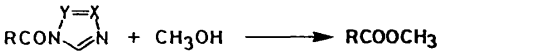

7a—7c

7a: R=$CH_3(CH_2)_4$-$(CH{=}CHCH_2)_2$-$(CH_2)_6$-
7b: R=$CH_3(CH_2CH{=}CH)_3$-$(CH_2)_7$-
7c: R=$CH_3(CH_2)_4$-$(CH{=}CHCH_2)_4CH_2CH_2$-

Fig. 3.

Only 1,1-carbonyldiimidazole,which is fairly expensive for a large-scale reaction, and 1,1-carbonyldiazole,[4] whose preparation requires severe poisonous phosgene, have been used for the activation of

TABLE 1. REACTION OF 1,1′-OXALYLDIAZOLE (**1**, **2**, AND **3**) WITH A CARBOXYLIC ACID

substrate	oxalyldiazole	conditions solv	conditions temp/°C	product[a] (% yield[b])
Linoleic acid	**1**	$CHCl_3$	40	1-Linoleoylimidazole (89)
Sodium linoleate	**1**	DMF	60	1-Linoleoylimidazole (88)
Lithium linoleate	**1**	DMF	60	1-Linoleoylimidazole (74)
Linolenic acid	**1**	$CHCl_3$	40	1-Linolenoylimidazole (79[c])
Linoleic acid	**2**	$CHCl_3$	20	1-Linoleoyltriazole (82)
Sodium linoleate	**2**	DMF	30	1-Linoleoyltriazole (75)
Linoleic acid	**3**	$CHCl_3$	0	1-Linoleoyltetrazole (72)
Lithium linoleate	**3**	DMF	25	1-Linoleoyltetrazole (78)
Arachidonic acid	**3**	$CHCl_3$	0	1-Arachidonoyltetrazole (82[c])

a) Triazole and tetrazole refer to 1,2,4-triazole and 1,2,3,4-tetrazole, respectively. b) Isolated yield. c) Isolated yield of the methyl ester which was obtained in the treatment with methanol.

carboxylic acids. Since 1,1'-oxalyldiazoles **1**—**3** can be prepared safely from easily available reagents and work in the mild conditions almost same as 1,1-carbonyldiimidazole, the utilization of **1**—**3** is suggested to be more suitable for a large-scale experiment.

Experimental

General. IR spectra were recorded on a JASCO IR A-102 spectrometer. ^{1}H NMR spectra were measured on JEOL PMX-60Si and Fx-90Q instruments. GLC analyses were done on a Gasukuro Kogyo Model 370 instrument using a capillary column of PEG 20 M (0.25 mm×25 m). Elemental analyses were performed at the Analytical Center of Faculty of Agriculture in Nagoya University. 1*H*-Azoles were dried over P_2O_5 *in vacuo*.

A General Procedure for 1-Acylazoles **4**—**6**. To a 1:1 mixture of a 1*H*-azole and *N,N'*-diisopropylethylamine in dry $CHCl_3$ or DMF (2—2.5 ml for 1 mmol) was added oxalyl dichloride (0.5 equiv), drop-by-drop, at −30—−10 °C. After 1—2h stirring, a fatty acid (or its salt) was added to the resulting mixture containing **1**, **2**, or **3**. This was stirred for 1 h at 0 °C, then warmed and maintained at an appropriate temperature for several hours. Three times the volume of petroleum ether or pentane was added to the solutions. A yellow-brown emulsion was separated into a colorless-yellow clear solution and a dark oil by centrifuge. Then, the oil was rinsed twice with the light petroleum. Concentration (40 °C, 6500 Pa) of the combined petroleum solutions yielded **4**—**6** as colorless-yellow oils. Bulb-to-bulb distillation of the oil gave an analytically pure sample.

1-Linoleoylimidazole[5] *(4a).* **4a** (89% (2.92 g) from linoleic acid, 88% (3.03 g) from sodium linoleate, 74% (0.28 g) from lithium linoleate): bp 230 °C (bath)/130 Pa; IR (neat) 1745 cm^{-1} (C=O); ^{1}H NMR ($CDCl_3$) 8.15 (1H, brs, H(C5) of imidazole), 7.43 (1H, dd, J=1.3 Hz, H(C2)), 7.08 (1H, m, H(C3)), 5.37 (4H, m, CH=CH), 2.82 (2H, m, =CCH_2C=), 2.05 (6H, m, CH_2C= and CH_2CO), 1.37 (16H, br, CH_2), 0.89 (3H, brt, CH_3).

Found: C, 76.53; H, 10.58; N, 8.23%. Calcd for $C_{21}H_{34}N_2O$: C, 76.31; H, 10.37; N, 8.48%.

1-Linoleoyl-1,2,4-triazole (5a). **5a** (82% (0.29 g) from linoleic acid, 75% (0.03 g) from sodium linoleate): bp 180 °C (bath)/130 Pa; IR (neat) 1760 cm^{-1} (C=O); ^{1}H NMR ($CDCl_3$) 8.90 (1H, s, H(C5) of triazole), 8.00 (1H, s, H(C3)), 5.37 (4H, m, HC=CH), 3.11 (2H, dd, J=7.2 Hz, =CCH_2C=), 2.78 (2H, brt, CH_2CO), 2.05 (4H, m, CH_2C=), 1.36 (14H, m, CH_2), 0.88 (3H, brt, CH_3).

Found: C, 72.21; H, 10.05; N, 12.41%. Calcd for $C_{20}H_{33}N_3O$: C, 72.46; H, 10.03; N, 12.68%.

1-Linoleoyl-1,2,3,4-tetrazole (6a). **6a** (72% (0.28 g) from linoleic acid, 78% (0.03 g) from lithium linoleate): bp 180 °C (bath)/7 Pa; IR (neat) 1770 cm^{-1} (C=O); ^{1}H NMR ($CDCl_3$) 9.28 (1H, s, H(C5) of tetrazole), 5.40 (4H, m, HC=CH), 3.33 (2H, dd, J=6.0 Hz, =CCH_2C=), 2.82 (2H, brt, CH_2CO), 2.1 (4H, m, CH_2C=), 1.4 (16H, m, CH_2), 0.93 (3H, brt, CH_3).

Found: C, 68.93; H, 9.85; N, 16.55%. Calcd for $C_{19}H_{32}N_4O$: C, 68.64; H, 9.70; N, 16.85%.

Reaction of 4 with Methanol. A mixture of **4**, which was prepared *in situ* or isolated, and 0.05 M *t*-C_4H_9OK/CH_3OH (0.5 ml for 1 mmol) was stirred at 25 °C for 6 h. A column of silica gel eluting with 5% ethyl acetate in petroleum ether gave **7**.

Reaction of 5 and 6 with Methanol. Methanol (0.5 ml for 1 mmol) was added to the solution of **5** or **6** prepared *in situ*. After 3—8 h at 25 °C, **7** was obtained by a silica-gel column.

Methyl Linoleate (7a). **7a** (93% from **4a**): IR (neat) 1740 cm^{-1} (C=O); ^{1}H NMR (CCl_4) 5.33 (4H, m, CH=CH), 3.66 (3H, s, CH_3O), 2.78 (2H, m, =CCH_2C=), 2.05 (6H, m, CH_2C= and CH_2CO), 1.35 (16H, br, CH_2), 0.90 (3H, brt, CH_3); GLC (170 °C) t_R=10.5 min (authentic sample[6] 10.5 min).

Methyl Linolenate (7b). **7b** (79% from linolenic acid): IR (neat) 1743 cm^{-1} (C=O). ^{1}H NMR (CCl_4) 5.35 (6H, m, HC=CH), 3.63 (3H, s, CH_3O), 2.79 (4H, m, =CCH_2C=), 2.4—1.9 (6H, m, CH_2CO and CH_2C=), 1.7—1.2 (10H, m, CH_2), 0.98 (3H, t, CH_3); GLC (170 °C) t_R=10.3 min (10.3 min[6]).

Methyl Arachidonate (7c). **7c** (82% from arachidonic acid): IR (neat) 1745 cm^{-1} (C=O); ^{1}H NMR ($CDCl_3$) 5.36 (8H, m, HC=CH), 3.68 (3H, s, CH_3O), 2.80 (6H, br, =CCH_2C=), 2.4—1.5 (6H, m, CH_2CO and CH_2C=), 1.3 (8H, br, CH_2), 0.89 (3H, brt, CH_3); GLC (185 °C) t_R=12.7 min (12.7 min[6]).

The work was supported by the Grant-in-Aids for Scientific Research, No. 58740224, from the Ministry of Education, Science and Culture. I deeply acknowledge Professors Ryoji Noyori and Sadao Matsuura from Nagoya University for their kind permission to use their instruments.

References

1) H. A. Staab, *Chem. Ber.*, **89**, 1927 (1956); H. A. Staab, *Angew. Chem., Int. Ed. Engl.*, **1**, 351 (1962); G. S. Bates, J. Diskur, and S. Masamune, *Tetrahedron Lett.*, **1976**, 4423; S. Ohta and M. Okamoto, *J. Synth. Org. Chem. Jpn.*, **41**, 38 (1983).

2) W. Walter and M. Radke, *Liebigs Ann. Chem.*, **1979**, 1756.

3) S. Murata, *Chem. Lett.*, **1983**, 1819.

4) H. C. Beyerman and W. M. Van Den Brink, *Rec. Trav.*, **80**, 1372 (1961).

5) T. G. Warner and A. A. Benson, *J. Lipid Res.*, **18**, 548 (1977); J. G. Lammers, J. Liefkens, J. Bus, and J. van der Meer, *Chem. Phys. Lipids*, **22**, 293 (1978).

6) The authentic methyl esters were obtained from Sigma Chemical Co.

Orbital Phase Explanation of Regioselectivity of Organic Reactions

Satoshi INAGAKI
Department of Chemistry, Faculty of Engineering, Gifu University, Yanagido, Gifu 501-11
(Received May 7, 1984)

Synopsis. The regioselectivity of such fundamental organic reactions as electrophilic addition to olefins, Diels-Alder cycloaddition, and electrophilic aromatic substitution, can be explained by the phase continuity-discontinuity properties of orbitals involved in cyclic interaction for acyclic delocalization of electrons.

Electron delocalization in acyclic conjugated systems was recently found to involve cyclic interaction of orbitals of subsystems.[1] The acyclic delocalization is under control of the continuity-discontinuity property of orbital phase. The phase continuity requirement is simultaneous satisfaction of the following conditions: (i) the occupied orbitals out of phase; (ii) the vacant orbitals in phase; (iii) the occupied and vacant orbitals in phase. The concept of cyclic orbital interaction in acyclic conjugation has been applied[1-2] to explaining why cross-conjugation is thermodynamically more favorable than linear conjugation in polyanions while the thermodynamic preference is opposite for polyenes. The phase continuity-discontinuity properties of orbitals involved in acyclic delocalization have been employed to design a variety of interesting electron-localizing and delocalizing conjugated systems.[3] We show that acyclic delocalization under control of orbital phase covers the regioselectivity of fundamental organic reactions.

Addition of electrophile (E) to C=C bond (A) with electron-releasing (R) and -withdrawing (W) substituents selectively occurs at the β- and α-carbon, respectively. The transition state is considered as a system where three subsystems, R or W, A, and E interact in an acyclic manner. The electron delocalization from R to E *via* A can be expected to control the regioselectivity of the reactions. The orbitals involved in the delocalization are the occupied orbital (r) of R, the vacant orbital (e*) of E, and the bonding (a) and antibonding (a*) orbital of A. For the β- addition (**1**) the delocalization is favored by the orbital phase continuity (**2**), whereas the phase is discontinuous (**4**) for the α addition (**3**).[4] Similarly, the transition state of the electrophilic addition to W-substituted olefins is considered to be an interacting system composed of W, A, and E. The acyclic delocalization from A to W and E can be expected to

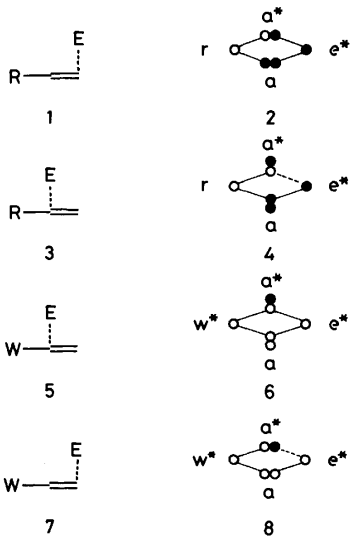

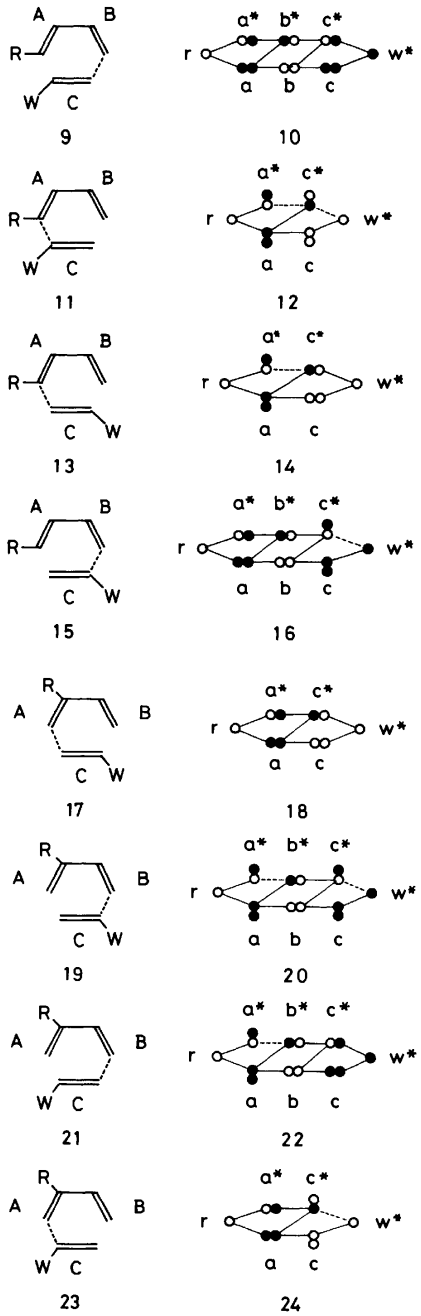

control the regioselectivity. The cyclic orbital interaction involves, a, a*, e*, and w*. The α-addition (**5**) is favored by the orbital phase continuity (**6**), the β-addition (**7**) being disfavored by the phase property (**8**).

A diene with R at a terminal carbon reacts with a W-substituted dienophile to preferentially give an "ortho"-cycloadduct. An R-substituent on an inner carbon leads to a "para"-cycloadduct. There are two pathways for the delocalization from R to W at cyclic transition state. The delocalization occurs through a long path *via* the substituted (A) and unsubstituted (B) double bonds in the diene and that (C) in the dienophile and through a short path *via* A and C. The delocalization along the long R-A-B-C-W path contains cyclic interaction among the occupied orbital (r) of R, the vacant orbital (w*) of W, the bonding (a, b, c) and antibonding (a*, b*, c*) orbitals of A, B, and C. The delocalization along the short R-A-C-W path involves the interaction among r, a, c, w*, c*, and a* orbitals. For the ortho-adduct formation from 1-R-diene the R-A-B-C-W delocalization (**9**) is favored by the orbital phase continuity (**10**), the R-A-C-W delocalization (**11**) being disfavored by the phase property (**12**). Neither is favored by phase property (**14**, **16**) for the meta-adduct formation (**13** and **15**). As a result, the orbital phase favors an acyclic delocalization path (**9**) at the transition state to the ortho-adduct.

A similar argument holds for the Diels-Alder reaction involving 2-R-diene. At the transition state to the para-product the delocalization along the R-A-C-W path (**17**) is favored by the orbital phase continuity (**18**), that along the R-A-B-C-W path (**19**) disfavored (**20**). The acyclic delocalization is disfavored (**22**, **24**) for both paths (**21** and **23**) at the transition state to the meta-cycloadduct.

The transition state model for the aromatic substitution can be formally generated from that for the Diels-Alder reactions as illustrated in Scheme. The

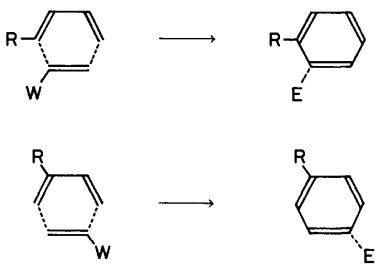

Scheme

incipient σ-bonds between diene and dienophile and π-type interaction between dienophile and W are replaced by π-type interactions in benzene and an incipient σ-bond between benzene and E. The preferential formation of ortho- and para-adducts in Diels-Alder reactions has been shown to be controlled by the acyclic delocalization. At the same qualitative level we can say that the ortho/para-orientation arises from the orbital phase properties for acyclic delocalization.

We gratefully acknowledge support of this work by a grant from the Ministry of Education, Science, and Culture.

References

1) a) S. Inagaki and Y. Hirabayashi, *Chem. Lett.*, **1982**, 709; b) S. Inagaki, H. Kawata, and Y. Hirabayashi, *Bull. Chem. Soc. Jpn.*, **55**, 3724 (1982).

2) a) S. Inagaki, H. Kawata, and Y. Hirabayashi, *J. Org. Chem.*, **48**, 2928 (1983); b) S. Inagaki, K. Iwase, and N. Goto, *J. Chem. Soc., Perkin Trans. 2*, in press.

3) S. Inagaki, K. Iwase, and H. Kawata, submitted for publication.

4) The neighboring orbitals which meet the phase continuity requirements are linked by solid lines, and otherwise by broken lines.

Reactions of Trifluoromethanesulfonyl Azide with Aromatic Compounds

Nobumasa KAMIGATA,* Kazutoshi YAMAMOTO, Osamu KAWAKITA, Kiyoyuki HIKITA, Haruo MATSUYAMA, Masato YOSHIDA, and Michio KOBAYASHI

Department of Chemistry, Faculty of Science, Tokyo Metropolitan University, Fukazawa, Setagaya-ku, Tokyo, 158

(Received June 7, 1984)

Synopsis. Thermolysis of trifluoromethanesulfonyl azide in solvents composed of 1:1 mixtures of benzene and substituted benzenes gives trifluoromethanesulfonanilide and substituted trifluoromethanesulfonanilides. The isomer ratios, the total rate ratios, and the partial rate factors for the sulfonamidation have been determined. By the intramolecular and intermolecular selectivities, the reaction mechanism involving trifluoromethanesulfonyl nitrene intermediate is discussed.

The thermal decomposition of sulfonyl azides in aromatic solvents was first reported by Curtius and Schmidt.[1] Abramovitch *et al.* studied the thermal reactions of methanesulfonyl azide with substituted benzenes and determined the isomer ratios, total rate ratios, and partial rate factors for the sulfonamidation.[2] We have studied the thermal reaction of trifluoromethanesulfonyl azide with monosubstituted benzenes since we have interest in the reactivities and selectivities of sulfonyl nitrenes possessing a strong electron-withdrawing group.

Thermal reactions of trifluoromethanesulfonyl azide in an equimolar mixture of benzene and substituted benzenes at 120 °C in a degassed sealed tube were carried out. The reaction products were trifluoromethanesulfonanilide and substituted trifluoromethanesulfonanilides which were analyzed on a silica-gel-column-packed HPLC using chloroform–ethanol as an eluent. The isomer ratio, the total rate ratios, and the partial rate factors for the trifluoromethanesulfonamidation were determined and the results are summarized in the Table together with those for sulfonamidation with methanesulfonyl azide.[2]

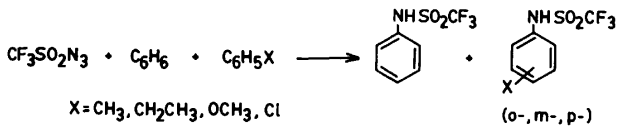

As shown in the Table, the partial rate factors for the trifluoromethanesulfonamidation of anisol are smaller than those for the methanesulfonamidation. Similar results were obtained in the sulfonamidation of toluene. Unfortunately, in the case of the sulfonamidation of toluene or ethylbenzene, ortho and meta or meta and para isomers of trifluoromethanesulfonanilides, respectively, could not be separated under various HPLC separating conditions. This implies that trifluoromethanesulfonyl nitrene intermediate formed by the thermolysis is more reactive and less selective than a methanesulfonyl nitrene. The fact that the total rate ratios for the trifluoromethanesulfonamidation of any substituted benzenes (especially that of chlorobenzene) are close to unity compared with methanesulfonamidation supports this interpretation. The trifluoromethanesulfonamidation has electrophilic nature since the total rate ratios are larger value in the electron-donating group (k_{OMe}/k, k_{Me}/k, and k_{Et}/k were 1.53, 1.12, and 1.10, respectively) and smaller value in the electron-withdrawing group (k_{Cl}/k=0.64). And also, no trifluoromethanesulfonamidation was observed in the reaction of triflazide with nitrobenzene. The ionic character indicates the trifluoromethanesulfonyl nitrene reacts in a singlet state.

$$CF_3SO_2N_3 \xrightarrow[-N_2]{} CF_3SO_2\ddot{N}$$

According to the frontier molecular orbital theory, the electrophilic reactions of a singlet carbene with olefins are directed by the interaction with lowest unoccupied molecular orbital (LUMO) of the carbene and highest occupied molecular orbital (HOMO) of the olefin.[3] This conception could be applied in the reaction of electrophilic nitrene with olefins as shown below. Trifluoromethyl group should decrease the

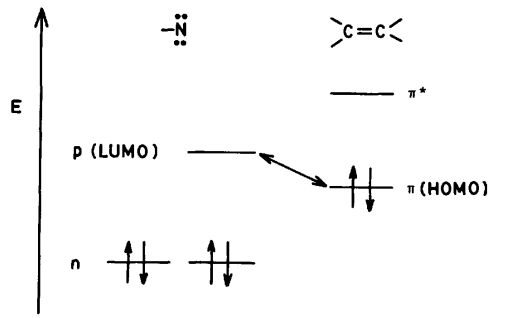

energy level of the LUMO (vacant p orbital) of the trifluoromethanesulfonyl nitrene in the singlet state compared with that of methanesulfonyl nitrene, thus the interaction of LUMO of trifluoromethanesulfonyl nitrene and HOMO of benzene becomes easier. Consequently, the trifluoromethanesulfonyl nitrene intermediate showed higher reactivities and lower selectivities (partial rate factors and total rate ratios are closer to unity) in the sulfonamidation of arenes compared with methanesulfonamidation.

The isomer ratios of the trifluoromethanesulfonamidation were similar to those for the methanesulfonamidation. According to the mechanism for the methanesulfonamidation of arenes proposed by Abramovitch *et al.*,[2] a singlet sulfonyl nitrene adds to the aromatic ring giving aziridine, followed by opening of the three membered ring affording the final product *via* a carbonium ion intermediate. If we assume a similar mechanism for the trifluoromethanesulfonamidation as shown below, the ring opening will be directed by the stability of carbonium ion which is effected by the substituent X in the aromatic ring and does not depend on the group attached on the sulfonyl group (methyl or trifluoromethyl). Therefore, intramolecular selectivities (isomer ratios) of sulfonamidation of monosubstituted benzenes are quite similar in the cases of trifluoro-

TABLE 1. THE ISOMER RATIOS, PARTIAL RATE FACTORS, AND TOTAL RATE RATIOS FOR THE SULFONAMIDATION OF ARENES IN THE THERMOLYSIS OF SULFONYL AZIDE AT 120°C

Sulfonyl Azide	Arene	Isomer Ratio (%)			Partial Rate Factor			Total Rate Ratio
		o-	*m*-	*p*-	k_o/k	k_m/k	k_p/k	k_x/k
$CF_3SO_2N_3$	$C_6H_5OCH_3$	53.1	3.5	43.5	2.43	0.16	3.99	1.53
$CH_3SO_2N_3$[2]	$C_6H_5OCH_3$	55.5	1.2	43.3	4.23	0.09	6.6	2.54
$CF_3SO_2N_3$	$C_6H_5CH_3$	57.0[a]		43.0	2.10[b]		3.15	1.12
$CH_3SO_2N_3$[2]	$C_6H_5CH_3$	65.4	2.4	32.2	3.65	0.13	3.59	1.86
$CF_3SO_2N_3$	$C_6H_5CH_2CH_3$	49.2		59.8[c]	1.63		3.36[d]	1.10
$CF_3SO_2N_3$	C_6H_5Cl	51.9	4.0	44.1	1.01	0.08	1.70	0.64
$CH_3SO_2N_3$[2]	C_6H_5Cl	57.4	0.9	41.7	0.76	0.01	1.10	0.44

a) ortho+meta, b)k_{o+m}/k, c) meta+para, d)k_{m+p}/k

methanesulfonamidation and methanesulfonamidation.

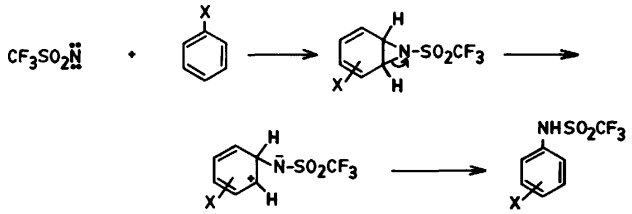

Experimental

Materials. Trifluoromethanesulfonyl chloride was prepared from 25.0 g of trifluoromethanesulfonic acid treated with 50.0 g of phosphorus pentachloride at 100°C. The volatile component was trapped by an ice-bath and distilled to give 24.0 g (85%) of trifluoromethanesulfonyl chloride: bp 33°C. Trifluoromethanesulfonyl azide was prepared by dropping 8.4 g of trifluoromethanesulfonyl chloride into a slurry of 4.2 g of sodium azide in 60 cm^3 of acetonitrile with stirring at 0°C and the mixture was stirred for additional 3 h. The organic layer was extracted with decalin, the extract washed with water and dried over anhydrous magnesium sulfate. Careful distillation of the extract gave 6.8 g (78%) of trifluoromethanesulfonyl azide: bp 45°C/350 Torr (52.2°C/444 Torr:[4] 1 Torr=133.322 Pa); IR (neat) 1130, 1160, 1220, 1420, and 2150 cm^{-1}; Mass *m/z* 175 (M^+).

Preparation of Authentic Trifluoromethanesulfonimides. The general procedure described by Marvel *et al.* was used.[5] To a dichloromethane solution of 2 molar equiv of the amine was added 1 equiv of trifluoromethanesulfonyl chloride in dichloromethane at 0°C. The solution was stirred at room temperature for 3 h, and refluxed for 5 h. The reaction mixture was washed with 5% hydrochloric acid and water, then the organic layer was dried with anhydrous magnesium sulfate. Evaporation of the solvent left a residue which was subjected to Florisil column chromatography using benzene as eluent. The amide isolated was recrystallized from hexane.

Trifluoromethanesulfonanilide. Mp 65.5—66.0°C (66—67°C[6]); IR (KBr) 1140, 1200, 1360, and 3300 cm^{-1}; NMR ($CDCl_3$) δ=6.52 (1H, s) and 7.37 (5H, s); Mass *m/z* 226 (M^++1).

o-*Trifluoromethanesulfontoluidide.* Mp 55—56°C; IR (KBr) 1140, 1190, 1360, and 3280 cm^{-1}; Mass *m/z* 239 (M^+).

m-*Trifluoromethanesulfontoluidide.* Mp 64.5—65.5°C; IR (KBr) 1145, 1210, 1360, and 3280 cm^{-1}; Mass *m/z* 240 (M^++1).

p-*Trifluoromethanesulfontoluidide.* Mp 42.5—43.5°C; IR (KBr) 1140, 1210, 1355, and 3290 cm^{-1}; Mass *m/z* 239 (M^+).

N-(o-*Ethylphenyl*)*trifluoromethanesulfonamide.* Mp 61—62°C; IR (KBr) 1140, 1210, 1360, and 3260 cm^{-1}; NMR ($CDCl_3$) δ=1.18 (3H, t, J=7.2 Hz), 2.58 (2H, q, J=7.2 Hz), and 7.00 (4H, s); Mass *m/z* 254 (M^++1).

N-(m-*Ethylphenyl*)*trifluoromethanesulfonamide.* IR (KBr) 1140, 1215, 1365, and 3295 cm^{-1}; NMR ($CDCl_3$) δ=1.18 (3H, t, J=7.8 Hz), 2.55 (2H, q, J=7.8 Hz), 6.41 (1H, s), and 6.8—7.6 (4H, m); Mass *m/z* 253 (M^+).

N-(p-*Ethylphenyl*)*trifluoromethanesulfonamide.* Mp 33—34°C; IR (neat) 1145, 1215, 1365, and 3300 cm^{-1}; NMR ($CDCl_3$) δ=1.17 (3H, t, J=7.2 Hz), 2.55 (2H, q, J=7.2 Hz), 6.58 (1H, s), 7.09 (4H, s); Mass *m/z* 254 (M^++1).

o-*Trifluoromethanesulfonanisidide.* Mp 60—61°C; IR (KBr) 1150, 1205, 1370, and 3300 cm^{-1}; Mass *m/z* 255 (M^+).

m-*Trifluoromethanesulfonanisidide.* Mp 64.5—65.5°C; IR (KBr) 1140, 1195, 1380, and 3170 cm^{-1}; Mass *m/z* 255 (M^+).

p-*Trifluoromethanesulfonanisidide.* Mp 39.5—40.0°C; IR (KBr) 1150, 1210, 1375, and 3300 cm^{-1}; Mass *m/z* 256 (M^++1).

N-(o-*Chlorophenyl*)*trifluoromethanesulfonamide.* Mp 74.5—75.5°C; IR (KBr) 1140, 1215, 1370, and 3270 cm^{-1}; Mass *m/z* 262 and 260 (M^++1).

N-(m-*Chlorophenyl*)*trifluoromethanesulfonamide.* Mp 76.5—77.5°C; IR (KBr) 1140, 1210, 1360, and 3270 cm^{-1}; Mass 261 and 259 (M^+).

N-(p-*Chlorophenyl*)*trifluoromethanesulfonamide.* Mp 50—51°C; IR (KBr) 1135, 1215, 1410, and 3320 cm^{-1}; Mass *m/z* 261 and 259 (M^+).

The Reaction of Trifluoromethanesulfonyl Azide with Substituted Benzenes. A solution of trifluoromethanesulfonyl azide (105 mg, 0.6 mmol) in benzene (2.34 g, 30 mmol) and monosubstituted benzene (30 mmol) was heated at 120°C in a degassed sealed tube for 24 h. The reaction mixture was subjected to Florisil column chromatography using hexane-ethyl acetate as eluent to remove the resinous by-product. The trifluoromethanesulfonanilide and substituted trifluoromethanesulfonanilides formed were analyzed by HPLC using silica-gel column and chloroform-ethanol as eluent. The isomer ratios and partial rate factors for the trifluoromethanesulfonamidation were determined. The overall yield of the amidation based on the trifluoromethanesulfonyl azide used was 50—80%. The results are summarized in Table 1.

References

1) A. Bertho, T. Curtius, and F. Schmidt, *Chem. Ber.*, **60**, 1717 (1927); T. Curtius and F. Schmidt, *Chem. Ber.*, **55**, 1571 (1922); A. Bertho, *J. Prakt. Chem.*, **120**, 89 (1928).

2) R. A. Abramovitch, G. N. Knaus, and V. Uma, *J. Am. Chem. Soc.*, **91**, 7532 (1969); R. A. Abramovitch, J. Roy and V. Uma, *Can. J. Chem.*, **43**, 3407 (1965).

3) R. A. Moss, *Accounts Chem. Res.*, **13**, 58 (1980); N. G. Randon, N. H. Houk, and R. A. Moss, *J. Am. Chem. Soc.*, **102**, 1770 (1980).

4) J. K. Ruff, *Inorg. Chem.*, **4**, 567 (1965).

5) C. S. Marvel, M. D. Helfrick, and J. P. Belsley, *J. Am. Chem. Soc.*, **51**, 1272 (1929).

6) J. B. Hendrickson and R. Bergeron, *Tetrahedron Lett.*, **1973**, 3839.

A Simple Synthesis of Methyl 2,3,6- and 2,4,6-Tri-*O*-benzyl-α-D-mannosides

Shinkiti KOTO,* Kazuhiro TAKENAKA, Naohiko MORISHIMA, Akiko SUGIMOTO, and Shonosuke ZEN
School of Pharmaceutical Sciences, Kitasato University, Shirokane, Minato-ku, Tokyo 108
(Received June 12, 1984)

Synopsis. Cotrolled benzylation of methyl α-D-mannopyranoside with benzyl chloride and LiOH selectively gave the 2,3,6-tribenzyl ether in a 53% yield. Such a reaction using benzyl chloride and KOH afforded mainly the 2,4,6-tribenzyl ether in a 41% yield. The products were allylated and then hydrolyzed to give the corresponding 1-OH derivatives.

Various methods for the synthesis of partially benzylated carbohydrates have been proposed.[1] This kind of compound, however, has often been prepared through direct benzylation[2] of readily available methyl glycosides.[3-5]

Benzylation of methyl α-D-mannopyranoside (**1**) in benzyl chloride (BnCl) and LiOH (8 equiv) at 140 °C for 9 h selectively gave the 2,3,6-tribenzyl ether **2** in a 53% yield. Benzylation of **1** in BnCl and KOH (4.5 equiv) at 140 °C for 3 h mainly furnished the 2,4,6-tribenzyl ether **3**[6] in a 41% yield.

A trace (<1%) of the 3,4,6-tribenzyl ether **4**[7] and an appreciable quantity (3—8%) of the 2,3,4-tribenzyl ether **5**[8] were always isolated from the reaction mixture. Controlled benzylation of the 3,4-dibenzyl ether **7**[9] also gave **5** as the main product. These show that the 2-OH group, rather than the 6-OH group, of **1** has an unusual susceptibility to benzylation.

Other mannosides, benzyl,[10] allyl,[11] and phenyl α-D-mannopyranosides[12] (**8**, **12**, and **16**) afforded preferentially the corresponding 2,3,6-tribenzyl ethers *via* the benzylation with LiOH.

The tribenzyl ethers, **2** and **3**, were allylated and hydrolyzed to the respective 1-OH derivatives, **20** and **21**.[6c]

Experimental[3-5]

4-O-Allyl-2,3,6-tri-O-benzyl-D-mannopyranose (20). Compound **2** (157.7 mg, 0.34 mmol) was allylated in allyl bromide (Wako, 3 ml) in the presence of NaH (Wako, 60%, 95 mg) at 70 °C for 2 h. The allyl ether was hydrolyzed in a mixture of AcOH (5.4 ml) containing aq H_2SO_4 (3M, 0.75 ml (1 M=1 mol dm^{-3})) at 100 °C for 1.3 h to gave **20** (70.0 mg, 42%).

3-O-Allyl-2,4,6-tri-O-benzyl-D-mannopyranose (21). Compound **3** (145.9 mg) was converted into **21** (50.8 mg, 33%).

Methyl 2-O-Acetyl-3,4,6-tri-O-benzyl-α-D-mannopyranoside. 1,2,3,4,6-Penta-*O*-acetyl-α-D-mannopyranose (Kyowa, 250 mg, 0.64 mmol) was stirred in CH_2Cl_2 (0.65 ml) containing

TABLE 1. THE RESULTS OF BENZYLATION OF MANNOPYRANOSIDES

Run	Starting Material	Alkali(equiv)		Temp °C	Time h	Yield %							
						2,3,4,6-Bn$_4$		2,3,6-Bn$_3$		2,4,6-Bn$_3$		2,3,4-Bn$_3$	
1	**1**	LiOH	(8.0)	140	9	**6**	14	**2**	53	**3**	10	**5**	6
2	**1**	LiOH	(8.0)	140	24	**6**	24	**2**	38	**3**	3	**5**	4
3	**1**	LiOH	(13.5)	140	6	**6**	14	**2**	50	**3**	6	**5**	3
4	**1**	KOH	(4.5)	100	9	**6**	12	**2**	17	**3**	30	**5**	3
5	**1**	KOH	(4.5)	140	3	**6**	20	**2**	18	**3**	41	**5**	8
6	**1**	RbOH	(4.5)	70	5.5	**6**	9	**2**	19	**3**	33	**5**	5
7	**8**	LiOH	(8.0)	140	9	**11**	8	**9**	31	**10**	5		—[a]
8	**8**	KOH	(4.5)	140	3	**11**	14	**9**	13	**10**	17		—[a]
9	**12**	LiOH	(8.0)	140	9	**15**	20	**13**	35	**14**	3		—[a]
10	**12**	KOH	(4.5)	100	3	**15**	21	**13**	21	**14**	19		—[a]
11	**16**	LiOH	(8.0)	140	9	**19**	4	**17**	35	**18**	4		—[a]
12	**16**	KOH	(4.5)	100	3	**19**	10	**17**	23	**18**	19		—[a]

a: Not isolated.

TABLE 2. PHYSICAL AND ANALYTICAL DATA OF COMPOUNDS

Compd	$[\alpha]_D^{20}$(*c*, $CHCl_3$) deg	R_f	Toluene / Butanone	Mol. Form.	Anal/% Calcd C	Calcd H	Found C	Found H
2	+2(2.0)	0.54					71.73	6.91
3	+17(0.2)	0.60	(5/1)	$C_{28}H_{32}O_6$	72.39	6.94	72.04	6.94 a
4	+56(3.0)	0.23					72.53	6.95 b
5	+29(0.2)	0.27					72.39	6.92 c
9	+30(0.3)	0.47	(10/1)	$C_{34}H_{36}O_6$	75.53	6.71	75.23	6.71
10	+33(0.2)	0.56					75.50	6.93
13	+3(1.6)	0.51					73.43	6.97
14	+46(0.2)	0.62	(6/1)	$C_{30}H_{34}O_6$	73.45	6.99	72.92	6.83
20	+21(1.0)	0.42					73.18	7.00
21	+21(1.7)	0.38					73.73	6.81
17	+35(0.4)	0.60	(7/1)	$C_{33}H_{34}O_6$	75.26	6.51	75.36	6.43
18	+66(0.2)	0.70					75.35	6.49
11	+51(0.3)	0.65	(10/1)	$C_{41}H_{42}O_6$	78.07	6.71	77.81	6.63
15	+51(0.3)	0.70	(6/1)	$C_{37}H_{40}O_6$	76.53	6.94	76.18	6.94
19	+71(0.3)	0.84	(7/1)	$C_{40}H_{40}O_6$	77.90	6.55	77.71	6.53

a Ref. 7a: $[\alpha]_D^{31}$+59.7°(*c* 1.85, CH_2Cl_2), Ref. 7b: $[\alpha]_D^{25}$+57.7°(*c* 0.485, $CHCl_3$). b Ref. 6a: $[\alpha]_D^{25}$+14.4°(*c* 1, $CHCl_3$), Ref. 6b: $[\alpha]_D^{29}$+16.9°(*c* 1.5, $CHCl_3$), Ref. 6c: $[\alpha]_D^{25}$+17.2°(*c* 1.0, $CHCl_3$). c Ref. 8: $[\alpha]_D$+30°(*c* 0.49, $CHCl_3$).

TABLE 3. ^{1}H NMR DATA FOR THE ACETATES OF THE TRIBENZYL ETHERS OF MANNOPYRANOSIDES[a]

Compd	(ppm) H-1 (Hz)	J_{12}	H-2	J_{23}	H-3	J_{34}	H-4	J_{45}	Ac-3	Ac-4
Acetates[b] of.										
2	4.61	2.1	—	—	—	9.0	5.20	9.0	—	1.82
3	4.61	1.8	3.77	3.2	5.03	8.7	3.80	9.6	1.84	—
9	4.76	2.0	—	—	—	9.0	5.22	9.0	—	1.80
10	4.75	2.0	3.80	3.0	5.12	8.1	3.92	8.1	1.87	—
13	4.60	1.6	—	—	—	9.0	5.17	9.0	—	1.80
14	4.73	2.0	—	3.5	5.08	8.5	—	—	1.89	—
17	5.37	1.6	3.81	3.0	3.87	8.7	5.31	9.8	—	1.80
18	5.37	2.3	3.97	3.0	5.22	8.4	4.00	9.6	1.85	—

a: At 90 Mz in CCl_4 with Me_4Si. b: Acetylation of a sample with excess Ac_2O in pyridine at room temperature overnight, followed by chromatography on silica gel using benzene -2- butanone system gave a homogeneous acetate.

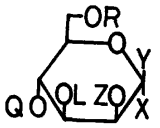

All=allyl
Bn=benzyl

Compd	X	Y	Z	L	Q	R
1	OMe	H	H	H	H	H
2	OMe	H	Bn	Bn	H	Bn
3	OMe	H	Bn	H	Bn	Bn
4	OMe	H	H	Bn	Bn	Bn
5	OMe	H	Bn	Bn	Bn	H
6	OMe	H	Bn	Bn	Bn	Bn
7	OMe	H	H	Bn	Bn	H
8	OBn	H	H	H	H	H
9	OBn	H	Bn	Bn	H	Bn
10	OBn	H	Bn	H	Bn	Bn
11	OBn	H	Bn	Bn	Bn	Bn
12	OAll	H	H	H	H	H
13	OAll	H	Bn	Bn	H	Bn
14	OAll	H	Bn	H	Bn	Bn
15	OAll	H	Bn	Bn	Bn	Bn
16	OPh	H	H	H	H	H
17	OPh	H	Bn	Bn	H	Bn
18	OPh	H	Bn	H	Bn	Bn
19	OPh	H	Bn	Bn	Bn	Bn
20	OH, H		Bn	Bn	All	Bn
21	OH, H		Bn	All	Bn	Bn

AcBr (Wako, 0.55 ml) and H_2O (0.11 ml).[14] After stirring for 3 h at room temperature, evaporation and co-evaporation with toluene gave a syrup, which was treated in $MeNO_2$ (0.64 ml) with 2,6-dimethylpyridine (0.24 ml) and MeOH (0.20 ml) at room temperature overnight. The mixture was diluted with $CHCl_3$, washed with aq $NaHCO_3$ (5%) and the organic layer evaporated to give a syrup, which was stirred in BnCl (4 ml) containing crushed KOH (1.0 g) at 110—120 °C for 2 h. After filtration and evaporation, the mixture was chromatographed on alumina (Woelm, 02084) just with hexane–toluene and subsequently with diisopropyl ether–2-butanone systems to give a syrup (294.2 mg). This was treated in CH_2Cl_2 (4 ml) with $BF_3 \cdot Et_2O$ (5 μl) at room temperature for 5 min, followed by chromatography, to give the titled compound (232.3 mg, 72%, $[\alpha]_D^{20}$ +26 °(*c* 6, $CHCl_3$), lit,[7a] $[\alpha]_D^{27}$ +27.9 ° (*c* 2.24, CH_2Cl_2). Found: C, 71.42; H, 6.80%. Calcd for $C_{30}H_{34}O_7$: C, 71.13; H, 6.77%).

This was quantitatively deacetylated with dil methanolic NaOMe to give **4**.

Benzylation of Methyl 3,4-Di-O-benzyl-α-D-mannopyranoside (7). The dibenzyl ether **7**[9] (63.5 mg, 0.17 mmol) was stirred in BnCl (1.2 ml) containing LiOH (12.2 mg at 140 °C for 9 h. Chromatography gave a trace of **6**,[13] **5** (21.7 mg, 28%), **4** (4.1 mg, 5%), and unchanged **7**.

When **7** (63.2 mg), KOH (14.3 mg) and BnCl (1.2 ml) was stirred at 140 °C for 3 h, **5** (15.6 mg, 20%) and **4** (12%) were obtained after chromatography.

References

1) T. Ogawa and M. Matsui, *Carbohydr. Res.*, **62**, C 1 (1978); R. Taman, J. Rosik, and M. Zikmund, *ibid.*, **103**, 165 (1982); P. J. Garegg, T. Iversen, and S. Oscarson, *ibid.*, **50**, C12 (1976); R. Eby and C. Schuerch, *ibid.*, **100**, C41 (1982); A. Lipták, *Tetrahedron Lett.*, **1976**, 3551.

2) G. Zemplén, Z. Csüros, and S. Angyal, *Chem. Ber.*, **70**, 1848 (1937).

3) S. Koto, Y. Takebe, and S. Zen, *Bull. Chem. Soc. Jpn.*, **45**, 291 (1972).

4) N. Morishima, S. Koto, M. Oshima, A. Sugimoto, and S. Zen, *Bull. Chem. Soc. Jpn.*, **56**, 2849 (1983).

5) N. Morishima, S. Koto, C. Kusuhara, and S. Zen, *Bull. Chem. Soc. Jpn.*, **55**, 631 (1982).

6) a) V. K. Handa, J. J. Barlow, and K. L. Matta, *Carbohydr. Res.*, **76**, Cl (1979); b) A. J. Verma and C. Schuerch, *J. Org. Chem.*, **46**, 799 (1981); c) F. Kong and C. Schuerch, *Carbohydr. Res.*, **112**, 141 (1983).

7) a) N. E. Franks and R. Montgomery, *Carbohydr. Res.*, **6**, 286 (1968); b) T. Ogawa, K. Katano, K. Sasajima, and M. Matsui, *Tetrahedron*, **37**, 2779 (1981).

8) H. B. Borén, K. Eklind, P. J. Garegg, B. Lindberg, Å. Pilotti, *Acta Chem. Scand.*, **26**, 4143 (1972).

9) S. Koto, N. Morishima, T. Yoshida, M. Uchino, and S. Zen, *Bull. Chem. Soc. Jpn.*, **56**, 1171 (1983).

10) P. A. J. Gorin and A. S. Perlin, *Can. J. Chem.*, **39**, 2476 (1961).

11) F. M. Winnik, J. P. Carver, and J. J. Krepinsky, *J. Org. Chem.*, **47**, 2701 (1982).

12) B. Helferich and S. Winkler, *Chem. Ber.*, **66**, 1556 (1933).

13) S. Koto, N. Morishima, Y. Miyata, and S. Zen, *Bull. Chem. Soc. Jpn.*, **49**, 2639 (1976).

14) S. Koto, N. Morishima, T. Irisawa, Y. Hashimoto, M. Yamazaki, and S. Zen, *Nippon Kagaku Kaishi*, **1982**, 1651.

Studies of Unusual Amino Acids and Their Peptides. XV. The Chemistry of *N*-Carboxymethyl Amino Acids. III. The Synthesis of *N*-Tosyl-*N*-carboxymethyl Amino Acid Derivatives by *N*-Alkoxycarbonylmethylation

Toshifumi MIYAZAWA,* Takashi YAMADA, and Shigeru KUWATA
Department of Chemistry, Faculty of Science, Konan University, Okamoto, Higashinada-ku, Kobe 658
(Received June 22, 1984)

Synopsis. The alkoxycarbonylmethylation of the amide nitrogen of *N*-tosyl amino acid esters with iodoacetic acid esters in the presence of silver(I) oxide in *N*,*N*-dimethylformamide afforded the corresponding *N*-tosyl-*N*-carboxymethyl amino acid esters in good yields without racemization of the amino acids.

Previous publications[1,2] from this laboratory have dealt with the first systematic investigation regarding the preparation and properties of *N*-carboxymethyl (Cm-) amino acids and their derivatives, especially their peptides. On the synthetic routes adopted, a Cm-amino acid[3] (or its ester) was at first prepared from the corresponding parent amino acid, and then converted to an appropriate *N*-protected intermediate for further derivation. As a possible alternative, we examined the carboxymethylation of the amide nitrogen of *N*-protected amino acid derivatives for preparing Cm-amino acid derivatives.

The *N*-alkylation of tosylamides, which has often been used as a preparative reaction, may also be applicable to *N*-alkoxycarbonylmethylation. Attempts to react *N*-tosyl amino acids with methyl iodoacetate in aqueous alkaline solutions,[4] however, were unsuccessful. On the other hand, the *N*-alkoxycarbonylmethylation of an *N*-tosyl amino acid ester (**1**) with an iodoacetic acid ester (**2**) in the presence of silver(I) oxide[5] yielded an *N*-tosyl Cm-amino acid derivative (**3**).

$$\underset{\mathbf{1}}{\text{Tos-AA-OR}^1} + \underset{\mathbf{2}}{\text{ICH}_2\text{CO}_2\text{R}^2} \xrightarrow{\text{Ag}_2\text{O}} \underset{\mathbf{3}}{\text{Tos-}\overset{\text{OR}^2}{\overset{|}{\text{C}}}\text{mAA-OR}^1}$$

TABLE 1. *N*-ALKOXYCARBONYLMETHYLATION OF *N*-TOSYL AMINO ACID ESTERS

Product **3**				Yield[a]	$[\alpha]_D^{25}$ (MeOH)	TLC,
	AA	R^1	R^2	%		R_f[b]
3a	Ala	Me	Me	76	−54.7° (*c* 0.79)	0.44
3b	Asp(OMe)	Me	Me	71	−24.7° (*c* 1.0)	0.37
3c	Glu(OMe)	Me	Me	65	−55.7° (*c* 0.90)	0.35
3d[c]	Gly	Me	Me	73	—	0.36
3e[c]	Ile	Me	Me	83	−60.7° (*c* 1.0)	0.54
3f[c]	Leu	Me	Me	76	−46.0° (*c* 1.0)	0.53
3g	Phe	Me	Me	74	−13.7° (*c* 0.65)	0.52
3h	Val	Me	Me	82	−70.5° (*c* 1.0)	0.52
3i	Ala	Bzl	Bzl	72	−34.3° (*c* 0.92)	0.62
3j	Phe	Bzl	Bzl	63	−9.1° (*c* 1.0)	0.67
3k	Val	Bzl	Bzl	67	−38.3° (*c* 0.65)	0.68
3l	Ala	Bzl	Me	63	−34.5° (*c* 1.0)	0.51
3m	Phe	Bzl	Me	65	−5.3° (*c* 0.90)	0.56
3n	Val	Bzl	Me	73	−39.9° (*c* 1.2)	0.56

a) Isolated yield. b) Benzene–EtOAc (3:1). c) Obtained as crystals: **3d**, mp 100—101 °C ($CHCl_3$–hexane); **3e**, mp 47—49 °C (cyclohexane); **3f**, mp 60—61 °C (cyclohexane).

An investigation of the conditions for this reaction employing methyl *N*-tosylalaninate and methyl iodoacetate revealed that the best yield was obtained using the reactants in an 8:2:1 molar ratio (ICH_2CO_2-Me/Ag_2O/Tos-Ala-OMe) in *N*,*N*-dimethylformamide (DMF) after 24 h at room temperature. As can be seen from Table 1, several *N*-tosyl Cm-amino acid methyl esters (**3a—h**) were thus prepared from the methyl esters of *N*-tosyl monoamino mono- and dicarboxylic acids as substrates in a 70—80% isolated yield under the above reaction conditions. All the compounds, except **3d**, **3e**, and **3f**, were obtained as oils. Their homogeneity was demonstrated by elemental analyses, TLC on silica gel, and ^1H NMR spectral data. In the NMR spectra the absorption attributable to the methylene protons in the *N*-alkoxycarbonylmethyl group appeared at δ=3.8—4.4, in many cases as an AB quartet with J=18—19 Hz.

The above reaction conditions were also applicable to cases where R^1 on **1** and/or R^2 on **2** were groups other than the methyl group (**3i—n**). The Cm-amino acid derivatives carrying two different ester groups, such as **3l—n**, are practically useful intermediates for further derivation. When an *N*-tosyl amino acid itself was used as a substrate instead of its ester, *O*-alkoxycarbonylmethylation occurred simultaneously with the *N*-alkoxycarbonylmethylation. The analytical and spectral data were compatible with the assigned structures (**4**) of the products (Table 2, **4a—c**).

$$\text{Tos-}\overset{\text{OMe}}{\overset{|}{\text{C}}}\text{mAA-OCH}_2\text{CO}_2\text{Me}$$
4

The specific rotation of the *N*-tosyl Cm-amino acid dimethyl ester (**3a**, **3g**, or **3h**) prepared by the present method was in good accordance with that of a sample prepared by esterification with diazomethane of the corresponding *N*-tosyl Cm-amino acid synthesized previously.[2] Furthermore, the *N*-tosyl Cm-amino acid prepared by the catalytic hydrogenation of its dibenzyl ester (**3i** or **3k**) was identical in its specific rotation

TABLE 2. METHOXYCARBONYLMETHYLATION OF *N*-TOSYL AMINO ACIDS

Product **4**		Yield[a]	$[\alpha]_D^{25}$	TLC,
	AA	%	(MeOH)	R_f[b]
4a	Ala	66	−37.3° (*c* 0.67)	0.38
4b	Phe	73	−9.0° (*c* 1.6)	0.48
4c	Val	72	−68.4° (*c* 1.4)	0.49

a) Isolated yield. b) Benzene–EtOAc (3:1).

with an authentic sample.[2] These results indicate that no appreciable racemization occurred during *N*-alkoxycarbonylmethylation. In addition, since the yields for *N*-tosylation of free Cm-amino acids were rather low,[2] the present route to *N*-tosyl Cm-amino acid derivatives is a convenient alternative for preparing compounds containing Cm-amino acids.

The *N*-alkoxycarbonylmethylation of *N*-benzyloxycarbonyl amino acid esters would not proceed smoothly under the above conditions, nor even at an elevated temperature, in contrast to the corresponding *N*-methylation.[5]

Experimental

Optical rotations were measured with a JASCO DIP-4 polarimeter. Melting points are uncorrected. ^{1}H NMR spectra were recorded on a Hitachi R-24B spectrometer. TLC and preparative TLC were performed on Merck Kieselgel 60 F_{254} and Kieselgel GF_{254} (Type 60), respectively. All new compounds (**3a—n** and **4a—c**) gave satisfactory microanalysis (C, H, N ±0.3%).

General Procedure for the N-*Alkoxycarbonylmethylation of* N-*Tosyl Amino Acids and Their Esters.* *Methyl* N-*Tosyl*-N-*(methoxycarbonylmethyl)alaninate (**3a**)*: A solution of Tos-Ala-OMe (130 mg, 0.5 mmol) and ICH_2CO_2Me (800 mg, 4 mmol) in DMF (4 ml) was stirred at room temperature with Ag_2O (232 mg, 1 mmol) in the dark for 24 h. The reaction mixture was filtered, and the filtrate was mixed with $CHCl_3$, washed with 5% $Na_2S_2O_3$ and water, and dried over Na_2SO_4. Evaporation of the solvent *in vacuo* afforded a syrup, which was chromatographed on preparative layers of silica gel with benzene–EtOAc (49:1); yield, 125 mg (76%); syrup, $[\alpha]_D^{25}$ −54.7° (*c* 0.79, MeOH).

Methoxycarbonylmethyl N-*Tosyl*-N-*(methoxycarbonylmethyl)alaninate (**4a**)*: Tos-Ala (130 mg, 0.5 mmol) was reacted with ICH_2CO_2Me (800 mg, 4 mmol) in the presence of Ag_2O (464 mg, 2 mmol) in DMF (4 ml) for 36 h. After a work-up similar to the above, the final purification was performed by preparative TLC with benzene–EtOAc (9:1); yield, 130 mg (66%); syrup, $[\alpha]_D^{25}$ −37.3° (*c* 0.67, MeOH).

Preparation of the Dimethyl Esters from N-*Tosyl Cm-amino Acids by Treatment with Diazomethane.* *Tos-CmAla-OMe*: Tos-CmAla[2] (215 mg) was dissolved in EtOAc and treated with an ethereal solution of CH_2N_2 as usual. Purification by preparative TLC with benzene–EtOAc (49:1) afforded a syrup; yield, 219 mg (93%); $[\alpha]_D^{25}$ −55.2° (*c* 1.0, MeOH).

Tos-CmPhe-OMe ($[\alpha]_D^{25}$ −13.2° (*c* 0.66, MeOH)) and Tos-CmVal-OMe ($[\alpha]_D^{25}$ −70.8° (*c* 0.96, MeOH)) were prepared from Tos-CmPhe[2] and Tos-CmVal,[2] respectively, in the same manner as above.

N-*Tosyl Cm-amino Acids Prepared by Catalytic Hydrogenation of Their Dibenzyl Esters.* *Tos-CmVal*: **3k** (285 mg) was hydrogenated in dioxane (15 ml) in the presence of 5% Pd-C (140 mg). After the absorption of hydrogen had ceased, the catalyst was filtered off and the filtrate evaporated *in vacuo*. The residue was dissolved in ether and extracted with 5% $NaHCO_3$. The extracts were combined, washed with ether, and acidified with 4 M HCl (1 M=1 mol dm^{-3}) to pH 2. The turbid mixture was extracted with EtOAc. The extracts were combined, washed with water, and dried over Na_2SO_4. Evaporation of the solvent afforded crystals; yield, 140 mg (76%); mp 179.5—181 °C (EtOAc–hexane), $[\alpha]_D^{25}$ −55.4° (*c* 0.70, MeOH). Lit,[2] mp 179.5—181 °C, $[\alpha]_D^{25}$ −55.6° (*c* 1.0, MeOH).

Tos-CmAla was prepared from **3i** in the same manner as above; $[\alpha]_D^{25}$ −33.2° (*c* 0.62, MeOH). Lit,[2] $[\alpha]_D^{25}$ −33.7° (*c* 0.82, MeOH).

^{1}H NMR Spectra (CDCl$_3$) of Products, 3 and 4. **3a**: δ=1.31 (3H, d), 2.39 (3H, s), 3.47 (3H, s), 3.62 (3H, s), 3.95 and 4.12 (2H, ABq), 4.36 (1H, q), 7.19 and 7.65 (4H, ABq).

3b: δ=2.40 (3H, s), 2.7—3.0 (2H, 4 peaks), 3.50 (3H, s), 3.55 (3H, s), 3.59 (3H, s), 4.02 (2H, s), 4.68 (1H, *t*-like), 7.21 and 7.65 (4H, ABq).

3c: δ=1.6—2.8 (4H, m), 2.40 (3H, s), 3.47 (3H, s), 3.61 (3H, s), 3.69 (3H, s), 3.92 and 4.19 (2H, ABq), 4.46 (1H, q), 7.25 and 7.69 (4H, ABq).

3d: δ=2.40 (3H, s), 3.61 (6H, s), 4.16 (4H, s), 7.25 and 7.65 (4H, ABq).

3e: δ=0.7—1.0 (6H, m), 1.1—2.0 (3H, m), 2.39 (3H, s), 3.41 (3H, s), 3.64 (3H, s), 3.86 (1H, d), 4.00 and 4.30 (2H, ABq), 7.22 and 7.70 (4H, ABq).

3f: δ=0.83 and 0.86 (6H, 2× d), 1.1—2.0 (3H, m), 2.40 (3H, s), 3.47 (3H, s), 3.69 (3H, s), 4.11 (2H, s), 4.38 (1H, *t*-like), 7.26 and 7.72 (4H, ABq).

3g: δ=2.36 (3H, s), 2.86 and 2.99 (2H, *d*-like), 3.30 (3H, s), 3.59 (3H, s), 4.11 and 4.13 (2H, 2× *s*-like), 4.42 (1H, *t*-like), 7.04 (5H, s), 7.12 and 7.61 (4H, ABq).

3h: δ=0.85 and 0.96 (6H, 2× d), 1.5—2.2 (1H, m), 2.39 (3H, s), 3.37 (3H, s), 3.57 (3H, s), 3.83 (1H, d), 3.84 and 4.20 (2H, ABq), 7.17 and 7.63 (4H, ABq).

3i: δ=1.35 (3H, d), 2.32 (3H, s), 4.04 and 4.27 (2H, ABq), 4.60 (1H, q), 4.89 (2H, s), 5.10 (2H, s), 7.1—7.35 (10H, m), 7.10 and 7.67 (4H, ABq).

3j: δ=2.34 (3H, s), 2.95 and 3.07 (2H, *d*-like), 4.30 (2H, s), 4.62 (1H, *t*-like), 4.73 (2H, s), 5.11 (2H, s), 6.9—7.35 (17H, m), ~7.65 (2H, half of ABq).

3k: δ=0.83 and 0.94 (6H, 2× d), 1.6—2.3 (1H, m), 2.33 (3H, s), 4.01 (2H, d), 4.08 and 4.39 (2H, ABq), 4.74 and 4.88 (2H, ABq), 5.08 (2H, s), 7.1—7.35 (10H, m), 7.09 and 7.70 (4H, ABq).

3l: δ=1.39 (3H, d), 2.35 (3H, s), 3.66 (3H, s), 4.01 and 4.23 (2H, ABq), 4.54 (1H, q), 4.91 (2H, s), 7.23 (5H, s), 7.16 and 7.68 (4H, ABq).

3m: δ=2.33 (3H, s), 2.96 and 3.08 (2H, *d*-like), 3.62 (3H, s), 4.23 (2H, s), 4.63 (1H, *t*-like), 4.77 (2H, s), 6.85—7.3 (10H, m), 7.16 and 7.65 (4H, ABq).

3n: δ=0.86 and 0.97 (6H, 2× d), 1.6—2.3 (1H, m), 2.35 (3H, s), 3.60 (3H, s), 4.01 (1H, d), 4.02 and 4.32 (2H, ABq), 4.78 and 4.92 (2H, ABq), 7.13 and 7.69 (4H, ABq), 7.24 (5H, s).

4a: δ=1.39 (3H, d), 2.38 (3H, s), 3.64 (6H, s), 3.99 and 4.08 (2H, 2× *s*-like), 4.36 (2H, s), 4.48 (1H, q), 7.18 and 7.65 (4H, ABq).

4b: δ=2.38 (3H, s), 3.0—3.2 (2H, 4 peaks), 3.64 (6H, s), 4.21 (2H, s), 4.37 (2H, s), 4.71 (1H, *t*-like), 7.12 (5H, s), 7.17 and 7.68 (4H, ABq).

4c: δ=0.93 and 1.04 (6H, 2× s), 1.7—2.3 (1H, m), 2.40 (3H, s), 3.63 (3H, s), 3.68 (3H, s), 4.06 (1H, d), 4.02 and 4.26 (2H, ABq), 4.26 and 4.43 (2H, ABq), 7.22 and 7.74 (4H, ABq).

References

1) T. Miyazawa, *Bull. Chem. Soc. Jpn.*, **53**, 2555 (1980).
2) T. Miyazawa, *Bull. Chem. Soc. Jpn.*, **53**, 3661 (1980).
3) The amino acid derivatives used here are all of the L-configuration. The following abbreviations are used for Cm-amino acids and their derivatives: CmAA for a Cm-amino acid derived from an amino acid (AA), and X^1-CmAA-X^3 for its derivative (X^1-NCHCO-X^3). Abbreviations given by the IUPAC-IUB Commission (*J. Biol. Chem.*, **247**, 977 (1972)) are used throughout.
4) *Cf.* E. Fischer and W. Lipschitz, *Ber.*, **48**, 360 (1915).
5) *Cf.* R. K. Olsen, *J. Org. Chem.*, **35**, 1912 (1970).

The Synthesis of Racemic Dihydroageratone. Efficient Demethylation by Magnesium Iodide Etherate

Seiji YAMAGUCHI, Kyoichi SUGIURA, Reiko FUKUOKA, Kazumi OKAZAKI, Mie TAKEUCHI, and Yoshiyuki KAWASE*

Department of Chemistry, Faculty of Science, Toyama University, Gofuku 3,190, Toyama 930

(Received June 23, 1984)

Synopsis. 2-Isopropenyl-6-methoxy-2,3-dihydrobenzofuran, prepared from *m*-methoxyphenol and 1,4-dibromo-2-methyl-2-butene, was converted to racemic dihydroageratone *via* oxidation with selenium dioxide, the acetylation with acetic acid–trifluoroacetic anhydride, and the demethylation with magnesium iodide etherate.

Some syntheses of 2-isopropenyl-2,3-dihydrobenzofuran derivatives were reported. They mainly consisted of two methods; one was the dehydration of 2-(1-hydroxy-1-methylethyl)-2,3-dihydrobenzofurans and the other was our one-step cyclization of the phenols and 1,4-dibromo-2-methyl-2-butene.[1] We have already reported the synthesis of 5-acetyl-2-[1-(hydroxymethyl)-vinyl]-2,3-dihydrobenzofuran (**1**) having an oxidized isopropenyl group.[2] Dihydroageratone (**2**), isolated from *Ageratum houstnianum* by Anthonsen and Chanthrasakul, also exhibited an oxidized side chain.[3] Here, we describe the synthesis of the dihydroageratone (**2**) having an oxidized isopropenyl and a phenolic hydroxyl group.

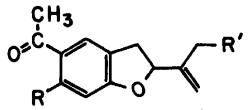

1 R=H, R′=OAc
2 R=OH, R′=OAc
3 R=OH, R′=H

Chart 1.

For the synthesis of **2**, a key step was to remove the protection of the phenolic hydroxyl group. In the syntheses of hydroxytremetone (**3**), Oda *et al.* used alkaline hydrolysis for the removal of the acetyl group[4] and Harada *et al.* used hydrogenolysis for the removal of the benzyl group.[5] However, in our one-step cyclization using sodium metal, the protection by *O*-acetylation was unsuitable, and the deprotection of a benzyl group by hydrogenolysis or acidic cleavage might have caused a hydrogenation or an isomerization on the isopropenyl side chain. However, we were able to remove the protection by demethylation with magnesium iodide etherate without affecting the isopropenyl group.

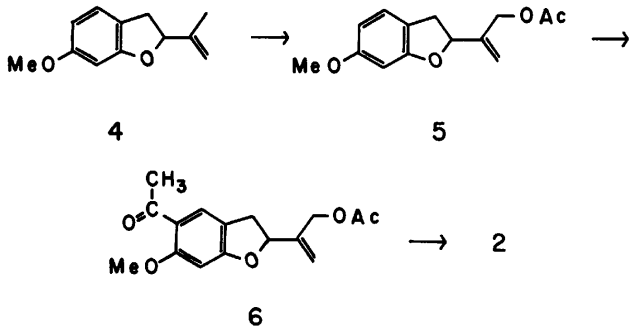

Chart 2.

We have already described the preparation of 2-isopropenyl-6-methoxy-2,3-dihydrobenzofuran (**4**) from *m*-methoxyphenol and 1,4-dibromo-2-methyl-2-butene.[1] When the dihydrobenzofuran **4** was heated with selenium dioxide in refluxing acetic anhydride for 7 h, 2-[1-(acetoxymethyl)vinyl]-6-methoxy-2,3-dihydrobenzofuran (**5**) was obtained in 7.1% yield. A carbonyl absorption at 1740 cm^{-1} in the IR spectrum and a methyl signal at δ 1.9 in the ^1H NMR spectrum showed the exsistence of an acetoxyl group. Further, a methylene signal at δ 4.6 showed that the acetoxyl group was on the methyl carbon in the isopropenyl group. Acylation of the acetate **5** with acetic acid–trifluoroacetic anhydride at room temperature for 3 h gave 2-[1-(acetoxymethyl)vinyl]-5-acetyl-6-methoxy-2,3-dihydrobenzofuran (**6**) in 48.3% yield. A new carbonyl absorption in the IR spectrum and two singlets at δ 6.5 and 7.7 in the ^1H NMR specturm indicated that the acetylation was at position 5. Refluxing the keto-acetate **6** with magnesium iodide etherate in dry benzene for 3 h gave the corresponding demethylated product **3** in 20.5% yield without any isomerization. Carbonyl absorption at 1635 cm^{-1} in the IR specturum and a signal at δ 13.0 in the ^1H NMR indicated the formation of intramolecular hydrogen bonding. This reagent was very useful for the demethylation of a methoxyl group in the ortho position of an acyl group in mild conditions. The spectral data of this demethylated product **3** were identical with reported data of natural dihydroageratone.[3]

Two methoxy ketones, 5-acetyl-2-isopropenyl-4-methoxy- and -6-methoxy-2,3-dihydrobenzofuran (**7** and **8**) have already been reported.[1] They were similarly demethylated with magnesium iodide etherate to give corresponding hydroxy ketones, **9** and **3**. The spectral data of the hydroxyketone **3** were identical with those of natural hydroxytremetone.[6] However, the other hydroxy ketone, 5-acetyl-6-hydroxy-2-isopropenyl-2,3-dihydrobenzofuran (**9**), did not agree with the natural compound[7] in the spectral data. Both samples showed intramolecular hydrogen bonding in their IR and ^1H NMR spectra. However, in the ^1H NMR spectra, our synthetic sample showed aromatic signals at δ 6.3 and 7.5, while the natural sample showed them at δ 6.81 and 6.99. This indicated that the natural compound had another structure, 4-acetyl-5-hydroxy-2-isopropenyl-2,3-dihydrobenzofuran or 7-acetyl-6-hydroxy-2-isopropenyl-2,3-dihydrobenzofuran, having a hydrogen-bonding between a phenolic hydroxyl group and an acetyl group and no aromatic proton in ortho position of an acetyl group.[8]

Experimental

The boiling points were uncorrected (in boiling points:

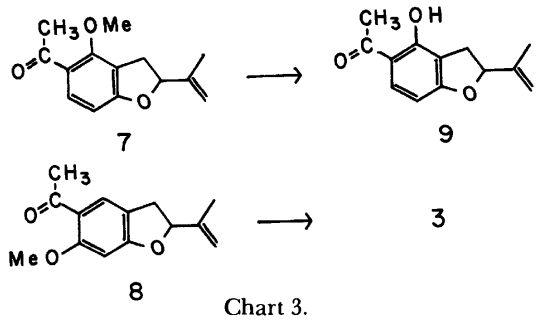

Chart 3.

1 mmHg=133.322 Pa). The IR spectra were measured on a Hitachi EPI-S2 spectrophotometer in a liquid film and the UV spectra were taken on a Hitachi 220 A spectrophotometer in an ethanolic solution. The ^{1}H NMR spectra were recorded on a JEOL JNM-MH-60 NMR spectrometer and the mass spectra were recorded on a JEOL JMS-OISG-2 mass spectrometer.

2-[1-(Acetoxymethyl)vinyl]-6-methoxy-2,3-dihydrobenzofuran (5). To a solution of 2-isopropenyl-6-methoxy-2,3-dihydrobenzofuran (**4**)[1] (1.08 g, 5.68 mmol) in acetic anhydride (15 ml), powdered selenium dioxide (578 mg, 5.21 mmol) was added, and the mixture was refluxed for 7 h. After cooling, the mixture was diluted with ether and filtered. The ether and the excess acetic anhydride was removed from the filtrate under reduced pressure. The residue was dissolved in ether and the ethereal solution was washed with saturated sodium hydrogencarbonate solution and then with saturated sodium chloride solution, and dried over anhydrous sodium sulfate. After the removal of the ether, the residual oil was purified on a silica-gel column. Fractions eluted with benzene gave pure 2-[1-(acetoxymethyl)vinyl]-6-methoxy-2,3-dihydrobenzofuran (**5**) (100 mg, 7.1%) as an oil; IR (neat) 1740 cm^{-1}. ^{1}H NMR (CCl_4) δ=2.0 (3H s), 3.0 (1H, dd, J=16 and 9 Hz), 3.3 (1H, dd, J=16 and 9 Hz), 3.7 (3H, s), 4.6 (2H, broad s), 5.1 (1H, broad s), 5.2 (1H, t, J=9 Hz), 5.3 (1H, broad s), 6.3 (2H, m), and 6.9 (1H, d, J=9 Hz).

Found: C, 67.57; H, 6.73%; M$^+$ 248. Calcd for $C_{14}H_{16}O_4$: C, 67.73; H, 6.50%; M$^+$ 248.

2-[1-(Acetoxymethyl)vinyl]-5-acetyl-6-methoxy-2,3-dihydrobenzofuran (6). By a method similar to one described in our previous parer,[1] 2-[1-(acetoxymethyl)vinyl]-6-methoxy-2,3-dihydrobenzofuran (**5**)(200 mg, 0.806 mmol) was acetylated with acetic acid (97 mg, 1.6 mmol) and trifluoroacetic anhydride (500 mg, 2.38 mmol) at room temperature for 3 h, and gave a crude oil (229 mg). The crude oil was purified on a silica-gel column. Fractions eluted with chloroform gave pure 2-[1-(acetoxymethyl)vinyl]-5-acetyl-6-methoxy-2,3-dihydrobenzofuran (**6**) (113 mg, 48.3%) as an oil; bp 230—250 °C/15 mmHg (bath temp). IR (neat) 1740 and 1660 cm^{-1}. ^{1}H NMR ($CDCl_3$) δ=2.1 (3H, s), 2.6 (3H, s), 3.2 (1H, dd, J=16 and 9 Hz), 3.4 (1H, dd, J=16 and 9 Hz), 3.9 (3H, s), 4.7 (2H, s), 5.3 (1H, broad s), 5.4 (1H, broad s), 5.4 (1H, t, J=9 Hz), 6.5 (1H, s), and 7.7 (1H, s).

Found: C, 66.42; H, 6.31%; M$^+$ 290. Calcd for $C_{16}H_{18}O_5$: C, 66.19; H, 6.25%; M$^+$ 290.

2-[1-(Acetoxymethyl)vinyl]-5-acetyl-6-hydroxy-2,3-dihydrobenzofuran (Racemic Dihydroageratone) (2). To magnesium metal (21 mg, 0.80 mmol) in dry ether (0.24 ml) and dry benzene (0.5 ml), iodine crystals (108 mg, 0.850 mmol) were added in small portions. The mixture was stirred until the iodine color disappeared (*ca.* 3 h). A solution of 2-[1-(acetoxymethyl)-vinyl]-5-acetyl-6-methoxy-2,3-dihydrobenzofuran (**6**) (165 mg, 0.638 mmol) in dry benzene was added to the benzene solution of magnesium iodide etherate prepared previously. The mixture was then refluxed for 3 h. After cooling, the mixture was poured onto 10% hydrochloric acid and extracted with ether. The ethereal solution was washed with a saturated sodium hydrogencarbonate solution and dried over anhydrous sodium sulfate. After the removal of the ether and benzene, the residual oil was purified on a silica-gel column. Fractions eluted with chloroform gave pure 2-[1-(acetoxymethyl)vinyl]-5-acetyl-6-hydroxy-2,3-dihydrobenzofuran (**2**) as an oil; bp 247—255 °C/15 mmHg. IR (neat) 1740 and 1635 cm^{-1}. UV (EtOH) 238 (log ε 4.47), 277 (4.29), and 325 nm 4.11). ^{1}H NMR (CCl_4) δ=2.0 (3H, s), 2.5 (3H, s), 3.1 (1H, dd, J=16 and 9 Hz), 3.4 (1H, dd, J=16 and 9 Hz), 4.5 (2H, s), 5.4 (2H, broad s), 5.4 (1H, t, J=9 Hz), 6.5 (1H, s), 7.5 (1H, s), and 13.0 (1H, s). Mass m/z 276 (M$^+$), 216 (M$^+$—$C_2H_4O_2$), and 176 (M$^+$—$C_5H_8O_2$).

Found: C, 65.29; H, 6.06%; M$^+$ 276. Calcd for $C_{15}H_{16}O_5$: C, 65.21; H, 5.84%; M$^+$ 276.

Those spectral data agreed with the reported data of natural dihydroageratone.[3]

Demethylation of 5-Acetyl-2-isopropenyl-4-methoxy- and -6-methoxy-2,3-dihydrobenzofuran (7 and 8). By a method similar to that described for the preparation of **2**, 5-acetyl-2-isopropenyl-4-methoxy- or -6-methoxy-2,3-dihydrobenzofuran (**7** or **8**) was demethylated with magnesium iodide etherate to give 5-acetyl-4-hydroxy-2-isopropenyl-2,3-dihydrobenzofuran (**9**); yield 42.1%; bp 190—215 °C/15 mmHg (bath temp); IR (neat) 1645 cm^{-1}; UV (EtOH) 234 (logε 3.94), 241 (3.94), and 288 nm (4.19); ^{1}H NMR (CCl_4) δ=1.8 (3H, broad s), 2.5 (3H, s), 3.0 (1H, dd, J=16 and 10 Hz), 3.3 (1H, dd, J=16 and 10 Hz), 4.9 (1H, broad s), 5.1 (1H, broad s), 5.3 (1H, t, J=10 Hz), 6.3 (1H, d, J=10 Hz), 7.5 (1H, d, J=10 Hz), and 12.7 (1H, s); Mass m/z 218 (M$^+$) and 203 (M$^+$ —CH_3). Found: C, 71.35; H, 6.38%; M$^+$ 218. Calcd for $C_{13}H_{14}O_3$: C, 71.54; H, 6.47%; M$^+$ 218; and 5-acetyl-6-hydroxy-2-isopropenyl-2,3-dihydrobenzofuran (**3**); yield 44.7%; IR (neat) 1640 cm^{-1}; ^{1}H NMR (CCl_4) δ=1.7 (3H, broad s), 2.4 (3H, s), 2.9 (1H, dd, J=16 and 9 Hz), 3.2 (1H, dd, J=16 and 9 Hz), 4.9 (1H, broad s), 5.0 (1H, broad s), 5.2 (1H, t, J=9 Hz), 6.2 (1H, s), 7.4 (1H, s), and 12.7 (1H, s).

The hydroxy ketone **3** was identical to natural hydroxytremetone[6] in their IR and ^{1}H NMR spectra, but the other hydroxy ketone **9** did not agreed with that of the natural compound (reported by Bohlmann *et al.*).[7,8]

We wish to thank Professer Dr. Ferdinand Bohlmann for providing copies of the IR and ^{1}H NMR spectra of natural compound.

References

1) S. Yamaguchi, A. Miyata, M. Ueno, T. Hase, K. Yamamoto, and Y. kawase, *Bull. Chem. Soc. Jpn.*, **57**, 617 (1984).

2) Y. Kawase, S. Yamaguchi, S. Kondo, and K. Shimokawa, *Chem. Lett.*, **1978**, 253; Y. Kawase, S. Yamaguchi, S. Kondo, O. Inoue, and M. Sannomiya, *Bull. Chem. Soc. Jpn.*, **55**, 2500 (1982).

3) T. Anthonsen and S. Chantharasakul, *Acta Chem. Scand.*, **24**, 721 (1970). The optical activity of natural dihydroageratone was not reported, but it must be an active form (probably —).

4) J. Oda, H. Fukami, and M. Nakajima, *Agric. Biol. Chem.*, **30**, 59 (1966).

5) I. Harada, Y. Hirose, and M. Nakazaki, *Tetrahedron Lett.*, **1968**, 5463.

6) J. I. DeGraw, Jr., and M. A. Bonner, *J. Org. Chem.*, **27**, 3917 (1962).

7) F. Bohlmann, J. Jakupovic, A. Schuster, R. M. King, and H. Robinson, *Phytochemistry*, **21**, 161 (1982).

8) Recentry, we found, this natural compound had 4-acetyl-5-hydroxy-2-isopropenyl-2,3-dihydrobenzofuran, by another preparation. It will be reported soon.

^{1}H-NMR Study of the Aromatic-ring Motion in 3,12-Dithia-[4.4]metaparacyclophanes

Kazuhiko TSUCHIYA, Tetsuo TAKEMURA, and Nobuo MORI*
Department of Chemistry, Science University of Tokyo, Kagurazaka, Shinjuku-ku, Tokyo 162
(Received June 27, 1984)

Synopsis. In 10-substituted 3,12-dithia[4.4]metaparacyclophanes, the free energy barrier to the rotation of the para-bridged ring increases with the substituent in the order: H<F<CH_3O<Cl, whereas for the flipping of the meta-bridged ring, the order of CH_3O and Cl is reversed. This is discussed in terms of the steric-size anisotropy of the CH_3O group.

There have been several ^{1}H-NMR and stereochemical studies of the aromatic-ring motion in [2.2]- and 2,11-dithia[3.3]metaparacyclophanes. In [2.2]metaparacyclophane itself, the meta-ring can flip[1] even with a sizable energy barrier to flipping,[1-4] but the para-ring can not rotate because of the severe nonbonded interaction between the para-ring and the 8-hydrogen atom.[1,3,4] In the dithia[3.3]phanes,[4,5] where there is a much weaker interaction between the para-ring and a substituent at the 9-position, it becomes easier for both rings to move, the facility being dependent on the steric size of the 9-substituent.[5]

In the present work, we have investigated the relative motility of the two benzene rings in 3,12-dithia-[4.4]- and 4,13-dithia[5.5]metaparacyclophanes, **1—5**, by means of ^{1}H-NMR spectroscopy.

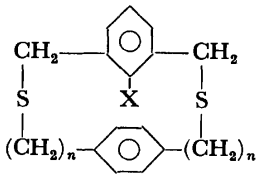

Compound	n	X
1	2	H
2	2	F
3	2	Cl
4	2	CH_3O
5	3	CH_3O

In **1—5**, the rotation of the para-ring and the flipping of the meta-ring were followed separately, as was done in the dithia[3.3]phanes,[5] by variable-temperature measurements of the 100-MHz spectra of the para-ring protons and of the meta-bridged benzylic methylene protons.

In **1**, the para-ring and the 4,11-methylene protons showed sharp, temperature-independent singlets at δ 6.83 and 3.45 respectively down to −51 °C, indicating a rapid rotation of the para-ring and a rapid flipping of the meta-ring in the temperature range examined. The bridging ethylene protons also showed a temperature-independent AA'BB' multiplet down to −51 °C.

In **2**, the para-ring and the methylene protons showed sharp singlets at δ 6.70 and 3.44 respectively at room temperature; each of them became broader as the temperature dropped down to −51 °C. The ethylene protons showed an AA'BB' multiplet at room temperature; this multiplet approached an ABCD system with the drop in the temperature.

In **3**, the para-ring protons showed two narrow AA'XX' multiplets centered at δ 6.44 and 6.87 at room temperature; they coalesced to a broad singlet at 88 °C and became a sharp singlet at 120 °C. On the other hand, at room temperature the 4,11-methylene protons showed an AB quartet (δ 3.35, 3.69; J=15 Hz) which coalesced at 133 °C. The ethylene protons showed a very wide, unsymmetrical, finely split ABCD multiplet at low temperature; this multiplet approached an AA'BB' multiplet with the rise in the temperature.

The low-temperature spectrum of **4** was very similar to that of **3**. The two multiplets due to the para-ring protons (δ 6.48, 6.80) coalesced at 54 °C, whereas the AB quartet due to the two-methylene protons (δ 3.29, 3.64; J=15 Hz) was temperature-independent up to 162 °C. The ethylene protons gave an ABCD multiplet at low temperatures; this multiplet approached an AA'BB' system with the rise in the temperature.

In **5**, the para-ring protons showed a temperature-independent sharp singlet down to −51 °C, whereas the 5,12-methylene protons gave, at −40 °C, an AB quartet (δ 3.38, 3.84; J=15 Hz) which coalesced at 15 °C.

The table gives the free-energy barriers to ring motion (ΔG^*), estimated using the chemical-shift difference at a low temperature ($\Delta\nu$) and the coalescence temperature (T_c).[6] It can be noticed that, in **1—4**, the free-energy barrier to rotation of the para-ring increases with X in the order: H<F<CH_3O<Cl, whereas for the flipping of the meta-ring the order of CH_3O and Cl

TABLE 1. ^{1}H-NMR DATA FOR COMPOUNDS **1—5**

Compound	X	Solvent	Protons concerned	$\Delta\nu$/Hz	T_c/°C	ΔG^*/kcal mol^{-1}[b]
1	H	$CDCl_3$	*p*-ArH	—	$\ll -51$	—[c]
			m-$ArCH_2$	—	$\ll -51$	—[c]
2	F	$CDCl_3$	*p*-ArH	—	< -51	—[c]
			m-$ArCH_2$	—	< -51	—[c]
3	Cl	DMSO-d_6	*p*-ArH	43.0[a]	88	18
			m-$ArCH_2$	33.8[a]	133	21
4	CH_3O	DMSO-d_6	*p*-ArH	32.0	54	16
			m-$ArCH_2$	34.9	$\gg 162$	>22
5	CH_3O	$CDCl_3$	*p*-ArH	—	$\ll -51$	—
			m-$ArCH_2$	46.3	15	14

a) Values in $CDCl_3$. b) 1 cal=4.184 J. c) Since the spectrum of **2** was temperature-dependent but that of **1** was temperature-independent, ΔG^* for **2** can be expected to be larger than that for **1**.

is reversed.[7] This may be explained in terms of the anisotropy of the steric size of the methoxyl group. If the para-ring rotation is influenced dominantly by the nonbonded interaction of X with the para-ring, the free-energy barrier should correlate with the net size of the C-X moiety, which can be approximately estimated as the sum of the bond length of C_{sp^2}–X and the steric size (or the van der Waals radius) of X. This is the case only, however, when X is a single atom: the order of the net size is 2.2 for H<2.7 for F<3.5 Å for Cl. For CH_3O, the net size is estimated to be *ca.* 4.0 Å in the direction along the C–OCH_3 bond axis, but this is too large. Molecular models suggest that, in **4**, the CH_3 moiety of the CH_3O group is not a severe obstacle to the rotating of the para-ring when it is not very much distorted out of the plane of the attached meta-ring. Neglecting the steric size of the CH_3 moiety, the size estimation leads to a net size of *ca.* 2.8 Å (the sum of the bond length of C_{sp^2}–O and the van der Waals radius of O), a value between those for F and Cl. Thus, this or a somewhat larger size seems rather reasonable.

On the other hand, the meta-ring flipping may be influenced not only by the above X···para-ring interaction, but also by the nonbonded interaction of X with the bridging chains. This interaction should be dependent on the van der Waals radius of X, if X is a single atom. Of importance for CH_3O is the net size in the direction along the O–CH_3 bond axis, when the CH_3 moiety is substantially coplanar with the attached meta-ring. The order of the size of X estimated in this way is 1.2 for H<1.35 for F<1.8 for Cl<3.4 Å for CH_3O, in agreement with the order of $\Delta G^{\neq}$.

The lower $\Delta G^{\neq}$ values for **5** give further evidence for the dependence of the ring motions on the length of the bridging chains or on the nonbonded interaction between X and the para-ring.

Experimental

Samples. **1** was prepared by the literature method:[8] Mp 81.0°C. **2**—**5** are unknown and were similarly prepared using the corresponding 2-substituted *m*-xylenes.

2: Mp 113.3—113.8°C; Found: C, 67.78; H, 6.02; S, 19.51%; M^+, 318. Calcd for $C_{18}H_{19}S_2F$: C, 67.89; H, 6.01; S, 20.13%; M^+, 318.

3: Mp 132.1—132.4°C; Found: C, 64.70; H, 5.73; S 19.05%; M^+, 334. Calcd for $C_{18}H_{19}S_2Cl$: C, 64.55; H, 5.72; S, 19.15%; M^+, 334.

4: Mp 93.4—94.2°C; Found: C, 69.00; H, 6.79; S, 19.08%; M^+, 330. Calcd for $C_{19}H_{22}S_2O$: C, 69.05; H, 6.71; S, 19.40%; M^+, 330.

5: Mp 80.2—81.3°C; Found: C, 70.75; H, 7.35; S, 17.90%; M^+, 358. Calcd for $C_{21}H_{26}S_2O$: C, 70.34, H, 7.31; S, 17.89%; M^+, 358.

^{1}H-NMR spectra were recorded on a JEOL JNM-FX 100 spectrometer (100 MHz) for solutions of *ca.* 10 w/v% in dimethyl-d_6 sulfoxide or chloroform-*d*; the measurement temperature was that in the probe. Mass spectra were recorded on a HITACHI M-80 spectrometer.

References

1) D. T. Hefelfinger and D. J. Cram, *J. Amer. Chem. Soc.*, **92**, 1073 (1970); **93**, 4767 (1971).

2) F. Vögtle, *Chem. Ber.*, **102**, 3077 (1969); S. Akabori, S. Hayashi, M. Nawa, and K. Shiomi, *Tetrahedron Lett.*, **1969**, 3727; S. A. Sherrod and V. Boekelheide, *J. Am. Chem. Soc.*, **94**, 5513 (1972).

3) S. A. Sherrod, R. L. da Costa, R. A. Barnes, and V. Boekelheide, *J. Am. Chem. Soc.*, **96**, 1565 (1974).

4) V. Boekelheide, P. H. Anderson, and T. A. Hylton, *J. Am. Chem. Soc.*, **96**, 1558 (1974).

5) F. Vögtle, *Tetrahedron Lett.*, **1969**, 3193.

6) H. S. Gutowsky and C. H. Holm, *J. Chem. Phys.*, **25**, 1228 (1956).

7) In the cyclohexane system, the generally accepted order is Cl<CH_3O, but the reverse is also known. J. A. Hirsh, "Topics in Stereochemistry," ed by N. L. Allinger and E. L. Eliel, Interscience, New York (1967), Vol. 1, p. 199.

8) T. Otsubo, M. Kitasawa, and S. Misumi, *Chem. Lett.*, **1977**, 977.